Biomimetic aromatization of Hantzsch 1,4-dihydropyridines with sodium periodate catalyzed by a new polystyrene-bound manganese porphyrin

Majid Moghadam, Masoud Nasr-Esfahani, Shahram Tangestaninejad, Valiollah Mirkhani, and Mohammad Ali Zolfigol

Abstract: Efficient oxidation of Hantzsch 1,4-dihydropyridines with sodium periodate catalyzed by a polystyrene-bound manganese(III) porphyrin is reported. This catalyst shows high activity in the oxidation of various 1,4-dihydropyridines at room temperature. This heterogeneous catalyst can be reused five times without significant loss of its activity.

Key words: biomimetic oxidation, supported metalloporphyrin, periodate, 1,4-dihydropyridine.

Résumé : On a effectué l'oxydation efficace des 1,4-dihydropyridines de Hantzsch par le biais d'une réaction avec du periodate de potassium catalysée par une porphyrine de manganèse(III) liée à du polystyrène. Ce catalyseur présente une grande activité pour l'oxydation, à la température ambiante, de diverses 1,4-dihydropyridines. Ce catalyseur hétérogène peut être réutilisé jusqu'à cinq fois dans perte significative de son activité.

Mots clés : oxydation biomimétique, métalloporphyrine déposée sur un support, periodate, 1,4-dihydropyridine.

[Traduit par la Rédaction]

Introduction

In the last two decades, metalloporphyrins have been successfully used as models for the cytochrome P-450 enzyme with respect to the oxidation of organic compounds such as hydrocarbons (1–3). Development in this area is based on different strategies with the aim of designing selective, stable, and high turnover catalytic systems (4). Several simple oxidants such as iodosylbenzene, hypochlorite, *m*-chloroperbenzoic acid, hydrogen peroxide, and periodates have been extensively studied in oxygenation reactions catalyzed by metal complexes to understand the mechanism of the cytochrome P-450 monooxygenation enzyme (5–10). Great efforts have been made toward the chemical modification of the metalloporphyrin microenvironment in the studies of the cytochrome P-450 model. One method is to immobilize the metalloporphyrins onto solid supports. Such immobilization not only modifies the metalloporphyrin microenvironment, but also increases the catalytic activity of metalloporphyrins, so one can prepare the catalysts, which are easier to handle and easily separate from reaction medium. Among the metalloporphyrin microenvironment models, polystyrene derivatives are often utilized because they can provide a suitable microenvironment for the "accommodation" of the porphyrin catalytic center.

Amlodepine besylate, nifedepine, and related dihydropyridines are Ca^{2+} channel blockers and are rapidly emerging as one of the most important classes of drugs for the treatment of cardiovascular diseases, including hypertension cardiac arrhythmias (11). In the human body, it has been observed that these compounds undergo oxidation to form pyridine derivatives by the action of cytochrome P-450 in the liver. This observation led us to investigate the ability of this biomimetic catalyst to act in the oxidation of 1,4-dihydropyridines. These oxidized compounds are largely devoid of the pharmacological activity of the parent compounds (12, 13).

Recently, we reported on the oxidation of 1,4-dihydropyridines with tetra-*n*-butylammonium periodate catalyzed by homogeneous Mn(TPP)Cl (14). In this paper, we report on the efficient oxidation of 1,4-dihydropyridines with sodium periodate at room temperature catalyzed by a Mn(TPyP) supported on chloromethylated polystyrene (CMP) (Scheme 1).

Results and discussion

The manganese(III) tetrapyridylporphyrin supported on polystyrene (Mn(TPyP)–CMP) is easily prepared from commercially available porphyrin and chloromethylated polystyrene (Fig. 1).

The high catalytic activity of this heterogeneous catalyst in the alkene epoxidation and alkane hydroxylation and oxidation of alcohols (15, 16) prompted us to investigate its ability in the oxidation of 1,4-dihydropyridines with sodium periodate at mild reaction conditions. The oxidation of 1,4-dihydropyridines by Mn(TPyP)–CMP and sodium periodate yielded the corresponding pyridine derivative in CH_3CN–

Received 6 July 2005. Published on the NRC Research Press Web site at http://canjchem.nrc.ca on 3 February 2006.

M. Moghadam[1] and M. Nasr-Esfahani. Department of Chemistry, Yasouj University, Yasouj 75914-353, Iran. **S. Tangestaninejad and V. Mirkhani.** Department of Chemistry, Isfahan University, Isfahan 81746-73441, Iran. **M.A. Zolfigol.** Department of Chemistry, Bu-Ali Sina University, Hamadan 65173, Iran.

[1]Corresponding author (e-mail: moghadamm@mail.yu.ac.ir).

 doi:10.1139/V05-255 © 2006 NRC Canada

Scheme 1.

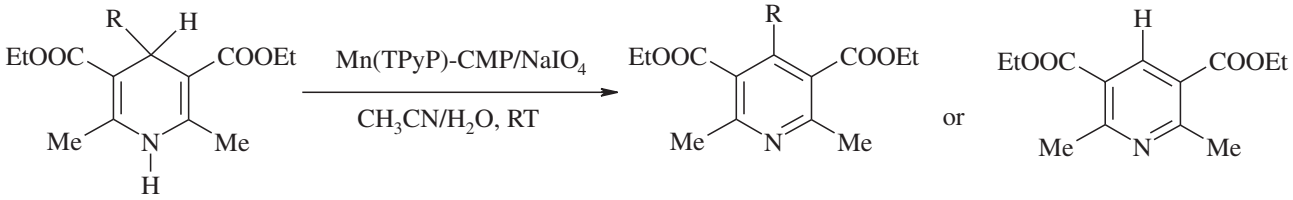
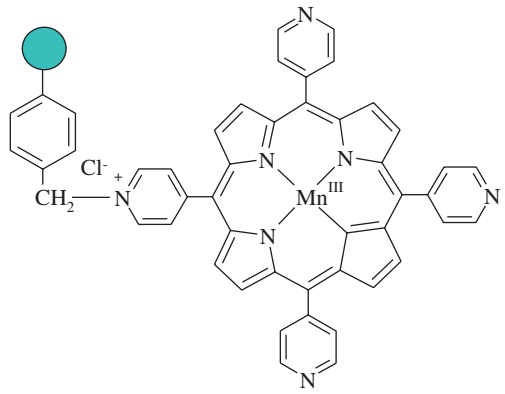


Fig 1. The catalyst used in this study.



H_2O (1:1) as solvent, whereas trace amounts of the product was detected when the identical reaction was carried out in the absence of periodate. The effects of other oxidants were also studied in the oxidation of 4-phenyl derivatives of 1,4-dihydropyridines. The obtained results showed that $NaIO_4$ is more effective than H_2O_2, NaOCl, *t*-BuOOH, and urea-hydrogen peroxide adduct (UHP) (Table 1). To choose the reaction media, different solvents were investigated in the oxidation of 4-phenyl derivatives of 1,4-dihydropyridines. As shown in Table 2, among the studied solvents, the 1:1 mixture of CH_3CN–H_2O was chosen as solvent because a higher amount of pyridine derivative was observed. The blank experiment, in the absence of catalyst, showed that the presence of catalyst is crucial in oxidation reactions. In biomimetic systems using metalloporphyrins as catalyst, addition of an axial base is necessary to obtain high catalytic activity. One observation is that this catalytic system shows higher catalytic activity in the absence of imidazole. When imidazole is added as axial ligand to this catalytic system, the reaction times become longer in the oxidation of 1,4-dihydropyridines. For instance, the oxidation of 4-phenyl and 4-nitrophenyl derivatives was completed in 60 and 90 min, respectively; but addition of imidazole as co-catalyst led to longer reaction times of 90 and 150 min for 4-phenyl and 4-nitrophenyl derivatives, respectively. These observations show that the 1,4-dihydropyridines can play the axial ligand role. The Mn(TPyP)–CMP–$NaIO_4$ catalytic system can be used for oxidizing a wide variety of 1,4-dihydropyridine derivatives to their corresponding pyridine derivatives giving excellent yields at room temperature. All reactions were completed during the appropriate time (until no starting material is detected by TLC) and gave only the corresponding pyridine derivatives. The results are summarized in Table 3. As shown in Table 3, the oxidation of the 4-isopropyl derivative accompanied by expulsion of this substituent gave the dealkylated pyridine derivative (Table 3, entry 12), which was previously reported by Ortiz de Montellano et al. (17) in the oxidation of 1,4-dihydropyrines by cytochrome P-450. This approach shows that this synthetic model behaves in the same way as cytochrome P-450.

Table 1. Effect of various oxidants on the oxidation of 4-phenyl derivatives of 1,4-dihydropyridines.

Oxidant	Solvent	Yield (%)[a]
$NaIO_4$	CH_3CN–H_2O	97
H_2O_2	CH_3CN	40
H_2O_2–urea	CH_3CN	32
NaOCl	CH_3CN	17
t-BuOOH	CH_3CN	10

[a]Isolated yields.

Table 2. Effect of solvent oxidation of 4-phenyl derivatives of 1,4-dihydropyridines.

Solvent	Yield (%)[a] after 60 min
CH_3CN–H_2O	97
CH_3COCH_3–H_2O	75
CH_3OH–H_2O	58
CH_3CH_2OH–H_2O	42
$CHCl_3$–H_2O	15
CH_2Cl_2–H_2O	33
CCl_4–H_2O	8

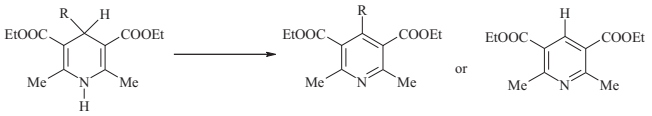
[a]Isolated yields.

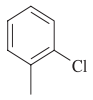
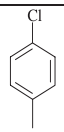
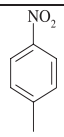
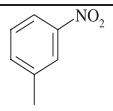
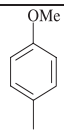
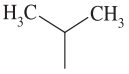
We also studied recycling of the used Mn(TPyP)–CMP in the repeated oxidation reactions. After the first run, the polymer was recovered by filtration followed by washing with water and acetonitrile and then reused. The catalyst was reused five consecutive times without loss of its activity. No manganese was detectable in the filtrates by atomic absorption spectrometry.

From a synthetic point of view, the oxidation of Hantzsch 1,4-dihydropyridines is an old reaction in synthetic organic chemistry. In recent years, several new methods have been reported for dehydrogenation of Hantzsch 1,4-dihydropyridines with ferric or cupric nitrates on a solid support: ceric ammonium nitrate, pyridinium chlorochromate, *t*-BuOOH, photochemical oxidation, NO gas, inorganic acidic salts – $NaNO_3$ – wet SiO_2, and $NaHSO_4$–$NaNO_2$ (18). Most of the reported procedures suffer from disadvantages such as producing by-products that are difficult to remove from the desired product, using the reagents that are either highly toxic or present serious environmental problems (or both such as NO), and nonreusability of heterogeneous catalysts. The comparison of our reported system with the previously re-

© 2006 NRC Canada

Table 3. Oxidation of Hantzsch 1,4-dihydropyridines with $NaIO_4$ catalyzed by Mn(TPyP)–CMP.



Row	R	Time (min)
1	H	60
2	CH_3	60
3		60
4		120
5		90
6		90
7		130
8		120
9		140
10		140
11		60
12		60[a]
13		90
14		70

Note: All products were identified by comparison with authentic samples (IR, ^{1}H NMR, and mp).

[a]The product is dealkylated.

ported systems shows that the Mn(TPyP)–CMP–$NaIO_4$ catalytic system has the following advantages: mild reaction conditions, robustness of the catalyst, nontoxicity of reagents, and reusability of the catalyst without loss of its activity.

Experimental

All materials were commercial reagent grade. The tetrapyridylporphyrin ligand (TPyP) was purchased from the Fluka Chemical Company (Dubai, UAE), and metalated and supported according to literature procedures (19, 14). All Hantzsch 1,4-dihydropyridines were synthesized by the reported procedures (20). ^{1}H NMR spectra were obtained with a Bruker AW80 (80 MHz) spectrometer.

General procedure for oxidation of 1,4-dihydropyridines with $NaIO_4$ catalyzed by Mn(TPyP)–CMP

All of the reactions were carried out at room temperature under air in a 25 mL flask equipped with a magnetic stirrer bar. A solution of $NaIO_4$ (2 mmol) in H_2O (10 mL) was added to a mixture of 1,4-dihydropyridines (1 mmol) and MnTPyP–CMP (20 μmol) in CH_3CN (10 mL). The progress of the reaction was monitored by TLC. After the reaction was completed, the reaction mixture was filtered and the pyridine derivative was extracted with CH_2Cl_2 (2 × 20 mL). The pyridine derivatives were obtained after evaporation of the solvent. Further purification was followed using a silica gel plate. IR and ^{1}H NMR spectral data confirmed the identities of the products.

References

1. B. Meunier. Chem. Rev. **92**, 1411 (1992).
2. R.A. Sheldon (*Editor*). Metalloporphyrins in catalytic oxidations. Marcel Dekker, New York. 1994.
3. B. Meunier, A. Robert, G. Pratviel, and J. Bernadou. The porphyrins handbook. Vol. 4. *Edited by* K. Kadish, K.M. Smith, and R. Guilard. Academic Press, New York. 2000.
4. R.A. Sheldon. Biomimetic oxidations catalyzed by transition metal complexes. *Edited by* B. Meunier. Imperial College Press, London. 2000.
5. M.J. Coon and R.E. White. Dioxygen binding and activation by metal centers. *Edited by* T.G. Spiro. Wiley, New York. 1980.
6. J.T. Groves and T.E. Nemo. J. Am. Chem. Soc. **105**, 5786 (1983).
7. O. Bortolini and B. Meunier. J. Chem. Soc. Perkin Trans. 2, 1967 (1984).
8. B. Meunier, E. Guilmet, M.E. De Carvalho, and R. Poilblanc. J. Am. Chem. Soc. **106**, 6668 (1984).
9. D. Mohajer and S. Tangestaninejad. J. Chem. Soc. Chem. Commun. 240 (1993).
10. D. Mohajer and S. Tangestaninejad. Tetrahedron Lett. **35**, 945 (1994).
11. D.J. Triggle. Comprehensive medicinal chemistry. *Edited by* J.C. Emmet. Pergamon, Oxford. 1990.
12. R.H. Böcker and F.P. Guengerich. J. Med. Chem. **29**, 1596 (1986).
13. F.P. Guengerich, W.R. Brian, M. Iwasaki, M.A. Sari, C. Bäärnhielm, and P. Berntsson. J. Med. Chem. **34**, 1838 (1991).

© 2006 NRC Canada

14. M. Nasr-Esfahani, M. Moghadam, S. Tangestaninejad, and V. Mirkhani. Bioorg. Med. Chem. Lett. **15**, 3276 (2005).
15. M. Moghadm, S. Tangestaninejad, M.H. Habibi, and V. Mirkhani. J. Mol. Catal. A: Chem. **217**, 9 (2004).
16. M. Moghadam, S. Tangestaninejad, V. Mirkhani, I. Mohammadpoor-Baltork, and H. Kragar. Bioorg. Med. Chem. **13**, 2901 (2005).
17. P.R. Ortiz de Montellano, H.S. Beilan, and K.L. Kunze. J. Biol. Chem. **256**, 6708 (1981).
18. (*a*) S.P. Chavan, S.W. Dantale, U.R. Kalkote, U.R. Jyothirmai, and R.K. Kharul. Synth. Commun. **28**, 2789 (1998); (*b*) T. Itoh, K. Nagata, Y. Matsuya, M. Miyazaki, and A. Ohsawa. J. Org. Chem. **62**, 3582 (1997); (*c*) M. Balogh, I. Hermecz, Z. Meszaros, and P. Laszlo. Helv. Chem. Acta, **67**, 2270 (1984); (*d*) B. Khadikar and S. Borka. Synth. Commun. **28**, 207 (1998); (*e*) J.R. Pfister. Synthesis, 689 (1990); (*f*) J.J.V. Eynde, A. Mayence, and A. Maquestiau. Tetrahedron, **48**, 463 (1992); (*g*) H.R. Memarian, M.M. Sadeghi, and H. Alian. Indian J. Chem. **37B**, 219 (1998); (*h*) M.A. Zolfigol, M. Kiany-Borazjani, M.M. Sadeghi, H.R. Memarian, and I. Mohammadpoor-Baltork. J. Chem. Res. Synop. 167 (2000); (*i*) M.A. Zolfigol, M. Kiany-Borazjani, M.M. Sadeghi, H.R. Memarian, and I. Mohammadpoor-Baltork. Synth. Commun. **30**, 2945 (2000).
19. A. Harriman and G. Porter. J. Chem. Soc. Faraday Trans. 2, **75**, 1532 (1979).
20. M.A. Zolfigol and M. Safaiee. Synlett, **5**, 827 (2004).

© 2006 NRC Canada

Prediction of the photoelectron spectrum for XPY_2 (X = H, F, Cl; Y = O, S) type of molecules by ab initio and DFT methods

Didier Bégué, Jean-marc Sotiropoulos, Claude Pouchan, and Daisy Y. Zhang

Abstract: The present study reports the theoretical vertical ionization potentials (IPs) for all the valence electrons in six XPY_2 molecules by utilizing the corrected orbital energies calculated with three theoretical methods, namely, the ab initio Hartree–Fock (HF), and both the pure and hybrid density functional theory (DFT) methods at, respectively, the BLYP/6-311+G* and B3lYP/6-311+G* levels of theory. Evaluation of the numerical corrections to the orbital energies was achieved by comparisons with the IP values obtained via explicit computation of the energy differences between the neutral molecules and the corresponding radical cations (the ΔSCF method) and shows values from –0.9 to –1.9 eV for the HF, and positive values from 2.9 to 3.9 eV and from 1.8 to 2.4 eV for the pure and hybrid DFT methods, respectively. In contrast to the orbital energies, the ΔSCF method is shown to give consistent values among the three methods, as well as reasonable agreement with the experimental IP values.

Key words: ionization potential, phosphorane, Koopmans' theorem, Janak's theorem.

Résumé : Dans ce travail, on a calculé les potentiels théoriques d'ionisation (PI) verticale pour tous les électrons de valence de six molécules XPY_2 en faisant appel à des énergies d'orbitales corrigées calculées par trois méthodes théoriques, soit les méthodes de Hartree–Fock (HF) ab initio ainsi que par des méthodes pure ainsi qu'hybride de la théorie de la densité fonctionnelle (TDF) aux niveaux respectivement BLYP/6-311+G* et B31YP/6-311+G*. On a réalisé l'évaluation des corrections numériques des énergies d'orbitales par des comparaisons avec des valeurs de PI obtenues par des calculs explicites de différences d'énergie entre les molécules neutres et les cations radicaux correspondants (la méthode de différences autocohérentes, ΔCAC) et les valeurs s'étalent entre –0,9 et –1,9 eV pour la méthode HF et entre +2,9 et 3,9 eV et +1,8 et 2,4 eV pour les méthodes de la TDF respectivement pure et hydride. Par opposition aux énergies d'orbitales, on montre que la méthode des ΔCAC conduit à des valeurs qui en accord entre elles pour chacune des trois méthodes et, de plus, elles sont en bon accord avec les valeurs expérimentales de PI.

Mots clés : potentiel d'ionisation, phosphorane, théorème de Koopmans, théorème de Janak.

[Traduit par la Rédaction]

Introduction

The title molecules, known as monomeric metaphosphate (RPO_2) and dithioxophosphorane (RPS_2), have been the focus of much research. As Nobel Prize laureate Arthur Kornberg wrote in his recollections on ATP and inorganic pyro- and poly-phosphate in 1993 (1), "My attachment to poly P withstood 35 years of a devotion to DNA replication … Unlike children and friends, shaped and altered by passage of time, the face of poly P has remained fresh with the mystery and allure of a new acquaintance".[2] As well as the essential roles that metaphosphate plays in the ATP hydrolysis mechanism (2–4), these phosphorus-containing molecules are fundamentally important to the study of chemistry, in particular, the study of bonding theory. As π and σ bond models, they are ideal systems for the investigation of bonding structures; the results provide insights into the role of the 3d orbitals in valence bonding (5–8), and furthermore, help to discern the much debated issue of normal valency vs. hypervalency.

Experimental potential energy surfaces (PESs) of FPS_2, $ClPS_2$, and $ClPO_2$ were recorded by Bock and co-workers (9, 10) using thermal decomposition (around 500 K) of pyridinium-FPS_2 betaine compounds. The spectra of FPS_2 and $ClPS_2$ were clearly identified with bands at mainly 10.1, 10.5, 11.3 and 9.8, 10.2, 10.7 eV, respectively. For the oxygen analogue, the bands were stabilized at 11.9, 12.4, 13.0, and 13.5 eV. The assignments were supported by Koopmans' correlations with MNDO eigenvalues from geometry-optimized semiempirical ΔSCF calculations. More elaborate analysis was necessary to reinvestigate the photoelectron spectra, and in light of a better quantum calculation, we assigned the four previous PESs and predicted bands for the other compounds.

Recognizing that quantum mechanical calculations have become an essential tool in chemical research, many re-

Received 13 September 2005. Published on the NRC Research Press Web site at http://canjchem.nrc.ca on 3 February 2006.

D. Bégué, J.-m. Sotiropoulos, C. Pouchan, and D.Y. Zhang.[1] Laboratoire de Chimie Théorique et de Physico-Chimie Moléculaire, UMR 5624, FR 2606 IPREM, Université de Pau et de Pays de l'Adour, F-64000 Pau, France.

[1]Corresponding author (e-mail: daisyz@spu.edu).

[2]Poly P refers to the polymeric metaphosphate.

 doi:10.1139/V05-257 © 2006 NRC Canada

searchers have been engaged in the evaluation of various theoretical methods in the calculation of the ionization potentials (IPs) (11–13). Reliable predictions for the IPs are certainly invaluable in understanding the chemical structures, as well as helping to identify the molecules in photoelectron spectroscopy experiments.

The most commonly used practice to produce the IP data by theoretical methods is to use the orbital energy values. As is known, the negative values of the Hartree–Fock (HF) orbital energies can be used to predict the vertical IPs via the application of Koopmans' theorem (14), and in the DFT analogy of Janak's theorem (15). However, it is also known that those orbital energies do not always match the IP values accurately. In Koopmans' theorem, it is due to the assumption that the orbitals for the cation are identical to those in the neutral molecule, which results in neglecting two major changes in the electronic structure of the radical, namely, the orbital relaxation after the ionization process and the overestimation of the electron correlation in the cation. In Janak's theorem, it is due to the self-interaction error, as the exchange–correlation functionals do not completely cancel the spurious Coulomb interaction of an electron with itself. Therefore, a more accurate way to predict the vertical IP is by using the so-called ΔSCF method, which calculates the IPs via explicit computation of the energy difference between the neutral molecule and the corresponding radical cation. While this method yields much more accurate IP values, its application is limited by the fact that it is time-consuming and is not practical for large systems if high levels of theory for the calculations are desired.

Herein, we report a case study of six title molecules on the numerical corrections to the orbital energies generated by three computational procedures, namely, the ab initio HF and both the pure (BLYP) and hybrid (B3LYP) DFT methods. With these values, a complete photoelectron spectrum is therefore constructed theoretically for each of the six molecules. We believe that these numerical values provide some general information that would allow for a more accurate prediction of the IP values by applying Koopmans' or Janak's theorem.

Computation methodology

All calculations were carried out using the Gaussian 98 suite of programs (16). Full geometry optimization was performed at the BLYP/6-311+G*, B3LYP/6-311+G* (17–19), and CCSD(T)/cc-pVTZ (20–22) levels of theory, and all molecules were found to be of C_{2v} symmetry at the optimized structures, each of which was further confirmed as a stationary point on the PES by the vibrational analysis calculations, such that all frequencies were found to be real.

The vertical IPs were computed by taking the electronic energy difference (ΔSCF) between the neutral molecule and the corresponding radical cation at the same geometry but by using the unrestricted method. Zero-point energy (ZPE) corrections were included for the neutral molecules but not for the cations. The size of ZPE ranges from 0.29 eV for the largest molecule of series, namely, $ClPS_2$, to 0.80 eV for the smallest molecule of HPO_2. With this procedure, the four lowest possible ionization energies were computed at the (U)B3LYP/6-311+G* and (U)CCSD(T)/cc-pVTZ levels of theory, which correspond to having the unpaired electron in the radical cation occupying the MOs of $^2A_1$, $^2A_2$, $^2B_1$, and $^2B_2$ symmetries.

Table 1. Structural data for the six XPY_2 molecules computed at the B3LYP/6-311+G* and CCSD(T)/cc-pVTZ levels of theory.

XPY_2	r (X—P)	r (P—Y)	α (Y-P-Y) (°)
FPO_2	1.58/1.55	1.46/1.45	136.5/135.8
$ClPO_2$	2.02/2.00	1.46/1.46	134.7/134.5
HPO_2	1.41/1.40	1.47/1.47	135.2/134.8
FPS_2	1.61/1.57	1.91/1.90	135.6/136.1
$ClPS_2$	2.07/2.04	1.92/1.91	132.7/134.0
HPS_2	1.41/1.41	1.92/1.92	133.6/134.3

Results and discussion

The computed structural results at the B3LYP/6-311+G* and CCSD(T)/cc-pVTZ levels of theory are listed in Table 1. The energy data are summarized in Tables 2–7. There, ε_i stands for the negative value of the orbital energy; in the notations for the MOs, *n* stands for the orbital space in the region of a specific atom; σ or π corresponds to the symmetry of the orbital with respect to the molecular plane; and the negative and positive signs indicate the out-of-phase and in-phase interactions among the orbitals, respectively. Photoelectron spectroscopy data from the literature for the ionization energies for $ClPO_2$ (9), $ClPS_2$ (9), and FPS_2 (10) have also been included in these tables.

The structural results

Both the ab initio values at the CCSD(T)/cc-pVTZ level and the DFT method at the B3LYP/6-311+G* level yield structural data similar to each other, as well as to the experimental results (9, 10, 23, 24). As is shown, the P—Y bond length is insensitive to the nature of X, in spite of the large differences in electronegativity among F, Cl, and H. In all three molecules, the P—O and P—S bond lengths are consistently around 1.46 and 1.91 Å, respectively, which are close to the typical P=O and P=S bond lengths (25). In contrast, the X—P bonds are predicted to be slightly shorter in XPO_2 than in XPS_2, with X being a halogen. This can be understood as the reduced back-electron donating from X to P in XPS_2, where P bears a less positive charge than in XPO_2. The substituent effect on the bond lengths supports a conventional hypervalent Lewis structure of these molecules.

Explicit computation of the ionization energies

Explicit computation of the energy difference between the neutral molecule and the radical cation in one of the four electronic states are listed under ΔSCF in Tables 2–7. As the first four frontier molecular orbitals (FMOs) in all cases are of the four different symmetries for a C_{2v} molecule, these four ΔSCF values, therefore, correspond to the four lowest ionization energies in a photoelectron spectrum.

Both (U)B3LYP/6-311+G* and (U)CCSD(T)/cc-pVTZ calculations yield very similar ΔSCF values. In most cases, the ΔSCF values vary by less than 0.2 eV. Among the total of 24 ΔSCF values, only four cases show a difference of greater than 0.3 eV.

© 2006 NRC Canada

Table 2. Orbital energy (ε_i), ΔSCF, and predicted IP values (in parentheses) for $ClPO_2$.

	ε_i			ΔSCF		
MO of $ClPO_2$	BLYP	B3LYP	HF	B3LYP	CCSD(T)	Exp.[a]
$(n_O^{\sigma-}/n_{Cl}^{\sigma})^-$ (B_2)	8.2	9.6	13.7	12.0	11.9	11.9
$\pi_{P=O}^-$ (A_2)	9.0	10.4	14.2	12.7	12.6	12.4
$(n_{Cl}^{\pi}/\pi_{P=O}^+)^-$ (B_1)	9.2	10.6	14.5	13.1	13.1	13.0
$(n_O^{\sigma+}/n_{Cl}^{\sigma})^-$ (A_1)	9.2	10.7	14.8	13.1	12.9	13.5
$(n_{Cl}^{\sigma}/n_O^{\sigma-})^+$ (B_2)	9.6	11.1	15.3	(13.6)	(13.6)	13.9
$(n_O^{\sigma-}/n_{Cl}^{\sigma})^+$ (B_2)	11.3	12.9	17.0	(15.3)	(15.3)	15.4
$(n_{Cl}^{\pi}/\pi_{P=O}^+)^+$ (B_1)	11.2	12.8	17.5	(15.4)	(15.4)	16.5
$(n_O^{\sigma+}/n_{Cl}^{\sigma})^+$ (A_1)	12.0	13.6	18.1	(16.1)	(16.1)	17.3
$(n_{Cl}^{\sigma}/n_O^{\sigma+})^+$ (A_1)	14.6	16.3	21.2	(18.9)	(18.9)	19.2

Note: All values are in eV.
[a]Reference 10.

Table 3. Orbital energy (ε_i), ΔSCF, and predicted IP values (in parentheses) for $ClPS_2$.

	ε_i			ΔSCF		
MO of $ClPS_2$	BLYP	B3LYP	HF	B3LYP	CCSD(T)	Exp.[a]
$(n_S^{\sigma-}/n_{Cl}^{\sigma})^-$ (B_2)	6.6	7.6	10.5	9.7	9.5	9.8
$\pi_{P=S}^-$ (A_2)	7.1	8.0	10.4	10.0	9.8	10.2
$(n_S^{\sigma+}/n_{Cl}^{\sigma})^-$ (A_1)	7.4	8.6	11.4	10.6	10.4	10.8
$(\pi_{P=S}^+/n_{Cl}^{\pi})^-$ (B_1)	8.2	9.4	12.5	11.5	11.3	11.8
$(n_{Cl}^{\sigma}/n_S^{\sigma-})^-$ (B_2)	8.6	10.0	13.5	(12.1)	(12.1)	12.8
$(n_{Cl}^{\pi}/\pi_{P=S}^+)^+$ (B_1)	9.8	11.3	15.0	(13.4)	(13.4)	14.1
$(n_S^{\sigma-}/n_{Cl}^{\sigma})^+$ (B_2)	10.4	11.7	15.3	(13.8)	(13.8)	14.7
$(n_S^{\sigma+}/n_{Cl}^{\sigma})^+$ (A_1)	11.1	12.5	16.0	(14.6)	(14.6)	15.9
$(n_{Cl}^{\sigma}/n_S^{\sigma+})^+$ (A_1)	13.9	15.4	19.7	(17.7)	(17.7)	17.2

Note: All values are in eV.
[a]Reference 11.

Table 4. Orbital energy (ε_i), ΔSCF, and predicted IP values (in parentheses) for FPO_2.

	ε_i			ΔSCF	
MO of FPO_2	BLYP	B3LYP	HF	B3LYP	CCSD(T)
$(n_O^{\sigma-}/n_F^{\sigma})^-$ (B_2)	8.6	10.1	14.6	12.8	12.6
$\pi_{P=O}^-$ (A_2)	9.2	10.6	14.5	13.2	13.0
$(n_O^{\sigma+}/n_F^{\sigma})^-$ (A_1)	9.8	11.4	16.0	13.2	13.9
$(\pi_{P=O}^+/n_F^{\pi})^-$ (B_1)	10.6	12.2	16.5	14.1	14.8
$(n_O^{\sigma-}/n_F^{\sigma})^-$ (B_2)	10.9	12.5	17.2	(15.0)	(15.0)
$(n_O^{\sigma+}/n_F^{\sigma})^+$ (A_1)	12.5	14.4	19.4	(16.9)	(16.9)
$(n_F^{\sigma}/n_O^{\sigma-})^+$ (B_2)	12.7	14.7	21.2	(17.7)	(17.7)
$(n_F^{\pi}/\pi_{P=O}^+)^+$ (B_1)	12.8	14.9	21.1	(17.7)	(17.7)
$(n_F^{\sigma}/n_O^{\sigma+})^+$ (A_1)	15.8	17.8	24.1	(20.7)	(20.7)

Note: All values are in eV.

Furthermore, these ΔSCF values are also in reasonably good agreement with the experimental values, with a difference in the range of 0.1–0.6 eV. In all cases, when the difference is significant, i.e., 0.6 eV, the ΔSCF values are always less than the experimental IP values. This could be explained by the possible over-excitation of the electrons in the photoelectron experiments, as the radical cations are often formed in a vibrationally excited state. Therefore, extra energy is absorbed during the formation of the cation, resulting in a higher IP in comparison to the ΔSCF values, which corresponds to the energy difference between the two electronic states at the vibrationally ground states.

Orbital energies

The orbital energies for the FMOs containing all the valence electrons are listed for the halogen- and hydrogen-containing XPY_2 molecules. Overall, the two methods predict the same pattern for the layout of the relative energies of the FMOs. In only a few cases where the orbitals are very close in energy, the order of the highest occupied molecular orbital (HOMO) and HOMO-1 are switched between the two methods. For example, the HOMOs are of the B_2 symmetry for all six XPY_2 molecules according to the B3LYP calculations, but are predicted to be of A_2 symmetry for four out the six molecules by the CCSD(T) method. Nevertheless, the first and the third band were assigned to the ionization of a chalcogen–chlorine antibonding combination in the σ plane, and the second band was well-resolved with the antibonding combination of the $\pi_{P=O\ (S)}$. All of the next assignments are listed in Tables 2–7.

Consistent with the understanding that the atomic orbitals in O are more low-lying than in S, the FMOs are consistently lower in the XPO_2 molecules by around 2 eV in com-

© 2006 NRC Canada

Table 5. Orbital energy (ε_i), ΔSCF, and predicted IP values (in parentheses) for FPS_2.

	ε_i			ΔSCF		
MO of FPS_2	BLYP	B3LYP	HF	B3LYP	CCSD(T)	Exp.[a]
$(n_S^{\sigma-}/n_F^{\sigma})^-$ (B_2)	6.7	7.8	10.7	10.0	9.7	10.1
$\pi_{P=S}^-$ (A_2)	7.1	8.1	10.6	10.6	10.0	10.5
$(n_S^{\sigma+}/n_F^{\sigma})^-$ (A_1)	7.7	9.0	12.0	11.1	10.8	11.3
$(\pi_{P=S}^+/n_F^{\pi})^-$ (B_1)	8.8	10.1	13.1	12.2	11.8	12.1
$(n_S^{\sigma-}/n_F^{\sigma})^-$ (B_2)	9.8	11.1	14.4	(13.3)	(13.3)	13.5
$(n_S^{\sigma+}/n_F^{\sigma})^+$ (A_1)	11.7	13.4	17.4	(15.7)	(15.7)	16.0
$(n_F^{\sigma}/n_S^{\sigma-})^+$ (B_2)	11.8	13.8	20.2	(16.8)	(16.8)	16.5
$(n_F^{\pi}/\pi_{P=S}^+)^+$ (B_1)	12.0	13.9	20.2	(16.8)	(16.8)	16.9
$(n_F^{\sigma}/n_S^{\sigma+})^+$ (A_1)	14.8	16.7	22.7	(19.6)	(19.6)	

Note: All values are in eV.
[a]Reference 12.

Table 6. Orbital energy (ε_i), ΔSCF, and predicted IP values (in parentheses) for HPO_2.

	ε_i			ΔSCF	
MO of HPO_2	BLYP	B3LYP	HF	B3LYP	CCSD(T)
$n_O^{\sigma-}$ (B_2)	8.3	9.8	14.3	12.2	12.1
$n_O^{\sigma+}$ (A_1)	8.4	10.0	14.4	12.4	12.3
$\pi_{P=O}^-$ (A_2)	8.5	10.0	13.9	12.3	12.3
$\pi_{P=O}^+$ (B_1)	10.6	12.2	16.3	14.7	14.4
$n_O^{\sigma-}$ (B_2)	10.7	12.3	17.3	(14.9)	(14.9)
$n_O^{\sigma+}$ (A_1)	11.6	13.3	18.3	(15.9)	(15.9)

Note: All values are in eV.

Table 7. Orbital energy (ε_i), ΔSCF, and predicted IP values (in parentheses) for HPS_2.

	ε_i			ΔSCF	
MO of HPS_2	BLYP	B3LYP	HF	B3LYP	CCSD(T)
$n_S^{\sigma-}$ (B_2)	6.5	7.6	10.5	9.5	9.2
$n_S^{\sigma+}$ (A_1)	6.7	7.7	10.1	9.6	9.3
$\pi_{P=S}^-$ (A_2)	6.8	7.9	10.9	9.9	9.5
$\pi_{P=S}^+$ (B_1)	8.9	10.1	13.0	12.1	11.4
$n_S^{\sigma-}$ (B_2)	9.8	11.1	14.3	(12.9)	(12.9)
$n_S^{\sigma+}$ (A_1)	10.8	12.2	15.8	(14.1)	(14.1)

Note: All values are in eV.

parison to XPS_2. This is also consistent with the high reactivities reported for dithioxophosphoranes.

Data in Tables 2–7 show that the orbital energies obtained by the pure GGA BLYP method are consistently lower than the ΔSCF values by 3 to 4 eV, and those obtained by the hybrid method of B3LYP are lower by a less amount of around 2 eV. These results are consistent with the well-known fact that the DFT methods usually give orbital eigenvalues that are too high in energy and, therefore, give ionization energy values that are too low (26–28). In contrast, the HF values are all higher than the ΔSCF values by 1 to 2 eV. This is also understandable, as electron correlation is not involved in the HF method, the lack of consideration of the orbital relaxation in the cation results in the overestimate of the energy of the cation and, therefore, gives IP values that are too high.

Numerical corrections to the orbital energies

Table 8 lists the numerical corrections to the orbital energies so that the corrected orbital energies match with the IP values calculated by the ΔSCF method. They were obtained by taking the averaged differences between the orbital energies and the average of the two ΔSCF values, which are extremely close to each other. The size of the corrections is insensitive to the nature of X for the DFT methods, but demonstrates a slight variation in the ab initio method. The corrections are smaller in the sulfur series by 0.5–1.0 eV, in comparison with the oxygen analogs.

By using these corrections, we have attempted to evaluate the IP values for the IPs involving exciting lower-lying electrons. These results are listed under ΔSCF as values in parentheses in Tables 2–7. These values were taken as the averaged values of the orbital energies computed by the three methods, with the corresponding corrections included.

Table 8. Averaged numerical corrections (eV) to the orbital energies.

Molecules		BLYP	B3LYP	HF
XPO_2	$ClPO_2$	3.8	2.4	–1.5
	FPO_2	3.9	2.4	–1.9
	HPO_2	3.9	2.4	–1.9
XPS_2	$ClPS_2$	3.0	2.0	–0.9
	FPS_2	3.2	2.1	–0.8
	HPS_2	2.9	1.8	–1.3

As is shown, these high IP values match remarkable well with the experimental values, especially among those of relatively lower IP values. For instance, the first two IP values calculated with this approach vary between 0.1 and 0.4 eV from the experimental values.

Conclusions

We have shown that the theoretical IPs predicted by the ΔSCF method agree very well with the experimental values, both by ab initio and DFT methods at the (U)CCSD(T)/cc-

© 2006 NRC Canada

pVTZ and B3LYP/6-311+G* levels of theory, respectively. With these values, corrections to the orbital energies were evaluated and were therefore used to predict the IP values for all the valence electrons by the application of the Koopmans'and Janak's theorem. Re-evaluation of the experimental results occurred, and the numerical corrections from this study provide some general information that would allow for a better prediction of the IP values in systems where ΔSCF calculations are not practical.

Acknowledgement

DYZ gratefully acknowledges a one-year grant from the Conseil Regional d'Aquitaine and Fulbright Research Award, which allowed her to spend her sabbatical year in France, during which time this work was carried out.

References

1. A. Kornberg. Protein Sci. **2**, 131 (1993).
2. S. Freeman, J.M. Friedman, and J.R. Knowles. J. Am. Chem. Soc. **109**, 3166 (1987).
3. S.L. Buchwald, J.M. Friedman, and J.R. Knowles. J. Am. Chem. Soc. **106**, 4911 (1984).
4. J.M. Friedman and J.R. Knowles. J. Am. Chem. Soc. **107**, 6125 (1985).
5. A.E. Reed and P.v.R. Schleyer. J. Am. Chem. Soc. **112**, 1434 (1990).
6. E.J. Baran. J. Mol. Struct. **245**, 155 (1991).
7. S. Mathieu, J. Navech, and J.C. Barthelat. Inorg. Chem. **28**, 3099 (1989).
8. S. Noury, B. Silvi, and R. Gillespie. J. Inorg. Chem. **41**, 2164 (2002).
9. M. Meisel, H. Bock, B. Solouki, and M. Kremer. Angew. Chem. Int. Ed. Engl. **28**, 1373 (1989).
10. H. Bock, M. Kremer, B. Solouki, M. Binnewies, and M. Meisel. J. Chem. Soc. Chem. Commun. 9 (1992).
11. O.V. Gritsenko and E.J. Baerends. J. Chem. Phys. **117**, 9154 (2002).
12. D.P. Chong, O.V. Gritsenko, and E.J. Baerends. J. Chem. Phys. **116**, 1760 (2002).
13. S. Joanteguy, G. Pfister-Guillouzo, and H. Chermette. J. Phys. Chem. A, **103**, 3505 (1999).
14. A. Koopmans. Physica, **1**, 104 (1933).
15. J.F. Janak. Phys. Rev. B, **18**, 7165 (1978).
16. M.J. Frisch, G.W. Trucks, H.B. Schlegel, G.E. Scuseria, M.A. Robb, J.R. Cheeseman, V.G. Zakrzewski, J. Montgomery, R.E. Stratmann, J.C. Burant, S. Dapprich, J.M. Millam, A.D. Daniels, K.N. Kudin, M.C. Strain, O. Farkas, J. Tomasi, V. Barone, M. Cossi, R. Cammi, B. Menucci, C. Pomelli, C. Adamo, S. Clifford, J. Ochterski, G.A. Petersson, P.Y. Ayala, Q. Cui, K. Morokuma, D.K. Malick, A.D. Rabuck, K. Raghavachari, J.B. Foresman, J. Cioslowski, J.V. Ortiz, B.B.J. Stefanov, G. Liu, A. Liashenko, P. Piskorz, I. Koaromi, R. Gomperts, R.L. Martin, D.J. Fox, T. Keith, M.A. Al-Laham, C.Y. Peng, A. Nanayakkara, C. Gonzalez, M. Challcombe, P.M.W. Gill, B.G. Johnson, W. Chen, M.W. Wong, J.L. Andres, M. Head-Gordon, E.S. Replogle, and J.A. Pople. Gaussian 98. Revision A.7 [computer program]. Gaussian Inc., Pittsburgh, Penn. 1998.
17. A.D. Becke. J. Chem. Phys. **98**, 5648 (1993).
18. C. Lee, W. Yang, and R.G. Parr. Phys. Rev. B, **37**, 785 (1988).
19. T. Clark, J. Chandrasekhar, and P.v.R. Schleyer. J. Comput. Chem. **4**, 294 (1983).
20. T.H. Dunning, Jr. J. Chem. Phys. **90**, 1007 (1989).
21. D.E. Woon and T.H. Dunning, Jr. J. Chem. Phys. **98**, 1358 (1993).
22. D.E. Woon and T.H. Dunning, Jr. J. Chem. Phys. **100**, 2975 (1994).
23. B. Brupbacher-Gatehouse. J. Am. Chem. Soc. **122**, 4171 (2000).
24. R. Ahlrichs, C. Ehrhardt, M. Lakenbrink, S. Schunck, and H. Schnockel. J. Am. Chem. Soc. **108**, 3596 (1986).
25. N.N. Greenwood and A. Earnshaw. *In* Elements of chemistry. 2nd ed. Butterworth-Heinemann, Oxford. 1997.
26. H. Chermette, I. Ciofini, F. Mariotti, and C. Daul. J. Chem. Phys. **114**, 1447 (2001).
27. H. Chermette, I. Ciofini, F. Mariotti, and C. Daul. J. Chem. Phys. **115**, 11068 (2001).
28. Y. Zhang and W. Yang. J. Chem. Phys. **109**, 2604 (1998).

© 2006 NRC Canada

Steric effects in the phototransposition reactions of dialkylbenzenes

C.M. Gonzalez and J.A. Pincock

Abstract: The photochemistry, photophysical properties, and temperature dependence (–25 to +65 °C) of fluorescence by quantum yields and excited singlet state lifetimes in acetonitrile have been examined for three sets of dialkylbenzene derivatives: Set 1 — *ortho*-xylene (**10**), tetralin (**11**), and indan (**12**); Set 2 — 2,3-dimethylbenzonitrile (**9-23**), 5-cyanotetralin (**T-23**), and 4-cyanoindan (**I-23**); and Set 3 — 3,4-dimethylbenzonitrile (**9-34**), 6-cyanotetralin (**T-34**), and 5-cyanoindan (**I-34**). Phototransposition reactions occur for **10**, **9-23**, **9-34**, and **T-34**. Fitting of the temperature-dependent fluorescence data to an Arrhenius expression gave A and E_a values for all substrates studied except **I-23** and **I-34**. The fluorescence intensity of these two compounds was essentially independent of temperature. For the other compounds, the data revealed that the activation barrier separating the excited singlet state (S_1) from the reactive intermediate, a prefulvene biradical, was the important one in determining the reaction efficiency. The dominant mode of decay of the reactive intermediate was internal return to the starting material. Moreover, the general observation was made that nitrile substitution ortho to one of the alkyl groups in these dialkylbenzene derivatives reduced the rate at which they were converted to the reactive intermediate and, therefore, also the efficiency of the phototransposition reactions.

Key words: phototranspositions, substituted benzenes, temperature-dependent fluorescence, activation parameters.

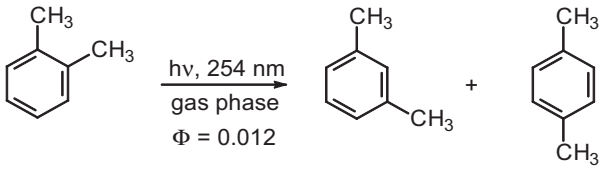
Résumé : En se basant sur les rendements quantiques ainsi que les temps de vie de l'état singulet excité observés lors de réactions dans l'acétonitrile, on a étudié la photochimie, les propriétés photophysiques et la relation entre la température (–25 à +65 °C) et les rendements quantiques pour trois ensembles de dérivés benzéniques dialkylés, soit l'ensemble 1 formé d'*ortho*-xylène (**10**), de tétraline (**11**) et d'indane (**12**); l'ensemble 2 formé de 2,3-diméthylbenzonitrile (**9-23**), de 5-cyanotétraline (**T-23**) et de 4-cyanoindane (**I-23**); l'ensemble 3 formé de 3,4-diméthylbenzonitrile (**9-34**), de 6-cyanotétraline (**T-34**) et de 5-cyanoindane (**I-34**). Il se produit des réactions de phototransposition pour les composés **10**, **9-23**, **9-34** et **T-34**. Un ajustement des données de fluorescence influencées par la température à une expression d'Arrhenius permet de calculer les valeurs A et E_a pour tous les substrats étudiés, à l'exception de **I-23** et **I-34**. L'intensité de la fluorescence de ces deux composés est essentiellement indépendante de la température. Pour les autres composés, les données ont permis de déterminer que la barrière d'activation qui sépare S_1, l'état singulet excité, de l'intermédiaire réactif, un biradical préfulvène, est celle qui est importante dans la détermination de l'efficacité de la réaction. Le mode dominant dans la désactivation de l'intermédiaire réactif est le retour interne vers le produit de départ. De plus, on a observé que la présence d'un substituant nitrile en position ortho par rapport aux groupes alkyles de ces dialkylbenzènes provoque une réduction de la vitesse avec laquelle ils se transforment en intermédiaires réactifs et que, en conséquence, l'efficacité des réactions de phototransposition est aussi réduite.

Mots clés : phototranspositions, benzènes substitués, fluorescence dépendante de la température, paramètres d'activation.

[Traduit par la Rédaction]

Introduction

Phototransposition reactions were first reported in 1964 by Wilzbach and Kaplan (1) for the xylenes (eq. [1]) and by Burgsthaler et al. (2) for di-*tert*-butylbenzenes. It was demonstrated (3), by photolysis of [1,3,5-$^{14}C_3$]-mesitylene (eq. [2]), that these rearrangements occurred by a fundamental transposition of the ring carbons and not by alkyl group detachment. These, and related reactions, lead to a proposed mechanism involving formation of a prefulvene (or substituted prefulvene) biradical **1** from S_1 followed by ring closure to form benzvalene (or substituted benzvalenes) **2**, as outlined in Scheme 1 (path A) for benzene itself. Either opening of the benzvalene intermediate by cleavage of the

[1] 

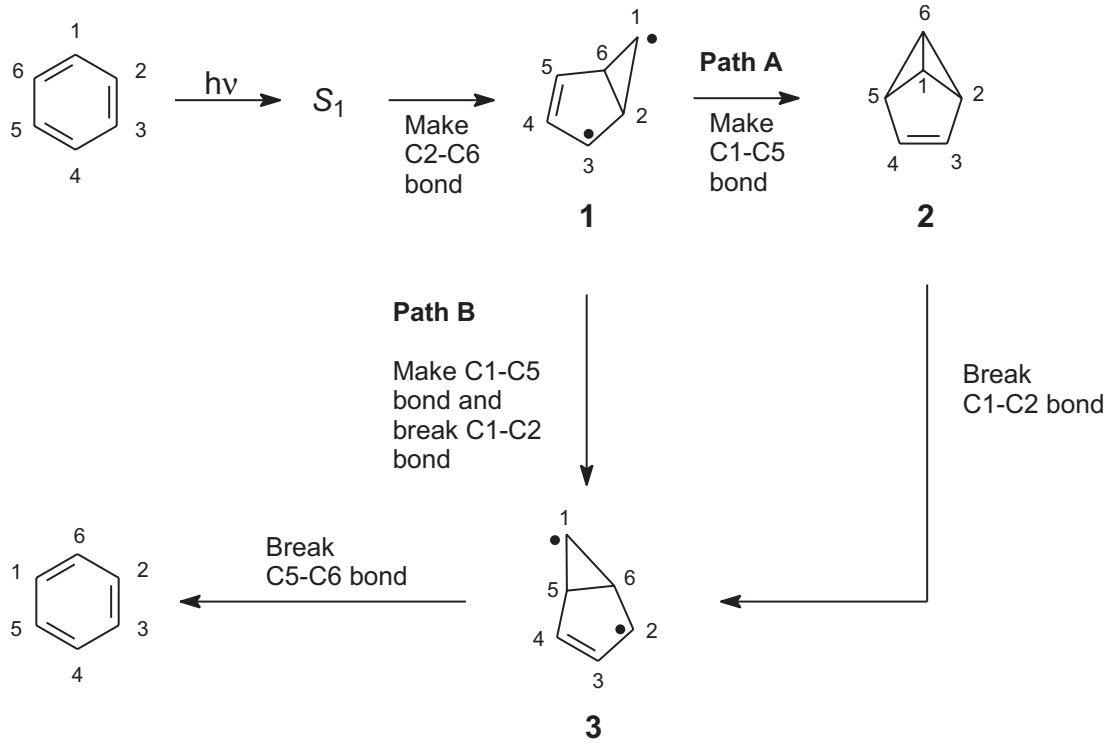
Received 15 September 2005. Published on the NRC Research Press Web site at http://canjchem.nrc.ca on 11 February 2006.

C.M. Gonzalez and J.A. Pincock.[1] Department of Chemistry, Dalhousie University, Halifax, NS B3H 4J3, Canada.

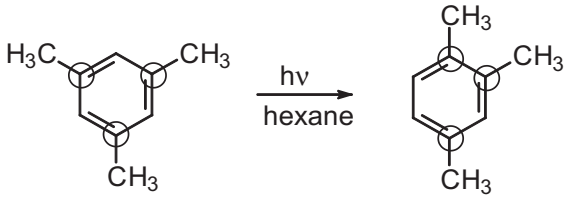
[1]Corresponding author (e-mail: james.pincock@dal.ca).

 doi:10.1139/V05-258 © 2006 NRC Canada

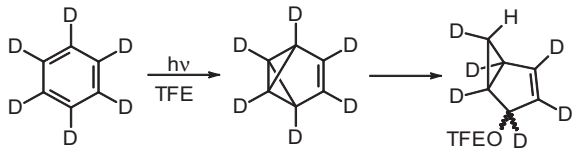
Scheme 1. Proposed mechanism for the photochemical formation of benvalene and the phototransposition reactions of benzene itself.



C1—C2 bond or a 1,5-migration of C1 in the prefulvene biradical (path B) leads to a rearranged biradical **3** that then returns to benzene but with interchange of two adjacent carbons, C1 and C6.

[2] 

This mechanism received strong support by the isolation of benzvalene from the photolysis of benzene (4) and by the formation of bicyclo[3.1.0]hexenyl derivatives (eq. [3]) for benzene-d_6 in 2,2,2-trifluoroethanol (TFE) on photolysis in alcohol solvents (5, 6). Research in this area up until 1980 has been the subject of several reviews (7–10).

[3] 

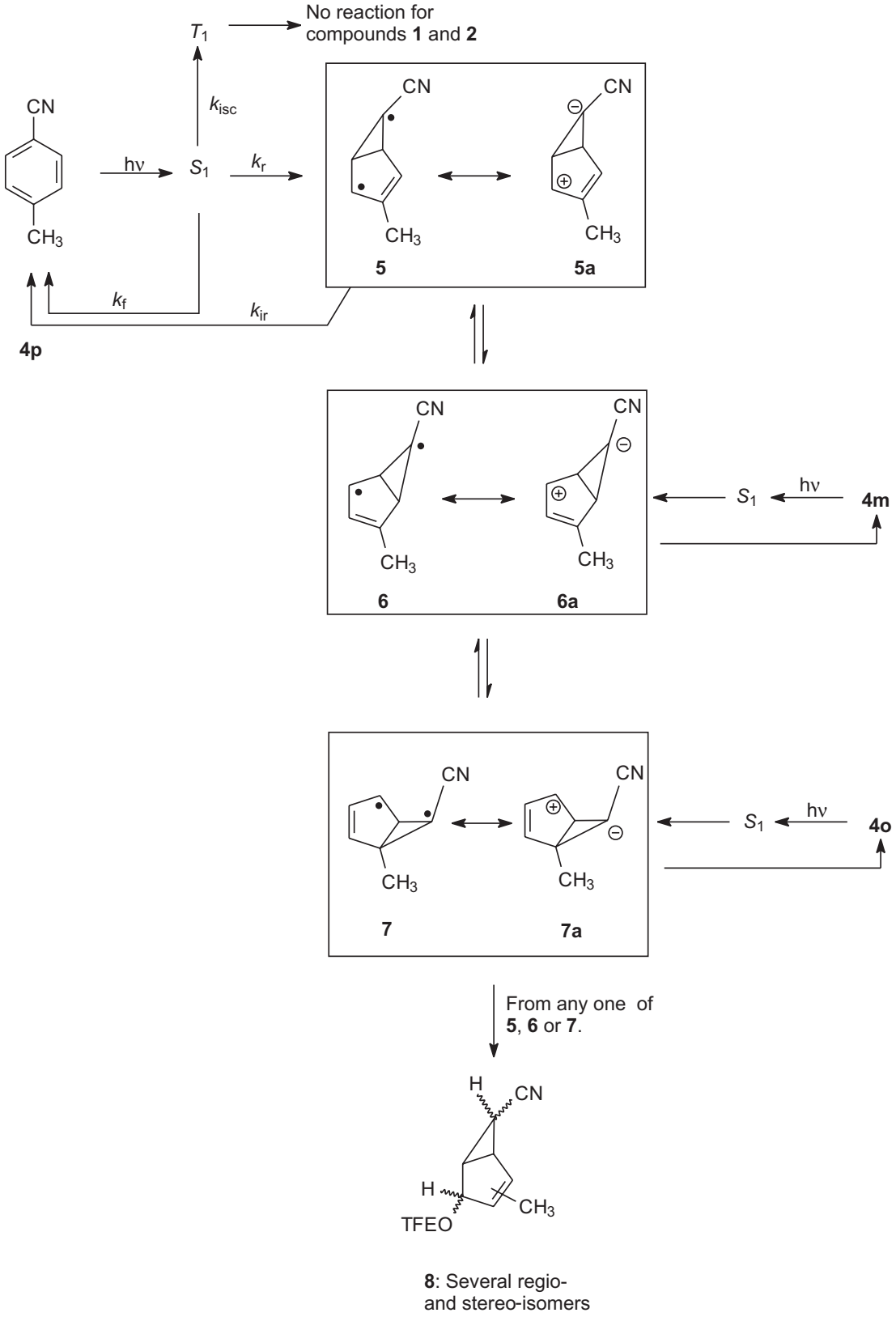
More recently, we have observed both phototransposition reactions in acetonitrile (AN) (11) and photoaddition reactions of TFE (12) for nitrile-substituted benzene compounds. Scheme 2 summarizes the results for the three isomers (para (**4p**), meta (**4m**), and ortho (**4o**)) of methylbenzonitrile. Photolysis of labelled 2,6-dideuterio-**4p** gave 5,6-dideuterio-**4m**, consistent with the nitrile-substituted carbon being the active one in the phototransposition reactions, that is, the critical intermediates are **5**, **6**, and **7**. This mechanism was strongly supported by isolation of the bicyclo[3.1.0]hexene adducts **8** (several stereo- and regio-isomers) by photolysis of **4p** in TFE, indicating that the intermediates may have considerable ionic character, as shown in **5a**, **6a**, and **7a**. This also implies that these intermediates are singlet states in agreement with the fact that they are formed from the excited singlet state (S_1) of starting materials. Substituted benzvalenes have not been included in this scheme because no evidence has been obtained for their formation as intermediates in these transformations. The more recent results on phototransposition and photoaddition reactions to substituted benzenes have also been recently reviewed (13, 14).

Further support for the importance of the nitrile-substituted carbon came from the photochemistry of the set of six dimethylbenzonitriles **9-34**, **9-23**, **9-26**, **9-35**, **9-24**, and **9-25** (15). The results indicated that these compounds are divided into two independent triads as shown in eqs. [4] and [5]. For instance, photolysis of **9-34** in AN gave only **9-23** and **9-26** (eq. [4]), with no mixing with the other triad. This result is easily explained if the phototransposition reactions involve the nitrile-substituted carbon exchanging position with either of its two neighbours.

During these studies, we observed that substrates with methyl groups ortho to the nitrile-substituted carbon were quite unreactive. For instance, the relative reactivity of **4p**:**4m**:**4o** = 32:4:1 and **9-34**:**9-23**:**9-26** ≅ 50:1:0. These observations suggested that the rate-determining step in these photoreactions was the conversion of S_1 of the substrate to the prefulvene biradical and that this step was slowed by the presence of a methyl group occupying a bridgehead position in the biradical. However, as shown in Fig. 1 for **4p**, several

© 2006 NRC Canada

Scheme 2. Proposed mechanism and products formed from the photochemistry of the benzonitriles **4p**, **4m**, and **4o** in AN and TFE.

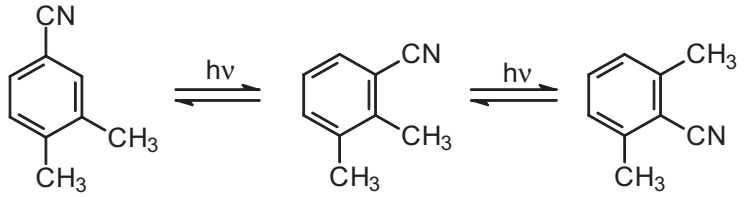


barriers on the reaction coordinate diagram need to be considered: first, the one from S_1 to intermediate **5**, and second, the ones that allow conversions among **5**, **6**, and **7**. Which of these barriers is more important can, at least partially, be assessed by examining the barrier separating S_1 and **5**.

To probe this question, we have examined the photochem-

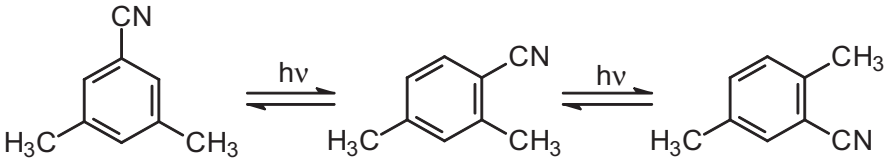
© 2006 NRC Canada

[4]



9-34 **9-23** **9-26**

[5]



9-35 **9-24** **9-25**

istry and photophysics of the three sets of substrates: Set 1 — *ortho*-xylene (**10**), tetralin (**11**), and indan (**12**); Set 2 — 2,3-dimethylbenzonitrile (**9-23**), 5-cyanotetralin (**T-23**), and 4-cyanoindan (**I-23**); and Set 3 — (3,4-dimethylbenzonitrile (**9-34**), 6-cyanotetralin (**T-34**), and 5-cyanoindan (**I-34**).[2] Set 1 was included to provide results for the cases without the nitrile group and because some previous literature values are available for comparison. We expected that the geometric changes required to form the bicyclic diradical intermediate (the important one in the phototransposition reactions) would be inhibited moving from left to right in each set.

Results and discussion

Synthesis of compounds

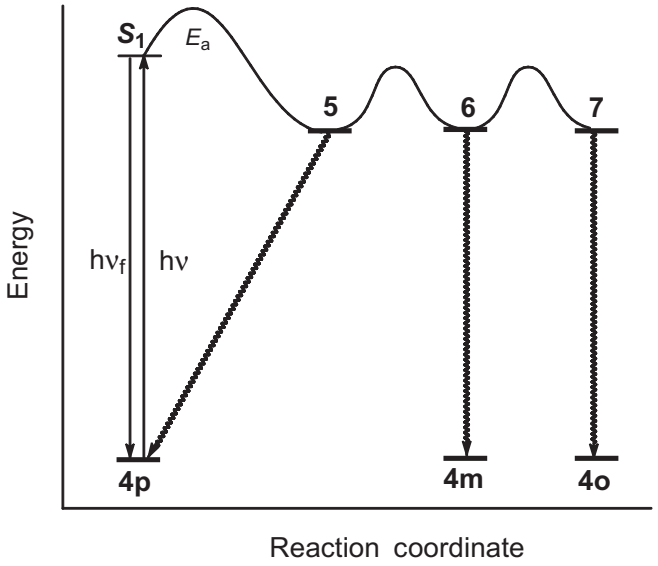
Compounds **10**, **11**, and **12** are commercially available. Compounds **9-23** and **9-34** were prepared in our laboratory previously (15). Compounds **T-23**, **I-23**, and **I-34** were synthesized in the same way by Sandmeyer reaction with CuCN from the corresponding amines, as described previously (16, 17). The amine precursor for **T-34** was prepared by nitration of tetralin, reduction of the mixture of 5- and 6-nitrotetralin to the mixture of amines with Sn–HCl, and separation of the amines by column chromatography with Florisil and 1% ethyl acetate in hexanes as the eluant.

Photolysis of compounds

Set 1

The phototransposition reactions of **10** have been described in the early literature (1, 18) and have been repeated in AN by Pincock and co-workers more recently (13). The ratio of meta to para isomers is 11:1 (obtained at very low conversion), indicating that both one-step and two-step phototranspositions are occuring in the primary photochemical event. This result is explained by rapid interconversion of the reactive intermediates, as in Scheme 2 for the methylbenzonitriles. Moreover, the addition of TFE to give the bicyclo[3.1.0]hexene addition products is efficient (13). Both **11** and **12** are photochemically unreactive in AN. However, any phototransposition reaction occurring would be undetectable.

Fig. 1. Proposed reaction coordinate diagram for the phototransposition reaction of methylbenzonitriles **4p** to **4m** and **4o**.

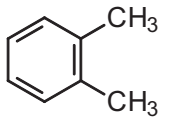


Set 2

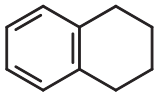
As described in the Introduction, **9-23** is very unreactive to phototransposition in AN and is only very slowly converted at 25 °C to a mixture of **9-34** (2.8%) and **9-26** (2.3%) after 760 min of irradiation. Photolysis at 50 °C is somewhat more efficient, giving 10.2% of **9-23** and 1.3% of **9-26** after the same length of time, indicating that the phototransposition reaction is an activated one as expected. Neither **T-23** nor **I-23** show any conversion to the possible transposi-

[2] The numbering system used is chosen to indicate the analogy of the position of the nitrile substituent relative to the two alkyl groups in each set with the acyclic compounds, *ortho*-xylene (**10**), 2,3-dimethylbenzonitrile (**9-23**), and 3,4-dimethylbenzonitrile (**9-34**) being the basis for comparison.

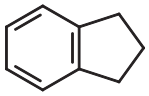
© 2006 NRC Canada



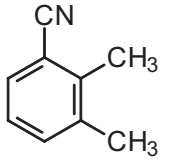
10



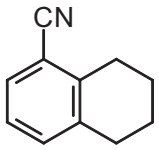
11



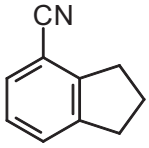
12



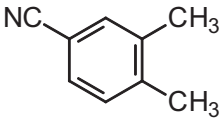
9-23



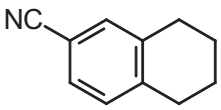
T-23



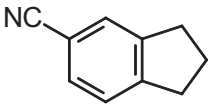
I-23



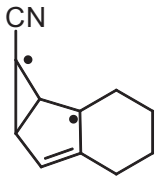
9-34



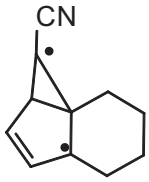
T-34



I-34



13



14

tion products **T-34** or **I-34**, respectively, in AN even on irradiation at 50 °C.

Set 3

In contrast to Set 2, the acyclic compound, **9-34**, is quite reactive. After 760 min of irradiation in AN at 25 °C, only 40% remained, giving **9-23** (53%) and **9-26** (7%). Surprisingly, a very similar conversion was obtained after the same time of irradiation at 50 °C. The cyclic tetralin **T-34** also reacts in AN giving the only possible phototransposition product **T-23**, although not quite as efficiently as for **9-34** with 36% conversion after 750 min irradiation. After 2500 min of irradiation, a photostationary state is reached with the ratio of **T-34**:**T-23** = 41:59. The indane derivative **I-34** again does not undergo phototransposition in AN or photoaddition in TFE, even at 50 °C.

Photophysical properties of the compounds of Sets 1–3

Values of λ_{max} (nm), ε ((mol/L)$^{-1}$ cm^{-1}), $E_{0,0}$ (kJ mol^{-1}, from overlap of the fluorescence and excitation spectra), Φ_f, τ (from nanosecond single photon counting), k_f (from $k_f = \Phi_f/\tau$), and k_f^{calc} (from eq. [6], the Strickler–Berg relationship (19), and $k_t = 1/\tau$) are given in Table 1.

$$[6] \qquad k_f = 2.88 \times 10^{-9} n^2 < \bar{\upsilon}_f^{-1} > \int \varepsilon d \ln \bar{\upsilon} = n^2 k_f^0$$

In eq. [6], the general theoretical relationship between the radiative lifetime ($\tau_f = 1/k_f$) and the absorbance spectrum, n is the refractive index of the solvent, υ_f is the expectation value for the frequency of the fluorescence spectrum, and the final term is the integrated molar absorptivity over the S_0 to S_1 transition in the absorbance spectrum. The constant gives k_f in units of s^{-1} if the frequency values are expressed in wavenumber (cm^{-1}) and molar absorptivity ε in the usual units ((mol/L)$^{-1}$ cm^{-1}). This equation is derived on the basis of the oscillator strength model and the important assumption that the excited singlet state and the ground state have similar geometries. The agreement in Table 1 between k_f (from experimental measurement of Φ_f and τ) and k_f^{calc} is excellent and confirms that the singlet excited state of each of these compounds is a spectroscopic minimum with little change in geometry from the ground state. We have made similar observations in the past for the use of eq. [6] for aryl-substituted methyl, allyl (20), and adamantyl (21) ethers. The one exception in Table 1 is for **I-23** with k_f^{calc} (3.8×10^7 s^{-1}) significantly larger than the experimental value (2.6×10^7 s^{-1}). However, the ε value, which is directly related to the calculated value of k_f by eq. [6], also seems anomalously high. Although we have rechecked the ε value several times for this compound, including with a repurified sample, and both NMR spectra and GC analysis indicated no

© 2006 NRC Canada

Table 1. Photophysical properties of the compounds of Sets 1–3 in AN at 25 °C.

Cmpd.	λ_{max} (nm) (ε ((mol/L)$^{-1}$cm^{-1}))	$E_{0,0}$ (kJ/mol)[a]	Φ_f	τ (ns)	k_f (10^7 s^{-1})[b]	k_f^{calc} (10^7 s^{-1})[c]
10	266 (268)	435	0.12	23.8	0.50	0.48
11	266 (437)	432	0.20	23.1	0.86	0.81
12	265 (577)	432	0.24	17.5	1.4	1.5
9-23	280 (1660)	404	0.22	9.3	2.4	2.4
T-23	282 (1880)	405	0.24	9.4	2.6	2.8
I-23	283 (2600)	404	0.23	8.8	2.6	3.8
9-34	273 (882)	418	0.16	8.9	1.8	1.3
T-34	275 (1320)	414	0.18	10.9	1.7	1.8
I-34	275 (882)	417	0.21	9.9	2.1	2.1

[a]From overlap of the excitation and emission spectra.
[b]$k_f = \Phi_f/\tau$.
[c]Calculated from eq. [6].

impurities, we suspect that this value is incorrect. The important conclusion reached from the data in Table 1 is that for these nitrile-substituted benzene derivatives, the photophysical properties (absorption spectra, excited singlet state energy, fluorescence quantum yields, and fluorescence rate constants (k_f)) are essentially the same for each compound of Sets 2 and 3.

Measurement of rate constants of reaction of S_1 by the temperature dependence of fluorescence

Recently, we have shown that the measurement of excited singlet state lifetimes (τ) or quantum yields of fluorescence (Φ_f) as a function of temperature provide a simple method for obtaining rate constants of reaction and other modes of decay of the excited singlet states of substituted benzene derivatives (22, 23). This method has also been used very effectively by the laboratories of Lewis for arylalkenes (24) and Zachariasse for arylamines (25).

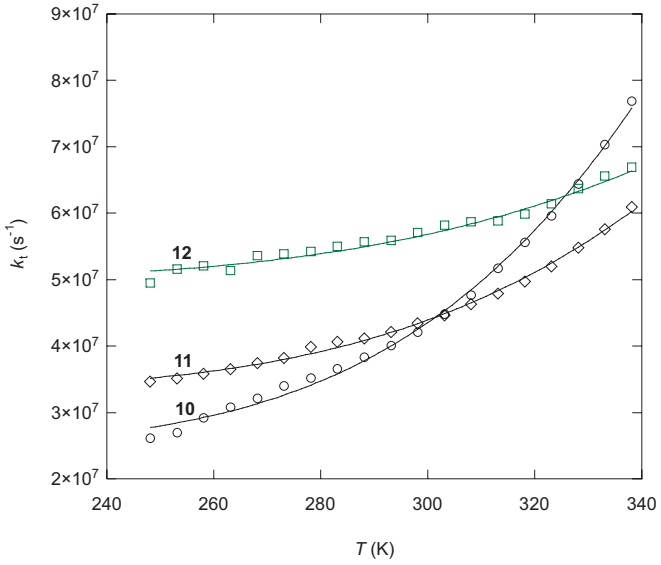
The basic concept is described by eqs. [7] and [8], where the total rate constant of decay of the excited singlet state (k_t) is the sum of all the rate constants of the individual processes: fluorescence (k_f), internal conversion (k_{ic}), intersystem crossing (k_{isc}), and the reaction itself (k_r). Equation [8] results from the assumptions that nonactivated internal conversion for substituted benzenes is very slow (~10^3 s^{-1}) (26), and that k_r is the only activated process and follows an Arrhenius expression. From Scheme 2 and Fig. 1, the k_r process leads to a reactive intermediate, which may proceed to rearranged products or return to S_0 by internal return (k_{ir}). This latter process has the same outcome as internal conversion but does not occur directly from S_1 and, therefore, is part of k_r. This possibility demonstrates that the measurement of quantum yields of formation of products cannot, in general, give reliable values of k_r.

$$[7] \qquad k_t = k_f + k_{ic} + k_{isc} + k_r$$

$$[8] \qquad k_t = k_f + k_{isc} + A \exp(-E_a/RT)$$

Values for k_t as a function of temperature for applying eq. [8] have normally been obtained by measuring S_1 lifetimes (τ_s), but this is a very time-consuming process. Nevertheless, we used that method for Sets 2 and 3, and the results are given in Tables S2 and S3.[3] A more rapid method is to use τ_s and Φ_f at 25 °C (Table 1) to obtain $k_f = \Phi_f/\tau_s$. Then measurement of relative fluorescence quantum yields over a wide temperature range (–25 to 65 °C) gives k_t (t °C) = [k_t (25 °C) Φ_f (25 °C) / Φ_f (t)]. This method assumes that k_f is a constant, independent of temperature. The values for the compounds of Set 1 were obtained by this method and are given in Table S1.[3]

Fig. 2. Fits of k_t vs. T according to eq. [8] for the compounds of Set 1.



Plots of k_t vs. T are shown in Figs. 2, 3, and 4 for Sets 1, 2, and 3, respectively. The plots for the two cyanoindan derivatives **I-23** (Fig. 3) and **I-34** (Fig. 4) are different from the rest, as they have very low, but negative, slopes. The fits shown in Figs. 2–4 are to a linear expression. Considering the experimental scatter, these slopes may not be significantly different from zero. However, negative slopes are, in

[3]Supplementary data for this article are available on the journal Web site (http://canjchem.nrc.ca) or may be purchased from the Depository of Unpublished Data, Document Delivery, CISTI, National Research Council Canada, Building M-55, 1200 Montreal Road, Ottawa, ON K1A 0R6, Canada. DUD 4069. For more information on obtaining material refer to http://cisti-icist.nrc-cnrc.gc.ca/irm/unpub_e.shtml.

© 2006 NRC Canada

Table 2. Fits to eq. [8] and derived rate constants and quantum yields at 25.0 °C for the compounds of Sets 1–3 in AN.

Cmpd.	A^a (10^{11} s^{-1})	$E_a{}^a$ (kJ/mol)	$(k_f + k_{isc})^a$ (10^7 s^{-1})	$k_f{}^b$ (10^7 s^{-1}) $\Phi_f{}^c$	k_{isc} (10^7 s^{-1}) Φ_{isc}	$k_r{}^d$ (10^7 s^{-1}) Φ_r	$k_t{}^d$ (10^7 s^{-1})
10	1.4	22.2	2.5	0.50	2.0	1.8	4.2
	(0.5)	(1.0)	(0.1)	0.12	0.45	0.42	
11	0.4	20.6	3.3	0.86	2.4	1.0	4.3
	(0.1)	(1.0)	(0.1)	0.20	0.56	0.23	
12	0.11	18.1	5.0	1.4	3.6	0.68	5.7
	(0.14)	(2.7)	(0.1)	0.24	0.63	0.12	
9-23	1.4	23.3	9.5	2.4	7.1	1.1	10.8
	(0.5)	(1.2)	(0.1)	0.22	0.66	0.10	
T-23	0.001	6.5	9.6	2.6	7.0	0.9	10.5
	(0.001)	(3.8)	(0.5)	0.24	0.67	0.09	
I-23	—	—	11.4	2.6	8.8	0.0	11.5
				0.22	0.77		
9-34	3.0	21.6	6.4	1.8	4.6	5.0	11.2
	(0.7)	(0.6)	(0.1)	0.16	0.40	0.45	
T-34	4.6	25.6	7.6	1.7	5.9	1.5	9.2
	(1.3)	(0.8)	(0.1)	0.24	0.64	0.16	
I-34	—	—	11.2	2.1	9.1	0.0	10.1
				0.21	0.79		

[a]From fits to eq. [8]. Errors are given in parentheses.
[b]$k_f = \Phi_f/\tau$, see Table 1.
[c]Estimated errors in Φ are ±10% and, therefore, also in k_f.
[d]Calculated from fits to eq. [8].

Fig. 3. Fits of k_t vs. T according to eq. [8] for the compounds of Set 2. The plot for **I-23** is a linear one.

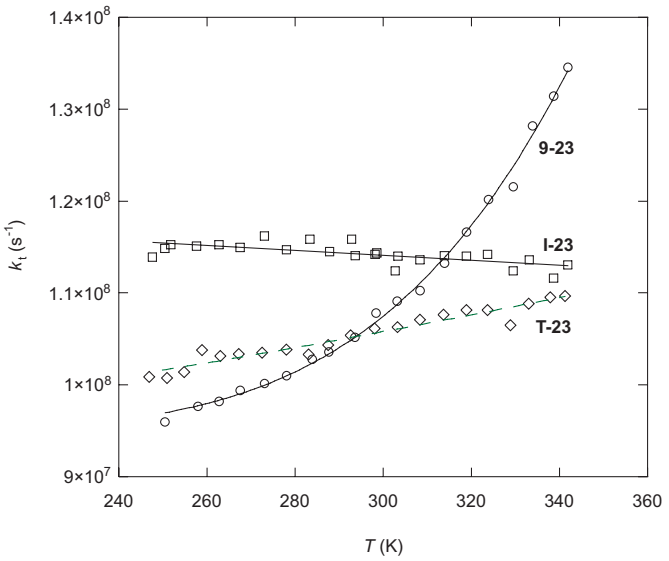
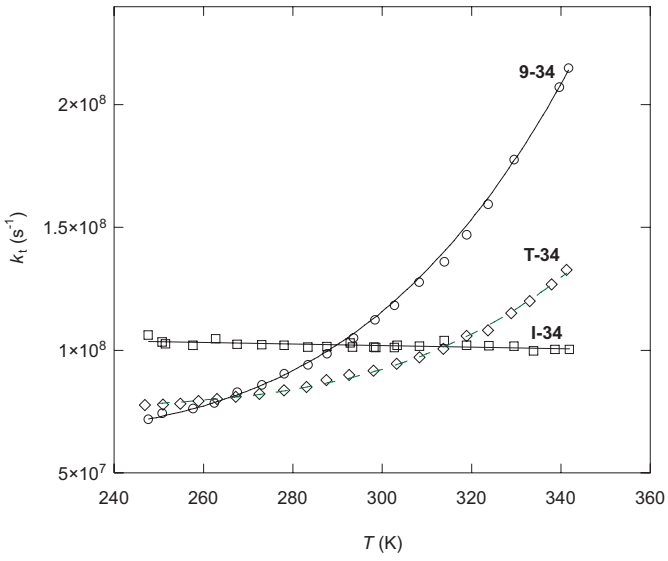


Fig. 4. Fits of k_t vs. T according to eq. [8] for the compounds of Set 3. The plot for **I-34** is a linear one



fact, expected, even if all of the rate constants of eq. [8] are temperature independent. The reason for this is given by eq. [9], where n is the refractive index of the solvent and n^0 is the refractive index of vacuum. Therefore, k_f should decrease slightly with temperature because n also decreases slightly with temperature (27). Equation [9] has been used previously to show that k_f^0 is independent of temperature for aromatics like benzene, toluene, *ortho*-xylene, and tetralin in hydrocarbon solvents (28). For other compounds studied with significant positive dependence of k_t with temperature, the very small negative changes in k_f with temperature were ignored and k_f was assumed to be constant.

$$[9] \qquad k_f = k_f^0 n^2$$

The more significant point to make about the plots for these two cyanoindan derivatives is that the plots have slopes that are essentially zero. Therefore, the activation energy for any aromatic ring deformation that could lead to reactive intermediates like the bicyclic structures of Scheme 2 must be too high over the temperature range examined for those processes to compete with fluorescence and intersystem crossing for deactivation of S_1. However, from the data in Table 2, the k_f values for each compound of Sets 2 and 3 are essentially the same. Therefore, the higher values of k_t for

© 2006 NRC Canada

compounds **I-23** and **I-34** at the lower temperatures reflect faster rates of intersystem crossing for the indan derivatives compared with their tetralin and acyclic analogues for each set. We have no explanation for this observation.

For the remaining compounds studied, the plots have obvious upward curvature, some more than others. Excellent fits of this data to eq. [8] were obtained ($r > 0.988$ in all cases), giving an intercept equal to $k_f + k_{isc}$ (assuming $k_{ic} = 0$) and Arrhenius A and E_a values from the curved portion. These values are given in Table 2. Previous literature values (28) for k_t obtained from –70 to +80 °C in methylcyclohexane for **10** gave $k_f + k_{isc} = (1.5 \pm 0.1) \times 10^7$ s^{-1}, $A = (2.1 \pm 1.8) \times 10^{11}$ s^{-1}, and $E_a = (25 \pm 3)$ kJ/mol in good agreement with our values in AN: $k_f + k_{isc} = (2.5 \pm 0.1) \times 10^7$ s^{-1}, $A = (1.4 \pm 0.5) \times 10^{11}$ s^{-1}, and $E_a = (22 \pm 1)$ kJ/mol. An important observation from similar measurements for benzene (28) is that although the k_f value obtained ((0.16 ± 0.01) $\times 10^7$ s^{-1}) is independent of the solvent, Φ_f (0.06, 0.05, 0.04, 0.029, and 0.025) and τ (34, 30, 28, 20, and 15 ns) decrease significantly as the solvent polarity increases (cyclohexane, methylcyclohexane, ethanol, methanol, and acetonitrile). The reason for this must be that k_r, the rate of formation of the prefulvene biradical **1** in Scheme 1, increases with solvent-ionizing ability. We have observed the same effect for the methylbenzonitriles (23) and arylboronate esters (29) on going from AN to TFE.

Surprisingly, the plot for indan itself (Fig. 2), in contrast to the other two indane derivatives with the nitrile substitutent, does show a slight upward curvature indicating a temperature-dependent process is occurring. However, in a recent publication (23), we used artificial data to assess the reliability of the temperature vs. fluorescence method for obtaining rate constants of reaction for S_1. The conclusion reached from our experimental method, which involves a limited temperature range (–25 to +65 °C), was that reliable values of k_r can only be obtained if $A > 0.5 \times 10^{11}$ s^{-1} and $E_a <$ 25 kJ/mol in order that the k_r process contributes significantly enough over the temperature range examined to compete with the other modes of deactivation. Zachariasse and co-workers (25) have overcome this problem by measuring Φ_{isc} (by laser flash photolysis of triplet yields), τ, and Φ_f from –151 to +284 °C for aminobenzonitriles in hydrocarbon solvents (25*d*). The low temperature data was analyzed to determine the temperature dependence of intersystem crossing because k_r (which, in the absence of any observable photochemical conversion, is described as an activated internal conversion (k_{ic})) did not contribute significantly to the overall rate of decay of the excited singlet state. At higher temperatures, the internal conversion process became the dominant one and its activation parameters could then be separated from those for intersystem crossing. Unfortunately, we cannot make measurements over such a wide temperature range because of the limitations of our instruments and quartz cuvettes. Nevertheless, we have shown that this method provides values for rate constants and quantum yields for the reactions of excited singlet states for benzene, toluene, and *ortho*-xylene that agree with those obtained by much more difficult experimental methods, particularly for intersystem crossing (22).

On this basis, the data for **12** and **T-23** (Table 2) do not satisfy the criteria that we have established. **T-23** is particularly obvious because of the very low A and E_a values obtained. Similar low values of A (~10^8 s^{-1}) and E_a (<10 kJ/mol) have been reported previously for activated intersystem crossing (23, 25). Therefore, the k_r value obtained from eq. [8] for the tetralin **T-23** is expected to be the contribution that activated k_{isc} makes to intersystem crossing. At room temperature for **T-23**, the total rate of intersystem crossing will then be $k_{isc} + k_r = 7.9 \times 10^7$ s^{-1} and $\Phi_{isc} = 0.76$, the remainder of the deactivation of S_1 being fluorescence, $\Phi_f = 0.24$. The activation parameters for **12** suggest that some activated bond deformation is leading to a low value of k_r; a surprising observation in view of the complete lack of reactivity of the cyanoindan derivatives **I-23** and **I-24**. However, photolysis at 254 nm of even the more highly strained benzocyclobutene yields two bicyclo[3.3.0]octatriene (also known as "dihydropentalenes") derivatives and the proposed mechanism included prefulvene (also known as "prebenzvalenes") as the critical intermediates (30).

Reliable values of k_r should be obtained for **10**, **11**, **9-23**, **9-34**, and **T-34**. The first conclusion to be reached, one that reinforces our previous reports (22, 23), is the general one that although the k_r process results in significant quantum yields, the actual quantum yields of reaction are considerably smaller. Therefore, internal return of the prefulvene biradical **1** (Scheme 1) is one of the dominant modes of deactivation of S_1 for substituted benzenes.

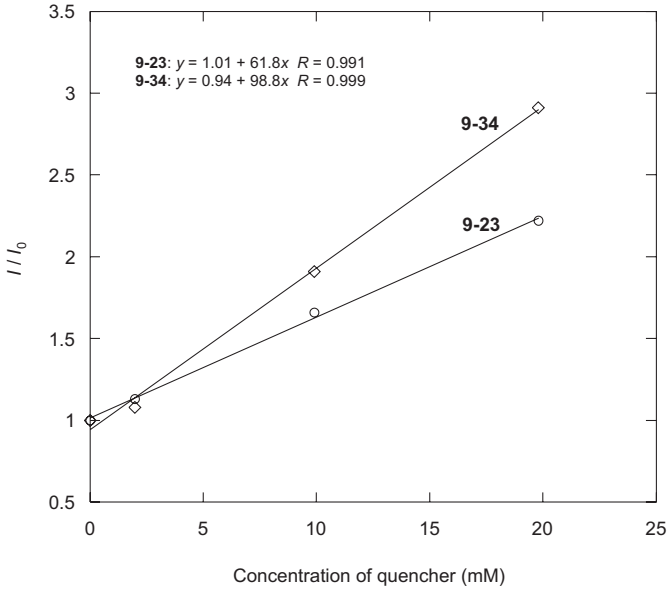
Also, the effect of ortho nitrile substitution is very evident for the tetralin derivatives, with both the unsubstituted case **11** and **T-34** having similar rates of reaction (1.0 and 1.5 × 10^7 s^{-1}, respectively); whereas for **T-23** this pathway is completely shut off and only intersystem crossing occurs. The preferred reaction pathway for nitrile-substituted benzene rings involves an intermediate with the nitrile group at C6 of the bicylic intermediate (Scheme 2). This geometry change looks possible for formation of **13** from **T-34**, but because of bridgehead strain, improbable for formation of **14** from **T-23**. For the acyclic nitrile-substituted cases, a similar steric effect is present but much less severe, k_r for **9-34** (5.0×10^7 s^{-1}) is only a factor of five times greater than for **9-23** (1.0×10^7 s^{-1}), in agreement with the observation from the preparative scale photochemistry that **9-34** is converted efficiently to **9-23**, but **9-23** is converted very slowly, even at 50 °C, back to **9-34**.

Triplet state reactivity of 9-23 and 9-34

Because of the very high quantum yields of intersystem crossing of 0.66 and 0.40 for **9-23** and **9-34**, respectively, the possibility of triplet state (T_1) reactivity must be considered. Previously, we have shown that the methylbenzonitriles **4p** and **4m** do not react from the triplet state and, therefore, S_1 was the reactive state for their phototransposition reactions. This was done by selective quenching of T_1 by 2,3-dimethyl-1,3-butadiene. The fluorescence of AN of **9-23** and **9-34** is also quenched by this diene giving Stern–Volmer ($k_q\tau$) slopes of 61.8 and 99.0 (mol/L)$^{-1}$, respectively (Fig. 5), and k_q values of 6.6 and 11.1×10^9 (mol/L)$^{-1}$ s^{-1}, respectively, close to the diffusional limit. Therefore, at a quencher concentration of 1.0×10^{-3} mol/L, the percentage of excited singlet states that are being quenched is 6% for **9-23** and 11% for **9-34**. Making the usual assumption that T_1 will be much longer lived than S_1 and that the quenching will also be dif-

© 2006 NRC Canada

Fig. 5. Stern–Volmer plots for the fluorescence quenching of **9-23** and **9-34** by 2,3-dimethyl-1,3-butadiene.



fusion controlled, the percentage of triplet states being quenched should be much higher. Irradiation of either **9-23** or **9-34** under these conditions resulted in only minor decreases in the efficiencies of the phototransposition reactions, suggesting that T_1 is, at most, a minor contributor to the phototransposition reactions of these two substrates. Irradiation of **9-34** at a higher concentration of the diene gave cycloaddition products (*m*/*z* 213 by GC–MS) as expected for quenching of the excited singlet states of substituted methylbenzonitriles by dienes (11).

Conclusions

The results presented clearly show that for compounds that undergo phototransposition reactions, significant barriers exist on the surface that connects S_1 to the reactive intermediate (E_a in Fig. 1). The major pathway for reaction of this substituted prefulvene biradical is return to the starting material by cleavage of the bond that was formed (meta bonding) from S_1. The first formed reactive intermediate equilibrates with its isomeric forms, which allows phototransposition to occur (Scheme 2). The barriers on this surface will not be easy to determine experimentally, but perhaps can be modelled by high level computational methods.

As expected, the effect of incorporating the substituted benzene into a bicyclic structure, as in the tetralin and indan derivatives, decreases the efficiency of formation of the reactive intermediate, particularly for the cyanoindans, **I-23** and **I-34**. Ortho substitution of the nitrile group to the alkyl groups also decreases reactivity for **9-23** and particularly for cyanotetralin, **T-23**.

Experimental

General procedures

Routine proton (^{1}H) and carbon (^{13}C) nuclear magnetic resonance (NMR) spectra were obtained in $CDCl_3$ on a Bruker AC 250 F NMR spectrometer in automation mode. GC–MS analyses were performed on a PerkinElmer Autosystem XL instrument with a mass selective detector. The column used was a Supelco 30 m × 0.25 mm MDN-5S 5% phenyl methylsiloxane, film thickness 0.50 mm, temperature programmed: 60 °C for 1 min; 20 °C per minute to 240 °C; and 240 °C for 10 min. GC-FID analyses were done on the same instrument. Mass spectral data are reported in units of mass over charge (*m*/*z*) for all values between 50 and the molecular ion if greater than 10% of the base peak. Intensities are reported as a % of the base peak. HR-MS were obtained on a CEC 21-110 instrument with a resolution of 5×10^3 to 10×10^3. The acetonitrile (HPLC grade, Caledon, Georgetown, Ontario) used for photochemical reactions and fluorescence measurements was used as received.

Preparation of compounds

ortho-Xylene (**10**), tetralin (**11**), and the benzonitriles (**9-23** and **9-34**) were obtained from Aldrich and purified by bulb-to-bulb distillation. Indan (95%, Sigma-Aldrich, Oakville, Ontario) was purified by silica gel chromatography using hexanes as the solvent, followed by bulb-to-bulb distillation.

The cyanotetralins (**T-23** and **T-34**) and cyanoindans (**I-23** and **I-34**) have all been reported previously (16, 17). All were prepared by diazotization of the corresponding amines, followed by reaction with CuCN. All four of these compounds were at least 99% pure (GC-FID). UV spectra are reported in Table 1. Other spectral data, not reported in the initial publications describing their preparation, are given in the following.

5-Cyanotetralin (T-23)

^{1}H NMR ($CDCl_3$) δ: 7.43 (1H, d, *J* = 7.5 Hz), 7.27 (1H, d, *J* = 8.0 Hz), 7.16 (1H, t, *J* = 7.5 Hz), 2.95 (2H, t, *J* = 6.0 Hz), 2.78 (2H, t, *J* = 6.0 Hz), 1.89–1.79 (4H, m). ^{13}C NMR ($CDCl_3$) δ: 22.5, 22.5, 28.0, 29.7, 112.7 (-CN), 118.2, 125.8, 130.2, 133.6, 138.7, 140.8. GC–MS *m*/*z*: 157 (61), 156 (26), 142 (17), 130 (13), 129 (100), 128 (14), 116 (19). HR-MS calcd. for $C_{11}H_{11}N$: 157.0891; found: 157.0897.

6-Cyanotetralin (T-34)

^{1}H NMR ($CDCl_3$) δ: 7.33–7.34 (2H, m), 7.13 (1H, d, *J* = 8.5 Hz), 2.77–2.80 (4H, m), 1.79–1.83 (4H, m). ^{13}C NMR ($CDCl_3$) δ: 22.6 (two signals), 29.0, 29.7, 109.1 (-CN), 119.4, 128.9, 129.9, 132.8, 138.5, 143.0. GC–MS *m*/*z*: 159 (21), 158 (86), 157 (86), 156 (68), 154 (11), 142 (58), 141 (11), 140 (30), 130 (42), 129 (100), 128 (56), 127 (32), 126 (13), 117 (12), 116 (73), 115 (34), 114 (12), 103 (28), 102 (53), 101 (20), 89 (33), 88 (10), 78 (25), 77 (49), 76 (32), 75 (27), 74 (15), 71 (10), 65 (14), 64 (24), 63 (47), 62 (16), 52 (17), 51 (50), 50 (22). HR-MS calcd. for $C_{11}H_{11}N$: 157.0891; found: 157.0896.

4-Cyanoindan (I-23)

^{1}H NMR ($CDCl_3$) δ: 7.39–7.43 (2H, m), 7.18–7.24 (1H, m), 3.10 (2H, t, *J* = 7.3 Hz), 2.98 (2H, t, *J* = 7.3 Hz), 2.18 (2H, quintet, *J* = 7.3 Hz). ^{13}C NMR ($CDCl_3$) δ: 24.6, 32.4, 32.9, 108.5, 118.1 (-CN), 126.8, 128.8, 129.5, 145.6, 148.3. GC–MS *m*/*z*: 144 (38), 143 (93), 142 (100), 141 (21), 140 (66), 117 (32), 116 (77), 115 (86), 114 (32), 113 (31),

© 2006 NRC Canada

103 (13), 102 (10), 91 (12), 90 (18), 89 (60), 88 (27), 87 (22), 86 (11), 77 (18), 76 (23), 74 (17), 71 (72), 65 (22), 64 (25), 63 (61), 62 (38), 61 (14), 60 (26), 59 (16), 57 (43), 52 (15), 51 (45), 50 (21). HR-MS calcd. for $C_{10}H_9N$: 143.0735; found: 143.0728.

5-Cyanoindan (I-34)

^{1}H NMR ($CDCl_3$) δ: 7.48 (1H, s), 7.42 (1H, d, J = 8.0 Hz), 7.30 (1H, d, J = 8.0 Hz), 2.93–2.96 (4H, m), 2.12 (2H, quintet, J = 7.0 Hz). ^{13}C NMR ($CDCl_3$) δ: 25.1, 32.6, 33.2, 109.7, 119.6 (-CN), 125.1, 127.9, 130.3, 145.4, 150.0. GC–MS *m/z*: 144 (10), 143 (100), 142 (98), 140 (20), 116 (49), 115 (50), 114 (10), 89 (19), 71 (10), 63 (23), 62 (13), 51 (16). HR-MS calcd. for $C_{10}H_9N$: 143.0735; found: 143.0732.

Irradiations

A solution of ~100 mg of the appropriate compound in 100 mL of acetonitrile was purged with nitrogen and then irradiated in a Rayonet photochemical reactor using 16 lamps (75 W, 254 nm). The temperature was controlled at the desired value by circulating water in an immersion tube. Reaction progress was monitored by GC.

Absorbance measurements

Absorbance spectra were recorded at 1 nm resolution using a Cary 100 UV–vis spectrometer thermostatted at 25 °C. The integrated spectra needed to obtain k_f values from eq. [6] were obtained by summing the 1 nm incremental areas (the absorbance values converted to ε by dividing by the molar concentration) over the complete absorption band. These areas are somewhat uncertain at the short wavelength end because of the overlap with the long wavelength tail of the S_2 band so that the absorbance does not reach zero. The wavelength for the minimum in absorbance was used as the cut-off point for the S_1 band.

Fluorescence measurements

All samples were degassed by three freeze–pump–thaw cycles and then thermostatted at 25 °C. Fluorescence intensity measurements were done using a PTI-210M fluorescence spectrometer with dual model 101 monochromators, a 75W xenon lamp, and a model 814 photomultiplier detector. Corrected spectra were obtained. Fluorescence quantum yields were determined using solutions of matched absorbance by comparison with the known fluorescence quantum yield for anisole of 0.29 (31) in cyclohexane. As a result of uncertainties in the standards and accumulation of errors, absolute values at 25 °C are probably accurate to 10%. Relative values are probably considerably better. The expectation values necessary for calculating the k_f values from eq. [6] were obtained by summing the 1 nm incremental areas over the complete emission band. For temperature-dependent quantum yield measurements, a 1 cm cuvette was thermostatted with stirring in a cuvette holder equipped with a Quantum Northwest TLC 50 temperature controller, which allows relative fluorescence measurements at 5 °C intervals from –25 to 65 °C in acetonitrile over a 3 h time span. The stability of the lamp over this time period was normally confirmed by rerunning the fluorescence spectrum at 25 °C at the end. The values of ϕ_f as a function of T were obtained this way for **10**, **11**, and **12** and used to calculate k_t (see previous text and Table S1).[3]

Singlet lifetimes were measured by monitoring fluorescence decay using a PRA time-correlated single photon counting apparatus with a hydrogen flash lamp of pulse width about 1.8 ns. The temperature was controlled (±0.1 °C) by circulating methanol from an external constant-temperature bath and checked by measurement in the fluorescence cuvette with a digital thermocouple probe. The values of $k_t = 1/\tau$ reported for **9-23**, **I-23**, **T-23**, **9-34**, **T-34**, and **I-34** were obtained this way (see Tables S2 and S3).[3]

Acknowledgments

We thank the National Sciences and Engineering Research Council of Canada (NSERC) for financial support, Dalhousie University for a fellowship (CMG), the Killam foundation for the award of a Dalhousie University Faculty of Science Killam professorship (JAP), and Sepracor Canada Ltd., Windsor, Nova Scotia, for the donation of chemicals.

References

1. K.E. Wilzbach and L. Kaplan. J. Am. Chem. Soc. **86**, 2307 (1974).
2. A.W. Burgstahler, P.-L. Chein, and M.O. Abdel-Raman. J. Am. Chem. Soc. **86**, 5291 (1964).
3. L. Kaplan, K.E. Wiltzbach, W.G. Brown, and S.S. Yang. J. Am. Chem. Soc. **87**, 675 (1965).
4. K.E. Wiltzbach, J.S. Ritscher, and L. Kaplan. J. Am. Chem. Soc. **89**, 1031 (1967).
5. L. Kaplan, J.S. Ritscher, and K.E. Wiltzbach. J. Am. Chem. Soc. **88**, 2881 (1966).
6. L. Kaplan, D.J. Rausch, and K.E. Wiltzbach. J. Am. Chem. Soc. **94**, 8638 (1972).
7. D. Bryce-Smith and A. Gilbert. Tetrahedron, **32**, 1309 (1976).
8. D. Bryce-Smith and A. Gilbert. Tetrahedron, **33**, 2459 (1977).
9. D. Bryce-Smith and A. Gilbert. *In* Rearrangements in ground and excited states. Vol. 3. *Edited by* P. DeMayo. Academic Press, New York. 1980. p. 349.
10. A. Gilbert. *In* CRC handbook of organic photochemistry and photobiology. *Edited by* W.M. Horspool and P.-J. Song. CRC Press, Boca Raton, Florida. 1995. pp. 229–236.
11. P.J. MacLeod, A.L. Pincock, J.A. Pincock, and K.A. Thompson. J. Am. Chem. Soc. **120**, 6443 (1998).
12. J. Foster, A.L. Pincock, J.A. Pincock, and K.A. Thompson. J. Am. Chem. Soc. **120**, 13354 (1998).
13. J. Foster, A.L. Pincock, J.A. Pincock, S. Rifai, and K.A. Thompson. Can. J. Chem. **78**, 1019 (2000).
14. J.A. Pincock. *In* CRC handbook of organic photochemistry and photobiology. Vol. 2. *Edited by* W.M. Horspool and F. Lenci. CRC Press, Boca Raton, Florida. 2004. pp. 46-1–46-19.
15. N. Howell, J.A. Pincock, and R. Stefanova. J. Org. Chem. **65**, 6173 (2000).
16. O. Exner and Z. Friedl. Coll. Czech. Chem. Commun. **43**, 3227 (1978).
17. J. Houben and W. Fischer. Ber. **63B**, 2464 (1930).
18. P. Anderson. J. Phys. Chem. **74**, 1686 (1970).
19. S.J. Stickler and R.A. Berg. J. Chem. Phys. **37**, 814 (1962).
20. A.L. Pincock, J.A. Pincock, and R. Stefanova. J. Am. Chem. Soc. **124**, 9768 (2003).
21. A.L. Pincock and J.A. Pincock. Can. J. Chem. **83**, 1237 (2005).

© 2006 NRC Canada

22. C.M. Gonzalez and J.A. Pincock. J. Am. Chem. Soc. **26**, 8870 (2004).
23. C. Gonzalez and J. Pincock. Photochem. Photobiol. doi:10.1562/2005-04-27-RA-502.
24. (*a*) F.D. Lewis and X. Zuo. J. Am. Chem. Soc. **125**, 8806 (2003); (*b*) F.D. Lewis and X. Zuo. J. Am. Chem. Soc. **125**, 2046 (2003); (*c*) F.D. Lewis, X. Zuo, R.S. Kalgutkar, J.M. Wagenr-Brennan, M.A. Miranda, E. Font-Sanchis, and J. Perez-Orieto. J. Am. Chem. Soc. **123**, 11883 (2001); (*d*) F.D. Lewis and R.S. Kalgutkar. J. Phys. Chem. A, **105**, 285 (2001); (*e*) F.D. Lewis and W. Weigel. J. Phys. Chem. A, **104**, 8146 (2000); (*f*) F.D. Lewis, R.S. Kalgutkar, and J.-S. Yang. J. Am. Chem. Soc. **121**, 12045 (1999); (*g*) F.D. Lewis, D.M. Bassani, R.A. Caldwell, and D.J. Unett. J. Am. Chem. Soc. **116**, 10477 (1994).
25. (*a*) I. Rückert, A. Demeter, O. Morawski, W. Kühnle, E. Tauer, and K.A. Zachariasse. J. Phys. Chem. **103**, 1958 (1999); (*b*) K. Suzuki, A. Demeter, W. Kühnle, E. Tauer, K.A. Zachariasse, S. Tobita, and H. Shizuka. Phys. Chem. Chem. Phys. **2**, 981 (2000); (*c*) S.I. Druzhinin, Y.-B. Jiang, A. Demeter, and K.A. Zachariasse. Phys. Chem. Chem. Phys. **3**, 5213 (2001); (*d*) S.I. Druzhinin, A. Demeter, V.A. Galievsky, T. Yoshihara, and K.A. Zachariasse. J. Phys. Chem. **107**, 8075 (2003).
26. N.V. Nijegorodov, V. Ramachandran, and D.P. Winkoun. Spectrochim. Acta, Part A, **53**, 1813 (1997).
27. J. Timmermans. Physico-chemical constants of pure organic liquids. Vol. 1. Elsevier, New York. 1950.
28. R.B. Cundall and L.C. Pereira. J. Chem. Soc. Faraday Trans. **68**, 1152 (1972).
29. K.S. Cameron, A.L. Pincock, J.A. Pincock, and A. Thompson. J. Org. Chem. **69**, 4954 (2004).
30. N.J. Turro, Z. Zhang, W.E. Trahanovsky, and C.-H. Chou. Tetrahedron Lett. **29**, 2543 (1988).
31. I.B. Berlman. Handbook of fluorescence spectra of aromatic molecules. Academic Press, New York. 1971. p. 139.

© 2006 NRC Canada

Preparation, spectroscopic characterization, and deprotonation reactions of $Si(NHR)_4$ (R = *i*-Pr, *t*-Bu, *p*-tolyl) — EPR identification of persistent radicals formed by oxidation of polyimidosilicates

Andrea F. Armstrong, Tristram Chivers, and Jari Konu

Abstract: Treatment of $Cl_2Si(NH\text{-}t\text{-}Bu)_2$ (**6a**) with *t*-$BuNH_2$ in boiling toluene yields trisamino(chloro)silane $ClSi(NH\text{-}t\text{-}Bu)_3$ (**7**); formation of the tetraaminosilane $Si(NH\text{-}t\text{-}Bu)_4$ is not observed. The reaction of $SiCl_4$ with 4 equiv. of LiNHR produces the corresponding tetraaminosilanes $Si(NHR)_4$ (**2a**, R = *i*-Pr; **2b**, R = *t*-Bu; **2c**, R = *p*-tol) in good yields. When the sterically demanding adamantyl derivative LiHNAd is employed, only disubstitution occurs to form $Cl_2Si(NHAd)_2$ (**6b**). Oxidation of the dimeric imidosilicates $\{Li_3[Si(NR)_3(NHR)]\cdot THF\}_2$ (**3a**, R = *i*-Pr; **3b**, R = *t*-Bu) with 1 mol of iodine produces the persistent radicals $\{Li_2[Si(NR)_3(NHR)]\cdot LiI\cdot 3THF\}^{\cdot}$, which, on the basis of EPR spectra, exist as SiN_3Li_3I cubes in solution. The spirocyclic tetraimidosilicate monoanion radical $\{[(THF)_2Li(\mu\text{-}Nnaph)_2Si(\mu\text{-}Nnaph)_2Li(THF)_2]\}^{-\cdot}$ (**10**) is formed upon oxidation of the tetralithiated species $\{Li_4[Si(Nnaph)_4]\cdot 4Et_2O\}$ (**1**) and $\{[Li(12\text{-crown-}4)]_2[(Et_2O)_2Li(\mu\text{-}Nnaph)_2Si(\mu\text{-}Nnaph)_2Li(Et_2O)_2]\}$ (**8**) with iodine. The spectroscopic characterization of hexa(amino)disiloxane $(t\text{-}BuNH)_3SiOSi(NH\text{-}t\text{-}Bu)_3$ (**14**) formed from the reaction of $Cl_3SiOSiCl_3$ with 6 equiv. of LiNH-*t*-Bu is discussed.

Key words: imido ligands, silicate, radicals, EPR spectra, lithium.

Résumé : Le traitement du $Cl_2Si(NH\text{-}t\text{-}Bu)_2$ (**6a**) par de la *t*-$BuNH_2$ dans du toluène bouillant conduit à la formation de trisamino(chloro)silane, $ClSi(NH\text{-}t\text{-}Bu)_3$ (**7**); on n'a pas observé de formation du tétraaminosilane, $Si(NH\text{-}t\text{-}Bu)_4$. La réaction du $SiCl_4$ avec quatre équivalents de LiNHR conduit à la formation des tétraaminosilanes correspondants, $Si(NHR)_4$ (**2a**, R = *i*-Pr; **2b**, R = *t*-Bu; **2c**, R = *p*-tol), avec de bons rendements. Lorsqu'on effectue la réaction avec le LiHNAd, un dérivé de l'adamantane dont les contraintes stériques sont plus grandes, on ne se produit qu'une disubstitution conduisant à la formation du $Cl_2Si(NHAd)_2$ (**6b**). L'oxydation des imidosilicates dimères $\{Li_3[Si(NR)_3(NHR)\cdot THF\}_2$ (**3a**, R = *i*-Pr; **3b**, R = *t*-Bu) avec une mole d'iode conduit à la formation des radicaux persistants $\{Li_2[Si(NR)_3(NHR)\cdot LiI\cdot 3THF\}^{\cdot}$ qui, sur la base de leurs spectres RPE, existeraient en solution sous la forme de cubes de SiN_3Li_3I. L'oxydation par de l'iode des espèces tétralithiées $\{Li_4[SiNnaph)_4]\cdot 4Et_2O\}$ (**1**) et $\{Li[12\text{-couronne-}4]_2[(Et_2O)_2Li(\mu\text{-}Nnaph)_2Si(\mu\text{-}Nnaph)_2Li(Et_2O)_2]\}$ (**8**) conduit à la formation du radical monoanion tétraimidosilicate spirocyclique $\{[(THF)_2Li(\mu\text{-}Nnaph)_2Si(\mu\text{-}Nnaph)_2Li(THF)_2]\}^{-\cdot}$ (**10**). On discute de la caractérisation spectroscopique de l'hexa(amino)disiloxane $(t\text{-}BuNH)_3SiOSi(NH\text{-}t\text{-}Bu)_3$ (**14**) qui se forme par réaction du $Cl_3SiOSiCl_3$ avec six équivalents de LiNH-*t*-Bu.

Mots clés : ligands imido, silicate, radicaux, spectre RPE, lithium.

[Traduit par la Rédaction]

Introduction

An ongoing area of research in main group chemistry is the synthesis and characterization of imido $[NR]^{2-}$ (R = alkyl, aryl) analogues of common *p*-block oxoanions such as sulfate and phosphate (1–3). The chemistry of the tetraimidophosphate trianion $[P(NR)_4]^{3-}$, formally isoelectronic[2] with orthophosphate $[PO_4]^{3-}$, has been extensively explored. Both main group (4–7) and transition-metal (8) derivatives are known; the coordination behaviour (6, 7) and radical chemistry (6, 7, 9, 10) of this important member of the family of polyimido anions have been examined.

In contrast, the chemistry of the isoelectronic tetraimidosilicate tetraanion ($[Si(NR)_4]^{4-}$) remains essentially unknown; only one example, $\{Li_4[Si(Nnaph)_4]\cdot 4Et_2O\}_x$ (**1**), has been characterized (11). This naphthyl derivative was originally targeted because, unlike the majority of primary amines, 1-aminonaphthalene can be doubly deprotonated

Received 2 August 2005. Published on the NRC Research Press Web site at http://canjchem.nrc.ca on 22 February 2006.

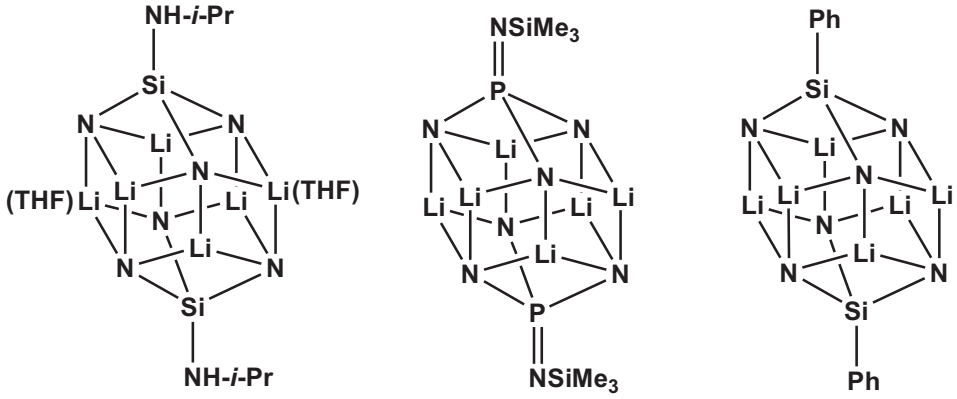
A.F. Armstrong, T. Chivers,[1] and J. Konu. Department of Chemistry, University of Calgary, Calgary, AB T2N 1N4, Canada.

[1]Corresponding author (e-mail: chivers@ucalgary.ca).

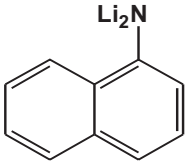
[2]The original definition of "isoelectronic" (isosteric) compounds restricts the term to species having the *same number of atoms* and the same number of electrons (I. Langmuir. J. Am. Chem. Soc. **41**, 1543 (1919)). Thus, according to this definition, N^{3-} is isoelectronic with O^{2-}. However, nitrides are compositionally different to oxides as a result of the different charges on the anions.

 doi:10.1139/V05-264 © 2006 NRC Canada

Fig. 1. Solid-state structures of **3a**, **4**, and **13**. The *i*-Pr (**3a**), *t*-Bu (**4a**, **13**), and Ad (**4b**) groups are omitted from cluster N atoms for clarity.



3a **4** **13**

[1] $SiCl_4 + 4$  $\xrightarrow[-4\ LiCl]{Et_2O} \{Li_4[Si(Nnaph)_4]\bullet 4Et_2O\}$

(12, 13). The metathesis reaction between dilithiated amide (Li_2Nnaph) and silicon tetrachloride ($SiCl_4$) in diethyl ether proceeds with the elimination of lithium chloride (LiCl) to yield **1** (eq. [1]) (11).

Unfortunately, it has not proven possible to grow crystals of **1** that are suitable for X-ray analysis; in consequence, the solid-state structure of **1** remains unknown. In an effort to structurally characterize a tetraimidosilicate, the preparation of the isopropyl analogue of **1** was also attempted by the reaction of tetraaminosilane $Si(NH\text{-}i\text{-}Pr)_4$ (**2a**) with 4 equiv. of *n*-butyllithium. Regardless of the reaction conditions, only trilithiation was achieved, resulting in the isolation of $\{Li_3[Si(N\text{-}i\text{-}Pr)_3(NH\text{-}i\text{-}Pr)]\cdot THF\}_2$ (**3a**) (11). This behaviour is reminiscent of observations reported for trisamino(imino)phosphoranes, for which only twofold deprotonation of $(i\text{-}PrNH)_3PNSiMe_3$ is observed under a variety of reaction conditions (10). However, it should be noted that the reaction of the *tert*-butyl analogue $(t\text{-}BuNH)_3PNSiMe_3$ with *n*-BuLi yields the tetraimidophosphate $[P(N\text{-}t\text{-}Bu)_3(NSiMe_3)]^{3-}$ via triple deprotonation under mild reaction conditions (5). Thus, it is of interest to attempt the tetralithiation of $Si(NH\text{-}t\text{-}Bu)_4$ (**2b**) to determine whether a similar increase in reactivity over **2a** is observed.

An examination of the extant literature (14) regarding **2b** revealed that no practical synthetic route to this compound has been reported, though **2a** is well-known and can be prepared by the reaction of excess isopropylamine with $SiCl_4$ (15). However, only a 6% yield of the desired product **2b** is recovered from the analogous reaction of $SiCl_4$ with excess *tert*-butylamine, even at elevated reaction temperatures (14). Thus, the synthesis of **2b** has been reinvestigated, as only minimal experimental detail is available from previous work.

The isoelectronic relationship between the tetraimidosilicate tetraanion $[Si(NR)_4]^{4-}$ of **1** and the tetraimidophosphate trianion $[P(NR)_4]^{3-}$ is especially intriguing in light of the remarkably stable radicals formed upon oxidation of $\{Li_3[P(NR)_3(NSiMe_3)]\}_2$ (**4a**, R = *t*-Bu; **4b**, R = Ad) with halogens (9, 10). As the synthesis of radicals of the p-block elements is a topical area of research (16), it will, thus, be of interest to examine the one-electron oxidation of **1** to see if similar behaviour is observed. Furthermore, the fact that **3a** is isostructural with **4** (Fig. 1) suggests that the oxidation of **3a** may well result in the formation of cubic radicals that are isostructural with the tetraimidophosphate radicals $\{Li_2[P(NR)_3(NSiMe_3)]\cdot LiX\cdot 3THF\}^{\cdot}$ (**5a**, R = *t*-Bu; **5b**, R = Ad; X = Cl, Br, I) described previously (9, 10).

In this contribution, we describe the synthesis and multinuclear NMR spectroscopic characterization of (*i*) the tetraaminosilanes $Si(NHR)_4$ (**2a**, R = *i*-Pr; **2b**, R = *t*-Bu; **2c**, R = *p*-tol), (*ii*) the aminochlorosilanes $Cl_2Si(NHAd)_2$ (**6b**) and $ClSi(NH\text{-}t\text{-}Bu)_3$ (**7**), and (*iii*) the hexa(amino)disiloxane $(t\text{-}BuNH)_3SiOSi(NH\text{-}t\text{-}Bu)_3$ (**14**) and the tetraimidosilicate complex $\{[Li(12\text{-crown-}4)]_2[(Et_2O)_2Li(\mu\text{-}Nnaph)_2Si(\mu\text{-}Nnaph)_2\text{-}Li(Et_2O)_2]\}$ (**8**). We also report the characterization, by EPR spectroscopy, of persistent radicals formed by oxidation of tetramido- and aminotris(imido)-silicates with iodine.

Experimental

Reagents and general procedures

All experiments were carried out under an argon atmosphere using standard Schlenk techniques. Toluene, diethyl ether, and tetrahydrofuran (THF) were dried over Na–benzophenone, distilled, and stored over molecular sieves prior to use. 12-Crown-4 (98%), $Cl_3SiOSiCl_3$ (>98%), *n*-BuLi (2.5 mol/L solution in hexanes), *tert*-butylamine, and $SiCl_4$ (99%) were used as received from Aldrich. The lithiated amides LiHNR (R = *i*-Pr, *t*-Bu, *p*-tol) were prepared by standard procedures involving the reaction of the corresponding primary amines with *n*-BuLi in hexane (*i*-Pr, *t*-Bu) or Et_2O (*p*-tol) at –78 °C. Iodine was sublimed prior to use. Com-

© 2006 NRC Canada

pounds **1** (11), **3b** (11), and **13** (17) were prepared by the methods reported in the literature.

Instrumentation

^{1}H, ^{7}Li, ^{13}C, ^{29}Si, and ^{31}P NMR spectra were collected on a Bruker DRX-400 spectrometer with ^{1}H and ^{13}C chemical shifts referenced internally to ^{1}H impurities and natural abundance ^{13}C in the deuterated solvents, respectively; external standards were used for the ^{7}Li (LiCl in D_2O), ^{29}Si ($SiMe_4$ in $CDCl_3$), and ^{31}P (85% H_3PO_4 in D_2O) spectra. All spectra were collected at 22 °C (unless otherwise noted). IR spectra were recorded as Nujol or Fluorolube mulls on KBr plates using a Nicolet Nexus 470 FT IR spectrometer in the range 4000–400 cm^{-1}. Mass spectra were recorded on a Bruker Esquire 3000 ESI ion trap mass spectrometer. Elemental analyses were provided by the Analytical Services Laboratory, Department of Chemistry, University of Calgary, Calgary, Alberta and by Canadian Microanalytical Service Ltd., Vancouver, British Columbia. EPR spectra were recorded at 22 °C on a Bruker EMX 113 spectrometer; spectral simulations were carried out using WINEPR SimFonia; spectra were plotted using WinEPR (18). The *g* values of the radicals were calculated using the field–frequency ratio of each sample.

Preparation of Si(NH-*i*-Pr)$_4$ (2a)

$SiCl_4$ (1.3 mL, 1.93 g, 11.3 mmol) was added dropwise to a white slurry of LiHN-*i*-Pr (3.040 g, 46.74 mmol) in diethyl ether (50 mL) at 0 °C. The reaction mixture was stirred for 3 h, then warmed slowly to 22 °C and stirred for an additional 15 h. The pale yellow slurry was centrifuged; the supernatant liquid was filtered, leaving a colourless filtrate. The solvent was removed in vacuo and the product was washed with hexane (5 mL), giving Si(NH-*i*-Pr)$_4$ as a white powder (2.292 g, 8.80 mmol, 78%). ^{1}H NMR (C_6D_6) δ: 3.22 (sept, 1H, CH_3-C*H*, ^{3}J(H,H) = 7 Hz), 1.10 (d, 6H, C*H*$_3$-CH, ^{3}J(H,H) = 7 Hz, Me). $^{13}C\{^{1}H\}$ NMR (C_6D_6) δ: 42.65 (s, CH), 28.34 (s, CH_3). Literature values (from ref. 15): ^{1}H NMR (C_6D_6) δ: 3.21 (sept, 1H, CH_3-C*H*, ^{3}J(H,H) = 6.7 Hz), 1.10 (d, 6H, C*H*$_3$-CH, ^{3}J(H,H) = 6.7 Hz, Me). $^{13}C\{^{1}H\}$ NMR (C_6D_6) δ: 42.6 (s, CH), 28.3 (s, CH_3).

Preparation of Si(NH-*t*-Bu)$_4$ (2b)

A solution of $SiCl_4$ (0.79 mL, 6.90 mmol) in diethyl ether (15 mL) was added to a white slurry of LiHN-*t*-Bu (2.191 g, 27.71 mmol) in diethyl ether (50 mL) at 0 °C. The reaction mixture was stirred for 1 h, then warmed slowly to 22 °C and stirred for an additional 3.5 h. The white slurry was filtered, and the solvent was removed from the colorless filtrate in vacuo, giving Si(NH-*t*-Bu)$_4$ as a white powder (1.830 g, 5.78 mmol, 84%). ^{1}H NMR (C_6D_6) δ: 1.28 (s, *t*-Bu). $^{13}C\{^{1}H\}$ NMR (C_6D_6) δ: 48.69 (s, *C*Me$_3$), 33.99 (s, C*Me*$_3$). $^{29}Si\{^{1}H\}$ NMR (C_6D_6) δ: –52.9 (s). MS (EI): 316.6 ($[M]^+$). Anal. calcd. for $C_{16}H_{40}N_4Si$: C 60.70, H 12.73, N 17.70; found: C 60.28, H 11.47, N 17.97.

Preparation of Si(NH-*p*-tol)$_4$ (2c)

$SiCl_4$ (0.11 mL, 0.16 g, 0.96 mmol) was added dropwise to a white slurry of LiHN-*p*-tol·Et_2O (0.606 g, 3.723 mmol) in diethyl ether (35 mL) at 0 °C. The reaction mixture was stirred for 2 h, then warmed slowly to 22 °C and stirred for an additional 15 h. The pale orange slurry was centrifuged; the supernatant liquid was filtered, leaving a yellow filtrate. The solvent was removed in vacuo, giving Si(NH-*p*-tol)$_4$ as a pale orange powder (0.338 g, 0.747 mmol, 78%). ^{1}H NMR (C_6D_6) δ: 6.90, 6.71 (d of d, 4H, C_6H_4, $^{2}J(^{1}H,^{1}H)$ = 76.8 Hz, $^{3}J(^{1}H,^{1}H)$ = 8.2 Hz), 3.80 (s, 1H, N*H*), 2.11 (s, 3H, *p*-CH_3). $^{13}C\{^{1}H\}$ NMR (C_6D_6) δ: 142.66 (s, *C*-NH), 130.22 (s, *o*-*C*H), 128.53 (*m*-*C*H), 117.59 (*C*-CH_3), 20.53 (CH_3). $^{29}Si\{^{1}H\}$ NMR (C_6D_6) δ: –52.9 (s). Anal. calcd. for $C_{28}H_{32}N_4Si$: C 74.29, H 7.13, N 12.38; found: C 73.22, H 7.13, N 11.91.

Preparation of Cl$_2$Si(NH-*t*-Bu)$_2$ (6a)

A solution of $SiCl_4$ (4.0 mL, 34.9 mmol) in diethyl ether (20 mL) was added to a solution of *t*-$BuNH_2$ (25.0 mL, 0.238 mol) in diethyl ether (150 mL) at 22 °C over 5 min, resulting in a dense white slurry. The reaction mixture was stirred for 16 h, then filtered through a sintered glass frit, yielding a clear colourless filtrate. The white solid (*t*-$BuNH_3$)Cl was washed with diethyl ether (100 mL). The solvent was removed from the filtrate in vacuo, giving $Cl_2Si(NH$-*t*-Bu$)_2$ as a colourless liquid (7.024 g, 28.88 mmol, 83%). ^{1}H NMR (C_6D_6) δ: 1.48 (br, N*H*), 1.11 (s, *t*-Bu). $^{13}C\{^{1}H\}$ NMR (C_6D_6) δ: 50.61 (s, *C*Me$_3$), 32.63 (s, C*Me*$_3$). $^{29}Si\{^{1}H\}$ NMR (C_6D_6) δ: –38.9 (s). Literature values (from ref. 18): ^{1}H NMR (C_6D_6) δ: 1.49, 1.11. $^{13}C\{^{1}H\}$ NMR (C_6D_6) δ: 50.6, 32.5.

Preparation of Cl$_2$Si(NHAd)$_2$ (6b)

$SiCl_4$ (0.26 mL, 2.27 mmol) was added to a white slurry of LiHNAd (0.714 g, 4.54 mmol) in toluene (30 mL) at 0 °C. The reaction mixture was allowed to warm to 22 °C and stirring was continued for 28 h. The reaction mixture was filtered and the solvent was removed from the filtrate in vacuo, giving $Cl_2Si(NHAd)_2$ as a white solid (0.731 g, 1.83 mmol, 81%). ^{1}H NMR (C_6D_6) δ: 1.90 (br, 1H, C*H*), 1.79 (d, 2H, *CH*$_2$-C-NH), 1.49 (t, 2H, CH-*CH*$_2$-CH). $^{13}C\{^{1}H\}$ NMR (C_6D_6) δ: 51.20 (s, *C*-NH), 46.25 (s, *C*H), 36.45 (s, *CH*$_2$-C-NH), 30.35 (s, CH-*CH*$_2$-CH). $^{29}Si\{^{1}H\}$ NMR (C_6D_6) δ: –38.8 (s). Anal. calcd. for $C_{20}H_{30}N_2SiCl_2$: C 60.13, H 8.07, N 7.01; found: C 59.85, H 8.24, N 7.13.

Preparation of ClSi(NH-*t*-Bu)$_3$ (7)

tert-Butylamine (10.0 mL, 95.16 mmol) was added to a solution of $Cl_2Si(NH$-*t*-Bu$)_2$ (3.078 g, 12.65 mmol) in toluene (20 mL) at 22 °C, resulting in a clear colorless solution. The reaction mixture was refluxed at 113 °C for 24 h. The resulting white slurry was cooled to 22 °C and filtered through a sintered glass frit, resulting in a clear colorless filtrate. The white solid (*t*-$BuNH_3$·HCl) was washed with toluene (5 mL). The solvent was removed from the filtrate in vacuo, giving spectroscopically pure $ClSi(NH$-*t*-Bu$)_3$ as a colourless liquid (3.138 g, 11.21 mmol, 89%). ^{1}H NMR (C_6D_6) δ: 1.20 (s, *t*-Bu). $^{13}C\{^{1}H\}$ NMR (C_6D_6) δ: 49.47 (s, *C*Me$_3$), 33.28 (s, C*Me*$_3$). $^{29}Si\{^{1}H\}$ NMR (C_6D_6) δ: –45.2 (s).

Preparation of {[Li(12-crown-4)]$_2$[(Et$_2$O)$_2$Li(μ-Nnaph)$_2$Si(μ-Nnaph)$_2$Li(Et$_2$O)$_2$]} (8)

n-Butyllithium (4.65 mL, 11.62 mmol) was added to a solution of 1-aminonaphthalene (0.833 g, 5.817 mmol) in diethyl ether (30 mL) at –78 °C and stirred for 1 h. $SiCl_4$

© 2006 NRC Canada

(0.17 mL, 1.484 mmol) was added to the reaction mixture dropwise. After 30 min, the reaction mixture was warmed to 22 °C and stirred for an additional 24 h. The resulting yellow slurry was then filtered, yielding a clear yellow solution. 12-Crown-4 (0.48 mL, 3.024 mmol) was added to the solution at 22 °C, resulting in a yellow slurry, which was stirred for 1 h. The solvent was then removed in vacuo, giving **8** as a bright yellow powder (1.489 g, 1.166 mmol, 80%). ^{1}H NMR (d_8-THF) δ: 8.5 (br), 8.10 (d, 4H), 7.44 (d, 4H), 7.09 (t, 4H), 7.02 (t, 4H), 6.90 (t, 4H), 6.40 (t, 4H), 3.40 (q, 16H, Et_2O), 3.33 (s, 24H, 12-crown-4), 1.14 (t, 24H, Et_2O). ^{13}C{^{1}H} NMR (d_8-THF) δ: 162.37, 137.44, 128.61, 128.24, 127.06, 124.63, 124.19, 120.70, 108.46, 106.92, 68.82 (s, 12-crown-4), 65.52 (s, $(CH_3CH_2)_2O$), 14.59 (s, $(CH_3CH_2)_2O$). ^{7}Li NMR (d_8-THF) δ: 0.63 (s). Anal. calcd. for $C_{72}H_{100}N_4SiO_{12}Li_4$: C 68.12, H 7.94, N 4.41; found: C 67.20, H 8.00, N 4.83.

Preparation of (*t*-BuNH)$_3$SiOSi(NH-*t*-Bu)$_3$ (14)

A solution of $Cl_3SiOSiCl_3$ (1.479 g, 5.191 mmol) in diethyl ether (10 mL) was added to a white slurry of LiHN-*t*-Bu (2.463 g, 31.15 mmol) in diethyl ether (40 mL) at 0 °C. After 30 min, the white slurry was warmed to 22 °C and stirred for an additional 15 h. The resulting pale yellow slurry was filtered and the solvent was removed from the filtrate in vacuo, giving (*t*-BuNH)$_3$SiOSi(NH-*t*-Bu)$_3$ as a pale yellow solid (1.770 g, 3.505 mmol, 68%). Sublimation of the crude product at 135 °C under reduced pressure resulted in the isolation of a white powder (1.177 g, 2.331 mmol, 45%). IR (cm^{-1}) ν: 3412 (m, (N-H)), 1230 (vs, (Si-O-Si)). ^{1}H NMR (C_6D_6) δ: 1.34 (s, *t*-Bu), 1.31 (s, *t*-Bu, minor resonance) (relative intensities ca. 5:1), 1.21 (N*H*). ^{13}C{^{1}H} NMR (C_6D_6) δ: 49.10 (s, *C*Me$_3$), 33.84 (s, C*Me*$_3$), 48.80, 33.87 (minor resonances). ^{29}Si{^{1}H} NMR (C_6D_6) δ: –54.5 (s). Anal. calcd. for $C_{24}H_{60}N_6Si_2O$ (**14**): C 57.09, H 11.98, N 16.64; $C_{28}H_{71}N_7Si_2O$ (**14** + *t*-BuNH$_2$): C 58.17, H 12.38, N 16.96; found: C 56.32, H 12.19, N 15.99, Cl < 0.3.

Results and discussion

Preparation and NMR characterization of Cl$_2$Si(NHAd)$_2$ (6b), ClSi(NH-*t*-Bu)$_3$ (7), and Si(NHR)$_4$ (2a, R = *i*-Pr; 2b, R = *t*-Bu; 2c, R = *p*-tol)

With only limited information available (14) regarding previous attempts to synthesize **2b**, the reaction of $SiCl_4$ with *t*-BuNH$_2$ was reinvestigated. As reported in the literature (19), treatment of $SiCl_4$ with an excess of *tert*-butylamine at room temperature results in the aminolysis of two silicon–chlorine bonds and the formation of **6a** in 83% yield. Further treatment of **6a** with an excess of *t*-BuNH$_2$ in boiling toluene resulted in the formation of **7**, a colourless liquid, in 89% yield. While several physical properties of **7** have been determined, including the boiling point and refractive index (14), no spectroscopic data for this compound have been reported. The *tert*-butyl ^{1}H NMR resonance of **7** (1.20 ppm) is shifted slightly downfield as compared with that of **6a** (1.11 ppm), while the ^{29}Si NMR signal (–45.2 ppm) of **7** appears at higher field than the corresponding resonance of **6a** (–38.9 ppm). The α-carbon signal in the ^{13}C NMR spectrum of **7** is shifted to higher field (49.5 vs. 50.6 ppm), while the methyl groups resonate at lower field (33.3 vs. 32.6 ppm).

Attempts to prepare **2b** by the reaction of **7** with an excess of *tert*-butylamine at elevated temperatures were unsuccessful; in all cases, no reaction could be detected by ^{1}H NMR spectroscopy. In consequence, an alternative synthetic route, based on the method by which the trisamino(imino)phosphoranes (RNH)$_3$PNSiMe$_3$ (R = *i*-Pr, Cy, *t*-Bu, Ad) have been prepared (5, 10) (eq. [2]), was adopted whereby $SiCl_4$ was treated with 4 equiv. of LiHN-*t*-Bu at 22 °C (eq. [3]). This reaction proceeds with the elimination of 4 equiv. of LiCl and produces the desired compound **2b** in 84% yield. The identity of **2b** was established by multinuclear NMR, mass spectrometry (M^+ at 316.6), and elemental (C, H, N) analysis. The trends in multinuclear NMR data that were observed on moving from the bisamino compound **6a** to the trisamino species **7** continue with this tetraaminosilane: the ^{1}H NMR signal is at still lower field (1.28 ppm) as is the C*Me*$_3$ peak in the ^{13}C NMR spectrum (34.0 ppm), while the second ^{13}C NMR resonance (48.7 ppm) and the ^{29}Si NMR signal (–52.9 ppm) appear at higher field. No trace of contamination from unreacted **6a** or **7** was detected in the NMR spectra of this compound.

[2] $$Cl_3PNSiMe_3 + 3LiHNR \xrightarrow[0\ ^\circ C]{Et_2O} (RNH)_3PNSiMe_3 + 3LiCl$$

[3] $$SiCl_4 + 4LiHN\text{-}t\text{-}Bu \xrightarrow[0\ ^\circ C]{Et_2O} Si(NH\text{-}t\text{-}Bu)_4 + 4LiCl$$

The ease with which this reaction (eq. [3]) occurs indicates that electronic effects rather than the steric influence of the bulky *t*-BuNH$_2$ group, as previously postulated (14), preclude the formation of **2b** in solvothermal reactions between $SiCl_4$ and *t*-BuNH$_2$. The formation of LiCl presumably provides a sufficient driving force for complete aminolysis to occur. The utility of this synthetic approach is not limited to the *tert*-butyl group: the known derivatives **2a** and **2c** have also been prepared in ca. 80% yields by this procedure and identified by multinuclear NMR spectra.

Following the success of this synthetic methodology for producing **2b**, it was of interest to determine whether other, perhaps even more sterically hindered tetraaminosilanes, could be prepared in the same manner. To that end, the synthesis of "Si(NHAd)$_4$" (**2d**) was attempted via the analogous reaction of $SiCl_4$ with lithium adamantylamide (LiHNAd). However, the disubstituted compound **6b** was isolated in 81% yield in this case. As the electron-withdrawing effects of NHAd and NH-*t*-Bu groups are expected to be quite similar to one another, this failure to generate tris- or tetra-(adamantylamino)silanes must be attributed to the greater steric bulk of the adamantyl cages as compared with that of the *tert*-butyl substituents of **2b**.

Attempted preparation of {Li$_4$[Si(NR)$_4$]} (R = *t*-Bu, *p*-tol) — Synthesis and NMR characterization of {[Li(12-crown-4)]$_2$[(Et$_2$O)$_2$Li(μ-Nnaph)$_2$Si(μ-Nnaph)$_2$Li(Et$_2$O)$_2$]} (8)

With an efficient synthetic route to Si(NH-*t*-Bu)$_4$ established, an attempt to tetralithiate this species with *n*-BuLi was carried out. The two reagents were combined in hexane

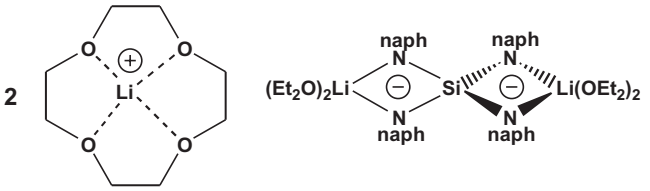
© 2006 NRC Canada

at 22 °C. The ^{1}H NMR spectrum of the product of this reaction, a fine white powder, contained two *t*-Bu resonances at 1.64 and 1.48 ppm in a 1:3 ratio, as well as a broad signal attributable to a NH fragment; unreacted *n*-BuLi was also detected. These spectroscopic data are consistent with the formation of a trilithiated species $\{Li_3[Si(N\text{-}t\text{-}Bu)_3(NH\text{-}t\text{-}Bu)]\}_2$ (**3b**) (11), which is isostructural with **3a**. The reaction was repeated under various conditions. In all cases, a significant amount of unreacted *n*-BuLi was observed in the ^{1}H NMR spectrum of the product, along with a broad signal that was attributed to a NH fragment, the presence of which was confirmed by IR spectroscopy. Reactions between **2b** and Mg-*n*-Bu_2 under a variety of conditions also resulted in incomplete deprotonation, as revealed by sharp N–H stretching vibrations in the IR spectra of the products.

In light of the limited reactivity of **2b** toward *n*-BuLi, it was decided to undertake similar reactions with Si(NH-*p*-tol)$_4$ (**2c**), as the increased acidity of the NH protons of arylamino substituents compared with that of alkylamino groups has been observed to facilitate complete lithiation in related trisamino(thio)phosphate systems (20). The spectroscopic data obtained from these experiments were inconclusive, but did not provide any strong evidence to support the formation of "$\{Li_4[Si(N\text{-}p\text{-}tol)_4]\}$". Based on these results, it is proposed that fourfold deprotonation of $Si(NHR)_4$ (R = alkyl, aryl) is not possible using alkyl lithium reagents, as they are not sufficiently basic to effect the removal of the fourth proton. The synthesis of **1** requires the double deprotonation of 1-aminonaphthalene prior to reaction with $SiCl_4$ (11); since H_2Nnaph is the only primary amine that can be dilithiated, the naphthyl derivative **1** may be a unique example of a tetralithiated tetraimidosilicate.

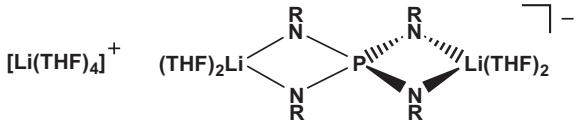
With the library of viable R groups thus curtailed, the preparation of a crown ether complex of **1** was undertaken, with the expectation that the resulting material would be more crystalline than the diethyl etherate **1**. The synthesis of **1** by the literature procedure (11) was modified by the addition of 2 equiv. of 12-crown-4 after filtration to remove the LiCl by-product. The resulting bright yellow powder was characterized by ^{1}H and ^{13}C NMR spectroscopy, as well as by an elemental (C, H, N) analysis. The overlapping multiplets in the aromatic region of the ^{1}H NMR spectrum of the product render it difficult to interpret. However, only 10 distinct signals were observed in the aromatic region (106.9–162.4 ppm) of the ^{13}C NMR spectrum, in addition to the resonances for 12-crown-4 and diethyl ether ligands, indicating the equivalence of the four Nnaph substituents. Based on these data, this novel tetraimidosilicate complex is thought to exist in a spirocyclic conformation $\{[Li(12\text{-crown-}4)]_2[(Et_2O)_2Li(\mu\text{-Nnaph})_2Si(\mu\text{-Nnaph})_2Li(Et_2O)_2]\}$ (**8**), with two Li^+ cations sequestered by 12-crown-4; the remaining two Li^+ cations are each *N*,*N*′-chelated by the naphthylimido groups and bis-solvated by two diethyl ether ligands.

Though single crystals of **8** are readily obtained from THF–hexane solutions, they are not of sufficient quality for X-ray analysis; thus, the proposed structure of **8** has not been confirmed in the solid state. However, the proposed



8

spirocyclic geometry has been observed in the solid state for the isoelectronic tetra(naphthylimido)phosphate $\{[Li(THF)_4][(THF)_2\text{-}Li(\mu\text{-Nnaph})_2P(\mu\text{-Nnaph})_2Li(THF)_2]\}$ (**9a**) (4) and in solution for the *tert*-butyl analogue $\{[Li(THF)_4]\{Li(THF)_2[(\mu\text{-N-}t\text{-Bu})_2P(\mu\text{-N-}t\text{-Bu})_2]Li(THF)_2\}$ (**9b**) (10).



9

Surprisingly, only one signal (0.63 ppm) was observed in the ^{7}Li NMR spectrum of **8** in d_8-THF, indicating that the chemically inequivalent lithium cations exchange rapidly in solution despite the presence of 12-crown-4. This can be rationalized by taking into account the presence of four highly nucleophilic imido groups and the large negative charge of the tetraimidosilicate tetraanion. These two factors combine to render chelation by the $[Si(Nnaph)_4]^{4-}$ preferable to, or at least competitive with, an η_4 mode of coordination by the crown ether. A variable-temperature ^{7}Li NMR study in d_8-THF showed that the spectrum is highly dependent upon temperature, confirming that the lithium cations are in dynamic equilibrium in solution. The single resonance broadens significantly even at 0 °C, then resolves into several sharp resonances at lower temperatures (–45 to –60 °C). It is expected that further lowering of the temperature would eventually result in two singlets in a 1:1 ratio attributed to the *N*,*N*′-chelated lithium ions and the $[Li(12\text{-crown-}4)]^+$ cations. However, this resolution could not be achieved above the temperature at which the NMR solvent began to gel.

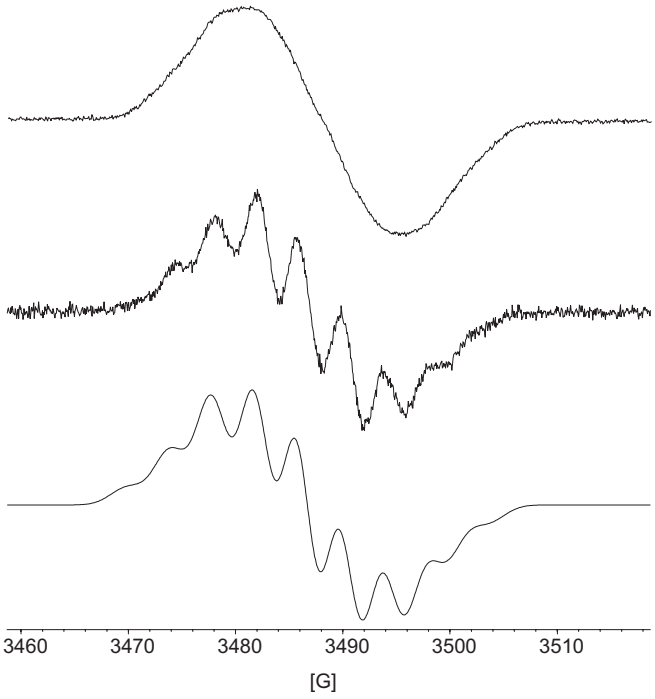
Formation and EPR characterization of persistent polyimidosilicate radicals

Oxidation reactions of the tetraimidosilicate **1** were explored to determine whether **1** is capable of forming stable radicals,[3] in a manner similar to that reported for the isoelectronic tetraimidophosphates $\{Li_3[P(NR)_3(NSiMe_3)]\}_2$ (**4a**, R = *t*-Bu; **4b**, R = Ad) (6, 9, 10). The addition of 0.5 mol of iodine to a bright yellow solution of **1** in THF resulted in a deep green-brown solution, indicating the formation of a paramagnetic species, presumably a lithiated derivative of trianion radical $[Si(Nnaph)_4]^{3-\cdot}$. An EPR spectrum of this solution (Fig. 2) at 22 °C displayed a single broad resonance (ca. 15 G), with no resolved hyperfine coupling (HFC) to the four nitrogen nuclei of the tetraimidosilicate radical. Though this was initially surprising, it

[3] In this article, a "stable" radical is one that is inherently stable as an isolated species and does not decompose under an inert atmosphere at room temperature (16). A "persistent" radical is one that has a relatively long lifetime under the conditions that are used to generate it; radicals less stable than this are termed "transient".

© 2006 NRC Canada

Fig. 2. Experimental EPR spectra of iodine-oxidized **1** (top) and **10** (middle); simulated EPR spectrum of **10** (bottom).

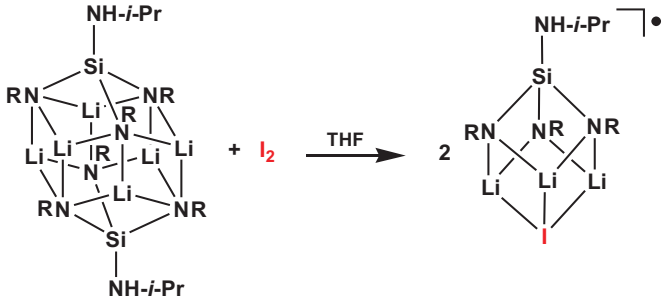


should be noted that extensive line broadening is often observed in fluxional radical systems: the variable-temperature ^{7}Li NMR data obtained for the related crown ether complex **8** are certainly indicative of considerable solution dynamics, and lithium exchange is expected to occur still more readily in the absence of any crown ether.

In an attempt to resolve the nitrogen and lithium HFCs in the EPR spectrum of the $[Si(Nnaph)_4]^{3-\bullet}$ radical, the crown ether complex **8**, believed to be less fluxional than **1**, was oxidized with iodine. An EPR spectrum (Fig. 2) of this dark-green reaction mixture revealed a nine-line pattern, which is consistent with coupling to four equivalent ^{14}N (I = 1, 99.6%) nuclei; the g value of this radical is 2.0037. The pronounced "S-curve" shape of the spectrum and the broadness of the spectral lines are attributed to unresolved HFC (21) to the lithium cations (^{7}Li, I = 3/2, 92.6%) in the spirocyclic radical monoanion $\{[(THF)_2Li(\mu\text{-}Nnaph)_2Si(\mu\text{-}Nnaph)_2Li(THF)_2]\}^{-\bullet}$ (**10**).

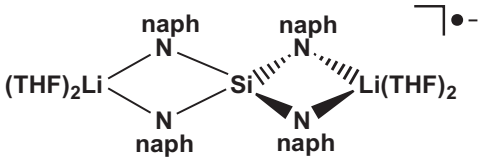
A good simulation of this spectrum (Fig. 2) was obtained by using hyperfine coupling constants (HFCCs) of 3.8 G to four nitrogen atoms and 0.7 G to two lithium cations. These HFCCs are slightly smaller than those observed for the isostructural tetraimidophosphate radical $[(THF)_2Li(\mu\text{-}N\text{-}t\text{-}Bu)_2P(\mu\text{-}N\text{-}t\text{-}Bu)Li(THF)_2]^{\bullet}$ (**11**) for which the corresponding HFCCs are 4.30 G (^{14}N) and 1.08 G (^{7}Li) (10). However, the value of the ^{7}Li HFCC for **10** should be regarded as approximate, since the broadness of the spectral lines precludes direct measurement of this coupling. The striking difference between the line widths produced by the two symmetrical spirocyclic radicals **10** (ca. 3 G) and **11** (ca. 0.5 G) is thought to be caused by spin delocalization into the naphthyl groups of **10**, and the resultant presence of numerous inequivalent ^{1}H hyperfine couplings. This is not an unreasonable hypothesis, since Li_2Nnaph is reported to be paramagnetic and the EPR spectrum contains sufficiently large ^{1}H HFCCs to produce a signal that is approximately 17 G in width (12).

Scheme 1. Oxidation of **3a** by iodine to form two cubic radicals **12** (R = *i*-Pr).

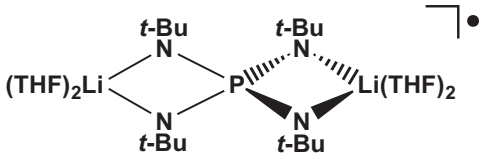


While the green colour formed upon oxidation of **1** and **8** persists for more than 24 h in both instances, the EPR signals were surprisingly weak, indicating the presence of only a small amount of paramagnetic material in the solutions. This observation suggests that either the tetraimidosilicate radical has only a short lifetime or that radical formation is not quantitative, i.e., that the radical **10** is not the exclusive product of these oxidation reactions. Attempts to isolate the tetraimidosilicate radical were unsuccessful owing to the limited stability of this persistent radical. Overall, the stability of **10** is comparable to that of the isostructural neutral radical **11** (10).

Previous work with tetraimidophosphate radicals has shown that cubic derivatives are significantly more stable than spirocycles such as **10** and **11** (6, 7, 9, 10). Oxidation of the dimeric aminotris(imido)silicate **3a** with iodine is expected to proceed in an analogous fashion to oxidations of the structurally similar cluster **4**. As depicted in Scheme 1, this process can be viewed to involve disruption of the Li_6N_6 core of **3a**, yielding two molecules of the cubane radical $\{Li_2[Si(N\text{-}i\text{-}Pr)_3(NH\text{-}i\text{-}Pr)]\cdot LiI\cdot 3THF\}^{\bullet}$ (**12**). In practice, the addition of 1 equiv. of I_2 to a slurry of **3a** in THF yields an intensely yellow solution that gives rise to a somewhat stronger EPR signal than do the products of the corresponding reactions with **1** and **8**. The EPR spectrum of the reaction mixture is primarily a seven-line pattern with multiple smaller HFCs present as well (Fig. 3); the g value of this radical is 2.0044. The best simulation of this spectrum was obtained by including HFCCs to three equivalent nitrogen atoms (8.1 G), one unique nitrogen atom (2.0 G), three lith-



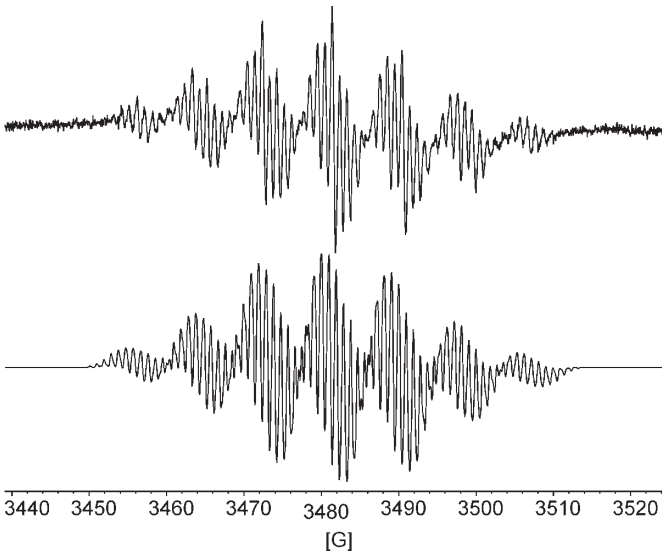
10



11

© 2006 NRC Canada

Fig. 3. Experimental (top) and simulated (bottom) EPR spectra of **12**.



ium cations (0.9 G), and an iodine atom (0.4 G) (Fig. 3). Thus, this EPR spectrum is consistent with the formation of the cubic radical **12** and confirms that **3a** undergoes an analogous reaction to **4** when oxidized.

Like the tetraimidosilicate radical **10**, the amidotris(imido)silicate **12** is considered to be a persistent radical, since it decomposes in solution within 72 h.[3] This is somewhat surprising, as cubic tetraimidophosphate radicals are more stable than related spirocyclic species and they can be isolated and structurally characterized in the solid state (6, 7, 9, 10). However, it must be noted that the isopropyl substituents of **10** provide only modest steric protection to prevent dimerization of the radical: stable tetraimidophosphate radicals occur only when bulkier *tert*-butyl or adamantyl groups are in place (10). Thus, oxidation of the *tert*-butyl derivative **3b** with 1 mol of iodine was undertaken, with the expectation that a highly persistent or stable radical would result. Surprisingly, the paramagnetic species generated from this reaction was found to be even less stable than **12**, persisting in solution for only a few seconds. An EPR spectrum of the reaction mixture produced a very weak signal, consisting of a poorly resolved seven-line pattern. While this suggests HFC of the unpaired electron to three equivalent ^{14}N nuclei, consistent with the formation of a cubic radical, the experimental parameters used to acquire this spectrum were not optimal owing to the low sample concentration. Oxidation of the related dimer $\{Li_3[PhSi(N\text{-}t\text{-}Bu)_3]\}_2$ (**13**) (17), an organic derivative of a trisimidosilicate that exists as a Li_6N_6 hexagonal prism bicapped by the two Si–Ph units (cf. **3a** in Fig. 1), also yielded a transient radical. The lower stability of this radical as compared with that of **12** can be attributed to a combination of the smaller steric bulk of the phenyl group (cf. the NH-*i*-Pr unit), combined with the fewer number of electronegative (i.e., N) atoms over which the unpaired electron can be delocalized. However, no explanation can be given at the present time as to why the oxidation of the more sterically protected **3b** leads to less stable radicals than the corresponding reactions of the isopropyl derivative **3a**.

Preparation and characterization of $(t\text{-}BuNH)_3SiOSi(NH\text{-}t\text{-}Bu)_3$ (14)

As an alternative precursor to polyimidosilicate radicals, we targetted hexa(*tert*-butylamino)disiloxane $(t\text{-}BuNH)_3SiOSi(NH\text{-}t\text{-}Bu)_3$ (**14**), which was synthesized by the reaction of hexachlorodisiloxane with 6 equiv. of LiHN-*t*-Bu at 0 °C in diethyl ether (eq. [4]) and purified by sublimation. The resultant white powder was characterized by IR and multinuclear NMR spectra, GC–MS, and elemental analyses.

$$[4]\qquad Cl_3SiOSiCl_3 + 6LiHN\text{-}t\text{-}Bu \xrightarrow{Et_2O} (t\text{-}BuNH)_3SiOSi(NH\text{-}t\text{-}Bu)_3 + 6LiCl$$

The ^1H NMR spectrum of the product exhibits a minor resonance at 1.31 ppm in addition to the major peak at 1.34 ppm. The integrated relative intensities of these two resonances exhibit an approximately 1:5 ratio. The ^{13}C NMR spectrum is consistent with this observation, showing one major set of *tert*-butyl resonance (49.10 and 33.84 ppm) and a second set of minor resonances at 48.80 and 33.87 ppm. These minor resonances, with the same relative intensities, persist in the NMR spectra of samples purified by either sublimation or recrystallization. The ^{29}Si NMR spectrum of the product exhibits a single sharp resonance at –54.6 ppm. Furthermore, the GC–MS revealed only a single component. Since the two signals in the ^1H NMR spectrum are very close together, the integration of the relative intensities must be regarded as approximate, and we have considered the possibility that the ratio of the intensities is 1:6 with the smaller resonance attributed to a component with a single *t*-BuN group. The possible candidates for the "single *t*-BuN" species include *t*-BuNHLi, $t\text{-}BuNH_2$, or $[t\text{-}BuNH_3]Cl$, each of which could form a hydrogen-bonded adduct with the O atom of **14**. The product shows no resonance in the ^7Li NMR spectrum, thus ruling out *t*-BuNHLi as an additional component. Elemental analyses show that the product contains insignificant amounts of Cl (<0.3%), thus excluding $[t\text{-}BuNH_3]Cl$ as an impurity. Although we cannot count out the possibility of one molecule of $t\text{-}BuNH_2$ as a hydrogen-bonded component of the product, the IR spectrum (Fluorolube mull) shows only extremely weak, broad bands in the 3120–3240 cm^{-1} region, which could be assigned to hydrogen-bonded $t\text{-}BuNH_2$, in addition to a sharp, medium-intensity band at 3412 cm^{-1} attributed to υ(N-H) of **14**. We also note that the CHN analyses are in better agreement with the calculated values for **14** than with the alternative (**14** + $t\text{-}BuNH_2$). We are led to the tentative conclusion, therefore, that the best explanation of the combined spectroscopic and analytical data for **14** involves some sort of intermolecular interaction in solution that leads to inequivalence of one of the N-*t*-Bu groups. Unfortunately, numerous crystals of **14** obtained by recrystallization or sublimation were only weakly diffracting, and consequently, we have been unable to obtain a solid-state structure by X-ray crystallography. In view of the uncertainty about the structure of **14**, we have not pursued the hexalithiation.

Conclusions

The reaction of $SiCl_4$ with lithiated primary amides LiHNR (R = alkyl, aryl) in diethyl ether provides a versatile

© 2006 NRC Canada

and efficient route to tetraaminosilanes $Si(NHR)_4$. Fourfold deprotonation of $Si(NHR)_4$ does not appear to be possible using either *n*-BuLi or $MgBu_2$, suggesting that the preparation of tetraimidosilicates $[Si(NR)_4]^{4-}$ can only be achieved if the amine is doubly deprotonated prior to reaction with $SiCl_4$, i.e., by the use of Li_2NR. EPR studies of the products of the one-electron oxidation of tetraimido or amidotris(imido)silicates with iodine indicate the formation of persistent spirocyclic and cubic radicals, respectively. The reasons for the lower stability of these polyimidosilicate radicals as compared with that of the analogous tetraimidophosphate radicals are not yet fully understood and merit further investigation.

Acknowledgements

We thank the University of Calgary, the Natural Sciences and Engineering Research Council of Canada (NSERC), and the Academy of Finland (JK) for funding. The assistance of J.S. Ritch and J.F. van Humbeck in obtaining the IR spectrum and GC–MS of **14**, respectively, is gratefully acknowledged.

References

1. T. Chivers. Top. Curr. Chem. **229**, 143 (2003).
2. G.M. Aspinall, M.C. Copsey, A.P. Leedham, and C.A. Russell. Coord. Chem. Rev. **227**, 217 (2002).
3. J.K. Brask and T. Chivers. Angew. Chem. Int. Ed. **40**, 3960 (2001).
4. P.R. Raithby, C.A. Russell, A. Steiner, and D.S. Wright. Angew. Chem. Int. Ed. Engl. **36**, 649 (1997).
5. A. Armstrong, T. Chivers, M. Krahn, M. Parvez, and G. Schatte. Chem. Commun. (Cambridge), 2332 (2002).
6. A. Armstrong, T. Chivers, M. Parvez, and R.T. Boeré. Inorg. Chem. **43**, 3453 (2004).
7. A.F. Armstrong, T. Chivers, H.M. Tuononen, and M. Parvez. Inorg. Chem. **44**, 5778 (2005).
8. A. Armstrong, T. Chivers, M. Krahn, and M. Parvez. Can. J. Chem. **83**, 1768 (2005).
9. A. Armstrong, T. Chivers, M. Parvez, and R.T. Boeré. Angew. Chem. Int. Ed. **43**, 502, (2004).
10. A.F. Armstrong, T. Chivers, H.M. Tuononen, M. Parvez, and R.T. Boeré. Inorg. Chem. **44**, 7981 (2005).
11. J.K. Brask, T. Chivers, and M. Parvez. Inorg. Chem. **39**, 2505 (2000).
12. D.A. Armstrong, D. Barr, W. Clegg, S.R. Drake, R.J. Singer, R. Snaith, D. Stalke, and D.S. Wright. Angew. Chem. Int. Ed. Engl. **30**, 1707 (1991).
13. W.J. Grigsby, T. Hascall, J.J. Ellison, M.M. Olmstead, and P.P. Power. Inorg. Chem. **35**, 3254 (1996).
14. H. Breederveld and H.I. Waterman. Research (London), **6**, 43S (1953).
15. M. Söldner, A. Schier, and H. Schmidbaur. Inorg. Chem. **37**, 510 (1998).
16. P. Power. Chem. Rev. **103**, 789 (2003).
17. D.J. Brauer, H. Bürger, and G.R. Liewald. J. Organomet. Chem. **308**, 119 (1986).
18. Bruker AXS. Versions 1.25 [computer program]; WinEPR. Version 2.11 [computer program]. Bruker Analytische Messtechnik GmbH, Rheinstetten, Germany. 1996.
19. V. Passarelli, G. Carta, G. Rossetto, and P. Zanella. Dalton Trans. 413 (2003).
20. T. Chivers, M. Krahn, M. Parvez, and G. Schatte. Inorg. Chem. **42**, 3994 (2003).
21. J.A. Weil, J.R. Bolton, and J.E. Wertz. Electron paramagnetic resonance: Elementary theory and practical applications. Wiley-Interscience, New York. 1994.

© 2006 NRC Canada

Total synthesis of 14β-fluorosteroids via a transannular Diels–Alder reaction

Sylvie Beaubien and Pierre Deslongchamps

Abstract: 14β-Fluorosteroids **3** and **4** were synthesized to give a new class of unnatural cardenolides. The total synthesis of racemic 14β-fluorosteroids was accomplished using a highly diastereoselective transannular Diels–Alder reaction on a trans-cis-cis macrocyclic triene. The α-fluoro analog **4** provided a comparable inhibitory activity to natural digitoxigenin **1**.

Key words: fluorosteroid, bioisostere, cardiovascular diseases, transannular Diels–Alder reaction (TADA), macrocyclization.

Résumé : Les 14β-fluorostéroïdes **3** et **4** ont été synthétisés en vue d'obtenir une nouvelle classe de cardénolides non-naturels. La synthèse totale racémique des 14β-fluorostéroïdes a été accomplie en utilisant la réaction diastéréosélective de Diels–Alder transannulaire à partir d'un triène macrocyclique trans-cis-cis. L'α fluoro-analogue **4** donne une activité inhibitrice comparable à la digitoxigénine **1**.

Mots clés : fluorostéroïde, bioisostère, maladies cardiovasculaires, réaction de Diels–Alder transannulaire (DATA), macrocyclisation.

Introduction

The (+)-digitoxigenin **1** is derived from the biologically active trisaccharide digitoxin **2**, which is extracted from the *Digitalis purpura* plant (1) (Fig. 1). These cardenolide steroids belong to the large digitalis family, and the principal use of this type of molecule is the treatment of cardiovascular diseases (2).

Compounds from the digitalis family are considered to be dangerous because the therapeutic dose can correspond to up to 60% of the lethal dose. The therapeutic dose for cardiovascular disease is very small (1) (0.2 mg for digitoxin **2**). For this reason, many efforts have been made to synthesize cardenolide analogs to diminish the toxicity of this type of compound.

Bioisosterism is an approach used to decrease the toxicity of a drug (3). Based on this method, we decided to consider fluoro analogs of digitoxigenin **1**, since fluorine is a bioisostere of the hydroxyl group. In addition, some analogs of digitoxigenin **1** are known to possess an α,β-unsaturated ester instead of butenolide at the C-17 position (4). We, therefore, decided to synthesize the racemic fluoro analogs **3** and **4** of digitoxigenin **1** with a fluorine atom at the C-14 position and an α,β-unsaturated ester at the C-17 position. The biological activity of these analogs could then be measured and compared with that of digitoxigenin **1**.

To synthesize these two fluoro analogs, we used the transannular Diels–Alder (TADA) (5) reaction to construct the tetracyclic skeleton. Our past studies on the TADA reaction (6, 7) have shown that a 13-membered ring with a trans-cis-cis olefin geometry can lead to an A.B.C.[6.6.5] tricycle having a trans-syn-cis (TSC) ring junction configuration (8). In this reaction, four asymmetric centers are created simultaneously with high stereoselectivity. The challenging synthesis of the fluorinated compound, which represents a new class of unnatural cardenolides, is reported herein.

Received 26 July 2005. Published on the NRC Research PressWeb site at http://canjchem.nrc.ca on 25 February 2006.

S. Beaubien and P. Deslongchamps.[1] Laboratoire de synthèse organique, Département de chimie, Institut de Pharmacologie de Sherbrooke, Université de Sherbrooke, 3001, 12e Avenue nord, Sherbrooke, QC J1H 5N4, Canada.

[1]Corresponding author (e-mail: Pierre.Deslongchamps@USherbrooke.ca).

Results and discussion

Retrosynthesis

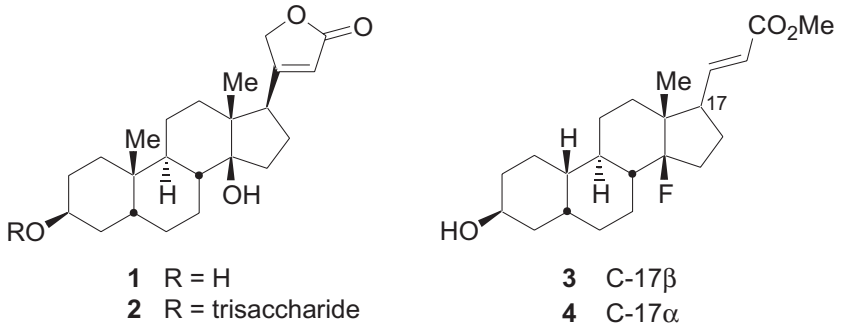
The retrosynthetic analysis of fluoro analogs **3** and **4** is presented in Scheme 1. These fluoro analogs can be obtained by Birch reduction of the aromatic ring and by homologation of the C-17 ketone of tetracycle **5** to form the α,β-unsaturated esters **3** and **4**. Tetracycle **5** (TSC) can be obtained via the TADA reaction of trienic macrocycle **6** possessing an *E,E*-diene and an *E*-dienophile. Macrocycle **6** can be formed from the β-keto ester **7** by macrocyclization. This β-keto ester can be obtained from compound **8** by alkylation. Homologation of diol **9** with two different Horner–Emmons reactions can produce compound **8**. Finally, the diol **9** can be prepared from commercially available compound **10** in a few steps.

Synthesis of β-keto ester 7

The synthesis of β-keto ester **7** starts with the reduction of the commercially available ketone **10** with lithium aluminium hydride to give the corresponding alcohol followed

 doi:10.1139/V05-259 © 2006 NRC Canada

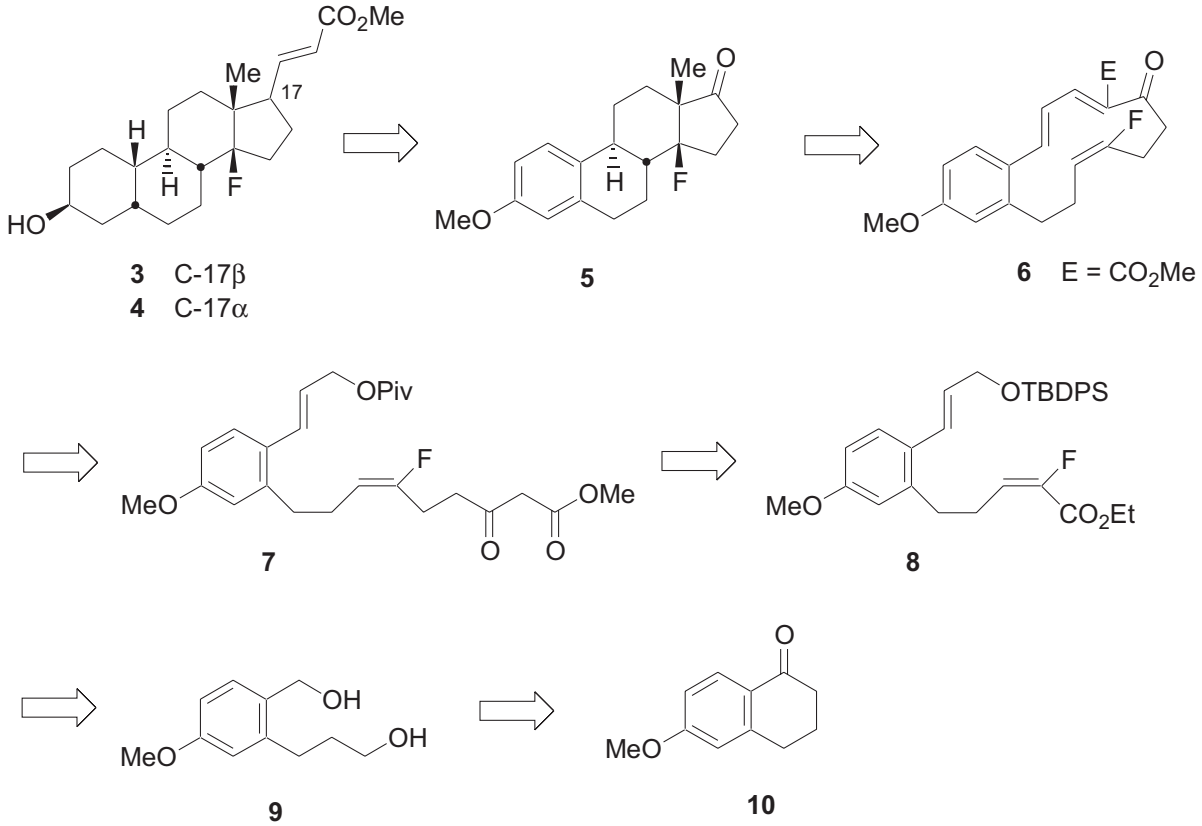
Fig. 1. Target structures.



1 R = H
2 R = trisaccharide

3 C-17β
4 C-17α

Scheme 1.



3 C-17β
4 C-17α

5

6 E = CO_2Me

7

8

9

10

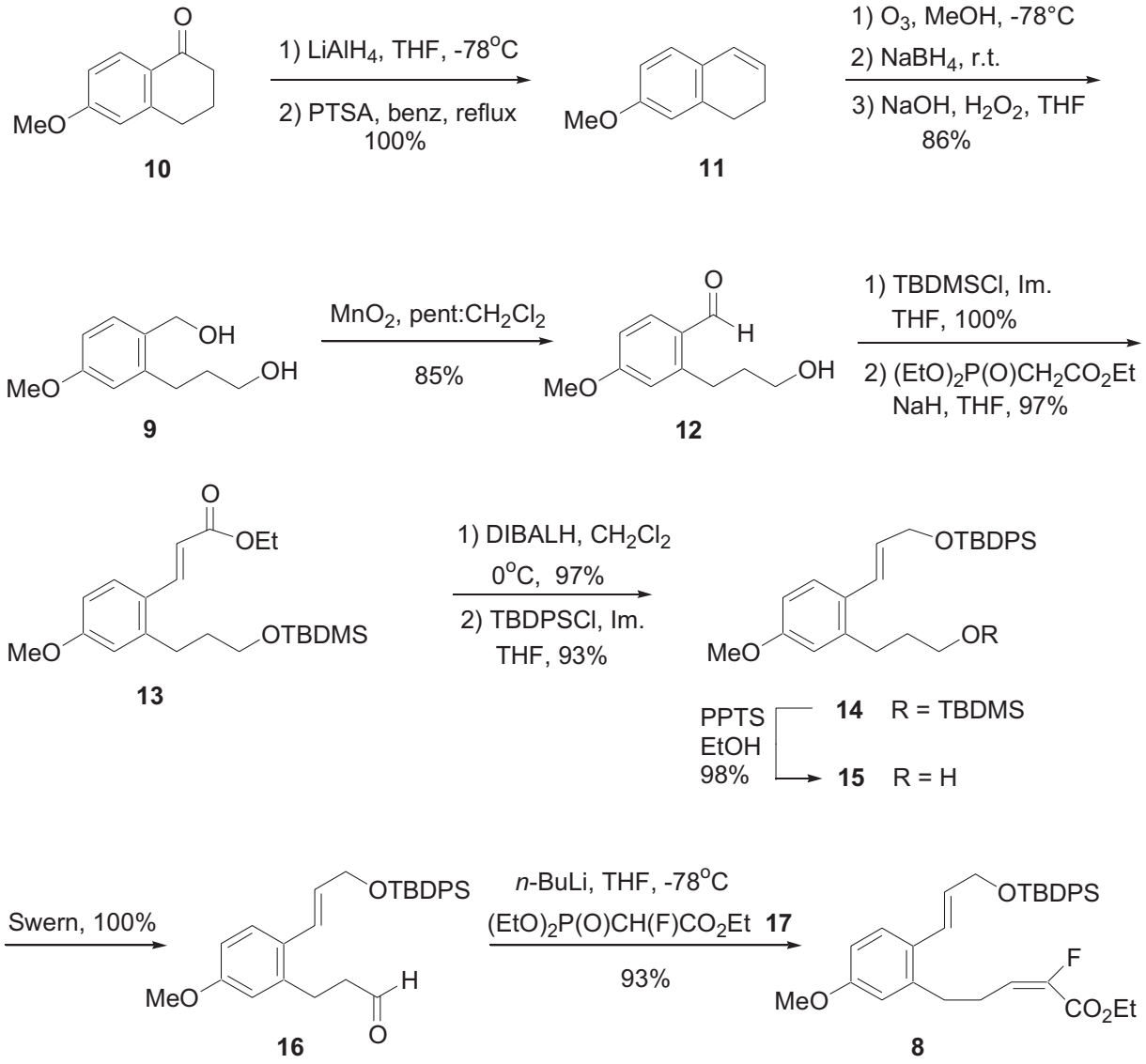
by dehydratation to produce the olefin **11** in a quantitative yield (Scheme 2). Ozonolysis of this olefin was performed followed by treatment with sodium borohydride (9) to give diol **9** in 86% yield. The selective oxidation of the benzylic alcohol of diol **9** was accomplished with manganese dioxide and the hydroxyaldehyde **12** was obtained in 85% yield. This hydroxyaldehyde was protected as a TBDMS ether and a Horner–Emmons (10) reaction was performed to produce the α,β-unsaturated ester **13** with very good yield as a single detectable geometrical isomer. Reduction with DIBALH of the α,β-unsaturated ester **13** afforded the corresponding alcohol, which was protected as a TBDPS ether to give disilylated compound **14**. The selective deprotection of TBDMS in the presence of the TBDPS ether was performed with a catalytic amount of PPTS in ethanol, and alcohol **15** was obtained in 98% yield. Swern oxidation (11) then led to aldehyde **16** in quantitative yield.

The fluorine atom, which is required at the 14β position in the final targets **3** and **4**, was introduced at this step with a Horner–Emmons (10) reaction. The aldehyde **16** was treated with the anion of fluorophosphonate **17** (12), and α,β-unsaturated ester **8** was obtained in 93% yield (Scheme 2). The isomer with the E geometry (12) was the only compound observed by ^{1}H NMR. With this key intermediate in hand, we could synthesize β-keto ester **7** for the macrocyclization reaction.

To this end, α,β-unsaturated ester **8** was reduced with lithium aluminium hydride to provide a quantitative yield of the alcohol, which was converted to the allylic chloride **18** with hexachloroacetone and triphenylphosphine (13). The introduction of the β-keto ester was accomplished by treating allylic chloride **18** with the dianion of methyl acetoacetate (14) to afford β-keto ester **19** in 65% yield. Deprotection of the silyl ether was carried out with TBAF, and the resulting

© 2006 NRC Canada

Scheme 2.



alcohol was converted to a pivaloate ester to give β-keto ester **7**, the desired macrocyclization precursor (Scheme 3).

Macrocyclization and TADA reaction

The key steps in this synthesis are the macrocyclization and the TADA reaction. To achieve macrocyclization, the silyl enol ether of β-keto ester **7** was prepared with *N*,*N*-bistrimethylsilylacetamide and subsequent slow addition (14 h) of this silyl enol ether to a solution of palladium catalyst at a high dilution (2 mmol/L). This concentration is essential to eliminate polymer formation. Under these reaction conditions (8, 15), the macrocyclization took place to afford the 13-membered ring macrocycle **20** in an excellent yield of 88% (Scheme 4). Now, we have to introduce an *E*-olefin to make the necessary diene for the TADA reaction. Macrocycle **20** was thus treated with benzeneseleninic anhydride (16, 17), and the trienic macrocycle **6** was obtained in 91% yield.

The macrocycle **6** contains the *E*-dienophile and *E,E*-diene that are necessary to obtain the TSC tetracycle after the TADA reaction. This key step was accomplished by heating macrocycle **6** at 165 °C in the presence of triethylamine in a sealed tube for 4 h. The TSC tetracycle **21** was obtained in 78% yield as a single isomer. In this step, four new chiral centers were formed simultaneously with a high degree of stereoselectivity.

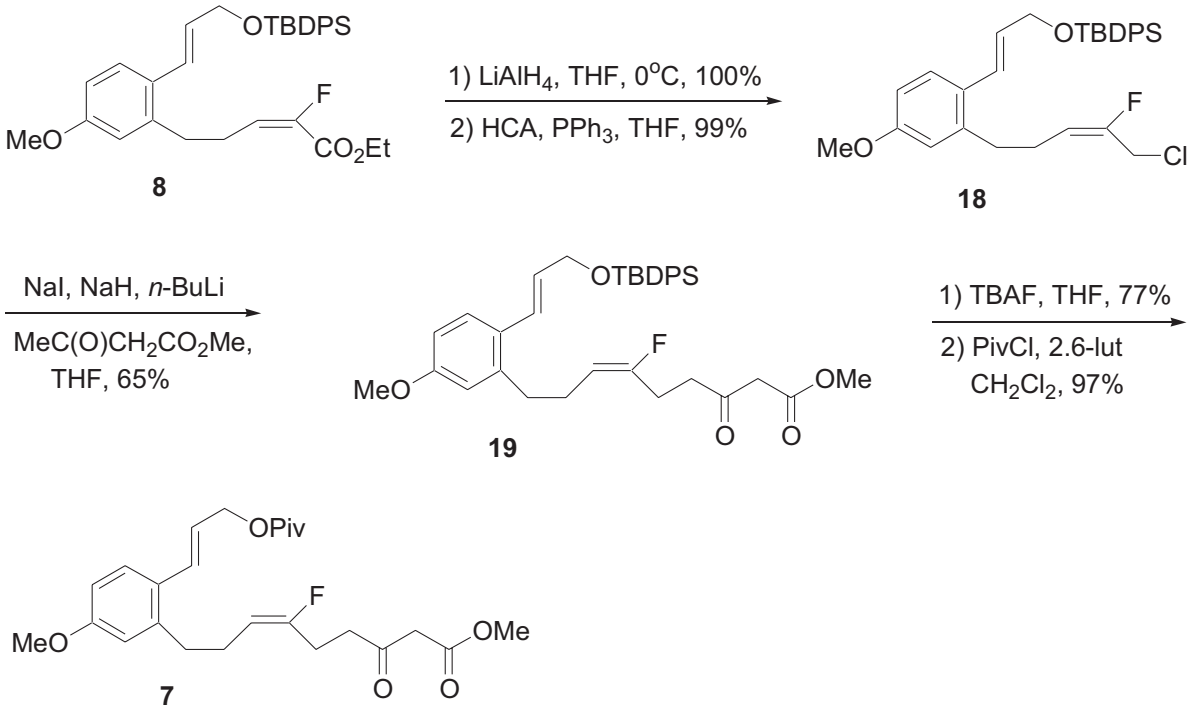
The selective formation of the TSC tetracycle can be explained by considering the transition state of the TADA reaction. As seen in Scheme 5, in transition state **22**, the olefins are perfectly aligned for the TADA reaction without any severe steric interaction. The other possible TADA product, CST tetracycle **21a**, cannot be obtained owing to improper orbital alignment (transition state **22a**). Thus, this transannular process allows complete control in the formation of TSC tetracycle **21** (18). The desired key 17β-fluoro racemic intermediate was thus obtained with a very good yield at each step.

Installation of the C-13 methyl group and a model study for the homologation at the C-17 position

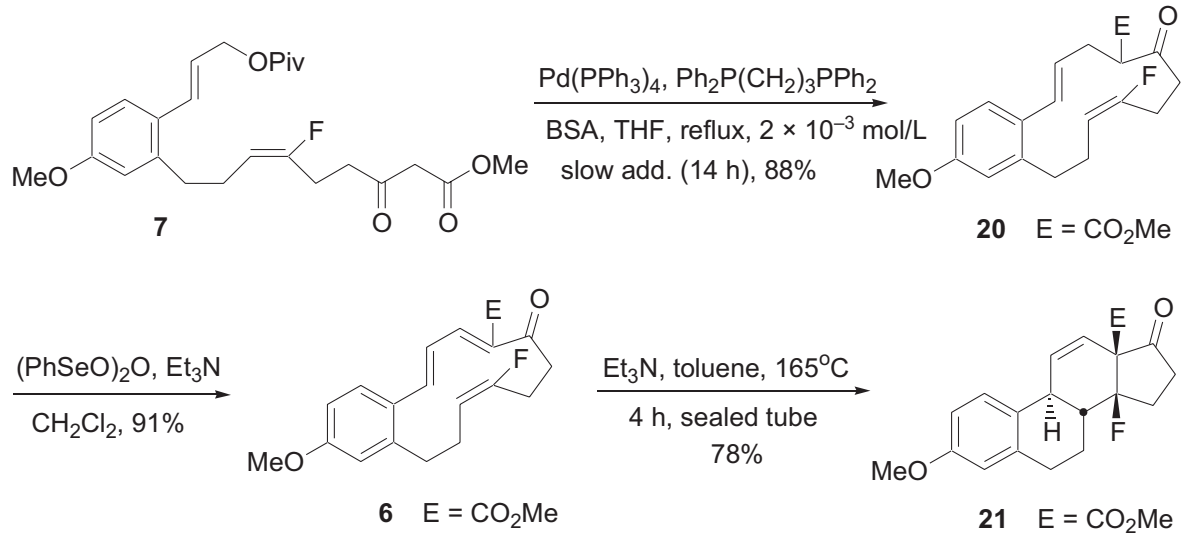
Having built the key intermediate **21**, the next step was to

© 2006 NRC Canada

Scheme 3.



Scheme 4.



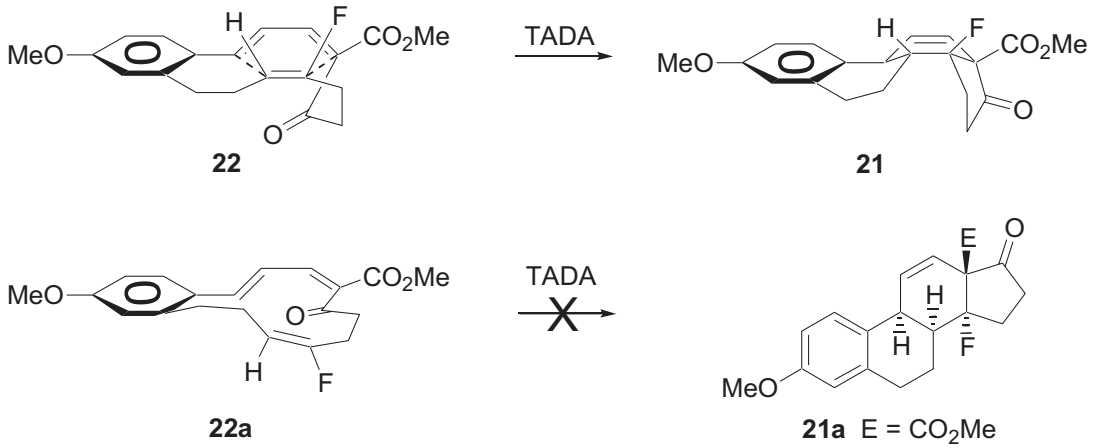
obtain a methyl group at the C-13 position and explore the homologation at the C-17 position.

Hydrogenation of the olefin in tetracycle **21** (Scheme 6) was carried out, and compound **23** was obtained in quantitative yield. Reduction of the ester and ketone moieties was performed to give diol **24** as a 9:1 mixture of α:β isomers at C-17, which could not be separated. Selective tosylation of the primary alcohol of this diol mixture was then achieved in two steps (19). First, the diol **24** was treated with dibutyltin oxide at reflux in a mixture of benzene and DMF with a Dean–Stark trap and the corresponding ketal tin intermediate was formed. Tosyl chloride was then added to produce a 9:1 mixture (α:β isomers) of tosylate **25** in 87% yield. This mixture was reduced with sodium borohydride, and compound **26** was obtained pure in 85% yield after chromatography. Oxetane **27** was also obtained as a side product in 10% yield. This compound must come from the intramolecular displacement of the C-17 tosylate by the β-secondary alcohol of the minor β isomer of **25**.

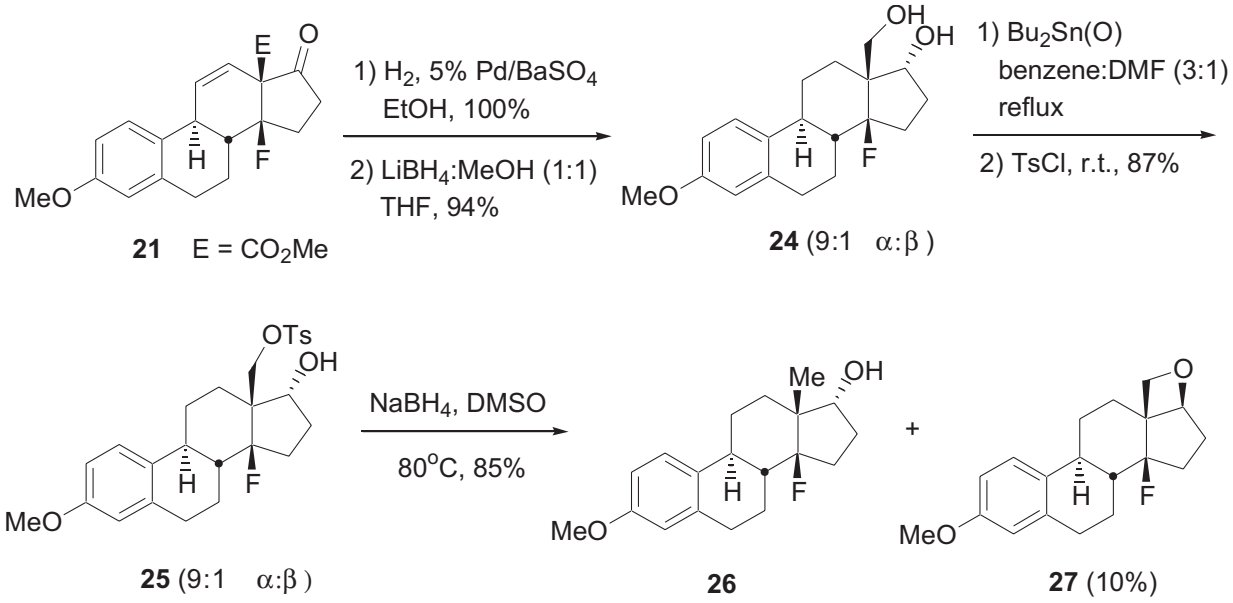
Having tetracycle **26** with the desired methyl group at the C-13 position in hand, homologation at the C-17 position was then investigated. Many types of reactions for C-17 homologation of steroids are known in the literature (20). In our case, many attempts were made to add one carbon at this position. Several homologation methods were tried (Wittig (21), epoxidation (22, 23), S_N2 reaction, etc.), but the best results were obtained with a coupling reaction. The alcohol was first oxidized with TPAP–NMO (24) to give ketone **5** in 87% yield (Scheme 7). This ketone was treated with KHMDS to form the corresponding enolate. Comins reagent (25) was

© 2006 NRC Canada

Scheme 5.



Scheme 6.



then added, and the triflic enol ether **28** was obtained in 84% yield.

Palladium-catalyzed coupling of **28** was then investigated. Carbonylation (26) of compound **28** catalyzed by $Pd(OAc)_2$ led to the α,β-unsaturated ester **29** in 81% yield. This unsaturated ester was reduced with a catalytic amount of palladium to give ester **30** in a quantitative yield as a single isomer. Unfortunately, the isomer obtained at the C-17 center was α rather than the desired β isomer (confirmed by ^{1}H NMR shift of the β proton). To obtain the C-17 β isomer **31**, epimerization conditions were explored but without success. A survey of the literature (27) indicated that with an ester at C-17, both the kinetic and thermodynamic isomers correspond to the α isomer when the C–D ring junction is cis.

The only method to obtain the β C-17 center with the C–D cis ring junction is by using a nitrile (28). The coupling reaction was therefore performed on the triflic enol ether **28** with $Pd(PPh_3)_4$ and LiCN (29) from which α,β-unsaturated nitrile **32** was obtained in 79% yield (Scheme 8). Hydrogenation of this α,β-unsaturated nitrile provided a mixture of α- (**33a**, 37%) and β- (**33b**, 58%) nitriles, which were separated by chromatography. The structure of β-nitrile **33b** was confirmed by a X-ray diffraction analysis (Fig. 2). Having obtained the desired β-nitrile, the model study for the C-17 homologation was thus completed (Table 1).[2]

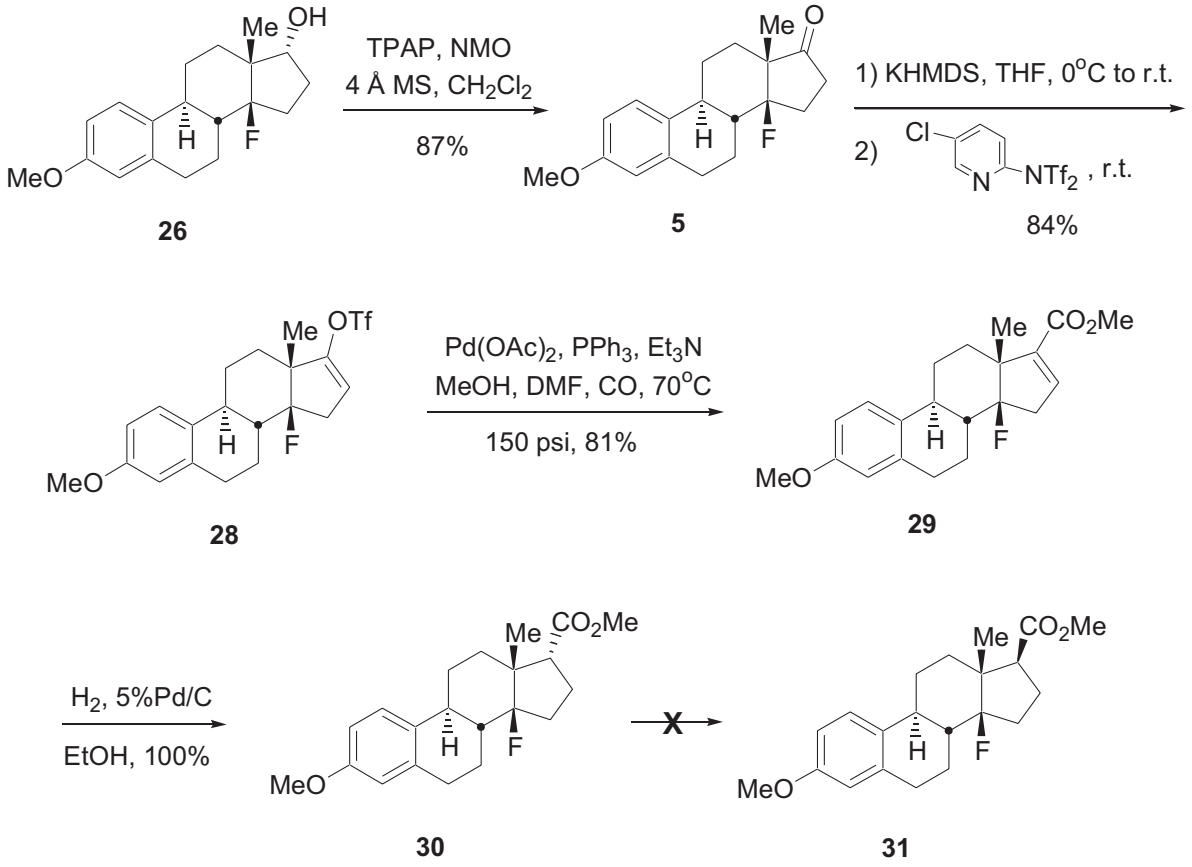
Functionalization of ring A

Starting from alcohol **26**, Birch reduction (30) with lithium metal was performed at –78 °C, and the corresponding enol ether was hydrolyzed with 1 N HCl to afford the α,β-

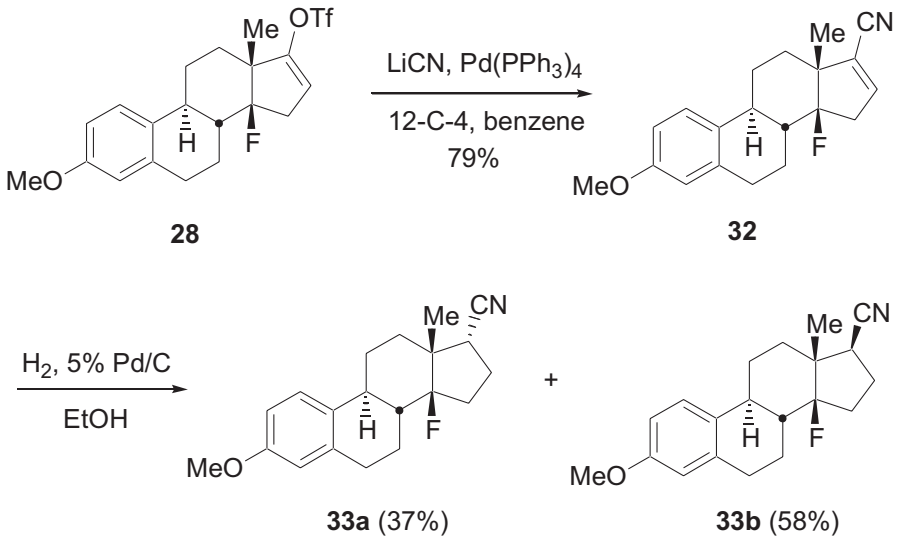
[2] Supplementary data for this article are available on the journal Web site (http://canjchem.nrc.ca) or may be purchased from the Depository of Unpublished Data, Document Delivery, CISTI, National Research Council Canada, Building M-55, 1200 Montreal Road, Ottawa, ON K1A 0R6, Canada. DUD 4073. For more information on obtaining material refer to http://cisti-icist.nrc-cnrc.gc.ca/irm/unpub_e.shtml. CCDC 264404 and 264405 contain the crystallographic data for this manuscript. These data can be obtained, free of charge, via http://www.ccdc.cam.ac.uk/conts/retrieving.html (or from the Cambridge Crystallographic Data Centre, 12 Union Road, Cambridge CB2 1EZ, UK; fax +44 1223 336033; or deposit@ccdc.cam.ac.uk).

© 2006 NRC Canada

Scheme 7.



Scheme 8.



unsaturated ketone **34** in 77% yield (Scheme 9). The proton at the C-10 position was β, as expected. We were pleased to see that the fluorine atom was not hydrogenolyzed at –78 °C, since this had occured at –30 °C.

To obtain the desired cis A–B ring junction, hydrogenation of the α,β-unsaturated ketone **34** was accomplished with a catalytic amount of palladium (Scheme 9) to yield the cis and trans isomers **36** and **35** in 60% and 37% yields, respectively. The two isomers were easily separated and the synthesis was continued with tetracycle **36**, which had the A–B cis ring junction. Oxidation of tetracycle **36** with TPAP–NMO (23) furnished the diketone **37** in 99% yield.

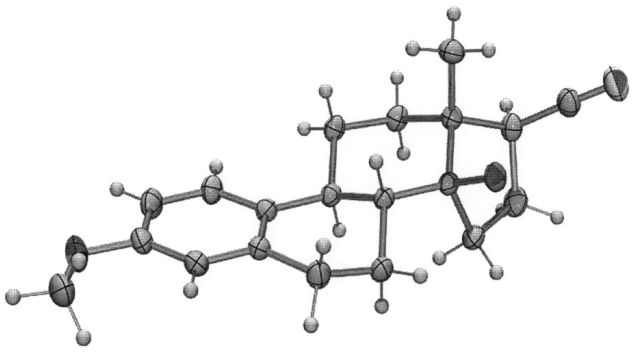
Selective reduction of the ketone at the C-3 position should be possible with a hydride source sensitive to the steric hindrance (31). In addition, with such a hydride source, the reduction of the C-3 center to afford the β alco-

© 2006 NRC Canada

Table 1. X-ray crystallographic information for nitrile **33b** and nitro **47**.

Crystal	Nitrile **33b**	Nitro **47**
Empirical formula	$C_{20}H_{24}FNO$	$C_{26}H_{31}FN_2O_4$
Formula mass	313.40	454.53
Colour, habit	Colourless, plate	Colourless, plate
Crystal dimension (mm^3)	0.4 × 0.3 × 0.3	0.05 × 0.40 × 0.50
Crystal system	Prism	Triclinic
Space group	*P*1	*P*1
Z	4	2
a (Å)	9.601(2)	6.6631(10)
b (Å)	16.891(4)	9.5374(15)
c (Å)	10.3300(19)	18.128(3)
α (°)	90.00	92.969(3)
β (°)	98.40(4)	94.269(3)
γ (°)	90.00	102.600(3)
Collection ranges	$-11 < h < 11, 0 < k < 20, 0 < l < 12$	$-8 < h < 8, -12 < k < 11, -23 < l < 21$
Temperature (K)	293(2)	173(1)
Volume ($Å^3$)	1657.3(6)	1118.4(3)
D_{calcd} (Mg m^{-3})	1.256	1.350
Abs. coeff. (μ) (mm^{-1})	0.673	0.096
F(000)	672	484
θ Range for data collection (°)	5.05–71.76	2.19–27.50
No. of obsrvd. reflns.	3220	7872
No. of ind. reflns.	2873	4952
No. of data/restr./params.	3220/0/209	4952/0/422
Max. shift/error	0.002/0.000	0.000/0.000
Goodness-of-fit on F^2	1.031	1.083
Final *R* indices [$l > 2\sigma(l)$]	$R_1 = 0.0420$, $wR_2 = 0.1123$	$R_1 = 0.0491$, $wR_2 = 0.1362$
R indices (all data)	$R_1 = 0.0383$, $wR_2 = 0.1092$	$R_1 = 0.0617$, $wR_2 = 0.1429$
Max. diff. peak and hole (e $Å^{-3}$)	0.283 and –0.148	0.396 and –0.226

Fig. 2. Single crystal X-ray structure of nitrile β-**33b**.



hol should be favored (32). Indeed, the use of L-Selectride as the reducing agent on diketone **37** gave a quantitative yield of the β C-3 alcohol **38** (Scheme 9).

Fluoro analog synthesis and biological activities

To complete the synthesis of the fluoro analogs, we had to carry out the nitrile homologation at the C-17 position developed in the model study and to introduce the α,β-unsaturated ester at the C-17 position.

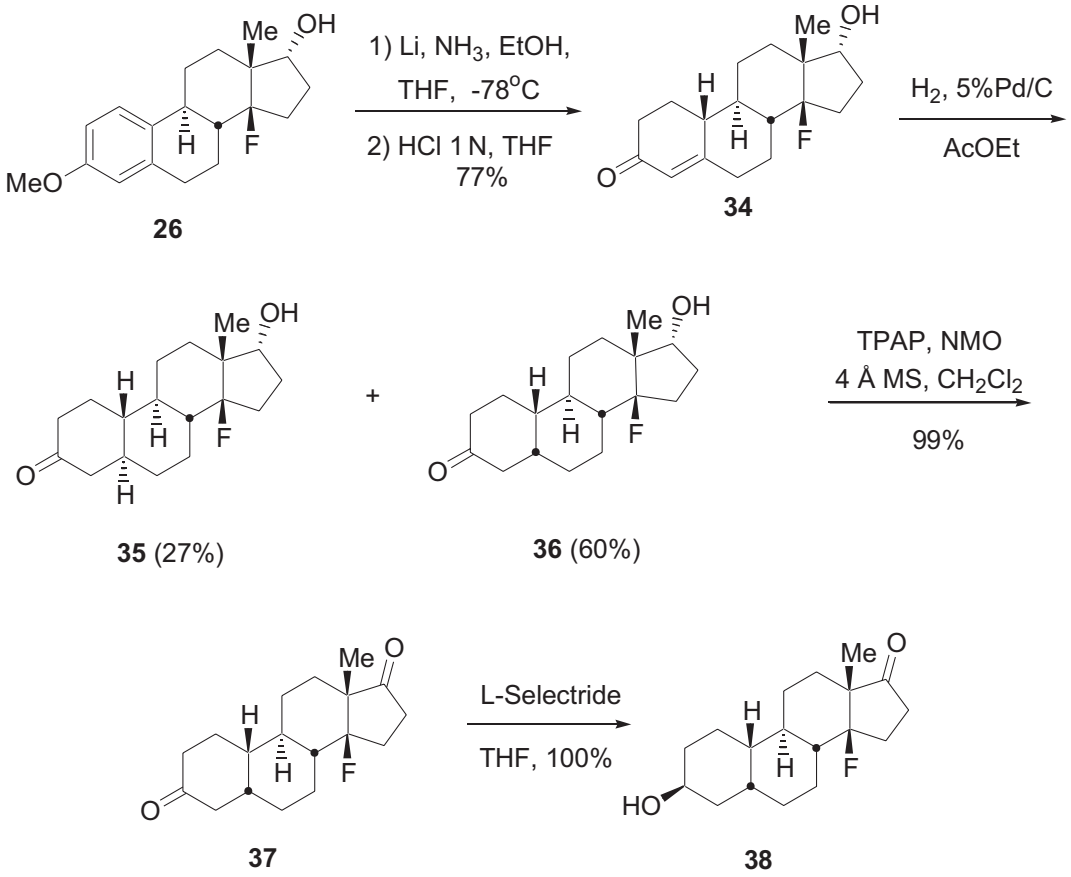
Alcohol **38** was protected with TBDMSOTf (Scheme 10), and a mixture of the desired silyl ether **40** and silyl enol ether **39** was obtained. This mixture was treated with TBAF, and the silyl ether **40** was the only compound obtained in 92% yield for the two steps. This compound was treated under the same conditions used for the model compound **5** (Scheme 7) to prepare the triflic enol ether **41** without success. The starting material was recovered with some decomposition. We tried other bases (LiHMDS, NaHMDS, and LDA) to make this triflic enol ether, but the same negative results were obtained. We therefore looked for an alternative method via a vinyl iodide intermediate (33).

Starting with ketone **38**, the corresponding hydrazone was formed with hydrazine at reflux over 5 days, and this hydrazone was treated with iodine to provide the desired vinylic iodide **42** in 91% yield for the two steps (Scheme 11). The coupling reaction (LiCN, $Pd(PPh_3)_4$, 12-C-4) on this compound having a free alcohol was attempted, but gave a very poor yield. Thus, the alcohol was protected with TBDMSOTf to give compound **43** in a quantitative yield. The same coupling reaction (LiCN, $Pd(PPh_3)_4$, 12-C-4) was performed with vinylic iodide **43**, and the desired α,β-unsaturated nitrile **44** was obtained in 45% yield. This unsaturated nitrile was then hydrogenated to give the β-nitrile **45b** (53%) and the α-nitrile **45a** (47%), which were separated by chromatography.

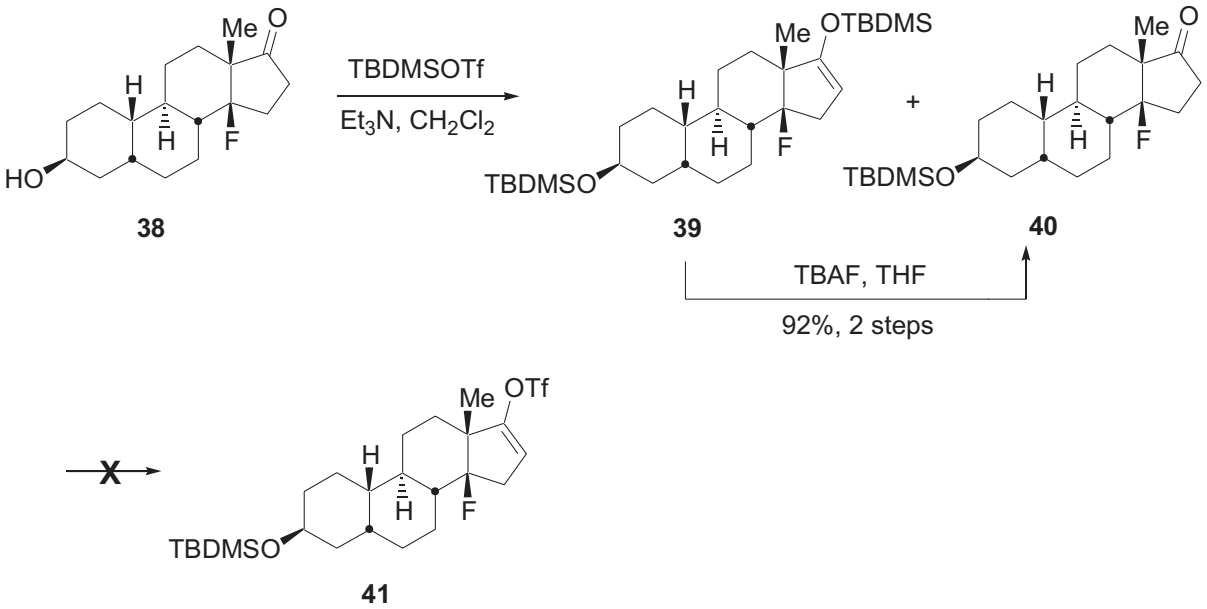
Deprotection of the silyl ethers **45a** and **45b** was accomplished under acidic conditions to furnish the corresponding compounds **46a** and **46b** in a quantitative yield. To confirm the stereochemistry of the β-nitrile **46b**, the *p*-nitrobenzoate **47** was prepared and an X-ray diffraction analysis was ob-

© 2006 NRC Canada

Scheme 9.



Scheme 10.



tained, which confirmed the stereochemistry of all the asymmetric centers (Fig. 3).

To complete the synthesis, only two steps were required: the reduction of the nitrile to an aldehyde, and a Horner–Emmons reaction to introduce the α,β-unsaturated ester at the C-17 center. DIBALH was used to reduce the nitriles **46a** and **46b**. Reduction of the α-nitrile **46a** at 0 °C gave two compounds (Scheme 12), which were identified as aldehydes **48** and **49**, each containing an olefin. Clearly, the fluoride is sensitive to the presence of Lewis acid. In an attempt to resolve this problem, many other reducing agents were tried ($LiAlH(OEt)_3$, $LiAlH_4$, Raney Ni), but in each

© 2006 NRC Canada

Scheme 11.

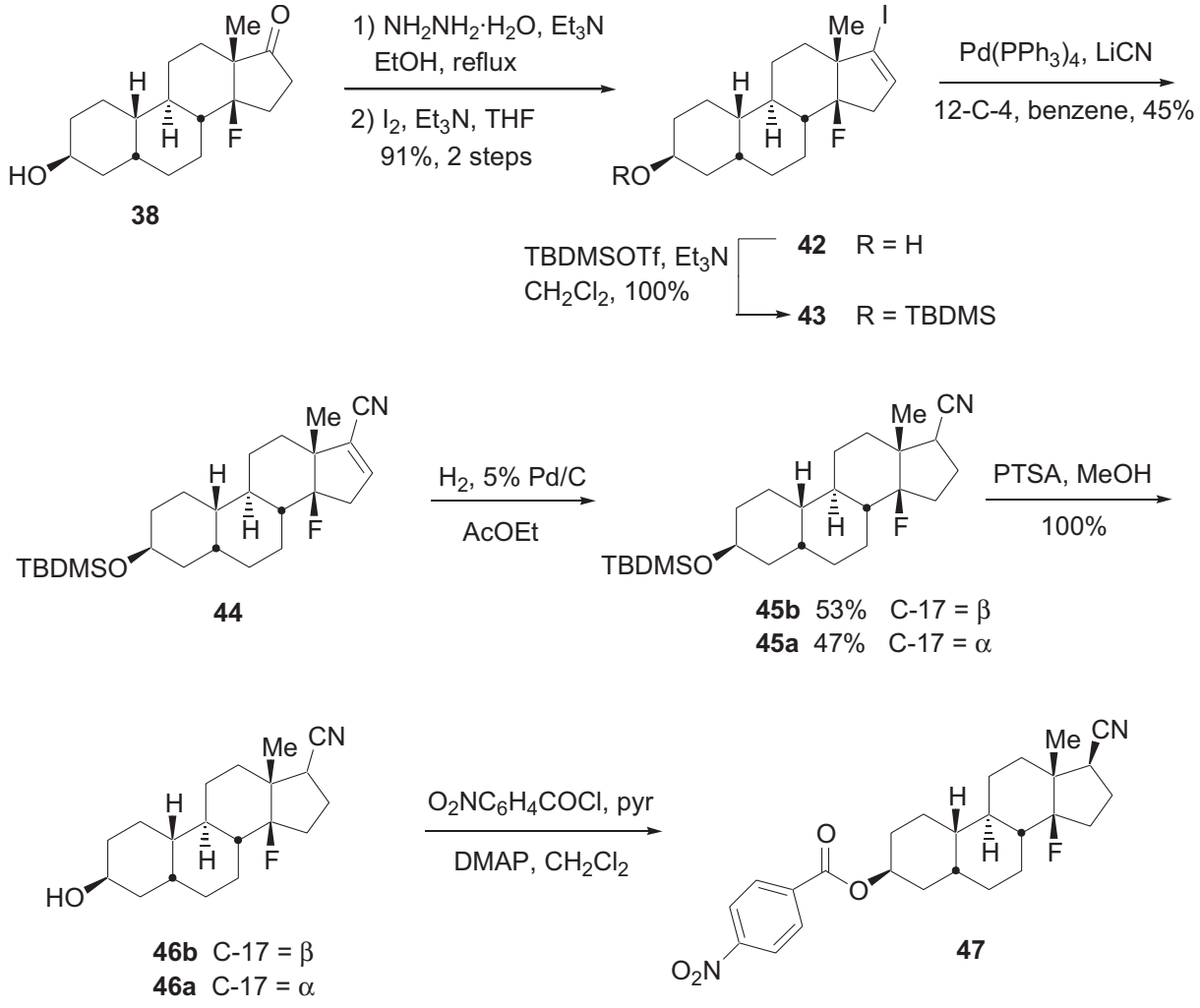
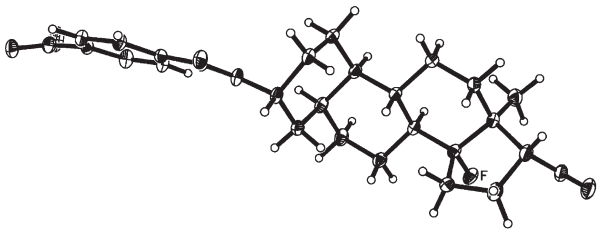


Fig. 3. Single crystal X-ray structure of *p*-nitrobenzoate **47**.



case, the starting material was recovered with some decomposition products. After considering these results, we decided to attempt the reduction of the α-nitrile **46a** with DIBALH at a lower temperature. When the reduction was performed at –78 °C, the starting material was recovered. The corresponding imine was obtained when the reaction was performed at –60 °C with 10 equiv. of DIBALH. To hydrolyze this imine, the residue was passed through a silica gel pad and α-aldehyde **50a** was obtained. The Horner–Emmons reaction was carried out on this aldehyde to furnish the desired α-fluoro analog **4** in 60% yield for the two last steps.

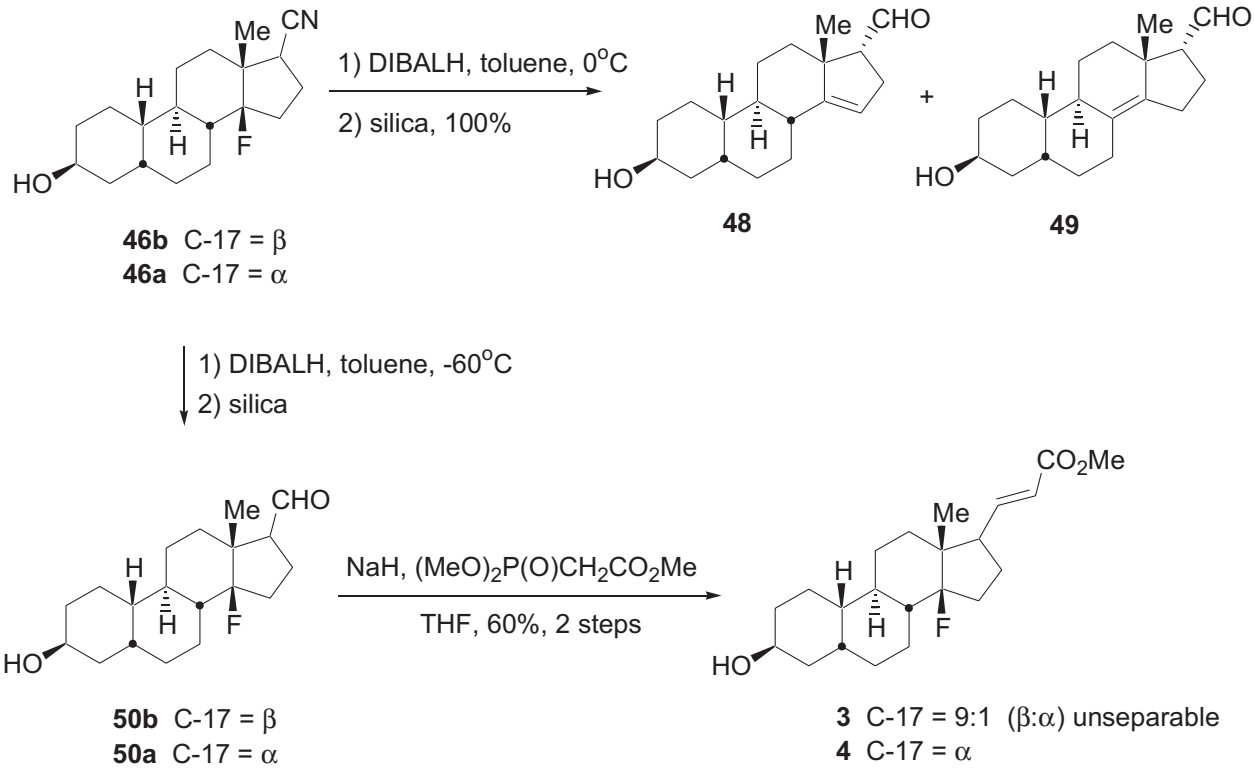
To complete the synthesis of the β-fluoro analog **3**, we had to repeat the last two steps previously discussed on the β-nitrile **46b**. Reduction of β-nitrile **46b** with DIBALH worked well to give the corresponding imine, but when this imine was passed through the silica gel pad, partial isomerization of the β- to α-aldehyde took place (Scheme 12).

To resolve this problem of epimerization, we tried to use aqueous conditions to hydrolyze the β-imine but with no success. Better results were obtained when the β-imine was passed rapidly through a short silica gel pad, and the corresponding aldehyde was obtained as a mixture of β-aldehyde **50b** and α-aldehyde **50a** (9:1). The Horner–Emmons reaction was performed on this mixture of aldehydes to give an unseparable 9:1 mixture of the β-fluoro analog **3** and α-fluoro analog **4**. This mixture was used to study the biological activity for the β-fluoro analog.

The biological activities of these two racemic fluoro analogs **3** and **4** were studied and compared with digitoxigenin **1**. Radioligand binding studies were performed to measure ligand–receptor affinities for **1**, **3**, and **4** at the ouabain receptor (i.e., ATPase (Na^+/K^+) expressed in the MDCK (dog kidney) cell line). [^{3}H]ouabain was used as the radioligand for competitive displacement. Compound binding affinities are reported as IC_{50} values, indicative of the drug concentration needed to inhibit 50% of [^{3}H]ouabain binding to the Na^+,K^+-ATPase. The results are very surpris-

© 2006 NRC Canada

Scheme 12.



ing. We expected that the inhibitory activity of the β-fluoro analog **3** would be superior to that α-fluoro analog **4**, but it was not the case. The β-fluoro analog **3** exhibited no activity, while the α-fluoro analog **4** had an IC_{50} of 12 μmol/L, in comparison to the natural product digitoxigenin **1** (IC_{50} of 0.35 μmol/L). No explanation can be provided to rationalize this result. However, the primary result obtained with the α-fluoro analog **4** has encouraged us to continue with the synthesis of other analogs to optimize the biological activity of this class of fluoro-steroids, and the results will be presented in another publication.

Summary

In summary, the synthesis of the fluoro analogs **3** and **4** was carried out via the formation of β-keto ester **7** with excellent yields. The macrocyclization reaction with this β-keto ester afforded the 13-membered macrocycle **6** with the trans-cis-cis olefin geometry, the precursor needed for the TADA reaction. The key step of the synthesis, the TADA reaction, was performed on this macrocycle to give the steroidal tetracycle **21** with the desired TSC configuration at the ring junction. With this TADA reaction, four new centers were created in one step to give the expected tetracycle **21**. This key tetracycle was obtained in 19 steps with very high yields and complete control of the diastereoselectivity. The functionalization of the A ring was accomplished and the homologation of the C-17 position was performed to give the desired α- and β-fluoro analogs.

The fluoro analog syntheses have been achieved in 35 steps in a linear sequence with 0.7% overall yield. The chemoselectivity, regioselectivity, and stereochemistry were controlled at each step of the synthesis except for the reduction of the β-nitrile **46b** to the corresponding aldehyde at the end of the sequence that gives 10% epimerization. The biological activity was measured for the two fluoro analogs. Surprisingly, the α-fluoro analog **4** provided 5% of the inhibitory potency of natural digitoxigenin **1**.

Experimental section

General

All reactions were performed under a nitrogen atmosphere with oven (150 °C) or flame-dried glassware. All solvents were distilled prior to use: ether and tetrahydrofuran from sodium–benzophenone; toluene, dichloromethane, and dimethyl sulfoxyde were distilled over calcium hydride, and methanol from magnesium–iodine. Most amines were dried over calcium hydride and distilled. All other starting materials and reagents were obtained commercially and used as such. For reaction workups, all organic phases were dried over magnesium sulphate. Analytical TLC was carried out on precoated glass plates (0.25 mm) with silica gel 60 (230–400 mesh). The following abbreviations were used for NMR data: singlet (s), doublet (d), triplet (t), quadruplet (q), multiplet (m), broad (br). Chemical shifts are reported in ppm δ units relative to chloroform (7.26 ppm for ^{1}H NMR and 77.0 ppm for decoupled ^{13}C NMR) as internal standard. ^{1}H and ^{13}C NMR spectra are referenced with respect to the residual signals of the solvent; they are described using standard abbreviations. ^{13}C NMR spectra of fluoro compounds give more carbon signals (one to five) owing to fluorine coupling with carbon. Melting points (mp) are uncorrected. Mass spectra (MS) were obtained with electronic ionization (70 eV).

© 2006 NRC Canada

Olefin 11

To a stirred solution of ketone **10** (20 g, 113 mmol) in tetrahydrofuran (500 mL) at –78 °C was added lithium aluminium hydride (2.2 g, 57 mmol). The mixture was stirred at –78 °C for 1 h and sodium sulfate decahydrate was added. The mixture was stirred at room temperature for 1 h and the precipitate was filtrated and washed with dichloromethane. The solvent was evaporated and crude alcohol was diluted in benzene. *p*-Toluenesulfonic acid (215 mg, 1.13 mmol) was added and the mixture was stirred at reflux with a Dean–Stark for 1.5 h. Satd. aq. $NaHCO_3$ was added and the aqueous phase was extracted with ethyl acetate. The combined organic phases were dried, filtered, and evaporated. The crude compound was filtered on a silica gel pad and washed with ethyl acetate – hexanes (3:7) to give olefin **11** as a colorless oil (19 g, 100%). IR ($CHCl_3$, cm^{-1}) ν: 3030, 2933, 2830, 1606, 1569, 1500, 1464, 1428, 1253. ^{1}H NMR (300 MHz, $CDCl_3$, ppm) δ: 6.96 (1H, d, J = 9.1 Hz, Ph), 6.71–6.68 (2H, m, Ph), 6.42 (1H, dt, J = 9.3, 1.9 Hz, PhCH=C*H*CH_2), 5.90 (1H, dt, J = 9.3, 4.4 Hz, PhC*H*=$CHCH_2$), 3.80 (3H, s, $ArOCH_3$), 2.78 (2H, t, J = 8.2 Hz, $PhCH_2CH_2$), 2.33–2.26 (2H, m, $PhCH{=}CHCH_2$). ^{13}C NMR (75 MHz, $CDCl_3$, ppm) δ: 158.53, 137.08, 127.32, 127.14, 126.78, 125.81, 113.79, 111.02, 55.13, 27.97, 22.96. MS (*m*/*e*): 160 ($[M]^+$). HR-MS calcd. for $C_{11}H_{16}O_3$: 160.0888 ($[M]^+$); found: 160.0887 ± 0.0005.

Diol 9

To a stirred solution of olefin **11** (26.0 g, 160.3 mmol) in methanol (2 L) at –78 °C, O_3 was bubbled at –78 °C for 1.5 h. Nitrogen was bubbled for 15 min and sodium borohydride (12.1 g, 319.9 mmol) was added. The mixture was stirred at room temperature for 2 h and sodium borohydride (6.1 g, 160.0 mmol) was added. The mixture was stirred for 1 h and solvent was evaporated. The crude compound was diluted in tetrahydrofuran (1 L) and an aqueous solution of 2.5 mol/L NaOH (330 mL) and 30% hydrogen peroxide (230 mL) were added. The mixture was stirred at room temperature for 18 h. Aqueous sodium thiosulfate solution (10%) was added and the aqueous phase was extracted with chloroform. The combined organic phases were dried, filtered, and evaporated to give diol **9** as an amorphous white solid (27.1 g, 86%). IR ($CHCl_3$, cm^{-1}) ν: 3327, 2939, 2875, 1610, 1580, 1500, 1460, 1256, 1160, 1111, 1055, 1031, 942, 819. ^{1}H NMR (300 MHz, $CDCl_3$, ppm) δ: 7.22 (1H, d, J = 8.3 Hz, Ph), 6.78 (1H, d, J = 2.7 Hz, Ph), 6.72 (1H, dd, J = 8.3, 2.7 Hz, Ph), 4.63 (2H, s, $ArCH_2OH$), 3.80 (3H, s, $ArOCH_3$), 3.57 (2H, t, J = 5.9 Hz, CH_2CH_2OH), 2.82 (2H, t, J = 7.3 Hz, $ArCH_2CH_2$), 2.49 (2H, broad, $ArCH_2OH$, CH_2CH_2OH), 1.93 (2H, quint, J = 6.1 Hz, $CH_2CH_2CH_2$). ^{13}C NMR (75 MHz, $CDCl_3$, ppm) δ: 159.34, 142.05, 131.06, 130.80, 115.02, 110.88, 62.41, 60.74, 55.17, 33.63, 27.26. MS (*m*/*e*): 196 ($[M]^+$). HR-MS calcd. for $C_{11}H_{16}O_3$: 196.1099 ($[M]^+$); found: 196.1108 ± 0.0006.

Hydroxyaldehyde 12

To a stirred solution of diol **9** (9.5 g, 48.5 mmol) in a mixture of pentane–dichloromethane (4:1) (100 mL) was added MnO_2 (21.0 g, 242.5 mmol) and the mixture was stirred at room temperature for 30 min. MnO_2 was added in portions of 21.0 g every 30 min until the reaction was finished. The mixture was filtered on a silica gel pad and was further washed with ethyl acetate. The solvent was evaporated to give hydroxyaldehyde **12** as a yellow oil (8.0 g, 85%). IR ($CHCl_3$, cm^{-1}) ν: 3414, 2942, 2872, 1682, 1599, 1566, 1496, 1463, 1431, 1290, 1251, 1121, 1057, 1025, 813. ^{1}H NMR (300 MHz, $CDCl_3$, ppm) δ: 10.06 (1H, s, C*H*O), 7.78 (1H, d, J = 8.6 Hz, Ph), 6.89 (1H, dd, J = 8.6, 2.5 Hz, Ph), 6.82 (1H, d, J = 2.5 Hz, Ph), 3.90 (3H, s, $ArOCH_3$), 3.68 (2H, t, J = 6.1 Hz, CH_2CH_2OH), 3.15 (2H, t, J = 7.8 Hz, $ArCH_2CH_2$), 2.06–1.85 (3H, m, $CH_2CH_2CH_2OH$). ^{13}C NMR (75 MHz, $CDCl_3$, ppm) δ: 191.54, 163.85, 147.53, 135.56, 127.29, 116.40, 111.68, 61.52, 55.44, 34.50, 28.93. MS (*m*/*e*): 194 ($[M]^+$). HR-MS calcd. for $C_{11}H_{14}O_3$: 194.0943 ($[M]^+$); found: 194.0948 ± 0.0006.

Ester 13

To a stirred solution of hydroxyaldehyde **12** (8.7 g, 44.8 mmol) in tetrahydrofuran (200 mL) were added imidazole (7.6 g, 112 mmol) and *tert*-butyldimethylsilyl chloride (10.1 g, 67.2 mmol). The mixture was stirred at room temperature for 45 min and satd. aq. NH_4Cl was added. The aqueous phase was extracted with ethyl acetate. The combined organic phases were dried, filtered, and evaporated. The residue was purified by flash chromatography (10% ethyl acetate, 90% hexanes) to give the corresponding silyl ether as a yellow oil (13.8 g, 100%). IR ($CHCl_3$, cm^{-1}) ν: 2959, 2929, 2856, 2734, 1689, 1600, 1463, 1225, 1102, 1029, 836. ^{1}H NMR (300 MHz, $CDCl_3$, ppm) δ: 10.14 (1H, s, C*H*O), 7.80 (1H, d, J = 8.6 Hz, Ph), 6.85 (1H, dd, J = 8.6, 2.6 Hz, Ph), 6.77 (1H, d, J = 2.6 Hz, Ph), 3.87 (3H, s, $ArOCH_3$), 3.68 (2H, t, J = 6.1 Hz, $CH_2CH_2OTBDMS$), 3.07 (2H, dd, J = 7.9, 6.1 Hz, $ArCH_2CH_2$), 1.84 (2H, dt, J = 9.5, 6.1 Hz, $CH_2CH_2CH_2OTBDMS$), 0.91 (9H, s, $Si\text{-}C(CH_3)_3$), 0.06 (6H, s, $Si(CH_3)_2$). ^{13}C NMR (75 MHz, $CDCl_3$, ppm) δ: 190.75, 163.7, 147.8, 134.31, 127.5, 116.18, 111.71, 62.19, 55.43, 34.84, 29.95, 25.95, 18.3, –5.3. MS (*m*/*e*): 251 ($[M - C_4H_9]^+$). HR-MS calcd. for $C_{13}H_{19}O_3Si$: 251.1103 ($[M - C_4H_9]^+$); found: 251.1108 ± 0.0007.

To a suspension of sodium hydride 60% in oil (2.5 g, 61.8 mmol) in tetrahydrofuran (350 mL) was added triethyl phosphonoacetate (12.3 mL, 61.8 mmol). The mixture was stirred at room temperature for 15 min and a solution of aldehyde (12.7 g, 41.2 mmol) in tetrahydrofuran (50 mL) was added. The mixture was stirred at room temperature for 20 min and satd. aq. NH_4Cl was added. The aqueous phase was extracted with ethyl acetate. The combined organic phases were dried, filtered, and evaporated. The residue was filtered on a silica gel pad and washed with 10% ethyl acetate in hexanes to give ester **13** as a yellow oil (15.2 g, 97%). IR ($CHCl_3$, cm^{-1}) ν: 2954, 2857, 1712, 1603, 1495, 1464, 1366, 1295, 1257, 1159, 1105, 1032, 979, 837. ^{1}H NMR (300 MHz, $CDCl_3$, ppm) δ: 7.95 (1H, d, J = 15.8 Hz, PhC*H*=CH), 7.56 (1H, d, J = 9.2 Hz, Ph), 6.76–6.73 (2H, m, Ph), 6.28 (1H, d, J = 15.8 Hz, PhCH=C*H*), 4.27 (2H, q, J = 7.1 Hz, $CO_2CH_2CH_3$), 3.84 (3H, s, $ArOCH_3$), 3.77 (2H, t, J = 6.3 Hz, $CH_2CH_2OTBDMS$), 2.81 (2H, dd, J = 9.7, 6.1 Hz, $ArCH_2CH_2$), 1.81 (2H, dt, J = 9.7, 6.1 Hz, $CH_2CH_2CH_2OTBDMS$), 1.35 (3H, t, J = 7.1 Hz, $CO_2CH_2CH_3$), 0.93 (9H, s, $SiC(CH_3)_3$), 0.08 (6H, s, $Si(CH_3)_2$). ^{13}C NMR (75 MHz, $CDCl_3$, ppm) δ: 167.26, 161.01, 143.91, 141.48, 128.14, 125.57, 116.95, 115.15,

© 2006 NRC Canada

112.17, 62.17, 60.22, 55.16, 34.34, 29.67, 25.95, 18.30, 14.36, –5.31. MS (*m*/*e*): 363 [M – CH_3]$^+$, 321 ([M – C_4H_9]$^+$). HR-MS calcd. for $C_{20}H_{31}O_4Si$: 363.1991 ([M – CH_3]$^+$); found: 363.1995 ± 0.0011.

Disilyl ether 14

To a stirred solution of ester **13** (18.4 g, 48.7 mmol) in dichloromethane (450 mL) at 0 °C was added 1 mol/L diisobutylaluminium hydride in dichloromethane (121.8 mL, 121.8 mmol). The mixture was stirred at 0 °C for 1 h and sodium sulfate decahydrate was added. The mixture was stirred for 1 h. The precipitate was filtered and washed with dichloromethane. The solvent was evaporated to give the corresponding alcohol as a yellow oil (15.9 g, 97%). IR ($CHCl_3$, cm^{-1}) ν: 3356, 2952, 2857, 1607, 1494, 1464, 1256, 1098, 1033, 967, 836. ^{1}H NMR (300 MHz, $CDCl_3$, ppm) δ: 7.43 (1H, d, *J* = 8.4 Hz, Ph), 6.83 (1H, d, *J* = 15.7 Hz, PhC*H*=CH), 6.77–6.72 (2H, m, Ph), 6.18 (1H, dt, *J* = 15.7, 6.0 Hz, PhCH=C*H*), 4.32 (2H, dd, *J* = 6.0, 1.3 Hz, CH_2OH), 3.82 (3H, s, ArOCH_3), 3.67 (2H, t, *J* = 6.2 Hz, CH_2CH_2OTBDMS), 2.76–2.71 (2H, m, ArCH_2CH_2), 1.79 (2H, dt, *J* = 9.9, 6.1 Hz, $CH_2CH_2CH_2$OTBDMS), 1.60 (1H, massif, CH_2O*H*), 0.94 (9H, s, SiC(CH_3)$_3$), 0.09 (6H, s, Si(CH_3)$_2$). ^{13}C NMR (75 MHz, $CDCl_3$, ppm) δ: 159.13, 141.29, 128.50, 128.11, 128.06, 127.27, 114.85, 111.74, 64.06, 62.44, 55.18, 34.02, 29.76, 25.98, 18.35, –5.25. MS (*m*/*e*): 336 ([M]$^+$). HR-MS calcd. for $C_{19}H_{32}O_3Si$: 336.2121 ([M]$^+$); found: 336.2123 ± 0.0010.

To a stirred solution of alcohol (15.9 g, 47.3 mmol) in tetrahydrofuran (400 mL) were added imidazole (8.1 g, 118.3 mmol) and *tert*-butyldiphenylsilane chloride (18.5 mL, 71.0 mmol). The mixture was stirred at room temperature for 1.5 h and satd. aq. NH_4Cl was added. The aqueous phase was extracted with ethyl acetate. The combined organic phases were dried, filtered, and evaporated. The residue was purified by flash chromatography (5% ethyl acetate, 95% hexanes) to give disilyl ether **14** as a yellow oil (25.0 g, 93%). IR ($CHCl_3$, cm^{-1}) ν: 3048, 2934, 2858, 1607, 1495, 1466, 1254, 1106, 1062, 967, 837. ^{1}H NMR (300 MHz, $CDCl_3$, ppm) δ: 7.74 (4H, dd, *J* = 7.5, 1.7 Hz, Ph), 7.48–7.36 (7H, m, Ph), 6.87 (1H, d, *J* = 15.7 Hz, PhC*H*=CH), 6.76–6.72 (2H, m, Ph), 6.10 (1H, dt, *J* = 15.7, 4.9 Hz, PhCH=C*H*), 4.39 (2H, dd, *J* = 6.7, 1.8 Hz, CH_2OTBDPS), 3.82 (3H, s, ArOCH_3), 3.63 (2H, t, *J* = 6.3 Hz, CH_2CH_2OTBDMS), 2.71 (2H, dd, *J* = 9.7, 7.7 Hz, ArCH_2CH_2), 1.84–1.74 (2H, m, $CH_2CH_2CH_2$OTBDMS), 1.58 (9H, s, SiC(CH_3)$_3$), 1.11 (9H, s, SiC(CH_3)$_3$), 0.06 (6H, s, Si(CH_3)$_2$). ^{13}C NMR (75 MHz, $CDCl_3$, ppm) δ: 158.92, 141.09, 135.59, 133.79, 129.69, 128.22, 127.73, 127.65, 127.16, 126.46, 114.86, 111.77, 64.84, 62.45, 55.23, 33.97, 29.87, 26.91, 26.02, 19.32, 19.35, –5.20. MS (*m*/*e*): 574 ([M]$^+$). HR-MS calcd. for $C_{35}H_{50}O_3Si_2$: 574.3298 ([M]$^+$); found: 574.3303 ± 0.0017.

Alcohol 15

To a stirred solution of disilyl ether **14** (40.3 g, 70.2 mmol) in ethanol 95% (500 mL) was added *p*-toluenesulfonate pyridinium salt (1.8 g, 7.02 mmol) and the mixture was stirred at room temperature overnight. Satd. aq. $NaHCO_3$ was added and the aqueous phase was extracted with ethyl acetate. The combined organic phases were dried, filtered, and evaporated. The residue was purified by flash chromatography (50% ethyl acetate, 50% hexanes) to give alcohol **15** as a yellow oil (31.5 g, 98%). IR ($CHCl_3$, cm^{-1}) ν: 3390, 3048, 2937, 2859, 1607, 1496, 1465, 1380, 1256, 1202, 1110, 1057, 967. ^{1}H NMR (300 MHz, $CDCl_3$, ppm) δ: 7.75 (4H, dd, *J* = 7.5, 1.7 Hz, Ph), 7.48–7.38 (7H, m, Ph), 6.89 (1H, dt, *J* = 15.6, 1.7 Hz, PhC*H*=CH), 6.78–6.73 (2H, m, Ph), 6.11 (1H, dt, *J* = 15.6, 4.7 Hz, PhCH=C*H*), 4.41 (2H, dd, *J* = 4.7, 1.9 Hz, CH_2OTBDPS), 3.82 (3H, s, ArOCH_3), 3.65 (2H, t, *J* = 6.3 Hz, CH_2CH_2OH), 2.75 (2H, dd, *J* = 7.9, 6.2 Hz, ArCH_2CH_2), 1.89–1.80 (2H, m, $CH_2CH_2CH_2$), 1.61 (1H, massif, CH_2O*H*), 1.11 (9H, s, SiC(CH_3)$_3$). ^{13}C NMR (75 MHz, $CDCl_3$, ppm) δ: 158.94, 140.71, 135.56, 133.72, 129.71, 128.63, 128.35, 127.73, 127.25, 126.29, 114.84, 111.85, 64.68, 62.19, 55.25, 33.78, 29.74, 26.86, 19.32. MS (*m*/*e*): 403 ([M – C_4H_9]$^+$). HR-MS calcd. for $C_{25}H_{27}O_3Si$: 403.1729 ([M – C_4H_9]$^+$); found: 403.1734 ± 0.0012.

Aldehyde 16

To a stirred solution of DMSO (14.6 mL, 205.5 mmol) in dichloromethane (700 mL) at –78 °C were slowly added oxalyl chloride (12.0 mL, 137.0 mmol) and the alcohol **15** (31.5 g, 68.5 mmol) in dichloromethane. The mixture was stirred at –78 °C for 45 min and triethylamine (38.5 mL, 274.0 mmol) was added. The mixture was stirred at room temperature for 1 h and satd. aq. NH_4Cl was added. The aqueous phase was extracted with dichloromethane. The combined organic phases were dried, filtered, and evaporated. The residue was filtered on a silica gel pad and washed with 50% ethyl acetate in hexanes to give aldehyde **16** as a yellow oil (31.5 g, 100%). IR ($CHCl_3$, cm^{-1}) ν: 3078, 2935, 2857, 2721, 1925, 1607, 1496, 1428, 1256, 1110, 967. ^{1}H NMR (300 MHz, $CDCl_3$, ppm) δ: 9.78 (1H, s, C*H*O), 7.73 (4H, dd, *J* = 7.5, 1.6 Hz, Ph), 7.49–7.38 (7H, m, Ph), 6.83 (1H, dt, *J* = 15.6, 1.8 Hz, PhC*H*=CH), 6.77 (1H, dd, *J* = 5.8, 2.8 Hz, Ph), 6.71 (1H, d, *J* = 2.8 Hz, Ph), 6.11 (1H, dt, *J* = 15.5, 4.7 Hz, PhCH=C*H*), 4.41 (2H, dd, *J* = 4.7, 1.9 Hz, CH_2OTBDPS), 3.82 (3H, s, ArOCH_3), 2.98 (2H, dt, *J* = 7.4 Hz, ArCH_2CH_2), 2.71 (2H, t, *J* = 7.24 Hz, CH_2CH_2CHO), 1.11 (9H, s, SiC(CH_3)$_3$). ^{13}C NMR (75 MHz, $CDCl_3$, ppm) δ: 201.26, 139.06, 135.56, 133.68, 129.76, 129.03, 128.54, 127.83, 127.76, 127.67, 127.51, 125.70, 114.77, 112.26, 64.57, 55.27, 44.74, 26.87, 25.97, 19.33. MS (*m*/*e*): 458 ([M]$^+$), 401 ([M – C_4H_9]$^+$). HR-MS calcd. for $C_{29}H_{34}O_3Si$: 458.2277 ([M]$^+$); found: 458.2282 ± 0.0014.

Ester 8

To a stirred solution of fluorophosphonate **17** (10.2 g, 42.3 mmol) in tetrahydrofuran (700 mL) at –78 °C was added a 1.4 mol/L solution of *n*-butyl lithium in hexanes (32.0 mL, 42.3 mmol). The mixture was stirred at –78 °C for 10 min and aldehyde **16** (12.9 g, 28.2 mmol) in tetrahydrofuran was added. The mixture was stirred at –78 °C for 45 min and satd. aq. NH_4Cl was added. The aqueous phase was extracted with ethyl acetate. The combined organic phases were dried, filtered, and evaporated. The residue was purified by flash chromatography (10% ethyl acetate, 90% hexanes) to give ester **8** as a colorless oil (14.3 g, 93%). IR ($CHCl_3$, cm^{-1}) ν: 3048, 2935, 2858, 1728, 1607, 1496, 1465,

© 2006 NRC Canada

1376, 1254, 1112, 1047, 967, 822. ^{1}H NMR (300 MHz, $CDCl_3$, ppm) δ: 7.75 (4H, dd, *J* = 7.5, 1.6 Hz, Ph), 7.46–7.37 (7H, m, Ph), 6.89 (1H, dt, *J* = 15.6, 1.7 Hz, PhC*H*=CH), 6.78 (1H, dd, *J* = 8.5, 2.7 Hz, Ph), 6.72 (1H, d, *J* = 2.7 Hz, Ph), 6.12 (1H, dt, *J* = 15.5, 4.8 Hz, PhCH=C*H*), 5.97–5.84 (1H, m, CH_2CH=$CFCO_2Et$), 4.42 (2H, dd, *J* = 4.8, 1.8 Hz, CH_2OTBDPS), 4.26 (2H, q, *J* = 7.1 Hz, $CO_2CH_2CH_3$), 3.83 (3H, s, $ArOCH_3$), 2.80–2.79 (4H, m, $ArCH_2CH_2$), 1.33 (3H, t, *J* = 7.1 Hz, $CO_2CH_2CH_3$), 1.12 (9H, s, $SiC(CH_3)_3$). ^{13}C NMR (75 MHz, $CDCl_3$, ppm) δ: 158.96, 148.99, 145.65, 139.41, 135.56, 134.84, 133.74, 129.72, 128.71, 127.73 127.36, 126.02, 122.35, 122.10, 114.87, 112.16, 64.68, 61.36, 55.25, 32.83, 26.87, 26.59, 19.33, 14.15. MS (*m*/*e*): 546 ($[M]^+$). HR-MS calcd. $C_{33}H_{39}O_4SiF$: 546.2601 ($[M]^+$); found: 546.2596 ± 0.0016.

Chloride 18

To a solution of ester **8** (33.4 g, 61.2 mmol) in tetrahydrofuran (600 mL) at 0 °C was added lithium aluminium hydride (2.32 g, 61.2 mmol). The mixture was stirred at 0 °C for 20 min and sodium sulfate decahydrate was added. The mixture was stirred for 1 h and the precipitate was filtered and washed with dichloromethane. The solvent was evaporated to give the alcohol as a colorless oil (30.8 g, 100%). IR ($CHCl_3$, cm^{-1}) ν: 3433, 3047, 2936, 2858, 1735, 1607, 1496, 1429, 1253, 1111, 967, 854. ^{1}H NMR (300 MHz, $CDCl_3$, ppm) δ: 7.77 (4H, dd, *J* = 7.5, 1.7 Hz, Ph), 7.50–7.40 (7H, m, Ph), 6.90 (1H, dt, *J* = 15.6, 1.6 Hz, PhC*H*=CH), 6.79 (1H, dd, *J* = 8.6, 2.7 Hz, Ph), 6.69 (1H, d, *J* = 2.7 Hz, Ph), 6.14 (1H, dt, *J* = 15.5, 4.6 Hz, PhCH=C*H*), 5.23 (1H, dt, *J* = 20.6, 8.4 Hz, CH_2CH=$CFCH_2OH$), 4.44 (2H, dd, *J* = 4.6, 1.9 Hz, CH_2OTBDPS), 3.98 (2H, d, *J* = 21.4 Hz, CH_2OH), 3.83 (3H, s, $ArOCH_3$), 2.76 (2H, t, *J* = 7.3 Hz, $ArCH_2CH_2$), 2.30 (2H, q, *J* = 7.6 Hz, $ArCH_2CH_2$), 1.49 (1H, massif, CH_2OH), 1.15 (9H, s, $SiC(CH_3)_3$). ^{13}C NMR (75 MHz, $CDCl_3$, ppm) δ: 160.58, 158.82, 157.32, 139.64, 135.55, 133.65, 129.76, 128.77, 127.76, 127.40, 125.97, 115.45, 112.15, 107.54, 107.58, 65.00, 57.27, 56.87, 55.30, 33.68, 26.88, 19.34. MS (*m*/*e*): 504 ($[M]^+$). HR-MS calcd. for $C_{31}H_{37}O_3SiF$: 504.2496 ($[M]^+$); found: 504.2488 ± 0.0015.

To a stirred solution of the alcohol (8.6 g, 17.1 mmol) in tetrahydrofuran (200 mL) at –40 °C were added triphenylphosphine (4.9 g, 18.8 mmol) and hexachloroacetone (2.6 mL, 17.1 mmol). The mixture was stirred at –40 °C for 20 min and the solvent was evaporated. The residue was purified by flash chromatography (100% hexanes to 20% ethyl acetate, 80% hexanes) to give chloride **18** as a yellow oil (8.8 g, 99%). IR ($CHCl_3$, cm^{-1}) ν: 3017, 2936, 2859, 1732, 1607, 1496, 1465, 1429, 1254, 1217, 1111, 1047, 967. ^{1}H NMR (300 MHz, $CDCl_3$, ppm) δ: 7.75 (4H, dd, *J* = 7.6, 1.6 Hz, Ph), 7.50–7.39 (7H, m, Ph), 6.87 (1H, dt, *J* = 15.6, 1.8 Hz, PhC*H*=CH), 6.79 (1H, dd, *J* = 8.6, 2.7 Hz, Ph), 6.68 (1H, d, *J* = 2.7 Hz, Ph), 6.13 (1H, dt, *J* = 15.6, 4.7 Hz, PhCH=C*H*), 5.31 (1H, dt, *J* = 18.8, 8.3 Hz, CH_2CH=$CFCH_2Cl$), 4.44 (2H, dd, *J* = 4.7, 1.9 Hz, CH_2OTBDPS), 3.94 (2H, d, *J* = 21.4 Hz, CH_2Cl), 3.83 (3H, s, $ArOCH_3$), 2.76 (2H, t, *J* = 7.3 Hz, $ArCH_2CH_2$), 2.30 (2H, q, *J* = 7.8 Hz, $ArCH_2CH_2$), 1.13 (9H, s, $SiC(CH_3)_3$). ^{13}C NMR (75 MHz, $CDCl_3$, ppm) δ: 158.92, 156.83, 153.55, 139.27, 135.54, 133.67, 129.74, 128.86, 128.55, 127.74, 127.47, 125.88, 115.14, 112.17, 110.16, 109.89, 64.60, 55.29, 37.64, 37.20, 33.39, 26.86, 19.33. MS (*m*/*e*): 520 ($[M]^+$). HR-MS calcd. for $C_{31}H_{36}O_2SiFCl$: 522.2157 ($[M]^+$); found: 522.2153 ± 0.0016.

β-Keto ester 19

Solution 1

To a suspension of 60% sodium hydride in oil (592 mg, 14.8 mmol) in tetrahydrofuran (20 mL) at 0 °C was added methyl acetoacetate (2.8 mL, 26.3 mmol) and the mixture was stirred at 0 °C for 30 min. A solution of 1.6 mol/L *n*-butyl lithium in hexanes (8.6 mL, 13.8 mmol) was added and the mixture was stirred at 0 °C for 30 min.

Solution 2

To a stirred solution of chloride **18** (1.03 g, 1.97 mmol) in tetrahydrofuran (20 mL) was added sodium iodide (885 mg, 5.9 mmol) and the mixture was stirred at room temperature for 30 min.

Solution 1 was added to solution 2 and the mixture was stirred at room temperature overnight. Satd. aq. NH_4Cl was added and the aqueous phase was extracted with ethyl acetate. The combined organic phases were dried, filtered, and evaporated. The residue was purified by flash chromatography (30% ethyl acetate, 70% hexanes) to give β-keto ester **19** as a yellow oil (770 mg, 65%). IR ($CHCl_3$, cm^{-1}) ν: 3020, 2955, 2860, 1745, 1720, 1608, 1496, 1433, 1315, 1217, 1110, 967, 756. ^{1}H NMR (300 MHz, $CDCl_3$, ppm) δ: 12.05 (RC(O)C*H*=C(OH)R′), 7.75 (4H, dd, *J* = 7.4, 1.7 Hz, Ph), 7.49–7.37 (7H, m, Ph), 6.92–6.87 (1H, m, CH=C*H*Ph), 7.77 (1H, dd, *J* = 8.5, 2.7 Hz, Ph), 6.70 (1H, d, *J* = 2.7 Hz, Ph), 6.11 (1H, dt, *J* = 15.5, 4.6 Hz, C*H*=CHPh), 5.06 (1H, dt, *J* = 21.7, 8.1 Hz, C*H*=CFR), 4.43 (2H, dd, *J* = 4.6, 1.8 Hz, CH_2OTBDPS), 3.82 (3H, s, $ArOCH_3$), 3.73 (3H, s, CO_2CH_3), 3.39 (2H, s, $C(O)CH_2C(O)$), 2.72 (2H, t, *J* = 7.3 Hz, $ArCH_2CH_2$), 2.55–2.20 (6H, m, $CH_2CH_2C(O)$, $CH_2CH_2C(O)$, CH_2CH=CFR), 1.13 (9H, s, Si-$C(CH_3)_3$). ^{13}C NMR (75 MHz, $CDCl_3$, ppm) δ: 167.36, 160.38, 158.83, 157.12, 139.99, 135.54, 133.72, 129.71, 128.70, 128.61, 127.73, 127.25, 126.01, 115.17, 112.07, 105.57, 105.28, 64.58, 55.25, 52.35, 48.89, 39.14, 33.58, 26.86, 22.02, 21.65, 19.31. MS (*m*/*e*): 602 ($[M]^+$). HR-MS calcd. for $C_{36}H_{43}O_5FSi$: 602.2864 ($[M]^+$); found: 602.2870 ± 0.0018.

Pivaloate ester 7

To a stirred solution of β-keto ester **19** (1.72 g, 2.85 mmol) in tetrahydrofuran (30 mL) was added 1 mol/L tetrabutylammonium fluoride in tetrahydrofuran (5.7 mL, 5.70 mmol). The mixture was stirred at room temperature for 1.5 h and solvent was evaporated. The residue was purified by flash chromatography (70% ethyl acetate, 30% hexanes) to give the corresponding alcohol as a colorless oil (798 mg, 77%). IR ($CHCl_3$, cm^{-1}) ν: 3425, 2949, 2867, 1744, 1716, 1608, 1496, 1441, 1372, 1254, 1084, 1008, 912, 733. ^{1}H NMR (300 MHz, $CDCl_3$, ppm) δ: 7.41 (1H, d, *J* = 8.6 Hz, Ph), 6.83 (1H, d, *J* = 15.7 Hz, CH=C*H*Ph), 6.76 (1H, dd, *J* = 8.6, 2.7 Hz, Ph), 6.68 (1H, d, *J* = 2.7 Hz, Ph), 6.18 (1H, dt, *J* = 15.6, 5.6 Hz, C*H*=CHPh), 5.10 (1H, dt, *J* = 21.6, 8.2 Hz, C*H*=CFR), 4.34 (2H, dd, *J* = 5.6, 1.5 Hz, CH_2OH), 3.82 (3H, s, $ArOCH_3$), 3.76 (3H, s, CO_2CH_3), 3.46 (2H, s, $C(O)CH_2C(O)$), 2.72 (2H, t, *J* = 8.0 Hz, $ArCH_2CH_2$),

© 2006 NRC Canada

2.63–2.58 (2H, m, $CH_2CH_2C(O)$), 2.48–2.36 (2H, m, $CH_2CH_2C(O)$), 2.23 (2H, q, J = 7.8 Hz, CH_2CH=CFR), 1.67 (1H, br, O*H*). ^{13}C NMR (75 MHz, $CDCl_3$, ppm) δ: 201.71, 167.53, 160.32, 158.96, 157.05, 140.21, 128.88, 128.38, 127.35, 115.10, 112.03, 105.68, 105.40, 63.56, 55.18, 52.39, 48.84, 39.12, 33.73, 26.81, 21.96. MS (*m*/*e*): 364 ($[M]^+$). HR-MS calcd. for $C_{20}H_{25}O_5F$: 364.1686 ($[M]^+$); found: 364.1683 ± 0.0011.

To a stirred solution of the alcohol (798 mg, 2.19 mmol) in dichloromethane (20 mL) were added 2,6-lutidine (765 μL, 6.57 mmol) and trimethylacetyl chloride (809 μL, 6.57 mmol) and the mixture was stirred at room temperature overnight. Satd. aq. NH_4Cl was added and the aqueous phase was extracted with dichloromethane. The combined organic phases were dried, filtered, and evaporated. The residue was purified by flash chromatography (30% ethyl acetate, 70% hexanes) to give pivaloate ester **7** as a colorless oil (952 mg, 97%). IR ($CHCl_3$, cm^{-1}) ν: 3020, 2957, 2873, 1744, 1719, 1606, 1495, 1438, 1282, 1216, 1158, 1090, 1040, 695, 853, 756. ^{1}H NMR (300 MHz, $CDCl_3$, ppm) δ: 12.05 (RC(O)C*H*=C(OH)R′), 7.40 (1H, d, J = 8.6 Hz, Ph), 6.83 (1H, d, J = 15.7 Hz, CH=C*H*Ph), 6.75 (1H, dd, J = 8.6, 3.0 Hz, Ph), 6.67 (1H, d, J = 2.7 Hz, Ph), 6.06 (1H, dt, J = 15.6, 6.2 Hz, C*H*=CHPh), 5.11 (1H, dt, J = 21.6, 8.1 Hz, C*H*=CFR), 4.73 (2H, dd, J = 6.2, 1.3 Hz, CH_2OPiv), 3.80 (3H, s, ArOCH_3), 3.73 (3H, s, CO_2CH_3), 3.41 (2H, s, C(O)CH_2C(O)), 2.71 (2H, t, J = 7.5 Hz, ArCH_2CH_2), 2.54–2.49 (2H, m, $CH_2CH_2C(O)$), 2.43–2.31 (2H, m, $CH_2CH_2C(O)$), 2.24 (2H, m, CH_2CH=CFR), 1.23 (9H, s, C(CH_3)$_3$). ^{13}C NMR (75 MHz, $CDCl_3$, ppm) δ: 200.94, 167.35, 160.39, 159.29, 157.13, 140.38, 130.54, 127.90, 127.43, 123.48, 115.16, 112.11, 105.48, 105.19, 65.09, 55.22, 52.33, 48.89, 39.05, 38.79, 33.53, 27.21, 26.84, 21.96. MS (*m*/*e*): 448 ($[M]^+$). HR-MS calcd. for $C_{25}H_{33}O_6F$: 448.2261 ($[M]^+$); found 448.2270 ± 0.001.

Macrocycle 20

Solution 1

To a stirred solution of pivaloic ester **7** (1.67 g, 3.73 mmol) in tetrahydrofuran (15 mL) degassed with Ar was added *N*,*O*-bis(trimethylsilyl)acetamide (1.8 mL, 7.46 mmol). The mixture was stirred at reflux for 5 h.

Solution 2

To a stirred solution of tetrakis(triphenylphosphine) palladium(0) (1.07 g, 0.93 mmol) in tetrahydrofuran (1.9 L) degassed with Ar was added 1,3-bis(diphenylphospino)propane (384 mg, 0.93 mmol) and the mixture was stirred at reflux for 1 h.

Solution 1 was slowly added to solution 2 at reflux for 14 h and the resulting mixture was heated for 4 h. The solvent was evaporated and the residue was purified by flash chromatography (5% ethyl acetate, 35% dichloromethane, 60% hexanes) to give macrocycle **20** as a white solid (1.14 g, 88%); mp 129–131 °C. IR ($CHCl_3$, cm^{-1}) ν: 3020, 2956, 1743, 1714, 1607, 1493, 1436, 1250, 1216, 1165, 1115, 1078, 1041, 970, 762. ^{1}H NMR (300 MHz, $CDCl_3$, ppm) δ: 7.21 (1H, d, J = 8.4 Hz, Ph), 6.73 (1H, dd, J = 8.4, 2.8 Hz, Ph), 6.67 (1H, d, J = 2.8 Hz, Ph), 6.57 (1H, d, J = 15.7 Hz, PhC*H*=CH), 5.77 (1H, ddd, J = 15.6, 8.6, 5.3 Hz, C*H*=CHPh), 5.00 (1H, dt, J = 20.7, 7.7 Hz, C*H*=CFR), 3.80 (3H, s, ArOCH_3), 3.77 (3H, s, CO_2CH_3), 3.80–3.75 (1H, m, C(O)C*H*C(O)), 3.04–1.86 (10H, m, PhCH_2CH_2CH=CFR, CH=C(F)CH_2CH_2C(O), CH_2C(H)CO_2Me). ^{13}C NMR (75 MHz, $CDCl_3$, ppm) δ: 204.00, 169.54, 160.98, 159.09, 157.11, 140.77, 131.98, 129.24, 128.38, 126.07, 114.54, 111.63, 105.80, 105.52, 57.71, 55.19, 52.58, 39.06, 33.90, 32.01, 27.89, 22.42. MS (*m*/*e*): 346 ($[M]^+$). HR-MS calcd. for $C_{20}H_{23}O_4F$: 346.1580 ($[M]^+$); found: 346.1576 ± 0.0010.

Triene 6

To a stirred solution of 70% benzeneseleninic anhydride (10.2 g, 19.8 mmol) in dichloromethane (200 mL) was added triethylamine (4.6 mL, 32.9 mmol) and the mixture was stirred for 15 min. A solution of macrocycle **20** (2.30 g, 6.65 mmol) in dichloromethane was added and the mixture was stirred for 15 min. Satd. aq. $NaHCO_3$ was added and the aqueous phase was extracted with dichloromethane. The combined organic phases were dried, filtered, and evaporated. The residue was purified by flash chromatography (5% ethyl acetate, 95% dichloromethane) to give triene **6** as a yellow solid (2.05 g, 91%); mp 147–149 °C. IR ($CHCl_3$, cm^{-1}) ν: 3020, 2954, 1696, 1603, 1583, 1436, 1275, 1241, 1158, 1077, 1045. ^{1}H NMR (300 MHz, $CDCl_3$, ppm) δ: 7.43 (1H, d, J = 11.5 Hz, PhCH=CH=C*H*), 7.21 (1H, d, J = 8.5 Hz, Ph), 6.96 (1H, d, J = 16.2 Hz, CH=C*H*Ph), 6.76 (1H, dd, J = 8.4, 2.7 Hz, Ph), 6.71 (1H, d, J = 2.7 Hz, Ph), 6.64 (1H, dd, J = 16.2, 11.5 Hz, PhCH=C*H*), 5.26 (1H, dt, J = 22.1, 8.7 Hz, C*H*=CFR), 3.82 (3H, s, ArOCH_3), 3.81 (3H, s, CO_2CH_3), 2.97–2.93 (2H, m, $CH_2CH_2C(O)$), 2.87–2.81 (2H, m, PhCH_2CH_2), 2.58 (2H, dt, J = 22.1, 6.9 Hz, $CH_2CH_2C(O)$), 2.22–2.14 (2H, m, PhCH_2CH_2). ^{13}C NMR (75 MHz, $CDCl_3$, ppm) δ: 203.17, 164.94, 160.41, 159.01, 155.73, 144.16, 142.15, 136.13, 131.88, 126.46, 123.62, 117.45, 111.76, 107.23, 106.93, 55.29, 52.14, 39.48, 37.15, 26.02, 23.61. MS (*m*/*e*): 344 ($[M]^+$). HR-MS calcd. for $C_{20}H_{21}O_4F$: 344.1424 ($[M]^+$); found: 344.1426 ± 0.0010.

Tetracycle 21

To a solution of triene **6** (500 mg, 1.45 mmol) in toluene (70 mL) degassed with Ar was added triethylamine (1.0 mL, 7.25 mmol) and the mixture was heated in a sealed tube at 165 °C for 4 h. The solvent was evaporated and the residue was purified by flash chromatography (20% ethyl acetate, 80% hexanes) to give tetracycle **21** as a white solid (389 mg, 78%); mp 162–164 °C. IR ($CHCl_3$, cm^{-1}) ν: 3019, 2954, 1761, 1734, 1609, 1502, 1436, 1258, 1216, 1045. ^{1}H NMR (300 MHz, $CDCl_3$, ppm) δ: 7.28 (1H, d, J = 8.9 Hz, *Ph*), 6.76 (1H, dd, J = 8.9, 2.7 Hz, *Ph*), 6.70 (1H, d, J = 2.7 Hz, *Ph*), 6.53 (1H, d, J = 9.9 Hz, CH=C*H*C(CO_2Me)R), 5.64 (1H, ddd, J = 9.9, 5.6, 3.0 Hz, C*H*=CHC(CO_2Me)R), 3.79 (3H, s, ArOCH_3), 3.72 (3H, s, CO_2CH_3), 3.23 (1H, d, J = 11.5 Hz, PhC*H*CH=CH), 3.00–2.94 (2H, m, PhCH_2CH_2), 2.91–2.77 (1H, m, C*H*C(F)R), 2.51–2.23 (4H, m, C(O)CH_2CH_2C(F)R), 2.14–1.92 (1H, m, PhCH_2CH*H*), 1.73–1.57 (1H, m, PhCH_2C*H*H). ^{13}C NMR (75 MHz, $CDCl_3$, ppm) δ: 209.92, 167.91, 157.95, 137.43, 132.10, 128.26, 125.88, 122.52, 114.30, 111.89, 105.07, 102.64, 65.61, 55.25, 52.88, 40.66, 40.37, 40.01, 35.60, 29.51, 26.43, 21.36. MS (*m*/*e*): 344 ($[M]^+$). HR-MS calcd. for $C_{20}H_{21}O_4F$: 344.1424 ($[M]^+$); found: 344.1413 ± 0.0010.

© 2006 NRC Canada

Diol 24

To a stirred solution of tetracycle **21** (594 mg, 1.73 mmol) in ethanol 95% (75 mL) was added 5% palladium(0) on barium sulfate (745 mg, 0.35 mmol) and hydrogen was bubbled through this solution for 15 min. The resulting mixture was stirred at room temperature overnight under a hydrogen atmosphere. N_2 was bubbled through this mixture and the solution was filtered on a silica gel pad to give the corresponding tetracycle as a beige solid (594 mg, 100%); mp 154–157 °C. IR ($CHCl_3$, cm^{-1}) ν: 3055, 2954, 1754, 1731, 1611, 1502, 1435, 1266, 1043, 896. ^1H NMR (300 MHz, $CDCl_3$, ppm) δ: 7.19 (1H, d, *J* = 8.6 Hz, *Ph*), 6.74 (1H, dd, *J* = 8.6, 2.7 Hz, *Ph*), 6.65 (1H, d, *J* = 2.7 Hz, *Ph*), 3.78 (3H, s, ArOCH_3), 3.73 (3H, s, CO_2CH_3), 2.94–2.89 (2H, m, PhCH_2CH_2), 2.83–2.70 (1H, m, PhC*H*), 2.58–2.49 (2H, m, RC(O)CH_2), 2.38–1.90 (7H, m), 1.65–1.77 (2H, m). ^{13}C NMR (75 MHz, $CDCl_3$, ppm) δ: 211.61, 169.27, 157.77, 137.43, 130.21, 127.05, 113.72, 112.08, 106.08, 103.66, 62.19, 61.94, 55.16, 52.30, 42.70, 42.40, 39.37, 34.97, 30.05, 29.79, 26.73, 26.19, 22.04. MS (*m*/*e*): 346 ($[M]^+$). HR-MS calcd. for $C_{20}H_{23}O_4F$: 346.1580 ($[M]^+$); found: 346.1576 ± 0.0010.

To a stirred solution of this tetracycle (575 mg, 1.66 mmol) in tetrahydrofuran (40 mL) were added lithium borohydride (180 mg, 8.30 mmol) and methanol (336 μL, 8.30 mmol) and the mixture was stirred at room temperature for 2 h. Lithium borohydride (72 mg, 3.32 mmol) and methanol (134 μL, 3.32 mmol) were added and the mixture was stirred for 1 h. Satd. aq. NH_4Cl was added and the aqueous phase was extracted with ethyl acetate. The combined organic phases were dried, filtered, and evaporated. The residue was purified by flash chromatography (100% ethyl acetate) to give a mixture (α:β = 9:1) of diol **24** as a white solid (539 mg, 94%). Diol α-**24**: ^1H NMR (300 MHz, $CDCl_3$, ppm) δ: 7.22 (1H, d, *J* = 8.6 Hz, *Ph*), 6.72 (1H, dd, *J* = 8.6, 2.7 Hz, *Ph*), 6.64 (1H, d, *J* = 2.7 Hz, *Ph*), 4.74 (1H, t, *J* = 8.2 Hz, RR′C*H*OH), 4.00 (1H, d, *J* = 10.3 Hz, C*H*HOH), 3.90 (1H, d, *J* = 10.3 Hz, CH*H*OH), 3.78 (3H, s, ArOCH_3), 2.85 (2H, dd, *J* = 8.9, 3.8 Hz, PhCH_2CH_2), 2.47 (1H, t, *J* = 11.6 Hz, PhC*H*), 2.38–2.05 (5H, m), 1.92–1.62 (3H, m), 1.87 (2H, br, CHO*H*, CH_2OH), 1.50–1.28 (3H, m). MS (*m*/*e*): 320 ($[M]^+$). HR-MS calcd. for $C_{19}H_{25}O_3F$: 320.1788 ($[M]^+$); found: 320.1779 ± 0.0010. Diol β-**24**: ^1H NMR (300 MHz, $CDCl_3$, ppm) δ: 7.18 (1H, d, *J* = 8.6 Hz, *Ph*), 6.73 (1H, dd, *J* = 8.6, 2.7 Hz, *Ph*), 6.64 (1H, d, *J* = 2.7 Hz, *Ph*), 4.18 (1H, d, *J* = 11.7 Hz, RC*H*HOH), 4.01 (1H, dd, *J* = 7.3, 2.2 Hz, RR′C*H*OH), 3.78 (3H, s, ArOCH_3), 3.71 (1H, d, *J* = 11.7 Hz, CH*H*OH), 2.86 (2H, dd, *J* = 8.6, 3.5 Hz, PhCH_2CH_2), 2.49–2.35 (2H, m), 2.31–1.83 (10H, m), 1.74 (1H, qd, *J* = 11.7, 2.0 Hz), 1.53–1.34 (1H, m), 1.05–0.96 (1H, m).

Tosylate 25

To a stirred solution of diol **24** (460 mg, 1.4 mmol) in a mixture of benzene–DMF (3:1, 12 mL) was added dibutylstannane oxide (430 mg, 1.73 mmol) and the mixture was stirred at reflux with a Dean–Stark for 1.5 h. The mixture was cooled down and *p*-toluenesulfonyle chloride (320 mg, 1.68 mmol) was added. The mixture was stirred at room temperature for 1 h. Satd. aq. NH_4Cl was added and the aqueous phase was extracted with ether–hexanes (1:1). The combined organic phases were dried, filtered, and evaporated. The residue was purified by flash chromatography (50% ethyl acetate, 50% hexanes) to give a mixture (α:β = 9:1) of tosylates **25** unseparable as a white solid (539 mg, 94%). Tosylate α-**25**: IR ($CHCl_3$, cm^{-1}) ν: 3602, 3551, 2951, 2872, 1610, 1501, 1464, 1361, 1176, 1097, 1045, 944, 816. ^1H NMR (300 MHz, $CDCl_3$, ppm) δ: 7.78 (2H, d, *J* = 8.2 Hz, Ph), 7.34 (2H, d, *J* = 8.2 Hz, Ph), 7.16 (1H, d, *J* = 8.6 Hz, *Ph*), 6.72 (1H, dd, *J* = 8.6, 2.5 Hz, *Ph*), 6.62 (1H, d, *J* = 2.5 Hz, *Ph*), 4.81 (1H, massif, RR′CHO*H*), 4.57 (1H, t, *J* = 8.0 Hz, RR′C*H*OH), 4.30 (1H, d, *J* = 9.9 Hz, C*H*HOTs), 4.23 (1H, d, *J* = 9.9 Hz, CH*H*OTs), 3.78 (3H, s, ArOCH_3), 2.86–2.79 (2H, m, PhCH_2CH_2), 2.44 (3H, s, PhCH_3), 2.37–2.15 (2H, m), 2.08–2.01 (3H, m), 1.88–1.52 (4H, m), 1.46–1.33 (2H, m), 1.29–1.09 (1H, m). MS (*m*/*e*): 474 ($[M]^+$). HR-MS calcd. for $C_{26}H_{31}O_5FS$: 474.1876 ($[M]^+$); found: 474.1880 ± 0.0014.

Alcohol 26 and oxetane 27

To a stirred solution of tosylate **25** (650 mg, 1.37 mmol) in dimethylsulfoxide (80 mL) was added sodium borohydride (260 mg, 6.85 mmol) and the mixture was stirred at 80 °C overnight. Satd. aq. NH_4Cl was added and the aqueous phase was extracted with ethyl acetate. The combined organic phases were dried, filtered, and evaporated. The residue was purified by flash chromatography (50% ethyl acetate, 50% hexanes) to give alcohol **26** as colorless oil (353 mg, 85%) and about 10% of oxetane **27**. Alcohol **26**: IR ($CHCl_3$, cm^{-1}) ν: 3386, 2942, 2870, 1610, 1501, 1466, 1261, 1235, 1042. ^1H NMR (300 MHz, $CDCl_3$, ppm) δ: 7.22 (1H, d, *J* = 8.6 Hz, *Ph*), 6.73 (1H, dd, *J* = 8.6, 2.8 Hz, *Ph*), 6.65 (1H, d, *J* = 2.8 Hz, *Ph*), 4.28 (1H, t, *J* = 8.0 Hz, RR′C*H*OH), 3.78 (3H, s, ArOCH_3), 2.90–2.85 (2H, m, PhCH_2CH_2), 2.46–2.39 (1H, m, PhC*H*), 2.32–2.00 (4H, m), 1.90–1.74 (2H, m), 1.72–1.57 (3H, m), 1.53–1.36 (3H, m), 1.08 (3H, d, *J* = 1.3 Hz, CH_3). ^{13}C NMR (75 MHz, $CDCl_3$, ppm) δ: 157.58, 137.76, 131.39, 126.83, 113.71, 111.88, 109.08, 106.71, 80.43, 55.21, 47.48, 47.25, 42.40, 42.11, 40.23, 29.97, 28.42, 28.22, 27.58, 27.24, 25.68, 22.13, 16.33. MS (*m*/*e*): 304 ($[M]^+$). HR-MS calcd. for $C_{19}H_{25}O_2F$: 304.1838 ($[M]^+$); found: 304.1843 ± 0.0009. Oxetane **27**: IR ($CHCl_3$, cm^{-1}) ν: 3018, 2945, 2882, 1610, 1502, 1465, 1215, 1038, 974. ^1H NMR (300 MHz, $CDCl_3$, ppm) δ: 7.12 (1H, d, *J* = 8.6 Hz, *Ph*), 6.72 (1H, dd, *J* = 8.6, 2.8 Hz, *Ph*), 6.62 (1H, d, *J* = 2.8 Hz, *Ph*), 4.95 (1H, d, *J* = 5.9 Hz, C*H*HOCHRR′), 4.72 (1H, d, *J* = 5.9 Hz, CH*H*OCHRR′), 4.35 (1H, dd, *J* = 5.6, 4.7 Hz, RR′C*H*OCH_2), 3.78 (3H, s, ArOCH_3), 2.90–2.84 (2H, m, PhCH_2CH_2), 2.48–1.25 (12H, m). ^{13}C NMR (75 MHz, $CDCl_3$, ppm) δ: 157.51, 137.58, 131.72, 127.84, 113.38, 112.33, 106.60, 104.18, 91.12, 74.36, 74.16, 55.20, 51.18, 50.95, 44.32, 43.97, 36.51, 32.33, 32.16, 32.12, 30.31, 29.05, 27.83, 23.94. MS (*m*/*e*): 302 $([M])^+$. HR-MS calcd. for $C_{19}H_{23}O_2F$: 302.1682 ($[M]^+$); found: 302.1399 ± 0.0009.

Ketone 5

To a stirred solution of alcohol **26** (312 mg, 1.03 mmol) in dichloromethane (50 mL) were added molecular sieve 4 Å (515 mg), 4-methylmorpholine-*N*-oxide (241 mg, 2.06 mmol), and tetrapropylammonium perruthenate (35 mg, 0.10 mmol). The resulting mixture was stirred at room temperature for

© 2006 NRC Canada

2 h and filtered on a silica gel pad. The solvent was evaporated and the residue was purified by flash chromatography (30% ethyl acetate, 70% hexanes) to give ketone **5** as an amorphous white solid (269 mg, 87%). IR ($CHCl_3$, cm^{-1}) ν: 2944, 2869, 1741, 1611, 1502, 1464, 1274, 1232, 1093, 1043, 936. ^1H NMR (300 MHz, $CDCl_3$, ppm) δ: 7.19 (1H, d, *J* = 8.6 Hz, *Ph*), 6.74 (1H, dd, *J* = 8.6, 2.8 Hz, *Ph*), 6.67 (1H, d, *J* = 2.8 Hz, *Ph*), 3.79 (3H, s, $ArOCH_3$), 2.93 (2H, dd, *J* = 9.0, 3.9 Hz, $PhCH_2CH_2$), 2.59–2.48 (3H, m, PhC*H*, $RC(O)CH_2$), 2.42–2.13 (4H, m), 1.92 (1H, qd, *J* = 11.9, 2.1 Hz), 1.65–1.41 (4H, m), 1.13 (3H, d, *J* = 1.5 Hz, CH_3). ^{13}C NMR (75 MHz, $CDCl_3$, ppm) δ: 219.62, 157.80, 137.56, 130.58, 126.78, 113.82, 112.03, 107.01, 104.64, 55.21, 52.94, 52.67, 42.19, 41.90, 40.27, 33.30, 32.42, 29.90, 25.57, 25.21, 21.97, 12.72. MS (*m*/*e*): 302 ($[M]^+$). HR-MS calcd. for $C_{19}H_{23}O_2F$: 302.1682 ($[M]^+$); found: 302.1689 ± 0.0009.

Triflic enol ether 28

To a stirred solution of ketone **5** (22 mg, 0.073 mmol) in tetrahydrofuran (2 mL) at 0 °C was added 0.5 mol/L potassium bis(trimethylsilyl)amide in toluene (740 μL, 0.37 mmol) and the mixture was stirred at 0 °C for 15 min then at room temperature for 45 min. *N*-(5-Chloro-2-pyridyl)triflimide (93 mg, 0.22 mmol) in tetrahydrofuran (1 mL) was added and the resulting mixture was stirred at room temperature for 30 min. Satd. aq. NH_4Cl was added and the aqueous phase was extracted with ethyl acetate. The combined organic phases were dried, filtered, and evaporated. The residue was purified by flash chromatography (5% ethyl acetate, 95% hexanes) to give triflic enol ether **28** as a yellow oil (27 mg, 84%). IR ($CHCl_3$, cm^{-1}) ν: 2944, 2868, 1650, 1611, 1502, 1423, 1218, 1141, 1085, 1044, 884. ^1H NMR (300 MHz, $CDCl_3$, ppm) δ: 7.22 (1H, d, *J* = 8.6 Hz, *Ph*), 6.74 (1H, dd, *J* = 8.6, 2.7 Hz, *Ph*), 6.65 (1H, d, *J* = 2.7 Hz, *Ph*), 5.59 (1H, t, *J* = 2.7 Hz, C*H*=C(OTf)R), 3.79 (3H, s, $ArOCH_3$), 2.93–2.86 (2H, m, $PhCH_2CH_2$), 2.71 (1H, td, *J* = 17.1, 1.8 Hz, PhC*H*), 2.61–2.40 (2H, m), 2.30–2.05 (3H, m), 1.87 (1H, qd, *J* = 12.0, 2.1 Hz), 1.57–1.26 (3H, m), 1.18 (3H, d, *J* = 2.7 Hz, CH_3). ^{13}C NMR (75 MHz, $CDCl_3$, ppm) δ: 157.77, 155.04, 137.57, 130.16, 127.23, 120.65, 116.40, 113.76, 112.12, 108.48, 105.33, 102.86, 55.21, 49.48, 49.22, 43.00, 42.70, 40.25, 37.15, 34.05, 33.68, 29.57, 25.54, 22.27, 13.31. MS (*m*/*e*): 434 ($[M]^+$). HR-MS calcd. for $C_{20}H_{22}O_4F_4S$: 434.1175 ($[M]^+$); found: 434.1181 ± 0.0013.

α,β-Unsaturated ester 29

To a stirred solution of triflic enol ether **28** (20 mg, 0.046 mmol) in dimethylformamide (3 mL) were added triethylamine (32 μL, 0.23 mmol), methanol (233 μL, 4.60 mmol), triphenylphophine (0.7 mg, 0.0028 mmol), and palladium(II) acetate (0.3 mg, 0.0014 mmol). CO_2 was bubbled through the solution and the resulting mixture was stirred at 70 °C under a pressure of 150 psi (1 psi = 6.894 757 kPa) overnight. Satd. aq. NH_4Cl was added and the aqueous phase was extracted with ether. The combined organic phases were dried, filtered, and evaporated. The residue was purified by flash chromatography (10% ethyl acetate, 90% hexanes) to give the α,β-unsaturated ester **29** as an amorphous white solid (13 mg, 81%). IR ($CHCl_3$, cm^{-1}) ν: 2944, 2565, 1717, 1612, 1501, 1436, 1336, 1243, 1191, 1044, 885. ^1H NMR (300 MHz, $CDCl_3$, ppm) δ: 7.24 (1H, d, *J* = 8.7 Hz, *Ph*), 6.75–6.70 (2H, m, *Ph*, C*H*=CRCO_2Me), 6.65 (1H, d, *J* = 2.7 Hz, *Ph*), 3.78 (3H, s, $ArOCH_3$), 3.76 (3H, s, CO_2CH_3), 2.93–2.88 (2H, m, $PhCH_2CH_2$), 2.84–2.59 (2H, m), 2.46–2.32 (2H, m), 2.26–2.05 (2H, m), 2.00–1.86 (1H, m), 1.55–1.22 (3H, m), 1.35 (3H, d, *J* = 3.2 Hz, CH_3). ^{13}C NMR (75 MHz, $CDCl_3$, ppm) δ: 164.98, 157.64, 143.61, 137.89, 137.69, 130.70, 127.27, 113.71, 112.01, 108.74, 106.32, 55.21, 51.25, 42.52, 42.22, 40.58, 38.13, 37.70, 37.34, 30.03, 25.77, 23.07, 14.85. MS (*m*/*e*): 344 ($[M]^+$). HR-MS calcd. for $C_{21}H_{25}O_3F$: 344.1788 ($[M]^+$); found: 344.1779 ± 0.0010.

Ester 30

To a stirred solution of α,β-unsaturated ester **29** (15 mg, 0.044 mmol) in ethanol (2 mL) was added 5% palladium(0) on activated carbon (9 mg, 0.0044 mmol) and hydrogen was bubbled through the solution for 10 min. The mixture was stirred for 1 h under a hydrogen atmosphere and filtered on a silica gel pad. The solvent was evaporated to give ester **30** as a colorless oil (15 mg, 100%). IR ($CHCl_3$, cm^{-1}) ν: 2945, 2862, 1732, 1610, 1502, 1466, 1260, 1199, 1166, 1044, 961. ^1H NMR (300 MHz, $CDCl_3$, ppm) δ: 7.18 (1H, d, *J* = 8.6 Hz, *Ph*), 6.72 (1H, dd, *J* = 8.6, 2.8 Hz, *Ph*), 6.64 (1H, d, *J* = 2.8 Hz, *Ph*), 3.78 (3H, s, $ArOCH_3$), 3.71 (3H, s, CO_2CH_3), 3.05 (1H, t, *J* = 9.2 Hz, C*H*CO_2Me), 2.91–2.86 (2H, m, $PhCH_2CH_2$), 2.50–2.42 (1H, m, PhC*H*), 2.29–1.78 (7H, m), 1.58–1.30 (4H, m), 1.21 (3H, d, *J* = 1.1 Hz, CH_3). ^{13}C NMR (75 MHz, $CDCl_3$, ppm) δ: 174.38, 157.62, 137.69, 131.23, 126.80, 113.69, 111.90, 110.58, 55.20, 53.16, 51.47, 42.10, 41.81, 40.05, 31.15, 30.06, 29.69, 29.29, 28.96, 26.05, 23.01, 22.22, 17.58. MS (*m*/*e*): 346 $([M])^+$. HR-MS calcd. for $C_{21}H_{27}O_3F$: 346.1944 ($[M]^+$); found: 346.1940 ± 0.0010.

α,β-Unsaturated nitrile 32

To a stirred solution of triflic enol ether **28** (41 mg, 0.094 mmol) in benzene (10 mL) were added lithium cyanide (18 mg, 0.56 mmol), tetrakis(triphenylphosphine) palladium(0) (11 mg, 0.0094 mmol), and 12-C-4 ether (2 μL, 0.0094 mmol). The resulting mixture was stirred at room temperature overnight and a catalytic amount of palladium (11 mg, 0.0094 mmol) was added. The mixture was stirred for an additional 24 h and water was added. The aqueous phase was extracted with ethyl acetate. The combined organic phases were dried, filtered, and evaporated. The residue was purified by flash chromatography (10% ethyl acetate, 90% hexanes) to give α,β-unsaturated nitrile **32** as an amorphous solid (23 mg, 79%). IR ($CHCl_3$, cm^{-1}) ν: 3054, 2932, 2568, 2219, 1610, 1502, 1422, 1265, 1041, 883. ^1H NMR (300 MHz, $CDCl_3$, ppm) δ: 7.22 (1H, d, *J* = 8.6 Hz, *Ph*), 6.74 (1H, dd, *J* = 8.6, 2.7 Hz, *Ph*), 6.65 (1H, d, *J* = 2.7 Hz, *Ph*), 6.59 (1H, t, *J* = 2.6 Hz, C*H*=C(CN)R), 3.79 (3H, s, $ArOCH_3$), 2.93–2.88 (2H, m, $PhCH_2CH_2$), 2.84–2.68 (1H, m), 2.47–2.38 (1H, m), 2.31–2.10 (3H, m), 1.90 (1H, qd, *J* = 11.9, 2.1 Hz), 1.57–1.22 (4H, m), 1.31 (3H, d, *J* = 2.6 Hz, CH_3). ^{13}C NMR (75 MHz, $CDCl_3$, ppm) δ: 157.79, 142.09, 137.52, 130.03, 127.22, 125.12, 115.38, 113.78, 112.12, 107.07, 104.62, 55.22, 52.57, 52.31, 42.78, 42.48, 40.35, 38.99, 38.63, 37.93, 29.94, 25.69, 23.10, 14.96. MS

© 2006 NRC Canada

(*m*/*e*): 311 ([M]$^+$). HR-MS calcd. for $C_{20}H_{22}OFN$: 311.1585 ([M]$^+$); found: 311.1678 ± 0.0009.

Nitriles 33a and 33b

To a stirred solution of α,β-unsaturated nitrile **32** (20 mg, 0.064 mmol) in ethanol (2 mL) was added 5% palladium(0) on activated carbon (28 mg, 0.013 mmol) and hydrogen was bubbled through the solution for 10 min. The mixture was stirred for 2 h under a hydrogen atmosphere and filtered on a silica gel pad. The solvent was evaporated and the residue was purified by flash chromatography (20% ethyl acetate, 80% hexanes) to give nitrile α-**33a** as a white solid (7 mg, 35%) and nitrile β-**33b** as a white solid (12 mg, 60%). Nitrile β-**33b**: IR ($CHCl_3$, cm^{-1}) ν: 2932, 2868, 2238, 1610, 1501, 1466, 1236, 1161, 1038. ^{1}H NMR (300 MHz, $CDCl_3$, ppm) δ: 7.16 (1H, d, *J* = 8.6 Hz, *Ph*), 6.74 (1H, dd, *J* = 8.6, 2.8 Hz, *Ph*), 6.65 (1H, d, *J* = 2.8 Hz, *Ph*), 3.78 (3H, s, ArOC*H*$_3$), 2.92–2.87 (2H, m, PhC*H*$_2$CH$_2$), 2.74 (1H, t, *J* = 7.7 Hz, R(CN)C*H*CH$_2$), 2.50–2.42 (1H, m, PhC*H*), 2.35–2.15 (5H, m), 2.10–2.03 (1H, m), 1.86 (1H, qd, *J* = 11.8, 2.2 Hz), 1.71–1.64 (1H, m), 1.57–1.36 (3H, m), 1.33 (3H, d, *J* = 1.1 Hz, C*H*$_3$). ^{13}C NMR (75 MHz, $CDCl_3$, ppm) δ: 157.76, 137.61, 130.64, 126.70, 121.71, 113.73, 112.05, 109.19, 106.78, 55.21, 48.52, 48.26, 42.03, 41.75, 39.93, 36.85, 30.32, 30.02, 26.64, 25.72, 23.17, 16.38. MS (*m*/*e*): 313 ([M]$^+$). HR-MS calcd. for $C_{20}H_{24}OFN$: 313.1842 ([M]$^+$); found: 313.1849 ± 0.0009. Nitrile α-**33a**: IR ($CHCl_3$, cm^{-1}) ν: 2938, 2239, 1610, 1502, 1467, 1320, 1236, 1043, 957. ^{1}H NMR (300 MHz, $CDCl_3$, ppm) δ: 7.20 (1H, d, *J* = 8.6 Hz, *Ph*), 6.74 (1H, dd, *J* = 8.6, 2.8 Hz, *Ph*), 6.65 (1H, d, *J* = 2.8 Hz, *Ph*), 3.78 (3H, s, ArOC*H*$_3$), 3.04 (1H, t, *J* = 9.2 Hz, R(CN)C*H*CH$_2$), 2.91–2.86 (2H, m, PhC*H*$_2$CH$_2$), 2.47 (1H, td, *J*= 11.2, 3.5 Hz, PhC*H*), 2.36–1.77 (8H, m), 1.53–1.33 (3H, m), 1.18 (3H, d, *J* = 1.0 Hz, C*H*$_3$). ^{13}C NMR (75 MHz, $CDCl_3$, ppm) δ: 157.77, 137.47, 130.64, 126.78, 120.51, 113.78, 111.99, 55.21, 42.02, 41.73, 40.10, 39.13, 31.64, 29.90, 29.68, 29.35, 25.85, 24.31, 22.88, 16.81. MS (*m*/*e*): 313 ([M]$^+$). HR-MS calcd. for $C_{20}H_{24}OFN$: 313.1842 ([M]$^+$); found: 313.1849 ± 0.0009.

α,β-Unsaturated ketone 34

To a stirred solution of tetracycle **26** (227 mg, 0.75 mmol) in tetrahydrofuran (10 mL) at –78 °C was added 95% ethanol (1 mL), and gaseous ammonia was condensed (20 mL). Metallic lithium was added by portion until the solution was blue and the resulting mixture was stirred at –78 °C for 2 h. Solid NH_4Cl was added slowly until the blue color disappeared and ammoniac was evaporated at room temperature. Water was added and the aqueous phase was extracted with ether. The combined organic phases were dried, filtered, and evaporated. The residue was dissolved in tetrahydrofuran (10 mL) and 1 mol/L HCl (1 mL) was added. The mixture was stirred at room temperature overnight. Satd. aq. $NaHCO_3$ was added and the aqueous phase was extracted with ether. The combined organic phases were dried, filtered, and evaporated. The residue was purified by flash chromatography (60% ethyl acetate, 40% hexanes) to give α,β-unsaturated ketone **34** as a colorless oil (168 mg, 77%). IR ($CHCl_3$, cm^{-1}) ν: 3611, 3432, 3016, 2949, 2874, 1662, 1619, 1454, 1364, 1220, 1067, 1007, 952. ^{1}H NMR (300 MHz, $CDCl_3$, ppm) δ: 5.81 (1H, s, C*H*=CRR′), 4.18 (1H, t, *J* = 7.6 Hz, RR′C*H*OH), 2.52–1.46 (17H, m), 1.26–1.10 (3H, m), 1.05 (3H, s, C*H*$_3$). ^{13}C NMR (75 MHz, $CDCl_3$, ppm) δ: 199.85, 165.58, 124.76, 108.73, 106.36, 80.00, 47.23, 47.00, 45.78, 43.74, 43.45, 42.73, 36.36, 35.04, 27.91, 27.84, 26.34, 25.26, 25.02, 15.93. MS (*m*/*e*): 292 ([M]$^+$). HR-MS calcd. for $C_{18}H_{25}O_2F$: 292.1838 ([M]$^+$); found: 292.1832 ± 0.0008.

Ketones 35 and 36

To a stirred solution of α,β-unsaturated ketone **34** (126 mg, 0.43 mmol) in ethyl acetate (10 mL) was added 5% palladium(0) on activated carbon (91 mg, 0.043 mmol) and hydrogen was bubbled for 10 min. The mixture was stirred for 1 h under a hydrogen atmosphere and filtered on a silica gel pad. The solvent was evaporated and the residue was purified by flash chromatography (50% ethyl acetate, 50% hexanes) to give ketone **36** (cis) as a colorless oil (76 mg, 60%) and ketone **35** (trans) as a colorless oil (33 mg, 27%). Ketone **36** (cis): IR ($CHCl_3$, cm^{-1}) ν: 3444, 3019, 2932, 2882, 1706, 1466, 1216, 1077, 958. ^{1}H NMR (300 MHz, $CDCl_3$, ppm) δ: 4.22 (1H, t, *J* = 7.8 Hz, RR′C*H*OH), 2.52 (1H, t, *J* = 13.9 Hz, RC(O)CH$_2$C*H*), 2.31–1.44 (19H, m), 1.39–1.10 (3H, m), 1.07 (3H, s, C*H*$_3$). ^{13}C NMR (75 MHz, $CDCl_3$, ppm) δ: 212.42, 108.91, 106.54, 80.33, 44.79, 44.51, 42.75, 40.31, 37.70, 36.43, 34.95, 30.10, 28.25, 28.00, 27.89, 27.80, 27.30, 24.42, 19.32, 16.12. MS (*m*/*e*): 294 ([M]$^+$). HR-MS calcd. for $C_{18}H_{27}O_2F$: 294.1995 ([M]$^+$); found: 294.1989 ± 0.0009. Ketone **35** (trans): ^{1}H NMR (300 MHz, $CDCl_3$, ppm) δ: 4.23 (1H, t, *J* = 8.2 Hz, RR′C*H*OH), 2.44–0.89 (23H, m), 1.07 (3H, d, *J* = 0.8 Hz, C*H*$_3$). MS (*m*/*e*): 294 ([M]$^+$). HR-MS calcd. for $C_{18}H_{27}O_2F$: 294.1995 ([M]$^+$); found: 294.1989 ± 0.0009.

Diketone 37

To a stirred solution of alcohol **36** (76 mg, 0.26 mmol) in dichloromethane (5 mL) were added molecular sieve 4 Å (130 mg), 4-methylmorpholine-*N*-oxide (61 mg, 0.52 mmol), and tetrapropylammonium perruthenate (9 mg, 0.026 mmol). The resulting mixture was stirred at room temperature for 1 h and filtered on a silica gel pad. The solvent was evaporated to give diketone **37** as a colorless oil (76 mg, 99%). IR ($CHCl_3$, cm^{-1}) ν: 3020, 2930, 2879, 1740, 1708, 1461, 1215, 929, 746. ^{1}H NMR (300 MHz, $CDCl_3$, ppm) δ: 2.59–2.37 (2H, m), 2.32–2.08 (6H, m), 1.88–1.05 (14H, m), 1.12 (3H, d, *J* = 1.5 Hz, C*H*$_3$). ^{13}C NMR (75 MHz, $CDCl_3$, ppm) δ: 219.46, 211.74, 106.80, 104.42, 44.52, 44.24, 42.63, 40.28, 37.45, 36.32, 35.06, 33.07, 31.91, 30.11, 27.20, 26.09, 25.75, 24.22, 19.10, 12.62. MS (*m*/*e*): 292 ([M]$^+$). HR-MS calcd. for $C_{18}H_{25}O_2F$: 292.1838 ([M]$^+$); found: 292.1844 ± 0.0008.

Alcohol 38

To a stirred solution of diketone **37** (71 mg, 0.24 mmol) in tetrahydrofuran (10 mL) at –78 °C was added a solution of 1 mol/L L-Selectride in tetrahydrofuran (360 µL, 0.36 mmol). The mixture was stirred at –78 °C for 1.5 h. A 2 mol/L NaOH solution and a 30% hydrogen peroxide solution were added and the aqueous phase was extracted with ethyl acetate. The combined organic phases were dried, filtered, and evaporated. The residue was purified by flash chromatography (70% ethyl acetate, 30% hexanes) to give

© 2006 NRC Canada

alcohol **38** as an amorphous white solid (72 mg, 100%). IR ($CHCl_3$, cm^{-1}) ν: 3611, 3451, 2933, 2878, 1739, 1447, 1266, 1061, 1001, 922. ^1H NMR (300 MHz, $CDCl_3$, ppm) δ: 4.14 (1H, t, J = 2.7 Hz, RR′C*H*OH), 2.51–2.40 (2H, m), 2.29–2.05 (3H, m), 1.86–1.15 (18H, m), 1.08 (3H, d, J = 1.3 Hz, CH_3). ^{13}C NMR (75 MHz, $CDCl_3$, ppm) δ: 220.09, 107.25, 104.88, 66.75, 44.74, 44.47, 41.27, 34.51, 33.18, 32.13, 30.81, 29.26, 26.95, 26.07, 25.74, 24.30, 20.97, 19.60, 12.62. MS (*m*/*e*): 294 ($[M]^+$). HR-MS calcd. for $C_{18}H_{27}O_2F$: 294.1995 ($[M]^+$); found: 294.2000 ± 0.0009.

Silyl ether 40

To a stirred solution of alcohol **38** (36 mg, 0.12 mmol) in dichloromethane (3 mL) were added triethylamine (84 μL, 0.60 mmol) and *tert*-butyldimethylsilane trifluoromethanesulfonate (41 μL, 0.18 mmol). The mixture was stirred at room temperature for 1 h. Satd. aq. NH_4Cl was added and the aqueous phase was extracted with dichloromethane. The combined organic phases were dried, filtered, and evaporated. The residue was dissolved in tetrahydrofuran (2 mL) and tetrapropylammonium fluoride (1 mol/L) in tetrahydrofuran (60 μL, 0.060 mmol) was added. The mixture was stirred at room temperature for 15 min. Satd. aq. NH_4Cl was added and the aqueous phase was extracted with ethyl acetate. The combined organic phases were dried, filtered, and evaporated. The residue was purified by flash chromatography (10% ethyl acetate, 90% hexanes) to give silyl ether **40** as a colorless oil (46 mg, 92%). IR ($CHCl_3$, cm^{-1}) ν: 3020, 2931, 2882, 1739, 1471, 1446, 1252, 1212, 1050, 930. ^1H NMR (300 MHz, $CDCl_3$, ppm) δ: 4.06 (1H, t, J = 2.6 Hz, RR′C*H*OTBDMS), 2.47–2.34 (2H, m), 2.29–2.05 (3H, m), 1.89–1.13 (17H, m), 1.09 (3H, d, J = 1.4 Hz, CH_3), 0.89 (9H, s, SiC(CH_3)$_3$), 0.02 (6H, s, Si(CH_3)$_2$). ^{13}C NMR (75 MHz, $CDCl_3$, ppm) δ: 220.18, 107.37, 105.00, 67.10, 44.83, 44.57, 41.43, 34.70, 34.58, 34.14, 33.15, 32.21, 32.13, 31.10, 29.28, 27.70, 26.07, 25.84, 25.81, 25.73, 24.38, 21.01, 19.73, 18.06, 12.65, 12.55, –4.89. MS (*m*/*e*): 208 ($[M]^+$), 351 ($[M - C_4H_9]^+$). HR-MS calcd. for $C_{24}H_{41}O_2FSi$: 408.2860 ($[M]^+$); found: 408.2863 ± 0.0012.

Vinylic iodide 42

To a stirred solution of ketone **38** (101 mg, 0.34 mmol) in ethanol (7 mL) were added triethylamine (952 μL, 6.80 mmol) and hydrated hydrazine (165 μL, 3.40 mmol). The mixture was stirred at reflux for 5 days and water was added. The aqueous phases were extracted with dichloromethane and the combined organic phases were dried, filtered, and evaporated. The residue was dissolved in tetrahydrofuran (5 mL) and triethylamine (1 mL) was added. Iodide was added until a brown color appeared and the mixture was stirred for 5 min. Water was added and the aqueous phase was extracted with dichloromethane. The combined organic phases were washed with saturated aqueous sodium thiosulfate and the organic phase was dried, filtered, and evaporated. The residue was purified by flash chromatography (40% ethyl acetate, 60% hexanes) to give vinylic iodide **42** as an amorphous white solid (125 mg, 91%). IR ($CHCl_3$, cm^{-1}) ν: 3386, 2931, 2873, 1459, 1447, 1380, 1263, 1000. ^1H NMR (300 MHz, $CDCl_3$, ppm) δ: 6.06 (1H, t, J = 2.5 Hz, C*H*=CIR), 4.14 (1H, t, J = 2.8 Hz, RR′C*H*OH), 2.62–2.40 (2H, m, CH_2CH=CIR), 2.19–2.13 (1H, m), 1.86–1.10 (16H, m), 1.08 (3H, d, J = 2.8 Hz, CH_3), 1.05–0.83 (2H, m). ^{13}C NMR (75 MHz, $CDCl_3$, ppm) δ: 132.48, 109.80, 105.63, 103.18, 66.85, 45.97, 45.68, 40.96, 40.63, 40.27, 37.36, 34.93, 33.17, 30.90, 29.28, 27.03, 24.26, 21.13, 20.75, 17.11. MS (*m*/*e*): 404 ($[M]^+$). HR-MS calcd. for $C_{18}H_{26}OFI$: 404.1012 ($[M]^+$); found: 404.1008 ± 0.0012.

Silyl ether 43

To a stirred solution of alcohol **42** (148 mg, 0.37 mmol) in dichloromethane (10 mL) were added triethylamine (1.3 mL, 1.85 mmol) and *tert*-butyldimethylsilane trifluoromethanesulfonate (94 μL, 0.41 mmol). The mixture was stirred at room temperature for 1 h. Satd. aq. NH_4Cl was added and the aqueous phase was extracted with dichloromethane. The combined organic phases were dried, filtered, and evaporated. The residue was purified by flash chromatography (10% ethyl acetate, 90% hexanes) to give silyl ether **43** as an amorphous white solid (190 mg, 100%). IR ($CHCl_3$, cm^{-1}) ν: 3019, 2930, 2856, 1509, 1424, 1364, 1217, 1048. ^1H NMR (300 MHz, $CDCl_3$, ppm) δ: 6.07 (1H, t, J = 2.4 Hz, C*H*=CIR), 4.05 (1H, t, J = 2.4 Hz, RR′C*H*OTBDMS), 2.62–2.43 (2H, m, CH_2CH=CIR), 2.22–2.13 (1H, m), 1.89–0.91 (17H, m), 1.08 (3H, d, J = 2.8 Hz, CH_3), 0.89 (9H, s, SiC(CH_3)$_3$), 0.02 (6H, s, Si(CH_3)$_2$). ^{13}C NMR (75 MHz, $CDCl_3$, ppm) δ: 132.48, 109.92, 105.70, 103.24, 67.17, 54.23, 53.98, 46.08, 45.80, 41.13, 40.65, 40.29, 37.44, 35.11, 34.11, 31.20, 29.28, 27.80, 25.83, 24.35, 21.17, 20.90, 17.14, –4.87. MS (*m*/*e*): 461 ($[M - C_4H_9]^+$). HR-MS calcd. for $C_{20}H_{31}OFISi$: 461.1173 ($[M - C_4H_9]^+$); found: 461.1178 ± 0.0014.

α,β-Unsaturated nitrile 44

To a stirred solution of vinylic iodide **43** (47 mg, 0.091 mmol) in benzene (3 mL) were added lithium cyanide (18 mg, 0.55 mmol), tetrakis(triphenylphosphine) palladium(0) (11 mg, 0.0091 mmol), and 12-C-4 ether (2 μL, 0.0091 mmol). The resulting mixture was stirred at reflux for 30 min and water was added. The aqueous phase was extracted with dichloromethane. The combined organic phases were dried, filtered, and evaporated. The residue was purified by flash chromatography (7% ethyl acetate, 93% hexanes) to give α,β-unsaturated nitrile **44** as an amorphous white solid (17 mg, 45%). IR ($CHCl_3$, cm^{-1}) ν: 3019, 2930, 2546, 2127, 1610, 1504, 1368, 1215, 1168, 1086, 1049. ^1H NMR (300 MHz, $CDCl_3$, ppm) δ: 6.54 (1H, t, J = 2.6 Hz, C*H*=C(CN)R), 4.05 (1H, massif, RR′C*H*OTBDMS), 2.83–2.54 (2H, m, CH_2CH=C(CN)R), 2.24–2.20 (1H, m), 2.03–1.96 (1H, m), 1.90–0.90 (16H, m), 1.26 (3H, d, J = 2.5 Hz, CH_3), 0.88 (9H, s, SiC(CH_3)$_3$), 0.02 (6H, s, Si(CH_3)$_2$). ^{13}C NMR (75 MHz, $CDCl_3$, ppm) δ: 141.97, 125.37, 115.51, 107.41, 104.95, 67.06, 52.47, 52.21, 45.28, 45.00, 41.02, 39.55, 39.18, 37.4, 34.81, 34.07, 31.10, 29.18, 27.76, 25.80, 24.33, 21.16, 18.06, 14.81, –4.89. MS (*m*/*e*): 402 ($[M - CH_3]^+$), 360 ($[M - C_4H_9]^+$). HR-MS calcd. for $C_{21}H_{31}OFNSi$: 360.2159 ($[M - C_4H_9]^+$); found: 360.2166 ± 0.0014.

Nitriles 45a and 45b

To a stirred solution of α,β-unsaturated nitrile **44** (15 mg, 0.036 mmol) in ethyl acetate (2 mL) was added a catalytic amount of 10% palladium(0) on activated carbon and hydro-

© 2006 NRC Canada

gen was bubbled through the solution for 15 min. The mixture was stirred for 2 h under a hydrogen atmosphere and filtered on a silica gel pad. The solvent was evaporated and the residue was purified by flash chromatography (10% ethyl acetate, 90% hexanes) to give nitrile β-**45a** as an amorphous white solid (8 mg, 53%) and nitrile α-**45b** as an amorphous white solid (7 mg, 47%). Nitrile α-**45a**: IR ($CHCl_3$, cm^{-1}) ν: 2930, 2856, 2363, 1460, 1444, 1252, 1216, 1047. ^1H NMR (300 MHz, $CDCl_3$, ppm) δ: 4.05 (1H, t, J = 2.6 Hz, RR′C*H*OTBDMS), 2.98 (1H, t, J = 9.0 Hz, RR′C*H*CN), 2.27–0.95 (22H, m), 1.15 (3H, s, CH_3), 0.88 (9H, s, SiC(CH_3)$_3$), 0.02 (6H, s, Si(CH_3)$_2$). ^{13}C NMR (75 MHz, $CDCl_3$, ppm) δ: 120.70, 109.17, 106.76, 67.1, 48.42, 48.18, 44.74, 44.48, 41.38, 39.18, 34.52, 34.14, 31.27, 31.18, 30.25, 29.92, 29.26, 27.67, 25.81, 24.82, 24.14, 20.96, 18.07, 16.66, –4.90. MS (*m*/*e*): 404 ([M – CH_3]$^+$), 362 ([M – C_4H_9]$^+$). HR-MS calcd. for $C_{24}H_{39}OFNSi$: 404.2785 ([M – CH_3]$^+$); found: 404.2773 ± 0.0012. Nitrile β-**45b**: IR ($CHCl_3$, cm^{-1}) ν: 3019, 2930, 2856, 2240, 1527, 1477, 1426, 1215, 1048. ^1H NMR (300 MHz, $CDCl_3$, ppm) δ: 4.05 (1H, t, J = 2.5 Hz, RR′C*H*OTBDMS), 2.65 (1H, t, J = 6.0 Hz, RR′C*H*CN), 2.28–1.96 (5H, m), 1.87–1.03 (17H, m), 1.30 (3H, s, CH_3), 0.88 (9H, s, SiC(CH_3)$_3$), 0.02 (6H, s, Si(CH_3)$_2$). ^{13}C NMR (75 MHz, $CDCl_3$, ppm) δ: 121.92, 109.58, 107.18, 67.10, 48.46, 48.21, 44.71, 44.44, 41.46, 40.04, 36.65, 34.25, 34.12, 31.23, 30.85, 30.51, 29.24, 27.69, 25.80, 25.59, 21.17, 20.97, 18.06, 16.20, –4.88. MS (*m*/*e*): 404 ([M – CH_3]$^+$), 362 ([M – C_4H_9]$^+$). HR-MS calcd. for $C_{24}H_{39}OFNSi$: 404.2785 ([M – CH_3]$^+$); found: 404.2773 ± 0.0012.

Alcohols 46a

To a stirred solution of nitrile **45a** (7 mg, 0.017 mmol) in methanol was added a catalytic amount of PTSA and the mixture was stirred at room temperature for 3 h. Satd. aq. $NaHCO_3$ was added and the aqueous phase was extracted with dichloromethane. The combined organic phases were dried, filtered, and evaporated. The residue was purified by flash chromatography (50% ethyl acetate, 50% hexanes) to give alcohol **46a** as an amorphous white solid (5 mg, 100%). ^1H NMR (300 MHz, $CDCl_3$, ppm) δ: 4.15 (1H, t, J = 2.8 Hz, RR′C*H*OH), 2.98 (1H, t, J = 9.5 Hz, RR′C*H*CN), 2.23–2.16 (2H, m), 2.04–1.06 (21H, m), 1.15 (3H, s, CH_3). ^{13}C NMR (75 MHz, $CDCl_3$, ppm) δ: 120.68, 109.07, 106.67, 66.83, 48.46, 48.22, 44.70, 44.43, 41.27, 39.21, 34.38, 33.24, 31.33, 30.93, 30.29, 29.96, 29.29, 27.00, 24.80, 24.16, 20.97, 16.68. MS (*m*/*e*): 287 ([M – H_2O]$^+$). HR-MS calcd. for $C_{19}H_{26}FN$: 287.2049 ([M – H_2O]$^+$); found: 287.2045 ± 0.0008.

Alcohol 46b

The procedure used for the synthesis of alcohol **46a** was used with alcohol **46b** to give alcohol **46b** as an amorphous white solid (5 mg, 100%). IR ($CHCl_3$, cm^{-1}) ν: 3423, 3019, 2933, 2360, 1523, 1423, 1216, 928. ^1H NMR (300 MHz, $CDCl_3$, ppm) δ: 4.14 (1H, t, J = 2.8 Hz, RR′C*H*OH), 2.66 (1H, t, J = 7.7 Hz, RR′C*H*CN), 2.28–1.96 (6H, m), 1.82–1.00 (17H, m), 1.30 (3H, s, CH_3). ^{13}C NMR (75 MHz, $CDCl_3$, ppm) δ: 121.86, 109.46, 107.42, 66.79, 48.45, 48.21, 44.62, 44.35, 41.30, 40.02, 36.56, 34.19, 33.22, 30.94, 30.51, 29.69, 29.23, 26.93, 25.51, 21.04, 20.94, 16.18. MS (*m*/*e*): 287 ([M – H_2O]$^+$). HR-MS calcd. for $C_{19}H_{26}FN$: 287.2049 ([M – H_2O]$^+$); found: 287.2045 ± 0.0008.

p-Nitrobenzoate 47

To a stirred solution of alcohol **46b** (1 mg, 0.0033 mmol) in dichloromethane (250 μL) were added pyridine (250 μL), *p*-nitrobenzoyle chloride (6 mg, 0.033 mmol), and 4-dimethylaminopyridine (catalytic amount). The resulting mixture was stirred at room temperature for 3 h. HCl (1 mol/L) was added and the aqueous phase was extracted with dichloromethane. The combined organic phases were dried, filtered, and evaporated. The residue was purified by flash chromatography (30% ethyl acetate, 70% hexanes) to give *p*-nitrobenzoate **47** as a white solid (1 mg); mp 210 to 211 °C. IR ($CHCl_3$, cm^{-1}) ν: 2934, 2856, 2244, 1719, 1280, 1118. ^1H NMR (300 MHz, $CDCl_3$, ppm) δ: 8.30 (2H, d, J = 9.0 Hz, Ph), 8.21 (2H, d, J = 9.0 Hz, Ph), 5.40 (1H, t, J = 2.4 Hz, RR′C*H*OC(O)Ar), 2.68 (1H, t, J = 6.6 Hz, RR′C*H*CN), 2.31–1.07 (22H, m), 1.32 (3H, s, CH_3). MS (*m*/*e*): 472 ([MNH_4]$^+$). HR-MS calcd. for $C_{26}H_{35}O_4FN_3$: 472.2611 ([MNH_4]$^+$); found: 472.2623 ± 0.0014.

α,β-Unsaturated ester 4

To a stirred solution of nitrile **46a** (4 mg, 0.013 mmol) in toluene (1 mL) at –60 °C was added a 1.5 mol/L solution of DIBALH in toluene (26 μL, 0.039 mmol) and the mixture was stirred at –60 °C for 1 h. Sodium sulfate decahydrate was added and the mixture was stirred at room temperature for 1 h. The residue was filtered and the solvent was evaporated to give the corresponding imine. This imine was passed rapidly through a short silica gel pad to give aldehyde **50a** (4 mg) as a crude material. To a stirred suspension of 60% NaH in oil (5 mg, 0.13 mmol) in tetrahydrofuran (1 mL) was added trimethyl phosphonoacetate (21 μL, 0.13 mmol). The mixture was stirred at room temperature for 15 min and crude aldehyde **50a** (4 mg, 0.013 mmol) in tetrahydrofuran (1 mL) was added. The resulting mixture was stirred at room temperature for 30 min. Satd. aq. NH_4Cl was added and the aqueous phase was extracted with dichloromethane. The combined organic phases were dried, filtered, and evaporated. The residue was purified by flash chromatography (40% ethyl acetate, 60% hexanes) to give α,β-unsaturated ester **4** as a colorless oil (3 mg, 60% for two steps). IR ($CHCl_3$, cm^{-1}) ν: 3501, 2932, 2875, 1718, 1654, 1540, 1558, 1437, 1281, 1216, 1002. ^1H NMR (300 MHz, $CDCl_3$, ppm) δ: 6.91 (1H, dd, J = 15.6, 8.7 Hz, C*H*=CHCO$_2$Me), 5.83 (1H, J = 15.6 Hz, CH=C*H*CO$_2$Me), 4.14 (1H, t, J = 2.6 Hz, RR′C*H*OH), 3.73 (3H, s, CO$_2$CH_3), 2.81 (1H, q, J = 8.7 Hz, RR′C*H*CH=CHCO$_2$Me), 2.22–1.03 (23H, m), 1.00 (3H, d, J = 1.1 Hz, CH_3). ^{13}C NMR (75 MHz, $CDCl_3$, ppm) δ: 149.70, 149.57, 121.97, 66.93, 51.45, 51.33, 49.00, 45.09, 44.81, 41.27, 34.39, 34.27, 33.26, 31.00, 30.41, 30.06, 29.96, 29.37, 26.97, 25.04, 24.69, 20.98, 20.74, 16.81. MS (*m*/*e*) (source temperature: 100 °C): 364 ([M]$^+$), 344 ([M – HF]$^+$). HR-MS (source temperature: 100 °C) calcd. for $C_{22}H_{33}O_3F$: 364.2414 ([M]$^+$); found: 364.2403 ± 0.0011.

α,β-Unsaturated ester 3

The procedure used for the synthesis of α,β-unsaturated ester **4** was used for α,β-unsaturated ester **3** to give an

© 2006 NRC Canada

unseparable mixture of α,β-unsaturated ester **3** and α,β-unsaturated ester **4** (9:1) as an amorphous white solid (3 mg, 60%). IR ($CHCl_3$, cm^{-1}) ν: 3501, 2931, 2865, 1718, 1654, 1541, 1458, 1437, 1269, 1221, 1000. ^1H NMR (300 MHz, $CDCl_3$, ppm) δ: 7.01 (1H, ddd, J = 15.5, 10.7, 1.8 Hz, C*H*=CHCO$_2$Me), 5.65 (1H, J = 15.5 Hz, CH=C*H*CO$_2$Me), 4.14 (1H, t, J = 2.7 Hz, RR′C*H*OH), 3.71 (3H, s, CO$_2$C*H*$_3$), 2.38 (1H, td, J = 8.5, 3.2 Hz, R′RC*H*CH=CHCO$_2$Me), 2.17–1.03 (23H, m), 0.90 (3H, s, C*H*$_3$). ^{13}C NMR (75 MHz, $CDCl_3$, ppm) δ: 153.55, 153.49, 119.75, 66.93, 53.93, 51.35, 45.09, 44.81, 41.43, 38.08, 37.98, 34.18, 33.27, 31.09, 30.75, 29.37, 26.97, 26.66, 25.42, 21.09, 21.01, 15.63. MS (*m*/*e*) (source temperature: 100 °C): 364 ([M]$^+$), 344 ([M – HF]$^+$). HR-MS (source temperature: 100 °C) calcd. for $C_{22}H_{33}O_3F$: 364.2414 ([M]$^+$); found: 364.2403 ± 0.0011.

Acknowledgments

The authors thank Mr. Andreas Decken and Marc Drouin for X-ray diffraction analysis and Tranzyme Pharma Inc. for biological activity. Financial support from Shire BioChem Inc. and the Natural Sciences and Engineering Research Council of Canada (NSERC) are highly appreciated.

References

1. L.F. Fieser and M. Fieser. Steroids. Reinhold Publishing Corporation, Baltimore, Md. 1959.
2. T.R. Watson, H.T.A. Cheung, and R.E. Thomas. Natural products and drug development, Alfred Benzon symposium 20. Munksgaard, Copenhagen. 1984.
3. R.B. Silverman. The organic chemistry of drug design and drug action. Academic Press Inc., San Diego. 1992.
4. S.D. Munari, P. Barassi, A. Cerri, G. Fedrezzi, M. Gobbini, M. Mabilia, and P. Melloni. J. Med. Chem. **41**, 3033 (1998).
5. O. Diels and K. Alder. Justus Liebigs Ann. Chem. **98**, 460 (1928).
6. (*a*) P. Deslongchamps. Aldrichimica Acta, **24**, 43 (1991); (*b*) P. Deslongchamps. Pure Appl. Chem. **64**, 1831 (1992).
7. E. Marsault, A. Toro, P. Nowak, and P. Deslongchamps. Tetrahedron, **57**, 4243 (2001).
8. L. Ouellet, P. Langlois, and P. Deslongchamps. Synlett, 689 (1997).
9. F.L Greenwood. J. Org. Chem. **20**, 803 (1955).
10. J. Boutagy and R. Thomas. Chem. Rev. **74**, 87 (1974).
11. A.J. Mancuso and D. Swern. Synthesis, 165 (1981).
12. A. Thenappan and D.J. Burton. J. Org. Chem. **55**, 4639 (1990).
13. R.M. Magid, O. Frucfey, W.L. Johnson, and T.G. Allen. J. Org. Chem. **44**, 359 (1979).
14. N. Stuart, H. Weiler, and L. Weiler. J. Am. Chem. Soc. **96**, 1082 (1974).
15. J.A. Marshall, R.C. Andrews, and L. Lebioda. J. Org. Chem. **52**, 2378 (1987).
16. D.H.R. Barton, D.J. Lester, and V.J. Leys. J. Chem. Soc. Chem. Commun. 130 (1978).
17. L.A Paquette and H. Kang. J. Am. Chem. Soc. **133**, 2610 (1991).
18. (*a*) S. Lamothe, A. Ndibwani, and P. Deslongchamps. Tetrahedron Lett. **29**, 1639 (1988); (*b*) S. Lamothe, A. Ndibwani, and P. Deslongchamps. Tetrahedron Lett. **29**, 1641 (1988).
19. X. Kong and T.B. Grindley. Can. J. Chem. **72**, 2396 (1994).
20. (*a*) J.R. Kutney, K. Piotrowska, J. Somerville, S.-P. Hyang, and S.J. Rettig. Can. J. Chem. **67**, 580 (1989); (*b*) M. Adamczyk, E.K. Dolence, and D.S. Watt. J. Org. Chem. **49**, 1378 (1984); (*c*) P. Drasar, V. Pouzar, I. Cerny, M. Havel, V.V. Egorova, S.N. Ananchemko, I.V. Torgov, and F. Turesek. Steroids, **53**, 107 (1989).
21. B. Maryanoff and A.B. Reitz. Chem. Rev. **89**, 863 (1989).
22. P. Mosset and R. Grée. Synth. Commun. 749 (1985).
23. G. Tsuchihashi and K. Ogura. Bull. Chem. Soc. Jpn. **45**, 2023 (1972).
24. W.P. Griffith and S.V. Ley. Aldrichimica Acta, **23**, 13 (1990).
25. D.L. Comins and A. Dehghani. Tetrahedron Lett. **33**, 6299 (1992).
26. (*a*) S. Cacchi, E. Morera, and G. Ortar. Tetrahedron Lett. **26**, 1109 (1985); (*b*) M.A. Tuis and S.K. Kannangara. J. Org. Chem. **55**, 5711 (1990).
27. (*a*) J.F. Templeton, V.P.S. Kumar, D. Dose, and F.S. Labella. J. Med. Chem. **32**, 1977 (1989); (*b*) N. Daniele, Y. Mazur, and F. Sondheimer. J. Am. Chem. Chem. **84**, 875 (1962); (*c*) A. Hastier, A. Pancrazi, and Q. Khuong-Huu. Bull. Soc. Chim. Fr. 1581 (1976).
28. G. Stork, F. West, H.Y. Lee, R.C.A. Isaacs, and S. Manabe. J. Am. Chem. Soc. **118**, 10660 (1996).
29. E. Piers and F.F. Fleming. Can. J. Chem. **71**, 1867 (1993).
30. H.L. Dryden, G.M. Webber, R.R. Burtner, and J.A. Cella. J. Org. Chem. **26**, 3237 (1961).
31. G. Goendoes and J.C. Orr. J. Chem. Soc. Chem. Commun. 1239 (1982).
32. R. Contreras and L. Mendoza. Steroids, **34**, 121 (1979).
33. D.H.R. Barton, G. Bashiardes, and J.-L. Fourrey. Tetrahedron Lett. **24**, 1605 (1983).

© 2006 NRC Canada

Oxyhalogen-sulfur chemistry — Kinetics and mechanism of the oxidation of cysteamine by acidic iodate and iodine

Alice Chanakira, Edward Chikwana, David H. Peyton, and Reuben H. Simoyi

Abstract: The oxidation of cysteamine by iodate and aqueous iodine has been studied in neutral to mildly acidic conditions. The reaction is relatively slow and is heavily dependent on acid concentration. The reaction dynamics are complex and display clock behavior, transient iodine production, and even oligooscillatory production of iodine, depending upon initial conditions. The oxidation product was the cysteamine dimer (cystamine), with no further oxidation observed past this product. The stoichiometry of the reaction was deduced to be $IO_3^- + 6H_2NCH_2CH_2SH \rightarrow I^- + 3H_2NCH_2CH_2S\text{-}SCH_2CH_2NH_2 + 3H_2O$ in excess cysteamine conditions, whereas in excess iodate the stoichiometry of the reaction is $2IO_3^- + 10H_2NCH_2CH_2SH \rightarrow I_2 + 5H_2NCH_2CH_2S\text{-}SCH_2CH_2NH_2 + 6H_2O$. The stoichiometry of the oxidation of cysteamine by aqueous iodine was deduced to be $I_2 + 2H_2NCH_2CH_2SH \rightarrow 2I^- + H_2NCH_2CH_2S\text{-}SCH_2CH_2NH_2 + 2H^+$. The bimolecular rate constant for the oxidation of cysteamine by iodine was experimentally evaluated as 2.7 $(\text{mol L}^{-1})^{-1}\ \text{s}^{-1}$. The whole reaction scheme was satisfactorily modeled by a network of 14 elementary reactions.

Key words: cysteamine, cystamine, Dushman reaction, oligooscillations.

Résumé : L'oxydation de la cystéamine par l'iodate et l'iode aqueux a été étudiée dans des conditions allant de neutre à faiblement acides. La réaction est relativement lente et dépend fortement sur la concentration en acide. La dynamique de la réaction est complexe et présente un comportement d'horloge avec production transitoire d'iode allant jusqu'à une production oligooscillatoire d'iode suivant les conditions initiales. Le produit de l'oxydation est le dimère de la cystéamine, la cystamine, sans oxydation apparente ultérieure de ce produit. On a déduit que, dans les conditions où la cystéamine est en excès la stoechiométrie de la réaction est $IO_3^- + 6H_2NCH_2CH_2SH \rightarrow I^- + 3H_2NCH_2CH_2S\text{-}SCH_2CH_2NH_2 + 3H_2O$ alors que lorsque l'iodate est en excès, la stoechiométrie de la réaction est de la forme $2IO_3^- + 10H_2NCH_2CH_2SH \rightarrow I_2 + 5H_2NCH_2CH_2S\text{-}SCH_2CH_2NH_2 + 6H_2O$. On a établi que la stoechiométrie de la réaction d'oxydation de la cystéamine par l'iode aqueux est de la forme $I_2 + 2H_2NCH_2CH_2SH \rightarrow 2I^- + H_2NCH_2CH_2S\text{-}SCH_2CH_2NH_2 + 2H^+$. La valeur établie expérimentalement pour la constante de vitesse bimoléculaire d'oxydation de la cystéamine par l'iode est de 2,7 $(\text{mol L}^{-1})^{-1}\ \text{s}^{-1}$. On peut faire une modélisation complète du schéma réactionnel sur la base de quatorze réactions élémentaires.

Mots clés : cystéamine, cystamine, réaction de Dushman, oligooscillations.

[Traduit par la Rédaction]

Introduction

Organosulfur compounds dominate much of synthetic, analytical, and medicinal chemistry. Oxidations of organic sulfur compounds appear to be involved in many cellular functions, including regulation of protein synthesis and protection of the cell from oxidative damage (1). Owing to the nucleophilic nature of the thiol group, a better understanding of the biological activities of these compounds can be derived from their oxidation mechanisms. Studies of the oxidation mechanisms of organosulfur compounds have been hampered by the propensity of sulfur chemistry to produce complex and exotic dynamics (2), which are fueled by free-radical mechanisms (3), autoxidations, and production of varied products and intermediates (4, 5). With the sulfur center having an oxidation state range of –2 to +6, it is easy for these intermediates to assert themselves.

Cysteamine is a very important biological molecule. Medically known as Cystagon, it can be used as oral therapy for prevention of hypothyroidism and enhances growth in patients with nephropathic cystinosis (6, 7). This is a lysosomal storage disorder that was long considered primarily a renal disease but is now recognized as a systemic disorder that eventually affects many organ systems in children (8). This disorder is characterized by cystine accumulation within cellular lysosomes, and cysteamine converts this disulfide into cysteine and a mixed disulfide, cysteamine–cysteine, which can easily be eliminated from the cystinotic lysosomes, thus effecting depletion of cellular cystine (9).

Received 4 April 2005. Published on the NRC Research Press Web site at http://canjchem.nrc.ca on 25 February 2006.

A. Chanakira,[1] E. Chikwana, D.H. Peyton, and R.H. Simoyi.[2] Department of Chemistry, Portland State University, Portland, OR 97207-0751, USA.

[1]Present address: College of St. Catherine, St. Paul, MN 55105, USA.
[2]Corresponding author (e-mail: rsimoyi@pdx.edu).

 doi:10.1139/V05-263 © 2006 NRC Canada

Cysteamine and its disulfide, cystamine, can also be used in topical eye drops to dissolve corneal cystine crystals (10).

Cysteamine is an excellent scavenger of ·OH and HOCl; it also reacts with H_2O_2 and other oxygen-based toxic metabolites (11). In addition to protection against radical damage in DNA, cysteamine can also act as a repair agent for DNA through the formation of the protective $RSSR^{-}$, which reacts with the DNA^{+} radical ion to regenerate DNA and form cystamine (12). It has been shown that cysteamine and its metabolite hypotaurine are far more likely to act as antioxidants in vivo than is taurine, provided that they are present in sufficient concentration at sites of oxidant generation (13). Cysteamine is oxidized to the sulfinic derivative (hypotaurine) only in the presence of cofactorlike compounds such as sulfide, methylene blue, and hydroxyalamine (14). Most metabolic pathways give hypotaurine as a precursor to taurine (15, 16).

In some of our recent work, we examined the reactivity of the cysteamine metabolites: hypotaurine (cysteamine sulfinic acid) and taurine (cysteamine sulfonic acid) (17). Oxidation of hypotaurine by chlorite and chlorine dioxide occurred simultaneously at the sulfur center (giving taurine) and at the nitrogen center (to give the chloramines) (18). On the other hand, taurine is relatively inert to oxidation by chlorine dioxide, a reactive radical species, and acidified bromate (19). When subjected to the strong oxidizing agent HOCl, the C—S bond is not cleaved, and reaction occurs exclusively at the nitrogen center, giving chlorotaurine (17).

The key to understanding the physiological role of cysteamine is through its oxidation pathway: its reactive intermediates and oxidation products. In this manuscript we report on the oxidation of cysteamine by the mild oxidizing agents acidic iodate and aqueous iodine. In a nonenzymatic pathway, could the oxidation of cysteamine yield hypotaurine or go all the way to taurine? Specifically, we are aware that the action of most goitrogenic mechanisms involves the consumption of the iodine atom, which is needed for thyroid activity (20). What then, is the rate and mechanism by which cysteamine reacts with molecular iodine?

Experimental

Materials

Cysteamine hydrochloride (CA, 2-aminoethanethiol hydrochloride) (98%), iodine, potassium iodide (Aldrich), sodium perchlorate (98%) (Acros), cystamine dihydrochloride (MP Biomedical), potassium iodate, perchloric acid (72%), soluble starch, sodium thiosulfate, and hydrochloric acid (Fisher) were used without further purification. The concentration of iodine was determined by standardization against thiosulfate with starch as indicator. This standardization allowed us to evaluate the absorptivity coefficient of iodine at its isosbestic point of 460 nm with triiodide as 770 $(\text{mol L}^{-1})^{-1}$ cm^{-1}. This standardization was carried out before each series of kinetic experiments were performed because of the volatile nature of iodine. CA solutions were prepared just before use and not kept for more than 24 h. All solutions were prepared using distilled–deionized water from a Barnstead Sybron Corporation water purification unit. Inductively coupled plasma mass spectrometry (ICPMS) was used to show that our aqueous reaction media did not contain enough metal ions to affect the overall reaction kinetics and mechanism (21). The highest metal ion concentration was cadmium at 1.5 ppb, followed by lead at 0.43 ppb.

Methods

All experiments were carried out at 25.0 ± 0.5 °C and at a constant ionic strength of 1.0 mol L^{-1} ($NaClO_4$). CA, sodium perchlorate, and perchloric acid solutions were mixed in one reactant vessel and iodate (or iodine) solutions in another. All kinetics measurements were performed on a Hi-Tech Scientific SF61–DX2 double mixing stopped-flow spectrophotometer. Spectrophotometric determinations were performed on a PerkinElmer Lambda 25 UV–vis spectrophotometer.

Stoichiometric determinations

The stoichiometry for the CA–IO_3^- was determined both in excess iodate and in excess CA. In excess iodate the total oxidizing power was determined by titration. Excess acidified iodide was added to the reaction solution, and the released iodine was titrated against standard thiosulfate. Spectrophotometry was also used to determine the amount of iodine formed in excess iodate by its absorbance at 460 nm. In the I_2–CA reaction the stoichiometry was determined by titrating standardized iodine solution from a burette into a solution of CA of known strength. The end point, which was enhanced by starch indicator, was detected as the point where the blue-black color lingered.

Results

Stoichiometry

The stoichiometry of the reaction was strictly 1:6, with 6 mol of cysteamine reacting with 1 mol iodate. This suggested a one-electron oxidation of the sulfur center, and the only product possible after one-electron oxidation of an organosulfur center was the disulfide ($H_2NCH_2CH_2S$-$SCH_2CH_2NH_2$, RSSR). Both spectrophotometric and titrimetric techniques were used to deduce the following stoichiometry:

$$[R1]\quad IO_3^- + 6H_2NCH_2CH_2SH \rightarrow I^- + 3H_2NCH_2CH_2S\text{-}SCH_2CH_2NH_2 + 3H_2O$$

Stoichiometry [R1] was obtained only at the stoichiometric ratio of 1:6. In lower concentrations of iodate, the reaction mixture produced a mixture of both cysteamine and cystamine. These products were confirmed by the NMR spectrum of the mixture. In stoichiometric excess of iodate, the reaction products included iodine, which was then spectrophotometrically examined to deduce the overall stoichiometry of [R2]:

$$[R2]\quad 2IO_3^- + 10H_2NCH_2CH_2SH + 2H^+ \rightarrow I_2 + 5H_2NCH_2CH_2S\text{-}SCH_2CH_2NH_2 + 6H_2O$$

If the iodate-to-substrate ratio was greater than 1:5, then the amount of iodine produced was determined by the amount of cysteamine as the limiting reagent. There was an increase in the amount of iodine produced as the ratio was

© 2006 NRC Canada

increased from 1:6. At 1:5, however, the increase saturated, and no further increase in the production of iodine was observed. The direct reaction of aqueous iodine and cysteamine was determined by a rapid and careful titration aided by starch indicator. Although the end point of the titration shifted upon prolonged standing, the correct stoichiometry was attained at the first end point of 1:2, as shown below.

$$[R3] \quad I_2 + 2H_2NCH_2CH_2SH \rightarrow 2I^- + H_2NCH_2CH_2S\text{-}SCH_2CH_2NH_2 + 2H^+$$

The complications observed after allowing the titrated solution to incubate arose from two equilibria: the sulfide–disulfide equilibrium (22), which sought to reestablish itself after the depletion of the iodine because of titration with thiosulfate, and the iodine–thiol equilibrium (23, 24), which is well-known and has been extensively discussed in this manuscript under "charge-transfer" complex formation (see below). Stoichiometry [R3] could also be obtained spectrophotometrically in an excess of iodine and under high acid conditions, where both of these complicating equilibria were suppressed.

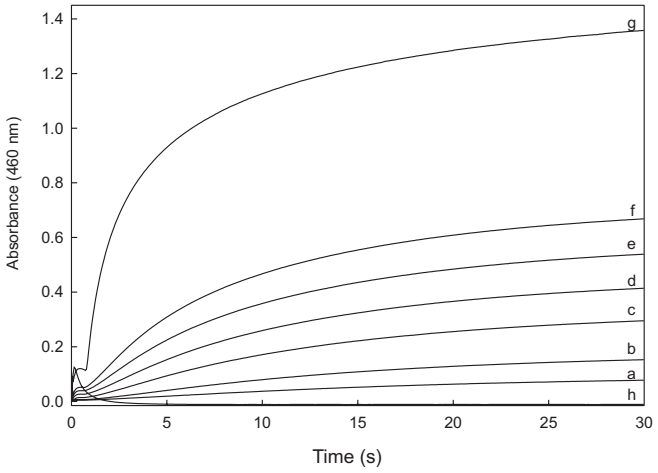
Confirmation of products

Reactions run in excess iodate did not afford sulfate as a product, as shown by the lack of precipitation of barium sulfate with barium chloride. Before barium chloride was added, excess iodate was removed by the use of excess acidified iodide, followed by evaporation of the iodine formed to avoid precipitation of barium iodate. Standard proton NMR spectra were also used to confirm the formation of the disulfide. Reagent grade cysteamine gave the expected spectrum of two triplets owing to the methylene proton sets on the carbon skeleton. This reagent-grade quality cysteamine also showed some cystamine impurity. Addition of DCl destroyed the resolution of the cysteamine triplets and also shifted them downfield because of the protonation of the amino center. The NMR spectrum of the product confirmed that the product was the dimeric cystamine. These product identities were confirmed by an HPLC technique, which utilized an isocratic 98%:2% water–methanol medium. The aqueous medium was 0.05 mol L^{-1} phosphate at pH 4.0. Both cysteamine and cystamine were modified by addition of acid, and so a control spectrum was initially obtained with cystamine mixed with acid before product UV spectral analyses were performed.

Reaction dynamics

The reaction dynamics were complex, with oligo-oscillatory production of iodine (25), transient formation of iodine, and clock reaction behavior (26). Figure 1 shows all three types of complex dynamics. This is much more evident if the region between $t = 0$ and 5 s is expanded and magnified. Trace h, for example, is at the 1:6 stoichiometric ratio of rxn. [R1] and should produce no aqueous iodine at the end of the reaction. Trace h shows, however, an initial rapid formation of iodine, followed by an equally rapid consumption, all within 3 s. The rest of the traces, a–g, have stoichiometric excess of iodate according to [R1], while only traces a and b have the stoichiometric ratio that satisfies stoichiometry [R2]. Traces a–e display clock reaction characteristics: an initial quiescent period followed by formation of iodine. Trace g, on the other hand, shows two peaks in iodine concentrations (oligooscillations), with one peak after approximately 1 s and the other peak (which represented the maximum concentrations obtained) at 60 s (truncated from Fig. 1). The only difference in the traces shown in Fig. 1 is the oxidant-to-reductant ratio, $R = [IO_3^-]_0/[CA]_0$. The increase in final iodine concentrations formed in going from trace a to g is justified from the premise that stoichiometry [R2] is a stepwise combination of rxn. [R1] and the Dushman reaction, [R4] (5[R1] + [R4]) (27).

Fig. 1. CA variation in excess oxidant shows higher rates of iodine production, as well as higher final concentrations of iodine, at the end of the reaction as the CA concentration is increased. Trace h shows that at the stoichiometric ratio there is just a transient formation of iodine. $[IO_3^-]_0 = 0.005$ mol L^{-1}, $[H^+]_0 =$ 0.02 mol L^{-1}, $[CA]_0$ = (a) 0.0005, (b) 0.001, (c) 0.002, (d) 0.003, (e) 0.004, (f) 0.005, (g) 0.015, (h) 0.03 mol L^{-1}.

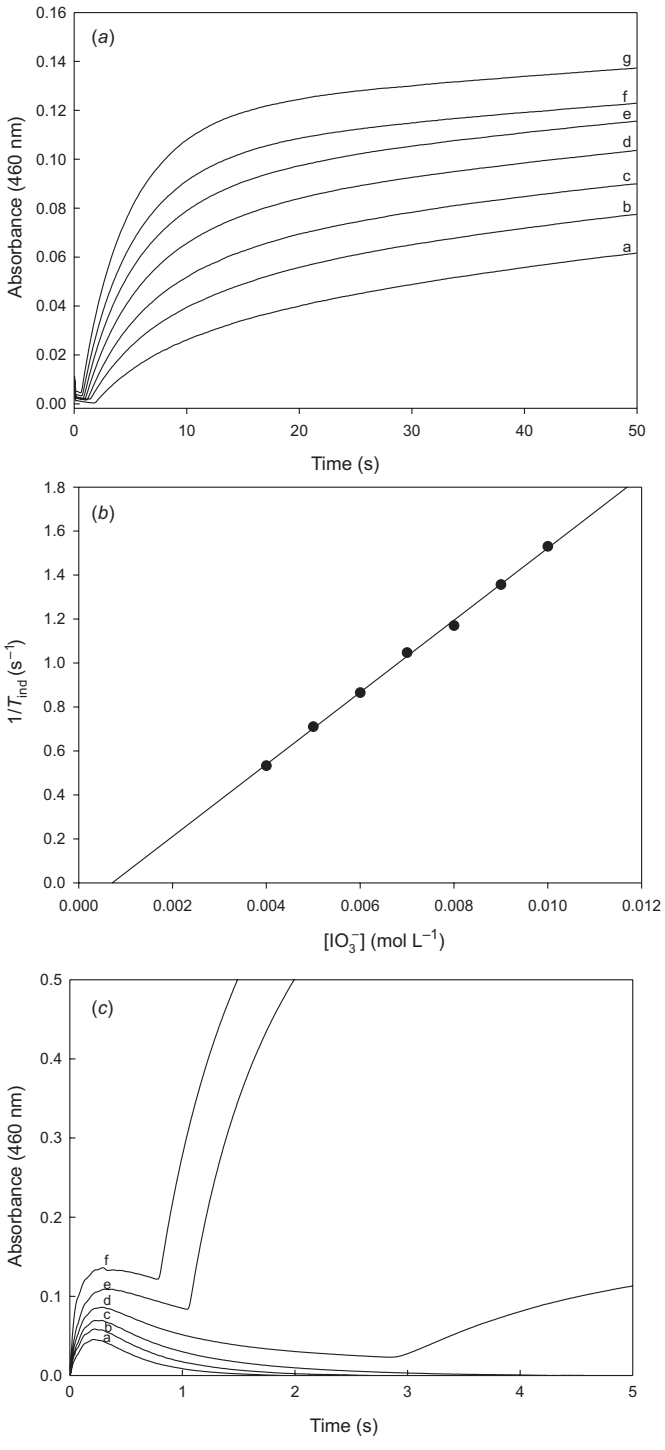


$$[R4] \quad IO_3^- + 5I^- + 6H^+ \rightarrow 3I_2 + 3H_2O$$

The collapse of observed iodine concentration in increasing $[CA]_0$ to trace h arises from the decrease in R (which is $[IO_3^-]_0/[CA]_0$) to below that expected for stoichiometry [R2]. Figure 2*a* shows a series of experimental traces obtained by varying initial iodate concentrations while keeping all other species concentrations constant. Traces c–g satisfy stoichiometry [R2], and thus, at $t = \infty$ all these traces give the same iodine absorbance. Expansion of the first 4 s of the reaction shows a distinct induction period, which could be related to the initial concentration of iodate. We define an induction period as the time taken before a rapid and monotonic formation of iodine commences. A linear relationship (see Fig. 2*b*) exists between the inverse of this induction period and initial iodate concentrations. The intercept on the iodate axis, the concentration of iodate for an induction period of $t = \infty$ ($1/t = 0$), confirmed stoichiometry [R1]. The intercept is approximately 0.0005 mol L^{-1} iodate for an initial concentration of 0.003 mol L^{-1} CA (a 1:6 ratio). An induction time of infinity indicates that no iodine is formed. Any higher iodate concentration over 0.0005 mol L^{-1} will yield iodine as a final product and stoichiometry will shift from [R1] towards [R2]. In Fig. 2*c*, increasing the initial acid concentration relative to Fig. 2*a* and amplifying the first 5 s

© 2006 NRC Canada

Fig. 2. (*a*) Effect of $[IO_3^-]$ variation at constant $[H^+]$ and [CA] showing a finite and measurable induction period before formation of iodine. The initial rate of reaction increased as $[IO_3^-]_0$ increased; $[CA]_0 = 0.003$ mol L^{-1}, $[H^+]_0 = 0.001$ mol L^{-1}, $[IO_3^-]_0$ = (a) 0.004, (b) 0.005, (c) 0.006, (d) 0.007, (e) 0.008, (f) 0.009, (g) 0.01 mol L^{-1}; (*b*) Linear plot of reciprocal induction time vs. $[IO_3^-]_0$ for data shown in Fig. 2*a*; (*c*) Effect of progressively increasing $[IO_3^-]$ at constant acid and [CA] close to stoichiometry show oligooscillations. Traces below stoichiometry and at stoichiometry a–c show just the transient formation of iodine. $[CA]_0 = 0.015$ mol L^{-1}, $[H^+] = 0.02$ mol L^{-1}, $[IO_3^-]_0$ = (a) 0.0015, (b) 0.002, (c) 0.0025, (d) 0.003, (e) 0.004, (f) 0.005 mol L^{-1}.



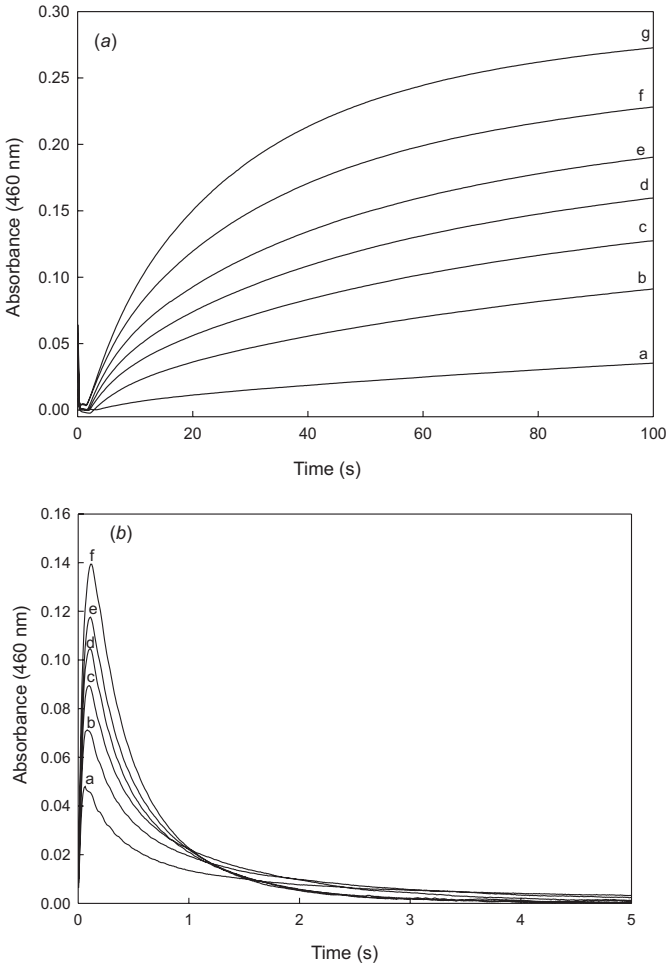
shows, instead of an induction period, a transient peak in iodine concentrations, followed by a final and rapid formation of iodine. In all cases shown in Fig. 2*c*, the reactions that form iodine initially dominate those that consume iodine (even in stoichiometric excess of CA), and hence the observed initial iodine peak. Iodine formation is also almost instantaneous. The onset of prolonged and monotonic iodine formation is determined by the initial iodate concentrations. For traces e and f, for example, the high ratio ensures rapid consumption of the substrate, leaving only the Dushman reaction, [R4], to form iodine without any other reactions in the reaction medium that consume iodine.

Lower acid concentrations did not produce such oligooscillatory behavior: only a period of no iodine formation is observed, followed by monotonic iodine formation. The strong catalytic effect of acid on the Dushman reaction is responsible for the olligooscillations. The effect of acid on the reaction appears much more complex than that of iodate (see Figs. 3*a* and 3*b*). There are several reactions that are viable in this reaction mixture, and it would appear all of them are affected by acid; hence, a clean assessment of the effect of acid is not easily obtained. However, what is obvious from Fig. 3*a* is that acid concentrations catalyze the formation of iodine after the induction period. In all traces shown in Fig. 3*a*, the final iodine concentrations were the same (6×10^{-4} mol L^{-1}, absorbance ~ 0.46). While trace g went to completion in less than 250 s, it took more than 2000 s for trace a to go to completion. A very interesting set of data are shown in Fig. 3*b*. In this set of data the reaction conditions are set to the stoichiometric ratio of [R1], and at $t = \infty$ no iodine is (nor should be) observed. Acid variations at these conditions show that acid catalyzes the formation of iodine and retards the consumption of iodine. Hence, high acid concentrations will show a wider "excursion" away from the equilibrium conditions before settling down to stoichiometry [R1].

Figure 4 shows the expected catalytic effect of iodide ions. In this case, very low iodide ion concentrations can drastically reduce the induction period (upon expanding the first 2 s of the reaction). They also increase the rate and amount of iodine obtained. This is expected in conditions where the oxidant to reductant ratio (R) is greater than 0.2, where the iodide ions initially added to the reaction mixture combine with those formed in stoichiometry [R1] to fuel the Dushman reaction, [R4]. This is also evident from Fig. 4, which shows a long enough time evolution of the reaction. Other experimental data (not shown) demonstrated a saturation of the reduction of the induction period when the added iodide ions equaled or exceeded the concentrations of the substrate. Iodide acts solely as a catalyst: in stoichiometric excess of the substrate (stoichiometry [R1]), it is used and released intact at the end of the reaction. Iodide ultimately does not participate in the overall stoichiometry except in high excess of iodate conditions, where it is ultimately converted to molecular iodine. Strictly speaking, the Dushman reaction (27) is an extraneous reaction that only asserts itself after stoichiometry [R1] of our fiduciary reaction has been satiated. No simple relationship could be deduced between induction period and (or) rate of formation of iodine with iodide (see Fig. 2*b* for the iodate dependency). This is due to the fact that the effect of iodide on the whole reaction is

© 2006 NRC Canada

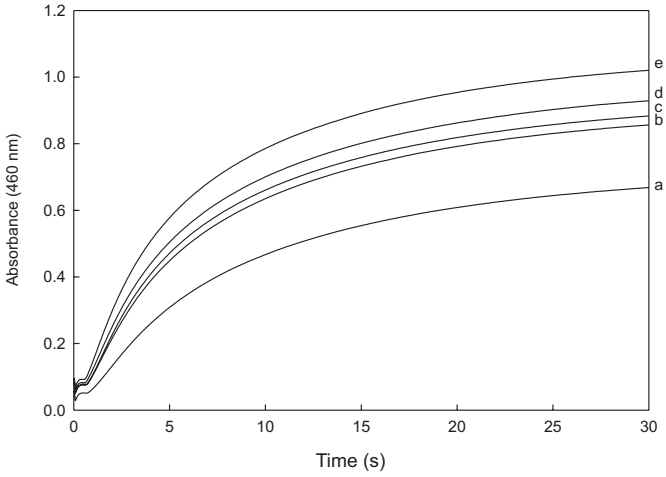
Fig. 3. (*a*) Effect of varying acid concentration on the oxidation of CA by iodate. There is an increase in rate of iodine formation as acid concentration is increased. $[CA]_0$ = 0.003 mol L^{-1}, $[IO_3^-]_0$ = 0.003 mol L^{-1}, $[H^+]_0$ = (a) 0.001, (b) 0.0015, (c) 0.002, (d) 0.0025, (e) 0.003, (f) 0.00375, (g) 0.005 mol L^{-1}; (*b*) Effect of acid variation at stoichiometric point (trace h from Fig. 1). The effect of acid can be seen in the form of a higher maximum iodine concentration. $[CA]_0$ = 0.03 mol L^{-1}, $[IO_3^-]_0$ = 0.005 mol L^{-1}, $[H^+]_0$ = (a) 0.005, (b) 0.0075, (c) 0.01, (d) 0.0125, (e) 0.015, (f) 0.02 mol L^{-1}.



complex and most likely involves a multiterm rate law. Alternatively (as proved later) iodide ions most likely affect both the formation and consumption of iodine reactions.

The simple and direct oxidation of CA by aqueous iodine was also studied spectrophotometrically at 460 nm. Figure 5*a* shows that this reaction is relatively slow and is mildly inhibited by acid. Under low acid concentrations, Fig. 5*b* shows that there is an inverse relationship between the acid concentrations and rate of consumption of iodine. The positive intercept is important: it suggests two pathways, one inhibited by acid and one that is not. The gentle slope of the plot suggests very mild inhibition by acid. This linearity is lost at high acid concentrations (Fig. 5*c*). The effect of iodide was much more complex (Fig. 6). After mixing iodine and CA, a rapid equilibrium sets up, which forms some adduct that also absorbs at 460 nm. We could not locate a wavelength where this adduct did not adversely affect

Fig. 4. $[I^-]$ effect on the iodate oxidation of CA. The effect of iodide can be seen on the reduced induction period and increased final absorbance of iodine as the iodide concentration is increased. $[CA]_0$ = 0.005 mol L^{-1}, $[H^+]_0$ = 0.02 mol L^{-1}, $[IO_3^-]_0$ = 0.005 mol L^{-1}, $[I^-]_0$ = (a) no iodide, (b) 0.00025, (c) 0.0005, (d) 0.00075, (e) 0.001 mol L^{-1}.



the optical observation of the iodine–CA reaction. Hence, data interpretation of the iodide effect was not possible, although a cursory glance showed that the iodide effect was mildly inhibitory.

Mechanism

The mechanistic basis of the oxidation of CA by iodate–iodine had fewer possible intermediates in going from CA (reactant) to cystamine (product) when compared with other organosulfur oxidations in which the oxidation pathway involves formation of sulfinic and sulfonic acids, as well as cleavage of the C—S bond to yield sulfate (28, 29). There are only two possible pathways towards formation of the dimer: through the cysteamine-thiyl radical (30) and (or) the cysteamine sulfenic acid. In metal–ion mediated oxidation of cysteamine, the radical pathway is highly favored (31).

[R5] $H_2NCH_2CH_2SH + M^{n+} \rightleftharpoons H_2NCH_2CH_2S^{\cdot} + M^{(n-1)+} + H^+$

Our reaction environment has been stripped of metal ions, making the radical pathway unlikely. Oxyiodine species are known to predominantly oxidize via two-electron steps, making the pathway through the unstable sulfenic acid the most likely pathway (32).

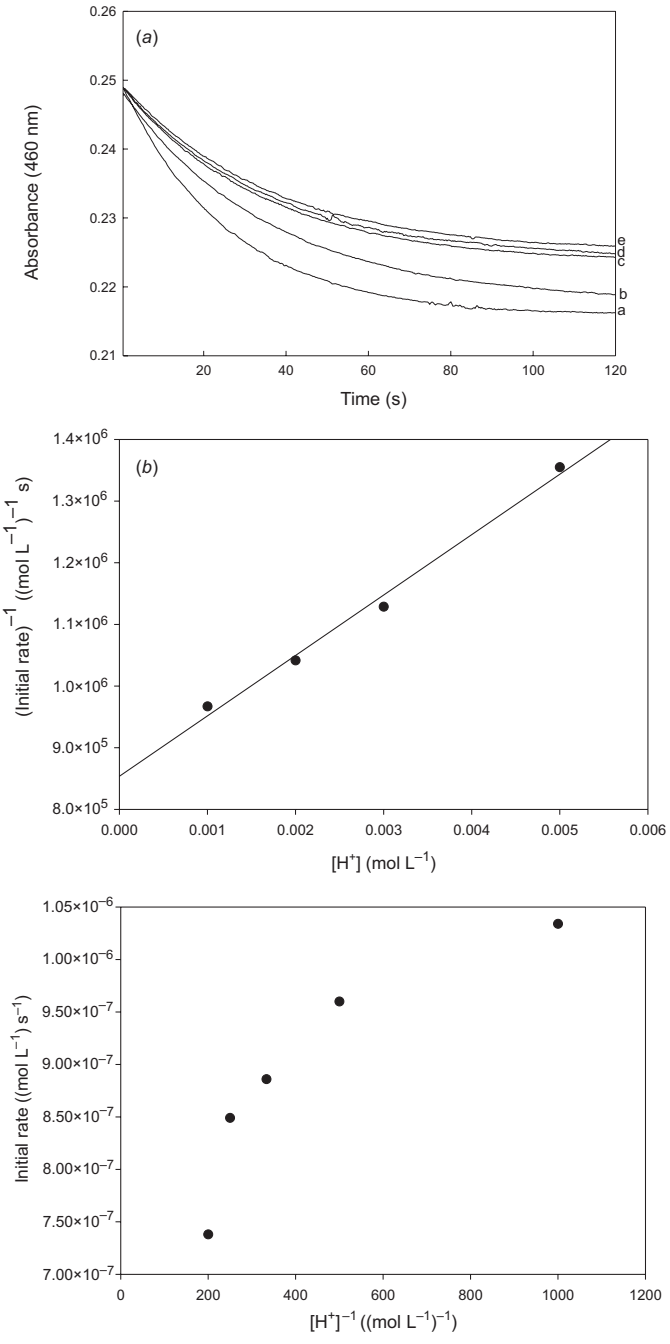
[R6] $H_2NCH_2CH_2SH + H_2O \rightarrow H_2NCH_2CH_2SOH + 2H^+ + 2e^-$

The sulfenic acid should rapidly combine with an unoxidized CA molecule (a condensation reaction) to form cystamine.

[R7] $H_2NCH_2CH_2SOH + H_2NCH_2CH_2SH \rightarrow H_2NCH_2CH_2S\text{-}SCH_2CH_2NH_2 + H_2O$

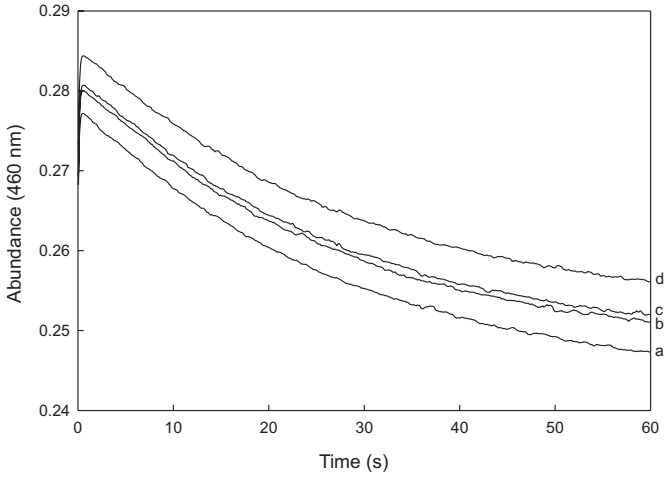
© 2006 NRC Canada

Fig. 5. (*a*) Effect of varying acid concentration on the reaction of CA and iodine. The initial rate of reaction decreases as the acid concentration is increased. $[CA]_0$ = 0.001 mol L^{-1}, $[I_2]_0$ = 0.00044 mol L^{-1}, $[H^+]_0$ = (a) 0, (b) 0.001, (c) 0.002, (d) 0.003, (e) 0.004 mol L^{-1}; (*b*) Plot of inverse of the initial rate vs. acid concentrations of the I_2–CA reaction for low acid variations for the type of data shown in Fig. 5*a*. $[CA]_0$ = 0.001 mol L^{-1}, $[I_2]_0$ = 0.00044 mol L^{-1}; (*c*) Types of initial rates vs. inverse acid dependence plots for the I_2–CA reaction for a wider range of acid concentrations than those selected for Fig. 5*b*. $[CA]_0$ = 0.001 mol L^{-1}, $[I_2]_0$ = 0.00044 mol L^{-1}.



Any uncondensed sulfenic acid left after all the CA has been consumed will rapidly disproportionate through standard pathways to form thiosulfinates (33) as well as CA.

Fig. 6. Effect of iodide variation on the I_2–CA reaction. There is an increase in the initial absorbance with addition of iodide, but no parallel nature of the absorbance traces shows little effect of iodide on the reaction rate, only a change in the equilibrium position of the I_2–CA reaction mixture. $[CA]_0$ = 0.0002 mol L^{-1}, $[I_2]_0$ = 0.00044 mol L^{-1}, $[I^-]_0$ = (a) 4.0×10^{-5}, (b) 6.0×10^{-5}, (c) 8.0×10^{-5}, (d) 1.0×10^{-4} mol L^{-1}.



This can bring about some stoichiometric uncertainties, but if rxn., [R7] is very rapid, there will be very little deviation in the expected 1:6 stoichiometry.

Iodate oxidations are strongly acid-catalyzed and will not proceed except in low pH environments (34). All iodate oxidations reported in this manuscript were at pH conditions lower than 3.0. We expect, at these pH conditions, that the amino group of the cysteamine will be protonated and that the prevailing form of cysteamine will be $[H_3NCH_2CH_2SH]^+$. The accepted pK_a value of $[H_3NCH_2CH_2SH]^+$ is 10.8, with a K_b of the amino group of cysteamine as 6.3×10^{10} (mol L^{-1})$^{-1}$, which calculates to a full protonation of the amino group in pH conditions lower than 4.0. Thus any further protonation to cysteamine will be in addition to the one already resident on the amino group. Since this protonation is distal to the active thiol group, it does not strongly influence its reactivity. We shall represent cysteamine, in this manuscript, however, as the neutral form.

Sulfenic acids are stronger acids than thiols and, if they are long-lived, would exist predominantly as zwitterions (produced in rxn. [R6] and others), $^+N(H)_3CH_2CH_2SO^-$. However, the strongly acidic environment would protonate the oxygen atom, and it would exist predominantly as $^+N(H)_3CH_2CH_2SOH$.

Oxyiodine oxidizing species

The chemistry of oxyiodine species has been extensively studied, and it is well-established that the major oxidizing species are HIO_2, HOI, and molecular iodine (I_2). These species are derived from iodate through a series of well-known reactions (35, 36).

[R8] $IO_3^- + 2H^+ + I^- \rightleftharpoons HIO_2 + HOI$

[R9] $HOI + H^+ + I^- \rightleftharpoons I_2 + H_2O$

In the absence of iodide, the initiation reaction involves the direct oxidation of CA by iodic acid.

© 2006 NRC Canada

[R10] $IO_3^- + H^+ \rightleftharpoons HIO_3$

[R11] $HIO_3 + H_2NCH_2CH_2SH \rightarrow H_2NCH_2CH_2SOH + HIO_2$

[R12] $HIO_2 + H_2NCH_2CH_2SH \rightarrow H_2NCH_2CH_2SOH + HOI$

[R13] $HOI + H_2NCH_2CH_2SH \rightarrow H_2NCH_2CH_2SOH + H^+ + I^-$

Equations [R10]–[R13] are relevant at the beginning of the reaction before iodide ions accumulate. After iodide concentrations have built up to effective levels, the reaction will proceed through rxn. [R8], as it is the overall rate-determining step in the consumption of CA. In the presence of added iodide ions, as in Fig. 4, eqs. [R10]–[R13] are completely shunted out and are insignificant. The sum of rxns. [R8] + [R10] + [R11] + [R12] + 2[R13] shows that in each initial reaction cycle, 1 mol of iodide ultimately produces 2 mol of iodide in a quadratic autocatalytic sequence. This is obvious because each iodate ion, whose reactivity is triggered off by iodide, will ultimately end up as iodide, effectively doubling the number of iodide ions initially present. Reaction [R13] is the major oxidation route. This leaves two important oxyiodine reactions, which involve the disproportionation of HOI (37). This disproportionation ensures that there is no accumulation of HOI in the reaction medium, especially after all the reducing substrate has been consumed. The stable species allowable at the end of the reaction are iodate, iodine, and iodide.

[R14] $HIO_2 + I^- + H^+ \rightleftharpoons 2HOI$

[R15] $IO_3^- + HOI + H^+ \rightleftharpoons 2HIO_2$

Iodine oxidation

Acid dependence experiments (Figs. 5*a* and 5*b*) clearly indicate an electrophilic mechanism with an initial attack by iodine on the nucleophilic sulfur atom of CA.

[R16] $H_2NCH_2CH_2SH + I\text{-}I \rightarrow H_2NCH_2CH_2S(H)I^+ + I^-$

[R17] $H_2NCH_2CH_2S(H)I^+ + H_2O \rightarrow H_2NCH_2CH_2SOH + 2H^+ + I^-$

The product is then formed by rxn. [R7]. This step ([R16] + [R17]) was qualitatively proved by the experimental observations of an immediate drop in pH upon mixing iodine and CA. Thus, acid dependence experiments can be justified from the basis of an initial protonation of the thiol group, which subsequently reacts much more slowly with the electrophilic iodine atom.

[R18] $H_2NCH_2CH_2SH + H^+ \rightleftharpoons [H_2NCH_2CH_2SH_2]^+$; K_b

[R19] $H_2NCH_2CH_2SH + I_2 + H_2O \rightarrow H_2NCH_2CH_2SOH + 2I^- + 2H^+$; k_1

[R20] $[H_2NCH_2CH_2SH_2]^+ + I_2 + H_2O \rightarrow H_2NCH_2CH_2SOH + 2I^- + 3H^+$; k_2

In this reaction scheme we are ignoring the iodine–triiodide equilibrium (38, 39) by assuming that triiodide reacts just as rapidly as iodine.

[R21] $I_2 + I^- \rightleftharpoons I_3^-$; $K_I = 770\ (\text{mol L}^{-1})^{-1}$

This assertion was based on our experiments that showed that the effect of iodide on the reaction rate was inconclusive. Addition of iodide to the reaction medium changed the original absorbance, but did not alter the subsequent rate of consumption of iodine (see Fig. 6).

Using [R18]–[R20], we can derive the following overall rate law for the consumption of iodine.

$$[1] \qquad \text{Rate} = -\frac{d[I_2]}{dt} = \frac{[CA]_0[I_2]}{(1 + K_b[H^+])}(k_1 + k_2K_b[H^+]$$

In eq. [1], $[CA]_0$ represents the amount of cysteamine added to the reaction mixture. This is then partitioned between the protonated and unprotonated forms of the thiol, based on the acid concentrations and K_b. Equation [1] will give different acid dependence behavior depending upon the relative values of k_1 and k_2. If $k_1 >> k_2$, the general form of the equation for the initial rate of reaction vs. the inverse of the acid concentration will give a nearly straight line at acid concentrations where $K_b[H^+] << 1$, with the second term in eq. [1] assumed to be negligible. The plot shown in Fig. 5*b* was restricted to low acid concentrations. The high acid concentration kinetics data were discarded. The low acid concentrations plot allows us to estimate the values of k_1 and K_b by assuming that the observed retardation is due to the removal of active cysteamine by the protonation equilibrium. After deleting the second term in eq. [1], the equation can then be rearranged and written as:

$$[2] \qquad \frac{1}{\text{mod(rate)}} = \left(\frac{K_b}{k_1[CA]_0[I_2]_0}\right)[H^+] + \left(\frac{1}{k_1[CA]_0[I_2]_0}\right)$$

Equation [2] is then used to plot the inverse of the modulus of the initial rate vs. the acid concentrations (see Fig. 5*b*), from where we can evaluate values of k_1 and K_b. From the intercept, a value of $k_1 = 2.7 \pm 0.3\ (\text{mol L}^{-1})^{-1}\ \text{s}^{-1}$ was deduced. The slope gave $K_b = 117 \pm 15\ (\text{mol L}^{-1})^{-1}$. This value of K_b has no thermodynamic significance apart from the fact that it fits kinetics data through eq. [2]. This is a value that is only relevant for the conditions used for Figs. 5*a* and 5*b*. Literature quotes the pK_a of the thiol group of cysteamine as 8.6, but the protonation of the amino group precludes an accurate measurement of pK_a for $[H_2NCH_2CH_2SH_2]^+$, should this exist. Another possible mechanism for the observed acid retardation of iodine oxidation is the loss of nucleophilicity of the water molecules, owing to the formation of the hydronium ions. However, this retardation would be kinetically indistinguishable to the one suggested through rxn. [R20]. A plot of inverse acid dependence, which includes both high and low acid concentrations, is shown in Fig. 5*c*. This is not a linear plot, as expected from the form of eq. [1]. We could then work with the curve generated in Fig. 5*c* and curve-fit it to variables k_1, k_2, and K_b. This fitting procedure gave $k_2 = 0.37\ (\text{mol L}^{-1})^{-1}\ \text{s}^{-1}$.

© 2006 NRC Canada

Table 1. Cysteamine–iodate–iodine reaction.

Reaction No.	Reaction	k_f and k_r
M1	$H^+ + IO_3^- \rightleftharpoons HIO_3$	1×10^7, 1×10^9
M2	$HIO_3 + RSH \rightarrow HIO_2 + RSOH$	2.5×10^2
M3	$HIO_2 + RSH \rightarrow HOI + RSOH$	5×10^2
M4	$HOI + RSH \rightarrow I^- + H^+ RSOH$	1×10^3
M5	$RSOH + RSH \rightarrow RSSR + H_2O$	5×10^8
M6	$IO_3^- + I^- + 2H^+ \rightleftharpoons HIO_2 + HOI$	2.8, 1.44×10^3
M7	$HIO_2 + I^- + H^+ \rightleftharpoons 2HOI$	2.1×10^8, 90
M8	$HOI + I^- + H^+ \rightleftharpoons I_2 + H_2O$	3.1×10^{12}, 2.2
M9	$IO_3^- + HOI + H^+ \rightleftharpoons 2HIO_2$	8.6×10^2, 2.00
M10	$I_2 + I^- \rightleftharpoons I_3^-$	6.2×10^9, 8.5×10^6
M11	$I_2 + RSH + H_2O \rightarrow RSOH + 2H^+ + 2I^-$	2.7
M12	$I_3^- + RSH + H_2O \rightarrow RSOH + 2H^+ + 3I^-$	1.5
M13	$RSH + H^+ \rightleftharpoons RSH_2^+$	1×10^8, 8.5×10^5
M14	$RSH_2^+ + I_2 + H_2O \rightarrow RSOH + 3H^+ + 2I^-$	0.37

Note: RSH = cysteamine; RSOH = unstable cysteamine sulfenic acid intermediate; RSSR = cystamine.

Computer modeling

The reaction scheme was modeled using the Kintecus software generated by James Ianni. The whole reaction scheme is shown in Table 1. The 14-reaction scheme was able to model satisfactorily all of the reaction dynamics observed in Figs. 1–4. The data for the direct reaction of iodine and CA could also be simulated by the same model after nullifying rxns. [M1]–[M7] (i.e., setting all their rate constants to zero).

Charge-transfer complexes

While the calculations were able to simulate the general dynamics of the data shown in Figs. 1–4, they gave much lower absorbance readings than those shown in these figures. The absorbance readings only matched the calculations at the beginning and at the end of the simulations. The experimentally observed intermediate values were much higher, owing to the expected charge-transfer complexes that cysteamine is known to form with molecular iodine (23, 40).

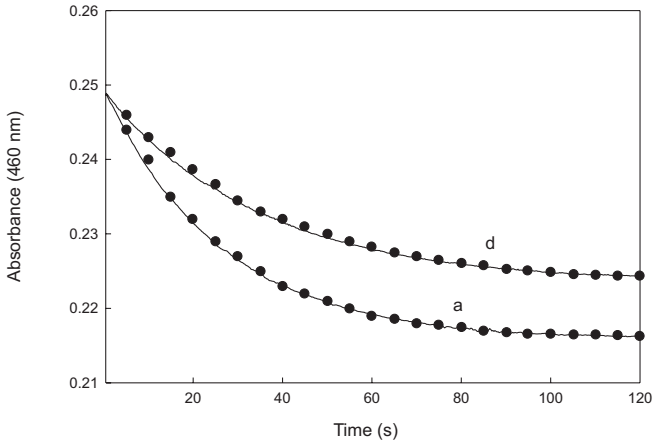
[R22] $H_2NCH_2CH_2SH + I_2 \rightleftharpoons [H_2NCH_2CH_2SH\text{-}I^+][I^-]$

Absorbance readings from experiments and simulations coincided under conditions where iodate was in stoichiometric excess over cysteamine such that at the end of the reaction cysteamine concentrations had vanished, thus precluding the possibility of rxn. [R22]. While reactions of the [R22]-type have been reported (40), no specific measurements have been performed for the cysteamine–iodine mixtures. Reaction [R22] is suppressed in high acid conditions, such that it was easier to fit simulations to the data in Fig. 5*a*. Figure 7 shows a typical fit to the experimental data in Fig. 5*a* at separate acid concentrations.

Adoption of rate constants

The model presented had very few rate constants that needed to be guessed for the best simulations fit. For example, kinetics constants for reactions [M6]–[M10] were obtained from well-established literature values (27, 35, 37, 41, 42). In the absence of added iodide ions (as in data in Fig. 4), the most important reaction in the whole model was

Fig. 7. Comparison of experimental and calculated absorbance traces for the I_2–CA reaction data shown in Fig. 5*a* (traces a and d). The symbols represent calculations.



[M2]. After setting up an initial guess value for k_{M2}, the kinetics parameters for the rest of the reactions in that chain, [M3] and [M4], became instantly irrelevant for as long as they were faster than the set value for k_{M2} and with the relative magnitudes in the order of $k_{M3} < k_{M4}$. Any reversal in this order generated large amounts of HIO_2 (in excess iodate conditions), which never decayed as the reaction reached its end point with respect to iodine production. The data shown in Fig. 4 could be modeled without reactions [M1] through [M4]. We settled on a value of k_{M2} of 250 $(\text{mol L}^{-1})^{-1}\ \text{s}^{-1}$ as the one that gave us the best fit to the induction period. The two protolytic reactions, [M1] and [M13], were set to be faster than all reactions in the mechanism. The role of [M1] was to ensure bimolecular kinetics for rxn. [M2]. The role of [M13] was to simulate acid retardation observed in the direct oxidation of CA by iodine. The values of k_{M13} and k_{-M13} were linked together by the value of K_b derived in this study. The fact that reaction [M13] was rapid in both directions made it insignificant with respect to the sequence [M1]–[M4], since k_{M2}, the rate-determining step for that sequence, was only 250 $(\text{mol L}^{-1})^{-1}\ \text{s}^{-1}$. The effect of sequence [M10] + [M12] was not utilized in the derivation of rate for

© 2006 NRC Canada

eq. [1] and was not very effective in the mechanism for the overall iodate–CA reaction. A very small degree of retardation was observed in the iodine–CA reaction upon asserting this sequence (see Fig. 6). The possible direct reaction of the protonated thiol with triiodide was also not included in the mechanism.

Conclusion

Our study shows that cysteamine, the well-known precursor to taurine (14), is not easily oxidized to taurine by the mild oxidizing agent iodine and without the standard P450-type enzymes and the flavin-containing monooxygenases (43). In its goitrogenic role (9), cysteamine most likely abstracts the iodine atom in a reversible process to form the disulfide, which can be converted back to the thiol by a very mild redox potential.

Acknowledgement

We would like to thank Itai Chipinda for performing the HPLC analysis for us. This work was supported by research grant Nos. CHE 0137435 and CHE 0341769 from the National Science Foundation and research grant No. R01 AI051509-01A2 from the National Institutes of Health.

References

1. R.B. Freedman. FEBS Lett. **97**, 201 (1979).
2. C.R. Chinake and R.H. Simoyi. J. Phys. Chem. **98**, 4012 (1994).
3. B. Kalyanaraman. Biochem. Soc. Symp. **61**, 55 (1995).
4. I.R. Wilson and G.M. Harris. J. Am. Chem. Soc. **82**, 4515 (1960).
5. I.R. Wilson and G.M. Harris. J. Am. Chem. Soc. **83**, 286 (1961).
6. J.M. Geelen, L.A. Monnens, and E.N. Levtchenko. Nephrol. Dial. Transplant. **17**, 1766 (2002).
7. W.A. Gahl. Eur. J. Pediatr. **162** (Suppl. 1), S38 (2003).
8. R.L. Pisoni, G.Y. Park, V.Q. Velilla, and J.G. Thoene. J. Biol. Chem. **270**, 1179 (1995).
9. V.E. Kimonis, J. Troendle, S.R. Rose, M.L. Yang, T.C. Markello, and W.A. Gahl. J. Clin. Endocrinol. Metab. **80**, 3257 (1995).
10. F. Iwata, E.M. Kuehl, G.F. Reed, L.M. Mccain, W.A. Gahl, and M.I. Kaiser-Kupfer. Mol. Genet. Metab. **64**, 237 (1998).
11. O.I. Aruoma, B. Halliwell, B.M. Hoey, and J. Butler. Biochem. J. **256**, 251 (1988).
12. D. Becker, S. Summerfield, S. Gillich, and M.D. Sevilla. Int. J. Radiat. Biol. **65**, 537 (1994).
13. M.M. Oosthuizen and D. Greyling. Redox Rep. **4**, 277 (1999).
14. D. Cavallini, C. De Marco, R. Scandurra, S. Dupre, and M. Graziani. J. Biol. Chem. **241**, 3189 (1966).
15. J.H. Fellman, T.R. Green, and A.L. Eicher. Adv. Exp. Med. Biol. **217**, 39 (1987).
16. G. Ricci, R. Chiaraluce, G. Pitari, S. Dupre, O. Fujii, Y. Hosokawa, and K. Yamaguchi. J. Nutr. Sci. Vitaminol. **35**, 143 (1989).
17. C.R. Chinake and R.H. Simoyi. J. Phys. Chem. B, **101**, 1207 (1997).
18. B.S. Martincigh, C. Mundoma, and R.H. Simoji. J. Phys. Chem. A, **102**, 9838 (1998).
19. R.H. Simoyi, K. Streete, C. Mundoma, and R. Olojo. S. Afr. J. Chem. **55**, 136 (2002).
20. C.C. Capen. Toxicol. Lett. **64/65**, 381 (1992).
21. C.J. Doona and D.M. Stanbury. J. Phys. Chem. **98**, 12630 (1994).
22. P.J. Hogg. Redox Rep. **7**, 71 (2002).
23. J.P. Danehy. Q. Rep. Sulfur Chem. **2**, 325 (1967).
24. J. Kurzawa and K. Janowicz. Acta Chim. Hung. **125**, 147 (1988).
25. G. Rabai and M.T. Beck. J. Chem. Soc. Dalton Trans. 1669 (1985).
26. M. Melichercik, A. Olexova, and L. Treindl. J. Mol. Catal. A: Chem. **127**, 43 (1997).
27. H.A. Liebhafsky and G.M. Roe. Int. J. Chem. Kinet. **11**, 693 (1971).
28. T.R. Chigwada, E. Chikwana, and R.H. Simoyi. J. Phys. Chem. A, **109**, 1081 (2005).
29. T.R. Chigwada and R.H. Simoyi. J. Phys. Chem. A, **109**, 1094 (2005).
30. T. Nauser and C. Schoneich. Chem. Res. Toxicol. **16**, 1056 (2003).
31. L. Pecci, G. Montefoschi, G. Musci, and D. Cavallini. Amino Acids, **13**, 355 (1997).
32. R. Okazaki and K. Goto. Heteroat. Chem. **13**, 414 (2002).
33. G. Capozzi and G. Modena. Oxidation of thiols. *In* The chemistry of the thiol group. *Edited by* S. Patai. Wiley and Sons, New York. 1974. p. 791.
34. Y. Xie, M.R. McDonald, and D.W. Margerum. Inorg. Chem. **38**, 3938 (1999).
35. G. Schmitz. Phys. Chem. Chem. Phys. **1**, 1909 (1999).
36. K. Kustin and M. Eigen. J. Am. Chem. Soc. **84**, 1355 (1962).
37. L. Kolaranic and G. Schmitz. J. Chem. Soc. Faraday Trans. **88**, 2343 (1992).
38. M.-F. Ruasse, J. Aubard, B. Galland, and A. Adenir. J. Phys. Chem. **90**, 4382 (1986).
39. D.H. Turner, G.W. Flynn, N. Sutin, and J.V. Beitz. J. Am. Chem. Soc. **94**, 1554 (1972).
40. W.H. Miller, R.O. Roblin, and E.B. Astwood. J. Am. Chem. Soc. **67**, 2201 (1945).
41. G. Schmitz. Phys. Chem. Chem. Phys. **2**, 4041 (2000).
42. E.T. Urbansky, B.T. Cooper, and D.W. Margerum. Inorg. Chem. **36**, 1338 (1997).
43. W.X. Guo, L.L. Poulsen, and D.M. Ziegler. Biochem. Pharmacol. **44**, 2029 (1992).

© 2006 NRC Canada

Ditopic receptors of hexaamide derivatives derived from hexahomotrioxacalix[3]arene triacetic acid

Takehiko Yamato, Shofiur Rahman, Zeng Xi, Fumika Kitajima, and Jeong Tae Gil

Abstract: The lower rim functionalized hexahomotrioxacalix[3]arene hexaamide **7** having an amino acid moiety with cone conformation was synthesized from triol **1** by a stepwise reaction. The different extractability for alkali metal ions, transition metal ions, and alkylammonium ions from water into dichloromethane was discussed. Owing to the strong intramolecular hydrogen bond between the neighboring NH and CO groups in hexaamide **7**, its affinity to metal cations was weakened. Hexaamide **7** shows a single selectivity to n-$BuNH_3^+$. The anion complexation of hexaamide **7** was also studied by ^{1}H NMR titration experiments. Hexaamide **7** binds halides through the intermolecular hydrogen bond among the NH hydrogens of the amide in a 1:1 fashion in $CDCl_3$. Thus, hexaamide **7** serves as a heteroditopic receptor that can complex with halides (Cl^-, Br^-) and n-$BuNH_3^+$ at the same time. The association constants calculated from the chemical shift changes of the amide protons are K_a = 536 ± 32 $(mol/L)^{-1}$ for Cl^- and K_a = 230 ± 17 $(mol/L)^{-1}$ for Br^-.

Key words: hexahomotrioxacalix[3]arenes, ionophores, molecular recognition, ammonium ion, ditopic receptor.

Résumé : Utilisant le triol **1** comme produit de départ, on a réalisé la synthèse par étape de l'hexahomotrioxacalix[3]arène hexaamide **7** dont la ceinture inférieure fonctionnalisée porte une portion d'acide aminé avec conformation en cône. On discute des possibilités de l'extraire de solutions aqueuses vers du dichlorométhane à l'aide de divers ions métalliques alcalins ou métalliques et avec des ions alkylammonium. En raison de la forte liaison hydrogène intramoléculaire entre les groupes voisins NH et CO dans l'hexaamide **7**, son affinité pour les cations métalliques est réduite. L'hexaamide **7** présente une sélectivité particulière pour le n-$BuNH_3^+$. La complexation anionique de l'hexaamide **7** a aussi été étudiée par des expériences de titrage par RMN du ^{1}H. Dans le $CDCl_3$, l'hexaamide **7** se lie aux halogénures par le biais d'une liaison hydrogène intermoléculaire 1 : 1 avec les atomes d'hydrogène NH de l'amide. L'hexaamide **7** peut donc servir de récepteur hétéroditopique qui peut complexer en même temps les halogénures (Cl^-, Br^-) et le n-$BuNH_3^+$. Les constantes d'association obtenues à partir des changements du déplacement chimique des protons de l'amide sont K_a = 536 ± 32 $(mol/L)^{-1}$ pour Cl^- et K_a = 230 ± 17 $(mol/L)^{-1}$ pour Br^-.

Mots clés : hexahomotrioxacalix[3]arène, ionophores, reconnaissance moléculaire, ion ammonium, récepteur ditopique.

[Traduit par la Rédaction]

Introduction

Calixarene and related macrocycles have received considerable attention for their host–guest chemistry as ionophoric receptors and potential enzyme mimics in biology. Chemical modification of calixarene represents a simple though effective and versatile way of producing receptors with highly selective cation-binding properties (1). Shinkai and co-workers (2) reported the complexation of alkali metals to hexahomotrioxacalix[3]arene derivatives with alkylated phenolic oxygens. Hexahomotrioxacalix[3]arene derivatives with C_3 symmetry can selectively bind ammonium ions, which play important roles in both chemistry and biology (3). Thus, Takeshita and Shinkai (2*b*) reported the construction of C_3 symmetry pyrene-functionalized hexahomotrioxacalix[3]arenes, which selectively recognize primary ammonium ions.

On the other hand, the hydrogen bond plays an important role in the self-assembly of molecular recognition and has been investigated in calixarene systems. An intermolecular hydrogen-bonded duplex was formed through the interaction between a calix[4]arene with four carboxyl groups, and a calix[4]arene with stilbazole moieties was reported (4). Arduini et al. (5) also described the formation of a hydrogen-bonded dimer in $CDCl_3$ based on the self-complementarity of carboxylic acid. The intramolecular hydrogen bonding also formed among opposing urea groups, which can bind anionic species, in calix[4]arene (6). Thus, the design of new ditopic ligands (7) for the simultaneous complexation of anionic and cationic guest species is a new exciting area of coordination chemistry of significant relevance to the selective extraction and (or) transportation of metal salts across lipophilic membranes. Rare examples of receptors contain-

Received 16 September 2005. Published on the NRC Research Press Web site at http://canjchem.nrc.ca on 25 February 2006.

T. Yamato,[1] S. Rahman, Z. Xi, F. Kitajima, and J.T. Gil. Department of Applied Chemistry, Faculty of Science and Engineering, Saga University, Honjo-machi 1, Saga-shi, Saga 840-8502, Japan.

[1]Corresponding author (e-mail: yamatot@cc.saga-u.ac.jp).

 doi:10.1139/V05-260 © 2006 NRC Canada

Scheme 1.

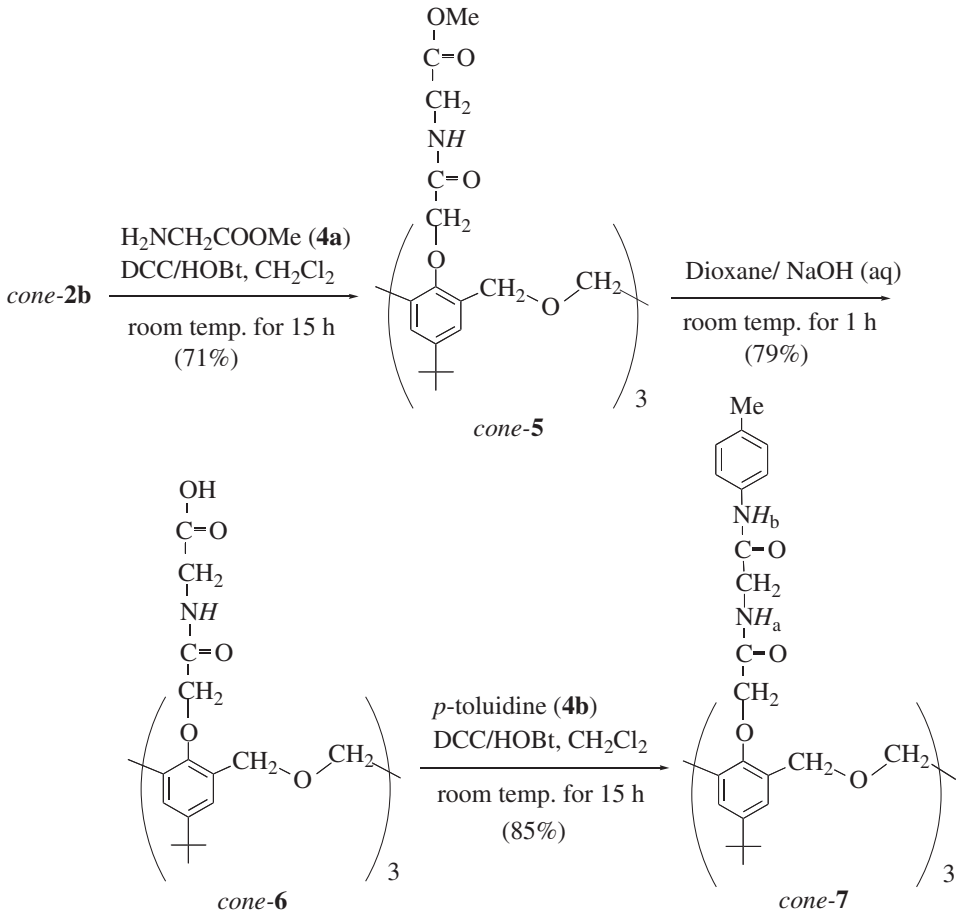
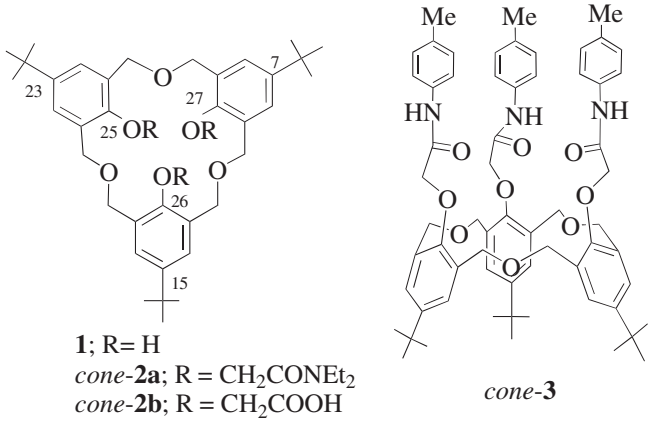


Chart 1.



ing appropriate covalently linked binding sites for anions and cations include Lewis acidic boron (8), uranyl (9), polyammonium (10) centers combined with crown ether moieties, and crown ether or urea-functionalized calix[4]arene ionophores (11), which are capable of solubilizing alkali metal salts into organic media (Chart 1).

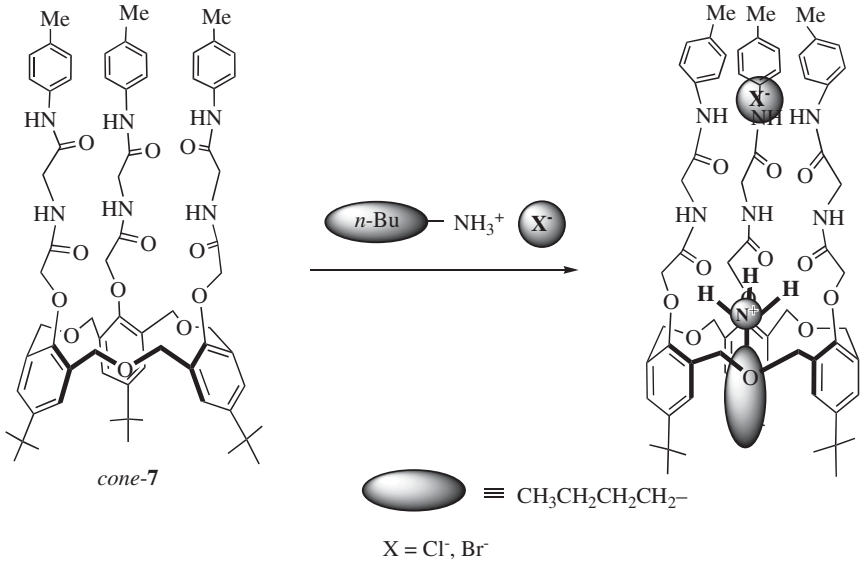
Recently, we reported a ditopic receptor (*cone*-**3**) incorporating these two types of recognition sites by introducing three amide groups to the phenolic oxygens of homotrioxacalix[3]arene, which can simultaneously bind alkyl ammonium ions and halides (12*a*). On the other hand, the introduction of multiple binding sites for cations and anions is important for the construction of the allosteric host–guest inclusion systems. In the present paper, we describe the synthesis, conformations, and metal and ammonium ion complexation properties of the additional amino acid linked cone *p*-methylphenyl amide derivative having two hydrogen-bonding systems and C_3-symmetric ionophoric cavities.

Results and discussion

cone-Hexahomotrioxacalix[3]arene tricarboxylic acid (*cone*-2**b**) was prepared by hydrolysis of *cone*-[(*N*,*N*-diethylaminocarbonyl)methoxy]hexahomotrioxacalix[3]arene (*cone*-**2a**) with aq. KOH in a mixture of dioxane and water, which was prepared by O-alkylation of **1** with *N*,*N*-diethylchloroacetoamide in the presence of NaH according to the reported procedures (2*d*, 12). *cone*-Hexahomotrioxacalix[3]arene triamide (*cone*-**5**) was prepared by a condensation reaction of *cone*-**2b** with glycine methyl ester (**4a**) in the presence of dicyclohexylcarbodiimide (DCC) and 1-hydroxybenzotriazole (HOBt) at room temperature for 15 h in CH_2Cl_2. *cone*-**5** was converted to triacid *cone*-**6** by hydrolysis with aq. NaOH in a mixture of dioxane and water at room temperature. *cone*-**6** was treated with *p*-toluidine (**4b**) in the presence of DCC and HOBt similar to that of *cone*-**5** to afford

© 2006 NRC Canada

Fig. 1. Binding mode of host *cone*-**7** and *n*-$BuNH_3X$.



the desired compound *cone*-hexahomotrioxacalix[3]arene hexaamide (*cone*-**7**) in 85% yield (Scheme 1).

From the singlet peaks of *tert*-butyl protons and calix benzene protons for *cone*-**7**, it could be seen that the conformation remained in the desired compound with the cone conformation. To investigate the intramolecular hydrogen bond between the neighboring NH and CO groups of *cone*-**7** in detail, a reference compound **9c** was synthesized from 4-*tert*-butyl-2,6-dimethylphenoxyacetic acid (**8**) following a method similar to that used in the preparation of *cone*-**7**.

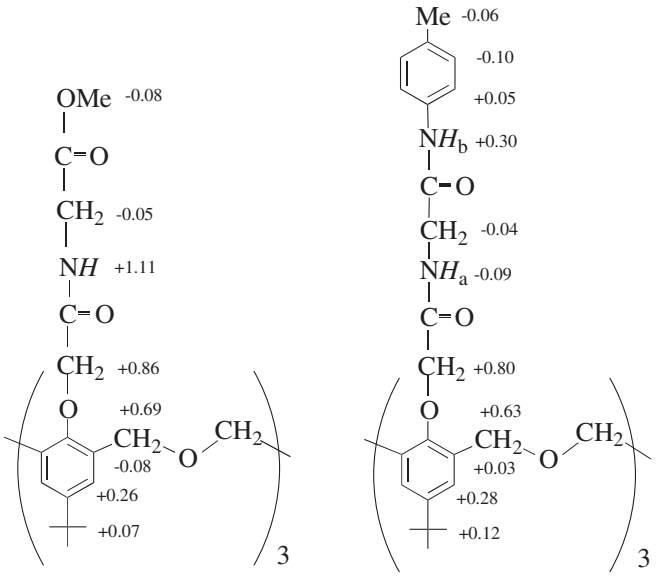
Conformation assignment for the new hexahomotrioxacalix[3]arene hexaamide (*cone*-**7**) is firmly established by the presence of AB quartets for the bridging methylene protons with a $\Delta\delta$ separation between H_{ax} and H_{eq} of 0.45 ppm in its ^{1}H NMR spectrum ($CDCl_3$). In the calix[4]arenes, the $\Delta\delta$ values of the ArCH_2Ar protons have been correlated to the orientation of adjacent aromatic rings, i.e., $\Delta\delta > 1$ ppm with cone conformation or syn orientation, $\Delta\delta$ of approximately 0.5 ppm with flattened cone or out orientation, and $\Delta\delta$ of 0 ppm with 1,3-alternate or anti orientation (13). The same findings were observed in hexahomotrioxacalix[3]arenes (2*a*). Thus, we can deduce that *cone*-**7** prefers a flattened cone conformation in which hydrogen bonding can form. The intramolecular hydrogen bond was formed between neighboring NH and C=O groups, which induced a large downfield shift for the NH_a proton (δ 8.45 ppm, $\Delta\delta$ = +0.69 ppm) and NH_b proton (δ 9.21 ppm, $\Delta\delta$ = +0.85 ppm) in *cone*-**7** compared with compound **9c** (NH_a proton, δ 7.76 ppm; NH_b proton, δ 8.36 ppm). When the concentration of *cone*-**7** in $CDCl_3$ was diluted about 40 times, there was no change in the chemical shifts for both NH_a and NH_b protons, which is attributed to the concentration-independent intramolecular hydrogen bonds formed in this compound. Interestingly, the chemical shift of the NH_b protons in *cone*-**7** was shifted to a lower magnetic field to δ 9.91 ppm in DMSO-d_6 than in $CDCl_3$ (δ 9.21 ppm, $\Delta\delta$ = +0.70 ppm). This phenomenon was attributed to the intermolecular hydrogen bonding formed between the NH_b proton and DMSO-d_6. The intramolecular hydrogen bonding formed in compound *cone*-**7** was broken, and the new intermolecular hydrogen bonding was formed.

Interestingly, hexaamide *cone*-**7** shows low efficiency for metal cations compared with *cone*-**2a** (2*d*). The ionophoric activity of *cone*-**7** was almost absent. Hexaamide *cone*-**7** shows a single affinity only to *n*-butylammonium ion owing to the C_3-symmetric structure. However, no extractability for isobutyl- or *tert*-butyl-ammonium ion was observed under the conditions used. The ionophores usually form loose ion pairs with metal picrates, which produced the maximum absorption peak at 377 nm (14, 15). Interestingly, the hexaamide *cone*-**7** also forms a contact ion pair with *n*-$BuNH_3^+$ and shows the maximum absorption peak at 365 nm. In comparison with *cone*-**7**, *N*,*N*-diethylamide derivative *cone*-**2a** has a higher affinity to alkali metal ions (Na^+ (93.0% extraction) and K^+ (71.6%)), transition metal ions (Ag^+ (90.4%) and Cu^{2+} (27.5%)), and typical metal ion (Al^{3+} (19.1%)). Higher extractabilities of the *cone*-*N*,*N*-diethylamide derivative for *n*-butyl- (97.8%), isobutyl- (48.1%), and *tert*-butylammonium ion (35.4%) were observed and are attributable to the higher electron density of the oxygen of the carbonyl group by the electron donation ability of the amide group through conjugation N–C=O $\leftrightarrow$ N^+=C–O^- (2*d*, 12*a*, 12*b*). These findings clearly indicate that because of the strong hydrogen-bonding formation between NH and neighboring CO groups in hexaamide *cone*-**7**, there is no affinity shown for either hard or soft metal cations.

The present binding mode can be demonstrated more clearly by using ^{1}H NMR spectroscopy. There are two modes for *cone*-**7** to bind with *n*-butylammonium ion (Fig. 1), i.e., from the lower rim through substituent moieties or from the upper rim through the π cavity formed by three aromatic rings. As shown in Fig. 2, the chemical shifts of *cone*-**7** are different in the absence or presence of *n*-butylammonium ion. After adding an equivalent of *n*-$BuNH_3Cl$ to a solution of *cone*-**7** (5×10^{-3} (mol/L)$^{-1}$) in $CDCl_3$ at 27 °C, methylene protons of Ar$CH_2O CH_2$Ar and Ar′OCH_2CONHCH_2CONH$C_6H_4CH_3$ were dramatically shifted to a lower magnetic field, indicating that the binding mode is occurring through

© 2006 NRC Canada

Fig. 2. Chemical shift changes (Δδ) of *cone*-**5** and *cone*-**7** (5×10^{-3} mol/L) induced in the presence of *n*-$BuNH_3Cl$ (5×10^{-3} mol/L) in $CDCl_3$ at 27 °C. A plus sign (+) denotes a shift to lower magnetic field, whereas a minus sign (–) denotes a shift to higher magnetic field.



the π cavity formed by the three aromatic rings. This binding is attributed to the π effect of aromatic rings on the C-H protons of the alkyl group because both the host and guest molecules have a C_3-symmetric conformation. With an excess of *n*-$BuNH_3Cl$, the free guest molecule and the encapsulated guest molecule were clearly observed by ^{1}H NMR spectroscopy in which the encapsulated one was shifted upfield: CH_3 (δ 0.95–0.26 ppm, Δδ = –0.69 ppm), CH_3CH_2 (δ 1.45–0.30 ppm, Δδ = –1.05 ppm), $CH_3CH_2CH_2$ (δ 1.77 to –0.25 ppm, Δδ = –2.02 ppm), and CH_2N (δ 3.00–0.30 ppm, Δδ = –2.70 ppm). The NH_b proton in *cone*-**7** was shifted to a lower magnetic field (δ 9.21–9.51 ppm, Δδ = +0.30 ppm) while NH_a was shifted to an upper field (δ 8.45–8.36 ppm, Δδ = –0.09 ppm). This observation indicates that the complexation of the anionic guest Cl^- occurred at the *p*-methylphenyl amide moiety but not at the glycine amide moiety. This is different from the observation that N*H* of the glycine amide in *cone*-**5** was shifted strongly to a lower magnetic field (δ 8.03–9.14 ppm, Δδ = +1.11 ppm).

As mentioned above, Δδ between H_{ax} and H_{eq} of the ArCH_2Ar methylene protons in calix[4]arene serves as a measure of the "flattening". The Δδ value increases from 0.37 to 0.92 ppm in *cone*-**7** upon the binding of *n*-$BuNH_3^+$. These findings imply that *cone*-**7** stands up when the guest is included because *n*-$BuNH_3^+$ enters into the π cavity formed by the three aromatic rings and Cl^- complexes with NH_b by hydrogen-bonding interaction. Similar findings were observed in the case of *cone*-**5** and *n*-$BuNH_3Cl$ (the Δδ value increases from 0.40 to 1.15 ppm).

Intramolecular hydrogen bonding in *cone*-**7** weakens the affinity of *cone*-**7** to metal ions, which were encapsulated through the lower rim of the homotrioxacalix[3]arene derivative. When *cone*-**7** was complexed with *n*-$BuNH_3^+$ through the π cavity, the conformation was changed and intramolecular hydrogen bonding was broken. Thus, the complexation of the anionic guest Cl^- through hydrogen bonding is possible (16). Upon the addition of *n*-Bu_4NI and $PhMe_3NCl$ to a solution of *cone*-**7** in $CDCl_3$ (5×10^{-3} (mol/L)$^{-1}$), no complexation of halide anions was observed. This is due to the strong intramolecular hydrogen bonding, which breaks the anion binding site.

Table 1. Association constants (K_a, (mol/L)$^{-1}$) and free energies of association (ΔG, kJ mol^{-1}) of hosts *cone*-**3**, *cone*-**5**, and *cone*-**7** with halide anions.

	Cl^-		Br^-	
Hosts	K_a	$-\Delta G°$	K_a	$-\Delta G°$
cone-**3**	8520±510	22.6	1731±122	18.6
cone-**5**	1060±60	17.4	220±16	13.4
cone-**7**	536±32	15.7	230±17	13.6

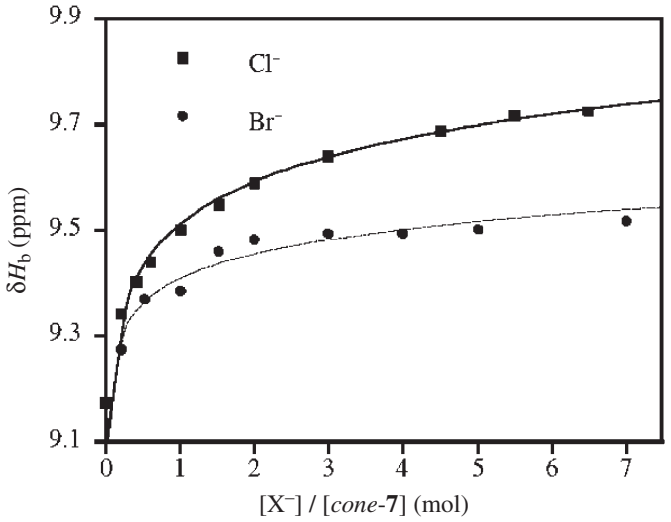
Note: In $CDCl_3$ at 27 °C; host concentration was 5 mmol/L.

Based on this observation, we investigated the complexation of *cone*-**7** with *n*-butylammonium halide counterions. With the addition of ammonium halide counterions, the proton peaks in *cone*-**7** were separated into complex and uncomplex. The downfield shift of NH_b might be attributed to the presence of the anionic guest close to the NH_b group by the intramolecular hydrogen bonding. The chloride anion induces a larger downfield shift for the amide hydrogen of *cone*-**7** than the bromide anion does. For example, significant downfield shifts of Δδ = +0.60 ppm for the NH_b proton in the case of Cl^- and Δδ = +0.40 ppm in the case of Br^- were observed. As the electronegativity of the halogen atom decreased with the series of Cl, Br, and I atoms, the intensity of hydrogen bonding formed between their anions and N*H* protons should be decreased following the same order. In fact, in ^{1}H NMR spectrum of a mixture of *cone*-**7** and *n*-$BuNH_3^+X^-$, a larger downfield chemical shift in the complex of NH_b with Cl^- was observed as compared with Br^- and I^-. The association constants calculated from these changes in chemical shifts of the amide protons are K_a = 536 ± 32 (mol/L)$^{-1}$ ($\Delta G°$ = 15.7 kJ mol^{-1}) for Cl^- and K_a = 230 ± 17 (mol/L)$^{-1}$ ($-\Delta G°$ = 13.6 kJ mol^{-1}) for Br^-. The smaller K_a values for the halide anions than for those of *cone*-**3** and *cone*-**5** might be attributable to the reduced electrostatic attractive interaction between *n*-butylammonium ion and the halide anions arising from the longer distance (Table 1).

Similar to triamide *cone*-**3**, hexaamide *cone*-**7** shows a preference for Cl^- over Br^- complexation (Fig. 3). This finding suggests that the cavity formed by the threefold amide moieties is more complementary to the size of the Cl^- than to that of Br^-, as well as the higher electronegativity of Cl^- than that of Br^-. In the case of tri(urea)-functionalized calix[6]arene, the anion complexation is prefered for Br^- because it has a large calix cavity and the three functionalized moieties in the 1, 3, and 5 positions of calix[6]arene are more complementary to the size of Br^- than to that of Cl^- (16*b*). Calix[5]arene derivatives were reported to complex with alkylammonium ions and to display an enzymelike selectivity (17) towards biologically important ammonium substrates. Since hexahomotrioxacalix[3]arenes and their de-

© 2006 NRC Canada

Fig. 3. Dependence of halide anion on chemical shift values of proton NH_b in *cone*-**7**.



rivatives have the C_3-symmetric conformation, they can bind with primary ammonium ions, having a potential function not only in chemical but also in biological systems (3).

Conclusions

We have demonstrated that the relationship between the properties of ionophore hosts and their intramolecular hydrogen bonding was taken into account in C_3-symmetric conformation. Owing to the intramolecular hydrogen bonding, the affinities of ionophore *cone*-**7** to metal ions were weakened; *cone*-**7** does not bind alkali metal ions because the binding site was blocked. However, hexaamide *cone*-**7** can bind *n*-butylammonium ion through the π cavity formed by three aryl rings, which can provide functional moieties in biological systems with good affinity and high selectivity. Interestingly, hexaamide *cone*-**7** binds a halide through the intermolecular hydrogen bonding among the NH_b hydrogens of *p*-methyphenyl amide in a 1:1 fashion in $CDCl_3$ in spite of the reduced electrostatic attractive interaction between *n*-butylammonium ions and the halide anions arising from the longer distance. Thus, hexaamide *cone*-**7** serves as a heteroditopic receptor that can complex with Cl^- and *n*-$BuNH_3^+$ at the same time. These results give some insight into the molecular design of new synthetic receptors for use in anion-controlled biomimetic systems.

Experimental

All melting points (Yanagimoto MP-S1) were uncorrected. ^{1}H NMR spectra were recorded on a Nippon Denshi JEOL FT-270 spectrometer. Chemical shifts are reported as δ values (ppm) relative to internal Me_4Si. Mass spectra were obtained on a Nippon Denshi JMS-01SG-2 mass spectrometer at an ionization energy of 70 eV using a direct inlet system through GLC; *m*/*z* values reported include the parent ion peak. IR spectra were obtained on a Nippon Denshi JIR-AQ2OM spectrophotometer as KBr disks. Elemental analyses were performed using a Yanaco MT-5. UV spectra were measured by a Hitachi 220A spectrophotometer.

Materials

cone-Hexahomotrioxacalix[3]arene triacetic acid (*cone*-**2b**) and (4-*tert*-butyl-2,6-dimethyl)phenoxyacetic acid (**8**) were prepared according to the previously reported procedures (2*d*, 12*a*, 12*b*).

Preparation of *cone*-7,15,23-tri-*tert*-butyl-25,26,27-tris[(methoxyacetylaminocarbonyl)methoxy]-2,3,10,11,18,19-hexahomo-3,11,19-trioxacalix[3]arene (*cone*-5)

To a solution of *cone*-hexahomotrioxacalix[3]arene triacetic acid (*cone*-**2b**) (400 mg, 0.532 mmol) and glycine methyl ester (**4a**) (427 mg, 4.80 mmol) in CH_2Cl_2 (30 mL) was added 1-hydroxybenzotriazole (HOBt) (94 mg, 0.697 mmol). To the mixture was added a solution of dicyclohexylcarbodiimide (DCC) (684 mg) in CH_2Cl_2 (10 mL) dropwise at 0 °C. Then the solution was stirred for 15 h at room temperature. After reaction, the solvent was removed; then the residue was dissolved with AcOEt and filtered; the filtrate was washed with 10% citric acid, water, 5% sodium bicarbonate, water, and brine, dried with Na_2SO_4, and condensed under reduced pressure. The residue was chromatographed over silica gel (Wako, C-300; 100 g) with AcOEt as the eluent to give a colorless solid. The solid was recrystallized from methanol to give *cone*-**5** (365 mg, 70.5%) as colorless prisms, mp 90–92 °C. IR (KBr) ν_{max}: 3350, 2958, 2871, 1752, 1678, 1540, 1484, 1200, 1076. ^{1}H NMR ($CDCl_3$) δ: 1.13 (27H, s, *t*-Bu), 3.78 (9H, s, *CH*$_3$), 4.15 (6H, d, *J* = 5.86 Hz, N-*CH*$_2$), 4.38 (6H, d, *J* = 12.7 Hz, Ar*CH*$_2$O), 4.78 (6H, d, *J* = 12.7 Hz, Ar*CH*$_2$O), 4.23 (6H, s, ArO*CH*$_2$), 6.95 (6H, s, Ar-*H*), 8.03 (3H, s, N*H*). *m*/*z*: 964 ([M]$^+$). Anal. calcd. for $C_{51}H_{69}O_{15}N_3$ (964.12): C 63.54, H 7.21, N 4.36; found: C 63.75, H 7.35, N 4.26.

Preparation of *cone*-7,15,23-tri-*tert*-butyl-25,26,27-tris[(hydroxyacetylaminocarbonyl)methoxy]-2,3,10,11,18,19-hexahomo-3,11,19-trioxacalix[3]arene (*cone*-6)

To a mixture of *cone*-**5** (225 mg, 0.23 mmol) in dioxane (35 mL) was added an aqueous 1 mol/L NaOH solution (25 mL), the mixture was stirred at room temperature for 1 h, then the solvent was removed under reduced pressure. The residue was acidified to neutral pH. The dispersion was extracted with ethyl acetate (30 mL × 2). The combined extracts were washed with 10% citric acid (20 mL × 2), 5% sodium bicarbonate (20 mL), water (20 mL), and saturated brine (20 mL), dried with Na_2SO_4, and condensed under reduced pressure. The residue was washed with hexane to give *cone*-**6** (170 mg, 79%) as a colorless solid, mp 215–217 °C. IR (KBr) ν_{max}: 3500–3250, 2958, 2867, 1736, 1661, 1540, 1457, 1363, 1231, 1197, 1093. ^{1}H NMR ($CDCl_3$–MeOH[D_4], 3:1 *v*/*v*) δ: 1.13 (27H, s, *t*-Bu), 4.13 (6H, s, ArO*CH*$_2$), 4.20 (6H, d, *J* = 5.86 Hz, N-*CH*$_2$), 4.42 (6H, d, *J* = 12.7 Hz, Ar*CH*$_2$O), 4.80 (6H, d, *J* = 12.7 Hz, Ar*CH*$_2$O), 6.97 (6H, s, Ar-*H*), 8.18 (3H, t, *J* = 5.86 Hz, *NH*). *m*/*z*: 922 ([M]$^+$). Anal. calcd. for $C_{48}H_{63}O_{15}N_3$ (922.05): C 62.53, H 6.89, N 4.56; found: C 62.72, H 6.73, N 4.40.

Preparation of the hexaamide derivative of homooxacalix[3]arene (*cone*-7)

To a solution of cone triacid homocalix[3]arene (*cone*-**6**) (491 mg, 0.532 mmol) and *p*-toluidine (**4b**) (514 mg, 4.80 mmol) in CH_2Cl_2 (30 mL) was added HOBt (94 mg,

© 2006 NRC Canada

0.697 mmol). To the mixture was added a solution of DCC (684 mg) in CH_2Cl_2 (10 mL) dropwise at 0 °C. Then the solution was stirred for 15 h at room temperature. After reaction, the solvent was removed; then the residue was dissolved with AcOEt and filtered; the filtrate was washed with 10% citric acid, water, 5% sodium bicarbonate, water, and brine, dried with Na_2SO_4, and condensed under reduced pressure. The residue was chromatographed over silica gel (Wako, C-300; 100 g) with AcOEt as the eluent to give a colorless solid. The solid was recrystallized from methanol to give *cone*-**7** (538 mg, 85%) as colorless prisms, mp 147–149 °C. IR (KBr) ν_{max}: 3476, 3410, 3312, 2958, 2867, 1664, 1609, 1541, 1516, 1482, 1197, 818. ^{1}H NMR ($CDCl_3$) δ: 1.11 (27H, s, *t*-Bu), 2.29 (9H, s, Ar′-CH_3), 4.09 (6H, s, ArOCH_2), 4.20 (6H, d, *J* = 5.86 Hz, N-CH_2), 4.34 (6H, d, *J* = 12.7 Hz, ArCH_2O), 4.79 (6H, d, *J* = 12.7 Hz, ArCH_2O), 6.95 (6H, s, Ar-*H*), 7.08 (6H, d, *J* = 8.8 Hz, Ar′-H_a), 7.43 (6H, d, *J* = 8.8 Hz, Ar′-H_b), 8.45 (3H, t, *J* = 5.86 Hz, NH_a), 9.21 (3H, s, NH_b); (DMSO-d_6) δ: 1.23 (27H, s, *t*-Bu), 2.23 (9H, s, Ar′-CH_3), 4.01 (6H, d, *J* = 5.86 Hz, N-CH_2), 4.19 (6H, s, ArOCH_2), 4.47 (6H, d, *J* = 12.7 Hz, ArCH_2O), 4.77 (6H, d, *J* = 12.7 Hz, ArCH_2O), 6.94 (6H, s, Ar-*H*), 7.06 (6H, d, *J* = 8.8 Hz, Ar′-H_a), 7.39 (6H, d, *J* = 8.8 Hz, Ar′-H_b), 8.25 (3H, t, *J* = 5.86 Hz, NH_a), 9.91 (3H, s, NH_b). ^{13}C NMR ($CDCl_3$) δ: 20.89, 31.44, 34.28, 43.98, 70.28, 73.26, 120.20, 127.79, 129.52, 129.52, 131.05, 134.18, 135.16, 147.39, 153.51, 167.74, 170.99. *m*/*z*: 1189 ([M]$^+$). Anal. calcd. for $C_{69}H_{84}O_{12}N_6$ (1189.47): C 69.68, H 7.12, N 7.07; found: C 69.51, H 7.23, N 7.14.

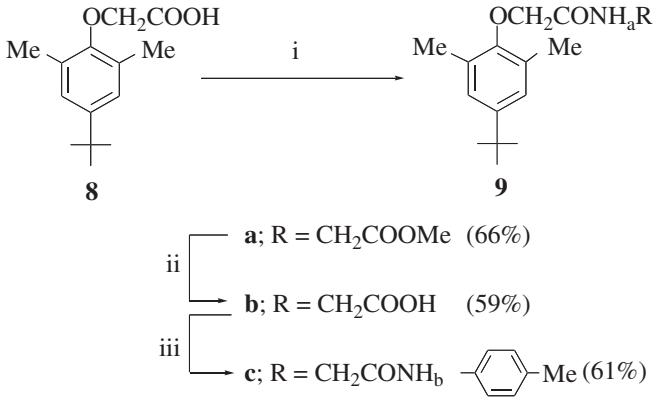
Preparation of 4-*tert*-butyl-2,6-dimethyl[(methoxyacetylaminocarbonyl)methoxy]benzene (9a)

To a solution of (4-*tert*-butyl-2,6-dimethyl)phenoxyacetic acid (**8**) (100 mg, 0.43 mmol), glycine methyl ester (**4a**) (114 mg, 1.28 mmol), and HOBt (75 mg, 0.17 mmol) in CH_2Cl_2 (12 mL) was added a solution of DCC (560 mg) in CH_2Cl_2 (5 mL) dropwise at 0 °C. After the mixture was stirred for 7 h at room temperature, it was condensed under reduced pressure. The residue was extracted with ethyl acetate (30 mL × 2). The combined extracts were washed with 10% citric acid (20 mL × 2), 5% sodium bicarbonate (20 mL), water (20 mL), and saturated brine (20 mL), dried with Na_2SO_4, and condensed under reduced pressure. The residue was recrystallized from methanol to give the title compound **9a** (Scheme 2) (87 mg, 66%) as colorless prisms, mp 101 to 102 °C. IR (KBr) ν_{max}: 3337, 3320, 2968, 2865, 1755, 1734, 1667, 1534, 1488, 1277, 1197, 1182, 1056. ^{1}H NMR ($CDCl_3$) δ: 1.29 (9H, s, *t*-Bu), 2.27 (6H, s, CH_3), 3.80 (3H, s, OCH_3), 4.20 (2H, d, *J* = 5.37 Hz, N-CH_2), 4.33 (2H, s, ArOCH_2), 7.03 (2H, s, Ar-*H*), 7.46 (1H, t, *J* = 5.37 Hz, *NH*). *m*/*z*: 307 ([M]$^+$). Anal. calcd. for $C_{17}H_{25}O_4N$ (307.39): C 66.43, H 8.2, N 4.56; found: C 66.23, H 8.35, N 4.68.

Preparation of 4-*tert*-butyl-2,6-dimethyl[(hydroxyacetylaminocarbonyl)methoxy]benzene (9b)

To a solution of **9a** (150 mg) in dioxane (30 mL) was added an aqueous 1 mol/L NaOH solution (30 mL) at room temperature. After the mixture was stirred at room temperature for 1 h, it was condensed under reduced pressure. The residue was then acidified to neutral condition. The precipitate was extracted with ethyl acetate (30 mL × 2). The combined extracts were washed orderly with water (20 mL) and saturated brine (20 mL), dried with Na_2SO_4, and condensed under reduced pressure. The residue was washed with hexane to give **9b** (Scheme 2) (81 mg, 59%) as a colorless solid, mp 193–195 °C. IR (KBr) ν_{max}: 3383, 2963, 2925, 2867, 1730, 1635, 1540, 1436, 1245, 1229, 1124. ^{1}H NMR ($CDCl_3$) δ: 1.29 (9H, s, *t*-Bu), 2.27 (6H, s, CH_3), 3.10 (1H, broad, COO*H*), 4.25 (2H, d, *J* = 5.37 Hz, N-CH_2), 4.35 (2H, s, ArOCH_2), 7.03 (2H, s, Ar-*H*), 7.46 (1H, t, *J* = 5.37 Hz, *NH*). *m*/*z*: 293 ([M]$^+$). Anal. calcd. for $C_{16}H_{23}O_4N$ (293.37): C 65.51, H 7.9, N 4.77; found: C 65.63, H 7.87, N 4.64.

Scheme 2. Reagents and conditions: (*i*) H_2NCH_2COOMe (**4a**), DCC–HOBt, CH_2Cl_2, room temp. for 15 h; (*ii*) Dioxane–NaOH(aq), room temp. for 1 h; (*iii*) *p*-toluidine (**4b**), DCC–HOBt, CH_2Cl_2, room temp. for 15 h.



Preparation of 4-*tert*-butyl-2,6-dimethyl[(4-methylphenylaminocarbonyl)methoxy]benzene (9c)

To a solution of **9b** (50 mg, 0.17 mmol), *p*-toluidine (**4b**) (55 mg, 0.51 mmol), and HOBt (23 mg, 0.17 mmol) in CH_2Cl_2 (12 mL) was added a solution of DCC (171 mg) in CH_2Cl_2 (5 mL) dropwise at 0 °C. After the mixture was stirred for 15 h at room temperature, it was condensed under reduced pressure. The residue was extracted with ethyl acetate (30 mL × 2). The combined extracts were washed with 10% citric acid (20 cm^3 × 2), 5% sodium bicarbonate (20 mL), water (20 mL), and saturated brine (20 mL), dried with Na_2SO_4, and condensed under reduced pressure. The residue was recrystallized from hexane–CH_2Cl_2 (3:1) to give **9c** (Scheme 3) (83 mg, 61.2%) as colorless prisms, mp 233 to 234 °C. IR (KBr) ν_{max}: 3383, 3320, 3289, 2962, 2948, 2851, 1699, 1609, 1526, 1312, 1195. ^{1}H NMR ($CDCl_3$) δ: 1.29 (9H, s, *t*-Bu), 2.27 (6H, s, CH_3), 2.31 (3H, s, ArCH_3), 4.25 (2H, d, *J* = 5.37 Hz, N-CH_2), 4.36 (2H, s, ArOCH_2), 7.02 (2H, s, Ar-*H*), 7.13, 7.42 (each 2H, d, *J* = 8.8 Hz, Ar-H_a, Ar-H_b), 7.76 (1H, t, *J* = 5.37 Hz, NH_a), 8.36 (1H, s, NH_b). *m*/*z*: 382 ([M]$^+$). Anal. calcd. for $C_{23}H_{30}O_3N_2$ (382.51): C 72.22, H 7.91, N 7.32; found: C 72.45, H 7.73, N 7.48.

Picrate extraction measurements

Alkali metal picrates (2.5×10^{-4} mol/L) were prepared in situ by dissolving 0.1 mol/L of alkali metal hydroxide in 2.5×10^{-4} mol/L of picric acid; triply distilled water was used for all aqueous solutions. Similarly, metallic picrates

© 2006 NRC Canada

were prepared in situ by dissolving 0.1 mol/L of metallic nitrate ($AgNO_3$, $Cu(NO_3)_2{\cdot}3H_2O$, $Al(NO_3)_3{\cdot}9H_2O$) in 2.5×10^{-4} mol/L of picric acid. Alkyl ammonium picrates were prepared by mixing an equimolar amount of alkylamine and picric acid in methanol.

Two-phase solvent extraction was carried out between water (5 mL, [alkali picrate] = 2.5×10^{-4} mol/L) and CH_2Cl_2 (5 mL, [ionophore] = 2.5×10^{-4} mol/L). The two-phase mixture was shaken in a stoppered flask for 24 h at 25 °C. We confirmed that this period is sufficient to attain the distribution equilibrium. This was repeated 3 times, and the solutions were left standing until phase separation was complete. The extractability was determined spectrophotochemically from the decrease in the absorbance of the picrate ion in the aqueous phase as described by Pedersen (18).

Determination of association constants

The measurements were performed by ^{1}H NMR titration experiments in a varying guest concentration of 0–50 mmol/L and a constant concentration of host receptors (5 mmol/L). As a probe, the chemical shift of the amide protons [C(O)NH_b] signal was used. The association constant values were calculated by the integral intensity of NH protons in the complex and free host molecules according to the literature (19).

References

1. (*a*) V. Böhmer. Angew. Chem. Int. Ed. Engl. **34**, 713 (1995); (*b*) C.D. Gutsche. Calixarene. Royal Society of Chemistry, Cambridge. 1989; (*c*) J. Vicens and V. Böhmer (*Editors*). CALIXARENES: A versatile class of macrocyclic compounds. Kluwer Academic Publishers, Cambridge. 1990; (*d*) C.D. Gutsche. Calixarenes revisited. Royal Society of Chemistry, Cambridge. 1998.
2. (*a*) K. Araki, N. Hashimoto, H. Otsuka, and S. Shinkai. J. Org. Chem. **58**, 5958 (1993); (*b*) M. Takeshita and S. Shinkai. Chem. Lett. 125 (1994); (*c*) K. Araki, K. Inaba, H. Otsuka, and S. Shinkai. Tetrahedron, **49**, 9465 (1993); (*d*) H. Matsumoto, S. Nishio, M. Takeshita, and S. Shinkai. Tetrahedron, **51**, 4647 (1995); (*e*) K. Araki, K. Akao, H. Otsuka, K. Nakashima, F. Inokuchi, and S. Shinkai. Chem. Lett. 125 (1994); (*f*) K. Araki, K. Inada, and S. Shinkai. Angew. Chem. Int. Ed. Engl. **35**, 72 (1996).
3. (*a*) A. Casnati, P. Minari, A. Pochini, and R. Ungaro. J. Chem. Soc. Chem. Commun. 1413 (1991); (*b*) S. Chang, M. Jang, S. Han, J. Lee, M. Kang, and K. No. Chem. Lett. 1937 (1992).
4. K. Koh, K. Araki, and S. Shinkai. Tetrahedron Lett. **35**, 8255 (1994).
5. A. Arduini, M. Fabbi, M. Mantovani, L. Mirone, A. Pochini, A. Secchi, and R. Ungaro. J. Org. Chem. **60**, 1454 (1995).
6. (*a*) J. Scheerder, J.P.M. van Duynhoven, J.F.J. Engbersen, and D.N. Reinhoudt. Angew. Chem. Int. Ed. Engl. **35**, 1090 (1996); (*b*) D.M. Rudkevich, W. Verboom, and D.N. Reinhoudt. J. Org. Chem. **59**, 3683 (1994); (*c*) J. Scheerder, R.H. Vreekamp, J.F.J. Engbersen, W. Verboom, J.P.M. van Duynhoven, and D.N. Reinhoudt. J. Org. Chem. **61**, 3476 (1996).
7. J.-M. Lehn. Angew. Chem. Int. Ed. Engl. **27**, 89 (1988).
8. M.T. Reetz, C.M. Niemeyer, and K. Harris. Angew. Chem. Int. Ed. Engl. **30**, 1472 (1991).
9. D.M. Rudkevich, Z. Brzozka, M. Palys, H.C. Visser, W. Verboom, and D.N. Reinhoudt. Angew. Chem. Int. Ed. Engl. **33**, 467 (1994).
10. K.I. Kinner, D.P. Mousley, E. Arafar, and J.C. Lockhart. J. Chem. Soc. Dalton Trans. 3637 (1994).
11. (*a*) P.D. Beer, M.G.B. Drew, R.J. Knubley, and M.I. Ogden. J. Chem. Soc. Dalton Trans. 3117 (1995); (*b*) J. Scheerder, J.P.M. van Duynhoven, J.F.J. Engbersen, and D.N. Reinhoudt. Angew. Chem. Int. Ed. Engl. **35**, 1090 (1996).
12. (*a*) T. Yamato and F. Zhang. J. Inclusion Phenom. **42**, 55 (2001); (*b*) T. Yamato, F. Zhang, H. Tsuzuki, and Y. Miura. Eur. J. Org. Chem. 1069 (2001); (*c*) T. Yamato, M. Haraguchi, J. Nishikawa, and S. Ide. J. Chem. Soc. Perkin Trans. 1, 609 (1998); (*d*) T. Yamato, M. Haraguchi, J. Nishikawa, S. Ide, and H. Tsuzuki. Can. J. Chem. **76**, 989 (1998).
13. (*a*) S. Kanamathareddy and C.D. Gutsche. J. Org. Chem. **57**, 2160 (1992); (*b*) F. Cunsolo, M. Piattelli, and P. Neti. J. Chem. Soc. Chem. Commun. 1977 (1994).
14. K. Kita, T. Kida, Y. Nakatsuji, and I. Ikeda. Chem. Lett. 405 (1997).
15. (*a*) A. Anduni, A. Pochini, S. Reverber, R. Ungaro, G.D. Andretti, and F. Ugozzoli. Tetrahedron, **42**, 2089 (1986); (*b*) S.K. Chang and I. Cho. J. Chem. Soc. Perkin Trans. 1, 211 (1986).
16. (*a*) J. Scheerder, M. Fochi, J.F.J. Engbersen, and D.N. Reinhoudt. J. Org. Chem. **59**, 7815 (1994); (*b*) J. Scheerder, J.F.J. Engbersen, A. Casnati, R. Ungaro, and D.N. Reinhoudt. J. Org. Chem. **60**, 6448 (1995).
17. (*a*) F.J. Castellino and J.R. Powell. Methods Enzmol. **80**, 365 (1981); (*b*) J.L. Hoover-Plow, L.A. Miles, G.M. Fless, A.M. Scanu, and E.F. Plow. Biochemistry, **32**, 13681 (1993); (*c*) J.M. Marshall, A.J. Brown, and C.P. Ponting. Biochemistry, **33**, 3599 (1994).
18. C.J. Pedersen. J. Am. Chem. Soc. **89**, 2495 (1967).
19. H.A. Benesi and J.H. Hildebrand. J. Am. Chem. Soc. **71**, 2073 (1949).

© 2006 NRC Canada

Solubilities of H_2 in H_2O and D_2 in D_2O with dissolved boric acid and lithium hydroxide

Uncharat Setthanan, David R. Morris, and Derek H. Lister

Abstract: The solubilities of hydrogen (H_2 and D_2) in aqueous (H_2O and D_2O) solutions of lithium hydroxide or boric acid have been measured in the temperature range 25–80 °C. Lithium hydroxide and boric acid cause a salting-out effect for H_2 and D_2. The solubilities of H_2 and D_2 in aqueous electrolyte solutions exhibit similar responses to temperature changes as those for pure water. The solute specific parameter (h_i) for boric acid in light and heavy water is 0.07 ± 0.02 and 0.48 ± 0.26 m^3 $kmol^{-1}$, respectively.

Key words: hydrogen solubility, deuterium solubility, salting-out effect.

Résumé : Opérant à des températures allant de 25 à 80 °C, on a mesuré les solubilités de l'hydrogène (H_2 et D_2) dans des solutions aqueuses (H_2O et D_2O) d'hydroxyde de lithium ou d'acide borique. L'hydroxyde de lithium et l'acide borique provoquent un effet de relargage pour le H_2 et le D_2. Les solubilités du H_2 et du D_2 dans des solutions aqueuses d'électrolyte présentent des réponses semblables aux changements de températures que ceux pour l'eau pure. Les valeurs du paramètre spécifique de soluté (h_i) pour l'acide borique dans l'eau normale et lourde sont respectivement de 0,07 ± 0,02 et de 0,48 ± 0,26 m^3 $kmol^{-1}$.

Mots clés : solubilité de l'hydrogène, solubilité du deutérium, effet de relargage.

[Traduit par la Rédaction]

Introduction

Light and heavy water are used as moderators and heat transport media in nuclear power reactors and may contain dissolved boric acid and lithium hydroxide for reactivity and pH control. In addition, hydrogen is introduced to suppress radiolysis and to minimize oxygen concentration to reduce corrosion of the system components. In this paper, solubilities are reported for H_2 in H_2O and D_2 in D_2O in the presence of dissolved boric acid or lithium hydroxide.

Several models have been proposed to explain salting-in and salting-out phenomena in which gas solubility is, respectively, increased and decreased. These models include the hydration theory, electrostatic theory, van der Waals theory, and the internal pressure concept. However, because of the complexity of the electrolyte–water–gas interactions, it is inconclusive as to which model is most reliable.

The effect of a dissolved species on the solubility of a gas in a solution can be described by the Sechenov relation:

$$[1] \qquad \log_{10}\left(\frac{c_{G,0}}{c_G}\right) = Kc_s$$

The Sechenov constant (K) is an empirical parameter for a specific gas, solute, solvent, and temperature. A shift from the salting-out to salting-in effect was reported by Sergeeva (1) as the ionic radius of a solute increases.

Based upon an extensive analysis of published data for the solubilities of gases in liquids in the presence of dissolved species, Schumpe (2) and Weisenberger and Schumpe (3) derived the expressions

$$[2] \qquad \log_{10}\left(\frac{c_{G,0}}{c_G}\right) = \sum_i (h_i + h_G)\, c_i$$

$$[3] \qquad h_G = h_G^0 + h_T(T - 298.15\ \mathrm{K})$$

The temperature effect is included in the gas-specific parameter, h_G. The solute-specific and (or) ion-specific parameter (h_i) is temperature independent.

Experimental

The solubilities of H_2 and D_2 in light and heavy water, respectively, were measured using apparatus and procedures according to ASTM D2780 (4). The experiments were performed at ambient atmospheric pressure over the temperature range 25–80 °C. The atmospheric pressure was corrected to the standard atmospheric pressure by using data from Weather Underground Inc. (www.weatherunderground.com). The lithium and boron concentrations were in the range 0–1000 ppm and 0–2000 ppm, respectively. The solute-specific parameter (h_i) for boron was then calculated from the experimental data at various temperatures and boron concentrations. The precision of the solubility measurements was estimated as 3%, based upon the uncertainties of measurements of the volume of gas and the system pressure and temperature.

Received 2 May 2005. Published on the NRC Research Press Web site at http://canjchem.nrc.ca on 28 February 2006.

U. Setthanan,[1] D.R. Morris, and D.H. Lister. Department of Chemical Engineering, University of New Brunswick, Fredericton, NB E3B 5A3, Canada.

[1]Corresponding author (e-mail: Uncharat_S@yahoo.ca).

 doi:10.1139/V06-010 © 2006 NRC Canada

Table 1. Solubility for H_2 in H_2O, H_2O + $B(OH)_3$, and H_2O + LiOH + $B(OH)_3$ solutions.

Expt. No.	Temp (°C)	Li content (ppm)	B content (ppm)	No. of expts.	H_2 solubility (10^{-5} mol fraction)	Standard deviation (10^{-5})
1.1	25.0	0	0	9	1.38	0.029
1.2	40.0	0	0	9	1.36	0.023
1.3	60.0	0	0	9	1.31	0.020
1.4	80.0	0	0	15	1.38	0.071
2.1	25.0	0.5	350	9	1.36	0.043
2.2	30.0	0.5	350	4	1.34	0.025
2.3	40.0	0.5	350	6	1.30	0.047
2.4	80.0	0.5	350	8	1.32	0.097
3.1	25.0	290	0	5	1.39	0.052
3.2	40.0	290	0	4	1.28	0.052
3.3	60.0	290	0	4	1.33	0.051
3.4	70.0	290	0	5	1.32	0.040
4.1	25.0	1000	0	4	1.36	0.059
4.2	40.0	1000	0	4	1.25	0.048
4.3	60.0	1000	0	5	1.28	0.049
4.4	70.0	1000	0	5	1.30	0.046
5.1	30.0	0	1000	4	1.37	0.042
5.2	40.0	0	1000	5	1.33	0.048
5.3	50.0	0	1000	5	1.30	0.041
5.4	60.0	0	1000	5	1.31	0.042
5.5	70.0	0	1000	5	1.31	0.063
6.1	30.0	0	2000	5	1.35	0.049
6.2	40.0	0	2000	5	1.31	0.048
6.3	50.0	0	2000	5	1.29	0.051
6.4	60.0	0	2000	5	1.30	0.043
6.5	70.0	0	2000	5	1.32	0.057

Results and discussion

The measured solubilities of H_2 in H_2O with dissolved boric acid or lithium hydroxide are presented in Table 1 and Figs. 1 and 2. Published data on the solubilities in H_2O have been reviewed by Wilhelm et al. (5). The measured solubilities of H_2 in H_2O reported in this work agree within 6%. Solubilities in lithium hydroxide solutions agree with the data of Weisenberger and Schumpe (3) within 7%. Standard deviation on the solubility measurements averages 4.7%.

The concentrations of various boron species in aqueous solution were calculated using the dissociation constants from Baes and Mesmer (6). Boron is present in solution primarily as $B(OH)_3$. The concentrations of charged species $B(OH)_4^-$, $B_2(OH)_7^-$, $B_3(OH)_{10}^-$, and $B_4(OH)_{14}^{2-}$ are very low and were neglected.

The specific parameter (h_i) for $B(OH)_3$ in the H_2 + H_2O system was calculated from the concentration of $B(OH)_3$, the measured solubilities of H_2 in the $B(OH)_3$ + H_2O solutions, and the correlation of published data from Wilhelm et al. (5) for the H_2 + H_2O system. The gas-specific parameter for H_2 and ion-specific parameters for H^+ and OH^- were obtained from Weisenberger and Schumpe (3).

The measured solubilities of D_2 in D_2O with dissolved boric acid are presented in Table 2 and Fig. 3. Solubilities in D_2O agree with published data within 8% (Scharlin and Battino (7)). Standard deviation on the solubility measurements averages 4.3%.

The solubility of D_2 in D_2O shows a minimum value of 1.70×10^{-5} mol fraction D_2 at about 323 K. This solubility minimum is significantly higher than that for the H_2 + H_2O system (1.30×10^{-5} mol fraction H_2 at about 325 K (5)). The solubilities of D_2 in D_2O are substantially lowered by dissolved boric acid. The combined effects of increasing boric acid concentration and increasing temperature are contrasting (see Fig. 3). At temperatures below that of the minimum solubility for the D_2 + D_2O system (323 K), increasing boric acid concentration causes a progressive decrease of the D_2 solubility. By contrast, at temperatures above 323 K, increasing boric acid concentration from 350 ppm B to 1000 ppm B causes the D_2 solubilities to increase. However, the magnitudes of the standard deviations on the measurements of D_2 solubility are such that the effects described, are not clear.

The specific parameter (h_i) for $B(OD)_3$ in the D_2 + D_2O system was calculated from the concentration of $B(OD)_3$, the measured solubilities of D_2 in the $B(OD)_3$ + D_2O solutions and in D_2O. D_2 was assumed to have the same gas-specific parameter (h_G) as H_2, and $B(OD)_3$ was assumed to dissociate in D_2O to the same extent as $B(OH)_3$ in H_2O. Also, the ion-specific parameters for D_3O^+ and OD^- were assumed to be the same as the values for H_3O^+ and OH^- in H_2O. No comparable data have been found in the literature.

Conclusions

The specific parameter (h_i) for the salting-out effect of $B(OH)_3$ in the H_2 + H_2O system is $h_{B(OH)_3}$ = 0.07 ±

© 2006 NRC Canada

Fig. 1. Solubility of H_2 in H_2O and LiOH + H_2O solutions. 0 ppm Li (ref. 5) (—); 0 ppm Li (this work) (◆); 290 ppm Li (■); 1000 ppm Li (▲).

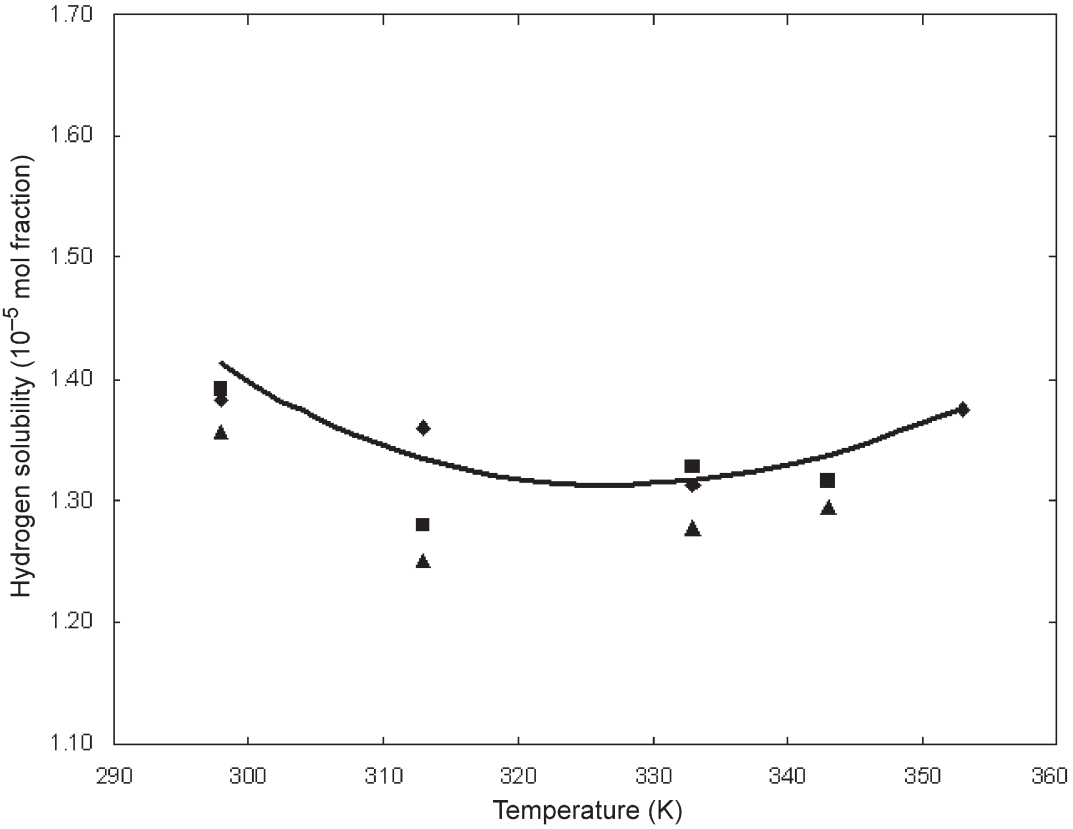
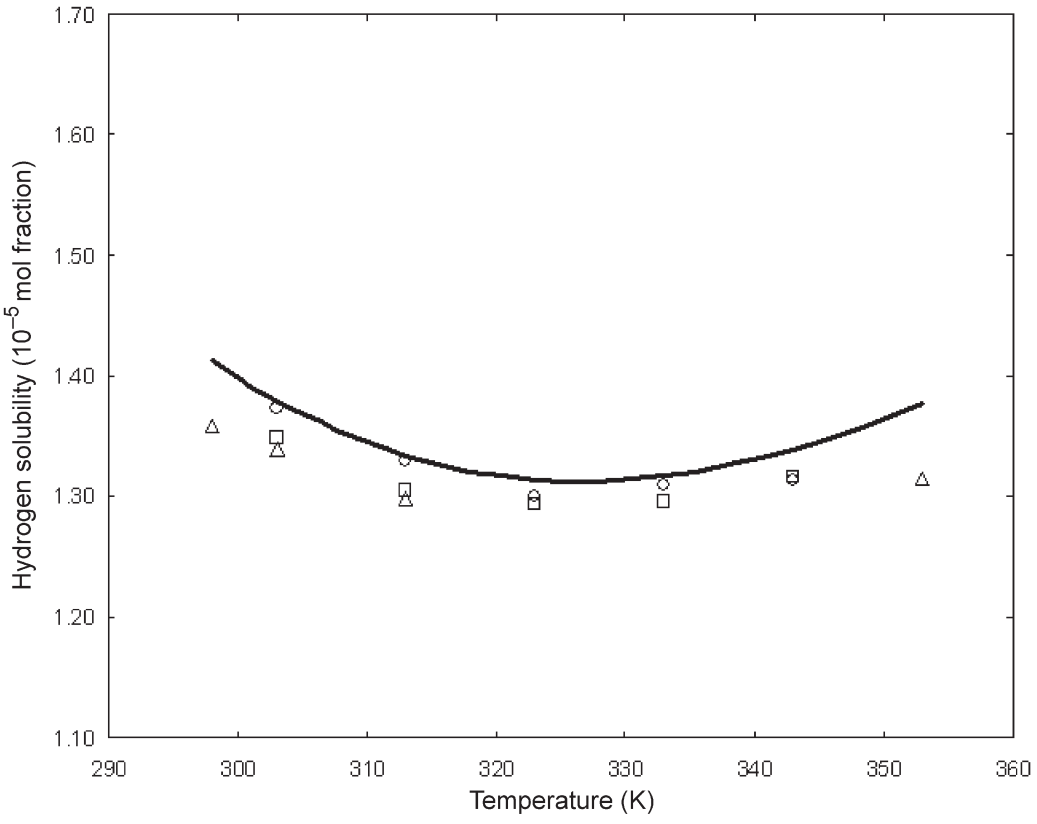


Fig. 2. Solubility of H_2 in H_2O and $B(OH)_3$ + H_2O solutions. 0 ppm B (ref. 5) (—); 1000 ppm B (this work) (○); 2000 ppm B (□); 350 ppm B + 0.5 ppm Li (△).



© 2006 NRC Canada

Fig. 3. Solubility of D_2 in D_2O and $B(OD)_3$ + D_2O solutions. 0 ppm B (ref. 7) (●); 0 ppm B (this work) (◆); 350 ppm B (□); 1000 ppm B (△).

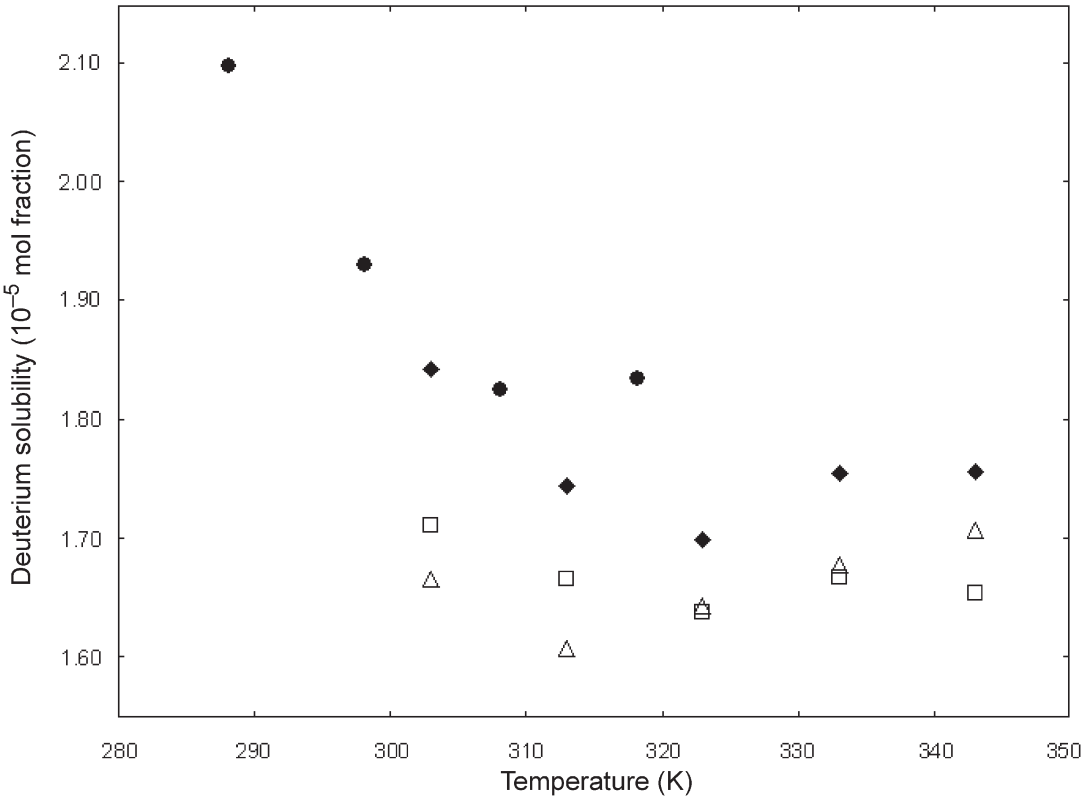


Table 2. Solubility for D_2 in D_2O and D_2O + $B(OD)_3$ solutions.

Expt. No.	Temp (°C)	B content (ppm)	No. of expts.	D_2 solubility (10^{-5} mol fraction)	Standard deviation (10^{-5})
7.1	30.0	0	8	1.84	0.099
7.2	40.0	0	8	1.74	0.031
7.3	50.0	0	9	1.70	0.071
7.4	60.0	0	11	1.76	0.050
7.5	70.0	0	5	1.76	0.066
8.1	30.0	350	9	1.71	0.047
8.2	40.0	350	9	1.67	0.057
8.3	50.0	350	9	1.64	0.079
8.4	60.0	350	8	1.67	0.074
8.5	70.0	350	8	1.65	0.077
9.1	30.0	1000	4	1.67	0.092
9.2	40.0	1000	4	1.61	0.078
9.3	50.0	1000	4	1.64	0.092
9.4	60.0	1000	4	1.68	0.081
9.5	70.0	1000	4	1.71	0.091

0.02 m^3 $kmol^{-1}$. The specific parameter (h_i) for the salting-out effect of $B(OD)_3$ in the D_2 + D_2O system is $h_{B(OD)_3}$ = 0.48 ± 0.26 m^3 $kmol^{-1}$. The reasons for the high value of $h_{B(OD)_3}$ relative to the value of $h_{B(OH)_3}$ are not known. The large uncertainty value for $h_{B(OD)_3}$ arises from the contrasting effects of increasing temperature and increasing B concentration above and below the temperature of minimum solubility of D_2 in the solutions.

Acknowledgements

The Natural Sciences and Engineering Research Council of Canada (NSERC) and the CANDU Owners Group are thanked for providing financial support.

References

1. V.F. Sergeeva. Russ. Chem. Rev. **32**, 309 (1965).
2. A. Schumpe. Chem. Eng. Sci. **48**, 153 (1993).
3. S. Weisenberger and A. Schumpe. AIChE J. **42**, 298 (1996).
4. ASTM International. Standard test method for solubility of fixed gas. Standard D2780-92 (1997).
5. E. Wilhelm, R. Battino, and R.J. Wilcock. Chem. Rev. **77**, 219 (1977).
6. C.F. Baes and R.E. Mesmer. The hydrolysis of cations. Wiley, New York. 1976. pp. 104–111.
7. P. Scharlin and R. Battino. J. Solution Chem. **21**, 67 (1992).

List of symbols

c_G gas solubility in solution (mol fraction)
$c_{G,0}$ gas solubility in pure water (mol fraction)
c_i concentration of solute (or ion) species i (kmol m^{-3})
c_s solute (or ion) concentration (kmol m^{-3})
h_G^0 gas-specific parameter at 298.15 K (m^3 $kmol^{-1}$)
h_G gas-specific parameter (m^3 $kmol^{-1}$)
h_i solute-specific and (or) ion-specific parameter (m^3 $kmol^{-1}$)
h_T gas-specific for temperature effect (m^3 $kmol^{-1}$ K^{-1})
K Sechenov constant (m^3 $kmol^{-1}$)
T temperature (K)

© 2006 NRC Canada

Regioselective synthesis of *vic*-halo alcohols and symmetrical or unsymmetrical *vic*-dihalides from epoxides using triphenylphosphine – *N*-halo imides

Nasser Iranpoor, Habib Firouzabadi, Roya Azadi, and Farzaneh Ebrahimzadeh

Abstract: A simple, novel, and highly regioselective cleavage of epoxides into vicinal halo alcohols and symmetrical or unsymmetrical dihalides is described using different stoichiometries of triphenylphosphine (PPh_3) and *N*-halo succinimide (NXS) or *N*-halo saccharine (NXSac).

Key words: *N*-halo succinimide (NXS), *N*-halo saccharine (NXSac), triphenylphosphine (PPh_3), epoxide, *vic*-halo alcohol, symmetrical dihalide, unsymmetrical dihalide.

Résumé : On a effectué un nouveau clivage simple et hautement régiosélectif d'époxydes qui conduit à des halogénoalcools et des dihalogénures symétriques et non symétriques vicinaux et qui a été réalisé en utilisant des stoechiométries diverses de triphénylphosphine, de *N*-halogénosuccinimide (NXS) ou de *N*-halogénosaccharine (NXSac).

Mots clés : *N*-halogénosuccinimide (NXS), *N*-halogénosaccharine (NXSac), triphénylphosphine (PPh_3), époxyde, halogénoalcool vicinal, dihalogénure symétrique, dihalogénure non symétrique.

[Traduit par la Rédaction]

Introduction

Epoxides are suitable starting materials for the preparation of different functional groups (1). Owing to the importance of vicinal halo alcohols in organic synthesis (2, 3), diverse methods have been developed for their preparation from epoxides. The conventional reagents for epoxide ring opening to halo alcohols are hydrogen halides and hypohalite–water (4). However, the disadvantages of these procedures are an intolerance to acid-sensitive moieties and by-product formation (5). A great effort has been made in the last few years to find milder procedures for converting epoxides into halo alcohols. For example, silyl halides can be added to epoxides to give *O*-silyl protected halo alcohols (6). Other methods include the use of a halogen and triphenylphosphine (PPh_3) (7), or disubstituted borane halogenides (8), β-bromo bis(dimethylamino)borane (9), monochloroborane – dimethyl sulfide (10), $Li_nM_nX_n$ (M = Ni, Cu, Ti) (11), and MX_n (12). Also, different metal salts (13–17) in the presence of halide ions, TMSCl, and phosphaferrocene as the catalyst (18); lithium halides in the presence of silica gel or Amberlyst 15 (19, 20); a combination of elemental halogen and 2-phenyl-2-(2-pyridyl)imidazolidine (PPI) (21), phenyl hydrazine (22), or crown ethers (23); PPh_3–CBr_4 (24), and acyl methylimidazolium halide ([AcMIm]X) (25) are among the reagents used for this transformation. Although there are many methods reported for the conversion of epoxides into vicinal halo alcohols, their conversion to symmetrical or unsymmetrical *vic*-dihalides is rarely found in the literature. The use of reagents such as PPh_3–CCl_4 (26) and PPh_3–X_2 (X = Cl, Br) (27) is reported for the preparation of symmetrical *vic*-dihalides and PPh_3–X_2 (X = Cl, Br) followed by using HCl–THF for the preparation of unsymmetrical *vic*-dihalides (27).

Received 30 August 2005. Published on the NRC Research Press Web site at http://canjchem.nrc.ca on 28 February 2006.

N. Iranpoor,[1] H. Firouzabadi,[2] R. Azadi, and F. Ebrahimzadeh. Department of Chemistry, College of Sciences, Shiraz University, Shiraz, 71454, Iran.

[1]Corresponding author (e-mail: iranpoor@chem.susc.ac.ir).
[2]Corresponding author (e-mail: firouzabibi@chem.susc.ac.ir).

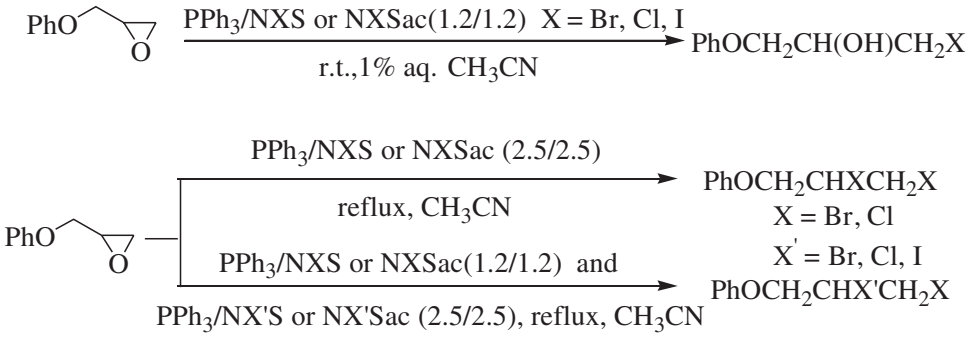
Results and discussion

Recently, we reported a method for the preparation of *vic*-halo alcohols or symmetrical or unsymmetrical dihalides (28) from epoxides using a combination of PPh_3–DDQ–R_4NX (X = Cl, Br, I). In conjunction with this research and in continuation of our previous work on the use of PPh_3 – *N*-halo succinimide (NXS) (29), we now introduce a new, mild, regioselective, and simpler method for the efficient conversion of epoxides to *vic*-halo alcohols or symmetrical or unsymmetrical *vic*-dihalides. In this method, epoxides in the presence of PPh_3–NXS or PPh_3 – *N*-halo saccharine (NXSac) are converted to *vic*-halo alcohols or symmetrical or unsymmetrical *vic*-dihalides depending on the molar ratio and the type of halo imide used (Scheme 1).

We took oxiranylmethyl phenyl ether (Table 1, entry 1) as an example and optimized the reaction conditions for its conversion to *vic*-bromo alcohol. It was observed that the mixture of oxiranylmethyl phenyl ether – PPh_3 – NBS or NBSac with the molar ratio of 1:1.2:1.2 in 1% aqueous acetonitrile at room temperature is suitable for the quantita-

 doi:10.1139/V05-261 © 2006 NRC Canada

Scheme 1.



tive conversion of oxiranylmethyl phenyl ether to 1-bromo-3-phenoxy-2-propanol. Aqueous acetonitrile is required to hydrolyze the intermediate to the corresponding vicinal halohydrine. Similar reaction conditions were then applied for the conversion of structurally different epoxides to their corresponding *vic*-halo alcohols. The results are shown in Table 1.

Under these reaction conditions, the ethereal bonds, ester groups, carbon–carbon double bond, and activated aromatic ring do not interfere with the formation of halo alcohols and remain intact. Electronic and steric factors control the orientation of the attack of halide ion. In the case of styrene oxide, owing to electronic factors, the attack of the halide ion occurs mainly at the more substituted position. However, in other epoxides that bear alkyl or electron-withdrawing groups, owing to the combination of steric and electronic factors, the attack occurs at the less hindered site of the ring and 1-halo-2 alcohols are produced as the major product (Table 1).

We also investigated the possibility of converting epoxides to symmetrical vicinal dihalides using PPh_3–NXS or PPh_3–NXSac (X = Cl, Br). For this purpose, oxiranylmethyl phenyl ether (Table 2, entries 1 and 2) was treated as a model compound with the PPh_3–NBS or PPh_3–NBSac reagent system using the optimized molar ratio of 2.5:2.5 in refluxing acetonitrile, and the corresponding dibromide was obtained in high yield. The use of NCS or NCSac in this method under the same reaction conditions as used for the preparation of dibromide offers the possibility of producing *vic*-dichlorides. We extended this procedure to other epoxides to obtain symmetrical *vic*-dihalides. The results of this investigation are shown in Table 2.

However, the preparation of *vic*-diiodides by this method was not successful. This result is in accordance with the literature (30), which indicates that alkene formation is favoured owing to the ease of elimination of molecular iodine. In all the reactions of epoxides with PPh_3–NIS or PPh_3–NISac (2.5:2.5), alkene formation was the only pathway. For example, the addition of oxiranylmethyl phenyl ether to the mixture of PPh_3–NBS or PPh_3–NBSac (2.5:2.5) in refluxing acetonitrile produced allyl phenyl ether as the only product after 0.5 h. Therefore, the use of a PPh_3–NIS or PPh_3–NISac mixture offers a new mixed reagent system for the deoxygenation of epoxides into their corresponding alkenes.

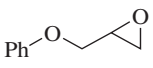
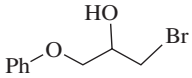
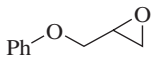
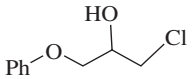
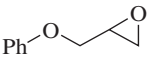
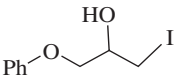
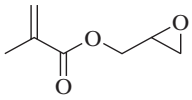
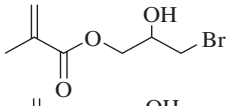
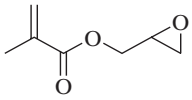
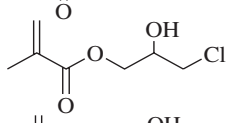
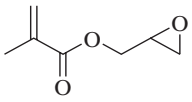
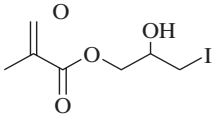
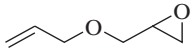
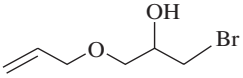
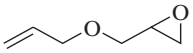
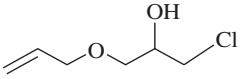
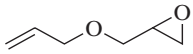
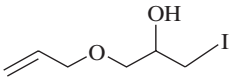
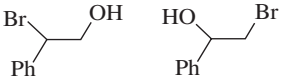
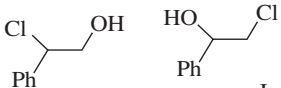
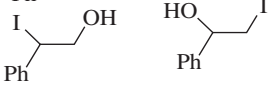
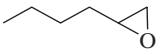
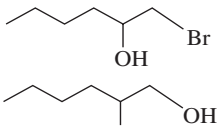
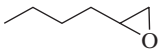
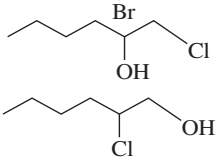
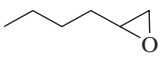
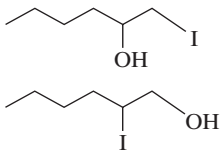
To overcome the problems of using highly acidic conditions for the conversion of epoxides to *vic*-dihalides (27), and to introduce a mild and novel method for this transformation, we applied our method to epoxides. For this transformation, the successive use of two *N*-halo imides having different halide ions produces the desired unsymmetrical *vic*-dihalide in high yield. To optimize the reaction conditions, oxiranylmethyl phenyl ether was added to a mixture of PPh_3–NCS or PPh_3–NCSac with the molar ratio of 1.2:1.2 in acetonitrile at room temperature. When all the epoxide was consumed, the mixture was poured into another mixture containing PPh_3–NBS or PPh_3–NBSac (2.5:2.5) in acetonitrile and refluxed for 8 h. After completion of the reaction, 2-bromo-1-chloro-3-phenoxypropane was obtained in 85% yield (Table 3, entry 2). Since this attempt was successful, we applied it to the preparation of unsymmetrical *vic*-dihalides from other epoxides. By using the proper halide anion in each step, we could easily control the formation of *vic*-dihalides with high regioselectivity. The results obtained for this study are tabulated in Table 3. In these reactions, as we expected, in the first step, the first halide ion attacks the epoxide ring from the same side of the formation of *vic*-halo alcohols. In the second step, the resulting halo alcohol reacts with the mixture of PPh_3–NXS or PPh_3–NXSac and the second halide anion displaces the hydroxyl group to produce the desired unsymmetrical dihalide. It was observed that when one of the nucleophiles was iodide, because of the possibility of the elimination of IX (X = Cl, Br), alkene formation was a competing pathway and lowered the yield of *vic*-dihalides considerably (Table 3, entries 3 and 6).

Although the exact mechanism of these reactions is not clear, it is suggested that, at first, a positively charged adduct (**I**) (31) is formed from the reaction of PPh_3 with NBS (Scheme 2). This positively charged adduct interacts with the oxygen atom of the epoxide and produces (**II**). When *R*-(–)-styrene oxide, the formation of the corresponding β-bromohydrin, which did not show any optical rotation, accounts for the formation of the racemic product through the intermediacy of a benzylic carbocation. Nucleophile attack of the halide ion on (**II**) produces the intermediate (**III**). This intermediate in the presence of water could produce triphenylphosphine oxide, succinimide, and the corresponding *vic*-halo alcohol. Similarly, the attack of another halide ion on this intermediate produces the corresponding vicinal symmetrical or unsymmetrical dihalide.

As shown in Table 3, entries 1 and 4, when the first nucleophile used was bromide, a mixture of two regioisomers was obtained. It is assumed that, in these cases,

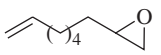
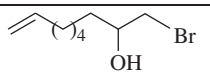
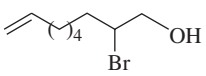
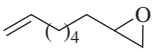
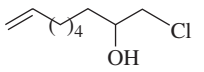
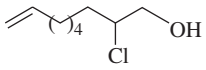
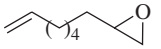
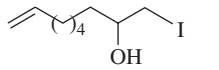
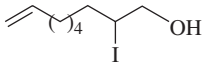
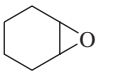
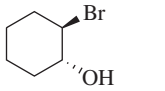
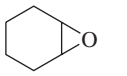
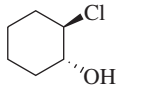
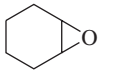
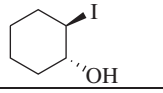
© 2006 NRC Canada

Table 1. Conversion of epoxides to *vic*-halo alcohols with PPh_3–NXS or PPh_3–NXSac (X = Br, C1, I) in 1% aqueous acetonitrile at room temperature.

Entry	Substrate	Product [a]		Time (min)	Yield (%)[b]
1			NBS	40	93
			NBSac	8	95
2			NCS	6	88
			NCSac	15	92
3			NIS	5	90
			NISac	7	85
4			NBS	20	82
			NBSac	3	90
5			NCS	3	95
			NCSac	8	85
6			NIS	5	80
			NISac	3	86
7			NBS	3	96
			NBSac	3	85
8			NCS	10	82
			NCSac	6	93
9			NIS	3	90
			NISac	10	88
10			NBS	30	80(16)[c]
			NBSac	3	90(8)[c]
11			NCS	3	78(18)[c]
			NCSac	5	85(8)[c]
12			NIS	8	80(15)[c]
			NISac	5	78(10)[c]
13			NBS	3	65(15)[c]
			NBSac	3	70(16)[c]
14			NCS	8	75(20)[c]
			NCSac	3	66(20)[c]
15			NIS	3	65(15)[c]
			NISac	10	76(15)[c]

© 2006 NRC Canada

Table 1 *(concluded)*.

Entry	Substrate	Product [a]		Time (min)	Yield (%)[b]
16			NBS	3	69(15)[c]
			NBSac	5	75(20)[c]
17			NCS	3	70(18)[c]
			NCSac	10	75(10)[c]
18			NIS	5	65(25)[c]
			NISac	10	70(20)[c]
19			NBS	10	95
			NBSac	8	90
20			NCS	3	87
			NCSac	10	92
21			NIS	3	90
			NISac	5	90

[a]All the products are known compounds (16, 20, 21, 24, 28) and are identified by their physical or spectral data.
[b]Isolated yield.
[c]Yield % in parentheses shows the formation of the other regioisomer.

the intermediate (**a**) can release $OPPh_3$ through the anchimeric assistance of bromide to form the bromonium ion (**b**). An attack of the second nucleophile to either side of (**b**) can produce a mixture of two regioisomers (Scheme 3).

In summary, the present investigation has demonstrated that the use of a PPh_3–NXS or PPh_3–NXSac system offers a simple, novel, and convenient method for the selective conversion of epoxides to either their corresponding *vic*-halo alcohols or symmetrical or unsymmetrical *vic*-dihalides.[3]

Experimental section

All the solvents and reagents were purchased from Fluka (Switzerland) or Merck (Germany) Chemical Companies. The products were purified by column or thick layer chromatography techniques. FT-IR spectra were recorded on a Shimadzu DR-8001 spectrometer. NMR spectra were recorded on a Brucker Avance DPX 250 MHz instrument. Mass spectra were recorded on a Shimadzu GC–MS-QP 1000PX.

Typical procedure for the conversion of oxiranylmethyl phenyl ether to 1-bromo-3-phenoxy-2-propanol by PPh_3–NBS

Oxiranylmethyl phenyl ether (0.15 g, 1 mmol) was added to a flask containing PPh_3 (0.314 g, 1.2 mmol) and NBS (0.213 g, 1.2 mmol) in 1% aq. CH_3CN (5 mL) at room temperature. TLC monitoring showed the completion of the reaction after 40 min. (This reaction with 1.2 mmol of NBSac takes 8 min, Table 1, entry 1.) After evaporation of the solvent, column chromatography of the crude mixture on silica gel using *n*-hexane – ethyl acetate afforded 1-bromo-3-phenoxy-2-propanol as a yellow oil in 93% yield. ^{1}H NMR ($CDCl_3$, 250 MHz, ppm) δ: 2.6 (d, 1H, J = 5 Hz), 3.6–3.7 (m, 2H), 4.07–4.10 (m, 2H), 4.15–4.25 (m, 1H), 6.90–7.10 (m, 3H), 7.3–7.6 (m, 1H). ^{13}C NMR ($CDCl_3$, 62.9 MHz, ppm) δ: 35.0, 69.5, 70.3, 114.5, 121.4, 129.6, 158.1. Mass spectra *m/e* (%): 232 ([M + 2], 33.1), 230 ([M], 35.6), 151 ([M – Br], 20.3).

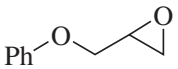
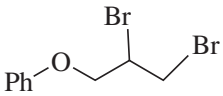
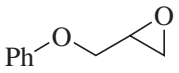
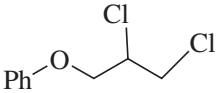
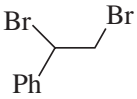
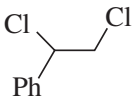
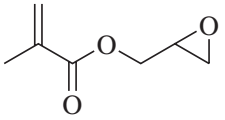
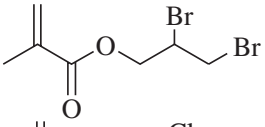
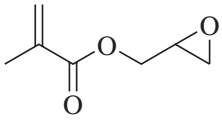
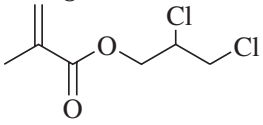
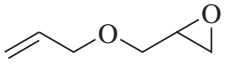
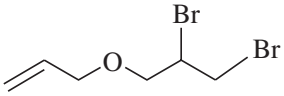
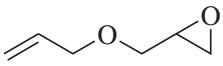
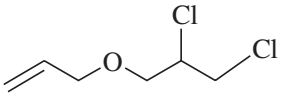
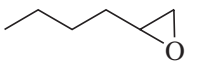
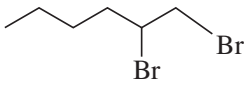
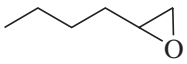
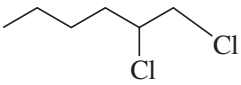
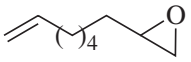
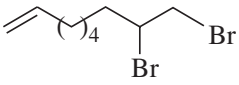
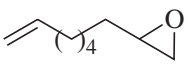
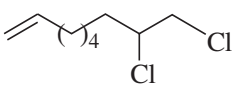
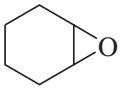
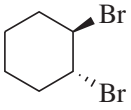
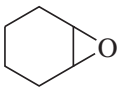
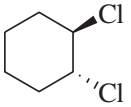
Typical procedure for the conversion of oxiranylmethyl phenyl ether to 1,2-dibromo-3-phenoxy propane by PPh_3–NBS

PPh_3 (0.654 g, 2.5 mmol) was added to a flask containing NBS (0.443 g, 2.5 mmol) in refluxing acetonitrile. Then oxiranylmethyl phenyl ether (0.15 g, 1 mmol) was added. TLC or GC analysis showed the completion of the conversion of oxiranylmethyl phenyl ether to 1,2-dibromo-3-phenoxypropane after 3 h. After completion of the reaction, the solvent was evaporated. 1,2-Dibromo-3-phenoxy propane was obtained in 88% yield after column chromatography of the crude mixture using *n*-hexane – ethyl acetate (5:1) as eluent. ^{1}H NMR ($CDCl_3$, 250 MHz, ppm) δ: 3.8–3.9 (m,

[3] Supplementary data for this article are available on the journal Web site (http://canjchem.nrc.ca) or may be purchased from the Depository of Unpublished Data, Document Delivery, CISTI, National Research Council Canada, Building M-55, 1200 Montreal Road, Ottawa, ON K1A 0R6, Canada. DUD 4096. For more information on obtaining material refer to http://cisti-icist.nrc-cnrc.gc.ca/irm/unpub_e.shtml.

© 2006 NRC Canada

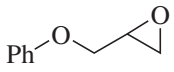
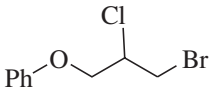
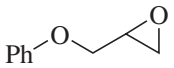
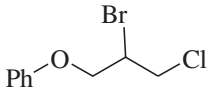
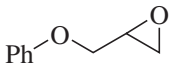
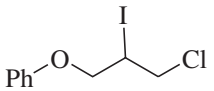
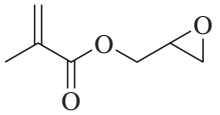
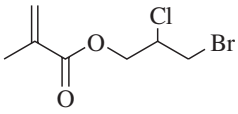
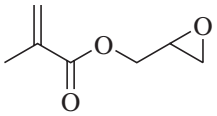
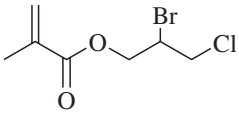
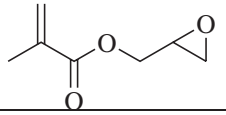
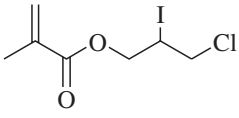
Table 2. Conversion of epoxides to *vic*-dihalides with PPh_3–NXS or PPh_3–NXSac (X = Br, C1) in acetonitrile under reflux conditions.

Entry	Substrate	Product[a]	Time (h)	Yield (%)[b]
1			3.5	88
2			3	90
3			3	80
4			2	87
5			3.5	89
6			2	79
7			5.5	82
8			5	75
9			5	80
10			4	78
11			3	80
12			2	85
13			4.5	83[c]
14			4	88

[a]All the products are known compounds (28) and are identified by their physical or spectral data.
[b]Isolated yield.
[c]The stereochemistry of product was determined by the comparison of its ^{1}H NMR spectrum with the literature (32).

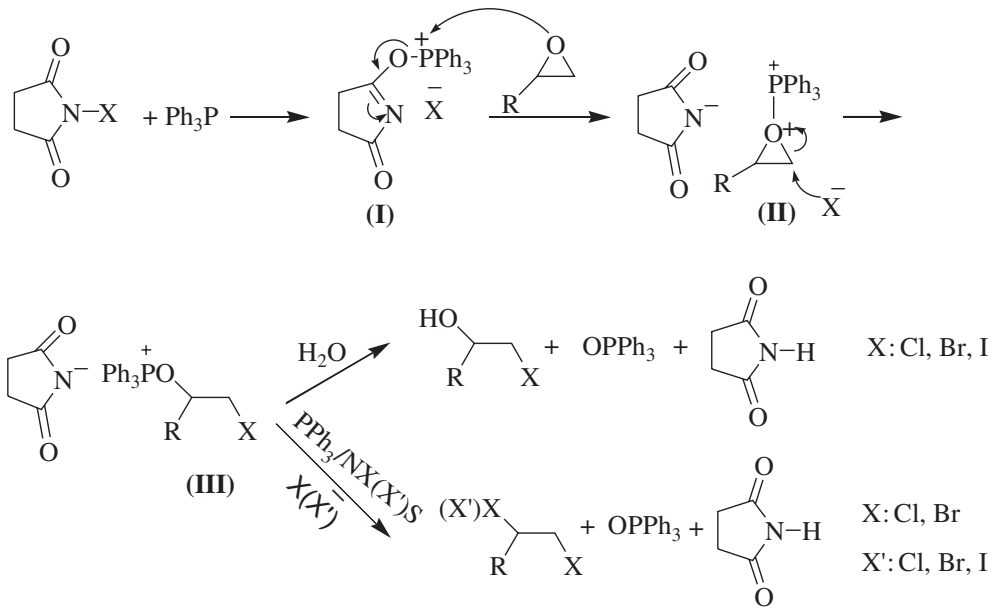
© 2006 NRC Canada

Table 3. Conversion of epoxides to unsymmetrical *vic*-dihalides with PPh_3–NXS of different halides.

Entry	Substrate	Product[a]	Time (h)[b]	Yield (%)[c]
1			5	65[d]
2			8	85
3			8.5	52
4			7	68[d]
5			9	90
6			10	44

[a]All the products are known compounds (28) and are identified by their physical or spectral data.
[b]These reactions were performed in the presence of PPh_3–NXSac with similar results.
[c]Isolated yield.
[d]The other isomeric product was also formed in 25% yield.

Scheme 2.



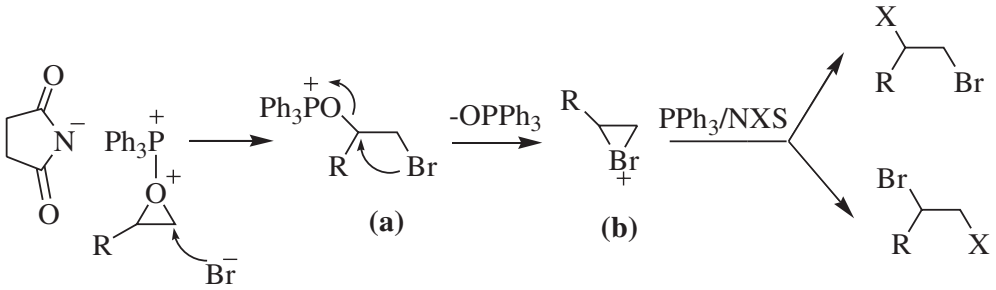
2H), 4.3–4.4 (m, 3H), 6.9–7.0 (m, 3H), 7.2–7.32 (m, 2H). ^{13}C NMR ($CDCl_3$, 62.9 MHz, ppm) δ: 31.7, 46.7, 68.0, 113.8, 120.6, 128.6, 156.9. Mass spectra *m/e* (%): 296 ([M + 4], 16.2), 294 ([M + 2], 41.7), 292 ([M], 14.1), 203 ([M + 4 – PhO], 3.2), 201 ([M + 2 – PhO], 8.7), 199 ([M – PhO], 5.3).

Typical procedure for the conversion of oxiranylmethyl phenyl ether to 2-bromo-1-chloro-3-phenoxypropane

PPh_3 (0.314 g, 1.2 mmol) was added to a flask containing of NCS (0.159 g, 1.2 mmol) in CH_3CN at room temperature. Then oxiranylmethyl phenyl ether (0.15 g, 1 mmol) was

© 2006 NRC Canada

Scheme 3.



gradually added to the reaction mixture over a period of 1.5 h. TLC or GC analysis showed the completion of the conversion of oxiranylmethyl phenyl ether to 1-chloro-3-phenoxy-2-propanol. Then the reaction mixture was transferred to another flask containing a solution of PPh_3 (0.654 g, 2.5 mmol) and NBS (0.443 g, 2.5 mmol) in CH_3CN (5 mL) and refluxed for 8 h to produce 2-bromo-1-chloro-3-phenoxypropane. After completion of the reaction, the solvent was evaporated. 2-Bromo-1-chloro-3-phenoxypropane was obtained in 85% yield after column chromatography of the crude mixture using *n*-hexane – ethyl acetate (5:1) as eluent. ^{1}H NMR ($CDCl_3$, 250 MHz, ppm) δ: 3.9–4.0 (m, 2H), 4.25–4.4 (m, 3H), 6.8–7.1 (m, 3H), 7.2–7.3 (m, 2H). ^{13}C NMR ($CDCl_3$, 62.9 MHz, ppm) δ: 45.0, 48.1, 68.3, 114.8, 121.6, 129.6, 157.9. Mass spectra *m/e* (%): 252 ([M + 4], 8.7), 250 ([M + 2], 29.3), 248 ([M], 24), 171 ([M + 2 – ^{79}Br] and [M + 4 – ^{81}Br], 7.2), 169 ([M + 2 – ^{81}Br] and [M – ^{79}Br], 12.9).

Acknowledgments

We are thankful to the Organization of Management and Planning of Iran and the Shiraz University Research Council for the support of this work.

References

1. T. Katsuki and V.S. Martin. Org. React. **48**, 1 (1996).
2. P.A. Bartlett. *In* Asymmetric synthesis. Vol. 3. *Edited by* J.D. Morrison. Academic Press, New York. 1984. p. 411.
3. R.E. Erickson. *In* Marine natural products. Vol. 5. *Edited by* P.J. Scheuer. Academic Press, New York. 1986. p. 131.
4. J.G. Smith and M. Fieser. Fieser and Fieser's reagent for organic synthesis. Vols. 1–12. John Wiley and Sons, New York. 1990.
5. (*a*) C.A. Stewart and C.A. Vanderwerf. J. Am. Chem. Soc. **76**, 1259 (1954); (*b*) L.N. Owen and G.S. Saharia. J. Chem. Soc. 2582 (1953).
6. (*a*) H.R. Kricheldorf, G. Morber, and W. Regel. Synthesis, 383 (1981); (*b*) G.C. Andrews, T.C. Crawford, and L.G. Contillo. Tetrahedron Lett. **22**, 3803 (1981); (*c*) M.R. Detty and M.D. Seidler. Tetrahedron Lett. **23**, 2543 (1982).
7. (*a*) G. Palumbo, C. Ferreri, and R. Caputo. Tetrahedron Lett. **24**, 1307 (1983); (*b*) R. Caputo, C. Ferreri, S. Noviello, and G. Palumbo. Synthesis, 499 (1986).
8. (*a*) Y. Guindon, M. Therien, Y. Girard, and C. Yoakim. J. Org. Chem. **52**, 1680 (1987); (*b*) N.N. Joshi, M. Srebnik, and H.C. Brown. J. Am. Chem. Soc. **110**, 6246 (1988).
9. T.W. Bell and J.A. Ciaccio. Tetrahedron Lett. **27**, 827 (1986).
10. P. Bovicelli, E. Mincione, and G. Ortaggi. Tetrahedron Lett. **32**, 3719 (1991).
11. (*a*) J.A. Ciaccio, E. Heller, and A. Talbot. Synlett, 248 (1991); (*b*) M. Shimizu, A. Yoshida, and T. Fujisawa. Synlett, 204 (1992); (*c*) Z.X. Guo, A.H. Haines, and R.J.K. Taylor. Synlett, 607 (1993).
12. (*a*) J.S. Bajwa and R.C. Anderson. Tetrahedron Lett. **32**, 3021 (1991); (*b*) H. Kotsuki and T. Shimanouchi. Tetrahedron Lett. **37**, 1845 (1996).
13. Y.-G. Suh, B.A. Koo, J.-A. Ko, and Y.-S. Cho. Chem. Lett. 1907 (1993).
14. Y. Ueda and S.C. Maynard. Tetrahedron Lett. **29**, 5197 (1988).
15. T. Inokuchi, H. Kawafuchi, and S. Torii. Synlett, 510 (1992).
16. N. Iranpoor, F. Kazemi, and P. Salehi. Synth. Commun. **27**, 1247 (1997).
17. N. Iranpoor and H. Adibi. Bull. Chem. Soc. Jpn. **73**, 675 (2000).
18. C.E. Garrett and G.C. Fu. J. Org. Chem. **62**, 4534 (1997).
19. H. Kotsuki, T. Shimanouchi, R. Ohshima, and S. Fujiwara. Tetrahedron, **54**, 2709 (1998).
20. (*a*) C. Bonini and G. Righi. Synthesis, 225 (1991); (*b*) C. Bonini, C. Giuliano, G. Righi, and L. Rossi. Synth. Commun. **22**, 1863 (1922).
21. H. Sharghi and H. Naeimi. Synlett, 1343 (1998).
22. H. Sharghi and M.M. Eskandari. Synthesis, 1519 (2002).
23. H. Sharghi, A.R. Massah, H. Eshghi, and K. Niknam. J. Org. Chem. **63**, 1455 (1998).
24. D. Diaz, T. Martin, and V.S. Martin. J. Org. Chem. **66**, 7231 (2001).
25. B.C. Ranu and S. Banerjee. J. Org. Chem. **70**, 4517 (2005).
26. N.S. Isaacs and D. Kirkpatric. Tetrahedron Lett. **13**, 3869 (1972).
27. P.E. Sonnet and J.E. Oliver. J. Org. Chem. **41**, 3279 (1976).
28. N. Iranpoor, H. Firouzabadi, G. Aghapour, and A. Nahid. Bull. Chem. Soc. Jpn. **77**, 1885 (2004).
29. N. Iranpoor, H. Firouzabadi, and G. Aghapour. Synlett, **19**, 1176 (2001).
30. Z. Paryzek and R. Wydra. Tetrahedron Lett. **25**, 2601 (1984).
31. S. Trippett. J. Chem. Soc. 2337 (1962).
32. T.J. Davies, A.C. Garner, S.G. Davies, and R.G. Compton. J. Electroanal. Chem. **570**, 171 (2004).

© 2006 NRC Canada

Organo(organooxo)mercury(II) chemistry — Synthesis and structure of methyl(phenoxo)mercury(II)[1]

Allan J. Canty, Janette W. Devereux, Brian W. Skelton, and Allan H. White

Abstract: Methyl(phenoxo)mercury(II) may be obtained from the reaction of methyl(chloro)mercury(II) with silver(I) oxide, followed by addition of phenol. The dominant motif of the structure is a pair of independent MeHgOPh aggregates (Hg—C,O 2.05(2) Å, 2.06(1) Å (x2); C-Hg-O 176.6(5)°, 176.3(5)°) loosely associated about a quasi-inversion centre by Hg···O interactions (2.702(9) Å, 2.719(9) Å) to form a dimer (Hg-O-Hg′ 106.0(4)°, 106.5(4)°; O-Hg-O′ 73.0(3)°, 72.6(3)°), the dimer stacking up the short crystallographic *c* axis (= 6.914(1) Å) at spacings *c*/2. Vibrational spectroscopic studies are insensitive to the associative interactions.

Key words: mercury, methylmercury, organomercury, structure, aryloxide, phenoxide.

Résumé : On peut obtenir du méthyl(phénoxo)mercure(II) par réaction du méthyl(chloro)mercure(II) avec de l'oxyde d'argent(I), suivie d'une addition de phénol. Le motif dominant de la structure est une paire d'agrégats indépendants de MeHgOPh (Hg—C,O 2,05(2) Å, 2,06(1) Å (x2); C-Hg-O 176,6(5)°, 176,3(5)°) faiblement associés autour d'un centre de quasi-inversion par des interactions Hg···O (2,702(9) Å, 2,719(9) Å) qui permettent de former le dimère (Hg-O-HgN 106,0(4)°, 106,5(4)°; O-Hg-ON 73,0(3)°, 72,6(3)°) qui s'empile le long de l'axe cristallographique *c* (= 6,914(1) Å) à des distances de *c*/2. Les études spectroscopiques vibrationnelles sont insensibles aux interactions associatives.

Mots clés : mercure, méthylmercure, organomercure, structure, aryloxyde, phénolate.

[Traduit par la Rédaction]

Introduction

The coordination chemistry of monoorganomercury(II) complexes has been reviewed (1, 2); for arylalkoxides and aryloxides, structural studies are limited to the early study of the 4-bromo-2-chlorophenoxo complex $PhHgOC_6H_3ClBr$ (3, 4), although the structure of a trimethylsiloxo complex, $MeHgOSiMe_3$, has also been described (5). Vibrational spectroscopic data have been interpreted in terms of monomeric structures for MeHgOPh and PhHgOPh in both the solid state and in dichloromethane (**1** in Scheme 1), consistent with osmometric studies in dichloromethane (6). However, in the less polar solvent benzene, ebullioscopic studies indicate that PhHgOPh and relatives PhHgOR′ (R′ = Me, *i*-Pr, *s*-Bu, CMe_2Ph) are associated and consistent with a monomer (**1**) – dimer (**2**) equilibrium (7), and it has also been suggested that PhHgOPh can adopt both dimeric (**2**) and trimeric (**3**) forms (8). Vibrational spectra are also consistent with a dimeric structure in the solid state for PhHgOR′ (R′ = Me, Et) (6). The complex $MeHgOSiMe_3$ is monomeric in benzene (osmometry) (9), and in the solid state an incomplete X-ray structure determination (280 "observed" reflections, R = 0.21) indicated a tetrameric structure (**4**) with short Hg—O (2.11 Å) and long Hg···O (2.75 Å) interactions (5). A weak intermolecular Hg···O interaction is also observed in $PhHgOC_6H_3ClBr$ (2.85(2) Å), although the molecule is essentially a monomer with C-Hg-O 174(1)°, where this angle is opposite a weak intramolecular Hg···Cl interaction (3.03 Å) (3). Noting the additional weak interactions present in these structures and the marked tendency for unsymmetrical coordination geometries for monoorganomercury(II) complexes, geometries for **2**–**4** are drawn to illustrate this behaviour, and additional weak interactions could be anticipated for monomers (**1**) (Scheme 1). Archetypal examples of unsymmetrical geometry are illustrated by the 2,2′-bipyridine complex $[MeHg(bpy)]NO_3$, which has C-Hg-N 164(1)°, Hg—N 2.24(3) Å, Hg···N 2.43(3) Å (10); the D,L-penicillamine complex $MeHgSCMe_2CH(CO_2)NH_2HgMe$, which has C-Hg-N 168.1°, Hg—N 2.216(5) Å, Hg···O 2.708(4) Å (11); and the closely related D,L-selenocysteine complex $MeHgSeCH_2CH(CO_2)NH_3{\cdot}H_2O$, which has C-Hg-Se 177.8(11)°, with associated more distant approaches Hg···O 2.93(2) Å and Hg···Se 3.737(4) Å (12).

In view of the lack of structural characterization for fundamental aryloxo complexes, the propensity for organomercury(II) compounds to adopt unusual geometries for mercury, the various structures proposed on the basis of physical and spectroscopic studies (**1**–**3**), and the structure

Received 17 January 2005. Published on the NRC Research Press Web site at http://canjchem.nrc.ca on 14 February 2006.

In honour of our colleague and friend Arthur J. Carty.

A.J. Canty[2] and J.W. Devereux. School of Chemistry, University of Tasmania, Hobart, Tasmania, Australia 7001.
B.W. Skelton and A.H. White. Chemistry M313, University of Western Australia, Crawley, Western Australia, Australia 6009.

[1]This article is part of a Special Issue dedicated to Professor Arthur Carty.
[2]Corresponding author (e-mail: allan.canty@utas.edu.au).

 doi:10.1139/V05-219 © 2006 NRC Canada

Scheme 1.

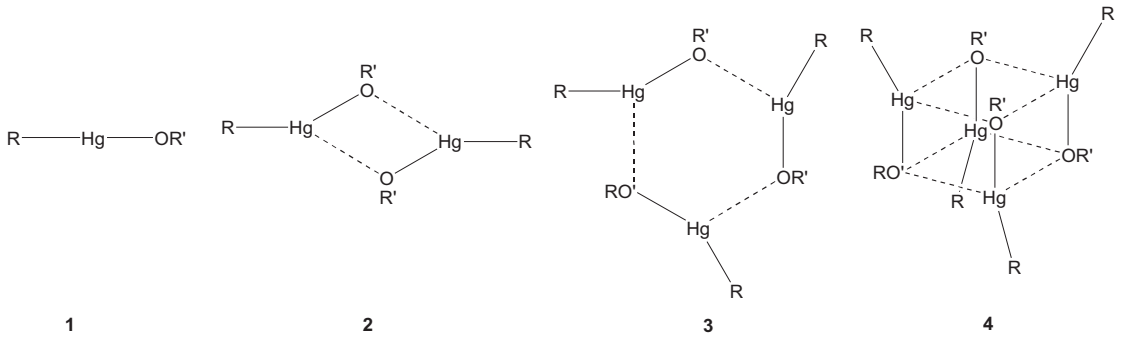


Table 1. Selected geometries for MeHgOPh.

	Parameter			Parameter	
Atoms	n = 1	n = 2	Atoms	n = 1	n = 2
Bond lengths (Å)					
Hg(n)—C(n)	2.046(16)	2.049(18)	Hg(n)—O(2)	2.702(9)	2.063(10)
Hg(n)—O(1)	2.060(11)	2.719(9)	C(n1)—O(n)	1.369(16)	1.364(16)
Bond angles (°)					
C(n)-Hg(n)-O(n)	176.6(5)	176.3(5)	Hg(1)-O(n)-Hg(2)	106.0(4)	106.5(4)
C(n)-Hg(n)-O(n')	109.4(5)	109.3(5)	C(11)-O(1)-Hg(n)	120.7(8)	123.5(8)
O(1)-Hg(n)-O(2)	73.0(3)	72.6(3)	C(21)-O(2)-Hg(n)	120.6(8)	121.4(8)

reported for the trimethylsiloxo complex (**4**), we have synthesized MeHgOPh and determined its structure in the solid state.

Results and discussion

Although the complex MeHgOPh was prepared by the reported method, the preparation is given in detail here in view of the brief description reported previously (13). Crystals were obtained from dichloromethane – light petroleum. Selected geometries are given in Table 1, and views of the structure are shown in Fig. 1.

The results of the low-temperature single crystal X-ray structure determination are consistent with the formulation of the complex, in terms of stoichiometry and connectivity, as neutral MeHgOPh. Two formula units, devoid of crystallographic symmetry, comprise the asymmetric unit of the structure. These may be viewed essentially as single molecules with almost linear C-Hg-O coordination (Hg—O 2.060(11) Å, 2.063(10) Å; Hg—C 2.046(16) Å, 2.049(18) Å; C-Hg-O 176.6(5)°, 176.3(5)°). The mercury environments lie side-by-side, quasi-inversion related (Fig. 1*a*), with long Hg···O interactions (2.702(9) Å, 2.719(9) Å), appreciably less than the van der Waals radii sum (O, 1.4 Å (14); Hg, ca. 1.73 Å (15)) that perturb the linearity of the C-Hg-O arrays. The $Hg(\mu\text{-}O)_2Hg$ arrays are quasi-planar (χ^2 523) with a fold angle across the Hg···Hg line of 17.4(6)° (Fig. 1*b*). The mercury atoms lie out of the associated C_6 ring planes by 0.17(3) Å and 0.20(2) Å, the Hg(n)-O(n)-C(n1)-C(n2) torsion angles being –8(2)° and –9(2)°. C(11, 21) lie out of the Hg_2O_2 "plane" by 0.22(2) Å and 0.32(2) Å. Despite these distortions, the quasi-dimeric arrays may be considered approximately planar and, as such, stack up the *c* axis of the almost orthogonal cell — Hg above O — these contacts being much longer and at the van der Waals limit (Hg(1)···O(1) (x, 1/2 – y, z – 1/2) 3.318(9) Å; Hg(2)···O(2) (x, 1/2 – y, z – 1/2) 3.368(10) Å) (Fig. 1*c*).

Although the structure determination reveals several interesting features in crystal chemistry, the structure of MeHgOPh conforms broadly to model **1** with the additional presence of weak intermolecular interactions, consistent with the monomeric behaviour exhibited in dichloromethane (6). Structural assignments for the solid state based on IR and Raman spectroscopic data (6), are supported by the structural determination, the spectroscopic data being insensitive to the weak intermolecular Hg···O interactions.

Experimental

Synthesis of MeHgOPh

Freshly precipitated silver(I) oxide (from an aqueous solution of silver(I) nitrate and sodium hydroxide) was collected and repeatedly washed and centrifuged until the pH of the solution was 7. An excess of Ag_2O was added to MeHgCl (6.28 g) in a small volume of water. The resulting aqueous solution was filtered, and phenol (2.35 g) was added. The white crystalline precipitate that formed was collected, washed with water, and dried over phosphorus pentoxide. The product was recrystallized from dichloromethane and then from dichloromethane – light petroleum (bp 40–60 °C) to give the pure complex (3.86 g, 50%). IR spectra are as reported (6).

X-ray data collection, structure determination, and refinement

Following earlier unsuccessful attempts at data acquisition at room temperature using a four-circle instrument (the ma-

© 2006 NRC Canada

Fig. 1. (*a*) The asymmetric unit of the structure of MeHgOPh projected down *c* and (*b*) oblique to the central plane; (*c*) Unit cell contents projected down *c*. 50% Probability amplitude displacement envelopes are shown for the non-hydrogen atoms, hydrogen atoms where shown having arbitrary radii of 0.1 Å.

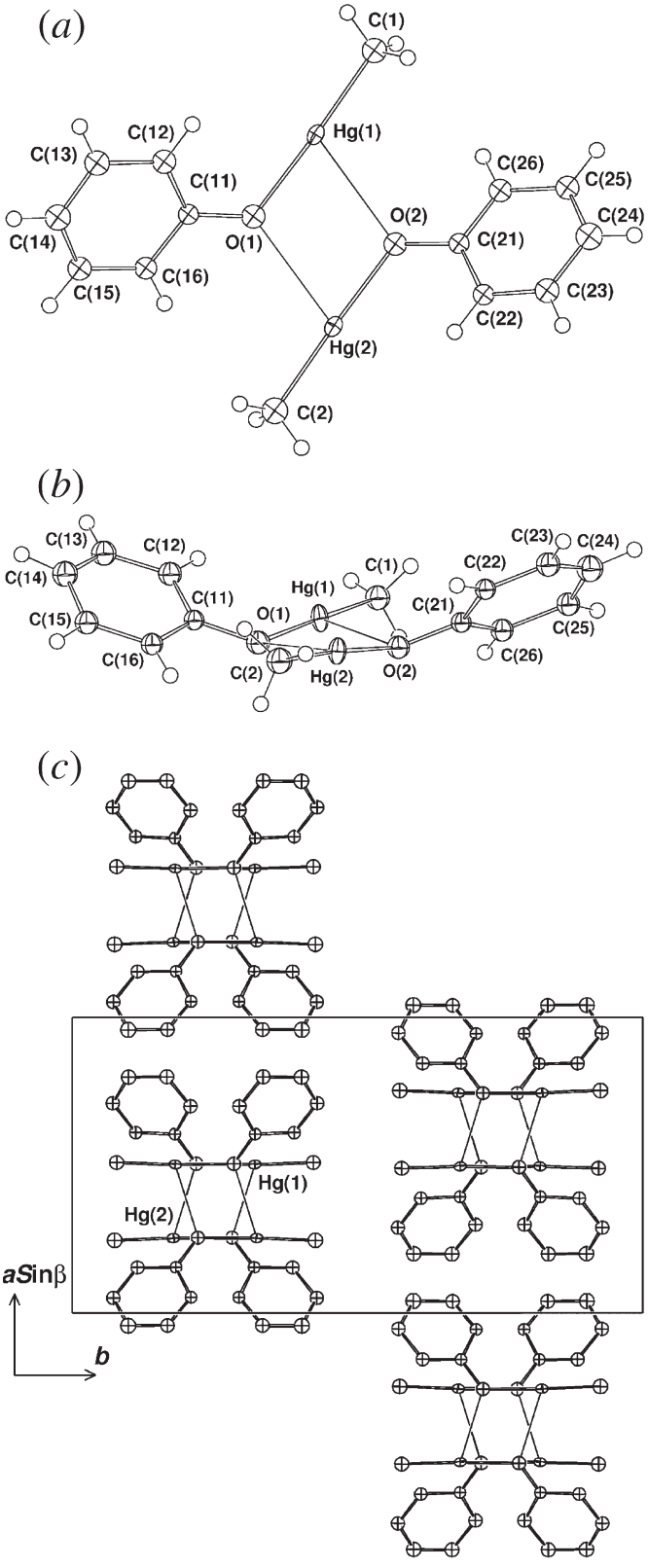


Table 2. Crystal data and structure refinement for MeHgOPh.

Empirical formula	$C_{14}H_{16}Hg_2O_2$
Formula mass	617.5
Crystal dimensions (mm^3)	0.30 × 0.07 × 0.06
Crystal system	Monoclinic
Space group	$P2_1/c$ (No. 14)
Z	4
a (Å)	10.340(2)
b (Å)	19.886(1)
c (Å)	6.914(1)
β (°)	91.200(4)
Collection ranges	$-13 \le h \le 13$; $-11 \le k \le 11$; $-8 \le l \le 8$
Temperature (K)	ca. 150
Volume ($Å^3$)	1421.4(4)
D_{calcd} (Mg m^{-3})	2.88_5
Radiation	Mo Kα (λ = 0.7107_3 Å)
Absorption coefficient (μ) (mm^{-1})	21.6
$F(000)$	1104
θ range for data collection (°)	1–27.5
Measured reflections	27 505
Independent reflections	3 196 (R_{int} = 0.072)
Data/restraints/parameters	2 345/(see text)/83
Maximum shift/error	9×10^{-4}
Goodness-of-fit	0.98
Final R indices ($I > 4\sigma(I)$)	R_1 = 0.064, wR_2 = 0.086
R indices (all data)	R_1 = 0.079, wR_2 = 0.096
Largest diff. peak and hole (e $Å^{-3}$)	–6.1, 5.3(2)

terial being fine whiskers), a full sphere of low-temperature CCD area-detector diffractometer data were measured (Bruker AXS instrument), "empirical"–multiscan absorption correction (proprietary software) being applied ($T_{min/max}$ = 0.28) (Table 2). The full-matrix least-squares refinement would support meaningful anisotropic displacement parameter form refinement for the mercury atoms only (x, y, z $U_{iso})_H$, being included and constrained at estimated values (reflection weights: $(\sigma^2(F) + 0.005F^2)^{-1}$). Neutral atom complex scattering factors were employed within the Xtal 3.7 program system (16).[3]

Acknowledgements

We thank the Australian Research Council for financial support.

[3]Supplementary data for this article are available on the journal Web site (http://canjchem.nrc.ca) or may be purchased from the Depository of Unpublished Data, Document Delivery, CISTI, National Research Council Canada, Ottawa, ON K1A 0R6, Canada. DUD 4077. For more information on obtaining material refer to http://cisti-icist.nrc-cnrc.gc.ca/irm/unpub_e.shtml. CCDC 234052 contains the crystallographic data for this manuscript. These data can be obtained, free of charge, via www.ccdc.cam.ac.uk/conts/retrieving.html (Or from the Cambridge Crystallographic Data Centre, 12 Union Road, Cambridge CB2 1EZ, UK; fax +44 1223 336033; or deposit@ccdc.cam.ac.uk).

© 2006 NRC Canada

References

1. J.L. Wardell. *In* Comprehensive organometallic chemistry. Vol. 1. *Edited by* G. Wilkinson, F.G.A. Stone, and E.W. Abel. Pergamon Press, Oxford. 1982. p. 863.
2. J.S. Casas, M.S. García-Tasende, and J. Sordo. Coord. Chem. Rev. **193–195**, 283 (1999).
3. L.G. Kuz′mina, N.G. Bokii, Y.T. Struchkov, D.N. Kravtsov, and L.G. Golovchenko. Zh. Strukt. Khim. **14**, 508 (1973).
4. D.C. Bradley, R.C. Mehrotra, I.P. Rothwell, and A. Singh. Alkoxo and aryloxo derivatives of metals. Academic Press, San Diego. 2001.
5. G. Dittmar and E. Hellner. Angew. Chem. **81**, 707 (1969).
6. A.J. Canty and J.W. Devereux. Spectrochim. Acta, **36A**, 495 (1980).
7. A.J. Bloodworth. J. Chem. Soc. C, 2051 (1970).
8. G. Holan. Tetrahedron Lett. 1985 (1966).
9. H. Schmidbaur and F. Schindler. Angew. Chem. Int. Ed. Engl. **4**, 876 (1965).
10. A.J. Canty and B.M. Gatehouse. J. Chem. Soc. Dalton Trans. 2018 (1976).
11. Y.S. Wong, P.C. Chieh, and A.J. Carty. Can. J. Chem. **51**, 2597 (1973).
12. A.J. Carty, S.F. Malone, N.J. Taylor, and A.J. Canty. J. Inorg. Biochem. **18**, 291 (1983).
13. L.F. Sytsma and R.J. Kline. J. Organomet. Chem. **54**, 15 (1973).
14. L. Pauling. The nature of the chemical bond. 3rd ed. Cornell University Press, Ithaca, New York. 1960. p. 260.
15. A.J. Canty and G.B. Deacon. Inorg. Chim. Acta, **45**, L225 (1980).
16. S.R. Hall, D.J. du Boulay, and R. Olthof-Hazekamp. The XTAL 3.7 system [computer program]. University of Western Australia, Crawley, Australia. 2001.

© 2006 NRC Canada

Synthesis and coordination chemistry of 2,2′-diboratabiphenyls[1]

Ioan Ghesner, Warren E. Piers, Masood Parvez, and Robert McDonald

Abstract: Dianionic 2,2′-diboratabiphenyl derivatives were prepared as a new class of binucleating ligands. Preliminary investigations into their coordination chemistry involved Rh complexes. Their solution and solid state structures were studied and confirm the preference for η^6–η^6 coordination of the novel ligands, rendering them isoelectronic analogues of the ubiquitous bicyclopentadienyl system. Comparative studies suggest stronger donor properties for the fulvalene ligand as compared with the 2,2′-diboratabiphenyl system.

Key words: dinucleating ligands, bimetallic complexes, rhodium complexes, boron heterocycles, X-ray structure.

Résumé : On a préparé des dérivés dianioniques du 2,2′-diboratabiphényle comme nouvelle classe de ligands binucléaires. Les études préliminaires de leur chimie de coordination ont été réalisées à l'aide de complexes du ruthénium. On a étudié leurs solutions et les structures cristallines et ces études confirment la préférence de ces nouveaux ligands pour une coordination η^6–η^6, ce qui en fait des analogues isoélectroniques du système bicyclopentadiényle qu'on retrouve partout. Des études comparatives suggèrent que, par comparaison avec le système 2,2′-boratabiphényle, le ligand fulvalène est un meilleur donneur.

Mots clés : ligands binucléaires, complexes bimétalliques, complexes du rhodium, hétérocycles du bore, structures par diffraction des rayons X.

[Traduit par la Rédaction]

Introduction

It is well-documented that organometallic bi- and polynuclear complexes can promote reactions with no precedence in mononuclear systems, or show increased reactivity compared with monometallic species (1). In addition, the physical properties (nonlinear optical (NLO) activity, luminescence, redox properties) of bimetallic complexes can be easily tuned, rendering them suitable candidates for certain applications in materials science (2). These differences in physical properties and chemical behavior, both in stoichiometric and catalytic reactions, are due to cooperative interactions between the two metals present in close proximity. Among the many bimetallic systems that have been studied, bimetallic fulvalene (bicyclopentadienyl) complexes have attracted the most attention and are still a subject of continuous investigation (3). The special position occupied by the fulvalene system in such research is due to the strong binding properties of the cyclopentadienyl ligand, and also to the fact that it can mediate the electronic communication between adjacent metal centers even in the absence of a direct metal–metal bond. Attempts to modulate the nature and extent of metal–metal communication have led to variations in the nature of the coordinating ligand, as well as the bridging ligand framework.

In this context, we became interested in 2,2′-diboratabiphenyls as dinucleating isoelectronic analogues of fulvalene ligands and report here their synthesis and coordination chemistry. The advantages of using boratabenzene ligands as cyclopentadienyl surrogates are well-documented; they are isoelectronic to Cp^- donors (both are monoanionic 6p electron donors), but offer the possibility for more control of the electronic influence of the boratabenzene ligand in catalytic reactions by adjusting the exocyclic substituents on boron (4). As a result, numerous monometallic complexes containing boratabenzene ligands have been prepared and their reactivity studied in detail (5). Bimetallic D-p-A (D = donor, p = conjugated bridge, A = acceptor) complexes containing boratabenzene ligands have also been prepared and examined for their potential application as heterobimetallic nonlinear optical chromophores (6). For these complexes in which the (boratabenzene)metal fragment acts as an electron acceptor, unexpectedly high first-order hyperpolarizability β values have been measured. More recently, a bimetallic co-

Received 6 April 2005. Published on the NRC Research Press Web site at http://canjchem.nrc.ca on 14 February 2006.

This paper is dedicated to Dr. Arthur Carty for his mentorship, outstanding contributions to organometallic chemistry, and leadership in the Canadian science community.

I. Ghesner, W.E. Piers,[2] and M. Parvez. Department of Chemistry, University of Calgary, 2500 University Drive NW, Calgary, AB T2N 1N4, Canada.
R. McDonald. X-ray Structure Laboratory, Department of Chemistry, University of Alberta, Edmonton, AB T6G 2G2, Canada.

[1]This article is part of a Special Issue dedicated to Doctor Arthur Carty.
[2]Corresponding author (e-mail: wpiers@ucalgary.ca).

 doi:10.1139/V05-220 © 2006 NRC Canada

balt complex featuring a bis(boratabenzene)benzene ligand was prepared and the ability of the novel binucleating ligand to facilitate electronic communication between the cobalt centers was evaluated (7).

Results and discussion

Synthesis and characterization of 2,2′-diboratabiphenyl ligands

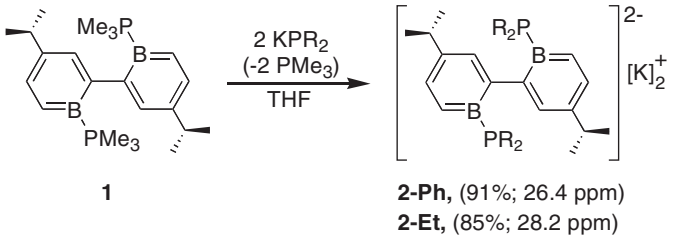
We have previously reported the synthesis of precursors to Lewis base adducts of 2,2′-diborabiphenyl (8). In this study, we explored the reactivity of bisPMe_3 adducts of 2,2′-diborabiphenyl towards a variety of nucleophiles, as a potentially useful synthetic method leading to dianionic 2,2′-diboratabiphenyl derivatives. This strategy is based on a previous observation that borabenzene–trimethylphosphine reacts with a wide range of anionic nucleophiles providing a versatile route to 1-substituted boratabenzenes (9). First we reacted the bisPMe_3 adduct **1** with KPR_2 (R = Ph, Et) as representative examples of anionic phosphorus nucleophiles and isolated the corresponding dianionic 2,2′-diboratabiphenyls in good yields (Scheme 1; chemical shifts in the schemes throughout indicate ^{11}B NMR data). The progress of the reaction was easily monitored by ^{31}P NMR by following the disappearance of the signal at –23 ppm corresponding to **1**, which was accompanied by increasing intensity for the signals corresponding to products **2-Ph** (–34 ppm) or **2-Et** (–66 ppm) and free PMe_3 (–58 ppm).

Whereas $KPEt_2$ already reacts with **1** at room temperature, prolonged heating at 75 °C is required for the reaction with $KPPh_2$. This difference in reactivity reflects the different donor strengths of the two phosphides. Nucleophilic aromatic substitution of **1** is a convenient way to access 2,2′-diboratabiphenyl derivatives since it requires a single precursor, the product is obtained in a single step, and the PMe_3 by-product is easily removed under vacuum because of its high volatility.

Compounds **2-Ph** and **2-Et** represent dianionic analogs of chelating biaryl diphosphine ligands like Fu's diphenylphosphinoboratabenzene is an anionic version of PPh_3 (10). Unlike Fu's monodentate phosphinoboratabenzene, which coordinates early, mid- and late-transition metals through the phosphorus atom in a "phosphine-like" bonding mode (10) (as opposed to through the boratabenzene π system in a "Cp-like" bonding arrangement), we were unable to coordinate either **2-Ph** or **2-Et** to a transition metal via salt elimination protocols. We investigated the reactivity of compounds **2** towards several transition metal or main group dihalides; in some cases, dissociation of the phosphide ligand with concomitant decomposition of the diborabiphenyl framework was observed.

To expand the scope of this chemistry to include other 2,2′-diboratabiphenyls, we reacted **1** with anionic carbon, nitrogen, oxygen, and sulphur nucleophiles, but were unable to isolate clean products from these reactions. It appears that while nucleophilic substitution is a direct approach, it is sensitive to solubility, steric bulk, and basicity of the incoming nucleophile, and unknown side reactions lead to complex product mixtures. Similar observations were reported by

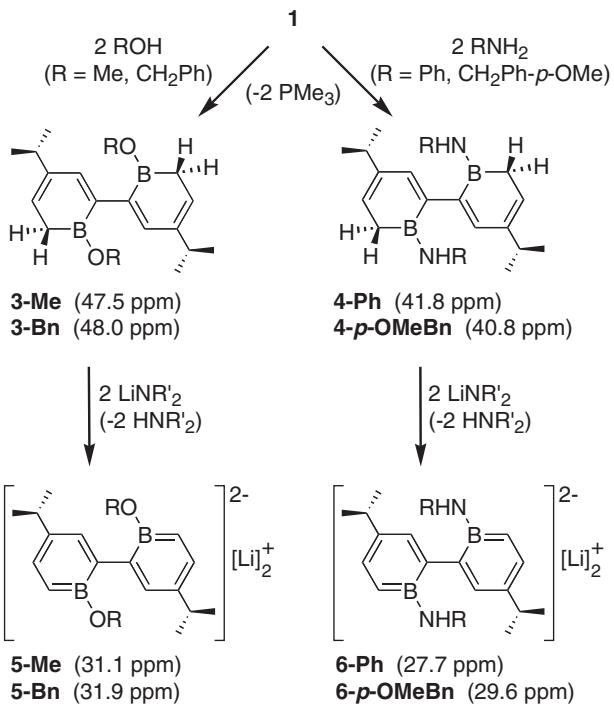
Scheme 1.



1

2-Ph, (91%; 26.4 ppm)
2-Et, (85%; 28.2 ppm)

Scheme 2.



3-Me (47.5 ppm)
3-Bn (48.0 ppm)

4-Ph (41.8 ppm)
4-*p*-OMeBn (40.8 ppm)

5-Me (31.1 ppm)
5-Bn (31.9 ppm)

6-Ph (27.7 ppm)
6-*p*-OMeBn (29.6 ppm)

Bazan and co-workers (11) for the synthesis of alkoxy- and aryloxy-boratabenzene complexes.

An alternative synthetic approach has therefore been developed based on observations that neutral, base-stabilized borabenzene and diborabiphenyl derivatives undergo reaction with protic acids via addition of AH (A = conjugate base) across the B=C bond of the borabenzene framework; deprotonation of the cyclic diboranes restores the aromaticity of the ring, providing a facile route to anionic boron heterocycles (11, 12). This method was applied successfully in the present study using alcohols and primary amines (Scheme 2). Addition of the protic acids to **1** occurred smoothly at room temperature to give bis(alkoxy) boranes **3-Me** and **3-Bn** and bis(amido) boranes **4-Ph** and **4-*p*-OMeBn** within 10 min in excellent yields. In practice, these cyclic diboranes are not isolated but are deprotonated at room temperature using bulky lithium amides, yielding the corresponding dianionic 2,2′-diboratabiphenyl derivatives **5-Me/Bn** and **6-Ph/*p*-OMeBn**. Complete removal of the PMe_3 by-product prior to deprotonation is essential for the success of the reaction. In the case of the bis(amido)diboranes, despite the presence of an acidic proton on nitrogen, selective deprotonation of the cyclic borane can be achieved in good

© 2006 NRC Canada

yields with lithium bis(trimethylsilyl)amide or lithium 2,2,6,6-tetramethylpiperidine. Using less bulky bases such as lithium dimethylamide or lithium diisopropylamide resulted in the formation of mixtures of products.

All compounds were characterized by multinuclear NMR spectroscopy and mass spectrometry. The ^{11}B NMR spectra of the neutral boranes contain diagnostic resonances at ≈48 ppm (**3-Me/Bn**) and ≈41 ppm (**4-Ph/*p*-OMeBn**), which are in the usual range for three-coordinate amino- and alkoxy-boranes. After deprotonation, these signals are significantly upfield shifted to ≈31 ppm (**5-Me/Bn**) and ≈28 ppm (**6-Ph/*p*-OMeBn**), as expected owing to the presence of a delocalized negative charge in the diboratabiphenyl rings. The room-temperature ^{1}H NMR spectra also support the proposed structures with no unexpected features being revealed. However, in the case of **6-Ph** the ^{1}H NMR spectrum measured at room temperature in THF-d^8 contained only broad signals, which made their assignment difficult. Dilution or increasing the temperature to 63 °C greatly simplified the spectrum making the assignment of the signals possible. At this temperature, three signals were observed for the hydrogens in the boratabenzene ring and one doublet centered at 1.21 ppm owing to the methyl protons, indicating a symmetrical structure. Furthermore, the N-*H* protons were observed at 5.48 ppm as a broad singlet, which became weaker in intensity upon prolonged heating because of slow decomposition of **6-Ph** to the previously reported 9,11-diboratacarbazole (12) and free aniline. Upon cooling to −40 °C, two overlapping doublets were observed for the methyl protons of the isopropyl groups, whereas no significant changes in the resonances of the boratabenzene protons were observed. While the variable-temperature NMR data are suggestive of dynamic behavior for **6-Ph** in THF-d^8, probably an equilibrium between monomeric and dimeric species, no assertion can be made on whether a structure with contact ion pairs or solvent-separated ion pairs is operative. The ^{7}Li NMR spectra, which contain one broad singlet between −4.50 and −3.54 ppm at all accessible temperatures, do not shed any further light on the solution structures.

To gain further insight into the structural details of the neutral and dianionic compounds **3**–**6**, single crystals of **3-Bn**, **4-Ph**, **5-Bn**, and **6-Ph** were grown and subjected to X-ray diffraction analysis.[3] Molecular diagrams are shown in Figs. 1 and 2, along with selected metrical parameters. Despite the presence of an sp^3 carbon atom in the boracyclohexadiene rings of structures **3-Bn** and **4-Ph**, the atoms of the two cycles are essentially coplanar. The two boracycles are twisted by 42.3° (**3-Bn**) and 77.5° (**4-Ph**), such that the boron atoms are pointing in opposite directions, which is the most sensible steric arrangement for the benzyloxy and amido groups on boron. In the structure of **4-Ph**, the boron and the nitrogen atoms are both trigonal-planar coordinated and the B—N bond length (1.412(2) Å) is slightly shorter than the 1.45 Å found in lithium 1-(dimethylamido)boratabenzene (13) for which significant double-bond character was assigned. The B—O bond distances of **3-Bn** (1.368(3) and 1.364(3) Å) are only slightly shorter than that found in the structure of $[C_5H_5B\text{-}OPh]_2ZrCl_2$ (1.385(4) Å) (11). The B—C bond lengths are in the range found for single bonds (14), while the C—C bonds of the cyclic boranes alternate between short (C(9)—C(10), C(11)—C(12), C(24)—C(25), and C(26)—C(27) for **3-Bn** and C(7)—C(8) and C(9)—C(10) for **4-Ph**) and long (C(8)—C(9), C(10)—C(11), C(23)—C(24), and C(25)—C(26) for **3-Bn** and C(8)—C(9) and C(10)—C(11) for **4-Ph**), indicating localization of the π bonds in these systems.

The structure adopted by dianionic **5-Bn** and **6-Ph** in the solid state is that of dimers with lithium atoms coordinated exocyclic and endocyclic to the boratabenzene rings (Fig. 2). The endocyclic lithiums are sandwiched by two boratabenzene rings from two diboratabiphenyl molecules and are asymmetrically bonded to the various atoms of the rings. There is a slip distortion of the endocyclic lithiums away from boron and toward the more electron-rich carbons of the ring, i.e., the carbons meta and para to the boron. The exocyclic lithium atoms are η^6 coordinated by a $O_2B_2C_2$ (Fig. 2*b*) or $N_2B_2C_2$ (Fig. 2*a*) framework of the bis(benzyloxy)- and bis(amido)-diboratabiphenyl ligands. The coordination enviroment around each exocyclic lithium atom is further completed by two molecules of THF. The Li—B distances range from 2.497(7) to 2.671(7) Å for **5-Bn** and 2.598(4) to 2.628(5) Å for **6-Ph** and are somewhat longer than the Li—C distances, which range from 2.338(6) to 2.797(23) Å for **5-Bn** and 2.367(4) to 2.484(4) Å for **6-Ph**. Upon deprotonation, the exocyclic B—O and B—N bonds (B—O = 1.418(4)–1.446(4) Å, B—N = 1.481(3) and 1.477(3) Å) are slightly elongated, indicating a less effective B—O and B—N π interaction in **5-Bn** and **6-Ph**.

Rhodium complexes

As inferred from the crystal structures of **5-Bn** and **6-Ph**, π coordination through the boratabenzene rings, as well as chelate coordination through the exocyclic substituents on boron, are possibilities for the coordination chemistry of ligands **5** and **6**. As mentioned earlier, the latter coordination mode could not be demonstrated for the phosphido boratabiphenyls (**2**). Furthermore, the presence of potentially reactive N-H functions in ligands **6** were deemed to be problematic. Therefore, initial investigations into the coordination chemistry of the ligands **5** and **6** focused on the reactions of **5-Bn** with univalent binuclear rhodium species with a view to preparing binuclear complexes bridged by the diboratabenzene framework.

Reaction of the dilithio compound **5-Bn** with 1 molar equiv. of the binuclear rhodium complexes $[(\mu\text{-Cl})\text{-}RhL_2]_2$ (L = CO, L_2 = cod) in THF occurred at room temperature to give complexes *syn*/*anti*-**7-CO** and *syn*/*anti*-**7-COD** as 1:1

[3] Supplementary data for this article are available on the journal Web site (http://canjchem.nrc.ca) or may be purchased from the Depository of Unpublished Data, Document Delivery, CISTI, National Research Council Canada, Ottawa, ON K1A 0R6, Canada. DUD 4075. For more information on obtaining material refer to http://cisti-icist.nrc-cnrc.gc.ca/irm/unpub_e.shtml. CCDC 267251–267258 (**6-Ph**, *anti*-**7-COD**, *anti*-**8-COD**, **5-Bn**, **3-Bn**, *syn*-**7-CO**, *syn*-**8-CO**, **4-Ph**) contain the crystallographic data for this manuscript. These data can be obtained, free of charge, via www.ccdc.cam.ac.uk/conts/retrieving.html (Or from the Cambridge Crystallographic Data Centre, 12 Union Road, Cambridge CB2 1EZ, UK; fax +44 1223 336033; or deposit@ccdc.cam.ac.uk).

© 2006 NRC Canada

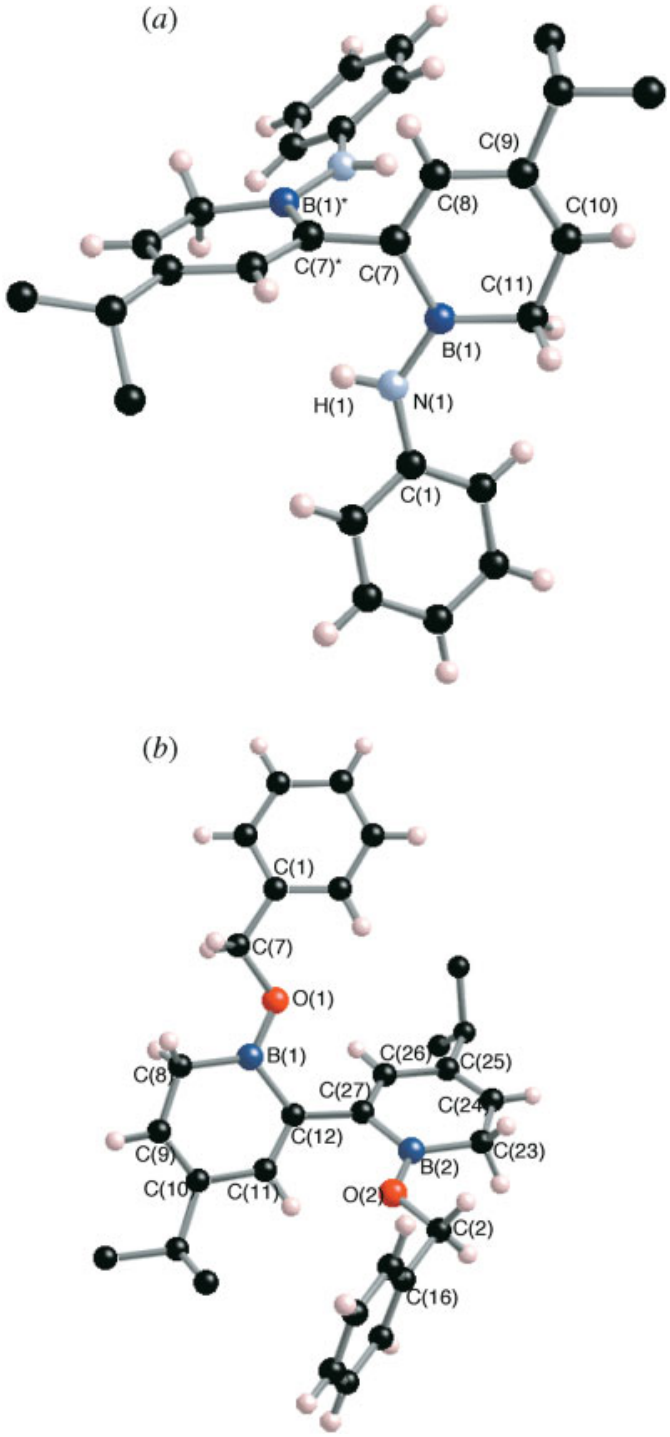


Fig. 1. CrystalMaker representation of the structure of (*a*) **4-Ph** and (*b*) **3-Bn**. Isopropyl hydrogen atoms are omitted for clarity. **4-Ph**: Selected bond lengths (Å): N(1)—B(1), 1.412(2); N(1)—C(1), 1.404(2); B(1)—C(11), 1.572(3); B(1)—C(7), 1.560(3); C(11)—C(10), 1.506(2); C(10)—C(9), 1.334(2); C(9)—C(8), 1.472(2); C(8)—C(7), 1.352(2); C(7)—(7)*, 1.493(3). Selected bond angles (°): C(1)-N(1)-B(1), 134.30(15); C(7)-B(1)-C(11), 117.52(15); N(1)-B(1)-C(7), 116.58(15); N(1)-B(1)-C(11), 125.90(17). **3-Bn**: Selected bond lengths (Å): B(1)—O(1), 1.368(3); B(2)—O(2), 1.364(3); B(1)—C(8), 1.565(4); B(2)—C(23), 1.566(4); B(1)—C(12), 1.547(4); B(2)—C(27), 1.552(4); C(8)—C(9), 1.486(4); C(9)—C(10), 1.338(4); C(10)—C(11), 1.462(4); C(11)—C(12), 1.359(3); C(23)—C(24), 1.475(4); C(24)—C(25), 1.334(4); C(25)—C(26), 1.458(4); C(26)—C(27), 1.364(4); C(12)—C(27), 1.487(3). Selected bond angles (°): C(7)-O(1)-B(1), 120.9(2); C(22)-O(2)-B(2), 120.8(2).

mixtures of syn- and anti-facial isomers in high yields (Scheme 3). These isomers arise depending on the relative facial coordination of the second metal fragment once the first is in place; the isomers do not undergo exchange under thermal or photochemical duress. Since their relative abundance is to some degree dependent on the conditions employed in the reaction (for example, in the case of the carbonyl complex **7-CO**, using toluene instead of THF as the reaction medium resulted in an increase in the ratio of the syn product to 3:1), these mixtures are likely kinetic product mixtures. In idealized structures where the B-C_{ipso}-C_{ipso}-B torsion angle is 180 °C, the syn isomers have C_2 symmetry and are present as a pair of enantiomers, while the anti isomers are C_i symmetric, with a centre of inversion at the C_{ipso}-C_{ipso} midpoint, and therefore achiral. In reality, there is some variation in the B-C_{ipso}-C_{ipso}-B torsion angle in the syn isomers (see the following), but they retain C_2 symmetry.

Attempts to separate the isomers by column chromatography were unsuccessful. Enriched samples of s*yn*-**7-CO** could be obtained by fractional crystallization from the 3:1 mixtures prepared in toluene, but complete separation of syn from anti was not possible by this method. In the case of **7-COD**, most of the syn isomer was extracted in isopentane, whereas the anti isomer and small amounts of the syn isomer remained undissolved and were separated by filtration. All complexes were characterized by NMR spectroscopy and high-resolution mass spectrometry, and two examples were studied by X-ray crystallographic methods.

Single crystals of both **7-CO** and **7-COD** were obtained from isopentane solutions and analyzed by X-ray diffraction. CrystalMaker diagrams of *syn*-**7-CO** and of the *anti*-**7-COD** isomer are shown in Figs. 3 and 4 along with selected metrical data. In both complexes, the metal is π coordinated to the boratabenzene rings in an η^6 fashion. The two boracycles are twisted by 73.7° in *syn*-**7-CO**, but are aligned essentially coplanar in anti-**7-COD** such that the substituents on boron are pointing in opposite directions. In both complexes, the Rh—B and Rh—C bond distances are suggestive of slip distortion of the rhodium atom away from boron and toward the carbons meta and para to the boron. For Rh complexes, the magnitude of the $^1J_{RhC}$ coupling constants, as determined from ^{13}C NMR measurements, can be used as an indication of the extent of ring slippage in solution (15). Accordingly, the slippage from η^6 to η^3 coordination is accompanied by smaller $^1J_{RhC}$ observed coupling constants for the less-coordinated atoms. The coupling constant for the bonds between Rh and the C atoms ortho to boron could not be determined owing to broadening of these signals by the quadrupolar boron nucleus. The remaining $^1J_{RhC}$ coupling constants are in the range of 3.1–4.1 Hz for *syn*/*anti*-**7-CO** and 2.8–4.1 Hz for *syn*/*anti*-**7-COD**, with the smaller coupling constants assigned to Rh—C(4) (Fig. 3) and Rh—

© 2006 NRC Canada

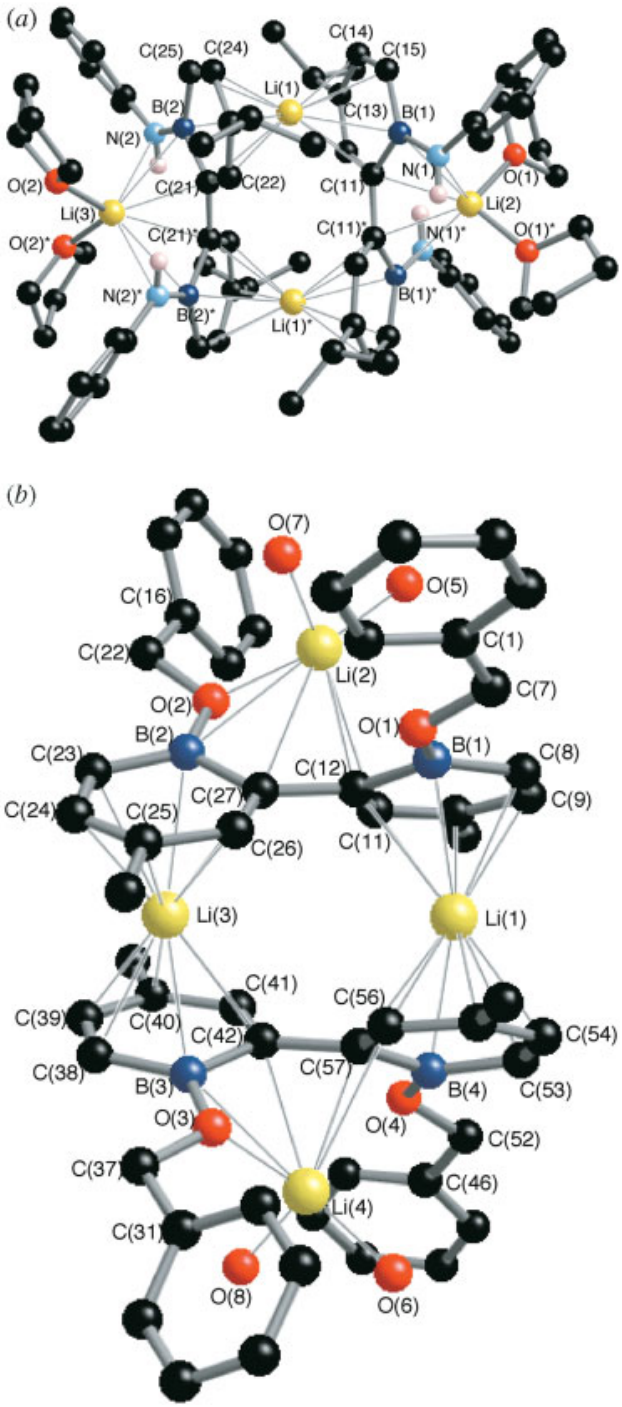
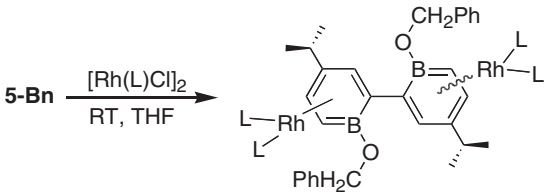


Fig. 2. CrystalMaker representation of the structure of (*a*) [**6-Ph**·$(THF)_2]_2$ and (*b*) [**5-Bn**·$(THF)_2]_2$. In the case of [**5-Bn**·$(THF)_2]_2$ only the central part of the dimer is shown. [**6-Ph**·$(THF)_2]_2$: Selected bond lengths (Å): N(1)—B(1), 1.481(3); N(2)—B(2), 1.477(3); B(1)—C(11), 1.528(3); B(1)—C(15), 1.505(3); B(2)—C(21), 1.536(3); B(2)—C(25), 1.512(3); Li(1)—B(1), 2.612(4); Li(1)—C(11), 2.484(4); Li(1)—C(12), 2.386(4); Li(1)—C(13), 2.380(4); Li(1)—C(14), 2.375(4); Li(1)—C(15), 2.473(4); Li(1)—B(2), 2.598(4); Li(1)—C(21), 2.470(4); Li(1)—C(22), 2.367(4); Li(1)—C(23), 2.392(4); Li(1)—C(24), 2.390(4); Li(1)—C(25), 2.472(4); Li(2)—O(1), 1.901(4); Li(2)—N(1), 2.595(3); Li(2)—B(1), 2.601(5); Li(2)—C(11), 2.404(6); Li(3)—N(2), 2.684(3); Li(3)—B(2), 2.628(5); Li(3)—(21), 2.379(6). Selected bond angles (°): C(31)-N(1)-B(1), 127.47(16); C(41)-N(2)-B(2), 130.83(17); N(1)-B(1)-C(11), 119.01(17); N(1)-B(1)-C(15), 125.42(17); N(2)-B(2)-C(21), 119.54(17); N(2)-B(2)-C(25), 125.03(18). $C_5B(1)/C_5B(1)$*, 50.7 (°); $C_5B(2)/C_5B(2)$*, 44.9 (°). [**5-Bn**·$(THF)_2]_2$: Selected bond lengths (Å): O(1)—B(1), 1.418(4); Li(1)—B(1), 2.598(7); Li(1)—C(8), 2.477(6); Li(1)—C(9), 2.377(6); Li(1)—C(10), 2.356(6); Li(1)—C(11), 2.366(6); Li(1)—C(12), 2.488(6); O(2)—B(2), 1.446(4); Li(2)—O(2), 1.976(6); Li(2)—B(2), 2.671(7); Li(2)—C(27), 2.739(6); Li(2)—C(12), 2.413(6); Li(2)—C(11), 2.676(7); Li(3)—B(2), 2.536(7); Li(3)—C(23), 2.449(6); Li(3)—C(24), 2.370(7); Li(3)—C(25), 2.401(6); Li(3)—C(26), 2.384(6); Li(3)—C(27), 2.425(6); O(3)—B(3), 1.440(4); Li(3)—B(3), 2.497(7); Li(3)—C(38), 2.365(6); Li(3)—C(39), 2.338(6); Li(3)—C(40), 2.421(6); Li(3)—C(41), 2.438(6); Li(3)—C(42), 2.472(6); O(4)—B(4), 1.433(4); Li(1)—C(53), 2.499(6); Li(1)—C(54), 2.388(6); Li(1)—C(55), 2.358(6); Li(1)—C(56), 2.352(6); Li(1)—C(57), 2.470(6); Li(4)—O(3), 1.969(7); Li(4)—B(3), 2.526(8); Li(4)—C(42), 2.604(7); Li(4)—C(57), 2.447(7); Li(4)—C(56), 2.797(23). Selected bond angles (°): C(7)-O(1)-B(1), 119.2(3); C(22)-O(2)-B(2), 117.8(3); C(37)-O(3)-B(3), 118.9(3); C(52)-O(4)-B(4), 118.0(3). $C_5B(1)/C_5B(2)$, 45.2 (°), $C_5B(3)/C_5B(4)$, 39.7 (°).

Scheme 3.



syn/anti-**7-CO**, L = CO
syn/anti-**7-COD**, L_2 = cyclooctadiene

C(12) (Fig. 4). Consistent with this observation, the bond lengths of the metal to the carbon atoms C(4) and C(12) are longer than those to C(5), C(6) and C(13), C(14). The average bonding distance of rhodium to the CO ligands in *syn*-**7-CO** is 1.872(3) Å and is slightly longer than the values found in the structure of the fulvalene dirhodium complex $(\eta^5{:}\eta^5\text{-}C_{10}H_8)Rh_2(CO)_4$ (1.861(4) and 1.866(4) Å) (16). In keeping with this finding, carbonyl stretching frequencies in *anti*-**7-COD** were found at higher values (2158 and 2120 cm^{-1}) than those reported for the fulvalene system (2037 and 1978 cm^{-1}) (16), suggesting stronger donor properties for the fulvalene ligand as compared with the 2,2′-diboratabiphenyl system. The related mononuclear complexes cyclooctadiene boratabenzene rhodium $(C_5H_5B\text{-}R)Rh(cod)$ (R = Ph, Me) (17) and bis(ethylene)boratabenzene rhodium $(C_5H_5B\text{-}R)Rh(C_2H_4)_2$ (R = Ph, NMe_2) (18) have been also prepared. These complexes were structurally characterized and show Rh—B distances shorter (2.398 Å, R = Ph) and longer (2.516 Å, R = NMe_2) than those found in *syn*-**7-CO** (2.488(3) Å) and *anti*-**7-COD** (2.439(2) Å), consistent with the differences in π-donating abilities of the exocyclic substituents on boron.

Interestingly, the mononuclear bis(ethylene)boratabenzene rhodium complexes were found to be efficient catalysts for

© 2006 NRC Canada

Fig. 3. CrystalMaker representation of the structure of *syn*-**7-CO**. Hydrogen atoms are omitted for clarity. Selected bond lengths (Å): O(3)—B(1), 1.392(4); B(1)—C(3), 1.536(4); B(1)—C(7), 1.534(4); Rh(1)—C(1), 1.866(3); Rh(1)—C(2), 1.878(3); C(1)—O(1), 1.139(4); C(2)—O(2), 1.135(4); Rh(1)—B(1), 2.488(3); Rh(1)—C(3), 2.393(2); Rh(1)—C(4), 2.331(3); Rh(1)—C(5), 2.246(3); Rh(1)—C(6), 2.304(3); Rh(1)—C(7), 2.360(3); C(3)—C(3)*, 1.497(4). Selected bond angles (°): C(12)-C(11)-O(3), 112.9(2); C(11)-O(3)-B(1), 122.9(2); O(3)-B(1)-C(3), 117.8(2); O(3)-B(1)-C(7), 127.2(2); C(1)-Rh(1)-C(2), 89.95(13).

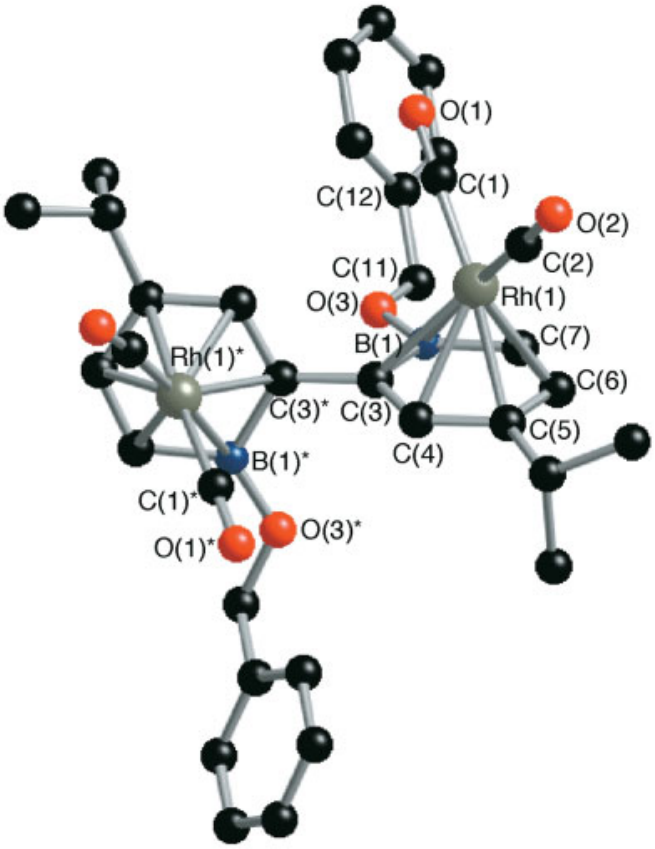
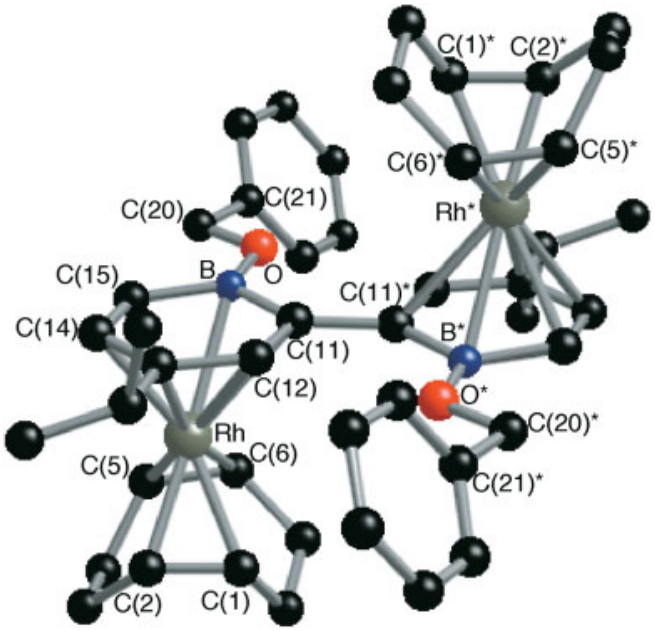


Fig. 4. CrystalMaker representation of the structure of *anti*-**7-COD**. Hydrogen atoms are omitted for clarity. Selected bond lengths (Å): O—B, 1.399(3); B—C(11), 1.550(3); B—C(15), 1.528(3); C(11)—C(11)*, 1.500(4); Rh-B, 2.439(2); Rh—C(1), 2.150(2); Rh—C(2), 2.140(2); Rh—C(5), 2.114(2); Rh—C(6), 2.119(2); Rh—C(11), 2.428(2); Rh—C(12), 2.302(2); Rh—C(13), 2.241(2); Rh—C(14), 2.273(2); Rh—C(15), 2.273(2). Selected bond angles (°): C(21)-C(20)-O, 109.0(2); C(20)-O-B, 120.93(18); O-B-C(11), 121.8(2); O-B-C(15), 122.2(2).



the C-H activation of alkanes (18). Therefore, the reaction chemistry of **7-CO** was also briefly investigated. First, it should be noted that solutions of *syn*- or *anti*-**7-CO** or **7-COD** cannot be converted to their opposite stereoisomer at any accessible temperature. Photolysis of carbonyl complexes **7-CO** or reactions with trimethylamine-*N*-oxide, showed no evidence for the formation of any products as determined by NMR and IR spectroscopy, the starting materials being fully recovered. Similarly, no product was obtained when **7-CO** was photolysed in the presence of excess cyclooctadiene. On the other hand, $(\eta^5{:}\eta^5\text{-}C_{10}H_8)Rh_2(CO)_4$ was found to react with trimethylamine-*N*-oxide and cyclooctatetraene, yielding the tricarbonyl species $(\eta^5{:}\eta^5\text{-}C_{10}H_8)(\mu\text{-}CO)(CO)_2Rh_2$ and the bis(cyclooctatetraene) complex $(\eta^5{:}\eta^5\text{-}C_{10}H_8)(\eta^4\text{-}1,2,5,6\text{-cyclooctatetraene})_2Rh_2$, respectively (16). Attempts to study the electrochemistry of *syn*-**7-CO** and *anti*-**7-COD** indicate that these compounds undergo irreversible oxidation to unidentified products. This contradicts the findings for the fulvalene system $(\eta^5{:}\eta^5\text{-}C_{10}H_8)Rh_2(CO)_4$ for which reversible oxidation to the corresponding dication with concomitant formation of a Rh—Rh bond was reported (19). These observations can be explained by the poorer donor properties of the diboratabenzene ligands relative to the fulvalene bridge. The present ligand system is thus unable to stabilize coordinatively unsaturated intermediates or higher oxidation state complexes, resulting in relatively unreactive compounds in comparison to the fulvalene congeners.

In previous work, we reported the synthesis of dilithio 9,11-diboratacarbazole heterocycles (12). The structure of this dilithio derivative and computational exploration of the distribution of charge in this novel heterocyclic framework suggested η^6 bonding as the preferential coordination mode as opposed to η^5 coordination through the $B_2N_2C_2$ core. On the other hand, the η^5 mode is emphasized in the coordination chemistry of the isoelectronic fluorenyl anion (20). Indeed, reaction of 10-phenyl-9,11-diboratacarbazole with 1 equiv. of Cp^*ZrCl_3 showed no evidence for the formation of the η^5-coordination product, giving rather complicated mixtures of products. However, similar reactions to those described above with $[(\mu\text{-}Cl)\text{-}RhL_2]_2$ (L = CO, L_2 = cod) in THF allowed us to isolate complexes *syn*/*anti*-**8-CO** and *anti*-**8-COD** in high yields as the only products (Scheme 4). Interestingly, because the diborabiphenyl framework is locked into a chelating arrangement by the bridging $[NR]^{2-}$ fragment, in these compounds the syn isomer is the meso compound (idealized C_s symmetry), while the anti isomer is of C_2 symmetry and therefore present as a pair of enantiomers.

© 2006 NRC Canada

Scheme 4.

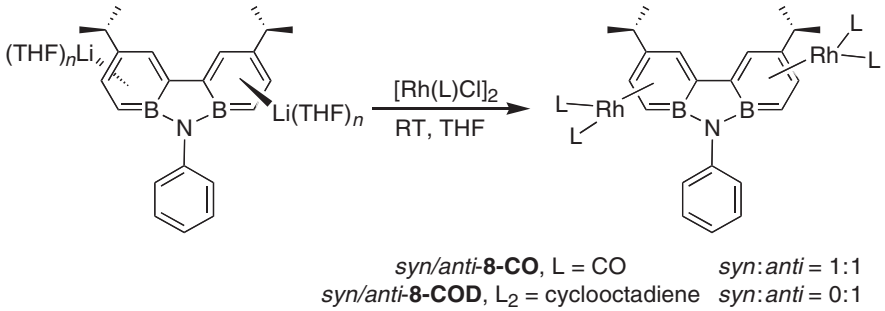


Fig. 5. CrystalMaker representation of the structure of *syn*-**8-CO**. Hydrogen atoms are omitted for clarity. Selected bond lengths (Å): N(1)—B(1), 1.457(6); N(1)—B(2), 1.461(6); Rh(1)—C(1), 1.847(4); Rh(1)—C(2), 1.862(5); C(1)—O(1), 1.160(5); C(2)—O(2), 1.147(6); Rh(1)—B(1), 2.494(4); Rh(1)—C(5), 2.303(4); Rh(1)—C(6), 2.257(4); Rh(1)—C(7), 2.214(4); Rh(1)—C(8), 2.383(4); Rh(1)—C(9), 2.527(4); Rh(2)—B(2), 2.486(4); Rh(2)—C(3), 1.862(6); Rh(2)—C(4), 1.853(5); C(3)—O(3), 1.138(6); C(4)—O(4), 1.156(6); Rh(2)—C(10), 2.389(4); Rh(2)—C(11), 2.330(4); Rh(2)—C(12), 2.211(5); Rh(2)—C(13), 2.278(4); Rh(2)—C(14), 2.395(4). Selected bond angles (°): C(21)-N(1)-B(1), 126.1(3); C(21)-N(1)-B(2), 125.8(4); B(1)-N(1)-B(2), 108.0(3); C(1)-Rh(1)-C(2), 91.41(18); C(3)-Rh(2)-C(4), 92.0(2). Mean deviation from planarity $C_{10}B_2N$: 0.0733 Å. $C_{10}B_2N/C_6$, 45.3 (°).

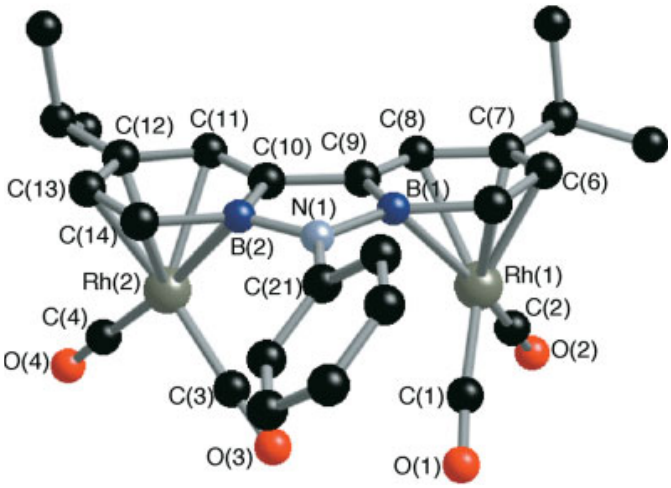
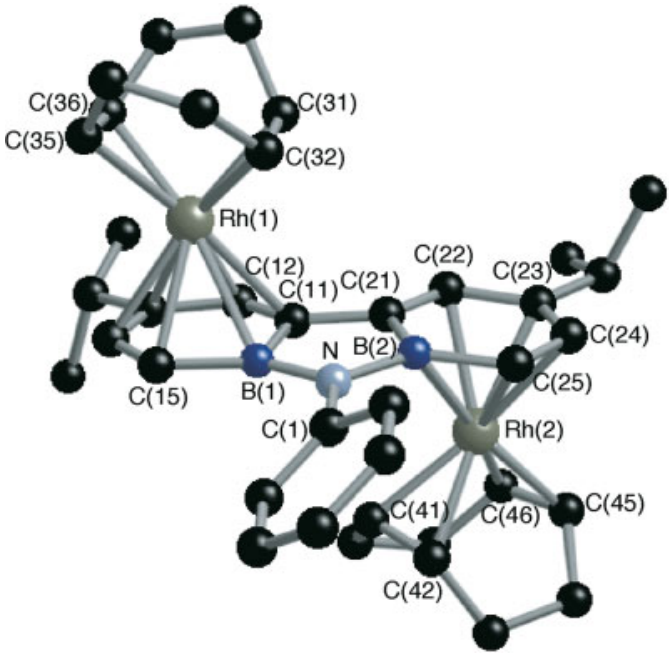


Fig. 6. CrystalMaker representation of the structure of *anti*-**8-COD**. Hydrogen atoms are omitted for clarity. Selected bond lengths (Å): C(1)—N, 1.412(3); N—B(1), 1.466(3); N—B(2), 1.465(3); Rh(1)—B(1), 2.457(3); Rh(1)—C(11), 2.294(2); Rh(1)—C(12), 2.311(2); Rh(1)—C(13), 2.261(2); Rh(1)—C(14), 2.246(2); Rh(1)—C(15), 2.376(2); Rh(1)—C(31), 2.106(3); Rh(1)—C(32), 2.098(3); Rh(1)—C(35), 2.131(3); Rh(1)—C(36), 2.123(3); Rh(2)—B(2), 2.441(2); Rh(2)—C(21), 2.354(2); Rh(2)—C(22), 2.314(2); Rh(2)—C(23), 2.232(2); Rh(2)—C(24), 2.290(2); Rh(2)—C(25), 2.397(2); Rh(2)—C(41), 2.135(2); Rh(2)—C(42), 2.167(2); Rh(2)—C(45), 2.134(2); Rh(2)—C(46), 2.147(2). Selected bond angles (°): C(1)-N-B(1), 125.47(19); C(1)-N-B(2), 126.52(19); B(1)-N-B(2), 107.81(18). Mean deviation from planarity $C_{10}B_2N$: 0.0515 Å. $C_{10}B_2N/C_6$, 39.0 (°).



While complex **8-CO** forms as a 1:1 mixture of syn and anti isomers, only the anti isomer of **8-COD** was detected by NMR spectroscopy. Our attempts to isolate the isomers of *syn/anti*-**8-CO** by column chromatography or fractional crystallization failed. However, cooling solutions of *syn/anti*-**8-CO** in isopentane at –35 °C afforded orange single crystals. X-ray diffraction analysis revealed the compound to be the syn isomer (Fig. 5). Single crystals of *anti*-**8-COD** were also grown from a CH_2Cl_2–pentane mixture and also subjected to X-ray diffraction analysis. A molecular diagram is provided in Fig. 6 along with selected metrical data.

The molecular structures of *syn*-**8-CO** and *anti*-**8-COD** confirm the predicted η^6-coordination mode for the 9,11-diboratacarbazole ligand. Related (fluorenyl)rhodium complexes have not been structurally characterized, but the η^5 binding was confirmed by X-ray diffraction for a (fluorenyl)Co(COD) complex (20*a*). Slip distortion of the rhodium atoms, similar to those observed in the structures of *syn*-**7-CO** and *anti*-**7-COD**, is also found in the structures of *syn*-**8-CO** and *anti*-**8-COD**. Accordingly, the Rh—C distances are not equivalent and range from 2.211(5) to 2.527(4) Å for *syn*-**8-CO** and 2.232(2) to 2.397(2) Å for *anti*-**8-COD**, with bonds from rhodium to the carbons ortho to boron being the longest. Distances and angles within the $C_{10}B_2N$ ring are comparable to those found in the structure

© 2006 NRC Canada

of the dilithio 10-phenyl-9,11-diboratacarbazole (12). Using $^1J_{RhC}$ coupling constants as a measure of the Rh—C interaction in solution, one can find values ranging from 2.5–4.4 Hz (**8-CO**) and 2.5–3.9 Hz (**8-COD**), with the smaller values assigned to Rh(1)—C(8) and Rh(2)—C(11) in **8-CO** and Rh(1)—(C12) and Rh(2)—C(22) in **8-COD**. These findings suggest that a similar slip distortion to that found in the solid state is maintained in solution.

Conclusions

2,2′-Diboratabiphenyl derivatives bearing alkoxy, amido, or phosphido exocyclic substituents on boron were prepared and their structural details in solution and the solid state examined. The coordination chemistry of the novel ligands and of the previously reported 9,11-diboratacarbazole was investigated in view of their isoelectronic relationship with the fulvalene and fluorenyl anions. Reactions of 9,11-diboratacarbazole ligand with dinuclear Rh complexes resulted in η^6 coordination of Rh to the flanking six-membered rings of the diboratacarbazole framework. These observations confirm the predicted coordination chemistry of this ligand with transition metals, as the η^5 mode is emphasized in the coordination chemistry of the fluorenyl anion. While preliminary reactions of phosphido-substituted 2,2′-diboratabiphenyl with transition metal dihalides or monohalides gave no isolable products, the η^6-coordination mode was confirmed in the case of the benzyloxy derivatives by the isolation of their Rh complexes as mixtures of syn and anti isomers. Electrochemical studies on these Rh complexes showed no evidence for reversible redox events suggesting that the 2,2′-diboratabiphenyl ligand is not capable of sustaining electronic communication between adjacent Rh centers. This is probably due to the slip distortion of the rhodium atom away from boron and the bridging carbon atoms observed in the solid state and in solution.

Experimental

General considerations

All manipulations were performed under an argon atmosphere using standard glovebox and Schlenk techniques. Toluene, hexane, and THF solvents were dried and purified by passing through activated alumina and Q5 columns (21). Isopentane was dried and distilled from Na. Benzyl alcohol, methanol, aniline, 4-methoxybenzylamine, and lithium bis(trimethylsilyl)amide were purchased from Aldrich Chemical Co. and distilled prior to use. $[Rh(COD)Cl]_2$ and $[Rh(CO)_2Cl]_2$ were purchased from Strem Chemicals. Solid lithium diisopropylamide (LDA) was prepared by addition of a 1.6 mol L^{-1} *n*-hexane solution of *n*-BuLi (100 mL, 0.16 mol) to HN-*i*-Pr_2 (23.5 mL, 0.17 mol) in *n*-hexane (50 mL), followed by evaporation to dryness. Potassium diethylphosphide was prepared as a white solid by addition of $KCH_2C_6H_5$ to Et_2PH at 0 °C. The mixture was stirred for 3 h at room temperature, the volatiles removed under vacuum, and the solid washed with *n*-hexane. The bisPMe_3 adduct of 2,2′-diborabiphenyl **1** (8) and lithium 2,2,6,6-tetramethylpiperidene (22) were prepared according to a reported procedure.

All NMR spectra were performed in dry, oxygen-free C_6D_6 or THF-d_8. ^{1}H, $^{13}C\{^1H\}$, DEPT-135, ^{11}B, ^{7}Li, COSY, and HMQC NMR experiments were recorded on a Bruker DRX-400 spectrometer. ^{1}H and $^{13}C\{^1H\}$ NMR spectra were calibrated using signals from the solvent and are reported downfield from $SiMe_4$, whereas ^{11}B and ^{7}Li NMR spectra are referenced to external $BF_3{\cdot}OEt_2$ and LiCl, respectively.

Mass spectra were recorded on Esquire 3000, Kratos MS80RFA, or Micromass VG7070 spectrometers. The pattern of boron-containing ions was compared with theoretical values.

Melting points were determined by DSC-TG analysis on a Netzsch STA 449C from 25 to 600 °C at a heating rate of 5 K/min.

Synthesis of 2-Ph

Potassium diphenylphosphide (1.14 mL, 0.5 mol L^{-1} in THF) was added at room temperature to a solution of the bisPMe_3 adduct of 2,2′-diborabiphenyl (110 mg, 0.28 mmol) in 6 mL THF. The solution was stirred for 24 h under reflux, and the volatiles were removed under vacuum. The solid was slurred in *n*-hexane, sonicated and then filtered to collect a yellow solid (177 mg, 91%), mp 79 °C. ^{1}H NMR (THF-d_8, 400 MHz) δ: 0.95 (d, 12H, CH_3-*i*-Pr, $^3J_{HH}$ = 6.9 Hz), 2.50 (sept., 2H, C*H*-*i*-Pr, $^3J_{HH}$ = 6.9 Hz), 6.33 (dd, 2H, CH^3, $^3J_{PH}$ = 9.9, 4.4 Hz), 6.82 (d, 2H, CH^6, $^4J_{PH}$ = 5.2 Hz), 6.91 (d, 2H, CH^4, $^3J_{HH}$ = 9.9 Hz), 7.01 (t, 4H, C_6H_5-para, $^3J_{HH}$ = 6.9 Hz), 7.09 (dd, 8H, C_6H_5-meta, $^3J_{HH}$ = 7.2, 7.2 Hz), 7.47 (dd, 8H, C_6H_5-ortho, $^3J_{HH}$ = 6.5, 6.5 Hz). $^{13}C\{^1H\}$ NMR (THF-d_8, 100 MHz) δ: 22.56 (s, CH$_3$-*i*-Pr), 32.80 (s, *C*H-*i*-Pr), 122.74 (s, C_6H_5-para), 124.98 (d, C_6H_5-meta, $^3J_{PC}$ = 6.0 Hz), 125.52 (d, CH^4, $^3J_{PC}$ = 5.0 Hz), 129.04 (s, br, CH^3), 131.22 (dd, CH^6, $^3J_{PC}$ = 9.2 Hz, $^4J_{PC}$ = 3.7 Hz), 132.58 (d, C_6H_5-ortho, $^2J_{PC}$ = 13.1 Hz), 144.46 (s, br, *C*-ipso). ^{11}B NMR (THF-d_8, 128 MHz) δ: 26.42 (s, br). ^{31}P NMR (THF-d_8, 162 MHz) δ: –34.15 (s, *P*Ph_2). ESI-MS *m*/*z*: 721 $[M + K]^+$, 497 $[M - PPh_2]^+$.

Synthesis of 2-Et

Potassium diethylphosphide (134 mg, 1.05 mmol) in 2 mL THF was added at room temperature to a solution of the bisPMe_3 adduct of 2,2′-diborabiphenyl (202 mg, 0.52 mmol) in 6 mL THF. The solution was stirred for 2 h at room temperature, and the volatiles were removed under vacuum. The product was obtained as an orange solid after recrystallization from THF–pentane (217 mg, 85%), mp 92 °C. ^{1}H NMR (THF-d_8, 400 MHz) δ: 1.00 (dt, 12H, PCH_2CH_3, $^3J_{HH}$ = 7.5 Hz, $^3J_{PH}$ = 12.6 Hz), 1.22 (d, 12H, CH_3-*i*-Pr, $^3J_{HH}$ = 6.9 Hz), 1.59 (m, 8H, PCH_2CH_3), 2.77 (sept., 2H, C*H*-*i*-Pr, $^3J_{HH}$ = 6.9 Hz), 6.57 (dd, 2H, CH^3, $^3J_{HH}$ = 9.9 Hz, $^3J_{PH}$ = 3.8 Hz), 6.87 (ddd, 2H, CH^6, $^4J_{PH}$ = 5.6 Hz, $^4J_{HH}$ = 1.6 Hz, $^5J_{PH}$ = 1.6 Hz), 6.97 (dd, 2H, CH^4, $^4J_{HH}$ = 1.5 Hz, $^3J_{HH}$ = 9.8 Hz). $^{13}C\{^1H\}$ NMR (THF-d_8, 100 MHz) δ: 13.55 (d, PCH_2CH_3, $^2J_{PC}$ = 10.0 Hz), 19.37 (d, br, PCH_2CH_3, $^1J_{PC}$ = 6.1 Hz), 26.09 (s, CH$_3$-*i*-Pr), 36.20 (s, *C*H-*i*-Pr), 127.39 (s, br, CH^3), 127.57 (d, CH^4, $^3J_{PC}$ = 4.6 Hz), 130.79 (s, *C*-ipso), 133.79 (dd, CH^6, $^3J_{PC}$ = 8.4 Hz, $^4J_{PC}$ = 2.3 Hz). ^{11}B NMR (THF-d_8, 128 MHz) δ: 28.26 (s, br). ^{31}P NMR (THF-d_8, 162 MHz) δ: –65.85. ESI-MS *m*/*z*: 529 $[M + K]^+$, 491 $[M + H]^+$, 453 $[M - K + 2H]^+$, 401 $[M - PEt_2K + K]^+$.

© 2006 NRC Canada

Synthesis of 3-Me

Methanol (48 mg, 1.50 mmol) in 2 mL toluene was added dropwise to a stirred solution of the bisPMe$_3$ adduct of 2,2′-diborabiphenyl (290 mg, 0.75 mmol) in 6 mL toluene at room temperature over a period of 10 min. The solution was stirred for 30 min at room temperature, and the volatiles were removed under vacuum. The product was obtained as a colourless solid after recrystallization from isopentane at –35 °C (210 mg, 94%), mp 52 °C. ^{1}H NMR (C_6D_6, 400 MHz) δ: 1.18 (d, 12H, CH_3-*i*-Pr, $^3J_{HH}$ = 6.9 Hz), 1.61 (d, 4H, BCH_2^3, $^3J_{HH}$ = 4.3 Hz), 2.50 (sept., 2H, C*H*-*i*-Pr, $^3J_{HH}$ = 6.8 Hz), 3.30 (s, 6H, O-CH_3), 5.86 (t, 2H, CH^4, $^3J_{HH}$ = 4.5 Hz), 7.37 (d, 2H, CH^6, $^4J_{HH}$ = 1.6 Hz). ^{13}C{^{1}H} NMR (C_6D_6, 100 MHz) δ: 20.57 (s, br, BCH_2^3), 22.55 (s, CH_3-*i*-Pr), 35.11 (s, *C*H-*i*-Pr), 52.97 (s, O-CH_3), 123.85 (s, CH^4), 143.48 (s, *C-ipso*), 147.25 (s, CH^6). ^{11}B NMR (C_6D_6, 128 MHz) δ: 47.49 (s, br). EI-MS *m*/*z*: 298 [M$^+$], 283 [M$^+$ – CH_3], 266 [M$^+$ – OCH_3Ph], 255 [M$^+$ – $CH(CH_3)_2$], 149 [M$^+$/2], 73 [$(CH_3)_2COCH_3^+$], 43 [$CH(CH_3)_2^+$]. EI-HR-MS calcd. for $C_{18}H_{28}O_2{}^{11}B_2$ (amu): 298.22754; found: 298.22960.

Synthesis of 3-Bn

Benzyl alcohol (112 mg, 1.04 mmol) in 2 mL toluene was added dropwise to a stirred solution of the bisPMe$_3$ adduct of 2,2′-diborabiphenyl (200 mg, 0.52 mmol) in 5 mL toluene at room temperature over a period of 10 min. The solution was stirred for 30 min at room temperature, and the volatiles were removed under vacuum. The product was obtained as a light-brown solid in quantitative yield. Suitable crystals for X-ray diffraction study were grown by cooling a solution of **3-Bn** in isopentane at –35 °C, mp 84 °C. ^{1}H NMR (C_6D_6, 400 MHz) δ: 1.15 (d, 12H, CH_3-*i*-Pr, $^3J_{HH}$ = 6.9 Hz), 1.69 (d, 4H, BCH_2^3, $^3J_{HH}$ = 3.6 Hz), 2.51 (sept., 2H, C*H*-*i*-Pr, $^3J_{HH}$ = 6.6 Hz), 4.66 (s, 4H, O-CH_2-C_6H_5), 5.85 (t, 2H, CH^4, $^3J_{HH}$ = 3.6 Hz), 7.09 (m, 6H, C_6H_5-meta + para), 7.25 (m, 4H, C_6H_5-ortho), 7.59 (d, 2H, CH^6, $^4J_{HH}$ = 1.8 Hz). ^{13}C{^{1}H} NMR (C_6D_6, 100 MHz) δ: 21.27 (s, br, BCH_2^3), 22.58 (s, CH_3-*i*-Pr), 35.18 (s, *C*H-*i*-Pr), 67.66 (s, O-CH_2-C_6H_5), 124.12 (s, CH^4), 126.91 (s, C_6H_5-ortho), 127.34 (s, C_6H_5-para), 128.50 (s, C_6H_5-meta), 139.93 (s, *C*-ipso), 142.44 (s,br, *C*-ipso), 143.54 (s, *C*-ipso), 148.41 (s, CH^6). ^{11}B NMR (C_6D_6, 128 MHz) δ: 48.07 (s, br). EI-MS *m*/*z*: 450 [M$^+$], 359 [M$^+$ – CH_2Ph], 267 [M$^+$ – CH_2Ph, – CH_3Ph], 225 [M$^+$ – $2CH_2Ph$ – $CH(CH_3)_2$], 91 [CH_2Ph^+]. EI-HR-MS calcd. for $C_{30}H_{36}O_2{}^{11}B_2$ (amu): 450.29014; found: 450.29381.

Synthesis of 4-Ph

201 mg (0.52 mmol) of the bisPMe$_3$ adduct of 2,2′-diborabiphenyl in 4 mL toluene was added over a period of 10 min to a solution of aniline (97 mg, 1.04 mmol) in 6 mL toluene at room temperature. The solution was stirred for 10 min at room temperature, and the volatiles were removed under vacuum. The product was obtained as a colourless solid after recrystallization from pentane at –35 °C (212 mg, 97%), mp 145 °C. ^{1}H NMR (C_6D_6, 400 MHz) δ: 1.12 (d, 12H, CH_3-*i*-Pr, $^3J_{HH}$ = 6.9 Hz), 2.29 (d, 4H, BCH_2^3, $^3J_{HH}$ = 4.3 Hz), 2.43 (sept., 2H, C*H*-*i*-Pr, $^3J_{HH}$ = 6.9 Hz), 5.92 (t, 2H, CH^4, $^3J_{HH}$ = 4.1 Hz), 6.54 (s, br, 2H, N*H*C_6H_5), 6.84 (m, 6H, C_6H_5-meta + para), 6.94 (d, 2H, CH^6, $^4J_{HH}$ = 1.4 Hz), 7.06 (m, 4H, C_6H_5-ortho). ^{13}C{^{1}H} NMR (C_6D_6, 100 MHz) δ: 21.71 (s, br, BCH_2^3), 22.38 (s, CH_3-*i*-Pr), 34.91 (s, *C*H-*i*-Pr), 46.72 (s, NHCH_2), 120.93 (s, C_6H_5-meta), 122.52 (s, C_6H_5-para), 124.49 (s, CH^4), 129.28 (s, C_6H_5-ortho), 142.21 (s, *C*-ipso), 143.51 (s, CH^6), 144.00 (s, br, *C*-ipso), 144.36 (s, *C*-ipso). ^{11}B NMR (C_6D_6, 128 MHz) δ: 41.83 (s, br). EI-MS *m*/*z*: 420 [M$^+$], 377 [M$^+$ – $CH(CH_3)_2$], 327 [M$^+$ – $C_6H_5NH_2$], 284 [M$^+$ – $C_6H_5NH_2$ – $CH(CH_3)_2$], 242 [M$^+$ – $C_6H_5NH_2$ – $2CH(CH_3)_2$], 93 [$C_6H_5NH_2^+$]. EI-HR-MS calcd. for $C_{28}H_{34}N_2{}^{11}B_2$ (amu): 420.29081; found: 420.29420.

Synthesis of 4-*p*-OMeBn

4-Methoxybenzylamine (106 mg, 0.77 mmol) in 2 mL toluene was added over a period of 10 min to a solution of the bisPMe$_3$ adduct of 2,2′-diborabiphenyl (150 mg, 0.38 mmol) in 10 mL toluene. The solution was stirred for 10 min at room temperature, and the volatiles were removed under vacuum. The product was obtained as a light brown solid after recrystallization from isopentane at –28 °C (169 mg, 86%), mp 93 °C. ^{1}H NMR (C_6D_6, 400 MHz) δ: 1.09 (d, 12H, CH_3-*i*-Pr, $^3J_{HH}$ = 6.9 Hz), 1.95 (d, 4H, BCH_2^3, $^3J_{HH}$ = 4.3 Hz), 2.43 (sept., 2H, C*H*-*i*-Pr, $^3J_{HH}$ = 6.8 Hz), 3.32 (s, 6H, C_6H_4-O-CH_3, $^1J_{CH}$ = 143.3 Hz), 3.85 (d, 4H, NHCH_2, $^3J_{HH}$ = 7.5 Hz), 4.55 (t, 2H, N*H*CH_2, $^3J_{HH}$ = 7.4 Hz), 5.87 (t, 2H, CH^4, $^3J_{HH}$ = 4.2 Hz), 6.72 (m, 4H, C_6H_4), 6.82 (d, 2H, CH^6, $^4J_{HH}$ = 1.3 Hz), 6.96 (m, 4H, C_6H_4). ^{13}C{^{1}H} NMR (C_6D_6, 100 MHz) δ: 18.94 (s, br, BCH_2^3), 22.38 (s, CH_3-*i*-Pr), 35.13 (s, *C*H-*i*-Pr), 46.72 (s, NHCH_2), 54.75 (s, C_6H_4-O-CH_3), 114.120 (s, C_6H_4), 123.71 (s, CH^4), 128.38 (s, C_6H_4), 133.85 (s, *C*-ipso), 141.12 (s, CH^6), 142.69 (s, *C*-ipso), 144.59 (s, br, *C*-ipso), 159.10 (s, *C*-ipso). ^{11}B NMR (C_6D_6, 128 MHz) δ: 40.86 (s, br). EI-MS *m*/*z*: 508 [M$^+$], 387 [M$^+$ – $CH_2C_6H_4OCH_3$], 371 [M$^+$ – $H_2NCH_2C_6H_4OCH_3$], 328 [M$^+$ – $CH_2C_6H_4OCH_3$ – $CH(CH_3)_2$], 121 [$CH_2C_6H_4OCH_3^+$]. EI-HR-MS calcd. for $C_{32}H_{42}N_2{}^{11}B_2$ (amu): 508.34324; found: 508.34562.

Synthesis of 5-Me

Lithium bis(trimethylsilyl)amide (118 mg, 0.70 mmol) in 4 mL THF was added dropwise to a stirred solution of **3-Me** (105 mg, 0.30 mmol) in 4 mL THF at room temperature. The solution was stirred for 1 h at room temperature, and the volatiles removed under vacuum. The product was obtained as a yellow solid in quantitative yield, mp 72 °C. ^{1}H NMR (THF-d_8, 400 MHz) δ: 1.16 (d, 12H, CH_3-*i*-Pr, $^3J_{HH}$ = 6.9 Hz), 2.67 (sept., 2H, C*H*-*i*-Pr, $^3J_{HH}$ = 6.9 Hz), 3.49 (s, 6H, O-CH_3), 5.68 (d, 2H, CH^3, $^3J_{HH}$ = 10.5 Hz), 6.82 (d, 2H, CH^6, $^4J_{HH}$ = 1.9 Hz), 7.01 (dd, 2H, CH^4, $^3J_{HH}$ = 10.5 Hz, $^4J_{HH}$ = 1.9 Hz). ^{13}C{^{1}H} NMR (THF-d_8, 100 MHz) δ: 26.35 (s, CH_3-*i*-Pr), 35.85 (s, *C*H-*i*-Pr), 52.47 (s, O-CH_3), 107.15 (s, br, CH^3), 125.36 (s, *C*-ipso), 130.43 (s, *C*-ipso), 131.71 (s, CH^4), 133.81 (s, CH^6). ^{11}B NMR (THF-d_8, 128 MHz) δ: 31.12 (s, br). ^{7}Li NMR (THF-d_8, 155 MHz) δ: –3.45 (s). EI-MS *m*/*z*: 281 [M$^+$ – 2Li – CH_3], 254 [M$^+$ – 2Li – $CH(CH_3)_2$].

Synthesis of 5-Bn

Lithium diisopropylamide (109 mg, 1.04 mmol) in 5 mL THF was added dropwise to a stirred solution of **3-Bn** (233 mg, 0.52 mmol) in 10 mL THF at room temperature. The solution was stirred for 1 h at room temperature, and the

© 2006 NRC Canada

volatiles removed under vacuum. The product was obtained as a yellow solid in quantitative yield. Suitable crystals for X-ray diffraction study were grown by cooling a solution of **5-Bn** in hexane–toluene (20:1) at –35 °C; mp 119 °C. ^{1}H NMR (THF-d_8, 400 MHz) δ: 1.16 (d, 12H, CH_3-*i*-Pr, $^3J_{HH}$ = 6.9 Hz), 1.78 (m, 6H, THF), 2.69 (sept., 2H, C*H*-*i*-Pr, $^3J_{HH}$ = 6.9 Hz), 3.62 (m, 6H, THF), 4.96 (s, 4H, O-CH_2-C_6H_5), 5.74 (d, 2H, C*H*^{3}, $^3J_{HH}$ = 10.6 Hz), 6.94 (d, 2H, C*H*^{6}, $^4J_{HH}$ = 2.1 Hz), 7.00 (dd, 2H, C*H*^{4}, $^3J_{HH}$ = 10.6 Hz, $^4J_{HH}$ = 2.1 Hz), 7.16 (m, 6H, C_6H_5-meta + para), 7.48 (d, 4H, C_6H_5-ortho, $^3J_{HH}$ = 7.3 Hz). ^{13}C{^{1}H} NMR (THF-d_8, 100 MHz) δ: 25.40 (s, THF), 25.48 (s, *C*H$_3$-*i*-Pr), 35.02 (s, *C*H-*i*-Pr), 67.20 (s, O-*C*H$_2$-C$_6$H$_5$), 67.25 (s, THF), 108.44 (s, br, *C*H^3), 125.41 (s, *C*-ipso), 126.05 (s, *C*$_6$H$_5$-para), 127.15 (s, *C*$_6$H$_5$-ortho), 127.53 (s, *C*$_6$H$_5$-meta), 131.66 (s, *C*H^4), 133.50 (s, *C*H^6), 142.82 (s, *C*-ipso). ^{11}B NMR (THF-d_8, 128 MHz) δ: 31.98 (s, br). ^{7}Li NMR (THF-d_8, 155 MHz) δ: –1.30 (s). ESI-MS *m*/*z*: 527 [**5-Bn**·THF – Li]$^-$.

Synthesis of 6-Ph

Lithium 2,2,6,6-tetramethylpiperidene (44 mg, 0.33 mmol) in 2 mL THF was added dropwise to a stirred solution of **4-Ph** (63 mg, 0.15 mmol) in 4 mL THF at room temperature. The solution was stirred for 1 h at room temperature, and the volatiles removed under vacuum. In the ^{1}H NMR spectrum of the crude product besides **6-Ph**, aniline and the dilithium salt of 9,11-diboratacarbazole were identified as by-products. Recrystallization of the crude product from THF–*n*-pentane gave clean **6-Ph** as light-yellow single crystals (72 mg, 84%), mp 170 °C (dec.). ^{1}H NMR (THF-d_8, 400 MHz, 20 °C) δ: 1.22 (d, br, 12H, CH_3-*i*-Pr, $^3J_{HH}$ = 6.6 Hz), 1.73 (m, 4H, THF), 2.74 (sept., 2H, C*H*-*i*-Pr, $^3J_{HH}$ = 6.9 Hz), 3.58 (m, 4H, THF), 5.40 (s, br, 2H, N*H*Ph), 6.28 (d, br, 2H, C*H*^{3}, $^3J_{HH}$ = 10.5 Hz), 6.37 (s, br, 2H, C_6H_5-para), 6.89 (m, 8H, C_6H_5-ortho + meta), 6.98 (d, br, 2H, C*H*^{4}, $^3J_{HH}$ = 10.0 Hz), 7.02 (s, br, 2H, C*H*^{6}). ^{1}H NMR (THF-d_8, 400 MHz, 63 °C) δ: 1.21 (d, 12H, CH_3-*i*-Pr, $^3J_{HH}$ = 6.8 Hz), 1.73 (m, 4H, THF), 2.76 (sept., 2H, C*H*-*i*-Pr, $^3J_{HH}$ = 6.8 Hz), 3.58 (m, 4H, THF), 5.48 (s, br, 2H, N*H*Ph), 6.27 (d, 2H, C*H*^{3}, $^3J_{HH}$ = 10.5 Hz), 6.39 (m, 2H, C_6H_5-para), 6.91 (m, 8H, C_6H_5-ortho + meta), 6.96 (d, 2H, C*H*^{4}, $^3J_{HH}$ = 10.3 Hz), 7.14 (s, br, 2H, C*H*^{6}). ^{1}H NMR (THF-d_8, 400 MHz, –40 °C) δ: 1.23 (d, 6H, CH_3-*i*-Pr, $^3J_{HH}$ = 6.9 Hz), 1.21 (d, 6H, CH_3-*i*-Pr, $^3J_{HH}$ = 6.9 Hz), 1.74 (m, 4H, THF), 2.68 (sept., 2H, C*H*-*i*-Pr, $^3J_{HH}$ = 6.7 Hz), 3.58 (m, 4H, THF), 5.50 (s, 2H, N*H*Ph), 6.21 (d, 2H, C*H*^{3}, $^3J_{HH}$ = 10.2 Hz), 6.32 (m, 2H, C_6H_5-para), 6.87 (m, 12H, C_6H_5-ortho + meta, C*H*^{4}, C*H*^{6}). ^{13}C{^{1}H} NMR (THF-d_8, 100 MHz, 20 °C) δ: 26.36 (s, THF), 26.66 (s, br, *C*H$_3$-*i*-Pr), 35.89 (s, br, *C*H-*i*-Pr), 68.21 (s, THF), 112.72 (s, br, *C*H^3), 115.20 (s, br, *C*$_6$H$_5$-para), 117.02 (s, br, *C*$_6$H$_5$-ortho or meta), 125.69 (s, br, *C*-ipso), 128.85 (s, br, *C*$_6$H$_5$-ortho or meta), 130.09 (s, br, *C*H^4), 133.08 (s, br, *C*H^6), 136.14 (s, br, *C*-ipso), 151.80 (s, *C*-ipso). ^{13}C{^{1}H} NMR (THF-d_8, 100 MHz, 63 °C) δ: 25.83 (s, THF), 26.00 (s, br, *C*H$_3$-*i*-Pr), 35.45 (s, *C*H-*i*-Pr), 68.20 (s, THF), 112.66 (s, br, *C*H^3), 115.68 (s, *C*$_6$H$_5$-para), 117.36 (s, *C*$_6$H$_5$-ortho or meta), 124.95 (s, br, *C*-ipso), 128.93 (s, br, *C*$_6$H$_5$-ortho or meta), 129.77 (s, *C*H^4), 133.21 (s, *C*H^6), 135.80 (s, br, *C*-ipso), 151.62 (s, *C*-ipso). ^{11}B NMR (THF-d_8, 128 MHz, 20 °C) δ: 25.83 (s, br). ^{11}B NMR (THF-d_8, 128 MHz, 63 °C) δ: 27.73 (s, br). ^{7}Li NMR (THF-d_8, 155 MHz, 20 °C) δ: –4.05 (s, br). ^{7}Li NMR (THF-d_8, 155 MHz, 63 °C) δ: –3.63 (s, br). ^{7}Li NMR (THF-d_8, 155 MHz, –40 °C) δ: –3.54 (s). ESI-MS *m*/*z*: 419 [**6-Ph**, –2Li + H$^+$]$^-$.

Synthesis of 6-*p*-OMeBn

Lithium bis(trimethylsilyl)amide (33 mg, 0.20 mmol) in 1 mL THF was added dropwise to a stirred solution of **4-*p*-OMeBn** (50 mg, 0.10 mmol) in 3 mL THF at room temperature. The solution was stirred for 1 h at room temperature, and the volatiles removed under vacuum. The product was obtained as a yellow solid after washing with pentane (46 mg, 90%), mp 55 °C (decomp.). ^{1}H NMR (C_6D_6, 400 MHz) δ: 1.18 (d, 12H, CH_3-*i*-Pr, $^3J_{HH}$ = 6.8 Hz), 1.79 (m, 4H, THF), 2.49 (s, br, 2H, N*H*CH_2), 2.70 (sept., 2H, C*H*-*i*-Pr, $^3J_{HH}$ = 6.8 Hz), 3.63 (m, 4H, THF), 3.71 (s, 6H, C_6H_4-O-CH_3), 4.01 (s, br, 4H, NHCH_2), 5.84 (d, br, 2H, C*H*^{3}, $^3J_{HH}$ = 10.3 Hz), 6.71 (d, 4H, C_6H_4, $^3J_{HH}$ = 8.2 Hz), 6.90 (s, br, 2H, C*H*^{6}), 6.95 (d, br, 2H, C*H*^{4}, $^3J_{HH}$ = 9.6 Hz), 7.18 (d, 4H, C_6H_4, $^3J_{HH}$ = 8.2 Hz). ^{13}C{^{1}H} NMR (C_6D_6, 100 MHz) δ: 26.53 (s, THF), 26.62 (s, br, *C*H$_3$-*i*-Pr), 36.17 (s, *C*H-*i*-Pr), 48.85 (s, NH*C*H$_2$), 55.43 (s, C$_6$H$_4$-O-*C*H$_3$), 68.38 (s, THF), 112.28 (s, *C*H^3), 114.40 (s, *C*$_6$H$_4$), 125.80 (s, *C*-ipso), 129.22 (s, *C*-ipso), 129.59 (s, *C*$_6$H$_4$), 132.04 (s, *C*H^6), 132.79 (s, *C*H^4), 138.75 (s, *C*-ipso), 159.29 (s, *C*-ipso). ^{11}B NMR (C_6D_6, 128 MHz) δ: 29.62 (s, br). ^{7}Li NMR (THF-d_8, 155 MHz) δ: –2.38 (s, br). ESI-MS *m*/*z*: 513 [**6-*p*-OMeBn** – Li]$^-$.

Synthesis of *syn*/*anti*-7-CO

5-Bn (222 mg, 0.37 mmol) in 4 mL THF was added dropwise to a stirred solution of [Rh(CO)$_2$Cl]$_2$ (143 mg, 0.37 mmol) in 4 mL THF at room temperature. The solution was stirred for 30 min. at room temperature, and the volatiles removed under vacuum. The residue was dissolved in pentane and filtered through a frit covered with Celite to remove the LiCl. The ^{1}H NMR spectrum of an aliquot from the reaction mixture showed the formation of an 1:1 mixture of the syn and anti isomers (274 mg, 97%). A syn:anti ratio of 3:1 could be obtained if the reaction was carried out in toluene instead of THF. Clean syn product was obtained as a light brown solid by dissolving the 3:1 mixture of the two isomers in isopentane followed by cooling the solution at –35 °C. However, part of the syn isomer dissolves in isopentane and clean anti product could not be obtained. Single crystals for X-ray diffraction studies of the syn isomer were grown by cooling an isopentane solution of the syn isomer at –35 °C. syn Isomer: IR (KBr, cm^{-1}): 2158 vs, 2120 vs (ν CO). ^{1}H NMR (C_6D_6, 400 MHz) δ: 1.05 (d, 6H, CH_3-*i*-Pr, $^3J_{HH}$ = 6.9 Hz), 1.07 (d, 6H, CH_3-*i*-Pr, $^3J_{HH}$ = 6.9 Hz), 2.20 (sept., 2H, C*H*-*i*-Pr, $^3J_{HH}$ = 6.9 Hz), AB spin system: A 4.93 (d, 2H, O-CH_2Ph, $^2J_{HH}$ = 12.7 Hz), B 5.02 (d, 2H, O-CH_2Ph, $^2J_{HH}$ = 12.7 Hz), 5.00 (d, 2H, C*H*^{3}, $^3J_{HH}$ = 9.4 Hz), 6.02 (d, 2H, C*H*^{4}, $^3J_{HH}$ = 9.4 Hz), 7.17 (m, 2H, C_6H_5-para), 7.19 (d, 2H, C*H*^{6}, $^4J_{HH}$ = 1.6 Hz), 7.28 (m, 4H, C_6H_5-meta), 7.49 (m, 4H, C_6H_5-ortho). ^{13}C{^{1}H} NMR (C_6D_6, 100 MHz) δ: 23.83 (s, *C*H$_3$-*i*-Pr), 24.13 (s, *C*H$_3$-*i*-Pr), 33.51 (s, *C*H-*i*-Pr), 68.02 (s, O-*C*H$_2$Ph), 87.13 (s, br, *C*H^3), 106.84 (d, *C*-ipso, $^1J_{RhC}$ = 3.8 Hz), 110.34 (d, *C*H^4, $^1J_{RhC}$ = 4.1), 118.02 (d, *C*H^6, $^1J_{RhC}$ = 3.1 Hz), 123.33 (s, *C*-ipso), 127.34 (s, *C*$_6$H$_5$-ortho), 127.40 (s, *C*$_6$H$_5$-para), 128.57 (s,

© 2006 NRC Canada

C_6H_5-meta), 140.75 (s, br, *C*-ipso), 190.34 (d, Rh-*C*O, $^1J_{RhC}$ = 84). ^{11}B NMR (C_6D_6, 128 MHz) δ: 23.60 (s, br). anti Isomer: ^{1}H NMR (C_6D_6, 400 MHz) δ: 1.01 (d, 6H, CH_3-*i*-Pr, $^3J_{HH}$ = 6.9 Hz), 1.10 (d, 6H, CH_3-*i*-Pr, $^3J_{HH}$ = 6.9 Hz), 2.15 (sept., 2H, C*H*-*i*-Pr, $^3J_{HH}$ = 6.9 Hz), AB spin system: A 4.85 (d, 2H, O-CH_2Ph, $^2J_{HH}$ = 12.8 Hz), B 4.89 (d, 2H, O-CH_2Ph, $^2J_{HH}$ = 12.8 Hz), 5.07 (d, 2H, CH^3, $^3J_{HH}$ = 9.6 Hz), 5.87 (dd, 2H, CH^4, $^3J_{HH}$ = 9.7 Hz, $^4J_{HH}$ = 1.4 Hz), 7.04 (d, 2H, CH^6, $^4J_{HH}$ = 1.6 Hz), 7.13 (m, 2H, C_6H_5-para), 7.21 (m, 4H, C_6H_5-meta), 7.39 (m, 4H, C_6H_5-ortho). ^{13}C{^{1}H} NMR (C_6D_6, 100 MHz) δ: 23.65 (s, *C*H_3-*i*-Pr), 24.13 (s, *C*H_3-*i*-Pr), 33.51 (s, *C*H-*i*-Pr), 67.93 (s, O-*C*H_2Ph), 90.07 (s, br, *C*H^3), 106.52 (d, *C*-ipso, $^1J_{RhC}$ = 3.8 Hz), 110.75 (d, *C*H^4, $^1J_{RhC}$ = 3.7), 117.88 (d, *C*H^6, $^1J_{RhC}$ = 3.3 Hz), 127.33 (s, C_6H_5-ortho), 127.38 (s, C_6H_5-para), 128.57 (s, C_6H_5-meta), 140.73 (s, br, *C*-ipso), 190.60 (d, Rh-*C*O, $^1J_{RhC}$ = 84). ^{11}B NMR (C_6D_6, 128 MHz) δ: 24.20 (s, br). EI-MS *m*/*z*: 710 [M^+ – 2CO], 654 [M^+ – 4CO]. EI-HR-MS calcd. for $C_{30}H_{34}O_2{}^{11}B_2Rh_2$ (amu): 654.08550; found: 654.08514.

Synthesis of *syn*/*anti*-7-COD

$[Rh(COD)Cl]_2$ (64 mg, 0.13 mmol) in 2 mL THF was added dropwise to a stirred solution of **5-Bn** (79 mg, 0.13 mmol) in 2 mL THF at room temperature. The solution was stirred for 1 h at room temperature, and the volatiles removed under vacuum. The residue was dissolved in CH_2Cl_2 and filtered through a frit covered with Celite to remove the LiCl. Removal of the CH_2Cl_2 under vacuum gave 110 mg (97%) of **7-COD** as a 1:1 mixture of syn and anti isomers. Clean syn product was obtained by dissolving the mixture of the two isomers in isopentane followed by filtration of the undissolved solid. However, part of the syn isomer dissolved in isopentane and clean anti could not be obtained. Single crystals for X-ray diffraction studies of the anti isomer were grown by slow evaporation of an isopentane solution containing both isomers. Attempts to separate the two isomers by column chromatography using Al_2O_3 activity level I failed. syn Isomer: ^{1}H NMR (C_6D_6, 400 MHz) δ: 1.13 (d, 6H, CH_3-*i*-Pr, $^3J_{HH}$ = 6.8 Hz), 1.17 (d, 6H, CH_3-*i*-Pr, $^3J_{HH}$ = 6.8 Hz), 1.91 (m, 4H, CH_2-COD), 2.09 (m, 10H, CH_2-COD + C*H*-*i*-Pr), 2.30 (m, 4H, CH_2-COD), 4.09 (m, 8H, C*H*-COD), 4.72 (d, 2H, CH^3, $^3J_{HH}$ = 9.1 Hz), AB spin system: A 4.82 (d, 2H, O-CH_2Ph, $^2J_{HH}$ = 13.0 Hz), B 4.89 (d, 2H, O-CH_2Ph, $^2J_{HH}$ = 13.0 Hz), 5.93 (d, 2H, CH^4, $^3J_{HH}$ = 9.1 Hz), 6.57 (s, 2H, CH^6), 7.08 (t, 2H, C_6H_5-para, $^3J_{HH}$ = 7.2 Hz), 7.18 (dd, 4H, C_6H_5-meta, $^3J_{HH}$ = 7.4 Hz, $^3J_{HH}$ = 7.4 Hz), 7.44 (d, 4H, C_6H_5-ortho, $^3J_{HH}$ = 7.5 Hz). ^{13}C{^{1}H} NMR (C_6D_6, 100 MHz) δ: 22.58 (s, *C*H_3-*i*-Pr), 24.05 (s, *C*H_3-*i*-Pr), 32.24 (s, *C*H_2-COD), 32.59 (s, *C*H-*i*-Pr), 33.02 (s, *C*H_2-COD), 67.61 (s, O-*C*H_2Ph), 69.33 (d, *C*H-COD, $^1J_{RhC}$ = 12.8 Hz), 71.09 (d, *C*H-COD, $^1J_{RhC}$ = 13.1 Hz), 85.95 (s, br, *C*H^3), 103.75 (d, *C*-ipso, $^1J_{RhC}$ = 4.1 Hz), 105.52 (d, *C*H^4, $^1J_{RhC}$ = 3.5), 112.32 (d, *C*H^6, $^1J_{RhC}$ = 2.8 Hz), 119.44 (s, br, *C*-ipso), 126.82 (s, C_6H_5-para), 127.14 (s, C_6H_5-ortho), 128.29 (s, C_6H_5-meta), 142.18 (s, *C*-ipso). ^{11}B NMR (C_6D_6, 128 MHz) δ: 23.40 (s, br). anti Isomer: ^{1}H NMR (C_6D_6, 400 MHz) δ: 1.14 (d, 6H, CH_3-*i*-Pr, $^3J_{HH}$ = 6.9 Hz), 1.16 (d, 6H, CH_3-*i*-Pr, $^3J_{HH}$ = 6.9 Hz), 1.75 (m, 4H, CH_2-COD), 1.91 (m, 4H, CH_2-COD), 2.06 (m, 4H, CH_2-COD), 2.19 (m, 6H, CH_2-COD + C*H*-*i*-Pr), 3.85 (m, 4H, C*H*-COD), 4.09 (m, 4H, C*H*-COD), 4.83 (d, 2H, CH^3, $^3J_{HH}$ = 9.0 Hz), AB spin system: A 4.88 (d, 2H, O-CH_2Ph, $^2J_{HH}$ = 12.5 Hz), B 4.97 (d, 2H, O-CH_2Ph, $^2J_{HH}$ = 12.5 Hz), 6.03 (dd, 2H, CH^4, $^3J_{HH}$ = 9.0 Hz, $^4J_{HH}$ = 1.6 Hz), 7.15 (t, 2H, C_6H_5-para, $^3J_{HH}$ = 7.6 Hz), 7.25 (dd, 4H, C_6H_5-meta, $^3J_{HH}$ = 7.4 Hz, $^3J_{HH}$ = 7.4 Hz), 7.38 (d, 2H, CH^6, $^4J_{HH}$ = 1.6 Hz), 7.54 (d, 4H, C_6H_5-ortho, $^3J_{HH}$ = 7.4 Hz). ^{13}C{^{1}H} NMR (C_6D_6, 100 MHz) δ: 23.27 (s, *C*H_3-*i*-Pr), 23.71 (s, *C*H_3-*i*-Pr), 31.78 (s, *C*H_2-COD), 32.59 (s, *C*H-*i*-Pr), 32.79 (s, *C*H_2-COD), 68.07 (s, O-*C*H_2Ph), 70.05 (d, *C*H-COD, $^1J_{RhC}$ = 12.8 Hz), 72.78 (d, *C*H-COD, $^1J_{RhC}$ = 12.9 Hz), 85.64 (s, br, *C*H^3), 105.02 (d, *C*H^4, $^1J_{RhC}$ = 3.6), 105.82 (d, *C*-ipso, $^1J_{RhC}$ = 4.0 Hz), 112.74 (d, *C*H^6, $^1J_{RhC}$ = 3.0 Hz), 113.98 (s, br, *C*-ipso), 127.17 (s, C_6H_5-para), 127.64 (s, C_6H_5-ortho), 128.41 (s, C_6H_5-meta), 142.02 (s, *C*-ipso). ^{11}B NMR (C_6D_6, 128 MHz) δ: 23.84 (s, br). EI-MS *m*/*z*: 870 [M^+], 760 [M^+ – cyclooctene]. EI-HR-MS calcd. for $C_{58}H_{46}O_2{}^{11}B_2Rh_2$ (amu): 870.27330; found: 870.27847.

Synthesis of *syn*/*anti*-8-CO

Dilithium 9,11-diboratacarbazole (77 mg, 0.16 mmol) in 4 mL THF was added dropwise to a stirred solution of $[Rh(CO)_2Cl]_2$ (62 mg, 0.16 mmol) in 4 mL THF at room temperature. The solution was stirred for 30 min at room temperature, and the volatiles removed under vacuum. The residue was dissolved in isopentane and filtered through a frit covered with Celite to remove the LiCl. The ^{1}H NMR spectrum of an aliquot from the reaction mixture showed the formation of an 1:1 mixture of the syn and anti isomers as the only products of the reaction. Attempts to separate the two isomers by cooling an isopentane solution of the mixture at –35 °C failed. Instead several single crystals of the syn isomer together with an orange solid formed (93 mg, 91%). ^{1}H NMR (C_6D_6, 400 MHz) δ: 0.95 (d, 6H, CH_3-*i*-Pr, $^3J_{HH}$ = 6.9 Hz), 0.99 (d, 6H, CH_3-*i*-Pr, $^3J_{HH}$ = 6.9 Hz), 1.03 (d, 6H, CH_3-*i*-Pr, $^3J_{HH}$ = 6.9 Hz), 1.05 (d, 6H, CH_3-*i*-Pr, $^3J_{HH}$ = 6.9 Hz), 2.16 (sept., 2H, C*H*-*i*-Pr, $^3J_{HH}$ = 6.9 Hz), 2.21 (sept., 2H, C*H*-*i*-Pr, $^3J_{HH}$ = 6.9 Hz), 5.56 (d, 2H, CH^3, $^3J_{HH}$ = 9.4 Hz), 5.77 (d, 2H, CH^3, $^3J_{HH}$ = 9.6 Hz), 5.92 (d, 2H, CH^4, $^3J_{HH}$ = 9.6 Hz), 5.93 (d, 2H, CH^4, $^3J_{HH}$ = 9.4 Hz), 6.88 (s, 2H, CH^6), 6.95 (s, 2H, CH^6), 7.07 (m, 2H, C_6H_5), 7.40 (m, 4H, C_6H_5-meta), 7.66 (m, 2H, C_6H_5-ortho). ^{13}C{^{1}H} NMR (C_6D_6, 100 MHz) δ: 23.78 (s, *C*H_3-*i*-Pr), 24.05 (s, *C*H_3-*i*-Pr), 24.18 (s, *C*H_3-*i*-Pr), 24.27 (s, *C*H_3-*i*-Pr), 33.68 (s, *C*H-*i*-Pr), 33.75 (s, *C*H-*i*-Pr), 89.01 (s, br, *C*H^3), 94.59 (s, br, *C*H^3), 103.14 (d, *C*H^6, $^1J_{RhC}$ = 2.6 Hz), 105.31 (d, *C*-ipso, $^1J_{RhC}$ = 3.7 Hz), 105.31 (d, *C*H^6, $^1J_{RhC}$ = 2.5 Hz), 105.71 (d, *C*-ipso, $^1J_{RhC}$ = 3.8 Hz), 110.31 (d, *C*H^4, $^1J_{RhC}$ = 4.4), 111.38 (d, *C*H^4, $^1J_{RhC}$ = 4.0), 122.66 (s, C_6H_5-para), 122.76 (s, C_6H_5-para), 123.91 (s, C_6H_5-ortho), 123.95 (s, C_6H_5-ortho), 129.65 (s, C_6H_5-meta), 129.66 (s, C_6H_5-meta), 147.86 (s, *C*-ipso), 147.95 (s, *C*-ipso), 189.15 (d, Rh-*C*O, $^1J_{RhC}$ = 84.3), 189.42 (d, Rh-*C*O, $^1J_{RhC}$ = 84.4). ^{11}B NMR (C_6D_6, 128 MHz) δ: 25.00 (s, br). EI-MS *m*/*z*: 643 [M^+], 615 [M^+ – CO], 588 [M^+ – 2CO]. EI-HR-MS calcd. for $C_{26}H_{25}N^{11}B_2O_4Rh_2$ (amu): 643.00798; found: 643.00991.

Synthesis of *anti*-8-COD

$[Rh(COD)Cl]_2$ (54 mg, 0.11 mmol) in 2 mL THF was added dropwise to a stirred solution of dilithium 9,11-diboratacarbazole (53 mg, 0.11 mmol) in 2 mL THF at room

© 2006 NRC Canada

temperature. The solution was stirred for 1 h at room temperature, and the volatiles removed under vacuum. The residue was dissolved in CH_2Cl_2 and filtered through a frit covered with Celite to remove the LiCl. Removal of the CH_2Cl_2 under vacuum gave 78 mg (95%) of *anti*-**8-COD** as an orange solid. Only the anti isomer was detected. Single crystals for X-ray diffraction studies were grown by slow diffusion of pentane into a solution of *anti*-**8-COD** in CH_2Cl_2. ^{1}H NMR (C_6D_6, 400 MHz) δ: 1.06 (d, 6H, CH_3-*i*-Pr, $^3J_{HH}$ = 6.9 Hz), 1.24 (d, 6H, CH_3-*i*-Pr, $^3J_{HH}$ = 6.9 Hz), 1.58 (m, 4H, CH_2-COD), 1.94 (m, 8H, CH_2-COD), 2.06 (sept., 2H, C*H*-*i*-Pr, $^3J_{HH}$ = 6.9 Hz), 2.22 (m, 4H, CH_2-COD), 3.40 (m, 8H, C*H*-COD), 5.32 (d, 2H, CH^4, $^3J_{HH}$ = 9.5 Hz), 6.06 (d, 2H, CH^3, $^3J_{HH}$ = 9.5 Hz), 6.85 (s, 2H, CH^6), 7.05 (t, 1H, C_6H_5-para, $^3J_{HH}$ = 7.3 Hz), 7.48 (dd, 2H, C_6H_5-meta, $^3J_{HH}$ = 7.4 Hz, $^3J_{HH}$ = 7.4 Hz), 7.94 (d, 2H, C_6H_5-ortho, $^3J_{HH}$ = 8.3 Hz). ^{13}C{^{1}H} NMR (C_6D_6, 100 MHz) δ: 22.14 (s, *C*H_3-*i*-Pr), 25.00 (s, *C*H_3-*i*-Pr), 31.30 (s, *C*H_2-COD), 32.71 (s, *C*H-*i*-Pr), 33.64 (s, *C*H_2-COD), 73.60 (d, *C*H-COD, $^1J_{RhC}$ = 12.9 Hz), 74.12 (d, *C*H-COD, $^1J_{RhC}$ = 12.9 Hz), 92.33 (s, br, *C*H^3), 95.65 (d, *C*H^6, $^1J_{RhC}$ = 2.5 Hz), 107.16 (d, *C*-ipso, $^1J_{RhC}$ = 3.9 Hz), 107.52 (d, *C*H^4, $^1J_{RhC}$ = 3.4), 108.81 (s, br, *C*-ipso), 120.63 (s, C_6H_5-para), 123.41 (s, C_6H_5-ortho), 129.39 (s, C_6H_5-meta), 150.76 (s, *C*-ipso). ^{11}B NMR (C_6D_6, 128 MHz) δ: 24.45 (s, br). EI-MS *m*/*z*: 747 [M$^+$]. EI-HR-MS calcd. for $C_{38}H_{49}N^{11}B_2Rh_2$ (amu): 747.21612; found: 747.21738.

Acknowledgements

Funding for this work was provided by the Natural Sciences and Engineering Research Council of Canada (NSERC) through a Discovery grant to WEP and the Alberta Ingenuity Fund through an Associateship to IG.

References

1. Recent examples: (*a*) H. Li, L. Li, and T.J. Marks Angew. Chem. Int. Ed. **43**, 4937 (2004); (*b*) C.R. Baar, L.P. Carbray, M.C. Jennings, and R.J. Puddephatt. Organometallics, **19**, 2482 (2000); (*c*) A.J. Carty, G. Hogarth, G.D. Enright, J.W. Steed, and D. Georganopoulou. Chem. Commun. (Cambridge), 1499 (1999).
2. (*a*) S. Di Bella. Chem. Soc. Rev. **30**, 355 (2001); (*b*) I.R. Whittall, A.M. McDonagh, and M.G. Humphrey. Adv. Organomet. Chem. **42**, 291 (1998).
3. (*a*) S. Barlow and D. O'Hare. Chem. Rev. **97**, 637 (1997); (*b*) A. Ceccon, S. Santi, L. Orian, and A. Bisello. Coord. Chem. Rev. **248**, 683 (2004).
4. J.S. Rogers, G.C. Bazan, and C.K. Sperry. J. Am. Chem. Soc. **119**, 9305 (1997).
5. (*a*) G.E. Herberich and H. Ohst. Adv. Organomet. Chem. **25**, 199 (1986); (*b*) G.C. Fu. Adv. Organomet. Chem. **47**, 101 (2001).
6. (*a*) U. Hagenau, J. Heck, E. Hendricks, A. Persoons, T. Schuld, and H. Wong. Inorg. Chem. **35**, 7863 (1996); (*b*) U. Behrens, T. Meyer-Friedrichsen, and J. Heck. Z. Anorg. Allg. Chem. **629**, 1421 (2003).
7. T. Hascall, V. Beck, S. Barlow, A.R. Cowley, and D. O'Hare. Organometallics, **23**, 3808 (2004).
8. D.J.H. Emslie, W.E. Piers, and M. Parvez. Angew. Chem. Int. Ed. **42**, 1252 (2003).
9. S. Qiao, D.A. Hoic, and G.C. Fu. J. Am. Chem. Soc. **118**, 6329 (1996).
10. D.A. Hoic, W.M. Davis, and G.C. Fu. J. Am. Chem. Soc. **118**, 8176 (1996).
11. J.S. Rogers, R.J. Lachicotte, and G.C. Bazan. J. Am. Chem. Soc. **121**, 1288 (1999).
12. I. Ghesner, W.E. Piers, M. Parvez, and R. McDonald. Organometallics, **23**, 3085 (2004).
13. G.E. Herberich, B. Schmidt, U. Englert, and T. Wagner. Organometallics, **12**, 2891 (1993).
14. J.J. Eisch. Adv. Organomet. Chem. **39**, 355 (1995).
15. R.T. Baker and T.H. Tulip. Organometallics, **5**, 839 (1986).
16. M.D. Rausch, W.C. Spink, B.G. Conway, R.D. Rogers, and J.L. Atwood. J. Organomet. Chem. **383**, 227 (1990).
17. (*a*) G.E. Herberich and H.J. Becker. Angew. Chem. Int. Ed. Engl. **14**, 184 (1975); (*b*) G.E. Herberich, H.J. Becker, K. Carsten, C. Engelke, and W. Koch. Chem. Ber. **109**, 2382 (1976).
18. D.H. Woodmansee, X. Bu, and G.C. Bazan. Chem. Commun. (Cambridge), 619 (2001).
19. T.E. Bitterwolf, W.C. Spink, and M.D. Rausch. J. Organomet. Chem. **363**, 189 (1989).
20. (*a*) A. Gutnov, H.-J. Drexler, A. Spannenberg, G. Oehme, and B. Heller. Organometallics, **23**, 1002 (2004); (*b*) S. Tirapattur, M. Belletete, N. Drolet, M. Leclerc, and G. Durocher. Macromolecules, **35**, 8889 (2002), and refs. therein.
21. A.B. Pangborn, M.A. Giardello, R.H. Grubbs, R.K. Rosen, and F.J. Timmers. Organometallics, **15**, 1518 (1996).
22. M.F. Lappert, M.J. Slade, and A. Singh. J. Am. Chem. Soc. **105**, 302 (1983).

© 2006 NRC Canada

Use of ^{1}H NMR chemical shifts to determine the absolute configuration and enantiomeric purity for enantiomers of 3,3′-disubstituted-MeO-BIPHEP derivatives[1]

Evgueni Gorobets, Masood Parvez, Bronwen M.M. Wheatley, and Brian A. Keay

Abstract: The absolute configuration of a series of 3,3′-disubstituted-MeO-BIPHEP derivatives can be determined by the ^{1}H NMR chemical shift of the methoxyl group when the 3,3′-disubsituted-MeO-BIPHEP derivative is mixed with (–)-(2*R*,3*R*)-dibenzoyltartaric acid ((–)-DBTA) (1:2) and its NMR spectrum is run in $CDCl_3$. The chemical shift of the methoxyl group in the S_{ax} enantiomer always occurred at higher field than the corresponding R_{ax} enantiomer. Integration of the corresponding methoxyl signals provides the enantiomeric purity of any mixtures.

Key words: assignment of absolute configuration, 2,2′-bis(diphenylphosphino)-1,1′-biaryls, MeO-BIPHEP derivatives, asymmetric Heck reaction, ^{1}H NMR chemical shifts.

Résumé : La configuration absolue d'une série de dérivés MeO-BIBHEP 3,3′-disubstitués peut être déterminée par RMN du ^{1}H, en utilisant le déplacement chimique du groupe méthoxyle et en procédant à la détermination des spectres RMN des dérivés MeO-BIBHEP 3,3′-disubstitués en présence d'acide (–)-(2*R*,3*R*)-dibenzoyltartrique (1 : 2) dans du $CDCl_3$. Le déplacement chimique du groupe méthoxyle dans l'énantiomère S_{ax} se trouve toujours à un champ plus élevé que celui de l'énantiomère R_{ax} correspondant. L'intégration des signaux des groupes méthoxyles correspondants permet d'évaluer la pureté énantiomérique de tous les mélanges.

Mots clés : attribution d'une configuration absolue, 2,2′-bis(diphénylphosphino)-1,1′-biaryles, dérivés MeO-BIPHEP, réaction de Heck asymétrique, déplacements chimiques en RMN du ^{1}H.

[Traduit par la Rédaction]

Introduction

Over the past few years, we have been interested in the development of synthetic routes towards the preparation of 3,3′-disubstituted-MeO-BIPHEP derivatives **4**–**11** for use as chiral ligands in a variety of transition-metal-catalyzed asymmetric transformations involving palladium and rhodium (1, 2).[3] During the course of these studies it became necessary to not only resolve the resulting racemic mixtures of biaryl products **2** obtained from Ullmann couplings of the corresponding aryl halides **1** (Scheme 1), but also to assign the absolute configuration to each of the enantiomers. The standard method reported for the optical resolution of **3** is via the mixing of (±)-**3** and (–)-(2*R*,3*R*)-dibenzoyltartaric acid ((–)-DBTA) (1:1.5) in DCM–EtOAc, followed by the crystallization of the (*R*)-**3**:(–)-DBTA complex from the solution (3). We tried to resolve compounds **3**–**6**, **8**, and **10** using this resolution method; however, we were only successful with compounds **4**, **5**, and **8** using either (–)-DBTA or (–)-(2*R*,3*R*)-ditoluoyltartaric acid (DTTA). Two solutions to the resolution problem were developed. The first was to attach the chiral auxiliary (R = $OSiMe_2$-(L)-menthol) to **2** (R^1 = Me, R^2 = OH) to create diastereomers that could then be separated by silica gel chromatography (1*a*). Removal of the chiral auxiliary then gave enantiomers of **2** (R^1 = Me, R^2 = OH) that were then converted to **7**. The second solution was to replace the methyl moiety in **1** (R^1 = Me) with the chiral auxiliary ((*S*)-$H_3CCH(OAc)C{=}O$) and then perform the Ullmann coupling to give a mixture of diastereomers **2** that were easily separated by silica gel chromatography (1*b*). The chiral auxiliary was then replaced by a methyl group, thereby providing biaryls **3**–**10**. However, the absolute configuration of the axis of chirality in biaryls **3**–**11** still had to be determined. This paper describes how the absolute con-

Received 9 May 2005. Published on the NRC Research Press Web site at http://canjchem.nrc.ca on 14 February 2006.

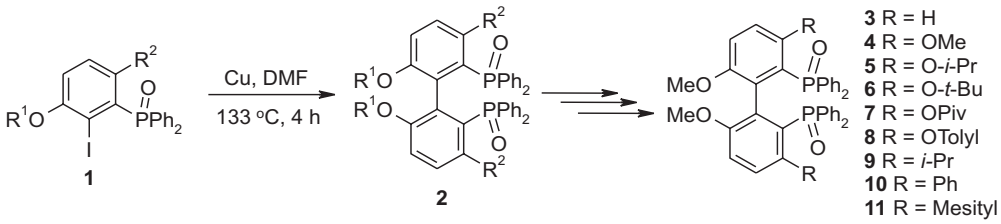
This manuscript is dedicated to Dr. Arthur J. Carty for his contributions to the field of organometallic chemistry, his work for the chemistry community throughout Canada, and for being an inspiration in the classroom.

E. Gorobets, M. Parvez, B.M.M. Wheatley, and B.A. Keay.[2] Department of Chemistry, University of Calgary, Calgary, AB T2N 1N4, Canada.

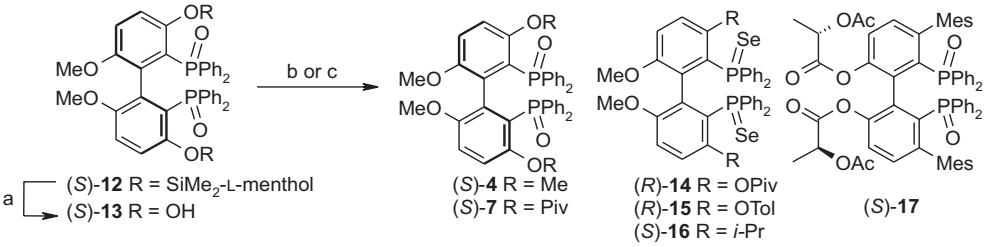
[1]This article is part of a Special Issue dedicated to Professor Arthur Carty.
[2]Corresponding author (e-mail: keay@ucalgary.ca).
[3]J.M. Hopkins, M. Parvez, and B.A. Keay. Unpublished results.

 doi:10.1139/V05-230 © 2006 NRC Canada

Scheme 1.



Scheme 2. (*a*) HF-pyr, THF, –70 °C to rt, 1 h (89%); (*b*) MeI, DMF, K_2CO_3, rt, 24 h (95%); (*c*) pivalyl chloride, Et_3N, DCM (94%).



figuration for biaryls **3–11** were assigned and how the absolute configuration of a series of 3,3′-disubstituted-MeO-BIPHEP derivatives can be determined by the ^{1}H NMR chemical shift of the methoxyl group when the 3,3′-disubstituted-MeO-BIPHEP derivative is mixed with (–)-DBTA (1:2).

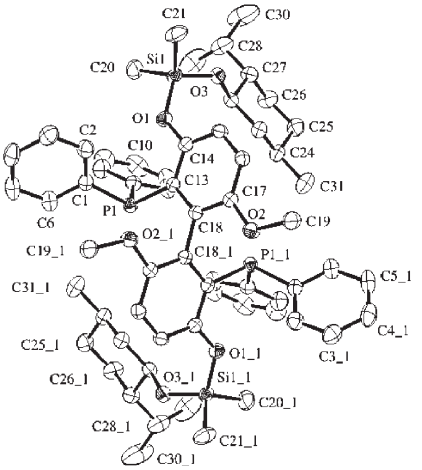
Results and discussion

Determining the absolute configuration of the axis of chirality in biaryls 3–11

The absolute configurations of biaryls **3–11** were determined by obtaining the X-ray crystal structure of some derivatives of biaryls **3–5** and **7–11** that contain a chiral auxiliary, by using the Flack parameter (4) or using ^{1}H NMR chemical shifts of the methoxy group when the 3,3′-disubstituted-MeO-BIPHEP derivative is mixed with (–)-DBTA (1:2).[4]

The absolute configuration of synthesized MeO-BIPHEP **3** was assigned by comparing the sign of the optical rotation obtained from the synthesized sample with that reported by Schmid et al. (3). Biaryls (*S*)-**4** and (*S*)-**7** were prepared from the corresponding 3,3′-dihydroxybiaryl system (*S*)-**13** (Scheme 2). The absolute configuration of (*S*)-**13** was determined from the X-ray crystal structure of the $SiMe_2$-(L)-menthol derivative **12** (Fig. 1). Figure 1 indicates that **12** has an axis of chirality of *S*. The absolute configuration of (*S*)-**5** was determined by obtaining an X-ray crystal structure of (*S*)-**5** when complexed with two molecules of (L)-DTTA (Fig. 2). The absolute configurations of (*R*)-**7**, (*R*)-**8**, and (*S*)-**9** were determined from the Flack parameter (4) of the X-ray crystal structure of their corresponding phosphine-selenides (*R*)-**14**, (*R*)-**15**, and (*S*)-**16** (Scheme 2 and Figs. 3–5). Finally the absolute configuration of (*R*)-**10** and (*S*)-**11** were determined by the Flack parameter (4) of the X-ray crystal structure of the phosphine oxide (*R*)-**10** (Fig. 6) and the lactate derivative (*S*)-**17** (Scheme 2 and Fig. 7), respectively.

Fig. 1. ORTEP diagram of (–)-(*S*)-**12** drawn with 30% probability ellipsoids. Hydrogen atoms are represented as spheres of arbitrary size.



Use of ^{1}H NMR chemical shifts of the methoxy group to determine the absolute configuration of MeO-BIPHEP derivatives

As mentioned above, the reported (3) procedure for the resolution of MeO-BIPHEP **3** is by the mixing of (±)-**3** and (–)-DBTA (1:1.5) in DCM–EtOAc, followed by the crystallization of the complex (*R*)-**3**:(–)-DBTA from the solution. While we were successful with the resolution of **8** with (–)-DBTA, we found **4** and **5** were better resolved using

[4] Supplementary data for this article are available on the journal Web site (http://canjchem.nrc.ca) or may be purchased from the Depository of Unpublished Data, Document Delivery, CISTI, National Research Council Canada, Ottawa, ON K1A 0R6, Canada. DUD 4079. For more information on obtaining material refer to http://cisti-icist.nrc-cnrc.gc.ca/irm/unpub_e.shtml. CCDC 239964, 285584, 285585, 285586, 285587, 285588, and 285589 contain the crystallographic data for this manuscript. These data can be obtained, free of charge, via www.ccdc.cam.ac.uk/conts/retrieving.html (Or from the Cambridge Crystallographic Data Centre, 12 Union Road, Cambridge CB2 1EZ, UK; fax +44 1223 336033; or deposit@ccdc.cam.ac.uk).

© 2006 NRC Canada

Fig. 2. ORTEP diagram of (–)-(*S*)-**5** complexed with two molecules of (L)-DTTA drawn with 30% probability ellipsoids. Hydrogen atoms are represented as spheres of arbitrary size.

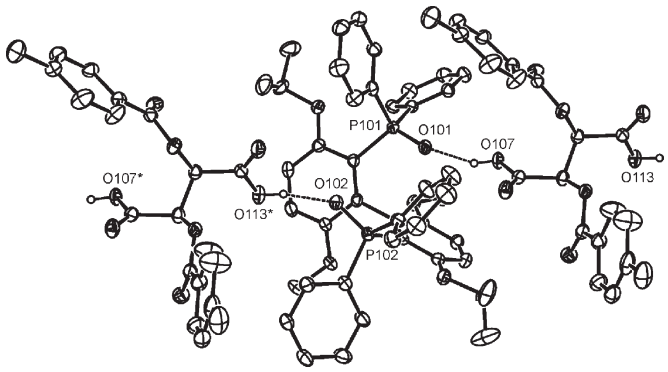
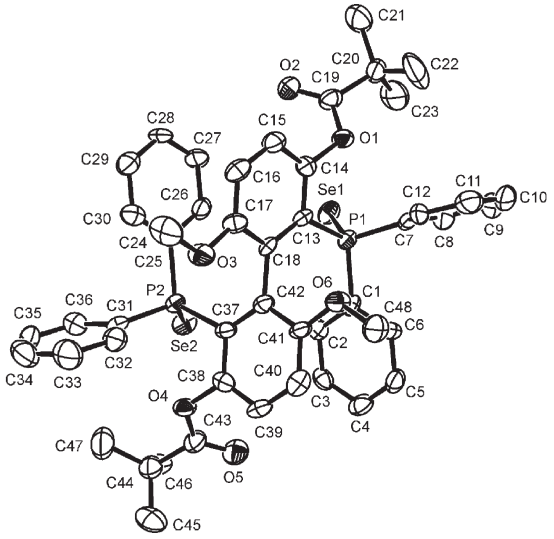


Fig. 3. ORTEP diagram of (+)-(*R*)-**14** drawn with 30% probability ellipsoids. Hydrogen atoms are represented as spheres of arbitrary size.



(+)-DTTA. Attempts to resolve compounds **3**, **6**, and **10** by this procedure failed even after trying modified resolution conditions. While trying to resolve the latter grouping of biaryls, we decided to examine the ^{1}H NMR spectrum of compounds (±)-**3**–**6**, **8**, and **10** in the presence of 2 equiv. of (–)-DBTA to determine if indeed diastereomeric complexes were formed. In all cases, a pair of singlets integrating for 3H each were observed between 2.8 and 3.6 ppm. The two signals corresponded to the methoxy groups[5] for each of the diastereomeric complexes in solution. Although the diastereomeric complexes were formed in solution with compounds (±)-**6** and **10** and 2 equiv. of (–)-DBTA, the crystals obtained were always a mix of both diastereomers. Thus enantiomerically pure **3**, **6**, **7**, and **9**–**11** were prepared by alternative methods (1). Once compounds **3**–**11** were obtained, the enantiopurity of the compounds was determined by complexing them with 2 equiv. of (–)-DBTA and observing the region between 2.8 and 3.6 ppm in the ^{1}H NMR spectrum. Once resolved, only one methoxy signal was ob-

Fig. 4. ORTEP diagram of (+)-(*R*)-**15** drawn with 30% probability ellipsoids. Hydrogen atoms are represented as spheres of arbitrary size.

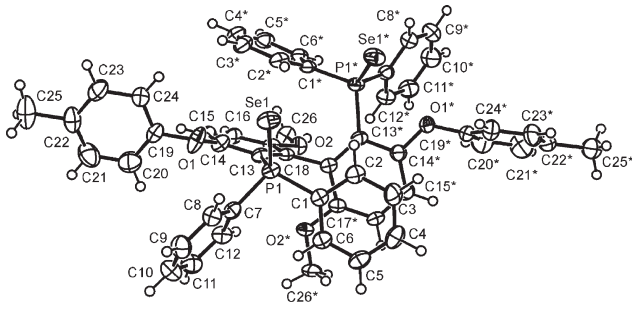


Fig. 5. ORTEP diagram of (+)-(*S*)-**16** drawn with 30% probability ellipsoids. Hydrogen atoms are represented as spheres of arbitrary size.

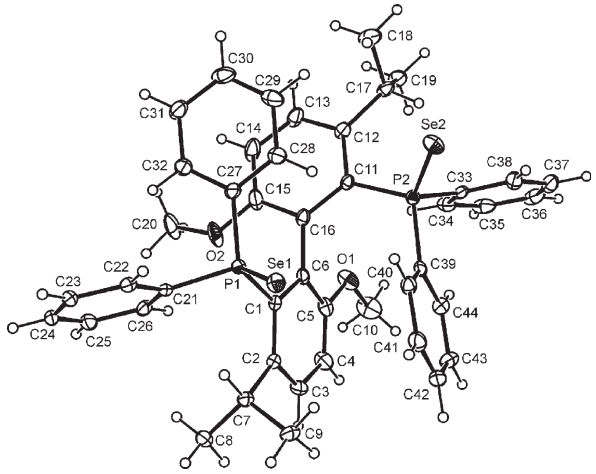
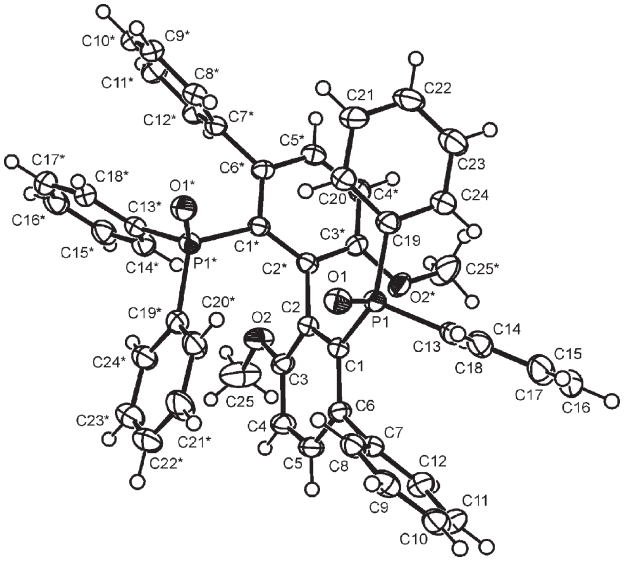


Fig. 6. ORTEP diagram of (+)-(*R*)-**10** drawn with 30% probability ellipsoids. Hydrogen atoms are represented as spheres of arbitrary size.



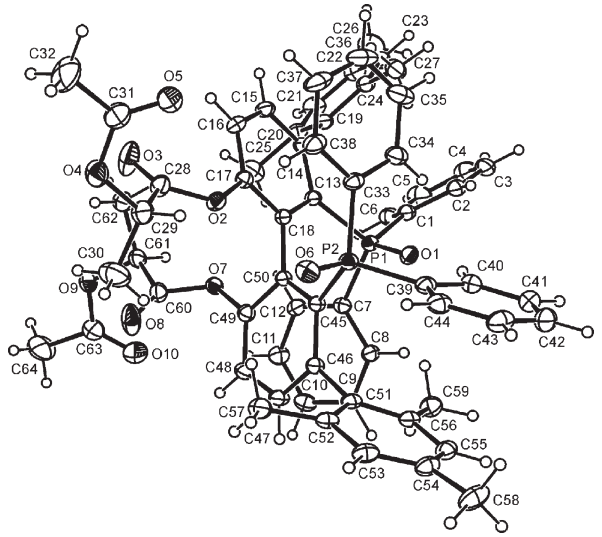
[5] Each methoxy signal arising from the two diastereomeric complexes corresponds to both the C6 and C6′ methoxy groups within one complex. The C6 and C6′ methoxy groups are homotopic by virtue of a C2 axis, even when complexed with (–)-DBTA.

© 2006 NRC Canada

Table 1. ^{1}H NMR shifts of the methoxy group for complexes of **3–11** with 2 equiv. of (–)-DBTA.

Compound	3,3′-Group	$[\alpha]_D^{20}$ (c solvent) for (*S*)-enantiomer	Chemical shift (ppm) ($CDCl_3$) (*S*)-enantiomer	(*R*)-enantiomer
3	H	–130.4 (1.00, $CHCl_3$)	2.90	3.04
4	OMe	–130.1 (1.05, $CHCl_3$)	2.87	3.07
5	O-*i*-Pr	–80.1 (0.53, $CHCl_3$)	2.84	3.09
6	O-*t*-Bu	–44.1 (1.42, $CHCl_3$)	2.75	3.05
7	OPiv	–1.1 (2.70, $CHCl_3$)	2.98	3.11
8	OTolyl	–124.0 (1.40, $CHCl_3$)	2.82	3.13
9	*i*-Pr	+17.1 (0.76, $CHCl_3$)	3.02	3.30
10	Ph	+347.0 (1.04, $CHCl_3$)	3.54	3.58
11	Mesityl	+47.0 (0.82, $CHCl_3$)	3.30	3.35

Fig. 7. ORTEP diagram of (+)-(*S*)-**17** drawn with 30% probability ellipsoids. Hydrogen atoms are represented as spheres of arbitrary size.



served for each of compounds **3–11**, indicating the samples were enantiopure. What was interesting is that when we correlated the absolute configuration of the axis of chirality to the chemical shift of the methoxy signals complexed with 2 equiv. of (–)-DBTA, we found that the chemical shift of the methoxy group of the (*S*)-enantiomer was always upfield of the methoxy signal for the (*R*)-enantiomer (Table 1).

The only 3,3′-disubstituted compound in Table 1 whose absolute configuration was not determined by X-ray crystallography was biaryl **6** (3,3′-diO-*t*-Bu-MeO-BIPHEP). The absolute stereochemistry was assigned based on the ^{1}H NMR shifts of the methoxy groups when complexed with 2 equiv. of (–)-DBTA (Table 1). The individual enantiomers of **6** were separated as previously described (1*b*). Additional support for the hypothesis that the absolute configuration of compound **6** was *R* (based on the NMR shifts in Table 1) came when the corresponding bisphosphine, (+)-(*R*)-**26** (made by the reduction of bisphosphine oxide (+)-(*R*)-**6** (1)) was used in the Heck arylation of 2,3-dihydrofuran (Table 2) (5). With all the reactions recorded with compounds **23–25** and **27–30**, the biaryl enantiomer with the *R*-axis of chirality always gave (*R*)-**20** as the major product. This was also observed with (*R*)-BINAP (entry 9). The reaction with the enantiomer assigned as (*R*)-**26** from the ^{1}H NMR data (Table 1) also provided (*R*)-**20** as the major product, thereby providing additional evidence (although not entirely conclusive) that the absolute configuration of **6** could be assigned by following the general trend shown in Table 1.

Conclusions

We have shown that the absolute stereochemistry of 3,3′-disubstituted-MeO-BIPHEP derivatives can be correlated to the chemical shift of the methoxy signal when the BIPHEP derivative is complexed with 2 equiv. of (–)-DBTA. In all cases the methoxy signal from the *S*-enantiomer:(–)-DBTA complex appeared at higher field than the *R*-enantiomer:(–)-DBTA complex. In addition, the enantiomeric purity of scalemic mixtures of MeO-BIPHEP derivatives can be obtained by integration of methoxy signals when the MeO-BIPHEP derivative is complexed with 2 equiv. of (–)-DBTA.

Experimental procedures

Compounds **3–11** were prepared as previously described (1). ^{1}H NMR spectra were obtained on a 300 MHz NMR spectrometer. All spectra were obtained in $CDCl_3$, and the chemical shifts (ppm) are relative to the C*H*Cl_3 peak as an internal reference (7.27 ppm for ^{1}H). X-ray crystal structures were determined by Dr. Masood Parvez at the University of Calgary, Calgary, Alberta.

General procedure for preparation of the 1:2 complexes of biaryls 3–11:(–)-DBTA

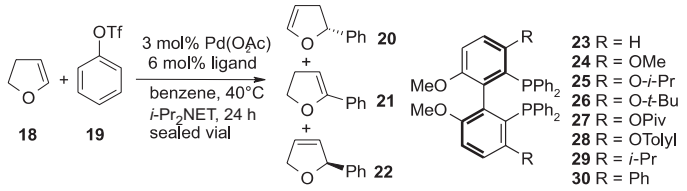
To a solution of phosphine oxide **3–11** (~10 μmol) in $CDCl_3$ was added a solution of (–)-DBTA (~20 μmol) in $CDCl_3$ (0.4 mL). The clear solution was then analyzed by NMR.

General procedure for the Heck reaction with 2,3-dihydrofuran (18)

Under a nitrogen atmosphere, the chiral phosphine (0.03 equiv.) and $Pd(OAc)_2$ (0.067 equiv.) were placed in a scintillation vial equipped with a magnetic stirring bar. The vial was sealed with a Teflon-faced silicone septum under nitrogen. The reagents were dissolved in dry benzene (1.65 mL/equiv. PhOTf) and stirred at room temperature for 10 min. Phenyl triflate (1 equiv.), DIPEA (3.39 equiv.), and 2,3-dihydrofuran (5.60 equiv.) were added sequentially, and the vial was placed in a preheated, thermostatically controlled 40 °C oil bath for 24 h. Hexanes (8.26 mL/equiv.

© 2006 NRC Canada

Table 2. Asymmetric Heck results with ligands **3**–**10**.



			Ratio of products		
Entry	Ligand	Conversion (%)	(***R***)-**20** (% ee)	**21**	(*S*)-**22** (% ee)
1	(+)-(*R*)-**23**	65	83 (92)	7	10 (63)
2	(+)-(*R*)-**24**	6	100 (9)	0	0
3	(+)-(*R*)-**25**	37	93 (77)	0	7 (0)
4	(+)-(*R*)-**26**	100	96 (89)	0	4 (11)[a]
5	(+)-(*R*)-**27**	100	99 (90)	0	1 (10)
6	(+)-(*R*)-**28**	57	97 (20)	0	3 (85)
7	(–)-(*R*)-**29**	12	66 (51)	0	34 (25)
8	(–)-(*R*)-**30**	60	99 (>99)	0	1 (>99)[a,b]
9	(+)-(*R*)-BINAP	41	91 (81)	0	9 (61)[c]

[a]The major enantiomer of **22** had the *R*-configuration.
[b]10 mol% $Pd(OAc)_2$, 20 mol% (–)-(*R*)-9.
[c]Results reported by Hayashi and co-workers (5).

ligand) were then added, and the resulting slurry was filtered through a plug of silica gel. The filtrate was analyzed by chiral GC (Cyclodex B column, 80 °C start temperature, 2 min initial hold time, 1 °C/min ramp rate, 160 °C final temperature, helium carrier gas at 2.0 mL/min, FID detection), with the reaction components eluting in the following order: phenyl triflate (10.81 min), (*S*)-2-phenyl-2,3-dihydrofuran (26.57 min), (*R*)-2-phenyl-2,3-dihydrofuran (26.97 min), 2-phenyl-4,5-dihydrofuran (29.11 min), (*S*)-2-phenyl-2,5-dihydrofuran (31.51 min), (*R*)-2-phenyl-2,5-dihydrofuran (31.91 min).

X-ray crystal data for compound (*S*)-12

Monoclinic *C*2; a = 28.3813(7) Å, b = 9.6063(2) Å, c = 11.1778(4) Å, β = 105.3695(10)°, V = 2938.52(14) Å^3; Z = 2; R = 0.042; wR = 0.083.

X-ray crystal data for compound (*S*)-5

Monoclinic $P2_1$; a = 13.0510(10) Å, b = 23.083(2) Å, c = 21.525(3) Å, β = 95.548(4)°, V = 6454.2(12) Å^3; Z = 4, R = 0.054; wR = 0.147. The asymmetric unit is composed of two independent pairs of molecules of $C_{44}H_{44}O_6P_2$ and $C_{20}H_{18}O_8$, an ordered molecule of CH_3CN, and three disordered half molecules of CH_3CN. The non-hydrogen atoms of the complex molecules and ordered solvate were refined anisotropically; the C and N atoms of the disordered solvates were allowed isotropic displacement parameters. Phenyl rings were constrained as regular hexagons with C—C 1.39 Å and C-C-C 120°. Hydrogen atoms were included at geometrically idealized positions and were not refined; H-atoms of the disordered CH_3CN molecules were ignored.

X-ray crystal data for compound (*R*)-14

Orthorhombic $P2_12_12_1$; a = 18.334(2) Å, b = 18.530(2) Å, c = 33.367(6) Å, V = 11 336(3) Å^3; Z = 8. The asymmetric unit is composed of two independent molecules of $C_{48}H_{48}O_6P_2Se_2$, an ordered molecule of $C_3H_6O_3$, and two disordered half molecules of $C_3H_6O_3$. A *t*-Bu group and an O11,C91-C95 moiety in one of the $C_{48}H_{48}O_6P_2Se_2$ molecules are disordered. Most of the non-hydrogen atoms were refined anisotropically. Phenyl rings were constrained as regular hexagons with C—C = 1.39 Å and C-C-C = 120°. Hydrogen atoms were included at geometrically idealized positions and were not refined; H-atoms of the disordered $C_3H_6O_3$ half molecules were ignored. The final cycle of full-matrix least-squares refinement using SHELXL97 (6) converged with unweighted and weighted agreement factors, R = 0.074; wR = 0.212 (all data), respectively, and goodness of fit, S = 1.01. The absolute configuration was established by the Flack method (4). The Flack parameter for the inverted structure was 0.992(13). Therefore, the inverted structure was rejected as the one present in the crystal.

X-ray crystal data for compound (*R*)-15

Orthorhombic $C222_1$; a = 12.1890(10) Å, b = 17.261(2) Å, c = 22.239(4) Å, α = β = γ = 90°, V = 4679.0(11) Å^3, Z = 4. The final cycle of full-matrix least-squares refinement using SHELXL97 (6) converged with unweighted and weighted agreement factors R = 0.033, wR = 0.072 (all data), respectively, and goodness of fit, S = 1.03. The absolute configuration was established by the Flack method (4). The Flack parameter for the inverted structure was 0.995(6). Therefore, the inverted structure was rejected as the one present in the crystal.

X-ray crystal data for compound (*S*)-16

Monoclinic $P2_1$; a = 13.577(2) Å, b = 18.990(4) Å, c = 17.459(3) Å, α = γ = 90°, β = 98.903(10)°, V = 4447.2(14) Å^3; Z = 2. The asymmetric unit is composed of two molecules of the complex, a CH_3CN of solvation and a half molecule of C_6H_{14} of solvation that was disordered over two sites with partial occupancy factors of 0.25 each. The non-hydrogen atoms were refined anisotropically. Hydrogen atoms were included at geometrically idealized positions and were not

© 2006 NRC Canada

refined; H-atoms of the disordered C_6H_{14} were ignored. The final cycle of full-matrix least-squares refinement using SHELXL97 (6) converged with unweighted and weighted agreement factors $R = 0.038$, $wR = 0.095$ (all data), respectively, and goodness of fit, $S = 1.09$. The absolute configuration was established by the Flack method (4). The Flack parameter for the inverted structure was 0.976(5). Therefore, the inverted structure was rejected as the one present in the crystal.

X-ray crystal data for compound (*R*)-10

Monoclinic *C*2; $a = 22.090(6)$ Å, $b = 9.557(3)$ Å, $c = 12.174(2)$ Å, $\alpha = \gamma = 90°$, $\beta = 103.889(15)°$, $V = 2495.0(11)$ Å^3; $Z = 2$. The asymmetric unit is composed of a half molecule of the complex lying about a twofold axis, a CH_2Cl_2 of solvation on a general position, and a disordered half molecule of CH_2Cl_2 of solvation lying on a special position. The non-hydrogen atoms were refined anisotropically. Hydrogen atoms were included at geometrically idealized positions and were not refined; H-atoms of the disordered CH_2Cl_2 were ignored. The final cycle of full-matrix least-squares refinement using SHELXL97 (6) converged with unweighted and weighted agreement factors, $R = 0.0548$, $wR = 0.113$ (all data), respectively, and goodness of fit, $S = 1.04$. The absolute configuration was established by the Flack method (4). The Flack parameter for the inverted structure was 0.95(8). Therefore, the inverted structure was rejected as the one present in the crystal.

X-ray crystal data for compound (*S*)-17

Monoclinic $P2_1$; $a = 11.8900(10)$ Å, $b = 21.565(4)$ Å, $c = 22.128(15)$ Å, $\alpha = \gamma = 90°$, $\beta = 93.399(10)°$, $V = 5663.8(15)$ Å^3; $Z = 4$. The asymmetric unit contains two molecules of the complex and a water of solvation. In one of the molecules, C160-C164 and O18-O20 were disordered over two sites each. Most of the non-hydrogen atoms were refined anisotropically. Hydrogen atoms were included at geometrically idealized positions and were not refined. The final cycle of full-matrix least-squares refinement using SHELXL97 (6) converged with unweighted and weighted agreement factors $R = 0.05$, $wR = 0.125$ (all data), respectively, and goodness of fit, $S = 1.03$. The absolute configuration was established by the Flack method (4). The Flack parameter for the inverted structure was 0.97(6). Therefore, the inverted structure was rejected as the one present in the crystal.

Acknowledgements

We thank Merck Frosst (Pointe Claire, Quebec), the Natural Sciences and Engineering Research Council of Canada (NSERC) CRD program, and the University of Calgary for financial support. In addition, NSERC and the Alberta Ingenuity Fund are thanked for postgraduate scholarships (for BMMW).

References

1. (*a*) E. Gorobets, G.-R. Sun, B.M.M. Wheatley, M. Parvez, and B.A. Keay. Tetrahedron Lett. **45**, 3597 (2004); (*b*) E. Gorobets, B.M.M. Wheatley, J.M. Hopkins, R. McDonald, and B.A. Keay. Tetrahedron Lett. **46**, 3843 (2005).
2. (*a*) N.G. Andersen, M. Parvez, R. McDonald, and B.A. Keay. Can. J. Chem. **82**, 145 (2004); (*b*) N.G. Andersen, R. McDonald, and B.A. Keay. Tetrahedron: Asymmetry, **12**, 263 (2001); (*c*) N.G. Andersen, M. Parvez, and B.A. Keay. Org. Lett. **2**, 2817 (2000); (*d*) D. Che, N.G. Andersen, S.Y.W. Lau, M. Parvez, and B.A. Keay. Tetrahedron: Asymmetry, **11**, 1919 (2000).
3. (*a*) R. Schmid, M. Cereghetti, B. Heiser, P. Schonholzer, and H.-J. Hansen. Helv. Chim. Acta, **71**, 897 (1988); (*b*) R. Schmid, J. Foricher, M. Cereghetti, and P. Schönholzer. Helv. Chim. Acta **74**, 370 (1991).
4. H.D. Flack. Acta Crystallogr. Sect. A, **A39**, 876 (1983).
5. (*a*) F. Ozawa, A. Kubo, Y. Matsumoto, and T. Hayashi. Organometallics, **12**, 4188 (1993); (*b*) F. Ozawa, A. Kubo, and T. Hayashi. J. Am. Chem. Soc. **113**, 1417 (1991).
6. G.M. Sheldrick. SHELXL97 [computer program]. University of Göttingen, Göttingen, Germany. 1997.

© 2006 NRC Canada

A critical evaluation of homo- and hetero-leptic cadmium complexes using bond valence sums[1]

Gus J. Palenik

Abstract: The effect of the donor atoms in Cd complexes on the determination of R_0 values for the bond valence sum (BVS) is reported. A total of 1321 CdX_mY_n fragments with X and Y = O, N, S, Cl, Br, and I were used to calculate the R_0 values for Cd—X bonds from both homoleptic and heteroleptic fragments. The R_0 values determined from mixed CdX_mY_n fragments agree with those determined from the homoleptic species, with no significant differences in the values as a function of either electronegativity or hard–soft character of the atoms. The new R_0 values derived from the homoleptic series recommended for use in calculating the BVS are as follows: Cd(II)—O of 1.875(13) Å, Cd(II)—N of 1.951(15) Å, Cd(II)—S of 2.279(7) Å, Cd(II)—Cl of 2.216(17) Å, Cd(II)—Br of 2.334(7) Å, and Cd(II)—I of 2.525(7) Å. These R_0 values can be used to calculate the oxidation state of Cd in complexes where Cd is bonded to any combination of O, N, S, Cl, Br, and I donor atoms. Cases where the BVS does not agree with the expected oxidation state are discussed. In particular, the planarity of Cd porphyrins is discussed in terms of the BVS.

Key words: bond valence sums, cadmium complexes, cadmium porphyrins, cadmium distances.

Résumé : On a déterminé l'effet des atomes donneurs présents dans des complexes de cadmium sur la détermination des valeurs de R_0 de la somme des liaisons de valence « SLV ». On a utilisé un total de 1321 fragments CdX_mY_n (dans lesquels X et Y peuvent être égaux à O, N, S, Cl, Br et I) pour calculer les valeurs de R_0 pour des liaisons Cd—X appartenant à des fragments homoleptiques et hétéroleptiques. Les valeurs de R_0 déterminées à partir de fragments CdX_mY_n mixtes sont en bon accord avec celles déterminées à partir d'espèces homoleptiques, sans différences significatives dans les valeurs en fonction de l'électronégativité ou du caractère dur ou mou des atomes. Les nouvelles valeurs de R_0, dérivées des séries homoleptiques et dont l'usage est recommandé dans les calculs de « SLV » sont: Cd(II)—O, 1,875(13) Å; Cd(II)—N, 1,951(15) Å; Cd(II)—S, 2,279(7) Å; Cd(II)—Cl, 2,216(17) Å; Cd(II)—Br, 2,334(7) Å et Cd(II)—I, 2,525(7) Å. Ces valeurs de R_0 peuvent être utilisées pour calculer l'état d'oxydation du cadmium dans des complexes où il est lié à O, N, S, Cl, Br et I comme atomes donneurs. On discute de cas où la somme des liaisons de valence ne conduit pas aux valeurs attendues pour l'état d'oxydation. En particulier, on discute de la planéité du cadmium dans les porphyrines en termes de la somme des liaisons de valence.

Mots clés : somme des liaisons de valence, complexes du cadmium, cadmium dans les porphyrines, distances du cadmium.

[Traduit par la Rédaction]

Introduction

The concepts of electronegativity (1), hard–soft acid–bases or HSAB (1, 2), and the bond valence sum or BVS (3, 4) have been very useful in many areas of inorganic chemistry. Soft acids bond more readily with soft bases than with hard bases and vice versa. The question is whether the HSAB effect would be manifested in the BVS. The postulate that the BVS is equal to the oxidation state (z_j, as shown in eq. [1]) has been applied to a variety of problems in coordination chemistry (3–6), particularly to verify a postulated oxidation state. The calculation of the valences of the individual bonds (s_{ij} in eq. [1]) from the observed bond lengths can be accomplished using either eq. [2] or eq. [3], where r_{ij} is the observed bond length and R_0 and N are constants dependent upon the nature of the ij pair.

$$[1] \quad z_j = \Sigma_j s_{ij}$$

$$[2] \quad s_{ij} = \exp[(R_0 - r_{ij})/b]$$

$$[3] \quad s_{ij} = (r_{ij}/R_0)^{-N}$$

The R_0 value[2] can be viewed as a bond length of unit valence. One of the first compilations of R_0 values used data in the Inorganic Crystal Structural Database or ICSD (7) with eq. [2] and assumed that $b = 0.37$ (8), a value that has been generally accepted as an almost universal constant (9). Recently, the validity of the universal nature of $b = 0.37$ was investigated using data from alkali halides and chalcogenides (10) and considering not only the distances in the first coordination sphere but neighboring atoms as well. One conclusion was that the assumption that $b = 0.37$ is acceptable for most applications of the BVS. A more extensive discussion

Received 18 March 2005. Published on the NRC Research Press Web site at http://canjchem.nrc.ca on 14 February 2006.

G.J. Palenik. Chemistry Department, The University of Florida, PO Box 117200, Gainesville, FL 32611-7200, USA. (e-mail: palenik@chem.ufl.edu).

[1]This article is part of a Special Issue dedicated to Professor Arthur Carty.

[2]An italicized R_0 refers to the constant in eqs. [2] and [3] and is not the usual crystallographic R value, which is simply capital *R*.

 doi:10.1139/V05-227 © 2006 NRC Canada

Table 1. Summary of the R_0 values for Cd—X bonds determined from CdX and CdXY complexes.

	X					
	O	N	S	Cl	Br	I
Y = O	1.875(13)	1.968(3)	2.291(6)	2.224(7)	2.336(9)	2.537(12)
n/*t*	92/122	315/327	54/56	48/48	17/17	23/23
Y = N	1.875(3)	1.951(15)	2.277(10)	2.216(9)	2.344(10)	2.530(25)
n/*t*	315/327	138/178	106/107	48/48	18/18	20/22
Y = S	1.899(6)	1.957(10)	2.279(7)	2.251(14)	2.334(14)	2.526(10)
n/*t*	54/56′	106/111	96/145	44/44	20/20	17/17
Y = Cl	1.877(7)	1.972(9)	2.263(14)	2.216(17)		
n/*t*	48/48	48/48	44/44	54/55		
Y = Br	1.856(9)	1.966(10)	2.284(15)		2.334(7)	
n/*t*	17/17	18/18	20/20		27/37	
Y = I	1.897(12)	1.945(25)	2.280(10)			2.525(7)
n/*t*	23/23	20/22	17/17			32/33
Avg.	1.880(16)	1.953(23)	2.274(22)	2.214(35)	2.337(5)	2.530(5)
BA	1.904		2.304	2.212		
OB	1.842	1.959	2.278	2.215	2.362	2.572
χ(X)	3.44	3.04	2.58	3.16	2.96	2.66
η(X)	6.08	7.23	4.14	4.68	4.22	3.69

Note: For a given X, the R_0 value is given followed by the estimated standard deviation in parentheses, calculated using *n* of the *t* total number of entries. Avg. is the average R_0 value for Cd—X, calculated from the individual R_0 with the estimated standard deviation in parentheses. BA gives the R_0 values from ref. 8; OB gives the R_0 values calculated from the parameters in ref. 9, χ(X) is the Pauling electronegativity from ref. 1(*b*), and η(X) is the hardness from ref. 2.

of the BVS method can be found elsewhere (3, 4, 8–11, and refs. therein).

Although some R_0 values have been obtained by empirical expressions or by extrapolation from known values (3, 8, 9), the majority of the experimental R_0 values have been determined from species containing only one type of donor atom using data initially from the ICSD (7) and later from the Cambridge Structural Base or CSD (12). This restrictive approach was useful in obtaining R_0 values from structural data in the CSD and has led to an appreciation of the usefulness of the BVS and an understanding of the effect of the coordination number and oxidation state on the R_0 value. More recently, the observation was made that the R_0 values obtained from the CSD file appeared to be smaller than the values obtained from the ICSD. The questions were whether the R_0 derived from mixed compounds would differ from those obtained from homoleptic complexes and whether electronegativity and (or) the HSAB characteristics of the atoms would affect the experimentally determined R_0 values.

To answer these questions, the determination of R_0 values has been extended to complexes containing two different atoms in the coordination sphere. This report demonstrates that R_0 values obtained from mixed complexes CdX_nY_m (where X and Y are the donor atoms O, N, S, Cl, Br, and I) are identical, within the calculated standard deviations, to those obtained from homoleptic fragments. These results provide further support for the use of the BVS in inorganic chemistry. The Cd case was chosen to avoid the problems of different oxidation and (or) spin states. We have operated under the assumption that the BVS should always be "correct" and have used the reported bond distances to determine the R_0 value only when the observed and calculated oxidation states are in agreement. Any discrepancies can usually be explained by a careful examination of crystallographic and (or) experimental data, vide infra.

Experimental section

Cd—X bond distances

The Cd—X bond length data for X = O, N, S, Cl, Br, and I were retrieved from the April 2004 release of the CSD with no restrictions. This approach ensures that all the relevant Cd—X distances could be retrieved for further analysis, since one goal of the project was to demonstrate the usefulness of the BVS as a simple diagnostic tool for the noncrystallographer. The fact that structures with a low crystallographic R value can still be incorrect also argues against retrieving only those structures with low R values.

BVS calculations

The R_0 values for the homoleptic fragments were determined using procedures described earlier (5, 13). For the CdX_nY_m fragments, a least-squares procedure was used with all entries given equal weight. The R_0 values, with the number of fragments used for the various X, Y combinations, together with literature values, electronegativities, and HSAB character are given in Table 1. The Cd—X distances from the homoleptic species used in the analysis are summarized in Table 2.

Results and discussion

R_0 values for Cd—X bonds

The values in Table 1 show that an R_0 value for a Cd—X bond determined from homoleptic Cd—X data is the same, within the estimated standard deviation, as that obtained

© 2006 NRC Canada

Table 2. Summary of Cd—X distances, X = O, N, S, Cl, Br, and I, used in the analysis.

X	CN	No.	Min	Max	Avg(σ)	Val	CN×Val
O	4	4	1.979	2.32	2.138(150)	0.491	1.965
	5	10	2.147	2.346	2.217(66)	0.397	1.985
	6	306	2.193	2.509	2.281(47)	0.334	2.002
	7	133	2.213	2.736	2.355(102)	0.273	1.912
	8	152	2.251	2.705	2.404(92)	0.240	1.917
N	4	32	2.180	2.243	2.204(19)	0.504	2.016
	5	25	2.166	2.390	2.297(63)	0.393	1.965
	6	726	2.176	2.731	2.361(62)	0.330	1.979
	7	14	2.247	2.572	2.421(96)	0.280	1.963
	8	16	2.349	2.745	2.493(96)	0.231	1.850
S	3	6	2.417	2.453	2.427(13)	0.670	2.011
	4	300	2.413	2.708	2.538(44)	0.497	1.987
	5	65	2.513	2.897	2.628(102)	0.389	1.944
	6	36	2.518	3.068	2.713(130)	0.310	1.859
Cl	4	96	2.361	2.565	2.459(34)	0.518	2.073
	5	10	2.438	2.773	2.581(109)	0.373	1.863
	6	174	2.466	2.822	2.639(54)	0.319	1.912
Br	4	112	2.522	2.712	2.588(36)	0.503	2.013
	5	10	2.538	3.055	2.730(199)	0.343	1.716
	6	42	2.578	3.082	2.780(71)	0.299	1.796
I	4	128	2.679	2.900	2.785(48)	0.496	1.983

Note: CN is the coordination number; No. is the number of bonds found; Min is the minimum Cd—X distance found for that coordination number; Max is the maximum Cd—X distance found for that coordination number; Avg(σ) is the average Cd—X distance for that coordination number with the estimated standard deviation in parentheses; Val is the valence of the average distance calculated using eq. [2] with b = 0.37 and R_0 = 1.875 Å for X = O, 1.951 Å for X = N, 2.279 Å for X = S, 2.216 Å for X = Cl, 2.334 Å for X = Br, and 2.525 Å for X = I.

from mixed CdX_nY_m fragments. The R_0 values for Cd—X bonds determined from homoleptic fragments are slightly shorter than the experimental values found in ref. 8, as has been noted (14). The reasons for the difference in the R_0 values from the CSD file vs. data from only inorganic structures is not obvious. A comparison of R_0 from homoleptic and mixed species shows no discernable trend with either electronegativity or with hardness. Finally, the values determined experimentally from the CSD data are surprisingly close to the values calculated from the empirical atomic constants (9). Therefore, the values from CSD data for either homoleptic or mixed donor complexes can be used to derive the desired R_0 values, and these values can be used in complexes containing more than one type of donor atom. A final point is that the empirical atomic constant parameter can be used to calculate R_0 values for pairs in which there are very little or no experimental bond distance data.

Cd—X distances

The Cd—X distances in the homoleptic CdX_n complexes used in the analysis are tabulated in Table 2. The range of Cd—X distances is very large; however, the average distance for any bond and coordination number is dictated by the oxidation state and the number of bonds, so that the valence times the number of bonds equals the oxidation state. One implication is that a comparison of a Cd—X distance in a particular complex may not be very meaningful, but the BVS should always equal the oxidation state. The final distances in any coordination complex represent a balance between the donor ability and the steric constraints imposed by the ligand.

Calculation of the oxidation state of Cd(XY) complexes

For the 1321 complexes used in the analysis, the oxidation state of the Cd ion was calculated using the R_0 values given in Table 1 for the homoleptic species. There are only 59 cases, or 4.5%, where the BVS differs from the expected value of 2 by more than 0.30 valence units (vu). The 0.30 is a somewhat arbitrary difference that has been used to determine which structures are to be investigated in more detail. A large deviation of the BVS from the expected value has been a good indication that there are problems, which can include disorder in the crystal, an incorrect space group assignment, an incorrectly assigned oxidation state, a misidentified atom, or weak interactions that may have been overlooked.

BVS and cadmium tetraphenylporphyrins

There is a group of Cd-N and Cd-ON complexes that have a BVS > 2.0, and these are all cadmium tetraphenylporphyrins, or CdTPP, complexes. These include a series of CdTPP clathrate complexes, JIVROV (15),[3] BVS = 2.48; JIVRUB (15), BVS = 2.50; JIVSOW (15), BVS = 2.48; and HALXIB (16), BVS = 2.45, where the Cd ion is on a center of symmetry and therefore in the plane of the TPP ligand, which is very unlikely. The TPP cavity is too small for the large Cd ion, as was nicely illustrated in DIPXAB (17),

[3] We shall give the refcode used in the CSD file in capital letters and the compound name in the reference list.

© 2006 NRC Canada

BVS = 2.11, where the Cd ion is 0.568 Å from the plane of the four nitrogen atoms. If the Cd(II) is coplanar with the TPP ring, the Cd—N distances are too short, and the corresponding BVS too large, as seen in the above examples. The TPP cavity has been examined in some detail by various groups (18–20), and the cavity radius is unlikely to be larger than 2.11 Å, with 2.01 Å being approximately strain free. A Cd—N bond with a valence of 0.5 would be 2.207 Å, and if the ring center to N distance were 2.10 Å, the Cd(II) ion would be 0.70 Å out of the TPP plane. A larger, but unlikely, distortion of the TPP ligand could lower the displacement of the Cd ion relative to the plane of the four nitrogen atoms. Therefore, the BVS suggests that the Cd should not lie in the plane of the TPP ligand, but is displaced by about 0.6 Å from the center of the TPP ligand.

The situation with PHPNCD (21) (BVS = 2.55) is somewhat more complicated since the authors state that the Cd is only 0.028 Å from the plane of the four nitrogen atoms. However, the thermal ellipsoid for Cd is elongated in the direction perpendicular to the TPP plane, suggesting that the Cd is disordered, a view noted in DIPXAB (17). There are also some questions about the formulation of PHPNCD, since the observed and calculated densities differ markedly. The problem in most cases is that the Cd should not be on a center of symmetry and coplanar with the TPP ligand, see DOFXOL (22). Whether the displacement of the Cd from the TPP ring can be resolved becomes a question of the quality of the X-ray data and the effort put into the refinement.

Cd complexes where the BVS << 2

Of the CdO_n complexes used in the analysis, there are only four cases were the BVS differs from the expected value by more than 0.30 vu. Two of the four are the same complex determined by two different groups at two different temperatures, SIGJUN (23) at 298 K (BVS = 1.59) and SIGJUN01 (24) at 193 K (BVS = 1.59). The complex is one of a series of bis(2,6-disubstituted phenoxo)Cd(II) complexes with O bases that includes NULVUL01 (24) (BVS = 1.79) and SEYLIR (24) (BVS = 1.77). The complexes SIGJUN, NULVUL01, and SEYLIR have a BVS that is less than 2, probably resulting from the different steric constraints of the phenoxide ligands. In both NULVUL01 and SEYLIR, there appear to be fewer steric constraints, and the corresponding values are closer to 2. The complexes were described in terms of obviously short or dative bonds (25), with additional longer or secondary bonds (26) used to complete the coordination sphere. A simple description could be made using BVS arguments by stating that the best donor atoms contribute a larger share to the BVS and that the overall result is a balance between steric and electronic constraints. When very bulky ligands are used to synthesize low CN complexes, the severe steric constraints imposed by the ligands usually yield longer bond distances and, consequently, a BVS that is less than the expected value.

In YAYREV (27), the BVS of 1.50 appears to be too small. The crystals were mounted in glass capillaries, but the question of absorption corrections was not discussed in the paper. The effect of absorption on bond distances is usually small, but the thermal parameters can reflect absorption effects. Consequently, at this time the complex appears to be one of the few examples where there does not seem to be any apparent reason for the low BVS value.

The CdS and Cd(NI) complexes afford several examples where the BVS is less than the expected value of 2, but weak interactions increase the BVS to the expected value. The complexes JUXTAX (28) (BVS = 1.65), LOLXUF (29) (BVS = 1.64), and PAGBAA (30) (BVS = 1.64 and 1.65) were classified in the CSD as three-coordinate CdS complexes, while KABPEI (31) (BVS = 1.53) and VIJXOB (32) (BVS = 1.53) were four-coordinate. However, in all cases there are additional weak interactions that increase the BVS to a value close to 2. A similar situation exists with WUQHAR (33) (BVS = 1.57), but when two additional Cd···I interactions are included, the BVS = 1.79. The problem is that the weak interactions are not always recognized by investigators and are difficult to justify and include in the CSD. However, in many of the above cases, the authors recognized the importance of these secondary interactions.

Another example of a low BVS was the two-coordinate complex ZIFKUU (34) (BVS = 0.52). The authors noted two additional Cd···S interactions of 2.918 and 2.972. Å, but these only add 0.60 vu to the BVS. The authors reported the stochiometry as containing 0.66Cd without any discussion of a charge balance. Of the 14 compounds reported in two papers (34, 35), ZIFKUU is the only one that does not have +1 or +3 metal ions. The thermal parameters for the NCS group suggest a disorder about the central C atom, although this would make the BVS even smaller. This paper has been cited for errors in two different publications (36, 37), although not for the complex ZIFKUU. In summary, there are so many questions regarding this paper that the results should be viewed with caution.

For the complex HAXJOF (38) (BVS = 1.32) the number of missing bits of information raises doubts about the validity of the structure report. The compound was prepared by a novel electrochemical method. The solid formed was removed, and the solution was allowed to evaporate. Although the "crystal formed was characterized by elemental analysis", these data were not given. The U_{eq} for the Cd of 0.0522 is larger than that for the coordinated O and N atoms, 0.043–0.050, an unusual result. The molecule is surprisingly distorted for a spherical d^{10} ion. One might speculate that an impurity such as Pb in the Cd electrode was concentrated in the solution and that the metal ion is not Cd but Pb.

ZUSBUK (39) (BVS = 1.50) and ZUSCAR (39) (BVS = 1.59) are azacryptand complexes with either tetrafluoroborate or acetate as the anions. ZUSBUK was assigned the high symmetry space group *P*31*c*, No. 163, and the authors determined that the cation consisted of 85% of the right-handed and 15% of the left-hand molecule, and that the anions were also disordered. The authors apparently did not consider whether a lower symmetry space group would yield an ordered structure. Consequently, the low BVS may reflect the disorder and the choice of the high symmetry space group. In ZUSCAR, the space group is *C*2/*c*, but the authors do not give an ORTEP drawing showing the thermal ellipsoids. An inspection of the deposited data shows that the thermal parameters do not look reasonable, and the structural results should be viewed with some skepticism.

© 2006 NRC Canada

QIZFUA01 (40) (BVS = 1.54) and QIZFOU01 (40) (BVS = 1.98) are both Cd-Mo-S cluster compounds with slightly different S groups, and QIZFUA01 also contains a "disordered" $Co(H_2O)_6^{2+}$ cation. The disordered cation is surprising since there are 22 H_2O molecules, as well as various donors and acceptors on the cluster that would be expected to hydrogen bond to the cation. The question of whether the Co and Cd are disordered was apparently not considered and could account for the lower BVS in QIZFUA01. The thermal parameters, which were not published, might be helpful in evaluating this hypothesis.

The series of complexes MEJQUN (41) (BVS = 1.51), MEJRAU (41) (BVS = 1.66), MEJROI (41) (BVS = 1.64), and MEJRUO (41) (BVS = 1.89) have the same hexadentate macrocyclic ligand with two ether linkages. Only in the case of MEJRUO do the authors postulate that there is an O···Cd bond. However, an examination of the distances in these compounds suggests weak interactions (with both ether O atoms in MEJQUN and MEJRAU and one of the O links in MEJROI) that increase the BVS to 1.76, 1.81, and 1.75, respectively. We see that the BVS provides experimental evidence for an interaction with the O atoms of the macrocycle in all cases.

Cd complexes where the BVS >> 2

The majority of the cases where the BVS was >> 2.0 were discussed above in the TPP examples. There are other factors that can cause the BVS to be larger than the expected, such as a misidentification of the metal atom (42, 43), high thermal motion, and disorder in the crystal structure, all leading to apparently shorter bonds. An incorrect space group assignment masking a disorder, as noted above, can also give a BVS greater than the expected value.

The case of ZETFUZ (44) (BVS = 2.50) is difficult to evaluate since the publication was not available. However, the choice of the space group *F*-43*c* is unusual since only 23 of the 272 066 entries in the CSD file have this high symmetry space group. An incorrect space group assignment could give rise to disordered groups and unusually short distances and a corresponding large BVS.

The tris(ethylenediamine)cadmium(II) cation appears in both ENCDSS (45) (BVS = 1.67) and ENDACD (46) (BVS = 2.62) in the space group *P*31*c* with different anions. Two problems arise with both of the complexes: the high symmetry space group and the large *R* values of 0.177 for ENCDSS and 0.145 for ENDACD. In both structures the anions are "disordered", again reflecting the fact that a lower symmetry space group might be more appropriate. In essence, these two structures should be viewed with caution.

A problem with the choice of a space group arises with RACFEG01 (47) (BVS = 2.32) where the choice of *Cm* in the original report (48) was questioned, and the centric choice *C*2/*m* and averaged parameters were used in the CSD file. There is also a remark in the CSD file that an I and CN group are disordered. The BVS suggests that the data may not be as reliable as the crystallographic *R* factor of 0.080 might suggest.

Conclusions and recommendations

The results presented here demonstrate that the BVS constant R_0 derived from homoleptic Cd-X complexes does not differ significantly from those derived from heteroleptic fragments and appears to be independent of the hard–soft character or electronegativities of the atom pair. Therefore, the homoleptic-derived constants can be used to calculate the BVS for Cd-X complexes, which should be 2.0 ± 0.30 vu. However, the use of R_0 values derived from the data in the ICSD file (7) are usually slightly larger, see Table 1 for examples, and will give larger values for the BVS. The R_0 values derived from empirical atomic constants can provide a reasonable starting value for other atom pairs if no other values are available.

The BVS is recommended as a check of the reliability of a crystal structure report rather than a comparison with other metal atom — X distances. Although for a given coordination number, the bond distances vary over a wide range (see Table 2), the bond order of the average M—X distance is the coordination number divided by the valence. The BVS is particularly useful in recognizing a disorder in the metal atom position, as was noted for the CdTPP complexes. A final recommendation is the use of the BVS to provide experimental data to support the postulate of weak interactions in the solid state.[4]

References

1. See any current inorganic textbook for a discussion of electronegativity or hard–soft acid–base concepts, such as: (*a*) C.E. Housecroft and A.G. Sharpe. Inorganic chemistry. Pearson Educational Limited, Essex, UK. 2005; (*b*) D. Shriver and P. Atkins. Inorganic chemistry. 3rd ed. W.H. Freeman and Company, New York. 1999.
2. R.G. Pearson. Inorg. Chem. **27**, 734 (1988).
3. I.D. Brown. The chemical bond in inorganic chemistry. Oxford University Press Inc., New York. 2002.
4. I.D. Brown. J. Chem. Educ. **77**, 1070 (2000).
5. G.J. Palenik. Inorg. Chem. **42**, 2725 (2003).
6. K.H. Tyyko, J. Mehmke, and D. Kurad. Struct. Bonding (Berlin), **93**, 1 (1999).
7. G. Bergerhoff, R. Hundt, R. Sievers, and I.D. Brown. J. Chem. Inf. Comput. Sci. **23**, 66 (1983).
8. I.D. Brown and D. Altermatt. Acta Crystallogr. Sect. B: Struct. Sci. **B41**, 244 (1985).
9. M. O'Keeffe and N.E. Brese. J. Am. Chem. Soc. **113**, 3226 (1991).
10. S. Adams. Acta Crystallogr. Sect. B: Struct. Sci. **B57**, 276 (2001).
11. F. Mohri. Acta Crystallogr. Sect. B: Struct. Sci. **B59**, 190 (2003).
12. F.H. Allen. Acta Crystallogr. Sect. B: Struct. Sci. **B58**, 380 (2002).
13. N.E. Brese and M. O'Keeffe. Acta Crystallogr. Sect. B: Struct. Sci. **B47**, 192 (1991).

[4] Supplementary data for this article are available on the journal Web site (http://canjchem. nrc.ca) or may be purchased from the Depository of Unpublished Data, Document Delivery, CISTI, National Research Council Canada, Ottawa, ON K1A 0R6, Canada. DUD 4091. For more information on obtaining material refer to http://cisti-icist.nrc-cnrc.gc.ca/irm/unpub_e.shtml.

© 2006 NRC Canada

14. A. Trzesowska, R. Kruszynski, and T. Bartczak. Acta Crystallogr. Sect. B: Struct. Sci. **B60**, 174 (2004).
15. JIVROV is (5,10,15,20-tetraphenylporphinato)cadmium(II) bis(*o*-xylene) clathrate: M.P. Byrn, C.J. Curtis, I. Goldberg, Y. Hsiou, S.I. Khan, P.A. Sawin, S.K. Tendick, and C.E. Strouse. J. Am. Chem. Soc. **113**, 6549 (1991); JIVRUB is (5,10,15,20-tetraphenylporphinato)cadmium(II) bis(*m*-xylene) clathrate; JIVSOW is (5,10,15,20-tetraphenylporphinato)cadmium(II) bis(methyl benzoate) clathrate.
16. HALXIB is 4-picoline(5,10,15,20-tetraphenylporphinato)cadmium(II) bis(picoline) clathrate: M.P. Byrn, C.J. Curtis, Y. Hsiou, S.I. Khan, P.A. Sawin, S.K. Tendick, A. Terzis, and C.E. Strouse. J. Am. Chem. Soc. **115**, 9480 (1993).
17. DIPXAB is (5,10,15,20-tetraphenylporphinato)cadmium(II): A. Hazell. Acta Crystallogr. Sect. C: Cryst. Struct. **C42**, 296 (1986).
18. W.R. Scheidt and Y.J. Lee. Struct. Bonding (Berlin), **64**, 1 (1987).
19. D.M. Collins, W.R. Scheidt, and J.L. Hoard. J. Am. Chem. Soc. **94**, 6689 (1972).
20. D.M. Collins and J.L. Hoard. J. Am. Chem. Soc. **92**, 3761 (1970).
21. PHPNCD is bis(dioxane)(5,10,15,20-tetraphenylporphinato)cadmium(II): P.F. Rodesiler, E.H. Griffith, P.D. Ellis, and E.L. Amma. Chem. Commun. 492 (1980).
22. DOFXOL is piperdine(5,10,15,20-tetraphenylporphinato)cadmium(II): P.F. Rodesiler, E.A.H. Griffith, N.G. Charles, L. Lieboda, and E.L. Amma. Inorg. Chem. **24**, 4595 (1985).
23. SIGJUN is bis[2,6-di(*tert*-butyl)phenoxy] bis(tetrahydrofuran)cadmium(II): S.C. Gol, M.Y. Chiang, and W.E. Buhro. J. Am. Chem. Soc. **112**, 6724 (1990).
24. SIGJUN01 is *trans*-bis[2,6-di(*tert*-butyl)phenoxy] bis(tetrahydrofuran)cadmium(II) and is **1**: D.J. Darensbourg, S.A. Niezgoda, J.D. Draper, and J.H. Reibenspies. J. Am. Chem. Soc. **120**, 4690 (1998); NULVUL01 is *trans*-bis[2,6-diphenylphenoxy] bis(tetrahydrofuran)cadmium(II) is **3**; SEYLIR is *trans*-bis[2,6-di(*tert*-butyl)phenoxy] bis(propylenecarbonate)cadmium(II) is **6**.
25. N.W. Alcock. Adv. Inorg. Chem. Radiochem. **15**, 1 (1972).
26. A. Haaland. Angew. Chem. Int. Ed. Engl. **28**, 992 (1989).
27. YAYREV is (μ_2-triethyleneglycol)bis(triethyleneglycol)dicadmium(II) tetrachloride dihydrate: R.D. Rogers, A.H. Bond, S. Aguinaga, and A. Reyes. Inorg. Chim. Acta, **212**, 225 (1993).
28. JUXTAX is tetramethylammonium hexakis(μ_2-thiobenzoato)-dicadmium-sodium: J.J. Vittal and P.A.W. Dean. Inorg. Chem. **32**, 791 (1993).
29. LOLXUF is tetramethylammonium potassium bis(tris(μ_2-thiobenzoato, *O*,*S*)cadmium(II): T.C. Deivaraj, P.A.W. Dean, and J.J. Vittal. Inorg. Chem. **39**, 3071 (2000).
30. PAGBAA is bis((μ_2-tri-*tert*-butoxysilanethiolato) (tri-*tert*-butoxysilanethiolato)cadmium(II): W. Wojnowski, B. Becker, L. Waltz, K. Peters, E.-M. Peters, and H.V. Von Schnering. Polyhedron, **11**, 607 (1992).
31. KABPEI is bis(methoxyethylxanthate-*S*,*S*′)cadmium(II): B.F. Abrahams, B.F. Hoskins, E.R.T. Tiekink, and G. Winter. Aust. J. Chem. **41**, 1117 (1988).
32. VIJXOB is potassium bis(dimercaptomethylenemalononitrile)cadmium(II): H.Y. Li and E.L. Amma. Inorg. Chim. Acta, **177**, 5 (1990).
33. WUQHAR is bis(4-aminobenzoic acid-*N*)diiodocadmium(II): R. Wang, M. Hong, J. Luo, R. Cao, Q. Shi, and J. Weng. Eur. J. Inorg. Chem. 2904 (2002).
34. ZIFKUU is α-bis(ethylenedithio)tetrathiafulvalenium bis(isothiocyanato)cadmium(II): H. Mori, S. Tanaka, T. Mori, and Y. Maruyama. Bull. Chem. Soc. Jpn. **68**, 1136 (1995).
35. H. Mori, S. Tanaka, T. Mori, A. Kobayashi, and H. Kobayashi. Bull. Chem. Soc. Jpn. **71**, 797 (1998).
36. R.E. Marsh and A.L. Spek. Acta Crystallogr. Sect. B: Struct. Sci. **B57**, 800 (2001).
37. F.H. Herbstein, S. Hu, and M. Kapon. Acta Crystallogr. Sect. B: Struct. Sci. **B58**, 884 (2002).
38. HAXJOF is dihydroxy-bis(1,10-phenanthroline)cadmium(II): E. Labisbal, J. Romero, J.A. Garcia-Vazquez, A. Sousa, and A. Castineiras. J. Crystallograph. Spectrosc. Res. **23**, 895 (1993).
39. ZUSBUK is (2.2.2-octaazacryptand)cadmium(II) tetrafluoroborate and is **1a**: J.A. Thompson, M.E. Barr, D.K. Ford, L.A. Silks III, J. McCormick, and P.H. Smith. Inorg. Chem. **35**, 2025 (1996); ZUSCAR is (2.2.2-octaazacryptand)cadmium(II) acetate dihydrate is **1b**.
40. QIZFUA01 is bis(hexaaquacobalt(II) octakis(μ_3-sulfido)hexakis(nitrilo(diacetato) acetic acid-*N*,*O*,*O*′)cadmium-hexamolybdenum hydrate is **5**′: G. Sakane, H. Kawasaki, T. Oomori, M. Yamasaki, H. Adachi, and T. Shibahara. J. Cluster Sci. **13**, 75 (2002); QIZFOU01 is **4**.
41. MEJQUN is *trans*-(10,16-dioxa-3,13,23,28 -tetraazatetracyclo-(23.3.1.0 ^{4,9}.0 ^{17,22}) nonacosa-1(29),2,4(9)5,7,17,19,21,23,25,27-undecaene)(nitrato-*O*)(nitrato-*O*,*O*′)cadmium(II) and is **1**: H. Adams, R. Bastida, D.E. Fenton, A. Macias, S.E. Spey, and L. Valencia. J. Chem. Soc. Dalton Trans. 4131 (1999); MEJRAU is **2**; MEJROI is **4**; MEJRUO is **5**.
42. R.M. Wood and G.J. Palenik. Inorg. Chem. **38**, 1031 (1999).
43. R.M. Wood and G.J. Palenik. Inorg. Chem. **38**, 3926 (1999).
44. ZETFUZ is hexaaquacadmium(II) [(μ_4-sulfido)dodecakis(μ_2-phenylthiolato)tetrachloroocta cadmium(II)]: K.-L. Tang, X.-L. Jin, S.-J. Jia, and Y.-Q. Tang. Jiegou Huaxue, **14**, 399 (1995); see Chem. Abstr. **124**, 20319t (1996).
45. ENCDSS is tris(ethylenediamine)cadmium(II) selenosulfate: N.V. Podberezskaya and S.V. Borisov. Zh. Strukt. Khim. **12**, 1114 (1971); see Chem. Abstr. **76**, 64706 (1972).
46. ENDACD is tris(ethylenediamine)cadmium(II) thiosulfate: N.V. Podberezskaya and S.V. Borisov. Zh. Strukt. Khim. **10**, 847 (1969); see Chem. Abstr. **72**, 26155 (1970).
47. RACFEG01 is bis(tetramethylammonium) catena(hexa((μ_2-cyano)diiodotricadmium(II)) tetrachloroethene) clathrate. R.E. Marsh, M. Kapon, S. Hu, and F.H. Herbstein. Acta Crystallogr. Sect. B: Struct. Sci. **B58**, 62 (2002).
48. T. Kitazawa, S. Nishikiori, and T. Iwamoto. Mater. Sci. Forum, **91–93**, 257 (1992).

© 2006 NRC Canada

Hexaruthenium and octaruthenium carbonyl cluster complexes derived from 2-amino-6-methylpyridine — Novel coordination modes for 2-imidopyridines[1]

Javier A. Cabeza, Ignacio del Río, Pablo García-Álvarez, and Daniel Miguel

Abstract: The hexanuclear ruthenium cluster $[Ru_6(\mu_3\text{-}H)_2(\mu\text{-}H)_2(\mu_4\text{-}\kappa^2\text{-ampy})_2(CO)_{14}]$ (**1**) and the octanuclear one $[Ru_8(\mu\text{-}H)(\mu_4\text{-}\kappa^2\text{-ampy})_3(\mu_3\text{-}\kappa^2\text{-Hampy})(\mu\text{-}CO)_2(CO)_{15}]$ (**2**) have been prepared by treating $[Ru_6(\mu_3\text{-}H)_2(\mu_5\text{-}\kappa^2\text{-ampy})(\mu\text{-}CO)_2(CO)_{14}]$ with 2-amino-6-methylpyridine (H_2ampy) in decane at reflux temperature. Their metal atoms are supported by ligands that derive from the activation of one (complex **2**) or both N—H bonds (complexes **1** and **2**) of the H_2ampy amino fragment. Both contain at least one ampy ligand featuring an unprecedented coordination type: the imido N atom caps a triangle of metal atoms while the pyridine nitrogen is attached to an additional metal atom. One of the ampy ligands of cluster **2** also displays another unprecedented coordination type: it caps a distorted square of metal atoms through the imido N atom while the pyridine nitrogen is attached to one of the atoms included in that square.

Key words: ruthenium, cluster compounds, amido ligands, imido ligands.

Résumé : En faisant réagir du $[Ru_6(\mu_3\text{-}H)_2(\mu_5\text{-}\kappa^2\text{-ampy})(\mu\text{-}CO)_2(CO)_{14}]$ avec de la 2-amino-6-méthylpyridine (H_2ampy), dans du décane au reflux, on obtenu les agrégats de ruthénium hexanucléaire $[Ru_6(\mu_3\text{-}H)_2(\mu\text{-}H)_2(\mu_4\text{-}\kappa^2\text{-ampy})_2(CO)_{14}]$ (**1**) et octanucléaire $[Ru_8(\mu\text{-}H)(\mu_4\text{-}\kappa^2\text{-ampy})_3(\mu_3\text{-}\kappa^2\text{-Hampy})(\mu\text{-}CO)_2(CO)_{15}]$ (**2**). Les atomes métalliques sont supportés par les ligands qui dérivent de l'activation d'une (complexe **2**) ou des deux liaisons N—H (complexes **1** et **2**) du fragment aminé H_2ampy. Les deux contiennent chacun au moins un ligand ampy comportant un type jusque là inconnu de coordination: les atomes d'azote imido recouvrent un triangle d'atomes métalliques alors que l'azote de la pyridine est attaché à un atome métallique additionnel. Un des ligands ampy de l'agrégat **2** présente en plus un autre type jusque là inconnu de coordination: l'atome d'azote imido recouvre un carré déformé d'atomes métalliques alors que l'azote de la pyridine est attaché à un des atomes inclus dans le carré.

Mots clés : ruthénium, agrégats, ligands amido, ligands imido.

[Traduit par la Rédaction]

Introduction

An extensive derivative chemistry of triruthenium carbonyl clusters containing 2-amidopyridine ligands has been developed during the last decade. These studies have demonstrated that such ligands help maintain the cluster integrity because they act as strong anchors that hold the three metal atoms in close proximity, preventing cluster fragmentations (1).

We have recently reported that the trinuclear cluster $[Ru_3(\mu\text{-}H)(\mu_3\text{-}\kappa^2\text{-Hampy})(CO)_9]$ (H_2ampy = 2-amino-6-methylpyridine) undergoes condensation with $[Ru_3(CO)_{12}]$ at 110–140 °C to give the hexanuclear derivative $[Ru_6(\mu_3\text{-}H)_2(\mu_5\text{-}\kappa^2\text{-ampy})(\mu\text{-}CO)_2(CO)_{14}]$ in high yield (2, 3) (Scheme 1). This reaction afforded the first example of a 2-imidopyridine ligand in which the imido N atom caps a metallic square. Subsequent reactivity studies using $[Ru_6(\mu_3\text{-}H)_2(\mu_5\text{-}\kappa^2\text{-ampy})(\mu\text{-}CO)_2(CO)_{14}]$ as starting material have shown that its apical $Ru(CO)_3$ fragment, which is not anchored by the N atoms, is labile and that this fact is responsible for the observation of pentanuclear and heptanuclear derivatives on some occasions (4).

Prompted by the fact that the number of known ruthenium carbonyl cluster complexes of nuclearity greater than five that contain N-donor ligands is as yet small (2–6), and having in mind the ability of 2-aminopyridines to undergo N—H bond cleavage processes under thermal conditions when treated with $[Ru_3(CO)_{12}]$ (2, 7, 8), we decided to attempt the

Received 26 May 2005. Published on the NRC Research Press Web site at http://canjchem.nrc.ca on 17 February 2006.

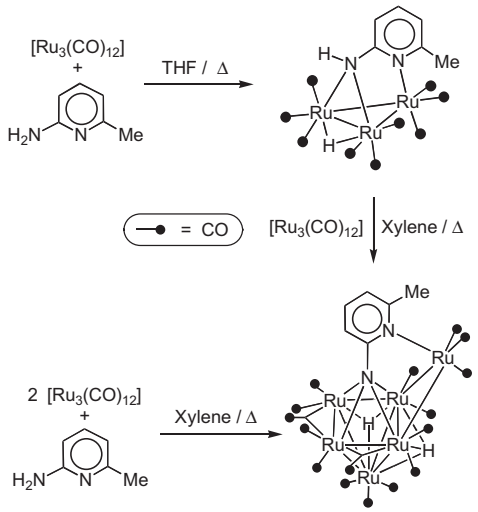
Dedicated to Professor Arthur J. Carty, for his outstanding contributions to organometallic cluster chemisty.

J.A. Cabeza,[2] I. del Río, and P. García-Álvarez. Departamento de Química Orgánica e Inorgánica, Instituto de Química Organometálica "Enrique Moles", Universidad de Oviedo-CSIC, E-33071 Oviedo, Spain.
D. Miguel. Área de Química Inorgánica, Facultad de Ciencias, Universidad de Valladolid, E-47005 Valladolid, Spain.

[1]This article is part of a Special Issue dedicated to Professor Arthur Carty.
[2]Corresponding author (e-mail: jac@fq.uniovi.es).

 doi:10.1139/V05-228 © 2006 NRC Canada

Scheme 1.



synthesis of new high nuclearity ruthenium carbonyl clusters containing ligands derived from 2-amino-6-methylpyridine. The reason for using a methyl-substituted 2-aminopyridine is that the methyl group facilitates the monitoring of the reactions by ^{1}H NMR spectroscopy (1).

We now report that the treatment of $[Ru_6(\mu_3\text{-}H)_2(\mu_5\text{-}\kappa^2\text{-ampy})(\mu\text{-}CO)_2(CO)_{14}]$ with H_2ampy at high temperature has provided two new high-nuclearity ruthenium carbonyl cluster complexes featuring two novel coordination modes for 2-imidopyridine ligands.

Results and discussion

The reaction of the hexanuclear complex $[Ru_6(\mu_3\text{-}H)_2(\mu_5\text{-}\kappa^2\text{-ampy})(\mu\text{-}CO)_2(CO)_{14}]$ with H_2ampy (1:3 molar ratio) in refluxing decane for 50 min afforded a mixture of carbonyl products along with some intractable black solid. Shorter reaction times resulted in the observation of considerable amounts of unreacted hexanuclear starting complex. A chromatographic workup revealed the presence of trace amounts of several complexes accompanying two major products, which were subsequently identified as the hexanuclear and octanuclear derivatives $[Ru_6(\mu_3\text{-}H)_2(\mu\text{-}H)_2(\mu_4\text{-}\kappa^2\text{-ampy})_2(CO)_{14}]$ (**1**) and $[Ru_8(\mu\text{-}H)(\mu_4\text{-}\kappa^2\text{-ampy})_3(\mu_3\text{-}\kappa^2\text{-Hampy})(\mu\text{-}CO)_2(CO)_{15}]$ (**2**), respectively (Scheme 2).

The X-ray diffraction structure of compound **1** is shown in Fig. 1. A selection of interatomic distances is given in Table 1. The molecule can be described as being formed by two trinuclear moieties related to each other by a noncrystallographic twofold axis. The metal atoms of each trinuclear fragment are capped by an ampy ligand that is also attached to one of the metal atoms of the other trinuclear fragment through the N atom of its imido fragment. The cluster shell is completed by four hydrides (two edge-bridging and two face-capping) and 14 terminal CO ligands. The electron count for this cluster is 92 for which the 18-electron rule predicts eight M—M bonds. However, nine Ru—Ru bonding interactions between the atoms of a double wing edge-bridged butterfly metallic skeleton are clearly observed, two of them are shorter than 2.70 Å and four are longer than 2.95 Å (9). These long distances suggest that a considerable amount of electron density is residing in Ru—Ru antibonding orbitals.

Scheme 2.

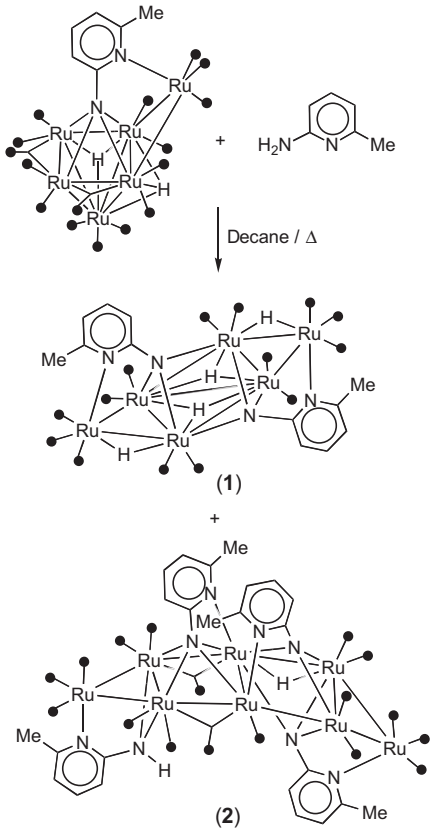
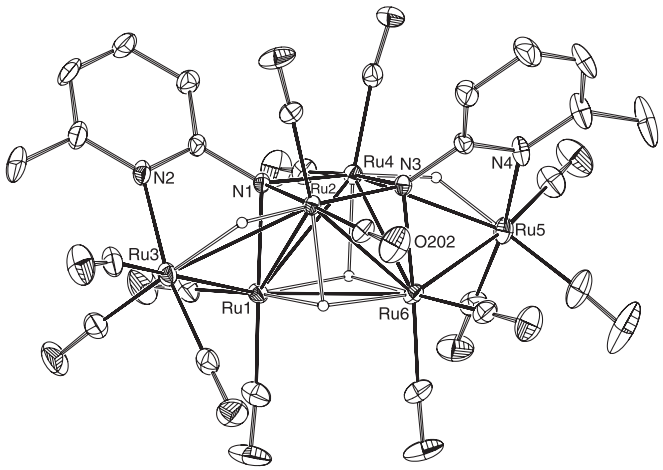


Fig. 1. Molecular structure of compound **1** (H atoms, except hydrides, omitted for clarity).



A remarkable feature of the structure of compound **1** is that its ampy ligands bridge four metal atoms, being attached to one Ru atom through their pyridine N atom and to three additional Ru atoms through the imido N atom. Although triply bridging imido ligands are well-known in cluster chemistry (10), this coordination mode displayed by the ampy ligands in complex **1** is unprecedented for 2-imidopyridine ligands.

© 2006 NRC Canada

Table 1. Selected interatomic distances (Å) in compound **1**.

Interatomic distances (Å)	
Ru(1)—Ru(2)	2.8795(8)
Ru(1)—Ru(3)	2.6961(8)
Ru(1)—Ru(4)	2.9559(8)
Ru(1)—Ru(6)	2.9164(8)
Ru(2)—Ru(3)	2.9598(9)
Ru(2)—Ru(6)	2.9701(8)
Ru(4)—Ru(5)	2.9808(8)
Ru(4)—Ru(6)	2.8731(8)
Ru(5)—Ru(6)	2.6946(8)
Ru(1)—N(1)	2.067(5)
Ru(2)—N(1)	2.102(5)
Ru(2)—N(3)	2.088(5)
Ru(3)—N(2)	2.182(5)
Ru(4)—N(1)	2.087(4)
Ru(4)—N(3)	2.109(5)
Ru(5)—N(4)	2.197(5)
Ru(6)—N(3)	2.064(5)

The solution ^{1}H NMR spectrum of complex **1** corroborates that the symmetric molecular structure found in the solid state is maintained in solution because it only shows the resonances of one ampy ligand and two hydrides (–14.27 and –17.89 ppm, J = 1.7 Hz).

The X-ray diffraction structure of the octanuclear cluster **2** is shown in Fig. 2. A selection of interatomic distances is given in Table 2. Its metallic skeleton can be described as formed by two distorted edge-sharing squares having their most distant edges spanned by two additional metal atoms. Three metal atoms of one of the squares (Ru(1), Ru(2), and Ru(3)) are doubly capped by the imido N atoms of two ampy ligands, one of which has the pyridyl fragment attached to the remaining Ru atom of that square (Ru(4)), while the other has its pyridyl group bonded to the edge-bridging atom Ru(8). An additional ampy ligand is attached to the remaining square in such a way that it caps the four metal atoms with the imido N atom, while the pyridyl fragment is attached to one of these atoms (Ru(1)). The unique Hampy ligand caps the remaining metal triangle, since its amido N atom spans the Ru(5)—Ru(6) edge and its pyridine N atom is attached to Ru(7). The cluster shell is completed with one hydride ligand, which spans the Ru(1)—Ru(3) edge, and 17 carbonyl ligands, two of which asymmetrically span two edges of the imido-capped square. It can be considered that the cluster obeys the 18-electron rule, since its electron count is 122 and has 11 M—M bonds. The long Ru(1)—Ru(4) distance (3.178(1) Å) seems to be compensated for with four distances shorter than 2.72 Å.

The way by which the unique ampy ligand of compound **2** coordinates to the square of metal atoms Ru(1), Ru(4), Ru(5), and Ru(6) is remarkable because, although a few examples of quadruply bridging imido ligands are already known in cluster chemistry (2–4, 6*d*–6*f*, 11), it represents an unprecedented coordination mode for 2-imidopyridine ligands.

The ^{1}H NMR spectrum of cluster **2** is in agreement with its solid state structure, since it shows the resonances of four different 6-methylpyrid-2-yl fragments, along with those of one NH proton (–0.20 ppm) and one hydride ligand (–10.18 ppm).

Fig. 2. Molecular structure of compound **2** (H atoms, except hydride and NH, omitted for clarity).

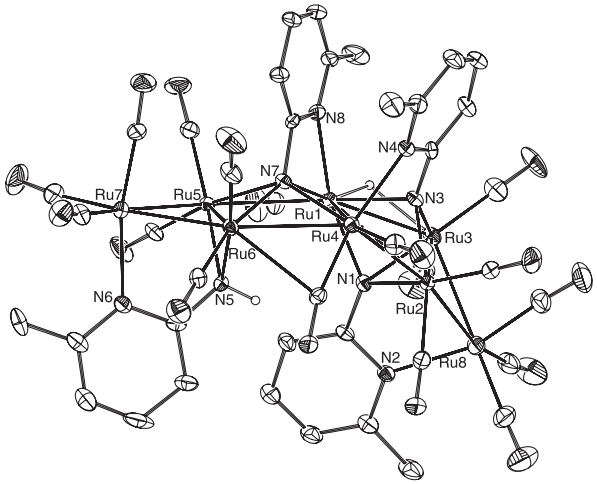


Table 2. Selected interatomic distances (Å) in compound **2**.

Interatomic distances (Å)	
Ru(1)—Ru(3)	2.703(1)
Ru(1)—Ru(4)	3.178(1)
Ru(1)—Ru(5)	2.897(1)
Ru(2)—Ru(3)	2.656(1)
Ru(2)—Ru(4)	2.771(1)
Ru(2)—Ru(8)	2.741(1)
Ru(3)—Ru(8)	2.754(1)
Ru(4)—Ru(6)	2.805(1)
Ru(5)—Ru(6)	2.846(1)
Ru(5)—Ru(7)	2.711(1)
Ru(6)—Ru(7)	2.711(1)
Ru(1)—N(1)	2.081(6)
Ru(1)—N(3)	2.122(6)
Ru(1)—N(8)	2.100(7)
Ru(1)—N(7)	2.213(6)
Ru(2)—N(1)	2.118(7)
Ru(2)—N(3)	2.042(6)
Ru(3)—N(1)	2.113(6)
Ru(3)—N(3)	2.062(6)
Ru(4)—N(4)	2.193(6)
Ru(4)—N(7)	2.210(7)
Ru(5)—N(5)	2.123(6)
Ru(5)—N(7)	2.230(6)
Ru(6)—N(5)	2.175(6)
Ru(6)—N(7)	2.192(6)
Ru(7)—N(6)	2.217(7)
Ru(8)—N(2)	2.210(7)

Concluding remarks

The reaction of the hexanuclear complex $[Ru_6(\mu_3\text{-}H)_2(\mu_5\text{-}\kappa^2\text{-ampy})(\mu\text{-}CO)_2(CO)_{14}]$ with H_2ampy has provided two

© 2006 NRC Canada

Table 3. Selected crystal, measurement, and refinement data for the X-ray structures of **1** and **2**·0.25(CH_2Cl_2).

Compound	**1**	**2**·0.25(CH_2Cl_2)
Empirical formula	$C_{26}H_{16}N_4O_{14}Ru_6$	$C_{41}H_{26}N_8O_{17}Ru_8$·0.25($CH_2Cl_2$)
Formula mass	1 214.85	1 732.49
Color, habit	Dark red, block	Black, block
Crystal dimensions (mm)	0.12 × 0.09 × 0.08	0.18 × 0.10 × 0.08
Crystal system	Monoclinic	Triclinic
Space group	$P2_1/c$	P–1
Z	4	2
a (Å)	22.545(4)	11.219(3)
b (Å)	9.051 6(16)	13.020(3
c (Å)	17.678(3)	19.787(5)
α (°)	90	74.711(4)
β (°)	90.600(4)	86.421(6)
γ (°)	90	72.977(5)
Collection ranges	$-21 < h < 25$, $-10 < k < 10$, $-19 < l < 19$	$-11 < h < 12$, $-14 < k < 14$, $-21 < l < 17$
Temperature (K)	293(2)	296(2)
Volume (Å^3)	3 607.4(11)	2 665.6(12)
D_{calcd} (Mg m^{-3})	2.237	2.159
Radiation (λ, Å)	Mo Kα (0.710 73)	Mo Kα (0.710 73)
Absorption coeff. (μ) (mm^{-1})	2.515	2.300
Absorption correction	SADABS	SADABS
F(000)	2 304	1 653
θ Range for data collection (°)	0.90 to 23.27	1.07 to 23.29
Observed reflns	15 464	11 953
Independent reflns	5 170 (R_{int} = 0.040 7)	7 588 (R_{int} = 0.026)
Data/restraints/parameters	5 170 / 0 / 463	7 588 / 0 / 699
Maximum shift/error	0.001	0.001
Goodness-of-fit on F^2	0.993	0.998
Final R indices ($I > 2\sigma(I)$)	R_1 = 0.028 0, wR_2 = 0.052 1	R_1 = 0.038 2, wR_2 = 0.100 9
R indices (all data)	R_1 = 0.046 8, wR_2 = 0.062 3	R_1 = 0.059 4, wR_2 = 0.112 2
Largest diff. peak and hole (e Å^{-3})	0.474 and –0.479	1.156 and –0.640

new high-nuclearity ruthenium carbonyl clusters and has allowed us to observe two new coordination types for 2-imidopyridine ligands.

In the reaction, once coordinated, the H_2ampy ligand undergoes one or two N—H bond activation processes that results in the formation of new ligands containing amido (as in **2**) or imido fragments (as in **1** and **2**). As these new ligands are excellent donors, they easily replace carbonyl ligands of the same metallic fragment (as in **1**) or bind to other metallic fragments that are present in solution (as in **2**).

Experimental

General

Solvents were dried over sodium (hydrocarbons) or CaH_2 (dichloromethane) and distilled under nitrogen prior to use. The hexanuclear cluster $[Ru_6(\mu_3\text{-}H)_2(\mu_5\text{-}\kappa^2\text{-ampy})(\mu\text{-}CO)_2(CO)_{14}]$ was prepared as described elsewhere (3). H_2ampy was purchased from Aldrich. Instrumentation: IR: PerkinElmer FT Paragon 1000X; NMR: Bruker DPX-300, with $SiMe_4$ as internal standard (δ 0); microanalyses: PerkinElmer 2400.

Synthesis of $[Ru_6(\mu_3\text{-}H)_2(\mu\text{-}H)_2(\mu_4\text{-}\kappa^2\text{-ampy})_2(CO)_{14}]$ (1) and $[Ru_8(\mu\text{-}H)(\mu_4\text{-}\kappa^2\text{-ampy})_3(\mu_3\text{-}\kappa^2\text{-Hampy})(\mu\text{-}CO)_2(CO)_{15}]$ (2)

A solution of $[Ru_6(\mu_3\text{-}H)_2(\mu_5\text{-}\kappa^2\text{-ampy})(\mu\text{-}CO)_2(CO)_{14}]$ (150 mg, 0.129 mmol) and H_2ampy (42 mg, 0.387 mmol) in decane (20 mL) was stirred under nitrogen at reflux temperature for 50 min. At this time, the IR spectrum of the solution did not show any starting material. A change in the color of the solution from dark brown to reddish brown was accompanied by the formation of some black solid. The solvent was removed under vacuum. The solid residue was extracted into dichloromethane (10 mL) and the solution was supported on silica gel (ca. 6 g). The resulting solid was placed onto a silica gel chromatographic column (2 cm × 20 cm) packed in hexane. Three bands, A (brown), B (brown), and C (red-brown), were eluted with hexane–dichloromethane (10:1). Subsequent elution of the column with hexane–dichloromethane (5:1) afforded band D (greenish yellow). Further elution of the column with hexane–dichloromethane (3:1) afforded band E (violet-brown). Bands A and D contained trace amounts of compounds that were not characterized. Band B contained 5 mg of the starting material, $[Ru_6(\mu_3\text{-}H)_2(\mu_5\text{-}\kappa^2\text{-ampy})(\mu\text{-}CO)_2(CO)_{14}]$. Band C

© 2006 NRC Canada

afforded 10 mg of compound **1** (6.4%). Band E gave 7 mg of compound **2** (4.2%).

Data for compound 1

IR (CH_2Cl_2) ν_{CO}: 2089 (m), 2075 (vs), 2038 (s, sh), 2031 (vs), 2013 (vs), 1983 (m), 1944 (w), 1929 (w). ^{1}H NMR ($CDCl_3$, 293 K, 300 MHz) δ: 7.45 (t, *J* = 7.8 Hz, 1H), 7.28 (d, *J* = 7.8 Hz, 1H), 6.65 (d, *J* = 7.8 Hz, 1H), 2.56 (s, 3H), –14.27 (d, *J* = 1.7 Hz, 1H), –17.89 (d, *J* = 1.7 Hz, 1H). Anal. calcd. for $C_{26}H_{16}N_4O_{14}Ru_6$: C 25.71, H 1.33, N 4.61; found: C 25.54, H 1.35, N 4.55.

Data for compound 2

IR (CH_2Cl_2) ν_{CO}: 2070 (w), 2054 (vs), 2009 (vs), 2000 (s, sh), 1987 (m, sh), 1948 (w, br), 1924 (w, sh), 1869 (w, br). ^{1}H NMR ($CDCl_3$, 293 K, 300 MHz) δ: 7.15–6.95 (m, 4H), 6.70 (d, *J* = 7.8 Hz, 1H), 6.57 (d, *J* = 7.8 Hz, 1H), 6.42 (d, *J* = 7.8 Hz, 1H), 6.25 (d, *J* = 7.8 Hz, 1H), 6.05 (d, *J* = 7.8 Hz, 1H), 5.93 (d, *J* = 7.8 Hz, 1H), 5.79 (d, *J* = 7.8 Hz, 1H), 5.06 (d, *J* = 7.8 Hz, 1H), 2.82 (s, 3H), 2.72 (s, 3H), 2.31 (s, 3H), 2.01 (s, 3H), –0.20 (s, 1H, NH), –10.18 (s, 1H). Anal. calcd. for $C_{41}H_{26}N_8O_{17}Ru_8$: C 28.78, H 1.53, N 6.55; found: C 28.56, H 1.66, N 6.38.

X-ray diffraction studies

A selection of crystal, measurement, and refinement data for **1** and **2**·0.25(CH_2Cl_2) is given in Table 3. Diffraction data were collected at room temperature on a Bruker AXS SMART 1000 diffractometer, using graphite-monochromated Mo Kα radiation. Absorption corrections were applied with SADABS (12). The structures were solved by direct methods and refined by full matrix least-squares against F^2 with SHELXTL (13). All non-hydrogen atoms were refined anisotropically. Hydrogen atoms were refined isotropically. The edge-bridging hydrides of **1** were located on difference Fourier maps and were freely refined. The positions of the face-capping hydrides of **1** and the hydride of **2**·0.25(CH_2Cl_2) were calculated with XHYDEX (14) and were freely refined. The molecular plots were made with the PLATON program package (15). The WINGX program system (16) was used throughout the structure determinations.[3]

Acknowledgements

This work has been supported by the Spanish Ministry of Education and Science through grants BQU2002-2623 (to JAC) and BQU2002-3414 (to DM). PG-A is also grateful to the FPI program (Programa de Formación de Personal Investigador) for a doctoral fellowship.

References

1. For a review on the reactivity of triruthenium carbonyl clusters containing 2-amidopyridine ligands, see: J.A. Cabeza. Eur. J. Inorg. Chem. 1559 (2002).
2. J.A. Cabeza, I. del Río, P. García-Álvarez, V. Riera, M. Suárez, and S. García-Granda. Dalton Trans. 2808 (2003).
3. J.A. Cabeza, I. del Río, P. García-Álvarez, D. Miguel, and V. Riera. Inorg. Chem. **43**, 5450 (2004).
4. J.A. Cabeza, I. del Río, P. García-Álvarez, and D. Miguel. Organometallics, **24**, 665 (2005).
5. For a review on medium- and high-nuclearity clusters of ruthenium, see: M.P. Cifuentes and M.G. Humphrey. *In* Comprehensive organometallic chemistry II. Vol. 7. *Edited by* D.F. Shriver and M.I. Bruce. Pergamon, Oxford. 1995. Chap. 16. p. 907.
6. For additional examples of ruthenium cluster complexes of nuclearity greater than five containing N-donor ligands, see: (*a*) L. Hoferkamp, G. Rheinwald, H. Stoeckli-Evans, and G. Süss-Fink. Inorg. Chem. **34**, 5786 (1995); (*b*) L. Hoferkamp, G. Rheinwald, H. Stoeckli-Evans, and G. Süss-Fink. Organometallics, **15**, 1122 (1996); (*c*) U. Bodensieck, L. Hoferkamp, H. Stoeckli-Evans, and G. Süss-Fink. J. Chem. Soc. Dalton Trans. 127 (1993); (*d*) S.W. Han, S.T. Nguyen, G.L. Geoffroy, and A.L. Rheingold. Organometallics, **7**, 2034 (1988); (*e*) K.K.H. Lee and W.T. Wong. J. Organomet. Chem. **503**, C43 (1995); (*f*) K.K.H. Lee and W.T. Wong. J. Chem. Soc. Dalton Trans. 1707 (1996); (*g*) J.A. Cabeza, J.M. Fernández-Colinas, S. García-Granda, A. Llamazares, F. López-Ortiz, V. Riera, and J.F. Van der Maelen. Organometallics, **14**, 3342 (1995); (*h*) J.A. Cabeza, I. del Río, V. Riera, and F. Grepioni. Organometallics, **14**, 3124 (1995); (*i*) J.A. Cabeza, I. da Silva, I. del Río, L. Martínez-Méndez, D. Miguel, and V. Riera. Angew. Chem. Int. Ed. **43**, 3464 (2004).
7. P.L. Andreu, J.A. Cabeza, V. Riera, Y. Jeannin, and D. Miguel. J. Chem. Soc. Dalton Trans. 2201 (1990).
8. N. Lugan, F. Laurent, G. Lavigne, T.P. Newcomb, E.W. Liimatta, and J.J. Bonnet. Organometallics, **11**, 1351 (1992).
9. The Ru—Ru distances in [$Ru_3(CO)_{12}$] are in the range 2.8595 to 2.8515 Å: M.R. Churchill, F.J. Hollander, and J.P. Hutchinson. Inorg. Chem. **16**, 2655 (1977).
10. For examples of clusters having μ_3-imido ligands, see: (*a*) M.I. Bruce, M.P. Cifuentes, and M.G. Humphrey. Polyhedron, **10**, 277 (1991), and refs. cited therein; (*b*) J.S. Song, S.H. Han, S.T. Nguyen, G.L. Geoffroy, and A.L. Rheingold. Organometallics, **9**, 2386 (1990), and refs. cited therein; (*c*) D.M. Ramage, G.L. Geoffroy, A.L. Rheingold, and B.S. Haggerty. Organometallics, **11**, 1242 (1992); (*d*) A.J. Deeming. *In* Comprehensive organometallic chemistry II. Vol. 7. *Edited by* D.F. Shriver and M.I. Bruce. Pergamon, Oxford. 1995. Chap. 12. p. 683; (*e*) L.A. Oro, M.A. Ciriano, C. Tejel, Y.M. Shi, and F. Modrego. *In* Metal clusters in chemistry. *Edited by* P. Braunstein, L.A. Oro, and P.R. Raithby. Wiley-VCH, Weinheim. 1999. p. 381.
11. For additional examples of clusters having μ_4-imido ligands, see: (*a*) H. Link and D.Z. Fenske. Anorg. Allg. Chem. **625**, 1878 (1999); (*b*) P. Reiβ and D. Fenske. Z. Anorg. Allg. Chem. **626**, 2245 (2000); (*c*) M.L. Blohm and W.L. Gladfelter. Organometallics, **5**, 1049 (1986); (*d*) G. Gervasio, R. Rossetti, and P.L. Stanghellini. J. Chem. Res. **334**, 3943 (1979); (*e*) E.N.M. Ho and W.T. Wong. J. Chem. Soc. Dalton Trans.

[3] Supplementary data for this article are available on the journal Web site (http://canjchem.nrc.ca) or may be purchased from the Depository of Unpublished Data, Document Delivery, CISTI, National Research Council Canada, Ottawa, ON K1A 0R6, Canada. DUD 4083. For more information on obtaining material refer to http://cisti-icist.nrc-cnrc.gc.ca/irm/unpub_e.shtml. CCDC 272943 (**1**) and 272944 (**2**) contain the crystallographic data for this manuscript. These data can be obtained, free of charge, via http://www.ccdc.cam.ac.uk/conts/retrieving.html (Or from the Cambridge Crystallographic Data Centre, 12 Union Road, Cambridge CB2 1EZ, UK; fax +44 1223 336033; or deposit@ccdc.cam.ac.uk).

© 2006 NRC Canada

4215 (1998); (*f*) E.N.M. Ho and W.T. Wong. J. Chem. Soc. Dalton Trans. 513 (1998); (*g*) E.N.M. Ho, Z. Lin, and W.T. Wong. J. Eur. J. Inorg. Chem. 1321 (2001); (*h*) S.W.H. Han, S.T. Nguyen, G.L. Geoffroy, and A.L. Rheingold. Organometallics, **7**, 2034 (1988); (*i*) L. Scoles, B.T. Sterenberg, K.A. Udachin, and A.J. Carty. Chem. Commun. (Cambridge), 320 (2002); (*j*) J.A. Cabeza, I. del Río, S. García-Granda, M. Moreno, V. Riera, M.J. Rosales-Hoz, and M. Suárez. Eur. J. Inorg. Chem. 2899 (2001); (*k*) W.Y. Yeh, C. Stern, and D.F. Shriver. Inorg. Chem. **35**, 7857 (1996); (*l*) B. Hansert, A.K. Powell, and H. Vahrenkamp. Chem. Ber. **124**, 2697 (1991).

12. G.M. Sheldrick. SADABS [computer program]. University of Göttingen, Göttingen, Germany. 1997.
13. G.M. Sheldrick. SHELXTL. Version 5.1 [computer program]. Bruker AXS Inc., Madison, Wis. 1998.
14. A.G. Orpen. J. Chem. Soc. Dalton Trans. 2509 (1980).
15. A.L. Spek. PLATON [computer program]. University of Göttingen, Göttingen, Germany. 1997.
16. L.J. Farrugia. J. Appl. Crystallogr. **32**, 837 (1999).

© 2006 NRC Canada

Organogold(I) macrocycles and [2]catenanes containing pyridyl and bipyridyl substituents — Organometallic catenanes as ligands[1]

Nicolle C. Habermehl, Fabian Mohr, Dana J. Eisler, Michael C. Jennings, and Richard J. Puddephatt

Abstract: The synthesis of achiral gold(I) macrocycles [RCH(4-$C_6H_4OCH_2C{\equiv}CAu)_2$(μ-$Ph_2PZPPh_2$)] and the corresponding chiral gold(I) [2]catenanes, bearing substituents R = 2-pyridyl, 4-pyridyl, and 4-(2,2′-bipyridyl), is reported. The gold(I) compounds form by self-assembly on reaction of oligomeric digold(I) diacetylides [{RCH(4-$C_6H_4OCH_2C{\equiv}CAu)_2\}_n$] or the isocyanide complexes [RCH(4-$C_6H_4OCH_2C{\equiv}CAuC{\equiv}N$-*t*-Bu)$_2$] with diphosphine ligands Ph_2PZPPh_2, Z = CC or $(CH_2)_n$ with n = 2–5, or on reaction of [$Au_2(O_2CCF_3)_2$(μ-Ph_2PZPPh_2)] with diacetylenes RCH(4-$C_6H_4OCH_2C{\equiv}CH)_2$ in the presence of a base. The equilibrium between macrocycles and chiral [2]catenanes in solution was established by NMR spectroscopy, while the structures of several [2]catenanes in the solid state were established crystallographically. The coordination of the gold(I) compounds with R = 4-(2,2′-bipyridyl) to platinum(IV), by formation of the corresponding [$PtIMe_3$(bipy)] units, is established, showing that organometallic [2]catenanes can act as ligands.

Key words: gold, macrocycle, catenane, platinum.

Résumé : On a réalisé la synthèse des macrocycles achiraux d'or(I) de formule générale [RCH(4-$C_6H_4OCH_2C{\equiv}CAu)_2$-(μ-$Ph_2PZPPh_2$)] et des [2]caténanes chiraux d'or(I) correspondants portant les groupes R = 2-pyridyle, 4-pyridyle et 4-(2,2′-bipyridyle). Les composés d'or(I) forment des produits d'autoassemblage par réaction des diacétylures de dior(I) oligomères de formule générale [{(RCH(4-$C_6H_4OCH_2C{\equiv}CAu)_2\}_n$] ou des complexes d'isocyanures de formule générale [RCH(4-$C_6H_4OCH_2C{\equiv}CAuC{\equiv}N$-*t*-Bu)$_2$] avec des ligands diphosphine Ph_2PZPPh_2 (Z = CC ou $(CH_2)_n$ avec n = 2, 3, 4, 5) ou par réaction de [$Au_2(O_2CCF_3)_2$(μ-Ph_2PZPPh_2)] avec des dérivés diacétylènes RCH(4-$C_6H_4OCH_2C{\equiv}CH)_2$, en présence de base. On a établit la nature de l'équilibre entre les macrocycles et les [2]caténanes chiraux en solution à l'aide de la spectroscopie RMN alors que plusieurs structures de [2]caténanes à l'état solide ont été établies par diffraction des rayons X. En montrant que les [2]caténanes organométalliques peuvent agir comme ligands avec formation des unités correspondantes [$PtIMe_2$(bipy)], on a démontré que les composés d'or(I) avec R = 4-(2,2′-bipyridyle) peuvent donner une coordination avec le platine(IV).

Mots clés : or, macrocycle, caténane, platine.

[Traduit par la Rédaction]

Introduction

The field of chemistry that encompasses the design, synthesis, and functionalization of mechanically interlocked molecules such as catenanes, rotaxanes, and knots has undergone great advances in recent decades, with the use of the coordinate bond allowing the directed self-assembly of these molecules in high yields (1–7). A natural extension to this field is the synthesis of coordination polymers (8–11) such as poly[2]catenanes (12–15). For example, a poly(bis-[2]catenane) that contains covalent, coordinate, and mechanical linkages has been reported in which a bipyridine unit was incorporated into the backbone of a [2]catenane and then used to coordinate to silver(I) (15). This example suggests a general method for growing more complex architectures from [2]catenane building blocks by introducing donor groups as substituents and then using these donor groups to form complexes with transition metals, as shown in Scheme 1. In the simplest case **A**, a macrocycle can act as a ligand, but a metal centre can also act as template to assemble two or more macrocycles as in case **B**. If the macrocycles form a [2]catenane, then the analogous forms of coordination will give a [2]catenane coordinated to two metal centres (case **C**) or to a polymer of [2]catenanes (case

Received 16 June 2005. Published on the NRC Research Press Web site at http://canjchem.nrc.ca on 21 February 2006.

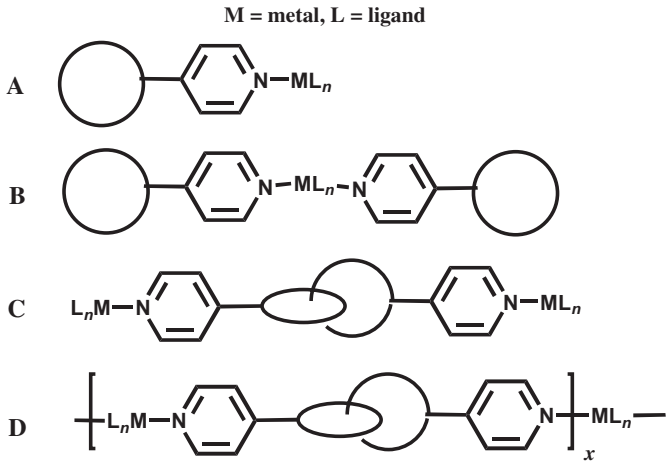
This article is dedicated to Dr. Arthur J. Carty in recognition of his pioneering research in cluster chemistry and his outstanding service to science in Canada.

N.C. Habermehl, F. Mohr, D.J. Eisler, M.C. Jennings, and R.J. Puddephatt.[2] Department of Chemistry, University of Western Ontario, London, ON N6A 5B7, Canada.

[1]This article is part of a Special Issue dedicated to Professor Arthur Carty.
[2]Corresponding author (e-mail: pudd@uwo.ca).

 doi:10.1139/V05-229 © 2006 NRC Canada

Scheme 1.



D). This article describes attempts to develop this chemistry by using organogold macrocycles and [2]catenanes with pyridyl or bipyridyl groups as substituents, and reports the first example of the use of an organometallic [2]catenane as a ligand.

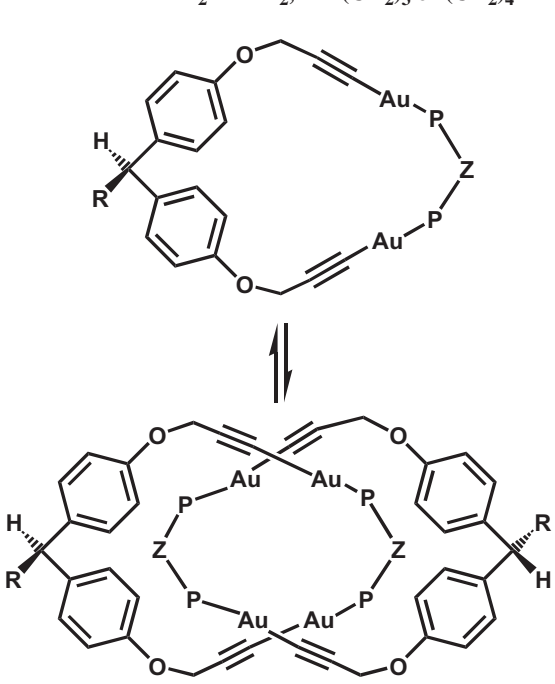
The ligands pyridine and 2,2′-bipyridyl (bipy) form stable complexes with transition-metal ions (16), and appropriate substitution of the two pyridyl rings in 2,2′-bipyridyl has given many symmetrical or unsymmetrical derivatives that are useful for the synthesis of helicates, ladders, rods, catenanes, and coordination polymers (2, 16–24). In earlier papers, we have reported that macrocyclic organogold(I) complexes, such as $[RCH(C_6H_4OCH_2C{\equiv}CAu)_2(\mu\text{-}Ph_2P(CH_2)_nPPh_2)]$ with R,R′ = H, alkyl, or aryl and n = 3 or 4, may spontaneously and reversibly form [2]catenanes $[RCH(C_6H_4OCH_2C{\equiv}CAu)_2(\mu\text{-}Ph_2P(CH_2)_nPPh_2)]_2$, probably by a mechanism involving cleavage of a gold–phosphorus bond followed by threading/unthreading and recoordination (Scheme 2) (25, 26). It is then a natural extension to prepare the corresponding organogold complexes with R = pyridyl or 2,2′-bipyridyl, to form organometallic [2]catenanes that have the potential to act as ligands. Another important feature of these compounds is that the macrocycles are achiral but the [2]catenanes are chiral, and so the pyridyl and 2,2′-bipyridyl donors may act as chiral ligands (25). The syntheses and structures of the organogold complexes with pyridyl and bipyridyl substituents, and some preliminary studies of their properties, are described in the following.

Results and discussion

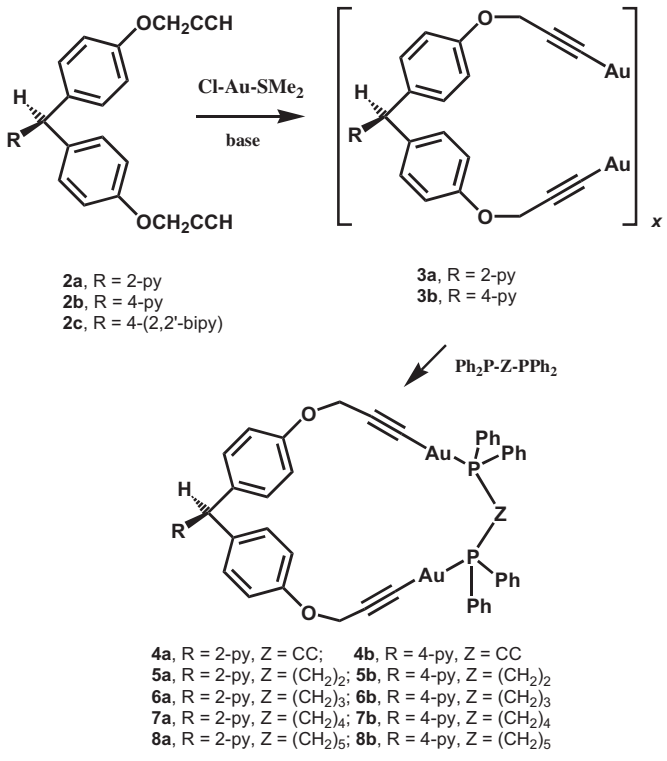
Synthesis of gold(I) compounds

The ligands $RCH(C_6H_4OCH_2C{\equiv}CH)_2$, containing substituents R = 2-pyridyl (**2a**), 4-pyridyl (**2b**), and 4-(2,2′-bipyridyl) (**2c**), were prepared by condensation of phenyl propargyl ether with the corresponding carboxaldehydes (RCH=O), **1a** (R = 2-pyridyl), **1b** (R = 4-pyridyl), and **1c** (R = 4-(2,2′-bipyridyl) (27, 28)) by the established general method (25, 26). Reaction of the diacetylene ligands **2a** and **2b** with chloro(dimethylsulfide)gold(I) in the presence of a base gave the insoluble oligomeric digold(I) diacetylides ($[RCH(C_6H_4OCH_2C{\equiv}CAu)_2]_x$) **3a**, R = 2-pyridyl, and **3b**, R = 4-pyridyl, as shown in Scheme 3. The C≡C stretching frequencies observed by IR spectroscopy (**3a**, 2000 cm^{-1}; **3b**, 2013 cm^{-1}) are about 100 cm^{-1} lower than the corresponding C≡C stretching frequencies for the free ligands (**2a**, 2120 cm^{-1}; **2b**, 2118 cm^{-1}), which indicates that the

Scheme 2.



Scheme 3.



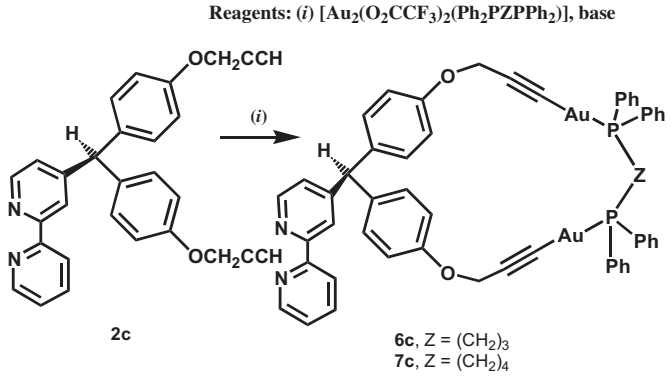
2a, R = 2-py
2b, R = 4-py
2c, R = 4-(2,2'-bipy)

3a, R = 2-py
3b, R = 4-py

4a, R = 2-py, Z = CC; **4b**, R = 4-py, Z = CC
5a, R = 2-py, Z = $(CH_2)_2$; **5b**, R = 4-py, Z = $(CH_2)_2$
6a, R = 2-py, Z = $(CH_2)_3$; **6b**, R = 4-py, Z = $(CH_2)_3$
7a, R = 2-py, Z = $(CH_2)_4$; **7b**, R = 4-py, Z = $(CH_2)_4$
8a, R = 2-py, Z = $(CH_2)_5$; **8b**, R = 4-py, Z = $(CH_2)_5$

© 2006 NRC Canada

Scheme 4.



diacetylenes are both σ bonded and π bonded to the gold(I) centres to form oligomeric structures (29, 30). Reaction of these oligomeric digold(I) complexes (**3a** and **3b**) with diphosphine ligands then gave the macrocyclic digold(I) complexes, $[RCH(C_6H_4OCH_2C{\equiv}CAu)_2\{\mu\text{-}Ph_2P\text{-}Z\text{-}PPh_2\}]$ (**4**–**8**) (Scheme 3), many of which exist as an equilibrium mixture of the macrocyclic complexes depicted in Scheme 3 and the corresponding [2]catenane. An alternative route to the complexes **4**–**8** is to react the oligomers **3** with *tert*-butyl isocyanide to give the soluble isocyanide derivatives $RCH(C_6H_4OCH_2C{\equiv}CAuC{\equiv}N\text{-}t\text{-}Bu)_2$ and then to displace the isocyanide ligands by the appropriate diphosphine ligand (Ph_2P-Z-PPh_2).

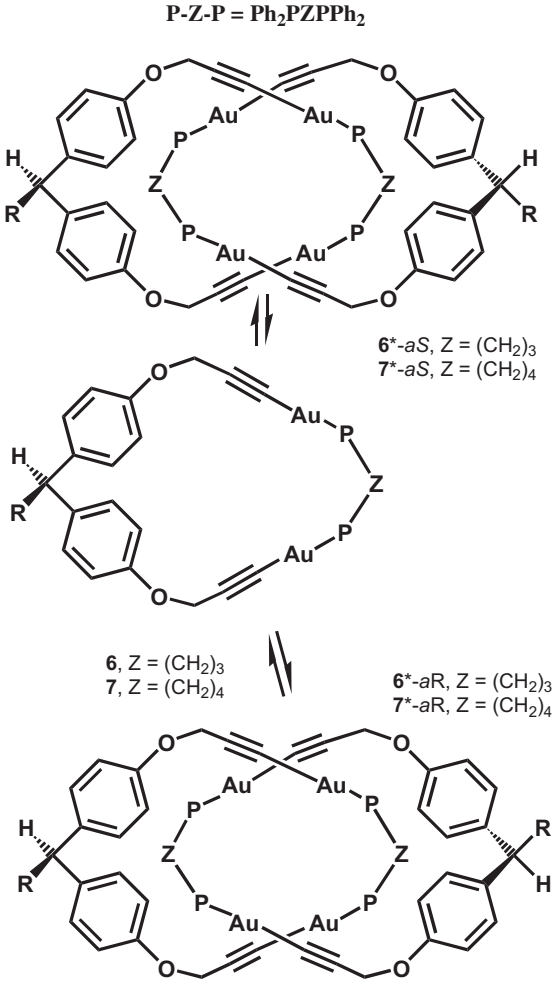
Attempts to prepare the corresponding complexes with R = 4-(2,2′-bipy) by this procedure were unsuccessful because the desired products, $[RCH(C_6H_4OCH_2C{\equiv}CAu)_2\{\mu\text{-}Ph_2P\text{-}Z\text{-}PPh_2\}]$, were always formed as a mixture with the chloride complex $[Au_2Cl_2(\mu\text{-}Ph_2P\text{-}Z\text{-}PPh_2)]$, and this chlorogold impurity was not easily separated. The pure digold(I) complexes containing the 4-(2,2′-bipy) group were therefore prepared by reaction at low temperature of the diacetylene ligand **2c** with $[Au_2(O_2CCF_3)_2(\mu\text{-}Ph_2P\text{–}Z\text{–}PPh_2)]$, which is conveniently prepared in situ from $[Au_2Cl_2(\mu\text{-}Ph_2P\text{–}Z\text{–}PPh_2)]$ and silver trifluoroacetate (Scheme 4).

In cases where the macrocyclic complexes **6** and **7** are in equilibrium with the [2]catenane isomers, the presence of a prochiral carbon at the hinge group (*C*HR) leads to formation of [2]catenanes **6*** and **7***, which are axially chiral with C_2 symmetry (25). These chiral [2]catenanes are formed as racemates, which have the stereochemical descriptors a*R* and a*S* (the symbol "a" in a*R*/a*S* indicates axial chirality (31, 32)), as illustrated in Scheme 5. The interconversion of ring and catenane is known to be catalysed by traces of free phosphine and so probably involves ring-opening by cleavage of an Au—P bond, followed by threading or dethreading (25, 26).

Characterization of the gold(I) complexes

The structures of the singly braided [2]catenane complexes **6a*** (R = 2-py), **6b*** (R = 4-py), **6c*** (R = 4-(2,2′-bipy), and **7a*** (R = 2-py) were determined crystallographically and are shown in Figs. 1–4. They form by [2+2] self-assembly of the appropriate digold(I) diacetylide unit and diphosphine ligand to give two mechanically interlocked rings. The [2]catenanes **6a***, **6b***, and **6c*** are each comprised of two interlocked 24-membered rings, while **7a*** is comprised of two 25-membered rings.

Scheme 5.

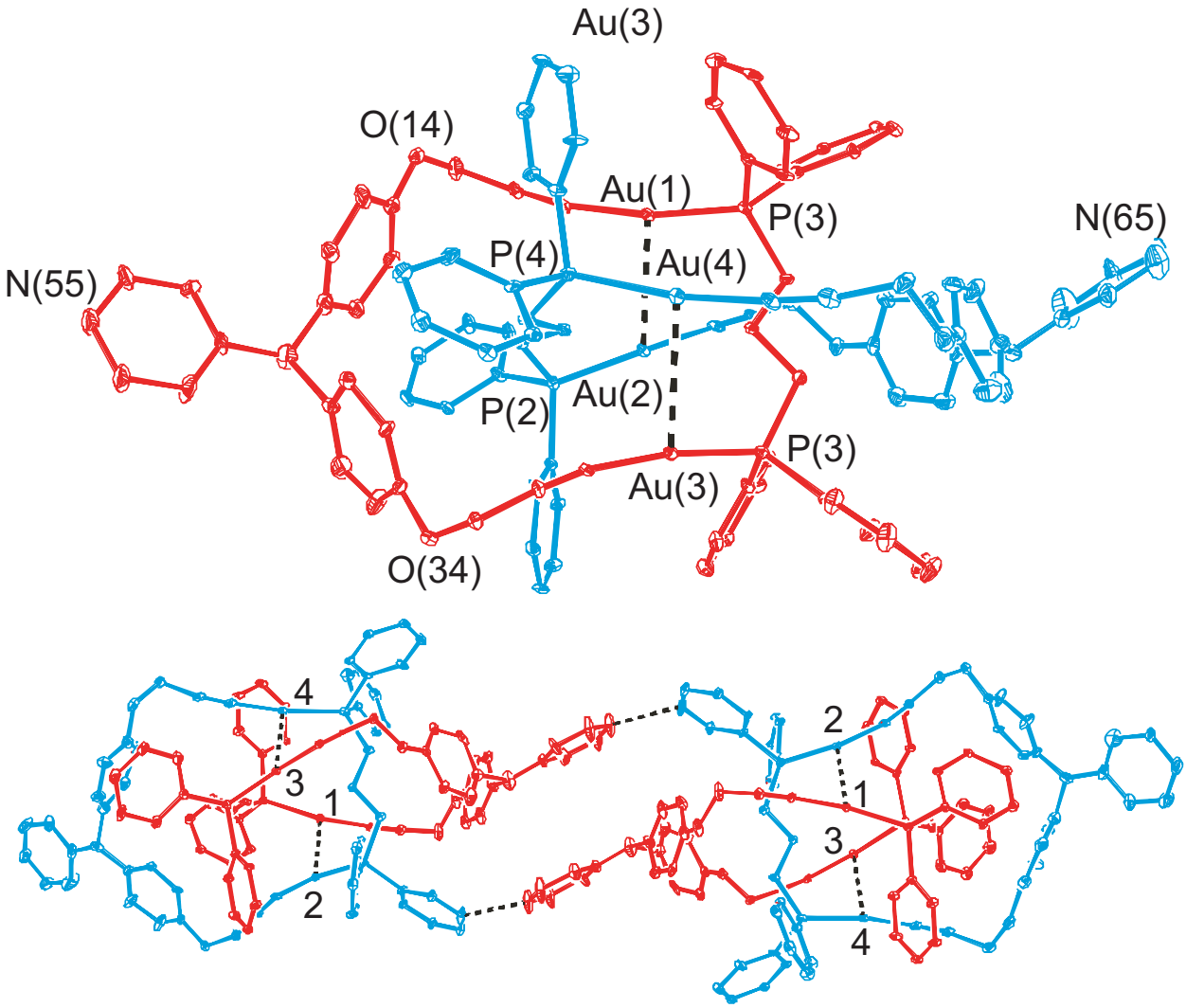


Of the complexes studied, only **6b*** (R = 4-pyridyl, Z = $(CH_2)_3$, Fig. 1) showed no disorder, so its structure will be discussed first. The complex crystallized in space group $P2_1/c$ with $Z = 4$, and hence contains equal amounts of the enantiomers **6b***-*aR* and **6b***-*aS*. As seen in previous examples of gold(I) [2]catenanes (25, 26, 33–35), an intermacrocycle aurophilic interaction is observed for the [2]catenane, with Au(1)—Au(2) = 3.2097(8) Å, while the second gold···gold distance (Au(3)—Au(4) = 3.404 Å) indicates only a weak Au···Au interaction (36). A combination of the secondary Au···Au bonding and several intermacrocycle aryl···aryl bonding interactions provides the driving force for the catenation (25, 26, 33–36). There is significant bowing of the P-Au-C-C-C groups away from linearity with angles P-Au-C, Au-C-C, and C-C-C in the ranges 169.3(5)°–171.4(4)°, 167(2)°–174(2)°, and 169(2)°–178(2)°, respectively, and this bowing appears to be correlated to the short Au···Au contacts.

The aryl twist angles, defined as the angles between the planes of the C_6H_4 groups and the C-C-C plane of the "hinge carbon atom", are important in determining the favorability of [2]catenane formation (25, 26). Optimum aryl

© 2006 NRC Canada

Fig. 1. Molecular structure of [2]catenane **6b*** (R = 4-pyridyl, Z = $(CH_2)_3$): above, a single chiral [2]catenane, and below, a racemic pair of [2]catenanes with connecting N···HC hydrogen bonds (only the gold atoms are numbered). Selected bond distances (Å) and angles (°): Au(1)—Au(2) 3.2097(8); Au(1)—P(1) 2.269(4); Au(2)—P(2) 2.275(4); Au(3)—P(3) 2.268(4); Au(4)—P(4) 2.275(5); Au(1)—C(11) 1.97(2); Au(2)—C(21) 2.01(2); Au(3)—C(31) 2.02(2); Au(4)—C(41) 1.93(2); C(11)—C(12) 1.19(2); C(21)—C(22) 1.16(2); C(31)—C(32) 1.15(2); C(41)—C(42) 1.18(2); P(1)-Au(1)-C(11) 169.3(5); P(2)-Au(2)-C(21) 171.4(4); P(3)-Au(3)-C(31) 171.2(4); P(4)-Au(4)-C(41) 170.1(6); Au(1)-C(11)-C(12) 170(2); Au(2)-C(21)-C(22) 167(1); Au(3)-C(31)-C(32) 170(1); Au(4)-C(41)-C(42) 174(2); C(11)-C(12)-C(13) 177(2); C(21)-C(22)-C(23) 178(2); C(31)-C(32)-C(33) 175(2); C(41)-C(42)-C(43) 169(2).



twist angles are in the range 45°–90° (25, 26) and in complex **6b*** these angles are 83° and 82° in one macrocycle and 72° and 71° in the other (the corresponding twist angles in the parent bis(phenol) are 44° and 87°). In the structures of all other known complexes with unsymmetrical hinge groups (R*C*H), there is disorder of the substituent R on either side of the plane of the macrocycle. The well-ordered structure of **6b*** appears to result from favorable pairwise hydrogen bonding between the nitrogen atom of one of the 4-pyridyl substituents and a *meta*-hydrogen atom of a phenylphosphorus group on a neighbouring molecule (37), as shown in Fig. 1. The nitrogen atom N(55) of the 4-pyridyl group of one ring interacts with an aryl CH group of a neighbour with N(55)···C(2C) = 3.22 Å, N···H = 2.35 Å, and angle C-H···N = 154°. No close intermolecular aryl–aryl interactions were observed (38, 39). The pairs of chiral hydrogen-bonded [2]catenanes (Fig. 1) are related by an inversion centre and so comprise a racemic *aR–aS* couple.

The structures of complexes **6a*** and **6c*** (Figs. 2 and 3) are similar to that of **6b*** but they each show disorder in the $RCH(C_6H_4)_2$ region. The aryl twist angles associated with the two disorder components ***A*** and ***B*** in **6a***were for component ***A***: 88°,25° (ring 1) and 85°,29° (ring 2); and for component ***B***: 85°,43° (ring 1) and 89°,41° (ring 2). The values of the aryl twist angles of 25° and 29° are the smallest yet observed in a [2]catenane (25, 26). For comparison, the aryl twist angles in the related bis(phenol) $RCH(C_6H_4OH)_2$ (R = 2-pyridyl) were 87°,44°. The closest gold···gold contacts in **6a*** are the intermacrocycle distances Au(1)—Au(4) = 3.1574(5) Å and Au(2)—Au(3) = 3.555 Å.

© 2006 NRC Canada

Fig. 2. Molecular structure of [2]catenane **6a*** (R = 2-pyridyl, Z = $(CH_2)_3$) showing only the ***A*** disorder component. Selected bond distances (Å) and angles (°): Au(1)—Au(4) 3.1574(5); Au(1)—P(1) 2.276(2); Au(2)—P(2) 2.275(2); Au(3)—P(3) 2.280(2); Au(4)—P(4) 2.273(2); Au(1)—C(11) 1.990(8); Au(2)—C(21) 1.991(7); Au(3)—C(31) 2.008(8); Au(4)—C(41) 1.990(8); C(11)—C(12) 1.18(1); C(21)—C(22) 1.19(1); C(31)—C(32) 1.18(1); C(41)—C(42) 1.19(1); P(1)-Au(1)-C(11) 170.4(2); P(2)-Au(2)-C(21) 168.3(2); P(3)-Au(3)-C(31) 173.0(2); P(4)-Au(4)-C(41) 168.9(2); Au(1)-C(11)-C(12) 170.4(8); Au(2)-C(21)-C(22) 172.2(7); Au(3)-C(31)-C(32) 175.3(7); Au(4)-C(41)-C(42) 171.7(8); C(11)-C(12)-C(13) 178.9(9); C(21)-C(22)-C(23A) 171(1); C(21)-C(22)-C(23B) 176(1); C(31)-C(32)-C(33) 175.1(9); C(41)-C(42)-C(43A) 173(1); C(41)-C(42)-C(43B) 158(1).

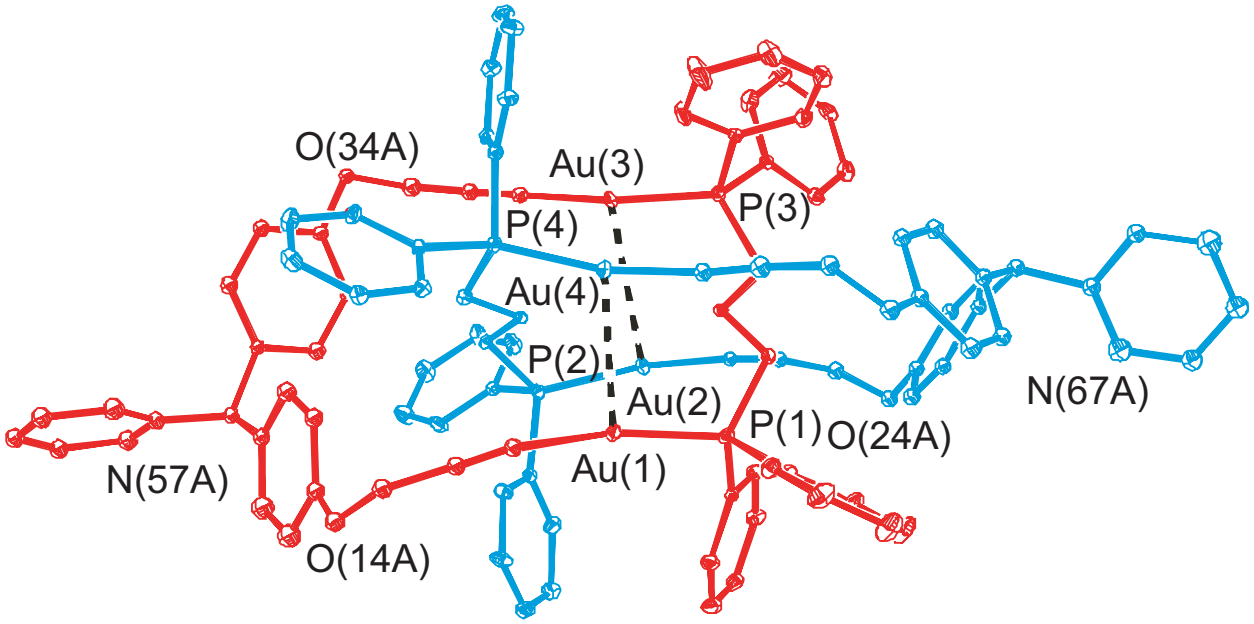
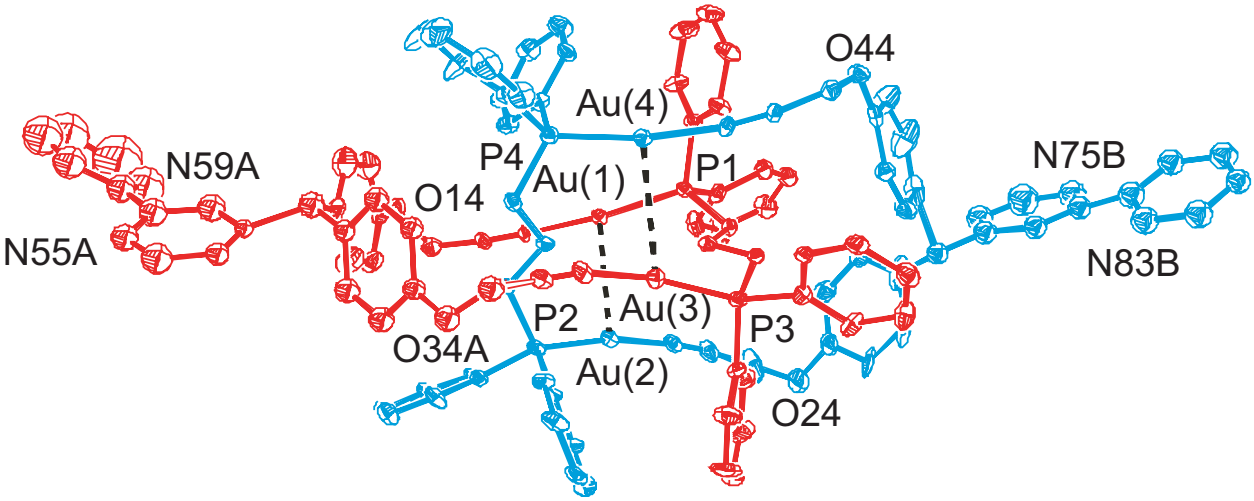


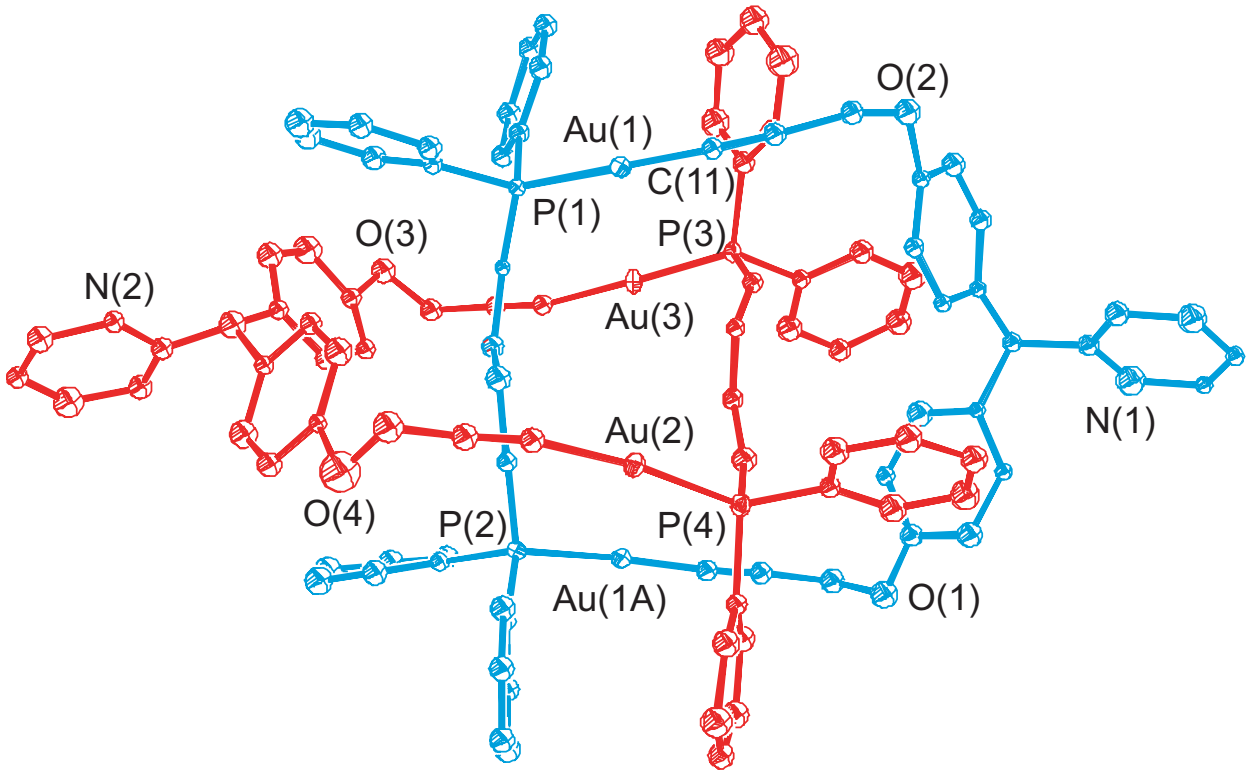
Fig. 3. Molecular structure of [2]catenane **6c*** (R = 4-(2,2′-bipyridyl), Z = $(CH_2)_3$); only one disorder component is shown. Selected bond distances (Å) and angles (°): Au(1)—Au(2) 3.2195(7); Au(1)—P(1) 2.269(3); Au(2)—P(2) 2.281(3); Au(3)—P(3) 2.271(4); Au(4)—P(4) 2.266(3); Au(1)—C(11) 2.02(1); Au(2)—C(21) 1.99(2); Au(3)—C(31) 2.00(2); Au(4)—C(41) 2.04(1); C(11)—C(12) 1.16(2); C(21)—C(22) 1.18(2); C(31)—C(32) 1.18(2); C(41)—C(42) 1.17(2); P(1)-Au(1)-C(11) 170.8(4); P(2)-Au(2)-C(21) 170.2(4); P(3)-Au(3)-C(31) 170.5(4); P(4)-Au(4)-C(41) 171.2(4); Au(1)-C(11)-C(12) 170(1); Au(2)-C(21)-C(22) 174(1); Au(3)-C(31)-C(32) 166(1); Au(4)-C(41)-C(42) 171(1); C(11)-C(12)-C(13) 177(1); C(21)-C(22)-C(23) 174(2); C(31)-C(32)-C(33A) 177(2); C(41)-C(42)-C(43) 175(1).



Complex **6c*** (Fig. 3) was also disordered around the two CH(4-(2,2′-bipy))$(C_6H_4)_2$ units of the [2]catenane and the disorder was modeled as ***A/B*** = 51/49 for each component of the interlocked rings. The aryl twist angles for the two distributions were found to be: ***A***: 88°,52° (ring 1) and 70°,56° (ring 2); and ***B***: 69°,36° (ring 1) and 50°,45° (ring

© 2006 NRC Canada

Fig. 4. Molecular structure of [2]catenane **7a*** (R = 2-pyridyl, Z = $(CH_2)_4$) with only one disorder component shown. Selected bond distances (Å) and angles (°): Au(1)—P(1) 2.361(6); Au(2)—P(4) 2.277(6); Au(1A)—P(2) 2.272(6); Au(3)—P(3) 2.256(7); Au(1)—C(11) 1.94(3); Au(2)—C(22) 2.00(3); Au(1A)—C(5) 1.98(3); Au(3)—C(16) 2.09(3); P(1)-Au(1)-C(11) 176.4(6); P(4)-Au(2)-C(22) 173.1(8); P(2)-Au(1A)-C(27) 176.1(7); P(3)-Au(3)-C(16) 177.8(7); Au(1)-C(11)-C(10) 169(2); Au(2)-C(21)-C(22) 166(3); Au(1A)-C(5)-C(6) 169(2); Au(3)-C(16)-C(17) 168(2); C(5)-C(6)-C(7) 176(3); C(9)-C(10)-C(11) 176(3); C(16)-C(17)-C(18) 170(3); C(20)-C(21)-C(22) 174(3).



2). In complex **6c***, the nitrogen atoms of the two pyridyl rings in each 4-(2,2′-bipy) group adopt an approximately planar s-trans conformation, as is typical for free 2,2′-bipyridyl ligands (16). In the disordered structure, the angles between the two pyridyl rings of each 2,2′-bpy group were: ***A***: 31° and 9°; and ***B***: 34° and 17°. As in the complexes **6a*** and **6b***, there was one strong and one weak Au···Au interaction (36) with Au(1)···Au(2) = 3.2195(7) Å and Au(3)···Au(4) = 3.442 Å in **6c***. No significant intercatenane hydrogen bonding or π stacking of aryl groups was observed in the crystal structure of complex **6c***.

The structure of **7a*** showed disorder at the $RCH(C_6H_4)_2$ units, similar to that in **6a*** and **6c***, but there was a second form of disorder arising from the presence of an inversion centre at the midpoint of the Au(1)···Au(1A) unit. The interlocked 25-membered rings in **7a*** (Fig. 4) are much less congested than the 24-membered rings in **6a***–**6c*** and there are no short gold···gold distances. The shortest intracatenane Au···Au distance is Au(1A)—Au(2) = 5.138 Å, which is too long to be indicative of an aurophilic interaction (36). The main forces favoring catenation in this case are aryl···aryl attractions (25, 26).

NMR spectroscopy

It is possible to distinguish between the macrocycle and [2]catenane structures by NMR spectroscopy based on the molecular symmetry. Thus, the achiral ring complexes **4**–**8** have C_s symmetry so that the two phosphorus atoms are equivalent and will resonate as a singlet in the ^{31}P NMR spectrum. In contrast, the chiral [2]catenanes **6*** and **7*** have C_2 symmetry and so the two phosphorus atoms in each interlocked ring of the [2]catenane will be nonequivalent and will resonate as two doublets in the ^{31}P NMR spectrum (25, 26). The gold(I) complexes **4**, **5**, **7**, and **8**, containing the diphosphines Ph_2P-Z-PPh_2 with Z = C≡C, $(CH_2)_2$, $(CH_2)_4$, and $(CH_2)_5$, respectively, all give a singlet resonance in their ^{31}P NMR spectra and so are presumed to exist in solution as the macrocyclic complexes. In the solid state, the gold(I) complex with R = 2-pyridyl and Z = $(CH_2)_4$ exists as a [2]catenane **7a***, but this is presumed to dissociate back to the macrocycle **7a** in solution. However, the gold(I) complexes **6**, with Z = $(CH_2)_3$, give several resonances in the ^{31}P NMR spectra, indicating that they exist as a mixture of isomers in solution. For example, the macrocyclic complex **6a** (R = 2-py) gave a singlet resonance at δ(^{31}P) 35.93 and was in equilibrium with the [2]catenane **6a***, which gave an "AB" multiplet with δ(^{31}P) 31.89 and 32.18, with coupling $^4J(P^AP^B)$ = 6 Hz. In the ^1H NMR spectra, there are some significant differences in chemical shift between the macrocyclic and [2]catenane structures. For example, **6a** has δ(C*H*py) 5.54 and δ(C_6H_4) 7.01 and 7.12, whereas **6a*** has δ(C*H*py) 5.07 and δ(C_6H_4) 6.16 and 6.78. Ring current effects from the adjacent phenylphosphorus groups in the [2]catenane cause these diagnostic shifts. Slow crystalliza-

© 2006 NRC Canada

tion of this complex (**6a/6a***) gave the pure [2]catenane **6a***, which, on dissolution in CD_2Cl_2, gave only the resonances of the [2]catenane. Equilibration occurred slowly in solution, over a period of several days at room temperature. In dilute solution the equilibrium favours the macrocycle **6a** but, at high concentration, more of the [2]catenane **6a*** and other higher molecular weight isomers (25, 26) are observed. The slow equilibration of **6a** and **6a*** is expected, based on earlier studies (25, 26), and is assumed to result from the very compact structure of **6a*** in which the gold atoms are sterically protected from external reagents.

The NMR features described for **6a** and **6a*** were typical of all the macrocycles and [2]catenanes studied, and full details are given in the Experimental section. In particular, the proton resonances of the [2]catenanes with the diphosphine ligand $Ph_2P(CH_2)_3PPh_2$ occurred at higher field than in the macrocyclic complexes, with large upfield shifts observed for the RC*H* ($\Delta\delta$ ca. 0.45) and C_6H_4 ($\Delta\delta$ ca. 0.4 and 0.8) proton resonances. The shielding arises from the close contacts with the phenyl groups of the interlocked gold macrocycle and is a useful indicator of [2]catenane formation (25, 26).

Coordination and quaternization studies

As shown in Scheme 1 for the 4-pyridyl derivative, the gold(I) macrocyclic complexes and [2]catenanes can, in principle, form extended structures by coordination of the pyridyl or bipyridyl groups to suitable metal ions. By variation of the stoichiometry of the reaction (pyridyl:metal) and by use of either the macrocyclic complex or the [2]catenane, the resulting products are the molecularly discrete complexes **A**, **B**, and **C**, and the polymeric complex **D**. Similar chemistry could be achieved by quaternization of the pyridyl nitrogen atoms by reaction with alkyl halides. However, the chemistry proved to be difficult as a result of the lability of the gold(I) centres, especially with respect to cleavage of the gold–acetylide bonds.

The reaction of complex **6b/6b*** with benzyl bromide or with 1,4-bis(bromomethyl)benzene gave only $[Au_2Br_2(\mu\text{-}Ph_2P(CH_2)_3PPh_2)]$ as the isolated gold-containing product. Attempts were then made to quaternize the pyridyl nitrogen atom of the parent diacetylene ligand **2b** with 1,4-bis(bromomethyl)benzene, but this too was unsuccessful. A milder form of self-assembly might be possible by using hydrogen bond donors, such as phenol derivatives, to form secondary bonds to the pyridyl substituents of **6b/6b***. Attempts were made to crystallize **6b/6b*** in the presence of 1,4-$C_6H_4(OH)_2$ and other bis(phenol) derivatives, but they were not successful. Slow decomposition of **6b/6b*** occurred instead. The reaction of complex **6b/6b*** with metal halides MBr_2 (M = Zn, Cd, or Hg) led only to acetylide for bromide exchange reactions to give $[Au_2Br_2(\mu\text{-}Ph_2P(CH_2)_3PPh_2)]$. The 2,2′-bipyridyl complex **6c/6c*** gave similar results, and this complex also reacted with $AgPF_6$ to give an intractable black precipitate. It seems clear then that most electrophiles react with the gold–acetylide bond instead of or in addition to reacting with the free pyridyl or bipyridyl group.

The reaction of 2,2′-bipyridyl with $[PtMe_2(\mu\text{-}SMe_2)]_2$ occurs by displacement of the dimethylsulfide ligands to give $[PtMe_2(bipy)]$ (42), but the reaction of **7c** with $[PtMe_2(\mu\text{-}SMe_2)]_2$ occurred primarily by methyl for acetylide exchange to give $[Au_2Me_2(\mu\text{-}Ph_2P(CH_2)_4PPh_2)]$, identified by comparison of its ^1H and ^{31}P NMR spectra with those of an authentic sample (40, 41). The organoplatinum product was an insoluble solid, whose IR spectrum (KBr disc) showed a band owing to $\nu(C{\equiv}C)$ at 2120 cm^{-1} (cf. **7c**, 2131 cm^{-1}), but which was not fully characterized.

The only successful reaction was that of *fac*-$[PtMe_3I]_4$ (42), which is inert to methyl transfer reactions, with the 2,2′-bipyridine complex **6c/6c***, which gave the products $[PtMe_3I(\mathbf{6c})]$, **9** and $[(PtMe_3I)_2(\mu\text{-}\mathbf{6c}^*)]$, **9***, shown in Scheme 6. The mixture of complexes **9/9*** was isolated as an air-stable, pale-orange solid, but attempts to separate the isomers by recrystallization were unsuccessful, so they were characterized spectroscopically.

The presence of the $PtIMe_3$ group reduces the symmetry of **9** with respect to **6c**, by loss of the plane of symmetry containing the bipyridyl group in **6c**, and so there are also more potential isomers of **9*** compared with **6c***. The nonequivalence that arises from the presence of the $PtIMe_3$ group causes broadening rather than splitting of most resonances as described in the following. The NMR spectra were recorded as a mixture of **9/9*** in about a 3:1 molar ratio, but assignments were possible based on correlations in the COSY ^1H NMR spectrum and on peak intensities. The ^{31}P NMR spectrum of **9** contained a broad singlet shifted from the corresponding resonance of the macrocyclic gold complex **6c** [**9**, δ 34.67; **6c**, δ 35.92]. The ^1H NMR spectrum of **9** contained two broad resonances assigned to the methylplatinum groups in a 1:2 ratio at δ 0.62, $^2J(PtH)$ = 74 Hz and δ 1.46, $^2J(PtH)$ = 70 Hz. In principle, each isomer should give three Me-Pt resonances since the bipyridine is unsymmetrical, but there is evidently accidental degeneracy of the resonances of the methylplatinum groups trans to nitrogen. These ^1H NMR parameters of **9** are typical of complexes $[PtIMe_3(LL)]$ with LL = 2,2 bipyridyl or its derivatives (40–43). The ^{31}P NMR spectrum of **9*** contained a broad AB multiplet resonance shifted from the corresponding resonance of the gold [2]catenane **6c** (**9***, δ 32.73, 32.82, $^4J(PP)$ not resolved; **6c***, δ 31.83, 32.34, $^4J(PP)$ = 6 Hz). The methylplatinum resonances for **9*** were at δ 0.43, $^2J(PtH)$ = 74 Hz and δ 1.14, $^2J(PtH)$ = 70 Hz, significantly shifted from those of the macrocyclic complex **9** as a result of the catenation. The bipyridyl protons and several protons of the macrocycles of **9** and **9*** showed significant deshielding on coordination of the bipyridyl to platinum(IV), as listed in the Experimental section.

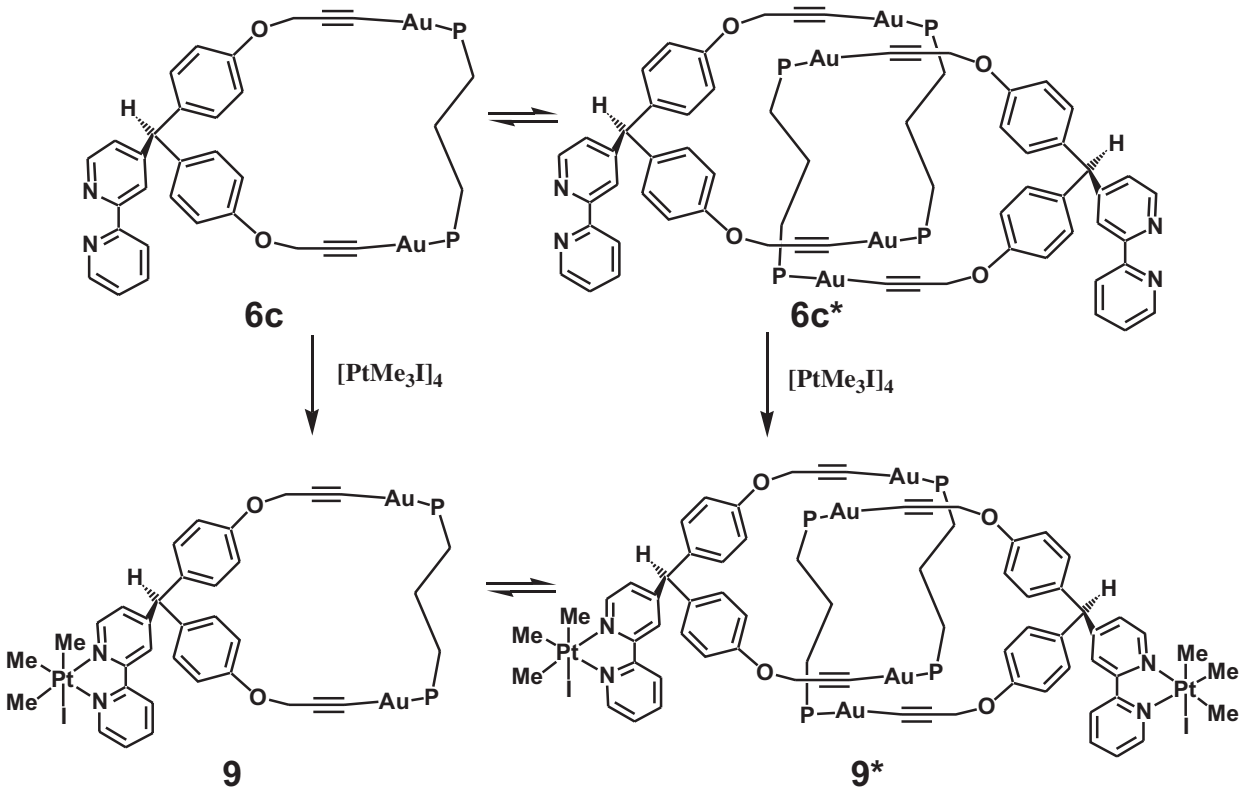
Further evidence for coordination of the bipyridyl group to platinum(IV) was obtained by ESI-MS of the mixture of **9/9*** in dichloromethane solution. As expected, based on the easy cleavage of the mechanical link (25, 26), no peaks for the [2]catenane were observed, but a low intensity envelope of peaks was observed at *m*/*z* 1602, assigned to $[\mathbf{9}{\cdot}H]^+$, and a major peak was observed at *m*/*z* = 1474, assigned to $[\mathbf{9} - I]^+$. The IR spectrum of the mixture of **9/9*** gave a single peak owing to $\nu(C{\equiv}C)$ at 2129 cm^{-1}, shifted only slightly from the corresponding peak for **6/6*** at $\nu(C{\equiv}C)$ = 2132 cm^{-1}.

Conclusions

Achiral digold(I) macrocycles and chiral tetragold(I)

© 2006 NRC Canada

Scheme 6.



[2]catenanes, each bearing 2-pyridyl, 4-pyridyl, or 4-(2,2′-bipyridyl) substituents at the hinge group, have been prepared and the structures of four [2]catenane complexes have been determined. The presence of the pyridyl or bipyridyl functional substituent does not complicate the synthesis. However, preliminary studies suggest that the ability of the new gold macrocycles and [2]catenanes to give an extensive coordination chemistry through use of the pendant nitrogen-donor groups will be limited as a result of the lability of the Au—C and Au—P bonds. One successful example was established in the use of the bipyridyl derivative **6c/6c*** as ligand for the inert $PtIMe_3$ group, and this appears to be the first example of the use of an organometallic [2]catenane as a ligand. The aim of using the coordination chemistry to prepare an organometallic poly[2]catenane according to Scheme 1, **D**, is yet to be achieved.

Experimental

NMR spectra were recorded by using Varian Mercury 400 and Varian Inova 400 spectrometers. ^{1}H and ^{13}C NMR chemical shifts are reported with respect to TMS reference and ^{31}P NMR chemical shifts are reported relative to 85% H_3PO_4 as an external standard. IR spectra were recorded as KBr discs or as Nujol mulls between NaCl plates using a PerkinElmer 2000 FT-IR spectrometer. High-resolution mass spectra were measured by using a Finnigan MAT 8400 spectrometer, and ESI-MS by using a Micromass LCT spectrometer, often using formic acid or CsI to aid ionization.

The complexes $[AuCl(SMe_2)]$, $[Au_2Cl_2(\mu\text{-}Ph_2P(CH_2)_3PPh_2)]$, $[Au_2Cl_2(\mu\text{-}Ph_2P(CH_2)_4PPh_2)]$ (44), $[PtMe_2(\mu\text{-}SMe_2)]_2$ (45), and $[(PtIMe_3)_4]$ (42) were prepared according to the literature. Gold compounds were protected from light by use of darkened reaction flasks.

Caution: Some gold acetylides are potentially explosive; they should be prepared in small quantities and not subjected to shock.

(2-C_5H_4N)CH(4-$C_6H_4OCH_2C{\equiv}CH)_2$ (2a)

A solution of 2-pyridinecarboxaldehyde (**1a**, 0.78 g, 7.3 mmol) and phenyl propargyl ether (46) (2.00 g, 15.1 mmol) in glacial acetic acid (5 mL) was cooled to 0 °C. Concentrated sulfuric acid (2 mL) was added slowly, then the mixture was heated for 5 h at 100 °C. The mixture was cooled, water was added, and the solution was neutralized by addition of aq. NaOH. The aqueous phase was extracted with diethyl ether, then the combined organic phases were washed with saturated aqueous sodium bicarbonate and then with water. The organic phase was dried over Na_2SO_4, filtered, and the solvent removed under reduced pressure to give an orange oil. Purification by flash chromatography gave the product as a yellow oil. Yield: 1.66 g (65%). IR (Nujol mull, cm^{-1}): 2120 (C≡C stretch). ^{1}H NMR ($CDCl_3$) δ: 2.51 (t, 2H, $^4J_{HH}$ = 2 Hz, C≡C*H*), 4.65 (d, 4H, $^4J_{HH}$ = 2 Hz, OCH_2), 5.61 (s, 1H, C*H*py), 6.90 (d, 4H, $^3J_{HH}$ = 9 Hz, C_6H_4), 7.08 (m, 5H, C_6H_4 + py-H3), 7.13 (ddd, 1H, $^3J_{HH}$ = 8, 5 Hz, $^4J_{HH}$ = 1 Hz, py-H5), 7.60 (dt, 1H, $^3J_{HH}$ = 8 Hz, $^4J_{HH}$ = 2 Hz, py-H4), 8.59 (ddd, 1H, $^3J_{HH}$ = 5 Hz, $^4J_{HH}$ = 2 Hz, $^5J_{HH}$ = 1 Hz, py-H6). ^{13}C NMR δ: 55.77 (OCH_2), 57.56 (*C*Hpy), 75.42 (C≡*C*H), 78.61 (*C*≡CH), 114.72,

© 2006 NRC Canada

130.23, 135.93, 156.16 (C_6H_4), 121.39, 123.62, 136.55, 149.34, 163.42 (py). EI-MS (*m*/*z*) calcd. for $C_{24}H_{19}NO_2$: 353.1415; found: 353.1413.

(4-C_5H_4N)CH(4-$C_6H_4OCH_2C{\equiv}CH)_2$ (2b)

Prepared following the procedure described for **2a**, using 4-pyridinecarboxaldehyde (**1b**, 1.4 mL, 14.7 mmol), phenyl propargyl ether (4.0 g, 30.3 mmol), glacial acetic acid (20 mL), and concd. sulfuric acid (4 mL). The product was isolated as a dark orange oil. Yield: 3.81 g (74%). IR (Nujol mull, cm^{-1}): 2118 (C≡C stretch). ^1H NMR ($CDCl_3$) δ: 2.53 (t, 2H, $^4J_{HH}$ = 2 Hz, C≡C*H*), 4.67 (d, 4H, $^4J_{HH}$ = 2 Hz, OCH_2), 5.40 (s, 1H, C*H*py), 6.91 (d, 4H, $^3J_{HH}$ = 8 Hz, C_6H_4), 7.00 (d, 4H, $^3J_{HH}$ = 8 Hz, C_6H_4), 7.02 (d, 2H, $^3J_{HH}$ = 5 Hz, py-H3 + py-H5), 8.48 (d, 2H, $^3J_{HH}$ = 5 Hz, py-H2 + py-H6). ^{13}C NMR δ: 54.85 (*C*Hpy), 56.04 (O*C*H_2), 75.74 (C≡*C*H), 78.74 (*C*≡CH), 115.09, 130.47, 135.56, 156.58 (C_6H_4), 124.74, 149.98, 153.42 (py). EI-MS (*m*/*z*) calcd. for $C_{24}H_{19}NO_2$: 353.1415; found: 353.1413.

4-(2,2′-bpy)CH(4-$C_6H_4OCH_2C{\equiv}CH)_2$ (2c)

To a solution of phenyl propargyl ether (46) (3.34 g, 25.3 mmol) and 2,2′-bipyridine-4-carboxaldehyde (27, 28) (1.86 g, 10.1 mmol) in glacial acetic acid (25 mL) was added concd. sulfuric acid (15 mL). The reaction mixture was stirred for 17 h then poured into water (150 mL) and neutralized by addition of sodium hydroxide. A brown oil separated and was extracted into diethyl ether (3 × 50 mL). The combined organic phases were washed with aqueous sodium carbonate, then the organic phase was dried ($MgSO_4$), filtered, and the solvent removed under reduced pressure. Chromatography of the residue on a silica gel column with 1:1 petroleum spirits (bp 60–90 °C) – ethyl acetate as eluant gave the product as a yellow oil. Yield: 1.94 g (45%). IR (neat, cm^{-1}): 2121 (C≡C stretch). ^1H NMR ($CDCl_3$) δ: 2.51 (t, 2H, $^4J_{HH}$ = 2 Hz, C≡C*H*), 4.66 (d, 4H, $^4J_{HH}$ = 2 Hz, OCH_2), 5.53 (s, 1H, C*H*bpy), 6.91 (d, 4H, $^3J_{HH}$ = 9 Hz, C_6H_4), 7.02 (d, 1H, $^3J_{HH}$ = 5 Hz, bpy-H5), 7.05 (d, 4H, $^3J_{HH}$ = 9 Hz, C_6H_4), 7.28 (dd, 1H, $^3J_{HH}$ = 8, 5 Hz, bpy-H5′), 7.79 (dt, 1H, $^3J_{HH}$ = 8 Hz, $^4J_{HH}$ = 1 Hz, bpy-H4′), 8.23 (s, 1H, bpy-H3), 8.37 (d, 1H, $^3J_{HH}$ = 8 Hz, bpy-H3′), 8.58 (d, 1H, $^3J_{HH}$ = 5 Hz, bpy-H6), 8.63 (dd, 1H, $^3J_{HH}$ = 5 Hz, $^4J_{HH}$ = 1 Hz, bpy-H6′). ^{13}C NMR δ: 54.90 (*C*Hbpy), 55.77 (O*C*H_2), 75.53 (C≡*C*H), 78.50 (*C*≡CH), 114.83, 130.27, 135.39, 156.30 (C_6H_4), 121.27 (bpy-*C*3′), 121.95 (bpy-*C*3), 123.66 (bpy-*C*5′), 124.40 (bpy-*C*5), 136.87 (bpy-*C*4′), 149.08 (bpy-*C*6′), 149.23 (bpy-*C*6), 154.32, 156.00, 156.15 (bpy-*C*2, -*C*2′, -*C*4). EI-MS (*m*/*z*) calcd. for $C_{29}H_{22}N_2O_2$: 430.1681; found: 430.1674.

Digold(I) diacetylide 3a

To a solution of [AuCl(SMe_2)] (0.73 g, 2.48 mmol) in THF (40 mL) and MeOH (30 mL) was added a solution of **2a** (0.44 g, 1.31 mmol) and Et_3N (0.2 mL) in THF (5 mL). The mixture was stirred for 30 min, and the pale yellow precipitate of the product was isolated by filtration, washed with THF, MeOH, and ether, and dried under vacuum. Yield: 0.86 g (88%). IR (KBr disc, cm^{-1}): 2000 ν(C≡C). Anal. calcd. for $C_{24}H_{17}Au_2NO_2$: C 38.68, H 2.30, N 1.88; found: C 38.21, H 2.00, N 1.69.

Digold(I) diacetylide 3b

This was prepared similarly and isolated as a beige solid. Yield: 95%. IR (KBr disc, cm^{-1}) : 2013 ν(C≡C). Anal. calcd. for $C_{24}H_{17}Au_2NO_2$: C 38.68, H 2.30, N 1.88; found: C 39.14, H 2.05, N 2.34.

(2-C_5H_4N)CH(4-$C_6H_4OCH_2C{\equiv}CAuC{\equiv}N$-*t*-Bu)$_2$

A mixture of **3a** (0.075 g, 0.10 mmol) and *t*-BuNC (22 mL, 0.195 mmol) in CH_2Cl_2 (10 mL) was stirred for 3 h. The mixture was filtered through Celite, the volume was reduced to 2 mL under vacuum, and pentane (10 mL) was added to precipitate the product as a pale yellow solid. Yield: 0.07 g (90%). IR (KBr disc, cm^{-1}): 2228 ν(N≡C), 2141 ν(C≡C). ^1H NMR (CD_2Cl_2) δ: 1.54 (s, 18H, Bu), 4.73 (s, 4H, OCH_2), 5.53 (s, 1H, C*H*py), 7.89 (d, 4H, $^3J_{HH}$ = 9 Hz, C_6H_4), 7.08 (d, 4H, $^3J_{HH}$ = 9 Hz, C_6H_4), 7.11–7.13 (m, 2H, py-H3 + py-H5), 7.62 (m, 1H, py-H4), 8.55 (d, 1H, $^3J_{HH}$ = 5 Hz, py-H6). Anal. calcd. for $C_{34}H_{35}Au_2N_3O_2$: C 44.80, H 3.87, N 4.61; found: C 44.71, H 3.30, N 4.56.

(4-C_5H_4N)CH(4-$C_6H_4OCH_2C{\equiv}CAuC{\equiv}N$-*t*-Bu)$_2$

This was prepared in a similar way from **3b** (0.075 g, 0.10 mmol). Yield: 0.065 g (71%). IR (KBr disc, cm^{-1}): 2226 ν(N≡C), 2139 ν(C≡C). ^1H NMR (CD_2Cl_2) δ: 1.54 (s, 18H, Bu), 4.73 (s, 4H, OCH_2), 5.53 (s, 1H, Chpy), 7.89 (d, 4H, $^3J_{HH}$ = 9 Hz, C_6H_4), 7.08 (d, 4H, $^3J_{HH}$ = 9 Hz, C_6H_4), 7.11–7.13 (m, 2H, py-H3 + py-H5), 7.62 (m, 1H, py-H4), 8.55 (d, 1H, $^3J_{HH}$ = 5 Hz, py-H6). MALDI-TOF MS *m*/*z*: 912 $[P + H]^+$. Anal. calcd. for $C_{34}H_{35}Au_2N_3O_2$: C 44.80, H 3.87, N 4.61; found: C 45.28, H 3.63, N 4.67.

Macrocyclic complex 4a (R = 2-pyridyl, Z = C≡C)

A mixture of **3a** (0.05 g, 0.067 mmol) and $Ph_2PCCPPh_2$ (0.023 g, 0.058 mmol) in CH_2Cl_2 (10 mL) was stirred for 1 h. The mixture was filtered through Celite, the volume was reduced to 2 mL under vacuum, and pentane (10 mL) was added to precipitate the product as a cream solid. Yield: 0.057 g (85%). IR (KBr disc, cm^{-1}): 2133 ν(C≡C). ^1H NMR (CD_2Cl_2) δ: 4.78 (s, 4H, OCH_2), 5.53 (s, 1H, C*H*py), 7.00 (d, 4H, $^3J_{HH}$ = 8 Hz, C_6H_4), 7.08–7.13 (m, 6H, C_6H_4 + py-H3 + py-H5), 7.45–7.62 (m, 13H, P*Ph* + py-H4), 7.67–7.82 (m, 8H, P*Ph*), 8.53 (d, 1H, $^3J_{HH}$ = 4 Hz, py-H6). ^{31}P NMR δ: 18.85 (s). ESI-MS *m*/*z*: 1272 [**4a** + Cs^+]. Anal. calcd. for $C_{50}H_{37}Au_2O_2NP_2$: C 52.69, H 3.27, N 1.23; found: C 52.21, H 2.91, N 1.28. The following complexes were similarly prepared.

Macrocyclic complex 4b (R = 4-pyridyl, Z = C≡C)

Pale orange solid. Yield: 85%. IR (KBr disc, cm^{-1}): 2132 ν(C≡C). ^1H NMR (CD_2Cl_2) δ: 4.80 (s, 4H, OCH_2), 5.40 (s, 1H, C*H*py), 6.92–7.04 (m, 10H, C_6H_4 + py-H3 + py-H5), 7.46–7.60 (m, 12H, P*Ph*), 7.68–7.78 (m, 8H, P*Ph*), 8.44 (d, 2H, $^3J_{HH}$ = 5 Hz, py-H2 + py-H6).^{31}P NMR δ: 18.82 (s). MALDI-TOF MS *m*/*z*: 1140 (**4b** + H)$^+$. Anal. calcd. for $C_{50}H_{37}Au_2O_2NP_2$: C 52.69, H 3.27, N 1.23; found: C 52.99, H 3.13, N 1.47.

Macrocyclic complex 5a (R = 2-pyridyl, Z = $(CH_2)_2$)

Pale pink solid. Yield: 65%. IR (KBr disc, cm^{-1}): 2132 ν(C≡C). ^1H NMR (CD_2Cl_2) δ: 2.51 (s, 4H, PCH_2), 4.78 (s,

© 2006 NRC Canada

4H, OCH_2), 5.52 (s, 1H, C*H*py), 7.02 (d, 4H, $^3J_{HH}$ = 9 Hz, C_6H_4), 7.13 (m, 2H, py-H3 + py-H5), 7.19 (d, 4H, $^3J_{HH}$ = 9 Hz, C_6H_4), 7.42–7.68 (m, 21H, P*Ph* + py-H4), 8.55 (d, 1H, $^3J_{HH}$ = 4 Hz, py-H6). ^{31}P NMR δ: 40.38 (s). ESI-MS *m*/*z*: 1276 (**5a** + Cs^+). Anal. calcd. for $C_{50}H_{41}Au_2O_2NP_2$: C 52.51, H 3.61, N 1.22; found: C 52.21, H 3.62, N 1.22.

Macrocyclic complex 5b (R = 4-pyridyl, Z = $(CH_2)_2$)

Cream solid. Yield: 73%. IR (KBr disc, cm^{-1}): 2132 ν(C≡C). ^{1}H NMR (CD_2Cl_2) δ: 2.51 (s, 4H, PCH_2), 4.79 (s, 4H, OCH_2), 5.40 (s, 1H, C*H*py), 7.00–7.06 (m, 6H, C_6H_4 + py-H3 + py-H5), 7.11 (d, 4H, $^3J_{HH}$ = 8 Hz, C_6H_4), 7.41–7.69 (m, 20H, P*Ph*), 8.45 (d, 2H, $^3J_{HH}$ = 6 Hz, py-H2 + py-H6). ^{31}P NMR δ: 40.37 (s). ESI-MS *m*/*z*: 1276 (**5b** + Cs^+). Anal. calcd. for $C_{50}H_{41}Au_2O_2NP_2$: C 52.51, H 3.61, N 1.22; found: C 52.95, H 3.31, N 1.97.

Macrocyclic complex 6a and [2]catenane 6a* (R = 2-pyridyl, Z = $(CH_2)_3$)

Cream solid. Yield: 88%. IR (KBr disc, cm^{-1}): 2132 ν(C≡C). **6a**: ^{1}H NMR (CD_2Cl_2) δ: 1.80 (br, 2H, PCH_2CH_2), 2.46 (br, 4H, PCH_2), 4.77 (s, 4H, OCH_2), 5.54 (s, 1H, C*H*py), 7.01 (d, 4H, $^3J_{HH}$ = 9 Hz, C_6H_4), 7.09 (m, 2H, py-H3 + py-H5), 7.12 (d, 4H, $^3J_{HH}$ = 9 Hz, C_6H_4), 7.41–7.69 (m, 21H, P*Ph* + py-H4), 8.54 (d, 1H, $^3J_{HH}$ = 4 Hz, py-H6). ^{31}P NMR (CD_2Cl_2) δ: 35.93 (s). **6a***: ^{1}H NMR δ: 2.25 (br, 4H, PCH_2CH_2), 2.75 (br, 8H, PCH_2), 4.65 (br m, 8H, OCH_2), 5.07 (s, 2H, C*H*py), 6.16 (d, 8H, $^3J_{HH}$ = 7 Hz, C_6H_4), 6.78 (d, 8H, $^3J_{HH}$ = 7 Hz, C_6H_4), 6.90 (m, 2H, py-H3), 7.16 (m, 2H, py-H5), 7.30–7.65 (m, 42H, P*Ph* + py-H4), 8.42 (d, 2H, $^3J_{HH}$ = 4 Hz, py-H6). ^{31}P NMR δ: 31.89 (d, $^4J_{PP}$ = 6 Hz), 32.18 (d, $^4J_{PP}$ = 6 Hz). ESI-MS *m*/*z*: 1290 (**6a** +H)$^+$. Anal. calcd. for $C_{51}H_{43}Au_2O_2NP_2$: C 52.91, H 3.74, N 1.21; found: C 52.74, H 3.71, N 1.24.

Macrocyclic complex 6b and [2]catenane 6b* (R = 4-pyridyl, Z = $(CH_2)_3$)

Cream solid. Yield: 89%. IR (KBr disc, cm^{-1}): 2132 ν(C≡C). **6b**: ^{1}H NMR (CD_2Cl_2) δ: 1.82 (br, 2H, PCH_2CH_2), 2.47 (m, 4H, PCH_2), 4.78 (s, 4H, OCH_2), 5.41 (s, 1H, C*H*py), 6.97 (d, 4H, $^3J_{HH}$ = 8 Hz, C_6H_4), 7.01 (d, 4H, $^3J_{HH}$ = 8 Hz, C_6H_4), 7.05 (d, 2H, $^3J_{HH}$ = 6 Hz, py-H3 + py-H5), 7.42–7.64 (m, 20H, P*Ph*), 8.45 (d, 2H, $^3J_{HH}$ = 6 Hz, py-H2 + py-H6). ^{31}P NMR (CD_2Cl_2) δ: 35.92 (s). **6b***: ^{1}H NMR δ: 1.82 (br, 4H, PCH_2CH_2), 2.76 (br, 8H, PCH_2), 4.67 (s, 8H, OCH_2), 4.96 (s, 2H, C*H*py), 6.19 (d, 8H, $^3J_{HH}$ = 8 Hz, C_6H_4), 6.63 (d, 8H, $^3J_{HH}$ = 8 Hz, C_6H_4), 6.74 (d, 4H, $^3J_{HH}$ = 6 Hz, py-H3 + py-H5), 7.42–7.64 (m, 40H, P*Ph*), 8.32 (d, 4H, $^3J_{HH}$ = 6 Hz, py-H2 + py-H6). ^{31}P NMR δ: 31.83 (d, $^4J_{PP}$ = 6 Hz), 32.15 (d, $^4J_{PP}$ = 6 Hz). ESI-MS *m*/*z*: 1290 (**6a** +H)$^+$. Anal. calcd. for $C_{51}H_{43}Au_2O_2NP_2$: C 52.91, H 3.74, N 1.21; found: C 53.37, H 3.42, N 1.54.

Macrocyclic complex 7a (R = 2-pyridyl, Z = $(CH_2)_4$)

Cream solid. Yield: 88%. IR (KBr disc, cm^{-1}): 2132 ν(C≡C). ^{1}H NMR (CD_2Cl_2) δ: 1.73 (br s, 4H, PCH_2CH_2), 2.35 (br, 4H, PCH_2), 4.77 (s, 4H, OCH_2), 5.53 (s, 1H, C*H*py), 7.01 (d, 4H, $^3J_{HH}$ = 9 Hz, C_6H_4), 7.12 (m, 2H, py-H3 + py-H5), 7.15 (d, 4H, $^3J_{HH}$ = 9 Hz, C_6H_4), 7.42–7.52 (m, 12H, P*Ph*), 7.57–7.65 (m, 9H, P*Ph* + py-H4), 8.53 (d, 1H, $^3J_{HH}$ = 3 Hz, py-H6). ^{31}P NMR δ: 38.89 (s). ESI-MS *m*/*z*: 1304 (**7a** + Cs^+). Anal. calcd. for $C_{52}H_{45}Au_2O_2NP_2$: C 53.30, H 3.87, N 1.20; found: C 52.97, H 3.91, N 1.23. Slow crystallization of **7a** gave the [2]catenane **7a***, but on dissolution it quickly reverted back to **7a**.

Macrocyclic complex 7b (R = 4-pyridyl, Z = $(CH_2)_4$)

Cream solid. Yield: 76%. IR (KBr disc, cm^{-1}): 2132 ν(C≡C). ^{1}H NMR (CD_2Cl_2) δ: 1.73 (br s, 4H, PCH_2CH_2), 2.35 (br, 4H, PCH_2), 4.78 (s, 4H, OCH_2), 5.40 (s, 1H, C*H*py), 6.88–7.06 (m, 6H, C_6H_4 + py-H3 + py-H5), 7.08 (d, 4H, $^3J_{HH}$ = 8 Hz, C_6H_4), 7.41–7.51 (m, 12H, P*Ph*), 7.56–7.65 (m, 8H, P*Ph*), 8.44 (d, 2H, $^3J_{HH}$ = 6 Hz, py-H2 + py-H6). ^{31}P NMR δ: 38.90 (s). Anal. calcd. for $C_{52}H_{45}Au_2O_2NP_2$: C 53.30, H 3.87, N 1.20; found: C 53.13, H 3.54, N 1.33.

Macrocyclic complex 8a (R = 2-pyridyl, Z = $(CH_2)_5$)

Cream solid. Yield: 85%. IR (KBr disc, cm^{-1}): 2132 ν(C≡C). ^{1}H NMR (CD_2Cl_2) δ: 1.57 (br, 6H, $PCH_2CH_2CH_2$), 2.36 (br, 4H, PCH_2), 4.78 (s, 4H, OCH_2), 5.57 (s, 1H, C*H*py), 7.02 (d, 4H, $^3J_{HH}$ = 9 Hz, C_6H_4), 7.10–7.15 (m, 6H, C_6H_4 + py-H3 + py-H5), 7.42–7.54 (m, 12H, P*Ph*), 7.59–7.70 (m, 9H, P*Ph* + py-H4), 8.55 (d, 1H, $^3J_{HH}$ = 4 Hz, py-H6). ^{31}P NMR δ: 37.56 (s). ESI-MS *m*/*z*: 1318 (**8a** + Cs^+). Anal. calcd. for $C_{53}H_{47}Au_2O_2NP_2$: C 53.68, H 3.99, N 1.18; found: C 53.44, H 3.73, N 1.22.

Macrocyclic complex 8b (R = 4-pyridyl, Z = $(CH_2)_5$)

Cream solid. Yield: 72%. IR (KBr disc, cm^{-1}): 2132 ν(C≡C). ^{1}H NMR (CD_2Cl_2) δ: 1.56 (br, 6H, $PCH_2CH_2CH_2$), 2.35 (br, 4H, PCH_2), 4.77 (s, 4H, OCH_2), 5.42 (s, 1H, C*H*py), 6.89–7.08 (m, 10H, C_6H_4 + py-H3 + py-H5), 7.42–7.52 (m, 12H, P*Ph*), 7.58–7.68 (m, 8H, P*Ph*), 8.46 (d, 2H, $^3J_{HH}$ = 6 Hz, py-H2 + py-H6). ^{31}P NMR δ: 37.56 (s). Anal. calcd. for $C_{53}H_{47}Au_2O_2NP_2$: C 53.68, H 3.99, N 1.18; found: C 53.94, H 3.74, N 1.23.

Synthesis from t-BuNC derivatives — 6a/6a*

To a solution of (2-C_5H_4N)CH(4-$C_6H_4OCH_2C{\equiv}CAuC{\equiv}N$-*t*-Bu)$_2$ (0.022 g, 0.024 mmol) in CH_2Cl_2 (10 mL) was added $Ph_2P(CH_2)_3PPh_2$ (0.01 g, 0.023 mmol). The mixture was stirred for 1 h, the volume was reduced to 2 mL, and pentane (10 mL) was added to precipitate the product. Yield: 0.024 g (89%). Spectroscopic data were as described above for **6a/6a***. **6b/6b*** (90%), **7a** (73%), and **8a** (65%) were similarly prepared.

Macrocyclic complex 6c and [2]catenane 6c* (R = 4-(2,2′-bipyridyl), Z = $(CH_2)_3$)

To a solution of [Au_2Cl_2(μ-$Ph_2P(CH_2)_3PPh_2$)] (0.505 g, 0.58 mmol) in CH_2Cl_2 (20 mL) was added AgO_2CCF_3 (0.254 g, 1.15 mmol). The mixture was stirred for 2 h, then filtered through Celite to remove AgCl. The filtrate was added to a solution of **2c** (0.58 mmol) and Et_3N (3.2 mL) in CH_2Cl_2 (40 mL) at –78 °C, and the mixture was stirred for 2 h then allowed to warm to room temperature. The organic phase was washed with water (50 mL), then dried over $MgSO_4$, and the volume was reduced to 5 mL, and pentane (80 mL) was added to precipitate the product as a pale-orange solid, identified as a mixture of **6c** and **6c***. Yield: 73%. Recrystallization from CH_2Cl_2–pentane gave the pure [2]catenane as a white solid. IR (KBr disc, cm^{-1}): 2132

© 2006 NRC Canada

ν(C≡C). **6c**: ^{1}H NMR (CD_2Cl_2) δ: 1.84 (m, 2H, PCH_2CH_2), 2.47 (m, 4H, PCH_2), 4.79 (s, 4H, OCH_2), 5.52 (s, 1H, C*H*bpy), 7.05 (d, 4H, $^3J_{HH}$ = 9 Hz, C_6H_4), 7.07 (d, 1H, bpy-H5), 7.11 (d, 4H, $^3J_{HH}$ = 9 Hz, C_6H_4), 7.28 (m, 1H, bpy-H5′), 7.35–7.60 (m, 20H, P*Ph*), 7.80 (dt, 1H, $^3J_{HH}$ = 7, 8 Hz, $^4J_{HH}$ = 2 Hz, bpy-H4′), 8.21 (s, 1H, bpy-H3), 8.40 (d, 1H, $^3J_{HH}$ = 8 Hz, bpy-H3′), 8.54 (d, 1H, $^3J_{HH}$ = 5 Hz, bpy-H6), 8.59 (d, 1H, $^3J_{HH}$ = 4 Hz, bpy-H6′). ^{31}P NMR δ: 35.92 (s). **6c***: ^{1}H NMR δ: 1.80 (br, 4H, PCH_2CH_2), 2.29 (br, 8H, PCH_2), 4.68 (br s, 8H, OCH_2), 5.08 (s, 2H, C*H*bpy), 6.20 (dd, 8H, $^3J_{HH}$ = 8 Hz, $^4J_{HH}$ = 3 Hz, C_6H_4), 6.69 (d, 8H, $^3J_{HH}$ = 8 Hz, C_6H_4), 6.82 (br, 2H, bpy-H5), 7.10–7.49 (m, 42H, P*Ph* + bpy-H5′), 7.77 (t, 2H, $^3J_{HH}$ = 8 Hz, bpy-H4′), 7.96 (s, 2H, py-H3), 8.35 (br, 2H, bpy-H3′), 8.42 (d, 2H, $^3J_{HH}$ = 6 Hz, py-H6), 8.52 (d, 2H, $^3J_{HH}$ = 4 Hz, bpy-H6′). ^{31}P NMR δ: 31.83 (d, $^4J_{PP}$ = 6.0 Hz), 32.23 (d, $^4J_{PP}$ = 6.0 Hz). ESI-MS *m*/*z*: 1235 (**6c** + H^+). Anal. calcd. for $C_{56}H_{46}Au_2N_2O_2P_2$: C 54.47, H 3.75, N 2.27; found: C 54.25, H 3.96, N 2.11.

Macrocyclic complex 7c (R = 4-(2,2′-bipyridyl), Z = $(CH_2)_4$)

This was prepared in a similar way to **6b** but using $Ph_2P(CH_2)_4PPh_2$. Orange solid. Yield: 78%. IR (KBr disc, cm^{-1}): 2131 ν(C≡C). ^{1}H NMR (CD_2Cl_2) δ: 1.73 (br, 4H, PCH_2CH_2), 2.34 (br, 4H, PCH_2), 4.80 (s, 4H, OCH_2), 5.52 (s, 1H, C*H*bpy), 7.05 (m, 5H, C_6H_4 + bpy-H5), 7.14 (d, 4H, $^3J_{HH}$ = 9 Hz, C_6H_4), 7.27 (m, 1H, bpy-H5′), 7.42–7.50 (m, 12H, P*Ph*), 7.57–7.63 (m, 8H, P*Ph*), 7.79 (dt, 1H, $^3J_{HH}$ = 8 Hz, $^4J_{HH}$ = 2 Hz, bpy-H4′), 8.19 (s, 1H, bpy-H3), 8.39 (d, 1H, $^3J_{HH}$ = 8 Hz, bpy-H3′), 8.53 (d, 1H, $^3J_{HH}$ = 5 Hz, bpy-H6), 8.58 (d, 1H, $^3J_{HH}$ = 5 Hz, bpy-H6′). ^{31}P NMR δ: 38.90 (s). ESI-MS *m*/*z*: 1249 (**7c** + H^+). Anal. calcd. for $C_{57}H_{48}Au_2N_2O_2P_2$: C 54.82, H 3.87, N 2.24; found: C 54.43, H 3.77, N 2.09.

Complexes 9/9*

To a solution of $[PtMe_3I]_4$ (1.5×10^{-5} mol) in CH_2Cl_2 (10 mL) was added **6c**/**6c*** (6.0×10^{-5} mol) and the solution stirred for 1 h. The volume of the solution was concentrated to ~2 mL at reduced pressure, then diethyl ether (40 mL) was added to precipitate the product as a pale-orange solid. Yield: 0.08 g (84%). IR (KBr disc, cm^{-1}): 2129 ν(C≡C). ESI-MS (*m*/*z*): 1602, [**9** + H]$^+$; 1474, [**9** – I]$^+$. **9**: ^{1}H NMR (CD_2Cl_2) δ: 0.62 (s, 3H, $^2J_{PtH}$ = 74 Hz, *Me*Pt trans to I), 1.46 (s, 6H, $^2J_{PtH}$ = 70 Hz, *Me*Pt trans to N), 1.82 (m, 2H, PCH_2CH_2), 2.64 (m, 4H, PCH_2), 4.80 (s, 4H, OCH_2), 5.61 (s, 1H, C*H*bpy), 6.98 (d, 4H, $^3J_{HH}$ = 9 Hz, C_6H_4), 6.95 (m, 1H, bpy-H5), 7.10 (d, 4H, $^3J_{HH}$ = 9 Hz, C_6H_4), 7.28 (m, 1H, bpy-H5′), 7.2–7.5 (m, 20H, P*Ph*), 7.97 (m, 1H, bpy-H4′), 8.20 (s, 1H, bpy-H3), 8.40 (m, 1H, bpy-H3′), 8.80 (d, 1H, $^3J_{HH}$ = 5 Hz, bpy-H6), 8.91 (m, 1H, bpy-H6′). ^{31}P NMR δ: 34.67 (s). **9***: ^{1}H NMR δ: 0.43 (s, 6H, $^2J_{PtH}$ = 74 Hz, *Me*Pt trans to I), 1.10 (s, 12H, $^2J_{PtH}$ = 70 Hz, *Me*Pt trans to N), 1.80 (br, 4H, PCH_2CH_2), 2.46 (br, 8H, PCH_2), 4.41 (br, 8H, OCH_2), 5.04 (s, 2H, C*H*bpy), 6.01 (m, 8H, C_6H_4), 6.62 (m, 8H, C_6H_4), 7.1–7.5 (m, 44H, P*Ph* + bpy-H5+ bpy-H5′), 7.77 (m, 2H, bpy-H4′), 8.01 (s, 2H, py-H3), 8.32 (br, 2H, bpy-H3′), 8.72 (m, 2H, py-H6), 8.87 (m, 2H, bpy-H6′). ^{31}P NMR δ: 32.82, 32.73 (br). Anal. calcd. for $C_{59}H_{55}Au_2IN_2O_2P_2Pt$: C 44.24, H 3.46, N 1.75; found: C 43.87, H 3.27, N 1.54.

X-ray crystal structure determinations

Crystals of **6a***·$Cl(CH_2)_2Cl$ were grown by slow diffusion of hexane into a solution of **6a*** in 1,2-dichloroethane. Similarly, crystals of **6b***·CH_2Cl_2 were obtained from dichloromethane–pentane; crystals of **6c***·H_2Cl_2 from dichloromethane–hexane; and crystals of **7a*** from 1,2-dichloroethane – diethyl ether. Data were collected using a Nonius Kappa-CCD diffractometer with Mo-Kα radiation (λ = 0.710 73 Å) at 150 K with COLLECT software (47). The unit cell parameters were calculated and refined from the full data set. Crystal cell refinement and data reduction were carried out with the DENZO package (47). The data were scaled using SCALEPACK (47). The SHELXTL-NT V6.1 package (47) was used to solve the structures of **6a***, **6b***, and **6c*** by direct methods, and to solve the structure of **7a*** by Patterson methods. The structure solutions were followed by successive difference Fourier transformations and refined with full-matrix least-squares on F^2. Non-hydrogen atoms were refined anisotropically. The hydrogen atoms were calculated geometrically, riding on their respective carbon atoms. Crystal data and refinement parameters are listed in Table 1.[3]

2-pyCH(C$_6$H$_4$OH)$_2$

No crystallographic complexity.

6a*·C$_2$H$_4$Cl$_2$

There was disorder associated with the acetylide ligands and they were modeled as 50/50 isotropic for one ring of the [2]catenane and as 65:35 for the other ring of the [2]catenane.

6b*·3CH$_2$Cl$_2$

The molecule showed no disorder. There were three dichloromethane molecules of solvation: one was refined anisotropically, one was refined isotropically, and one was disordered. The disordered dichloromethane molecule was modeled as a 55:45 mixture of isotropic atoms complete with hydrogens. The C—Cl distance was fixed at 1.65 Å, and some of the Cl—Cl distances were fixed at 2.74 Å.

6c*·CH$_2$Cl$_2$

The molecule showed some disorder for the bipyridyl–diacetylide ligands. For one ring of the [2]catenane, the bipyridyl group was modeled as a 51:49 isotropic mixture; in the other ring of the [2]catenane, there was more extensive disorder and the bipyridyl group and one phenylene group were modeled as a 51:49 mixture. There were three

[3] Supplementary data for this article are available on the journal Web site (http://canjchem.nrc.ca) or may be purchased from the Depository of Unpublished Data, Document Delivery, CISTI, National Research Council Canada, Ottawa, ON K1A 0R6, Canada. DUD 4084. For more information on obtaining material refer to http://cisti-icist.nrc-cnrc.gc.ca/irm/unpub_e.shtml. CCDC 275188–275192 contain the crystallographic data for this manuscript. These data can be obtained, free of charge, via http://www.ccdc.cam.ac.uk/conts/retrieving.html (Or from the Cambridge Crystallographic Data Centre, 12 Union Road, Cambridge CB2 1EZ, UK; fax +44 1223 336033; or deposit@ccdc.cam.ac.uk).

© 2006 NRC Canada

Table 1. Crystallographic data and experimental parameters for X-ray structure analyses of the 2-pyridylbis(phenol) and of [2]catenanes **6a***, **6b***, **6c***, and **7a***.

Compound	2-pyCH(C_6H_4OH)$_2$	**6a***·Cl(CH_2)$_2$Cl	**6b***·3CH_2Cl_2	**6c***·CH_2Cl_2	**7a***
Formula	$C_{18}H_{15}NO_2$	$C_{104}H_{90}Au_4Cl_2N_2O_4P_4$	$C_{105}H_{92}Au_4Cl_6N_2O_4P_4$	$C_{56.5}H_{47}Au_2ClN_2O_2P_2$	$C_{104}H_{90}Au_4N_2O_4P_4$
Fw	277.31	2 414.43	2 570.25	1 277.28	1 171.76
Cryst. Syst.	Monoclinic	Triclinic	Monoclinic	Monoclinic	Triclinic
Space group	*C*2/*c*	*P*-1	*P*2(1)/*c*	*P*2(1)/*n*	*P*-1
a (Å)	19.2706(5)	12.4285(1)	12.2843(3)	12.2811(2)	10.7552(3)
b (Å)	9.8267(2)	12.6883(1)	22.4961(6)	22.4781(4)	14.5857(3)
c (Å)	17.4670(4)	29.8997(4)	35.9454(9)	38.6828(7)	15.7336(4)
α (°)	90	92.062(1)	90	90	115.413(1)
β (°)	121.059(1)	101.313(1)	96.180(1)	95.255(1)	96.354(1)
γ (°)	90	104.334(1)	90	90	90.744(1)
V (Å^3)	2 833.5(1)	4 461.76(8)	9 875.7(4)	10 633.7(3)	2 210.6(1)
Z	8	2	4	8	1
d_{calcd} (g cm^{-3})	1.300	1.797	1.729	1.596	1.760
μ (mm^{-1})	0.085	6.743	6.203	5.664	6.743
F(000)	1 168	2 340	4 984	4 968	1 136
Reflections	14 668	59 523	82 874	95 071	23 677
Unique refl. (R_{int})	3 249	16 290 (0.080)	17 433 (0.112)	18 691 (0.091)	7 775 (0.062)
Parameters	192	747	987	905	348
θ range (°)	2.56–27.53	2.55–25.35	2.91–25.03	2.55–25.02	2.55–25.00
GOF on F^2	1.074	1.009	1.014	1.018	1.048
R, R_w ($I > 2\sigma(I)$)	0.0417, 0.0985	0.0456, 0.0871	0.069, 0.145	0.064, 0.148	0.067, 0.132
R, R_w (all data)	0.0688, 0.1094	0.0886, 0.0976	0.1836, 0.1797	0.1429, 0.1774	0.1272, 0.1838

sites of solvation that were modeled isotropically at reduced occupancy (site 200 (15%:10%); site 300 (25%); site 400 (25%:25%)) with fixed bond distances.

7a*

The [2]catenane was 50:50 disordered as a result of an inversion centre at the midpoint of the Au(1)···Au(1A) vector, with all other atoms at 50% occupancy. In addition, 50:50 disorder of the individual pyCH(C_6H_4)$_2$ groups was observed. Because of the extensive disorder, only the gold and phosphorus atoms were refined with anisotropic parameters.

Acknowledgments

We thank the Natural Sciences and Engineering Research Council of Canada (NSERC) for financial support. RJP thanks the Government of Canada for a Canada Research Chair.

References

1. M. Fujita. Acc. Chem. Res. **32**, 53 (1999).
2. G.F. Swiegers and T.J. Malefetse. Chem. Rev. **100**, 3483 (2000).
3. D.B. Amabilino and J.F. Stoddart. Chem. Rev. **95**, 2725 (1995).
4. V. Balzani, M. Gómez-López, and J.F. Stoddart. Acc. Chem. Res. **31**, 405 (1998).
5. J.-P. Sauvage. Acc. Chem. Res. **31**, 611 (1998).
6. J.-P. Sauvage (*Editor*). Transition metals in supramolecular chemistry. Wiley, Chichester. 1999.
7. J.-P. Sauvage and C. Dietrich-Buchecker (*Editors*). Molecular catenanes, rotaxanes and knots. Wiley-VCH, Weinheim. 1999.
8. L. Carlucci, G. Ciani, and D.M. Proserpio. Coord. Chem. Rev. **246**, 247 (2003).
9. B. Moulton and M.J. Zaworotko. Chem. Rev. **101**, 1629 (2001).
10. C. Janiak. Dalton Trans. 2781 (2003).
11. H.W. Roesky and M. Andruh. Coord. Chem. Rev. **236**, 91 (2003).
12. T. Takata, N. Kihara, and Y. Furusho. Adv. Polym. Sci. **171**, 1 (2004).
13. A. Godt. Eur. J. Org. Chem. 1639 (2004).
14. D.A. Leigh and R.A. Smith. Cyclic polymers. 2nd ed. *Edited by* J.A. Semlyen. Kluwer Academic, Dordrecht. 2000. Chap.13.
15. C. Hamers, O. Kocian, F.M. Raymo, and J.F. Stoddart. Adv. Mater. **10**, 1366 (1998).
16. E.C. Constable. Adv. Inorg. Chem. **34**, 1 (1989).
17. C. Kaes, A. Katz, and M.W. Hosseini. Chem. Rev. **100**, 3553 (2000).
18. U.S. Schubert and C. Eschbaumer. Angew. Chem. Int. Ed. **41**, 2892 (2002).
19. A.C. Benniston, P.R. Mackie, L.J. Farrugia, S. Parsons, W. Clegg, and S.J. Teat. Platinum Met. Rev. **42**, 100 (1998).
20. A.C. Try, M.M. Harding, D.G. Hamilton, and J.K.M. Sanders. Chem. Commun. (Cambridge), 723 (1998).
21. Y.-Z. Hu, D. van Loyen, O. Schwarz, S. Bossmann, H. Dürr, V. Huch, and M. Veith. J. Am. Chem. Soc. **120**, 5822 (1998).
22. P.F.H. Schwab, B.C. Noll, and J. Michl. J. Org. Chem. **67**, 5476 (2002).
23. J.P. Schneider and J.W. Kelly. Chem. Rev. **95**, 2169 (1995).
24. K.M. Stewart, J. Rojo, and L.W. McLaughlin. Angew. Chem. Int. Ed. **43**, 5808 (2004).
25. C.P. McArdle, S. Van, M.C. Jennings, and R.J. Puddephatt. J. Am. Chem. Soc. **124**, 3959 (2002).
26. C.P. McArdle, M.C. Jennings, J.J. Vittal, and R.J. Puddephatt. Chem. Eur. J. **7**, 3572 (2001).
27. S.M. Treffert-Ziemelis, J. Golus, D.P. Strommen, and J.R. Kincaid. Inorg. Chem. **32**, 3890 (1993).
28. B. Imperiali, T.J. Prins, and S.L. Fisher. J. Org. Chem. **58**, 1613 (1993).

© 2006 NRC Canada

29. G.E. Coates and C. Parkin. J. Chem. Soc. 3220 (1962).
30. K. Nakamoto. Infrared and Raman spectra of inorganic and coordination compounds. 3rd ed. Wiley-Interscience, New York. 1978. p. 387.
31. E.L. Eliel, S.H. Wilen, and L.N. Mander. Stereochemistry of organic compounds. Wiley-Interscience, New York. 1994. pp. 1119–1121.
32. G. Schill. Catenanes, rotaxanes, and knots. Academic Press, New York. 1971.
33. F. Mohr, M.C. Jennings, and R.J. Puddephatt. Eur. J. Inorg. Chem. 217 (2003).
34. (*a*) C.P. McArdle, M.J. Irwin, M.C. Jennings, and R.J. Puddephatt. Angew. Chem. Int. Ed. **38**, 3376 (1999); (*b*) C.P. McArdle, M.J. Irwin, M.C. Jennings, J.J. Vittal, and R.J. Puddephatt. Chem. Eur. J. **8**, 723 (2002).
35. F. Mohr, D.J. Eisler, C.P. McArdle, K. Atieh, M.C. Jennings, and R.J. Puddephatt. J. Organomet. Chem. **670**, 27 (2003).
36. H. Schmidbaur. Gold: Progress in chemistry, biochemistry and technology. Wiley, Chichester. 1999.
37. T. Steiner. Angew. Chem. Int. Ed. **41**, 48 (2002).
38. C. Janiak. J. Chem. Soc. Dalton Trans. 3885 (2000).
39. N.W. Alcock, P.R. Barker, J.M. Haider, M.J. Hannon, C.L. Painting, Z. Pikramenou, E.A. Plummer, K. Rissanen, and P. Saarenketo. J. Chem. Soc. Dalton Trans. 1447 (2000).
40. J.K. Jawad, R.J. Puddephatt, and M.A. Stalteri. Inorg. Chem. **21**, 332 (1982).
41. G.W. Rice and R.S. Tobias. Inorg. Chem. **14**, 2402 (1975).
42. (*a*) R.J. Puddephatt and J.D. Scott. Organometallics, **4**, 1221 (1985); (*b*) P.K. Monaghan and R.J. Puddephatt. Organometallics, **3**, 444 (1984).
43. D.E. Clegg, J.R. Hall, and G.A. Swile. J. Organomet. Chem. **38**, 403 (1972).
44. M.-C. Brandys, M.C. Jennings, and R.J. Puddephatt. J. Chem. Soc. Dalton Trans. 4601 (2000).
45. G.S. Hill, M.J. Irwin, C.J. Levy, L.M. Rendina, and R.J. Puddephatt. Inorg. Synth. **32**, 149 (1998).
46. I. Iwai and J. Ide. Chem. Pharm. Bull. **11**, 1042 (1963).
47. Computer programs: (*a*) Nonius B.V. COLLECT, DENZO, SCALEPACK. Nonius B.V., Amsterdam. 1998; (*b*) G.M. Sheldrick. SHELXTL-NT. Version 6.1. Madison, Wisconsin. 2000.

© 2006 NRC Canada

Hydrothermal synthesis, crystal structure, and vibrational and Mössbauer spectra of a new tricationic orthophosphate — $KCo_3Fe(PO_4)_3$[1]

Hassane Assaaoudi, Zhen Fang, Dominic H. Ryan, Ian S. Butler, and Janusz A. Kozinski

Abstract: Crystals of a new potassium cobalt(II) iron(II) triorthophosphate salt, $KCo_3Fe(PO_4)_3$, as well as amorphous nanoparticles of the same material have been produced by hydrothermal reactions, under supercritical water (SCW) conditions, of equivalent quantities of aq. $CoCl_2 \cdot 6H_2O$ (2 mol/L) and $K_4P_2O_7$ (1 mol/L) in concd. HCl in a stainless steel batch reactor at 400–450 °C and 25–32 MPa. The dark-violet crystals of the new salt have been characterized by single-crystal X-ray diffraction and IR, Raman, and Mössbauer spectroscopy. The Fe(II) in the new orthophosphate salt must derive from leaching of iron from the stainless steel walls of the reactor by concd. HCl under the SCW conditions. The salt crystallizes in the orthorhombic space group *Pnnm*, $Z = 4$, with unit cell parameters as follows: $a = 9.672(1)$ Å, $b = 16.457(2)$ Å, $c = 6.2004(8)$ Å, $V = 986.97$ Å^3. Microporous $KCo_3Fe(PO_4)_3$ exhibits infinite chains of corner-sharing [PO_4^{3-}], [FeO_6], and [CoO_5] units, which form two large rhombus tunnels, occupied by K^+ ions, running parallel to [100] in the unit cell. The vibrational spectra have been interpreted partly on the basis of factor group effects and are in accord with the centrosymmetric structure of the material. The particle sizes of this new nanomaterial and their distribution have been determined by scanning electron micrography and laser scattering particle size distribution analysis, while the amorphous nanomaterial has also been characterized by X-ray powder diffraction and Raman spectroscopy.

Key words: crystal structure, vibrational and Mössbauer spectra, orthophosphate, nanomaterial.

Résumé : Les cristaux du nouveau sel tri-orthophosphate de potassium, cobalt(II) et fer(II), $KCo_3Fe(PO_4)_3$, ainsi que des nano particules amorphe du même matériel, ont été produites par réactions hydrothermal dans des conditions supercritique de l'eau. Ils sont obtenus à partir d'un mélange équimolaire des solutions aqueuses $CoCl_2 \cdot 6H_2O$ (2 mol/L), et $K_4P_2O_7$ (1 mol/L), en milieu acide HCl concentré dans un tube en acier inoxydable à températures 400–450 °C, et à pression 25–32 MPa. Les cristaux violets foncés du nouveau sel ont été caractérisés par diffraction des rayons-X sur monocristal, et par spectroscopie IR, Raman et Mössbauer. Le Fe(II) du nouveau sel d'orthophosphate provient d'une infiltration à partir de la parois interne du réacteur en acier inoxydable, sous l'effet de l'acide HCl concentré dans les conditions supercritique de l'eau. Le sel cristallise dans le système orthorhombique de groupe d'espace *Pnnm*, avec $Z = 4$. Les paramètres cristallographiques de la maille sont : $a = 9.672(1)$ Å, $b = 16.457(2)$ Å, $c = 6.2004(8)$ Å, $V = 986.97$ Å^3. La structure microporeuse de $KCo_3Fe(PO_4)_3$ se présente sous forme de chaînes formées des groupements [PO_4^{3-}], [CoO_5] et [FeO_6]. Ils partageant des atomes en commun, créant ainsi deux larges tunnels par maille élémentaire. Ils sont alignés le long de l'axe [100], en forme rhomboèdre, logés par des cations K^+. Les spectres de vibration ont été interprétés en utilisant l'analyse du groupe facteur des groupements PO_4^{3-}. L'absence de coïncidence entre la plupart des fréquences de vibrations IR et Raman est en accord avec la structure centro-symétrique du matériau. La taille et la répartition des nouvelles nanoparticules amorphes ont été déterminées par la micrographie SEM, et l'analyseur de distribution de taille des particules par diffusion laser. Ce matériau est caractérisé par diffraction des rayons-X sur poudre et par spectroscopie Raman.

Mots clés : structure cristalline, spectres de vibration et Mössbauer, orthophosphate, nanomatériau.

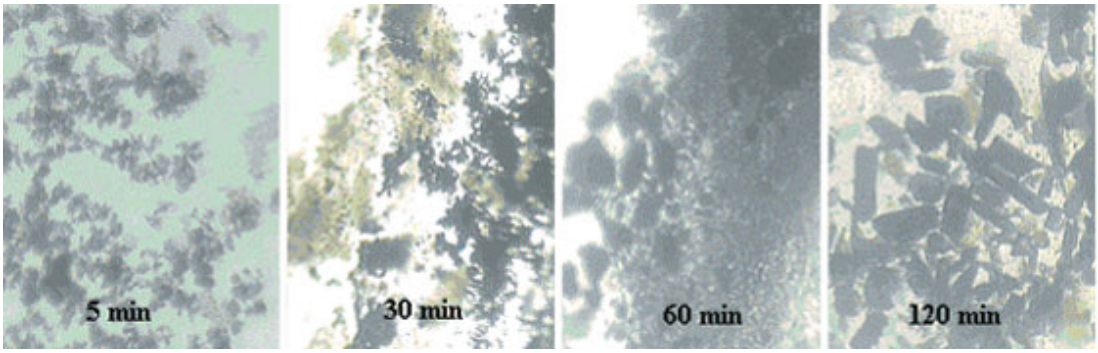
Received 1 March 2005. Published on the NRC Research Press Web site at http://canjchem.nrc.ca on 22 February 2006.

H. Assaaoudi. Department of Chemistry, Otto Maass Building, McGill University, 801 Sherbrooke Street West, Montreal, QC H3A 2K6, Canada and Energy and Environmental Research Group, Department of Mining, Metals and Materials Engineering, Wong Building, Room 2290, McGill University, 3610 University St., Montreal, QC H3A 2B2, Canada.
I.S. Butler.[2] Department of Chemistry, Otto Maass Building, McGill University, 801 Sherbrooke Street West, Montreal, QC H3A 2K6, Canada.
Z. Fang and J.A. Kozinski. Energy and Environmental Research Group, Department of Mining, Metals and Materials Engineering, Wong Building, Room 2290, McGill University, 3610 University St., Montreal, QC H3A 2B2, Canada.
D.H. Ryan. Department of Physics and Centre for the Physics of Materials, 3600 University St., McGill University, Montreal, QC H3A 2T8, Canada.

[1]This article is part of a Special Issue dedicated to Professor Arthur Carty.
[2]Corresponding author (e-mail: ian.butler@mcgill.ca).

 doi:10.1139/V05-235 © 2006 NRC Canada

Fig. 1. Evolution of products obtained from reaction under SCW conditions (450 °C, 32 MPa, and vol(HCl):vol(Co) = 2:5) after 5, 30, 60, and 120 min.



Introduction

Hydrothermal synthesis has been carried out since the end of the 19th century, mainly in the production of synthetic minerals to imitate natural geothermal processes (1, 2). More recently, both near-critical and supercritical water (SCW) have been used as reaction media for the synthesis of highly crystalline metal oxides (2–5). The use of the SCW approach has only just been demonstrated for phosphate materials in the formation of highly crystalline, micro-sized particles of $LiFePO_4$ (6). Numerous orthophosphates built from discrete PO_4^{3-} tetrahedra (7) have been characterized over the past 20 years, prompted by the discovery of the vast structural variety in aluminum, beryllium, and zinc phosphates. Some new potassium–iron and potassium–cobalt triorthophosphates have also been described, e.g., $KCo_4(PO_4)_3$ (8), $KFe_4(PO_4)_3$ (9), and $K_3Fe_2(PO_4)_3$ (10), and can be obtained from molten mixtures of Co(II) or Fe(II) sulfates or oxides and KBr or KCl in the presence of potassium hydrogen phosphate, at 350 °C and 1000 atm (1 atm = 101.325 kPa). Several cobalt and iron phosphates with similarities to open mineral-type frameworks have also been reported (11, 12).

The design, synthesis, and characterization of new micro- and nano-porous materials, such as polyphosphates, is of enormous interest because of the many potential industrial applications, e.g., heterogeneous catalysis, gas absorption, and ion exchange. Micro- and nano-porous catalysts often display high selectivity because the channel apertures may allow only certain reactants to access the catalytically active interior of the material and only certain products to leave (13, 14). Transition-state selectivity may also be related to the position and degree of substitution of catalytically active sites in the framework structure, where the active site can be a transition metal that might function by selective oxidation, e.g., Fe(II) and Co(II) (15). Further knowledge of the mechanism by which transition metals substitute into the framework structures of porous materials is, therefore, of considerable importance, both for controlling the number of catalytically active sites in such materials and also for fine tuning their function by manipulating the specific positions and coordination environments of the active centers (16).

In this paper, we present analytical, structural, and spectroscopic data for a new crystalline, open framework, tricationic orthophosphate salt, $KCo_3Fe(PO_4)_3$, and amorphous nanoparticles of the same material produced under SCW conditions. The effects of temperature, pH, and reaction time on the size and size distribution of the particles have also been investigated.

Experimental section

Synthesis

Crystals of $KCo_3Fe(PO_4)_3$, as well as nanoparticles of the same material, were obtained from the reaction between equivalent amounts of aqueous cobalt $CoCl_2{\cdot}6H_2O$ (2 mol/L) and $K_4P_2O_7$ (1 mol/L) in a predetermined volume of concd. HCl (35%), (vol(HCl):vol(Co) = 2:5 or 3:5). The final red solution obtained was transferred quickly to a stainless steel batch reactor (volume = 6 mL; length = 105 mm, o.d. = 12.7 mm (1/2 in)). Both temperature and pressure were measured with a pressure transducer fitted with a J-type thermocouple (Dynisco E242). The pressure was also calculated by first calculating the density of water ((weight of water added)/(volume of batch reactor) ≈ 1.6 g/mL), assuming that only water contributed to the pressure. Bassett et al. (17) have compared the pressures obtained by such calculations with the *P–T* boundary of the α–β transition in quartz and have shown that the pressure difference is less than 4% between the two methods. Approximately 1 mL of the final solution was loaded into the reactor, which, after being sealed and connected to a data acquisition system, was submerged in a fluidized sand bath (Omega FSB- 3) or placed into a tubular furnace. The reactor was heated at a rate of 3.5 °C/s to 400–450 °C and then held at this temperature for 5, 10, 30, 60, or 120 min. After each given period, the reactor was quenched in cold water, and the reaction mixture was emptied into a flask. The reactor was washed with water, and the washings were added to the same flask. The solution in the flask was filtered through a membrane filter to yield a solid phase, which was dried at room temperature. Well-shaped, dark-violet crystals (Fig. 1) were produced under the conditions reported in Table 1. The aqueous phase was left at room temperature for about 1 to 2 h, after which a grey-violet powder appeared, which was subsequently filtered and analyzed (Table 1).

© 2006 NRC Canada

Table 1. Experimental conditions and results.

	Run				
	1	2	3	4	5
HCl (mol/L)	0.6	0.6	0.6	0.4	0.4
T (°C)	25	400	450	400	450
P (MPa)	0.1	25	32	25	32
Products					
0 min	—	—	—	—	—
5 min	—	P	P	P	P
10 min	—	P	P	P	P
30 min	—	P	P	P	P
60 min	$Co_2P_2O_7{\cdot}6H_2O$[a]	P	$KCo_3Fe(PO_4)_3$	$KCo_3Fe(PO_4)_3$	$KCo_3Fe(PO_4)$
120 min	$Co_2P_2O_7{\cdot}6H_2O$[a]	P	$KCo_3Fe(PO_4)_3$	$KCo_3Fe(PO_4)_3$	$KCo_3Fe(PO_4)$
Chemical analysis of powder P					
Co (%)	—	≈0	≈0	≈0	≈0
Fe (%)	—	15–17	25–30	14–17	25–30
P (%)	—	9–11.5	18–22	9–11	18–20
K (%)	—	2.5–5	2.5–5	2.5–5	3–5

[a]Reference 18.

Spectroscopic and crystallographic analyses

The powders obtained in the experiments were characterized by X-ray powder diffraction (XRD),[3] ICP chemical analyses, scanning electronic microscopy (SEM), and Raman spectroscopy. Crystalline $KCo_3Fe(PO_4)_3$ was analyzed by SEM and X-ray energy dispersive analysis (EDS) and was further characterized by IR, Raman, and Mössbauer spectroscopy, as well as by single-crystal X-ray diffraction.

A Philips model PW1710, vertical goniometer, X-ray powder diffractometer with a Cu Kα radiation source was used for the powder diffraction measurements. The samples were scanned over the range from 5° or 10° to 60° at a step size (2θ) of 0.02° and a measurement time of 0.5 s/step. Chemical analyses were performed using ICP-AES on a Thermo Jarrell Ash TraceScan axial torch sequential ICP system. The morphology of the particles was investigated using a field emission SEM (model JSM-840), while EDS (model EDAX) was used to characterize the materials (powder and crystals). The size distribution of the particles was determined using a laser scattering particle size distribution analyzer (model Horiba LA-920), which can measure particle size distributions over a wide range of sizes — from 0.02 to 2000 μm — in dry or slurry form.

Infrared spectra were recorded at ambient temperature on a Bomem MB100 FT-IR spectrometer at 2 cm^{-1} resolution (50 scans), using the KBr pellet technique. The wavenumber accuracy is considered to be within ±1 cm^{-1} for sharp bands. Raman spectra were measured on a Renishaw 3000 Raman microscope (20× objective), using the 514.5 nm line of an Ar^+-ion laser for excitation (5–100 mW laser power; 1 cm^{-1} spectral slit width; 5 s exposure time; 10 accumulations). The band positions are considered to be accurate to at least ±1 cm^{-1}. The Mössbauer effect measurements were made at room temperature with a Wissel spectrometer. The spectra were recorded using the radiation from ^{57}Co in Rh with a 512 multichannel analyzer. The velocity was calibrated using iron metal as a standard.

A summary of the X-ray data collection and refinement is given in Table 2. A Bruker D8 Discover diffractometer was used for examination of the crystal. The structure was solved by direct methods using SHELXS97 (19) and was refined by a full-matrix, least-squares technique, SHELXL97 (20). The molecular drawings obtained with ORTEP III (21) were manipulated using the WINGX system of programs (22) and the program Molview (23). The X-ray data resulted in the formula $KCo_3Fe(PO_4)_3$ for the compound after checking the final residuals R, R_w ($I > 2\sigma(I_{obs})$), and GOF for different ratios of Co and Fe atoms and taking anisotropic thermal parameters into account.

Results

Identification of materials

The XRD patterns of the powders obtained from the SCW reactions under the conditions reported in Table 1 showed that the materials were amorphous. The Fe, Co, K, and P analyses of these powders were performed using ICP-AES. The results obtained correspond to the composition shown in Table 1. The morphology of the particles and the distribution of their sizes were determined by SEM (Fig. 2*a*). The composition of crystalline $KCo_3Fe(PO_4)_3$ and the powder were determined using EDS analysis, and the results showed that their compositions were essentially identical except for the amount of Co present (Figs. 2*b* and 2*c*) because, irrespective

[3] Supplementary data for this article are available on the journal Web site (http://canjchem.nrc.ca) or may be purchased from the Depository of Unpublished Data, Document Delivery, CISTI, National Research Council Canada, Ottawa, ON K1A 0R6, Canada. DUD 4080. For more information on obtaining material refer to http://cisti-icist.nrc-cnrc.gc.ca/irm/unpub_e.shtml. CCDC 415778 contains the crystallographic data for this manuscript. These data can be obtained, free of charge, via www.ccdc.cam.ac.uk/conts/retrieving.html (Or from the Cambridge Crystallographic Data Centre, 12 Union Road, Cambridge CB2 1EZ, UK; fax +44 1223 336033; or deposit@ccdc.cam.ac.uk).

© 2006 NRC Canada

Table 2. Crystal data and structure refinement for KCo_3FePO_4.

Crystal data	
Formula	$KCo_3FeO_{12}P_3$
MW	556.66
V (Å^3)	987.0(2)
Z	4
Colour, habit	Dark violet, block
Crystal dimensions (mm^3)	0.10 × 0.10 × 0.10
D_x (Mg m^{-3})	3.746
Crystal system	Orthorhombic
Space group	*Pnnm* (No. 58)
a (Å)	9.6722(12)
b (Å)	16.457(2)
c (Å)	6.2004(8)
T (K)	153(2)
μ (mm^{-1})	4.221
Radiation	Mo Kα
l (Å)	0.710 73
Data collection	
Instrument	Bruker D8 Discover
Scans	w-2q
Reflections collected	4619
Independent reflections	1074 ($R_{(int)}$ = 0.1028)
q_{max}	26.73
Collection ranges	$-11 \le h \le 7$; $-19 \le k \le 20$; $-7 \le l \le 7$
R_{int}	0.1028
Refinement	
Refinement	On F^2
R ($F^2 > 2s(F^2)$)	0.0339
R (F^2, all data)	0.0356
wR (F^2)	0.0924
Dr_{max} (e Å^{-3})	1.171
Dr_{min} (e Å^{-3})	–0.945
Parameters	104

of the SCW experimental conditions employed, the powders obtained did not contain any Co. The carbon peak in Figs. 2*b* and 2*c* is associated with the agent used to immobilize the particles for analysis. The powder nanoparticles are spherical, and the particle size ranges from 100 to 800 nm, with an average size of about 500 nm (Fig. 2*a*).

Iron(III) has five electrons in the 3d valence subshell, which makes it spherically symmetric, thereby practically eliminating any electric field gradient and quadrupole splitting (QS). On the other hand, Fe(II) has one extra electron in the 3d valence subshell, thus introducing an asymmetry resulting in an electric field gradient and a detectable QS. From the Mössbauer effect measurements undertaken in this work (Fig. 3), the values obtained for both the isomer shift (IS) and the QS for the iron atoms present in the new orthophosphate material are typical of Fe(II) (24). The expected Fe(II) doublet is observed with IS = 1.2 and QS = 2.9 mm/s. This definitive demonstration of the presence of Fe(II) means that the cobalt atoms in $KCo_3Fe(PO_4)_3$ must be in the Co(II) state to charge compensate for the three PO_4^{3-} ions. The Fe(II) ions must have been produced by iron being leached from the stainless steel walls of the reactor by concd. HCl under the SCW conditions employed.

Effect of synthesis temperature

Two temperatures under SCW conditions (400 and 450 °C) were investigated. From the quantity of crystals obtained at these two different temperatures, the production of crystalline $KCo_3Fe(PO_4)_3$ was much more favorable at 450 °C than at 400 °C. The particles produced at 450 °C (with all the other conditions being kept constant) have a slightly narrower size distribution than do those obtained at 400 °C (Fig. 4*a*). This figure also shows that the particles decrease in size with increasing temperature, although the size distribution is quite broad.

Effect of pH

The effect of pH was investigated by adjusting the amount of HCl added. The reaction between equivalent quantities of aqueous cobalt $CoCl_2{\cdot}6H_2O$ (2 mol/L) and $K_4P_2O_7$ (1 mol/L) was limited by the amount of concd. HCl that could be added while avoiding instantaneous precipitation from solution and yet still permitting synthesis of $KCo_3Fe(PO_4)_3$ crystals under SCW conditions (vol(HCl):vol(Co) = 2:5 and 3:5). The particles synthesized at a vol(HCl):vol(Co) ratio of 3:5 tended to exhibit a narrower size distribution than did those obtained for a vol(HCl):vol(Co) ratio of 2:5. The particles had an average size range of 100 μm to submicron (Fig. 4*b*). Compared to the influence of other parameters on the particle sizes produced under SCW conditions and their distribution, the effect of pH was by far the most important.

Effect of residence time

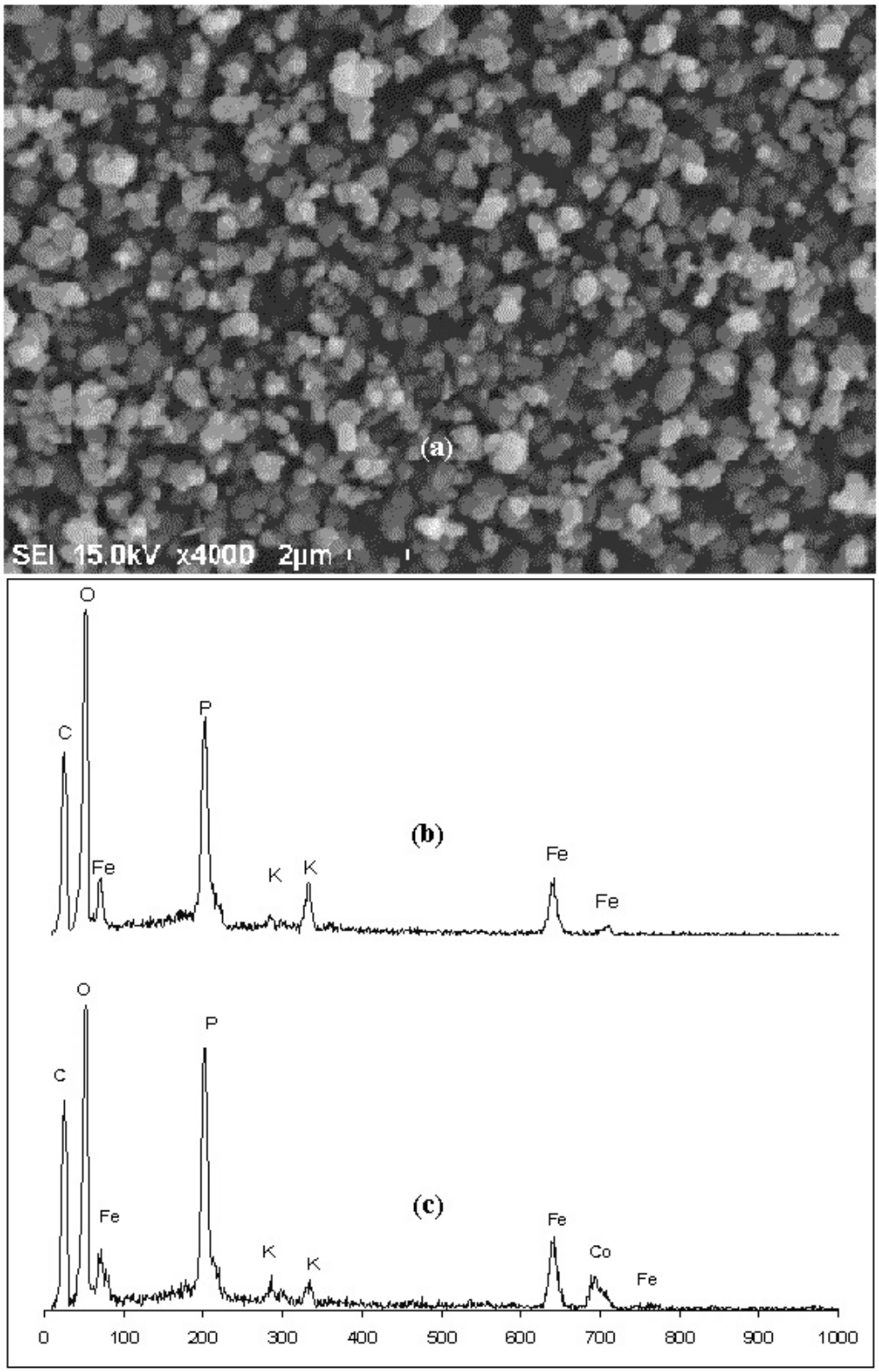
The influence of residence time (τ) in the reactor was investigated by carrying out hydrothermal reactions at 400 °C with τ = 0, 5, 10, 30, 60, and 120 min. The vol(HCl):vol(Co) ratio was maintained at 3:5 to keep the pH of the reactant mixture constant. No significant difference in morphology was observed with changing residence time. The particles produced when τ = 120 min, however, had a narrower size distribution than did those obtained after 10 min (Fig. 4*c*). Similar results were obtained when the reaction temperature was 450 °C, with all other conditions being kept constant.

Crystal structure

The structure of the new orthophosphate is built up from [FeO_6] octahedra, [CoO_5] pentahedra, [KO_8] heptahedra, and [PO_4^{3-}] tetrahedra sharing corners and edges to form a 3-D open framework (Fig. 5). There are three crystallographically distinct P atoms, all with tetrahedral coordination, and two distinct Co atoms. The Co(2), O(3), O(4), and O(7) atoms occupy general positions. All the other atoms occupy special positions on mirror plane symmetry. Atomic coordinates and isotropic thermal parameters are given in Table 3 and selected interatomic distances in Table 4. The Co atoms are arranged in five-vertex polyhedra, like distorted square-based pyramids for both the Co(1) and Co(2) atoms. Their average bond distances are Co(1)—O_{av} = 2.056 Å and Co(2)—O_{av} = 2.084 Å; the Co atoms are surrounded by O atoms from four and five different phosphate anions, respec-

© 2006 NRC Canada

Fig. 2. (*a*) Scanning electron micrographs of powder obtained after reaction at 400 °C, 120 min; (*b*) EDS analysis of powder obtained after reaction at SCW; and (*c*) EDS analysis of crystalline $KCo_3Fe(PO_4)_3$.



© 2006 NRC Canada

Fig. 3. Room-temperature ^{57}Fe Mössbauer spectrum of crystalline $KCo_3Fe(PO_4)_3$.

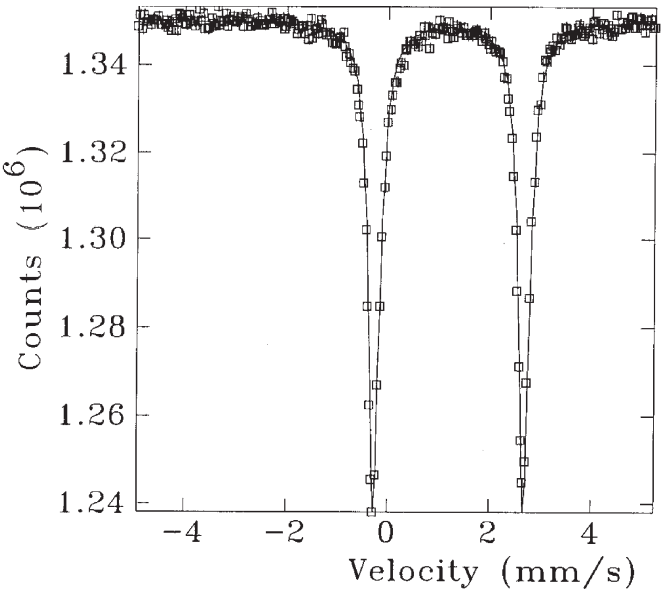


Table 3. Atomic coordinates (×10^4) and equivalent isotropic displacement parameters (Å^2 × 10^3) for $KCo_3Fe(PO_4)_3$.

Atom	Site	*x*	*y*	*z*	U_{eq}[a]
Co(1)	4g	5360(1)	4064(1)	0	4(1)
Co(2)	8h	2508(1)	2964(1)	–2515(1)	7(1)
Fe	4g	–179(1)	3609(1)	0	5(1)
K	4g	2948(1)	329(1)	0	12(1)
P(1)	4g	2117(2)	4621(1)	0	6(1)
P(2)	4g	4578(1)	2170(1)	0	6(1)
P(3)	4g	437(1)	1662(1)	0	5(1)
O(1)	4g	3674(4)	4777(2)	0	9(1)
O(2)	4g	–1411(4)	4563(2)	0	12(1)
O(3)	8h	1676(3)	4103(2)	1967(4)	10(1)
O(4)	8h	4016(3)	1773(2)	–2044(5)	10(1)
O(5)	4g	6167(4)	2243(2)	0	8(1)
O(6)	4g	3939(4)	3051(2)	0	8(1)
O(7)	8h	5897(3)	3787(2)	–3003(4)	8(1)
O(8)	4g	1140(4)	2530(2)	0	8(1)
O(9)	4g	3846(4)	3212(2)	–5000	8(1)

[a] U_{eq} is defined as one-third of the trace of the orthogonalized U_{ij} tensor.

tively (Table 4). The Fe coordination is tetrahedral with Fe—O in the range 1.97–2.18 Å. This tetrahedron is somewhat distorted, however, because of two additional weak Fe···O(3) and Fe···O(3)^I interactions, which are 2.316 Å in length (Table 4). Thus, the Fe coordination can be interpreted as either tetrahedral or octahedral. The latter is used in the figures for simplicity and clarity. The difference in Fe coordination observed here is similar to that in the isotype $KFe_4(PO_4)_3$ (9). The $[Co(1)O_5]$ pentahedron is more distorted than is the $[Co(2)O_5]$ one because of corner sharing via the oxygen atom O(6). But both pentahedra are less distorted than is the $[FeO_6]$ octahedron, which is involved in corner sharing via the oxygen atom O(8) and also has two weak bonds with oxygen atoms O(3) and O(3)^I. The distor-

Table 4. Selected bond distances (Å) for $KCo_3Fe(PO_4)_3$.

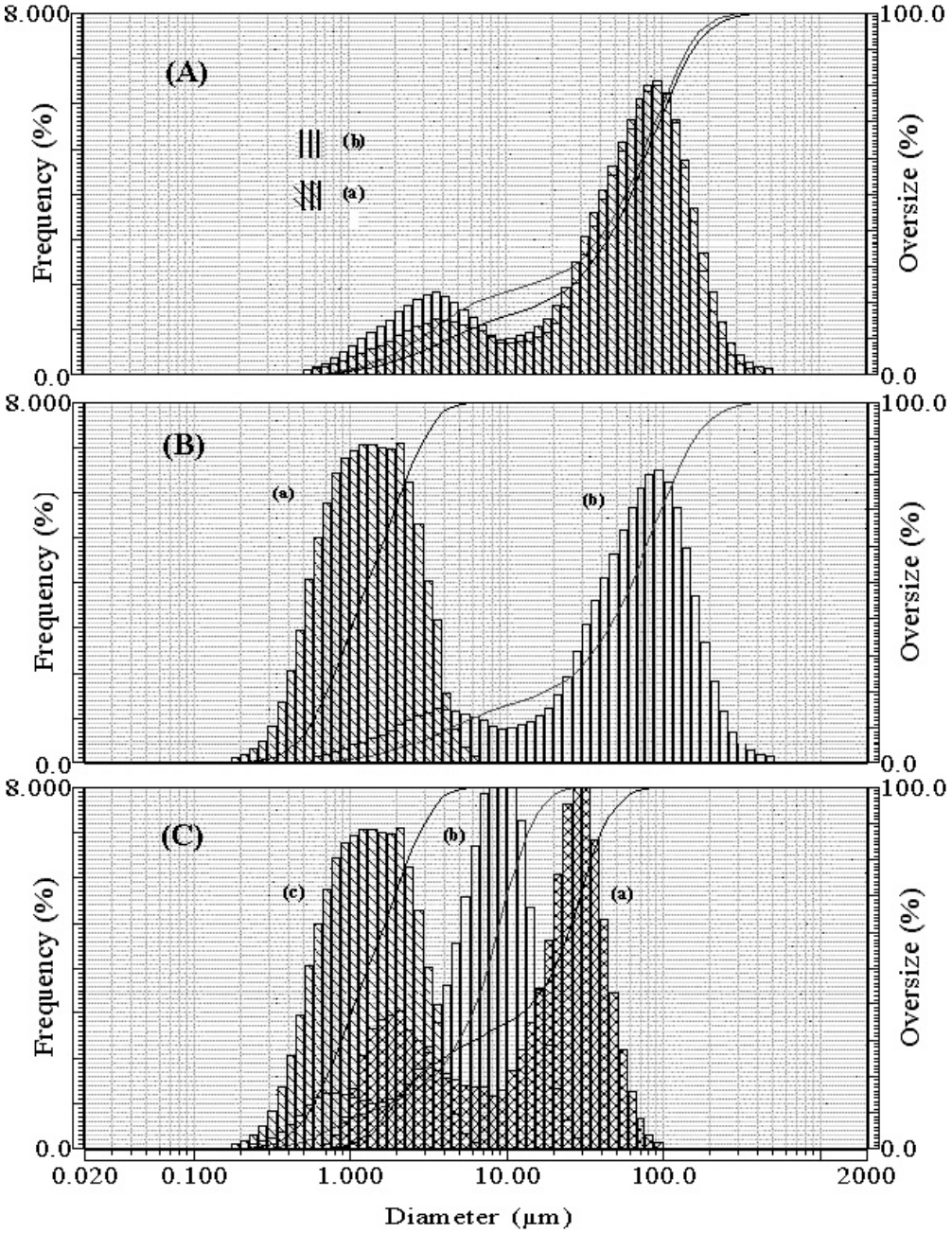
P(1)—O(1)	1.528(4)	P(2)—O(4)	1.526(3)
P(1)—O(2)^{XI}	1.507(4)	P(2)—O(4)^I	1.526(3)
P(1)—O(3)	1.548(3)	P(2)—O(5)	1.542(4)
P(1)—O(3)^I	1.548(3)	P(2)—O(6)	1.576(4)
<P—O>	1.5327	<P—O>	1.5327
P(3)—O(9)^{IV}	1.553(4)	Fe—O(2)	1.971(4)
P(3)—O(7)^{III}	1.509(3)	Fe—O(4)^{III}/O(4)^{IV}	2.088(3)
P(3)—O(7)^{IV}	1.509(3)	Fe—O(8)	2.187(4)
P(3)—O(8)	1.582(4)	Fe—O(3)/O(3)^I	2.316(3)
<P—O>	1.5382	<Fe—O>	2.161
Co(1)—O(7)/O(7)^I	1.980(3)	Co(2)—O(3)^I	2.068(3)
Co(1)—O(1)	2.029(4)	Co(2)—O(5)^V	2.042(2)
Co(1)—O(1)^{II}	2.113(4)	Co(2)—O(6)	2.090(3)
Co(1)—O(6)	2.176(4)	Co(2)—O(8)	2.166(3)
<Co(1)—O>	2.0556	Co(2)—O(9)	2.053(2)
K—O(2)^{VIII}/O(2)^{IX}	3.1665(10)	<Co(2)—O>	2.0838
K—O(3)^{VI}/O(3)^{VII}	2.783(3)	K—O(4)^I/O(4)	2.885(3)
<K—O>	2.8971	K—O(7)^{III}/O(7)^{IV}	2.754(3)

Note: Symmetry transformations used to generate equivalent atoms: ^{I}: *x*, *y*, –*z*; ^{II}: –*x* + 1, –*y* + 1, –*z*; ^{III}: *x* – 1/2, –*y* + 1/2, –*z* – 1/2; ^{IV}: *x* – 1/2, –*y* + 1/2, *z* + 1/2; ^{V}: *x* – 1/2, –*y* + 1/2, *z* – 1/2; ^{VI}: –*x* + 1/2, *y* – 1/2, *z* – 1/2; ^{VII}: –*x* + 1/2, *y* – 1/2, –*z* + 1/2; ^{VIII}: *x* + 1/2, –*y* + 1/2, *z* + 1/2; ^{IX}: *x* + 1/2, –*y* + 1/2, *z* – 1/2; ^{X}: –*x* + 1/2, *y* – 1/2, –*z* – 1/2; ^{XI}: –*x*, –*y* + 1, –*z*.

tion indices, $[(\text{cation-O})_{max} - (\text{cation-O})_{min}]/(\text{cation-O})_{av}$ (25), for Co(1), Co(2), and Fe are 0.095, 0.059, and 0.160, respectively. The $[Co(1)O_5]$ pentahedra share cis-edges with one $[Co(2)O_5]$ pentahedron via oxygen atom O(6), which belongs to a *P*(2) tetrahedron. The $[Co(2)O_9]$ dimer has different angles from an eclipsed conformation when viewed along the Co(1)—Co(2) axis, which confers a general site symmetry to this dimer. There are additional links at the shared corners to $[FeO_6]$ via O(8) and O(3). The structure results in alternating layers of $[Co_4O_{18}]$ units in a flat "S" form (or like "∫") and its opposite face in the *ab* plane, which is linked from those ends to two $[FeO_6]$ octahedra. The K atom is surrounded by six oxygen atoms at the vertices of a distorted trigonal prism (K—O = 2.754–2.885 Å) plus two other oxygen atoms at a distance of 3.166 Å. The K atoms involve a strong network between interlayers holding the structure together. Based on the work of Dumas et al. (26), who consider the K—O threshold bond to be 3.19 Å, the K atoms in $KCo_3Fe(PO_4)_3$ can be considered to form irregular $[KO_8]$ polyhedra (distortion index = 0.142). The K^+ ion, because of its large dimensions (ionic radii = 1.38, 1.46, and 1.51 Å for coordination numbers 6, 7, and 8, respectively (27)), forms more complex polyhedra with the distortion indices being extremely variable, ranging from 0.080 up to 0.199 (28–30). As can be seen from Fig. 6*c*, alternating Co, Fe, and P polyhedra form two large rhombus tunnels, occupied by K^+ ions, running parallel to < 100 > in a unit cell with diagonal lengths 5.49 Å (along the *c* axis) and 5.80 Å (along the *b* axis). Perpendicular to these axes, along the *c* axis, the structure presents other different tunnels with different shapes and sizes (Fig. 6*a*). In the previously reported crystal structures for iron phosphates, such as $LiFePO_4$ (31), Fe_2FPO_4 (32), $(Fe,Zn)_3(PO_4)_2$ (33), $Na_2(Fe_{0.5}^{3+}Fe_{0.5}^{2+})_2Fe^{2+}(PO_4)_3$ (34), $KFeFPO_4$ (35), and $KFe_4(PO_4)_3$ (9), there is

© 2006 NRC Canada

Fig. 4. (A) Size distribution for particles synthesized with τ = 120 min, vol(HCl):vol(Co) = 2:5, and temperature equal to (*a*) 400 °C and (*b*) 450 °C; (B) size distribution for particles synthesized at 400 °C with τ = 120 min and ratio vol(HCl):vol(Co) = (*a*) 3:5 and (*b*) 2:5; (C) size distribution for particles synthesized at 400 °C with ratio vol(HCl):vol(Co) = 3:5, after (*a*) 0 min, (*b*) 10 min, and (*c*) 120 min.



typically at least one unit cell constant that is approximately equal to six or to multiples of this value. The pertinent parameter in our case, c = 6.2004, determines the lattice spacing along the c axis of the unit cell. This value is due to chains of alternating [FeO_6] octahedra and [PO_4^{3-}] tetrahedra, linked by their vertices (Fig. 6*b*).

Vibrational spectra

The new orthophosphate salt, $KCo_3Fe(PO_4)_3$, crystallizes in the orthorhombic space group *Pnnm* (D_{2h}^{12}) with Z = 4. The P atoms lie on C_s sites. The proposed vibrational band assignments for the IR and Raman spectra of the salt are given in Table 5. The absence of the symmetric stretching and antisymmetric H–O(P) bending vibrations at ~2300 and ~1447 cm^{-1}, respectively, confirms that the salt does not contains H atoms. The nature of the four normal vibrations (ν_1, ν_2, ν_3, and ν_4 in Herzberg notation (36)) of the PO_4^{3-} groups was determined by the site group method of Halford (37), in which the normal modes of the free ion are correlated to the vibrations in the site and crystal symmetry.

© 2006 NRC Canada

Table 5. Proposed vibrational band assignments for $KCo_3Fe(PO_4)_3$ (cm^{-1}).

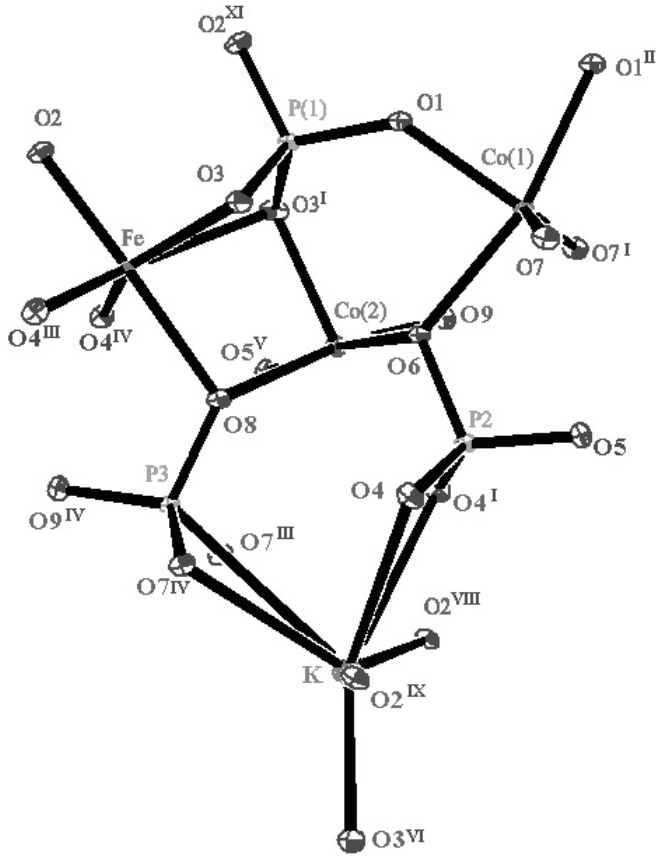
IR	Raman	Assignment	
	1070	A_g+B_g	$\nu_{asym}PO$
1067		$B_{1u}+B_2u+B_{3u}$	
	1039	A_g+B_g	
980		B_{1u}	$\nu_{sym}PO$
	970	A_g	
920		B_{1u}	
	915	B_{1g}	
629	608	$B_{1u}+B_2u+B_{3u}$	$\delta_{asym}PO_2$
587	560sh		
533			
520	470sh		
439		$B_{1u}+B_2u+B_{3u}$	
	390	$A_g+B_{1g}+B_{2g}+B_{3g}$	$\delta_{sym}PO_2$
380	300		External modes
365	235		
355	205		
	180		

Theoretically, each vibrational mode of the PO_4^{3-} ions could be split into four components by dynamic coupling between the four anions in the primitive unit cell. The full influence of the site and factor groups on the internal vibrations of the PO_4^{3-} ions is, however, not observed for each mode. If the vibrations of the three different PO_4^{3-} groups were equivalent, only one vibration would be expected in both the IR and Raman spectra under the influence of the site effect. If the factor group effect is predominating, there should be two Raman bands and one IR band observed. However, two bands were observed in the Raman spectrum and another two bands in the IR spectrum, thereby confirming that the PO_4^{3-} groups are indeed different, in agreement with the crystallographic results. Finally, most of the IR bands are noncoincident with those observed in the Raman spectrum, in accord with the centrosymmetric nature of the crystal.

The Raman spectra of the amorphous powders obtained under different SCW conditions indicate the presence of orthophosphate groups, and as expected for amorphous materials, the spectra are characterized by weak, extremely broad bands and a relatively high and featureless background. The bands observed at ~1000 cm^{-1} correspond to the A_g symmetric P–O stretching mode.

Vibrational spectroscopy often plays a prominent role in the structural study of inorganic crystals, especially in cases where X-ray diffraction fails to give unequivocal results, such as for glasses and amorphous materials. The correlation between X-ray diffraction results and vibrational spectroscopy has become of practical importance. A linear empirical correlation was established recently (38) for inorganic crystalline phosphates between the wavenumbers of the Raman-active P–O stretching modes and the associated P—O bond lengths. This correlation has been tested and extended with success to glassy and amorphous phosphate materials, such as $Na_5Ti(PO_4)_3$ glass (39). The unpolarized vibrational spectra of crystals and their amorphous or glassy analogues are often quite similar because the vibrational spectra are determined largely by short-range order. There are two established empirical equations used nowadays (38) to calculate P—O bond lengths (in pm), as follows:

Fig. 5. ORTEP view of asymmetric unit with atomic numbering scheme (ellipsoids drawn at 60% probability level). Symmetry codes ^{I}: x, y, $-z$, ^{II}: $-x+1$, $-y+1$, $-z$, ^{III}: $x-1/2$, $-y+1/2$, $-z-1/2$, ^{IV}: $x-1/2$, $-y+1/2$, $z+1/2$, ^{V}: $x-1/2$, $-y+1/2$, $z-1/2$, ^{VI}: $-x+1/2$, $y-1/2$, $z-1/2$, ^{VII}: $-x+1/2$, $y-1/2$, $-z+1/2$, ^{VIII}: $x+1/2$, $-y+1/2$, $z+1/2$, ^{IX}: $x+1/2$, $-y+1/2$, $z-1/2$, ^{X}: $-x+1/2$, $y-1/2$, $-z-1/2$, ^{XI}: $-x$, $-y+1$, $-z$.



[1] $\nu = 6.3 \times 10^3 - 34.3R$

[2] $\nu_w = 224\,500 \exp(-R/28.35)$

These two equations were used in our case to predict the P—O bond lengths in the amorphous orthophosphates obtained under different SCW experimental conditions. The results agree well with the values found for other orthophosphates (Table 6). The precision in the estimation of a P—O bond length from a measured Raman wavenumber using the bond length – stretching wavenumber correlation is 1 pm. The standard deviation in the estimate of a Raman stretching wavenumber from an absolute P—O bond length is 37 cm^{-1}. The observed Raman bands exhibited slight shifts, but noticeably broadened and decreased in intensity, with the increasing SCW reaction time. For the experiment run at 450 °C for 120 min, a new phase was produced (Fig. 7*d*), which is different from those obtained previously (Fig. 7*a*–7*c*), and this material has yet to be identified.

© 2006 NRC Canada

Table 6. Raman stretching wavenumbers for P—O bonds in amorphous orthophosphate powders obtained under SCW conditions and the predicted P—O bond lengths from eqs. [1] and [2].

Reaction conditions	Stretching wavenumbers	P—O bond lengths from eq. [1] (Å)	P—O bond lengths from eq. [2] (Å)
450 °C, 120 min	998 νs	1.546	1.535
	1060 νas	1.527	1.518
450 °C, 30 min	1040 νs	1.533	1.524
450 °C, 10 min	1005 νs	1.544	1.533
	1045 νs	1.532	1.522

Note: Equations [1] and [2] predict the bond lengths in picometers. These values have been converted to angstroms (100 pm = 1 Å) for more ready comparison with the X-ray results. For stretching wavenumbers, s is symmetric frequency and as is asymmetric frequency.

Fig. 6. Three-dimensional view of the structure of $KCo_3Fe(PO_4)_3$ viewed down the (*a*) *c* axis; (*b*) *b* axis; and (*c*) *a* axis (program Molview).

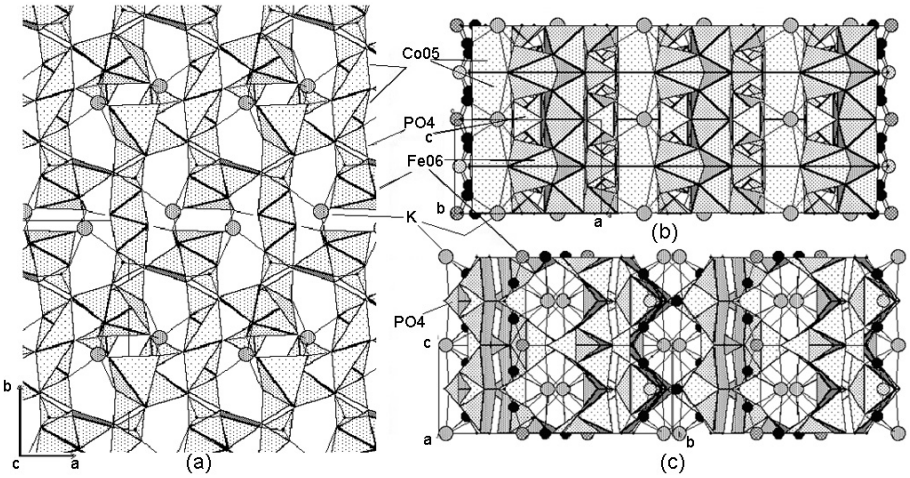
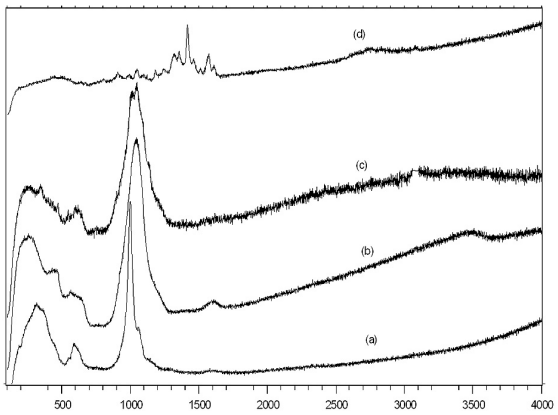


Fig. 7. Raman spectra of powder obtained after reaction under different SCW conditions: (*a*) 450 °C, 120 min; (*b*) 450 °C, 30 min; (*c*) 450 °C, 10 min; and (*d*) 450 °C, 120 min (an extra phase).



Acknowledgements

This research was supported by operating and equipment grants from the Natural Sciences and Engineering Research Council of Canada (NSERC) and Le fonds québécois de la recherche sur la nature et les technologies (FQRNT).

References

1. G.W. Morey and P. Niggli. J. Am. Chem. Soc. **35**, 1086 (1913).
2. A. Rabenau. Angew. Chem. Int. Ed. Engl. **24**, 1026 (1986).
3. T. Adschiri, K. Kanazawa, and K. Arai. J. Am. Ceram. Soc. **75**, 2615 (1992).
4. J.A. Darr and M. Poliakoff. Chem. Rev. **99**, 495 (1999).
5. A. Cabanas, J.A. Darr, T. Ilkenhans, and M. Poliakoff. In Proceedings of 6th meeting on supercritical fluids. *Edited by* M. Poliakoff. Chemistry and Materials, Nottingham, England. 1999.
6. J. Lee and A.S. Teja. Supercrit. Fluids. **35**, 83 (2005).
7. D.E.C. Corbridge. Bull. Soc. Fr. Mineral. Cristallogr. **94**, 271 (1971).
8. S. Apinitis. Latv. Kim. Z. **6**, 664 (1991).
9. E.N. Matvienko, O.V. Yakubovich, M.A Simonov, and N.V. Belov. Dokl. Akad. Nauk SSSR, **259(3)**, 591 (1981).
10. M. Pintard-Screpel, F. D'Yvoire, and J. Durand. Acta Cryst. **C39**, 9 (1983).
11. S. Neeraj, M.L. Noy, C.N.R. Rao, and A.K. Cheetham. J. Solid State Chem. **167**, 344 (2002).
12. K.-H. Lii and Y.-F. Huang. Chem. Commun. **9**, 839 (1997).
13. J.M. Thomas, R. Raja, G. Sankar, and R.G. Bell. Nature (London), **398**, 227 (1999).
14. J. Chen and J.M. Thomas. J. Chem. Soc. Chem. Commun. 603 (1994).
15. J.M. Thomas and W.J. Thomas. Principles and practice of heterogeneous catalysis. VCH verlagsgesellschart mbH, Weinheim, Germany. 1997.

© 2006 NRC Canada

16. P.A. Barrett, R.H. Jones, J.M. Thomas, G. Sankar, I.J. Shannon, and C.R.A. Catlow. J. Chem. Soc. Chem. Commun. 2001 (1996).
17. W.A. Bassett, A.H. Shen, M. Bucknum, and I.-M. Chou. Rev. Sci. Instrum. **64**, 2340 (1993).
18. F. Capitelli, M. Harcharras, H. Assaaoudi, A. Ennaciri, A.G.G. Moliterni, and V. Bertolasi. Z. Kristallogr. **218**, 345 (2003).
19. G.M. Sheldrick. SHELXS97 [computer program]. University of Göttingen, Göttingen, Germany. 1997.
20. G.M. Sheldrick. SHELXL97 [computer program]. University of Göttingen, Göttingen, Germany. 1997.
21. M.N. Burnett and C.K. Johnson. ORTEP-III [computer program]. Oak Ridge National Laboratory Report ORNL-6895, Oak Ridge, Tenn. 1996.
22. L.J. Farrugia. J. Appl. Crystallogr. **30**, 565 (1997).
23. T.J. Smith. J. Mol. Graphics, **13**, 122 (1995).
24. D.P.E. Dickson and F.J. Berry. Mossbauer spectroscopy. Cambridge University Press, New York. 1986.
25. D. Kobashi, S. Kohara, J. Yamakawa, and A. Kawahara. Acta Crystallogr. **C53**, 1523 (1997).
26. Y. Dumas, J.L. Galigne, and J. Falgueirettes. Acta Crystallogr. **B29**, 1623 (1973).
27. R.D. Shannon. Acta Crystallogr. **A32**, 751 (1976).
28. O.V. Yakubovich, M.S. Dadashov, and B.N. Litvin. Sov. Phys. Crystallogr. **33**, 16 (1988).
29. Y. Dumas, J. Lapasset, and J. Vicat. Acta Crystallogr. **B36**, 2754 (1980).
30. A.A. Tahiri, R. Oursanal, M. Lachnar, B. El Bali, and M. Bolte. Acta Crystallogr. **E58**, 91 (2002).
31. O.V. Yakubovich, M.A. Simonov, and N.V. Belov. Sov. Phys. Dokl. **22**, 347 (1977)
32. O.V. Yakubovich, M.A. Simonov, E.N. Matvienko, and N.V. Belov. Sov. Phys. Dokl. **23**, 11 (1978); Dokl. Akad. Nauk SSSR, **238**(3), 576 (1978).
33. K. Yu, M.A. Kabalov, O.V. Simonov, N.A. Yakubovich, N.V. Yamnova, and N.A. Belov. Sov. Phys. Dokl. **18**, 362 (1973); Dokl. Akad. Nauk SSSR, **210**, 830 (1973).
34. O.V. Yakubovich, M.A. Simonov, K. Yu, N. Egorov-Tismenko, and N.V. Belov. Sov. Phys. Dokl. **22**, 570 (1977); Dokl. Akad. Nauk SSSR, **236**, 1123 (1977).
35. E.N. Matvienko, O.V. Yakubovich, M.A. Simonov, and N.V. Belov. Sov. Phys. Dokl. **24**, 411 (1979); Dokl. Akad. Nauk SSSR, **246**, 875 (1979).
36. G. Herzberg. Infrared and raman spectra of polyatomic molecules. Van Nostrand, Princeton, New Jersey. 1946.
37. R.S. Halford. J. Chem. Phys. **14**, 8 (1946).
38. L. Popovic, D. de Waal, and J.C.A. Boeyens. J. Raman Spectrosc. **36**, 2 (2005).
39. S. Krimi, A. El Jazouli, L. Rabardel, M. Couzi, I. Mansouri, and G. Le Flem. J. Solid State Chem. **102**, 400 (1993).

© 2006 NRC Canada

Thermodynamic investigations of zeolites NaX and NaY[1]

Liyan Qiu, Patricia A. Laws, Bi-Zeng Zhan, and Mary Anne White

Abstract: Understanding of the thermodynamic stability of zeolites is important in the prediction of thermodynamic equilibrium. Therefore, we have undertaken an investigation of the thermodynamic stability of the zeolites NaX and NaY through heat capacity measurements from ca. 30 to 300 K. No phase transitions were observed, and zeolite NaX does not show a significant particle size effect when the particle size is reduced to ca. 30 nm. The results show that the specific heat capacity increases with the Al content in the zeolite. Both NaX and NaY are found to be thermodynamically stable with respect to their elements because of enthalpic stabilization and with slight entropic destabilization. These data are used along with literature data for many other zeolitic materials to show that the thermodynamic stability of zeolites is enhanced with increasing aluminum content.

Key words: zeolite, heat capacity, thermodynamic stability, nano effects.

Résumé : Une compréhension de la stabilité thermodynamique des zéolites est importante pour pouvoir prédire leur équilibre thermodynamique. Nous avons donc entrepris une étude de la stabilité thermodynamique des zéolites NaX et NaY par le biais de mesures de capacité calorifique entre environ 30 et 300 K. Aucune transition de phase n'a été observée et le zéolite NaX ne présente pas d'effet significatif de taille des particules lorsque cette taille est réduite jusqu'à environ 30 nm. Les résultats montrent que la capacité calorifique spécifique augmente avec la teneur en aluminium dans le zéolite. Il a été observé que les zéolites tant NaX que NaY sont thermodynamiquement stables par rapport à leurs éléments en raison d'une stabilisation enthalpique accompagnée d'une déstabilisation entropique. Ces données ont été utilisées de concert avec celles retrouvées dans la littérature pour plusieurs autres zéolites pour montrer que la stabilité thermodynamique des zéolites est rehaussée par une augmentation de la teneur en aluminium.

Mots clés : zéolite, capacité calorifique, stabilité thermodynamique, effets nano.

[Traduit par la Rédaction]

Introduction

Zeolites are aluminosilicates composed of TO_4 (T = Si, Al) primary building blocks, with about 100 different architectures based on vertex-sharing $[SiO_4]^{4-}$ and $[AlO_4]^{5-}$ tetrahedra (1). Zeolites are very useful materials, with applications including catalysis, ion exchange, molecular sieves, photochemistry, and solar energy conversion (2).

The large number of well-established zeolite structures offers an excellent opportunity to explore the relationships between structure and properties of materials. From a thermodynamic perspective, it is interesting that so many structures exist, with rather subtle compositional differences. Since understanding of the thermodynamic stability of zeolites is important to the prediction of thermodynamic equilibrium, we have undertaken an investigation of the thermodynamic stability of several zeolites to learn more of the generalities of their thermodynamic stability. The results are reported herein.

Zeolites and characterization

NaX

Zeolite NaX (also called zeolite X, NaX, Linde X, and molecular sieve 13X) is an analogue of the natural zeolite faujasite. Its structure is shown schematically in Fig. 1.

Zeolite NaX was purchased from Aldrich, calcined in air (4 h, T = 773 K) to remove any organic template residue, and then dehydrated in a quartz tube (24 h vacuum, T = 473 K); DSC showed <0.1 mass% water (limit of detection). Powder X-ray diffraction indicated a well-defined crystalline material with a cubic lattice parameter of 24.7701(1) Å, with the expected diffraction pattern (3) both before and after heating. From X-ray fluorescence analysis, we determined

Received 14 June 2005. Published on the NRC Research Press Web site at http://canjchem.nrc.ca on 22 February 2006.

Dedicated to Dr. Arthur J. Carty, National Science Advisor to the Prime Minister of Canada, in honour of his contributions to science in Canada and internationally.

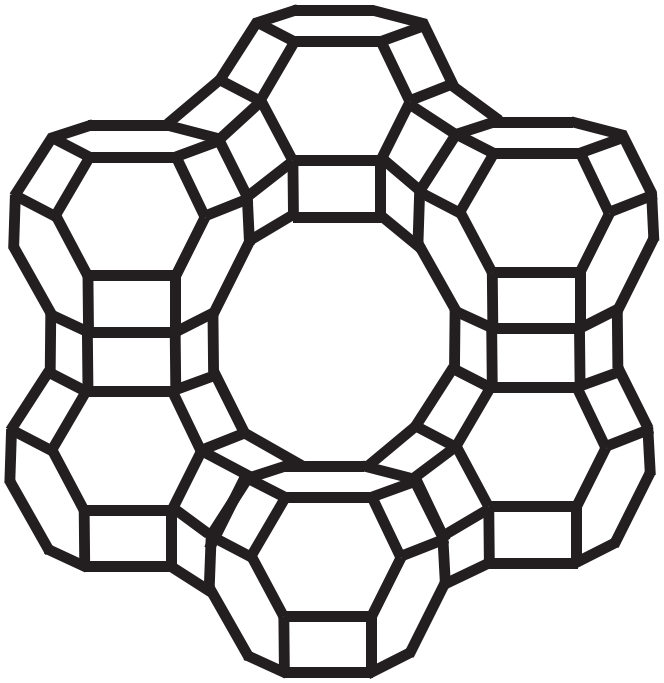
L. Qiu, P.A. Laws, B.-Z. Zhan, and M.A. White.[2] Department of Chemistry and Institute for Research in Materials, Dalhousie University, Halifax, NS B3H 4J3, Canada.

[1]This article is part of a Special Issue dedicated to Professor Arthur Carty.

[2]Corresponding author (e-mail: mary.anne.white@dal.ca).

 doi:10.1139/V05-244 © 2006 NRC Canada

Fig. 1. Framework structure of zeolites NaX and NaY.

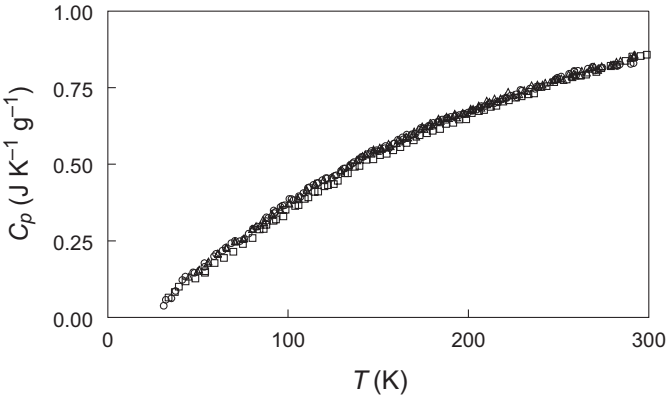


that the Si–Al mole ratio was 1.21 ± 0.02. The unit cell is considered to have the ideal chemical formula $Na_{87}Al_{87}Si_{105}O_{384}$. Hereafter, this sample is referred to as *bulk*-NaX.

We have recently developed techniques to produce zeolites with controlled particle sizes: nano- and micro-sized NaX were synthesized from fumed silica (11 nm, Sigma), NaOH (Aldrich), and $Al(OH)_3$ (McArthur Chemical) by these hydrothermal methods (4, 5). *Nano*-NaX was synthesized by crystallization in a shaker (rotation rate 250 rpm) at T = 60 °C for 4 days. *Micro*-NaX was synthesized by heating the fumed silica and sodium aluminate mixture at 90 °C for 2 days without shaking. The powdered products were recovered with centrifugation, washed with distilled water until pH < 8, and then dried at room temperature for 24 h. The samples were dehydrated in vacuum (3 h, T = 473 K). Power X-ray diffraction indicated well-defined crystalline materials with the same structure as for bulk-NaX. From X-ray fluorescence analysis, we found an Si–Al mole ratio of 1.25 ± 0.02 for both nano-NaX and micro-NaX, indicating an empirical formula of $Na_{85}Al_{85}Si_{107}O_{384}$.

High-resolution scanning electron microscopy (uncoated samples, Hitachi S4700 cold-field emission SEM) showed nano-NaX, micro-NaX, and bulk-NaX particle sizes in the range 20–100 nm, ≈800 nm, and ≈2 μm, respectively. Scherrer analysis (6) for the [111], [331], and [642] peaks of nano-NaX gave an average crystallite size of 23 ± 4 nm, indicating that the particles seen in the SEM are predominantly single grains. In the IR spectrum, nano-NaX is distinguished by the presence of a broad band at 860 cm^{-1}, attributed (5) to the silanol (Si-OH) bending mode for Si in a

Fig. 2. Experimentally determined heat capacities of zeolite NaX: nano-NaX (○); micro-NaX (△); bulk-NaX (□).[3]



Q^3 environment, i.e., three Si-O-T (T = Si-O-T) and one Si-O-H linkage, consistent with the high surface-to-volume ratio. The Q^3 species in nano-NaX also were confirmed by solid-state magic angle spinning ^{29}Si (single-pulse and cross-polarization) NMR spectroscopy (5).

NaY

Zeolite Y (also called molecular sieve Y and Linde Y) has the same framework topology as zeolite X, but with a higher Si–Al ratio, typically in the range 1.5 to 3.0 (compared with 1.1 to 1.5 for X). Thus, zeolite Y has fewer exchangeable cations.

Zeolite NaY (Aldrich), dehydrated as for NaX, showed no detectable water (DSC, <0.1 mass% water) and a well-defined crystalline lattice, cubic lattice parameter 24.6609(5) Å. The Si–Al ratio (X-ray fluorescence) was 2.65 ± 0.02, giving an ideal empirical formula of $Na_{53}Al_{53}Si_{139}O_{384}$.

Thermodynamic methods

The heat capacities of nano-NaX, micro-NaX, bulk-NaX, and NaY were determined using adiabatic calorimetry (7). After dehydration, all further sample handling was in vacuum or in a helium atmosphere. Sample masses for bulk-NaX, micro-NaX, nano-NaX, and NaY, respectively, were: 2.908, 2.038, 2.787, and 2.062 g. These masses are relatively small for this calorimeter and were limited by the low density of the zeolites and the volume (≈5 cm^3) of the sealed calorimeter. The small masses of the zeolitic samples here led to rather small contributions of the sample to the total heat capacity, and concomitantly large uncertainties in the heat capacities, namely ±6% for T < 100 K and ±4% for T > 100 K.

Particle size dependence in NaX

The heat capacities of bulk-NaX, micro-NaX, and nano-NaX are shown in Fig. 2.[3] All show smooth heat capacities, with no evidence of phase transitions.

Enhancement of the heat capacity of a material is expected as its particle size is decreased because of the increased motion of the surface atoms relative to the atoms in

[3] Supplementary data (Tables S1–S5) for this article are available on the journal Web site (http://canjchem.nrc.ca) or may be purchased from the Depository of Unpublished Data, Document Delivery, CISTI, National Research Council Canada, Ottawa, ON K1A 0R6, Canada. DUD 4086. For more information on obtaining material refer to http://cisti-icist.nrc-cnrc.gc.ca/irm/unpub_e.shtml.

© 2006 NRC Canada

Table 1. Heat capacities of dehydrated zeolites at T = 298.15 K as a percentage of the Dulong–Petit value and Al content.

Zeolite	Formula	Al/(Al+Si)	D–P value (%)	Reference
MTT	SiO_2	0	59	15
BEA	SiO_2	0	61	15
MFI	SiO_2	0	61	16
Faujasite	SiO_2	0	61	15
NaY	$Na_{53}Al_{53}Si_{139}O_{384}$	0.276	63	Present work
nano-NaX	$Na_{85}Al_{85}Si_{107}O_{384}$	0.443	69	Present work
micro-NaX	$Na_{85}Al_{85}Si_{107}O_{384}$	0.443	70	Present work
bulk-NaX	$Na_{87}Al_{87}Si_{105}O_{384}$	0.453	70	Present work
4A	$Na_{96}Al_{96}Si_{96}O_{384}$	0.500	75	14

the bulk. However, it is not clear, a priori, how large this effect would be.

While there might be some enhancement of the heat capacity of NaX with decreasing particle size at the lowest temperatures, it appears to be similar for both nano-NaX and micro-NaX and to be at the limits of uncertainty of the experiment, given the small contribution of the samples to the total heat capacity. Although nano-NaX does exhibit an enhanced external surface area compared with micro-NaX and bulk-NaX, the internal surface area comprises the majority of the total surface area of these open framework porous materials (80% for nano-NaX and 90%–95% for micro-NaX and bulk-NaX) (5). Thus, the external surface energy would have to be significantly different from the internal surface energy to give a large difference in the heat capacity with particle size. Recent calculations have shown only a small difference between the internal and external surface energies for zeolitic materials (8). Therefore, it is not surprising that we find only a small, perhaps negligible, enhancement of heat capacity of NaX as the particle size decreases from ≈1 μm to ≈30 nm.

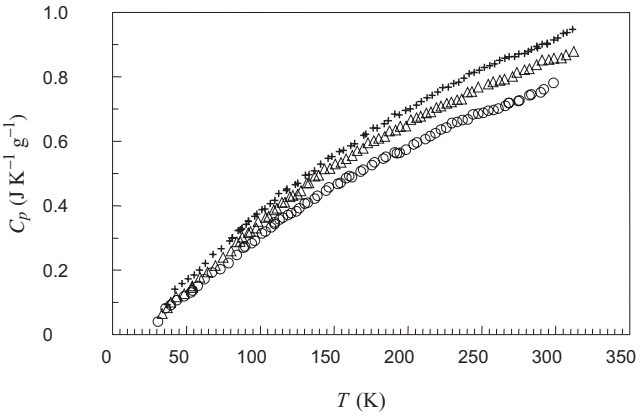
Dugdale et al. (9) found that the heat capacity of the rutile form of TiO_2 was enhanced only up to 3% for 14 nm particles, in comparison with the bulk. While there has been a report of 6%–11% enhancement of the heat capacity of zeolite ZSM-5 (75 nm particles, compared with 1 μm) (10), TGA characterization of that sample appears to show water loss, indicating incomplete dehydration, which also could account for the apparent heat capacity enhancement. A report of significant (≈20%) enhancement of the heat capacity of the anatase form of TiO_2 with ca. 15 nm particles (11, 12) has been shown to be unphysical and likely owing to a few % of adsorbed water (13).

Relationship between Al content and heat capacity

The heat capacity of NaY as a function of temperature is shown in Fig. 3,[3] in comparison with the heat capacities of bulk-NaX and zeolite 4A (14). Again, the heat capacity of NaY is smooth, showing no evidence of any phase transition in this temperature range. However, it is considerably less than that of NaX or zeolite 4A, for reasons we now consider.

The T = 298.15 K heat capacities of several well-characterized zeolites are presented in Table 1 as a percentage of the Dulong–Petit value and as a function of Al content. The results indicate that the heat capacity increases

Fig. 3. Experimentally determined heat capacities of zeolites: 4A (+) (14); NaX (bulk) (△);[3] and NaY (○).[3]



(vibrational modes are more excited) as the Al content increases. This can be understood in terms of lattice dynamics, considering that the Si—O bond is stiffer than the Al—O bond (17, 18). Therefore, for a given temperature, the vibrational modes will be more activated in zeolites with higher Al content.

The trend of changing heat capacity with Al content also can be understood by estimating the heat capacity by the constituent additivity method (19). This method is based on consideration of the heat capacity of the complex inorganic compound as a combination of the contributions of simpler constituents. At T = 298.15 K, the heat capacities of the constituents for zeolites containing sodium as the charge-balancing cation are as follows: $C_p(SiO_2)$ = 44.97 J K^{-1} mol^{-1} (20), $C_p(Al_2O_3)$ = 78.80 J K^{-1} mol^{-1} (21), and $C_p(Na_2O)$ = 69.10 J K^{-1} mol^{-1} (22). As the proportion of Al increases in a zeolite, the concentration of Na^+ also must increase to balance the framework charge. Therefore the contributions to the specific heat capacity from Al_2O_3 and Na_2O will also increase, resulting in an overall increase in heat capacity.

Thermodynamic stability

The availability of temperature-dependent heat capacities of these zeolites allows quantification of their thermodynamic functions, as presented in Tables 2 and 3.

Using a method similar to the constituent additivity for heat capacity, we can calculate the Gibbs energy of formation of NaX based on the values for zeolitic SiO_2 and

© 2006 NRC Canada

Table 2. Thermodynamic functions for NaX, $Na_{87}Al_{87}Si_{105}O_{384}$ (as determined from the bulk sample).

T (K)	C_p (J K^{-1} mol^{-1})	$(H_T–H_0)$ (kJ mol^{-1})	$(S_T–S_0)$ (J K^{-1} mol^{-1})	$(G_T–G_0)$ (kJ mol^{-1})
10	29	0.0906	10.9	–0.018
20	229	1.23	79.4	–0.362
30	689	5.67	252	–1.88
40	1 280	15.5	529	–5.66
50	1 810	30.9	871	–12.6
60	2 380	51.9	1 250	–23.1
70	2 960	78.6	1 660	–37.6
80	3 550	111	2 100	–56.9
90	4 120	150	2 550	–80
100	4 680	194	3 010	–108
110	5 210	243	3 480	–140
120	5 710	298	3 960	–178
130	6 190	357	4 430	–219
140	6 640	421	4 910	–266
150	7 060	490	5 380	–317
160	7 460	562	5 850	–374
170	7 830	639	6 310	–434
180	8 180	719	6 770	–500
190	8 520	802	7 220	–570
200	8 840	889	7 660	–643
220	9 450	1072	8 540	–807
240	10 030	1267	9 380	–984
260	10 570	1473	10 210	–1182
280	11 080	1689	11 010	–1394
298.15	11 500	1894	11 720	–1600
300	11 540	1916	11 790	–1621

Note: The required extrapolation of the heat capacity to $T = 0$ K was carried out by fitting the data below 100 K to the function $C_v/3R = mC_E + nC_D$, where C_E and C_D are, respectively, Einstein and Debye heat capacity functions represented by their characteristic temperatures, θ_E and θ_D. Here $m = 166$, $n = 497$, $\theta_E = 579 \pm 5$ K, and $\theta_D = 227 \pm 2$ K.

Table 3. Thermodynamic functions for NaY, $Na_{53}Al_{53}Si_{139}O_{384}$.

T (K)	C_p (J K^{-1} mol^{-1})	$(H_T–H_0)$ (kJ mol^{-1})	$(S_T–S_0)$ (J K^{-1} mol^{-1})	$(G_T–G_0)$ (kJ mol^{-1})
10	23.2	0.0724	8.69	–0.015
20	184	0.981	63.5	–0.29
30	566	4.6	204	–1.51
40	1090	12.9	436	–4.59
50	1560	26.1	729	–10.4
60	2040	44.1	1060	–19.5
70	2530	66.9	1410	–31.8
80	3010	94.6	1780	–47.8
90	3470	127	2160	–67.4
100	3920	164	2550	–91
110	4340	205	2940	–118
120	4740	251	3340	–150
130	5130	300	3730	–185
140	5500	353	4120	–224
150	5850	410	4520	–268
160	6190	470	4900	–314
170	6510	534	5290	–366
180	6830	600	5670	–420
190	7140	670	6050	–479
200	7430	743	6420	–541
220	7980	897	7150	–676
240	8480	1060	7870	–829
260	8930	1240	8570	–988
280	9370	1420	9250	–1170
298.15	9840	1590	9850	–1350
300	9890	1610	9910	–1360

Note: The required extrapolation of the heat capacity to $T = 0$ K was carried out as for NaX, with $m = 157$, $n = 472$, $\theta_E = 629 \pm 8$ K, and $\theta_D = 236 \pm 3$ K.

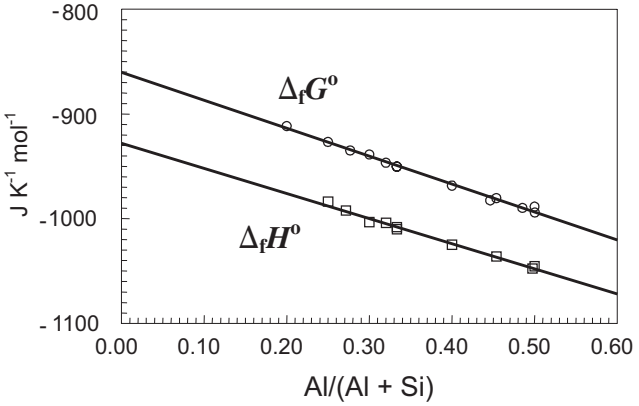
$Na_2O{\cdot}Al_2O_3$ (23). This gives $\Delta_f G°$(NaX, $Na_{87}Al_{87}Si_{105}O_{384}$) of $–(1.866 \pm 0.002) \times 10^8$ J mol^{-1}, in excellent agreement (within 0.2%) of the value from solubility studies (24). Similarly, the Gibbs energy of formation of NaY can be determined from the present NaX value and SiO_2 (23), giving $\Delta_f G°$(NaY, $Na_{53}Al_{53}Si_{139}O_{384}$) = $–(1.791 \pm 0.002) \times 10^8$ J mol^{-1}.

The entropies of formation for NaX and NaY can be calculated from the data for the elements (22, 23, 25–28) along with the present entropy data, correcting for residual entropy for random Si–Al disorder (S_0(NaX) = 5.79 J K^{-1} mol^{-1}; S_0(NaY) = 4.96 J K^{-1} mol^{-1}). This gives $\Delta_f S°$(NaX, $Na_{87}Al_{87}Si_{105}O_{384}$) = –36.52 ± 0.06 kJ K^{-1} mol^{-1} and $\Delta_f S°$(NaY, $Na_{53}Al_{53}Si_{139}O_{384}$) = –38.43 ± 0.06 kJ K^{-1} mol^{-1}.

Combining these results, we determined $\Delta_f H°$(NaX, $Na_{87}Al_{87}Si_{105}O_{384}$) = $–(1.97 \pm 0.002) \times 10^8$ J mol^{-1} and $\Delta_f H°$(NaY, $Na_{53}Al_{53}Si_{139}O_{384}$) = $–(1.91 \pm 0.002) \times 10^8$ J K^{-1} mol^{-1}. Therefore, we see that the thermodynamic stability of both zeolites NaX and NaY arise from enthalpic and not entropic factors.

It is qualitatively known that thermodynamic stability of zeolites depends on the Si–Al ratio (29), but it appears that there are few quantitative discussions of this matter. In Fig. 4, the values of $\Delta_f G°$ and $\Delta_f H°$ of some dehydrated zeolites (synthetic and natural) and related materials with different Si–Al ratios are presented.[3] The values of the thermodynamic functions depend more strongly on the Si–Al ratio than on the structural details. (Similarly, the thermodynamic stability of pure silica molecular sieves has been found to be nearly independent of structure (30). For exam-

Fig. 4. Thermodynamic formation functions for zeolites as a function of Al content based on the general formula $Na_xAl_xSi_{(1-x)}O_2$, expressed per mol of x. See deposited[3] Table S5 for data and references.



© 2006 NRC Canada

ple, the natural zeolite analcime has almost the same Gibbs energy of formation as the nonzeolitic jadeite (Al/(Al + Si)) = 0.333 and 0.320; $\Delta_f G°$ = –946.6 and –950.3 kJ mol^{-1}, respectively). Overall, the relationship can be expressed in kJ mol^{-1} as:

[1] $\Delta_f G° = -859.6 - 268.4\ [Al/(Al + Si)]$

where the intercept, corresponding to SiO_2, is –860 ± 7 kJ mol^{-1}, very close to the $\Delta_f G°$ of quartz, –856.4 kJ mol^{-1} (22).

The enthalpy of formation of zeolites (Fig. 4) also exhibits a linear relationship with the Al content, which can be expressed in kJ mol^{-1} as:

[2] $\Delta_f H° = -921.4 - 258.3\ [Al/(Al + Si)]$

and again the SiO_2 intercept, –921 kJ mol^{-1}, corresponds well to the $\Delta_f H°$ of quartz, –910.0 kJ mol^{-1} (22).

In Fig. 4, the difference between $\Delta_f G°$ and $\Delta_f H°$ represents the entropy change in the formation of the zeolites, $T\Delta_f S°$. It can be seen that the entropy change is negative, and hence entropy factors decrease the thermodynamic stability of zeolites. Therefore, the thermodynamic stability of zeolites comes from the enthalpic effect, not the entropic effect. Equations [1] and [2] indicate that the entropic effect is almost independent of Al–Si ratio, but not negligible.

From Fig. 4, it can be seen that increasing the aluminum content increases the thermodynamic stability of zeolites. As Si^{4+} is replaced by Al^{3+}, the framework requires more nonframework cations (e.g., Na^+) to compensate. Since the Gibbs energy of formation of 1 mol of SiO_2 (–865.4 kJ mol^{-1} for quartz (22)) is less negative than that of (0.5 mol Al_2O_3 + 0.5 mol Na_2O), –980.7 kJ mol^{-1} (22), increasing the concentration of Al^{3+} decreases the Gibbs energy and, hence, increases the thermodynamic stability of the zeolite. Similar results were found for the dehydrated sodium faujasite frameworks with different Si–Al ratios at T = 977 K (31). An important related matter is that templates are required to synthesize high-Si-content zeolites because they are not as thermodynamically favoured as lower-Si-content zeolites. This finding also reconciles the fact that natural zeolites generally have higher Al content. Furthermore, DTA experiments show (31) that the decomposition temperature of zeolites increases with increasing Si content. This is because Si—O bonds are stronger than Al—O bonds. In this case, thermodynamic stability relative to the constituent elements also corresponds with overall thermal stability.

For further comparison, the formation of relevant proportions of Na_2O, SiO_2, and Al_2O_3 has been considered (as in Fig. 4), and the results are as follows:

[3] $\Delta_f G° = -857 - 123\ [Al/(Al + Si)]$

and

[4] $\Delta_f H° = -912 - 135\ [Al/(Al + Si)]$

indicating the following: lesser thermodynamic stability than the zeolites; enthalpic (not entropic) stability; less dependence of $\Delta_f G°$ and $\Delta_f H°$ on the Al–Si ratio than for the zeolites; nearly the same entropy of formation as the zeolites and with similar independence of the Al–Si ratio.

Conclusions

Experimental heat capacity measurements of zeolite NaX do not show a significant particle size effect. The present measurements show that the specific heat capacity increases with the Al content in the zeolite. Both NaX and NaY are found to be thermodynamically stable with respect to their elements, owing to enthalpic stabilization, with slight entropic destabilization. These data are used along with literature data for many other zeolitic materials to show that the thermodynamic stability of zeolites is enhanced with increasing aluminum content.

Acknowledgements

We gratefully acknowledge the following: the Atlantic Region Magnetic Resonance Centre for NMR analyses; A. George and K. Robertson for assistance; R.L. White and J. Dahn for use of their facilities; J. Boerio-Goates for a useful comment; the Natural Sciences and Engineering Research Council of Canada (NSERC) and the Killam Trusts for financial support.

References

1. R. Szostak. Molecular sieves: principles of synthesis and identification. Van Nostrand Reinhold, New York. 1989.
2. A. Corma. Chem. Rev. **95**, 559 (1995); W. Hölderich, M. Hesse, and F. Näumann. Angew. Chem. Int. Ed. Engl. **27**, 226 (1988); M.E. Davis. Ind. Eng. Chem. Res. **30**, 1675 (1991).
3. C.A.E. Kirschhock, B. Hunger, J. Martens, and P.A. Jacobs. J. Phys. Chem. B, **104**, 439 (2000).
4. B.-Z. Zhan, M.A. White, K.N. Robertson, T.S. Cameron, and M. Gharghouri. Chem. Commun. (Cambridge), 1176 (2001).
5. B.-Z. Zhan, M.A. White, M. Lumsden, J. Mueller-Neuhaus, K.N. Robertson, T.S. Cameron, and M. Gharghouri. Chem. Mater. **14**, 3636 (2002).
6. B.D. Cullity. Elements of X-ray diffraction. Addison-Wesley, Reading, Mass. 1978.
7. M.J.M. Van Oort and M.A. White. Rev. Sci. Instrum. **58**, 1239 (1987).
8. E.C. Moloy, L.P. Davila, J.J. Shackelford, and A. Navrotsky. Microporous Mesoporous Mater. **54**, 1 (2002).
9. J.S. Dugdale, J.A. Morrison, and D. Patterson. Proc. R. Soc. London, **224**, 228 (1954).
10. L. Wang, S. Meng, Z. Tan, D. Liang, X. Guo, and X. Wang. Chin. J. Catal. **22**(5), 491 (2001).
11. X.-M. Wu, L. Wang, Z.-C. Tan, G.-H. Li, and S.-S. Qu. J. Solid State Chem. **156**, 220 (2001).
12. X.-M. Wu, Y.-Y. Di, Z.-C. Tan, and S.-S. Qu. J. Inorg. Mater. **16**, 159 (2001).
13. P. Laws. M.Sc. thesis, Department of Chemistry, Dalhousie University, Halifax, N.S. 2002.
14. L. Qiu, V. Murashov, and M.A. White. Solid State Sci. **2**, 841 (2000).
15. J. Boerio-Goates, R. Stevens, B.K. Hom, B.F. Woodfield, P.M. Piccione, M.E. Davis, and A. Navrotsky. J. Chem. Thermodyn. **34**, 205 (2002).
16. I.E. Paukov, I.A. Belitskii, and G.A. Berezovskii. Geochem. Int. **36**, 565 (1998).
17. P.K. Dutta and B. Del Barco. J. Chem. Soc. Chem. Commun. 1297 (1985).

© 2006 NRC Canada

18. K. Nakamoto. Infrared and Raman spectra of inorganic and coordination compounds. Part A: Theory and applications in inorganic chemistry. 5th ed. John Wiley & Sons Inc., New York. 1997.
19. L. Qiu and M.A. White. J. Chem. Educ. **78**, 1076 (2001).
20. C.T. Anderson. J. Am. Chem. Soc. **58**, 568 (1936).
21. D.A. Ditmars, S. Ishihara, S.S. Chang, G. Berstein, and E.D. West. J. Res. Natl. Bur. Stand. (US), **87**, 159 (1982).
22. W.M. Chase, Jr. J. Phys. Chem. Ref. Data Monogr. **9**, 1 (1998).
23. A. La Iglesia and A.J. Aznar. Zeolites, **6**, 26 (1986).
24. P. Caullet, J.-L. Guth, and R. Wey. Bull. Minéral. **103**, 330 (1980).
25. D.B. Downie and J.F. Martin. J. Chem. Thermodyn. **12**, 779 (1980).
26. P. Flubacher, A.J. Leadbetter, and J.A. Morrison. Philos. Mag. **4**, 275 (1959).
27. J. Hilsenrath, C.W. Beckett, W.S. Benedict, L. Fano, H.J. Hoge, J.F. Masi, R.L. Nuttall, Y.S. Touloukian, and H.W. Woolley. Tables of thermal properties of gases. Nat. Bur. Stand. Circ. (US), 564 (1955).
28. C.B. Alcock, M.W. Chase, and V.P. Itkin. J. Phys. Chem. Ref. Data, **23**, 415 (1994).
29. C.Y. Li and L.V.C. Rees. Zeolites, **6**, 60 (1986).
30. P.M. Piccione, B.F. Woodfield, J. Boerio-Goates, A. Navrotsky, and M.E. Davis. J. Phys. Chem. B, **105**, 6025 (2001).
31. I. Petrovic and A. Navrotsky. Microporous Mater. **9**, 1 (1997).

© 2006 NRC Canada

Two new high-nuclearity copper(II) chloride oligomers with herringbone stacking patterns synthesized by in situ templation[1]

Zhiyong Fu and Tristram Chivers

Abstract: The use of trichloroiminophosphoranes $Cl_3P{=}NR$ to control the concurrent release of the templating cation $[RNH_3]^+$ and chloride ligand via in situ P—N and P—Cl bond cleavage produced two new copper(II) chloride oligomers. The nature of the organic substituent R was a factor in determining the chain lengths. For *n*-propyltrichloroiminophosphorane, the hexanuclear cluster $[n\text{-}PrNH_3]_2[Cu_6Cl_{14}]$ (**1**) was obtained, while *p*-tolyltrichloroiminophosphorane generated the tetranuclear copper chloride salt $[4\text{-}CH_3C_6H_4NH_3][2\text{-}Cl\text{-}4\text{-}CH_3C_6H_3NH_3][Cu_4Cl_{10}]$ (**2**). In both structures a two-dimensional framework displaying a herringbone arrangement is created by Cu—Cl secondary bonding interactions. The direct addition of the $[n\text{-}PrNH_3]^+$ cation to a $CuCl_2{\cdot}2H_2O$ solution under the same reaction conditions produced $[n\text{-}PrNH_3]_2[CuCl_4]$.

Key words: copper halides, templation, oligomers, two-dimensional frameworks.

Résumé : L'utilisation de trichloroiminophosphoranes $Cl_3P{=}NR$ pour contrôler la libération simultanée du cation $[RNH_3]^+$ servant de gabarit et le ligand chlorure par le biais d'un clivage in situ de liaisons P—N et P—Cl conduit à la formation de deux nouveaux oligomères du chlorure de cuivre(II). La nature du substituant organique R est un facteur dans la détermination des longueurs des chaînes. Avec le *n*-propyltrichloroiminophosphorane, il y a formation de l'agrégat hexanucléaire $[n\text{-}PrNH_3]_2[Cu_6Cl_{14}]$ (**1**) alors que le *p*-tolyltrichloroiminophosphorane génère la formation du chlorure de cuivre tétranucléaire $[4\text{-}CH_3C_6H_4NH_3][2\text{-}Cl\text{-}4\text{-}CH_3C_6H_3NH_3][Cu_4Cl_{10}]$ (**2**). Dans les deux structures, il y a création d'un squelette bidimensionnel comportant un arrangement en chevrons formé par des interactions de liaisons secondaires Cu—Cl. L'addition directe du cation $[n\text{-}PrNH_3]^+$ à une solution de $CuCl_2{\cdot}2H_2O$ dans les mêmes conditions réactionnelles conduit à la formation de $[n\text{-}PrNH_3]_2[CuCl_4]$.

Mots clés : halogénures de cuivre, gabarit, oligomères, squelettes bidimensionnels.

[Traduit par la Rédaction]

Introduction

The use of templating reagents is a common technique in the synthesis of inorganic materials (1, 2). This method employs a cation, e.g., alkylammonium $[RNH_3]^+$, to provide charge balance and to regulate the structural arrangement of anionic frameworks through forces such as hydrogen bonding or van der Waals repulsion (3). The traditional procedure for the synthesis of oligomeric copper(II) halide frameworks involves mixing the copper(II) halide with an appropriate organic cation in a concentrated hydrohalic acid solution (4–6). Willett and co-workers (7–9) have used this approach to produce many copper halide oligomers with fascinating structural features and interesting physical properties. Much of their work has focused on the characterization of quasi-planar bibridged Cu_nX_{2n+2} systems (n = 2–7, 10) (10–16). The "softness" of the copper coordination sphere and the nonstereospecific bridging capability of the halide ions allow the formation of secondary bonding interactions (SBIs) between the oligomers, which give rise to various stacking patterns (17).

Recently, some new open-framework zinc phosphates were prepared under solvothermal conditions by using P—N bond cleavage in hexamethylphosphoramide $OP(NMe_2)_3$ to control the simultaneous release of an organic amine and phosphoric acid (18). As part of our investigations of novel inorganic materials, we are particularly interested in the in situ templation synthesis of new copper(II) halide frameworks. In addition to generating new functional compounds, this indirect templation method may contribute to an understanding of the mechanism of network formation. For example, we have shown that the tris(alkylamido)phosphate $OP[N(H)\text{-}t\text{-}Bu]_3$ functions both as an indirect source of the templating $[t\text{-}BuNH_3]^+$ cation and as a proton acceptor in the

Received 7 July 2005. Published on the NRC Research Press Web site at http://canjchem.nrc.ca on 22 February 2006.

Dedicated to Dr Arthur Carty for his outstanding contributions to Canadian science.

Z. Fu and T. Chivers.[2] Department of Chemistry, University of Calgary, Calgary, AB T2N 1N4, Canada.

[1]This article is part of a Special Issue dedicated to Professor Arthur Carty.
[2]Corresponding author (e-mail: chivers@ucalgary.ca).

 doi:10.1139/V05-237 © 2006 NRC Canada

Table 1. Crystal data and structure refinement for **1**, **2**, and **3**.

	1	**2**	**3**
Empirical formula	$C_6H_{20}Cl_{14}Cu_6N_2$	$C_{14}H_{19}Cl_{11}Cu_4N_2$	$C_7H_9Cl_2N$
fw (g)	997.78	859.42	178.05
T (K)	298(2)	298(2)	298(2)
Crystal system	Monoclinic	Monoclinic	Monoclinic
Space group	$P2_1/c$	$P2_1/c$	$P2_1/c$
a (Å)	9.3454(19)	13.031(3)	5.2178(10)
b (Å)	6.0319(12)	6.1151(12)	8.6191(17)
c (Å)	24.159(5)	17.191(3)	18.111(4)
β (°)	97.79(3)	95.66(3)	97.40(3)
V (Å^3)	1349.3(5)	1363.1(5)	807.7(3)
Z	2	2	4
D_{calcd} (g cm^{-3})	2.456	2.094	1.464
μ (mm^{-1})	6.032	4.165	0.724
F(000)	964	840	368
θmin–θmax (°)	3.78–27.50	3.14–25.02	2.62–25.03
Reflections collected	4644	8189	1667
Independent reflections	3075	2362	1154
R(int)	0.0331	0.0537	0.0426
Goodness-of-fit on F^2	1.033	1.101	1.067
Final R indices [$I > 2\sigma(I)$]; R_1, wR_2	0.0393, 0.0804	0.0521, 0.1460	0.0673, 0.1676
R indices (all data); R_1, wR_2	0.0656, 0.0907	0.0654, 0.1568	0.0815, 0.1786
Largest diff. peak and hole (e Å^{-3})	0.732, –0.638	0.786, –0.890	0.521, –0.556

production of a novel copper chloride structural motif that is different from the network synthesized by the direct addition of [t-BuNH$_3$]Cl (19). In the current work we have investigated the use of trichloroiminophosphoranes Cl_3P=NR (R = n-Pr, p-tolyl) as an in situ source of both the organic ammonium cation and the Cl^- ligand in the formation of novel copper halide frameworks. We report here the formation and X-ray structures of two high-nuclearity copper chloride oligomers [n-PrNH$_3$]$_2$[Cu_6Cl_{14}] (**1**) and [4-$CH_3C_6H_4NH_3$][2-Cl-4-$CH_3C_6H_3NH_3$][Cu_4Cl_{10}] (**2**), both of which exhibit a herringbone structure. For the quasi-planar bibridged Cu_nX_{2n+2} oligomers, this stacking pattern has only been reported in the pentanuclear cluster [Cu_5Cl_{10}(n-C_3H_7OH)$_2$] (20). For comparison, the direct addition of [n-PrNH$_3$]$^+$ to a $CuCl_2 \cdot 2H_2O$ solution under the same reaction conditions produced the known copper chloride complex [n-PrNH$_3$]$_2$[$CuCl_4$] (21). The structure of [2-Cl-4-$CH_3C_6H_3NH_3$]$^+Cl^-$ (**3**), a by-product of the reaction involving Cl_3P=N-p-tolyl, is also reported.

Experimental section

Reagents and general procedures

n-Propyltrichloroiminophosphorane and 4-tolyltrichloroiminophosphorane were prepared according to the literature procedure (22). Tetrachloroethane was dried over CaH_2 and fractionally distilled. Copper chloride dihydrate, phosphorus pentachloride, and chlorobenzene were used as received.

Synthesis of 1

A mixture of copper chloride dihydrate (0.170 g, 1.00 mmol), n-propyltrichloroiminophosphorane (0.194 g, 1.00 mmol), water (0.054 g, 3.00 mmol), and 10 mL toluene were placed in a sealed 23 mL Teflon vessel and heated at 90 °C for 12 h. The reaction vessel was allowed to cool to 23 °C, and yellow crystals of **1** (0.020 g, 12%) were isolated from the yellow precipitate manually.

Syntheses of 2 and 3

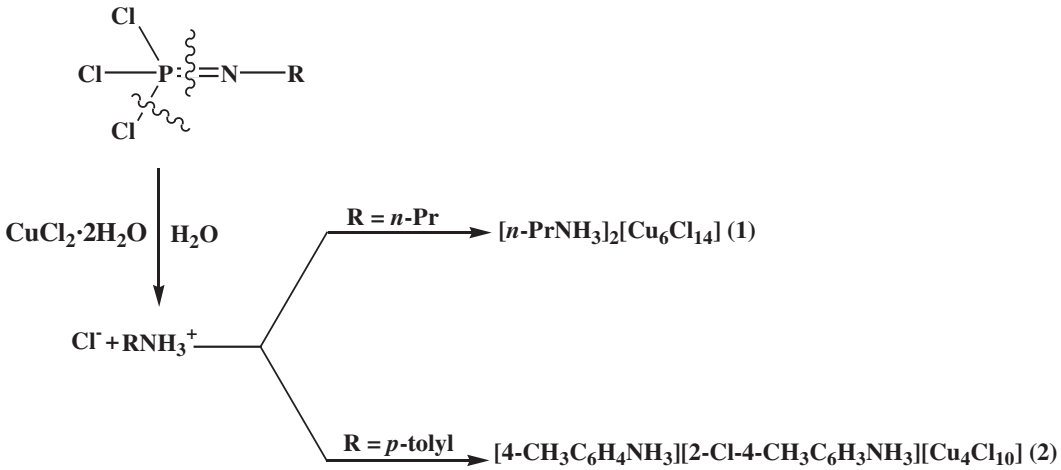
A mixture of copper chloride dihydrate (0.170 g, 1.00 mmol), p-tolyltrichloroiminophosphorane (0.243 g, 1.00 mmol), water (0.054 g, 3.00 mmol), and 10 mL toluene were placed in a sealed 23 mL Teflon vessel and heated at 90 °C for 12 h. The reaction vessel was allowed to cool to 23 °C. Yellow crystals of **2** (0.040 g, 18%) and a few pale yellow crystals of **3** were separated from the black precipitate manually.

X-ray structural analyses

Suitable crystals of the complexes (**1**, yellow block (0.18 × 0.12 × 0.12 mm^3); **2**, yellow plate (0.20 × 0.04 × 0.04 mm^3); **3**, pale yellow plate (0.24 × 0.08 × 0.08 mm^3)) were selected, coated with oil (Paratone 8277, Exxon), and mounted on glass fibres. The measurements were made on a Nonius KappaCCD diffractometer with graphite-monochromated Mo Kα radiation. Data were collected at 25 °C, using the ω and ϕ scans to a maximum θ value of 27.5°, 25.02°, and 25.03° for **1**, **2**, and **3**, respectively. The data were corrected for Lorentz and polarization effects and for absorption using the multiscan method (23). Since the crystals did not show any sign of decay during data collection, a decay correction was deemed unnecessary. The structures were solved by direct methods SHELXS-97 (24). The C atoms of the n-propyl groups in **1** were disordered over three positions with unequal site occupancy factors in an approximate ratio of 2:1:1; the C3 and C2a atoms were also disordered at the same position in a 1:1 ratio. In **2**, the cations [4-$CH_3C_6H_4NH_3$] and [2-Cl-4-$CH_3C_6H_3NH_3$] were disordered at the same position with equal site occupancy

© 2006 NRC Canada

Scheme 1.



factors. All non-hydrogen atoms were refined anisotropically except the disordered atoms. All the hydrogen atoms were included at geometrically idealized positions. Crystallographic data for **1**, **2**, and **3** are summarized in Table 1. Additional data are available in the Supporting information.[3]

Results and discussion

The products obtained from the solvothermal reactions of trichloroiminophosphoranes $Cl_3P{=}NR$ with $CuCl_2{\cdot}2H_2O$ in toluene at 90 °C exhibit distinctly different structural motifs depending on the identity of the R group (Scheme 1). In the case of R = *n*-Pr, the hexanuclear copper chloride chain $[Cu_6Cl_{14}]^{2-}$ is isolated as the $[n\text{-}PrNH_3]^+$ salt, whereas for the aryl subsituent (R = *p*-tolyl), the tetranuclear $[Cu_4Cl_{10}]^{2-}$ fragment is obtained in conjunction with the $[4\text{-}CH_3C_6H_4NH_3]^+$ and $[2\text{-Cl-4-}CH_3C_6H_3NH_3]^+$ cations. The chloride ions in these syntheses are generated by in situ hydrolysis of the P—Cl bonds in $Cl_3P{=}NR$, which is achieved by the addition of a stoichiometric amount of water to the reaction mixture. Concomitantly, the in situ generated organoammonium cations $[RNH_3]^+$ exhibit an indirect templation function in the generation of these anionic copper halide frameworks. The formation of bibridged Cu_nX_{2n+2} oligomers in previous reports is viewed to involve fragments cut from infinite CuX_2 chains by charge-compensating cations acting as "molecular scissors" (10, 12). The weak interaction between the Cl^- ion and the cation results in the termination of the CuX_2 chains. This is a common modification in the formation of copper halide oligomers. In the new synthesis described herein the copper chloride oligomers are built up by replacement of the aqua ligands in the $CuCl_2{\cdot}2H_2O$ monomer (25) by the stronger chloride ligands provided by the hydrolysis of $Cl_3P{=}NR$. The formation of the new cation $[2\text{-Cl-4-}CH_3C_6H_3ClNH_3]^+$ in the synthesis of **2** presumably occurs by the chlorination of the $[4\text{-}CH_3C_6H_4NH_3]^+$ cation during the solvothermal process. The chloride salt $[2\text{-Cl-4-}CH_3C_6H_3NH_3]^+Cl^-$ (**3**) was also isolated from the reaction products and characterized by X-ray crystallography (vide infra). A similar observation has been reported for the bromination of the 3-chloroanilinium cation by $CuBr_2$ in HBr solution to give the 6-bromo-3-chloroanilinium cation (26).

The direct reaction of $[n\text{-}PrNH_3]Cl$ and $CuCl_2{\cdot}2H_2O$ under the solvothermal conditions employed for the synthesis of **1** generated the known mononuclear anion $[CuCl_4]^-$ (21) as the $[n\text{-}PrNH_3]^+$ salt, demonstrating the structure-directing effect of the indirect templation method, as previously reported for the generation of a novel anionic copper halide framework by in situ templation employing $[t\text{-}BuNH_3]^+$, which is provided by the amidophosphate reagent $OP(NH\text{-}t\text{-}Bu)_3$] (19). Interestingly, the outcome of the indirect templation method is sensitive to reaction conditions, notably the polarity of the solvent. When the reaction of $Cl_3P{=}N\text{-}n\text{-}Pr$ with $CuCl_2{\cdot}2H_2O$ takes place in ethanol at 90 °C, the final product is $[n\text{-}PrNH_3]_2[CuCl_4]$. This difference may be attributable to the faster rate of hydrolysis of $Cl_3P{=}N\text{-}n\text{-}Pr$ in the more polar solvent ethanol compared with that in toluene. The rapid cleavage of P—Cl and P—N bonds apparently results in a templation effect similar to that observed for the direct addition of Cl^- and $[n\text{-}PrNH_3]^+$ (in the form of the salt $[n\text{-}PrNH_3]Cl$).

Complexes **1** and **2** were identified by single-crystal X-ray analyses (Tables 2 and 3). As illustrated in Fig. 1, compound **1** contains an anionic hexanuclear copper chloride oligomer with a different stacking pattern from that found in $[C_7H_{10}N]_2[Cu_6Cl_{14}]$ (11). In **1**, the $[Cu_6Cl_{14}]^{2-}$ dianion connects to four neighbours of adjacent stacks via two long Cu—Cl bonds (Cl2—Cu2c = 2.6266(12) Å) and two Cu—Cl secondary bonding interactions (Cl2—Cu1d = 2.8080(13) Å), which extend the structure to a 2D herringbone motif. By contrast, the stacks of oligomers in

[3] Supplementary data for this article are available on the journal Web site (http://canjchem.nrc.ca) or may be purchased from the Depository of Unpublished Data, Document Delivery, CISTI, National Research Council Canada, Ottawa, ON K1A 0R6, Canada. DUD 4081. For more information on obtaining material refer to http://cisti-icist.nrc-cnrc.gc.ca/irm/unpub_e.shtml. CCDC 277576 (**1**), 277577 (**2**), and 277578 (**3**) contain the crystallographic data for this manuscript. These data can be obtained, free of charge, via www.ccdc.cam.ac.uk/conts/retrieving.html (Or from the Cambridge Crystallographic Data Centre, 12 Union Road, Cambridge CB2 1EZ, UK; fax +44 1223 336033; or deposit@ccdc.cam.ac.uk).

© 2006 NRC Canada

Table 2. Selected bond lengths (Å) and bond angles (°) for **1**.

Bond lengths (Å)			
Cu(3)—Cl(6)	2.2631(13)	Cu(2)—Cl(4)	2.2674(13)
Cu(3)—Cl(7)	2.2674(13)	Cu(2)—Cl(3)	2.2807(12)
Cu(3)—Cl(7a)	2.2809(12)	Cu(2)—Cl(6)	2.2933(12)
Cu(3)—Cl(5)	2.2880(12)	Cu(2)—Cl(5)	2.3070(13)
Cu(1)—Cl(1)	2.2581(14)	Cu(2)—Cl(2b)	2.6266(12)
Cu(1)—Cl(2)	2.2723(12)	Cl(2)—Cu(2c)	2.6266(12)
Cu(1)—Cl(4)	2.3116(12)	Cl(7)—Cu(3a)	2.2809(12)
Cu(1)—Cl(3)	2.3381(13)	Cl(2)—Cu(1d)	2.8080(13)
Bond angles (°)			
Cl(6)-Cu(3)-Cl(7)	179.47(5)	Cl(3)-Cu(2)-Cl(6)	170.30(4)
Cl(6)-Cu(3)-Cl(7a)	92.72(4)	Cl(4)-Cu(2)-Cl(5)	167.35(4)
Cl(7)-Cu(3)-Cl(7a)	87.28(4)	Cl(3)-Cu(2)-Cl(5)	93.16(4)
Cl(6)-Cu(3)-Cl(5)	86.73(4)	Cl(6)-Cu(2)-Cl(5)	85.58(4)
Cl(7)-Cu(3)-Cl(5)	93.29(4)	Cl(4)-Cu(2)-Cl(2b)	95.25(4)
Cl(7a)-Cu(3)-Cl(5)	177.93(5)	Cl(3)-Cu(2)-Cl(2b)	97.72(4)
Cl(1)-Cu(1)-Cl(2)	96.52(5)	Cl(6)-Cu(2)-Cl(2b)	91.98(4)
Cl(1)-Cu(1)-Cl(4)	88.95(4)	Cl(5)-Cu(2)-Cl(2b)	97.30(4)
Cl(2)-Cu(1)-Cl(4)	170.83(4)	Cu(3)-Cl(6)-Cu(2)	94.07(5)
Cl(1)-Cu(1)-Cl(3)	172.53(5)	Cu(3)-Cl(5)-Cu(2)	93.04(4)
Cl(2)-Cu(1)-Cl(3)	89.69(4)	Cu(2)-Cl(4)-Cu(1)	94.51(5)
Cl(4)-Cu(1)-Cl(3)	84.37(4)	Cu(2)-Cl(3)-Cu(1)	93.45(4)
Cl(4)-Cu(2)-Cl(3)	86.71(4)	Cu(1)-Cl(2)-Cu(2c)	97.54(4)
Cl(4)-Cu(2)-Cl(6)	92.42(4)	Cu(3)-Cl(7)-Cu(3a)	92.72(4)

Note: Symmetry transformations used to generate equivalent atoms: $a = -x - 1, -y + 1, -z$; $b = x, y - 1, z$; $c = x, y + 1, z$; $d = -1 - x, 1/2 + y, 1/2 - z$.

Table 3. Selected bond lengths (Å) and bond angles (°) for **2**.

Bond lengths (Å)			
Cu(2)—Cl(3)	2.2743(18)	Cu(1)—Cl(2)	2.2589(17)
Cu(2)—Cl(5)	2.2846(18)	Cu(1)—Cl(4)	2.3143(18)
Cu(2)—Cl(4)	2.2897(16)	Cu(1)—Cl(3)	2.3187(17)
Cu(2)—Cl(5a)	2.2975(16)	Cl(5)—Cu(2a)	2.2975(16)
Cu(2)—Cl(2b)	2.6764(17)	Cl(2)—Cu(2c)	2.6764(17)
Cu(1)—Cl(1)	2.237(2)	Cl(2)—Cu(1d)	3.0724(18)
Bond angles (°)			
Cl(3)-Cu(2)-Cl(5)	170.35(7)	Cl(1)-Cu(1)-Cl(2)	95.53(8)
Cl(3)-Cu(2)-Cl(4)	85.68(6)	Cl(2)-Cu(1)-Cl(4)	92.10(7)
Cl(5)-Cu(2)-Cl(4)	93.02(6)	Cl(1)-Cu(1)-Cl(3)	89.37(7)
Cl(3)-Cu(2)-Cl(5a)	92.79(6)	Cl(2)-Cu(1)-Cl(3)	169.85(7)
Cl(5)-Cu(2)-Cl(5a)	86.87(6)	Cl(4)-Cu(1)-Cl(3)	84.11(6)
Cl(4)-Cu(2)-Cl(5a)	170.29(6)	Cu(2)-Cl(5)-Cu(2a)	93.13(6)
Cl(3)-Cu(2)-Cl(2b)	94.48(7)	Cu(2)-Cl(4)-Cu(1)	94.41(6)
Cl(5)-Cu(2)-Cl(2b)	95.18(6)	Cu(2)-Cl(3)-Cu(1)	94.70(6)
Cl(4)-Cu(2)-Cl(2b)	97.97(6)	Cu(1)-Cl(2)-Cu(2c)	99.70(6)
Cl(5a)-Cu(2)-Cl(2b)	91.71(6)		

Note: Symmetry transformations used to generate equivalent atoms: $a = -x - 4, -y - 3, -z - 2$; $b = x, y + 1, z$; $c = x, y - 1, z$; $d = -4 - x, -1/2 + y, -3/2 - z$.

$[C_7H_{10}N]_2[Cu_6Cl_{14}]$ are interlocked to give a layer pattern parallel to the *ab* plane. Each copper centre in **1** is coordinated to four chloride ligands. All the copper ions protrude from the ligand plane, displaying a square pyramidal distortion. The central Cu3 atom shows the smallest distortion with a dihedral angle of 2.0° between the Cl7-Cu3-Cl5 and Cl7a-Cu3-Cl6 planes. The most significant deviation from the square plane is observed at the Cu2 center with a dihedral angle of 16.3° between the Cl5-Cu2-Cl3 and Cl6-Cu2-Cl4 planes. The terminal Cu1 atom has a dihedral angle of 8.0° between the Cl4-Cu1-Cl1 and Cl3-Cu1-Cl2 planes. The terminal copper(II)—chloride bond lengths are 2.2581(14) (Cu1—Cl1) and 2.2723(12) Å (Cu1—Cl2), whereas the bridging copper(II)—chloride bond lengths are 2.3381(13) Å

© 2006 NRC Canada

Fig. 1. Molecular structure and atomic numbering scheme for **1**. Thermal ellipsoids are shown at the 70% level.

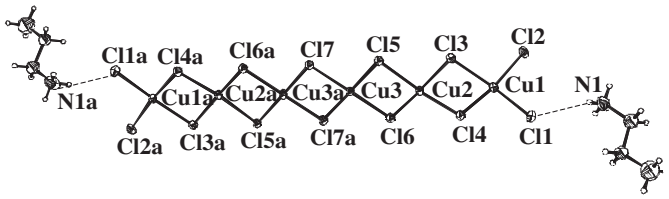
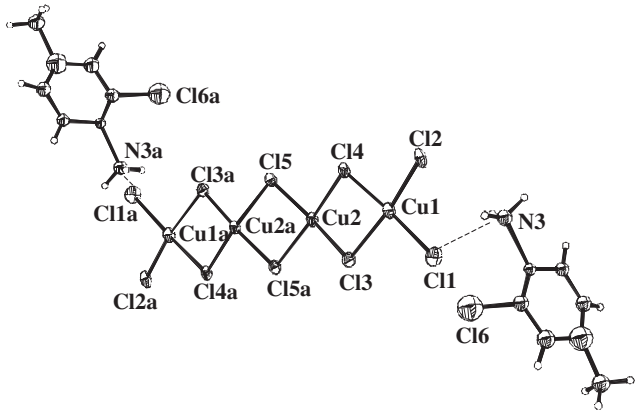


Fig. 2. Molecular structure and atomic numbering scheme for **2**. Thermal ellipsoids are shown at the 50% level.



(Cu1—Cl3), 2.3116 Å (Cu1—Cl4), 2.2674(13) Å (Cu2—Cl4), 2.2807(12) Å (Cu2—Cl3), 2.3070(13) Å (Cu2—Cl5), 2.2933(12) Å (Cu2—Cl6), 2.2880(12) Å (Cu3—Cl5), 2.2631(13) Å (Cu3—Cl6), 2.2809 (12) Å (Cu3—Cl7a), and 2.2674(13) Å (Cu3—Cl7), respectively. These values are in agreement with the rule of variations in in-plane bond lengths of bibridged Cu_nX_{2n+2} oligomers, demonstrating a short-long-short··· alternation for the t-b1-b2··· sequence.[4] The bridging Cu-Cl-Cu bond angles range from 94.51° for the terminal fragment to 92.72° for the central units.

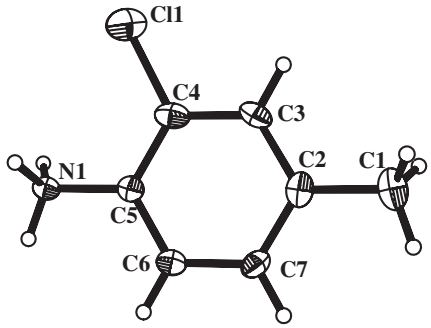
The structural characteristics of compound **2** are similar to those of **1** except that the anion is tetranuclear (Fig. 2). The $[Cu_4Cl_{10}]^{2-}$ fragment in $[Me_4N]_2[Cu_4Cl_{10}]$ has the same stacking pattern as that in **2**, but with a different mode of anion–cation interactions. In **2**, the oligomer is linked to four neighbours of adjacent stacks (Cl2—Cu2c = 2.6764(17) Å, Cl2—Cu1d = 3.0724(18) Å), whereas in $[Me_4N]_2[Cu_4Cl_{10}]$ the influence of the cations restricts these interactions to two neighbours (12). The Cu1 atom in **2** displays a small tetrahedral distortion, while the Cu2 atom exhibits a square pyramidal distortion with a dihedral angle of 14.0° between the Cl4-Cu2-Cl5 and Cl3-Cu2-Cl5a planes. The terminal Cl1 and Cl2 ligands coordinate with the Cu1 atom (Cu1—Cl1 = 2.237(2) Å, Cu1—Cl2 = 2.2589(17) Å), whereas the bridging ligands Cl3, Cl4, and Cl5 connect the adjacent copper atoms with a mode (Cu1—Cl3 = 2.3187(17) Å, Cu1—Cl4 = 2.3143(18) Å, Cu2—Cl3 = 2.2743(18) Å, Cu2—Cl4 = 2.2897(16) Å, and Cu2—Cl5 = 2.2846(18) Å). These values are typical and show the short-long-short alternation observed for **1**. The bridging Cu-Cl-Cu bond angles vary from 94.70° to 93.13°.

The X-ray analysis of compound **3** (Table 4) revealed that

Table 4. Bond lengths (Å) and bond angles (°) for **3**.

Bond lengths (Å)			
Cl(1)—C(4)	1.719(5)	C(5)—C(3)	1.397(8)
C(7)—C(6)	1.379(7)	C(4)—C(2)	1.394(8)
C(7)—C(5)	1.396(8)	C(3)—C(2)	1.399(8)
C(6)—C(4)	1.387(7)	C(3)—C(1)	1.497(8)
C(6)—N(1)	1.454(7)		
Bond angles (°)			
C(6)-C(7)-C(5)	120.5(5)	C(2)-C(4)-Cl(1)	118.0(4)
C(7)-C(6)-C(4)	119.3(5)	C(6)-C(4)-Cl(1)	121.6(4)
C(7)-C(6)-N(1)	120.6(4)	C(5)-C(3)-C(2)	117.6(5)
C(4)-C(6)-N(1)	120.2(4)	C(5)-C(3)-C(1)	121.8(5)
C(3)-C(5)-C(7)	121.1(5)	C(2)-C(3)-C(1)	120.6(5)
C(2)-C(4)-C(6)	120.4(5)	C(4)-C(2)-C(3)	121.1(5)

Fig. 3. Molecular structure and atomic numbering scheme for the cation in **3**. Thermal ellipsoids are shown at the 50% level.



chlorination occurred in the position ortho to the NH_3^+ group to give the $[2\text{-Cl-4-}CH_3C_6H_3NH_3]^+$ cation (Fig. 3). The bond lengths and bond angles in this cation (C—Cl = 1.719(5) Å, C6—N1 = 1.454(7) Å; C2-C4-Cl1 = 118.0(4)°, C6-C4-Cl1 = 121.6(4)°) are similar to those reported for the related anilinium cation, $[3\text{-Cl-6-Br}C_6H_3NH_3]^+$ (26).

As illustrated in Fig. 4, the structures of **1** and **2** are both extended into two-dimensional networks by SBIs that give rise to a herringbone motif. The terminal chloride ligand Cl2 in **1** acts as a μ_2 bridge connecting to the copper centres located in the adjacent fragments. The Cu1 and Cu2 atoms adopt a 4+1+1 coordination mode, while the Cu3 atom has a 4+2 coordination geometry, in which the secondary bonding interactions for Cu1, Cu2, and Cu3 are 2.808 and 3.008 Å, 2.627 and 3.213 Å, and 2.981 and 2.960 Å, respectively. In compound **2**, the Cu1 atom adopts a 4+2 coordination mode with SBIs of 3.072 and 3.127 Å. The Cu2 atom has a 4+1+1 coordination mode with SBIs of 2.676 and 3.194 Å. The stacking patterns of **1** and **2** are denoted as 6(3/2, 1/2) and 4(3/2, 1/2), respectively, according to the notation of Willett and co-workers (17). Like most bibridged Cu_nX_{2n+2} oligomers, the charge-compensating cations $[n\text{-PrNH}_3]^+$ in **1** and $[2\text{-Cl-4-}CH_3C_6H_3NH_3]^+$ and $[4\text{-}CH_3C_6H_4NH_3]^+$ in **2** form hydrogen bonds with a pair of trans terminal chloride ligands (N—Cl = 3.245 Å for **1** and 3.253 Å for **2**).

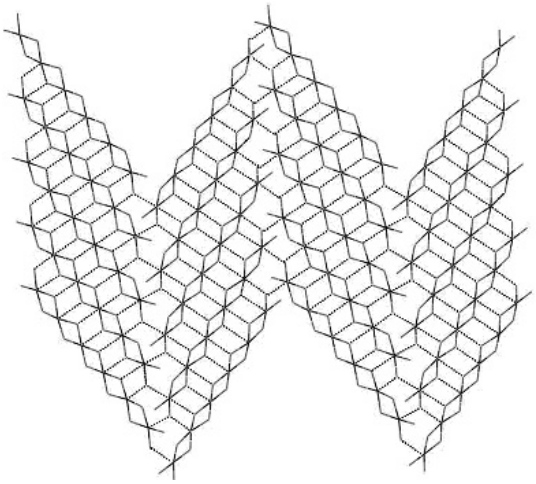
In summary, a new synthetic approach involving the simultaneous in situ generation of Cl^- and $[RNH_3]^+$ ions for

[4] The Ith Cu—Cl bond length is denoted by bI, starting from the terminal atom; b = bridging, t = terminal (27).

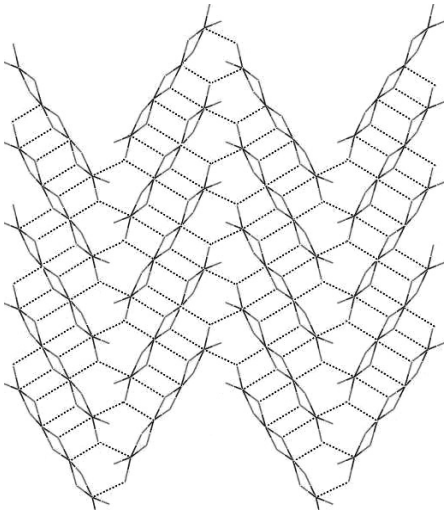
© 2006 NRC Canada

Fig. 4. Packing diagrams of compounds **1** and **2**. The Cu—Cl secondary bonding interactions are represented by broken lines.

1



2



the production of anionic copper chloride oligomers is introduced in this study. Variation of the R group in the precursors $Cl_3P{=}NR$ creates different lengths of the anionic chains. The structures of both oligomers exhibit a herringbone stacking pattern. These findings provide another example of the generation of new inorganic structural frameworks via *indirect* templation using P-N reagents (18, 19). There is considerable scope for the construction of novel inorganic architectures via variation in reaction conditions in these solvothermal processes, as indicated by the influence of solvent polarity in the current work.

Acknowledgements

We thank the Alberta Ingenuity Fund and the Natural Sciences and Engineering Research Council of Canada (NSERC) for financial support.

References

1. A.K. Cheetham, G. Férey, and T. Loiseau. Angew. Chem. Int. Ed. **38**, 3268 (1999).
2. J.D. Martin, A.M. Dattelbaum, T.A. Thornton, R.M. Sullivan, J. Yang, and M.T. Peachey. Chem. Mater. **10**, 2699 (1998).
3. C.N.R. Rao, S. Natarajan, and S. Neeraj. J. Am. Chem. Soc. **122**, 2810 (2000).
4. M. Wei, R.D. Willett, D. Teske, K. Subbaraman, and J.E. Drumheller. Inorg. Chem. **35**, 5781 (1996).
5. S. Haddad and R.D. Willett. Inorg. Chem. **40**, 809 (2001).
6. C. Horn, I. Dance, D. Craig, M. Scudder, and G. Bowmaker. J. Am. Chem. Soc. **120**, 10549 (1998).
7. M. Wei, R.D. Willett, and C.J. Gómez-García. Inorg. Chem. **43**, 4534 (2004).
8. M. Wei and R.D. Willett. Inorg. Chem. **35**, 6381 (1996).
9. M. Wei, R.D. Willett, and K.W. Hipps. Inorg. Chem. **35**, 5300 (1996).
10. S. Haddad, F. Awwadi, and R.D. Willett. Cryst. Growth Des. **3**, 501 (2003).
11. M.R. Bond, H. Place, Z. Wang, R.D. Willett, Y. Liu, T.E. Grigereit, J.E. Drumheller, and G.F. Tuthill. Inorg. Chem. **34**, 3134 (1995).
12. K.E. Halvorson, T. Grigereit, and R.D. Willett. Inorg. Chem. **26**, 1716 (1987).
13. T.E. Grigereit, B.L. Ramakrishna, H. Place, R.D. Willett, G.C. Pellacani, T. Manfredini, L. Menabue, A. Bonomartini-Corradi, and L.P. Battaglia. Inorg. Chem. **26**, 2235 (1987).
14. A. Colombo, L. Menabue, A. Motori, G.C. Pellacani, W. Porzio, F. Sandrolini, and R.D. Willett. Inorg. Chem. **24**, 2900 (1985).
15. R. Fletcher, J.J. Hansen, J. Livermore, and R.D. Willett. Inorg. Chem. **22**, 330 (1983).
16. M.R. Bond, R.D. Willett, R.S. Rubins, P. Zhou, C.E. Zaspel, S.L. Hutton, and J.E. Drumheller. Phys. Rev. B, **42**, 10280 (1990).
17. U. Geiser, R.D. Willett, M. Lindbeck, and K. Emerson. J. Am. Chem. Soc. **108**, 1173 (1986).
18. S. Neeraj and A.K.Cheetham. Chem. Commun. (Cambridge), 1738 (2002).
19. T. Chivers, Z. Fu, and L.K. Thompson. Chem. Commun. (Cambridge, U.K.), 2339 (2005).
20. R.D. Willett and R.E. Rundle. J. Chem. Phys. **40**, 838 (1964).
21. (*a*) B. Doudin and G. Chapuis. Acta Crystallogr. Sect. B, **46**, 175 (1990); (*b*) B. Doudin and G. Chapuis. Acta Crystallogr. Sect. B, **46**, 180 (1990).
22. S.A. Bell, T.Y. Meyer, and S.J. Geib. J. Am. Chem. Soc. **124**, 10698 (2002).
23. Z. Otwinowski and W. Minor. Methods Enzymol. **276**, 307 (1997).
24. G.M. Sheldrick. SHELXS-97 [computer program]. University of Göttingen, Göttingen, Germany. 1997.
25. M. Kakiuchi, T. Abe, and H. Nakayama, Geochem. J. **35**, 285 (2001).
26. R.D. Willett. Inorg. Chem. **40**, 966 (2001).
27. R.D. Willett. Acta Crystallogr. Sect. B, **44**, 503 (1988).

© 2006 NRC Canada

Rhodium(I) acetylacetonato complexes containing phosphinoalkynes as catalysts for the hydroboration of vinylarenes[1]

Christopher M. Vogels, Andreas Decken, and Stephen A. Westcott

Abstract: Three novel rhodium(I) acetylacetonato (acac) complexes bearing phosphinoalkynes ($Ph_2PC{\equiv}C$-*t*-Bu, $Ph_2PC{\equiv}CPPh_2$, and $Ph_2PC{\equiv}CC{\equiv}CPPh_2$) have been prepared and characterized fully. Addition of B_2cat_3 (cat = 1,2-$O_2C_6H_4$) to Rh(acac)($Ph_2PC{\equiv}C$-*t*-Bu)$_2$ (**1a**) led to zwitterionic Rh(η^6-catBcat)($Ph_2PC{\equiv}C$-*t*-Bu)$_2$ (**2a**), the first example of this type of compound to contain monodentate phosphine ligands. All new rhodium complexes have been investigated for their ability to catalyse the hydroboration of vinylarenes.

Key words: catalysis, hydroboration, phosphinoalkynes, regioselectivity, rhodium.

Résumé : On a préparé et complètement caractérisé trois nouveaux complexes acétylacétonato du rhodium(I) portant des phosphinoalcynes ($Ph_2PC{\equiv}C$-*t*-Bu; $Ph_2PC{\equiv}CPPh_2$ et $Ph_2PC{\equiv}CC{\equiv}CPPh_2$). L'addition de B_2cat_3 (cat = 1,2-$O_2C_6H_4$) au Rh(acac)($Ph_2PC{\equiv}C$-*t*-Bu)$_2$ (**1a**) conduit à la formation du composé zwitterionique Rh(η^6-catBcat)($Ph_2PC{\equiv}C$-*t*-Bu)$_2$ (**2a**), le premier exemple de ce type de composé à contenir des ligands phosphines monodentates. On a examiné l'utilité potentielle de tous les nouveaux complexes du rhodium comme catalyseurs pour l'hydroboration de vinylarènes.

Mots clés : catalyse, hydroboration, phosphinoalcynes, régiosélectivité, rhodium.

[Traduit par la Rédaction]

Introduction

One of the most important synthetic methodologies to emerge from organic chemistry in the last century has been the discovery that boron–hydrogen bonds add to unsaturated organic molecules to form a class of compounds known as organoboranes (1). Organoboranes possess an incredibly diverse chemistry and are remarkably useful intermediates in organic synthesis today. Indeed, organoboranes can be transformed into any number of functional groups. The simplest boron hydride agent is borane, BH_3, which reacts rapidly with unhindered alkenes to afford initially monoalkylboranes, then dialkylboranes, and finally trialkylboranes. For sterically hindered alkenes, the second and third hydroboration steps become increasingly sluggish. Addition occurs in a controlled cis-fashion (syn-addition), where the boryl (BR_2) fragment adds preferentially to the least hindered carbon of the unsymmetrically substituted double bond. While borane adds rapidly to alkenes at –80 °C (2), some hydroborating agents, such as polyhedral boranes, are slow to react even at room temperature. Likewise, addition of $H_3B{\cdot}THF$ to catechol affords catecholborane (HBcat, cat = 1,2-$O_2C_6H_4$), a relatively stable hydroborating agent, which adds to alkenes and alkynes only at elevated temperatures (ca. 100 and 70 °C, respectively) (3). Catecholborane decomposes thermally or by addition of nucleophiles to give a number of boron-containing products (4).

That transition metals accelerate the addition of B—H bonds to unsaturated organic moieties was initially reported for catalysed hydroborations of alkenes and alkynes using polyhedral boranes (5). Männig and Nöth (6) then demonstrated that rhodium complexes could be used to catalyse the hydroboration of alkenes with HBcat under mild conditions and with *chemoselectivity differing from that of the uncatalysed reaction* (Scheme 1). Indeed, in the catalysed hydroboration of 5-hexen-2-one, addition of HBcat occurred preferentially at the C=C double bond, even in the presence of the more reactive ketone group.

Since this seminal discovery, a considerable amount of research has focused on investigating the mechanism and scope of late metal catalysed hydroboration reactions (7). Although other metals have been found to catalyse hydroborations with HBcat, rhodium-based catalyst systems are usually the most effective for reactions of vinylarenes (8). Unfortunately, these reactions often suffer from poor selectivities or competing pathways (i.e., hydrogenation), and as a result, a considerable amount of research has focused on designing new catalyst systems (9). We report herein on the synthesis and hydroboration of rhodium(I) acetylacetonato complexes containing phosphinoalkyne ligands.

Received 14 June 2005. Published on the NRC Research Press Web site at http://canjchem.nrc.ca on 22 February 2006.

Dedicated to Dr. A.J. Carty in recognition of his outstanding contributions to chemistry and for being an exceptional and encouraging teacher and mentor.

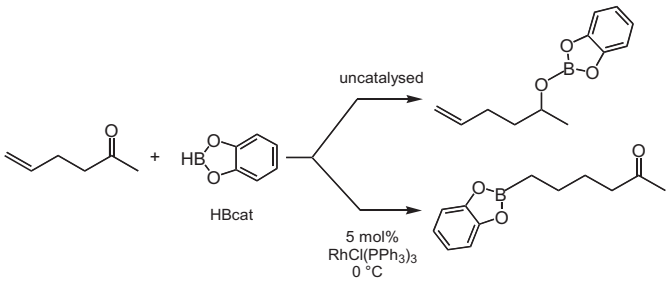
C.M. Vogels and S.A. Westcott.[2] Department of Chemistry, Mount Allison University, Sackville, NB E4L 1G8, Canada.
A. Decken. Department of Chemistry, University of New Brunswick, Fredericton, NB E3B 5A3, Canada.

[1]This article is part of a Special Issue dedicated to Professor Arthur Carty.

[2]Corresponding author (e-mail: swestcott@mta.ca).

 doi:10.1139/V05-242 © 2006 NRC Canada

Scheme 1. Hydroboration of 5-hexen-2-one.



Experimental

General

Reagents and solvents used were purchased from Aldrich Chemicals. NMR spectra were recorded on a JEOL JNM-GSX270 FT spectrometer. ^{1}H NMR chemical shifts are reported in parts per million (ppm) and referenced to residual solvent protons in deuterated solvent at 270 MHz. ^{11}B NMR chemical shifts are reported in ppm and are referenced to $BF_3{\cdot}OEt_2$ as an external standard at 87 MHz. ^{13}C NMR chemical shifts are referenced to solvent carbon resonances as internal standards at 68 MHz and are reported in ppm. ^{31}P NMR chemical shifts are reported in ppm and are referenced to H_3PO_4 as an external standard at 109 MHz. Multiplicities are reported as singlet (s), doublet (d), triplet (t), multiplet (m), broad (br), and overlapping (ov). All reactions were carried out under an atmosphere of dinitrogen. Microanalyses for C and H were carried out at Guelph Chemical Laboratories (Guelph, Ontario). Phosphines were prepared as described previously and donated as a generous gift from Dr. J.F. Corrigan (10). Rh(acac)(coe)$_2$ was prepared as described previously (11).

Rh(acac)(Ph$_2$PC≡C-*t*-Bu)$_2$ (1a)

A solution of Ph$_2$PC≡C-*t*-Bu (0.25 g, 0.95 mmol) in toluene (1 mL) was added to a solution of Rh(acac)(coe)$_2$ (0.20 g, 0.47 mmol) in toluene (2 mL), and the mixture was stirred for 18 h. The removal of solvent under vacuum afforded an orange solid, which was washed with hexane (3 × 3 mL) and collected by suction filtration to give **1a** (0.31 g, 88%). Spectroscopic NMR data (in C_6D_6): ^{1}H δ: 8.25–8.18 (ov m, 8H, Ar), 7.17–7.04 (ov m, 12H, Ar), 5.20 (s, 1H, C=C*H*), 1.53 (s, 6H, C(O)*Me*), 0.93 (s, 18H, *tert*-butyl). ^{13}C{^{1}H} δ: 184.3, 137.0 (app. quint, $J_{C\text{-}P\text{-}Rh}$ = 26 Hz), 133.9 (t, $J_{C\text{-}P}$ = 6 Hz), 128.7, 127.3 (t, $J_{C\text{-}P}$ = 5 Hz), 114.4 (t, $J_{C\text{-}P}$ = 6 Hz, PC*C*), 99.6, 75.7 (td, $J_{C\text{-}P}$ = 153, 46 Hz, P*C*C), 29.9, 28.2, 26.8. ^{31}P{^{1}H} δ: 31.4 (d, $J_{P\text{-}Rh}$ = 196 Hz). Anal. calcd. for $C_{41}H_{45}O_2P_2Rh$ (%): C 67.02, H 6.19; found: C 66.79, H 6.45.

[{Rh(acac)}$_2$(μ-Ph$_2$PC≡CPPh$_2$-κ^2*P*)$_2$] (1b)

A solution of Ph$_2$PC≡CPPh$_2$ (0.14 g, 0.36 mmol) in toluene (1 mL) was added to a solution of Rh(acac)(coe)$_2$ (0.15 g, 0.36 mmol) in toluene (2 mL), and the mixture was stirred for 18 h. The solvent was removed under vacuum, and the resulting orange precipitate was washed with hexane (3 × 3 mL) and collected by suction filtration to give **1b** (0.18 g, 82%). Spectroscopic NMR data (in C_6D_6): ^{1}H δ: 7.95–7.88 (ov m, 16H, Ar), 7.01–6.89 (ov m, 24H, Ar), 5.26 (s, 2H, C=C*H*), 1.57 (s, 12H, C(O)*Me*). ^{13}C{^{1}H} δ: 184.6, 134.1 (app. quint, $J_{C\text{-}P\text{-}Rh}$ = 27 Hz), 133.4 (t, $J_{C\text{-}P}$ = 6 Hz), 128.9, 127.5 (t, $J_{C\text{-}P}$ = 5.2 Hz), 102.4 (td, $J_{C\text{-}P}$ = 109, 36 Hz, P*C*C), 99.8, 26.9. ^{31}P{^{1}H} δ: 32.1 (d, $J_{P\text{-}Rh}$ = 191 Hz). Anal. calcd. for $C_{62}H_{54}O_4P_4Rh_2$ (%): C 62.42, H 4.57; found: C 62.26, H 4.25.

[{Rh(acac)}$_2$(μ-Ph$_2$PC≡CC≡CPPh$_2$-κ^2*P*)$_2$] (1c)

A solution of Ph$_2$PC≡CC≡CPPh$_2$ (0.22 g, 0.52 mmol) in THF (1 mL) was added to a solution of Rh(acac)(coe)$_2$ (0.20 g, 0.47 mmol) in THF (2 mL), and the mixture was stirred for 1 h. The resulting orange precipitate was collected by suction filtration and washed with hexane (3 × 3 mL) to give **3** (0.28 g, 95%). Spectroscopic NMR data (in C_6D_6): ^{1}H δ: 7.94–7.90 (ov m, 16H, Ar), 6.98–6.90 (ov m, 24H, Ar), 5.25 (s, 2H, C=C*H*), 1.52 (s, 12H, C(O)*Me*). ^{31}P{^{1}H} δ: 35.5 (d, $J_{P\text{-}Rh}$ = 193 Hz). Anal. calcd. for $C_{66}H_{54}O_4P_4Rh_2$ (%): C 63.87, H 4.39; found: C 63.42, H 4.49.

Rh(η^6-Bcat$_2$)(Ph$_2$PC≡C-*t*-Bu)$_2$ (2a)

A solution of B_2cat_3 (0.05 g, 0.14 mmol) in toluene (0.5 mL) was added to a solution of Rh(acac)(Ph$_2$PC≡C-*t*-Bu)$_2$ (0.10 g, 0.14 mmol) in toluene (2 mL), and the mixture was stirred for 18 h. The precipitate that formed was removed by suction filtration, and hexane (3 mL) was added to the filtrate, and the solution was stored at –25 °C for 3 days. The resulting red precipitate was collected by suction filtration to afford **2a** (0.080 g, 66%). Spectroscopic NMR data (in C_6D_6): ^{1}H δ: 7.89–7.81 (ov m, 8H, Ar), 7.15–6.96 (ov m, 16H, Ar), 4.83 (m, 4H, η^6-cat), 0.80 (s, 18H, *tert*-butyl). ^{11}B δ: 15.0. ^{31}P{^{1}H} δ: 23.6 (d, $J_{P\text{-}Rh}$ = 213 Hz). Anal. calcd. for $C_{48}H_{46}BO_4P_2Rh$ (%): C 66.83, H 5.39; found: C 67.17, H 5.62.

General procedure for the hydroboration of vinylarenes

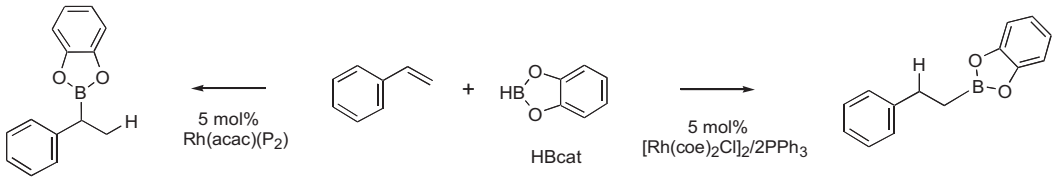
Under an atmosphere of dinitrogen, 1 equiv. of catecholborane in 0.5 mL of C_6D_6 was added to a 0.5 mL C_6D_6 solution of the appropriate catalyst and vinylarene. The reactions were allowed to proceed for 18 h, at which point NMR data were collected. Product distributions were confirmed by GC–MS.

X-ray crystallography

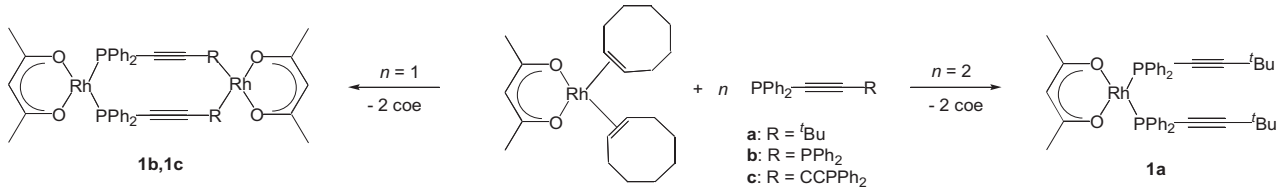
Crystals of **1a** and **2a** were grown from satd. Et_2O and toluene–hexane (1:1) solutions, respectively, at –30 °C. Single crystals were coated with Paratone-N oil, mounted using a glass fibre, and frozen in the cold stream of the goniometer. A hemisphere of data were collected on a Bruker AXS P4/SMART 1000 diffractometer using ω and θ scans with a scan width of 0.3° and exposure times of 30 s (**1a**) and 10 s (**2a**). The detector distances were 5 cm (**2a**) and 6 cm (**1a**). Crystals of **1a** were multiple twins; however, only the data for the major isomer lead to a successful structure refinement. The data were reduced (12*a*) and corrected for absorption (12*b*). The structures were solved by direct methods and refined by full-matrix least-squares on F^2 (12*c*). All non-hydrogen atoms were refined anisotropically. Hydrogen atoms were located in Fourier difference maps and refined isotropically.

© 2006 NRC Canada

Scheme 2. The rhodium-catalysed hydroboration of styrene with HBcat.



Scheme 3. Synthesis of rhodium complexes **1a**–**1c**.



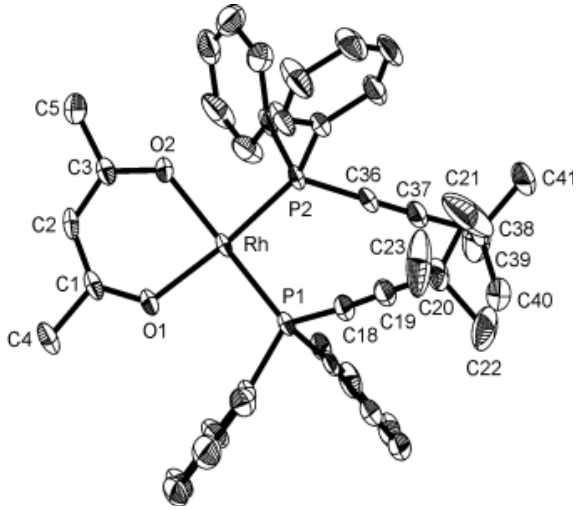
Results and discussion

Rhodium phosphine complexes are versatile and efficient catalysts for the hydroboration of alkenes using catecholborane (HBcat). Among this group, complexes of the type $Rh(acac)(P_2)$ (acac = acetylacetonato; P_2 = diphosphine) are unique in that they are the only catalyst precursors to have been used in the hydroboration of a tetrasubstituted alkene (13*a*). These complexes are also active and selective catalysts for the hydroboration of a wide range of vinylarenes using HBcat, giving predominantly the corresponding branched isomers (Scheme 2). Although a considerable amount of research has focused on using these complexes as catalysts for this reaction (13), all examples have used chelating bidentate phosphines. In this study, we have prepared the analogous rhodium acetylacetonato complexes bearing monodentate phosphinoalkynes and examined their ability to catalyze the hydroboration of vinylarenes.

Rhodium complexes

The coordination chemistry of bis(diphenylphosphino)acetylene and related alkynyl phosphines is an area of considerable interest (14–17). Although the normal mode of coordination is via the phosphine groups, examples where the alkyne unit is bound to a metal in a η^2-π fashion are also known (15*i*). We have found that alkynyl phosphines **a**–**c** add to $Rh(acac)(coe)_2$ (coe = *cis*-cyclooctene) to give $Rh(acac)(Ph_2PC{\equiv}C\text{-}t\text{-}Bu)_2$ (**1a**), $[\{Rh(acac)\}_2(\mu\text{-}Ph_2PC{\equiv}CPPh_2\text{-}\kappa^2P)_2]$ (**1b**), and $[\{Rh(acac)\}_2(\mu\text{-}Ph_2PC{\equiv}CC{\equiv}CPPh_2\text{-}\kappa^2P)_2]$ (**1c**), respectively (Scheme 3). All new complexes have been characterized by a number of physical methods, including multinuclear NMR spectroscopy. The $^{31}P\{^1H\}$ NMR spectra all showed doublets with coupling to rhodium with ca. $J_{P\text{-}Rh}$ = 195 Hz. Complex **1a** has also been characterized by a single crystal X-ray diffraction study (Fig. 1),[3] confirming that ligand **a** is bound to the metal centre via the phosphine groups. The rhodium atom lies in a distorted square-planar geometry with typical rhodium–oxygen distances of Rh—O(1) 2.057(3) and Rh—O(2) 2.061(3) Å

Fig. 1. The molecular structure of **1a** showing probability ellipsoids at 30% and hydrogen atoms omitted for clarity. Selected bond distances (Å) and angles (°): Rh—O(1) 2.057(3), Rh—O(2) 2.061(3), Rh—P(1) 2.173(1), Rh—P(2) 2.182(1), C(18)—C(19) 1.186(6), C(36)—C(37) 1.180(6); O(1)-Rh-O(2) 88.3(1), O(1)-Rh-P(1) 90.98(8), O(2)-Rh-P(1) 176.24(9), O(1)-Rh-P(2) 174.28(8), O(2)-Rh-P(2) 86.04(9), P(1)-Rh-P(2) 94.72(4), P(1)-C(18)-C(19) 174.2(4), P(2)-C(36)-C(37) 178.8(4).



found in other rhodium acetylacetonato complexes (18). Likewise, bond distances and angles within the phosphine ligands are similar to those reported previously, with C≡C bond lengths of C(18)—C(19) 1.186(6) and C(36)—C(37) 1.180(6) Å (17). Crystallographic data are given in Table 1. For complexes **1b** and **1c**, coordination of both phosphine groups to rhodium is observed by ^{31}P NMR spectroscopy.

As mentioned previously, phosphinorhodium acetylacetonato complexes are active and selective catalysts for the hydroboration of a wide range of alkenes. However, the catalyst resting state in these systems is believed to be the zwit-

[3] Supplementary data for this article are available on the journal Web site (http://canjchem.nrc.ca) or may be purchased from the Depository of Unpublished Data, Document Delivery, CISTI, National Research Council Canada, Ottawa, ON K1A 0R6, Canada. DUD 4088. For more information on obtaining material refer to http://cisti-icist.nrc-cnrc.gc.ca/irm/unpub_e.shtml. CCDC 275010 and 275011 contain the crystallographic data for this manuscript. These data can be obtained, free of charge, via www.ccdc.cam.ac.uk/conts/retrieving.html (Or from the Cambridge Crystallographic Data Centre, 12 Union Road, Cambridge CB2 1EZ, UK; fax +44 1223 336033; or deposit@ccdc.cam.ac.uk).

© 2006 NRC Canada

Table 1. Crystallographic data collection parameters for **1a** and **2a**.

	1a	**2a**
Formula	$C_{41}H_{45}O_2P_2Rh$	$C_{48}H_{46}BO_4P_2Rh$
fw	734.62	862.51
Crystal system	Triclinic	Triclinic
Space group	$P\bar{1}$	$P\bar{1}$
a (Å)	12.151(3)	11.749 9(9)
b (Å)	12.820(3)	14.204 1(11)
c (Å)	13.875(3)	14.348 2(11)
α (°)	97.010(3)	85.954(1)
β (°)	96.656(4)	70.850(1)
γ (°)	117.772(3)	71.777(1)
V (Å^3)	1861.0(7)	2 147.3(3)
Z	2	2
ρ_{calcd} (mg m^{-3})	1.311	1.334
Crystal size (mm^3)	0.225×0.2×0.05	0.40×0.35×0.15
Temperature (K)	173(1)	173(1)
Radiation	Mo Kα (λ = 0.710 73 Å)	Mo Kα (λ = 0.710 73 Å)
μ (mm^{-1})	0.578	0.515
Total reflections	8835	15 025
Total unique reflections	5824	9 365
No. of variables	454	541
R_{int}	0.034 1	0.015 7
θ Range (°)	1.83–24.99	1.50–27.49
Largest difference peak/hole (e Å^{-3})	2.529/–2.163	0.887/–0.239
S (GoF) on F^2	1.013	1.067
R_1[a] ($I>2\sigma(I)$)	0.060 1	0.028 6
wR_2[b] (all data)	0.156 4	0.077 9

[a] $R_1 = \Sigma||F_o| - |F_c||/\Sigma|F_o|$.
[b] $wR_2 = (\Sigma[w(F_o^2 - F_c^2)^2]/\Sigma[wF_o^4])^{1/2}$, where $w = 1/[\sigma^2(F_o^2) + (0.1223P)^2]$ (**1a**) and $w = 1/[\sigma^2(F_o^2) + (0.0436P)^2 + (0.6575P)]$ (**2a**), where $P = (\max(F_o^2, 0) + 2F_c^2)/3$.

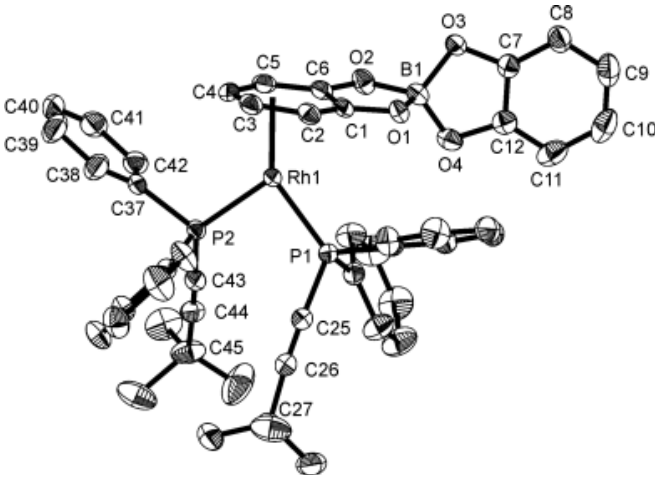
terionic complexes Rh(η^6-catBcat)(P_2), arising from the redistribution of substituents on HBcat. Indeed, hydroborations using these zwitterionic complexes give similar selectivities to those observed for the acetylacetonato precursors (13). In an elegant study, Marder and co-workers (13*d*) found that addition of B_2cat_3 to Rh(acac)(P_2) led to the zwitterionic complexes Rh(η^6-catBcat)(P_2) in high yields, along with concomitant formation of acacBcat. The diboron species B_2cat_3 is generated as an unwanted decomposition product in nucleophilic reactions with HBcat or when HBcat is heated to elevated temperatures (7*f*). We have found that addition of B_2cat_3 to **1a** gave the corresponding zwitterionic complex Rh(η^6-catBcat)($Ph_2PC{\equiv}C$-*t*-Bu)$_2$ (**2a**), which represents the first example of this type of compound to bear monodentate phosphine ligands (13*d*) to be structurally characterized by X-ray diffraction. The $^{31}P\{^1H\}$ NMR spectrum shows a doublet with coupling to rhodium at $J_{P\text{-}Rh}$ = 213 Hz and the ^{11}B NMR has a sharp peak at 15 ppm, consistent with the boron atom being four coordinate (19, 20). The molecular structure of **2a** has been confirmed by a single crystal X-ray diffraction study (Fig. 2) and shows that the P_2Rh fragment is bound to the catBcat$^-$ anion via one of the catecholato groups in a η^6 fashion. As with related systems (19), there appears to be considerable slippage of the P_2Rh group with respect to the π-bound arene ring. Indeed, two bond distances, Rh(1)—C(4) and Rh(1)—C(3), are considerably shorter (2.254(2) and 2.275(2) Å) than the remaining Rh—C bonds (ranging from 2.336(2) to 2.497(2) Å). The potential surface for such distortions is reputably quite shallow. Initial attempts to prepare **1b** and **1c** via this route were complicated by considerable degradation to give rhodium metal and a number of unidentified rhodium phosphine complexes. Interestingly, the reactivity of related rhodium β-diketonate diphosphine complexes with chlorinated solvents has been reported previously (21).

Hydroboration studies

To compare complexes **1a**–**1c** against other rhodium catalysts, we have examined their ability to catalyse the hydroboration of a series of vinylarenes. Initial studies were done on 4-vinylanisole in C_6D_6 (**3**, Table 2), and as with many other rhodium catalysts, all new phosphinoalkyne complexes gave selective formation of the branched isomer **3a**. Interestingly, hydroborations with isolated **2a** also gave exclusive formation of this product. In reactions of 4-fluorostyrene (**4**), however, complexes **1a** and **1c** gave small amounts of diboration product **4c** and hydrogenation product **4d**. Diborated product **4c** presumably arises from hydroboration of the transient vinyl boronate ester 4-F-C_6H_4CH=CHBcat, which is generated from a competing dehydrogenative borylation reaction (22). The vinyl boronate ester products are not observed to any extent, via ^1H NMR spectroscopy, in reactions using these relatively unhindered alkenes. Dehydrogenative borylations are generally believed to occur via initial coordination of the alkene to the metal centre followed by insertion into the Rh—B, and not the Rh—H, bond, with subsequent

© 2006 NRC Canada

Fig. 2. The molecular structure of **2a** showing probability ellipsoids at 30% and hydrogen atoms omitted for clarity. Selected bond distances (Å) and angles (°): Rh(1)—P(2) 2.2129(5), Rh(1)—P(1) 2.2260(5), Rh(1)—C(4) 2.254(2), Rh(1)—C(3) 2.275(2), Rh(1)—C(2) 2.336(2), Rh(1)—C(1) 2.392(2), Rh(1)—C(5) 2.429(2), Rh(1)—C(6) 2.497(2), B(1)—O(4) 1.461(3), B(1)—O(3) 1.469(2), B(1)—O(2) 1.494(3), B(1)—O(1) 1.511(2), C(25)—C(26) 1.193(3), C(43)—C(44) 1.185(3); P(2)-Rh(1)-P(1) 91.85(2), O(4)-B(1)-O(3) 106.1(2), O(4)-B(1)-O(2) 112.7(2), O(3)-B(1)-O(2) 113.8(2), O(4)-B(1)-O(1) 111.5(2), O(3)-B(1)-O(1) 109.8(2), O(2)-B(1)-O(1) 103.2(2).



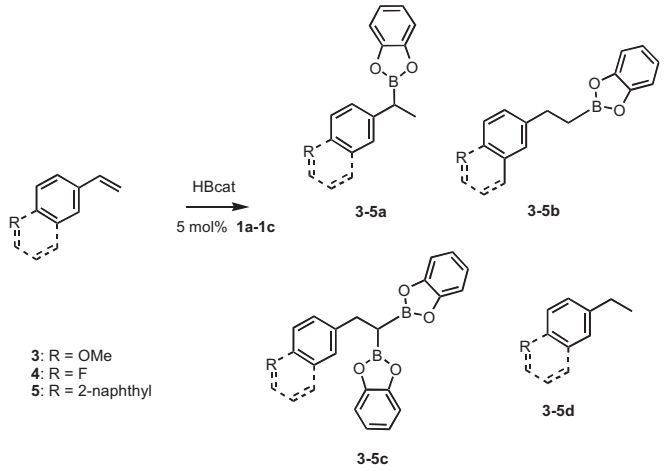
β-H elimination to give the corresponding vinyl boronate ester and an active rhodium dihydride species. This latter dihydride is presumably responsible for the hydrogenation of the starting alkene to give **4d**. Similar selectivities were observed in hydroborations of 2-vinylnaphthylene (**5**). Interestingly, dirhodium complex **1b** gave the best selectivities of the three new rhodium complexes examined for these reactions. Ratios of products were determined by multinuclear NMR spectroscopy and confirmed by GC–MS (7*e*, 13*a*).

Hydroborations of electron-deficient 2,3,4,5,6-pentafluorostyrene (**6**) were also examined, and selectivities are similar to that observed in reactions with 4-vinylanisole (Table 3). These results suggest the electronic nature of the arene group does not play a significant role in these hydroborations. Increasing the steric bulk around the alkene group by addition of fluorine groups in the 2 and 6 positions also did not seem to affect selectivities.

We then decided to investigate reactions of 2,4,6-trimethylstyrene (**7**), where the methyl groups further increase the steric crowding around the vinyl group. As expected, catalysed hydroborations of this bulkier vinylarene gave a mixture of branched (**7a**) and linear product (**7b**), along with a considerable amount of diborated product (**7c**), when complex **1a** was used (Table 4). Minor amounts of vinyl boronate ester product are observed by ^{1}H NMR spectroscopy (<1%). Rhodium complex **1c**, containing the dialkyne units, gave a significant amount of the linear product **7b**. It is plausible that reactions using **1b** and **1c** are complicated by addition of HBcat to the sterically uncongested dialkyne unit. Indeed, severe degradation of the starting rhodium complex is often observed in these reactions.

While results with vinylarene **7** show that steric hindrance caused by methyl groups ortho to the arene ring can alter

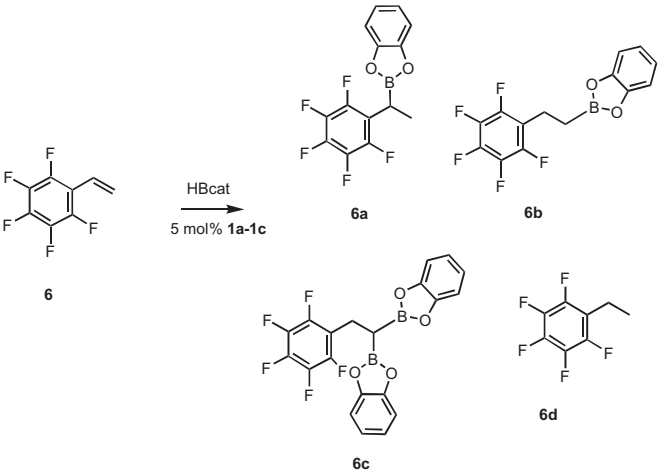
Table 2. Rhodium catalysed hydroboration of vinylarenes **3–5** using 1.1HBcat.



Catalyst	a	b	c	d
4-Vinylanisole	**3a**	**3b**	**3c**	**3d**
1a	>98	—	—	—
1b	>98	—	—	—
1c	>98	—	—	—
4-Fluorostyrene	**4a**	**4c**	**4c**	**4d**
1a	95	—	2	3
1b	>98	—	—	—
1c	98	—	2	—
2-Vinylnaphthalene	**5a**	**5b**	**5c**	**5d**
1a	90	—	—	10
1b	>98	—	—	—
1c	97	—	—	3

Note: Ratios were determined by ^{1}H NMR spectroscopy.

Table 3. Rhodium catalysed hydroboration of **6** using 1.1HBcat.

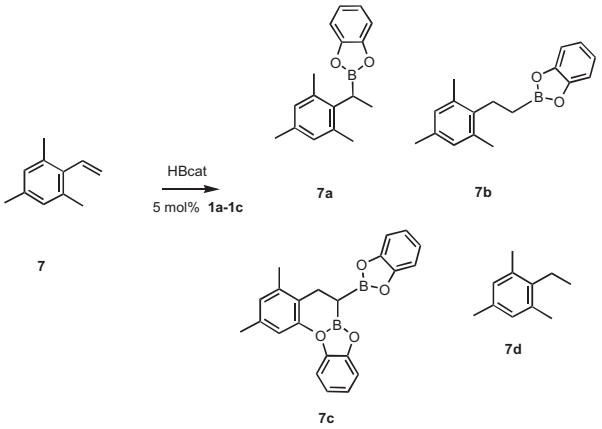


Catalyst	6a	6b	6c	6d
1a	96	—	2	2
1b	96	—	2	2
1c	96	—	2	2

Note: Ratios were determined by ^{1}H NMR spectroscopy.

© 2006 NRC Canada

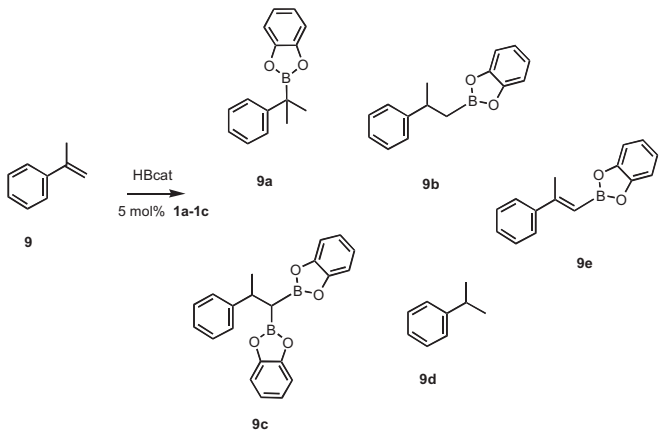
Table 4. Rhodium catalysed hydroboration of **7** using 1.1HBcat.



Catalyst	7a	7b	7c	7d
1a	40	40	15	5
1b	40	55	—	5
1c	5	85	10	—

Note: Ratios were determined by ^{1}H NMR spectroscopy.

Table 5. Rhodium catalysed hydroboration of **9** using 1.1HBcat.



Catalyst	9a	9b	9c	9d	9e
1a	40	30	20	5	5
1b	50	25	10	5	10
1c	40	30	15	10	5

Note: Ratios were determined by ^{1}H NMR spectroscopy.

hydroboration selectivities, reactions with *trans*-β-methylstyrene (**8**), where a methyl group is substituted for a hydrogen in the β position of the vinyl group, gave selective formation of $C_6H_5CH(Bcat)CH_2CH_3$ (**8a**) regardless of the choice of catalyst used to affect this transformation. The other isomer ($C_6H_5CH_2CH(Bcat)CH_3$, **8b**) was not observed to any significant extent. Reactions with α-methylstyrene (**9**), however, where substitution occurs in the α position, gave extremely complicated product distributions (Table 5). The corresponding vinyl boronate ester ($C_6H_5CMe{=}CH(Bcat)$, **9e**) was also observed to a considerable extent in these reactions, especially when complex **1b** was used to catalyse this reaction. Although linear product **9b** could be generated from a traditional catalysed hydroboration reaction, it is also plausible that this product arises from the catalysed hydrogenation of vinyl boronate ester **9e**.

Conclusions

Three novel rhodium(I) acetylacetonato (acac) complexes bearing phosphinoalkynes ($Ph_2PC{\equiv}C$-*t*-Bu, $Ph_2PC{\equiv}CPPh_2$, and $Ph_2PC{\equiv}CC{\equiv}CPPh_2$) have been prepared and characterized fully, including an X-ray diffraction study for $Rh(acac)(Ph_2PC{\equiv}C$-*t*-$Bu)_2$ (**1a**). Addition of B_2cat_3 (cat = 1,2-$O_2C_6H_4$) to $Rh(acac)(Ph_2PC{\equiv}C$-*t*-$Bu)_2$ (**1a**) led to zwitterionic $Rh(\eta^6$-catBcat$)(Ph_2PC{\equiv}C$-*t*-$Bu)_2$ (**2a**), which was also characterized by an X-ray diffraction study. This represents a novel zwitterionic rhodium complex bearing monodentate phosphine ligands. All new rhodium complexes are active catalysts for the hydroboration of a wide range of vinylarenes. Selectivities are excellent for reactions using unhindered vinylarenes (including *trans*-β-methylstyrene) and favour the formation of the corresponding branched hydroboration products. Reactions with hindered vinylarenes, however, give complicated product distributions, arising from a competing dehydrogenative borylation reaction.

Acknowledgements

Thanks are gratefully extended to the Natural Sciences and Engineering Research Council of Canada (NSERC), Canada Research Chairs Programme, Canadian Foundation for Innovation-Atlantic Innovation Fund, and Mount Allison University for financial support. We also thank Roger Smith and Dan Durant for their expert technical assistance, Professor J.F. Corrigan (The University of Western Ontario, London, Ontario) for the generous gift of phosphinoalkynes, and anonymous reviewers for helpful comments.

References

1. H.C. Brown. Hydroborations. Wiley-Interscience, New York. 1962.
2. A. Pelter, K. Smith, and H.C. Brown. Borane reagents. Academic Press, New York. 1988.
3. C.F. Lane and G.W. Kabalka. Tetrahedron, **32**, 981 (1976).
4. D. Männig and H. Nöth. J. Chem. Soc. Dalton Trans. 1689 (1985).
5. (*a*) R. Wilczynski and L.G. Sneddon. J. Am. Chem. Soc. **102**, 2857 (1980); (*b*) E.W. Corcoran, Jr. and L.G. Sneddon. J. Am. Chem. Soc. **106**, 7793 (1984); (*c*) J.D. Hewes, C.W. Kreimendahl, T.B. Marder, and M.F. Hawthorne. J. Am. Chem. Soc. **106**, 5757 (1984).
6. D. Männig and H. Nöth. Angew. Chem. Int. Ed. Engl. **24**, 878 (1985).
7. (*a*) D.A. Evans, G.C. Fu, and A.H. Hoveyda. J. Am. Chem. Soc. **114**, 6671 (1992); (*b*) K. Burgess and M.J. Ohlmeyer. Chem. Rev. **91**, 1179 (1991); (*c*) C.M. Crudden and D. Edwards. Eur. J. Org. Chem. 4695 (2003); (*d*) I. Beletskaya and A. Pelter. Tetrahedron, **53**, 4957 (1997); (*e*) K. Burgess, W.A. van der Donk, S.A. Westcott, T.B. Marder, R.T. Baker, and J.C. Calabrese. J. Am. Chem. Soc. **114**, 9350 (1992); (*f*) S.A. Westcott, H.P. Blom, T.B. Marder, R.T. Baker, and J.C. Calabrese. Inorg. Chem. **32**, 2175 (1993); (*g*) M.G.L. Mirabelli and L.G. Sneddon. J. Am. Chem. Soc. **110**, 449 (1988); (*h*) Y.

© 2006 NRC Canada

Matsumoto, M. Naito, and T. Hayashi. Organometallics, **11**, 2732 (1992); (*i*) N. Miyaura, T. Ishiyama, H. Sasaki, M. Ishikawa, M. Satoh, and A. Suzuki. J. Am. Chem. Soc. **111**, 314 (1989); (*j*) J.R. Knorr and J.S. Merola. Organometallics, **9**, 3008 (1990); (*k*) J.M. Brown. Modern rhodium catalyzed organic reactions. *Edited by* P.A. Evans. Wiley-VCH, Weinheim. 2004; (*l*) C. Fu, M. Beller, and C. Bolm. Transition metals for organic synthesis. Wiley-VCH, Weinheim. 1998; (*m*) A.-M. Carroll, T.P. O'Sullivan, and P.J. Guiry. Adv. Synth. Catal. **347**, 609 (2005).

8. (*a*) E. Daura-Oller, A.M. Segarra, J.M. Poblet, C. Claver, E. Fernández, and C. Bo. J. Org. Chem. **69**, 2669 (2004), and refs. cited therein; (*b*) C. Widauer, H. Grützmacher, and T. Ziegler. Organometallics, **19**, 2097 (2000); (*c*) A.M. Segarra, R. Guerrero, C. Claver, and E. Fernández. Chem. Commun. (Cambridge), 1808 (2001); (*d*) A.M. Segarra, F. Guirado, C. Claver, and E. Fernández. Tetrahedron: Asymmetry, **14**, 1611 (2003); (*e*) M. Diéguez, A. Ruiz, C. Claver, M.M. Pereira, M.T. Flor, J.C. Bayón, M.E.S. Serra, and A.M. d'A. Rocha Gonsalves. Inorg. Chim. Acta, **295**, 64 (1999).
9. (*a*) D.L. Connolly, P.M. Lacey, M. McCarthy, C.P. Saunders, A.-M. Carroll, R. Goddard, and P.J. Guiry. J. Org. Chem. **69**, 6572 (2004); (*b*) S. Gladiali, G. Loriga, S. Medici, and R. Taras. J. Mol. Catal. A, **196**, 27 (2003); (*c*) R.J. Kloetzing, M. Lotz, and P. Knochel. Tetrahedron: Asymmetry, **1**4 255 (2003); (*d*) F.Y. Kwong, Q. Yang, T.C.W. Mak, A.S.C. Chan, and K.S. Chan. J. Org. Chem. **67**, 2769 (2002); (*e*) T.A. Betley and J.C. Peters. Angew. Chem. Int. Ed. **42**, 2385 (2003); (*f*) C. Borriello, M.E. Cucciolito, A. Panunzi, and F. Ruffo. Inorg. Chim. Acta, **353**, 238 (2003); (*g*) G. Chelucci, G. Orrù, and G.A. Pinna. Tetrahedron, **59**, 9471 (2003); (*h*) A. Korostylev, I. Gridnev, and J.M. Brown. J. Organomet. Chem. **680**, 329 (2003); (*i*) P.J. Guiry, M. McCarthy, P.M. Lacey, C.P. Saunders, S. Kelly, and D.J. Connolly. Curr. Org. Chem. **4**, 821 (2000).
10. [$Ph_2PC{\equiv}C$-*t*-Bu]: A.J. Carty, N.K. Hota, T.W. Ng, H.A. Patel, and T. O'Connor. Can. J. Chem. **49**, 2706 (1971); [$Ph_2PC{\equiv}CPPh_2$]: D.R.M. Walton and F. Waugh. J. Organomet. Chem. **37**, 45 (1972); [$Ph_2PC{\equiv}CC{\equiv}CPPh_2$]: M.I. Bruce, J.M. Patrick, A.H. White, and M.L. Williams. J. Chem. Soc. Dalton Trans. 1229 (1985).
11. J.M. Burke, R.B. Coapes, A.E. Goeta, J.A.K. Howard, T.B. Marder, E.G. Robins, and S.A. Westcott. J. Organomet. Chem. **649**, 199 (2002).
12. (*a*) Bruker AXS, Inc. SAINT 6.02 [computer program]. Bruker AXS, Inc., Madison, Wisconsin 1997–1999; (*b*) G.M. Sheldrick. SADABS [computer program]. Bruker AXS, Inc., Madison, Wisconsin. 1999; (*c*) G.M. Sheldrick. SHELXTL 5.1 [computer program]. Bruker AXS, Inc., Madison, Wisconsin. 1997.
13. (*a*) S.A. Westcott, H.P. Blom, T.B. Marder, and R.T. Baker. J. Am. Chem. Soc. **114**, 8863 (1992); (*b*) P. Nguyen, R.B. Coapes, A.D. Woodward, N.J. Taylor, J.M. Burke, J.A.K. Howard, and T.B. Marder. J. Organomet. Chem. **652**, 77 (2002); (*c*) R.T. Baker, P. Nguyen, T.B. Marder, and S.A. Westcott. Angew. Chem. Int. Ed. Engl. **34**, 1336 (1995); (*d*) C. Dai, E.G. Robins, A.J. Scott, W. Clegg, D.S. Yufit, J.A.K. Howard, and T.B. Marder. Chem. Commun. (Cambridge), 1983 (1998).
14. (*a*) A.J. Carty and A. Efraty. Can. J. Chem. **46**, 1598 (1968); (*b*) A.J. Carty and A. Efraty. Can. J. Chem. **47**, 2573 (1969); (*c*) A.J. Carty and A. Efraty. Inorg. Chem. **8**, 543 (1969); (*d*) A.J. Carty and A. Efraty. Inorg. Nucl. Chem. Lett. **4**, 427 (1968); (*e*) A.J. Carty, A. Efraty, and T.W. Ng. Can. J. Chem. **47**, 1429 (1969); (*f*) A.J. Carty, T.W. Ng, W. Carter, G.J. Palenik, and T. Birchall. J. Chem. Soc. Chem. Commun. 1101 (1969); (*g*) A.J. Carty and T.W. Ng. J. Chem. Soc. Chem. Commun. 149 (1970); (*h*) A.J. Carty, A. Efraty, T.W. Ng, and T. Birchall. Inorg. Chem. **9**, 1263 (1970); (*i*) W.A. Anderson, A.J. Carty, and A. Efraty. Can. J. Chem. **47**, 3361 (1969); (*j*) A.J. Carty, S.A. MacLaughlin, J. Van Wagner, and N.J. Taylor. Organometallics, **1**, 1013 (1982); (*k*) Y.S. Wong, S. Jacobson, P.C. Chieh, and A.J. Carty. Inorg. Chem. **13**, 284 (1974).
15. (*a*) K.S. Wheelock, J.H. Nelson, and H.B. Jonassen. Inorg. Chim. Acta, **7**, 1063 (1971); (*b*) G.R. Eaton and R.H. Holm. Inorg. Chem. **10**, 805 (1971); (*c*) R.B. King, L.W. Houk, and P.N. Kapoor. Inorg. Chem. **8**, 1792 (1969); (*d*) G. Hogarth and T. Norman. J. Chem. Soc. Dalton Trans. 1077 (1996); (*e*) G. Hogarth and J.Y. Pang. J. Organomet. Chem. **515**, 193 (1996); (*f*) G. Minghetti, M.A. Cinellu, S. Stoccoro, A. Zucco, and M. Manassero. J. Chem. Soc. Dalton Trans. 777 (1995); (*g*) K. Dillinger, W. Oberhauser, C. Bachmann, and P. Brueggeller. Inorg. Chim. Acta, **223**, 13 (1994); (*h*) M.E. Wright, L. Lawson, R.T. Baker, and D.C. Roe. Polyhedron, **11**, 323 (1992); (*i*) C. Elschenbroich, J. Sebbach, B. Metz, and G. Heikenfeld. J. Organomet. Chem. **426**, 173 (1992); (*j*) M.I. Bruce, J.M. Patrick, A.H. White, and M.L. Williams. J. Chem. Soc. Dalton Trans. 1229 (1985); (*k*) G. Jia, R.J. Puddephatt, J.D. Scott, and J.J. Vittal. Organometallics, **12**, 3565 (1993); (*l*) D. Rodewald, C. Schulzke, and D. Rehder. J. Organomet. Chem. **498**, 29 (1995).
16. (*a*) J.R. Galsworthy, C.E. Housecroft, and A.L. Rheingold. J. Chem. Soc. Dalton Trans. 2917 (1996); (*b*) M.P. Cifuentes, M.G. Humphrey, and A.C. Willis. J. Organomet. Chem. **513**, 85 (1996); (*c*) E. Louattini, J. Suades, K. Urtiaga, M.I. Arriortua, and X. Solans. Organometallics, **15**, 468 (1996); (*d*) S.M. Draper, C.E. Housecroft, J.S. Humphrey, and A.L. Rheingold. J. Chem. Soc. Dalton Trans. 3789 (1995); (*e*) J. Lee, M.G. Humphrey, D.C.R. Hockless, B.W. Skelton, and A.H. White. Organometallics, **12**, 3468 (1993); (*f*) C.J. Adams, M.I. Bruce, B.W. Skelton, and A.H. White. J. Organomet. Chem. **447**, 91 (1993).
17. (*a*) A.I. Wallbank and J.F. Corrigan. Can. J. Chem. **80**, 1592 (2002); (*b*) M. Semmelmann, D. Fenske, and J.F. Corrigan. J. Chem. Soc. Dalton Trans. 2541 (1998); (*c*) J.R. Berenguer, M. Bernechea, J. Forniés, A. García, and E. Lalinde. Organometallics, **23**, 4288 (2004); (*d*) F.-E. Hong, Y.-J. Ho, Y.-C. Chang, and Y.-C. Lai. Tetrahedron, **60**, 2639 (2004); (*e*) D.F. Jones, P.H. Dixneuf, T.G. Southern, J.-Y. Le Marouille, D. Grandjean, and P. Guenot. Inorg. Chem. **20**, 3247 (1981); (*f*) F.-E. Hong, Y.-C. Chang, R.-E. Chang, S.-C. Chen, and B.-T. Ko. Organometallics, **21**, 961 (2002); (*g*) L. Li, N. Reginato, M. Urschey, M. Stradiotto, and J.D. Liarakos. Can. J. Chem. **81**, 468 (2003); (*h*) H.C. Clark, G. Ferguson, P.N. Kapoor, and M. Parvez. Inorg. Chem. **24**, 3924 (1985); (*i*) J.-L. Chen, L.-Y. Zhang, Z.-N. Chen, L.-B. Gao, M. Abe, and Y. Sasaki. Inorg. Chem. **43**, 1481 (2004); (*j*) M.-C. Brandys and R.J. Puddephatt. J. Am. Chem. Soc. **124**, 3946 (2002); (*k*) D. Xu, H.J. Murfee, W.E. van der Veer, and B. Hong. J. Organomet. Chem. **596**, 53 (2000); (*l*) A.J. Amoroso, B.F.G. Johnson, J. Lewis, A.D. Massey, P.R. Raithby, and W.T. Wong. J. Organomet. Chem. **440**, 219 (1992).
18. (*a*) N.A. Bailey, E. Coates, G.B. Robertson, F. Bonanit, and R. Ugo. J. Chem. Soc. Chem. Commun. 1041 (1967); (*b*) G.G. Aleksandrov, Yu.T. Struchikov, V.S. Khandkarova, and S.P. Gubin. J. Organomet. Chem. **25**, 243 (1970); (*c*) D.R. Russell and P.A. Tucker. J. Chem. Soc. Dalton Trans. 841 (1976); (*d*) M.J. Chetcuti, P.A.M. Chetcuti, J.C. Jeffrey, R.M. Mills, P.

© 2006 NRC Canada

Mitrprachachon, S.J. Pickering, F.G.A. Stone, and P. Woodward. J. Chem. Soc. Dalton Trans. 699 (1982); (*e*) J.G. Leipoldt, G.J. Lamprecht, and G.J. Van Zyl. Inorg. Chim. Acta, **96**, L31 (1985); (*f*) V.A. Nikanorow, V.I. Rozenberg, A.I. Yanovsky, Yu.T. Struchkov, O.A. Reutov, B.I. Ginsburg, V.V. Kaverin, and V.P. Yur'ev. J. Organomet. Chem. **307**, 363 (1986); (*g*) E.E. Nifantyev, A.T. Teleshev, T.A. Shikovets, A.R. Bekker, A.N. Chernega, M.Yu. Antipin, and Yu.T. Struchkov. J. Organomet. Chem. **336**, 237 (1987); (*h*) D.W. Price, M.G.B. Drew, K.K. Hii, and J.M. Brown. Chem. Eur. J. **6**, 4587 (2000); (*i*) M.A. Esteruelas, F.J. Lahoz, M. Martin, E. Onate, and L.A. Oro. Organometallics, **16**, 4572 (1997); (*j*) S. Otto, A. Roodt, J.J.C. Erasmus, and J.C. Swarts. Polyhedron, **17**, 2447 (1998); (*k*) M.B. Dinger and M.J. Scott. Inorg. Chem. **40**, 856 (2001); (*l*) M.A. Esteruelas, F.J. Lahoz, E. Onate, L.A. Oro, and L. Rodrguez. Organometallics, **15**, 3436 (1996); (*m*) F. Agbossou, J.-F. Carpentier, C. Hatat, N. Kokel, A. Mortreux, P. Betz, R. Goddard, and C. Kuger. Organometallics, **14**, 2480 (1995).

19. (*a*) M.J. Nolte and G. Gafner. Acta Crystallogr. Sect. B, **30**, 738 (1974); (*b*) S.A. Westcott, N.J. Taylor, T.B. Marder, R.T. Baker, N.J. Jones, and J.C. Calabrese. J. Chem. Soc. Chem. Commun. 304 (1991).
20. H. Nöth and B. Wrackmeyer. *In* Nuclear magnetic resonance spectroscopy of boron compounds. Springer-Verlag, Berlin. 1978.
21. P.J. Fennis, P.H.M. Budzelaar, J.H.G. Frijns, and A.G. Orpen. J. Organomet. Chem. **393**, 287 (1990).
22. (*a*) B. Marciniec, M. Jankowska, and C. Pietraszuk. Chem. Commun. (Cambridge, U.K.), 663 (2005); (*b*) J.M. Brown and G.C. Lloyd-Jones. J. Chem. Soc. Chem. Commun. 710 (1992); (*c*) S.A. Westcott, T.B. Marder, and R.T. Baker. Organometallics, **12**, 975 (1993); (*d*) J.M. Brown and G.C. Lloyd-Jones. J. Am. Chem. Soc. **116**, 866 (1994); (*e*) D.H. Motry, A.G. Brazil, and M.R. Smith III. J. Am. Chem. Soc. **119**, 2743 (1997); (*f*) M. Murata, S. Watanabe, and Y. Masuda. Tetrahedron Lett. **40**, 2585 (1999); (*g*) M. Murata, K. Kawakita, T. Asana, S. Watanabe, and Y. Masuda. Bull. Chem. Soc. Jpn. **75**, 825 (2002); (*h*) C. Morrill, T.W. Funk, and R.H. Grubbs. Tetrahedron Lett. **45**, 7733 (2004); (*i*) C.M. Vogels, P.G. Hayes, M.P. Shaver, and S.A. Westcott. Chem. Commun. (Cambridge), 51 (2000); (*j*) R.B. Coapes, F.E.S. Souza, R.Ll. Thomas, J.J. Hall, and T.B. Marder. Chem. Commun. (Cambridge), 614 (2003); (*k*) P. Nguyen, R.B. Coapes, A.D. Woodward, N.J. Taylor, J.M. Burke, J.A.K. Howard, and T.B. Marder. J. Organomet. Chem. **652**, 77 (2002).

© 2006 NRC Canada

The synthesis, structure, and electrochemical properties of Fe(C≡CC≡N)(dppe)Cp and related compounds[1]

Mark E. Smith, Richard L. Cordiner, David Albesa-Jové, Dmitri S. Yufit, František Hartl, Judith A.K. Howard, and Paul J. Low

Abstract: The cyanoacetylide complex Fe(C≡CC≡N)(dppe)Cp (**3**) is readily obtained from sequential reaction of $Fe(C{\equiv}CSiMe_3)(dppe)Cp$ with methyllithium and phenyl cyanate. Complex **3** is a good metalloligand, and coordination to the metal fragments $[RhCl(CO)_2]$, $[Ru(PPh_3)_2Cp]^+$, and $[Ru(dppe)Cp^*]^+$ affords the corresponding cyanoacetylide-bridged heterobimetallic complexes. In the case of the 36-electron complexes $[Cp(dppe)Fe\text{-}C{\equiv}CC{\equiv}N\text{-}ML_n]^{n+}$, spectroscopic and structural data are consistent with a degree of charge transfer from the iron centre to the rhodium or ruthenium centre via the C_3N bridge, giving rise to a polarized ground state. Electrochemical and spectroelectrochemical methods reveal significant interactions between the metal centres in the oxidized (35 electron) derivatives, $[Cp(dppe)Fe\text{-}C{\equiv}CC{\equiv}N\text{-}ML_n]^{(n+1)+}$.

Key words: cyanide, cyanoacetylide, crystal structure.

Résumé : Le complexe cyanoacétylure Fe(C≡CC≡N)(dppe)Cp (**3**) est facilement préparé par la réaction séquentielle du $Fe(C{\equiv}CSiMe_3)(dppe)Cp$ avec le méthyllithium et le cyanate de phényle. Le complexe **3** est un bon métalloligand et sa coordination aux fragments métalliques $[RhCl(CO)_2]$, $[Ru(PPh_3)_2Cp]^+$ et $[Ru(dppe)Cp^*]^+$ conduit à la formation des complexes hétérobimétalliques à point cyanoacétylure. Dans le cas des complexes à 36 électrons $[Cp(dppe)Fe\text{-}C{\equiv}CC{\equiv}N\text{-}ML_n]^{n+}$, les données spectroscopiques et structurales sont en accord avec un certain degré de transfert de charge du centre ferrique à rhodium ou au centre ruthénium par le biais du pont C_3N, ce qui conduit à un état fondamental polarisé. Les méthodes électrochimiques et spectroélectrochimiques révèlent l'existence d'interactions importantes entre les centres métalliques des dérivés oxydés (à 35 électrons) de formule générale $[Cp(dppe)Fe\text{-}C{\equiv}CC{\equiv}N\text{-}ML_n]^{(n+1)+}$.

Mots clés : cyanure, cyanoacétylure, structure cristalline.

[Traduit par la Rédaction]

Introduction

The chemistry of organometallic complexes featuring unsaturated ligands has been a source of interest for decades, owing to the unusual physical properties and chemical reactivity that arises from the mixing of metal d and ligand π orbitals. Acetylides and acetylenes are among the most structurally simple unsaturated ligands, offering cylindrical symmetry about the C≡C moiety, and a polarizable π system. However, these structurally simple ligands are remarkably electronically diverse, being capable of formally donating one to six electrons to metal fragments and frameworks through various combinations of the filled ligand σ and π orbitals.

Our interests in complexes featuring C≡C based ligands stem from the rich electrochemical response of bimetallic polyyndiyl systems (1), the coordinative flexibility of (poly)yne ligands (2), and the chemical, physical, and spectroscopic properties of metal complexes featuring polycarbon ligands that depend heavily on the mixing of metal and carbon orbitals (3). In seeking to extend these studies, and at the same time to explore the relationships that exist between acetylide, $[C{\equiv}CR]^-$, and isoelectronic cyanide, $[C{\equiv}N]^-$, based unsaturated ligands, we were drawn to the cyanoacetylide ligand, $[C{\equiv}CC{\equiv}N]^-$.

We have recently developed convenient syntheses of several ruthenium complexes featuring the cyanoacetylide ligand, such as $[Ru(C{\equiv}CC{\equiv}N)(PPh_3)_2Cp]$ (4). In the process

Received 13 June 2005. Published on the NRC Research Press Web site at http://canjchem.nrc.ca on 23 February 2006.

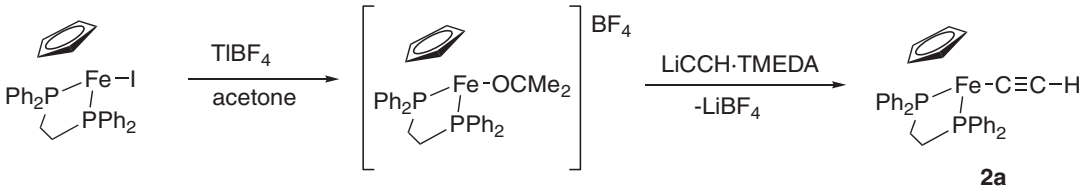
Dedicated to Arthur J. Carty, a respected mentor and valued friend, in recognition of his outstanding contributions to science.

M.E. Smith, R.L. Cordiner, D. Albesa-Jové, D.S. Yufit, J.A.K. Howard, and P.J. Low.[2] Department of Chemistry, University of Durham, South Rd, Durham DH1 3LE, UK.
F. Hartl. Van't Hoff Institute for Molecular Sciences, University of Amsterdam, Nieuwe Achtergracht 166, 1018 WV Amsterdam, The Netherlands.

[1]This article is part of a Special Issue dedicated to Professor Arthur Carty.
[2]Corresponding author (e-mail: p.j.low@durham.ac.uk).

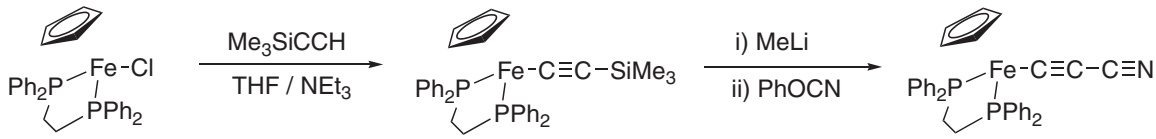
 doi:10.1139/V05-238 © 2006 NRC Canada

Scheme 1.

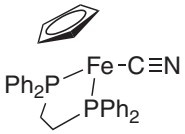


2a

Scheme 2.



1 **2b** **3**



4

of extending the synthetic methodology, we have had cause to prepare the related iron complex [Fe(C≡CC≡N)(dppe)Cp] (**3**). In this paper we describe the synthesis, molecular structure, and electrochemical response of **3**, together with those of several related complexes.

Results and discussion

Acetylide complexes featuring the elementary structure [Fe(C≡CR)(dppx)Cp] (dppx = bis(diphenylphosphino)methane, dppm; 1,2-bis(diphenylphosphino)ethane, dppe) are well-known (5), yet in recent times the development of the chemistry of this system has fallen behind that of the more electron-rich and sterically encumbered [Fe(C≡CR)(dppe)Cp*] analogues (Cp* = η^5-C_5Me_5) (6). This is somewhat surprising given the quite straightforward synthesis of the key reagent [FeCl(dppe)Cp] (**1a**) (7).

In seeking to access an iron cyanoacetylide complex of the general form [Fe(C≡CC≡N)(dppe)Cp], we required access to a synthon for the nucleophilic acetylide anion [Fe(C≡C$^-$)(dppe)Cp]. Although Fe(C≡CH)(dppe)Cp (**2a**) is a known compound (5*b*), the existing synthesis (reaction of Fe(dppe)Cp]$^+$ with [LiC≡CH·TMEDA]) (Scheme 1) was not considered to be optimal given the many advances in synthetic transition metal acetylide chemistry that have been made since the original report of this compound.

We chose instead to examine the possibility of preparing either **2a** or [Fe(C≡CSiMe_3)(dppe)Cp] (**2b**) by formation of the analogous vinylidene, and deprotonation in situ (8). Thus, reaction of [FeCl(dppe)Cp] with excess (4 equiv.) HC≡CSiMe_3 in THF–NEt_3 (1:1 volumetric ratio) resulted in a gradual colour change in the solution from dark purple to orange. Workup gave the orange trimethylsily-protected acetylide complex **2b** in high (~80%) yield (Scheme 2).

Further reaction of **2b** with MeLi (1.6 mol/L in diethyl ether) at low temperature gave an orange-yellow coloured solution containing the intermediate acetylide anion [Fe(C≡C$^-$)(dppe)Cp], which was not isolated but treated in situ with PhOCN to afford the cyanoacetylide complex [Fe(C≡CC≡N)(dppe)Cp] (**3**) as a mustard-yellow coloured solid in 88% yield after chromatography and crystallization (Scheme 2). The cyanoacetylide complex was readily characterized from solution spectroscopic data, which included sharp singlets in the ^{1}H and ^{13}C NMR spectra arising from the Cp ligand (δ_H 4.29, δ_C 80.42), the phosphine resonance in the ^{31}P NMR spectrum (δ_P 104.91), and three carbon resonances arising from the cyanoacetylide ligand (δ_C 153.95, J_{CP} = 37 Hz (C_α); 106.13 (*C*N); 87.02 (C_β)). The C_α resonance, which was unambiguously assigned on the basis of the coupling to the dppe phosphorus nuclei, falls at the higher end of frequencies found in other acetylide complexes, [Fe(C≡CR)(dppe)Cp*] (6*c*). The cyanoacetylide ligand gave rise to two bands of moderate intensity at 2174 and 1991 cm^{-1}, which can be approximated as isolated ν(CN) and ν(CC) vibrations, but could also be a combination of vibrational modes.

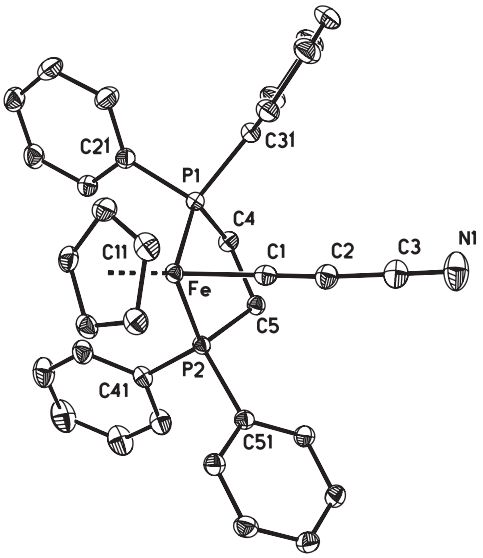
The molecular structure of **3** (Fig. 1) was determined by single crystal X-ray diffraction (Table 1), and selected bond lengths and angles are summarized in Table 2. For purposes of comparison, the structure of the related cyanide complex [Fe(C≡N)(dppe)Cp] (**4**) (9) was also determined (Fig. 2), while the complex [Fe(C≡C$C_6H_4NO_2$)(dppe)Cp] (**8**) provides a convenient set of metrical parameters associated with a metal acetylide featuring an electron-withdrawing group (10). The structures of **3**, **4**, and **8** show the expected gross similarities, with the iron centre adopting a pseudo-octahedral environment supported by the Cp ring, the chelating dppe ligand, and the C_nN (*n* = 1 (**4**), 3 (**3**)) or acetylide fragments.

© 2006 NRC Canada

Table 1. Crystallographic data for **3**, **4**, **[6]PF_6**, and **[7]PF_6**.

Compound code	**3**	**4**	**[6]PF_6**	**[7]PF_6**
Empirical formula	$C_{35}H_{31}Cl_2FeNP_2$	$C_{33}H_{31}Cl_2FeNP_2$	$C_{75.50}H_{65}ClF_6FeN\ P_5Ru$	$C_{75.50}H_{65}ClF_6\ FeNP_5Ru$
Formula weight	654.30	630.28	1 447.50	1 447.50
Temperature (K)	120(2)	120(2)	30(2)	120(2)
Crystal system	Triclinic	Monoclinic	Monoclinic	Monoclinic
Space group	*P*-1	$P2_1/n$	$P2_1/c$	$P2_1/c$
a (Å)	9.718(2)	12.8588(4)	14.6918(6)	14.6968(4)
b (Å)	12.415(3)	8.8080(3)	23.6085(9)	23.7690(7)
c (Å)	13.013(3)	25.7235(9)	19.5215(7)	19.6918(6)
α (°)	87.444(4)	90.00	90.00	90.00
β (°)	88.471(4)	90.862(2)	106.9440(10)	106.61(1)
γ (°)	76.206(4)	90.00	90.00	90.00
Volume (Å^3)	1 523.1(5)	2 913.12(17)	6 477.1(4)	6 591.9(3)
Z	2	4	4	4
D_c (Mg/m^3)	1.427	1.437	1.437	1.459
μ (mm^{-1})	0.802	0.835	0.649	0.673
Crystal size (mm)	0.25 × 0.24 × 0.16	0.26 × 0.24 × 0.22	0.40 × 0.32 × 0.16	0.20 × 0.18 × 0.18
θ Range (°)	2.81–30.51	1.58–30.52	1.45–30.45	1.68–28.00
Reflections collected	18 007	23 428	60 279	59 855
Independent reflections	9 055	8 857	19 302	15 905
$R_{(int)}$	0.0151	0.0427	0.1633	0.0446
$wR(F^2)$ ($I > 2\sigma(I)$)	0.0829	0.1229	0.0856	0.1719
$R(F)$ ($I > 2\sigma(I)$)	0.0317	0.0549	0.0755	0.0768
Refined parameters	458	352	882	807
GOF	1.068	1.154	1.227	1.192
$\Delta\rho_{min,max}$ (e Å^{-3})	0.832 and –0.466	0.841 and –0.578	1.376 and –1.327	1.014 and –1.338

Fig. 1. The molecular structure of Fe(C≡CC≡N)(dppe)Cp (**3**), showing the atom labelling scheme. In this and all subsequent figures hydrogen atoms are omitted for clarity. Selected bond lengths (Å): Fe—C(1), 1.8526(13); C(1)—C(2), 1.2278(19); C(2)—C(3), 1.3672(19); C(3)—N(1), 1.1547(19); Fe—P(1), 2.1726(5); Fe—P(2), 2.1736(5); Fe—Cp(centroid), 1.711(1). Selected bond angles (°): Fe-C(1)-C(2), 176.03(11); C(1)-C(2)-C(3), 176.22(15); C(2)-C(3)-N(1), 178.97(17); P(1)-Fe-P(2), 86.27(2).



The Fe—Cp distances in **3** (2.086(1)–2.105(1) Å, avg. 2.09_5 Å) and **4** (2.093(2)–2.107(2) Å, avg. 2.10_1 Å) are longer than those in **8** (2.060(9)–2.088(10) Å, avg. 2.07_8 Å), as

Table 2. Spectroelectrochemically generated IR data for compounds **3**, **3**$^+$, **[6]**$^+$, **[6]**$^{2+}$, **[7]**$^+$, and **[7]**$^{2+}$.

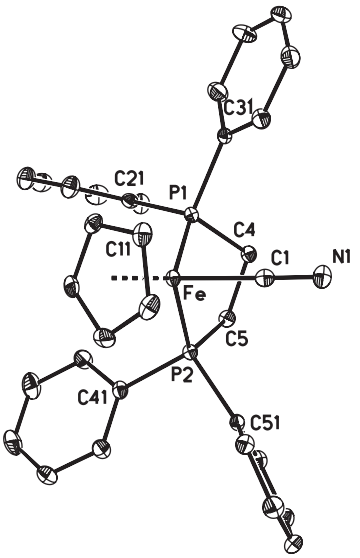
Compound	ν(C≡CC≡N) (cm^{-1})
3	2174, 1991
3$^+$	2201 (No other band observed)
[6]$^+$	2191, 1976
[6]$^{2+}$	2136, 1932
[7]$^+$	2189, 1984
[7]$^{2+}$	2121, 1946

are the the Fe—P (1, 2) bond lengths (**3**: 2.1736(5), 2.1726(5) Å; **4**: 2.1798(7), 2.1807(7) Å; **8**: 2.158(2), 2.157(2) Å). Interestingly, the intraring C—C distances in the cyclopentadienyl ring (**3**: avg. 1.42_1 Å; **4**: avg. 1.42_3 Å; **8**: avg. 1.37_6 Å) also display a degree of variation between the C_nN and acetylide complexes. Given the significance of back-bonding effects in M—Cp and M—P interactions, the structural trends in M—P and M—Cp bond lengths are consistent with either the decreased σ donation from the C_nN ligands relative to the acetylide ligand in **8**, and (or) a greater degree of iron-to-C_nN back-bonding. The Fe—C_α distance in all three complexes (**3**, **4**, and **8**) are similar (**3**: 1.853(1) Å; **4**: 1.893(2) Å; **8**: 1.856(8) Å), while the acetylide C≡C distance in **3** (1.228(2) Å) is indistinguishable from that in **8** (1.216(10) Å). Both observations argue against any statistically significant structural variation owing to a significant increase in back-bonding in **3** relative to **8**.

Numerous donor ligands (L) are known to react with the dimeric complex $[RhCl(CO)_2]_2$ resulting in cleavage of the chloride bridge, affording monomeric species *cis*-

© 2006 NRC Canada

Fig. 2. The molecular structure of Fe(C≡N)(dppe)Cp (**4**), showing the atom labelling scheme. Selected bond lengths (Å): Fe—C(1), 1.893(2); C(1)—N(1), 1.167(3); Fe—P(1), 2.1807(7); Fe—P(2), 2.1798(7); Fe—Cp(centroid), 1.717(1). Selected bond angles (°): Fe-C(1)-N(1), 178.6(2); P(1)-Fe-P(2), 84.84(2).

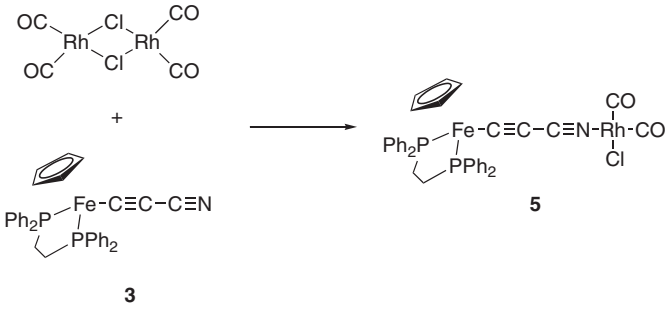


[RhCl(L)$(CO)_2$] or *cis*-[RhCl(L_2)(CO)] (11). The reaction of **3** with [RhCl$(CO)_2]_2$ proceeded smoothly in MeOH to afford *cis*-[RhCl{N≡CC≡CFe(dppe)Cp}$(CO)_2$] (**5**) as a pale orange solid after purification of the reaction mixture by chromatography (Scheme 3).

The cis geometry about the rhodium centre was unequivocally established from the IR spectrum, which revealed ν(CO) bands at 2085 and 2015 cm^{-1} in addition to the characteristic bands of the C≡CC≡N fragment at 2199 and 1978 cm^{-1}, and the ^{13}C NMR spectrum that contained a pair of doublets at 182.28 and 179.25 ppm arising from the two carbonyl ligands that are coupled to the Rh nucleus (Fig. 3). Similar data are associated with complexes derived from aminophosphines and point to the considerable donor character of the iron cyanoacetylide "metalloligand" (11). The ^{13}C NMR spectrum also revealed the remarkably high-frequency C_α resonance, which was observed as a triplet (J_{CP} = 36 Hz) at 177.23 ppm. Whilst the IR data clearly argue against a cumulenic description of the cyanocarbon ligand, the high-frequency ^{13}C shift of C_α supports the concept of a considerably polarized structure, with the electron-rich Fe(dppe)Cp fragment donating considerable electron density to the RhCl$(CO)_2$ fragment via the C≡CC≡N bridge, which also carries a dipole moment in the same orientation.

We have recently described the synthesis of the 36-electron ruthenium and mixed iron–ruthenium diyndiyl complexes [{Cp′(L_2)Ru}(μ-C≡CC≡C){Ru(L_2)Cp′}] and [{Cp*(dppe)Fe}(μ-C≡CC≡C){Ru(L_2)Cp′}] (L = PPh_3, Cp′ = Cp; L_2 = dppe, Cp′ = Cp*), together with the properties of the electrochemically accessible 35- and 34-electron oxidation products (1*b*, 1*c*, 12). The demonstration of considerable interaction between the heterometallic centres in **5** and predominant role of the ruthenium centre in determining the electronic properties of the mixed-metal diyndiyl system prompted us to consider the use of **3** in the preparation of

Scheme 3.



the cyanoacetylide-bridged complex, [{Cp(dppe)Fe}(μ-C≡CC≡N){Ru$(PPh_3)_2$Cp]PF_6 (**[6]PF_6**).

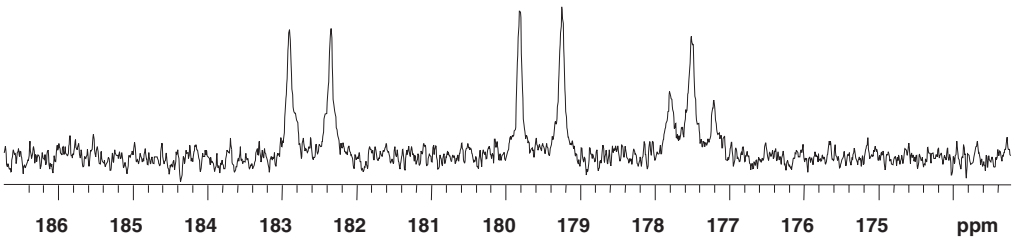
Reaction of **3** with RuCl$(PPh_3)_2$Cp in MeOH containing NH_4PF_6 afforded a red solution from which **[6]PF_6** was isolated as a bright yellow crystalline solid after extraction (CH_2Cl_2) and precipitation (hexane) (Scheme 4). Coordination of the Ru$(PPh_3)_2$Cp fragment to the nitrogen centre in **3** was evident from comparison of the spectroscopic data with the properties of model complexes such as **3** and [Ru(NCPh)$(PPh_3)_2$Cp]PF_6 (13, 14). IR spectroscopy revealed a shift in the characteristic cyanoacetylide bands from 2174 and 1991 cm^{-1} in **3** to 2192 and 1977 cm^{-1} in **[6]PF_6**. The presence of the distinct Cp ligands associated with iron and ruthenium were clearly observed in the ^1H NMR spectra (**[6]PF_6**: δ_H(Fe) 4.35; δ_H(Ru) 4.21; **3**: δ_H(Fe) 4.29; δ_H [Ru(NCPh)$(PPh_3)_2$Cp]PF_6 4.55), while the dppe and PPh_3 ligands in **[6]PF_6** gave rise to two singlet resonances in the ^{31}P NMR spectrum at 103.91 (cf. **3**: δ_P 104.91) and 42.20 ppm (cf. [Ru(NCPh)$(PPh_3)_2$Cp]PF_6: δ_P 42.89 ppm), respectively. The complex cation **[6]$^+$** was observed in the ES(+)-MS at *m*/*z* 1260.

The complex [{Cp$(PPh_3)_2$Ru}(μ-C≡CC≡N){Fe(dppe)Cp}]PF_6 (**[7]PF_6**), a coordination (C/N bond) isomer of **[6]PF_6**, was prepared on a previous occasion from the reaction of [Ru(C≡CC≡N)$(PPh_3)_2$Cp] with **1a** (4) (Scheme 5). The spectroscopic properties of **[6]PF_6** and **[7]PF_6** are distinct, which rules out the possibility of ligand isomerism processes occurring during the syntheses. However, as complexes **[6]PF_6** and **[7]PF_6** are the first C/N bond isomers featuring the cyanoacetylide ligand, a concerted effort was made to crystallize both complexes, resulting in samples suitable for single crystal X-ray diffraction (Table 1).

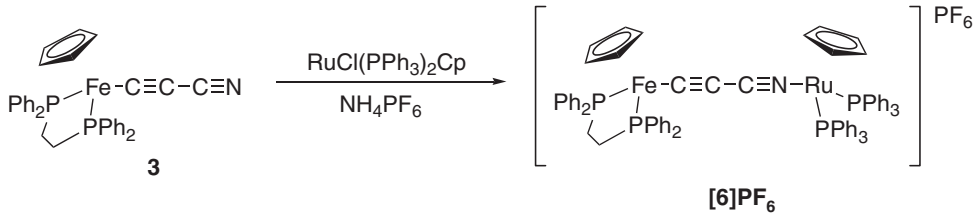
The structures of the cations **[6]$^+$** (Fig. 4) and **[7]$^+$** (Fig. 5) illustrate a number of unusual features. The compounds are isostructural and in both of them the molecules of the metal complex are disordered over two positions (Fig. 4, Fig. 5). The disorder is rather unusual and the two possible orientations differ by interchange of the positions of the ethane bridge and FeCp moiety. Inevitably, three out of four atoms of the central C_3N link in both compounds are also disordered, while the atom coordinated to the Ru centre (N1 (**[6]$^+$**); C1 (**[7]$^+$**)) has large anisotropic displacement parameters. At the same time, the P(1)Ph_2 and P(2)Ph_2 fragments, which are coordinated to the iron centre, are identical in both conformations. The disorder is static, with the structure of **[6]PF_6** remaining disordered in the same fashion at temperatures between 120 and 30 K. The structures of **[6]PF_6**

© 2006 NRC Canada

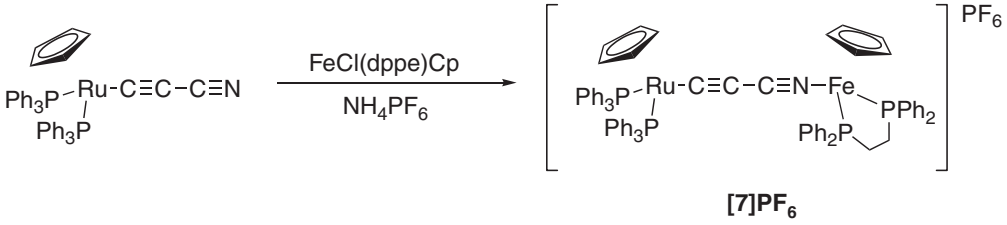
Fig. 3. The 175–185 ppm region of the ^{13}C NMR spectrum of **5** showing the distinct CO and C_α resonances.



Scheme 4.



Scheme 5.



and **[7]PF$_6$** also contain disordered PF_6 anions and molecules of the crystallization solvent, CH_2Cl_2.

Although variations in the relative disposition of the metal fragments about a diyndiyl (C≡CC≡C) ligand are common (15), demonstrating the low energy of rotation of the metal fragment about the M—C_α bond, the observation of both cisoid and transoid forms within the same crystal lattice in the case of **[6]PF$_6$** and **[7]PF$_6$** is most unusual. It is also unusual that the same disorder results from the rotation of the Fe(dppe)Cp fragment about both Fe—C (**[6]PF$_6$**) and Fe—N (**[7]PF$_6$**) bonds.

In spite of the disorder, the distinct metal–C/N bond lengths in **[6]PF$_6$** and **[7]PF$_6$** reflect the different metal fragment coordinated at the C and N termini of the C_3N bridge, e.g., Ru—N(1) = 2.054(4) Å in **[6]PF$_6$** and Ru—C(1) = 1.971(5) Å in **[7]PF$_6$**; Fe—C(1) = 1.845(8) Å (transoid) and 1.86(1) (cisoid) Å in **[6]PF$_6$**, Fe—N(1) = 1.904(6) Å (transoid) and 1.92(1) Å (cisoid) in **[7]PF$_6$**. The C(2)≡N(1) bond length in each conformation of **[6]$^+$** (1.183(9), 1.18(1) Å) is longer than the C(3)≡N(4) bond length in the corresponding conformation of **[7]$^+$** (1.16(2), 1.161(9) Å), but the other parameters are generally similar. Curiously, the Fe—P bond lengths are significantly longer in the cisoid conformation of **[6]$^+$** (2.138(2), 2.140(2) Å) than the transoid form (2.117(2), 2.116(2) Å). Back-bonding interactions will influence these Fe—P bond lengths, and we speculate that these Fe—P bond lengths indicate the different conformations observed in the solid state might arise from better transmission of electronic effects among the metal centres in the transoid geometry.

The combination of spectroscopic and structural data associated with the bimetallic complexes provides clear evidence for a degree of interaction between the metal centres through the polarized C≡CC≡N bridging ligand. In an effort to further quantify these interactions, combined electrochemical and spectroelectrochemical (UV–vis–NIR, IR) investigations were carried out. Potentials reported here are referenced against internal ferrocene or decamethyl ferrocene standards as detailed in the Experimental section.

Complex **3** undergoes a single, reversible oxidation event at +0.53 V, which compares to that of the cyanide complex **4** at +0.55 V (16). Under the same conditions, the oxidation potential of [Ru(C≡CC≡N)(PPh_3)$_2$Cp] falls at +0.92 V (4). The bimetallic complexes **[6]PF$_6$** and **[7]PF$_6$** each undergo two oxidation processes, the reversibility of which improves at subambient temperatures. The oxidation potentials of both heterobimetallic complexes, **[6]PF$_6$** (+0.66, +1.34 V) and **[7]PF$_6$** (+0.62, +1.22 V), are similar and do not correlate with a simple model based upon metal-centred oxidation events, but rather indicate a significant donor–acceptor interaction between the iron and ruthenium centres in agreement with the structural data described above.

To access spectroscopic data from the mono- and dioxidized forms of **3**, **[6]PF$_6$**, and **[7]PF$_6$** we turned to spectroelectrochemical methods. Although the oxidation events associated with each complex were reversible on the CV timescale at room temperature, bulk electrolysis reactions in the spectroelectrochemical cells were carried out at ca. –30 °C to restrict complications arising because of decomposition of the electrogenerated oxidation products. Oxi-

© 2006 NRC Canada

Fig. 4. Plots of the cation **[6]**$^+$ illustrating (*a*) the atom labelling scheme and (*b*) the disordered nature of the iron end-cap. Selected bond lengths (transoid/cisoid) (Å): Fe—C(1), 1.849(7)/1.864(10); C(1)—C(2), 1.237(10)/1.217(14); C(2)—C(3), 1.374(10)/1.370(13); C(3)—N(1), 1.184(8)/1.183(10); Ru(1)—N(1), 2.056(4); Fe—P(1), 2.1265(17)/2.151(2); Fe—P(2), 2.1248(14)/2.1493(19); Ru—P(3), 2.3423(10); Ru—P(4), 2.3367(11). Selected bond angles (°): Fe-C(1)-C(2), 163.7(5)/179.2(9); C(2)-C(3)-N(1), 175.7(8)/170.8(11); C(3)-N(1)-Ru, 163.7(5)/159.9(6); P(1)-Fe-P(2), 88.95(6)/87.68(7); P(3)-Ru-P(4), 104.21(4).

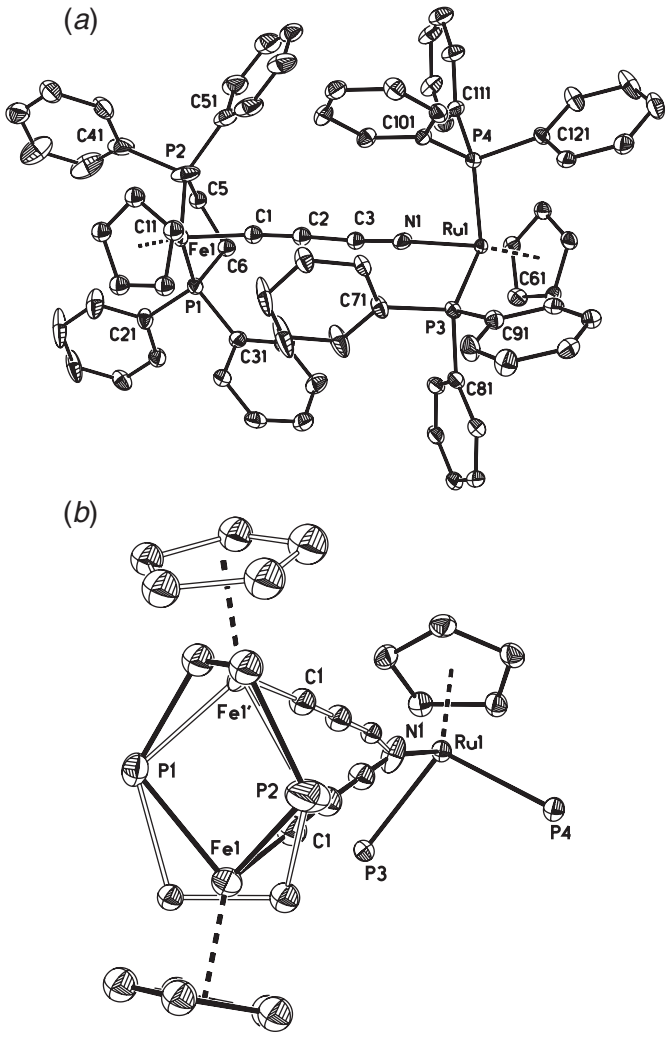
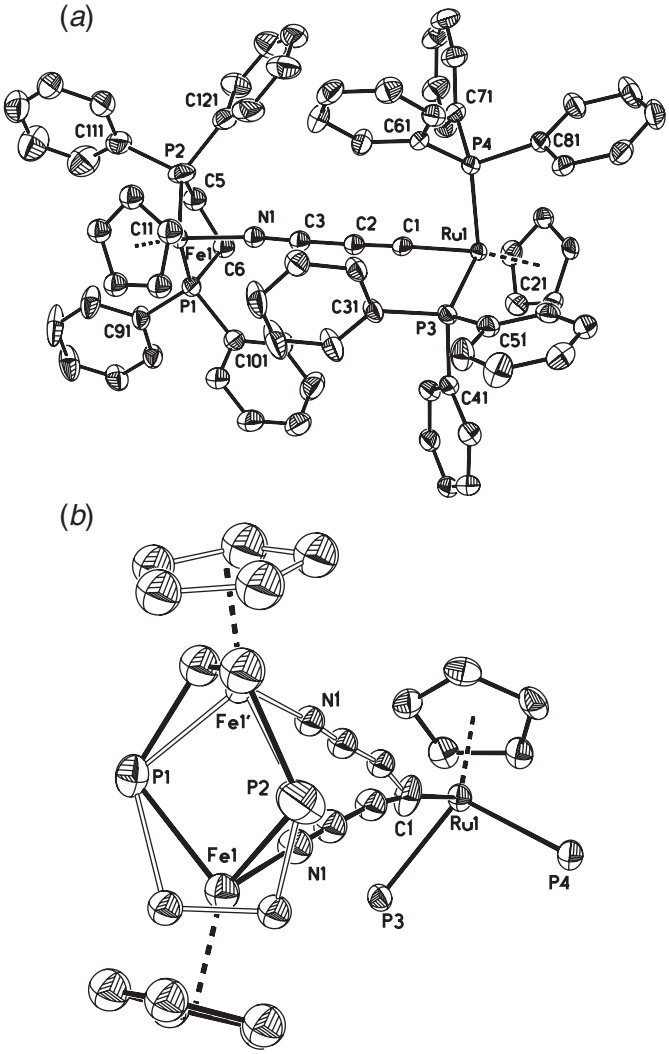


Fig. 5. An illustration of the disordered cation **[7]**$^+$ showing (*a*) the atom labelling scheme and (*b*) the disordered nature of the iron end-cap. Selected bond lengths (transoid/cisoid) (Å): Ru—C(1), 1.971(5); C(1)—C(2), 1.226(9)/1.318(16); C(2)—C(3), 1.374(10)/1.36(2); C(3)—N(1), 1.161(9)/1.16(3); Fe—N(1), 1.904(6)/1.916(13); Ru—P(3), 2.3093(13); Ru—P(4), 2.3090(13); Fe—P(1), 2.1310(18)/2.117(3); Fe—P(2), 2.147(2)/2.136(3). Selected bond angles (°): Ru-C(1)-C(2), 172.1(6)/157.1(8); C(1)-C(2)-C(3), 173.0(8)/168.6(16); C(2)-C(3)-N(1), 178.4(8)/176.7(17); C(3)-N(1)-Fe, 172.8(6)/175.9(13).



dation of [Fe(C≡CC≡N)(dppe)Cp] (**3**) resulted in the collapse of the characteristic ν(C≡CC≡N) bands of the unsaturated ligand and observation of a band at 2201 cm^{-1} of significantly lower intensity (Table 2). The pseudo ν(C≡C) band in this oxidized species, **[3]**$^+$, was not apparent, perhaps because of its low intensity. In contrast, two bands were observed following oxidation of the bimetallic complexes **[6]PF$_6$** and **[7]PF$_6$**, which were shifted to lower energy by ca. 40–70 cm^{-1} in comparison with the spectra of the precursors, and therefore supporting the notion of an oxidation event that involves an orbital with an appreciable degree of ligand as well as metal character. In each case the original spectral profile was recovered after back-reduction of the oxidized samples.

The electronic (UV–vis–NIR) spectrum of **3** changed little upon oxidation, and recovery of the original spectrum after back-reduction demonstrated the chemical reversibility of the electrochemical oxidation. Crucially, the NIR region of the spectrum remained transparent before and after oxidation of **3**. More interestingly, the one-electron oxidation products derived from **[6]PF$_6$** and **[7]PF$_6$** exhibited intense absorptions in the NIR region, each of which could be deconvoluted into three Gaussian-shaped absorption bands (Fig. 6, Table 3). Of these, the particularly low energy band of low intensity ($\bar{\nu}_{max}$(cm^{-1})/ε_{max} = 5260 cm^{-1}/140 (mol/L)$^{-1}$ cm^{-1} (**[6]**$^{2+}$); 5980 cm^{-1}/190 (mol/L)$^{-1}$ cm^{-1} (**[7]**$^{2+}$)) was approximated as a forbidden ligand–field transition associated with the oxidized iron centre (6*h*, 6*k*, 17), which indicates that the

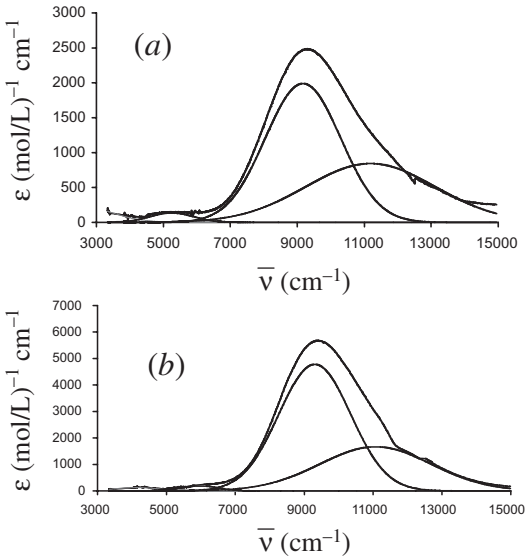
© 2006 NRC Canada

Table 3. Selected experimental and calculated band-shape parameters associated with the NIR bands exhibited by the 35-electron species, **[6]**$^{2+}$ and **[7]**$^{2+}$.

Band	$\bar{\nu}$ (cm^{-1}), ε ((mol/L)$^{-1}$ cm^{-1})	$\Delta\bar{\nu}_{1/2}$ (cm^{-1}, obs)	$\Delta\bar{\nu}_{1/2}$ (cm^{-1}, Hush)	H_{ab} (class II)[a]
[6]$^{2+}$ Band 1	9 175, 1 990	2650	4600	590
[6]$^{2+}$ Band 2	11 185, 840	4550	5080	555
[7]$^{2+}$ Band 1	9 310, 4 780	2445	4640	890
[7]$^{2+}$ Band 2	11 040, 1 665	3815	5050	710

[a]Calculated using eq. [1] and assuming $d_{MM'}$ = 7.62 Å, the average Fe—Ru separation obtained for both crystallographically determing cisoid and transoid conformations of **[6]PF$_6$** and **[7]PF$_6$**.

Fig. 6. The deconvoluted NIR band envelopes associated with (*a*) **[6]**$^{2+}$ and (*b*) **[7]**$^{2+}$.



first oxidation event has some iron character in both C/N bond isomers.

Demandis et al. (18) have recently reviewed the properties of strongly coupled, ligand-bridged bimetallic mixed valence complexes, and described the various contributions of metal–ligand orbital mixing, spin-orbit coupling, and low symmetry, which lead to the three transitions that are in principle allowed between d^6 and d^5 metal ions to gather appreciable intensity. While the 35-electron, heterobimetallic dications **[6]**$^{2+}$ and **[7]**$^{2+}$ are not true mixed-valence species, similar considerations apply to the electronic spectra of these complexes. Since spin-orbit effects are relatively minor in lighter first and second row transition elements, the observation of multiple transitions in the NIR region of both species provides further evidence that the electronic structure of these heterometallic systems features a considerable degree of metal–ligand mixing. The band energy and shape are remarkably similar for both **[6]**$^{2+}$ and **[7]**$^{2+}$, and consequently similar transitions, and hence underlying electronic structures, are involved in both isomers.

The relationships originally derived by Hush (19) provide a vehicle for comparison of the electron-transfer processes occurring through the cyanoacetylide ligand in the complexes reported here with those observed in a large number of cyanide-bridged examples (20). Using the deconvoluted band shapes, and assuming that electron-transfer distance is approximated by the crystallographically determined metal–metal separation, a coupling parameter (H_{ab}) may be calculated for each band using the expression give in eq. [1] (Table 3) (19).

$$[1] \qquad H_{ab} = \frac{0.0205\sqrt{\bar{\nu}_{max}\varepsilon\Delta\bar{\nu}_{1/2}}}{d'_{MM}}$$

Typically, values of H_{ab} for heterometallic cyanide bridged d^5/d^6 bimetallic complexes are in the range 1000–1700 cm^{-1} when the NIR band shape data is treated in an entirely similar fashion. We note, however, that the use of the metal–metal distance is only a crude approximation of the electron-transfer distance, and given the involvement of the ligand orbitals in the SOMO, the real electron-transfer distance is likely to be considerably shorter. The values of H_{ab} reported in Table 3 represent a lower limit for the value of this parameter.

Whilst the availability of these 35-electron species as isolated samples would have greatly facilitated this study by allowing ready measurement of the solvent dependence of the NIR bands and permitted access to Mössbauer and magnetic data, it is unfortunate that at the present time we have been unable to chemically isolate samples of **[6]**$^{2+}$ or **[7]**$^{2+}$ as salts with common counterions. However, efforts in this area are ongoing, and with the possibility of exchanging the Cp for Cp* and related substituted cyclopentadienyl ligands, together with the large variety of phosphine ligands that may be introduced at either metal centre, we are hopeful that further information regarding the electronic structure of these unusual cyanoacetylide-bridged heterobimetallic complexes will become available in due course.

Conclusion

The readily prepared substrate FeCl(dppe)Cp is a convenient reagent for the preparation of both acetylide and cyanoacetylide iron complexes. The iron–cyanoacetylide complex, [Fe(C≡CC≡N)(dppe)Cp], is a good metalloligand, readily coordinating to $RhCl(CO)_2$ or $Ru(PPh_3)_2Cp$ fragments to afford heterometallic complexes featuring the μ-η^1(C),η^1(N)-C≡CC≡N ligand. Spectroscopic data are consistent with a significant degree of polarization in the structures of the 36-electron species, and relatively large values of the coupling constant H_{ab} in the electrochemically generated 35-electron (d^5/d^6) dication, [{Cp(dppe)Fe}(μ-C≡CC≡N){Ru(PPh$_3$)$_2$Cp}]$^{2+}$, and its C/N bond isomer, [{Cp(PPh$_3$)$_2$Ru}(μ-C≡CC≡N){Fe(dppe)Cp}]$^{2+}$.

© 2006 NRC Canada

Experimental

All reactions were carried out using standard Schlenk techniques under dry high-purity nitrogen. Solvents were dried using an Innovative Technologies solvent purification system, and degassed prior to use. Preparative TLC was carried out on 20 cm × 20 cm glass plates coated with silica gel (Merck G_{254}, 0.5 mm thick). Reagents were purchased and used as received. Compounds **1a** (7), **4** (9), and **[7]PF$_6$** (4) were prepared according to the literature methods. Crystals of **4** and **[7]PF$_6$** suitable for X-ray diffraction were obtained from CH_2Cl_2–hexane and CH_2Cl_2–MeOH, respectively. IR spectra were recorded on a Nicolet Avatar FT IR spectrophotometer using solution cells fitted with CaF_2 windows. NMR spectra were obtained from solutions in $CDCl_3$ using Varian VXR-400 (^{1}H, 399.97 MHz; ^{13}C, 100.57 MHz; ^{31}P, 161.1 MHz) or Bruker DRX-400 (^{1}H, 400.13 MHz; ^{13}C, 100.61 MHz; ^{31}P, 162.05 MHz) spectrometers. Electrochemical experiments were conducted in CH_2Cl_2 solution containing 0.1 mol/L NBu_4PF_6 using a standard three-electrode cell (all Pt electrodes) and an EcoChemie Autolab PGSTAT-30. Potentials were corrected to SCE using an internal ferrocene/ferrocinium (Fc/Fc^+ = 0.46 V) or decamethylferrocene/decamethylferrocinium couple as standard (Fc^*/Fc^{*+} = 0.084 V).

IR spectroelectrochemical studies

IR spectroelectrochemical experiments at low temperatures were performed with a cryostated, optically transparent thin-layer electrochemical (OTTLE) cell equipped with CaF_2 windows and a Pt minigrid working electrode (32 wires/cm) (21). The electrolyses at room temperature were conducted with another homemade demountable OTTLE cell (22). The CH_2Cl_2 employed solutions were typically 3×10^{-1} mol/L in the supporting electrolyte (NBu_4PF_6) and 10^{-3} mol/L in the analyte. The working electrode potential of the spectroelectrochemical cell was controlled with a PA4 potentiostat (EKOM, Polná, Czech Republic). The IR spectra were recorded with Bio-Rad FTS-7 and Bruker Vertex 70 FT IR spectrometers (16 scans, 1 to 2 cm^{-1} spectral resolution).

UV–vis–NIR spectroelectrochemical studies

UV–vis–NIR were carried out using a Varian Cary 5 spectrophotometer in an OTTLE cell similar to that described previously (23) from solutions in CH_2Cl_2 containing 10^{-1} mol/L NBu_4BF_4 as supporting electrolyte. Typically analyte concentrations were 10^{-1} mmol/L.

[Fe(C≡CSiMe$_3$)(dppe)Cp] (2b)

A Schlenk flask was charged with [FeCl(dppe)Cp] (2.0 g, 3.60 mmol), $NaBPh_4$ (1.48 g, 4.32 mmol), THF (75 mL), and NEt_3 (75 mL), and the resulting dark solution treated with $Me_3SiC{\equiv}CH$ (1.77 g, 2.54 mL, 18.0 mmol). After stirring for 16 h the solution colour had turned deep orange. The solvent was removed and the residue extracted with Et_2O and pentane added. The combined solvent was removed resulting in precipitation of a dark orange solid (1.75 g, 79%). IR (CH_2Cl_2, cm^{-1}): 1984 ν(C≡C). ^{1}H NMR ($CDCl_3$) δ: 0.06 (s, 9H, $SiMe_3$), 2.12 (m, 2H, dppe), 2.81 (m, 2H, dppe), 4.32 (s, 5H, Cp), 7.04–8.11 (m, 20H, Ph). ^{13}C{H} NMR ($CDCl_3$) δ: 1.00 (s, $SiMe_3$), 27.96–28.32 (m, CH_2 dppe), 79.52 (s, Cp), 103.85 (s, C_β), 127.87 (dt, J_{CP} = 58, 4 Hz, m-Ph), 129.13 (d, J_{CP} = 42 Hz, p-Ph), 133.14 (dt, J_{CP} = 248, 5 Hz, o-Ph), 138.00–142.64 (m, i-Ph), 151.39 (t, J_{CP} = 39 Hz, C_α). ^{31}P{H} NMR ($CDCl_3$) δ: 107.71 (s, dppe). ES(+)-MS (*m*/*z*): 616.9 [M + H]$^+$. Anal. calcd. for $C_{36}H_{38}FeP_2Si$ (%): C 70.13, H 6.21; found: C 69.94, H 6.32.

[Fe(C≡CC≡N)(dppe)Cp] (3)

A Schlenk flask was charged with [Fe(C≡CSiMe$_3$)(dppe)Cp] (500 mg, 0.81 mmol) in THF (20 mL). The orange/yellow solution was cooled to –78 °C and MeLi (0.6 mL, 0.96 mmol of a 1.6 mol/L solution in Et_2O) was added at such a rate as to prevent the temperature exceeding –50 °C. After stirring for 1 h the solution was warmed to –20 °C before being cooled again. To the orange/yellow solution was added PhOCN (0.5 mL, 0.9 mmol) and the solution allowed to come slowly to room temperature before the solvent was removed. The dark red/brown residue was dissolved in CH_2Cl_2 and purified by column chromatography on silica, the product eluting with acetone–hexane (30:70). Concentration of the dark red fraction resulted in the formation of a mustard yellow precipitate, which was collected, washed with hexane, and air dried to afford **3**, which was recrystallized from CH_2Cl_2–Et_2O (yield: 400 mg, 88%). IR (CH_2Cl_2, cm^{-1}): 2174, 1991 ν(C≡CC≡N). ^{1}H NMR ($CDCl_3$) δ: 2.32 (m, 2H, dppe), 2.60 (m, 2H, dppe), 4.29 (s, 5H, Cp), 7.74–6.85 (m, 20H, Ph). ^{13}C{H} NMR ($CDCl_3$) δ: 27.88–28.35 (m, CH_2 dppe), 80.42 (s, Cp), 87.02 (s, C_β), 106.13 (s, CN), 127.99 (dt, J_{CP} = 26, 4 Hz, m-Ph), 129.58 (d, J_{CP} = 53 Hz, p-Ph), 132.23 (dt, J_{CP} = 167, 4 Hz, o-Ph), 135.55–140.21 (m, i-Ph), 153.95 (t, J_{CP} = 37 Hz, C_α). ^{31}P{H} NMR ($CDCl_3$) δ: 104.91 (s, dppe). ES(+)-MS (*m*/*z*): 570.1 [M + H]$^+$. Anal. calcd. for $C_{34}H_{29}FeNP_2$ (%): C 71.72, H 5.13, N 2.46; found: C 71.67, H 5.07, N 1.72.

[{Cp(dppe)Fe}(μ-C≡CC≡N){*cis*-RhCl(CO)$_2$}] (5)

A Schlenk flask was charged with [Fe(C≡CC≡N)(dppe)Cp] (73 mg, 0.129 mmol), $[RhCl(CO)_2]_2$ (25 mg, 0.065 mmol), NH_4PF_6 (35 mg, 0.215 mmol), and MeOH (25 mL), and the resulting solution stirred for 48 h. The solvent was then removed and the residue extracted with CH_2Cl_2 and filtered through a small pad of silica. Addition of hexane to the CH_2Cl_2 solution and concentration resulted in an orange precipitate, which was collected, washed with pentane, and air dried (yield: 50 mg, 51%). IR (CH_2Cl_2, cm^{-1}): 2199, 1991 ν(C≡CC≡N); 2085, 2015 ν(CO). ^{1}H NMR ($CDCl_3$) δ: 2.37 (m, 2H, dppe), 2.60 (m, 2H, dppe), 4.36 (s, 5H, Cp), 7.68–7.17 (m, 20H, Ph). ^{13}C{H} NMR ($CDCl_3$) δ: 28.24–28.59 (m, CH_2 dppe), 81.58 (s, Cp), 85.32 (s, C_β), 106.27 (s, CN), 128.30–139.41 (m, Ph), 177.23 (t, J_{CP} = 36 Hz, C_α), 179.25 (d, J_{RhC} = 70 Hz, CO cis to NC), 182.28 (d, J_{RhC} = 70 Hz, CO trans to NC). ^{31}P{H} NMR ($CDCl_3$) δ: 103.45 (s, dppe). Anal. calcd. for $C_{36}H_{29}ClFeNO_2P_2Rh$ (%): C 56.61, H 3.83, N 1.83; found: C 56.22, H 3.96, N 1.37.

[{Fe(dppe)Cp}(C≡CC≡N){Ru(PPh$_3$)$_2$Cp}]PF$_6$ ([6]PF$_6$)

A Schlenk flask was charged with [Fe(C≡CC≡N)(dppe)Cp] (75 mg, 0.132 mmol), $[RuCl(PPh_3)_2Cp]$ (96 mg, 0.132 mmol), and NH_4PF_6 (86 mg, 0.528 mmol). The mixture was suspended in MeOH (15 mL) and refluxed for 1 h after which time a dark red solution had formed. This was

© 2006 NRC Canada

allowed to cool and the solvent removed. The red/brown residue was extracted with CH_2Cl_2 and filtered into hexane. The resulting yellow precipitate was collected, washed with hexane, and air dried to afford **[6]PF$_6$** (yield: 105 mg, 57%). Crystals suitable for X-ray diffraction were obtained from CH_2Cl_2–hexane. IR (CH_2Cl_2, cm^{-1}): 2192, 1977 ν(C≡CC≡N). ^1H NMR ($CDCl_3$) δ: 1.62 (br, 8H, dppe), 4.21, 4.35 (2 × s, 10H, 2 × Cp), 6.97–7.64 (m, 40H, Ph). $^{31}P\{H\}$ NMR ($CDCl_3$) δ: –143.11 (ht, J_{PF} = 711 Hz, PF_6^-), 42.20 (s, PPh_3), 103.91 (s, dppe). ES(+)-MS (*m/z*): 1260 [{Fe(dppe)-Cp}(C≡CC≡N){Ru(PPh_3)$_2$Cp}]$^+$; 691 [Ru(PPh_3)$_2$Cp]$^+$ Despite repeated efforts to remove solvent from the analytical sample, this compound consistently analysed with 1/2 molecule of the CH_2Cl_2 crystallization solvent. Anal. calcd. for $C_{75}H_{64}F_6FeNP_5Ru{\cdot}0.5CH_2Cl_2$ (%): C 62.64, H 4.53, N 0.97; found: C 62.29, H 4.43, N 0.91.

Crystallography

The X-ray data sets for compounds **3**, **4**, **[6]PF$_6$**, and **[7]PF$_6$** were collected on Bruker 3-circle diffractometers with Bruker ProteumM diffractomer and Bede Microsource® (for **3**, **4**, and **[6]PF$_6$**) or SMART 6K (for **[7]PF$_6$**) CCD area detectors using graphite-monochromated sealed-tube Mo K_α radiation. The data collection was carried out at 120 K using cryostream (Oxford cryosystem) open flow N_2 cryostats. Reflection intensities were integrated using the SAINT program, version 6.02a (for **3** and **[6]PF$_6$**) and version 6.45 (for **4** and **[7]PF$_6$**) (24). The crystal structures were solved using direct-methods and refined by full matrix least-squares against F^2 of all data using SHELXTL software (25). All non-hydrogen atoms where refined in anisotropic approximation (for **3** and **4**). In the case of **[6]PF$_6$** and **[7]PF$_6$**, the non-hydrogen atoms located in two different sites, PF_6^- anions, and solvent molecules where refined in isotropic approximation.

Hydrogen atoms were placed in calculated positions and refined using a riding model (for **4**, **[6]PF$_6$**, and **[7]PF$_6$**) or located by different Fourier maps and refined unconstrained (for **3**). All four crystal structures present dichloromethane molecules, and for **[6]PF$_6$** and **[7]PF$_6$** the solvent molecules are highly disordered with connectivity between atoms only visible for one dichloromethane molecule.

Crystal data and experimental details are listed in Table 1.[3]

Acknowledgements

We thank Taasje Mahabiersing (University of Amsterdam) for assistance with the electrochemical and spectroelectrochemical work. Financial assistance from the Engineering and Physical Sciences Research Council (EPSRC), OneNorthEast, and the EU ESSD HPMT-CT-2001-0311 Marie Curie Training Site (Amsterdam, The Netherlands) is gratefully acknowledged. RLC held a scholarship from the University of Durham Chemistry EPSRC Doctoral Training Account.

References

1. (*a*) M.I. Bruce and P.J. Low. Adv. Organomet. Chem. **50**, 179 (2004); (*b*) M.I. Bruce, P.J. Low, K. Costuas, J.F. Halet, S.P. Best, and G.A. Heath. J. Am. Chem. Soc. **122**, 1949 (2000); (*c*) M.I. Bruce, B.G. Ellis, P.J. Low, B.W. Skelton, and A.H. White. Organometallics, **22**, 3184 (2003).
2. (*a*) P.J. Low and M.I. Bruce. Adv. Organomet. Chem. **48**, 71 (2002); (*b*) P.J. Low, K.A. Udachin, G.D. Enright, and A.J. Carty. J. Organomet. Chem. **578**, 103 (1999); (*c*) P.J. Low, T.M. Hayes, K.A. Udachin, A.E. Goeta, J.A.K. Howard, G.D. Enright, and A.J. Carty. J. Chem. Soc. Dalton Trans. 1455 (2002); (*d*) P.J. Low, K.A. Udachin, and A.J. Carty. J. Cluster Sci. **15**, 277 (2004); (*e*) O.F. Koentjoro, P.J. Low, R. Rousseau, C. Nervi, D.S. Yufit, J.A.K. Howard, and K.A. Udachin, Organometallics, **24**, 1284 (2005).
3. (*a*) O.F. Koentjoro, R. Rousseau, and P.J. Low. Organometallics, **20**, 4502 (2001); (*b*) P.J. Low, R. Rousseau, P. Lam, K.A. Udachin, G.D. Enright, J.S. Tse, D.D.M. Wayner, and A.J. Carty. Organometallics, **18**, 3885 (1999); (*c*) P.J. Low, A.J. Carty, K.A. Udachin, and G.D. Enright. Chem. Commun. (Cambridge), 411 (2001); (*d*) M.I. Bruce, K. Costuas, J.F. Halet, B.C. Hall, P.J. Low, B.K. Nicholson, B.W. Skelton, and A.H. White. J. Chem. Soc. Dalton Trans. 383 (2002); (*e*) R.L. Roberts, H. Puschmann, J.A.K. Howard, J.H. Yamamoto, A.J. Carty, and P.J. Low. Dalton Trans. 1099 (2003).
4. R.L. Cordiner, D. Corcoran, D.S. Yufit, A.E. Goeta, J.A.K. Howard, and P.J. Low. Dalton Trans. 3541 (2003).
5. (*a*) R. Nast. Coord. Chem. Rev. **47**, 89 (1982); (*b*) A. Davison and J.P. Selegue. J. Am. Chem. Soc. **100**, 7763 (1978); (*c*) S. Abbott, S.G. Davies, and P. Warner. J. Organomet. Chem. **246**, C65 (1983); (*d*) C.E. Powell, M.P. Cifuentes, A.M. McDonagh, S.K. Hurst, N.T. Lucas, C.D. Delfs, R. Stranger, M.G. Humphrey, S. Houbrechts, I. Asselberghs, A. Persoons, and D.C.R. Hockless. Inorg. Chim. Acta, **352**, 9 (2003); (*e*) N.G. Connelly, M.P. Gamasa, J. Gimeno, C. Lapinte, E. Lastra, J.P. Maher, N. Le Narvor, A.L. Rieger, and P.H. Rieger. J. Chem. Soc. Dalton Trans. 2575 (1993); (*f*) M.P. Gamasa, J. Gimeno, E. Lastra, M. Lanfranchi, and A. Tiripicchio. J. Organomet. Chem. **405**, 333 (1991).
6. (*a*) X.H.S. Gu and M.B. Sponsler. Organometallics, **17**, 5920 (1998); (*b*) L. Dahlenburg, A. Weiss, M. Bock, and A. Zahl. J. Organomet. Chem. **541**, 465 (1997); (*c*) R. Denis, T. Weyland, F. Paul, and C. Lapinte. J. Organomet. Chem. **546**, 615 (1997); (*d*) S. Le Stang, D. Lenz, F. Paul, and C. Lapinte. J. Organomet. Chem. **572**, 189 (1999); (*e*) N. Le Narvor and C. Lapinte. Organometallics, **14**, 634 (1995); (*f*) F. Paul and C. Lapinte. Coord. Chem. Rev. **178**, 431 (1998); (*g*) S. Le Stang, F. Paul, and C. Lapinte. Organometallics, **19**, 1035 (2000); (*h*) T. Weyland, K. Costuas, L. Toupet, J.-F. Halet, and C. Lapinte. Organometallics, **19**, 4228 (2000); (*i*) F. Paul, W.E. Meyer, L. Toupet, H. Jiao, J.A. Gladysz, and C. Lapinte. J. Am. Chem. Soc. **122**, 9405 (2000); (*j*) T. Weyland, I. Ledoux, S. Brasselet, J. Zyss, and C. Lapinte. Organometallics, **19**, 5235

[3] Supplementary data for this article are available on the journal Web site (http://canjchem.nrc.ca) or may be purchased from the Depository of Unpublished Data, Document Delivery, CISTI, National Research Council Canada, Ottawa, ON K1A 0R6, Canada. DUD 4087. For more information on obtaining material refer to http://cisti-icist.nrc-cnrc.gc.ca/irm/unpub_e.shtml. CCDC 274245–274248 contain the crystallographic data for this manuscript. These data can be obtained, free of charge, via http://www.ccdc.cam.ac.uk/conts/retrieving.html (Or from the Cambridge Crystallographic Data Centre, 12 Union Road, Cambridge CB2 1EZ, UK; fax +44 1223 336033; or deposit@ccdc.cam.ac.uk).

© 2006 NRC Canada

(2000); (*k*) S. Roué, C. Lapinte, and T. Bataille. Organometallics, **23**, 2558 (2004); (*l*) F. Coat, F. Paul, C. Lapinte, L. Toupet, K. Costuas, and J.-F. Halet. J. Organomet. Chem. **683**, 368 (2003); (*m*) M. Guillemot, L. Toupet, and C. Lapinte. Organometallics, **17**, 1928 (1998); (*n*) S. Roue and C. Lapinte. J. Organomet. Chem. **690**, 594 (2005).
7. M.J. Mays and P.L. Sears. J. Chem. Soc. Dalton Trans. 1873 (1973).
8. (*a*) N. Le Narvor, L. Toupet, and C. Lapinte. J. Am. Chem. Soc. **117**, 7129 (1995); (*b*) F. Coat, P. Thominot, and C. Lapinte. J. Organomet. Chem. **629**, 39 (2001).
9. G.J. Baird and S.G. Davies. J. Organomet. Chem. **262**, 215 (1984).
10. M.H. Garcia, M.P. Robalo, A.R. Dias, M.T. Duarte, W. Wenseleers, A. Aerts, E. Goovaerts, M.P. Cifuentes, S. Hurst, M.G. Humphrey, M. Samoc, and B. Luther-Davies. Organometallics, **21**, 2107 (2002).
11. P.W. Dyer, J. Fawcett, M.J. Hanton, R.D.W. Kemmitt, R. Padda, and N. Singh. Dalton Trans. 104 (2003).
12. M.I. Bruce, K. Costuas, T. Davin, B.G. Ellis, J.F. Halet, C. Lapinte, P.J. Low, M.E. Smith, B.W. Skelton, L. Toupet, and A.H. White. Organometallics. **24**, 3864 (2005).
13. G.S. Ashby, M.I. Bruce, I.B. Tomkins, and R.C. Wallis. Aust. J. Chem. **32**, 1003 (1979).
14. R.L. Cordiner, D. Albesa-Jové, R.L. Roberts, J.D. Farmer, H. Puschmann, D. Corcoran, A.E. Goeta, J.A.K. Howard, and P.J. Low. J. Organomet. Chem. **690**, 4908 (2005).
15. M.I. Bruce, B.G. Ellis, M. Gaudio, C. Lapinte, G. Melino, F. Paul, B.W. Skelton, M.E. Smith, L. Toupet, and A.H. White. Dalton Trans. 1601 (2004).
16. G.N. Richardson, U. Brand, and H. Vahrenkamp. Inorg. Chem. **38**, 3070 (1999).
17. S. Le Stang, F. Paul, and C. Lapinte. Inorg. Chim. Acta, **291**, 403 (1999).
18. K.D. Demandis, C.M. Hartshorn, and T.J. Meyer. Chem. Rev. **101**, 2655 (2001).
19. (*a*) C. Creutz, M.D. Newton, and N. Sutin. J. Photochem. Photobiol. A: Chem. **82**, 47 (1994); (*b*) J.-P. Launay. Chem. Soc. Rev. **30**, 386 (2001).
20. C. Díaz and A. Arancibia. Inorg. Chim. Acta, **269**, 246 (1998).
21. (*a*) F. Hartl, H. Luyten, H.A. Nieuwenhuis, and G.C. Schoemaker. Appl. Spectrosc. **4**8 1522 (1994); (*b*) T. Mahabiersing, H. Luyten, R.C. Nieuwendam, and F. Hartl. Coll. Czech. Chem. Commun. **6**8 1687 (2003).
22. M. Krejcík, M. Danek, and F. Hartl. J. Electroanal. Chem. **31**7 179 (1991).
23. C.M. Duff and G.A. Heath. Inorg. Chem. **30**, 2528 (1991).
24. (*a*) SAINT. Version 6.02a [computer program]. Bruker AXS, Madison, Wisconsin. 2001; (*b*) SAINT. Verision 6.45 [computer program]. Bruker AXS, Madison, Wisconsin. 1998.
25. SHELXTL. Version 5.10 [computer program]. Bruker AXS, Madison, Wisconsin. 1997.

© 2006 NRC Canada

An acidity scale of phosphonium tetraphenylborate salts and ruthenium dihydrogen complexes in dichloromethane[1]

Tianshu Li, Alan J. Lough, Cristiano Zuccaccia, Alceo Macchioni, and Robert H. Morris

Abstract: Equilibrium constants (K^{DM}) for reactions between acids and bases of the title compounds in CD_2Cl_2 (DM) have been determined by ^{31}P and ^{1}H NMR spectroscopy at room temperature. $[HPCy_3]BPh_4$ and $[HPCy_3]BF_4$, with pK^{DM} assigned by literature convention to 9.7, have been used as the anchor compounds for the pK^{DM} determinations. A continuous scale of pK^{DM} values covering the range 9.7 to 5.7 is created with the acidic compounds $[HPR_3]BPh_4$. Those acids with pK^{DM} greater than 6 are stable, while those with more acidic cations HPR_3^+ protonate BPh_4^- to produce R_3PBPh_3 and benzene. The literature pK^{THF} values reported for $[HPBu_2Ph]BPh_4$, $[HPMePh_2]BPh_4$, and $[HPEtPh_2]BPh_4$ are questionable because of this protonation reaction. NOE and PGSE ^{1}H NMR techniques are used to show that $[HPCy_2Ph]BPh_4$ in DM exists as ion pairs and higher aggregates up to quadrupoles at the concentrations used in the acid–base studies. The new dihydrogen complexes $[Ru(H_2)Cl(PPh_3)_2(dach)]BF_4$ (dach = (1*R*,2*R*)-(–)-diaminocyclohexane) and $[Ru(H_2)Cl\{tmeP_2(NH)_2\}]BF_4$ ($tmeP_2(NH)_2$ = $PPh_2C_6H_4CH_2NHCMe_2CMe_2NHCH_2C_6H_4PPh_2$) were prepared by reaction of $RuHCl(PPh_3)_2(dach)$ and $RuHCl\{tmeP_2(NH)_2\}$ with HBF_4. Their crystal structures are reported, and the pK^{DM} values of their BPh_4^- salts were determined to be 8.6 and 6.9, respectively.

Key words: acidity, dihydrogen complex, hydride, phosphonium, dichloromethane.

Résumé : Opérant à la température et dans le CD_2Cl_2 (DM) comme solvant et faisant appel à la spectroscopie RMN du ^{1}H et du ^{31}P, on a déterminé les constantes d'équilibre, K^{DM}, des réactions entres les acides et les bases des composés mentionnés dans le titre. La valeur de 9,7 attribuée par convention dans la littérature pour les composés $[HPCy_3]BPh_4$ et $[HPCy_3]BF_4$ a été utilisé comme composés de référence pour les déterminations des pK^{DM}. On a créé une échelle continue de valeurs de pK^{DM} s'étalant de 9,7, à 5,7 en faisant appel aux composés acides $[HPR_3]BPh_4$. Ces acides dont les valeurs de pK^{DM} sont supérieures à 6 sont stables alors que ceux des cations plus acides HPR_3^+ se protonent au BPh_4^- pour conduire à la formation de R_3PBPh_3 et de benzène. Les valeurs de pK^{THF} rapportées dans la littérature pour les $[HPBu_2Ph]BPh_4$, $[HPMePh_2]BPh_4$ et $[HPEtPh_2]BPh_4$ ne sont pas fiables en raison de cette réaction de protonation. On a utilisé les techniques d'effet Overhauser nucléaire et d'écho de spin a champ pulsé PGSE en RMN du ^{1}H pour montrer que dans le DM, aux concentrations utilisées pour les études acide–base, le $[HPCy_2Ph]BPh_4$ existe sous la forme de paire d'ions et d'agrégats plus importants allant jusqu'à des quadrupoles. La réaction du $RuHCl(PPh_3)_2(dach)$ et $RuHCl\{tmeP_2(NH)_2\}$ avec du HBF_4 a permid de préparer les deux nouveaux complexes de dihydrogène suivants $[Ru(H_2)Cl(PPh_3)_2(dach)]BF_4$ (dach = (1*R*,2*R*)-(–)-diaminocyclohexane) et $[Ru(H_2)Cl\{tmeP_2(NH)_2\}]BF_4$ ($tmeP_2(NH)_2$ = $PPh_2C_6H_4CH_2NHCMe_2CMe_2NHCH_2C_6H_4PPh_2$) dont on a déterminé les structures cristallines et les valeurs de pK^{DM} de leurs sels BPh_4^- qui s'établissent respectivement à 8,6 et 6,9.

Mots clés : acidité, complexe de dihydrogène, hydrure, phosphonium, dichlorométhane.

[Traduit par la Rédaction]

Introduction

The quantitative study of the acidity of transition metal hydride and dihydrogen complexes serves to better the understanding of the reactions of these species in catalytic reactions, including those of hydrogenases. Our previous work focused mainly on the use of tetrahydrofuran (THF) as a useful solvent in the study of metal hydride and dihydrogen

Received 9 June 2005. Published on the NRC Research Press Web site at http:canjchem.nrc.ca on 1 March 2006.

Dedicated to Dr. Arthur Carty, National Science Advisor to the Prime Minister of Canada, for his exemplary contributions to and support of science in Canada.

T. Li, A.J. Lough, and R.H. Morris.[2] Department of Chemistry, University of Toronto, 80 St. George Street, Toronto, ON M5S 3H6, Canada.
C. Zuccaccia and A. Macchioni. Dipartimento di Chimica, Università di Perugia, Via Elce di Sotto, 8-06123 – Perugia, Italy.

[1]This article is part of a Special Issue dedicated to Professor Arthur Carty.
[2]Corresponding author (e-mail: rmorris@chem.utoronto.ca).

 doi:10.1139/V05-236 © 2006 NRC Canada

complexes with a wide range of pK_α^{THF} values (1). The use of α in this acidity symbol indicates that the effects of ion pairing on the acid–base equilibria are approximately accounted for by use of the Fuoss equation. This approach has since been used by Leito and co-workers (2). Tetrahydrofuran cannot be used as a solvent for very acidic compounds because it can be protonated and undergo ring-opening reactions. Dichloromethane is a good solvent for this purpose because it is relatively noncoordinating and it dissolves many neutral and cationic metal complexes without reaction, as long as they are not too reducing or nucleophilic. Several pK^{DM} values of metal hydride and dihydrogen complexes in CH_2Cl_2 have been reported by the groups of Jia, Morris, and co-workers (3–7). Only a short continuous ladder of acids in the range of 9.7 to 7.0 was built on the basis of equilibria referenced to $[HPCy_3]BPh_4/PCy_3$ as a standard with pK = 9.7 (Fig. 1) (4). This is the same reference value used for the pK_α^{THF} scale (and pseudo pK_a^{aq} scale) (4, 8), but it will have to be redefined when an absolute value is determined relative to the solvated proton in CH_2Cl_2. There is no continuous ladder based on cationic acids with exclusively one type of anion (e.g., BPh_4^-) in CD_2Cl_2. In this study, we make a limited scale of acidic compounds with BPh_4^- anions. In a second paper we will describe a more extensive ladder involving BF_4^- salts. Although phosphonium salts are of utility as air-stable sources of air-sensitive trialkylphosphines (9), we show here that the tetraphenylborate salts of the more acidic aryl phosphonium compounds are unstable.

We also report the pK^{DM} of two new ruthenium dihydrogen trans-to-chloride complexes. These were prepared while exploring the application of such ruthenium hydrides for the catalytic hydrogenation of compounds with polar bonds (10, 11). Cationic ruthenium dihydrogen complexes have attracted interest with the recent report of Noyori and co-workers (12) that *trans*-[Ru(H_2)(H)((*R*)-binap)((*R,R*)-dpen)]$^+$ is an intermediate in the asymmetric catalytic H_2-hydrogenation of prochiral ketones catalyzed by RuH(BH_4)((*R*)-binap)((*R,R*)-dpen) in isopropanol. Bergens and co-workers (13) spectroscopically identified this unstable dihydrogen complex in deuterated isopropanol and reported that at least 1 equiv. of base is necessary to convert this complex to a catalytically active species.

Results and discussions

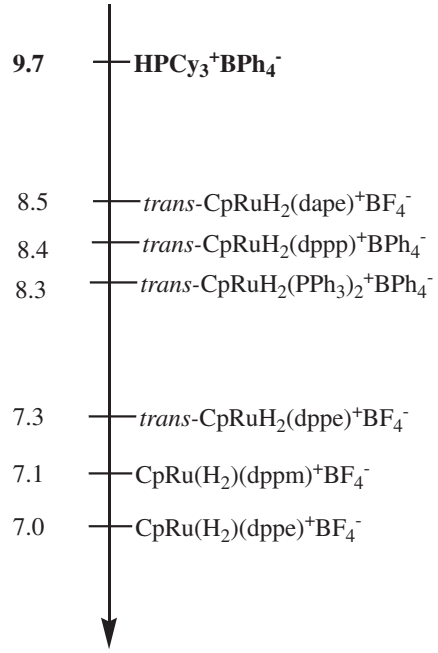
The preparation of $[HPR_3]BPh_4$

The tetrafluoroborate salts $[HPR_3]BF_4$ can be readily prepared by protonation of PR_3 (PR_3 = PCy_3, P-*n*-Bu_3, PCy_2Ph, P-*t*-Bu_2Ph) with $H(Et_2O)BF_4$ in diethyl ether (eq. [1]). As reported previously (1), these salts react with $NaBPh_4$ in ethanol to form the corresponding salts $[HPR_3]BPh_4$ (eq. [2]). However, we found that there is a limitation to this preparation. When the phosphonium salts HPR_3^+ (PR_3 = PBu_2Ph, PMe_2Ph, $PEtPh_2$, P(*p*-toly)$_3$, PPh_3) are more acidic than $HPCy_2Ph^+$, the borane adducts $PR_3{\cdot}BPh_3$ are isolated instead of the tetraphenylborate salts $[HPR_3]BPh_4$. A phenyl group of the BPh_4^- is protonated to form benzene (eq. [3]). The $PR_3{\cdot}BPh_3$ compounds were identified by ^{31}P and ^1H NMR.

[1] $PR_3 + H(Et_2O)BF_4 \rightarrow [HPR_3]BF_4$

[2] $[HPR_3]BF_4 + NaBPh_4 \rightarrow [HPR_3]BPh_4 + NaBF_4$

Fig. 1. The acidity ladder of pK^{DM} values of the cationic ruthenium complexes with $[HPCy_3]BPh_4$ as a standard.



[3] $[HPR_3]BPh_4 \rightarrow C_6H_6 + PR_3{\cdot}BPh_3$

There have been scattered reports of the protonation of the tetraphenylborate anion. Our group encountered it in the preparations of cationic hydrogen isocyanide complexes that were sometimes produced instead of the complexes Fe(TIM)$(CNBPh_3)_2$ (14) and RuH$(CNBPh_3)(dppe)_2$ (15), for example. This has also been reported by Pombeiro and co-workers (16) in the preparation of *trans*-[FeH$(CNBPh_3)(dppe)_2$]. The acidic dihydrogen complex [Ir(H_2)H(triphos)]BPh_4 decomposes to IrH_3(triphos), BPh_3, and benzene (17). However, several cationic dihydrogen and hydride complexes with tetraphenylborate counterions have been reported (for example, refs. 18–28), and so these are likely to be less acidic than $HPCy_2Ph^+$.

NOE and PGSE NMR measurements of $[HPCy_2Ph]BPh_4$

Ion pairing in low dielectric constant solvents like CH_2Cl_2 can lead to changes in reactivity and catalytic activity and selectivity (29). Table 1 shows the results of the study of NOE between ions (31) of the compound $[HPCy_2Ph]BPh_4$. Only the *meta*-aryl hydrogens of the anion (mH_a) can be used as a "reporter", since the resonances of oH_c and oH_a are superimposed. These meta protons are at about the same distance from both the hydrogen on the phosphorus and the hydrogen (H1) on each of the two ipso carbons of the cyclohexyl groups (Fig. 2, Table 1), thus demonstrating the interpenetration of the cation and anion. It is not surprising that more acidic salts can readily undergo transfer of the phosphorus proton to a phenyl ring carbon of the BPh_4^- anion, resulting in B—C bond cleavage.

The pulsed field gradient spin-echo (PGSE) NMR diffusion method (32, 33) is a powerful technique in determining the solution properties of ion pairs (34–36). From the mea-

© 2006 NRC Canada

Fig. 2. ^{1}H NOESY spectrum of $[HPCy_2Ph]BPh_4$ (27 mmol L^{-1}, CD_2Cl_2, 400 MHz, 299 K).

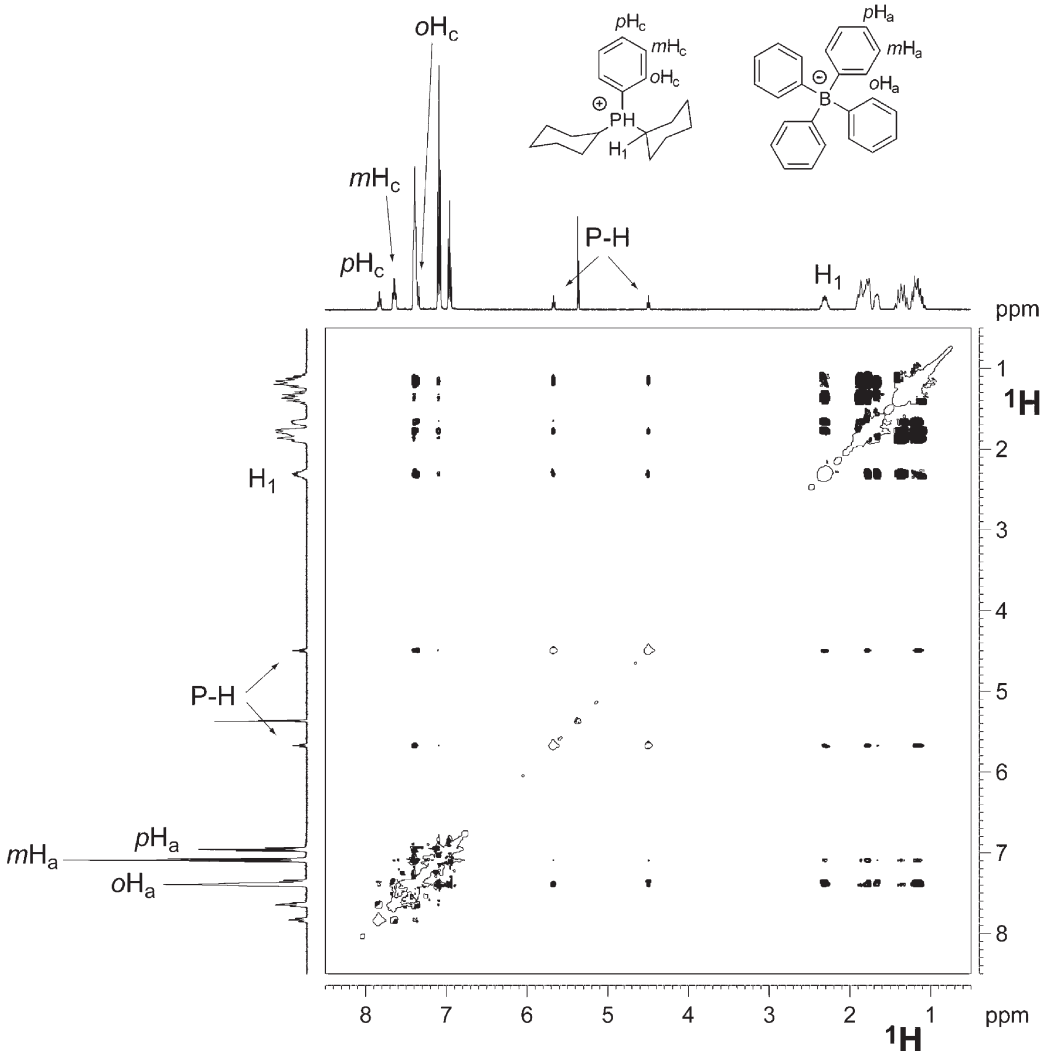


Table 1. Experimental NOE (au) and average interionic distances ($<r>_{exp}$ (Å)) determined using a 27 mmol L^{-1} solution of $[HPCy_2Ph]BPh_4$ in CD_2Cl_2 (the distance between pH$_a$ and oH$_a$ has been used as reference distance).

Pairs	NOE_{exp}	NOE_{corr}[a]	$<r>_{exp}$
pH_a/oH_a	2.66	1	4.04[b]
oH_c/P-H	4.02	6.03	2.99
mH_a/P-H	0.63	0.71	4.27
oH_a/P-H	1.76	1.98	3.60
P-H/H1	3.48	5.2	3.06
mH_a/mH_c	0.45	0.17	5.43
mH_a/H1	0.98	0.54	4.47

[a]Reference 30.
[b]Reference distance.

sured self-diffusion coefficients (D_t), the average hydrodynamic radius (r_H) and volume (V_H) of the diffusing particles were derived, taking advantage of the Stokes–Einstein equation that relates D_t with $1/r_H$. TMSS [tetrakis(trimethylsilyl)silane], whose r_H and V_H are known from the literature (37), was used as internal standard. The methodology to obtain accurate r_H and V_H values has been described elsewhere (38). The average hydrodynamic volumes for cation (V_H^+) and anion (V_H^-) determined from ^{1}H PGSE experiments were contrasted with the van der Waals volume of the ion pair (V_{IP}). The cationic and anionic aggregation numbers (N^+ and N^-) were calculated as the ratios V_H^+/V_{IP} and V_H^-/V_{IP} (Table 2).

The salt $[HPCy_2Ph]BPh_4$ in CH_2Cl_2 forms aggregates higher than ion pairs even at the lowest concentration investigated (entry 1, Table 2). The aggregation number for the cations, N^+, is 1.2 and that of the anions, N^-, is 1.6, indicating a dynamic equilibration of ion pairs, triples (e.g., $(HPCy_2Ph^+)(BPh_4^-)_2$), and quadrupoles. The tendency to aggregate increases as the concentration increases, resulting in N^+ and N^- values of 1.8 and 2.0, respectively, at 0.03 mol L^{-1} (entries 1–3 in Table 2). This is the range of concentrations used in our acid equilibrium studies, and so, such aggregation is a potential complication in interpreting our results.

pK^{DM} determination

The acid (BH^+) and base (B) reaction equilibria are built based on eq. [4]. The equilibrium constants K_{eq} for reactions

© 2006 NRC Canada

Fig. 3. An acidity scale ladder of phosphonium tetraphenylborate salts in CD_2Cl_2 showing pK^{DM} values.

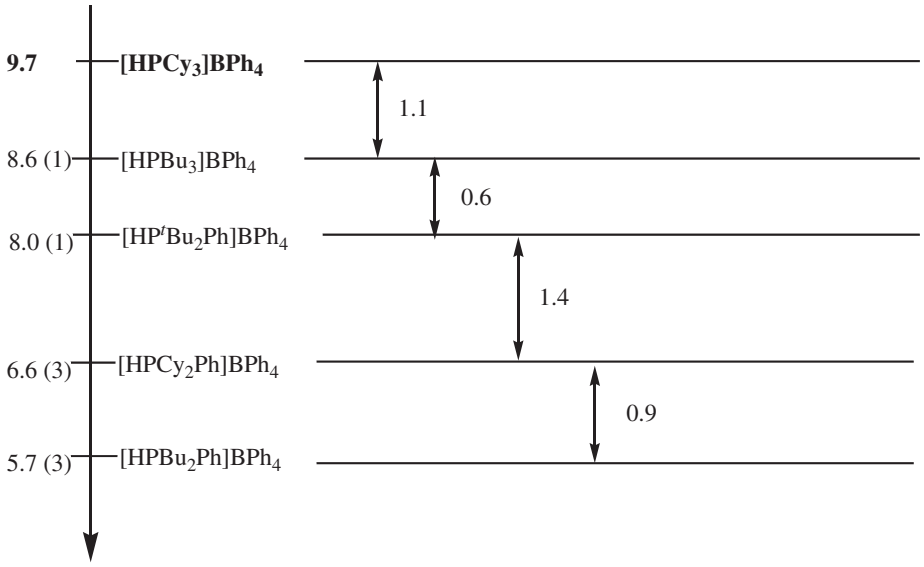


Table 2. Diffusion coefficients (D (10^{-10} m^2 s^{-1})), hydrodynamic radii (r_H (Å)), hydrodynamic volumes (V_H (Å^3)), and aggregation number values (N) for $[HPCy_2Ph]BPh_4$ in CD_2Cl_2.

Entry	Concn. (mmol L^{-1})	D^+	D^-	r_H^+	r_H^-	V_H^+	V_H^-	N^+	N^-
1	1.5	11.1	9.90	5.37	5.88	648	850	1.19	1.56
2	9	10.3	9.72	5.68	5.97	767	892	1.40	1.63
3	27	9.42	9.04	6.13	6.35	967	1072	1.77	1.97

Note: N is the ratio between the experimentally determined hydrodynamic volume and the van der Waals volume of the ion pair; + and – refer to the cation and anion of $[HPCy_2Ph]BPh_4$, respectively.

in CD_2Cl_2 were measured by use of quantitative $^{31}P\{^1H\}$ and ^1H NMR at room temperature. In view of the PGSE experiments, eq. [4] is a simplification of the actual ion-pairing equilibria that are present. However the ^{31}P NMR experiment measures the total phosphorus concentration, and these species are all in rapid equilibrium. If the extent and nature of ion pairing is the same for $B_1H^+X^-$ and $B_2H^+X^-$, then eq. [4] represents a practical, first-order description of the chemistry. K_{eq} in the range 10^3 to 10^{-3} can be measured with a 10%–30% error. The difference in pK^{DM} between the two acids $B_1H^+BPh_4^-$ and $B_2H^+BPh_4^-$ is calculated from the equilibrium constants (K_{eq}) by use of eq. [5].

$$[4] \quad B_1 + B_2H^+X^- \overset{K_{eq}}{\rightleftharpoons} B_1H^+X^- + B_2$$

$$[5] \quad \Delta pK^{DM} = \Delta pK_{eq} = pK^{DM}(B_1H^+X^-) - pK^{DM}(B_2H^+X^-)$$

$$[6] \quad \Delta pK^{DM} = \Delta pK_{fi}^{DM} = pK_{fi}^{DM}(B_1H^+) - pK_{fi}^{DM}(B_2H^+)$$

Ideally, we want the pK_{fi}^{DM} values for the free ions BH^+, independent of the counterion X^-, and not the ion-paired species BH^+X^- and its aggregates. If the extent of ion pairing is the same for $B_1H^+X^-$ and $B_2H^+X^-$, then pK^{DM} and pK_{fi}^{DM} values will be approximately the same (eq. [6]). $[HPCy_3]BPh_4$, with a free ion $pK_{fi}^{DM}(HPCy_3^+) = 9.7$, was chosen as the anchor for the scale in CD_2Cl_2, as in the THF scale (1). Overlapping equilibria were examined with more acidic compounds to create a continuous ladder of values (e.g., eqs. [7] and [8]).

$$[7] \quad PCy_3 + [HBu_3]BPh_4 \underset{pK_{eq} = -1.1}{\rightleftharpoons} \underset{9.7}{[HPCy_3]BPh_4} + PBu_3$$

$$[8] \quad pK_{fi}^{DM}(HPBu_3^+) = 9.7 + pK_{eq} = 8.6$$

A short acidity scale ladder of phosphonium tetraphenylborate salts in CD_2Cl_2 was built by this method (shown in Fig. 3). The estimated errors for the equilibrium constants are listed in Tables 3 and 4. The cumulative error in pK^{DM} value is calculated by eq. [9]. The errors in the last digit are shown in parentheses in Fig. 3. They represent the combination of the cumulative errors relative to the reference value of 9.7 and the estimated errors for K_{eq}.

$$[9] \quad \text{Cumulative error in } pK^{DM} = \pm 0.08\ |pK^{DM} - 9.7|$$

The equilibrium constant K_{eq} in the reaction between $HPCy_2Ph^+$ and PBu_2Ph has to be obtained by the immediate measurement of the NMR spectrum after mixing. Right after mixing, a signal due to $HPBu_2Ph^+$ can be observed. Longer standing (1 h) of the mixture causes a decay of $HPBu_2Ph^+$ to produce the $PBu_2Ph{\cdot}BPh_3$ species (Scheme 1). This suggests that $HPCy_2Ph^+$ with the pK^{DM} value of 6.6 is the most acidic BPh_4^- salt that can be obtained.

© 2006 NRC Canada

Table 3. Equilibrium constants for acid–base reaction of phosphonium salts in CD_2Cl_2.

Acid	Concn. (mmol L^{-1})	Base	Concn. (mmol L^{-1})	Time to reach equilibrium (h)	Error[a] (%)	K_{eq}	pK_{eq}
$[HPBu_3]BPh_4$	35	PCy_3	33	<4	5	11.8	–1.1
[HP-*t*-Bu_2Ph]BPh_4	38	PBu_3	35	<4	5	4.0	–0.6
[HP-*t*-Bu_2Ph]BPh_4	43	PCy_2Ph	46	<1	10	0.037	1.4
$[HPCy_2Ph]BPh_4$	43	PBu_2Ph	43	<1	5	0.12	0.9

[a]The error in the equilibrium constant determination is estimated from the magnitude of the constant and the *S/N* of each species in the spectrum of the equilibrium mixture.

Table 4. Equilibrium constants for reactions of ruthenium hydride complexes in CD_2Cl_2.

Entry	Acid (pK^{DM})	Concn. (mmol L^{-1})	Base	Concn. (mmol L^{-1})	Time to reach equilibrium (h)	K_{eq}	pK_{eq}	pK^{DM}
1	[HP-*t*-Bu_2Ph]BPh_4 (8.0)	21	$RuHCl(PPh_3)_2$(dach)	19	<1	6	–0.8	8.8
2	$[HPBu_3]BPh_4$ (8.6)	18	$RuHCl(PPh_3)_2$(dach)	16	<1	0.65	0.19	8.4
3	$[Ru(H_2)Cl(PPh_3)_2(dach)]BF_4$	14	PBu_3([$HPBu_3$]BF_4 8.2)	18	<1	0.50	–0.3	8.5
4	$[HPCy_2Ph]BPh_4$ (6.6)	20	$RuHCl(PPh_3)_2$(dach)	18	<1	153	–2.2	8.8
5	$[HPCy_2Ph]BPh_4$ (6.6)	16	$RuHCl\{tmeP_2(NH)_2\}$	20	<1	2.6	–0.4	7.0
6	$[HPBu_3]BPh_4$ (8.6)	21	$RuHCl\{tmeP_2(NH)_2\}$	20	<1	0.019	1.7	6.8
7	[HP-*t*-Bu_2Ph]BPh_4 (8.0)	17	$RuHCl\{tmeP_2(NH)_2\}$	20	<1	0.08	1.1	6.9
8	$[HPBu_2Ph]BF_4$ (5.8)	21	$RuHCl\{tmeP_2(NH)_2\}$	20	<1	5.9	–0.8	6.6
9	$[HPCy_2Ph]BF_4$ (6.7)	22	$RuHCl\{tmeP_2(NH)_2\}$	20	<1	1.0	0	6.7

Scheme 1.

$$PBu_2Ph + [HPCy_2Ph]BPh_4 \underset{K = 0.12}{\rightleftharpoons} [HPBu_2Ph]BPh_4 + PCy_2Ph \quad (10\ min)$$

$$\downarrow -C_6H_6$$

$$Bu_2PhP \cdot BPh_3 \quad (1\ h)$$

The pK^{DM} values of Fig. 3 show the expected substituent effect of an increase in acidity of the phosphonium with a change from alkyl to phenyl group. Replacing Cy or Bu by Ph causes a decrease of approx 3 units of pK^{DM}. The pK^{DM} values for phosphonium salts with pK^{DM} value greater than 6.5 are in reasonable agreement with the corresponding pK_α^{THF} values (Fig. 4). However, the reported values (1) of pK_α^{THF} for $[HPBu_2Ph]BPh_4$ (6.7), $[HPMePh_2]BPh_4$ (6.3), and $[HPEtPh_2]BPh_4$ (5.3) are questionable, and these equilibria may in fact involve the protonation of tetraphenylborate.

Synthesis and structure of ruthenium dihydrogen complexes

The complex $RuHCl(dach)(PPh_3)_2$ is a precursor to an active ketone hydrogen catalyst, $RuH_2(dach)(PPh_3)_2$ (11). The protonation of $RuHCl(dach)(PPh_3)_2$ by $HBF_4{\cdot}Et_2O$ in THF gives the new dihydrogen complex $[Ru(\eta^2\text{-}H_2)Cl(dach)(PPh_3)_2]BF_4$ (Scheme 2). The molecular structure of this dihydrogen complex is shown in Fig. 5.

The overall geometry is octahedral. The η^2-dihydrogen ligand is situated trans to the chloride. The Ru—H distances to the dihydrogen ligand are both 1.63(5) Å. The H—H distance is 0.78 (6) Å. Hydrogen-bonding interactions of $F_3BF\cdots HN$ (F···H 2.0 and 2.2 Å) and $C_4H_8O\cdots HN$ (O···H 2.1 Å) are observed in the X-ray crystal structure.[3] The trans geometry of the complex appears to be maintained in solution on the basis of the observation of a singlet in the $^{31}P\{^1H\}$ NMR spectrum. The dihydrogen resonance for this complex is a singlet at –10.8 ppm, and it is broad because of the rapid dipolar relaxation of the nuclei in the η^2-dihydrogen ligand.

The dihydrogen complex $[Ru(H_2)Cl(PPh_3)_2(dach)]BF_4$ in C_6D_6 reacts with D_2 gas to give isotopomers, including $[Ru(HD)Cl(PPh_3)_2(dach)]BF_4$. This probably proceeds via H–D exchange with the dach N—H bonds. The observation of $^1J_{HD}$ = 28.5 Hz in the Ru(HD) isotopomer provides more evidence of the side-on-bonded H_2-coordination. This corresponds to an H—H distance of 0.94 Å on the basis of eq. [10] (39). The X-ray derived value of 0.78(6) Å is probably underestimated because of the problem of locating hydrogen atoms by this method and the rotation of the H_2 ligand.

$$[10] \quad d(H\text{—}H) = -0.0167\ (^1J_{HD}) + 1.42$$

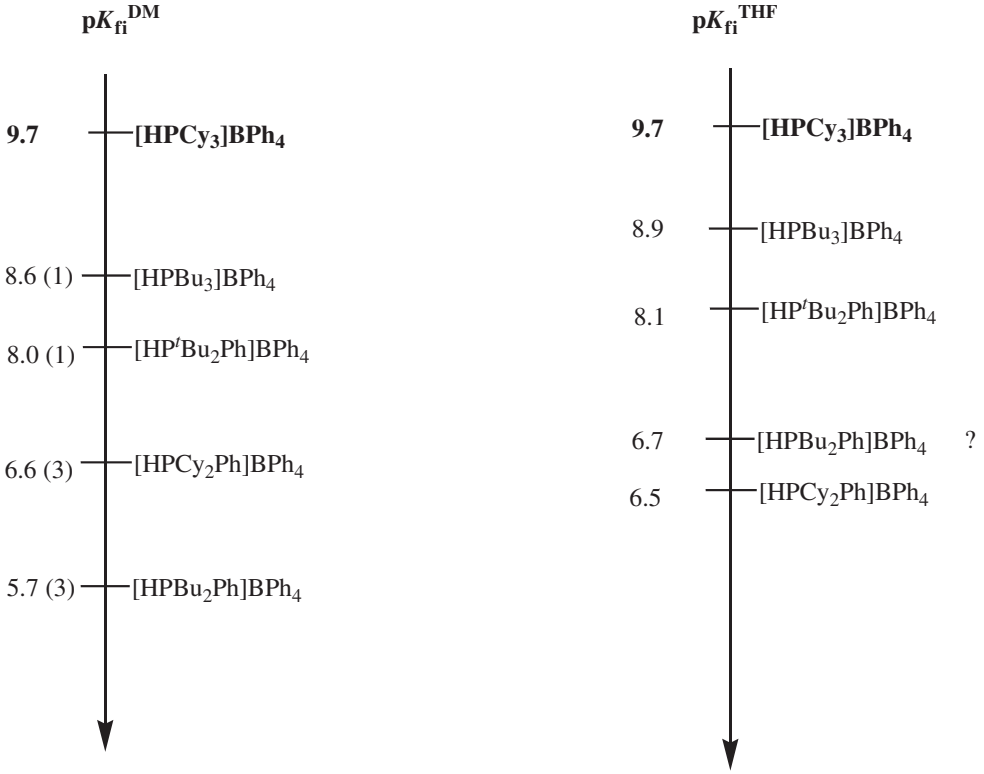
Synthesis and structure of $[Ru(\eta^2\text{-}H_2)Cl\{tmeP_2(NH)_2\}]BF_4$

$[Ru(\eta^2\text{-}H_2)Cl\{tmeP_2(NH)_2\}]BF_4$ is observed in the reaction of $RuHCl\{tmeP_2(NH)_2\}$ with HBF_4 in CD_2Cl_2 by NMR

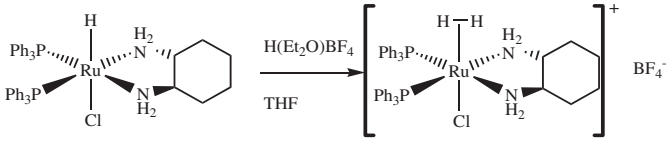
[3]Supplementary data for this article are available on the journal Web site (http://canjchem.nrc.ca) or may be purchased from the Depository of Unpublished Data, Document Delivery, CISTI, National Research Council Canada, Ottawa, ON K1A 0R6, Canada. DUD 4082. For more information on obtaining material refer to http://cisti-icist.nrc-cnrc.gc.ca/irm/unpub_e.shtml. CCDC 274511 and 274512 contain the crystallographic data for this manuscript. These data can be obtained, free of charge, via www.ccdc.cam.ac.uk/conts/retrieving.html (Or from the Cambridge Crystallographic Data Centre, 12 Union Road, Cambridge CB2 1EZ, UK; fax +44 1223 336033; or deposit@ccdc.cam.ac.uk).

© 2006 NRC Canada

Fig. 4. A comparison of the acidity ladders for $[HPR_3]BPh_4$ salts in CD_2Cl_2 and THF.



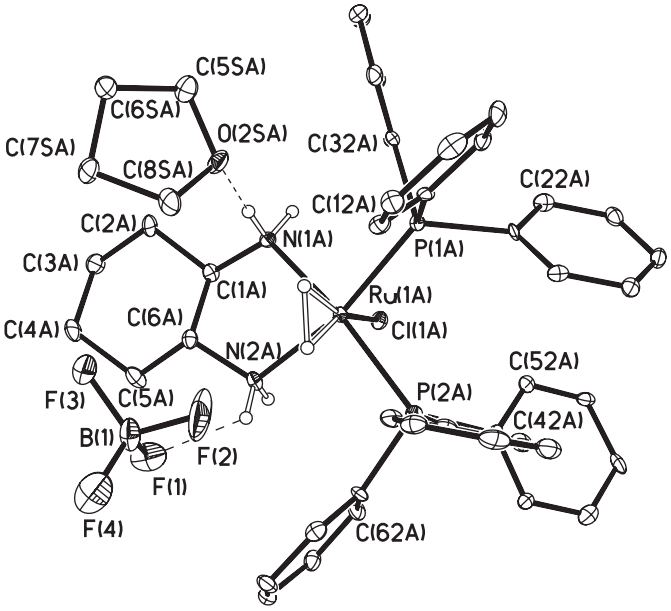
Scheme 2.



spectroscopy. There are two isomers, A and B, of the RuHCl complex in the ratio of 3:2 (40). Isomer A is believed to have two NH hydrogen atoms that are syn to the hydride. Isomer B has one NH hydrogen atom syn to the hydride and the other NH hydrogen atom syn to the chloride. Therefore, two isomers of the Ru dihydrogen complex are formed by protonation of isomers A and B (shown in Scheme 3).

A crystal of one isomer of the dihydrogen complexes was obtained from the reaction. The molecular structure of the dihydrogen complex (Fig. 6) is derived from isomer B with one NH hydrogen atom syn to the chloride. The distances Ru—H1 and Ru—H2 are 1.79(2) and 1.79(3) Å, respectively. These long Ru—H distances might signal a weak Ru—H_2 interaction, and this interaction might explain why the dihydrogen ligand is usually lost during isolation. There is an intramolecular electrostatic NH···Cl interaction observed in the structure with an H···Cl distance of 2.5 Å. $[Ru(\eta^2\text{-}H_2)Cl(dach)(PPh_3)_2]BF_4$ has an NH···Cl distance of 2.8 Å. The other NH hydrogen atom is syn to the dihydrogen ligand and hydrogen bonds with the BF_4 anion (NH···F distance of 2.0 Å). The ^{31}P NMR spectrum suggests that two isomers are formed in the ratio of 1:2 (A:B). Isomer A exhibits a singlet at 36.4 ppm. Isomer B exhibits two doublets at 40.6 and 30.5 ppm. The dihydrogen resonance for this complex is similar to that of $[Ru(\eta^2\text{-}H_2)Cl(dach)(PPh_3)_2]^+$ and

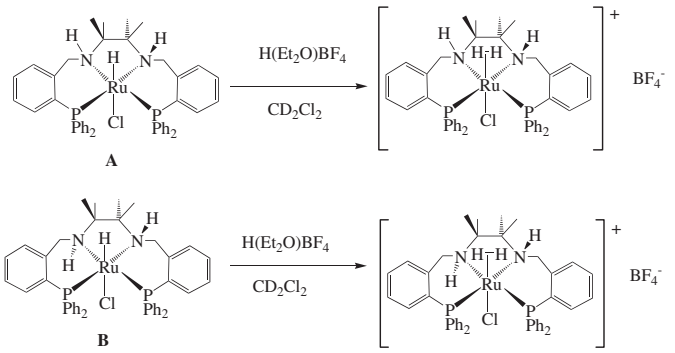
Fig. 5. Structure of $[Ru(\eta^2\text{-}H_2)Cl(dach)(PPh_3)_2]BF_4 \cdot THF$ as determined by single crystal X-ray diffraction.



exhibits a broad singlet at –10.9 ppm. $[Ru(HD)Cl\{tmeP_2(NH)_2\}]BF_4$ was prepared by the reaction of $RuHCl\{tmeP_2(NH)_2\}$ and HBF_4–D_2O in CD_2Cl_2. The observation of $^1J_{HD}$ = 28 Hz in the Ru(HD) isotopomer suggests an H—H distance of 0.95 Å on the basis of eq. [10]. When

© 2006 NRC Canada

Scheme 3.



$[Ru(\eta^2\text{-}H_2)Cl\{tmeP_2(NH)_2\}]BF_4$ reacts with D_2, there is no hydride signal in the ^1H NMR spectrum, consistent with the formation of $[Ru(\eta^2\text{-}D_2)Cl\{tmeP_2(NH)_2\}]BF_4$. Apparently there is no D–H exchange between D_2 and the NH groups.

The pK^{DM} measurements for the dihydrogen complexes

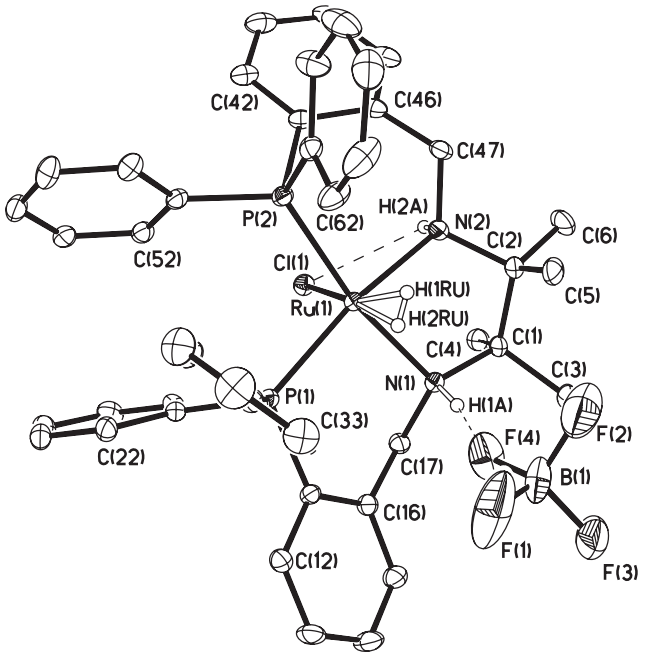
The equilibria between the hydrido complexes $RuHCl(dach)(PPh_3)_2$ or $RuHCl\{tmeP_2(NH)_2\}$ and the phosphonium salts were established within 1 h at 20 °C (Figs. 7 and 8). The equilibria involving the BPh_4^- salts $[HPBu_3]BPh_4$, $[HP\text{-}t\text{-}Bu_2Ph]BPh_4$, and $[HPCy_2Ph]BPh_4$ produced an average pK^{DM} value of 8.6 ± 0.2 for the dihydrogen complex $[Ru(\eta^2\text{-}H_2)Cl(dach)(PPh_3)_2]BPh_4$. A corresponding reaction with $[HPBu_3]BF_4$ gave a pK^{DM} value of 8.5 ± 0.2 for the corresponding BF_4^- salt of the dihydrogen complex. The variation in the values obtained could be a result of ion-pairing effects and NH···FBF_3^- hydrogen bonding in the case of equilibria involving the BF_4^- anion.

Three equilibria were established between $RuHCl\{tmeP_2(NH)_2\}$ and phosphonium tetraphenylborate salts $[HPBu_3]BPh_4$, $[HP\text{-}t\text{-}Bu_2Ph]BPh_4$, and $[HPCy_2Ph]BPh_4$, to give a consistent pK^{DM} value of 6.9 for $[Ru(\eta^2\text{-}H_2)Cl\{tmeP_2(NH)_2\}]BPh_4$. Two equilibria between $RuHCl\{tmeP_2(NH)_2\}$ and $[HPBu_2Ph]BF_4$ and $[HPCy_2Ph]BF_4$ suggest an average pK^{DM} value of 6.7 for $[Ru(\eta^2\text{-}H_2)Cl\{tmeP_2(NH)_2\}]BF_4$.

Comparison of the acidity of ruthenium dihydrogen complexes

The pK^{DM} values of some related dihydrogen complexes are listed in Table 5. The complexes $[Ru(H_2)Cl(dppe)_2]PF_6$ and $[Ru(H_2)Cl(dppp)_2]PF_6$ are dihydrogen complexes with four phosphorus (phosphine) donors and have pK^{DM} values of approximately 4.7 and 3.3, respectively (entries 1 and 2, Table 5) (41, 42).[4] $[Ru(H_2)Cl\{tmeP_2(NH)_2\}]BPh_4$ and $[Ru(H_2)Cl(dach)(PPh_3)_2]BPh_4$ are a different class of dihydrogen complex with two phosphorus (phosphine) and two nitrogen (amine) ligands, and they have pK^{DM} 6.9 and 8.6, respectively (entries 4 and 5, Table 5). The replacement of phosphine ligands with more electron-donating amine ligands decreases the acidity of the complexes. However, $[Ru(H_2)Cl(PPh_3)(PMP)]BF_4$ with three phosphorus (phosphine) ligands and one nitrogen (pyridyl) ligand (6) does not follow this trend (entry 3, Table 5), suggesting that the pyridine donor is more like a phosphine than an amine on ruthenium.

Fig. 6. Structure of $[Ru(H_2)Cl\{tmeP_2(NH)_2\}]$ BF_4 as determined by single crystal X-ray diffraction.



Conclusions

A continuous acidity ladder of five phosphonium tetraphenylborate salts in CD_2Cl_2 at room temperature has now been established by use of ^{31}P NMR spectroscopy. The pK^{DM} values are generally consistent with values previously measured in THF. NOE and PGSE measurements show that ion pairs and higher aggregates are present in solution, complicating the interpretation of the results. When the pK^{DM} is lower than 6.6, the BPh_4^- salts tend to decompose. The acidities of the new dihydrogen complexes, $[Ru(H_2)Cl(PPh_3)_2(dach)]BPh_4$ and $[Ru(H_2)Cl\{tmeP_2(NH)_2\}]BPh_4$, are determined to be p$K^{DM}$ 8.6 and 6.9, respectively, through the use of several consistent equilibria with phosphonium salts. The pK^{DM} values for the BF_4^- salts are similar. The crystal structures of $[Ru(H_2)Cl(PPh_3)_2(dach)]BF_4$ and $[Ru(H_2)Cl\{tmeP_2(NH)_2\}]BF_4$ are determined. We will describe elsewhere the use of tetrafluoroborate salts to extend the ladder to lower pK^{DM} values, below the limit set by the decomposition of BPh_4^- salts.

Experimental

General methods

All preparations and manipulations were carried out under hydrogen, nitrogen, or argon atmospheres with the use of standard Schlenk, vacuum line, and glovebox techniques in dry, oxygen-free solvents. Tetrahydrofuran (THF), diethyl ether (Et_2O), and hexanes were dried and distilled from sodium benzophenone ketyl. Dichloromethane was dried and distilled from calcium hydride. Deuterated solvents were degassed and dried over activated molecular sieves. NMR

[4] T. Li, A.J. Lough, and R.H. Morris. In preparation.

© 2006 NRC Canada

Fig. 7. The equilibria established between $RuHCl(dach)(PPh_3)_2$ and phosphonium salts in 1 h at 20 °C.

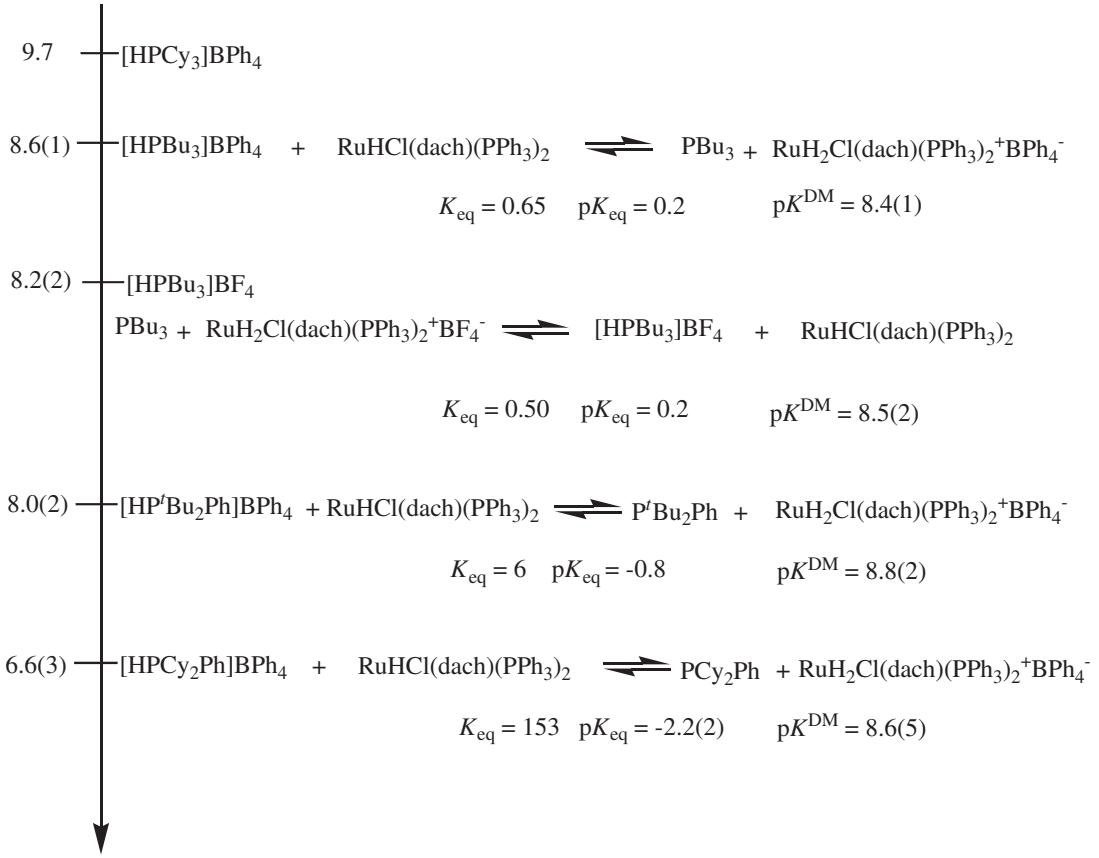


Table 5. Comparison of the acidity of ruthenium dihydrogen complexes.

Entry	Type	Complex	pK^{DM}	Ref.
1	$[RuP_4(H_2)Cl]X$	$[Ru(H_2)Cl(dppe)_2]PF_6$[a]	4.7	42
2		$[Ru(H_2)Cl(dppp)_2]PF_6$[b]	3.3	41
3	$[RuP_3N(H_2)Cl]X$	$[Ru(H_2)Cl(PPh_3)(PMP)]BF_4$[c]	4.0[d]	6
4	$[RuP_2N_2(H_2)Cl]X$	$[Ru(H_2)Cl\{tmeP_2(NH)_2\}]BPh_4$	6.9	This work
5		$[Ru(H_2)Cl(dach)(PPh_3)_2]BPh_4^-$	8.6	This work

[a]dppe = 1,2-bis(diphenylphosphine)ethane.
[b]dppp = 1,3-bis(diphenylphosphine)propane.
[c]PMP = 2,6-$(Ph_2PCH_2)_2C_5H_3N$.
[d]The literature value of 5.1 has been adjusted (42).

spectra were recorded on a Varian Unity-500 (500 MHz for ^1H), a Varian Unity-400 (400 MHz for ^1H), or on a Varian Gemini 300 MHz spectrometer (300 MHz for ^1H and 121.5 MHz for ^{31}P). All ^{31}P chemical shifts were measured relative to 10% $P(OMe)_3$ in C_6D_6. This reference solution was placed in a 2 mm capillary tube inside the 5 mm sample NMR tube. ^1H chemical shifts were measured relative to partially deuterated solvent peaks but are reported relative to tetramethylsilane. The phosphine compounds were received from commercial suppliers (Aldrich Chemical Co., Stem Co.) and used without further purification. $NaBPh_4$ was supplied by Aldrich Chemical Co. $RuCl_3$ hydrate was obtained from Johnson Matthey. The compounds $RuHCl(PPh_3)_2$-(dach) (10) and *trans*-$RuHCl\{tmeP_2(NH)_2\}$ (40) were prepared according to literature procedures. Protonated salts that have not already been reported in the literature have been found to have the correct elemental analyses by the Analyst Laboratory of the University of Toronto.

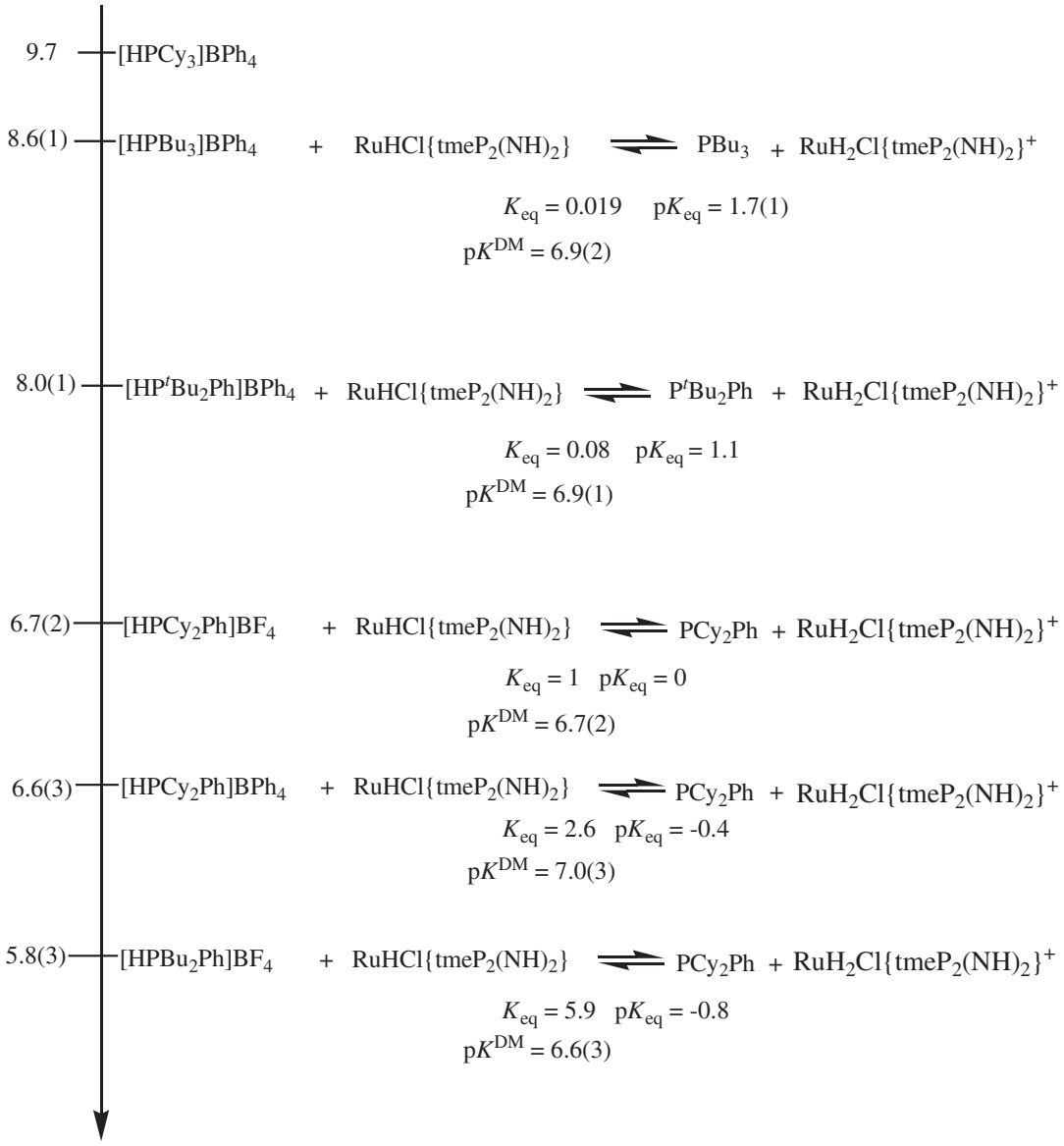
$[HPR_3]BPh_4$

All phosphonium salts $[HPR_3]BPh_4$ (PR_3 = PCy_3, P-*n*-Bu_3, P-*t*-Bu_2Ph, PCy_2Ph) were isolated by use of the reported preparation (4), with typical yields of 80%–90%. The attempted preparations of $[HPR_3]BPh_4$ (PR_3 = PBu_2Ph, PMe_2Ph, $PEtPh_2$, PPh_3) were unsuccessful as these decompose. $PR_3 \cdot BPh_3$ (PR_3 = PBu_2Ph, PMe_2Ph, $PEtPh_2$, PPh_3) compounds were obtained instead. The ^{31}P NMR chemical shifts are reported in Table 6. NMR data for $[HPCy_2Ph]BPh_4$ (CD_2Cl_2, 299 K, *J* values in Hz, refer to Fig. 2 for the labelling) follow.

^1H NMR δ: 7.83 (t, $^3J_{HH}$ = 7.7, pH_c), 7.64 (td, $^3J_{HH}$ = 7.8, $^4J_{HP}$ = 3.3, mH_c), 7.39 (m, oH_a), 7.36 (dd, $^3J_{PH}$ = 19.4,

© 2006 NRC Canada

Fig. 8. The equilibria established between $RuHCl\{tmeP_2(NH)_2\}$ and the phosphonium salt in 1 h at 20 °C.



$^3J_{HH}$ = 7.8, *o*H_c), 7.09 (t, $^3J_{HH}$ = 7.5, *m*H_a), 6.95 (tt, $^3J_{HH}$ = 7.3, $^4J_{HH}$ = 1.3 *p*H_a), 5.08 (dt, $^1J_{PH}$ = 471.0, $^3J_{HH}$ = 6.3, P-H), 2.30 (m, H_1), 1.81, 1.66, 1.35, 1.15 (m, cyclohexyl resonances).

$[Ru(H_2)Cl(PPh_3)_2(dach)]BF_4$

$RuHCl(PPh_3)_2$(dach) (203 mg, 0.26 mmol) was dissolved in THF (2 mL). HBF_4 (54 wt% in Et_2O, 90 mg, 0.30 mmol) was added to the solution under Ar and stirred for 0.5 h. Et_2O (6 mL) was added to give a yellow-green precipitate. The solid was filtered and washed with diethyl ether (2 × 3 mL). The solid product was obtained by filtration and dried under vacuum. Crystals of $[Ru(H_2)Cl(PPh_3)_2(dach)]BF_4$ were prepared by slow diffusion of diethyl ether into a saturated solution of the complex in THF. Yield: 190 mg, 87%. ^{1}H NMR (C_6D_6) δ: 7.4–7.0 (m, 30H, Ph), 3.3 (br, 2H, NH_2), 2.8–2.6 (m, 8H, CH_2), 2.2 (br, 2H, NH_2), 1.2 (m, 2H, C*H*), –10.75 (br, 2H, RuH_2). ^{31}P NMR δ: 46.1 (s). Anal.

Table 6. ^{31}P NMR chemical shifts of phosphines and phosphonium salts in CD_2Cl_2.

Bases	δ ^{31}P	Acids	δ ^{31}P
PCy_3	9.8	$[HPCy_3]BPh_4$	29.5
		$[HPCy_3]BF_4$	29.5
PBu_3	–31.1	$[HPBu_3]BPh_4$	10.7
P-*t*-Bu_2Ph	39.4	[HP-*t*-Bu_2Ph]BPh_4	52.3
PCy_2Ph	2.9	$[HPCy_2Ph]BPh_4$	27.1
		$[HPCy_2Ph]BF_4$	27.0
PBu_2Ph	–24.6	$[HPBu_2Ph]BF_4$	14.9
		$PBu_2Ph{\cdot}BPh_3$	–4.4
$PMePh_2$	–27.1	$[HPMePh_2]BF_4$	2.0
		$PMePh_2{\cdot}BPh_3$	–9.5
$PEtPh_2$	–11.8	$[HPEtPh_2]BF_4$	12.5
		$PEtPh_2{\cdot}BPh_3$	–4.0

© 2006 NRC Canada

calcd. for $C_{42}H_{46}N_2P_2BClF_4Ru$: C 58.08, H 5.46, N 3.33; found: C 58.40, H 5.33, N 3.24.

The reaction of RuHCl{tmeP_2(NH)$_2$} with HBF_4

A mixture of two isomers (see Discussion) of RuHCl{tmeP_2(NH)$_2$} (10 mg, 0.012 mmol) was dissolved in CD_2Cl_2 (1 mL) in an NMR tube under Ar. HBF_4 (54 wt% in Et_2O, 10 mg, 0.06 mmol) was added to the solution. ^{1}H NMR δ: 7.6–6.8 (m, 28H, Ph), 4.8 (m, C*H*$_2$), 4.6 (m, C*H*$_2$), 4.4 (m, N*H*), 3.9 (m, N*H*), 1.8–1.2 (m, 12H, C*H*$_3$), –10.9 (brs, 2H, Ru*H*$_2$); T_1 = 19 ms at 400 MHz NMR spectrometer at 293 K. ^{31}P NMR δ: 41.0 (d, $^2J_{PP}$ = 25 Hz, 40%, isomer B), 30.5 (d, 37%, isomer B), 37.0 (s, 23%, isomer A). Crystals of [Ru(H$_2$)Cl{tmeP_2(NH)$_2$}]BF_4 were prepared by slow diffusion of diethyl ether into the NMR solution of the complex in CD_2Cl_2 under Ar.

The reaction of [Ru(H$_2$)Cl(PPh$_3$)$_2$(dach)]BF_4 with D_2

[Ru(H$_2$)Cl(PPh$_3$)$_2$(dach)]BF_4 (10 mg, 0.011 mmol) was dissolved in C_6D_6 (1 mL) in a 5 mm NMR tube under Ar. The solution was frozen in liquid N_2 and degassed – refilled with D_2 gas for three cycles. The NMR tube was sealed with a flame under D_2 and warmed up to room temperature. An ^{1}H NMR spectrum was collected immediately and after 15 h. A 1:1:1 triplet of 1:2:1 triplets at –10.74 ppm ($^1J_{HD}$ = 28.5 Hz, $^2J_{HP}$ = 8.7 Hz) was observed over time due to Ru(HD).

The reaction of [Ru(H$_2$)Cl{tmeP_2(NH)$_2$}]BF_4 with D_2

The procedure used for the dach complex was followed. No H–D coupling was observed. The hydride signal at –10.9 ppm disappeared after 15 h.

The reaction of RuHCl{tmeP_2(NH)$_2$} with HBF_4(Et$_2$O)–D_2

RuHCl{tmeP_2(NH)$_2$} (isomer A, 10 mg, 0.012 mmol) was dissolved in CD_2Cl_2 (1 mL) in an NMR tube. DBF_4 (1 drop, prepared by mixing HBF_4, 54 wt% in Et_2O, 0.40 g, 0.025 mol and degassed D_2O, 1.1 g, in a Schlenk flask) was added to the solution. A 1:1:1 triplet of triplets was observed over time due to Ru(HD). ^{1}H NMR δ: –10.9 (tt, RuHD, $^1J_{HD}$ = 28.5 Hz, $^2J_{HP}$ = 8.4 Hz). ^{31}P NMR δ: 40.6 (d, $^2J_{PP}$ = 25 Hz, isomer B), 30.5 (d, isomer B).

Determination of equilibrium constants in CD_2Cl_2

Solutions of samples were mixed under N_2 as described in Tables 3 and 4. In general, equilibrium constants were determined by ^{1}H and ^{31}P{^{1}H} NMR. Usually, signals for all of the species in equilibrium could be located and integrated in the ^{31}P{^{1}H} NMR and, in the case of hydride complexes, in the ^{1}H NMR spectra as well. The chemical shifts for the pure phosphines and phosphonium salts (Table 6) were determined and referenced to the P(OMe)$_3$ standard at 141.5 ppm. In some cases, when the chemical shifts of two species are very similar, mass-balance arguments can be used to estimate the equilibrium concentration of the species from their starting concentrations. Thermodynamic data for the equilibria in CD_2Cl_2 are shown in Tables 3 and 4.

NOE measurements

The ^{1}H NOESY NMR experiment was acquired by the standard three-pulse sequence (43). Each transient (direct dimension) was acquired using 2K points; the number of transients (indirect dimension) was 1K, and the number of scans was set at 16. A relaxation delay of 2 s and a mixing time of 0.5 s were used. The average interionic distances were obtained taking into account that the volumes of the NOE cross peaks are proportional to ($n_I n_S/n_I+n_S$), where n_I and n_S are the number of equivalent I and S nuclei, respectively (30).

PGSE measurements

^{1}H PGSE NMR measurements were performed using the standard stimulated echo pulse sequence (32) on a Bruker AVANCE DRX 400 spectrometer equipped with a GREAT 1/10 gradient unit and a QNP probe with a Z-gradient coil, at 299 K without spinning. The shape of the gradients was rectangular, their duration was 5 ms, and their strength (G) was varied during the experiments. All the spectra were acquired using 32K points, a spectral width of 5000 Hz, and processed with a line broadening of 1.0 Hz. The semilogarithmic plots of $\ln(I/I_0)$ vs. G^2 (where I and I_0 are the intensities of the observed spin echo in the presence or in the absence of the field gradient, respectively) (34, 35) were fitted using a standard linear regression algorithm; the R factor was always higher than 0.99. r_H, V_H, and N values were derived from experimentally determined D_t data as described in ref. 31.

X-ray diffraction structure determination of [Ru(H$_2$)Cl(PPh$_3$)$_2$(dach)]BF_4 and [Ru(H$_2$)Cl{tmeP_2(NH)$_2$}]BF_4

Crystals suitable for X-ray diffraction were obtained by vapor diffusion. Data were collected on a Nonius Kappa-CCD diffractometer using monochromated Mo Kα radiation and were measured using a combination of ϕ scans and ω scans with κ offsets, to fill the Ewald sphere. The data were processed using the Denzo-SMN package (44). For the second structure (the tmeP_2(NH)$_2$ complex), absorption corrections were carried out using SORTAV (45). The structures were solved and refined using SHELXTL V6.1 (46) for full-matrix least-squares refinements that are based on F^2. The H atoms of the dihydrogen were refined independently with isotropic displacement parameters, but in the first structure these parameters were tied to the U_{eq} values of the Ru atoms. All other H atoms were included in calculated positions and allowed to refine in riding-motion approximation with U_{iso} tied to the carrier atom. Crystallographic data for the compounds are given in Tables 7 and 8, and selected bond distances and angles in Tables 9 and 10.

Acknowledgment

This work was supported by a discovery grant to RHM from the Natural Sciences and Engineering Research Council of Canada (NSERC) and by a grant to AM from the Ministero dell'Istruzione, dell'Università e della Ricerca (MUIR) (PRIN 2004-2005). We thank J. Matthey for a loan of ruthenium salts and Dr. K. Abdur-Rashid for assistance with some experiments.

© 2006 NRC Canada

Table 7. Crystallographic data for $[Ru(\eta^2H_2)Cl(dach)(PPh_3)_2]BF_4 \cdot THF$.

a (Å)	12.0771(5)	Formula	$C_{46}H_{54}N_2P_2BClF_4ORu$
b (Å)	12.2479(4)	Formula weight	936.18
c (Å)	16.5468(5)	Space group	$P\bar{1}$
α (°)	70.917(2)	T (K)	100(1)
β (°)	89.536(2)	λ (Å)	0.710 73
γ (°)	69.588(2)	ρ_{calc} (mg/m^3)	1.445
V (Å^3)	2152.28(13)	R_1 (all data)	0.071
Z	2	wR_2	0.123

Table 8. Crystallographic data for $[Ru(H_2)Cl\{tmeP_2(NH)_2\}]BF_4$.

a (Å)	14.7990(3)	Formula	$C_{44}H_{48}BClF_4N_2P_2Ru$
b (Å)	12.6530(3)	Formula weight	890.11
c (Å)	21.7310(4)	Space group	$P2_1/c$
α (°)	90	T (K)	150(1)
β (°)	92.670(1)	λ (Å)	0.710 73
γ (°)	90	ρ_{calc} (mg/m^3)	1.455
V (Å^3)	4064.8(2)	R_1 (all data)	0.074
Z	4	wR_2	0.109

Table 9. Selected bond distances and angles for $[Ru(\eta^2\text{-}H_2)Cl(dach)(PPh_3)_2]BF_4$.

Distances (Å)			
Ru(1)—H(1Ru)	1.63(5)	Ru(1)—H(2Ru)	1.63(5)
H(1Ru)—H(2Ru)	0.78(6)	Ru(1)—P(1A)	2.3242(8)
Ru(1)—P(2A)	2.3537(8)	Ru(1)—N(1A)	2.17(1)
Ru(1)—N(2A)	2.19(1)	Ru(1)—Cl(1)	2.4143(8)
Angles (°)			
H(1Ru)-Ru(1)-H(2Ru)	27(2)	H(1Ru)-Ru(1)-N(1)	81(2)
H(2Ru)-Ru(1)-N(1)	103(2)	H(1Ru)-Ru(1)-N(2)	90(2)
H(2Ru)-Ru(1)-N(2)	70(2)	N(1)-Ru(1)-N(2)	78.1(3)
P(1)-Ru(1)-P(2)	98.14(3)	N(1)-Ru(1)-P(1)	90.4(2)
N(2)-Ru(1)-P(1)	167.1(2)	N(1)-Ru(1)-P(2)	169.7(4)
N(2)-Ru(1)-P(2)	93.9(2)	H(1Ru)-Ru(1)-Cl(1)	163(2)
H(2Ru)-Ru(1)-Cl(1)	164(2)	P(1)-Ru(1)-Cl(1)	96.94(3)
P(2)-Ru(1)-Cl(1)	91.43(3)	N(1)-Ru(1)-Cl(1)	81.9(5)
N(2)-Ru(1)-Cl(1)	87.2(4)		

Table 10. Selected bond distances and angles for $[Ru(H_2)Cl\{tmeP_2(NH)_2\}]BF_4$.

Distances (Å)			
Ru(1)—H(1Ru)	1.79(2)	Ru(1)—P(2)	2.3205(8)
Ru(1)—H(2Ru)	1.79(3)	Ru(1)—P(1)	2.3412(7)
Ru(1)—N(2)	2.150(2)	Ru(1)—Cl(1)	2.4210(8)
Ru(1)—N(1)	2.175(2)		
Angles (°)			
H(1Ru)-Ru(1)-H(2Ru)	19(2)	H(2Ru)-Ru(1)-P(1)	81(2)
H(1Ru)-Ru(1)-N(2)	85(2)	N(2)-Ru(1)-P(1)	170.38(7)
H(2Ru)-Ru(1)-N(2)	100(2)	N(1)-Ru(1)-P(1)	92.48(6)
H(1Ru)-Ru(1)-N(1)	90(2)	P(2)-Ru(1)-P(1)	97.81(3)
H(2Ru)-Ru(1)-N(1)	82(2)	H(1Ru)-Ru(1)-Cl(1)	165(2)
N(2)-Ru(1)-N(1)	78.05(9)	H(2Ru)-Ru(1)-Cl(1)	174(2)
H(1Ru)-Ru(1)-P(2)	86(2)	N(2)-Ru(1)-Cl(1)	81.39(7)
H(2Ru)-Ru(1)-P(2)	97(2)	N(1)-Ru(1)-Cl(1)	91.86(7)
N(2)-Ru(1)-P(2)	91.73(7)	P(2)-Ru(1)-Cl(1)	89.52(3)
N(1)-Ru(1)-P(2)	169.35(6)	P(1)-Ru(1)-Cl(1)	97.41(3)
H(1Ru)-Ru(1)-P(1)	97(2)		

References

1. K. Abdur-Rashid, T.P. Fong, B. Greaves, D.G. Gusev, J.G. Hinman, S.E. Landau, A.J. Lough, and R.H. Morris. J. Am. Chem. Soc. **122**, 9155 (2000).
2. I. Kaljurand, T. Rodima, A. Pihl, V. Mämets, I. Leito, I.A. Koppel, and M. Mishima. J. Org. Chem. **68**, 9988 (2003).
3. G. Jia, R.H. Morris, and C.T. Schweitzer. Inorg. Chem. **30**, 593 (1991).
4. G. Jia and R.H. Morris. J. Am. Chem. Soc. **113**, 875 (1991).
5. G. Jia and R.H. Morris. Inorg. Chem. **29**, 581 (1990).
6. G. Jia, H.M. Lee, I.D. Williams, C.-P. Lau, and Y. Chen. Organometallics, **16**, 3941 (1997).
7. G. Jia and C.-P. Lau. Coord. Chem. Rev. **190–192**, 83 (1999).
8. S.S. Kristjansdottir, A.J. Loendorf, and J.R. Norton. Inorg. Chem. **30**, 4470 (1991).
9. M. Netherton and G. Fu. Org. Lett. **3**, 4295 (2001).

© 2006 NRC Canada

10. K. Abdur-Rashid, A.J. Lough, and R.H. Morris. Organometallics, **19**, 2655 (2000).
11. R. Abbel, K. Abdur-Rashid, M. Faatz, A. Hadzovic, A.J. Lough, and R.H. Morris. J. Am. Chem. Soc. **127**, 1870 (2005).
12. C.A. Sandoval, T. Ohkuma, K. Muñiz, and R. Noyori. J. Am. Chem. Soc. **125**, 13490 (2003).
13. R.J. Hamilton, C.G. Leong, G. Bigam, M. Miskolzie, and S.H. Bergens. J. Am. Chem. Soc. **127**, 4152 (2005).
14. P.I. Amrhein, A.J. Lough, and R.H. Morris. Inorg. Chem. **35**, 4523 (1996).
15. E. Rocchini, P. Rigo, A. Mezzetti, T. Stephan, R.H. Morris, A.J. Lough, C.E. Forde, T.P. Fong, and S.D. Drouin. J. Chem. Soc. Dalton Trans. 3591 (2000).
16. S.S.P.R. Almeida, M.F.C. Guedes da Silva, J.J.R. Fraùsto da Silva, and A.J.L. Pombeiro. J. Chem. Soc. Dalton Trans. 467 (1999).
17. C. Bianchini, S. Moneti, M. Peruzzini, and F. Vizza. Inorg. Chem. **36**, 5818 (1997).
18. A. Albinati, W. Klooster, T.F. Koetzle, J.B. Fortin, J.S. Ricci, J. Eckert, T.P. Fong, A.J. Lough, R.H. Morris, and A. Golombek. Inorg. Chim. Acta, **259**, 351 (1997).
19. J.S. Ricci, T.F. Koetzle, M.T. Bautista, T.M. Hofstede, R.H. Morris, and J.F. Sawyer. J. Am. Chem. Soc. **111**, 8823 (1989).
20. M.G. Basallote, M. Besora, J. Durán, M.J. Fernández-Trujillo, A. Lledós, M.A. Máñez, and F. Maseras. J. Am. Chem. Soc. **126**, 2320 (2004).
21. C. Bianchini, D. Masi, M. Peruzzini, M. Casarin, C. Maccato, and G.A. Rizzi. Inorg. Chem. **36**, 1061 (1997).
22. D.L. Hughes, G.J. Leigh, and C.N. McMahon. J. Chem. Soc. Dalton Trans. 909 (1999).
23. M. Jimenez-Tenorio, M.C. Puerta, and P. Valerga. J. Chem. Soc. Chem. Commun. 1750 (1993).
24. R.M. Henry, R.K. Shoemaker, R.H. Newell, G.M. Jacobsen, D.L. DuBois, and M. Rakowski DuBois. Organometallics, **24**, 2481 (2005).
25. J.A. Ayllon, S.F. Sayers, B. Donnadieu, B. Chaudret, and E. Clot. Organometallics, **18**, 3981 (1999).
26. F. Estevan, M. Feliz, R. Llusar, J.A. Mata, and S. Uriel. Polyhedron, **20**, 527 (2001).
27. M.G. Basallote, F. Estevan, M. Feliz, M.J. Fernández-Trujillo, D.A. Hoyos, R. Llusar, S. Uriel, and C. Vicent. J. Chem. Soc. Dalton Trans. 530 (2004).
28. T. Takao, S. Yoshida, and H. Suzuki. Chem. Lett. **138**, 1100 (2001).
29. A. Macchioni. Chem. Rev. **105**, 2039 (2005).
30. S. Macura and R.R. Ernst. Mol. Phys. **41**, 95 (1980).
31. A. Macchioni. Eur. J. Inorg. Chem. 195 (2003).
32. P. Stilbs. Prog. Nucl. Magn. Reson. Spectrosc. **19**, 1 (1987).
33. C.S. Johnson, Jr. Prog. Nucl. Magn. Res. Spectrosc. **34**, 203 (1999).
34. M. Valentini, H. Rüegger, and P.S. Pregosin. Helv. Chim. Acta, **84**, 2833 (2001).
35. B. Binotti, A. Macchioni, C. Zuccaccia, and D. Zuccaccia. Comments Inorg. Chem. **23**, 417 (2002).
36. E. Martinez-Viviente, P.S. Pregosin, L. Vial, C. Herse, and J. Lacour. Chem. Eur. J. **10**, 2912 (2004).
37. R.E. Dinnebier, W.A. Dollase, X. Helluy, J. Kümmerlen, A. Sebald, M.U. Schmidt, S. Pagola, P.W. Stephens, and S. van Smaalen. Acta Crystallogr. Sect. B, **B55**, 1014 (1999).
38. D. Zuccaccia and A. Macchioni. Organometallics, **24**, 3476 (2005).
39. K.A. Earl, G. Jia, P.A. Maltby, and R.H. Morris. J. Am. Chem. Soc. **113**, 3027 (1991).
40. T. Li, R. Churlaud, A. Lough, K. Abdur-Rashid, and R.H. Morris. Organometallics, **23**, 6239 (2004).
41. E. Rocchini, A. Del Zotto, P. Martinuzzi, P. Rigo, A. Mezzetti, H. Rüegger, U. Burckhardt, and V. Gramlich. Inorg. Chem. **36**, 711 (1997).
42. B. Chin, A.J. Lough, R.H. Morris, C.T. Schweitzer, and C. D'Agostino. Inorg. Chem. **33**, 6278 (1994).
43. J. Jeener, B.H. Meier, P. Bachmann, and R.R. Ernst. J. Chem. Phys. **71**, 4546 (1979).
44. Z.M. Otwinowski and W. Minor. *In* Methods in enzymology. *Edited by* C.W. Carter and R.M. Sweet. Academic Press, London. 1997. pp. 307.
45. R.H. Blessing. Acta Cryst. **A51**, 33 (1995).
46. G.M. Sheldrick. SHELXTL/PC. Version 6.1 [computer program] Windows NT Version. Bruker AXS Inc., Madison, Wisconsin. 2001.

© 2006 NRC Canada

The series $Os_4(\mu_x\text{-}\eta^2\text{-}C_2Ph_2)(CO)_{14-n}$ (n = 0, 1, 2; x = n + 2) — Models for site-specific surface catalysts[1]

John P. Canal, Michael C. Jennings, Glenn P.A. Yap, and Roland K. Pomeroy

Abstract: The cluster $Os_4(\mu\text{-}\eta^2\text{-}C_2Ph_2)(CO)_{14}$ (**1**) has been prepared from the reaction of $Os_4(CO)_{14}$ and C_2Ph_2 in CH_2Cl_2 at 25 °C. Other minor products include the known clusters $Os_3(\mu_3\text{-}\eta^2\text{-}C_2Ph_2)(CO)_{10}$ and $Os_3(\mu\text{-}\eta^4\text{-}C_4Ph_4)(CO)_9$. The structure of **1** reveals an approximately planar C_2Os_4 skeleton with a dimetallacyclobutene ring (C—C = 1.32(4) Å) and a flat butterfly Os_4 unit (Os—Os range = 2.859(2)–2.916(2) Å). The $^{13}C\{^1H\}$ NMR spectrum of **1** indicates the carbonyl ligands are rigid at room temperature. Stirring **1** in CH_2Cl_2 for 2 days (ambient temperature) afforded $Os_4(\mu_3\text{-}\eta^2\text{-}C_2Ph_2)(CO)_{13}$ (**2**). The Os atoms in **2** also have an almost flat butterfly arrangement (Os—Os range = 2.7392(7)–2.8947(6) Å) with the alkyne ligand located over one of the Os_3 triangles. The ^{13}C NMR data for **2** are consistent with rapid rotation on the NMR timescale of the hinge $Os(CO)_3$ units at 21 °C, but slow rotation at –50 °C. Heating **2** at 40 °C gave $Os_4(\mu_4\text{-}\eta^2\text{-}C_2Ph_2)(CO)_{12}$ (**3**) after 2 days. Cluster **3** has the common butterfly arrangement of Os atoms with the C_2Ph_2 bound to all four metal atoms (Os—Os range = 2.7457(5)–2.8742(5) Å). The $^{13}C\{^1H\}$ NMR spectra of **3** at 21 and 90 °C indicate there is rapid CO exchange of the carbonyls of the two types of $Os(CO)_3$ units, but not between the units. The spectrum at –90 °C indicates one of the rotations (presumed to be that involving the carbonyls of the wingtip $Os(CO)_3$ units) is slowed on the NMR timescale. Compounds **1**–**3** form a unique series of clusters that have an alkyne ligand bound to two, three, and four metal atoms. Compound **1** is a model for a corner, compound **2** for a planar surface, and compound **3** a step site, in site-specific surface catalysts.

Key words: osmium cluster, diphenylacetylene, dimetallacyclobutene, carbonyl exchange, surface catalysis.

Résumé : On a préparé l'agrégat $Os_4(\mu\text{-}\eta^2\text{-}C_2Ph_2)(CO)_{14}$ (**1**) par réaction du $Os_4(CO)_{14}$ avec du C_2Ph_2, dans le CH_2Cl_2, à 25 °C; il était accompagné d'autres produits mineurs, dont les agrégats connus $Os_3(\mu_3\text{-}\eta^2\text{-}C_2Ph_2)(CO)_{10}$ et $Os_3(\mu\text{-}\eta^4\text{-}C_4Ph_4)(CO)_9$. La structure de **1** comporte un squelette C_2Os_4 approximativement plan avec un cycle dimétallacyclobutène (C—C = 1,32(4) Å) et une unité de Os_4 en forme de papillon applati (Os—Os = 2,859(2) à 2,916(2) Å). Les spectres RMN $^{13}C\{^1H\}$ du composé **1** indiquent que les ligands carbonyles sont rigides à la température ambiante. Par agitation pendant deux jours dans du CH_2Cl_2, à la température ambiante, le composé **1** conduit au $Os_4(\mu_3\text{-}\eta^2\text{-}C_2Ph_2)(CO)_{13}$ (**2**). Les atomes d'osmium dans le composé **2** adoptent aussi un arrangement en forme de papillon pratiquement plat (Os—Os = 2,7392(7) à 2,8947(6) Å) dans lequel le ligand alcyne se trouve au-dessus de l'un des triangles Os_3. Les données de la RMN du ^{13}C pour le composé **2** sont en accord avec une rotation rapide, à l'échelle de temps de la RMN et à 21 °C, des unités charnières $Os(CO)_3$; la rotation est toutefois lente à –50 °C. Par chauffage à 40 °C pendant deux jours, le composé **2** conduit à la formation du $Os_4(\mu_4\text{-}\eta^2\text{-}C_2Ph_2)(CO)_{12}$ (**3**). Dans l'agrégat **3**, les atomes d'osmium adoptent l'arrangement habituel en forme de papillon et le C_2Ph_2 est lié aux quatre atomes métalliques (Os—Os = 2,7457(5) à 2,8742(5) Å). Les spectres RMN $^{13}C\{^1H\}$ du composé **3** à 21 et 90 °C indiquent qu'il se produit un échange rapide de CO des carbonyles des deux types d'unités $Os(CO)_3$, mais qu'il n'y a pas d'échange entre les unités. Le spectre à –90 °C indique qu'une des rotations (probablement celle impliquant les carbonyles des unités $Os(CO)_3$ au bout des ailes) est ralentie à l'échelle de temps de la RMN. Les composés **1**, **2** et **3** forment une série unique d'agrégats comportant un ligand alcyne lié à deux, trois et quatre atomes métalliques. Les composés **1**, **2** et **3** sont respectivement un modèle pour un coin, pour une surface plane et pour un site étagé dans les catalyseurs de surface à site spécifique.

Mots clés : agrégat d'osmium, diphénylacétylène, dimétallacyclobutène, échange de carbonyle, catalyseur de surface.

[Traduit par la Rédaction]

Received 15 June 2005. Published on the NRC Research Press Web site at http://canjchem.nrc.ca on 28 February 2006.

This paper is dedicated to Professor Arthur J. Carty for his contributions to Canadian chemistry.

J.P. Canal and R.K. Pomeroy.[2] Department of Chemistry, Simon Fraser University, Burnaby, BC V5A 1S6, Canada.
M.C. Jennings. Department of Chemistry, University of Western Ontario, London, ON N6A 5B7, Canada.
G.P.A. Yap.[3] Department of Chemistry, University of Ottawa, Ottawa, ON K1N 6N5, Canada.

[1]This article is part of a Special Issue dedicated to Professor Arthur Carty.
[2]Corresponding author (e-mail: pomeroy@sfu.ca).
[3]Present address: Department of Chemistry and Biochemistry, University of Delaware, Newark, DE 19716, USA.

 doi:10.1139/V05-239 © 2006 NRC Canada

Introduction

Alkynes form a plethora of complexes with group 8 metal carbonyls that have a remarkable structural diversity (1–3). For example, over 20 types of complexes have been isolated from the reaction of alkynes with $Fe_3(CO)_{12}$; they possess up to five metal atoms and three alkyne units (2, 4). Carty and co-workers (5, 6) have made notable contributions to the area, particularly alkyne derivatives of carbonyl clusters of ruthenium. The reaction of alkynes with $Os_3(CO)_{12}$ also provides novel products (3, 7–10).

In contrast to $Os_3(CO)_{12}$, the common carbonyl cluster of osmium (11), $Os_4(CO)_{14}$ readily undergoes substitution with two-electron donor ligands under mild conditions (12, 13). Here we describe the reaction of the tetraosmium cluster with diphenylacetylene to give the unique series $Os_4(\mu_x\text{-}\eta^2\text{-}C_2Ph_2)(CO)_{14-n}$ (n = 0, 1, 2; $x = n + 2$) in which a C_2Ph_2 molecule is successively bound to two, three, and four metal atoms. The dimetallacyclobutene cluster (i.e., the μ_2 compound) is of particular interest and is proposed as a model of corner sites of site-specific surface catalysts.

Experimental section

Unless otherwise stated, manipulations of starting materials and products were carried out under a nitrogen atmosphere with the use of standard Schlenk techniques. Hydrocarbon solvents were refluxed over potassium, distilled, and stored over molecular sieves before use. Dichloromethane was dried in a similar manner except that P_2O_5 was employed as the drying agent. The $Os_4(CO)_{14}$ was prepared by a literature procedure (13). The reactions were carried out in Carius tubes of volumes between 25–50 mL; each was fitted with a Teflon valve. NMR spectra were recorded on a Bruker AMX400 spectrometer at the appropriate operating frequencies for the ^1H and $^{13}C\{^1H\}$ NMR spectra. Samples of the complexes used for $^{13}C\{^1H\}$ NMR spectra were enriched to ~30% ^{13}CO. The samples were prepared from ^{13}CO-enriched $Os_4(CO)_{14}$, which in turn was prepared from ^{13}CO-enriched $Os_3(CO)_{12}$ (~40% ^{13}CO) (14).

Preparation of $Os_4(\mu\text{-}\eta^2\text{-}C_2Ph_2)(CO)_{14}$ (1)

To a solution of $Os_4(CO)_{14}$ (25 mg, 0.017 mmol) in CH_2Cl_2 (25 mL) at room temperature was added an excess of C_2Ph_2 (~20×) (C_2Ph_2 = diphenylacetylene). The solution was stirred for 105 min during which time the color of the solution changed from a red-brown to a deep red. The solvent was removed on the vacuum line and the remaining solid subjected to chromatography on a silica gel column (1.5 cm × 15 cm). Elution with hexanes removed the excess C_2Ph_2. Elution with hexanes–CH_2Cl_2 (90:10 by volume) gave several colored bands. The first (yellow) band was a trace amount of the known cluster $Os_3(\mu_3\text{-}\eta^2\text{-}C_2Ph_2)(CO)_{10}$. (In the preparations described below, the orange band of $Os_4(\mu_4\text{-}\eta^2\text{-}C_2Ph_2)(CO)_{12}$ (**3**) eluted next). This was followed by a red band that afforded $Os_4(\mu_3\text{-}\eta^2\text{-}C_2Ph_2)(CO)_{13}$ (**2**) in approximately 25% yield, then a purple band of another known cluster, $Os_3(\mu\text{-}\eta^4\text{-}C_4Ph_4)(CO)_9$, in <5% yield. Finally, a deep red band of the desired cluster **1** was obtained in about 70% yield. The analytical sample of **1** was obtained as air-stable, dark red (almost black) needles by recrystallization from CH_2Cl_2 and dried overnight under vacuum. IR (hexanes, cm^{-1}): ν(CO) 2126 (vw), 2080 (s), 2071 (m), 2065 (vw), 2044 (vs), 2025 (m), 1995 (m), 1909 (m). ^1H NMR (CD_2Cl_2) δ: 7.15–7.10 (m), 7.01–6.92 (m), 6.85–6.83 (dd). ^{13}C NMR (CD_2Cl_2, RT) δ: 192.13 (2C), 192.08 (2C), 185.6 (2C), 184.6 (1C), 176.6 (1C), 175.4 (2C), 172.5 (1C), 169.4 (1C), 169.3 (1C), 168.8 (1C), 128.1 (1C, Ph-*C*), 128.0 (2C, Ph-*C*), 126.6 (2C, Ph-*C*). MS (LI-MS) *m/z*: 1331.9 [M^+] (calcd. for M^+ = 1332 (100%), 1331 (81.5%)). Anal. calcd. for $C_{28}H_{10}O_{14}Os_4$: C 25.26, H 0.76; found: C 25.22, H 0.86.

$Os_3(\mu_3\text{-}\eta^2\text{-}C_2Ph_2)(CO)_{10}$

IR (hexanes, cm^{-1}): ν(CO) 2100 (m), 2066 (vs), 2047 (s), 2028 (s), 2011 (s), 1996 (m), 1982 (sh), 1965 (w) (in agreement with the literature values (7*a*)). ^{13}C NMR (CO region, RT) δ: 187.4 (2C), 186.8 (2C), 179.0 (1C), 174.5 (2C), 169.4 (1C), 168.0 (1C). MS (LI-MS) *m/z*: 1179.9 [M^+] (calcd. for M^+ = 1180 (100%), 1179 (86.1%)).

$Os_3(\mu\text{-}\eta^4\text{-}C_4Ph_4)(CO)_9$

IR (hexanes, cm^{-1}): ν(CO) 2113 (s), 2057 (vs), 2043 (vs), 2036 (sh), 2011 (vs), 1999 (m), 1990 (sh), 1974 (m), 1930 (m) (in agreement with the literature values (8*a*)). ^{13}C NMR (RT) δ: 175.7 (br s), 129.3 (2C, Ph-*C*), 128.1 (2C, Ph-*C*), 127.4 (1C, Ph-*C*). ^{13}C NMR (–60 °C) δ: 181.6 (~1C), 178.3 (~1C), 176.6 (~2C), 174.7 (~2C), 173.0 (~2C), 172.5 (~2C). MS (LI-MS) *m/z*: 1029.9 [M^+] (calcd. for M^+ = 1030 (100%), 1029 (83.3%)).

Preparation of $Os_4(\mu_3\text{-}\eta^2\text{-}C_2Ph_2)(CO)_{13}$ (2)

Cluster **2** was prepared in the same manner used to prepare **1**, except only a slight excess of C_2Ph_2 was used (~1:1.1) and the solution was allowed to stir at room temperature for 2 days. Again the solution changed from brown-red to a red over the reaction period. The desired product was isolated as described previously in about 60% yield. The analytical sample of **2** was obtained as air-stable, deep red crystals by recrystallization from CH_2Cl_2–hexanes. IR (hexanes, cm^{-1}): ν(CO) 2117 (m), 2078 (vs), 2046 (vs), 2040 (vs), 2012 (m), 1998 (m), 1987 (w), 1981 (w), 1963 (w), 1956 (w, sh). ^1H NMR (CD_2Cl_2) δ: 7.15–7.07 (m), 6.98–6.96 (m). ^{13}C NMR (CD_2Cl_2, RT) δ: 185.6 (1C, J_{CC} = 38.7 Hz), 182.6 (1C, J_{CC} = 37.2 Hz), 180.5 (1C), 176.5 (6C), 173.2 (1C), 169.3 (1C), 130 (2C, Ph-*C*), 127.8 (2C, Ph-*C*), 127.6 (1C, Ph-*C*). ^{13}C NMR (CD_2Cl_2, –50 °C) δ: 185.6 (1C), 181.8 (1C), 180.2 (1C), 177.6 (2C), 175.8 (2C), 175.2 (2C), 172.8 (2C), 169.0 (2C). MS (LI-MS) *m/z*: 1303.6 [M^+] (calcd. for M^+ = 1304 (100%), 1303 (87.4%)). Anal. calcd. for $C_{27}H_{10}O_{13}Os_4$: C 24.85, H 0.77; found: C 25.01, H 0.98.

Preparation of $Os_4(\mu_4\text{-}\eta^2\text{-}C_2Ph_2)(CO)_{12}$ (3)

The same reaction conditions used to produce **2** were employed except the reaction mixture was heated to 40 °C for 2 days. Over the time period the solution went from brown-red through dark red to orange-red as the initially produced **1** went to **2** and then **3**. The desired product in ~90% yield was isolated in the normal manner. (In an alternate procedure, **3** was isolated in 90% yield when either **1** or **2** was allowed to stir at room temperature in hexanes for 18 days). The analytical sample of **3** was obtained as air-stable, sparkling red-orange crystals by recrystallization from CH_2Cl_2. IR (hexanes, cm^{-1}): ν(CO) 2098 (m), 2071 (vs), 2046 (vs), 2041 (vs), 2019 (s), 2000 (s), 1982 (w), 1971 (m). ^1H NMR

© 2006 NRC Canada

Table 1. Details of the crystal structure determinations of **1**·CH_2Cl_2, **2**, and **3**.

Structure name	**1**·CH_2Cl_2	**2**	**3**
Compound	$C_{28}H_{10}O_{14}Os_4$	$C_{27}H_{10}O_{13}Os_4$	$C_{26}H_{10}O_{12}Os_4$
Formula weight	1416.09	1 303.15	1275.14
Crystal system	Monoclinic	Triclinic	Monoclinic
T (°C)	–123	–70	–70
Space group	$P2_1/n$	P-1	$P2_1/c$
a (Å)	8.8718(6)	12.492(1)	9.634(1)
b (Å)	25.138(2)	15.179(1)	16.743(2)
c (Å)	14.814(1)	15.923(1)	17.127(2)
α (°)	90	78.215(1)	90
β (°)	97.564(2)	85.257(1)	90.390(2)
γ (°)	90	84.797(2)	90
Cell volume (Å^3), Z	3275.0(4), 4	2 937.0(4), 4	2762.7(5), 4
$D_{calcd.}$ (Mg m^{-3})	2.872	2.947	3.066
Abs. coeff (mm^{-1})	15.701	17.315	18.402
Unique data ($I > 2\sigma$)	3053	12 503	6466
R^a	0.0622	0.0539	0.0424
$R_w{}^b$	0.1063	0.1584	0.1101

[a] $R = \Sigma(|F_o| - |F_c|)/\Sigma|F_o|$.
[b] $R_w = [\Sigma(w(|F_o| - |F_c|)^2)/\Sigma(wF_o^2)]^{1/2}$, $w = [\sigma^2(F_o)^2 + kF_o^2]^{-1}$.

(CD_2Cl_2) δ: 7.21–7.17 (m), 7.14–7.10 (m). ^{13}C NMR (toluene-d_8, 90 °C) δ: 180.4 (s, 6C), 175.5 (s, 6C). ^{13}C NMR (CD_2Cl_2, RT) δ: 180.5 (6C, J_{OsC} (^{187}Os) = 106.9 Hz), 175.5 (6C, J_{OsC} = 117.5 Hz), 132.5 (2C, Ph-*C*), 129.3 (1C, Ph-*C*), 127.2 (2C, Ph-*C*). ^{13}C NMR (CD_2Cl_2, –90 °C) δ: 180.5 (s, 6C), 175.5 (w/broad, 6C). MS (LI-MS) *m*/*z*: 1275.6 [M$^+$] (calcd. for M$^+$ = 1276 (100%), 1275 (87.4%)). Anal. calcd. for $C_{26}H_{10}O_{12}Os_4$: C 24.45, H 0.78; found: C 24.65, H 0.88.

X-ray structural determinations

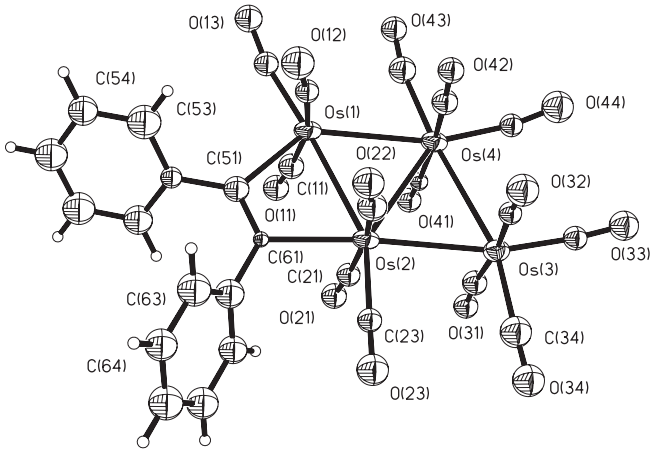
The structure of **1** was determined at the University of Western Ontario, London, Ontario. Crystals of **1**·CH_2Cl_2 were grown from a concentrated dichloromethane solution. A red-orange, flat needle was cut and mounted on a glass fiber. Data were collected at low temperature (–123 °C) on a Nonius Kappa-CCD diffractometer. The unit cell parameters were calculated and refined from the full data set. Crystal cell refinement and data reduction were carried out with the program DENZO and the data were scaled with the program SCALEPACK. The crystal data and refinement parameters for **1**·CH_2Cl_2 are listed in Table 1. The reflection data and systematic absences were consistent with a monoclinic space group, $P2(1)/n$. The SHELXTL-NT V6.1 (G. Sheldrick) suite of programs was used to solve the structure by direct methods. Subsequent difference Fourier syntheses allowed the remaining atoms to be located. The osmium atoms were refined with anisotropic thermal parameters. The remaining atoms were refined isotropically. The hydrogen atom positions were calculated geometrically and were included as riding on their respective carbon atoms. The solvent molecule was refined fully anisotropically and the C—Cl distances were fixed at 1.72 Å. Due to the poor quality of the crystal, good data was only obtained to 20° on θ. The largest residue electron density peak (2.02 e/Å^3) was associated with one of the osmium–osmium bonds. Full-matrix least-squares refinement on F^2 gave R_1 = 6.22 for 2σ data and wR_2 = 12.64 for all data (GOF = 1.134).

The structures of **2** and **3** were determined at the University of Ottawa, Ottawa, Ontario. Suitable crystals were selected, mounted with Paratone oil on glass fibres, and flash-cooled to the data collection temperature of –70 °C. Unit-cell parameters were obtained from 60 data frames, 0.3° θ, from three different sections of the Ewald sphere. No symmetry higher than triclinic was observed in the diffraction data for **2** and solution in the centrosymmetric space group option, *P*-1, yielded chemically reasonable and computationally stable results of refinement. The unit-cell parameters and systematic absences in the diffraction data of **3** were uniquely consistent with the space group $P2_1/c$. The data sets were corrected for absorption with the Bruker SADABS program based on redundant data. Two symmetry-unique, but chemically equivalent molecules were located in the asymmetric unit of **2**. Features remaining in the final difference Fourier electron density map of **2** were located <0.9 Å from osmium atoms and were ignored as noise artifacts. All non-hydrogen atoms were refined with anisotropic displacement parameters. All hydrogen atoms were treated as idealized contributions. Structure factors are contained in the SHELXTL 6.12 program library. A summary of the data collection and refinement for each structure are given in Table 1.[4]

[4] Supplementary data for this article are available on the journal Web site (http://canjchem.nrc.ca) or may be purchased from the Depository of Unpublished Data, Document Delivery, CISTI, National Research Council Canada, Ottawa, ON K1A 0R6, Canada. DUD 4089. For more information on obtaining material refer to http://cisti-icist.nrc-cnrc.gc.ca/irm/unpub_e.shtml. CCDC 279768–279770 contain the crystallographic data for this manuscript. These data can be obtained, free of charge, via http://www.ccdc.cam.ac.uk/conts/retrieving.html (Or from the Cambridge Crystallographic Data Centre, 12 Union Road, Cambridge CB2 1EZ, UK; fax +44 1223 336033; or deposit@ccdc.cam.ac.uk).

© 2006 NRC Canada

Fig. 1. Molecular structure of $Os_4(\mu\text{-}\eta^2\text{-}C_2Ph_2)(CO)_{14}$ (**1**).



Results and discussion

$Os_4(\mu\text{-}\eta^2\text{-}C_2Ph_2)(CO)_{14}$ (1)

Compound **1** was isolated as dark red needles in about 70% yield from the reaction of $Os_4(CO)_{14}$ in CH_2Cl_2 with an excess of C_2Ph_2 at room temperature (eq. [1]).

[1] $$Os_4(CO)_{14} + C_2Ph_2 \xrightarrow[CH_2Cl_2]{25\ ^\circ C} Os_4(\mu\text{-}\eta^2\text{-}C_2Ph_2)(CO)_{14}\ (\mathbf{1}) + \text{other products}$$

(By comparison, the reaction of $Os_3(CO)_{12}$ with C_2Ph_2 requires temperatures of 160 °C or above to proceed at a measurable rate (9)). An excess of the acetylene ensured that **1** formed quickly as it slowly loses CO to give $Os_4(\mu_3\text{-}\eta^2\text{-}C_2Ph_2)(CO)_{13}$ (**2**). Besides **2**, other products isolated from the reaction shown in eq. [1] were the known clusters $Os_3(\mu_3\text{-}\eta^2\text{-}C_2Ph_2)(CO)_{10}$ (7) and $Os_3(\mu\text{-}\eta^4\text{-}C_4Ph_4)(CO)_9$ (8, 9). The stereochemical nonrigidity of the former cluster has been investigated by variable-temperature $^{13}C\{^1H\}$ NMR spectroscopy (15) and found similar to the nonrigidity exhibited by $Os_3(\mu_3\text{-}\eta^2\text{-}C_2R_2)(CO)_{10}$ (R = Me, Et) (10). All products are brightly colored and were readily separated by column chromatography. The derivatives appeared air stable, although crystals of **1** deteriorated on standing. This can be attributed to either loss of CO (to give **2**) or loss of the CH_2Cl_2 of crystallization. (Crystals of **1** suitable for the structural determination were obtained only after some difficulty).

Compound **1** was characterized by C/H/N analysis, IR, mass (parent ion), ^1H and ^{13}C NMR spectroscopy, and X-ray crystallography. The structure of **1** (as the CH_2Cl_2 solvate) reveals an approximately planar Os_4C_2 unit (Fig. 1); selected bond lengths and angles for **1** are given in Table 2. The Os_4 unit adopts a flat butterfly arrangement with five Os—Os bonds that range in length from 2.859(2) to 2.916(2) Å. These lengths are typical for open Os carbonyl clusters and may be compared with the average Os—Os bond distance in $Os_3(CO)_{12}$ of 2.877 Å (16). If it is assumed that the Os—Os bonds are single nondative covalent bonds, then Os(1) has a 17 electron count and Os(4) a 19 electron count. The Os(1)—Os(4) can therefore be regarded as a dative metal–metal bond with the Os(4) atom donating two electrons to Os(1) (17). Interestingly, it is the shortest Os—Os bond in **1**. We have reported numerous complexes that contain unsupported Os—M (M = transition metal) dative bonds (18).

Table 2. Selected bond lengths (angstroms) and angles (degrees) for **1**.

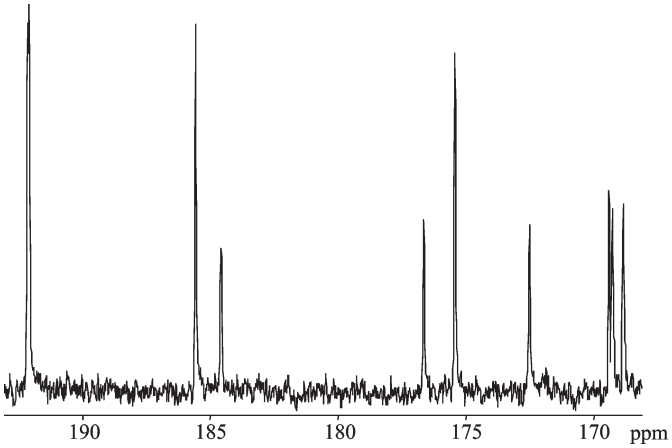
Bond lengths (Å)	
Os(1)—Os(2)	2.866(2)
Os(1)—Os(4)	2.859(2)
Os(2)—Os(3)	2.880(2)
Os(2)—Os(4)	2.916(2)
Os(3)—Os(4)	2.907(2)
C(51)—C(61)	1.32(4)
Os(1)—C(51)	2.13(3)
Os(2)—C(61)	2.28(3)
Os—C(CO) range	1.84(3)–1.96(3)
Bond angles (°)	
Os(1)-Os(2)-Os(3)	119.44(6)
Os(1)-Os(2)-Os(4)	59.25(5)
Os(1)-Os(4)-Os(2)	59.51(4)
Os(1)-Os(4)-Os(3)	118.77(6)
Os(2)-Os(1)-Os(4)	61.25(5)
Os(2)-Os(3)-Os(4)	60.52(4)
Os(2)-Os(4)-Os(3)	59.28(4)
Os(3)-Os(2)-Os(4)	60.20(4)
Os(1)-Os(2)-C(61)	65.5(6)
Os(2)-Os(1)-C(51)	73.5(8)
Os(1)-C(51)-C(52)	126(2)
Os(1)-C(51)-C(61)	108(2)
Os(2)-C(61)-C(51)	113(2)
Os(2)-C(61)-C(62)	119(2)
C(52)-C(51)-C(61)	126(3)
C(62)-C(61)-C(51)	128(3)

Cluster **1** possesses a dimetallacyclobutene ring (i.e., Os(1)-Os(2)-C(61)-C(51)). The geometry about each C atom of the unit is approximately trigonal planar, although the internal Os-C-C angles (108(2)° and 113(2)°) are somewhat compressed from the ideal value of 120°. The C—C bond length of 1.32(4) Å is consistent with an uncoordinated C=C double bond. The Os—C bond lengths to the alkyne are 2.13(3) (to Os(1)) and 2.28(3) Å (to Os(2)). Because of the somewhat poor quality of the data, it is not clear that the difference is significant, or a genuine electronic effect: Os(1) is six-coordinate, whereas Os(2) is seven-coordinate. The lengths may be compared with the Os—C lengths to the carbonyl ligands in **1** that are in the range 1.84(4) to 1.95(3) Å.

Dimetallacyclobutene compounds are comparatively rare and a search of the literature (SciFinder Scholar) of this term yielded only 11 publications containing compounds with this bonding motif (1, 19–23). Some recent examples are $Ir_2(\mu\text{-}\eta^2\text{-}C_2R_2)(\eta^5\text{-}C_9H_7)_2(CO)_2$ (R = Ph, Tol) (20) and $Re_2Cp^*_2(\mu\text{-}\eta^2\text{-}C_2(CO_2CH_3)_2(CO)_4$ (21). Only one compound, $Ir_4[(\mu\text{-}\eta^2\text{-}C_2(MeCO_2)_2]_2[(\mu_4\text{-}\eta^2\text{-}C_2(MeCO_2)_2]_2(CO)_8$, contains more than two metal atoms, that is, it is a cluster compound (22). The bond lengths and angles in **1** are comparable to those found in $Os_2[\mu\text{-}\eta^2\text{-}C_2(CO_2Me)_2](CO)_8$ (C—C bond = 1.33(1) Å; both Os—C bonds = 2.138(5) Å; Os-C-C angle = 111.2(2)°) (23). The C—C bond length in **1** may be also be compared with the corresponding length (1.53(3) Å) in the saturated Os-C-C-Os unit in $Os_2(\mu\text{-}\eta^2\text{-}C_2H_4)(CO)_8$ (24).

© 2006 NRC Canada

Fig. 2. The $^{13}C\{^1H\}$ NMR spectrum (CO region) of **1** (^{13}CO enriched) in CH_2Cl_2–CD_2Cl_2 (4:1) at 21 °C.



The $^{13}C\{^1H\}$ NMR spectrum of **1** (^{13}CO enriched) in CD_2Cl_2–CH_2Cl_2 at ambient temperature exhibits four signals of intensity 2 and six signals of intensity 1 in the carbonyl region (Fig. 2). This observation is consistent with the view that **1** has the same structure in solution as that in the solid state, and the carbonyls are rigid on the NMR timescale at this temperature. Typically, resonances due to axial carbonyl ligands come to low field of those due to equatorial carbonyls (14, 25). As can be seen from Fig. 2, one signal of intensity 2 is shifted to higher field and one signal of intensity 1 to lower field. These atypical signals are tentatively assigned to the carbonyls attached to Os(1) because of the unusual bonding at this atom.

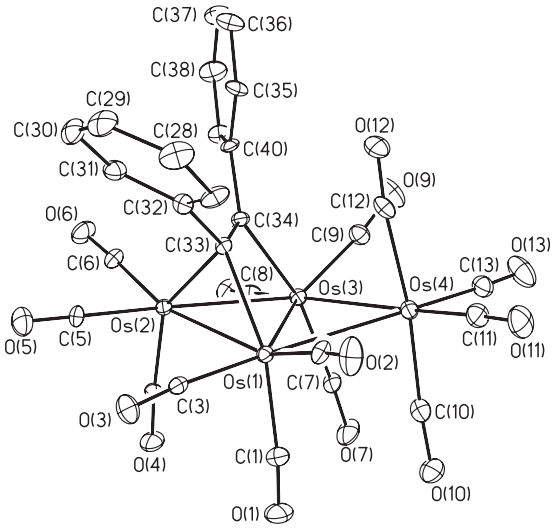
$Os_4(\mu_3\text{-}\eta^2\text{-}C_2Ph_2)(CO)_{13}$ (2)

When **1** was stirred in CH_2Cl_2 at room temperature for 2 days cluster **2** was produced in good yield (eq. [2]). The product was isolated after chromatography as red crystals that were characterized by C/H/N analysis, IR, mass (parent ion), ^1H and ^{13}C NMR spectroscopy, and X-ray crystallography.

[2] $$Os_4(\mu\text{-}\eta^2\text{-}C_2Ph_2)(CO)_{14} \xrightarrow[2\text{ days}]{25\ ^\circ C} Os_4(\mu_3\text{-}\eta^2\text{-}C_2Ph_2)(CO)_{13}\ (\mathbf{2}) + CO$$

The structure of **2** has two independent molecules in the unit cell that differ in the orientation of the phenyl rings, but are otherwise identical. A view of one of the molecules (molecule **2A**) is given in Fig. 3; selected bond lengths and angles for each molecule are collected in Table 3. The structure of **2** consists of an almost flat butterfly arrangement, as found in **1**, with the alkyne spanning one of the Os_3 triangles. The peripheral Os—Os lengths associated with the alkyne in each molecule (range = 2.7392(7)–2.7740(7) Å) are significantly shorter than the peripheral Os—Os lengths that involve Os atoms not directly bound to the C_2Ph_2 (range 2.8665(6)–2.8947(6) Å). The shorter Os—Os bonds can be attributed to the bonding requirements of the bridging C_2Ph_2 ligand. The unbridged Os—Os bonds are typical for open Os clusters. The hinge Os—Os bonds in each molecule are of intermediate length (2.8204(6) and 2.8007(7) Å).

Fig. 3. Molecular structure of $Os_4(\mu_3\text{-}\eta^2\text{-}C_2Ph_2)(CO)_{13}$ (**2**).



The 18-electron rule requires that the alkyne fragment donates two electrons to the wingtip Os atom (e.g., Os(2) in molecule **2A**) and one electron to each hinge Os atom (e.g., Os(1) and Os(3) in **2A**). The Os—C(alkyne) lengths that involve the wingtip Os atoms (e.g., Os(2) and Os(6)) are in the range 2.27(1)–2.29(1) Å and are somewhat longer than the other Os—C(alkyne) lengths in **2** (range 2.15(1)–2.18(1) Å). The bonding may be viewed as a dimetallacyclobutene unit with the C=C double bond acting as a typical alkene ligand toward the wingtip Os atom. The length of the C—C bond (1.42 Å) of the alkyne unit suggests a formal bond order less than two, as observed in similar compounds (7, 10, 26, 27). The bonding of the alkyne to the Os_3 triangle in **2** is similar to that in compounds such as $Os_3(\mu_3\text{-}\eta^2\text{-}C_2R_2)(CO)_{10}$ (R = Et (10), R = Ph (7)), $Os_5(\mu_3\text{-}\eta^2\text{-}C_2H_2)(CO)_{17}$ (26), and $Os_7(\mu_3\text{-}\eta^2\text{-}C_2Me_2)(CO)_{19}$ (27).

The $^{13}C\{^1H\}$ NMR spectra in the carbonyl region of **2** (^{13}CO enriched) in CD_2Cl_2–CH_2Cl_2 at –50 and 21 °C are shown in Fig. 4. The lower temperature spectrum exhibits eight signals in an approximate 1:1:1:2:2:2:2:2 (low to high field). This is consistent with the view that **2** has the same structure in solution as in the crystalline state, and that the carbonyls are rigid on the NMR timescale at –50 °C. The two signals at lowest field (i.e., at δ 185.6 and 181.8) exhibit satellites and are therefore readily assigned to the C atoms of the two chemically different axial CO ligands on the unbridged wingtip Os atom (i.e., the C atoms C(23) and C(25) in Fig. 3). This is because only these peaks would be expected to exhibit observable ^{13}C–^{13}C coupling owing to the mutual trans arrangement of these carbonyls. (Recall the complex was ^{13}CO enriched.) The remaining signal of intensity 1 (at δ 180.2) is attributed to the axial carbonyl atom on the bridged wingtip Os atom (i.e., C(17)). The signal at δ 177.6 is assigned to the two C atoms of the axial carbonyls on the hinge Os atoms (i.e., C(14) and C(20)). As stated previously, ^{13}C NMR resonances due to C atoms of axial carbonyls usually appear to lower field than the corresponding signals of equatorial carbonyls. The resonances at δ 175.8 and 175.2 are assigned to the C atoms of the equatorial carbonyls on the hinge Os atoms on the basis of their exchange behavior described in the following paragraph. The remain-

© 2006 NRC Canada

Table 3. Selected bond lengths (angstroms) and angles (degrees) for **2**.

Molecule **A**		Molecule **B**	
Bond lengths (Å)			
Os(1)—Os(2)	2.7586(6)	Os(5)—Os(6)	2.7392(7)
Os(1)—Os(3)	2.8204(6)	Os(5)—Os(7)	2.8007(7)
Os(1)—Os(4)	2.8665(6)	Os(5)—Os(8)	2.8871(7)
Os(2)—Os(3)	2.7454(6)	Os(6)—Os(7)	2.7740(7)
Os(3)—Os(4)	2.8947(6)	Os(7)—Os(8)	2.8939(7)
C(33)—C(34)	1.42(2)	C(47)—C(48)	1.42(2)
Os(5)—C(47)	2.17(1)	Os(5)—C(47)	2.17(1)
Os(6)—C(47)	2.29(1)	Os(6)—C(47)	2.29(1)
Os(6)—C(48)	2.29(1)	Os(6)—C(48)	2.29(1)
Os(7)—C(48)	2.16(1)	Os(7)—C(48)	2.16(1)
Os—C(CO) range	1.88(1)–1.99(1)		
Bond angles (°)			
Os(1)-Os(2)-Os(3)	61.65(2)	Os(5)-Os(6)-Os(7)	61.06(2)
Os(1)-Os(3)-Os(2)	59.41(2)	Os(5)-Os(7)-Os(6)	58.86(2)
Os(1)-Os(3)-Os(4)	60.19(2)	Os(5)-Os(7)-Os(8)	60.90(2)
Os(1)-Os(4)-Os(3)	58.62(2)	Os(5)-Os(8)-Os(7)	57.96(2)
Os(2)-Os(1)-Os(3)	58.94(2)	Os(6)-Os(5)-Os(7)	60.08(2)
Os(2)-Os(1)-Os(4)	118.26(2)	Os(6)-Os(5)-Os(8)	118.54(2)
Os(2)-Os(3)-Os(4)	117.74(2)	Os(6)-Os(7)-Os(8)	117.15(2)
Os(3)-Os(1)-Os(4)	61.19(2)	Os(7)-Os(5)-Os(8)	61.14(2)
Os(1)-Os(2)-C(33)	49.2(3)		
Os(1)-C(33)-Os(2)	76.8(3)		
Os(2)-Os(1)-C(33)	54.0(3)		
Os(2)-Os(3)-C(34)	53.5(3)		
Os(2)-C(34)-Os(3)	76.1(4)		
Os(3)-Os(2)-C(33)	70.6(3)		
Os(1)-Os(3)-C(34)	71.1(3)		
Os(3)-Os(1)-C(33)	71.0(3)		
Os(1)-C(33)-C(34)	110.4(8)		
Os(3)-C(34)-C(33)	107.5(8)		
Os(2)-C(33)-C(34)	71.2(6)		
Os(2)-C(34)-C(33)	72.6(6)		
C(33)-Os(2)-C(34)	36.1(4)		
Os(1)-C(33)-C(32)	124.2(8)		
Os(2)-C(33)-C(32)	120.7(8)		
Os(2)-C(34)-C(40)	125.2(8)		
Os(3)-C(34)-C(40)	125.4(8)		
C(32)-C(33)-C(34)	125(1)		
C(40)-C(34)-C(33)	126(1)		

Note: Two independent molecules in the unit cell.

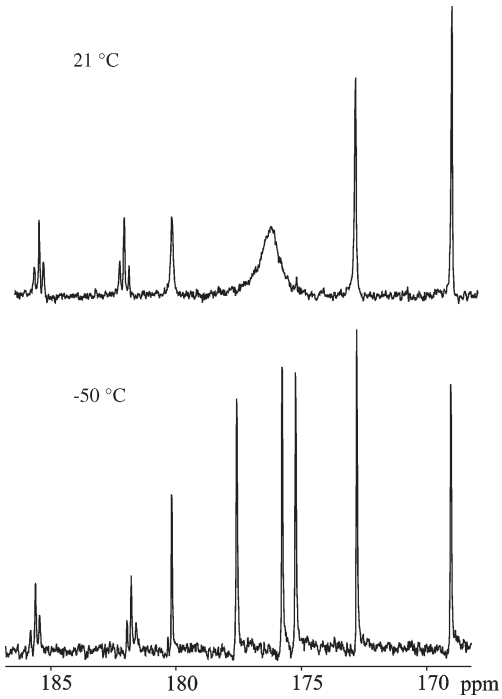
ing resonances at δ 172.8 and 169.0 are attributed to the C atoms of the equatorial carbonyls on the wingtip Os atoms. The latter signal is attributed to the carbonyls of the $Os(CO)_4$ grouping since it remains sharp in the spectrum at ambient temperature (see the following paragraph).

In the spectrum at 21 °C, three of the resonances have coalesced to a broad singlet (Fig. 4), indicative of exchange between the carbonyls that give rise to the signals in the spectrum at lower temperature. This is attributed to carbonyl exchange of the hinge $Os(CO)_3$ groupings. Rotation of $Os(CO)_3$ units in condensed Os carbonyl clusters is common. Examples are $Os_6(CO)_{17}(L)$ (L = CO, PPh_3) (28, 29) and $Os_7(CO)_{21}$ (30). The hinge Os atoms are seven-coordinate, whereas the wingtip Os atoms are nominally six-coordinate (if the bond to the C_2Ph_2 is a conventional metal–alkene bond). It is well-known that mononuclear six-coordinate complexes are usually rigid, whereas the corresponding seven-coordinate complexes are invariably nonrigid in solution.

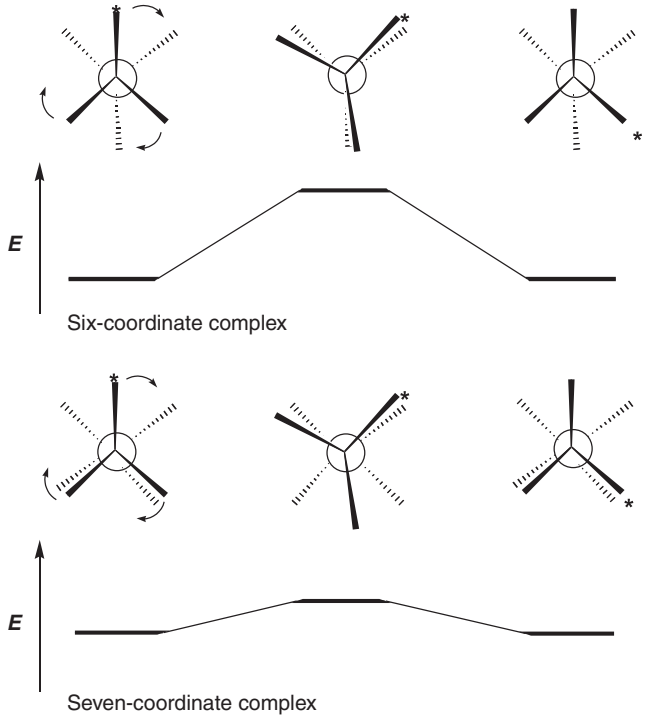
Although the reason for the difference in activation barriers to exchange may be based upon electronic considerations, it can be rationalized by using simple steric arguments. We have shown that the ground-state and transition-state energies are both important in determining a barrier to rotation of the arene ring in (η^6-arene)$Fe(CO)_2(SiCl_3)$ complexes (31). In six-coordinate complexes, the trigonal prismatic transition state for $M(CO)_3$ rotation has three eclipsing interactions as depicted in Scheme 1. Also of importance is that in the ground state all the substituents are perfectly staggered with their nearest neighbors and hence it is at a low

© 2006 NRC Canada

Fig. 4. The $^{13}C\{^1H\}$ NMR spectrum (CO region) of **2** (^{13}CO enriched) in CH_2Cl_2–CD_2Cl_2 (4:1) at 21 and –50 °C.



Scheme 1.



energy. In a seven-coordinate complex, the transition state to rotation of a trigonal unit only has two close eclipsing interactions in the transition state and therefore might be expected to be at a lower energy than the transition-state energy in the six-coordinate case (Scheme 1). What may not be realized is that in the seven-coordinate configuration the ground state is destabilized relative to the six-coordinate configuration because in the higher coordination case there are still close interactions in the lowest energy conformation.

In the spectrum at 21 °C, the signals attributed to the wingtip $Os(CO)_3$ group have broadened relative to the signals owing to the wingtip $Os(CO)_4$ unit. This probably indicates the onset of rotation on the NMR timescale of this $Os(CO)_3$ group and is relevant to the discussion on the rotation of the $Os(CO)_3$ units in **3** discussed in the following. The NMR spectrum of **2** at higher temperatures was not investigated because of its ready decarbonylation to **3**.

$Os_4(\mu_4\text{-}\eta^2\text{-}C_2Ph_2)(CO)_{12}$ (3)

When the reaction shown in eq. [2] was carried out at 40 °C, $Os_4(\mu_4\text{-}\eta^2\text{-}C_2Ph_2)(CO)_{12}$ (**3**) was isolated in ~90% yield (eq. [3]). The cluster, as bright orange-red, air-stable crystals, was characterized by C/H/N analysis, IR, mass (parent ion), ^1H and ^{13}C NMR spectroscopy, and by X-ray crystallography. Compound **3** has remarkable thermal stability. Overnight pyrolysis of **3** in C_6F_6 under vacuum at 230 °C had little effect on the cluster; decomposition (in part to $Os_3(CO)_{12}$) only commenced at 250 °C. Even after 4 days at 250 °C **3** had not completely decomposed.

[3] $Os_4(\mu_3\text{-}\eta^2\text{-}C_2Ph_2)(CO)_{13} \xrightarrow[2\text{ days}]{40\text{ °C}} Os_4(\mu_4\text{-}\eta^2\text{-}C_2Ph_2)(CO)_{12} + (\mathbf{3})\ CO$

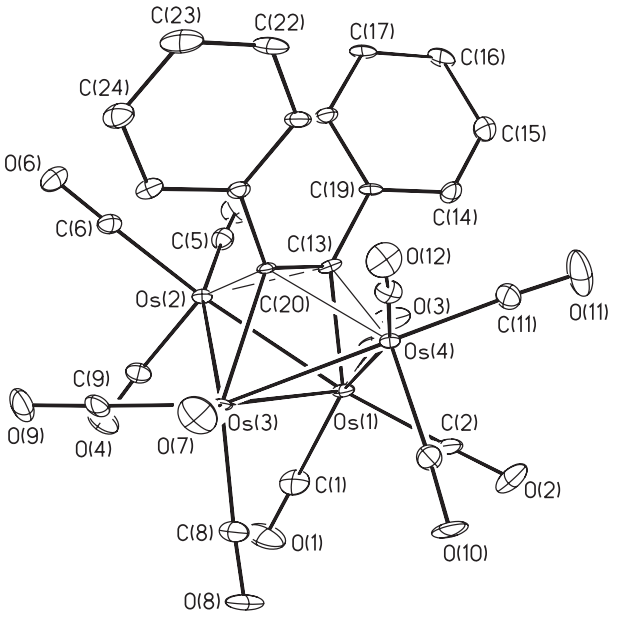
Although the Ru analogue of **3** has been known since 1977 (32), the Os compound has not been previously reported (SciFinder Scholar). A view of the structure of **3** is shown in Fig. 5. The structure is typical of clusters of the formula, $M_4(\mu_4\text{-}\eta^2\text{-}C_2RR')(CO)_{12}$ (M = Fe, Ru, Os) (1–3, 6, 32–34). These clusters may be viewed as electron-deficient butterfly clusters with 60 cluster valence electrons, or as *closo* octahedral clusters with seven skeletal electron pairs according to PSEPT (6). In **3** the peripheral Os—Os bonds range in length from 2.7457(5) to 2.7652(5) Å (Table 4), lengths that are typical of Os—Os lengths in condensed Os clusters. The hinge Os(1)—Os(3) bond is longer at 2.8742(5) Å. The four Os—C lengths of the alkyne unit to the wingtip Os atoms (Os(2) and Os(4)) are slightly longer (2.251(7)–2.274(8) Å) than the Os—C lengths to the hinge Os atoms (2.179(8), 2.201(8) Å). The pattern of the Os—Os and Os—C lengths closely match those previously found in $Ru_4(\mu_4\text{-}\eta^2\text{-}C_2Ph_2)(CO)_{12}$ (32) and $Os_4(\mu_4\text{-}\eta^2\text{-}C_2H_2)(CO)_{12}$ (34). The C—C bond length (1.49(1) Å) of the alkyne ligand in **3** is the longest of the three alkyne C—C lengths determined in this study and is close to that of a C—C single bond length.

Carbon-13 NMR spectra in the carbonyl region of **3** (^{13}CO enriched) at different temperatures are shown in Fig. 6. If the carbonyl groups were rigid, each chemically distinct $Os(CO)_3$ (i.e., wingtip and hinge moieties) unit would give rise to a 2:1 or 1:1:1 pattern of signals in the NMR spectrum (32). It is apparent that at 21 and 90 °C there is rapid rotation of the two different types of $Os(CO)_3$ groupings in **3**, but that migration of CO ligands between the wingtip and hinge Os atoms does not occur on the NMR timescale. This is also observed in clusters such as $Os_6(CO)_{18}$ (28).

In the spectrum at –90 °C, one of the signals has collapsed almost to the baseline, indicative of slowed exchange

© 2006 NRC Canada

Fig. 5. Molecular structure of $Os_4(\mu_4\text{-}\eta^2\text{-}C_2Ph_2)(CO)_{12}$ (**3**).



of one of the pairs of $Os(CO)_3$ units. This was also observed in the variable-temperature ^{13}C NMR spectra of $Ru_4(\mu_4\text{-}\eta^2\text{-}C_2Ph_2)(CO)_{12}$ (32). Given the fluxional behavior of the $Os(CO)_3$ units in **2**, it is probable that the carbonyls that are still undergoing rapid exchange in **3** are those of the hinge $Os(CO)_3$ units.

Clusters 1–3 as models for surface catalysts

As mentioned in the Introduction, **1**–**3** form a unique series of clusters in which an alkyne ligand is successively bound to two, three, and four metal atoms. Indeed, any series of structurally characterized clusters that involves the stepwise loss of two carbonyls are rare. One such series, however, is $Co_4(CO)_x(PNR_2)_2$ (x = 8, 9, or 10) recently reported by Carty and co-workers (35).

Muetterties et al. (36, 37) first pointed out that the structures of molecular clusters may provide insight to the understanding of surface catalysis. Despite its importance and intense study, the precise nature of the active sites in surface catalysts is still unknown (38–42). Recent investigations by physical techniques indicate that the catalytic properties of small particles depend on their size and imperfections (43, 44). For example, a recent study by Wei and Iglesia (44) of CH_4 reactions on Ru-based catalysts concluded that edge and corner atoms, with fewer Ru neighbors than those on terraces, were primarily responsible for C-H activation. We believe that compounds **1**–**3** may provide insight to the understanding of these active sites. In Table 5 the C—C and Os—C bond lengths for **1**–**3** are collected together for ready comparison. Scheme 2 summarizes the preparation of the clusters from $Os_4(CO)_{14}$.

Cluster **1** is a model for an alkyne bound to a corner site of a metal surface; compound **2** is a model for an alkyne bound to a planar metal surface; whereas **3**, with its butterfly arrangement of metal atoms, is a model for an alkyne bound to a step site of a metal surface. Although step sites have been proposed as the active sites of surface catalysts (6, 37, 38), the data in Table 5 indicates that the alkyne is tightly bound to the Os atoms in **3** and as such would be unreactive. Consider, for example, the thermal stability of **3**. The alkyne also appears to be tightly bound to the Os_4 unit in **2**, although less so than in **3**

On the other hand, the C_2Ph_2 molecule in **1** is bound to the Os_4 nucleus via two σ bonds, one of which is long (Table 5). It might be expected that there would also be considerable ring strain in the diosmacyclobutene unit. Furthermore, because of the proximity of the osmium atoms the frontier orbitals about the C atoms in the bound C_2Ph_2 will

Table 4. Selected bond lengths (angstroms) and angles (degrees) for **3**.

Bond lengths (Å)	
Os(1)—Os(2)	2.7515(5)
Os(1)—Os(3)	2.7592(5)
Os(1)—Os(4)	2.8742(5)
Os(2)—Os(3)	2.7652(5)
Os(3)—Os(4)	2.7457(5)
Os—C(CO) range	1.908(9)–1.95(1)
C(13)—C(20)	1.49(1)
Os(1)—C(13)	2.179(8)
Os(2)—C(13)	2.274(8)
Os(2)—C(20)	2.265(7)
Os(3)—C(20)	2.201(7)
Os(4)—C(13)	2.255(8)
Os(4)—C(20)	2.251(7)
Bond angles (°)	
Os(1)-Os(2)-Os(3)	62.80(1)
Os(1)-Os(3)-Os(2)	58.37(1)
Os(2)-Os(1)-Os(3)	58.83(1)
Os(1)-Os(3)-Os(4)	58.76(1)
Os(1)-Os(4)-Os(3)	62.95(1)
Os(3)-Os(1)-Os(4)	58.30(1)
Os(1)-Os(2)-C(13)	50.3(2)
Os(1)-C(13)-Os(2)	76.3(3)
Os(2)-Os(1)-C(13)	53.4(2)
Os(1)-Os(4)-C(13)	52.7(2)
Os(4)-Os(1)-C(13)	52.7(2)
Os(1)-C(13)-Os(4)	76.9(2)
Os(2)-Os(3)-C(20)	52.8(2)
Os(3)-Os(2)-C(20)	50.7(2)
Os(2)-C(20)-Os(3)	76.5(2)
Os(3)-Os(4)-C(20)	51.1(2)
Os(4)-Os(3)-C(20)	52.7(2)
Os(3)-C(20)-Os(4)	76.2(2)
Os(2)-C(13)-C(20)	70.5(4)
Os(2)-C(20)-C(13)	71.1(4)
C(13)-Os(2)-C(20)	38.4(3)
Os(4)-C(13)-C(20)	70.5(4)
Os(4)-C(20)-C(13)	70.8(4)
C(13)-Os(4)-C(20)	38.7(3)
Os(2)-Os(1)-Os(4)	91.67(1)
Os(1)-C(13)-C(19)	125.1(6)
Os(3)-C(20)-C(26)	125.6(6)
C(19)-C(13)-C(20)	126.3(7)
C(13)-C(20)-C(26)	126.0(7)

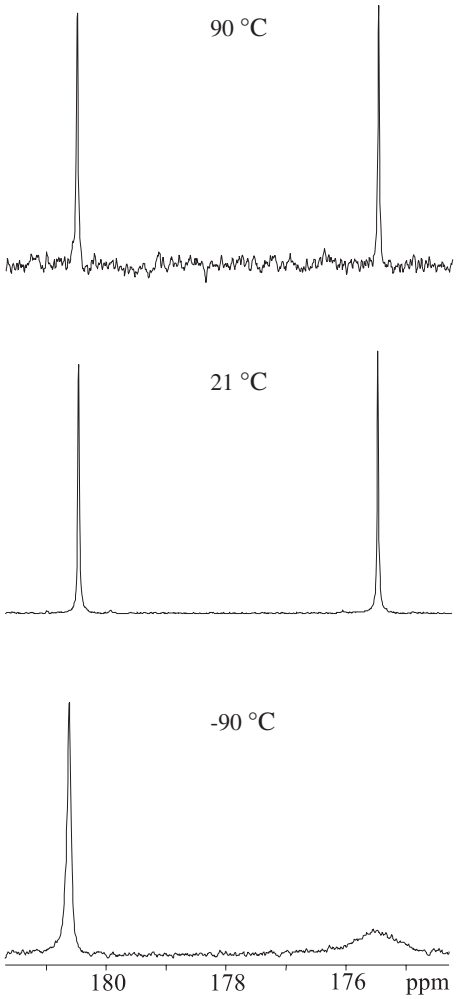
© 2006 NRC Canada

Table 5. The C—C and Os—C bond lengths of the alkyne-Os unit in **1**–**3**.

Compound	C—C bond lengths (Å)	Os—C bond lengths (Å) (σ)	Os—C bond lengths (Å) (π)
1	1.32(4)	2.13(3), 2.28(3)	—
2A[a]	1.42(2)	2.15(1), 2.18(1)	2.27(1), 2.29(1)
2B[a]	1.42(2)	2.17(1), 2.16(1)	2.29(1), 2.29(1)
3	1.49(1)	2.179(8), 2.201(7)	2.251(7), 2.255(8), 2.265(7), 2.274(8)

[a]Two independent molecules in the unit cell.

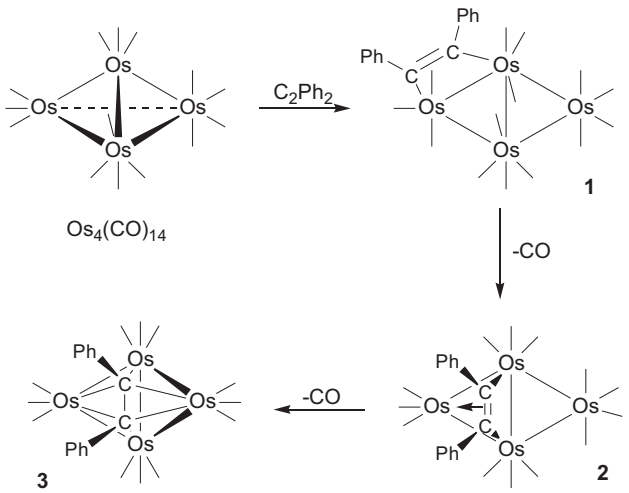
Fig. 6. The $^{13}C\{^1H\}$ NMR spectrum (CO region) of **3** (^{13}CO enriched) in CH_2Cl_2–CD_2Cl_2 (4:1) at 21 and –90 °C, and at 90 °C in C_7D_8.



be different from uncoordinated C_2Ph_2 that may also result in enhanced reactivity of the coordinated alkyne.

The catalytic half-hydrogenation of alkynes to *cis*-alkenes is an important industrial process and is normally carried out with solid Pd catalysts that have been poisoned (e.g., Lindlar's catalyst) (40, 45). Some homogeneous half-hydrogenation catalysts are however known (46). The mechanism of the hydrogenation is not fully understood, but a mechanism that involves a dimetallacyclobutene unit appears to be an attractive possibility. Partial hydrogenation of the alkyne in the dimetallacyclobutene unit could take place by reaction with coordinated hydrogen (the Langmuir–Hinshelwood mechanism) or by direct attack by molecular H_2 (the Rideal mechanism) (38, 47).

Scheme 2.



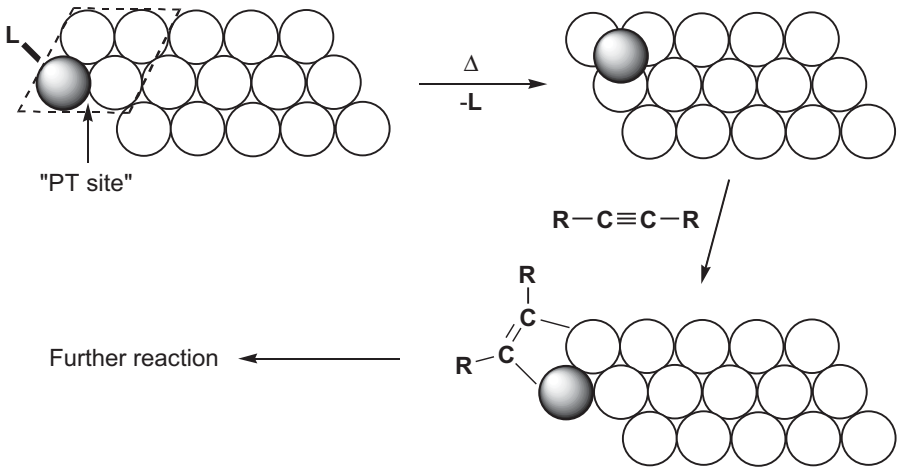
The intermediacy of an organic substrate bound to two low-coordinate metal atoms on a surface may have more general applicability to the understanding of the action of site-specific surface catalysis. The precursory cluster $Os_4(CO)_{14}$ (that has a tetrahedral Os_4 nucleus) is prepared by pyrolysis of $Os_4(CO)_{15}$. The latter cluster has a planar structure and hence is a model for a metal surface. Both $Os_4(CO)_{14}$ and $Os_4(CO)_{15}$ have unusual bonding that is not found in higher nuclearity Os clusters (48, 49).

Some corners and imperfect edges of metal surfaces resemble these clusters. This is shown in Scheme 3 for a corner site; the active site is designated a "PT" (planar-tetrahedral) site. To allow the unique metal atom to hop from the planar to the tetrahedral site (Scheme 3) probably requires the atom not to be coordinated to a metal atom below the plane it originates from.

There would be more of these atoms the greater the surface area and in freshly prepared catalysts. It is a general observation for surface catalysts that they are usually more active the more finely divided they are and if they are freshly prepared (38). It may be that after the surface and step sites are saturated (i.e., analogous to **2** and **3**) there must be surface reformation in order for the PT sites to be activated. A ligand must also dissociate from the dangling atom to allow formation of the tetrahedral form of the PT site. Both steps might explain the lag time that some catalysts exhibit before catalysis begins (38). The model also explains why only certain metals are active and why bimetallic catalysts can be more active than catalysts comprised of the individual atoms (38). The metal atoms of the PT site have few metal–metal

© 2006 NRC Canada

Scheme 3.



contacts and might be expected to have frontier orbitals like the corresponding metal atoms in mononuclear complexes. The most active metals for surface catalysts usually contain metal atoms that are present in the most active homogeneous mononuclear catalysts (e.g., Rh and Pd) (50). In the model, the substrate is bound to just two metal atoms and therefore it will have different susceptibilities to attack depending on whether it is coordinated to metals that are identical or different. Catalysts are often more effective with oxide promoters (38). If the atoms directly below or adjacent to the PT site were oxide ions, then the reactivity of the site would be strongly influenced by the ions.

Studies on the reactivity of clusters **1**–**3** (and derivatives thereof) with hydrogen and other small molecules are currently in progress.

Acknowledgements

We thank the Natural Sciences and Engineering Research Council of Canada (NSERC) for financial support.

References

1. (*a*) E. Sappa, A. Tiripiccio, and P. Braustein. Chem. Rev. **83**, 203 (1983); (*b*) P.R. Raithby and M.J. Rosales. Adv. Inorg. Radiochem. **29**, 169 (1985); (*c*) S. Deabate, R. Giordano, and E. Sappa. J. Cluster Sci. **8**, 407 (1997); (*d*) E. Sappa. J. Organomet. Chem. **573**, 139 (1999); (*e*) P.J. Low and M.I. Bruce. Adv. Organomet. Chem. **48**, 71 (2001).
2. Fe: (*a*) G. Wilkinson, F.G.A. Stone, and E.W. Abel (*Editors*). Comprehensive organometallic chemistry. Vol. 4. Pergamon, Oxford. 1982. Chap. 31.3–31.5; (*b*) G. Wilkinson, F.G.A. Stone, and E.W. Abel (*Editors*). Comprehensive organometallic chemistry II. Vol. 7. Pergamon, Oxford. 1995. Chap. 2–4; Some recent examples: (*c*) P.J. Low, A.J. Carty, K.A. Udachin, and G.D. Enright. J. Chem. Soc. Chem. Commun. 411 (2001); (*d*) A.J. Carty, G. Hogarth, G.D. Enright, J.W. Steed, and D. Georganopoulou. J. Chem. Soc. Chem. Commun. 1499 (1999).
3. Ru/Os: (*a*) G. Wilkinson, F.G.A. Stone, and E.W. Abel (*Editors*). Comprehensive organometallic chemistry. Vol. 4. Pergamon, Oxford. 1982. Chap. 32.3–32.6 and 33; (*b*) G. Wilkinson, F.G.A. Stone, and E.W. Abel (*Editors*). Comprehensive organometallic chemistry II. Vol. 7. Pergamon, Oxford. 1995. Chap. 8 and 13–16; Some recent examples: (*c*) M.I. Bruce, A.C. Meier, B.W. Skelton, A.H. White, and N.N. Zaitseva. Aust. J. Chem. **54**, 319 (2001); (*d*) R.L. Mallors, A.J. Blake, P.J. Dyson, B.F.G. Johnson, and S. Parsons. Organometallics, **16**, 1668 (1997); (*e*) M. Deng and W.K. Leong. Organometallics, **21**, 1221 (2002); (*f*) S.P. Tunik, V.D. Khripun, I.A. Balova, E. Nordlander, M. Haukka, T.A. Pakkanen, and P.R. Raithby. Organometallics, **20**, 3854 (2001); (*g*) J.A. Cabeza, I. del Río, P. García-Álverez, and D. Miguel. Organometallics, **24**, 665 (2005)
4. (*a*) V. Busetti, G. Granozzi, S. Aime, R. Gobetto, and D. Osella. Organometallics, **3**, 1510 (1984); (*b*) S. Brait, G. Gervasio, D. Marabello, and E. Sappa. J. Chem. Soc. Dalton Trans. 989 (2000); (*c*) E. Gatto, G. Gervasio, D. Marabello, and E. Sappa. J. Chem. Soc. Dalton Trans. 1448 (2002).
5. Recent examples: (*a*) P.J. Low, K.A. Udachin, and A.J. Carty. J. Cluster Sci. **15**, 1040 (2005); (*b*) P.J. Low, T.M. Hayes, K.A. Udachin, A.E. Goeta, J.A.K. Howard, D. Gary, and A.J. Carty. J. Chem. Soc. Dalton Trans. 1455 (2002); (*c*) M.I. Alcalde, A.J. Carty, Y. Chi, E. Delgado, B. Donnadieu, E. Hernandez, K. Dallmann, and J. Sanchez-Nieves. J. Chem. Soc. Dalton Trans. 2502 (2001); (*d*) P.J. Low, K.A. Udachin, G.D. Enright, and A.J. Carty. J. Organomet. Chem. **578**, 103 (1999); (*e*) P. Blenkiron, G.D. Enright, P.J. Low, J.F. Corrigan, N.J. Taylor, Y. Chin, J.-Y. Saillard, and A.J. Carty. Organometallics, **17**, 2447 (1998); (*f*) E. Delgado, Y. Chi, W. Wang, G. Hogarth, P.J. Low, G.D. Enright, S.-M. Peng, G.-H. Lee, and A.J. Carty. Organometallics, **17**, 2936 (1998); (*g*) P.J. Low, G.D. Enright, and A.J. Carty. J. Organomet. Chem. **565**, 279 (1998).
6. E. Sappa, A. Tiripicchio, A.J. Carty, and G.E. Toogood. Prog. Inorg. Chem. **35**, 437 (1987).
7. (*a*) M. Tachikawa, J.R. Shapley, and C.G. Pierpont. J. Am. Chem. Soc. **97**, 7172 (1975); (*b*) C.G. Pierpont. Inorg. Chem. **16**, 636 (1977);
8. (*a*) O. Gambino, G.A. Vaglio, R.P. Ferrari, and G. Cetini. J. Organomet. Chem. **30**, 381 (1971); (*b*) G. Ferraris and G. Gervasio. J. Chem. Soc. Dalton Trans. 1813 (1974); (*c*) A.J. Poë, D.H. Farrar, R. Ramachandran, and C. Moreno. Inorg. Chem. Acta, **274**, 82 (1998); (*d*) A.J. Poë and C. Moreno. Organometallics, **18**, 5518 (1999).
9. A.J. Poë, C.N. Sampson, and R.T. Smith. J. Am. Chem. Soc. **108**, 5459 (1986).
10. E. Rosenberg, J. Bracker-Novak, R.W. Gellert, S. Aime, R. Gobetto, and D. Osella. J. Organomet. Chem. **365**, 163 (1989).
11. A.J. Deeming. Adv. Organomet. Chem. **26**, 1 (1986).

© 2006 NRC Canada

12. (*a*) C.-Y. Lu, F.W.B. Einstein, V.J. Johnston, and R.K. Pomeroy. Inorg. Chem. **28**, 4212 (1989); (*b*) W. Wang, R.J. Batchelor, F.W.B. Einstein, C.-Y. Lu, and R.K. Pomeroy. Organometallics, **12**, 3598 (1993).
13. J.P. Canal, G.P.A. Yap, and R.K. Pomeroy. Organometallics, **22**, 3439 (2003).
14. R.F. Alex and R.K. Pomeroy. Organometallics, **41**, 2437 (1987).
15. J.P. Canal. Ph.D. thesis, Simon Fraser University, Burnaby, British Columbia. 2004.
16. M.R. Churchill and B.G. DeBoer. Inorg. Chem. **16**, 878 (1977).
17. G.R. John, B.F.G. Johnson, and J. Lewis. J. Organomet. Chem. **181**, 143 (1979).
18. For example: (*a*) H.B. Davis, F.W.B. Einstein, P.G. Glavina, T. Jones, R.K. Pomeroy, and P. Rushman. Organometallics, **8**, 1030 (1989); (*b*) F. Jiang, J.L. Male, K. Biradha, W.K. Leong, R.K. Pomeroy, and M.J. Zaworotko. Organometallics, **17**, 5810 (1998); (*c*) F. Jiang, H.A. Jenkins, K. Biradha, H.B. Davis, R.K. Pomeroy, and M.J. Zaworotko. Organometallics, **19**, 5049 (2000).
19. (*a*) D.M. Hoffman and R. Hoffmann. J. Chem. Soc. Dalton Trans. 1471 (1982); (*b*) M.R. Gagné and J. Takats. Organometallics **7**, 561 (1988); (*c*) A. Krebs, A. Jacobsen-Bauer, E. Haupt, M. Veith, and V. Huch. Angew. Chem. **101**, 640 (1989); (*d*) A.A. Cherkas, N. Hadj-Bagheri, A.J. Carty, E. Sappa, M.A. Pellinghelli, and A. Tiripicchio. Organometallics, **9**, 1887 (1990); (*e*) H.A. Mirza, J.J. Vittal, and R.J. Puddephatt. Organometallics, **13**, 3063 (1994); (*f*) C.P. Casey, W.T. Boese, R.S. Carino, and P.C. Ford. Organometallics, **15**, 2189 (1996); (*g*) C.P. Casey, R.S. Carino, H. Sakaba, and R.K. Hayashi. Organometallics, **15**, 2640 (1996); (*h*) H.A. Mirza, J.J. Vittal, and R.J. Puddephatt. J. Coord. Chem. **37**, 131 (1996); (*i*) S. Doherty, M. Waugh, T.H. Scanlan, M.R.J. Elsegood, and W. Glegg. Organometallics, **18**, 679 (1999).
20. M.C. Comstock and J.R. Shapley. Organometallics, **16**, 4816 (1997).
21. C.P. Casey, R.S. Carino, R.K. Hayashi, and K.D. Schladetzky. J. Am. Chem. Soc. **118**, 1617 (1996).
22. P.F. Heveldt, B.F.G. Johnson, J. Lewis, P.R. Raithby, and G.M. Sheldrick. J. Chem. Soc. Chem. Commun. 340 (1978).
23. M.R. Burke and J. Takats. Organomet. Chem. **302**, C25 (1986).
24. O.P. Anderson, B.R. Bender, J.R. Norton, A.C. Larson, and P.J. Vergamini. Organometallics, **10**, 3145 (1991).
25. B.E. Mann and B.F. Taylor. ^{13}C NMR data for organometallic compounds. Academic Press, New York. 1981.
26. B.F.G. Johnson, J Lewis, P.R. Raithby, and M.J. Rosales. J. Chem. Soc. Dalton Trans. 2645 (1983).
27. D. Braga, F. Grepioni, B.F.G. Johnson, J. Lewis, and J.A. Lunniss. J. Chem. Soc. Dalton Trans. 1101 (1992).
28. C.R. Eady, W.G. Jackson, B.F.G. Johnson, J. Lewis, and T.W. Matheson. J. Chem. Soc. Chem. Commun. 958 (1975).
29. B.F.G. Johnson, J. Lewis, M.-A. Pearsall, and L.G. Scott. J. Organomet. Chem. **413**, 337 (1991).
30. C.R. Eady, B.F.G. Johnson, J. Lewis, R. Mason, P.B. Hitchcock, and K.M. Thomas. J. Chem. Soc. Chem. Commun. 385 (1977).
31. V.M. Hansen, R.J. Batchelor, F.W.B Einstein, J.L. Male, and R.K. Pomeroy. Organometallics, **16**, 4875 (1997).
32. B.F.G Johnson, J. Lewis, B.E. Reichert, K.T. Schorpp, and G.M. Sheldrick. J. Chem. Soc. Dalton Trans. 1417 (1977).
33. (*a*) H. Bantel, B. Hansert, A.K. Powell, M. Tasi, and H. Vahrenkamp. Angew. Chem. Int. Ed. Engl. **28**, 1059 (1989); (*b*) H. Chen, B.F.G. Johnson, J. Lewis, and P.R. Raithby. J. Chem. Soc. Chem. Commun. 373 (1990); (*c*) G. Chen, M. Deng, C.H. Lee, and W.K. Leong. Organometallics, **21**, 1227 (2002).
34. R. Jackson, B.F.G Johnson, J. Lewis, P.R. Raithby, and S.W. Sankey. J. Organomet. Chem. **193**, C1 (1980).
35. J. Sanchez-Nieves, B.T. Sterenberg, K.A. Udachin, and A.J. Carty. Can. J. Chem. **82**, 1507 (2004).
36. (*a*) E.L. Muetterties. Bull. Soc. Chim. Belg. **84**, 959 (1975); (*b*) E.L. Muetterties, T.N. Rhodin, E. Band, C.F. Brucker, and W.R. Pretzer. Chem. Rev. **79**, 91 (1979).
37. E.L. Muetterties, W.R. Pretzer, M.G. Thomas, B.F. Beier, D.L. Thorn, V.W. Day, and A.B. Anderson. J. Am. Chem. Soc. **100**, 2090 (1978).
38. G.A. Somorjai. Introduction to surface chemistry and catalysis. Wiley, New York. 1994.
39. (*a*) G.A. Somorjai and M. Yang. Top. Catal. **24**, 61 (2003); (*b*) G.A. Somorjai. J. Phys. Chem. B, **106**, 9201 (2002); (*c*) P.S. Cremer, X. Su, Y.R. Shen, and G.A. Somorjai. J. Am. Chem. Soc. **118**, 2942 (1996); (*d*) G.A. Somorjai. J. Phys. Chem. B, **106**, 9201 (2002).
40. G.V. Smith and F. Notheisz. Heterogeneous catalysis in organic chemistry. Academic Press, San Diego. 1999.
41. C.R. Henry. Surf. Sci. Rep. **31**, 231(1998).
42. (*a*) A.M. Doyle, S.K. Shaikhutdinov, S.D. Jackson, and H.-J. Freud. H. Angew. Chem. Int. Ed. **42**, 5240 (2003); (*b*) V. Johánek, S. Schauermann, M. Laurin, J. Libuda, and H.-J. Freund. Angew. Chem. Int. Ed. **42**, 3035 (2003).
43. (*a*) J. Wei and E. Iglesia. J. Phys. Chem. B, **108**, 4094 (2004); (*b*) J. Wei and E. Iglesia. J. Catal. **225**, 116 (2004).
44. J. Wei and E. Iglesia. J. Phys. Chem. B, **108**, 7253 (2004).
45. J.G. Ulan, W.F. Maier, and D.A. Smith. J. Org. Chem. **52**, 3132 (1987).
46. For example: (*a*) J.A. Cabeza, I. del Río, J.M. Fernández-Colinas, and V. Riera. Organometallics, **15**, 449 (1996); (*b*) R. Giordano, E. Sappa, and S.A. Knox. J. Cluster Sci. **7**, 179 (1996).
47. M. Farina, C. Morandi, E. Mantica, and D. Botta. J. Chem. Soc. Chem. Commun. 816 (1976).
48. (*a*) F.W.B. Einstein, V.J. Johnston, A.K. Ma, and R.K. Pomeroy. Can. J. Chem. **73**, 1223 (1995); (*b*) V.J. Johnston, F.W.B. Einstein, and R.K. Pomeroy. J. Am. Chem. Soc. **109**, 7220 (1987).
49. V.J. Johnston, F.W.B. Einstein, and R.K. Pomeroy. Organometallics, **7**, 1867 (1988).
50. (*a*) D.D. Shriver, H.D. Kaesz, and R.D. Adams (*Editors*). The chemistry of metal clusters. VCH, New York. 1990; (*b*) B.C. Gates, L. Guczi, and H. Knözinger (*Editors*). Metal clusters in catalysis. Elsevier, Amsterdam. 1986.

© 2006 NRC Canada

The synthesis and characterization of the pendant-armed ligand *N*,*N*′-bis(2′-pyridylmethyl)-1,7-dithia-4,11-diazacyclotetradecane (L_4) and crystal structures of L_4 and the copper(II) complex $[Cu(L_4)](ClO_4)_2$ — Crystal structure of the nickel(II) complex of *N*-(2′-pyridylmethyl)-1,4,7-trithia-11-azacyclotetradecane (L_2), $[Ni(L_2)(CH_3CN)](ClO_4)_2 \cdot CH_3CN$[1]

B.C.M. Chak and A. McAuley

Abstract: The synthesis and characterization of the mixed donor ligand *N*,*N*′-bis(2′-pyridylmethyl)-1,7-dithia-4,11-diazacyclotetradecane (**L_4**) containing two pendant pyridine arms is described. The macrocycle formation involves reaction of *N*-tosylbis(2-bromoethyl)amine with *N*-tosylbis(3-mercaptopropyl)amine at high dilution followed by detosylation at the nitrogen atoms using $LiAlH_4$ in view of the presence of the thioether groups. An X-ray study of the ligand shows the sulphur atoms lie exo to the macrocyclic ring. The nickel(II) and copper(II) complexes of **L_4** have been characterized and the X-ray structure of the Cu(II) ion exhibits a five-coordinate copper ion despite the presence of six available donor atoms. In the case of ligand *N*-(2-pyridylmethyl)-1,4,7-trithia-11-azacyclotetradecane (**L_2**), with a single pendant N donor, the Ni(II) complex is distorted octahedral with a molecule of acetonitrile in the sixth site. Details of UV–vis, ESR spectra, and electrochemical studies on the complexes are presented.

Key words: synthesis, pendant-armed, mixed donor S,N macrocycles, copper, nickel.

Résumé : On décrit la synthèse et la caractérisation du ligand donneur mixte *N*,*N*′-bis(2′-pyridylméthyl)-1,7-dithia-4,11-diazacyclotétradécane (**L_4**) qui contient deux noyaux pyridines comme bras pendants. La formation du macrocycle implique la réaction du *N*-tosylbis(2-bromoéthyl)amine avec la *N*-tosylbis(3-mercaptopropyl)amine à dilution élevée, suivie d'une détosylation des atomes d'azote à l'aide de $LiAlH_4$ en raison de la présence de groupes thioéthers. Une étude par diffraction des rayons X du ligand montre que les atomes de soufre se trouvent en position exo par rapport au cycle macrocyclique. Les complexes du **L_4** avec le nickel(II) et le cuivre(II) ont été caractérisés et la structure de l'ion Cu(II) telle que déterminée par diffraction des rayons X comporte un ion cuivre pentacoordiné malgré la présence de six atomes donneurs disponibles. Dans le cas du ligand *N*-(2-pyridylméthyl)-1,4,7-trithia-11-azacyclotétradécane (**L_2**) qui ne comporte qu'un seul azote donneur pendant, le complexe de nickel(II) se présente sous la forme d'un octaèdre déformé comportant une molécule d'acétonitrile sur le sixième site. On rapporte aussi les détails des données UV–vis, des spectres RPE et des études électrochimiques des complexes.

Mots clés : synthèse, bras pendant, macrocycles à donneurs mixtes S,N, cuivre, nickel.

[Traduit par la Rédaction]

Introduction

Historically, the most commonly studied macrocyclic ligands are tetraazatetradentate with cyclam as a typical example. X-ray diffraction studies show that most of these complexes have square-planar geometry in which the ligand cyclam encircles the metal ion in the equatorial plane (1–4). The coordination chemistry of the thia analogue (i.e.,

Received 6 July 2005. Published on the NRC Research Press Web site at http://canjchem.nrc.ca on 28 February 2006.

It is a pleasure to recognize the many continuing contributions to chemistry in Canada by colleague and friend Arthur Carty.

B.C.M. Chak and A. McAuley.[2] Chemistry Department, University of Victoria, Victoria, BC V8W 3V6, Canada.

[1]This article is part of a Special Issue dedicated to Professor Arthur Carty.
[2]Corresponding author (e-mail: amcauley@uvic.ca).

 doi:10.1139/V05-241 © 2006 NRC Canada

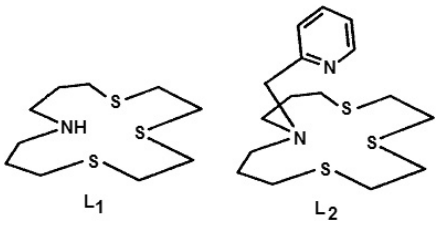
[14]aneS_4) has been investigated (5) and solid-state studies show the free ligand isomorphs exhibit exo conformations of the S lone pairs. The chemistry of thioether ligands has also been reviewed (6).

In contrast to the N_4 and S_4 donor sets, there have been relatively fewer studies on macrocyclic ligands involving sulphur and nitrogen mixed donor sets (7, 8). Black and McLean (9) synthesized the macrocyclic sexadentate ligand 1,4,10,13-tetrathia-7,16-diazacyclooctadecane ([18]aneN_2S_4). The associated Co(II) and Ni(II) complexes were assumed to be octahedral with the N donors in the apical sites. Rorabacher and co-workers (10) have prepared a series of N_xS_{4-x} donor sets (where x = 1–3) and also Cu complexes of cyclic polythiaethers. Kaden and co-workers (11, 12) have provided details of two sets of 12-, 14-, and 16-membered N_2S_2 macrocycles, dependent on the cis and trans arrangement of the donors within the ring, and have described the synthesis and solution chemistry of the Cu(II) and Ni(II) complexes. The use of mixed donor macrocycles as ligands for the selective interaction of Ag(I) has also been explored (13). In these laboratories, a focus has been on the synthesis of polymacrocylic ligands with these donors and the nature of the various oxidation states that may be stabilized owing to the mixed donor systems (14–16). Continuing interest in the coordination chemistry of these systems arises from the potential similarity of the coordination environment around metal centres in copper proteins. A recent review (17) has focussed on the role of macrocyclic ligands with pendant arms as Cu models related to electron transport and activation of small molecules in biological systems. In this paper, the synthesis of two macrocycles with attached pyridine moieties is described in an ongoing investigation of nitrogen and sulphur mixed donor macrocycles. The ability to complex a variety of metal ions in differing oxidation states is increased by the presence of both hard and soft donor centres within the macrocyclic framework.

Experimental

Ligand syntheses

The preparation of 1,4,7-trithia-11-azacyclotetradecane **L_1** and the pendant-armed methylpyridine derivative **L_2** have been reported previously (18).



L_1 L_2

N-*Tosylbis(2-(tosyloxy)ethyl)amine (2)*

Diethanolamine (**1**, 27.5 g, 0.262 mol) was dissolved in 500 mL of distilled CH_2Cl_2 in a three-necked flask. The solution was cooled to 0 °C in a stream of dry nitrogen and 122 mL of triethylamine (88.6 g, 0.88 mol) was added. With the temperature maintained at 0 °C, solid *p*-toluenesulfonyl chloride (157 g, 0.823 mol) was added in portions with vigorous stirring over the course of 5 h. The reaction mixture was stirred at ambient temperature overnight. The Et_3NHCl formed was filtered off and the resulting pale yellow filtrate was washed three times with 1 mol/L HCl, followed by 5 × 200 mL portions of water and 5 × 200 mL portions of satd. $NaHCO_3$ solution. The organic layer was dried over anhydr. $MgSO_4$. Removal of the solvent by rotatory evaporation gave a white product (**2**). Yield: 120 g (ca. 80%), mp 98 °C. ^{1}H NMR (90 MHz, $CDCl_3$) δ: 7.2–7.9 (m, 12H, ArH), 4.14 (t, J = 6 Hz, 4H, CH_2OTs), 3.4 (t, J = 6 Hz, 4H, CH_2NTs), 2.47 (two singlets, 9H, $ArCH_3$). MS (CI): 568 [M + 1], 396 [M – OTs].

N-*Tosylbis(2-bromoethyl)amine (3)*

To a solution of the tritosylate **2** (43 g, 0.076 mol) in 250 mL of DMF was added NaBr (40 g, 0.39 mol). The resulting suspension was stirred in an oil bath at 120 °C for 4 h. After cooling to room temperature, the reaction mixture was concentrated to about 50 mL. The viscous milky product mixture was poured into a rapidly stirred ice–water mixture (1 L) where a white solid separated out. This material was filtered, washed with water, and air dried. Yield: 24 g (ca. 80%), mp 56–58 °C. ^{1}H NMR (90 MHz, $CDCl_3$) δ: 7.36–7.75 (m, 4H, ArH), 3.5 (s, 8H, CH_2NTs, CH_2Br), 2.45 (s, 3H, CH_3Ar). MS (EI): 383, 385, 387 [M^+ in a ratio of 1:2:1].

N-*Tosylbis(3-(tosyloxy)propyl)amine (4)*

Bis(3-hydroxypropyl)amine (65 g, 0.488 mol) was dissolved in 800 mL of distilled CH_2Cl_2 in a 2 L, three-necked round bottom flask. The solution was cooled to –5 °C in a stream of dry nitrogen and triethylamine (218 mL, 1.56 mol) was added. With the temperature kept below 0 °C, solid *p*-toluenesulphonyl chloride (285 g, 1.49 mol) was added in portions to the above solution over the course of 2 h. The reaction mixture was stirred in an ice bath for 3 h and then at ambient temperature overnight. The white triethylamine hydrochloride formed was filtered off and washed with CH_2Cl_2. The pale yellow filtrate was washed with water (5 × 250 mL), 1 mol/L HCl (5 × 250 mL), water (5 × 250 mL), and satd. $NaHCO_3$ solution. The CH_2Cl_2 layer was dried over anhydr. $MgSO_4$. Removal of the solvent by rotatory evaporation resulted in a pale yellow viscous oil that was triturated to a white solid by the addition of diethyl ether. Yield: 232 g (80%), mp 68 to 69 °C. ^{1}H NMR (250 MHz, $CDCl_3$) δ: 7.74 (d, J = 8 Hz, 4H, ArH), 7.58 (d, J = 8 Hz, 4H, ArH), 7.25–7.39 (m, 6H, ArH), 4.00 (t, J = 7 Hz, 4H, CH_2OTs), 3.05 (t, J = 7 Hz, 4H, CH_2NTs), 2.42 (s, $ArCH_3$, 6H), 2.40 (s, $ArCH_3$, 3H), 1.84 (tt, J = 7 Hz, 4H, $CH_2CH_2CH_2$). ^{13}C{^{1}H} NMR ($CDCl_3$) δ: 144.9, 143.6, 135.4, 132.7 (quat. ArC), 129.9, 129.8, 127.8, 127.1 (ArC), 67.62 (CH_2OTs), 45.76 (CH_2NTs), 28.62 ($CH_2CH_2CH_2$), 21.54, 21.41 ($ArCH_3$). MS (CI) 596 [M + 1], 424 [M + 1 – 172]. An analytically pure sample was obtained by recrystallizing the white solid twice with hot ethanol. Anal. calcd. for $C_{27}H_{33}NS_3O_8$ (%): C 54.44, H 5.58, N 2.35, S 16.14; found: C 54.33, H 5.43, N 2.38, S 16.53.

N-*Tosylbis(3-mercaptopropyl)amine (5)*

To a solution of tritosylate (**4**) (20.2 g, 0.034 mol) dissolved in 200 mL of 95% ethanol in a 500 mL round-bottomed flask was added thiourea (5.6 g, 0.074 mol). The

© 2006 NRC Canada

suspension was refluxed for 12 h. After cooling to room temperature, the reaction mixture was concentrated (rotovap) and pump-dried. A crystalline white solid of the isothiouronium salt was obtained. A solution of NaOH (13 g, 0.325 mol) in 215 mL of water (6% NaOH) was prepared and bubbled with nitrogen for 15 min. To the isothiouronium salt was added the deaerated 6% NaOH solution and the reaction mixture was well-stirred and refluxed in a nitrogen atmosphere for 2 h. After the mixture was cooled to room temperature, and subsequently in an ice bath, 6 mol/L HCl was added dropwise until the pH of the solution reached 1. The milky solution obtained was saturated with NaCl and extracted with 3 × 100 mL CH_2Cl_2. The organic layers were combined and dried with anhydr. $MgSO_4$, concentrated by rotovap, and pumped dry. The desired product was isolated as a colorless viscous oil. Yield: 90%. ^{1}H NMR (90 MHz, $CDCl_3$) δ: 7.35–7.75 (m, 4H, ArH), 3.20 (t, 4H, J = 6 Hz, CH_2NTs), 2.6 (q, 4H, J = 6 Hz, CH_2S), 2.40 (s, 3H, CH_2Ar), 1.90 (m, 4H, $CH_2CH_2CH_2$), 1.45 (t, 2H, J = 6 Hz, SH). MS (CI): 318 [M + 1], 348 [M + 29], 360 [M + 41].

N,N′-*Bistosyl-1,7-dithia-4,11-diazacyclotetradecane (6)*

To a 5 L three-necked round flask equipped with a mechanical stirrer, condenser, and a dropping funnel was added oven-dried Cs_2CO_3 (14.8 g, 0.0454 mol) and 1 L of freshly opened DMF. The resulting suspension was stirred vigorously in a nitrogen atmosphere and warmed to 50 °C. A solution containing the dibromide (**3**) (4.82 g, 0.0125 mol) and dithiol (**5**) (4 g, 0.0125 mol) in 500 mL of DMF was prepared and bubbled in nitrogen for 20 min. This solution was then added to the Cs_2CO_3–DMF suspension via high dilution a rate of 4 to 5 mL/h. After the addition of all reactants, the mixture was stirred overnight. Upon cooling to room temperature, DMF was removed by rotatory evaporation. After extraction of the residual pale yellow solid with $CHCl_3$ several times, the resultant yellow solution obtained was taken to dryness and evacuated, yielding a pale brown oil that was purified by column chromatography (silica gel, CH_2Cl_2–EtOAc, 95%:5%). Fractions with R_f = 0.7 were collected. The desired product was isolated as a white crystalline solid. Yield: 30%. ^{1}H NMR (90 MHz, $CDCl_3$) δ: 7.8 (m, ArH), 7.35 (m, ArH), 3.00–3.5 (m, CH_2NTs), 2.5–2.9 (m, CH_2S), 2.45 (s, CH_3Ar), 2.00 (m, $CH_2CH_2CH_2$). MS (CI): 543 [M + 1], 571 [M + 29].

1,7-Dithia-4,11-diazacyclotetradecane (L_3)

A sample of (**6**) (0.5 g, 0.92 mmol) was added slowly under a nitrogen atmosphere to a stirred suspension of $LiAlH_4$ (0.41 g, 10.8 mmol) in 40 mL of dry THF. The reaction mixture was stirred under reflux for 72 h. After cooling to room temperature, the excess $LiAlH_4$ was destroyed by dropwise addition of 30 mL of THF–H_2O (2:1 *v*/*v*). The mixture was filtered and the precipitate was carefully washed with CH_2Cl_2. Evaporation of the solvent afforded 150 mg of $\mathbf{L_3}$ as a white crystalline waxy solid, which was used for subsequent reactions without further purification. ^{1}H NMR (90 MHz, $CDCl_3$) δ: 2.6–2.8 (m, 16H, CH_2S, CH_2N), 1.8 (m, 4H, $CH_2CH_2CH_2$), 1.45 (s, 2H, NH). MS (CI): 235 [M + 1], 263 [M + 29], 275 [M + 41].

N,N′-*Bis(2′-pyridylmethyl)-1,7-dithia-4,11-diazacyclotetradecane (L_4)*

To a two-necked, round-bottomed flask equipped with a magnetic stirrer, reflux condenser, and nitrogen inlet was added a solution of $\mathbf{L_3}$ (1.30 g, 6.1 mmol), triethylamine (4.5 mL, 32.3 mmol, 5 equiv.), and 2-(chloromethyl)pyridine hydrochloride (2 g, 12.2 mmol) in 50 mL of absolute ethanol. The solution was heated to a gentle reflux under a nitrogen atmosphere for 12 h. After cooling to room temperature, $CHCl_3$ (3 × 100 mL) was added to the orange-red reaction mixture. The organic phase was washed with water (5 × 100 mL) and dried over anhydr. Na_2SO_4. $CHCl_3$ was removed by rotoevaporation and the brown oil obtained was purified by column (silica gel, EtOAc–CH_2Cl_2, 60%:40%). Fractions with a R_f value of 0.2 were collected. The title product was obtained as a pale yellow oil that yielded clear white crystals. Yield: 500 mg, 20%. ^{1}H NMR (250 MHz, $CDCl_3$) δ: 8.42, 7.61, 7.56, 7.38, 7.07 (m, 8H, pyridine Hs), 3.74 (s, 2H, CH_2-pyridine), 3.62 (s, 2H, CH_2-pyridine), 2.60–2.73 (m, 8H, CH_2S), 2.51 (t, J = 7 Hz, 8H, CH_2N), 1.75 (tt, J = 7 Hz, 4H, $CH_2CH_2CH_2$). ^{13}C{^{1}H} NMR ($CDCl_3$) δ: 159.9, 159.6 (quat. ArC), 148.8, 136.3, 136.1, 122.7, 122.6, 121.8, 121.7 (ArC), 61.3, 61.0 (*C*H_2-pyridine), 52.6, 52.1 (*C*H_2N), 29.3, 29.2 (S*C*H_2), 27.1 (CH_2*C*H_2CH_2). MS (CI): 417 [M + 1], 445 [M + 29].

Syntheses of Co(II), Ni(II), and Cu(II) complexes

[Co(L_2)(CH_3CN)(NO_3)$_2$]·CH_3CN (complex A)

An acetonitrile solution of $\mathbf{L_2}$ (0.06 g, 0.175 mmol) in a round-bottomed flask was purged with nitrogen for 20 min. A solution of [Co(H_2O)$_6$](NO_3)$_2$ (0.0496 g, 0.17 mmol) in acetonitrile was added dropwise to the ligand solution. The reaction mixture, now pink, was stirred at room temperature under a nitrogen atmosphere overnight to ensure complete complexation before concentration to ~1 mL on the rotovap. Slow evaporation of the solvent at room temperature yielded pink crystals of X-ray quality. Yield: 40 mg. Anal. calcd. for $C_{20}H_{32}N_6S_3O_6Co$ (%): C 39.51, H 5.31, N 13.83; found: C 38.91, H 5.20, N 13.46.

[Co(L_2)(ClO_4)](ClO_4) (complex B)

A solution of 0.57 g (0.156 mmol) of [Co(H_2O)$_6$](ClO_4)$_2$ in dry nitromethane was added dropwise to a similar N_2-purged solution of the ligand (0.0546 g, 0.159 mmol). The mixture turned deep red instantly and was refluxed gently under N_2 for about 1 h. After cooling, the solvent was removed and the resultant red oil was triturated with EtOH to a reddish-brown solid that was dried in vacuo. Yield: 0.089 g (92%). Anal. calcd. for $C_{16}H_{26}N_2S_3O_8Cl_2Co$ (%): C 31.07, H 4.56, N 4.53; found: C 30.97, H 4.26, N 4.67.

Compounds A and B are stable in air and, when dissolved in acetonitrile or nitromethane, show different spectroscopic characteristics and electrochemical behavior.

[Ni(L_2)(CH_3CN)](ClO_4)$_2$·CH_3CN

An acetonitrile solution of $\mathbf{L_2}$ (0.170 g, 0.496 mmol) was purged with nitrogen for 20 min and a solution of [Ni(H_2O)$_6$](ClO_4)$_2$ (0.145 g, 0.396 mmol) in acetonitrile was added dropwise to the ligand solution. The reaction mixture changed to purple and was stirred at room temperature under

© 2006 NRC Canada

nitrogen overnight to ensure complete complexation after which it was concentrated to ~1 mL. Slow evaporation of the solvent at room temperature yielded purple crystals of X-ray quality. Yield: 200 mg (83%). Anal. calcd. for $C_{18}H_{32}N_4S_3Cl_2O_8Ni$ (%): C 35.20, H 4.73, N 8.21; found: C 35.05, H 4.60, N 7.79.

[Cu(L$_2$)](ClO$_4$)$_2$

A solution of **L$_2$** (0.059 g, 0.172 mmol) in CH_2Cl_2 in a round-bottomed flask was purged with nitrogen for 20 min. An ethanolic solution of $[Cu(H_2O)_6](ClO_4)_2$ (0.060 g, 0.16 mmol) was added dropwise to the ligand solution. The reaction mixture changed to bluish green and was stirred at room temperature under nitrogen overnight to ensure complete complexation. The green precipitate formed was filtered, washed with diethyl ether, and air dried. Yield: 55 mg (57%). The green powder was recrystallized by dissolving it in EtOH–CH_3CN, yielding a microcrystalline green solid. Anal. calcd. for $C_{16}H_{26}N_2S_3O_8Cl_2Cu$ (%): C 31.76, H 4.33, N 4.63; found: C 31.86, H 4.18, N 4.69.

[Cu(L$_4$](ClO$_4$)$_2$

A method similar to that described previously using solutions of **L$_4$** (0.068 g, 0.164 mmol) in CH_2Cl_2 and $[Cu(H_2O)_6](ClO_4)_2$ (0.058 g, 0.156 mmol) in ethanol was used. Yield: 66 mg (66%). The powder was recrystallized by dissolving it in EtOH–CH_3CN, giving green crystals of X-ray quality. Anal. calcd. for $C_{22}H_{32}N_4S_2O_8Cl_2Cu$ (%): C 38.91, H 4.75, N, 8.25; found: C 38.83, H 4.69, N 8.19.

[Ni(L$_4$](ClO$_4$)$_2$

To a solution of the ligand (0.11 g, 0.0264 mmol) dissolved in a CH_2Cl_2–MeCN (1:1) solution was added dropwise an acetonitrile solution of $[Ni(H_2O)_6](ClO_4)_2$ (0.096 g, 0.262 mmol). The colour changed to blue and the mixture was stirred under N_2 at room temperature. After reduction to dryness, the resultant solid was dissolved in a MeOH–H_2O–acetone solution and a mixture of blue and purple solids was obtained. The latter was reduced to dryness, yielding a brown oil and a blue solid. Isolation of the blue material and dissolution in a minimum volume of ethanol yielded a blue solid that was washed with Et_2O and dried in vacuo. Anal. calcd. for $C_{22}H_{32}N_4S_2O_8Cl_2Ni$ (%): C 39.19, H 4.78, N 8.31; found: C 39.08, H 4.85, N 8.22.

(Caution: Perchlorate complexes may be hazardous and should be prepared in small quantities).

Electrochemistry

Cyclic voltammograms were recorded with a Princeton Applied Research model 273 potentiostat/galvanostat interfaced to an IBM PC computer. All measurements were carried out in acetonitrile, which was dried before use by distilling over calcium hydride overnight under a nitrogen atmosphere. A solution of 0.1 mol/L *n*-Bu_4NPF_6 in acetonitrile was used as the supporting electrolyte. Platinum beads were used as the working electrode and counter electrode. The reference electrode was $Ag/AgNO_3$ (0.01 mol/L in CH_3CN) linked to the cell via a salt bridge containing an acetonitrile solution of *n*-Bu_4NPF_6 (0.1 mol/L).

Crystallography

Crystals were mounted in glass Lindemann tubes. The unit cells and space groups were determined by using Weissenberg and precession photography after which the crystals were transferred to a Picker four-circle diffractometer automated with a PDP 11/10 computer or an Enraf Nonius CAD4 diffractometer to collect the data. Intensity measurements were obtained with Zr-filtered Mo radiation, λ = 0.710 69 Å, or Cu radiation (1.542 Å). Background counting was introduced at the end of each scan. A set of three internal standard reflections preceded each batch of 50 measurements, with no noticeable change in intensity observed during the collection. The solution of the phase problem was achieved with MULTAN (19) and refined by direct methods with SHELX-76 (20). The atomic scattering factors used were those included in the SHELX-76 program together with the metal *f* curve from the *International Tables* (21). Completion and refinement of the structure was carried out by using difference electron density maps and least-squares techniques. All atoms were refined anisotropically except for hydrogen atoms, which were observed and refined isotropically when possible; otherwise the H-atom positions were calculated. In general, the refinement converged with a maximum shift/esd of less than 0.2 on the final cycle.

Electron spin resonance

ESR spectra were obtained by use of a Varian E6 ESR spectrometer using DPPH as the external standard. Spectra were obtained at 77 K using a quartz insert dewar.

Nuclear magnetic resonance

^{1}H NMR spectra were recorded on a 90 MHz PerkinElmer R-32 instrument; high-field ^{1}H and ^{13}C NMR spectra were obtained on either a Bruker WM 250 or AMX 360 instrument. Two-dimensional NMR spectra (e.g., ^{1}H COSY and ^{1}H–^{13}C correlated spectra) were recorded on the Bruker AMX 360 instrument. All chemical shifts are reported relative to tetramethylsilane (TMS). Simulated ^{1}H and ^{13}C NMR spectra were calculated using NMRPLOT (22).

Elemental analyses were performed by Canadian Microanalytical Services, Vancouver, British Columbia.

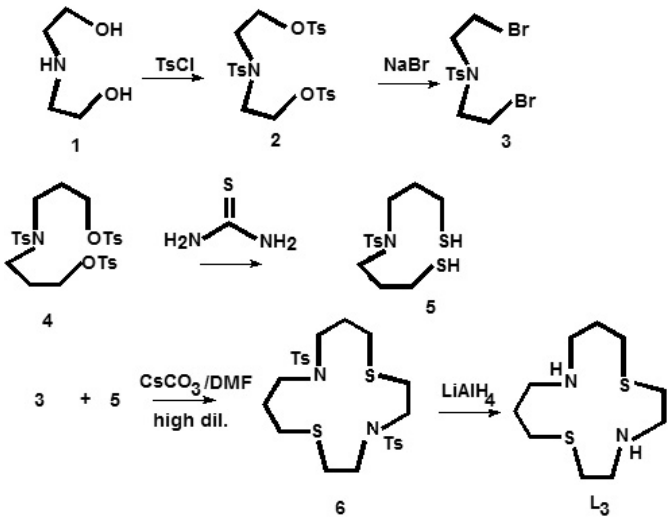
Results and discussion

Syntheses

The synthetic route leading to **L$_3$** is summarized in Scheme 1. The tosylated amine **2** can be used directly for the cyclization or converted to the corresponding dibromide (Scheme 1) via nucleophilic substitution of tosyl oxy groups by NaBr in DMF. Both can serve as the leaving groups in the formation of C—S bonds in the cyclization. The dithiol (**5**) required for the cyclization was obtained in good yield (ca. 85%) by refluxing an ethanolic solution of **4** and thiourea for 12 h, followed by the base hydrolysis of the isothiuronium salt. The cyclization reaction leading to **6** was carried out under medium dilution conditions (final concentration of reagents ca. 0.01 mol/L) using Cs_2CO_3 as the base in dry DMF. Detosylation of **6** was complicated by the presence of thioether functional groups that are prone to cleavage when acidic procedures sufficient to remove tosyl groups were used. To avoid this problem, a reductive

© 2006 NRC Canada

Scheme 1.



detosylation involving $LiAlH_4$ was employed (23). Ligand $\mathbf{L_3}$ was obtained in satisfactory yields (ca. 70%). The preparation of the bispyridine adduct ($\mathbf{L_4}$) is shown in Scheme 2.

Two isomers of $\mathbf{L_3}$ have been prepared previously (11, 12), and comparisons with the present metal–ion complexes are made. The nickel(II) and copper(II) complexes of $\mathbf{L_2}$ were prepared by the reaction of equimolar quantities of the ligand with $[Ni(H_2O)_6](ClO_4)_2$ or $[Cu(H_2O)_6](ClO_4)_2$ in dry CH_3CN under a nitrogen atmosphere. X-ray quality crystals were obtained by slow diffusion of diethyl ether into the acetonitrile solution of the complexes. In the case of the cobalt(II) complex of $\mathbf{L_2}$, two compounds were isolated vide infra.

Crystal structures

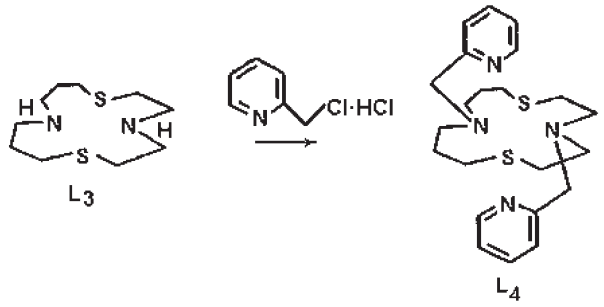
Experimental crystallographic data for three molecules are provided in Table 1.

$[Ni(L_2)CH_3CN)](ClO_4)_2$

The molecular structure is shown in Fig. 1, and significant interatomic distances and bond angles are given in Table 2. Complete details on distances and bond angles are provided in Supplementary tables S1–S5.[3]

As illustrated, the nickel centre is located in a pseudo-octahedral environment, coordinated to the three thioether sulphur atoms and three nitrogen atoms (from the macrocycle, the pyridine ring, and acetonitrile) with differing Ni—N bond lengths observed. The Ni—N(1)pyr (2.04 Å) is slightly shorter than the ideal strain-free Ni—N bond length (2.10 Å) (24). However, it is close to the values found for related high spin mixed donor macrocyclic complexes reported (8, 11, 25). Three distinct Ni—S bond distances, ranging from 2.37 to 2.48 Å, are observed in the cation. The shortest, Ni(1)—S(1) trans to the pyridine N(1), the results from the trans influence of a S atom being greater than the nitrogen donor. For S(3), trans to N(3), the bond length of Ni—S is 2.40 Å. This value is comparable to other mixed donor macrocyclic complexes such as $Ni([9]aneNS_2)_2]^{2+}$ ($[9]aneNS_2)_2$ = 1-aza-4,7-dithiacyclononane) (2.41 Å) (26). The longest (Ni—S(2)) bond is consistent with earlier findings of the trans influence sequence thioether S > N(tert) > N(py). The folded structure has been observed in the Pd and Pt analogues (18).

Scheme 2.



$[Co(L_2)(NO_3)_2{\cdot}CH_3CN]{\cdot}CH_3CN$

Attempts made at characterizing this complex crystallographically were not completely successful (R = 0.115, R_w = 0.114). However, the broad outlines of the structure are identifiable and the proposed molecular structure is shown in Fig. S1,[3] where it is seen that the cobalt ion is in an octahedral environment. It is coordinated to three nitrogen atoms from the macrocycle, the pyridyl ring, and the solvent acetonitrile. However, the remaining coordination sites are occupied by a monodentate and bidentate nitrate ion. These two modes of coordination have also been established by IR spectroscopy, with N—O stretches at 1360 and 1461 cm^{-1} corresponding to a monodentate nitrate ion (27) and those at 1285 and 1021 cm^{-1} consistent with a bidentate configuration. In contrast to the structure of the nickel(II) complex of $\mathbf{L_2}$ discussed previously, none of the thioether sulphur atoms in the macrocycle $\mathbf{L_2}$ is coordinated to the metal. The ligand adopts a conformation similar to that observed in the free ligand [14]aneS_4 (5), consistent with the lone pairs on the thioether atoms being directed out of the ring. This species is of interest in that it is an example of a rare precursor to complexation with the macrocyclic ligand.

Ligand L_4 and $[Cu(L_4)](ClO_4)_2$

Both the free ligand $\mathbf{L_4}$ and its Cu(II) complex have been characterized crystallographically. The molecular structures are shown in Figs. 2 and 3, respectively, and crystallographic parameters for the copper(II) ion are listed in Table 2. Complete interatomic distances and bond angles of $\mathbf{L_4}$ are provided in Tables S7–S9,[3] and those of $[Cu(\mathbf{L_4})](ClO_4)_2$ are presented in Tables S10–S13.[3]

For the free ligand $\mathbf{L_4}$, the interatomic distances between the nitrogen and sulphur donor atoms inside the macrocyclic

[3] Supplementary data for this article are available on the journal Web site (http://canjchem.nrc.ca) or may be purchased from the Depository of Unpublished Data, Document Delivery, CISTI, National Research Council Canada, Ottawa, ON K1A 0R6, Canada. DUD 4093. For more information on obtaining material refer to http://cisti-icist.nrc-cnrc.gc.ca/irm/unpub_e.shtml. CCDC 277077–277079 contain the crystallographic data for this manuscript. These data can be obtained, free of charge, via http://www.ccdc.cam.ac.uk/conts/retrieving.html (Or from the Cambridge Crystallographic Data Centre, 12 Union Road, Cambridge CB2 1EZ, UK; fax +44 1223 336033; or deposit@ccdc.cam.ac.uk).

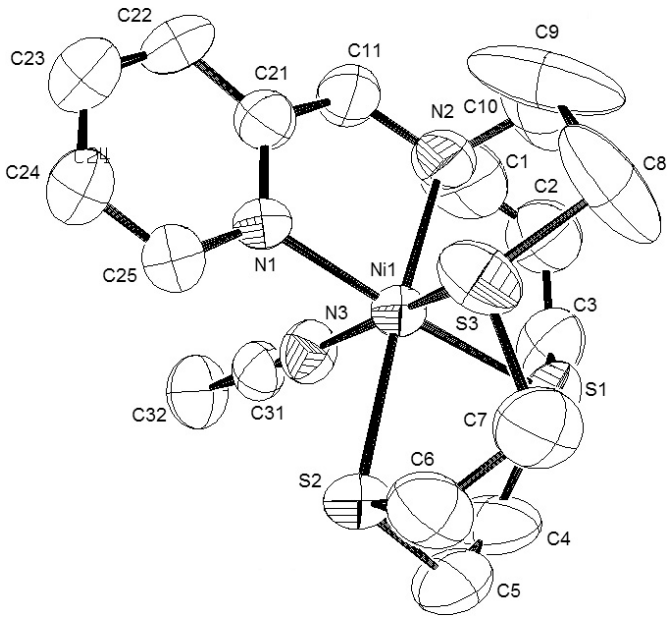
© 2006 NRC Canada

Table 1. Crystallographic data for the macrobicyclic complexes.

Complex	$\mathbf{L_4}$	$[Cu(\mathbf{L_4})](ClO_4)_2$	$[Ni(\mathbf{L_2})\cdot CH_3CN](ClO_4)_2\cdot CH_3CN$
Empl. form.	$C_{22}H_{32}N_4S_2$	$C_{22}H_{32}Cl_2N_4O_8S_2Cu$	$C_{20}H_{32}Cl_2N_4O_8S_3Ni$
Mol. wt.	416.64	679.1	682.3
Crystal colour, habit	Clear white	Emerald green	Royal purple
Crystal system	Monoclinic	Monoclinic	Monoclinic
Space group	$P2_1$ (No. 4)	$P2_1/n$ (No. 14)	$P2_1/n$ (No. 14)
Cell dimensions			
a (Å)	10.593(4)	15.632(1)	12.152(5)
b (Å)	17.195(9)	9.753(3)	14.445(2)
c (Å)	6.401(2)	18.713(2)	17.194(5)
α (°)	90	90	90
β (°)	97.72(4)	96.21(1)	109.84(3)
γ (°)	90	90	90
V (Å)	1155.29	2836.2	2839.1
Z	2	4	4
$D_{calcd.}$ (g cm^{-3})	1.198	1.716	1.595
F(000)	1104	1100.00	1896.00
λ (Å)	0.710 69	1.542	0.710 69
μ (cm^{-1})	2.44	44.5	11.07
Crystal dimens. (mm)	1.051×0.098×0.427	0.105×0.136×0.546	0.64×0.20×0.25
Transmission factors	0.893–0.927		0.598–0.664
2θ Range (°)	2–50	2–120	4.0–45
No. reflections measd.	2134	3774	3828
No. reflections with $I > x\sigma(I)$	1464[a]	2197[a]	2992[b]
No. parameters	252	352	343
R	0.085	0.0938	0.078
R_w	0.084 7	0.0936	0.086

Note: $T = 20°$. $R = \Sigma||F_o| - ||F_c||/\Sigma|F_o|$; $R_w = [(\Sigma w(|F_o| - |F_c|)^2/\Sigma wF_o^2)]^{1/2}$.
[a] $x = 6$.
[b] $x = 4$.

Fig. 1. Crystal structure of $[Ni\mathbf{L_2}(CH_3CN)]^{2+}$.



cavity are: N(1)···S(1) = 3.011 Å, S(1)···N(2) = 4.511 Å, N(1)···S(2) = 4.099 Å, N(2)···S(2) = 4.737 Å, N(1)···N(2) = 5.762 Å, and S(1)···S(2) = 5.905 Å. The average of the C—S bond distance is 1.833 Å, which is similar to that observed in [14]aneS$_4$ (5). The geometry of the ligand in the solid state indicates that the S lone pairs are exocyclic and those on the nitrogen atoms are oriented in different directions such that binding to the metal centre requires conformational changes within the ligand.

In the complex ion $[Cu(\mathbf{L_4})]^{2+}$, the copper ion is in a distorted square-pyramidal environment (Fig. 3). It is coordinated by three nitrogen atoms and two thioether sulphur atoms. One tertiary nitrogen atom in the macrocycle is not coordinated. The Cu—N bond distances range from 2.00 to 2.14 Å. The apical Cu—S(1) bond distance is 2.51 Å, which is very close to the value in 17-thia-1,5,8,12-tetrazaabicyclo[10.5.2]nonadecane ($[Cu(bicycloSN_4)]^{2+}$, 2.55 Å) (14*b*) where there is a similar N,S five-membered chelate ring. A comparison with the interatomic bond distances in $\mathbf{L_4}$ indicates that there are no major changes in bond lengths within the macrocycle upon coordination to copper. From the mean plane calculation (Table S12),[3] the copper ion is 0.258 Å above the plane defined by the basal atoms N(1), N(3), and N(4). In addition, S(2) is 0.9059 Å below this plane. A consequence of the nonplanarity between the copper ion and the nitrogen and sulphur donor atoms is that the bond angle S(1)-Cu-S(2) is 130.5°. The bond angles in the equatorial plane are: N(4)pyr-Cu-S(2) = 90.2°, N(4)pyr-Cu-N(3) = 91.7°, S(2)-Cu-N(1)pyr = 86.8°, and N(1)-Cu-N(3)pyr = 81.7°, consistent with deviations from an ideal square-pyramidal structure that probably arises from the strain imposed by the ligand.

© 2006 NRC Canada

Table 2. Interatomic distances (Å) and bond angles (°) (standard deviations in parenthesis) for complex cations.

	$[Ni(\mathbf{L_2})CH_3CN)]^{2+}$	$[Cu(\mathbf{L_4})]^{2+}$
Interatomic distances (Å)		
Ni(1)—S(1)	2.371(3)	
Ni(1)—S(2)	2.481(2)	
Ni(1)—S(3)	2.398(3)	
Ni(1)—N(1)	2.037(7)	
Ni(1)—N(2)	2.133(7)	
Ni(1)—N(3)	2.085(8)	
Cu(1)—S(1)		2.511(4)
Cu(1)—S(2)		2.339(4)
Cu(1)—N(1)		2.135(11)
Cu(1)—N(3)		2.066(11)
Cu(1)—N(4)		2.000(11)
Bond angles (°)		
S(2)-Ni(1)-S(1)	84.8(1)	
N(1)-Ni(1)-S(1)	174.2(2)	
N(2)-Ni(1)-S(1)	91.9(2)	
N(3)-Ni(1)-S(1)	92.4(2)	
S(3)-Ni(1)-S(1)	96.2(1)	
N(1)-Ni(1)-S(2)	100.8(2)	
N(2)-Ni(1)-S(2)	176.0(2)	
N(3)-Ni(1)-S(2)	87.7(2)	
S(3)-Ni(1)-S(2)	82.6(1)	
N(1)-Ni(1)-S(3)	86.3(2)	
N(2)-Ni(1)-S(3)	95.5(3)	
N(3)-Ni(1)-S(3)	166.4(2)	
S(2)-Cu(1)-S(1)		130.5(2)
N(1)-Cu(1)-S(1)		85.3(4)
N(4)-Cu(1)-S(1)		107.8(3)
N(4)-Cu(1)-N(3)		91.7(4)
N(3)-Cu(1)-S(1)		84.3(3)
N(1)-Cu(1)-S(2)		86.8(4)
N(4)-Cu(1)-S(2)		90.2(3)
N(3)-Cu(1)-S(2)		142.3(3)
N(3)-Cu(1)-N(1)		81.7(5)
N(4)-Cu(1)-N(1)		164.8(5)

ESR spectra

The ESR spectral data for the Cu(II) and Co(II) complexes studied in this work are listed in Table 3. For the complexes $[Cu(\mathbf{L_1})]^{2+}$ and $[Cu(\mathbf{L_3})]^{2+}$ (L_3 = 1,7-diaza-4,10-dithiacyclotetradecane), the ESR spectra are characteristic of a tetragonally distorted d^9 ion in a tetragonal elongated environment, with $g_\parallel > g_\perp$. Hyperfine lines are also observed in the $g_\parallel$ region, with the coupling constants ranging from 115 to 125 G. The $g_\parallel$ value of $[Cu(\mathbf{L_1})]^{2+}$ is greater than for $[Cu([14]aneS_4)]^{2+}$ ($g_\parallel$ = 2.10; $A_\parallel$ = 165 G) and also other Cu(II) N_2S_2 complexes prepared by Kaden and co-workers (12). Isotropic spectra were obtained even at 77 K for the copper(II) complexes with pyridine pendant arms, $[Cu(\mathbf{L_2})]^{2+}$ and $[Cu(\mathbf{L_4})]^{2+}$. The signals span a range of 500 G, and no hyperfine coupling was observed. A possible explanation for the spectra is that consistent with the structure of $[Cu(\mathbf{L_4})]^{2+}$ shown in Fig. 3, the possibility exists of a dynamic exchange between the Cu-coordinated nitrogen atom from the pyridine and that of the tertiary amine. Although the crystal structure of $[Cu(\mathbf{L_2})]^{2+}$ is not available currently, a five-coordinate geometry is anticipated and a fluxional process may be present.

For the Co(II) complexes of $\mathbf{L_2}$, only ion B, $[Co(\mathbf{L_2})(ClO_4)]^+$, is active. The spectrum at 77 K exhibits characteristics of a low spin d^7 ion in a distorted octahedral environment, with $g_\parallel$ = 2.020 and $g_\perp$ = 2.290. This is consistent with a Co(II) ion coordinated to the N and S donor at-

Fig. 2. Crystal structure of the ligand $\mathbf{L_4}$.

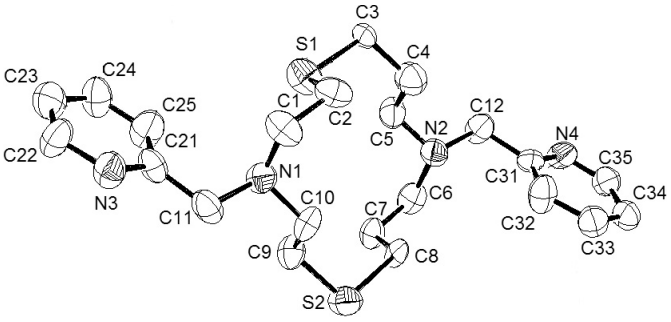


Fig. 3. Crystal structure of the $[CuL_4]^{2+}$ ion.

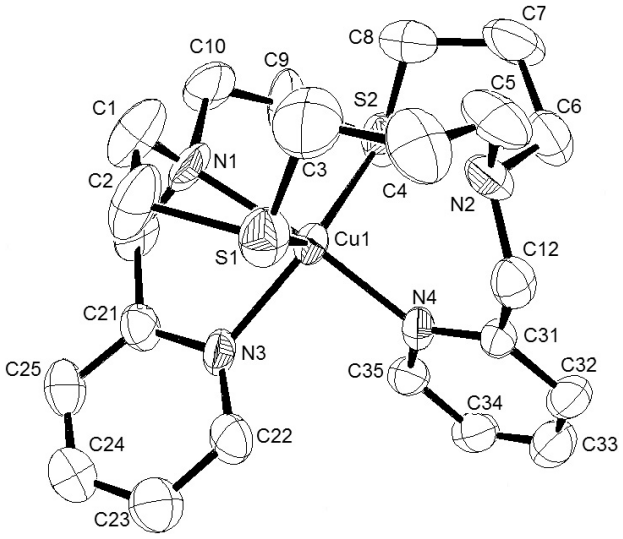


Table 3. ESR data for Cu(II) and Co(II) complexes (T = 77 K).

Complex	$g_\parallel$ ($A_\parallel$ in Gauss)	$g_\perp$
$[Cu(\mathbf{L_1})]^{2+}$	2.467 (115)	2.121
$[Cu(\mathbf{L_2})]^{2+}$	2.070[a]	
$[Cu(\mathbf{L_4})]^{2+}$	2.100[a]	
$[Cu(\mathbf{L_3})]^{2+}$	2.167 (125)	1.983
$[Cu(\mathbf{L_5})]^{2+}$	2.146 (170)	2.121[b]
$[Cu(\mathbf{L_6})]^{2+}$	2.162 (161)	2.121[b]
$[Co(\mathbf{L_2})]^{2+}$	2.020 (75)	2.290

Note: $\mathbf{L_3}$ = 1,7,dithia-4,11-diazacyclotetradecane, $\mathbf{L_5}$ = 1,4,dithia-8,11-diazacyclotetradecane, and $\mathbf{L_6}$ = 4,12-diaza-1,8-dithiacyclotetradecane.
[a] g_{iso} value shown.
[b] Reference 11.

© 2006 NRC Canada

Table 4. UV–vis spectra of metal complexes in acetonitrile.

Complex	Anion	λ_{max} (nm) (ε_{max}, (mol/L)$^{-1}$ cm^{-1})
$[Ni(\mathbf{L_1})]^{2+}$	PF_6^-	282 (1700), 373 (38), 578 (23), 900 (31)
$[Ni(\mathbf{L_2})]^{2+}$	PF_6^-	282 (4870), 556 (28), 820 (24)
$[Ni(\mathbf{L_6})]^{2+}$	ClO_4^-	375 (32), 585 (17), >800[a]
$[Ni(\mathbf{L_7})_2]^{2+}$[b]	ClO_4^-	297 (680), 524 (15), 840 (22)[c]
$[Cu(\mathbf{L_1})]^{2+}$[a]	PF_6^-	278 (2100), 368 (4500), 750 (430)
$[Cu(\mathbf{L_2})]^{2+}$	ClO_4^-	380 (5610), 704 (540), 871 (570)
$[Cu(\mathbf{L_4})]^{2+}$	ClO_4^-	356 (3020), 737 (390)
$[Co(\mathbf{L_2})(ClO_4)]^+$	ClO_4^-	261 (4410), 531 (32)
$[Co(\mathbf{L_2})(NO_3)_2(MeCN)$	—	500 (396), 800 (153)[b]

[a]Reference 11.
[b]Spectrum recorded in nitromethane.
[c]$\mathbf{L_7}$ = 7-aza-1,4-dithiacyclononane (26).

oms from $\mathbf{L_2}$ and perchlorate ion in a tetragonal elongated geometry. Since no hyperfine coupling from the nitrogen atoms was observed, the tertiary amine and pyridine moiety from the ligand are most likely coordinated in the equatorial plane of the distorted octahedron in a manner similar to the corresponding nickel(II) complex (Fig. 1). The eight hyperfine lines observed in the $g_\perp$ region arise from the interaction of the unpaired electron with the Co nucleus (^{59}Co, I = 7/2). For the complex $[Co(\mathbf{L_2})(NO_3)_2(CH_3CN)]$, no ESR signal was detected. Instead, a paramagnetic ^{1}H NMR spectrum spanning from –30 to +50 ppm was obtained, consistent with the persistence of the crystalline structure (Fig. S1)[3] in solution, although the paramagnetic spectrum was not amenable to further analysis.

UV–vis spectra

The UV–vis spectral data for various Ni(II), Cu(II), and Co(II) complexes studied in this work are presented in Table 4. The Ni(II) complexes exhibit typical octahedral geometry, with solvent coordinated axially. Molar extinction coefficients, ranging in the visible from 20 to 40 (mol/L)$^{-1}$ cm^{-1}, are very similar to the Ni(II) complex of 1,8-dithia-5,11-diazacyclotetradecane, a ligand isomer reported in the literature (12), and are typical of octahedral geometry with solvent participation in the axial sites. This is confirmed by the similarity with the six-coordinate $Ni(\mathbf{L_7})_2^{2+}$ ion ($\mathbf{L_7}$ = 7-aza-1,4-dithiacyclononane) (26).

The Cu(II) complexes are green in acetonitrile and their UV–vis spectra show absorptions bands in the regions 324–380 nm and 704–760 nm that are assigned as ligand-to-metal charge transfer (LMCT) and d–d transitions, respectively. However, the presence of axial donors apparently induces a difference in spectra from the planar N_2S_2 systems (12).

The spectra of the two Co(II) complexes of $\mathbf{L_2}$ show slightly different characteristics. Although both isomers have an absorption band around 500 nm, compound B has a slightly larger extinction coefficient. In addition, it has an additional absorption band at 800 nm. These observations can be rationalized by the different coordination environment at the cobalt centre in the two species. The ESR spectrum of B at 77 K is consistent with a Co(II) ion coordinated to all of the donor atoms in $\mathbf{L_2}$ with weak interaction with an axial perchlorate ion. For A (Fig. S1),[3] the nature of the primary coordination sphere is expected to produce a different ligand field at the metal centre.

Table 5. Electrochemical data.

Complex	E vs. Fc/Fc$^+$	ΔE (V)
Cu(II)/(I)		
$[Cu(\mathbf{L_2})]^{2+}$	$E_{1/2}$ = –0.024	0.077
$[Cu(\mathbf{L_4})]^{2+}$	$E_{1/2}$ = –0.137	0.086
$[Cu(\mathbf{L_5})]^{2+}$	$E_{1/2}$ = –0.045	0.150
Ni(II)/(I)		
$[Ni(\mathbf{L_2})]^{2+}$	$E_{1/2}$ = –1.18	a
$[Ni(\mathbf{L_4})]^{2+}$	$E_{1/2}$ = –1.23	0.14
$[Ni(\mathbf{L_1})]^{2+}$	$E_{1/2}$ = –1.29	a
Co(II)/(III)		
$[Co(\mathbf{L_2})]^{2+}$ (B)	$E_{1/2}$ = 0.18	0.23
$[Co(\mathbf{L_2})(NO_3)_2MeCN]$ (A)	$E_{1/2}$ = 1.71	b
	E_{red} = –1.83	a

Note: a = irreversible oxidation, b = irreversible reduction.

Electrochemistry

The redox chemistry of the Cu(II), Ni(II), and Co(II) complexes of $\mathbf{L_2}$–$\mathbf{L_4}$ was studied by cyclic voltammetry. The results are summarized in Table 5. For the Cu(II) complexes, the reduction to Cu(I) is, at best, quasi-reversible. It has been shown (28) that coordination geometry greatly influences redox potentials for these couples. Since Cu(II) complexes are generally tetragonal distorted and Cu(I) species prefer tetrahedral coordination, rearrangement of the structure of the complexes is required when Cu(II) is reduced to Cu(I). This process probably involves the "square scheme" discussed recently (10) that will contribute to the value of ΔE being greater than the theoretical value for a reversible one-electron reduction.

Both the cyclic voltammograms of $[Ni(\mathbf{L_2})]^{2+}$ and $[Ni(\mathbf{L_1})]^{2+}$ show irreversible reduction waves to Ni(I) at –1.18 and –1.29 V vs. Fc/Fc$^+$, respectively. However, for the complex $[Ni(\mathbf{L_4})]^{2+}$, a quasi-reversible reduction from Ni(II) to Ni(I) is observed at –1.23 V with peak potentials separated by 0.14 V. In this case, since the ligand can impose octahedral geometry on the metal centre, there is less reorganizational energy required for the electron transfer.

For the complex $[Co(\mathbf{L_2})(ClO_4)]^+$ (compound B), a quasi-reversible oxidation to Co(III) was observed at $E_{1/2}$ = 0.18 V vs. Fc/Fc$^+$. The peak to peak separation is 0.23 V. This Co(II)/Co(III) couple occurs at a more positive value relative

© 2006 NRC Canada

to other thioether complexes such as $[Co([9]aneS_3)]^{2+}$ (0.02 V vs. Fc/Fc^+) (29) and $[Co([10]aneS_3)_2]^{2+}$ (0.01 V vs. Fc/Fc^+) (30). A much more reversible situation is observed in preliminary observations of the reduction Co(II)/Co(I) of the hexacoordinate $Co(\mathbf{L_4})^{2+}$ ion ($E_{1/2}$ = –1.33 V, ΔE = 80 mV).

Conclusion

The preparation of mixed N,S-coordinating macrocycles has been achieved by reaction of thiols with either tosylated amines or the corresponding dibromides, where either can serve as the leaving groups in the formation of C—S bonds in the cyclization. Reductive detosylation, under mild conditions, results in satisfactory yields (ca. 70%). Complexes with pendant arms exhibit thermodynamic stabilities similar to their aza analogues. Interesting differences have been observed in the formation of cobalt(II) species dependent on the solvent used in the reaction. Although in the potentially hexacoordinating ligand with two pendant arms the S donors are exocyclic, in the copper(II) ion they are coordinated to the metal centre as are only three of the four other aza donors, confirming the preference for five-coordinate geometry at this metal centre. This observation contrasts with the corresponding Ni(II) complex where the octahedral ion permits possible access to Ni(I) and Ni(III) species.

Acknowledgements

One of us (BCMC) wishes to thank the University of Victoria and the Natural Sciences and Engineering Council of Canada (NSERC) for post-graduate awards. We thank Ms. K. Beveridge for the crystallographic analysis and the University of Victoria and NSERC for support.

References

1. G.A. Melson (*Editor*). Coordination chemistry of macrocyclic compounds. Plenum Press, New York. 1979.
2. L. Lindoy. The chemistry of macrocyclic ligand complexes. University Press, Cambridge, UK. 1989.
3. M. Zimmer. Coord. Chem. Rev. **212**, 133 (2001).
4. (*a*) E.K. Barefield, A. Bianchi, E.J. Billo, P.J. Connolly, P. Paoletti, J.S. Summers, and D.G. Van Derveer. Inorg. Chem. **25**, 4197 (1986); (*b*) V.J. Thöm, C.C. Fox, J.C.A. Boeyens, and R.D. Hancock. J. Am. Chem. Soc. **106**, 5947 (1984); (*c*) L.S. Sabatini and L. Fabbrizzi. Inorg. Chem. **18**, 438 (1979).
5. (*a*) S.R. Cooper and S.C. Rawle. Struct. Bonding (Berlin), **72**, 1 (1990); (*b*) S.R. Cooper. Acc. Chem. Res. **21**, 141 (1988).
6. A.J. Blake and M. Schröder. Adv. Inorg. Chem. **29**, 2830 (1990).
7. H.-J. Kruger and R.H. Holm. Inorg. Chem. **26**, 3467 (1986).
8. U. Kallert and R. Mattes. Inorg. Chim. Acta, **180**, 263 (1991).
9. D.St.C. Black and I.A. McLean. J. Chem. Soc. Chem. Commun. 1004 (1968); Tetrahedron Lett. **10**, 3961 (1969); Aust. J. Chem. **24**, 1401 (1971).
10. (*a*) B.C. Westerby, K.L. Juntunen, G.H. Leggett, V.B. Pett, M.J. Koenigbauer, M.D. Purgett, M.J. Taschner, L.A. Ochrymowycz, and D.B. Rorabacher. Inorg. Chem. **30**, 2109 (1991); (*b*) K. Krylova, C.P. Kulatilleke, M.J. Heeg, C.A. Salhi, L.A. Ochrymowycz, and D.B. Rorabacher. Inorg. Chem. **38**, 4322 (1999).
11. L. Siegfried and Th. Kaden. Helv. Chim Acta, **67**, 29 (1984).
12. M. Micheloni, P. Paoletti, L. Siegfried-Hertli, and Th. Kaden. J. Chem. Soc. Dalton Trans. 1169 (1985).
13. J.D. Chartres, A.M. Groth, L.F. Lindoy, and G.V. Meehan. J. Chem. Soc. Dalton Trans. 405 (2002).
14. (*a*) D.G. Fortier and A. McAuley. J. Am. Chem. Soc. **112**, 2640 (1990); (*b*) D.G. Fortier and A. McAuley. Inorg. Chem. **28**, 655 (1989); (*c*) K.A. Beveridge, A. McAuley, and C. Xu. Inorg. Chem. **30**, 2074 (1991).
15. A.I. Ingham, M. Rodopoulos, K.R. Coulter, T. Rodopoulos, S. Subramanian, and A. McAuley. Coord. Chem. Rev. **233–234**, 255 (2002).
16. T.M. Barclay, A. McAuley, and S. Subramanian. J. Chem. Soc. Chem. Commun. 170 (2002).
17. J. Costamagna, G Ferraudi, B. Matsuhiro, M. Campos-Vallette, J. Canala, M. Villagrán, J. Vargas, and M.J. Aguirre. Coord. Chem. Rev. **196**, 125 (2000).
18. B. Chak, A. McAuley, and T.W. Whitcombe. Inorg. Chim. Acta, **246**, 349 (1996).
19. P. Main, L. Lessinger, M.M. Woolfson, G. Germain, and J.P. Declarecq. MULTAN77 [computer program]. The University of York, Heslington, York, UK and Université cathollique de Louvain, Louvain-la-Neuve, Belgium. 1977.
20. G.M. Sheldrick. SHELX-76 [computer program]. University of Cambridge, Cambridge, UK. 1976.
21. J.A. Ibers and W.C. Hamilton (*Editors*). International tables for X-ray crystallography. Vol. IV. Kynoch Press, Birmingham, UK. 1974.
22. J.D. Swalen. *In* Computer programs for chemistry. Vol. 1. *Edited by* D.F. Detar. W.A. Benjamin Inc., New York. 1968.
23. P.L. Anelli, F. Montanari, and S. Quici. J. Org. Chem. **53**, 5291 (1988).
24. G.J. McDougall, R.D. Hancock, and J.C.A. Boeyens. J. Chem. Soc. Dalton Trans. 1438 (1978).
25. L. Fabbrizzi and D.M. Proserpio. J. Chem. Soc. Dalton Trans. 229 (1989).
26. A. McAuley and S. Subramanian. Inorg. Chem. **29**, 2830 (1990).
27. K. Nakamoto and P.J. McCarthy. Spectroscopy and structure of metal chelate compounds. John Wiley and Sons, New York. 1968.
28. E.A. Ambundo, M.-V. Deydier, A.J. Grall, N. Aguera-Vega, L.T. Dressel, T.H. Cooper, M.J. Heeg, L.A. Ochrymowycz, and D.B. Rorabacher. Inorg. Chem. **38**, 4233 (1999).
29. J.R. Hartman, E.J. Hintsa, and S.R. Cooper. J. Chem. Soc. Chem. Commun. 386 (1984).
30. S. Chandrasekhar and A. McAuley. Inorg. Chem. **31**, 480 (1992).

© 2006 NRC Canada

Copper tellurolate clusters in trimethylsilylated MCM-41 — Preparation and condensation[1]

Collin M. Kowalchuk, Harald Rösner, Dieter Fenske, Yining Huang, and John F. Corrigan

Abstract: The copper tellurolate cluster $[(Cu_6(TePh)_6(PEtPh_2)_5]$ (**1**) has been loaded into the pores of a trimethylsilylated MCM-41 (TMS–MCM-41) framework. Solutions of **1** in tetrahydrofuran lead to good impregnation weight % (~10 wt%, **1**). The resulting material was analysed by powder X-ray diffraction (PXRD), nitrogen sorption isotherms, thermogravimetric analysis (TGA), energy dispersive X-ray (EDX) analysis, ^{31}P CP MAS NMR spectroscopy, and transmission electron microscopy (TEM). It was observed that the loading process proceeds with the intact cluster **1** being present within the hexagonal architecture. The intact nature of **1** makes it an ideal candidate for condensation by photochemical or thermal means. Both of these condensation treatments increase the Cu:Te ratio of **1** to approach that observed in binary semiconductor Cu_2Te. The condensation process was analysed by GC–MS spectrometry and characterization of the condensed, isolated composites was performed by TGA, EDX analysis, ^{31}P CP MAS NMR spectroscopy, nitrogen adsorption, and TEM measurements. Thermal condensation results in the formation of Cu_2Te particles, whereas photochemical condensation yields larger copper-tellurolate nanoclusters.

Key words: copper, tellurium, cluster, MCM-41, trimethylsilylated, photolysis, thermolysis, Cu_2Te, composite, mesoporous material.

Résumé : L'agrégat de tellurolate de cuivre $[(Cu_6(TePh)_6(PEtPh_2)_5]$ (**1**) a été introduit dans les pores d'un squelette de MCM-41 triméthylsilylé (TMS–MCM-41). Des solutions du composé **1** dans le tétrahydrofurane conduisent à de bonnes imprégnations allant jusqu'à 10% de **1**, en poids. On a analysé le produit qui en est résulté par diffraction des rayons X par des poudres, par des isothermes de sorption d'azote, par analyse thermogravimétrique (ATG), par analyse de la dispersion d'énergie de rayons X (DEX), par spectroscopie RMN du ^{31}P, à l'angle magique de rotation avec polarisation croisée (RMN du ^{31}P « CP MAS ») et par la microscopie de transmission électronique (MTE). On a observé que le processus d'imprégnation se produit tout en maintenant l'agrégat **1** intact dans l'architecture hexagonale. La nature intacte du composé **1** en fait un candidat idéal pour des condensations par des méthodes photochimiques ou thermiques. Ces deux traitements de condensation augmentent le rapport Cu : Te du composé **1** pour lui permettre d'approcher celui observé dans le semiconducteur binaire Cu_2Te. On a analysé le processus de condensation par le biais de la spectroscopie de masse liée à la chromatographie gazeuse et on a procédé à une caractérisation des composites qui ont été isolés de la condensation par le biais de l'ATG, d'analyses de DEX, de RMN du ^{31}P CP MAS, d'adsorption d'azote et de mesures de MTE. La condensation thermique conduit à la formation de particules de Cu_2Te alors que la condensation photochimique conduit à des nano-agrégats plus gros de tellurolate de cuivre.

Mots clés : cuivre, tellure, agréagat, MCM-41, triméthylsilylé, photolyse, thermolyse, Cu_2Te, composite, matériel mésoporeux.

[Traduit par la Rédaction]

Introduction

A wide array of transition-metal–chalcogen nanoclusters has been prepared and characterized with diverse composition, size, and structure (1). Numerous routes to metal–chalcogenide particles have been described from the controlled decomposition of the appropriate metal–chalcogenolate precursor, although the reports detailing copper telluride nanocomposites with this method are relatively rare (2). Copper telluride (Cu_2Te) is a photoemmissive semiconductor with a band gap energy calculated to be 0.673 eV (3). Copper tellurolate clusters represent convenient "premixed"

Received 28 February 2005. Published on the NRC Research Press Web site at http://canjchem.nrc.ca on 1 March 2006.

C.M. Kowalchuk, Y. Huang,[2] and J.F. Corrigan.[3] Department of Chemistry, The University of Western Ontario, London, ON N6A 5B7, Canada.
H. Rösner and D. Fenske. Institut für Nanotechnologie, Forschungszentrum Karlsruhe GmbH, Hermann-von-Helmholtz-Platz 1, 76344 Eggenstein-Leopoldshafen, Germany.

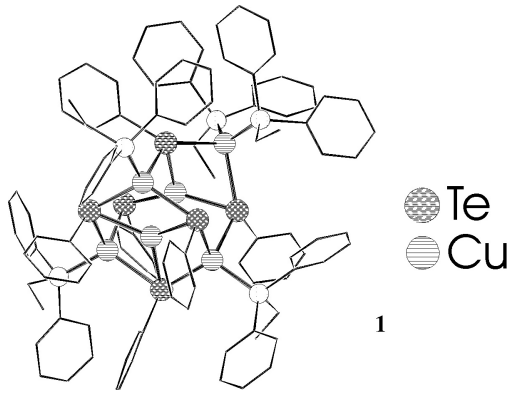
[1]This article is part of a Special Issue dedicated to Professor Arthur Carty.
[2]Corresponding author (e-mail: yhuang@uwo.ca).
[3]Corresponding author (e-mail: jfcorrig@uwo.ca).

 doi:10.1139/V05-221 © 2006 NRC Canada

single source precursors that exhibit ease of handling (4, 5) and represent facile, viable routes for the preparation of solid copper telluride. These Cu(TeR) precursors decompose via the established tellurolate–telluride decomposition pathway (eq. [1]) (6, 7).

[1] $Cu(TeR)_2 \xrightarrow{\Delta} CuTe + TeR_2$

$Cu_6(TePh)_6(PEtPh_2)_5$ (**1**) is a model cluster for the investigation of thermal decomposition reactions (4). It may be prepared in high yield (80%) from Cu(1) salts, it is stable for short durations under atmospheric conditions and exhibits good solubility in common organic solvents. The cluster **1** consists of a Cu_6Te_6 core, which is shielded by aryl and alkyl groups with a roughly spherical ~1.6 nm structure.



1

Similar metal–chalcogenolate species have been shown to produce nanometer-sized particles (8), accessed from molecular complexes via the thermal ejection of ER_2 from $M(ER)_2$ centers (E = S, Se, and Te) (4–6, 9). Cluster **1** also condenses via photolytic treatment to produce the layered structure, $[Cu_{50}(TePh)_{20}Te_{17}(PEtPh_2)_8]^{4-}$, formed via the ejection of $PEtPh_2$ and TeR_2 from the Cu(TeR) centers present in **1** (4). As cluster **1** may condense both thermally and photochemically, it represents an ideal model as a single source precursor to larger copper tellurium nanomaterials and the condensation of such a cluster in a size-restricted environment may allow for general control of particle size.

MCM-41 is a silicate material consisting of one-directional, nonintersecting channels arranged in a hexagonal fashion (10). The favourable framework architecture of mesoporous MCM-41 makes it an ideal host for the encapsulation and subsequent preparation of one-directional ordered nanomaterials, and this has allowed for particle sizes to be controlled within the mesopore, which may be varied between 2 and 10 nm. Diverse size-restricted nanocomposites have been generated within mesoporous materials from small molecular precursors (11), and preformed nanoparticles have also been deposited within the pore architecture of mesoporous materials (12, 13). It is known that solutions diffuse through mesoporous materials and that these frameworks may be utilized as separation media both for small contaminants (14) and large molecules, with demonstrated size exclusion properties of inorganic nanomaterials (12). A trimethylsilyl-modified mesoporous framework has been demonstrated to be effective for solution phase infiltration where larger impregnation wt% were absorbed into the organic/inorganic functionalized framework vs. the unmodified siliceous counterpart (15). We recently reported the loading of **1** into the pores of MCM-41 via a solid-state impregnation technique (16). This method is, however, rather specific for **1** and it proceeded with cluster modification through loss of the phosphine shell, although the copper tellurolate core was maintained. A more general and facile impregnation technique was targeted that would provide access to a wider array of metal–chalcogen nanoclusters. Herein, we present the full details of the solution impregnation of **1** into trimethylsilylated MCM-41 (TMS–MCM-41), which proceeds with the cluster integrity being maintained. This intact cluster was subsequently condensed by thermal and photochemical means to form larger copper tellurium composites.

Experimental section

General

All experimental manipulations were performed with standard Schlenk techniques under an inert nitrogen atmosphere. Prior to all combinations of TMS–MCM-41 with **1**, dehydration of the mesoporous framework was performed at 130 °C and 10^{-3} Torr (1 Torr = 133.3224 Pa) for 4 h.

Preparation of starting materials

MCM-41 was prepared according to the literature procedure under hydrothermal conditions and calcined at 540 °C to remove the surfactant (10). Trimethylsilylated MCM-41 (TMS–MCM-41) was synthesized according to the literature procedure (10), after 1.50 g of calcined MCM-41 was rehydrated for 6 days from atmospheric humidity. The cluster $Cu_6(TePh)_6(PPh_2Et)_5$ (**1**) was prepared according to the literature procedure (4).

Preparation of the mesoporous matrices

Matrix I was prepared from the combination of 25.00 mL of a 8.14×10^{-6} mol L^{-1} solution of **1** in tetrahydrofuran with 0.10 g of TMS–MCM-41 under stirring for 24 h. The mother liquor was removed via pipet and filtered to eliminate any residual I. UV–vis spectra were obtained on the filtered mother liquor and compared with the 8.14×10^{-6} mol L^{-1} stock solution. A higher concentration solution of **1** (1.9×10^{-2} mol L^{-1} of **1**) in THF was utilized to prepare matrix II. The solution of **1** was combined with 0.50 g TMS–MCM-41 and stirred for 3 days. Following an adequate settling process, removal of residual nonabsorbed **1**–THF solution was performed by pipet and treatment in vacuo for 1 h yielded the desolvated matrix II. Matrix II was a yellow microcrystalline powder.

Preparation of PPh_2Et–TMS–MCM-41 (III)

TMS–MCM-41 (0.08 g) was combined with 0.018 mL of $PEtPh_2$ and 2.0 mL of THF. The sample was stirred for 3 days at room temperature, followed by removal of the solvent by pipet and treatment in vacuo for 1 h.

Preparation of $Ph_2EtP{=}O$–TMS–MCM-41 (IV)

TMS–MCM-41 (0.10 g) was combined with 0.025 g of $Ph_2EtP{=}O$ and 5 mL of CH_2Cl_2. The mixture was stirred overnight and then the solvent was removed in vacuo and dried for 1 h.

© 2006 NRC Canada

Condensation reactions of II (1–TMS–MCM-41)

Photolysis of the **1**–TMS–MCM-41 matrix II was carried out on two different scales, both in the solid state. Firstly, 0.05 g (10.4 wt% of **1**) was combined with ~0.2 g dry KBr and photolysed in a diffuse reflectance cell fitted with a quartz window for 3.5 h; UV–vis-DR (diffuse reflectance) measurements were obtained at regular intervals. Matrix V was prepared from 0.20 g of II (11.4 wt% of **1**) in a slurry of hexanes, photolysed behind a Pyrex filter ($\lambda > 350$ nm) for 3 h. Excess hexane was subsequently removed via pipet and the sample dried in vacuo for 4 h. Isolated matrix V was an orange-brown microcrystalline powder. Condensed matrix VI was prepared by solvothermal treatment in heptane at reflux temperature (98 °C) on 0.20 g of II (11.4 wt% of **1**) for 3 h. After condensation treatment the mother liquor was removed from VI by pipet and the brown-black powder treated in vacuo for 24 h.

Instrumentation

Powder X-ray diffraction patterns were obtained on a Rigaku diffractometer with Co Kα radiation ($\lambda = 1.799\ 260$ Å). Nitrogen sorption data were obtained on a Micromeritics ASAP 2010 isotherm instrument. Prior to nitrogen adsorption measurements, the calcined MCM-41 and TMS–MCM-41 complexes were outgassed at room temperature (~25 °C) overnight (24 h) to eliminate any water from the sample introduced during sample transfer under atmospheric conditions. Adsorption/desorption measurements were performed at 77 K. The BET surface area, pore diameter, and the BJH pore volume were obtained using the Micromeritics ASAP V5.01 software. Thermogravimetric analyses were performed on a Mettler Toledo TGA/SDTA851^e analyzer. TGA measurements were carried out with a dynamic temperature program of 25–1000 °C with a heating rate of 10 °C/min. The ^{31}P cross polarization MAS spectra were obtained on a Varian/Chemagnetic Infinitypulse 400 wide bore spectrometer at the field strength of 9.4 T, with resonance frequencies of 399.491 and 161.719 MHz for ^{1}H and ^{31}P, respectively. A Varian/Chemagnetic 3.2 mm double-tuned MAS probe was used. The rotor frequency was 22 kHz. ^{31}P CP MAS NMR spectra were referenced to 85% H_3PO_4 using $(NH_4)H_2PO_4$ as a secondary reference. The Hartmann–Hahn condition was determined using $(NH_4)H_2PO_4$. The proton 90° pulse length was typically 2 μs with an optimized contact time of 2 ms. The variable amplitude CP (17) and two pulse phase modulated (TPPM) decoupling (18) methods were utilized. The proton recycle delay was 10 s. The samples for the TEM characterization were prepared by dropping a suspension of ethanol containing the samples onto carbon-coated copper grids. TEM investigations were performed in a Philips Tecnai F20 ST operated at 200 kV using an extraction voltage of 4.1 keV for the field emission gun. The point resolution of this microscope is about 0.235 nm at Scherzer focus and an information limit of about 0.14 nm was obtained. The TEM was equipped with an EDAX® energy-dispersive X-ray SiLi detector with a S-UTW (super-ultra-thin window). EDX analyses were carried out in the STEM (scanning transmission electron microscopy) mode using nanometre-sized probes (1 nm spot size for the presented EDX measurements). For this purpose, an extraction voltage of 4.5 keV was used. Use of a double tilt holder (Gatan) was made. High-resolution micrographs were taken with a 1K × 1K CCD camera and analysed with the software package Digital Micrographs (version 3.5.2, Gatan Company, Pleasanton, California) to perform Fourier transformations.

EDX analyses were also obtained on an EDAX® Phoenix model EDX system with light element detection capability coupled to a Hitachi S-4500 SEM. A 20 kV electron beam rastered over a 100 μm × 100 μm area was used to obtain semiquantitative analysis with the manufacturer's standardless software. UV–vis measurements were performed on a Varian Cary Bio 100 spectrometer with a scan rate of 600 nm/min and a sweep width from 700 to 200 nm. A Varian diffuse reflectance attachment was utilized for the UV–vis-DR studies.

Results and discussion

Solution UV–vis spectra of **1** display two absorption maxima at 278 and 350 nm (4). The high energy absorption at 278 nm is assigned to π–π* transitions of the aromatic rings, whereas the peak at 350 nm has been ascribed to ligand-to-metal charge transfer (LMCT) (4). This assignment is consistent with what has been observed for other copper–chalcogenolate complexes (19). Matrix I was prepared from the treatment of TMS–MCM-41 with an 8.14×10^{-6} mol L^{-1} solution of **1** in THF for 24 h. This treatment was deemed sufficient to allow loading within mesopores of cluster **1**. Figure 1 demonstrates that the intensity of the absorptions in the UV–vis spectra of the mother liquor after the preparation of the **1**–TMS–MCM-41 matrix (I) decreased (Fig. 1*b*) as compared with the initial stock solution (Fig. 1*a*). This concentration decrease of **1** in solution was measured from the absorption maxima at 260 nm to be ~45%. These data demonstrate that **1** is taken up from the solution when allowed to interact with TMS–MCM-41. When a similar UV–vis study was performed with silicalite-1 (a siliceous zeolite with a small pore) in place of TMS–MCM-41, no detectable decrease of intensity was observed in the UV–vis spectrum of the filtered mother liquor vs. the stock solution after identical treatment (not shown). TMS–MCM-41 and silicalite-1 have very similar external surfaces, but silicalite-1 has much smaller micropores (~5.1 Å), which are too small to allow penetration of **1** into the internal surface area. Therefore, we conclude that the majority of **1** must be restricted within the pores of the TMS–MCM-41 framework following the preparation of matrix I.

Thermogravimetric analysis of TMS–MCM-41 was performed to obtain a decomposition profile for the grafted trimethylsilyl organic groups (Fig. 2*a*). The framework is hydrophobic as demonstrated by the minimal quantity of water adsorbed from the atmosphere during transfer to the TGA (0.73 wt%). There is a much larger weight loss observed upon heating from 200 to 900 °C, which arises from the decomposition of grafted TMS groups (6.56 wt%). Chemisorbed water is also expected to be ejected over this temperature region, as TMS groups do not graft to these units (20). When TMS–MCM-41 is treated with a THF solution of **1** (1.9×10^{-2} mol L^{-1}, matrix II), the TGA curve of II (Fig. 2*b*) displays a marked change vs. that for TMS–MCM-41. A single, new decomposition is observed between 120 and 220 °C, which overlaps with the thermal decomposition

© 2006 NRC Canada

Fig. 1. UV–vis absorption spectra of the absorption of **1** in a **1**–THF solution into TMS–MCM-41: (*a*) 8.14×10^{-6} mol L^{-1} of **1** stock solution; (*b*) filtered mother liquor after the 1 day treatment of 0.10 g of TMS–MCM-41 with the 8.14×10^{-6} mol L^{-1} of **1** solution (I).

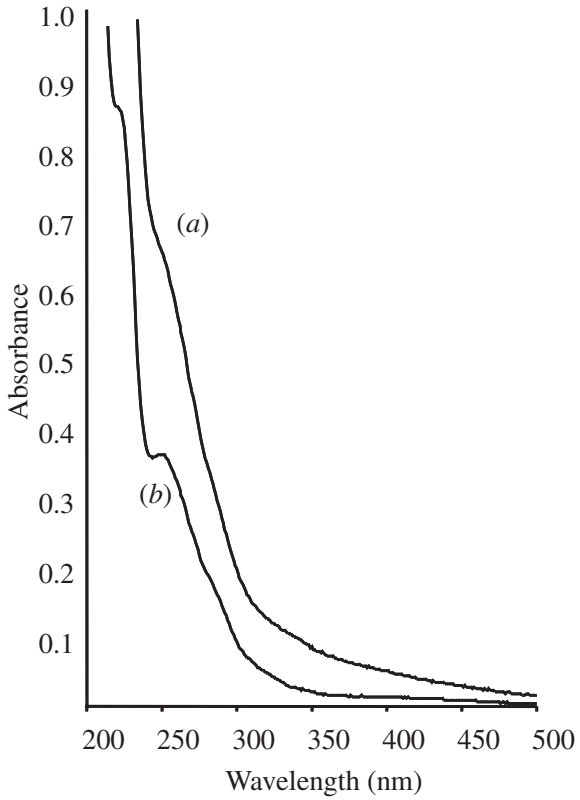
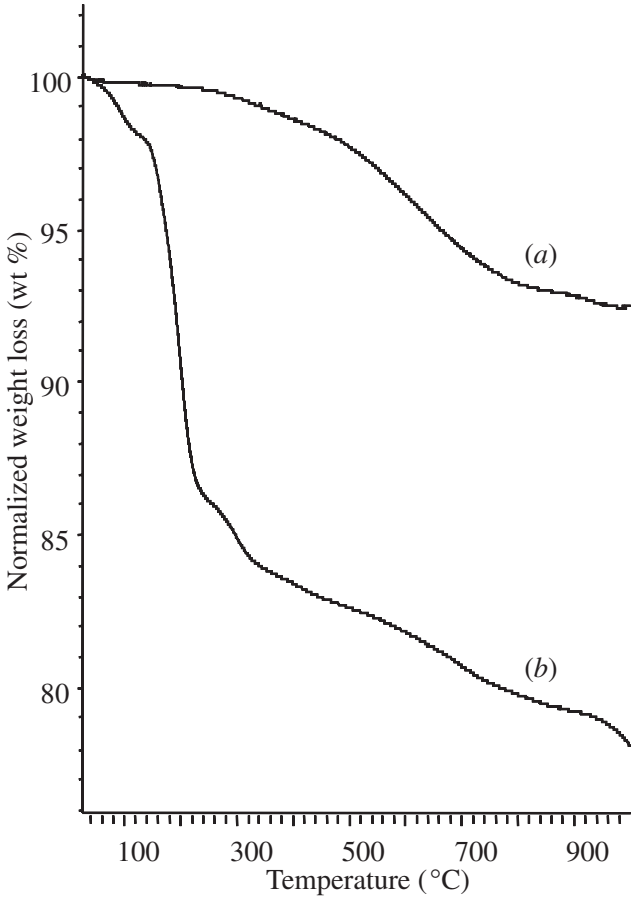


Fig. 2. Normalized TGA curves, 25–1000 °C, 10 °C/min heating rate: (*a*) TMS–MCM-41; (*b*) **1**–TMS–MCM-41 (II).



of crystalline **1** (not shown). This feature is consistent with the formation and ejection of $TePh_2$ and the elimination of $PEtPh_2$, as observed for crystalline **1** (16*c*). A calculated loading of 11.4 wt% of **1** associated with matrix II can be obtained from this decomposition. To verify that the decomposition of II arises from the presence of **1** and not an interaction of THF (the solvent utilized for loading) with TMS–MCM-41, THF was allowed to interact with TMS–MCM-41. The TGA of THF–TMS–MCM-41 displays a high temperature decomposition (see Supplemental information, Fig. S1),[4] which has previously been assigned to chemisorbed THF on dehydrated silica (21). Due to the greatly different temperatures at which weight loss occurs in II vs. THF–TMS–MCM-41, the decomposition displayed in Fig. 2*b* can be assigned to the presence of **1** within TMS–MCM-41 (II).

The individual atomic components that constitute cluster **1**, namely Cu, Te, P, and C, and the framework Si and O of II, were simultaneously probed by EDX analysis on 100 × 100 nm^2 areas (see Supplemental information, Fig. S2).[4] The relative wt% and atomic ratios obtained from the EDX provide a semiquantitative determination of the elements present. The relative atomic ratios are as expected, with a 1:2 ratio of Si:O and a ~1:~1:~1 ratio of Cu:Te:P, which remains close to the stoichiometry of pure cluster **1**. From this data, an approximate formula for II of $0.15Cu_6(TePh)_6(PEtPh_2)_5{:}38SiO_2$ is obtained. This is in agreement with the TGA data.

Powder X-ray diffraction (PXRD) is an effective technique to probe the microcrystalline one-dimensional ordered porous environment of MCM-41 and when electron dense materials such as **1** are present, provide evidence of occlusion (22). The PXRD pattern of TMS–MCM-41 (Fig. 3*a*) has the characteristic pattern of this framework with the reflections h_{100}, h_{110}, and h_{200} being observed (10). The presence of the higher ordered diffractions suggests a well-ordered architecture with long length pores. The PXRD pattern of II (Fig. 3*b*) exhibits identical diffractions albeit with decreased intensity. Since II does not have large quantities of occluded THF as determined by TGA, the intensity decrease is a result of contrast matching (22) because of the presence of **1** within the pores. The position of the d_{100} peak is similar for II and TMS–MCM-41, which translates into an identical $a_o d_{100}$ calculation ($a_o d_{100} = 2/3^{1/2} d_{100}$). Framework integrity

[4] Supplementary data for this article are available on the journal Web site (http://canjchem.nrc.ca) or may be purchased from the Depository of Unpublished Data, Document Delivery, CISTI, National Research Council Canada, Ottawa, ON K1A 0R6, Canada. DUD 4076. For more information on obtaining material refer to http://cisti-icist.nrc-cnrc.gc.ca/irm/unpub_e.shtml.

© 2006 NRC Canada

Fig. 3. PXRD patterns, 2°–18°2θ, normalized to the d_{100} diffraction of TMS–MCM-41: (*a*) TMS–MCM-41; (*b*) **1**–TMS–MCM-41 (II).

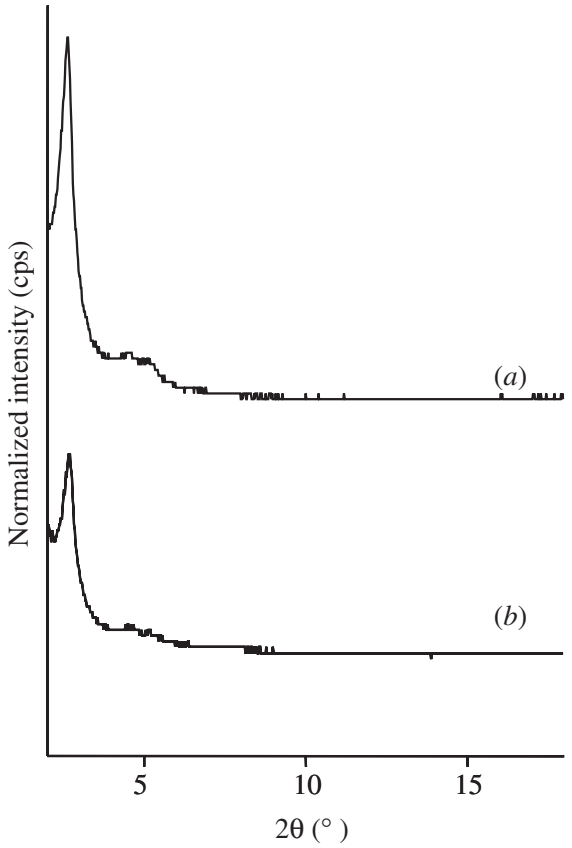
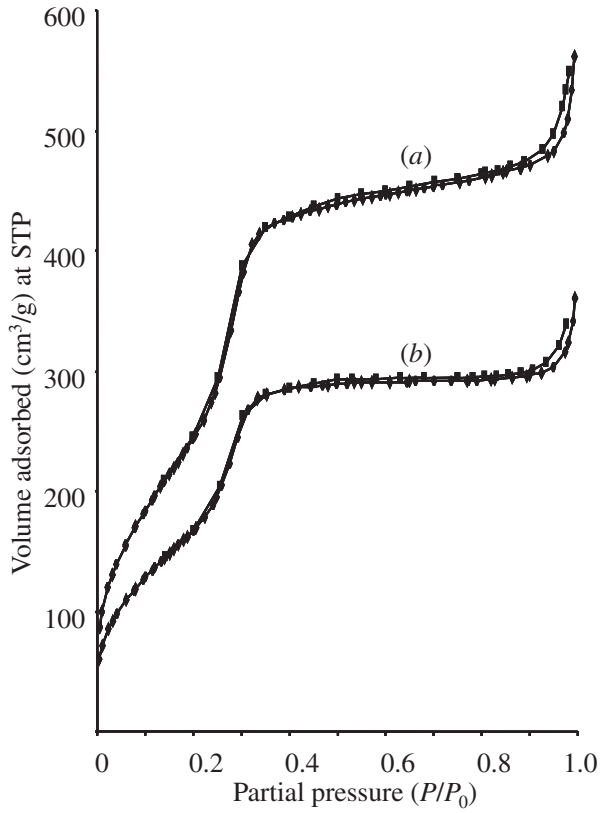


Fig. 4. Nitrogen adsorption/desorption isotherms at 77 K; samples subjected to outgassing prior to adsorption at 25 °C for 24 h: (*a*) TMS–MCM-41; (*b*) **1**–TMS–MCM-41 (II).



is therefore maintained. No reflections owing to **1** are present, suggesting that cluster **1** in the channels has no long-range ordering.

Nitrogen adsorption/desorption isotherms of II provide additional evidence for the occlusion of **1** within the pores of TMS–MCM-41. The N_2 isotherm of TMS–MCM-41 (Fig. 4*a*) is type IV with distinct capillary condensation and no hysteresis, characteristic of mesoporous M41s materials (23). The nitrogen adsorption isotherm of II (Fig. 4*b*) remains type IV and therefore is mesoporous, although II adsorbs a decreased volume of nitrogen vs. TMS–MCM-41. The structural parameters extracted from these two isotherms demonstrate that **1** is in fact occluded within the pores of TMS–MCM-41 for II. The BET surface area decreases from 746 m^2/g for TMS–MCM-41 to 498 m^2/g for II. Similarly, the BJH pore volume decreases by 0.19 cm^3/g for II vs. TMS–MCM-41.

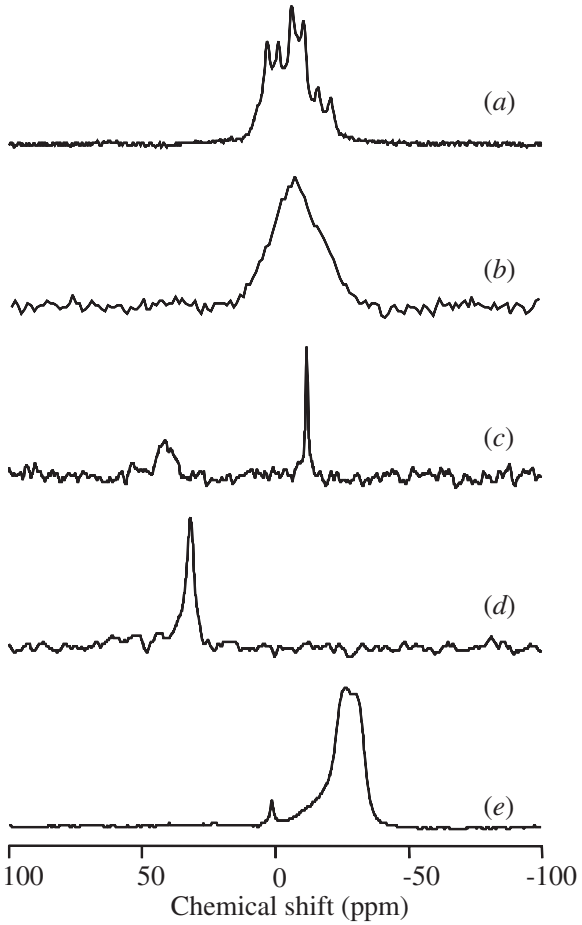
TEM images and the corresponding electron diffraction patterns (by fast Fourier transformation) of II parallel to the pores verify the previous analysis by PXRD and nitrogen adsorption that the hexagonal porous structured architecture is maintained during the impregnation of **1** (see Supplementary information, Fig. S3).[4] Expectedly, no occluded clusters are visible within the channel network nor is there any apparent electron-dense material on the TMS–MCM-41 surface. It was previously observed that the solid-state impregnation of **1** into MCM-41 proceeded with loss of the phosphine shell and formation of several surface phosphorus-containing species (16*c*). To probe the structural integrity of cluster **1** within TMS–MCM-41, a ^{31}P CP MAS NMR study was performed on II. The ^{31}P CP MAS spectrum of pure crystalline **1** (Fig. 5*a*) exhibits *J* coupling between ^{31}P and $^{63/65}Cu$ (I = 3/2). The observed coupling constants are 1–1.5 kHz, which are consistent with those reported in the literature (24). The ^{31}P CP MAS NMR spectrum displayed in Fig. 5*b* of II has an identical chemical shift as observed for the pure cluster, however without the ^{31}P–$^{63/65}Cu$ *J* coupling being resolved. A large FWHH (full width at half height, 3.2–3.4 kHz) for the peak centered at –8 ppm indicates cluster-coordinated phosphines with broad FWHH originating from orientational disorder in slightly different environments.

To verify that the ^{31}P NMR peak at –8 ppm for II arises from copper-bonded phosphine ligands, the phosphine-loaded samples $PEtPh_2$–TMS–MCM-41 (III) and $Ph_2EtP{=}O$–TMS–MCM-41 (IV) were prepared and analysed by ^{31}P CP MAS NMR spectroscopy (Figs. 5*c* and 5*d*, respectively). Spectra of III display a sharp peak at –11 ppm that results from physiosorbed phosphine within the framework (an identical solution shift in C_6D_6 is obtained, not shown), and demonstrates what feature would be present in the ^{31}P CP MAS NMR of II if $PEtPh_2$ was not coordinated to copper. The formation of $Ph_2EtP{=}O$ is not observed during the preparation of II, as the ^{31}P NMR spectra of IV displays a peak at +33 ppm, which is also not observed for II.

The occlusion of intact **1** within the pores of TMS–MCM-41 presents an opportunity to probe condensation reactions

© 2006 NRC Canada

Fig. 5. ^{31}P CP MAS NMR spectra, –150 to 150 ppm, referenced to H_3PO_4: (*a*) crystallites of cluster **1**; (*b*) **1**–TMS–MCM-41 (II); (*c*) $PEtPh_2$–TMS–MCM-41 (III); (*d*) $Ph_2EtP{=}O$–TMS–MCM-41 (IV); (*e*) II after photolysis for 3 h in a slurry of hexanes, internal standard of $H_2PO_4^-$ at δ +0.81 ppm.



of the cluster, to generate larger clusters or a copper telluride composite. It has been demonstrated that photochemical condensation of **1** in solution results in the generation of the larger condensed cluster, $[Cu_{50}(TePh)_{20}Te_{17}(PEtPh_2)_8][PEtPh_3]_4$, through ejection of $TePh_2$ and phosphine moieties and NMR spectra of the photolysis mixture also suggested that other CuTe clusters were present, but these species were not isolated (4). Controlled thermolysis of other metal–chalcogenolate complexes has also yielded nanometer-sized particles via the elimination of ER_2 from $M(ER)_2$ centers (E = S, Se, and Te) (6, 7, 9). Suspending II in hydrocarbon solvent allows for even treatment of the sample and elimination through solvent transport of condensation by-products out of the pores. Cluster **1** is insoluble in hydrocarbon solvents and is not likely to be leached out of the mesoporous host, whereas expected by-products from condensation reactions should be. Photolysis of II suspended in hexanes (Pyrex filter, λ > 350 nm) using a Hg lamp leads to a gradual darkening of the sample to yield V. Thermolysis was achieved by solvothermal treatment of II in heptane at reflux temperature (98 °C) to produce VI. A similar thermolysis procedure is commonly utilized to produce binary composites from metal–chalcogen coordination complexes (25).

A UV–vis-DR time-resolved experiment was performed on II (10.4 wt% of **1**), evenly distributed throughout a KBr matrix. It is observed that over 3 h of irradiation through a quartz window that II darkens in colour from an initial yellow to a dark brown, which is accompanied by a red shift of the band edge region as irradiation time increases (see Supplementary information, Fig. S4).[4] The effect that photolytic treatment of II has on the sample colour and the red shift observed by UV–vis-DR suggests that a condensation process does indeed occur. From V (photolysis of II (11.4 wt%) suspended in hexanes, 3 h), GC–MS spectra of the reaction solvent identified four distinct species: EtTePh, EtTeTePh, $TePh_2$, and $PEtPh_2$. GC–MS analysis of the reaction solvent of composite VI (thermolysis of II (11.4 wt%) suspended in heptane, 3 h) proved to proceed with the ejection of only $TePh_2$ and $PEtPh_2$. The effect of both thermal and photochemical condensation treatments on the unmodified TMS–MCM-41 host was examined. It was found that the TMS–MCM-41 framework is inert toward both photolysis and thermolysis under identical treatment as for the preparation of V and VI as determined via PXRD (not shown). Since no decrease in the intensity of the d_{100} peak occurred, it may be concluded that the solvent used for thermolysis experiments can be completely removed from TMS–MCM-41 by treatment in vacuo.

TGA of V and VI (not shown) indicated that for both condensed composites a single weight loss occurred over an identical temperature range as for II, but the magnitude of weight loss was 5.5 wt% for V (vs. 8.2 wt% in II) and 5.2 wt% for VI. Complete condensation of **1** would presumably result in the formation of Cu_2Te, however this does not occur and residual cluster/nanocluster fragments are likely present.

The deconvoluted atom % of P, Cu, and Te from composite V (photolysis) and VI (thermolysis) as obtained from EDX analysis are summarized in Table 1. The initial 1:1 ratio of Te:Cu within II is reduced by the condensation reactions. The ratio of Cu:Te after photolysis suggests that the Cu:Te stoichiometry in the final composite approaches the binary semiconductor Cu_2Te. Thermolysis of II produces an end product in which the Cu:Te is 2:1.

The phosphorus content retained within composites V and VI was probed with ^{31}P CP MAS NMR spectroscopy. The ^{31}P CP MAS NMR spectrum of V suggests very different phosphorus chemical environments of the photolysed product (Fig. 5*e*). The original peak for the cluster-coordinated phosphines (Fig. 5*b*) at –8 ppm is no longer present as only new peaks in the region of –30 ppm are observed. The broad nature of these peaks for V suggests that the phosphorus-31 nucleus may be bonded to copper in a disordered environment. As the photolysis of II leads to the formation of EtTePh and EtTeTePh, phoshido (μ-PPh_2) complexes may be present. Phosphido groups that bridge copper have been reported in the literature (25–28). Phosphorus-31 NMR spectra of these Cu_2(μ-PPh_2) coordination complexes are not commonly demonstrated because of their atmospheric instability and insolubility in common organic solvents (27), although recently a resonance of δ –25 ppm has been determined (28). Cu_2(μ-PPh_2) coordination complexes may also undergo

© 2006 NRC Canada

Table 1. Results from the EDX analysis for the photolysis of **1**–TMS–MCM-41 using a Pyrex filter in a slurry of hexanes to generate V and thermolysis in a slurry of heptane to generate VI.

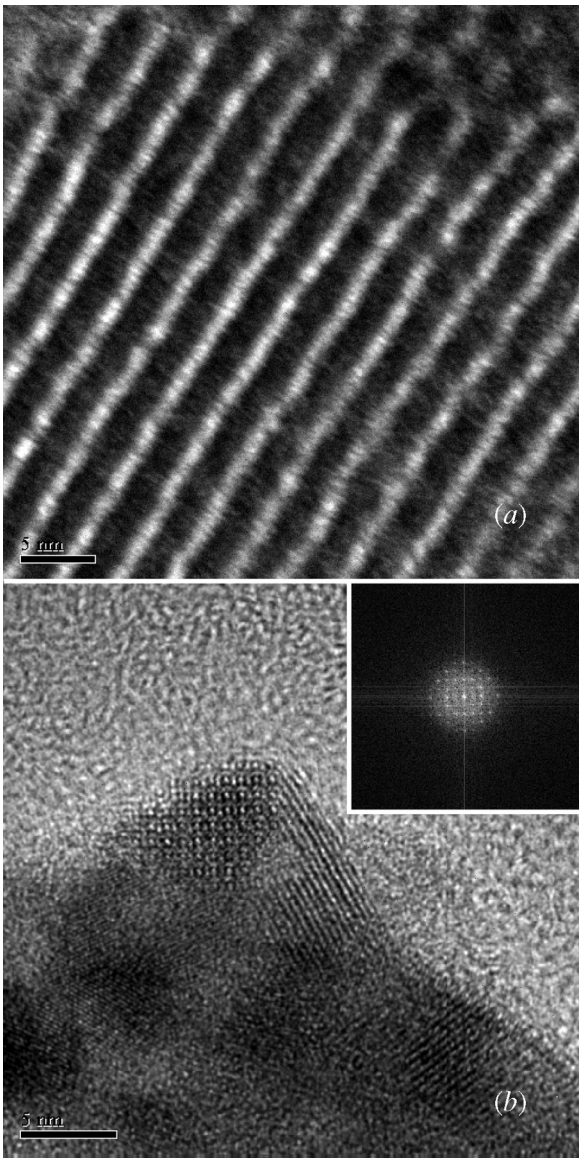
Compound	P (atom %)	Te (atom %)	Cu (atom %)	Cu:Te ratio
1–TMS–CM-41	1.58	1.70	1.87	1.1:1
Composite V (photolysis)	0.27	0.25	0.40	1.6:1
Composite VI (thermolysis)	0.35	0.28	0.55	2.0:1

chalcogen insertion reactions into the Cu—P bonds (26, 27); this is less likely however for tellurium. EDX analysis of composite VI also suggests some phosphorus is present, however no phosphorus-31 signals were observed in the ^{31}P CP MAS NMR spectrum.

Type IV isotherms are retained for V and VI, although a smaller quantity of nitrogen is adsorbed vs. II (not shown). BET surface areas of 498 m^2/g for II decrease to 421 and 384 m^2/g for composites V and VI, respectively. A similar trend is obtained for the pore volume assessment as it decreased from the initial 0.36 to 0.30 cm^3/g for composite V and 0.24 cm^3/g for composite VI.

HR-TEM images of V and VI were obtained in an attempt to directly observe the condensed metal–chalcogen material (Fig. 6). The TEM images for V demonstrate that the TMS–MCM-41 framework remains intact (Fig. 6*a*). There is no direct evidence of nanoparticles or nanowires within the pores. This is likely due to a poor electron density (better contrast) difference between photolysed **1** and the framework and small amounts present. The micrograph, however, illustrates that no noticeable leaching of the copper telluride composite has occurred from the pores. Leaching does appear to present a problem for the thermolysed sample, as illustrated in Fig. 6*b*. The HR-TEM image of VI demonstrates that thermal treatment results in the formation of particles outside of the porous framework. This electron-dense material has smaller spacing and different periodicity than that of TMS–MCM-41. From the electron diffraction pattern (by fast Fourier transformation), the material has two axes of equal length (Fig. 6*b*, inset) and a corresponding *d*-spacing value of 0.76 nm (29). The electron-dense material has a rodlike morphology. During the thermal condensation of cluster **1**, limited solubility in hot heptane likely results in partial leaching from the TMS–MCM-41 framework where it aggregates and condenses to form Cu_2Te particles. This condensed Cu_2Te particle, however, does not represent the majority of the sample as PXRD of this composite only exhibits peaks for the TMS–MCM-41 framework.

Fig. 6. HR-TEM analysis of the condensed composites (measurement bars displayed on the micrographs represent 5 nm): (*a*) V produced by photolysis of II; (*b*) VI produced by thermolysis of II. The inset is the electron diffraction pattern (by fast Fourier transformation) of the large piece of condensed material.



Conclusions

The preparation of occluded $Cu_6(TePh)_6(PEtPh_2)_5$ (**1**), which remains completely intact within the TMS–MCM-41, has been demonstrated. Subsequent condensation chemistry of **1** has been determined to be possible either by photochemical or thermal means, both of which reduce the Cu:Te ratio to approach the 2:1 observed for the binary semiconductor Cu_2Te. Photolysis and thermolysis proceeds with condensed material being present within the pores, although thermal condensation also resulted in limited leaching. Similar impregnation and condensation studies could potentially allow access to virtually any size-restricted metal–chalcogen material of interest through the utilization of other metal–chalcogenolate clusters.

Acknowledgements

We thank the Natural Sciences and Engineering Research Council of Canada (NSERC), the Canada Foundation for Innovation, and the Academic Development Fund (UWO) for

© 2006 NRC Canada

financial support. Dr. Chris W. Kirby (UWO) is thanked for his assistance with the MAS NMR spectra. CMK thanks the Ontario government for an OGSST scholarship and JFC thanks the Forschungszentrum Karlsruhe for a research fellowship. YH acknowledges funding from the Canada Research Chairs program.

References

1. For selected reviews, see: (*a*) I. Dance and K. Fisher. Prog. Inorg. Chem. **41**, 637 (1994); (*b*) D. Fenske. *In* Clusters and colloids, From theory to applications. *Edited by* G. Schmid. VCH, Weinheim. 1994. p. 217; (*c*) T. Saito. *In* Early transition metal clusters with π-donor ligands. *Edited by* M.H. Chisholm. VCH, New York. 1995. p. 63; (*d*) I.G. Dance. Polyhedron, **5**, 1037 (1986); (*e*) B. Krebs and G. Henkel. Angew. Chem. Int. Ed. Engl. **30**, 769 (1991); (*f*) A. Müller and E. Diemann. *In* Comprehensive coordination chemistry. Vol. 2. *Edited by* G. Wilkinson, R.D. Gillard, and J.A. McCleverty. Pergamon, Oxford. 1987. p. 515; (*g*) L.C. Roof and J.W. Kolis. Chem. Rev. **93**, 1037 (1993); (*h*) M.A. Ansari and J.A. Ibers. Coord. Chem. Rev. **100**, 223 (1990); (*i*) J. Arnold. Prog. Inorg. Chem. **43**, 353 (1995); (*j*) M.W. Degroot and J.F. Corrigan. *In* Comprehensive coordination chemistry II. Vol. 7. *Edited by* J.A. McCleverty and T.J. Meyer. 2004. p. 57.
2. (*a*) O. Palchik, R. Kerner, Z. Zhu, and A. Gedanken. J. Solid State Chem. **154**, 530 (2000); (*b*) Y. Zhang, Z.-P. Qiao, and X.-M. Chen. J. Mater. Chem. **12**, 2747 (2002); (*c*) K. Sridhar and K. Chattopadhyay. J. Alloys Compd. **264**, 293 (1998); (*d*) Y. Jiang, B. Xie, J. Wu, S. Yuan, Y. Wu, H. Huang, and Y. Qian. J. Solid State Chem. **167**, 28 (2002); (*e*) G. Henshaw, I.P. Parkin, and G.A. Shaw. J. Chem. Soc. Dalton Trans. 231 (1997); (*f*) J. Yang, S.-H. Yu, Z.-H. Han, Y.T. Qian, and Y.-H. Zhang. J. Solid State Chem. **387**–**389**, 387 (1999).
3. (*a*) S. Kashida, W. Shimosaka, M. Mori, and D. Yoshimura. J. Phys. Chem. Solids, **64**, 2357 (2003); (*b*) S.N. Mostafa, S.R. Selim, S.A. Soliman, and E.G. Gadalla. Electrochim. Acta, **38**, 1699 (1993).
4. J.F. Corrigan and D. Fenske. Angew. Chem. Int. Ed. Engl. **36**, 1981 (1997).
5. (*a*) D. Fenske and J.F. Corrigan. *In* Metal clusters in chemistry. Vol. 3. *Edited by* P. Braunstein, L.A. Oro, and P.R. Raithby. Wiley-VCH, Weinheim. 1999. p. 1302; (*b*) M.W. DeGroot, M.W. Cockburn, M.S. Workentin, and J.F. Corrigan. Inorg. Chem. **40**, 4678 (2001).
6. (*a*) J.G. Brennan, T. Siegrist, P.J. Carroll, S.M. Stuczynski, P. Reynders, L.E. Brus, and M.L. Steigerwald. Chem. Mater. **2**, 403 (1990); (*b*) V. Christou and J. Arnold. J. Am. Chem. Soc. **114**, 6240 (1992); (*c*) D.R. Cary and J. Arnold. J. Am. Chem. Soc. **115**, 2520 (1993); (*d*) A.L. Seligson and J. Arnold. J. Am. Chem. Soc. **115**, 8214 (1993); (*e*) D.R. Cary and J. Arnold. Inorg. Chem. **33**, 1791 (1994); (*f*) A.R. Strzelecki, C.L. Likar, B.A. Helsel, T. Utz, M. Lin, and P.A. Bianconi. Inorg. Chem. **33**, 5188 (1994); (*g*) M. Bochmann, G.C. Bwembya, A.K. Powell, and X. Song. Polyhedron, **14**, 3495 (1995).
7. (*a*) W. Piers, L.R. MacGillivray, and M. Zaworotko. Organometallics, **12**, 4723 (1993); (*b*) W.E. Piers, D.J. Parks, L.R. MacGillivray, and M.J. Zaworotko. Organometallics, **13**, 4547 (1994); (*c*) D.E. Gindelberger and J. Arnold. Organometallics, **13**, 4462 (1994); (*d*) L.K. Knight, W.E. Piers, and R. McDonald. Chem. Eur. J. **6**, 4322 (2000).
8. (*a*) S.L. Cumberland, K.M. Hanif, A. Javier, G.A. Khitrov, G.F. Strouse, S.M. Woessner, and C.S. Yun. Chem. Mater. **14**, 1576 (2002); (*b*) J.R. Babcock, R.W. Zehner, and L.R. Sita. Chem. Mater. **10**, 2027 (1998); (*c*) S.R. Bahr, P. Boudjouk, and G.J. McCarthy. Chem. Mater. **4**, 383 (1992); (*d*) Y.-W. Jun, C.-S. Choi, and J. Cheon. Chem. Commun. (Cambridge), 101 (2001).
9. (*a*) M.L. Steigerwald and C.R. Sprinkle. J. Am. Chem. Soc. **109**, 7200 (1987); (*b*) J.G. Brennan, T. Siegrist, P.J. Carroll, S.M. Stuczynski, L.E. Brus, and M.L. Steigerwald. J. Am. Chem. Soc. **111**, 4141 (1989); (*c*) M. Bochmann, K. Webb, M. Harman, and M.B. Hursthouse. Angew. Chem. Int. Ed. Engl. **29**, 638 (1990); (*d*) M.A. Malik and P.L. O'Brien. Chem. Mater. **3**, 999 (1991); (*e*) P. O'Brien and R. Nomura. J. Mater. Chem. **5**, 1761 (1995); (*f*) S.L. Stoll and A.R. Barron. Chem. Mater. **10**, 650 (1998); (*g*) M. Chunggaze, J. McAleese, P. O'Brien, and D.J. Otway. Chem. Commun. (Cambridge), 833 (1998); (*h*) M. Lazell, P. O'Brien, D.J. Otway, and J.-H. Park. J. Chem. Soc. Dalton Trans. 4479 (2000).
10. J.S. Beck, J.C. Vartuli, W.J. Roth, M.E. Leonowicz, C.T. Kresge, K.D. Schmitt, C.T.-W. Chu, D.H. Olson, E.W. Sheppard, S.B. McCullen, J.B. Higgins, and J.L. Schlenker. J. Am. Chem. Soc. **114**, 10834 (1992).
11. J.-L. Shi, Z.-L. Hua, and L.-X. Zhang. J. Mater. Chem. **14**, 795 (2004).
12. T. Hirai, H. Okubo, and I. Komasawa. J. Phys. Chem. B, **B103**, 4228 (1999).
13. (*a*) T. Hirai, H. Okubo, and I. Komasawa. J. Colloid Interface Sci. **235**, 358 (2001); (*b*) W.-S. Chae, J.-H. Ko, I.-W. Hwang, and Y.-R. Kim. Chem. Phys. Lett. **365**, 49 (2002); (*c*) T. Hirai, M. Nanba, and I. Komasawa. J. Colloid Interface Sci. **268**, 394 (2003); (*d*) J. Zhang, B. Han, Z. Hou, Z. Liu, J. He, and T. Jiang. Langmuir **19**, 7616 (2003); (*e*) D.S. Shephard, T. Maschmeyer, G. Sankar, J.M. Thomas, D. Ozkaya, B.F.G. Johnson, R. Raja, R.D. Oldroyd, and G.B. Bell. Chem. Eur. J. **4**, 1214 (1998); (*f*) W. Zhou, J.M. Thomas, D.S. Shephard, B.F.G. Johnson, D. Ozkaya, T. Maschmeyer, R.G. Bell, and Q. Ge. Science (Washington, D.C.), **280**, 705 (1998); (*g*) S. Hermans, S. Sadasivan, C.M.G. Judkins, B.F.G. Johnson, S. Mann, and D. Kushalani. Adv. Mater. **15**, 1853 (2003); (*h*) J. Zhang, B. Han, Z. Hou, Z. Liu, J. He, and T. Jiang. Langmuir, **19**, 7616 (2003).
14. (*a*) X. Feng, G.E. Fryxell, L.-Q. Wang, A.Y. Kim, J. Liu, and K.M. Kemner. Science (Washington, D.C.), **276**, 923 (1997); (*b*) J. Liu, X. Feng, G.E. Fryxell, L.-Q. Wang, A.Y. Kim, and M. Gong. Adv. Mater. **10**, 161 (1998); (*c*) A.M. Liu, K. Hidajat, S. Kawi, and D.Y. Zhao. Chem. Commun. (Cambridge), 1145 (2000); (*d*) B. Lee, Y. Kim, H. Lee, and J. Yi. Microporous Mesoporous Mater. **50**, 77 (2001); (*e*) R.I. Nooney, M. Kalyanaraman, G. Kennedy, and E.J. Maginn. Langmuir, **17**, 528 (2001).
15. (*a*) L. Washmon-Kriel, V.L. Jimenez, and K.J. Balkus. J. Mol. Catal. B: Enzym. **10**, 453 (2000); (*b*) J.M. Kisler, G.W. Stevens, and A.J. O'Conner. Mater. Phys. Mech. **4**, 89 (2001).
16. (*a*) C. Kowalchuk, Y. Huang, and J.F. Corrigan. Chem. Commun. (Cambridge), 1811 (2000); (*b*) C.M. Kowalchuk, Y. Huang, and J.F. Corrigan. Stud. Surf. Sci. Catal. **129**, 303 (2000); (*c*) C.M. Kowalchuk, G. Schmid, W. Meyer-Zaika, Y. Huang, and J.F. Corrigan. Inorg. Chem. **43**, 173 (2004).
17. O.B. Peerson, X. Wu, I. Kustanovich, and S.O. Smith. J. Magn. Reson. Ser. A, **104**, 334 (1993).
18. A.E. Bennett, C.M. Rienstra, M. Auger, K.V. Lakshme, and R.G. Griffen. J. Chem. Phys. **103**, 6951 (1995).
19. (*a*) V.W.-W. Yam and K.K.-W. Lo. Chem. Soc. Rev. **28**, 323 (1999); (*b*) V.W.-W. Yam, C.-H. Lam, W.K.-M. Fung, and K.-K. Cheung. Inorg. Chem. **40**, 3435 (2001); (*c*) V.W.-W. Yam,

© 2006 NRC Canada

C.-H. Lam, and K.-K. Cheung. Chem. Commun. (Cambridge), 545 (2001).
20. D.J. Macquarrie, D.B. Jackson, J.E.G. Mdoe, and J.H. Clark. New J. Chem. **23**, 539 (1999).
21. R.E. Day, A.V. Kiselev, B.V. Kuznetsov, and Y.S. Nikitin. Kinet. Catal. **10**, 529 (1969).
22. B. Marler, U. Oberhangemann, S. Vortmann, and H. Gies. Microporous Mater. **6**, 375 (1996).
23. (*a*) P.J. Branton, P.G. Hall, and K.S. Sing. J. Chem. Soc. Chem. Commun. 1257 (1993); (*b*) K.S.W. Sing, D.H. Everett, R.A.W. Haul, L. Moscou, R.A. Pierotti, J. Rouquérol, and T. Siemieniewska. Pure Appl. Chem. **57**, 603 (1985).
24. (*a*) A. Olivieri. J. Am. Chem. Soc. **114**, 5758 (1992); (*b*) A.C. Kolbert, H.J.M. de Groot, D. van der Putten, H.B. Brom, L.J. de Jongh, G. Schmid, H. Krautscheid, and D. Fenske. Z. Phys. D, **26**, 24 (1993); (*c*) S. Kroeker, J.V. Hanna, R.E. Wasylishen, E.W. Ainscough, and A.M. Brodie. J. Magn. Reson. **135**, 208 (1998).
25. J. Li, Z. Chen, R.-J. Wang, and D.M. Proserpio. Coord. Chem. Rev. **190–192**, 707 (1999).
26. T.A. Annan, R. Kumar, and D.G. Tuck. J. Chem. Soc. Chem. Commun. 446 (1988).
27. T.A. Annan, R. Kumar, and D.G. Tuck. J. Chem. Soc. Dalton. Trans. 11 (1991).
28. C. Meyer, H. Grützmacher, and H. Pritzkow. Angew. Chem. Int. Ed. Engl. **36**, 2471 (1997).
29. N. Vouroutzis, N. Frangis, and C. Manolikas. Phys. Status Solidi, **202**, 271 (2005).

© 2006 NRC Canada

Preparation of hydrido(vinyl)iridium(III) complexes from functionalized olefins by C—H activation[1]

Bernd Papenfuhs, Thomas Dirnberger, and Helmut Werner

Abstract: The four-coordinate iridium(I) precursor *trans*-[IrCl(N_2)(PPh_3)$_2$] (**1**) reacts with functionalized olefins RCH=C(R′)C(O)R″ by displacement of the dinitrogen ligand and oxidative addition of the C—H bond to the metal center to give six-coordinate hydrido(vinyl)iridium(III) complexes [IrH(Cl){κ^2(*C*,*O*)-C(R)=C(R′)C(R″)=O}(PPh_3)$_2$] (**2**–**12**) in good to excellent yields. The reaction of [IrH(Cl){κ^2(*C*,*O*)-CH=CHC(Me)=O}(PPh_3)$_2$] (**2**) with $AgClO_4$ affords the cationic compound [IrH{κ^2(*C*,*O*)-CH=CHC(Me)=O}(PPh_3)$_2$]ClO_4 (**15**), which in solution equilibrates with the uncharged isomers [IrH($OClO_3$){κ^2(*C*,*O*)-CH=CHC(Me)=O}(PPh_3)$_2$] (**15a** and **15b**). In contrast, five-coordinate [IrH{κ^2-(*C*,*O*)-CH=CHC(Et)=O}(PPh_3)$_2$]ClO_4 (**16**), prepared from **3** and $AgClO_4$, is stable and undergoes addition reactions with CO, PPh_3, C_2H_4, $CH_3C{\equiv}CH$, MeCN, and PhCN to give the six-coordinate complexes [IrH(L){κ^2(*C*,*O*)-CH=CHC-(Et)=O}(PPh_3)$_2$]ClO_4 (**17**–**22**). The neutral hydrido(thiolato) compound [IrH(SPh){κ^2(*C*,*O*)-CH=CHC(Et)=O}(PPh_3)$_2$] (**23**) was obtained on treatment of **21** with NaSPh.

Key words: iridium, C—H activation, hydrido complexes, vinyl complexes, phosphine complexes.

Résumé : Le précurseur tétracoordiné de l'iridium(I), *trans*-[IrCl(N_2)(PPh_3)$_2$] (**1**), réagit avec les oléfines fonctionnalisées RCH=C(R′)C(O)R″ par déplacement du ligand diazote et par addition oxydante de la liaison C—H du centre métallique pour conduire à la formation des complexes hexacoordinés hydrido(vinyl)iridium(III) [IrH(Cl){κ^2(*C*,*O*)-C(R)=C(R′)C(R″)=O}(PPh_3)$_2$] (**2**–**12**) avec de bons rendements. La réaction du [IrH(Cl){κ^2(*C*,*O*)-CH=CHC(Me)=O}(PPh_3)$_2$] (**2**) avec du $AgClO_4$ conduit à la formation du composés cationique [IrH{κ^2(*C*,*O*)-CH=CHC(Me)=O}(PPh_3)$_2$]ClO_4 (**15**) qui s'équilibre en solution avec formation des isomères non chargés [IrH($OClO_3$){κ^2(*C*,*O*)-CH=CHC(Me)=O}(PPh_3)$_2$] (**15a** and **15b**). Par opposition, le composé pentacoordiné [IrH{κ^2(*C*,*O*)-CH=CHC(Et)=O}(PPh_3)$_2$]ClO_4 (**16**) qui a été préparé à partir du composé **3** et de $AgClO_4$ est stable et il donne des réactions d'additions avec le CO, le PPh_3, le C_2H_4, le $CH_3C{\equiv}CH$, le MeCn et le PhCN pour conduire à la formation de complexes hexacoordinés [IrH(L){κ^2(*C*,*O*)-CH=CHC(Et)=O}(PPh_3)$_2$]ClO_4 (**17**–**22**). Le traitement du composé **21** avec du NaSPh conduit à la formation du composé neutre [IrH(SPh){κ^2(*C*,*O*)-CH=CHC(Et)=O}(PPh_3)$_2$] (**23**).

Mots clés : iridium, activation de C—H, complexes hydrido, complexes de vinyle, complexes de phosphine.

[Traduit par la Rédaction]

Introduction

As part of our investigations on the reactivity of low-valent iridium complexes containing alkenes and alkynes as ligands, we reported (1) that upon low-temperature UV irradiation in toluene the four-coordinate ethene derivative *trans*-[IrCl(C_2H_4)(P-*i*-Pr_3)$_2$] partly rearranges to the five-coordinate hydrido(vinyl) isomer [IrH(Cl)($CH{=}CH_2$)(P-*i*-Pr_3)$_2$]. This compound is thermodynamically unstable and on warming to room temperature reconverts to the starting material. If, however, instead of the ethene complex *trans*-[IrCl(C_2H_4)(P-*i*-Pr_3)$_2$] the related methyl acrylate and dimethyl fumarate derivatives *trans*-[IrCl($CH_2{=}CHCO_2Me$)(P-*i*-Pr_3)$_2$] and *trans*-[IrCl{(*E*)-$CH(CO_2Me){=}CH(CO_2Me)$}(P-*i*-Pr_3)$_2$] are used as the precursors, UV irradiation in benzene leads to a quantitative conversion to the six-coordinate isomers [IrH(Cl){κ^2(*C*,*O*)-C(R)=CH(OMe)=O}(P-*i*-Pr_3)$_2$] in which the hydrido(vinyl)iridium moiety is stabilized by an additional linkage of one C=O group to the metal center (2).

The present paper describes a synthetic protocol for a series of neutral and cationic hydrido(vinyl)iridium(III) complexes with Ir(PPh_3)$_2$ as a building block in which the substituted vinyl group also behaves as a bidentate ligand. Due to this coordination mode, the order of thermodynamic stability [Ir](H)(CH=CHR) < [Ir](η^2-CH_2=CHR), found by Bergman (3) and Perutz (4) and their co-workers for [Ir] = (η^5-C_5Me_5)Ir(PMe_3) and (η^5-C_5H_5)Ir(C_2H_4), is reversed and the hydrido(vinyl) compounds can be isolated as stable enti-

Received 16 June 2005. Published on the NRC Research Press Web site at http://canjchem.nrc.ca on 28 February 2006.

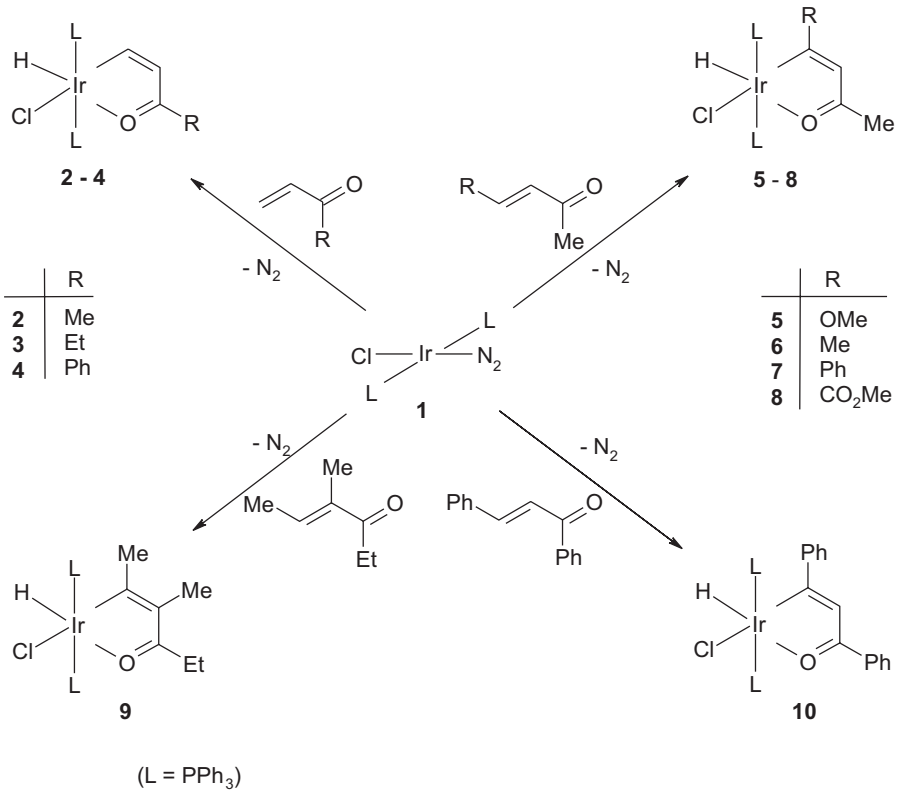
This paper is dedicated to Professor Arthur J. Carty, in recognition of his manifold and important contributions to organometallic chemistry.

H. Werner,[2] B. Papenfuhs, and T. Dirnberger. Institut für Anorganische Chemie der Universität, Am Hubland, D-97074 Würzburg, Germany.

[1]This article is part of a Special Issue dedicated to Professor Arthur Carty.
[2]Corresponding author (e-mail: helmut.werner@mail.uni-wuerzburg.de).

 doi:10.1139/V05-234 © 2006 NRC Canada

Scheme 1.



ties. Some preliminary results related to this study have already been communicated (5).

Results and discussion

The dinitrogen complex *trans*-[IrCl(N_2)(PPh_3)$_2$] (**1**), prepared by Collman and Kang (6) from *trans*-[IrCl(CO)(PPh_3)$_2$] and benzoyl azide, reacts in benzene with the Michael acceptors CH_2=CHC(O)R (R = Me, Et, Ph) to give the six-coordinate hydrido(vinyl)iridium(III) compounds **2**–**4** in about 80%–90% yield (Scheme 1). Although the displacement of the dinitrogen ligand proceeds slowly at room temperature, attempts to detect the olefin species *trans*-[IrCl{η^2-CH_2=CHC(R)=O}(PPh_3)$_2$], supposed to be generated in one of the initial steps of the reaction, by NMR spectroscopy failed. Nevertheless, we assume that these compounds are formed as intermediates but presumably are short-lived and react by intramolecular C—H activation to give the thermodynamically more stable products. In this context we note that recently Esteruelas, Oro, and co-workers (7) reported the preparation of the four-coordinate iridium(I) complex [Ir(κ^2-acac){η^2-CH_2=CHC(O)Me}(PCy_3)] from [Ir(κ^2-acac)(C_8H_{14})(PCy_3)] and methyl(vinyl) ketone, which is stable and upon heating rearranges to a mixture of two six-coordinate hydrido(vinyl)iridium(III) stereoisomers.

The hydrido(vinyl) complexes **2**–**4** are yellow or orange solids, which are not air-sensitive and readily soluble in common polar organic solvents. A characteristic feature in the IR spectra of **2**–**4** is the ν(C=O) stretching mode at 1525–1550 cm^{-1}, which is shifted by ca. 120–150 cm^{-1} to lower wavenumbers compared with the free ketones. Since this shift is consistent with a coordination of the carbonyl group to the metal center, an octahedral geometry for compounds **2**–**4** (as shown in Scheme 1) can be assumed. The ^{1}H NMR spectra of **2**–**4** display two doublets at about δ 9.60 and 6.20 (for **2** and **3**) and δ 9.97 and 6.86 (for **4**), which in agreement with results by Nesmeyanov et al. (8) and one of us (9) are assigned to the vinylic protons in α and β positions. For the hydrido ligand, there appears in the high-field region a triplet resonance at, respectively, δ –22.42 (for **2**), –22.55 (for **3**), and –21.88 (for **4**), which is split into a triplet owing to ^{1}H–^{31}P coupling. Since the chemical shift of these signals is quite similar to that of the bis(triisopropylphosphine) complex [IrH(Cl){κ^2(*C*,*O*)-$C(CO_2Me)$=CHC(OMe)=O}(P-*i*-Pr_3)$_2$], which has been characterized crystallographically (10), we assume that the hydrido ligand is trans to the oxygen and not to the carbon atom of the chelate ring. The observation of only one signal in the ^{31}P NMR spectra of **2**–**4** confirms that the phosphine ligands are trans disposed. The ^{13}C NMR spectrum of **2** displays the signals for the vinyl carbon atoms at δ 197.3 and 133.1 ppm. Due to the cis disposition of the α-C atom and the PPh_3 groups, the signal at δ 197.3 ppm is split into a triplet, while the resonance at δ 133.1 ppm appears as a singlet.

The starting material **1** not only reacts with the ketones CH_2=CHC(O)R (R = Me, Et, Ph), but also with the related derivatives RCH=CHC(O)Me (R = OMe, Me, Ph, CO_2Me), MeCH=C(Me)C(O)Et, and PhCH=CHC(O)Ph to give the corresponding hydrido(vinyl)iridium(III) complexes **5**–**10** in good to excellent yields. These reactions are considerably slower than those leading to **2**–**4**, and thus the corresponding reaction mixture has to be stirred for 18 h at 80 °C in toluene. In contrast to the conditions employed to obtain **2**–**7**, for the preparation of **8**–**10** an excess of the olefinic sub-

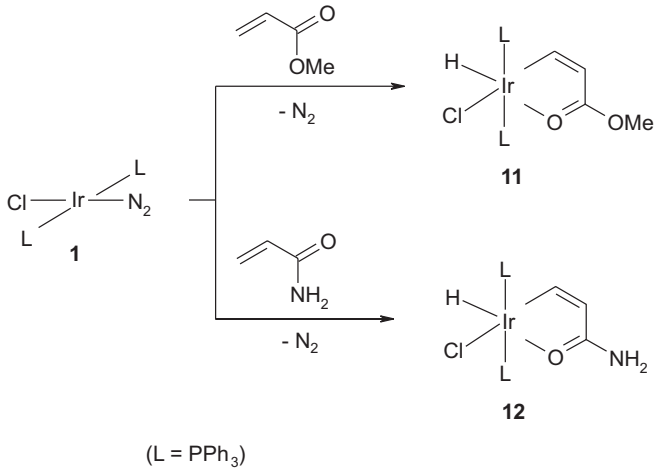
© 2006 NRC Canada

strate has to be used. If the dinitrogen complex **1** was treated with an equimolar amount of MeCH=C(Me)C(O)Et, the carbonyl iridium(I) compound *trans*-[IrCl(CO)(PPh_3)$_2$] (11) is generated as the dominant product. With regard to the formation of **8** from **1** and MeC(O)CH=$CHCO_2$Me, the remarkable feature is that the oxidative addition of the C—H bond adjacent to the CO_2Me functionality occurs exclusively. Moreover, it is worth mentioning that upon treatment of **1** with PhCH=CHC(O)Ph only the activation of the olefinic C—H and not that of an aromatic C—H bond is observed. The reactivity of **1** is thus different to that of the bis(triisopropylphosphine)iridium(I) derivative *trans*-[IrCl(C_8H_{14})(P-*i*-Pr_3)$_2$], which reacts with PhCH=CHC(O)Ph to give a 1:1 mixture of the two isomers [IrH(Cl){κ^2(*C*,*O*)-C(Ph)=CHC(Ph)=O}(P-*i*-Pr_3)$_2$] and [IrH(Cl){κ^2(*C*,*O*)-C_6H_4C(CH=CHPh)=O}(P-*i*-Pr_3)$_2$] (12). The ^{13}C NMR spectrum of **10** displays a triplet resonance at δ 215.0 (with ^2J(PC) = 6.1 Hz), which appears at a similar chemical shift (δ 209.4, ^2J(PC) = 5.3 Hz) as that of [IrH(Cl){κ^2(*C*,*O*)-C(Ph)=CHC(Ph)=O}(P-*i*-Pr_3)$_2$] (12) and thus supports the proposed structure.

Similarly to the Michael acceptors used for the preparation of **2**–**10**, methyl acrylate and acrylic acidamide also react with the dinitrogen compound **1** to afford the air-stable hydrido(vinyl) complexes **11** and **12** in 66% and 89% yield, respectively (Scheme 2). The IR spectrum of **12** shows the band for the ν(C=O) stretching mode at 1555 cm^{-1}, which is at nearly the same position as for **2** and **3**. In the ^{1}H NMR spectra of **11** and **12**, the hydride resonance appears at δ –25.07 (**11**) and δ –24.19 (**12**) and is significantly shifted upfield compared with **2**–**10**. We assume that this shift is due to the stronger electron-donating effect of the OMe and NH_2 functionalities compared with that of the alkyl and phenyl groups. The reaction of **1** with acrylonitrile does not lead to a stable iridium(I) or iridium(III) complex, but yields a pale yellow solid, which, according to the IR spectrum, presumably is a polymer with terminal CH_2CN and $CH(CH_3)CN$ groups (13).

To obtain a coordinatively unsaturated hydrido(vinyl)iridium(III) compound, considered to be a potential precursor for addition/insertion reactions, we attempted to eliminate the chloro ligand from **2** by using $AgPF_6$ and $AgClO_4$, respectively. The reaction of **2** with $AgPF_6$ in dichloromethane is quite rapid at room temperature and yields, after separation of AgCl and chromatographic workup of the solution, a brownish solid that owing to the ^{1}H and ^{31}P NMR spectra consists mainly (ca. 90%) of the expected compound [IrH{κ^2(*C*,*O*)-CH=CHC(Me)=O}(PPh_3)$_2$]PF_6 (**13**). Attempts to separate the by-products by fractional crystallization or repeated column chromatography failed. Typical spectroscopic data of **13** are the ^{1}H NMR resonances for the vinylic protons at δ 9.73 and 6.02 (see **2**: δ 9.58 and 6.18), the hydride signal at δ –21.38 (see **2**: δ –22.42), and the singlet in the ^{31}P NMR spectrum at δ 21.7 (see **2**: δ 14.7). Treatment of **2** with $AgPF_6$ in the presence of CO gave the cationic six-coordinate hydrido(vinyl)iridium(III) carbonyl **14** (Scheme 3) for which a correct elemental analysis was obtained. The IR spectrum of **14** (being an off-white, air-stable solid) displays a strong band for the CO ligand at 2060 cm^{-1} and a medium-to-strong absorption for the ν(C=O) stretching mode at 1580 cm^{-1}. The latter is shifted by 30 cm^{-1} to higher

Scheme 2.



wavenumbers compared with the coordinatively unsaturated compound **13**. The hydride signal appears in the ^{1}H NMR spectrum of **14** at δ –19.09 and is thus shifted by ca. 2.3 ppm to lower fields compared with **13**.

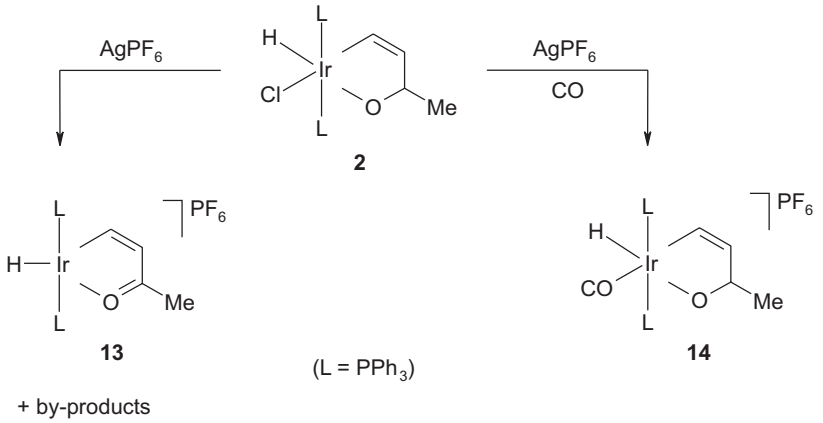
The reaction of **2** with $AgClO_4$ was carried out under similar conditions as with $AgPF_6$ and resulted in the formation of the hydrido(vinyl) complex **15** (Scheme 4). While the poor solubility of **15** in hydrocarbons is in agreement with the formulation as an ionic compound analogous to **13**, the molar conductivity (Λ) in nitromethane (36 $cm^2\ \Omega^{-1}\ mol^{-1}$) is considerably lower than expected for a 1:1 electrolyte (see **14**: Λ = 65 $cm^2\ \Omega^{-1}\ mol^{-1}$). The ^{31}P NMR spectrum of **15** in $CDCl_3$ at room temperature shows two singlets at δ 23.1 (sharp) and δ 17.5 (broad), which after decoupling change into doublets. In CD_2Cl_2 at –80 °C three doublets appear, two of which collapse to a broadened resonance after increasing the temperature to 0 °C. Although these results have to be interpreted with caution, we assume that in solution an equilibrium between the cationic species **15** and the uncharged isomers **15a** and **15b** exists. It is well-known that not only for iridium (14), but also for various other transition metals (15), the perchlorate anion can behave as a weakly coordinated ("noninnocent") ligand that is readily replaced by better nucleophiles. It should be mentioned that the ^{1}H NMR spectrum of the product obtained from **2** and $AgClO_4$ also displays two sets of signals for the =CH, CH_3, and IrH protons, which is in agreement with the equilibrium between **15** and the nonionic species **15a** and **15b**.

Similarly to **2**, the corresponding iridium(III) counterpart **3** reacts with $AgClO_4$ in CH_2Cl_2 to give the cationic complex **16** (Scheme 5), which, however, appears to have no tendency to coordinate the perchlorate anion. The ^{1}H as well as the ^{31}P NMR spectrum of **16** shows only one sharp resonance for the IrH proton and the phosphine ligands, respectively, and these resonances do not broaden or split into two signals by decreasing the temperature. We note that the chemical shifts of the signals observed in the ^{1}H and ^{31}P NMR spectra of **16** are nearly identical to those assigned to the cation of **15**, and thus we are convinced that the proposed structure with a five-coordinate metal center is correct.

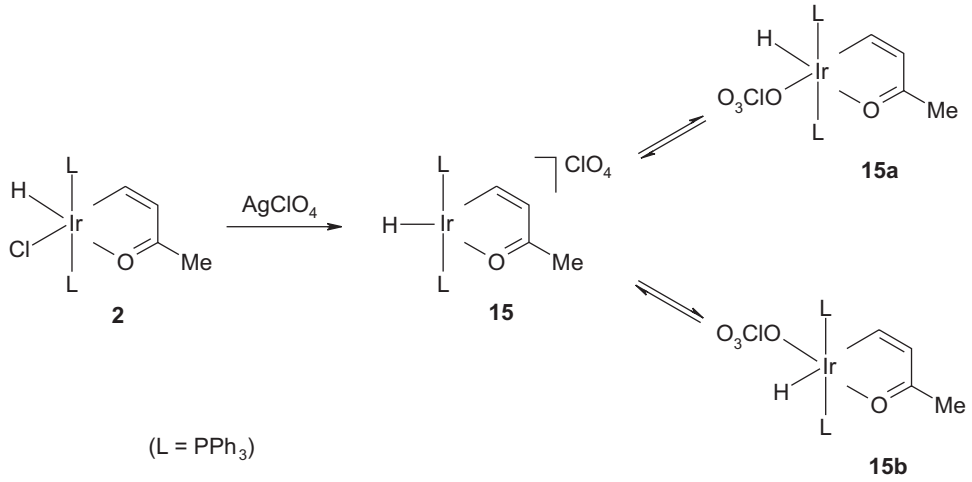
The open coordination site in the cation of **16** can easily be occupied by CO, PPh_3, ethene, propyne, acetonitrile, and

© 2006 NRC Canada

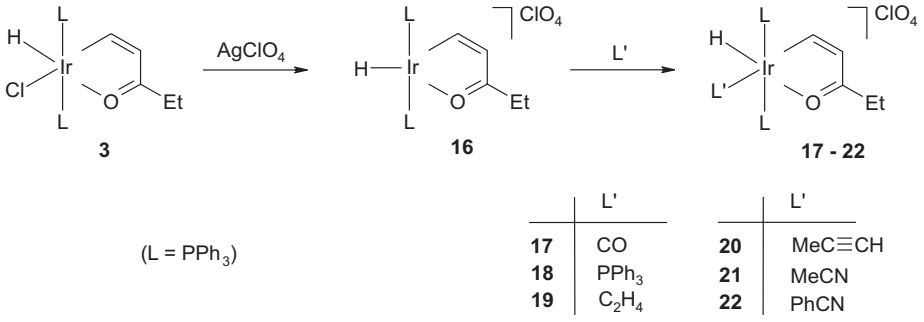
Scheme 3.



Scheme 4.



Scheme 5.

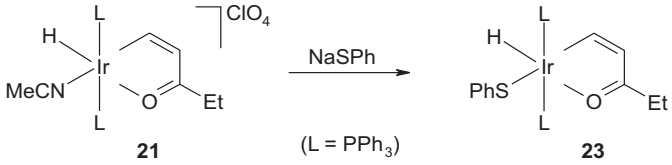


benzonitrile. With the exception of **19**, the related hydrido(vinyl)iridium(III) compounds **17**, **18**, and **20**–**22** are exceedingly stable and decompose between 112 (**20**) and 179 °C (**21**). Owing to the ionic nature, they are soluble in acetone, nitromethane, CH_2Cl_2, and $CHCl_3$, but almost insoluble in benzene and other hydrocarbons. Conductivity measurements confirm the presence of 1:1 electrolytes. The ethene complex **19** is only stable under a C_2H_4 atmosphere and has been characterized by ^1H and ^{31}P NMR spectroscopy. Typical features of **19** are the ^1H NMR signal for the ethene protons at δ 3.55 (triplet with $^3J(PH)$ = 3.1 Hz) and the singlet resonance for the ^{31}P NMR nuclei at δ 13.9, the latter being shifted upfield by 8.6 ppm compared with **16**. When we attempted to remove the volatiles and isolate compound **19**, the precursor **16** was regenerated.

In contrast to **19**, the analogous propyne complex **20** is rather inert and neither undergoes an insertion of the alkyne ligand into the Ir—H bond nor rearranges to the vinylidene isomer [IrH(=C=CHCH$_3$){κ^2(*C*,*O*)-CH=CHC(Et)=O}(PPh$_3$)$_2$]ClO$_4$ (16). However, compound **20**, as well as the nitrile iridium(III) analogues **21** and **22**, smoothly react with CO to afford the corresponding carbonyl complex **17**.

© 2006 NRC Canada

Scheme 6.



The acetonitrile ligand in **21** can not only be replaced by CO but also by thiophenolate. The reaction of **21** with NaSPh in THF proceeds slowly at room temperature and gives the neutral hydrido(thiophenolato) complex **23** in 78% yield (Scheme 6). **23** is an orange air-stable solid that has been characterized by elemental analysis and spectroscopic techniques. Attempts to also displace the acetonitrile ligand in **21** by methyl xanthogenate, K[SC(S)OMe], led to the formation of a mixture of compounds that could not be separated by fractional crystallization or column chromatography.

In summarizing, the present work has shown that, provided the olefinic substrate RCH=CHR′ possesses a substituent R′ such as C(O)R, C(O)NH_2, or C(O)OMe, the reaction of the starting material *trans*-[IrCl(N_2)(PPh_3)$_2$] (**1**) with RCH=CHR′ leads preferentially to the hydrido(vinyl)-iridium(III) complexes **2**–**12**. These compounds are remarkably stable and neither thermally nor photochemically react by intramolecular reductive elimination to give the four-coordinate olefin iridium(I) isomers *trans*-[IrCl(η^2-RCH=CHR′)(PPh_3)$_2$]. A rearrangement of this type does not occur with the cationic species [IrH(L){κ^2(*C*,*O*)-CH=CHC(R)=O}(PPh_3)$_2$]$^+$, independent of whether the ligand L is a good σ donor (MeCN, PhCN) or a destinctive π-acceptor ligand (CO, $CH_3C{\equiv}CH$). There is no doubt that the driving force for the formation of **2**–**12** from **1** and the functionalized olefin is the formation of the chelating five-membered IrC_3O ring, which remains intact even in the presence of excess CO. In this context, we note that in contrast to [IrH(Cl)(CH=CH_2)(P-*i*-Pr_3)$_2$], the related hydrido(phenyl) complex [IrH(Cl)(C_6H_5)(P-*i*-Pr_3)$_2$] is also quite stable and reacts with CO by addition and not by reductive elimination (17).

Experimental

All experiments were carried out under an atmosphere of argon by using standard Schlenk techniques. The starting material **1** was prepared as described in the literature (6). IR spectra were recorded on a PerkinElmer 1420 IR spectrometer and NMR spectra on Jeol FX 90 Q as well as Bruker AC 200 and Bruker AMX 400 instruments. Melting points (dec. temp.) were determined by DTA. Conductivity measurements were carried out in nitromethane with a Schott Konduktometer CG 851. Abbreviations used: singlet (s), doublet (d), triplet (t), quartet (q), multiplet (m), broadened signal (br); $N = {}^1J(PC) + {}^3J(PC)$.

Preparation of [IrH(Cl){κ^2(*C*,*O*)-CH=CHC(Me)=O}(PPh_3)$_2$] (2)

A solution of **1** (94 mg, 0.12 mmol) in 6 mL of benzene was treated with methyl(vinyl)ketone (11 μL, 0.12 mmol) and stirred for 2 h at room temperature. The solvent was evaporated in vacuo, the residue was dissolved in 3 mL of benzene–hexane (1:1), and the solution chromatographed on Al_2O_3 (neutral, activity grade V, length of column 6 cm). With benzene–hexane (1:1) a yellow fraction was eluted, which was brought to dryness in vacuo. The remaining yellow, air-stable solid was washed twice with 5 mL portions of hexane (30 °C) and dried. Yield: 78 mg (80%), mp 184 °C (dec.). IR (KBr, cm^{-1}): 2190 ν(IrH), 1550 ν(C=O). ^{1}H NMR (90 MHz, $CDCl_3$) δ: 9.58 (d, 1H, *J*(HH) = 7.5 Hz, IrCH), 7.59–7.19 (m, 30H, C_6H_5), 6.18 (d, 1H, *J*(HH) = 7.5 Hz, IrCH=C*H*), 1.53 (t, 3H, *J*(PH) = 1.4 Hz, CH_3), –22.42 (t, 1H, *J*(PH) = 16.4 Hz, IrH). ^{13}C NMR (50.3 MHz, $CDCl_3$) δ: 208.0 (s, C=O), 197.3 (t, *J*(PC) = 7.0 Hz, IrCH), 133.1 (s, IrCH=*C*H), 134.3 (vt, *N* = 11.6 Hz, *ortho*-C of PC_6H_5), 131.9 (vt, *N* = 54.7 Hz, ipso-C of PC_6H_5), 129.6 (s, *para*-C of PC_6H_5), 127.7 (vt, *N* = 10.1 Hz, *meta*-C of PC_6H_5), 24.0 (s, C(O)*C*H_3). ^{31}P NMR (36.2 MHz, $CDCl_3$) δ: 14.7 (s, d in off-resonance). Anal. calcd. for $C_{40}H_{36}ClIrOP_2$: C 58.42, H 4.41; found: C 58.34, H 4.55.

Preparation of [IrH(Cl){κ^2(*C*,*O*)-CH=CHC(Et)=O}(PPh_3)$_2$] (3)

A solution of **1** (140 mg, 0.18 mmol) in 15 mL of toluene was treated with ethyl(vinyl)ketone (18 μL, 0.18 mmol) and stirred for 6 h at room temperature. The solvent was evaporated in vacuo, the remaining yellow, air-stable solid was washed twice with 5 mL portions of hexane (50 °C) and dried. Yield: 137 mg (91%), mp 178 °C (dec.). IR (KBr, cm^{-1}): 2240 ν(IrH), 1540 ν(C=O). ^{1}H NMR (90 MHz, $CDCl_3$) δ: 9.60 (d, 1H, *J*(HH) = 7.6 Hz, IrCH), 7.58–7.28 (m, 30H, C_6H_5), 6.21 (d, 1H, *J*(HH) = 7.6 Hz, IrCH=C*H*), 1.95 (q, 2H, *J*(HH) = 7.3 Hz, CH_2CH_3), 0.69 (t, 3H, *J*(HH) = 7.3 Hz, CH_2CH_3), –22.55 (t, 1H, *J*(PH) = 16.5 Hz, IrH). ^{31}P NMR (36.2 MHz, $CDCl_3$) δ: 13.6 (s, d in off-resonance). Anal. calcd. for $C_{41}H_{38}ClIrOP_2$: C 58.88, H 4.58; found: C 58.37, H 4.51.

Preparation of [IrH(Cl){κ^2(*C*,*O*)-CH=CHC(Ph)=O}(PPh_3)$_2$] (4)

A solution of **1** (140 mg, 0.18 mmol) in 15 mL of toluene was treated with phenyl(vinyl)ketone (23 μL, 0.18 mmol) and stirred for 18 h at room temperature. (Owing to the high tendency of PhC(O)CH=CH_2 to polymerize, preparation of the ketone (18) in situ from β-chloropropiophenone is recommended). The reaction mixture was worked up analogous to that described for **3**. An orange, air-stable solid was obtained. Yield: 134 mg (84%), mp 189 °C (dec.). IR (KBr, cm^{-1}): 2145 ν(IrH), 1525 ν(C=O). ^{1}H NMR (90 MHz, $CDCl_3$) δ: 9.97 (d, 1H, *J*(HH) = 7.4 Hz, IrCH), 7.72–7.17 (m, 35H, PC_6H_5 and CC_6H_5), 6.86 (d, 1H, *J*(HH) = 7.4 Hz, IrCH=C*H*), –21.88 (t, 1H, *J*(PH) = 16.5 Hz, IrH). ^{31}P NMR (36.2 MHz, $CDCl_3$) δ: 13.4 (s, d in off-resonance). Anal. calcd. for $C_{45}H_{38}ClIrOP_2$: C 61.11, H 4.33; found: C 60.74, H 4.35.

Preparation of [IrH(Cl){κ^2(*C*,*O*)-C(OMe)=CHC(Me)=O}(PPh_3)$_2$] (5)

A solution of **1** (140 mg, 0.18 mmol) in 15 mL of toluene was treated with 4-methoxybut-3-en-2-one (18 μL, 0.18 mmol) and stirred for 18 h at 80 °C. After the solution was cooled to room temperature, the solvent was evaporated

© 2006 NRC Canada

in vacuo, the remaining pale yellow, air-stable solid was washed twice with 5 mL portions of hexane (50 °C) and dried. Yield: 120 mg (78%), mp 226 °C (dec.). IR (KBr, cm^{-1}): 2175 ν(IrH), 1515 ν(C=O). ^1H NMR (90 MHz, $CDCl_3$) δ: 7.71–7.22 (m, 30H, C_6H_5), 5.17 (s, 1H, C*H*C(Me)=O), 2.54 (s, 3H, IrC(OC*H*$_3$)=CH), 1.76 (s, 3H, C(CH_3)=O), –21.92 (t, 1H, *J*(PH) = 16.0 Hz, IrH). ^{31}P NMR (36.2 MHz, $CDCl_3$) δ: 9.8 (s, d in off-resonance). Anal. calcd. for $C_{41}H_{38}ClIrO_2P_2$: C 57.77, H 4.49; found: C 57.44, H 4.67.

Preparation of [IrH(Cl){κ^2(*C*,*O*)-C(Me)=CHC(Me)=O}-(PPh_3)$_2$] (6)

The procedure was analogous to that described for **5**, using **1** (140 mg, 0.18 mmol) and pent-3-en-2-one (17 μL, 0.18 mmol) as starting materials. A yellow, air-stable solid was obtained. Yield: 125 mg (83%), mp 191 °C (dec.). IR (KBr, cm^{-1}): 2200 ν(IrH), 1535 ν(C=O). ^1H NMR (90 MHz, $CDCl_3$) δ: 7.78–7.23 (m, 30H, C_6H_5), 6.07 (s, 1H, C*H*C(Me)=O), 1.83 (s, 3H, C(CH_3)=O), 0.92 (s, 3H, IrC(C*H*$_3$)=CH), –22.67 (t, 1H, *J*(PH) = 16.4 Hz, IrH). ^{31}P NMR (36.2 MHz, $CDCl_3$) δ: 11.6 (s, d in off-resonance). Anal. calcd. for $C_{41}H_{38}ClIrOP_2$: C 58.88, H 4.58; found: C 59.37, H 4.71.

Preparation of [IrH(Cl){κ^2(*C*,*O*)-C(Ph)=CHC(Me)=O}-(PPh_3)$_2$] (7)

The procedure was analogous to that described for **5**, using **1** (140 mg, 0.18 mmol) and 4-phenylbut-3-en-2-one (25 μL, 0.18 mmol) as starting materials. An orange, air-stable solid was obtained. Yield: 133 mg (82%), mp 194 °C (dec.). IR (KBr, cm^{-1}): 2230 ν(IrH), 1540 ν(C=O). ^1H NMR (90 MHz, $CDCl_3$) δ: 7.68–7.11 (m, 30H, PC_6H_5), 7.01–6.56 (m, 5H, CC_6H_5), 1.95 (t, 3H, *J*(PH) = 1.2 Hz, C(CH_3)=O), –22.10 (t, 1H, *J*(PH) = 15.9 Hz, IrH), signal of =CH proton probably covered by signal of CC_6H_5 protons. ^{31}P NMR (36.2 MHz, $CDCl_3$) δ: 10.7 (s, d in off-resonance). Anal. calcd. for $C_{46}H_{40}ClIrOP_2$: C 61.50, H 4.49; found: C 61.43, H 4.37.

Preparation of [IrH(Cl){κ^2(*C*,*O*)-C(CO_2Me)=CHC(Me)=O}-(PPh_3)$_2$] (8)

The procedure was analogous to that described for **3**, using **1** (107 mg, 0.14 mmol) and methyl-4-oxo-2-pentenoate (24 mg, 0.28 mmol) as starting materials. An orange, air-stable solid was obtained. Yield: 97 mg (79%), mp 228 °C (dec.). IR (KBr, cm^{-1}): 2210 ν(IrH). ^1H NMR (400 MHz, $CDCl_3$) δ: 7.59–6.81 (m, 30H, PC_6H_5), 2.89 (s, 3H, CO_2CH_3), 2.03 (t, 3H, *J*(PH) = 1.2 Hz, C(CH_3)=O), –22.89 (t, 1H, *J*(PH) = 16.0 Hz, IrH), signal of =CH proton probably covered by signal of C_6H_5 protons. ^{31}P NMR (36.2 MHz, $CDCl_3$) δ: 11.5 (s, d in off-resonance). Anal. calcd. for $C_{42}H_{38}ClIrO_3P_2$: C 57.30, H 4.35; found: C 57.49, H 4.46.

Preparation of [IrH(Cl){κ^2(*C*,*O*)-C(Me)=C(Me)C(Et)=O}-(PPh_3)$_2$] (9)

The procedure was analogous to that described for **5**, using **1** (140 mg, 0.18 mmol) and 4-methylhex-4-en-3-one (69 μL, 0.54 mmol) as starting materials. A yellow, air-stable solid was obtained. Yield: 123 mg (79%), mp 218 °C (dec.). IR (KBr, cm^{-1}): 2145 ν(IrH), 1550 ν(C=O). ^1H NMR (90 MHz, $CDCl_3$) δ: 7.69–7.23 (m, 30H, PC_6H_5), 2.10 (q, 2H, *J*(HH) = 7.3 Hz, C*H*$_2$CH$_3$), 1.10 (s, 3H, IrC(CH_3)=C), 0.79 (t, 3H, *J*(HH) = 7.3 Hz, CH_2C*H*$_3$), 0.75 (s, 3H, =C(CH_3)C), –21.91 (t, 1H, *J*(PH) = 16.1 Hz, IrH). ^{31}P NMR (36.2 MHz, $CDCl_3$) δ: 11.7 (s, d in off-resonance). Anal. calcd. for $C_{43}H_{42}ClIrOP_2$: C 59.75, H 4.90; found: C 59.80, H 4.68.

Preparation of [IrH(Cl){κ^2(*C*,*O*)-C(Ph)=CHC(Ph)=O}-(PPh_3)$_2$] (10)

The procedure was analogous to that described for **5**, using **1** (140 mg, 0.18 mmol) and benzylidenacetophenone (75 mg, 0.36 mmol) as starting materials. An orange, air-stable solid was obtained. Yield: 131 mg (76%), mp 212 °C (dec.). IR (KBr, cm^{-1}): 2160 ν(IrH), 1520 ν(C=O). ^1H NMR (90 MHz, $CDCl_3$) δ: 7.96–6.62 (br m, 40H, C_6H_5), –21.43 (t, 1H, *J*(PH) = 16.4 Hz, IrH), signal of =CH proton probably covered by the broad signal of phenyl protons. ^{13}C NMR (50.3 MHz, $CDCl_3$) δ: 215.0 (t, *J*(PC) = 6.1 Hz, IrC), 199.3 (s, C=O), 144.7 (s, IrC(Ph)=*C*H), 136.9, 131.5, 131.0, 129.4, 128.5, 128.1, 126.7, 125.2 (all s, CC_6H_5), 134.7 (vt, *N* = 11.1 Hz, *ortho*-C of PC_6H_5), 131.4 (vt, *N* = 53.8 Hz, ipso-C of PC_6H_5), 129.5 (s, *para*-C of PC_6H_5), 127.3 (vt, *N* = 10.2 Hz, *meta*-C of PC_6H_5). ^{31}P NMR (36.2 MHz, $CDCl_3$) δ: 10.3 (s, d in off-resonance). Anal. calcd. for $C_{51}H_{42}ClIrOP_2$: C 63.77, H 4.41; found: C 63.39, H 4.13.

Preparation of [IrH(Cl){κ^2(*C*,*O*)-CH=CHC(OMe)=O}-(PPh_3)$_2$] (11)

A solution of **1** (94 mg, 0.12 mmol) in 6 mL of benzene was treated with methyl acrylate (11 μL, 0.12 mmol) and stirred for 2 h at 80 °C. After the solution was cooled to room temperature, it was worked up analogously to that described for **2**. A yellow, air-stable solid was obtained. Yield: 67 mg (66%), mp 159 °C (dec.). IR (KBr, cm^{-1}): 2205 ν(IrH), 1580 ν(C=O). ^1H NMR (90 MHz, $CDCl_3$) δ: 9.17 (d, 1H, *J*(HH) = 8.7 Hz, IrCH), 7.66–7.24 (m, 30H, C_6H_5), 5.77 (d, 1H, *J*(HH) = 8.7 Hz, IrCH=C*H*), 3.15 (s, 3H, OCH_3), –25.07 (t, 1H, *J*(PH) = 16.1 Hz, IrH). ^{31}P NMR (36.2 MHz, $CDCl_3$) δ: 14.7 (s, d in off-resonance). Anal. calcd. for $C_{40}H_{36}ClIrO_2P_2$: C 57.30, H 4.33; found: C 57.68, H 4.11.

Preparation of [IrH(Cl){κ^2(*C*,*O*)-CH=CHC(NH_2)=O}-(PPh_3)$_2$] (12)

A solution of **1** (94 mg, 0.12 mmol) in 6 mL of benzene was treated with methyl acrylate (9 mg, 0.12 mmol) and stirred for 3 h at room temperature. The solvent was evaporated in vacuo and the residue was recrystallized from dichloromethane–hexane (1:5) to give a white, air-stable solid. Yield: 88 mg (89%), mp 181 °C (dec.). IR (KBr, cm^{-1}): 3320, 3215 ν(NH), 2205 ν(IrH), 1555 ν(C=O). ^1H NMR (90 MHz, $CDCl_3$) δ: 8.82 (d, 1H, *J*(HH) = 7.9 Hz, IrCH), 7.53–7.16 (m, 30H, C_6H_5), 5.57 (d, 1H, *J*(HH) = 7.9 Hz, IrCH=C*H*), –24.19 (t, 1H, *J*(PH) = 16.8 Hz, IrH), signal for NH_2 protons not exactly located. ^{31}P NMR (36.2 MHz, $CDCl_3$) δ: 13.6 (s, d in off-resonance). Anal. calcd. for $C_{39}H_{35}ClIrNOP_2$: C 56.89, H 4.28, N 1.70; found: C 56.96, H 3.99, N 1.66.

Preparation of [IrH(CO){κ^2(*C*,*O*)-CH=CHC(Me)=O}-(PPh_3)$_2$]PF_6 (14)

A solution of **2** (100 mg, 0.12 mmol) in 10 mL of dichloromethane was treated with $AgPF_6$ (31 mg, 0.12 mmol)

© 2006 NRC Canada

and stirred for 15 min at room temperature in the dark under CO. After replacing the CO atmosphere for argon, the solution was filtered and the residue was washed twice with 1 mL portions of CH_2Cl_2. The filtrate was brought to dryness in vacuo, the residue was dissolved in 6 mL of hexane–CH_2Cl_2 (1:5), and the solution was chromatographed on Al_2O_3 (neutral, activity grade V, length of column 5 cm). A brownish fraction was eluted with hexane–CH_2Cl_2 (1:5) and the solvent was evaporated in vacuo. After the residue was recrystallized from CH_2Cl_2–hexane (1:5), an off-white, air-stable solid was obtained. Yield: 105 mg (91%), mp 111 °C (dec.). Conductivity (CH_3NO_2) Λ = 65 $cm^2\ \Omega^{-1}\ mol^{-1}$. IR (KBr, cm^{-1}): 2190 ν(IrH), 2060 ν(CO), 1580 ν(C=O). ^1H NMR (90 MHz, $CDCl_3$) δ: 9.47 (d, 1H, *J*(HH) = 9.2 Hz, IrCH), 7.87–7.49 (m, 30H, PC_6H_5), 6.71 (d, 1H, *J*(HH) = 9.2 Hz, IrCH=C*H*), 1.23 (s, 3H, $C(CH_3)$=O), –19.09 (t, 1H, *J*(PH) = 12.5 Hz, IrH). ^{31}P NMR (36.2 MHz, $CDCl_3$) δ: 11.7 (s, d in off-resonance). Anal. calcd. for $C_{41}H_{36}ClF_6IrO_2P_3$: C 51.30, H 3.78; found: C 51.52, H 3.67.

Preparation of [IrH{κ²(*C*,*O*)-CH=CHC(Me)=O}-(PPh₃)₂]ClO₄ (15)

A solution of **2** (140 mg, 0.17 mmol) in 15 mL of dichloromethane was treated with $AgClO_4$ (35 mg, 0.17 mmol) and stirred for 15 min at room temperature in the dark. The solution was filtered and the residue was washed twice with 1 mL portions of CH_2Cl_2. The filtrate was brought to dryness in vacuo, the remaining brown-yellow solid was washed three times with 5 mL portions of hexane and dried. Yield: 130 mg (86%), mp 131 °C (dec.). Conductivity (CH_3NO_2) Λ = 36 $cm^2\ \Omega^{-1}\ mol^{-1}$. IR (KBr, cm^{-1}): 2180 ν(IrH), 1550 ν(C=O). ^1H NMR (90 MHz, $CDCl_3$) δ: 9.72 (d, 1H, *J*(HH) = 7.4 Hz, IrCH), 7.56–7.12 (m, 30H, PC_6H_5), 5.96 (d, 1H, *J*(HH) = 7.4 Hz, IrCH=C*H*), 1.43 (s, 3H, $C(CH_3)$=O), –21.14 (t, 1H, *J*(PH) = 15.3 Hz, IrH); data for isomers **15a** and **15b** (see Scheme 3): δ: 9.59 (d, *J*(HH) = 7.4 Hz, IrCH), 6.22 (d, *J*(HH) = 7.4 Hz, IrCH=C*H*), 1.48 (s, $C(CH_3)$=O), –21.90 (br t, *J*(PH) ~ 15 Hz, IrH). ^{31}P NMR (36.2 MHz, $CDCl_3$) δ: 23.1 (s, d in off-resonance; at –80 °C in CD_2Cl_2 two doublets in off-resonance with δ 22.1 and 21.4). Anal. calcd. for $C_{40}H_{36}ClIrO_5P_2$: C 55.17, H 4.41; found: C 55.24, H 4.32.

Preparation of [IrH{κ²(*C*,*O*)-CH=CHC(Et)=O}(PPh₃)₂]-ClO₄ (16)

The procedure was analogous to that described for **15**, using **3** (140 mg, 0.17 mmol) and $AgClO_4$ (35 mg, 0.17 mmol) as starting materials. An orange, moderately air-sensitive solid was obtained. Yield: 133 mg (87%), mp 128 °C (dec.). Conductivity (CH_3NO_2) Λ = 50 $cm^2\ \Omega^{-1}\ mol^{-1}$. IR (KBr, cm^{-1}): 2185 ν(IrH), 1545 ν(C=O). ^1H NMR (90 MHz, $CDCl_3$) δ: 9.74 (d, 1H, *J*(HH) = 6.9 Hz, IrCH), 7.44–7.12 (m, 30H, PC_6H_5), 6.04 (d, 1H, *J*(HH) = 6.9 Hz, IrCH=C*H*), 1.75 (q, 2H, *J*(HH) = 7.4 Hz, CH_2CH$_3$), 0.64 (t, 3H, *J*(HH) = 7.4 Hz, CH$_2$CH_3), –21.10 (t, 1H, *J*(PH) = 15.6 Hz, IrH). ^{31}P NMR (36.2 MHz, $CDCl_3$) δ: 22.5 (s, d in off-resonance). Anal. calcd. for $C_{41}H_{38}ClIrO_5P_2$: C 54.70, H 4.25; found: C 54.51, H 4.41.

Preparation of [IrH(CO){κ²(*C*,*O*)-CH=CHC(Et)=O}-(PPh₃)₂]ClO₄ (17)

A solution of **16**, generated in situ from **3** (100 mg, 0.12 mmol) and $AgClO_4$ (25 mg, 0.12 mmol) in 10 mL of dichloromethane, was stirred for 15 min at room temperature in the dark. The solution was filtered and a slow stream of CO was passed through the filtrate for 1 min. The solvent was evaporated in vacuo, the remaining yellow solid was washed twice with 1 mL portions of CH_2Cl_2 and three times with 5 mL portions of hexane and dried. Yield: 100 mg (89%), mp 118 °C (dec.). Conductivity (CH_3NO_2) Λ = 56 $cm^2\ \Omega^{-1}\ mol^{-1}$. IR (KBr, cm^{-1}): 2195 ν(IrH), 2040 ν(CO), 1575 ν(C=O). ^1H NMR (200 MHz, $CDCl_3$) δ: 9.42 (d, 1H, *J*(HH) = 9.1 Hz, IrCH), 7.81–7.47 (m, 30H, PC_6H_5), 6.73 (dt, 1H, *J*(HH) = 6.9, *J*(PH) = 2.1 Hz, IrCH=C*H*), 1.80 (qt, 2H, *J*(HH) = 7.2, *J*(PH) = 2.4 Hz, CH_2CH$_3$), 0.53 (t, 3H, *J*(HH) = 7.2 Hz, CH$_2$CH_3), –19.20 (t, 1H, *J*(PH) = 12.4 Hz, IrH). ^{31}P NMR (36.2 MHz, $CDCl_3$) δ: 11.1 (s, d in off-resonance). Anal. calcd. for $C_{42}H_{38}ClIrO_6P_2$: C 54.34, H 4.13; found: C 54.71, H 4.25.

Preparation of [IrH{κ²(*C*,*O*)-CH=CHC(Et)=O}(PPh₃)₃]-ClO₄ (18)

A solution of **16**, generated in situ from **3** (100 mg, 0.12 mmol) and $AgClO_4$ (25 mg, 0.12 mmol) in 10 mL of dichloromethane, was treated with PPh_3 (32 mg, 0.12 mmol) and stirred for 5 min at room temperature in the dark. The solution was filtered, the filtrate was brought to dryness in vacuo, and the remaining white, air-stable solid was washed three times with 5 mL portions of toluene and twice with 5 mL portions of hexane and dried. Yield: 114 mg (82%), mp 136 °C (dec.). Conductivity (CH_3NO_2) Λ = 59 $cm^2\ \Omega^{-1}\ mol^{-1}$. IR (KBr, cm^{-1}): 2215 ν(IrH), 1550 ν(C=O). ^1H NMR (90 MHz, $CDCl_3$) δ: 8.43 (ddt, 1H, *J*(HH) = 7.3, *J*(P_{eq}H) = 7.3, *J*(P_{ax}H) = 4.2 Hz, IrCH), 7.39–6.82 (m, 30H, PC_6H_5), 6.66 (d, 1H, *J*(HH) = 7.3 Hz, IrCH=C*H*), 2.25 (m, 2H, CH_2CH$_3$), 1.11 (t, 3H, *J*(HH) = 7.1 Hz, CH$_2$CH_3), –21.47 (td, 1H, *J*(P_{ax}H) = 18.1, *J*(P_{eq}H) = 10.3 Hz, IrH). ^{31}P NMR (36.2 MHz, $CDCl_3$) δ: 2.5 (d, *J*(PP) = 17.6 Hz, dd in off-resonance, ax-PPh_3), –3.1 (d, *J*(PP) = 17.6 Hz, dt in off-resonance, eq-PPh_3). Anal. calcd. for $C_{59}H_{53}ClIrO_5P_3$: C 60.95, H 4.59; found: C 60.34, H 4.25.

Preparation of [IrH(C₂H₄){κ²(*C*,*O*)-CH=CHC(Et)=O}-(PPh₃)₂]ClO₄ (19)

A solution of **16**, generated in situ from **3** (100 mg, 0.12 mmol) and $AgClO_4$ (25 mg, 0.12 mmol) in 10 mL of $CDCl_3$, was stirred for 15 min at room temperature in the dark. The solution was filtered and a slow stream of ethene was passed through the filtrate for 5 min. The solution was concentrated to ca. 1 mL in vacuo and the product, which is only stable in an ethene atmosphere, characterized by NMR spectroscopy. ^1H NMR (90 MHz, $CDCl_3$) δ: 10.04 (d, 1H, *J*(HH) = 8.6 Hz, IrCH), 7.51–7.18 (m, 30H, PC_6H_5), 6.45 (dt, 1H, *J*(HH) = 8.6, *J*(PH) = 2.2 Hz, IrCH=C*H*), 3.55 (t, 4H, *J*(PH) = 3.1 Hz, C_2H_4), 1.97 (qt, 2H, *J*(HH) = 7.3, *J*(PH) = 2.4 Hz, CH_2CH$_3$), 0.83 (t, 3H, *J*(HH) = 7.3 Hz, CH$_2$CH_3), –20.85 (t, 1H, *J*(PH) = 14.2 Hz, IrH). ^{31}P NMR (36.2 MHz, $CDCl_3$) δ: 13.9 (s, d in off-resonance).

Preparation of [IrH(CH₃C≡CH){κ²(*C*,*O*)-CH=CHC(Et)=O}-(PPh₃)₂]ClO₄ (20)

A solution of **16**, generated in situ from **3** (100 mg, 0.12 mmol) and $AgClO_4$ (25 mg, 0.12 mmol) in 10 mL of

© 2006 NRC Canada

dichloromethane, was stirred for 15 min at room temperature in the dark. The solution was filtered and a slow stream of propyne was passed through the filtrate for 1 min. The solvent was evaporated in vacuo, the residue was dissolved in 4 mL of CH_2Cl_2–hexane (3:1) and chromatographed on Al_2O_3 (neutral, activity grade V, length of column 5 cm). With CH_2Cl_2–hexane (3:1) a brown fraction was eluted, which was concentrated to ca. 2 mL in vacuo. A brown, slightly air-sensitive solid precipitated, which was washed three times with 5 mL portions of hexane and dried. Yield: 100 mg (87%), mp 112 °C (dec.). Conductivity (CH_3NO_2) Λ = 52 $cm^2\ \Omega^{-1}\ mol^{-1}$. IR (KBr, cm^{-1}): 2185 ν(IrH), 1820 ν(C≡C), 1540 ν(C=O). ^{1}H NMR (90 MHz, $CDCl_3$) δ: 9.60 (d, 1H, *J*(HH) = 7.6 Hz, IrCH), 7.66–7.00 (m, 30H, PC_6H_5), 6.21 (d, 1H, *J*(HH) = 7.6 Hz, IrCH=C*H*), 2.55–0.61 (br m, 9H, $CH_3C{\equiv}CH$ and C_2H_5), –22.54 (t, 1H, *J*(PH) = 16.6 Hz, IrH). ^{31}P NMR (36.2 MHz, $CDCl_3$) δ: 13.7 (s, d in off-resonance). Anal. calcd. for $C_{44}H_{42}ClIrO_5P_2$: C 56.20, H 4.50; found: C 56.14, H 4.23.

Preparation of [IrH(MeCN){κ²(*C*,*O*)-CH=CHC(Et)=O}-(PPh_3)$_2$]ClO_4 (21)

A solution of **16**, generated in situ from **3** (100 mg, 0.12 mmol) and $AgClO_4$ (25 mg, 0.12 mmol) in 10 mL of dichloromethane, was added dropwise to a solution of acetonitrile (19 μL, 0.36 mmol) in 5 mL of dichloromethane. After the reaction mixture was stirred for 5 min at room temperature, the solution was filtered. The filtrate was brought to dryness in vacuo, the remaining white, air-stable solid was washed three times with 5 mL portions of hexane and dried. Yield: 101 mg (87%), mp 179 °C (dec.). Conductivity (CH_3NO_2) Λ = 61 $cm^2\ \Omega^{-1}\ mol^{-1}$. IR (KBr, cm^{-1}): 2175 ν(CN), 1565 ν(C=O). ^{1}H NMR (90 MHz, $CDCl_3$) δ: 9.77 (d, 1H, *J*(HH) = 8.3 Hz, IrCH), 7.51–7.23 (m, 30H, PC_6H_5), 6.37 (dt, 1H, *J*(HH) = 8.3, *J*(PH) = 1.7 Hz, IrCH=C*H*), 1.82 (qt, 2H, *J*(HH) = 7.6, *J*(PH) = 2.2 Hz, CH_2CH_3), 1.69 (t, 3H, *J*(PH) = 1.0 Hz, CH_3CN), 0.69 (t, 3H, *J*(HH) = 7.6 Hz, CH_2CH_3), –21.72 (t, 1H, *J*(PH) = 14.9 Hz, IrH). ^{31}P NMR (36.2 MHz, $CDCl_3$) δ: 17.3 (s, d in off-resonance). Anal. calcd. for $C_{43}H_{41}ClIrNO_5P_2$: C 54.86, H 4.39, N 1.49; found: C 54.85, H 4.88, N 1.49.

Preparation of [IrH(PhCN){κ²(*C*,*O*)-CH=CHC(Et)=O}-(PPh_3)$_2$]ClO_4 (22)

The procedure was analogous to that described for **21**, using **16** (100 mg, 0.12 mmol) and benzonitrile (37 μL, 0.36 mmol) as starting materials. A pale yellow, moderately air-sensitive solid was obtained. Yield: 108 mg (90%), mp 148 °C (dec.). Conductivity (CH_3NO_2) Λ = 59 $cm^2\ \Omega^{-1}\ mol^{-1}$. IR (KBr, cm^{-1}): 2200 ν(CN), 1555 ν(C=O). ^{1}H NMR (90 MHz, $CDCl_3$) δ: 9.75 (d, 1H, *J*(HH) = 7.3 Hz, IrCH), 7.79–7.15 (m, 35H, C_6H_5CN and PC_6H_5), 6.47 (d, 1H, *J*(HH) = 7.3 Hz, IrCH=C*H*), 1.84 (q, 2H, *J*(HH) = 7.3 Hz, CH_2CH_3), 0.65 (t, 3H, *J*(HH) = 7.3 Hz, CH_2CH_3), –21.33 (t, 1H, *J*(PH) = 15.2 Hz, IrH). ^{31}P NMR (36.2 MHz, $CDCl_3$) δ: 17.1 (s, d in off-resonance). Anal. calcd. for $C_{48}H_{43}ClIrNO_5P_2$: C 57.45, H 4.32, N 1.40; found: C 57.68, H 4.60, N 1.44.

Preparation of [IrH(SPh){κ²(*C*,*O*)-CH=CHC(Et)=O}-(PPh_3)$_2$] (23)

A suspension of **21** (120 mg, 0.13 mmol) in 15 mL of THF was treated with NaSPh (17 mg, 0.13 mmol) and stirred for 15 h at room temperature. The solvent was evaporated in vacuo, the residue was suspended in 10 mL of toluene, and the solution was filtered. The filtrate was brought to dryness in vacuo, the remaining orange, air-stable solid was washed twice with 10 mL portions of hexane and dried. Yield: 92 mg (78%), mp 157 °C (dec.). IR (KBr, cm^{-1}): 2180 ν(IrH), 1570 ν(C=O). ^{1}H NMR (90 MHz, $CDCl_3$) δ: 9.68 (d, 1H, *J*(HH) = 8.0 Hz, IrCH), 7.62–7.21 (m, 30H, PC_6H_5), 6.78–6.58 (m, 5H, SC_6H_5), 6.47 (d, 1H, *J*(HH) = 8.0 Hz, IrCH=C*H*), 1.64 (q, 2H, *J*(HH) = 7.1 Hz, CH_2CH_3), 0.35 (t, 3H, *J*(HH) = 7.1 Hz, CH_2CH_3), –22.53 (t, 1H, *J*(PH) = 15.4 Hz, IrH). ^{31}P NMR (36.2 MHz, $CDCl_3$) δ: 16.8 (s, d in off-resonance). Anal. calcd. for $C_{47}H_{43}ClIrO_5P_2S$: C 62.03, H 4.76; found: C 61.83, H 4.55.

Acknowledgements

We thank the Deutsche Forschungsgemeinschaft (SFB 347) and the Fonds der Chemischen Industrie for financial support. We also gratefully acknowledge support by Mrs. R. Schedl and Mr. C.P. Kneis (DTA measurements and elemental analyses) and BASF AG (Ludwigshafen, Germany, chemicals).

References

1. M. Schulz and H. Werner. Organometallics, **11**, 2790 (1992).
2. H. Werner, T. Dirnberger, and M. Schulz. Angew. Chem. Int. Ed. Engl. **27**, 948 (1988).
3. (*a*) P.O. Stoutland and R.G. Bergman. J. Am. Chem. Soc. **107**, 4581 (1985); (*b*) P.O. Stoutland and R.G. Bergman. J. Am. Chem. Soc. **110**, 5732 (1988).
4. (*a*) D.M. Haddleton and R.N. Perutz. J. Chem. Soc. Chem. Commun. 1734 (1986); (*b*) T.W. Bell, S.-A. Brough, M.G. Partridge, R.N. Perutz, and A.D. Rooney. Organometallics, **12**, 2933 (1993).
5. H. Werner, B. Papenfuhs, and P. Steinert. Z. Anorg. Allg. Chem. **627**, 1807 (2001).
6. J.P. Collman and J.W. Kang. J. Am. Chem. Soc. **88**, 3459 (1966).
7. R. Castarlenas, M.A. Esteruelas, M. Martín, and L.A. Oro. J. Organomet. Chem. **564**, 241 (1998).
8. A.N. Nesmeyanov, M.I. Rybinskaya, L.V. Rybin, V.S. Kaganovich, and P.V. Petrovskii. J. Organomet. Chem. **31**, 257 (1971).
9. H. Werner, M.A. Esteruelas, and H. Otto. Organometallics, **5**, 2295 (1986).
10. M. Schulz. Ph.D. thesis, Universität Würzburg, Würzburg, Germany. 1991.
11. L. Vaska and J.W. Di Luzio. J. Am. Chem. Soc. **83**, 2784 (1961).
12. T. Dirnberger. Ph.D. thesis, Universität Würzburg, Würzburg, Germany. 1990.
13. M. Masamoto. Nippon Kagaku Kaishi, **5**, 825 (1976).
14. J. Peone and L. Vaska. Angew. Chem. Int. Ed. Engl. **10**, 511 (1971).
15. Reviews: (*a*) N.M.N. Gowda, S.B. Naikar, and G.K.N. Reddy. Adv. Inorg. Chem. Radiochem. **28**, 255 (1984); (*b*) W. Beck and K.H. Sünkel. Chem. Rev. **88**, 1405 (1988); (*c*) S.H. Strauss. Chem. Rev. **93**, 927 (1993).
16. For the isomerization of alkyne iridium(I) to vinylidene iridium(I) complexes, see: (*a*) F.J. Garcia Alonso, A. Höhn, J. Wolf, H. Otto, and H. Werner. Angew. Chem. Int. Ed. Engl. **24**, 406

© 2006 NRC Canada

(1985); (*b*) A. Höhn and H. Werner. Angew. Chem. Int. Ed. Engl. **25**, 737 (1986); (*c*) A. Höhn and H. Werner. J. Organomet. Chem. **382**, 255 (1990); (*d*) H. Werner, R.W. Lass, O. Gevert, and J. Wolf. Organometallics, **16**, 4077 (1997).

17. H. Werner, A. Höhn, and M. Dziallas. Angew. Chem. Int. Ed. Engl. **25**, 1090 (1986).
18. H. Möhrle, T. Platzek, R. Wille, and D. Wendisch. Z. Naturforsch. B: Chem. Sci. **40b**, 524 (1985).

© 2006 NRC Canada

Ethylene and 1-hexene polymerization using zirconium iminophosphonamide complexes[1]

Robert Tomaszewski, Rainer Vollmerhaus, Abdulaziz Al-Humydi, Qinyan Wang, Nicholas J. Taylor, and Scott Collins

Abstract: Ethylene polymerization was studied using a variety of iminophosphonamide (PN_2) complexes of zirconium. Bis(PN_2) dichloride complexes $[Ph_2P(NR')_2]_2ZrX_2$ (X = Cl; **1a**: R′ = *p*-tolyl; **1b**: R′ = Bn; **1c**: R′ = C_6F_5) or dimethyl complexes (X = Me; **2a**: R′ = *p*-tolyl; **2b**: R′ = Bn) and cyclopentadienyl(PN_2)zirconium dichloride complexes $[\eta^5\text{-}C_5R''_5][R_2P(NR')_2]ZrCl_2$ (**3a**: R′ = *p*-tolyl, R = Ph, R″ = H; **3b**: R′ = $SiMe_3$, R = Et, R″ = H; **3c**: R′ = C_6F_5, R = Ph, R″ = H; **3e**: R′ = 3,5-$(CF_3)_2$Ph, R = Ph, R″ = H; **3f**: R′ = 3,5-$(CF_3)_2$Ph, R = Ph, R″ = Me) or dimethyl analogs $[\eta^5\text{-}C_5H_5][R_2P(NR')_2]ZrMe_2$ (**4a**: R′ = *p*-tolyl, R = Ph; **4b**: R′ = $SiMe_3$, R = Et) were evaluated under a range of conditions using methylaluminoxane (PMAO) activator. Complexes **1** and **2** behave as precursors to single-site polymerization catalysts under the conditions studied, while complexes **3** or dialkyls **4** show more complex behavior and formation of poly(ethylene) with a bimodal molecular weight distribution. In contrast, activation of dialkyl complexes **4** with $[Ph_3C][B(C_6F_5)_4]$ and polymerization in the presence of small amounts of PMAO or TIBAL as scavenger, led to single-site behavior. PMAO reacts with the neutral dialkyls via ligand abstraction to produce a number of P-containing species that may explain the multi-site behavior observed when using this activator. Dialkyls **4** react cleanly with $[Ph_3C][B(C_6F_5)_4]$ in haloarene or even dichloromethane solution to furnish the corresponding cationic alkyls **5**, which were characterized by multinuclear NMR spectroscopy. Fluxional dinuclear species are formed in the presence of excess dialkyl and these are susceptible to C—H activation to form μ-Me,μ-CH_2 complexes one of which could be isolated in pure form. The cationic alkyls initiate the polymerization of 1-hexene at room temperature in chlorobenzene solution, but extensive chain transfer occurs and the systems are not living.

Key words: single site, early metal olefin polymerization catalysis.

Résumé : On a étudié la polymérisation de l'éthylène à l'aide d'une variété de complexes à base d'iminophosphonamide (PN_2) du zirconium. Utilisant le méthylaluminoxane (PMAO) comme activateur dans une grande variété de conditions, on a évalué les complexes avec le dichlorure de bis(PN_2) $[Ph_2P(NR')_2]_2ZrX_2$ (X = Cl, **1a** : R′ = *p*-tolyl; **1b** : R′ = Bn; **1c** : R′ = C_6F_5) ou les complexes diméthylés (X = Me; **2a** : R′ = *p*-tolyl; **2b** : R′ = Bn), et le dichlorure de cyclopentadiényl(PN_2) $[\eta^5\text{-}C_5R''_5][R_2P(NR')_2]ZrCl_2$ (**3a** : R′ = *p*-tolyl, R = Ph, R″ = H; **3b** : R′ = $SiMe_3$, R = Et, R″ = H; **3c** : R′ = C_6F_5, R = Ph, R″ = H; **3e** : R′ = 3,5-$(CF_3)_2$Ph, R = Ph, R″ = H; **3f** : R′ = 3,5-$(CF_3)_2$Ph, R = Ph, R″ = Me) ou de leurs analogues diméthylés $[\eta^5\text{-}C_5H_5][R_2P(NR')_2]ZrMe_2$ (**4a** : R′ = *p*-tolyle, R = Ph; **4b** : R′ = $SiMe_3$, R = Et). Dans les conditions étudiées, les complexes **1** et **2** se comportent comme des précurseurs de catalyseurs à site unique alors que les complexes **3** ou les dialkyles **4** présentent un comportement plus complexe avec une formation de poly(éthylène) présentant une distribution bimodale des poids moléculaires. Par ailleurs, l'activation des complexes de dialkyles avec du $[Ph_3C][B(C_6F_5)_4]$ avec des polymérisations en présence de faibles quantités de PMAO ou de TIBAL comme piège conduit à un comportement à site unique. Le PMAO réagit avec les dialkyles neutres par le biais d'un enlèvement de ligand conduisant à la formation de diverses espèces contenant du phosphore qui peuvent expliquer le comportement multisite observé quand on utilise ce composé pour faire l'activation. Les complexes dialkyles **4** réagissent proprement avec le $[Ph_3C][B(C_6F_5)_4]$ en solution dans des halogénoarènes et même dans le dichlorométhane et ces réactions conduisent à la formation des complexes cationiques alkyles correspondants **5** qui ont été caractérisés par spectroscopie RMN multinucléaire. Il se forme des espèces binucléaires fluxionnelles en présence d'excès de dérivés dialkyles et ces espèces sont susceptibles à une activation C—H conduisant à la formation de complexes μ-Me et μ-CH_2 desquels un a pu être isolé dans une forme pure. Les complexes alkyles cationiques initient la polymérisation du

Received 17 May 2005. Published on the NRC Research Press Web site at http://canjchem.nrc.ca on 7 March 2006.

To Arthur Carty, one of the wisest (and most exuberant) scientists I have ever met.

R. Tomaszewski, R. Vollmerhaus, and N.J. Taylor. Department of Chemistry, University of Waterloo, Waterloo, ON N2L 3G1, Canada.
A. Al-Humydi and S. Collins.[2] Department of Polymer Science, University of Akron, Akron, OH 44325-3909, USA.
Q. Wang. Nova Chemicals Corporation, 2928-16th St. N.E., Calgary, AB T2E 7K7, Canada.

[1]This article is part of a Special Issue dedicated to Professor Arthur Carty.
[2]Corresponding author (e-mail: collins@uakron.edu).

 doi:10.1139/V05-246 © 2006 NRC Canada

hex-1-ène à la température ambiante, en solution dans le chlorobenzène, mais il se produit beaucoup de transfert de chaîne et les systèmes ne sont pas vivants.

Mots clés : précurseurs de catalyseurs à site unique de la polymérisation d'alcènes par des métaux de transition.

[Traduit par la Rédaction]

Introduction

The synthesis of novel group 4 complexes is of considerable interest in the context of olefin polymerization using "non-metallocene" catalysts (1). A wide variety of complexes based on the use of surrogates for the Cp ligand have been prepared and many are active in ethylene or α-olefin polymerization. However, the polymerization activities of isoelectronic (or even isolobal) complexes differ dramatically and often in a contradictory manner. Establishing fundamental trends in, e.g., catalyst activity with respect to parameters such as total electron count, and the steric and electronic effect of ligand substituents has been problematic. These difficulties arise through a number of complicating factors such as the efficiency of activation of catalyst precursors with typical cocatalysts, particularly methyl aluminoxane (PMAO), the stability of the active catalyst (or precatalyst) with respect to irreversible deactivation or reversible inhibition processes, and intrinsic electronic or steric effects on monomer coordination and insertion rates.

Some time ago, a number of workers elected to study group 4 complexes based on the amidinate ligand [$RC(NR')_2$=CN_2] as catalysts in ethylene or propylene polymerization. This ligand is a hard σ donor, which can contribute up to 5e ($3\sigma + 2\pi$) on coordination to a d^0 metal (2). On activation with PMAO in hydrocarbon media, both bis(CN_2) (3) and mixed Cp(CN_2) (4) complexes of Ti and Zr were active in ethylene, while the former were also active in propylene polymerization; however, compared with Cp_2ZrX_2 complexes, these 14 electron complexes were approximately 10^2–10^3 times less active under similar conditions of temperature and pressure. Further, some of these complexes (e.g., Cp(CN_2)$ZrCl_2$, R = $SiMe_3$, R′ = Ph) were said to be almost inactive in olefin polymerization (4*a*, 4*b*); in these cases, thermal instability of cationic alkyls generated in situ from neutral catalyst precursors was believed responsible for this finding.

More recently, less-hindered versions of mixed Cp(CN_2)$ZrMe_2$ complexes (Cp = η^5-C_5H_5, η^5-Cp*; R = Me and R′ = Et, *c*-Hx, *t*-Bu, etc.) have been shown to effect the living polymerization of 1-hexene or other sterically hindered alkenes in chlorobenzene solution on activation with either [$PhNMe_2H$][$B(C_6F_5)_4$] or [Ph_3C][$B(C_6F_5)_4$] (5). Detailed study of these cationic alkyl–Zr complexes has indicated that they are reasonable stable in such media and are less prone to β-H elimination than their Cp_2 counterparts. Further, bimolecular alkyl group exchange processes are facile at higher Zr concentrations (5*e*, 5*f*) and are responsible for erosion of tacticity seen using chiral initiators of this type. Although the polymerization of ethylene or propylene has not been reported in the open literature using these initiators, the activity in hexene polymerization (≤10^5 g C_6H_{12} / (mol Zr × h)) suggests that values in the range of 10^6–10^7 g monomer / (mol Zr × h) at 25 °C in this polar solvent are not unlikely.

Several years ago we were intrigued by the origins for the low activities observed for CN_2 complexes of group 4 in ethylene polymerization, at least when activated under conventional conditions using PMAO in hydrocarbon media. We suspected that either the precatalysts were inefficiently activated using PMAO, were insufficiently stable under the conditions studied, or that unfavorable steric and (or) electronic effects were at play here. Further, although the CN_2 ligand is sterically demanding with a cone angle comparable to Cp or Cp* depending on substitution (2), it is an inherently two-dimensional ligand that might make such complexes more susceptible to bimolecular inhibition and (or) degradation processes, compared with their Cp analogues.

We reasoned that a more three-dimensional analogue, such as the iminophosphonamide [$R_2P(NR')_2$=PN_2] ligand (6), where the tetrahedral P(V) atom is thought to represent a minimal electronic perturbation to trigonal C(IV), would be a suitable choice of ligand to investigate such issues. Preliminary work revealed that zirconium complexes derived from these ligands had ethylene polymerization activities that rivaled bent metallocene complexes when activated by PMAO under comparable conditions (7). In a recent paper, we provided detailed syntheses and structural characterization of a variety of bis(PN_2) and mixed Cp(PN_2) complexes of titanium and zirconium (8). Herein we report full details on the use of the zirconium complexes (Chart 1) in ethylene polymerization,[3] some solution chemistry of the cationic alkyls derived from these complexes, and their use for the polymerization of 1-hexene.

Results and discussion

Ethylene polymerization using PN_2 complexes and PMAO activator

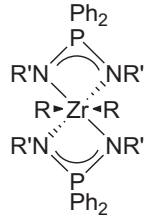
Bis(PN_2) complexes **1** and **2**, along with the mixed cyclopentadienyl(PN2) complexes **3** and **4**, were initially evaluated in toluene slurry using PMAO as activator at a 2000:1 or 1000:1 Al:Zr ratio, respectively.[4] The ethylene polymerization results are summarized in Tables 1 and 2.

The bis(PN_2) dichloride or dialkyl complexes **1** and **2** behave as single-site catalysts on activation with PMAO. They furnish poly(ethylene) with a somewhat broadened, but unimodal molecular weight distribution (MWD), where polydispersity is generally higher at higher temperatures. The activity of these complexes is actually higher at lower

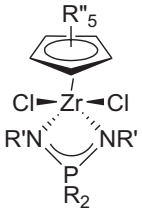
[3] The titanium complexes have been evaluated in ethylene polymerization (ref. 7), but they are all much less active than their Zr analogs.
[4] These catalysts were also evaluated at Nova Chemicals Corporation under conditions relevant to their industrial processes for polyethylene manufacture. Details of these tests are contained with a patent (7*b*).

© 2006 NRC Canada

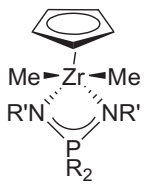
Chart 1.



1a: R' = *p*-tolyl, R = Cl
1b: R' = CH_2Ph, R = Cl
1c: R' = C_6F_5, R = Cl
2a: R' = *p*-tolyl, R - Me
2b: R' = CH_2Ph, R = Me



3a: R' = *p*-tolyl, R = Ph, R" = H
3b: R' = $SiMe_3$ R = Et, R" = H
3c: R' = C_6F_5, R = Ph, R" = H
3d: R' = 3,5-$(CF_3)_2$Ph, R = Ph, R" = H
3e: R' = 3,5-$(CF_3)_2$Ph, R = Ph, R" = Me



4a: R' = *p*-tolyl, R = Ph
4b: R' = $SiMe_3$ R = Et

Table 1. Ethylene polymerization using bis(PN_2) complexes **1** and **2**.

Entry	Catalyst (μmol)	*T* (°C)	Act.[a]	M_n (K)	M_w/M_n
1	**1a** (5)	40	7.90	143.8	2.07
2	**1a** (5)	70	2.50	78.7	3.55
3	**1c** (5)	40	0.16	331	3.02
4	**1c** (5)	70	0.34	133	1.98[b]
5	**2b** (5)	70	2.20	213.2	2.27
6	**2a** (5)	40	6.90	190.4	2.68
7	**2a** (5)	70	2.90	—	—

Note: For structures of complexes **1** and **2**, see Chart 1. Reaction conditions: 0.5 L toluene solvent, 75 psig ethylene, Al:Zr (2000:1), 1000 rpm.
[a]Polymerization activity in 10^6 g PE / (mol Zr × h).
[b]Bimodal molecular weight distribution. M_n and PDI are for analysis of the major component.

Table 2. Ethylene polymerization using Cp(PN_2) complexes **3** and **4** activated with PMAO.

Entry	Catalyst (μmol/L)	*T* (°C)	Act.[a]	M_n (K)[b]	M_w/M_n	M_n (K)[c]	M_w/M_n	Ratio[d]
1	**3a** (5)[e]	40	8.48	359	1.6	2.9	2.6	21:79
2	**4a** (5)[e]	40	0.95	235	1.9	3.6	2.6	54:46
3	**4a** (5)[f]	70	14.3	104	3.0	2.8	2.4	87:13
4	**3b** (10)	70	8.40	93.4	2.45	—	—	~100
5	**4b** (5)[e]	40	0.51	334	1.6	54.1	1.1	41:59
6	**4b** (5)[f]	70	8.44	137	1.8	3.1	2.0	70:30
7	**3c** (10)	40	6.0	760	2.1	18.2	2.2	16:84
8	**3c** (10)	70	11.0	—	—	11.6	2.62	~100
9	**3d** (10)	40	7.00	398	3.0	7.0	4.0	68:32
10	**3d** (10)	70	44.0	106	2.8	1.6	3.1	91:9
11	**3e** (10)	40	40.0	331	2.1	3.2	2.1	73:27

Note: For structures of complexes **3** and **4**, see Chart 1. Reaction conditions: toluene 0.5 L, 75 psig ethylene, Al:Zr (1000:1) unless otherwise noted, 1000 rpm.
[a]Polymerization activity in 10^6 g PE / (mol Zr × h).
[b]Bimodal MWD, high MW component.
[c]Bimodal MWD, low MW component.
[d]Ratio of high to low MW components.
[e]Al:Zr (4000:1).
[f]Al:Zr (8000:1).

temperatures suggesting limited thermal stability of the propagating species. Electron-deficient complexes **1c** are less active than electron-rich analogs **1a**, which may reflect intrinsic insertion rates and (or) the effectiveness of alkylation/ionization by PMAO. Since the activity of dialkyl **2a** is largely indistinguishable from that of dichloride **1a** (Table 1, entries 1 and 2 vs. 6 and 7), we suspect that the differences in activity between electron-deficient and electron-rich dichloride complexes is largely intrinsic.

In contrast, activation of the Cp(PN_2) dichloride or dialkyl complexes **3** and **4** with PMAO led to multisite behavior and formation of polymer with a broad and (or) bimodal MWD (Table 2). Also, in contrast to the bis(PN_2) complexes, activity was generally much higher at more elevated temperatures

© 2006 NRC Canada

Table 3. Ethylene polymerization using complexes **4a** and **4b** and $[Ph_3C][B(C_6F_5)_4]$.

Entry	Catalyst	AlR_3 (mmol)	Zr (μmol)	Act.[a]	M_n (K)	M_w/M_n
1	**3a**	PMAO (40)[b]	5	14.3	77.7	3.92[c]
2	**4a**	PMAO (4.0)	5	18.8	150	1.90
3	**4b**	PMAO (3.3)[b]	5	8.4	16.4	12.6[c]
4	**4b**	TMA (1.5×10^{-2})	11	0.41	29.9	7.53[c]
5	**4b**	TMA (1.5×10^{-2})[d]	11	2.20	110	2.87
6	**4b**	PMAO (3.3)	11	5.30	115	3.09
7	**4b**	TIBAL (6.5×10^{-2})	11	1.50	76.1	2.88
8	**4b**	TIBAL (2.50×10^{-2})	11	0.57	121	2.03

Note: Conditions: toluene (0.5 L), 75 psig ethylene, 70 °C, 1000 rpm. Complex **4** and $[Ph_3C][B(C_6F_5)_4]$ premixed in toluene prior to introduction into the reactor, presaturated with monomer in the presence of AlR_3 unless otherwise noted.

[a]Activity in 10^6 g PE / (mol Zr × h).

[b]PMAO used as both scavenger and activator (for conditions, see Table 2).

[c]Bimodal MWD with low and high MW components.

[d]Complex **4b** injected into a solution of cocatalyst and TMA in toluene, presaturated with monomer; MAO subsequently introduced after a period of several minutes with no monomer uptake.

(Table 2, compare entries 2 and 3, 5 and 6, 7 and 8, or 9 and 10). The relative amounts of the two different MW polymers formed was sensitive to both catalyst structure and temperature. Generally speaking, the amount of higher MW polymer increased with increasing temperature (Table 2, entries 2 vs. 3, 5 vs. 6, and 9 vs. 10), although the C_6F_5-substituted catalyst **3c** shows the opposite behavior (Table 2, entry 7 vs. 8); surprisingly, in two cases, the use of a dichloride vs. dialkyl precursor of the *same* $Cp(PN_2)$ complex led to different behavior (Table 2, entries 1 vs. 2 and 4 vs. 6).

It is largely a matter of speculation as to why different catalyst precursors show different activities and produce polymer of differing MW, etc., since based on these results it is not even clear which are the active catalysts! Possible explanations for the behavior observed include time-dependent chain transfer to PMAO as has been observed with Fe catalysts (9), aluminoxane-mediated degradation of the neutral precursors into different precatalysts, and (or) thermally induced or aluminoxane-induced transformation of one active catalyst into another. As the relative amount and MW of both polymer components was rather insensitive to Al:Zr ratios (over the range 500:1 to 8000:1) or polymerization time, it would appear that the latter two explanations are more likely.

With a view to clarifying the situation, ethylene polymerization using catalyst precursors **4a** and **4b** and $[Ph_3C][B(C_6F_5)_4]$ as activator in the presence of various alkylaluminum scavengers was studied and the results are summarized in Table 3. Generally speaking, single-site behavior was observed when **4a** or **4b** were premixed with the trityl borate activator prior to introduction into the reactor and highest activities were generally seen when using PMAO as scavenger. The use of trimethylaluminum as a scavenger strongly inhibited polymerization activity (Table 3, entry 3 vs. 4), while addition of PMAO ameliorated this behavior (Table 3, entry 4 vs. 5 vs. 6). Triisobutylaluminum was less inhibitory than $AlMe_3$, but appears to function as a chain-transfer agent at higher concentration (Table 3, entries 7 and 8). Tentatively, it would appear that the species responsible for polymer formation on ionization with $[Ph_3C][B(C_6F_5)_4]$ is the same as that responsible for formation of high MW polymer in PMAO-activated catalysts (Table 2, entry 3 vs. Table 3, entry 2, and Table 2, entry 6 vs. Table 3, entry 6) based on the similarity in MW of the polymer formed.

Qualitatively, the results appear similar to those observed when using β-diketimine complexes of group 4 (10), where PMAO as scavenger serves to assist with complete ionization of the neutral dialkyl precursors (through reversible formation of heterodinuclear Zr, Al adducts) and also as an agent for sequestration of excess $AlMe_3$ in the reactor, thus regulating the concentration of this inhibitor. Unfortunately, unlike the diketimine complexes (10), the dialkyl precursors and their derived ion pairs are incompatible[5] with the principle hydrolysis product of $MeAl(BHT)_2$ (2,6-di-*tert*-butyl-4-methylphenol) (11) and polymerization is not observed in the presence of this otherwise "noninteracting" scavenger.

Cationic alkyls **5** could be cleanly prepared from either **4a** or **4b** and $[Ph_3C][B(C_6F_5)_4]$ in bromobenzene or chlorobenzene solution (Scheme 1). These compounds are even stable in CH_2Cl_2 for short periods of time at room temperature and can be isolated as off-white solids from this solvent, following extraction of triphenylethane with hexane. Solutions of these cationic alkyls appear stable for indefinite periods of time at room temperature in haloarene solvent, although the ion pairs decompose on heating to furnish a variety of unidentified products, including methane. Spectroscopic data for ion pairs **5a** and **5b** are summarized in the Experimental section.

Key features in the ^1H NMR spectrum of **5b** that distinguish it from its neutral precursor **4b** are that the Et groups on P are inequivalent (*both* the CH_2 and CH_3 groups) on the NMR timescale at room temperature (Figs. 1*c* vs. 1*a*). Evidently, either rotation of the PN_2 ligand about the P—Zr axis or ion-pair reorganization are slow (with the other process being rapid) on the NMR timescale. Since the latter scenario seems unlikely, especially in a polar solvent like bromobenzene, we suspect there is hindered rotation about the P—

[5]A. Al-Humydi. Unpublished results.

© 2006 NRC Canada

Scheme 1.

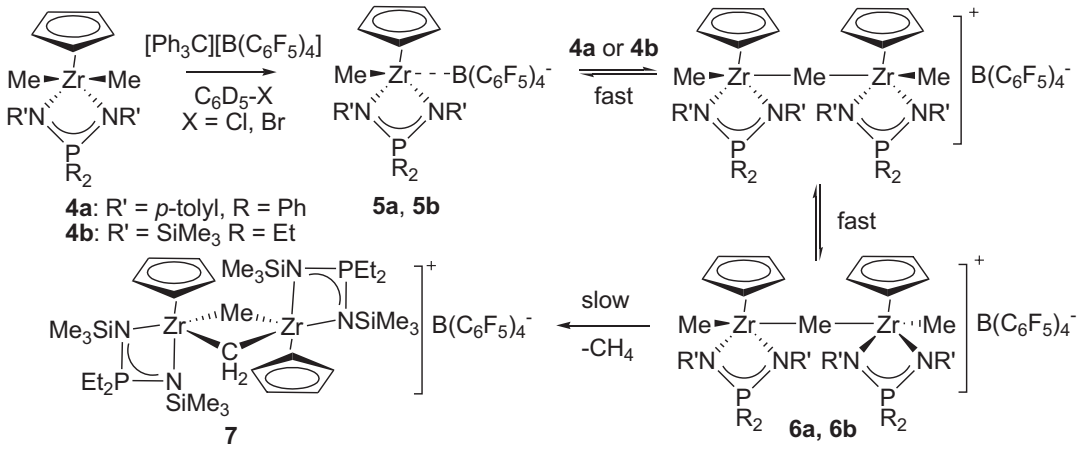
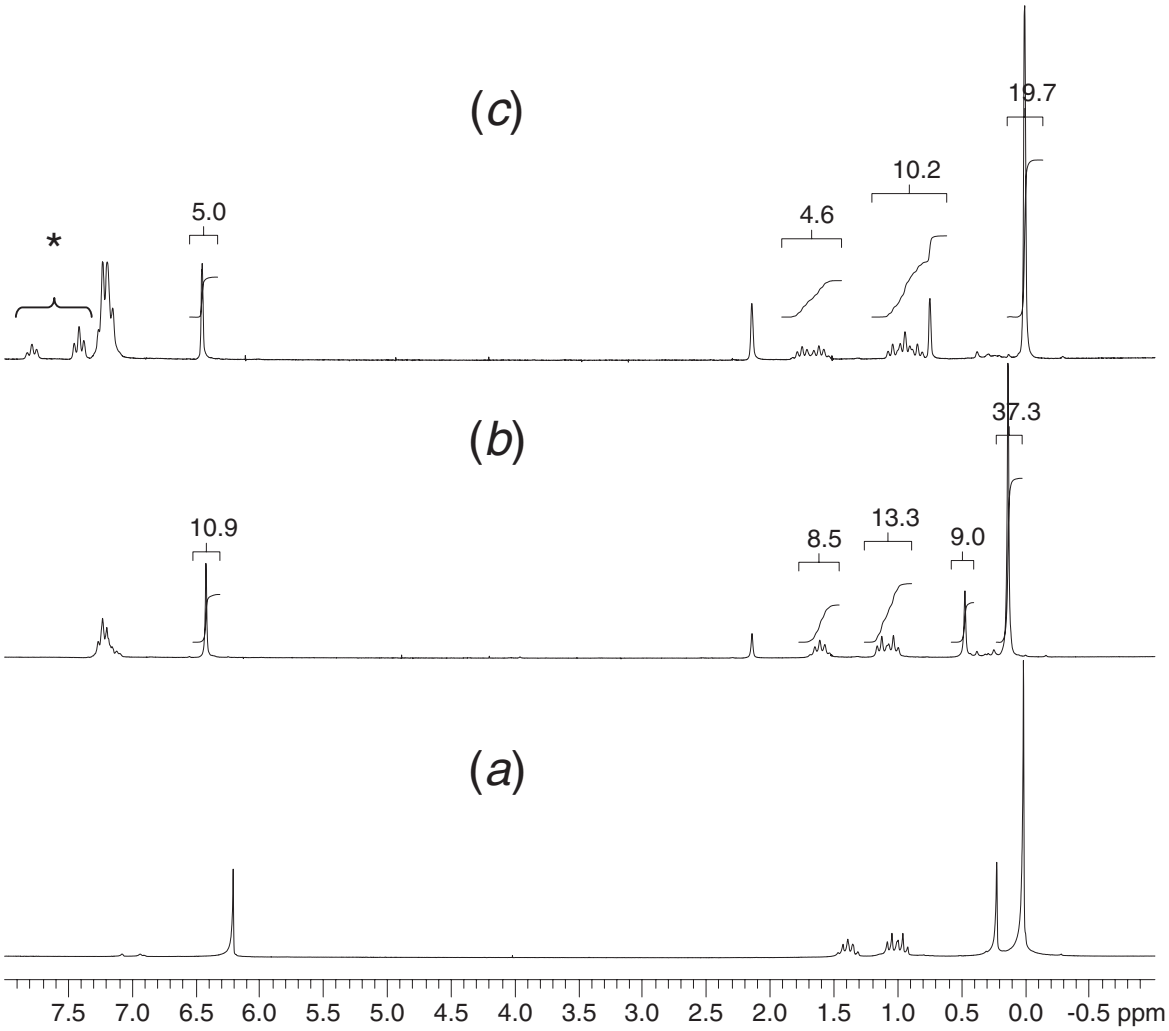


Fig. 1. ^{1}H NMR spectra (200 MHz, C_6D_5Br, 25 °C) of: (*a*) neutral dialkyl complex **4b**, (*b*) a 2:1 mixture of **4b** and $[Ph_3C][B(C_6F_5)_4]$, and (*c*) a mixture of **4b** and excess $[Ph_3C][B(C_6F_5)_4]$. Signals owing to the latter compound are marked with an asterisk.

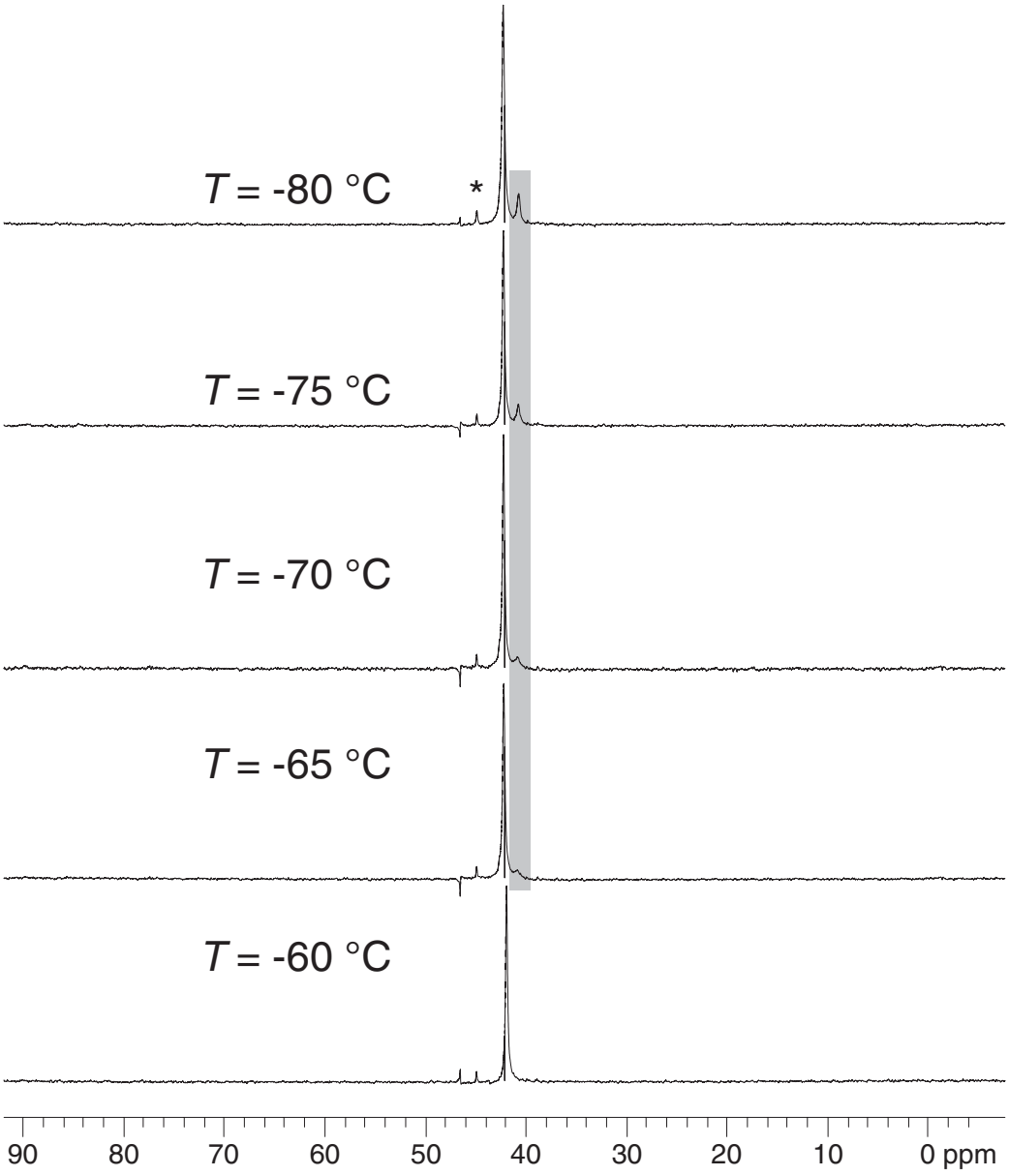


Zr axis as has been postulated to occur in analogous amidinate complexes (5). The spectra are unchanged on warming above 25 °C suggesting a significant barrier for this process.

In the presence of excess dialkyl, complex **5** forms fluxional dinuclear species **6** that appear analogous to those reported by Sita and co-workers (5) for the corresponding amidinate complexes and which are important in degenera-

© 2006 NRC Canada

Fig. 2. Variable-temperature ^{31}P NMR spectra (80.96 MHz, CD_2Cl_2) of a ca. 2:1 mixture of **4b** and $[Ph_3C][B(C_6F_5)_4]$. The signal owing to excess **4b** is marked with an asterisk, while the exchange-broadened signal for the minor isomer of **6b** (Scheme 1) is highlighted in grey.

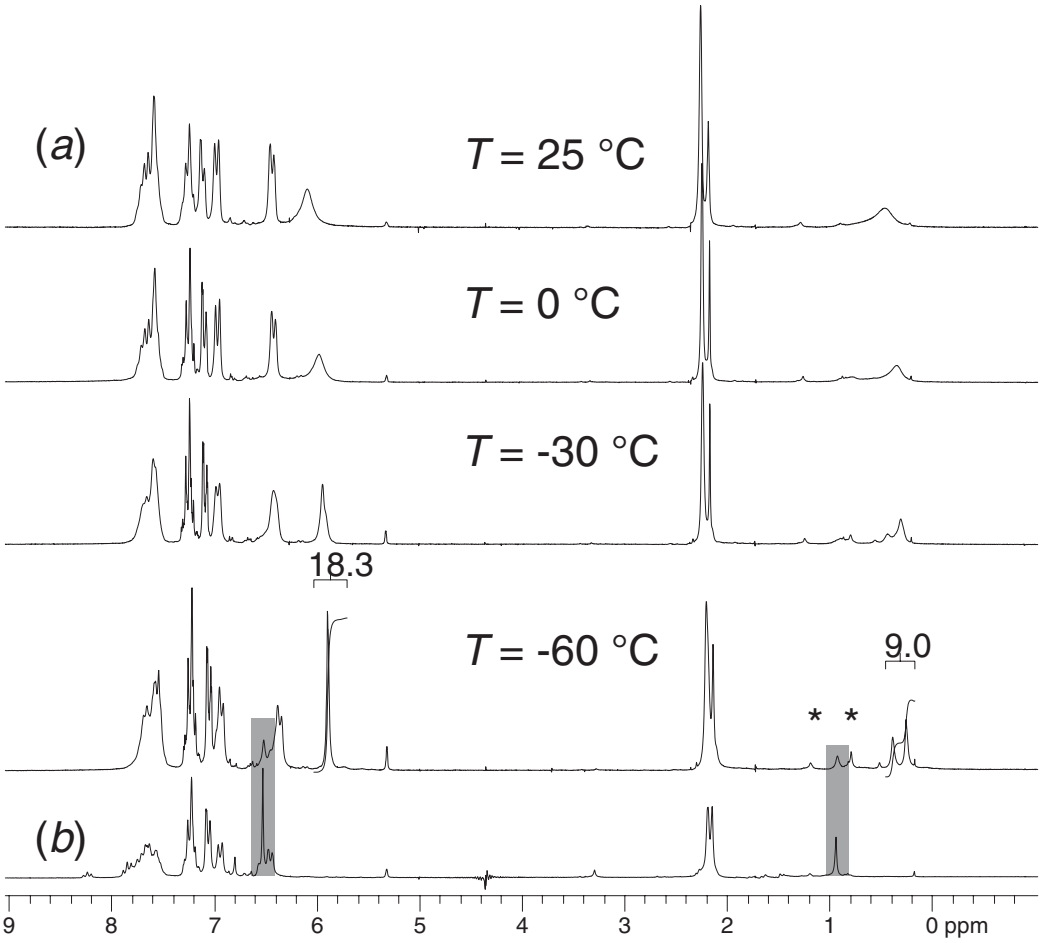


tive chain transfer processes with these quasi-living initiators. The ^1H NMR spectra of **6** are deceptively simple with equivalent PEt_2 groups in the case of **6b** at room temperature (Fig. 1*b*). Since complex **5b** appears static on the NMR timescale at room temperature, while complexes **4b** are fluxional and with a low barrier to rotation about the PN_2 ligand in solution (8, 12), it is possible that degenerate Me exchange (5) is the process responsible for higher effective symmetry observed for complexes **6** at room temperature. Both isomers (Scheme 1) should otherwise exhibit inequivalent PEt_2 groups even if intramolecular exchange between isomers were fast on the NMR timescale; alternately, it could be that as with **4**, rotation of the PN_2 ligand about the Zr—P axis is rapid in these dinuclear complexes.

Although we were unable to attain the slow exchange limit on the ^1H NMR timescale, separate ^{31}P NMR signals in an ~9:1 ratio and which may correspond to the different stereoisomers expected for **6b** (Scheme 1), were observed on cooling a solution of **4b**:$[Ph_3C][B(C_6F_5)_4]$ (~2:1) to –80 °C in CD_2Cl_2 (Fig. 2, signal owing to the minor isomer at δ 40.8 highlighted in grey). We did not observe a separate signal for **5b** at this temperature, although a signal owing to a slight excess of **4b** is evident in this experiment (Fig. 2, signal at δ 44.8 indicated by an asterisk). Thus, exchange between **4b** and **6b** appears slow on the NMR timescale at low temperature (only a single ^{31}P resonance is seen at room temperature) implying that the fluxional behavior observed at this low temperature is intramolecular and involves the

© 2006 NRC Canada

Fig. 3. (*a*) Variable-temperature ^{1}H NMR spectra (200 MHz, CD_2Cl_2) of a 2:1 mixture of **4a** and $[Ph_3C][B(C_6F_5)_4]$ and (*b*) ^{1}H NMR spectrum (200 MHz, CD_2Cl_2, –60 °C) of a 1:1 mixture of **4a** and $[Ph_3C][B(C_6F_5)_4]$. Signals marked with an asterisk are due to *n*-hexane.



two stereoisomers possible for **6b**. However, as the ^{1}H NMR spectrum exhibits equivalent, but line-broadened PEt_2 signals at –80 °C, we have been unable to confirm this hypothesis.

Similar behavior was observed for the *p*-tolyl analogues **4a** and **5a**, although it would appear that the rates (and mechanisms) of fluxional behavior are sensitive to the nature of the substituents on N. Thus, the room-temperature spectrum of a ca. 2:1 mixture of **4a** and $[Ph_3C][B(C_6F_5)_4]$ exhibits line-broadened resonances for the CpH and Zr-Me groups (Fig. 3*a*), and on cooling, decoalescence of the Cp and Zr–Me resonances were observed. At low temperature, separate signals owing to residual **5a** are observed (Fig. 3*a* vs. 3*b*), while the two remaining Zr-Me and one Cp-H signals are consistent with there being one isomer of **6a** present in solution. The signals owing to terminal and bridging Zr-Me groups of **6a** should be in a 2:1 ratio, but integration of these exchange-broadened resonances at –60 °C is only approximately consistent with this (Fig. 3*a*). An alternative explanation in which there are two isomers present in slow exchange with each other but featuring rapid exchange between terminal and bridging methyl groups for each isomer has to be rejected since this process would *also* interconvert the two stereoisomers.

On attempted crystallization of **6b**, crystals of dinuclear complex **7** (Scheme 1) separated on standing in CH_2Cl_2–chlorobenzene solution after several days at –30 °C. Although the X-ray structure of the cation is disordered (the anion is perfectly ordered),[6] this complex is also analogous to a μ-Me, μ-CH_2 dinuclear bis(amidinate) complex reported by Sita and co-workers (5). In the present case, this must form by a intramolecular C—H activation reaction involving dinuclear complexes **6** since there is no $PhNMe_2$ present as in the reaction reported by Sita and co-workers. Similar behavior was exhibited by **4a** and $[Ph_3C][B(C_6F_5)_4]$ in concentrated toluene solution (ca. 0.05 mol/L); a complex analogous to **7** is formed directly along with methane. We suspect that dissociation of **6** is unfavorable in nondonor media so that intramolecular C—H activation is more facile than complete ionization of **4a** by $[Ph_3C][B(C_6F_5)_4]$.

[6] Space group *C*2/*c*, *Z* = 4 based on $[C_{32}H_{71}N_4Si_4P_2Zr_2][C_{24}BF_{20}]$-$CH_2Cl_2$: Unit cell: *a* = 29.128(3) Å, *b* = 10.690(1) Å, *c* = 23.627(2) Å, β = 103.916(3)°; *V* = 7141(2) Å^3 at 180 K. The dinuclear cation sits on an inversion centre, while the borate counteranion and methylene chloride sit on diads. The disorder appears to arise from the coexistence of two different phases (ca. 80:20) in the lattice. N.J. Taylor. Unpublished results.

© 2006 NRC Canada

Fig. 4. ^{31}P NMR spectra (121.44 MHz, C_6D_5Br, 25 °C) of: (*a*) a 50:1 mixture of PMAO and **4a**, (*b*) a 1:1 mixture of **4a** and $[Ph_3C][B(C_6F_5)_4]$, (*c*) complex **4a**, and (*d*) a 1:1 mixture of $AlMe_3$ and $Ph_2P(=NAr)NHAr$ (Ar = *p*-tolyl).

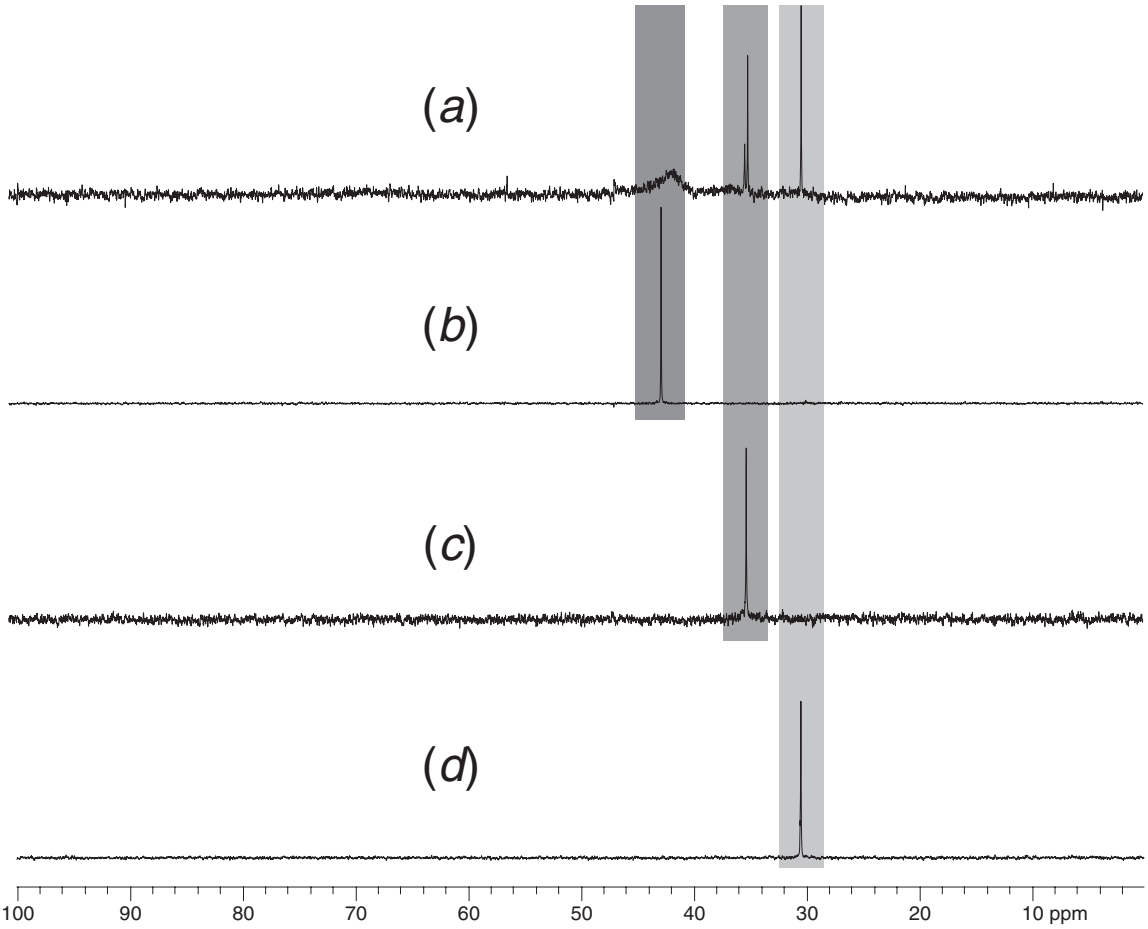


Table 4. Polymerization data for 1-hexene using complex **4a** and various activators.

Entry	Cocat.[a]	[**4a**] (mmol/L)	Zr:B	[1-Hx] (mol/L)	*t* (min)	*T* (°C)	Act.[b]	Conv. (%)	M_n (K)	M_w/M_n	*f*[c] (%)
1	A	2.4	1:1	5.4	0	60	0.24	1.3	13.1	1.35	19
2	A	3.6	1:1	4.0	30	25	1.70	9.0	5.95	1.22	141
3[d]	A	3.0	1:1	1.6	15	25	11.0	68.9	32.6	1.50	95
4	B	4.8	1:1	2.7	60	25	2.26	48.3	2.34	1.74	979
5	B	4.8	2:1	2.7	60	25	2.62	55.9	3.28	1.34	807
6	B	4.8	1:2	2.7	60	25	2.31	49.3	4.55	1.40	513
7	B	2.9	1:1	6.4	60	25	—	—	3.90	1.54	—
8	C	4.8	1:1	2.7	60	25	1.07	22.8	1.62	1.42	665

Note: Conditions: polymerizations were conducted for 60 min at 25 °C by adding 1-hexene to a solution of **4a** and the cocatalyst in chlorobenzene.
[a]Cocatalyst: A = $[PhNMe_2H][B(C_6F_5)_4]$; B = $[Ph_3C][B(C_6F_5)_4]$; C = $B(C_6F_5)_3$.
[b]Activity in 10^4 g polymer / (mol Zr × h).
[c]Initiator efficiency $f = \frac{M_n^{theor}}{M_n^{exp}} \times 100$ with $M_n^{theor} = \frac{[1-Hx]}{[\mathbf{4a}]} \times \frac{Conv.(\%)}{100} \times 84.18$.
[d]Initiator was $Cp[MeC(NEt)(N\text{-}t\text{-}Bu)]ZrMe_2$ (see ref. 5).

As for the multisite behavior exhibited by alkyls **4** (or halides **3**) on activation with PMAO (Table 2), it would seem that side reactions between PMAO and alkyls **4** is partly responsible for the behavior seen. As shown in Fig. 4, a mixture of ^{31}P-containing compounds is produced on treatment of **4a** with 50.0 equiv. of PMAO in bromobenzene-d_5 solution at room temperature. The major product present has a broadened resonance at a chemical shift similar to that **5a** in this solvent, while unreacted alkyl **4a** is seen and also the product of PN_2 ligand abstraction by $AlMe_3$ viz. $Me_2Al(N\text{-}p\text{-tolyl})_2PPh_2$ as verified by reaction of the PN_2 ligand with $AlMe_3$ (Fig. 4*d*). It is unclear whether this compound forms from **4a** or **5a**, but the expected Zr by-product in either case (i.e., $CpZrMe_3$ or $[CpZrMe_2][PMAO\text{-}X]$) is known to be a viable polymerization catalyst (13), and which could account for the bimodal MWD seen.

© 2006 NRC Canada

We also evaluated complex **4a** and various activators for the living polymerization of 1-hexene at or above room temperature. The results are summarized in Table 4. The activity of this complex when activated with $[PhNMe_2H][B(C_6F_5)_4]$ is about 6.5 times lower than that reported for the less sterically hindered amidinate complex Cp[MeC(NEt)(N-*t*-Bu)]$ZrMe_2$ when evaluated under the same conditions (Table 4, entry 2 vs. 3). Activity was a function of the activator employed, where $[Ph_3C][B(C_6F_5)_4]$ gave rise to the most active systems and $B(C_6F_5)_3$ the least active as might be expected based on the coordinating ability of the counterion.

However, as can be appreciated from the results summarized in Table 4, complex **4a** provides much lower MW polymer than the amidinate system, even at similar levels of conversion. As can be seen from the last column of Table 4, initiator efficiencies are all well over 100% at room temperature with this catalyst, and thus there is extensive chain transfer occurring despite the relatively narrow polydispersity observed. We suspect the narrow MWD reflects inefficient fractionation of these low MW hexene oligomers by the GPC column set and the use of a light-scattering detector rather than anything intrinsic.

Analysis of these polymers by ^{13}C NMR spectroscopy revealed the presence of unsaturated alkylidene end groups. Tentatively, it would appear that alkyl complexes homologous to **5a** have an increased tendency towards β-H elimination compared with their amidinate analogues, which must be intrinsic. Although steric effects are undoubtedly important here, it would seem that the more electron-rich PN_2 complexes (PN_2 ligands are about 10^3 times less acidic than their amidinate analogues (14)) are more prone to chain transfer at least relative to their tendency towards incorporation of monomer through insertion.

Conclusions

Bis(PN_2) and Cp(PN_2) complexes of Zr (**2** and **3**, respectively) are a promising new class of polymerization catalyst with ethylene polymerization activities that approach that of bent metallocene complexes on activation with PMAO or single component activators such as $[Ph_3C][B(C_6F_5)_4]$. The use of an excess of aluminum alkyl (or the corresponding Zr–dialkyl) as scavenger in polymerizations involving the latter activator inhibits activity, probably through formation of hetero- or homo-dinuclear complexes. Multisite behavior is observed on activation of the complexes **3** with PMAO and this appears at least in part related to side reactions of the neutral precursor with $AlMe_3$ or PMAO present. Although stable cationic alkyls **5** can be prepared from precursors **3**, and appear to be one of the active species in PMAO-activated systems, they do not elicit living polymerization of 1-hexene under conditions analogous to those reported by Sita and co-workers (5) for amidinate complexes. Evidently, the more electron-rich PN_2 complexes suffer from faster chain transfer via β-H elimination relative to insertion.

Experimental

All reactions were conducted under an atmosphere of dry N_2. Standard techniques for the manipulation of air-sensitive compounds were employed (15). All solvents were reagent grade and were purified using a solvent purification system similar to that described in the literature (16). Complexes **2**–**4** were prepared and characterized as described in the literature (8).

^1H and ^{13}C NMR spectra (referenced to residual protonated solvent) were recorded on Bruker AC 200, AM 250, AC 300, or Varian Innova 400 MHz spectrometers. Chemical shifts are referenced to residual undeutrated solvent. ^{31}P NMR spectra (referenced to external 85% H_3PO_4) and ^{19}F NMR spectra (referenced to external $CFCl_3$) were obtained in the solvent indicated on a Bruker AC 200 or Varian Innova 400 MHz spectrometer. IR spectra were recorded on a Bomem MB-100 FT-IR instrument. Elemental analyses were performed by Oneida Research Services, Whitesboro, New York.

General polymerization procedure

Propylene polymerizations were conducted in either a 1 or 2 L Autoclave Engineers Zipperclave reactor. The temperature of the reactor was controlled using a Neslab RTE-110 constant temperature bath by circulation of coolant (ethylene glycol – water, 50:50 *v*/*v*) through an external jacket. The consumption of monomer (propylene) during the course of polymerization was monitored using a calibrated Matheson mass flow meter, which was controlled by a Matheson Dynablender model 8219 power supply / readout device. The progress of polymerization was monitored using Labtech Acquire data acquisition software, which converted the digital input reading to the desired value (mmol/s of monomer) using appropriate conversion factors.

Prior to each polymerization, the reactor was conditioned by evacuation for ~4 h at 100 °C, and then cooled under nitrogen after three refill–evacuation cycles. Two general procedures were followed for the polymerization of ethylene. Method A was followed when PMAO was used as cocatalyst, whereas method B was used for activators such as $[Ph_3C][B(C_6F_5)_4]$.

Method A

The reactor was charged with 450 mL of toluene followed by PMAO in 25 mL of toluene via syringe under an atmosphere of N_2 through a septum port. The reactor was then saturated with C_2H_4 at 75 psig (26 kPa) and at the indicated temperature. After 30 min at process temperature and pressure, the zirconium complex dissolved in toluene (25 mL) was injected by using a sample cylinder, pressurized to ca. 80 psig using dry N_2.

Method B

The reactor was conditioned as above. Instead of PMAO, the reactor was charged with trimethylaluminum (15 mmol) or triisobutylaluminum (65 mmol) and 475 mL toluene followed by saturation with C_2H_4. The dialkyl (11 μmol) was added to a slight excess of $[Ph_3C][B(C_6F_5)_4]$ in toluene solution (25 mL) and the mixture was then added to the reactor using a sample cylinder.

Reactions were halted by venting the monomer and emptying the reactor contents into methanol. The polyethylene was filtered off and washed with methanolic HCl and methanol and then dried in a vacuum oven at ca. 65 °C. Polymer characterization procedures have been reported in detail elsewhere (17).

© 2006 NRC Canada

NMR characterization of [{CpZr[(*p*-$CH_3(C_6H_4)N)_2PPh_2$]}-CH_3][$B(C_6F_5)_4$] (5a)

A NMR tube was loaded with dialkyl complex **4a** (32 mg, 0.055 mmol) and [Ph_3C][$B(C_6F_5)_4$] (51 mg, 0.055 mmol) and cooled to –78 °C. Methylene chloride-d_2 (0.6 mL) was syringed into the tube resulting in an orange solution. ^{1}H NMR spectra over the temperature range –90 to 25 °C revealed a quantitative 1:1 reaction had taken place to form the title complex. ^{1}H NMR (CD_2Cl_2, ambient) δ: 7.60, 7.25 (m, 10 H, Ph), 7.10, 6.51 (d, 8H, J = 6.5 Hz, *p*-$CH_3(C_6H_4)$N), 6.60 (s, 5H, Cp), 2.20 (s, 6H, *p*-$CH_3(C_6H_4)$N), 1.03 (s, 3H, Zr-Me). ^{19}F NMR (CD_2Cl_2, ambient) δ: –132.8 (br m, 8F), –163.4 (t, 4F), –167.2 (m, 8F). ^{31}P NMR (bromobenzene-d_5, ambient) δ: 41.5.

Synthesis of [CpZr{$Et_2P(NTMS)_2$}Me][$B(C_6F_5)_4$] (5b)

Complex **4b** (0.118 g, 0.262 mmol) and [Ph_3C][$B(C_6F_5)_4$] (0.242 g, 0.262 mmol) were weighed into a Schlenk flask and stirred for 2 min to mix the two solids. Then methylene chloride (20 mL) was added and the mixture was stirred at room temperature for 10 min to give a pale yellow solution. The solvent was removed in vacuo to give an off-white solid. The solid was stirred with hexane (20 mL) for 2 h and the resulting white solid filtered off (0.257 g, 88%). ^{1}H NMR (CD_2Cl_2, ambient) δ: 6.85 (s, 5H, Cp), 2.04 (overlapping dq, total 4H, CH_2CH_3), 1.22 (overlapping dt, total 6H, CH_2CH_3), 0.91 (s, 3H, Zr-CH_3), 0.24 (s, 18H, $SiCH_3$). ^{19}F{^{1}H} NMR (CD_2Cl_2, ambient) δ: –132.0 (br dd, 8F), –163.7 (t, 4F, J = 24.5 Hz), –167.4 (br m, 8F). ^{31}P{^{1}H} NMR (CD_2Cl_2, ambient) δ: 34.0 (s). Attempted recrystallization from dichloromethane–hexane led to oiling out and (or) decomposition; a satisfactory combustion analysis was not obtained.

NMR characterization of [{CpZr[(*p*-$CH_3(C_6H_4)N)_2PPh_2$]}$_2$-(μ-Me_3)][$B(C_6F_5)_4$] (6a)

A NMR tube was loaded with complex **4a** (30 mg, 0.052 mmol) and [Ph_3C][$B(C_6F_5)_4$] (24 mg, 0.026 mmol) and cooled to –78 °C. Methylene chloride-d_2 (0.6 mL) was syringed into the tube resulting in an pale yellow solution. Variable-temperature (–90 to 25 °C) ^{1}H NMR spectra revealed a quantitative 2:1 reaction had taken place to provide the title complex. ^{1}H NMR (CD_2Cl_2, ambient) δ: 7.68 and 7.24 (m, 20H, Ph), 7.00, 6.44 (d, 16H, J = 6.8 Hz, *p*-$CH_3(C_6H_4)$N), 6.09 (s, br, 10H, Cp), 2.18 (s, 12H, CH_3), 0.50 (br s, 9H, μ-CH_3). ^{19}F NMR (CD_2Cl_2, ambient) δ: –132.8 (s, br, 8F), –163.4 (m, 4F), –167.2 (s, br, 8F).

Synthesis of [{CpZr[$Et_2PN_2TMS_2$]}$_2$(μ-$Me)_3$][$B(C_6F_5)_4$] (6b)

Complex **4b** (0.225 g, 0.500 mmol) and [Ph_3C][$B(C_6F_5)_4$] (0.231 g, 0.250 mmol) were weighed into a Schlenk flask and stirred for 2 min to mix the two solids. Then methylene chloride (15 mL) was added and the mixture was stirred at room temperature for 10 min to give an orange-yellow solution. The solvent was removed in vacuo to give an orange solid, which was slurried in hexane and filtered to give the crude material (0.389 g, 88%). ^{1}H NMR (CD_2Cl_2, ambient) δ: 6.54 (s, 10H, Cp), 1.89 (dq, 8H, J = 8.2 Hz, CH_2CH_3), 1.23 (dt, 12H, J = 7.5 Hz, CH_2CH_3), 0.27 (s, 9H, μ-CH_3), 0.18 (s, 36H, $SiCH_3$). ^{19}F NMR (CD_2Cl_2, ambient) δ: –132.9 (br m, 8F), –163.7 (t, 4F), –167.5 (br m, 8F). ^{31}P{^{1}H} NMR (CD_2Cl_2, ambient) δ: 42.2 (s). Attempted recrystallization of **6b** from chlorobenzene – methylene chloride led to the formation of complex **7** (see the following).

Synthesis of [{CpZr[$Ph_2PN_2TMS_2$]}$_2$(μ-CH_2)(μ-CH_3)]-[$B(C_6F_5)_4$] (7)

$CpZr[Ph_2PN_2TMS_2]Me_2$ (0.200 g, 0.444 mmol) and [Ph_3C][$B(C_6F_5)_4$] (0.205 g, 0.222 mmol) were weighed into a Schlenk flask and stirred for 2 min to mix the two solids. Then methylene chloride (15 mL) was added and the mixture was stirred at room temperature for 10 min. The solvent was removed in vacuo and the remaining orange solid was stirred with hexane (20 mL) for 1 week. The solvent was removed in vacuo to give an orange solid, which was dissolved in a chlorobenzene – methylene chloride mixture (1 mL : 0.5 mL) and placed in a –30 °C freezer to give orange crystals (0.199 g, 52%). Alternatively, placement of a chlorobenzene – methylene chloride solution of complex **6b** in a –30 °C freezer also gave the title complex. ^{1}H NMR (CD_2Cl_2, ambient) δ: 6.49 (s, 10H, Cp), 2.17 (m, 4H, CH_2CH_3), 1.60 (m, 4H, CH_2CH_3), 1.44 (dt, 6H, J = 7.3 Hz, CH_2CH_3), 1.10 (dt, 6H, J = 7.3 Hz, CH_2CH_3), 0.47 (s, 2H, μ-CH_2), 0.28 (s, 3H, μ-CH_3), 0.20 (s, br, 36H, $SiCH_3$). ^{19}F NMR (CD_2Cl_2, ambient) δ: –133.0 (br m, 8F), –163.7 (t, 4F), –167.5 (m, 8F). Anal. calcd. for $C_{56}H_{71}N_4P_2Si_4BF_{20}Zr_2 \cdot CH_2Cl_2$: C 41.93, H 4.50, N 3.43; found: C 41.52, H 4.11, N 3.08.

Acknowledgments

The authors would like to thank the Natural Sciences and Engineering Research Council of Canada (NSERC), Nova Chemicals Corporation of Calgary, Alberta, and The University of Akron, Akron, Ohio for financial support of this work. Scott Collins would also like to acknowledge the efforts of Dean of Research, Arthur J. Carty, who was instrumental in establishing the NSERC/Nova Industrial Research Chair at the University of Waterloo.

References

1 . (*a*) V.C. Gibson and S.K. Spitzmesser. Chem. Rev. **103**, 283 (2003); (*b*) G.J.P. Britovsek, V.C. Gibson, and D.F. Wass. Angew. Chem. Int. Ed. **38**, 428 (1999).
2. (*a*) J. Barker and M. Kilner. Coord. Chem. Rev. **133**, 219 (1994); (*b*) F.T. Edelmann. Coord. Chem. Rev. **137**, 403 (1994).
3. (*a*) D. Herskovics-Korine and M.S. Eisen. J. Organomet. Chem. **503**, 307 (1995); (*b*) J.C. Flores, J.C.W. Chien, and M.D. Rausch. Organometallics, **14**, 1827 (1995); (*c*) A. Littke, N. Sleiman, C. Bensimon, D.S. Richeson, G.P.A. Yap, and S.J. Brown. Organometallics, **17**, 446 (1998); (*d*) V. Volkis, M. Shmulinson, C. Averbuj, A. Lisovskii, F.T. Edelmann, and M.S. Eisen. Organometallics, **17**, 3155 (1998); (*e*) C. Averbuj, E. Tish, and M.S. Eisen. J. Am. Chem. Soc. **120**, 8640 (1998).
4. (*a*) A.N. Chernega, R. Gomez, and M.L.H.J. Green. Chem. Soc. Chem. Commun. 1415 (1993); (*b*) R. Gomez, M.L.H. Green, and J.L. Haggitt. Chem. Soc. Chem. Commun. 2607 (1994); (*c*) R. Gomez, R. Duchateau, A.N. Chernega, A. Meetsma, F.T. Edelmann, J.H. Teuben, and M.L.H. Green. J. Chem. Soc. Dalton Trans. 217 (1995).
5. (*a*) K.C. Jayaratne and L.R. Sita. J. Am. Chem. Soc. **122**, 958 (2000); (*b*) K.C. Jayaratne, R.J. Keaton, D.A. Henningsen, and L.R. Sita. J. Am. Chem. Soc. **122**, 10490 (2000); (*c*) R.J.

© 2006 NRC Canada

Keaton, K.C. Jayaratne, J.C. Fettinger, and L.R. Sita. J. Am. Chem. Soc. **122**, 12909 (2000); (*d*) R.J. Keaton, K.C. Jayaratne, D.A. Henningsen, L.A. Koterwas, and L.R. Sita. J. Am. Chem. Soc. **123**, 6197 (2001); (*e*) K.C. Jayaratne and L.R. Sita. J. Am. Chem. Soc. **123**, 10754 (2001); (*f*) Y. Zhang, R.J. Keaton, and L.R. Sita. J. Am. Chem. Soc. **125**, 9062 (2003); (*g*) Y. Zhang and L.R. Sita. J. Am. Chem. Soc. **126**, 7776 (2004).

6. (*a*) M. Witt, H.W. Roesky, D. Stalke, F. Pauer, T. Henkel, and G.M. Sheldrick. J. Chem. Soc. Dalton Trans. 2173 (1989); (*b*) A. Recknagel, M. Witt, and F.T. Edelmann. J. Organomet. Chem. **371**, C40 (1989); (*c*) A. Recknagel, A. Steiner, M. Noltemeyer, S. Brooker, D. Stalke, and F.T. Edelmann. J. Organomet. Chem. **414**, 327 (1991); (*d*) U. Kilimann, M. Noltemeyer, M. Schafer, R. Herbst-Irmer, H.-G. Schmidt, and F.T. Edelmann. J. Organomet. Chem. **469**, C27 (1994); (*f*) E. Muller, J. Muller, F. Olbrich, W. Bruser, W. Knapp, D. Abeln, and F.T. Edelmann. Eur. J. Inorg. Chem. 87 (1998), and refs. cited therein.
7. (*a*) Preliminary communication: R. Vollmerhaus, P. Shao, N.J. Taylor, and S. Collins. Organometallics, **18**, 2731 (1999); (*b*) R. Vollmerhaus, S. Collins, and Q. Wang. US Patent 6 268 448, 2001.
8. R. Vollmerhaus, R. Tomaszewski, P. Shao, K. Wiacek, S.P. Lewis, A. Al-Humydi, N.J. Taylor, and S. Collins. Organometallics, **24**, 494 (2005).
9. G.J.P. Britovsek, M. Bruce, V.C. Gibson, B.S. Kimberley, P.J. Maddox, S. Mastroianni, S.J. McTavish, C. Redshaw, G.A. Solan, S. Stroemberg, A.J.P. White, and D.J. Williams. J. Am. Chem. Soc. **121**, 8728 (1999).
10. R. Vollmerhaus, M. Rahim, R. Tomaszewski, S. Xin, N.J. Taylor, and S. Collins. Organometallics, **19**, 2161 (2000).
11. R.A. Stapleton, B.R. Galan, S. Collins, R.S. Simons, J.C. Garrison, and W.J. Youngs. J. Am. Chem. Soc. **125**, 9246 (2003).
12. For a definitive study using amidinate complexes, see: L.A. Koterwas, J.C. Fettinger, and L.R. Sita. Organometallics, **18**, 4183 (1999), and refs. cited therein.
13. (*a*) J.C.W. Chien and B.P. Wang. J. Polym. Sci. Part A: Polym. Chem. **28**, 15 (1990); for discrete examples, see: (*b*) D.J. Gillis, M.-J. Tudoret, and M.C. Baird. J. Am. Chem. Soc. **115**, 2543 (1993), and refs. cited therein.
14. (*a*) G. Genkina, B. Korolev, V. Gilyarov, B. Stepanov, and M. Kabachnik. Russ. J. Gen. Chem. **39**, 306 (1969); (*b*) A. Kraft, L. Peters, and H. Powell. Tetrahedron, **58**, 3499 (2002).
15. D.F. Shriver and M.A. Drezdon. The manipulation of air-sensitive compounds. 2nd ed. Wiley, New York. 1986.
16. A.B. Pangborn, M.A. Giardello, R.H. Grubbs, R.K. Rosen, and F.J. Timmers. Organometallics, **15**, 1518 (1996).
17. A.M. Bravakis, L.E. Bailey, M. Pigeon, and S. Collins. Macromolecules, **31**, 1000 (1998).

© 2006 NRC Canada

Syntheses, characterization, and crystal structures of the tetramethylammonium salts of the novel weakly coordinating anions $[MeCO_2\{B(C_6F_5)_3\}]^-$ and $[MeCO_2\{B(C_6F_5)_3\}_2]^-$ [1]

Simona Mitu and Michael C. Baird

Abstract: The novel compounds $[Me_4N][MeCO_2\{B(C_6F_5)_3\}]$ and $[Me_4N][MeCO_2\{B(C_6F_5)_3\}_2]$ are prepared and characterized spectroscopically and crystallographically. The compounds are salts of the unisolable acids $MeCO_2H{\cdot}B(C_6F_5)_3$ and $MeCO_2H{\cdot}2B(C_6F_5)_3$, respectively, which are sufficiently strong that they can protonate isobutene and initiate its carbocationic polymerization. The 1:1 adduct contains a conventional, monodentate acetate ion coordinated to the $B(C_6F_5)_3$, while the 2:1 adduct contains a bridging acetate ligand.

Key words: weakly coordinating anions, carbocationic polymerization, isobutene, polyisobutene.

Résumé : On a préparé les nouveaux composés $[Me_4N][MeCO_2\{B(C_6F_5)_3\}]$ et $[Me_4N][MeCO_2\{B(C_6F_5)_3\}_2]$ et on les a caractérisés sur des bases spectroscopiques et cristallographiques. Les composés sont respectivement des acides $MeCO_2H{\cdot}B(C_6F_5)_3$ et $MeCO_2H{\cdot}2B(C_6F_5)_3$ qui ne peuvent pas être isolés, mais qui sont suffisamment forts pour protoner l'isobutène et initier sa polymérisation carbocationique. L'adduit 1 : 1 contient un ion acétate monodentate conventionnel qui est lié par coordination au $B(C_6F_5)_3$ alors que l'adduit 2 : 1 comporte un ligand acétate qui agit comme pont.

Mots clés : anions faiblement coordinés, polymérisation carbocationique, isobutène, polyisobutène.

[Traduit par la Rédaction]

Recent years have seen extraordinary developments in the once esoteric field of "weakly coordinating anions" (1). For present purposes, weakly coordinating anions may be defined loosely, if narrowly, as anions that, in solution, bind sufficiently weakly to cationic species such as H^+, carbocations, or metal ions that they are readily displaced by such normally poor electron pair donors as unsaturated hydrocarbons (1). Of great relevance here are the clearly similar, important properties of weakly coordinating anions in the complementary fields of the coordination polymerization of olefins such as ethylene and 1-alkenes (2) and of the carbocationic polymerization of, e.g., the more sterically hindered, electron-rich isobutene (3). As well-known examples of coordination polymerization catalysis, active catalysts are often generated from neutral zirconocene precursors, as in Scheme 1 (2).

Since monomer access to the active metal site of $[Cp'ZrMe]^+$ may be effectively blocked if the counteranion X^- binds too strongly to the metal, it is clearly important that X^- be an exceedingly poor ligand if olefin coordination and subsequent polymerization are to occur (Scheme 2).

In a similar vein, initiation of carbocationic polymerization of an olefin such as isobutene involves interaction of a molecule of monomer with, e.g., a strong acid, as in Scheme 3.

The carbocationic center so formed is stabilized by solvent and (or) counteranion X^-, and the latter must be a very poor Lewis base, otherwise the ions will combine to give the neutral compound Me_3CX. Chain propagation involves displacement of X^- by monomer and repeated additions of alkene molecules to the carbocationic center, which migrates well away from the site of initial attack (Scheme 4).

Weakly coordinating counteranions result in higher molecular weights (3*d*, 3*e*), and thus, in chemistry reminiscent of coordination polymerization, the C=C bond must be the most nucleophilic species in the system. Indeed, many cationic transition metal complexes function as both coordination catalysts and carbocationic initiators (3*f*, 4).

Much attention has been paid to the development of catalysts utilizing the chemistry of Scheme 1 (2, 5–8), and many new weakly coordinating anions X^- have been designed on the premise that delocalization of negative charge over as many atoms as possible in a large anion should be of advantage (5–8). Thus, there have been reported several very bulky anions in which the perfluorophenyl groups of $[BMe(C_6F_5)_3]^-$ have been substituted by more complex perfluoroaryl groups (5*g*–5*p*). Alternative, synthetically less

Received 8 June 2005. Published on the NRC Research Press Web site at http://canjchem.nrc.ca on 14 March 2006.

Dedicated to Dr. Arthur Carty, an excellent scientist, a visionary, a bon vivant, and a very generous friend.

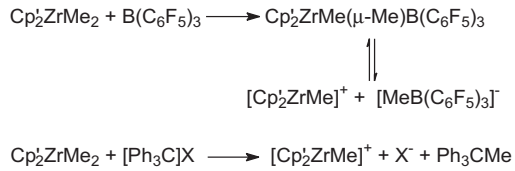
S. Mitu and M.C. Baird.[2] Department of Chemistry, Queen's University, Kingston, ON K7L 3N6, Canada.

[1]This article is part of a Special Issue dedicated to Professor Arthur Carty.

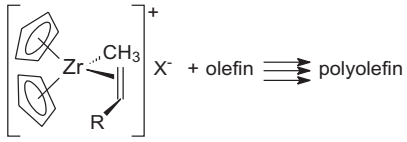
[2]Corresponding author (e-mail: bairdmc@chem.queensu.ca).

 doi:10.1139/V05-245 © 2006 NRC Canada

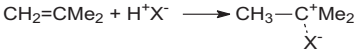
Scheme 1. Cp′ = substituted cyclopentadienyl, X^- = weakly coordinating anion.



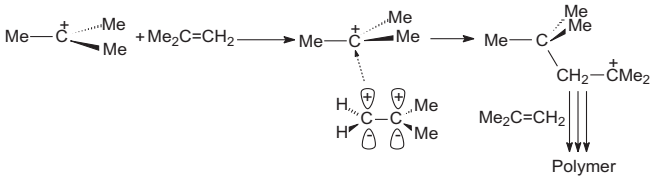
Scheme 2. R = H, alkyl.



Scheme 3.

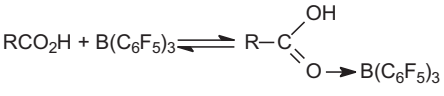


Scheme 4.

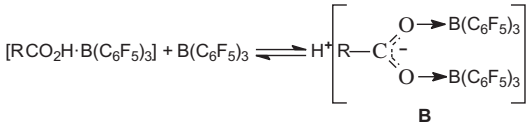


challenging procedures involve interaction of $B(C_6F_5)_3$ with various anions Y^- (Y^- = e.g., OH^- (6), CN^- (5*f*, 7*a*), N_3^- (7*b*), OR^- (6*b*–6*d*, 6*j*), SR^- (6*b*–6*d*), imidazolate (7*c*)) to form complex anions of the types $[YB(C_6F_5)_3]^-$ and $[(\mu\text{-}Y)\{B(C_6F_5)_3\}_2]^-$. In addition, we have recently reported utilization of $[Me_3CH_2B(C_6F_5)_3]^-$ in which the sterically demanding neopentyl group renders the borate anion much less weakly coordinating than is the above-mentioned methyl analogue, $[BMe(C_6F_5)_3]^-$ (8).

Complementing aspects of the above-mentioned research, we have reported the synthesis and utilization for isobutene polymerization of strong acids of the types $[ROH\{B(C_6F_5)_3\}_{1,2}]$ and $[RCO_2H\{B(C_6F_5)_3\}_{1,2}]$ (R = alkyl, aryl) (9, 10). Carboxylic acids, RCO_2H, do not by themselves initiate isobutene polymerization but are apparently activated via formation of adducts with $B(C_6F_5)_3$, as in eqs. [1] and [2].

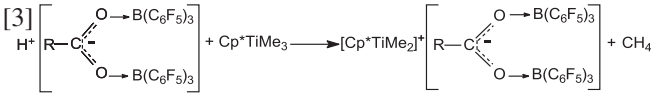
[1] 

A

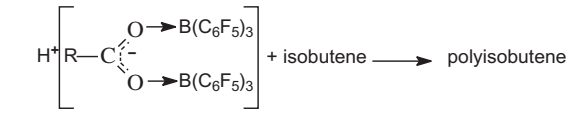
[2] 

B

These can then react with metallocene-type compounds, as in eq. [3], generating the cationic $[Cp^*TiMe_2]^+$, a known initiator for both coordination and carbocationic olefin polymerization reactions (10*a*), or they can be used directly to initiate the carbocationic polymerization of, e.g., isobutene and similarly polymerizable olefins (eq. [4]) (10*b*–10*d*).

[3] 

C

[4] 

The species formed when a carboxylic acid is combined with 2 equiv. of the borane is thus a novel type of Brønsted acid, sufficiently strong to protonate isobutene; presumably its conjugate base, $[RCO_2\{B(C_6F_5)_3\}_2]^-$, is stabilized by extensive delocalization of the negative charge. However, to this point the nature of the species in solution had been inferred only from the chemistry observed, and we have possessed only spectroscopic information concerning the structures of the putative products of eqs. [1] and [2].

Complicating our attempts to investigate spectroscopically the nature of the species in solution, we have found that the 1:1 and 2:1 adducts **A** and **B** are sufficiently acidic that cleavage of the B—C_6F_5 bonds occurs readily above about –30 °C to give pentafluorobenzene. We wished, however, to determine unequivocally the nature of the borane–carboxylate species in solution, and we have now accomplished this by isolating and characterizing salts of the conjugate bases of the products of eqs. [1] and [2]. Although the best carbocationic polymerization initiators found previously have involved long-chain carboxylic acids (10), we decided that we might have better success obtaining crystalline materials if we were to use short-chain carboxylic acids, and we have now accomplished the successful syntheses and characterization of the 1:1 and 2:1 acetato compounds $[Me_4N][MeCO_2\{B(C_6F_5)_3\}]$ and $[Me_4N][MeCO_2\{B(C_6F_5)_3\}_2]$. Crystal structures of both tetramethylammonium salts confirm their structures. A subsequent paper will consider the nature of the conjugate acids of these types of anions and their roles in initiating carbocationic polymerization of isobutene.

We note reports elsewhere of isobutene polymerizations being effected in the presence of other dinuclear counteranions (4*g*, 11), and it seems clear that counteranions, which are weakly coordinating because of combinations of steric factors and extensive delocalization of charge, do indeed play a role similar to those mentioned above for coordination polymerization catalysts.

Experimental

Most synthetic procedures, unless otherwise noted, were carried out under an atmosphere of nitrogen or argon purified by passing through a column of BASF catalyst heated to 140 °C and a column of 5 Å molecular sieves. Manipulation of air-sensitive materials employed standard Schlenk line techniques and an Mbraun Labmaster glovebox. Solvents were dried by passing them through activated alumina col-

© 2006 NRC Canada

Table 1. Crystallographic data for $[Me_4N][MeCO_2\{B(C_6F_5)_3\}]$ and $[Me_4N][MeCO_2\{B(C_6F_5)_3\}_2]$.

	$[Me_4N][MeCO_2\{B(C_6F_5)_3\}]$	$[Me_4N][MeCO_2\{B(C_6F_5)_3\}_2]$
Empirical formula	$C_{25}H_{17}BC_{12}F_{15}NO_2$	$C_{44.72}H_{20.43}B_2C_{15.43}F_{30}NO_2$
	$(C_{24}H_{15}BF_{15}NO_2{\cdot}CH_2Cl_2)$	$([N(CH_3)_4]\{[(C_6F_5)_3B]_2(OOCCH_3)\}{\cdot}2.72CH_2Cl_2)$
Formula weight	730.11	1 387.99
Temperature (K)	180(2)	150(2)
Wavelength (Å)	0.710 73	0.710 73
Crystal system	Monoclinic	Triclinic
Space group	$P2_1/c$	$P\bar{1}$
Unit cell dimensions		
a (Å)	9.659(2)	11.682(2)
b (Å)	14.080(3)	15.629(3)
c (Å)	21.244(5)	17.363(3)
α (°)	90	100.132(3)
β (°)	90.137(4)	108.095(3)
γ (°)	90	108.198(3)
Volume (Å^3)	2 889.1(12)	2 728.7(8)
Z	4	2
Density (calcd.) (Mg/m^3)	1.679	1.689
Absorption coefficient (mm^{-1})	0.349	0.429
F(000)	1 456	1 368
Crystal size (mm^3)	0.3 × 0.3 × 0.2	0.4 × 0.4 × 0.3
θ Range for data collection (°)	1.74–28.24	1.44–28.30
Index ranges	$-12 \le h \le 12$,	$-14 \le h \le 14$,
	$-17 \le k \le 17$,	$-20 \le k \le 19$,
	$-28 \le l \le 27$	$-22 \le l \le 21$
Reflections collected	20 046	19 369
Independent reflections	6 686 [R(int) = 0.033 1]	12 259 (R(int) = 0.016 9]
Completeness to θ = 25.00° (%)	100.0	99.5
Absorption correction	Empirical (Bruker SADABS)	Empirical (Bruker SADABS)
Max. and min. transmission	1.000 0 and 0.744 7	1.000 0 and 0.912 1
Refinement method	Full-matrix least-squares on F^2	Full-matrix least-squares on F^2
Data / restraints / parameters	6 686 / 0 / 474	12 259 / 667 / 871
Goodness-of-fit on F^2	0.844	1.103
Final R indices $I > 2\sigma(I)$	R_1 = 0.038 1, wR_2 = 0.077 4	R_1 = 0.062 6, wR_2 = 0.194 9
R indices (all data)	R_1 = 0.083 9, wR_2 = 0.087 4	R_1 = 0.086 5, wR_2 = 0.208 4
Largest diff. peak and hole (e Å^{-3})	0.233 and –0.307	1.246 and –0.994

umns (Innovative Technology). All chemicals were purchased from Aldrich and were purified as appropriate before use. The compound $B(C_6F_5)_3$ was prepared as described in the literature (12).

The ^{1}H, ^{11}B, and ^{19}F NMR spectra were run on an Avance 400 NMR spectrometer, the residual proton resonances of the deuterated solvents serving as internal references. Mass spectra were obtained on a Quatro Fisons Pro Quadrupole mass spectrometer in EI mode with CH_2Cl_2 as solvent. Canadian Microanalytical Services of Delta, British Columbia, performed elemental analyses. X-ray crystallographic structure determinations were carried out using a Siemens P4 diffractometer with a Bruker SMART CCD 1000 detector and graphite-monochromated Mo Kα radiation (λ = 0.710 73 Å) controlled with a Crysostream controller 700. Typically a crystal was mounted on a glass fibre with epoxy glue. No significant decay was observed during data collection, and the data were processed on a Pentium PC using the Bruker AXS Windows NT SHELXTL software package (version 5.10) (13*a*). Neutral atom scattering factors were taken from Cromer and Waber (13*b*). The raw intensity data were converted to structure amplitudes and their esds using the program SAINT-plus, which corrects for *L*p and decay. Absorption corrections were applied using the program SADABS. The crystals are monoclinic space group $P2_1/c$ for $[Me_4N][MeCO_2\{B(C_6F_5)_3\}]$ and triclinic space group $P\bar{1}$ for $[Me_4N][MeCO_2\{B(C_6F_5)_3\}_2]$ based on the systematic absences, E statistics, and successful refinement of the structure. The structure was solved by direct methods. Full-matrix least-square refinements minimizing the function $\sum w(F_o^2 - F_c^2)^2$ were applied to the compound. For the structure of $[Me_4N][MeCO_2\{B(C_6F_5)_3\}]$, all non-hydrogen atoms in the structure were refined anisotropically, and only the hydrogen atoms of the solvent molecule were calculated; all the other hydrogen atoms were located directly from the difference Fourier map. For the structure of $[Me_4N][MeCO_2\{B(C_6F_5)_3\}_2]$, the solvent molecules ($2.72CH_2Cl_2$) in the crystal are severely disordered, and the SHELXL commands SIMU, DFIX, SAME, and PART were thus used to refine the structure. All non-hydrogen atoms in the structure (**II**) (except C47, C49, Cl13, and Cl14) were refined anisotropically. All hydrogen atoms were calculated,

© 2006 NRC Canada

Table 2. Important bond lengths and bond angles for $[Me_4N][MeCO_2\{B(C_6F_5)_3\}]$ and $[Me_4N][MeCO_2\{B(C_6F_5)_3\}_2]$.

Compound	$[Me_4N][MeCO_2\{B(C_6F_5)_3\}]$	$[Me_4N][MeCO_2\{B(C_6F_5)_3\}_2]$
Bond lengths (Å)		
C(1)—C(2)	1.499(3)	1.496(4)
C(2)—O(1)	1.324(2)	1.279(4)
C(2)—O(2)	1.217(2)	1.260(4)
B(1)—O(1)	1.514(2)	1.543(4)
B(2)—O(2)	—	1.568(4)
B(1)—C(3)	1.654(3)	1.649(5)
B(1)—C(9)	1.651(3)	1.650(5)
B(1)—C(15)	1.644(3)	1.628(4)
B(2)—C(21)	—	1.644(4)
B(2)—C(27)	—	1.636(5)
B(2)—C(33)	—	1.645(5)
Bond angles (°)		
C(1)-C(2)-O(1)	112.84(18)	114.8(3)
C(1)-C(2)-O(2)	123.32(19)	124.5(3)
O(1)-C(2)-O(2)	123.84(17)	120.7(3)
C(2)-O(1)-B(1)	119.74(14)	128.0(2)
C(2)-O(2)-B(2)	—	127.8(2)
O(1)-B(1)-C(15)	112.20(14)	108.8(2)
O(1)-B(1)-C(9)	105.93(14)	103.3(2)
O(1)-B(1)-C(3)	106.33(14)	109.9(2)
O(2)-B(2)-C(27)	—	105.9(2)
O(2)-B(2)-C(33)	—	103.7(2)
O(2)-B(2)-C(21)	—	112.1(3)
C(15)-B(1)-C(9)	116.35(15)	111.3(2)
C(15)-B(1)-C(3)	104.42(14)	116.7(2)
C(9)-B(1)-C(3)	111.28(15)	105.9(2)
C(21)-B(2)-C(27)	—	116.3(2)
C(21)-B(2)-C(33)	—	104.0(2)
C(27)-B(2)-C(33)	—	114.3(3)

and their contributions were included in the structure factor calculations with isotropic thermal parameters 1.2 times that of the attached carbon atoms (1.5 times for methyl hydrogens). Crystallographic data for the two compounds studied are summarized in Table 1, with selected bond distances and angles in Table 2. Molecular structures are shown in Figs. 1 and 2, and complete crystallographic data are given in the supporting information.[3]

Preparation of $[Me_4N][MeCO_2\{B(C_6F_5)_3\}]$

$[Me_4N][MeCO_2]$ was prepared by neutralizing tetramethylammonium hydroxide (6 mL, 25 wt% aqueous solution) with glacial acetic acid (1.43 mL, 0.0250 mol) (14). The solution was evaporated to dryness, and the solid residue was recrystallized from acetone and dried under reduced pressure for 12 h at 150 °C to give 2.1 g of $[Me_4N][MeCO_2]$ (95% yield). IR (Fluorolube mull, cm^{-1}) ν(CO): 1681, 1491. ^1H NMR (CD_2Cl_2) δ: 3.43 (s, 12H, MeN), 1.80 (s, 3H, MeC). To prepare $[Me_4N][MeCO_2\{B(C_6F_5)_3\}]$, a mixture of $B(C_6F_5)_3$ (250 mg, 0.49 mmol) and $[Me_4N][MeCO_2]$ (64.9 mg, 0.49 mmol) in dry CH_2Cl_2 (20 mL) was stirred at room temperature for 1 h, after which the solvent was removed under reduced pressure. The resulting white solid was recrystallized from a mixture of CH_2Cl_2 (5 mL) and hexanes (15 mL), filtered off, washed with hexanes, and dried to give 253 mg (80% yield) of product. IR (Fluorolube mull, cm^{-1}) ν(CO): 1682, 1491. ^1H NMR (CD_2Cl_2) δ: 3.13 (s, 12H, MeN), 1.94 (s, 3H, MeC). ^{11}B NMR (CD_2Cl_2) δ: –5.1 (sharp). ^{19}F NMR (CD_2Cl_2) δ: –135.9 (*o*-F), –163.6 (*p*-F), –168.2 (*m*-F). HR-MS (EI) calcd. for $[(CH_3)_4N]$: 74.1460; found: 74.0784. HR-MS (EI) calcd. for $[MeCO_2\{B(C_6F_5)_3\}]$: 571.0296; found: 571.0672. Anal. calcd. for $C_{24}H_{15}BF_{15}O_2 \cdot CH_2Cl_2$: C 41.13, H 2.35, N 1.92; found: C 41.58, H 2.38, N 1.88. Crystallographic quality crystals were grown by layering a solution of $[Me_4N][MeCO_2\{B(C_6F_5)_3\}]$ in CH_2Cl_2 with hexanes.

Preparation of $[Me_4N][MeCO_2\{B(C_6F_5)_3\}_2]$

A mixture of $B(C_6F_5)_3$ (500 mg, 0.98 mmol) and $[Me_4N][MeCO_2]$ (64.9 mg, 0.49 mmol) in CH_2Cl_2 (30 mL)

[3] Supplementary data for this article are available on the journal Web site (http://canjchem.nrc.ca) or may be purchased from the Depository of Unpublished Data, Document Delivery, CISTI, National Research Council Canada, Ottawa, ON K1A 0R6, Canada. DUD 4085. For more information on obtaining material refer to http://cisti-icist.nrc-cnrc.gc.ca/irm/unpub_e.shtml. CCDC 275372 and 275373 contain the crystallographic data for this manuscript. These data can be obtained, free of charge, via www.ccdc.cam.ac.uk/conts/retrieving.html (Or from the Cambridge Crystallographic Data Centre, 12 Union Road, Cambridge CB2 1EZ, UK; fax +44 1223 336033; or deposit@ccdc.cam.ac.uk).

© 2006 NRC Canada

Fig. 1. X-ray structure of $[Me_4N][MeCO_2\{B(C_6F_5)_3\}]$.

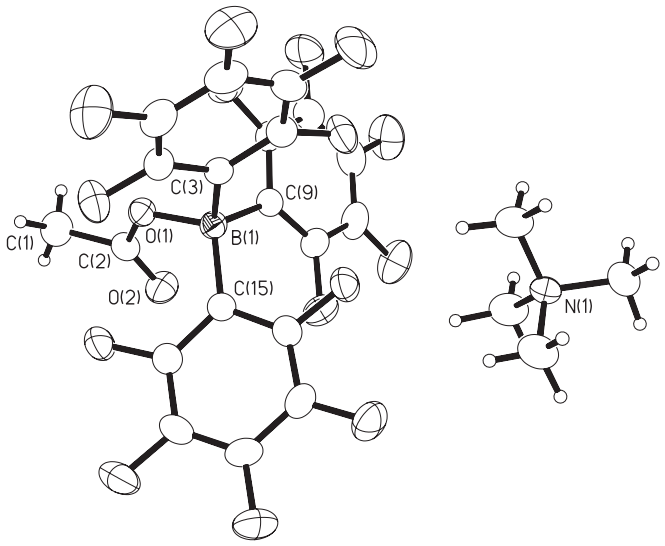
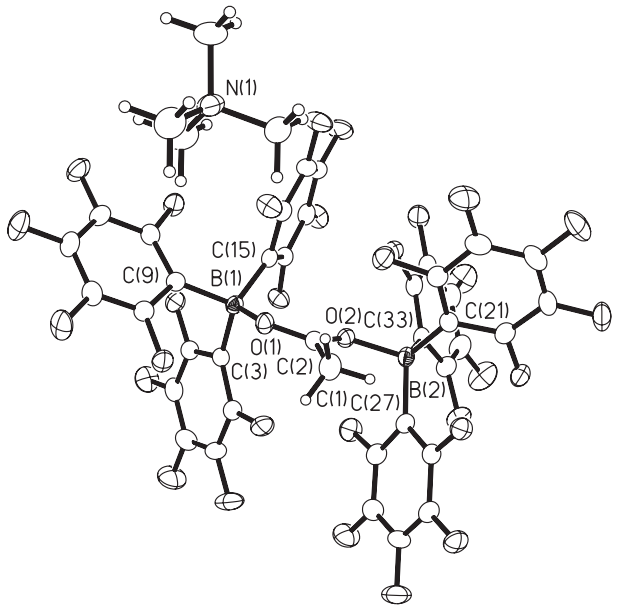


Fig. 2. X-ray structure of $[Me_4N][MeCO_2\{B(C_6F_5)_3\}_2]$.



was stirred at room temperature for 1 h, after which the solvent was removed under reduced pressure. The resulting white solid was recrystallized from a mixture of CH_2Cl_2 (5 mL) and hexanes (15 mL), filtered off, washed with hexanes, and dried to give 398 mg (70% yield) of product. IR (Fluorolube mull, cm^{-1}) ν(CO): 1566, 1417. ^1H NMR (CD_2Cl_2) δ: 3.22 (s, 12H, MeN), 2.19 (s, 3H, MeC). ^{11}B NMR (CD_2Cl_2) δ: –1.6 (broad). ^{19}F NMR (CD_2Cl_2) δ: –135.6 (*o*-F), –161.0 (*p*-F), –167.1 (*m*-F). HR-MS (EI) calcd. for $[(CH_3)_4N]$: 74.1460; found: 74.0832. HR-MS (EI) calcd. for $[MeCO_2\{B(C_6F_5)_3\}_2]$: 1083.0147; found: 1083.0642. Anal. calcd. for $C_{42}H_{15}B_2F_{30}O_2$: C 43.59, H 1.31, N 1.21; found: C 43.28, H 1.26, N 1.52. Crystallographic quality crystals were grown by layering a solution of $[Me_4N][MeCO_2\{B(C_6F_5)_3\}_2]$ in CH_2Cl_2 with hexanes.

Results and discussion

The combination of carboxylic acids and $B(C_6F_5)_3$, especially in a 2:1 $B(C_6F_5)_3$ – carboxylic acid ratio, results in an acid system sufficiently strong to protonate isobutene (IB) and to initiate its carbocationic polymerization (10). Carboxylic acids themselves are too weak to effect this chemistry, of course, and furthermore carboxylate anions are expected to bind very effectively to the carbocation intermediates. However, the inductive effects of carboxylic acid coordination to the strongly electrophilic borane in a species such as **B** would very likely result in an acid much stronger than the free carboxylic acid itself (10), as has been observed elsewhere with other potentially acidic Lewis base donors (6*j*, 15), and it seemed very likely that the reactions described in eqs. [1] and [2] would pertain. The purpose of this research was to prepare, characterize, and determine the structures of salts of the putative counteranions of species **A** and **B**.

Syntheses of $[Me_4N][MeCO_2\{B(C_6F_5)_3\}]$ and $[Me_4N][MeCO_2\{B(C_6F_5)_3\}_2]$

These two compounds were synthesized by reacting $[Me_4N][MeCO_2]$ with 1 and 2 molar equiv. of $B(C_6F_5)_3$, respectively. Both compounds were characterized fully by elemental analyses and IR and NMR spectroscopy; the crystals of the 1:1 adduct contained one molecule of CH_2Cl_2, as shown by the elemental analyses and X-ray crystallography. The IR spectra are illustrated in Figs. 3 and 4, and we note especially that the observed values of ν(CO) of 1682 and 1491 cm^{-1} for the 1:1 adduct and of 1566 and 1417 cm^{-1} for the 2:1 adduct are consistent with the literature for monodentate and bridging acetato ligands as in **D** and **E**, respectively (16).



D **E**

The positions of the symmetric stretches are in both cases uncertain because absorptions of the $B(C_6F_5)_3$ (indicated in the spectra by **B**) and the $[Me_4N]^+$ ion also appear in the region 1300–1800 cm^{-1}.

The ^1H, ^{19}F, and ^{11}B NMR spectra are shown in Figs. 5, 6, and 7, respectively, where they are compared with the spectra of $[Me_4N][MeCO_2]$ (^1H) and $B(C_6F_5)_3$ (^{19}F, ^{11}B). The electron-withdrawing power of the borane is evident in the acetate methyl ^1H resonances, and the changes in the ^{19}F chemical shifts on going from free to coordinated $B(C_6F_5)_3$ are characteristic (5–10). The ^{11}B chemical shifts of the adducts are similar to those of other adducts with O-donors, and the observed narrowing of the resonances is consistent with tetrahedral structures (6*h*, 17*b*–17*d*), although it is not at all clear why the 2:1 complex has a much broader resonance than does the 1:1 complex.

Crystal structures of $[Me_4N][MeCO_2\{B(C_6F_5)_3\}]$ and $[Me_4N][MeCO_2\{B(C_6F_5)_3\}_2]$

Crystal structures were obtained for both compounds, with the 1:1 complex containing a molecule of CH_2Cl_2. Selected bond distances and angles are shown in Table 2, and

© 2006 NRC Canada

Fig. 3. IR spectrum (Fluorolube mull) of $[Me_4N]\{[MeCO_2][B(C_6F_5)_3]\}$: * identifies ν(CO); **B** identifies peaks assignable to $B(C_6F_5)_3$.

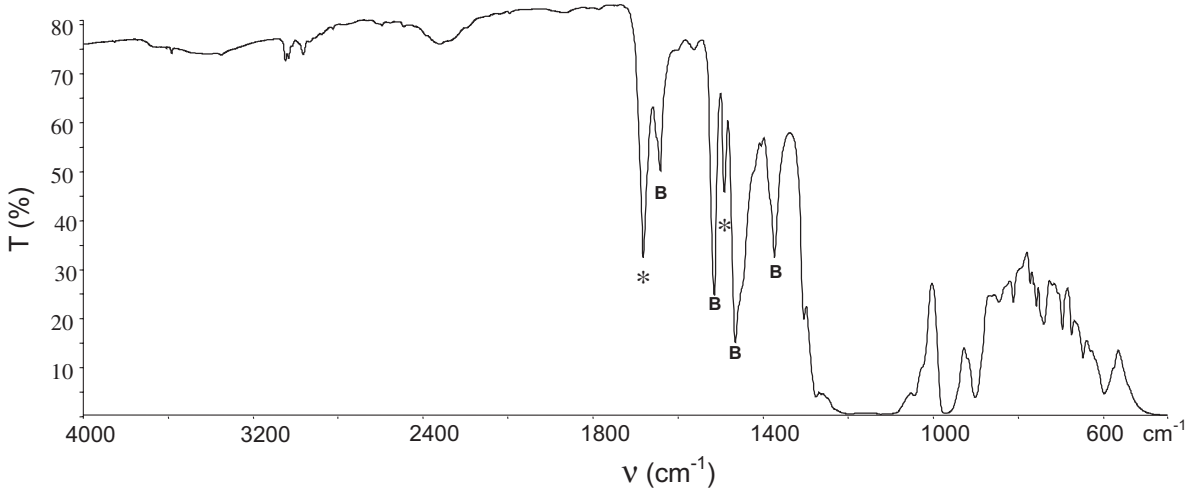


Fig. 4. IR spectrum (Fluorolube mull) of $[Me_4N]\{[MeCO_2][B(C_6F_5)_3]_2\}$: * identifies ν(CO); **B** identifies peaks assignable to $B(C_6F_5)_3$.

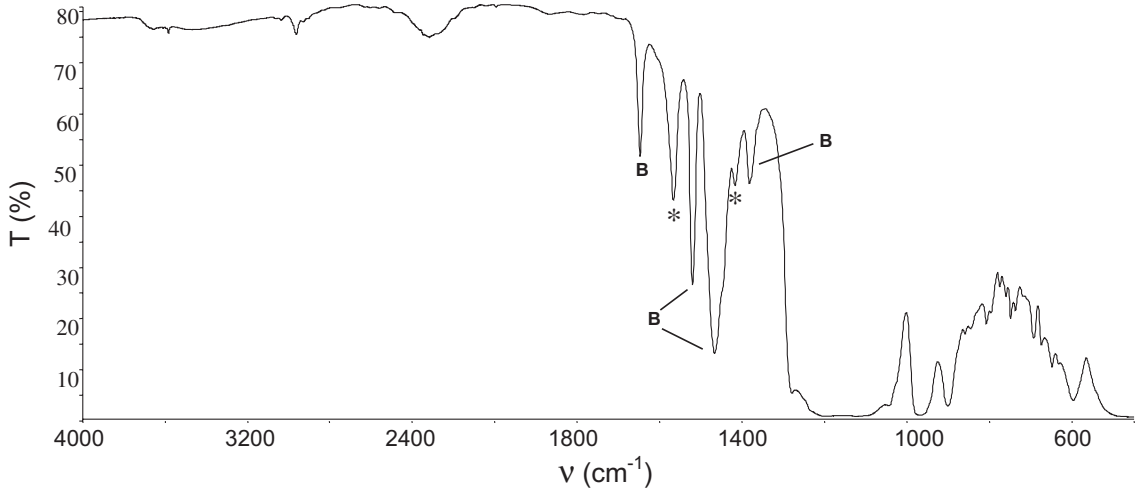
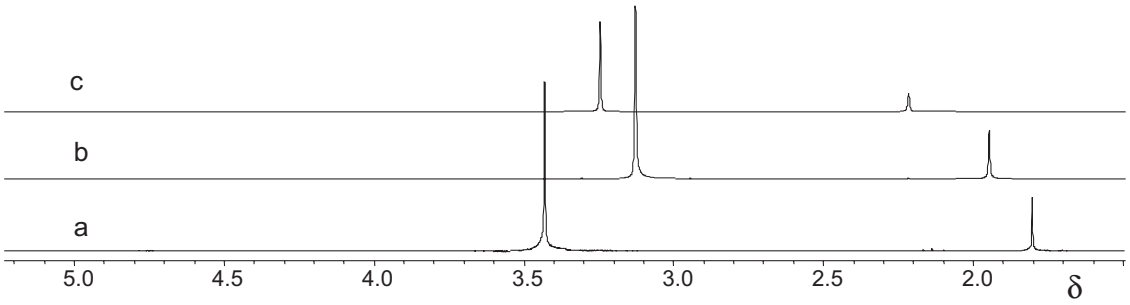


Fig. 5. ^1H NMR spectra of (*a*) $[Me_4N][MeCO_2]$, (*b*) $[Me_4N][MeCO_2\{B(C_6F_5)_3\}]$, and (*c*) $[Me_4N][MeCO_2\{B(C_6F_5)_3\}_2]$ (CD_2Cl_2).



molecular structures are shown in Figs. 1 and 2. As can be seen, the crystal structures are completely in accord with the modes of bonding suggested by **D** and **E**. Thus the carbon–oxygen bond lengths of the 1:1 adduct are 1.216(2) and 1.321(2) Å, as expected for a double and a single bond, respectively. On the other hand, the two carbon–oxygen distances of the 2:1 adduct are intermediate between these two values and are very similar to each other. Interestingly, the boron–oxygen distance in the 1:1 adduct is significantly shorter than that of the 2:1 adduct, consistent with the expected stronger B—O bond in the former. However, all three B—O distances fall in the range established for a variety of adducts of $B(C_6F_5)_3$ with a variety of other O-donors (6*h*, 6*j*, 17).

Possibly complementing the stronger donor–acceptor interaction in the 1:1 adduct, the average of the B—C_6F_5 bond lengths in this adduct is marginally longer than the average of the 2:1 adduct, although steric repulsions should be more

© 2006 NRC Canada

Fig. 6. ^{19}F NMR spectrum of (*a*) $B(C_6F_5)_3$, (*b*) $[Me_4N][MeCO_2\{B(C_6F_5)_3\}]$, and (*c*) $[Me_4N][MeCO_2\{B(C_6F_5)_3\}_2]$ in CD_2Cl_2.

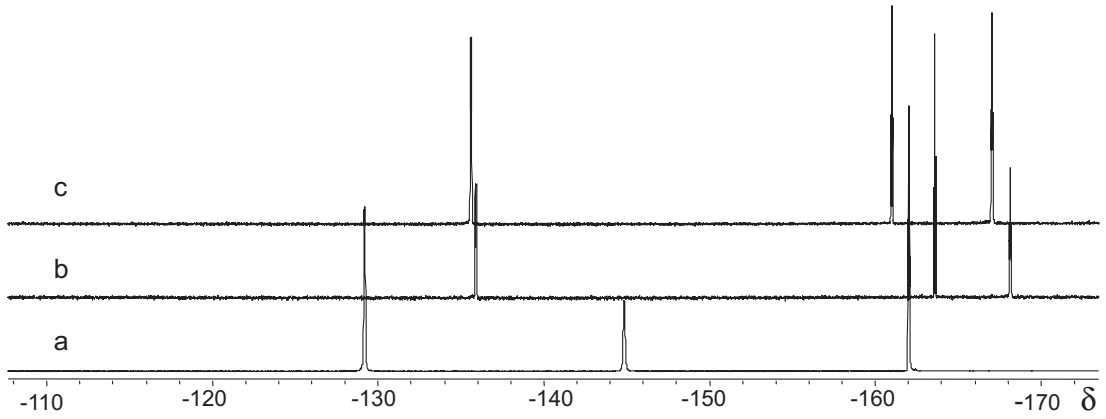
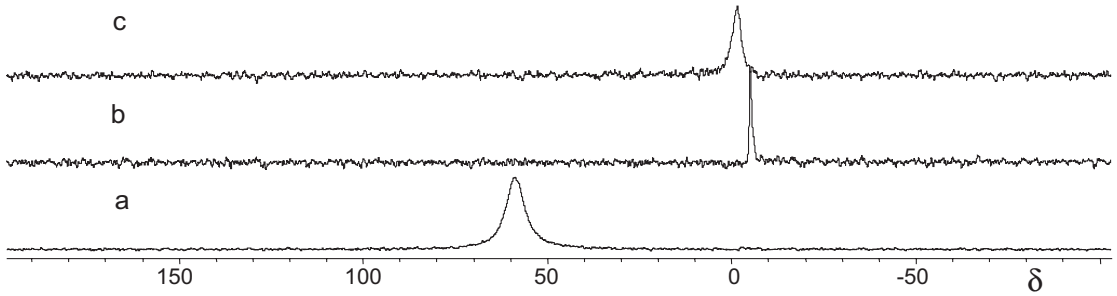


Fig. 7. ^{11}B NMR spectra of (*a*) $B(C_6F_5)_3$, (*b*) $[Me_4N][MeCO_2\{B(C_6F_5)_3\}]$, and (*c*) $[Me_4N][MeCO_2\{B(C_6F_5)_3\}_2]$ (CD_2Cl_2).



important in the latter. The acetate ions are essentially planar in both adducts, but the bond angles vary widely. Thus the O-C-O bond angle of the 1:1 adduct is significantly less than 120°, the two Me-C-O bond angles both being significantly greater. In contrast, the O-C-O bond angle of the 2:1 adduct is 120.7(3)°, while the two (chemically equivalent) Me-C-O bond angles vary widely. The O-B-C_6F_5 and C_6F_5-B-C_6F_5 bond angles vary considerably, but the latter variations seem to be normal (18).

Acknowledgements

We thank Queen's University, the Natural Sciences and Engineering Research Council of Canada (NSERC), and Lanxess Inc. for financial support, and Drs. A. Carr and M. Drewitt for helpful discussions and advice. We also thank Dr. R. Wang for his crystallographic expertise and help.

References

1. (*a*) M. Bochmann. Top. Catal. **7**, 9 (1999); (*b*) C.A. Reed. Acc. Chem. Res. **31**, 133 (1998); (*c*) M. Bochmann. Curr. Opin. Solid State Mater. Sci. **2**, 639 (1997); (*d*) M. Sperrle and G. Consiglio. Chem. Ber. Recl. **130**, 1557 (1997); (*e*) S.H. Strauss. Chem. Rev. **93**, 927 (1993); (*f*) W. Beck and K. Suenkel. Chem. Rev. **88**, 1405 (1988); (*g*) B. Stibr and B. Wrackmeyer. J. Organomet. Chem. **657**, 3 (2002); (*h*) H. Kobayashi. J. Fluorine Chem. **105**, 201 (2000).
2. (*a*) P.C. Möhring and N.J. Coville. J. Organomet. Chem. **479**, 1 (1994); (*b*) V.K. Gupta, S. Satish, and I.S. Bhardwaj. J. Macromol. Sci. Rev. Macromol. Chem. Phys. **C34**, 439 (1994); (*c*) H.H. Brintzinger, D. Fischer, R. Mülhaupt, B. Rieger, and R.M. Waymouth. Angew. Chem. Int. Ed. Engl. **34**, 1143 (1995); (*d*) M. Bochmann. J. Chem. Soc. Dalton Trans. 255 (1996); (*e*) W. Kaminsky and M. Arndt. Adv. Polym. Sci. **127**, 143 (1997); (*f*) J.C.W. Chien. *In* Topics in catalysis. Vol. 7. *Edited by* T.J. Marks and J.C. Stevens. Baltzer AG, Science Publishers, Switzerland. 1999. p. 23; (*g*) H.G. Alt and A. Köppl. Chem. Rev. **100**, 1205 (2000); (*h*) G.W. Coates. Chem. Rev. **100**, 1223 (2000); (*i*) L. Resconi, L. Cavallo, A. Fait, and F. Piemontesi. Chem. Rev. **100**, 1253 (2000); (*j*) K. Angermund, G. Fink, V.R. Jensen, and R. Kleinschmidt. Chem. Rev. **100**, 1457 (2000); (*k*) J. Scheirs and W. Kaminsky. *In* Metallocene-based polyolefins. John Wiley and Sons, UK. 2000.
3. (*a*) J.P. Kennedy and E. Maréchal. *In* Carbocationic polymerization. John Wiley and Sons, New York. 1982; (*b*) J.P. Kennedy and B. Iván. *In* Designed polymers by carbocationic macromolecular engineering: Theory and practice. Hanser Publishers, Munich. 1991; (*c*) T.D. Shaffer and J.R. Ashbaugh. J. Polymer Sci. A, **35**, 329 (1997); (*d*) S. Jacob, Z.J. Pi, and J.P. Kennedy. Polym. Bull. (Berlin), **41**, 503 (1998); (*e*) Z. Pi, S. Jacob, and J.P. Kennedy. *In* Ionic polymerizations and related processes. *Edited by* J.R. Puskas. Kluwer, Dordrecht, The Netherlands. 1999. p. 1; (*f*) M.C. Baird. Chem. Rev. **100**, 1471 (2000).
4. (*a*) F. Barsan and M.C. Baird. J. Chem. Soc. Chem. Commun. 1065 (1995); (*b*) Q. Wang and M.C. Baird. Macromolecules, **28**, 8021 (1995); (*c*) Q. Wang, R. Quyoum, D.J. Gillis, M.-J. Tudoret, D. Jeremic, B.K. Hunter, and M.C. Baird. Organometallics, **15**, 693 (1996); (*d*) F. Barsan, A.R. Karam, M.A. Parent, and M.C. Baird. Macromolecules, **31**, 8439 (1998); (*e*) T.D. Shaffer and J.R. Ashbaugh. J. Polym. Sci. Part A: Polym. Chem. **35**, 329 (1997); (*f*) T.D. Shaffer, J.A.M. Canich, and K.R. Squire. Macromolecules, **31**, 5145 (1998); (*g*) A.G.

© 2006 NRC Canada

Carr, D.M. Dawson, M. Thornton-Pett, and M. Bochmann. Organometallics, **18**, 2933 (1999); (*h*) A.G. Carr, D.M. Dawson, and M. Bochmann. Macromol. Rapid Commun. **19**, 205 (1998); (*i*) X. Song, M. Thornton-Pett, and M. Bochmann. Organometallics, **17**, 1004 (1998); (*j*) A.G. Carr, D.M. Dawson, and M. Bochmann. Macromolecules, **31**, 2035 (1998).

5. (*a*) L. Jia, X. Yang, C.L. Stern, and T.J. Marks. Organometallics, **16**, 842 (1997); (*b*) P.A. Deck, C.L. Beswick, and T.J. Marks. J. Am. Chem. Soc. **120**, 1772 (1998); (*c*) C.L. Beswick and T.J. Marks. Organometallics, **18**, 2410 (1999); (*d*) L. Luo and T.J. Marks. *In* Topics in catalysis. Vol. 7. *Edited by* T.J. Marks and J.C. Stevens. Baltzer AG, Science Publishers, Switzerland. 1999. p. 97; (*e*) E.Y.-X. Chen and T.J. Marks. Chem. Rev. **100**, 1391 (2000); (*f*) J. Zhou, S.J. Lancaster, D.A. Walker, S. Beck, M. Thornton-Pett, and M. Bochmann. J. Am. Chem. Soc. **123**, 223 (2001); (*g*) L. Jia, X. Yang, C.L. Stern, and T.J. Marks. Organometallics, **13**, 3755 (1994); (*h*) L. Jia, X. Yang, A. Ishihara, and T.J. Marks. Organometallics, **14**, 3135 (1995); (*i*) L. Li and T.J. Marks. Organometallics, **17**, 3996 (1998); (*j*) Y.-X. Chen, M.V. Metz, L. Li, C.L. Stern, and T.J. Marks. J. Am. Chem. Soc. **120**, 6287 (1998); (*k*) L. Li, C.L. Stern, and T.J. Marks. Organometallics, **19**, 3332 (2000); (*l*) M.V. Metz, D.J. Schwartz, C.L. Stern, P.N. Nickias, and T.J. Marks. Angew. Chem. Int. Ed. **39**, 1312 (2000); (*m*) K. Köhler, W.E. Piers, A.P. Jarvis, S. Xin, Y. Feng, A.M. Bravakis, S. Collins, W. Clegg, G.P.A. Yap, and T.B. Marder. Organometallics, **17**, 3557 (1998); (*n*) V.C. Williams, W.E. Piers, W. Clegg, M.R. Elsegood, S. Collins, and T.B. Marder. J. Am. Chem. Soc. **121**, 3244 (1999); (*o*) V.C. Williams, G.J. Irvine, W.E. Piers, Z. Li, W. Clegg, M.R.J. Elsegood, S. Collins, and T.B. Marder. Organometallics, **19**, 1619 (2000); (*p*) W.E. Piers, G.J. Irvine, and V.C. Williams. Eur. J. Inorg. Chem. 2131 (2000); (*q*) W.E. Piers, Y. Sun, and L.W.M. Lee. *In* Topics in catalysis. Vol. 7. *Edited by* T.J. Marks and J.C. Stevens. Baltzer AG, Science Publishers, Switzerland. 1999. p. 133; (*r*) G. Lanza, I.L. Fragala, and T. Marks. J. Am. Chem. Soc. **122**, 12764 (2000).
6. (*a*) A.R. Siedle, R.A. Newmark, W.M. Lamanna, and J.C. Huffman. Organometallics, **12**, 1491 (1993); (*b*) A.R. Siedle, W.M. Lamanna, R.A. Newmark, J. Stevens, D.E. Richardson, and M. Ryan. Makromol. Chem. Macromol. Symp. **66**, 215 (1993); (*c*) A.R. Siedle and W.M. Lamanna (Minnesota Mining and Manufacturing Co). US Patent 5296433, 1994; (*d*) A.R. Siedle and W.M. Lamanna (Minnesota Mining and Manufacturing Co). US Patent 5416177, 1995; (*e*) T.D. Shaffer. *In* ACS symposium series 665. Cationic polymerization. *Edited by* R. Faust and T.D. Shaffer. 1997. p. 96; (*f*) G.S. Hill, L. Manojlovic-Muir, K.W. Muir, and R.J. Puddephatt. Organometallics, **16**, 525 (1997); (*g*) A.A. Danopoulos, J.R. Galsworthy, M.L.H. Green, S. Cafferkey, L.H. Doerrer, and M.B. Hursthouse. J. Chem. Soc. Chem. Commun. 2529 (1998); (*h*) L.H. Doerrer and M.L.H. Green. J. Chem. Soc. Dalton Trans. 4325 (1999); (*i*) J.L. Priego, L.H. Doerrer, L.H. Rees, and M.L.H. Green. J. Chem. Soc. Chem. Commun. 779 (2000); (*j*) C. Bergquist, B.M. Bridgewater, C.J. Harlan, J.R. Norton, R.A. Friesner, and G. Parkin. J. Am. Chem. Soc. **122**, 10581 (2000).
7. (*a*) S.J. Lancaster, D.A. Walker, M. Thornton-Pett, and M. Bochmann. J. Chem. Soc. Chem. Commun. 1533 (1999); (*b*) R.E. LaPointe (Dow Chemical Co). PCT Int. Application WO 9942467. 1999; (*c*) R.E. LaPointe, G.R. Roof, K.A. Abboud, and J. Klosin. J. Am. Chem. Soc. **122**, 9560 (2000).
8. N. Bavarian and M.C. Baird. J. Chem. Soc. Dalton Trans. 4089 (2004).
9. (*a*) M.J. Drewitt, M. Niedermann, R. Kumar, and M.C. Baird. Inorg. Chim. Acta, **335**, 43 (2002); (*b*) R. Kumar, A. Penciu, M.J. Drewitt, P.J. McInenly, and M.C. Baird. J. Polym. Sci. Part A: Polym. Chem. **40**, 3302 (2002); (*c*) K.R. Kumar, A. Penciu, M.J. Drewitt, and M.C. Baird. J. Organomet. Chem. **689**, 2900 (2004).
10. (*a*) C.K.W. Tse, K.R. Kumar, M.J. Drewitt, and M.C. Baird. Macromol. Chem. Phys. **205**, 1439 (2004); (*b*) C.K.W. Tse, A. Penciu, P.J. McInenly, K.R. Kumar, M.J. Drewitt, and M.C. Baird. Eur. Polymer J. **40**, 2653 (2004); (*c*) A. Cordoneanu and M.C. Baird. Macromolecules, **37**, 6744 (2004); (*d*) P.J. McInenly, M.A. Drewitt, and M.C. Baird. Macromol. Chem. Phys. **205**, 1707 (2004).
11. (*a*) S. Garratt, A.G. Carr, G. Langstein, and M. Bochmann. Macromolecules, **36**, 4276 (2003); (*b*) S.P. Lewis, L.D. Henderson, B.D. Chandler, M. Parvez, W.E. Piers, and S. Collins. J. Am. Chem. Soc. **127**, 46 (2005); (*c*) S.P. Lewis, N.J. Taylor, W.E. Piers, and S. Collins. J. Am. Chem. Soc. **125**, 14686 (2003); (*d*) L.D. Henderson, W.E. Piers, G.J. Irvine, and R. McDonald. Organometallics, **21**, 340 (2002).
12. (*a*) J.L. Pohlmann and F.E. Brinckmann. Z. Naturforsch. **20b**, 5 (1965); (*b*) A.G. Massey and A.J. Park. J. Organomet. Chem. **2**, 245 (1964).
13. (*a*) Bruker AXS Inc. SHELXTL NT. Version 5.10 [computer program]. Bruker AXS Inc., Madison, Wis. 1999; (*b*) D.T. Cromer and J.T. Waber. *In* International tables for X-ray crystallography. Vol. 4. Kynoch Press, Birmingham, UK. 1974. Table 2.2 A.
14. H.L. Goering, T.D. Nevitt, and E.F. Silversmith. J. Am. Chem. Soc. **77**, 4042 (1955).
15. (*a*) T. Beringhelli, D. Maggioni, and G. D'Alfonso. Organometallics, **20**, 4927 (2001); (*b*) S. Guidotti, I. Camurati, F. Focante, L. Angellini, G. Moscardi, L. Resconi, R. Leardini, D. Nanni, P. Mercandelli, A. Sironi, T. Beringhelli, and D. Maggioni. J. Org. Chem. **68**, 5445 (2003); (*c*) F. Focante, I. Camurati, D. Nanni, R. Leardini, and L. Resconi. Organometallics, **23**, 5135 (2004); (*d*) A. Bonazza, I. Camurati, S. Guidotti, N. Mascellari, and L. Resconi. Macromol. Chem. Phys. **205**, 319 (2004).
16. G.B. Deacon and R.J. Phillips. Coord. Chem. Rev. **33**, 227 (1980).
17. (*a*) C. Janiak, L. Braun, T.G. Scharmann, and F. Girgsdies. Acta Crystallogr. **C54**, 1722 (1998); (*b*) D.J. Parks, W.E. Piers, M. Parvez, R. Atencio, and M.J. Zawarotko. Organometallics, **17**, 1369 (1998); (*c*) D. Vagedes, R. Fröhlich, and G. Erker. Angew. Chem. Int. Ed. **38**, 3362 (1999); (*d*) G. Barrado, L. Doerrer, M.L.H. Green, and M.A. Leech. J. Chem. Soc. Dalton Trans. 1061 (1999).
18. (*a*) X. Yang, C.L. Stern, and T.J. Marks. J. Am. Chem. Soc. **116**, 10015 (1994); (*b*) S. Beck, S. Lieber, F. Schaper, A. Geyer, and H.H. Brintzinger. J. Am. Chem. Soc. **123**, 1483 (2001); (*c*) B.E. Bosch, G. Erker, R. Fröhlich, and O. Meyer. Organometallics, **16**, 5449 (1997); (*d*) H.C. Strauch, G. Erker, and R. Fröhlich. Organometallics, **17**, 5746 (1998).

© 2006 NRC Canada

1-Bromoindene — A new synthon for the preparation of (indenyl)Ni(II)(PPh_3)Br[1]

Sylvain Boucher and Davit Zargarian

Abstract: The oxidative addition of the carbon–bromine bond in 1-bromoindene to $Ni(PPh_3)_4$ gives the complex (indenyl)$Ni(PPh_3)Br$ (**1**) in 95% yield. In contrast, other nickel(0) species such as $Ni(PMe_3)_4$ and $Ni(COD)_2$ promote the oxidative coupling of 1-bromoindene to 1,1′-biindene. Complex **1** has been characterized by NMR spectroscopy (^1H, ^{13}C, ^{31}P) and single-crystal X-ray structural analysis.

Key words: indenyl complexes, oxidative addition, oxidative coupling.

Résumé : L'addition oxydante du lien carbone–brome du 1-bromoindène sur le $Ni(PPh_3)_4$ permet d'obtenir le complexe (indényle)$Ni(PPh_3)Br$ (**1**) avec un rendement de 95 %. Par contraste, d'autres espèces du nickel(0) comme le $Ni(PMe_3)_4$ et le $Ni(COD)_2$ promeuvent le couplage oxydatif du 1-bromoindène en 1,1′-biindène. Le complexe **1** a été caractérisé par la spectroscopie de RMN (^1H, ^{13}C, ^{31}P) et par la diffraction des rayons-X d'un cristal unique.

Mots clés : complexes indényles, addition oxydante, couplage oxydatif.

Introduction

A number of transition metal complexes bearing indenyl (Ind) ligands possess greater reactivity, both in catalysis (1) as well as in stoichiometric ligand exchange (2) and insertion (3) reactions, than their cyclopentadienyl (Cp) analogues. The most common synthetic route to Ind complexes is based on the reaction of metal halide precursors with M[Ind] (M = Li, Na, and K), but in some cases the synthesis is complicated by undesirable side reactions such as reduction of the metal precursor. Such complications are particularly prevalent in the syntheses of relatively electron-rich group 10 metal complexes; as a result, generally poor yields are obtained for Ind complexes of Ni (4) and Pd (5) from the reaction of LiInd with their halide precursors.

Our interest in the preparation and catalytic reactivities of Ind complexes of group 10 metals (6) prompted us to seek alternative synthetic procedures that avoid using indenyl anions as the source of Ind ligand. Given the propensity of zerovalent precursors of group 10 metals to oxidatively add alkyl (7), allyl (8), aryl (9), and Cp (10) halides, we set out to explore the feasibility of preparing IndM(II) complexes via oxidative addition of a suitable Ind-halide to L_nM^0 precursors. A search of the literature revealed that 1-bromoindene (1-Br-Ind) can be conveniently prepared from the reaction of 1-(trimethylsilyl)indene and the dioxane·Br_2 adduct (11); moreover, the relatively weak C—Br bond in 1-Br-Ind should make this reagent suitable for our purposes. A preliminary study has indicated that reacting 1-Br-Ind with $Ni(PPh_3)_4$ gives (indenyl)$Ni(PPh_3)Br$ in good yield. The preparation and characterization of this compound is reported herein along with an account of a study on the potential of 1-Br-Ind as a synthon for the synthesis of other Ind-Ni complexes.

Results and discussion

The recently reported catalytic reactivities of (R-Ind)Ni-(PPh_3)Cl make these the most commonly studied group 10 metal Ind complexes. Therefore, we selected the bromo analogue Ind$Ni(PPh_3)Br$ as our first synthetic target. Stirring a toluene solution of 1-Br-Ind and $Ni(PPh_3)_4$ for 1 h at ambient temperature gave Ind$Ni(PPh_3)Br$ (**1**) in 95% yield (Scheme 1), which represents a significant improvement over the 25%–60% yields obtained from the reaction of $(PPh_3)_2$-NiX_2 (X = Cl, Br) with LiInd (4). We envisage this new synthetic route proceeding according to the sequence of steps shown in Scheme 1: oxidative addition of 1-Br-Ind to $Ni(PPh_3)_3$ (12) forms $(PPh_3)_2Ni(\eta^1$-Ind)Br, which undergoes $\eta^1 \rightarrow \eta^{3/5}$ slippage of the indenyl ring to give the observed product. To our knowledge, **1** is the first Ind complex to be obtained through oxidative addition of 1-X-Ind (X = halogens).

Subsequent attempts to apply the above reaction to other precursors have not been successful so far. Thus, reaction of 1-Br-Ind with $Ni(PMe_3)_4$ or $Ni(COD)_2$ did not result in the formation of Ind$Ni(L)Br$; instead, both of these compounds converted 1-Br-Ind to 1,1′-biindene, which was obtained with d,l:meso ratios of ca. 1:1 ($Ni(PMe_3)_4$) and 4:1

Received 20 June 2005. Published on the NRC Research Press Web site at http://canjchem.nrc.ca on 16 March 2006.

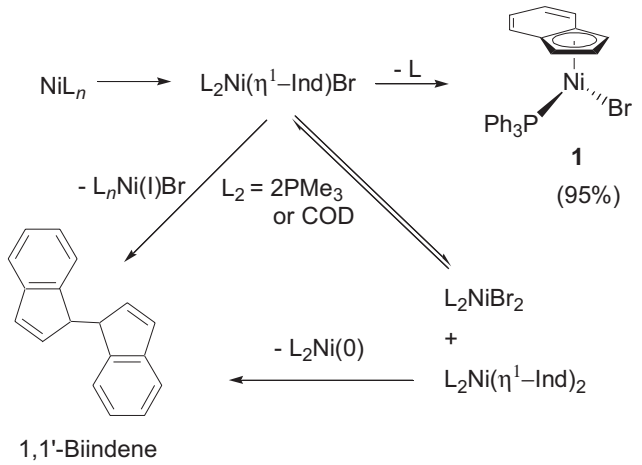
This report is dedicated to Dr. A.J. Carty for his numerous contributions to chemistry in Canada.

S. Boucher and D. Zargarian.[2] Département de chimie, Université de Montréal, Montréal, QC H3C 3J7, Canada.

[1]This article is part of a Special Issue dedicated to Professor Arthur Carty.
[2]Corresponding author (e-mail: zargarian.davit@umontreal.ca).

 doi:10.1139/V05-248 © 2006 NRC Canada

Scheme 1.



(Ni(COD)$_2$) (13). This coupling reaction is reminiscent of the homocoupling of benzyl bromide to 1,2-diphenylethane in the presence of Ni(PMe$_3$)$_4$.[3] In addition, Carmona et al. (14) have reported that the complex *trans*-(PMe$_3$)$_2$Ni(η^1-PhCH$_2$)Cl decomposes in the presence of excess PMe$_3$ to give Ni(PMe$_3$)$_3$Cl$_2$, Ni(PMe$_3$)$_4$, and 1,2-diphenylethane. These findings are consistent with our observation that the reaction of beige-coloured Ni(PMe$_3$)$_4$ and colourless 1-Br-Ind gives a deep blue mixture consistent with the formation of (PMe$_3$)$_3$NiBr$_2$ (15). In the reaction involving Ni(COD)$_2$, the formation of 1,1′-biindene was concomitant with the precipitation of an insoluble, orange solid that seems to be NiBr$_2$; the ^{1}H NMR spectrum of the reaction mixture also showed the presence of free COD.

On the basis of the above precedents and observations, we propose the following scenario (Scheme 1) to explain why the reactions with PMe$_3$ and COD derivatives did not lead to the desired Ind complexes. We believe that the initial intermediates arising from the oxidative addition of 1-Br-Ind to Ni(0)L$_n$, i.e., L$_2$Ni(η^1-Ind)Br, do not undergo the requisite η^1→η$^{3/5}$ slippage of the indenyl ring at a sufficiently rapid rate; this is likely caused by the unfavourable dissociation of the more nucleophilic PMe$_3$ and the chelating COD ligands. The hindered slippage then makes possible side reactions that lead to the formation of 1,1′-biindene.[4] There is much debate on the precise mechanism for the Ni-catalyzed coupling of organohalides R-X (16). The most reasonable mechanism for the formation of 1,1′-biindene from Ni(0) precursors involves the redistribution of the initial intermediate L$_2$Ni(η^1-Ind)Br to L$_2$NiBr$_2$ and L$_2$Ni(η^1-Ind)$_2$ (17); reductive elimination of the latter would furnish 1,1′-biindene. Alternatively, a binuclear reductive elimination from L$_2$Ni(η^1-Ind)Br could give 1,1′-biindene and L$_2$Ni^{I}Br; the latter would then be expected to disproportionate to Ni(II) and Ni(0) species (Scheme 1).[5]

Characterization of 1

Complex **1** was fully characterized to allow structural comparisons with previously studied analogues of this family of complexes. Thus, the ^{31}P{^{1}H} NMR spectrum of **1** consisted of a singlet at ca. 31.0 ppm, somewhat downfield of the corresponding signal in the chloride analogue IndNi(PPh$_3$)Cl (**2**, 28.2 ppm). Such deshielding of the P nucleus with the heavier halide has also been observed in the analogous complexes (1-Me-Ind)Ni(PPh$_3$)X (δ: 31.2 for Cl, 33.9 for Br, and 38.6 for I) (18). We have shown a correlation between the deshielding of the ^{31}P signals in these complexes and the extent of PPh$_3$ donation to Ni, greater donation resulting in more downfield signals (6). This correlation can be attributed to two phenomena: (*i*) the longer Ni—Br and Ni—I bond lengths result in less efficient X → Ni π donation, which reduces the cis-weakening normally associated with such π donation and allows greater R$_3$P → Ni donation (4*b*); (*ii*) the ionic character of the Ni—X bond diminishes on going from Cl to I, which in turn reduces the hardness of the Ni centre and results in greater covalent interaction with the soft PR$_3$ ligand (19).

The ^{1}H NMR spectrum was also valuable for structural comparisons. As was the case for the previously studied chloro analogue **2**, the room-temperature spectrum of **1** contained broad signals for the symmetry-related protons of Ind (H1/H3, H4/H7, H5/H6); the broadness of these signals results from the hindered rotation of Ind. Cooling the sample to ca. 218 K resulted in the appearance of well-resolved signals for these protons, indicating that in the low-temperature regime the complex adopts the C_1 symmetry expected in the solid state (vide infra). The signals rebroadened and eventually disappeared into the baseline (ca. 338 K) with the gradual warming of the sample, indicating that the symmetry of the complex changes to C_s as a result of Ind rotation; unfortunately, however, the coalescence temperature for the two-site exchange process brought about by the hindered rotation of Ind could not be determined because the compound decomposed at around 348 K. Thus, we can only assign a lower limit of ca. 15 kcal/mol (1 cal = 4.184 J) for the energy barrier (20); this value is comparable to the barrier of ca. 16 kcal/mol measured for complex **2** (4*a*).

Other structural information can be inferred from ^{1}H NMR data and especially the chemical shift of H3, which has been found to reflect the solution hapticity of the Ind ligand, with upfield shifts implying greater η^5 → η^3 slippage (6). Thus, the H3 signal of **1** resonates at 3.55 ppm, slightly downfield of the corresponding signal for its chloride analogue (3.31 ppm). Although this chemical shift difference is small (Δδ = 0.24 ppm), its direction is consistent with the previously noted trend in the chemical shifts of H3 signals in the complexes (1-Me-Ind)Ni(PPh$_3$)X (δ: 3.38 for Cl, 3.55 for Br, and 3.86 for I) (18) and (1-Et-Ind)Ni(PPh$_3$)X (δ: 3.37 for Cl, 3.61 for Br, and 3.93 for I) (21), and signals greater Ind hapticity in solution for the Ni-Br analogue.

The ^{13}C{^{1}H} NMR data were also quite valuable for structural comparisons, especially the chemical shift of the ring junction carbons C3a and C7a, which are thought to reflect the hapticity of the Ind ligand. This is based on the

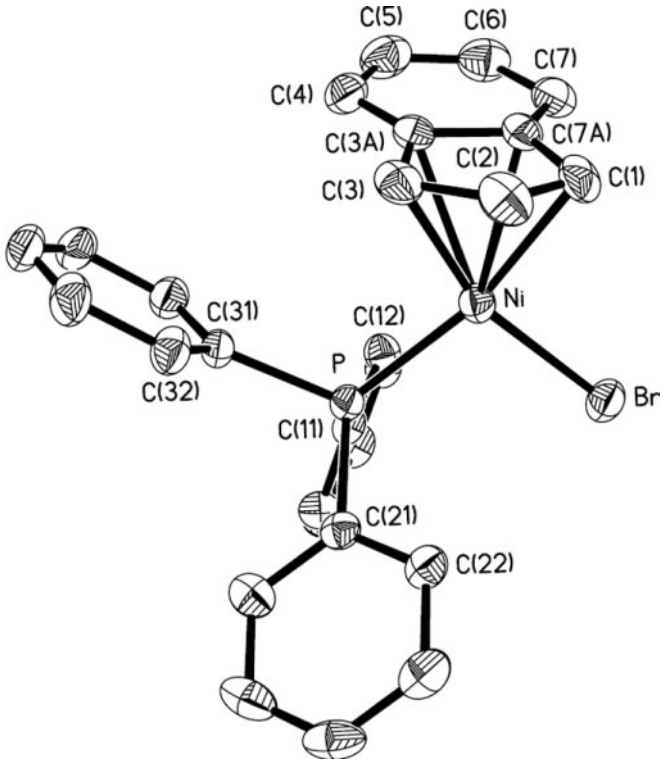
[3] S. Beaudoin and D. Zargarian. Unpublished results.

[4] Unsuccessful attempts were made to circumvent the nearly instantaneous formation of 1,1′-biindene from the Ni(PMe$_3$)$_4$ reaction by placing the reaction vessel under reduced pressure to remove volatile PMe$_3$ from the reaction mixture.

[5] It is worth noting that the coupling of 1-Br-Ind by the PMe$_3$ and COD precursors might proceed through two different mechanisms. Indeed, the different selectivities observed in these reactions for the formation of the *d*,*l*- over *meso*-1,1′-biindene support this possibility.

© 2006 NRC Canada

Fig. 1. ORTEP view of **1**. The thermal ellipsoids are shown at 30% probability and the hydrogen atoms have been omitted for clarity.



notion that coordination of the Cp moiety of Ind to metals disrupts the aromaticity of the benzene moiety, thereby resulting in upfield shifts of C3a and C7a signals (22). The magnitude of this shift in a given complex can be estimated from the $\Delta\delta^{13}C$ parameter[6] as follows: compounds bearing nearly perfectly pentahapto Ind ligands have $\Delta\delta^{13}C$ values as low as –43.7 ppm (Ind_2Fe) (22*c*) and –32.4 ppm ($[Ind_2Co]^+$) (22*c*), whereas those bearing trihapto Ind ligands give values as high as +26 ppm ($IndIr(PMe_2Ph)_3$) (23) and +27 ppm ($[IndFe(CO)_3]^-$) (24), and those featuring intermediate hapticities (η^3–η^5) show near zero values of $\Delta\delta^{13}C$ (e.g., +3.6 ppm for Ind_2Ni) (22*c*). The $\Delta\delta^{13}C$ values for **1** (–3 ppm) and **2** (–2 ppm) indicate that the Ind ligands in these complexes adopt intermediate hapticities (η^3–η^5).

Finally, complex **1** was subjected to an X-ray crystallographic study to confirm the conclusions inferred from the NMR spectra and compare some of its important structural features to those of related compounds (Fig. 1). The crystal data and details of measurement and refinement are given in Table 1, while the most pertinent structural parameters are tabulated in Table 2; the latter also lists the corresponding data for **2** to facilitate comparisons.[7]

The geometry around the Ni center in **1** may be described as being intermediate between a two-legged piano stool (assuming η^5-Ind) and a distorted square-planar (assuming η^3-Ind). The planes formed by the atoms P, Ni, and Br, on the one hand, and C1, C2, C3, C3a, and C7a on the other, are nearly perpendicular to each other (ca. 87°). The atoms P, Br, C1, C2, and C3 are within the expected bonding distance from Ni, while C3a and C7a are considerably farther away. The difference in the Ni—P bond distances in **1** and **2** is

Table 1. X-ray crystallographic data for **1**.

Formula, mol wt.	$C_{27}H_{22}BrNiP$, 516.03
Crystal color and habit	Red, parallelepiped
Crystal dimensions (mm)	0.25 × 0.20 × 0.07
Cell setting and space group	Triclinic, *P*-1
a (Å)	8.933 0(2)
b (Å)	10.170 9(2)
c (Å)	14.473 9(3)
α (°)	104.046(2)
β (°)	98.256(2)
γ (°)	113.636(2)
V (Å^3)	1124.96(5)
Z	2
D(calcd.) (g cm^{-1})	1.523
λ (Cu Kα, cm^{-1})	1.541 78
Temp (K)	220(2)
Diffractometer	Nonius CAD-4
$2\theta_{max}$ (°)	146
Data collection method	ω/2θ
No. of reflns. used ($I > 2\sigma(I)$)	4292
R, R_w	0.036 6, 0.091 8
Max residual (e Å^{-3})	0.517

Table 2. Selected bond distances (Å) and structural parameters (22*c*) for **1** and **2** (4*a*).

	1	**2**
Bond distances (Å)		
Ni—P	2.1754(8)	2.1835(7)
Ni—Br/Cl	2.3272(6)	2.1822(7)
Ni—C1	2.079(3)	2.094(2)
Ni—C2	2.051(3)	2.061(2)
Ni—C3	2.053(3)	2.042(2)
Ni—C3a	2.338(3)	2.318(2)
Ni—C7a	2.339(3)	2.344(2)
C1—C2	1.401(5)	1.399(4)
C2—C3	1.431(5)	1.417(4)
C3—C3a	1.448(4)	1.449(3)
C3a—C7a	1.421(4)	1.422(3)
C7a—C1	1.458(4)	1.459(3)
HA (°)	11.1	10.9
FA (°)	11.1	11.7
ΔM-C (Å)	0.27	0.26

[6] $\Delta\delta^{13}C$ = δ[C(3a/7a) of MInd] – δ[C(3a/7a) of NaInd] (ppm), where δC(3a/7a) of NaInd in THF-d^8= 130.7. See refs. 22*b* and 22*c*.

[7] Supplementary data for this article are available on the journal Web site (http://canjchem.nrc.ca) or may be purchased from the Depository of Unpublished Data, Document Delivery, CISTI, National Research Council Canada, Ottawa, ON K1A 0R6, Canada. DUD 4097. For more information on obtaining material refer to http://cisti-icist.nrc-cnrc.gc.ca/irm/unpub_e.shtml. CCDC 287367 contains the crystallographic data for this manuscript. These data can be obtained, free of charge, via http://www.ccdc.cam.ac.uk/conts/retrieving.html (Or from the Cambridge Crystallographic Data Centre, 12 Union Road, Cambridge CB2 1EZ, UK; fax +44 1223 336033; or deposit@ccdc.cam.ac.uk).

© 2006 NRC Canada

small but significant (10 times esd); the shorter bond in **1** is consistent with the somewhat stronger Ni—PPh_3 interaction inferred on the basis of the more downfield ^{31}P NMR signal obtained in the solution (vide supra).

Perhaps the most important structural feature of **1** concerns the Ni–Ind interactions and the extent of $\eta^5 \rightarrow \eta^3$ slip-fold distortions. Varying degrees of such distortions occur in most η-Ind complexes, but in the present case they can be attributed to the tendency of Ni(II) to avoid forming 18-electron complexes. As was inferred from the $\Delta\delta^{13}C$ values above, the Ni–Ind interactions in solid state structures of **1** and **2** appear to be fairly similar at first glance. For example, the extent of $\eta^5 \rightarrow \eta^3$ slippage is comparable in both complexes, as indicated by the much shorter Ni—C distances involving the allylic carbons (C1–C3) compared with those involving the ring junction carbons (C3a and C7a). The degree of slip-fold distortion can be defined more quantitatively in terms of the slip value (ΔM-C) and the hinge and fold angles (HA and FA);[8] larger ΔM-C, HA, and FA values generally imply greater "slippage" away from the idealized η^5-coordination mode (22*b*, 22*c*). A comparison of these parameters (Table 2) points to a slightly more slip-folded Ind in **1**. In addition, a closer inspection of the Ni—C bond distances reveals a more pronounced "sideways slippage" in **2** (Ni—C1 > Ni—C2 > Ni—C3; Ni—C7a > Ni—C3a) compared with more symmetrical interactions in **1** (Ni—C1 > Ni—C2 ≈ Ni—C3; Ni—C3a ≈ Ni—C7a).

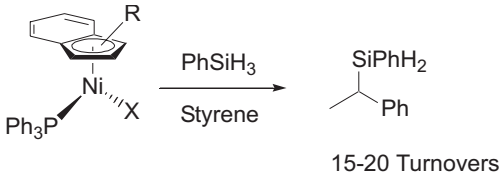
Catalytic reactivity of 1

The complexes (1-R-Ind)Ni(PPh_3)X (R = Me, *i*-Pr; X = Cl, Me) have been shown to catalyze the hydrosilylation of styrene with $PhSiH_3$, giving high regioselectivities for the addition of the $PhSiH_2$ fragment at the α-C (Scheme 2) (25). Previous studies demonstrated that the choice of X in the precursor has some bearing on the catalytic activities, with the Ni-Cl precursor catalyzing the hydrosilylation more efficiently (in the presence of $NaBPh_4$). We have briefly studied the catalytic activity of **1** in the hydrosilylation of styrene to assess the impact of the Ni-Br moiety on the catalysis. The results of this study indicate that **1** is less active than **2**. Thus, a number of catalytic runs using **1** as the catalyst precursor gave 27%–36% yields for the reaction, compared with 42%–82% yields for the reactions catalyzed by **2** under similar conditions. We believe that the higher reactivities of **2** might originate from the more facile formation of Ni-H intermediates from the weaker Ni—Cl bond, whereas the more labile Ni—Cl bond can be attributed to its less covalent nature or to destabilizing X → Ni η-interactions that are greater with Cl vs. Br (vide supra).

Conclusion

The oxidative addition of 1-bromoindene to Ni(PPh_3)$_4$ has provided a convenient and very high yield method for the preparation of IndNi(PPh_3)Br. This new methodology should be particularly practical for the preparation of Ind complexes of those transition metals that are susceptible to side reactions encountered commonly when using various sources of indenyl anions. Despite the unsuccessful attempts to prepare IndNi(II) complexes from Ni(PMe_3)$_4$ and Ni(COD)$_2$, we plan to explore the suitability of this new synthetic route for the preparation of a wide range of Ind complexes, including IndM(CO)$_n$.

Scheme 2.



Experimental section

All manipulations and experiments were performed under an inert atmosphere of nitrogen using standard Schlenk techniques and (or) in an argon-filled glovebox. Dry, oxygen-free solvents were employed throughout. A Bruker AV-300 spectrometer was employed for recording the ^1H (300.1 MHz), $^{13}C\{^1H\}$ (75.5 MHz), and $^{31}P\{^1H\}$ (121.5 MHz) NMR spectra with $SiMe_4$ and H_3PO_4 (85%) as external standards. Ni(COD)$_2$ was purchased from Sigma-Aldrich and used as received; synthetic procedures for the preparation of 1-Br-Ind (11) (from 1-$SiMe_3$-Ind (26) and dioxane dibromide (27)), Ni(PMe_3)$_4$ (28), and Ni(PPh_3)$_4$ (29) have been reported elsewhere.

IndNi(PPh_3)Br

A toluene solution (10 mL) of 1-Br-Ind (88 mg, 0.451 mmol) was added slowly to a stirring solution of Ni(PPh_3)$_4$ (500 mg, 0.451 mmol) in toluene (40 mL) at ambient temperature. The resultant red-brown mixture was stirred for 1 h after the addition and the solvent evaporated to dryness. The residue was washed with hexane (3 × 10 mL) to remove excess PPh_3 and other by-products, then dried under vacuum for a few hours to give the title compound as a brown powder (221 mg, 95%). Recrystallization of a small portion of this solid from a cold (–30 °C) toluene–hexane solution yielded crystals suitable for X-ray diffraction and elemental analysis. ^1H NMR (C_6D_6, 300.1 MHz) δ: 7.62 (m, PPh_3), 7.33 (br, H4/H7), 7.03 (br, H5/H6), 6.98 (m, PPh_3), 6.84 (br, H5/H6), 6.37 (t, J = 3 Hz, H2), 6.10 (br, $\Delta\nu_{1/2}$ = 20 Hz, H4/H7), 5.90 (br, $\Delta\nu_{1/2}$ = 21 Hz, H1), 3.55 (br, $\Delta\nu_{1/2}$ = 19 Hz, H3). $^{13}C\{^1H\}$ NMR (C_6D_6, 75.5 MHz) δ: 134.7 (d, J = 11 Hz, *o*-C of PPh_3), 133.0 (C5/C6), 132.6 (d, J = 44 Hz, *i*-C of PPh_3), 131.7 (C5/C6), 130.4 (d, J = 2 Hz, *p*-C of PPh_3), 128.8 (C3a/C7a), 126.4 (C3a/C7a), 120.8 (C4/C7), 117.1 (C4/C7), 103.0 (C2), 89.2 (C1), 73.0 (C3) ppm; the missing resonances for the *m*-C of PPh_3 are obscured under the residual solvent at ca. 128 ppm. $^{31}P\{^1H\}$ NMR (C_6D_6, 121.5 MHz) δ: 31.0 (s, PPh_3) ppm. Anal. calcd. for $C_{27}H_{22}NiPBr \cdot C_7H_8$ (toluene): C 67.15, H 4.97; found: C 67.23, H 4.97.

[8] HA is the angle between the planes formed by the atoms C(1), C(2), C(3) and C(1), C(3), C(3a), C(7a); FA is the angle between the planes formed by the atoms C(1), C(2), C(3) and C(3a), C(4), C(5), C(6), C(7), C(7a); ΔM-C = [1/2(M-C3a + M-C7a) – 1/2(M-C1 + M-C3)]. See ref. 22*c* for details.

© 2006 NRC Canada

Catalytic hydrosilylation of styrene

The catalytic runs were carried out on NMR scale, in C_6D_6 at ambient temperature for 18–21 h with a Ni–styrene–$PhSiH_3$ ratio of 1 : 50 : (50 or 100). In some runs, 10 equiv. of $NaBPh_4$ were used as an initiator for abstracting Br to generate the catalytically active Ni cation (25). The product of the catalysis was characterized on the basis of its ^1H NMR spectrum; the yields were determined as described previously (30).

Acknowledgments

We are grateful to the Natural Sciences and Engineering Research Council of Canada (NSERC), Fonds pour la formation des chercheurs et l'aide à la recherche (Québec, FCAR), and Université de Montréal for financial support.

References

1. (*a*) P. Caddy, M. Green, L.E. Smart, and N. White. J. Chem. Soc. Chem. Commun. 839 (1978); (*b*) A. Borrini, P. Diversi, G. Ingrosso, A. Lucherini, and G. Serra. J. Mol. Catal. **30**, 181 (1985); (*c*) P. Cioni, P. Diversi, G. Ingrosso, A. Lucherini, and P. Ronca. J. Mol. Catal. **40**, 337 (1987); (*d*) T.B. Marder, C.D. Roe, and D. Milstein. Organometallics, **7**, 1451 (1988); (*e*) R.S. Tanke and R.H. Crabtree. J. Am. Chem. Soc. **112**, 7984 (1990); (*f*) H. Brunner and K. Fisch. Angew. Chem. Int. Ed. Engl. **29**, 1131 (1990); (*g*) A. Ceccon, A. Gambaro, S. Santi, and A. Venzo. J. Mol. Catal. **69**, L1 (1991); (*h*) R.L. Halterman. Chem. Rev. **92**, 965 (1992); (*i*) B.M. Trost and R.J. Kulawiec. J. Am. Chem. Soc. **114**, 5579 (1992); (*j*) E. Hauptman, S. Sabo-Etienne, P.S. White, M. Brookhart, J.M. Garner, P.J. Fagan, and J.C. Calabrese. J. Am. Chem. Soc. **116**, 8038 (1994); (*k*) B.Y. Lee and Y.K. Chung. J. Am. Chem. Soc. **116**, 8793 (1994).
2. For a few leading references, see: (*a*) T.M. Frankcom, J.C. Green, A. Nagy, A.K. Kakkar, and T.B. Marder. Organometallics, **12**, 3688 (1993); (*b*) M.P. Gamasa, J. Gimeno, C. Gonzalez-Bernardo, B.M. Martìn-Vaca, D. Monti, and M. Bassetti. Organometallics, **15**, 302 (1996).
3. (*a*) T. Foo and R.G. Bergman. Organometallics, **11**, 1801 (1992); (*b*) T. Foo and R.G. Bergman. Organometallics, **11**, 1811 (1992); (*c*) P. Caddy, M. Green, J.A.K. Howard, J.M. Squire, and N.J. White. J. Chem. Soc. Dalton Trans. 400 (1981).
4. (*a*) T.A. Huber, F. Bélanger-Gariépy, and D. Zargarian. Organometallics, **14**, 4997 (1995); (*b*) T.A. Huber, M. Bayrakdarian, S. Dion, I. Dubuc, F. Gariépy-Bélanger, and D. Zargarian. Organometallics, **16**, 5811 (1997).
5. C. Sui-Seng, G.D. Enright, and D. Zargarian. Organometallics, **23**, 1236 (2004).
6. For a recent review of the chemistry of group 10 metal Ind complexes, see: D. Zargarian. Coord. Chem. Rev. **233–234**, 157 (2002).
7. N.L. Bauld. Tetrahedron Lett. **27**, 1841 (1963).
8. (*a*) G.A. Molander and D.C. Shubert. Tetrahedron Lett. **27**, 787 (1986); (*b*) E. Carmona, P. Palma, and M.L. Poveda. Polyhedron, **9**, 757 (1990).
9. M. Hidai, T. Kashiwagi, T. Ikeuchi, and Y. Uchida. J. Organomet. Chem. **30**, 279 (1971).
10. P. Jutzi and A. Mix. Chem. Ber. **123**, 1043 (1990).
11. J.B. Woell and P. Boudjouk. J. Org. Chem. **45**, 5213 (1980).
12. It is known that $Ni(PPh_3)_4$ is converted to $Ni(PPh_3)_3$ almost completely at room temperature. C.A. Tolman, W.C. Seidel, and D.H. Gerlsah. J. Am. Chem. Soc. **94**, 2669 (1972).
13. For direct synthetic routes to 1,1′-biindene and its characterization by NMR, see: P. Nicolet, J.-Y. Sanchez, A. Benaboura, and M.J.M. Abadie. Synthesis, 202 (1987).
14. E. Carmona, M. Paneque, and M.L. Poveda. Polyhedron, **8**, 285 (1989).
15. For identification of $(PMe_3)_2NiBr_2$, see the following report: O. Dahl. Acta Chem. Scand. **23**, 2342 (1969).
16. For leading accounts of this topic, see: (*a*) T.T. Tsou and J.K. Kochi. J. Am Chem. Soc. **101**, 7547 (1979); (*b*) I. Colon and D.R. Kelsey. J. Org. Chem. **51**, 2627 (1986); (*c*) M. Iyoda, H. Otsuka, K. Sato, N. Nisato, and M. Oda. Bull. Chem. Soc. Jpn. **63**, 80 (1990); (*d*) M.F. Semmelhack, P.M. Helquist, and L.D. Jones. J. Am. Chem. Soc. **93**, 5908 (1971).
17. Redistribution reactions of $L_2Ni(R)X$ to L_2NiR_2 and L_2NiX_2 occur fairly commonly. For a few examples, see: (*a*) W.J. Marshall and V.V. Grushin. Can. J. Chem. **83**, 640 (2005); (*b*) D.R. Fahey and J.E. Mahan. J. Am. Chem. Soc. **98**, 4499 (1976).
18. M.-A. Dubois. M.Sc. thesis, Université de Montréal, Montréal, Québec. 2000.
19. For a detailed discussion of the interplay between electrostatic-covalent terms and their effects on Ni—X bonds, see: P.L. Holland, R.A. Andersen, R.G. Bergman, J. Huang, and S.P. Nolan. J. Am. Chem. Soc. **119**, 12800 (1997).
20. The energy barrier can be calculated from the Eyring equation for a two-site exchange process involving a molecular rotation, $\Delta G^{\ddagger}/RT_c = 22.96 + \ln(T_c/\delta\nu)$: R.J. Abraham and P. Loftus. Proton and carbon-13 NMR spectroscopy. Wiley, New York. 1985. Chap. 7. pp. 165–168 (eq. [7.11]).
21 W.-F. Li, H.-M. Sun, Q. Shen, Y. Zhang, and K.-B. Yu. Polyhedron, **23**, 1473 (2004).
22. (*a*) F.H. Köhler. Chem. Ber. **107**, 570 (1974); (*b*) R.T. Baker and T.H. Tulip. Organometallics, **5**, 839 (1986); (*c*) S.A. Westcott, A.K. Kakkar, G. Stringer, N.J. Taylor, and T.B. Marder. J. Organomet. Chem. **394**, 777 (1990).
23. J.S. Merola, R.T. Kacmarcik, and D.V. Engen. J. Am. Chem. Soc. **108**, 329 (1986).
24. T.C. Forschner, A.R. Cutler, and R.K. Kullnig. Organometallics, **6**, 889 (1987).
25. F.-G. Fontaine, R.-V. Nguyen, and D. Zargarian. Can. J. Chem. **81**, 1299 (2003).
26. T.E. Ready, J.C.W. Chien, and M.D. Rausch. J. Organomet. Chem. **519**, 21 (1996).
27. J.D. Billimoria and N.F. Maclagan. J. Chem. Soc. 3257 (1954).
28. C.A. Tolman. J. Am. Chem. Soc. **92**, 2956 (1970).
29. R.A. Schunn. Inorg. Synth. **13**, 124 (1973).
30. Y. Chen, C. Sui-Seng, S. Boucher, and D. Zargarian. Organometallics, **24**, 149 (2005).

© 2006 NRC Canada

Arene–perfluoroarene interactions in crystal engineering. Part 14. 1:1 Complexes of octafluoronaphthalene with fluorene and 9,10-dihydrophenanthrene[1,2]

Jonathan C. Collings, Andrei S. Batsanov, Judith A.K. Howard, and Todd B. Marder

Abstract: The 1:1 molecular complexes of octafluoronaphthalene (OFN) with fluorene (**1**) and with 9,10-dihydrophenanthrene (**2**) were prepared by cocrystallization of the components and characterized by single-crystal X-ray diffraction. The structure of **1** can be described as a mixed-stack or a laminar checkerboard motif of alternating OFN and fluorene molecules, whilst slanted mixed-stack, herringbone, and face-to-face heteromolecular dimer motifs can all be recognised in **2**.

Key words: single crystal, X-ray structure, π stacking, fluoroarene.

Résumé : Nous avons préparé les complexes moléculaires 1:1 de l'octafluoronaphtalène (OFN) avec le fluorène (**1**) et le 9,10-dihydrophénanthrène (**2**) par cocristallisation des constituants, et nous les avons caractérisés par diffraction des rayons X sur un cristal unique. La structure du composé **1** peut être comparée à celle d'un échiquier laminaire ou à un empilement mixte à motif de molécules d'OFN et de fluorène en alternance, alors que dans celle du composé **2** on peut reconnaître des motifs de dimères hétéromoléculaires inclinés en empilement mixte, en face à face et en chevrons.

Mots clés : cristal unique, détermination d'une structure par diffraction des rayons X, empilement π, fluoroarène.

[Traduit par la Rédaction]

Introduction

Arenes and perfluoroarenes have been known for over 40 years to form complexes with each other. The simplest example is the complex formed between benzene and hexafluorobenzene (HFB), which has a crystal structure composed of infinite stacks of alternating benzene and HFB molecules (2), in contrast to the crystal structures of the pure component molecules that are arranged in a herringbone fashion (3). Similar stacked arrangements occur in complexes of HFB with various benzene derivatives and related molecules (4), or in complexes of octafluoronaphthalene (OFN) with various fused-ring polyaromatic molecules (5, 6), tolan (diphenylethyne) (7), biphenyl (8), biphenylene (8), TTF (9), sulfur–nitrogen containing molecules (both acyclic and heterocyclic) (10), etc. Almost always, the components cocrystallize to acquire, spontaneously, a 1:1 stoichiometry, although OFN has also been shown to form a 3:2 complex with ferrocene in which some of the OFN molecules do *not* take part in stacking (11). The mixed-stack motif seems remarkably robust and able to absorb much distortion. Thus, the OFN·naphthalene (5), OFN·acenaphthene (12), and OFN·1,8-diaminonaphthalene (13) complexes form isomorphous crystals, notwithstanding substantial differences in the shapes of arene molecules. Indeed, the latter complex adopts the stacked structure in spite of it being singularly unsuitable for hydrogen bonding.

The causes of such complexation are still under debate. One hypothesis, suggested long ago (14) and recently supported by DFT calculations on the crystal lattices (4*b*), explains parallel stacking of arene and perfluoroarene molecules by electrostatic effects, C—H and C—F bonds having substantial polarity in the opposite sense. Calculations of isolated dimers show that although van der Waals energy contribution is larger than the electrostatic energy contribution (15), it is the latter that makes heterodimers more stable than homodimers (16). On the other hand, Dunitz (16) emphasised the importance of dispersion interactions, and therefore of the anomalously low atomic polarizability of fluorine.

It has been suggested that intermolecular H···F attractions (weak hydrogen bonds) play a significant role in stabilizing the structures (4*a*, 17). Dunitz pointed out that the same reasoning should apply to alkanes and perfluoroalkanes, which

Received 7 April 2005. Published on the NRC Research Press Web site at http://canjchem.nrc.ca on 16 March 2006.

Dedicated to an outstanding scientist, leader, and friend, Professor Arthur J. Carty. We present a paper that is "a little different" in its subject matter, in recognition of Arthur's broad interests in the field of chemistry.

J.C. Collings, A.S. Batsanov, J.A.K. Howard, and T.B. Marder.[3] Department of Chemistry, University of Durham, South Road, Durham, DH1 3LE, UK.

[1]This article is part of a Special Issue dedicated to Professor Arthur Carty.
[2]For part 13, see ref. 1
[3]Corresponding author (e-mail: Todd.Marder@durham.ac.uk).

 doi:10.1139/V06-007 © 2006 NRC Canada

Table 1. Analytical and crystallographic data.

Complex	**1**	**2**
Formula	$C_{10}F_8 \cdot C_{13}H_{10}$	$C_{10}F_8 \cdot C_{14}H_{12}$
Formula weight	438.31	452.34
Analysis calcd. (%)	C 63.02, H 2.30	C 63.73, H 2.67
Analysis found (%)	C 63.06, H 2.25	C 63.79, H 2.63
Melting point (°C)	132–134	53–55
Crystal system	Triclinic	Orthorhombic
Space group (No.)	$P\bar{1}$ (2)	$P2_12_12_1$ (19)
a (Å)	6.798(2)	6.457(2)
b (Å)	7.872(3)	8.808(2)
c (Å)	9.414(4)	32.253(8)
α (°)	101.74(1)	90
β (°)	105.96(1)	90
γ (°)	103.89(1)	90
V (Å^3)	450.2(3)	1 834.3(8)
Z	1	4
ρ_{calcd} (g cm^{-3})	1.617	1.638
μ (mm^{-1})	0.15	0.15
Temperature of data collection (K)	120	120
Total reflections	2533	20 054
Unique reflections	1925	2 456
R_{int}	0.095	0.061
Refined parameters	139	337
$R(F)$, $I > 2\sigma(I)$	0.070	0.030
$wR(F^2)$, all data	0.223	0.070
CCDC deposit no.	276491	276492

in fact have negative mixing enthalpy and neither mix in the liquid state nor cocrystallize (16). Indeed, partially fluorinated alkanes crystallize in such fashion that fluorinated and non-fluorinated parts form segregated domains in the crystal (18). All this suggests a (relatively) nonstabilizing character of C-H···F interactions. However, gas-phase spectroscopic studies have shown that $CH_3F \cdot CHF_3$, $CH_2F_2 \cdot CH_2F_2$, and similar dimers are held together exclusively by C-H···F bridges (19).

To clarify this topic requires, inter alia, testing the limits of stability of the mixed-stack motif, and of the face-to-face arene–perfluoroarene synthon generally, against various steric distortions. In particular, all previously studied molecules were either entirely planar or planar except for a few hydrogen atoms. In the present work, we have studied complexation of OFN with planar (except for two methylene H atoms) fluorene and with rigidly nonplanar 9,10-dihydrophenanthrene.

Experimental

Synthesis

Octafluoronaphthalene (Bristol Organics), fluorene, and 9,10-hydrophenanthrene were tested for purity by GC–MS and used without further purification. GC–MS was carried out using a Hewlett-Packard HP-5890 series II gas chromatograph equipped with a HP-5971A mass selective detector. A 12 m fused silica (5% crosslinked phenylmethylsilicone) capillary column was used with UHP helium as the carrier gas.

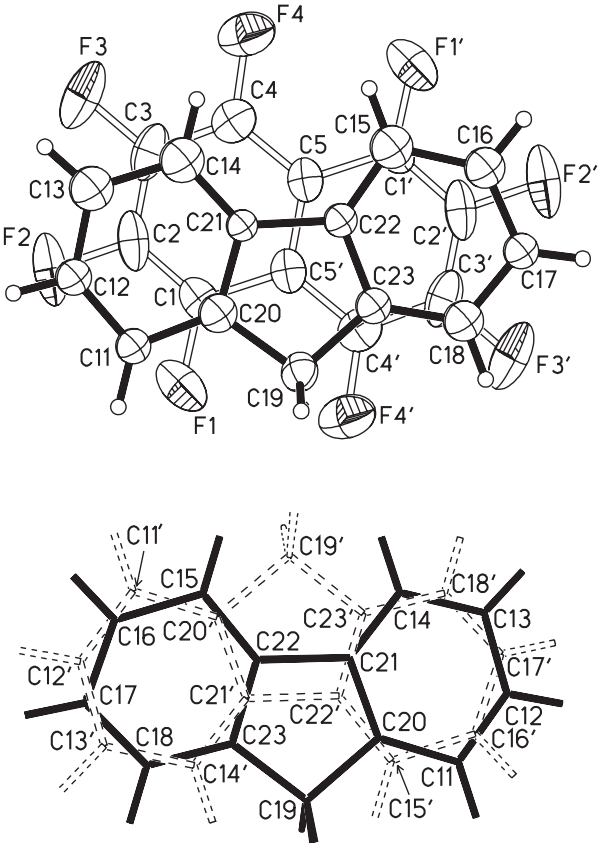
Single crystals of OFN·fluorene (**1**) were obtained as regular blocks by slow evaporation of a solution containing OFN (0.1 mmol) and fluorene (0.1 mmol) in 1 mL of dichloromethane (DCM). Single crystals of OFN·9,10-dihydrophenanthrene (**2**) were obtained by slow evaporation of a solution containing OFN (0.1 mmol) and 9,10-dihydrophenathrene (0.1 mmol) in 1 mL of DCM. Elemental analyses and melting points are presented in Table 1.

X-ray crystallography

X-ray diffraction experiments were carried out on Bruker 3-circle diffractometers with APEX ProteumM (**1**) or SMART 6K (**2**) CCD area detectors, using graphite-monochromated Mo Kα radiation (λ = 0.710 73 Å) from a 60 W microfocus Bede Microsource® with glass polycapillary optics (**1**) or a sealed tube (**2**). The crystals were cooled to 120 K using Cryostream (Oxford Cryosystems) open-flow N_2 cryostats. The structures were solved by direct methods and refined by full-matrix least-squares against F^2 of all data, using SHELXTL software (20). In **1**, all atoms of the OFN molecule were easily located and refined in anisotropic mode, but the Fourier map in the plane midway between the OFN planes showed a blurred pattern, which was rationalized by fitting a fluorene molecule of the literature dimensions (and hence its inversion equivalent) with 50% occupancy. This molecule was refined initially as a rigid body, then all C atoms were refined independently in isotropic approximation with all H atoms included in the "riding" model. The lengths of the C—C bonds related by the *molecular* twofold symmetry were constrained to be identical. All non-H atoms of the molecule proved coplanar within experi-

© 2006 NRC Canada

Fig. 1. Top: The molecules of OFN and fluorene (one possible position) in the structure of **1**, viewed down the *a* axis; bottom: disorder of the fluorene molecule. Primed atoms are generated by inversion centres; thermal ellipsoids are drawn at the 50% probability level.

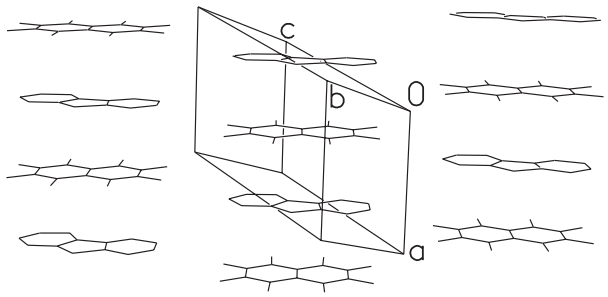


mental error; the mean plane passes through the inversion centre, which falls within the five-membered ring; hence, the alternative position of the molecule lies in the same plane. In **2**, all C and F atoms were refined in anisotropic mode, and all H atoms were located in a difference Fourier map and refined in isotropic approximation. Crystal data and other experimental details are listed in Table 1.[4]

Results and discussion

In both cases, cocrystallization gave the usual 1:1 stoichiometry. The structure of **1** contains infinite stacks of alternating OFN and fluorene molecules, which overlap as shown in Fig. 1. The asymmetric unit comprises half of the chemical formula unit. The OFN molecule has crystallographic C_i symmetry, whereas the fluorene molecule is statistically disordered between two overlapping positions related by an inversion centre (Fig. 1). Such disorder of fluorene has been observed in its cocrystals with

Fig. 2. Crystal packing of complex **1** (H atoms are omitted).



trinitrobenzene (21*a*) and various tetracyano-substituted molecules (21*b*), and phenanthrene is similarly disordered in its complex with OFN (6). Both the OFN and fluorene molecules are planar within experimental error (cf. fluorene is folded by 1.3° in its pure solid (22)), and their mean planes are parallel within 1.6(1)°. The two alternative positions of the disordered fluorene molecule are also coplanar within experimental error. The structure being triclinic implies that all molecules in the crystal are parallel within this range. The mean direction of the stack is parallel to the crystallographic *a* axis and nearly normal to the molecular planes, forming an angle of 85.6(1)° with the OFN plane and 87.3(1)° with the fluorene plane, i.e., the stack is practically columnar rather than slanted. All interplanar separations (*d*) in the stack are uniform, of 3.39 Å. Not surprisingly, the shortest intermolecular contact within a stack (C(19)-H···F4 of 2.53 Å) involves an out-of-plane methylene H atom.

The stacks are combined in the crystal in such a way that each fluorene molecule is closer to OFN than to fluorene molecules of adjacent stacks (Fig. 2). Therefore, the structure can be alternatively described as laminar, containing 2D sheets wherein each fluorene molecule is surrounded by six OFN molecules and vice versa. The sheets are substantially puckered; adjacent (dissimilar) molecules are not strictly coplanar but are shifted above or below the sheet plane by *d*/3. Nevertheless, such packing results in a number of close intermolecular C-H···F contacts (Fig. 3). Whereas the sum of van der Waals radii (23) of F and H is 2.56 Å, structure **1** contains six symmetrically independent interstack distances in the range 2.49–2.60 Å (but none between 2.60 and 2.68 Å), and two even shorter contacts, of 2.31 and 2.41 Å, respectively.[5]

The asymmetric unit of OFN·9,10-dihydrophenanthrene (**2**) is identical with the formula unit, both component molecules having no crystallographic symmetry (Fig. 4). The 9,10-dihydrophenanthrene molecule contains two planar fragments, each comprising a benzene ring with an adjacent methylene carbon atom. The dihedral angle between these moieties is 19.5(1)° (cf. 20.7° in the pure solid 9,10-dihydrophenanthrene (25)), hence, it is meaningless to refer to the mean plane of this molecule. Unlike biphenyl (8), dihydrophenanthrene cannot be easily planarized by

[4] Supplementary data for this article are available on the journal Web site (http://canjchem.nrc.ca) or may be purchased from the Depository of Unpublished Data, Document Delivery, CISTI, National Research Council Canada, Ottawa, ON K1A 0R6, Canada. DUD 5007. For more information on obtaining material refer to http://cisti-icist.nrc-cnrc.gc.ca/irm/unpub_e.shtml. CCDC 276491 and 276492 contain the crystallographic data for this manuscript. These data can be obtained, free of charge, via www.ccdc.cam.ac.uk/conts/retrieving.html (or from the Cambridge Crystallographic Data Centre, 12 Union Road, Cambridge CB2 1EZ, UK; fax +44 1223 336033; or deposit@ccdc.cam.ac.uk).

[5] After correcting the C(sp^2)—H bonds lengths to 1.08 Å, the standard value obtained from neutron diffraction data (24).

© 2006 NRC Canada

Fig. 3. Laminar packing in structure **1**, showing the distances of OFN molecules from the fluorene plane and H···F contacts of <2.6 Å.

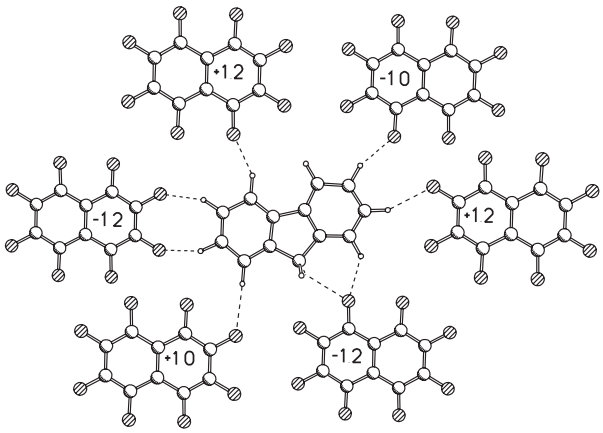
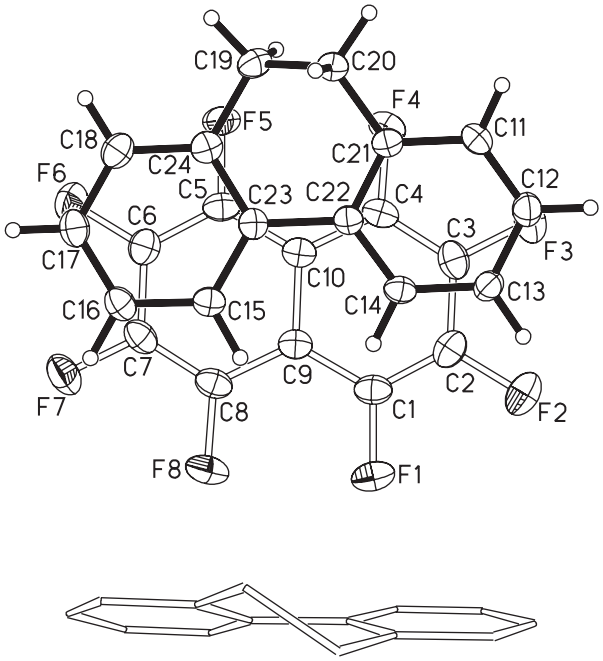


Fig. 4. Top: The molecules of OFN and 9,10-dihydrophenathrene in the structure of **2**, projection on the OFN plane. Bottom: Conformation of the 9,10-dihydrophenathrene molecule (H atoms are omitted).



intermolecular forces, thus its combination with the essentially planar OFN results in an awkward packing motif (Fig. 5) that cannot be described by any simple scheme. One can distinguish a strongly slanted stack, or rather a "ladder" of face-to-face heteromolecular dimers. In the dimer, the central C(21)—C(22) bond of the dihydrophenanthrene is parallel to the OFN plane within 3.3(1)°, and the two benzene rings are inclined to this plane by 17.0(1)° and 5.5(1)°. Contacts between the stacks resemble a distorted herringbone pattern with the dihedral angles of 48.3(1)° between contacting OFN molecules. Each dihydrophenanthrene molecule forms seven H···F contacts in the 2.40–2.60 Å range: six in-plane (Fig. 6) and one between stacked molecules, but no such contacts in the 2.60–2.71 Å range.

Fig. 5. Crystal packing of complex **2** (H atoms are omitted).

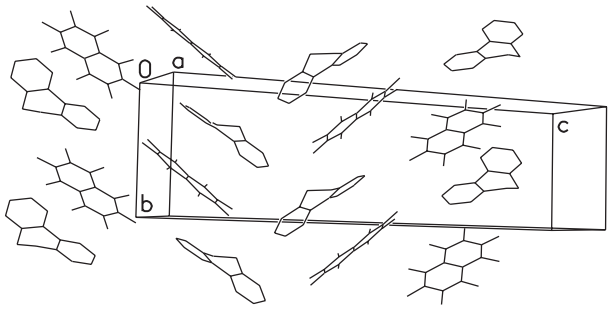
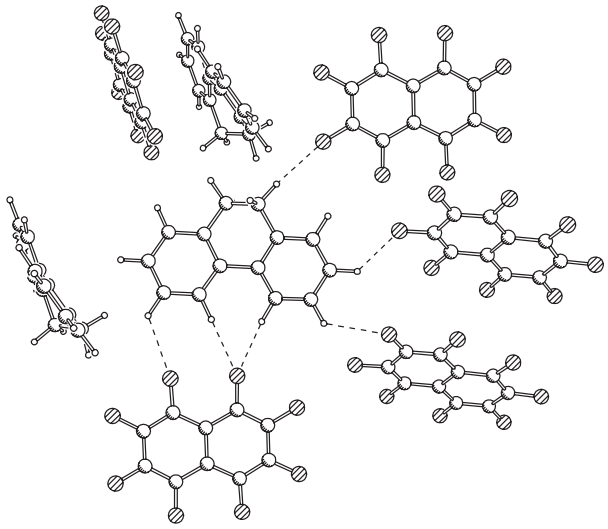


Fig. 6. H···F contacts (≤2.6 Å) in the structure of **2**.



Thus, the crystal packing of **1** is similar to those observed between OFN and *planar* arenes (while contrasting starkly with the herringbone packing of both pure OFN (10) and pure fluorene (22)), especially in the OFN·pyrene complex, which also crystallizes in the space group $P\bar{1}$ with $Z = 1$ and with roughly similar lattice parameters. In the latter, the site occupied by the disordered fluorene molecule in **1** is taken by an ordered pyrene molecule that possesses a crystallographic inversion centre. The molecular volume of OFN·pyrene (477 Å^3) is only 27 Å^3 larger than that of **1**, although the usual rule of 18 Å^3 per non-hydrogen atom requires a difference twice as big. Thus, fluorene does produce a somewhat looser packing, although it is not clear whether it is the effect of the disorder or of the out-of plane hydrogen atoms. In any case, the structure of **1** (and also of OFN·acenaphthene (12)) shows that the latter do not disrupt the typical mixed-stack pattern of arene–perfluoroarenes substantially. On the contrary, the constrained nonplanarity of the 9,10-dihydrophenanthrene molecule causes a complete departure from this pattern and an evident thermodynamic destabilization of the cocrystal, as indicated by its much lower melting point (Table 2). Most arene–perfluoroarene complexes, beginning with the seminal $C_6F_6{\cdot}C_6H_6$, have higher melting points than either of the components (although there are exceptions). Whereas complex **1** conforms to this rule, **2** has a melting point only slightly higher than that of the mean of the components.

© 2006 NRC Canada

Table 2. Melting temperatures (T_m, °C) of arene–perfluoroarene complexes.

	T_m			
Complex Φ·A	A	Φ	A·Φ	ΔT_m
$C_6F_6 \cdot C_6H_6$	5.4	5.0	23.7	18.5
OFN·naphthalene (5)	81	87	132	48
OFN·pyrene (6)	156	87	249	127.5
OFN·biphenyl (8)	71	87	97	18
OFN·biphenylene (8)	110	87	148	49.5
OFN·acenaphthene (12)	96	87	162	81
OFN·phenanthrene (6)	101	87	173	79
OFN·fluorene (**1**) (this work)	116	87	133	31.5
OFN·9,10-dihydrophenanthrene (**2**) (this work)	32.5	87	54	6

Note: $\Delta T_m = T_m(A \cdot \Phi) - 1/2[T_m(A) + T_m(\Phi)]$.

Conclusions

This study has confirmed that arene–perfluoroarene complexes are formed between OFN and two constrained biphenyl derivatives, the planar fluorene and nonplanar 9,10-dihydrophenathrene. However, the packing arrangements of the two complexes differ significantly, in that the OFN·fluorene structure comprises infinite stacks of approximately planar molecules, whereas the OFN·dihydrophenanthrene structure consists of a herringbone arrangement of OFN–dihydrophenanthrene dimers. The cause of this discrepancy is postulated to be due to the rigid nonplanarity of the dihydrophenanthrene molecules. In both structures, there are close intermolecular H···F contacts.

Acknowledgements

We thank Ms. Jaroslava Dostal for performing the elemental analyses. JCC and JAKH thank the Engineering and Physical Sciences Research Council (EPSRC) for a studentship and Senior Research Fellowship, respectively. TBM thanks the University of Durham for a Sir Derman Christopherson Foundation Fellowship. TBM and JAKH thank One NorthEast for funding under the Nanotechnology UIC program.

References

1. J.C. Collings, A.S. Batsanov, J.A.K. Howard, D.A. Dickie, J.A.C. Clyburne, H.A. Jenkins, and T.B. Marder. J. Fluorine Chem. **126**, 515 (2005).
2. (*a*) J.S.W. Overell and G.S. Pawle. Acta Crystallogr. Sect. B, **38**, 1966 (1982); (*b*) J.H. Williams, J.K. Cockcroft, and N. Finch. Angew. Chem. Int. Ed. Engl. **31**, 1655 (1992).
3. (*a*) G.R. Desiraju and A. Gavezzotti. Acta Crystallogr. Sect. B, **45**, 473 (1989); (*b*) N. Boden, P.P. Davis, C.H. Stam, and G.A. Wesselink. Mol. Phys. **25**, 81 (1973).
4. (*a*) T. Dahl. Acta Chem. Scand. Ser. A, **A42**, 1 (1988); (*b*) J.C. Collings, K.P. Roscoe, E.G. Robins, A.S. Batsanov, L.M. Stimson, J.A.K. Howard, S.J. Clark, and T.B. Marder. New J. Chem. **26**, 1740 (2002).
5. J. Potenza and D. Mastropaolo. Acta Crystallogr. Sect. B, **31**, 2527 (1975).
6. J.C. Collings, K.P. Roscoe, R.Ll. Thomas, A.S. Batsanov, L.M. Stimson, J.A.K. Howard, and T.B. Marder. New J. Chem. **25**, 1410 (2001).
7. J.C. Collings, A.S. Batsanov, J.A.K. Howard, and T.B. Marder. Acta Crystallogr. Sect. C, **57**, 870 (2001).
8. J.C. Collings, P.S. Smith, D.S. Yufit, A.S. Batsanov, J.A.K. Howard, and T.B. Marder. CrystEngComm. **6**, 25 (2004).
9. A.S. Batsanov, J.C. Collings, J.A.K. Howard, T.B. Marder, and D.F. Perepichka. Acta Crystallogr. Sect. C, **57**, 1306 (2001).
10. I.Y. Bagryanskaya, Y.V. Gatilov, E. Lork, R. Mews, M.M. Shakirov, P.G. Watson, and A.V. Zibarev. J. Fluorine Chem. **116**, 149 (2002).
11. J.A.C. Clybourne, T. Hamilton, and H.A. Jenkins. Cryst. Eng. **4**, 1 (2001).
12. J.C. Collings, A.S. Batsanov, J.A.K. Howard, and T.B. Marder. Cryst. Eng. **5**, 37 (2002).
13. A.S. Batsanov, J.C. Collings, J.A.K. Howard, and T.B. Marder. Acta Crystallogr. Sect. E, **57**, o950 (2001).
14. N.M.D. Brown and F.L. Swinton. J. Chem. Soc. Chem. Commun. 770 (1974).
15. S. Lorenzo, G.R. Lewis, and I. Dance. New J. Chem. **24**, 295 (2000); O.R. Lozman, R.J. Bushby, and J.G. Vinter. J. Chem. Soc. Perkin Trans. 2, 1446 (2001).
16. J.D. Dunitz. Chem. Bio. Chem. **5**, 614 (2004).
17. (*a*) L. Shimoni and J.P. Glusker. Struct. Chem. **5**, 383 (1994); (*b*) V.R. Thalladi, H.-C. Weiss, D. Blaser, R. Boese, A. Nangia, and G.R. Desiraju. J. Am. Chem. Soc. **120**, 8702 (1998); (*c*) G.R. Desiraju. Acc. Chem. Res. **35**, 565 (2002).
18. J. Lapasset, J. Moret, M. Melas, A. Collet, M. Vigeur, and H. Blancou. Z. Kristallogr. **211**, 945 (1996).
19. W. Caminati, J.C. Lopez, J.L. Alouso, and J.-U. Grabow. Angew. Chem. Int. Ed. **44**, 3840 (2005), and refs. therein.
20. G.M. Sheldrick. SHELXTL. Version 6.12 [computer program]. Bruker AXS, Madison, Wisconsin. 2001.
21. (*a*) R.A. Mariezcurrena, S. Russi, A.W. Mombru, L. Suescun, H. Pardo, O.L. Tombesi, and M.A. Frontera. Acta Crystallogr. Sect. C, **55**, 1170 (1999); (*b*) A. Arrais, E. Boccaleri, G. Crosie, M. Milanesio, R. Orlando, and E. Diana. CrystEngComm. **5**, 388 (2003).
22. R.E. Gerkin, A.P. Lundstedt, and W.J. Repport. Acta Crystallogr. Sect. C, **40**, 1892 (1984).
23. R.S. Rowland and R. Taylor. J. Phys. Chem. **100**, 7384 (1996).
24. F.H. Allen, O. Kennard, D.G. Watson, L. Brammer, A.G. Orpen, and R.J. Taylor. J. Chem. Soc. Perkin Trans. 2, S1 (1987).
25. (*a*) V.K. Belskii, V.E. Zavodnik, and V.M. Vozzhenrika. Acta Crystallogr. Sect. C, **40**, 1210 (1984); (*b*) R. Cosmo, T.W. Hambley, and S. Sternhell. J. Org. Chem. **52**, 3119 (1987).

© 2006 NRC Canada

Formation and X-ray structure of the host–guest adduct $[Pd_3(dppm)_3(CO)(NO_3)]^+$ and the mechanism of its electrochemical reduction[1]

David Brevet, Dominique Lucas, Philippe Richard, Alain Vallat, Yves Mugnier, and Pierre D. Harvey

Abstract: $[Pd_3(dppm)_3(CO)]^{2+}$, $[Pd_3]^{2+}$, reacts with NO_3^- to form the host–guest adduct $[Pd_3(dppm)_3(CO)(NO_3)]^+$, $[Pd_3(NO_3)]^+$. The presence of NO_3^- inside the cavity is confirmed by X-ray crystallography. Using a qualitative relationship between λ_{max} (UV–vis) and the association constant of various adducts, the relative binding between NO_3^- and $[Pd_3]^{2+}$ is in the same order of magnitude of that between $CF_3CO_2^-$ and $[Pd_3]^{2+}$. Based on Pd···O distances, the NO_3^- ion is relativity more weakly associated to $[Pd_3]^{2+}$ in comparison with the known $[Pd_3(CF_3CO_2)]^+$. Using variation of $[NO_3^-]$ in the presence of $[Pd_3](PF_6)_2$ and variation of scan rates, the resulting cyclic voltammogramms (CV) were simulated to extract both kinetic and thermodynamic constants associated to a square scheme. Both the anodic and cathodic scans of the title cluster exhibits ECE mechanisms (E = electrochemical process; C = chemical process). For the anodic scan, the EEC event is not ruled out, at least as a minor process.

Key words: nitrate, palladium cluster, adduct, electrochemistry, X-ray structure, rate constant, equilibrium constant.

Résumé : Le $[Pd_3(dppm)_3(CO)]^{2+}$, $[Pd_3]^{2+}$ réagit avec l'anion NO_3^- pour former l'adduit hôte–invité $[Pd_3(dppm)_3(CO)(NO_3)]^+$, $[Pd_3(NO_3)]^+$. La présence de l'anion NO_3^- dans la cavité est confirmée par diffraction des rayons X. Utilisant une relation qualitative entre λ_{max} (UV–vis) et la constante d'association de divers adduits, on a déterminé que les fixations relatives entre NO_3^- et $[Pd_3]^{2+}$ sont du même ordre de grandeur que celles entre $CF_3CO_2^-$ et $[Pd_3]^{2+}$. Sur la base des distances Pd···O, l'ion NO_3^- est associé relativement plus faiblement au $[Pd_3]^{2+}$ que dans le produit connu $[Pd_3(CF_3CO_2)]^+$. Utilisant une variation de la concentration de NO_3^- en présence de $[Pd_3](PF_6)_2$ et une variation des vitesses de balayage, on a pu simuler les voltampérogrammes cycliques pour en tirer les constantes cinétiques ainsi que thermodynamiques associées à un schéma carré. Les balayages tant anodique que cathodique de l'agrégat mentionné dans le titre présentent tous les deux des mécanismes ECE (E = processus électrochimique; C = processus chimique). Pour le balayage anodique, il n'est pas possible d'éliminer la possibilité d'un processus EEC, au moins comme processus mineur.

Mots clés : nitrate, agrégat de palladium, adduit, électrochimie, détermination de structure par diffraction des rayons X, constante de vitesse, constante d'équilibre.

[Traduit par la Rédaction]

Introduction

The use of NO_3^- in electrosynthesis is well-known (1–3) and involves the electrochemical one-electron oxidation to generate the highly reactive intermediate $NO_3^{\cdot}$ via the reaction, $NO_3^- \rightarrow NO_3^{\cdot} + 1\ e^-$. Its properties, whether it reacts with itself or with organics are also well-documented (4–7). The possibility of mediating the electrochemical one-electron oxidation of NO_3^- via a transition metal complex intermediate is interesting, if the oxidation potential to perform this reaction occurs at a lower potential than that of NO_3^- alone. We have recently extensively explored the electrochemical and electrocatalytic properties of the unsaturated cluster, $[Pd_3]^{2+}$ (8–12). The NO_3^- ion can exhibit multiple forms of binding onto metal atoms (13–18). On the other hand, host–guest association complexes of an anion inside the cavity of a metal-containing host are scarce (19). The $[Pd_3]^{2+}$ cluster is one of the rare examples of a host capable of accepting anions inside its cavity formed by the dppm–phenyl groups above the Pd_3 plane (anion = $PO_2F_2^-$ (9),

Received 17 June 2005. Published on the NRC Research Press Web site at http://canjchem.nrc.ca on 16 March 2006.

This paper is dedicated to Arthur Carty.

D. Brevet,[2] D. Lucas, P. Richard, A. Vallat, and Y. Mugnier. Laboratoire de Synthèse et d'Electrosynthèse Organométallique LSEO UMR 5188, faculté des Sciences Mirande, Allée Savary, 21000 Dijon, France.
P.D. Harvey.[3] Département de Chimie, Université de Sherbrooke, Sherbrooke, QC J1K 2R1, Canada.

[1]This article is part of a Special Issue dedicated to Professor Arthur Carty.
[2]Corresponding author (e-mail: David.Brevet@u-bourgogne.fr).
[3]Corresponding author (e-mail: Pierre.Harvey@USherbrooke.ca).

 doi:10.1139/V05-249 © 2006 NRC Canada

$CF_3CO_2^-$ (20), PF_6^- for $[Pd_3(dpam)_3(CO)]^{2+}$, where dpam = $(Ph_2As)_2CH_2$ (21)). In relation with the comments made above, the structural analysis of the title cluster, $[Pd_3(NO_3)]^+$, along with analysis of the electrochemical properties, both in oxidation and reduction, are in order. We now wish to report the X-ray structure of $[Pd_3(NO_3)]^+$ and its behaviour upon its reduction by cyclic voltammetry (CV) and rotating disk electrode (RDE). The overall results are interpreted with a six-member square scheme (in which one species is absent or not observed), and the CV and RDE are simulated to extract the reaction rates and equilibrium constants for NO_3^- dissociation in $[Pd_3(NO_3)]^{n+}$ (n = 1 or 0).

Experimental section

Materials

$[Pd_3(dppm)_3(CO)](PF_6)_2$ was prepared according to a literature procedure (20). NBu_4NO_3 was purchased from Fluka and was used as received. Tetrahydrofuran (THF) was distilled under Ar over Na and benzophenone, while CH_2Cl_2 was distilled over P_2O_5. The supporting electrolyte used in each experiment was NBu_4PF_6 (Aldrich). The salt was recrystallized twice in ethanol and dried at 80 °C for at least 2 days before use.

Preparation of ($[Pd_3(dppm)_3(CO)(NO_3)](PF_6)$

The $[Pd_3(dppm)_3(CO)](PF_6)_2$ starting material (10.4 mg, 0.005 81 mmol) was added to a degassed THF solution (10 mL). A mother solution of 177 mg (0.582 mmol) of NBu_4NO_3 in THF (1 mL) was prepared. Ten microlitres of this solution (corresponding to 1 equiv. of NBu_4NO_3) was added to the $[Pd_3(dppm)_3(CO)](PF_6)_2$ solution, which was stirred for 15 min. The deep red solution turned brown immediately. UV–vis (THF, nm) λ: 480. IR (KBr, cm^{-1}) ν(CO): 1816. ^{1}H NMR (acetone-d_6, ppm) δ: 5.08, 4.80 (m, ^2J (H^aH^b) = 14.09 Hz, ($CH^aH^bP_2$)). ^{31}P NMR (acetone-d_6, ppm) δ: –6.93. Anal. calcd. for $C_{76}H_{66}O_1P_6Pd_3{\cdot}(NO_3)_{1.3}(PF_6)_{0.7}{\cdot}1THF{\cdot}1.33H_2O$: C 53.64, H 4.31, N 1.02; found: C 53.23, H 4.48, N 1.07. The presence of THF and H_2O molecules was confirmed by ^{1}H NMR. Additionally, the presence of THF was also observed in the X-ray structure.

Electrochemical experiments

All manipulations were performed using Schlenk techniques in an atmosphere of dry, oxygen-free argon gas. The supporting electrolyte was degassed under vacuum before use and then solubilized at a concentration of 0.2 mol/L. For cyclic voltammetry experiments, the concentration of the analyte was nearly 10^{-3} mol/L. Voltammetric analyses were carried out in a standard three-electrode cell with a EG&G Princeton Applied Research (PAR) model 273A potentiostat, connected to an interfaced computer employing Electrochemistry Power Suite software. The reference electrode was a saturated calomel electrode (SCE) separated from the solution by a sintered glass disk. The auxiliary electrode was a platinum wire. For all voltammetric measurements, the working electrode was a vitreous carbon electrode (ϕ = 3 mm). In these conditions, when operating in THF, the formal potential for the ferrocene$^{\pm}$ couple was found to be +0.56 V vs. SCE.

Digital simulation

The computations were performed using the commercially available program called Digisim (Bioanalytical Systems). The potential increase was set to 10 mV. The uncompensated resistance, here R_u = 1500 Ω, was determined with a PAR 373A potentiostat using the same experimental conditions as for the CV measurements. The double-layer capacitance value was estimated as Cdl/A = 10^{-4} F cm^{-2} using a blank solution prior to voltammetric measurements. The experimental curves were corrected for residual current, also determined using voltammetric measurements of blank solutions.

Crystallography

Crystal suitable for X-ray analysis were obtained from slow diffusion between ether and a THF solution containing the adduct. Data was collected with a Nonius Kappa CCD diffractometer at 110 K. The structure was solved in the $P2_1$ space group via a Patterson search program and refined with full-matrix least-squares methods based on F^2 (SHELX-97) (22) with the aid of the WINGX (23) program. Except for one disordered THF solvate molecule, all non-hydrogen atoms were refined with anisotropic thermal parameters. All H atoms were placed in idealized positions and refined using a riding model [Uiso(H) = 1.2Ueq(C)]. One of the two THF molecules is disordered, the oxygen atom occupies several positions of the ring, and this molecule was modelized by a five-carbon ring with an overall isotropic temperature factor and a common restrained variable C—C distance. The Flack parameter converged to 0.65(2) and could suggest a racemic twin. Table 1 presents a summary of the crystal data, data collection, and refinement parameters.[4]

Results and discussion

Adduct formation

The addition of NBu_4NO_3 to $[Pd_3](PF_6)_2$ induces a PF_6^-/NO_3^- metathesis. Because of the planar geometry and smaller size of NO_3^-, this anion should be trapped by the dppm cavity, hence converting $[Pd_3](PF_6)_2$ into the desired adduct $[Pd_3(NO_3)](PF_6)$. Because of the excess of NO_3^- ion used, some of the counter ion (PF_6^-) was also exchanged based on the chemical analysis. Full exchange into $[Pd_3(NO_3)](NO_3)$ or precise conversion into $[Pd_3(NO_3)](PF_6)$ were unsuccessfully attempted several times, and no further effort was made. It was not necessary for this work since we were only interested in the X-ray structure of the $[Pd_3(NO_3)]^+$ adduct. Nonetheless, from the analysis (and ^{1}H NMR spectra), the formulation $[Pd_3(dppm)_3(CO)(NO_3)](NO_3)_{0.3}(PF_6)_{0.7}{\cdot}THF{\cdot}1.3H_2O$ is obtained for the sample that provided crystals suitable for X-ray studies. Indeed, X-ray crystallography and electrochemistry confirm the presence

[4] Supplementary data for this article are available on the journal Web site (http://canjchem.nrc.ca) or may be purchased from the Depository of Unpublished Data, Document Delivery, CISTI, National Research Council Canada, Ottawa, ON K1A 0R6, Canada. DUD 4098. For more information on obtaining material refer to http://cisti-icist.nrc-cnrc.gc.ca/irm/unpub_e.shtml. CCDC 287167 contains the crystallographic data for this manuscript. These data can be obtained, free of charge, via http://www.ccdc.cam.ac.uk/conts/retrieving.html (Or from the Cambridge Crystallographic Data Centre, 12 Union Road, Cambridge CB2 1EZ, UK; fax +44 1223 336033; or deposit@ccdc.cam.ac.uk).

© 2006 NRC Canada

Table 1. Crystal data and data parameters for $[Pd_3(dppm)_3(CO)(NO_3)](PF_6)$.

Compound	$[Pd_3(dppm)_3(CO)(NO_3)](PF_6)\cdot 2THF$
Formula	$C_{84}H_{82}O_6NF_6P_7Pd_3$
MW	1 851.5
T (K)	110(2)
Crystal system	Monoclinic
Space group	$P2_1$
a (Å)	10.715 2(1)
b (Å)	26.521 8(2)
c (Å)	14.162 5(1)
β (°)	100.803(1)
V (Å^3)	3 953.46(6)
Z	2
F(000)	1 876
D_{calcd} (g/cm^3)	1.555
Diffractometer	Enraf-Nonius KappaCCD
Scan type	Mixture of ϕ rotations and ω scans
λ (Å)	0.710 73
μ (mm^{-1})	0.885
Crystal size (mm^3)	0.50 × 0.35 × 0.25
sin(θ)/λ max (Å^{-1})	0.65
Index ranges	$-13 \le h \le 13$
	$-34 \le k \le 33$
	$-18 \le l \le 18$
Absorption correction	SCALEPACK
RC = Refl. collected	17 517
IRC = independent RC	17 517
IRCGT = IRC and [$I > 2\sigma(I)$]	16 646
Refinement method	Full-matrix least-squares on F^2
Data / restraints / parameters	17 517 / 6 / 912
R for IRCGT	$R1$ = 0.041 4,[a] $wR2$ = 0.105 8[b]
R for IRC	$R1$ = 0.044 4,[a] $wR2$ = 0.108 1[b]
Goodness-of-fit[c]	1.024
Abs. structure parameter	0.65(2)
Largest diff. peak and hole (e Å^{-3})	1.13 and –0.83

[a] $R1 = \Sigma(||F_o| - |F_c||)/\Sigma|F_o|$.
[b] $wR2 = [\Sigma w(F_o^2 - F_c^2)^2/\Sigma[w(F_o^2)^2]]^{1/2}$, where $w = 1/[\sigma^2(F_o^2) + 5.54P + (0.0677P)^2]$, where $P = (\max(F_o^2,0) + 2F_c^2)/3$.
[c] Goodness-of-fit = $[\Sigma w(F_o^2 - F_c^2)^2/(N_o - N_v)]^{1/2}$.

of NO_3^- in the cavity. THF is also found in the lattice as solvate molecule (Experimental section). The electrochemical studies were performed with $[Pd_3](PF_6)_2$.

The UV–vis spectrum of $[Pd_3(NO_3)]^+$ in THF is compared to $[Pd_3]^{2+}$ and other adducts in Table 2. The previously reported binding constants (K_1) for the $[Pd_3(X)]^+$ adducts indicate that the interactions increase as $PF_6^- < CF_3CO_2^- < Cl^- < Br^- < I^-$ (20, 21, 24). Interestingly, λ_{max} follows the same trend in reverse order: 496 > 484 > 463 > 459 > 456 nm, respectively, and can serve as a qualitative tool to compare the relative strength of $Pd_3^{2+}\cdots X^-$ interactions. The λ_{max} for $[Pd_3(NO_3)]^+$ is 480 nm, which indicates that the binding strength of NO_3^- is similar to that of $CF_3CO_2^-$. This trend is qualitative because of the broadness of the bands.

X-ray structure

The X-ray data and selected bond distances and angles are presented in Tables 1 and 3. An ORTEP representation is shown in Fig. 1. The NO_3^- ion is placed inside the cavity where the closest distance (Pd···O) is 2.801 Å ($Pd_1\cdots O_2$), which is indicative of electrostatic interactions. The skeleton bond distances are normal as compared to other $[Pd_3(X)]^+$ adducts (Table 4). The O-N-O angles are 118.45° (O_4NO_2), 119.06° (O_2NO_3), and 122.46° (O_4NO_3), and the N—O distances are 1.224 Å (N—O_4), 1.245 Å (N—O_2), and 1.248 Å (N—O_3). There is an obvious deviation from the expected ideal triangular structure, which seems to be associated with steric interactions between the NO_3^- ion and the phenyl groups (Fig. 1). The 2.801 Å distance for Pd···O interactions is longer than that for the $CF_3CO_2^-$ adduct (shortest Pd···O distances are 2.752 and 2.682 Å) (20). The weaker host–guest interactions deduced from X-ray data are entirely consistent with the residual charge on each oxygen atom (1/2 and 1/3 for $CF_3CO_2^-$ and NO_3^-, respectively), reinforcing the electrostatic model.

Electrochemistry

Our group has previously investigated the electrochemical behaviour of $[Pd_3]^{2+}$ (25) and $[Pd_3(X)]^+$ (X = Br (10), I (26)). The CV of $[Pd_3](PF_6)_2$ in a mixture of THF–NBu_4PF_6

© 2006 NRC Canada

Table 2. Comparison of selected spectroscopic and electrochemical data for the $[Pd_3(X)]^+$ adducts.

Type of data	$[Pd_3]^{2+a}$	$[Pd_3(p\text{-}TS)]^{+a,b}$	$[Pd_3(HSO_4)]^{+a}$	$[Pd_3(CF_3CO_2)]^{+c}$	$[Pd_3(NO_3)]^{+a}$	$[Pd_3(Cl)]^{+a}$	$[Pd_3(Br)]^{+a}$	$[Pd_3(I)]^{+a}$
^{31}P NMR[d]	–3.43	–7.84	–6.82	–9.23	–6.93	–8.55	–8.32	–8.42
UV–vis[e]	496	490	489	484	480	463	459	456
Reduction potential[f,g]	–0.34 (A_1), –0.60 (A_2)	$A_3 > -0.50$	–0.445 (A_3)	–0.60 (A)	–0.44 (A_1), –0.60 (A_2)	–0.87 (A_3)	–0.81 (A_3)	–0.89 (A_3)
Standard potential[f,g]	–0.29 (E°_1), –0.55 (E°_2)				–0.515 (E°_3)			

[a]With PF_6^- as the counterion.
[b]*p*-TS = *p*-$CH_3C_6H_4SO_3^-$.
[c]With $CF_3CO_2^-$ as the counterion.
[d]In acetone-d_6; δ (ppm).
[e]In THF; λ (nm).
[f]Reference electrode: V vs. SCE.
[g]In THF–NBu_4PF_6 (0.2 mol/L) solution.

Table 3. Selected bond lengths and angles for $[Pd_3(dppm)_3(CO)(NO_3)](PF_6)$.

Bond lengths (Å)		Bond angles (°)	
N—O(2)	1.245(6)	O(2)-N-O(3)	119.4(5)
N—O(3)	1.247(6)	O(2)-N-O(4)	118.3(5)
N—O(4)	1.229(7)	O(3)-N-O(4)	122.3(5)
C(1)—O(1)	1.155(5)	O(1)-C(1)-Pd(1)	136.0(4)
C(1)—Pd(1)	2.095(4)	O(1)-C(1)-Pd(2)	134.0(3)
C(1)—Pd(2)	2.127(4)	O(1)-C(1)-Pd(3)	133.5(4)
C(1)—Pd(3)	2.100(4)	Pd(1)-C(1)-Pd(2)	76.34(13)
C(2)—P(1)	1.838(4)	Pd(1)-C(1)-Pd(3)	76.26(13)
C(2)—P(2)	1.839(4)	Pd(2)-C(1)-Pd(3)	76.22(14)
C(3)—P(4)	1.831(4)	P(1)-C(2)-P(2)	110.1(2)
C(3)—P(3)	1.844(4)	P(3)-C(3)-P(4)	110.9(2)
C(4)—P(5)	1.837(5)	P(5)-C(4)-P(6)	109.8(2)
C(4)—P(6)	1.853(5)	C(2)-P(1)-Pd(1)	110.65(15)
P(1)—Pd(1)	2.3213(11)	C(2)-P(2)-Pd(2)	109.32(15)
P(2)—Pd(2)	2.3117(11)	C(3)-P(3)-Pd(2)	110.31(15)
P(3)—Pd(2)	2.3248(11)	C(3)-P(4)-Pd(3)	112.25(15)
P(4)—Pd(3)	2.3113(11)	C(4)-P(5)-Pd(3)	109.66(15)
P(5)—Pd(3)	2.3211(11)	C(4)-P(6)-Pd(1)	109.87(14)
P(6)—Pd(1)	2.3185(11)	P(1)-Pd(1)-P(6)	107.90(4)
Pd(1)—Pd(3)	2.5903(4)	P(2)-Pd(2)-P(3)	111.32(4)
Pd(1)—Pd(2)	2.6094(4)	P(4)-Pd(3)-P(5)	107.56(4)
Pd(2)—Pd(3)	2.6092(4)	Pd(2)-Pd(1)-Pd(3)	60.238(12)
		Pd(1)-Pd(2)-Pd(3)	59.518(11)
		Pd(1)-Pd(3)-Pd(2)	60.244(12)

(0.2 mol/L) (Fig. 2) exhibits the two electrochemically reversible one-electron reduction waves A_1/A_1' and A_2/A_2' at $E_{1/2}$ = –0.29 and –0.54 V vs. SCE ($E_{1/2} = 0.5(E_{pa} + E_{pc})$; E_p = peak potential, a = anodic, c = cathodic), respectively. THF is used for comparison purposes with previous works (10, 25, 26). The addition of 1 equiv. of NBu_4NO_3 slightly modifies the reduction waves witnessing quantitative formation of $[Pd_3(NO_3)]^+$ according to (eq. [1]).

[1] $$[Pd_3]^{2+} + NO_3^- \rightarrow [Pd_3(NO_3)]^+$$

Both reduction waves are still eletrochemically reversible, but a new reduction wave system (A_3/A_3') appears at $E_{1/2}$ = –0.357 V vs. SCE at the expense of the current intensity of wave (A_1/A_1'). Using spectroscopy, this reaction is easily monitored. The UV–vis spectra exhibit the disappearance of the 496 nm band characteristic to $[Pd_3]^{2+}$ and the appearance of the 480 nm band of the $[Pd_3(NO_3)]^+$ adduct. For ^{31}P NMR, the –3.43 ppm resonance of $[Pd_3]^{2+}$ is replaced by the new one at –6.93 ppm associated with $[Pd_3(NO_3)]^+$. Further addition of NO_3^- ions induces further modification of the CV. System A_3/A_3' moves towards more negative potentials. This can be explained by the EC (E = electrochemical process; C = chemical process) process for the reduction step, where the chemical step corresponds to the dissociation (eq. [2]).

[2] $$[Pd_3(NO_3)]^0 \rightleftharpoons [Pd_3]^+ + NO_3^-$$

In the presence of excess NO_3^- the equilibrium is shifted to the left, so the reduction of $[Pd_3(NO_3)]^+$ becomes more difficult. In an excess of NO_3^-, the system A_3/A_3' super-

© 2006 NRC Canada

Fig. 1. ORTEP representation of $[Pd_3(NO_3)]^+$. The thermal ellipsoids are represented at 50% probability. The THF molecules and H atoms are not shown for more clarity.

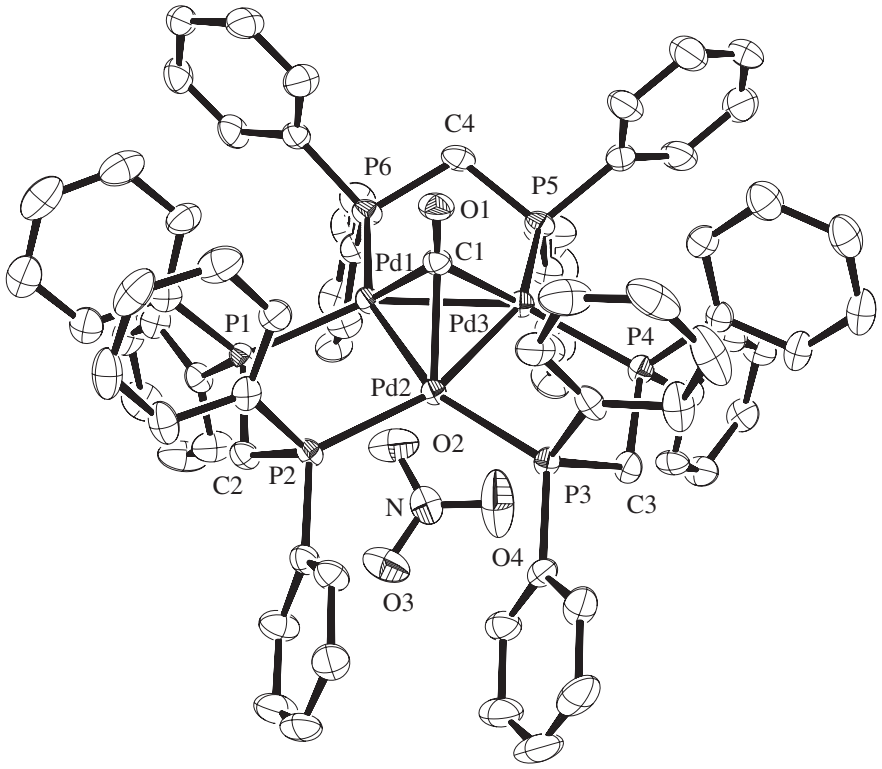
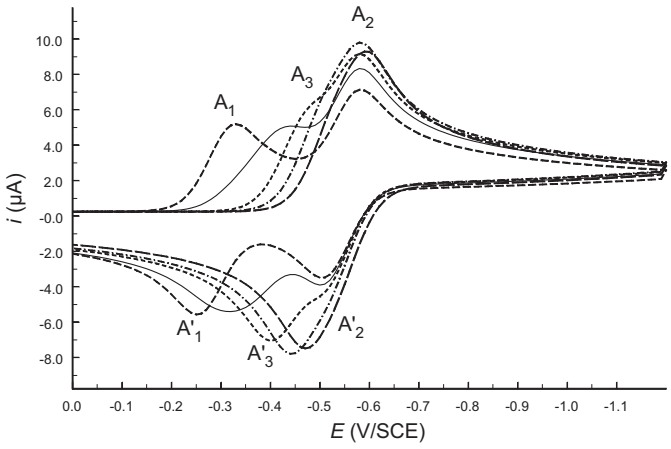


Table 4. Comparison of average bond distances in the skeleton of the Pd_3^{2+} core.

Skeleton	*d*(Pd—Pd) (Å)	*d*(Pd—P) (Å)	*d*(Pd—C) (Å)	*d*(C=O) (Å)	Ref.
$[Pd_3(NO_3)]PF_6$	2.603	2.318	2.106	1.16	This work
$[Pd_3(PF_2O_2)]PF_6$	2.612	2.322	2.104	1.17	9
$[Pd_3(CF_3CO_2)]PF_6$	2.595	2.311	2.08	1.17	20
$[Pd_3(Cl)]BF_4$	2.595	2.312	2.104	1.15	27
$[Pd_3](PF_6)_2$	2.613	2.318	2.104	1.16	20

Fig. 2. CV of $[Pd_3]^{2+}$ in THF–NBu_4PF_6 (0.2 mol/L) in the presence of 0, 1, 10, 50, and 200 equiv. of NO_3^- anions. Initial potential: 0 V. Scan rate: 50 mV s^{-1}.



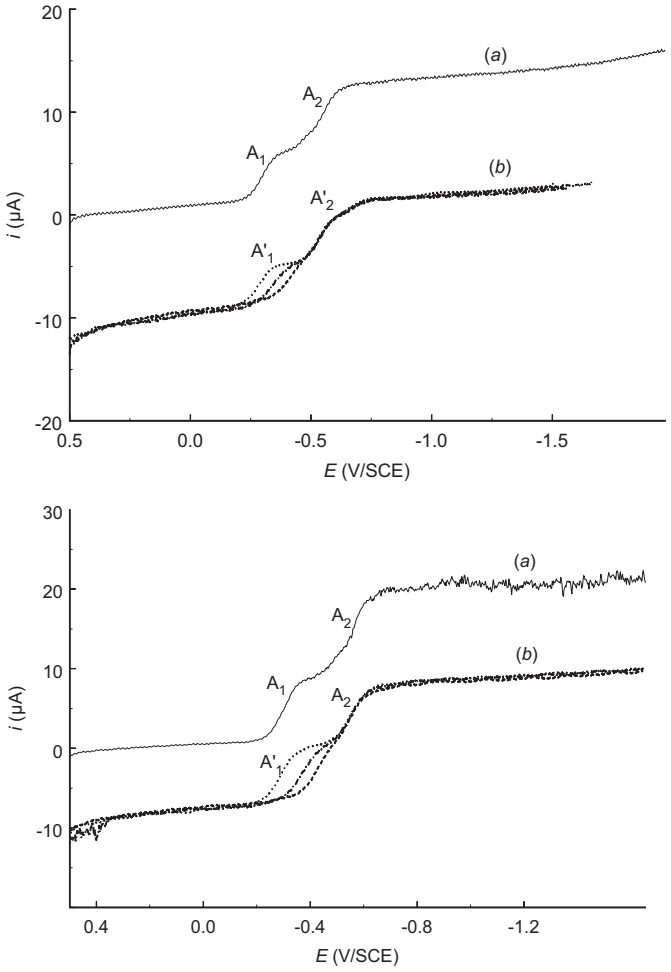
poses wave A_2/A'_2, which makes the evolution of E°_3 impossible from direct measurements in the CV traces.

The reactivity of NO_3^- towards the electrogenerated species $[Pd_3]^+$ and $[Pd_3]^0$ was also investigated. $[Pd_3]^0$ exhibits two oxidation waves, A'_1 and A'_2. In the presence of NO_3^-, no modification of wave A'_2 occurs, but wave A_1' shifts towards more negative potentials. This behaviour indicates that $[Pd_3]^0$ is stable in the presence of NO_3^-. For the second oxidation wave, a clear curve modification is observed with the change in $[NO_3^-]$, demonstrating that an EE mechanism operates in the absence of NO_3^- anion, but becomes an ECE process in the presence of this anion. A similar behaviour is also observed with the electrogenerated $[Pd_3]^+$ species, which exhibits wave A_2 and A'_1 (Fig. 3, bottom).

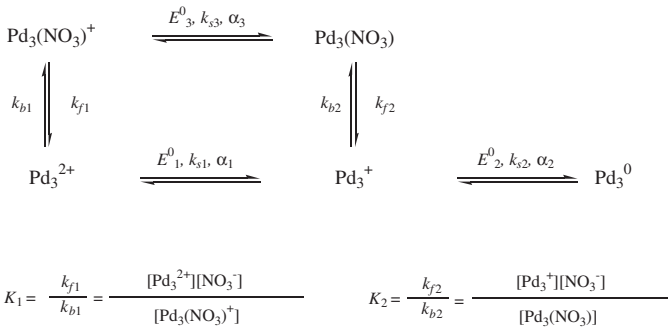
Both CV and RDE were simulated to establish the reduction mechanism and to extract the kinetic and thermodynamic parameters based on a six-member square scheme (Scheme 1). The $[Pd_3(NO_3)]^-$ species does not exist in this work, so this member is not represented.

© 2006 NRC Canada

Fig. 3. (Top graph): RDE voltammogramms of: (*a*) $[Pd_3]^{2+}$; (*b*) (solid line) after two-electron reduction and formation of $[Pd_3]^0$; (b_1) (dotted line) in the presence of 1 equiv. of NO_3^-; (b_2) (dashed line) in the presence of 10 equiv. of NO_3^-. (Bottom graph): RDE voltammogramms of: (*a*) $[Pd_3]^{2+}$; (*b*) (solid line) after one-electron reduction and formation of $[Pd_3]^0$; (b_1) (dashed line) in the presence of 1 equiv. of NO_3^-; (b_2) (dotted line) in the presence of 10 equiv. of NO_3^-.



Scheme 1.



The standard potentials (E_1^o and E_2^o), the heterogeneous rate constants (k_{s1} and k_{s2}), the charge transfer coefficients (α_1 and α_2), and the diffusion constant for $[Pd_3]^{2+}$ were evaluated previously (26). The potential E_3^o is not obtained as the potential is influenced by the chemical process. To estimate this value for E_3^o, the following experiments and comparisons were performed.

Table 5. Comparison of $E_{1/2}(A_1/A_1')$ and $E_{1/2}(A_2/A_2')$ of Pd_3^{2+} + NO_3^- in THF and CH_2Cl_2 (V vs. SCE).

Potential	THF (V)	CH_2Cl_2 (V)
$E_{1/2}(A_1/A_1')^a$	–0.298	–0.362
$E_{1/2}(A_3/A_3')^a$	–0.357	–0.410

[a]SCE as reference electrode.

In CH_2Cl_2, the CV exhibits a better separation of the A_2/A_2' and A_3/A_3' waves (eqs. [3] and [4]). The CVs are no longer modified when 250 equiv. of NO_3^- ion are added. In this solvent, $E^o_{(A_3/A_3')} = E_{1/2} = -0.564$ V. By assuming that the potential difference between wave A_1/A_1' and wave A_3/A_3' remains the same for THF and CH_2Cl_2, we can approximatively evaluate E_3^o for $[Pd_3(NO_3)]^+$.

[3] $[Pd_3]^{2+} + 1\ e^- \rightleftharpoons [Pd_3]^+\ A_1/A_1'$

[4] $[Pd_3(NO_3)]^+\ 1\ e^- \rightleftharpoons [Pd_3(NO_3)]\ A_3/A_3'$

The comparison was also made for $[Pd_3]^{2+}$ + 1 equiv. of NO_3^- in THF and in CH_2Cl_2. This comparison of $E_{1/2}(A_1/A_1')$ and $E_{1/2}(A_3/A_3')$ is shown in Table 5. The differences between $E_{1/2}(A_1/A_1')$ and $E_{1/2}(A_3/A_3')$ in THF and CH_2Cl_2 are 0.064 and 0.053 V, respectively. The fact that these values are similar is reassuring. In the presence of 250 equiv. of NO_3^-, $E°(CH_2Cl_2)$ is –0.564 V. By subtracting these values (0.064 and 0.053 V) from –0.564 V, we can then estimate $E° = E_{1/2}(A_3/A_3')$ for $[Pd_3(NO_3)]^+$ in THF (–0.500 V if 0.064 is used, and –0.511 V if 0.053 is employed). At best fits, the simulations predicted $E° = E_{1/2}(A_3/A_3') = -0.515$ V vs. SCE in THF (see the following and Table 6). The transfer coefficient (α_3) was arbitrarily set at 0.5 for the simulation, a value typical for this type of system. The fits were performed with seven variables (k_{s1}, k_{s2}, k_{s3}, K_1, K_2, k_{f1}, and k_{f2}; see Scheme 1 for their description) and were tested against curves that were measured at various $[NO_3^-]$ and scan rates. The variables k_{s1}, k_{s2}, and k_{s3} were generally observed within a small window (Table 6). These seven variables were extracted at best fits (Tables 6 and 7 and Fig. 4), except for k_{f1}, which turned out to have no effect on the computed curves in the explored window ($v <$ 500 mV s^{-1}). The diffusion constant was determined by RDE to be 4×10^{-6} cm^2 s^{-1}.

The cathodic scan is described by an ECE mechanism since the reduction of the $[Pd_3(NO_3)]^0$ species was not observed. This contrasts with the mechanism determined for the stronger $[Pd_3(I)]^+$ adduct (26). For the anodic scan, one must consider two possibilities, ECE and EEC mechanisms. No shift should be observed for the A_2/A_2' wave in an EEC process, while a shift toward more negative potentials should be observed for an ECE mechanism. Experimentally, the ECE mechanism was observed for both anodic and cathodic scans (i.e., there was a shift for both cases). This observation was confirmed from the curve simulation, particularly from the comparison of the K_1 and K_2 values ($K_1 << K_2$). For the anodic scan, the EEC mechanism is not excluded, but must be a minor process if it is present.

© 2006 NRC Canada

Fig. 4. Simulations (solid line) and experimental (symbols) CVs for $[Pd_3(NO_3)]^+$ in THF–Bu_4NPF_6 (0.2 mol/L). (*a*) Alone; (*b*) with 10 equiv. of NO_3^-; (*c*) with 50 equiv. of NO_3^-; (*d*) with 200 equiv. of NO_3^-. Initial potential: 0 V. Scan rate: 50 mV s^{-1}.

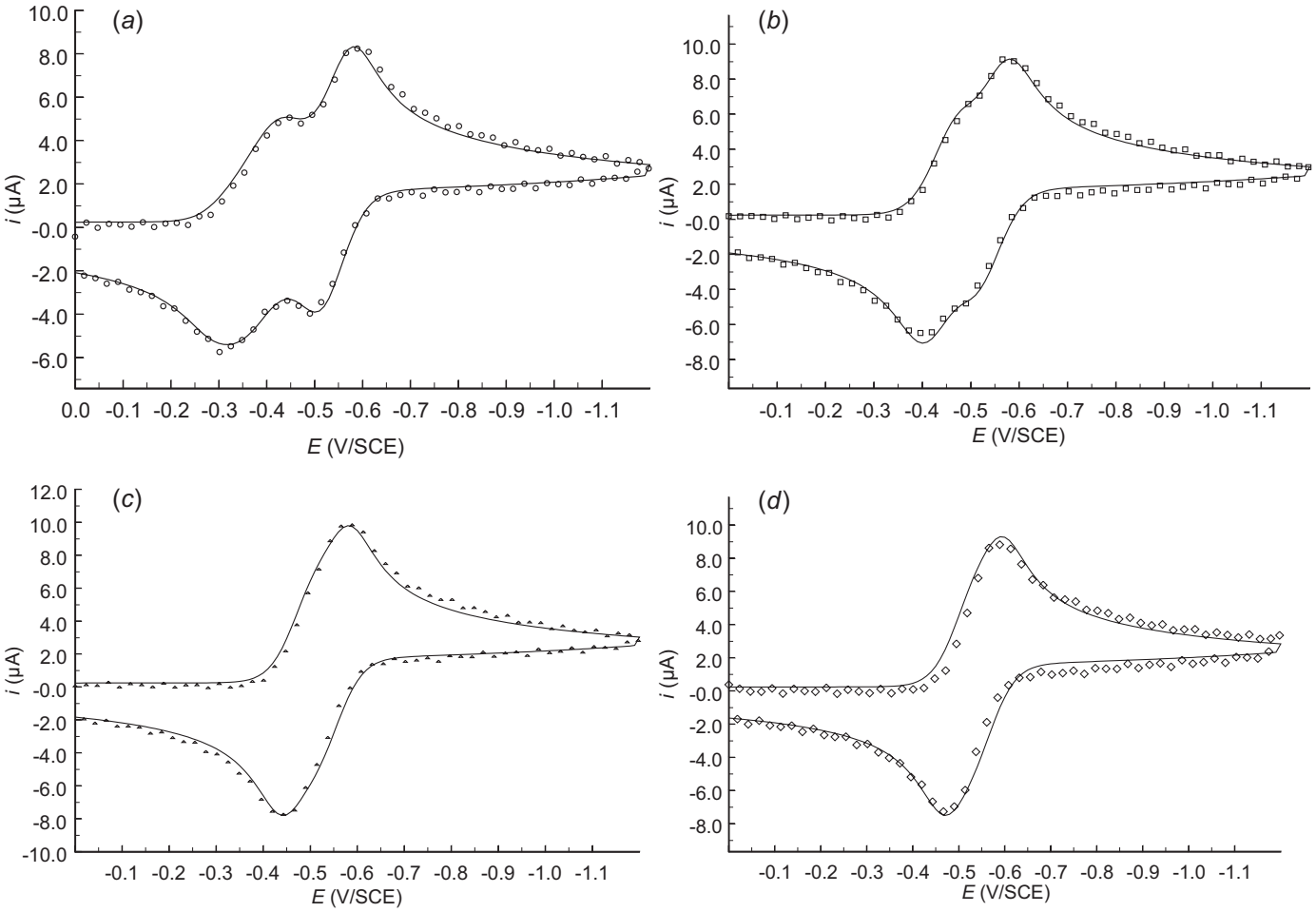


Table 6. Input data for best fits.

E_i^o (V)[a]	k_{si} (cm s^{-1})	α_i
E_1^o = –0.290	k_{s1} = 0.2	α_1 = 0.5
E_2^o = –0.545	k_{s2} = 0.2	α_2 = 0.5
E_3^o = –0.515	k_{s3} = 0.1	α_3 = 0.5

[a]SCE as reference electrode.

Table 7. Simulation results at best fits.

K_i (mol L^{-1})	k_{fi} (s^{-1})
$K_1 = 1.575\times10^{-5}$[a]	k_{f1} = ?[b]
K_2 = 0.1	$k_{f2} = 10^9$

[a]K_1 depend on the E_1^o, E_3^o, and K_2 parameters and was obtained by the relation $E_1^o - E_3^o = \frac{RT}{nF}\ln\frac{K_2}{K_1}$.

[b]This value has no effect within the explored window.

Interactions with RSO_3^- and HSO_4^-

Similar host–guest interactions are observed for *p*-toluenesulfonate and hydrogenosulfate ions with $[Pd_3]^{2+}$. The corresponding adducts, $[Pd_3(p\text{-}CH_3C_6H_5SO_3)]^+$ and $[Pd_3(HSO_4)]^+$, were generated and characterized (Table 2) after the addition of 1 equiv. of the anion on the cluster. Based on the λ_{max} trend discussed, these two substrates bind $[Pd_3]^{2+}$ less strongly than the NO_3^- analogue. Steric hindrance could be at the origin of this difference. Similar conclusions are anticipated for electrochemical properties of adducts, except that both kinetic and thermodynamic parameters should be different.

Conclusion

The properties of the $[Pd_3(NO_3)]^+$ adduct, notably, the structure, the ^{31}P NMR and UV–vis spectroscopy, and the electrochemical reduction behaviour were described. The ECE mechanism is the dominant process, both in the cathodic and anodic scans. Future works will focus on the oxidation of this adduct to find useful catalytic processes. Preliminary results show a large increase in oxidative current at ~+1 V vs. SCE, which represents a decrease of ~0.5 V with respect to that for NO_3^- alone, with the increase of $[NO_3^-]$. This behaviour is indicative of a catalytic process ($NO_3^- \rightarrow NO_3^{\cdot} + 1\ e^-$), presumably mediated by the $[Pd_3]^{2+}$ cluster, via the host–guest interactions established in this work.

Acknowledgements

PDH thanks the Natural Sciences and Engineering Re-

© 2006 NRC Canada

search Council of Canada (NSERC) and Fonds Québecois pour la Recherche en Sciences Naturelles et en Technologie (FQRNT) for funding. YM is grateful to the Centre National de la Recherche Scientifique (CNRS) and the Conseil Régional de Bourgogne for funds.

References

1. T. Shono, Y. Yamamoto, K. Takigawa, H. Maekawa, M. Ishifune, and S. Kashimura. Chem. Lett. **6**, 1045 (1994).
2. T. Shono, M. Chuankamnerdkarn, H. Maekawa, M. Ishifune, and S. Kashimura. Synthesis, **9**, 895 (1994).
3. S. Tatsuya, T. Takigawa, Y. Yoshihide, M. Hirofumi, and K. Shigenori. Tetrahedron Lett. **35**, 4161 (1994).
4. S.I. Bannov and V.A. Nevostruev. Radiat. Phys. Chem. **68**, 917 (2003).
5. G. Fantechi, N.R. Jensen, J. Hjorth, and J. Peeters. Atmos. Environ. **32**, 3547 (1998).
6. A. Boughriet and M. Wartel. Electrochim. Acta, **36**, 889 (1991).
7. O. Ito, S. Akiho, and M. Iino. J. Phys. Chem. **93**, 4079 (1989).
8. D. Lucas, F. Lemaitre, B. Gallego-Gomez, C. Cugnier, P. Richard, Y. Mugnier, and P.D. Harvey. Eur. J. Inorg. Chem. 1011 (2005).
9. F. Lemaitre, D. Lucas, K. Groison, P. Richard, Y. Mugnier, and P.D. Harvey. J. Am. Chem. Soc. **125**, 5511 (2003).
10. D. Brevet, Y. Mugnier, F. Lemaitre, D. Lucas, S. Samreth, and P.D. Harvey. Inorg. Chem. **42**, 4909 (2003).
11. D. Brevet, D. Lucas, H. Cattey, F. Lemaitre, Y. Mugnier, and P.D. Harvey. J. Am. Chem. Soc. **123**, 4340 (2001).
12. P.D. Harvey, Y. Mugnier, D. Lucas, D. Evrard, F. Lemaitre, and A. Valain. J. Cluster Sci. **15**, 63 (2004).
13. H. Oberhammer. J. Mol. Struct. **605**, 177 (2002).
14. Y.K. Gun'ko, S.D. Elliot, P.B. Hitchcock, and M.F. Lappert. J. Chem. Soc. Dalton Trans. 1852 (2002).
15. X. Liu, J.A. McAllister, M.P. de Miranda, E.J.L. McInnes, C.A. Kilner, and M.A. Halcrow. Chem. Eur. J. **10**, 1827 (2004).
16. V.V. Sharrutin, O.K. Sharutina, N.V. Nasonova, A.P. Pakusina, A.N. Zakharova, D.V. Krivolapov, A.T. Gubaidullin, and I.A. Litvinov. Russ. J. Gen. Chem. **71**, 1238 (2001).
17. D.J. Rose, Q. Chen, and J. Zubieta. Inorg. Chim. Acta, **268**, 163 (1998).
18. M. Maekawa, M. Munakata, T. Kuroda-Sowa, and Y. Suenaga. Anal. Sci. **14**, 447 (1998).
19. R.D. Schnebeck, E. Freisinger, and B. Lippert. Angew. Chem. Int. Ed. **38**, 168 (1999).
20. R. Provencher, K.T. Aye, M. Drouin, J. Gagnon, N. Boudreault, and P.D. Harvey. Inorg. Chem. **33**, 3689 (1994).
21. T. Zhang, M. Drouin, and P.D. Harvey. Chem. Commun. (Cambridge), **7**, 877 (1996).
22. G.M. Sheldrick. SHELX97 (includes SHELXs97 and SHELX97). Release 97-2 [computer program]. University of Göttingen, Göttingen, Germany. 1998.
23. L.J. Farrugia. J. Appl. Crystallogr. **32**, 837 (1999).
24. P.D. Harvey, K. Hierso, P. Braunstein, and X. Morise. Inorg. Chim. Acta, **250**, 337 (1996).
25. I. Gautheron, Y. Mugnier, K. Hierso, and P.D. Harvey. Can. J. Chem. **75**, 1182 (1997).
26. F. Lemaitre, D. Brevet, D. Lucas, A. Vallat, Y. Mugneir, and P.D. Harvey. Inorg. Chem. **41**, 2368 (2002).
27. P.D. Harvey, R. Provencher, J. Gagnon, T. Zhang, D. Fortin, K. Hierso, M. Drouin, and S.M. Socol. Can. J. Chem. **74**, 2268 (1996).

© 2006 NRC Canada

A simple synthetic route to the formation of tetracopper(I) 2-mercaptothiazoline compounds — The crystal structures of $[Cu_4(S\text{-}thiaz)_4(PEt_2Ph)_2]$, $[Cu_4(S\text{-}thiaz)_4(PEt_3)_2]$, $[Cu_4(S\text{-}thiaz)_4]_2$, and $[Cu_4(S\text{-}thiaz)_4]_4$[1]

Olaf Fuhr, Lucia Fernandez-Recio, and Dieter Fenske

Abstract: Reactions of copper(I) acetate with 2-mercaptothiazoline (HS-thiaz) in the presence of tertiary phosphines lead to the formation of tetranuclear sulphur-bridged copper complexes. Depending on the reaction conditions, isolated clusters ($[Cu_4(S\text{-}thiaz)_4(PR_3)_2]$ (PR_3 = PPh_3 (**1**), PEt_2Ph (**2**), PEt_3 (**3**)), oligomeric compounds ($[Cu_4(S\text{-}thiaz)_4]_2$ (**4**) and $[Cu_4(S\text{-}thiaz)_4]_4$ (**5**)), or a one-dimensional polymer ($[Cu_4(S\text{-}thiaz)_4]_\infty$ (**6**)) are formed. The structures of the compounds **2**–**5** have been determined by single crystal X-ray analysis.

Key words: copper, 2-mercaptothiazoline, single crystal X-ray analysis.

Résumé : Les réactions de l'acétate de cuivre(I) avec la 2-mercaptothiazoline (HS-thiaz), en présence de phosphines tertiaires, conduisent à la formation de complexes de cuivre tétranucléaires comportant des ponts de soufre. Suivant les conditions réactionnelles, il y a formation d'agrégats isolés, ($[Cu_4(S\text{-}thiaz)_4(PR_3)_2]$ (PR_3 = PPh_3 (**1**); PEt_2Ph (**2**); PEt_3 (**3**)), des composés oligomères, ($[Cu_4(S\text{-}thiaz)_4]_2$ (**4**) ou $[Cu_4(S\text{-}thiaz)_4]_4$ (**5**)), ou d'un polymère unidimensionnel, $[Cu_4(S\text{-}thiaz)_4]_\infty$ (**6**). Les structures des composés **2**, **3**, **4** et **5** ont été déterminées par diffraction des rayons X sur un cristal unique.

Mots clés : cuivre, 2-mercaptothiazoline, diffraction des rayons X par un cristal unique.

[Traduit par la Rédaction]

Introduction

The chemistry of copper(I) in combination with chalcogen derivatives provides a large variety of compounds. Many clusters with increasing numbers of metal atoms have been synthesized, the biggest cluster to date being $[Cu_{146}Se_{73}(PPh_3)_{30}]$ (1). Typically, such clusters reflect the transition from separated molecules or complexes to the infinite bulk phase. Not only structural aspects are of interest, but many polynuclear d^{10} compounds also show interesting photophysical features (2). A third aspect is the fact that many enzymes contain copper–sulphur clusters (3). Therefore, researchers have spent considerable effort on the synthesis of copper(I) complexes with 2-mercaptothiazoline and its derivatives as ligands (4–9).

In this work, we describe a simple route to tetracopper(I) 2-mercaptothiazoline compounds. Those that were unknown so far were characterized by single crystal X-ray analysis.

Experimental

All reactions were performed in a dry, oxygen-free nitrogen atmosphere using standard Schlenk techniques. Solvents were dried with sodium/benzophenone and freshly distilled. Copper(I) acetate (CuOAc) was synthesized by reduction of copper(II) acetate with copper tunings in acetonitrile (10), PEt_3, P-*n*-Pr_3, and PEt_2Ph by common Grignard reactions (11). PPh_3 and 2-mercaptothiazoline were used as received from the commercial source (Sigma-Aldrich).

IR-spectra were recorded as KBr pellets using a FT-IR spectrometer Spectrum GX from PerkinElmer.

Received 28 September 2005. Published on the NRC Research Press Web site at http://canjchem.nrc.ca on 17 March 2006.

Dedicated to Professor Arthur J. Carty.

O. Fuhr[2] and L. Fernandez-Recio. Forschungszentrum Karlsruhe, Institut für Nanotechnologie, Postfach 36 40, D-76021 Karlsruhe, Germany.
D. Fenske. Universität Karlsruhe (TH), Institut für Anorganische Chemie, Engesserstraße 15, Geb. 30.45D-76128 Karlsruhe, Germany.

[1]This article is part of a Special Issue dedicated to Professor Arthur Carty.
[2]Corresponding author (e-mail: olaf.fuhr@int.fzk.de).

 doi:10.1139/V06-003 © 2006 NRC Canada

Table 1. Crystallographic data for **2**–**5**.

Compound	**2**	**3**·C_7H_8	**4**	**5**·$2C_7H_8$
Empirical formula	$C_{32}H_{46}Cu_4N_4P_2S_8$	$C_{31}H_{54}Cu_4N_4P_2S_8$	$C_{24}H_{32}Cu_8N_8S_{16}$	$C_{62}H_{80}Cu_{16}N_{16}S_{32}$
Formula mass	1 059.31	1 055.36	1 453.86	3 091.98
Colour, habit	Colourless, block	Colourless, block	Colourless, plate	Colourless, block
Crystal system	Monoclinic	Tetragonal	Monoclinic	Monoclinic
Space group	*C*2/*c*	$P4_32_12$	$P2_1/c$	$P2_1/c$
Z	4	4	4	2
a (Å)	23.672(5)	12.278(2)	16.846(3)	20.363(4)
b (Å)	11.354(2)	12.278(2)	11.234(2)	11.296(2)
c (Å)	16.063(3)	29.192(6)	24.336(5)	21.928(4)
α (°)	90	90	90	90
β (°)	94.99(3)	90	110.01(3)	95.11(3)
γ (°)	90	90	90	90
Volume (Å^3)	4 300.8(15)	4 400.7(12)	4 327.4(15)	5 023.8(18)
D_{calcd} (g cm^{-3})	1.636	1.593	2.232	2.044
Temperature (K)	180	200	180	180
μ(MoKα) (mm^{-1})	2.443	2.387	4.659	4.020
2θ range of data collection (°)	2.0–54.2	3.6–52	2.3–52	3.8–52
F(000)	2 160	2 168	2 880	3 080
Observed reflections	10 770	11 516	18 544	23 594
Independent reflections	4 687 (R_{int} = 0.0403)	4 273 (R_{int} = 0.0528)	8 272 (R_{int} = 0.0475)	9 709 (R_{int} = 0.0905)
Independent reflections with $I > 2\sigma(I)$	3 439	3 603	6 832	5 268
Restraints/parameters	0, 228	12, 209	0, 506	0, 571
Goodness of fit on F^2	0.912	0.963	1.172	0.831
Final *R* indices [$I > 2\sigma(I)$]	R_1 = 0.0386	R_1 = 0.0395	R_1 = 0.0756	R_1 = 0.0444
	wR_2 = 0.0950	wR_2 = 0.0945	wR_2 = 0.1941	wR_2 = 0.0767
R indices (all data)	R_1 = 0.0542	R_1 = 0.0475	R_1 = 0.0847	R_1 = 0.1051
	wR_2 = 0.0994	wR_2 = 0.0973	wR_2 = 0.1967	wR_2 = 0.0904
Largest diff. peak and hole (e Å^{-3})	0.601, –0.684	0.613, –0.666	2.037, –1.078	0.805, –0.727
Flack parameter		0.00(2)		

X-ray structure determination

Crystals were removed from the reaction flask under a stream of N_2 gas and immediately covered with a layer of perfluoropolyether oil (Riedel de Häen). A suitable crystal was selected, attached to a glass fibre, and immediately placed in the low-temperature nitrogen stream. The data were collected with a STOE IPDS II diffractometer using MoKα (λ = 0.710 73 Å) radiation produced by a common X-ray tube (2 kW). Structure solution and refinement against F^2 were carried out using SHELXS and SHELXL software (12). Molecular drawings were prepared with Diamond 2.1 (13) and PaintShopPro 7AE (14).

The crystal and refinement data of **2**–**5** are summarized in Table 1.[3]

Synthesis of $[Cu_4(S\text{-}thiaz)_4(PPh_3)_2]$ (1)

A solution of copper(I) acetate (390 mg, 3.18 mmol) and triphenylphosphine (830 mg, 3.18 mmol) PPh_3 in THF (30 mL) was layered with a solution of 2-mercaptothiazoline (380 mg, 3.18 mmol) in THF (5 mL). Within 4 days, colourless plates of **1**·2THF crystallized. Yield: 1.1 g (98%). IR (KBr, cm^{-1}): 3049 (m), 2941 (m), 2850 (m), 1958 (w), 1585 (w), 1571 (w), 1523 (vs), 1480 (s), 1448 (m), 1434 (s), 1304 (s), 1261 (w), 1189 (m), 1157 (w), 1093 (s), 1067 (m), 1026 (vs), 968 (vs), 934 (s), 852 (w), 746 (s), 694 (s), 619 (w), 574 (w), 518 (s), 432 (m). Anal. calcd. for $C_{56}H_{62}Cu_4N_4O_2P_2S_8$: C 48.19, H 4.48, N 4.01, S 18.38; found: C 48.53, H 4.60, N 4.16, S 18,61.

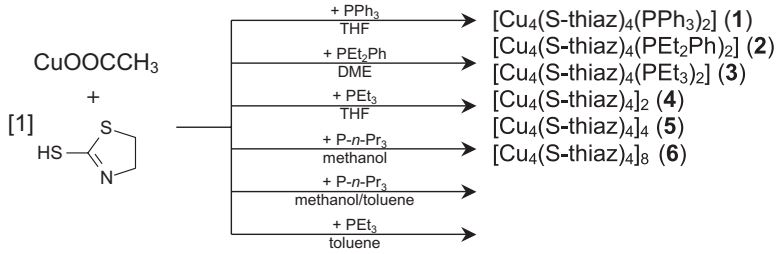
Synthesis of $[Cu_4(S\text{-}thiaz)_4(PEt_2Ph)_2]$ (2)

Copper(I) acetate (150 mg, 1.22 mmol), PEt_2Ph (0.21 mL, 1.22 mmol), and 2-mercaptothiazoline (145 mg, 1.22 mmol) were dissolved in DME (60 mL). After stirring for 1 day, the volume of the reaction mixture was reduced to 10 mL and *n*-heptane (15 mL) was added. From this solution **2** crystallized within 2 h as colourless blocks. Yield: 80 mg (25%). IR (KBr, cm^{-1}): 3084 (w), 2958 (m), 2927 (m), 2870 (m), 2850 (m), 2361 (m), 2342 (m), 1522 (vs), 1453 (m), 1433

[3] Supplementary data for this article are available on the journal Web site (http://canjchem.nrc.ca) or may be purchased from the Depository of Unpublished Data, Document Delivery, CISTI, National Research Council Canada, Ottawa, ON K1A 0R6, Canada. DUD 5006. For more information on obtaining material refer to http://cisti-icist.nrc-cnrc.gc.ca/irm/unpub_e.shtml. CCDC 290083–290086 contain the crystallographic data for this manuscript. These data can be obtained, free of charge, via http://www.ccdc.cam.ac.uk/conts/retrieving.html (Or from the Cambridge Crystallographic Data Centre, 12 Union Road, Cambridge CB2 1EZ, UK; fax +44 1223 336033; or deposit@ccdc.cam.ac.uk).

© 2006 NRC Canada

Scheme 1.



(s), 1375 (w), 1306 (m), 1259 (w), 1187 (w), 1101 (w), 1023 (vs), 967 (vs), 933 (s), 855 (w), 767 (m), 755 (m), 734 (m), 699 (m), 669 (m), 574 (w), 490 (w), 432 (w), 418 (w). Anal. calcd. for $C_{32}H_{46}Cu_4N_4P_2S_8$: C 36.28, H 4.38, N 5.29, S 24.21; found: C 36.51, H 4.29, N 5.16, S 23.74.

Synthesis of $[Cu_4(S\text{-thiaz})_4(PEt_3)_2]$ (3)

Copper(I) acetate (312 mg, 2.55 mmol) was dissolved in THF (60 mL) by adding triethylphosphine (0.38 mL, 2.55 mmol) to give a light yellow solution. After addition of 2-mercaptothiazoline (300 mg, 2.55 mmol), the reaction mixture turned colourless and was stirred for 6 h. All volatile compounds were removed under reduced pressure and the resulting oily residue was recrystallized from toluene. The product was isolated as big colourless crystals of $\mathbf{3}\cdot C_7H_8$. Yield: 175 mg (26%). IR (KBr, cm^{-1}): 2954 (m), 2929 (m), 2872 (m), 1525 (vs), 1450 (m), 1376 (m), 1304 (m), 1259 (w), 1194 (w), 1025 (vs), 970 (s), 933 (s), 768 (m), 729 (w), 669 (w), 576 (w), 433 (w). Anal. calcd. for $C_{31}H_{54}Cu_4N_4P_2S_8$: C 35.28, H 5.16, N 5.31, S 24.31; found: C 34.94, H 5.31, N 5.62, S 23.78.

Synthesis of $[Cu_4(S\text{-thiaz})_4]_2$ (4)

A solution of 2-mercaptothiazoline (80 mg, 0.7 mmol) in methanol (10 mL) was added at room temperature to a solution of CuOAc (86 mg, 0.7 mmol) and P-*n*-Pr_3 (0.07 mL, 0.35 mmol) in methanol (20 mL). After 30 min, the pale yellow solution was separated from a white precipitate. Within several days compound **4** crystallized from the filtrate as colourless plates. Yield: 50 mg (39%). IR (KBr, cm^{-1}): 3430 (w), 1636 (m), 1532 (s), 1505 (m), 1309 (m), 1026 (s), 970 (m), 931 (m). Anal. calcd. for $C_{24}H_{32}Cu_8N_8S_{16}$: C 19.83, H 2.22, N 7.71, S 35.29; found: C 20.47, H 1.81, N 7.34, S 35.81.

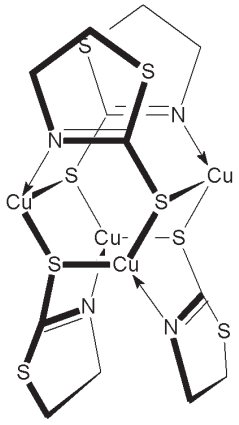
Synthesis of $[Cu_4(S\text{-thiaz})_4]_4$ (5)

A solution of 2-mercaptothiazoline (160 mg, 1.31 mmol) in methanol (10 mL) was added at room temperature to a solution of CuOAc (161 mg, 1.31 mmol) and P-*n*-Pr_3 (0.13 mL, 0.66 mmol) in methanol (40 mL). After 30 min, the pale yellow solution was separated from a white precipitate. Toluene (30 mL) was added to the filtrate; within the next 2 weeks, compound **4** and **5** crystallized from this solution.

Synthesis of $[Cu_4(S\text{-thiaz})_4]_\infty$ (6)

2-Mercaptothiazoline (360 mg, 3.06 mmol) was added to a solution of copper(I) acetate (375 mg, 3.06 mmol) and triethylphosphine (0.45 mL, 3.06 mmol) in toluene (60 mL).

Fig. 1. Principal drawing of the $[Cu_4(S\text{-thiaz})_4]$ cage found in compounds **1**–**6**.



Within a short time a white precipitate was formed, which was redissolved by mild heating. After several hours the product crystallized as colourless bars as $\mathbf{6}\cdot C_7H_8$. Yield: 280 mg (45%). IR (KBr, cm^{-1}): 2852 (w), 1524 (vs), 1447 (m), 1304 (m), 1189 (w), 1025 (s), 970 (s), 937 (s), 737 (m), 697 (w), 676 (w), 469 (w), 427 (w). Anal. calcd. for $C_{19}H_{24}Cu_4N_4S_8$: C 27.86, H 2.95, N 6.84, S 31.32; found: C 27.81, H 2.88, N 6.55, S 33.20.

Results and discussion

When 2-mercaptothiazoline (HS-thiaz) reacts with copper(I) acetate it is deprotonated and sulphur-bridged copper clusters are formed. The main structural motif of these compounds is a $[Cu_4(S\text{-thiaz})_4]$ cage, which is shown in Fig. 1.

The four copper atoms of this unit are bridged by the four exocyclic sulphur atoms of the 2-mercaptothiazoline ligands forming an eight-membered, folded ring. In addition, the heterocycles coordinate via the lone pairs of the nitrogen atoms to the copper atoms of the Cu_4S_4 core. Depending on the reaction conditions — especially the solvent used — different substances can be synthesized: compounds with isolated $[Cu_4(S\text{-thiaz})_4]$ cages (**1**–**3**), as well as oligomeric (**4**, **5**) and polymeric (**6**) products (Scheme 1). All reactions have been carried out in the presence of tertiary phosphines as additional donor components.

In ethereal solvents two phosphine molecules are coordinated to one Cu_4 unit forming clusters of the type $[Cu_4(S\text{-thiaz})_4(PR_3)_2]$ (PR_3 = PPh_3 (**1**), PEt_2Ph (**2**), PEt_3 (**3**)). **1** has been synthesized before starting from copper(II) acetate under reductive conditions (**4**); the crystallographic data pub-

© 2006 NRC Canada

Fig. 2. Molecular structure of **2** (H atoms are omitted for clarity).

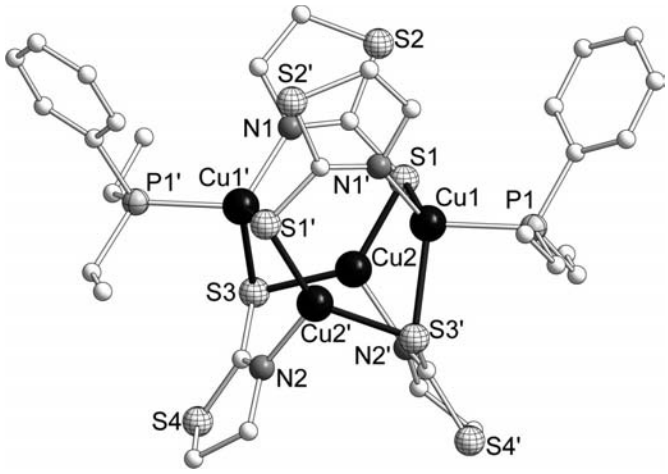


Fig. 3. Molecular structure of **4** (H atoms are omitted for clarity).

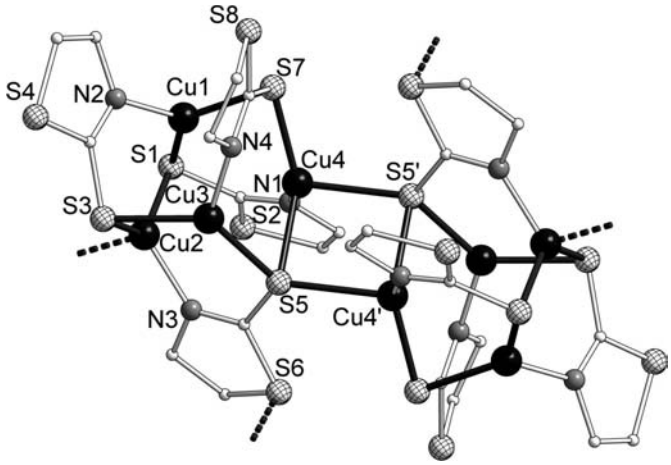
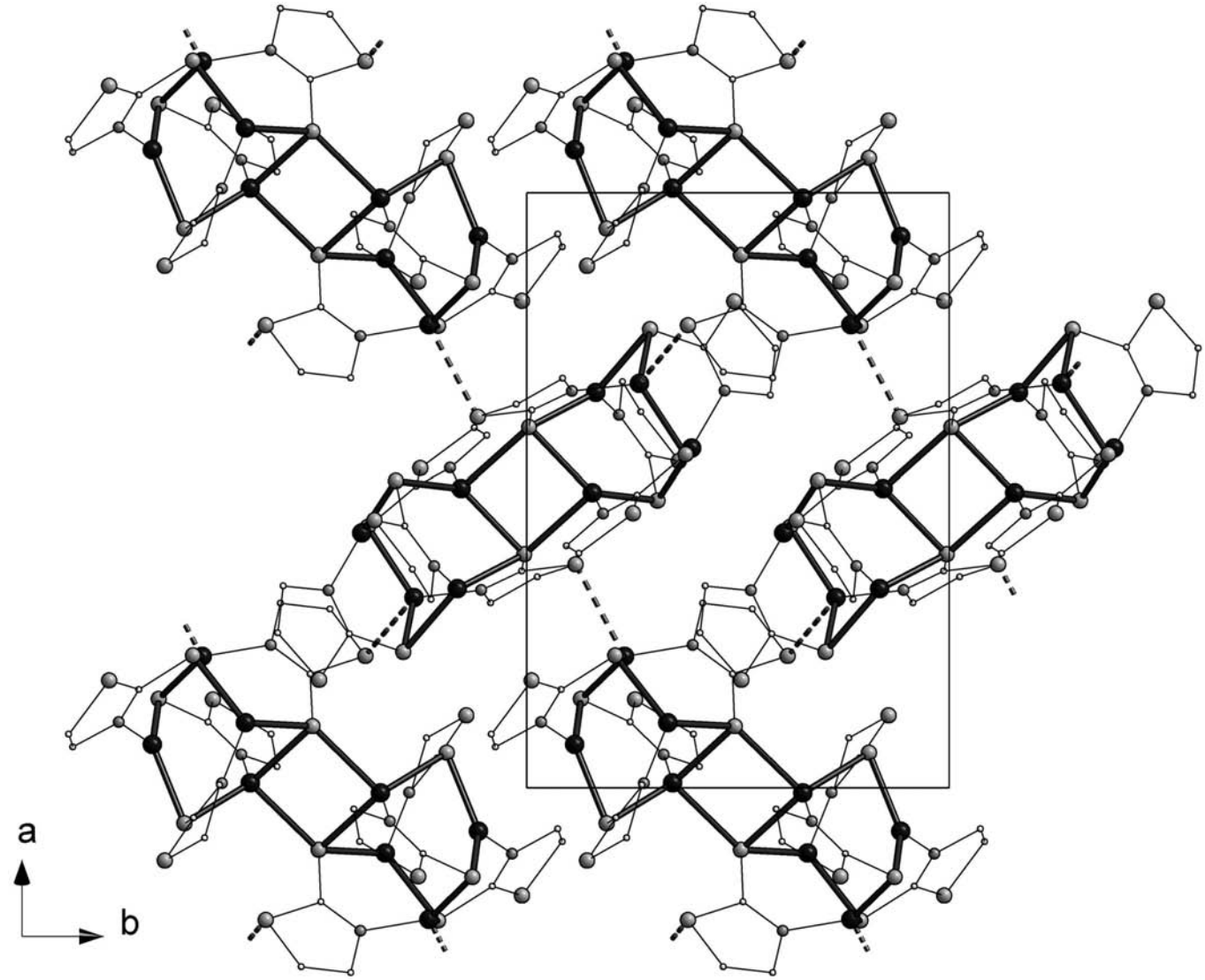
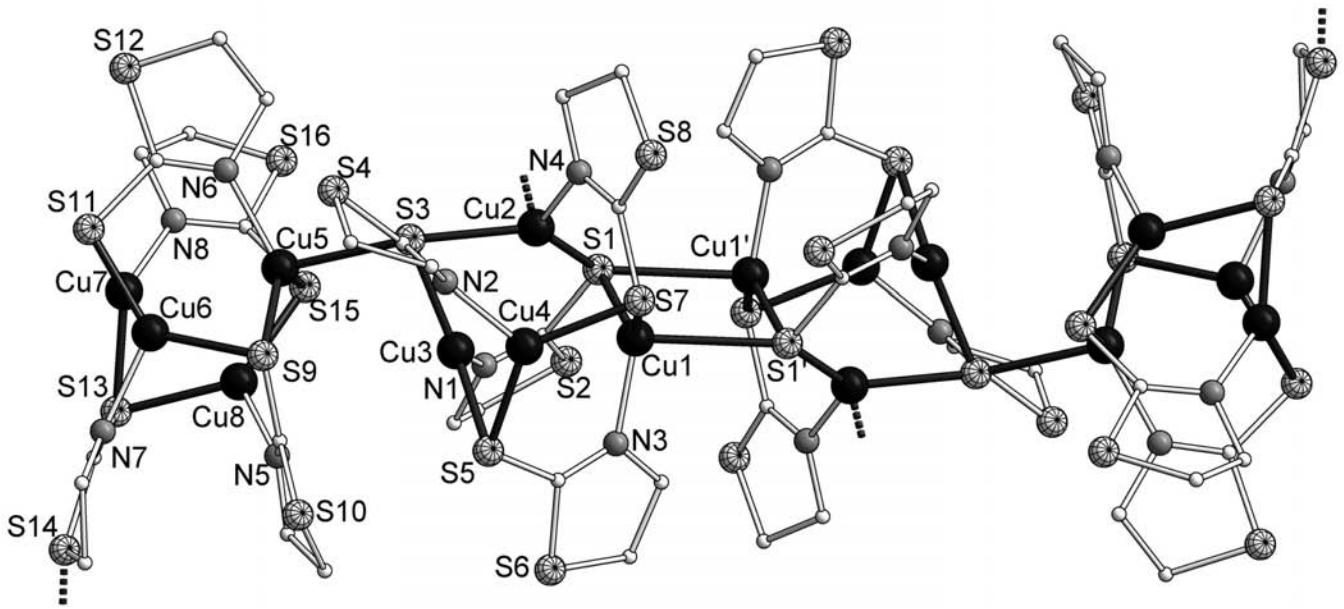


Fig. 4. A section of the layer structure of **4** showing the Cu—S_{endo} interactions (dashed lines).



© 2006 NRC Canada

Fig. 5. Molecular structure of **5** (H atoms are omitted for clarity).



lished could be proven by our samples. Using methanol as solvent, a dimer, $[Cu_4(S\text{-thiaz})_4]_2$ (**4**), is formed, a mixture of methanol and toluene leads to the formation of a tetramer, $[Cu_4(S\text{-thiaz})_4]_4$ (**5**). Finally, in pure toluene a one-dimensional polymer, $[Cu_4(S\text{-thiaz})_4]_\infty$ (**6**), is formed, which is also already described in the literature, obtained via an electrochemical synthesis (5). Again the crystallographic data published there fit with our sample.

Crystal structures of 2–5

The colourless compound **2** (Fig. 2) crystallizes in the monoclinic space group *C*2/*c* with four molecules per unit cell. There is a twofold axis running through each molecule. The Cu—S distances in the Cu_4S_4 cycle range between 220.2(1) pm (Cu2—S1) and 250.3(1) pm (Cu1—S3′); Cu—N distances are Cu1—N1′, 203.4(3) pm, and Cu2—N2′, 201.4(3) pm. Cu2 and Cu2′ have a nearly trigonal planar coordination sphere (the sum of the bond angles is 358.8°). Both Cu1 and Cu1′ are additionally bonded to a phosphine ligand (Cu1—P1, 227.0(1) pm), whereby these copper atoms achieve a distorted tetrahedral coordination.

3 crystallizes as colourless blocks in the tetragonal space group $P4_32_12$ with four molecules per unit cell and one toluene molecule per formula unit. The molecular structure of **3** is analogous to **2** except for the different phosphine ligands. Therefore, further discussions of the structure are unnecessary.

There is one example in the literature of a similar tetranuclear copper compound with no further coordinating ligands or aggregation of cages, where chiral benzyl-substituted 2-mercaptothiazoline is used as chelating ligand. Indeed, this compound has been published twice, once discussed as a copper(II) species (CCDC no. 174127) (15) and 1 year later as a copper(I) compound (CCDC no. 174125) (16). Though the compounds have been synthesized in different ways, the crystallographic parameters are the same. As both are described as colourless, and each ligand should carry one negative charge, we assume that the description as a copper(I) compound is the right one.

Compound **4** crystallizes as colourless plates in the monoclinic space group $P2_1/c$ with four formula units per elementary cell. Figure 3 shows one dimeric unit of **4**; another crystallographically independent molecule is found in the asymmetric unit having, within experimental errors, the same bonding parameters.

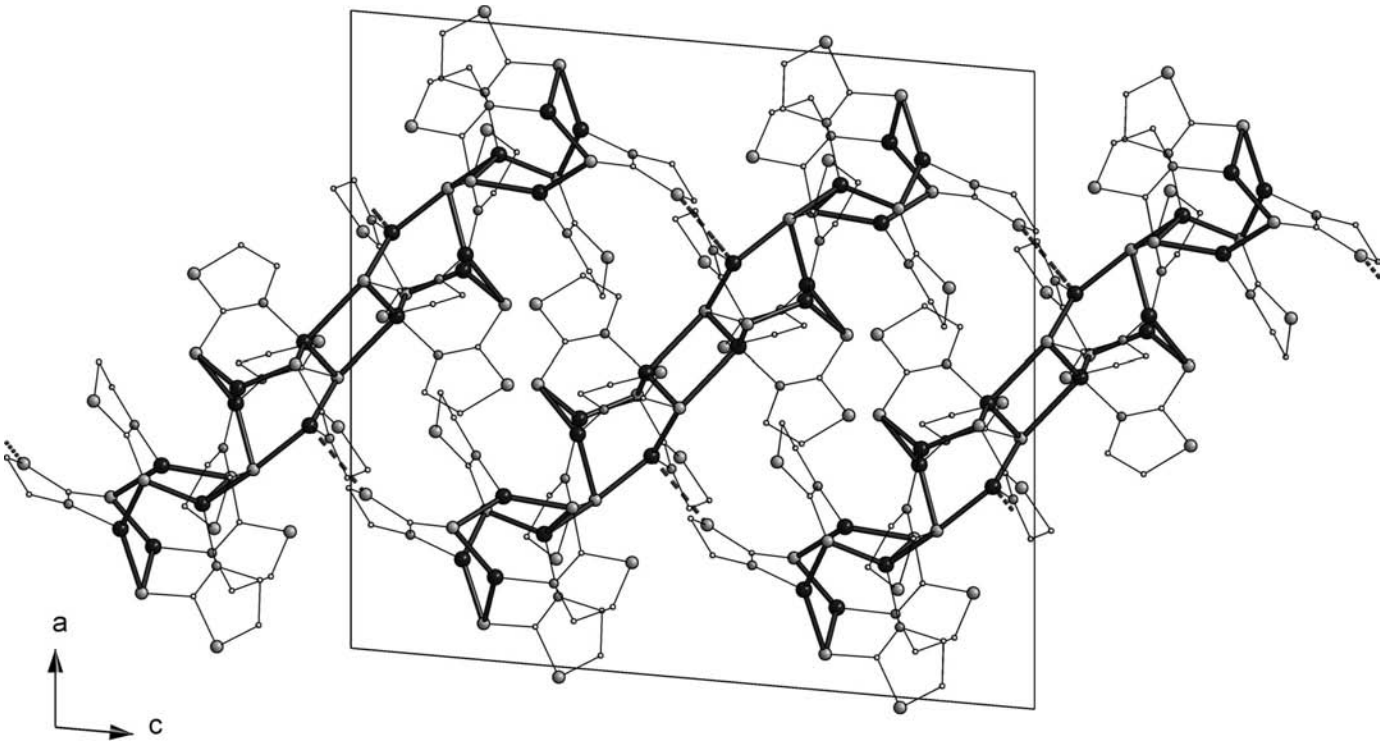
4 consists of two $[Cu_4(S\text{-thiaz})_4]$ clusters connected via the atoms Cu4 and S5. There is an inversion centre in the middle of the so formed Cu_2S_2 ring. Cu—S distances within a Cu_4S_4 cycle range from 223.7(4) to 244.8(3) pm, the Cu4—S5′ bond is slightly longer (255.4(3) pm). This kind of cluster agglomeration is also found in **6** where the Cu_4 units form infinite strands (5). In contrast to **1**–**3** and **6** where no intermolecular bonds are present, the dimers in **4** are interconnected by donor bonding of two endocyclic sulphur atoms (S6, S6′) to copper atoms of neighbouring molecules. In this way layers are formed and this is illustrated in Fig. 4. Therefore, Cu2 is shifted out of the centre of the triangle formed by S1, S3, and N3, whereas Cu1 and Cu3, which have no intermolecular contacts, are nearly in plane with their neighbouring atoms. The average Cu—S_{endo} distances are 289.7 pm, which is significantly shorter than the sum of the van der Waals radii of copper and sulphur (320 pm (17)). The same kind of intermolecular linking was also found in the compound $[Cu_4(S\text{-thiaz})_4(NC_5H_5)]$ (4).

In **5** (Fig. 5) four $[Cu_4(S\text{-thiaz})_4]$ units are bound together forming a tetramer. Compound **5** crystallizes in the monoclinic space group $P2_1/c$ with two molecules per elementary cell and two molecules of toluene per formula unit.

The middle part of **5** is identical with **4**: two $[Cu_4(S\text{-thiaz})_4]$ units being connected via two Cu—S bonds (Cu1—S1′ and Cu1′—S1, 279.0(2) pm). The two additional subunits are both bonded to this inner part by one Cu—S bond (Cu5—S3, 253.6(2) pm). Altogether, the tetramer has a length of 2.16 nm. As in **4** the molecules are agglomerated by interactions between copper atoms (Cu2) and endocyclic

© 2006 NRC Canada

Fig. 6. A section of the layer structure of **5** showing the Cu—S_{endo} interactions (dashed lines).



sulphur atoms (S14) of neighbouring molecules (Cu—S_{endo}, 302.6(1) pm). Layers are also formed in this case as illustrated in Fig. 6.

Conclusion

Tetranuclear copper(I) 2-mercaptothiazoline complexes can be easily synthesized starting from copper(I) acetate by deprotonation of the ligand. Depending on the reaction conditions the [Cu_4(S-thiaz)$_4$] cages are either monomeric (**1**–**3**) with two additional phosphine ligands, or they form oligomeric (**4**, **5**) or polymeric (**6**) aggregates. In **4** and **5** additional intermolecular interactions between endocyclic sulphur atoms and copper atoms of neighbouring molecules are found.

References

1. S. Dehnen, A. Eichhöfer, and D. Fenske. Eur. J. Inorg. Chem. 279 (2002), and refs. cited therein.
2. (*a*) P.C. Ford, E. Cariati, and J. Bourassa. Chem. Rev. **99**, 3625 (1999); (*b*) V.W.W. Yam and K.K.W. Lo. Chem. Soc. Rev. **28**, 323 (1999), and refs. cited therein.
3. K.A. Koch, M.M.O. Pena, and D.J. Thiele. Chem. Biol. **4**, 549 (1997), and refs. cited therein.
4. J.P. Fackler, Jr., C.A. López, R.J. Staples, S. Wang, R.E.P. Winpenny, and R.P. Lattimer. J. Chem. Soc. Chem. Commun. 146 (1992).
5. E.S. Raper, J.R. Creighton, and W. Clegg. Inorg. Chim. Acta, **237**, 87 (1995).
6. E.S. Raper, J.R. Creighton, W. Clegg, L. Cucurull-Sanchez, M.N.S. Hill, and P.D. Akrivos. Inorg. Chim. Acta, **271**, 57 (1998).
7. P. Aslanidis, S.K. Hadjikakou, P. Karagiannidis, and P.J. Cox. Inorg. Chim. Acta, **271**, 243 (1998).
8. J.-M. Du, H.-Y. Zeng, Z.-C. Dong, G.-C. Guo, and J.-S. Huang, Acta Crystallogr. Sect. C, **C58**, M396 (2002).
9. P. Aslanidis, P.J. Cox, P. Karagiannidis, S.K. Hadjikakou, and C.D. Antoniadis. Eur. J. Inorg. Chem. 2216 (2002).
10. D.A. Edwards and R. Richards. J. Chem. Soc. Dalton Trans. 2463 (1973).
11. K. Sasse. *In* Houben–Weyl: Methoden der Organischen Chemie. Part 1. Thieme Verlag, Stuttgart. 1963. p. 32f.
12. (*a*) G.M. Sheldrick. SHELXS-97 [computer program]. University of Göttingen, Göttingen, Germany. 1997; (*b*) G.M. Sheldrick. SHELXL-97 [computer program]. University of Göttingen, Göttingen, Germany. 1997.
13. K. Brandenburg. Diamond 3.1 (visual crystal structure information system) [computer program]. Crystal Impact GbR, Bonn, Germany. 2005.
14. Jasc Software. Paint Shop Pro 7AE [computer program]. Jasc Software, Eden Prairie, Minnesota. 2001.
15. M. Shi and J.-K. Jiang. J. Organomet. Chem. **650**, 274 (2002).
16. M. Shi and J.-K. Jiang. Chirality, **15**, 605 (2003).
17. A.F. Hollemann and E. Wiberg. *In* Lehrbuch der Anorganischen Chemie. de Gruyter, Berlin, Germany. 1995. p. 1839f.

© 2006 NRC Canada

Chiral lithium amides on polymer support — Synthesis and use in deprotonation of ketones[1]

Marek Majewski, Agnieszka Ulaczyk-Lesanko, and Fan Wang

Abstract: A number of chiral secondary amines attached to Merrifield resin or to noncrosslinked (soluble) polystyrene support were synthesized. The corresponding lithium amides, generated from these amines by treatment with BuLi, react with tropinone, a model symmetrical ketone, to give the corresponding enolates enantioselectively (ee up to 75%). The enolates were trapped either as the corresponding aldol adducts by a reaction with benzaldehyde or as ring-opening products in a reaction with a chloroformate.

Key words: chiral lithium amides, polymer-supported reagents, deprotonation, enolates, tropinone.

Résumé : On a réalisé la synthèse d'un certain nombre d'amines secondaires chirales liées à une résine de Merrifield ou à un support de polystyrène non réticulé (soluble). Les sels de lithium des amides correspondants obtenus à partir de ces amines par traitement avec du BuLi réagissent avec la tropinone, une cétone symétrique modèle, pour conduire d'une façon énantiosélective (ee allant jusqu'à 75 %) à la formation des énolates correspondants. Les énolates ont été piégés sous la forme d'adduits aldoliques correspondants par réaction avec du benzaldéhyde ou sous la forme de produits d'ouverture par réaction avec un chloroformiate.

Mots clés : sels de lithium d'amides chiraux, réactifs supportés par un polymère, déprotonation, énolates, tropinone.

[Traduit par la Rédaction]

Introduction

There is a lot of interest in developing chemistry that involves reactants on polymer support that are often described in terms of solid phase synthesis (SPS) for insoluble polymers, and liquid phase synthesis (LPS) for soluble resins (the differences between "solid-phase", "liquid-phase" and "solution-phase" chemistry were discussed in a seminal paper by Janda in 1997) (1) and often the challenge involves adaptation of solution-phase reactions to work on the resin (2). As the popularity of the polymer-supported scaffolds and reagents grows, the more difficult aspects of synthetic chemistry such as stereoselective reactions, and especially their catalytic versions, are developed in the SPS and LPS context (3). It should be noted that applications of substrates and reagents on polymer support are not limited to combinatorial chemistry, there is also a number of potential benefits that could arise from using such reagents including easy recovery of expensive chemicals, easier control of environmental contamination, and new reactor design (2, 3).

We have been interested in development of chiral lithium amide bases for several years (4). Analogous amides supported on a resin are interesting because of a potential connection to solid phase synthesis. At the onset of this work it was not clear if chemistry involving reagents on polymer support would be compatible with highly reactive reagents such as butyllithium or carbanions, since there had been very few precedents (5). Fortunately, no major problems on this score were encountered. The preliminary results of this study have been reported in a communication (6). Recently, other researchers have taken up the theme of lithium amides on polymer support achieving very interesting and useful results in different systems (7). Below, we present a full account of the synthesis of a number of chiral lithium amides on polymer support and their reactions as bases in selected systems.

Results and discussion

Synthesis of chiral amines on insoluble polymer support

Chloromethyl polystyrene **1** (Merrifield resin, 200–400 mesh) was chosen as the solid support for the initial studies. The general method elaborated for the direct attachment of a chiral amine to the resin is shown in Scheme 1.

Replacement of chlorine in **1** with iodine was done using the Finkelstein reaction (8). The N-alkylation of chiral primary amines (**3**–**5**) proceeded smoothly when the amine was used in excess. After the reaction was completed, the resins (**6**–**8**) were separated by filtration, washed with the follow-

Received 4 July 2005. Published on the NRC Research Press Web site at http://canjchem.nrc.ca on 17 March 2006.

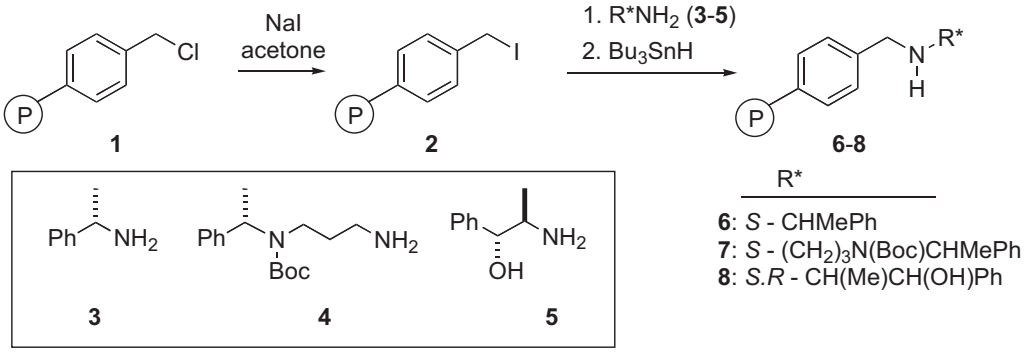
Dedicated to Professor Arthur Carty in recognition of his contributions to chemistry and the sciences in Canada.

M. Majewski,[2] A. Ulaczyk-Lesanko, and F. Wang. Department of Chemistry, University of Saskatchewan, Saskatoon, SK S7N 5C9, Canada.

[1]This article is part of a Special Issue dedicated to Professor Arthur Carty.
[2]Corresponding author (e-mail: majewski@usask.ca).

 doi:10.1139/V06-006 © 2006 NRC Canada

Scheme 1.



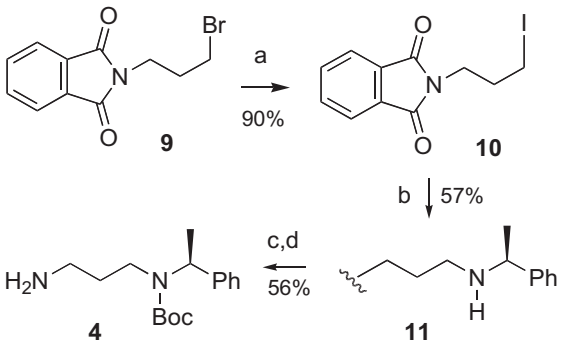
ing solvents: THF, MeOH, aq. MeOH (50%), H_2O, NaOH, H_2O, MeOH, Et_2O, and were dried under vacuum to the constant weight. The rather involved washing procedure results from the fact that the polymers of this type swell in THF or Et_2O, but do not swell in polar protic solvents such as MeOH or H_2O. Thus, the resins were washed with a swelling solvent first, to remove organic impurities absorbed on the polymer. The wash with THF was followed by washing with solvents that do not have good swelling properties, but which remove inorganic and acidic impurities.

Next, a method for determination of the amount of nitrogen (loading) in the polymer-supported reagents had to be elaborated. The Volhard titration method was tried first (9). A known amount of standard HCl solution was added to the polymer-supported amine sample, which gave the corresponding salt. The chloride ions that were not trapped by the amine moieties were precipitated by addition of a known excess of a standard solution of $AgNO_3$. After several experiments, it was found that HCl was being incorporated into the polymer matrix and the apparent N-loading of the resin was higher than the Cl-loading of the original Merrifield resin. This absorption of HCl on the polymer was confirmed by several "blind titration" experiments, i.e., the commercially available Merrifield resin was treated with a known amount of the standard HCl solution, the resin was separated by filtration, and the filtrate was titrated using the Volhard method. Overall, contrary to some reports (9*b*), the Volhard method was not effective. Another method of titration that was tried was the Fajans method, which works in a similar fashion, but relies on the analysis of sulfate ions (9*a*). This method allowed a reasonably accurate determination of the amine loading.

The third method used for determination of the nitrogen content in polymeric amines was elemental analysis. The loading values of all insoluble polymer-supported amines ranged between 0.4 and 1.1 mmol of NH per gram (cf., the Experimental section). Nitrogen loading clearly indicated that, in many cases, the N-alkylation reaction did not go to completion. Since the halide groups attached to the polymer could interfere with subsequent reactions, a dehalogenation procedure was performed according to the method described by Leznoff that involves using an excess of Bu_3SnH (10). A quick, qualitative test of amine incorporation into the polymer structure was done by using a solution of bromophenol blue, similar to the test developed by Lam to monitor progress of reactions of peptides connected to resin beads (11).

Amine **4**, needed for synthesis of the corresponding resin **7**, which was envisaged as the precursor of the bidentate chiral lithium amide, was synthesized as shown in Scheme 2.

Scheme 2. Reagents and conditions: (*a*) NaI, Me_2CO, reflux; (*b*) **3a**, K_2CO_3, THF, reflux; (*c*) Et_3N, $(Boc)_2O$, MeOH; (*d*) 95% NH_2NH_2, EtOH.

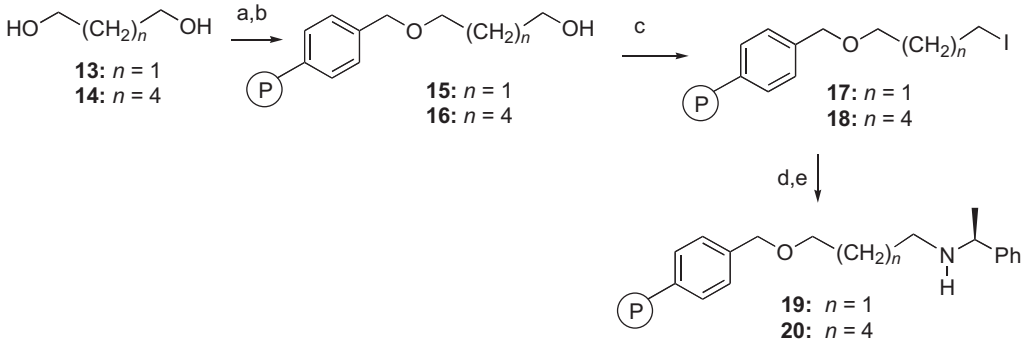


Most of the reacting groups in an insoluble polymer-supported reagent are situated inside the polymer bead. These reacting sites are not easily accessible to reagents in solution, but the situation could be improved by distancing the reactive groups from the rigid polymer matrix by a linker. Selection of the proper linker can be critical to the success of SP chemistry (1, 2*b*). Initially, two simple linkers derived from 1,3-propanediol (**13**) and 1,6-hexanediol (**14**) were used. They were attached to the polymer-supported benzyl chloride **1** by a modified literature method (12), involving O-alkylation, followed by functional group manipulation using reactions that are well-known in the context of solution chemistry (Scheme 3) (13). Iodides **17** and **18** served as precursors for the polymer-supported amines **19** and **20**, which were obtained by simple N-alkylation of (*S*)-α-methylbenzyl amine (**3**) with these compounds.

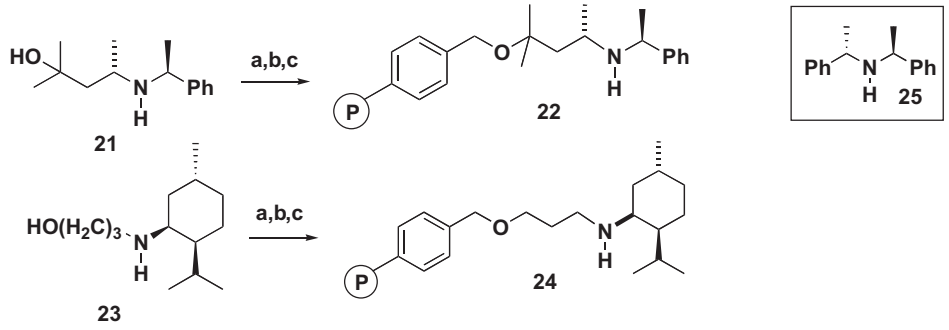
Some examples of attaching a chiral amine moiety to an insoluble polymer support via a linker that had been incorporated into the amine structure as the corresponding amino alcohol were published by other groups working on developing catalysts for stereoselective addition of nucleophiles to aldehydes (2*a*, 12, 14–16). We have synthesized amines **22** and **24** hoping that they might be effective in enantioselective deprotonation (Scheme 4). Compound **22** seemed especially promising owing to its structural similarity to the C_2 symmetrical amine **25** — the lithium amide of this amine is one of the most versatile and effective chiral bases (4). Compounds **21** and **23** used in these studies were synthesized from chiral primary amines by the reductive

© 2006 NRC Canada

Scheme 3. Reagents and conditions: (*a*) NaH, 0 °C, DMF; (*b*) **1**, 60 °C; (*c*) PhP_3, I_2, imidazole, CH_2Cl_2, rt; (*d*) **3a**; (*e*) Bu_3SnH.



Scheme 4. Reagents and conditions: (*a*) NaH, 0 °C, DMF; (*b*) **2**, K_2CO_3; (*c*) Bu_3SnH, THF.



amination method (starting from 4-hydroxy-4-methyl-2-pentanone or menthone, respectively).

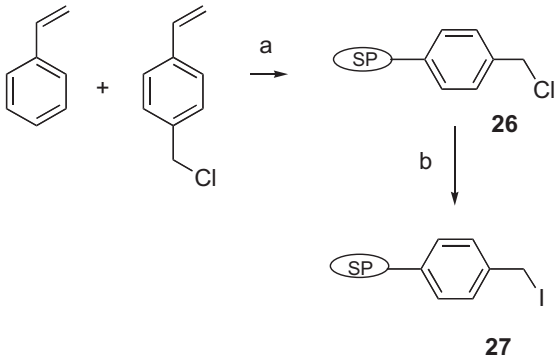
Synthesis of chiral amines supported on a soluble polymer

Reagents that are bound to soluble polymers offer a number of advantages while suffering less from reactivity problems often associated with a two-phase system (1). The soluble polymer supports selected for our studies were the noncrosslinked copolymer of styrene and chloromethyl styrene **26**, which was synthesized by free radical polymerization following the procedure of Narita (9*b*, 17) and the corresponding iodo derivative **27** (Scheme 5).

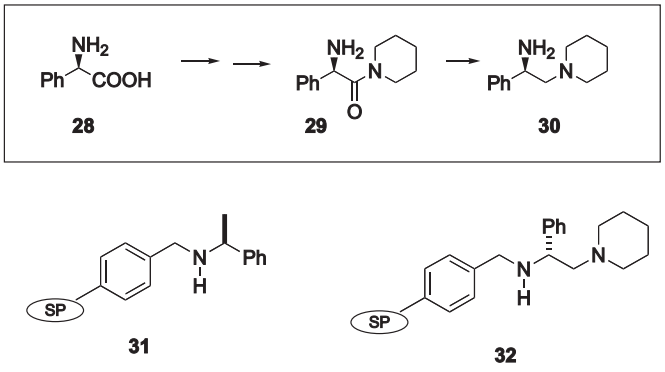
Compound **26** has a number of advantages: it can be easily prepared from the commercially available starting materials; it is soluble in common organic solvents such as THF, CH_2Cl_2, $CHCl_3$, AcOEt, and benzene even at low temperatures, but it is insoluble in MeOH and H_2O. The products of reactions involving this polymer can be purified using aqueous extraction and polymer precipitation. Chiral amines **3** and **30** (the latter was prepared as shown in Scheme 6, using literature procedures, refs. 4*b*, 18) were attached to the polymer backbone using the iodo derivative **27** analogously to the method described above for compounds derived from the Merrifield resin (Scheme 6; cf., Scheme 1). All reactions were easy to carry out, and the resulting resins (**31**, **32**) were isolated by precipitation from cold MeOH.

Attachment of chiral amines to the soluble support via linkers was realized by a three-step procedure shown in Scheme 7. The linker was attached first to the soluble polymer (**26** or **27**) followed by the well-precedented functional group manipulations and attachment of the chiral amine. The linker was expected to distance the amine from the polymer

Scheme 5. Reagents and conditions: (*a*) AIBN, benzene, 70 °C, 48 h; (*b*) NaI, acetone.



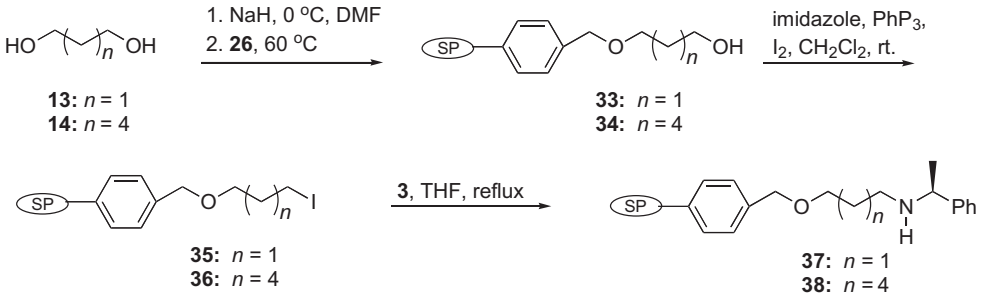
Scheme 6.



matrix and it was hoped that this should make it more accessible to BuLi during the generation of the corresponding lithium amide, and also should result in less steric hindrance

© 2006 NRC Canada

Scheme 7.



during the subsequent deprotonation step. Polymers **37** and **38** were synthesized according to the procedure analogous to that described above for the insoluble amines **19** and **20**.

Synthesis and reactions of polymer-supported lithium amides

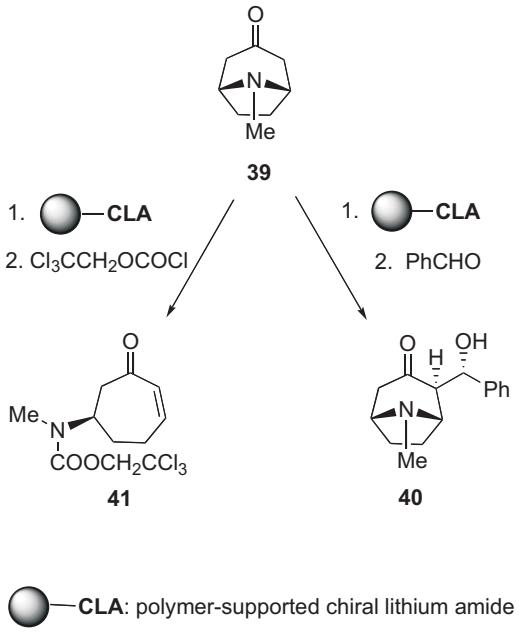
After the synthesis of the series of polymer-supported chiral amines was completed, the stage was set for generation of the corresponding lithium amides. Polymer-supported reagents could offer several advantages over the chiral lithium amides generated in solution. Some of these could involve: simplified reaction procedures, possibility of easy regeneration of the polymer bound reagent, and undesired side reactions such as crosslinking could be suppressed by using more solvent (the principle of high dilution) (2*b*). Polymer-bound reagents are usually more stable, and a possibility for the automation of reactions exists when dealing with polymer-supported chiral lithium amides. Generation of lithium amides from secondary amines is a relatively simple reaction in solution and numerous procedures have been described. The reader's attention is directed to a few recent references that illustrate a certain variety of conditions (4, 19). The procedure for generation of polymer-supported lithium amides was designed by analogy with chemistry in solution (cf., Experimental) and involved treatment of the parent amine with BuLi at 0 °C in THF. In the case of insoluble polymer-supported chiral lithium amides, it should be noted that THF is the solvent that swells the polymer matrix the most, which implies that the conditions of the subsequent reaction should be similar to homogenous conditions.

During the generation of both the insoluble and soluble polymer-supported lithium amides from the corresponding chiral amines, color changes were observed (the suspension of the polymer changed color from yellow to light reddish-brown in the case of insoluble reagents and to red or purple in the case of soluble ones). This could be attributed to the formation of unidentified by-products. It was determined experimentally that if the color change did not occur, the subsequent reactions did not proceed well; if the color became dark brown, the yield of the reaction was usually low.

Deprotonation of carbonyl compounds

Chiral lithium amide bases are powerful reagents that are often used for enantioselective deprotonation of symmetrical cyclic ketones (4). The resulting enolates are usually trapped by various electrophiles and the reaction selectivity is measured on the product. Tropinone (**39**), a bicyclic ketone of C_s symmetry provides a good model for deprotonation studies

Scheme 8.



and is also a useful scaffold for construction of tropane alkaloids (4). The aldol addition of tropinone enolate to benzaldehyde is well-known to give only one diastereoisomer of the corresponding aldol (**40**), which simplifies the analysis, and the enantioselectivity can by easily and accurately measured by ^{1}H NMR with chiral solvating agents such as (*S*)-(+)-2,2,2-trifluoro-1-(9-anthryl)ethanol (4). Tropinone enolate undergoes ring opening with chloroformates to give cycloheptenone derivatives (**41**); the enantiomer ratio of these products can be analyzed by NMR or by HPLC (Scheme 8) (4*e*).

Developing proper conditions for reactions involving polymer-supported reagents can be complicated because of a number of variables. The polymer matrix could react with the reagents in solution in an undesirable fashion giving rise to by-products and microenvironmental effects of an unknown nature could be present (20). The reagents that are supported on a polymer have restricted mobility owing to the rigidity of the polymer matrix, and, usually, longer times are required for reactions in which such reagents are employed. After some experimentation we established that generation of lithium amides attached to insoluble polymer supports (i.e., derived from amines **6** or **20**) required up to 8 h, and the subsequent deprotonation of tropinone required

© 2006 NRC Canada

Table 1. Deprotonation of tropinone with chiral lithium amides on polymer support, followed by the aldol reaction of the corresponding enolate.

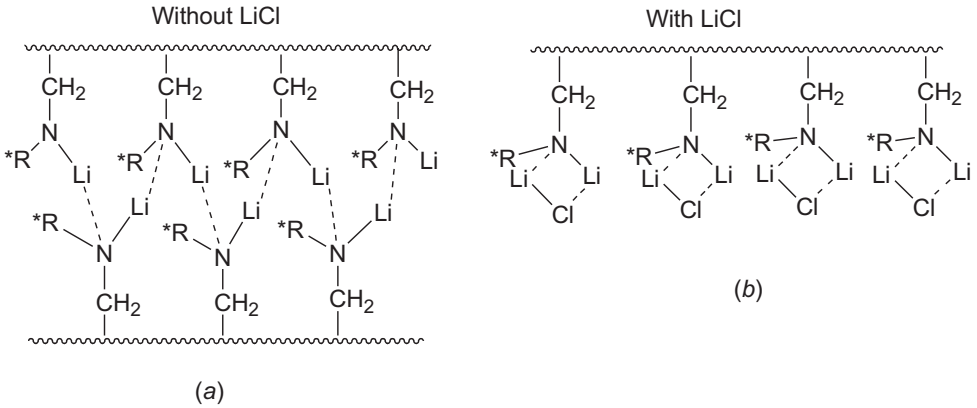
Entry	Lithium amide	Additive	Yield of **40** (%)	ee of **40**[a] (%)
1	**Li-6**	—	38	14
2	**Li-6**[b]	—	40	20
3	**Li-6**	LiCl (1 equiv.)	45	24
4	**Li-20**	—	30	10
5	**Li-20**	LiCl (1 equiv.)	35	20
6	**Li-31**	LiCl (2 equiv.)	83	75
7	**Li-32**	LiCl (1 equiv.)	51	70
8	**Li-37**	LiCl (1 equiv.)	35	26
9	**Li-38**	LiCl (1 equiv.)	40	35

Note: All reactions were done in THF, the lithium amides were generated at 0 °C, and the aldol reaction was done at –78 °C (cf., the Experimental).

[a]All products were dextrarotatory and the absolute configuration is as drawn for structure **40**.

[b]The ketone was added slowly (over 45 min).

Fig. 1. Hypothetical structures of (*a*) a dimer involving the chiral lithium amide supported on soluble polymer and (*b*) mixed aggregates involving lithium amide and LiCl connected to the polymer.



up to 15 h to proceed to completion (detailed procedures are described in the Experimental section). The analogous reactions in solution are much faster (1 h and 1–2.5 h are usually sufficient for the two steps, respectively).

The second task was to elaborate a proper workup for reactions involving polymer-supported amides. Aldol reactions in solution are usually quenched with an aqueous solution of a weak acid, followed by an extraction. However, with insoluble polymer-supported reagents the reaction mixture could not be extracted before the removal of the polymeric reagent. In the end the following procedure proved to be effective: the reaction was quenched by addition of an aqueous solution of NH_4Cl, the polymers were separated off by filtration and washed with THF. The aqueous layer of the filtrate was then extracted with Et_2O. Both the insoluble polymer reagents **6** and **20** and soluble amines (such as **30**) were recycled, purified, and could be reused without loss of reactivity.

In most cases, both the yield and the enantiomeric purity of the tropinone aldol (**40**) were modest. As far as the insoluble polymers were concerned (Table 1, entries 1–5), we speculated that the heterogeneous conditions were lowering the efficiency and selectivity of the reaction. Soluble polymers proved somewhat better (Table 1, entries 6–10). In this case, the extraction was applied before the precipitation of the polymer, which made the workup much easier. After quenching the reaction, the mixture was simply diluted with AcOEt, and the aqueous layer was further extracted with AcOEt. (cf., the Experimental section).

Lithium chloride appears to be a necessary additive in reactions involving amides on soluble polymeric support. In some cases lithium amides could not be generated without LiCl because of the formation of a gel, which made the reaction mixture heterogeneous. This was especially evident in experiments involving the lithium amide generated from amine **31** — the reaction in the absence of LiCl did not work at all because of gel formation, while when LiCl was added the enantioselectivity increased (albeit slightly) with increasing amounts of LiCl (at 0.5 equiv. of LiCl the ee was 66% and at 2 equiv. of LiCl, it was 75%). This behaviour parallels the reaction in solution (4*a*, 4*e*). It is possible that formation of the gel could be caused by a noncovalent crosslinking of the polymer chains owing to aggregation of the lithium amide moieties. After addition of a LiCl solution, the gel disappears presumably because formation of the mixed aggregates breaks the crosslinking (Fig. 1). The possibility of such phenomena occurring in solution had been previously pointed out by Seebach (21).

Another reaction of tropinone that had been studied is the somewhat unusual ring opening with chloroformates (Scheme 8) (4*e*). The reaction is easy to carry out in solution, and the methods for measuring the enantiomeric excess of product **41** are known (4).

© 2006 NRC Canada

Table 2. Deprotonation of tropinone with lithium amides on polymer support, followed by the ring opening of the corresponding enolate.

Entry	Lithium amide	Additive	Yield of **41** (%)	ee of **41** (%)
1	**Li-6**	—	13	2
2	**Li-6**	LiCl (1 equiv.)	37	59
3	**Li-7**	—	10	–13[a]
4	**Li-7**	LiCl (1 equiv.)	15	36
5[b]	**Li-8**	—	5	–1.5[a]
6	**Li-8**	—	7	–6.5[a]
7	**Li-8**	LiCl (1 equiv.)	10	–13[a]
8	**Li-19**	—	42	3
9	**Li-19**	LiCl (1 equiv.)	48	6
10	**Li-20**	—	22	2
11	**Li-20**	LiCl (1 equiv.)	25	22
12	**Li-22**	—	5	–11[a]
13	**Li-22**	LiCl (1 equiv.)	11	9
14	**Li-24**	—	5	3
15	**Li-32**	LiCl (1 equiv.) and *n*-BuLi (1 equiv.)	57	30

Note: Enantioselectivity was measured with HPLC using a Chiralpack AD column and 15% isopropanol in hexane as the solvent system. All reactions were done in THF, the lithium amides were generated at 0 °C, and the ring-opening reaction was done at 0 °C (cf., the Experimental).

[a]Levorotatory enantiomer of **41** was the major product.

[b]The reaction was done in 2,2,5,5-tetramethyltetrahydrofuran.

The yields and enantioselectivities varied from mediocre to low with only a few exceptions. The highest ee in this series of experiments was obtained with lithium amide derived from amine **6** in the presence of LiCl (Table 2, entry 2). The incorporation of a linker into amine structures, to separate the chiral lithium amide moiety from the polymeric rigid backbone, did not seem to make a difference. Obviously, the steric hindrance that reagent **6** exhibits is necessary for the reaction to proceed with a useful degree of selectivity.

Interesting results were obtained with lithium amides **Li-7** (Table 2, entries 3 and 4) and **Li-22** (Table 2, entries 12 and 13). In both cases, in the absence of LiCl, the major product was the levorotatory enantiomer of **41**; however, after the addition of LiCl the dextrarotatory enantiomer was the major product. The mechanism of deprotonation of ketones with chiral lithium amides is not well understood. It could be suggested that the origins of the LiCl effects lie in a different lithium amides species acting as the deprotonating agent (22). There is much interest in identifying the role of different possible aggregates in deprotonation (23). It should be noted, however, that formation of a dimer by an insoluble, polymer-supported lithium amide is unlikely because of the rigid nature of the polymer matrix. The explanation why different enantiomers form at different conditions has to wait for a detailed mechanistic study.

Table 2 contains only one entry that refers to a lithium amide attached to soluble support (entry 15). We investigated all the lithium amides corresponding to the chiral amines attached to the soluble support in the ring-opening reaction, however, the yields were uniformly very low. In a few cases, such as that involving lithium amide **Li-32**, we were able to improve the yield to a moderate level by adding an extra equivalent of BuLi prior to addition of the electrophile. The overall low yields and the improvement that was realized through addition of extra BuLi were rationalized by the internal proton return. This phenomenon was had been observed by Seebach and co-workers (24) and others (25) and usually appears during attempts to deuterate enolates resulting in low deuterium incorporation. The process can, in principle, manifest itself also when different electrophiles are used. We had recovered substantial amounts of tropinone from experiments that gave low yields of the ring-opening products, suggesting that the internal proton return might be the culprit.

In summary, we synthesized a number of chiral amines attached to polymer supports that were either insoluble or soluble in organic solvents. The corresponding lithium amides were generated efficiently from these amines. The lithium amides were used in the deprotonation of tropinone, resulting, in several cases, in an efficiency and enantioselectivity similar to reactions in solution. These studies comprise a preliminary step towards development of practical lithium amide reagents on polymer support.

Experimental

General

For a general description of solvent and reagent purification and ee measurements see the previous contributions from our group (4*b*, 4*c*). Chiral amines used in this study were either commercially available (compounds **3** and **5**), or were synthesized according to previously published procedures (compound **30**) (4*b*, 18), or are described in the following.

The insoluble resin used as polymer support was the commercially available Merrifield resin (PS-Cl from Argonaut Technologies) and the soluble noncrosslinked polystyrene resin was synthesized as described before (9*b*). All NMR spectra were acquired in $CDCl_3$ on a 300 MHz instrument (Bruker).

© 2006 NRC Canada

General and typical procedures

Conversion of chlorobenzyl to the iodobenzyl moiety on polymer support

Sodium iodide (5.00 g, 33.4 mmol) was added to the preswollen (acetone) Merrifield resin (4.00 g, 4.00 mmol, original loading: 1.00 mmol of Cl per gram) in acetone (50 mL), and the resulting suspension was refluxed for 48 h. The polymer was then separated by filtration and washed with 100 mL of each of the following solvents: acetone, THF, EtOH, MeOH, methanol–water (1:1), 2 N NaOH, water, MeOH, and EtOH. (Note: in the case of soluble, noncrosslinked polymer **27**, the product was washed with water and then MeOH). Polymer **2** was dried to constant weight under high vacuum, yielding 3.862 g of the product.

Amination (typical procedure)

S-(–)-α-Methylbenzyl amine (3.645 g, 3.880 mL, 30.12 mmol) was added to the preswollen polymer **2** (6.026 g, 6.026 mmol, original loading of 1.00 mmol of halide per gram) in THF (100 mL). The mixture was refluxed under N_2 for 48 h. After the reaction was completed, polymer **6** was separated by filtration and washed with the following solvents (150 mL): THF, acetone, methanol, methanol–water (1:1), water, NaOH, water, methanol, ethanol, and Et_2O. The polymer was dried under high vacuum to constant weight, and 6.000 g of the corresponding resin was obtained. The loading of polymeric amine **6** was determined by Fajans titration method and by elemetal analysis and was 0.604 mmol of N per gram. ^{1}H NMR δ: 8.05–5.75 (m, 28H, Ar), 3.87–3.11 (m, 3H, $PhCH_2$-N and CH-N), 2.14–0.44 (m, 12H, CH_2, CH, polymer matrix, and CH_3, amine moiety). ^{13}C NMR δ: 145.8 (C-Ar), 128.1 (C-Ar), 126.9 (C-Ar), 125.9 (C-Ar), 58.1 (CH-N), 52.3 ($PhCH_2$-N), 40.6 (CH, polymer matrix), 24.7 (CH_3). Found: C 81.43, H 6.55, N 1.83, which indicated loading to be 0.604 mmol/g.

Dehalogenation

This procedure was applied in cases involving insoluble polymers only. A solution of tributyltin hydride (3.645 g, 3.300 mL, 12.54 mmol) was added to a suspension of polymer **6** (6.122 g, 4.180 mmol, loading of 0.604 mmol of N per gram) in THF (125 mL), and the reaction mixture was refluxed under N_2 for 48 h. The polymer was separated by filtration and washed with the following solvents (150 mL): hexane, THF, methanol, methanol–water (1:1), water, 2 N NaOH, water, methanol, ethanol, hexane, and Et_2O. The product was dried under reduced pressure to constant weight, yielding 5.387 g of polymer-supported amine **6**.

Connection of the linker using a diol (typical procedure)

1,3-Propanediol (10.94 g, 10.40 mL, 144.0 mmol) was added slowly to a suspension of NaH prewashed with dry pentane (1.728 g, 75.13 mmol) in DMF (100 mL), and the reaction mixture was stirred at 0 °C under N_2 for 2 h. Chloromethyl polystyrene **1** (8.00 g, 8.80 mol, 1.10 mmol of Cl per gram) was then added and the reaction mixture was refluxed under N_2 for 48 h. The reaction was quenched by the addition of water (100 mL) at 0 °C, and polymer **15** was separated by filtration and washed with the following solvents: water, methanol, ethanol, and Et_2O, followed by Soxhlet extraction with a 1:1 mixture of THF and ethanol (150 mL) for 4 h, and drying to the constant weight under high vacuum (8.125 g). (Note: during the synthesis of soluble noncrosslinked polymers **33** and **34**, the product was washed with water and then MeOH only in each case). The loading, as determined by gravimetric analysis, was 0.825 mmol of OH per gram. ^{1}H NMR δ: 8.57–6.30 (m, 24H, Ar), 4.28–3.37 (m, 8H, CH_2Cl, polymer matrix, and $PhCH_2O$-, -OCH_2 and -CH_2OH, alcohol moiety), 2.18–1.09 (m, 8H, CH_2, CH polymer matrix and CH_2, alcohol moiety); ^{13}C NMR δ: 128.4 (C-Ar), 68.1 ($PhCH_2O$-), 62.5 (OCH_2-), 40.5 (CH, polymer matrix), 25.8 (CH_2).

Activation of the linker by iodination (typical procedure)

Imidazole (1.138 g, 16.74 mmol) was added to a solution of triphenyl phosphine (4.386 g, 16.74 mmol) in dry CH_2Cl_2 (150 mL). Iodine (4.252 g, 16.74 mmol) was added next, followed by the addition of polymer **15** (6.973 g, 5.753 mmol, 0.825 mmol of OH per gram). The reaction mixture was protected from light and was stirred under N_2 for 96 h. After the reaction was completed, the polymer was separated by filtration and washed with 200 mL of each of the following solvents: diethyl ether, benzene, water, methanol, and diethyl ether. (Note: during the synthesis of soluble noncrosslinked polymers **35** and **36**, the product was washed with water and then MeOH only in each case). Product **17** was dried to constant weight under high vacuum, yielding 7.210 g of the resin. The loading of the polymer was estimated by gravimetric analysis and was 0.750 mmol of iodine per gram of compound. ^{1}H NMR δ: 8.50–5.90 (m, 148H, Ar), 4.93–4.13 (m, 4H, CH_2Cl, polymer matrix, and $PhCH_2O$-), 3.82–2.85 (m, 12H, -OCH_2 and CH_2I), 2.35–0.80 (m, 52H, CH_2, CH, polymer matrix, and CH_2, iodide moiety). ^{13}C NMR δ: 128.8 (C-Ar), 68.1 ($PhCH_2$-O), 41.0 (CH, polymer matrix), 33.8 (CH_2), 3.7 (CH_2I).

N-(3-Iodopropyl)phthalimide (10) (ref. 26)

A solution of *N*-(3-bromopropyl)phthalimide (0.500 g, 1.86 mmol) in acetone (2 mL) was added to a suspension of sodium iodide (1.40 g, 9.30 mmol) in acetone (15 mL), and the reaction mixture was refluxed for 2.5 h. Acetone was evaporated and the residue was diluted with Et_2O (35 mL), and a saturated solution of $Na_2S_2O_3$ (30 mL) was added. The aqueous layer was extracted with Et_2O (3 × 35 mL). The organic layers were combined, dried with $MgSO_4$, and the solvent was removed in vacuo giving the crude product (0.600 g), which was purified by flash chromatography (hexane, hexane–AcOEt 4:1) yielding pure **10** (0.530 g, 90%); mp 84–86 °C (lit. value (26) mp 86–88 °C). ^{1}H NMR δ: 7.85–7.57 (m, 4H), 3.71 (t, J = 6.76 Hz, 2H), 3.11 (t, J = 7.19 Hz, 2H), 2.19 (quint, J = 7.00 Hz). ^{13}C NMR δ: 168.3, 134.1, 132.0, 123.4, 38.7, 32.6, 1.4.

(*S*)-(–)-(3-Phthalimidopropyl)-1-phenylethylamine (11)

A solution of (*S*)-α-methylbenzylamine (0.363 g, 3.00 mmol) in THF (5 mL) was added to a solution of iodide **10** (0.473 g, 1.50 mmol) in THF (15 mL). The reaction was refluxed for 1.5 h and potassium carbonate (0.207 g, 1.50 mmol) was added. The reflux was continued overnight. The reaction mixture was cooled down to room temperature, a

© 2006 NRC Canada

saturated solution of sodium bicarbonate (20 mL) was added, and the mixture was extracted with Et_2O (3 × 30 mL). The organic layers were combined, washed with brine, and dried with $MgSO_4$. The solvent was removed in vacuo yielding the crude product (0.650 g). The crude product was purified by flash chromatography (hexane, hexane–AcOEt 1:1) yielding pure **11** (0.265 g, 57%); mp 82–85 °C. $[\alpha]^{25}_D$ –34.2° (*c* 1.15, CH_2Cl_2). IR (cm^{-1}): 2958, 1708, 1395. ^1H NMR δ: 7.80–7.70 (m, 2H), 7.65–7.57 (m, 2H), 7.27–7.08 (m, 5H), 3.80–3.52 (m, 3H), 2.70–2.31 (m, 2H), 1.77 (quint., 2H, *J* = 6.65 Hz, *J* = 13.39 Hz), 1.48 (br s, 1H, NH), 1.27 (d, 3H, *J* = 6.55 Hz). ^{13}C NMR δ: 168.3, 145.7, 133.8, 132.1, 128.3, 126.7, 126.5, 123.0, 58.2, 44.6, 35.9, 28.8, 24.3. MS (EI): 293 (M – 1, 97), 231 (6), 188 (32), 160 (42), 134 (16), 105 (100), 79 (11). Anal. calcd. for $C_{19}H_{20}N_2O_2$: C 74.00, H 6.54, N 9.08; found: C 73.98, H 6.49, N 8.94.

(*S*)-(–)-[*N*-*tert*-Butoxycarbonyl-(3-phthalimidopropyl)]-1-phenylethylamine (12)

A solution of 30% Et_3N in MeOH (2.5 mL) was added to a solution of amine **11** (0.500 g, 1.62 mmol) in MeOH (20 mL), followed by the addition of $(Boc)_2O$ (1.769 g, 8.110 mmol) in MeOH (10 mL) during which time the reaction was stirred vigorously. The reaction mixture was refluxed overnight. The mixture was cooled down to room temperature and the solvent was removed in vacuo giving the crude product (0.454 g), which was purified by DFC (hexane, hexane–AcOEt 1:1), giving the pure product **12** (0.433 g, 70% yield); bp 150–152 °C at 0.05 Torr (1 Torr = 133.322 4 Pa). $[\alpha]^{25}_D$ –56.3° (*c* 1.38, CH_2Cl_2). IR (cm^{-1}): 2974, 1710, 1687, 1394, 1365. ^1H NMR δ: 7.80–7.60 (m, 4H), 7.25–7.00 (m, 5H), 5.65–5.14 (br s, 1H), 3.53–3.36 (m, 2H), 3.03–2.85 (br s, 2H), 1.89–1.68 (m, 2H), 1.50–1.41 (d, 3H, *J* = 7.07 Hz), 1.41–1.30 (s, 9H). ^{13}C NMR δ: 167.6, 155.2, 141.2, 133.5, 131.8, 127.9, 126.8, 122.7, 79.2, 59.8, 35.4, 28.0, 20.6, 16.9, 13.9. Anal. calcd. for $C_{24}H_{28}N_2O_4$: C 70.57, H 6.91, N 6.86; found: C 70.30, H 7.08, N 6.75.

(*S*)-(–)-3-[*tert*-Butoxycarbonylamino-(1-phenylethyl)]-1-propylamine (4)

A solution of 95% hydrazine (1 mL) was added to a solution of **12** (0.200 g, 0.490 mmol) in EtOH (10 mL), and the reaction was stirred at room temperature overnight. A white solid (phthalazine-1,4-dione) was filtered off and washed with EtOH (10 mL). The filtrate was concentrated in vacuo. The residue was diluted with Et_2O (10 mL), and a saturated solution of sodium bicarbonate was added (10 mL). The aqueous layer was extracted with Et_2O (2 × 10 mL). The organic layers were combined, washed with brine (30 mL), and dried with $MgSO_4$. The solvent was removed in vacuo, and the crude product was obtained (0.150 g). The crude product was purified by DFC (hexane, hexane–AcOEt 1:1), giving pure **4** (0.110 g, 81% yield); bp 235 °C at 15 Torr. $[\alpha]^{25}_D$ –77.3° (*c* 1.11, CH_2Cl_2). IR (cm^{-1}): 2973, 2931, 1685, 1406, 1365, 699. ^1H NMR δ: 7.45–7.09 (m, 5H), 5.59–4.98 (br s, 1H), 3.23–2.70 (m, 2H), 2.65–2.35 (m, 2H), 1.55–1.47 (d, 3H, *J* = 7.00 Hz), 1.47–1.23 (m, 11H). ^{13}C NMR δ: 155.9, 141.9, 128.3, 127.0, 79.6, 53.7, 49.7, 41.4, 39.7, 33.7, 28.5, 17.5. Anal. calcd. for $C_{16}H_{26}N_2O_2$: C 69.03, H 9.41, N 10.06; found: C 69.07, H 9.16, N 9.99.

(*S*)-*N*-(1-Phenylethyl-3-propyl)amino-1-propoxymethyl polystyrene (19)

S-(–)-α-Methylbenzylamine (3.225 g, 3.43 mL, 26.65 mmol) was added to a slurry of polymer **2** (5.331 g, 6.930 mmol) in THF (150 mL). The reaction mixture was refluxed under N_2 for 72 h. After the reaction was completed, polymeric amine **19** was separated by filtration and washed with the following solvents (150 mL): THF, acetone, methanol, methanol–water (1:1), water, NaOH, water, methanol, ethanol, and ether, and then was dried under vacuum to constant weight and 5.00 g of product was obtained. The loading of the polymer was calculated from elemental analysis and was 0.636 mmol of N per gram. Dehalogenation was conducted according to the Dehalogenation procedure. The resulting pure polymeric amine **19** was dried to constant weight under reduced pressure and 4.85 g was obtained. The loading was determined to be the same as before the dehalogention procedure. ^1H NMR δ: 8.35–6.50 (m, 25H, Ar), 4.04–3.15 (m, 5H, $PhCH_2O$, O-CH_2, CH-N), 2.10–0.70 (m, 10H, CH_3, CH_2, CH, polymer matrix, and CH_3, CH_2, amine moiety). ^{13}C NMR δ: 128.5 (C-Ar), 126.7 (C-Ar), 68.8 ($PhCH_2O$-), 66.2 (OCH_2), 58.6 (CH-N), 45.5 (CH_2N), 40.6 (CH, polymer matrix), 31.0 (CH_2), 24.7 (CH_3). Found: C 87.68, H 7.57, N 0.92.

(*S*)-*N*-(1-Phenylethyl-6-hexyl)amino-1-hexoxymethyl polystyrene (20)

The amine **20** was synthesized according to the procedure described for amine **19**. Loading was calculated from elemental analysis and was 0.707 mmol of NH per gram. Dehalogenation was conducted according to the procedure for **19**. ^1H NMR δ: 7.60–6.13 (m, 32H, Ar, polymer matrix and amine moiety), 4.50–4.27 (br s, 2H, $PhCH_2O$-), 3.95–3.70 (br s, 1H, N-CH), 3.58–3.15 (br s, O-CH_2), 2.70–0.70 (m, 25H, CH_3, CH_2, CH, polymer matrix, and CH_3, CH_2, amine moiety). ^{13}C NMR δ: 145.4 (C-Ar), 128.2 (C-Ar), 127.9 (C-Ar), 125.9 (C-Ar), 73.0 ($PhCH_2O$-), 58.6 (CH-N), 45.4 (CH_2N), 44.0 (CH_2), 42.0 (CH_2, polymer matrix), 40.7 (CH, polymer matrix), 29.9 (CH_2), 26.4 (CH_2). Found: C 86.25, H 7.80, N 0.903.

(*S*,*S*)-(+)-4-(1-Phenylethylamino)-2-methyl-1-pentanol (21)

This compound was prepared according to a general procedure for reductive amination of ketones (27). A solution of 4-hydroxy-4-methyl-2-pentanone (1.00 g, 1.07 mL, 8.62 mmol) in MeOH (5 mL) was added to a solution of (*S*)-α-methylbenzylamine (0.949 g, 1.00 mL, 7.84 mmol) in MeOH (25 mL), followed by the addition of $NaBH_3CN$ (0.518 g, 8.23 mmol). The reaction was stirred at room temperature overnight. The solvent was removed in vacuo, a 10% solution of hydrochloric acid (50 mL) was added to the residue, and the aqueous layer was extracted with Et_2O (30 mL). The acidic aqueous layer was cooled down to 0 °C and was made basic by the slow addition of NaOH (ca. 4 g). The basic solution was extracted with Et_2O (3 × 50 mL). The organic layers were combined, washed with brine (75 mL), and dried with $MgSO_4$. The solvent was removed in vacuo giving a mixture of two products in a 5:1 ratio (GC). The products were separated by chromatography (hexane, hexane–AcOEt 1:1), and the major one was obtained (0.866 g, 50% yield); bp 135–139 °C at 6 mmHg (1 mmHg = 133.322 4 Pa). Only the major isomer was fully characterized. $[\alpha]^{26}_D$ +67.7°

© 2006 NRC Canada

(*c* 3.06, CH_2Cl_2). IR (cm^{-1}): 3310, 2943, 2913, 2865, 1454, 1071. ^1H NMR δ: 7.28–7.05 (m, 5H), 3.82 (q, 1H, *J* = 6.45 Hz), 3.20–3.04 (m, 1H), 1.41–1.33 (m, 2H), 1.28 (d, 3H, *J* = 6.45 Hz), 1.23 (s, 3H), 1.11 (s, 3H), 0.99 (d, 3H, *J* = 6.19 Hz). ^{13}C NMR δ: 145.6, 128.5, 127.2, 126.3, 70.2, 54.7, 48.3, 31.8, 28.5, 22.1, 21.3. MS: (NH_3): 222 (M + 1, 100), 148 (9), 105 (5). Anal. calcd. for $C_{14}H_{23}NO$: C 75.97, H 10.47, N 6.33; found: C 75.87, H 10.51, N 6.60.

(*S*,*S*)-(+)-4-(1-Phenylethylamino)-2-methyl-1-pentanol on polystyrene support (22)

A solution of amine **21** (2.00 g, 9.05 mmol) in dry DMF (5 mL) was added to a prewashed suspension of NaH (0.350 g, 14.6 mmol) in DMF (80 mL) at 0 °C under N_2. The reaction mixture was stirred for 1 h at 0 °C, and the polymer-supported benzyl iodide (**2**, 6.50 g, 7.15 mmol, 1.1 mmol of halide per gram) was added, followed by the addition of dry K_2CO_3 (2.498 g, 18.10 mmol). The reaction mixture was heated at 80 °C for 72 h. The mixture was cooled down to room temperature, and polymer **22** was separated by filtration, washed with H_2O (500 mL), followed by washing with 150 mL of each of the following solvents: MeOH, EtOH, THF, MeOH, and Et_2O. Polymer **22** was dried to constant weight under vacuum (7.0 g). ^1H NMR δ: 8.55–4.80 (m, 105H, Ar and CH-N), 3.70–3.10 (m, 4H, $PhCH_2$-N and N-CH_2), 2.64–0.00 (m, 110H, CH_3, CH_2, CH, polymer matrix, and CH_3, CH_2, amine moiety). ^{13}C NMR δ: 128.2 (C-Ar), 65.3 (C-O), 40.5 (CH, polymer matrix), 28.5 (CH_3-C), 17.3 (CH_3). Found: C 84.12, H 8.07, N 2.72, which indicated the loading of the resin to be 0.414 mmol of NH per gram.

3-[(1*R*,2*R*,5*S*)-2-Isopropyl-5-methylcyclohexylamino]-1-propanol (23)

A solution of 3-aminopropanol (2.212 g, 2.250 mL, 29.50 mmol) in dry MeOH (10 mL) was added to a solution of (–)-menthone (5.00 g, 5.60 mL, 32.5 mmol) in dry MeOH (50 mL), followed by the addition of $NaBH_3CN$ (2.047 g, 32.50 mmol). The pH of the reaction was adjusted to 6 by addition of glacial acetic acid, and the reaction mixture was stirred at room temperature overnight. The mixture was diluted with water (30 mL), and Et_2O (75 mL) was added. The organic layer was extracted with a 10% solution of HCl (3 × 50 mL). The acidic aqueous layers were made basic by slow addition of solid NaOH. The basic solution was extracted with Et_2O (3 × 50 mL). The organic layers were combined, dried with $MgSO_4$, and the solvent was removed in vacuo giving the crude product as two diastereomers in a 1:6 ratio (determined by GC; 7.00 g). The crude product was purified by chromatography (hexane, hexane–AcOEt 1:1) giving pure **23** (3.50 g, 55% yield); bp 145–147 °C at 7 mmHg. $[\alpha]^{29}_D$ +22.4° (*c* 1.14, CH_2Cl_2). IR (cm^{-1}): 3250, 2969, 1600, 1374, 700. ^1H NMR δ: 3.63 (dd, 2H, *J* = 5.15, 5.15 Hz), 2.86 (dt, 1H, *J* = 5.39, 11.20 Hz), 2.73 (d, 1H, *J* = 2.91 Hz), 2.47 (dt, 1H, *J* = 5.70, 11.50 Hz), 1.81 (dd, 1H, *J* = 2.43, 13.78 Hz), 1.61–1.48 (m, 4H), 1.48–1.35 (m, 1H), 1.30 (ddd, *J* = 6.63, 3.23, 13.21 Hz), 1.04–0.87 (m, 1H), 0.75 (d, 3H, *J* = 2.58 Hz), 0.74–0.69 (m, 9H). ^{13}C NMR δ: 64.4, 54.3, 48.1, 47.9, 37.5, 35.2, 31.5, 28.9, 25.6, 24.8, 22.5, 21.4, 20.5. MS: (CI, NH_3): 214 (M + 1, 100), 128 (22). Anal. calcd. for $C_{13}H_{27}NO$: C 73.18, H 12.75, N 6.56; found: C 73.13, H 12.91, N 6.87.

(1*S*,2*R*,5*S*)-*N*-[(2-Isopropyl-5-methyl)cyclohexylamino]-3-propyl-1-propoxymethyl polystyrene (24)

A solution of amine **23** (3.443 g, 16.20 mmol) in DMF (10 mL) was added to a suspension of prewashed NaH (0.450 g, 18.75 mmol) at 0 °C, and the reaction was stirred under N_2 for 2 h. The reaction was warmed up to room temperature, and Merrifield resin (**1**) was added (6.50 g, 7.15 mmol, 1.1 mmol of Cl per gram), followed by the addition of dry K_2CO_3 (2.235 g, 16.20 mmol). The reaction mixture was heated at 80 °C for 72 h. The reaction mixture was cooled down to room temperature, and polymeric amine **24** was separated by filtration. The polymer was then washed with water (500 mL), followed by the following solvents (200 mL): 50% aq. MeOH, MeOH, EtOH, THF, MeOH, Et_2O, and THF, dried under vacuum to constant weight, and 7.0 g of the polymer were obtained. The loading of the polymer was calculated from elemental analysis and was 0.536 mmol of NH per gram. ^1H NMR δ: 8.40–5.60 (m, 44H, Ar), 3.90–3.70 (m, 4H, CH_2Cl, polymer matrix, and $PhCH_2O$-), 3.70–3.40 (m, 8H, OCH_2 and CH_2N), 2.70–1.42 (m, 4H, CH, polymer matrix, CH_2 in the ring), 1.42–0.60 (m, 10H, CH_2, polymer matrix, and CH_3, CH_2, CH, amine moiety). ^{13}C NMR δ: 128.1 (C-Ar), 66.0 ($PhCH_2O$-), 54.5 (CH-i-Pr), 48.8 (CH-N), 45.5 (CH_2N), 40.7 (CH, polymer matrix), 25.8 (CH_3), 15.5 (CH_3). Found: C 88.70, H 8.42, N 0.75.

Generation of the lithium enolate of tropinone using polymer-supported chiral lithium amides

Insoluble polymers

A solution of *n*-BuLi in hexanes (1.45 mol/L, 1.4 mL, 2.049 mmol) was added to a slurry of an insoluble polymer-supported chiral amine (2.049 mmol) in THF (20–25 mL) at 0 °C, and the resulting suspension was stirred for 8 h. Lithium chloride in THF (0.63 mol/L, 2.95 mL, 1.86 mmol) was added, and the stirring was continued for an additional 2 h. After cooling to –78 °C, tropinone (0.258 g, 1.86 mmol) in THF (2 mL) was added dropwise over ca. 3 min, and the resulting mixture was stirred overnight.

Soluble polymers

A solution of *n*-BuLi in hexanes (1.9 mol/L, 0.58 mL, 1.1 mmol) was added to a solution of a soluble polymer-supported chiral amine (1.1 mmol) in THF (25 mL) at 0 °C, and the resulting solution was stirred for 2.5 h. Lithium chloride in THF (1.0 mmol) was added, and the stirring was continued for an additional hour. After cooling to –78 °C, tropinone (0.139 g, 1.00 mmol) in THF (2 mL) was added dropwise for over a period of 3 min, and the resulting mixture was stirred for 3 h. If necessary, a second equivalent of *n*-BuLi (1.9 mol/L, 0.58 mL, 1.1 mmol) was added at this time, and the reaction mixture was warmed up to 0 °C. The stirring was continued for 30 min, followed by cooling down of the reaction mixture to –78 °C before the addition of an electrophile.

© 2006 NRC Canada

Noncrosslinked (*S*)-*N*-(methyl-1-phenylethyl)amino polystyrene (31)

A solution of (*S*)-(–)-α-methylbenzylamine (10.00 g, 10.64 mL, 82.64 mmol) in benzene (20 mL) was added to a solution of polymer **27** (20 g, 20 mmol, 1.0 mmol of halide per gram) in benzene (100 mL), and the reaction was refluxed for 48 h. The reaction was cooled down to room temperature, and the solvent was removed in vacuo. The residue was cooled down to –45 °C and methanol was added (300 mL). Amine **31** precipitated, was separated by filtration and washed with water (100 mL) and MeOH (500 mL), and then was dried to constant weight under vacuum and 20.5 g were obtained. The loading of the polymer **31** was calculated from elemental analysis and was 0.69 mmol of N per gram. ^{1}H NMR δ: 7.41–6.98 (m, 102 H, Ar), 6.98–6.45 (m, 66H, Ar), 4.74–4.54 (br s, 2H, CH_2X), 4.29 (q, J = 6.4 Hz, 2H, CH-N), 4.01–3.55 (m, 9 H, CH_2 and NH), 2.20–1.86 (m, 30H, CH, polymer matrix), 1.78–1.40 (m, 72H, CH_3, amine moiety and CH_2, CH_3, polymer matrix). ^{13}C NMR δ: 145.2 (C-Ar), 128.8 (C-Ar), 128.6 (C-Ar), 128.4 (C-Ar), 128.1 (C-Ar), 127.8 (C-Ar), 127.0 (C-Ar), 126.1 (C-Ar), 125.8 (C-Ar), 57.6 (-CH-N), 51.1 (CH_2N), 46.4 (CH_2Cl), 43.9 (CH_2, polymer matrix), 40.5 (CH, polymer matrix), 24.4 (CH_3, amine moiety). Found: C 89.16, H 7.74, N 1.47

Noncrosslinked (*R*)-[1-phenyl-2-(-1-piperidino)ethylmethyl]amino polystyrene (32)

A solution of (*R*)-(1-amino-1-phenyl)ethyl-1-piperidine (3.023 g, 15.00 mmol) in benzene (25 mL) was added to a solution of soluble polymer-supported benzyl iodide **27** (15.0 g, 15.0 mmol, 1.0 mmol of halide per gram) in benzene (150 mL), followed by the addition of K_2CO_3 (8.28 g, 60.0 mmol). The reaction mixture was refluxed under N_2 for 48 h. The solvent was removed in vacuo, and the residue was cooled down to –45 °C. Methanol (300 mL) was added and amine **32** precipitated. Polymer **32** was separated by filtration and washed with MeOH (200 mL), water (500 mL), and MeOH (750 mL), and then dried to constant weight under vacuum (16.099 g). The loading of amine **32** was estimated by subtracting the molar amount of unreacted amine from the total molar amount of amine used for the attachment to the polymer and was 0.944 mmol of N per gram. ^{1}H NMR δ: 7.25–6.25 (m, 70H, Ar), 3.90–3.65 (m, 2H, CH_2-N), 3.53–3.18 (m, 3H, CH_2-N, CH-N), 2.83–2.58 (m, 2H, CH_2), 2.58–2.28 (m, 4H, CH_2), 2.20–1.10 (m, 40H, CH_2, CH, polymer matrix and CH_2 amine moiety). ^{13}C NMR δ: 145.5 (C-Ar), 143.3 (C-Ar), 128.5 (C-Ar), 128.1 (C-Ar), 127.8 (C-Ar), 127.3 (C-Ar), 125.8 (C-Ar), 66.7 (CH_2N), 55.1 (CH-N), 54.7 (CH_2-N), 40.6 (CH, polymer matrix), 26.4 (CH_2), 24.7 (CH_2). Found: C 87.81, H 7.42, N 1.91.

Noncrosslinked 3-hydroxy-1-propoxymethyl polystyrene (33)

A solution of 1,3-propanediol (6.84 g, 6.58 mL, 90.0 mmol) in THF (20 mL) was added to a suspension of prewashed NaH (1.2 g, 50 mmol) in THF (100 mL) at 0 °C under N_2. After stirring for 2 h, a solution of soluble polymer **26** (15 g, 15 mmol, 1.0 mmol of Cl per gram) in THF (75 mL) was added dropwise, and the reaction was refluxed for 48 h. The reaction was cooled down to 0 °C and water (50 mL) was added. The layers were separated and the aqueous layer was extracted with AcOEt (3 × 300 mL). The organic layers were combined, dried with $MgSO_4$, and the bulk of the solvents were removed in vacuo. The residue was added to cold (–45 °C) MeOH (300 mL) and polymer **33** precipitated and was separated by filtration, washed with water (500 mL) and MeOH (750 mL). The polymer was dried under vacuum to constant weight and 15.5 g were obtained. The loading of **33** was calculated by gravimetric analysis (0.9 mmol of OH per gram). ^{1}H NMR δ: 7.40–6.86 (m, 79 H, Ar), 6.86–6.30 (m, 50H, Ar), 4.55–4.35 (m, 2H, CH_2Cl), 3.89–3.73 (m, 2H, CH_2OH), 3.73–3.55 (m, 2H, CH_2O), 3.45–3.25 (m, 1H, OH), 2.35–2.10 (m, 10 H, CH_2), 2.05–1.73 (m, 25 H, CH, polymer matrix), 1.70–1.24 (m, 47 H, CH_2, CH_3, polymer matrix). ^{13}C NMR δ: 145.4 (C-Ar), 131.2 (C-Ar), 128.9 (C-Ar), 128.1 (C-Ar), 127.8 (C-Ar), 125.8 (C-Ar), 73.3 (CH_2-OAr), 69.3 (-OCH_2), 62.1 (CH_2OH), 45.5 (CH_2Cl), 44.0 (CH_2, polymer matrix), 40.6 (CH, polymer matrix), 32.4 (CH_2, alcohol moiety). Found: C 87.63, H 7.87.

Noncrosslinked 6-hydroxy-1-hexoxymethyl polystyrene (34)

A solution of 1,6-hexanediol (9.912 g, 84.00 mmol) in dry DMF (30 mL) was added to a cold (0 °C) suspension of prewashed NaH (1.2 g, 50 mmol) in DMF (150 mL), and the reaction was stirred under N_2 for 2 h. Soluble polymer **26** (12 g, 12 mmol, 1.0 mmol of Cl per gram) was added. The reaction was heated at 80 °C for 48 h. The bulk of DMF was distilled off under reduced pressure. The residue was cooled down to –45 °C and MeOH (500 mL) was added. Polymer **34** precipitated and was separated by filtration, washed with water (250 mL) and MeOH (500 mL), and dried under vacuum to constant weight and 12.5 g were obtained. The loading of the polymer was calculated by the OH titration method and was 0.98 mmol of OH per gram. ^{1}H NMR δ: 7.45–6.35 (m, 55H, Ar), 4.55–4.34 (m, 2H, CH_2Cl), 3.75–3.60 (m, 2H, O-CH_2Ph), 3.55–3.30 (m, 4H, OCH_2, CH_2OH), 2.35–1.25 (m, 41H, CH_2, CH, CH_3, polymer matrix), 1.1–0.85 (m, 8H, CH_2). ^{13}C NMR δ: 145.4 (C-Ar), 138.0 (C-Ar), 128.1 (C-Ar), 127.8 (C-Ar), 125.8 (C-Ar), 73.5 (CH_2-OAr), 64.3 (OCH_2), 63.0 (CH_2OH), 45.5 (CH_2Cl), 44.4 (CH_2, polymer matrix), 40.6 (CH, polymer matrix), 32.9 (CH_2), 29.9 (CH_2), 26.3 (CH_2), 25.8 (CH_2). Found: C 85.82, H 7.93.

Noncrosslinked 3-iodo-1-propoxymethyl polystyrene (35)

Imidazole (2.652 g, 39.00 mmol) was added to a solution of triphenylphosphine (10.218 g, 39.00 mmol) in dry CH_2Cl_2 (200 mL), followed by the addition of iodide (9.906 g, 39.00 mmol) and polymeric alcohol **33** (10 g, 9.0 mmol, 0.9 mmol of OH per gram). The reaction was protected from light and stirred under N_2 at room temperature for 48 h. The reaction mixture was extracted with a saturated solution of $Na_2S_2O_3$ (3 × 100 mL). The organic layers were dried with $MgSO_4$ and the bulk of CH_2Cl_2 was removed in vacuo. The residue was cooled down to –45 °C and MeOH (500 mL) was added. The polymer precipitated, was separated by filtration, and washed with H_2O (200 mL) and MeOH (500 mL). The polymer was dried under vacuum to constant weight (11.5 g). The loading of the polymer was not determined at this stage. ^{1}H NMR δ: 7.27–6.27 (m, 84 H, Ar), 4.55–4.33 (m, 2H, CH_2Cl), 4.25–3.92 (m, 2H, CH_2-OAr), 3.60–3.41 (m, 2H, OCH_2), 3.39–3.20 (m, 2H, CH_2I), 3.89–3.50 (m, 2H, CH_2), 2.15–1.18 (m, 44 H, CH, CH_2, CH_3,

© 2006 NRC Canada

polymer matrix). ^{13}C NMR δ: 145.3 (C-Ar), 132.1 (C-Ar), 128.1 (C-Ar), 127.8 (C-Ar), 125.8 (C-Ar), 73.2 (CH_2-OAr), 69.5 (O-CH_2), 44.3 (CH_2Cl), 42.0 (CH_2, polymer matrix), 40.6 (CH, polymer matrix), 33.7 (CH_2), 3.7 (CH_2I). Found: C 77.75, H 6.54.

Noncrosslinked 6-iodo-1-hexoxymethyl polystyrene (36)

Compound **36** was prepared according to the procedure described for polymer **35**. The loading of starting alcohol **33** was 0.98 mmol of OH per gram. Polymer **36** was dried under vacuum to constant weight and 10.68 g were obtained; the loading was not determined at this stage. ^{1}H NMR δ: 7.40–6.25 (m, 120H, Ar), 4.57–4.32 (m, 2H, CH_2Cl), 4.3–3.92 (m, 2H, O-CH_2Ar), 3.62–3.35 (m, 2H, OCH_2), 3.30–3.11 (m, 2H, CH_2I), 2.98–2.54 (m, 4H, CH_2, alcohol moiety), 2.38–1.05 (m, 80H, CH_2, CH, polymer matrix, and CH_2 alcohol moiety). ^{13}C NMR δ: 145.4 (C-Ar), 132.2 (C-Ar), 128.6 (C-Ar), 128.0 (C-Ar), 127.8 (C-Ar), 125.8 (C-Ar), 73.0 (CH_2-OAr), 70.3 (OCH_2), 40.5 (CH, polymer matrix), 33.6 (CH_2), 30.4 (CH_2), 29.7 (CH_2), 25.5 (CH_2), 7.5 (CH_2I). Found: C 75.92, H 6.27.

Noncrosslinked (*S*)-*N*-[(1-phenylethyl-3-propyl)amino]-1-propoxymethyl polystyrene (37)

A solution of (*S*)-(–)-α-methylbenzylamine (4.588 g, 4.88 mL, 37.90 mmol) in benzene (10 mL) was added to a solution of polymer **35** (6.321 g, 5.690 mmol, 0.9 mmol of halide per gram) in benzene (150 mL), and the reaction was refluxed under N_2 for 48 h. The reaction was cooled down to room temperature and the bulk of the benzene was removed in vacuo. The residue was cooled down to –45 °C and MeOH (300 mL) was added slowly. Polymeric amine **37** precipitated, was separated by filtration, and washed with water (250 mL) and MeOH (300 mL), and then was dried to constant weight under vacuum and 6.0 g were obtained. The loading was determined from elemental analysis and was 0.985 mmol per gram. ^{1}H NMR δ: 7.50–6.40 (m, 142 H, Ar), 4.59–4.33 (m, 2H, CH_2Cl), 4.28–4.16 (m, 1H, CH-OAr), 3.98–3.80 (m, 1H, CH-OAr), 3.70–3.35 (m, 3H, OCH_2, CH-N), 2.85–2.57 (m, 2H, N-CH_2), 2.53–1.13 (m, 80H, CH_2, CH, CH_3, polymer matrix and CH_2, CH_3, amine moiety). ^{13}C NMR δ: 145.3 (C-Ar), 135.0 (C-Ar), 128.6 (C-Ar), 128.1 (C-Ar), 127.8 (C-Ar), 126.8 (C-Ar), 125.8 (C-Ar), 72.9 (CH_2-OAr), 68.9 (OCH_2), 64.4 (CH-N), 58.7 (CH_2-N), 45.4 (CH_2Cl), 44.1 (CH_2, polymer matrix), 40.5 (CH, polymer matrix), 30.0 (CH_2), 24.5 (CH_3). Found: C 87.50, H 8.03, N 1.17.

Noncrosslinked (*S*)-*N*-[(1-phenylethyl-6-hexyl)amino]-1-hexoxymethyl polystyrene (38)

Amine **38** was prepared according to the procedure described for amine **37**. The product was dried to constant weight under vacuum and 9.5 g were obtained. The loading of polymer **38** was calculated from elemental analysis and was 0.742 mmol N per gram. ^{1}H NMR δ: 7.25–6.25 (m, 179H, Ar), 4.60–4.35 (m, 2H, CH_2Cl), 4.25–4.13 (m, 1H, ArO-CH_2), 3.95–3.70 (m, 1H, ArO-CH_2), 3.55–3.30 (m, 4H, OCH_2, CH-N, NH), 2.65–0.90 (m, 115H, CH_2, CH polymer matrix, and CH_2N, CH_2, CH_3, amine moiety). ^{13}C NMR δ: 145.4 (C-Ar), 134.0 (C-Ar), 128.6 (C-Ar), 128.1 (C-Ar), 125.8 (C-Ar), 73.2 (CH_2-OAr), 70.5 (OCH_2), 64.3 (CH-N), 58.5 (CH_2N), 45.4 (CH_2, polymer matrix), 40.6 (CH, polymer matrix), 29.5 (CH_2), 27.3 (CH_2), 26.2 (CH_3). Found: C 87.62, H 7.69, N 1.05.

(1*S*,2*R*,1′*S*)-2-(1′-Hydroxybenzyl)-8-methyl-8-azabicyclo[3.2.1]octan-3-one (40) (ref. 28)

Synthesis using insoluble polymer-supported chiral lithium amides

Benzaldehyde (0.217 g, 0.208 mL, 2.049 mmol) was added to a solution of tropinone lithium enolate (1.86 mmol) at –78 °C, generated as described previously, and the reaction mixture was stirred for 4 h. The mixture was quenched with a saturated solution of NH_4Cl (10 mL). The polymer was separated by filtration and washed with NH_4Cl solution and Et_2O. The aqueous layer was separated and extracted with Et_2O (3 × 50.00 mL). The organic extracts were combined and dried with $MgSO_4$. The solvents were removed in vacuo and the crude product was obtained. The crude product was purified by chromatography (hexane–AcOH (4:1), CH_2Cl_2–MeOH (85:15)) and the reaction yield and enantioselectivity were determined as described before (28).

Synthesis using soluble polymer-supported chiral lithium amides

Benzaldehyde (117 mg, 0.11 mL, 1.10 mmol) was added to a solution of tropinone enolate at –78 °C (1.0 mmol) generated as described previously, and the reaction mixture was stirred for 1 h. The mixture was quenched with a saturated solution of NH_4Cl (10 mL), and quickly extracted with AcOEt (3 × 100 mL). The organic extracts were combined, dried with $MgSO_4$, and the solvents were removed in vacuo. The residue was cooled down to –40 °C and MeOH (100 mL) was added. A soluble polymer-supported amine precipitated out, and was separated by filtration. The filtrate was concentrated in vacuo, and the crude product was obtained. The crude product was purified by chromatography (hexane–AcOH (4:1), CH_2Cl_2–MeOH (85:15)), and the reaction yield and enantioselectivity were determined as described before (28).

6-[*N*-(2,2,2-Trichloroethoxycarbonyl)-*N*-methyl]-amino-2-cyclohepten-1-one (41) (ref. 4*e*)

With insoluble polymer-supported chiral lithium amides

2,2,2-Trichloroethyl chloroformate (0.434 g, 0.28 mL, 2.05 mmol) was added to a solution of tropinone lithium enolate (1.86 mmol), generated as described previously, and the reaction mixture was stirred for 8 h. The reaction was quenched with a saturated solution of K_2CO_3 (10 mL), and the polymeric amine was separated by filtration and washed with a saturated solution of K_2CO_3 (100 mL) and Et_2O (100 mL). The aqueous layer was separated and extracted with Et_2O (3 × 50.00 mL). The organic extracts were combined and dried with $MgSO_4$. The solvents were removed in vacuo, and the crude product was purified by DFC (hexane, hexane–AcOEt 1:1) and pure **41** was obtained. Spectral characterisctics of compound **41** and the method for measuring ee were described before (4*e*).

With soluble polymer-supported chiral lithium amides

2,2,2-Trichloroethyl chloroformate (277 mg, 0.18 mL, 1.30 mmol) was added to a solution of tropinone lithium

© 2006 NRC Canada

enolate (1.0 mmol), generated by as described previously (with a second equivalent of *n*-BuLi), and the reaction mixture was stirred for 2 h. The mixture was quenched with a saturated solution of K_2CO_3 (10 mL) and was then allowed to warm up to room temperature. The mixture was then extracted with AcOEt (3 × 100 mL). The organic extracts were combined, dried with $MgSO_4$, and the solvents were evaporated. The residue was cooled down to –40 °C and methanol (100 mL) was added. A soluble polymer-supported amine precipitated out and was separated by filtration. The filtrate was concentrated in vacuo, and the crude product was obtained. The crude product was purified by chromatography (hexane, hexane–AcOEt 1:1).

Acknowledgements

The authors thank the Natural Sciences and Engineering Research Council of Canada (NSERC) and the University of Saskatchewan, Saskatoon, Saskatchewan, for financial support.

References

1. D.J. Gravert and K.D. Janda. Chem. Rev. **97**, 489 (1997).
2. (*a*) C.R. Harrison, P. Hodge, B.J. Hunt, E. Khoshedel, and G. Richardson. J. Org. Chem. **48**, 3721 (1983); (*b*) J.S. Fruchtel and G. Jung. Angew. Chem. Int. Ed. Engl. **35**, 17 (1996); (*c*) A.R.Vaino and K.D. Janda. J. Comb. Chem. **2**, 579 (2000); (*d*) C.W. Harwing, J. Gravert, and K.D. Janda. Chemtracts, **12**, 1 (1999); (*e*) P.H. Toy and K.D. Janda. Acc. Chem. Res. **33**, 546 (2000).
3. J.A. Gladysz. Chem. Rev. **102**, 3215 (2002), and other papers in this special issue
4. (*a*) M. Majewski. *In* Advances in asymmetric synthesis. Vol. 3. *Edited by* A. Hassner. JAI Press, London. 1998, p. 39; (*b*) M. Majewski and F. Wang. Tetrahedron, **58**, 4567 (2002); (*c*) M. Majewski, M. DeCaire, P. Nowak, and F. Wang. Can. J. Chem. **79**, 1792 (2001); (*d*) M. Majewski and P. Nowak. J. Org. Chem. **65**, 5152 (2000); (*e*) M. Majewski, R. Lazny, and A. Ulaczyk. Can. J. Chem. **75**, 754 (1997); (*f*) M. Majewski and R. Lazny. Synlett, 785 (1996); (*g*) Review of enantioselective deprotonation with chiral lithium amide bases: P.J. O'Brien. J. Chem. Soc. Perkin Trans. 1, 1439 (1998).
5. B.J. Cohen, M.A. Kraus, and A. Patchornik. J. Am. Chem. Soc. **103**, 7620 (1981).
6. M. Majewski, A. Ulaczyk, and F. Wang. Tetrahedron Lett. **40**, 8755 (1999).
7. (*a*) A. Seki, Y. Takizawa, F. Ishiwata, and M. Asami. Chem. Lett. **32**, 342 (2003); (*b*) A. Johansson, P. Abrahamsson, and O. Davidsson. Tetrahedron: Asymmetry, **14**, 1261 (2003); (*c*) M. Asami and A. Seki. Chem. Lett. 160 (2002); (*d*) A. Seki and M. Asami. Tetrahedron, **58**, 4655 (2002).
8. M.B. Smith and J. March. March's advanced organic chemistry. Wiley, Toronto. 2001. p. 517
9. (*a*) D. Harris. Quantitative chemical analysis. Freeman, New York. 1987; (*b*) M. Narita. Bull. Chem. Soc. Jpn. **51**, 1477 (1978).
10. C.R. McArthur, P.M. Worster, J. Jiang, and C.C. Leznoff. Can. J. Chem. **60**, 1836 (1982).
11. K.S. Lam, M. Lebl, and V. Krchnak. Chem. Rev. **97**, 411 (1997).
12. M. Watanabe and K. Soai. J. Chem. Soc. Perkin Trans. 1, 837 (1994).
13. G.L. Lange and C. Gottardo. Synth. Commun. **10**, 1473 (1990).
14. G. Liu and J.A. Ellman. J. Org. Chem. **60**, 7712 (1995).
15. A. Vidal-Ferran, N. Bampos, A. Moyano, M.A. Pericas, A. Riera, and J.K.M Sanders. J. Org. Chem. **63**, 6309 (1998).
16. K.D. Shimizu, M.L. Snapper, and A.H. Hoveyda. Eur. J. Chem. **4**, 1885 (1998).
17. P. Wentworth, Jr. and K.D. Janda. Chem. Commun. 1917 (1999).
18. K. Shirai, K. Aoki, D. Sato, H.-D. Kim, M. Murakata, T. Yasuka, and K. Koga. Chem. Pharm. Bull. **42**, 690 (1994).
19. (*a*) T. Honda, S. Ono, H. Mizutani, and K.O. Hallinan. Tetrahedron: Asymmetry, **8**, 181 (1997); (*b*) O. Muraoka, B.Z. Zheng, K. Okumura, E. Tabata, G. Tanabe, and M. Kubo. J. Chem. Soc. Perkin Trans. 1, 113 (1997); (*c*) M. Nowakowski and H.M.R. Hoffmann. Tetrahedron Lett. **38**, 1001 (1997); (*d*) M. Asami, T. Ishizaki, S. Inoue. Tetrahedron Lett. **36**, 1893 (1995); (*e*) K. Mori and N. Murata. Liebigs Ann. Chem. 2089 (1995); (*f*) M. Tsukazaki, M. Tinkl, A. Roglans, B.J. Chapell, N.J. Taylor, and V. Snieckus. J. Am. Chem. Soc. **118**, 685 (1996); (*g*) A.J. Blake, S.M. Westaway, and N.S. Simpkins. Synlett, 919 (1997).
20. P. Hodge. Chem. Soc. Rev. **26**, 417 (1997).
21. D. Seebach. Angew. Chem. Int. Ed. Engl. **27**, 1624 (1988).
22. M. Majewski, R. Lazny, and P. Nowak. Tetrahedron Lett. **36**, 5465 (1995).
23. X. Sun and D.B. Collum. J. Am. Chem. Soc. **122**, 2452 (2000).
24. T. Laube, J.D. Dunitz, and D. Seebach. Helv. Chim. Acta, **68**, 1373 (1985).
25. (*a*) E. Vedejs and N. Lee. J. Am. Chem. Soc. **113**, 5483 (1991); (*b*) E. Vedejs and N. Lee. J. Am. Chem. Soc. **117**, 891 (1995).
26. K. Martinkus, C.-H. Tann, and S.J. Gould. Tetrahedron, **39**, 3493 (1983).
27. R.F. Borch, M.D. Bernstein, and H.D. Durst. J. Am. Chem. Soc. **93**, 2897 (1971).
28. (*a*) M. Majewski and G.-Z. Zheng. Can. J. Chem. **70**, 2618 (1992); (*b*) M. Majewski and R. Lazny. J. Org. Chem. **60**, 5825 (1995).

© 2006 NRC Canada

Synthesis and characterization of N-silylated, C_1-symmetric benzamidinates of lithium, sodium, and tin(II)[1]

Floria Antolini, Peter B. Hitchcock, Alexei V. Khvostov, and Michael F. Lappert

Abstract: The synthesis and characterization of complexes obtained from the reactions between Li[*N*-*t*-Bu(SiMe$_3$)] (**A**) or the sodium analogue Na[*N*-*t*-Bu(SiMe$_3$)] (**B**) and the cyanoarene RCN (R = Ph or 4-MeOC$_6$H$_4$) are discussed. These are the THF adduct [Li{μ-*cis*-N(*t*-Bu)C(Ph)N(SiMe$_3$)}(THF)]$_2$ (**1**), the TMEDA adduct Li[N(*t*-Bu)C(Ph)N(SiMe$_3$)](TMEDA) (**2**), the neutral ligand-free lithium benzamidinate Li[N(*t*-Bu)C(C$_6$H$_4$OMe-4)N(SiMe$_3$)] (**3**), and the THF adduct Li[N(*t*-Bu)C(C$_6$H$_4$OMe-4)N(SiMe$_3$)](THF) (**3a**). The preparation and structure of the crystalline compound [Na{μ-*cis*-N(*t*-Bu)C(Ph)N(SiMe$_3$)}(OEt$_2$)]$_2$ (**4**) is described. From the lithium benzamidinate **1** and Sn(II) chloride the tin(II) complex [Sn{N(*t*-Bu)C(Ph)N(SiMe$_3$)}$_2$] (**5**) was obtained. The molecular structures of the crystalline compounds **1**, **4**, and **5** were established by X-ray diffraction. In **1** and **4** the benzamidinato ligand is both chelating and bridging, with the Me$_3$Si-substituted nitrogen atom as the bridging site. The central planar (MN)$_2$ four-membered ring is a rhombus in **1**, with almost equal Li—N bond lengths, whereas in **4** the bonds to Na(1) are significantly longer than those to Na(2). In **5**, the ligand is N,N′-chelating.

Key words: alkali metals, tin(II), benzamidinates, NMR spectra, X-ray structures.

Résumé : On discute de la synthèse et de la caractérisation de complexes obtenus par les réactions du Li[*N*-*t*-Bu(SiMe$_3$)] (**A**) ou de analogue sodique Na[*N*-*t*-Bu(SiMe$_3$)] (**B**) avec des cyanoarènes RCN (R = Ph ou 4-MeOC$_6$H$_4$) et isolés sous la forme de benzamidinate de lithium neutre, sans ligand, [Li[N(*t*-Bu)C(C$_6$H$_4$OMe-4)N(SiMe$_3$)] (**3**) ou sous la forme d'adduits avec le THF [Li{μ-*cis*-N(*t*-Bu)C(Ph)N(SiMe$_3$)}(THF)]$_2$ (**1**) ou [Li[N(*t*-Bu)C(C$_6$H$_4$OMe-4)N(SiMe$_3$)](THF) (**3a**) et avec le TMEDA Li[N(*t*-Bu)C(Ph)N(SiMe$_3$)](TMEDA) (**2**). On a aussi préparer le composé [Na{μ-*cis*-N(*t*-Bu)C(Ph)N(SiMe$_3$)}(OEt$_2$)]$_2$ (**4**) dont on a déterminé la structure cristalline. La réaction du benzamidinate de lithium (**1**) avec le chlorure d'étain(II) permet d'obtenir le complexe d'étain(II) [Sn{N(*t*-Bu)C(Ph)N(SiMe$_3$)}$_2$] (**5**). On a déterminé les structures moléculaires des composés cristallins **1**, **4** et **5** par diffraction des rayons X. Dans les composés **1** et **4**, le ligand benzamidinato agit à la fois comme pont et comme agent chélatant alors que l'atome d'azote substitué par un groupe Me$_3$Si agit comme pont. Le cycle central planaire à quatre chaînons (MN)$_2$ est rhombique dans le composé **1** et les longueurs de ses liaisons Li—N sont pratiquement égales alors que dans le composé **4** les longueurs des liaisons vers le Na(1) sont beaucoup plus longues que celles vers la Na(2). Dans le composé **5**, le ligand est N,N′-chélatant.

Mots clés : métaux alcalins, étain(II), benzamidinates, spectres RMN, structures déterminées par diffraction des rayons X.

[Traduit par la Rédaction]

Introduction

Amidines and amidinates are valuable reagents in organic synthesis (1). The amidinato ligand [N(R^1)C(R^2)N(R^3)]$^-$ (Am$^-$) is widely employed in coordination chemistry; there have already been more than 100 publications in the 21st century. Its role often is that of a spectator ligand. Attractive features are that (*i*) its steric and electronic properties can be widely varied by judicious selection of the substituents R^1, R^2, and R^3, (*ii*) it can display a diversity of bonding modes in its binding to the metal or metals, and (*iii*) it often is firmly bound to the latter. Reviews have dealt with transition metal amidinates (2*a*), s-, p-, d-, and f-block metal *N*,*N*′-bis(trimethylsilyl)benzamidinates (R^1 = SiMe$_3$ = R^3, R^2 = an aryl group) (2*b*), and "paddle-wheel" dinuclear formamidinates of formula [M$_2${N(R^1)C(H)N(R^3)}$_4$(L$_{ax}$)$_n$] (M = Mo, Rh, Ni, or Ru; R^1 = an aryl group = R^3, L$_{ax}$ is the axial ligand; *n* = 0–2) (2*c*).

Received 3 June 2005. Published on the NRC Research Press Web site at http://canjchem.nrc.ca on 17 March 2006.

This paper is dedicated to Dr. Arthur J. Carty, in recognition of his many important contributions to organometallic chemistry, and as a mark of esteem and (by MFL) friendship.

F. Antolini, P.B. Hitchcock, A.V. Khvostov, and M.F. Lappert.[2] The Chemical Laboratory, University of Sussex, Brighton BN1 9QJ, UK.

[1]This article is part of a Special Issue dedicated to Professor Arthur Carty.

[2]Corresponding author (e-mail: M.F.Lappert@sussex.ac.uk).

 doi:10.1139/V05-250 © 2006 NRC Canada

Some group 4 metal amidinates are catalysts for olefin polymerization, as summarized in a recent survey on advances in non-metallocene olefin polymerization (3). For example, isotactic polypropylene was obtained using tris(amidinato)zirconium(IV) complexes bearing a chiral N-substituted ligand (4); and C_1-symmetric amidinates, $[Zr(Am)_2Me_2]$ (Am: $R^1 \neq R^3$), were moderately active for formation of isotactic poly(1-hexene) (5). Cationic aluminium amidinates, such as $[Al\{(N\text{-}i\text{-}Pr)_2C\text{-}t\text{-}Bu\}Me][B(C_6F_5)_3Me]$, were shown to be active single site catalysts for the living polymerization of ethylene (6). Lanthanide metal amidinates, $[Ln\{(N(c\text{-}C_6H_{11}))_2CR^2\}_3]$ (Ln = Nd, Gd, Yb; R^2 = Me or Ph), were highly active catalysts for the ring-opening polymerization of ε-caprolactam (7).

The more important methods that have been used to prepare metal amidinates are (*i*) metallation of the amidine $HN(R^1)C(R^2)N(R^3)$, (*ii*) ligand transfer reactions from either an alkali metal (8) or trimethylsilyl (9) amidinate and a metal chloride, (*iii*) addition of a metal hydrocarbyl to a carbodiimide (e.g., LiR^2 to $R^1N{=}C{=}NR^3$, $R^1 = SiMe_3 = R^3$, R^2 = aryl), and (*iv*) the reaction between a metal bis(trimethylsilyl)amide and a cyanoarene. As for (*iv*), Sanger (in our laboratory) found in 1973 that $Li[N(SiMe_3)_2]$ and PhCN in Et_2O readily yielded $Li[\{N(SiMe_3)\}_2CPh]$, which was characterized by treatment with Me_3SiCl, yielding the benzamidine $N(SiMe_3)_2C(Ph){=}N(SiMe_3)$ (10); substantial extensions to this methodology up to 1990 have been summarized (5*b*). In the present paper are described reactions of the related, but C_1-symmetric, alkali metal amides M[*N*-*t*-Bu($SiMe_3$)] (M = Li (**A**) (11), M = Na (**B**) (12)) with PhCN or 4-$MeOC_6H_4CN$.

Our prior publications in this area dealt with $[K\{N(SiMe_3)C(C_6H_3Me_2\text{-}2,5){=}C(H)SiMe_3\}]_2$ and $[\{UCl(\mu\text{-}Cl)(L)N(SiMe_3)\}_2][UCl_2(L)(Am)]_2$ (L = $\{N(SiMe_3)C(Ph)\}_2CH$, Am = $N(SiMe_3)C(Ph)NC(Ph){=}C(H)SiMe_3$) (13*a*), M[{N-(CH=$NSiMe_3$)}$_2$CH]$_n$ [*n* = 3 and M = Li (13*b*), Na (13*c*); *n* = 4, Tl (13*c*)); $[Li(Am)(CNPh)]_2$ (13*d*), $[K(Am)]_2$, [SnCl(Am)], $[Sn(Am)_2]$, and $[Hg(Am)_2]$ (Am = $N(SiMe_3)C(Ph)$-$NC(Ph){=}C(SiMe_3)_2$) (13*e*); $Li[N(SiMe_3)C(Ar)NC(Ar){=}C(H)$-$SiMe_3]$(D) (D = TMEDA or THF with Ar = Ph; or D = TMEDA, Ar = 4-MeC_6H_4) (13*f*); $[Li(Am)]_2$, $[M(Am)Cl_2]$ (M = Al or Ga) and $[\{Ln(Am)_2(\mu\text{-}Cl)\}_2]$ (Am = $N(SiMe_3)C$-$(Ph)N(CH_2)_3NMe_2$, Ln = La or Ce) (13*g*); $Li[N(SiMe_3)C$-$(H)NC(H){=}C(H)C(t\text{-}Bu){=}NSiMe_3]$ (13*h*); and $Li[N(Si$-$Me_2OMe)C(C_6H_3Me_2\text{-}2,5)NC(C_6H_3Me_2\text{-}2,5){=}C(H)SiMe_3]$-(TMEDA) (13*i*).

Experimental

General remarks

All manipulations were performed under argon using standard Schlenk techniques. Hexane was dried and distilled over sodium–potassium alloy, THF and diethyl ether were dried and distilled over sodium–benzophenone and stored over a sodium mirror under argon. TMEDA (Aldrich) was distilled from CaH_2 prior use. Nitriles (Aldrich) were dried over molecular sieves. The alkali metal amides M[N-*t*-Bu($SiMe_3$)] (M = Li (**A**) (14), Na (**B**) (12)) were synthesized by published procedures. The NMR spectra were recorded on a Bruker DPX 300 (300.1 MHz for ^{1}H, 75.5 MHz for ^{13}C, and 116.6 MHz for ^{7}Li) or an AMX 500 (49.7 MHz for ^{29}Si) instrument, and referenced externally (^{7}Li, using LiCl; ^{29}Si, using $SiMe_4$) or internally to the residual solvent resonances. Unless otherwise stated, all NMR spectra were measured at 298 K and other than ^{1}H were proton-decoupled. Electron impact mass spectra were taken from solid samples using a Kratos MS 80 RF instrument. Melting points were taken in sealed capillaries and are uncorrected. Elemental analyses were determined by Medac Ltd., Brunel University, Uxbridge, Middlesex, UK.

Preparations

[Li{μ-cis-N(t-Bu)C(Ph)N(SiMe$_3$)}(THF)]$_2$ (1)

A solution of PhCN (0.46 cm^3, 4.49 mmol) in diethyl ether (5 cm^3) was added slowly to a cooled (–78 °C) solution of **A** (1.01 g, 4.49 mmol) in diethyl ether (15 cm^3). The resulting yellow mixture was allowed to warm to room temperature and was stirred for 12 h. The slightly cloudy mixture was filtered and the filtrate was concentrated and stored at –25 °C for 24 h, yielding colorless crystals of the 1:1 ether adduct (0.58 g, 44.7%). As the diethyl ether was not strongly bonded to the molecule, during the drying in vacuo the complex gradually lost the coordinated solvent, compromising the credibility of the analysis. Thus, the diethyl ether adduct was recrystallized from a satd. THF solution and a few colorless crystals of compound **1** were obtained (mp 55–80 °C). ^{1}H NMR (C_6D_6) δ: 0.06 (s, 9H, $SiMe_3$), 1.26 (s, 9H, *t*-Bu), 1.35 (m, 4H, THF), 3.59 (m, 4H, THF), 7.09 (d, 1H, $^3J_{HH}$ = 7.20 Hz), 7.12 (m, 2H, Ph), 7.29 (d, 2H, $^3J_{HH}$ = 7.12 Hz). ^{13}C NMR (C_6D_6) δ: 2.91 ($SiMe_3$), 25.43 (THF), 33.49 (CMe_3), 51.38 (CMe_3), 68.11 (THF), 126.59, 127.49, and 127.83 (Ph), 145.37 (ipso-C), 175.65 (NCN). ^{7}Li NMR (C_6D_6) δ: –0.48. ^{29}Si NMR (C_6D_6) δ at 323 K: –8.08 and –10.65; at 298 K, δ –10.69. MS (*M* denotes the monomer) *m*/*z* (% and assignment): 508 (8%, $[M_2 - 2THF]^+$), 451 (72%, $[M_2 - 2THF - t\text{-}Bu]^+$), 395 (8%, $[M_2 - 2THF - 2t\text{-}Bu + H]^+$), 375 (48%, $[M_2 - 2THF - Ph + H]^+$).

[Li{N(t-Bu)C(Ph)N(SiMe$_3$)}(TMEDA)] (2)

A solution of PhCN (0.32 cm^3, 3.11 mmol) in hexane (5 cm^3), was added to a cooled (0 °C) solution of **A** (0.47 g, 3.11 mmol) in hexane (25 cm^3). The reaction mixture was allowed to warm to room temperature and was stirred for 4 h. TMEDA (0.61 cm^3, 4.04 mmol) was added to the mixture, which was stirred for 12 h. The mixture was filtered; the filtrate was concentrated and stored at 10 °C for 12 h. Being cloudy, it was again filtered; the filtrate was concentrated and stored at 10 °C for a further 12 h to furnish yellow crystals of compound **2** (0.71 g, 61.3%), mp 132–135 °C. ^{1}H NMR (C_6D_6) δ: 0.09 (s, 9H, $SiMe_3$), 1.25 (s, 9H, *t*-Bu), 1.78 (s, 4H, TMEDA), 2.02 (s, 12H, TMEDA), 7.06 (tt, 1H, *p*-H of Ph, $^3J_{HH}$ = 7.6 Hz, $^4J_{HH}$ = 1.2 Hz), 7.15 (m, 2H, *m*-H of Ph), 7.35 (dd, 2H, *p*-H of Ph, $^3J_{HH}$ = 7.9 Hz, $^4J_{HH}$ = 1.2 Hz). ^{13}C NMR (C_6D_6) δ: 4.05 ($SiMe_3$), 34.32 (CMe_3), 50.67 (CMe_3), 125.80, 127.18 (*C*H of Ph), 146.47 (ipso-C), 174.56 (NCN). ^{29}Si NMR (C_6D_6) δ at 50 °C: –15.19. ^{7}Li NMR (C_6D_6) δ: –0.34. MS *m*/*z* (% and assignment): 375 (34%, $[M + Li - H]^+$), 262 (37%, $[M - TMEDA + Li + H]^+$), 247 (79%, $[M - Li - TMEDA]^+$), 191 (100%, $[247 - t\text{-}Bu]^+$).

© 2006 NRC Canada

[Li{N(t-Bu)C(C_6H_4OMe-4)N($SiMe_3$)}] (3)

4-$MeOC_6H_4CN$ (0.49 g, 3.62 mmol) was added in small portions to a cooled (–78 °C) solution of **A** (0.55 g, 3.63 mmol) in diethyl ether (45 cm^3). The reaction mixture was allowed to warm to room temperature and was stirred for 12 h. The cloudy mixture was filtered and the filtrate concentrated and stored at –25 °C for 12 h to afford an amorphous, ether-solvated product (Et_2O–benzamidinate, 1:2; calculated from the NMR integrals), recrystallized from a saturated hexane solution yielding compound **3** (0.29 g, 28%), as a yellow crystalline material (not suitable for X-ray analysis); mp 127–130 °C. ^{1}H NMR (C_6D_6) δ: 0.01 (s, 9H, $SiMe_3$), 1.25 (s, 9H, *t*-Bu), 3.30 (s, 3H, MeO), 6.75 (d, 2H, $^3J_{HH}$ = 8.37 Hz), 7.17 (d, 2H, $^3J_{HH}$ = 9.42 Hz). Anal. calcd. for $C_{15}H_{25}LiN_2OSi$ (%): C 63.5, H 9.41, N 9.83; found: C 62.5, H 8.49, N 9.81.

Variable temperature (V.T.) experiments

IR (cm^{-1}): 2246 ν(CN). ^{1}H NMR ($C_6D_5CD_3$ at ca. 231 K) δ: 0.09, 0.18, 0.23 (s, 9H, $SiMe_3$), 1.28, 1.32, 1.35 (s, 9H, *t*-Bu), 3.17, 3.22, 3.34 (s, 3H, MeO), 6.66 (m, 2H), 7.18 (d, 1H, $^3J_{HH}$ = 8.21 Hz), 7.30 (d, 1H, $^3J_{HH}$ = 7.95 Hz); at ca. 243 K δ: 0.08, 0.16, 0.21 (s, 9H, $SiMe_3$), 1.26, 1.31, 1.34 (s, 9H, *t*-Bu), 3.17, 3.22, 3.24, 3.30 (s, 3H, MeO), 6.65 (d, 1H, $^3J_{HH}$ = 7.93 Hz), 6.67 (d, 1H, $^3J_{HH}$ = 6.86 Hz), 7.16 (d, 1H, $^3J_{HH}$ = 8.24 Hz), 7.25 (d, 1H, $^3J_{HH}$ = 7.97 Hz); at ca. 253 K δ: 0.07, 0.14, 0.19 (s, 9H, $SiMe_3$), 1.24, 1.29, 1.34 (s, 9H, *t*-Bu), 3.17, 3.22, 3.24, 3.27 (s, 3H, MeO), 6.72 (m, 2H), 7.17 (m, 2H); at ca. 273 K δ: 0.90 (m, 9H, $SiMe_3$), 1.20 (s, 9H, *t*-Bu), 3.23, 3.25 (m, 3H, MeO), 6.67 (m, 3H, (d, 2H, $^3J_{HH}$ = 6.92 Hz)), 7.13 (d, 1H, $^3J_{HH}$ = 7.27 Hz); at ca. 298 K δ: 0.01 (s, 9H, $SiMe_3$), 1.18 (s, 9H, *t*-Bu), 3.26 (s, 3H, MeO), 6.66 (d, 2H, *o*-H, $^3J_{HH}$ = 7.44 Hz), 7.09 (m, 2H, *m*-H); at ca. 338 K δ: 0.09 (s, 9H, $SiMe_3$), 1.25 (s, 9H, *t*-Bu), 3.43 (s, 3H, MeO), 6.66 (d, 2H, $^3J_{HH}$ = 6.82 Hz), 7.25 (d, 2H, $^3J_{HH}$ = 8.52 Hz). ^{13}C NMR (C_6D_6 at ca. 298 K) δ: 2.78 ($SiMe_3$), 33.41 (C*Me*$_3$), 54.68 (*C*Me_3), 113.05 (MeO), 126.32, 128.40, 129.23 (Ph), 158.95 (CN). ^{7}Li NMR (C_6D_6 at ca. 298 K) δ: –0.24. ^{29}Si NMR (C_6D_6 at 338 K) δ: –9.92. MS *m*/*z* (% and assignment): 277 (85%, [*M* – Li]$^+$), 263 (38%, [*M* – Li – Me]$^+$), 221 (100%, [*M* – *t*-Bu – H]$^+$), 206 (65%, [*M* – *t*-Bu – Me – H]$^+$), 73 (100%, [$SiMe_3$]$^+$), 57 (12%, [*t*-Bu]$^+$).

[Li{μ-cis-N(t-Bu)C(C_6H_4OMe-4)N($SiMe_3$)}(THF)] (3a)

Evaporation of a THF solution of **3** produced the amorphous complex **3a**. ^{1}H NMR (C_6D_6) δ: 0.11 (s, 9H, $SiMe_3$), 1.29 (s, 9H, *t*-Bu), 1.39 (m, 4H, CH_2 of THF), 3.33 (s, 3H, MeO), 3.64 (m, 4H, OCH_2 of THF), 6.78 (d, 2H, *m*-H of C_6H_4, $^3J_{HH}$ = 8.65 Hz), 7.22 (d, 2H, *o*-H of C_6H_4, $^3J_{HH}$ = 8.48 Hz). ^{13}C NMR (C_6D_6) δ: 3.22 ($SiMe_3$), 25.51 (THF), 33.65 (C*Me*$_3$), 51.35 (*C*Me_3), 54.63 (MeO), 68.16 (THF), 112.90 (*m*-C of C_6H_4), 129.05 (*o*-C of C_6H_4), 138.07 (ipso-C of C_6H_4), 158.75 (*p*-C of C_6H_4), 175.58 (NCN). ^{7}Li NMR (C_6D_6) δ: 1.86. ^{29}Si NMR (inverse gated, d_1 = 25 s, C_6D_6) δ: –11.30. ^{1}H NOE (C_6D_6, η, %) irradiation of MeO: 5.7 (*m*-H of C_6H_4). ^{1}H{^{7}Li} NOE (C_6D_6, – η, %): 0.08 ($SiMe_3$), 0.12 (OCH_2 of THF), 0.15 (*o*-H of C_6H_4).

[Na{μ-cis-N(t-Bu)C(Ph)N($SiMe_3$)}(OEt_2)]$_2$ (4)

A solution of PhCN (0.98 cm^3, 9.56 mmol) in diethyl ether (5 cm^3) was added slowly to a cooled (0 °C) solution of **B** (1.60 g, 9.56 mmol) in diethyl ether (50 cm^3). The resulting solution was allowed to warm to room temperature, stirred for 12 h, concentrated and stored at –25 °C for 24 h, yielding colorless crystals of compound **4** (2.24 g, 69%). ^{1}H NMR (C_6D_6) δ: 0.04 (s, 9H, $SiMe_3$), 1.20 (t, 6H, Et_2O), 1.25 (s, 9H, *t*-Bu), 3.24 (q, 4H, Et_2O), 7.00–7.25 (m, 5H, Ph). ^{13}C NMR (333 K, C_6D_6) δ: 3.70 ($SiMe_3$), 15.30 (C*Me*$_3$), 34.12 (Et_2O), 51.38 (*C*Me_3), 65.91 (Et_2O), 126.28, 127.49, 129.08 (Ph), 146.23 (ipso-C), 175.10 (NCN). ^{23}Na NMR (C_6D_6) δ: 8.54 ($\Delta\nu_{1/2} \approx 2.6$ kHz). ^{29}Si NMR (ineptrd, C_6D_6) δ: –13.37. Anal. calcd. for $C_{18}H_{33}N_2NaOSi$ (%): C 62.8, H 9.65, N 8.13; found: C 62.3, H 9.38, N 8.09.

[Sn{N-t-BuC(Ph)N($SiMe_3$)}$_2$] (5)

$SnCl_2$ (0.481 g, 2.54 mmol) was added to a cooled (0 °C) solution of **1** (1.48 g, 5.08 mmol) in diethyl ether (40 cm^3). The mixture was warmed to room temperature and stirred for 12 h. The volatiles were removed at 30 °C and 10^{-2} Torr (1 Torr = 133.3224 Pa). The residue was extracted into diethyl ether. The extract was filtered and the filtrate concentrated and stored at –25 °C for 4 months to furnish pale yellow crystals of compound **5** (1.0 g, 64%), mp 73–80 °C. ^{1}H NMR (C_6D_6) δ: 0.11 (s, 9H, $SiMe_3$), 1.24 (s, 9H, *t*-Bu), 7.01 (m, 5H, Ph). ^{13}C NMR (C_6D_6) δ: 2.86 ($SiMe_3$), 33.22 (C*Me*$_3$), 53.94 (*C*Me_3), 126.88, 128.32, 128.99 (Ph), 142.15 (ipso-C), 170.01 (NCN). ^{29}Si NMR (C_6D_6) δ: –1.75. ^{119}Sn NMR (C_6D_6) δ: –258.5. MS *m*/*z* (% and assignment): 614 (25%, [*M*]$^+$), 557 (6%, [*M* – *t*-Bu]$^+$), 367 (27%, [*M* – (*N*-*t*-Bu)C(Ph)$NSiMe_3$)]$^+$), 247 (48%, [(*N*-*t*-Bu)C(Ph)($NSiMe_3$)]$^+$), 233 (50%, [(*N*-*t*-Bu)C(Ph)($NSiMe_3$) – *t*-Bu]$^+$), 191 (100%, [$SiMe_3$N=CPh]$^+$). Anal. calcd. for $C_{28}H_{46}N_4Si_2Sn$ (%): C 54.8, H 6.59, N 9.11; found: C 54.0, H 7.57, N 9.13.

X-ray crystallographic analysis of [Li{μ-*cis*-N(*t*-Bu)C(Ph)N($SiMe_3$)}(THF)]$_2$ (1), [Na{μ-*cis*-N(*t*-Bu)C(Ph)N($SiMe_3$)}(OEt_2)]$_2$ (4), and [Sn{η^3-N(*t*-Bu)C(Ph)N($SiMe_3$)}$_2$] (5)

Diffraction data for compound **1** were collected on a Nonius CAD4 and for **4** and **5** on a Nonius Kappa-CCD diffractometer using monochromated Mo Kα radiation (λ = 0.710 73 Å). Crystals were directly mounted on the diffractometer under a stream of cold nitrogen gas. In complex **4** there was unresolved end-for-end disorder in one ligand giving rise to partial Si/C occupancy for the sites labeled Si(2) and C(25) and some unrealistic ADPs for this ligand. DELU restraints were applied. Dimensions in the disordered ligand are unreliable. In both ligands of complex **5** there was unresolved end-for-end disorder of the $SiMe_3$ and *t*-Bu groups; 0.86:0.14 for Si1 and C8, and 0.65:0.35 for Si2 and C22. Bonds and angles involving these atoms are therefore unreliable. The structures were refined on all F^2 using SHELXL 97 (15). Further details are in Table 1.

Results and discussion

Reactions between Li[*N*-*t*-Bu($SiMe_3$)] (A) and the nitrile RCN (R = Ph or 4-$MeOC_6H_4$)

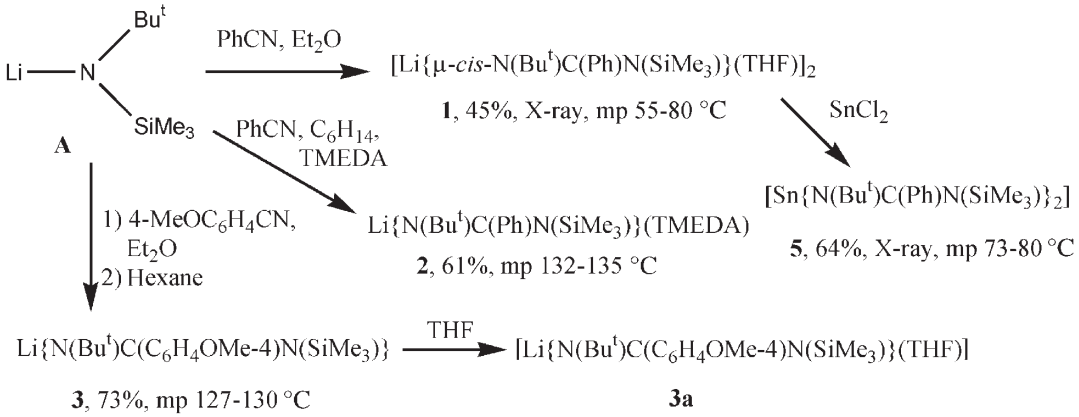
The initial targets in the nitrile reactions were lithium amidinates derived from Li[*N*-*t*-Bu($SiMe_3$)] (**A**) (11). This was based on an analogy with reactions of Li[N($SiMe_3$)$_2$] (14) with a cyanoarene (10, 2*b*). The results of treating **A** with PhCN and 4-$MeOC_6H_4CN$ are summarized in Scheme 1.

© 2006 NRC Canada

Table 1. Crystal data and structure refinements for **1**, **4**, and **5**.

Compound	**1**	**4**	**5**
Empirical formula	$C_{36}H_{62}Li_2N_4O_2Si_2$	$C_{36}H_{66}N_4Na_2O_2Si_2$	$C_{28}H_{46}N_4Si_2Sn$
Formula weight	652.96	689.09	613.56
Crystal system	Monoclinic	Tetragonal	Triclinic
Space group	*C2/c* (No. 15)	$P4_3$ (No. 78)	$P\bar{1}$ (No. 2)
a (Å)	11.413(2)	12.0845(4)	10.7754(2)
b (Å)	17.370(3)	12.0845(4)	11.9247(3)
c (Å)	20.526(4)	29.6425(6)	14.0436(4)
α (°)	90	90	67.740(1)
β (°)	99.27(2)	90	73.941(1)
γ (°)	90	90	86.438(2)
V (Å^3)	4016.3(13)	4 328.8(2)	1 603.01(7)
Z	4	4	2
D_c (Mg m^{-3})	1.08	1.06	1.27
μ(Mo Kα) (mm^{-1})	0.12	0.13	0.89
Reflections collected	3712	12 138	25 339
Independent reflections	3533 [*R*(int) = 0.029]	7 216 [*R*(int) = 0.043]	9 307 [*R*(int) = 0.035]
Reflections with $I > 2\sigma(I)$	2376	5 783	7 955
Data/restraints/parameters	3533/0/208	7 216/209/416	9 307/0/318
Final *R* indices [$I > 2\sigma(I)$]	*R*1 = 0.057, *wR*2 = 0.120	*R*1 = 0.062, *wR*2 = 0.148	*R*1 = 0.033, *wR*2 = 0.072
R indices (all data)	*R*1 = 0.098, *wR*2 = 0.139	*R*1 = 0.084, *wR*2 = 0.164	*R*1 = 0.044, *wR*2 = 0.077

Scheme 1. Synthesis of complexes **1**–**3** and **5**.



The colorless, crystalline, binuclear THF-bound lithium benzamidinate [Li{μ-*cis*-N(*t*-Bu)C(Ph)N(SiMe$_3$)}(THF)]$_2$ (**1**) was obtained after crystallizing the initially formed weakly bound diethyl ether adduct from THF. Alternatively, by carrying out the reaction between **A** and PhCN in hexane, followed by addition of TMEDA, the product was the yellow, crystalline, and probably (MS) mononuclear TMEDA adduct, Li[N(*t*-Bu)C(Ph)N(SiMe$_3$)](TMEDA) (**2**), as in the X-ray-characterized compounds, [Li{N(SiMe$_3$)C(Ph)N(SiMe$_3$)}-(TMEDA)] (16), [Li{N(myrtanyl)C(Ph)N(SiMe$_3$)}(TMEDA)] (4), and [Li{N(*i*-Pr)C(terpenyl)N(*i*-Pr)}(TMEDA)] (17).

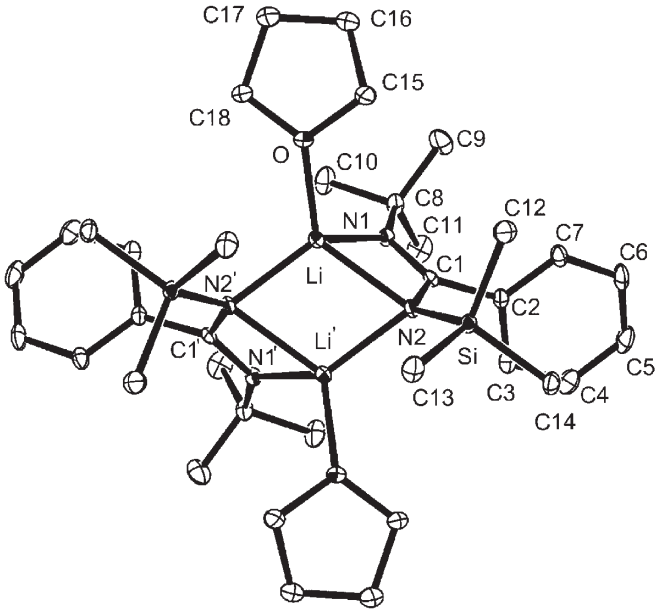
The reaction between **A** and 4-MeOC$_6$H$_4$CN in diethyl ether yielded the expected lithium benzamidinate as an amorphous powder containing weakly bound diethyl ether; crystallization from hexane afforded the neutral donor-free, pale-yellow, crystalline compound [Li{N(*t*-Bu)C(C$_6$H$_4$OMe-4)N(SiMe$_3$)}] (**3**), which in THF solution yielded the adduct [Li{N(*t*-Bu)C(C$_6$H$_4$OMe-4)N(SiMe$_3$)}(THF)] (**3a**).

Compounds **1**, **2**, and **3** gave satisfactory multinuclear (^{1}H, ^{13}C, ^{7}Li and ^{29}Si) NMR and mass (EI) spectra, as well as microanalysis for **3**. Complex **1** was further authenticated by its molecular structure determination by single crystal X-ray diffraction; X-ray quality crystals were not obtained for **2**, **3**, and **3**·THF. Whereas the mass spectrum of **3** was consistent with it being a mononuclear complex, the ^{1}H NMR spectrum in $C_6D_5CD_3$ at ambient temperature gave broad signals, which sharpened only upon heating. In the 231–338 K range, there appeared to be three species present. The heteronuclear ^{1}H{^{7}Li} NOE experiment of the THF adduct **3a** suggests that in benzene solution the compound has the cis-dimeric structure, as found in the crystalline THF adduct **1** (Fig. 1).

The THF-solvated lithium benzamidinate [Li{μ-*cis*-N(*t*-Bu)C(Ph)N(SiMe$_3$)}(THF)]$_2$ (**1**) was crystallized after storage for 1 day at –25 °C. An ORTEP representation of complex **1** is depicted in Fig. 1. Selected bond distances (Å) and angles (°) are reported, together with data for the related

© 2006 NRC Canada

Fig. 1. Molecular structure of [Li{μ-*cis*-N(*t*-Bu)C(Ph)N(SiMe$_3$)}(THF)]$_2$ (**1**) (20% ellipsoids, H atoms are omitted for clarity).



compound, [Li{μ-N(SiMe$_3$)C(C$_6$H$_4$OMe-4)N(SiMe$_3$)$_2$}(THF)]$_2$ (**6**) (18, 19), in Table 2.

A fused array of three, four-membered rings forms the core of molecule **1**. The dihedral angles between each of the outer rings and the central are 129.85° and 112.19°. The central [LiN(2)Li′N(2)′] rhomboid core is puckered, being folded by 13.7° around the Li(1)-Li(2) vector. The presence of a *tert*-butyl group imposes a distinct asymmetry on the N-C-N system (N(1)—C(1) = 1.302(3) Å and C(1)—N(2) = 1.370(3) Å). This corresponds to differences in the Li—N(1) and Li—N(2) bond lengths. The two nitrogen atoms of each benzamidinate ligand differ in that the *tert*-butyl-bound N is three-coordinate, whereas the four-coordinated trimethylsilyl-bound N atom bridges the two lithium atoms; thus, each ligand is N,N′-chelating, but also N(SiMe$_3$)-bridging. Due to steric impediments, the *tert*-butyl groups in complex **1** are arranged in a cis fashion. This creates narrower folding angles of the ladder structure core (112.89° and 129.85°) than in **6** (130.4° and 145.3°) (19). Thus, compound **1** exhibits a more compact architecture than that of **6**, evident also in the narrower N(1)-C(1)-N(2) angle in **1** than in **6** (19). A further structural detail concerns the orientation of the phenyl rings. The steric influence of the SiMe$_3$ and *t*-Bu groups imposes, at the aromatic substituents, a nearly orthogonal orientation (80.5° for one phenyl group and 78.2° for the other) with respect to the N-C-N heteroallylic units, which precludes any significant conjugation between the two π systems.

Other examples of dimeric crystalline N-silylated lithium benzamidinates include [Li{μ-N(*n*-Pr)C(Ph)N(SiMe$_3$)}(OEt$_2$)]$_2$ (20*a*), [Li(Am)]$_2$ (Am = N(SiMe$_3$)C(Ph)N(CH$_2$)$_n$NMe$_2$, *n* = 2 (20*b*) or 3 (13*g*)), [Li{N(SiMe$_3$)C(Ph)NC(Ph)=C(SiMe$_3$)$_2$}(NCPh)]$_2$ (13*d*), [Li{N(SiMe$_3$)C(Ph)NC(Ph)=C(H)SiMe$_3$}(THF)]$_2$ (13*f*), [Li{N((1*R*,2*R*)-(–)-2-(trimethylsilylamino)-cyclohexyl)propyl)C(Ph)N(SiMe$_3$)}]$_2$ (20*c*), several phenyl-fluorinated benzamidinates (20*d*), [Li{N(SiMe$_3$)C(4-MeC$_6$H$_4$)N(SiMe$_3$)}(NCC$_6$H$_4$Me-4)]$_2$ (20*e*), and [Li{N-(SiMe$_3$)C(Ph)N(SiMe$_3$)}(NCPh)]$_2$ (20*f*).

Table 2. Selected bond distances (Å) and angles (°) for compounds **1** and [Li{μ-N(SiMe$_3$)C(C$_6$H$_4$OMe-4)N(SiMe$_3$)$_2$}(THF)]$_2$ (**6**) (19).

Compounds	**1**	**6** (19)
Bond distances (Å)		
Li—N(1)	2.035(5)	2.099(9)
Li—N(2)	2.199(5)	2.145(8)
Li—N(2)′	2.063(5)	2.073(8)
Bond angles (°)		
N(1)-C(1)-N(2)	117.5(2)	120.1(4)
N(1)-Li-N(2)	65.2(2)	65.5(3)

Reactions between Na[*N*-*t*-Bu(SiMe$_3$)] (B) and PhCN

It had previously been shown that the sodium benzamidinate, [Na{μ-N(SiMe$_3$)C(Ph)N(SiMe$_3$)}(OEt$_2$)]$_2$-(OEt$_2$), had been obtained from the reaction of Na[N-(SiMe$_3$)$_2$] with PhCN (21). Hence, Na[*N*-*t*-Bu(SiMe$_3$)] (**B**) was treated with PhCN in Et$_2$O–hexane at low temperature; an inseparable mixture of starting materials and insertion products was formed. Various attempts to isolate the sodium benzamidinate (the presence of which was inferred by means of ^{13}C NMR spectroscopy of the reaction mixture (δ 174.8 NCN)) failed. It may be that some of the unidentified products consisted of oligomerized PhCN, as in the case of treating PhCN with Li-*n*-Bu (10, 22). In contrast, when the reaction was carried out in Et$_2$O, the expected product, [Na{μ-*cis*-N(*t*-Bu)C(Ph)N(SiMe$_3$)}(OEt$_2$)]$_2$ (**4**), was obtained (eq. [1]).

$$[1]\quad [Na\{N\text{-}t\text{-}Bu(SiMe_3)\}]_3 + 3PhCN \xrightarrow{Et_2O} 3/2[Na\{\mu\text{-}cis\text{-}N(t\text{-}Bu)C(Ph)N(SiMe_3)\}(OEt_2)]_2$$

(**4**, 69%, X-ray)

The sodium benzamidinate **4** was crystallized from the reaction mixture at –25 °C. An ORTEP representation of its molecular structure is shown in Fig. 2. Selected bond distances (Å) and angles (°), together with data for the related compound, [Na{μ-N(SiMe$_3$)C(Ph)N(SiMe$_3$)}(OEt$_2$)]$_2$(OEt$_2$) (**7**) (21), are listed in Table 3.

There is disorder between the silicon and carbon atoms (Si2 and C25) attached to N3 and N4, respectively, of one of the benzamidinato ligands. The N-silylated, four-coordinate nitrogen atom N1 bridges the sodium atoms Na1 and Na2, whereas the *tert*-butyl-bound nitrogen atom N2 is in a three-coordinate environment. Thus, the ligand is both N1,N2-chelating and N1-bridging. The difference between the Na1—N bond lengths of the bridging (N1) and terminal (N2) atoms is 0.38 Å, whereas the corresponding value for compound **7** is 0.19 Å (21). While the angle N1-Na1-N2 is similar in **4** and **7**, the angle N1-C1-N2 is slightly smaller in **4** than in **7** (21). The dihedral angle between the C2-C7 phenyl ring plane and the N1-C1-N2 plane is 78.1°.

Synthesis and characterization of [Sn{*N*(*t*-Bu)C(Ph)N(SiMe$_3$)}$_2$] (5)

As indicated in Scheme 1, the reaction between **1** and SnCl$_2$ in diethyl ether yielded crystalline [Sn{N(*t*-Bu)C(Ph)N(SiMe$_3$)}$_2$] (**5**), which was characterized by ele-

© 2006 NRC Canada

Fig. 2. Molecular structure of [Na{μ-*cis*-N(*t*-Bu)C(Ph)N(SiMe$_3$)}(OEt$_2$)]$_2$ (**4**) (20% ellipsoids, H atoms are omitted for clarity).

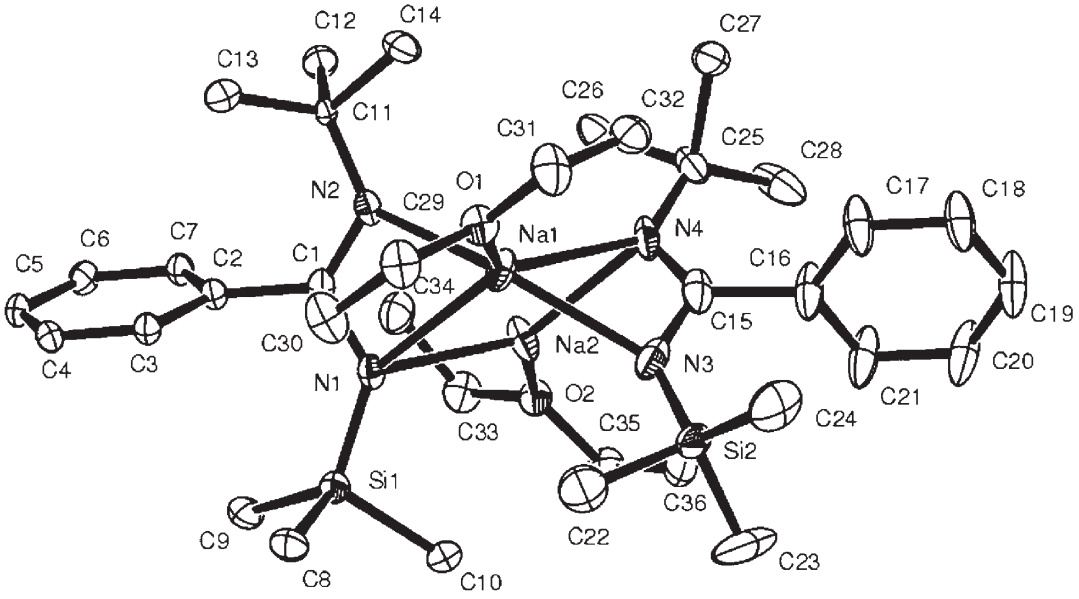


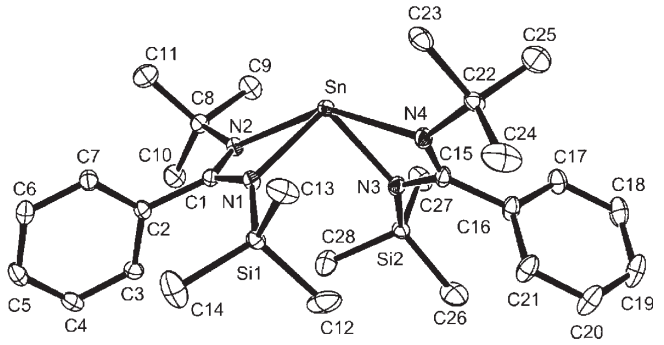
Table 3. Selected bond distances (Å) and angles (°) for compounds **4** and [Na{μ-N(SiMe$_3$)C(Ph)N-(SiMe$_3$)}(OEt$_2$)]$_2$(OEt$_2$) (**7**) (21).

Compounds	**4**	**7** (21)
Bond distances (Å)		
Na(1)—N(1)	2.752(4)	2.671(5)
Na(1)—N(2)	2.376(4)	2.482(5)
Na(1)—N(3)	2.412(4)	2.426(5)
Na(1)—N(4)	2.758(5)	2.725(5)
Na(2)—N(1)	2.380(4)	2.459(5)
Na(2)—N(4)	2.336(4)	2.397(5)
Bond angles (°)		
N(1)-Na(1)-N(2)	52.07(12)	52.8(2)
N(3)-Na(1)-N(4)	51.02(19)	52.8(2)
N(1)-Na(1)-N(4)	100.02(12)	105.9(2)
N(1)-Na(2)-N(4)	127.07(16)	124.9(2)
N(1)-C(1)-N(2)	118.3(3)	121.0(5)
N(3)-C(15)-N(4)	118.8(5)	121.0(5)

mental analysis, multinuclear NMR spectra in C_6D_6, and its EI mass spectrum. The ^{119}Sn NMR chemical shift value of δ –258.5 for **5** may be compared with the δ –387 for the tin(II) azaallyl Sn[N(SiMe$_3$)C(*t*-Bu)C(H)SiMe$_3$]$_2$, which like **5** has a four-coordinate tin(II) atom at the spiro junction of two strained four-membered rings (23).

An ORTEP representation of complex **5** is depicted in Fig. 3. A list of selected bond distances (Å) and angles (°), together with complementary data on [Sn{N(SiMe$_3$)C(Ph)N-(SiMe$_3$)}$_2$] (**8**) (24), is presented in Table 4.

Fig. 3. Molecular structure of [Sn{*N*-*t*-BuC(Ph)N(SiMe$_3$)}$_2$] (**5**) (20% ellipsoids, H atoms are omitted for clarity).



Crystalline **5** is a monomer with N,N′-chelating benzamidinato ligands. In each of the latter, there is unresolved end-for-end disorder of the SiMe$_3$ and CMe$_3$ groups: 0.86:0.14 for Si1 and C8, and 0.65:0.35 for Si2 and C22; bond lengths and angles involving these atoms are therefore unreliable. The structure of **5** is closely similar to that of **8** (24). The geometric parameters of each of the two Sn-N-C-N′ rings in both **5** and **8** are almost identical. The dihedral angle between the N1-Sn-N2 and N3-Sn-N4 planes in **5** is 86°, while that between each N-C-N plane and the attached aromatic C_6 plane is ca. 78°. There clearly is a stereochemically active lone pair of electrons at the Sn atom.

Other Sn(II) benzamidinates related to **5** and **8** (24) that have been reported include [Sn{N(SiMe$_3$)C(Ph)NC-(Ph)=C(SiMe$_3$)$_2$}$_2$] (13*d*), [Sn{N(SiMe$_2$Ph)C(Ph)N(SiMe$_2$-Ph)}$_2$] (24), [Sn{N(SiMe$_3$)C(Me)N(SiMe$_3$)}$_2$] (25), and [Sn{N(SiMe$_3$)C(C$_6$H$_4$Ph-4)N(Ph)}$_2$] (26).[3]

[3] Supplementary data for this article are available on the journal Web site (http://canjchem.nrc.ca) or may be purchased from the Depository of Unpublished Data, Document Delivery, CISTI, National Research Council Canada, Ottawa, ON K1A 0R6, Canada. DUD 5000. For more information on obtaining material refer to http://cisti-icist.nrc-cnrc.gc.ca/irm/unpub_e.shtml. CCDC 273350–273352 contain the crystallographic data for this manuscript. These data can be obtained, free of charge, via http://www.ccdc.cam.ac.uk/conts/retrieving.html (Or from the Cambridge Crystallographic Data Centre, 12 Union Road, Cambridge CB2 1EZ, UK; fax +44 1223 336033; or deposit@ccdc.cam.ac.uk).

© 2006 NRC Canada

Table 4. Selected bond distances (Å) and angles (°) for **5** and [Sn{N($SiMe_3$)C(Ph)N($SiMe_3$)}$_2$] (**8**) (24).

Compounds	**5**	**8** (24)
Bond distances (Å)		
Sn—N(1,3)	2.224(2), 2.229(2)	2.239(2), 2.245(2)
Sn—N(2,4)	2.384(2), 2.382(2)	2.375(2), 2.374(4)
Bond angles (°)		
N(1)-Sn-N(3)	94.9(1)	93.3(1)
N(2)-Sn-N(3)	97.5(1)	95.3(1)
N(2)-Sn-N(4)	146.3(1)	143.1(1)
N(1)-Sn-N(4)	98.1(1)	94.2(1)
N(1,3)-Sn-N(2,4)	58.2(1)	58.7 (1) and 58.9(1)
N(1)-C(1)-N(2) [N(4)-C(15)-N(3)]	115.1(2)	117.2(2) [117.4(2)]

Conclusions

Five new crystalline benzamidinates bearing the C_1 symmetric [N(*t*-Bu)C(R)N($SiMe_3$)]$^-$ ligand (Am$^-$) have been prepared and characterized: [Li(Am)(THF)]$_2$ (**1**), Li(Am)(TMEDA) (**2**), Li(Am) (**3**), [Na(Am)(OEt_2)]$_2$ (**4**), and [Sn(Am)$_2$] (**5**) (R = Ph in **1**, **2**, **4**, and **5**; R = 4-$MeOC_6H_4$ in **3**). The X-ray structures of **1**, **4**, and **5** are reported. The Am$^-$ ligand in **1** and **4** is both chelating and via N($SiMe_3$) is also bridging. The two structures differ in that the core of the planar M-N-CN′-M′ ring is rhomboidal in **1** (M = Li), but C_2 symmetric with unequal contiguous Na—N bond lengths in **4**. The Am$^-$ ligand in **5** functions as a chelate.

Acknowledgments

We thank Dr. A.G. Avent for recording ^{1}H NOE, ^{1}H{^{7}Li} NOE, ^{29}Si-, ^{119}Sn-, and ^{23}Na-NMR spectra, the EU, and the University of Bologna, Bologna, Italy for provision of a studentship for FA, and the UK Engineering and Physical Sciences Research Council (EPSRC) for a fellowship for AVK.

References

1. S. Patai (*Editor*). The chemistry of amidine and amidinates. John Wiley, New York. 1975.
2. (*a*) J. Barker and M. Kilner. Coord. Chem. Rev. **133**, 219 (1994); (*b*) F.T. Edelmann. Coord. Chem. Rev. **137**, 403 (1994); (*c*) T. Ren. Coord. Chem. Rev. **175**, 43 (1998).
3. V.C. Gibson and S.K. Spitzmesser. Chem. Rev. **103**, 283 (2003).
4. C. Averbuj, E. Tish, and M.S. Eisen. J. Am. Chem. Soc. **120**, 8640 (1998).
5. K.C. Jayaratne and L.R. Sita. J. Am. Chem. Soc. **122**, 958 (2000).
6. (*a*) M.P. Coles and R.F. Jordan. J. Am. Chem. Soc. **119**, 8125 (1997); (*b*) M.P. Coles, D.C. Swenson, R.F. Jordan, and V.G. Young, Jr. Organometallics, **16**, 5183 (1997).
7. Y. Luo, Y. Yao, Q. Shen, J. Sun, and L. Weng. J. Organomet. Chem. **662**, 144 (2002).
8. G. Fraenkel, S. Dayagi, and S. Kobayashi. J. Phys. Chem. **72**, 953 (1968).
9. G. Ergezinger, F. Weller, and K. Dehnicke. Z. Naturforsch. B, **43**, 1621 (1988).
10. A.R. Sanger. Inorg. Nucl. Chem. Lett. **9**, 351 (1973).
11. (*a*) R.P Bush, N.C. Lloyd, and C.A. Pearce. J. Chem. Soc. Chem. Commun. 1270 (1967); (*b*) R. Brüning, W. Kalk, and I. Schumann-Ruidisch. Z. Naturforsch. B, **23**, 307 (1968).
12. F. Antolini, P.B. Hitchcock, A.V. Khvostov, and M.F. Lappert. Eur. J. Inorg. Chem. 3391 (2003).
13. (*a*) P.B. Hitchcock, M.F. Lappert, and D.-S. Liu. J. Organomet. Chem. **488**, 241 (1995); (*b*) W.M. Boesveld, P.B. Hitchcock, and M.F. Lappert. J. Chem. Soc. Dalton Trans. 4041 (1999); (*c*) W.M. Boesveld, P.B. Hitchcock, and M.F. Lappert. Angew. Chem. Int. Ed. **39**, 222 (2000); (*d*) P.B. Hitchcock, M.F. Lappert, and M. Layh. J. Chem. Soc. Dalton Trans. 3113 (1998); (*e*) C.F. Caro, P.B. Hitchcock, M.F. Lappert, and M. Layh. Chem. Commun. (Cambridge), 1297 (1998); (*f*) P.B. Hitchcock, M.F. Lappert, M. Layh, D.-S. Liu, R. Sablong, and T. Shun. J. Chem. Soc. Dalton Trans. 2301 (2000); (*g*) D. Doyle, Yu.K. Gun'ko, P.B. Hitchcock, and M.F. Lappert. J. Chem. Soc. Dalton Trans. 4093 (2000); (*h*) W.M. Boesveld, P.B. Hitchcock, and M.F. Lappert. J. Chem. Soc. Perkin Trans. 1, 1103 (2001); (*i*) P.B. Hitchcock, M.F. Lappert, and X.-H. Wei. J. Organomet. Chem. **683**, 83 (2003).
14. (*a*) D. Mootz, A. Zinnius, and B. Böttcher. Angew. Chem. Int. Ed. Engl. **8**, 378 (1969); (*b*) R.D. Rogers, J.L. Atwood, and R. Grüning. J. Organomet. Chem. **157**, 229 (1978).
15. G.M. Sheldrick. SHELXL-97 [computer program]. University of Göttingen, Göttingen, Germany. 1997.
16. J. Barker, D. Barr, N.D.R. Barnett, W. Clegg, I. Cragg-Hine, M.G. Davidson, R.P. Davies, S.M. Hodgson, J.A.K. Howard, M. Kilner, C.W. Lehmann, I. Lopez-Solera, R.E. Mulvey, P.R. Raithby, and R. Snaith. J. Chem. Soc. Dalton Trans. 951 (1997).
17. J.A.R. Schmidt and J. Arnold. Chem. Commun. (Cambridge), 2149 (1999).
18. K. Dehnicke. Chem. Ztg. **114**, 5000 (1990).
19. M. Wedler, F. Knösel, U. Pieper, D. Stalke, F.T. Edelmann, and H.-D. Amberger. Chem. Ber. **125**, 2171 (1992).
20. (*a*) C.L. Boyd, B.R. Tyrrell, and P. Mountford. Acta Crystallogr. Sect. E: Struct. Rep. Online, **58**, m597 (2002); (*b*) H.-B. Tong, X.-H. Wei, D.-S. Liu, and S.-P. Huang. Acta Crystallogr. Sect. E: Struct. Rep. Online, **60**, m825 (2004); (*c*) J.-F. Li, S.-P. Huang, L.-H. Weng, and D.-S. Liu. Eur. J. Inorg. Chem. 810 (2003); (*d*) C. Knapp, E. Lork, P.G. Watson, and R. Mews. Inorg. Chem. **41**, 2014 (2002); (*e*) M.S. Eisen and M. Kapon. J. Chem. Soc. Dalton Trans. 3507 (1994); (*f*) V. Volkis, E. Nelkenbaum, A. Lisovski, G. Hasson, R. Semiat, M. Kapon, M. Botoshansky, Y. Eishen, and M.S. Eisen. J. Am. Chem. Soc. **125**, 2179 (2003).

© 2006 NRC Canada

21. D. Stalke, M. Wedler, and F.T. Edelmann. J. Organomet. Chem. **431**, C1 (1992).
22. R.P. Davies, P.R. Raithby, G.P. Shields, R. Snaith, and A.E.H. Wheatley. Organometallics, **16**, 2223 (1996).
23. P.B. Hitchcock, J. Hu, M.F. Lappert, M. Layh, and J.R. Severn. J. Chem. Soc. Chem. Commun. 1189 (1997).
24. K.B. Aubrecht, M.A. Hillmyer, and W.B. Tolman. Macromolecules, **35**, 644 (2002).
25. S.R. Foley, Y. Zhou, G.P.A. Yap, and D.S. Richeson. Inorg. Chem. **39**, 924 (2000).
26. U. Kilimann, M. Noltemeyer, and F.T. Edelmann. J. Organomet. Chem. **443**, 35 (1993).

© 2006 NRC Canada

Hexaethylbenzene complexes of ruthenium and manganese — X-ray crystal structures and NMR spectra of $[(HEB)_2Ru_2(\mu\text{-}Cl)_3][C_5(CO_2Me)_5]$, $[(HEB)Ru(H_2O)_3][BF_4]_2$, $(HEB)RuCl_2[P(OMe)_3]$, *trans*-$RuCl_2(PMe_3)_4$, and $(HEB)Mn(CO)_2Br$[1]

Hari K. Gupta, Philippa E. Lock, Nada Reginato, James F. Britten, and Michael J. McGlinchey

Abstract: Hexaethylbenzene (HEB) and $[(p\text{-cymene})RuCl_2]_2$ react in the melt to yield $[(HEB)RuCl_2]_2$ (**6**), the NMR spectra of which reveal the presence of $[(HEB)_2Ru_2(\mu\text{-}Cl)_3]Cl$ in solution. In $[(HEB)_2Ru_2(\mu\text{-}Cl)_3][C_5(CO_2Me)_5]$ (**7**), the cation has D_{3h} symmetry with alternating proximal and distal ethyl groups. Bridge cleavage of **6** with trimethyl phosphite or with trimethylphosphine gives $(HEB)RuCl_2[P(OMe)_3]$ (**9**) or $(HEB)RuCl_2(PMe_3)$ (**10**), respectively. The latter reaction also yields $RuCl_2(Me_3P)_4$ (**11**), whose structure represents a relatively rare example of a crystallographically characterized trans isomer of this type. In **9**, five of the ethyl ligands are distal, whereas in **10** all six substituents are distal. Attempts to prepare the sandwich dication $[(HEB)_2Ru]^{2+}$ gave instead $[(HEB)Ru(H_2O)_3](BF_4)_2$ (**8**), whose NMR and X-ray data reveal the 1,3,5-distal–2,4,6-proximal arrangement of ethyls both in the solid state and in solution. $(HEB)Mn(CO)_2Br$ (**13**) likewise adopts the 1,3,5-distal–2,4,6-proximal structure in the solid state but, surprisingly, there is no evidence for slowed ethyl rotation in solution.

Key words: hexaethylbenzene conformations, hindered rotations, crystallography, NMR, ruthenium, manganese.

Résumé : L'hexaéthylbenzène (HEB) et le $[(p\text{-cymène})RuCl_2]_2$ réagissent à l'état fondu pour conduire à la formation de $[(HEB)RuCl_2]_2$ (**6**) dont le spectre RMN en solution révèle la présence de $[(HEB)_2Ru_2(\mu\text{-}Cl)_3]Cl$. Dans le $[(HEB)_2Ru_2(\mu\text{-}Cl)_3][C_5(CO_2Me)_5]$ (**7**), le cation est de symétrie D_{3h} avec, en alternance, des groupes éthyles de type distal et proximal. Le clivage du pont du composé **6** avec du phosphite de triméthyle ou avec de la triméthylphosphine conduit, selon le cas, au $(HEB)RuCl_2[P(OMe)_3]$ (**9**) ou au $(HEB)RuCl_2(PMe_3)$ (**10**). La dernière réaction fournit aussi du $RuCl_2(Me_3P)_4$ (**11**) dont la structure correspond à un rare exemple d'un isomère trans de type à être caractérisé par cristallographie. Dans le composé **9**, cinq sur six ligands sont de type distal alors que dans le composé **10** les six ligands sont tous de type distal. Des essais en vue de préparer le dication sandwich $[(HEB)_2Ru]^{2+}$ on plutôt conduit à la formation de $[(HEB)Ru(H_2O)_3](BF_4)_2$ (**8**) dans lequel, selon les données de la RMN et de la diffraction des rayons X, on observe un arrangement 1,3,5-distal–2,4,6-proximal des groupes éthyles tant à l'état solide qu'en solution. La structure du $(HEB)Mn(CO_2)Br$ (**13**) adopte aussi une structure 1,3,5-distal–2,4,6-proximal à l'état solide, mais il est surprenant d'observer que, en solution, on n'observe aucune donnée laissant croire à un ralentissement de la rotation des groupes éthyles.

Mots clés : conformation de l'hexaéthylbenzène, rotations empêchées, cristallographie, RMN, ruthénium, manganèse.

[Traduit par la Rédaction]

Received 15 June 2005. Published on the NRC Research Press Web site at http://canjchem.nrc.ca on 17 March 2006.

This paper is dedicated to Professor Arthur Carty in recognition of his major achievements in inorganic and organometallic chemistry, and also for his many outstanding contributions to science in Canada.

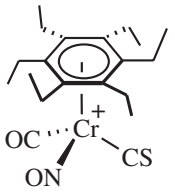
H.K. Gupta, P.E. Lock, N. Reginato, and J.F. Britten. Department of Chemistry, McMaster University, Hamilton, ON L8S 4M1, Canada.
M.J. McGlinchey.[2] School of Chemistry and Chemical Biology, University College Dublin, Belfield, Dublin 4, Ireland.

[1]This article is part of a Special Issue dedicated to Professor Arthur Carty.
[2]Corresponding author (e-mail: michael.mcglinchey@ucd.ie).

 doi:10.1139/V06-005 © 2006 NRC Canada

Introduction

Hexaethylbenzene (HEB) is a conformationally versatile ligand! When bonded to organometallic fragments, such as $Cr(CO)_3$ (1), $[Fe(C_5H_5)]^+$ (2), or $[Mo(CO)_3Cl]^+$ (3), the ethyl groups can adopt a variety of conformational patterns (4). The favoured structure — and the one found for the free ligand (5, 6) — is the 1,3,5-distal–2,4,6-proximal isomer exemplified by $[(\eta^6\text{-HEB})Cr(CO)(CS)NO]^+$ (**1**).



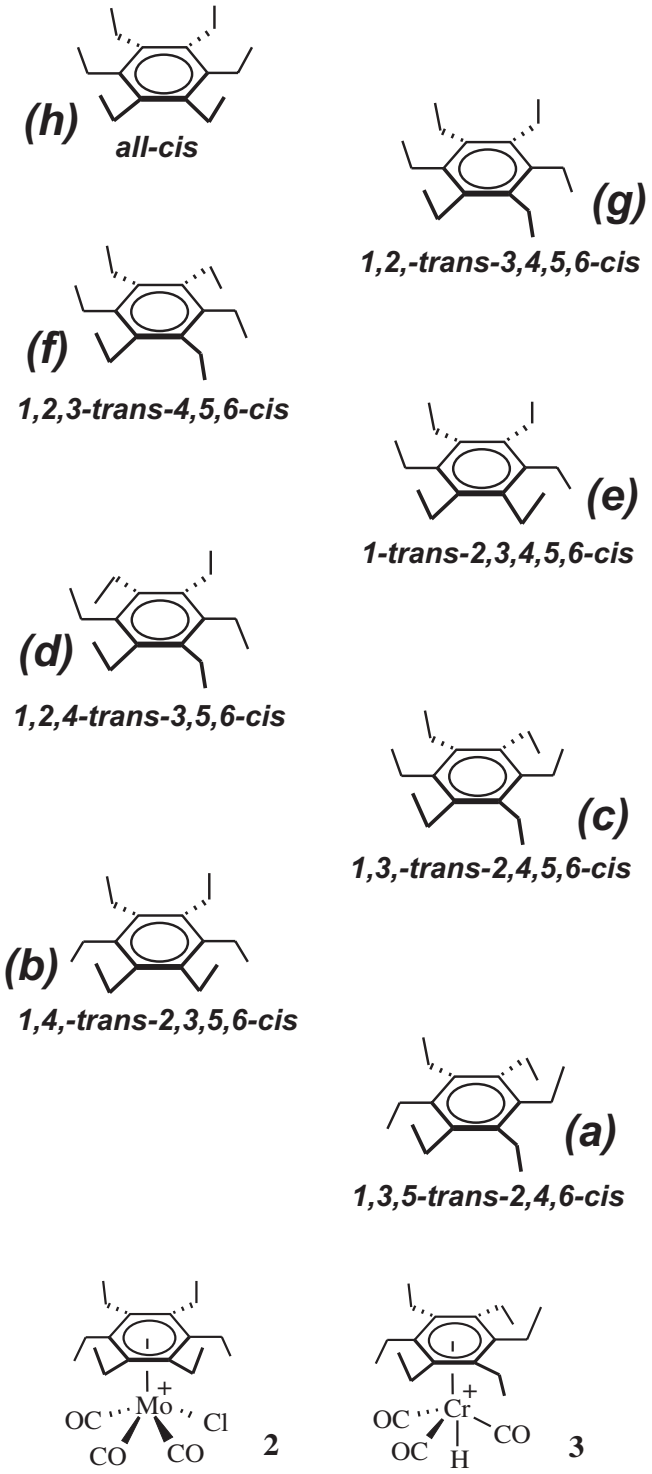
1

This particular system, which possesses a chiral tripod, was specifically designed to probe the molecular dynamics of both the HEB ligand and also the ML_3 fragment (7). In the series $(\eta^6\text{-HEB})Cr(CO)L'L''$, where L′ and L″ are CO, CS, or NO^+, the ethyls exhibit uncorrelated proximal–distal exchange with a $\Delta G^{\ddagger}$ value of ≈11.5 kcal mol^{-1} (6–8) (1 cal = 4.184 J). In contrast, tripodal rotation has a markedly lower barrier (≈9.5 kcal mol^{-1}) (7, 8). These studies are complemented, not only by our own work on (pentaethylacetophenone)$Cr(CO)_3$ (9), but also by an elegant series of experiments by Kilway and Siegel (10) who independently measured the alkyl and tripodal rotation barriers in 1,4-bis(4,4-dimethyl-3-oxopentyl)-2,3,5,6-tetraethylbenzene and its tricarbonylchromium complex.

The relative energies of the conformations of hexaethylbenzene have been computed; these are depicted in Fig. 1 together with the labeling scheme originally used by Mislow and co-workers (6). Moreover, it has been shown that in the molecules $(\eta^6\text{-HEB})Cr(CO)_2(PR_3)$, there is a clear correlation between the size of the phosphine and the ratio of distal to proximal ethyl substituents. Thus, X-ray crystallographic data for the complexes $(\eta^6\text{-HEB})Cr(CO)_2(PMe_3)$ (11), $(\eta^6\text{-HEB})Cr(CO)_2(PEt_3)$ (12), and $(\eta^6\text{-HEB})Cr(CO)_2(PPh_3)$ (6), yield structures *c*, *e*, and *h*, respectively.

The ^1H and ^{13}C NMR data for $(\eta^6\text{-HEB})ML_n$ complexes provide a convenient probe for the symmetry of the system. For example, Flood's low-temperature NMR measurements have shown that protonation of a series of $(\eta^6\text{-arene})Cr(CO)_2PR_3$ complexes leads to a square-based pyramidal structure for the corresponding $[(\eta^6\text{-arene})Cr(CO)_2(PR_3)H]^+$ systems (13); likewise, protonation of $(\eta^6\text{-}C_6H_5OMe)Cr(CO)_3$ yields a 2:1 pattern for the ^{13}CO resonances, consistent with a square-pyramidal $Cr(CO)_3H$ unit (14). Since the X-ray crystal structure of $[(\eta^6\text{-HEB})Mo(CO)_3Cl][MoCl_6]$ (**2**) reveals that the ML_4 moiety is square pyramidal and that the hexaethylbenzene ligand in the cation adopts conformer *b* (Fig. 1) (3), one might have anticipated a similar arrangement of ethyls for $[(\eta^6\text{-HEB})Cr(CO)_3H]^+$ (**3**). However, the ^1H and ^{13}C NMR data for **3** show unambiguously that the ethyls adopt the 1,3,5-distal–2,4,6-proximal conformation *a* (Fig. 1), indicating that the proton has attacked along the threefold axis of the molecule (15).

Fig. 1. Relative energies of conformers of hexaethylbenzene (HEB) (data from ref. 6).



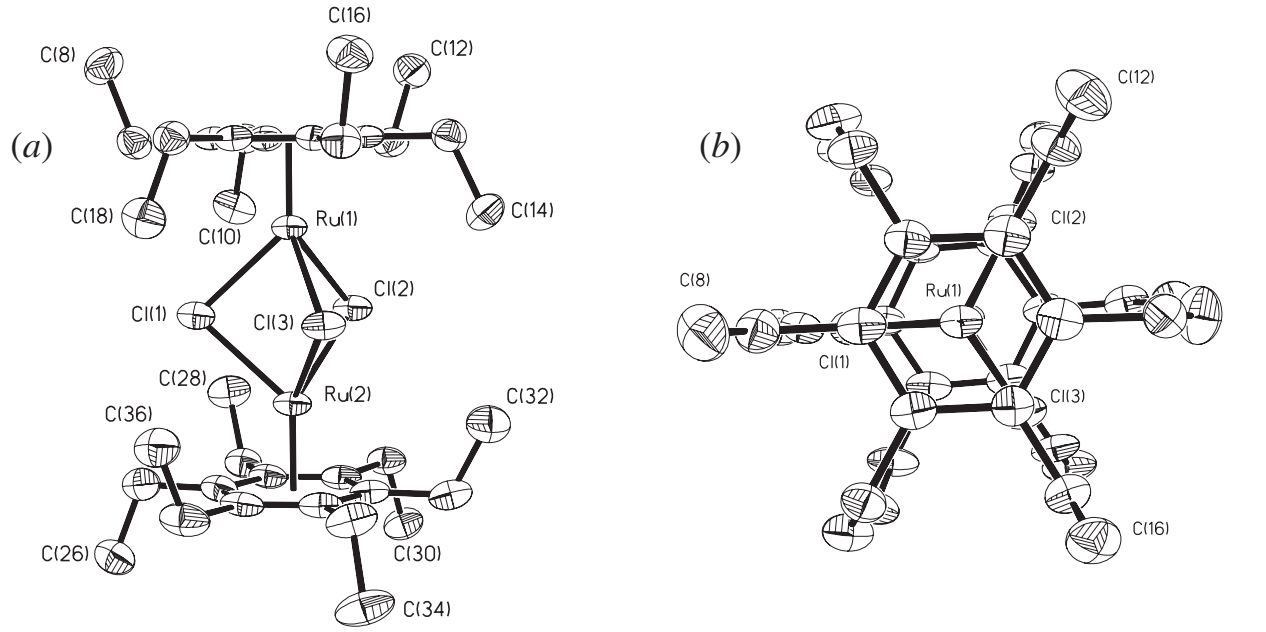
2

3

In a continuation of our ongoing program aimed at rationalizing the structures and dynamic NMR behaviour of hexaethylbenzene–metal complexes (4), and in light of our more recent work (16) on ruthenium complexes of trindane, (tris(cyclopentano)benzene, the condensation trimer of cyclopentanone), we had initiated a study of the syntheses, NMR spectra, and X-ray crystal structures of a series of

© 2006 NRC Canada

Fig. 2. Molecular structure of the cation $[(\eta^6\text{-HEB})_2Ru_2(\mu\text{-}Cl)_3]^+$ in **7** showing (*a*) the alternating proximal and distal ethyl groups and (*b*) eclipsing of the tripod of chlorines relative to the distal ethyl groups. Thermal ellipsoids are drawn at the 50% probability level, and hydrogen atoms are omitted for clarity.

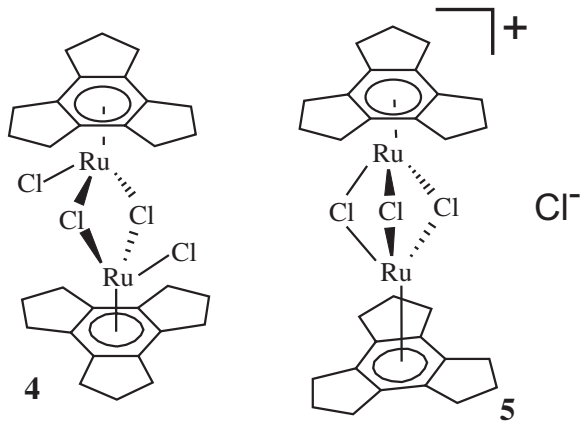


$(C_6Et_6)RuCl_2L$ complexes to explore whether their ^1H and ^{13}C NMR spectra correlated with the solid state structures of these molecules. In a 1997 review on ruthenium–arene systems (17), Bennett made passing mention of some HEB–Ru complexes and, more recently, he and his co-workers (18) have published a fuller account of this work. This prompts us to describe our own findings, which, in some cases, overlap with and confirm Bennett's observations. We therefore describe in detail only those aspects that have not hitherto been reported.

Results and discussion

Molecules of the type $[(\eta^6\text{-arene})RuCl_2]_2$ are generally prepared by the replacement of cymene in $[(\eta^6\text{-cymene})RuCl_2]_2$ (19); this latter system is readily available by reaction of $RuCl_3$ with dipentene, an inexpensive diene (20). We have previously reported (16) the synthesis, X-ray crystal structure, and variable-temperature NMR spectra of $[(\eta^6\text{-trindane})RuCl_2]_2$ (**4**), which dissociates in polar solvents into $[(\eta^6\text{-trindane})_2Ru_2(\mu\text{-}Cl)_3]^+$ Cl^- (**5**). Although trindane is a hexa-alkylated arene, and bears a superficial resemblance to hexaethylbenzene, it lacks the subtle stereochemical probes for molecular symmetry that HEB can, in principle, provide.

When $[(\eta^6\text{-cymene})RuCl_2]_2$ and hexaethylbenzene were melted together at 170 °C in a sealed tube, a product **6**, with empirical formula $(C_6Et_6)RuCl_2$, was obtained. The room-temperature ^1H and ^{13}C NMR spectra of **6** exhibited resonances for only a single ethyl environment, but at –90 °C there was clear decoalescence into two equally populated ethyl groups. Such behaviour appeared to be analogous to that of the trindane–ruthenium complexes (**4** and **5**), whereby dissociation into a triply bridged cation and a chloride anion had occurred. Moreover, the coalescence behaviour of these ethyl resonances is entirely reminiscent of the

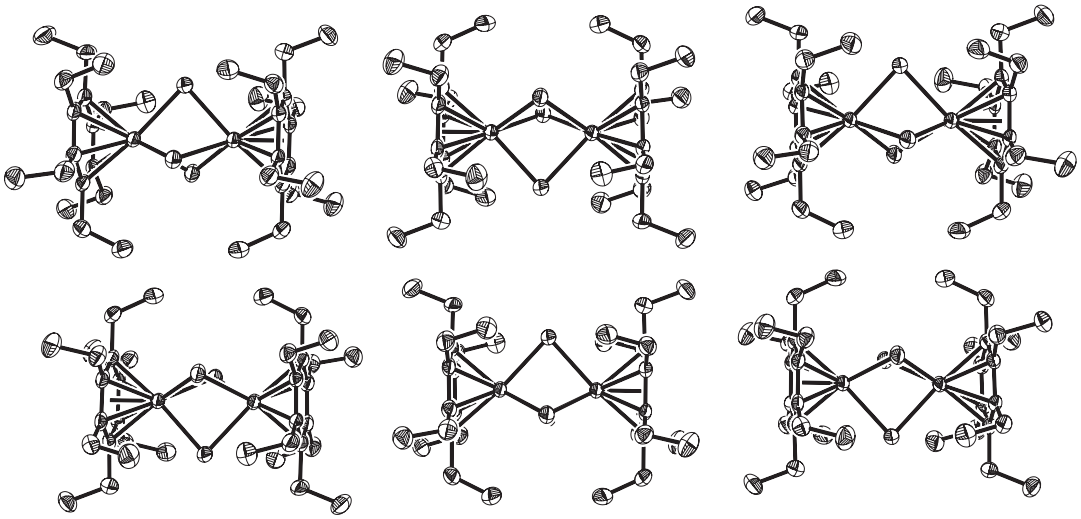


previously discussed systems that adopt the 1,3,5-distal–2,4,6-proximal conformation; gratifyingly, the calculated $\Delta G^{\ddagger}$ value of 11.5 ± 0.4 kcal mol^{-1} is in the normal range for such ethyl rotation barriers. We were therefore drawn to the conclusion that **6** exists in solution primarily as $[(\eta^6\text{-HEB})_2Ru_2(\mu\text{-}Cl)_3]^+Cl^-$, and that the arene adopts conformation *a* (Fig. 1).

To determine whether this same structure could be found in the solid state, **6** was treated with the potassium salt of penta(carbomethoxy)cyclopentadienide, $K[C_5(CO_2Me)_5]$ (21). Removal of KCl and recrystallization from hexane–dichloromethane yielded X-ray quality crystals of $[(\eta^6\text{-HEB})_2Ru_2(\mu\text{-}Cl)_3][C_5(CO_2Me)_5]$ (**7**), and the structure of the cation appears as Fig. 2. $[(\eta^6\text{-HEB})_2Ru_2(\mu\text{-}Cl)_3]^+$ has effective D_{3h} symmetry in which each HEB ligand adopts the alternating proximal–distal arrangement of ethyls such that the three bridging chlorines eclipse distal substituents and so minimize steric interactions.

© 2006 NRC Canada

Fig. 3. Packing of the $[(\eta^6\text{-HEB})_2Ru_2(\mu\text{-Cl})_3]^+$ cations in **7**.



The ruthenium–arene centroid distance of 1.648 Å is comparable to those observed in systems such as $[(\eta^6\text{-arene})_2Ru_2(\mu\text{-Cl})_3]^+$, where the arene is benzene, toluene, or cymene (22). Interestingly, in $[(\eta^6\text{-benzene})_2Ru_2(\mu\text{-Cl})_3]^+$ the $RuCl_3$ tripod is staggered with respect to the benzene ligand, while in $[(\eta^6\text{-cymene})_2Ru_2(\mu\text{-Cl})_3]^+$ the chlorine atoms eclipse arene ring carbon atoms. As predicted by molecular orbital calculations at the extended Hückel level (22*a*), the methylene substituents are bent slightly towards the metal atoms (an average of 2.5° for distal ethyls and 0.5° for proximal ethyl groups). This enhances the overlap between the arene π manifold and the ruthenium d orbitals. This minor distortion is, however, not as significant as the 6° bend observed in $[(\eta^6\text{-benzene})_2Ru_2(\mu\text{-Cl})_3]^+$ (22*a*). The average Ru—Cl distance in **7** is 2.442 Å and the average Ru—C(arene) distance is 2.183 Å, similar to those observed, for example, in $[(\eta^6\text{-trindane})RuCl_2]_2$ (**4**) (16). Thus, the Ru—Cl distance is similar to that found in the other arene systems mentioned above, but the Ru—C(arene) bond is slightly longer than that in $[(\eta^6\text{-benzene})_2Ru_2(\mu\text{-Cl})_3]^+$ (2.163 Å) or in $[(\eta^6\text{-cymene})_2Ru_2(\mu\text{-Cl})_3]^+$ (2.168 Å) (22).

The penta(carbomethoxy)cyclopentadienide counterion in the structure of **7** is highly disordered, as is sometimes the case for this isolated anion in crystal structures (21), and it has not proved possible to determine its conformation in the solid state. Nevertheless, it is evident from an examination of the packing that the anions and cations form alternating layers as is also seen for $[C_7H_7][C_5(CO_2Me)_5]$ (21). The program PLATON (23) was used to subtract the averaged diffractional contribution of the disordered $[C_5(CO_2Me)_5]^-$ anion from the X-ray intensity data collected for **7**. This not only allowed a more accurate determination of the structure of the $[(\eta^6\text{-HEB})_2Ru_2(\mu\text{-Cl})_3]^+$ cation, but also reveals (see Fig. 3) that the cations are arranged in layers such that the intermolecular contacts between distal ethyls are minimized.

The structure of the $[(\eta^6\text{-HEB})_2Ru_2(\mu\text{-Cl})_3]^+$ cation in **7** parallels closely the data previously reported by Bennett and co-workers (18) for the corresponding hexafluorophosphate salt. Those workers had also obtained independently synthesized **6** by treating $(\eta^6\text{-HEB})Ru(\eta^4\text{-1,5-COD})$ with HCl and had shown definitively that, in the solid state, it adopted the doubly bridged structure $[(\eta^6\text{-HEB})Ru(\mu\text{-Cl})Cl]_2$, akin to **4**, whereby all the ethyl substituents are distal, as in conformation *h* (Fig. 1). Finally, since the variable-temperature NMR spectra of **7** in the ethyl region parallel exactly the behavior of **6**, one may conclude that the triply bridged isomer is the major species present in solution in both cases.

We have previously prepared the sandwich cation $[(\eta^6\text{-trindane})_2Ru]^{2+}$ by treatment of $[(\eta^6\text{-trindane})RuCl_2]_2$ with $AgBF_4$ in acetone; the presumed intermediate, $[(\eta^6\text{-trindane})Ru(acetone)_3]^{2+}$, reacted with excess trindane to yield the $[bis(\eta^6\text{-arene})Ru]^{2+}$ dication (16). Interestingly, the $[(\eta^6\text{-arene})Ru(solvent)_3]^{2+}$ structure type is rare; one such molecule for which a crystal structure has been reported is $[(\eta^6\text{-1,3,5-}C_6H_3Me_3)Ru(acetone)_3][BF_4]_2$ in which two of the acetone molecules have coupled (24).

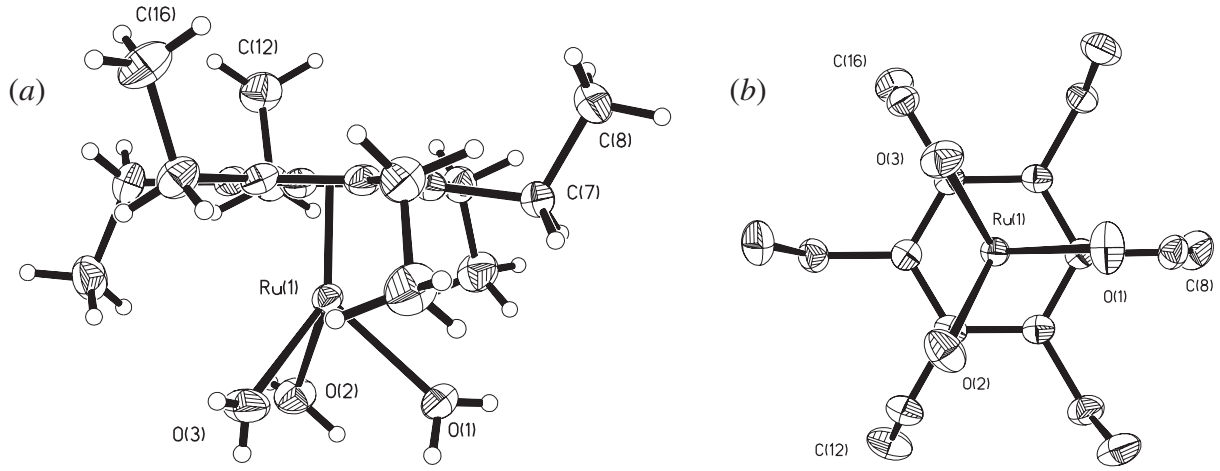
In an attempt to prepare $[(\eta^6\text{-}C_6Et_6)_2Ru]^{2+}$, treatment of "$(C_6Et_6)RuCl_2$" (**6**) with $AgBF_4$ in acetone gave a remarkably stable crystalline material (**8**), whose ^1H and ^{13}C NMR spectra are entirely consistent with a molecule possessing threefold symmetry; once again, at low temperature the familiar pattern of alternating proximal and distal ethyls is apparent. As shown in Fig. 4*a*, the product was characterized by X-ray crystallography as $[(\eta^6\text{-}C_6Et_6)Ru(H_2O)_3][BF_4]_2\cdot H_2O$. In **8**, the cation possesses almost ideal C_{3v} symmetry in which the HEB ligand adopts conformation *a* — the 1,3,5-distal–2,4,6-proximal arrangement — whereby each water ligand is partially encapsulated by two ethyl groups. Figure 3*b* shows the eclipsed tripod of oxygen atoms with respect to the distal ethyl groups. In the closely related structure of $[(\eta^6\text{-}C_6H_6)Ru(H_2O)_3]^{2+}$, the RuO_3 tripod is staggered with respect to the benzene ligand (25).

The ruthenium–arene centroid distance of 1.650 Å in **8** is in the expected range and, while the average Ru—C(arene) of 2.183 Å is very similar to that seen in **7**, it is slightly longer than that observed in $[(\eta^6\text{-}C_6H_6)Ru(H_2O)_3]^{2+}$ (2.164 Å). Moreover, the average Ru—O distance of 2.145 Å in **8** is also slightly longer than the value of 2.127 Å reported for $[(\eta^6\text{-}C_6H_6)Ru(H_2O)_3]^{2+}$ (25).

There is extensive hydrogen bonding observed in the packing diagram for **8** such that water ligands bonded to ruthenium have contacts to fluorine atoms of tetrafluoroborate

© 2006 NRC Canada

Fig. 4. Molecular structure of the cation $[(\eta^6\text{-HEB})Ru(H_2O)_3]^{2+}$ in **7** showing (*a*) the alternating proximal and distal ethyl groups and (*b*) eclipsing of the tripod of oxygens relative to the distal ethyl groups. Thermal ellipsoids are drawn at the 50% probability level.



anions, and also to lattice water molecules. The lone water of crystallization also has contacts to tetrafluoroborate anions. For example, in one layer, a lattice water molecule has contacts through its hydrogens to two neighbouring BF_4^- anions such that O—H_a is 0.966 Å, and $H_a\cdots F_1$ is 1.889 Å, while the $O\cdots F_1$ distance is 2.742 Å. For the other hydrogen of the same water molecule, O—H_b is 0.822 Å, $H_b\cdots F_2$ is 1.934 Å, and the $O\cdots F_2$ contact is now 2.733 Å. This oxygen also interacts with a neighbouring H_2O ligand bonded to ruthenium, with O···H′ at 1.748 Å, and an O···O′ contact of 2.616 Å. Furthermore, some BF_4^- anions show a long contact to a methylene hydrogen atom of a neighbouring distal ethyl group (e.g., F···H is 2.539 Å). Layers of contacts of the types described above persist throughout the structure, and these interactions are depicted in Fig. 5.

To test the steric limits of the $(\eta^6\text{-HEB})RuL_n$ system, **6** was treated with trimethyl phosphite and with trimethylphosphine to give $(\eta^6\text{-HEB})RuCl_2[P(OMe)_3]$ (**9**) and $(\eta^6\text{-HEB})RuCl_2(PMe_3)$ (**10**), respectively. The ^1H and ^{13}C NMR spectra of both complexes exhibited only a single ethyl environment, even at low temperature. This result suggested that neither molecule possessed the alternating proximal–distal arrangement labelled as *a* in Fig. 1. On the basis of the relative cone angles of $P(OMe)_3$ (107°) and PMe_3 (118°) (26), one might have predicted that the phosphine complex **10** would tend to have the greater number of distal ethyl substituents, and this is indeed the case. As shown in Fig. 6, $(\eta^6\text{-HEB})RuCl_2[P(OMe)_3]$ (**9**) prefers isomer *e* in which there is a single proximal ethyl substituent; in contrast, $(\eta^6\text{-HEB})RuCl_2(PMe_3)$ (**10**) adopts the "all-distal" conformer *h*.

The all-distal structure for $(\eta^6\text{-HEB})RuCl_2(PMe_3)$ (**10**) has already been described by Bennett and co-workers (17, 18, 27) and our data are in accord with theirs. The single proximal ethyl in $(\eta^6\text{-HEB})RuCl_2[P(OMe)_3]$ (**9**) is the one furthest from the relatively bulky phosphite ligand and is analogous to the structure of $(\eta^6\text{-HEB})Cr(CO)_2(PEt_3)$, which likewise exhibits the 5:1 distal-to-proximal ratio (12). In **10**, the $RuCl_2(PMe_3)$ tripod is staggered with respect to the HEB ring, and follows the pattern found in $(\eta^6\text{-HEB})Cr(CO)_2(PPh_3)$, which also adopts conformation *h* (Fig. 1) (6). The orientations of the $RuCl_2(PR_3)$ tripods in **9** and **10** with respect to the HEB ligands are illustrated in Fig. 7. Interestingly, the trimethyl phosphite ligand in **9** crystallizes in a propeller conformation rendering the molecule chiral, whereas in $(\eta^6\text{-HEB})Cr(CO)_2(PEt_3)$ the Et_3P ligand lies in a molecular mirror plane (12).

The reaction of **6** with trimethylphosphine yielded a second crystalline product that was shown by mass spectrometry, and also by ^1H and ^{31}P NMR spectroscopy, to be the known compound *trans*-dichlorotetrakis(trimethylphosphine)-ruthenium(II) (**11**) (28). A search of the Cambridge Crystallographic Database revealed that structures of trans isomers of the type $(Me_3P)_4RuXY$ are rare, although a number of cis complexes have been reported (29). Since we had suitable crystals in hand, the structure was determined and appears as Fig. 8.

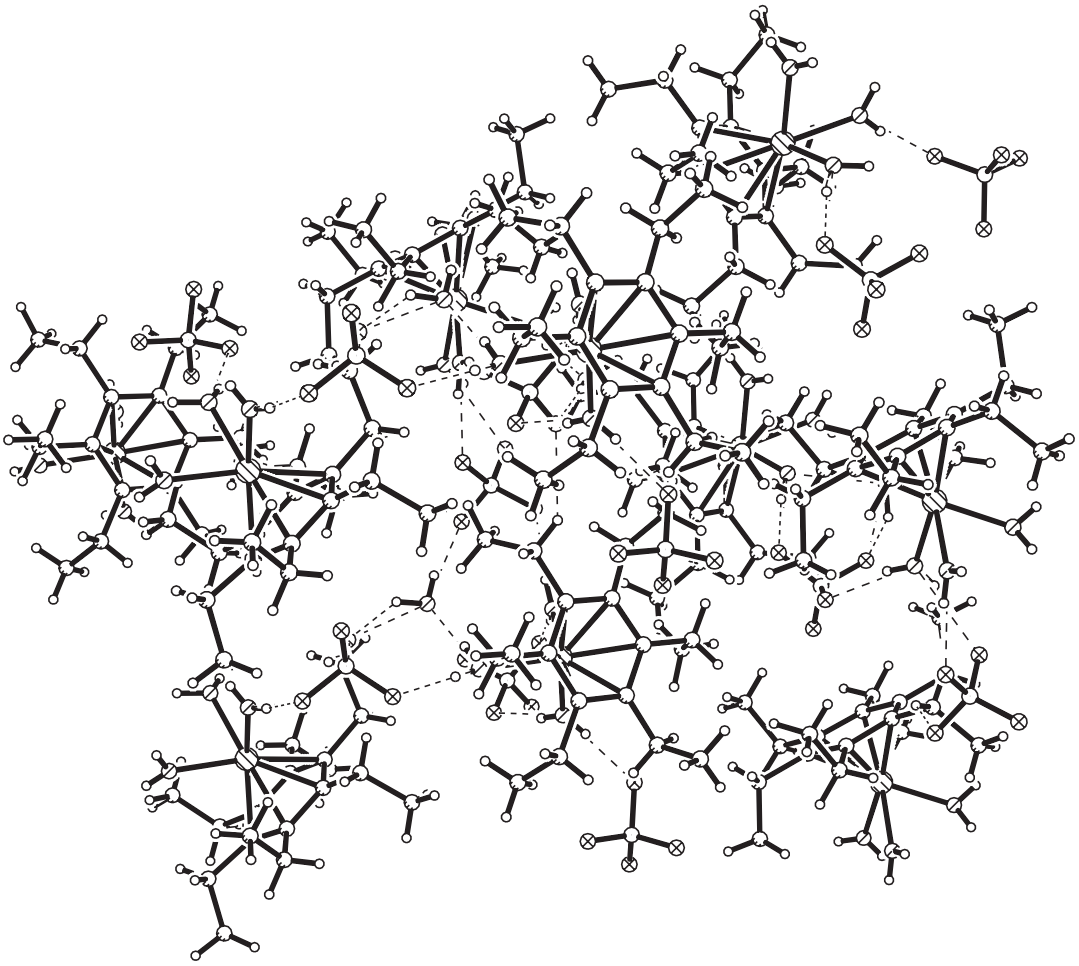
While the structure solves to give two independent half-molecules in the asymmetric unit, the symmetry operator of the space group completes the full molecules, and the successful structure gives the trans isomer. The steric problems that arise with four equatorially disposed trimethylphosphines are immediately evident. The PMe_3 ligands undergo a tetragonal distortion such that they are placed alternately above and below their mean plane. The P-Ru-P angles found in the two independent molecules are 165.86(2)° and 165.38(11)°. The nonlinearity is, however, somewhat less than the corresponding P-Rh-P angles (151.46(5)° and 148.29(5)°) found in $[(Me_3P)_4Rh]^+ Cl^-$ (28), and in the P-Ru-P angle (161.41°) found in $trans\text{-}RuH_2[(C_6H_5)P(OC_2H_5)_2]_4$ (30). Apparently, the out-of-plane distortion of the phosphines in $trans\text{-}(Me_3P)_4RuCl_2$ (**11**) is limited by the presence of the two axial chlorine ligands. The cis P-Ru-P angles are close to 90° (with a range of 90.05(3)° to 92.11(4)°).

In a closely related system, $trans\text{-}(PMe_3)_4Ru(N_3)_2$, the molecule crystallizes in the space group *C*2/*c*. All four phosphine ligands are located individually, and there is no ambiguity about the assignment as a cis or trans isomer; it is clearly a trans system (31). Moreover, the P-Ru-P angles between the *trans*-phosphines (163.1° and 163.4°) agree closely with those found in **11**, and so reinforce the structural assignment presented here.

As was the case with ruthenium, our studies on trindane complexes of manganese (32) led us to prepare the analogous hexaethylbenzene derivatives. The cationic complex

© 2006 NRC Canada

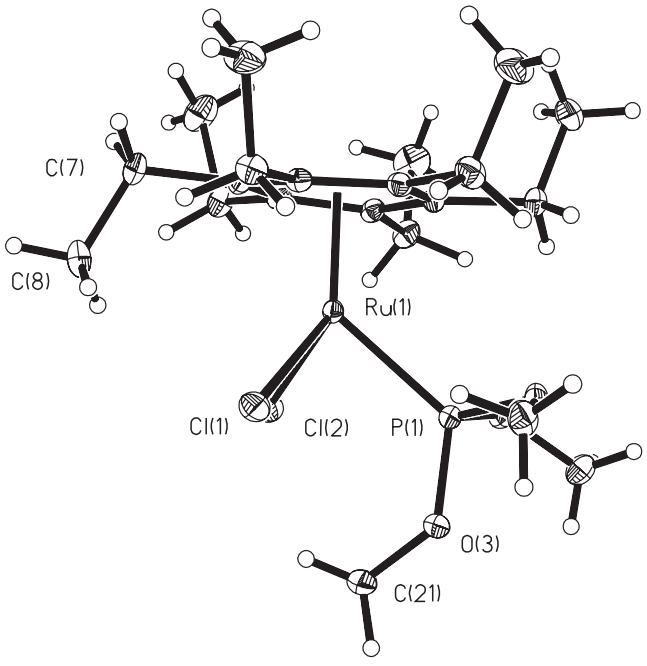
Fig. 5. The extensive hydrogen bonding network in $[(\eta^6\text{-}C_6Et_6)Ru(H_2O)_3][BF_4]_2\cdot H_2O$ (**8**).



$[(HEB)Mn(CO)_3]^+$ behaves entirely analogously to its neutral $(HEB)Cr(CO)_3$ counterpart. The room-temperature ^1H and ^{13}C NMR spectra that exhibit a single ethyl environment show clear decoalescence as the temperature is lowered, and once again reveal that the ligand adopts the favoured 1,3,5-distal–2,4,6-proximal structure; the barrier towards this fluxional behaviour is the usual 11.5 kcal mol^{-1}. With the goal of breaking the threefold symmetry of the tripod, as had been done previously in the $(HEB)Cr(CO)_2L$ series (6–8), $[(HEB)Mn(CO)_3][BF_4]$ (**12**) was treated with trimethylamine *N*-oxide, and subsequently with KBr to yield the neutral complex $(C_6Et_6)Mn(CO)_2Br$ (**13**). (This follows the route described by Eyman and co-workers (33) for the preparation of $(C_6Me_6)Mn(CO)_2Br$.) The ^1H and ^{13}C NMR spectra of the bromo-compound **13** exhibited only a single ethyl environment and were invariant even down to –90 °C. We had anticipated seeing a 2:1:2:1 pattern of ethyl groups attributable to slowed ethyl rotation and slowed tripodal rotation on the NMR timescale; this would have matched the known behaviour of $(HEB)Cr(CO)_2L$, where L is CS or NO^+ (7). However, when the X-ray crystal structure of **13** was determined, it was of the commonly observed 1,3,5-distal–2,4,6-proximal type (see Fig. 9), and it is tempting to propose that several rotameric structures undergo ready exchange with a low barrier in solution, as is known for $[(C_6Et_6)Fe(C_5H_5)]^+$ (2, 34).

In closing, we note that in those cases where the

Fig. 6. Molecular structure of $(\eta^6\text{-}HEB)RuCl_2[P(OMe)_3]$ (**9**) showing the 1-proximal–2,3,4,5,6-distal conformer *e*. Thermal ellipsoids are shown at the 50% probability level.



© 2006 NRC Canada

Fig. 7. Orientations of the $RuCl_2P$ tripods (*a*) almost eclipsed in (η^6-HEB)$RuCl_2[P(OMe)_3]$ (**9**) and (*b*) staggered in (η^6-HEB)$RuCl_2(PMe_3)$ (**10**).

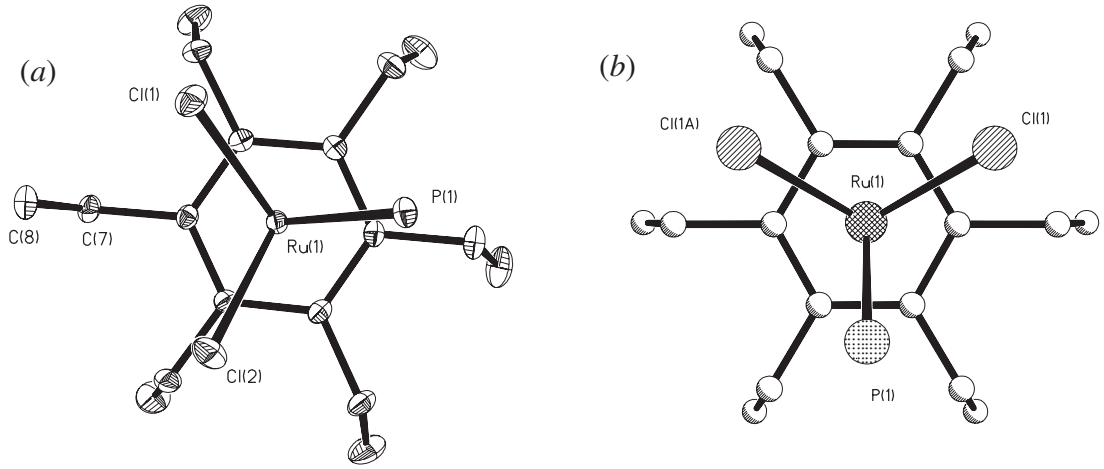


Fig. 8. Molecular structure of *trans*-$(Me_3P)_4RuCl_2$ (**11**) showing both of the independent molecules in the unit cell.

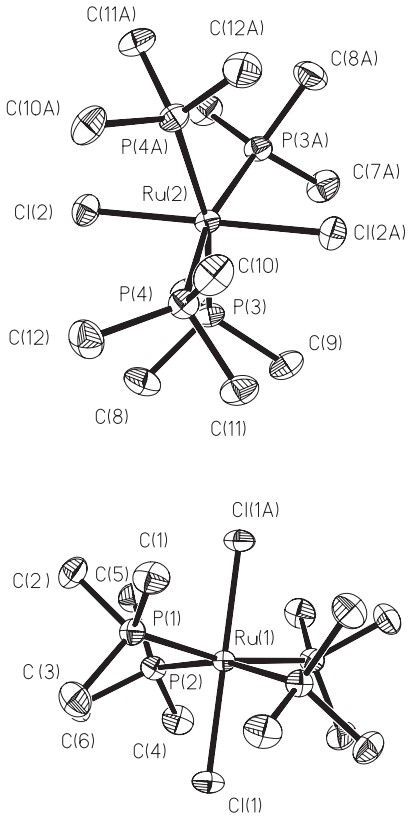
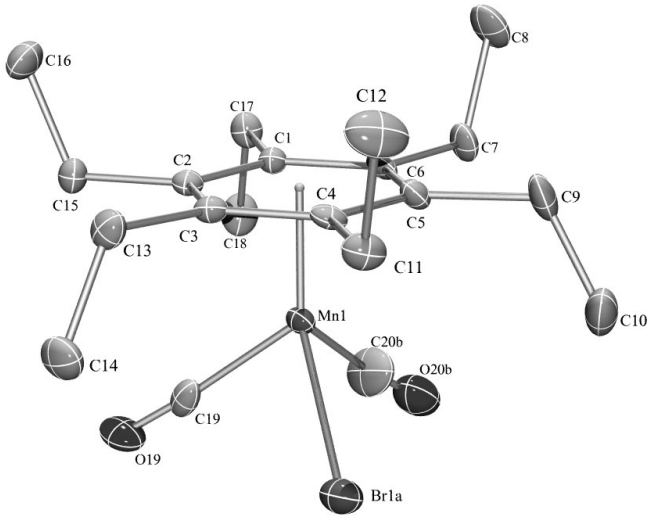


Fig. 9. Molecular structure of (HEB)$Mn(CO)_2Br$ (**13**) showing the alternating proximal and distal ethyl substituents. Thermal ellipsoids are shown at the 30% probability level.



organometallic moiety imposes a particular conformation, such as 1,3,5-distal–2,4,6-proximal arrangement, on a hexaalkylbenzene ligand, this can be of synthetic advantage, and elegant applications in supramolecular chemistry have been described (35).

Experimental section

All reactions were carried out under an atmosphere of dry nitrogen with use of conventional bench top and glovebag techniques. Silica gel (particle size 20–45 μm) was used for flash column chromatography. ^1H, ^{13}C, and ^{31}P NMR spectra were acquired on Bruker DRX 500, AC 300, or AC 200 spectrometers, and were referenced to the residual proton or ^{13}C signal of the solvent, or to external 85% H_3PO_4. Mass spectra (DEI, DCI, and electrospray) were obtained on a VG analytical ZAB-SE spectrometer with an accelerating potential of 8 KV and a resolving power of 10 000. Where applicable, *m*/*z* values listed are for $^{35}Cl/^{102}Ru$ isotopomers; all peak clusters showed correct isotopic abundance patterns. Infrared spectra were recorded on a Bio-Rad FTS-40 spectrometer, using NaCl windows. Melting points (uncorrected) were determined on a Fisher-Johns melting apparatus. Elemental analyses were performed either by Guelph Chemical Laboratories in Guelph, Ontario or by the Microanalytical Laboratory at University College Dublin.

$RuCl_3 \cdot 3H_2O$, $Mn_2(CO)_{10}$, and $AgBF_4$ were purchased from Sigma-Aldrich Chemical Co., Inc., and used as received. $AlCl_3$ was sublimed before use, and [(*p*-cy-

© 2006 NRC Canada

mene)$RuCl_2]_2$ was prepared as described in the literature (20).

Preparation of [(η^6-hexaethylbenzene)$RuCl_2]_2$ (6)

A mixture of [(*p*-cymene)$RuCl_2]_2$ (1.0 g, 1.63 mmol) and hexaethylbenzene (8.04 g, 32.7 mmol) was sealed under vacuum, immersed in an oil bath at 170 °C for 72 h, and then cooled to room temperature. The residue was washed with a large excess of hexane (250 mL) to remove the unreacted HEB and dissolved in dry CH_2Cl_2 (10 mL). Addition of hexane (25 mL) brought about precipitation of a dark purple-red compound that was filtered, dried, and recrystallized from dichloromethane–hexane to give **6** (0.680 g, 0.81 mmol, 50%); mp 240 °C (dec). ^{1}H NMR (500 MHz, CD_2Cl_2, 30 °C) δ: 2.53 (12H, broadened quartet, J = 7.5 Hz, CH_2), 1.42 (18H, t, J = 7.5 Hz, CH_3). At –90 °C these signals resolve into broadened singlets at δ 2.57 and 2.27 ppm, 1.40 and 1.27 ppm, respectively. ^{13}C NMR (125 MHz, CD_2Cl_2, 30 °C) δ: 94.2 (arene *C*), 20.5 (*C*H_2), 14.2 (*C*H_3). At –90 °C these signals resolve into singlets at δ 99.1, 85.1; 20.3, 17.6; 15.0, 11.2. MS (EI, *m*/*z*) (%): 418 [(HEB)$RuCl_2]^+$ (50), 348 [(HEB)Ru]$^+$ (12), 246 [HEB]$^+$ (52). MS (CI, *m*/*z*) (%): 436 [(HEB)$RuCl_2$ + $NH_4]^+$ (18), 247 [HEB + H]$^+$ (100). MS (+ve ion electrospray, *m*/*z*) (%): 801 [M – Cl]$^+$ (85), 383 [(HEB)RuCl]$^+$ (100).

Preparation of [(η^6-hexaethylbenzene)$_2Ru_2(\mu$-$Cl_3)$]-[$C_5(CO_2CH_3)_5$] (7)

To a solution of [(HEB)$RuCl_2]_2$ (**6**, 0.418 g, 0.5 mmol) in CH_2Cl_2 (25 mL) was added K[$C_5(CO_2CH_3)_5$] (0.792 g, 2.0 mmol) in methanol (50 mL), and the reaction mixture was heated at 70 °C for 3 h during which time the color of the solution gradually became greenish-yellow. After cooling and removal of solvents under reduced pressure, the residue was taken up in CH_2Cl_2 (25 mL) and filtered. Hexane (20 mL) was added and the solution was left to crystallize for 3 days after which time yellow-orange microcrystals were separated and dried to give **7** (305 mg, 0.26 mmol, 53%); mp 216 °C. ^{1}H NMR (500 MHz, CD_2Cl_2, 30 °C) δ: 3.69 (15H, s, OCH_3), 2.39 (12H, quartet, J = 7.5 Hz, CH_2), 1.29 (18H, t, J = 7.5 Hz, CH_3). ^{13}C NMR (125 MHz, CD_2Cl_2, 30 °C) δ: 167.9 (CO), 95.3 (arene *C*), 51.4 (O*C*H_3) 21.5 (*C*H_2), 15.0 (*C*H_3). MS (+ve ion electrospray, *m*/*z*) (%): 801 [(HEB)$_2Ru_2Cl_3]^+$ (30), 383 [(HEB)RuCl] $^+$ (100). Anal. calcd. for $C_{51}H_{75}Ru_2Cl_4O_{10}$ (%): C 52.92, H 6.49; found: C 53.13, H 6.83.

Preparation of [(η^6-hexaethylbenzene)$Ru(H_2O)_3](BF_4)_2$ (8)

To a purple-red solution of [(HEB)$RuCl_2]_2$ (**6**, 0.105 g, 0.125 mmol) in CH_2Cl_2 (10 mL) was added $AgBF_4$ (0.100 g, 0.5 mmol) and the mixture was stirred for 1 h at room temperature during which time the colour of the solution became orange-yellow. After filtration and concentration to a volume of approximately 5 mL, hexane (5 mL) was added, and the mixture left at 0 °C to crystallize. The resulting yellow-orange crystalline solid was separated and dried to give **8** (100 mg, 0.17 mmol, 69%); mp 155 °C. ^{1}H NMR (500 MHz, CD_2Cl_2, 30 °C) δ: 4.14 (broad s, H_2O), 2.66 (12H, broad s, CH_2), 1.39 (18H, t, J = 7.4 Hz, CH_3). At –74 °C these signals resolve into broadened singlets at δ 2.55 and 2.25 and 1.36 and 1.21 ppm, respectively. ^{13}C NMR (125 MHz, CD_2Cl_2, 30 °C) δ: 95.3 (arene *C*), 21.6 (*C*H_2), 14.2 (*C*H_3). MS (+ve ion electrospray in CH_3CN–H_2O, *m*/*z*) (%): 408 [M + H + CH_3CN – $2H_2O]^+$ (100), 192 [M – $H_2O]^{2+}$ (32). Anal. calcd. for $C_{18}H_{36}RuO_3B_2F_8{\cdot}H_2O$ (%): C 36.41, H 6.40; found: C 36.66, H 6.51. Addition of excess HEB to **8**, followed by heating at reflux overnight, led merely to the recovery of starting materials.

Preparation of [(η^6-hexaethylbenzene)$RuCl_2P(OMe)_3$] (9)

To a solution of [(HEB)$RuCl_2]_2$ (**6**, 0.167 g, 0.2 mmol) in dry CH_2Cl_2 (10 mL) was added trimethyl phosphite (100 mg, 0.8 mmol) via syringe and the mixture was stirred at room temperature for 3 h. The resulting orange-red solution was concentrated to about 3 mL under reduced pressure and hexane (5 mL) was added. Recrystallization overnight produced a red crystalline solid, which was separated from the solution and dried to give **9** (174 mg, 0.32 mmol, 80%); mp 150 °C. ^{1}H NMR (200 MHz, CD_2Cl_2) δ: 3.71 (9H, d, $^3J(^1H$-$^{31}P)$ = 10.2 Hz, OCH_3), 2.57 (12H, quartet, J = 7.6 Hz, CH_2), 1.31 (18H, t, J = 7.6 Hz, CH_3). ^{13}C NMR (50 MHz, CD_2Cl_2) δ: 103.7 (arene *C*), 54.6 (O-*C*H_3), 22.5 (*C*H_2), 14.9 (*C*H_3). MS (EI, *m*/*z*) (%): 542 [M]$^+$ (37), 507 [M – Cl]$^+$ (14), 418 [M – P(OMe)$_3]^+$ (100), 383 [(HEB)RuCl]$^+$ (44), 348 [(HEB)Ru]$^+$ (37). MS (CI, *m*/*z*) (%): 436 [(HEB)$RuCl_2$ + $NH_4]^+$ (158), 247 [HEB + H]$^+$ (35), 125 [P(OMe)$_3$ + H]$^+$ (100). Anal. calcd. for $C_{21}H_{39}RuCl_2O_3P$ (%): C 46.45, H 7.19; found: C 46.23, H 7.37.

Preparation of [(η^6-hexaethylbenzene)$RuCl_2(PMe_3)$] (10)

To a solution of [(HEB)$RuCl_2]_2$ (**6**, 0.418 g, 0.5 mmol) in dry CH_2Cl_2 (50 mL) was added trimethylphosphine (0.3 mL, 0.24 mmol) via syringe, and the mixture was stirred at room temperature for 24 h. The resulting orange-red solution was concentrated to about 3 mL under reduced pressure and hexane (10 mL) was added. Recrystallization overnight produced a red crystalline solid, which was separated from the solution and dried to give **10** (400 mg, 0.81 mmol, 81%); mp 192 °C. ^{1}H NMR (200 MHz, CD_2Cl_2, 30 °C) δ: 2.55 (12H, quartet, J = 7.6 Hz, CH_2), 1.40 (9H, d, $^2J(^1H$-$^{31}P)$ = 10.5 Hz, P-CH_3), 1.32 (t, J = 7.6 Hz, CH_3), 1.32 (18H, t, J = 7.6 Hz, CH_3). ^{13}C NMR (50 MHz, CD_2Cl_2) δ: 100.9 (arene *C*), 23.5 (*C*H_2), 15.9 (d, $^1J(^{13}C$-$^{31}P)$ = 34 Hz, P-CH_3), 15.2 (*C*H_3). ^{31}P NMR (121.5 MHz, CD_2Cl_2) δ: 3.08 (decet, $^2J(^1H$-$^{31}P)$ = 10.5 Hz, *P*-CH_3). MS (EI, *m*/*z*) (%): 494 [M]$^+$ (40), 459 [M – Cl]$^+$ (16), 418 [M – $PMe_3]^+$ (100), 383 [M – PMe_3-Cl]$^+$ (67), 246 [HEB]$^+$ (38), 76 [$PMe_3]^+$ (98). MS (CI, *m*/*z*) (%): 495 [M + H]$^+$ (28), 460 [M – Cl + H]$^+$ (50), 77 [PMe_3 + H]$^+$ (100). From the crystalline sample, red crystals of a minor product were separated and shown by NMR and X-ray crystallography to be the known compound *trans*-$RuCl_2(PMe_3)_4$ (**11**).

Preparation of [(η^6-hexaethylbenzene)$Mn(CO)_3](BF_4)$

A mixture of $Mn(CO)_5Br$ (2.48 g, 9.03 mmol) and $AgBF_4$ (1.75 g, 9.03 mmol) in dry CH_2Cl_2 (50 mL) was heated to reflux for 3 h under nitrogen and then cooled to room temperature. To the reaction mixture, a solution of hexaethylbenzene (2.23 g, 9.03 mmol) in dry CH_2Cl_2 (20 mL) was added, and heating was continued for 16 h. After cooling

© 2006 NRC Canada

Table 1. Crystallographic collection and refinement parameters for **7–9**, **11**, and **13**.

Identification code	**7**	**8**	**9**	**11**	**13**
Empirical formula	$C_{51}H_{75}Cl_3O_{10}Ru_2$	$C_{18}H_{38}B_2F_8O_4Ru$	$C_{21}H_{39}Cl_2O_3PRu$	$C_{12}H_{36}Cl_2P_4Ru$	$C_{20}H_{30}BrO_2Mn$
Formula weight	1 156.60	593.17	542.46	476.26	437.29
Temperature (K)	210(2)	210(2)	210(2)	210(2)	173(2)
Wavelength (Å)	0.710 73	0.710 73	0.710 73	0.710 73	0.710 73
Crystal system	Triclinic	Orthorhombic	Triclinic	Monoclinic	Monoclinic
Space group	$P\bar{1}$	$P2_12_12_1$	$P\bar{1}$	$P2/n$	$P2_1/n$
a (Å)	13.410 60(10)	10.072 60(10)	9.828 0(10)	15.677 30(10)	9.004(6)
b (Å)	14.919 4(2)	13.828 4(2)	10.252 0(10)	9.447 60(10)	16.690(11)
c (Å)	14.983 30(10)	18.362 9(2)	13.364(2)	15.681 2(2)	14.135(9)
α (°)	103.250 0(10)	90	71.768(4)	90	90
β (°)	94.771 0(10)	90	85.496(3)	111.578 0(10)	105.688(10)
γ (°)	110.832 0(10)	90	68.657 0(10)	90	90
Volume (Å^3)	2 682.21(4)	2 557.73(5)	1 190.3(2)	2 159.81(4)	2 045.0(22)
Z	2	4	2	4	4
Density (calcd.) (Mg/m^3)	1.432	1.540	1.514	1.465	1.420
Absorption coefficient (mm^{-1})	0.766	0.692	0.969	1.259	2.608
F(000)	1 200	1 216	564	984	904
Crystal size (mm^3)	0.30 × 0.20 × 0.08	0.40 × 0.30 × 0.20	0.30 × 0.18 × 0.08	0.40 × 0.28 × 0.09	0.55 × 0.32 × 0.25
θ range for data collection (°)	1.42–26.51	1.84–26.54	2.23–28.43	1.40–26.47	1.93–27.53
Index ranges	$-16 \le h \le 16$, $-15 \le k \le 18$, $-18 \le l \le 18$	$-12 \le h \le 12$, $-17 \le k \le 17$, $-19 \le l \le 22$	$-13 \le h \le 13$, $-13 \le k \le 13$, $-17 \le l \le 17$	$-19 \le h \le 19$, $-9 \le k \le 11$, $-19 \le l \le 19$	$-11 \le h \le 11$, $-20 \le k \le 21$, $-18 \le 1 \le 18$
Reflections collected	22 408	21 529	14 274	17 943	17 809
Independent reflections	10 095 [R(int) = 0.032 52]	5 246 [R(int) = 0.017 5]	5 358 [R(int) = 0.022 9]	4 408 [R(int) = 0.042 2]	4 705 [R(int) = 0.074 4]
Absorption correction	SADABS	SADABS	SADABS	SADABS	SADABS
Max. and min. transmission	0.946 870 and 0.758 383	0.899 6 and 0.773 8	0.934 773 and 0.760 503	1.000 0 and 0.825 625	0.936 7 and 0.854 2
Refinement method	Full-matrix least-squares on F^2	Full-matrix least-squares on F^2	Full-matrix least-squares on F^2	Full-matrix least-squares on F^2	Full-matrix least-squares on F^2
Data/restraints/parameters	10 095 / 0 / 370	5 245 / 0 / 451	5 358 / 0 / 410	4 408 / 0 / 174	4 705 / 0 / 223
Goodness-of-fit on F^2	0.997	1.040	1.042	1.051	1.049
Final R indices [$I > 2\sigma(I)$]	$R1$ = 0.037 3, $wR2$ = 0.096 2	$R1$ = 0.014 8, $wR2$ = 0.038 3	$R1$ = 0.022 4, $wR2$ = 0.060 3	$R1$ = 0.023 1, $wR2$ = 0.060 4	$R1$ = 0.049 0, $wR2$ = 0.114 8
R indices (all data)	$R1$ = 0.058 6, $wR2$ = 0.104 5	$R1$ = 0.015 2, $wR2$ = 0.039 0	$R1$ = 0.024 7, $wR2$ = 0.061 4	$R1$ = 0.024 8, $wR2$ = 0.061 4	$R1$ = 0.107 0, $wR2$ = 0.142 4
Extinction coefficient		0.000 2(2)	0.003 0(6)		0.002 4(6)
Absolute structure parameter		–0.012(14)			
Largest diff. peak and hole (e Å^{-3})	0.677 and –0.690	0.333 and –0.296	0.558 and –0.689	0.665 and –0.620	0.583 and –0.783

© 2006 NRC Canada

and filtration, the filtrate was passed through Celite and concentrated to approximately one-third its volume under pressure, and excess hexane (100 mL) was added. The resulting orange-yellow solid was filtered and dried in vacuo furnishing [(HEB)$Mn(CO)_3$](BF_4) (3.34 g, 7.08 mmol, 79%); mp 266 °C (dec). ^{1}H NMR (500 MHz, CD_2Cl_2) δ: 1.41 (12H, broad singlet, CH_2), 2.68 (18H, broad singlet, CH_3). At 173 K, the methylene protons are resolved into broad singlets at 2.56 and 2.45 ppm. ^{13}C NMR (125 MHz, CD_2Cl_2) δ: 217.8 (Mn-*C*O), 120.3 (arene *C*), 22.6 (*C*H_3), 17.1 (*C*H_2). At 203 K, the aromatic, methylene, and methyl resonances are each resolved into two peaks at 124.0 and 113.6, 23.2 and 19.7, and 20.0 and 13.6 ppm, respectively. IR (NaCl windows, $CDCl_3$, cm^{-1}): υ_{CO} 2058 (s), 1996 (s). MS (+ve ESI, *m*/*z*) (%): 385 $[M]^+$ (100), 386 ($[M + H]^+$ (24), 357 $[M - CO]^+$ (0.5), 329 $[M - 2CO]^+$ (1.2), 301 $[M - 3CO]^+$ (0.5).

Preparation of [(η^6-hexaethylbenzene)$Mn(CO)_2Br$ (13)

A mixture of [(η^6-hexaethylbenzene)$Mn(CO)_3$](BF_4) (0.559 g, 1.187 mmol), Me_3NO (0.089 g, 1.187 mmol), and (n-Bu)$_4$NBr (0.462 g, 1.463 mmol) were placed in a two-neck round-bottom flask that was then evacuated. Upon addition of dry CH_2Cl_2 (30 mL), the resulting solution became deep red in colour, and the solution was stirred for 2 h under N_2. After removal of solvent under reduced pressure, the crude product was chromatographed on a silica gel column (eluent: hexane–acetone, 50:50) to give a thermally sensitive, red-purple solid, **13** (0.356 g, 0.819 mmol, 69%); mp 127–129 °C. (During the acquisition of the NMR spectra, some decomposition into HEB was evident.) IR (NaCl windows, $CDCl_3$, cm^{-1}): υ_{CO} 1974 (s), 1927 (s). ^{1}H NMR (500 MHz, CD_2Cl_2) δ: 2.67 (12H, br. s, CH_2), 1.21 (18H, br. s, CH_3). ^{13}C NMR (50 MHz, CD_2Cl_2) δ: 230.3 (Mn-*C*O), 112.0 (arene *C*), 22.6 (*C*H_2), 16.3 (*C*H_3). MS (DEI, *m*/*z*) (%): 357 $[M - Br]^+$ (1), 329 $[M - Br - CO]^+$ (2), 301 $[M - Br - 2CO]^+$ (5), 246 $[HEB]^+$ (100). MS (CI, NH_3, *m*/*z*) (%): 357 $[M - Br]^+$ (1), 329 $[M - Br - CO]^+$ (2), 301 $[M - Br - 2CO]^+$ (14), 246 (100, $[HEB]^+$ (100)). An X-ray quality crystal was obtained by repeated recrystallization from pentane–acetone by slow evaporation at room temperature under an atmosphere of nitrogen.

Crystallographic data for 7–9, 11, and 13

X-ray crystallographic data for **7**–**9**, **11**, and **13** (Table 1) were collected from suitable samples mounted with epoxy on the end of thin glass fibers. Data were collected on a P4 Bruker diffractometer equipped with a Bruker SMART 1K CCD area detector (employing the program SMART) (36) and a rotating anode utilizing graphite-monochromated Mo Kα radiation (λ = 0.710 73 Å). Data processing was carried out by use of the program SAINT (37), while the program SADABS (38) was utilized for the scaling of diffraction data, the application of a decay correction, and an empirical absorption correction based on redundant reflections. Structures were solved by using the direct-methods procedure in the Bruker SHELXTL (39) program library and refined by full-matrix least-squares methods on F^2. All non-hydrogen atoms were refined using anisotropic thermal parameters (except for the disordered anion $C_5(CO_2Me)_5$ in **7**, as discussed in the text), and hydrogen atoms were added as fixed contributors at calculated positions, with isotropic thermal parameters based on the carbon atom to which they are bonded.[3]

Acknowledgements

Financial support from the Natural Sciences and Engineering Research Council of Canada (NSERC) is gratefully acknowledged. Mass spectra were obtained courtesy of Dr. Richard Smith of the McMaster Regional Centre for Mass Spectrometry, Hamilton, Ontario.

References

1. G. Hunter, D.J. Iverson, K. Mislow, and J.F. Blount. J. Am. Chem. Soc. **102**, 5942 (1980).
2. (*a*) J.-R. Hamon, J.-Y. Saillard, A. LeBeuze, M.J. McGlinchey, and D. Astruc. J. Am. Chem. Soc. **104**, 7549 (1982); (*b*) R.H. Dubois, M.J. Zaworotko, and P.S. White. J. Organomet. Chem. **362**, 155 (1989).
3. W.A. Herrmann, W.R. Thiel, and E. Herdtweck. Polyhedron, **7**, 2027 (1988).
4. M.J. McGlinchey. Adv. Organomet. Chem. **34**, 285 (1992),
5. H.K. Pal and A.C. Guha. Z. Kristallogr. Kristallgeom. Kristallphys. Kristallchem. **92**, 392 (1935).
6. D.J. Iverson, G. Hunter, J.R. Damewood, Jr., J.F. Blount, and K. Mislow. J. Am. Chem. Soc. **103**, 6073 (1981).
7. B. Mailvaganam, C.S. Frampton, S. Top, B.G. Sayer, and M.J. McGlinchey. J. Am. Chem. Soc. **113**, 1177 (1991).
8. M.J. McGlinchey, P. Bougeard, B.G. Sayer, R. Hofer, and C.J.L. Lock. J. Chem. Soc. Chem. Commun. 789 (1984).
9. P.A. Downton, B. Mailvaganam, C.S. Frampton, B.G. Sayer, and M.J. McGlinchey. J. Am. Chem. Soc. **112**, 27 (1990).
10. (*a*) K.V. Kilway and J.S. Siegel. J. Am. Chem. Soc. **113**, 2332 (1991); (*b*) K.V. Kilway and J.S. Siegel. J. Am. Chem. Soc. **114**, 255 (1992).
11. J.F. Blount, G. Hunter, and K. Mislow. J. Chem. Soc. Chem. Commun. 170 (1984).
12. G. Hunter, J.F. Blount, J.R. Damewood, Jr., D.J. Iverson, and K. Mislow. Organometallics, **1**, 448 (1981).
13. T.C. Flood, E. Rosenberg, and A. Sarhangi. J. Am. Chem. Soc. **99**, 4335 (1977).
14. G.A. Olah and H. Yu. J. Org. Chem. **41**, 717 (1976).
15. B. Mailvaganam, B.G. Sayer, and M.J. McGlinchey. Organometallics, **9**, 1089 (1990).
16. H.K. Gupta, P.E. Lock, D.W. Hughes, and M.J. McGlinchey. Organometallics, **16**, 4335 (1997).
17. M.A. Bennett. Coord. Chem. Rev. **166**, 225 (1997).

[3] Supplementary data for this article are available on the journal Web site (http://canjchem.nrc.ca) or may be purchased from the Depository of Unpublished Data, Document Delivery, CISTI, National Research Council Canada, Ottawa, ON K1A 0R6, Canada. DUD 5010. For more information on obtaining material refer to http://cisti-icist.nrc-cnrc.gc.ca/irm/unpub_e.shtml. CCDC 292775–292778 contain the crystallographic data for this manuscript. These data can be obtained, free of charge, via http://www.ccdc.cam.ac.uk/conts/retrieving.html (Or from the Cambridge Crystallographic Data Centre, 12 Union Road, Cambridge CB2 1EZ, UK; fax +44 1223 336033; or deposit@ccdc.cam.ac.uk).

© 2006 NRC Canada

18. R. Baldwin, M.A. Bennett, D.C.R. Hockless, P. Pertici, A. Verrazzini, G.U. Barretta, F. Marchetti, and P. Salvadori. J. Chem. Soc. Dalton Trans. 4488 (2002).
19. (*a*) H. Le Bozec, D. Touchard, and P.H. Dixneuf. Adv. Organomet. Chem. **29**, 163 (1989); (*b*) L.C. Porter and J.R. Polam. Organometallics, **13**, 2092 (1994); (*c*) S. Suravajjala, L.C. Porter, and J.R. Polam. Organometallics, **13**, 37 (1994).
20. (*a*) R.A. Zelonka and M.C. Baird. Can. J. Chem. **50**, 3063 (1972); (*b*) M.A. Bennett, T.W. Matheson, G.B. Robertson, A.K. Smith, and P.A. Tucker. Inorg. Chem. **19**, 1014 (1980); (*c*) M.A. Bennett, T.-N. Huang, T.W. Matheson, and A.K. Smith. Inorg. Synth. **21**, 75 (1982).
21. M.I. Bruce. Aust. J. Chem. **43**, 949 (1990).
22. (*a*) F. Grepioni, D. Braga, P.J. Dyson, B.F.G. Johnson, F.M. Sanderson, M.J. Calhorda, and L.F. Veiros. Organometallics, **14**, 121 (1995); (*b*) F.B. McCormick and W.B. Gleason. Acta Crystallogr. Sect. C: Struct. Crystallogr. Cryst. Chem. **49**, 1493 (1993); (*c*) D. Tocher and M.D. Walkinshaw. Acta Crystallogr. Sect. B: Struct. Crystallogr. Cryst. Chem. **38**, 3083 (1982).
23. A.L. Spek. PLATON. Version 200296 [computer program]. University of Utrecht, Utrecht, The Netherlands. 1996.
24. M.A. Bennett, T.W. Matheson, G.B. Robertson, W.L. Steffen, and T.W. Turney. J. Chem. Soc. Chem. Commun. 32 (1979).
25. H.-B. Bürgi. Inorg. Chem. **27**, 1358 (1988).
26. (*a*) C.A. Tolman. Chem. Rev. **77**, 313 (1977); (*b*) J.P. Collman and L.S. Hegedus. Principles and applications of organotransition metal chemistry. University Science Books, Mill Valley, California. 1980. pp. 57 to 58.
27. The X-ray crystal structures of (arene)$RuCl_2(PMePh_2)$, where arene = benzene or cymene, have been previously reported: M.A. Bennett, G.B. Robertson, and A.K. Smith. J. Organomet. Chem. **43**, C41 (1972).
28. R.A. Jones, F.M. Real, G. Wilkinson, A.M.R. Galas, M.B. Hursthouse, and K.M.A. Malik. J. Chem. Soc. Dalton Trans. 511 (1980).
29. See, for example: (*a*) J.A. Statler, G. Wilkinson, M. Thornton-Pett, and M.B. Hursthouse. J. Chem. Soc. Dalton Trans. 1731 (1984); (*b*) W.-K. Wong, K.W. Chiu, J.A. Statler, and G. Wilkinson. Polyhedron, **3**, 1255 (1984); (*c*) J.F. Hartwig, R.A. Andersen, and R.G. Bergman. J. Am. Chem. Soc. **112**, 5670 (1990); (*d*) K. Osakada, K. Ohshiro, and A.Yamamoto. Organometallics, **10**, 404 (1991); (*e*) J.F. Hartwig, R.G. Bergman, and R.A. Andersen. J. Am. Chem. Soc. **113**, 3404 (1991); (*f*) J.F. Hartwig, R.A. Andersen, and R.G. Bergman. Organometallics, **10**, 1875 (1991); (*g*) J.F. Hartwig, R.G. Bergman, and R.A. Andersen. Organometallics, **10**, 3326 (1991); (*h*) J.F. Hartwig, R.G. Bergman, and R.A. Andersen. Organometallics, **10**, 3344 (1991); (*i*) L. Dahlenberg and K.-M. Frosin. Polyhedron, **12**, 427 (1993).
30. L.J. Guggenberger. Inorg. Chem. **12**, 1317 (1973).
31. H.G.L. Siebald, P.L. Fabre, M. Dartiguenave, Y. Dartiguenave, M. Simard, and A.L. Beauchamp. Polyhedron, **15**, 4241 (1996).
32. (*a*) H.K. Gupta, P.E. Lock, and M.J. McGlinchey. Organometallics, **16**, 3628 (1997); (*b*) N. Reginato and M.J. McGlinchey. Organometallics, **20**, 4147 (2001).
33. (*a*) R.J. Bernhardt and D.P. Eyman. Organometallics, **3**, 1445 (1984); (*b*) R.J. Bernhardt, M.A. Wilmoth, J.J. Weers, D.M. LaBrush, D.P. Eyman, and J.C. Huffman. Organometallics, **5**, 883 (1986).
34. J.F. Blount, G. Hunter, and K. Mislow. J. Chem. Soc. Chem. Commun. 170 (1984).
35. (*a*) G. Hennrich, V.M. Lynch, and E.V. Anslyn. Chem. Eur. J. **10**, 2274 (2002); (*b*) G. Hennrich and E.V. Anslyn. Chem. Eur. J. **10**, 2219 (2002), and refs. therein.
36. G.M. Sheldrick. SMART. Release 4.05 [computer program]. Siemens Energy and Automation Inc., Madison, Wisconsin. 1996.
37. G.M. Sheldrick. SAINT. Release 4.05 [computer program]. Siemens Energy and Automation Inc., Madison, Wisconsin. 1996.
38. G.M. Sheldrick. SADABS [computer program]. Siemens Energy and Automation Inc., Madison, Wisconsin. 1996.
39. G.M. Sheldrick. SHELXTL. Version 5.03 [computer program]. Siemens Crystallographic Research Systems, Madison, Wisconsin. 1994.

© 2006 NRC Canada

Metallocenes as references for the determination of redox potentials by cyclic voltammetry — Permethylated iron and cobalt sandwich complexes, inhibition by polyamine dendrimers, and the role of hydroxy-containing ferrocenes[1]

Jaime Ruiz Aranzaes, Marie-Christine Daniel, and Didier Astruc

Abstract: Measurement of the redox potentials ($E_{1/2}$) of ferrocene (**1**), decamethylferrocene (**2**), decamethylcobaltocene (**3**), and [$Fe^{I}Cp^{*}(\eta^{6}$-$C_6Me_6)$] (**4**) ($Cp^{*} = \eta^{5}$-C_5Me_5) in DMF, CH_3CN, THF, DME, CH_2Cl_2, and DMSO were recorded vs. the saturated calomel electrode (SCE), showing that the $E_{1/2}$ value of **1** was more solvent dependent than those of **2**–**4**, and that the difference in $E_{1/2}$ values among **2**–**4** was solvent independent, unlike those found between **1** and **2**–**4**. This shows that **2**–**4** are much more reliable internal references for determining redox potentials than **1**, but using data from this article, one can convert the literature values reported vs. **1** into values vs. **2**, **3**, or **4**. The electrochemistry of **1** and **2** is all the more inhibited by polyamine dendrimers as the dendrimer generation is higher. On the other hand, ferrocenes or other iron sandwich compounds containing hydroxy groups can reestablish reversible cyclic voltammograms. It is shown, using a tetra(ferrocenylmethylamine), that this phenomenon is due to hydrogen bonding between the amido and phenol groups rather than bonding of hydroxy groups to the electrode surface.

Key words: ferrocene, reference, electrochemistry, metallocene, sandwich complex, iron, dendrimer, passivation, hydrogen bond.

Résumé : Utilisant une électrode de calomel saturée (ECS) et opérant dans le DMF, le CH_3CN, le THF, le DME, le CH_2Cl_2 et de DMSO, on a mesuré les potentiels redox ($E_{1/2}$) du ferrocène (**1**), du décaméthylferrocène (**2**), du décaméthylcobaltocène (**3**) et du [$Fe^{I}Cp^{*}(\eta^{6}$-$C_6Me_6)$] (**4**) ($Cp^{*} = \eta^{5}$-C_5Me_5). Les résultats obtenus montrent que la valeur $E_{1/2}$ du composé **1** est plus influencée par le solvant que celles des composés **2**–**4** et que la différence entre les valeurs de $E_{1/2}$ entre les composés **2**–**4** est indépendante du solvant, ce qui n'est pas le cas pour celles observées entre le composé **1** et les composés **2**–**4**. Ces observations montrent que, par comparaison avec le composé **1**, les composés **2**–**4** sont des références internes beaucoup plus fiables pour déterminer les potentiels redox. Il est toutefois possible, en utilisant les données de cet article, de convertir les valeurs obtenues par rapport à la référence **1** et rapportées antérieurement dans la littérature en valeurs par rapport aux références **2**, **3** ou **4**. L'électrochimie des composés **1** et **2** est d'autant plus inhibée par les dendrimères polyamides que la génération de dendrimère est élevée. Par ailleurs, les ferrocènes et les autres composés sandwichs contenant des groupes hydroxyles peuvent rétablir les voltampérogrammes cycliques réversibles. On a démontré, à l'aide de tétra(ferrocénylméthylamine), que ce phénomène est dû à une liaison hydrogène entre les groupes amido et phénol plutôt qu'à une liaison des groupes hydroxyles à la surface de l'électrode.

Mots clés : ferrocène, référence, électrochimie, métallocène, complexe sandwich, fer, dendrimère, passivation, liaison hydrogène.

[Traduit par la Rédaction]

Received 18 July 2005. Published on the NRC Research Press Web site at http://canjchem.nrc.ca on 21 March 2006.

This article is dedicated to our distinguished colleague and friend Professor Arthur Carty.

J. Ruiz Aranzaes, M.-C. Daniel, and D. Astruc.[2] Molecular Nanosciences and Catalysis Group, LCOO, UMR CNRS N°5802, Université Bordeaux I, 33405 Talence CEDEX, France.

[1]This article is part of a Special Issue dedicated to Professor Arthur Carty.

[2]Corresponding author (e-mail: d.astruc@lcoo.u-bordeaux1.fr).

 doi:10.1139/V05-262 © 2006 NRC Canada

Introduction

The determination of standard redox potentials of compounds is a "Holy Graal" in electrochemistry. The average of the cathodic and anodic peak potentials ($E_{1/2} = (E_{pa} + E_{pc})/2$) in cyclic voltammetry is an excellent approximation of standard redox potential (E^0) (eq. [1], (1)).

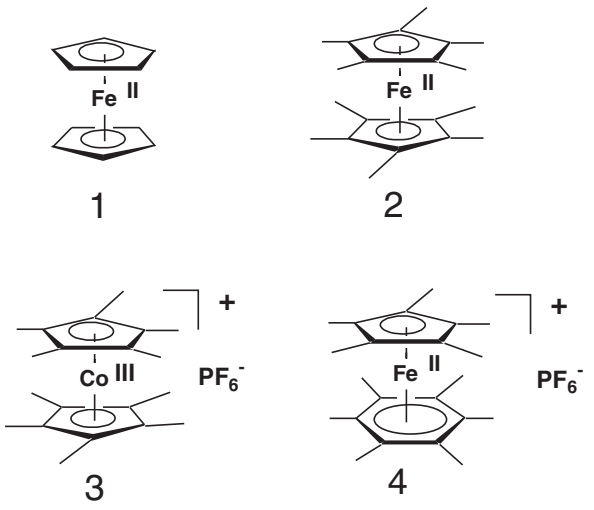
$$[1] \qquad E^0 = E_{1/2} - (RT/nF)\ \ln(D_{red}/D_{ox})^{1/2}$$

Indeed, the diffusion coefficient of the reduced and oxidized forms are usually not very different, so the square root of their ratio is not very different from unity, at least in reversible redox systems for which the structures of the reduced and oxidized forms are not very different. The saturated calomel electrode is unstable (2, 3), however, and therefore electrochemists have been seeking internal reference compounds to determine standard redox potentials of compounds more accurately in nonaqueous solvents (1, 4). Internal references overcome the problem of potential variations owing to changes in liquid junction potentials between the solution and the reference electrode (5).

Ferrocene/ferrocenium ($1/1^+$) has been considered as the prototype of electrochemically reversible systems (6). Indeed, its reduced Fe^{II} and oxidized Fe^{III} (ferrocenium) forms are both low spin, therefore the difference in Fe—C bond length between these two compounds is not larger than 0.05 Å (7). Although ferrocenium salts react with nucleophiles (8–10) and dioxygen (11), these reactions usually do not perturb the redox potential because they are slow on the relatively fast electrochemical timescale of cyclic voltammetry and the $Fe^{II/III}$ system remains reversible; even partial chemical irreversibility does not modify the potential (1). Ferrocene now is a popular reference compound commonly used as such by the community of molecular chemists, especially because, in addition, it is a cheap, stable, and easily available compound, and the location of its redox potential is conveniently located in the electrochemical scale. Finally, for these reasons, it has been recommended by IUPAC (12). The use of ferrocene as an internal reference is indeed adequate when a single solvent is used. However, it has been found that the ferrocene/ferrocenium couple was the subject of specific solvation effects that questioned the so-called "ferrocene assumption" (13–15). Therefore, the redox potential of ferrocene varies with the nature of the solvent, this variation reaching up to 0.56 V (16, 17). This is due to the thermodynamics of the ion paring between ferrocenium cation and the anion of the supporting electrolyte in specific solvents. Indeed, the central iron atom is not well-protected against side binding, especially because even large tilting of the ferrocene rings can occur almost without energy change, such as in the protonated form of ferrocene, the Fe^{IV} hydride $[FeCp_2(H)]^+$ (18, 19). This ion pairing decreases the energy necessary to reduce ferrocenium cation, causing a cathodic shift of the redox potential that depends on the natures of both the solvent and anion of the supporting electrolyte. More specifically, it has been shown that two types of solvation effects are involved in ferrocene/ferrocenium: those directed towards the iron center and those directed towards the rings (15, 20, 21).

Clearly, this inconvenience almost vanishes in decamethylferrocene (**2**) (Chart 1) whose electrochemistry of the fully reversible redox $Fe^{III/II}$ system has been largely reported (22–37) including the electrochemical reversibility (fast electron-transfer kinetics) (25, 26).

Chart 1.



The $Cp^*_2Fe^{III/II}$ redox couple has indeed been proposed as an internal standard taking these reasons into account (36, 37). In particular, the shell of the 10 methyl groups encapsulate the iron center in such a way that it is protected against close interactions with substrates. This is ascertained upon scrutiny of the X-ray data for $[Cp^*_2Fe^{II}]$ ($Cp^* = \eta^5\text{-}C_5Me_5$) showing that the inter-ring methyl group contacts are within van der Waals distances (38). As a result, the solvent effects have been found to be very weak as compared with those observed with the $FeCp_2^{II/III}$ redox system (37). Other permethylated first-row, transition-metal sandwich compounds such as $[CoCp^*_2]$ (**3**) and $[Fe^ICp^*(\eta^6\text{-}C_6Me_6)]$ (**4**) that have been called electron-reservoir complexes also fulfill this property. Indeed, the $Fe^{II/I}$ redox change in compounds of the family of **4** involves an e^*_1 orbital that has a high metal character, and the central metal undergoing the redox change is fully protected sterically (39–44). The radii of the permethylmetallocenes $[FeCp^*_2]$ and $[Cp^*_2Co]$ and of $[Fe^ICp^*(\eta^6\text{-}C_6Me_6)]$ are much larger than those of the parent metallocenes, and the ion pairing energy (45) is an order of magnitude lower in permethylmetallocenium salts compared with metallocenium salts. Therefore, we suggest their use as internal references that are more accurate than ferrocene and independent of the solvent and supporting electrolyte. An interest in addressing these three compounds is that they cover the redox scale, which allows using the one that does not overlap with the substrate under study. Detailed studies demonstrate this feature here including the absence of variation of the differences among the redox potentials of these compounds upon changing the solvent (unlike with ferrocene) and how to connect ferrocene to permethylated sandwich references even if ferrocene is continuously used as an internal reference.

In the present context of nanosciences, we have also found that commercial polyamine dendrimers inhibit the electrochemistry of ferrocene and decamethylferrocene (46). Thus, in addition, the reference problem needed to be addressed again. We show that hydroxy-containing ferrocene deriva-

© 2006 NRC Canada

Table 1. $E_{1/2}$ values (V) of transition-metal sandwich complexes determined vs. SCE.

$E_{1/2}$ vs. SCE	DMF	CH_3CN	THF	CH_2Cl_2	DMSO	DME
$FeCp_2^{+/0}$	0.470	0.382	0.547	0.475	0.435	0.580
$FeCp^*_2{}^{+/0}$	–0.125	–0.125	0.102	–0.070	–0.030	0.140
$CoCp^*_2{}^{+/0}$	–1.402	–1.525	–1.295	–1.497	–1.425	–1.260
$FeCp^*(C_6Me_6)^{+/0}$	–1.762	–1.865	–1.645		–1.775	–1.605

Note: $E_{1/2}$ values were determined using the cationic form: $E^0 \sim E_{1/2} = (E_{pa} + E_{pc})/2$. n-$Bu_4N^+PF_6^-$ (0.1 mol/L); cationic complex: 10^{-3} mol/L; v = 400 mV/s, to 20 °C; working and counter electrodes: Pt; reference electrode: SCE; $\Delta E_p = E_{pa} - E_{pc}$ = 40–45 mV (DMF), 45–50 mV (MeCN), 50–55 mV (THF), 50–60 mV (CH_2Cl_2), 50–60 mV (DMSO), 60–70 mV (DME). The shifts vs. the theoretical value of 58 mV at 20 °C are due to variations in ohmic compensation. $E_{1/2}$ values were recorded with an accuracy of ±0.005 V except the $E_{1/2}$ value of $FeCp^*(C_6Me_6)^{+/0}$ in CH_2Cl_2, which is not accurate because of the interference with the reduction of the solvent. In CH_2Cl_2, n-Bu_4N^+ salts with various counteranions and concentrations (vide infra) were used, but the difference between the $E_{1/2}$ values of $FeCp^*_2{}^{+/0}$ and $CoCp^*_2{}^{+/0}$ remained constant (1.390 V). The difference between the $E_{1/2}$ values of $FeCp_2^{+/0}$ and $FeCp^*_2{}^{+/0}$ varied, however, between 0.460 and 0.545 V. The $E_{1/2}$ values vs. SCE obtained for $FeCp_2^{+/0}$ and $FeCp^*_2{}^{+/0}$, respectively, are as follows (V): n-$Bu_4N^+PF_6^-$ (0.1 mol/L: 0.475 and –0.070; 0.4 mol/L: 0.425 and –0.100); n-$Bu_4N^+BF_4^-$ (0.1 mol/L: 0.585 and 0.045; 0.4 mol/L: 0.555 and 0.035); n-$Bu_4N^+Br^-$ (0.1 mol/L: 0.490 and –0.010; 0.4 mol/L: 0.480 and 0.000); n-$Bu_4N^+HSO_4^-$ (0.1 mol/L: 0.545 and 0.065; 0.4 mol/L: 0.515 and 0.055); n-$Bu_4N^+Cl^-$ (0.1 mol/L: 0.590 and 0.070; 0.4 mol/L: 0.570 and 0.070).

Table 2. $E_{1/2}$ values (V) of transition-metal sandwich complexes determined vs. $FeCp^*_2{}^{+/0}$.

$E_{1/2}$ vs. $FeCp^*_2{}^{+/0}$	DMF	CH_3CN	THF	CH_2Cl_2	DMSO	DME
$FeCp^*_2{}^{+/0}$	0	0	0	0	0	0
$FeCp_2^{+/0}$	0.480	0.510	0.440	0.545	0.470	0.440
$CoCp^*_2{}^{+/0}$	1.390	1.390	1.400	1.390	1.395	1.400
$FeCp^*(C_6Me_6)^{+/0}$	1.750	1.745	1.750		1.750	1.750

Note: $E_{1/2}$ values were determined using the cationic form: $E^0 \sim E_{1/2} = (E_{pa} + E_{pc})/2$. n-$Bu_4N^+PF_6^-$ (0.1 mol/L); cationic complex: 10^{-3} mol/L; v = 400 mV/s, to 20 °C; working and counter electrodes: Pt; reference electrode: SCE; $\Delta E_p = E_{pa} - E_{pc}$ = 40–45 mV (DMF), 45–50 mV (MeCN), 50–55 mV (THF), 50–60 mV (CH_2Cl_2), 50–60 mV (DMSO), 60–70 mV (DME). The shifts vs. the theoretical value of 58 mV at 20 °C are due to variations in ohmic compensation. $E_{1/2}$ values were recorded with an accuracy of ±0.005 V except the $E_{1/2}$ value of $FeCp^*(C_6Me_6)^{+/0}$ in CH_2Cl_2, which is not accurate because of the interference with the reduction of the solvent. In CH_2Cl_2, n-Bu_4N^+ salts with various counteranions and concentrations (vide infra) were used, but the difference between the $E_{1/2}$ values of $FeCp^*_2{}^{+/0}$ and $CoCp^*_2{}^{+/0}$ remained constant (1.390 V). The difference between the $E_{1/2}$ values of $FeCp_2^{+/0}$ and $FeCp^*_2{}^{+/0}$ varied, however, between 0.460 and 0.545 V. The $E_{1/2}$ values vs. SCE obtained for $FeCp_2^{+/0}$ and $FeCp^*_2{}^{+/0}$, respectively, are as follows (V): n-$Bu_4N^+PF_6^-$ (0.1 mol/L: 0.475 and –0.070; 0.4 mol/L: 0.425 and –0.100); n-$Bu_4N^+BF_4^-$ (0.1 mol/L: 0.585 and 0.045; 0.4 mol/L: 0.555 and 0.035); n-$Bu_4N^+Br^-$ (0.1 mol/L: 0.490 and –0.010; 0.4 mol/L: 0.480 and 0.000); n-$Bu_4N^+HSO_4^-$ (0.1 mol/L: 0.545 and 0.065; 0.4 mol/L: 0.515 and 0.055); n-$Bu_4N^+Cl^-$ (0.1 mol/L: 0.590 and 0.070; 0.4 mol/L: 0.570 and 0.070).

tives can reestablish a reasonably good and reliable cyclic voltammetry in the presence of these dendrimers allowing the use of these ferrocenes as reference systems. The competition between binding amino groups and hydroxy groups to the Pt electrode has been examined using ferrocenyl amine dendrimers previously reported by Salmon and Jutzi (47) to better understand this positive hydroxy group effect.

Results and discussion

Permethylated iron and cobalt sandwich complexes as references

We have selected the permethylated transition-metal sandwich redox systems decamethylferrocene/decamethylferrocenium $[FeCp^*_2]^{+/0}$, decamethylcobaltocene/decamethylcobaltocenium $[CoCp^*_2]^{+/0}$, and $[FeCp(\eta^6\text{-}C_6Me_6)]^{+/0}$ as alternative and complementary reference systems. The redox potential values of these redox couples are reported in Table 1 vs. SCE in different solvents. Therefore, the mixture of these compounds was analyzed in different solvents. The average values of $E_{1/2}$ between the anodic and cathodic peak potentials recorded by cyclic voltammetry in dimethylformamide (DMF), acetonitrile (CH_3CN), tetrahydrofurane (THF), dimethoxyethane (DME), dichloromethane (CH_2Cl_2), and dimethylsulfoxide (DMSO) are reported vs. SCE in Table 1 and are in accord with previous literature data within 0.2 V. These data show that the variations of $E_{1/2}$ values with the nature of the solvent are smaller with $[FeCp^*_2]$ than with $[FeCp_2]$, as noted by Lay's group who recorded the variation of the $E_{1/2}$ value of **1** and **2** with a large number of solvents (37). These variations vs. SCE are still significant with the three permethylated sandwich compounds because of the different solvent interactions with the cationic forms or to the variations of the SCE electrode reference in different solvents or both. A way to answer this uncertainty consists of determining the potentials ($E_{1/2}$) of the different permethylmetallocenes ($MCp^*_2{}^{+/0}$) vs. one of them, for instance $FeCp^*_2{}^{+/0}$, in the different solvents. In this way, the data will be free of the SCE reference electrode. These values have been determined vs. $FeCp^*_2{}^{+/0}$ using the experimental values of Table 1 and are reported in Table 2. Notice that the less polar solvent CH_2Cl_2 is the one giving the larger difference between the potential values of $[FeCp_2]^{+/0}$ vs. $FeCp^*_2{}^{+/0}$. This is due to the fact that, in such a solvent, the ion pairs are not separated (tight ion pairs), therefore, the anion influence on the cation containing the redox center is

© 2006 NRC Canada

Table 3. Formal potentials (V) of the main reductants.

Reductant	Solvent	E^0 vs. $FeCp^*_2{}^{+/0}$	E^0 vs. SCE	E^0 vs. NHE	E^0 vs. $FeCp_2{}^{+/0}$
$[C_{10}H_8]^{\bullet-}$	THF	–2.66	–2.76	–2.52	–3.10
	DMF	–2.56	–2.68	–2.44	–3.05
Na	THF, DME	–2.60	–2.72	–2.58	–3.04
Li(Hg)	H_2O	–2.13	–2.16	–1.92	–2.60
[Anthracene]$^{\bullet-}$	THF	–2.08*	–1.98		
$[FeCp^*(C_6Me_6)]$	CH_2Cl_2	–1.75*	–1.85	–1.61	–2.30
	DMF	–1.75*	–1.76	–1.62	–2.24
[Perylene]$^{\bullet-}$	THF	–1.75*			
[Benzophenone]$^{\bullet-}$	THF	–1.75	–1.86	–1.62	–2.30
	MeCN	1.68*	–1.69	–1.45	–2.17
$[FeCp(C_6Me_6)]$	DMF	–1.54	–1.55	–1.31	–2.02
	THF	–1.53*			
	DMSO	–1.52*	–1.56	–1.32	–1.99
$C_{60}{}^{3-}$	MeCN–PhMe	–1.41*	–1.36	1.12	–1.87
$[CoCp^*_2]$	DMF	–1.39*	–1.40	–1.16	–1.87
$[FeCp(C_6H_6)]$	THF	–1.34*			
$C_{60}{}^{2-}$	MeCN–PhMe	–0.915*	–0.91	–0.67	–1.37
$[CoCp_2]$	DME	–0.74*	–0.86	–0.62	–1.33
$C_{60}{}^{-}$	MeCN–PhMe	–0.515*	–0.51	–0.27	–0.98
$[FeCp^*_2]$	DMF	0	–0.012	0.23	–0.49
	CH_2Cl_2	0	–0.105	0.13	–0.55
Hydrazine	DMSO	0.06	–0.03	0.21	–0.41

Note: Direct measurements vs. $FeCp^*_2{}^{+/0}$ are noted by *. The mono-, di-, and tri-anions of C_{60} are accessible by reduction of C_{60} using $[Fe^{I}Cp(C_6Me_6)]$ (17). The other values vs. $FeCp_2{}^{*+/0}$ are: $C_{60}{}^{3-/4-}$: –1.895 V; $C_{60}{}^{4-/5-}$: –2.39 V; and $C_{60}{}^{5-/6-}$: –2.39 V. The two later values were deduced from the values vs. $FeCp_2{}^{+/0}$ reported in ref. 48. Other standard redox potentials E^0 (V) of oxidants and reductants vs. various references were extracted from ref. 16 and corrected from the $FeCp_2{}^{+/0}$ to the $FeCp^*_2{}^{+/0}$ reference using the ΔE^0 values of Table 2.

more substantial, especially because there is space for interaction between the non-methylated rings in ferrocenium. It now becomes clear from Table 2 that the $E_{1/2}$ values measured vs. $FeCp^*_2{}^{+/0}$ are independent of the solvent for these three permethylated metal sandwich complexes within the accuracy of our experiments. Variations of up to 0.11 V for ferrocene were found, however, showing the significant influence of the solvent on the redox potential of ferrocene compared with the permethylated complexes. The fact that the $FeCp_2{}^{+/0}$ reference is not quite accurate enough in this respect does not mean that the many results that have been reported in the recent literature vs. $FeCp_2{}^{+/0}$ have to be remeasured vs. the more accurate $FeCp^*_2{}^{+/0}$ reference. Indeed, it is possible to take advantage of all the results obtained vs. $FeCp_2{}^{+/0}$ (16) using the conversion of values vs. $FeCp_2{}^{+/0}$ to values vs. $FeCp^*_2{}^{+/0}$ of Tables 2 and 3 in various solvents. Likewise, it is possible to continue using ferrocene as the internal reference and yet to have a solvent- and electrolyte-independent redox potential by conversion using Tables 2 and 3. Accordingly, the standard redox potentials of the main reductants and oxidants, $E^{0\prime}$ vs. $FeCp_2{}^{+/0}$, $FeCp^*_2{}^{+/0}$, SCE, and the normal hydrogen electrode (NHE), are now given in Tables 3 and 4, respectively.

Inhibition of the electrochemistry of ferrocene and decamethylferrocene by polyamine dendrimers

Dendrimers (49) might be essential parts of future biomedical, electronic, optical, and magnetic nanodevices (sensors, switches, memories, transistors) (50). Therefore, electrochemistry involving these nanomolecules is crucial to the analysis of electron-transfer properties (17, 51–54). Among the dendritic redox probes (55–61), ferrocenes occupy a central place, for the same reasons involving physical properties and conveniency that led to its choice as an internal reference for the determination of redox potentials (vide supra). Ferrocenes are also used as mediators between electrodes and buried metal centers of metalloenzymes, a property that has been applied to glucose sensors (62).

The well-known commercial DSM polyamine — or so-called poly(propylene imine) — dendrimers (Chart 2) (63) are shown here to inhibit the electrochemistry of simple ferrocene derivatives such as ferrocene itself and decamethylferrocene.

We will also indicate how this electrochemical activity is reestablished using hydrogen bonding (64–77) between the primary amino groups of these dendrimers and metallocenyl alcohols and phenols (72–76).

Despite the well-known electrochemical behavior of ferrocene, Fig. 1 shows that the electrochemical activity of **2** in CH_2Cl_2 on a Pt electrode at a fixed return potential is all the more inhibited by the presence of a polyamine dendrimer as the dendrimer generation increases, i.e., this inhibition is subjected to a dramatic dendritic effect. Although the cyclic voltammogram (CV) is hardly perturbed in the presence of propylamine (Fig. 1*a*), it almost completely vanishes in the presence of G_4 dendr-$(NH_2)_{64}$ (Fig. 1*d*). Thus, the Pt elec-

© 2006 NRC Canada

Table 4. Formal potentials (V) of the main oxidants.

Oxidant	Solvent	E^0 vs. $FeCp^*_2{}^{+/0}$	E^0 vs. SCE	E^0 vs. NHE	E^0 vs. $FeCp_2{}^{+/0}$
$[N(C_6H_2Br_3\text{-}2,4,6)_3]^{\cdot+}$	MeCN	1.87	1.74	1.98	1.36
$[N(C_6H_3Br_2\text{-}2,4)_3]^{\cdot+}$	MeCN	1.65	1.52	1.76	1.14
$[NO]^+$	CH_2Cl_2	1.55	1.44	1.68	1.00
$[RuL_3]^{3+}$, L = bpy or phen	MeCN	1.40*	1.25	1.49	0.87
[Thianthrene]$^{\cdot+}$	MeCN	1.32*	1.24	1.48	0.86
$[N(C_6H_4Br\text{-}4)_3]^{\cdot+}$	MeCN	1.21*	1.05	1.29	0.70
$[Fe(bipy)_3]^{3+}$	MeCN	1.17	1.04	1.28	0.66
Ag^+	CH_2Cl_2	1.16	1.05	1.29	0.65
$[FeCp(\eta^5\text{-}C_5H_4COMe)]^+$	MeCN	0.75*	0.71	0.95	0.27
Cl_2	MeCN	0.69	0.56	0.80	0.18
DDQ	MeCN	0.635*	0.51	0.75	0.13
Br_2	MeCN	0.58	0.45	0.69	0.07
$[FeCp_2]$	MeCN	0.51*	0.38	0.62	0
	CH_2Cl_2	0.55*	0.42	0.66	0
$[N_2C_6H_4F\text{-}4]^+$	MeCN	0.44	0.31	0.55	–0.07
$[Fe\{C_5(CH_2Ph)_5\}_2]$	CH_2Cl_2	0.49*	0.50	0.74	–0.06
	THF, MeCN	0.41*			
	DMF	0.34*	0.215	0.455	–0.14
I_2	MeCN	0.37	0.24	0.48	–0.14
TCNE	MeCN	0.345*	0.11	0.35	–0.27
TCNQ	MeCN	0.32*	0.08	0.32	–0.30
$[FeCp^*_2]$	MeCN	0	–0.13	0.11	–0.51
$[FeCp^*_2]$	CH_2Cl_2	0	–0.105	0.13	–0.55

Note: Direct measurements vs. $FeCp^*_2{}^{+/0}$ are noted by *. The mono-, di-, and tri-anions of C_{60} are accessible by reduction of C_{60} using $[Fe^ICp(C_6Me_6)]$ (17). The other values vs. $FeCp_2{}^{*+/0}$ are: $C_{60}{}^{3-/4-}$: –1.895 V; $C_{60}{}^{4-/5-}$: –2.39 V; and $C_{60}{}^{5-/6-}$: –2.39 V. The two later values were deduced from the values vs. $FeCp_2{}^{+/0}$ reported in ref. 48. Other standard redox potentials E^0 (V) of oxidants and reductants vs. various references were extracted from ref. 16 and corrected from the $FeCp_2{}^{+/0}$ to the $FeCp^*_2{}^{+/0}$ reference using the ΔE^0 values of Table 2.

trode is passivated by the polyamine dendrimer that shields the redox-active compounds in solution.

The inhibition is all the more marked as the return potential is more positive. This results from modification of the electrode by scanning beyond the potential at which the dendritic polyamine is oxidized (Fig. 2). Thus, the large polyamine dendrimers adsorbed on the passivated Pt electrode are insulating barriers between the Pt electrode and $[FeCp_2]$ (**1**) or $[FeCp^*_2]$ (**2**). What is left in the CV of Fig. 1*d* is reminiscent of the electrochemistry observed with metalloproteins on electrodes, and the shape of the CV might be explainable similarly. If the dendrimer has holes in the surface coverage, then the bulk electrode acts as a microelectrode and the signal that is observed corresponds to a hemispherical diffusion (mixing hemispherical and linear diffusion) (77).

Figure 3 compares the CVs of **2** together with those of various ferrocene derivatives in the presence of G_3 dendr-$(NH_2)_{16}$. First, Figs. 3*a* and 3*b* compare the CVs of a mixture of **1** and **2** in the presence of propylamine (Fig. 3*a*) vs. G_3 dendr-$(NH_2)_{16}$ (Fig. 2*b*) showing that the ferrocene wave is rectified (i.e., the return reduction wave of ferrocenium is strongly reduced or lost) only in the presence of the dendrimer.

The scan rate has little influence on the passivation phenomenon, as shown in Fig. 4. On the other hand, nondendritic amines such as dodecylamine and triethylenetetramine do not show the inhibition phenomenon, which is indicative of the specificity of polyamine dendrimers (Fig. 5).

The key role of hydrogen bonding with the hydroxy group in hydroxy-containing ferrocene references to reestablish the electrochemical activity

In Figs. 3*c* and 3*d*, ferrocene is replaced by a ferrocenyl derivative containing a hydroxymethyl substituent in **5a** (Chart 3, Fig. 3*c*) or a hydroxybenzyl substituent in **6** (Chart 3, Fig. 3*d*) showing that the reversibility is reestablished when a hydroxymethyl or phenol group is present on the ferrocene substituent.

The complex **5b** is less efficient than **5a** owing to the steric effect of the methyl group. Figure 2*d* shows that the effect is more marked with the more acidic phenol-group-containing ferrocene derivative [Fc-CH_2p·C_6H_4-OH] (**6**) (78) that forms stronger hydrogen bonds with amines than **5a**. Altogether, the magnitude of the inhibition follows the sequence:

$$[FeCp^*_2] > [FeCp_2] > FcCH(Me)OH\text{-}Me > [Fc\text{-}CH_2OH] > [Fc\text{-}CH_2p\cdot C_6H_4\text{-}OH]$$

For instance, it is remarkable that the ferrocenyl estradiol derivative **8** (79) gives a reversible CV wave in the presence of G_3 dendr-$(NH_2)_{16}$ (Fig. 6), whereas the CVs of the standard references **1** and **2** themselves are inhibited or strongly rectified under the same conditions. Note, however, that the CV of **8** is slightly rectified by comparison to those of **6**. Indeed, the rigid steroidal frame keeps the redox center away from the phenol group, unlike in **6**. This is also in accord

© 2006 NRC Canada

Chart 2.

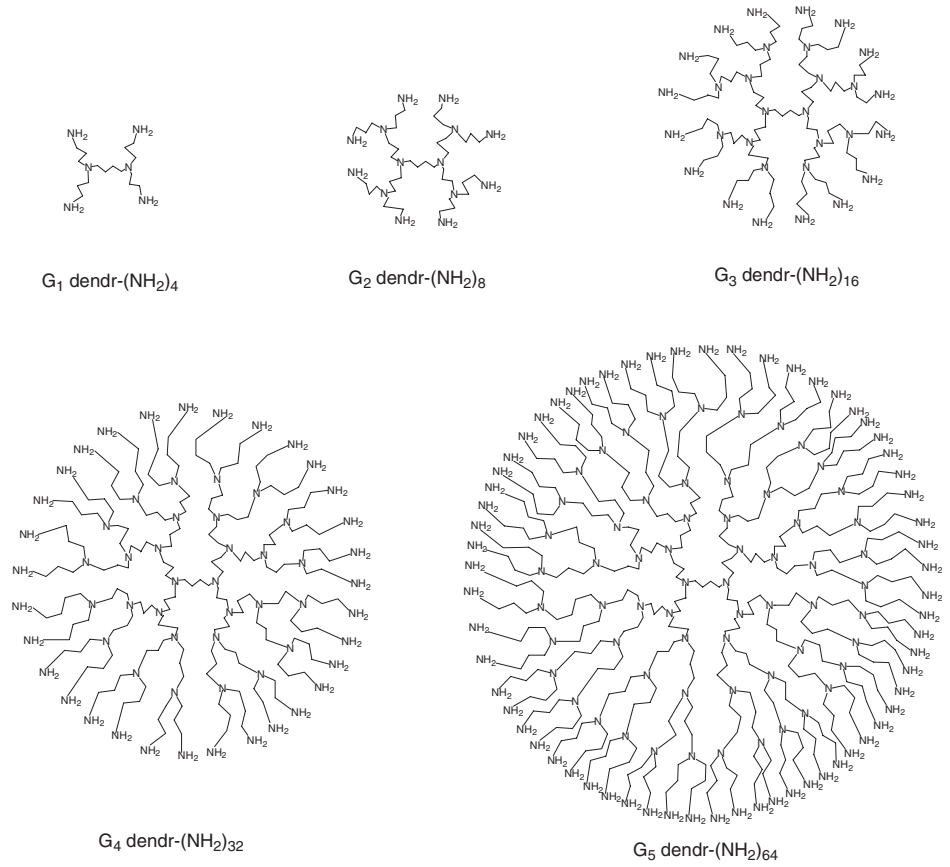


Fig. 1. Cyclic voltammograms (CVs) of $FeCp_2^*$ (**2**, 10^{-3} mol/L), CH_2Cl_2; *n*-Bu_4NPF_6 (0.1 mol/L); reference electrode: Ag/Ag^+; working and counter electrodes: Pt; scan rate: 0.2 V s^{-1}; (*a*) **2** in the presence of 1 equiv. propylamine; (*b*) **2** in the presence of 1/4 equiv. G_1 dendr-$(NH_2)_4$; (*c*) **2** in the presence of 1/16 equiv. G_3 dendr-$(NH_2)_{16}$; (*d*) **2** in the presence of 1/64 equiv. G_5 dendr-$(NH_2)_{64}$.

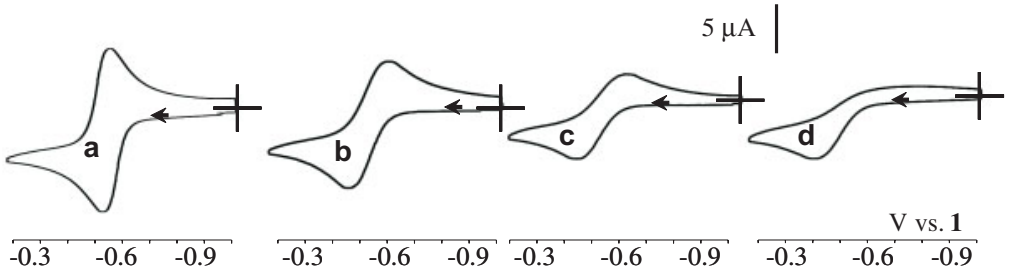
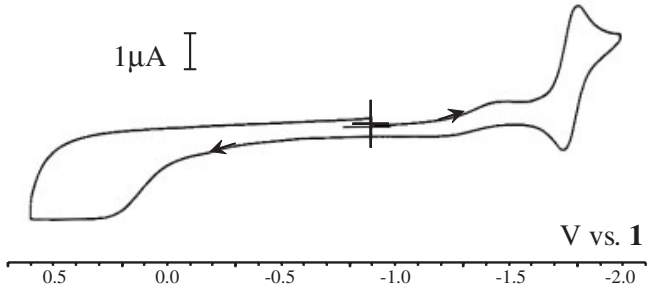


Fig. 2. Cyclic voltammogram (CV) of G_5 dendr-$(NH_2)_{64}$ (10^{-3} mol/L): CH_2Cl_2; *n*-Bu_4NPF_6 (0.1 mol/L); reference electrode: Ag/Ag^+; internal reference: **7** (see Chart 3); working and counter electrodes: Pt; scan rate: 0.2 V s^{-1}.



with the selective OH···H_2N hydrogen bonding with the distal phenol rather than with the tertiary alcohol near the redox center of **8**. The recovery of the CV in hydroxy-containing redox-active compounds can tentatively be taken into account by the dendrimeric linkage between **8** and the Pt electrode via the amino termini of the polyamine dendrimer represented in Fig. 6.

This suggestion implies that the hydrogen bonding between the hydroxy groups and the dendrimer amino group brings **5a**, **6**, or **8** near the electrode, so that they are close enough to remain electroactive. Indeed, it is well-known that dendrimers adsorb strongly (80, 81) and flatten (82, 83) on metal surfaces. It has also been shown that, in the dendrimers containing ferrocenyl termini (84), all the ferrocenyl centers are electroactive with fast electron transfer even in the solid state owing to electron hopping. This is

© 2006 NRC Canada

Fig. 3. Cyclic voltammograms (CVs) of **2** (10^{-3} mol/L): CH_2Cl_2; *n*-Bu_4NPF_6 (0.1 mol/L); reference electrode: Ag^+/Ag; working and counter electrodes: Pt; scan rate: 0.2 V s^{-1}; (*a*) **1** + **2** + 1 equiv. propylamine; (*b*) **1** + **2** + 1/16 equiv. G_3 dendr-$(NH_2)_{16}$; (*c*) **2** + **5a** + 1/16 equiv. G_3 dendr-$(NH_2)_{16}$; (*d*) **2** + **6** + 1/16 equiv. G_3 dendr-$(NH_2)_{16}$.

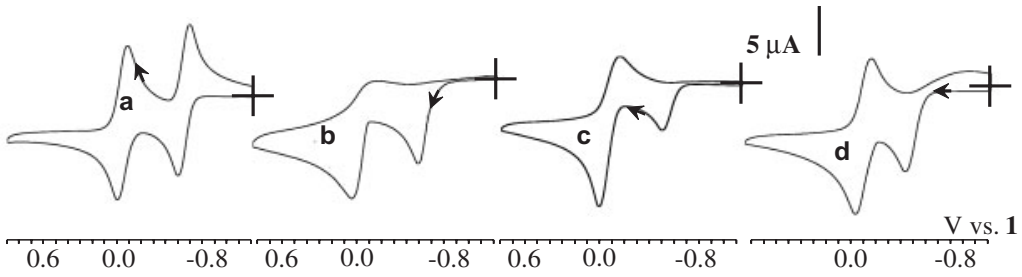


Fig. 4. Cyclic voltammogram (CV) of **2** and G_5 dendr-$(NH_2)_{64}$ (10^{-3} mol/L): CH_2Cl_2; *n*-Bu_4NPF_6 (0.1 mol/L); reference electrode: Ag^+/Ag; working and counter electrodes: Pt. (*a*) Scan rate: 0.1 V s^{-1}. (*b*) Scan rate: 0.5 V s^{-1}.

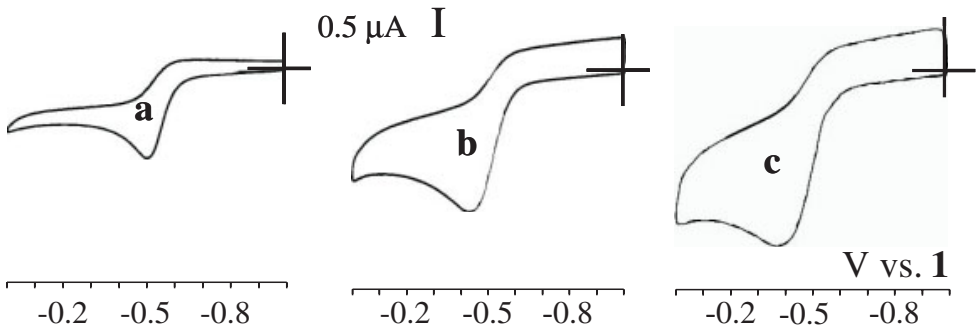
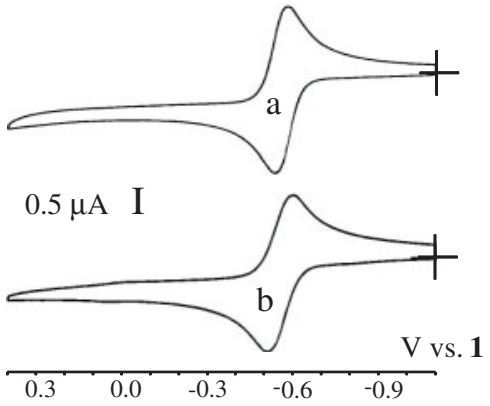


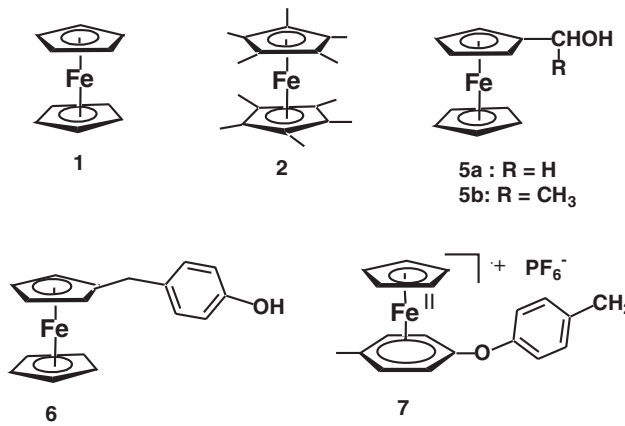
Fig. 5. Cyclic voltammogram (CV) of **2** in the presence of dodecylamine and triethylenetetramine. CVs of **2** (10^{-3} mol/L), CH_2Cl_2; *n*-Bu_4NPF_6 (0.1 mol/L); reference electrode: Ag^+/Ag; working and counter electrodes: Pt; scan rate: 0.2 V s^{-1}. (*a*) **2** in the presence of 1 equiv. dodecylamine. (*b*) **2** in the presence of 1 equiv. triethylenetetramine.



true even with ferrocenyl dendrimers containing several hundred ferrocenyl groups (85, 86). A similar situation is found here in supramolecular dendrimers.

This reversible hydrogen bonding between polyamine dendrimers and phenols is shown by comparison of the ^1H NMR spectra of the phenol derivative **6** and G_3 dendr-$(NH_2)_{16}$ alone with that of a mixture of these compounds (equimolar mixture of hydroxy and amino groups, Fig. 7). Thus, in the ^1H NMR spectrum of the mixture, the signals of the OH and NH_2 groups of the isolated compounds have disappeared and a new broad average signal common to the

Chart 3.

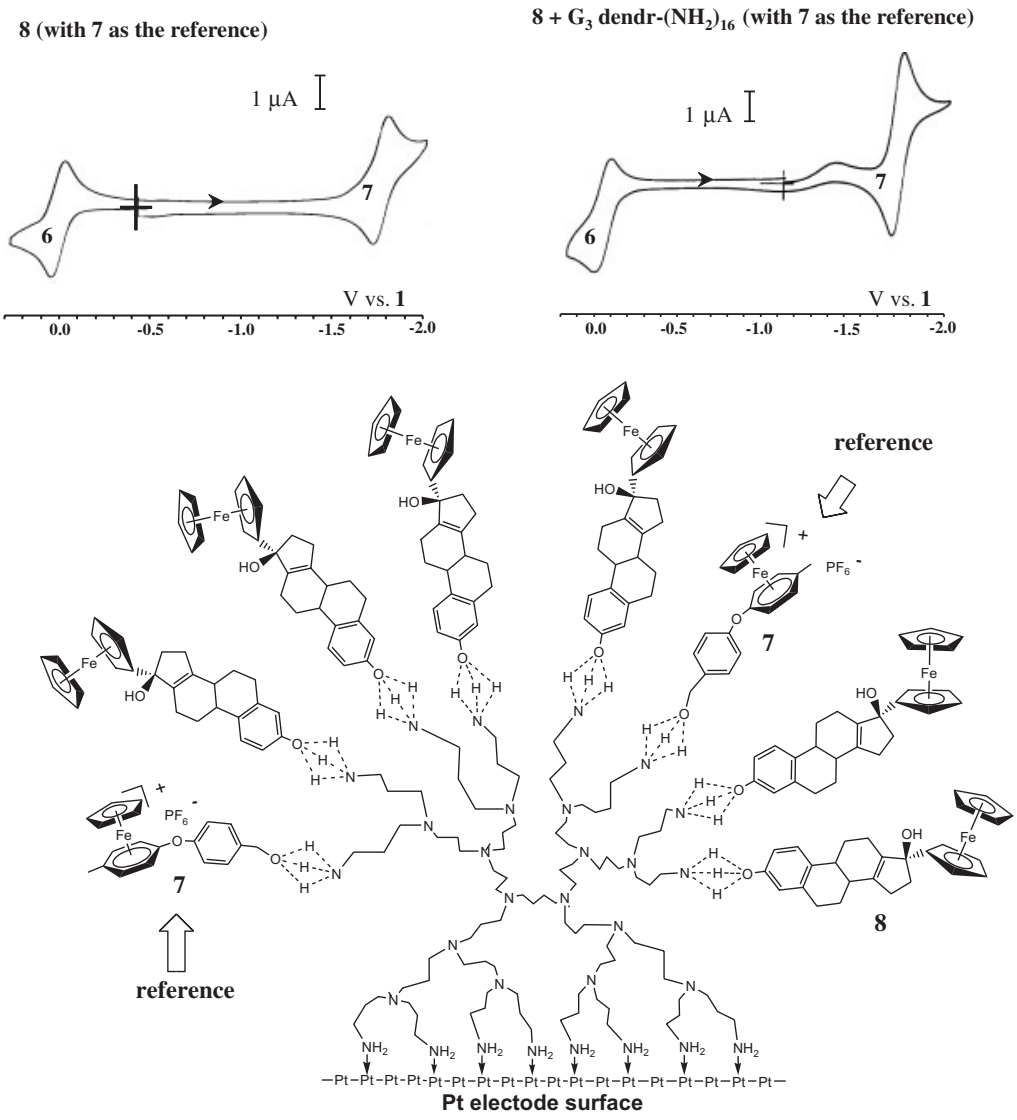


OH + NH_2 groups has appeared. Even though this H-bonding is reversible (as indicated by the concentration dependence of the signal location) owing to the low energy of the hydrogen-bonding interaction, the process is efficient on the relatively large electrochemical timescale of the CV.

To confirm that the OH···NH_2 hydrogen bonding is responsible for the CV of the hydroxy-containing ferrocenes, we considered the other possibility: preferential direct interaction of the hydroxy group of a phenol with the electrode in the presence of a polyamine dendrimer. For this purpose, we recorded the CV of the tetra ferrocenyl dendrimer, G_1 dendr-$(NHCH_2Fc)_4$ (**9**) (Fc = ferrocenyl), already reported together with its detailed electrochemical study by Jutzi (47). It provides additional evidence of the observation of electrochemical redox activity of a ferrocenyl group when it is linked to a polyamine dendrimer (Fig. 8*a*), as already shown by this

© 2006 NRC Canada

Fig. 6. CH_2Cl_2; *n*-Bu_4NPF_6 (0.1 mol/L); reference electrode: Ag^+/Ag; working and counter electrodes: Pt; scan rate: 0.2 V s^{-1}. (*a*) Cyclic voltammogram (CV) of the steroid derivative **8** (5×10^{-4} mol/L) in the presence of the reference compound **7** (5×10^{-4} mol/L), both containing hydroxy groups without (top left) and with (top right) G_3 dendr-$(NH_2)_{16}$ (6.25×10^{-4} mol/L); note the slight rectification for **8**. (*b*) Linkage of redox-active groups to the Pt electrode via G_3 dendr-$(NH_2)_{16}$ (bottom).



author. We have also compared the CV of **9** and *p-tert*-butylphenol with that of their mixture. No dramatic difference was found for the CV of **7** in the presence and absence of *p-tert*-butylphenol (compare Figs. 8*b* and 8*d*). Then, the oxidation wave of *p-tert*-butylphenol at 1 V vs. **1** is no longer observed when **7** is present in the electrochemical cell. The ferrocenyl and amine groups are anodically oxidized at close potentials, giving a broad anodic wave. Scanning beyond this wave is necessary to reach the phenol oxidation wave, but the electrode is modified or passivated by the polyamine dendrimer acting as an insulator, which prevents the observation of this phenol oxidation wave (compare Figs. 8*c* and 8*d*).

These experiments indicate that the phenol is not adsorbed onto the Pt electrode preferentially to the polyamine dendrimer, even a small one. It is also probable that hydrogen bonding with the secondary amine **9** is much less efficient than with primary amines for steric reasons (vide supra **5b** vs. **5a**). Since the adsorption of the polyamine dendrimer is all the stronger as the generation is higher, the electroactivity of redox-active compounds containing a hydroxy group cannot be explained by the direct interaction of the hydroxy group with the Pt electrode in the presence of the polyamine dendrimer. Consequently, the hydrogen bonding shown by NMR and the above experiment indicates that the dendrimer linkage shown in Fig. 4 is responsible for the electroactivity of the hydroxy-bonded redox-active ferrocenes in the presence of polyamine dendrimers.

Figure 8*e* shows the CV of the hexaammonium hexaundecanoate salt resulting from the protonation of **9** by undecanoic acid. The electrochemistry of the hexaammonium hexachloride salt resulting from the protonation of **9** by HCl in DMSO has already been reported (47), but the undecanoate ion now provides solubility in CH_2Cl_2 for comparison with the CV of **9**. This comparison (Fig. 8 including 8*e*) also confirms that *p-tert*-butylphenol does not protonate **9**,

© 2006 NRC Canada

Fig. 7. ^{1}H NMR (300 MHz) spectra of **6** (top), G_3-dendr-$(NH_2.)_{32}$ (middle), and their mixture (1 equiv. of **6** per amino group of the dendrimer; bottom) in $CDCl_3$.

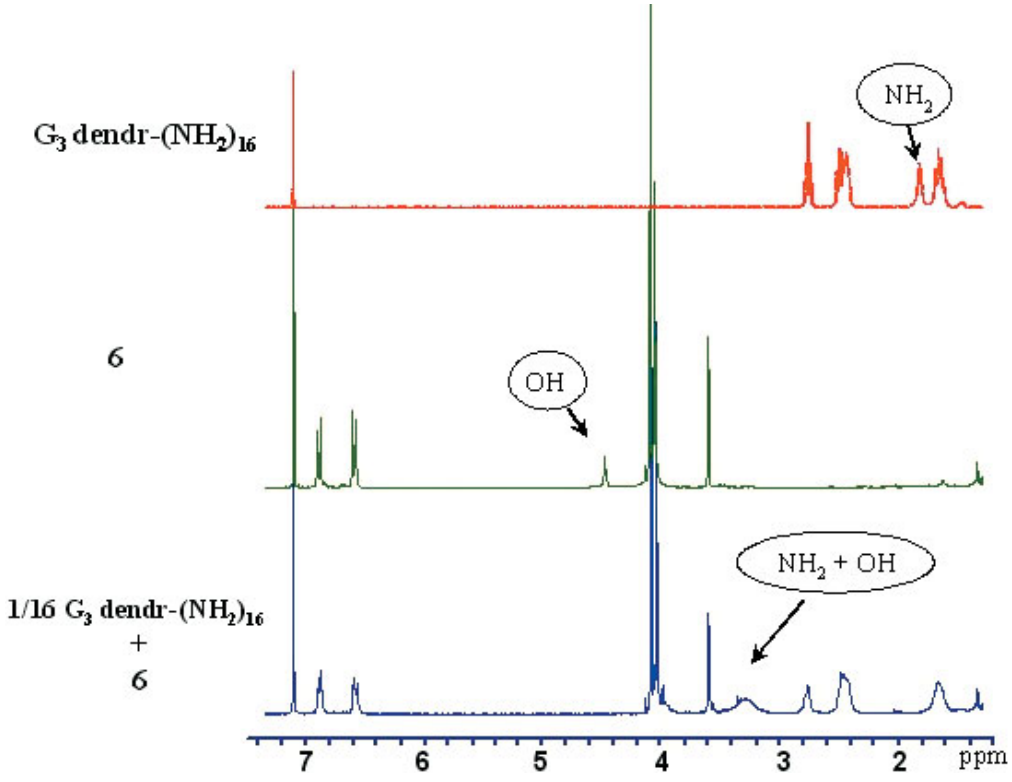
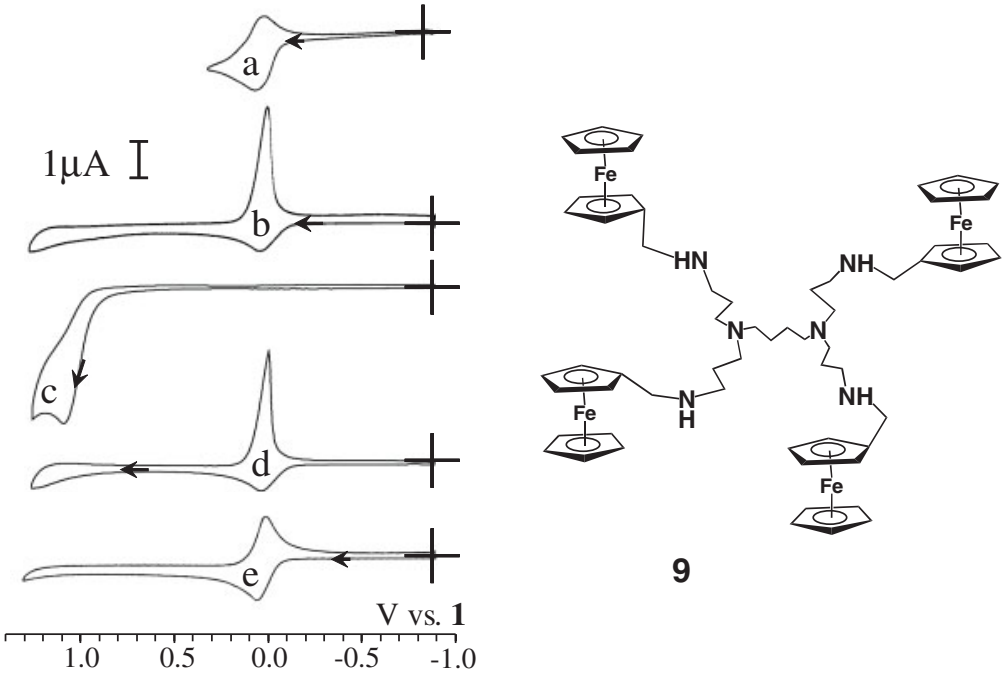


Fig. 8. (*a*) Cyclic voltammogram (CV) of **9** showing the overlap between the reversible oxidation of the ferrocenyl groups and the irreversible oxidation of the primary and tertiary amine groups on the anodic side (compare with Fig. 2). (*b*) Cyclic voltammogram (CV) of **9** with scanning up to 1.4 V vs. **1** showing the strong adsorption on the cathodic side. (*c*) Cyclic voltammogram (CV) of *p-tert*-butylphenol. (*d*) Cyclic voltammogram (CV) of **9** scanned up to 1.4 V vs. **1** in the presence of *p-tert*-butylphenol. (*e*) Cyclic voltammogram (CV) of the hexaamine **9** protonated by 6 equiv. undecanoic acid. The shift of potential of the hexaammonium salt vs. the hexaamine **9** results from both the hydrophobic and electronic effects.



© 2006 NRC Canada

as shown by the disappearance of the anodic oxidation in the CV of this salt, contrary to that of **9** in the presence of *p-tert*-butylphenol. Thus, since the secondary amino groups of **9** are more basic than the primary amino groups of the DSM polyamine dendrimers, the H-bonding responsible for the CV of OH-containing ferrocenes in the presence of a DSM dendrimer does not involve protonation of the amino groups by the phenol.

Conclusion

It has been shown here that (*i*) the difference in $E_{1/2}$ values between the permethylated Fe and Co sandwich complexes are solvent independent within the accuracy of our experiments, in agreement with prior work by Lay's group (37) and our preliminary study (43); (*ii*) this allows using them as solvent-independent internal references for the determination of redox potentials and linking the solvent dependent $E_{1/2}$ obtained in the literature vs. ferrocene $E_{1/2}$ to values vs. decamethylferrocene that are solvent independent (37, 43); (*iii*) polyamine dendrimers inhibit (or strongly rectify) the electrochemistry of simple redox-active compounds such as the ferrocenes **1** and **2** because of their adsorption on Pt electrodes upon anodic oxidation. They do all the more so as they are larger and as the potential is scanned toward more positive values; (*iv*) this CV can be reestablished by bonding between the primary amino groups of the dendrimer and the redox-active compound either by hydrogen bonding or by covalent bonding. Thus, although polyamine dendrimers inhibit the electrochemistry of simple redox-active compounds, they form redox-active dendritic systems by $NH_2\cdots HO$ hydrogen bonding resembling redox-active dendrimers well-known with covalent bonding between the core and redox-active termini. Finally, two or several hydroxymethyl- or phenol-containing redox-active compounds can simultaneously show redox activity, which could potentially be used in combinatorial ways. For instance, a simple application shown here is that compounds such as **8** or **9** are excellent internal references to determine redox potentials in the presence of polyamine dendrimers (see Figs. 2 and 4), whereas the use of the classic references **1** or **2** is not possible under these conditions.

Experimental section

General data

Tetrahydrofuran and diethyl ether were purified before use by distillation from sodium/benzophenone ketyl under nitrogen. Acetonitrile was stirred under nitrogen overnight on phosphorus pentoxide, distilled from sodium carbonate, and stored under nitrogen. Dichloromethane was distilled from calcium hydride just before use. Anhydrous *N*,*N*-dimethylformamide (DMF), [$FeCp_2$], [$FeCp_2$*], DSM polyamine dendrimers G_n-DAB-dend-$(NH_2)x$ were purchased from Aldrich and [$CoCp^*_2$]PF_6 and [$FeCp_2$*]PF_6 were purchased from Strem and used as received. Tetrabutylammonium tetrafluoroborate (Bu_4NBF_4) and tetrabutylammonium hexaflurophosphate (Bu_4NPF_6) were purchased from Fluka. The former salt was crystallized in a methanol–water mixture to eliminate traces of iodide ions and dried under vacuum.

Cyclic voltammetry

Cyclic voltammetry data were recorded with a PAR 273 potentiostat galvanostat. Care was taken in the CV experiments to minimize the effects of the solution resistance on the measurements of potential peaks (the use of positive feedback *iR* compensation and dilute solution (10^{-4} mol/L) maintained currents between 1 and 10 μA). The working electrode and counter electrode were platinum (Pt). The working electrode was a disc of 1 mm diameter and was treated by immersion in 0.1 mol/L HNO_3, then polished before use and between each recording if necessary.

Acknowledgments

We are grateful to Dr. M. Szlosek (University of Bordeaux I, Talence, France) for a sample of tetraferrocenyl dendrimer **9**. Financial support from the Institut Universitaire de France (IUF, D. Astruc), the Centre National de la Recherce Scientifique (CNRS), and the Ministère de la Recherche et de la Technologie (MRT, Ph.D. grant to M.-C. Daniel) and the University of Bordeaux I is gratefully acknowledged.

References

1. A.J. Bard and L.R. Faulkner. Electrochemical methods. Wiley, New York. 1980.
2. G.J. Hills. *In* Reference electrodes. *Edited by* D. Ives and J.G. Janz. Academic Press, New York. 1961.
3. J.F. Coetzee and G.R. Padmanablan. J. Phys. Chem. **66**, 7708 (1962).
4. V.D. Parker. Adv. Phys. Org. Chem. **19**, 131 (1983)
5. W.E. Geiger. J. Organomet. Chem. **22**, 142 (1990).
6. G. Wilkinson. J. Organomet. Chem. **100**, 273 (1952).
7. Ch. Elschenbroich and A. Salzer. Organometallics. 4th ed. Wiley-VCH, Weinheim, Germany. 2005.
8. R. Prins, A.R. Korswagen, and A.G.T.G. Kortbeck. J. Organomet. Chem. **39**, 335 (1972).
9. Z.J. Karpinsky, C. Nanjundiah, and R.A. Osteryoung. Inorg. Chem. **23**, 3358 (1984).
10. A.J. Zara, S.S. Machado, L.O.S. Bulhoes, A.V. Benedetti, and T. Rabockai. J. Electroanal. Chem. **221**, 165 (1987).
11. J.P. Hurvois and C. Moinet. J. Organomet. Chem. **690**, 1829 (2005).
12. G. Grizner and J. Kuta. Pure Appl. Chem. **56**, 461 (1984).
13. S. Sahami and M.J. Weaver. J. Solution Chem. **10**, 199 (1981).
14. J.T. Hupp. Inorg. Chem. **29**, 5010 (1990).
15. P.A. Lay. J. Phys. Chem. **90**, 878 (1986).
16. N.G. Connelly and W.E. Geiger. Chem. Rev. **96**, 877 (1996).
17. D. Astruc. Electron transfer and radical processes in transition metal chemistry. VCH, New York. 1995. Chap. 2.
18. T.J. Curphey, J.O. Santer, M. Rosenblum, and J.H. Richards. J. Am. Chem. Soc. **82**, 5249 (1960).
19. J.W. Lauer and R. Hoffmann. J. Am. Chem. Soc. **98**, 1729 (1976).
20. H. Morisaki, A. Nishikawa, H. Ono, and K. Yazawa. J. Electrochem. Soc. **137**, 2759 (1990).
21. P.A. Lay and W.H.F. Sasse. Inorg. Chem. **24**, 4707 (1985).
22. U. Kölle and F. Khouzami. Angew. Chem. Int. Ed. Engl. **19**, 640 (1980).

© 2006 NRC Canada

23. J.L. Robbins, N. Edelstein, B. Spencer, and J.C. Smart J. Am. Chem. Soc. **104**, 1882 (1982).
24. P.G. Gassman, D.W. Macomber, and J.W. Hershberger. Organometallics, **2**, 1470 (1983).
25. T. Gennett, D.F. Milner, and M.J. Weaver. Phys. Chem. **89**, 2787 (1985).
26. S.F. Nelson, M.T. Ramm, R.F. Ismagilov, M.A. Nagy, D.A. Trieber, D.R. Powell, X. Chen, J.J. Gengler, Q. Qu, J.L. Brandt, and J.R. Pladziewitcz. J. Am. Chem. Soc. **119**, 5900 (1997).
27. W.E. Britton, R. Kahyap, M. El-Hashah, and M. El-Kady. Organometallics, **5**, 1029 (1986).
28. M.P. Castellani, J.M. Wright, S.J. Geib, A.L. Rheingold, and W.C. Troggler. Organometallics, **5**, 1116 (1986).
29. C.R. Cabrera and A.J. Bard. J. Electroanal. Chem. Interfacial Electrochem. **273**, 147 (1989).
30. C.P. Andrieux, P. Audebert, and F. Michalak. J. Electroanal. Chem. Interfacial Electrochem. **296**, 117 (1990).
31. S. Ching, J.T. McDewitt, S.R. Peck, and R.W. Murray. J. Electrochem. Soc. **138**, 2308 (1991).
32. J.C. Gallucci, G. Opromolla, L.A. Paquette, L. Pardi, P.F.T. Schirch, M.R. Sivik, and P. Zanello. Inorg. Chem. **32**, 2292 (1993).
33. P. Zanello, A. Cinquantini, S. Mangani, and G. Opromolla. J. Organomet. Chem. **471**, 171 (1994).
34. P. Zanello. Inorganic electrochemistry: Theory, practice and applications. Royal Society of Chemistry, Cambridge. 2003.
35. J.N. Richardson, J. Harvey, and R.W. Murray. J. Phys. Chem. **98**, 13396 (1994).
36. J.K. Bashkin and P.J. Kinlen. Inorg. Chem. **29**, 4507 (1990).
37. I. Noviandri, K.N. Brown, D.S. Fleming, P.T. Gulyas, P.A. Lay, A.F. Masters, and L.J. Phillips. J. Phys. Chem. B, **103**, 6713 (1999).
38. D.P. Freyberg, J.L. Robbins, K.N. Raymond, and J.C. Smart. J. Am. Chem. Soc. **101**, 892 (1979).
39 D. Astruc, J.-R. Hamon, G. Althoff, E. Román, P. Batail, P. Michaud, J.-P. Mariot, F. Varret, and D. Cozak. J. Am. Chem. Soc. **101**, 5445 (1979).
40. M.V. Rajasekharan, S. Giezynski, J.H. Ammeter, N. Oswald, J.-R. Hamon, P. Michaud, and D. Astruc. J. Am. Chem. Soc. **104**, 2400 (1982).
41. D. Astruc. Acc. Chem. Res. **19**, 377 (1986).
42. D. Astruc. Chem. Rev. **88**, 2253 (1988).
43. J. Ruiz and D. Astruc. C. R. Acad. Sci. Ser. IIc, **1**, 21 (1998).
44. H.A. Trujillo, C.M. Casado, J. Ruiz, and D. Astruc. J. Am. Chem. Soc. **121**, 5674 (1999).
45. A. Loupy, B. Tchoubar, and D. Astruc. Chem. Rev. **92**, 1141 (1992).
46. M.-C. Daniel, J. Ruiz Aranzaes, and D. Astruc. Chem. Commun. (Cambridge, U.K.), 1569 (2005).
47. A. Salmon and P. Jutzi. J. Organomet. Chem. **637–639**, 595 (2001).
48. Q. Xie, E. Pérez-Cordero, and L. Echegoyen. J. Am. Chem. Soc. **114**, 3978 (1992).
49. G.R. Newkome, C.N. Moorefield, and F. Vögtle. Dendrimers and dendrons. Concepts, synthesis and applications. VCH-Wiley, Weinheim, Germany. 2001.
50. D. Astruc (*Guest editor*). Dendrimers and nanosciences. Vols. 8–10. C.R. Chimie, Elsevier, Paris. 2003.
51. A.E. Kaifer and M. Gomez-Kaifer. Supramolecular electrochemistry. Wiley-VCH, Weinheim, Germany. 1999. Chap. 16.
52. V. Balzani, S. Campagna, G. Denti, A. Juris, S. Serroni, and M. Venturi. Acc. Chem. Res. **32**, 25 (1998).
53. R. Sadamoto, N. Tomioka, and T. Aida. J. Am. Chem. Soc. **118**, 3978 (1996).
54. J. Isberner, F. Vögtle, L. de Cola, and V. Balzani. Chem. Eur. J. **3**, 706 (1997).
55. C.B. Gorman, B.L. Parkhurst, W.Y. Su, and K.Y. Che. J. Am. Chem. Soc. **119**, 1141 (1997).
56. G.R. Newkome, E. He, and Moorefield. Chem. Rev. **99**, 1689 (1999).
57. I. Cuadrado, M. Moran, C.M. Casado, B. Alonso, and J. Losada. Coord. Chem. Rev. **193**, 395 (1999).
58. G.R. Newkome, L.A. Narayanan, and L.A. Godinez. J. Org. Chem. **65**, 643 (2000).
59. J.J. Apperlo, R.A. Jansse, P.R.L. Malenfant, L. Groenendal, and J.M.J. Fréchet. J. Am. Chem. Soc. **122**, 7042 (2000).
60. C.B. Gorman and J.C. Smith. Acc. Chem. Res. **34**, 60 (2001).
61. V. Balzani, P. Ceroni, A. Juris, M. Venturi, S. Campagna, F. Puntoriero, and S. Serroni. Coord. Chem. Rev. **219–221**, 545 (2001).
62. A. Heller. Acc. Chem. Res. **23**, 228 (1990).
63. E.M.M. de Brabander-van den Berg and E.W. Meijer. Angew. Chem. Int. Ed. Engl. **32**, 1308 (1993).
64. J.C. Hummelen, J.L.J. van Dongen, and E.W. Meijer. Chem. Eur. J. **3**, 1489 (1997).
65. A.W. Bosman, H.M. Janssen, and E.W. Meijer. Chem. Rev. **99**, 1665 (1999).
66. J.-W. Weener, M.W.P.L. Baars, and E.W. Meijer. *In* Dendrimers and other dendritic polymers. *Edited by* D. Tomalia and J.M.J. Fréchet. Wiley-VCH, New York. 2002.
67. J.-M. Lehn. Supramolecular chemistry: Concepts and perspectives. VCH, Weinheim, Germany. 1995.
68. H.M. Janssen, E.M.M. de Brabander-van den Berg, and E.W. Meijer. Science (Washington, D.C.), **265**, 1226 (1994).
69. H.M. Janssen and E.W. Meijer. J. Am. Chem. Soc. **117**, 4417 (1995).
70. S.C. Zimmerman, F. Zeng, D.E.C. Reichert, and S. Kolotuchin. Science (Washington, D.C.), **272,** 1095 (1996).
71. D. De Groot, B.F.M. de Waal, J.N.H. Reek, A.P.H.J. Schenning, P.C.J. Kamer, E.W. Meijers, and P.W.N.M. van Leeuwen. J. Am. Chem. Soc. **123**, 8453 (2001).
72. For hydrogen bonding between alcohols and amines, see refs. 73–76 and: O. Ermer and A. Eling. J. Chem. Soc. Perkin Trans. 2, 925 (1994).
73. E.A. Melwyn-Hugues. Physical chemistry. 2nd ed. Pergamon, Oxford. 1961. p. 1960.
74. S. Hanessian, M. Simard, and S. Roelens. J. Am. Chem. Soc. **117**, 7630 (1995).
75. For ^{1}H NMR and electrochemical evidence for H-bonding between dendritic polyamines and phenols, see ref. 76 and : M.-C. Daniel, J. Ruiz, and D. Astruc. J. Am. Chem. Soc. **125**, 1150 (2003).
76. M.-C. Daniel, F. Ba, J. Ruiz, and D. Astruc. Inorg. Chem. **43**, 8649 (2004).
77. F.A. Amstrong, A.M. Bond, H.A.O. Hill, B.N. Oliver, and I.S.M. Psalti. J. Am. Chem. Soc. **111**, 9185 (1989); A.M. Bond and H.A.O. Hill. Met. Ions Biol. **27**, 431 (1991); F.N. Buechi, A.M. Bond, R. Codd, L.N. Huc, and H.C. Freeman. Inorg. Chem. **31**, 5007 (1992); D.D.N. McLeod, D.D. Niles, H.C. Freeman, I. Harvey, P.A. Lay, and A.M. Bond. Inorg. Chem. **35**, 7156 (1996); H.A.O. Hill, N.I. Hunt, and A.M. Bond. J. Electroanal. Chem. **436**, 17 (1997).
78. M. Ota, Y. Ushijima, M. Horiguchi, Y. Kawai, and S. Otani. Mol. Cryst. Liq. Cryst. **232**, 313 (1993).
79. D. Vichard, M. Gruselle, G. Jaouen, I.A. Nefedova, I.A. Mamedyarova, V.I. Sokolov, and J. Vaissermann. J. Organomet. Chem. **484**, 1 (1994).
80. K. Takada, D.J. Diaz, H. Abruna, I. Cuadrado, C.M. Casado,

© 2006 NRC Canada

B. Alonso, M. Moran, and J. Losada. J. Am. Chem. Soc. **119**, 19763 (1997).
81. R.M. Crooks, M. Zhao, L. Sun, V. Chechik, and L.K. Yeung. Acc. Chem. Res. **34**, 181 (2001).
82. A. Hierlemann, J.K. Campbell, L.A. Baker, R.M. Crooks, and A.J. Ricco. J. Am. Chem. Soc. **120**, 5323 (1998).
83. J. Li, L.T. Piehler, D. Qin, J.R. Baker, Jr., D.A. Tomalia, and D.J. Meier. Langmuir, **16**, 5613 (2000).
84. For a review on ferrocenyl dendrimers, see: C.M. Casado, I. Cuadrado, M. Moràn, B. Alonso, B. Garcia, J. Gonzales, and J. Losada. Coord. Chem. Rev. **185/186**, 53 (1999); for supramolecular interactions in the electrochemistry of ferrocenyl dendrimers, see ref. 51 and C.M. Cardona, and A.E. Kaifer. J. Am. Chem. Soc. **120**, 4023 (1998).
85. S. Nlate, J. Ruiz, V. Sartor, R. Navarro, J.-C. Blais, and D. Astruc. Chem. Eur. J. **6**, 2544 (2000).
86. M.-C. Daniel, J. Ruiz, S. Nlate, J.-C. Blais, and D. Astruc. J. Am. Chem. Soc. **125**, 2617 (2003).

© 2006 NRC Canada

NMR spectroscopy of the solid-state isomerization of nitrito- and nitro-pentamminecobalt(III) chloride[1]

Kristopher J. Ooms and Roderick E. Wasylishen

Abstract: Cobalt-59 and nitrogen-15 NMR spectra of the *nitrito*pentamminecobalt(III) chloride, $[(NH_3)_5Co\text{-}ONO]Cl_2$, and *nitro*pentamminecobalt(III) chloride, $[(NH_3)_5Co\text{-}NO_2]Cl_2$, isomers in the solid state have been obtained at several applied magnetic field strengths. The ^{59}Co NMR line shapes indicate that both the cobalt nuclear quadrupolar coupling constant (C_Q) and the span of the chemical shift tensor (Ω) decrease when the complex isomerizes from $[(NH_3)_5Co\text{-}ONO]^{2+}$ to $[(NH_3)_5Co\text{-}NO_2]^{2+}$; C_Q decreases from 23 to 10.3 MHz and Ω changes from 1650 to 260 ppm. The ^{15}N NMR line shapes also show a significant change in the nitrogen magnetic shielding tensor upon isomerization, with Ω decreasing from 710 to 547 ppm; also, an indirect spin-spin coupling, $^1J(^{59}Co,^{15}N) = 63$ Hz, is observed in the ^{15}N NMR spectra of the nitro isomer. The NMR parameters are rationalized based on differences in the molecular structure of the two isomers. NMR spectra have also been recorded as the isomerization progresses with time and demonstrate the practicality of the technique for the study of solid-state isomerizations.

Key words: ^{15}N, ^{59}Co, solid-state NMR, linkage isomerization, chemical shift tensor, electric field gradient tensor.

Résumé : Opérant en phase solide et à plusieurs forces de champ magnétique appliqué différentes, on a déterminé les spectres RMN du ^{59}Co et du ^{15}N d'isomères du chlorure de *nitrito*pentamminecobalt(III), $[(NH_3)_5Co\text{-}ONO]Cl_2$ et du chlorure de *nitro*pentamminecobalt(III), $[(NH_3)_5Co\text{-}NO_2]Cl_2$. Les formes des raies des spectres RMN du ^{59}Co indiquent que la constante de couplage quadripolaire nucléaire du cobalt (C_Q) ainsi que l'envergure du tenseur du déplacement chimique (Ω) diminuent toutes les deux lorsque le complexe s'isomérise de $[(NH_3)_5Co\text{-}ONO]^{2+}$ à $[(NH_3)_5Co\text{-}NO_2]^{2+}$; la valeur de C_Q diminue de 23 à 10,3 MHz alors que la valeur de Ω passe de 1650 à 260 ppm. Lors de l'isomérisation, les formes des raies en RMN du ^{15}N présentent aussi un changement significatif dans le tenseur de blindage magnétique de l'azote, avec Ω, qui passe de 710 à 547 ppm; de plus, on observe un couplage spin-spin indirect, $^1J(^{59}Co,^{15}N) = 63$ Hz, dans le spectre RMN du ^{15}N de l'isomère nitro. Les différences dans les paramètres RMN sont rationalisées sur la base de différences dans la structure moléculaire de chacun des isomères. On a aussi enregistré les spectres RMN alors qu'ils s'isomérisent en fonction du temps et on démontrent que cette technique peut être pratique pour l'étude d'isomérisations à l'état solide.

Mots clés : ^{15}N, ^{59}Co, RMN à l'état solide, isomérisation de liaison, tenseur du déplacement chimique, tenseur du gradient du champ électrique.

[Traduit par la Rédaction]

Introduction

Reactions that occur in the solid state are of interest in many areas of research such as pharmaceutical chemistry (1, 2), organometallic chemistry (3), and organic synthesis (4–6). Linkage isomerizations are one class of solid-state reactions that involve a change in the bond(s) between a ligand and a metal centre. The linkage isomerization involving the nitrite anion (NO_2^{-1}) in *nitrito*pentamminecobalt(III) chloride (nitrito), which isomerizes to form the more thermodynamically stable *nitro*pentamminecobalt(III) chloride (nitro), $[(NH_3)_5Co\text{-}ONO]^{2+} \rightarrow [(NH_3)_5Co\text{-}NO_2]^{2+}$, has been known for over 100 years (7). This reaction has been studied in depth by numerous techniques, including solution NMR spectroscopy (8), IR spectroscopy (9–14), single-crystal and powder X-ray diffraction (15–17), and recently, DFT quantum chemical methods (18, 19).

Several studies, primarily employing IR spectroscopy, have determined the rate constants, equilibrium values, and activation energies of the reaction in the solid state (11, 15, 20–23). Typically the isomerization half-life is on the order of hours to days depending on the temperature. One problem with the solid-state investigations to date is that the temperatures at which the kinetic data are measured are usually

Received 21 September 2005. Published on the NRC Research Press Web site at http://canjchem.nrc.ca on 21 March 2006.

Dedicated to Dr. Arthur J. Carty for his contributions to science in Canada.

K.J. Ooms and R.E. Wasylishen.[2] Department of Chemistry, University of Alberta, Edmonton, AB T6G 2G2, Canada.

[1]This article is part of a Special Issue dedicated to Professor Arthur Carty.
[2]Corresponding author (e-mail: roderick.wasylishen@ualberta.ca).

 doi:10.1139/V06-001 © 2006 NRC Canada

above room temperature, while the X-ray diffraction data has been obtained well below room temperature. This makes it difficult to draw connections between the kinetic data and the crystal structures. In addition, there are significant discrepancies in the rate constants reported by different investigators. In principle, solid-state NMR spectroscopy can provide a valuable link between the structural and thermodynamic properties of this system at the same temperature; however, only the solid-state ^{59}Co NMR of the more stable nitro isomer has been reported (24).

In the current study we have determined the ^{59}Co and ^{15}N NMR parameters of both the nitrito and nitro complexes of pentamminecobalt(III) chloride using solid-state NMR. Cobalt-59 is a spin $I = 7/2$ quadrupolar nucleus and has one of the largest chemical shift ranges in the periodic table, >18 000 ppm (25), making it ideally suited for solid-state NMR investigations of cobalt complexes because of its sensitivity to subtle changes in molecular structure (25–29). Nitrogen-15, which is a spin $I = 1/2$ nucleus, is well-suited to follow the effect that structural changes have on the NO_2^- ligand (30, 31). We present the ^{59}Co and ^{15}N solid-state NMR parameters for the $[(NH_3)_5Co\text{-}ONO]^{2+}$ isomer followed by those for the $[(NH_3)_5Co\text{-}NO_2]^{2+}$ isomer. We have also monitored the thermal isomerization reaction using solid-state ^{59}Co and ^{15}N NMR spectroscopy in an effort to determine whether this technique has the potential to provide the relative amounts of each isomer in the solid state.

Experimental

The pink nitrito, $[(NH_3)_5Co\text{-}ONO]Cl_2$, and yellow nitro, $[(NH_3)_5Co\text{-}NO_2]Cl_2$, isomers were synthesized according to literature methods, and the product purity was verified using IR spectroscopy (10, 12). The isotopically enriched ^{15}N samples were prepared using 99% ^{15}N-labelled sodium nitrite obtained from C/D/N Isotopes Inc., Pointe-Claire, Quebec. The precursor compound for the synthesis (chloropentamminecobalt(III) chloride) was synthesized by the addition of 15 mL of concentrated aqueous hydrochloric acid to 5 g of cobalt(II) carbonate in 35 mL of distilled water. The precipitate was filtered twice and 5.05 g of ammonium chloride and 50 mL of concentrated aqueous ammonia were added. The solution was cooled and 80 mL of 6% hydrogen peroxide was slowly added. When bubbling ceased, nitrogen was bubbled through the solution for 1 h. The solution was neutralized with hydrochloric acid, after which an additional 20 mL of concentrated hydrochloric acid were added and the solution was set in a hot water bath for 2 h. The purple precipitate was filtered and washed with water and ethanol, yielding approximately 9 g of sample.

Solid-state NMR spectroscopy was performed on three spectrometers with field strengths of 4.70 T (Chemagnetics CMX Infinity 200), 7.05 T (Bruker Avance 300), and 11.75 T (Bruker Avance 500). Bruker double or triple resonance probes (4 mm o.d. MAS) were used on the Bruker systems, while Chemagnetics double resonance probes (4 mm o.d. MAS and 5 mm o.d. solenoid) were used on the Chemagnetics system. All ^{59}Co NMR chemical shifts were referenced with respect to a 1.0 mol/L aqueous solution of $K_3Co(CN)_6$ at 0.0 ppm, while the ^{15}N NMR chemical shifts were referenced with respect to liquid NH_3 (20 °C) by setting the ammonium peak of labelled, solid $^{15}NH_4NO_3$ to 23.8 ppm (32). Magic angle spinning (MAS) rates were controlled using automated MAS controllers to within ±2 Hz. The ^{59}Co nonselective $\pi/2$ pulse lengths were determined for the setup sample (1.0 mol/L $K_3Co(CN)_6$) and were 4.5, 2.0, and 1.9 μs at 4.70, 7.05, and 11.75 T, respectively. A one-pulse or echo-pulse sequence was used for acquiring ^{59}Co NMR spectra with pulse lengths ($\tau_{p(sel)}$), that selectively excited the central transition ($\tau_{p(sel)} = \tau_{p(nonsel)}/(I + 1/2)$) (33). Nitrogen-15 NMR spectra were acquired using a cross polarization (CP) pulse sequence ($\pi/2(^1H) = 4.5$ μs) and a contact time of 8.0 ms, which was initially setup on solid $^{15}NH_4NO_3$ and then optimized for the samples. High-power proton decoupling was performed during the acquisition of all spectra using the TPPM method (34). The sample temperature was determined using a Chemagnetics temperature controller that had been calibrated using the ^{207}Pb NMR peak of solid lead nitrate (32, 35).

Typically, Gaussian line-broadening functions of 20–50 Hz and 500–3000 Hz were applied when processing the spectra of MAS and stationary samples, respectively. The calculated and experimental spectra were fit by visual inspection using the program WSOLIDS (36).

Ab initio calculations of the nitrogen magnetic shielding tensors were performed using Gaussian 98W (revision A.7) (37) employing the B3LYP method (38, 39) to determine the orientation of the tensor in the molecular frame of reference. Either the 6-311++G(d,p) basis set, or the LANL2DZ basis set with an effective core potential, was used on the cobalt (40); 6-311++G(d,p) basis sets were used on all other atoms. Calculations with both basis sets yielded the same orientation of the magnetic shielding tensor. The calculated magnetic shielding values (σ) were converted to chemical shifts relative to the reference compound, NH_3(*l*, 20 °C), by applying the formula $\delta = \sigma_{ref} - \sigma$, where $\sigma_{ref} = 244.6$ ppm (41). The atomic coordinates of the cations used were calculated from the X-ray crystal structures determined by Boldyreva et al. (15) and Grenthe and Nordin (17); chloride ions were not included in the DFT calculations.

Results and discussion

Solid-state NMR results

Nitritopentamminecobalt(III) chloride

Figure 1 shows the ^{59}Co NMR spectra for the central transition ($m_I = 1/2 \leftrightarrow -1/2$) of stationary samples of the nitrito isomer, $[(NH_3)_5Co\text{-}ONO]^{2+}$, acquired at 4.70, 7.05, and 11.75 T. The parameters used to calculate the spectra are presented in Table 1 and are defined in the table footnote. The spectra in Fig. 1 are influenced by both the ^{59}Co quadrupolar interaction and anisotropic magnetic shielding at all three fields. At 4.70 T the second-order quadrupolar broadening (i.e., the line width without the addition of anisotropic magnetic shielding to the simulation) accounts for approximately 90% of the total breadth, while at 11.75 T it accounts for approximately 33%. The spectra are all between 180 and 220 kHz broad, making uniform excitation of the powder pattern difficult and magic angle spinning impractical.

The ^{59}Co isotropic chemical shift (δ_{iso}) of the nitrito isomer in the solid state is 8650 ± 50 ppm, the span is 1650 ±

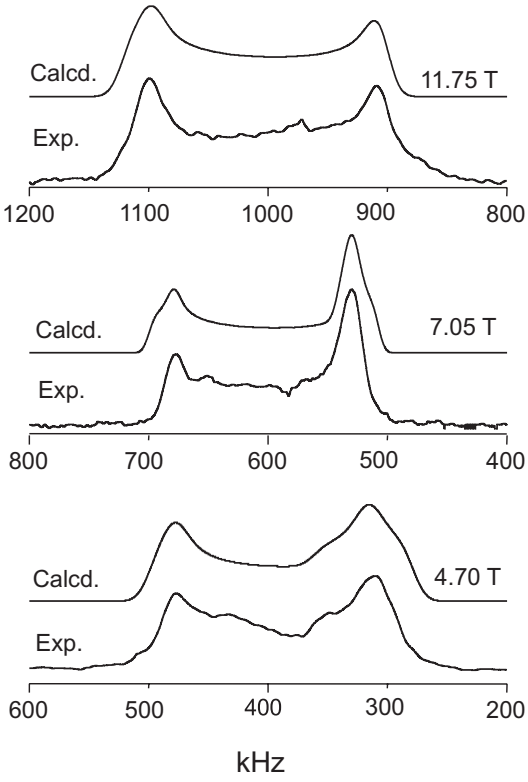
© 2006 NRC Canada

Table 1. The experimental chemical shift and EFG parameters determined by fitting the ^{15}N and ^{59}Co NMR spectra for nitrito- and nitro-pentamminecobalt(III) chloride.

		^{59}Co NMR parameters							
Isomer	Structure	δ_{iso} (ppm)	Ω (ppm)	κ	C_Q (MHz)	η	α (°)	β (°)	γ (°)
Nitrito	$[(NH_3)_5Co\text{-}ONO]^{2+}$	8650±50	1650±100	0.8±0.1	±23±1	0.20±0.05	0±5	0±5	0±2
Nitro	$[(NH_3)_5Co\text{-}NO_2]^{2+}$	7505±5	260±20	–0.20±0.05	+10.3±0.1	0.35 0.05	90±5	90±5	3±1
		^{15}N NMR parameters							
Isomer	Structure	δ_{iso} (ppm)	Ω (ppm)	κ	$^1J(^{59}Co,^{15}N)$ (Hz)	α (°)	β (°)		
Nitrito	$[(NH_3)_5Co\text{-}ONO]^{2+}$	611±1	710±6	–0.95±0.05					
Nitro	$[(NH_3)_5Co\text{-}NO_2]^{2+}$	470±1	547±6	0.5±0.1	±63±2	90±2	90±2		

Note: The chemical shift parameters are defined as follows: $\delta_{33} \le \delta_{22} \le \delta_{11}$, $\delta_{iso} = (\delta_{11} + \delta_{22} + \delta_{33})/3$, $\Omega = \delta_{11} - \delta_{33}$, $\kappa = 3(\delta_{22} - \delta_{iso})/\Omega$ (62). The components of the chemical shift tensor are $\delta_{ii} = (\nu_{ii} - \nu_{ref})/\nu_{ref}$ (ii = 11, 22, 33). The EFG parameters are $C_Q = eQV_{ZZ}/h$ and $\eta_Q = (V_{XX} - V_{YY})/V_{ZZ}$, where $|V_{ZZ}| \ge |V_{YY}| \ge |V_{XX}|$. The Euler angles α, β, and γ describe the rotations illustrated in Fig. 2.

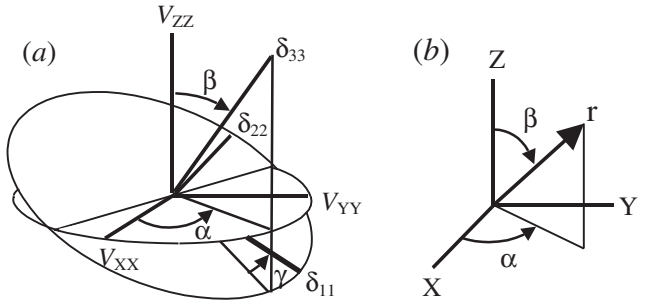
Fig. 1. Calculated and experimental ^{59}Co NMR spectra of stationary samples of $[(NH_3)_5Co\text{-}ONO]Cl_2$ acquired at 4.70, 7.05, and 11.75 T. Each experimental spectrum is the sum of 10 000 – 50 000 scans collected with a 0.1 s pulse delay. The spectrum acquired at 7.05 T has a small amount of nitro isomer present.



100 ppm, and the skew of the tensor is 0.8 ± 0.1. Since ^{59}Co has a large chemical shift range, the large span is not unexpected. In solution, the chemical shift of the nitrito isomer is 7532 ppm (26), corresponding to an 1118 ppm solution-to-solid shift. This is a large change in δ_{iso}, and highlights the sensitivity of the cobalt chemical shift to changes in the local structure (25, 42).

The cobalt electric field gradient (EFG) tensor is nearly axially symmetric ($\eta_Q = 0.20 \pm 0.05$). The fact that a deviation from axial symmetry is observed can be explained by the deviation from C_4 symmetry in the immediate coordination sphere. The quadrupolar coupling constant (C_Q) is 23 ± 1 MHz. While the error is large, it reflects the fact that the

Fig. 2. (*a*) The counter-clockwise rotations defined by the Euler angles α, β, and γ required to bring the PAS of the EFG tensor (V_{XX}, V_{YY}, V_{ZZ}) into coincidence with the PAS of the chemical shift tensor (δ_{11}, δ_{22}, δ_{33}). (*b*) Relative orientation of the ^{59}Co-^{15}N internuclear vector (r) with respect to a tensor.



^{59}Co NMR spectra may not be of the pure nitrito form. Any nitro isomer present in the sample would cause a distortion of the low frequency discontinuity, leading to some uncertainty in the analysis. The Euler angles, which describe the relative orientations of the ^{59}Co EFG and chemical shift tensors, are also obtained from the experiments and are all 0°, placing δ_{11} along V_{XX} and δ_{33} along V_{ZZ} (Fig. 2*a* shows how the angles are defined, ref. 43).

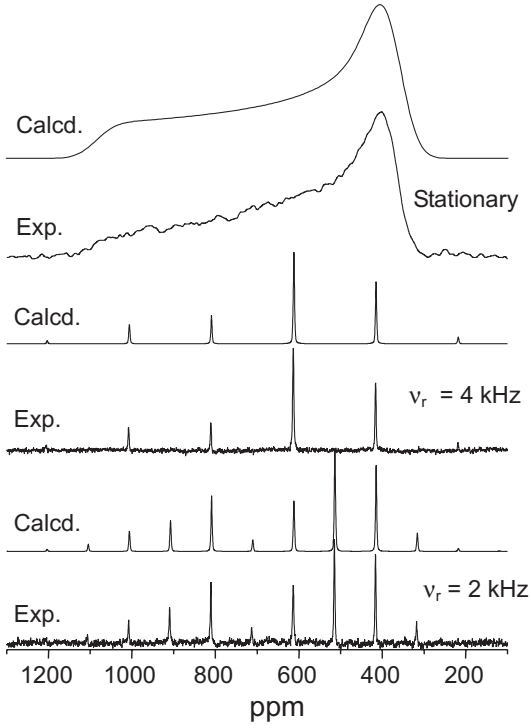
Figure 3 shows the experimental and calculated ^{15}N NMR spectra of nitritopentamminecobalt(III) chloride, with 99% ^{15}N-labelled nitrite, obtained at 4.70 T with MAS rates of 2.0 and 4.0 kHz. The observed spectra were fit with calculated spectra based on the procedure developed by Herzfeld and Berger (44) as implemented in the WSOLIDS program. The experimental and calculated spectra of a stationary sample acquired at 4.70 T are also shown in Fig. 3. Analysis of the spectra yields the experimental NMR parameters listed in Table 1. The tensor is approximately axially symmetric ($\kappa = -0.95 \pm 0.05$), has a span of 710 ± 6 ppm, and the δ_{iso} (611 ± 1 ppm) is only slightly less than that of the nitrogen in sodium nitrite (625.4 ppm) (45). The near axial symmetry is probably fortuitous given the lack of rotational symmetry at the nitrogen of this compound.

Nitropentamminecobalt(III) chloride

The ^{59}Co central transition NMR spectra of freshly synthesized nitro isomer, $[(NH_3)_5Co\text{-}NO_2]^{2+}$, collected at three fields (4.70, 7.05, and 11.75 T) are shown in Fig. 4; the parameters derived from the calculated spectra are given in Ta-

© 2006 NRC Canada

Fig. 3. Calculated and experimental ^{15}N NMR spectra of MAS and stationary samples of $[(NH_3)_5Co\text{-}ONO]Cl_2$ acquired at 4.70 T using CP. Each experimental spectrum was acquired using a pulse delay of 5.0 s and is the sum of 612 and 6144 scans for the MAS and stationary samples, respectively.



ble 1. The spectra suffered from a general broadening, which obscured some of the features, most likely because of direct and indirect spin-spin coupling to the six directly bonded ^{14}N nuclei. From the spectrum of an MAS sample, ν_r = 13 kHz, collected at 7.05 T (Fig. 4*b*), it is straightforward to determine the quadrupolar parameters because the chemical shift anisotropy is averaged by spinning at the magic angle. The values obtained are C_Q = 10.3 ± 0.1 MHz and η_Q = 0.35 ± 0.05. This corresponds to a significant decrease in the ^{59}Co quadrupolar coupling upon conversion from the nitrito isomer (C_Q = 23 ± 1 MHz). δ_{iso} also changes upon isomerization from 8650 ± 50 to 7505 ± 5 ppm.

With the C_Q, η_Q, and δ_{iso} determined from the ^{59}Co NMR spectra obtained with MAS, the spectra of the stationary samples (Figs. 4*a* and 4*c*) were analysed, and the chemical shift tensor and its orientation relative to the EFG tensor were determined. The span of the chemical shift tensor is 260 ± 20 ppm and the skew is –0.20 ± 0.05. The Euler angles are 90 ± 5°, 90 ± 5°, and 3 ± 1° for α, β, and γ, respectively, making the EFG and chemical shift tensors nearly coincident with δ_{11} parallel to V_{ZZ} and δ_{33} parallel to V_{YY}. These ^{59}Co EFG and chemical shift parameters differ from those previously reported (24): C_Q = 11.25 MHz, η_Q = 0.55, Ω = 270 ppm, κ = 0.519, and α = 7°, β = 88°, and γ = 7°. The differences can be related primarily to the different C_Q values; in the previous study, measurements of samples under MAS were not carried out.

Figure 5 shows the centre band region of the ^{15}N NMR spectrum acquired for a sample of the nitro isomer under MAS conditions at 4.70 T. The centre band, as well as the spinning side bands (not shown), are split by indirect spin-spin coupling to the ^{59}Co, $|^1J(^{59}Co, ^{15}N)|$, which is 63 ± 2 Hz. Previous solid-state $^1J(^{59}Co, ^{15}N)$ values have been reported for a series of cobaloxime complexes with either pyridine-^{15}N or aniline-^{15}N ligands; the magnitudes range from 36 to 75 Hz (46). The splitting pattern in the ^{15}N NMR spectrum is influenced by the cobalt quadrupolar coupling parameters because the ^{59}Co–^{15}N dipolar coupling can not be completely averaged by MAS (46–48). For the ^{59}Co–^{15}N pair, the peaks in the ^{15}N spectra are split into eight peaks, corresponding to the eight possible spin states of the ^{59}Co (m_I = –7/2 to +7/2). The peak intensities and splittings are dictated by $^1J(^{59}Co,^{15}N)$, the ^{59}Co–^{15}N dipolar coupling constant, R_{eff}, the ^{59}Co C_Q, η_Q, and the orientation of the ^{59}Co EFG tensor with respect to the ^{59}Co–^{15}N dipolar vector. With the magnitude of the ^{59}Co quadrupolar coupling and η_Q determined from the ^{59}Co NMR spectra and the value of R_{eff} = –402 Hz, calculated based on the Co—N distance obtained from the crystal structure (assuming ΔJ = 0), the experimental spectrum in Fig. 5 can be best fit when the sign of C_Q is positive and the Euler angles that orient the Co-N dipolar vector in the PAS of the ^{59}Co EFG are both 0°, placing V_{ZZ} along the dipolar vector (Fig. 2*b* shows how the angles are defined for a vector with respect to a tensor).

Analysis of the ^{15}N NMR spectrum of a stationary sample of the nitro isomer (Fig. 6) indicates that the span of the nitrogen chemical shift tensor is 547 ± 6 ppm and that the skew is 0.5 ± 0.1 (Table 1). This is a significant change from the nitrito isomer and is accompanied by a change in δ_{iso} from 611 ± 1 to 470 ± 1 ppm. The ^{15}N NMR isotropic chemical shift value of the nitrite ligand in the nitro isomer is significantly less than that reported for the nitrite ion in $NaNO_2$ (δ_{iso} = 625.4 ppm) (45). Also, the span of the nitro nitrogen shielding tensor in the cobalt complex is less than that of the nitrite ion in $NaNO_2$ (Ω = 951 ppm, κ = 0.37) (45).

The^{15}N NMR line shape of a stationary sample of an isolated spin pair, such as ^{15}N coupled to ^{59}Co, depends on the ^{15}N chemical shift tensor, R_{eff}, $^1J(^{59}Co,^{15}N)$, and the orientation of the dipolar vector in the principal axis system (PAS) of the ^{15}N chemical shift tensor (46, 49). The angles that relate the Co-N dipolar vector to the ^{15}N chemical shift tensor, determined from the analysis of the ^{15}N NMR spectrum in Fig. 6 are α = 90° and β = 90°; the δ_{22} component of the nitrogen chemical shift tensor is along the Co—N bond, while δ_{33} is perpendicular to the Co-NO_2 plane.

Relationship between molecular structure and the EFG and chemical shift tensors

To examine the relationship between the molecular structures and the cobalt and nitrogen NMR parameters of the two isomers, it is important to look at the three principal components of the tensors and their orientation in the molecular frame. As mentioned, the magnitude of the cobalt C_Q decreases when the nitrito isomer changes to the nitro form, from 23 to 10.3 MHz. This change indicates that the electronic distribution about the cobalt is more symmetric in the nitro isomer, where the cobalt atom is bonded to six nitrogen atoms, compared with the nitrito isomer, where the cobalt is bonded to five nitrogen atoms and one oxygen atom.

The orientation of the EFG tensors at the cobalt nuclei can

© 2006 NRC Canada

Fig. 4. Cobalt-59 NMR spectra of $[(NH_3)_5Co\text{-}NO_2]Cl_2$ acquired at (*a*) 11.75 T, (*b*) 7.05 T, and (*c*) 4.70 T. The spectrum acquired at 7.05 T is of a MAS sample (ν_{rot} = 13 kHz), while those acquired at the other two fields are ^{59}Co NMR spectra of stationary samples. The spectra are the sum of 359, 869, and 6227 scans for the three fields, respectively, with a 0.1 s pulse delay. The distortions in the baseline of the spectrum obtained with MAS are a result of not being able to spin rapidly enough to completely average the second-order quadrupolar interaction and chemical shift anisotropy.

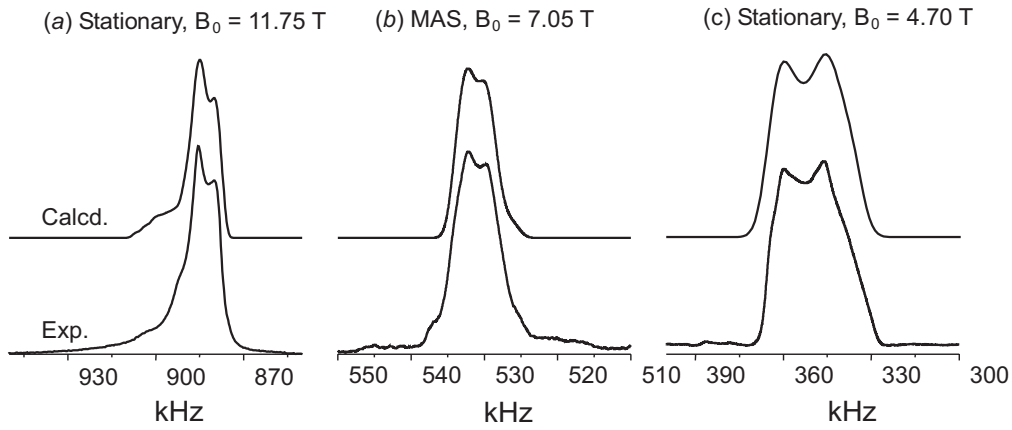


Fig. 5. Calculated and experimental ^{15}N NMR spectra of a MAS sample of $[(NH_3)_5Co\text{-}NO_2]Cl_2$ spinning at 8 kHz obtained using CP acquired at 4.70 T showing the $^1J(^{59}Co,^{15}N)$ coupling to the ^{59}Co. The intensities of the spinning side bands were added to the centre band.

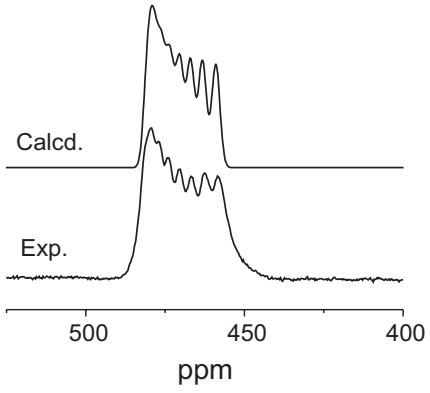
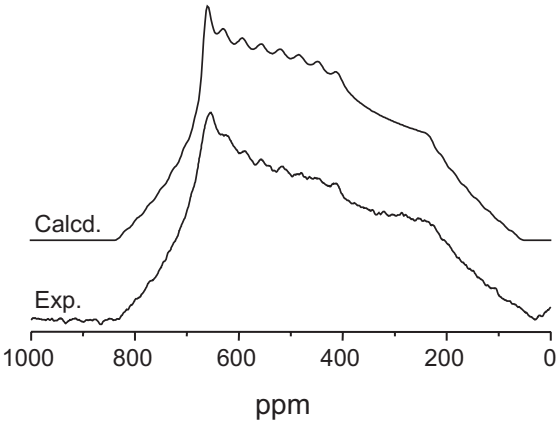


Fig. 6. Calculated and experimental ^{15}N NMR spectra of a stationary sample of $[(NH_3)_5Co\text{-}NO_2]Cl_2$ acquired using CP at 4.70 T. The spectrum is the sum of 17 692 scans using a 5.0 s pulse delay.



be understood based on symmetry arguments. While it was not possible to obtain the orientation of the ^{59}Co EFG in the molecular frame from the experimental data of the nitrito isomer, the pseudo-C_4 symmetry of the molecule suggests that the unique component of the EFG (V_{ZZ}) is approximately along the *Co—O*NO bond, and the two components that are nearly equal in magnitude are perpendicular to this bond. For the nitro isomer, the ^{15}N spectrum for the sample under MAS indicates that the ^{59}Co EFG tensor orientation is the same: the V_{ZZ} component is parallel to the *Co—N*O_2 bond. The lack of change in the orientation of the EFG tensor and the asymmetry parameter indicates that the isomerization simply results in a scaling of the EFG at the cobalt nucleus.

The orientations of the ^{59}Co chemical shift tensors in both isomers can be fixed in the molecular frame based on their relative orientation to the EFG tensor. The Euler angles determined from the ^{59}Co stationary line shapes of the nitrito isomer indicate that δ_{11} is along V_{XX} and δ_{33} is along V_{ZZ}. Since the tensor is close to axially symmetric, this places the "unique" component of the cobalt chemical shift tensor along the *Co—O*NO bond, as would be expected. The component of the cobalt chemical shift along the bond is 7605 ± 50 ppm, while the two components of the chemical shift tensor that lie in the $Co(NH_3)_4$ plane, perpendicular to the *Co—O*NO bond, are 9255 ± 50 and 9099 ± 50 ppm. The ^{59}Co chemical shift tensor of the nitro isomer is oriented such that the direction of least shielding is along the *Co—*NO_2 bond; δ_{11} has a value of 7643 ± 10 ppm and the two components perpendicular to the bond have values of 7487 ± 10 and 7383 ± 10 ppm. By comparing the values of the components for the two isomers, it is clear that the cobalt shielding along the Co—X bond (δ = 7605 ppm, X = ONO and δ = 7643 ppm, X = NO_2) does not change significantly when the compound isomerizes. In contrast, the shielding perpendicular to the bond increases by approximately 1750 ppm in the nitro isomer.

Correlation of cobalt chemical shifts to octahedral crystal field splitting (Δ_O) has been used for many years to explain the isotropic chemical shifts of octahedral cobalt complexes

© 2006 NRC Canada

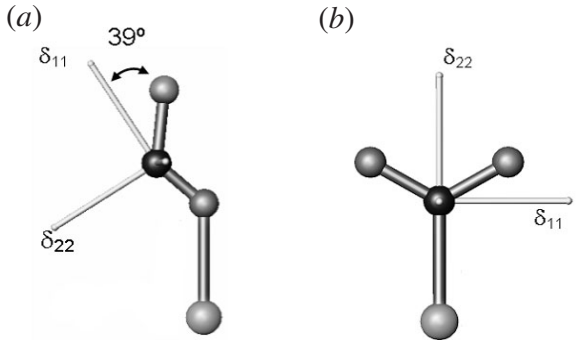
in solution and in the solid state (50–53). The paramagnetic shielding term, as described by Ramsey (54) in his original formalism, depends on the energy difference between electronic states that undergo symmetry-allowed mixing in the presence of a magnetic field and is generally deshielding. The good correlation between the cobalt chemical shifts and the excitation wavelength of the $^1A_{1g} \rightarrow {}^1T_{1g}$ electronic transition in octahedral cobalt(III) complexes was one of the early confirmations of Ramsey's formalism. In the solid state, the correlation can be used for octahedral complexes of high symmetry. Equations describing the dependence of shielding on the transition energies have been derived for numerous symmetries including D_3, C_{4v}, D_{4v}, C_{2v}, etc. (55, 56). In the present study, however, neither complex has high symmetry at the cobalt atom, which limits the application of the derived equations for determining the individual components or isotropic values of the chemical shift tensor. Despite this, an approximate correlation can be made between the overall shielding that occurs as the complex isomerizes and an increase in the Δ_O. The change in colour, from the pink nitrito isomer to the yellow nitro isomer, indicates an increase in Δ_O. The increase in Δ_O leads to a smaller paramagnetic shielding of the cobalt in the nitro isomer and results in the smaller chemical shift. This change is noticed primarily in the components of the shielding tensor perpendicular to the Co—X bond.

The orientation of the nitrogen chemical shift tensor in the nitrito isomer is unavailable from the NMR experiments. In other two-coordinate nitrogen compounds, such as sodium nitrite and bent nitrosyl compounds (45, 57), the nitrogen chemical shift tensor is oriented such that δ_{22} is approximately along the formal nitrogen lone pair and δ_{33} is perpendicular to the ONO plane. Quantum chemical calculations were performed and predict the same orientation for the nitrito isomer (Fig. 7*a*). The calculations reproduced the relative magnitudes of the δ_{11} and δ_{22} tensor components to within approximately 100 and 33 ppm, respectively, using both the 6-311++G(d,p) and LANL2DZ basis sets on the cobalt. Given that the chemical shift range of nitrogen is around 1200 ppm, the errors in δ_{11} and δ_{22} are reasonable and lend confidence to the orientations calculated for these two components. The δ_{33} component was underestimated by approximately 250 ppm, which is quite a large discrepancy. The origin of this difference between theory and experiment most likely arises from the neglect of intermolecular effects in the calculations.

The individual components of the nitrogen chemical shift tensor can be related to the electronic states that are responsible for the paramagnetic term in δ. For certain nitrosyl compounds (57), as well as in this case, mixing of the nitrogen *n* and π* electronic states is expected to be responsible for the paramagnetic shielding term associated with the δ_{11} component of the chemical shift tensor (30). It has also been reported that the orientation of the intermediate component of the nitrogen chemical shift tensor (δ_{22}) is in most cases parallel to the formal nitrogen lone pair for nitrogen atoms bonded to two other atoms such as nitrosyl compounds, oximes, and azides (58–61). The direction of greatest shielding is nearly perpendicular to the ONO plane and arises from the mixing of the in-plane σ and σ* states (57).

The orientation of the nitrogen chemical shift tensor of the nitro isomer as determined from the analysis of the ^{15}N NMR line shape of the stationary sample indicates that δ_{33} is perpendicular to the Co-NO_2 plane and δ_{22} is along the Co—N bond (Fig. 7*b*). The calculations with both the 6-311++G(d,p) and LANL2DZ basis sets on the Co yielded values for δ_{11}, δ_{22}, and δ_{33} that were in excellent agreement with the experimental values, within 11, 16, and 62 ppm of the experimental values, respectively. The process of coordination to the cobalt metal has the most profound effect on δ_{11}, which decreases by 412 ppm when the isomer changes from the nitrito to the nitro form. This is a result of the changes in the nonbonding molecular orbitals of the nitrito isomer as they coordinate to the cobalt centre to form the Co—N σ bond in the nitro isomer. The chemical shift component along the Co—N bond (δ_{22}) in the nitro isomer changes relatively little as a consequence of the coordination, increasing by 103 ppm with respect to the nitrito isomer. This is expected because the δ_{22} component does not involve mixing with the orbitals that form the Co—N σ bond. Finally, δ_{33} in the nitro isomer decreases by approximately 169 ppm with respect to the nitrito isomer.

Fig. 7. Orientation of the nitrogen CS tensor in the molecular frame of reference for: (*a*) the nitrito isomer, obtained from DFT calculations, and (*b*) the nitro isomer, obtained from DFT calculations and experiment.



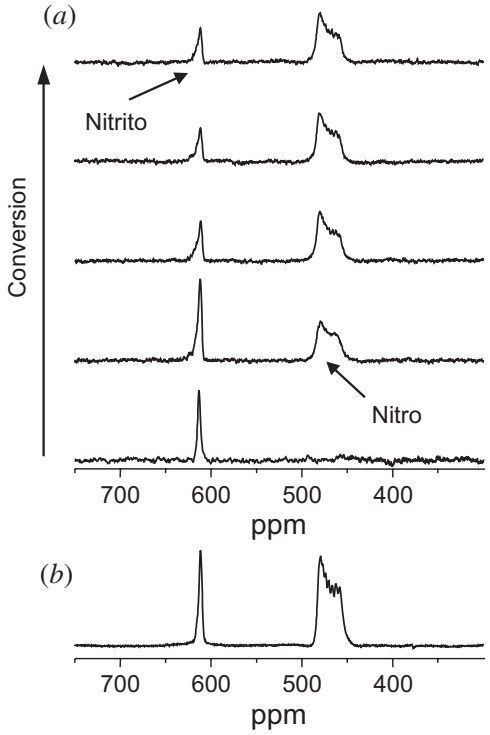
Monitoring the isomerization reaction

The isomerization from the nitrito to the nitro isomer was monitored directly using both ^{15}N and ^{59}Co solid-state NMR. The spectra acquired at 4.70 T as the reaction progressed are shown in Figs. 8 and 9 for ^{15}N and ^{59}Co, respectively. For the ^{15}N MAS spectra a heating scheme was used. The temperature was raised from room temperature (293 K) to 353 K in 5 min, where it was held for 8 min then cooled to room temperature before the spectra were acquired (Fig. 8*a*). In an attempt to drive the reaction to completion, the sample that yielded the top spectrum in Fig. 8*a* was heated at 413 K for 40 min yielding the spectrum in Fig. 8*b*; the sample was allowed to equilibrate at room temperature for 2 h prior to data collection.

The results show the benefit of using NMR to monitor the extent of the reaction. The ^{15}N peak from the nitrito isomer slowly decreases in intensity while a second peak appears at 470 ± 3 ppm, corresponding to the formation of the nitro isomer (Fig. 8*a*). It is clear that in the initial preparation there is very little of the nitro isomer present. Due to the breadth of the peak from the nitro isomer there could be as much as 10% of this form that is not detected because of the

© 2006 NRC Canada

Fig. 8. Nitrogen-15 NMR spectra of a MAS sample of the compound, acquired at 4.70 T. The spectra in (*a*) were obtained at room temperature after successive applications of the heating scheme described (see text). The sample that yielded the top spectrum in (*a*) was then heated at 413 K for an additional 40 min to drive the reaction to equilibrium and the NMR spectrum in (*b*) was acquired. Each spectrum in (*a*) is the sum of 612 scans and (*b*) is the sum of 10 050 scans, both using a 5.0 s pulse delay.

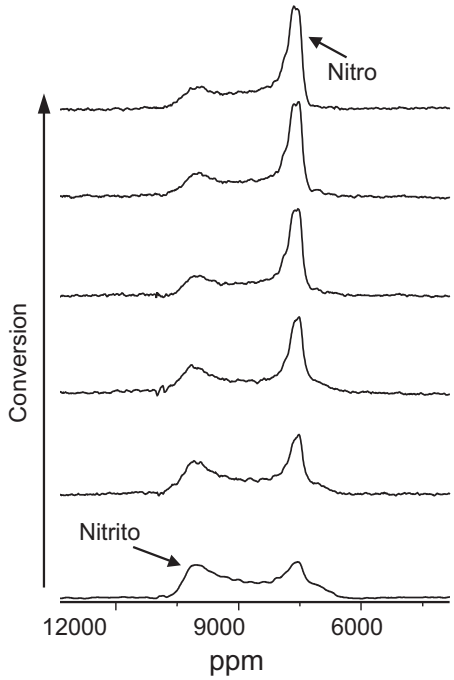


baseline noise. This illustrates one drawback to the ^{15}N NMR of this system; since the peak from the nitro isomer is much broader than that from the nitrito isomer under MAS conditions, when only small amounts of nitro are present it is difficult to get an accurate estimate of the relative amounts of each isomer. However, this is offset by the ability to measure very small quantities of nitrito isomer in a mixture.

While the use of CP generally does not result in completely quantitative peak intensities, the optimal CP parameters were almost identical for the two isomers; hence, it is assumed that the comparison of the integrated peak intensities is a good approximation of the relative amounts of the two isomers. The analysis of the intensities for the spectrum in Fig. 8*b* shows that a final nitro/nitrito equilibrium ratio of 5.0 is reached after the sample was heated at 413 K. This is in excellent agreement with a previous study that measured the equilibrium values based on the reaction rates (11). From the spectra in Fig. 8*a*, it is apparent that the reaction is close to equilibrium after the second heating step.

The ^{59}Co NMR spectra (Fig. 9) were collected on a second sample preparation without any heating to investigate the sensitivity of the experiment to the isomerization over times consistent with the room temperature rate of reaction. Every 2.75 h a spectrum was acquired over a time of

Fig. 9. The ^{59}Co NMR spectra of a stationary sample of the compound, acquired at 4.70 T, collected at room temperature without heating and with 2.75 h between each spectrum; 10 000 scans were added using a 0.1 s pulse delay.



16.7 min. The ^{59}Co NMR spectra show a decrease in the broad nitrito peak, while a new peak from the nitro isomer appears at 7505 ± 10 ppm. Since the line width of the nitro peak is much smaller than that of the nitrito isomer, the ^{59}Co NMR spectra show the opposite sensitivities to those of the ^{15}N NMR spectra. Whereas the ^{15}N NMR spectra are sensitive to small amounts of the nitrito isomer and less so to the presence of the nitro isomer, the ^{59}Co spectra are more sensitive to the presence of the nitro isomer. These two nuclei therefore offer complementary methods of analyzing the relative quantities of the two isomers.

Conclusions

The ^{59}Co and ^{15}N NMR parameters of nitritopentamminecobalt(III) chloride and nitropentamminecobalt(III) chloride have been determined in the solid state. There is a change in both the ^{59}Co quadrupolar coupling constants (23 to 10 MHz), and the spans of the chemical shift tensor (1650 to 260 ppm), for the nitrito and nitro isomers, respectively. The principal components of the ^{59}Co chemical shift tensor that are perpendicular to the Co—X (X = ONO or NO_2) bond decrease by approximately 1750 ppm upon isomerization, while the components parallel to the bond are similar in both isomers. The nitrogen chemical shift tensor also shows significant variations; δ_{iso} moves from 611 to 470 ppm and Ω decreases from 710 to 547 ppm as the ligand changes from the nitrito to nitro form. The orientations of the ^{15}N and ^{59}Co chemical shift tensors and the ^{59}Co EFG tensor in the molecular frame have been related to the molecular structure. The isomerization reaction was monitored directly using both ^{59}Co and ^{15}N NMR and the results suggest that solid-state NMR can be used to measure isomer ratios during the reac-

© 2006 NRC Canada

tion. These results highlight the value of solid-state NMR studies and the potential to use NMR to monitor reactions that occur in the solid state.

Acknowledgments

The authors wish to thank members of the solid-state NMR group at the University of Alberta, Edmonton, Alberta, as well as Dr. Klaus Eichele for helpful discussions. Dr. Guy Bernard, in particular, is thanked for his comments. REW is a Canada Research Chair in Physical Chemistry at the University of Alberta and thanks the Natural Sciences and Engineering Research Council of Canada (NSERC), Alberta Ingenuity, and the University of Alberta for research grants. KJO thanks NSERC, the Alberta Ingenuity Fund, and the University of Alberta for post-graduate scholarships.

Finally, REW thanks Arthur Carty for several fruitful scientific collaborations, and personal encouragement dating back to the late 1960s at the University of Waterloo.

References

1. S.R. Byrn, R.R. Pfeiffer, G. Stephenson, D.J.W. Grant, and W.B. Gleason. Chem. Mater. **6**, 1148 (1994).
2. M.C. Lai and E.M. Topp. J. Pharm. Sci. **88**, 489 (1999).
3. N.J. Coville and L. Cheng. J. Organomet. Chem. **571**, 149 (1998).
4. S.D.M. Atkinson, M.J. Almond, P. Hollins, and S.L. Jenkins. Spectrochim. Acta Part A, **A59**, 629 (2003).
5. L.R. MacGillivray, J.L. Reid, J.A. Ripmeester, and G.S. Papaefstathiou. Ind. Eng. Chem. Res. **41**, 4494 (2002).
6. S.D.M. Atkinson, M.J. Almond, S.J. Hibble, P. Hollins, S.L. Jenkins, M.J. Tobin, and K.S. Wiltshire. Phys. Chem. Chem. Phys. **6**, 4 (2004).
7. S.M. Jörgenson. Z. Anorg. Allg. Chem. **5**, 169 (1894).
8. W.G. Jackson, G.A. Lawrence, P.A. Lay, and A.M. Sargeson. J. Chem. Soc. Chem. Commun. 70 (1982).
9. W.G. Jackson, G.A. Lawrance, P.A. Lay, and A.M. Sargeson. J. Chem. Educ. **58**, 734 (1981).
10. R.B. Penland, T.J. Lane, and J.V. Quagliano. J. Am. Chem. Soc. **78**, 887 (1956).
11. W.M. Phillips, S. Choi, and J.A. Larrabee. J. Chem. Educ. **67**, 267 (1990).
12. W.H. Hohman. J. Chem. Educ. **51**, 553 (1974).
13. R.K. Murmann and H. Taube. J. Am. Chem. Soc. **78**, 4886 (1956).
14. R.G. Pearson, P.M. Henry, J.G. Bergmann, and F. Basolo. J. Am. Chem. Soc. **76**, 5920 (1954).
15. E.V. Boldyreva, J. Kivikoski, and J.A.K. Howard. Acta Crystallogr. Sect. C: Cryst. Struct. Commun. **53**, 523 (1997).
16. M. Kubota and S. Ohba. Acta Crystallogr. Sect. B: Struct. Sci. **48**, 627 (1992).
17. I. Grenthe and E. Nordin. Inorg. Chem. **18**, 1869 (1979).
18. J.C.C. Chan, P.J. Wilson, S.C.F. Au-Yeung, and G.A. Webb. J. Phys. Chem. A, **101**, 4196 (1997).
19. I. Ciofini and C. Adamo. J. Phys. Chem. A, **105**, 1086 (2001).
20. V.E. Dulepov and E.V. Boldyreva. React. Kinet. Catal. Lett. **53**, 289 (1994).
21. D.A. Johnson and K.A. Pashman. Inorg. Nucl. Chem. Lett. **11**, 23 (1975).
22. I.R. Beattie and D.P.N. Satchell. Trans. Faraday Soc. **52**, 1590 (1956).
23. E.V. Boldyreva. Russ. J. Coord. Chem. **27**, 297 (2001).
24. C.W. Kirby and W.P. Power. Can. J. Chem. **79**, 296 (2001).
25. R. Goodfellow. *In* Multinuclear NMR. *Edited by* J. Mason. Plenum, New York. 1989. pp. 521.
26. J.C.C. Chan and S.C.F. Au-Yeung. J. Chem. Soc. Faraday Trans. **92**, 1121 (1996).
27. J.C.C. Chan and S.C.F. Au-Yeung. Annu. Rep. NMR Spectrosc. **41**, 1 (2000).
28. A. Medek and L. Frydman. J. Am. Chem. Soc. **122**, 648 (2000).
29. W.P. Power, C.W. Kirby, and N.J. Taylor. J. Am. Chem. Soc. **120**, 9428 (1998).
30. J. Mason. *In* Nuclear magnetic shielding and molecular structure. *Edited by* J.A. Tossell. Kluwer Academic Publishers, Dordrecht. 1993. pp. 449.
31. J. Mason, L.F. Larkworthy, and E.A. Moore. Chem. Rev. **102**, 913 (2002).
32. D.L. Bryce, G.M. Bernard, M. Gee, M.D. Lumsden, K. Eichele, and R.E. Wasylishen. Can. J. Anal. Sci. Spectrosc. **46**, 46 (2001).
33. P.R. Bodart, J.-P. Amoureux, Y. Dumazy, and R. Lefort. Mol. Phys. **98**, 1545 (2000).
34. A.E. Bennett, C.M. Rienstra, M. Auger, K.V. Lakshmi, and R.G. Griffin. J. Chem. Phys. **103**, 6951 (1995).
35. L.C.M. van Gorkom, J.M. Hook, M.B. Logan, J.V. Hanna, and R.E. Wasylishen. Magn. Reson. Chem. **33**, 791 (1995).
36. K. Eichele and R.E. Wasylishen. WSOLIDS NMR simulation package. Version 1.17.26. 2000.
37. M.J. Frisch, G.W. Trucks, H.B. Schlegel, G.E. Scuseria, M.A. Robb, J.R. Cheeseman, V.G. Zakrzewski, J.A. Montgomery, Jr., R.E. Stratmann, J.C. Burant, S. Dapprich, J.M. Millam, A.D. Daniels, K.N. Kudin, M.C. Strain, O. Farkas, J. Tomasi, V. Barone, M. Cossi, R. Cammi, B. Mennucci, C. Pomelli, C. Adamo, S. Clifford, J. Ochterski, G.A. Petersson, P.Y. Ayala, Q. Cui, K. Morokuma, D.K. Malick, A.D. Rabuck, K. Raghavachari, J.B. Foresman, J. Cioslowski, J.V. Ortiz, B.B. Stefanov, G. Liu, A. Liashenko, P. Piskorz, I. Komaromi, R. Gomperts, R.L. Martin, D.J. Fox, T. Keith, M.A. Al-Laham, C.Y. Peng, A. Nanayakkara, C. Gonzalez, M. Challacombe, P.M.W. Gill, B.G. Johnson, W. Chen, M.W. Wong, J.L. Andres, M. Head-Gordon, E.S. Replogle, and J.A. Pople. Gaussian 98W. Revision A.7 [computer program]. Gaussian Inc., Pittsburgh, Penn. 1998.
38. A.D. Becke. J. Chem. Phys. **98**, 5648 (1993).
39. C. Lee, W. Yang, and R.G. Parr. Phys. Rev. B, **37**, 785 (1988).
40. W.R. Wadt and P.J. Hay. J. Chem. Phys. **82**, 284 (1985).
42. P.S. Pregosin. Transition metal nuclear magnetic resonance. Elsevier, Amsterdam. 1991.
43. M. Duer (*Editor*). Solid-state NMR spectroscopy: principles and applications. Blackwell Science, Oxford. 2002.
44. J. Herzfeld and A.E. Berger. J. Chem. Phys. **73**, 6021 (1980).
45. P.J. Barrie, C.J. Groombridge, J. Mason, and E.A. Moore. Chem. Phys. Lett. **219**, 491 (1994).
46. R.W. Schurko and R.E. Wasylishen. J. Phys. Chem. A, **104**, 3410 (2000).
47. R.K. Harris and A.C. Olivieri. Prog. Nucl. Magn. Reson. Spectrosc. **24**, 435 (1992).
48. P. Grondona and A.C. Olivieri. Concepts Magn. Reson. **5**, 319 (1993).
49. R.E. Wasylishen, R.D. Curtis, K. Eichele, M.D. Lumsden, G.H. Penner, W.P. Power and G. Wu. *In* Nuclear chemical shifts and molecular structure. Nato ASI Series Vol. 386. *Edited by* J.A. Tossel. Kluwer Academic Publishers, Dordrecht. 1993. pp. 297.
50. J.S. Griffith and L.E. Orgel. Trans. Faraday Soc. **53**, 601 (1957).

© 2006 NRC Canada

51. R. Freeman, G.R. Murray, and R.E. Richards. Proc. R. Soc. London. **A242**, 455 (1957).
52. N. Juranić. Coord. Chem. Rev. **96**, 253, (1989).
53. K. Eichele, J.C.C. Chan, R.E. Wasylishen, and J.F. Britten. J. Phys. Chem. A, **101**, 5423 (1997).
54. N.F. Ramsey. Phys. Rev. **78**, 699 (1950).
55. N. Juranić. J. Serb. Chem. Soc. **56**, 723 (1991).
56. N. Juranić, M.B. Ćelap, D. Vučelić, M.J. Malinar. and P.N. Radivojša. J. Magn. Reson. **35**, 319 (1979).
57. M.D. Lumsden, G. Wu, R.E. Wasylishen, and R.D. Curtis. J. Am. Chem. Soc. **115**, 2825 (1993).
58. R.D. Curtis, G.H. Penner, W.P. Power, and R.E. Wasylishen. J. Phys. Chem. **94**, 4000 (1990).
59. R.E. Wasylishen, G.H. Penner, W.P. Power, and R.D. Curtis. J. Am. Chem. Soc. **111**, 6082 (1989).
60. D. Schweitzer and H.W. Spiess. J. Magn. Reson. **15**, 529 (1974).
61. R.E. Wasylishen, W.P. Power, G.H. Penner, and R.D. Curtis. Can. J. Chem. **67**, 1219 (1989).
62. J. Mason. Solid State Nucl. Magn. Reson. **2**, 285 (1993).

© 2006 NRC Canada

Room-temperature NIR phosphorescence of new iridium (III) complexes with ligands derived from benzoquinoxaline[1]

Hsing-Yi Chen, Cheng-Han Yang, Yun Chi, Yi-Ming Cheng, Yu-Shan Yeh, Pi-Tai Chou, Hsi-Ying Hsieh, Chao-Shiuan Liu, Shie-Ming Peng, and Gene-Hsiang Lee

Abstract: A new series of new iridium (III) complexes (**1**–**5**) bearing ligands derived from benzoquinoxaline were designed and synthesized. X-ray structural analyses of **1** reveal a distorted octahedral geometry around the Ir atom in which the pyrazolate chelate is located opposite to the cis-oriented carbon donor atoms of benzoquinoxaline, while the benzoquinoxaline ligands adopt an eclipse configuration and their coordinated nitrogen atoms and carbon adopt trans- and cis-orientation, respectively. Complexes **1**–**5** exhibit moderate NIR phosphorescence with peak maxima located at around 910–930 nm. As supported by the TDDFT approach, the transition mainly involves benzoquinoxaline $^3\pi$–π^* intraligand charge transfer (ILCT) and metal (Ir) to benzoquinoxaline charge transfer (MLCT) of which the spectroscopy and dynamics of relaxation have been thoroughly investigated. The relatively weak NIR emission can be tentatively rationalized by the low energy gap of which the radiationless deactivation may be governed by nearly temperature-independent, weak-bonding motions in combination with a minor channel incorporating small torsional motions associated with phenyl ring in the benzoquinoxaline sites.

Key words: phosphorescence, NIR, iridium, benzoquinoxaline, isoquinoline, bipyridine, pyrazolate, acetylacetonate.

Résumé : On a préparé une nouvelle série de complexes de l'iridium(III) (**1**–**5**) portant des ligands dérivés de la benzoquinoxaline. L'analyse des données structurales du composé **1**, obtenues par diffraction des rayons X, révèle la présence d'une géométrie octaédrique déformée autour de l'atome d'iridium dans laquelle le chélate pyrazolate se trouve à l'opposé des atomes de carbone donneurs de la benzoquinoxaline orientés en cis, alors que les ligands benzoquinoxaline adoptent une conformation éclipsée et que leurs atomes d'azote coordonnés adoptent respectivement des orientations cis et trans. Les complexes **1**–**5** présentent de la phosphorescence modérée dans le proche infrarouge (PIR) avec un pic maximal situé autour de 910 à 930 nm. Tel que le prédit l'approche TDDFT, la transition implique principalement un transfert de charge interligand (TCIL) $^3\pi$–π^* de la benzoquinoxaline et un transfert de charge du métal (iridium) à la benzoquinoxaline (TCML) dont on a étudié à fond la spectroscopie et la dynamique de relaxation. L'émission relativement faible dans le proche infrarouge pourrait être rationalisée en fonction d'une discontinuité de faible énergie de laquelle la désactivation sans rayonnement pourrait être orientée par des mouvements de faible liaison, pratiquement indépendants de la température, en combinaison avec une voie mineure qui incorporerait de faibles mouvements de torsion du noyau phényle dans les sites benzoquinoxalines.

Mots clés : phosphorescence, PIR, iridium, benzoquinoxaline, isoquinoléine, bipyridine, pyrazolate, acétylacétonate.

[Traduit par la Rédaction]

Received 30 June 2005. Published on the NRC Research Press Web site at http://canjchem.nrc.ca on 21 March 2006.

This paper is dedicated to Professor Arthur J. Carty; he has been our mentor, collaborator, and friend for the past 15 years.

H.-Y. Chen, C.-H. Yang, and Y. Chi.[2] Department of Chemistry, National Tsing Hua University, Hsinchu 300, Taiwan.
Y.-M. Cheng, Y.-S. Yeh, P.-T. Chou,[3] **S.-M. Peng, and G.-H. Lee.** Department of Chemistry and Instrumentation Center, National Taiwan University, Taipei 106, Taiwan.
H.-Y. Hsieh.[4] Department of Food Nutrition, Chung Hwa College of Medical Technology, Tainan 717, Taiwan.
C.-S. Liu. Department of Chemistry, SooChow University, Taipei 111, Taiwan.

[1]This article is part of a Special Issue dedicated to Professor Arthur Carty.
[2]Corresponding author (e-mail: ychi@mx.nthu.edu.tw).
[3]Corresponding author (e-mail: chop@ntu.edu.tw).
[4]Corresponding author (e-mail: simn1628@ms26.hinet.net).

 doi:10.1139/V05-253 © 2006 NRC Canada

Introduction

Transition metal complexes, which exhibit strong emission in fluid solution at room temperature, have been extensively investigated owing to their fundamental interest and key roles in the design of novel systems for solar energy conversion (1), telecommunication and other optical technologies (2), as well as fabrication of high efficiency phosphorescent organic light emitting devices (OLEDs) (3). So far, most of the reported luminescent metal complexes emit in the visible region, while studies of emission properties in the NIR region are relatively rare. One reason lies in that decreasing the energy gap toward NIR may trigger a much faster radiationless decay channel because of the interaction between ground and emitting states, i.e., the so-called energy gap law, giving rise to poor quantum efficiencies (4).

The first class of complexes showing notable NIR luminescence should be credited to the lanthanide complexes incorporating the Nd(III), Yb(III), and Er(III) ions (5). Sharp emission signals for lanthanide complexes are expected simply because the 4f orbitals in the lanthanide elements are buried deep within the atom and would not be seriously coupled with the ligand vibration motions, as opposed to the broad d–d transitions of the transition metals. As a second class, the Pd porphyrinate types of complexes are documented as exhibiting moderate NIR phosphorescence in the fluid state at room temperature, a property which is desirable for application as oxygen sensors for biomedical applications in vivo (6). The third class consists of the polypyridyl complexes involving the Re(I), Ru(II), and Os(II) metal ions with the d^6 electronic configuration (7). Their systematic synthesis has remained as the outstanding issue in view of applications. These complexes typically absorb appreciably in the high energy region of the spectra, accompanied by the MLCT absorptions at lower energy, as well as a certain degree of contribution from direct ^{3}MLCT absorption, a result of the heavy atom enhanced spin-orbit coupling. Accordingly, NIR phosphorescent emissions are achievable for systems with extended electronic delocalization between the metal and ligands in both ground and excited states, making them important as light harvesting sensitizers for solar cell applications.

As an extension of our contribution to the third-row metal phosphorescent materials, we have embarked on the development of Ir(III)-based metal complexes showing detectable luminescence in the NIR spectral region. The key designing feature is to utilize a diphenyl substituted benzoquinoxaline ligand that allows formation of a highly extended π conjugation. The choice of Ir as the central atom renders the advantages of linking the benzoquinoxaline ligand through facile orthometalation, affording a desirable metal–chelate bonding interaction and a presumably rigid molecular skeleton. Along this line, the emission gaps are expected to shift significantly toward the lower energy, i.e., the NIR region, without drastic reduction to the corresponding emission efficiency.

Experimental section

General experiments

The pyrazole ligands, 3-trifluoromethyl-5-(2-pyridyl)pyrazole (fppz)H and 1-(5-*tert*-butyl-2*H*-pyrazol-3-yl)isoquinoline (bpiq)H, were prepared according to the literature methods (8). Commercially available chemicals were used without further purification. All reactions were monitored by TLC with Merck silica gel plates (0.20 mm with fluorescent indicator UV_{254}). Compounds were visualized with 254 or 365 nm UV irradiation. Column chromatography was carried out using silica gel purchased from Merck (230–400 mesh). Mass spectra were obtained on a JEOL SX-102A instrument operating in electron impact (EI) or fast atom bombardment (FAB) mode. ^{1}H and ^{13}C NMR spectra were recorded on a Varian INOVA-500 instrument; chemical shifts are quoted with respect to the internal standard tetramethylsilane for ^{1}H and ^{13}C NMR data. Elemental analysis was carried out with a Heraeus CHN-O rapid elementary analyzer.

Cyclic voltammetry (CV)

CV measurements were performed using a BAS 100 B/W electrochemical analyzer. The oxidation and reduction measurements were recorded, respectively, in anhydr. CH_2Cl_2 and anhydr. THF containing 0.1 mol/L $TBAPF_6$ as the supporting electrolyte, at a scan rate of 100 mV s^{-1}. The potentials were measured against a Ag/Ag^+ (0.01 mol/L $AgNO_3$) reference electrode with ferrocene as the internal standard.

Preparation of 2,3-diphenyl benzo[*g*]quinoxaline

An anhydrous ethanol solution (30 mL) of 2,3-naphthalenediamine (1.0 g 6.33 mmol) and benzil (1.34 g, 6.33 mmol) was heated to reflux for 5 h. Then the solution was gradually cooled to room temperature. The solid deposited from solution was then filtered, washed with a few drops of ethanol, and dried in vacuum overnight to afford 1.8 g of yellow-green 2,3-diphenyl benzo[*g*]quinoxaline (5.42 mmol, 86%), denoted as (dpbq)H. The yellow-colored derivative 2,3-di-*p*-tolyl benzo[*g*]quinoxaline, (dtbq)H, was obtained from 4,4′-dimethylbenzil in a similar fashion.

Spectral data for (dpbq)H

^{1}H NMR (400 MHz, $CDCl_3$, 298 K) δ: 8.72 (s, 2H), 8.07 (dd, 2H, J_{HH} = 6.4, 2.8 Hz), 7.56 (d, 4H, J_{HH} = 7.2 Hz), 7.52 (dd, 2H, J_{HH} = 6.4, 2.8 Hz), 7.38–7.32 (m, 6H). MS (EI) *m/z*: 332 [M^+]. Anal. calcd. for $C_{24}H_{16}N_2$: N 8.43, C 86.72, H 4.85; found: N 8.48, C 86.63, H 5.05.

Spectral data for (dtbq)H

^{1}H NMR (400 MHz, $CDCl_3$, 298 K) δ: 8.69 (s, 2H), 8.09–8.06 (m, 2H), 7.54–7.51 (m, 2H), 7.46 (d, 4H, J_{HH} = 10 Hz), 7.15 (d, 4H, J_{HH} = 10 Hz), 2.37 (s, 6H). MS (EI) *m/z*: 360 [M^+]. Anal. calcd. for $C_{26}H_{20}N_2$: N 7.77, C 86.64, H 5.59; found: N 7.41, C 86.65, H 5.26.

Preparation of $[(dpbq)_2IrCl]_2$

The chloride-bridged complex $[(dpbq)_2IrCl]_2$ was synthesized according to the method reported by Nonoyama (9), involving treatment of $IrCl_3 \cdot 3H_2O$ (1.0 g, 2.84 mmol) with (dpbq)H (2.83 g, 8.5 mmol) in 2-methoxyethanol (30 mL) for 24 h. Then the solution was treated with water (30 mL) to induce precipitation of a dark brown solid. The solid was then filtered, washed with methanol, and dried under vacuum (1.8 g, 1.22 mmol, 71%).

© 2006 NRC Canada

Preparation of $[(dtbq)_2IrCl]_2$

On the basis of a procedure similar to that described for $[(dpbq)_2IrCl]_2$, the *p*-tolyl-substituted complex $[(dtbq)_2IrCl]_2$ was synthesized in ~75% yield.

Preparation of $[(dpbq)_2Ir(fppz)]$ (1)

A mixture of $[(dpbq)_2IrCl]_2$ (300 mg, 0.168 mmol), 3-trifluoromethyl-5-(2-pyridyl)pyrazole (fppzH, 80 mg, 0.38 mmol), and Na_2CO_3 (100 mg, 0.94 mmol) in 2-methoxyethanol (20 mL) was heated to reflux for 4 h. An excess of deionized water was added after cooling the solution to room temperature (RT). The precipitate was collected by filtration and washed with methanol (10 mL), followed by diethyl ether (10 mL). Black crystals of $[(dpbq)_2Ir(fppz)]$ (**1**) were obtained from a mixture of CH_2Cl_2 and methanol at RT (210 mg, 0.19 mmol, 58%).

Spectral data for 1

^{1}H NMR (400 MHz, $CDCl_3$, 298 K) δ: 8.77 (s, 1H), 8.64 (d, 1H, J_{HH} = 5.6 Hz), 8.54 (s, 1H), 8.49 (s, 1H), 8.05 (s, 1H), 7.94–7.88 (m, 4H), 7.75 (d, 1H, J_{HH} = 8.0 Hz), 7.72–7.61 (m, 5H), 7.61–7.55 (m, 3H), 7.45–7.38 (m, 4H), 7.35 (t, 1H, J_{HH} = 6.0 Hz), 7.27–7.32 (m, 2H), 7.25–7.20 (m, 3H), 6.78 (d, 1H, J_{HH} = 7.6 Hz), 6.72 (t, 1H, J_{HH} = 8.0 Hz), 6.65 (t, 1H, J_{HH} = 7.6 Hz), 6.60 (t, 1H, J_{HH} = 7.2 Hz), 6.50–6.47 (m, 2H), 6.36 (d, 1H, J_{HH} = 7.2 Hz). MS (FAB, ^{193}Ir) *m/z*: 1067 [M^+]. Anal. calcd. for $C_{57}H_{35}F_3IrN_7$: N 9.19, C 64.15, H 3.31; found: N 9.09, C 64.21, H 3.62.

Preparation of $[(dpbq)_2Ir(bpiq)]$ (2)

Procedures identical to that of **1** were followed, using 200 mg of $[(dpbq)_2IrCl]_2$ (0.112 mmol), 71 mg of (bpiq)H (0.28 mmol), and 60 mg of Na_2CO_3 (0.57 mmol) in 20 mL of 2-methoxyethanol. Black crystals of $[(dpbq)_2Ir(bpiq)]$ (**2**) were obtained from a mixture of CH_2Cl_2 and hexane at RT (74 mg, 0.085 mmol, 33%).

Spectral data for 2

^{1}H NMR (400 MHz, $CDCl_3$, 298 K) δ: 9.00 (s, 1H), 8.50–8.43 (m, 5H), 8.30 (s, 1H), 7.97 (b, 2H), 7.87 (d, 2H, J_{HH} = 8.0 Hz), 7.82 (d, 1H, J_{HH} = 8.0 Hz), 7.72 (d, 1H, J_{HH} = 8.0 Hz), 7.69–7.58 (m, 7H), 7.52 (t, 1H, J_{HH} = 7.2 Hz), 7.44–7.28 (m, 4H), 7.26–7.18 (m, 5H), 6.74–6.66 (m, 2H), 6.64–6.53 (m, 3H), 6.45 (t, 1H, J_{HH} = 7.6 Hz), 6.31 (d, 1H, J_{HH} = 8.0 Hz), 1.37 (s, 9H). MS (FAB, ^{193}Ir) *m/z*: 1105 [M^+]. Anal. calcd. for $C_{64}H_{46}F_3IrN_7$: N 8.87, C 69.54, H 4.19; found: N 8.79, C 69.48, H 4.56.

Preparation of $[(dpbq)_2Ir(bpy)]$ (3)

A mixture of $[(dpbq)_2IrCl]_2$ (200 mg, 0.11 mmol), 2,2′-bipyridine (bpy, 45 mg, 0.29 mmol), and $AgBF_4$ (100 mg, 0.51 mmol) in CH_2Cl_2 (25 mL) was stirred at RT for 3 h. The solution was filtered and the filtrate was evaporated to give the crude product. Black crystals of $[(dpbq)_2Ir(bpy)][BF_4]$ (**3**) were obtained from a mixture of CH_2Cl_2 and hexane at RT (110 mg, 0.09 mmol, 41%).

Spectral data for 3

^{1}H NMR (400 MHz, $CDCl_3$, 298 K) δ: 8.71 (d, 2H, J_{HH} = 4.8 Hz), 8.60 (s, 2H), 8.55 (d, 2H, J_{HH} = 8.8 Hz), 8.20 (t, 2H, J_{HH} = 7.6 Hz), 7.96 (d, 2H, J_{HH} = 8.0 Hz), 7.86–7.80 (m, 8H), 7.68–7.64 (m, 8H), 7.49 (t, 2H, J_{HH} = 3.6 Hz), 7.40 (t, 2H, J_{HH} = 7.6 Hz), 7.03 (d, 2H, J_{HH} = 8.0 Hz), 6.75 (t, 2H, J_{HH} = 7.6 Hz), 6.63 (t, 2H, J_{HH} = 7.2 Hz), 6.54 (d, 2H, J_{HH} = 7.6 Hz). MS (FAB, ^{193}Ir) *m/z*: 1011 [M^+]. Anal. calcd. for $C_{58}H_{38}F_4IrN_6$: N 7.65, C 63.45, H 3.49; found: N 7.71, C 63.25, H 3.57.

Preparation of $[(dtbq)_2Ir(fppz)]$ (4)

Procedures identical with that of **1** were followed, using 200 mg of $[(dtbq)_2IrCl]_2$ (0.106 mmol), 113 mg of (fppz)H (0.53 mmol), and 100 mg of Na_2CO_3 (0.94 mmol) in 20 mL of 2-methoxyethanol. Black crystals of $[(dtpz)_2Ir(fppz)]$ (**4**) were obtained from a mixture of CH_2Cl_2 and methanol at RT (120 mg, 0.107 mmol, 50%).

Spectral data for 4

^{1}H NMR (400 MHz, $CDCl_3$, 298 K) δ: 8.69 (s, 1H), 8.57 (d, 1H, J_{HH} = 8.0 Hz), 8.49 (s, 1H), 8.44 (s, 1H), 7.98 (s, 1H), 7.91 (d, 1H, J_{HH} = 8.0 Hz), 7.86 (d, 1H, J_{HH} = 8.0 Hz), 7.81 (d, 2H, J_{HH} = 5.2 Hz), 7.72 (d, 1H, J_{HH} = 8.0 Hz), 7.54 (t, 1H, J_{HH} = 1.2 Hz), 7.50–7.41 (m, 5H), 7.40 (t, 3H, J_{HH} = 1.2 Hz), 7.31–7.24 (m, 4H), 7.20–7.12 (m, 3H), 6.63 (s, 1H), 6.57 (d, 1H, J_{HH} = 8.0 Hz), 6.48 (d, 1H, J_{HH} = 8.0 Hz), 6.44 (s, 1H), 6.20 (s, 1H), 2.54 (s, 3H), 2.51 (s, 3H), 1.86 (s, 3H), 1.79 (s, 3H). MS (FAB, ^{193}Ir) *m/z*: 1123 [M^+]. Anal. calcd. for $C_{61}H_{43}F_3IrN_7$: N 8.73, C 65.23, H 3.86; found: N 8.64, C 64.89, H 3.81.

Preparation of $[(dtbq)_2Ir(acac)]$ (5)

A mixture of $[(dtbq)_2IrCl]_2$ (200 mg, 0.106 mmol), acetylacetone (acacH, 300 mg, 3.0 mmol), and Na_2CO_3 (100 mg, 0.94 mmol) in CH_2Cl_2 (20 mL) was stirred at RT for 24 h. After stopping the reaction, the solution was washed with water (3 × 50 mL), dried over $MgSO_4$, and concentrated to dryness. Black crystals of $[(dtbq)_2Ir(acac)]$ (**5**) were recrystallized from CH_2Cl_2 and hexane at RT (90 mg, 0.89 mmol, 42%).

Spectral data for 5

^{1}H NMR (400 MHz, $CDCl_3$, 298 K) δ: 8.84 (s, 2H), 8.65 (s, 2H), 8.03 (d, 2H, J_{HH} = 8.0 Hz), 7.94–7.89 (m, 6H), 7.49–7.42 (m, 8H), 7.06 (d, 2H, J_{HH} = 8.4 Hz), 6.41 (d, 2H, J_{HH} = 8.4 Hz), 6.32 (s, 2H), 4.63 (s, 1H), 2.52 (s, 6H), 1.79 (s, 6H), 1.61 (s, 6H). MS (FAB, ^{193}Ir) *m/z*: 1010 [M^+]. Anal. calcd. for $C_{57}H_{45}IrN_4O_2$: N 5.55, C 67.77, H 4.49; found: N 5.51, C 67.63, H 4.83.

X-ray structural analysis

Single crystal X-ray diffraction data were measured on a Bruker Smart CCD diffractometer using (Mo Kα) radiation (λ = 0.710 73 Å). The data collection was executed using the SMART program. Cell refinement and data reduction were made with the SAINT program. The structure was determined using the SHELXTL/PC program and refined using full-matrix least-squares. All non-hydrogen atoms were refined anisotropically, whereas hydrogen atoms were placed at the calculated positions and included in the final stage of refinements with fixed parameters. The crystallographic refinement parameters for complexes **1** and **3** are summarized in Table 1, and selected bond distances and angles of these complexes are listed in Tables 2 and 3, respectively.

© 2006 NRC Canada

Table 1. Crystal data and refinement parameters for complexes **1** and **3**.

Compound	**1**	**3**
Formula	$C_{57}H_{35}F_3N_7Ir\cdot CH_2Cl_2$	$C_{58}H_{38}N_6Ir\cdot BF_4\cdot CH_2Cl_2$
Molecular weight	1 152.05	1 182.88
Crystal system	Triclinic	Triclinic
Space group	*P*-1	*P*-1
Crystal size (mm^3)	0.4×0.15×0.12	0.18×0.15×0.05
a (Å)	11.9568(4)	16.3626(6)
b (Å)	12.0739(5)	17.2949(6)
c (Å)	17.1667(7)	19.5430(7)
α (°)	74.820(1)	73.631(1)
β (°)	82.535(1)	72.197(1)
γ (°)	84.788(1)	70.003(1)
V ($Å^3$)	2 367.4(2)	4 850.1(3)
Z	2	4
ρ_{calcd} (g cm^{-3})	1.616	1.620
Temp (K)	295(2)	150(1)
μ (mm^{-1})	2.994	2.927
Reflections collected	31 690	64 361
Independent reflections	10 878 (*R*(int) = 0.0419)	22 242 (*R*(int) = 0.0680)
R_F, $R_w(F^2)$ (all data)	0.0445, 0.0928	0.0873, 0.1475
R_F, $R_w(F^2)$ [I > 2σ(I)]	0.0360, 0.0860	0.0606, 0.1319
GOF	1.043	1.144

Note: $R_F = \Sigma||F_o - F_c||/\Sigma|F_o|$ and $R_w(F^2) = [\Sigma w|F_o^2 - F_c^2|^2/\Sigma w(F_o^4)]^{1/2}$.

Table 2. Selected bond lengths (Å) and angles (°) for complex **1**.

Bond lengths (Å)	
Ir—N(1)	2.201(3)
Ir—N(4)	2.065(3)
Ir—C(10)	1.990(4)
C(25)···N(2)	3.013(7)
C(49)···N(1)	3.165(6)
Ir—N(2)	2.116(3)
Ir—N(6)	2.047(3)
Ir—C(34)	1.991(4)
C(25)···N(3)	3.381(6)
C(49)···C(1)	3.439(6)
Bond angles (°)	
N(1)-Ir-N(2)	75.02(13)
N(6)-Ir-C(34)	79.47(15)
N(2)-Ir-C(10)	174.19(14)
N(4)-Ir-C(10)	79.21(15)
N(1)-Ir-C(34)	170.85(14)
N(4)-Ir-N(6)	178.16(12)

Table 3. Selected bond lengths (Å) and angles (°) for complex **3**.

Bond lengths (Å)	
Ir(1)—N(1)	2.062(6)
Ir(1)—N(5)	2.171(6)
Ir(1)—C(1)	1.992(7)
C(23)···N(6)	2.995(8)
C(47)···N(5)	3.146(9)
Ir(1)—N(3)	2.076(5)
Ir(1)—N(6)	2.160(6)
Ir(1)—C(25)	1.999(6)
C(23)···C(58)	3.336(8)
C(47)···C(49)	3.438(8)
Bond angles (°)	
N(1)-Ir(1)-C(1)	79.4(3)
N(5)-Ir(1)-N(6)	75.2(2)
N(6)-Ir(1)-C(1)	171.7(2)
N(3)-Ir(1)-C(25)	79.3(2)
N(1)-Ir(1)-N(3)	173.7(2)
N(5)-Ir(1)-C(25)	174.9(2)

The crystallographic data for complexes **1** and **3** (excluding structure factors) have been deposited.[5]

Spectral and dynamic measurement

Steady-state absorption and emission spectra were recorded with a Hitachi (U-3310) spectrophotometer. The NIR emission spectra were acquired by exciting the sample solution under a rectangular excitation configuration using an Ar ion laser (488 or 514 nm, Innova 90, Coherent Inc., Santa Clara, California) and the continuous wave was chopped by

[5] Supplementary data for this article are available on the journal Web site (http://canjchem.nrc.ca) or may be purchased from the Depository of Unpublished Data, Document Delivery, CISTI, National Research Council Canada, Ottawa, ON K1A 0R6, Canada. DUD 5002. For more information on obtaining material refer to http://cisti-icist.nrc-cnrc.gc.ca/irm/unpub_e.shtml. CCDC 276875 and 276876 contain the crystallographic data for this manuscript. These data can be obtained, free of charge, via http://www.ccdc.cam.ac.uk/conts/retrieving.html (Or from the Cambridge Crystallographic Data Centre, 12 Union Road, Cambridge CB2 1EZ, UK; fax +44 1223 336033; or deposit@ccdc.cam.ac.uk).

© 2006 NRC Canada

a mechanic chopper operated at 200 Hz. To minimize the reabsorption effect, the excitation beam was focused as closely as possible to the front wall of the quartz cell. The NIR emission was measured by the photomultiplier tube (Hamamatzu R5509-72, operated at –80 °C) coupled with a Lock-in amplifier (SR830, Stanford Research Systems, Sunnyvale, California) and a monochromator (SpectraPro-275, Acton Research Corporation, Acton, Massachusetts) in that the grating was blazed at 1200 nm. IR125 (Exciton Inc., Dayton, Ohio) with $\Phi \sim 0.11$ ($\lambda_{max} \sim 925$ nm) in DMSO solution was used as a standard to calculate the emission quantum yield (10). For the NIR lifetime measurement, the sample was excited by a 532 nm pulse (2nd harmonic of Nd:YAG, 6 ns). The emission trace was detected by a photomultiplier tube (Hamamatzu R5509-72) operated at –80 °C and recorded by a sampling oscilloscope (TDS 3012, Tektronix, Beaverton, Oregon). An average of 100 shots was taken in the lifetime measurement, unless specified elsewhere.

Computational methodology

Calculations on the electronic ground state of complexes **1** and **3** were carried out using B3LYP density functional theory (11, 12). A double-ζ quality basis set consisting of Hay and Wadt's effective core potentials (LANL2DZ) (13) was employed for the Ir atom and a 6-31G* (14) basis for the H, C, N, and F atoms. A relativistic effective core potential (ECP) replaced the inner core electrons of Ir(III), leaving the outer core ($5s^25p^6$) electrons and the $5d^6$ valence electrons. Time-dependent DFT (TDDFT) calculations (15) using the B3LYP functional were then performed based on the structural optimized geometries. Typically, the lowest 10 triplet and 10 singlet roots of the nonhermitian eigenvalue equations were obtained to determine the vertical excitation energies. Oscillator strengths were deduced from the dipole transition matrix elements (for singlet states only). The ground-state B3LYP and excited-state TDDFT calculations were carried out using Gaussian03 (16).

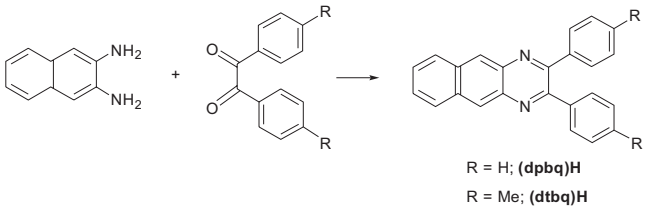
Results and discussion

Syntheses and structural characterization

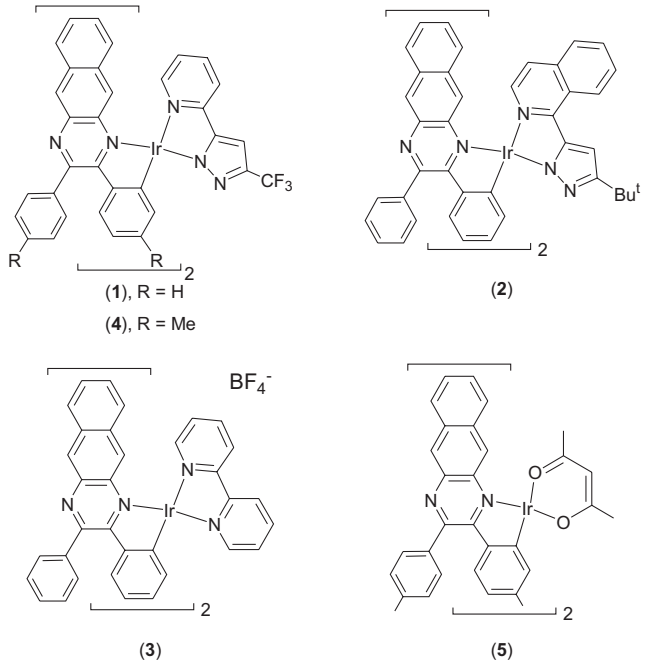
The preparation of highly conjugated ligand chromophores is necessary to achieve the NIR-emitting iridium complexes. As depicted in Scheme 1, the required ligands can be synthesized by treatment of 2,3-naphthalenediamine and dibenzil to produce 2,3-diphenyl-or di-*p*-tolyl-substituted benzo[*g*]quinoxaline in good yields. This synthetic approach follows the literature procedure utilized for the analogous diphenylquinoxaline, and is best prepared from related *o*-phenylenediamine and the corresponding α-diketone in refluxing ethanol (17).

Subsequent reactions of $IrCl_3 \cdot nH_2O$ with (dpbq)H or (dtbq)H in refluxing ethoxyethanol afforded chloride-bridged dimers $[(dpbq)_2IrCl]_2$ or $[(dtbq)_2IrCl]_2$, respectively. These dimer complexes can easily react with the pyrazole chelate ligand (fppz)H in the presence of Na_2CO_3 to afford black-colored complexes $[(dpbq)_2Ir(fppz)]$ (**1**) and $[(dtbq)_2Ir(fppz)]$ (**4**), where (fppz)H = 3-trifluoromethyl-5-(2-pyridyl)pyrazole. Similar reactions towards other bidentate chelates such as 1-(5-*tert*-butyl-2*H*-pyrazol-3-yl)isoquinoline ((bpiq)H), 2,2′-bipyridine (bpy), and acetylacetone (acacH) yielded the corresponding Ir(III) complexes, $[(dpbq)_2Ir(bpiq)]$ (**2**), $[(dpbq)_2Ir(bpy)][BF_4]$ (**3**), and $[(dtbq)_2Ir(acac)]$ (**5**), respectively (see Scheme 2).

Scheme 1.



Scheme 2.

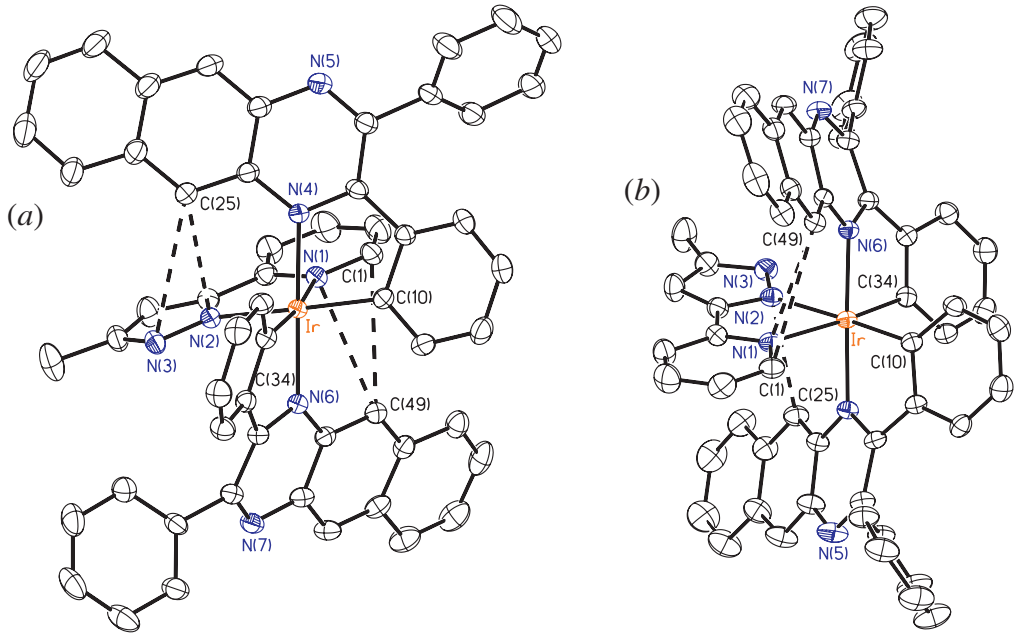


All iridium complexes were easily soluble in organic solvents such as CH_2Cl_2, THF, and acetone, and the corresponding solutions showed negligible decomposition for a period of over 24 h, upon exposure to air. Routine characterizations were conducted using microanalysis, mass spectrometry, and ^1H NMR spectroscopy. Moreover, the fppz complex **1** was further characterized by single crystal X-ray diffraction analysis. Its ORTEP diagram is depicted in Fig. 1, while crucial bond distances and angles are listed in Table 1.

As depicted in Fig. 1, complex **1** reveals a distorted octahedral geometry around the Ir atom, consisting of two cyclometalated phenylbenzoquinoxaline fragments and one (2-pyridyl) pyrazolate ligand. The unique pyrazolate chelate is located opposite to the cis-oriented carbon donor atoms of benzoquinoxaline, while the benzoquinoxaline ligands adopt an eclipse configuration and their coordinated nitrogen atoms (N(4) and N(6)) and carbon atoms (C(10) and C(34)) adopt trans and cis orientation, respectively. This coordinative arrangement is akin to those of the parent phenyl pyridine ligands observed for the chloride-bridged dimer

© 2006 NRC Canada

Fig. 1. (*a*) ORTEP diagram of **1** with thermal ellipsoids shown at the 30% probability level; fluorine atoms of the CF_3 substituent were omitted for clarity. (*b*) Same ORTEP diagram with an emphasis on the spatial distortion of dpbq ligands.



complex $[(ppy)_2Ir(\mu\text{-}Cl)]_2$ (18), the diketonate complex $(ppy)_2Ir(acac)$ (19), and even the pyrazolate derivatives, suggesting that the incoming fppz ligand occupies the positions of the bridging chloride ligands in its starting material, $[(dpbp)_2IrCl]_2$. Moreover, the uncoordinated and cyclometalated phenyl groups show twisting angles of 40°–54°, as well as unusually large deformation angles of 23°–28° with respect to the middle benzoquinoxaline fragments. The deformation angles reveal an unfavorable steric interaction between the chelating ligands and can be gauged by the least-squares calculation using planes defined by the cyclometalated phenyl group and the middle C_6 hexagon of the benzoquinoxaline. It appears to us that the nonbonding repulsion between benzoquinoxaline and pyridyl pyrazolate ligands is the main driving force causing such a large distortion at the cyclometalated phenyl groups, as most of the interligand C···C and C···N nonbonding contacts listed in Table 2 are shorter than a limited value of ca. 3.4 Å, i.e., the sum of the van der Waals radii of the carbon atoms.

For a further comparison, the X-ray structural study on the cationic dipyridine complex **3** was also examined. Comparison of the ORTEP diagram (Fig. 2) and the metric parameters (Table 3) with those of **1** shows no significant variation on the overall molecular architecture, except for the formation of an approximate C_2 rotational axis that bisects the bipyridine ligand and passes through the central Ir metal atom. This increasing molecular symmetry is consistent with the simplification of the ^1H NMR spectral pattern observed in solution at RT (see the Experimental section).

Electrochemistry

The electrochemical properties of these Ir complexes were investigated by CV using ferrocene as the internal standard, and the respective redox data are listed in Table 4. During the anodic scan, all iridium complexes exhibited a reversible oxidation wave with potentials in the region 0.50–0.77 V. It is believed that the oxidation process mainly occurred at the metal center and, in part, with a slight contribution from the surrounding chelate ligands (20). Thus, the formal oxidation potential was strongly dependent on the electronic environment of the Ir(III) cation, i.e., a better electron donor would shift the oxidation potential to a less positive value. This hypothesis was verified by the increased π conjugation of the anionic bpiq ligand in **2**, which decreased the oxidative potential from 0.77 (in **1**) to 0.61 V (in **2**), while the attachment of the 2,2′-bipyridine ligand in **3** led to the complete suppression of the metal oxidation signal owing to its cationic nature. Moreover, replacement of the phenyl substituents with tolyl substituents of benzoquinoxaline also slightly altered the oxidation potential, as supported by the fact that the oxidation potential of **4** is cathodically shifted to 0.70 V in comparison with that of the parent complex **1**. Owing to the presence of an extra methyl substituent, this result could possibly be attributed to a slightly better σ-donor ability of the cyclometalated tolyl group.

Upon switching to the cathodic sweep in THF, two reversible reduction processes, with potentials ranging from –1.33 to –1.96 V, were detected for all complexes (**1**–**5**). We assigned these signals to a sequential reduction of the cyclometalated benzoquinoxaline fragments. For dtbq complex **4**, the first reduction peak is shifted to –1.65 V in comparison with that of the dpbq counterpart **1** (–1.54 V) because of the electron-releasing effect of the *para*-methyl substituents. Conversely, complex **3** showed the lowest reduction potentials, owing to its cationic nature, while complexes **2** and **5** gave the highest reduction potential among the whole series. The results indicate that the third ancillary ligand also significantly affects the redox properties of these Ir complexes, possibly via their enhanced donor capability as well as the extended π conjugation. Qualitatively, this observation is consistent with both the photophysical properties and theoretical predictions elaborated as follows.

© 2006 NRC Canada

Fig. 2. (*a*) ORTEP diagram of **3** with thermal ellipsoids shown at the 50% probability level. (*b*) Same ORTEP diagram with an emphasis on the spatial distortion of dpbq ligands.

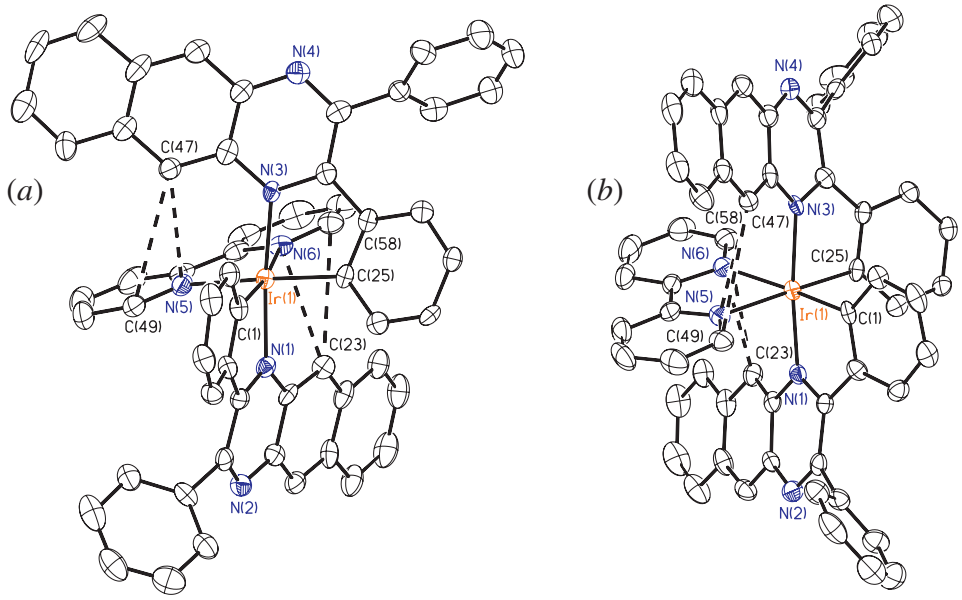
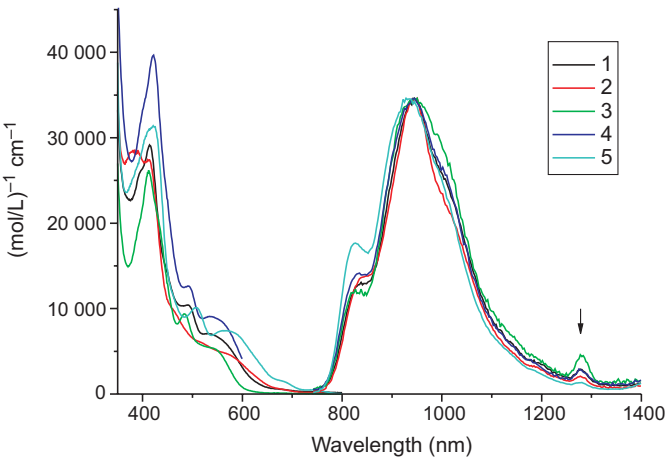


Table 4. One-electron redox potentials of complexes **1**–**5**.

Complex	$E_{1/2}^{ox}$ (V)[a]	$E_{1/2}^{red}$ (V)[a]
1	0.77 [100][b]	–1.54 [110], –1.81 [100]
2	0.61 [80]	–1.64 [100], –1.91 [100]
3	—	–1.31 [80], –1.61 [80]
4	0.70 [100]	–1.65 [110], –1.91 [120]
5	0.50 [90]	–1.73 [90], –1.96 [100]

[a]Potential values referenced vs. Fc/Fc^+.
[b]Data in square bracket denotes the $|E_{pa} - E_{pc}|$ values in mV.

Fig. 3. The absorption and emission spectra of complexes **1**–**5** in CH_2Cl_2. The peak intensities were normalized. λ_{ex} = 514 nm. The arrow indicates the peak for $^1O^2\,^1\Delta g(v' = 0) \rightarrow \Sigma_g^-(v'' = 0)$ 1276 nm emission.



Photophysical properties

Figure 3 shows the absorption and emission spectra of complexes **1**–**5** in CH_2Cl_2. As supported by CV measurements as well as the frontier orbital analyses (see the following section), it is reasonable to assign the first S_0–S_1 transition to absorption peaks around 500–600 nm ($\varepsilon \sim 5 \times 10^3$ $(mol/L)^{-1}$ cm^{-1}) to a metal to ligand (benzoquinoxaline part) charge transfer (MLCT) overlapping with the interligand phenyl to benzoquinoxaline transition. Due to a large molecular framework, the composition of higher electronic states is complicated, so that any corresponding assignments for complexes **1**–**5** may not be meaningful. Furthermore, the Ir-metal-enhanced spin-orbit coupling should result in nonnegligible absorptivity for the triplet transition, as indicated by a corresponding small absorption hump around 650–700 nm. However, absorption bands ascribed to the triplet manifolds could not be distinctly resolved mainly owing to their hiding inside the UV region of the strong singlet transitions. Detailed discussion regarding the transition in the triplet manifold will be given in the Theoretical approach section.

Figure 3 also depicts the emission spectra of complexes **1**–**5** in CH_2Cl_2. The spectral feature, quantum efficiency and relaxation dynamics (vide infra) of complexes **1**–**5** show concentration independence up to 10^{-3} mol/L, indicating a negligible aggregation effect in fluid solution. To reveal any differences in the spectral profile, the emission spectra were normalized at the peak wavelength. In comparison, for all complexes studied, only a slight variation was observed in view of the emission spectral feature and peak position. As listed in Table 5, the relaxation dynamics of **1**–**5** are O_2 concentration dependent. For example, the decay time of complex **1** was measured to be 286 ns in the degassed CH_2Cl_2, while it was decreased to 200 ns upon aeration. In the O_2 dependent study, in which the O_2 concentration was monitored by its vapor pressure filled in the vacuum line and deduced by Henry's law, a straight Stern–Volmer plot could be formulated (not shown here), and an oxygen-quenching rate constant of 1.7×10^9 $(mol/L)^{-1}$ s^{-1} was deduced, which is nearly one-nineth of the diffusion-controlled rate of 2.0×10^{10} $(mol/L)^{-1}$ s^{-1} calculated from the Stokes–Einstein equa-

© 2006 NRC Canada

Table 5. Photophysical properties of complexes **1**–**5** in CH_2Cl_2 at room temperature.

Complex	λ_{abs} (nm) (ε, 10^3 (mol/L)$^{-1}$ cm^{-1})	λ_{em} (nm)	Φ_{aer} ($\times 10^3$)[a]	τ_{aer} (ns)	τ_{deg} (ns)
1	535 (7), 491 (10), 414 (29)	916	6.48	200	286
2	575 (5), 464 (10), 414 (27)	922	9.53	195	276
3	540 (5), 484 (9), 412 (26)	922	3.59	245	403
4	541 (9), 491 (13), 422 (40)	916	10.2	209	302
5	570 (7), 508 (10), 421 (31)	904	21.8	216	290

[a]Quantum efficiencies were measured in aerated CH_2Cl_2.

Fig. 4. HOMO and LUMO of complex **1** involved in the low-lying transition.

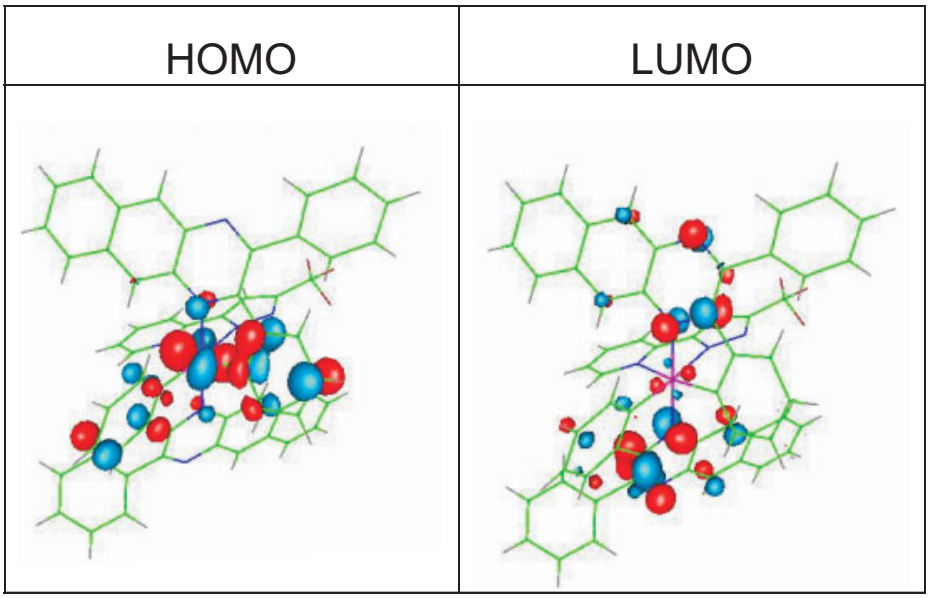


Table 6. The calculated lowest excited singlet and triplet states of complex **1**.

State	Assignment	λ (nm)	*E* (eV)	*f*
S_1	HOMO → LUMO (+95%)	618.3	2.01	0.0067
T_1	HOMO–1 → LUMO (+42%) HOMO → LUMO (+37%) HOMO–1 → LUMO+1 (23%) HOMO–2 → LUMO (11%)	743.6	1.67	~0

tion in CH_2Cl_2. The result is consistent with the O_2-quenching triplet state according to the theory of electron-exchange type (Dexter type) of energy transfer expressed as (21):

$$T + {}^3O_2 \xrightarrow{k_{O_2}} S_0 + {}^1O_2$$

The overall spin must be conserved upon forming a collisional complex. Accordingly, the possibility of each collision producing $^1O_2$ is statistically one-nineth. Perhaps the strongest support for the O_2 quenching is given by the observation of $^1O_2$ ($^1\Delta_g$ ($v'' = 0$) → $^1\Sigma^-_g$($v' = 0$) emission with a peak wavelength at ~1276 nm (22) for complexes **1**–**5** in aerated CH_2Cl_2 (see the arrow in Fig. 3). The results, in combination with the rather small radiative decay rate of $<10^6$ s^{-1}, lead us to unambiguously assign the dominant emission in complexes **1**–**5** to be of phosphorescence character. The spectra show a distinctly 0–0 vibronic onset of the transition, a profile that normally appears in a $^3\pi$–π^* transition of aromatic chromophores with high symmetry. The results provide a clue that the observed phosphorescence possesses, in part, a $^3\pi$–π^* character plausibly originating from a ligand-center chromophore of long conjugation such as benzoquinoxaline. Nevertheless, the involvement of other transitions such as ^{3}MLCT is also possible. Furthermore, the observation of rather small changes in spectral features, as well as peak positions, implies that frontier orbitals responsible for the T_1–S_0 transition may be mainly derived from the same origin for complexes **1**–**5**. It is thus of fundamental importance to gain more detailed insights into the transition properties of the phosphorescence based on the theoretical approaches elaborated as follows.

Theoretical approach

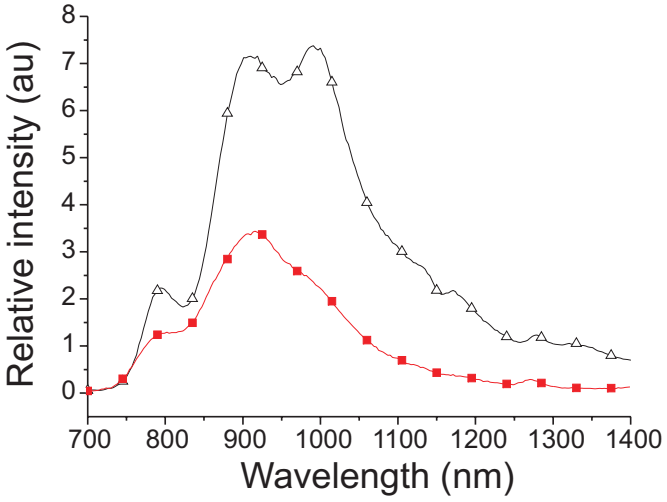
Theoretical confirmation of the photophysical properties of complex **1** was provided by the DFT calculations. In this study, the crystallographic data for **1** was used as the framework for the extended Hückel formalism, and the calculation

© 2006 NRC Canada

was performed via a CACAO program (see the Experimental section). Figure 4 depicts the features of the HOMO to HOMO–3 and LUMO to LUMO+3 frontier orbitals mainly involved in the lower-lying transition, while the descriptions and the energy gaps of each transition are listed in Table 6. The validity of the TDDFT approach can be readily perceived by the calculated $T_1 \rightarrow S_0$ emission peak at 745 nm, which is very close to the 0–0 onset peak (~785 nm) observed experimentally. Based on the results (see Fig. 4 and Table 6), the electron densities of the HOMO are mainly located on the Ir(III) metal center and, to a small extent, the cyclometalated phenyl ligand, while a large portion of the electron densities of HOMO–1 and HOMO–2 is attributed to the π orbitals of benzoquinoxaline overlapping with certain d_π orbitals of the Ir(III) atom. Conversely, the electron densities of LUMO and LUMO+1 are distributed mostly on the benzoquinoxaline moiety. The $S_0 \rightarrow S_1$ and $S_0 \rightarrow S_2$ transitions mainly incorporate HOMO → LUMO (+95%) and HOMO → LUMO+1 (+93%), respectively, and thus are dominated by MLCT (d_π (Ir) → π* (benzoquinoxaline)) overlapping with π–π* ILCT (mainly cyclometalated phenyl site (π) → benzoquinoxaline pyridine site (π*)) in character. As supported by the data shown in Table 6, the higher excited states in the singlet manifold, $S_0 \rightarrow S_n$ ($n > 3$), are relatively much more complicated, the results of which make a definitive frontier orbital assignment meaningless. In contrast, the lowest electronic transition in the triplet manifold, i.e., $S_0 \rightarrow T_1$, mainly incorporates the ligand center benzoquinoxaline $^3\pi$–π^* transition and ^{3}MLCT (d_π (Ir) → π* (benzoquinoxaline)).

The contribution of the $^3\pi$–π* transition is manifested by the low-temperature (77 K) approach to complex **1**. Figure 5 shows the luminescence spectrum of **1** in a 77 K CH_2Cl_2 matrix. Two salient remarks can be pointed out promptly according the spectral layout. First, in comparison to that measured at 298 K, the enhancement of the vibronic progression at 77 K is obvious, showing the notable population switching from perhaps ^{3}MLCT/$^3\pi$–π mixing character to the $^3\pi$–π dominating state under this condition. Nevertheless, one cannot eliminate the possibility that the increase in vibronic resolution upon cooling may just indicate an increase in rigidity of the molecule, making the vibrational levels more identical to one another, as well as the disappearance of hot bands. Secondly, the phosphorescence intensity at 77 K is increased ~2.5-fold with respect to that at 298 K. Similar structural phosphorescence with 2- to ~3-fold increases in intensity was observed for complexes **2**–**5** in 77 K CH_2Cl_2. Thus, temperature-dependent radiationless deactivation pathways may only play a minor role to the relaxation dynamics. Moreover, as listed in Table 5, substitution at non-benzoquinoxaline sites causes neither spectral change nor large alternation of the quantum efficiency. The latter implies that the large amplitude vibration or any torsional motion at non-benzoquinoxaline sites, which generally quenches emission in the NIR region, are not actively involved in the deactivation process. This viewpoint can be rationalized by the negligible contribution of non-benzoquinoxaline ligands to both HOMO (or HOMO–1 and HOMO–2) and LUMO (or LUMO+1). Since complexes **1**–**5** all bear aryl substituents at benzoquinoxaline sites, it is plausible that the torsional motion of phenyl (or tolyl) substituents, the relaxation dynamics of which should be temperature dependent, partly induces the radiationless transition. However, one ought to realize that because of the much smaller NIR energy gap, excitation that causes any weakening of the bond strength may result in crossing of the potential energy surface between T_1 and S_0 states and eventually trigger the rapid radiationless deactivation. In the case of complexes **1**–**5**, these nearly temperature-independent, weak vibrational motions play a key role in accounting for the dominant radiationless deactivation.

Fig. 5. The luminescence spectrum of **1** at room temperature (■) and in the 77 K CH_2Cl_2 matrix (Δ). Note that both spectra were analyzed using the same absorbance and excitation wavelength (514 nm). Thus, the intensity ratio can be directly estimated from the spectral integration.



Conclusion

In summary, we report the syntheses and characterization of a new series of NIR Ir(III) complexes (**1**–**5**). These complexes exhibit moderate NIR phosphorescence with peak wavelengths around 910–920 nm at RT. As supported by the TDDFT approach, the transition mainly involves benzoisoquinoline $^3\pi$–π^* intraligand charge transfer and metal (Ir) to benzoisoquinoline charge transfer. The relatively weak NIR emission can be tentatively rationalized by the low energy gap of which the radiationless deactivation may be governed by the large amplitude vibration and, in part, the phenyl torsional motions at the benzoquinoxaline sites. Knowing that current interest in Ir(III) types of phosphorescence emitter is focused on the Ir(III)-type OLED, to switch gears in research orientation, future applications of the titled NIR complexes and (or) relevant derivatives may be motivated by the strategy of using these complexes in the fabrication of photovoltaic devices (23). Focus on this approach is in progress.

Acknowledgment

We thank the National Science Council of Taiwan, Republic of China, for financial support (grant Nos. NSC 91-2119-M-002-016) and (NSC 91-2113-M-007-006).

© 2006 NRC Canada

References

1 (*a*) B. O'Regan and M. Graetzel. Nature (London), **353**, 737 (1991); (*b*) A. Hagfeldt and M. Gratzel. Acc. Chem. Res. **33**, 269 (2000); (*c*) D. Kuciauskas, M.S. Freund, H.B. Gray, J.R. Winkler, and N.S. Lewis. J. Phys. Chem. B, **105**, 392 (2001); (*d*) M. Gratzel. Nature (London), **414**, 338 (2001).

2. (*a*) R.J. Mears and S.R. Baker. Opt. Quantum Electron. **24**, 517 (1992); (*b*) E. Desurvire. Phys. Today, **97**, 20 (1994); (*c*) N. Ono, S. Ito, C.H. Wu, C.H. Chen, and T.C. Wen. Chem. Phys. **262**, 467 (2000).
3. (*a*) M.A. Baldo, D.F. O'Brien, Y. You, A. Shoustikov, S. Sibley, M.E. Thompson, and S.R. Forrest. Nature (London), **395**, 151 (1998); (*b*) Y.-L. Tung, S.-W. Lee, Y. Chi, Y.-T. Tao, C.-H. Chien, Y.-M. Cheng, P.-T. Chou, S.-M. Peng, and C.-S. Liu. J. Mater. Chem. **15**, 460 (2005); (*c*) A. Tsuboyama, H. Iwawaki, M. Furugori, T. Mukaide, J. Kamatani, S. Igawa, T. Moriyama, S. Miura, T. Takiguchi, S. Okada, M. Hoshino, and K. Ueno. J. Am. Chem. Soc. **125**, 12971 (2003); (*d*) Y.-L. Tung, S.-W. Lee, Y. Chi, L.-S. Chen, C.-F. Shu, F.-I. Wu, A.J. Carty, P.-T. Chou, S.-M. Peng, and G.-H. Lee. Adv. Mater. **17**, 1059 (2005).
4. (*a*) E.M. Kober, J.V. Caspar, R.S. Lumpkin, and T.J. Meyer. J. Phys. Chem. **90**, 3722 (1986); (*b*) L. Della Ciana, W.J. Dressick, D. Sandrini, M. Maestri, and M. Ciano. Inorg. Chem. **29**, 2792 (1990).
5. (*a*) T.J. Foley, B.S. Harrison, A.S. Knefely, K.A. Abboud, J.R. Reynolds, K.S. Schanze, and J.M. Boncella. Inorg. Chem. **42**, 5023 (2003); (*b*) W.-K. Wong, A. Hou, J. Guo, H. He, L. Zhang, W.-Y. Wong, K.-F. Li, K.-W. Cheah, F. Xue, and T.C.W. Mak. J. Chem. Soc. Dalton Trans. 3092 (2001); (*c*) A. Vogler and H. Kunkely. Top. Curr. Chem. **213**, 143 (2001); (*d*) N.M. Shavaleev, L.P. Moorcraft, S.J.A. Pope, Z.R. Bell, S. Faulkner, and M.D. Ward. Chem. Eur. J. **9**, 5283 (2003); (*e*) A.M. Klonkowski, S. Lis, M. Pietraszkiewicz, Z. Hnatejko, K. Czarnobaj, and M. Elbanowski. Chem. Mater. **15**, 656 (2003).
6. (*a*) I.B. Rietveld, E. Kim, and S.A. Vinogradov. Tetrahedron, **59**, 3821 (2003); (*b*) V.V. Rozhkov, M. Khajehpour, and S.A. Vinogradov. Inorg. Chem. **42**, 4253 (2003).
7. (*a*) A. Juris, V. Balzani, S. Campagna, G. Denti, S. Serroni, G. Frei, and H.U. Guedel. Inorg. Chem. **33**, 1491 (1994); (*b*) A. Mamo, A. Juris, G. Calogero, and S. Campagna. Chem. Commun. (Cambridge), 1225 (1996); (*c*) M.K. Nazeeruddin, R. Humphry-Baker, M. Gratzel, and B.A. Murrer. Chem. Commun. (Cambridge), 719 (1998).
8. (*a*) W.R. Thiel and J. Eppinger. Chem. Eur. J. **3**, 696 (1997); (*b*) S.P. Singh, D. Kumar, B.G. Jones, and M.D. Threadgill. J. Fluorine Chem. **94**, 199 (1999).
9. M. Nonoyama. J. Organomet. Chem. **86**, 263 (1975).
10. R.C. Benson and H.A. Jues. J. Chem. Eng. Data, **22**, 379 (1977).
11. C. Lee, W. Yang, and R.G. Parr. Phys. Rev. B, **37**, 785 (1988).
12. A.D. Becke. J. Chem. Phys. **98**, 5648 (1993).
13. (*a*) P.J. Hay and W.R. Wadt. J. Chem. Phys. **82**, 270 (1985); (*b*) W.R. Wadt and P.J. Hay. J. Chem. Phys. **82**, 284 (1985); (*c*) P.J. Hay and W.R. Wadt. J. Chem. Phys. **82**, 299 (1985).
14. P.C. Hariharan and J.A. Pople. Mol. Phys. **27**, 209 (1974).
15. (*a*) C. Jamorski, M.E. Casida, and D.R. Salahub. J. Chem. Phys. **104**, 5134 (1996); (*b*) M. Petersilka, U.J. Grossmann, and E.K.U. Gross. Phys. Rev. Lett. **76**, 1212 (1996); (*c*) R. Bauernschmitt, R. Ahlrichs, F.H. Hennrich, and M.M. Kappes. J. Am. Chem. Soc. **120**, 5052 (1998); (*d*) M.E. Casida. J. Chem. Phys. **108**, 4439 (1998); (*e*) R.E. Stratmann, G.E. Scuseria, and M.J. Frisch. J. Chem. Phys. **109**, 8218 (1998).
16. M.J. Frisch, G.W. Trucks, H.B. Schlegel, G.E. Scuseria, M.A. Robb, J.R. Cheeseman, J.A. Montgomery, Jr., T. Vreven, K.N. Kudin, J.C. Burant, J.M. Millam, S.S. Iyengar, J. Tomasi, V. Barone, B. Mennucci, M. Cossi, G. Scalmani, N. Rega, G.A. Petersson, H. Nakatsuji, M. Hada, M. Ehara, K. Toyota, R. Fukuda, J. Hasegawa, M. Ishida, T. Nakajima, Y. Honda, O. Kitao, H. Nakai, M. Klene, X. Li, J.E. Knox, H.P. Hratchian, J.B. Cross, V. Bakken, C. Adamo, J. Jaramillo, R. Gomperts, R.E. Stratmann, O. Yazyev, A.J. Austin, R. Cammi, C. Pomelli, J.W. Ochterski, P.Y. Ayala, K. Morokuma, G.A. Voth, P. Salvador, J.J. Dannenberg, V.G. Zakrzewski, S. Dapprich, A.D. Daniels, M.C. Strain, O. Farkas, D.K. Malick, A.D. Rabuck, K. Raghavachari, J.B. Foresman, J.V. Ortiz, Q. Cui, A.G. Baboul, S. Clifford, J. Cioslowski, B.B. Stefanov, M.A.G. Liu, A. Liashenko, P. Piskorz, I. Komaromi, R.L. Martin, D.J. Fox, T. Keith, Al-Laham, C.Y. Peng, A. Nanayakkara, M. Challacombe, P.M.W. Gill, B. Johnson, W. Chen, M.W. Wong, C. Gonzalez, and J.A. Pople. Gaussian 03. Revision C.02 [computer program]. Gaussian, Inc., Wallingford, Conn. 2004.
17. G.B. Caygill, R.M. Hartshorn, and P.J. Steel. J. Organomet. Chem. **382**, 455 (1990).
18. F.O. Graces, K.A. King, and R.J. Watts. Inorg. Chem. **27**, 3464 (1988).
19. S. Lamansky, P. Djurovich, D. Murphy, F. Abdel-Razzaq, H.-E. Lee, C. Adachi, P.E. Burrows, S.R. Forrest, and M.E. Thompson. J. Am. Chem. Soc. **123**, 4304 (2001).
20. (*a*) Y. Ohsawa, S. Sprouse, K.A. King, M.K. DeArmond, K.W. Hanck, and R.J. Watts. J. Phys. Chem. **91**, 1047 (1987); (*b*) P.J. Hay. J. Phys. Chem. A, **106**, 1634 (2002); (*c*) F.-M. Hwang, H.-Y. Chen, P.-S. Chen, C.-S. Liu, Y. Chi, C.-F. Shu, F.-I. Wu, P.-T. Chou, S.-M. Peng, and G.-H. Lee. Inorg. Chem. **44**, 1344 (2005).
21. D.L. Dexter. J. Chem. Phys. **21**, 836 (1953).
22. For example, see: P.T. Chou, Y.C. Chen, C.Y. Wei, S.J. Chen, H.L. Lu, and T.H. Wei. J. Phys. Chem. A, **101**, 8581 (1997), and refs. therein.
23. (*a*) P.A. Anderson, F.R. Keene, T.J. Meyer, J.A. Moss, G.F. Strouse, and J.A. Treadway. J. Chem. Soc. Dalton Trans. 3820 (2002); (*b*) M.K. Nazeeruddin, S.M. Zakeeruddin, J.-J. Lagref, P. Liska, P. Comte, C. Barolo, G. Viscardi, K. Schenk, and M. Graetzel. Coord. Chem. Rev. **248**, 1317 (2004).

© 2006 NRC Canada

Small bite-angle diphosphines — Synthesis and structure of low-valent complexes of bis(di-*ortho*-tolylphosphino)methane (dotpm) and related ligands[1]

Maria Filby, Antony J. Deeming, Graeme Hogarth, and Mo-yin (Venus) Lee

Abstract: The coordination chemistry of bis(di-*ortho*-tolylphosphino)methane (dotpm) has been studied. It is an excellent chelating ligand and a range of low-valent mononuclear complexes have been prepared; *cis*-[$M(CO)_4(\eta^2$-dotpm)] (M = Cr, Mo, W; **1**–**3**), [$CpRuCl(\eta^2$-dotpm)] (**4**), and *cis*-[$MX_2(\eta^2$-dotpm)] (M = Pt, X = Cl, Br, I; **5a**–**5c**, M = Pd, X = Cl; **6**). The backbone protons are relatively acidic and can be deprotonated using *n*-BuLi or $LiN(SiMe_3)_2$. Subsequent alkylation by RX (X = halogen; R = Me, Et, CH_2Ph) affords *cis*-[$M(CO)_4(\eta^2$-Rdotpm)] (M = Cr, Mo, W, R = Me; **7**–**9**, M = Mo, W, R = Et, CH_2Ph; **12**–**15**), [$CpRuCl(\eta^2$-Medotpm)] (**10**), and *cis*-[$PtI_2(\eta^2$-Medotpm)] (**11**). Thermolysis of *cis*-[$Mo(CO)_4(\eta^2$-Medotpm)] (**8**) yields what is believed to be the coordinately and electronically unsaturated complex [$Mo(CO)_3(\eta^2$-Medotpm)] (**16**), suggesting that derivatives of dotpm (cone angle 194°) are bulky enough to stabilize a 16-electron complex. Crystal structures of **2**, **3**, **7**–**9**, **13**, and **14** have been determined (diphosphine bite angles ranging from 66.58(3)° to 70.96(5)°.

Key words: diphosphine, transition metal, bulky, carbonyl, *ortho*-tolyl.

Résumé : On a étudié la chimie de coordination du bis(di-*ortho*-tolylphosphino)méthane (dotpm). C'est un excellent ligand chélatant et on en a préparé un large éventail de complexes mononucléaires de faible valence, dont les *cis*-[$M(CO)_4(\eta^2$-dotpm)] (M = Cr, Mo, W; **1**–**3**), [$CpRuCl(\eta^2$-dotpm)] (**4**) et *cis*-[$MX_2(\eta^2$-dotpm)] (M = Pt, X = Cl, Br, I; **5a**–**5c**, M = Pd, X = Cl; **6**). Les protons du squelette sont relativement acides et peuvent être déprotonés en utilisant du *n*-BuLi ou du $LiN(SiMe_3)_2$. Des alkylations subséquentes par du RX (X = halogène; R = Me, Et, CH_2Ph) conduisent à la formation des *cis*-[$M(CO)_4(\eta^2$-Rdotpm)] (M = Cr, Mo, W, R = Me; **7**–**9**, M = Mo, W, R = Et, CH_2Ph; **12**–**15**), [$CpRuCl(\eta^2$-Medotpm)] (**10**) et *cis*-[$PtI_2(\eta^2$-Medotpm)] (**11**). La thermolyse du *cis*-[$Mo(CO)_4(\eta^2$-Medotpm)] (**8**) conduit à la formation d'un composé qu'on croit être le complexe coordonné et électroniquement insaturé [$Mo(CO)_3(\eta^2$-Medotpm)] (**16**) qui suggère que les dérivés dotpm (angle du cône de 194°) sont suffisamment encombrants pour stabiliser un complexe à 16 électrons. On a déterminé les structures cristallines des composés **2**, **3**, **7**–**9**, **13** et **14** dans lesquels l'angle de morsure de la diphosphine varie de 66,58(3)° à 70,96(5)°.

Mots clés : diphosphine, métal de transition, encombrant, carbonyle, *ortho*-tolyle.

[Traduit par la Rédaction]

Introduction

Diphosphines are an important subclass of tertiary phosphines that find widespread use in homogeneous catalysis. A key to their success in this area is the ability to tune their spatial demands by variation of substituents at phosphorus and also the nature of the adjoining backbone (1). When metal bound, they can chelate to a single metal atom or act as a bridge between two, thus forming a binuclear complex. In general, the optimum ring size for a diphosphine ligand is five, and while bis(diphenylphosphino)ethane (dppe) is an excellent chelating ligand, in contrast bis(diphenylphosphino)methane (dppm) behaves predominantly as a bridging ligand since chelatation results in the formation of a highly strained four-membered ring (2, 3). Small changes to dppm can, however, lead to marked changes in its coordination chemistry. For example, substitution of both backbone hydrogens for methyl groups, as in 2,2-bis(diphenylphosphino)propane (2,2-dppp), results in a pronounced change in behavior. While dppm acts as a bridg-

Received 5 July 2005. Published on the NRC Research Press Web site at http://canjchem.nrc.ca on 23 March 2006.

Dedicated to Professor Arthur J. Carty in recognition of his unwavering enthusiasm for chemistry and unselfish dedication to the scientific community.

M. Filby, A.J. Deeming, G. Hogarth,[2] and M.-Y. Lee. Department of Chemistry, University College London, 20 Gordon Street, London, WC1H 0AJ, UK.

[1]This article is part of a Special Issue dedicated to Professor Arthur Carty.
[2]Corresponding author (e-mail: g.hogarth@ucl.ac.uk).

 doi:10.1139/V05-254 © 2006 NRC Canada

ing ligand in the binuclear complex $[Fe_2(CO)_6(\mu\text{-}CO)(\mu\text{-}dppm)]$ (4), 2,2-dppp in contrast, forms exclusively, and in high yields, the chelate complex $[Fe(CO)_3(\eta^2\text{-}2,2\text{-}dppp)]$ (5).

While the chemistry of diphosphines with two or more backbone atoms has been extensively studied, the effect of varying the steric and electronic properties of dppm and related ligands are far more limited (6–10). Such properties can be fine-tuned in a systematic way by varying both backbone and nonbackbone substituents. In general greater steric crowding at the backbone will lead to a reduction in the bite angle and thus a stronger tendency to chelate. Recently, a number of important developments have been made in this area of small bite-angle diphosphines. Hoge et al. (11) at Pfizer have shown that $[Rh(t\text{-}Bu_2PCH_2P\text{-}t\text{-}BuMe)(COD)]^+$ exhibits superior enantioselectivity with lower catalyst loading than conventional asymmetric catalysts in asymmetric hydrogenation reactions, while Pringle and co-workers (12) have shown that nickel(II) complexes of $Ar_2PN(Me)NAr_2$ (Ar = Ph, *o*-tolyl, *o*-*i*-PrC_6H_4) are very efficient ethylene polymerization catalysts, giving high-molecular-weight linear polymer. Further, while the work described herein was in progress, Pringle's group also showed that nickel complexes with small bite-angle diphosphines based on a methylene backbone were also active towards ethylene polymerization, but produced highly branched low-molecular-weight polymer (13). This report prompted us to describe our work in the area of small bite-angle diphosphines. In this contribution we describe the synthesis of a number of low-valent bis(di-*ortho*-tolylphosphino)methane (dotpm) transition metal complexes together with related backbone substituted (Rdotpm) species. We have used VT NMR spectroscopy and X-ray crystallography to probe the effect of the changes in substituents on the bite angle and conformational preference of the metal-bound ligand.

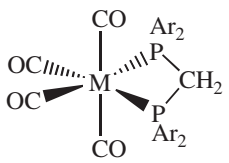
Results and discussion

Synthesis and characterization

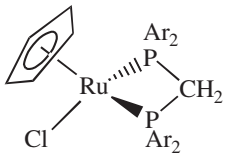
Bis(di-*ortho*-tolylphosphino)methane (dotpm) has previously been prepared by Clark and Mulraney (14) upon lithiation of di-*ortho*-tolylphosphinous chloride. We also prepared dotpm via this route, but found the lithiation of commercially available tri-*ortho*-tolylphosphine to be preferable. This method gave higher yields and proved easier to carry out mainly because of the ease of weighing out the tertiary phosphine. In contrast, di-*ortho*-tolylphosphinous chloride as we prepared it was very sticky and proved difficult to fully purify and handle. Dotpm is a white crystalline solid that can be stored indefinitely in air at room temperature. Characterization was straightforward and as found for dppm, the equivalent methylene protons couple only weakly to the phosphorus atoms ($J_{P\text{-}H}$ = 2.5 Hz).

Addition of dotpm to $[NEt_4][Cr(CO)_5]$ or *cis*-$[M(CO)_4(pip)_2]$ (pip = piperidine) afforded the expected tetracarbonyl complexes *cis*-$[M(CO)_4(\eta^2\text{-}dotpm)]$ (M = Cr, Mo, W) (**1**–**3**) in good yields (15). Likewise, thermolysis with $[CpRuCl(PPh_3)_2]$ at 110 °C gave $[CpRuCl(\eta^2\text{-}dotpm)]$ (**4**) in 76% yield after chromatography. Heating dotpm and $[MCl_2(PhCN)_2]$ (M = Pt, Pd) in dry dichloromethane cleanly afforded *cis*-$[PtCl_2(\eta^2\text{-}dotpm)]$ (**5a**) and *cis*-$[PdCl_2(\eta^2\text{-}dotpm)]$ (**6**), while the former was rapidly converted into the analogous dibromide, *cis*-$[PtBr_2(\eta^2\text{-}dotpm)]$ (**5b**), and diiodide, *cis*-$[PtI_2(\eta^2\text{-}dotpm)]$ (**5c**) upon addition of excess NaBr and NaI, respectively.

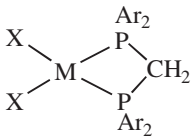
Characterization was relatively straightforward, key spectroscopic features being the downfield shift observed in the ^{31}P NMR spectrum upon coordination and the increase in the phosphorus-proton coupling constant to the methylene protons ($J_{P\text{-}H}$ = 7.9, 10.2 Hz). In all compounds (except **4**) the methylene protons are equivalent, being observed as a triplet in the ^1H NMR spectrum as expected for approximate C_{2v} symmetry. In **4** (C_s symmetry), the methylene protons are inequivalent being observed as two multiplets at δ 4.94 and 4.54 at 308 K. The different symmetries are also apparent in the tolyl resonances, with all exhibiting a single methyl resonance, except **4** where two methyl resonances are observed at room temperature.



1 M = Cr
2 M = Mo
3 M = W



4



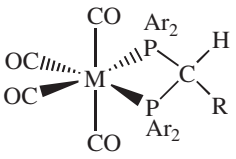
5a M = Pt, X = Cl
5b M = Pt, X = Br
5c M = Pt, X = I
6 M = Pd, X = Cl

All proton NMR spectra show a temperature dependency with most being at the high temperature limit at room temperature or just above. We attribute these changes to the restricted rotation of the aryl groups about the phosphorus–carbon bonds. Variable-temperature ^1H NMR measurements were made for a number of examples; data for **4** being most useful. At 308 K, two sharp equal intensity singlets at δ 2.08 and 2.05 are assigned to the methyl substituents on the aryl rings. The aromatic region is complex at this temperature with some sharp and some broad signals, but each individual component (when identifiable) integrated to two protons. Clear signals at the low field (δ 8.08) and high field (δ 6.73) of this region integrated to two protons. Upon cooling, significant broadening of most of the spectrum is noted to 268 K, below which the peaks begin to sharpen again. At 228 K, three methyl signals are observed at δ 2.21, 2.13, and 1.87 in the ratio 1:1:2 — although application of a Gaussian function to the high-field signal shows that it consists of two closely spaced resonances. Further, the low-field aromatic resonance seen at δ 8.08 at 308 K splits into two equal intensity signals at δ 8.51 and 7.57 at 228 K, while the high-field aromatic signal at δ 6.73 splits into two resonances at δ 6.43 and 6.36. These changes are interpreted in terms of the freezing out of the restricted rotation of the *ortho*-tolyl

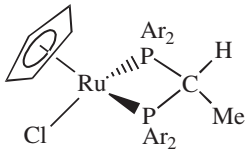
© 2006 NRC Canada

groups about the carbon–phosphorus bonds and taking the coalescence temperature for the δ 8.08 as 268 K, a rotational barrier of 50.6 (±1) kJ mol^{-1} can be estimated.

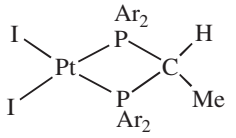
Shaw and co-workers (16–19) have previously shown that when dppm is coordinated to low-valent metal centres the backbone protons become relatively acidic. This is useful since it allows facile backbone functionalization. We have utilized this to prepare a number of backbone-substituted derivatives of dotpm (denoted Rdotpm). For example, backbone deprotonation of **1**–**3** using *n*-BuLi followed by a quench with methyliodide afforded the Medotpm complexes *cis*-[M(CO)$_4$(η^2-Medotpm)] (M = Cr, Mo, W) (**7**–**9**) in good yields, while [CpRuCl(η^2-Medotpm)] (**10**) was prepared similarly from **4** using LiN(SiMe$_3$)$_2$ as a base. Deprotonation of *cis*-[PtCl$_2$(η^2-dotpm)] (**5a**) by LiN(SiMe$_3$)$_2$ followed by addition of methyliodide afforded *cis*-[PtI$_2$(η^2-Medotpm)] (**11**), whereby the halides had also exchanged, while quenching the deprotonated molybdenum and tungsten complexes with ethyliodide or benzylbromide gave *cis*-[M(CO)$_4$(η^2-Etdotpm)] (M = Mo, W) (**12** and **13**) and *cis*-[M(CO)$_4$(η^2-Bzdotpm)] (M = Mo, W) (**14** and **15**), respectively.



7 M = Cr, R = Me
8 M = Mo, R = Me
9 M = W, R = Me
12 M = Mo, R = Et
13 M = W, R = Et
14 M = Mo, R = Bz
15 M = W, R = Bz



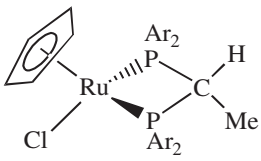
10



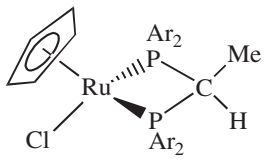
11

Characterization was again relatively straightforward. For all complexes, the remaining backbone proton was observed as a multiplet resonance being shifted slightly downfield of the analogous signal in dotpm complexes. The introduction of the substituent changes the symmetry of the complexes, such that those previously with C_{2v} symmetry are now in the C_s point group. This results in two sets of *ortho*-tolyl groups; those lying towards the substituent and those pointing away from it, which is reflected in the observation of two distinct methyl resonances in the ^{1}H NMR spectra. We have analyzed the spectrum of *cis*-[Mo(CO)$_4$(η^2-Bzdotpm)] (**14**) in some detail and this has allowed assignment of the benzyl and individual aryl protons (see the Experimental section). The methyl resonance at δ 2.15 is assigned to the aryl groups (Ar$_A$) that lie on the same side of the diphosphine as the benzyl group, while that at δ 1.82 is assigned to the *ortho*-tolyl groups that lie proximal to the remaining backbone proton. All ^{1}H NMR spectra are temperature dependent, which is again attributed to the restricted rotation of the aryl groups. For example, cooling **14** leads to a significant broadening of all peaks in the spectrum except those associated with the benzyl substituent. However, even at 213 K splitting into individual proton signals was not yet observed.

For [CpRuCl(η^2-Medotpm)] (**10**) two possible isomers are possible, with the methyl group pointing towards the chloride (**10a**) or the cyclopentadienyl group (**10b**). The ^{1}H NMR spectrum at room temperature is both complex and broad, making full assignment impossible. However, some regions are quite clear, most notably two sharp singlet resonances at δ 5.21 and 5.15 in an approximate 1:3 ratio being assigned to the cyclopentadienyl protons. This suggests that both isomers are formed and on the basis of adverse steric interactions we suggest that the major isomer is **10a** in which the methyl group points towards the chloride. The tolyl methyl substituents are broad at room temperature and only those assigned to the major isomer can be clearly distinguished, appearing as two broad singlets at δ 2.60 and 2.56. Upon cooling a number of changes occur. Most significantly at 278 K, the δ 2.56 signal splits into two new singlets at δ 2.70 and 2.51, while the δ 2.60 signal broadens significantly. By 258 K, four sharp singlets are seen at δ 2.96, 2.70, 2.50, and 2.22. With coalescence temperatures as 288 and 268 K, respectively, free energies of activation of 54.4 and 53.4 kJ mol^{-1} are calculated, suggesting that a single process with an activation energy of ca. 54 2 kJ mol^{-1} is responsible for the observed changes. This value is similar to that of 50.6 1 kJ mol^{-1} estimated for **4**, the higher barrier in **10a** relating to the greater steric hindrance. At 258 K, two further broad resonances can be seen at δ 2.79 and 2.34, which we assign to the methyl groups in **10b**.



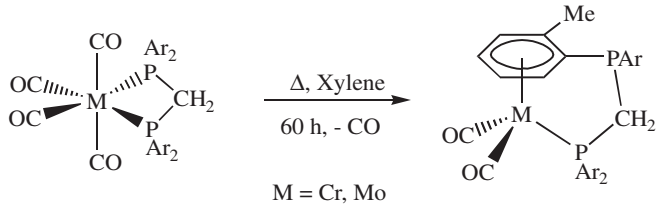
10a



10b

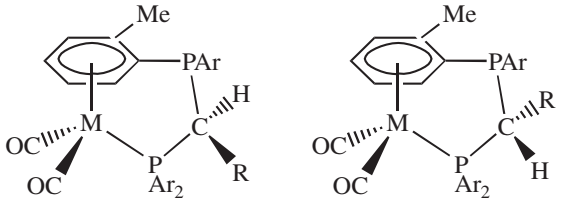
All attempts to replace a second backbone proton were unsuccessful. This is probably a result of the decreasing acidity of the remaining proton upon addition of an electron-releasing substituent and also the decreased kinetic acidity resulting from the increased steric crowding. We did, however, obtain some evidence for a partial deprotonation of [Cr(CO)$_4$(η^2-Medotpm)] (**7**). Addition of an excess of *n*-BuLi followed by a quench with D$_2$O lead to a ^{1}H NMR spectrum in which the backbone proton signal integrated to ca. 60% of that expected for full occupancy.

Complexes **1**–**3** have previously been prepared by Clark and Clark (15). The chromium and molybdenum complexes are reported to slowly lose CO upon heating in decalin to afford novel π-arene complexes.

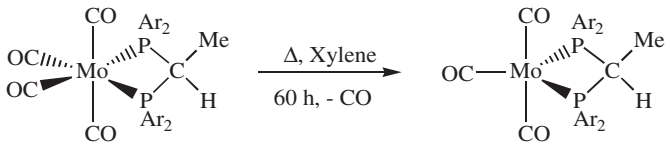


© 2006 NRC Canada

We were interested in trying to make similar complexes with substituents on the backbone since such species would contain two chiral centres, and we envisaged that high diastereomeric control may occur because of the differing steric interactions between the methyl substituent on the bound arene ring and the backbone substituent.



Heating a toluene solution of **8** for 3 days resulted in no discernable change, however, heating a xylene solution of **8** for 2.5 days resulted in the formation of a dark solid, which we tentatively propose to be the 16-electon complex, $[Mo(CO)_3(\eta^2\text{-Medotpm})]$ (**16**). Characterization was based primarily on the observation of a singlet in the ^{31}P NMR spectrum, an M–CO ion in the +ve FAB mass spectrum, and two absorptions in the carbonyl region of the IR spectrum, the latter being indicative of a tricarbonyl arrangement. Similar properties have been observed for the related 16-electron complex, $[W(CO)_3(P\text{-}i\text{-}Pr_3)_2]$, which is black, poorly soluble in hexane, and shows a singlet in the ^{31}P NMR spectrum (20). In contrast to **16**, however, $[W(CO)_3(P\text{-}i\text{-}Pr_3)_2]$ and related 16-electron tricarbonyl complexes exhibit three carbonyl bands in the IR spectrum. This difference may be due to the differing symmetry at the metal centre. For example, the crystal structure of $[W(CO)_3(P\text{-}i\text{-}Pr_3)_2]$ shows that the P-W-P angle is 160.94(4)° (i.e., approximately trans), while in **16** it is likely to be nearer 66° to 67° observed in the crystallographically characterized molybdenum complexes described in the following section. Unfortunately, owing to the air-sensitive nature of **16** we have not been able to obtain a satisfactory elemental analysis.



8 **16**

While **16** is the major product of the prolonged heating of **8**, close scrutiny of the crude ^1H NMR spectrum of the reaction mixture reveals the formation of a small amount (<10%) of a second species presumed to be the expected π-bound arene complex. A series of unresolved signals between δ 5.5–4.5 is indicative of a π-bound arene, and there are a series of sharp singlets in the methyl region of the spectrum. While it is not possible to fully discern the nature of this species, there appears to be eight resonances between δ 5.5–4.5 falling into two sets in an approximate 2:1 ratio, suggesting that both diastereoisomers are formed.

Structural studies

To gain more insight into the precise structural features of dotpm and Rdotpm ligands we have carried out crystallographic studies on isostructural *cis*-$[M(CO)_4(\eta^2\text{-dotpm})]$ (M = Mo, W) (**2**, **3**), isostructural *cis*-$[M(CO)_4(\eta^2\text{-Medotpm})]$ (M = Cr, Mo, W) (**7**–**9**), *cis*-$[W(CO)_4(\eta^2\text{-Etdotpm})]$ (**13**), and *cis*-$[Mo(CO)_4(\eta^2\text{-Bzdotpm})]$ (**14**). The results of these are summarized in Figs. 1–4 and Tables 1 and 2. In all, the diphosphine subtends a small bite angle, ranging between 66.58(3)° and 70.96(5)°, with molybdenum and tungsten complexes being at the bottom end, and chromium and ruthenium compounds at the top end of the range. The best comparison of dppm and dotpm complexes is that between **2** and *cis*-$[Mo(CO)_4(\eta^2\text{-dppm})]$ (21); bite angles of 67.20(3)° and 67.3(1)°, respectively, being essentially the same, as are most of the other structural parameters except the P-C-P angle, which at 99.9(2)° in **2** is significantly greater than that of 95.6(4)° in *cis*-$[Mo(CO)_4(\eta^2\text{-dppm})]$. This results from a slight elongation (0.037 avg.) of the molybdenum–phosphorus bonds in **2** vs. those in the dppm complex, probably resulting from the greater steric demands of the *ortho*-tolyl vs. phenyl substituents. Introduction of a methyl or ethyl substituent on the backbone leads to a slight increase in the bite angle and a more significant reduction in the P-C-P an-

Fig. 1. Molecular structure of *cis*-$[Mo(CO)_4(\eta^2\text{-dotpm})]$ (**2**).

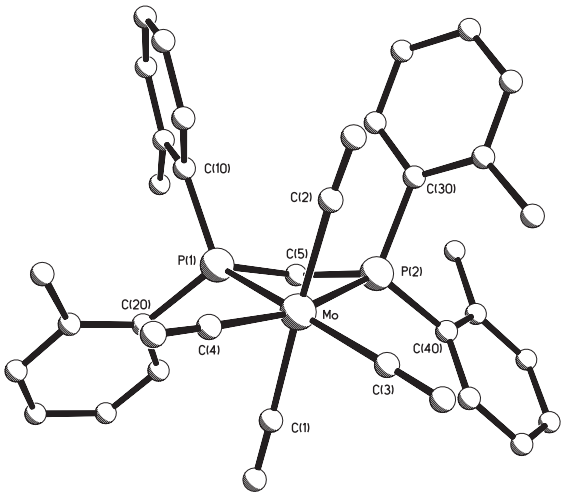
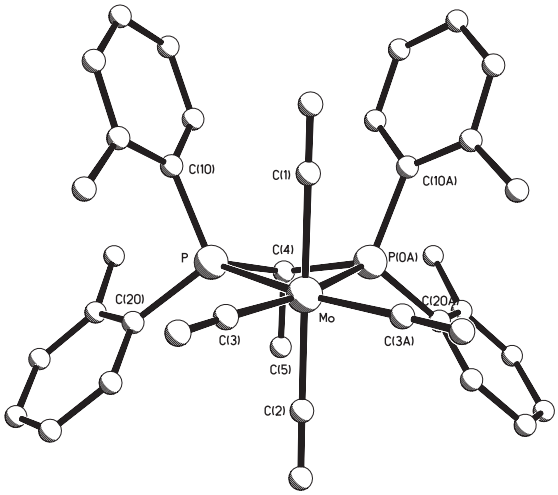


Fig. 2. Molecular sturcture of *cis*-$[Mo(CO)_4(\eta^2\text{-Medotpm})]$ (**7**).



© 2006 NRC Canada

Table 1. Selected bond lengths (Å) and angles (°) for dtopm and Rdotpm complexes and related compounds.

Compound	M—CO (cis) (Å)	M—CO (trans) (Å)	M—P (Å)	P-M-P (°)	P-C-P (°)
cis-[Mo(CO)$_4$(η^2-dotpm)] (**2**)	2.028(5), 2.051(5)	1.979(4), 1.981(5)	2.5338(11), 2.5561(10)	67.20(3)	99.2(2)
cis-[W(CO)$_4$(η^2-dotpm)] (**3**)	2.039(11), 2.046(11)	1.980(10), 1.989(11)	2.524(2), 2.545(2)	67.00(7)	98.2(4)
cis-[Cr(CO)$_4$(η^2-Medotpm)] (**7**)	1.873(7), 1.903(7)	1.847(5)	2.3995(12)	70.96(5)	95.5(2)
cis-[Mo(CO)$_4$(η^2-Medotpm)] (**8**)	1.993(8), 2.042(8)	1.972(5)	2.5502(12)	67.66(5)	97.6(3)
cis-[W(CO)$_4$(η^2-Medotpm)] (**9**)	2.012(14), 1.979(14)	1.978(10)	2.527(2)	67.68(8)	96.6(4)
cis-[W(CO)$_4$(η^2-Etdotpm)] (**13**)	2.00(2), 2.03(2)	2.00(2), 2.00(2)	2.522(4), 2.536(4)	67.65(13)	95.7(6)
cis-[Mo(CO)$_4$(η^2-Bzdotpm)] (**14**)	2.021(3), 2.031(4)	1.963(4), 1.990(3)	2.5378(8), 2.5767(9)	66.58(3)	96.33(13)
cis-[Mo(CO)$_4$(η^2-dppm)][a]	2.07(1), 2.02(2)	1.92(1), 1.94(1)	2.501(2), 2.535(3)	67.3(1)	95.6(4)
mer-[Cr(CO)$_3$(η^2-dppm)(η^1-dppm)][b]	1.87(1), 1.86(1)	1.80(1)	2.298(4), 2.395(4)	71.1(1)	94.0(5)
fac-[W(CO)$_3$(MeCN)(η^2-dppm)][c]	1.929(6)	1.962(6), 1.970(8)	2.512(2), 2.514(2)	67.5(1)	98.1(3)
[PtCl$_2$(η^2-Ar$_2$PCH$_2$PAr$_2$)] (Ar = *o*-*i*-PrC$_6$H$_4$)[d]			2.2202(9), 2.2301(9)	75.96(3)	—

[a]Reference 21.
[b]Reference 22.
[c]Reference 23.
[d]Reference 13.

Fig. 3. Molecular structure of *cis*-[W(CO)$_4$(η^2-Edotpm)] (**13**).

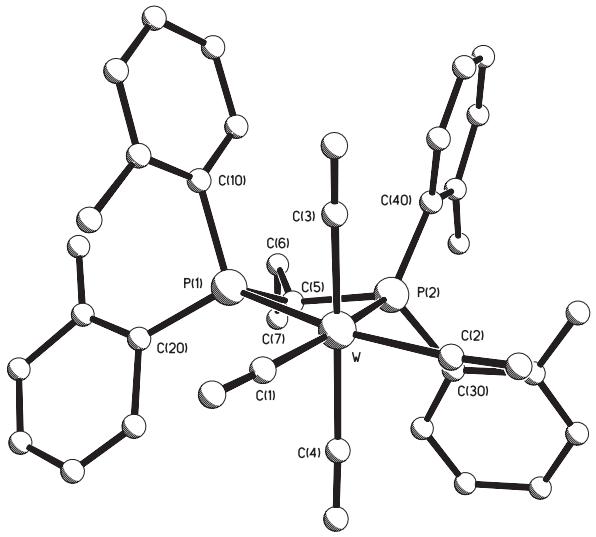
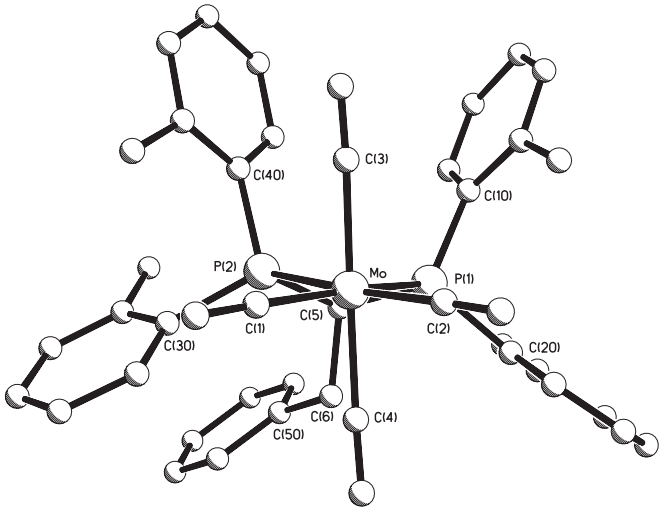


Fig. 4. Molecular structure of *cis*-[Mo(CO)$_4$(η^2-Bzdotpm)] (**14**).



gle of ca. 2°, while introduction of the bulky benzyl group leads to the smallest bite angle of 66.58(3)° observed in **14**.

In all the structures, the two *ortho*-tolyl groups on each phosphorus atom adopt a staggered-type arrangement, whereby the methyl groups are orientated in opposite directions, presumably to minimize adverse steric interactions. Further, for complexes carrying a backbone substituent, as expected, the *ortho*-tolyl groups lying on the same side as the substituent point away from it and thus the presence of the substituent dictates the orientational preference of the diphosphine ligand. The benzyl substituent in *cis*-[Mo(CO)$_4$-(η^2-Bzdotpm)] (**14**) is orientated such that there is a relatively close contact with one on the tolyl ligands, indicative of a π-stacking-type interaction. The structural arrangement adopted renders all the *ortho*-tolyl groups inequivalent. The appearance of two sets of aryl resonances at room temperature in solution shows that rotation of the benzyl group must be facile at this temperature and it may well be associated with a geared rotation of the *ortho*-tolyl groups.

© 2006 NRC Canada

Table 2. Crystallographic data for new compounds.

Compound	**2**	**3**	**7**	**8**	**9**	**13**	**14**
Chemical formula	$MoP_2O_4C_{34}H_{32}Cl$	$WP_2O_4C_{34}H_{32}Cl$	$CrP_2O_4C_{35}H_{34}Cl_2$	$MoP_2O_4C_{35}H_{34}Cl_2$	$WP_2O_4C_{35}H_{34}Cl_2$	$WP_2O_4C_{35}H_{34}$	$MoP_2O_4C_{40}H_{36}$
MW	697.93	785.84	03.46	747.40	835.31	764.41	738.57
Crystal system	Monoclinic	Monoclinic	Monoclinic	Monoclinic	Monoclinic	Orthorhombic	Monoclinic
Space group	$P2_1/c$	$P2_1/c$	$P2_1/m$	$P2_1/m$	$P2_1/m$	*Pbca*	$P2_1/c$
a (Å)	11.522(2)	11.526(2)	8.604(2)	8.639(2)	8.604(2)	17.167(3)	11.778(2)
b (Å)	18.292(4)	18.230(4)	19.750(4)	19.797(4)	19.708(4)	17.596(4)	15.230(3)
c (Å)	15.739(3)	15.717(3)	10.338(2)	10.501(2)	10.424(2)	21.436(4)	20.307(4)
α (°)	90	90	90	90	90	90	90
β (°)	99.45(3)	99.59(3)	92.37(3)	92.26(3)	92.44(3)	90	104.87(3)
γ (°)	90	90	90	90	90	90	90
Volume (Å^3)	3272.1(11)	3256.3(11)	1755.2(6)	1794.6(6)	1766.0(6)	6475(2)	3520.7(11)
Z	4	4	2	2	2	8	4
ρ_{calcd} (g cm^{-3})	1.417	1.603	1.331	1.383	1.571	1.568	1.393
μ(Mo Kα) (mm^{-1})	0.616	3.764	0.605	0.639	3.548	3.703	0.504
F(000)	1428	1566	728	764	828	3040	1520
Measured reflections	6104	5945	3436	3432	3445	5598	6531
Independent reflections	5801	5646	3218	3210	3229	5598	6211
Obs. reflections ($I > 2\sigma(I)$)	4660	4326	2417	2791	2914	2822	5005
R_1 ($F > 2\sigma(I)$)	0.0454	0.0545	0.0614	0.0587	0.0536	0.0949	0.0366
wR_2 (all data)	0.1242	0.1547	0.1799	0.1589	0.1412	0.2269	0.0944
Goodness-of-fit	1.063	1.100	1.037	1.066	1.079	0.947	1.049

© 2006 NRC Canada

In conclusion, this work shows that dotpm is an excellent chelating ligand. While similar in some respects to dppm when acting in this capacity, the enhanced steric bulk leading to restricted rotation about the carbon–phosphorus bonds potentially offers a more clearly defined reaction pocket at the metal centre. This can also be easily tuned upon modification of a backbone substituent leading to the facile synthesis of a wide range of derivatives with different spatial properties. In future work we aim to concentrate on the catalytic activity of Rdotpm and related ligands with other ortho substituents, particular focus being placed on group 8 and 10 complexes.

Experimental

All reactions were carried out under a nitrogen atmosphere in dried degassed solvents unless otherwise stated. *ortho*-Bromotoluene and P(*o*-tolyl)$_3$ were purchased from Aldrich and used as supplied, and (*o*-tolyl)$_2$PCl was prepared according to standard procedures (14). NMR spectra were run on Bruker AC300, AMX400, or Avance500 spectrometers and referenced internally to the residual solvent peak (^{1}H and ^{13}C) or externally to P(OMe)$_3$ (^{31}P). Infrared spectra were run on Nicolet 205 or Shimadzu 8700 FT-IR spectrometers. Solid-state spectra were recorded as KBr discs and solution spectra using a cell fitted with calcium fluoride plates, subtraction of the solvent absorptions being achieved by computation. The fast atom bombardment and electron impact mass spectra were recorded on a VG ZAB-SE high-resolution mass spectrometer in the Chemistry Department of University College London, and elemental analyses were performed in house. Chromatography was carried out on deactivated alumina (6% *w*/*w* distilled water) or silica wet packed with light petroleum unless otherwise stated. The solution to be separated was added to the support (3–5 g) and the solvent removed under reduced pressure. The resulting solids were then deposited on top of the prepared column and separation effected by elution with progressively more polar solvents.

Preparation of bis(di-*ortho*-tolylphosphino)methane (dotpm)

(*o*-Tolyl)$_2$PCl (13.17 g, 0.053 mol) was dissolved in dry THF (100 cm^3). Lithium metal (2.10 g, 0.265 mol) hammered and cut into strips was slowly added to the pale yellow solution. The mixture gradually turned blood red and was left to stir at room temperature for 20 h. After cooling to 0 °C, dry dichloromethane (1.7 cm^3, 0.027 mol) was slowly added, the solution turning brown. After 1 h the solution was warmed to room temperature and then refluxed for a further 1 h. After removal of volatiles, the yellow-brown solid produced was redissolved in dichloromethane and washed thoroughly with distilled water. The organic layer was dried over $MgSO_4$ and removal of volatiles under reduced pressure gave a cream solid (3.02 g, 26%). Recrystallization from dichloromethane and methanol afforded dotpm as white needles.

Alternatively, dotpm was also prepared by lithiation of P(*o*-tolyl)$_3$. P(*o*-tolyl)$_3$ (6.0 g, 0.0197 mol) was dissolved in dry THF (100 cm^3). Lithium metal (0.3 g) hammered and cut into strips was slowly added and the mixture was stirred for 20 h. Finely ground NH_4Br (1.96 g, 0.02 mol) was added in small portions to the blood red solution causing the mixture to autoreflux. After 2 h, dry dichloromethane (3 cm^3) was added dropwise and the color turned to pale straw. Approximately 30 cm^3 of methanol was added to remove any remaining lithium. After removal of volatiles under reduced pressure, dissolution of the residue in dichloromethane gave a colorless solution that was washed with distilled water several times and dried over $MgSO_4$. Removal of volatiles under reduced pressure gave dotpm (2.80 g, 65%). ^{1}H NMR ($CDCl_3$) δ: 7.36–7.10 (m, 16H, Ar), 2.60 (t, 2H, *J* = 2.5 Hz, CH_2), 2.30 (s, 12H, Me). ^{31}P{^{1}H} NMR ($CDCl_3$) δ: –60.5 (s). Mass spectrum (EI) *m*/*z*: 440 [M$^+$], 425 [M$^+$ – CH_3], 349 [M$^+$ – *o*-tolyl). Anal. calcd. for $C_{29}H_{30}P_2 \cdot 0.5H_2O$: C 77.51, H 6.90, P 13.81; found: C 77.23, H 6.88, P 13.97.

Preparation of *cis*-[Cr(CO)$_4$(η^2-dotpm)] (1)

[$Cr(CO)_5Cl$][NEt_4] (0.59 g, 1.66 mmol) and dotpm (0.37 g, 0.83 mmol) were dissolved in dry dichloromethane (25 cm^3). The pale green solution was refluxed for 5 h and then filtered. The filtrate was washed thoroughly with distilled water and the dichloromethane extract was dried over $MgSO_4$. Removal of volatiles under reduced pressure yielded **1** as a yellow solid (0.37 g, 73%). IR ν(CO) (CH_2Cl_2, cm^{-1}): 2006 (s), 1896 (s), 1867 (s). ^{1}H NMR ($CDCl_3$) δ: 7.69 (dd, 4H, *J* = 12.4, 8.0 Hz, Ar), 7.30 (t, 4H, *J* = 7.4 Hz, Ar), 7.16 (t, 4H, *J* = 7.5 Hz, Ar), 7.11 (dd, 4H, *J* = 7.5, 1.0 Hz, Ar), 4.38 (t, 2H, *J* = 8.5 Hz, CH_2), 2.00 (s, 12H, Me). ^{31}P{^{1}H} NMR ($CDCl_3$) δ: 9.7 (s). Mass spectrum (FAB) *m*/*z*: 604 [M$^+$], 520 [M$^+$ – 3CO], 492 [M$^+$ – 4CO]. Anal. calcd. for $CrP_2O_4C_{33}H_{30}$: C 65.56, H 4.97, P 10.26; found: C 65.03, H 5.06, P 9.79.

Preparation of *cis*-[Mo(CO)$_4$(η^2-dotpm)] (2)

cis-[$Mo(CO)_4(pip)_2$] (0.10 g, 0.26 mmol) and dotpm (0.11 g, 0.26 mmol) were dissolved in dichloromethane (15 cm^3) and the orange solution was refluxed for 4 h. After cooling to room temperature, methanol (15 cm^3) was added and the solution was reduced under vacuum until a precipitate formed. The mixture was filtered and the residue washed with methanol and air-dried. The tan solid was recrystallized from dichloromethane and methanol to yield colorless crystals of **2** (0.10 g, 62%). IR ν(CO) (CH_2Cl_2, cm^{-1}): 2019 (s), 1909 (s), 1872 (s). ^{1}H NMR ($CDCl_3$) δ: 7.63 (dd, 4H, *J* = 13.2, 7.2 Hz, Ar), 7.29 (t, 4H, *J* = 7.5 Hz, Ar), 7.14 (t, 4H, *J* = 7.6 Hz, Ar), 7.11 (d, 4H, *J* = 7.6 Hz, Ar) 4.43 (t, 2H, *J* = 7.9 Hz, CH_2), 2.04 (s, 12H, Me). ^{31}P{^{1}H} NMR ($CDCl_3$) δ: –14.2 (s). Mass spectrum (FAB) *m*/*z*: 650 [M$^+$], 623 [M$^+$ – CO], 594 [M$^+$ – 2CO], 538 [M$^+$ – 4CO]. Anal. calcd. for $MoP_2O_4C_{33}H_{30}$: C 61.11, H 4.63, P 9.57; found: C 60.41, H 4.77, P 9.15.

Preparation of *cis*-[W(CO)$_4$(η^2-dotpm)] (3)

cis-[$W(CO)_4(pip)_2$] (0.23 g, 0.49 mmol) and dotpm (0.22 g, 0.49 mmol) were dissolved in dichloromethane (15 cm^3) and the solution was refluxed for 2.5 h. The resulting yellow solution was pumped to dryness to yield a yellow solid, which was recrystallized from dichloromethane and methanol. Yellow crystals of **3** (0.24 g, 66%) were formed. IR ν(CO) (CH_2Cl_2, cm^{-1}): 2015 (s), 1900 (s), 1866 (s). ^{1}H NMR ($CDCl_3$) δ: 7.62 (dd, 4H, *J* = 13.9, 7.3 Hz, Ar), 7.30 (t,

© 2006 NRC Canada

4H, J = 7.4 Hz, Ar), 7.17 (t, 4H, J = 7.5 Hz, Ar), 7.12 (d, 4H, J = 7.2 Hz, Ar), 4.91 (t, 2H, J = 8.4 Hz, CH_2), 2.03 (s, 12H, Me). $^{31}P\{^1H\}$ NMR ($CDCl_3$) δ: –37.7 (s, J_{WP} = 197 Hz). Mass spectrum (FAB) *m/z*: 736 [M^+], 707 [M^+ – CO], 680 [M^+ – 2CO], 622 [M^+ – 4CO]. Anal. calcd. for $WP_2O_4C_{33}H_{30}\cdot 0.5CH_2Cl_2$: C 51.64, H 3.98, P 7.96; found: C 52.45, H 3.98, P 7.69.

Preparation of [CpRuCl(η²-dotpm)] (4)

[$CpRuCl(PPh_3)_2$] (0.37 g, 0.51 mmol) and dotpm (0.224 g, 0.51 mmol) were refluxed in toluene (100 cm^3) for 24 h. Chromatography on silica eluting with diethyl ether – light petroleum (2:1) gave a yellow band of [$CpRuCl(PPh_3)_2$], which was discarded. Eluting with diethyl ether – light petroleum (1:1) gave an orange band, which yielded **4** as an orange solid (0.14 g, 76%). IR (KBr, cm^{-1}): 1448 (m), 1132 (m), 1091 (m), 1089 (m), 1066 (m), 804 (m), 748 (s), 725 (s), 709 (m), 461 (s). ^1H NMR (CD_2Cl_2, 308 K) δ: 8.08 (br, 2H, Ar), 7.42–7.15 (m, 8H, Ar), 7.08 (d, 2H, J = 7.4 Hz, Ar), 7.04 (br d, 2H, Ar), 6.73 (t, 2H, J = 7.4 Hz, Ar), 4.94 (dt, 1H, J = 13.8, 8.1 Hz, CH_2), 4.75 (s, 5H, Cp), 4.54 (q, 1H, J = 10.9 Hz, CH_2), 2.08 (s, 6H, Me), 2.05 (s, 6H, Me); (228 K) δ: 8.51 (br, 1H, Ar), 7.58 (br, 1H, Ar), 7.40–6.95 (m, 11H, Ar), 6.86 (t, 1H, J = 7.1 Hz, Ar), 6.43 (br, 1H, Ar), 6.36 (br, 1H, Ar), 4.76 (br, 1H, CH_2), 4.75 (s, 5H, Cp), 4.46 (br, 1H, CH_2), 2.24 (s, 3H, Me), 2.13 (s, 3H, Me), 1.86 (s, 6H, CH_3). $^{31}P\{^1H\}$ NMR ($CDCl_3$) δ: –4.7 (s). Mass spectrum (FAB) *m/z*: 642 [M^+], 607 [M^+ – Cl], 576 [M^+ – Cp]. Anal. calcd. for $C_{34}H_{35}P_2ClRu\cdot CHCl_3\cdot 2H_2O$: C 51.53, H 5.15; found: C 51.63, H 4.34.

Preparation of *cis*-[$PtCl_2$(η²-dotpm)] (5a)

cis-[$Pt(PhCN)_2Cl_2$] (0.21 g, 0.44 mmol) and dotpm (0.21 g, 0.44 mmol) were dissolved in dry dichloromethane (15 cm^3) and the solution was refluxed for 10 h. A white precipitate was formed and after cooling, hexane (ca. 15 cm^3) was added to precipitate more solids. The mixture was filtered and the residue was washed with hexane and air-dried. A white powder was obtained, which was recrystallized from dichloromethane and methanol to yield **5a** as colorless plates (0.28 g, 92%). IR ν(CH) (KBr, cm^{-1}): 3056 (w), 3011 (w), 2960 (w), 2919 (w), 2904 (w), 2856 (w). ^1H NMR ($CDCl_3$) δ: 7.96 (dd, 4H, J = 8.1, 7.9 Hz, Ar), 7.43 (t, 4H, J = 7.3 Hz, Ar), 7.23–7.20 (m, 8H, Ar), 4.59 (t, 2H, J = 10.0 Hz, CH_2), 2.26 (s, 12H, Me). $^{31}P\{^1H\}$ NMR ($CDCl_3$) δ: –77.9 (s, J_{PtP} = 3097 Hz). Mass spectrum (FAB) *m/z*: 1484 [$2M^+$+ 2Cl], 1409 [$2M^+$], 742 [M^+ + Cl], 671 [M^+ – Cl], 634 [M^+ – 2Cl]. Anal. calcd. for $PtP_2Cl_2C_{29}H_{30}$: C 49.29, H 4.25, Cl 10.06, P 8.78; found: C 48.70, H 4.08, Cl 10.75, P 8.48.

Preparation of *cis*-[$PtBr_2$(η²-dotpm)] (5b)

5a (0.05 g, 0.08 mmol) and LiBr (0.01 g, 0.15 mmol) were dissolved in dry THF (15 cm^3) and the mixture was stirred at room temperature for 20 h. The solvent was distilled off and the residue was redissolved in dichloromethane. This was washed thoroughly with distilled water and the dichloromethane extract was dried over $MgSO_4$. Removal of volatiles under reduced pressure gave **5b** as a yellow powder (0.05 g, 78%). ^1H NMR ($CDCl_3$) δ: 7.98 (q, 4H, J = 7.7 Hz, Ar), 7.44 (t, 4H, J = 7.3 Hz, Ar), 7.23–7.21 (m, 8H, Ar), 4.65 (t, 2H, J = 10.2 Hz, CH_2), 2.27 (s, 12H, Me). $^{31}P\{^1H\}$ NMR ($CDCl_3$) δ: –80.3 (s, J_{PtP} = 3056 Hz). Mass spectrum (FAB) *m/z*: 715 [M^+ – Br], 634 [M^+ – 2Br]. Anal. calcd. for $PtBr_2P_2C_{29}H_{30}\cdot CH_2Cl_2$: C 40.90, H 3.52, Br 18.18, P 7.04; found: C 40.92, H 4.44, Br 16.74, P 7.30.

Preparation of *cis*-[PtI_2(η²-dotpm)] (5c)

5a (0.05 g, 0.08 mmol) and LiI (0.02 g, 0.15 mmol) were dissolved in THF (15 cm^3) and the yellow solution was stirred at room temperature for 20 h. Removal of volatiles under reduced pressure yielded a yellow solid. This was redissolved in dichloromethane and was washed three times with water. The yellow solution was pumped to dryness under reduced pressure to give **5c** as a yellow powder (0.04 g, 62%). ^1H NMR ($CDCl_3$) δ: 7.97 (q, 4H, J = 7.7 Hz, Ar), 7.43 (t, 4H, J = 7.6 Hz, Ar), 7.23 (t, 8H, J = 7.7 Hz, Ar), 4.78 (t, 2H, J = 10.3 Hz, CH_2), 2.28 (s, 12H, Me). $^{31}P\{^1H\}$ NMR ($CDCl_3$) δ: –87.7 (s, J_{PtP} = 2876 Hz). Mass spectrum (FAB) *m/z*: 889 [M^+], 762 [M^+ – I]. Anal. calcd. for $PtP_2I_2C_{29}H_{30}$: C 39.15, H 3.37, I 28.57, P 6.97; found: C 39.08, H 3.69, I 28.63, P 7.18.

Preparation of *cis*-[$PdCl_2$(η²-dotpm)] (6)

cis-[$Pd(PhCN)_2Cl_2$] (0.16 g, 0.42 mmol) and dotpm (0.19 g, 0.42 mmol) were dissolved in dry dichloromethane (15 cm^3) and this was refluxed for 20 h. Removal of volatiles under reduced pressure gave **6** as a brown powder (0.19 g, 75%), which was washed with methanol and was air-dried. IR ν(CH) (KBr, cm^{-1}): 3055 (w), 2963 (w), 2920 (w). ^1H NMR ($CDCl_3$) δ: 7.97 (dd, 4H, J = 8.2 Hz, 7.7, Ar), 7.45 (t, 4H, J = 7.6 Hz, Ar), 7.23–7.19 (m, 8H, Ar), 4.33 (t, 2H, J = 9.9 Hz, CH_2), 2.32 (s, 12H, Me). $^{31}P\{^1H\}$ NMR ($CDCl_3$) δ: –69.0 (s). Mass spectrum (FAB) *m/z*: 583 [M^+ – Cl], 545 [M^+ – 2Cl]. Anal. calcd. for $PdP_2Cl_2C_{29}H_{30}\cdot 0.2$ PhCN: C 54.83, H 4.85, N 0.44, Cl 11.11, P 9.70; found: C 54.49, H 4.54, N 0.44, Cl 12.80, P 9.70.

Preparation of *cis*-[$Cr(CO)_4$(η²-Medotpm)] (7)

1 (0.33 g, 0.55 mmol) was dissolved in dry THF (25 cm^3). *n*-BuLi (0.7 cm^3, 1.09 mmol) was added and the yellow solution immediately darkened. After stirring at room temperature for 1 h, MeI (0.07 cm^3, 1.09 mmol) was added and the color lightened. The reaction mixture was stirred for 20 h and pumped to dryness under reduced pressure. The solid was redissolved in dichloromethane and was washed thoroughly with distilled water. The dichloromethane extract was dried over $MgSO_4$ and filtered. Removal of volatiles under reduced pressure yielded a yellow powder that was recrystallized from dichloromethane and methanol to give **7** as yellow crystals (0.33 g, 99%). IR ν(CO) (CH_2Cl_2, cm^{-1}): 2006 (s), 1913 (s), 1893 (s), 1865 (s). ^1H NMR ($CDCl_3$) δ: 8.27–8.26 (m, 4H, Ar), 7.38–7.33 (m, 8H, Ar), 7.05 (m, 4H, Ar), 5.39 (sextet, 1H, J = 7.2 Hz, CH), 2.09 (s, 6H, Me), 2.00 (s, 6H, Me), 1.06 (dt, 3H, J = 15.9, 7.3 Hz, Me). $^{31}P\{^1H\}$ NMR ($CDCl_3$) δ: 27.8 (s). Mass spectrum (FAB) *m/z*: 618 [M^+], 562 [M^+ – 2CO], 534 [M^+ – 3CO], 506 [M^+ – 4CO]. Anal. calcd. for $CrP_2O_4C_{34}H_{32}\cdot 0.75CH_2Cl_2$: C 61.17, H 4.91, P 9.09; found: C 60.64, H 4.96, P 9.21.

Preparation of *cis*-[$Mo(CO)_4$(η²-Medotpm)] (8)

2 (0.30 g, 0.46 mmol) was dissolved in dry THF (15 cm^3). *n*-BuLi (0.37 cm^3, 0.60 mmol) was added to the yellow solu-

© 2006 NRC Canada

tion, which immediately turned darker and was stirred at room temperature for 1 h. MeI (0.04 cm^3, 0.60 mmol) diluted in dry THF (1 cm^3) was then added and the reaction mixture was stirred for 20 h, the color gradually lightening. Removal of volatiles under reduced pressure gave a yellow solid. This was redissolved in dichloromethane, washed thoroughly with distilled water, and dried over $MgSO_4$. Removal of volatiles under reduced pressure gave a yellow solid that was recrystallized from dichloromethane and methanol to give **8** as yellow crystals (0.18 g, 59%). IR ν(CO) (CH_2Cl_2, cm^{-1}): 2020 (s), 1921 (s), 1905 (s), 1869 (s). ^{1}H NMR ($CDCl_3$) δ: 8.14–8.10 (m, 4H, Ar), 7.33–7.22 (m, 8H, Ar), 7.08–7.06 (m, 4H, Ar), 5.38 (sextet, 1H, *J* = 7.7 Hz, CH), 2.14 (s, 6H, Me), 2.07 (s, 6H, Me), 1.08 (dt, 3H, *J* = 14.8, 7.7 Hz, Me). ^{31}P{^{1}H} NMR ($CDCl_3$) δ: 4.9 (s). Mass spectrum (FAB) *m/z*: 664 [M^+], 608 M^+ – 2CO], 552 [M^+ – 4CO]. Anal. calcd. for $MoP_2O_4C_{34}H_{32}\cdot 0.5CH_2Cl_2$: C 58.76, H 4.88, P 8.80; found: C 58.18, H 5.69, P 9.43.

Preparation of *cis*-[W(CO)$_4$(η^2-Medotpm)] (9)

3 (0.11 g, 0.15 mmol) was dissolved in THF (10 cm^3). *n*-BuLi (0.08 cm^3, 0.19 mmol) was added to the yellow solution, which immediately darkened. After 1 h, MeI (0.012 cm^3, 0.19 mmol) was added and the reaction stirred at room temperature for 20 h. After removal of volatiles under reduced pressure, redissolving in dichloromethane gave a yellow solution that was washed three times with water and dried over $MgSO_4$. Removal of volatiles under reduced pressure gave **9** as a yellow powder, which was recrystallized from dichloromethane and methanol to give yellow crystals (0.07 g, 62%). IR ν(CO) (CH_2Cl_2, cm^{-1}): 2016 (s), 1895 (s), 1863 (s). ^{1}H NMR ($CDCl_3$) δ: 8.17–8.11 (m, 4H, Ar), 7.37 (t, 2H, *J* = 7.3 Hz, Ar), 7.32 (t, 2H, *J* = 8.5 Hz, Ar), 7.28 (t, 2H, *J* = 8.3 Hz, Ar), 7.23 (t, 2H, *J* = 7.3 Hz, Ar), 7.06 (d, 2H, *J* = 8.0 Hz, Ar), 7.03 (d, 2H, *J* = 7.0 Hz, Ar), 6.01 (sextet, 1H, *J* = 7.3 Hz, CH), 2.11 (s, 6H, Me), 2.04 (s, 6H, Me), 1.02 (dt, 3H, *J* = 15.5, 7.7 Hz, Me). ^{31}P{^{1}H} NMR ($CDCl_3$) δ: –18.0 (s, J_{WP} = 199 Hz). Mass spectrum (FAB) *m/z*: 750 [M^+], 722 [M^+ – CO], 694 [M^+ – 2CO], 666 [M^+ – 3CO], 636 [M^+ – 4CO – 2H]. Anal. calcd. for $WP_2O_4C_{34}H_{32}\cdot CH_2Cl_2$: C 50.30, H 4.07, P 7.43; found: C 50.23, H 4.01, P 7.46.

Preparation of [CpRuCl(η^2-Medotpm)] (10)

4 (0.10 g, 0.16 mmol) was dissolved in dry THF (5 cm^3) and ca. 0.16 mmol of $LiN(SiMe_3)_2$ was added dropwise. The solution was stirred for 20 h and 0.01 cm^3 of methyl iodide was added dropwise. After a further 2 h of stirring, volatiles were removed under reduced pressure and the residue redissolved in dichloromethane. This was washed with distilled water and dried with $MgSO_4$. Removal of volatiles under reduced pressure afforded **10** (0.07 g, 68%) as a slightly oily orange solid. ^{1}H NMR ($CDCl_3$, 298 K) δ: 8.3–6.2 (m, 16H, Ar), 5.21 (s, ca. 1.2H, Cp, **10b**), 5.15 (s, ca. 3.8H, Cp, **10a**), ca. 4.4 (vbr, 1H, CH), 2.60 (br, 6H, Me), 2.56 (br, 6H, Me), 0.90 (m, 3H, Me). ^{31}P{^{1}H} NMR ($CDCl_3$) δ: 20.5 (s, **10a**), 13.0 (s, **10b**). Mass spectrum (FAB) *m/z*: 656 [M^+], 621 [M^+ – Cl].

Preparation of *cis*-[PtI$_2$(η^2-Medotpm)] (11)

5a (0.178 g, 0.25 mmol) was dissolved in THF (5 cm^3) and $LiN(SiMe_3)_2$ (ca. 0.3 mmol) was added and the mixture was stirred for 20 h. MeI (0.016 cm^3, 0.26 mmol) was then added dropwise and the mixture was stirred for a further 2 h. Removal of volatiles under reduced pressure and redissolution in dichloromethane gave a yellow solution that was washed with distilled water and dried over $MgSO_4$. The volume of the extract was reduced (ca. 5 cm^3) under reduced pressure and **11** (0.156 g, 85%) was precipitated as a yellow solid upon addition of ethanol. ^{1}H NMR ($CDCl_3$) δ: 8.16 (br, 2H, Ar), 7.76 (br, 2H, Ar), 7.52–7.29 (m, 10H, Ar), 7.10 (br, 2H, Ar), 5.38 (dd, 1H, *J* = 18.7, 9.9 Hz, CH), 2.47 (br, 6H, CH_3), 2.34 (s, 6H, CH_3), 1.16 (dt, 3H, *J* = 20.5, 11.0 Hz, CH_3); ^{31}P{^{1}H} NMR ($CDCl_3$) δ: –71.4 (s, *J* = 2892 Hz). Mass spectrum (FAB) *m/z*: 903 [M^+], 776 [M^+ – I], 649 [M^+ – 2I]. Anal. calcd. for $C_{30}H_{32}I_2P_2Pt$: C 39.86, H 3.54; found: C 39.28, H 3.49.

Preparation of *cis*-[Mo(CO)$_4$(η^2-Etdotpm)] (12)

2 (0.33 g, 0.50 mmol) was dissolved in dry THF (25 cm^3) to form a pale yellow solution. *n*-BuLi (0.5 cm^3, 0.75 mmol) was added and the solution immediately darkened. After stirring at room temperature for 1 h, EtI (0.06 cm^3, 0.75 mmol) was added and the reaction mixture stirred for a further 20 h. The solvent was removed and the solid was redissolved in dichloromethane and washed thoroughly with distilled water. The dichloromethane extract was dried over $MgSO_4$ and the mixture was filtered. Removal of volatiles under reduced pressure gave **12** as a yellow solid (0.24 g, 72%). IR ν(CO) (CH_2Cl_2, cm^{-1}): 2018 (s), 1906 (s), 1870 (s). ^{1}H NMR (CD_2Cl_2, 308 K) δ: 7.99 (m, 2H, Ar), 7.87 (q, 2H, *J* = 7.5 Hz, Ar), 7.39 (t, 2H, *J* = 7.00 Hz, Ar), 7.33–7.27 (m, 4H, Ar), 7.24 (t, 2H, *J* = 7.4 Hz, Ar), 7.15 (d, 4H, *J* = 7.3 Hz, Ar), 4.83 (septet, 1H, *J* = 4.9 Hz, CH), 2.15 (s, 6H, Me), 2.08 (s, 6H, Me), 1.87 (doublet octets, 2H, *J* = 7.4 Hz, 5.1, CH_2), 0.78 (t, 3H, *J* = 7.4 Hz, CH_3). ^{31}P{^{1}H} NMR ($CDCl_3$) δ: 5.9 (s). Mass spectrum (FAB) *m/z*: 678 [M^+], 664 [M^+ – Me], 649 [M^+ – Et], 622 [M^+ – 2CO], 566 [M^+ – 4CO]. Anal. calcd. for $MoP_2O_4C_{35}H_{34}$: C 62.13, H 5.03, P 9.17; found: C 62.16, H 5.55, P 10.85.

Preparation of *cis*-[W(CO)$_4$(η^2-Etdotpm)] (13)

3 (0.25 g, 0.35 mmol) was dissolved in dry THF (25cm^3) to form a pale yellow solution. *n*-BuLi (0.3 cm^3, 0.52 mmol) was added and the solution immediately darkened. This was left to stir at room temperature for 1 h. EtI (0.04 cm^3, 0.52 mmol) was then added and the solution was stirred for 20 h. The solvent was removed and the solid was redissolved in dichloromethane. This was washed thoroughly with distilled water. The dichloromethane extract was dried over $MgSO_4$ and the mixture was filtered. Removal of volatiles under reduced pressure gave a yellow powder. This was recrystallized from dichloromethane and methanol to give **13** as yellow crystals (0.19 g, 72%). IR ν(CO) (CH_2Cl_2, cm^{-1}): 2016 (s), 1900 (s), 1866 (s). ^{1}H NMR ($CDCl_3$) δ: 7.99 (m, 2H, Ar), 7.89 (q, 2H, *J* = 7.5 Hz, Ar), 7.34 (t, 4H, *J* = 7.2 Hz, Ar), 7.26 (m, 4H, Ar), 7.09 (m, 4H, Ar), 5.29 (br, 1H, CH), 2.13 (s, 6H, Me), 2.01 (s, 6H, Me), 1.81 (m, 2H, CH_2), 0.79 (t, 3H, *J* = 7.3 Hz, Me). ^{31}P{^{1}H} NMR ($CDCl_3$) δ: –15.7 (s). Mass spectrum (FAB) *m/z*: 764 [M^+], 750 [M^+ – Me], 736 [M^+ – CO], 708 [M^+ – 2CO], 680 [M^+ –

© 2006 NRC Canada

3CO], 650 [M^+ – 4CO]. Anal. calcd. for $WP_2O_4C_{35}H_{34}$: C 54.97, H 4.45, P 8.12; found: C 54.36, H 4.84, P 7.51.

Preparation of *cis*-[Mo(CO)$_4$(η^2-Bzdotpm)] (14)

2 (0.33 g, 0.51 mmol) was dissolved in dry THF (25 cm^3). *n*-BuLi (0.5 cm^3, 0.77 mmol) was added and the solution immediately darkened. The reaction was stirred at room temperature for 1 h. Benzyl bromide (0.09 cm^3, 0.77 mmol) was added and the solution was stirred for another 20 h. The solvent was removed and the residue was redissolved in dichloromethane. This was washed thoroughly with distilled water. The organic layer was dried over $MgSO_4$ and the mixture was filtered. Removal of volatiles under reduced pressure gave an oil. This was recrystallized from dichloromethane and methanol to give **14** as yellow plates (0.13 g, 34%). IR ν(CO) (CH_2Cl_2, cm^{-1}): 2020 (s), 1898 (s), 1869 (s). ^{1}H NMR (CD_2Cl_2, 308 K) δ: 8.03 (q, 2H, *J* = 7.6 Hz, Ar_A), 7.93 (q, 2H, *J* = 7.0 Hz, Ar_B), 7.36 (t, 2H, *J* = 6.8 Hz, Ar_A), 7.31 (t, 2H, *J* = 6.4 Hz, Ar_B), 7.27 (t, 2H, *J* = 6.4 Hz, Ar_A), 7.21 (t, 2H, *J* = 7.4 Hz, Ar_B), 7.12 (dd, 2H, *J* = 7.5, 2.0 Hz, Ar_B), 7.08 (t, 1H, *J* = 7.2 Hz, Bz), 7.02 (t, 2H, *J* = 7.0 Hz, Bz), 6.96 (d, 2H, *J* = 7.0 Hz, Ar_A), 6.56 (d, 2H, *J* = 7.2 Hz, Bz), 5.53 (m, 1H, CH), 3.06 (dt, 2H, *J* = 14.2, 5.4 Hz, CH_2), 2.15 (s, 6H, Me_A), 1.82 (s, 6H, Me_B); (213 K) δ: 8.25 (br, 2H, Ar), 8.18 (br, 2H, Ar), 7.55–7.23 (m, 8H, Ar), 7.04 (brd, 2H, *J* = 6.7 Hz, Ar), 7.02 (t, 1H, *J* = 7.3 Hz, Bz), 6.92 (t, 2H, *J* = 7.1 Hz, Bz), 6.76 (brd, 2H, *J* = 6.8 Hz, Ar), 6.48 (d, 2H, *J* = 7.5 Hz, Bz), 5.80 (brs, 1H, CH), 2.84 (brdt, 2H, *J* = 14.9, 5.2 Hz, CH_2), 2.04 (brs, 6H, Me), 1.55 (brs, 6H, Me). ^{31}P{^{1}H} NMR ($CDCl_3$) δ: 6.9 (s). Mass spectrum (FAB) *m*/*z*: 740 [M^+], 713 [M^+ – CO], 684 [M^+ – 2CO], 628 [M^+ – 4CO]. Anal. calcd. for $MoP_2O_4C_{40}H_{36}\cdot 0.25CH_2Cl_2$: C 63.62, H 4.81, P 8.17; found: C 64.31, H 4.84, P 8.12.

Preparation of *cis*-[W(CO)$_4$(η^2-Bzdotpm)] (15)

3 (0.11 g, 0.15 mmol) was dissolved in dry THF (25 cm^3). *n*-BuLi (0.14 cm^3, 0.23 mmol) was added and the solution immediately darkened. The reaction was stirred at room temperature for 1 h. Benzyl bromide (0.03 cm^3, 0.23 mmol) was added and the solution was stirred for another 20 h. The solvent was removed and the residue was redissolved in dichloromethane. This was washed thoroughly with distilled water. The organic layer was dried over $MgSO_4$ and the mixture was filtered. Removal of volatiles under reduced pressure gave a yellow powder. This was recrystallized from dichloromethane and methanol to give **15** as yellow crystals (0.05 g, 40%). IR ν(CO) (CH_2Cl_2, cm^{-1}): 2016 (s), 1912 (s), 1896 (s), 1866 (s). ^{1}H NMR ($CDCl_3$) δ: 8.13 (brs, 2H, Ar), 8.02 (brs, 2H, Ar), 7.38–7.20 (m, 9H, Ar + Bz), 7.06 (d, 2H, *J* = 7.2 Hz, Ar), 7.00 (t, 2H, *J* = 7.7 Hz, Bz), 6.86 (d, 2H, *J* = 7.0 Hz, Ar), 6.55 (d, 2H, *J* = 7.3 Hz, Bz), 6.17 (brs, 1H, CH), 2.98 (dt, 2H, *J* = 15.0, 5.6 Hz, CH_2), 2.10 (s, 6H, Me), 1.71 (s, 6H, Me). ^{31}P{^{1}H} NMR ($CDCl_3$) δ: –15.6 (s). Mass spectrum (FAB) *m*/*z*: 826 [M^+], 798 [M^+ – CO], 770 [M^+ – 2CO], 742 [M^+ – 3CO], 712 [M^+ – 4CO]. Anal. calcd. for $WP_2O_4C_{40}H_{36}$: C 58.11, H 4.36, P 7.51; found: C 57.67, H 4.20, P 7.40.

Preparation of [Mo(CO)$_3$(η^2-Medotpm)] (16)

8 (0.19 g, 0.28 mmol) was refluxed in xylene (15 cm^3) for 60 h. Removal of volatiles under reduced pressure gave a black solid (0.11 g, 62%). IR ν(CO) (CH_2Cl_2, cm^{-1}): 1901 (vs), 1840 (s). ^{1}H NMR ($CDCl_3$) δ: 7.41–6.98 (m, 16H, Ar), 3.27 (q, 1H, *J* = 7.1 Hz, CH), 2.49 (s, 6H, Me), 2.23 (s, 6H, Me), 0.97 (dt, 3H, *J* = 11.1, 4.0 Hz, Me). ^{31}P{^{1}H} NMR ($CDCl_3$) δ: –46.7 (s). Mass spectrum (FAB) *m*/*z*: 606 [M^+ – CO], 592 [M^+ – Me – CO], 576 [M^+ – 2CO], 561 [M^+ – 2CO – Me], 552 [M^+ – 3CO].

X-ray data collection and solution

Single crystals were mounted on glass fibres and all geometric and intensity data were taken from these samples using an automated four-circle diffractometer (Nicolet R3mV) equipped with Mo Kα radiation (λ = 0.710 73 Å) at 293 ± 2 K. Lattice parameters were identified by application of the automatic indexing routine of the diffractometer to the positions of a number of reflections taken from a rotation photograph and centred by the diffractometer. The ω–2θ technique was used to measure reflections and three standard reflections (remeasured every 97 scans) showed no significant loss in intensity during data collection. The data was corrected for Lorenz and polarization effects and unique data with $I \geq 2\sigma(I)$ were used to solve and refine the structure. This was solved by direct methods and developed by using alternating cycles of least-squares refinement and difference-Fourier synthesis. All non-hydrogen atoms were refined anisotropically and placed in idealized positions (C—H, 0.96 Å) and assigned a common isotropic thermal parameter (U = 0.08 Å^2).[3]

Acknowledgements

We thank the Engineering and Physical Sciences Research Council (EPSRC, UK) for the provision of a research studentship to M.-Y. Lee and Dr. Abil Aliev for help with NMR experiments.

References

1. P. Dierkes and P.W.N.M. van Leeuwen. J. Chem. Soc. Dalton Trans. 1519 (1999), and refs. therein.
2. R.J. Puddephatt. Chem. Soc. Rev. **12**, 99 (1983).
3. B. Chaudret, B. Delavaux, and R. Poilblanc. Coord. Chem. Rev. **86**, 191 (1988).
4. F.A. Cotton and J.M. Troup. J. Am. Chem. Soc. **96**, 4422 (1974).

[3] Supplementary data for this article are available on the journal Web site (http://canjchem.nrc.ca) or may be purchased from the Depository of Unpublished Data, Document Delivery, CISTI, National Research Council Canada, Ottawa, ON K1A 0R6, Canada. DUD 5003. For more information on obtaining material refer to http://cisti-icist.nrc-cnrc.gc.ca/irm/unpub_e.shtml. CCDC 275347–275353 contain the crystallographic data for this manuscript. These data can be obtained, free of charge, via http://www.ccdc.cam.ac.uk/conts/retrieving.html (Or from the Cambridge Crystallographic Data Centre, 12 Union Road, Cambridge CB2 1EZ, UK; fax +44 1223 336033; or deposit@ccdc.cam.ac.uk).

© 2006 NRC Canada

5. N.M. Doherty, G. Hogarth, S.A.R. Knox, K.A. Macpherson, F. Melchior, D.A.V. Morton, and A.G. Orpen. Inorg. Chim. Acta, **198–200**, 257 (1992).
6. R. Appel, K. Geisler, and H.-F. Schöler. Chem. Ber. **112**, 648 (1979).
7. H.J. Colquhoun and W. McFarlane. J. Chem. Res. (S), 368 (1978).
8. H. Schmidbaur, S. Schnatterer, K.C. Dash, and A.A.M. Aly. Z. Naturforsch. B, **38B**, 62 (1983).
9. L.J. Al Hayaly. Trans. Met. Chem. **23**, 221 (1998).
10. A.F.M.J. Van der Ploeg and G. Van Koten. Inorg. Chim. Acta, **51**, 225 (1981).
11. G. Hoge, H.-P. Wu, W.S. Kissel, D.A. Pflum, D.J. Greene, and J. Bao. J. Am. Chem. Soc. **126**, 5966 (2004).
12. N.A. Cooley, S.M. Green, D.F. Wass, K. Heslop, A.G. Orpen, and P.G. Pringle. Organometallics, **20**, 4769 (2001).
13. J.N.L. Dennett, A.L. Gillon, K. Heslop, D.J. Hyett, J.S. Fleming, C.E. Lloyd-Jones, A.G. Orpen, P.G. Pringle, D.F. Wass, J.N. Scutt, and R.H. Weatherhead. Organometallics, **23**, 6077 (2004).
14. P.W. Clark and B.J. Mulraney. J. Organomet. Chem. **217**, 51 (1981).
15. G.R. Clark and P.W. Clark. J. Organomet. Chem. **255**, 205 (1983).
16. S. Al-Jibori and B. L. Shaw. Inorg. Chim. Acta, **65**, L123 (1982).
17. S. Al-Jibori and B.L. Shaw. Inorg. Chim. Acta, **74**, 235 (1983).
18. S. Al-Jibori, M. Hall, A.T. Hutton, and B.L. Shaw. J. Chem. Soc. Dalton Trans. 863 (1984).
19. G.R. Copper, D.M. McEwan, and B.L. Shaw. Inorg. Chim. Acta, **122**, 207 (1986).
20. H.J. Wasserman, G.J. Kubas, and R.R. Ryan. J. Am. Chem. Soc. **108**, 2294 (1986).
21. K.K. Cheung, T.F. Lai, and K S. Mok, J. Chem. Soc. A, 1644 (1971).
22. R. Colton, B.F. Hoskins, and K. McGregor, Aust. J. Chem. **40**, 1471 (1987).
23. D.J. Darensbourg, D.J. Zalewski, C. Plepys, and C. Campana. Inorg. Chem. **26**, 3727 (1987).

© 2006 NRC Canada

Reaction of H_2S with $MoRu(CO)_6(dppm)_2$ to give H_2 and a bridged-sulfide product via hydrido-sulfhydryl intermediates (dppm = $Ph_2PCH_2PPh_2$)[1]

Mozhgan Khorasani-Motlagh, Nasser Safari, Craig B. Pamplin, Brian O. Patrick, and Brian R. James

Abstract: Oxidative addition of H_2S to $MoRu(CO)_6(\mu\text{-dppm})_2$ (**1**) at ~20 °C in toluene yields an isolable complex formulated as $Mo(CO)_3(\mu\text{-SH})(\mu\text{-CO})(\mu\text{-dppm})_2RuH(CO)$ (**2**) via the possible intermediate $Mo(CO)_3(\mu\text{-H})(\mu\text{-CO})(\mu\text{-dppm})_2Ru(SH)(CO)$ (**4**) (dppm = $Ph_2PCH_2PPh_2$) that is detectable at lower temperatures. Over 2 days, species **2** in toluene loses H_2 (and CO) to yield the bridged-sulfide product, $Mo(CO)_2(\mu\text{-CO})(\mu\text{-S})(\mu\text{-dppm})_2Ru(CO)$ (**5**) that is also formed directly from the reaction of **1** with elemental sulfur. The solid-state molecular structure of **5** is determined by X-ray crystallography. A further hydrido-sulfhydryl species, possibly $Mo(CO)_3(\mu\text{-SH})(\mu\text{-H})(\mu\text{-dppm})_2Ru(CO)_2$ (**3**), is in equilibrium with **2** at ambient temperature.

Key words: molybdenum, ruthenium, bis(diphenylphosphino)methane, hydrogen sulfide, hydrido-sulfhydryl species, carbonyl complexes, bridged-sulfide complex.

Résumé : L'addition oxydante du H_2S au $MoRu(CO)_6(\mu\text{-dppm})_2$ (**1**), à ~20 °C, dans le toluène, conduit à la formation d'un complexe qui peut être isolé, dont la formule serait $Mo(CO)_3(\mu\text{-SH})(\mu\text{-CO})(\mu\text{-dppm})_2RuH(CO)$ (**2**) et qui se formerait par le biais d'un intermédiaire possible de formule $Mo(CO)_3(\mu\text{-H})(\mu\text{-CO})(\mu\text{-dppm})_2Ru(SH)(CO)$ (**4**) (dppm = $Ph_2PCH_2PPh_2$) qu'on peut détecter à des températures plus basses. Sur une période de deux jours, l'espèce **2** perd une molécule d'hydrogène (et du CO) pour conduire au produit à pont sulfure de formule $Mo(CO)_2(\mu\text{-CO})(\mu\text{-S})(\mu\text{-dppm})_2Ru(CO)$ (**5**) qui se forme aussi directement par réaction du composé **1** avec du soufre élémentaire. On a déterminé la structure moléculaire à l'état solide du composé **5** par diffraction des rayons X. À la température ambiante, une autre espèce hydrido-sulfhydryle, possible de formule $Mo(CO)_3(\mu\text{-SH})(\mu\text{-H})(\mu\text{-dppm})_2Ru(CO)_2$ (**3**) est aussi en équilibre avec le composé **2**.

Mots clés : molybdène, ruthénium, bis(diphénylphosphino)méthane, sulfure d'hydrogène, espèces hydrido-sulfhydryle, complexe de carbonyle, complexe à pont sulfure.

[Traduit par la Rédaction]

Introduction

Interest in the reactivity of hydrogen sulfide toward transition metal complexes continues, particularly because of its relevance in catalytic hydrodesulfurization (1–3), the potential conversion of H_2S into H_2 and elemental sulfur (4, 5), and the importance of metal–sulfur interactions in enzymes such as nitrogenase and hydrogenase (1, 2, 6). Reactions of H_2S with bimetallic complexes to yield a bridged-sulfide with liberation of H_2 is common (4, 7–10), and mechanisms for such processes typically invoke formation of an H_2S adduct, followed by oxidative addition to give a hydrido-sulfhydryl intermediate; a proton, formed from the coordinated SH can then react with the metal-hydride to produce H_2 and a μ-S species (4, 7), or a "second oxidative addition" of the SH moiety can give a dihydride species that subsequently reductively eliminates H_2 (9). Although there are cases where the hydrido-sulfhydryl intermediates are detected in such chemistry (7, 9), detection of any precursor H_2S adduct is relatively rare, and there are only five structurally characterized H_2S complexes, all of which are Ru species (11).

Because of the documented Ru–H_2S chemistry, the fact that Ru is the second-row analogue of Fe, and the key role

Received 17 May 2005. Published on the NRC Research Press Web site at http://canjchem.nrc.ca on 24 March 2006.

This paper is dedicated to Arthur Carty in recognition of his contributions to organometallic chemistry (particularly within Ru complexes), and his commitment to the promotion of chemistry in Canada.

M. Khorasani-Motlagh. Department of Chemistry, University of Sistan and Baluchestan, Zahedan, Iran.
N. Safari. Department of Chemistry, University of Shahid Beheshti, Tehran, Iran.
C.B. Pamplin, B.O. Patrick, and B.R. James.[2] Department of Chemistry, University of British Columbia, 2036 Main Mall, Vancouver, BC V6T 1Z1, Canada.

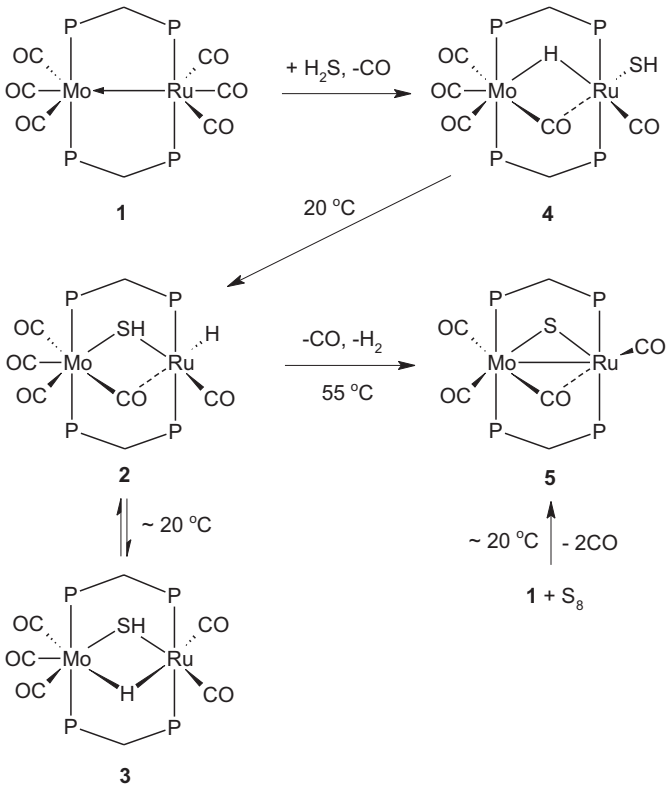
[1]This paper is part of a Special Issue dedicated to Professor Arthur Carty.
[2]Corresponding author (e-mail: brj@chem.ubc.ca).

 doi:10.1139/V06-002 © 2006 NRC Canada

of sulfur ligands in Mo–Fe enzyme systems, the complex $MoRu(CO)_6(\mu\text{-dppm})_2$ (**1**) (dppm = $Ph_2PCH_2PPh_2$)[3] seemed an attractive precursor for a study of reactivity toward H_2S, particularly in view of the success of our group and others in forming H_2S adducts with monometallic Ru(II) complexes (11). Subsequent to our first report on the reaction of H_2S with $Pd_2Cl_2(dppm)_2$ to generate H_2 and a bridged-sulfide complex (12), Cowie's group (9, 13, 14) has reported on the reaction of H_2S with several heterobinuclear complexes of the type $MM'(CO)_n(dppm)_2$ (n = 3 or 4, and M and M′ may be the same or different transition metals). Complex **1**, first synthesized by Chaudret and co-workers (15) is commonly written as $(CO)_3Mo(dppm)_2Ru(CO)_3$ containing a Mo—Ru bond, although an X-ray structure reveals five terminal CO ligands and one semi-bridged CO, the structure being complicated by half occupancy at each metal centre; in solution, however, the preferred structure is one with six terminal CO ligands as shown in Scheme 1 (15).

This paper reports on the interaction of the Mo–Ru complex (**1**) with H_2S to form, via several hydrido-sulfhydryl intermediates (tentatively assigned as **2**–**4**), the bridged-sulfide complex, $Mo(CO)_2(\mu\text{-CO})(\mu\text{-S})(dppm)_2Ru(CO)$ (**5**), that can be synthesized also from the reaction of **1** with elemental sulfur (S_8); however, no H_2S adduct was detected. The findings were first presented at a conference (16), which Arthur Carty attended, and so it seems appropriate to remind him of the details, particularly because his favourite metal is involved!

Scheme 1. Reaction of H_2S with $MoRu(CO)_6(dppm)_2$ (P = PPh_2).



Experimental section

All solvents were dried by refluxing over Na benzophenone under Ar, and were distilled immediately before use. Purified Ar (Praxair) and H_2S (Matheson) were used without further treatment. The primary Ru source was $RuCl_3{\cdot}3H_2O$ donated by Colonial Metals Inc., Elkton, Maryland; $Mo(CO)_6$, elemental sulfur, and all other chemicals (Aldrich products) were used as received. All manipulations were conducted under Ar using standard Schenk techniques. The complex $MoRu(CO)_6(dppm)_2$ (**1**) was prepared as reported previously (15).

NMR spectra were recorded in C_6D_6 or toluene-d_8 on a Bruker AV-300 spectrometer operating at 121.49 MHz for ^{31}P (referenced to external 85% aq. H_3PO_4), using an internal deuterated solvent lock; broad (br), singlet (s), triplet (t), quintet (qnt), multiplet (m), pseudo (ps); coupling constants are given in Hz. Deuterated solvents were dried over molecular sieves and freeze–pump–thaw degassed prior to vacuum transfer into 5 mm NMR tubes containing the sample; the NMR tube could be flushed with H_2S. For the variable-temperature NMR experiments, the temperature regulation of the probehead was calibrated using a standard curve based on the chemical shift separation of the resonances of 4% MeOH in MeOH-d_4 (17). IR spectra were recorded as KBr disks on an ATI Mattson Genesis FT IR instrument. Conductivity data (1.0 mmol/L of the complex in CH_2Cl_2), measured on a RCM151B Serfass conductance bridge (A.H. Thomas Co.) at 25 °C with a 3404 cell (Yellow Springs Instrument Co.), were calibrated using 0.0100 mol/L aq. KCl, and are given as Λ_M in units of Ω^{-1} mol^{-1} cm^2. Elemental analyses were performed by P. Borda (Department of Chemistry, University of British Columbia).

Syntheses

$Mo(CO)_3(\mu\text{-}SH)(\mu\text{-}CO)(dppm)_2RuH(CO)$ (2)

Complex **1** (100 mg, 0.084 mmol) was dissolved in toluene (10 mL) and H_2S (5 mL, 0.22 mmol) was added via a gas-tight syringe at room temperature (~20 °C). After ~15 min, the orange solution became dark orange, and addition of hexane (10 mL) yielded an orange precipitate that was collected, washed with hexane, and dried by passing a stream of CO over the product. The complex was stored under Ar. Yield: 88 mg (88%). IR (cm^{-1}): ν_{CO} 1959 (s), 1937 (s), 1880 (s), 1768 (s). ^1H NMR (C_7D_8, ~20 °C) δ: –8.13 (ps t, $^2J_{PH}$ = 18.8 Hz, 1H, Ru*H*), –0.98 (ps qnt, $^3J_{PH}$ = 9.3 Hz, 1H, S*H*), 2.80–3.45 (br m, 4H, CH_2). $^{31}P\{^1H\}$ NMR δ: 35.7 (br m). Anal. calcd. for $C_{55}H_{46}O_5P_4SMoRu$: C 57.95, H 4.07; found: C 57.43, H 4.29. (See Results and discussion section for low-temperature NMR data.) Λ_M = 2.2 (nonconducting).

$Mo(CO)_2(\mu\text{-}CO)(\mu\text{-}S)(dppm)_2Ru(CO)$ (5)

(*a*) Addition of excess sulfur (30 mg, 0.94 mmol "S") to a solution of **1** (100 mg, 0.084 mmol) in toluene (10 mL) im-

[3] In all the bimetallic complexes mentioned subsequently in this paper, the dppm ligands are bridging, but for convenience the μ symbol is omitted.

© 2006 NRC Canada

mediately generated an orange precipitate. The mixture was stirred for 1 h, when hexane (10 mL) was added to complete precipitation of the product that was collected, dried under Ar, and recrystallized from CH_2Cl_2–Et_2O. Yield: 88 mg (90%). IR (cm^{-1}): ν_{CO} 2010 (m), 1954 (s), 1866 (s), 1777 (m). ^1H NMR (C_6D_6, ~20 °C) δ: 2.17 (m, 2H), 5.36 (m, 2H). $^{31}P\{^1H\}$ NMR: AA′BB′ pattern centered at δ 16.3, 25.9 (see below). Anal. calcd. for $C_{54}H_{44}O_4P_4SMoRu{\cdot}0.5CH_2Cl_2$: C 56.80, H 3.94; found: C 56.66, H 4.24. Λ_M = 1.8 (nonconducting). (*b*) H_2S (5 mL, 0.22 mmol) was added via a gas-tight syringe to **1** (50 mg) dissolved in toluene (10 mL). The solution was stirred for 48 h, when addition of hexane (10 mL) precipitated the orange product. Yield: 68 mg (69%). The NMR data were identical to those listed above.

Crystallography

Brown crystals of **5**, grown by diffusion of hexane into a concentrated C_6D_6 solution of the complex, were mounted on a glass fibre. Measurements were made on a Rigaku/ADSC CCD area detector with graphite-monochromated Mo-Kα radiation (λ = 0.710 69 Å), data being collected at –100 ± 1 °C to a maximum 2θ value of 55.8°. A sweep of data was done using φ oscillations from 0.0° to 190.0° at χ = –90.0°, and a second sweep was performed using ω oscillations between –19.0° and 23.0° at χ = –90.0°. The crystal-to-detector distance was 40.51 mm, and the detector swing angle was –5.50°. Data were collected and processed using the d*TREK program (18), and the structure was solved by direct methods and expanded using Fourier techniques (19). The non-hydrogen atoms were refined anisotropically. The weighting scheme was based on counting statistics; the plot of $\Sigma w(|F_o| - |F_c|)^2$ vs. $|F_o|$, the reflection order in data collection sin θ/λ, and various classes of indices showed no unusual trends.

There was disorder in the site occupancy of both Ru1 and Mo1, with the metal at the Ru1 site consisting of disordered Ru and Mo with populations of 0.83 and 0.17, respectively. Residual electron density with geometry consistent with four CO ligands was found near Ru1 and Mo1 and was modeled as such. The populations of the CO ligands were refined, with the result that two of these had a population of ~1 (C52-O2 and C53-O3), while one CO ligand at Mo1 had a population of 0.83 (C51A-O1A), and the second CO ligand on Ru1 had a population of ~0.17 (C51B-O1B). Extra electron density consistent in geometry with a CO was found near S1, while one relatively large peak was found near the bridging C54-O4 ligand; the residual peaks near S1 were modeled as a bridging CO ligand (C54B-O4B), and the peak near C54-O4 as a bridging S ligand (S1B). Final occupancies were refined such that the major fragment consisted of (O3-C53)Ru1-C54A-Mo1(C51A-O1A)(C52-O2)-S1A. Final refinements on the populations gave a ratio of 0.83:0.17 between the major and minor fragments. The material also crystallizes with four molecules of C_6D_6. Some details of the data collection are given in Table 1, while complete crystallographic information is available.[4]

Table 1. Crystal data for $Mo(CO)_2(\mu\text{-}CO)(\mu\text{-}S)(dppm)_2Ru(CO)$ (**5**)·$4C_6D_6$.

Empircal formula	$C_{54}H_{44}O_4P_4SMoRu{\cdot}4C_6D_6$
Formula weight	1 446.37
Crystal size (mm^{-1})	0.50 × 0.35 × 0.35
Crystal system	Monoclinic
Space group	$P2_1$ (No. 4)
a (Å)	11.7314(3)
b (Å)	20.7675(4)
c (Å)	13.9807(4)
β (°)	98.346(2)
Volume ($Å^3$)	3 370.1(1)
Z	2
Density (calculated) ($Mg\ m^{-3}$)	1.425
F(000)	1 464.00
μ (cm^{-1})	5.86
Reflections collected	29 340
Independent reflections	12 913 (*R*(int) = 0.042)
Observed reflections	12 448 ($I > 2\sigma(I)$)
Variable	820
Goodness-of-fit on F^2	1.03
Final *R* indices ($I > 2\sigma(I)$)	*R*1 = 0.031, *wR*2 = 0.078
R indices (all data)	*R*1 = 0.042, *wR*2 = 0.080
Largest diff. peak and hole (e $Å^{-3}$)	0.71 and –0.87

Note: $R1 = \Sigma||F_o| - |F_c||/\Sigma|F_o|$, $wR2 = \sqrt{\Sigma(F_o^2 - F_c^2)^2/\Sigma w(F_o^2)^2}$.

Results and discussion

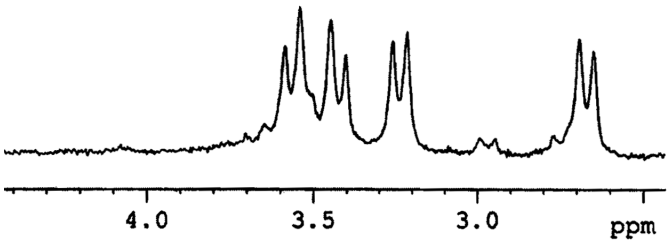
Isolated products from the reaction of H_2S with $MoRu(CO)_6(dppm)_2$ (1)

A toluene solution of complex **1** reacts rapidly with H_2S at ambient conditions to yield an isolable, orange product believed to be $Mo(CO)_3(\mu\text{-}SH)(\mu\text{-}CO)(dppm)_2RuH(CO)$ (**2**), formed via oxidative addition of H_2S with loss of one CO ligand (Scheme 1). The elemental analysis and spectroscopic data support this formulation. The room-temperature ^1H NMR spectrum shows one broad multiplet at δ 3.40 for the CH_2 protons, implying fluxional behaviour, but in a ^{31}P-decoupled spectrum at –75 °C four doublets are seen (Fig. 1), revealing the expected inequivalence of these protons; a ^1H(COSY) NMR experiment showed coupling between the proton signals at δ 2.67 and 3.24, and coupling between those at δ 3.42 and 3.56. (The room-temperature, broad multiplet must result from a combination of fluxionality and a temperature dependence of the chemical shifts bringing them close together.) A high-field hydride resonance (a pseudotriplet at δ –8.13 implying coupling to two P atoms) is attributed to a terminal hydride at the Ru, and a pseudoquintet at δ –0.98 (coupling to four P atoms) is attributed to a bridging SH. The $^2J_{PH}$ coupling constant for

[4] Supplementary data for this article are available on the journal Web site (http://canjchem.nrc.ca) or may be purchased from the Depository of Unpublished Data, Document Delivery, CISTI, National Research Council Canada, Ottawa, ON K1A 0R6, Canada. DUD 5005. For more information on obtaining material refer to http://cisti-icist.nrc-cnrc.gc.ca/irm/unpub_e.shtml. CCDC 272191 contains the crystallographic data for this manuscript. These data can be obtained, free of charge, via http://www.ccdc.cam.ac.uk/conts/retrieving.html (Or from the Cambridge Crystallographic Data Centre, 12 Union Road, Cambridge CB2 1EZ, UK; fax +44 1223 336033; or deposit@ccdc.cam.ac.uk).

© 2006 NRC Canada

Fig. 1. $^1H\{^{31}P\}$ NMR spectrum (CH_2 region) of a C_7D_8 solution of $Mo(CO)_3(\mu\text{-}SH)(\mu\text{-}CO)(dppm)_2RuH(CO)$ (**2**) at 198 K.



the hydride is about twice that for the $^3J_{PH}$ coupling for the sulfhydryl hydrogen, and both values are in the reported range (9, 13). The fluxionality of **2** is also evident in the $^{31}P\{^1H\}$ NMR spectrum; at ~20 °C, this shows a broad multiplet centred at δ ~ 35.7, but at 0 °C this resolves into several sharper peaks. Attempts to simulate the expected AA′BB′ spin pattern proved to be impossible, as solutions of **2** always contained an isomer (species **3**, see below) that also gave at room temperature a broad multiplet at δ ~ 40.0, which was also resolved at 0 °C. The lower temperature spectrum was thus extremely complex; data from Cowie's group reveal the complexity of such $^{31}P\{^1H\}$ NMR spectra (9, 13, 14). The H ligand in **2** is considered to be cis to the SH group because such geometry is essential for subsequent loss of H_2 to generate **5** (see below); the H could in principle be attached to the Mo, cis to the SH, but we consider Mo-monohydride formulations less likely. The inability to distinguish which ^{31}P resonances were associated with which metal (see below) made it impractical to carry out $^1H\{^{31}P\}$ decoupling NMR experiments that could have shed light on this problem. Well-resolved ^{13}C NMR data would also be of value; however, at room temperature, the natural abundance ^{13}C spectrum shows a broad single resonance for the carbonyl groups (again consistent with fluxionality), while low-temperature measurements were thwarted by insolubility of **2**. ^{13}C NMR spectra of ^{13}C-enriched samples are needed to substantiate a more definitive formulation for **2**.

The solid-state IR spectrum (which is essentially of pure **2**) displays three intense ν_{CO} bands in the 1959–1880 cm^{-1} region (attributed to the four terminal carbonyls), and an intense band at 1768 cm^{-1} for the bridging carbonyl. A very weak band at ~2360 cm^{-1} might be due to the μ-SH ligand. The corresponding reaction of **1** with D_2S gave an isolated solid that showed corresponding ν_{CO} bands at 1960, 1883, and 1772 cm^{-1}, but the IR spectrum was of no assistance in detecting a ν_{RuH} band in **2**, which must be buried under the ν_{CO} bands; a ν_{RuH} band for Ru(II) complexes is typically found in the 2000–1850 cm^{-1} region (20, 21), and a small band at 1340 cm^{-1} (not seen for **2**) could be the ν_{RuD} band.

A C_6D_6 solution of **2** on standing for ~30 min at room temperature generates new NMR signals, which are thought to correspond to a species such as **3**, an isomerization product of **2**, in which the terminal hydride has interchanged with the μ-CO ligand (see Scheme 1); the ratio of **2**:**3** equilibrates at a value of ~5:1. The high-field hydride resonance for the μ-H of **3** is seen as a multiplet at δ –11.12, while the μ-S*H* pseudoquintet resonance ($^3J_{PH}$ = 12.6 Hz) occurs at δ –1.38. The complex $^{31}P\{^1H\}$ NMR spectrum of **3** was mentioned previously.

The reaction of **1** with H_2S is similar to its reported oxidative addition reaction with H_2 when the isolated product, again formed with loss of a CO ligand, is $MoRu(H)_2(CO)_5(dppm)_2$; however, the structure was written with five terminal CO ligands (three on Mo and two on Ru) with both hydrides exchanging between bridging and Ru-terminal positions (15). The high-field hydride ^1H NMR signal appeared as a multiplet at δ –7.95, similar to those seen for **2** and **3**; indeed, the formulation of the dihydride was written (15) as $Mo(CO)_3(\mu\text{-}H)_2(dppm)_2Ru(CO)_2$, identical to the structure type assigned to **3** in Scheme 1.

Attempts to obtain single crystals of a hydrido-sulfhydryl species (such as **2** or **3**) led instead to isolation of the bridged-sulfide complex, $Mo(CO)_2(\mu\text{-}CO)(\mu\text{-}S)(dppm)_2Ru(CO)$ (**5**). The conversion of **2** (or a mixture of **2** and **3**) via loss of H_2 and CO to give **5** occurs on heating C_6D_6 (or toluene-d_8) solutions of **2** at ~55 °C for 1 h (Scheme 1), or leaving such solutions for 2 to 3 days under Ar at room temperature. Such conversions of hydrido-sulfhydryl species to bridged-sulfide complexes are well-established for homo- or hetero-bimetallic complexes containing μ-dppm ligands (4, 7, 9, 13, 14). The easiest route for isolation of the air-stable, orange **5** in high yield is via treatment of **1** with elemental sulfur at room temperature, the reaction being complete within a few minutes.

Complex **5**, characterized by X-ray crystallography, elemental analysis, and solution spectroscopic methods, is structurally analogous to $Mn(CO)_2(\mu\text{-}CO)(\mu\text{-}S)(dppm)_2Rh(CO)$ (9), but with Mo and Ru replacing the Mn and Rh, respectively. The IR spectra are also similar, showing three intense ν_{CO} bands in the 2010–1865 cm^{-1} region, and a ν_{CO} band at a lower wavenumber for the μ-CO.

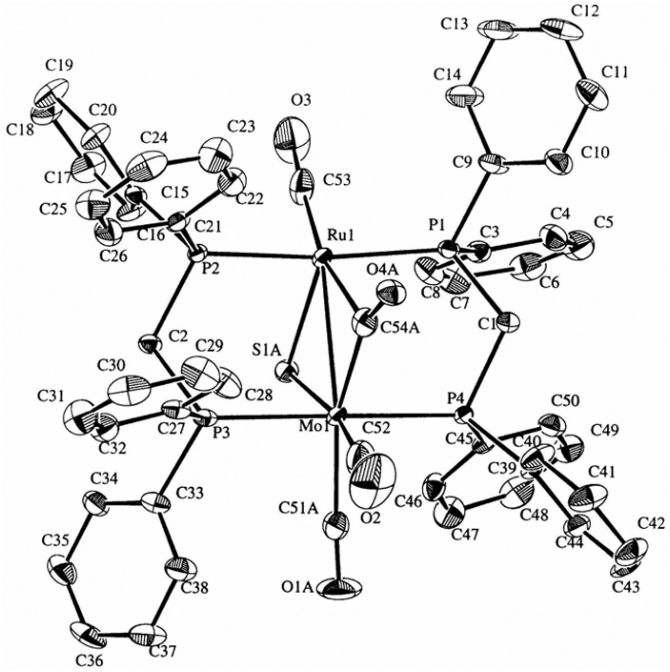
The solid state structure of **5** (Fig. 2), selected bond lengths and angles being reported in Table 2, shows the expected *trans*-$MoRu(\mu\text{-}dppm)_2$ unit, having P-M-P angles of 174.60° (M = Mo) and 172.10° (M = Ru). The P-Mo-P angle is close to that of 173.80° for our previously reported $[Mo(CO)_2(\mu\text{-}I)(\mu\text{-}CO)(dppm)_2Ru(CO)_2]^+$ cation (22), and is in between that of 171.39° for $Mo(CO)_2(\mu\text{-}Cl)(\mu\text{-}CO)(dppm)_2Rh(CO)$ (23) and that of 178.4° for $Mo(CO)_2(\mu\text{-}CO)(\mu\text{-}SO_2)(dppm)_2RhCl$ (24). The Mo—P bond lengths are within 0.05 Å of those in the above Mo–Ru and Mo–Rh analogues. The Ru—P distances (2.365 and 2.378 Å) and the P-Ru-P angle are close to those in $Ru(CO)_2(\mu\text{-}SO_2)(dppm)_2Ru(CO)_2$ (8) and the Mo–Ru cation noted above (22). The Mo—P distances are some 0.06–0.08 Å longer than the Ru—P distances, which is consistent with a Mo(0)–Ru(II) formulation, although an extra factor might be more steric crowding at the octahedral Mo centre as opposed to the formally five-coordinate Ru (ignoring any metal–metal interaction; see the following).

The $MoRuP_4C_2$ ring in complex **5** assumes a chair conformation, resulting in the presence of two distinct axial phenyl groups and two similarly sized cavities into which the μ-S and μ-CO ligands lie. Qualitatively, the situation is similar to that found in $Ru(S_2)(\mu\text{-}CO)(\mu\text{-}S)(dppm)_2Ru(CO)_2$, where similar cavities accommodate the μ-S and μ-CO ligands (8).

The nonlinearity of the Mo-C(54A)-O(4) moiety (153.4°), and Mo—C(54A) and Ru—C(54A) distances of 2.071 and 2.416 Å, respectively, correspond to a semibridging CO; these angles and distances are close to those reported for

© 2006 NRC Canada

Fig. 2. ORTEP representation (50% ellipsoids) of the molecular structure of $Mo(CO)_2(\mu\text{-}S)(\mu\text{-}CO)(dppm)_2Ru(CO)$ (**5**). H atoms omitted for clarity.

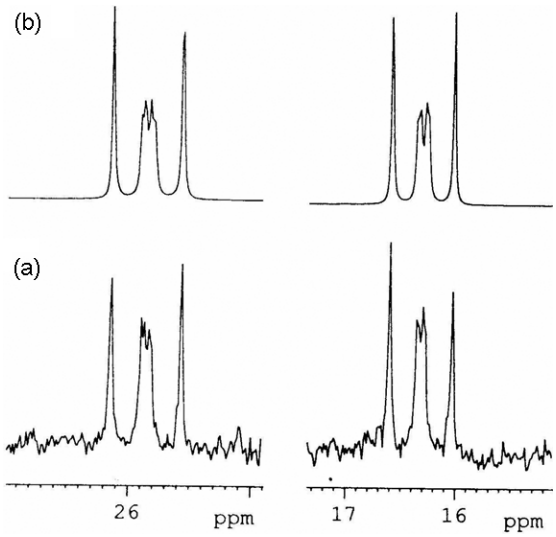


$[(Mo(CO)_2(\mu\text{-}I)(\mu\text{-}CO)(dppm)_2Ru(CO)_2]^+$ in which a semibridging CO is defined by the Mo-C-O angle (155.4°) and Mo—C and Rh—C distances of 2.08 and 2.45 Å, respectively (22). The $Mo(CO)_2(\mu\text{-}Cl)(\mu\text{-}CO)(dppm)_2Rh(CO)$ complex (23, 24) is another related species with a semibridging CO, and there are many others where a semibridging CO is similarly defined (e.g., refs. 8 and 9). That the C(54A)—O(4A) distance of 1.154 Å in **5** is still within 0.02 Å of the values for the terminal CO ligands is not unusual (23).

In complex **5**, the relatively short Mo—C(52) bond (1.953 Å) and somewhat longer C(52)—O(2) bond (1.167 Å), compared with the other metal-C-O linkages, presumably result from this CO being trans to the π-donor sulfide ligand. The metal–metal bond length in **5** (2.986 Å) is ~0.04 Å shorter than in the cationic Mo(μ-I)(μ-CO)Ru species mentioned above (22), and ~0.07 Å shorter than in the precursor complex **1**, where a weak metal–metal interaction is considered likely, especially in solution where all the CO ligands are considered to be terminal (15). Thus, a weak metal–metal interaction may be present in the solid state structure for **5**, but if this is ignored and the semibridged CO is considered as ligated to both metals, **5** is probably best described as consisting of a distorted octahedral Mo(0) centre and a trigonal-bipyramidal Ru(II) centre.

It may be unusual (as suggested by a reviewer of this paper) to have a vacant coordination site trans to a bridging sulfide. In this regard, the structure is complicated by several disorder problems (see the Experimental section) and only the "main fragment" is illustrated in Fig. 2; and, of note, the minor (18%) fragment does show a bridging S trans to the semibridging CO (S(1B)-Ru-C(53) = 152.7(2)°). The structure has been rechecked, and the solution offered is the optimum one; perhaps all we can conclude is that complex **5** in the solid state is a bridged-sulfide species containing four CO ligands.

Fig. 3. $^{31}P\{^1H\}$ NMR spectrum of a C_6D_6 solution of $Mo(CO)_2(\mu\text{-}S)(\mu\text{-}CO)(dppm)_2Ru(CO)$ (**5**) at room temperature. (*a*) Observed, (*b*) simulated with $J_{AA'(Mo)} \sim 87$, $J_{BB'(Ru)} \sim 225$, $J_{AB} = J_{A'B'} \sim 65$, $J_{A'B} = J_{AB'} \sim 4$ Hz.



The room-temperature, solution NMR data for **5** are typical of those for heterobimetallic complexes containing μ-dppm and μ-CO ligands, the closest analogue being complex **2** and $[(Mo(CO)_2(\mu\text{-}I)(\mu\text{-}CO)(dppm)_2Ru(CO)_2]^+$ (22), while related species with a μ-sulfide ligand include Rh–M species (M = Re, Mn, Rh, and Ir (9, 13, 14)), Ir_2 species (14), and Ru_2 species (8). The ^1H NMR spectrum of **5** shows multiplets at δ 5.36 and 2.17 owing to the inequivalent dppm-CH_2 protons. The $^{31}P\{^1H\}$ NMR spectrum displays an AA′BB′ spin pattern that was simulated using $^2J_{PP}$ values of ~225 and ~87 Hz for the *trans*-P atoms at Ru and at Mo, respectively, and values of ~65 and ~4 Hz for the cross-couplings (Fig. 3). These *J* values are comparable to those determined earlier (15) for the precursor **1** (~231 and ~112 Hz and ~90 and ~21 Hz, respectively).

In situ reactions of $MoRu(CO)_6(dppm)_2$ (1) with H_2S

To gain information about possible intermediates in the formation of $Mo(CO)_3(\mu\text{-}SH)(\mu\text{-}CO)(\mu\text{-}dppm)_2RuH(CO)$ (**2**), the title reaction was monitored in situ from –80 to ~20 °C by ^1H and $^{31}P\{^1H\}$ NMR. On exposure of a C_6D_6 solution of **1** to 1 atm H_2S (1 atm = 101.325 kPa) at room temperature, a species (**4**) begins to form "instantaneously" prior to formation of **2**, which is complete after ~15 min; at lower temperatures, **4** can be stabilized. The ^1H NMR spectrum of **4** shows a broad singlet at δ –2.76 (not noticeably changed by ^{31}P decoupling, but tentatively assigned to a terminal S*H* proton at Ru), a pseudoquintet at δ –14.77 ($^2J_{HP}$ = 15.5 Hz, assigned to a μ-H), and two multiplets at δ 3.76 and 4.61 for the dppm-CH_2 protons; the $^{31}P\{^1H\}$ NMR spectrum of **4** (Fig. S1)[4] shows an AA′BB′ pattern centred at δ 39.1 and 25.5 that can be simulated using $^2J_{PP}$ values of ~230, ~115, ~75, and ~35 Hz (cf. the data above for **1** and **5**). The favoured structure for **4** is that shown in Scheme 1 and is a

© 2006 NRC Canada

Table 2. Selected bond lengths (Å) and angles (°) of **5** (esds in parentheses).

Bond lengths (Å)		**Bond angles (°)**	
Ru(1)—S(1A)	2.5177(10)	P(1)-Ru(1)-P(2)	172.10(3)
Ru(1)—P(1)	2.3649(8)	Ru(1)-P(1)-C(1)	114.50(10)
Ru(1)—C(53)	1.840(4)	P(1)-Ru(1)-C(53)	89.03(12)
Ru(1)—C(54B)	2.080(11)	P(2)-Ru(1)-C(53)	91.26(12)
Ru(1)—Mo(1)	2.9857(3)	Ru(1)-P(1)-C(9)	114.45(12)
Mo(1)—S(1B)	2.563(7)	S(1A)-Ru(1)-P(1)	99.79(3)
Mo(1)—C(52)	1.953(4)	S(1A)-Ru(1)-P(2)	87.99(3)
Mo(1)—C(54B)	2.429(11)	S(1A)-Ru(1)-C(54A)	97.19(15)
Mo(1)—P(4)	2.4434(8)	S(1A)-Ru(1)-C(54A)	97.19(15)
O(1B)—C(51B)	1.23(3)	P(3)-Mo(1)-C(51A)	91.44(12)
O(3)—C(53)	1.160(5)	P(3)-Mo(1)-C(52)	89.05(13)
O(4B)—C(54B)	1.157(10)	P(3)-Mo(1)-C(54A)	96.55(14)
P(1)—C(3)	1.832(3)	P(4)-Mo(1)-C(51A)	87.00(12)
P(2)—C(2)	1.849(3)	P(4)-Mo(1)-C(52)	95.61(13)
P(2)—C(21)	1.820(3)	P(4)-Mo(1)-C(54A)	87.07(14)
P(3)—C(27)	1.840(3)	C(52)-Mo(1)-C(54A)	78.4(2)
P(4)—C(1)	1.849(3)	C(51A)-Mo(1)-C(52)	76.7(2)
P(4)—C(45)	1.840(3)	C(51A)-Mo(1)-C(54A)	153.8(2)
Ru(1)—S(1B)	2.479(9)	Ru(1)-C(53)-O(3)	176.7(4)
Ru(1)—P(2)	2.3777(8)	Ru(1)-C(54A)-O(4A)	123.2(4)
Ru(1)—C(51B)	2.00(2)	Ru(1)-S(1A)-Mo(1)	72.70(3)
Ru(1)—C(54A)	2.416(5)	P(3)-Mo(1)-P(4)	174.60(3)
Mo(1)—S(1A)	2.5197(11)	Ru(1)-P(2)-C(2)	113.01(11)
Mo(1)—C(51A)	2.014(5)	Ru(1)-P(2)-C(15)	114.04(10)
Mo(1)—C(54A)	2.071(6)	Ru(1)-P(2)-C(21)	120.27(11)
Mo(1)—P(3)	2.4434(8)	Ru(1)-P(1)-C(3)	120.42(11)
O(1A)—C(51A)	1.151(6)	S(1A)-Mo(1)-P(3)	83.26(3)
O(2)—C(52)	1.167(5)	S(1A)-Mo(1)-P(4)	91.86(3)
O(4A)—C(54A)	1.154(6)	S(1A)-Mo(1)-C(51A)	98.67(15)
P(1)—C(1)	1.837(3)	S(1A)-Mo(1)-C(52)	170.97(13)
P(1)—C(9)	1.824(3)	S(1A)-Mo(1)-C(54A)	107.06(16)
P(2)—C(15)	1.835(3)	Mo(1)-P(3)-C(2)	113.71(10)
P(3)—C(2)	1.838(3)	Mo(1)-P(3)-C(27)	121.15(12)
P(3)—C(33)	1.842(3)	Mo(1)-P(3)-C(33)	114.63(11)
P(4)—C(39)	1.834(3)	Mo(1)-P(4)-C(1)	112.41(10)
Mo(1)—Ru(1)	2.9857(3)	Mo(1)-P(4)-C(39)	115.81(11)
		Mo(1)-P(4)-C(45)	120.37(10)
		Mo(1)-C(52)-O(2)	175.2(5)
		Mo(1)-C(54A)-O(4A)	153.4(5)
		Mo(1)-C(51A)-O(1A)	173.2(5)
		Mo(1)-O(54A)-Ru(1)	83.04(19)
		P(1)-C(1)-P(4)	111.80(16)
		P(2)-C(2)-P(3)	111.24(16)

further isomer of species **2** and **3**. The H_2S reaction with **1** can be followed more leisurely at lower temperatures in C_7D_8, but no other intermediates such as an H_2S adduct were observed. Thus, in essence, oxidative addition of the H_2S is likely initiated at the Ru(0) centre with loss of a CO ligand, with the SH ligand found terminal at the Ru and the hydride first detected as a μ-H (species **4**); the SH- and H-ligands then exchange to generate **2**, which also equilibrates with species **3** in which the terminal H exchanges with a μ-CO ligand (see above for comparison with the reaction of H_2 with **1**). If solutions containing species **2**–**4** were subjected to 1 atm CO at room temperature, complex **1** was not regenerated, showing that the H_2S reaction is irreversible. Intermediates such as **4**, containing a bridging hydride and terminal sulfhydryl, have been observed in the reaction of H_2S with $Mn(CO)_2(\mu\text{-}CO)(\mu\text{-}S)(dppm)_2Rh(CO)$ (9) and the $M_2(CO)_3(dppm)_2$ complexes (M_2 = Ir_2 or RhIr) (14).

It is worth noting that the experimental elemental analysis for **2** (formulated as a pentacarbonyl) is in even better agreement with a tetracarbonyl formulation with an added solvate, water, i.e., $MoRu(H)(CO)_4(SH)(dppm)\cdot H_2O$ (calcd. for $C_{54}H_{46}O_4P_4SMoRu\cdot H_2O$: C 57.95, H 4.07). If **2** is a tetracarbonyl, then species **3** (and possibly **4**) would have to be formulated as tetracarbonyls, with likely one less CO at the Mo. However, no evidence was found for an associated water, and the fact that the oxidative addition of H_2S to **1** to

© 2006 NRC Canada

give **4** parallels that of H_2 addition, which involves loss of just one CO ligand (15), makes us favour a pentacarbonyl formulation for **4**. Definitive ^{13}C NMR or crystallographic data, which we were unable to collect, are needed to establish unambiguously the structure of **2** (and thus **3**).

Concluding remarks

Our findings add to the data base on reactions of H_2S with solutions of bimetallic-dppm complexes. Three types of systems could be recognized prior to our study: (*i*) In systems exemplified by $Rh_2(CO)_3(dppm)_2$ (14) and $Ru_2(CO)_5(dppm)_2$ (8), a bridging-sulfide product is formed with concomitant loss of H_2, and no intermediates are detected, even when using low-temperature NMR data. (*ii*) In systems such as $RhRe(CO)_4(dppm)_2$ (13), $Ir_2(CO)_3(dppm)_2$ (14), $RhMn(CO)_4(dppm)_2$ (9), and $Pd_2Cl_2(dppm)_2$ (4, 7), a bridged sulfide and H_2 are the final products, but hydrido-sulfhydryl intermediates, with the H^- and SH^- ligands being terminal or bridging, have been detected; migrations of these two ligands between terminal and bridging positions have also been seen (13, 14). (*iii*) A system such as $RhIr(CO)_3(dppm)_2$ that gives a hydrido-sulfhydryl as a final stable product (14). With all the carbonyl-containing precursors, a CO ligand is lost in the proposed first step, usually considered to involve formation of a H_2S complex, although direct ^1H NMR evidence for the coordinated H_2S in any of these systems is lacking. We were hoping that the $MoRu(CO)_6(dppm)_2$ system would generate a detectable H_2S adduct (see Introduction), but the study reveals that the system is of type (*ii*), with the hydrido-sulfhydryl intermediates being detectable at room temperature, a feature shared with the $RhMn(CO)_4(dppm)_2$ (9) and $Ir_2(CO)_3(dppm)_2$ (14) systems. It is not impossible that H_2S can react in a concerted manner with dimetallic precursors, without prior formation of an adduct.

Acknowledgements

We thank the Natural Sciences and Engineering Research Council of Canada (NSERC) for a research grant (BRJ), the Ministry of Science, Research and Technology of the Islamic Republic of Iran for financial support (MKM, NS), and Colonial Metals Inc. for the loan of Ru.

References

1. E.I. Steifel and K. Matsumoto. Transition metal sulfur chemistry; Biological and industrial significance. ACS Symposium Series 653. American Chemical Society, Washington, D.C. 1996.
2. D.E. Schwarz, J.A. Dopke, T.B. Rauchfuss, and S.R. Watson. Angew. Chem. Int. Ed. **40**, 2351 (2001), and refs. therein.
3. R.A. Sanchez-Delgado. Organometallic modeling of the hydrodesulfurization and hydrodenitrogenation reactions. Kluwer Academic, Dordrecht, The Netherlands. 2002.
4. B.R. James. Pure Appl. Chem. **69**, 2213 (1997), and refs. therein.
5. T.Y.H. Wong, S.J. Rettig, and B.R. James. Inorg. Chem. **38**, 2143 (1999).
6. (*a*) M. Hidai and Y. Mizobe. Chem. Rev. **95**, 1115 (1995); (*b*) R.H. Holm, P. Kennepohl, and E.I. Soloman. Chem. Rev. **96**, 2239 (1996); (*c*) M.C. Smith, J.E. Barclay, S.C. Davies, D.L. Hughes, and D.J. Evans. J. Chem. Soc. Dalton Trans. 4147 (2003); (*d*) D. Chong, J.P. Georgakaki, R. Mejia-Rodriguez, J. Sanabria-Chinchilla, M.S. Soriaga, and M.Y. Darensbourg. J. Chem. Soc. Dalton Trans. 4158 (2003).
7. A.F. Barnabas, D. Sallin, and B.R. James. Can. J. Chem. **67**, 2009 (1989).
8. J. Kuncheria, H.A. Mirza, H.A. Jenkin, J.J. Vihal, and R.J. Puddephatt. J. Chem. Soc. Dalton Trans. 285 (1998).
9. L.S. Wang, R. McDonald, and M. Cowie. Inorg. Chem. **33**, 3735 (1994), and refs. therein.
10. A. Müller and E. Diemann. *In* Comprehensive coordination chemistry. Vol. 2. *Edited by* G. Wilkinson, R.D. Gillard, and J.A. McCleverty. Pergamon Press, Oxford, UK. 1987. Chap. 16.1.
11. (*a*) D.C. Mudalige, E.S. Ma, S.J. Rettig, B.R. James, and W.R. Cullen. Inorg. Chem. **36**, 5426 (1997); (*b*) S.L. Chatwin, R.A. Diggle, R.F.R. Jazzar, S.A. Macgregor, M.F. Mahon, and M.K. Whittlesey. Inorg. Chem. **42**, 7695 (2003), and refs. therein.
12. C.-L. Lee, G. Besenyei, B.R. James, D.A. Nelson, and M.A. Lilga. J. Chem. Soc. Chem. Commun. 1175 (1985).
13. M.D. Antonelli and M. Cowie. Inorg. Chem. **29**, 3339 (1990).
14. R. McDonald and M. Cowie. Inorg. Chem. **32**, 1671 (1993).
15. H. Ben Laarab, B. Chaudret, F. Dahan, J. Devillers, R. Poilblanc, and S. Sabo-Etienne. New J. Chem. **14**, 321 (1990).
16. M. Khorasani-Motlagh, N. Safari, and B.R. James. Proceedings of the 13th International Symposium on Homogeneous Catalysis, Tarragona, Spain, 2003. Poster 324.
17. S. Braun, H.-O. Kalinowski, and S. Berger. 100 and more basic NMR experiments: A practical course. VCH Publishers, New York. 1996. p. 111.
18. d*TREK. Area detector software version 4.13 [computer program]. Molecular Structure Corporation, The Woodlands, Tex. 1996–1998.
19. (*a*) A. Altomare, A.M.C. Burla, G. Cammalli, M. Cascarano, C. Gaiacovazzo, A. Guagliardi, A.G.G. Moliterni, G. Polidori, and A. Spanga. J. Appl. Crystallogr. **32**, 115 (1999); (*b*) P.T. Beurskens, G. Admiraal, G. Beurskens, W.P. Bosman, R. de Gelder, R. Israel, and J.M.M. Smits. The DIRDIF94 program system. Technical Report of the Crystallography Laboratory, University of Nijmegen, Nijmegen, The Netherlands. 1994.
20. M. Khorasani-Motlagh, N. Safari, C.B. Pamplin, B.O. Patrick, and B.R. James. Inorg. Chim. Acta, **320**, 184 (2001), and refs. therein.
21. K. Osakada, T. Yamamoto, A. Yamamoto, A. Takenaka, and Y. Sasada. Inorg. Chim. Acta, **105**, L9 (1985), and refs. therein.
22. M. Khorasani-Motlagh, N. Safari, C. Pamplin, B.O. Patrick, and B.R. James. Inorg. Chem. Commun. **6**, 1175 (2003).
23. T.W. Graham, F.V. Gastel, R. McDonald, and M. Cowie. Organometallics, **18**, 2177 (1999).
24. O. Heyke, O.W. Hiller, and I.P. Lorenz. Chem. Ber. **124**, 2217 (1991).

© 2006 NRC Canada

Reactions of $Fe_3(CO)_{12}$ and $Fe(CO)_5$ with functionalized alkynes in CH_3OH–KOH solution — The crystal structure of $Fe_2(CO)_6(PPh_3)[\mu\text{-}\eta^3\text{-}(H_2CCCH_2)]$[1]

Giuliana Gervasio, Domenica Marabello, Enrico Sappa, and Andrea Secco

Abstract: The complex $Fe_2(CO)_7(H_2CCCH_2)$ (**1**) is obtained starting from a variety of functionalized alkynes that can release C_3 fragments during the reactions with $Fe_3(CO)_{12}$ or $Fe(CO)_5$ in CH_3OH–KOH solutions. Owing to the oily nature of **1**, it was reacted with triphenylphosphine, and the structure of the resulting title compound (**1a**) has been determined by X-ray analysis. Complex **1a** shows a new coordination mode of a $H_2C{=}C{=}CH_2$ ligand to a diiron centre and is, to our knowledge, unprecedented. We have also found that **1** (and **1a**) are by-products, and not intermediates in the formation of complex **3**. A discussion of the possible reaction pathways is given.

Key words: iron carbonyls, alkynols, CO and methanol activation, acetyl and acetate complexes, allenyl iron complexes, crystal structure.

Résumé : Le complexe $Fe_2(CO)_7(H_2CCCH_2)$ (**1**) a été préparé à partir d'une variété d'alcynes fonctionnalisés qui peuvent perdre des fragments en C_3 au cours de réactions avec du $Fe_3(CO)_{12}$ ou du $Fe(CO)_5$ dans des solutions de CH_3OH–KOH. En raison de la nature huileuse du composé **1**, on l'a fait réagir avec de la triphénylphosphine et on a fait appel à la diffraction des rayons X pour déterminer la structure cristalline du produit qui en résulte et qui est mentionné dans le titre (**1a**). Le complexe **1a** présente un nouveau mode de coordination du ligand $H_2C{=}C{=}CH_2$ au centre difer qui, à notre connaissance était inconnu jusqu'à maintenant. On a aussi trouvé que les composés **1** (et **1a**) sont des sous-produits et non pas des intermédiaires dans la formation du complexe **3**. On présente une discussion des voies réactionnelles potentielles.

Mots clés : fer carbonyles, alkynols, activation du CO et du méthanol, complexes acétyles et acétates, complexes d'allényl fer, structure cristalline.

[Traduit par la Rédaction]

Introduction

Propargyl alcohols react with $M_3(CO)_{12}$ carbonyls (M = Fe, Ru, or Os) both under thermal (hydrocarbons, reflux) and basic conditions (CH_3OH–KOH solution, followed by acidification with HCl) undergoing different processes, among which the more important is dehydration. Two main dehydration pathways leading, respectively, to coordinated ene-yne (or vinylacetylene) or to allenylidene ligands have been evidenced (1). The latter is apparently preferred when M = Fe, as discussed in the following. Most of the dehydration–hydration reactions are promoted by acids (2), silica surfaces (3), or silica and alumina slurries (4). Other processes observed are deoxygenation (5) and loss of functionalities (6).

We have recently reported the reactions of $Fe_3(CO)_{12}$ with propargyl alcohol ($HC{\equiv}CCH_2OH$) and propargyl chloride ($HC{\equiv}CCH_2Cl$), both under thermal and basic methanolic conditions. The products obtained were: $Fe_2(CO)_7(C_3H_4)$ (**1**), the allenylidenic $Fe_3(CO)_9(\mu\text{-}CO)(C{=}C{=}CH_2)$ (**2**) in very small yields, $Fe_2(CO)_6[H_2CCC(H)C(=O)OCH_3]$ (**3**), and $Fe_3(CO)_{10}[H_2CCC(H)C(=O)C\{CH_2(O)CH_3\}CCH_2]$ (**4**) (7). The structures of complexes **2**–**4** are shown in Scheme 1.

On the basis of previous results (8), the formation of com-

Received 31 May 2005. Published on the NRC Research Press Web site at http://canjchem.nrc.ca on 25 March 2006.

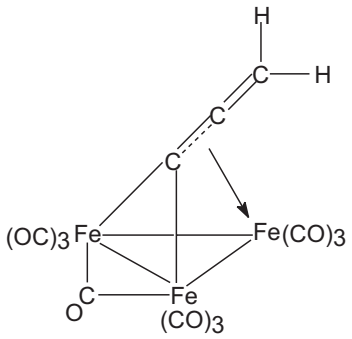
Dr. Carty is now at the top of a brilliant career. This paper is dedicated to the chemist who agreed to collaborate with us, the teacher who told me how to decently write a paper in English, and to the friend with whom we shared nice ski and walking runs in the Alps. In a word: Arthur Carty.

G. Gervasio and D. Marabello. Dipartimento di Chimica Inorganica, Chimica Fisica e Chimica dei Materiali, Universita' di Torino, Via Pietro Giuria 7, I-10125 Torino, Italy.
E. Sappa[2] and A. Secco. Dipartimento di Scienze e Tecnologie Avanzate, Universita' del Piemonte Orientale, Via Bellini 25/g, I-15100, Alessandria, Italy.

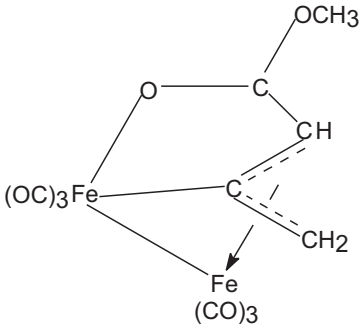
[1]This article is part of a Special Issue dedicated to Professor Arthur Carty.
[2]Corresponding author (e-mail: enrico.sappa@unipmn.it).

 doi:10.1139/V05-252 © 2006 NRC Canada

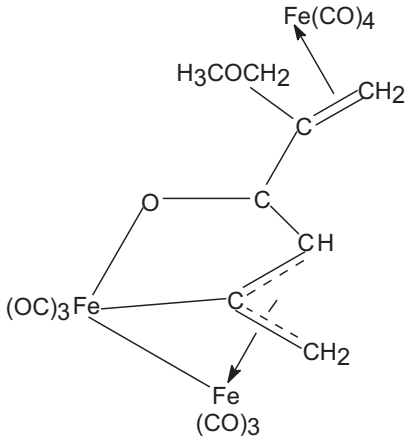
Scheme 1.



2



3



4

plexes such as **3** had been explained by invoking the intermediacy of complexes of type **2**, with no evidence for the role of complex **1** in the reaction sequence. In this work the attention has been paid to the synthetic pathways leading to complexes **1** and **3** and on some aspects of their reactivity with the aim of obtaining more details on the reaction mechanisms leading to methoxycarbonyl derivatives (**3**, **4**). The reactions of $Fe(CO)_5$ and $Fe_3(CO)_{12}$ with the alkynes collected in Table 1, under basic methanolic conditions, have been therefore considered. These alkynes, except for the last two, are characterized by $C{\equiv}CCH_2OH$ or $HC{\equiv}CCH_2$ moieties, which could form cumulene systems.

Reacting the oily complex **1** with triphenylphosphine, the title complex (**1a**) was obtained as the major product, and its structure was determined by X-ray analysis. The structural features for this unprecedented derivative are discussed.

Table 1. These alkynes, except for the last two, are characterized by $C{\equiv}CCH_2OH$ or $HC{\equiv}CCH_2$ moieties, which could form cumulene systems.

Ligand	Name
$HC{\equiv}CCH_2OH$	Propargylic alcohol
$ClC{\equiv}CCH_2OH$	Propargyl chloride
$PhC{\equiv}CCH_2OH$	3-Phenyl-2-propyn-1-ol
$(CH_3)_3SiC{\equiv}CCH_2OH$	Trimethylsilyl propargyl alcohol
$(CH_3)_3SiOCH_2C{\equiv}CH$	Propargyloxytrimethylsilane
$H_2NCH_2C{\equiv}CH$	Monopropargylamine
$(CH_3COO)CH_2C{\equiv}CH$	Propargyl acetate
$(Ph)_2(OH)CC{\equiv}CH$	1,1-Diphenyl-2-propyn-1-ol
$(CH_3)_3SiC{\equiv}CH$	Trimethylsilyl acetylene

Experimental

$Fe(CO)_5$, $Fe_3(CO)_{12}$ (Strem Chemicals), and the alkynes (Lancaster Syntheses) were used as received. Methanol, KOH (pellets), and HCl (37%) were laboratory grade chemicals. Solvents (hexane, heptane, toluene, and dietyl ether) were dehydrated (over sodium when possible). The reactions were performed under dry nitrogen in conventional three-necked flasks, equipped with a gas inlet, cooler, mercury check valve, and magnetic stirring.

All reactions of $Fe_3(CO)_{12}$ were performed in CH_3OH–KOH solution and the following "standard" conditions were adopted: dissolution of KOH (20 pellets, ca. 1.5 g) in 200 cm^3 of CH_3OH, then addition and dissolution of 5.0 g (ca. 10 mmol) of $Fe_3(CO)_{12}$, and warming at 40 °C for 10 min; addition of 4.0 cm^3 of the liquid alkynes (or of 1.0 g for the solid ones) and warming at 40 °C for a further 10–15 min. After cooling, the substrate was acidified with HCl (37%) to pH 1. After 1 h, the solution was extracted with three 75 cm^3 portions of *n*-heptane. The solution was then reduced to a small volume under reduced pressure and then purified using TLC (Kieselgel PF Merck; eluants were mixtures of light petroleum (40–70 °C) and diethyl ether in a 9:1 *v*/*v* ratio). Finally, the TLC bands were extracted with diethyl ether.

The reactions of $Fe(CO)_5$ with propargylic alcohol and propargyl chloride were performed under the following conditions: to a solution of 30 pellets of KOH in 200 cm^3 of methanol, 30 cm^3 (ca. 65 mmol) of $Fe(CO)_5$ was added. The resulting solution was stirred and warmed at 40 °C for 30 min after which time 6 cm^3 of the liquid alkynes were added. Stirring and warming were continued for a further 30 min. The resulting solution was allowed to cool and acidified (to pH 1) with HCl (32%). A violent evolution of gases and vapours was observed. After filtering, the solutions were extracted with three 75 cm^3 portions of heptane. After reduction to a small volume under vacuum, the solutions obtained were chromatographed as described previously.

Elemental analyses were performed in the laboratories of the DISTA (Università del Piemonte Orientale). The IR spectra were obtained on a Bruker Equinox 55 (KBr cells, path length 0.5 mm). The ^1H and ^{13}C NMR were obtained on a JEOL GX 270 spectrometer. The EI (and CI) mass spectra were obtained on a Finnigan Mat TSQ-700 mass

© 2006 NRC Canada

spectrometer (Servizio di Spettrometria di Massa, Dipartimento di Scienza e Tecnologia del Farmaco, Università di Torino).

Reactions of propargyl alcohol with $Fe(CO)_5$

After extraction with heptane, the following products were obtained: complex **1** (20%), $Fe_3(CO)_{12}$ (15%), and orange complex **3** (20%).

Complex 1

IR (heptane, cm^{-1}) ν_{CO}: 2098 (m), 2040 (vs), 2020 (vs), 2012 (s sh), 1989 (m), 1980 (m sh). ^1H NMR ($CDCl_3$, r.t.) δ: 3.77 (s, 2H), 2.42 (s, 2H). ^{13}C NMR δ: 70.87 (s), 75.86 (s, CH_2), 186.0 (s, b), 206.1 (s, b, terminal CO), 212.0 (s, CO). EI-MS: M^+ = 348 *m/z*, release of a fragment with 16 *m/z*, then release of 7CO; intense signal at 152 *m/z* [$Fe_2(C_3H_4)$]. Anal. calcd. (%): C 34.5, H 1.15, Fe 32.2; found: C 34.6, H 1.2, Fe 32.1.

Complex 3

IR (cm^{-1}): 2078 (m-s), 2033 (vs), 2008 (s, sh), 1996 (vs), 1979 (m-s). ^1H NMR δ: 4.08 (s, 1H), 3.68 (s, 3H, Me), 3.56 (s, 1H), 2.97 (s, 1H). ^{13}C NMR δ: 54.4 (s, Me), 58.8 (d, CH_2), 66.3 (d, CH), 189.1 (d, C ring?), 197.1 (s, CO), 212.0 (vb, CO acetate). EI-MS: M^+ = 378 *m/z*, release of 6CO, then complex fragmentation. Anal. calcd. (%) C 34.9, H 1.6, Fe 29.6; found: C 35.0, H 1.7, Fe 29.7. The analytical results for complexes **1** and **3** have already been reported in ref. 7. These are given here for comparison with the other complexes described.

Reaction of propargyl chloride with $Fe(CO)_5$

After filtration of the acidified solution a considerable amount of solid residual was observed; this was partially soluble in methanol. The methanolic solution was added to the filtrate. After extraction with heptane, TLC gave the following bands: yellow (ca. 10%, complex **1**), $Fe_3(CO)_{12}$ (30%), orange (ca. 10%, complex **3**) and red (tr, not collected).

Reaction of $Fe_3(CO)_{12}$ with trimethylsilyl propargyl alcohol

After acidification and extraction, the red, clear heptane solution was chromatographed on TLC plates and the following bands were obtained: yellow (10%, complex **1**), triiron dodecacarbonyl (10%), orange (25%, complex **3**), orange-red (20%, complex **5**), and some decomposition.

Complex 5

IR (heptane, cm^{-1}): 2100 (m), 2074 (m-s), 2032 (vs), 2006 (s), 1992 (s, sh), 1974 (m). ^1H NMR δ: 4.18 (d), 3.95 (d), 3.86 (s, 1H), 3.75 (d), 3.67 (d), 3.53 (s, 1H), 3.28 (d), 3.04 (q, 2H), 2.94 (s, 1H), 2.77 (s, 1H), 2.55 (s, 1H). EI-MS: M^+ = 586 *m/z*, release of 12 fragments with *m/z* = 28. Anal. calcd. (%) C 38.1, H 1.7, Fe 29.1; found: C 38.3, H 1.7, Fe 28.8.

Complex 4

IR (cm^{-1}): 2100 (m), 2075 (m-s), 2031 (vs), 2026 (vs), 1992 (s), 1973 (m). ^1H NMR δ: 4.16–4.12 (d, 2H), 3.89–3.78 (d, 2H), 3.68–3.66 (d, 1H), 3.29 (s, 3H, Me), 3.07–3.04 (d, 2H, CH_2). ^{13}C NMR δ: 37.3 (s), 58.4 (s), 66.4 (s), 68.2 (s), 72.3 (s), 203.3 (s), 206.6 (s), 220.0 (s). EI-MS: M^+ = 586 *m/z*, release of 12 fragments with *m/z* = 28. Anal. calcd. (%): C 38.1, H 1.7, Fe 29.1; found: C 38.2, H 1.8, Fe 28.0.

Reaction of $Fe_3(CO)_{12}$ with propargyloxytrimethylsilane

After extraction, the red-yellow heptane solution was chromatographed on TLC plates and the following bands were obtained: dark yellow (15%, complex **1**), $Fe_3(CO)_{12}$ (15%), orange (20%, complex **3**), red (**5**, 10%), trace amounts of a red and a yellow compound (not collected), and decomposition.

Reaction of $Fe_3(CO)_{12}$ with propargyl acetate

After extraction with heptane, TLC showed the following bands: yellow (20%, complex **1**), $Fe_3(CO)_{12}$ (20%), orange (20%, complex **3**), traces of a red compound, and decomposition.

Reaction of $Fe_3(CO)_{12}$ with monopropargylamine

After acidification, the dark yellow heptane extract was chromatographed and the following bands were observed: yellow (complex **1**, 13%), orange yellow (complex **3**, 30%) and some decomposition.

Reaction of $Fe_3(CO)_{12}$ with 3-phenyl-2-propyn-1-ol in methanol

After acidification and extraction, the greenish solution gave the following TLC bands: light yellow (10%, complex **6**), $Fe_3(CO)_{12}$ (15%), orange (15%, complex **7**), and orange, purple, purple (tr, not collected).

Complex 6

IR (cm^{-1}): 2074 (m), 2033 (vs), 2005 (s), 1996 (s, sh), 1978 (m, sh). ^1H NMR δ: 7.26–7.19 (m, 5H, Ph), 4.28 (s, 1H), 3.88 (s, 1H), 3.69 (s, 1H). EI-MS: M^+ = 424 *m/z*, loss of seven fragments with *m/z* = 28. Proposed formula: $Fe_2(CO)_7C_3H_3(Ph)$. Anal. calcd. (%): C 45.3, H 1.9, Fe 26.4; found: C 45.2, H 1.8, Fe 26.5.

Complex 7

IR (cm^{-1}): 2074 (m-s), 2033 (vs), 2005 (s), 1996 (s, sh), 1978 (m-s). ^1H NMR δ: 7.45–7.26 (m, 5H, Ph), 6.30 (s, 1H), 3.88 (s, 1H). EI-MS: M^+ = *m/z* 454, loss of 6CO (see ref. 7). Proposed formula: $Fe_2(CO)_6[RHC_3R'C(=O)OCH_3]$ (R, R′ = Ph, H). Anal. calcd. (%): C 45.0, H 2.2, Fe 24.6; found: C 45.1, H 2.3, Fe 24.5.

Reactions of complexes 1 and 3

Reaction of complex 1 with PPh_3 under thermal conditions

About 0.5 g of complex **1** (ca. 1.5 mmol) were dissolved in heptane; PPh_3 (0.5 g, ca. 1.9–2.0 mmol) and Me_3NO were added and the solution was warmed to reflux (10 min) under nitrogen. After 4 min reflux (after which time the colour turned from yellow to dark red), the suspension was allowed to cool, was reduced to a small volume under vacuum, and chromatographed on TLC plates. The following bands were obtained: orange (50%, complex **1a**) and red (50%, complex

© 2006 NRC Canada

1b). Complex **1b** is nearly insoluble in solvents commonly used for obtaining X-ray grade crystals.

*Complex **1a***

IR (cm^{-1}): 2061 (m-s), 2017 (s), 1988 (vs), 1978 (s, sh), 1946 (w). ^1H NMR δ: 7.56 (m), 7.45 (m), 7.32 (m, 15H, Ph), 3.55 (s, 2H), 2.86 (s, 2H). ^{31}P NMR δ: –4.50 (s). Anal. calcd. (%): C 55.67, H 3.26, Fe 19.24; found: C 55.8, H 3.3, Fe 19.1. (MW = 582).

*Complex **1b***

IR (cm^{-1}): 2050 (m b), 1970 (vs), 1900 (m b). ^1H NMR δ: 7.54 (m), 7.40 (m, 30H, Ph), 3.50 (s, 2H), 2.16 (s, 2H). ^{31}P NMR δ: 59.78 (s), 79.20 (s). CI-MS: M^+ = 842 *m/z* (exp. 844), loss of 5CO. Anal. calcd. (%): C 55.67, H 3.26, Fe 19.24; found: C 55.7, H 3.3, Fe 19.3. (MW = 844).

Reaction of complex 1 with CH_3OH under thermal conditions

Approximately 0.2 g of complex **1** (ca. 0.6 mmol) were dissolved in CH_3OH (10 cm^3), brought to reflux (3 min), and allowed to react for 15 min. The dark yellow suspension was brought to dryness under N_2 flow; after TLC purification, only parent **1** could be observed together with some decomposition.

Approximately 0.25 g of complex **1** (ca. 0.72 mmol) were dissolved in 10 cm^3 of CH_3OH (and 0.2 cm^3 of HCl were added), brought to reflux (5 min), and allowed to react for 13 min. No change in colour was observed. The suspension was dried under a nitrogen stream; TLC purification and spectroscopic analyses showed the presence of complex **1** only.

Reactions of 1a with methanol under thermal conditions

Approximately 25 mg of **1a** (crystals used for the X-ray study) were dissolved in 10 cm^3 of CH_3OH under N_2 and allowed to reflux for 5 min. No change in colour was observed. The mixture was brought to dryness under reduced pressure; after TLC separation, only one complex could be obtained (**1c**).

*Complex **1c***

IR (cm^{-1}): 2061 (m-s), 2018 (m-s), 1987 (vs), 1977 (s sh), 1946 (m). ^1H NMR δ: 7.70–7.28 (mm, Ph), 3.58 (s, 1H), 3.51 (s, 1H), 2.31 (s, 1H), 2.19 (s, 3H). CI-MS: M^+ = 584 *m/z*, loss of 6CO. Anal. calcd. (%): C 55.5, H 3.6, Fe 19.2; found: C 55.4, H 3.7, Fe 19.3.

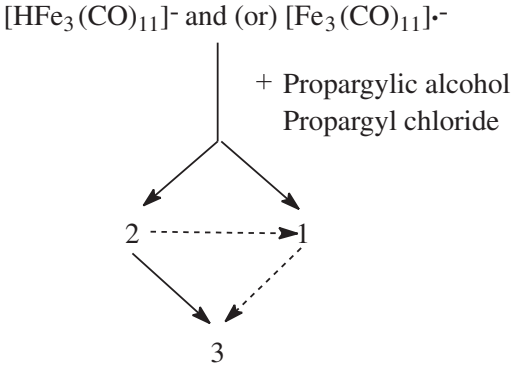
Reactions of 3 with triphenylphosphine

Approximately 0.5 g of complex **3** (ca. 1.3 mmol) were dissolved in heptane under N_2 and a 2:1 molar excess of PPh_3 was added. The suspension was brought to reflux (10 min) and allowed to reflux for 3 min. The colour of the clear solution turned from orange to red. TLC purification gave the following bands: dark yellow (**3**, ca. 10%), red (complex **3a**, ca. 40%) and impure PPh_3.

*Complex **3a***

IR (cm^{-1}): 2042 (vs), 1991 (vs), 1977 (s), 1963 (m), 1936 (m b). ^1H NMR δ: 7.55–7.25 (mm, Ph), 3.97 (s, 1H), 3.40 (s, 1H), 3.21 (s, 3H), 2.66 (s, 1H). ^{31}P NMR δ: 30.8 (s). Anal. calcd. (%): C 54.0, H 3.5, Fe 18.7; found: C 54.1, H 3.6, Fe 18.8.

Scheme 2.



X-ray structure analysis for complex 1a

The reflection data were collected on a Siemens P4 diffractometer equipped with a Bruker APEX CCD detector using graphite-monochromated Mo Kα radiation (λ = 0.710 73 Å). The complex **1a** ($C_{27}H_{19}Fe_2O_6P$) crystallized from *n*-heptane in a monoclinic $P2_1/n$ space group, with a = 12.7888(15) Å, b = 9.3735(10) Å, c = 21.4652(26) Å, β = 92.163(2)°, V = 2571.3(5) $Å^3$, MW = 582.09, Z = 4, Dcalcd. = 1.504 g cm^{-3}, μ = 1.230 mm^{-1}. The red crystal used was prismatic and had dimensions of 0.08 × 0.10 × 0.20 mm^3. The θ range for measurement was 1.90°–28.32°; 23 563 reflections were measured at 293 K and 5444 were unique (R_{int} = 0.077). The intensities were corrected semi-empirically for absorption, based on symmetry equivalent reflections. The refinement of 325 parameters was made using full-matrix least-squares on F^2. All non-hydrogen atoms were refined anisotropically. The hydrogen atoms were calculated and refined with U_{iso} set at 1.2 times U_{eq} of the corresponding C atom. The final parameters were: $R = \Sigma||F_o| - |F_c||/\Sigma|F_o| = 0.0732$ for 2975 "observed" reflections having $F_o^2 > 2\sigma(F_o^2)$, $Rw = [\Sigma(wF_o^2 - F_c^2)^2/\Sigma w(F_o^2)^2]^{1/2} = 0.127$, goodness-of-fit = $[\Sigma w(F_o^2 - F_c^2)^2/(\text{No. of unique reflections} - \text{No. of parameters})]^{1/2} = 0.959$. Programs used were SHELXTL (9) for structure solution, refinement, and molecular graphics, Bruker AXS SMART (diffractometer control), SAINT (integration), and SADABS (absorption correction) (10). The high R values are due to the poor quality of crystals; the intensity measurements were repeated on other crystals with the same results. Therefore, the calculated hydrogen atom positions must be considered with caution.

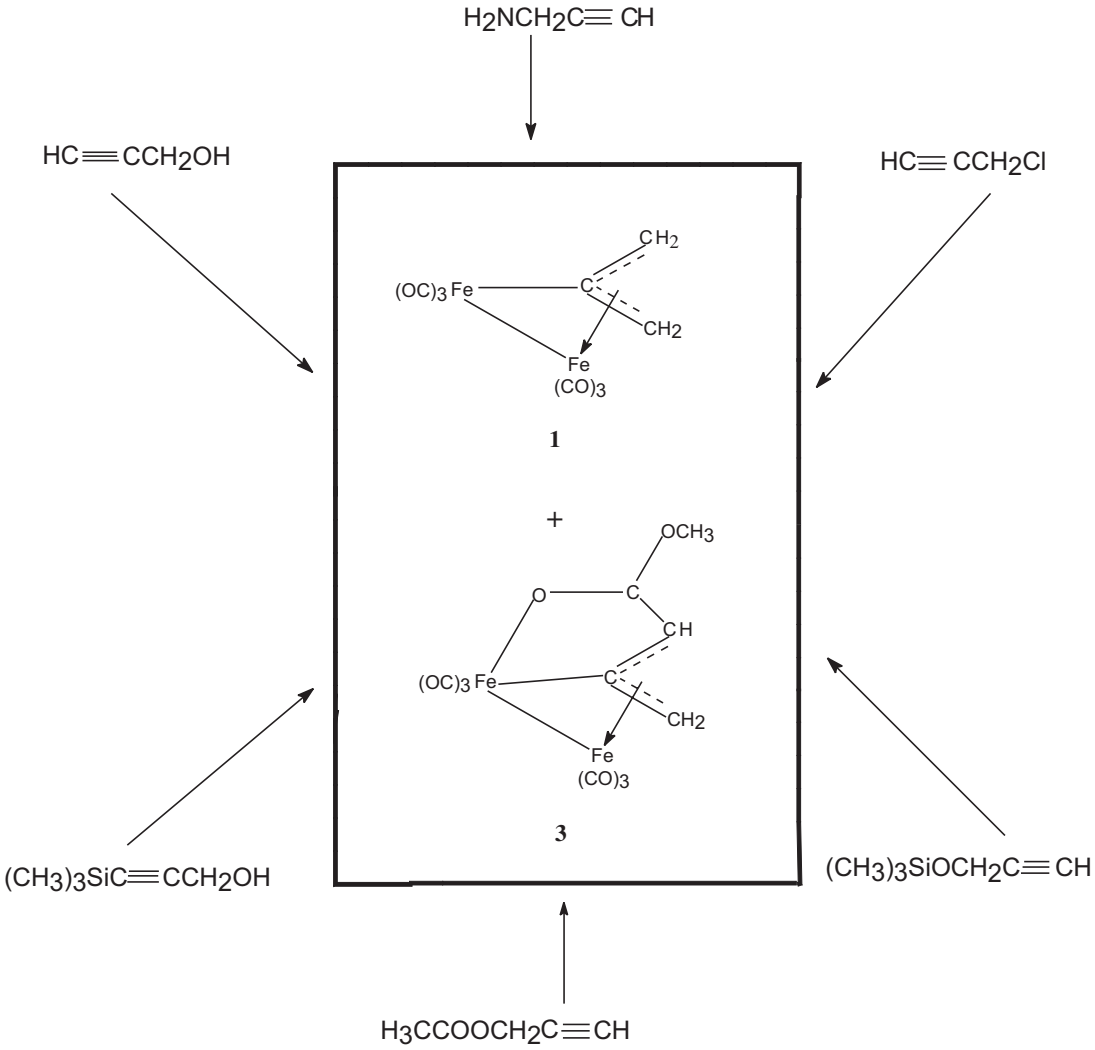
Results and discussion

Spectroscopic characterization of complexes 5–7

Complex **5** is obtained only from the isomeric ligands trimethylsilyl propargyl alcohol and propargyloxytrimethylsilane. The analytical and spectroscopic data (except for the ^1H NMR) are closely comparable with those of complex **4**. However, in view of the high complexity of the NMR spectrum, we cannot provide a structure. Complex **5** has an isomeric formula with respect to **4** (elemental analysis and mass spectrum) and the NMR spectrum could indicate that "**5**" is a nonseparated mixture of the two isomers. Attempts

© 2006 NRC Canada

Scheme 3.



at obtaining crystals suitable for X-ray analysis were unsuccessful.

Complexes **6** and **7** are the homologues of **1** and **3**, respectively, and contain a phenyl at the site of one of the hydrogens of the C_3 part of the organic ligand. The complexes are obtained from 3-phenyl-2-propyn-1-ol, which apparently behaves like the other alkynes, but does not lose the phenyl group. Complex **7** shows the same analytical data, but a different NMR with respect to the complex reported in ref. 7. Again, it could be an isomer obtained by a different position of the phenyl group in the structure.

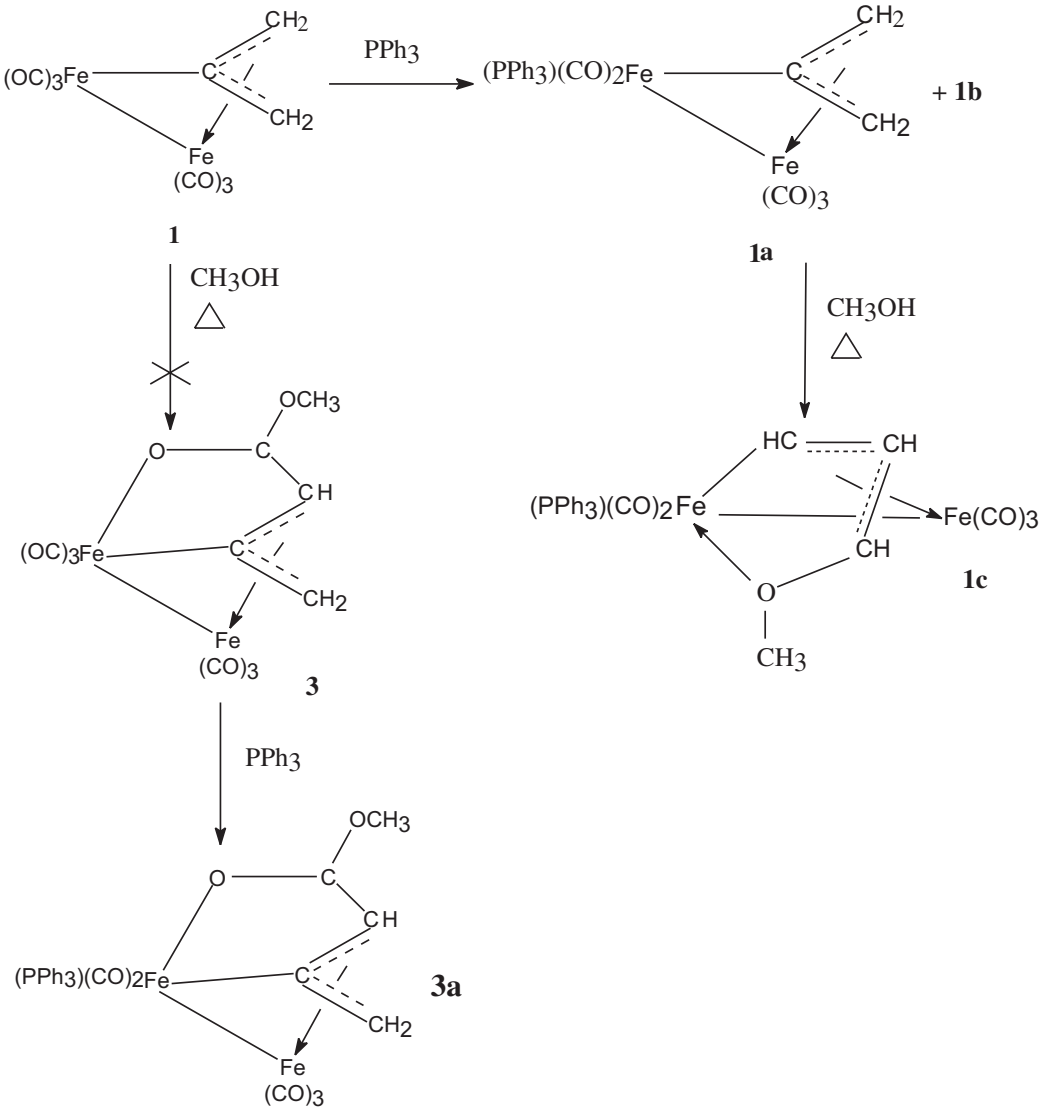
Reactions leading to complexes 1 and 3

As previously discussed, the reactions of $Fe_3(CO)_{12}$ with propargylic alcohol and propargyl chloride give, as the main products, complexes **1**, **3**, and **4** and much smaller amounts of the allenylidene complex **2**[7]. No unequivocal evidence, both for the structure of **1** and for its role in the reaction pathways leading to **3**, was obtained. As shown in Scheme 2, two hypotheses can be advanced: (*i*) **1** would be a fragmentation product derived from **2**; however, complex **2** was obtained in yields not allowing a reactivity study, only from the reactions of propargylic alcohol and propargyl chloride. It was observed only in trace amounts in other reactions leading to medium yields of **1**. This could represent indirect evidence for **2** being a labile intermediate in the formation of **1** (as a by-product) and of **3** in a direct reaction. (*ii*) An alternative possibility could be that **1** is an intermediate in the formation of **3**.

The formation of complexes **1** and **3** has been therefore taken into account. The results show that complexes **1** and **3** are obtained in medium yields starting from propargylic alcohol, propargyl chloride, trimethylsilyl propargyl alcohol, propargyloxytrimethylsilane, monopropargylamine, and propargyl acetate (see Table 1). These alkynes can release -C≡CCH_2OH or HC≡CCH_2-, three-carbon atom fragments that could rearrange (and uptake hydrogen atoms) to form the H_2C=C=CH_2 ligand observed in **1** and **1a**. In contrast, complexes **1** and **3** are not obtained from trimethylsilyl acetylene and 1,1-diphenyl-2-propyn-1-ol, which can release only C_2 fragments. The reaction of $Fe_3(CO)_{12}$ with 1,1-diphenyl-2-propyn-1-ol in the same conditions reported for the other alkyne ligands yields only two products in trace amounts (not collected). The reaction of $Fe_3(CO)_{12}$ with trimethylsilyl acetylene gives mostly $Fe_3(CO)_{12}$ and very small yields of a orange, yellow, and red bands showing IR

© 2006 NRC Canada

Scheme 4.



and NMR spectra different from those of **1** and of **3**. The "parent" alkynes forming complexes **1** and **3** are shown in Scheme 3.

Interestingly, 3-phenyl-2-propyn-1-ol, which would not easily release the C_6H_5 substituent, gives complexes **6** and **7**, which are the phenyl-containing homologues of **1** and **3**.

It is also worth noting that **1** and **3** are obtained from monopropargylamine: this also indicates that the NH_2 functionality can be lost. Finally, complex **3** is also obtained from propargyl acetate. Mathieu and co-workers (11) have described the synthesis of the acetate open-cluster derivative $Fe_3(CO)_{10}(PPh_2)[CHCCHC(OCH_3)O]$ containing a heterocyclic ring comparable with that of **3**. The complex was obtained from $[HFe_3(CO)_{11}]^-$ and $(CH_3COO)CH_2C{\equiv}CPPh_2$.

It is also interesting to observe that **1** (and **3**) are obtained when reacting propargylic alcohol and propargyl chloride both with $Fe_3(CO)_{12}$ and with $Fe(CO)_5$ in basic methanolic conditions. The intermediacy of the $[HFe_3(CO)_{11}]^-$ anion in these reactions can be hypothesized on the grounds of the following observations: (*i*) its formation from $Fe_3(CO)_{12}$ in the reaction conditions adopted was reported in the literature (1); (*ii*) its presence during the synthesis of $Fe_3(CO)_{12}$ starting from $Fe(CO)_5$ is well-established (12). It is also possible that, in the above reaction conditions, the radical anion $[Fe_3(CO)_{11}]^{\cdot-}$ (13) is present.

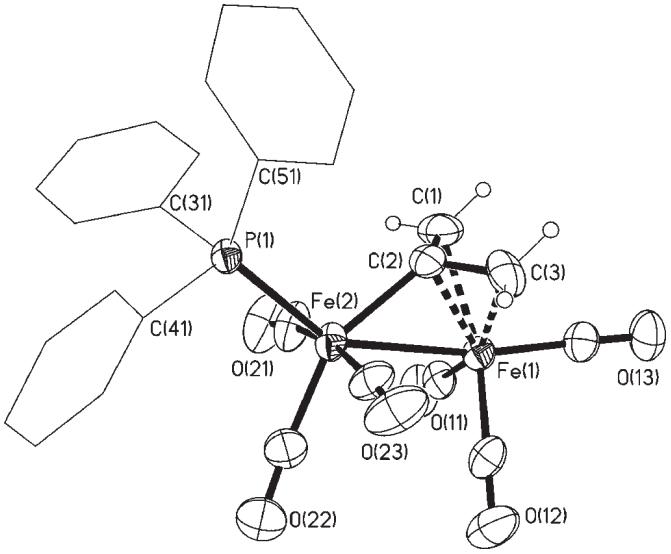
Reactions leading to 1a and 1b — Proposed structure of complex 1 on the basis of the X-ray structure of complex 1a

The reaction of complex **1** with triphenylphosphine leads to the monosubstituted **1a**, whose structure is discussed in the following, and to the disubstituted complex **1b** presumably bearing the two phosphine ligands on different iron atoms, as indicated by the ^{31}P NMR spectrum.

Complex **1**, when dissolved in heptane, heptane–toluene, or other solvents and kept at –30 °C, gives large and well-formed orange "crystals"; however, when the solvent is removed, even at low temperature, the crystals collapse quickly forming a thick oil. For **1** a structure is therefore proposed on the basis of analytical and spectroscopic data and on the

© 2006 NRC Canada

Fig. 1. ORTEP plot of $Fe_2(CO)_6(PPh_3)[\mu\text{-}\eta^3\text{-}(H_2CCCH_2)]$ (complex **1a**) with thermal ellipsoids (30% probability).



following observations: (*i*) **1** is formed from several alkynes that can loose a three-carbon atom fragment; (*ii*) in a recent report propargylic alcohol has been shown to react with triruthenium benzoquinoline complexes releasing a (coordinated) C_3H_4 unit (14), albeit different from that proposed for **1**; (*iii*) complex **1** shows a ^1H NMR spectrum indicating the presence of two nonequivalent CH_2 groups. Mass spectra of samples coming from reactions with different alkynes all showed a $P^+ = 348$ *m*/*z* corresponding to $Fe_2(CO)_7(C_3H_4)$. In the light of the structure of **1a** discussed in the following, we now think that the more probable structure is that shown in Scheme 3.

Reactions of complexes 1 and 1a with CH_3OH

Complex 1

These reactions have shown that under thermal conditions complex **1** does not react very easily with methanol. Only trace amounts of complex **3** were observed. Thus, complex **1** should be considered a side product, rather than an intermediate, in the formation of **3**.

Complex 1a

From this reaction, one can see that complex **1a** can add methanol, giving, however, a complex (**1c**) different from **3a**. For complex **1c**, we propose the structure shown in Scheme 4 on the basis of the analytical and spectroscopic results and by analogy with the previous reports of Mathieu and co-workers (11). Thus, complex **1a** is not an intermediate in the formation of the phosphine-substituted **3a**.

Reaction of complex 3 with PPh_3

The monosubstituted complex **3a** was isolated and characterized using spectroscopy; complex **3a** probably follows the behaviour of other ferrole-like complexes, where the phosphine substitution for CO occurs first at the iron atom σ bound to the organic ring (15).

Table 2. Some relevant bond distances (Å) and angles (°) for complex **1a**, $Fe_2(CO)_6(PPh_3)[\mu\text{-}\eta^3\text{-}(H_2CCCH_2)]$.

Bond distances (Å)	
Fe(1)—C(2)	1.952(5)
Fe(1)—C(3)	2.120(5)
Fe(1)—C(1)	2.123(6)
Fe(1)—Fe(2)	2.6479(10)
Fe(2)—C(2)	1.977(5)
Fe(2)—P(1)	2.2514(14)
P(1)—C(51)	1.824(4)
P(1)—C(31)	1.824(5)
P(1)—C(41)	1.835(5)
C(1)—C(2)	1.448(8)
C(2)—C(3)	1.384(8)
Bond angles (°)	
C(3)-C(2)-C(1)	112.5(6)
C(3)-C(2)-Fe(2)	119.4(5)
C(1)-C(2)-Fe(2)	117.9(5)

The crystal structure of 1a

The structure of **1a** is shown in Fig. 1 and significant distances and angles are given in Table 2. The complex is formed by two nonequivalent iron atoms, with an Fe—Fe distance of 2.648(1) Å.

The C_3H_4 ligand is coordinated both to Fe(1), as a formal $3e^-$ donor, and to Fe(2), as a formal $1e^-$ donor. Six COs are terminally bound to Fe(1) and to Fe(2), which is also bound to the PPh_3 ligand disposed cis with respect to C(2), in the less sterically and electronic demanding situation. When considering the C_3H_4 as a four-electron donor and the presence of an Fe—Fe bond, each iron atom would reach the 18-electron configuration. The Fe(2)-C(1)-C(2)-C(3) moiety deviates from planarity with a mean deviation of 0.10 Å. The Fe—C bond distances and their geometry agree with a formal description of a π interaction of Fe(1) with C(1)—C(2) and with C(2)—C(3) elongated double bonds and with a Fe(2)—C(2) σ interaction. This situation corresponds to a π-allyl moiety where a hydrogen atom is substituted by an iron atom. Allyl groups coordinated in this way are commonly found, especially in the nickel triad chemistry. Complex **1a** has been very presumably obtained upon simple substitution of a phosphine for a CO, suggesting a similar formula for **1**.[3]

Conclusions

The results obtained allow the unequivocal characterization of complex **1**. We have found that **1** is a by-product in the synthesis of **3**; it is presumably a fragmentation product of the allenylidenic complex **2**. Complex **1** does not react with methanol to give **3**. In contrast, **1a** gives a product (**1c**)

[3] Supplementary data for this article are available on the journal Web site (http://canjchem.nrc.ca) or may be purchased from the Depository of Unpublished Data, Document Delivery, CISTI, National Research Council Canada, Ottawa, ON K1A 0R6, Canada. DUD 5001. For more information on obtaining material refer to http://cisti-icist.nrc-cnrc.gc.ca/irm/unpub_e.shtml. CCDC 273281 contains the crystallographic data for this manuscript. These data can be obtained, free of charge, via http://www.ccdc.cam.ac.uk/conts/retrieving.html (Or from the Cambridge Crystallographic Data Centre, 12 Union Road, Cambridge CB2 1EZ, UK; fax +44 1223 336033; or deposit@ccdc.cam.ac.uk).

© 2006 NRC Canada

containing the fragments of methanol, albeit coordinated differently than in **3** or **3a**.

These results confirm the mechanism already proposed for the formation of **3** (see Scheme 2), that is, the intermediacy of complex **2** only. Formation of complexes containing methoxycarbonyl groups upon activation of CO under basic methanolic conditions seems to be a general trend. For example, recently we have observed that $Ru_3(CO)_{12}$ reacts with 1,4-dichloro-but-2-yne in basic methanolic conditions forming the complex $H_2Ru_3(CO)_9[H_2C{=}CC{\equiv}CC(=O)OCH_3]$ (16); the formation of this complex requires loss of chlorine and activation of CO. In our opinion, the mechanisms leading to this type of complex deserve further efforts towards being fully understood, especially in view of organometallic-mediated organic syntheses.

Last but not least, from the reactions described in this paper, complex **1a** was obtained. The structure of this complex is unprecedented and shows, once again, that alkynol-cluster chemistry may lead to unprecedented bonding modes for hydrocarbyls on metal clusters.

Acknowledgements

Financial support of this work was obtained (in part) from the Consorzio Interuniversitario Scienza e Tecnologia dei Materiali (INSTM) and from the Universita' del Piemonte Orientale, and from the Ministero per l'Istruzione, l'Università e la Ricerca (MIUR, Rome) as a part of the COFIN 2003 programme.

References

1. See, for example: S. Deabate, P.J. King, and E. Sappa. *In* Metal clusters in chemistry. Vol. 2. *Edited by* P. Braunstein, L.A. Oro, and P.R. Raithby. Wiley-VCH, Weinheim. 1999. Chap. 8. p. 796.
2. See, for example: J.P.H. Charmant, P. Crawford, P.J. King, R. Quesada-Pato, and E. Sappa. J. Chem. Soc. Dalton Trans. 4390 (2000).
3. G. Gervasio and E. Sappa. J. Organomet. Chem. **498**, 73 (1995).
4. See, for example: (*a*) J.P.H. Charmant, G. Davies, P.J. King, J.R. Wigginton, and E. Sappa. Organometallics, **19** (2000) 2330; (*b*) J.P.H. Charmant, P.J. King, R. Quesada-Pato, E. Sappa, and C. Schaefer. J. Chem. Soc. Dalton Trans. 46 (2001).
5. G. Gervasio and E. Sappa. Organometallics, **12**, 1458 (1993).
6. (*a*) G. Gervasio, D. Marabello, P.J. King, E. Sappa, and A. Secco. J. Organomet. Chem. **671**, 137 (2003);(*b*) G. Gervasio, D. Marabello, E. Sappa, and A. Secco. J. Organomet. Chem. **689**, 35 (2004).
7. G. Gervasio, D. Marabello, E. Sappa, and A. Secco. J. Organomet. Chem. **690**, 3755 (2005).
8. G. Gervasio, D. Marabello, and E. Sappa. J. Chem. Soc. Dalton Trans.1851 (1997).
9. G.M. Sheldrick. SHELXTL. Version 5.1 [computer program]. Bruker AXS Inc., Madison, Wisconsin. 1997.
10. SMART, SAINT, SADABS, and XPREP software for CCD diffractometers. Bruker AXS Inc., Madison, Wisconsin.
11. A. Elarraoui, J. Ros, R. Mathieu, and R. Yanez. J. Organomet. Chem. **678**, 117 (2003).
12. (*a*) R.B. King, F.G.A. Stone, R.S. Summitt, and W.E. Edgell. Inorg. Synth. **VII**, 193 (1965); (*b*) W. McFarlane, G. Wilkinson, and W. Hubel. Inorg. Synth. **VIII**, 181 (1966).
13. F. Ragaini, J.-S. Song, D.L. Ramage, G.L. Geoffroy, G.A.P. Yap, and A.L. Rheingold. Organometallics, **14**, 378 (1995).
14. J.A. Cabeza, I. del Rio, S. Garcia-Granda, V. Riera, and M. Suarez. Organometallics, **23**, 3501 (2004).
15. L.J. Todd, J.P. Huckey, J.R. Wilkinson, J.C. Huffman, and K. Folting. J. Organomet. Chem. **112**, 167 (1976).
16. G. Gervasio, D. Marabello, E. Sappa, and A. Secco. J. Organomet. Chem. **690**, 1594 (2005).

© 2006 NRC Canada

Determination of the location of naphthalene in the zeolite ZSM-5 host framework by solid-state $^{1}H/^{29}Si$ CP MAS NMR spectroscopy[1]

Colin A. Fyfe and Darren H. Brouwer

Abstract: The location of naphthalene in the zeolite ZSM-5 has been determined from solid-state $^{1}H/^{29}Si$ cross-polarization (CP) magic-angle-spinning (MAS) NMR data alone. With the peaks in the ^{29}Si spectrum assigned to the inequivalent Si sites in the zeolite from a two-dimensional INADEQUATE spectrum, the rates of cross polarization between the ^{1}H nuclei of the guest sorbate molecules and the ^{29}Si nuclei of the zeolite framework were used to determine the location of the naphthalene molecules by exploiting the proportional relationship between cross-polarization rate constants and $^{1}H/^{29}Si$ dipolar coupling second moments. The NMR structure determination was carried out on three different selectively deuterium-labeled naphthalene molecules (naphthalene-d_0, α-naphthalene-d_4, and β-naphthalene-d_4). The average of the molecule locations in agreement with all three sets of NMR data was found to be in excellent agreement with an existing single crystal XRD structure of the naphthalene–ZSM-5 complex.

Key words: solid-state NMR, cross polarization, zeolites, host–guest complexes, structure determination.

Résumé : On a déterminé la location du naphtalène dans le zéolite ZSM-5 en ne faisant appel qu'à des données de RMN à l'état solide, à l'angle magique de rotation et une polarisation croisée $^{1}H/^{29}Si$. Après avoir attribuer les pics du spectre de ^{29}Si aux sites de silicium inéquivalents de la zéolite en se basant sur un spectre bidimensionnel « INADEQUATE », on a utilisé les vitesses de polarisation croisée entre le noyau ^{1}H des molécules du sorbat invité et les noyaux de ^{29}Si du squelette de zéolite pour déterminer la location des molécules de naphtalène en exploitant la relation proportionnelle entre les constantes de vitesse de polarisation croisée et les deuxièmes moments du couplage dipolaire $^{1}H/^{29}Si$. On a déterminer la structure RMN sur trois molécules de naphtalènes marquées sélectivement de trois façons différentes (naphtalène-d_0, α-naphtalène-d_4, β-naphtalène-d_4). On a trouvé que les locations moyennes de la molécule dans les trois ensembles de données RMN sont en excellent accord avec une structure XRD sur un cristal unique qui a été déterminée antérieurement pour le complexe naphtalène–ZSM-5.

Mots clés : RMN à l'état solide, polarisation croisée, zéolites, complexes hôte–invité, détermination d'une structure.

[Traduit par la Rédaction]

Introduction

A full understanding of the interactions between guest species and host zeolite frameworks, central to the synthesis and applications of zeolites, requires detailed structures for these complexes. For most zeolites, structure determination by X-ray diffraction (XRD) is limited because of their microcrystalline nature and the weak contribution, relative to the framework, of the guest species to the X-ray scattering intensity. Solid-state NMR spectroscopy offers an alternative and complementary method for structure determinations of zeolite host–guest complexes.

We have developed an approach to determine the locations of rigid organic sorbate molecules in highly siliceous zeolite frameworks from solid-state $^{1}H/^{29}Si$ cross-polarization (CP) magic-angle-spinning (MAS) NMR data (1, 2).[4] The peaks in a high-resolution ^{29}Si MAS NMR spectrum of the zeolite framework are first assigned to the inequivalent Si sites in the structure by performing (3) and analyzing (4, 5) a two-dimensional ^{29}Si INADEQUATE correlation experiment (6, 7). The relative rates of $^{1}H/^{29}Si$ cross polarization measured between the ^{1}H nuclei of the sorbate molecules and the ^{29}Si nuclei of the zeolite framework (8) are then used to determine the location of the sorbate molecule by exploiting the proportional relationship (9) that exists between these experimentally measured CP rate constants and calculated $^{1}H–^{29}Si$ dipolar coupling second moments (10).

This proportional relationship between CP rate constants and second moments in zeolite–sorbate complexes was first demonstrated for the high-loaded *p*-xylene–ZSM-5 complex (1, 2), a complex with a previously known structure, and then used to determine the previously unknown location of

Received 15 June 2005. Published on the NRC Research Press Web site at http://canjchem.nrc.ca on 30 March 2006.

C.A. Fyfe[2] and D.H. Brouwer.[3] Department of Chemistry, Room 300, 6174 University Boulevard, University of British Columbia, Vancouver, BC V6T 1Z3, Canada.

[1]This article is part of a Special Issue dedicated to Professor Arthur Carty.

[2]Corresponding author (e-mail: fyfe@chem.ubc.ca).
[3]Present address: National Research Council of Canada, Steacie Institute for Molecular Sciences, 100 Sussex Drive, Ottawa, ON K1A OR6, Canada.

[4]C.A. Fyfe and D.H. Brouwer. Submitted for publication.

 doi:10.1139/V06-009 © 2006 NRC Canada

p-xylene in the low-loaded complex with ZSM-5 (2), which was shown to be correct by a subsequent structure determination from single crystal XRD data.[5] An improved protocol for this structure determination approach is described in detail in footnote 4 where the structure of the low-loaded *p*-dichlorobenzene–ZSM-5 complex was determined by solid-state NMR and again shown to be in excellent agreement with an existing single crystal XRD structure. It was also shown that this approach is quite robust, being relatively insensitive to temperature and the exact coordinates of the zeolite framework. We have also shown that paramagnetic molecular oxygen in the vacant spaces of the zeolite–sorbate complexes can give rise to severe line broadening of the ^{29}Si spectra (11) and that rapid ^{1}H $T_{1\rho}$ relaxation can lead to complications in the measurement of the CP rate constants (8).

In the present paper, we describe the determination of the exact location of naphthalene in zeolite ZSM-5 from ^{1}H/^{29}Si CP MAS NMR data using the general method that we have developed. Since a reliable single crystal XRD structure to which these results can be compared has been previously reported (12), this investigation serves to further evaluate the reliability of the approach There are also two lower-quality structures of the naphthalene–ZSM-5 complex derived from powder XRD, which are in general agreement with the single crystal XRD structure (13, 14).

Naphthalene is a very appropriate sorbate molecule with which to further evaluate the solid-state NMR structure determination method since it is a rigid molecule and is a significant departure, in terms of molecular structure, from the previously studied *p*-disubstituted aromatic molecules (2).[4] In addition, it is possible to obtain selectively deuterated naphthalenes so that ^{1}H/^{29}Si CP MAS NMR data can be collected on systems that have differently localized ^{1}H polarization sources, increasing the amount of structural information available from the solid-state NMR data. The experiments and analyses have been carried out on ZSM-5 complexes with three types of naphthalene molecule: completely protonated naphthalene (naph-d_0, **1**) and two complementary selectively deuterated naphthalenes (α-naph-d_4 (**2**) and β-naph-d_4 (**3**)). The polarization transfer profile to the framework ^{29}Si nuclei will be unique to each naphthalene and the acceptable locations will be those that best agree with the ^{1}H/^{29}Si CP MAS NMR data sets from all three naphthalene–ZSM-5 complexes (Scheme 1).

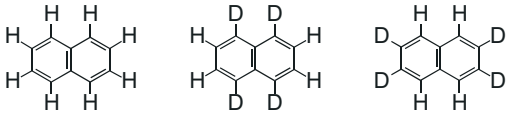
There is also practical interest in the structure of the naphthalene–ZSM-5 complex since the acid form of ZSM-5 has been reported to be a good catalyst for the shape-selective alkylation of naphthalene with methanol to give 2-methylnaphthalene, which is a good starting material for vitamin K synthesis (14).

Experimental section

Sample

The selectively deuterated naphthalene molecules (α-naphthalene-d_4 and β-naphthalene-d_4) were synthesized according to the procedure of Davis and Garnett (15), using a homogeneous $PtCl_4^-$ catalyst to selectively exchange the H or D atoms in the β positions of naphthalene and naphthalene-d_8 with D_2O and H_2O, respectively. The solutions for these selective exchanges consisted of 0.015 mol/L K_2PtCl_4 and 0.02 mol/L NaCl in 1:1 mixtures of H_2O–CH_3COOH or D_2O–CH_3COOD (made from 3:1 mixtures of H_2O or D_2O with acetic anhydride). A typical exchange reaction was carried out by mixing 0.4 g of naphthalene-d_8 or naphthalene-d_0 with 16 mL of the appropriate exchange solution and heating at 70 °C for about 24 h, after which the naphthalene was isolated by quenching with water and filtering. The exchanges were repeated four times with fresh solutions. Multiple exchanges of naphthalene-d_8 (Aldrich) with the $PtCl_4^-$ in H_2O–CH_3COOH solution resulted in α-naphthalene-d_4 as the β-deuterium atoms were selectively exchanged with protons. Likewise, multiple exchanges of naphthalene-d_0 (Aldrich) with $PtCl_4^-$ in D_2–CD_3COOD solution resulted in β-naphthalene-d_4 as the β protons were selectively exchanged with deuterium. The resulting samples were analyzed by ^{1}H solution NMR and mass spectrometry to confirm that the ^{1}H nuclei were primarily located in the desired locations and the majority of the molecules had three or four protons per molecule (see Supplementary data, Table S1).[6]

Scheme 1. Naphthalene molecules.



naph-d_0 **1** α-naph-d_4 **2** β-naph-d_4 **3**

A very highly siliceous and crystalline sample of ZSM-5 was used, which had peak widths of about 0.1 ppm in the ^{29}Si MAS NMR spectrum (16). The zeolite–naphthalene complexes had a maximum loading of four molecules per unit cell and were prepared by mixing an excess of the solid organic with about 200 mg of calcined zeolite powder in a prescored glass ampoule. The ampoule was evacuated on a vacuum line, flame-sealed, and then placed in an oven at between 80 and 100 °C for at least 12 h to equilibrate.

Solid-state NMR

Solid-state NMR experiments were carried out on a Bruker AVANCE DSX-400 NMR spectrometer operating at frequencies of 400.13 MHz for ^{1}H and 79.495 MHz for ^{29}Si, using a Bruker double-frequency CP MAS probe modified with a standard 7 mm stator system from Doty Scientific. ^{29}Si chemical shifts were referenced to tetramethylsilane using Q_8M_8 as a secondary reference (17). Low-temperature MAS was achieved by using precooled nitrogen gas as the bearing gas and room temperature air as the drive gas with the temperature controlled and monitored by a heater–thermocouple system in the probe. The Hartmann–Hahn CP match condition for ^{1}H/^{29}Si CP was initially set up on the

[5] C.A. Fyfe, A.R. Lewis, and W. Schweiger. Manuscript in preparation.

[6] Supplementary data for this article are available on the journal Web site (http://canjchem.nrc.ca) or may be purchased from the Depository of Unpublished Data, Document Delivery, CISTI, National Research Council Canada, Ottawa, ON K1A 0R6, Canada. DUD 5009. For more information on obtaining material refer to http://cisti-icist.nrc-cnrc.gc.ca/irm/unpub_e.shtml.

© 2006 NRC Canada

Q_8M_8 reference sample and subsequently checked on the sample itself. The power levels corresponding to the maximum of a relatively broad matching profile were approximately 30 kHz for both ^{1}H and ^{29}Si. ^{1}H decoupling applied during the acquisition time was found to have no noticeable effect on the width of the peaks in the ^{29}Si spectrum, even at the lowest temperatures used, so it was not applied (with the exception of the mixing and evolution times in the ^{29}Si INADEQUATE experiment). All spectra were collected using a spinning rate of approximately 2 kHz. Additional experimental details for the individual spectra are provided in the figure captions.

Data analysis

The deconvolution of the spectra, fitting of the CP and CP drain curves, and the determination of the guest molecule locations were performed using programs written for Mathematica version 3.0 (18).

Results and discussion

To determine the best temperature at which to carry out the experiments, a series of ^{29}Si MAS NMR spectra of the ZSM-5–naph-d_0 complex were collected at temperatures between 180 and 360 K, and selected spectra between 180 and 300 K are displayed in Fig. 1. The spectra are not as well-resolved as previous examples (2),[4] and the application of ^{1}H decoupling during the acquisition did not improve the resolution. The line broadening of the ^{29}Si resonances is most likely a result of short T_2 relaxation times arising from the presence of paramagnetic molecular oxygen in the zeolite cavities (11), with the temperature dependence of the line broadening reflecting the changing motions of the oxygen molecules. It should also be noted that the temperature dependence of the line broadening is different from ZSM-5 complexes with *p*-disubstituted aromatics in which the highest resolution is observed at room temperature and very broad spectra are observed around 200 K (11),[4] suggesting that the naphthalene molecules cause a different motional behavior of the oxygen molecules in the zeolite cavities.

The peaks are best resolved at 220 K, so all subsequent experiments were carried out at this temperature. In terms of spectral resolution, these spectra are on the limit from which one could hope to determine a reliable sorbate–zeolite framework structure by solid-state ^{1}H/^{29}Si CP MAS NMR, since only 5 of the 12 ^{29}Si peaks can be resolved with any reliability at all. However, by using data from the different deuterated naphthalene molecules, the number of independent observations is increased, thus increasing the reliability of the structure determination.

The assignment of the ^{29}Si spectrum at 220 K was accomplished using the two-dimensional INADEQUATE experiment (Fig. 2) with a previously described algorithm that was developed to obtain all possible assignment sets consistent with the 2D data (4, 5). Due to the large number of overlapping peaks in the present two-dimensional INADEQUATE spectrum, there are 34 possible sets of peak assignments that are consistent with the observed correlations. However, only three of these assignments are consistent with the assignments for other zeolite–sorbate complexes, with the low-field peaks assigned to Si8 and Si2 and a high-field peak

Fig. 1. Quantitative variable-temperature ^{29}Si MAS NMR spectra of the ZSM-5–naph-d_0 complex. For each spectrum, 16 scans were acquired with 45° pulses, 5 s recycle delay, and no ^{1}H decoupling applied during acquisition. The peak assignments shown for the spectrum at 220 K are from the INADEQUATE experiment shown in Fig. 2.

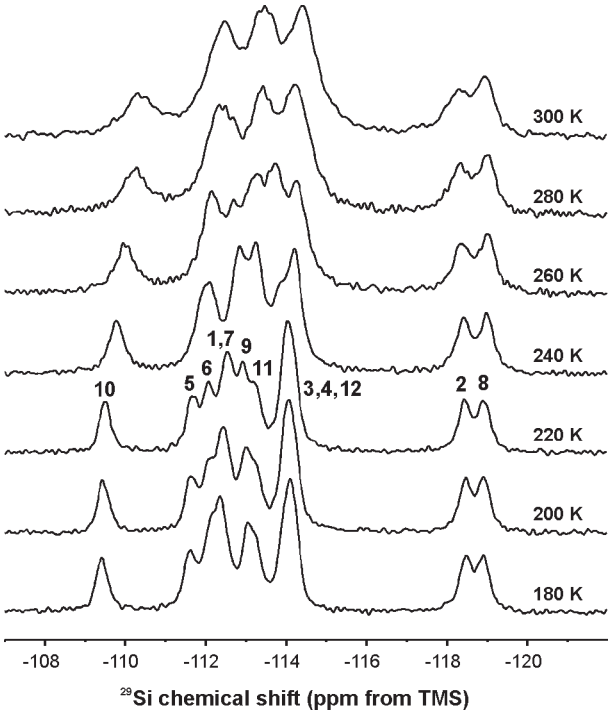
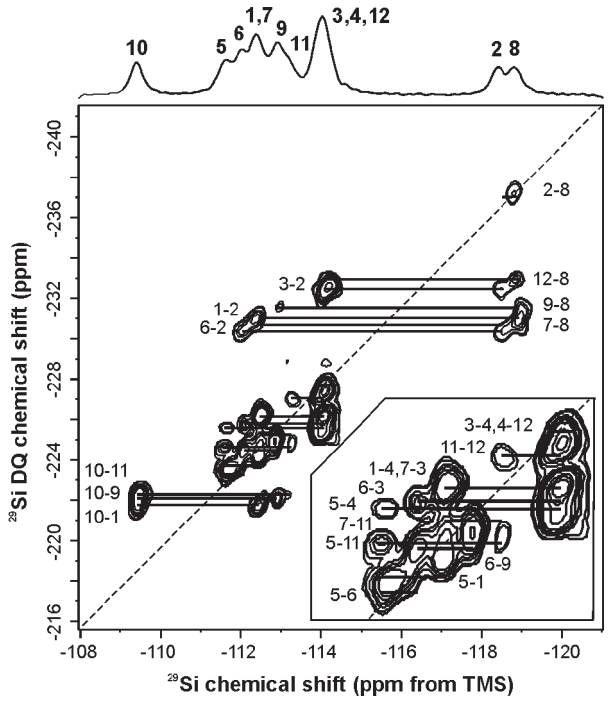


Fig. 2. Two-dimensional ^{29}Si INADEQUATE spectrum of the ZSM-5–α-naph-d_4 complex. See text for a discussion of the peak assignments. Forty experiments, each with 3200 scans and 2 s recycle delay, were acquired in t_1. The sweep widths in f_2 and f_1 were 1040 and 2080 Hz, respectively. The echo delay time during the double quantum preparation period was 14.4 ms.



© 2006 NRC Canada

assigned to Si10 (6).[4] Furthermore, only these three assignments show a strong correlation between ^{29}Si chemical shifts and mean Si—Si distances (19), using the ZSM-5–naphthalene single crystal structure data (12) as the source for the Si—Si distances. The three assignment sets are identical with respect to the identity of all of the resolved peaks, but are different with respect to the identity of the unresolved peaks at –112.4 and –114.0 ppm, which could be assigned to {1,7} and {3,4,12} or {1,12} and {3,4,7} or {1,3} and {4,7,12}. During the structure determination (see the following), all three assignment sets were tested and the assignment presented in Fig. 2 was found to give the best agreement between the predicted and experimental ^{1}H/^{29}Si cross-polarization spectra.

With the peaks in the ^{29}Si spectrum assigned to specific Si sites in the zeolite framework, it is now possible to use the ^{1}H/^{29}Si CP MAS NMR experiment to probe the locations of the ^{1}H nuclei with respect to these various Si sites, since the magnetization is transferred in a distance-dependent manner. In Fig. 3, the ^{1}H/^{29}Si CP MAS NMR spectra (collected at 220 K and with a contact time of 10 ms) for ZSM-5 loaded with naph-d_0, α-naph-d_4, and β-naph-d_4 are compared to a quantitative ^{29}Si MAS NMR spectrum. The relative intensities in these CP spectra reveal that some ^{29}Si nuclei are clearly closer to the source ^{1}H nuclei than others. For example, in all the CP spectra, the peaks for Si2 and Si8 are enhanced and that of Si10 is discriminated against, indicating that the naphthalene molecules are not located in the zigzag channels, but rather somewhere in the straight channels, since Si2 and Si8 are on the surface of the straight channel and Si10 is found on the surface of the zigzag channel. Furthermore, there are significant differences between the CP spectra when the ^{1}H nuclei are in different positions of the naphthalene molecules. For example, Si2 is enhanced more than Si8 for the α-naph-d_4 sample, while the signals for Si5 and Si6 are quite weak for the sample. It should be noted that the relative intensities of the peaks in the α- and β-naph-d_4 spectra cannotbe directly compared with those in the naph-d_0 spectrum owing to the larger number of protons involved in the interactions in the latter case.

The ^{29}Si relaxation times were also measured for the various ^{29}Si peaks (see Table 1). The spectra with the poorest resolution (Figs. 3*b* and 3*d*) have the shortest ^{29}Si T_2 relaxation times, indicating that the line broadening of the ^{29}Si resonances is a relaxation effect, most likely owing to paramagnetic molecular oxygen (11). The differences in the spectral resolution for these three samples may have arisen from the exact loading of the naphthalene molecules or the concentration of oxygen in the zeolite cavities. For all three samples, Si8 consistently has a much longer ^{29}Si T_1 relaxation time compared with the other Si peaks, especially compared with Si5 and Si6. If paramagnetic molecular oxygen is the relaxation source, this observation would suggest that the oxygen molecules are in the zigzag channels and the naphthalene molecules are in the channel intersection, as was previously found for the pDBB–ZSM-5 structure (11).

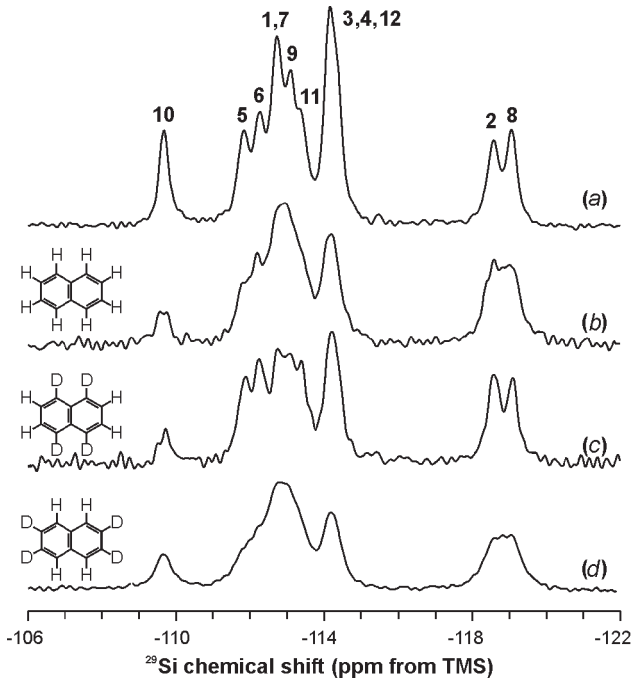
There are subtle details in the measurement of ^{1}H/^{29}Si CP rate constants in zeolite–sorbate complexes that must be accounted for (8). Normally, the rate of ^{1}H/^{29}Si cross polarization is measured by performing a variable contact time ^{1}H/^{29}Si CP MAS experiment and plotting the ^{29}Si peak areas as functions of the contact time. The contact time dependence of the S spin magnetization during $I \rightarrow S$ cross polarization (where the I spins (^{1}H) are abundant and the S spins (^{29}Si) are rare) is described by the following expression (20):

$$[1] \qquad S_{CP}(t) = I_0 \frac{k_{IS}}{(k_{IS} + k_S) - k_I}(e^{-k_I t} - e^{-(k_{IS}+k_S)t})$$

where k_I and k_S are the rate constants for spin-lock relaxation ($T_{1\rho}$) of the I and S spins, respectively, k_{IS} is the rate of cross polarization between the I and S spins, and I_0 reflects the initial magnetization of the I spins. For most systems, the increase in the S spin magnetization is governed by the CP rate constant k_{IS} (assuming k_S is small), and its decay is governed by k_I, the $T_{1\rho}$ relaxation of the I spins. This normal situation is termed the "fast CP regime". However, there exists a "slow CP regime" (21) in which the rate of I spin $T_{1\rho}$ relaxation is fast compared with the rate of $I \rightarrow S$ cross polarization ($k_I > k_{IS}$) such that the dynamics of the S spin magnetization in the CP curve is reversed from the usual assumptions: the rate of growth of the S spin magnetization is governed by k_I, while its decay is governed by $k_{IS} + k_S$.

Due to the presence of paramagnetic oxygen in the cavities of the zeolite–sorbate complexes (11), ^{1}H and ^{29}Si spin lock relaxation can occur quite rapidly, while the rate of ^{1}H/^{29}Si cross polarization can be slow since the dipolar interactions between the ^{1}H nuclei of the sorbate molecules and the ^{29}Si nuclei of the zeolite framework are quite weak. It is important to recognize the slow CP regime in order for

Fig. 3. Comparison of the ^{1}H/^{29}Si CP MAS NMR spectra to the quantitative ^{29}Si MAS NMR spectrum at 220 K. (*a*) Quantitative ^{29}Si MAS NMR spectrum of ZSM-5–α-naph-d_4 (64 scans, 12 s recycle delay, 90° pulses); ^{1}H/^{29}Si CP MAS NMR spectra of ZSM-5 loaded with (*b*) naph-d_0, (*c*) α-naph-d_4, and (*d*) β-naph-d_4 (10 ms contact times, 320–400 scans, 1 or 2 s recycle delays). ^{1}H decoupling was not applied during acquisition.



© 2006 NRC Canada

Table 1. NMR data for the ZSM-5–naphthalene complexes.

	Si8	Si2	Si6	Si5	Si10	Si4, Si12, Si3	Si11, Si9, Si1, Si7
naph-d_0							
Shift (ppm)[a]	–119.2	–118.7	–112.3	–111.9	–109.8	–114.5, –114.3, –114.2	–113.4, –113.1, –112.8, –112.8
Width (Hz)[a]	35.8	37.0	33.1	33.7	29.8	27.2, 27.2, 27.2	35.4, 35.4, 39.0, 39.0
T_1 (s)[b]	2.4	1.8	1.2	1.5	1.5	1.2	1.6
T_2 (ms)[b]	14.0	14.0	18.4	21.8	31.0	25.6	17.4
$T_{1\rho}$ (ms)[b]	157	110	111	112	142	140	133
k_{IS} (s^{-1})[c]	12.6	13.0	8.9	7.7	6.2	3.1	9.6
k_{IS}' (s^{-1})[c]	23.7	20.1	14.2	9.4	8.5	10.0	16.8
α-naph-d_4							
Shift (ppm)[a]	–119.1	–118.6	–112.3	–111.8	–109.7	–114.4, –114.2, –114.1	–113.4, –113.1, –112.7, –112.7
Width (Hz)[a]	24.9	28.6	28.6	28.9	22.9	22.3, 22.3, 22.3	29.3, 29.3, 28.1, 28.1
T_1 (s)[b]	3.8	2.3	1.5	1.8	2.1	1.7	2.2
T_2 (ms)[b]	29.2	23.8	24.0	26.9	47.0	31.6	29.0
$T_{1\rho}$ (ms)[b]	325	180	159	159	257	239	246
k_{IS} (s^{-1})[c]	4.8	7.2	6.4	6.2	2.6	3.9	4.3
k_{IS}' (s^{-1})[c]	30.5	39.0	35.4	28.6	10.0	18.4	23.0
β-naph-d_4							
Shift (ppm)[a]	–119.1	–118.6	–112.2	–111.8	–109.7	–114.3, –114.1, –114.0	–113.3, –113.0, –112.7, –112.7
Width (Hz)[a]	43.9	42.1	39.9	40.6	36.9	34.2, 34.2, 34.2	43.8, 43.8, 47.1, 47.1
T_1 (s)[b]	2.5	1.5	1.2	1.1	1.4	1.2	1.6
T_2 (ms)[b]	13.6	17.4	21.3	25.1	31.2	26.2	18.9
$T_{1\rho}$ (ms)[b]	170	114	111	114	124	144	136
k_{IS} (s^{-1})[c]	9.8	7.2	4.8	4.1	5.2	4.2	7.5
k_{IS}' (s^{-1})[c]	25.9	19.6	12.7	8.9	14.0	10.3	20.1

[a]Spectrum fitting parameters determined from a quantitative ^{29}Si MAS NMR spectrum.
[b]Relaxation parameters determined from ^{29}Si saturation recovery (T_1), spin echo (T_2), and spin-locking ($T_{1\rho}$) experiments.
[c]CP rate constants determined from ^{1}H/^{29}Si CP drain (k_{IS}) and standard CP (k_{IS}') experiments.

the measured CP rate constants to be correct, as an analysis assuming normal fast CP may lead to erroneous measurements.

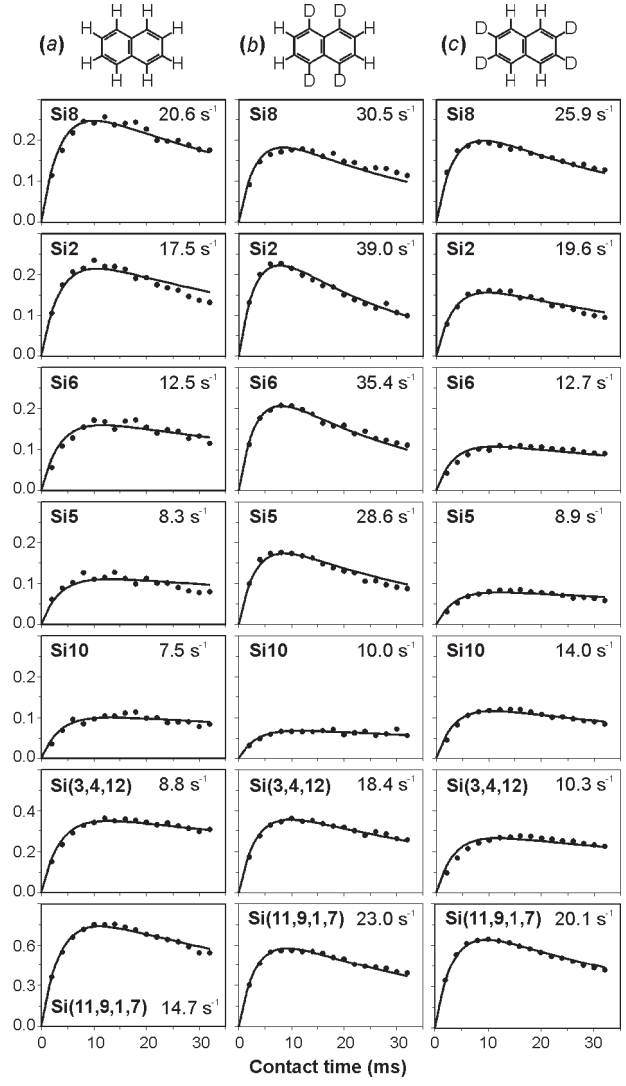
A series of ^{1}H/^{29}Si CP MAS NMR experiments at varying contact times were carried out on the three ZSM-5–naphthalene complexes at 220 K. The intensities for each Si peak were extracted, using peak positions and widths determined from quantitative ^{29}Si spectra, and plotted as functions of the contact time as shown in Fig. 4. There are a number of characteristics of these CP curves that indicate the CP dynamics are in the slow CP regime. Firstly, the CP signal intensities are only on the order of about 20% of those obtained in a quantitative ^{29}Si spectra (rather than being enhanced by up to a factor of $\gamma_H/\gamma_{Si} = 5$), indicating that the CP process is quite inefficient. Furthermore, all of the curves reach their maximum intensities at approximately the same contact time, indicating that the rate of growth of the curves is governed by k_I, the ^{1}H $T_{1\rho}$ relaxation time, which is the same for each curve since all ^{29}Si nuclei are polarized from the same ^{1}H source. An additional characteristic of the slow CP regime is that the maximum intensities of the curves vary. This arises mainly from the varying CP rate constants since the preexponential term in eq. [1] is largely determined by k_{IS} in the slow CP regime, assuming the ^{29}Si nuclei are polarized from the same ^{1}H source such that I_0 and k_I are the same for each curve. The final characteristic is that the rates of decay of the CP curves vary, indicating the slow CP regime since these rates of decay are governed by the different CP rate constants, and perhaps different ^{29}Si $T_{1\rho}$ relaxation times.

The CP rate constants for each Si peak were extracted from the CP curves presented in Fig. 4 by fitting the data to eq. [1], assuming the spin dynamics were in the slow CP regime, neglecting the contribution from ^{29}Si $T_{1\rho}$ relaxation ($k_S = 0$ s^{-1}), and using identical values of I_0 and k_I for all CP curves. In all three samples, the ^{1}H $T_{1\rho}$ relaxation is quite rapid ($k_I \sim 300$ s^{-1}; $T_{1\rho} \sim 3$ ms) compared with the CP rate constants ($k_{IS} \sim 10$ s^{-1}), clearly indicating the slow CP regime. However, even when the slow CP regime is correctly recognized, it is difficult to obtain absolute values for the CP rate constants from fits to standard CP curves, especially when $k_I < k_{IS} \approx k_S$, since k_{IS} is highly correlated to I_0, the contribution from ^{29}Si $T_{1\rho}$ relaxation (k_S) is ignored, and because it is difficult to obtain reliable data at very long contact times. Consequently, the CP rate constants obtained from these CP curves are considered to be relative values and are denoted by k_{IS}'.

To circumvent these potential problems, we have found that absolute CP rate constants in zeolite–sorbate complexes are best measured with ^{1}H/^{29}Si CP "drain" or "depolarization" experiments (22, 23), when possible (8). The dynamics of the S spin magnetization during a cross-polarization drain experiment are described by an exponential decay:

© 2006 NRC Canada

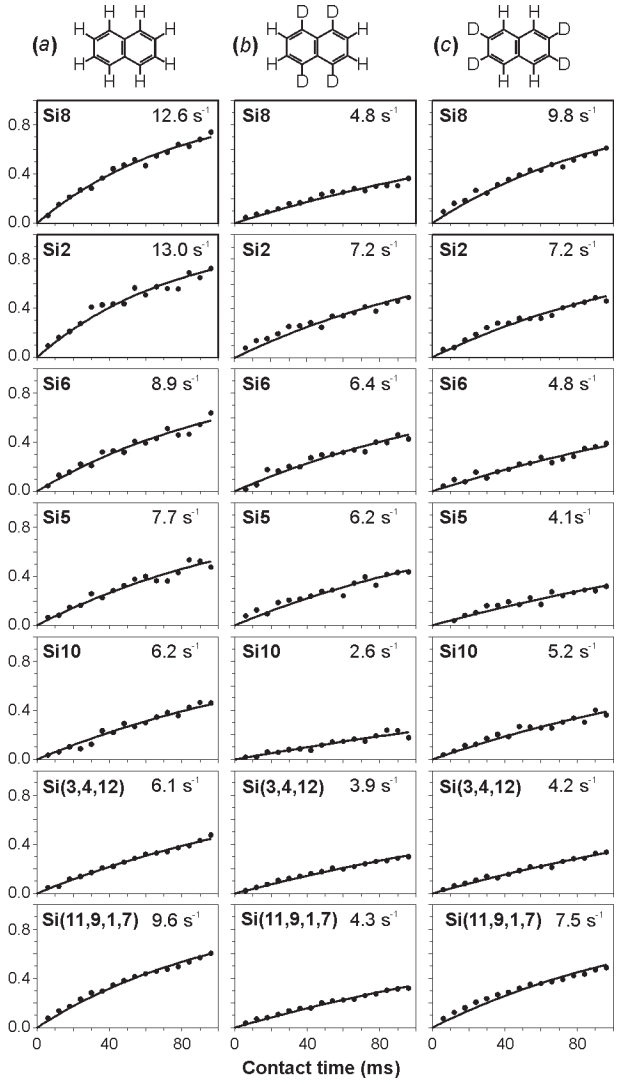
Fig. 4. $^1H/^{29}Si$ cross-polarization curves for the ZSM-5–naphthalene complexes at 220 K: (*a*) naph-d_0; (*b*) α-naph-d_4; and (*c*) β-naph-d_4. The signal intensities are plotted as S_{CP}/S_Q, where S_{CP} is the cross-polarization intensity and S_Q is the intensity of the peaks in the corresponding quantitative ^{29}Si MAS NMR spectrum. The curves were fit to eq. [3] (with $k_S = 0$) using the relative CP rate constants (k_{IS}') indicated and the following I_0 and k_I values: (*a*) $I_0 = 3.66$, $k_I = 275\ s^{-1}$ ($T_{1\rho} = 3.6$ ms); (*b*) $I_0 = 2.34$, $k_I = 303\ s^{-1}$ ($T_{1\rho} = 3.3$ ms); (*c*) $I_0 = 2.89$, $k_I = 300\ s^{-1}$ ($T_{1\rho} = 3.3$ ms). At each contact time, between 320 and 400 scans were collected with a recycle delay of 1 or 2 s.



$$[2] \qquad S(t) = S(0)e^{-(k_S + k_{IS})t}$$

where $S(0)$ is the initial magnetization of the S spins. The exponential decay resulting from the CP drain experiment without the contact pulse applied on the I spins ("reference" experiment, S_0) is due entirely to S spin $T_{1\rho}$ relaxation and has the rate constant k_S since $k_{IS} = 0$. The exponential decay resulting from the CP drain experiment with the contact pulse applied on the I spins (drain experiment, S_d) has the rate constant $k_{IS} + k_S$. The analysis of the CP drain dynamics can be simplified by plotting the data as a normalized difference plot (22), $\Delta S/S_0$, where $\Delta S = S_0 - S_d$, such that the CP rate constant is the only variable in the fit to the data.

Fig. 5. Normalized difference cross-polarization drain curves for the ZSM-5–naphthalene complexes at 220 K: (*a*) naph-d_0; (*b*) α-naph-d_4; and (*c*) β-naph-d_4. The signal intensities are plotted as $\Delta S/S_0$. The curves were fit to eq. [3] using the rate constants indicated. At each contact, reference and drain spectra were acquired with 48 scans with a 12 s recycle delay.



$$[3] \qquad \Delta S/S_0 = 1 - e^{-k_{IS}t}$$

Absolute values for the cross-polarization rates are thus obtained from these normalized CP drain curves, since the contributions from I_0 and both I and S $T_{1\rho}$ relaxation are removed

A series of $^1H/^{29}Si$ CP drain experiments at varying contact times were carried out on the three ZSM-5–naphthalene complexes at 220 K. The intensities for each Si peak were extracted using peak positions and widths determined from quantitative ^{29}Si spectra, and plotted as functions of the contact time as shown in Fig. 5. These curves were fit to eq. [3] to obtain absolute values for the CP rate constants, denoted as k_{IS}. All of the fitting parameters are summarized in Table 1. Although the CP rate constants obtained from both the

© 2006 NRC Canada

$^1H/^{29}Si$ CP and CP drain experiments could potentially be used for structure determination,[4] only the values determined from the CP drain data were subsequently used in the present work to determine the locations of naphthalene molecules in ZSM-5, since these values are considered to be more reliable.

The basis of the strategy to determine the locations of organic guest molecules in host zeolite frameworks from $^1H/^{29}Si$ cross-polarization experiments is the relationship between the measured CP rate constants and the $^1H—^{29}Si$ internuclear distances, via the heteronuclear second moments (M_2) of the dipolar line shapes (9).

$$[4] \qquad k_{IS} \propto M_2 \propto \sum r_{IS}^{-6}$$

If both the I and S nuclei are spin –1/2, the heteronuclear second moment for a powder can be calculated according to Van Vleck (10) as a pair-wise summation of the inverse sixth powers of the $I—S$ internuclear distances (in units of Hz^2).

$$[5] \qquad M_2 = \left(\frac{1}{2\pi}\right)^2 \frac{4}{5}\left(\tfrac{1}{2}\gamma_I\gamma_S\hbar\frac{\mu_0}{4\pi}\right)^2 \sum \frac{1}{r_{IS}^6}$$

The strategy for determining the guest molecule locations in host zeolite frameworks is essentially to find all possible locations of the guest molecule for which the condition in eq. [4], the proportionality between the set of experimental $^1H/^{29}Si$ CP rate constants and the set of heteronuclear second moments calculated from the H—Si distances, is satisfied (1, 2).[4]

Using the approach outlined in footnote 4, the void space of the ZSM-5 framework was searched for locations of the naphthalene molecules that (*a*) were physically reasonable, (*b*) had a strong linear correlation between the experimental CP rate constants and the calculated second moments, and (*c*) gave good agreement between experimental and the intensities of the groups of overlapping peaks predicted from the linear correlation between k_{IS} and M_2. The last condition was tested for each of the three possible sets of peak assignments that differed only in the identities of the overlapping peaks.

The coordinates for the ZSM-5 framework were taken from the single crystal XRD structure of the ZSM-5–naphthalene complex determined by van Koningsveld and Jansen (12). It should be noted that we have previously shown that it is not necessary to have the exact zeolite framework structure for the structure determination to be successful.[4] For the geometry of the naphthalene molecules, the C—H and C—C bond lengths were assumed to be 1.00 and 1.39 Å, respectively, while the C-C-C and H-C-C angles were assumed to be 120°. The locations of the rigid guest molecules are defined by six parameters: x, y, and z are fractional atomic coordinates of the centre of the molecule, and ϕ, θ, and ψ are Euler angles describing the rotational orientation of the molecule, as described in footnote 4.

Initial tests revealed that high degrees of linear correlation between k_{IS} and M_2 only existed for locations near the intersection of the straight and zigzag channels. Therefore, this region was investigated in detail with a total of 9.6×10^6 locations of the naphthalene molecules tested in the range $0.45 \le x \le 0.55$, $0.10 \le y \le 0.25$, and $-0.09 \le z \le 0.03$, in steps of 0.2 Å, and with Euler rotations of $20° \le \phi \le 80°$, $50° \le \theta \le 130°$, and $-40° \le \psi \le 40°$ in steps of 3° (ϕ) or 5° (θ and ψ). CP rate constants obtained from the $^1H/^{29}Si$ CP drain experiments were used. Structure determinations were performed for the three individual data sets of $^1H/^{29}Si$ CP drain experiments on the different deuterated naphthalene molecules. Locations were selected that had all atoms of the naphthalene molecule >2 Å from the zeolite framework atoms, gave a linear correlation of $r^2 \ge 0.96$ between experimental k_{IS} and calculated M_2 values, and predicted the intensities of the groups of overlapping peaks within the 95% prediction intervals. The intersection of the resulting three sets of naphthalene locations yielded the locations that are consistent across all three sets of cross polarization data.

Fig. 6. Distributions of the locations of naphthalene in ZSM-5 for naph-d_0 (squares), α-naph-d_4 (circles), and β-naph-d_4 (triangles), which are consistent with the $^1H/^{29}Si$ CP drain data (with $r^2 \ge 0.96$). The black diamonds indicate the distribution of locations that are consistent with *all three* sets of data. The arrows indicate the average of these locations that are consistent with all three sets of data (x = 0.492 ± 0.005, y = 0.199 ± 0.014, z = –0.040 ± 0.10, ϕ = 46° ± 3°, θ = 94° ± 6°, and ψ = 1° ± 8°).

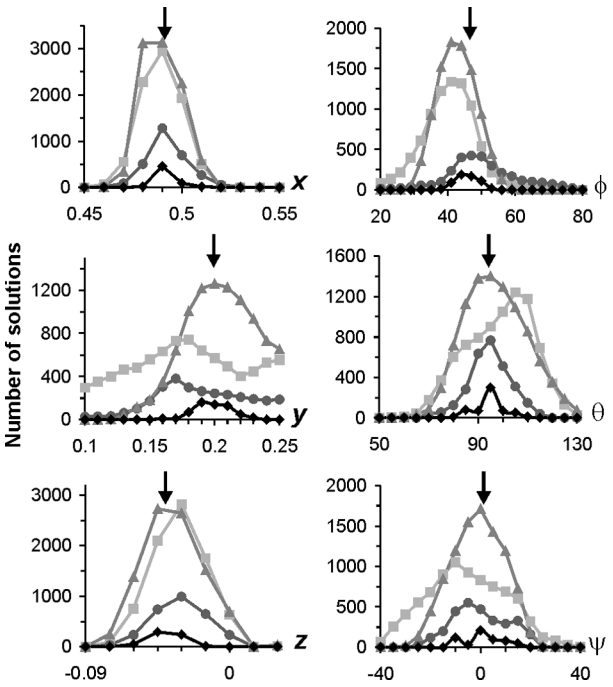
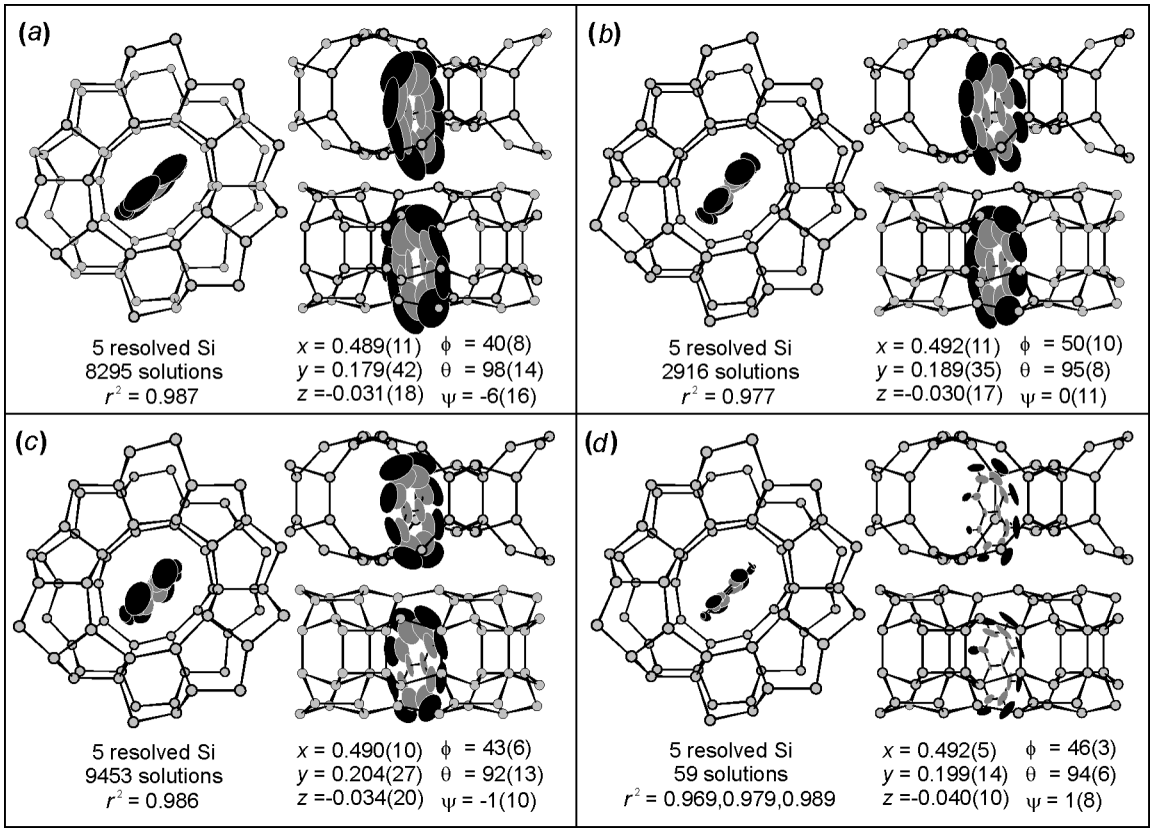


Figure 6 summarizes the range of possible locations that meet the three criteria (with $r^2 \ge 0.96$) found for each $^1H/^{29}Si$ CP drain data set. Each of these distributions was assumed to approximate a normal distribution, so that an "average" location (with standard deviations) could be proposed. These average locations (with error ellipsoids) in the ZSM-5 framework are presented in Fig. 7. The average structures derived from each data set are in quite good agreement. The structures from the completely protonated naph-d_0 data are the least defined, especially along the y axis. This is not unexpected since the eight protons are placed all round the periphery of the molecule. The structures from the deuterated naphthalene data are better defined, especially those from the α-naph-d_4 system,

© 2006 NRC Canada

Fig. 7. Average locations (with 50% error ellipsoids) of naphthalene in ZSM-5 determined from $^{1}H/^{29}Si$ CP drain data collected on ZSM-5 loaded with (*a*) naph-d_0, (*b*) α-naph-d_4, and (*c*) β-naph-d_4. (*d*) The average location of naphthalene in ZSM-5 consistent with all three sets of $^{1}H/^{29}Si$ CP drain data (the overlap between *a*, *b*, and *c*). The standard deviation in the last digits for each parameter is given in parentheses.

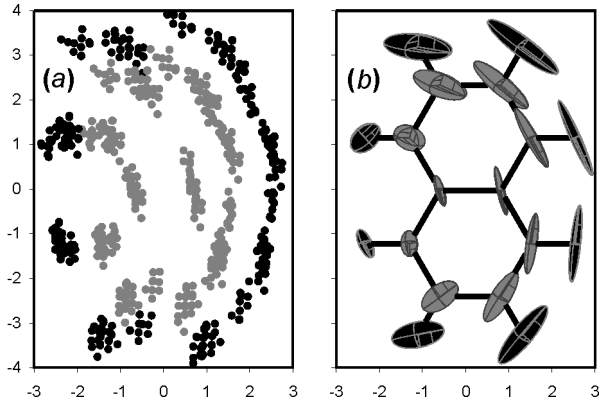


illustrating the benefit of having well-localized sources of polarization.

When these three sets of locations are examined, there are only 59 locations that fulfill all three criteria (with $r^2 \geq 0.96$) for all three sets of experimental CP drain data. The distributions of these locations are presented in Fig. 6. The average of these locations (indicated by the arrows in Fig. 6) is at $x = 0.492 \pm 0.005$, $y = 0.199 \pm 0.014$, $z = -0.040 \pm 0.10$, $\phi = 46° \pm 3°$, $\theta = 94° \pm 6°$, and $\psi = 1° \pm 8°$. This average location is compared to the average locations found for the three individual data sets in Fig. 7. By selecting the locations consistent with all three data sets, the location of the naphthalene molecule is very well-defined, especially considering the low resolution of the ^{29}Si MAS NMR spectra.

A scatter plot of all the atomic positions for each atom for all naphthalene locations consistent with all three data sets is shown in Fig. 8*a* and demonstrates visually the distribution of the solutions. The scatter for each atom can be represented by an ellipsoid in which the length of each principal axis is proportional to the root mean square distance from the mean position,[4] and Fig. 8*b* shows that these ellipsoids represent the error in the corresponding scatter plot quite well. The fractional atomic coordinates for this average location, along with the elements of the tensors that describe the error ellipsoid for each of the atoms are provided as Supplementary data (Table S2).[6] This average location of naphthalene in the ZSM-5 framework is displayed in Fig. 9, where it

Fig. 8. (*a*) Scatter plot of the atomic positions of all naphthalene locations that are consistent with all three sets of $^{1}H/^{29}Si$ CP drain data (with $r^2 \geq 0.96$). (*b*) Average location with 50% error ellipsoids to represent the distributions of the locations. Both plots are viewed in the plane of the molecule with the units in Å (hydrogen (black), carbon (grey)).



can be seen that this location determined by solid-state NMR is in excellent agreement with that previously found by single crystal XRD (12), the only minor difference being the exact location along the straight channel. The naphthalene locations, expressed in terms of fractional coordinates of the molecule's center and Euler rotations, determined by

© 2006 NRC Canada

Table 2. Comparison of naphthalene locations in ZSM-5 determined by various techniques.

Method	Ref.	*x*	y	z	ϕ	θ	ψ
Solid-state NMR	This work	0.492(5)	0.199(14)	–0.040(10)	46(3)	94(6)	1(8)
Single crystal XRD	12	0.486	0.237	–0.035	50	89	2
Powder XRD	13	0.494	0.248	–0.041	24	95	–5
Powder XRD	14	0.476	0.220	–0.046	44	95	5

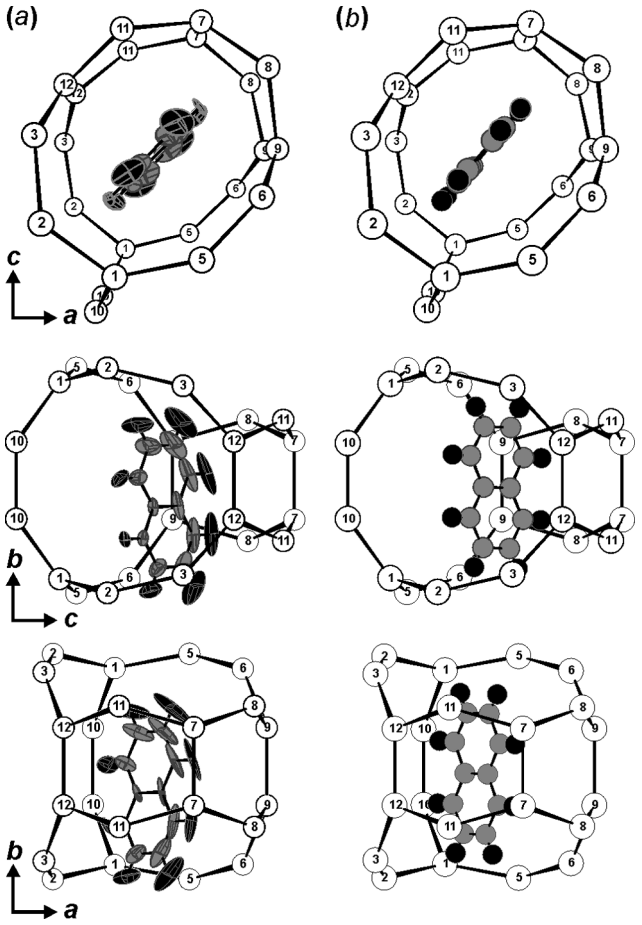


Fig. 9. (*a*) Average location (with 50% error ellipsoids) of the naphthalene molecule in ZSM-5 for solutions that are consistent with all three sets of $^{1}H/^{29}Si$ CP drain data ($r^2 \geq 0.96$) collected at 220 K. (*b*) Representation of the location of the naphthalene molecule determined by single crystal XRD (12). View down straight channels (top), view down zigzag channels (middle), and view perpendicular to straight and zigzag channels (bottom).

solid-state NMR, single crystal XRD (12), and powder XRD (13, 14), are compared in Table 2.

The linear correlation plots (experimental k_{IS} vs. calculated M_2) and the predicted $^{1}H/^{29}Si$ CP drain difference spectra, calculated using the correlation between k_{IS} and M_2, for the average naphthalene location are presented in Fig. 10. These plots demonstrate the high degree of linear correlation between the CP rate constants and the second moments calculated for this average location for all three types of naphthalene molecules, and the close agreement between the predicted and experimental spectra. This final test confirms that the naphthalene location is fully consistent with the experimental $^{1}H/^{29}Si$ cross-polarization data.

In the k_{IS} vs. M_2 plots, the linear correlation lines have non-zero intercepts, which is not entirely consistent with the proportional relationship between k_{IS} and M_2 (eq. [4]). The reason for this is not yet entirely clear to us, however, it is possible that the equations describing the CP dynamics and the relationship between CP rate constants and second moments, which were developed for $^{1}H/^{13}C$ spin systems in organic solids, are not completely valid for the $^{1}H/^{29}Si$ spin systems encountered in these zeolite–sorbate complexes. Nonetheless, this NMR method can correctly determine the location of guest molecules in these complexes.

Figure 11 displays the location of naphthalene in ZSM-5 determined from the solid-state $^{1}H/^{29}Si$ CP MAS NMR data, with several $^{1}H—^{29}Si$ internuclear distances indicated. The different distances between the Si sites and the α and β protons of naphthalene are the source of the different cross-polarization behaviors of these Si peaks in the $^{1}H/^{29}Si$ CP MAS NMR spectra of the naphthalene–ZSM-5 complexes with different deuterated naphthalene molecules (see Fig. 3). In the α-naph-d_4 sample, Si2, Si5, and Si6 have larger signals than Si8 and Si10 in the $^{1}H/^{29}Si$ CP MAS NMR spectra (Fig. 3*c*) owing to their proximity to the β protons (Fig. 11*a*). Likewise, in the β-naph-d_4 sample, the CP signals of Si2 and Si8 are larger than those of Si5, Si6, and Si10 (Fig. 3*d*), owing to their proximity to the α protons (Fig. 11*b*).

Conclusions

The location of naphthalene in ZSM-5 has been determined from solid-state $^{1}H/^{29}Si$ CP MAS NMR data and is in excellent agreement with the structure obtained from single crystal XRD, further demonstrating the usefulness and reliability of this solid-state NMR structure determination approach, particularly since naphthalene is significantly different in structure from the *p*-disubstituted aromatic molecules that to date have mainly been those studied by both NMR and XRD techniques. This example also demonstrates the importance of having localized sources of ^{1}H polarization as was achieved here by using differently deuterated naphthalene molecules, since the structure determined by the fully protonated naphthalene molecule was not very well-defined, particularly the location along the straight channel. Combining the information from samples made with differently deuterated naphthalene molecules increased the reliability of the structure determination, which was particularly important for this system as the resolution of the ^{29}Si spectrum was on the limit of being useful with only five reliably resolved peaks. These results further confirm the validity and reliability of this NMR method for structure determina-

© 2006 NRC Canada

Fig. 10. Correlation plots (with 95% prediction interval indicated by dashed lines) between the experimental CP rate constants from the drain experiments and the calculated second moments (upper) and the predicted $^{1}H/^{29}Si$ CP drain difference spectra (96 ms contact time) based on these correlations (lower) for (*a*) naph-d_0, (*b*) α-naph-d_4, and (*c*) β-naph-d_4, for the average location consistent with all three sets of $^{1}H/^{29}Si$ CP drain data.

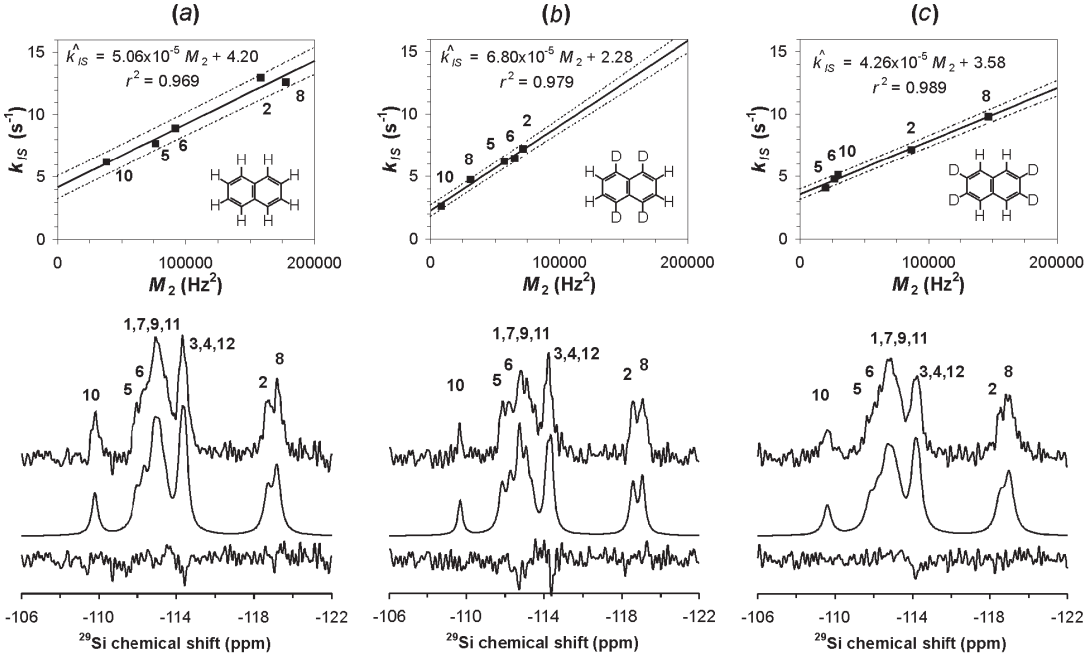
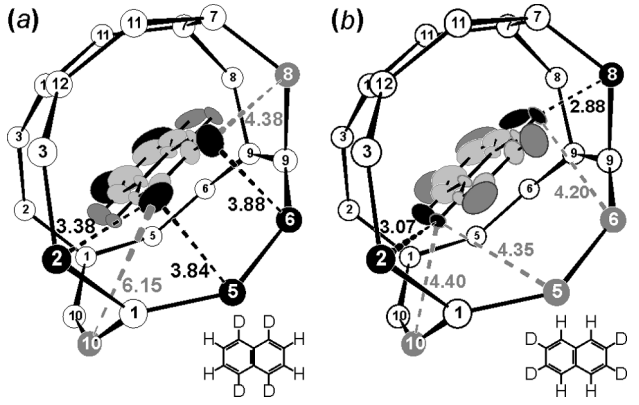


Fig. 11. The location of naphthalene in ZSM-5 (determined by solid-state NMR) showing selected $^{1}H–^{29}Si$ internuclear distances involving (*a*) the β protons and (*b*) the α protons.



tions and indicate that it can be applied with confidence to suitable systems of unknown structure where the use of diffraction techniques is precluded, and such studies are currently in progress.

Acknowledgements

The authors thank the Natural Sciences and Engineering Research Council of Canada (NSERC) for Discovery and Equipment grants (CAF), and for the award of a Postgraduate Fellowship (DHB). We would also like to acknowledge the contributions of Professor Carty to chemical research and his help and friendship as a colleague.

References

1. C.A. Fyfe, A.C. Diaz, A.R. Lewis, J.-M. Chézeau, H. Grondey, and G.T. Kokotailo. *In* Solid state NMR spectroscopy of inorganic materials. Vol. 717. *Edited by* J.J. Fitzgerald. ACS Symposium Series. American Chemical Society, Washington, D.C. 1999. p. 283.
2. C.A. Fyfe, A. Diaz, H. Grondey, A.R. Lewis, and H. Förster. J. Am. Chem. Soc. **127**, 7543 (2005).
3. A. Bax, R. Freeman, and S.P. Kempsell. J. Am. Chem. Soc. **102**, 4849 (1980).
4. D.H. Brouwer. J. Magn. Reson. **164**, 10 (2003).
5. D.H. Brouwer and E.K. Lloyd. J. Comput. Chem. Jpn. **3**, 103 (2004).
6. C.A. Fyfe, H. Grondey, Y. Feng, and G.T. Kokotailo. J. Am. Chem. Soc. **112**, 8812 (1990).
7. C.A. Fyfe, Y. Feng, H. Grondey, G.T. Kokotailo, and H. Gies. Chem. Rev. **91**, 1525 (1991).
8. C.A. Fyfe, D.H. Brouwer, and P. Tekely. J. Phys. Chem. A, **109**, 6187 (2005).
9. A. Pines, G. Gibby, and J.S. Waugh. J. Chem. Phys. **59**, 569 (1973).
10. J.H. van Vleck. Phys. Rev. **74**, 1168 (1948).
11. C.A. Fyfe and D.H. Brouwer. J. Am. Chem. Soc. **126**, 1306 (2004).
12. H. van Koningsveld and J.C. Jansen. Microporous Mater. **6**, 159 (1996).
13. B.F. Mentzen, M. Sacerdoté-Peronnet, J.-F. Bérar, and F. Lefebvre. Zeolites, **13**, 485 (1993).
14. H. Klein, H. Fuess, S. Ernst, and J. Weitkamp. Microporous Mater. **3**, 291 (1994).
15. K. Davis and J.L. Garnett. Aust. J. Chem. **28**, 1699 (1975).
16. C.A. Fyfe, J.H. O'Brien, and H. Strobl. Nature (London), **326**, 281 (1987).
17. P.A. Agaskar. Inorg. Chem. **29**, 1603 (1990).

© 2006 NRC Canada

18. S. Wolfram. Mathematica. Version 3.0 [computer program]. Wolfram Media, Champaign, Illinois. 1996.
19. C.A. Fyfe, Y. Feng, and H. Grondey. Microporous Mater. **1**, 393 (1993).
20. M. Mehring. Principles of high resolution NMR in solids. Springer-Verlag, Berlin. 1983.
21. I. Klur, J.-F. Jacquinot, F. Brunet, T. Charpentier, J. Virlet, C. Schneider, and P. Tekely. J. Phys. Chem. B, **104**, 10162 (2000).
22. E.O. Stejskal, J. Schaefer, and R.A. McKay. J. Magn. Reson. **57**, 471 (1984).
23. J. Schaefer, R.A. McKay, and E.O. Stejskal. J. Magn. Reson. **34**, 443 (1979).

© 2006 NRC Canada

(–)-Sparteine-mediated stereoselective directed ortho metalation of ferrocene diamides[1]

Radoslaw Laufer, Ulrich Veith, Nicholas J. Taylor, and Victor Snieckus

Abstract: The utility of (–)-sparteine-mediated directed ortho metalation (D*o*M) has been investigated in stereoselective preparation of planar chiral ferrocenes derived from 1,1′-*N*,*N*,*N*′,*N*′-tetraisopropylferrocenedicarboxamide (**5**). In the synthesis of C_2-symmetric analogs of **5**, the protocol (base, solvent, and two-step D*o*M) was found to be crucial for obtaining high enantio- and diastereo-selectivities of the products. A variety of highly enantioenriched mono and doubly functionalized derivatives of **5** have been synthesized. The synthetic applications of these compounds as chiral ligands in asymmetric alkylation of aldehydes and asymmetric palladium-catalyzed allylic substitutions have been demonstrated.

Key words: directed ortho metalation, stereoselective deprotonation, ferrocene ligands, asymmetric catalysis.

Résumé : On a étudié l'utilité de l'ortho métallation dirigée (*o*MD) orientée par la (–)-spartéine, dans la préparation stéréosélective de ferrocènes chiraux planaires dérivés du 1,1′-*N*,*N*,*N*′,*N*′-tétraisopropylferrocènedicarboxamide (**5**). Dans la synthèse d'analogues de symétrie C_2 du composé **5**, on a trouvé que le protocole expérimental (base, solvant et *o*MD en deux étapes) est crucial si on veut obtenir des valeurs élevées d'énantio- et de diastéréo-sélectivités des produits. On a pu synthétiser avec un degré d'énantioenrichissement élevé une grande variété de dérivés du composé **5** mono- et di-fonctionnalisés avec un degré d'énantioenrichissement élevé. On a démontré l'utilité synthétique de ces composés, en particulier comme ligands chiraux dans l'alkylation asymétrique d'aldéhydes et dans les substitutions allyliques asymétriques catalysées par le palladiium.

Mots clés : ortho métallation dirigée, déprotonation stéréosélective, ligands ferrocènes, catalyse asymétrique.

[Traduit par la Rédaction]

The disclosure, with an interesting socio-chemical history, of the correct structure of ferrocene over half a century ago constituted a landmark achievement that heralded an entirely new theme of organometallic chemistry (1). The continuing significance of the field of ferrocene chemistry (2) is attested by research in areas of asymmetric catalysis (3, 4), enantioselective synthesis (2, 5), diverse material science (2), and biological (6) areas and, most spectacularly, industrial applications (7). Shortly after the excellent summary of the field by Schlőgl (8), Ugi and co-workers (9) reported the effective preparation of optically active planar chiral ferrocenes, which proceeds by diastereoselective directed ortho metalation (D*o*M) and subsequent reaction with electrophiles and which relies on a chiral auxiliary directed metalation group (DMG) for the central to planar chirality transfer. Following these pioneering studies, Kagan and co-workers (10) demonstrated a high diastereoselective D*o*M reaction using chiral sulfoxide DMGs, which was followed by rapid accumulation of reports using other DMGs, providing convincing evidence for the generality of the diastereoinduction process (11, 12) (Scheme 1).

In 1996, stimulated by the results of Hoppe and Hense (13) and Beak et al. (14), we reported on the highly enantioselective synthesis of planar chiral ferrocenecarboxamides **1a** → **2a** by (–)-sparteine-mediated D*o*M chemistry (Scheme 2) (15). This constituted the first general and direct synthetic method to enantiomerically pure ferrocenyls that avoids substrate-specific resolution (9*a*, 16) and chiral auxiliary introduction and removal (10, 17). In subsequent work, we addressed a limitation of the diethyl amide DMG of "seldom allow(ing) functional group modification" (10*b*) by introducing the *N*-cumyl-*N*-ethylferrocenecarboxamide (**1b**), which behaved equally well in sparteine-mediated D*o*M chemistry to afford planar chiral ferrocenes in high yields and % ee, and served, after mild decumylation, as convenient syntheses of optically active Ugi amines, little-known esters, and new phosphines (18). Another limitation, "the disadvantage of the (availability of a) single enantiomeric form of (–)-sparteine" (19) was addressed by showing that 2-TMS-*N*-ethylferrocenecarboxamide (**3**, E = TMS) undergoes C-5 rather than C-1′ deprotonation and thereby allows a latent silicon protec-

Received 10 August 2005. Published on the NRC Research Press Web site at http://canjchem.nrc.ca on 30 March 2006.

Dedicated to friend and former colleague, Arthur Carty, in recognition of his forefront and continuing contributions to organometallic chemistry and chemistry in Canada, and for early fruitful collaboration in diazepine irontricarbonyl chemistry.

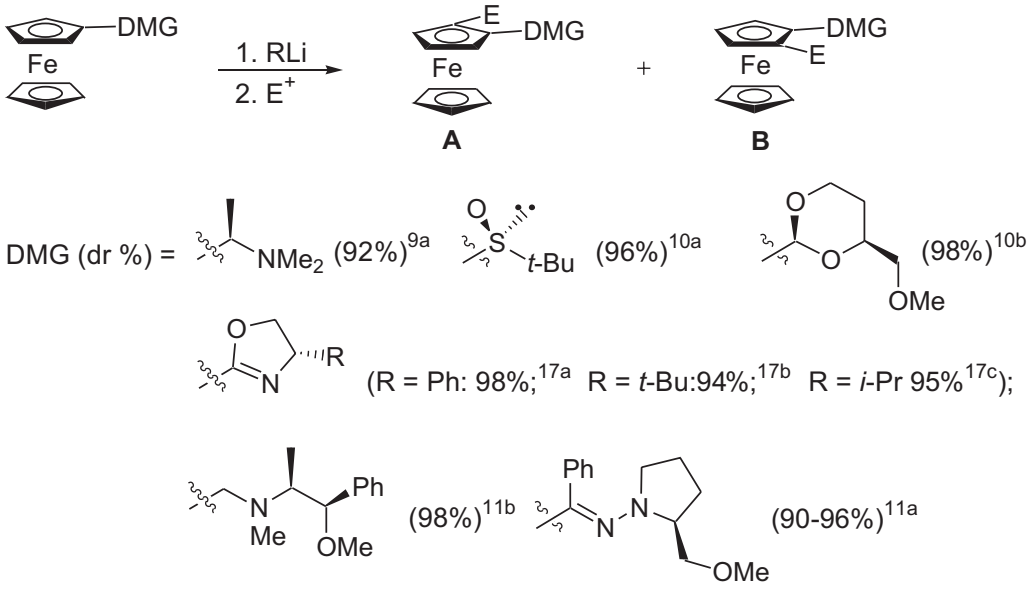
R. Laufer, U. Veith, N.J. Taylor, and V. Snieckus.[2,3] Department of Chemistry, University of Waterloo, Waterloo, ON N2L 3G1, Canada.

[1]This article is part of a Special Issue dedicated to Professor Arthur Carty.

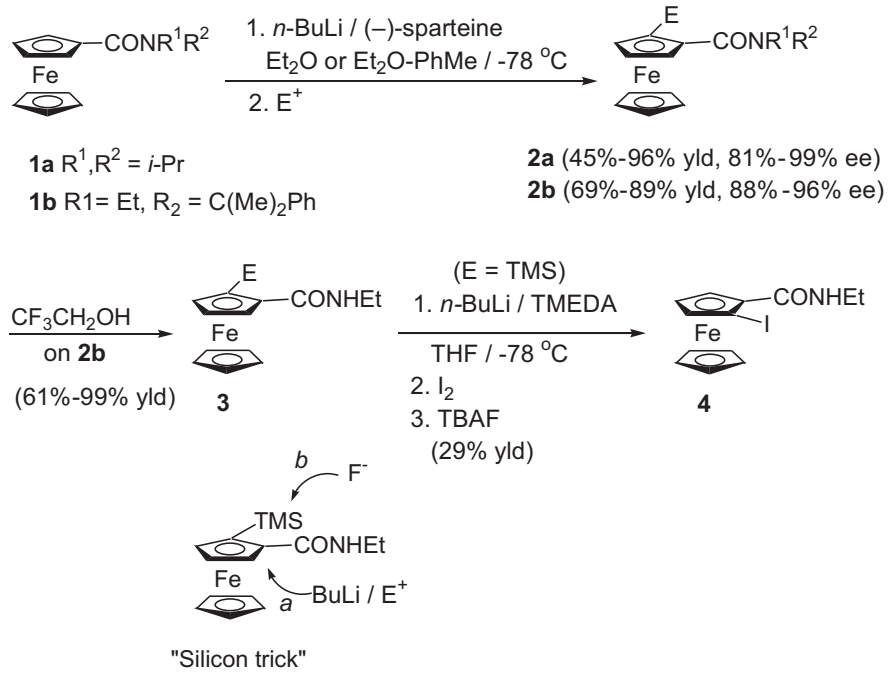
[2]Present address: Department of Chemistry, Queen's University, Kingston, ON KL7 3N6, Canada.
[3]Corresponding author (e-mail: snieckus@chem.queensu.ca).

 doi:10.1139/V06-008 © 2006 NRC Canada

Scheme 1.



Scheme 2.



tion route (4, 20, 21) to the valuable enantiomeric ferrocene (*S*) series (Scheme 2).

As part of efforts to expand the scope of the (–)-sparteine-mediated enantioinduction of planar chirality, we recently reported (22) on the synthesis of highly enantioenriched mono- and double-functionalized derivatives of ferrocenyl 1,1′-bisamides, **6** and **7** (Scheme 3) by combined D*o*M–Pd-catalyzed Suzuki–Miyaura and Stille cross-coupling reactions (23). Herein we present the full details of our studies.

At the outset of our initial investigation, we attempted to establish the optimal reaction conditions for D*o*M of ferrocenyldiamide **5** in Et_2O using chlorotrimethylsilane (TMSCl) as the electrophilic partner. Only later, we discovered that application of TMSCl led to exceptional results. As gleaned from the results in Table 1, use of more than 2 equiv. of both *n*-BuLi and (–)-sparteine led to effective electrophilic trapping of doubly deprotonated **5** (Table 1, entries 2 and 3) in very good yields, however, with unsatisfactory levels of both diastereoselectivity (dr meso:dl, 2:1, **7a**: E = TMS) and optical activity (54% optical purity).[4] Application of *s*-BuLi and (–)-sparteine allowed for quantitative conversions of **5** into **7a** (Table 1, entry 5), but the reaction

[4] Neither (±)-**6a** nor (±)-**7a** could be resolved on chiral HPLC. The requisite homochiral crystals of (+)-**7a** were obtained by recrystallizations of the enantioenriched **7a** from hexanes.

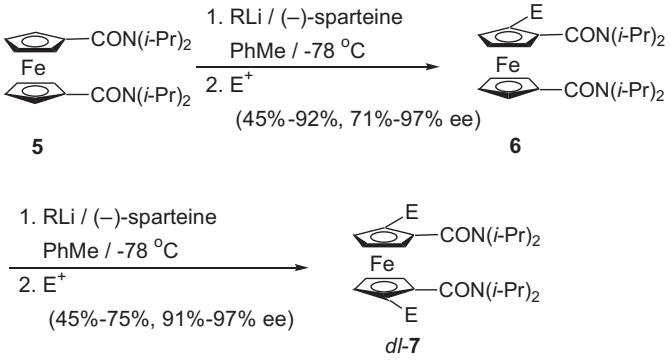
© 2006 NRC Canada

Table 1. Metalation of 1,1′-ferrocenyldiamide **5** in Et_2O (E^+ = TMSCl).

No.	Base	Equiv.	Yield (%)			
			6a	**7a**	**7a** dr[a] dl:meso	Op[b] (*dl*-**7a**)
1	*n*-BuLi–(–)-sparteine	2.1	10	Trace	46:54	—
2	*n*-BuLi–(–)-sparteine	3.1	3	88	30:70	54
3	*n*-BuLi–(–)-sparteine	4.2	Trace	87	37:63	—
4	*n*-BuLi–TMEDA	4.2	38	46	49:51	—
5	*s*-BuLi–(–)-sparteine	4.2	—	99	4:96	15
6	*s*-BuLi–TMEDA	4.2	—	99	25:75	—

Note: Conditions: RLi–(–)-sparteine or TMEDA; Et_2O at –78 °C for 2 h then excess TMSCl; –78 °C → rt.
[a]Determined by GC analysis of crude reaction mixtures.
[b]Op (optical purity); homochiral **7a**: $[\alpha]^{23}_{578}$ +49.2° (*c* 0.24, $CHCl_3$).

Scheme 3.



exhibited prohibitively strong preference for the meso diastereomer and very low optical induction for *dl*-**7a** (15% optical purity). Interestingly, in all cases D*o*M-trimethylsilylation of **5** utilizing *n*-BuLi or *s*-BuLi together with TMEDA led to modestly (Table 1, entries 3 vs. 4 and 5 vs. 6) improved contents of racemic *dl*-**7a**.

For electrophilies other than TMSCl, the reactions of 1,1′-ferrocenyldiamide (**5**) with 4.2 equiv. of *n*-BuLi–(–)-sparteine in Et_2O at –78 °C are markedly different. As illustrated in Table 2, the protocol furnished, almost exclusively, products from electrophilic trapping of monolithium anion in good yields but with moderate enantioselectivities. At present, the high yields for the double D*o*M of **5** in the reactions involving TMSCl are difficult to rationalize. Related reactions, involving deprotonation of hindered lithium dialkylamides and in situ TMSCl as the electrophilic trap, have been shown to give superior yields and stereoselectivities. Effects of the in situ generated LiCl has been suggested as the causative agent (24). Despite the apparent incompatibility of *n*-BuLi with TMSCl, we have observed a modest LiCl effect on D*o*M of **5**. Under unchanged reaction conditions, D*o*M of **5** with 4.2 equiv. of *n*-BuLi–(–)-sparteine in the presence of 2.0 equiv. of LiCl followed by a quench with an excess of MeI led to improved yields and greatly enhanced stereoselectivities for both the mono-**6b** (61% yield, 79% ee vs. Table 2, entry 1) and dimethylated **7b**. Compound **7b** was obtained in 16% yield (3:1 dr dl:meso, 80% ee), compared with only trace amounts observed under LiCl-free conditions.

Although double D*o*M–electrophile quench was effected much more efficiently with *s*-BuLi–(–)-sparteine, the same general trend for the unfavorable diastereoselectivities and low enantioinductions was observed with a number of different electrophiles (Table 3). Under these reaction conditions, monocarbinol **6d** was isolated as the only product in low yield and low enantiomeric excess (Table 3, entry 6). Interestingly, unlike 2,2′-bis(diphenylphosphine) (**7c**), which was obtained in respectable yield either directly from **5** utilizing *s*-BuLi (Table 3, entry 5) or stepwise, with *n*-BuLi via **6g** (vide infra, Table 4), all attempts to prepare the 2,2′-bis(diphenylhydroxymethyl) derivative by D*o*M of **5** or monocarbinol **6d** were unsuccessful.

Table 2. Monometalation of **5** in Et_2O (base is *n*-BuLi).

No.	E+	Product (E)	Yield (%)	ee (%)
1	MeI	**6b** (Me)	56	68
2	I_2	**6c** (I)	53	59
3	$Ph_2C{=}O$	**6d** (Ph_2C-OH)	77	64

Note: Conditions: 4.2 equiv. *n*-BuLi–(–)-sparteine; Et_2O; –78 °C for 2 h then 6 equiv. E^+, –78 °C → rt for 4 h.

Gratifyingly, use of solvents of lower coordinating abilities (Table 5, entries 1–3) allowed the preparation of 1,1′,2-trisubstituted derivatives (**6b**–**6i**) in augmented optical and chemical yields. Toluene was found to give the optimal balance between the level of enantioinduction and chemical yield, e.g., the diphenylphosphine derivative **6g** was obtained in 53% yield and 97% ee without a recrystallization (Table 5, entry 9). Interestingly, the opposite solvent effect on the entantioselectivty of (–)-sparteine-assisted D*o*M was observed in applications of *N*,*N*-diisopropylferrocenylcarboxamide (15). Reduction of the amount of *n*-BuLi–(–)-sparteine to 2.2 equiv. caused a slight decline in the chemical yield of the product **6d** (Table 5, entry 5 vs. 6), but did not lead to the erosion of ee. Again, utilization of TMSCl as the electrophile afforded 2,2′-disilylated product **7a** as the major product (71% yield, dr dl:meso, 3:1, 97% optical purity) when 4.2 equiv. of base was used (Table 5, entry 12). Lesser amount of the base (2.2 equiv.) resulted in formation of the monosilylated **6a** as the major product with **7a** isolated as a minor component (16% yield, dr dl:meso, 68:32, 99% optical purity) (Table 5, entry 13).

The enantiomeric excess for stannane **6f** (Table 5, entry 8) was determined by its transformation into carbinol **6d** in a sequence involving a lithiodestannylation–benzophenone quench. Under these unoptimized conditions, the relatively lower ee of **6d** (82% ee) derived from **6f** may be the result of partial racemization, occurring via an intermolecular Li-H

© 2006 NRC Canada

Table 3. Double D*o*M of **5** in Et_2O using *s*-BuLi and TMEDA or (–)-sparteine.

No.	E^+	Diamine	Product (E)	Yield (%)[a]	*dl*-**7**:*meso*-**7**	ee (%)
1	MeI	(–)-Sparteine	**7b** (Me)	70	24:76[b]	53[b]
2	MeI	TMEDA	**7b**	19	21:79[b]	—
3	TMSCl	(–)-Sparteine	**7a** (TMS)	99	4:96[c]	15[d]
4	TMSCl	TMEDA	**7a**	99	25:75[c]	—
5	PPh_2Cl	(–)-Sparteine	**7c** (PPh_2)	49	<5:>95[e]	—
6	$Ph_2C{=}O$	(–)-Sparteine	**6d** (Ph_2C-OH)	36[f]	NA	32[b]
7	Ph_2S_2	TMEDA	**7d** (PhS)	51	31:69[b]	—

Note: Conditions: 4.2 equiv. *s*-BuLi–(–)-sparteine or TMEDA; Et_2O at –78 °C for 2 h then 6 equiv. E^+ at –78 °C → rt for 4 h.
[a]Combined yields.
[b]Determined by chiral HPLC.
[c]Determined by GC analysis of crude reaction mixtures.
[d]As optical purity.
[e]Determined by ^{31}P NMR.
[f]Only the mono derivative **6d** was isolated.

Table 4. *n*-BuLi–(–)-sparteine-induced monometalation of 2-substituted derivatives, **6a**, **6g**, and **6h**.

(SM) ee (%)	E^+	Product	Yield (%)	dl:meso	ee (%)
(**6a**) 0	TMSCl[a]	**7a**	86	51:49	72[b]
(**6a**) —[c]	TMSCl[d]	**7a**	75	84:16	91[b]
(**6g**) 97	Ph_2PCl[e]	**7c**	45	>95:<5[f]	98[b]
(**6h**) 89	$(PhS)_2$[a]	**7d**	60	99:1[g]	97[g]

[a]2.1 equiv. of *n*-BuLi–(–)-sparteine were used.
[b]Determined as optical purity.
[c]$[\alpha]^{23}_{578}$ +67.5° (*c* 0.54, $CHCl_3$).
[d]4.2 equiv. of *n*-BuLi–(–)-sparteine were used.
[e]1.5 equiv. of *n*-BuLi–(–)-sparteine were used.
[f]Determined by ^{31}P NMR.
[g]Determined by chiral HPLC.

exchange. The heteroatom-tethered phenyl derivatives (thioether, diphenylphosphine, and phenylselenide) **6g**–**6i** (Table 5, entries 9–11) were found to surrender their optical integrity on standing in solution. For example, 2-(phenylthio)-1,1′-ferrocenediamide derivative **6h** undergoes racemization in a mixture of hexanes and *i*-PrOH at a faster rate ($t_{1/2} \approx 9$ h) (25) compared with the corresponding derivative of *N*,*N*-diisopropylferrocenylcarboxamide ($t_{1/2} \approx 24$ h) (15). Noteworthy is the fact that the solution of C_2-symmetric analog, chiral 2,2′-bis(diphenylthio)-1,1′-ferrocenediamide (**7d**), exhibited a very low tendency towards isomerization losing ~30% ee and de on standing at room temperature (rt) for 19 days (25).

Highly diastereo- and enantio-enriched, tetrasubstituted ferrocenyldiamides *dl*-**7** were prepared by subjecting 1,2,1′-trisubstituted ferrocenes **6** to a further asymmetric D*o*M (Table 4). This constituted the first reported preparation of C_2-symmetric ferrocenes outfitted exclusively with the element of planar chirality (26). Quench with electrophiles furnished products **7a**, **7c**, and **7d** with diastereoselective amplification of enantioselectivity as demonstrated by converting **6h** (89% ee) into optically active, 2,2′-bis(diphenylthio)-1,1′-ferrocenediamide (**7d**, 97% ee, 99:1 dl:meso) (27).

To demonstrate the combined potential of D*o*M-cross coupling strategy (28) as a route to aryl-substituted ferrocenes, the iodo (**6c**) and stannane (**6f**) ferrocenediamides were subjected to Suzuki–Miyaura and Gronowitz-modified Stille (29) cross-coupling conditions (Scheme 4). Thus, the reaction of **6c** (89% ee) with (2,4-dimethoxyphenyl)boronic acid afforded the aryl derivatives **6k** in a modest yield (20% yield, 89% ee) together with recovered **6c** (70% yield). Palladium coupling of **6f** and bromobenzene led to a formation of **6l** (35% yield) along with destannylated product **5** (51% yield).

X-ray crystallographic analysis of compounds 7a and 6d

The (*S*) absolute configuration (8), established by single crystal X-ray crystallography analysis of carbinol **6d** (Fig. 1),[5] was provisionally assigned to all of the 2-substituted ferrocenediamides **6a**–**6l**. This is the same sense of enantioinduction as previously seen in (–)-sparteine-assisted D*o*M of *N*-cumyl-*N*-ethyl and *N*,*N*-diisolpropyl ferrocenyl monoamides (15, 18). The (*R*,*R*) absolute configuration of the C_2-symmetric derivatives of **5** (**7a**, **7c**, and **7d**,

[5] Supplementary data for this article are available on the journal Web site (http://canjchem.nrc.ca) or may be purchased from the Depository of Unpublished Data, Document Delivery, CISTI, National Research Council Canada, Ottawa, ON K1A 0R6, Canada. DUD 5008. For more information on obtaining material refer to http://cisti-icist.nrc-cnrc.gc.ca/irm/unpub_e.shtml. CCDC 295149 and 602324 contain the crystallographic data for this manuscript. These data can be obtained, free of charge, via www.ccdc.cam.ac.uk/conts/retrieving.html (or from the Cambridge Crystallographic Data Centre, 12 Union Road, Cambridge CB2 1EZ, UK; fax +44 1223 336033; or deposit@ccdc.cam.ac.uk).

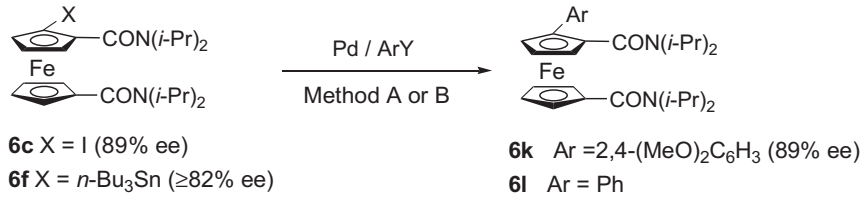
© 2006 NRC Canada

Table 5. *n*-BuLi–(–)-sparteine-induced monolithiation of **5**.

No.	E+	Product (E)	Solvent	Yield (%)	ee (%)
1	I_2	**6c** (I)	Et_2O	53	59
2	I_2	**6c**	*t*-BuOMe	77	70
3	I_2	**6c**	PhMe	70	89
4	MeI	**6b** (Me)	PhMe	71	92
5	Ph_2C=O	**6d** (Ph_2C-OH)	PhMe	92	94
6	Ph_2C=O	**6d**	PhMe	72[a]	96
7	Et_2C=O	**6e** (Et_2C-OH)	PhMe	45	91
8	Bu_3SnCl	**6f** (Bu_3Sn)	PhMe	58	≥82[b]
9	Ph_2PCl	**6g** (Ph_2P)	PhMe	53	97[c]
10	$(PhS)_2$	**6h** (PhS)	PhMe	71	89[c]
11	$(PhSe)_2$	**6i** (PhSe)	PhMe	82	71[c]
12	TMSCl	**6a** (TMS)	PhMe	16	—[d]
13	TMSCl	**6a**	PhMe	68[a]	—[e]

Note: Conditions: 4.2 equiv. *s*-BuLi–(–)-sparteine, solvent at –78 °C for 2 h then 6 equiv. E^+ at –78 °C → rt for 4 h.
[a]2.1 equiv. of both *n*-BuLi and (–)-sparteine were used.
[b]ee was determined after conversion into **6d** (1, *n*-BuLi; 2, Ph_2C=O).
[c]ee determination was carried out immediately after purification.
[d]$[\alpha]^{23}_{578}$ +64.3° (*c* 0.11, $CHCl_3$); **7a** was also isolated in 71% yield (dr dl:meso, 72:28); 97% optical purity.
[e]$[\alpha]^{23}_{578}$ +67.5° (*c* 0.54, $CHCl_3$); also **7a** was isolated in 16% yield (dr dl:meso, 68:32); 99% optical purity.

Scheme 4.



6c X = I (89% ee)
6f X = *n*-Bu_3Sn (≥82% ee)

6k Ar =2,4-$(MeO)_2C_6H_3$ (89% ee)
6l Ar = Ph

Methods: A. on **6c**: 2,4-$(MeO)_2C_6H_3B(OH)_2$ / $Pd(PPh_3)_4$ / 2 mol/L aq. Na_2CO_3 / DME / 85 °C / 5 d (20% yld)
B. on **6f**: PhBr / $PdCl_2$(dppf) / CuO / DMF /150 °C / 18 h (35% yld)

Table 4) must be derived from (*R*) stereochemistry of the corresponding chiral precursors (**6a**, **6g**, and **6h**). The formation of *meso*-**7** products necessitates that the second deprotonation occurs with the opposite stereoselectivity, which may be the result of a cooperative effect of the two DMGs.

In the crystal structure of **6d**, the Cp rings are almost eclipsed with respect to each other, deviating by 14.0° from a fully eclipsed conformation. A hydrogen bond between the carbonyl group of carboxamide and the proximal hydroxyl group (O16—H16, 1.94 Å) is evident. Presumably, owing to packing effects, the two carboxylamides remain in a relative proximity.

Compound *meso*-**7a** proved amenable to X-ray analysis and its crystal structure is shown in Fig. 1.[5] The center of inversion structure entails the staggered conformation for both Cp rings with minimum interactions among the four substituents.

Applications of the ferrocenediamides

In an initial study of utility the new planar chiral ferrocenes in asymmetric synthesis, 1,1′-bis(diphenylphosphino)-2,2′-ferrocenyldiamide (**7c**, 98% ee) was tested as an auxiliary ligand for enantioselective Pd-catalyzed allylic substitution of (±)-phenylcinnamyl acetate (Scheme 5) (30).

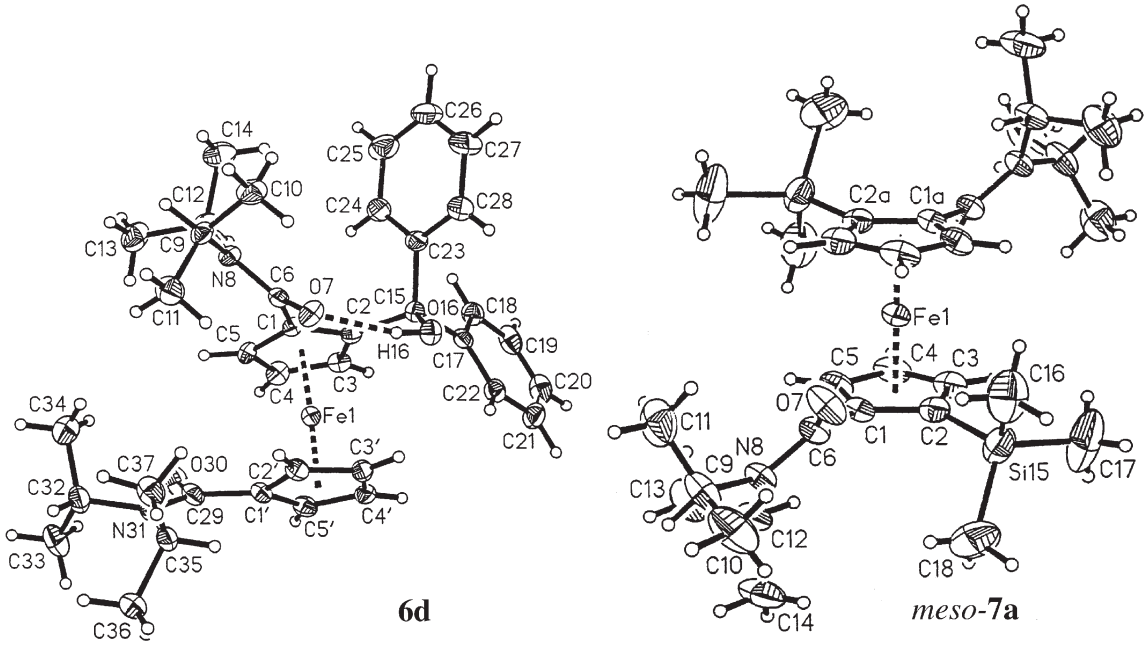
The reactions were conducted using palladium allyl chloride dimer (2.5 mol%) as the Pd source utilizing the Trost alkylation conditions (31) or sodiodimethylmalonate. In both cases, alkylated product **8** was obtained in essentially quantitative yield and with good enantiocontrol (96% yield, 84% ee (*R*)). The enantiomeric excess was determined by chiral HPLC and the absolute configuration of the product was assigned by comparison of the optical rotation with literature values (32).

In an additional classic test for enantioinduction, the 1,1′,2-ferrocenyldiamides (**6d**, **6e**, and **6k**) were shown to exhibit moderate to good catalytic activities in the reaction of diethylzinc with benzaldehyde (Scheme 6, Table 6) (33).

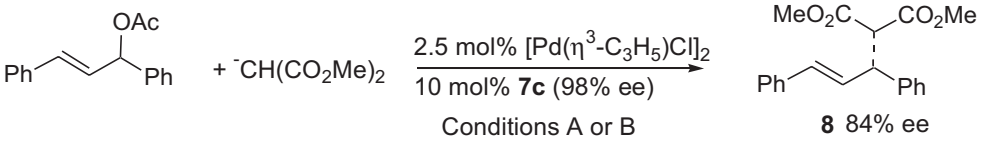
Thus, in a typical reaction, a stirred solution of benzaldehyde (1 mmol) and chiral additive (**6d**, **6e**, **6k**) (5 mol%) in either hexane or PhMe under argon, was treated with diethylzinc (1.6 equiv.) and the resultant mixture was stirred at rt for 48–72 h. The crude product was analyzed by chiral HPLC, purified by flash chromatography, and the absolute configuration was determined by a comparison of its

© 2006 NRC Canada

Fig. 1. X-ray crystallographic structures of **6d** and *meso*-**7a**.

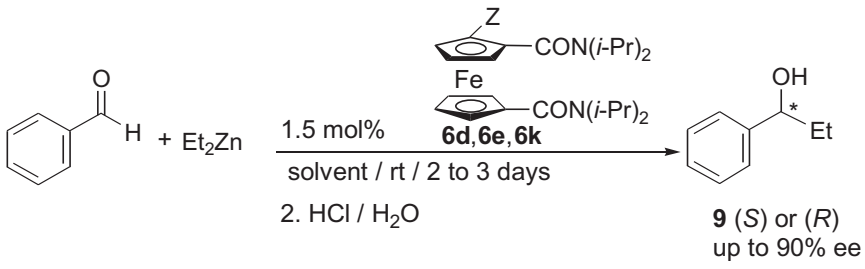


Scheme 5.



Conditions:
A. *N,O*-bis(trimethylsilyl)acetamide / AcOK / $CH_2(CO_2Me)_2$ / CH_2Cl_2 / rt / 10 h
B. $NaCH(CO_2Me)_2$ / THF / rt / 36 h

Scheme 6.



optical rotation with the literature values (34). The results are summarized in Table 6. Ethylations of benzaldehyde in hexanes catalyzed by carbinols **6d** and **6e** proceed with the same degree of enantioinduction; however, for **6e**, the chemical yield is greatly diminished, presumably as a consequence of the lower solubility of the catalyst (Table 6, entries 1 and 4). Quite unusual and, to our knowledge, previously unobserved, is the variation in the enantiotopicity of the reaction as a function of the solvent (Table 6, entry 1 vs. entry 2) and use of lithium salt of carbinol **6d** (Table 6, entry 2 vs. entry 3). The lithium salt of the **6d**-catalyzed reaction proceeded in PhMe with greater optical efficiency (47% ee) than the free carbinol **6d** (12% ee) and with a reversal of enantioselection (Table 6, entries 2 and 3). The best optical yield (90% ee) was observed for a nonprotic ligand **6k** (Table 6, entry 5). Attempts to lower the temperature of the process led to prohibitively long reaction times. These variations in the entantiotopiciy of the reaction are currently not understood.

In summary, direct and highly efficient enantioselective syntheses of mono- (**6a**–**6i**) and C_2-symmetric, homoleptic (**7a**, **7c**, and **7d**) ferrocene diamides from achiral ferrocenyldicarboxamide **5** using (–)-sparteine-mediated D*o*M and combined D*o*M-cross coupling (**6k**, and **6l**) have been demonstrated. The preliminary encouraging results in asymmetric synthesis and the current intense activity in ferrocene-

© 2006 NRC Canada

Table 6. 2-Substituted derivatives (**6d**, **6e**, **6k**) (catalyzed Et_2Zn addition to PhCHO).

No.	*Z*	Ligand (ee, %)	Solvent	Yield (%)	ee (%)[a]
1	$Ph_2C(OH)$	**6d** (96)	Hexanes	98	61 (*S*)
2	$Ph_2C(OH)$	**6d** (96)	PhMe	98	12 (*R*)
3	$Ph_2C(OLi)$	**6d**·Li (95)	PhMe	70	47 (*S*)[b]
4	$Et_2C(OH)$	**6e** (90)	Hexanes	37	60 (*S*)
5	2,4-$(MeO)_2C_6H_3$	**6k** (89)	PhMe	43	90 (*S*)

[a]Determined on a Chiracel OD column and compared to racemic material.
[b]$[\alpha]^{23}_D$ –21.7° (*c* 3.43, $CHCl_3$).

based catalysis (4, 35) may stimulate continuing efforts in the design, synthesis, and application of similar planar chiral ferrocenyl ligands.

Experimental section

General procedures

Melting points were determined on a Buchi SMP-20 or a Fisher hot stage melting point apparatus and were uncorrected. IR spectra were recorded on a BOMEM MB-100 and PerkinElmer 1600 FT-IR spectrophotometer as either neat film, a CH_2Cl_2 solution, or a KBr pellet. ^1H NMR and ^{13}C NMR spectra were recorded on either a Bruker AM-250 or an AC-200 instrument with tetramethylsilane or $CDCl_3$ as an internal standard. ^{31}P NMR spectra were recorded on an AC-200 instrument with H_3PO_4 as an external standard.

Mass spectra (MS) were determined on a high-resolution Varian MAT-CH7 instrument at 70 eV (Monsanto Co., St. Louis, Missouri and Guelph Centre for Mass Spectrometry Service, University of Waterloo Mass Spectrometry Service). Elemental analyses were performed by Chemisar Laboratories, Guelph, Ontario. Stereoselectivities of the reactions were determined using and a Waters HPLC system consisting of a 600E multisolvent delivery system, a Waters 486 UV detector (λ = 254 nm), and a Waters 746 integrator/recorder. The columns used were: Chiralpak, Chiracel OD, and Whelk-O1. Optical rotations were determined using a PerkinElmer 241 polarimeter at λ = 578 or 589 nm at rt. All dry solvents used were purified according to Perrin and Armarego (36): THF and Et_2O were freshly distilled from sodium benzophenone ketyl under nitrogen prior to use. Hexane and PhMe were distilled from CaH_2 and Na, respectively.

n-BuLi and *s*-BuLi were purchased from Sigma-Aldrich Chemical Co., as solutions in hexanes and cyclohexane, respectively. They were stored in resealable containers and titrated periodically against 2,5-dimethoxybenzyl alcohol (37) or *s*-butanol-1,10-phenanthroline (38). *N*,*N*,*N*′,*N*′-Tetramethylenethylenediamine (TMEDA) and (–)-sparteine were dried and distilled over CaH_2 and stored under argon. All commercial materials were purchased from Sigma-Aldrich Chemical Co. or Lancaster Synthesis Ltd. $Pd(PPh_3)_4$ was prepared following a literature procedure (39).

All the reactions were performed in oven-dried glassware under argon, using syringe-septum cap techniques. The –78 °C temperature designation is approximate and achieved by a dry ice – acetone bath. The phrase "standard workup" refers to addition of water or satd. aq. NH_4Cl, extraction with Et_2O, washing the organic extracts (brine), drying ($MgSO_4$), filtration, and concentration under reduced pressure. Flash column chromatography was carried out using Merck silica gel 60 (0.040–0.063 mm).

Standard methods

*(A) Lithiation of 1,1′-*N,N,N′,N′*-tetraisopropylferrocenedicarboxamide (5)*

A solution of (–)-sparteine (0.91 mL, 4.20 mmol) or TMEDA (0.64 mL, 4.20 mmol) in PhMe or Et_2O (20 mL) under Ar was stirred at rt (5 min), cooled to –78 °C, and treated with either *n*-BuLi or *s*-BuLi (4.20 mmol). After stirring (10 min) at –78 °C, a solution of **5** (0.44 g, 1.0 mmol) in either PhMe (4.5 mL) or Et_2O (10 mL) was added dropwise (ca. 1 drop / 10 s). After stirring for 2 h at –78 °C, the reaction mixture was quenched by an addition of electrophile (6 mmol) and then allowed to warm to rt over 4 h. Standard workup afforded the crude product.

*(B) Lithiation of 2-substituted derivatives of 1,1′-*N,N,N′,N′*-tetraisopropylferrocenedicarboxamide (6a, 6g, 6h)*

A solution of (–)-sparteine (0.45–0.91 mL, 2.1–4.2 mmol) in PhMe (20 mL) under Ar was stirred at rt (5 min), cooled to –78 °C, and treated with *n*-BuLi (4.2 mmol). After stirring (10 min) at –78 °C, a solution of a **6** (1.0 mmol) in PhMe (2.5 mL) was added slowly. After stirring for 2 h at –78 °C, the reaction mixture was quenched by addition of the electrophile (3.0–6.0 mmol), allowed to warm to rt over 4 h, and then subjected to standard workup to afford the crude product.

Experimental procedures

1,1′-Ferrocenedicarboxylic acid

A solution of *n*-BuLi (72.2 mL, 1.66 mol/L solution in hexane, 120 mmol) was added to a solution of ferrocene (10.1 g, 53.7 mmol) and TMEDA (20.0 mL, 132 mmol) in hexane (150 mL) under Ar at 0 °C. The reaction mixture was stirred for 12 h at rt. The hexane supernatant solution was removed via cannula and THF (150 mL) was added to dissolve the precipitate. The resultant solution was cooled to –78 °C and purged with carbon dioxide for 1 h. Later the reaction mixture was allowed to warm to rt and treated with H_2O (50 mL). THF was removed under reduced pressure. The aqueous residue was extracted with Et_2O (2 × 100 mL) and acidified with 2 N aq. HCl. The precipitate (bright yellow) was collected by filtration, dried in vacuo, and used without further purification (10.6 g, 72%); mp > 300 °C

© 2006 NRC Canada

(dec). IR (KBr) ν_{max}: 915, 1029, 1167, 1292, 1372, 1403, 1487, 1675, 2825 (br). ^{1}H NMR (DMSO-d_6) δ: 4.30 (s, 4H, Cp-*H*), 4.78 (s, 4H, Cp-*H*), 10.75–11.60 (br, 2H, COO*H*). ^{13}C NMR (DMSO-d_6) δ: 71.2, 72.5, 73.4, 171.0. MS *m*/*z* (rel intensity) (FAB): 274.2 (M^+, 8), 257.1 (11), 231.2 (8). HRMS calcd. for $C_{12}H_{10}{}^{56}FeO_4$: 273.9929; found: 273.9969.

1,1′-N,N,N′,N′-*Tetraisopropylferrocenedicarboxamide (5)*

To a stirred solution of 1,1′-ferrocenedicarboxylic acid (10.0 g, 36.2 mmol) in PhMe (100 mL) at rt, DMF (1.10 mL, 14.1 mmol) and oxalyl chloride (12.8 mL, 149 mmol) were added sequentially. The reaction mixture was stirred for 1 h at rt before PhMe and the excess of oxalyl chloride were removed under reduced pressure. The residue was dissolved in Et_2O (250 mL), cooled to 0 °C, and treated with an excess of HN(*i*-Pr)$_2$ (28.4 mL, 217 mmol). The reaction mixture was stirred for 8–12 h at rt. Standard workup followed by column chromatography (EtOAc–hexane, 1:2) and crystallization gave **5** as an orange solid (11.1 g, 80%); mp 133 to 134 °C (Et_2O–hexane) (lit. value (40) mp 127 to 128 °C). IR (KBr) ν_{max}: 1000, 1050, 1105, 1162, 1198, 1225, 1289, 1377, 1458, 1561, 1684, 2803, 2957, 3091. ^{1}H NMR ($CDCl_3$) δ: 1.05–1.70 (br, 24H, CH(C*H*$_3$)$_2$), 3.30–3.58, 4.35–4.55 (br, 2H, C*H*(CH$_3$)$_2$), 4.37 (t, *J* = 2.0 Hz, 4H, C$_5$*H*$_4$), 4.58 (t, *J* = 2.0 Hz, 4H, C$_5$*H*$_4$). ^{13}C NMR ($CDCl_3$) δ: 21.0, 70.9, 71.3, 83.2, 167.1. MS *m*/*z* (rel intensity) (EI): 440 (M^+, 100), 340 (16), 312 (9), 270 (6), 248 (20), 213 (10), 186 (11), 177 (5), 156 (12), 146 (9), 121 (19), 92 (10), 65 (7). HRMS calcd. for $C_{24}H_{36}{}^{54}FeN_2O_2$: 438.2169; found: 438.2173.

2-(Trimethylsilyl)-1,1′-N,N,N′,N′-*tetraisopropylferrocenedicarboxamide (6a)*

According to Standard method A, a solution of (–)-sparteine (0.49 mL, 2.2 mmol) and *n*-BuLi (1.4 mL, 1.65 mol/L solution in hexane, 2.2 mmol) was sequentially treated with a solution of **5** (0.47 g, 1.1 mmol) in PhMe and TMSCl (0.34 mL, 2.7 mmol). Standard workup followed by column chromatography (EtOAc–hexane, 1:30) afforded compound **6a** as an orange solid (0.42 g, 68%); mp 107.0–107.5 °C (hexanes). $[\alpha]^{23}_{578}$ +67.5° (*c* 0.54, $CHCl_3$). IR (KBr) ν_{max}: 2962, 2883, 1624, 1449, 1325, 1204, 1149, 1040, 829, 754. ^{1}H NMR ($CDCl_3$) δ: 0.23 (s, 9H, Si(C*H*$_3$)$_3$), 0.80–1.60 (br, 24H, CH(C*H*$_3$)$_2$)), 3.2–4.1 (br, 4H, C*H*(CH$_3$)$_2$), 4.20, 4.38, 4.43, 4.49, 4.57, 4.67 (m, 7H, Cp-*H*). ^{13}C NMR ($CDCl_3$) δ: 0.5, 20.7, 21.2, 71.0, 72.03, 72.23, 75.7, 82.4, 93.5, 168.6. MS *m*/*z* (rel intensity) (EI): 512 (M^+, 51), 510 (4), 497 (100), 439 (7), 220 (9), 149 (14), 73 (14). HRMS calcd. for $C_{27}H_{44}{}^{54}FeN_2O_2Si$: 510.2568; found: 510.2551. Two other isolated fractions contained *dl*-**4a** (0.032g, 5%), $[\alpha]^{23}_{578}$ +49.2° (*c* 0.49, $CHCl_3$), 99% op (optical purity) and *meso*-**4a** (0.015 g, 2%).

2-Methyl-1,1′-N,N,N′,N′-*tetraisopropylferrocenedicarboxamide (6b)*

According to Standard method A, a solution of (–)-sparteine (0.91 mL, 4.1 mmol) and *n*-BuLi (2.35 mL, 1.75 mol/L solution in hexane, 4.12 mmol) was sequentially treated with a solution of **5** (0.437 g, 0.98 mmol) in PhMe and MeI (0.37 mL, 5.9 mmol). Standard workup followed by column chromatography (EtOAc–hexane, 1:4) afforded **6b** as an orange solid (0.32 g, 71%); mp 123 to 124 °C. CSP HPLC analysis (Chiralcel OD; eluent: *n*-hexane–*i*-PrOH–Et_2NH (99:1:0.01, flow 0.75 mL/min) determined 92% ee (t_R(major *dl*) = 26.95 min, t_R(minor) = 29.35 min). $[\alpha]^{23}_{578}$ +63.2° (*c* 0.66, $CHCl_3$). IR (KBr) ν_{max}: 1025, 1044, 1111, 1137, 1157, 1204, 1316, 1372, 1453, 1615, 2954, 3001, 3086. ^{1}H NMR ($CDCl_3$) δ: 0.65–1.82 (br, 24H, CH(C*H*$_3$)$_2$)), 2.02 (s, 3H, CpC*H*$_3$), 3.25–3.55 and 3.70–4.05 (br, 4H, C*H*(CH$_3$)$_2$), 4.18 (m, 2H, Cp-*H*), 4.39 (m, 2H, Cp-*H*), 4.57 (m, 2H, Cp-H), 4.67 (br, 1H, Cp-*H*). ^{13}C NMR ($CDCl_3$) δ: 12.7, 20.1, 20.7, 20.9, 21.0, 45.3, 50.2, 67.8, 68.2, 70.8, 71.3, 71.4, 71.6, 72.0, 82.1, 85.1, 88.2, 169.2. MS *m*/*z* (rel intensity) (EI): 454 (27), 426 (4), 169 (6). HRMS calcd. for $C_{25}H_{38}{}^{56}FeN_2O_2$: 454.2283; found: 454.2242.

2-Iodo-1,1′-N,N,N′,N′-*tetraisopropylferrocenedicarboxamide (6c)*

According to Standard method A, a solution of (–)-sparteine (0.97 mL, 4.20 mmol) and *n*-BuLi (2.47 mL, 1.70 mol/L solution in hexane, 4.20 mmol) was sequentially treated with solutions of **5** (0.44 g, 1.0 mmol) and iodine (1.52 g, 6.00 mmol) in PhMe (4.5 mL and 14 mL, respectively). Standard workup followed by column chromatography (EtOAc–hexane, 1:10) afforded **6c** as a slowly solidifying orange oil (0.37 g, 70%); mp 113–115 °C. CSP HPLC analysis ((*S*,*S*)-Whelk-O1; eluent: *n*-hexane–*i*-PrOH (96:4, flow 0.5 mL/min) determined 89% ee (t_R(major) = 25.84 min, t_R(minor) = 21.68 min). $[\alpha]^{23}_D$ +33.2 (*c* 0.47, $CHCl_3$). IR (neat) ν_{max}: 807, 1037, 1206, 1316, 1369, 1460, 1635, 2931, 2966. ^{1}H NMR ($CDCl_3$) δ: 0.92–1.72 (m, 24H, CH(C*H*$_3$)$_2$), 3.38–3.70 (m 4H, C*H*(CH$_3$)$_2$), 4.26–6.60 and 4.82–4.88 (m, 7H, Cp*H*). ^{13}C NMR ($CDCl_3$) δ: 20.41, 20.54, 40.64, 45.6, 50.4, 68.9, 70.3, 72.8, 74.1, 74.7, 75.1, 83.7, 92.8, 165.6, 168.0. MS *m*/*z* (rel intensity) (EI): 566 (M^+, 0.5), 502 (8), 414 (6), 219 (25), 131 (40), 69 (100). HRMS calcd. for $C_{24}H_{35}{}^{56}FeIN_2O_2$: 566.1092; found: 566.1103.

2-(Diphenylhydroxymethyl)-1,1′-N,N,N′,N′-*tetraisopropylferrocenedicarboxamide (6d)*

Method 1

According to Standard method A, a solution of (–)-sparteine (0.91 mL, 4.1 mmol) and *n*-BuLi (2.36 mL, 1.75 mol/L solution in hexane, 4.1 mmol) was sequentially treated with solutions of **5** (0.433 g, 0.98 mmol) and benzophenone (1.07 g, 5.90 mmol) in PhMe (4.5 mL and 10.0 mL, respectively). Standard workup followed by column chromatography (EtOAc–hexane, 1:15) afforded the title compound (**6d**) as an orange solid (0.56 g, 92%); mp 179–182 °C (Et_2O). CSP HPLC analysis ((*S*,*S*)-Whelk-O1; eluent: *n*-hexane–*i*-PrOH 92:8, flow 0.75 mL/min) determined 94% ee (t_R(major) = 12.06 min, t_R(minor) = 15.15 min). $[\alpha]^{23}_D$ +161.1° (*c* 0.54, $CHCl_3$). IR (KBr) ν_{max}: 704, 752, 765, 818, 832, 1031, 1047, 1134, 1161, 1202, 1320, 1368, 1456, 1594, 2875, 2932, 2966, 3066, 3204. ^{1}H NMR ($CDCl_3$) δ: 0.65–1.48 (br, 24H, CH(C*H*$_3$)$_2$), 2.87, 3.15, 3.44, 4.20 (m, 4H, C*H*(CH$_3$)$_2$), 3.67, 4.29, 4.56, 4.63, 4.92 (m, 7H, Cp-*H*), 5.81 (s, 1H, O*H*), 7.06–7.40, 7.55 (m, 10H, Ph*H*), 7.94 (s, 1H, C*H*(OH)Ph$_2$). ^{13}C NMR ($CDCl_3$) δ: 20.4, 20.5, 40.6, 45.6, 50.4, 68.9, 70.3, 72.8, 74.07, 74.7, 75.1, 83.7, 92.8, 165.6, 168.0. MS *m*/*z* (rel intensity) (EI): 622 (M^+, 2), 614 (8), 502

© 2006 NRC Canada

(50), 414 (42), 354 (3), 218 (78), 131 (100), 70 (98). HRMS calcd. for $C_{37}H_{46}{}^{56}FeN_2O_3$: 622.2858; found: 622.2836.

Method 2

By Sn-Li exchange from 2-(tributylstannyl)-1,1′-N,N,N′,N′-tetraisopropylferrocenedicarboxamide (6f).

n-BuLi (0.09 mL, 1.67 mol/L solution in hexane, 0.15 mmol) was added to a cold (–78 °C), stirred solution of 2-(tributylstannyl)-1,1′-*N*,*N*,*N*′,*N*′-tetraisopropylferrocenedicarboxamide (**6f**) (0.10 g, 0.14 mmol) in PhMe (5 mL). The resulting solution was stirred for 15 min, benzophenone (0.052 g, 0.28 mmol) in PhMe (0.5 mL) was added, and stirring was continued for 40 min at –78 °C before the reaction mixture was allowed to warm to rt. Standard workup and flash chromatography (EtOAc–hexane, 8:1) afforded pure **6d** (0.022 g, 25%) and also **5** (3 mg, 5%) and unreacted 2-(tributylstannyl)-1,1′-*N*,*N*,*N*′,*N*′-tetraisopropylferrocenedicarboxamide (**6f**) (51 mg, 49%). The crude product was analysed by CSP HPLC ((*S*,*S*)-Whelk-O1; eluent: *n*-hexane–*i*-PrOH 97:3, flow 0.5 mL/min) and found to be 82% ee (t_R(major) = 22.88 min, t_R(minor) = 35.98 min).

2-(Diethylhydroxymethyl)-1,1′-N,N,N′,N′-tetraisopropylferrocenedicarboxamide (6e)

According to Standard method A, a solution of (–)-sparteine (0.97 mL, 4.4 mmol) and *n*-BuLi (2.31 mL, 1.90 mol/L solution in hexane, 4.40 mmol) was sequentially treated with solutions of **5** (0.459 g, 1.04 mmol) and 3-pentanone (0.63 mL, 6.2 mmol) in PhMe (4.5 and 5.0 mL, respectively). Standard workup followed by column chromatography (EtOAc–hexane, 1:6) afforded **6e** as an orange solid (0.25 g, 45%); mp 121 to 122 °C. CSP HPLC analysis (Chiralcel OD; eluent: *n*-hexane–*i*-PrOH 98:2, flow 0.15 mL/min) determined 90% ee (t_R(major) = 37.02 min, t_R(minor) = 39.18 min). $[\alpha]^{23}{}_{578}$ –31.2° (*c* 0.34, $CHCl_3$). IR (KBr) ν_{max}: 814, 970, 1038, 1038, 1113, 1135, 1157, 1200, 1340, 1453, 1604, 2939, 3343. ^{1}H NMR ($CDCl_3$) δ: 0.47 (t, *J* = 7.5 Hz, 3H, CH_2CH_3), 0.72–1.98 (m, 31H, $CH(CH_3)_2$, CH_2CH_3, CH_2CH_3, 3.29–3.55 (br, 4H, $CH(CH_3)_2$), 4.10–4.32 (m, 3H, Cp*H*), 4.47 (s, 1H, Cp*H*), 4.60 (s, 2H, Cp*H*), 4.73 (s, 1H, Cp*H*), 6.10 (s, 1H, O*H*). ^{13}C NMR ($CDCl_3$) δ: 7.6, 9.2, 20.3, 20.7, 20.9, 29.6, 33.9, 46.2, 50.8, 67.7, 69.5, 71.7, 72.2, 72.6, 82.0, 83.1, 101.4, 168.9, 171.4. MS *m*/*z* (rel intensity) (EI): 526 (M^+, 18), 508 (100), 446 (3), 338 (4), 316 (12), 306 (5), 265 (5), 231 (5), 161 (7), 105 (9), 91 (8), 86 (7). HRMS calcd. for $C_{29}H_{46}{}^{56}FeN_2O_3$: 526.2858; found: 526.2893. Anal. calcd. for $C_{29}H_{46}FeN_2O_3$: C 66.15, H 8.80, N 5.22; found: C 66.17, H 8.65, N 4.93.

2-(Tributylstannyl)-1,1′-N,N,N′,N′-tetraisopropylferrocenedicarboxamide (6f)

According to Standard method A, a solution of (–)-sparteine (0.92 mL, 4.2 mmol) and *n*-BuLi (5.17 mL, 1.68 mol/L solution in hexane, 8.69 mmol) was sequentially treated with a PhMe (4.5 mL) solution of **5** (0.903 g, 1.00 mmol) and neat tributyltin chloride (3.51 mL, 12.41 mmol). Standard workup followed by column chromatography (EtOAc–hexane, 1:10) afforded **6f** as a red oil, which was purified by Kugelrohr distillation (0.86 g, 58%). $[\alpha]^{23}{}_{578}$ +90.4° (*c* 0.44, $CHCl_3$). IR (neat) ν_{max}: 1039, 1158, 1204, 1280, 1323, 1372, 1457, 1614, 2930. ^{1}H NMR ($CDCl_3$) δ: 0.79–1.83 (br, 51H, $CH(CH_3)_2$, Bu-*H*), 3.19–3.68 (br, 4H, $CH(CH_3)_2$)), 4.22–4.33 (m, 3H, Cp- *H*), 4.30–4.52 (m, 2H, Cp-*H*), 4.52–4.68 (m, 2H, Cp-*H*). ^{13}C NMR ($CDCl_3$) δ: 11.22, 13.7, 14.6, 14.8, 21.0, 26.8, 27.4, 28.0, 29.2, 46.1, 50.0, 69.9, 70.4, 71.1, 71.5, 72.0, 74.2, 76.1, 82.3, 88.4, 168.9, 169.4. MS *m*/*z* (rel intensity) (FAB): 730 (M^+, 7), 673 (100), 630 (9), 558 (28), 495 (28), 426 (16), 368 (20). Anal. calcd. for $C_{36}H_{62}FeN_2O_2Sn$: C 59.28, H 8.57, N 3.84; found: C 58.99, H 8.49, N 3.80.

2-(Diphenylphosphino)-1,1′-N,N,N′,N′-tetraisopropylferrocenedicarboxamide (6g)

According to Standard method A, a solution of (–)-sparteine (1.04 mL, 4.20 mmol) and *n*-BuLi (2.40 mL, 1.75 mol/L solution in hexane, 4.20 mmol) was sequentially treated with a PhMe (4.5 mL) solution of **5** (0.440 g, 1.00 mmol) and neat chlorodiphenylphosphine (1.1 mL, 6.0 mmol). After stirring for 1 h at –78 °C, the reaction mixture was allowed to warm to 0 °C and quenched with satd. aq. NH_4Cl. Standard workup followed by column chromatography (SiO_2 deactivated by additon of 2% Et_3N, EtOAc–hexane 1:10) afforded **6g** as an orange solid (0.335 g, 54%); mp 142–144 °C (dec). CSP HPLC analysis (Chiracel OD; eluent: *n*-hexane–*i*-PrOH 98:2, flow 0.25 mL/min) determined 97% ee (t_R(major) = 31.31 min, t_R(minor) = 34.24 min). $[\alpha]^{23}{}_D$ +225.5° (*c* 0.31, CH_2Cl_2). IR (KBr) ν_{max}: 2963, 1624, 1449, 1336, 1206, 820, 751, 701. ^{1}H NMR ($CDCl_3$) δ: 0.32–1.75 (br, 24 $CH(CH_3)_2$), 3.03–3.48 (br, 4H, $CH(CH_3)_2$), 3.90, 4.26, 4.34, 4.37, 4.45, 4.51, 4.58, 4.65, 4.80 (m, 7H, Cp*H*), 7.18–7.62 (br, 10H, C_6H_5). ^{13}C NMR ($CDCl_3$) δ: 20.3, 21.4, 31.6, 71.7, 72.2, 73.4, 74.7, 76.9, 80.3, 82.7, 86.0, 98.3, 128.1, 128.2, 128.7, 133.0, 133.4, 134.1, 134.6, 137.9, 139.2, 166.7. MS *m*/*z* (rel. intensity) (EI): 625 (M^+, 62), 539 (71), 423 (100), 346 (84), 245 (69). HRMS calcd. for $C_{36}H_{46}{}^{56}FeN_2O_2P$: 625.2674; found: 625.2646.

2-(Phenylthio)-1,1′-N,N,N′,N′-tetraisopropylferrocenedicarboxamide (6h)

According to Standard method A, a solution of (–)-sparteine (0.93 mL, 4.2 mmol) and *n*-BuLi (2.76 mL, 1.52 mol/L solution in hexane, 4.2 mmol) was sequentially treated with solutions of **5** (0.440 g, 1.00 mmol) and Ph_2S_2 (1.30 g, 5.95 mmol) in PhMe (4.5 mL and 10.0 mL, respectively). Standard workup followed by column chromatography (EtOAc–hexane, 1:6) afforded **6h** (0.39 g, 71%); mp 135–137 °C. CSP HPLC analysis (Chiralcell OD; eluent: *n*-hexane–*i*-PrOH (0.1% solution of Et_2NH of 99.1:0.9, flow mL/min) determined 89% ee (t_R(major) = 17.54 min, t_R(minor) = 21.21 min). $[\alpha]^{23}{}_{578}$ +97.7° (*c* 1.41, $CHCl_3$). IR (KBr) ν_{max}: 738, 814, 814, 840, 1041, 1143, 1205, 1337, 1453, 1611, 2935. ^{1}H NMR ($CDCl_3$) δ: 0.33–1.61 (br, 24H, $CH(CH_3)_2$), 3.12–3.78 (br, 4H, $CH(CH_3)_2$), 4.35–4.98 (m, 7H, Cp-*H*), 7.01–7.37 (m, 5H, C_6H_5). ^{13}C NMR ($CDCl_3$) δ: 19.99, 20.4, 20.7, 20.9, 45.8, 50.5, 70.6, 71.7, 72.6, 72.9, 73.7, 73.9, 77.7, 79.0, 83.7, 92.8, 125.4, 127.3, 128.7, 139.7, 165.5, 168.6. MS *m*/*z* (rel intensity) (FAB): 548 (M^+, 45), 460 (62), 372 (72), 328 (31), 185 (100), 132 (88). Anal. calcd. for $C_{30}H_{40}FeN_2O_2S$: C 65.67, H 7.35, N 5.11; found: C 65.80, H 7.28, N 5.05.

© 2006 NRC Canada

2-(Phenylselenyl)-1,1′-N,N,N′,N′-tetraisopropylferrocenedicarboxamide (6i)

According to Standard method A, a solution of (–)-sparteine (0.92 mL, 4.2 mmol) and *n*-BuLi (2.49 mL, 1.68 mol/L solution in hexane, 4.19 mmol) was sequentially treated with solutions of **5** (0.439 g, 1.00 mmol) and Ph_2Se_2 (1.87 g, 5.98 mmol) in PhMe (4.5 and 2.5 mL, respectively). Standard workup followed by column chromatography (EtOAc–hexane, 1:4) afforded **6i** (0.36 g, 82%); mp 126 to 127 °C. CSP HPLC analysis (Chiralcel OD; eluent: *n*-hexane–*i*-PrOH 99:1, flow 0.3 mL/min) determined 71% ee (t_R(major) = 32.92 min, t_R(minor) = 35.90 min). $[\alpha]^{23}_{578}$ +216° (*c* 0.23, $CHCl_3$). IR (CH_2Cl_2) ν_{max}: 1037, 1135, 1160, 1205, 1266, 1322, 1372, 1463, 1475, 1621, 2971, 2934, 3053. ^{1}H NMR ($CDCl_3$) δ: 0.37–1.60 (br, 24H, $CH(CH_3)_2$)), 3.11–3.76 (br, 4H, $CH(CH_3)_2$)), 4.40 (dd, *J* = 2.8, 1.3 Hz, 1H, Cp-*H*), 4.48–4.70 (m, 3H, Cp-*H*), 4.68 (dt, *J* = 1.3, 2.6 Hz, 1H, Cp-*H*), 4.90 (dt, *J* = 1.3, 2.6 Hz, 1H, Cp*H*), 7.08–7.19 (m, 3H, C_6H_5), 7.27–7.35 (m, 2H, C_6H_5). ^{13}C NMR ($CDCl_3$) δ: 14.1, 21.0, 22.6, 31.5, 45.8, 49.8, 50.4, 71.1, 71.2, 72.2, 72.6, 73.4, 73.2, 74.2, 77.3, 83.4, 92.4, 126.1, 128.8, 130.3, 133.7, 166.0, 168.5. MS *m*/*z* (rel intensity) (FAB): 597 (M^+, 9), 553 (8), 517 (6), 461 (11), 369 (32), 356 (5), 277 (100), 241 (8). HRMS calcd. for $C_{30}H_{41}{}^{56}FeN_2O_2Se$: 597.1683; found: 597.1678.

2-(2,4-Dimethoxyphenyl)-1,1′-N,N,N′,N′-tetraisopropylferrocenedicarboxamide (6k)

A mixture of $Pd(PPh_3)_4$ (0.070 g, 0.06 mmol), 2-iodo-1,1′-*N*,*N*,*N*′,*N*′-tetraisopropylferrocenedicarboxamide (**6c**) (0.34 g, 0.61 mmol, 89% ee), degassed aq. Na_2CO_3 solution (1.80 mL, 2 mol/L, 3.66 mmol), and 2,4-dimethoxyphenylboronic acid (0.18 g, 0.97 mmol) in freshly distilled DME (15 mL) was refluxed for 5 days. The crude material was passed through Celite, and the filtrate was subjected to standard workup. Purification by column chromatography (EtOAc–hexane, 1:8) afforded **6k** as a brown-red solid (0.069 g, 20%); mp 161–163 °C. CSP HPLC analysis (Chiralcel OD; eluent: *n*-hexane–*i*-PrOH 98.5:1.5, flow 0.20 mL/min) determined 89% ee (t_R(major) = 67.93 min, t_R(minor) = 75.04 min). $[\alpha]^{23}_{578}$ +8.9° (*c* 0.18, $CHCl_3$). IR (KBr) ν_{max}: 817, 1036, 1151, 1205, 1317, 1370, 1454, 1533, 1619, 2936. ^{1}H NMR ($CDCl_3$) δ: 0.25–1.75 (br, 24H, $CH(CH_3)_2$), 3.05–3.65 (b, 2H, $CH(CH_3)_2$), 3.72 (s, 3H, OCH_3), 3.78 (s, 3H, OCH_3), 4.32–4.44 (m, 3H, Cp*H*), 4.54 (m, 2H, Cp*H*), 4.67–4.70 (m, 1H, Cp*H*), 4.76–4.79 (m, 1H, Cp*H*), 6.38 (d, *J* = 2.6 Hz, 1H, H(3)-C_6H_3), 6.45 (dd, *J* = 2.6, 8.4 Hz, 1H, H(5)-C_6H_3), 7.70 (d, *J* = 8.4 Hz, 1H, H(6)-C_6H_3). ^{13}C NMR ($CDCl_3$) δ: 19.5, 19.9, 20.9, 21.0, 45.5, 50.4, 55.4, 69.3, 69.8, 71.5, 71.7, 73.0, 73.4, 74.7, 81.4, 82.4, 90.0, 98.2, 104.2, 117.7, 127.9, 128.1, 130.4, 132.6, 134.7, 134.9, 157.9, 159.8, 167.7, 169.3. MS *m*/*z* (rel intensity) (CI): 577 (MH^+, 46), 576 (42), 476 (9), 441 (17), 349 (6), 330 (13), 309 (6), 253 (16), 233 (13), 194 (16), 145 (22), 131 (15), 117 (100), 100 (14), 86 (19), 71 (10). HRMS calcd. for $C_{32}H_{44}{}^{56}FeN_2O_4$: 576.2650; found: 576.2675.

2-Phenyl-1,1′-N,N,N′,N′-tetraisopropylferrocenedicarboxamide (6l)

A mixture of $PdCl_2$(dppf) (37 mg, 0.051 mmol), CuO (95 mg, 1.2 mmol), and PhBr (0.02 mL, 0.19 mmol) in DMF (3 mL) was heated to 150 °C for 30 min and treated with a solution of 2-(tributylstannyl)-1,1′-*N*,*N*,*N*′,*N*′-tetraisopropylferrocenedicarboxamide (**6f**) (0.107 g, 0.15 mmol, $[\alpha]^{23}_{578}$ +90.4° (*c* 0.44, $CHCl_3$), i.e., ≥82% ee) in DMF (0.3 mL). The resulting reaction mixture was stirred for 18 h at 100 °C, cooled to rt, passed through Celite, concentrated and subjected to standard workup followed by column chromatography (hexane–EtOAc, 6:1) to afford **6l** as a brown oil (27 mg, 35%) and separately 1,1′-*N*,*N*,*N*′,*N*′-tetraisopropylferrocenedicarboxamide (**5**) (24 mg, 51%). Compound **6l**: $[\alpha]^{23}_{578}$ –266.1° (*c* 0.17, $CHCl_3$). IR (neat) ν_{max}: 764, 815, 1038, 1111, 1135, 1159, 1207, 1261, 1318, 1372, 1457, 1508, 1623, 2926, 2964. ^{1}H NMR ($CDCl_3$) δ: 0.24–1.72 (br, 24H, $CH(CH_3)_2$), 3.13–3.60 (br, 4H, $CH(CH_3)_2$), 4.25–4.92 (br, 7H, Cp*H*), 7.25 (m, 3H, C_6H_5), 7.56 (m, 2H, C_6H_5). ^{13}C NMR ($CDCl_3$) δ: 19.5, 19.8, 20.8, 20.9, 21.0, 22.7, 29.7, 45.7, 50.6, 68.6, 70.0, 70.9, 72.0, 72.9, 73.4, 74.3, 82.4, 85.6, 90.1, 126.6, 128.1, 137.5, 167.5, 168.9. MS *m*/*z* (rel intensity) (FAB): 517 (MH^+, 22), 416 (5), 330 (3), 277 (8), 185 (100), 116 (5). HRMS calcd. for $C_{30}H_{41}{}^{56}FeN_2O_2$ (MH^+): 517.2518; found: 517.2495.

2,2′-Bis(trimethylsilyl)-1,1′-N,N,N′,N′-tetraisopropylferrocenedicarboxamide (7a)

Method 1

From 1,1′-*N*,*N*,*N*′,*N*′-tetraisopropylferrocenedicarboxamide (**5**). According to Standard method A, a solution of (–)-sparteine (0.51 mL, 2.30 mmol) and *n*-BuLi (1.36 mL, 1.69 mol/L solution in hexane, 2.30 mmol) in PhMe (20 mL) was sequentially treated with a solution of 1,1′-*N*,*N*,*N*′,*N*′-tetraisopropylferrocenedicarboxamide (**5**) (0.24 g, 0.55 mmol) PhMe (4.5 mL) and then TMSCl (0.42 mL, 3.3 mmol). Standard workup followed by column chromatography (EtOAc–hexane, 1:30) gave separately *dl*-**7a** (0.153 g, 50%), *meso*-**7a** (0.065 g, 21%), and 2-(trimethylsilyl)-1,1′-*N*,*N*,*N*′,*N*′-tetraisopropylferrocenedicarboxamide (**6a**) (0.043 g, 16%, $[\alpha]^{23}_{578}$ +64.3° (*c* 0.11, $CHCl_3$)) as orange solids.

dl-*2,2′-Bis(trimethylsilyl)-1,1′-N,N,N′,N′-tetraisopropylferrocenedicarboxamide (7a):* $[\alpha]^{23}_{578}$ +48.0° (*c* 0.51, $CHCl_3$). Optical purity: 97%; mp 192–194 °C (hexanes). IR (KBr) ν_{max}: 833, 1041, 1069, 1120, 1155, 1207, 1246, 1279, 1330, 1371, 1455, 1627, 2934. ^{1}H NMR ($CDCl_3$) δ: 0.25 (s, 18H, $Si(CH_3)_3$), 0.77–1.12 (br, 24H, $CH(CH_3)_2$), 3.15–3.50, 3.80–4.06 (br, 4H, $CH(CH_3)_2$), 4.15 (s, 2H, Cp-*H*), 4.60 (s, 4H, Cp-*H*). ^{13}C NMR ($CDCl_3$) δ: 0.6, 20.7, 45.9, 50.1, 73.0, 73.5, 74.0, 74.4, 92.6, 168.9. MS *m*/*z* (rel intensity) (EI): 585 (M^+, 76), 442 (26), 312 (16), 220 (22), 128 (17), 73 (95). Anal. calcd. for $C_{30}H_{52}{}^{56}FeN_2O_2Si_2$: C 61.62, H 8.96, N 4.79; found: C 61.50, H 8.73, N 4.79.

meso-*2,2′-Bis(trimethylsilyl)-1,1′-N,N,N′,N′-tetraisopropylferrocenedicarboxamide (7a):* mp 192–194 °C (Et_2O–hexane). IR (KBr) ν_{max}: 904, 1040, 1067, 1127, 1156, 1207, 1279, 1349, 1454, 1623, 2963, 3088. ^{1}H NMR ($CDCl_3$) δ: 1.32 (s, 18H, $Si(CH_3)_3$), 0.75–1.70 (br, 24H, $CH(CH_3)_2$), 3.15–3.44, 3.73–4.05 (br, 4H, $CH(CH_3)_2$), 4.34 (s, 2H, Cp-*H*), 4.43 (s, 2H, Cp-*H*), 4.52 (s, 2H, Cp-*H*). ^{13}C NMR ($CDCl_3$) δ: 0.0, 20.7, 45.7, 50.1, 70.5, 72.6, 74.8, 92.2, 168.7. MS (EI) *m*/*z* (rel intensity): 585 (M^+, 5), 370 (2), 204 (3), 100 (5), 73 (100). Anal. calcd. for $C_{30}H_{52}{}^{56}FeN_2O_2Si_2$: C 61.62, H 8.96, N 4.79; found: C 61.80, H 8.85, N 4.79.

© 2006 NRC Canada

Method 2

From 2-(trimethylsilyl)-1,1′-*N*,*N*,*N*′,*N*′-tetraisopropylferrocenedicarboxamide (**6a**). According to Standard method B, a solution of (–)-sparteine (0.71 mL, 3.23 mmol), and *n*-BuLi (1.96 mL, 1.65 mol/L solution in hexane, 3.23 mmol) in PhMe (20 mL) was sequentially treated with a solution of 2-(trimethylsilyl)-1,1′-*N*,*N*,*N*′,*N*′-tetraisopropylferrocenedicarboxamide (**6a**, 0.39 g, 0.76 mmol, $[\alpha]^{23}_{578}$ +67.5° (*c* 0.54, $CHCl_3$)) in PhMe (2.5 mL) and then TMSCl (0.60 mL, 4.6 mmol). Standard workup followed by column chromatography (EtOAc–hexane, 1:30) gave the title compounds (**7a**) as orange solids; *dl*-**7a** (0.336 g, 75%) and *meso*-**7a** (0.056 g, 12%), *dl*-**7a** ($[\alpha]^{23}_{578}$ +44.8° (*c* 0.42, $CHCl_3$)); 91% optical purity.

2,2′-Dimethyl-1,1′-N,N,N′,N′-*tetraisopropylferrocenedicarboxamide (7b)*

Method 1

From 1,1′-*N*,*N*,*N*′,*N*′-tetraisopropylferrocenedicarboxamide (**5**) using *s*-BuLi. According to Standard method A, a solution of (–)-sparteine (0.90 mL, 4.1 mmol) and *s*-BuLi (3.44 mL, 1.18 mol/L solution in cyclohexane, 4.06 mmol) in Et_2O (20 mL) was sequentially treated with a solution of 1,1′-*N*,*N*,*N*′,*N*′-tetraisopropylferrocenedicarboxamide (**5**) (0.447 g, 1.02 mmol) in Et_2O (10 mL) followed by MeI (0.38 mL, 6.1 mmol). Standard workup followed by column chromatography (EtOAc–hexane, 1:15) afforded a mixture of *meso*-**7b** and *dl*-**7b** diastereomers (0.33 g, 70%) as an orange solid. CSP HPLC analysis (Chiralcel OD; eluent: *n*-hexane–*i*-PrOH 99.4:0.6, flow 1.0 mL/min) determined dr (meso:dl, 76:24) and 52% ee (t_R(major dl) = 5.74 min, t_R(minor dl) = 6.96 min, t_R(meso diastereomer) = 9.30 min). IR (KBr) ν_{max}: 815, 1022, 1037, 1076, 1134, 1156, 1210, 1314, 1346, 1371, 1455, 1629, 2937, 3088. ^{1}H NMR ($CDCl_3$) δ: 0.62–1.78 (br, 24H, $CH(CH_3)_2$), 2.02 (s, 6H, $CpCH_3$), 3.18–4.00 (br, 4H, $CH(CH_3)_2$), 4.15 (m, 2H, Cp-*H*), 4.36 (m, 2H, Cp-*H*), 4.52 (m, 1H, Cp-*H*), 4.66 (m, 1H, Cp-*H*). ^{13}C NMR ($CDCl_3$) δ: [12.06], 12.44, 20.75, [20.48], 45.35, 49.85, [68.50], 69.41, [69.98], 72.11, 84.76, [86.76], 87.10, 167.90. MS *m*/*z* (rel intensity) (FAB): 468 (M^+, 100), 396 (2), 368 (35), 262 (26), 213 (5), 134 (13), 55 (11). HRMS calcd. for $C_{26}H_{40}{}^{56}FeN_2O_2$: 468.2439; found: 468.2390. Values in square parentheses indicate resonances assigned to the dl-diastereomer.

Method 2

From 1,1′-*N*,*N*,*N*′,*N*′-tetraisopropylferrocenedicarboxamide (**5**) using *n*-BuLi in the presence of LiCl. According to Standard method A, a solution of (–)-sparteine (0.49 mL, 2.2 mmol), vacuum-dried LiCl (0.048 g, 2.1 mmol), and *n*-BuLi (1.32 mL, 1.69 mol/L solution in hexane, 4.2 mmol) in Et_2O (10 mL) was sequentially treated with a solution of 1,1′-*N*,*N*,*N*′,*N*′-tetraisopropylferrocenedicarboxamide (**5**) (0.23 g, 0.53 mmol) in Et_2O (5 mL) and MeI (0.37 mL, 6.0 mmol). Standard workup followed by column chromatography (EtOAc–hexane, 1:15) afforded a mixture of *dl*-**7b** and *meso*-**7b** diastereomers (0.040 g, 16%). CSP HPLC analysis determined 80% ee and dr = 72:28 (dl:meso); 2) and separately 2-methyl-1,1′-*N*,*N*,*N*′,*N*′-tetraisopropylferrocenedicarboxamide (**6b**) (0.15 g, 61%), 79% ee by CSP HPLC analysis, as well as the starting material 1,1′-*N*,*N*,*N*′,*N*′-tetraisopropylferrocenedicarboxamide (**5**) (0.018 g, 8%).

2,2′-Bis(diphenylphosphino)-1,1′-N,N,N′,N′-*tetraisopropylferrocenedicarboxamide (7c)*

Preparation of *dl*-**7c** from 2-(diphenylphosphino)-1,1′-*N*,*N*,*N*′,*N*′-tetraisopropylferrocenedicarboxamide (**6g**). According to Standard method B, a solution of (–)-sparteine (0.30 mL, 1.4 mmol) and *n*-BuLi (0.67 mL, 2.00 mol/L solution in hexane, 1.3 mmol) in PhMe (20 mL) was sequentially treated with a solution of 2-(diphenylphosphino)-1,1′-*N*,*N*,*N*′,*N*′-tetraisopropylferrocenedicarboxamide (**6g**) (0.400 g, 0.91 mmol, 97% ee) in PhMe (2.5 mL) and Ph_2PCl (0.36 mL, 1.9 mmol). The reaction mixture was quenched with satd. aq. NH_4Cl and extracted with CH_2Cl_2. The organic extract was washed with brine and concentrated under reduced pressure. The residue was purified by column chromatography (SiO_2 pretreated with 2% Et_3N, EtOAc–hexane 1:6) to give compound **7c** as a bright yellow solid (0.29 g, 45%); dr(dl:meso) >95:<5 by ^{31}P NMR; mp 233–236 °C (dec) (lit. value (41) mp 228–230 °C). $[\alpha]^{20}_D$ +277° (*c* 0.76, CH_2Cl_2), 98% optical purity. IR (KBr) ν_{max}: 3088, 2938, 1625, 1531, 1454, 1371, 1333, 1279, 1244, 1204, 1154, 1039. ^{1}H NMR ($CDCl_3$) δ: 0.34–1.53 (br, 24H, $CH(CH_3)_2$), 3.04–3.26 and 3.92–4.13 (br, 4H, $CH(CH_3)_2$), 3.53 (s, 2H, Cp-*H*), 4.78–4.82 (m, 4H, Cp-*H*), 7.12–7.43 (br, 20H, C_6H_5). ^{13}C NMR ($CDCl_3$) δ: 13.7, 19.0, 20.3, 50.0, 72.7, 74.8, 76.7, 81.1, 90.5, 127.9, 128.0, 128.1, 128.2, 129.1, 130.0, 130.4, 132.7, 133.1, 133.5, 133.6, 133.9, 137.9, 138.1, 139.0, 167.0. ^{31}P NMR($CDCl_3$) δ: –22.27. Anal. calcd. for $C_{48}H_{54}{}^{56}FeN_2O_2P_2$: C 71.28, H 6.73, N 3.46: found: C 71.36, H 6.75, N 3.51.

Preparation of meso-**7c** *from 1,1′*-N,N,N′,N′-*tetraisopropylferrocenedicarboxamide (**5**) using* s-*BuLi*

According to Standard method A, a solution of (–)-sparteine (1.9 mL, 8.4 mmol) and *s*-BuLi (7.1 mL, 1.18 mol/L solution in cyclohexane, 8.4 mmol) in Et_2O (40 mL) was sequentially treated with a solution of 1,1′-*N*,*N*,*N*′,*N*′-tetraisopropylferrocenedicarboxamide (**5**) (0.883 g, 2.01 mmol) in Et_2O (20 mL) and Ph_2PCl (2.16 mL, 12.0 mmol). The reaction mixture was quenched with satd. aq. NH_4Cl and extracted with excess CH_2Cl_2. The organic extract was washed with brine and concentrated under reduced pressure. The residue was purified by column chromatography (SiO_2 pretreated with 2% Et_3N, EtOAc–hexane 1:6) to give *meso*-**7c** as a bright yellow solid (0.79 g, 49%). The diastereomeric composition was determined by ^{31}P NMR dr(meso:dl) >95:<5; mp 235–237 °C (dec). IR (KBr) ν_{max}: 3063, 2924, 1629, 1451, 1373, 1330, 1205, 1159, 1093, 822. ^{1}H NMR ($CDCl_3$) δ: 0.34–1.68 (br, 24H, $CH(CH_3)_2$), 2.92–3.25 and 3.43–3.96 (br, 4H, $CH(CH_3)_2$), 4.20 and 4.76 (m, 6H, Cp-*H*), 7.12–7.67 (br, 20H, C_6H_5). ^{13}C NMR ($CDCl_3$) δ: 20.3, 72.8, 81.1, 90.8, 91.2, 128.0, 128.0, 128.2, 128.9, 132.8, 133.1, 134.5, 134.9, 139.6, 139.9, 166.3. ^{31}P NMR ($CDCl_3$) δ: –22.68. MS *m*/*z* (rel intensity) (FAB): 808 (M^+, 3), 766 (8), 639 (16), 625 (47). Anal. calcd. for $C_{48}H_{54}{}^{56}FeN_2O_2P_2$: C 71.28, H 6.73, N 3.46; found: C 71.39, H 6.79, N 3.52.

Diphenylphosphine derivatives **6g** and **7c** were found to be air-sensitive, but could be stored for months as solids un-

© 2006 NRC Canada

der argon at low temperatures (–20 °C). Purification by column chromatography required deactivation of silica gel with Et_3N.

2,2′-Bis(phenylthio)-1,1′-N,N,N′,N′-tetraisopropylferrocenedicarboxamide (7d)

According to Standard method B, a solution of (–)-sparteine (0.07 mL, 0.31 mmol and *n*-BuLi (0.19 mL, 1.67 mol/L solution in hexane, 0.15 mmol) in PhMe (5 mL) was sequentially treated with a solution of 2-(phenylthio)-1,1′-*N*,*N*,*N*′,*N*′-tetraisopropylferrocenedicarboxamide (**6h**) (0.084 g, 0.15 mmol, 89% ee) in PhMe (0.5 mL) and Ph_2S_2 (0.131 g, 0.6 mmol) in PhMe (0.5 mL). Standard workup followed by column chromatography (EtOAc–hexane, 1:10) gave **7d** as an orange solid (0.06 g, 60%). CSP HPLC analysis (Chiralcel OD; eluent: *n*-hexane–*i*-PrOH 99:1, flow 0.4 mL/min) determined dr(dl:meso) = 98.5:1.5 and 97% ee (t_R(major dl) = 15.97 min, t_R(minor dl) = 19.14 min, t_R(meso diastereomer) = 22.00 min).

dl-*2,2′-Bis(phenylthio)-1,1′*-N,N,N′,N′-*tetraisopropylferrocenedicarboxamide (*dl-***7d***)*

mp 200–202 °C (dec). IR (KBr) ν_{max}: 2954, 1628, 1458, 1372, 1325, 1207, 1159, 1127, 1033. ^{1}H NMR ($CDCl_3$) δ: 0.42–1.71 (br, 24H, CH(CH_3)$_2$), 3.24 (sept, *J* = 11 Hz, 2H, C*H*(CH_3)$_2$), 3.72 (sept, *J* = 11 Hz, 2H, C*H*(CH_3)$_2$), 4.71 (s, 4H, Cp-*H*), 4.59 (m, 2H, Cp-*H*), 7.02–7.28 (br, 10H, C_6H_5). ^{13}C NMR ($CDCl_3$) δ: 20.9, 50.6, 74.0, 77.4, 80.6, 92.5, 125.5, 127.6, 128.6, 139.2, 165.3. MS *m*/*z* (rel intensity) (FAB): 657 (MH^+, 98), 656 (M^+, 100), 557 (17), 548 (14), 455 (34), 356 (16), 318 (28), 302 (89), 201 (69), 185 (59), 154 (69), 137 (59). HRMS calcd. for $C_{36}H_{45}{}^{56}FeN_2O_2S_2$ (MH^+): 657.2272; found: 657.2294. Anal. calcd. for $C_{36}H_{44}{}^{56}FeO_2N_2S_2$: C 65.84, H 6.75, N 4.26; found: C 66.02, H 6.68, N 4.32.

meso-*2,2′-Bis(phenylthio)-1,1′*-N,N,N′,N′-*tetraisopropylferrocenedicarboxamide (*meso-***7d***)*

mp 201–203 °C (dec). IR (KBr) ν_{max}: 2949, 1631, 1459, 1372, 1316, 1207, 1034. ^{1}H NMR ($CDCl_3$) δ: 0.26–1.79 (br, 24H, CH(CH_3)$_2$), 3.24 (m, 2H, C*H*(CH_3)$_2$), 3.67 (m, 2H, C*H*(CH_3)$_2$), 4.53, 4.70, 4.90 (m, 6H, Cp-*H*), 6.92–7.38 (br, 10H, C_6H_5). ^{13}C NMR ($CDCl_3$) δ: 20.0, 20.7, 45.8, 50.5, 71.4, 74.2, 79.1, 82.1, 125.5, 127.7, 128.7, 137.0, 165.1. MS *m*/*z* (rel intensity) (FAB): 657 (MH^+, 8), 656 (M^+, 7), 556 (2), 547 (2), 455 (5), 338 (5), 302 (14), 246 (16), 201 (9), 185 (100), 154 (59), 137 (65). HRMS calcd. for $C_{36}H_{45}{}^{56}FeN_2O_2S_2$ (MH^+): 657.2272; found: 657.2292.

Dimethyl 1,3-diphenylprop-2-enylmalonate (8) — Asymetric Pd-catalyzed allylic substitution

Method 1 (utilizing BSA and AcOK)

A solution of 1,3-diphenyl-1-acetoxy-2-propene (0.25 g, 1.0 mmol) (42), 2,2′-bis(diphenylphosphino)-1,1′-*N*,*N*,*N*′,*N*′-tetraisopropylferrocenedicarboxamide (**7c**, 0.071 g, 0.1 mmol, 96% ee), and allylpalladium chloride dimer (0.009 g, 0.025 mmol) in CH_2Cl_2 (3.5 mL) was stirred for 15 min at rt before a solution (CH_2Cl_2, 3.5 mL) of BSA (0.74 mL, 3.0 mmol), dimethyl malonate (0.40 g, 3.0 mmol), and AcOK (0.004 g, 0.04 mmol) was added. The reaction mixture was stirred for 10 h at rt, quenched with water, and subjected to the standard workup. Purification by column chromatography (EtOAc–hexane, 1:5) gave compound **8** as a pale yellow solid (0.313 g, 96%). CSP HPLC analysis (eluent: *n*-hexane–*i*-PrOH 99:1, flow 0.2 mL/min) determined 84% ee (t_R(major) = 58.78 min, t_R(minor) = 63.50 min). $[\alpha]^{23}_D$ +15.9° (*c* 0.71, EtOH). IR (neat) ν_{max}: 2995, 1758, 1605, 1493, 1454, 1316, 1259. ^{1}H NMR ($CDCl_3$) δ: 3.52 (s, 3H, CO_2CH_3), 3.70 (s, 3H, CO_2CH_3), 3.95 (d, *J* = 10.9 Hz, 1H, C*H*(CO_2CH_3)$_2$), 4.27 (dd, *J* = 10.9, 8.0 Hz, 1H, Ph-C*H*), 6.32 (dd, *J* = 8.0, 15.7 Hz, 1H, -C*H*=CH-Ph), 6.51 (d, *J* = 15.7 Hz, 1H, Ph-CH=), 7.19–7.33 (m, 10H, C_6H_5). ^{13}C NMR ($CDCl_3$) δ: 48.9, 52.0, 52.2, 57.3, 126.1, 126.9, 127.3, 127.6, 127.9, 128.2, 128.4, 128.9, 131.5, 136.5, 140.0, 167.4, 167.9. MS *m*/*z* (rel intensity) (EI): 324 (M^+, 56), 292 (29), 264 (37), 232 (41), 204 (84), 193 (98), 178 (53), 165 (39), 152 (18), 139 (12), 128 (42), 115 (100), 102 (43), 91 (74), 78 (42), 69 (43). HRMS calcd. for $C_{20}H_{20}O_4$: 324.1361; found: 324.1353.

Method 2 (utilizing NaH)

A solution of 1,3-diphenyl-1-acetoxy-2-propene (0.095 g, 0.38 mmol), 2,2′-bis(diphenylphosphino)-1,1′-*N*,*N*,*N*′,*N*′-tetraisopropylferrocenedicarboxamide (**7c**, 0.027 g, 0.038 mmol, 96% ee), allylpalladium chloride dimer (0.004 g, 0.011 mmol), and THF (2 mL) was stirred for 15 min at rt and then treated with a THF (3 mL) solution of NaCH(CO_2Me)$_2$ (prepared by the addition of NaH (60% in oil, 0.05 g, 1.13 mmol) to dimethylmalonate (0.15 g, 1.13 mmol) in THF (3 mL) at 0 °C) at rt. The reaction reaction mixture was stirred for 36 h at rt, quenched with water, and subjected to the standard workup. Purification by column chromatography afforded compound **8** (0.117 g, 96%), which, as determined by CSP HPLC, was 84% ee (R-enantiomer).

1-Phenylpropan-1-ol (9) (Et_2Zn addition to benzaldehyde)

To a stirred solution of benzaldehyde (0.10 mL, 1.6 mmol) and chiral ferrocenyl ligand (**6d**, **6e**, **6k**, **6l**) (0.05 mmol) in either hexane (15 mL) or PhMe (5 mL) was added a solution of Et_2Zn (1.60 mL, 1.0 mol/L in hexane, 1.60 mmol) at rt and the reaction mixture was further stirred for 1–3 days. The reaction mixture was quenched with excess 0.2 mol/L aq. HCl solution at 0 °C. After standard workup, the crude material was analyzed by CSP HPLC (Chiralcel OD column, eluent: *n*-hexane–isopropyl alcohol 99:1, flow 0.5 mL/min, t_R 29.66 min, t_R 27.20 min) and purified by column chromatography (hexane–EtOAc, 10:1) to yield compound **9** as a colorless oil. IR (CH_2Cl_2) ν_{max}: 700, 756, 1097, 1454, 1493, 2875, 2930, 2966, 3030, 3369. ^{1}H NMR ($CDCl_3$) δ: 0.92 (t, *J* = 7.3 Hz, 3H, CH_2CH_3), 1.81 (m, 2H, CH_2CH_3), 1.90–2.00 (br, 1H, O*H*), 4.59 (t, *J* = 6.6 Hz, 1H, C*H*(OH)CH_2), 7.20–7.40 (m, C_6H_5). ^{13}C NMR ($CDCl_3$) δ: 10.1, 31.8, 76.0, 126.0, 127.4, 128.3. MS *m*/*z* (rel intensity) (EI): 136 (M^+, 32), 117 (2), 107 (100), 97 (0.5). HRMS calcd. for $C_9H_{12}O$: 136.0888; found: 136.0897.

Et_2Zn addition to benzaldehyde catalyzed by the lithium salt of 2-(diphenylhydroxymethyl)-1,1′-N,N,N′,N′-tetraisopropylferrocenedicarboxamide (6d)

A solution of *n*-BuLi (0.05 mL, 1.67 mol/L in hexane, 0.85 mmol) was added to a cold (–78 °C) solution of **6d** (53.4 mg, 0.086 mmol) in PhMe (20 mL). PhCHO (0.19 mL,

© 2006 NRC Canada

0.86 mmol) and Et_2Zn (1.37 mL, 1.0 mol/L in hexane, 1.37 mmol) were added and stirring was continued at rt for 3 days. The reaction mixture was quenched with excess 0.2 mol/L HCl at 0 °C. Standard workup followed by flash chromatography afforded compound **9** (0.082 g, 70%, 47% ee).

Acknowledgements

We warmly thank Dr. Heiner Jendralla, Novartis (formerly Hoechst) for exchange of correspondence and insightful comments. We are grateful to the Natural Sciences and Engineering Research Council of Canada (NSERC) for support under the Industrial Research Chair (Monsanto Company) and Research Grant programs. RL was an Ontario Graduate Scholar, 1996 to 1997.

References

1. For a memorable quotation regarding the initial proposed structure attributed to G. Wilkinson, see: A. Yamamoto. Organotransition metal chemistry. Wiley-Interscience, New York. 1986. p. 103.
2. T. Hayashi and A. Togni (*Editors*). Ferrocenes: Homogenous catalysis, organic synthesis, material science. VCH, Weinheim, Germany. 1995.
3. T. Satyanarayana and H.B. Kagan. Adv. Synth. Catal. **347**, 737 (2005).
4. (*a*) L.-X.D. Li, T. Tu, S.-L. You, W.-P. Deng, and X.-L. Hou. Acc. Chem. Res. **36**, 659 (2003); (*b*) R.C.J. Atkinson, V.C. Gibson, and N.J. Long. Chem. Soc. Rev. **33**, 313 (2004).
5. (*a*) H.B. Kagan and O. Riant. Adv. Asymmetric Synth. **2**, 189 (1997); (*b*) I. Ojima. Catalytic asymmetric synthesis. VCH Publishers, New York. 1993.
6. (*a*) A. Heine, E.A. Stura, J.T. Yli-Kauhaluoma, C. Gao, Q. Deng, B.R. Beno, K.N. Houk, K.D. Janda, and I.A. Wilson. Science (Washington, D.C.), **279**, 1934 (1998); (*b*) J. Westwood, S.J. Coles, S.R. Collinson, G. Gasser, S.J. Green, M.B. Hursthouse, M.E. Light, and J.H.R. Tucker. Organometallics, **23**, 946 (2004); (*c*) B. Rudolf, J. Zakrzewski, M. Salmain, and G. Jaouen. Tetrahedron Lett. **39**, 4281 (1998).
7. (*a*) T. Sturm, W. Weissensteiner, and F. Spindler. Adv. Synth. Catal. **345**, 160 (2003); (*b*) U. Blaser. Adv. Synth. Catal. **17**, 344, (2002)
8. K. Schlögl. Top. Stereochem. **1**, 39 (1967).
9. (*a*) D. Marquarding, H. Klusacek, G. Gokel, P. Hoffmann, and I. Ugi. J. Am. Chem. Soc. **92**, 5389 (1970); (*b*) L.F. Battelle, R. Bau, G.W. Gokel, R.T. Oyakawa, and I. Ugi. J. Am. Chem. Soc. **95**, 482 (1973); (*c*) For a review on the CH_2NR_2 DMG, see: L. Xiao, K. Mereiter, W. Weissensteiner, and M. Widhalm. Synthesis, 9179 (2002); (*d*) For recent work: X. Hu, H. Chen, X. Hu, H. Dai, C. Bai, J. Wang, and Z. Zheng. Tetrahedron Lett. **43**, 9179 (2002); X. Hu, H. Chen, and Z. Zheng. Adv. Synth. Catal. **347**, 541 (2005).
10. (*a*) F. Rebière, O. Riant, L. Ricard, and H.B. Kagan. Angew. Chem. Int. Ed. Engl. **32**, 568 (1993); (*b*) O. Riant, O. Samuel, and H.B. Kagan. J. Am. Chem. Soc. **115**, 5835 (1993); (*c*) For more recent work, see: O. Riant, G. Argouarch, D. Guillaneux, S. Samuel, and H.B. Kagan. J. Org. Chem. **63**, 3511 (1998).
11. (*a*) D. Enders, R. Peters, R. Lochtman, and J. Runsink. Synlett, 1462, (1997); (*b*) L. Xiao, R. Kitzler, and W.J. Weissensteiner. J. Org. Chem. **66**, 8912 (2001); (*c*) L.E. Overman, C.E. Owen, and G.G. Zipp. Angew. Chem. Int. Ed. **41**, 3884 (2002); (*d*) M. Lotz, K. Polborn, J.M. Chong, and L.S. Hegedus. Organometallics, **23**, 1010 (2004); (*e*) O.G. Mancheño, R.G. Arrayás, and J.C. Carretero. Organometallics, **24**, 557 (2005); (*f*) R.G. Arrayás, I. Alonso, O. Familiar, and J.C. Carretero. Organometallics, **23**, 1991 (2004).
12. (*a*) P. Knochel. Angew. Chem. Int. Ed. **41**, 4708 (2002); (*b*) J. Kang, K.H. Yew, T.H. Kim, and D.H. Choi. Tetrahedron Lett. **43**, 9509, (2002); (*c*) J. Priego, O.G. Mancheño, S. Cabrera, and J.C. Carretero. J. Org. Chem. **67**, 1346, (2002); (*d*) S. Lu, X. Han, and Y. Zhou. Adv. Synth. Catal. **346**, 909 (2004); (*e*) T. Tu, X. Hou, and L. Dai. Org. Lett. **5**, 3651 (2003).
13. D. Hoppe and T. Hense. Angew. Chem. Int. Ed. Engl. **36**, 2283 (1997).
14. P. Beak, A. Basu, D.J. Gallagher, Y.S. Park, and S. Thayumanavan. Acc. Chem. Res. **29**, 552 (1996).
15. M. Tsukazaki, M. Tinkl, A. Roglans, B.J. Chapell, N.J. Taylor, and V. Snieckus. J. Am. Chem. Soc. **118**, 685 (1996).
16. (*a*) T. Hayashi and M. Kumada. Acc. Chem. Res. **15**, 395 (1982); (*b*) M. Sawamura, H. Hamashima, and Y. Ito. Tetrahedron: Asymmetry, **2**, 593 (1991); (*c*) For other methods to obtain ferrocenes with planar chirality, see: A. Ratajczak and B. Misterkiewicz. J. Organomet. Chem. **91**, 73 (1975); (*d*) T. Hayashi, T. Mise, and M. Kumada. Tetrahedron Lett. 4351 (1976); (*e*) Y.-F. Wang, J. Lalonde, M. Momongan, D.E. Bergbreiter, and C.-H. Wong. J. Am. Chem. Soc. **110**, 7200 (1988); (*f*) N.W. Boaz. Tetrahedron Lett. **30**, 2061 (1989); (*g*) D.M. David, L.A.P. Kane-Maguire, and S.G. Pyne. J. Chem. Soc. Chem. Commun. 888 (1990); (*h*) G. Nicolosi, A. Patti, R. Morrone, and M. Piattelli. Tetrahedron: Asymmetry, **5**, 1275 (1994).
17. (*a*) Y. Nishibayashi and S. Uemura. Synlett, 79 (1995); (*b*) T. Sammakia, H.A. Latham, and D.R. Schaad. J. Org. Chem. **60**, 10 (1995); (*c*) C.J. Richards, T. Damalidis, D.E. Hibbs, and M.B. Hursthouse. Synlett, 74 (1995).
18. C. Metallinos, H. Szillat, N.J. Taylor, and V. Snieckus. Adv. Synth. Catal. **345**, 370 (2003).
19. A. Togni. Angew. Chem. Int. Ed. Engl. **35**, 1475 (1996).
20. For recent adaption to other ferrocenyls, see: C. Metallinos and V. Snieckus. Org. Lett. **4**, 1935 (2002).
21. For previous use of this concept in ferrocene chemistry, see: (*a*) C. Ganter and T. Wagner. Chem. Ber. **128**, 1157 (1995); (*b*) K.H. Anh, C. Cho, H. Baek, J. Park, and S.J. Lee. J. Org. Chem. **61**, 4937 (1996).
22. R.S. Laufer, U. Veith; N.J. Taylor, and V. Snieckus. Org. Lett. **2**, 629 (2000).
23. New centrally chiral 1,1′-disubstituted ferrocenes and corresponding 1,1′,2-trisubstituted and 1,1′,2,2′-terasubstituted derivatives, mostly incorporating a chiral 1-oxazolinyl substituent, have been prepared by Ikeda, Knochel, and Dai and their coworkers and shown to give good enantioselectivities in several asymmetric reactions, see: (*a*) W. Zhang, Y. Adachi, T. Hirao, and I. Ikeada. Tetrahedron: Asymmetry, **7**, 451, (1996); (*b*) W. Zhang, T. Kida, Y. Nakayashi, and I. Ikeda. Tetrahedron Lett. **37**, 7995 (1996); (*c*) M. Lotz, T. Ireland, J.J. Almena, and P. Knochel. Tetrahedron: Asymmetry, **10**, 1839 (1999); (*d*) L. Schwink and P. Knochel. Chem. Eur. J. **4**, 950, (1998), and ref. 4, and refs. cited therein. As pointed out by Dai, while the 1,1′-disubstituted ferrocene ligands posses only central chirality, coordination with a metal results in systems with three chiral elements (central, axial, and planar), which leads to greater mechanistic interest in the manner of their participation in enantioinduction.
24. (*a*) Spectroscopic studies of LiX effect on hindered lithium dialkylamides: P.L. Hall, J.H. Gilchrist, A.T. Harrison, D.J. Fuller, and D.B. Collum. J. Am. Chem. Soc. **113**, 9575 (1991);

© 2006 NRC Canada

B.H. Lipshutz, M.R. Wood, and C.W. Lindsey. Tetrahedron Lett. **36**, 4385 (1995); (*b*) Application of LiX salts to stereoselective enolization of ketones, e.g.: M. Majewski, R. Lazny, and P. Nowak. Tetrahedron Lett. **36**, 5465 (1995); N.S. Simpkins. Pure Appl. Chem. **68**, 691, (1996); (*c*) Lateral lithiation of isooxazole, e.g.: D.J. Burkhart, P. Zhou, A. Blumenfeld, B. Twamley, and N.R. Natale. Tetrahedron, **57**, 8039 (2001).

25. R. Laufer. M.Sc. thesis, University of Waterloo, Waterloo, Ontario. 1998.
26. D*o*M has been used in a one-pot preparation of a racemic 2,2′-bis(diphenylphosphino) analog of 1,1′-dimethoxyferrocene: M.A. Caroll, D.A. Widdowson, and D.J. Williams. Synlett, 1025 (1994). 2,2′-Bis(diphenylphosphino)-1,1′-ferrocenecarboxylate was derived from the product of a diastereoselective D*o*M of chiral 1,1′-dioxazolinylferrocene (see ref. 23*b*).
27. P. Beak, S.T. Kerrick, S. Wu, and J. Chu. J. Am. Chem. Soc. **116**, 3231 (1994).
28. C.A. Quesnelle, O.B. Familioni, and V. Snieckus. Synlett, 349 (1994), and refs. therein.
29. S. Gronowitz, P. Bjork, J. Malm, and A.-B. Hornfeldt. J. Organomet. Chem. **460**, 127 (1993).
30. For reviews on catalyzed allylic substitution reactions, see: (*a*) B.M. Trost and D.L. Van Vranken. Chem. Rev. **96**, 395 (1996); (*b*) B.M. Trost. Acc. Chem. Res. **29**, 355 (1996); (*c*) G.J. Helmchen. J. Organomet. Chem. **576**, 203 (1999).
31. B.M. Trost and D.J. Murphy. Organometallics, **4**, 1143 (1985).
32. H. Kubota, M. Nakajamima, and K. Koga. Tetrahedron Lett. **34**, 8135 (1993).
33. (*a*) R. Noyori. Asymmetric catalysis in organic synthesis. Wiley, New York. 1994; (*b*) L. Pu and H.-B. Yu. Chem. Rev. **101**, 757 (2001).
34. M. Yoshioka, T. Kawakita, and M. Ohno. Tetrahedron Lett. **30**, 1657 (1989).
35. T.J. Colacot. Chem. Rev. **103**, 3101 (2003).
36. D.D. Perrin and W.L.F. Armarego. Purification of laboratory chemicals. 3rd ed. Pergamon Press, Oxford. 1988.
37. M.R. Winkle, J.M. Lansinger, and R.C. Ronald. J. Chem. Soc. Chem. Commun. 87 (1980).
38. S.C. Watson and J.F. Eastham. J. Organomet. Chem. **9**, 165 (1967).
39. R.F. Heck. Palladium reagents in organic synthesis. Academic Press, New York. 1985.
40. P.J. Hammond, P.D. Beer, C. Dudman, I.P. Danks, C.D. Hall, J. Knychala, and M.C. Grossel. J. Organomet. Chem. **305**, 367 (1986).
41. H. Jendralla and E. Paulus. Synlett, 471 (1997)
42. J.V. Allen, S.J. Coote, G.J. Dawson, C.G. Frost, C.J. Martin, and J.M.J. Williams. J. Chem. Soc. Perkin Trans. 1, 2065 (1994).

© 2006 NRC Canada

TRIBUTE / HOMMAGE

This special issue of the *Canadian Journal of Chemistry* is dedicated to Doctor Arthur J. Carty for his outstanding accomplishments in organotransition metal chemistry and also for his exceptional contributions to the advancement of science and technology in Canada. As all contributors to this issue will know, Arthur's status in the pantheon of eminent Canadian scientists and scientific administrators is unique, and his position in the history of science in Canada is secure.

Arthur attended Hookergate Grammar School, County Durham, England, from 1952 to 1959, obtaining the G.C.E. Advanced Level in Chemistry, Physics, and Mathematics, with distinction in chemistry and physics and scholarship level chemistry and physics. He held the position of Head Boy from 1958 to 1959 and was Captain of the school soccer and cricket teams from 1957 to 1959. He went on to study chemistry at the University of Nottingham, where he graduated with a First Class Honours B.Sc. in 1962. He then joined the research group of the late Dennis Tuck at Nottingham, obtaining his Ph.D. in inorganic chemistry in 1965.

After a two year period as Assistant Professor of Chemistry at Memorial University, St. John's, Newfoundland, Arthur joined the Department of Chemistry at the University of Waterloo, Waterloo, Ontario, where he rose through the ranks to become Professor in 1975, founding Director of the Guelph–Waterloo Centre for Graduate Work in Chemistry (1975–1979), Chairman of the Department of Chemistry (1983–1989), and Dean of Research (1989–1994). Arthur left Waterloo in 1994 to become President of the National Research Council of Canada (NRC), and left NRC in 2004 to become Canada's first National Science Advisor to the Prime Minister.

Arthur's doctoral studies with Dennis Tuck involved the development of the coordination chemistry of the group 13 metals. His independent research career was launched with spectroscopic (IR, Raman, NMR, and Mössbauer) studies of metal–halide complexes ligated to phosphorus donors, including phosphinoalkynes, and his contributions to chemistry have ultimately spanned the spectrum of the coordination chemistry of main group and transition metal elements, from the bioinorganic chemistry of mercury to organometallic chemistry and materials science.

In particular, his research program has involved the exploration of the chemistry of acetylenic phosphines and diphosphines, with leading edge research into the synthesis of a large series of organometallic complexes. His work with metal carbonyls of the late transition metals and their bonding to phosphinoacetylene ligands led to the development of a world-renowned research program in transition metal cluster chemistry, and his research on the facile phosphorus–carbon bond cleavage reactions of coordinated P-C≡CR ligands provided an elegant entry into metal–acetylide complexes. This work was widely recognized, and resulted in rankings in the 100 most-cited papers published in the world in pure and synthetic chemistry in both 1981 and 1982 (A.J. Carty, S.A. MacLaughlin, and N.J. Taylor. Open and closed ruthenium and osmium clusters with μ_3-acetylide and phosphido bridges. J. Organomet. Chem. **204**, C27 (1981); A.J. Carty. Structural chemistry and reactivity of cluster bound acetylides: Close relatives of the carbides? Pure Appl. Chem. **54**, 113 (1982)). Arthur and his co-workers led the development of C—C and C—N bond forming reactions of coordinated acetylide groups, helping to cement many of the ideas regarding the "cluster-surface analogy" proposed by Muetterties. This work continued its rapid growth through the 1980s and 1990s, with in-depth studies on the synthesis and reactivity patterns of polyunsaturated carbon ligands, including late transition metal allenyl (-C(R)=C=CR′$_2$) and butadiynyl (-C≡C-C≡C-R) complexes.

In most instances, the development of this chemistry was made possible by the flexible nature of ancillary phosphido (PR_2), phosphidoxo (R_2PO), and phosphinidene (PR) ligands, which function as supports to the metal centres, preventing or controlling metal–metal bond cleavage reactions. Arthur and his team also clearly demonstrated that such ligands can play an active role as mediators of reactions on cluster surfaces via P—C and P—O *bond forming* reactions. The reaction chemistry of metal-phosphinidenes also led to the unprecedented development of phosphorus monoxide (PO) chemistry via acid-catalysed hydrolysis of P—N bonds of coordinated aminophosphinidenes and the utility of electrophilic "Fischer-type" phosphinidene complexes in promoting novel P—X bond forming reactions.

Arthur has supervised or co-supervised 18 M.Sc. and 29 Ph.D. students, 35 post-doctoral fellows, and dozens of undergraduate researchers, and has hosted in his laboratories a large number of scientific visitors from Canada and abroad. He and his co-workers have reported their research findings in over 300 papers, five review articles, nine book chapters, and five patents, and Arthur has given an enormous number of invited presentations (over 20 in 2005 alone!). He has received numerous awards in recognition of his outstanding contributions to science, including a Royal Society-Nuffield Foundation Fellowship (1974), the Alcan Award of the Canadian Society for Chemistry (1984), the E.W.R. Steacie Award of the Canadian Society of Chemistry (1995), the Montreal Medal of the Chemical Institute of Canada (1996), the Purvis Award of the Society of Chemical Industry (1997), and the National Merit Award of the Ottawa Life Sciences Council (2000). He is a Fellow of the Royal Society of Canada, an Honorary Fellow of the Chemical Institute of Canada, an Officier de l'Ordre National du Mérite, France, an Honorary Member of the Engineering Institute of Canada, a Fellow of the Fields Institute for Research in Mathematical Sciences, and an Officer of the Order of Canada. He has received nine honorary doctoral degrees from universities in Canada (Carleton, Waterloo, Acadia, McMaster, Queen's, Ottawa, Memorial, Calgary, and Okanagan University College, now UBC Okanagan), as well as one from France (Rennes), and an honorary professorship from Taiwan (National Chiao-Tung University).

He has served as Vice-President and President of the Canadian Society for Chemistry, and as member or chair of over 30 organizations as diverse as the Executive Committee of the Society of Chemical Industry, the Atomic Energy Control Board of Directors, the R&D Advisory Council of the Department of National Defence, the Leaders' Forum on Innovation of The Conference Board of Canada, the Board of Directors of Canadian Light Source Inc., the Board of Directors of Genome Canada, the Canadian Space Agency Advisory Council, the Canadian Nuclear Safety Commission, the Board of Directors of the Ottawa Health Research Institute, the Selection Committee of the Network of Centres of Excellence, the editorial advisory boards of four scientific journals, the advisory boards

© 2006 NRC Canada

of eight international conferences, and the Board of Directors of Opera Lyra (National Arts Centre). Through these activities, as well as in his roles as President of the National Research Council and National Science Advisor to the Prime Minister, Dr. Carty has served and continues to serve as a preeminent advocate for the development of science and technology in Canada.

Despite these many commitments outside of the laboratory, however, and as a testament to his roots, Arthur also continues to maintain an enviable level of productivity in his research and continues to attract the brightest young minds to his research team. As is known to all who have worked with him, his dedication to chemistry, his excellent mentoring skills, and his sincerity, integrity, generosity, and vision have all been instrumental in launching numerous careers in industry and academia. We are very pleased to present this special issue as a token of our admiration and respect.

Mike Baird
John Corrigan

© 2006 NRC Canada

TRIBUTE / HOMMAGE

Ce numéro spécial de la *Revue canadienne de chimie* vise à saluer les réalisations exceptionnelles de M. Arthur J. Carty dans le domaine de la chimie des composés organométalliques ainsi que sa contribution remarquable à l'avancement des sciences et de la technologie au Canada. Comme tous les auteurs qui ont contribué au présent numéro le savent, M. Carty occupe une place unique au panthéon des grands savants et administrateurs scientifiques du Canada. Il est, sans aucun doute, un des grands personnages de l'histoire des sciences au Canada.

De 1952 à 1959, M. Carty a fréquenté l'école Hookergate Grammar School, dans le comté de Durham, en Angleterre, où il a obtenu un certificat général d'éducation (G.C.E.) au niveau avancé en chimie, en physique et en mathématiques, avec distinction et niveau de boursier en chimie et en physique. En 1958 et 1959, il a été capitaine de l'école, et de 1957 à 1959, il a également été capitaine des équipes de football et de cricket. Par la suite, il a étudié la chimie à l'Université de Nottingham, où il a obtenu, en 1962, un baccalauréat *ès* sciences avec spécialisation de première classe. Devenu membre du groupe de recherche de feu Dennis Tuck à Nottingham, il a obtenu son doctorat en chimie inorganique en 1965.

Après deux ans de travail en qualité de professeur adjoint de chimie à l'Université Memorial, à St. John's (Terre-Neuve-et-Labrador), M. Carty est devenu membre du département de chimie de l'Université de Waterloo, à Waterloo (Ontario). Il est monté progressivement dans la hiérarchie pour devenir professeur titulaire en 1975, directeur fondateur du centre Guelph-Waterloo des études supérieures en chimie (1975–1979), directeur du département de chimie (1983–1989) et doyen à la recherche (1989–1994). En 1994, M. Carty a quitté l'Université de Waterloo et a assumé la présidence du Conseil national de recherches du Canada (CNRC). Il a tiré sa révérence au CNRC en 2004 pour devenir le premier conseiller national des sciences auprès du premier ministre du Canada.

Dans le cadre de ses études de doctorat sous la direction de Dennis Tuck, M. Carty a contribué à l'avancement de la chimie de coordination des métaux du groupe 13. Au début de sa carrière de chercheur indépendant, il s'est livré à des études spectroscopiques (IR, Raman, RMN et Mössbauer) des complexes métal-halogénure ligandés au donneur de phosphore, y compris les phosphinoalcynes. Au cours de sa carrière de chercheur, il a contribué à l'avancement de la chimie dans tout le domaine de la chimie de coordination des éléments métalliques des groupes principaux et de transition, de la chimie bio-inorganique du mercure à la chimie organométallique et à la science des matériaux.

Plus particulièrement, ses recherches ont porté sur l'exploration de la chimie des phosphines et diphosphines acétyléniques, et ont donné lieu à des études de pointe sur la synthèse d'une grande série de complexes organométalliques. Ses travaux sur les carbonyles métalliques des métaux de transition lourds et la liaison de ceux-ci aux ligands de phosphinoacétylène ont mené à l'élaboration d'un programme de recherche de renommée mondiale axé sur la chimie des agrégats de métaux de transition. Dans le domaine des réactions faciles de clivage de la liaison phosphore-carbone des ligands coordonnés P-C≡CR, ses recherches ont offert une entrée élégante au domaine des complexes métal-acétylure. Ces recherches ont été chaudement accueillies, et en 1981 et 1982, les mémoires de M. Carty ont été classés parmi les 100 mémoires le plus cités du monde dans le domaine de la chimie pure et synthétique (A.J. Carty, S.A. MacLaughlin et N.J. Taylor, « Open and closed ruthenium and osmium clusters with μ_3-acetylide and phosphido bridges », J. Organomet. Chem. **204**, C27 (1981); A.J. Carty, « Structural chemistry and reactivity of cluster bound acetylides: Close relatives of the carbides? », Pure Appl. Chem. **54**, 113 (1982)). M. Carty et ses collèges ont été chefs de file de l'étude des réactions de formation de liaisons C—C et C—N des groupes d'acétylures coordonnés, ce qui a permis de conforter bon nombre de notions concernant l'analogie agrégat-surface proposée par Muetterties. Les travaux dans ce domaine, qui a connu un grand essor pendant les années 1980 et 1990, ont été caractérisés notamment par des études approfondies de la synthèse et des schémas de réactivité des ligands de carbone polyinsaturés, y compris des complexes allenyles (-C(R)=C=CR′$_2$) et butadiynyles (-C≡C-C≡C-R) des métaux de transition lourds.

Dans la plupart des cas, l'exploration de cette chimie a été rendue possible par la souplesse des ligands auxiliaires phosphido (PR_2), phosphidoxo (R_2PO) et phosphinidène (PR), qui supportent les centres métalliques de manière à empêcher ou à restreindre les réactions de clivage des liaisons métal-métal. Par ailleurs, M. Carty et son équipe ont démontré clairement que ces ligands peuvent jouer un rôle actif comme médiateurs des réactions sur les surfaces des agrégats par des réactions de *liaisons* P—C et P—O. Finalement, la chimie des réactions entre les métaux et les phosphinidènes a mené à l'expansion sans précédent de la chimie du monoxyde de phosphore (PO) au moyen de l'hydrolyse catalysée par acides des liaisons P—N aminophosphinidènes coordonnées et grâce à l'utilité des complexes électrophiles de phosphinidènes de type Fischer pour la promotion de nouvelles réactions de formation de la liaison P—X.

M. Carty a supervisé, seul ou en collaboration, 18 étudiants de maîtrise *ès* sciences, 29 doctorants, 35 boursiers de recherches postdoctorales et des dizaines de chercheurs au premier cycle des études universitaires. Dans ses laboratoires, il a accueilli un grand nombre de scientifiques invités du Canada et de l'étranger. M. Carty et ses collègues ont rapporté les résultats de leurs recherches dans plus de 300 communications, cinq rapports de synthèse, neuf chapitres de livre et cinq brevets. M. Carty lui-même a fait un très grand nombre d'exposés en tant que conférencier invité (plus de 20 en 2005 seulement!). En reconnaissance de ses contributions exceptionnelles à la science, il s'est vu décerner de nombreux prix, entre autres une bourse de la Royal Society et de la Nuffield Foundation (1974), le prix Alcan de la Société canadienne de chimie (1984), le prix E.W.R. Steacie de la Société canadienne de chimie (1995), la médaille de Montréal de l'Institut de chimie du Canada (1996), le prix Purvis de la Society of Chemical Industry (1997) et le prix d'excellence national du Conseil bioscentifique d'Ottawa (2000). Il est membre de la Société royale du Canada, membre honoraire de l'Institut de chimie du Canada, officier de l'Ordre national du mérite de France, membre honoraire de l'Institut canadien des ingénieurs, associé du Fields Institute for Research in Mathematical Sciences et officier de l'Ordre du Canada. Il a reçu neuf doctorats honorifiques d'universités canadiennes (Carleton, Waterloo, Acadia, McMaster, Queen's, Ottawa, Memorial, Cal-

© 2006 NRC Canada

gary et le collège universitaire Okanagan, aujourd'hui UBC Okanagan) et un de l'Université de Rennes, en France. En outre, l'Université nationale Chiao-Tung de Taiwan l'a nommé professeur honoraire.

M. Carty a été vice-président et président de la Société canadienne de chimie, ainsi que membre ou président de plus de 30 groupes très divers, entre autres : le comité de direction de la Society of Chemical Industry, le conseil d'administration de la Commission canadienne de sûreté nucléaire, le comité consultatif sur la R-D du ministère de la Défense nationale, le forum des chefs de file sur l'innovation du Conference Board du Canada, le conseil d'administration de Canadian Light Source Inc., le conseil d'administration de Génome Canada, le comité consultatif de l'Agence spatiale canadienne, la Commission canadienne de sûreté nucléaire, le conseil d'administration de l'Institut de recherche en santé d'Ottawa, le comité de sélection des Réseaux de centres d'excellence, le comité consultatif de rédaction de quatre revues scientifiques, la commission consultative de huit congrès internationaux et le conseil d'administration d'Opéra Lyra du Centre national des arts. En poursuivant toutes ces activités et en jouant ses rôles de président du Conseil national de recherches et de conseiller national des sciences auprès du premier ministre, M. Carty a été, et est toujours, un grand défenseur du développement des sciences et de la technologie au Canada.

Malgré ses nombreux engagements hors du laboratoire, M. Carty reste fidèle à ses origines, car il maintient un niveau enviable de productivité dans ses recherches et continue d'attirer à son équipe de recherche les jeunes scientifiques les plus brillants. Comme le savent ceux et celles qui ont travaillé à ses côtés, son dévouement à la chimie, ses grandes compétences de mentor et sa sincérité, sa probité, sa générosité et sa vision ont grandement contribué au lancement de nombreuses carrières dans les secteurs industriel et universitaire. C'est un grand plaisir pour nous de présenter ce numéro spécial, gage de notre admiration et de notre respect.

Mike Baird
John Corrigan

© 2006 NRC Canada

AWARD LECTURE / CONFÉRENCE D'HONNEUR

2005 Pure or Applied Inorganic Chemistry Award Lecture — Host–guest inclusion chemistry of electroactive, mesoporous transition metal oxides oxidation and 1-D confinement in one step and why amorphous is better

B.O. Skadtchenko and D.M. Antonelli

Abstract: The flexible oxidation states of mesoporous Nb, Ta, and Ti oxides make them unique amongst porous materials allowing reaction pathways and cascades that are not possible for mesoporous silica or microporous materials such as zeolites. This electronic activity coupled with the 20–30 Å pores and the amorphous wall structure, which provides greater bandwidth (*W*) and hence an even greater range of redox potentials, leads to a rich variety of host–guest inclusion chemistry, which serves as an unprecedented 1-D analogue to layered 2-D host–guest inclusion reactions studied for decades. In this paper we survey a series of reactions between these mesoporous hosts and a wide variety of organic and organometallic guest species including alkali fullerides, cobaltocene, and other organometallic sandwhich species, and discuss the electronic and magnetic properties of the resulting composites.

Key words: mesoporous materials, semiconductors, fullerides, superconductors, oxides, nanomaterials, metallocenes.

Résumé : Les états d'oxydation flexibles des oxydes de Nb, de Ta ou de Ti mésoporeux les rendent uniques parmi les matériaux poreux et rendent possibles des voies réactionnelles et des cascades qui ne sont pas possibles avec las silices mésoporeuses ou les matériaux microporeux, tels les zéolites. Cette activité électronique couplée à des pores de 20 à 30 Å et à une structure amorphe des parois qui rend possible une largeur de bande plus grande (*W*) et, en conséquence, des plages plus grandes de potentiels redox, conduit à une chimie d'inclusion hôte–invité riche et variée qui peut servir d'analogue 1-D sans précédent pour des réactions d'inclusion hôte–invité en couches 2-D qui ont été étudiées depuis plusieurs décades. Dans ce travail, on passe en revue une série de réactions entre ces hôtes mésoporeux et une grande variété d'espèces invitées, tant organiques qu'organométalliques, y compris des fullerures et des espèces cobaltocène et autres composés sandwiches organométalliques et on discute des propriétés électroniques et magnétiques des composites qui en résultent.

Mots clés : matériaux mésoporeux, semiconducteurs, fullerures, supraconducteurs, oxydes, nanomatériaux, métallocènes.

[Traduit par la Rédaction]

Introduction

The study and fabrication of materials on the nanoscale has recently attracted a great deal of attention from scientific disciplines as disparate as physics and medicine (1–4). One of the most important classes of nanoscale materials are those with a regular pore structure on the nanometer scale (5–7). The discovery of M41S mesoporous silica in 1992, a material with extremely high surface areas (up to 1400m^2/g) and pore sizes ranging from 2 to 10 nm (8, 9), represented the first synthesis of a material with ordered pores greater than 15 Å in size. This discovery also led to great strides in the fabrication of materials with ordered structural motifs ranging from the nanometer level all the way up to the micron level (10). While mesoporous silicas have great advantages over microporous zeolites in the diffusion of bulky molecules through the pore channels, their amorphous wall structure leads to a lack of local geometric control on the molecular level, limiting applications to catalysis. In 1995, Antonelli and Ying reported the first successful synthesis of stable, mesoporous transition metal oxides. These materials were based on Ti (11), Nb (12), and Ta (13) oxides and pos-

Received 10 July 2005. Published on the NRC Research Press Web site at http://canjchem.nrc.ca on 30 March 2006.

B.O. Skadtchenko and D.M. Antonelli.[1] Department of Chemistry and Biochemistry, University of Windsor, 401 Sunset Avenue, Windsor, ON N9B 3P4, Canada.

[1]Corresponding author (e-mail: danton@uwindsor.ca).

 doi:10.1139/V06-021 © 2006 NRC Canada

sessed pore sizes of 2–5 nm and surface areas up to 1200 m^2/g. The great advantage of these materials over traditional silica-based materials is that mesoporous transition metal oxides are capable of existing in various oxidation states, a property that could lead to interesting electronic, catalytic, and optical applications because of the presence of d electrons in the walls of the structure. To this end, our group showed that mesoporous Nb, Ti, and Ta can act as stochiometric electron acceptors (14, 15). This was the first example of a full one-electron transfer of a guest species to a porous host. While some Mn oxides possess channel structures and undergo some redox chemistry, these materials cannot accept a full electron equivalent without undergoing a phase change because of redox-induced local distortion (16). The greater capacity to accept electron density in mesoporous Nb, Ta, and Ti oxides is thought to be due to the amorphous nature of the walls, which impart fewer local constraints on the geometry of the transition metal centers (15). Therefore, in some applications, amorphous walls in a mesoporous structure are clearly an advantage. Like redox-active layered materials of the types MO_3 and MX_2 (M = Nb, Ta, Mo, V; X = S, Se), mesoporous Nb, Ta, and Ti oxides can also serve as hosts for a wide variety of guest molecules (17–21), where electron transfer from the guest to the host drives the intercalation process. An important difference, however, is that in the case of the mesoporous systems, the resulting product contains one-dimensional nanophases in the pores, rather than the two-dimensional sheets adopted by the guest phase in a layered host lattice. This may lead to unusual physical properties such as charge density waves and other phenomena associated with 1-D materials. Another interesting result of the amorphous walls in these materials is that an amorphous oxide has a broader distribution of reduction potentials than its crystalline counterpart. This enables mesoporous Nb oxide, for example, to react with up to 0.5 equiv. of cobaltocene (19), where crystalline Nb_2O_5 does not react with cobaltocene at all! More recent unpublished results in our group have also shown that these materials are useful in nitrogen activation and hydrogen storage. In the latter application, the amorphous walls appear to open up space for hydrogen molecules that would otherwise not exist in the crystalline oxide counterparts, again stressing the advantages in some cases of a loosely knit amorphous structure with potential to act as an electron acceptor or as multiple binding sites.

This review will focus on a wide range of host–guest inclusion chemistry of mesoporous Nb, Ta, and Ti oxides, focusing largely on encapsulated low-dimensional nanostructures, and in particular, our extensive efforts to rationalize the electronic properties of low-dimensional alkali fulleride superconductors confined in the host lattice, which have very different properties from bulk-phase fullerides.

Mesoporous transition metal oxides (Nb, Ta, Ti) reduced with alkali metals

In 2000, Vettraino et al. (14). reported the reduction of mesoporous Nb oxide with 0.2–1.0 equiv. of Na-naphthalene in THF to produce a series of new gray to black composites These reduced materials showed full retention of the mesostructure as determined by X-ray powder diffraction (XRD) and nitrogen adsorption/desorption. Systematic X-ray photoelectron spectroscopy (XPS) studies on these materials showed that the Nb 3d 5/2, 3/2 emission shifts monotonically to a lower binding energy corresponding to a decrease in the average oxidation state of the Nb from (V) to (IV) as the Na loading level increases. The observed lack of individual peaks for Nb(IV) and Nb(V) species was attributed to fast electron hopping between two adjacent Nb sites relative to the XPS timescale. This work was subsequently expanded to include all alkali metal reduced mesoporous Nb, Ti, and Ta (15). The order of stability of the mesostructure upon reduction with alkali metal established from the XRD data was found to be Ti < Nb < Ta. This observation is consistent with thermal stability of these mesostructures. XPS studies on the Nb material showed that the different alkali metals gave a progressively higher shift (ca. 0.5 eV per row) to lower binding energy in the 3d emission as the size of the alkali metal increased. This was attributed to the decrease in electronegativity of the alkali metal down the row leading to greater electron density around the transition metal center. The band gaps were calculated from UV–vis spectra and varied from 3.3 to 4.0 eV depending on the material. The closest distance from the impurity band, formed by overlapping of the *n*d transition metal orbital and the ms orbital of the alkali metal, to the conduction band was 2.1 eV. Room-temperature conductivity measurements performed on this series of composites showed that all Nb and Ta materials were insulating with conductivity values below 10^{-7} ohm^{-1} cm^{-1}. The Li/Ti materials, on the other hand, displayed conductivity values up to 10^{-6} ohm^{-1} cm^{-1}. The insulating nature of the Nb and Ta composites was attributed to Anderson localization, an electron localization phenomenon caused by random dislocations in the oxide structure, while the high conductivity of the Li/Ti material was attributed to an Anderson transition (Scheme 1), which occurs in many amorphous systems, including Na-doped Na_xWO_3 (22).

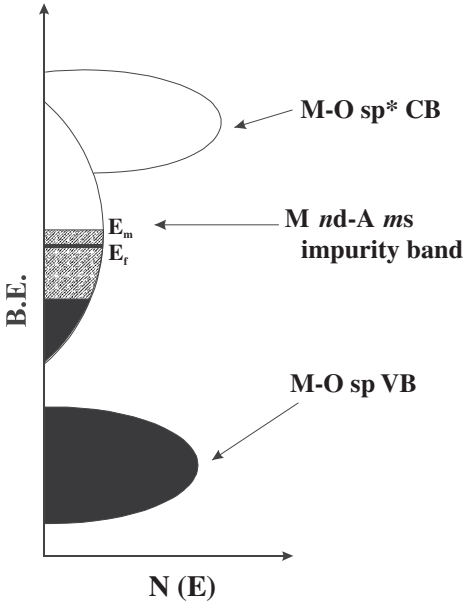
The superconducting quantum interference device (SQUID) magnetometry measurements of these materials revealed paramagnetic behavior. The presence of free electrons in this system was confirmed by electron paramagnetic resonance (EPR), however, no Nb coupling was observed, suggesting that the electrons are not tightly bound to one Nb center. To better understand the electrochemistry of Nb, Ta, and Ti oxides, a series of cyclic voltammograms (CVs) were employed. The Nb and Ta materials exhibited a high level of capacitance suggesting a possible application as supercapacitors. The CV run for the Ti material produced two clear peaks at 0.8 and 1.4 eV indicating reversible reduction/oxidation of the framework, suggesting its potential application in Li batteries and fuel cell fabrication. The difference in behavior of the Nb, Ta, and Ti materials was attributed to a charge mobility problem arising from greater electron localization in case of the Nb and Ta materials vs. the Ti material. This suggestion is consistent with conductivity measurements of the reduced Nb, Ta, and Ti materials.

Unusual magnetic properties in mesoporous Nb oxide – cobaltocene and nickelocene composites

Cobalt is known for its ability to influence magnetic prop-

© 2006 NRC Canada

Scheme 1. Graphic illustration of the energy level diagram of alkali A (A = Li, K, Na, Rb) reduced M-TMS1 (M = Ta, Nb, Ti). The electron resides in an *m*s (alkali metal) – *n*d (transition metal) impurity band between the valence and conduction bands of the mesostructure. E_F denotes the Fermi level, while E_m represents the mobility edge. Black areas are filled with electrons, while the area marked by grid lines represents a region of localized states extending down into the black filled levels of the impurity band.



erties of mixed alloy systems and often brings about strong ferromagnetic (23), superconducting (24), and superparamagnetic (25) properties, depending on the alloy or compound. The intercalation of cobaltocne into redox-active layered structures such as $NbSe_2$ has been extensively studied (26). In many ways cobaltocene can be viewed as a pseudo alkali metal, however, it has never been successfully intercalated into layered Nb_2O_5 because of the mismatch of reduction potentials between the host and guest. Since mesoporous Nb oxide possesses amorphous walls and amorphous structures are known to have a broader dispersion of reduction potentials than their crystalline counterparts, we attempted intercalation of cobaltocene into this structure. Surprisingly, mesoporous Nb oxide readily reacts with cobaltocene to give new dark gray solid that exhibits a sudden transition in magnetic behavior from paramagnetic to superparamagnetic on increase of cobaltocene loading at a critical molar ratio for Co–Nb of 0.5:1 (19, 27). These results are very unusual since superparamagnetism is normally observed only in nanometer-sized colloid grains of ferromagnetic transition metals or compounds, and neither cobaltocene or reduced mesoporous Nb oxide is ferromagnetic. XPS studies of this series of composites confirmed electron transfer from cobaltocene to the walls of the mesostructure by the presence of Nb in both the (IV) and (V) oxidation states. Clear emissions for both cobaltocene and cobaltocenium were also present, depending on the Co-loading level. While the materials at Co-loading levels below 0.5 equiv. showed only cobaltocinium, those at higher loading levels (up to 0.8 equiv.) showed a mixture of the oxidized and reduced metallocene. From the magnetic data, it was estimated that there was roughly 20 spins per superparamagnetic domain.

To understand which factors govern the onset of superparagnetism in these materials, a systematic study of the variation of pore size, wall thickness, and composition was conducted (27). The wall thickness and pore sizes were varied from 15 to 20 Å and 23 to 33 Å, respectively. In addition, mesoporous Ta and Ti cobaltocene composites were synthesized to gauge the effect of different mesostructure composition on the magnetic properties. The pore size and wall thickness seemed to have no effect on the magnetic properties of these materials. In contrast to the mesoporous Nb composites, the mesoporous Ta and Ti materials showed paramagnetic behavior and a much lower level of absorbed organometallic. This is not surprising because mesoporous Ti(IV) and Ta(V) oxides are more difficult to reduce than mesoporous Nb(V) oxide, and intercalation reactions are electron transfer driven. Thus, the host material must be reactive enough toward reduction by a guest species to absorb the critical amount of cobaltocene required to initiate superparamagnetic behavior. Initially, all the intercalated cobaltocene is oxidized to cobaltocinium by Nb sites of strong enough oxidizing strength (roughly half, according to the XPS). Additional cobaltocene is absorbed in the neutral form to give a mixed oxidation state cobaltocene/cobaltocinium phase trapped in a reduced mesoporous Nb oxide lattice. Once the critical absorption level is reached, the material undergoes a transition to superparamagnetic behavior owing to the increased density of unpaired electrons arising from neutral cobaltocene in the pore channels. The reason for superparamagnetism is still not understood, but may be related to ferromagnetic coupling induced by rapidly exchanging itinerant electrons, not bound exclusively to one Nb or Co site.

To gauge the effect of the overall spin of the organometallic guest species on the magnetic behavior of these composites, nickelocene, which has two unpaired electrons per Ni center, was introduced into the mesoporous Nb host (28). Similar to the cobaltocene composites, these materials revealed a loading dependent transition, however, in this case the transition was from paramagnetic to spin-glass behavior, which is normally associated with amorphous metal alloys in which the spins become "frozen" in a random orientation below a certain temperature. From the XPS it was found that the loading level of the organometallic species in case of the nickeltocene was much lower than in the case of the cobaltocene composites. This was rationalized by the higher ionization energy of nickelocene as compared with cobaltocene, i.e., fewer Nb sites are strong enough oxidizing agents to strip the electrons from the organometallic guest in the case of Ni as compared with Co.

Pseudo 1-D organometallic molecular wires supported by mesoporous Nb oxide

While intercalation of late metal metallocenes into mesoporous Nb oxide leads to materials that are insulating, but possess unusual magnetic properties, the impregnation of the pores of this material with early metal sandwich complexes leads to a new family of one-dimensional conducting

© 2006 NRC Canada

molecular nanowires in the case of Cp_2Cr, Cp_2V, $(C_6H_6)_2Cr$, and $(C_6H_6)_2V$ (17, 29–31). As in the case of cobaltocene, the mesoporous structure acts as an oxidizing agent and creates a mixed-valent cationic organometallic phase encapsulated in the negatively charged walls of the Nb oxide mesostructure. The spontaneity of this reaction is due to the broader distribution of redox potentials in the Nb oxide walls, since none of these organometallic species react with the crystalline bulk Nb oxide. In contrast to the Nb–cobaltocene composites, which are insulating, the electron transport measurements of these organometallic intercalates provided conductivity values as high as 10^{-4} ohm^{-1} cm^{-1}. A series of additional experiments (XPS, EPR, and NMR) suggested that conductivity in these systems arises only from the presence of the mixed oxidation state, low-dimensional organometallic phase, e.g., $(C_6H_6)_2Cr/(C_6H_6)_2Cr^+$. The conductivity in the V- and Cr-based composites was explained by a model where the hole in the mixed oxidation phase, arising from partial oxidation of the organometallic species by the mesostructure, is the charge carrier, since in all cases the presence of both cationic and neutral species were required for conductivity (17, 30), and the reduced mesostructure was previously shown to be insulating (15).

To better understand the nature of electron mobility in these organometallic composites, a systematic study of Cp_2V and Cp_2Cr intercalates using XPS, EPR, and UV–vis spectroscopy was performed (31). The Mott–Hubbard model, describing conductivity and electron localization in solids, was applied to rationalize the results. The estimated values of $W–U$ (W = bandwidth, U = Hubbard potential) for the V and Cr systems provided values of 1.38 and 2.32 eV with conductivities of 10^{-5} ohm^{-1} cm^{-1} and 10^{-6} ohm^{-1} cm^{-1}, respectively, as compared with $W \approx U = 0.05$ eV in the insulating cobaltocene system. The trend in conductivity from V and Cr to Co and Ni fits well into the Mott–Hubbard model. It also was found that in all these materials the electronic properties depend on the electronic configuration, mixed oxidation state of dopants, and the loading level of the organometallic. Solid-state ^{2}H NMR on the ^{2}H-labelled bis(benzene) Cr composite showed no evidence of close proximity between two adjacent organometallic species, suggesting that the Nb oxide walls may be involved in the local electron transfer between Cr(0) and Cr(I) (29).

Mesoporous Ta oxide reduced with bis(toluene) Ti — Metallic mesoporous oxides and dinitrogen cleavage

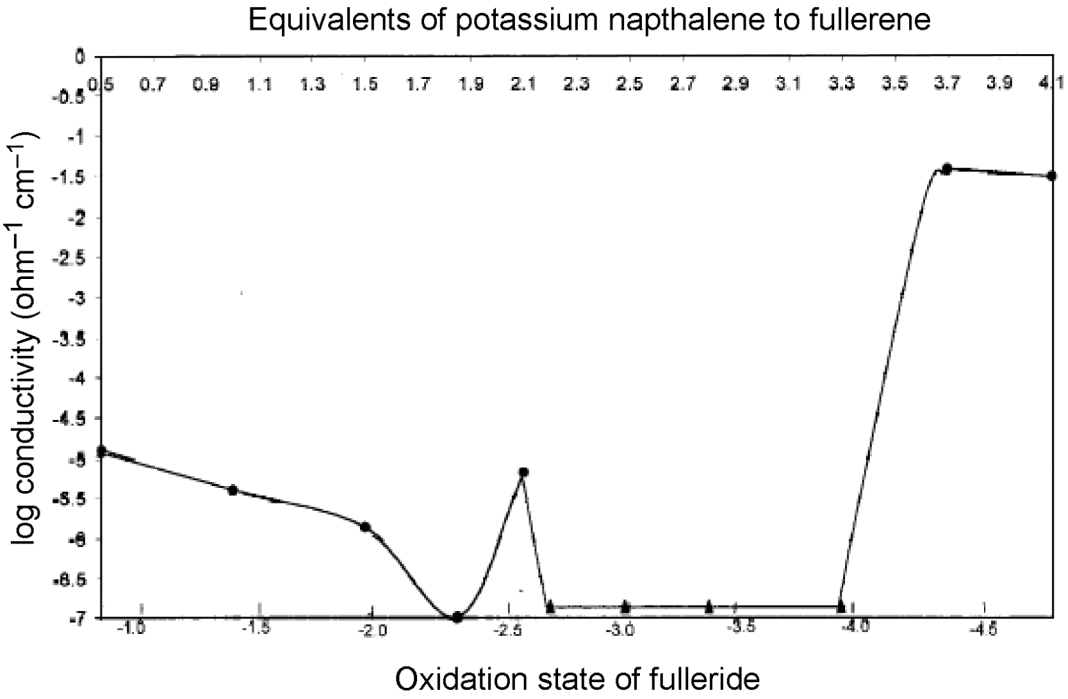
While sandwich complexes of mid- and late-transition metal species react with mesoporous Nb, Ta, and Ti oxides to give materials with mixed oxidation state organometallic phases in the pores, treatment of mesoporous Nb oxide with bis(toluene) Nb and mesoporous Ti oxides with bis(toluene) Ti leads to complete degradation of the organometallic structure and deposition of low-valent Nb or Ti on the surface of the respective mesostructure (32). The introduction of the organometallic into the pores is similar to a classical redox intercalation reaction in which an electron donor reduces the walls of the inorganic host to create a material with periodic charge regions consisting of an anionic metal oxide phase and a cationic dopant intercalate phase. In the case of bis(toluene) Ti and bis(toluene) Nb, the organometallic reduces the walls of the mesostructure, but does not retain its structural integrity on loss of electrons because the resulting cation is thermally unstable. The complex instead loses the toluene ligands and deposits Ti atoms on the inner and outer surface of the mesostructure. XPS studies of the material synthesized from mesoporous Nb oxide and bis(toluene) Nb reveal Nb(II) and Nb(IV). The XPS spectrum of the Ti analogue was less resolved, but showed emissions consistent with Ti(III) and Ti(II). There was also a broad hump at the Fermi level in both materials, suggesting metallic behavior. This was confirmed by variable-temperature conductivity measurements, which showed a slight increase in conductivity from the room-temperature values of 10^{-1} ohm^{-1} cm^{-1}. This was the first example of metallic behavior in a porous metal oxide structure. The metallic nature of this material can be attributed to the low-valent Nb or Ti coat on the surface (both NbO and TiO are metallic) of the mesostructure and suggests that there are continuous electronic pathways existing in the material that may be exploited in a catalytic process. An immediate example of the enormous potential of these materials in small molecule activation is the reaction of these materials with dinitrogen. Both the Nb and Ti analogues react spontaneously with dinitrogen to give surface nitride, which is subsequently protonated by incipient moisture to ammonia. ^{15}N-labeling studies confirmed that dinitrogen was indeed the source of ammonia. The ease of this reaction is surprising given the great stability of dinitrogen and the resistance to protonation of most metal nitrides. Treatment of mesoporous Ta oxide with bis(toluene) Ti also led to spontaneous ammonia formation in the presence of dinitrogen. Mechanistic studies on this system showed that both dinitrogen cleavage and protonation were fast steps, suggesting that the only barrier to making this process catalytic is the regeneration of the reduced active site on the surface.

Mesoporous Nb oxide as a host for K fulleride nanowires

Since mesoporous transition metal oxides function as insulating hosts for 1-D molecular nanowires and alkali fullerides have attracted much interest because of their metallic and superconducting properties, we began to explore the intercalation of these carbon-based materials into the pores of mesoporous Nb, Ta, and Ti oxides (20, 33–35). The role of the oxidation state in the metallic and superconducting behavior of alkali fullerides is still an area of much debate (36–38). However, it is widely believed that superconductivity in alkali fullerides, A_3C_{60} (A = K, Rb, Cs), arise from structural defects and the actual composition may be slightly different from the nominal A_3C_{60} composition (36). Recent theoretical advances suggest that the triple degeneracy of the t_{1u} band may lead to the removal of strong electron repulsion, the key factor of the Mott–Hubbard model, and thus might also be responsible for metallic and superconducting behavior in A_3C_{60}-type fullerides (39). Because of the subtleties of the solid-state chemistry involved, it is extremely difficult to study nonstoichiometry in C_{60}. The closest attempts to study noninteger oxidation states

© 2006 NRC Canada

Fig. 1. Plot of the oxidation state vs. the logarithm of conductivity as calculated from the Raman shift for reduced mesoporous Nb oxide – K_3C_{60} composites. The points represent an average measurement across 5–10 identically-prepared samples.



came from the group of Prassides, who showed that Li does not give complete charge transfer to fullerides (40).

With the goal in mind of using mesoporous Nb oxide as a kind of "quantum test tube" to study conductivity–oxidation state relationships in isolated fulleride nanophases, we developed methods to impregnate mesoporous Nb oxide with K_3C_{60} (33, 34). The pore size of mesoporous Nb oxide used in this study was 23 Å, which is ideal to fit one unit cell of K_3C_{60} (ca. 14 Å). The reaction between mesoporous Nb oxide and K_3C_{60} in tetrahydrofuran (THF) yields a material with the alkali fulleride inside the pores in an oxidation state of $n = 0.5$ (parent material), as judged by Raman spectroscopy. For fulleride salts of the type A_nC_{60} (A = K, Rb, Cs), the A_g mode shifts roughly 6 cm^{-1} for every integer increment in the value of n (41, 42). The oxidation state of the Nb mesostructure was probed by XPS and revealed a partial reduction equal to that of pure mesoporous Nb oxide reduced with 0.4 equiv. of potassium naphthalene. Attempts to intercalate alkali fullerides into mesoporous silica were unsuccessful, suggesting that charge transfer from the fulleride to the Nb oxide walls was a key feature of stabilizing the composite. The room-temperature conductivity of the Nb composite provided values of up to 1.25×10^{-3} ohm^{-1} cm^{-1}, 10 000 times greater than that observed for the potassium-reduced, fulleride-free samples of mesoporous Nb oxide (14).

To probe into the possible contributions to the bulk charge transport properties from surface conductivity pathways, a sample of nonporous, amorphous Nb oxide was treated with K_3C_{60} in THF. The XPS measurements indicated partial reduction of the surface by K_3C_{60}, but the conductivity of this was below the instrument threshold of 10^{-7} ohm^{-1} cm^{-1}. This suggests that the conductivity pathway in the mesoporous composites is through the fulleride units occluded in the channels, rather than through the Nb oxide walls of the structure, and the fulleride units are acting as a one-dimensional molecular wire. Since room-temperature conductivity provides only limited information on a material's transport properties, variable-temperature conductivity measurements were performed on this series of materials (20). These studies revealed that some materials behave as semiconductors with a transition to an insulating state below 210 K. The presence of metal–insulator or semiconductor–insulator transition in one-dimensional materials is normally attributed to a Peirls distortion in which electrons become localized in traps owing to charge density waves (22).

An intriguing feature of this material is that it can be sequentially reduced with potassium naphthalene and the oxidation states of the occluded fulleride and Nb oxide mesostructure controlled and monitored by Raman and XPS, respectively. This allows us to study the effect of the oxidation state. To probe into the dependence of conductivity on the oxidation state of the fulleride inside pores, a series of new composites with oxidation states up to $n = 4.5$ were synthesized from the parent material by gradual titration with potassium naphthalene. Surprisingly, two conductivity maximums at $n = 2.6$ and 4.1 with values of 10^{-4} and 10^{-1} ohm^{-1} cm^{-1}, respectively, were observed in these composites (Fig. 1) (35).

The maximum at $n = 2.6$ is unexpected on the basis of conductivity patterns in pure alkali fullerides, but may support the view that metallic behavior in pure K_3C_{60} arises from nonstoichiometry and oxidation state defects in the fcc lattice. The maximum at $n = 4.1$ is particularly intriguing as K_4C_{60} has a calculated density of states at the Fermi level close to that of K_3C_{60}, and according to most models should be metallic because of its 2/3 filled t_{1u} band (43), yet so far

© 2006 NRC Canada

all samples of K_4C_{60} prepared are insulating. Variable-temperature conductivity measurements indicated that the $n = 2.6$ composite behaves similarly to the parent material, while the $n = 4.1$ material displayed metallic behavior. The nature of the conductivity maximum at $n = 4.1$ was explained by an increase in cooperation between the walls of mesostructure and t_{1u} band of the fulleride and is consistent with an observed increase in the density of states near the Fermi level in the XPS. When the parent material was reduced back to the $n = 3.0$ state, the room-temperature conductivity of this composite was lower than 10^{-7} ohm^{-1} cm^{-1} and no further reduction of the mesostructure was observed. This composite proved too insulating to perform variable-temperature conductivity measurements. Such results are quite surprising when compared with bulk fullerides, but not unexpected on the basis of theory, since K_3C_{60}, in accordance with the Mott–Hubbard model, should be an insulator with a half-filled t_{1u} band (44), but shows metallic behavior, possibly owing to accidental vacancies in its structure or perhaps because of lattice distortions lifting the degeneracy of the t_{1u} band.

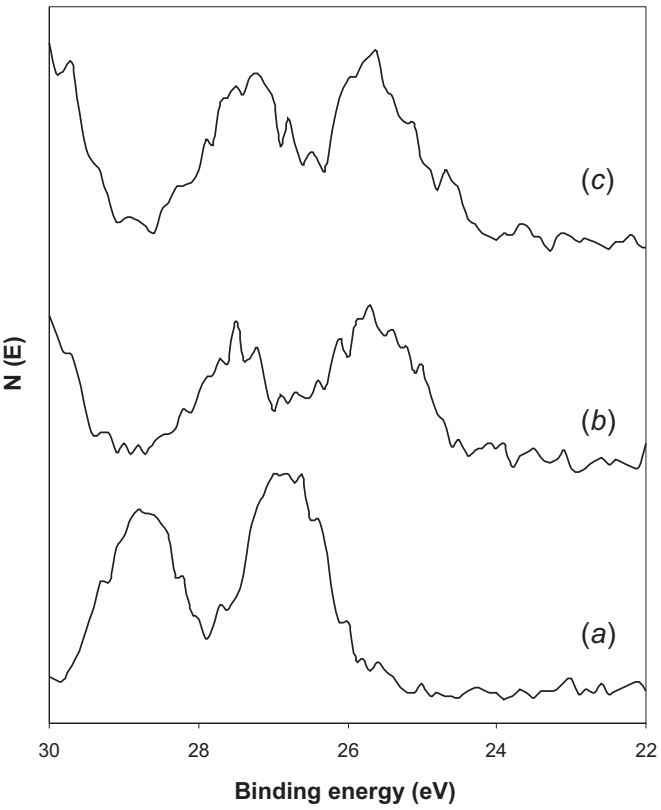
To better understand the unusual properties of this new family of composite materials, the effect of pore size and wall composition were studied. The pore size was expanded from 23 to 32 Å, sufficient to accommodate up to two fulleride units, while mesoporous Ti and Ta hosts were used in place of Nb. It was found that, in general, the change of host produces very little effect with a small difference in the position of the double maximum; however, this difference was too subtle to draw any definitive conclusions. Rather than providing enough room to accommodate two fullerides across the diameter of the pore channel, the expansion of pore size only makes it easier to wash out the fulleride, suggesting that restricted motion inside the narrow pores, and not just Coulombic attractions among the negatively charged walls, the alkali metal cations, and the anionic fullerides, are responsible for holding the structure together. SQUID magnetometry measurements revealed that all composites in this study were paramagnetic with no sign of a transition to superparamagnetic behavior at lower temperatures.

To make a more direct comparison between our mesoporous composites and the bulk materials and elucidate the role of the oxidation state of fulleride on conductivity, further information about the coordination geometry of the fulleride units and possible conductivity pathways was required. These materials are largely amorphous and solid-state NMR is perhaps the only way to gain information about the local structure of the material inside the pores. Since potassium is a difficult nucleus for NMR, we extended our study to include Na, Li, and Rb fulleride intercalates to perform ^{23}Na, ^{7}Li, and ^{87}Rb NMR. In these subsequent studies presented in the following sections, we also focused on mesoporous Ta, rather than Nb or Ti oxides, because of the greater thermal stability of the heavy metal based mesostructure, and its ability to resist reduction and reoxidation without any loss of structure.

Mesoporous Ta oxide impregnated with sodium fulleride

Because no known phase of sodium fulleride has yet demonstrated superconducting properties in the bulk phase, it was anticipated that sodium fulleride composites of mesoporous Ta oxide may have different electronic properties than the potassium analogues. Impregnation of the mesoporous oxide and subsequent Na-naphthalene reduction of the fulleride composites was performed in a manner similar to that used to synthesize the potassium fulleride composites. The oxidation state of fulleride after impregnation was estimated at $n = 0.5$ (parent material) by Raman spectroscopy, consistent with the value previously reported for the potassium analogues (21). XPS also showed a reduction of the Ta oxide walls to an oxidation state between (IV) and (V) (Fig. 2). Conductivity measurements of the parent material yielded values of 10^{-3} ohm^{-1} cm^{-1}, similar to those reported in the case of potassium fullerides.

Fig. 2. XPS spectra of the Ta 4f 7/2, 5/2 region for reduced mesoporous Ta oxide – Na_3C_{60} composites. (*a*) $n = 0.5$, (*b*) $n = 3.0$, and (*c*) $n = 4.5$ materials.

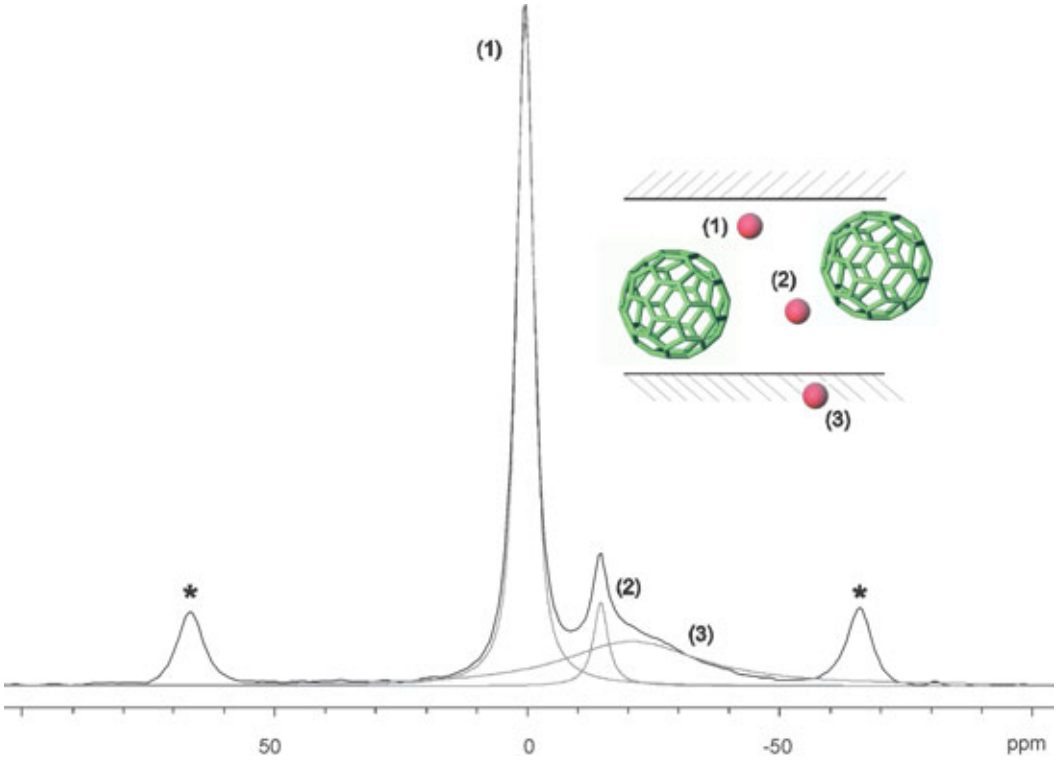


To explore the relationship between the fulleride oxidation state and conductivity in these materials, the parent intercalate was reduced sequentially with Na-naphthalene. The XPS spectra of the reduced materials showed a reduction of the Ta oxide walls of the mesostructure between the parent and $n = 3.0$ states, but almost no further reduction up to a level of $n = 4.5$ (Fig. 2*c*). This behavior is different from that observed in the K_3C_{60}/Nb system in which no reduction of the Nb oxide walls of the mesostructure upon addition of K-naphthalene was observed until the oxidation state of the fulleride units reached $n = 4.0$ (35). This behavior can be rationalized by the different reduction potentials of Nb vs. Ta and K-naphthalene vs. Na-naphthalene.

Room-temperature conductivity profiles for this series of

© 2006 NRC Canada

Fig. 3. ^{23}Na rotor-synchronized Hahn-echo MAS NMR spectrum of Na_3C_{60} intercalated into the mesoporous tantalum oxide acquired (spinning sidebands are denoted with asterisks). Inset: highly schematized representation of three different sodium cation sites: Na(1), sodium cations in the Ta oxide channels; Na(2), sodium cations associated with the fulleride species; and Na(3), sodium cations confined within the walls of the mesoporous Ta oxide.



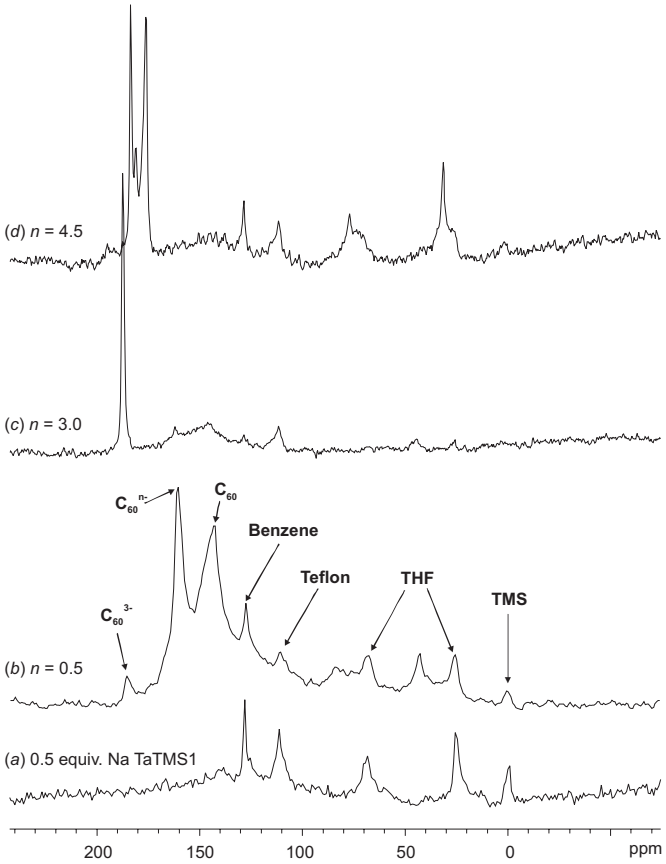
reduced materials showed a progressive decrease in conductivity with increasing anionic charge on the fulleride from the n = 0.5 to the n = 3.0 state, which is totally insulating. After this, there is a sharp rise to n = 4.5, which has a conductivity value of 10^{-2} ohm^{-1} cm^{-1}. The absence of the conductivity maxima at 2.5, observed in the K/Nb analogue, is not totally unexpected, as the electronic properties of Na fulleride are substantially different from that of K fulleride, and there are no reports of superconductivity or metallic behavior in Na_3C_{60}. Variable-temperature conductivity measurements performed on the n = 0.5 and 4.5 composites revealed that both of these materials are semiconductors. This is not unlike the results obtained for potassium fulleride materials, except that the maximum at n = 4.0 in the K/Nb system is metallic rather than semiconducting.

The elemental analysis data for the sodium fulleride materials is puzzling when compared with that of the K/Nb analogues. The %C analysis of composite materials showed that the carbon-loading level remains virtually the same, within only 3% to 4% difference for all materials. This trend is very different from the K_3C_{60}/Nb materials, where progressive leaching of carbon upon reduction was observed, and the insulating n = 3.0 state is more rich in C than the metallic n = 4.0 state. This suggests that the carbon-loading level does not significantly contribute to the conducting properties of the materials. The reason why progressive leaching of fulleride upon reduction does not occur in the Na_3C_{60}/Ta system is not clear, but may be due to the polymerization of the fulleride units in the pores of the mesostructure, which has been reported in bulk Na_4C_{60}.

Solid-state ^{23}Na and ^{13}C NMR studies were conducted in the hope of establishing structural information about the coordination geometry about the alkali metals in the pores of the intercalated materials. ^{23}Na NMR performed on the parent material showed the presence of three distinct sodium species in the series of Na/Ta materials (Fig. 3). These are: (*i*) mobile uncoordinated Na ions in the channels of mesostructure; (*ii*) sodium ions that are closely associated with fulleride cages, and (*iii*) sodium ions confined or buried in the walls of the mesostructure. ^{23}Na NMR measurements for the series of reduced materials revealed the following trends: (*i*) decrease of Na ions associated with fulleride units; and (*ii*) progressive increase in the population of confined and channel sodium ions. ^{13}C NMR of this new series of materials revealed the presence of multiple carbon-containing species (Fig. 4). Three distinct resonances corresponding to C_{60}, C_{60}^{3-}, and C_{60}^{n-} were observed in the parent materials. Of special interest, however, is the spectra of the n = 3.0 material (Fig. 4*c*), as it almost exclusively showed the presence of C_{60}^{3-}. This allows much more direct comparison with the bulk phase and represents the first isolated example of an insulating n = 3.0 fulleride, possibly supporting the view that C_{60}^{3-} is a Mott–Hubbard insulator. In the case of the n = 4.5 materials (Fig. 4*d*), several new C_{60} species were identified that could not be assigned to known fulleride phases. This could be due to polymerization

© 2006 NRC Canada

Fig. 4. ^{13}C MAS NMR spectra: (*a*) mesoporous Ta oxide reduced with 0.5 equiv. Na naphthalene TaTMS1, mesoporous Ta oxide intercalated with Na_3C_{60} and reduced to the oxidation states of (*b*) $n = 0.5$, (*c*) $n = 3.0$, and (*d*) $n = 4.5$.



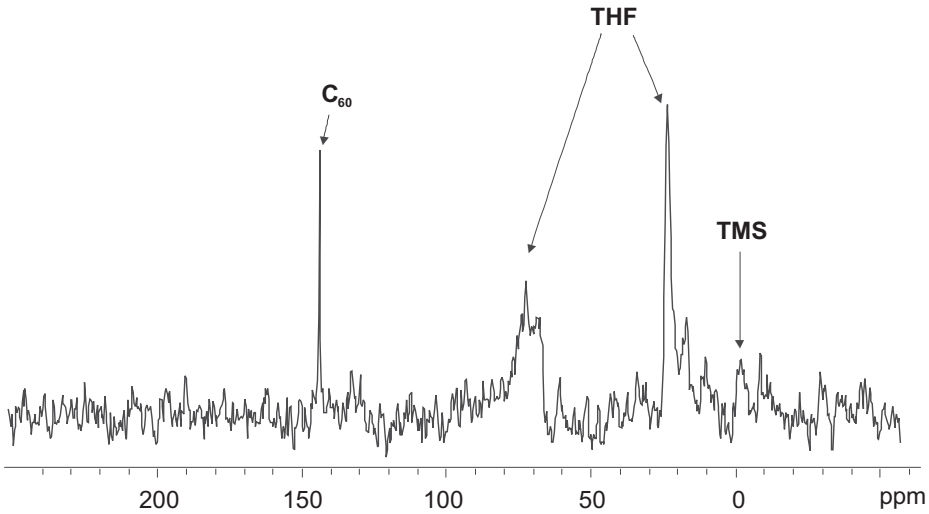
of C_{60} within the pores of the mesostructure, a picture supported further by the high level of carbon in this material. However, polymerization could not be verified, since the sp^3 resonance associated with polymerized fullerenes falls between 30 and 80 ppm (45) and this region of the spectrum is obscured by multiple solvent species. All of these data suggest a unique and unprecedented fulleride structure in the $n = 4.5$ material in which the fulleride units are surrounded by a double sheath composed of an inner layer of Na ions followed by the reduced anionic walls of the mesostructure comprising the outer layer.

Mesoporous Ta oxide – Li fulleride composites

As mentioned previously, mesoporous Ti oxide impregnated with Li fullerides may be useful in Li batteries owing to the high conductivity imparted by the C-phase to the insulating oxide (15). To improve charge transport to the active sites in insulating Fe phosphate cathodic materials, carbon coating of the insulating inorganic grains has been employed. In the case of mesoporous transition metal oxides, 1-D fulleride nanowires could potentially be used to improve charge transport through the otherwise insulating channels to the redox-active transition metal sites. Although mesoporous Ta oxide reduced with Li naphthalene is an insulator, impregnation of the mesostructure with alkali (K, Na) fullerides clearly leads to improved electron transport through the structure (20, 21, 35). Thus, it stands to reason that impregnation of a Ta oxide mesostructure with a Li fulleride phase could lead to the new cathodic materials with improved electron transport to the active sites. In this regard, we attempted to synthesize a new series of mesoporous Ta oxides impregnated with Li fulleride (46). On paper it seemed feasible to use a similar approach to that used for K and Na fulleride analogues, however, synthesis of Li_3C_{60} itself is extremely difficult and requires high temperature and pressure apparatus (47). Attempts to synthesize Li_3C_{60} in solution were unsuccessful and led to formation of insoluble products that could not be used for impregnation. Thus, an alternative route for the synthesis of these materials was developed. This involved the reduction of the mesostructure with Li naphthalene followed by the treatment of the reduced mesostructure with an excess of C_{60}. This method relies on the unique ability of the alkylated mesostructure to reduce the fullerene in solution and hence trap it as a fulleride in the pores, rather than using alkylated fulleride to reduce the mesostructure. It was established earlier (15) that the materials reduced with less than 1 equiv. of Li naphthalene are less effective reducing agents and absorb less C_{60}, while the materials reduced with more than 1 equiv. of Li naphthalene indicated a partial collapse of the mesostructure. Given these considerations, and for the sake of simplicity, material reduced with 1 equiv. of Li naphthalene and subsequently treated with the maximum amount of C_{60} was chosen for study. Raman spectra of this material revealed a very subtle shift in the position of the A_g band of C_{60} in this composite, indicating that no visible reduction of the fulleride phase had occurred. This was further confirmed by solid-state ^{13}C NMR (Fig. 5), which revealed the presence of a single C_{60} species with a chemical shift almost coincident with that of unreduced C_{60} (48). The absence of other resonances within the 140–170 ppm range, where chemical shifts for fulleride species are normally distributed, further demonstrated that no visible reduction of C_{60} had occurred. Solid-state ^7Li NMR for this material revealed a single broad resonance centered at around 0 ppm. Given the narrow distribution of chemical shifts in the ^7Li NMR, the assignment of a Li environment based on this single resonance is extremely difficult and could be misleading. Conductivity measurements for this composite gave values below 10^{-7} ohm^{-1} cm^{-1}, which is surprising given the conductive behavior of K- and Na-reduced fullerides (20, 21, 33–35). On the other hand, Raman and XPS data suggested that Li does not provide complete charge transfer to C_{60}, nor to the walls of mesostructure. SQUID measurements showed that this material is paramagnetic and contains approximately one unpaired electron per Ta. In our previous studies of K and Na fulleride intercalated systems it was possible to reduce these materials further by simple treatment with alkali naphthalene in THF. This allowed the charting of the dependence of the electronic and magnetic properties of these materials on the oxidation state of C_{60} and the absolute loading level of alkali metal, and hence to draw some comparison with bulk phase alkali fullerides (21, 34, 35). In the case of the Li fulleride material, all further attempts to reduce this material with Li naphthalene were unsuccessful and led to

© 2006 NRC Canada

Fig. 5. ^{13}C MAS NMR of the Li fulleride composite. TMS here refers to trimethylsilyl.



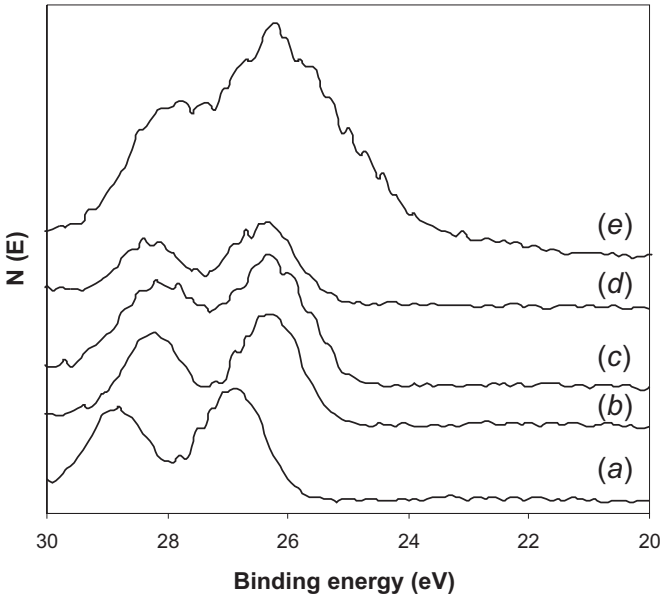
no observable reaction. Since Li naphthalene is a strong enough reducing agent to reduce either the walls of the mesostructure or the occluded C_{60}, the fulleride units in these composites are likely blocking the pores and preventing charge transfer to the inside the channels. Given that previous studies of K and Na fulleride materials would likely have the same pore restrictions, it is feasible that reduction in these materials likely occurs via a reaction on the outside of the channels followed by subsequent charge transfer through the channels, rather than gradual diffusion of alkali naphthalene through the pores to the active site. Impregnation of the pores with Li fulleride thus impedes charge transfer through the channels and prevents the possibility of further reduction.

Electrochemical studies were conducted to compare the Li insertion/deinsertion behaviors of this composite with a previously synthesized Na fulleride mesoporous Ta oxide composite and a pristine mesoporous Ta oxide. The results of these studies showed that Li insertion into the fullerene composites is rather irreversible in the Li material and more reversible in the more highly conducting Na analogue. This was attributed to a strong interaction between the inserted Li ions and the walls of the mesostructure, with fullerene doping suppressing the charge transfer owing to the nonconductive fullerene wires. This shows that impregnation of the pores of mesoporous Ta oxide does not improve charge transfer as anticipated, and that these materials would thus be a poor choice for cathodes in a Li battery.

Mesoporous Ta oxide impregnated with rubidium fulleride

Considering the extreme diversity in properties of alkali fullerides and because Rb fullerides have higher T_c as compared with K fullerides (Li and Na fullerides are not superconducting) we extended our study to include Rb fullerides (49). ^{87}Rb is an extremely receptive NMR probe and applying it to Rb composite materials may help reveal more relationships between local structure and the unusual conducting properties of the composite materials. A series of Rb fulleride materials was synthesized in a similar manner to

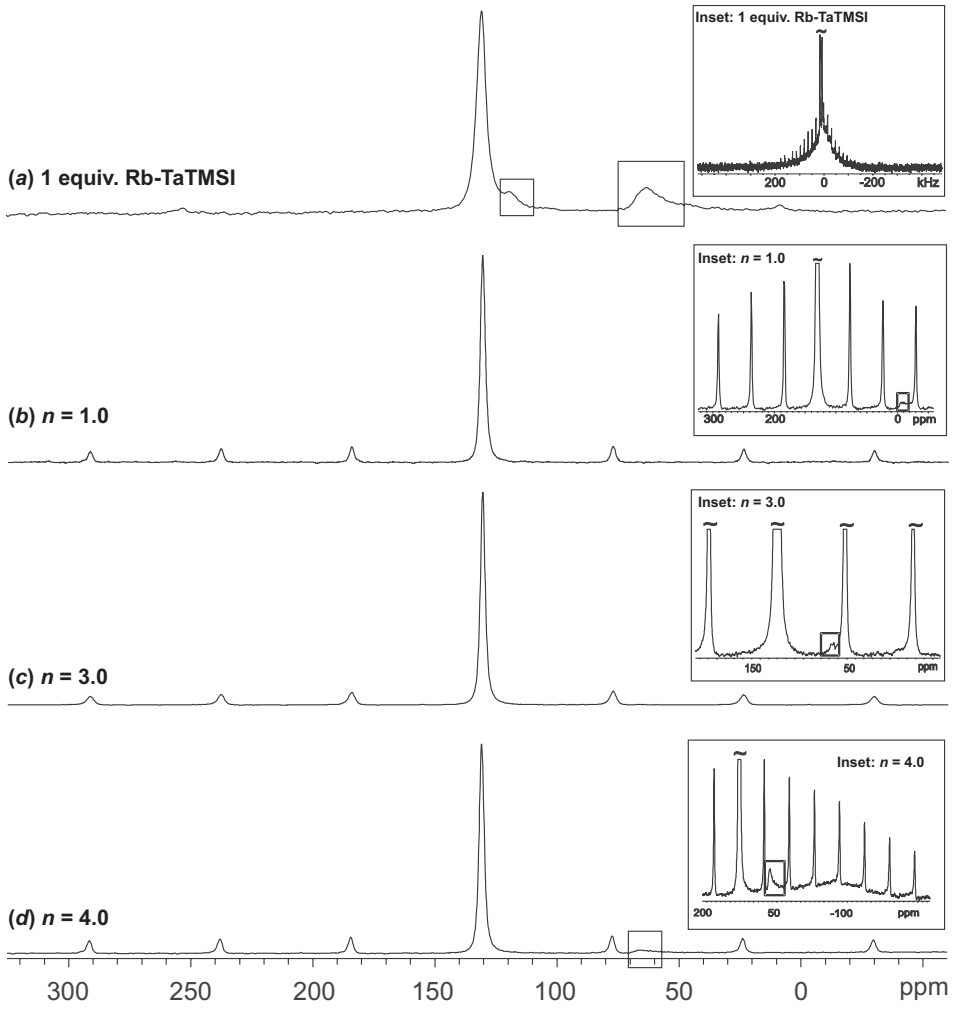
Fig. 6. XPS spectra showing the Ta 4f 7/2, 5/2 region for (*a*) pure mesoporous Ta oxide, mesoporous Ta oxide intercalated with Rb_3C_{60}, and reduced to the oxidation states of (*b*) n = 1.0, (*c*) n = 3.0, (*d*) n = 4.0, and (*e*) mesoporous Ta oxide reduced with only 1 equiv. of Rb-naphthalene (1 equiv. Rb-TaTMSl).



that of the K and Na fulleride analogues by impregnation in THF by the fulleride followed by sequential reduction by Rb naphthalene (35). For the sake of comparison, mesoporous Ta oxide reduced only with 1 equiv. of Rb naphthalene (1 equiv. Rb-TaTMSl), which is "fulleride-free", was also prepared. The oxidation state of C_{60} in the parent intercalate was estimated by Raman spectroscopy at n = 1.0 rather than n = 0.5 in the Na and K systems. This was attributed to the stronger reduction potential of Rb fullerides as compared with K and Na counterparts. XPS spectroscopy recorded for this series of new materials (Fig. 6) indicated that the walls of the mesostructure were reduced to an oxidation state between Ta(IV) and Ta(V) at the initial stage of impregnation of Rb_3C_{60} (Fig. 6*b*) and that no further reduction upon addi-

© 2006 NRC Canada

Fig. 7. ^{87}Rb MAS NMR spectra of (*a*) mesoporous Ta oxide reduced with only 1 equiv. of Rb-naphthalene (1 equiv. Rb-TaTMSl) and mesoporous Ta oxide intercalated with Rb_3C_{60}, and reduced to the oxidation states of (*b*) n = 1.0, (*c*) n = 3.0, and (*d*) n = 4.0 composites. Inset: Vertical expansions of the isotropic chemical shift regions.

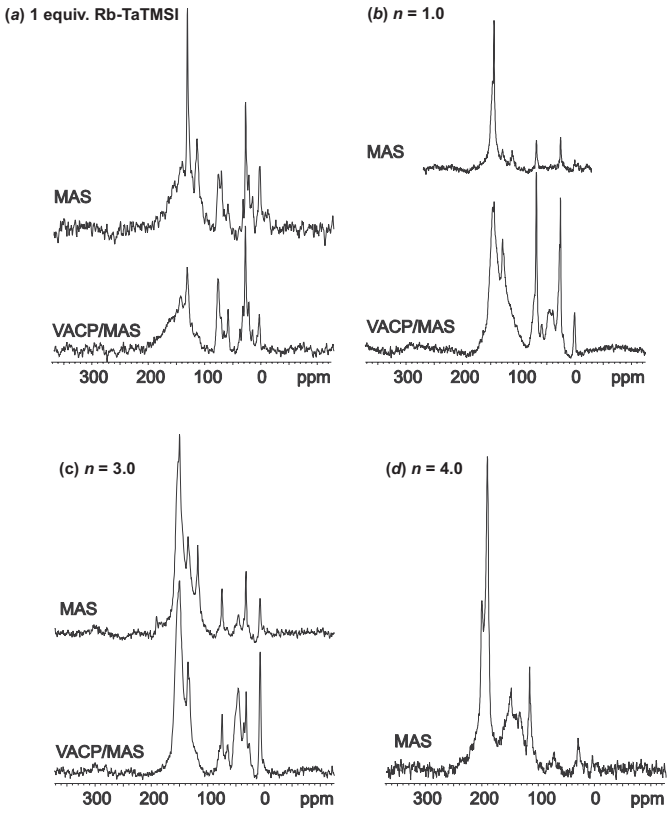


tion of Rb naphthalene to the parent material was detected. There was, however, substantial broadening of the emissions observed. This is indicative, again, of the presence of multiple Ta species at a higher reduction level. The conductivity measurements on a series of these materials revealed a pattern similar to that of Na fulleride materials with a single conductivity maxima at n = 4.0. There was no conductivity maxima at n = 2.5, and the n = 3.0 state was highly insulating. The reason for the lack of conductivity maxima at around n = 2.5 in the Rb and Na composites is not understood, but may be due to different electronic properties of Rb and Na fullerides and K fullerides. Once again, the absolute value of the carbon content in these composites has a negligible effect on conductivity, as the n = 4.0 material had the lowest carbon loading, yet the highest conductivity. Variable-temperature conductivity measurements were performed for the two most conductive samples, n = 1.0 and 4.0. The n = 1.0 material is a typical semiconductor, while the n = 4.0 material is a semi-metal or narrow band gap semiconductor.

Solid-state ^{87}Rb and ^{13}C NMR measurements were conducted to probe into the local geometry of alkali fullerides occluded in the pores of the mesostructure. ^{87}Rb NMR spectra of the parent material (Fig. 7*b*) allowed us to clearly identify two major environments: (*i*) Rb ions in the channels; and (*ii*) Rb ions confined into the walls of the mesostructure. These were not unexpected on the basis of NMR studies on the Na system. There were also several unresolved resonances that likely correspond to Rb ions coordinated to fulleride species. These resonances, however, were much lower in intensity than those observed for Na fullerides. A trend similar to that of Na fullerides was also observed upon reduction, i.e., the population of channel and confined Rb ions progressively grew on addition of Rb-naphthalene. There was, however, an additional resonance at around –75 ppm detected in the n = 4.0 material (Fig. 7*d*). This resonance was attributed to the presence of Rb ions associated with one or more fulleride species. ^{13}C NMR measurements (Fig. 8) revealed an even greater variation of carbon-containing species than in the Na system. In the parent n = 1.0 material (Fig. 8*b*), resonances at 144 and 148 ppm, corresponding to pure C_{60} and C_{60}^{n-}, respectively,

© 2006 NRC Canada

Fig. 8. ^{13}C MAS NMR spectra (ν_{rot} = 15 kHz) of materials from Fig. 7. Corresponding ^{13}C VACP/MAS spectra are shown for all samples with the exception of the n = 4.0 sample.



were observed. The spectra of the n = 3.0 material (Fig. 8*c*) is similar in appearance to that of the parent material, with a smaller amount of C_{60} and more C_{60}^{n-}. There is, however, an extremely small resonance at around 184 ppm, corresponding to C_{60}^{3-}. This very surprising result differs significantly from that of the n = 3.0 Na composite, which showed an almost exclusive presence of C_{60}^{3-}! This demonstrates that Raman spectroscopy cannot be relied on to assign fulleride oxidation states in these systems and that combinations of disparate species can lead to insulating behavior and the appearance of an n = 3.0 state. The appearance of the n = 4.0 spectra (Fig. 8*d*) was also intriguing, as it showed a significant amount of C_{60}^{3-} along with a smaller amount of C_{60}^{n-}. The high conductivity values of this material that n = 3.0 fullerides can function as semi-metals as long as they are mixed with a suitable amount of fulleride in a different oxidation state. This suggests that K_3C_{60}, although containing mostly insulating C_{60}^{3-}, may possibly be made metallic by the introduction of oxidation state defects in the lattice, an observation that lends some support to the hole-doped Mott–Hubbard insulator model.

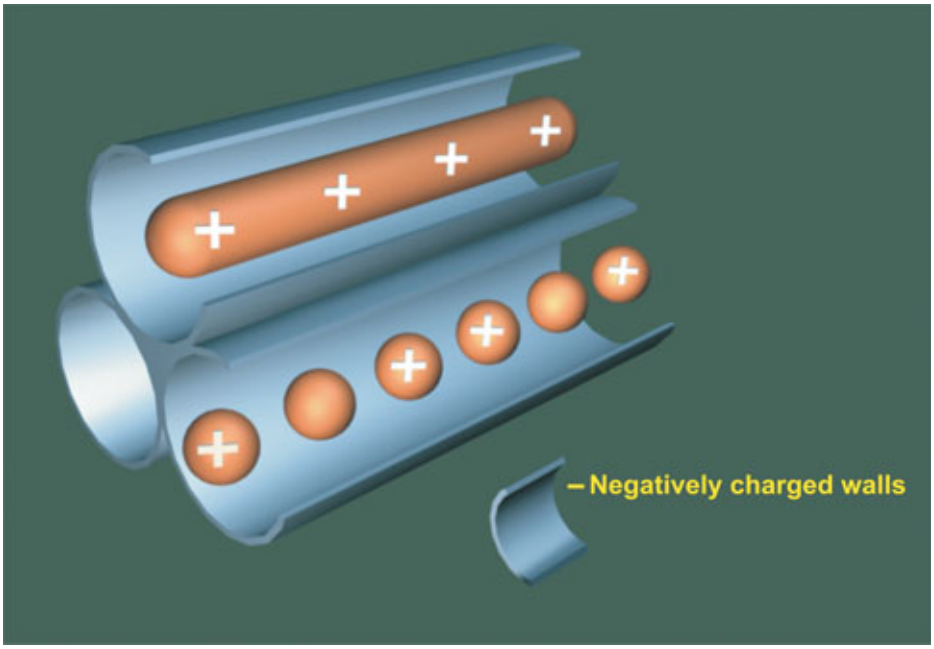
While this study revealed a wide range of electronic behavior and established many firm composition–property relationships, and also represented the first attempt to synthesize and rationalize physical properties of 1-D fullerides, direct comparisons of these composites with bulk fullerides are difficult because of the lack of order in the pores of these materials as well as the 1-D nature of the occluded phases. Low-dimensional solids often undergo temperature-related transitions to insulating behavior owing to the introduction of physical distortion in the conducting chain. In spite of this, the observation of metallic behavior in the n = 4.0 systems is of theoretical interest, while the insulating nature of the pure phase n = 3.0 Na/Ta and mixed-phase n = 3.0 Rb/Ta systems invites some comparisons to the bulk-phase materials. Since 1-D lattice distortions to insulating phases normally occur at lower temperatures, and room temperature provides enough energy for a thermal averaging of sites along a conducting chain, it is not likely that the insulating nature of the pure n = 3.0 Na/Ta phase is due to Peierl's distortion, especially since the n = 4.0 Rb/Ta and K/Nb materials are metallic or semi-metals under these same conditions and possess less C than the insulating n = 3.0 phase, which would tend to make them even more prone to electron localization effects. With this in mind, it appears that the most important conclusion that can be drawn from this long series of studies is that C_{60}^{3-} is indeed a Mott–Hubbard insulator, at least in a 1-D phase, and that addition of oxidation state defects can lead to transitions to semiconducting or even metallic behavior, apparently independent of the net C-loading level.

Summary

The synthesis and study of stable mesoporous transition metal oxides has led to a new series of intercalation reactions in which the guest species occupies a 1-D channel in the host lattice rather than a 2-D sheet, as is the case with layered materials. The redox activity of the walls allows for electron-transfer reactions to occur between the host and guest, similar to what is observed in the reactions of metal chalcogenides. The amorphous nature of the mesostructured walls also provides a broader range of redox potentials than the corresponding bulk oxides. As a result, mesoporous Nb, Ta, and Ti oxides are able to react with guest species that are not strong enough reducing agents for intercalation into the corresponding crystalline oxide. Thus, these materials combine the capacity for quantum confinement into 1-D channels with the capacity for oxidation or partial oxidation in the same step. This has already led to a series of mixed oxidation state, cationic molecular phases encapsulated within a 1-D anionic transition metal oxide lattice. This is illustrated in Scheme 2. Not surprisingly, these composites possess many unusual properties not observed for the corresponding bulk phases of the guest materials. For example, because of these unique properties, cobaltocene becomes superparamagnetic in the pores of mesoporous Nb oxide and metallic K_3C_{60} becomes an insulator, while insulating K_4C_{60} becomes metallic! There is also the possibility that the walls of the structure can cooperate with the guest phases, leading to properties not observed in the pure nanophases of the same encapsulated materials. The extension of this class of materials into continuous phase nanowires with cationic defects supported by the anionic host lattice is ongoing in our group and is almost certain to lead to materials with properties not observed in the bulk-phase or even pure-phase nanowires of the same substance.

© 2006 NRC Canada

Scheme 2. Schematic representation of cationically charged low-dimensional nanophase (continuous or molecular) encapsulated in a negatively charged anionic mesoporous transition metal oxide host lattice.



References

1. B.T. Holland, C.F. Blanford, and A. Stein. Science (Washington, D.C.), **281**, 538 (1998).
2. C.P. Collier, E.W. Wong, M. Belohradsky, F.M. Raymo, J.F. Stoddart, P.J. Kuekes, R.S. Williams, and J.R. Heath. Science, **285**, 391 (1999).
3. H. Noji. Science (Washington, D.C.), **282**, 1844 (1998).
4. N. Mosznert. Int. J. Nanotechnol. **1**, 130 (2004).
5. M.C. Roco and W.S. Bainbridge. *In* Societal implications of nanoscience and nanotechnology. *Edited by* M.C. Roco and W.S. Bainbridge. Kluwer, Dordrecht. 2001. pp. 1–24.
6. Y. Huang, X. Duan, Q. Wei, and C.M. Lieber. Science, **291**, 630 (2001).
7. G. Vissokov. Bulg. Chem. Ind. **74**, 1 (2003).
8. J.S. Beck, J.C. Vartuli, W.J. Roth, M.E. Leonowicz, C.T. Kresge, K.D. Schmitt, C.T.-W. Chu, D.H. Olson, E.W. Shepard, S.B. McCullen, J.B. Higgins, and J.L.J. Schlenker. J. Am. Chem. Soc. **114**, 10834 (1992).
9. C.T. Kresge, M.E. Leonowicz, W.J. Roth, J.C. Vartulli, and J.S. Beck. Nature (London), **359**, 710 (1992).
10. J.C. Vartuli, K.D. Schmitt, C.T. Kresge, W.J. Roth, M.E. Leonowicz, S.B. McCullen, S.D. Hellring, J.S. Beck, J.L. Schlenker, D.H. Olson, and E.W. Sheppard. Chem. Mater. **6**, 2317 (1994).
11. D.M. Antonelli and J.Y. Ying. Angew. Chem. Int. Ed. Engl. **34**, 2014 (1995).
12. D.M. Antonelli and J.Y. Ying. Angew. Chem. Int. Ed. Engl. **35**, 426 (1996).
13. D.M. Antonelli and J.Y. Ying. Chem. Mater. **8**, 874 (1996).
14. M. Vettraino, M. Trudeau, and D.M. Antonelli. Adv. Mater. **12**, 337 (2000).
15. M. Vettraino, M. Trudeau, and D.M. Antonelli. Inorg. Chem. **40**, 2088 (2001).
16. S.L. Brock, N. Duan, Z.R. Tian, O. Giraldo, H. Zhou, and S.L. Suib. Chem. Mater. **10**, 2619 (1998).
17. X. He, M. Trudeau, and D.M. Antonelli. Adv. Mater. **12**, 1036 (2000).
18. X. He, M. Trudeau, and D.M. Antonelli. J. Mater. Chem. **13**, 75 (2003).
19. S. Murray, M. Trudeau, and D.M. Antonelli. Adv. Mater. **12**, 1339 (2000).
20. B. Ye, M. Trudeau, and D.M. Antonelli. Chem. Mater. **14**, 2774 (2002).
21. B.O. Skadtchenko, M. Trudeau, R.W. Schurko, M.J. Willans, and D.M. Antonelli. Adv. Funct. Mater. **13**, 671 (2003).
22. P. Cox. Electronic structure and chemistry of solids. Oxford University Press, New York. 1987.
23. F. Imbierwitz, J. Pelzl, E. Arnscheidt, M. Acet, H. Zahres, H. Bach, and G.A. Saunders. Magn. Magn. Mater. **196**, 863 (1999).
24. A.M. Fogg, V.M. Green, and D. O'Hare. Chem. Mater. **11**, 216 (1999).
25. H.J. Blythe, V.M. Fedosyuk, O.I. Kasyutich, and W.J. Schwarzacher. Magn. Magn. Mater. **208**, 251 (2000).
26. D. O'Hare. Chem. Soc. Rev. **21**, 121 (1992).
27. S. Murray, M. Trudeau, and D.M. Antonelli. Inorg. Chem. **39**, 5901 (2000).
28. M. Vettraino, X. He, M. Trudeau, and D.M. Antonelli. J. Mater. Chem. **11**, 1755 (2001).
29. X. He, A.Y.H. Lo, R.W. Schurko, M. Trudeau, and D.M. Antonelli. Inorg. Chem. **42**, 335 (2003).
30. X. He, M. Trudeau, and D.M. Antonelli. Inorg. Chem. **40**, 6463 (2001).
31. X. He, M. Trudeau, and D.M. Antonelli. Chem. Mater. **13**, 4808 (2001).
32. A. Lezau, B. Skadtchenko, M. Trudeau, and D.M. Antonelli. Dalton Trans. **21**, 4115 (2003).
33. B. Ye, M. Trudeau, and D.M. Antonelli. Adv. Mater. **12**, 29 (2001).
34. B. Ye, M. Trudeau, and D.M. Antonelli. Adv. Mater. **13**, 561 (2001).
35. B. Ye, M. Trudeau, and D.M. Antonelli. Chem. Mater. **13**, 2730 (2001).

© 2006 NRC Canada

36. R.W. Lof, M.A. van Veenendaal, B. Koopmans, H.T. Jonkman, and G.A. Sawatzky. Phys. Rev. Lett. **68**, 3924 (1992).
37. T. Pichler, M. Matus, J. Kurti, and H. Kuzmany. Phys. Rev. B, **45**, 13841 (1992).
38. H.W. Kroto, J.R. Health, S.C. O'Brien, R.F. Curl, and R.E. Smalley. Nature (London), **318**, 162 (1985).
39. P. Durand, G.R. Darling, Y. Dubitsky, A. Zaopo, and M.J. Rosseinsky. Nat. Mater. **2**, 605 (2003).
40. M. Kosaka, K. Tanigaki, K. Prassides, S. Margedonna, A. Lappas, C.M. Brown, and A.N. Fitch. Phys. Rev. B, **59**, 6628 (1999).
41. H. Kuzmany, M. Matus, B. Burger, and J. Winter. Adv. Mater. **6**, 731 (1994).
42. J. Winter and H. Kuzmany. Solid State Commun. **84**, 935 (1992).
43. M.J. Rosseinsky. Chem. Mater. **10**, 2665 (1998).
44. N.F. Mott. Metal-insulator transition. Taylor and Francis, London. 1999.
45. K.-F. Thier, M. Mehring, and F. Rachdi. Phys. Rev. B, **55**, 124 (1997).
46. B.O. Skadtchenko, M. Trudeau, C.-W. Kwon, B. Dunn, and D.M. Antonelli. Chem. Mater. **16**, 2886 (2004).
47. G.U. Mitronova, A.P. Savchenkova, A.F. Mayorova, S.N. Mudretsova, and V.V. Avdeev. Russ. Ser. Chem. **48**, 491 (1996).
48. K. Tanigaki and K. Prassides. J. Mater. Chem. **5**, 1515 (1995).
49. B.O. Skadtchenko, M. Trudeau, R.W. Schurko, A.Y. Lo, and D.M. Antonelli. Chem. Mater. **17**, 1467 (2005).

© 2006 NRC Canada

LGA-Dock/EM-Dock — Exploring Lamarckian genetic algorithms and energy-based local search for ligand–receptor docking

E. Ashley Wiley, Michael MacDonald, Andreas Lambropoulos, D. Joseph Harriman, and Ghislain Deslongchamps

Abstract: We report the development of LGA-Dock and EM-Dock, two SVL-based docking programs for flexible ligand – rigid receptor docking applications. LGA-Dock is comprised of a stochastic population generator, a docking routine based on a Lamarckian genetic algorithm, and a local search function based on molecular mechanics (MM) energy minimization. Subsequent modifications of LGA-Dock to address performance issues produced EM-Dock, which proved to be as accurate and much faster than its predecessor despite the deletion of the genetic algorithm component. The basic performance of LGA-Dock and EM-Dock, compared with AutoDock and MOE™ 2004.03 docking routines is presented.

Key words: docking, Lamarckian genetic algorithm, molecular mechanics, simulated annealing, tabu search, local search.

Résumé : On a développé deux programmes d'arrimage à base de SVL, le LGA-Dock et le EM-Dock, qui peuvent être utilisés pour des applications d'arrimage entre un ligand flexible et un récepteur rigide. Le LGA-Dock comprend un générateur de population stochastique, une routine d'arrimage sur la base d'un algorithme génétique Lamarckien et une fonction de recherche locale basée sur une minimisation d'énergie de mécanique moléculaire (MM). Des modifications subséquentes du LGA-Dock faites dans le but d'en régler certains problèmes ont conduit au EM-Dock qui s'est avéré être aussi précis et beaucoup plus rapide que son prédécesseur, même si on en avait éliminé la composante de l'algorithme génétique. On présente une comparaison de la performance de base du LGA-Dock et du EM-Dock avec les routines d'arrimage AutoDock et MOE™ 2004.03.

Mots clés : arrimage, algorithme génétique Lamarckien, mécanique moléculaire, annelage, recherche tabu, recherche locale.

[Traduit par la Rédaction]

Introduction

Molecular docking programs are designed to predict the correct thermodynamic binding pose of a ligand within its target receptor (1). Fast, accurate, and general use docking routines promise to be powerful tools for rational drug design and virtual screening activities (2). Much effort has been invested in the development of methodologies for searching docking space and for scoring the resulting poses to identify the most energetically favorable ones (3). Systematic searching schemes are prone to combinatorial explosion, a problem compounded by the consideration of ligand flexibility during docking (4). Therefore, many docking methods perform a stochastic search to adequately sample the ligand's conformational space, as well as its translational and rotational position within the binding site.

The Monte Carlo method has been used to randomly generate docking poses, accepting or rejecting new poses based on the Metropolis criterion (5). Similarly, the Tabu search method randomly samples conformational space while maintaining a list of previously visited solutions, steering the algorithm toward new minima (6). Many of these stochastic methods have been paired with a local search function to home in on the minima within local energy wells. Such optimization approaches have included molecular dynamics, simulated annealing, random searching, and various minimization algorithms.

Genetic algorithms (GA) offer yet another approach to stochastic searching by encoding docking poses as "chromosome" bitstrings and subjecting these to evolutionary processes (7). Accordingly, populations of chromosomes are created, mutated, and subjected to crossovers under some evolutionary pressure to identify the "fittest" progeny. A Lamarckian genetic algorithm (LGA) takes this process one step further by allowing a docking pose, identified by local search, to be written back to a chromosome for further optimization by the GA (8). The popular docking program AutoDock (8), for example, uses an LGA with a pseudo

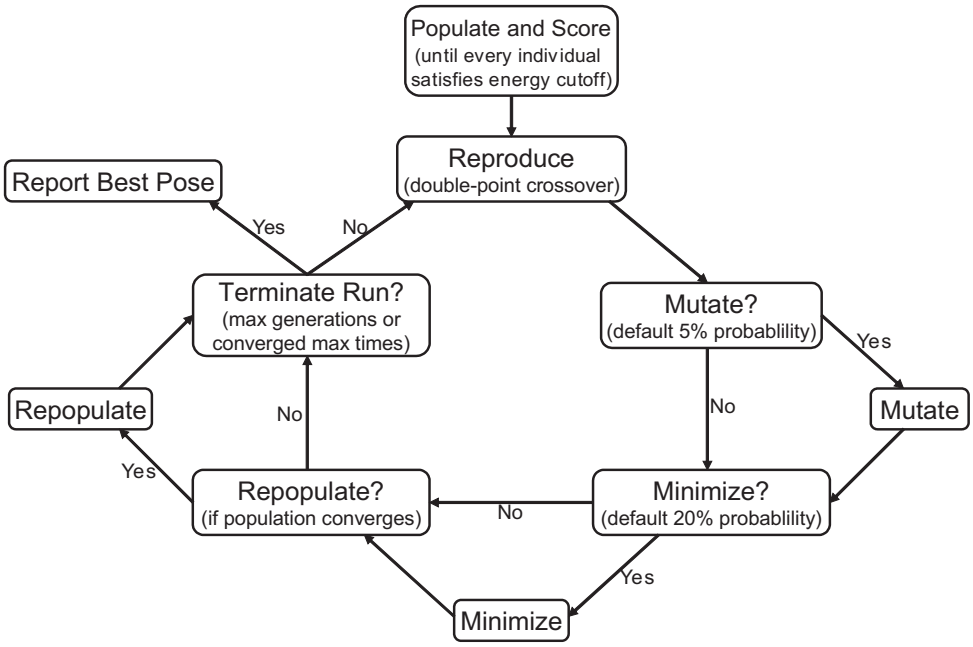
Received 16 September 2005. Published on the NRC Research Press Web site at http://canjchem.nrc.ca on 17 March 2006.

E.A. Wiley, M. MacDonald, A. Lambropoulos, D.J. Harriman, and G. Deslongchamps.[1] Department of Chemistry, University of New Brunswick, Fredericton, NB E3B 5A3, Canada.

[1]Corresponding author (e-mail: ghislain@unb.ca).

 doi:10.1139/V06-012 © 2006 NRC Canada

Fig. 1. LGA-Dock flowchart.



Solis and Wets local search (9), an adaptive stochastic minimization function.

Our interest in the docking arena began with our development of "reverse-docking", a novel approach for developing transition state models of asymmetric reactions catalyzed by conformationally flexible organocatalysts (10). Although AutoDock was used for the actual reverse-docking, all poses were subsequently reminimized, scored, and processed in MOE™ (11). To streamline the methodology, we sought to replace AutoDock with a fast docking algorithm written in scientific vector language (SVL), the native development language for MOE™.

Thus, the ultimate goal was to produce an SVL-based docking routine that performed at least as well as AutoDock for various docking applications. Our initial efforts resulted in LGA-Dock, a program that uses a stochastic population generator, an LGA-based docking routine, and a local search function based on molecular mechanics (MM) energy minimization. Subsequent modifications of LGA-Dock produced EM-Dock (energy minimization-dock), which proved to be much more efficient. Herein, we report the development of LGA-Dock and EM-Dock, and compare their basic performance in simple flexible ligand – rigid receptor docking with MOE™ 2004.03 and AutoDock 3.0.5.

Experimental

LGA-Dock and EM-Dock were written in SVL and implemented in MOE™ 2004.03. A simple GA routine with grid-based scoring was obtained from the Chemical Computing Group Inc. (moredock.svl) and served as the initial template for LGA-Dock development. The core components of LGA-Dock include population, reproduction, mutation, minimization, and repopulation functions (Fig. 1).

Genetic encoding

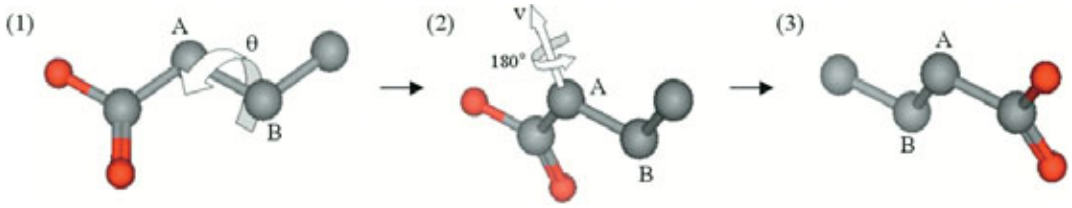
LGA-Dock incorporates a Lamarckian genetic algorithm with a MM energy-based local search. Key to this approach is the encoding of a ligand pose into a linear chromosome for subsequent genetic manipulation (crossover, mutation, etc.). In this context, the term "pose" refers to a ligand's translation/rotation within the receptor-binding site and to its conformation with respect to rotatable acyclic bonds. Each chromosome is comprised of nine elements. Elements 1–3 specify the molecular translation in Cartesian space (x, y, and z axes) relative to the position of a reference structure. Elements 4–7 specify the molecular rotation relative to that of the reference structure (an angle θ and a 3D vector, Fig. 2). Element 8 is a vector, which stores a dihedral angle for each of the rotatable bonds in the molecule (excluding amide C—N bonds, inter alia). Finally, element 9 stores the index of the reference structure to which transformation elements 1–8 are applied. This feature is required for the phenotype (Cartesian coordinates) to genotype (chromosome) conversion that is necessary for the Lamarckian component. In LGA-Dock, some docking poses (20% probability) are energy-minimized and must be converted from Cartesian space back to genotype for further manipulation by the GA. In short, each chromosome encodes a translational/rotational/conformational change (elements 1–8) to be applied to a reference structure (element 9), usually the starting pose.

Stochastic population generation

The stochastic population function randomly generates an initial population of ligand conformations (default is 50 chromosomes). Once an initial population has been generated, it is scored using the potential energy function of MOE™ (vide infra) and optimized prior to entering the LGA as follows: each individual score is compared with the average score of the five best individuals (hereafter referred to as the "reference score"). Only individuals with a score better than the reference score plus 10% (a relative energy cutoff) are retained otherwise the unfit individuals are eliminated and stochastically replaced with new candidates. The process continues until the scores of all the individuals meet

© 2006 NRC Canada

Fig. 2. Molecular rotation, a two-step procedure, as performed by LGA-Dock: (1) rotation about the A–B axis by angle θ (A is the atom closest to the ligand's Cartesian centroid and B is any one of the atoms bound to A); (2) 180° rotation about a random unit vector **v**; (3) the resultant pose. The whole process can be easily reversed to determine rotation from a given reference structure.



the energy cutoff. The population then enters a cycle involving the remaining four functions.

Scoring

Since a rigid-receptor model was used, docking scores are based on the sum of the MM energy of the ligand plus the ligand–receptor interaction energy. A faster but less accurate grid-based scoring is used to calculate van der Waals and electrostatic ligand–receptor interaction energies for every step of each run. MM-based scoring is used for the intramolecular ligand energy. At the end of each run, explicit scoring is used to calculate the full docking energy (intramolecular and intermolecular components) so as to obtain a more accurate final energy evaluation (which is then written to the output database). LGA-Dock utilizes the built-in functions of MOE™ for precalculating an interaction grid of the protein (van der Waals and electrostatic) and for computing the interaction energy of ligand poses by trilinear interpolation.

Crossover

The reproduction function performs crossovers among individuals using a modification of a strategy recently reported by Chapleur and co-workers (12). The population is divided into two equal halves, termed mothers and fathers. Each father is paired with a randomly chosen mother, and vice versa. Each parent pair undergoes random double-point crossover, producing two children. The best-scoring 10% of the children then replace the worst scoring individuals from the population if their scores are better.

Mutation

Every generation has a user-defined probability for mutation (default is 10%), which is performed on the best 10% of the population. For each chromosome, a random mutation site is chosen and a random perturbation applied. The resultant pose is scored and replaces the current worst scoring individual if it is better; otherwise, mutation is repeated until either a better-scoring individual is created or a maximum number of attempts have been made (default is five).

MM-based local search

Standard MM energy minimization functions, present in MOE™, are used to perform local searches and improve ligand poses within their rigid receptor (i.e., adjust the poses to the bottom of their respective potential wells). Steepest descent minimization is used in the first 25 generations of a run. In later generations, conjugate gradient and truncated Newton methods are also applied for finer minimization. Energy minimization is always performed on the best-scoring chromosome that had not already been minimized.

Repopulation

The final function of the cycle is repopulation. It is very much like the initial populate function, but is only called whenever the population converges. It retains the best-scoring individual and randomly generates the rest of the population until the energy cutoff is met.

Generation cycle

Once a population has been produced, it enters a common GA cycle (referred to as a "generation") of reproduction, mutation, energy minimization, and repopulation (Fig. 1). The cycle continues until either the maximum number of generations has been reached (default is 200) or minimization fails to produce better-scoring poses a number of times (default is 10). If either of these events occurs, the algorithm appends the best-scoring structure to a MOE™ database along with a breakdown of energies.

Ligand–receptor pairs

Ligand–receptor pairs were selected from the Protein Data Bank (http://www.wwpdb.org) to encompass a wide range of ligand size, conformational flexibility, and receptor environments, including several pairs sampled from the development data sets of other docking programs. For the LGA-Dock experiments, the following seven ligand–receptor complexes were chosen, including five described in the original AutoDock training set, five from the FlexX study (13), and three from the GOLD study (14): benzyldiamine–β-trypsin [3PTB], biotin–streptavidin [1STP], methotrexate – dihydrofolate reductase [4DFR], sialic acid – hemagglutinin [4HMG], TIBO-R86183 – HIV-1 reverse transcriptase [1HNV], VX-478 – HIV-1 protease [1HPV], and XK263 – HIV-1 protease [1HVR]. For the subsequent EM-Dock experiments, the set was expanded to include 10 additional ligand–receptor pairs, including five more from the FlexX study, and two more from the GOLD study: hydroxyethylene isostere – HIV-1 protease [1AAQ], D-fucose – L-arabinose-binding protein [1ABF], 1-deaza-adenosine – adenosine deaminase [1ADD], aetiocholanolone – Fab′ fragment of monoclonal antibody Db3 [1DBJ], folate – dihydrofolate reductase [1DRF], rapamycin – Fk506-binding protein [1FKB], L-histidine – histidine-binding protein [1HSL], benzene – lysozyme mutant [1L83], 3-phenylpropylamine–trypsin [1TNK], and palmitic acid – intestinal fatty acid binding protein [2IFB].

© 2006 NRC Canada

Table 1. LGA-Dock results.

PBD ID		LGA-Dock	AutoDock	MOE-SA	MOE-Tabu	MOE-GA
3PTB	RMSD of No. 1 rank	0.38	0.71	0.94	0.95	0.50
	Lowest RMSD	0.38	0.65	0.70	0.60	0.50
	(Rank)	(1)	(30)	(5)	(37)	(1)
1STP	RMSD of No. 1 rank	1.11	3.08	7.5	7.3	7.8
	Lowest RMSD	0.96	3.1	1.3	6.7	5.0
	(Rank)	(3)	(1)	(36)	(9)	(50)
4DFR	RMSD of No. 1 rank	0.86	2.1	12.2	9.4	12.0
	Lowest RMSD	0.86	0.81	12.1	9.4	7.6
	(Rank)	(1)	(6)	(49)	(1)	(41)
4HMG	RMSD of No. 1 rank	4.9	6.3	4.8	5.1	6.1
	Lowest RMSD	4.28	3.56	4.43	4.52	4.66
	(Rank)	(14)	(18)	(9)	(11)	(31)
1HNV	RMSD of No. 1 rank	0.74	2.61	4.94	0.84	1.56
	Lowest RMSD	0.64	0.70	1.14	0.56	1.55
	(Rank)	(14)	(26)	(10)	(2)	(2)
1HPV	RMSD of No. 1 rank	1.04	0.90	12.10	11.18	11.23
	Lowest RMSD	1.04	0.84	5.24	1.76	6.78
	(Rank)	(1)	(2)	(20)	(18)	(40)
1HVR	RMSD of No. 1 rank	0.94	0.87	6.13	6.00	12.71
	Lowest RMSD	0.66	0.83	5.83	5.19	4.21
	(Rank)	(2)	(6)	(4)	(4)	(13)

Receptor preparation

In MOE™, the ligand and all water molecules were deleted from the PDB file of a given receptor–ligand complex. Atom bonding was checked and corrected as needed; ionization states for all His, Lys, Arg, Asp, and Glu residues were set according to Pang et al. (15). Hydrogens were added and energy-minimized using the AMBER94 force field. Partial charges on the receptor were assigned with the AMBER94 force field in MOE™. For use in AutoDock, receptors were saved in the mol2 format.

Ligand preparation

Ligands were extracted from the corresponding PDB files. All ligands were checked manually for correct atom and bond type. Hydrogens were added and energy-minimized using the MMFF94x force field. Initial ligand geometries were optimized with Gaussian 03 (16) at the HF/6-31G* level to remove any bias from the crystallographic structure. Electrostatic potentials were calculated and used to derive RESP (17) charges with the Antechamber module of Amber 7 (18) for later use in MOE™. For AutoDock, ligand partial charges were computed with the Gasteiger PEOE method (19, 20), and the ligands were manipulated with AutoDockTools (21).

Docking

All docking tests were run against MOE™ 2004.03 and AutoDock 3.0.5. Default settings and the MMFF94x potential energy force field were used for MOE™'s two docking methods (Monte Carlo simulated annealing (MOE-SA) and Tabu search (MOE-Tabu), as well as an unreleased SVL-based genetic algorithm (MOE-GA). AutoDock runs were carried out using the same settings reported in its original publication.

Default settings were used for LGA-Dock: each ligand was tested with 50 runs, a population size of 50, and a maximum generation limit of 200. Mutation probability was set to 10% and minimization probability to 20%. The repopulation limit was set to 10, such that the run would terminate after that many populations converged. The docking boxes were centered on the bound crystallographic ligands and the box dimensions from whichever program created the largest box were applied to all the others (for example, the box size for 1HSL was 13.2 Å × 13.2 Å × 13.2 Å). Initial ligand translation, rotation, and conformation were generated randomly within the box to mitigate bias from their original crystallographic pose.

Results and discussion

To compare the different docking results, root-mean-square deviations (RMSD) were calculated from heavy atom positions in the docking poses relative to their respective crystallographic poses and are reported in Tables 1–4. With the understanding that comparing docking programs via RMSD calculations alone can be misleading (22), all docking poses were visually inspected by superposition to ensure that relative RMSDs within a comparison set were consistent with the observed structural deviations. Representative examples of pose comparisons are shown in Figs. 3 and 4.

For each Table, the following data are reported: 1-RMSD of No. 1 rank (ranked by scoring function), and 2-lowest RMSD with corresponding rank. Docking solutions were considered to be successful if the RMSD was <1.5 Å, which is more stringent than the common 2.0 Å standard. This was deemed important since the test sets included small ligands that might still meet the success cutoff by random placement in small active sites (22).

LGA-Dock

LGA-Dock was tested with seven ligand–receptor complexes. The results were compared with those of AutoDock

© 2006 NRC Canada

Table 2. Averages of LGA-Dock results.

Averaged result	LGA-Dock	AutoDock	MOE-SA	MOE-Tabu	MOE-GA
RMSD of No. 1 rank	1.43	4.32	6.94	5.82	7.41
Lowest RMSD	1.26	1.64	4.39	4.10	4.33
Rank of lowest RMSD	5.1	14.3	19.0	11.7	25.4

Table 3. EM-Dock results.

PBD ID		EM-Dock	AutoDock	MOE-SA	MOE-Tabu	MOE-GA
1AAQ	RMSD of No. 1 rank	11.92	4.70	8.27	5.55	15.74
	Lowest RMSD	2.78	2.38	5.51	3.29	4.12
	(Rank)	(109)	(55)	(125)	(3)	(104)
1ABF	RMSD of No. 1 rank	0.43	0.28	0.42	0.39	0.44
	Lowest RMSD	0.35	0.21	0.37	0.32	0.37
	(Rank)	(121)	(125)	(4)	(96)	(49)
1ADD	RMSD of No. 1 rank	0.59	0.68	1.80	2.56	2.92
	Lowest RMSD	0.23	0.62	1.69	1.94	1.92
	(Rank)	(28)	(38)	(8)	(126)	(39)
1DBJ	RMSD of No. 1 rank	0.54	5.89	6.09	4.93	0.75
	Lowest RMSD	0.33	1.10	0.69	0.56	0.31
	(Rank)	(24)	(48)	(11)	(26)	(2)
1DRF	RMSD of No. 1 rank	1.81	2.13	2.86	1.98	1.50
	Lowest RMSD	0.59	0.83	2.58	1.45	1.34
	(Rank)	(8)	(51)	(2)	(22)	(5)
1FKB	RMSD of No. 1 rank	7.02	7.31	8.43	9.16	8.22
	Lowest RMSD	6.69	5.15	8.03	8.24	7.58
	(Rank)	(150)	(2)	(3)	(134)	(71)
1HSL	RMSD of No. 1 rank	0.53	1.17	1.32	1.29	1.32
	Lowest RMSD	0.35	1.12	0.40	0.32	0.65
	(Rank)	(12)	(5)	(21)	(43)	(4)
1L83	RMSD of No. 1 rank	0.87	1.30	0.56	0.57	0.56
	Lowest RMSD	0.78	1.29	0.51	0.45	0.41
	(Rank)	(150)	(1)	(71)	(150)	(150)
1TNK	RMSD of No. 1 rank	1.49	2.67	2.46	2.62	2.94
	Lowest RMSD	1.32	1.39	0.80	1.95	1.01
	(Rank)	(150)	(150)	(88)	(13)	(78)
2IFB	RMSD of No. 1 rank	0.88	4.07	2.17	1.56	9.29
	Lowest RMSD	0.88	1.03	1.81	1.22	1.93
	(Rank)	(1)	(63)	(18)	(2)	(12)

Table 4. Averages of EM-Dock results.

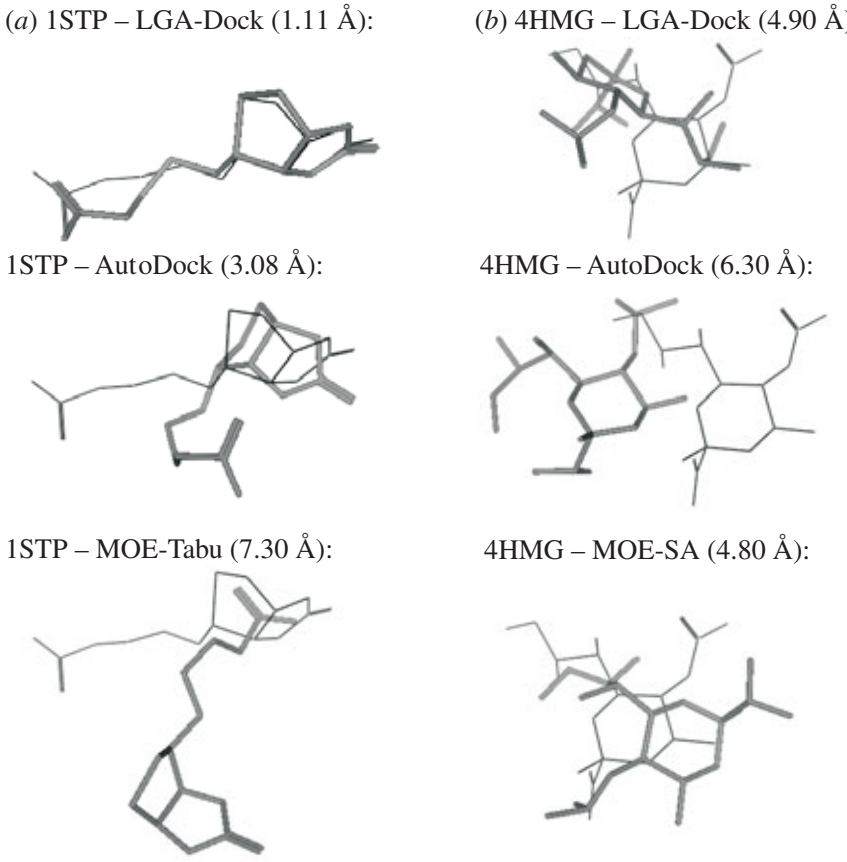
Averaged result	EM-Dock	AutoDock	MOE-SA	MOE-Tabu	MOE-GA
RMSD of No. 1 rank	2.72	3.01	3.43	3.06	4.37
Lowest RMSD	1.47	1.51	2.24	1.97	1.96
Rank of lowest RMSD	68.7	70.1	35.1	61.5	51.4

and current MOE™ docking programs and are reported in Table 1. LGA-Dock was found to perform at least as well as AutoDock when comparing RMSDs of the No. 1 ranked poses, and outperformed AutoDock in three cases (1STP, 4DFR, 1HNV). Three of the LGA-Dock cases did not assign a No. 1 rank to the lowest RMSD solution, but the RMSD differences were less than 0.28 and are negligible (1STP, 1HNV, 1HVR). Interestingly, LGA-Dock's only failure was with 4HMG, the only system that could not be properly docked by any of the five methods. Visual inspection of the best 4HMG poses superposed over the crystallographic pose of the sialic anion did not shed any light on the anomaly.

MOE-SA performed poorly, resulting in only one successful docking (3PTB). Similarly, MOE-Tabu produced only two successful dockings (3PTB, 1HNV), while MOE-GA only produced one hit (3PTB), perhaps two if the success threshold were relaxed by 0.1 Å (1HNV). All in all, this is an important result since it shows that LGA-Dock performed considerably better than the existing SVL-based docking routines available in MOE™ at the time.

© 2006 NRC Canada

Fig. 3. Representative docking poses of LGA-Dock vs. other docking methods. (*a*) Left column: 1STP; (*b*) right column: 4HMG. Docking poses are shown as cylinders and the crystallographic poses are shown as lines. RMSDs are in parentheses.



All docking results were visually inspected to ensure proper correlation with reported RMSDs. Two representative examples contrasting successful and unsuccessful dockings with LGA-Dock are illustrated in Fig. 3. In the case of 1STP, LGA-Dock was able to dock to a RMSD of 1.11 Å, compared with values of 3.08 and 7.30 Å for AutoDock and MOE-Tabu, respectively (Fig. 3*a*). Note the proper docking of the bicyclic moiety of biotin and general alignment of its carboxylate side chain by LGA-Dock. This is in sharp contrast to the 4HMG docking pair (Fig. 3*b*) in which the sialic acid ligand could not be properly positioned docked by LGA-Dock (4.90 Å) or any of the other docking routines (4.80–6.30 Å). Structural analysis did not reveal any insight into the difficulty of docking this particular ligand–receptor pair.

The numerical results were averaged (Table 2) and showed that, on the whole, LGA-Dock was as capable as AutoDock in producing lowest RMSD poses. LGA-Dock seems to score the poses more accurately, as its average RMSD for No. 1 ranked poses was considerably lower than for the other four docking programs. Although LGA-Dock met the accuracy test, calculation times took 20–30 times longer than AutoDock on some ligands. As such, LGA-Dock was certainly not deemed suitable for high-throughput docking or virtual screening applications.

AutoDock uses an empirical, grid-based scoring function, making for very fast energy calculations, while LGA-Dock uses complete MM-based energy for calculating ligand and interaction energy. In addition, LGA-Dock uses energy minimization for the local search, which will also contribute to the computation time. The performance impact of LGA-Dock's other routines including the stochastic population routine and the LGA itself remained to be established.

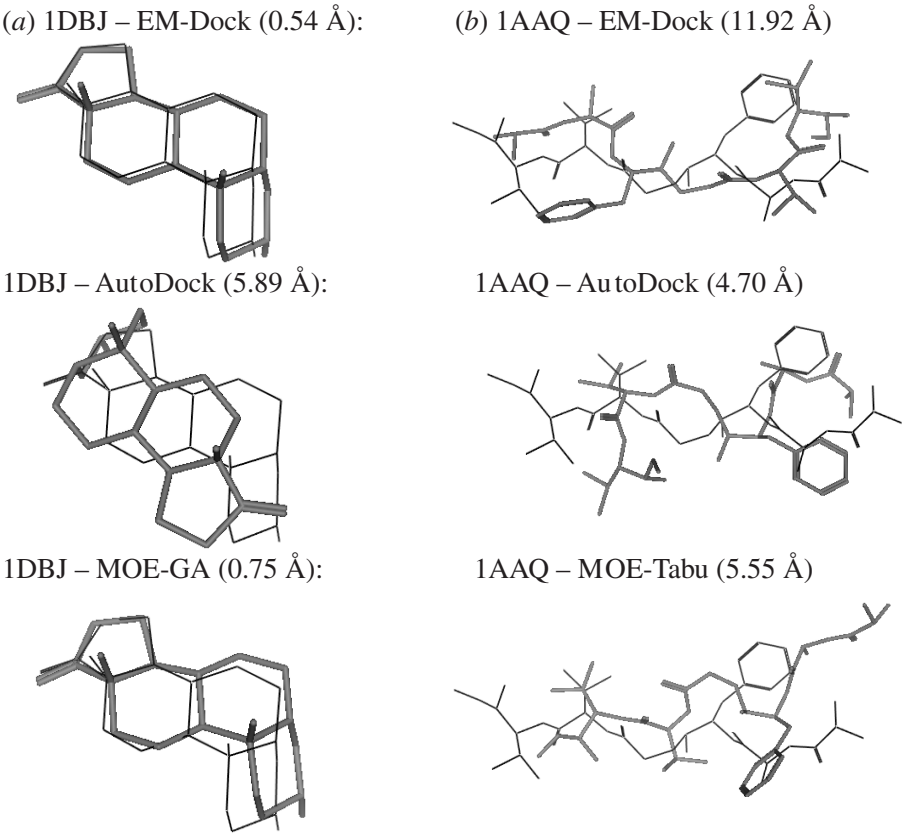
EM-Dock

In the process of exploring ways to improve the speed and performance of LGA-Dock, the reproduction and mutation functions were eliminated. These functions were found to be largely responsible for the long CPU times and it was unclear whether they made a significant contribution to the docking success. Preliminary tests using this truncated algorithm showed little loss of performance while speeding up docking times considerably. These tests prompted the development of EM-Dock (energy minimization dock), a second generation program that, ironically, did not retain any of the original genetic algorithm components. However, EM-Dock retained LGA-Dock's stochastic population engine and the MM-minimization-based local search program (23), with one minor modification: when EM-Dock generates an initial population of chromosomes, a simple distance-based test filters out initial ligand translations that collide with receptor atoms, improving the speed of the program. The population is then scored and regenerated until all individuals meet the energy cutoff.

Once the initial population is generated, the algorithm enters a cycle of minimization-based local search and repopu-

© 2006 NRC Canada

Fig. 4. Representative docking poses of EM-Dock vs. other docking methods. (*a*) Left column: 1DBJ; (*b*) right column: 1AAQ. Docking poses are shown as cylinders and the crystallographic poses are shown as lines. RMSDs are in parentheses.



lation. First, the lowest-energy conformation is minimized with MOE™'s minimization methods (the initial coarse minimization phase of LGA-Dock is omitted) and the resultant pose replaces the current worst-scoring individual. The second best chromosome is then minimized, scored, and compared with the first minimized structure. If the second minimized structure's energy is lower than that of the first, the next best pose is minimized and compared with the last; otherwise, the repopulation function is called, seeding the best pose back into the population and randomly recreating the other individuals. This cycle of minimization and repopulation continues until either a maximum number of generations are reached or the program has repopulated a maximum number of times (user-defined). When either of these criteria is met, the algorithm terminates and the best structure is reported.

EM-Dock was tested with the original seven ligand–receptor complexes and produced a series of poses almost identical to those of LGA-Dock. Testing was then extended to an additional set of 10 ligand–receptor complexes. The same docking settings were used, with the exception that 150 runs were performed (as opposed to 50 runs performed for LGA-Dock). EM-Dock results are reported in Table 3.

Analysis of the data in Table 3 revealed that EM-Dock, in similar fashion to LGA-Dock, performed well. For 7 of the 10 dockings, EM-Dock returned RMSDs for the No. 1 ranked poses that were within the 1.5 Å threshold (8/10 if including 1DRF at 41.81 Å). It also performed at least as well as AutoDock or the other MOE™-based programs. EM-Dock surpassed AutoDock in two cases (1DBJ, 2IBF) and MOE™'s three algorithms on over half of the systems.

Once again, all docking results were visually inspected to verify proper correlation with reported RMSDs. Two representative examples contrasting successful and unsuccessful dockings with EM-Dock are illustrated in Fig. 4. In the case of 1DBJ (Fig. 4*a*), EM-Dock's No. 1 ranked pose had a 0.54 Å RMSD and was very similar to that of MOE-GA (0.75 Å), and was much better than the AutoDock result (5.89 Å). In contrast, Fig. 4*b* illustrates the docking of the larger and considerably more flexible hydroxyethyl isostere peptidomimetic (1AAQ), which proved to be much more problematic. Indeed, EM-Dock flipped the ligand lengthwise, while AutoDock and MOE-Tabu rotated it around its longitudinal axis. This ligand was problematic for all docking routines, which is perhaps not surprising because of the large number of conformational rotors present.

Averaging the results (Table 4) reveals that EM-Dock, like LGA-Dock, performed at least as well as AutoDock. Of greater relevance, however, was the observation that EM-Dock calculation times were much shorter than for LGA-Dock (10–15 times faster for most ligands), much shorter than the other MOE™ docking routines, and almost as quick as AutoDock. Although EM-Dock is still not fast enough for virtual screening, its performance was deemed suitable for our reverse-docking and other applications.

An interesting outcome of this study was the efficiency and accuracy of EM-Dock even though its GA component had been culled completely from the program. One must

© 2006 NRC Canada

note that LGA-Dock contained two distinct stochastic engines (population generator and genetic algorithm), while EM-Dock retained only one (population generator); this suggests that LGA-Dock was perhaps overkill for searching the docking space. In the end EM-Dock was found to be an effective docking routine that was almost as fast as AutoDock while retaining a full MM-based scoring scheme (and local searching), resulting in improved overall accuracy.

Conclusion

A new program in the place-and-minimize spirit (EM-Dock) has emerged from modification and optimization of LGA-Dock, an intermediate Lamarckian genetic algorithm. LGA-Dock scored the poses more accurately than AutoDock or the MOE™-based methods, as the RMSD for No. 1 ranked poses was consistently lower for a range of ligand–receptor pairs. However, calculation times were 20–30 times longer than AutoDock on some ligands, prompting the development of EM-Dock. EM-Dock retained the stochastic population generation and MM-minimization-based local search routines while eliminating the genetic algorithm itself. Results showed that EM-Dock was at least as accurate as LGA-Dock. Thus, the deletion of the reproduction and mutation schemes produced a much faster algorithm without sacrificing docking accuracy. Although the default settings were parameterized for a general set of molecular systems, users should adjust values so as to best match particular docking situations.

We have since used EM-Dock successfully for a series of docking and reverse-docking studies and have appreciated its overall performance and integration into MOE™. Further development and applications of EM-Dock will be reported in due course.

Acknowledgements

Financial support from the Natural Sciences and Engineering Research Council of Canada (NSERC), the New Brunswick Innovation Foundation, and the University of New Brunswick is gratefully acknowledged. We are also grateful to the Chemical Computing Group Inc. for software licenses and SVL support. We thank the referees for helpful comments.

References

1. N. Brooijmans and I.D. Kuntz. Ann. Rev. Biophys. Biomol. Struct. **32**, 335 (2003).
2. G. Schneider and H.J. Bohm. Drug Discov. Today, **7**, 64 (2002).
3. M. Kontoyianni, L.M. McClellan, and G.S. Sokol. J. Med. Chem. **47**, 558 (2004).
4. J.A. Erickson, M. Jalaie, D.H. Robertson, R.A. Lewis, and M. Vieth. J. Med. Chem. **47**, 45 (2004).
5. R.D. Taylor, P.J. Jewsbury, and J.W. Essex. J. Comput. Aided Mol. Des. **16**, 151 (2002).
6. C.A. Baxter, C.W. Murray, D.E. Clark, D.R. Westhead, and M.D. Eldridge. Proteins: Struct. Funct. Gen. **33**, 367 (1998).
7. C.M. Oshiro, I.D. Kuntz, and J.S. Dixon. J. Comput. Aided Mol. Des. **9**, 113 (1995).
8. G.M. Morris, D.S. Goodsell, R.S. Halliday, H. Huey, W.E. Hart, R.K. Belew, and A.J. Olson. J. Comput. Chem. **19**, 1639 (1998).
9. F.J. Solis and R.J. Wets. Math. Oper. Res. **6**, 19 (1981).
10. D.J. Harriman and G. Deslongchamps. J. Comput. Aided Mol. Des. **18**, 303 (2004).
11. Molecular Operating Environment (MOE™) software. Version 2004.03 [computer program]. The Chemical Computing Group Inc., Montreal, Quebec.
12. N. Moitessier, C. Henry, C. Len, and Y. Chapleur. J. Org. Chem. **67**, 7275 (2002).
13. B. Kramer, M. Rarey, and Thomas Lengauer. Proteins: Struct. Funct. Bioinf. **37**, 228 (1999).
14. M.L. Verdonk, J.C. Cole, M.J. Hartshorn, C.W. Murray, and R.T. Taylor. Proteins: Struct. Funct. Genet. **52**, 609 (2003).
15. Y.P. Pang, E. Perola, K. Xu, and F.G. Prendergast. J. Comput. Chem. **22**, 1750 (2001).
16. M.J. Frisch, G.W. Trucks, H.B. Schlegel, G.E. Scuseria, M.A. Robb, J.R. Cheeseman, J.A. Montgomery, Jr., T. Vreven, K.N. Kudin, J.C. Burant, J.M. Millam, S.S. Iyengar, J. Tomasi, V. Barone, B. Mennucci, M. Cossi, G. Scalmani, N. Rega, G.A. Petersson, H. Nakatsuji, M. Hada, M. Ehara, K. Toyota, R. Fukuda, J. Hasegawa, M. Ishida, T. Nakajima, Y. Honda, O. Kitao, H. Nakai, M. Klene, X. Li, J.E. Knox, H.P. Hratchian, J.B. Cross, V. Bakken, C. Adamo, J. Jaramillo, R. Gomperts, R.E. Stratmann, O. Yazyev, A.J. Austin, R. Cammi, C. Pomelli, J.W. Ochterski, P.Y. Ayala, K. Morokuma, G.A. Voth, P. Salvador, J.J. Dannenberg, V.G. Zakrzewski, S. Dapprich, A.D. Daniels, M.C. Strain, O. Farkas, D.K. Malick, A.D. Rabuck, K. Raghavachari, J.B. Foresman, J.V. Ortiz, Q. Cui, A.G. Baboul, S. Clifford, J. Cioslowski, B.B. Stefanov, G. Liu, A. Liashenko, P. Piskorz, I. Komaromi, R.L. Martin, D.J. Fox, T. Keith, M.A. Al-Laham, C.Y. Peng, A. Nanayakkara, M. Challacombe, P.M.W. Gill, B. Johnson, W. Chen, M.W. Wong, C. Gonzalez, and J.A. Pople. Gaussian 03. Revision A.01 [computer program]. Gaussian, Inc., Wallingford, Connecticut. 2004.
17. C.I. Bayly, P. Cieplak, W.D. Cornell, and P.A. Kollman. J. Phys. Chem. **97**, 10269 (1993).
18. D.A. Case, D.A. Pearlman, J.W. Caldwell, T.E. Cheatham III, J. Wang, W.S. Ross, C.L. Simmerling, T.A. Darden, K.M. Merz, R.V. Stanton, A.L. Cheng, J.J. Vincent, M. Crowley, V. Tsui, H. Gohlke, R.J. Radmer, Y. Duan, J. Pitera, I. Massova, G.L. Seibel, U.C. Singh, P.K. Weiner, and P.A. Kollman. AMBER 7 [computer program]. University of California, San Francisco. 2002.
19. M. Marsili and J. Gasteiger. Croat. Chem. Acta, **53**, 601 (1980).
20. J. Gasteiger and M. Marsili. Tetrahedron, **36**, 3219 (1980).
21. AutoDockTools. Molecular Graphics Laboratory, Scripps Research Institute, La Jolla, California. Available from http://www.scripps.edu/~sanner/python/.
22. J.C. Cole, C.W. Murray, J.W.M. Nissink, R.D. Taylor, and R. Taylor. Proteins: Struct. Funct. Bioinf. **60**, 325 (2005).
23. C. McMartin and S.J. Bohacek. J. Comput. Aided Mol. Des. **11**, 333 (1997).

© 2006 NRC Canada

Concerted and stepwise mechanisms in the Diels–Alder and Michael reactions of furans with methyl 3-nitroacrylate — Experimental and theoretical studies

Kuniaki Itoh, Kazue Kitoh, and Shigehisa Kishimoto

Abstract: The Diels–Alder reactions of the furans (**1a**–**1c**) and methyl 3-nitroacrylate (**2**) produce the cycloadducts via a concerted mechanism. Then, the products subsequently undergo retro-Diels–Alder reactions to give the Michael adducts via a stepwise mechanism. We have used both experimental and theoretical methods to investigate the mechanism for, and the regio- and stereo-selectivity in, the Diels–Alder and Michael reactions. To account for the selectivity observed in these additions, we examined the frontier molecular orbitals involved, and to locate the transition states (TS), we employed a B3LYP/6-31G* level density functional calculation. We were able to explain the regio- and stereo-selectivity of the four possible Diels–Alder adducts observed in the experiments by a comparison of their calculated activation energies, which ranged from 11 to 18 kcal/mol (1 cal = 4.184 J). The s-cis forms of the dienophile (**2**) were found to be more stable than the s-trans forms, both in the ground state and in the transition state. In addition, the endo transition structures for the ester group exhibited a lower energy barrier by 0.3 kcal/mol than their exo counterparts, a value that is in disagreement with the experimental results. The presence of the nitro group in **2** may play an important role in determining the selectivity. Our attempts to find a stepwise mechanism leading to the Diels–Alder adduct via a zwitterion were unsuccessful. We did find that two stepwise processes lead to the formation of Michael adducts generated via an electrophilic attack by **2** at the α position of **1b** and **1c**, and an intramolecular proton-transfer mediated by the formation of a four-membered structure. The potential energies for these reactions showed values in the following ranges: 17 kcal/mol for **5a** and **5b**, and 11 to 12 kcal/mol for **7a** and **7b** for the first step, and, for the proton-transfer step, 48–51 kcal/mol for **5a** and **5b**, and 41–45 kcal/mol for **7a** and **7b**. Solvent effects in chloroform on the Michael addition did not appear in the electrophilic attack step (less than 4 kcal/mol), but the transition state of the later process was stabilized by 6–13 kcal/mol.

Key words: Diels–Alder reactions, Michael reactions, density functional method, furan, retro-Diels–Alder reactions, solvent effect.

Résumé : Les réactions de Diels–Alder entre les furanes (**1a**–**1c**) et le 3-nitroacrylate de méthyle (**2**) conduisent à la formation de cycloadduits par le biais d'un mécanisme concerté. Les produits formés subissent alors des réactions de rétro-Diels–Alder subséquentes qui conduisent à la formation d'adduits de Michael par le biais d'un mécanisme par étape. On a fait appel à des méthodes tant théoriques qu'expérimentales pour étudier les mécanismes des réactions de Diels–Alder et de Michael ainsi que leurs régio- et stéréo-sélectivités. Pour tenter d'expliquer la sélectivité observée au cours de ces additions, on a examiné les orbitales frontières impliquées alors que pour localiser les états de transition (ET), on a fait appel à des calculs de densité fonctionnelle au niveau B3LYP/6-31G*. On a aussi pu expliquer les régio- et stéréo-sélectivités des quatre adduits de Diels–Alder possibles par le biais d'une comparaison de leurs énergies d'activation calculées qui s'étalent de 11 à 18 kcal/mol (1 cal = 4,184 J). On a trouvé que les formes s-cis du diénophile (**2**) sont plus stables que les formes s-trans, tant dans l'état fondamental que dans l'état de transition. De plus, les structures de transition endo du groupe ester présentent une barrière d'énergie de 0,3 kcal/mol plus basse que celles de leurs contreparties exo; cette valeur n'est pas en accord avec les données expérimentales. La présence d'un groupe nitro dans le composé **2** joue peut-être un rôle important dans la détermination de la sélectivité. On n'a malheureusement pas pu trouver un mécanisme par étape pouvant conduire à l'adduit de Diels–Alder par le biais d'un zwitterion. On a toutefois trouvé deux processus par étape qui peuvent générer la formation d'adduits de Michael par le biais d'une attaque électrophile du composé **2** dans la position α des composés **1b** et **1c** suivie d'un transfert intramoléculaire de proton aidé par la formation d'une structure à quatre chaînons. Les énergies potentielles de ces réactions sont de l'ordre suivant: pour la première étape, 17 kcal/mol pour les composés **5a** et **5b**, 11 à 12 kcal/mol pour les composés **7a** et **7b**; et pour l'étape du transfert de proton, 48 à 51 kcal/mol pour les composés **5a** et **5b** et 41 à 45 kcal/mol pour

Received 19 September 2005. Published on the NRC Research Press Web site at http://canjchem.nrc.ca on 25 March 2006.

K. Itoh[1], K. Kitoh, and S. Kishimoto. Department of Chemistry, Faculty of Science, Kobe University, Nada-ku, Kobe 657-8501, Japan.

[1]Corresponding author (e-mail: kuitoh@kobe-u.ac.jp).

 doi:10.1139/V06-013 © 2006 NRC Canada

les composés **7a** et **7b**. Il ne semble pas que les effets de solvant dans le chloroforme sur l'attaque électrophile de l'addition de Michael semblent inexistants (moins de 4 kcal/mol), mais l'état de transition de l'étape suivante semble stabilisée par 6 à 13 kcal/mol.

Mots clés : réactions de Diels–Alder, réactions de Michael, méthode de la densité fonctionnelle, furane, réactions de rétro-Diels–Alder, effet de solvant.

[Traduit par la Rédaction]

Introduction

The Diels–Alder addition of furans, which are poor reactive dienes (1–3), provides an attractive approach to the synthesis of various cycloadducts that are useful building blocks for *C*-nucleosides (1, 4, 5). We have reported the synthesis of a ribofuranoside as a part of a program to synthesis *C*-nucleosides by use of the Diels–Alder reaction of furan with methyl 3-nitroacrylate (6). The reaction not only yielded the endo- and exo-cycloadducts, but also provided indications that these products and their yields changed with reaction times and temperatures (7). We also discussed the presence of an alternate pathway for the Diels–Alder reaction. This alternative involves a Michael reaction of a nitro methyl ester with the furans; here, the orbital energy difference between the HOMO of the diene and the LUMO of the dienophile seems to control the distribution of the Diels–Alder and Michael products of the reaction. In the present paper, we describe the time-dependent change in the reaction state (Scheme 1 and Figs. 1–3) using both experimental results and a theoretical study of frontier molecular orbital (FMO) energies, the orbital coefficients, the energies and geometries of the transition state, and solvent effects.

The mechanism of the Diels–Alder reaction has long been a topic of disussion (8). It may be either synchronous concerted or stepwise involving the formation of a zwitterion or biradical intermediate (9). Several recent theoretical studies devoted to the cycloaddition reaction of furans point out that the mechanism changes from concerted to stepwise with an increased electron deficiency in the dienophile (10, 11). Thus, the Diels–Alder reaction of furan with methyl vinyl ketone takes place in an asynchronous concerted manner. In this theoretical study, we attempt to understand the two pathways, the Diels–Alder and Michael reactions, which involve both regio- and stereo-selectivity.

Computational details

The density functional method computations for the gas-phase calculations were performed with the Spartan 4 for Windows package (12) implemented on an Endeavor MT 7000 workstation. The reactant, product,and transition state (TS) geometries for the above reactions were optimized by DFT calculations at the B3LYP/6-31G* level (13). After the optimization of all transitional structures, we carried out vibrational analyses to check the nature of the stationary points. The transition states are defined by exactly one imaginary frequency. Unless otherwise indicated, all energy changes in the B3LYP/6-31G* optimizations reported in this paper include zero-point energies without scaling. To calculate the free energies of solvation needed to understand the effect of the solvent on the stereoselectivities (14), we used the Q-chem version 2.1 package for Linux (15). To evaluate the solvent effect, we carried out a B3LYP/6-31G* single-point calculation, using the method based on the Onsager model (16). The solvent used in the experimental work was chloroform; therefore, we employed the dielectric constant ($\varepsilon = 4.81$) and the solute radius ($\alpha = 3.92$).

Results and discussion

Experimental reactivity results

Furan (**1a**) reacted with methyl 3-nitroacrylate (**2**) to give the two known Diels–Alder adducts, ***endo*-3a** and ***exo*-3b** (17). However, the adduct ratios (3:2–1:1) and the yields (30%–85%) depended upon the reaction conditions: the reactant concentrations, the ratios of the reactants, and the reaction times (18). The reaction of **1a** with **2** in chloroform at room temperature was followed by ^{1}H NMR for 1 month. The results are given in Fig. 1. They indicated that ***endo*-3a** was produced at up to a 28% yield during the initial stage of the reaction (8 days), at which point this adduct decomposed. In contrast, the yield of ***exo*-3b** slowly increased without decomposition, and after 18 days, an equilibrium composed of ***endo*-3a** (12%) and ***exo*-3b** (18%) was established.

The reaction of 2-methylfuran (**1b**) with **2** for 1 day yielded a product mixture containing the Diels–Alder adducts **4b** in a 16% yield, **4d** in a 23% yield, and a few concomitant products. The reaction, which took place under conditions similar to those used for furan (**1a**), was carefully followed by ^{1}H NMR at room temperature for 2 weeks. The results, presented in Fig. 2, indicate that the yields of the four Diels–Alder adducts (**4a**–**4d**) reached their maximum values (18%, 16%, 6%, and 23% yield, respectively) within 5 days; however, after 10 days, the amounts of these adducts noticeably declined. In contrast, the yield of the Diels–Alder adduct (**4a**) steadily increased up to 19% after 2 weeks. The yield of one of the Michael adducts (**5b**) rose rather slowly during the early stages of the reaction to reach a maximum of 5% at 4 days. Interestingly, the other Michael adduct (**5a**) was not detected during the early stage of the reaction, but was increasingly produced after the three Diels–Alder adducts began to decompose.

The compound 2-methoxyfuran (**1c**), a highly reactive diene for the Diels–Alder reaction, actually reacted with **2** in benzene at room temperature to very rapidly give the Michael adduct (**7a**) in a 72% yield. This reaction, in chloroform solvent, was also followed at a temperature of –10 °C for 50 min. The result obtained was similar to that observed for the reaction of **1b** with **2**. Only two Diels–Alder adducts (**6a** and **6b**) were found, and no other isomer was detected

© 2006 NRC Canada

Scheme 1.

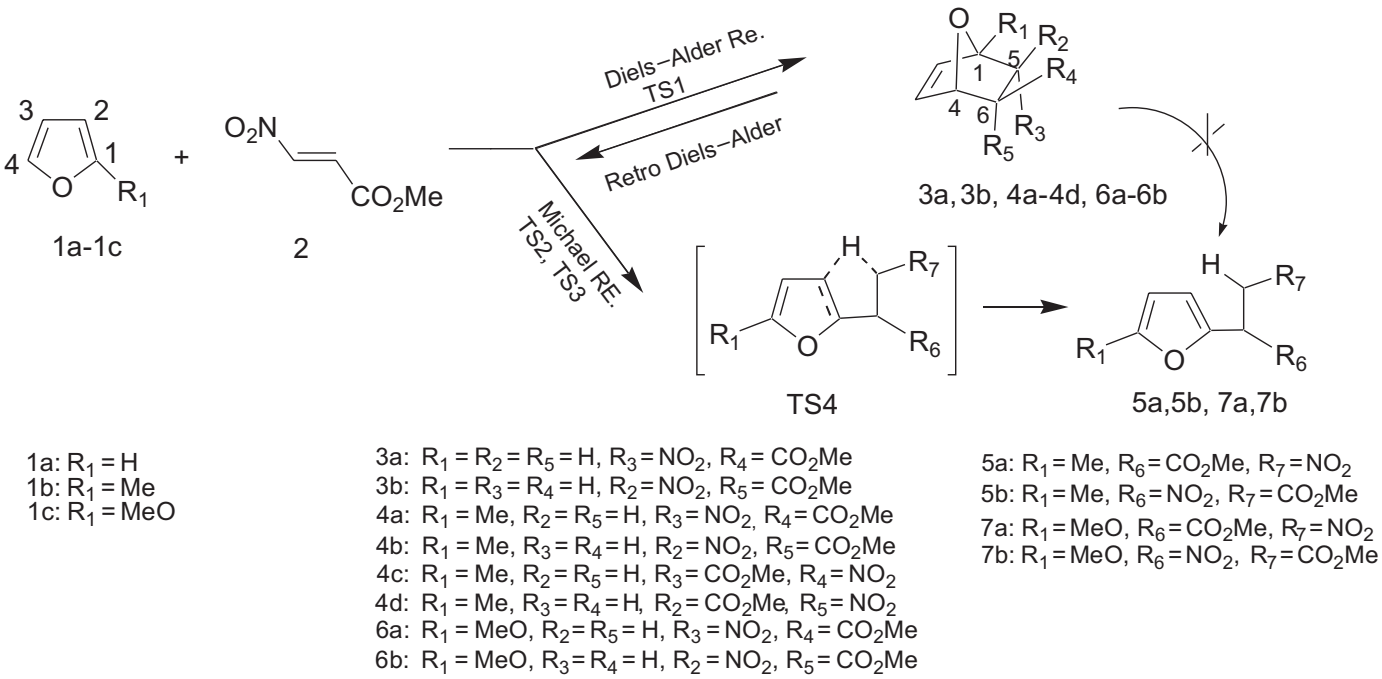
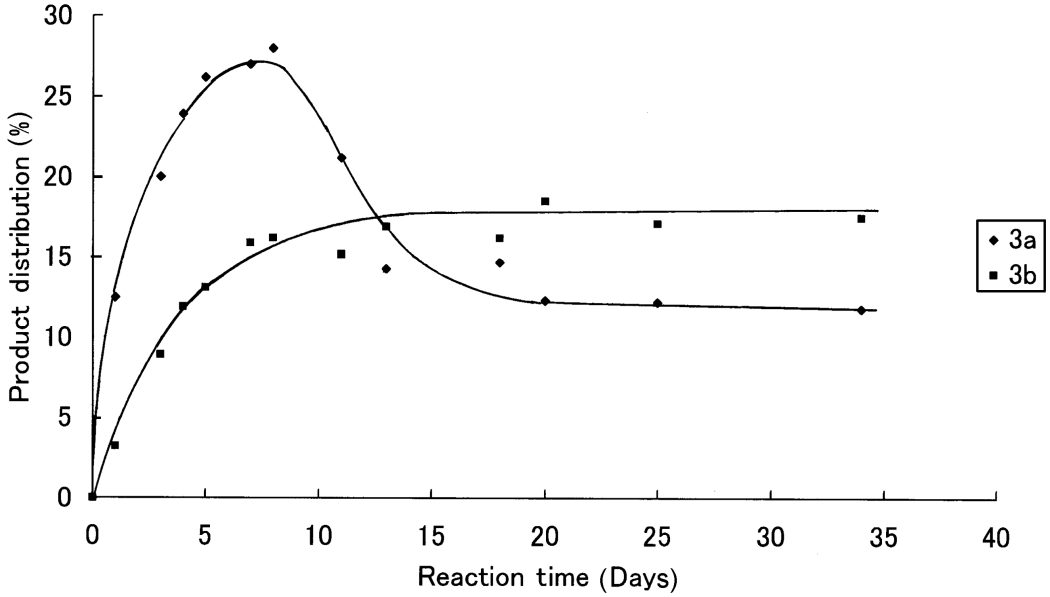


Fig. 1. The reaction of **1a** with **2**.



(Fig. 3). Indeed, one of the Diels–Alder adducts (**6a**, 37% yield at 30 min) was quickly generated, but soon began to disappear, while the other one (**6b**) steadily accumulated. One of the Michael adducts (**7b**) was produced from the beginning, but production of the other one (**7a**) was significantly delayed; it appeared during the course of the reaction (45 min).

The Diels–Alder adducts are known to be kinetic products that are subject to the retroreactions that yield the thermodynamically favored Michael adduct products (7, 19). Figures 2 and 3 clearly demonstrate the conversion of Diels–Alder adducts to Michael adducts. However, the formation of these Michael adducts may also occur directly from the furans (**1a**–**1c**) and the nitroacrylate (**2**). Thus, to check the formation process of the Michael reaction, we followed the thermal decomposition of the Diels–Alder adduct (**4a**) by ^{1}H NMR. The result was that adduct **4a** initially produced the starting materials (**1b** and **2**), and after 2 days, the Michael adduct (**5a**) was obtained.

Computational results

The conformation of methyl 3-nitroacrylate (2)

It is known that methyl acrylates exist as a mixture of s-cis and s-trans conformations involving the C—C bond between the C=O and C=C bonds. Konakaand co-workers (20)

© 2006 NRC Canada

Fig. 2. The reaction of **1b** with **2**.

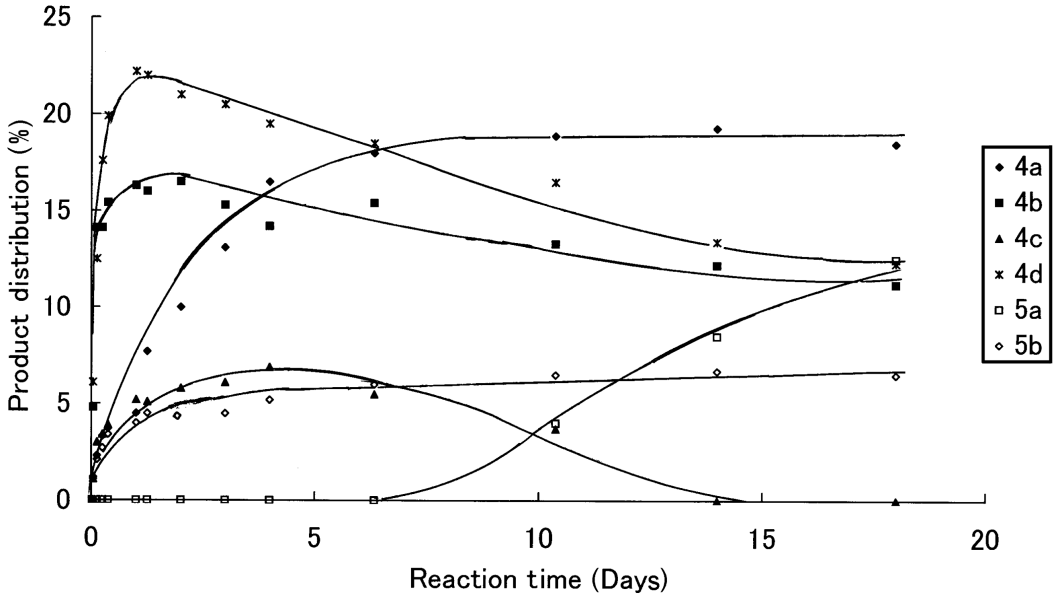
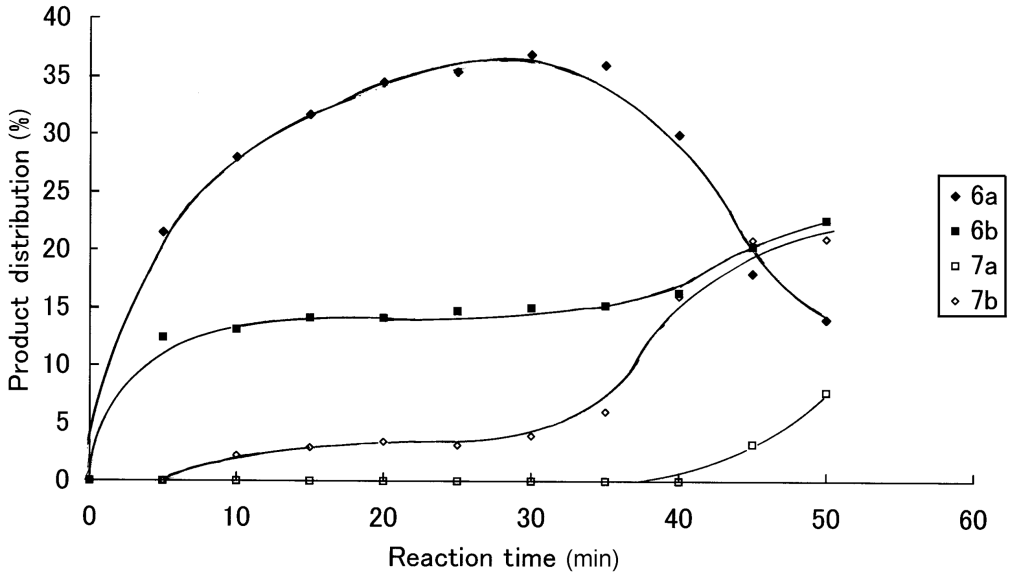


Fig. 3. The reaction of **1c** with **2**.



found that the relative abundance of the s-cis form of methyl acrylate is 67% in the gas phase, and that the vapor of methyl methacrylate exists in the s-trans form (64%). However, the conformations of methyl acrylates in general have never been unambiguously determined. Accordingly, we have compared the stabilities of the two forms of methyl 3-nitroacrylate by calculation. The rotational barriers around its C—C bond are shown in Table 1. The cis-form is more stable than the trans-form by 0.54 kcal/mol (1 cal = 4.184 J) at the HF/6-31G* level and by 0.69 kcal/mol at the DFT/B3LYP level. The cis-form preference can be explained in terms of an electrostatic effect: the lone-pair electrons on the oxygen avoid the π electrons of the double bond in the cis-conformation. The rotation from the s-trans form to the cis-form has a barrier of 6.07 kcal/mol by DFT and 14.05 kcal/mol by HF(6-31G*). Because the difference in stabilities of the two forms are small, we calculated the cycloadditions by both the s-trans,s-cis forms of the dienophiles. However, we considered only the reactions of the cis pathways in the present paper because the pairing of the s-cis,s-trans forms is different.

FMO results

To interpret our experimental results, we used the the PM3 method to calculate the FMO energies and coefficients of the dienes (furans, **1a**–**1c**) and of the dienophile (methyl 3-nitroacrylate, **2**). The LUMO–HOMO energy gaps are presented in Tables 2 and 3. We have found that the highest occupied molecular orbital (HOMO) of **2** is the nonbonding orbital in which the lone-pair electron of the nitrogen and the oxygen atoms are involved, as found in methyl acrylate (21). Therefore, this orbital is not suitable to be associated

© 2006 NRC Canada

Table 1. Comparison of energy differences between the two forms, ΔG (s-trans)–(s-cis) and rotational barriers, ΔG (rot,TS), at the 6-31G* and B3LYP levels.

	6-31G* (kcal/mol)	B3LYP (kcal/mol)	MA[a] (kcal/mol)	MMA[b] (kcal/mol)
ΔG ((s-trans)–(s-cis))	0.54	0.69	0.58	–0.32
ΔG (rot,TS)	14.05	6.07		

[a]Methyl acrylate, HP/6-31G* calculation by T. Tsuji et al. (20).
[b]Methyl methacrylate, B3LYP/6-31G* calculation by M. Avalos et al. (21).

Table 2. The HOMO and LUMO energies and orbital coefficients of **1a**–**1c** and **2**.

Compound	Level	Energy (eV)	C1	C2	C3	C4
1a	LUMO	0.603	–0.5698	0.3341	0.3341	–0.5698
	HOMO	–9.377	–0.5923	–0.3862	0.3862	0.5923
1b	LUMO	0.596	0.5723	–0.3531	–0.3075	0.5493
	HOMO	–9.104	–0.5712	–0.4152	0.3516	0.5661
1c	LUMO	0.664	0.5642	–0.3817	–0.2752	0.5651
	HOMO	–8.802	0.5423	0.2729	–0.4937	–0.4936
2	LUMO	–1.734	0.5471	–0.6004		
	HOMO	–12.000	0.0000	0.0000		
	$HOMO_{-1}$	–12.096	0.0830	0.0652		

Table 3. The MO gaps for the reaction of **2** with **1a**–**1c**.

	1a	**1b**	**1c**
HOMO–LUMO alkene	7.642	7.369	7.067
HOMOalkene–LUMO	12.705	12.692	12.76

with a (4+2) cycloaddition. The nearest occupied orbital to the latter ($HOMO_{-1}$) is 0.096 eV (in the s-cis) lower than the HOMO. Because it possesses a nodal plane coincident with the molecular plane of the dienophilic system, it has the right symmetry to react as a HOMO in a cycloaddition. From now on this orbital, $HOMO_{-1}$ will be considered as the reacting HOMO of **2**. The interactions between the diene HOMO and the LUMO of the dienophile, and between the LUMO of the diene and the dienophile $HOMO_{-1}$, should play significant roles in both the reactivity and regioselectivity of the cycloaddition (22–24). The most favorable FMO interaction is that of the HOMO diene – LUMO dienophile, as shown in Table 3. The reaction, then, is a LUMO dienophile-controlled Diels–Alder reaction.

On the basis of the orbital coefficients of the atoms forming the σ bond, we believe that the LUMO of **2** is quite polarized. However, because the atomic coefficients over both the carbons are similar in the case of furan (**1a**), the dienophile should exhibit no regiochemical preference. On the other hand, when the diene is methylfuran (**1b**), the overlap is the largest between the atom pair C diene – C dienophile, a situation leading to the regioisomers **4a** and **4b** as Diels–Alder adducts and **5a** as a Michael adduct. However, the orbital coefficients of each carbon in the diene are relatively close in magnitude. Therefore, six possible regioisomers (**4a**–**4d** and **5a** and **5b**) may be produced. Further, in the case of methoxyfuran (**1c**), the orbital coefficients of each carbon in the diene are fairly different in magnitude. As we observed experimentally, this difference leads to the selective formation of the regioisomers **6a** and **6b** as the Diels–Alder products and **7a** as the Michael product. Our FMO calculation produced sufficient information to allow us to successfully interpret our experimental results relating to the regioselectivity of the reaction.

A synchronous concerted mechanism for the production of the Diels–Alder adducts

There are several issues of selectivity to be considered in the Diels–Alder reaction of the furans (**1a**–**1c**) with methyl 3-nitroacrylate (**2**). First, there is the issue of regioselectivity in which the carbon bearing the side group of the diene is attached to either the carbon atom bonded to the nitro group (ortho) or to the carbon atom bonded to the ester group (meta, with respect to the nitro group). Second, there is the issue of stereoselectivity, involving the orientation of the dienophile (endo or exo) with respect to the diene. Four different products occur as ortho/endo (**4a**, **6a**), ortho/exo (**4b**, **6b**), meta/endo (**4c**, **6c**), or meta/exo (**4d**, **6d**) adducts. Third, as discussed earlier, the s-cis and s-trans conformations of the dienophile remain unexplained. Overall, this creates a set of eight possible transition structures from each dienophile (see Scheme 2). Figure 4 depicts the TS geometries of the adducts for **4b** of s-cis at TS1-2, on behalf of the geometries of the eight adducts for **4a**–**4d**: TS1-1, TS1-2, TS1-3, and TS1-4. The values of the activation energies and selected geometrical parameters, obtained through B3LYP/6-31G* (DFT) calculations, are given in Table 4.

The activation energies calculated for the Diels–Alder reaction decrease as the dienes change from furan to methoxyfuran (17 to 18 kcal → 16 to 17 kcal → 11 to 13 kcal). The tendencies for the energies and the differences among the energies to decrease in a similar manner are consistent with the experimental results. A comparison of the relative energies of the transition state structures for each reaction reveals a narrow range of 1 to 2 kcal/mol. However, comparing these values in more detail, we have found that

© 2006 NRC Canada

Scheme 2.

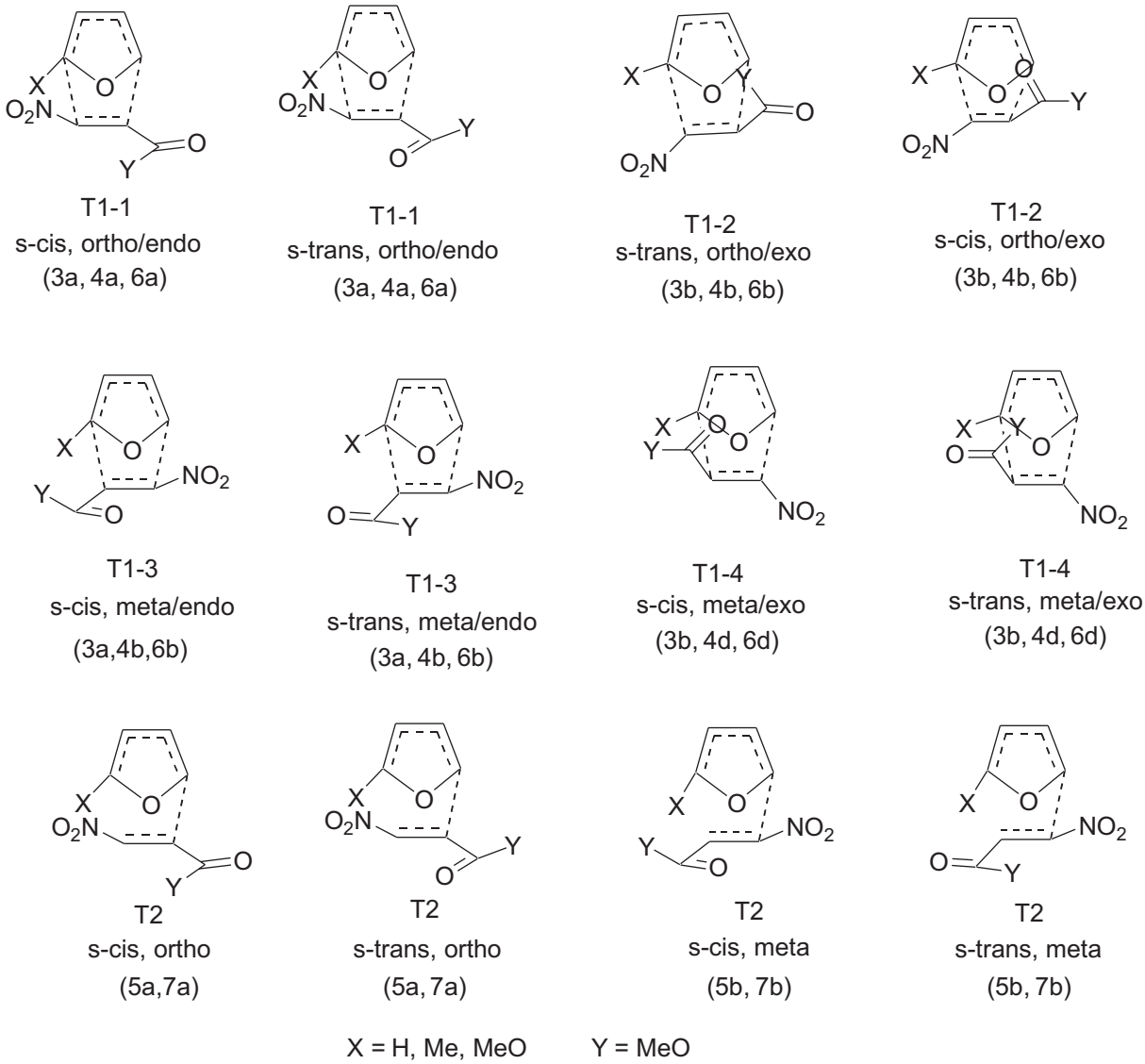
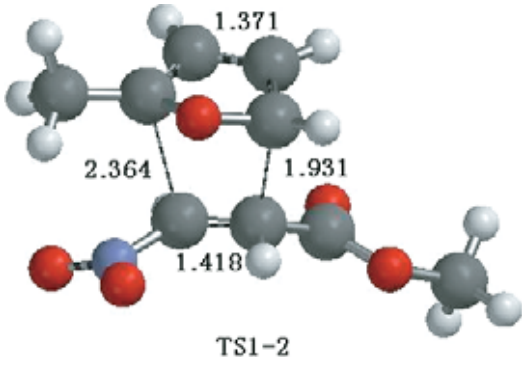


Fig. 4. Transition structure (TS1-2, ortho/exo, s-cis) for the Diels–Alder reaction between methylfuran (**1b**) and methyl 3-nitroacrylate (**2**) by DFT calculation at the B3LYP/6-31G* level. The distances of the C—C bonds are given in angstoms.



the endo/exo and ortho/meta pairings are only slightly different. The calculations suggest that the ortho isomer is more stable than the meta isomer by ca. 0.6 kcal/mol for **4** and 1 to 2 kcal/mol for **6**, a result in good agreement with the observed regio- and stereo-selectivity. As calculated, the endo isomer for the ester group (**4b**, **4d**, **6b**) is more reactive than the exo (**4a**, **4c**, **6a**) by 0.3 kcal/mol, while the experiment did not show good agreement for **4** and **6**. At first glance, this difference in isomer energy appears to be due to a steric effect. However, all of the transition state structures may be crowded to a similar extent, and so steric repulsion is probably not the main factor. The kinetic preference for endo adduct formation is often attributed to a second orbital interaction (25). In this case, there is an interaction between the orbital on the C2 or C3 atom of the furan ring and that on the carbon atom of the ester group at the endo position of the dienophile (see Fig. 4). This second orbital interaction may contribute to an acceleration of the rate. In addition, the endo approach presents a lower activation barrier than the exo ones, a finding which could be explained by the π-facial stereoselectivity of the carbonyl group.

In the case of furan (**1a**), both DFT calculations estimated a lower energy for TS1-1 (TS1-3) than for TS1-2 (TS1-4) by 0.7 kcal/mol. This small difference correlates with the obvi-

© 2006 NRC Canada

Table 4. The activation energies, imaginary frequencies, thermal parameters, and selected geometric parameters for TSs using calculations at the B3LYP/6-31G* level for Diels–Alder reactions between the furans (**1a**–**1c**) and 3-methyl nitroacrylate (**2**).

	3a	**3b**	**4a**	**4b**	**4c**	**4d**	**6a**	**6b**	**6c**	**6d**
Activation energy (kcal/mol)	17.25	17.91	16.14	16.53	16.97	17.28	11.05	10.90	12.08	12.99
Activation energy (kcal/mol)[a]	16.89	16.69	16.01	15.12	16.21	16.00	6.93	7.03	8.63	10.63
Energy difference (kcal/mol)[b]	0.36	1.22	0.13	1.41	0.76	1.28	4.12	3.87	3.45	2.36
Activation energy (kcal/mol)[c]	23.26	23.62	20.79	20.89	21.08	22.00	18.59	17.95	20.53	20.70
Frequency (cm^{-1})	476.33	486.64	457.89	411.67	447.93	483.28	278.07	270.44	277.64	367.00
ΔH (kcal/mol)	0.876	0.766	0.799	0.659	0.769	0.729	0.781	0.917	0.851	0.729
ΔS (cal/mol K)	–46.5	–55.0	–49.6	–47.7	–48.5	–49.7	–51.4	–50.4	–50.5	–49.4
ΔG (kcal/mol)	14.75	14.44	15.57	14.88	15.54	15.54	16.10	15.95	15.90	17.48
Bond distance (C1—C5, Å)	2.112	2.111	2.235	2.364	2.320	2.232	2.828	2.732	2.654	2.544
Bond distance (C4—C6, Å)	2.128	2.130	2.015	1.931	1.961	2.017	1.833	1.860	1.838	1.868
Asychronous indicator[d]	0.004	0.004	0.052	0.101	0.084	0.051	0.213	0.189	0.182	0.153
NBO (C1—C5)[e]	0.426	0.427	0.350	0.298	0.335	0.391	0.127	0.126	0.173	0.222
NBO (C4—C6)[e]	0.422	0.425	0.495	0.549	0.516	0.483	0.617	0.601	0.611	0.581
Bond angle (C2-C1-C5, °)	99.62	98.74	95.49	91.63	92.28	96.48	84.04	86.99	85.48	89.70
Bond angle (C3-C4-C6, °)	98.38	99.88	100.71	104.06	103.00	100.69	108.29	106.82	106.68	105.48
Dihedral angle (C1-C4-C6-C5, °)	–1.81	–1.75	–1.73	–8.27	–7.01	–0.83	–21.70	–11.16	–11.93	–8.04
Dihedral angle (C1-C5-C6-C4, °)	1.85	1.78	1.69	7.63	7.76	0.89	16.65	8.86	13.96	9.23

[a]Activation energy in $CHCl_3$.
[b]Activation energy difference between at gas phase and in the solvent.
[c]Activation energy in the retro-Diels–Alder reaction.
[d]Asychronous indicator: $(ra - rb)/(ra + rb)$; ra and rb are the lengths of the forming bonds.
[e]Wiberg index for the natural bond orbital.

ous adduct selectivity observed. In the case of methylfuran (**1b**), we found small TS energy differences of less than 0.7 kcal/mol; a low selectivity for adducts may account for them. On the other hand, in the case of methoxyfuran (**1c**), the energy gap between the TS1-1, TS1-2 group and the TS1-3, TS1-4 group was found to be ca. 1.5 kcal/mol. These large gaps indicate a clear selectivity preference for the products from the TS1-1 and TS1-2 group; in accord with this prediction and the previous FMO prediction, the products from TS1-3 and TS1-4 group were not observed experimentally. This discrepancy may be attributable to an electrostatic attraction between the nitro group and the neighbouring methoxy group of the furan. The more reliable density functional method produced fairly good agreement in selectivity with the experiment. Although we did not necessarily expect accurate quantitative reproductions of the experimental value for each reaction, the relative energies of the transition state, which are little affected by the presence of the solvent, should be well-modeled (26, 27). In addition, the important factor to note is the conformation of the dienophile in the transition structures. The preferred conformation is the same as that found in the starting material, the s-cis conformation. The difference of the energies at the transition structures is less than 0.5 kcal/mol. Due to the small magnitude of the energy variation with transition state structure, it is important to pinpoint the pertinent factors producing the preferred conformation. However, as pointed out by Jimenez and co-workers (21) for the case of methyl acrylate, there will be a relatively larger increase in the delocalization energy for the transition structure than for the reactants.

Intermolecular cycloadditions are entropically very unfavorable because of the geometry restrictions. Thus, the butadiene–ethylene cycloaddition has a very large negative activation entropy of –44.5 cal/mol K, which raises the free energy of activation to 37.4 kcal/mol. Thus, the process is very unfavorable, as can be seen by a production of 78% only under very drastic conditions (165 °C and 900 atm, 1 atm = 101.325 kPa) (28). A general similar large negative entropy (–46 to –55 cal/mol K) was found for the present intermolecular cycloaddition.

However, the free energy of activation was determined to be quite different from the butadiene–ethylene case, having a value of only 14–17 kcal/mol. In addition, the low activation enthalpy at the polar addition contributes to the low activation energy (29). Therefore, this low free energy provides an explanation for the spontaneous intermolecular cycloaddition with the furans under mild conditions without any Lewis acid catalyst.

As noted in the discussion in the Experimental section, the Diels–Alder adducts produce the starting materials (**1b**, **1c**, and **2**); that is, retro-Diels–Alder reactions take place. The activation energies calculated for the retro-Diels–Alder reaction are 21 to 22 kcal/mol for **4** and 18–21 kcal/mol for **6a** and **6b**. Evidently, the reaction has its equilibrium on the Diels–Alder adduct side.[2] Because both the forward and the reverse reactions possess lower activation energies, they are faster and reach equilibrium more quickly. Therefore, the theoretical predication agrees with the experimental observation that no Diels–Alder product could be isolated. In contrast to these findings, the alternative path to the retroreaction from the thermodynamically favored Michael

[2]In the Diels–Alder reaction between 2-methoxyfuran and methyl 3-nitroacrylate, the distances 1.883 and 2.828 Å indicate that only the C4—C6 bond is being formed at TS; the short distance is comparable to that at the TS associated with the Michael addition. Certainly, this cycloaddition is a Michael addition with concomitant ring closure to give the Diels–Alder adduct in a single step.

© 2006 NRC Canada

adduct has a high activation barrier, 37–44 kcal/mol for **5** and 20–29 kcal/mol for **7**. This reaction equilibrium, then, lies to the Michael adduct side.

Solvent effect on the Diels–Alder reaction

Solvent effects on cycloaddition are well-known (30) and have received considerable attention. Sustamann et al. (30*a*) studied the influence of the solvent effect on the stereoselectivity of Diels–Alder reactions and reported that it favors the transition structure that exhibits the higher dipolar moment. Table 4 shows the relative energies of the stationary points corresponding to the Diels–Alder reaction in chloroform used as the experimental solvent. The solvent effect increases with the polar zwitterionic character of the TS, which is related to the increase of the nucleophilic character of the furan derivative (0.4 kcal/mol → 1 kcal/mol → 4 kcal/mol). This poor solvent effect can be attributed to the low polar character of these cycloadditions. Inclusion of solvent effects does not substantially modify the geometries obtained in the gas phase. Therefore, the inclusion of the solvent effects in the experimental models does not alter the gas-phase analysis.

Geometry of the Diels–Alder reaction in the concerted mechanism

As pointed out by Houk et al. (31) in his discussion of the transition state structures, bond lengths other than those for newly forming bonds fall within small ranges. The TS bond distance C5—C6 increased from that in the starting dienophile to 1.31–1.33 Å and further rose to 1.55 Å in the Diels–Alder adducts. The C2—C3 distance in the diene TS lengthens to about 1.39 Å from that in the starting material, and becomes 1.35 Å in the adducts. The geometrical values obtained are shown in Table 4.

The geometries of the forming bonds reveal an asynchronous transition structure in which the shorter of the forming bonds is the one involving the carbon that attacked the methyl ester group, which corresponds to the more electrophilic site of methyl 3-nitroacrylate, and the nonsubstituted position of furan, the C5, which corresponds to the more nucleophilic site of the substituted furans. Furthermore, the bond length differences between the forming bonds, C1—C5 and C4—C6 in the transition states of the ortho structures of the TS1-1 and TS1-2 group are more asynchronous than those in the meta structure states of the TS1-3 and TS1-4 group. The degree of asynchronicity in the TS is defined as $\alpha = (ra - rb)/(ra + rb)$ (18). The values of this function are 0.15–0.21 at the TS structure in the case of methoxyfuran, much larger than of the TS formed by methylfuran (0.05–0.10). A more balanced measure of the extent of bond formation or bond breaking along a reaction pathway is provided by the bond order of the Wiberg index, derived from the natural bond orbital (NBO) basis (32), which is implemented in the Q-chem package. For **3a** and **3b**, the value of the C1—C5 BO is 0.43, whereas the value of the C4—C6 BO is 0.42. These data demonstrate a synchronous concerted bond formation. For the reaction of methylfuran (**1b**), the BOs of the forming bonds at the carbon bonded to the methyl group in furan are 0.30–0.39, and its other BOs are 0.48–0.55. These data give evidence for steric repulsion by the methyl group of the furan (**1b**). Furthermore, in the reaction of the methoxyfuran (**1c**), the tendency is increased, as the BOs at the carbon bonded to the methoxy group are 0.13–0.22, and the other BOs are 0.58–0.62. Similar tendencies are observed in the bond order of the furan rings. Thus, the values of C4—C6 are larger than the values of C1—C5, and the differences are greater in the methoxyfuran (0.36–0.49) than in the methylfuran (0.09–0.25). The decreasing BO found in the double bond at the olefin and increase obtained for the double bond of the furan are similar. The NBO analysis indicates a need to further evaluate the situation along the cycloaddition.

To achieve the maximum interaction, the π orbitals at the reactive portions should have maximal overlap. The indicators of such an interaction are not only the length of the forming bond but also the bond angles and the torsion angles. The optimal value of the bond angle and the torsion angle are 90° and 0°, respectively (33). Both the bond angles (C2-C1-C5 and C3-C4-C6) deviate only slightly from the optimal angle, so they appear to be sufficient to allow the reaction to take place. However, the deviation of the bond angle in the case of **6** is slightly larger than that seen in the case of **4**. On the other hand, a shift of –1° to –8° in the dihedral angle (C1-C4-C5-C6) was found in the case of **4** for the parallel conformation, and in the case of **6**, the angle showed a –8° to –21° change. Therefore, the vinyl group is almost parallel to the plane of the furan ring. Also, the twist angle produced between the forming bonds (the dihedral angle C1-C5-C4-C6) was found to be 1°–8° in the case of **4**, and 9°–17° in the case of **6**. The angles in the case of **4b** and **4c** (7.7°) when compared with those in **4a** and **4d** (1° to 2°) showed the steric interaction resulting from having the substituents groups located in the ortho position. On the other hand, in the case of the methoxyfuran, the twist angle shows similar larger values regardless of the position of the substituent groups, so the geometry of the TS of **6** is disfavored over that of **4**. Therefore, the asynchronicity of the TSs is not due to steric repulsion but to the more favorable nucleophile and electrophile interaction.

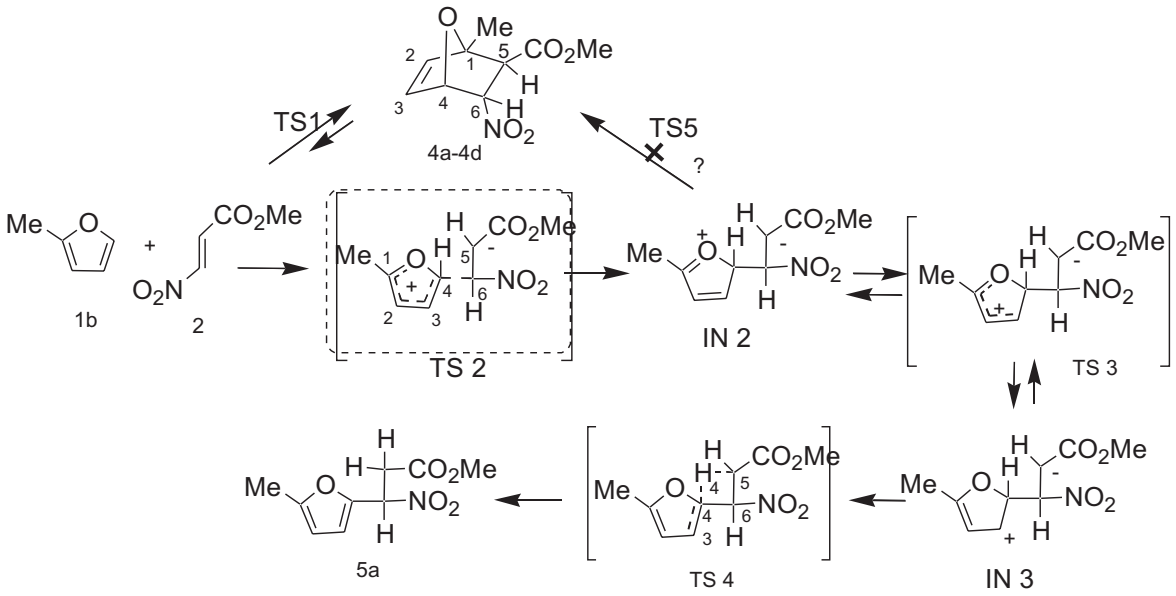
Stepwise mechanism to the Michael adducts

The process leading to the Michael adduct beginning from the electrophilic attack of methyl 3-nitroacrylate (**2**) on the furans (**1b** and **1c**) is shown in Scheme 3. Figure 5 presents the geometry of these transition structures. Tables 5 and 6 show the values of the activation energies and some selected geometrical parameters at the TS, while Fig. 6 and 7 display a schematic representation of the energy profile. Although generally the zwitterionic intermediate produced from the electrophilic attack of the nitroacrylate (**2**) is thought to adopt an anti-periplanar conformation, there may exist the possibility of it being generated in a syn-periplanar conformation because of the competitive Diels–Alder and Michael reactions (29).

The transition structure TS2 corresponds to a nucleophilic attack of the C4 center of the furan ring on the vinyl system of **2** to give the zwitterionic intermediate IN1. Furthermore, TS3 corresponds to the cation transfer from the oxygen atom of the furan to the atom of C3 to give the localized zwitterionic intermediate IN2. Both IN1 and IN2 have similar potential energies, and further, the structures of IN1 and IN2 are similar. However, it is not possible to associate the production of the Michael adduct via the transfer of the H4 atom from the C4 to the C5 center on IN1 without passing

© 2006 NRC Canada

Scheme 3. The reaction mechanism of the addition reaction of furan with methyl 3-acrylate.



through IN2. The energy barriers associated with TS2 are 16.5–17.3 kcal/mol for **5a** and **5b**, 10.9 kcal/mol for **7a**, and 12.3 kcal/mol for **7b**. The length of the new forming bond (C4—C6) linked in TS2 are 1.93–2.02 Å for **5a** and **5b** and 1.87 Å for **7a** and **7b**, whereas the distance of the spacing between C1 and C5 are more narrow (2.23 Å for **5a** and **5b** and 2.53 Å for **7a** and **7b**). These values are similar to that of TS1 for the concerted mechanism of the Diels–Alder reaction (1.93–2.02 Å for C4—C6, 2.23–2.36 Å for C1—C5 in **4a**–**4d**, 1.83–1.86 Å for C4—C6, and 2.73–2.83 Å for C1—C5 in **6a** and **6b**).

The bond angles C2-C1-C5 and C3-C4-C6 in TS2 are 91.4°–96.5° for **5a** and **5b** and 86.9°–90.0° for **7a** and **7b**, and 100.6°–104.3° for **5a** and **5b** and 105.2°–106.6° for **7a** and **7b**, respectively. These values are similar to that of TS1. Furthermore, the values of the C1-C4-C6-C5 dihedral angles in the TS are –0.8° to 8.6° for **5a** and **5b** and 9.9°–11.2° for **7a** and **7b**, again similar to that of TS1. In contrast to the Diels–Alder reaction, the angles in the Michael addition TS structures show the reverse twist. This twist may be caused by steric repulsion between the substituent groups at the side of the molecular opposite to the area where bonds form. Also, the differences between the distances and the angle are larger for the pair **5a**, **7a** than for **5b**, **7b**. This indicates that the vinyl group of the dienophile is twisted out of the plane of the furan ring to a slightly greater extent in the TS for the electrophilic attack of **2** on **5a** and **7a** than it is in the TS of **5b** and **7b**. This difference in conformation may result from a repulsive interaction between the nitro group of **2** and the substituent groups present on the furan ring. However, the activation energy for the formation of the TS for the Michael reaction seems to be smaller as the result of the electron-rich character of the nitro group. Finally, the reactivity may be determined by the balance between the steric repulsion and the electronic attraction. Our result may indicate that the nitro group predominates over an ester in controlling the direction of the Michael additions as has been pointed out by Patterson and McMurry (34).

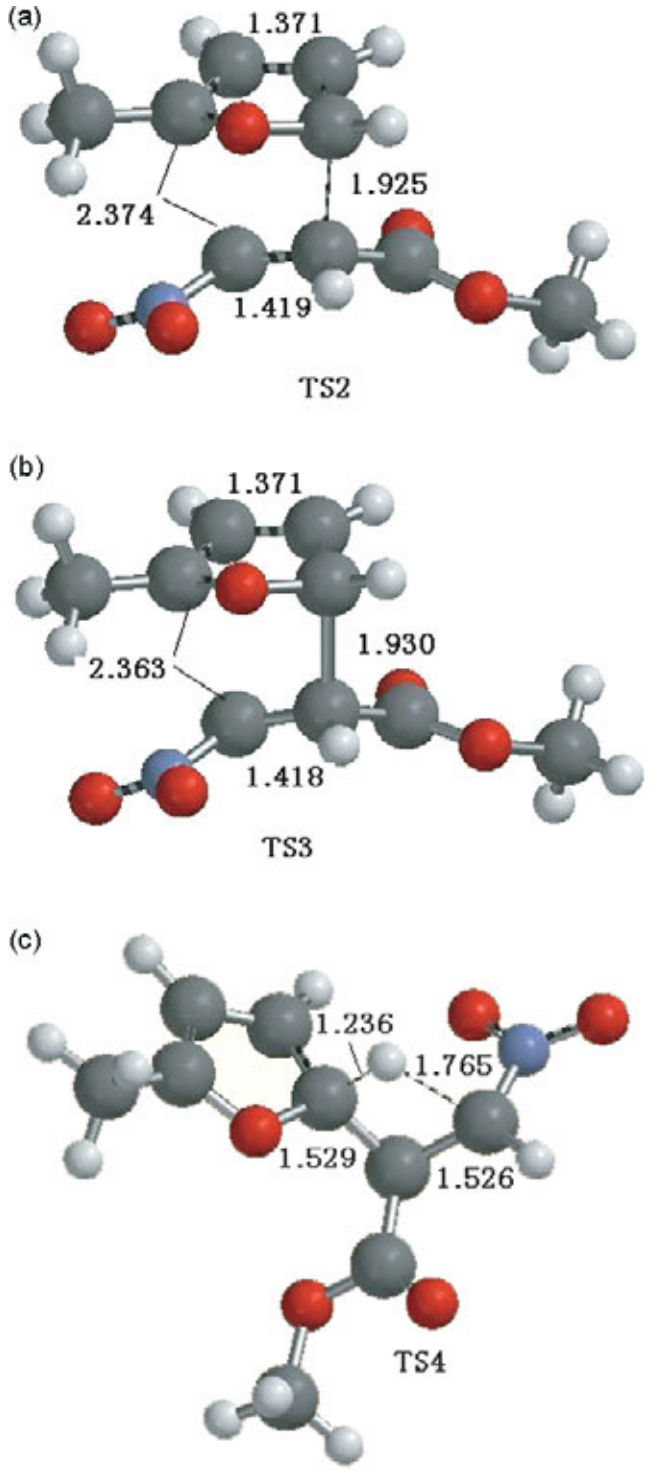
Previous studies of this reaction and the results summarized in the figures and tables of this paper reveal some interesting characteristic features. The presence of the nitro group on C5 may be necessary for the occurrence of the Michael addition reaction (35); the reaction of the furan (**1a**–**1c**) with diethyl malonate does not lead to a Michael adduct (36), but the reaction of **1b** with 1-nitro-3,3,3-trichloro-1-propene does (37). Furthermore, Just et al. (38) reported that the same reaction afforded Diels–Alder adducts, which were converted into Michael adducts with extended reaction times. It appears that the nitro group can delocalize the charge generated in the formation of the zwitterion (3) as suggested by the calculated high electron density on both C5 and C6.

The intermediate IN2 may undergo a process that leads to the formation of the last molecular adducts **5a**, **5b**, **7a**, and **7b**. This process (TS4) corresponds to an intramolecular proton-transfer process, which presents a high potential energy barrier (48 kcal/mol for **5a**, 50 to 51 kcal/mol for **5b**, 41 kcal/mol for **7a**, and 45 kcal/mol for **7b**) relative to the former steps (TS2, TS3) of the stepwise addition.

The transition structure TS4 corresponds to a four-membered transition structure in which the intramolecular proton (H4) transfers from the C4 to the C5 center. In the transition state, the length of the C4—H4 bond being broken is 1.23–1.28 Å and the C5—H4 bond being formed is 1.66–1.76 Å. These lengths suggest bond orders that indicate a concerted bond breaking – formation process for the intramolecular proton transformation. One of the causes of the high potential energy of TS4 relative to TS2, TS3 is the angular strain associated with the formation of this transition structure. The C3-C4-C6 bond angle is 125°–129° (ca. 104° at TS2, TS3) and the H4-C4-C6 bond angle is 84°–88° (ca. 106° at TS2, TS3). These values show that the C4 center is far from sp^3 hybridized. In addition, the C4-C6-C5 bond angle is associated with the strain that appears during the formation of this four-membered transition structure. To the contrary, the TS2, TS3 route has a lower energy owing to a favorable π–π electric interaction between the furan (**1b**, **1c**) and the olefin (**2**) taking a syn-periplanar conformation.

© 2006 NRC Canada

Fig. 5. Transition structures (TS2, TS3, TS4 at s-cis, ortho/exo) for the Michael reaction between methylfuran (**1b**) and methyl 3-nitroacrylate (**2**) by DFT calculation at the B3LYP/6-31G* level. The distances of the C—C bonds and C—H bonds are given in angstoms.



However, for this intramolecular process, the negative activation entropy is only –4 to –7 cal/mol K compared with the more entropically unfavorable value for the concerted Diels–Alder reaction. In addition, the computed free energy of activation is found to be 5 to 6 kcal/mol. These cooperative factors permit this intramolecular process with the smooth motion of the H4 atom from the C4 to the C5 center.

Solvent effect on the Michael reaction

Solvent effects on the Michael addition are interesting because of the presence of the polar zwitterion intermediate. Table 5 shows the B3LYP/6-31G* relative energies with the inclusion of the solvent effect. The data of TS2 and TS3 do not show a definite difference between carrying out the reaction in the gas phase and in solvent. These intermediates and transition structures are stabilized by 1 to 2 kcal/mol for **5a** and **5b** and 2–4 kcal/mol for **7a** and **7b**, similar to the concerted Diels–Alder reaction. These results are due to the low variation of the dipole moments along the reactive channels, and are related to the effective delocalization of the charge transferred during the nucleophilic attack of **2b** and **2c** to **1**. However, the energy differences of the transition state TS4 in solvent are stabilized by 6–13 kcal/mol over that in the gas phase. The transition structure involving proton transfer is preferentially stabilized relative to the reactants owing to the large charge transfer that is developed along this polar transfer path. The low energy barrier found for the Michael reaction is in good agreement with the fact that, experimentally, this reaction can be carried out completely at room temperature. The large difference in the solvent and gas-phase TS energies is related to localization of the charge around the transfer proton. Moreover, the solvent effect increase for **5a** and **7a** is more dramatic than that of **5b** and **7b**. Thus, inclusion of the solvent effect may accelerate this polar reaction by a larger stabilization of the transition state corresponding to the proton transfer.

Preparation of the Diels–Alder adduct from IN1 via TS5

As mentioned in the previous section, the geometries of the first intermediate (IN1) in the Michael reactions for **5** and **7** are similar to that of transition state of the concerted Diels–Alder reaction. Therefore, as Houk, Domingo and coworkers (9, 10, 39) reported, with a small change of the geometry, the Diels–Alder adduct may be produced from IN1 by the stepwise process. That is, the nucleophilic attack of the anionic C5 center on the C1 atom on IN1 via TS5 gives the cycloadducts **4** and **6** (Scheme 3 and Table 5). For **5a**, s-cis, in which the C1 position is substituted by the methyl group, this cyclization process presents a small potential energy barrier (15.4 kcal/mol). The length of the C1—C5 bond being formed in the TS is 1.60 Å. For **5b**, s-cis, where C6 possesses a NO_2 group, the potential energy barriers are 21.2 kcal/mol, and the forming bond length is 2.33 Å. For **7a** and **7b**, the forming bond lengths are longer, owing to the steric repulsion, at 2.74 and 2.65 Å, respectively. The potential energies (25.0 and 19.7 kcal/mol) are larger than that of **5**. Therefore, these values are different from the experiment results in which the rates of reaction of **6** are faster than that of **4**. After many attempts, we were able to find TS5 for the s-cis form. In addition, we tried to calculate the transition state for the s-trans form. However, the transition state had an unreasonable conformation of the ester group and unrealistic thermal parameters. Any attempts to find the true transition state were unsuccessful. Therefore, the Diels–Alder adducts may be not prepared via the stepwise mechanism via TS5.

© 2006 NRC Canada

Table 5. Relative energies (kcal/mol) and energies in $CHCl_3$ (kcal/mol) for the stationary points, and entropies (cal/mol K) and free energies at TS for the Michael reactions between the furans (**1b**–**1c**) and 3-methyl nitroacrylate (**2**).

	5a		**5b**		**7a**		**7b**	
Structure	Relative energy (kcal/mol)	Energy in $CHCl_3$ (kcal/mol)	Relative energy (kcal/mol)	Energy in $CHCl_3$ (kcal/mol)	Relative energy (kcal/mol)	Energy in $CHCl_3$ (kcal/mol)	Relative energy (kcal/mol)	Energy in $CHCl_3$ (kcal/mol)
TS2	16.54	15.13	17.31	15.10	10.92	7.22	12.35	10.61
IN1	–4.36	–4.92	–4.12	–3.80	–6.11	–9.90	–5.68	–6.86
TS3	16.52	15.10	16.97	16.21	10.92	7.10	12.08	8.64
IN2	–4.36	–4.91	–4.12	–3.80	–6.12	–9.89	–5.67	–6.85
TS4	47.74	34.77	50.93	42.16	41.48	32.84	44.58	38.37
TS5	15.42	15.41	21.18	20.24	25.00	18.01	19.70	15.50
ΔS (cal/mol K)	–3.70	–9.12	–7.00	–2.38	–3.86	–6.00	–6.11	–6.33
ΔG	5.44	6.23	6.48	5.81	5.22	5.65	5.94	6.04
5, **7**	–24.79	–23.43	–25.98	–26.07	–24.08	–26.12	–25.01	–26.26

Table 6. The selected geometric parameters for the TSs of the Michael reactions between the furans (**1a**–**1c**) and 3-methyl nitroacrylate (**2**).

	5a	**5b**	**7a**	**7b**
TS2				
Bond distance (C1—C5, Å)	2.374	2.230	2.735	2.531
Bond distance (C4—C6, Å)	1.925	2.018	1.869	1.876
Bond angle (C2-C1-C5, °)	91.42	96.54	86.91	90.04
Bond angle (C3-C4-C6, °)	104.28	100.60	106.63	105.16
Bond angle (C4-C6-C5, °)	105.03	103.12	108.87	108.58
Dihedral angle (H2-C2-C1-R1, °)	–16.07	–21.14	–6.29	–13.32
Dihedral angle (H3-C3-C4-H4, °)	34.52	28.56	42.59	38.7
Dihedral angle (C1-C4-C6-C5, °)	8.61	0.77	11.21	9.93
TS3				
Bond distance (C1—C5, Å)	2.363	2.317	2.727	2.649
Bond distance (C4—C6, Å)	1.930	1.965	1.861	1.839
Bond angle (C2-C1-C5, °)	91.64	92.37	87.06	85.50
Bond angle (C3-C4-C6, °)	104.07	102.89	106.71	106.83
Bond angle (C4-C6-C5, °)	104.85	105.65	108.91	110.84
Dihedral angle (H2-C2-C1-R1, °)	–16.56	–20.13	–6.47	–9.9
Dihedral angle (H3-C3-C4-H4, °)	34.21	30.37	42.75	39.89
Dihedral angle (C1-C4-C6-C5, °)	8.22	8.10	10.95	17.01
TS4				
Bond distance (C4—H4, Å)	1.236	1.235	1.282	1.275
Bond distance (C5—H4, Å)	1.765	1.767	1.662	1.703
Bond angle (C4-H4-C5, °)	100.38	100.34	103.41	102.02
Bond angle (C4-C6-C5, °)	99.42	99.45	98.66	99.17
Bond angle (C3-C4-C6, °)	129.58	127.78	127.8	125.14
Bond angle (H4-C4-C6, °)	87.64	87.70	84.00	84.98
TS5				
Bond distance (C4—C6, Å)	1.592	1.953	1.865	1.842
Bond distance (C1—C5, Å)	1.598	2.330	2.744	

Note: R1 = CH_3 (**5a**, **5b**); R1 = OCH_3 (**7a**, **7b**).

Experimental

The proportions of the cycloadducts have been determined by integration of the corresponding methyne and vinyl peaks in the ^1H NMR spectra of their mixtures. We did not fully succeed in separating the different cycloadducts by column chromatography. Their stereochemical assignments were established by a series of 1D and 2D COSY experiments (250 MHz, Tables 7 and 8) (36, 40). They were confirmed by the acquisition of the spectra of **3a**, **4a**, and **5a**.

General

The ^1H and ^{13}C NMR spectra were recorded on JEOR FX-90Q and Bruker AC-250 spectrometers in deuterochloroform. Tetramethylsilane was used as the internal references for the proton spectra. The IR spectra were recorded on a

© 2006 NRC Canada

Fig. 6. Potential energy profiles for the Michael reaction of **1b** and **2**.

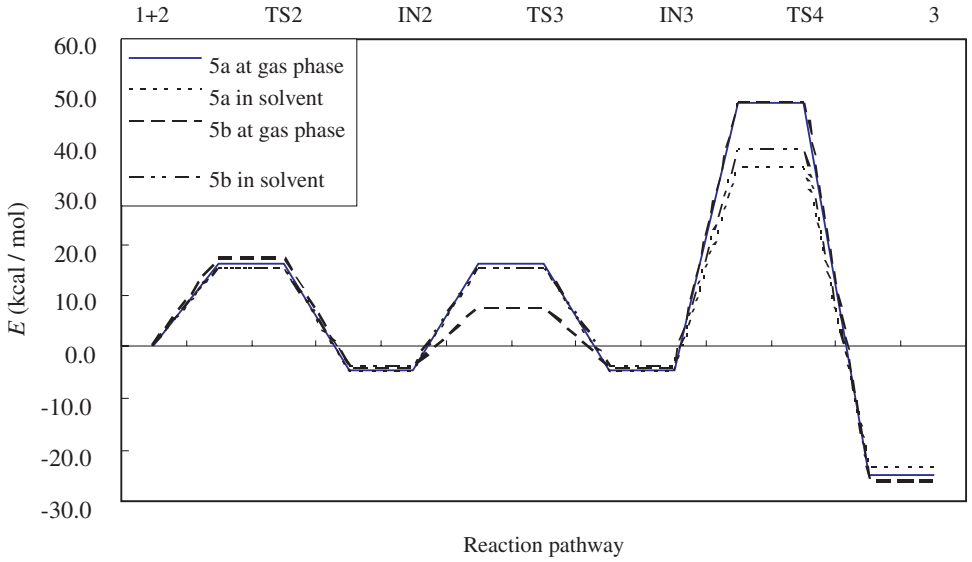
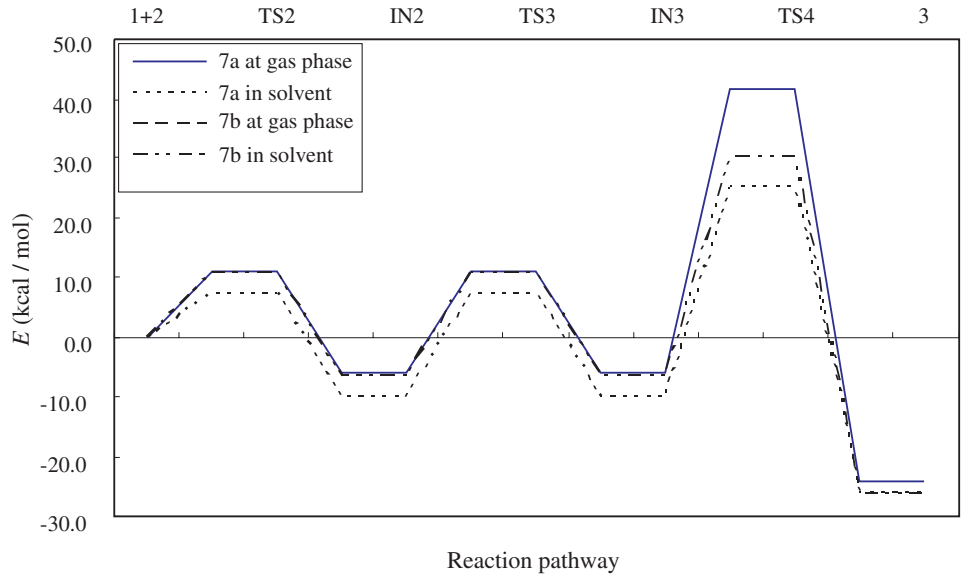


Fig. 7. Potential energy profiles for the Michael reaction of **1c** and **2**.



Hitachi I-2000 by sandwiching the materials between NaCl plates. The melting points were determined on a Yanako micro hot plate apparatus and are uncorrected.

Reactions

Synthesis of methyl 3-nitroacrylate (2) (ref. 41)

To a dimethyl ether solution (165 mL) of methyl acrylate (16.7 g, 0.2 mol) and iodine (31.5 g, 0.1 mol), silver nitrite (12.7 g, 0.1 mol) was added, and the solution was stirred for 5 days at room temperature. The reaction solution was washed with aqueous sodium thiosulfate, sodium carbonate, and sodium chloride solution. After evaporation of the solvent, methyl 2-iodo-3-nitro-propylate was obtained in a 18.5 g (87%) yield as yellow oil. The dried 2-iodo-3-nitropropylate (18.5 g, 0.1 mol) was added to sodium acetate (9.6 g, 0.1 mol) in dimethyl ether solution (120 mL) and left for 6 h at room temperature. The reaction mixture was then washed as previously described. Methyl 3-nitroacrylate was obtained in nearly quantitatively yield as a yellow oil. The liquid crystallized out on standing in a refrigerator. Yield: 8.0 g (87%); mp 32.0–33.0 °C.

Typical reaction procedure for furan (1a) with methyl 3-nitroacrylate (2)

Furan (18 mg, 0.3 mmol) and methyl 3-nitroacrylate (33 mg, 0.3 mmol) was placed in chloroform (3 mL) in a reaction flask and the reaction followed by ^{1}H NMR spectroscopy.

Separation of the products of the reaction of furan (1a) and methyl 3-nitroacrylate (2)

A mixture of **1a** (631 mg, 9.3 mmol) and **2** (105 mg, 0.8 mmol) was allowed to stand at room temperature for 1 day. After evaporation of the liquid, crystals were obtained from the reaction mixture by recrystallization from dimethyl ether.

© 2006 NRC Canada

Table 7. ^{1}H NMR data for Diels–Alder adducts (ppm).

Adduct	H1	H2	H3	H4	H5	H6
3a	5.35 (J = 1.4 Hz)	6.39 (J = 1.4, 5.8 Hz)	6.73 (J = 1.7, 5.8 Hz)	5.47 (J = 1.7, 4.8 Hz)	5.54 (J = 2.9, 4.8 Hz)	3.25 (J = 2.9 Hz)
3b	5.53 (m)	6.5 (J = 5.8 Hz)	6.5 (J = 5.8 Hz)	5.34 (J = 3.3 Hz)	3.97 (J = 3.0, 3.3 Hz)	4.85 (J = 3.0 Hz)
4a		6.35 (J = 5.8 Hz)	6.49 (J = 1.9, 5.8 Hz)	5.42 (J = 1.9 Hz)	3.60 (J = 3.0 Hz)	4.93 (J = 3.0 Hz)
4b		6.27 (J = 5.5 Hz)	6.57 (J = 1.6, 5.5 Hz)	5.29 (J = 1.6, 4.8 Hz)	4.05 (J = 3.4, 4.8 Hz)	4.88 (J = 3.4 Hz)
4c		6.35 (J = 5.6 Hz)	6.49 (J = 1.6, 5.6 Hz)	5.41 (J = 1.6, 4.8 Hz)	5.57 (J = 3.3, 4.8 Hz)	3.17 (J = 3.3 Hz)
4d		6.19 (J = 5.7 Hz)	6.69 (J = 1.8, 5.7 Hz)	5.24 (J = 1.8, 5.7 Hz)	5.15 (J = 3.1 Hz)	3.37 (J = 3.1 Hz)
6a		6.39 (J = 5.5 Hz)	6.85 (J = 2.1, 5.5 Hz)	5.20 (J = 2.1 Hz)	3.42 (J = 3.3 Hz)	5.39 (J = 3.3 Hz)
6b		6.45 (J = 5.7 Hz)	6.74 (J = 1.8, 5.7 Hz)	5.27 (J = 1.8, 5.0 Hz)	4.17 (J = 3.3, 5.0 Hz)	5.02 (J = 3.3 Hz)

Note: Spectra were recorded in $CDCl_3$ at 250 MHz.

Table 8. ^{1}H NMR data for the Michael adducts (ppm).

Adduct	H2	H3	H5	H6
5a	5.92 (J = 3.1 Hz)	6.15 (J = 3.1 Hz)	4.54 (J = 5.2, 9.3 Hz)	4.69 (J = 5.2, 14.5 Hz), 5.06 (J = 9.3, 14.5 Hz)
7a	5.09 (J = 3.3 Hz)	6.18 (J = 3.3 Hz)	4.47 (J = 5.0, 9.0 Hz)	4.65 (J = 5.0, 14.5 Hz), 5.03 (J = 9.0, 14.5 Hz)
7b	5.11 (J = 3.3 Hz)	6.23 (J = 3.3 Hz)	6.69 (J = 7.4 Hz)	4.83 (J = 7.4 Hz)

Note: Spectra were recorded in $CDCl_3$ at 250 MHz.

© 2006 NRC Canada

***3a**: Methyl 5*-endo-*nitro-7-oxabicyclo[2.2.1]hept-2-ene-6*-exo-*carboxylate (ref. 42)*

Yield: 34 mg (21%); mp 66.0–67.0 °C. ^{1}H NMR ($CDCl_3$) δ: 3.25 (1H, d, *J* = 2.9 Hz), 3.28 (3H, s), 5.35 (1H, d, *J* = 1.4 Hz), 5.47 (1H, dd, *J* = 1.7, 4.8 Hz), 5.54 (1H, dd, *J* = 2.9, 4.8 Hz), 6.39 (1H, dd, *J* = 1.4, 5.8 Hz), 6.73 (1H, dd, *J* = 1.7, 5.8 Hz). ^{13}C NMR ($CDCl_3$, ppm) δ: 48.9, 53.0, 75.7, 83.2, 84.4, 133.7, 138.9, 170.2.

Separation of the products of the reaction of 2-methylfuran (1b) and methyl 3-nitroacrylate (2)

A chloroform solution (5 mL) of **1b** (341 mg, 4.2 mmol) and **2** (357 mg, 2.7 mmol) was allowed to stand at room temperature for 5 days. The isomers were separated by HPLC (benzene–acetone, 50:1).

***4a**: Methyl 6*-endo-*nitro-7-oxabicyclo[2.2.1]hept-2-ene-1-methyl-5*-exo-*carboxylate*

Yield: 40 mg (7%); yellow oil. IR (cm^{-1}): 2960, 1740, 1554, 1440, 1374. ^{1}H NMR ($CDCl_3$) δ: 1.85 (3H, s), 3.60 (1H, d, *J* = 3.0 Hz), 3.73 (3H, s), 4.93 (1H, d, *J* = 3.0 Hz), 5.42 (1H, d, *J* = 1.9 Hz), 6.35 (1H, *J* = 5.8 Hz), 6.49 (1H, dd, *J* = 1.9, 5.8 Hz). ^{13}C NMR ($CDCl_3$, ppm) δ: 17.7, 52.6, 54.2, 83.1, 88.4, 89.4, 134.4, 141.2, 170.0. MS *m*/*z*: 213 (M^+), 167 ($M^+ - NO_2$), 135 ($M^+ - (NO_2 + CH_3OH)$).

***5a**: Methyl 2-[2-(5-methylfuranyl)]-3-nitropropylcarboxylate*

Yield: 68 mg (12%); yellow oil. IR (cm^{-1}): 1744, 1560, 1440, 1380, 1246, 1206. ^{1}H NMR ($CDCl_3$) δ: 2.25 (3H, s), 3.77 (3H, s), 4.54 (1H, dd, *J* = 5.2, 9.3 Hz), 4.69 (1H, dd, *J* = 5.2, 14.5 Hz), 5.06 (1H, dd, *J* = 9.3, 14.5 Hz), 5.92 (1H, d, *J* = 3.1 Hz), 6.15 (1H, d, *J* = 3.1 Hz). ^{13}C NMR ($CDCl_3$, ppm) δ: 13.5, 42.8, 53.1, 73.6, 106.8, 109.7, 144.1, 153.1, 169.1. MS *m*/*z*: 213 (M^+), 166 ($M^+ - NO_2 - H$), 108, 97.

Separation of the products of the reaction of 2-methoxylfuran (1c) and methyl 3-nitroacrylate (2)

A benzene solution (2 mL) of **1c** (17 mg, 1.7 mmol) and **2** (2.93 mg, 2.0 mmol) was allowed to stand at room temperature for 30 min. The product was separated by column chromatography (hexane – dimethyl ether, 1:1).

***7a**: Methoxy 2-[2-(5-methylfuranyl)]-3-nitropropyl carboxylate*

Yield: 282 mg (72%); yellow oil IR (cm^{-1}): 3436, 1726, 1310, 1208, 940, 740. ^{1}H NMR ($CDCl_3$) δ: 3.77 (3H, s), 3.83 (3H, s), 4.47 (1H, dd, *J* = 5.0, 9.0 Hz), 4.65 (1H, dd, *J* = 5.0, 14.5 Hz), 5.03 (1H, dd, *J* = 9.0, 14.0 Hz), 5.09 (1H, d, *J* = 3.3 Hz), 6.18 (1H, d, *J* = 3.3 Hz). ^{13}C NMR ($CDCl_3$, ppm) δ: 42.7, 53.0, 57.8, 73.5, 80.5, 110.5, 135.8, 161.8, 168.8. MS *m*/*z*: 229 (M^+), 182, 167, 124, 113.

References

1. (*a*) O.C. Kappe, S. Murphree, and A. Padwa. Tetrahedron, **53**, 4179 (1997); (*b*) R.L. Ellias, N.H. Niklson, F.E. Peaker, A.K. Table, C.M. Richardson, J.W. Tyler, J. White, M. Person, D.S. Eggleston, and R.C. Haltiwangor. J. Org. Chem. **62**, 4998 (1997); (*c*) M. Lautens, S. Ma, and P. Chi. J. Am. Chem. Soc. **119**, 6478 (1997); (*d*) W.M. Horspool, J.M. Tedder, and Z.U. Din. J. Chem. Soc. C, 1694 (1969).
2. J.M. Fraile, J.I. Garcia, M.A. Gomez, A. de la Hoz, J.A. Mayoral, A. Moreno, P. Prieto, L. Salvatella, and E. Vazquez. Eur. J. Org. Chem. 2891 (2001), and refs. cited therein.
3. H. Katsuki, K. Asano, and H. Ohnishi. Bull. Chem. Soc. Jpn. **57**, 3339 (1984).
4. P. Vogel, D. Fattori, F. Gasparini, and C.L. Drian. Synlett, 173 (1990).
5. (*a*) Y.H. Lai, Y.L. Yong, and S.W. Wong. J. Org. Chem. **62**, 4500 (1997); (*b*) A. Toyota, M. Uchiyama, and C.H. Kanako. Tetrahedron, **53**, 6327 (1997).
6. A. Sera, K. Itoh, and H. Yamada. Tetrahedron Lett. **31**, 6547 (1990).
7. K. Itoh, K. Kitoh, and A. Sera. Heterocycles, **51**, 243 (1999).
8. K.H. Houk, J. Gonzalez, and Y. Li. Acc. Chem. Res. **28**, 81 (1995).
9. (*a*) L.R. Domingo, M.T. Picher, J. Andres, V. Moliner, and V.S. Safont. Tetrahedron, **52**, 10093 (1996); (*b*) L.R. Domingo, M.T. Picher, J. Andres, and V.S. Safont. J. Org. Chem. **62**, 1775 (1997); (*c*) B.R. Beno, S. Wilsey, and K.N. Houk. J. Am. Chem. Soc. **121**, 4816 (1999).
10. (*a*) L.R. Domingo, M.T. Picher, and M.L. Aurell. J. Am. Chem. Soc. **122**, 390 (2000); L.R. Domingo, M.T. Picher, and M.L. Aurell. J. Phys. Chem. A, **103**, 11425 (1999); (*b*) M. Nendel, L.M. Tolbert, L.E. Herring, M.N. Islam, and K.N. Houk. J. Org. Chem. **64**, 976 (1999).
11. M. Avalos, R. Babiano, J.L. Bravo, P. Cintas, J.L. Jimenez, J.C. Palacios, and M.A. Silvia. J. Org. Chem. **65**, 6613 (2000).
12. B.J. Doppmeier, A.J. Driessen, T.S. Hehre, W.J. Hehre, J.A. Johnson, P.E. Khunzinger, J.M. Leonard, I.N. Pham, W.J. Pietro, and J. Yu. Spartan 2002. Version 1.5a [computer program]. Wavefunction, Inc., Irvine, Calif. 2002; B.J. Doppmeier, A.J. Driessen, T.S. Hehre, W.J. Hehre, J.A. Johnson, P.E. Khunzinger, J.M. Leonard, I.N. Pham, W.J. Pietro, and J. Yu. Spartan 2004. Version 1.0.0 [computer program]. Wavefunction, Inc., Irvine, Calif. 2004.
13. (*a*) C. Lee, W. Yang, and R.G. Parr. Phys. Rev. B, **37**, 785 (1988); (*b*) A.D. Becke. J. Chem. Phys. **98**, 5648 (1993).
14. C.C. Chambers, G.D. Hawkins, C.J. Cramer, and D.G. Truhlar. J. Phys. Chem. **100**, 16385 (1996).
15. J. Kong, C.A. White, A.I. Krylov, C.D. Sherrill, R.D. Adamson, T.R. Furlan, M.S. Lee, A.M. Lee, S.R. Gwaltuev, T.R. Adams, C. Ochsenfeld, A.T.B. Gilbert, G.S. Kedziord, V.A. Rasolov, D.R. Mourice, N. Nair, V. Shan, N.A. Besley, P.E. Maslen, J.P. Dombroski, H. Dachsef, W.M. Zhang, P.P. Korambath, J. Baber, E.F.C. Byrd, J. Van Voorhis, M. Oumi, S. Hirata, C.P. Hsu, N. Ishikawa, J. Florian, A. Warshed, B.G. Johnson, P.M.W. Gill, M. Head-Gerdon, and J.A. Pople. J. Comput. Chem. **21**, 1532 (2000).
16. (*a*) L. Onsager. J. Am. Chem. Soc. **58**, 1486 (1936); (*b*) J.B. Foresman, T.A. Keeth, K.B. Wiborg, J. Snoonian, and M.J. Frisch. J. Phys. Chem. **100**, 16098 (1996); (*c*) M.W. Wong, M.J. Frish, and K.B. Wiberg. J. Am. Chem. Soc. **112**, 4776 (1990).
17. T.M. Balthazor, B. Gaede, D.E. Korte, and H. Shieh. J. Org. Chem. **49**, 4547 (1984).
18. V. Branchadell, J. Orti, R.M. Ortuno, A. Oliva, J. Font, J. Bertran, and J.J. Danneberg. J. Org. Chem. **56**, 2190 (1991)
19. M. Koermerand and B. Rickborn. J. Org. Chem. **55**, 2662 (1990).
20. T. Tsuji, H. Takeuchi, and S. Konaka. J. Mol. Struct. **457**, 55 (1999).
21. M. Avalos, R. Babiana, F.R. Chemente, P. Cintas, R. Gordilla, J.I. Jimenez, and J.C. Palacios. J. Org. Chem. **65**, 8251 (2000).
22. R. Sustman, W. Müller, S. Mignani, R. Merenyi, Z. Janousck, and H.G. Vieke. New J. Chem. **13**, 557 (1989).
23. I. Fleming. Frontier orbitals and organic reactions. John Wiley and Sons, Chichester, UK. 1976.

© 2006 NRC Canada

24. K.N. Houk. Acc. Chem. Res. **8**, 361 (1975).
25. (*a*) M.A. Fox, R. Cardona, and N.J. Kiwiet. J. Org. Chem. **52**, 1469 (1987); (*b*) M. Avalos, R. Babiano, J.L. Bravo, P. Cintas, J.L. Jimenez, J.C. Palacios, and M.A. Silva. Chem. Eur. J. **6**, 267 (2000); (*c*) A. Arrieta, B. Lacea, and F.P. Cossio. J. Org. Chem. **66**, 6178 (2001).
26. S. Calvo-Losada and D. Suarez. J. Am.Chem. Soc. **122**, 390 (2000).
27. M.J. Dewar and A.B. Pierini. J. Am. Chem. Soc. **106**, 203 (1984).
28. O. Diels and K. Alder. Justus Liebigs Ann. Chem. **98**, 460 (1928).
29. L.R. Domingo, M. Arno, and J. Andres. J. Org. Chem. **64**, 5867 (1999).
30. (*a*) R. Sustman, W. Sicking, H. Lamy-Schelkens, and L. Ghosez. Tetrahedron Lett. **32**, 1401 (1991); R. Sustman, W. Sicking, H. Lamy-Schelkens, and L. Ghosez. Tetrahedron, **48**, 10293 (1992); (*b*) U. Pindur, G. Lutz, and C. Otto. Chem. Rev. **93**, 741 (1993); (*c*) C.-J. Li. Chem. Rev. **93**, 2023 (1993).
31. K.N. Houk, Y. Li, and J.D. Evanseck. Angew. Chem. Int. Ed. Engl. **31**, 682 (1992).
32. (*a*) A.E. Reed, R.B. Weinstock, and F. Weinhold. J. Chem. Phys. **83**, 735 (1985); (*b*) A.E. Reed, L.A. Curtiss, and F. Wenhold. Chem. Rev. **88**, 899 (1988); (*c*) E.D. Glendening, A.E. Reed, J.E. Carenter, and F. Weinhold. NBO. Version 4.0 [computer program]. Theoretical Chemistry Institute, University of Wisconsin, Madison, Wisconsin. 1996.
33. (*a*) G.M.J. Schmidt. Pure Appl. Chem. **27**, 647 (1971); (*b*) G.M.J. Schmidt. J. Chem. Soc. 2000 (1964); J. Chem. Soc. 2014 (1964).
34. J.W. Patterson and J.E. McMurry. J. Chem. Soc. Chem. Commun. 488 (1971).
35. F. Fringuelli and A. Taticchi. The Diels–Alder reaction, selected practical methods. John Wiley and Sons, Ltd., West Surrex, UK. 2002.
36. (*a*) H. Katsuki, H. Nishizawa, M. Ochi, and K. Matsuoka. Bull. Chem. Soc. Jpn. **55**, 496 (1982); (*b*) J. Rimmelim, G. Jenner, and P. Rimmelim. Bull. Soc. Chim. Fr. 461 (1978).
37. T.M. Balthazor, B. Gaede, D.E. Korte, and S. Shieh. J. Org. Chem. **49**, 4547 (1984).
38. G. Just, A. Martel, K. Grozinger, and M. Ramjeesingh. Can. J. Chem. **53**, 131 (1975).
39. (*a*) E. Goldstein, B. Beno, and K.N. Houk. J. Am. Chem. Soc. **118**, 6036 (1996); (*b*) L.R. Domingo and M.J. Aurell. J. Org. Chem. **67**, 959 (2002).
40. C.C. Chambers, G.D. Hawkins, C.J. Cramer, and D.G. Truhlet. J. Phys. Chem. **100**, 16385 (1996).
41. M.M. Campbell, A.D. Kaye, and M. Sainsbury. Tetrahedron, **38**, 2783 (1982).
42. J.E. McMurray, J.H. Musser, I. Fleming, J. Fortunak, and C. Nubling. Org. Synth. Coll. **6**, 799 (1988).

© 2006 NRC Canada

The effect of pressure and heating rate on the melting behavior of indium and tin

David E.G. Jones, Ruiping Wang, and Anne-Marie Turcotte

Abstract: The dependence of the phase transition behavior of indium and tin on pressure and heating rate has been investigated using heat flow calorimetry (HFC). The work has shown a significant influence of heating rate on the form of the melting curve, onset temperature for both indium and tin, as well as the enthalpy of fusion for indium. Based on the result for the dependence of onset temperature on pressure, the volume changes on fusion have been estimated using the Clausius–Clapeyron equation and compared with literature results.

Key words: indium, tin, high pressure, heat flow calorimetry calibration, fusion temperature, enthalpy of fusion.

Résumé : Faisant appel à la calorimétrie avec écoulement de chaleur (CEC), on a étudié la relation entre le comportement de la phase de transition de l'indium et de l'étain et la pression et la vitesse de chauffage. Ce travail a permis de montrer qu'il existe la vitesse de chauffage influence fortement la forme de la courbe de fusion, la température de mise en route tant pour l'indium que pour l'étain ainsi que l'enthalpie de fusion de l'indium. Sur la base des résultats relatifs à l'influence de la pression sur la température de mise en route, on a évalué les changements de volume lors de la fusion en faisant appel à l'équation de Clausius–Clapeyron et on les a comparés aux valeurs trouvées dans la littérature.

Mots clés : indium, étain, pression élevée, calibration de la calorimétrie à écoulement de chaleur, température de fusion, enthalpie de fusion.

[Traduit par la Rédaction]

Introduction

High-pressure thermal analysis has drawn increasing attention in order to better understand the influence of the pressure on the phase transitions and thermal decomposition of solid materials (1–3). Consequently, the pressure dependent properties of standard reference materials (SRMs) used for the calibration of temperature and heat flow are required to calibrate the thermal instruments used in these high-pressure studies. The phase transition behavior of indium and tin, the most commonly used SRMs, has been investigated by means of differential thermal analysis (DTA) (4–6), differential scanning calorimetry (DSC) (7), and X-ray diffraction techniques (8) under pressure. McDaniel et al. (9) developed a technique with a free piston pump to determine the melting curves for indium at pressures up to 10 GPa and for tin up to 0.5 GPa. In 1980, the melting curve of tin was redetermined by DTA with Chromel–Alumel thermocouples in an attempt to minimize the uncertainties of the data reported previously (4). Höhne et al. (7) have studied the pressure dependence of the fusion temperature and the volume change on fusion for indium using DSC with a high-pressure piston-cylinder-type dilatometer. However, due to the difficulties of accurately measuring melting curves under simultaneous application of both high temperature and high pressure, the available data on the changes of fusion temperature and enthalpy of fusion for the calibration substances, including indium and tin under pressure, are still limited, and furthermore, the results do not agree very well. Particularly, to our knowledge, no work on the phase-transition behavior of indium and tin using the heat flow calorimetry (HFC) technique at high pressure has been reported.

In our laboratory, HFC was used in a modified system to study the thermal properties of energetic materials at various pressures up to 69 MPa (10). Indium and tin were selected to calibrate the instrument. This paper describes the effects of pressure and heating rates on the form of the fusion curve, the fusion temperature (T_o), the enthalpy of fusion ($\Delta_{fus}H$), and the volume change (ΔV) on fusion of indium and tin measured using HFC.

Received 16 May 2005. Published on the NRC Research Press Web site at http://canjchem.nrc.ca on 30 March 2006.

D.E.G. Jones,[1] R. Wang, and A.-M. Turcotte. Canadian Explosives Research Laboratory, Natural Resources Canada, 555 Booth St., Ottawa, ON K1A 0G1, Canada.

[1]Corresponding author (e-mail: djones@nrcan.gc.ca).

Experimental section

Synthetic sapphire (~100% α-Al_2O_3), biphenyl (99.984%), indium (99.9999%), and tin (99.999%) were purchased from the National Institute of Standards and Technology (NIST, Gaithersburg, Maryland).

A Setaram C-80 heat-flux calorimeter was used to study the thermal properties of energetic materials at pressures up to 69 MPa. Currently, argon at high pressure (~40 MPa) is being used as a pressure source. Baseline experiments with empty vessels at 0.3 K min^{-1} and 0.17 and 33.2 MPa argon showed no significant influence of pressure on the baseline drift, which is on average approximately 4 mW over the temperature range from 370 to 570 K. At β = 1.0 K min^{-1},

 doi:10.1139/V05-256 © 2006 NRC Canada

Fig. 1. Heat flow of indium and tin at β = 0.1, 0.3, and 1.0 K min^{-1} and p = 0.2 MPa.

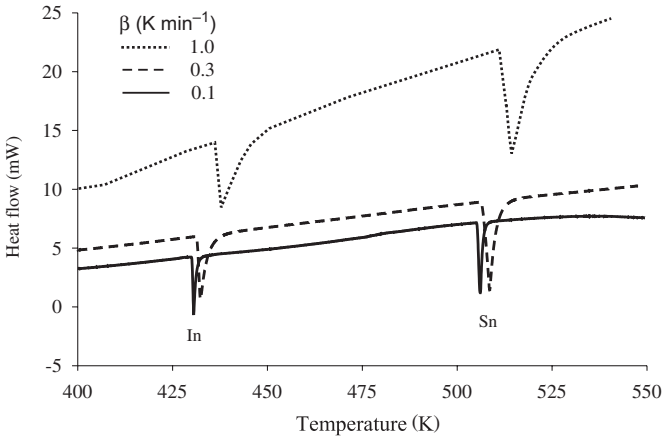
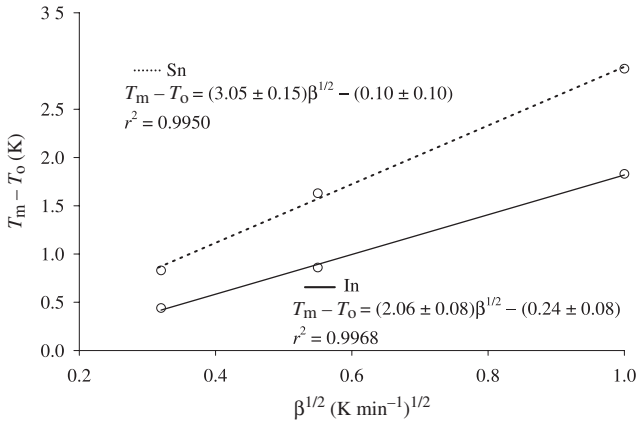


Fig. 2. Dependence of ($T_m - T_o$) of indium and tin on $\beta^{1/2}$ at p = 0.2 MPa.



where thermal lag is higher, the difference in heat capacity between the sample and reference cells is exacerbated, resulting in a slightly larger baseline drift.

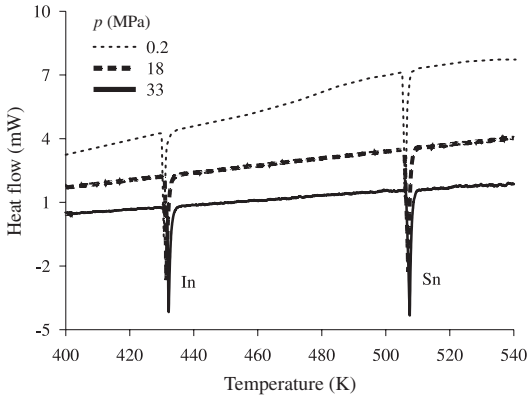
The verification experiments using biphenyl, indium, and tin at 0.3 K min^{-1} and 0.17 MPa argon demonstrated that T_o and $\Delta_{fus}H$ for biphenyl (341.38 K and 119.93 J g^{-1}) are comparable with the literature values[2] of 342.45 K and 120.41 J g^{-1} at β = 2.5 K min^{-1}; those for indium (429.9 K and 29.0 J g^{-1}) are in good agreement with the literature values[3] of 429.8 K and 28.7 J g^{-1}; those for tin (505.0 K and 60.1 J g^{-1}) agree well with the literature values[4] of 505.11 K and 60.20 J g^{-1}. A more detailed description of this Calvet type microcalorimeter fitted with a high-pressure manifold and vessels was reported elsewhere (10).

The experiments were performed as follows: 94.9 mg of indium was placed in an alumina liner, 71.8 mg of alumina powder was placed on top of the indium, and 71.1 mg of tin was placed on top of the alumina. An equivalent mass of alumina powder was contained in another liner and put into the reference cavity of the calorimeter. In this way, both SRM materials could be analyzed in one experiment. These materials were run at heating rates of β = 0.1, 0.3, and 1 K min^{-1} and various pressures up to about 33 MPa.

Results and discussion

Indium and tin partitioned by alumina were heated from 301 to 553 K at the desired heating rate and pressure of argon. Figure 1 shows an overlay graph of representative experiments at pressure p = 0.2 MPa and heating rates of β = 0.1, 0.3, and 1.0 K min^{-1}. It is noted that the fusion curves for both indium and tin become broader with an increase in the heating rate, which is in agreement with an observation by Van Miltenburg and Cuevas-Diarte (11), who have also reported that the width ($T_m - T_o$) of melting peaks of indium in DSC and DTA, where T_m is the temperature at minimum heat flow, depends on β by a square-root relation at β < 5 K min^{-1}. The HFC results also show that the width ($T_m - T_o$) of melting curves for both indium and tin varies linearly as a function of $\beta^{1/2}$ for β from 0.1 to 1.0 K min^{-1} and at pressures (p) up to 33 MPa. Figure 2 represents the linear dependence of the width ($T_m - T_o$) of melting curves on $\beta^{1/2}$ for indium and tin at p = 0.2 MPa measured using HFC. However, no significant effect of pressure on the width of peaks was observed within the employed pressure range (Fig. 3). The influence of β on the baseline drift was also observed, probably owing to the slight difference in the thermal environment of the reference and sample vessels in the calorimeter. The increase in baseline shift with β may be a result of the delay in equilibration between the sample and reference cells.

Fig. 3. Heat flow of indium and tin at p = 0.2, 18, and 33 MPa and β = 0.1 K min^{-1}.



Indium

The values of the onset temperatures (T_o), the minimum heat flow temperatures (T_m), and the enthalpies of fusion ($\Delta_{fus}H$) for the phase transition of indium at three heating rates and five pressures are summarized in Table 1. From these data, it was noted that there is no apparent effect of pressure on the fusion heat of indium within the employed pressure range at a fixed heating rate (Fig. 4), which is in ac-

[2] National Institute of Standards and Technology, Certificate of Analysis, SRM 2222.
[3] National Institute of Standards and Technology, Certificate of Analysis, SRM 2232.
[4] National Institute of Standards and Technology, Certificate of Analysis, SRM 2220.

© 2006 NRC Canada

Table 1. The onset temperature (T_o), the minimum heat flow temperatures (T_m), and the enthalpy of fusion ($\Delta_{fus}H$) for indium at various heating rates (β) and pressures (p).

β (K min^{-1})	p (MPa) at T_o	T_o (K) observed	T_o (K) from eq. [1]	T_m (K)	$\Delta_{fus}H$ (J g^{-1})
0.1	0.17	430.14		430.58	27.58
	11.13	430.70	430.69±0.01	431.16	26.65
	18.26	431.03	431.04±0.01	431.46	27.05
	25.45	431.37	431.39±0.02	431.80	27.41
	32.86	432.74	431.76±0.03	432.19	26.72
0.3	0.17	431.51		432.38	26.67
	10.97	432.05	432.05±0.01	432.85	26.42
	18.21	432.40	432.41±0.01	433.19	26.38
	25.49	432.73	432.76±0.02	434.52	26.49
	32.95	433.08	433.13±0.03	433.86	27.13
1.0	0.17	436.17		437.00	25.00
	10.85	436.64	436.70±0.01	438.35	24.57
	17.99	436.97	437.06±0.01	438.66	24.65
	25.42	437.31	437.42±0.02	438.99	24.67
	32.37	437.64	437.76±0.03	439.27	24.89

Fig. 4. Dependence of $\Delta_{fus}H$ on p for indium at β of 0.1, 0.3, and 1.0 K min^{-1}.

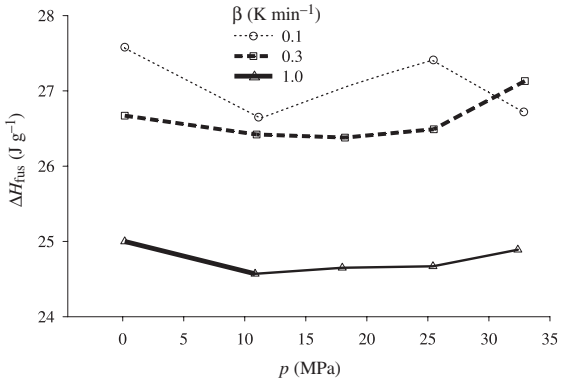
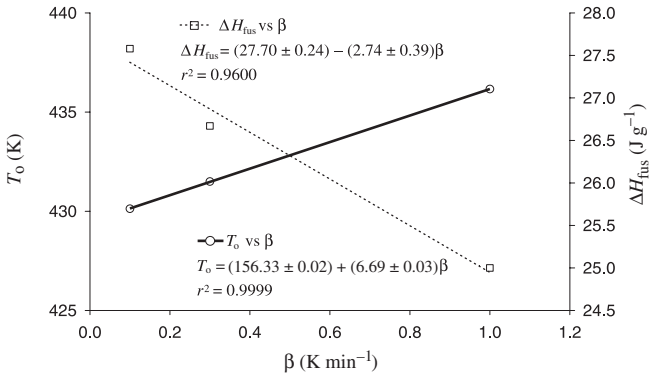


Fig. 5. Effect of β on T_o and $\Delta_{fus}H$ of phase transition for indium at p = 0.2 MPa.



cordance with the literature results obtained from high-pressure DSC measurements (7). However, the fusion enthalpies decrease with the heating rate at a constant pressure. Figure 5 demonstrates the decrease of enthalpy ($\Delta_{fus}H$) and the increase of onset temperature (T_o) measured at p = 0.2 MPa as a function of heating rate. Similar behavior is observed at other pressures up to 33 MPa.

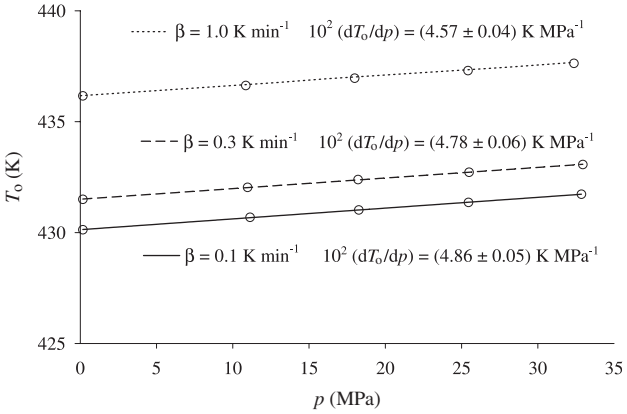
Figure 6 shows the linear increase of T_o with the increase in pressure (p) at heating rates of β = 0.1, 0.3, and 1 K min^{-1}, respectively. For all values of β, the dependence of the fusion temperature of indium on pressure agrees with the results measured by a high-pressure dilatometer at a heating rate of 5 K h^{-1}. This is illustrated in Table 1 by comparison of our observed results from HFC and those calculated from regression eq. [1] reported in the literature (7).

$$[1] \qquad T_f = T_o + (0.04929 \pm 0.0008)p - (3.9 \pm 2) \times 10^{-6}p^2$$

where p is the pressure in MPa and T_o is the onset temperature of indium measured by HFC at 0.17 MPa.

Based on the slope (dT_o/dp) of the plot of T_o vs. pressure (at T_o) and atmospheric-pressure fusion enthalpies, the fusion volume change was estimated at different heating rates

Fig. 6. Effect of p and β on onset temperature of phase transition of indium.



via the Clausius–Clapeyron equation and included in Table 2. These values are compatible with the values of 0.389 (p = 0.1 MPa) and 0.394 cm^3 mol^{-1} (p = 50 MPa) obtained in a high-pressure dilatometer (7). The value of V at

© 2006 NRC Canada

Table 2. Volume change (ΔV) for the phase transition of indium.

	ΔV (cm^3 mol^{-1})		
β (K min^{-1})	This work	Literature[a]	
0.0	0.36±0.04	0.389 (p = 0.1 MPa)	0.394 (p = 50 MPa)
0.1	0.358±0.004		
0.3	0.339±0.004		
1.0	0.301±0.003		

[a]Reference 4.

Table 3. The onset temperature (T_o), the minimum heat flow temperatures (T_m), and the enthalpy of fusion ($\Delta_{fus}H$) for tin at various heating rates (β) and pressures (p).

β (K min^{-1})	p (MPa) at T_o	T_o (K)	T_m (K)	$\Delta_{fus}H$ (J g^{-1})
0.1	0.18	505.28	506.11	55.56
	11.33	505.81	506.85	56.22
	18.59	506.04	507.05	55.19
	25.93	506.22	507.21	55.54
	33.41	506.47	507.49	55.16
0.3	0.18	506.91	508.54	54.90
	11.19	507.25	508.93	56.62
	18.65	507.50	509.10	56.31
	26.07	507.63	509.17	55.43
	33.88	507.91	509.52	56.90
1.0	0.18	511.55	514.47	54.11
	11.08	511.86	514.74	55.47
	18.42	512.02	514.90	55.35
	26.09	512.28	514.88	54.16
	33.29	512.47	515.28	54.27

β = 0.0 K min^{-1} was obtained by extrapolating the curve of ΔV vs. β to β = 0.0 K min^{-1}; the uncertainty in this value was determined by extrapolating the 95% confidence interval to β = 0.0 K min^{-1}. For β > 0.0 K min^{-1}, the uncertainties were calculated from the standard deviation of the fits.

Tin

Table 3 summarizes the onset temperatures (T_o), the temperatures of minimum heat flow (T_m), and the enthalpies of fusion ($\Delta_{fus}H$) for the phase change of tin at various heating rates and pressures measured along with indium by HFC. Figures 1 and 2 also show that the width of the fusion curve of tin varies as a function of the square root of heating rate at p = 0.2 MPa, and Fig. 3 demonstrates that no substantial influence of pressure on the width of the fusion curve of tin at p = 0.2 MPa was observed. Moreover, it is noted that there is no significant dependence of fusion enthalpy on pressure, as was also observed for indium (Fig. 4). However, the enthalpies of fusion for tin at specific pressures have not shown an obvious decrease with heating rate, which was observed for indium (Fig. 5). Similar to the observation for indium, T_o and T_m for the phase transition of tin increase with pressure at constant heating rate, and increase with heating rate at constant pressure. Zhou et al. (6) have also reported that the melting point of tin increases with increasing pressure. Figure 7 shows the dependence of T_o on β at p = 0.2 MPa; the derived equation of onset temperature as a function of heating rate has been included in this figure. Similar equations at other pressures have been regressed and are listed in Table 4.

Fig. 7. Dependence of T_o on β for tin at p = 0.2 MPa.

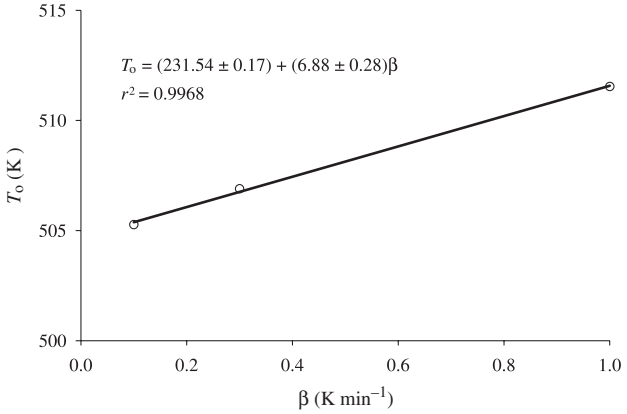


Table 4. Equations of T_o for tin as a function of β at various pressures (p).

p (MPa)	Equation (K)	r^2
11	T_o = (505.19±0.07) + (6.69±0.11)β	0.9994
18	T_o = (505.44±0.09) + (6.60±0.15)β	0.9989
26	T_o = (505.60±0.06) + (6.59±0.10)β	0.9995
33	T_o = (505.86±0.08) + (6.63±0.12)β	0.9993

Plots of T_o vs. pressure (at T_o) at heating rates of 0.1, 0.3, and 1 K min^{-1} in Fig. 8 suggest linear dependence of T_o on pressure with positive slopes (dT_o/dp) of (0.0348 ± 0.0027), (0.0290 ± 0.0014), and (0.0266 ± 0.0017) K MPa^{-1}, respectively, which is in accordance with the result of 0.03 K MPa^{-1} reported by Kennedy and Newton (12) and 0.032 K MPa^{-1} determined by Kingon and Clark (4) using DTA with a piston-cylinder for pressures up to 3.7 MPa.

Based on the slope dT_o/dp of the plot (Fig. 8) of onset temperature vs. pressure and the enthalpy measured at ambient pressure (0.2 MPa), the volume changes have been calculated via the Clausius–Clapeyron relation. These volume changes in Table 5 obtained in this work were compared with the value of 0.46 cm^3 mol^{-1} predicted by Kingon and Clark (4) via the Clausius–Clapeyron equation using the determined slope of 32 K GPa^{-1} for heating rates in the range of 30 to 54 K min^{-1} and the atmospheric-pressure enthalpy (60.80 J g^{-1}) of melting cited in ref. 4. The literature result for ΔV in Table 5 does not agree with the values obtained here, and in particular, it should be noted that the result reported by Kingon and Clark (4) shows an opposite trend

© 2006 NRC Canada

Fig. 8. Effect of p and β on onset temperature of the phase transition of tin.

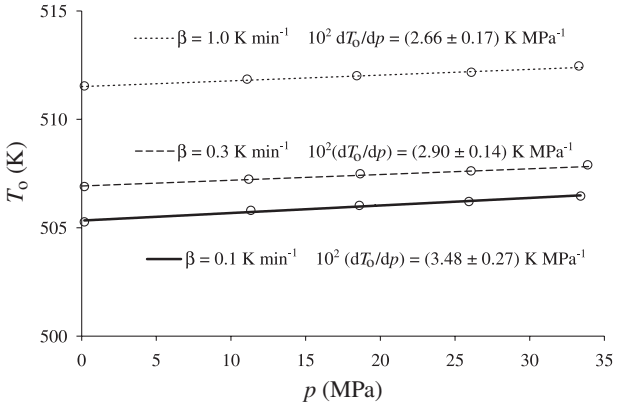


Table 5. Volume change (ΔV) for the phase transition of tin.

β (K min^{-1})	ΔV (cm^3 mol^{-1})	10^2 dT/dp (K MPa^{-1})
0.1	0.45±0.04	3.48±0.27
0.3	0.37±0.02	2.90±0.14
1.0	0.33±0.02	2.66±0.17
30–54[a]	0.46	3.2

[a]Reference 4.

with heating rate than expected on the basis of our HFC results. ΔV (β = 0.0 K min^{-1}) is not meaningful because of the scatter in the ΔV vs. β plot and thus has not been included in Table 5.

Conclusions

The observed melting curves for both indium and tin are broader at high heating rates than those at low heating rates, but the breadth of the thermal curves is independent of pressure within the studied pressure range of 0.2 to 33 MPa. A low heating rate favors generating sharper fusion curves and fusion temperatures closer to the International Practical Temperature Scale value at ambient temperature and less baseline drift in the HFC measurements. The onset temperatures for indium and tin increase with increasing heating rate, while the enthalpy of fusion of indium decreases, and there is no obvious change for tin. At a specific heating rate, no dependence of the enthalpy of fusion on pressure was observed, while the dependence of onset temperature on pressure shows a linear increase. The slope dT_o/dp of the onset temperature vs. pressure curve decreases with increasing heating rate. Based on the values of dT_o/dp and the enthalpy of fusion measured at ambient pressure, the volume changes on melting have been estimated via the Clausius–Clapeyron equation and the volume changes are in agreement with the literature results for indium but are not in agreement with those for tin. The results of this study may help us to calibrate HFC measurements more precisely when conducting thermal decomposition studies at elevated pressures.

References

1. Y. Sawada, H. Henmi, N. Mizutani, and M. Kato. Thermochim. Acta, **121**, 21 (1987).
2. C. Schmidt, M. Rittmerier-Kettner, H. Becker, J. Ellert, R. Krombach, and G.M. Schneider. Thermochim. Acta, **238**, 321 (1994).
3. G.J. Piermarini, S. Block, and P.J. Miller. *In* Proceedings of the 19th International Conference of ICT on Combustion and Detonation Phenomena. Karlsrühe, Germany. 29 June – 1 July 1988. Fraunhofer Institut Chemische Technologie, Karlsrühe, Germany. 1988. pp. 15-1 – 15-11.
4. A.I. Kingon and J.B. Clark. High Temp. — High Pressures, **12**, 75 (1980).
5. B. Turner. High Temp. — High Pressures, **5**, 273 (1973).
6. W. Zhou, Z. Shen, X. Yin, Y. Zhang, and M. Zhao. J. Less Common Met. **143**, 59 (1988).
7. G.W.H. Höhne, W. Dollhopf, K. Blankenhorn, and P.U. Mayr. Thermochim. Acta, **273**, 17 (1996).
8. G. Shen, N. Sata, N. Taberlet, M.L. Rivers, and S.R. Sutton. Appl. Phys. Lett. **78**, 3208 (2001).
9. M.L. McDaniel, S.E. Babb, Jr., and G.J. Scott. J. Chem. Phys. **37**, 822 (1962).
10. D.E.G. Jones, A.-M. Turcotte, and R.C. Fouchard. Thermochim. Acta, **401**, 63 (2003).
11. J.C. Van Miltenburg and M.A. Cuevas-Diarte. Thermochim. Acta, **156**, 291 (1989).
12. G.C. Kennedy and R.C. Newton (reported data by G.C. Vezzoli). Solids under Pressure. *Edited by* W. Paul and D.M. Warschauer. McGraw-Hill, New York. 1963. p. 163.

© 2006 NRC Canada

Dynamics of percolation and energetics in the clustering of water/AOT/oil microemulsions in the presence of ethanol amines

Andrew van Bommel, Andrew Glennie, Danielle Chisholm, and Rama M. Palepu

Abstract: Temperature-induced percolation in water/AOT/oil microemulsions in the presence of mono-, di-, and triethanol amines have been studied using conductometric measurements. The percolation temperature of water/AOT/oil microemulsions depends on the nature of the alkanol amine added. Mono- and di-ethanol amines hinder the percolation process, while triethanol amine promotes the process. Percolation studies were also conducted with varying $\omega = [H_2O]/[AOT]$ values and varying chain lengths of continuous oil phase (C_6–C_{10}). The results indicate that increases in both ω and the chain length of the oil decrease the percolation temperature. The microemulsion systems have been analyzed in terms of percolation temperature, scaling equation parameters, and activation energies. The energetic parameters of the clustering process have also been determined employing the phase–separation model. The influence of alkanol amines on the percolation phenomenon has been rationalized in terms of the changes in fluidity of the interfacial layer, the viscosity of the water micropool, and the attractive interactions of the microemulsion droplets. The influence of the alkanol amine additives on the stated parameters was discussed in view of the individual effects of the alcohol and amine moieties on the properties of water/AOT/oil microemulsions.

Key words: microemulsion, percolation, conductometry, alkanol amine, surfactant.

Résumé : On a étudié la percolation induite par la température de microémulsions d'eau/AOT/huile en présence de mono-, di- et tri-éthanolamines en se basant sur des mesures de conductométrie. La température de percolation des microémulsions d'eau/AOT/huile dépend de la nature de l'alcanolamine ajoutée. Les mono- et di-éthanolamines inhibent le processus de percolation alors que la triéthanolamine accélère le processus. On a aussi effectué des études de percolation en faisant varier les valeurs de $\omega = [H_2O]/[AOT]$ et en faisant varier les longueurs des chaînes de la phase huileuse continue (C_6–C_{10}). Les résultats indiquent que l'augmentation tant de la valeur de ω que de la longueur de la chaîne de la phase huileuse diminuent la température de percolation. On a analysé les systèmes de microémulsions en termes de température de percolation de paramètres de l'équation d'échelle et d'énergies d'activation. On a aussi déterminé les paramètres énergétiques du processus de formation d'agrégats à l'aide du modèle de séparation de phase. On a rationalisé l'influence des alcanolamines sur le phénomène de percolation en termes de changements dans la fluidité de la couche interfaciale, de la viscosité du microréservoir d'eau et des interactions attractives des gouttelettes de la microémulsion. On discute de l'influence des alcanolamines ajoutées sur les paramètres donnés en fonction des effets individuels des parties alcool et amine sur les propriétés des microémulsions d'eau/AOT/huile.

Mots clés : microémulsion, percolation, conductométrie, alcanolamine, agent de surface.

[Traduit par la Rédaction]

Introduction

Microemulsions are thermodynamically stable phase separations of water-in-oil (w/o) or oil-in-water (o/w) aided by a surfactant (and possibly a cosurfactant) (1, 2). They are polydisperse and isotropic, with droplet radii ranging from 5 to 100 nm (3). Many w/o microemulsions exhibit a dramatic increase in conductivity upon the increase of temperature or a volume fraction of water. This phenomenon is known as percolation (4–12), as a microemulsion undergoes an increase in conductivity, its droplets coalesce and a transfer of charge takes place. Proposed mechanisms of percolation include the hopping mechanism (in which ions hop among droplets) and the fusion–fission mechanism (in which a continuum of droplets forms where charge exchange occurs) (3).

Ion transport in w/o microemulsions is influenced by the presence of additives. The effect of additives on the percolation of microemulsions can be analyzed in terms of changes in various physicochemical parameters. For example, short-chained alcohols soften the interfacial layer, thereby increasing the ease of conduction (13), whereas compounds such as

Received 28 July 2005. Published on the NRC Research Press Web site at http://canjchem.nrc.ca on 25 March 2006.

A. van Bommel, A. Glennie, D. Chisholm, and R.M. Palepu.[1] Department of Chemistry, St. Francis Xavier University. Antigonish, NS B2G 2W5, Canada.

[1]Corresponding author (e-mail: rpalepu@stfx.ca).

 doi:10.1139/V06-011 © 2006 NRC Canada

cholesterols (13) and toluene (14) have been reported to block the transfer of ions, rigidifying the microemulsion interface. Other additives, such as electrolytes (15–18), organics (19–21), surfactants (22–24), and bile salts (25, 26), have also been studied in terms of their influence on the percolation phenomenon.

In the present study, percolation temperatures have been obtained for water/AOT/oil microemulsions in the presence of mono-, di-, and tri-ethanol amines. The presence of both amine and hydroxyl groups in alkanol amines make them versatile for industrial applications, particularly in textile, pharmaceutical, and household product industries (27, 28). Oil phase, water content, and percentage of alkanol amine additive have been varied in the present investigation. The scaling parameters, activation energies, and thermodynamics of the droplet clustering process have been determined. The results obtained have been analyzed in terms of changes in the physicochemical properties of the microemulsion, particularly the interfacial layer.

Materials

AOT (sodium bis(2-ethylhexyl) sulfosuccinate), *n*-alkanes, and alkanol amines were purchased from Sigma-Aldrich and were used as received. Solutions were prepared with triply deionized water.

Methods

Conductivity measurements (0.5% accuracy) were made on a CDM conductometer (Radiometer, Copenhagen) using a temperature-compensated cell with a constant of 0.978 cm^{-1} and a measuring frequency of 1 kHz. Microemulsions were prepared with varying amounts of water content and oil chain length (C_6–C_{10}). Conductivity measurements were taken as a function of temperature for the water/AOT/oil systems at a fixed AOT concentration of 0.5 mol/L. The solutions were held in a Haake F3 digital-temperature-controlled circulation water bath at a temperature accuracy of ±0.1 °C. The conductance of the microemulsion sample at a fixed composition was measured at increasing temperatures until a rapid rise in the conductance was observed. The conductivity measurements were made after careful equilibration of the system at each temperature. Similar sets of measurements were taken on samples with different compositions.

Results and discussion

Percolation courses and the threshold temperature of clustering

The amount of water content in the microemulsion can be stated as the molar ratio of water to AOT surfactant, given as:

$$[1] \qquad \omega = \frac{[H_2O]}{[AOT]}$$

The percolation courses upon varying the oil and ω values are given in Fig. 1. Percolation courses in the absence of additive and in the presence of mono-, di-, and tri-ethanol amine additive, as well as courses with varying amounts of additive, are shown in Fig. 2. For the determination of the threshold percolation temperature (θ_t), the sigmoidal Boltzmann equation (SBE) was employed (29):

$$[2] \qquad \ln\sigma = \frac{\ln\sigma_i - \ln\sigma_f}{[1 + \exp(\theta - \theta_t)/d\theta]} + \ln\sigma_f$$

where σ and θ represent conductance and temperature, and the subscripts i, f, and *t* represent the initial, final, and percolation stages, respectively. The value of dθ controls the rise or decay of the profile from $\ln\sigma_i$ to $\ln\sigma_f$.

The θ_t values of the studied microemulsions, which vary in terms of oil, additive, and ω value, are reported in Table 1. Table 1 illustrates that for all solvents, the increase in the ω value is associated with a decrease in the percolation temperature. This trend is in agreement with the trends reported in the literature (11), where greater water content is associated with larger microemulsions and greater attractive interactions among microemulsion droplets, thus forming a continuum structure at a lower thermal requirement.

Also, the increase in the chain length of the apolar solvent results in a decrease in the percolation temperature. This has been attributed to the greater droplet interaction with increasing microemulsion size, as well as an increased fluidity of the microemulsion interface (11).

Adding mono- and di-ethanol amines produces an increase in the percolation temperature. Replacing the additive with triethanol amine, however, resulted in a decrease in this threshold temperature. This can be resolved by viewing the nature of both the amine and alkanol functionality of the additives.

Garcia-Rio et al. (30) found that the addition of *n*-alkyl amines to a water/AOT/isooctane microemulsion system resulted in an increase in the percolation temperature, with the threshold percolation temperature increasing with increasing chain length of the *n*-alkyl amine.

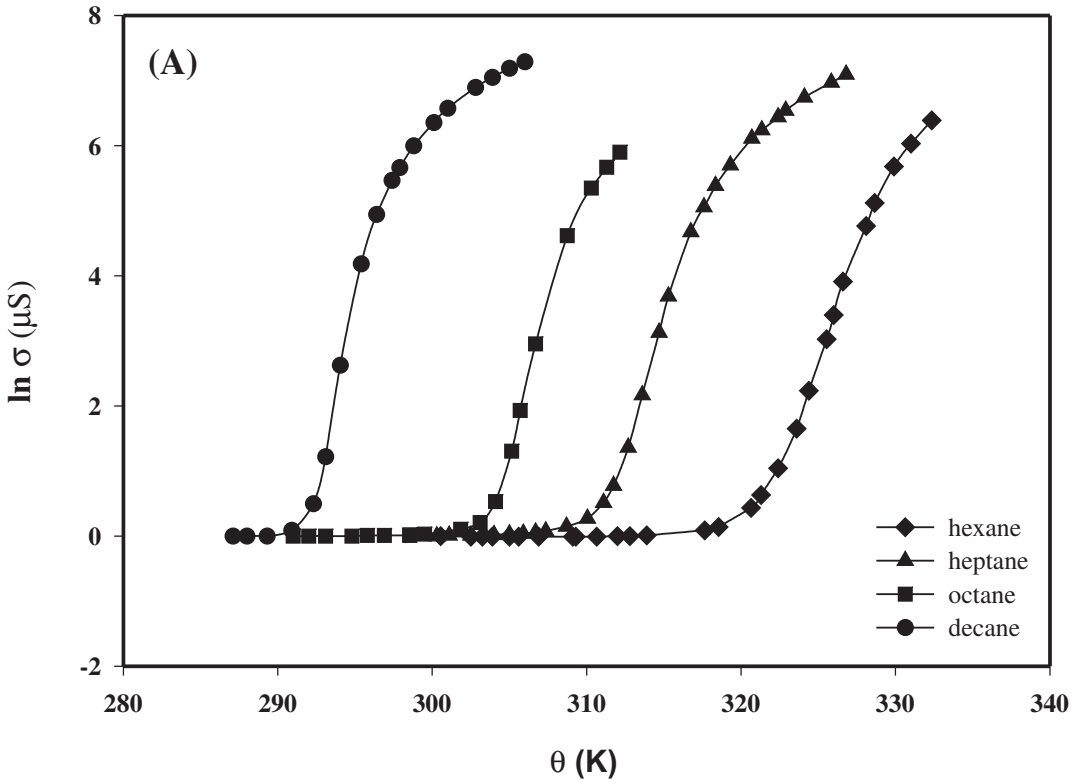
In terms of the ethanol moiety of the studied additive, it has been found that small organic molecules, such as short-chained alcohols, reduce the percolation temperature (27). In the present study, the increase in θ_t upon the addition of mono- and di-ethanol amines is due to the dominance of amine functionality in these molecules, while the decrease in θ_t upon the addition of triethanol amine may be attributed to the added effects of the ethanol moieties. Cazabat et al. (31) found that butanol decreases the temperature of percolation of AOT based microemulsions and Shubel and Ilgenfritz (32) stated that small alcohols such as ethanol forced the interfacial curvature to less negative values, decreasing the percolation temperature. Eicke et al. (33) assumed that these alcohols were located among the surfactant head groups, thus decreasing the effective wedge shape (Table 2).

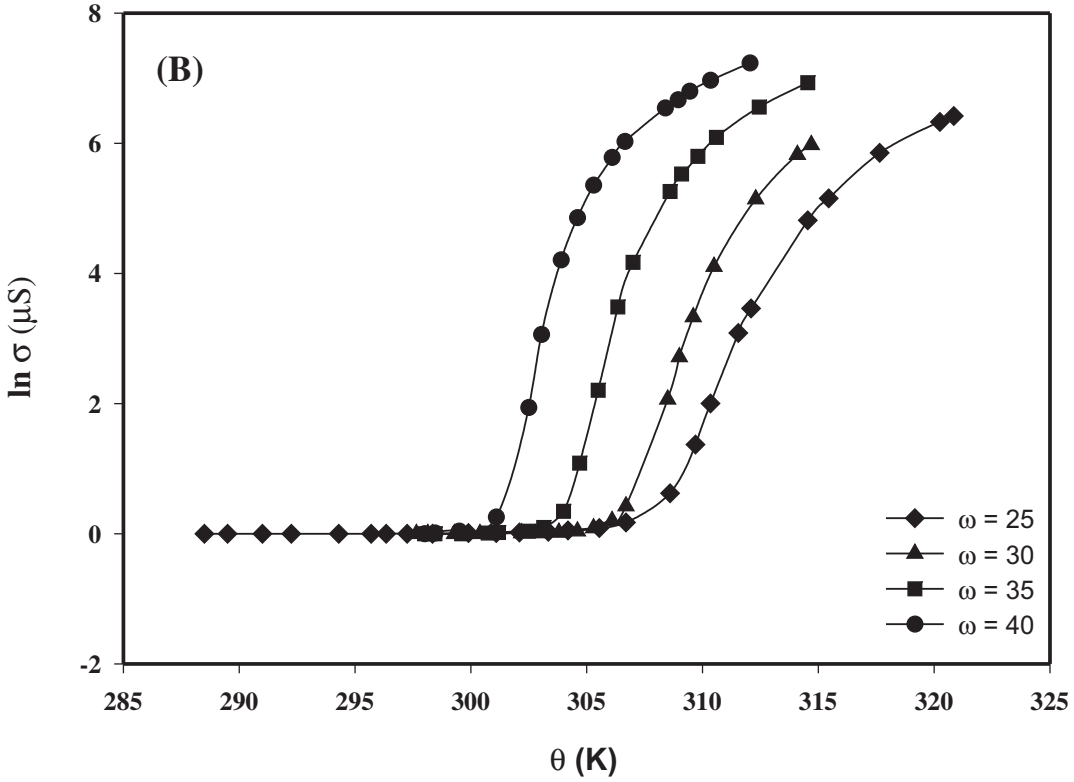
Garcia-Rio et al. (30) made the assumption that *n*-alkyl amines act as cosurfactants, as long chained alcohols do, rigidifying the interface of the microemulsion and increasing the percolation temperature, as observed by other workers (14, 33, 34). Short-chained amines have been reported to increase the percolation temperature (30), whereas short-chained alcohols decrease the percolation temperature. This is indicative of a more complex influence of the amine additives than that of a normal organic substrate (30).

In the case of monoethanol amine, the increase in percolation temperature indicates that it is acting as a short-chained

© 2006 NRC Canada

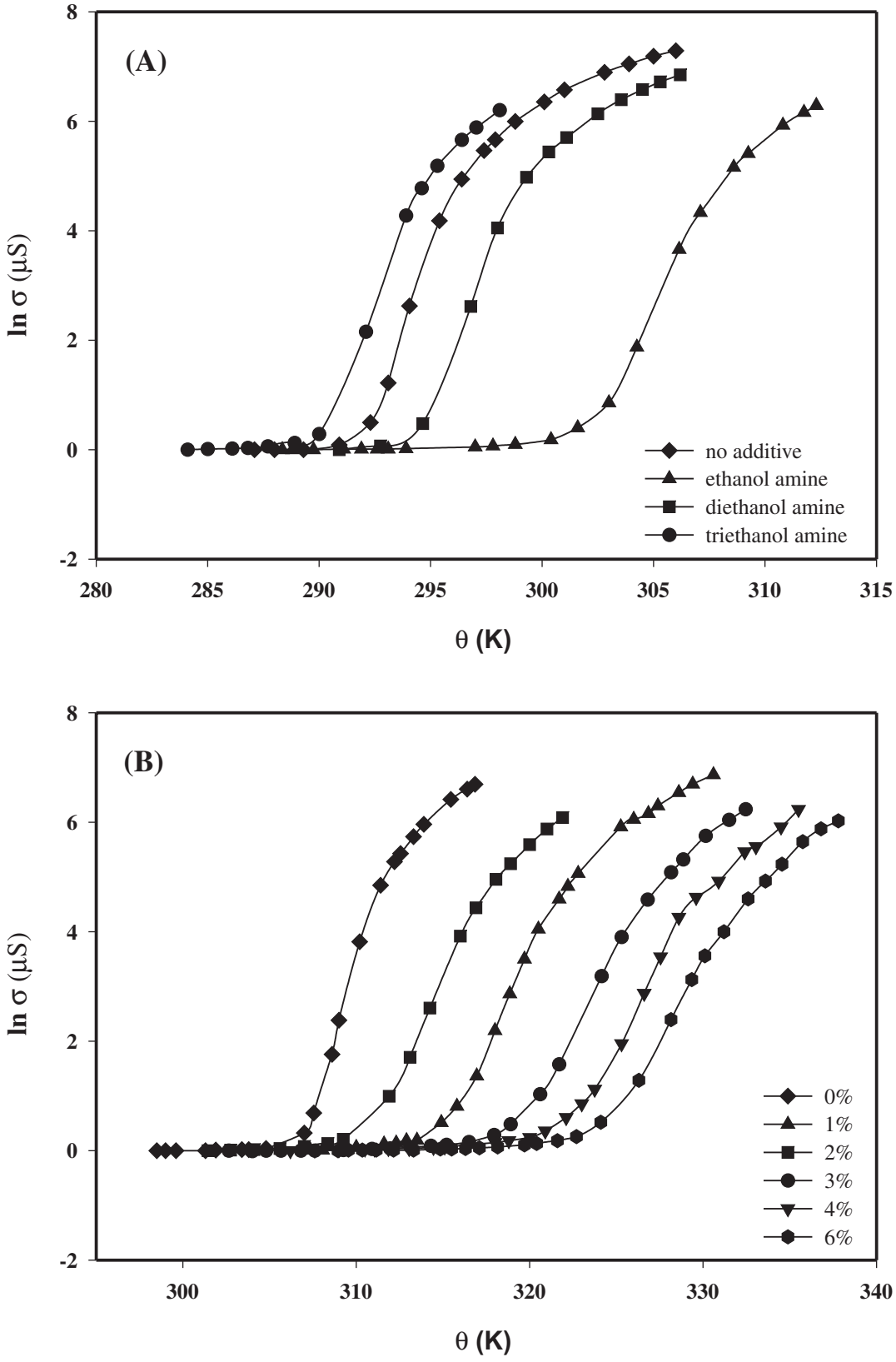
Fig. 1. Percolation courses of (A) water/AOT/oil microemulsions with varying oil, ω = 30, and no additive and (B) water/AOT/isooctane microemulsions with varying ω values and no additive.





© 2006 NRC Canada

Fig. 2. Percolation courses of (A) water/AOT/decane microemulsions with varying ethanol amine additives and $\omega = 30$ and (B) water/AOT/heptane microemulsions with varying % ethanol amine and $\omega = 30$.



© 2006 NRC Canada

Table 1. Percolation temperatures (θ_t) of water/AOT/oil microemulsions with varying oil, ω values, and alkanol amines.

		θ_t (K)				
Solvent	Additive	ω = 25	ω = 30	ω = 35	ω = 40	ω = 45
Hexane	—	326.3	325.4	321.9	318.1	314.8
	1% Ethanol amine	—	330.5	329.6	327.0	328.4
	1% Diethanol amine	—	—	322.2	321.4	319.4
	1% Triethanol amine	—	—	318.1	316.9	314.2
Heptane	—	315.9	314.4	311.0	307.2	305.0
	2% Ethanol amine	323.2	321.3	318.7	317.5	313.5
	2% Diethanol amine	318.1	316.7	315.1	313.9	311.6
	2% Triethanol amine	312.2	310.6	306.2	302.6	300.2
Octane	—	308.0	306.0	303.6	299.7	297.1
	2% Ethanol amine	315.4	316.3	315.5	—	—
	2% Diethanol amine	309.2	307.8	306.9	—	—
	2% Triethanol amine	305.5	305.0	302.1	—	—
Decane	—	297.5	294.4	292.5	—	—
	2% Ethanol amine	304.9	305.0	304.8	—	—
	2% Diethanol amine	297.9	296.6	295.5	—	—
	2% Triethanol amine	291.5	292.2	290.9	—	—
Isooctane	—	311.0	308.9	306.1	303.0	300.5
	2% Ethanol amine	316.9	315.2	313.4	311.2	306.4
	2% Diethanol amine	312.7	310.6	309.4	308.0	305.3
	2% Triethanol amine	309.2	305.2	304.0	300.5	299.0

Table 2. Percolation temperatures (θ_t) of water/AOT/heptane microemulsions with varying percentages of ethanol amine additive and ω values.

		θ_t (K)				
Solvent	% Ethanol amine	ω = 25	ω = 30	ω = 35	ω = 40	ω = 45
Heptane	—	315.9	314.4	311.0	307.2	305.0
	1	322.4	320.9	317.1	317.7	314.6
	2	323.2	321.3	318.7	317.5	313.5
	3	325.1	324.5	323.2	319.6	317.1
	4	—	326.5	326.0	323.4	323.9
	5	326.5	326.7	327.0	327.0	327.4
	6	—	329.7	328.6	327.3	326.4

alkylamine rather than as an alcohol. Triethanol amine, with three hydroxyl groups, promoted the percolation process while acting as a short-chained alcohol. The behavior of the diethanol amine falls in between these two alkanol amines. Another possible explanation for their distinct behavior towards the percolation process may be attributed to the effect of these additives on the water pool size of the droplet. The pool size may follow the order triethanol > diethanol > monoethanol amines. Further experimentation is required to exactly pinpoint the actual mechanism.

Performance of the scaling equation

The temperature-related conductivity in the percolation range obeys the following scaling equation

$$\sigma = P(\theta - \theta_t)^n \quad [3]$$

where σ is the specific conductivity corresponding to the temperature (θ), and P and n are constants. The value of n has been shown to be 1.9 for static percolation. However, both higher and lower values are reported in the literature (3). To evaluate ln P and n, the logarithmic form of the equation was used

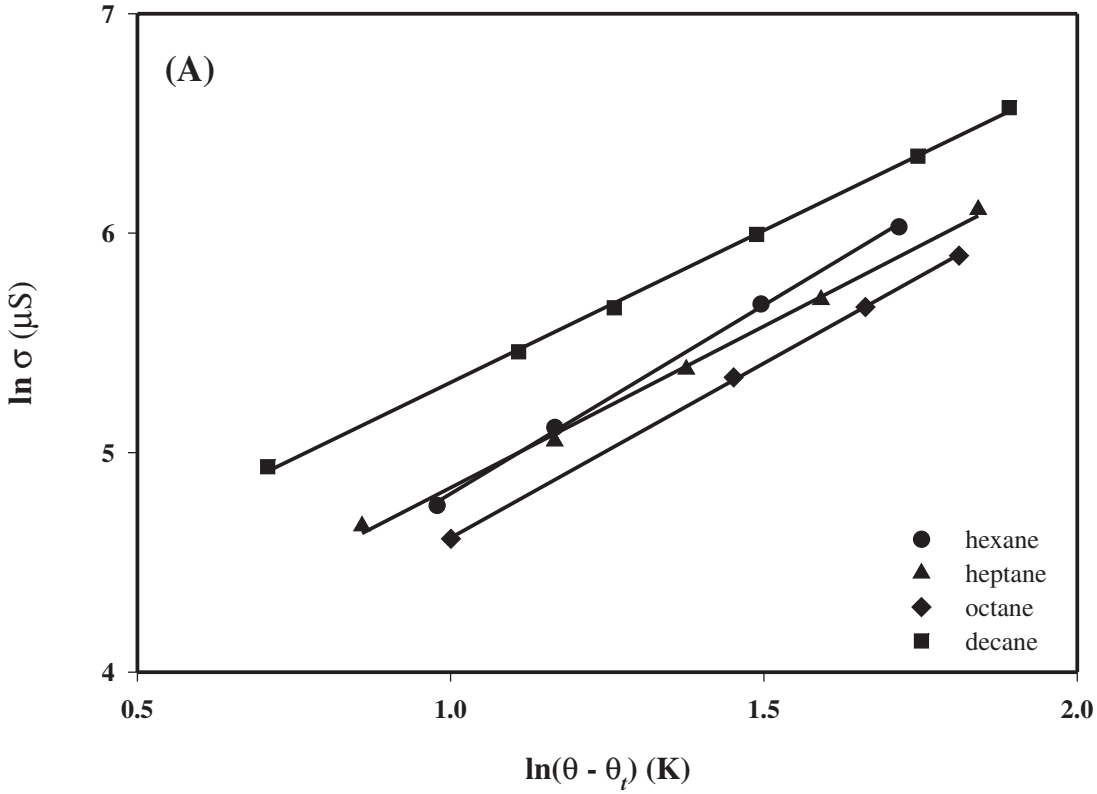
$$\ln \sigma = \ln P + n\ln(\theta - \theta_t) \quad [4]$$

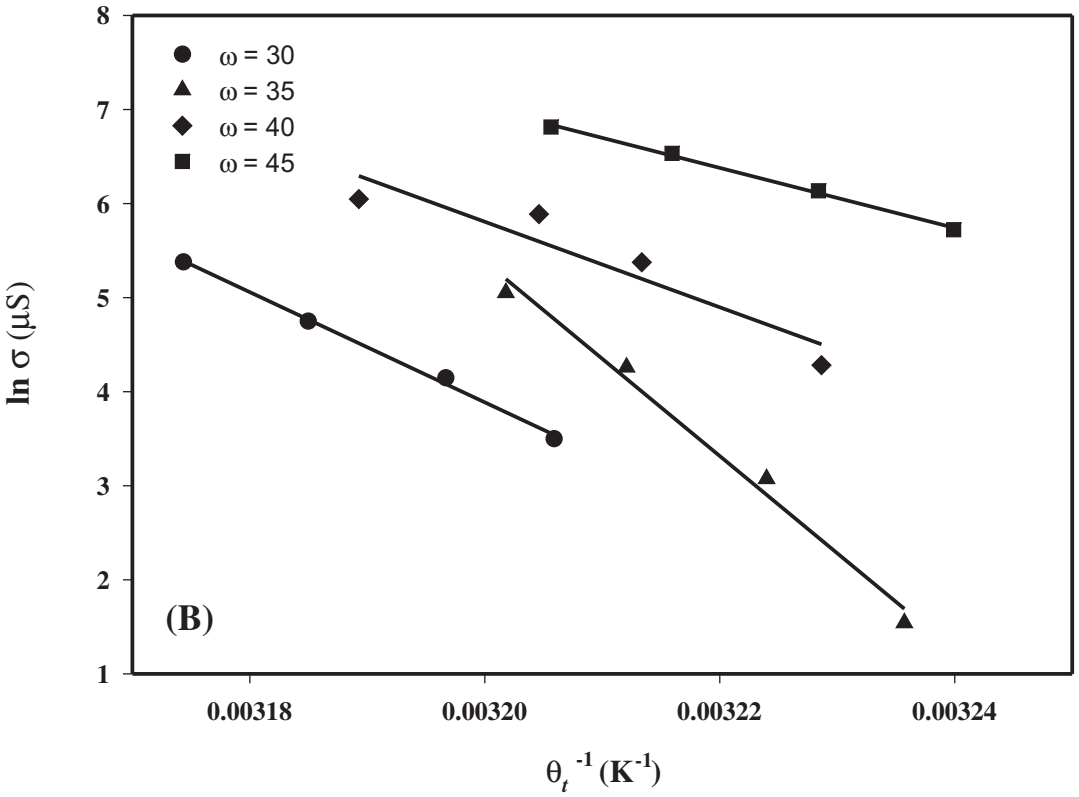
Therefore, a plot of ln σ vs. $\ln(\theta - \theta_t)$ results in a linear plot with slope and intercept corresponding to n and ln P scaling parameters, respectively. The performance of the scaling equation in the percolation region is illustrated in Fig. 3A. The resultant scaling parameters are given in Table 3.

The deviation of n from the predicted value of 1.9 for static percolation lies in the contribution of dynamic percolation to the microemulsion system. In static percolation, conductance remains virtually zero below the threshold temperature. In dynamic percolation, as is the case for w/o microemulsions, the droplets are constantly in motion and can randomly rearrange and approach each other, leading to conductance before the threshold temperature. In the present investigation, the values of n were lower than 1.9 in the

© 2006 NRC Canada

Fig. 3. (A) Scaling equation plots of water/AOT/oil microemulsions with varying oil, no additive, and ω = 30 and (B) activation energy plots of water/AOT/isooctane microemulsions with varying ω values and 2% diethanol amine additive.





© 2006 NRC Canada

Table 3. Scaling parameters (n and ln P) of water/AOT/oil microemulsions with varying oil, ω values, and alkanol amines.

		n, ln P				
Solvent	Additive	ω = 25	ω = 30	ω = 35	ω = 40	ω = 45
Hexane	—	1.6, 3.2	1.7, 3.1	1.7, 3.3	1.5, 3.8	1.5, 4.3
	1% Ethanol amine	—	1.4, 3.6	1.8, 2.7	1.8, 3.4	1.6, 3.6
	1% Diethanol amine	—	—	1.6, 3.6	1.5, 3.8	1.5, 3.8
	1% Triethanol amine	—	—	1.5, 3.5	1.6, 3.6	1.5, 4.0
Heptane	—	1.8, 2.2	1.5, 3.4	1.5, 3.8	1.4, 4.2	1.3, 4.4
	2% Ethanol amine	1.3, 2.9	1.6, 2.6	1.6, 2.8	1.4, 3.4	1.5, 3.7
	2% Diethanol amine	1.4, 3.0	1.5, 3.1	1.7, 3.1	1.5, 3.9	1.5, 3.8
	2% Triethanol amine	1.4, 3.0	1.5, 3.3	1.3, 4.1	1.4, 4.2	1.5, 4.2
Octane	—	1.4, 3.2	1.6, 3.0	1.5, 3.6	1.4, 4.0	1.4, 4.5
	2% Ethanol amine	1.7, 1.9	1.6, 3.0	1.4, 3.6	—	—
	2% Diethanol amine	1.5, 2.8	1.5, 3.3	1.5, 3.6	—	—
	2% Triethanol amine	1.4, 2.7	1.3, 3.4	1.4, 3.8	—	—
Decane	—	1.5, 2.6	1.4, 4.0	1.3, 4.3	—	—
	2% Ethanol amine	1.5, 2.9	1.6, 3.1	1.5, 3.5	—	—
	2% Diethanol amine	1.4, 3.1	1.5, 3.5	3.8, 1.4	—	—
	2% Triethanol amine	1.4, 3.9	1.5, 3.5	1.4, 4.1	—	—
Isooctane	—	1.6, 2.8	1.3, 3.7	1.4, 4.0	1.4, 4.2	1.3, 2.5
	2% Ethanol amine	1.4, 2.9	1.4, 3.4	1.4, 3.6	1.3, 4.1	1.3, 4.1
	2% Diethanol amine	1.5, 2.8	1.5, 3.3	1.4, 3.8	1.4, 4.0	1.4, 4.2
	2% Triethanol amine	1.5, 2.9	1.4, 3.9	1.5, 3.6	1.5, 4.0	1.4, 4.5

Table 4. Activation energies (E_p) of water/AOT/oil microemulsions with varying oil, ω values, and alkanol amines.

		E_p (kJ mol^{-1})				
Solvent	Additive	ω = 25	ω = 30	ω = 35	ω = 40	ω = 45
Hexane	—	408	522	285	741	273
	1% Ethanol amine	—	616	727	740	862
	1% Diethanol amine	—	—	675	515	928
	1% Triethanol amine	—	—	869	527	553
Heptane	—	271	305	258	374	252
	2% Ethanol amine	408	240	162	367	587
	2% Diethanol amine	339	602	371	499	250
	2% Triethanol amine	352	413	369	386	533
Octane	—	371	641	1114	663	767
	2% Ethanol amine	459	709	734	—	—
	2% Diethanol amine	547	327	565	—	—
	2% Triethanol amine	276	837	883	—	—
Decane	—	251	912	130	—	—
	2% Ethanol amine	662	391	372	—	—
	2% Diethanol amine	282	202	163	—	—
	2% Triethanol amine	253	355	216	—	—
Isooctane	—	879	500	217	1084	324
	2% Ethanol amine	267	396	478	337	396
	2% Diethanol amine	284	487	956	500	265
	2% Triethanol amine	339	302	226	549	241

presence of all additives, reflecting that the percolation process is more complex than predicted by the theory.

Activation energy of percolation

The activation energy of conductance percolation (E_p) has been determined using an Arrhenius-type equation

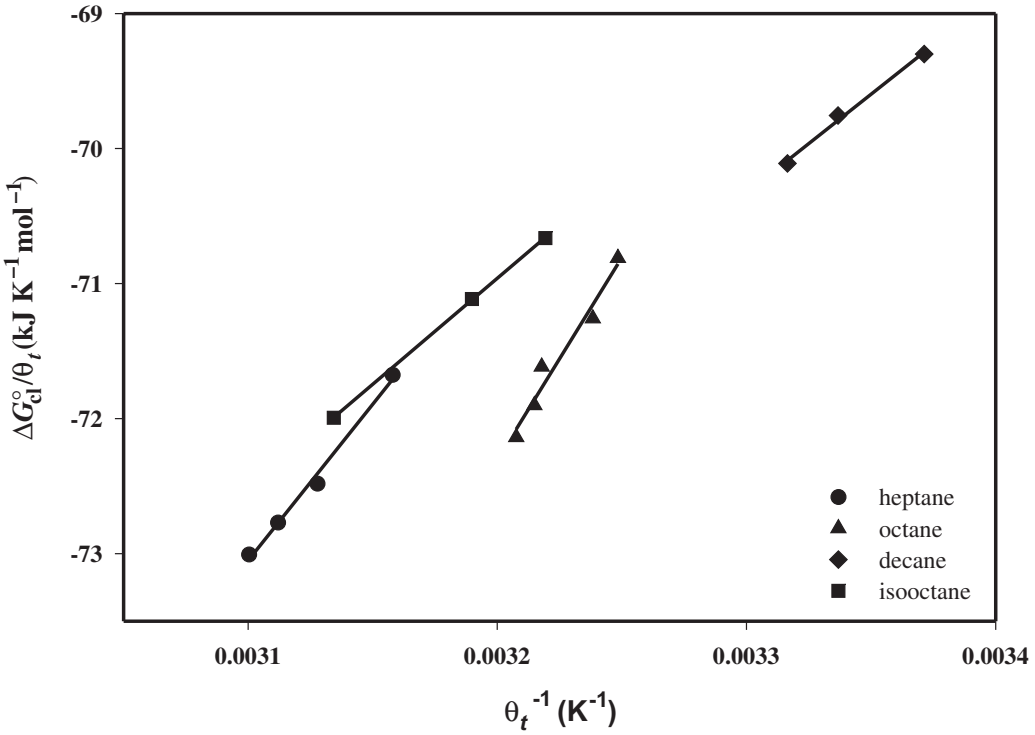
$$[5] \qquad \sigma = Ae^{-E_p/RT}$$

where A is a constant and R and T have their usual significance.

The E_p values have been obtained from the slope (E_p/R) of the ln σ vs. θ^{-1} plot shown in Fig. 3B. The activation energies of the clustering of water/AOT/oil microemulsions are presented in Table 4 with variations of oil chain length, ω value, and alkanol amine. Low activation energy suggests that channels facilitating charge transfer form in the droplet

© 2006 NRC Canada

Fig. 4. $\Delta G^{\circ}_{cl}/\theta_t$ vs. $1/\theta_t$ of water/AOT/oil microemulsions with varying oil in the determination of the enthalpy of clustering (2% diethanol amine, $\omega = 30$).



continuum structure. There has been no observed dependency of activation energy on oil, ω value, or alkanol amine in the present study.

Thermodynamics of droplet association

The phase separation model is employed in the determination of the thermodynamics of droplet clustering, as it is assumed that the droplets and the droplet continuum that is formed at the threshold percolation temperature exist in separate phases. This gives the standard Gibbs free energy change for the clustering process as the following equation:

$$[6] \qquad \Delta G^{\circ}_{cl} = RT \ln X_d$$

where X_d is the mole fraction of droplets in the microemulsion at the point of the percolation threshold. The X_d value can be obtained from the following relationship:

$$[7] \qquad X_d = \frac{n_d}{n_d + n_{oil}} = \frac{A_t M V_t}{(M A_t V_t + 4000\pi r_d^2 N_A V d}$$

where n_d and n_{oil} are the moles of droplet and oil, respectively, A_t is the total surface area covered by the AOT headgroup, and V_t is the total volume of the system. The terms V, d, and M are the volume, density, and molar mass of the oil, respectively, r_d is the average radius of the droplet, and N_A is Avagadro's number. Standard enthalpy changes of clustering follow from the first derivative of ΔG°_{cl} with respect to temperature and were obtained from the Gibbs–Helmholtz equation:

$$[8] \qquad \Delta H^{\circ}_{cl} = \frac{\left(\frac{\Delta G^{\circ}_{cl}}{T}\right)}{d\left(\frac{1}{T}\right)}$$

The entropy of clustering follows from the Gibbs equation:

$$[9] \qquad \Delta S^{\circ}_{cl} = \frac{\Delta H^{\circ}_{cl} - \Delta G^{\circ}_{cl}}{T}$$

To obtain ΔH°_{cl}, water/AOT/oil microemulsions at a fixed ω value of 30 were diluted with several portions of oil, and the θ_t values for all the diluted samples were determined from conductance measurements. The ΔG°_{cl} values were obtained from the sample compositions. $\Delta G^{\circ}_{cl}/\theta_t$ values for the samples were plotted as a function of $1/\theta_t$ to yield the values of ΔH°_{cl} (Fig. 4).

Thermodynamics of the clustering process for selected microemulsion systems are given in Table 5. The values show that the studied process is endothermic and entropically driven, as is depicted in the literature (11). The enthalpic contributions of the clustering process include the breaking of the interfacial layer (endothermic) and the formation of the continuous microemulsion structure at the temperature of percolation (exothermic). As ΔH°_{cl} is positive, the breaking of the interfacial layer serves as the predominating enthalpic contribution.

From the ΔG°_{cl} values, the observation was made that the process of clustering is spontaneous and the increase in the chain length of the oil phase of the microemulsion results in

© 2006 NRC Canada

Table 5. Thermodynamics of the clustering process of water/AOT/oil microemulsions with varying oil and alkanol amines (ω = 30).

Solvent	Additive	ΔG°_{cl} (kJ mol^{-1})	ΔH°_{cl} (kJ mol^{-1})	ΔS°_{cl} (J K^{-1} mol^{-1})
Heptane	1% Ethanol amine	–23.0	15.7	121
	1% Diethanol amine	–22.7	23.1	145
	1% Triethanol amine	–22.5	21.8	141
Octane	2% Ethanol amine	–22.4	26.1	153
	2% Diethanol amine	–21.8	30.0	168
	2% Triethanol amine	–21.6	31.9	175
Decane	2% Ethanol amine	–21.1	18.7	131
	2% Diethanol amine	–20.6	14.6	119
	2% Triethanol amine	–20.6	30.0	175
Isooctane	2% Ethanol amine	–22.4	13.9	114
	2% Diethanol amine	–22.0	15.7	121
	2% Triethanol amine	–21.6	12.7	112

the decrease in spontaneity of the clustering process. This result is consistent to that reported in the literature (11).

Conclusions

1. The percolation of water/AOT/oil microemulsions was restricted by the addition of ethanol amine additive. The addition of ethanol moieties to this additive further decreased the percolation temperature.
2. An increase in the percolation temperature of water/AOT/oil microemulsions was associated with a decrease in the chain length of the oil, a decrease in the microemulsion's ω value, and an increase in the percentage of alkanol amine additive.

Acknowledgements

RP acknowledges the Natural Sciences and Engineering Research Council of Canada (NSERC) for the support in the form of an operating grant. AG is grateful for the Undergraduate Student Research Awards (USRA) from NSERC (2002).

References

1. T.P. Hoar and J.H. Schulman. Nature (London), **152**, 103 (1943).
2. VI. Danielsson and B. Lindman. Colloids Surf. **3**, 391 (1981).
3. S.P. Moulik and B.K. Paul. Adv. Colloid Interface Sci. **78**, 99 (1998).
4. J. Sjoblom, R. Lindberg, and S.E. Friberg. Adv. Colloid Interface Sci. **95**, 125 (1996).
5. J. Fang and R. Venable. J. Colloid Interface Sci. **116**, 269 (1987).
6. S.R. Bisal, P.K. Bhattacharya, and S.P. Moulik. J. Phys. Chem. **94**, 350 (1990).
7. S. Pal, S.R. Bisal, and S.P. Moulik. J. Phys. Chem. **96**, 896 (1992).
8. S. Ray, S. Pal, and S.P. Moulik. J. Colloid Interface Sci. **183**, 6 (1996).
9. S. Ray, S.R. Bisal, and S.P. Moulik. J. Chem. Soc. Faraday Trans. **89**, 3277 (1993).
10. S.P. Moulik and S. Ray. Pure Appl. Chem. **66**, 521 (1994).
11. P. Alexandridis, J.F. Holzwarth, and T.A. Hatton. J. Phys. Chem. **99**, 8222 (1995).
12. I.D. Robb. *In* Microemulsions. Plenum Press, New York. 1982.
13. A.M. Cazabat, D. Chateney, F. Guering, D. Langevin, J. Meunier, D. Sorba, J. Lang, R. Zana, and M. Paillette. *In* Surfactants in solution. Plenum Press, New York. 1984.
14. A. Maitra, C. Mathew, and M. Varshney. J. Phys. Chem. **94**, 5290 (1990).
15. S.R. Bisal, P.K. Bhattacharya, and S.P. Moulik. J. Surf. Sci. Technol. **4**, 121 (1998).
16. L. Garcia-Rio, J.R. Leis, J.C. Mejuto, and M.E. Peña. Langmuir, **10**, 1676 (1994).
17. S.K. Mehta and Kawaljit. Colloids Surf. A, **136**, 35 (1998).
18. S.K. Mehta, R.K. Dewan, and K. Bala. Phys. Rev. E, **50**, 4759 (1994).
19. S.K. Mehta, S. Sherma, and K.K. Bhasin. J. Phys. Chem. B, **109**, 9751 (2005), and refs. cited therein.
20. L. Garcia-Rio, P. Hervés, J.R. Leis, and J.C. Mejuto. Langmuir, **13**, 6083 (1997).
21. J. Dasilva-Carvalhal, L. Garcia-Rio, D. Gómez-Diaz, J.C. Mejuto, and and P. Rodriguez-Dafonte. Langmuir, **19**, 5975 (2003).
22. R.K. Mitra and B.K. Paul. Colloids Surf. A, **255**, 165 (2005).
23. R.K. Mitra and B.K. Paul. Colloids Surf. A, **252**, 243 (2005).
24. L.M.M. Nazario, T.A. Hatton, and P.S.G. Crespo. Langmuir, **12**, 6326 (1996).
25. S.K. Hait, S.P. Moulik, M.P. Rodgers, S.P. Burke, and R. Palepu. J. Phys. Chem. B, **105**, 7145 (2001).
26. H. Yang, K. Erford, D.J. Kiserow, and L.B. McGown. J. Colloid Interface Sci. **262**, 531 (2003).
27. Dow Chemical Co. The alkanolamines handbook. Dow Chemical Company, Midland, Michigan. 1981.
28. B.R. Brown. *In* The organic chemistry of aliphatic nitrogen compounds. Oxford University Press, New York. 1994.
29. S.K. Hait, S.P. Moulik, and R. Palepu. Langmuir, **18**, 2471 (2002).
30. L. Garcia-Rio, P. Hervés, J.C. Mejuto, J. Pérez-Juste, and P. Rodriguex-Dafonte. J. Colloid Interface Sci. **225**, 259 (2000).
31. A.M. Cazabat, D. Chateney, F. Guering, D. Langevin, J. Meunier, D. Sorba, J. Lang, R. Zana, and M. Paillette. *In* Surfactants in solution. Plenum Press, New York. 1984.
32. D. Schubel and G. Ilgenfritz. Langmuir, **13**, 4250 (1997).
33. H.F. Eicke, R. Kubick, R. Haase, and I. Zschokke. *In* Proceedings of the International Symposium on Surfactants in Solution, Bordeaux, France. 9–13 July 1984. Plenum, New York. 1984.
34. L. Mukhopadhyay, P.K. Bhattacharya, and S.P. Moulik. Colloids Surf. **50**, 295 (1990).

© 2006 NRC Canada

Studies of structure and dynamics in a nominally symmetric twisted amide by NMR and electronic structure calculations

Alex D. Bain, Hao Chen, and Paul H.M. Harrison

Abstract: Amides that are twisted around the C—N bond show unusual spectroscopy and reactivity when compared with planar amides. The diacyl derivatives of 3,4,7,8-tetramethyl-2,5-dithioglycoluril are intriguing examples of this class, since the crystal structures show that the two acyl groups are twisted by different amounts on either side of the molecule owing to a combination of steric and electronic effects. However, the ^{1}H NMR spectra in solution at room temperature exhibit only one acyl resonance, so there must be fast interconversion among pairs of equivalent structures of each compound. We have prepared a number of derivatives with different acyl groups, both on the glycoluril framework as well as on its dithio analogue. The chemical exchange in solution was slowed down sufficiently by cooling to see individual sites for only two compounds: the dithiodipivaloyl and the dithiodiadamantyl derivatives. The barriers were estimated at 41 kJ mol^{-1} for the dipivaloyl derivative and 45 kJ mol^{-1} for diadamantyl derivative. The results show that rotation around the twisted amide bond is slowed by both the steric size of the acyl group and the presence of the thioureido group vs. the ureido group in the glycoluril core. In the solid-state ^{13}C NMR spectra, there is no evidence for any dynamics, even for the diacetyl derivative at ambient temperature. Electronic structure calculations predict a geometry for the dipivaloyl derivative very close to that observed in the crystal structure. These results indicate that the crystal confines, but does not distort the molecule. A mechanism for the exchange is proposed. The relevance of these results to the mechanism of Claisen-like condensations in diacylglycolurils is also discussed.

Key words: ^{1}H and ^{13}C NMR, exchange, dynamics, CP/MAS, solids, line shape analysis, amides, twisted amides, atropisomers, glycoluril.

Résumé : Par comparaison avec les propriétés correspondantes des amides planaires, les propriétés spectroscopiques et la réactivité des amides ayant subi une déformation autour de la liaison C—N présentent des caractéristiques inhabituelles. Les dérivés diaryles du 3,4,7,8-tétraméthyl-2,5-dithioglycouril sont des exemples intriguant de cette classe puisque leurs structures cristallines montrent la présence de deux groupes acyles décalés par des angles différents sur chaque côté de la molécule en raison d'une combinaison d'effets stérique et électronique. Toutefois, le spectre RMN du ^{1}H en solution, à la température ambiante ne présente qu'un seul signal de résonance pour un groupe acyle, ce qui implique qu'il se produit une interconversion rapide entre les paires de structures équivalentes de chaque composé. On a préparé un certain nombre de dérivés avec différents groupes acyles, tant dans le squelette du glycoluril que dans son analogue dithio. Le refroidissement des solutions afin de ralentir suffisamment l'échange chimique en solution ne nous a permis d'observer les sites individuels de deux que dans les cas de deux dérivés, le dithiodipyvaloyle et le dithiodiadamantyle. On a évalué que les barrières sont de 41 kJ mol^{-1} pour le dérivé dipivaloyle et de 45 kJ mol^{-1} pour le dérivé diadamantyle. Les résultats montrent que la rotation autour de la liaison amide déformée est ralentie tant par la grosseur stérique du groupe acyle que par la présence d'un groupe thiouréido vs. le groupe uréido du coeur de glycouril. Dans le spectre RMN du ^{13}C à l'état solide, on n'a relevé aucune donnée pour quelle que dynamique que ce soit, même avec le dérivé diacétyle à la température ambiante. Des calculs de structure électronique permettent de prédire une géométrie pour le dérivé dipivaloyle qui ressemble beaucoup à celle observée dans la structure cristalline. Les résultats indiquent que le cristal sert à confiner les molécules sans toutefois les déformer. On propose un mécanisme pour l'échange. On discute aussi de l'intérêt de ces résultats pour le mécanisme de condensations de type Claisen dans les diacétylglycolurils.

Mots clés : RMN du ^{1}H et ^{13}C, échange, dynamique, CP/MAS, solides, analyse de la forme des bandes, amides, amides déformés, atropisomères, glycoluril.

[Traduit par la Rédaction]

Received 27 July 2005. Published on the NRC Research Press Web site at http://canjchem.nrc.ca on 30 March 2006.

A.D. Bain,[1] H. Chen,[2] and P.H.M. Harrison. Department of Chemistry, McMaster University, 1280 Main St. West, Hamilton, ON L8S 4M1, Canada.

[1]Corresponding author (e-mail: bain@mcmaster.ca).
[2]Present address: National Research Council of Canada, Plant Biotechnology Institute, 110 Gymnasium Place, Saskatoon, SK S7N 0W9, Canada.

 doi:10.1139/V06-016 © 2006 NRC Canada

Introduction

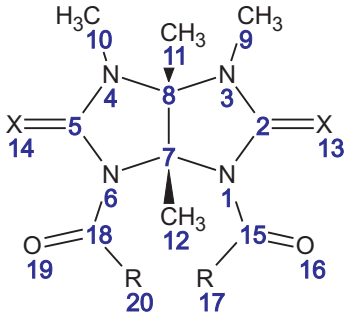
Amides are perhaps the most studied three-atom linkage in chemistry (1, 2). Their central role as the backbone of protein structure provides thousands of different examples of the peptide bond, and the dynamics of this bond is central to the protein folding problem. Chemically, amides are quite distinct in their reactivity from simple amines and ketones. Furthermore, there are a number of theoretical challenges in understanding the bonding. The classic model of resonance predicts an interaction of the lone pair on the nitrogen atom with the carbonyl π system, thus weakening the carbonyl bond and imparting partial double bond character to the C—N bond. This prediction is supported by the observation of significant barriers to rotation around the C—N bond. On all of these points, there is a vast literature.

The interaction of the lone pair on nitrogen and the π system is most efficient when the amide linkage is planar. We are assuming that both the carbonyl carbon and the amide nitrogen are sp^2 hybridized, so the local geometry is planar around each atom. In many amides, these two planes coincide (a planar linkage), but many twisted amides have been prepared and studied (3–9). This effect may result from twisting around the C—N bond (owing to the arrangement of covalent bonds or severe steric effects), or through bending of the amide functionality, for example, as a result of pyramidalization (and change of hybridization) at nitrogen. In these cases, the nitrogen lone pair and the attached carbonyl π system are not fully conjugated. The degree of twist gives us an experimental probe of the amide bond. These molecules are of intense theoretical interest because they allow aspects of amide electronic resonance structures to be explored (10–17). The loss of this N-C=O interaction makes the carbonyl carbon unusually electrophilic, so that twisted amides are often highly reactive (14, 15, 18, 19). As such, they have found utility as acylating agents (3, 4, 20–22). Further, they may act as stable model structures for intermediates or transition states in a variety of processes of biological relevance (1).

In the course of the investigations of the glycoluril framework as a scaffold for studying intramolecular Claisen-like reactions (23), we synthesized several 1,6-diacyl-3,4,7,8-tetramethylglycolurils and their 2,5-dithio congeners (e.g., **1**, **2**, and **4**, Fig. 1). The crystal structure (24) of **1** shows that the amides are significantly twisted and that the twisting is different on the two sides of this nominally symmetrical molecule. Compounds **2** and **4** in this series have shown similar, but less dramatic effects (25–27). In solution, however, the NMR spectra at room temperature of all the symmetrically substituted glycolurils prepared by us indicate symmetrical structures. This suggests that there are two mirror-image forms that interconvert quickly at ambient temperatures, but can be observed separately at low temperatures (24). Analysis of the chemical exchange allows us to probe the potential energy surface of these molecules.

Chemical systems that are apparently symmetric, but sterically crowded, relieve the stress by distorting. For example, Iwamura and Mislow (28) refer to molecular machinery in which the crowded groups undergo cogwheellike motions, and there are many further examples of this type of system (29–31). In some of the literature, these systems are often

Fig. 1. Structure of 1,6-dipivaloyl-3,4,7,8-tetramethyl-2,5-dithioglycoluril. The R groups at positions 17 and 20 in **1** are tertiary butyl, and the other derivatives are as described.



1	R = *t*-Bu	X = S
2	R = Me	X = S
3	R = *t*-Bu	X = O
4	R = Me	X = O
5	R = Et	X = S
6	R = *i*-Pr	X = S
7	R = adamantyl	X = S

referred to as atropisomers (32–37). However, the distortion need not retain any of the original symmetry. The published (24) crystal structure of 1,6-dipivaloyl-3,4,7,8-tetramethyl-2,5-dithioglycoluril (**1**, Figs. 1 and 2) shows that one of the pivaloyl groups attached to the glycoluril framework is twisted down (towards the endo face of the molecule) relative to an average plane through the attached tetrahydroimidazolone ring, but the other acyl group is almost perpendicular to its ring (Fig. 2) and twisted up (towards the exo face). Thus, both acyl groups are twisted, but to different extents and in opposite senses.

These previous results suggested that twisting the acyl groups in the ground-state structure might contribute significantly to the acidity of the acyl groups bearing α protons (18). Loss of the resonance interaction in an amide renders it more ketone-like, and simple ketones are significantly more acidic than amides. Since the first step in the Claisen-like condensation of diacylglycolurils involves deprotonation (38, 39), twisting in the substrates may be an important factor in activating one or both of the acyl groups, leading to the observed fast and efficient condensation.

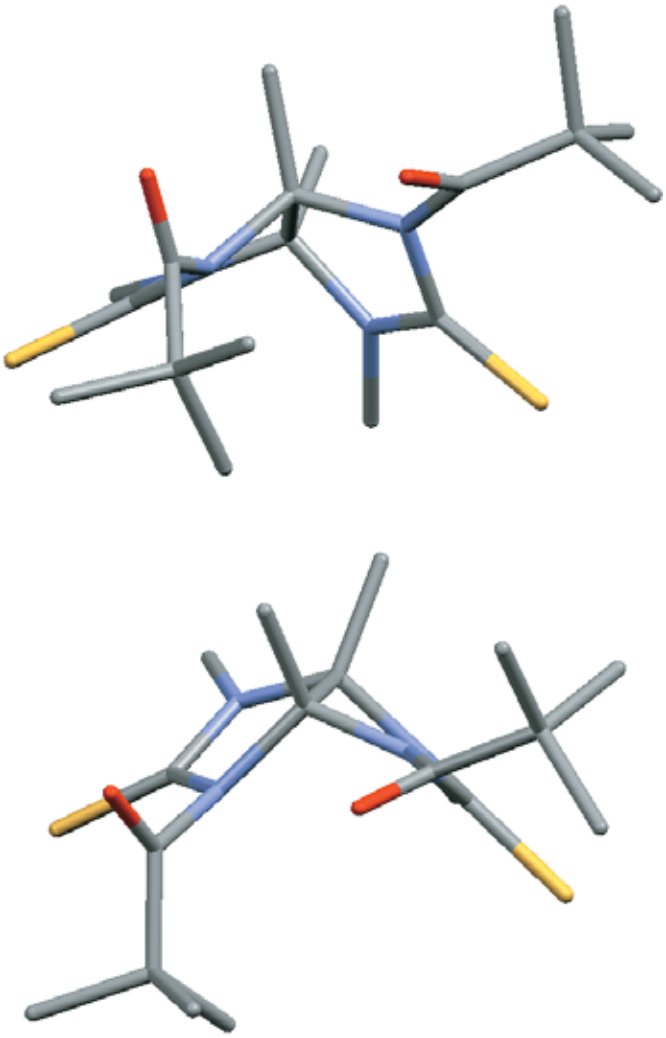
Therefore, we wished to examine the structures of the diacylglycolurils in greater detail. In this paper we extend our investigation of this phenomenon by looking at the dynamic NMR spectra of a number of derivatives (Fig. 1), supplemented with electronic structure calculations and solid-state NMR spectra.

Results and discussion

In the molecules in Fig. 1, both steric and electronic effects will strongly influence the geometry of the molecule (40, 41). The nitrogen lone pairs, the carbonyl (or

© 2006 NRC Canada

Fig. 2. Three-dimensional drawings of the crystal structure of **1**. The hydrogen atoms have been omitted for clarity. The acyl groups are facing out of the page, and the group N6-C18-O19-R20 is on the left-hand side. In the top figure, the page is roughly perpendicular to the plane of the left-hand ring, showing the twist of the N6-C18-O19-R20 group. In the lower figure, the right-hand ring is roughly perpendicular to the page, showing the opposite twist of the N1-C15-O16-R17 group.



thiocarbonyl) groups in the rings, and the carbonyls of the acyl groups could form conjugated π systems if each side of the molecule were planar, but twisting around the N1—C15 and N6—C18 bonds may remove some of that conjugation. However, planar amides might cause strong steric repulsions, e.g., among the tertiary butyl groups themselves or with the sulfur in the thiocarbonyl. The crystal structure of **1** (Fig. 2) shows the cis ring fusion, giving a butterflylike, but asymmetric, geometry with the two bridgehead methyl groups canted with respect to each other. The pivaloyl groups are also twisted asymmetrically. The twist angle in an amide (τ) was defined by Winkler and Dunitz (42) to give a single descriptive parameter of the torsion angles. It is the average of the two cisoid torsional angles, as defined in Table 1. Yamada (43) suggested restricting the angle to be in the range from 0° to 90° and positive, to make comparisons more clear. However, in the glycoluril derivatives, the sign of the twist is useful, but the signs of torsion angles require careful specification. We use a positive sign to indicate that the carbonyl is twisted upwards (in the view in Fig. 2) or towards the exo face of the molecule. Twisting of the carbonyl towards the endo face is signified by a negative twist angle.

Table 1 gives the relevant geometrical information from the published crystal structure and from electronic structure calculations at the 6-31G(d,p) level (restricted Hartree–Fock method). Density functional methods (B3LYP) were also used and gave essentially identical geometries. The close match between the geometry in the crystal and the calculated gas-phase geometry indicates that the crystal packing has relatively little influence on the geometry as seen in the crystal. However, we will see later that the lattice confines the dynamics greatly.

During a search for the ground-state geometry in the calculations, a local minimum in the potential energy surface was also detected. Approximately 20 random sets of amide twist angles were defined as initial conditions for the geometry optimization. Most converged to the global minimum, but one gave the metastable state. The glycoluril framework is much the same in this metastable state as in the ground state, but the amide incorporating N6 and C18 has a significantly different twist. The twist angle goes from +67° in the ground state to –77° in the metastable state. The change in sign of the twist angle shows that the carbonyl group has been rotated through almost 180° in going from one state to the other. The geometrical parameters for the metastable state are also given in Table 1. This metastable state is approximately 17 kJ mol^{-1} less stable than the true ground state and may represent an intermediate in the exchange reaction.

The effects of dynamics are often observed by NMR spectroscopy (37, 44–46). Similarly, solids can show considerable molecular motion, even though the molecules remain fixed in the crystal lattice (47, 48). The processes that can be studied in the solid may be the same as those in solution or they may be quite different. If the same process can be observed in both solid and liquid, then the role of the crystal lattice can be investigated.

To probe the steric and electronic effects of substituents on the barrier to interconversion of the two acyl sites, the derivatives listed in Fig. 1 were prepared. Changing the thiocarbonyl group to a carbonyl will alter the nature of the electronic π system (as well as change the steric interactions), and the steric bulk of the acyl group was varied from methyl to adamantyl. The low-temperature NMR spectra of **1**–**7** were recorded. As well, the room-temperature CP/MAS spectra of solid samples of the dipivaloyl derivative (**1**) and the diacetyl derivative (**2**) were measured to check for dynamics in the solid state.

In the dipivaloyl and diadamantyl dithio derivatives (**1** and **7**), the chemical exchange can be sufficiently slowed at low temperature in CD_2Cl_2 so that individual sites are observed. The free energies of activation for the positional exchange are approximately 41 (±2) kJ mol^{-1} at 210 K for the dipivaloyl derivative (**1**) and 45 (±2) kJ mol^{-1} at 230 K for the diadamantyl derivative (**7**). The accessible temperature range is not sufficient to separate the free energy into

© 2006 NRC Canada

Table 1. Geometrical parameters for the dipivaloyl derivative (**1**) and the diacetyl derivative (**2**) from crystal structures and electronic structure calculations (in the columns labeled Calcd.).

	Crystal (**1**)	Calcd. (**1**)	Metast. (**1**)	Crystal (**2**)	Calcd. (**2**)
Bond distances (Å)					
N1—C2	1.389	1.398	1.381	1.367	1.390
N1—C15	1.429	1.433	1.424	1.448	1.452
N1—C7	1.468	1.475	1.458	1.461	1.462
C2—S13	1.664	1.670	1.662	1.660	1.668
C5—N6	1.380	1.376	1.350	1.394	1.398
C5—S14	1.650	1.670	1.668	1.650	1.666
N6—C18	1.467	1.484	1.469	1.397	1.408
N6—C7	1.498	1.498	1.485	1.505	1.513
C15—O16	1.202	1.216	1.189	1.190	1.208
C18—O19	1.201	1.205	1.178	1.211	1.222
Bond angles (°)					
C2-N1-C15	125.4	127.3	128.6	122.6	126.7
C5-N6-C18	119.8	119.7	121.4	123.9	130.2
τ(N1-C15)	–54.3	–54.1	–45.7	55.0	45.6
τ(N6-C18)	66.3	68.4	–77.6	–3.8	8.6

Note: The column labeled Metast. indicates the geometry of a calculated local minimum 17 kJ mol^{-1} above the ground state. Distances are in Angstroms and angles are in degrees. The amide twist angle (τ) is based on the definitions of Winker and Dunitz (42) and Yamada (43), and is the average of the two cisoid torsion angles. For the N1-C15 amide, it is [(C2-N1-C15-C17) + (C7-N1-C15-O16)]/2 and for the N6-C18 amide, it is [(C5-N6-C18-C20) + (C7-N6-C18-O19)]/2. A positive sign indicates that the carbonyl is twisted towards the exo face and a negative sign indicates an endo twist. The experimental data for **1** is from ref. 24 and that for **2** is from ref. 25. For **2**, the numbering of the molecule has been changed from ref. 25 to be consistent with Fig. 1. In **2**, it is the N1-C15 amide that is the more twisted in the crystal, but in **1**, it is the N6-C18 amide that is more twisted. The calculated ground state (restricted Hartree–Fock at the 6-31G(d,p) level) for both molecules and metastable state for **1** are from this work.

enthalpy and entropy with any precision. All the other derivatives (**2**–**6**), with smaller acyl groups or with oxygen replacing the sulfur, showed no detectable exchange-based line broadening at the lowest temperature achieved (163 K).

These results can be compared with previous studies. As the substituent on nitrogen of a simple N,N-disubstituted amide is varied from methyl up to *tert*-butyl, there is a marked decrease in the barrier when the groups are *tert*-butyl (49, 50). The suggested cause in this case is that the planar ground state is destabilized by the steric interactions of the *tert*-butyl groups, whereas the transition states are much the same for all cases. Also, when the methyl group attached to the carbonyl in N,N-disubstituted acetamides is replaced by a *tert*-butyl group, the barrier is significantly decreased (2). Similar effects have been seen in other crowded systems (51). The simple amides show a decrease of the barrier when the substituent is changed from methyl to *tert*-butyl, but in the present molecule there is a significant increase.

The difference between the dithio and the dioxo derivatives is interesting. Thioamides tend to have higher barriers (by up to 10 kJ mol^{-1}) than the corresponding amides (12, 49, 52–55). This implies that the double bond character of the carbon–nitrogen bond is larger, and the nitrogen lone pair mixes strongly with the π bond of the thiocarbonyl in the simple thioamides. In the present glycoluril case, we assume that the bond from the nitrogen to the thiocarbonyl (such as **2**) is stronger than that to a carbonyl in an oxoglycoluril (such as **4**). Therefore, less of the lone pair would be available for overlap to the acyl carbonyl, implying less double bond character in the bond to the acyl group. This argument would imply a lower barrier to acyl rotation for the dithio derivative over the dioxo, but the reverse is observed. Therefore, there must be significant steric interaction when a large acyl group tries to rotate past the sulfur in the thiocarbonyl in the ring.

Attempts to find the true transition state for the interconversion by calculations have been unsuccessful, perhaps because there are many degrees of freedom in the *tert*-butyl group. However, the calculated metastable state for the dipivaloyl derivative suggests a route to the transition state. In the metastable state, both carbonyl groups are on the same face of the molecule, whereas they are opposed in the ground state. Furthermore, it appears as if the more twisted amide (Table 1) is the one that rotates to form the intermediate. The evidence of the metastable state and the suggested steric effects between the *tert*-butyl group and the thiocarbonyl lead us to the following mechanism. First, the more twisted amide twists from above the ring to below the ring, with the carbonyl group toward the centre of the molecule and the *tert*-butyl group brushing past the sulfur of the thiocarbonyl. The fact that the adamantyl group has a barrier of about 4 kJ mol^{-1} higher than the *tert*-butyl group of the dipivaloyl derivative implies that the barrier has a significant steric component. This rotation leads to the metastable state as an intermediate. Following that, the other acyl group twists up through the plane and the other *tert*-butyl group passes the sulfur to complete the exchange. It appears that the bridgehead methyl groups must also twist past each other, and the two five-membered rings must change their pucker in this step as well. The observed data are not sufficient to distinguish between the highest transition state lying

© 2006 NRC Canada

Table 2. ^{13}C chemical shifts for **1** in the solid state and in a CD_2Cl_2 solution.

^{13}C chemical shifts (ppm)		
Carbons	Solid	Solution
11, 12	19.5, 13.1	16.9, 15.9
17, 20 (methyl)	All in the range	28.8, 28.3
9, 10	of 31 to 29	30.9, 29.7
17, 20 (central)	45.7, 45.3	45.0, 44.6
7, 8	90.1, 88.2	88.7, 87.2
2, 5	179.6, 176.9	179.8, 176.3
15, 18	186.6, 184.9	186.9, 185.3

before or after the intermediate on the reaction coordinate. This mechanism fits all the available data.

By contrast, in the solid state there was no evidence for chemical exchange in the molecules studied. The ^{13}C NMR chemical shifts (Table 2, and Figs. 3 and 4) match quite well in the solid and in solution, indicating that the low-temperature solution species is similar to the crystal structure. Only the methyl groups on the bridgeheads have significantly different chemical shifts, presumably because of the different influences of the carbonyl groups). In the crystal, one carbonyl oxygen atom is twisted up from the approximate plane of the attached ring (towards the exo face of the glycoluril) and the other is twisted down (towards the endo face). In solution, there is significantly more motion, so the average magnetic environment will be quite different. The separate shifts for each carbon must be due to the asymmetry, since in the crystal (24), there is only one magnetic environment for the molecule in the unit cell. Separate peaks could arise from different polymorphs, but given the crystal structure this is unlikely. Two-dimensional EXSY experiments (56) on the dipivaloyl (**1**) and diacetyl (**2**) derivatives under CP/MAS conditions at ambient temperature showed no detectable cross peaks, even at mixing times approaching 1 s. It is clear that the crystal packing is sufficiently dense to prevent any exchange, even for the least sterically hindered case (structure **2**).

Conclusions

The acyl derivatives of glycoluril show puckered and asymmetric structures because of interactions among the acyl groups. However, in solution, the NMR spectra show symmetrical structures because of fast exchange among asymmetric conformations. Only for the derivatives with the most bulky groups (dipivaloyl or diadamantyl) and thiocarbonyls in the glycoluril skeleton was it possible to slow the exchange in solution sufficiently to observe separate signals in the NMR spectrum at temperatures around 200 K. The increased steric bulk of the diadamantyl group raised the barrier approximately 4 kJ mol^{-1} over the dipivaloyl group. A change from thiocarbonyl to carbonyl groups in the ring also significantly lowered the barrier. No evidence of exchange broadening was seen in the NMR of **3**, so that rate must be significantly faster. A very rough estimate is that the barrier must be lower by at least 10 kJ mol^{-1}. Therefore, both steric and electronic effects are important in determining the exchange rate. The observation of a metastable state in the cal-

Fig. 3. The ^{13}C CP/MAS spectrum of the solid (upper) and the solution spectrum at 190 K (lower) of 1,6-dipivaloyl-3,4,7,8-tetramethyl-2,5-dithioglycoluril. In the upper spectrum, the peaks marked with an asterisk are spinning sidebands; in the lower spectrum, the marked peaks belong to solvent (CD_2Cl_2).

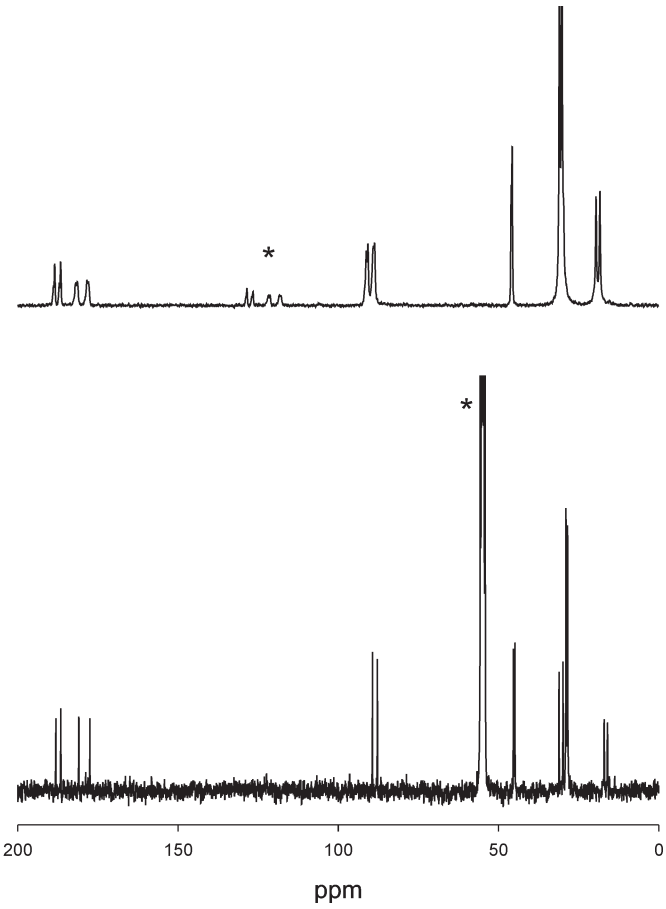
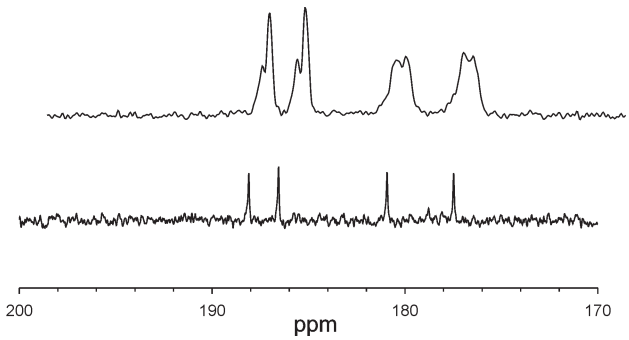


Fig. 4. Expansion of the high frequency region of the specta in Fig. 3, showing the fine structure of the carbonyl and thiocarbonyl peaks owing to dipolar coupling to ^{14}N (59–61). This dipolar coupling is not averaged by spinning at the magic angle, and gives a characteristic 1:2 ratio of peaks. The carbonyl peaks near 188 ppm show this structure in this figure. The thiocarbonyl peaks at lower frequency correspond to carbons bonded to two nitrogens, so they will have three peaks, roughly in the ratio of 1:3:3, as shown in the peaks near 180 ppm.



© 2006 NRC Canada

culations suggests that the exchange may go through this species as an intermediate. One acyl group rotates significantly so that both carbonyls are on the same face, then the other acyl group rotates to complete the exchange.

In the solid-state CP/MAS spectra, the diacetyl and the dipivaloyl derivatives showed no dynamics, even at temperatures of 330 K. Therefore, the crystal lattice plays an important role in restricting the motion of the acyl groups in the solid. This implies that the lattice may affect the geometry of the molecule to some small extent — the geometry in the crystal may not be the lowest-energy geometry of an isolated molecule. However, electronic structure calculations show that the gas-phase structure is very similar to that in solution. Therefore, the crystal lattice confines but does not distort the molecule.

These observations shed light on the intramolecular Claisen-like condensation reactions between the two acyl moieties. There appears to be little restriction on the ground-state conformation of the glycolurils, so the ground state will have little effect on the reaction outcome. Rather, the stability of the enolate formed by the initial deprotonation step is likely to be the major determinant of the regioselectivity of the reaction.

The glycoluril skeleton provides a versatile series of molecules with which to study the structure and dynamics of twisted amides. We are continuing with further investigations.

Experimental

1,6-Dipivaloyl-3,4,7,8-tetramethylglycoluril (3)

The molecule 1,6-dipivaloyl-3,4,7,8-tetramethyl-2,5-dithioglycoluril (**1**) was prepared as previously described (24). The preparation of compounds **2** and **4** are also in the literature (23, 39). The preparation of 1,6-dipivaloyl-3,4,7,8-tetramethylglycoluril (**3**) is reported here. Compound **3** was prepared as a side-product during the attempted sequential acylation of 3,4,7,8-tetramethylglycoluril. Thus, *n*-butyllithium (1.6 mol L^{-1} in hexane, 7.6 mL, 12.1 mmol) was added to a stirred suspension of 3,4,7,8-tetramethylglycoluril (800 mg, 4.04 mmol) in THF (200 mL) at room temperature. The mixture was heated at reflux for 2 h, then cooled to room temperature. Trimethylacetyl chloride (1.5 mL, 18 mmol) was added, and the resulting clear solution was concentrated to dryness. Flash column chromatography (ethyl acetate – hexanes, 30:70) gave pure **3** (120 mg, 8%) as a white solid; mp 138–140 °C. IR (υ_{max}, cm^{-1}): 2967 (C-H), 1733 (C=O), 1707 (C=O), 1436, 1313, 1111, 1077, 940. ^{1}H NMR (300 MHz, CD_2Cl_2, 190 K) δ: 2.81 (s, 6H, NCH_3), 1.69 (s, 3H, CH_3), 1.42 (s, 3H, CH_3), 1.15 (s, 18H, C(CH_3)$_3$). ^{13}C NMR (75 MHz, CD_2Cl_2, 190 K) δ: 181.34 (amide *C*=O), 152.75 (urea *C*=O), 81.71 (N*C*N), 78.57 (N*C*N), 42.98 (*C*Me$_3$), 27.41 (N*C*H$_3$), 26.48 (C(*C*H$_3$)$_3$), 19.69 (*C*H$_3$), 15.92 (*C*H$_3$). MS (EI) *m/e*: 367 (MH^+), 309, 225, 126.

General procedure for preparation of diacyl dithioglycolurils 5–7

To a solution of 2,5-dithio-3,4,7,8-tetramethylglycoluril in dry dichloromethane (7 mL) at room temperature was added the specified base. The mixture was stirred for 5–10 min, then the acyl chloride was added and stirring was continued for 30 min to 1 h. The mixture was extracted with 5% HCl. The organic layer was washed with water, dried over Na_2SO_4, filtered, and concentrated. The product was purified by flash column chromatography in the solvent described.

1,6-Dipropanoyl-2,5-dithioglycoluril (5)

Starting dithioglycoluril (500 mg, 2.43 mmol), proton sponge (501 mg, 2.27 mmol) and propanoyl chloride (0.6 mL, 6.5 mmol) gave, after flash chromatography in 50:50 EtOAc–hexanes, 1,6-dipropionyl-3,4,7,8-tetramethyl-2,5-dithioglycoluril (**5**) (126 mg, 17%). ^{1}H NMR ($CDCl_3$, 200 MHz) δ: 3.44 (m, 2H), 3.24 (s, 6H), 2.99 (m, 2H), 1.90 (s, 3H), 1.57 (s, 3H), 1.18 (t, *J* = 7.2 Hz, 6H). Also produced was 1-propionyl-3,4,7,8-tetramethyl-2,5-dithioglycoluril (150 mg, 23%): ^{1}H NMR ($CDCl_3$, 200 MHz) δ: 7.32 (s, 1H), 3.23–3.38 (m, 2H), 3.32 (s, 3H), 3.16 (s, 3H), 1.74 (s, 3H), 1.62 (s, 3H), 1.42 (t, *J* = 7.2 Hz, 3H).

1,6-Diisobutanoyl-2,5-dithioglycoluril (6)

Starting dithioglycoluril (500 mg, 2.43 mmol), triethylamine (0.9 mL, 6.5 mmol), and isobutanoyl chloride (0.7 mL, 6.5 mmol) gave, after flash chromatography in CH_2Cl_2, 328 mg (43%) of **6**. ^{1}H NMR ($CDCl_3$, 200 MHz) δ: 4.15 (m, 2H), 3.28 (s, 6H), 1.91 (s, 3H), 1.57 (s, 3H), 1.18 (d, *J* = 6.8 Hz, 6H), 1.14 (d, *J* = 6.9 Hz, 6H).

1,6-Di(adamantane-1′-carbonyl)-2,5-dithioglycoluril (7)

Starting dithioglycoluril (100 mg, 0.43 mmol), Et_3N (0.18 mL, 1.3 mmol), and 1-adamantanecarbonyl chloride (258 mg, 1.3 mmol) gave, after flash chromatography in CH_2Cl_2, 64 mg (30%) of **7**. ^{1}H NMR ($CDCl_3$, 200 MHz) δ: 3.23 (s, 6H), 2.03 (s, 3H), 1.57 (s, 3H), 1.19–2.13 (m, 30H).

NMR spectroscopy

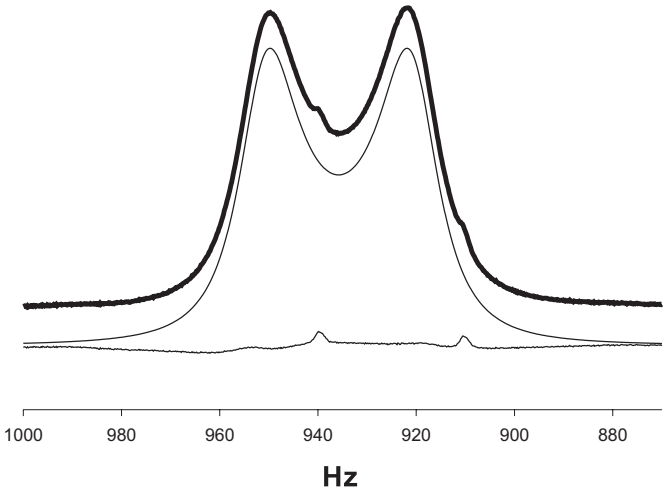
For solution-state NMR spectra, approximately 5 mg of material was dissolved in CD_2Cl_2 and put in a 5 mm NMR tube. Spectra were run on a Bruker AV 300 NMR spectrometer using a 5 mm broadband inverse probe. The 90° pulse for protons was 10 μs. The temperature of the sample was controlled with a BVT 3200 controller. Temperatures shown on the controller were checked against a thermocouple in an NMR tube and the two agreed within 1°. Spectra of the dipivaloyl and the diadamantyl derivatives were run at 183, 193, 215, 220, 225, 235, and 240 K. Both ^{1}H and ^{13}C spectra were acquired as a function of temperature.

Solid-state ^{13}C CP/MAS NMR spectra were run on a Bruker DSX 400 at the University of Toronto. A 4 mm rotor was packed with the material, and the spectra were run with a spinning speed of 6.0 kHz. The number of scans was 1000, the delay between scans was 6.0 s, and the contact time (for a ramped cross polarization) was 4 ms. The FID was apodized with a 20 Hz line broadening. Spectra were referenced to the carbonyl signal of glycine at 176.14 ppm.

Exchange rates were measured from the solution spectra using an iterative version of the MEXICO program (57) (Fig. 5). The natural line width was fixed, and the chemical shift difference and the rate were varied during the iteration. The program allows for both a universal natural line width (applied to all lines in the spectrum) and a specific line width for each spin. In a simple case such as this, the two

© 2006 NRC Canada

Fig. 5. Experimental and simulated ^{1}H NMR line shapes of the *N*-methyl signals in 1,6-dipivaloyl-3,4,7,8-tetramethyl-2,5-dithioglycoluril. The sample was dissolved in CD_2Cl_2, and the spectrum was measured at 200 K on a 300 MHz spectrometer. The heavy line represents the experimental spectrum, the lighter line represents the best fit, and the difference is shown at the bottom. The small peaks in the spectrum that remain in the difference spectrum are due to an unknown impurity.



can not readily be distinguished, so only their sum is significant.

Calculations

Electronic structure calculations were performed using the Gaussian03 suite of programs (58) running on an Intel Pentium-based personal computer under RedHat Linux version 9. The calculations were run with both restricted Hartree–Fock (RHF) and density functional methods (B3LYP) at the 6-31G(d,p) level of theory.

Acknowledgements

We would like to thank Brian G. Sayer and Hiltrud Grondey for help with the NMR measurements, and the Natural Sciences and Engineering Research Council of Canada (NSERC) for financial support.

References

1. A. Greenberg, C.M. Breneman, and J.F. Liebman (*Editors*). The amide linkage. Wiley Interscience, Hoboken, New Jersey. 2003.
2. W.E. Stewart and T.H. Siddall. Chem. Rev. **70**, 517 (1970).
3. S. Yamada. Rev. Heteroat. Chem. **19**, 203 (1999).
4. S. Yamada. *In* The amide linkage. Structural significance in chemistry, biochemistry and materials science. *Edited by* A. Greenberg, C.M. Breneman, and J.F. Liebman. Wiley Interscience, Hoboken, New Jersey. 2003.
5. Q.P. Wang, A.J. Bennet, R.S. Brown, and B.D. Santarsiero. J. Am. Chem. Soc. **113**, 5757 (1991).
6. Q.P. Wang, A.J. Bennet, and R.S. Brown. Can. J. Chem. **68**, 1732 (1990).
7. A.J. Kirby, I.V. Komarov, and N. Feeder. J. Chem. Soc. Perkin Trans. 2, 522 (2001).
8. K.M. Morgan, M.L. Rawlins, and M.N. Montgomery. J. Phys. Org. Chem. **18**, 310 (2005).
9. A.J. Bennet, Q.P. Wang, H. Slebocka-Tilk, V. Somayaji, R.S. Brown, and B.D. Santarsiero. J. Am. Chem. Soc. **112**, 6383 (1990).
10. K.E. Laidig and L.M. Cameron. Can. J. Chem. **71**, 872 (1993).
11. S. Ilieva, B. Hadjieva, and B. Galabov. J. Org. Chem. **67**, 6210 (2002).
12. B. Galabov, S. Ilieva, B. Hadjieva, and E. Dinchova. J. Phys. Chem. A, **107**, 5854 (2003).
13. P. Campomanes, M.I. Menendez, R. Lopez, and T.L. Sordo. J. Comput. Chem. **26**, 365 (2005).
14. J.I. Mujika, J.M. Mercero, and X. Lopez. J. Am. Chem. Soc. **127**, 4445 (2005).
15. X. Lopez, J.I. Mujika, G.M. Blackburn, and M. Karplus. J. Phys. Chem. A, **107**, 2304 (2003).
16. Y. Otani, O. Nagae, Y. Naruse, S. Inagaki, M. Ohno, K. Yamaguchi, G. Yamamoto, M. Uchiyama, and T. Ohwada. J. Am. Chem. Soc. **125**, 15191 (2003).
17. Y.R. Mo, P.V. Schleyer, W. Wu, M.H. Lin, Q. Zhang, and J.L. Gao. J. Phys. Chem. A, **107**, 10011 (2003).
18. P.R. Rablen and K.H. Bentrup. J. Am. Chem. Soc. **123**, 2142 (2003).
19. C.G. Bashore, I.J. Samardjiev, J. Bordner, and J.W. Coe. J. Am. Chem. Soc. **125**, 3268 (2003).
20. S. Yamada, T. Sugaki, and K. Matsuzaki. J. Org. Chem. **61**, 5923 (1996).
21. S. Yamada. Tetrahedron Lett. **33**, 2171 (1992).
22. S. Yamada and H. Katsumata. J. Org. Chem. **64**, 9365 (1999).
23. S. Sun, L. Edwards, and P.H.M. Harrison. J. Chem. Soc. Perkin Trans. 1, 437 (1998).
24. P.A. Duspara, C.F. Matta, S.I. Jenkins, and P.H.M. Harrison. Org. Lett. **3**, 495 (2001).
25. C.N. Cow, J.F. Britten, and P.H.M. Harrison. J. Chem. Soc. Chem. Commun. 1147 (1998).
26. S. Sun, J.F. Britten, C.N. Cow, C.F. Matta, and P.H.M. Harrison. Can. J. Chem. **76**, 301 (1998).
27. F. Borremans, M. Anteunis, U. Shmueli, L. Schleifer, H. Shvo, and B. Fuchs. Tetrahedron, **40**, 257 (1984).
28. H. Iwamura and K. Mislow. Acc. Chem. Res. **21**, 175 (1988).
29. S. Brydges, M.J. McGlinchey, and L.E. Harrington. Coord. Chem. Rev. **233**, 75 (2002).
30. L. Lunazzi, A. Mazzanti, and M. Minzoni. J. Org. Chem. **70**, 456 (2005).
31. T. Fekner, J. Gallucci, and M.K. Chan. J. Am. Chem. Soc. **126**, 223 (2004).
32. G.P. Moss. Pure Appl. Chem. **68**, 2193 (1996).
33. M.R. Plutino, L.M. Scolaro, A. Albinati, and R. Romeo. J. Am. Chem. Soc. **126**, 6470 (2004).
34. M.L. Magri, N. Vanthuyne, C. Roussel, M.B. Garcia, and L.R. Orelli. J. Chromatogr. A, **1069**, 203 (2005).
35. D. Casarini, C. Coluccini, L. Lunazzi, A. Mazzanti, and R. Rompietti. J. Org. Chem. **69**, 5746 (2004).
36. D. Casarini, C. Rosini, S. Grilli, L. Lunazzi, and A. Mazzanti. J. Org. Chem. **68**, 1815 (2003).
37. E. Kolehmainen. Annu. Rep. NMR Spectrosc. **49**, 1 (2003).
38. K. Kam, M. Rahimizadeh, R.S. McDonald, P.H.M. Harrison, H. Chen, S.I. Jenkins, and A. Pedrech. Can. J. Chem. **83**, 1253 (2005).
39. M. Rahimizadeh, K. Kam, S.I. Jenkins, R.S. McDonald, and P.H.M. Harrison. Can. J. Chem. **80**, 517 (2002).
40. Y. Jean, I. Demachy, A. Lledos, and F. Maseras. J. Mol. Struct: THEOCHEM, **632**, 131 (2003).
41. A. Muhlebach, G.P. Lorenzi, and V. Gramlich. Helv. Chim. Acta, **69**, 389 (1986).
42. F.K. Winkler and J.D. Dunitz. J. Mol. Biol. **59**, 169 (1971).

© 2006 NRC Canada

43. S. Yamada. Angew. Chem. Int. Ed. Engl. **32**, 1083 (1993).
44. L.M. Jackman and F.A. Cotton. Dynamic nuclear magnetic resonance spectroscopy. Academic Press, New York. 1975.
45. J. Sandstrom. Dynamic NMR spectroscopy. Academic Press, London. 1982.
46. A.D. Bain. Prog. Nucl. Magn. Reson. Spectrosc. **43**, 63 (2003).
47. J.R. Lyerla, C.S. Yannoni, and C.A. Fyfe. Acc. Chem. Res. **15**, 208 (1982).
48. Z. Dominguez, H. Dang, M.J. Strouse, and M.A. Garcia-Garibay. J. Am. Chem. Soc. **124**, 7719 (2002).
49. U. Berg and Z. Blum. J. Chem. Res (S), 206 (1983).
50. C.B. LeMaster and N.S. True. J. Phys. Chem. **93**, 1307 (1989).
51. T. Fauconnier, A.D. Bain, P. Hazendonk, R.A. Bell, and C.J.L. Lock. Can. J. Chem. **76**, 426 (1998).
52. S.M.N. Crawford, A.N. Taha, N.S. True, and C.B. LeMaster. J. Phys. Chem. A, **101**, 4699 (1997).
53. E. Kleinpeter. J. Mol. Struct. **380**, 139 (1996).
54. J. Sandstrom. J. Phys. Chem. **71**, 2318 (1967).
55. R.C. Neuman, D.N. Roark, and V. Jonas. J. Am. Chem. Soc. **89**, 3412 (1967).
56. J. Jeener, B.H. Meier, P. Bachmann, and R.R. Ernst. J. Chem. Phys. **71**, 4546 (1979).
57. A.D. Bain and G.J. Duns. Can. J. Chem. **74**, 819 (1996).
58. M.J. Frisch, G.W. Trucks, H.B. Schlegel, G.E. Scuseria, M.A. Robb, J.R. Cheeseman, J.A. Montgomery, Jr., T. Vreven, K.N. Kudin, J.C. Burant, J.M. Millam, S.S. Iyengar, J. Tomasi, V. Barone, B. Mennucci, M. Cossi, G. Scalmani, N. Rega, G.A. Petersson, H. Nakatsuji, M. Hada, M. Ehara, K. Toyota, R. Fukuda, J. Hasegawa, M. Ishida, T. Nakajima, Y. Honda, O. Kitao, H. Nakai, M. Klene, X. Li, J.E. Knox, H.P. Hratchian, J.B. Cross, C. Adamo, J. Jaramillo, R. Gomperts, R.E. Stratmann, O. Yazyev, A.J. Austin, R. Cammi, C. Pomelli, J.W. Ochterski, P.Y. Ayala, K. Morokuma, G.A. Voth, P. Salvadori, J.J. Dannenberg, V.G. Zakrzewski, S. Dapprich, A.D. Daniels, M.C. Strain, O. Farkas, D.K. Malik, A.D. Rabuck, K. Raghavachari, J.B. Foresman, J.V. Ortiz, Q. Cui, A.G. Baboul, S. Clifford, J. Cioslowski, B.B. Stefanov, G. Liu, A. Liashenko, P. Piskorz, I. Komaromi, R.L. Martin, D.J. Fox, T.A. Keith, M.A. Al-Laham, C.Y. Peng, A. Nanayakkara, M. Challacombe, P.M.W. Gill, B. Johnson, W. Chen, M.W. Wong, C. Gonzalez, and J.A. Pople. Gaussian03. Revison B.02 [computer program]. Gaussian Inc., Pittsburg, Penn. 2003.
59. M.H. Frey and S.J. Opella. J. Chem. Soc. Chem. Commun. 474 (1980).
60. P. Grondona and A.C. Olivieri. Concepts Magn. Reson. **5**, 319 (1993).
61. K. Eichele, M. Lumsden, and R.E. Wasylishen. J. Phys. Chem. **97**, 8909 (1993).

© 2006 NRC Canada

One-pot, solvent-free synthesis of α-aminonitriles under catalysis by magnesium bromide ethyl etherate

Mohammad M. Mojtahedi, M. Saeed Abaee, and Hassan Abbasi

Abstract: A three-component, efficient, and facile procedure has been developed for the synthesis of α-aminonitriles from aldehydes, amines, and trimethylsilyl cyanide using a catalytic amount of magnesium bromide ethyl etherate in the absence of solvent. Rapid formation of products is observed at room temperature in a one-pot procedure under very mild conditions giving excellent yields of the title compounds.

Key words: catalyzed Strecker's reaction, α-aminonitriles, magnesium bromide, solvent-free.

Résumé : On a développé une méthode simple et efficace pour réaliser la synthèse de α-aminonitriles par réaction monotope d'aldéhydes, d'amines et de cyanure de triméthylsilyle, en présence d'une quantité catalytique du complexe bromure de magnésium/éthérate d'éthyle, en l'absence de solvant. La formation rapide de produits se produit à la température ambiante, dans des conditions très douces et conduit aux composés mentionnés dans le titre avec d'excellents rendements.

Mots clés : réaction de Strecker catalysée, α-aminonitriles, bromure de magnésium, sans solvant.

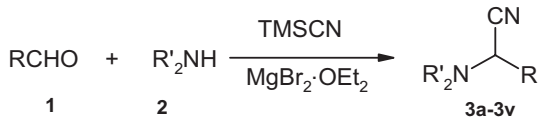
[Traduit par la Rédaction]

Introduction

A three-component combination of aldehydes, amines, and "cyanide", known as Strecker's reaction (1), facilitates the formation of α-aminonitriles (2), which are equivalent synthones to imminium moieties (3) and acyl anions (4). These compounds are very versatile intermediates for the synthesis of α-amino acids (5, 4*b*), 1,2-diamines (6), amides (7), and various nitrogen-containing heterocycles such as thiadiazoles and imidazoles (8). Recent progress such as the development of one-pot procedures for aminative cyanation of carbonyl compounds (9), use of Lewis acidic conditions (10), and employment of new cyanating reagents, especially trimethylsilyl cyanide (TMSCN) (11, 1*a*), have contributed outstanding elaborations (12) to the classical version of the Strecker's reaction (13). However, use of expensive reagents and strong acidic conditions, long reaction times, deactivation and decomposition of the catalytic systems under the reaction circumstances, and production of toxic disposals are still among the deficiencies of many of these methods. Thus, development of efficient, clean, and catalytic reactions for the synthesis of the title structures are still in demand.

In recent years, magnesium bromide ethyl etherate ($MgBr_2{\cdot}OEt_2$) has found many applications as a mild Lewis acid (14) because of its ease of preparation, oxophilic nature, and coordinating ability for bidentate chelation (15) that makes various chelation-controlled organic transformations easier. Our experiences with the use of such reaction conditions (16) prompted us to look for a mild medium for the synthesis of the title compounds. We would like to introduce here an efficient, three-component combination of aldehydes with various amines and TMSCN at room temperature for the synthesis of α-aminonitriles using a catalytic amount of $MgBr_2{\cdot}OEt_2$ (Scheme 1).

Scheme 1.



Results and discussion

Initial experiments were carried out by subjecting a benzaldehyde, pyrrolidine (piperidine), and $MgBr_2{\cdot}OEt_2$ mixture to reaction with TMSCN at room temperature in the absence of solvent (Table 1). Complete disappearance of the aldehyde and rapid formation of the product were monitored by TLC. Various amounts of the Lewis acid were used to optimize the reaction conditions. A catalytic quantity of $MgBr_2{\cdot}OEt_2$ (5 mol%) proved to be effective for the complete conversion of starting materials to the desired product (**3a** or **3b**) in 5 min (Table 1, entry 1). Use of smaller amounts of the catalyst down to 1 mol% only prolonged the reaction time up to 45 min, leading to nearly quantitative formation of **3a** (or **3b**). Similar reactions using various aromatic aldehydes bearing electron-withdrawing and electron-releasing groups with cyclic amines were conducted under the same conditions. Consequently, more than 90% yields of

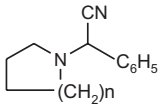
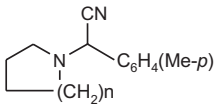
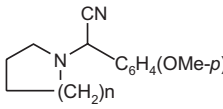
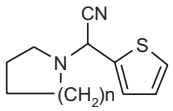
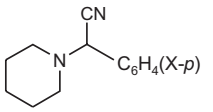
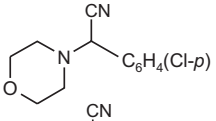
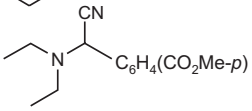
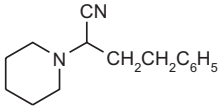
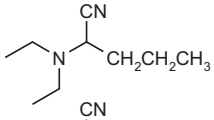
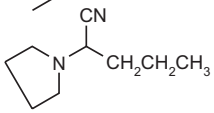
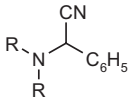
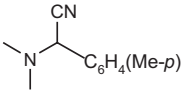
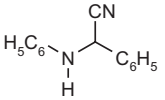
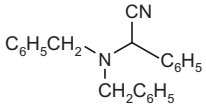
Received 30 December 2005. Published on the NRC Research Press Web site at http://canjchem.nrc.ca on 31 March 2006.

M.M. Mojtahedi,[1] M.S. Abaee, and H. Abbasi. Chemistry and Chemical Engineering Research Center of Iran, P.O. Box 14335-186, Tehran, Iran.

[1]Corresponding author (e-mail: mojtahedi@ccerci.ac.ir).

 doi:10.1139/V06-024 © 2006 NRC Canada

Table 1. Room-temperature $MgBr_2 \cdot OEt_2$-catalyzed synthesis of α-aminonitriles.

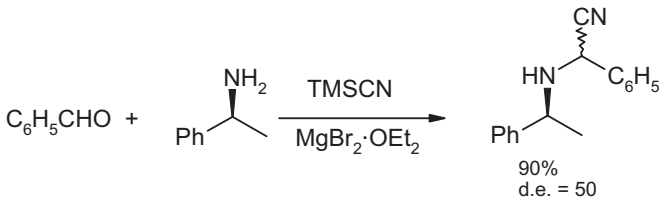
Entry	Aldehyde	Amine	Product		Yield (%)[a]
1	C_6H_5CHO	Pyrrolidine Piperidine		**3a**: *n* = 1 **3b**: *n* = 2	94 93
2	(*p*-Me)C_6H_4CHO	Pyrrolidine Piperidine		**3c**: *n* = 1 **3d**: *n* = 2	94 94
3	(*p*-OMe)C_6H_4CHO	Pyrrolidine Piperidine		**3e**: *n* = 2 **3f**: *n* = 2	93 96
4	2-Thiophen-CHO	Pyrrolidine Piperidine		**3g**: *n* = 2 **3h**: *n* = 2	91 93
5	(*p*-X)C_6H_4CHO	Piperidine		**3i**: X = F **3j**: X = Cl	98 93
6	(*p*-Cl)C_6H_4CHO	Morpholine		**3k**	94
7	(*p*-CO_2Me)C_6H_4CHO	$HNEt_2$		**3l**	96
8	$C_6H_5CH_2CH_2CHO$	Piperidine		**3m**	92
9	$CH_3CH_2CH_2CHO$	$HNEt_2$		**3n**	88
10	$CH_3CH_2CH_2CHO$	Pyrrolidine		**3o**	91
11	C_6H_5CHO	$TMSNMe_2$ $HNEt_2$ $HNBu_2$		**3p**: R = Me **3q**: R = Et **3r**: R = Bu	97 88 94
12	(*p*-Me)C_6H_4 CHO	$TMSNMe_2$		**3s**	91
13	C_6H_5CHO	Aniline		**3t**	88
14	C_6H_5CHO	$HN(CH_2C_6H_5)_2$		**3u**	90

[a]Isolated yields.

products **3c**–**3l** were all easily obtained in less than 10 min (Table 1, entries 2–7). The methodology proved to be equally effective for the smooth conversion of aliphatic aldehydes into α-aminonitriles when 3-phenyl-propionaldehyde or butyraldehyde were subjected to the reaction conditions (Table 1, entries 8–10).

© 2006 NRC Canada

Scheme 2.



The procedure was further explored using acyclic amines. Reactions between *N*-trimethylsilyldimethylamine ($TMSNMe_2$), diethylamine ($HNEt_2$), or dibuthylamine ($HNBu_2$) with benzaldehyde (Table 1, entry 11) and $TMSNMe_2$ with *p*-methylbenzaldehyde (Table 1, entry 12) resulted in rapid formation of products **3p** (97%), **3q** (88%), **3r** (94%), and **3s** (91%), respectively. Use of aromatic amines was successfully examined by a reaction between benzaldehyde and aniline leading to 88% formation of **3t** (Table 1, entry 13). Due to the synthetic importance of *N*,*N*-dibenzyl protected α-aminonitriles (17), the present procedure was employed to attempt the preparation of these compounds. As an example, the reaction between benzaldehyde and dibenzylamine in the presence of TMSCN and $MgBr_2{\cdot}OEt_2$ facilitated 90% formation of **3u** (Table 1, entry 14).

To test the diastereoselectivity of the process, a test reaction between (*S*)-1-phenylethylamine and benzaldehyde was conducted under the same sets of conditions leading to formation of **3v** in 90% yield within a few minutes. NMR spectroscopy of the reaction mixture revealed the formation of both possible products with a moderate diastereoselectivity of 3:1 (Scheme 2).

In summary, we have demonstrated a highly efficient, three-component conversion of aldehydes, amines, and TMSCN to α-aminonitriles at room temperature using a catalytic amount of $MgBr_2{\cdot}OEt_2$ in the absence of any solvent. The procedure is applicable to various aromatic and aliphatic aldehydes and amines. The versatility of the reaction, production of pure single compounds, easy procedure and work up, and no use of solvent or extra additives are among other benefits of the present method.

Experimental

General procedure

A mixture of aldehyde (2 mmol), amine (4 mmol), and $MgBr_2{\cdot}OEt_2$ (5 mol% in respect to aldehyde) was stirred at room temperature for 5 min. TMSCN (2.4 mmol) was added to this mixture and stirring continued for an appropriate length of time until TLC showed completion of the reaction. The product was extracted three times by 10 mL portions of diethyl ether and the combined etheral phases were washed with brine and dried over sodium sulphate. The solvent was removed under reduced pressure and the product was purified by column chromatography over silica gel using an EtOAc–hexane eluant, if necessary. The isolated yields of the products were 88%–98%. All products were identified by ^{1}H NMR, ^{13}C NMR, IR, and mass spectroscopic methods and the results were compared with those available in the literature.[2]

Selected spectral data

(4-Methoxy-phenyl)-piperidin-1-yl-acetonitrile (3f)

IR (neat, cm^{-1}) ν: 2219, 1513, 1250. ^{1}H NMR (80 MHz, $CDCl_3$) δ: 1.22–1.50 (m, 6H), 2.25–2.50 (m, 4H), 3.65 (s, 3H), 4.61 (s, 1H), 6.77 (d, J = 8 Hz, 2H), 7.27 (d, J = 8 Hz, 2H). ^{13}C NMR (20 MHz, $CDCl_3$) δ: 23.7, 25.5, 50.4, 54.9, 61.9, 113.7, 115.5, 125.3, 128.7, 159.5. MS *m*/*z*: 230 (M^+), 204, 146, 121, 84.

Piperidin-1-yl-thiophen-2-yl-acetonitrile (3h)

IR (neat, cm^{-1}) ν: 3107, 2937, 2368, 1442. ^{1}H NMR (80 MHz, $CDCl_3$) δ: 1.30–1.75 (m, 6H), 2.25–2.70 (m, 4H), 4.85 (s, 1H), 6.80–7.32 (m, 3H). ^{13}C NMR (20 MHz, $CDCl_3$) δ: 23.7, 25.5, 50.7, 58.5, 114.7, 126.2, 126.5, 126.7, 137.8. MS *m*/*z*: 206 (M^+), 122, 97, 84.

(4-Fluoro-phenyl)-piperidin-1-yl-acetonitrile (3i)

IR (neat, cm^{-1}) ν: 2928, 2808, 2224, 1608. ^{1}H NMR (80 MHz, $CDCl_3$) δ: 1.30–1.75 (m, 6H), 2.38–2.45 (m, 4H), 4.72 (s, 1H), 6.89–7.54 (m, 4H). ^{13}C NMR (20 MHz, $CDCl_3$) δ: 23.6, 25.5, 50.6, 63.4, 115.3, 116.4, 129.1, 129.5, 214.8. MS *m*/*z*: 218 (M^+), 217, 134, 123, 107.

4-Phenyl-2-piperidin-1-yl-butyronitrile (3m)

IR (neat, cm^{-1}) ν: 3027, 2937, 2222, 1684. ^{1}H NMR (80 MHz, $CDCl_3$) δ: 1.32–1.80 (m, 6H), 2.03 (t, J = 7 Hz, 2H), 2.20–2.82 (m, 6H), 3.40 (t, J = 8 Hz, 1H), 7.14–7.19 (m, 5H). ^{13}C NMR (20 MHz, $CDCl_3$) δ: 23.9, 25.6, 31.5, 32.2, 50.8, 57.1, 115.6, 126.1, 128.3, 139.8, 215.0. MS *m*/*z*: 228 (M^+), 201, 123, 110.

Acknowledgments

The Ministry of Science, Research, and Technology of Iran is gratefully acknowledged for partial financial support of this work.

References

1. (*a*) A. Strecker. Liebigs. Ann. Chem. **75**, 27 (1850); (*b*) H. Ishitani, S. Komiyama, Y. Hasegawa, and S. Kobayashi. J. Am. Chem. Soc. **122**, 762 (2000); (*c*) L. Yet. Angew. Chem. Int. Ed. **40**, 875 (2001).
2. (*a*) D. Enders and J.P. Shilvock. Chem. Soc. Rev. **29**, 359 (2000); (*b*) M. North. Angew. Chem. Int. Ed. **43**, 4126 (2004).
3. (*a*) D.B. Grotjahn, R.J. Albers, and J. Beckman. Synlett, 633 (2000); (*b*) G. Stork. Pure Appl. Chem. **61**, 439 (1989); (*c*) R.B. Woodward, F.E. Bader, H. Bickel, A.J. Frey, and R.W. Kierstead. J. Am. Chem. Soc. **78**, 2023 (1956); (*d*) R.B. Woodward, F.E. Bader, H. Bickel, A.J. Frey, and R.W. Kierstead. J. Am. Chem. Soc. **78**, 2657 (1956).
4. (*a*) C.R. Hauser, H.M. Taylor, and T.G. Ledford. J. Am. Chem. Soc. **82**, 1786 (1960); (*b*) J.D. Albright. Tetrahedron, **39**, 3207 (1983); (*c*) H.M. Taylor and C.R. Hauser. J. Am. Chem. Soc. **82**, 1790 (1960).

[2] Supplementary data for this article are available on the journal Web site (http://canjchem.nrc.ca) or may be purchased from the Depository of Unpublished Data, Document Delivery, CISTI, National Research Council Canada, Ottawa, ON K1A 0R6, Canada. DUD 5013.

© 2006 NRC Canada

5. (*a*) A.J. Davies, M.S. Ashwood, and I.F. Cottrell. Synth. Commun. **30**, 1095 (2000); (*b*) W.H.J. Boesten, J.P.G. Seerden, B. Lange, H.J.A. Dielemans, H.L.M. Elsenberg, B. Kaptein, H.N. Kellogg, and Q.B. Broxtermann. Org. Lett. **3**, 1121 (2001); (*c*) Y.M. Shafran, V.A. Bakulev, and V.S. Mokrushin. Russ. Chem. Rev. **58**, 148 (1989).
6. E. Leclerc, P. Mangency, and V. Henryon. Tetrahedron: Asymmetry, **11**, 3471 (2000).
7. (*a*) D. Enders, A.S. Amaya, and F. Pierre. New J. Chem. **23**, 261 (1999); (*b*) T.H. Chuang, C.C. Yang, C.J. Chang, and J.M. Fang. Synlett, 733 (1990).
8. (*a*) L.M. Weinstock, P. Davis, B. Handelsman, and R. Tull. J. Org. Chem. **32**, 2823 (1967); (*b*) W.L. Matier, D.A. Owens, W.T. Comer, D. Deitchman, H.C. Fergusen, R.J. Seidehamel, and J.R. Young. J. Med. Chem. **16**, 901 (1973); (*c*) J.P. Leblanc and H.W. Gibson. J. Org. Chem. **59**, 1072 (1994); (*d*) J.A. Gonzalez-Vera, M.T. Garcia-Lopez, and R. Herranz. J. Org. Chem. **70**, 3660 (2005).
9. (*a*) J.S. Yadav, B.V.S. Reddy, B. Eshwaraiah, and M. Srinivas. Tetrahedron, **60**, 1767 (2004); (*b*) W.Y. Chen and J. Lu. Synlett, 2293 (2005); (*c*) D.E. Fuerst and E.N. Jacobsen. J. Am. Chem. Soc. **127**, 8964 (2005); (*d*) E. Takahashi, H. Fujisawa, T. Yanai, and T. Mukaiyama. Chem. Lett. **34**, 604 (2005).
10. (*a*) S.K. De and R.A. Gibbs. Tetrahedron Lett. **45**, 7407 (2004); (*b*) L. Royer, S.K. De, and R.A. Gibbs. Tetrahedron Lett. **46**, 4595 (2005); (*c*) M. Suginome, A. Yamamoto, and Y. Ito. Chem. Commun. (Cambridge), 1392 (2002); (*d*) L. Bernardi, B.F. Bonini, E. Capit, G. Dessole, M. Fochi, M. Comes-Franchini, and A. Ricci. Synlett, 1778 (2003); (*e*) N. Azizi and M.R. Saidi. Synth. Commun. **34**, 1207 (2004); (*f*) R. Yousefi, N. Azizi, and M.R. Saidi. J Organomet. Chem. **690**, 76 (2005); (*g*) B.C. Ranu, S.S. Dey, and A. Hajra. Tetrahedron, **58**, 2529 (2002); (*h*) S.K. De. J. Mol. Catal. A: Chem. **225**, 169 (2005); (*i*) S.K. De and R.A. Gibbs. Synth. Commun. **35**, 961 (2005); (*j*) E. Takahashi, H. Fujisawa, T. Yanai, and T. Mukaiyama. Chem. Lett. **34**, 318 (2005); (*k*) S.K. De. Synth. Commun. **35**, 653 (2005); (*l*) S.K. De. Synth. Commun. **35**, 1577 (2005).
11. (*a*) A.S. El-Ahl. Synth. Commun. **33**, 989 (2003); (*b*) M. Takamura, Y. Hamashima, H. Usuda, M. Kanai, and M. Shibasaki. Angew. Chem. Int. Ed. **39**, 1650 (2000); (*c*) M. Takamura, Y. Hamashima, H. Usuda, M. Kanai, and M. Shibasaki. Chem. Pharm. Bull. **48**, 1586 (2000); (*d*) M. Chavarot, J.J. Byrne, P.Y. Chavant, and Y. Vallee. Tetrahedron: Asymmetry, **12**, 1147 (2001); (*e*) K. Mai and G. Patil. Tetrahedron Lett. **25**, 4583 (1984).
12. (*a*) J.T. Su, P. Vachal, and E.N. Jacobsen. Adv. Synth. Catal. **343**, 197 (2001); (*b*) F.A. Davis, S. Lee, H. Zhang, and D.L. Fanelli. J. Org. Chem. **65**, 8704 (2000); (*c*) F.A. Davis, P.S. Portonovo, R.E. Reddy, and Y.H. Chiu. J. Org. Chem. **61**, 440 (1996); (*d*) M.S. Sigman and E.N. Jacobsen. J. Am. Chem. Soc. **120**, 4901 (1998); (*e*) G. Jenner, R.B. Salem, J.C. Kim, and K. Matsumoto. Tetrahedron Lett. **44**, 447 (2003); (*f*) P.P. Sun, C.T. Qian, L.M. Wang, and R.F. Chen. Synth. Commun. **32**, 2973 (2002).
13. J.M. Fang, C.C. Yang, and Y.W. Wang. J. Org. Chem. **54**, 481 (1989).
14. (*a*) C. Malanga and S. Mannucci. Tetrahedron Lett. **42**, 2023 (2001); (*b*) S. Yamada, S. Yaguchi, and K. Matsuda. Tetrahedron Lett. **43**, 647 (2002); (*c*) S.K. Tipparaju, S.K. Mandal, S. Sur, V.G. Puranik, and A. Sarkar. Chem. Commun. (Cambridge), 1924 (2002); (*d*) B.Z. Zheng, M. Yamauchi, H. Dei, S. Kusaka, K. Matsui, and O. Yonemitsu. Tetrahedron Lett. **41**, 6441 (2000); (*e*) A. Vakalopoulos and H.M. Hoffmann. Org. Lett. **2**, 1447 (2000); (*f*) T. Onoda, R. Shirai, and S. Iwasaki. Tetrahedron Lett. **38**, 1443 (1997); (*g*) P. Lupattelli, C. Bonini, L. Caruso, and A. Gambacorta. J. Org. Chem. **68**, 3360 (2003); (*h*) S.K. Tipparaju, V.G. Puranik, and A. Sarkar, Org. Biomol. Chem. **1**, 1720 (2003); (*i*) D.E. Ward, M.J. Hrapchak, and M. Sales. Org. Lett. **2**, 57 (2000); (*j*) T. Abe, C. Sato, H. Ushirogochi, K. Sato, T. Takasaki, T. Isoda, A. Mihira, I. Yamamura, K. Hayashi, T. Kumagai, S. Tamai, M. Shiro, A.M. Venkatesan, and T.S. Mansour. J. Org. Chem. **69**, 5850 (2004); (*k*) H. Fujisava, Y. Saski, and T. Mukaiyama. Chem. Lett. **30**, 190 (2001).
15. S.K. Tipparaju. Synlett, 912 (2004).
16. (*a*) D.E. Ward and M.S. Abaee. Org. Lett. **2**, 3937 (2000); (*b*) M.S. Abaee, R. Sharifi, and M.M. Mojtahedi. Org. Lett. **7**, 5893 (2005); (*c*) M.S. Abaee, M.M. Mojtahedi, M.M. Zahedi, and R. Sharifi. Heteroatom Chem. In press.
17. (*a*) P. Sun, C. Qian, L. Wang, and R. Chen. Synth. Commun. **32**, 2973 (2002); (*b*) R. Martinez, D.J. Ramon, and M. Yus. Tetrahedron Lett. **46**, 8471 (2005).

© 2006 NRC Canada

Antimony(III) chloride impregnated on alumina — An efficient and economical Lewis acid catalyst for one-pot synthesis of dihydropyrimidinones under solvent-free conditions

Kamal. K. Kapoor, Bilal A. Ganai, Satish Kumar, and Charanjeet S. Andotra

Abstract: The antimony(III) chloride impregnated on alumina efficiently catalyses a one-pot, three-component condensation reaction among an aldehyde, a β-ketoester, and urea or thiourea to afford the corresponding dihydropyrimidinones in good to excellent yields. The reactions are probed in microwave (MW), ultrasonic, and thermal conditions and the best results are found using MW under solvent-free conditions.

Key words: Biginelli dihydropyrimidinones synthesis, $SbCl_3$–Al_2O_3, MW, sonication, solid supported.

Résumé : Le chlorure d'antimoine(III) imprégné sur de l'alumine catalyse efficacement la réaction de condensation monotope de trois composants, un aldéhyde, un β-cétoester et une urée ou une thiourée, pour conduire à la formation des dihydropyrimidinones correspondants avec des rendements allant de bons à excellents. Les réactions ont été réalisées sous l'influence de micro-ondes (MO), d'ultrasons ou de la chaleur et on a trouvé que les conditions de micro-ondes, sans solvant, donnent les meilleurs résultats.

Mots clés : synthèse de Biginelli de dihydropyrimidinones, $SbCl_3$–Al_2O_3, micro-ondes, soniquation, supporté sur un solide.

[Traduit par la Rédaction]

Introduction

The dihydropyrimidinones (DHPMs) and their derivatives have attracted considerable interest in organic and medicinal chemistry because of their fascinating array of pharmacological and therapeutic properties such as antiviral, antitumor, antibacterial, and antiinflammatory calcium channel blockers, antihypertensives, α_{1a}-adrenergic antagonists, and neuropeptide Y (NPY) antagonists (1, 2). Moreover, the potent HIVgp–120–CD_4 inhibitor batzelladine alkaloids (3) basically contain a dihydropyrimidine core unit. A simple synthesis of this biologically important pharmacophore was reported (4) by Biginelli in 1893 by one-pot reflux of a β-ketoester, an aromatic aldehyde, and urea in ethanol containing a catalytic amount of HCl. The major drawbacks of this protocol are low yields of products (20%–50%) and less functional group tolerance on the reactants. Consequently, this has led to the discovery of multistep strategies producing somewhat higher yields, but lacking the simplicity of original Biginelli reaction (5). Therefore, this reaction continues to be the focus of the researchers striving to find milder and more efficient procedures for the synthesis of DHPMs. This has led to the development of several synthetic methodologies using various catalysts (6) such as $BF_3{\cdot}OEt_2$, $InCl_3$, $BiCl_3$, $LiCl_4$, $ZrCl_4$, $La(OTf)_3$, $NiCl_2$, $FeCl_3$, KSF, $Yb(OTf)_3$, PPE, $Bi(OTf)_3$, CAN, $CuCl_2$, $CeCl_3$, $Cu(OTf)_2$, Me_3SiI, $LiBr_2$, $MgBr_2$, $InBr_3$, NH_4Cl, $SrCl_2$, silica-sulphuric acid, boric acid, and ionic liquids. However, in spite of their potential utility, many of these methods involve expensive reagents, a stoichiometric amount of catalysts, strongly acidic conditions, longer reaction times, high temperature, unsatisfactory yields, and tedious work-up.

The use of reagents impregnated on inorganic supports (7) offer advantages such as (*a*) simple work-up and product purification, (*b*) enhanced or reduced reactivity of the functional groups, (*c*) selectivity that may be different from that in solution, and (*d*) manipulative simplicity. Among the large number of Lewis acids used in organic synthesis, antimony(III) chloride has not been explored much for its catalytic activity. Recently, synthesis of some novel heterocycles catalyzed by antimony(III) chloride under solvent-free conditions has been reported from our laboratory (8). We wished to explore the use of antimony(III) chloride impregnated on alumina for the synthesis of DHPMs.

The condensation reaction between benzaldehyde (10 mmol), ethyl acetoacetate (10 mmol), and urea (10 mmol) was carried out in a microwave (MW) under solvent-free conditions for 1 min with 0.5 mmol (5 mol%, 0.05 equiv.) of antimony(III) chloride, (*i*) alone and (*ii*) impregnated on different amounts of alumina (1–8 g), which gave yields of 42%, 70%, 96%, 93%, 90%, 74%, 60%, and 45%, respectively, as shown in Fig. 1. In the absence of alumina, the reaction gave a low yield of the product (**4a**). However, increasing the amounts of antimony(III) chloride to 0.1, 0.2, 0.5, and 1.0 equiv. resulted in the formation of an unidentifiable tarry

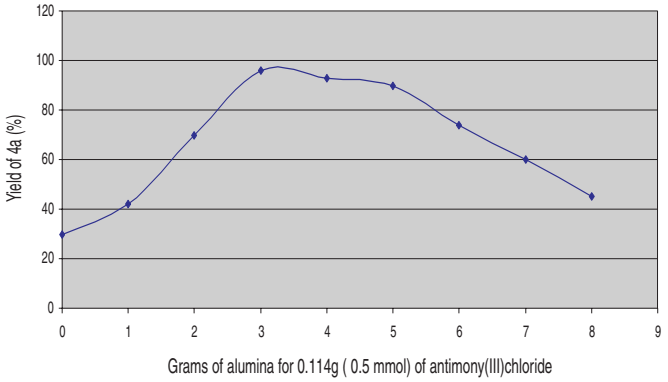
Received 7 December 2005. Published on the NRC Research Press Web site at http://canjchem.nrc.ca on 31 March 2006.

K.K. Kapoor,[1] B.A. Ganai, S. Kumar, and C.S. Andotra. Department of Chemistry, University of Jammu, Jammu Tawi-180 006, India.

[1]Corresponding author (e-mail: k2kapoor@yahoo.com).

 doi:10.1139/V06-019 © 2006 NRC Canada

Fig. 1. The influence of the amount of alumina on the yields of reaction.



material. It is evident that the amount of alumina used for impregnation is decisive in the completion of the three-component reaction. The results reveal that the most appropriate ratio of antimony(III) chloride and alumina is approximately 1:26 (*w*/*w*), which gives 96% isolated yield of **4a**. The decrease or increase of the amount of alumina led to the decrease in the yield of the desired product. It is presumed that the alumina acts as a carrier increasing the surface area of the heterogeneous reaction, and it is very probable that the antimony salt interacts with the oxide groups at the surface of the support forming new active sites on the alumina local structure.

In another set of experiments, when the reaction mixture comprised of benzaldehyde (10 mmol), ethyl acetoacetate (10 mmol), urea (10 mmol), and 5 mol% of antimony(III) chloride (0.5 mmol) impregnated on 3 g of alumina was (*i*) heated at 100 °C on an oil bath without any solvent, a clean conversion to **4a** (95% yield) was noticed in less than 1 h and (*ii*) sonicated in an ultrasonicator in a variety of solvents such as water, tetrahydrofuran, acetonitrile, chloroform, toluene, and THF–H_2O, produced the results summarized in Table 1. From Table 1, acetonitrile appears to be the best solvent (yield 94% in 1 h) of all the solvents tested under similar reaction conditions. The present findings in the ultrasonicator are superior in terms of yield and time to the earlier reported method (6*q*).

Encouraged by these results and to establish the versatility of antimony(III) chloride impregnated on alumina, various substrates were subjected to the optimized condensation reaction and the results are depicted in Table 2.

The efficiency of $SbCl_3$–Al_2O_3 as a Lewis acid catalyst is comparable to those reported in the literature (6), such as BF_3·OEt, $FeCl_3$, $Bi(OTf)_3$, $Yb(OTf)_3$, $InCl_3$, $Sc(OTf)_3$, $YbCl_3$, $MgBr_3$, and $SrCl_2$, as is evident from Table 3. The present catalyst, $SbCl_3$–Al_2O_3, enjoys benefits in terms of easy handling, economy, and simple workup (Scheme 1).

The reaction is believed to proceed through the acylimine intermediate formed in situ by reaction of the aldehyde with urea. The subsequent addition of the β-diketon enolate to the acylimine, followed by cyclization and dehydration, afforded the corresponding DHPMs (Scheme 2).

Conclusion

In conclusion, we have unraveled a newer application of $SbCl_3$ as a Lewis acid supported on alumina for the synthesis of DHPMs.The present catalyst is cheap, easily available, easy to handle, and works efficiently in MW, thermal, and ultrasonic conditions.

Table 1. Various solvents used for the synthesis of **4a** in an ultrasonicator.

Entry	Solvent	Time (h)	Yield (%)
1	H_2O	3	15
2	THF	4	40
3	THF–H_2O (3:2)	3	20
4	$CHCl_3$	5	45
5	CH_3CN	1	94
6	Toluene	5	50

Experimental

General

Melting points were measured in open capillaries on a Perfit melting point apparatus and are uncorrected. IR on KBr were recorded on a Bruker-4800 IR spectrometer. ^1H and ^{13}C NMR spectra were recorded on a Bruker AC-200 spectrometer. The mass spectra were obtained on a JEOL D-300 mass spectrometer. TLC was performed on 0.5 mm thick plates using BDH silica gel G as adsorbent and eluted in a 1:1 mixture of EtOAc and petroleum ether. The plates were developed with iodine vapors, 2,4-dinitrophenylhydrazone in acidic methanol solution, and anisaldehyde solution in acidic alcohol. All solvents were distilled before use. Microwave irradiation was carried out in an IFB microwave oven at the 5 power level and the sonication was carried out in a Bransonic-2510 ultrasonic cleaner.

General procedures

Preparation of the catalyst $SbCl_3$–Al_2O_3

To an antimony(III) chloride (2.28 g, 10 mmol) solution in 100 mL of distilled ethanol was added 60 g of neutral alumina. The mixture was stirred at room temperature for 1 h, followed by removal of solvent under reduced pressure on a rotovap. The resultant free-flowing powder was then activated at 110 °C in an oven for 2 h and was used throughout the experimentation.

Typical procedures for the three-component condensation reaction

(i) Under microwave irradiation

A mixture of ethyl acetoacetate (10 mmol), aryl aldehyde (10 mmol), urea (10 mmol), and the 3.1 g of the catalyst was placed in a 100 mL beaker. It was then irradiated in an IFB microwave oven at the 5 power level until the completion of reaction as monitored by TLC. The reaction mixture was cooled to room temperature and ethyl acetate (100 mL) was added, stirred well, and filtered through Celite under suction. The organic layer was washed twice with water (30 mL) and brine (30 mL). After drying over anhydr. Na_2SO_4, the solvent was evaporated under reduced pressure and the residue was recrystallized from ethanol to afford the pure product.

© 2006 NRC Canada

Table 2. $SbCl_3$–Al_2O_3 catalyzed synthesis of DHPMs.

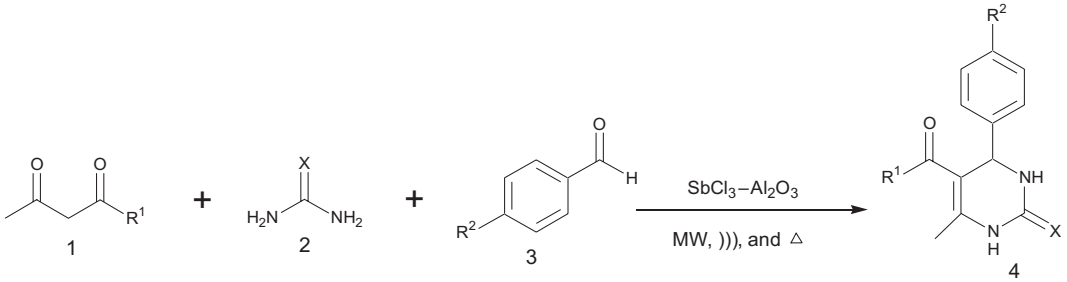
	Subsititution			Time (min), (yield in %)[b]			Melting point[c] (°C)	
Product[a]	R^1	R^2	X	Thermal	MW	Sonication	Obs.	Lit. (ref. 6)
4a	OEt	H	O	55 (95)	1.0 (96)	60 (94)	203 to 204	202–204
4b	OEt	OMe	O	70 (92)	1.5 (94)	75 (92)	201 to 204	201–203
4c	OEt	Cl	O	50 (89)	1.0 (90)	80 (90)	211–214	213–215
4d	OEt	F	O	75 (91)	1.5 (92)	90 (87)	177 to 178	175–177
4e	OEt	NO_2	O	60 (88)	2.0 (90)	60 (86)	210–212	208–211
4f	OEt	OH	O	65 (90)	2.5 (92)	90 (90)	233–235	232 to 233
4g	Me	H	O	45 (90)	1.0 (96)	75 (87)	240–242	242–244
4h	OMe	H	O	50 (83)	2.0 (96)	90 (84)	209–212	208–210
4i	OMe	OMe	O	75 (84)	2.0 (95)	90 (91)	193–195	192–194
4j	OMe	Cl	O	60 (91)	1.5 (94)	70 (89)	203–205	204–207
4k	OMe	NO_2	O	65 (80)	1.5 (82)	60 (93)	234 to 235	235–237
4l	OMe	F	O	70 (92)	2.0 (94)	65 (87)	190 to 191	192–194
4m	OEt	H	S	80 (89)	2.0 (95)	65 (89)	205–207	207 to 208
4n	OMe	H	S	80 (90)	1.5 (94)	85 (90)	235–237	236–238
4o	OEt	OMe	S	65 (81)	2.0 (91)	90 (84)	152 to 153	152 to 153

[a]All products were characterized by ^{1}H NMR, IR, and mass spectra.
[b]Isolated yields.
[c]Melting points are uncorrected.

Table 3. Comparison of various catalysts with $SbCl_3$–Al_2O_3 for the synthesis of **4a**.

Entry	Catalyst used	Reaction conditions	Amount of catalyst (mol%)	Yield (%)	Reference
1	$SbCl_3$–Al_2O_3	CH_3CN, sonication, 1 h	5	94	—
2	BF_3·OEt–CuCl	THF, reflux, 18 h	130	94	6*o*
3	$FeCl_3$–HCl	EtOH, reflux, 4 h	60	93	6*n*
4	$Bi(OTf)_3$	CH_3CN, rt, 1 h	2	90	6*b*
5	$Yb(OTf)_3$	CH_3CN, reflux, 6 h	5	83	6*r*
6	$InCl_3$	THF, Δ, 7 h	10	95	6*v*
7	$SbCl_3$–Al_2O_3	No solvent, 100 °C	5	95	—
8	$Sc(OTf)_3$	No solvent, 100 °C	5	96	6*r*
9	$YbCl_3$	No solvent, 100 °C	5	66	6*r*
10	MgBr	No solvent, 100 °C	10	92	6*u*
11	$La(OTf)_3$	No solvent, 100 °C	5	89	6*r*
12	$SbCl_3$	No solvent, MW	5	30	—
13	$SbCl_3$–Al_2O_3	No solvent, MW	5	96	—

Scheme 1.



(ii) Under thermal conditions

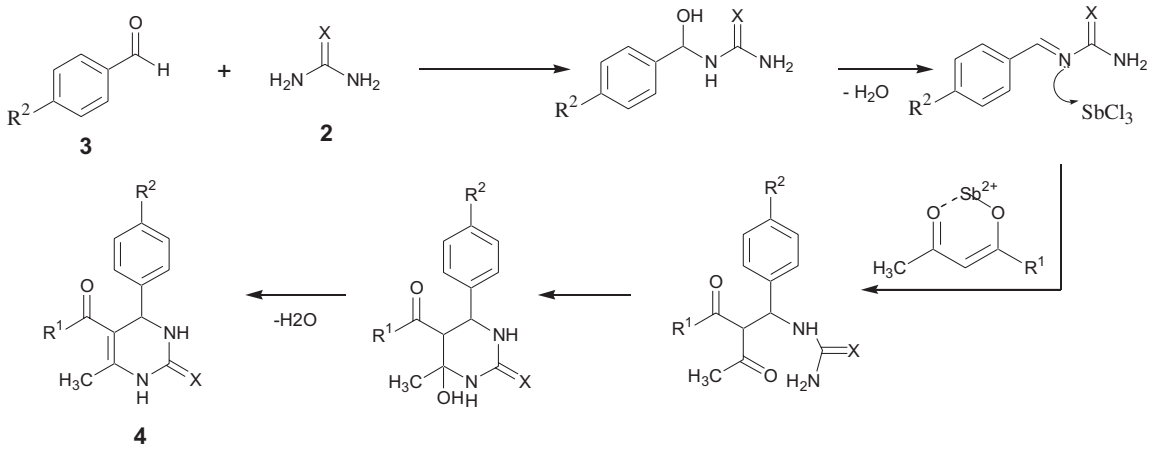
A mixture of ethyl acetoacetate (10 mmol), aryl aldehyde (10 mmol), urea (10 mmol), and 3.1 g of the catalyst was placed in a 100 mL round bottom flask was heated on an oil bath at 100 °C until the completion of the reaction as monitored by TLC. The reaction mixture was cooled to room temperature and worked up in the same manner as mentioned in (*i*).

(iii) Under sonication

A mixture of ethyl acetoacetate (10 mmol), aryl aldehyde (10 mmol), urea (10 mmol), and the 3.1 g of catalyst was

© 2006 NRC Canada

Scheme 2.



placed in a 100 mL round bottom flask containing 15 mL of acetonitrile. After the completion of the reaction (TLC), the solvent was removed and ethyl acetate was added to the residue and worked up in the same manner as mentioned in (*i*).

5-Ethoxycarbonyl-6-methyl-4-phenyl-3,4-dihydropyrimidin-2(1*H*)-one (4a)

Melting point 203 to 204 °C. IR (KBr, cm^{-1}): 3233, 3110, 2975, 2938, 1725, 1708, 1650, 1595. ^{1}H NMR (DMSO-d_6) δ: 1.12 (t, *J* = 7.2 Hz, 3H), 2.29 (s, 3H), 4.02 (q, *J* = 7.2 Hz, 2H), 5.19 (d, *J* = 2.7 Hz), 7.27–7.42 (m, 5H), 7.75 (d, *J* = 2.7 Hz, 1H), 9.21 (s, 1H). ^{13}C NMR (DMSO-d_6, 75 MHz) δ: 14.1, 17.9, 54.2, 59.3, 99.5, 126.4, 127.4, 128.5, 145.0, 148.5, 152.3, 165.5. MS *m*/*z*: 261 (M^+ + 1).

5-Ethoxycarbonyl-4-(4-methoxyphenyl)-6-methyl-3,4-dihydropyrimidin-2(1*H*)-one (4b)

Melting point 202 to 203 °C. IR (KBr, cm^{-1}): 3222, 3095, 2932, 2831, 1713, 1650, 1615, 1584, 1516. ^{1}H NMR (DMSO-d_6) δ: 1.09 (t, *J* = 7 Hz, 3H), 2.23 (s, 3H), 3.70 (s, 3H), 3.97 (q, *J* = 7 Hz, 2H), 5.09 (d, *J* = 3.1 Hz), 6.87–7.15 (m, 4H), 7.66 (s, 1H), 9.12 (s, 1H). ^{13}C NMR (DMSO-d_6) δ: 15.0, 18.6, 54.3, 55.9, 60.1, 100.5, 114.6, 128.3, 138.0, 148.9, 153.1, 159.4, 166.3. MS *m*/*z*: 291 (M^+ + 1).

4-(4-Chlorophenyl)-5-ethoxycarbonyl-6-methyl-3,4-dihydropyrimidin-2(1*H*)-one (4c)

Melting point 213 to 214 °C. IR (KBr, cm^{-1}): 3230, 3091, 2974, 2935, 1700, 1642. ^{1}H NMR (DMSO-d_6) δ: 1.10 (t, *J* = 6.7 Hz, 3H), 2.24 (s, 3H), 3.97 (q, *J* = 6.7 Hz, 2H), 5.14 (d, *J* = 3.1 Hz), 7.23–7.38 (m, 4H), 7.76 (s, 1H), 9.23 (s, 1H). ^{13}C NMR (DMSO-d_6) δ: 14.9, 18.7, 54.3, 60.1, 99.7, 129.0, 129.2, 132.7, 144.6, 149.6, 152.8, 166.2. MS *m*/*z*: 295 (M^+ + 1).

4-(4-Fluorophenyl)-5-ethoxycarbonyl-6-methyl-3,4-dihydropyrimidin-2(1*H*)-one (4d)

Melting point 177 to 178 °C. IR (KBr, cm^{-1}): 3235, 3090, 2975, 2930, 1705, 1645. ^{1}H NMR (DMSO-d_6) δ: 2.0 (t, *J* = 6.9 Hz, 3H), 2.26 (s, 3H), 3.99 (q, *J* = 6.9 Hz, 2H), 5.15 (d, *J* = 3.1 Hz), 7.21–7.40 (m, 4H), 7.76 (s, 1H), 9.23 (s, 1H). ^{13}C NMR (DMSO-d_6) δ: 14.5, 17.5, 53.3, 60.1, 99.1, 116.0, 129.2, 142.7, 148.6, 153.6, 165.2.

5-Ethoxycarbonyl-6-methyl-4-(4-nitrophenyl)-3,4-dihydropyrimidin-2(1*H*)-one (4e)

Melting point 208–211 °C. IR (KBr, cm^{-1}): 3232, 3108, 2977, 1701, 1641, 1591, 1522. ^{1}H NMR (DMSO-d_6) δ: 9.37 (s, 1H), 8.20–7.50 (m, 4H), 7.91 (d, *J* = 2.46 Hz, 1H), 5.27 (d, *J* = 1.6 Hz, 1H), 3.98 (q, *J* = 7.1 Hz, 2H), 2.27 (s, 3H), 1.09 (t, *J* = 7.1 Hz, 3H). ^{13}C NMR (DMSO-d_6) δ: 164.9, 151.9, 151.7, 149.3, 146.6, 127.5, 123.7, 59.3, 53.6, 17.8, 13.9. MS *m*/*z*: 306 (M^+ + 1).

5-Ethoxycarbonyl-6-methyl-4-(4-hydroxyphenyl)-3,4-dihydropyrimidin-2(1*H*)-one (4f)

Melting point 233–235 °C. IR (KBr, cm^{-1}): 3510, 3276, 3125, 2970, 1682, 1642. ^{1}H NMR (DMSO-d_6) δ: 1.06 (t, 3H, *J* = 6.90 Hz), 2.21 (s, 3H), 3.94 (q, 2H, *J* = 6.90 Hz), 5.02 (d, 1H, *J* = 2.76 Hz), 6.67–7.0 (m, 4H), 7.64 (s, 1H), 9.11 (s, 1H), 9.30 (s, 1H).

5-Acetyl-6-methyl-4-phenyl-3,4-dihydropyrimidin-2(1*H*)-one (4g)

Melting point 240–242 °C. IR (KBr, cm^{-1}): 3270, 3008, 2975, 2835, 1702, 1645, 1588. ^{1}H NMR (DMSO-d_6) δ: 2.12 (s, 3H), 2.30 (s, 3H), 5.28 (s, 1H), 7.24–7.32 (m, 5H), 7.82 (s, 1H), 9.20 (s, 1H).

5-Methoxycarbonyl-6-methyl-4-phenyl-3,4-dihydropyrimidin-2(1*H*)-one (4h)

Melting point 209–212 °C. IR (KBr, cm^{-1}): 3368, 3240, 3092, 3032, 2948, 1750, 1708, 1655. ^{1}H NMR (DMSO-d_6) δ: 8.06 (s, 1H), 7.32 (m, 5H), 5.74 (s, 1H), 5.40 (d, *J* = 2.7 Hz, 1H), 3.64 (s, 3H), 2.34 (s, 3H). ^{13}C NMR (DMSO-d_6) δ: 165.5, 152.2, 148.8 144.5, 128.3, 127.2, 126.0, 98.9, 53.9, 50.7, 17.8. MS *m*/*z*: 247 (M^+ + 1).

5-Methoxycarbonyl-4-(4-methoxyphenyl)-6-methyl-3,4-dihydropyrimidin-2(1*H*)-one (4i)

Melting point 192–194 °C. IR (KBr, cm^{-1}): 3238, 3102, 3000, 2952, 2838, 1692, 1640, 1609, 1516. ^{1}H NMR (DMSO-d_6) δ: 8.58 (s, 1H), 7.25–6.80 (m, 4H), 5.95 (s, 1H), 5.30 (d, *J* = 2.0 Hz, 1H), 3.76 (s, 3H), 3.65 (s, 3H), 2.30 (s, 3H). ^{13}C NMR ($CDCl_3$) δ: 163.5, 151.2, 143.6, 133.5, 125.4, 111.2, 52.7, 52.5, 48.5, 16.2. MS *m*/*z*: 277 (M^+ + 1).

© 2006 NRC Canada

4-(4-Chlorophenyl)-5-methoxycarbonyl-6-methyl-3,4-dihydropyrimidin-2(1*H*)-one (4j)

Melting point 204–207 °C. IR (KBr, cm^{-1}): 3240, 3114, 2950, 2875, 1702, 1645. ^1H NMR (DMSO-d_6) δ: 9.28 (s, 1H), 7.76 (s, 1H), 7.35–7.25 (m, 4H), 5.14 (d, J = 3.3 Hz, 1H), 3.53 (s, 3H), 2.25 (s, 3H). ^{13}C NMR (DMSO-d_6) δ: 165.5, 152.0, 148.8, 143.5, 131.8, 128.3, 128.0, 98.5, 53.2, 50.7, 17.6. MS m/z: 281 (M^+ + 1).

5-Methoxycarbonyl-6-methyl-4-(4-nitrophenyl)-3,4-dihydropyrimidin-2(1*H*)-one (4k)

Melting point 235–237 °C. IR (KBr, cm^{-1}): 3265, 3234, 3111, 2952, 1700, 1648, 1599, 1522. ^1H NMR (DMSO-d_6) δ: 9.36 (s, 1H), 8.22–7.52 (m, 4H), 7.95 (s, 1H), 5.26 (s, 1H), 3.54 (s, 3H), 2.28 (s, 3H). ^{13}C NMR (DMSO-d_6) δ: 165.5, 151.7, 149.5, 146.6, 127.5, 123.7, 97.9, 53.4, 50.8, 17.8. MS m/z: 292 (M^+ + 1).

4-(4-Fluorophenyl)-5-methoxycarbonyl-6-methyl-3,4-dihydropyrimidin-2(1*H*)-one (4l)

Melting point 190 to 191 °C. IR (KBr, cm^{-1}): 3260, 3135, 2992, 2898, 1725, 1658. ^1H NMR (DMSO-d_6) δ: 9.30 (s, 1H), 7.7 (s, 1H), 7.45–7.27 (m, 4H), 5.15 (d, J = 3.3 Hz, 1H), 3.55 (s, 3H), 2.26 (s, 3H). ^{13}C NMR (DMSO-d_6) δ: 164.6, 150.8, 147.9, 143.6, 130.9, 128.3, 128.2, 99, 53, 50.6, 17.6.

Ethyl 6-methyl-4-phenyl-2-thiooxo-1,2,3,4-tetrahydropyrimidine-5-carboxylate (4m)

Melting point 206–208 °C. IR (KBr, cm^{-1}): 3330, 3172, 3105, 2980, 1670, 1575, 1467. ^1H NMR (DMSO-d_6) δ: 1.08 (t, 3H, J = 7.02 Hz), 2.26 (s, 3H), 3.98 (q, 2H, J = 7.02 Hz), 5.15 (d, 1H, J = 3.57 Hz), 7.20–7.35 (m, 5H), 9.65 (s, 1H), 10.35 (s, 1H).

6-Methyl-4-phenyl-2-thioxo-1,2,3,4-tetrahydropyrimidine-5-carboxylic acid methyl ester (4n)

Melting point 235–237 °C. IR (KBr, cm^{-1}): 3296, 3203, 2994, 1610, 1577, 1462. ^1H NMR (DMSO-d_6) δ: 2.14 (s, 3H), 2.32 (s, 3H), 5.26 (d, 1H, J = 3.57 Hz), 7.20–7.38 (m, 5H), 9.75 (s, 1H), 10.28 (s, 1H). MS m/z: 247 (M^+ + 1).

Ethyl 6-methyl-4-methoxyphenyl-2-thiooxo-1,2,3,4-tetrahydropyrimidine-5-carboxylate (4o)

Melting point 152 to 153 °C. IR (KBr, cm^{-1}): 3446, 3315, 3178, 2965, 1669, 1619, 1578, 1512. ^1H NMR (DMSO-d_6) δ: 1.09 (t, 3H, J = 6.93 Hz), 2.26 (s, 3H), 3.74 (s, 3H), 3.98 (q, 2H, J = 6.93 Hz), 5.12 (d, 1H, J = 3.6 Hz), 6.88–7.10 (m, 4H), 9.62 (s, 1H), 10.30 (s, 1H).

Acknowledgement

One of the authors (S. Kumar) is thankful to the Council of Scientific and Industrial Research, New Delhi, India for a Junior Research Fellowship.

References

1. (*a*) C.O. Kappe. Tetrahedron, **49**, 6937 (1993); (*b*) C.O. Kappe. Acc. Chem. Res. **33**, 879 (2000).
2. (*a*) G.C. Rovnyak, S.D. Kimball, B. Beyer, G. Cucinotta, J.D. Di Marco, J. Goughoutas, A. Hedberg, M. Malley, J.P. McCarthy, R. Zhang, and S. Moreland. J. Med. Chem. **38**, 119 (1995); (*b*) C.O. Kappe, W.M.F. Fabian, and M.A. Semones. Tetrahedron, **53**, 2803 (1997).
3. (*a*) A.D. Patil, N.V. Kumar, W.C. Kokke, M.F. Bean, A.J. Freyer, C. De Brosse, S. Mai, A. Truneh, D.J. Faulkner, B. Carte, A.L. Breen, R.P. Hertzberg, R.K. Johnson, J.W. Westley, and B.C.M. Potta. J. Org. Chem. **60**, 1182 (1995); (*b*) A.V. Rama Rao, M.K. Gurjar, and J. Vasudevan. J. Chem. Soc. Chem. Commun. 1369 (1995); (*c*) B.B. Snider, J. Chen, A.D. Patil, and A.J. Freyer. Tetrahedron Lett. **37**, 6977 (1996).
4. P. Biginelli. Gazz. Chim. Ital. **23**, 360 (1893).
5. (*a*) B.C. O'Reilly and K.S. Atwa. Heterocycles, **26**, 1185 (1987); (*b*) K.S. Atwal, B.C. O'Reilly, J.Z. Gougoutas, and M.F. Malley. Heterocycles, **26**, 1189 (1987); (*c*) A.D. Shutalev, E.A. Kishko, N. Sivova, and A.Y. Kuznetsov. Molecules, **3**, 100 (1998).
6. (*a*) M. Gohain, D. Prajapati, and J.S. Sandhu. Synlett, **2**, 235 (2004); (*b*) R. Varala, M.M. Alam, and S.R. Adapa. Synlett, **1**, 67 (2003); (*c*) D. Subhas Bose, L. Fatima, and H.B. Mereyala. J. Org. Chem. **68**, 587(2003); (*d*) A.S. Paraskar, G.K. DewKar, and A. Sudalai. Tetrahedron Lett. **44**, 3305 (2003); (*e*) G. Sabitha, G.S.K.K. Reddy, C.S. Redy, and J.S. Yadav. Synlett, **1**, 58 (2003); (*f*) P. Salehi, M. Dabiri, M.A. Zolfigol, and M.A. Bodagh Ford. Tetrahedron Lett. **44**, 2889 (2003); (*g*) P.P. Baruah, S. Gadhwal, D. Prajapati, and J.S. Sandhu. Chem. Lett. 1038 (2002); (*h*) G. Maiti, P. Kundu, and C. Guin. Tetrahedron Lett. **44**, 2757 (2003); (*i*) S. Tu, F. Fang, C. Miao, H. Jiang, Y. Feng, D. Shi, and X. Wang. Tetrahedron Lett. **44**, 6153 (2003); (*j*) C.V. Reddy, M. Mahesh, K.V.P. Raju, T. Romeshbabu, and N.V.V. Reddy. Tetrahedron Lett. **43**, 2657 (2002); (*k*) N. Fu, Y. Yuan, Z. Cao, S. Wang, J. Wang, and C. Peppe. Tetrahedron, **58**, 4801 (2002); (*l*) J. Lu and Y. Bai. Synthesis, **4**, 466 (2002); (*m*) A. Shaabani, A. Bazgir, and F. Teimouri. Tetrahedron Lett. **44**, 857 (2003); (*n*) L. Jun and M. Huairang. Synlett, **1**, 63 (2000); (*o*) H.E. Hu, D.R. Sidler, and U.H. Dolling. J. Org. Chem. **63**, 3454 (1998); (*p*) F. Bigi, S. Carloni, B. Frulanti, R. Maggi, and G. Sartori. Tetrahedron Lett. **40**, 3465 (1999); (*q*) J.S. Yadav, B.V. Reddy, K.B. Reddy, K.S. Raj, and A.R. Prasad. J. Chem. Soc. Perkin Trans. 1, 1939 (2001); (*r*) Y. Ma, C. Qian, L. Wang, and M. Yang. J. Org. Chem. **65**, 3864 (2000); (*s*) C.O. Kappe and S.F. Falsome. Synlett, 718 (1998); (*t*) A.K. Kumar, M. Kasthuraiah, C.S. Reddy, and C.D. Reddy. Tetrahedron Lett. **42**, 7873 (2001); (*u*) H. Salehi and Q. Guo Xiang. Synth. Commun. **34**, 171 (2004); (*v*) B.C. Ranu, A. Hajra, and U. Janu. J. Org. Chem. **65**, 6270 (2000).
7. (*a*) V.S. Ley, I.R. Baxendale, and A.L. Lee. J. Chem. Soc. Perkin Trans. 1, 1850 (2002); (*b*) R.S. Varma. Green. Chem. **1**, 43 (1999); (*c*) J.O. Metzger. Angew. Chem. Int. Ed. **37**, 2975 (1998); (*d*) P. Laszlo. *In* Solid supports and catalysts in organic synthesis. *Edited by* K. Smith. Harwood, Chichester, UK. 1992. pp. 288–310.
8. B.A. Ganai, S. Koul, T.K. Razdan, and C.S. Andotra. Synth. Commun. **34**, 1823 (2004).

© 2006 NRC Canada

Synthesis of some new 1-aryl-4-formyl-3-(4-hydroxy-6-methyl-2-oxo-2*H*-pyran-3-yl)pyrazoles using the Vilsmeier–Haack reaction — Isolation of the key intermediate 1-aryl-3-(4-hydroxy-6-methyl-2-oxo-2*H*-pyran-3-yl)pyrazoles

Ajay Kumar, Om Prakash, Mayank Kinger, and Shiv P. Singh

Abstract: Arylhydrazones of dehydroacetic acid (DHA) underwent Vilsmeier–Haack reaction to generate the corresponding 1-aryl-4-formyl-3-(4-hydroxy-6-methyl-2-oxo-2*H*-pyran-3-yl)pyrazoles (**1**) with the pyrone moiety of the DHA remaining intact. However, when the reaction was performed using 1 equiv. of the reagent, compounds of 1-aryl-3-(4-hydroxy-6-methyl-2-oxo-2*H*-pyran-3-yl)pyrazoles (**2a**–**2f**) were obtained, which underwent smooth conversion to 1-aryl-4-formyl-3-(4-hydroxy-6-methyl-2-oxo-2*H*-pyran-3-yl)pyrazoles (**1**) on further treatment with another equivalent of the Vilsmeier–Haack reagent. This unreported observation suggests the intermediacy of 1-aryl-3-(4-hydroxy-6-methyl-2-oxo-2*H*-pyran-3-yl)pyrazoles (**2**) in Vilsmeier–Haack reactions of hydrazones with a pyrone moiety. Several analogous compounds were also prepared using arylhydrazones of DHA.

Key words: dehydroacetic acid, pyrazoles, Vilsmeier–Haack reaction, 3-acetyl-4-hydroxy-6-methyl-2*H*-pyran-2-one.

Résumé : Les arylhydrazones de l'acide déhydroacétique (DHA) subissent la réaction de Vilsmeier–Haack pour conduire à la formation des 1-aryl-4-formyl-3-(4-hydroxy-6-méthyl-2-oxo-2*H*-pyran-3-yl)pyrazoles (**1**) dans lesquelles la portion pyrone de l'acide DHA demeure intacte. Toutefois, lorsque la réaction est effectuée en utilisant un équivalent de réactif, on obtient plutôt les 1-aryl-3-(4-hydroxy-6-méthyl-2-oxo-2*H*-pyran-3-yl)pyrazoles (**2a**–**2f**) qui, sous l'influence d'un autre équivalent de réactif de Vilsmeier–Haack, se transforment facilement en 1-aryl-4-formyl-3-(4-hydroxy-6-méthyl-2-oxo-2*H*-pyran-3-yl)pyrazoles (**1**). Cette observation qui n'avait jamais été rapportée antérieurement suggère que les 1-aryl-3-(4-hydroxy-6-méthyl-2-oxo-2*H*-pyran-3-yl)pyrazoles (**2**) sont des intermédiaires dans les réactions de Vilsmeier-Haack comportant une portion pyrone. On a préparé plusieurs composés analogues à partir d'autres arylhydrazones de l'acide DHA.

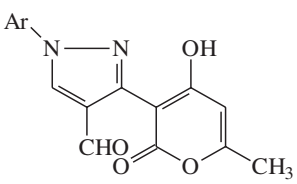
Mots clés : acide déhydroacétique, pyrazoles, réaction de Vilsmeier–Haack, 3-acétyl-4-hydroxy-6-méthyl-2*H*-pyran-2-one.

[Traduit par la Rédaction]

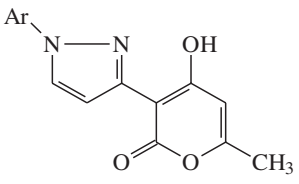
Introduction

Significant interest in the chemistry of pyrazoles is reflected by the design of new synthetic approaches, theoretical calculations on the reactions leading to their formation, applications of new spectroscopic techniques and their significance in pharmaceuticals, agrochemicals, and dye stuffs, etc. (1–3). In the course of our studies on the synthesis of heterocyclic compounds from the reactions of dehydroacetic acid (DHA) and its derivatives (4–6), we have reported the synthesis of pyrazoles (**2**) and bipyrazoles (**3**) from the rearrangement of hydrazones of DHA (**1**) (7) (Scheme 1).

In the conversion of **1** to **2**, there is involvement of the pyrone ring of DHA, leading to the formation of a β-dicarbonyl moiety through a novel rearrangement process. In continuation of our studies dealing with the synthesis and properties of new pyrazole derivatives, we became interested in the synthesis of the pyrazoles in which the pyrone moiety of the DHA remains intact. We now report herein the synthesis of pyrazoles **4** and **5** from DHA by using the Vilsmeier–Haack reagent.



4



5

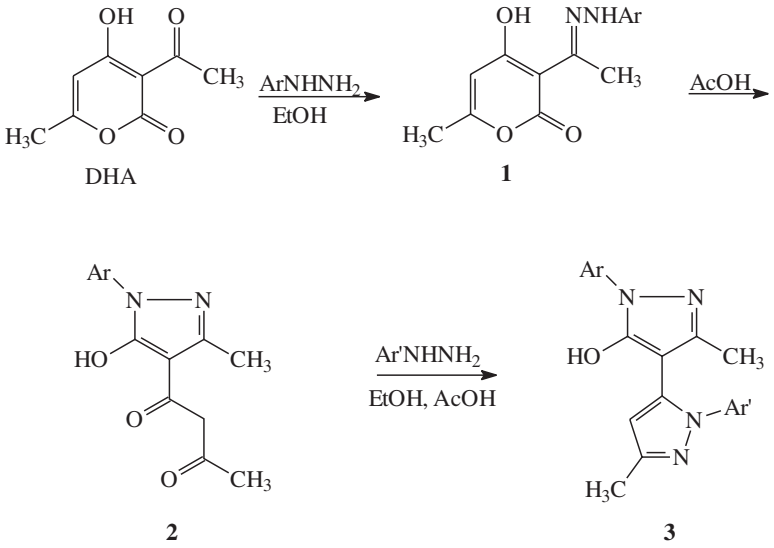
Received 8 December 2005. Published on the NRC Research Press Web site at http://canjchem.nrc.ca on 31 March 2006.

A. Kumar, O. Prakash,[1] M. Kinger, and S.P. Singh. Department of Chemistry, Kurukshetra University, Kurukshetra-136 119, Haryana, India.

[1]Corresponding author (e-mail: dromprakash50@rediffmail.com).

 doi:10.1139/V06-015 © 2006 NRC Canada

Scheme 1.



There are several recent reports involving the cyclization of some ketone hydrazones to 1-substituted 4-formylpyrazoles by using the Vilsmeier–Haack reagent ($POCl_3$–DMF, Scheme 2) (8–10). This transformation involves double formylation and its mechanistic pathways are not certain. Based on this important variation of the Vilsmeier–Haack reaction, we have adopted the same approach for the synthesis of **4**.

Scheme 2.



Results and discussion

1-Aryl-4-formyl-3-(4-hydroxy-6-methyl-2-oxo-2*H*-pyran-3-yl)pyrazoles (1a–1e)

Initially, DHA phenylhydrazone (**1a**) was prepared by the condensation of phenylhydrazine and DHA in ethanolic solution containing a small amount of acetic acid, and was subjected to the Vilsmeier–Haack reaction under standard conditions, i.e., treating 2 equiv. of $POCl_3$–DMF with hydrazone **4a** at 55–60 °C for 5 h. The usual work up, followed by the purification of the resulting crude product by recrystallization from ethanol, gave the expected 4-formylpyrazole derivative **1a** as a crystalline solid in 75% yield. Similarly, several DHA hydrazones (**1b**–**1e**), which were obtained by treating DHA with arylhydrazines, also underwent the Vilsmeier–Haack reaction to afford the corresponding 1-aryl-4-formyl-3-(4-hydroxy-6-methyl-2-oxo-2*H*-pyran-3-yl)pyrazoles (**4b**–**4e**) in good yields (Scheme 3). The structures of all products were established by their spectral properties, i.e., IR, ^{1}H NMR, MS, and elemental analyses.

The successful conversion of **3** to **4** reveals that the 4-hydroxy-6-methyl-2*H*-pyran-2-one system remains intact in the presence of the Vilsmeier–Haack reagent.

1-Aryl 3-(4-hydroxy-6-methyl-2-oxo-2*H*-pyran-3-yl)pyrazoles (5a–5e)

After the successful conversion of **1** to **4**, we focused our attention on the synthesis of the related compounds **5**. The reaction was carried out using controlled conditions, such as the use of 1 equiv. of Vilsmeier–Haack reagent to carry out the monoformylation of hydrazone **1a** to generate the pyrazole **5a**. Interestingly, the reaction afforded the desired product 1-aryl-3-(4-hydroxy-6-methyl-2-oxo-2*H*-pyran-3-yl)pyrazole (**5a**), in 60% yield (Scheme 4). Using identical reaction conditions, syntheses of similarly constituted pyrazoles (**5b**–**5e**) were achieved.

To the best of our knowledge, all the reported cases of Vilsmeier–Haack reactions of hydrazones give 4-formylpyrazoles, as shown in Scheme 2. This study represents the first example of the preparation of pyrazoles **5** from the corresponding hydrazones.

Conversion of 5 to 4

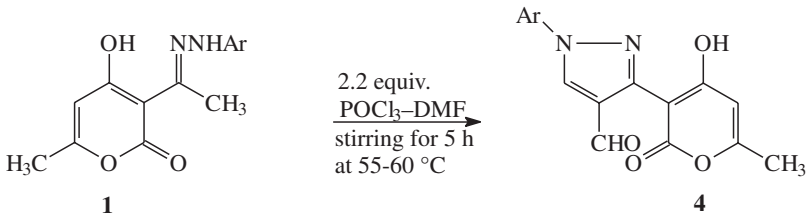
It is significant that pyrazoles **5a**–**5e** upon Vilsmeier–Haack reaction underwent smooth conversion into the corresponding 4-formylpyrazoles (**4a**–**4e**). The physical and spectral data of **4a**–**4e** were found to be identical with those obtained directly from **1**. The synthesis of **4** from **5**, not only provides additional examples of the Vilsmeier–Haack formylation of pyrazole derivatives, but also gives a clear indication of the involvement of **5** as an intermediate in the conversion of **1** to **4**.

Mechanistic pathways

Although the mechanism of the Vilsmeier–Haack reaction is not certain, two alternative pathways (Scheme 5) can be envisaged. According to Scheme 5 (path a), formation of the products **4** involves double formylation at the CH_3 group of the hydrazones **1**, followed by cyclization. In the second pathway (path b), single formylation at the CH_3 group followed by cyclization, initially gives 4-unsubstituted pyrazoles (**5**), which subsequently undergo another formylation to produce **4**.

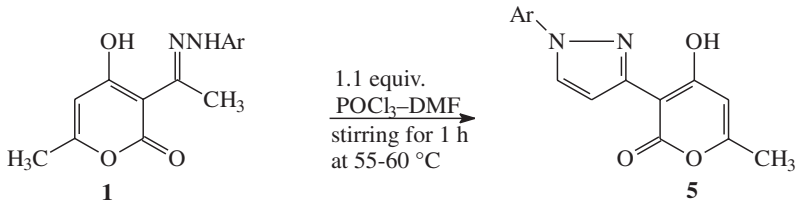
© 2006 NRC Canada

Scheme 3.



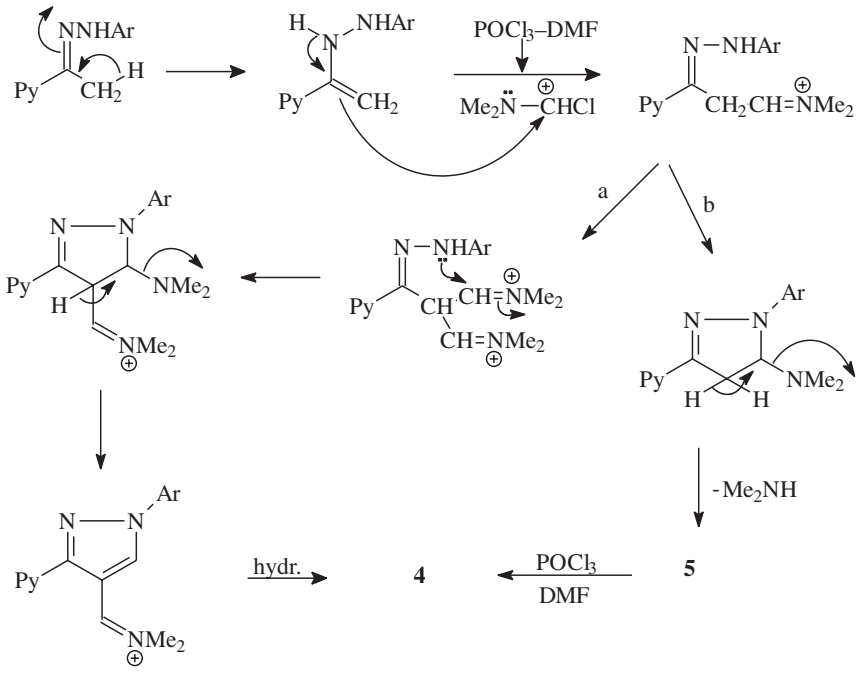
Compounds	Ar	Compounds	Ar
1a, 4a	C_6H_5	**1d, 4d**	4-$NO_2C_6H_4$
1b, 4b	4-$CH_3C_6H_4$	**1e, 4e**	2,4-$(NO_2)_2C_6H_3$
1c, 4c	4-ClC_6H_4		

Scheme 4.



Compounds	Ar	Compounds	Ar
1a, 5a	C_6H_5	**1d, 5d**	4-$NO_2C_6H_4$
1b, 5b	4-$CH_3C_6H_4$	**1e, 5e**	2,4-$(NO_2)_2C_6H_3$
1c, 5c	4-ClC_6H_4		

Scheme 5.

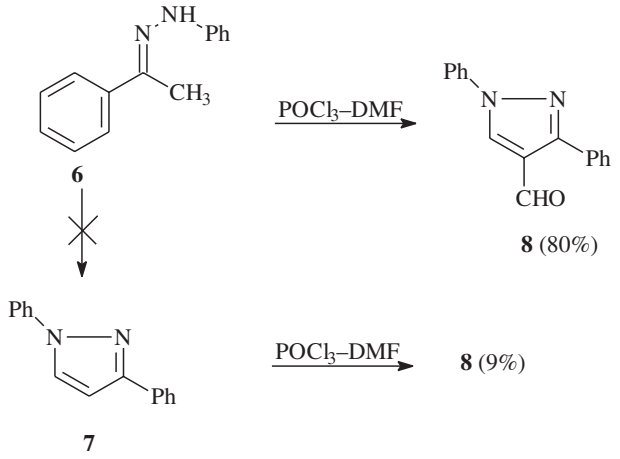


Since we were able to isolate the products **5** by using 1 equiv. of the Vilsmeier–Haack reagent (in this study), path b (Scheme 5) appears to be more reasonable. The observation in the present work that the second formylation of the pyrazole **5**, using similar reaction conditions and the reagent, indeed, afforded **4**, supports this pathway. However, in the presence of 2 equiv. of the Vilsmeier–Haack reagent, this study does not permit us to speculate on the operation of either of the two mechanisms as outlined in Scheme 5.

It is to be noted that in contrary to our observations, Kira

© 2006 NRC Canada

Scheme 6.



et al. (11) reported that in the case of Vilsmeier–Haack reaction of acetophenone phenylhydrazone (**6**), pyrazoles **7** are not intermediates in the reaction. They obtained 4-formyl-1,3-diphenylpyrazole (**8**) in 80% yield from the Vilsmeier–Haack reaction of **6**. However, formylation of 1,3-diphenylpyrazole (**7**) under identical conditions gave the same product (**8**), only in 9% yield (Scheme 6). Repetition of this work confirmed these observations.

Obviously, the presence of the 4-hydroxypyran-2-one moiety plays an important role in the conversions of **1** to **4** and of **5** to **4**. Further studies on related examples might be helpful to determine the actual effect of structural changes on the mechanistic pathways of these transformations.

Finally, noteworthy features of the present study are as follows:

(*i*) New pyrazole derivatives of **4** and **5** containing the 2-pyrone moiety are available through the Vilsmeier–Haack reaction using a simple experimental procedure. The mild reaction conditions do not allow attack at other nucleophilic positions (C(6) and C(4)-OH) of the pyrone moiety.

(*ii*) The synthesis of **5** represents the first example of monoformylation in the Vilsmeier–Haack reaction of the hydrazones of the $R(CH_3)C{:}NNHAr$ type.

(*iii*) The isolation of **5** and its subsequent formylation provides a valuable clue regarding the mechanistic pathways followed in these transformations.

(*iv*) The new pyrazole derivatives **4** and **5**, synthesized in the present work, are needed as precursors for the synthesis of several novel fused pyrazoloquinolone derivatives, particularly through the use of hypervalent iodine reagents.

Experimental

Instrumentation and general procedures

Melting points were taken in open capillaries and are uncorrected. ^{1}H NMR spectra were recorded on a Bruker 300 MHz instrument using TMS as an internal standard. IR spectra were recorded on a Buck Scientific IR M500 spectrophotometer. Elemental analyses were carried out in a PerkinElmer 2400 instrument, and mass spectra were recorded on a Kratos MS-50 mass spectrometer. Most of the common chemicals such as dehydroacetic acid, aldehydes, phenylhydrazine, 2,4-dinitrophenylhydrazine, etc., were obtained from commercial suppliers.

General procedure for the preparation of the hydrazone of DHA

DHA (0.02 molar equiv.) was dissolved in ethanol (50 mL) by warming, and arylhydrazine (0.02 molar equiv.) was added to the mixture while it was being shaken. The contents were stirred for 10 min and allowed to stand at room temperature for 2 h. The yellow solid (**1**) obtained was filtered and crystallized from acetonitrile.

Compounds **1a**–**1e** were similarly prepared.

General procedure for the preparation of 1-aryl-3-(4-hydroxy-6-methyl-2-oxo-2*H*-pyran-3-yl)pyrazoles (5)

Hydrazone **1** (0.004 molar equiv.) was added to the Vilsmeier–Haack reagent (prepared from DMF (10 mL) and $POCl_3$ (0.0044 molar equiv.)), and the reaction mixture was stirred at 55–60 °C for 1 h and then poured into ice-cold water. The solid that separated upon neutralization with $NaHCO_3$ was filtered, washed with water, and crystallized from ethanol to afford **5**.

Compounds **5a**–**5e** were similarly prepared.

*3-(4-Hydroxy-6-methyl-2-oxo-2*H*-pyran-3-yl)-1-phenylpyrazole (5a)*

Yield: 65%; mp 158 to 159 °C. IR (KBr, cm^{-1}): 1720 (C=O). ^{1}H NMR ($CDCl_3$, 300 MHz) δ: 2.4 (s, 3H, CH_3), 6.0 (s, 1H, C_5-H, DHA), 7.3 (d, 1H, C_4-H, J = 2.1 Hz), 7.31 (m, 1H, Ph), 7.50 (m, 2H, Ph), 7.62 (m, 2H, Ph), 8.0 (d, 1H, C_5-H, J = 2.1 Hz), 13.0 (s, 1H, OH). MS *m*/*z*: 268. Elemental anal. calcd. for $C_{15}H_{12}N_2O_3$: C 67.16, H 4.48, N 10.44; found: C 67.28, H 4.49, N 10.34.

*3-(4-Hydroxy-6-methyl-2-oxo-2*H*-pyran-3-yl)-1-(4-tolyl)pyrazole (5b)*

Yield 60%; mp 122 to 123 °C. IR (KBr, cm^{-1}): 1723 (C=O). ^{1}H NMR ($CDCl_3$, 300 MHz) δ: 2.3 (s, 3H, CH_3), 2.4 (s, 3H, CH_3), 6.0 (s, 1H, C_5-H, DHA), 7.3 (d, 1H, C_4-H, J = 2.1 Hz), 7.0 (d, 2H, Ph, J = 8.0 Hz), 7.1 (d, 2H, Ph, J = 8.0 Hz), 8.0 (d, 1H, C_5-H, J = 2.1 Hz), 13.0 (s, 1H, OH). MS *m*/*z*: 282. Elemental anal. calcd. for $C_{16}H_{14}N_2O_3$: C 68.08, H 4.96, N 9.92; found: C 68.24, H 4.95, N 9.94.

*1-(4-Chlorophenyl)-3-(4-hydroxy-6-methyl-2-oxo-2*H*-pyran-3-yl)pyrazole (5c)*

Yield 62%; mp 167 to 168 °C. IR (KBr, cm^{-1}): 1722 (C=O). ^{1}H NMR ($CDCl_3$, 300 MHz) δ: 2.4 (s, 3H, CH_3), 6.0 (s, 1H, C_5-H, DHA), 7.3 (d, 1H, C_4-H, J = 2.1 Hz), 7.1 (d, 2H, Ph, J = 8.1 Hz), 7.4 (d, 2H, Ph, J = 8.1 Hz), 8.0 (d, 1H, C_5-H, J = 2.1 Hz), 13.0 (s, 1H, OH). MS *m*/*z*: 302 (M^+), 304 (M^+ + 2). Elemental anal. calcd. for $C_{15}H_{11}ClN_2O_3$: C 59.50, H 3.63, N 9.25; found: C 59.53, H 3.64, N 9.29.

*3-(4-Hydroxy-6-methyl-2-oxo-2*H*-pyran-3-yl)-1-(4-nitrophenyl)pyrazole (5d)*

Yield 68%; mp 204 to 205 °C. IR (KBr, cm^{-1}): 1725 (C=O). ^{1}H NMR ($CDCl_3$, 300 MHz) δ: 2.4 (s, 3H, CH_3), 6.0 (s, 1H, C_5-H, DHA), 7.3 (d, 1H, C_4-H, J = 2.1 Hz), 7.6 (d, 2H, Ph, J = 8.4 Hz), 8.3 (d, 2H, Ph, J = 8.4 Hz), 8.0 (d, 1H,

© 2006 NRC Canada

C_5-H, J = 2.1 Hz), 13.0 (s, 1H, OH). MS *m/z*: 313. Elemental anal. calcd. for $C_{15}H_{11}N_3O_5$: C 57.51, H 3.51, N 13.42; found: C 57.55, H 3.49, N 13.44.

1-(2,4-Dinitrophenyl)-3-(4-hydroxy-6-methyl-2-oxo-2H-pyran-3-yl)pyrazole (5e)

Yield 60%; mp 221 to 222 °C. IR (KBr, cm^{-1}): 1728 (C=O). ^{1}H NMR ($CDCl_3$, 300 MHz) δ: 2.4 (s, 3H, CH_3), 6.0 (s, 1H, C_5-H, DHA), 7.3 (d, 1H, C_4-H, J = 2.1 Hz), 7.6 (m, 1H, Ph), 8.3 (d, 1H, Ph), 8.7 (s, 1H, Ph), 8.0 (d, 1H, C_5-H, J = 2.1 Hz), 13.0 (s, 1H, OH). MS *m/z*: 358. Elemental anal. calcd. for $C_{15}H_{10}N_4O_7$: C 50.27, H 2.79, N 15.64; found: C 50.30, H 2.77, N 15.60.

General procedure for the preparation of 1-aryl-4-formyl-3-(4-hydroxy-6-methyl-2-oxo-2*H*-pyran-3-yl)pyrazoles (4)

Hydrazone **1** (0.004 molar equiv.) was added to the Vilsmeier–Haack reagent (prepared from DMF (10 mL) and $POCl_3$ (0.0088 molar equiv.)), and the reaction mixture was stirred at 55–60 °C for 5 h and then poured into ice-cold water. The solid that separated upon neutralization with $NaHCO_3$ was filtered, washed with water, and crystallized from ethanol to afford **4**.

Compounds **4a**–**4e** were similarly prepared.

4-Formyl-3-(4-hydroxy-6-methyl-2-oxo-2H-pyran-3-yl)-1-phenylpyrazole (4a)

Yield 55%; mp 118 to 119 °C. IR (KBr, cm^{-1}): 1720, 1683 (C=O). ^{1}H NMR ($CDCl_3$, 300 MHz) δ: 2.4 (s, 3H, CH_3), 6.0 (s, 1H, C_5-H, DHA), 7.0–7.7 (m, 5H, Ph), 8.5 (s, 1H, C_5-H), 9.9 (s, 1H, CHO), 13.0 (s, 1H, OH). MS *m/z*: 296. Elemental anal. calcd. for $C_{16}H_{12}N_2O_4$: C 64.86, H 4.05, N 9.45; found: C 64.88, H 4.06, N 9.44.

4-Formyl-3-(4-hydroxy-6-methyl-2-oxo-2H-pyran-3-yl)-1-(4-tolyl)pyrazole (4b)

Yield 51%; mp 133 to 134 °C. IR (KBr, cm^{-1}): 1723, 1687 (C=O). ^{1}H NMR ($CDCl_3$, 300 MHz) δ: 2.3 (s, 3H, CH_3), 2.4 (s, 3H, CH_3), 6.0 (s, 1H, C_5-H, DHA), 7.0 (d, 2H, Ph, J = 8.0 Hz), 7.1 (d, 2H, Ph, J = 8.0 Hz), 8.5 (s, 1H, C_5-H), 9.9 (s, 1H, CHO), 13.0 (s, 1H, OH). MS *m/z*: 310. Elemental anal. calcd. for $C_{17}H_{14}N_2O_4$: C 65.80, H 4.51, N 9.03; found: C 65.81, H 4.49, N 9.06.

1-(4-Chlorophenyl)-4-formyl-3-(4-hydroxy-6-methyl-2-oxo-2H-pyran-3-yl)pyrazole (4c)

Yield 52%; mp 143 to 144 °C. IR (KBr, cm^{-1}): 1722, 1686 (C=O). ^{1}H NMR ($CDCl_3$, 300 MHz) δ: 2.4 (s, 3H, CH_3), 6.0 (s, 1H, C_5-H, DHA), 7.1 (d, 2H, Ph, J = 8.1 Hz), 7.4 (d, 2H, Ph, J = 8.1 Hz), 8.5 (s, 1H, C_5-H), 9.9 (s, 1H, CHO), 13.0 (s, 1H, OH). MS *m/z*: 330 (M^+), 332 (M^+ + 2). Elemental anal. calcd. for $C_{16}H_{11}ClN_2O_4$: C 58.09, H 3.32, N 8.47; found: C 58.08, H 3.34, N 8.44.

4-Formyl-3-(4-hydroxy-6-methyl-2-oxo-2H-pyran-3-yl)-1-(4-nitrophenyl)pyrazole (4d)

Yield 58%; mp 180 to 181 °C. IR (KBr, cm^{-1}): 1725, 1687 (C=O). ^{1}H NMR ($CDCl_3$, 300 MHz) δ: 2.4 (s, 3H, CH_3), 6.0 (s, 1H, C_5-H, DHA), 7.6 (d, 2H, Ph, J = 8.4 Hz), 8.3 (d, 2H, Ph, J = 8.4 Hz), 8.5 (s, 1H, C_5-H), 9.9 (s, 1H, CHO), 13.0 (s, 1H, OH). MS *m/z*: 341. Elemental anal. calcd. for $C_{16}H_{11}N_3O_6$: C 56.30, H 3.23, N 12.32; found: C 56.28, H 3.24, N 12.34.

1-(2,4-Dinitrophenyl)-4-formyl-3-(4-hydroxy-6-methyl-2-oxo-2H-pyran-3-yl)pyrazole (4e)

Yield 55%; mp 200 to 202 °C. IR (KBr, cm^{-1}): 1728, 1685 (C=O). ^{1}H NMR ($CDCl_3$, 300 MHz) δ: 2.4 (s, 3H, CH_3), 6.0 (s, 1H, C_5-H, DHA), 7.6 (m, 1H, Ph), 8.3 (d, 1H, Ph), 8.8 (s, 1H, Ph), 8.5 (s, 1H, C_5-H), 9.9 (s, 1H, CHO), 13.0 (s, 1H, OH). MS *m/z*: 386. Elemental anal. calcd. for $C_{15}H_{12}N_2O_3$: C 67.16, H 4.48, N 10.44; found: C 49.28, H 4.49, N 10.34.

General procedure for the preparation of 1-aryl-4-formyl-3-(4-hydroxy-6-methyl-2-oxo-2*H*-pyran-3-yl)pyrazoles (4) from 1-aryl-3-(4-hydroxy-6-methyl-2-oxo-2*H*-pyran-3-yl)pyrazole (5)

Compound **5** (0.004 molar equiv.) was added to the Vilsmeier–Haack reagent (prepared from DMF (10 mL) and $POCl_3$ (0.0044 molar equiv.)), and the reaction mixture was stirred at 55–60 °C for 4 h and then poured into ice-cold water. The solid that separated upon neutralization with $NaHCO_3$ was filtered, washed with water, and crystallized from ethanol to afford **4** in 50% yields.

Compounds **4a**–**4e** were similarly prepared.

Acknowledgement

We are thankful to the Defence Research and Development Organisation (DRDO, New Delhi) (ERIP/ER/0303447/M/01) for financial assistance.

References

1. S.F. Vasilevsky, E.V. Tretyakov, and J. Elguero. Adv. Heterocycl. Chem. **82**, 1 (2002).
2. R.M. Moriarty, R.K. Vaid, V.T. RaviKumar, T.E. Hopkins, and P. Farid. Tetrahedron, **45**, 1605 (1989).
3. J.S. Yadav, V.B. Reddy, and V. Geetha. Synlett, **3**, 513 (2002).
4. O. Prakash, A. Kumar, A. Sadana, and S.P. Singh. Synth. Commun. **32**, 2663 (2002).
5. O. Prakash, A. Kumar, and S.P. Singh. J. Indian Chem. Soc. **80**, 1035 (2003).
6. O. Prakash, A. Kumar, and S.P. Singh. Heterocycles, **63**, 1193 (2004).
7. S.P. Singh, O. Prakash, and R.K. Vaid. Indian J. Chem. **23B**, 191 (1984).
8. G. Jones and S.P. Stanforth. Organic reactions. Vol. 56. *Edited by* L.A. Paquette. John Wiley and Sons, New York. 2000. p. 355.
9. M.A. Kira, M.N. Aboul-Enein, and M.I. Korkor. J. Heterocycl. Chem. **7**, 25 (1970).
10. M.A. Kira, Z. Nofal, and K.Z. Gadella. Tetrahedron Lett. 4215 (1970).
11. M.A. Kira, M.C.A. Rahman, and K.Z. Gadella. Tetrahedron Lett. 109 (1969).

© 2006 NRC Canada

Reactions of $MAlH_4$ (M = Li, Na) with primary amines — Synthetic and structural studies of alkali metal tetrakis(amido)aluminates and related dinuclear complexes

Dana J. Eisler and Tristram Chivers

Abstract: The reactions of $MAlH_4$ (M = Li, Na) with primary amines NH_2R (R = *t*-Bu, *i*-Pr, *p*-tolyl) in a 1:4 molar ratio in THF produce the tetrakis(amido)aluminates, $[M(THF)_n][Al(NHR)_4]$, in yields of 46%–82% together with secondary products. The extent of solvation of the alkali-metal cation varies from none (n = 0) for $M[Al(NH\text{-}i\text{-}Pr)_4]$ (**2b**, M = Li; **3b**, M = Na) to n = 4 in the complex $[Li(THF)_4][Al(NH\text{-}p\text{-tolyl})_4]$ (**2c**), which exists as a solvent-separated ion pair. The complexes **2b**, **3b**, and $[Na(THF)][Al(NH\text{-}p\text{-tolyl})_4]_\infty$ (**3c**) all exhibit one-dimensional polymeric structures in which the bis-N,N′-chelating tetrakis(amido)aluminate anions are bridged by four- (**2b**, **3b**) and five-coordinate (**3c**) metal ions, respectively. The structures of two of the secondary products, $\{[Na(THF)_2][(NH\text{-}t\text{-Bu})Al(H)(\mu\text{-N-}t\text{-Bu})]\}_2$ (**4**) and $\{[Na(THF)_3][(NH\text{-}p\text{-tolyl})_2Al(\mu\text{-N-}p\text{-tolyl})]\}_2$ (**5**), were established by X-ray crystallography. Complex **4** is a dimer of the $[HAl(NH\text{-}t\text{-Bu})(N\text{-}t\text{-Bu})]^-$ anion, which forms a central Al_2N_2 ring with each monoanion N,N′-chelated to a $[Na(THF)_2]^+$ cation. Complex **5** is a dimer of the $[Al(NR)(NHR)_2]^-$ (R = *p*-tolyl) anion in which the bridging *p*-tolyl groups are coordinated in an N-monodentate fashion to the trisolvated $[Na(THF)_3]^+$ cations.

Key words: aluminohydrides, alkali metals, primary amines, tetrakis(amido)aluminates, structures.

Résumé : Les réactions des $MAlH_4$ (M = Li, Na) avec des amines primaires, NH_2R (R = *t*-Bu, *i*-Pr, *p*-tolyle), dans un rapport molaire de 1 : 4, dans le THF, conduit à la formation des tétrakis(amido)aluminates, $[M(THF)_n][Al(NHR)_4]$, avec des rendements allant de 46 % à 82 % aux côtés de produits secondaires. Le degré de solvatation du cation du métal alcalin varie de zéro (n = 0) pour $M[Al(NH\text{-}i\text{-Pr})_4]$ (**2b**, M = Li; **3b**, M = Na) à n = 4 pour le complexe $[Li(THF)_4]$-$[Al(NH\text{-}p\text{-tolyl})_4]$ (**2c**) qui existe sous la forme de paire d'ions séparés par le solvant. Les complexes **2b**, **3b** et $[Na(THF)][Al(NH\text{-}p\text{-tolyl})_4]_\infty$ (**3c**) présentent tous des structures polymériques monodimensionnelles dans lesquelles les anions tétrakis(amido)aluminates bis-N,N′-chélatants sont liés par des ponts d'ions métalliques respectivement tétra- (**2b**, **3b**) et penta-coordinés (**3c**). Les structures de deux des produits secondaires, le $\{[Na(THF)_2][(NH\text{-}t\text{-Bu})Al(H)(\mu\text{-N-}t\text{-Bu}]\}_2$ (**4**) et $\{[Na(THF)_3)][(NH\text{-}p\text{-tolyl})_2Al(\mu\text{-N-}p\text{-tolyl})]\}_2$ (**5**) ont été établies par diffraction des rayons X. Le complexe **4** est un dimère de l'anion $[HAl(NH\text{-}t\text{-Bu})(N\text{-}t\text{-Bu})]^-$ qui forme un cycle Al_2N_2 central dans chacun des monoanions N,N′-chélatés à un cation $[Na(THF)_2]^+$. Le complexe **5** est un dimère de l'anion $[Al(NR)(NHR)_2]^-$ (R = *p*-tolyle) dans lequel les groupes *p*-tolyles servant de pont sont coordinés d'une façon N-monodentate aux cations $[Na(THF)_3]^+$ trisolvatés.

Mots clés : hydrures d'aluminium, métaux alcalins, amines primaires, tétrakis(amido)aluminates, structures.

[Traduit par la Rédaction]

Introduction

The reactions of secondary amines with $LiAlH_4$ have been studied extensively (1–4). Several tetrakis(amido)aluminate complexes of the type $[L_2Li][Al(NR_2)_4]$ (L = electron-pair donor ligand) (1, 2) as well as the intermediate lithium amidohydridoaluminates formed in this process, e.g., $[H_3AlN(SiMe_3)_2Li(Et_2O)_2]_2$ (3) and $[Li(THF)_4][HAl(NPh_2)_3]$ (4), have been structurally characterized. Aluminum-nitrogen cage compounds of the type $(HAlNR)_n$ (imidoalanes) may be prepared by treatment of primary amines with $MAlH_4$ (M = Li, Na) in a 1:1 molar ratio in boiling hydrocarbon solvents (M = Li) or diethyl ether (M = Na) (5*a*) (eq. [1]) or by reaction of $RNH_2{\cdot}HCl$ with $LiAlH_4$ in diethyl ether at room temperature (5*b*). The value of n is determined by the nature of the R group and by the solvent used for the reaction (6). In 1997 Roesky and co-workers (7) prepared the first aluminum amides derived from primary amines via the reaction of $LiAlH_4$ with the sterically demanding amine, $DippNH_2$ (Dipp = 2,6-diisopropylphenyl). Molar ratios of 1:2 and 2:5

Received 17 November 2005. Published on the NRC Research Press Web site at http://canjchem.nrc.ca on 31 March 2006.

D.J. Eisler and T. Chivers.[1] Department of Chemistry, University of Calgary, Calgary, AB T2N 1N4, Canada.

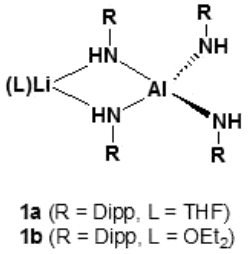
[1]Corresponding author (e-mail: chivers@ucalgary.ca).

 doi:10.1139/V06-018 © 2006 NRC Canada

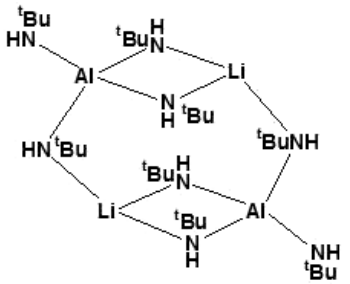
produced structurally characterized dinuclear complexes containing either one or two Al-H functionalities, respectively.

$$[1] \quad MAlH_4 + RNH_2 \rightarrow 1/n(HAlNR)n + 2H_2 + MH \ (M = Li, Na)$$

The reactions of lithium amides with aluminum(III) compounds have also been investigated. Tetrakis(amido)aluminates of the type $[Al(NHR)_4]^-$ are obtained as the monomeric ion-paired complex $[(DippNH)_2Al(\mu\text{-}NHDipp)_2\text{-}Li\cdot THF]$ (**1a**) (8) or the dimer $[(t\text{-}BuNH)Al(\mu\text{-}NH\text{-}t\text{-}Bu)_2Li(\mu\text{-}NH\text{-}t\text{-}Bu)]_2$ (**2a**) (9) from reactions of LiNHR (R = Dipp, *t*-Bu) with $AlCl_3$ in THF or hexane, respectively. The related complex, $[\{(Me_2N)_3SiNH\}_2Al(\mu\text{-}NHSi(NMe_2)_3\}_2\text{-}Li\cdot 2THF]$, which is structurally analogous to **1a** but incorporates a bis-solvated Li^+ cation, is prepared from $AlCl_3$ and $(Me_2N)_3SiNHLi$ in a 1:4 molar ratio in pentane (followed by recrystallization from THF) (10). The diethyl-ether-solvated complex, $[(DippNH)_2Al(\mu\text{-}NHDipp)_2Li\cdot OEt_2]$ (**1b**), isostructural with **1a**, was obtained as a minor product from the reaction of $H_3Al\cdot NMe_3$ with $DippNH_2$ (11). The open rhombododecahedral cage $[(HAl)_4(NPh)_6\{Li(OEt_2)\}_3]^-$ is formed by treatment of the adduct $AlH_3\cdot N(Me)C_5H_8$ with LiNHPh (12).



1a (R = Dipp, L = THF)
1b (R = Dipp, L = OEt_2)



2a

In connection with our interest in generating polyimido anions of p-block elements (13), we have previously investigated the reaction of the trialkylamidoalane dimer $[(t\text{-}BuNH)_2Al(\mu\text{-}NH\text{-}t\text{-}Bu)_2Al(NH\text{-}t\text{-}Bu)_2]$ with alkyl-lithium reagents and shown by NMR spectroscopy that the initial lithiation occurs at a bridging NH-*t*-Bu group to give mono- and di-lithiated derivatives, $Li_x[Al_2(N\text{-}t\text{-}Bu)_x(NH\text{-}t\text{-}Bu)_{6-x}]$ (x = 1, 2) (14). In the case of *n*-BuLi, the use of 5 equiv. of the organolithium reagent (per dimer) generates the trilithiated derivative, which acts as a template to trap the unsolvated dimer $(n\text{-}BuLi)_2$. By contrast, the reaction of the tris(arylamido) alane, $[Al(NHAr)_3]$ (Ar = 2-$MeOC_6H_4$), which is assumed to be dimeric (15), with 3 equiv. of *n*-BuLi (per monomer) leads to lithiation of all three N-H protons and nucleophilic addition of the *n*-Bu group to aluminum to give a tetraanionic organotriimidoaluminate, $[n\text{-}BuAl(NAr)_3]^{4-}$ (16). This anion, as the tetralithium derivative, forms the dimeric ion-separated cluster, $[Li(THF)_4]_2\text{-}[Li_6\{n\text{-}BuAl(NAr)_3\}_2]$ (16).

In view of the lack of a general, high-yield synthesis to tetrakis(amido)aluminates, we have undertaken a systematic investigation of the reactions of alkali metal aluminum hydrides, $M[AlH_4]$ (M = Li, Na), with primary amines, RNH_2 (R = *t*-Bu, *i*-Pr, *p*-tolyl), under mild conditions as a route to the potentially useful tetradentate, monoanionic ligands $[Al(NH\text{-}t\text{-}Bu)_4]^-$. We describe here the synthesis of six alkali metal tetrakis(amido)aluminates; the X-ray structures of four of them are compared with those of **1a**, **1b**, and **2a**. We also report the X-ray structures of two of the secondary products of these reactions, both of which are novel dinuclear clusters containing amido–imido aluminum anions.

Experimental section

Reagents and general procedures

Solvents were dried and distilled before use (*n*-hexane, THF, diethyl ether, and toluene (Na/benzophenone)). The reagents NH_2-*t*-Bu, NH_2-*i*-Pr, and NH_2-*p*-tolyl were commercial samples (Sigma-Aldrich) and used as received. A commercial sample of $NaAlH_4$ was dissolved in THF and, after 45 min at 23 °C, insoluble black material was removed by filtration to give pure $NaAlH_4$ as an off-white solid after the removal of solvent. $LiAlH_4$ was purified by recrystallization from diethyl ether. The handling of air- and moisture-sensitive materials was performed under an atmosphere of argon gas using standard Schlenk techniques or a glovebox.

^1H, ^7Li, ^{13}C, and ^{27}Al NMR spectra were collected on a Bruker AMX-300 spectrometer and chemical shifts are reported relative to Me_4Si in $CDCl_3$ (^1H, ^{13}C), LiCl in D_2O (^7Li), or $Al(NO_3)_3$ in D_2O (^{27}Al). All NMR spectra were collected at 23 °C unless otherwise stated. Fourier transform infrared (FT IR) spectra were obtained as Nujol mulls using KBr windows on a Mattson Genesis Series instrument. The Analytical Services Laboratory of the Department of Chemistry, University of Calgary, provided elemental analyses.

Preparation of Li[Al(NH-*t*-Bu)$_4$] (2a)

A slurry of $LiAlH_4$ (0.125 g, 3.30 mmol) in *n*-hexane or toluene (10 mL) was added to a clear colorless solution of NH_2-*t*-Bu (2.74 mL, 1.907 g, 26.1 mmol) in *n*-hexane or toluene (10 mL) at 23 °C. Immediate, vigorous bubbling was observed. The mixture was stirred for 3 h and then the volume of solution was reduced to 10 mL under vacuum. The resulting clear solution was cooled to –25 °C for 24 h to give colorless crystals of $LiAl(NH\text{-}t\text{-}Bu)_4$ (0.872 g, 2.70 mmol, 82%) with *n*-hexane as solvent and (0.810 mg, 2.51 mmol, 76%) when toluene was used. ^1H NMR (in C_6D_6) δ: 1.45 (s, C*Me*$_3$), cf. lit. δ 1.43 in C_6D_6 (7).

Preparation of Li[Al(NH-*i*-Pr)$_4$] (2b)

A solution of $LiAlH_4$ (0.223 g, 5.88 mmol) in THF (40 mL) was added to a solution of NH_2-*i*-Pr (2.00 mL, 1.388 g, 23.48 mmol) in THF (15 mL) at 23 °C resulting in immediate, vigorous evolution of H_2. The mixture was stirred for 1 h and the resulting slightly cloudy solution was filtered though a 0.45 μm pore size filter disk. The solvent was removed in vacuo and the residue was washed with diethyl ether (20 mL) leaving a white solid (0.892 g, 57%). IR (cm^{-1}): 3365 ν(N-H). ^1H NMR (in D_8-THF) δ: 3.05 (m, 1H, C*H*Me$_2$), 0.98 (d, 6H, CH*Me*$_2$, $^3J(^1H\text{-}^1H)$ = 6 Hz), –0.94 (d, 1H, N*H*, $^3J(^1H\text{-}^1H)$ = 11 Hz). ^{13}C NMR δ: 45.3 (*C*HMe$_2$), 31.0 (CH*Me*$_2$). ^{27}Al NMR δ: 107.1. ^7Li NMR δ: –1.31. Anal. calcd. for $C_{12}H_{32}AlLiN_4$ (%): C 54.12, H 12.11, N 21.01; found: C 53.60, H 13.08, N 20.92.

© 2006 NRC Canada

Preparation of [Li(THF)$_4$][Al(NH-*p*-tolyl)$_4$] (2c)

A solution of $LiAlH_4$ (0.089 g, 2.35 mmol) in THF (40 mL) was added slowly to a solution of *p*-toluidine (1.00 g, 9.33 mmol) in THF (15 mL) resulting in immediate, vigorous evolution of H_2. The mixture was stirred for 1 h and the resulting slightly cloudy solution was filtered though a 0.45 μm pore size filter disk and then concentrated to ca. 10 mL. Slow addition of *n*-hexane (25 mL) combined with vigorous stirring of the solution resulted in the precipitation of [Li(THF)$_4$][Al(NH-*p*-tolyl)$_4$] as a white solid. The solution was decanted and the solid dried in vacuo (1.385 g, 1.85 mmol, 79%). ^{1}H NMR (in D_8-THF) δ: 6.55 (m, 4H, C_6H_4), 3.63 (m, *THF*), 3.16 (s, 1H, N*H*), 2.08 (s, 3H, *Me*), 1.78 (m, *THF*). ^{13}C NMR δ: 154.1, 129.6, 120.2, 116.5 (C_6H_4), 68.4 (*THF*), 26.4 (*THF*), 20.8 (*Me*). ^{27}Al NMR δ: 96.7. ^{7}Li NMR δ: –2.68. Anal. calcd. for $C_{44}H_{64}AlLiN_4O_4$ (%): C 70.65, H 8.64, N 7.50; found: C 69.97, H 8.52, N 7.21.

Preparation of [Na(THF)][Al(NH-*t*-Bu)$_4$] (3a)

A solution of $NaAlH_4$ (0.251 g, 4.65 mmol) in THF (40 mL) was added to a solution of NH_2-*t*-Bu (2.0 mL, 1.358 g, 18.57 mmol) in THF (10 mL) at 23 °C resulting in immediate, slow evolution of H_2. The mixture was stirred for 3 h and the resulting slightly cloudy solution was filtered though a 0.45 μm pore size filter disk. The volume of solution was then reduced to 10 mL in vacuo and cooled to –10 °C for 2 h to give colorless crystals of [Na(THF)][Al(NH-*t*-Bu)$_4$] (0.872 g, 2.12 mmol, 46%). ^{1}H NMR (in D_8-THF) δ: 3.63 (m, 4H, *THF*), 1.78 (m, 4H, *THF*), 1.13 (s, 36H, C*Me*$_3$), –0.68 (s, 4H, N*H*). ^{13}C NMR δ: 68.4 (*THF*), 49.9 (*C*Me$_3$), 36.4 (C*Me*$_3$), 26.4 (*THF*). ^{27}Al NMR δ: 110.0. Anal. calcd. for $C_{20}H_{48}AlN_4NaO$ (%): C 58.50, H 11.78, N 13.65; found: C 56.15, H 10.74, N 13.10. The obtained carbon analysis for this complex was consistently low, however, the complex was pure by both ^{1}H and ^{13}C NMR spectroscopy.

Preparation of [Na][Al(NH-*i*-Pr)$_4$] (3b)

A solution of $NaAlH_4$ (0.315 g, 5.83 mmol) in THF (40 mL) was added to a solution of NH_2-*i*-Pr (2.00 mL, 1.388 g, 23.48 mmol) in THF (15 mL) at 23 °C resulting in immediate, vigorous evolution of H_2. The mixture was stirred for 1 h and the resulting slightly cloudy solution was filtered though a 0.45 μm pore size filter disk. The solvent was removed in vacuo and the residue was washed with diethyl ether (20 mL) leaving a white solid (1.068 g, 65%). ^{1}H NMR (in D_8-THF) δ: 3.12 (m, 1H, C*H*Me$_2$), 0.98 (d, 6H, CH*Me*$_2$, $^3J(^1H\text{-}^1H)$ = 6 Hz), –0.85 (d, 1H, N*H*, $^3J(^1H\text{-}^1H)$ = 9 Hz). ^{13}C NMR δ: 45.5 (*C*HMe$_2$), 31.1 (CH*Me*$_2$). ^{27}Al NMR δ: 108.5. Anal. calcd. for $C_{12}H_{32}AlN_4Na$ (%): C 51.04, H 11.42, N 19.84; found: C 50.31, H 11.81, N 19.44.

Preparation of [Na(THF)][Al(NH-*p*-tolyl)$_4$] (3c)

A solution of $NaAlH_4$ (0.126 g, 2.33 mmol) in THF (40 mL) was added slowly to a solution of *p*-toluidine (1.00 g, 9.33 mmol) in THF (15 mL) at 23 °C resulting in immediate, vigorous evolution of H_2. The mixture was stirred for 1 h and the resulting slightly cloudy solution was filtered though a 0.45 μm pore size filter disk. The solvent was removed in vacuo and the residue was washed with diethyl ether (40 mL) leaving a white solid (0.893 g, 70%). ^{1}H NMR (in D_8-THF) δ: 6.54 (m, 4H, C_6H_4), 3.63 (m, *THF*), 3.15 (s, 1H, N*H*), 2.06 (s, 3H, *Me*), 1.78 (m, *THF*). ^{13}C NMR δ: 154.0, 129.7, 120.6, 116.7 (C_6H_4), 68.4 (*THF*), 26.4 (*THF*), 20.8 (*Me*). ^{27}Al NMR δ: 95.4. Anal. calcd. for $C_{32}H_{40}AlN_4NaO$ (%): C 70.31, H 7.38, N 10.25; found: C 69.74, H 6.67, N 9.98.

Preparation of {[Na(THF)$_2$][(NH-*t*-Bu)Al(H)(μ-N-*t*-Bu)]}$_2$ (4)

This complex is a minor product (ca. 20%) obtained in the preparation of **3a**. In addition to complex **4**, an additional minor product (ca. 10%), which was not identified, is also present in reaction solutions of **3a**. Significantly larger quantities of **4** and this unidentified complex (ca. 50% combined) are observed when the reaction is carried in a 1:2 mixture of THF and *n*-hexane. An analytically pure sample of **4** could not be obtained, as this material was always contaminated with the other reaction products. X-ray quality crystals of **4** were isolated manually from a mixture of crystals of **3a** and **4** grown from a concentrated solution of the complexes in THF–hexane at –10 °C. ^{1}H NMR (in D_8-THF, 298 K) δ: 3.63 (m, *THF*), 1.78 (m, *THF*), 1.22 (s, 9H, C*Me*$_3$), 1.18 (s, 9H, C*Me*$_3$), 0.46 (s, 1H, N*H*). ^{13}C NMR δ: 68.4 (*THF*), 52.9, 50.9 (*C*Me$_3$), 38.9, 36.3 (C*Me*$_3$), 26.4 (*THF*). ^{1}H NMR (in D_8-THF, 233 K) δ: 4.38 (v br, $\Delta\omega_{1/2}$ ~ 70 Hz, 1H, Al-*H*), 3.63 (m, *THF*), 1.78 (m, *THF*), 1.19 (s, 9H, C*Me*$_3$), 1.14 (s, 9H, C*Me*$_3$), 0.60 (s, 1H, N*H*). ^{27}Al NMR δ: 110.0.

Preparation of {[Na(THF)$_3$][(NH-*p*-tolyl)$_2$Al(μ-N-*p*-tolyl)]}$_2$ (5)

This complex is the minor product (ca. 30%) obtained in the preparation of complex **3c**. An analytically pure sample of **5** could not be obtained, as this material was always contaminated with **3c**. X-ray quality crystals of **5** were isolated manually from a mixture of crystals of **3c** and **5** grown from a concentrated solution of the complexes in THF–hexane at –10 °C. ^{1}H NMR (in D_8-THF) δ: 6.72 (m, 8H, C_6H_4), 6.70 (m, 16H, C_6H_4), 3.63 (m, *THF*), 3.28 (s, 4H, N*H*) 2.06 (s, br, 18H, *Me*), 1.78 (m, *THF*). ^{13}C NMR δ: 157.4, 152.8, 130.4, 130.2, 122.5, 122.0, 117.3, 116.8 (C_6H_4), 68.4 (*THF*), 26.4 (*THF*), 20.6 (*Me*). ^{27}Al NMR δ: 97.2.

X-ray structural analyses

Crystal data for **2b**, **2c**, **3b**, **3c**, **4**, and **5** are summarized in Table 1.[2] A suitable crystal of the complex was selected, coated in Paratone oil, and mounted on a glass fibre. Data were collected at 173 K on a Nonius Kappa CCD diffractometer using Mo Kα radiation (λ = 0.710 73 Å) via ω and φ scans. The unit cell parameters were calculated and refined from the full data set. Crystal cell refinement and data

[2] Supplementary data for this article are available on the journal Web site (http://canjchem.nrc.ca) or may be purchased from the Depository of Unpublished Data, Document Delivery, CISTI, National Research Council Canada, Ottawa, ON K1A 0R6, Canada. DUD 5011. For more information on obtaining material refer to http://cisti-icist.nrc-cnrc.gc.ca/irm/unpub_e.shtml. CCDC 290050–290055 contain the crystallographic data for this manuscript. These data can be obtained, free of charge, via www.ccdc.cam.ac.uk/conts/retrieving.html (or from the Cambridge Crystallographic Data Centre, 12 Union Road, Cambridge CB2 1EZ, UK; fax +44 1223 336033; or deposit@ccdc.cam.ac.uk).

© 2006 NRC Canada

Table 1. Crystallographic data for **2b**, **2c**, **3b**, **3c**, **4**, and **5**.

Crystal	**2b**	**2c**	**3b**	**3c**	**4**	**5**
Empirical formula	$C_{12}H_{32}AlLiN_4$	$C_{44}H_{64}AlLiN_4O_4$	$C_{12}H_{32}AlN_4Na$	$C_{32}H_{40}AlN_4NaO$	$C_{32}H_{72}Al_2N_4Na_2O_4$	$C_{66}H_{94}Al_2N_6Na_2O_6$
Formula mass	266.34	746.91	282.39	546.65	676.88	1167.41
Colour, habit	Colourless, plate	Colourless, rod	Colourless, plate	Colourless, needle	Colourless, block	Colourless, block
Crystal size (mm)	0.16×0.12×0.08	0.12×0.07×0.05	0.08×0.06×0.03	0.14×0.05×0.03	0.20×0.16×0.14	0.12×0.08×0.06
Crystal system	Monoclinic	Monoclinic	Tetragonal	Monoclinic	Monoclinic	Monoclinic
Space group	*P*2/*c* (No. 13)	*C*2/*c* (No. 15)	$I4_1/a$ (No. 88)	$P2_1/c$ (No. 14)	$P2_1/n$ (No. 14)	$P2_1/c$ (No.14)
Z	4	4	4	4	2	2
a (Å)	9.047(2)	14.549(3)	16.888(2)	10.722(2)	10.898(2)	10.364(2)
b (Å)	11.157(2)	20.217(4)	16.888(2)	11.476(2)	18.400(4)	21.583(4)
c (Å)	19.156(4)	14.879(3)	6.275(1)	25.090(5)	11.074(2)	15.265(3)
β (°)	113.03(3)	90.69(3)		90.83(3)	110.19(3)	105.84(3)
Collection ranges	$-11 \le h \le 11$, $-13 \le k \le 13$, $-23 \le l \le 23$	$-17 \le h \le 17$, $-24 \le k \le 24$, $-17 \le l \le 17$	$-20 \le h \le 20$, $-20 \le k \le 20$, $-7 \le l \le 7$	$-11 \le h \le 12$, $-13 \le k \le 13$, $-29 \le l \le 29$	$-14 \le h \le 14$, $-23 \le k \le 21$, $-14 \le l \le 14$	$-12 \le h \le 12$, $-25 \le k \le 25$, $-18 \le l \le 18$
Volume ($Å^3$)	1 779.4(7)	4 376(2)	1 789.6(5)	3 087(1)	2 084.1(7)	3 285(1)
D_{calcd} (Mg/m^3)	0.994	1.134	1.048	1.176	1.079	1.180
μ (mm^{-1})	0.105	0.90	0.130	0.110	0.126	0.111
F(000)	592	1 616	624	1168	744	1 256
θ range for data collection (°)	3.26–26.37	10.24–25.02	3.41–25.02	2.48–25.04	2.96–27.51	2.92–25.03
Observed reflections	18 073	65 854	26 264	34 228	19 031	40 278
Independent reflections	3 614 (R_{int} = 0.043)	3 573 (R_{int} = 0.073)	789 (R_{int} = 0.091)	5 425 (R_{int} = 0.100)	4 756 (R_{int} = 0.038)	5 798 (R_{int} = 0.149)
Data/restraints/parameters	3 614 / 0 / 167	3 573 / 43/ 259	789 / 0 / 43	5 425 / 6 / 354	4 756 / 0 / 207	5 798 / 6 / 371
Maximum shift/error	0.00	0.00	0.00	0.00	0.00	0.00
GoF on F^2	1.046	1.036	1.042	1.016	1.089	1.029
Final *R* indices [$I > 2\sigma(I)$][a]	0.0652, 0.1781	0.0723, 0.1813	0.0383, 0.0929	0.0551, 0.1126	0.0504, 0.1337	0.0485, 0.1251
R indices (all data)[b]	0.0892, 0.1906	0.0923, 0.1985	0.0525, 0.1014	0.1248, 0.1385	0.0629, 0.1419	0.0840, 0.1397
Largest diff. peak and hole (e $Å^{-3}$)	0.454 and –0.366	0.516 and –0.273	0.194 and –0.236	0.193 and –0.241	0.389 and –0.262	0.729 and –0.292

[a] $R_1 = [\Sigma||F_o| - |F_c||]/[\Sigma|F_o|]$ for $[I > 2\sigma(I)]$.
[b] $wR_2 = \{[\Sigma w(F_o^2 - F_c^2)^2]/[\Sigma w(F_o^2)^2]\}^{1/2}$ (all data).

© 2006 NRC Canada

reduction were carried out using the Nonius DENZO package. After data reduction, the data were corrected for absorption based on equivalent reflections using SCALEPACK (Nonius, 1998). The structures were solved by direct methods using SHELXS-97 (17) and refinement was carried out on F^2 against all independent reflections by the full-matrix least-squares method using the SHELXL-97-2 program (18). The hydrogen atoms were calculated geometrically and were riding on their respective atoms unless otherwise noted. Except as mentioned, all non-hydrogen atoms were refined with anisotropic thermal parameters.

2b

The molecule was well-ordered and no special considerations for the refinement were necessary. The complex crystallizes with two independent, but chemically equivalent molecules in the unit cell, for which two independent halves of the molecules are present in the asymmetric unit (the other half in each case being generated by the crystallographic twofold axis). The lithium atoms were refined isotropically.

2c

The amidoaluminate anion was well-ordered, however the $[Li(THF)_4]^+$ cation was highly disordered around a crystallographic twofold rotation axis. Only one-half of the anion and cation are present in the asymmetric unit, with the second half of each being generated by the twofold axis. One of the THF molecules of the cationic moiety was modeled with a 75:25 disorder of the oxygen and one carbon atom; the 25% component of this disorder was refined isotropically. The second THF molecule was severely disordered and was modeled as a 25:25:25:25 isotropic mixture with geometric restraints applied.

3b

The molecule was well-ordered and no special considerations for the refinement were necessary. Due to symmetry only one-quarter of the molecule was located in the difference Fourier map, as the molecule is situated on a fourfold rotary inversion axis.

3c

The molecule was well-ordered with the exception of the coordinated THF molecule, which was modeled with a 65:35 isotropic mixture of two of the carbon atoms with mild geometric restraints.

4

The molecule was well-ordered and no special considerations for the refinement were necessary. The hydrogen atoms on the amido nitrogen and aluminum centers (H2D and H1D, respectively) were located and refined.

5

The molecule was well-ordered with the exception of one THF molecule, which was modeled with a 55:45 disorder of two of the carbon atoms that were refined with isotropic thermal parameters.

Results and discussion

Synthesis of lithium and sodium tetrakis(amido)aluminates

The reaction of lithium or sodium aluminum hydride with 4 equiv. of primary amine RNH_2 in THF at room temperature results in the immediate evolution of H_2 gas to give the corresponding lithium or sodium tetrakis(amido)aluminate (eq. [2]), as well as secondary products, which are observed in varying quantities (<5% to ca. 30%). However, the tetrakis(amido)aluminate complexes are readily purified owing to the higher solubility of the secondary products in diethyl ether, in comparison to the desired tetrakis(amido)aluminates. Although the quantities of the minor components formed vary with reaction conditions, the identities of the products do not change. All attempts to obtain analytically pure samples of the secondary products were unsuccessful owing to persistent contamination with the tetrakis(amido)aluminate complexes.

$$[2] \qquad MAlH_4 + 4NH_2R \rightarrow M[Al(NHR)_4] + 4H_2$$

(**2a**, M = Li, R = *t*-Bu; **3a**, M = Na, R = *t*-Bu; **2b**, M = Li, R = *i*-Pr; **3b**, M = Na, R = *i*-Pr; **2c**, M = Li, R = *p*-tolyl; **3c**, M = Na, R = *p*-tolyl)

Complex **2a** is obtained in 82% yield when *n*-hexane is used as solvent, cf. 60% yield of **2a** from the reaction of $AlCl_3$ with LiNH-*t*-Bu in hexane (9); it was identified by comparison of the ^{1}H NMR chemical shift (a broad singlet at δ 1.45) and unit cell constants with those reported in the literature (9).[3] The other tetrakis(amido)aluminate complexes (**2b**, **2c**, **3a**–**3c**), four of which have been identified by X-ray structural analyses (vide infra), were prepared in THF in yields ranging from 46% to 79%. They are accompanied by the formation of secondary products, and two of these have also been structurally characterized. The complexes **2b**, **2c**, and **3a**–**3c** are each obtained with a varying degree of THF-solvation of the alkali metal cations, as indicated by the ^{1}H NMR spectra. For example, the isopropyl complexes **2b** and **3b** are isolated as the unsolvated complexes $M[Al(NH\text{-}i\text{-}Pr)_4]$, whereas the arylamido complex **2c** is obtained as a highly solvated complex with four molecules of THF for each Li^+ ion.

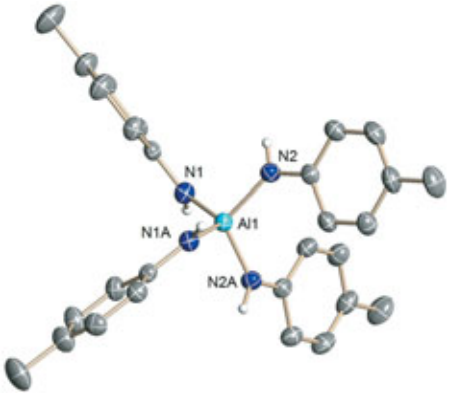
X-ray structures of lithium and sodium tetrakis(amido)aluminates

The solid-state structure of complex **2c**, which was determined crystallographically, confirmed the presence of an ion-separated complex consisting of a $[Li(THF)_4]^+$ cation and a $[Al(NH\text{-}p\text{-}tolyl)_4]^-$ anion, in contrast to the solvated monomeric structure of **1a** and the unsolvated dimeric structure of **2a**. The anion in **2c** is depicted in Fig. 1. The Al—N distances are identical within error (Al(1)—N(1) = 1.841(2) Å, Al(1)—N(2) = 1.844(2) Å), and are comparable to those observed for the terminal DippNH ligands in **1a** (1.845(9) Å) (8). The aluminum centre in **2c** adopts a distorted tetrahedral geometry with the N-Al-N bond angles ranging from 105.5(1)° to 116.6(2)°.

[3] As reported by Cowley and co-workers (9), the NH resonances of **2a** were not observed in the ^{1}H NMR spectrum. The broad singlet observed for the *t*-Bu groups at 23 °C is indicative of dynamic behaviour.

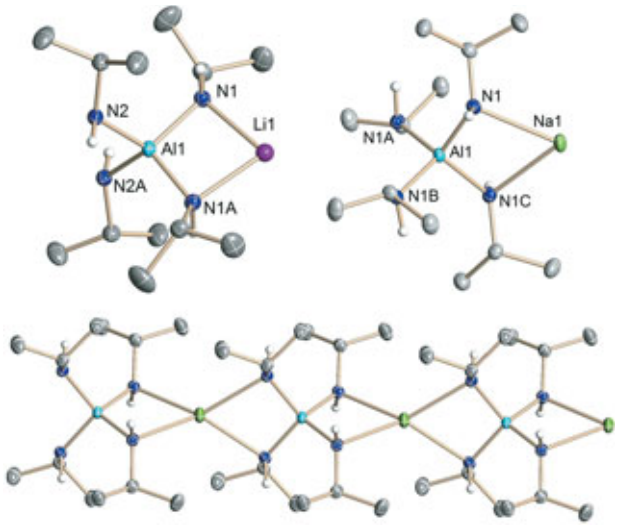
© 2006 NRC Canada

Fig. 1. Molecular structure of the anion $[Al(NH\text{-}p\text{-}tolyl)_4]^-$ in **2c**. Thermal ellipsoids are shown at 30% probability. Hydrogen atoms on carbon atoms have been removed for clarity. Selected bond lengths (Å) and angles (°): Al(1)—N(1), 1.841(2) Å; Al(1)—N(2), 1.844(2) Å; N(1)-Al(1)-N(1A), 116.6(2)°; N(1)-Al(1)-N(2), 107.3(1)°; N(1)-Al(1)-N(2A), 105.5(1)°; N(2)-Al(1)-N(2A), 115.2(2)°.



An X-ray analysis of the solid-state structures of complexes **2b** and **3b** verified that there are no solvent molecules present in either case (Fig. 2). The two structures are very similar, although there are variations that arise from the presence of different alkali metal cations. For complex **2b**, two independent, but chemically equivalent, molecules are present in the asymmetric unit, and only one is shown in Fig. 2. The two molecules are adjacent to each other, but are slightly skewed along the crystallographic twofold axis (torsion angles N-Al-Al-N, ca. 34°). In contrast, the $(HN\text{-}i\text{-}Pr)_2Al(HN\text{-}i\text{-}Pr)_2Na$ molecule in **3b** is highly symmetrical, with both the sodium and the aluminum centres situated on a fourfold rotary inversion axis. Presumably, the lower symmetry in **2b** arises owing to distortions resulting from the smaller size of the lithium cation in comparison to the sodium cation in **3b**. This rationale is supported by the observed distortions from regular tetrahedral geometry around the aluminum centres in **2b**. The smallest N-Al-N angles are those involved in the AlN_2Li rings (range 100.5(2)°–101.5(2)°). The exocyclic N-Al-N angles are considerably larger, ranging from 113.5(1)° to 114.2(1)°. By comparison, the aluminum centre in **3b** is only slightly distorted from tetrahedral, with bond angles in the narrow range of 107.61(9)°–110.41(5)°; the smallest angles are those in the AlN_2Na rings. The Al—N bond distances are identical within experimental error in both structures (**2b**, 1.857(2)–1.865(2) Å; **3b**, 1.862(2) Å) and are comparable to those observed for complex **2c**. Interestingly, the overall crystal structures of complexes **2b** and **3b** are one-dimensional polymers (Fig. 2, bottom). The polymeric structure is a result of the coordination of the lithium or sodium cation to two amido nitrogen centres from each of two adjacent tetrakis(amido)aluminate anions. The lithium and sodium cations are thus four-coordinate, and are highly distorted from tetrahedral (**2b**, N-Li-N bond angles 83.2(3)°–84.3(3)° in the AlN_2Li rings and exocyclic bond angles of 107.58(9)°–143.76(9)°; **3b**, N-Na-N bond angles of 72.80(7)° in the AlN_2Na rings and exocyclic N-Na-N bond angles of 130.38(4)°). A similar structure has been observed for the methyl derivative, $Li[Al(NHMe)_4]$ (19).

Fig. 2. Top left: Molecular structure of **2b**. Top right: Molecular structure of **3b**. Bottom: Polymeric crystal structure of **3b**. Thermal ellipsoids are shown at 30% probability. Hydrogen atoms on carbon atoms have been removed for clarity. Selected bond lengths (Å) and angles (°): **2b**: Al(1)—N(1), 1.857(2) Å; Al(1)—N(2), 1.863(2) Å; Li(1)—N(1), 2.166(6) Å; N(1)-Al(1)-N(2), 113.5(1)°; N(1)-Al(1)-N(1A), 101.5(2)°; N(1)-Al(1)-N(2A), 113.8(1)°; N(2)-Al(1)-N(2A), 101.4(2)°. **3b**: Al(1)—N(1), 1.862(2) Å; Na(1)—N(1), 2.532(2) Å; N(1)-Al(1)-N(1A), 107.61(9)°; N(1)-Al(1)-N(1B), 110.41(5)°.



The solid-state structure for **3c**, which is depicted in Fig. 3, was determined by X-ray crystallography; pertinent metrical parameters are given in Table 2. The molecular structure is similar to that of **3b** except that the sodium ion is monosolvated by THF. The four-coordinate aluminum centre adopts a distorted tetrahedral geometry, with the N-Al-N angles ranging from 106.9(1)° to 114.6(1)°. The Al—N bond lengths are equal within the limits of error, falling in the narrow range of 1.843(3)–1.855(3) Å.

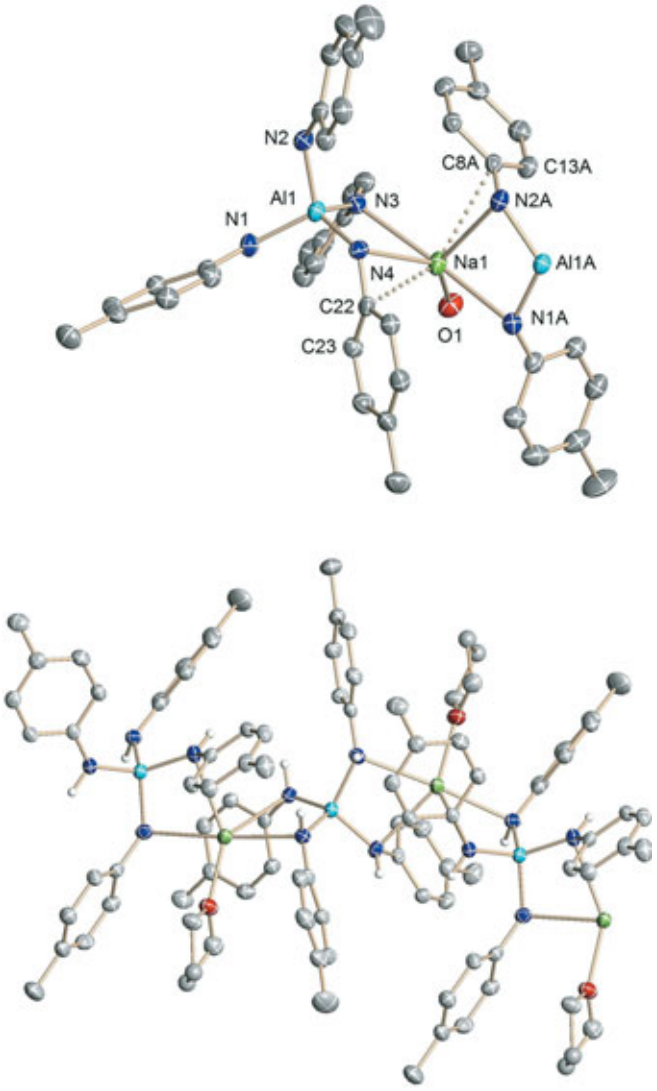
Similar to the structures of **2b** and **3b**, complex **3c** forms a one-dimensional polymer involving coordination of the sodium cations to amido groups of adjacent aluminate anions. In addition to the amido substituents and the single molecule of THF, each sodium ion displays interactions with the aromatic rings of two *p*-tolyl substituents. Thus, the sodium ions are overall seven-coordinate. The strongest Na—C interactions are with the ipso carbon atoms of the two rings with distances of 2.839(3) Å (C8A—Na1) and 2.868(3) Å (C22—Na1). There are also weaker contacts with one of the ortho carbon atoms (C13A—Na1 = 3.174(3) Å; C23—Na1 = 3.063(3) Å). These distances are within the typical range of 2.6–3.2 Å observed for Na—C aromatic interactions (20). The Na—N bond distances are considerably longer and more varied in **3c** (2.561(3)–2.785(3) Å) than those in **3b** (2.532(2) Å), presumably as a result of the higher coordination number of the sodium centre.

NMR spectra of lithium and sodium tetrakis(amido)aluminates

The NMR spectra for **2b**, **2c**, **3b**, and **3c** should provide a good indication of whether the solid-state structures (vide supra) are maintained in solution. In addition, the NMR

© 2006 NRC Canada

Fig. 3. Top: Molecular structure of **3c**; portions of an adjacent molecule are shown, and all hydrogen atoms and THF carbon atoms have been removed to clarify the full coordination environment of the sodium centre. Bottom: Polymeric crystal structure of **3c**; hydrogen atoms on carbon atoms have been removed for clarity. Thermal ellipsoids are shown at 30% probability.



spectra will furnish information about the solution structure of **3a**, which could not be determined in the solid state. The multinuclear NMR data obtained for **2c** were in keeping with the observed solid-state structure. For example, a single resonance was observed for the methyl groups of the *p*-tolyl substituents in the ^{1}H and ^{13}C NMR spectra, as well as a single resonance for the four equivalent N-H protons in the ^{1}H NMR spectrum. The integration of the ^{1}H NMR spectrum indicated the presence of four THF molecules of solvation. A single broad resonance ($\Delta\omega_{1/2}$ ~ 390 Hz) was observed in the ^{27}Al NMR spectrum, and a singlet was observed at δ –2.68 in the ^{7}Li NMR spectrum attributable to the $[Li(THF)_4]^+$ cation.

The NMR data obtained for the isopropyl derivatives **2b** and **3b** were consistent with the observed solid-state structures. There were no observable resonances in the ^{1}H or ^{13}C NMR spectra attributable to coordinated solvent molecules.

Table 2. Selected bond lengths (Å) and bond angles (°) for **3c**.

Bond lengths (Å)	
Al(1)—N(1)	1.855(3)
Al(1)—N(2)	1.843(3)
Al(1)—N(3)	1.853(2)
Al(1)—N(4)	1.847(2)
Na(1)—N(1A)	2.561(3)
Na(1)—N(2A)	2.785(3)
Na(1)—N(3)	2.613(3)
Na(1)—N(4)	2.625(3)
Bond angles (°)	
N(1)-Al(1)-N(2)	110.2(1)
N(1)-Al(1)-N(3)	108.0(1)
N(1)-Al(1)-N(4)	107.3(1)
N(2)-Al(1)-N(3)	106.9(1)
N(2)-Al(1)-N(4)	114.6(1)
N(3)-Al(1)-N(4)	109.7(1)
Al(1)-N(1)-Na(1)	93.6(1)
Al(1)-N(2)-Na(1)	86.9(1)
O(1)-Na(1)-N(1A)	92.79(9)
O(1)-Na(1)-N(3)	89.94(8)
O(1)-Na(1)-N(4)	139.59(9)
N(1A)-Na(1)-N(2A)	69.01(8)
N(1A)-Na(1)-N(3)	175.70(9)
N(2A)-Na(1)-N(3)	110.88(8)
N(2A)-Na(1)-N(4)	82.24(8)
N(3)-Na(1)-N(4)	70.57(8)

However, the complexes **2b** and **3b** are completely insoluble in noncoordinating solvents such as benzene and toluene, whereas they are freely soluble in THF. Presumably, there is some degree of solvation of the alkali metal cations that allows the complex to dissolve in the coordinating solvent, THF. In the respective ^{1}H NMR spectra for these isopropyl complexes, the methyl groups appear as a doublet owing to coupling with the methine protons. The resonances for the N-H protons appear as doublets owing to long-range coupling with the methine protons, which in turn appear as two overlapping septets. A single resonance is observed in each ^{27}Al NMR spectrum. In addition, a singlet is observed at δ –1.31 in the ^{7}Li NMR spectrum of **2b**, which is in keeping with a THF-solvated lithium ion (typical range ~δ –0.5 to –2.5) (21). These data suggest that these complexes exist in THF solution either as solvent-separated cation–anion pairs, as was observed for **2c**, or that the cation is partially solvated, and the complexes are present as contact-ion pairs. In the latter case, any association between the cation and the complex would have to be dynamic on the NMR timescale as all of the amido substituents are equivalent in solution, even down to –80 °C.

Complex **3c** is also insoluble in noncoordinating solvents, but it is freely soluble in THF. In keeping with the solid-state structure, resonances attributable to a single molecule of coordinated THF were present in the ^{1}H NMR spectrum of **3c**. However, in contrast to the solid-state structure, the multinuclear NMR data obtained for complex **3c** are consistent with a highly symmetrical structure, with only a single

© 2006 NRC Canada

Fig. 4. Molecular structure of **4**. Thermal ellipsoids are shown at 30% probability. Hydrogen atoms on carbon atoms have been removed for clarity.

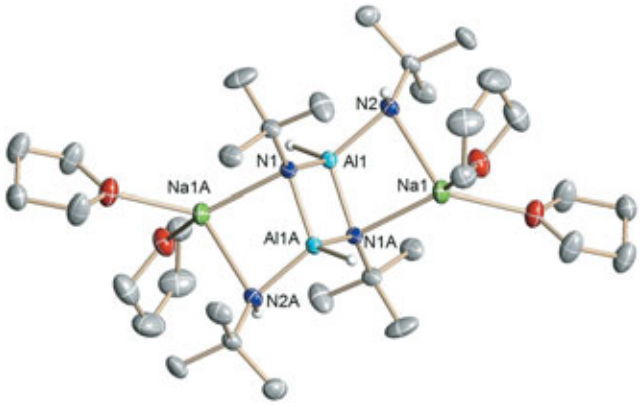


Table 3. Selected bond lengths (Å) and bond angles (°) for **4**.

Bond lengths (Å)	
Al(1)—N(1)	1.858(2)
Al(1)—N(1A)	1.869(2)
Al(1)—N(2)	1.891(2)
Na(1)—N(1A)	2.486(2)
Na(1)—N(2)	2.493(2)
Bond angles (°)	
N(1)-Al(1)-N(1A)	88.69(6)
N(1)-Al(1)-N(2)	111.86(7)
Al(1)-N(1)-Al(1A)	91.31(6)
Al(1)-N(1)-Na(1A)	98.06(7)
Al(1A)-N(1)-Na(1A)	84.68(6)

resonance observed for the N-H and methyl protons, for example. These data suggest that, like the isopropyl complexes, **3c** exists in solution as a solvent-separated cation–anion pair, or that the complex is present as a dynamic contact-ion pair.

All attempts to obtain crystals of **3a** suitable for X-ray diffraction studies were unsuccessful, and so the complex was characterized by multinuclear NMR spectra. In the ^{1}H NMR spectrum, a single resonance is observed for the *tert*-butyl methyl protons, as well as a single N-H resonance. Furthermore, the integrated ^{1}H NMR spectrum indicates that the complex is isolated in the solid state with a single molecule of THF, presumably coordinated to the sodium cation. A broad resonance is observed in the ^{27}Al NMR spectrum, similar to the resonances of the other complexes reported here. Thus, while the NMR data are in keeping with a symmetrical tetrakisimidoaluminate anion, the exact structure of the complex cannot be unambiguously established from these data.

X-ray structures and NMR spectra of the dinuclear complexes $\{[Na(THF)_2][(NH\text{-}t\text{-}Bu)Al(H)(\mu\text{-}N\text{-}t\text{-}Bu)]\}_2$ (4) and $\{[Na(THF)_3][(NH\text{-}p\text{-}tolyl)_2Al(\mu\text{-}N\text{-}p\text{-}tolyl)]\}_2$ (5)

As mentioned previously, the reactions of $MAlH_4$ with a primary amine result in the formation of small amounts of secondary products in addition to the desired tetrakis(amido)aluminate anion. We were able to unambiguously identify the minor products formed in two of the syntheses. The first of these is the dimeric complex $\{[Na(THF)_2][(NH\text{-}t\text{-}Bu)Al(H)(\mu\text{-}N\text{-}t\text{-}Bu)]\}_2$ (**4**), obtained from the reaction of $NaAlH_4$ with *t*-$BuNH_2$. Complex **4** was identified by an X-ray structural determination (Fig. 4); pertinent metrical parameters are given in Table 3.

Complex **4** can be viewed as a contact-ion pair involving the dianion $\{[(NH\text{-}t\text{-}Bu)Al(H)(\mu\text{-}N\text{-}t\text{-}Bu)]_2\}^{2-}$, a dimer of the $[AlH(N\text{-}t\text{-}Bu)(NH\text{-}t\text{-}Bu)]^-$ monoanion, and two THF-solvated sodium ions. The exocyclic amido groups in the dianion exhibit a slightly elongated Al—N bond (1.891(2) Å) in comparison to the bridging imido Al—N bonds (1.858(2) and 1.869(2) Å). The aluminum centres are highly distorted tetrahedral, with the bond angles ranging from 88.69(6)° to 111.86(7)°. The amido and imido Na—N bond distances are nearly identical (2.486(2) and 2.493(2) Å, respectively). The donation of the lone pair on the imido nitrogen centre to the sodium cation is evident from the pyramidal geometry of the nitrogen (bond angles range from 84.68(6)° to 98.06(7)°). The Na—N bond lengths are shorter than those observed for any of the previous complexes reported here. Presumably, the shorter distances are a reflection of the higher ionic character of these bonds in the dianionic complex **4** in comparison to that in the monoanionic complexes **3b** and **3c**.

The NMR data obtained for **4** indicate that the solid-state structure is maintained in solution. In the ^{1}H NMR spectrum, two resonances of equal intensity are apparent for the methyl groups of the two different *tert*-butyl substituents. A single resonance is observed for the N-H protons of the two amido substituents. At room temperature, no resonance was observed for the Al-H proton. However, at 233 K, a single broad resonance ($\Delta\omega_{1/2}$ ~ 70 Hz) at δ 4.38 was detected for this proton. While a large range of values has been reported for Al-H chemical shifts, values in the range of 4.3–5.8 ppm are typical (22), and the value observed for **4** correlates well with the shift δ 4.31 obtained for the structurally similar complex $[(SiMe_3N\text{-}CH_2CH_2\text{-}\mu\text{-}N\text{-}SiMe_3)AlH]_2$ (22*c*).

The by-product obtained from the reaction of *p*-toluidine with $NaAlH_4$ is related to complex **4**, and the structure is shown in Fig. 5 with selected bond distances and angles given in Table 4. In complex **5** a dimeric, dianionic aluminate core structure is observed, however, the hydrido ligand that was present in **4** has been replaced by an additional amido ligand. Thus, the dianion in **5** is $\{[(NH\text{-}p\text{-}tolyl)_2Al(\mu\text{-}N\text{-}p\text{-}tolyl)]_2\}^{2-}$, a dimer of the monoanion $[Al(NH\text{-}p\text{-}tolyl)_2(N\text{-}p\text{-}tolyl)]^-$. The Al—N bond distances fall in a narrow range (1.841(2)–1.860(2) Å), and the aluminum centres exhibit distorted tetrahedral geometries (Table 4). The Na—N distance of 2.493(2) Å is similar to that observed in complex **4**, presumably as a result of the ionic character of the bonding. The sodium centre is only coordinated to the pyramidal imido centre (and three molecules of THF), which suggests a preference for the more ionic imido nitrogen centre in comparison to the amido centres.

The multinuclear NMR data obtained for complex **5** are in accordance with the solid-state structure. In the ^{1}H NMR spectrum, two sets of resonances in a 2:1 ratio are apparent for the aromatic protons of the amido and imido *p*-tolyl substituents, respectively. Consistently, eight carbon resonances for these inequivalent *p*-tolyl groups were observed in the

© 2006 NRC Canada

Scheme 1. Possible pathways in the reactions of $MAlH_4$ with primary amines.

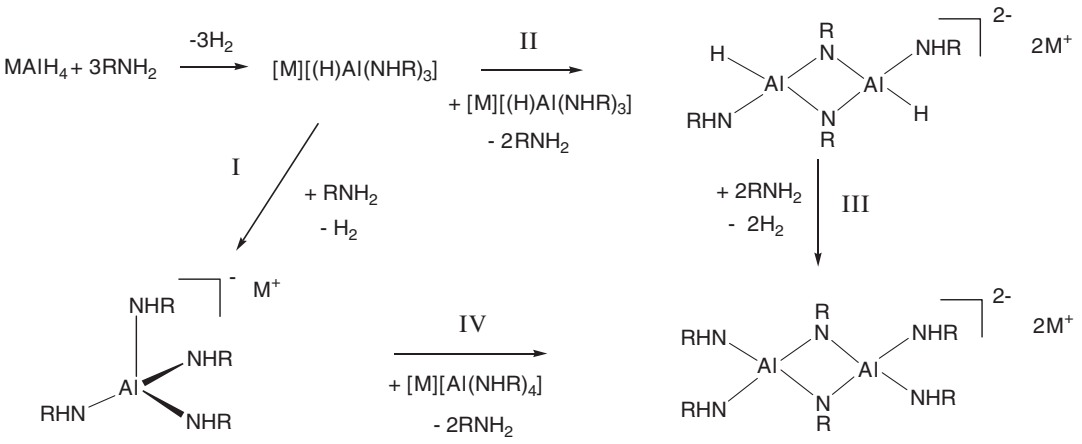


Fig. 5. Molecular structure of **5**. Thermal ellipsoids are shown at 30% probability. Hydrogen atoms on carbon atoms have been removed for clarity.

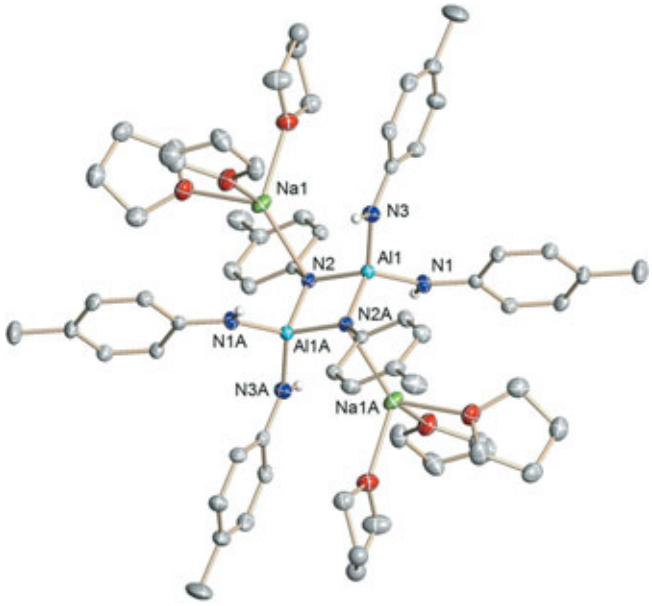


Table 4. Selected bond lengths (Å) and bond angles (°) for **5**.

Bond lengths (Å)	
Al(1)—N(1)	1.841(2)
Al(1)—N(2)	1.860(2)
Na(1)—N(2)	2.493(2)
Al(1)—N(2A)	1.862(2)
Al(1)—N(3)	1.857(2)
Bond angles (°)	
N(1)-Al(1)-N(2)	109.60(9)
N(1)-Al(1)-N(2A)	117.48(9)
N(1)-Al(1)-N(3)	115.69(9)
N(2)-Al(1)-N(2A)	87.86(8)
N(2)-Al(1)-N(3)	116.78(9)
N(2A)-Al(1)-N(3)	106.55(9)
Al(1)-N(2)-Al(1A)	92.14(8)
Al(1)-N(2)-Na(1)	99.06(8)
Al(1A)-N(2)-Na(1)	105.65(8)

^{13}C NMR spectrum. Curiously, however, the methyl groups of the *p*-tolyl substituents exhibit only a single resonance in both the ^{1}H and ^{13}C NMR spectra, indicating coincidental equivalence of these substituents.

The isolation and structural characterization of complexes **4** and **5** provides some insight into the possible different pathways for the reactions of $MAlH_4$ with primary amines. As illustrated in Scheme 1, under mild conditions these reactions likely proceed readily to the formation of the trisamido complex $[M][(RNH)_3Al(H)]$, cf. the formation of $[Li(THF)_4][HAl(NPh_2)_3]$ (4). Once this complex is formed, there is a competition among two possible reaction pathways. The first, predominant route involves reaction with a fourth equivalent of amine, resulting in the substitution of the final hydrido ligand with an amido ligand, to form the tetrakis(amido)aluminate complexes (**I**, Scheme 1). The second route, (**II**, Scheme 1), involves the condensation of two $[(RNH)_3Al(H)]^-$ anions, resulting in the elimination of 2 equiv. of primary amine (RNH_2) and the formation of the dianion $[(RNH)Al(H)(\mu\text{-}NR)]_2^{2-}$, as observed in complex **4** (R = *t*-Bu). Reaction of the Al-H functionality in this dianion with two additional equivalents of amine (**III**, Scheme 1) would result in the formation of the diamido imido dianion$[(RNH)_2Al(\mu\text{-}NR)]_2^{2-}$, which was identified in **5** (R = *p*-tolyl). Alternatively, condensation of two tetrakis(amido)aluminate anions, with the loss of primary amine (**IV**, Scheme 1), could also result in the production of the dianion $[(RNH)_2Al(\mu\text{-}NR)]_2^{2-}$. However, this pathway seems unlikely since it was possible to isolate the pure tetrakis(amido)aluminate complexes in good to excellent yields. Under more forcing conditions, the reactions of primary amines with $MAlH_4$ proceed according to eq. [1] (vide supra).

Conclusions

The reactions of alkali metal aluminum hydrides $MAlH_4$ (M = Li, Na) with primary alkyl- or aryl-amines produces tetrakis(amido)aluminate complexes in good to excellent yields. For the lithium derivatives, the established solid-state

© 2006 NRC Canada

structures of these complexes include mono- or bis-solvated monomeric contact-ion pairs, a solvent-separated ion pair, an unsolvated dimeric contact-ion pair, and a polymeric structure. By contrast, only polymeric structures, either unsolvated or monosolvated, are observed for sodium derivatives of the same primary amines. The $[Al(NHR)_4]^-$ anions represent potentially interesting tetradentate ligands. Although they have been known since 1998 (8, 9), their coordination chemistry has yet to be investigated. The facile synthetic procedure reported herein will facilitate such studies.

Acknowledgements

We thank P. Blais and Dr. G. Schatte for carrying out preliminary investigations of the reactions of primary amines with $LiAlH_4$. We gratefully acknowledge the Natural Sciences and Engineering Research Council of Canada (NSERC) and The Alberta Ingenuity Fund (AIF) for financial support.

References

1. (*a*) S. Böck, H. Nöth, and P. Rahm. Z. Naturforsch B: Chem. Sci. **43B**, 53 (1988); (*b*) G. Linti, H. Nöth, and P. Rahm. Z. Naturforsch B: Chem. Sci. **43B**, 1101 (1988).
2. M.M. Andrianarison, M.C. Ellerby, I.B. Gorrell, P.B. Hitchcock, J.D. Smith, and R.D. Stanley. J. Chem. Soc. Dalton Trans. 211 (1996).
3. A. Heine and D. Stalke. Angew. Chem. Int. Ed. Engl. **31**, 854 (1992).
4. J. Pauls and B. Neumüller. Inorg. Chem. **40**, 121 (2001).
5. (*a*) C. Cucinella, G. Dozzi, A. Mazzei, and T. Salvatori. J. Organomet. Chem. **90**, 257 (1975); (*b*) S. Cucinella, T. Salvatori, C. Busetto, G. Perego, and A. Mazzei. J. Organomet. Chem. **78**, 185 (1974).
6. M. Cesari and S. Cucinella. *In* The chemistry of inorganic homo- and heterocycles. Vol. 1. *Edited by* I. Haiduc and D.B. Sowerby. Academic Press, New York. 1987. pp. 167–190.
7. M.L. Montero, H. Wessel, H.W. Roesky, M. Teichert, and I. Usón. Angew. Chem. Int. Ed. Engl. **36**, 629 (1997).
8. M.A. Beswick, N. Choi, C.N. Harmer, M. McPartlin, M.E.G. Mosquera, P.R. Raithby, M. Tombul, and D.S. Wright. Chem. Commun. (Cambridge), 1383 (1998).
9. J.S. Silverman, C.J. Carmalt, D.A. Neumayer, A.H. Cowley, B.G. McBurnett, and A. Decken. Polyhedron, **17**, 977 (1998).
10. J.S. Bradley, F. Cheng, S.J. Archibald, R. Supplit, R. Rovai, C.W. Lehmann, C. Krüger, and F. Lefebvre. Dalton Trans. 1846 (2003).
11. T. Bauer, S. Schulz, H. Hupfer, and M. Nieger. Organometallics, **21**, 2931 (2002).
12. K.W. Henderson, A.R. Kennedy, A.E. McKeown, and R.E. Mulvey. Angew. Chem. Int. Ed. **39**, 3879 (2000).
13. For recent reviews, see: (*a*) J.K. Brask and T. Chivers. Angew. Chem. Int. Ed. **40**, 3960 (2001); (*b*) G.M. Aspinall, M.C. Copsey, A.P. Leedham, and C.A. Russell. Coord. Chem. Rev. **227**, 217 (2002).
14. J.K. Brask, T. Chivers, G. Schatte, and G.P.A. Yap. Organometallics, **19**, 5683 (2000).
15. J.K. Brask, T. Chivers, and G.P.A. Yap. Chem. Commun. (Cambridge), 2543 (1998).
16. M.C. Copsey, J.C. Jeffery, C.A. Russell, J.M. Slattery, and J.A. Straughan. Chem. Commun. (Cambridge), 2356 (2003).
17. G.M. Sheldrick. SHELXS-97. University of Göttingen, Göttingen, Germany. 1997.
18. G.M. Sheldrick. SHELXL-97-2. University of Göttingen, Göttingen, Germany. 1997.
19. S. Rings, V. Ischenko, and M. Jansen. Z. Naturforsch. B, **B55**, 730 (2000).
20. (*a*) M. Niemeyer and P.P. Power. Inorg. Chem. **35**, 7264 (1996); (*b*) C. Eaborn, W. Clegg, P.B. Hitchcock, M. Hopman, K. Izod, P.N. O'Shaughnessy, and J.D. Smith. Organometallics, **16**, 4728 (1997); (*c*) C.S. Weinert, P.E. Fanwick, and I.P. Rothwell. Dalton Trans. 1795 (2003).
21. (*a*) G. Fraenkel and M.P. Hallden-Abberton. J. Am. Chem. Soc. **103**, 5657 (1981); (*b*) J. Arnold. J. Chem. Soc. Chem. Commun. 976 (1990).
22. (*a*) W. Zheng, N.C. Mösch-Zanetti, H.W. Roesky, M. Noltemeyer, M. Hewitt, H.-G. Schmidt, and T.R. Schneider. Angew. Chem. Int. Ed. **39**, 4276 (2000); (*b*) W. Zheng, H.W. Roesky, and M. Noltemeyer. Organometallics, **20**, 1033 (2001); (*c*) M.G. Gradiner, G.A. Koutsantonis, S.M. Lawrence, and C.L. Raston. Inorg. Chem. **35**, 5696 (1996).

© 2006 NRC Canada

Effect of the nature of substituents on aromatic aldehydes in microwave induced *N*-cyclohexylamidine–aldehyde condensation reactions

Vipan Kumar, Manish Gupta, and M.P. Mahajan

Abstract: A simple, environmentally friendly protocol for the selective synthesis of the 4-aryl substituted acyclic 1,3-dienes and the medicinally potent triazines has been developed using a domestic microwave oven with excellent yields and reproducibility.

Key words: microwave, dihydrotriazine, triazine, imine metathesis.

Résumé : Utilisant un four microonde domestique, on a développé un protocole soucieux de l'environnement et reproductible pour la synthèse sélective, avec d'excellents rendements, de 1,3-diènes acycliques substitués par un groupe aryle en position 4 et de triazines efficaces d'un point de vue médicinal.

Mots clés : microonde, dihydrotriazine, triazine, métathèse d'imines.

[Traduit par la Rédaction]

Introduction

Azadienes have proved to be of great synthetic potential in heterocyclic synthesis, acting as 4π components in hetero Diels Alder cycloaddition reactions with various dienophiles (1). They have been explored in the synthesis of pyrimidines, pyrimidinones, thioxopyrimidines, and other aza-heterocyclic compounds. One of the crucial and common steps in most synthetic approaches for such heterocycles involves the formation of a new carbon–nitrogen double bond. The reaction of iminophosphoranes with carbonyl compounds is an excellent method for the construction of carbon–nitrogen double bonds under mild and neutral conditions (2). On the other hand, aza-Wittig type reactions with heterocumulenes like carbon dioxide, carbon disulphide, isocyanates, isothiocyanates, and ketenes, provide access to functionalized heterocumulenes, which are highly reactive intermediates able to undergo a plethora of heterocyclization reactions (3). It has been observed that 1-aryl-2-phenyl-5-alkyl/aryl-1,3-diazapenta-1,3,4-triene, generated in situ via aza-Wittig reactions of *N′*-aryl-*N*-(triphenylphosphoranilidene)carboximidamides, selectively undergo [4+2] cycloaddition and electrocyclization reactions leading to the formation of novel pyrimidinones and quinazolines with monosubstituted ketenes and diphenyl ketenes, respectively (4). A conceptually similar annulation involved the aza-Wittig reaction of *N*-imidoyliminophosphoranes with aldehydes to give 3,4-dihydroquinazolines and quinazolines via electrocyclization of initially formed 1,3-diazabuta-1,3-dienes as intermediates (5). Recent work from our laboratory has shown a simple and convenient version of the aza-Wittig reaction between *N*-imidoyliminophosphoranes and aldehydes using a domestic microwave oven (6). The strategy was further simplified by employing the condensation reactions of *N*-arylamidines with aldehydes (7). This simplified version to quinazolines is of significance because of the lack of reports on the condensation reactions of *N*-arylbenzamidines with aldehydes. Even the reported reactions of *N*-alkylamidines with aldehydes involve the use of Lewis acid catalysts (8), have longer reaction periods, suffer from the irreproducibility of the results, and have lower reaction yields (9). It was felt that the problem of spontaneous electrocyclization experienced with *N*-aryl-4-phenyl-1,3-diazabuta-1,3-dienes could be circumvented by the condensation reactions of *N*-alkylamidines with aldehydes.

Results and discussion

Thus, in continuation of our pursuits towards the synthesis and reactivity of azadienes (10), we report herein the results of a few condensation reactions of *N*-cyclohexylbenzamidines with various aldehydes using microwave irradiation. Interestingly, the reaction of *N*-cyclohexylbenzamidine with aromatic aldehydes containing p-electron-donating (-OCH_3) substituent under microwave irradiation resulted in a good yield of 1-(4-methoxy-benzyl)-2-(4-methoxy-phenyl)-4,6-

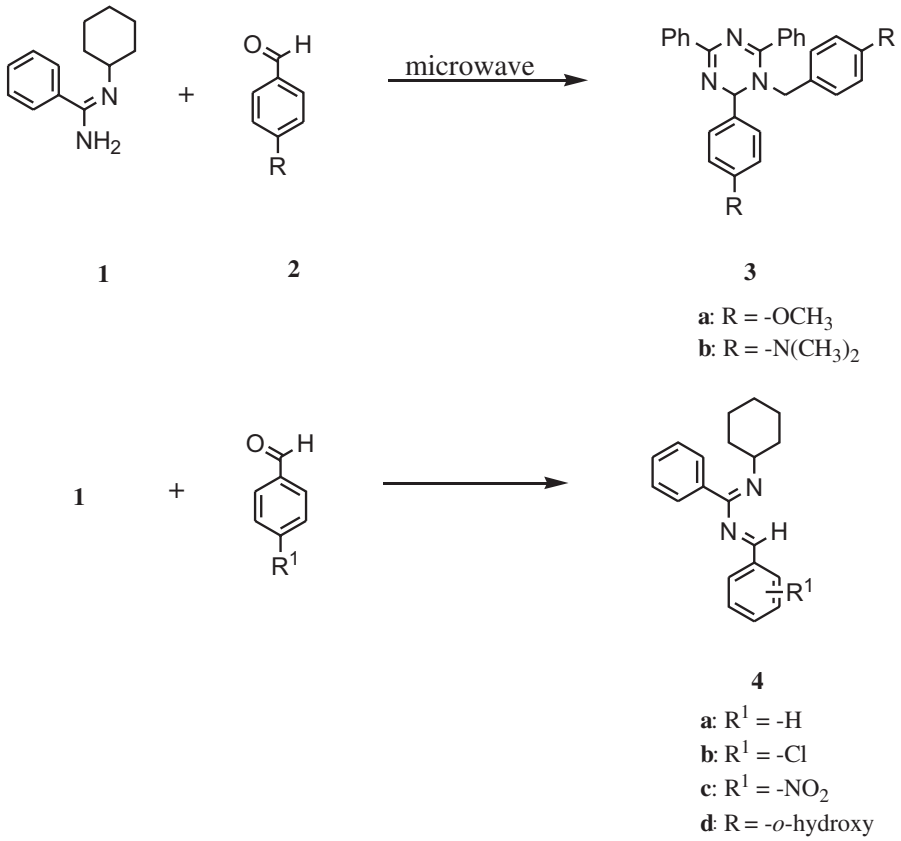
Received 1 May 2005. Published on the NRC Research Press Web site at http://canjchem.nrc.ca on 7 April 2006.

V. Kumar, M. Gupta, and M.P. Mahajan.[1] Department of Applied Chemistry, Guru Nanak Dev University, Amritsar-143005, Punjab, India.

[1]Corresponding author (e-mail: mahajanmohinderp@yahoo.co.in).

 doi:10.1139/V06-014 © 2006 NRC Canada

Scheme 1.



diphenyl-1,2-dihydro-[1,3,5]triazine (**3**), while other aldehydes led to the formation of *N*-cyclohexyl-1,3-diazabuta-1,3-dienes (**4**) (Scheme 1).

The structure of the dihydrotriazine (**3a**) was confirmed with the help of its spectral data. ^{1}H NMR spectrum of the compound showed the presence of a pair of doublets corresponding to methylene protons with a coupling constant of 14.8 Hz at δ 4.12 and 4.90 and a sharp singlet for a methine proton at δ 5.95. Its mass spectrum exhibited the molecular ion peak at 461.5. The structure of the product was further confirmed using ^{1}H–^{1}H correlation spectroscopic data.

In an attempt to generalize the previous observation, the reaction was repeated with another readily available aldehyde having a strong electron-donating substituent at its *p*-position (*p*-dimethylamino benzaldehyde), which also resulted in a good yield of the desired dihydrotriazine (**3b**). The probable mechanistic pathway leading to the formation of dihydrotriazines (**3a** and **3b**) is outlined in Scheme 2. In this scheme it is assumed that the initially formed 1,3-diazabuta-1,3-diene (**5**) and its tautomer (**6**) undergoes imine metathesis (imine exchange between the cyclohexylideneamine group of **6** and the cyclohexylimine group of **5**, forming *N*-cyclohexylcyclohexylideneamine and the 1,3,5-triaza-1,3,5-hexatriene derivative (**7**)). The 1,3,5-triaza-1,3,5-hexatriene thus formed underwent electrocyclization to yield dihydrotriazines (**3**). These dihydrotriazines were easily converted to the corresponding triazines (**8**) by their exposure to microwave irradiation (oxidative debenzylation) (11) at a power of 200 W for a period of 10 min (5 cycles of 2 min each) (Scheme 2).

Experimental

Melting points were determined by open capillary using a Veego Precision digital melting point apparatus (MP-D) and are uncorrected. IR spectra were recorded on a Shimadzu D-8001 spectrophotometer. ^{1}H NMR spectra were recorded in deuterochloroform with Bruker AC-E 200 (200 MHz) spectrometers using TMS as an internal standard. Chemical shift values are expressed as ppm downfield from TMS and *J* values are in Hz. Splitting patterns are indicated as singlet (s), doublet (d), triplet (t), multiplet (m), quartet (q), and broad peak (br). ^{13}C NMR spectra were also recorded with Bruker AC-200E (50.4 MHz) spectrometers, in deuterochloroform, and using TMS as an internal standard. Mass spectra were recorded on a Shimadzu GCMS-QP-2000 mass spectrometer. Elemental analyses were performed on a Heraus CHN-O-Rapid elemental analyzer.

General procedure

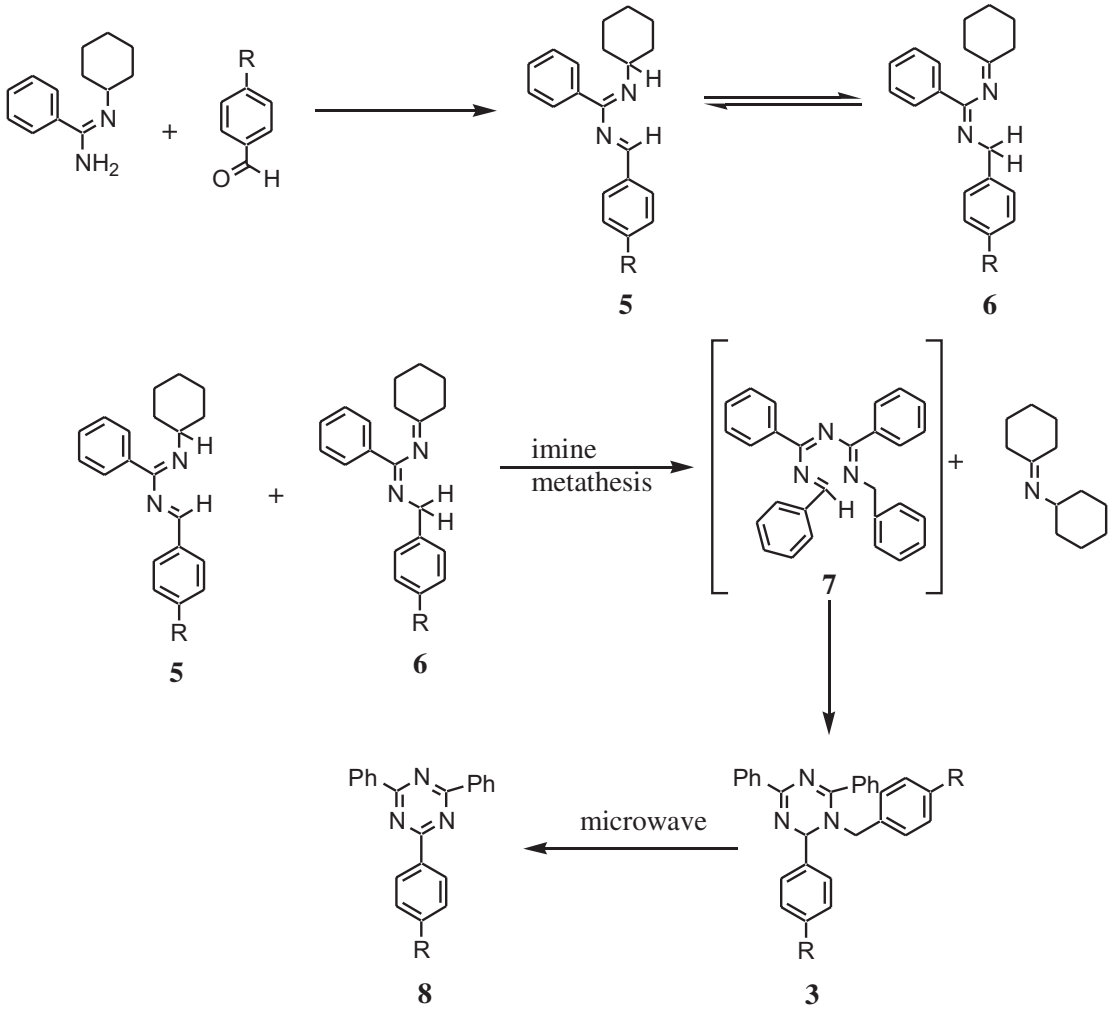
The typical procedure involved the irradiation of *N*-cyclohexylbenzamidine with 1.5 equiv. of aldehydes at a power of 100 W for a period of 20 min (10 cycles of 2 min each). The progress of the reaction was monitored using TLC. The product was then isolated by trituration using hexane and was recrystallized using an ethyl acetate – hexane mixture (1:10).

1-(4-Methoxy-benzyl)-2-(4-methoxy-phenyl)-4,6-diphenyl-1,2-dihydro-[1,3,5]triazine (3a)

Melting point: 166 to 167 °C. ^{1}H NMR (200 MHz) δ:

© 2006 NRC Canada

Scheme 2.



a: R = -OCH_3
b: R = -$N(CH_3)_2$

3.80 (s, 3H, -OCH_3), 3.84 (s, 3H, -OCH_3), 4.08–4.15 (d, 1H, *J* = 14.6 Hz, CH of CH_2), 4.86–4.93 (d, 1H, *J* = 15.0 Hz, CH of CH_2), 5.95 (s, 1H, -CH), 6.84–6.88 (d, 2H, *J* = 8.4 Hz, ArH), 6.92–6.96 (d, 2H, *J* = 8.6 Hz, ArH), 7.13–7.17 (d, 2H, *J* = 8.4 Hz, ArH), 7.41–7.51 (m, 8H, ArH), 7.63–7.67 (m, 2H, ArH), 8.27–8.32 (m, 2H, ArH). ^{13}C NMR (50.4 MHz) δ: 52.3 (CH2), 55.2 (-OCH_3), 73.2 (-CH), 114.2, 114.3, 127.4, 127.8, 127.9, 128.0, 128.7, 128.8, 130.1, 130.6, 133.8, 134.9, 137.0, 156.5, 159.4, 159.9 (C=N), 163.6 (C=N). MS *m/z*: 461.5 (M^+). Anal. calcd. for $C_{30}H_{27}N_3O_2$ (%): C 78.07, H 5.90, N 9.10; found: C 77.36, H 5.74, N 9.02.

1-(4-*N*,*N*-Dimethylamino-benzyl)-2-(4-dimethylamino-phenyl)-4,6-diphenyl-1,2-dihydro-[1,3,5]triazine (3b)

Melting point: 176 to 177 °C. ^{1}H NMR (200 MHz) δ: 3.11 (s, 6H, -$N(CH_3)_2$), 3.13 (s, 6H, -$N(CH_3)_2$), 4.06–4.13 (d, 1H, *J* = 14.4 Hz, CH of CH_2), 4.83–4.90 (d, 1H, *J* = 14.6 Hz, CH of CH_2), 5.92 (s, 1H, CH), 6.82–6.86 (d, 2H, *J* = 8.4 Hz, ArH), 6.90–6.94 (d, 2H, *J* = 8.6 Hz, ArH), 7.11–7.15 (d, 2H, *J* = 8.4 Hz, ArH), 7.36–7.46 (m, 8H, ArH), 7.60–7.64 (m, 2H, ArH), 8.24–8.29 (m, 2H, ArH). ^{13}C NMR (50.4 MHz) δ: 40.1 (-$N(CH_3)_2$), 40.3 (-$N(CH_3)_2$), 52.6 (CH_2), 73.2 (-CH), 114.1, 114.5, 127.5, 127.7, 127.9, 128.0, 128.5, 128.7, 130.5, 130.8, 133.8, 134.2, 137.2, 156.2, 159.3, 159.5 (C=N), 163.2 (C=N). MS *m/z*: 487 (M^+). Anal. calcd. for $C_{32}H_{33}N_5$ (%): C 78.82, H 6.82, N 14.36; found: C 78.91, H 6.64, N 14.45.

N-Benzylidene-*N′*-cyclohexylbenzamidine (4a)

Melting point: 148 to 149 °C. ^{1}H NMR (200 MHz) δ: 1.40–1.78 (m, 10H, cyclohexyl), 3.12 (m, 1H, cyclohexyl), 7.19–7.34 (m, 3H, ArH), 7.38–7.49 (m, 6H, ArH + olefinic), 7.77–7.80 (m, 2H, ArH). ^{13}C NMR (50.4 MHz) δ: 24.5, 27.2, 33.2, 54.5, 123.3, 127.1, 127.4, 129.1, 129.6, 129.8, 131.8, 137.4, 166.3 (C=N-), 174.1 (C=N). MS *m/z*: 290 (M^+).

N-(4-Chloro-benzylidene)-*N′*-cyclohexylbenzamidine (4b)

Melting point: 157 to 158 °C. ^{1}H NMR (200 MHz) δ: 1.32–1.68 (m, 10H, cyclohexyl), 3.13 (m, 1H, cyclohexyl), 7.20–7.24 (d, 2H, *J* = 8.4 Hz, ArH), 7.34–7.38 (d, 2H, *J* = 8.4 Hz, ArH), 7.40–7.48 (m, 3H, ArH), 8.02–8.06 (m, 2H,

© 2006 NRC Canada

ArH). ^{13}C NMR (50.4 MHz) δ: 24.3, 27.8, 34.0, 54.7, 123.2, 127.2, 127.6, 129.2, 130.0, 130.8, 131.6, 134.9, 161.8, 172.7. MS *m*/*z*: 324.5 (M^+).

N-Cyclohexyl-N′-(4-nitro-benzylidene)benzamidine (4c)

Melting point: 140 to 141 °C. ^{1}H NMR (200 MHz) δ: 1.42–1.88 (m, 10H, cyclohexyl), 3.29 (m, 1H, cyclohexyl), 7.16–7.20 (d, 2H, *J* = 8.2 Hz, ArH), 7.34–7.38 (d, 2H, *J* = 8.2 Hz, ArH), 7.40–7.46 (m, 3H, ArH), 8.00–8.04 (m, 2H, ArH). ^{13}C NMR (50.4 MHz) δ: 24.7, 28.0, 33.8, 54.5, 123.7, 126.8, 127.7, 129.4, 130.1, 131.0, 131.5, 135.0, 162.1, 171.9. MS *m*/*z*: 335 (M^+).

N-Cyclohexyl-N′-(2-hydroxy-benzylidene)benzamidine (4d)

Product: oily liquid. ^{1}H NMR (200 MHz) δ: 1.37–1.82 (m, 10H, cyclohexyl), 3.32 (m, 1H, cyclohexyl), 6.89–8.44 (m, 10H, 9H arom + 1H olefinic), 11.1 (s, 1H, -OH exchangeable with D_2O). ^{13}C NMR (50.4 MHz) δ: 24.57, 30.28, 34.73, 54.53, 127.23, 128.14, 129.20, 130.20, 131.53, 131.86, 133.38, 134.54, 135.0, 137.42, 165.24, 170.83. MS *m*/*z*: 306 (M^+).

2-(4-Methoxy-phenyl)-4,6-diphenyl-[1,3,5]triazine (8a)

Melting point: 198 to 199 °C. ^{1}H NMR (200 MHz) δ: 3.82 (s, 3H, $-OCH_3$), 6.82–6.86 (d, 2H, *J* = 8.6 Hz, ArH), 7.52–7.58 (m, 6H, ArH), 8.60–8.64 (d, 2H, *J* = 8.6 Hz, ArH), 8.70–8.76 (m, 4H, ArH). ^{13}C NMR (50.4 MHz) δ: 55.2 ($-OCH_3$), 111.1, 123.1, 128.1, 128.5, 130.2, 132.0, 136.2, 152.9, 170.8, 171.3. MS *m*/*z*: 339 (M^+). Anal. calcd. for $C_{22}H_{17}N_3O$ (%): C 77.86, H 5.05, N 12.38; found: C 77.72, H 5.11, N 12.46.

[4-(4,6-Diphenyl-[1,3,5]triazin-2-yl)phenyl]dimethylamine (8b)

Melting point: 211 to 212 °C. ^{1}H NMR (200 MHz) δ: 3.11 (s, 6H, $-N(CH_3)_2$), 6.87–6.91 (d, 2H, *J* = 8.8 Hz, ArH), 7.54–7.60 (m, 6H, ArH), 8.62–8.66 (d, 2H, *J* = 8.8 Hz, ArH), 8.74–8.79 (m, 4H, ArH). ^{13}C NMR (50.4 MHz) δ: 40.2 ($-N(CH_3)_2$), 111.3, 123.6, 128.4, 128.9, 130.7, 132.0, 136.9, 153.4, 171.0, 171.5. MS *m*/*z*: 352 (M^+). Anal. calcd. for $C_{23}H_{20}N_4$ (%): C 78.38, H 5.72, N 15.90; found: C 78.23, H 5.74, N 16.03.

Conclusion

The simple and convenient method presented for the synthesis of 1,3,5-triazines (12) is of significance because of the limited methods available and the broad range of their biological activities, including antiangiogenesis (13), herbicidal effects (14), antimetastatic effects (15), Erm methylenetransferase inhibition (16), and anti-microbial effects (17). The strategy is of further significance because of the lack of suitable methods for the synthesis of acyclic 1,3-diazabuta-1,3-dienes with aryl substituents at the C-4 position. Such acyclic dienes can prove to be useful substrates for studying the stereochemical aspects of their cycloaddition reactions.

Acknowledgements

Vipan Kumar is grateful to the Council of Scientific and Industrial Research (CSIR, New Delhi) for a Junior Research Fellowship under grant No. 01(1590)/99/EMR-II. The authors also gratefully acknowledge the support of Professor Takao Saito and Dr. Takashi Otani of the Tokyo University of Science (Japan) for providing high resolution NMR and ^{1}H–^{1}H correlation spectra.

References

1. For recent reviews on azadienes, see: (*a*) D.L. Boger. Tetrahedron, **39**, 2869 (1983); (*b*) D.L. Boger. Chemtracts: Org. Chem. **9**, 149 (1996); (*c*) J. Barluenga and M. Tomas. Adv. Heterocycl. Chem. **57**, 1 (1993); (*d*) M. Behforonz and M. Ahmadian. Tetrahedron, **56**, 5259 (2000); (*e*) S. Jayakumar, M.P.S. Ishar, and M.P. Mahajan. Tetrahedron, **58**, 379 (2002). Tetrahedron Report No. 595.
2. P. Molina and M.J. Vilaplana. Synthesis, 1197 (1994).
3. J. Barluenga and F. Palacios. Org. Prep. Proced. Int. **23**, 1 (1991).
4. S. Jayakumar, V. Kumar, and M.P. Mahajan. Tetrahedron Lett. **42**, 2235 (2001).
5. (*a*) E. Rossi and R. Stradi. Synthesis, 214 (1989); (*b*) E. Rossi, R. Stradi, and P. Visentin. Tetrahedron, **46**, 3581 (1990).
6. V. Kumar, A.K. Sharma, and M.P. Mahajan. Synth. Commun. **34**, 49 (2004).
7. V. Kumar, C. Mohan, M. Gupta, and M.P. Mahajan. Tetrahedron. In press.
8. (*a*) D.H. Hunter and S.K. Sim. Can. J. Chem. **50**, 669 (1972); (*b*) P. Luthardt, M.H. Moller, U. Rodeweld, and E.-U. Wurthwein. Chem. Rev. **122**, 1705 (1989); (*c*) A.C. Veronese, R. Callegari, and C.F. Morelli. Tetrahedron, **51**, 12277 (1995).
9. E. Rossi, G. Abbiati, and E. Pini. Tetrahedron, **53**, 14107 (1997).
10. (*a*) S.N. Mazumdar, I. Ibnusaud, and M.P. Mahajan. Tetrahedron Lett. **28**, 2641 (1987); (*b*) S.N. Mazumdar and M.P. Mahajan. Tetrahedron, **47**, 1473 (1991); (*c*) S.N. Mazumdar, S. Mukherjee, A.K. Sharma, D. Sengupta, and M.P. Mahajan. Tetrahedron, **50**, 7579 (1994); (*d*) S. Mukherjee, S.N. Mazumdar, A.K. Sharma, and M.P. Mahajan. Heterocycles, **47**, 933 (1998); (*e*) P.D. Dey, A.K. Sharma, P.V. Bharatam, and M.P. Mahajan. Tetrahedron, **53**, 13829 (1997); (*f*) A.K. Sharma, S. Jayakumar, M.S. Hundal, and M.P. Mahajan. J. Chem. Soc. Perkin. Trans. 1, 774 (2002), and refs. cited therein.
11. R.S. Verma, É. Rimán, and T. Patonay. ARKIVOC, Part (vii), 183 (2004).
12. (*a*) H. Bader. J. Org. Chem. **30**, 707 (1965); (*b*) C. Chen, R. Dagnino, and J.R. McCarthy. J. Org. Chem. **60**, 8428 (1995); (*c*) Y. Peng and G. Song. Tetrahedron Lett. **45**, 5313 (2004); (*d*) L.D.S. Yadav and R. Kapoor. Tetrahedron Lett. **44**, 8951 (2003).
13. M. Ono, N. Kawahara, D. Goto, Y. Wakahayashi, S. Ushiro, S. Yoshida, H. Izumi, M. Kuwano, and Y. Sato. Cancer Res. **56**, 1512 (1996).
14. W. Draber, K. Tietjen, J.F. Kluth, and A. Trebst. Angew. Chem. Int. Ed. Engl. **30**, 1621 (1991).
15. M. Maeda, M. Iogo, H. Tsuda, H. Fujita, Y. Yonemura, K. Nagakawa, Y. Endo, and T. Sasaki. Anti-Cancer Drug Des. **15**, 217 (2000).

© 2006 NRC Canada

16. P.J. Hajduk, J. Dinges, J.M. Schkeryantz, D. Janowick, M. Kaminski, M. Tufano, D.J. Aygeri, A. Petros, V. Nienaber, P. Zhong, R. Hammond, M. Coen, B. Beutal, L. Katz, and S.W. Fesik. J. Med. Chem. **42**, 3852 (1999).
17. J.L. Silen, A.T. Lu, D.W. Solas, M.A. Gore, D. Mcalean, N.H. Shah, L.M. Coffin, N.S. Bhinderwala, Y. Wang, K.T. Tsutsui, G.C. Look, D.A. Campbell, R.L. Hale, M. Navre, and C.R. Deluca-Flaherty. Antimicrob. Agents Chemother. **42**, 1447 (1998).

© 2006 NRC Canada

QSAR modeling of neonicotinoid insecticides for their selective affinity towards Drosophila nicotinic receptors over mammalian $\alpha_4\beta_2$ receptors

Anindya Basu, Shovanlal Gayen, Soma Samanta, Parthasarathi Panda, Kolloru Srikanth, and Tarun Jha

Abstract: Neonicotinoids are emerging as a major class of insecticides with promising insecticidal activity having a specific affinity towards the nicotinic acetylcholine receptors (nAChR). A quantitative structure–activity relationship (QSAR) study was performed on some azidopyridinyl neonicotinoids for their selective insecticidal activity over mammalian toxicity. The result showed that increased surface area of the molecules may help to increase the binding affinity of the compounds towards the Drosophila receptor and the presence of the azido group on the other hand may be detrimental towards the affinity. Compounds having low polarity, increased probability of nucleophilic attack at the particular position (N-1), and a higher positive charge at the C-12 position can reduce the binding affinity of these compounds towards the mammalian receptor.

Key words: QSAR, neonicotinoids, Drosophila nicotinic receptor, mammalian $\alpha_4\beta_2$ receptor, AM1.

Résumé : Les néonicotinoïdes émergent comme une classe majeure de composés possédant une activité insecticide intéressante et une activité spécifique pour les récepteurs de l'acétylcholine nicotinique (« nAChR »). Une étude de relation structure–activité quantitative (RSAQ) a été réalisée sur quelques néonicotinoïdes de l'azidopyridinyle pour évaluer leur activité insecticide sélective sur la toxicité mammifère. Le résultat montre que la superficie accrue de la surface des molécules pourrait éventuellement leur permettre d'augmenter les affinités de fixation des composés sur le récepteur Drosophila alors que, par ailleurs, la présence du groupe azido pourrait nuisible à cette affinité. Les composés de faible polarité augmentent la probabilité d'une attaque nucléophile à la position particulière (N-1) et d'une charge plus positive en position C-12 et peuvent réduire l'affinité de fixation de ces composés vis-à-vis des récepteurs mammifères.

Mots clés : RSTQ, néonicotinoïdes, récepteur nicotinique Drosophila, récepteur mammifère $\alpha_4\beta_2$, AM1.

[Traduit par la Rédaction]

Introduction

The neonicotinoids (1) are one of the major classes of insecticides, having very promising potency (2). They are nicotinic agonists that interact with nicotinic acetylcholine receptors (nAChR) in a different way than the conventional nicotinoids. Unlike the protonated nicotinoids, which require a cation–π interaction for binding to the vertebrate receptor, the neonicotinoids do not get protonated at physiological pH. This difference provides the neonictinoids with favourable toxicological profiles (3). The neonicotinoids act as agonists at the nAChR of insects and mammals (particularly the $\alpha_4\beta_2$ subtype) (3), which are mainly responsible for the toxicity of the compounds.

Nicotine, together with other nicotinoids, are also considered as candidate analgesics and for the treatment of neurodegenerative diseases (4–7). The potential activity of neonicotinoids is therefore of particular interest. However, the physical, chemical, or biological properties of a compound depend on the 3D arrangement of the atoms in the molecule. As a part of our composite program of rational drug design (8–22), an attempt was made to explore the quantitative structure–activity relationship (QSAR) study on a series of 20 azidopyridinyl neonicotinoids reported by Zhang et al. (1). Previously, we have reported the QSAR studies of these derivatives using topological descriptors, i.e., electrotopological state atom (ETSA) (8) and refractotopological state atom (RTSA) (9) indices. In the present QSAR study, we used semiempirical quantum descriptors, along with physicochemical and indicator parameters, to understand the structural and physicochemical properties requisite for insecticidal activity at the molecular level. The general structure

Received 23 November 2005. Published on the NRC Research Press Web site at http://canjchem.nrc.ca on 7 April 2006.

A. Basu, S. Gayen, S. Samanta, P. Panda, and T. Jha.[1] Division of Medicinal and Pharmaceutical Chemistry, Department of Pharmaceutical Technology, P.O. Box 17020, Jadavpur University, Kolkata 700 032, India.
K. Srikanth. Department of Medicinal Chemistry, College of Pharmacy, 8-125 Weaver Densford Hall, 308, Harvard St. SE, University of Minnesota, Minneapolis, MN 55455, USA.

[1]Corresponding author (e-mail: tjjupharm@yahoo.com; tarunjha123@yahoo.co.in).

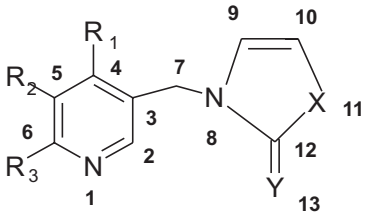
 doi:10.1139/V06-029 © 2006 NRC Canada

Table 1. Binding affinity data of neonicotinoids for mammalian ($\alpha_4\beta_2$, [$K_i(\alpha_4\beta_2)$] and Drosophila [K_i(Drosophila)] nicotinic receptors.

Cpd.[a]	Y	X	R_1	R_2	R_3	K_i[b] (nmol/L)	pK_i[c] ($\alpha_4\beta_2$)	K_i[d] (nmol/L)	pK_i[e] (Drosophila)
1*	NH	NH	H	H	Cl	2.2	–0.342	800	–2.903
2*	NH	NH	H	N_3	Cl	2.6	–0.415	5700	–3.756
3	NH	S	H	N_3	H	8.3	–0.919	7200	–3.857
4	NH	S	N_3	H	H	820	–2.914	30000	–4.477
5	NH	S	H	H	Cl	0.39	0.409	100	–2.000
6	NH	S	H	N_3	Cl	0.47	0.328	750	–2.875
7	NH	S	N_3	H	Cl	110	–2.041	3200	–3.505
8*	NNO_2	NH	H	H	Cl	720	–2.857	2.2	–0.342
9*	NNO_2	NH	H	N_3	Cl	340	–2.531	24	–1.380
10	NNO_2	NH	H	N_3	H	5400	–3.732	540	–2.732
11	NNO_2	NH	N_3	H	H	95800	–4.981	3600	–3.556
12	NNO_2	NH	H	H	Cl	470	–2.672	0.85	0.071
13	NNO_2	NH	H	N_3	Cl	300	–2.477	13	–1.114
14	NNO_2	NH	N_3	H	Cl	16900	–4.228	460	–2.663
15	NNO_2	S	H	H	Cl	170	–2.230	0.35	0.456
16	NNO_2	S	H	N_3	Cl	170	–2.230	3.9	–0.591
17*	$CHNO_2$	NH	H	H	Cl	60	–1.778	0.12	0.921
18*	$CHNO_2$	NH	H	N_3	Cl	40	–1.602	0.72	0.143
19	NCN	S	H	H	Cl	120	–2.079	1.4	–0.146
20	NCN	S	H	N_3	Cl	120	–2.079	28	–1.447

Note: For the compound numbers marked with an asterisk, CH_2-CH_2 at atom numbers 9 and 10.
[a]Taken from eq. [2].
[b]K_i value for $\alpha_4\beta_2$.
[c]pK_i for the K_i value of $\alpha_4\beta_2$ in molar units.
[d]K_i value for Drosophila.
[e]pK_i for the K_i value of Drosophila in molar units.

Fig. 1. General structure of the azidopyridinyl neonicotinoids with arbitrarily numbered common skeletal atoms.



of the neonicotinoids used in the present study is shown in Fig. 1.

Materials and methods

For the QSAR study, the binding affinities of azidopyridinyl neonicotinoids for mammalian $\alpha_4\beta_2$ [$K_i(\alpha_4\beta_2)$] and Drosophila [K_i Drosophila)] nicotinic receptors were taken as dependent parameters. Zhang et. al. (1) measured the binding affinities of these neonicotinoids. These were determined with mammalian $\alpha_4\beta_2$ and Drosophila nAChRs using radiopharmaceuticals. Semiempirical calculations of the neonicotinoids, whose activity data are shown in Table 1, were done according to the AM1 method (23) using the Hyperchem Release 7.0 Pro. Package. AM1 is a semiempirical, self-consistent implementation of the Hartree–Fock–Roothaan equations based on the neglect of differential diatomic overlap (NDDO) approximation. The AM1 method produces reliable total energies as a function of atomic positions and is able to probe the energy surface to find the minimum energy configurations (24). The structures of the compounds were drawn and model-built by the HyperChem software (25) to convert the 2D sketch into 3D structures. To shorten the total time required for energy minimization by the semiempirical method, the structures were first energy minimized using the molecular mechanics (MM+) method based on the classical force field without any cutoffs for nonbonded interactions, solvation, and constraints. These energy-minimized structures were then used as the starting structures for geometry optimization by the AM1 method using the Polak–Ribiere (conjugate gradient) algorithm with a RMS gradient of 0.1 kcal/Å mol (1 cal = 4.184 J). During calculations we used a Pentium IV 2.40 GHz computer with 512 MB RAM.

Quantum chemical descriptors such as atomic charges, molecular orbital energies (HOMO, LUMO), frontier electron density, approximate surface area (SA), polarizability, dipole moment, energies (total energy, binding energy, heat of formation), etc., were calculated by the method described in the previous paragraph.

These were subjected to a correlation study. Multiple linear regressions (MLR) were performed with different combinations of the parameters and the biological activity (mammalian $\alpha_4\beta_2$ and Drosophila nAChR agonistic activity) of the neonicotinoids. The correlation and regression analy-

© 2006 NRC Canada

Table 2. Values of the properties of azidopyridinyl neonicotinoids and indicator parameters.

Cpd.	SA[a]	IN3[b]	log P[c]	N1L[d]	qC12[e]
1	3.117	0.000	2.03	0.043	0.125
2	3.423	1.000	2.88	0.003	0.137
3	3.206	1.000	2.44	0.009	–0.010
4	2.811	1.000	2.44	0.183	–0.028
5	3.147	0.000	2.02	0.045	–0.009
6	3.487	1.000	2.87	0.001	–0.038
7	3.217	1.000	2.87	0.229	–0.038
8	3.535	0.000	4.93	0.073	0.262
9	4.056	1.000	6.31	0.002	0.255
10	3.696	1.000	5.36	0.006	0.262
11	3.154	1.000	5.36	0.215	0.266
12	3.541	0.000	4.93	0.073	0.262
13	3.828	1.000	5.78	0.000	0.261
14	3.689	1.000	5.78	0.156	0.056
15	3.748	0.000	5.45	0.007	0.004
16	3.990	1.000	6.3	0.003	0.001
17	3.716	0.000	1.6	0.046	0.239
18	4.200	1.000	2.44	0.000	0.223
19	3.610	0.000	2.56	0.054	–0.005
20	4.013	1.000	3.41	0.001	–0.005

[a]SA is the approximate surface area scaled by 0.01 (Å^2).
[b]IN3 is an indicator parameter indicating the presence of the azido group in the compounds.
[c]log P is the logarithm of the partition coefficient of the whole molecule.
[d]N1L is the frontier electron density for nucleophilic attack at the N1 position.
[e]qC12 is the charge at atom C-12.

ses were carried out by a computer program called Multi Regress, developed in our laboratory (26). The frontier electron densities, charge on the different atoms, approximate surface area (SA), and log P values were used to develop the QSAR equations and are recorded in Table 2.

The statistical quality of the regression equations were justified by parameters such as the correlation coefficient (R), the percentage of explained variance (%EV), the variance ratio (F), the probability factor related to the F ratio (p), and the standard error of estimate (s). The predictive powers of the equations were validated by the leave-one-out (LOO) cross validation method (20–23). Predicted residual sum of squares (PRESS), total sum of squares (SSY), cross-validated R^2 (R^2_{cv}), standard deviation error of prediction (SDEP), and standard error of PRESS (S_{PRESS}) were considered for the validation of the QSAR models.

Results and discussion

Attempts were made to develop QSAR models for the insecticidal activity (pK_i(Drosophila)) of azidopyridinyl neonicotinoids. The best univariate relation (eq. [1]) was obtained by taking the approximate surface area (SA) of the whole molecule as an independent parameter.

$$[1]\quad \text{p}K_i(\text{Drosophila}) = -12.675\ (\pm 2.776) + 3.059\ (\pm 0.776)\text{SA}$$

where n = 20; R = 0.681; %EV = 46.34; F(1,18) = 15.544; p < 0.001; s = 1.246; PRESS = 32.395; SSY = 52.101; R^2_{cv} = 0.378; SDEP = 1.273; and S_{PRESS} = 1.342.

Values within the parenthesis are the standard error of corresponding parameters. Equation [1] explains up to 46.34% of the variances in the activity data and suggests the importance of the approximate surface area of the whole molecules in biological activity. The positive coefficient of the approximate surface area implies that higher values of the whole molecular surface area correspond to higher binding affinity towards the Drosophila receptor.

An indicator parameter (IN3) was used to understand the importance of the azido moiety towards insecticidal activity. The indicator parameter was found to have a good correlation to the biological activity under consideration, and was thus used for the QSAR study. The model obtained is shown in eq. [2].

$$[2]\quad \text{p}K_i(\text{Drosophila}) = -12.775\ (\pm 1.208) - 2.271\ (\pm 0.257)\text{IN3} + 3.502\ (\pm 0.341)\text{SA}$$

where n = 20; R = 0.951; %EV = 90.40; F(2,17) = 80.038; p < 0.000; s = 0.542; PRESS = 7.338; SSY = 52.101; R^2_{cv} = 0.859; SDEP = 0.606; and S_{PRESS} = 0.657.

Compared with eq. [1], eq. [2] has a better statistical quality. It explains up to 90.44% of the variances of the activity data. The negative coefficient of IN3 strongly suggested the detrimental effect of the azido group towards insecticidal activity.

Attempts were also made to obtain QSAR models using the mammalian activity data. The different possible combinations of semiempirical and physicochemical parameters, together with the indicator parameter, were used for the study. Combinations of N1L, qC12, and log P (frontier electron density for nucleophilic attack at the N1 atom, charge at the C12 position, and the logarithm of the octanol–water partition coefficient of the compounds under consideration, respectively) values produced a model for mammalian $\alpha_4\beta_2$ agonistic activity as shown in eq. [3].

$$[3]\quad \text{p}K_i(\alpha_4\beta_2) = 0.708\ (\pm 0.472) - 9.909\ (\pm 2.315)\text{N1L} - 2.842\ (\pm 1.480)\text{qC12} - 0.486\ (\pm 0.115)\ \log P$$

where n = 20; R = 0.865; %EV = 74.87; F(3,16) = 15.885; p < 0.000; s = 0.765; PRESS = 14.020; SSY = 37.268; R^2_{cv} = 0.624; SDEP = 0.837; and S_{PRESS} = 0.936.

Equation [3] explains up to 74.87% of the variances of the activity data. However, the deletion of compounds **19** and **20**, which have different substituents than compounds **1**–**18** and may act through a different mechanism of action, produced eq. [4].

$$[4]\quad \text{p}K_i(\alpha_4\beta_2) = 1.089\ (\pm 0.443) - 10.878\ (\pm 2.092)\text{N1L} - 3.830\ (\pm 1.364)\text{qC12} - 0.507\ (\pm 0.102)\ \log P$$

where the deleted compounds (DC) = **19**, **20**; n = 18; R = 0.910; %EV = 82.84; F(3,14) = 22.529; p < 0.000; s = 0.676; PRESS = 10.443; SSY = 37.267; R^2_{cv} = 0.720; SDEP = 0.762; and S_{PRESS} = 0.864.

© 2006 NRC Canada

Table 3. Correlation matrices for the biological activity and independent parameters.

	SA	log *P*	NIL	q13	qC12	IN3	$\alpha_4\beta_2$[a]	DRO[b]
SA	1.00	0.44	–0.58	0.04	0.30	0.15	–0.14	0.68
log *P*		1.00	–0.03	0.16	0.37	0.24	–0.65	0.18
N1L			1.00	0.22	–0.10	0.09	–0.50	–0.42
q13				1.00	–0.46	0.18	–0.21	–0.21
qC12					1.00	–0.09	–0.41	0.31
IN3						1.00	–0.23	–0.56
$\alpha_4\beta_2$[a]							1.00	–0.03
DRO[b]								1.00

[a]$\alpha_4\beta_2$ stands for p$K_i(\alpha_4\beta_2)$.
[b]DRO stands for pK_i(Drosophila).

Table 4. *t*-value and *p*-value for the QSAR equations.

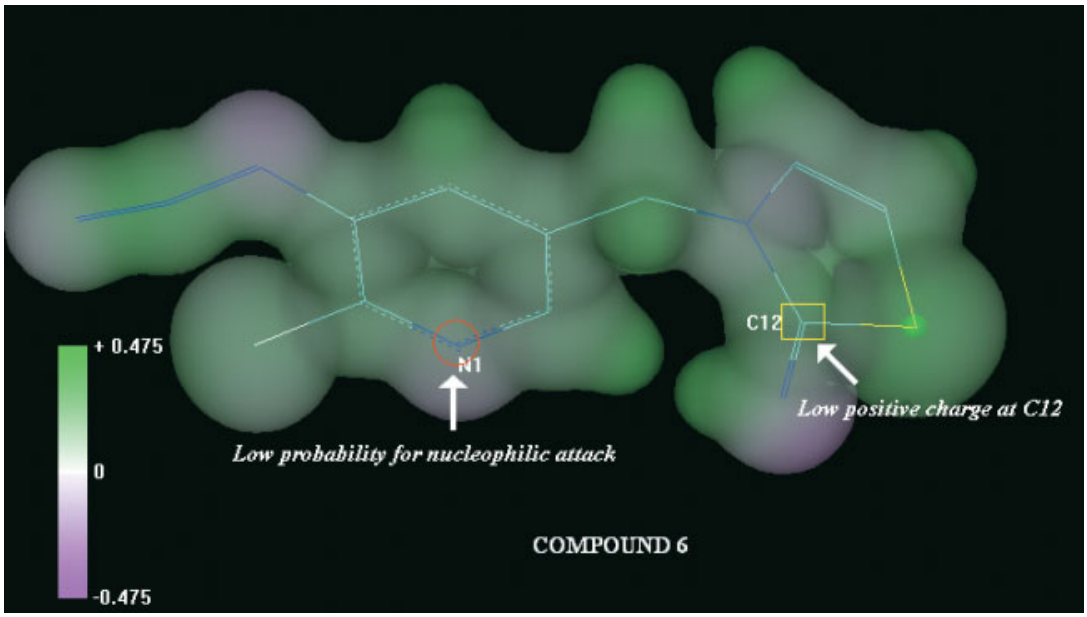
Equation	Intercepts and parameters	*t*-value	*p*-value
1	Intercept	–4.567	0.000
	SA	3.943	0.001
2	Intercept	–10.575	0.000
	IN3	–8.833	0.000
	SA	10.257	0.000
3	Intercept	1.502	0.153
	N1L	–4.281	0.001
	qC12	–1.919	0.073
	log *P*	–4.239	0.001
4	Intercept	2.458	0.028
	N1L	–5.201	0.000
	qC12	–2.807	0.014
	log *P*	–4.959	0.000

Table 5. Observed, calculated (Calcd.), residual (Res.), LOO-predicted (LOO Pred.), and predicted residual (Pres) activities of eqs. [2] and [4].

	Equation [2]					Equation [4]				
Cpd.	Observed [pK_i(*Drosophila*)]	Calcd.	Res.	LOO Pred.	Pres	Observed [p$K_i\alpha_4\beta_2$)]	Calcd.	Res.	LOO Pred.	Pres
1	–2.903	–1.874	–1.029	–1.620	–1.283	–0.342	–0.880	0.538	–0.973	0.631
2	–3.756	–3.060	–0.696	–2.9929	–0.764	–0.415	–0.921	0.506	–0.988	0.573
3	–3.857	–3.819	–0.038	–3.813	–0.044	–0.919	–0.211	–0.708	–0.056	–0.863
4	–4.477	–5.202	0.726	–5.547	1.070	–2.914	–2.035	–0.879	–1.713	–1.201
5	–2.000	–1.756	–0.244	–1.699	–0.301	0.409	–0.393	0.802	–0.556	0.965
6	–2.875	–2.834	–0.041	–2.830	–0.045	0.328	–0.232	0.560	–0.377	0.705
7	–3.505	–3.779	0.274	–3.821	0.316	–2.041	–2.710	0.669	–3.113	1.072
8	–0.342	–0.397	0.055	–0.407	0.065	–2.857	–3.205	0.348	–3.258	0.401
9	–1.380	–0.842	–0.538	–0.739	–0.641	–2.531	–3.104	0.573	–3.254	0.723
10	–2.732	–2.103	–0.629	–2.048	–0.684	–3.732	–2.692	–1.040	–2.503	–1.229
11	–3.556	–3.999	0.444	–4.081	0.525	–4.981	–4.989	0.008	–4.994	0.013
12	0.071	–0.375	0.446	–0.450	0.521	–2.672	–3.209	0.537	–3.290	0.618
13	–1.114	–1.641	0.527	–1.698	0.584	–2.477	–2.836	0.359	–2.914	0.437
14	–2.663	–2.127	–0.536	–2.080	–0.583	–4.228	–3.751	–0.477	–3.595	–0.632
15	0.456	0.352	0.104	0.330	0.126	–2.23	–1.763	–0.467	–1.617	–0.613
16	–0.591	–1.074	0.483	–1.151	0.560	–2.23	–2.143	–0.087	–2.098	–0.132
17	0.921	0.239	0.682	0.105	0.816	–1.778	–1.138	–0.640	–0.872	–0.907
18	0.143	–0.338	0.481	–0.474	0.617	–1.602	–1.001	–0.601	–0.848	–0.754
19	–0.146	–0.131	–0.014	–0.129	–0.017	–2.079	—	—	—	—
20	–1.447	–0.992	–0.455	–0.915	–0.532	–2.079	—	—	—	—

© 2006 NRC Canada

Fig. 2. Three-dimensional isosurface electrostatic potential map of compound **6**.



Equation [4] is of much better statistical quality and explains up to 82.84% of the variances. The equation suggests the importance of atoms N1 and C12 with respect to the toxicity of the compounds towards mammals. The negative coefficient of N1L in eq. [4] suggests that a higher probability of a nucleophillic attack at N1 reduces the binding affinity of the compound with the mammalian receptor, thus reducing the mammalian toxicity of the compounds under consideration. Further, the negative coefficient of qC12 suggests that increased positive charge at C12 diminishes the binding affinity of the compounds towards the mammalian receptor and thus helps in reducing the toxicity of the compounds. Another important parameter of eq. [4] is log *P*. A negative coefficient of this parameter in this equation indicates that compounds having low polarity will have reduced toxic effects on the mammals.

The correlation matrix of the dependent and independent variables used in this study are shown in Table 3. Table 4 represents the *t* and *p* values of the coefficients obtained in the different equations. The final equations obtained in both the cases, i.e., eqs. [2] and [4], were further validated by the LOO method. The LOO predicted values as obtained utilizing eqs. [2] and [4] and are shown in Table 5.

Conclusion

The QSAR study suggests that increased surface area of the molecules helps to increase the insecticidal properties of the compounds by increasing the binding affinity of the compound with the receptor nAChR (insect). The presence of the azido group on the other hand is detrimental to this activity. The study also reveals the importance of atoms N1 and C12 with respect to the binding affinity of the compounds towards the receptor nAChR (mammals). The model showed that a higher probability of a nucleophillic attack at the N1 position may reduce the binding affinity of the compound towards the mammalian receptor. It also explained that increased positive charge at C12 may diminish the binding affinity of the compounds towards the mammalian receptor and thus helps in reducing the toxicity of the compounds. The model also demonstrates that compounds having low polarity may inhibit the binding affinity of the compound to the mammalian nAChR receptor and may reduce the toxic effects to the mammals. Thus, designing compounds having low polarity, increased probability of nucleophilic attack at the N-1 position, and a higher positive charge at the C-12 position can reduce toxicity of these compounds towards the mammalian receptor.

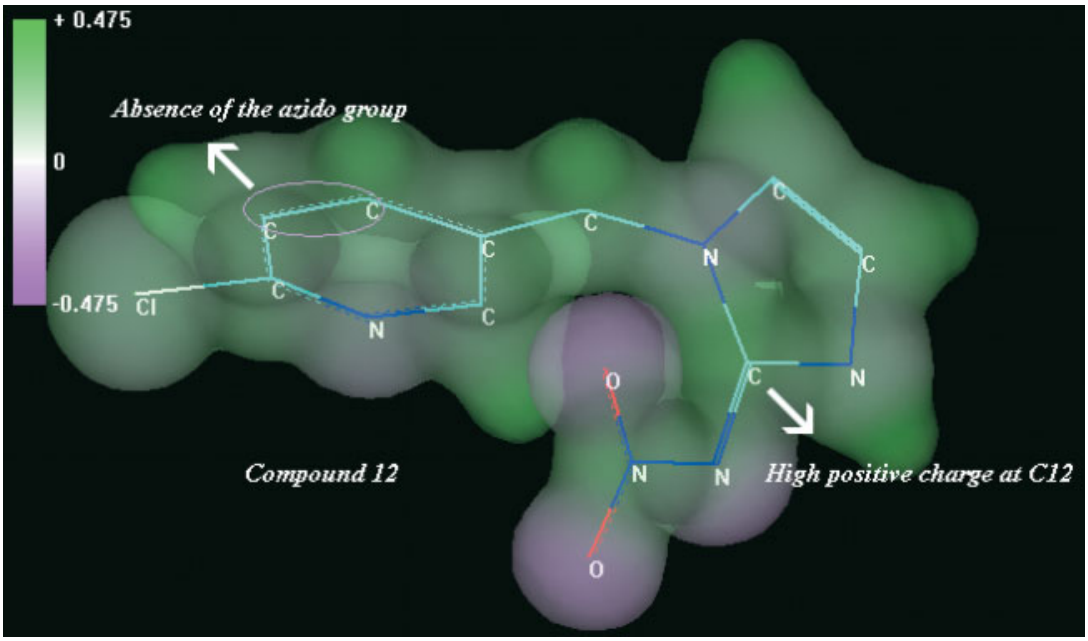
Our prediction is supported by the 3D isosurface electrostatic potential maps of compounds **6** and **12** obtained by AM1 calculations and shown in Figs. 2 and 3, respectively. The N1 atom of compound **6** possesses a low probability of nucleophilic attack as is evident from the value of the frontier electron density for nucleophilic attack at that particular position, recorded in Table 2. Compound **12**, on the other hand, possesses low toxicity towards mammals and a high insecticidal action. Fig. 3 clearly depicts the absence of the azido moiety in the compound, as well as the presence of a high positive charge at position C12, which according to our study should be one of the criteria for an ideal neonicotinoid insecticide. We have already shown that the binding affinity of these azido-pyridinyl neonicotinoids were quantitatively related with topological indices (8, 9). In this article, we also demonstrate that the pharmacological activity may also be explained with quantum chemical parameters.

Acknowledgements

The authors are thankful to the University Grants Commission (UGC), New Delhi and the All India Council for Technical Education (AICTE), New Delhi for providing financial support. Two of the authors (SG and SS) are grateful to the Indian Council of Medical Research (ICMR), New Delhi and the UGC for awarding a Senior Research Fellowship (SRF) and a Junior Research Fellowship (JRF), respec-

© 2006 NRC Canada

Fig. 3. Three-dimensional isosurface electrostatic potential map of compound **12**.



tively. Two of the authors (AB and PP) are grateful to the UGC for awarding Post Graduate Fellowships.

References

1. N. Zhang, M. Tomizawa, and J.E. Casida. J. Med. Chem. **45**, 2832 (2002).
2. W.D. Kollemeyer, R.F. Flattum, J.E. Powell, M.E. Schroeder, and S.B. Soloway. *In* Nicotinoid insecticides and the nicotinic acetylcholine receptor. *Edited by* I. Yamamoto and J.E. Casida. Springer-Verlag, Tokyo. 1999. pp. 71–89.
3. M. Tomizawa and J.E. Casida. Annu. Rev. Entomol. **48**, 339 (2003).
4. M.W. Decker and M.D. Meyer. Biochem. Pharmacol. **58**, 917 (1999).
5. G.K. Lloyd and M. Williams. J. Pharmacol. Exp. Ther. **292**, 461 (2000).
6. M. Cordero-Erausquin, L.M. Marubio, R. Klink, and J.-P. Changeux. Trends Pharmacol. Sci. **21**, 211 (2000).
7. M. Tomizawa, A. Cowan, and J.E. Casida. Toxicol. Appl. Pharmacol. **177**, 77 (2001).
8. B. Debnath, S. Gayen, S.K. Naskar, K. Roy, and T. Jha. Drug. Des. Discovery, **18**, 81 (2003).
9. B. Debnath, S. Gayen, A. Basu, B. Ghosh, K. Srikanth, and T. Jha. Bioorg. Med. Chem. **12**, 6137 (2004).
10. K. Srikanth, C.A. Kumar, D. Goswami, A.U. De, and T. Jha. Indian J. Biochem. Biophys. **38**, 120 (2001).
11. K. Srikanth, B. Debnath, and T. Jha. Bioorg. Med. Chem. **10**, 1841 (2002).
12. K. Srikanth, B. Debnath, and T. Jha. Bioorg. Med. Chem. Lett. **12**, 899 (2002).
13. K. Srikanth, C.A. Kumar, B. Ghosh, and T. Jha. Bioorg. Med. Chem. **10**, 2119 (2002).
14. B. Debnath, K. Srikanth, S. Banarjee, and T. Jha. Internet Electron. J. Mol. Des. **1**, 488 (2002) [online]. Available from http://www.biochempress.com.
15. B. Debnath, S.P. Vishnoi, B. Sa, and T. Jha. Internet Electron. J. Mol. Des. **1**, 128 (2003) [online]. Available from http://www.biochempress.com.
16. B. Debnath, S. Samanta, K. Roy, and T. Jha. Bioorg. Med. Chem. **11**, 1615 (2003).
17. B. Debnath, S. Samanta, S.K. Naskar, K. Roy, and T. Jha. Bioorg. Med. Chem. Lett. **13**, 2837 (2003).
18. T. Jha, B. Debnath, S. Samanta, and A.U. De. Internet Electron. J. Mol. Des. **2**, 539 (2003) [online]. Available from http://www.biochempress.com.
19. B. Debnath, S. Gayen, S. Samanta, and T. Jha. Bioorg. Med. Chem. **11**, 5493 (2003).
20. S. Gayen, B. Debnath, S. Samanta, and T. Jha. Bioorg. Med. Chem. **12**, 1493 (2004).
21. S. Samanta, K. Srikanth, S. Banarjee, B. Debnath, S. Gayen, and T. Jha. Bioorg. Med. Chem. **12**, 1413 (2004).
22. S. Samanta, B. Debnath, S. Gayen, B. Ghosh, K. Srikanth, and T. Jha. Farmaco, **10**, 818 (2005).
23. M.J.S. Dewar, E.G. Zoebisch, E.F. Healy, and J.J.P. Stewart. J. Am. Chem. Soc. **107**, 3902 (1985).
24. M. Besson and E.P. Batchelor. J. Biol. Phys. **30**, 161 (2004).
25. Hypercube, Inc. HyperChem Professional Release 7.0 [computer program]. Hypercube, Inc., Gainesville, Florida. Available from http://www.hyper.com
26. S.K. Naskar and B. Debnath. Multi Regress [computer program]. Department of Computer Science and Engineering, Jadavpur University, Kolkata, India. A computer program written in C^{++} language.

© 2006 NRC Canada

Chiral shift reagent catalyzed, diastereoselective imino Diels–Alder reaction — Synthesis of pyrazolyltetrahydroquinolines

Radhakrishnan Sridhar and Paramasivan T. Perumal

Abstract: A new, target oriented, highly diastereoselective synthesis of pyrazolyltetrahydroquinolines was attempted successfully. The chiral shift reagent Eu(tfc) was found to be a better choice for inducing diasteroselectivity.

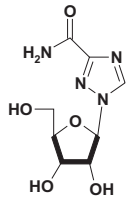
Key words: imino Diels–Alder reaction, chiral shift reagent catalyst, pyrazolyltetrahydroquinolines, diastereoselectivity, antibacterial activity.

Résumé : On a réalisé avec succès une nouvelle synthèse hautement diastéréosélective orientée en fonction de la cible de pyrazolyltétrahydroquinoléines. On a trouvé que le réactif chiral de déplacement chimique Eu(tfc) est le meilleur choix pour induire la diastéréosélectivité.

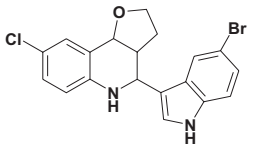
Mots clés : réaction imino de Diels–Alder, catalyseur à base de réactif chiral de déplacement chimique, pyrazolyltétrahydroquinoléines, diastéréosélectivité, activité antibactérienne.

[Traduit par la Rédaction]

Ribavirin (1-β-D-ribofuranosyl-1,2,4-triazole-3-carboxamide) **1**, a synthetic nucleoside analogue, possesses broad spectrum activity against both RNA and DNA viruses in vitro and in vivo (1). Several modifications were carried out in the sugar as well as in the base units to explore more of these nucleosides and their biological efficiency (2, 3). During our studies on the synthesis of similar base units (4, 5), we found that pyrazole-3-ester posses bacterial and fungal inhibition (4).



1



2

A number of tetrahydroquinoline derivatives exhibit a wide range of biological properties (6–8). Substituted tetrahydroquinolines are the core structures in many important pharmacological agents and drug molecules, such as antiarrhythmic and cardiovascular agents, anticancer drugs, immunosuppressants, and ligands for 5-HT1A and NMDA receptors (9). Hence, there has been considerable interest in the development of new and efficient methodologies for the synthesis of tetrahydroquinoline derivatives (8, 10).

The frequency of methicillin-resistant *Staphylococcus aureus* (MRSA) infections has been increasing for the last decade and has developed into a problem throughout the world. Novel antibacterial agents, 2-(1*H*-indol-3-yl)tetrahydroquinolines **2**, were prepared using hetero Diels–Alder chemistry and were found to be effective in vitro against MRSA. From the SAR study it was observed that among the two diastereomers, the *cis*-2-(1*H*-indol-3-yl)tetrahydroquinolines was found to be more potent in antibacterial inhibition than the trans isomer (11).

The imino Diels–Alder reaction provides a useful entry to the preparation of tetrahydroquinoline derivatives (8). Generally, Lewis acids (12–14) are known to catalyze the imino Diels–Alder reaction to produce quinoline derivatives. A few reports are available on the imino Diels–Alder reaction catalyzed by lanthanide catalysts (15). Lanthanide shift reagents have been shown to act as efficient catalysts for the inverse electron demand Diels–Alder reactions with complete diastereoselectivity (16). It was also observed that the usage of $Eu(thd)_3$ showed a dramatical reversal in diastereoselectivity (17). Cycloaddition reactions between the chiral 2-pyrone derivatives and various dienophiles were also reported with lanthanide shift reagents to afford bicyclic lactones in high diastereomeric excesses (18). A catalytic asymmetric version of these reactions, using optically active lanthanide catalysts, was also successfully investigated by Markó and co-workers (19).

Based on the report available on the antibacterial inhibition of tetrahydroquinolines (11) and results of our earlier studies on the antibacterial inhibition of pyrazole-3-esters (4), we planned to synthesize pyrazolyl tetrahydroquinolines

Received 24 May 2005. Published on the NRC Research Press Web site at http://canjchem.nrc.ca on 7 April 2006.

R. Sridhar and P.T. Perumal.[1] Organic Chemistry Division, Central Leather Research Institute, Adyar, Chennai – 600 020, India.

[1]Corresponding author (e-mail: ptperumal@hotmail.com).

 doi:10.1139/V06-017 © 2006 NRC Canada

Scheme 1. Synthesis of pyrazolyltetrahydrocyclopentaquinolines.

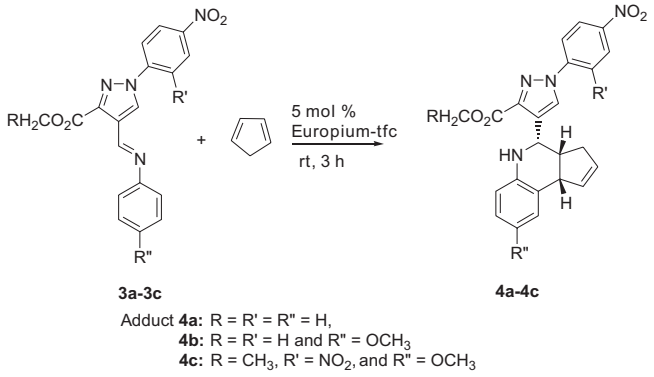


Table 1. Synthesis of pyrazolyltetrahydrocyclopentaquinolines using Eu(tfc).

Entry	R	R′	R″	Yield[a] (%)	Time (h)
4a	H	H	H	88	3.5
4b	H	H	OCH_3	89	3
4c	CH_3	NO_2	OCH_3	86	4

[a]Column chromatographic yield.

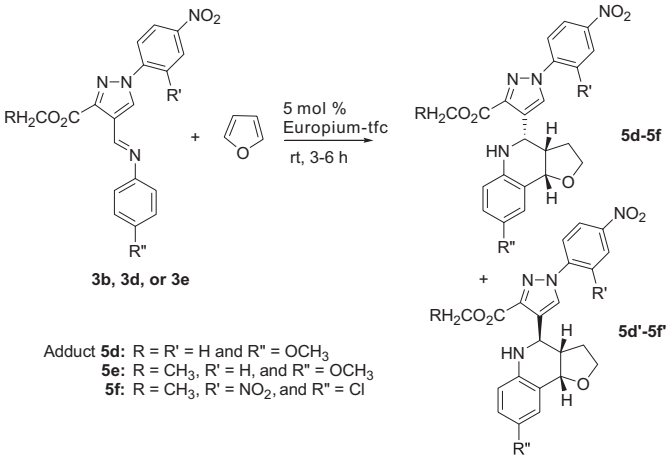
that we expect to be effective bactericides, through imino Diels–Alder reaction using the chiral shift reagent. Also, our aim was to synthesize the cis diastereomer in excess over the less potent antibacterial trans isomer, which we intend to achieve through the versatility of the chiral shift reagent (19).

Pyrazole aldimines were prepared from 4-formyl-1*H*-pyrazole-3-carboxylate (4, 5) and aniline using $InCl_3$ as catalyst following the reported procedure for the preparation of imines (20). These imines upon stirring at room temperature with cyclopentadiene (Scheme 1) in the presence of 5 mol% Eu(tfc) gave corresponding pyrazolyl tetrahydro-3*H*-cyclopenta[*c*]quinolines in excellent yield as a single product (Table 1). Pyrazolyl tetrahydrofuroquinolines (Scheme 2) or pyrazolyltetrahydropyranoquinoline (Scheme 3) were obtained in good to excellent yields by treating the respective imines with 2,3-dihydrofuran or 3,4-dihydropyran in the presence of 5 mol% Eu(tfc) at room temperature.

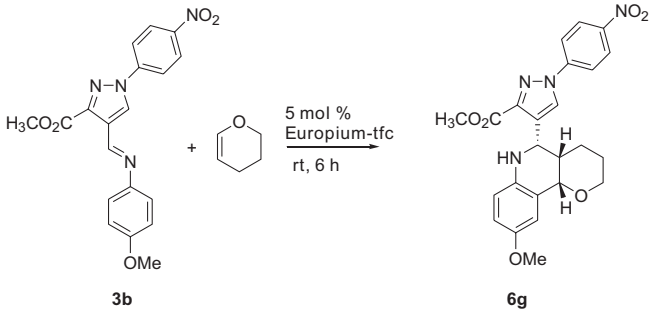
The structures of the products were confirmed through IR, NMR, and mass spectral data (see Experimental), and the diastereomeric excess of the products was determined based on column chromatographic yield. All the pyrazolyltetrahydroquinolines exhibited a resultant optical rotation owing to the excess of one enantiomer over the other, but the detailed study on enantiomeric excess will be demonstrated using chiral HPLC technique in due course.

In the case of tetrahydrofuroquinolines, two diastereomers were obtained and the orientation of H-3a and H-4 corresponding to cis and trans diastereomers were confirmed by their coupling constant values, J = 3.4 Hz and J = 10.3 Hz, respectively, from the NMR spectra. Further, the diastereomers show different fragmentation patterns in mass spectra (see Experimental). Our observations (Table 2) showed that the diastereoselectivity was improved by exchanging the catalyst $InCl_3$ with Eu(tfc). Hence, by employing Eu(tfc) the

Scheme 2. Synthesis of pyrazolyltetrahydrofuroquinolines.



Scheme 3. Synthesis of pyrazolyltetrahydropyranoquinolines.



yield of the more potent antibacterial cis diastereomer (8) was selectively increased over the trans.

Only one isomer was isolated and it was found to be in cis orientation (J = 2.3 Hz) for the tetrahydropyranoquinolines.

One-pot synthesis of tetrahydroquinolines was also attempted starting directly from pyrazole aldehydes, substituted anilines, and dienophiles in the presence of Eu(tfc) (Table 3). The yield obtained and diastereoselectivities from the table also clearly indicate the versatility of the europium D-3-trifluoroacetyl camphorate catalyst over the $InCl_3$ catalyst in the multicomponent reaction.

The higher diastereoselectivity in the product formation depending on the chiral catalyst used may be due to the unsymmetric nature of the aldehydic portion of the imine and the bulkiness of the chiral catalyst. The same reason can be extended for the formation of the product **6g** in 99% diastereomeric excess. On the other hand, this reason will be invalid in the use of $InCl_3$ as the catalyst because of its symmetric nature.

From the investigation it is clear that the catalyst is more versatile in selectivity and, hence, in the synthesis of the cis isomer, which we expect to be more potent over the trans (11). Herein we have synthesized pyrazolyltetrahydroquinolines and our ultimate goal is to prove them as novel and potent bactericides, which will be demonstrated in future articles. In summary, we report a target-oriented, highly diastereoselective synthesis for pyrazolyltetrahydroquinolines using Eu(tfc) catalyst.

© 2006 NRC Canada

Table 2. Synthesis of pyrazolyltetrahydrofuroquinolines and pyrazolyltetrahydropyranoquinolines.

Entry	R	R′	R″	Yield[a] (%)	Time (h)	Product ratio (cis:trans)
5d	H	H	OCH_3	82	3	80:20
5e	CH_3	H	OCH_3	85	3	83:17
5f	CH_3	NO_2	Cl	88	4.5	88:12
6g	H	H	OCH_3	62	6	99% **6g**

[a]Isolated yield after column chromatography.

Table 3. Comparison of Eu(tfc)- and $InCl_3$-catalyzed syntheses of pyrazolyltetrahydroquinolines.

	Yield[a] (%)		Time (h)		Product ratio (cis:trans)	
Entry	Eu(tfc)[b]	$InCl_3$[c]	Eu(tfc)	$InCl_3$	Eu(tfc)	$InCl_3$
5d	75	67	4	8.5	82:18	55:45
5e	79	63	3.5	8	84:16	52:48
5f	82	70	5	10	88:12	63:37
6g	58	—	6	—	—	—

[a]Isolated yield after column chromatography.
[b]Eu(tfc)-catalyzed, one-pot synthesis.
[c]$InCl_3$-catalyzed synthesis of pyrazolyltetrahydroquinolines starting from aldehyde and amine.

Experimental

General procedure for the synthesis of pyrazolyl tetrahydroquinolines from corresponding imines

To a solution of an imine (2 mmol) in acetonitrile (10 mL), was added 5 mmol of dienophile (cylopentadiene, 2,3-dihydrofuran, or 3,4-dihydropyran) and 5 mol% of Eu(tfc) or 20 mol% of $InCl_3$. The reaction mixture was stirred for an adequate time at room temperature until TLC showed the completion of the reaction. Water was then added to the mixture and extracted with $CHCl_3$. The combined organic layers were treated with brine solution, then with water, and the product dried over anhydrous sodium sulfate. After evaporation of the solvent, the residue was column chromatographed with 15% ethyl acetate – petroleum ether mixture to afford the pure cycloadduct.

*Methyl 4-(3a,4,5,9b-tetrahydro-3*H*-cyclopenta[*c*]quinolin-4-yl)-1-(4-nitrophenyl)-1*H*-pyrazole-3-carboxylate (4a)*

Red-coloured solid (15% ethyl acetate – petroleum ether); mp 240 °C. IR (KBr, cm^{-1}): 3331, 2923, 2857, 1719, 1595, 1465, 1335, 1227, 1108, 751. ^{1}H NMR (500 MHz, $CDCl_3$) δ: 8.35–8.37 (d, J = 9.2 Hz, 2H), 8.20 (s, 1H, pyrazole-CH), 7.96–7.98 (d, J = 9.2 Hz, 2H), 7.08–7.09 (m, 1H, phenyl), 6.98–7.02 (m, 1H, phenyl), 6.78–6.81 (m, 1H, phenyl), 6.63–6.64 (m, 1H, phenyl), 5.85–5.87 (m, 1H), 5.64–5.65 (m, 1H), 5.17–5.18 (d, J = 2.9 Hz, 1H), 4.14–4.16 (d, J = 8.6 Hz, 1H), 3.98 (s, 3H), 3.76 (brs, 1H), 3.26–3.32 (doublet of quartet, J_1 = 2.9 and J_2 = 8.6 Hz, 1H), 2.54–2.61 (m, 1H), 1.93–1.98 (m, 1H). ^{13}C NMR (125 MHz, $CDCl_3$, ppm) δ: 162.5, 146.5, 145.1, 143.6, 142.6, 134.5, 130.8, 129.9, 129.2, 126.9, 126.6, 126.5, 125.5, 120.0, 119.7, 116.2, 52.5, 49.9, 45.9, 42.6, 32.4. MS (*m*/*z*): 416 (M^+). Anal. calcd. for $C_{23}H_{20}N_4O_4$: C 66.34, H 4.84, N 13.45; found: C 66.28, H 4.76, N 13.38.

*Methyl 4-(8-methoxy-3a,4,5,9b-tetrahydro-3*H*-cyclopenta[*c*]quinolin-4-yl)-1-(4-nitrophenyl)-1*H*-pyrazole-3-carboxylate (4b)*

Red-coloured solid (15% ethyl acetate – petroleum ether); mp 200 °C. IR (KBr, cm^{-1}): 3347, 2952, 2843, 1722, 1597, 1505, 1341, 1235, 1110, 751. ^{1}H NMR (500 MHz, $CDCl_3$) δ: 8.35–8.37 (d, J = 9.2 Hz, 2H), 8.20 (s, 1H, pyrazole-CH), 7.94–7.96 (d, J = 9.2 Hz, 2H), 6.65–6.66 (m, 1H, *p*-methoxyphenyl), 6.59–6.60 (m, 2H, *p*-methoxyphenyl), 5.83–5.84 (m, 1H), 5.64–5.65 (m, 1H), 5.08–5.09 (d, J = 2.9 Hz, 1H), 4.10–4.12 (d, J = 8.6 Hz, 1H), 3.98 (s, 3H), 3.75 (s, 3H), 3.60 (brs, 1H), 3.23–3.29 (doublet of quartet, J_1 = 2.9 and J_2 = 8.6 Hz, 1H), 2.54–2.59 (m, 1H), 1.92–1.97 (m, 1H). ^{13}C NMR (125 MHz, $CDCl_3$, ppm) δ: 162.5, 153.5, 146.5, 143.6, 142.5, 138.8, 134.2, 130.8, 130.1, 127.7, 126.9, 125.5, 119.6, 117.0, 114.1, 112.6, 55.8, 52.5, 50.3, 46.3, 42.3, 32.3. MS (*m*/*z*): 446 (M^+). Anal. calcd. for $C_{24}H_{22}N_4O_5$: C 64.57, H 4.97, N 12.55; found: C 64.59, H 4.95, N 12.51.

*Ethyl 4-(8-methoxy-3a,4,5,9b-tetrahydro-3*H*-cyclopenta[*c*]quinolin-4-yl)-1-(2,4-dinitrophenyl)-1*H*-pyrazole-3-carboxylate (4c)*

Red-coloured solid (15% ethyl acetate – petroleum ether); mp 115 °C. IR (KBr, cm^{-1}): 3374, 2926, 2852, 1719, 1609, 1542, 1347, 1238, 1105, 753. ^{1}H NMR (500 MHz, $CDCl_3$) δ: 8.80–8.81 (d, J_1 = 2.3 Hz, 1H), 8.55–8.58 (dd, J_1 = 2.3 and J_2 = 8.6 Hz, 1H), 7.92–7.94 (d, J_2 = 8.6 Hz, 1H), 7.89 (s, 1H, pyrazole-CH), 6.75–6.76 (d, J_3 = 2.9 Hz, 1H, *p*-methoxyphenyl), 6.61–6.63 (dd, J_3 = 2.9 and J_4 = 8.6 Hz, 1H, *p*-methoxyphenyl), 6.55–6.56 (d, J_4 = 8.6 Hz, 1H, *p*-methoxyphenyl), 5.87–5.89 (m, 1H), 5.72–5.74 (m, 1H), 5.08–5.09 (d, J = 2.8 Hz, 1H), 4.40–4.46 (m, 2H), 4.09–4.11 (d, J = 8.6 Hz, 1H), 3.75 (s, 3H), 3.57 (brs, 1H), 3.25–3.28 (doublet of quartet, J_5 = 2.8 and J_6 = 8.6 Hz, 1H), 2.50–2.57 (m, 1H), 1.95–2.17 (m, 1H), 1.40–1.43 (t, J = 7.11 Hz, 3H). ^{13}C NMR (125 MHz, $CDCl_3$, ppm) δ: 161.6, 153.4, 146.6, 143.8, 143.7, 138.6, 137.2, 134.0, 130.7, 130.2, 129.9, 127.9, 127.8, 127.5, 121.2, 117.0, 114.0, 112.5, 61.7, 55.7, 50.1, 46.1, 42.3, 32.1, 14.3. MS (*m*/*z*): 505 (M^+). Anal. calcd. for $C_{25}H_{23}N_5O_7$: C 59.40, H 4.59, N 13.85; found: C 59.42, H 4.56, N 13.81.

*Methyl 4-[(3aα,4β,9bα)-8-methoxy-2,3,3a,4,5,9b-hexahydrofuro[3,2-*c*]quinolin-4-yl]-1-(4-nitrophenyl)-1*H*-pyrazole-3-carboxylate (5d)*

Yellow-coloured solid (first fraction in 15% ethyl acetate – petroleum ether); mp 146 °C. IR (KBr, cm^{-1}): 3374, 2957, 2843, 1722, 1598, 1510, 1343, 1236, 1113, 756. ^{1}H NMR (500 MHz, $CDCl_3$) δ: 8.34–8.36 (d, J = 9.2 Hz, 2H), 8.25 (s, 1H, pyrazole-CH), 7.94–7.96 (d, J = 9.2 Hz, 2H), 6.92–6.93 (d, J_1 = 2.9 Hz, 1H, *p*-methoxyphenyl), 6.70–6.72 (dd, J_1 = 2.9 and J_2 = 8.6 Hz, 1H, *p*-methoxyphenyl), 6.56–6.57 (d, J_2 = 8.6 Hz, 1H, *p*-methoxyphenyl), 5.21–5.23 (d, J = 8.0 Hz, 1H), 5.15–5.16 (d, J = 3.4 Hz, 1H), 4.01–4.04 (m, 1H), 3.98 (s, 3H), 3.81–3.87 (m, 1H), 3.76 (brs, 1H), 3.67 (s, 3H), 3.05–3.11 (m, 1H), 2.06–2.14 (m, 1H), 1.60–1.66 (m,

© 2006 NRC Canada

1H). ^{13}C NMR (125 MHz, $CDCl_3$, ppm) δ: 162.5, 153.6, 146.0, 143.6, 141.8, 138.5, 130.2, 127.2, 125.5, 123.9, 119.7, 116.6, 116.0, 113.8, 75.7, 66.6, 55.8, 52.6, 49.3, 42.5, 25.4. MS (*m*/*z*): 450 (M^+). Anal. calcd. for $C_{23}H_{22}N_4O_6$: C 61.33, H 4.92, N 12.44; found: C 61.25, H 4.96, N 12.41.

Methyl 4-[(3aα,4α,9bα)-8-methoxy-2,3,3a,4,5,9b-hexahydrofuro[3,2-c]quinolin-4-yl]-1-(4-nitrophenyl)-1H-pyrazole-3-carboxylate (5d′)

Yellow-coloured solid (second fraction in 15% ethyl acetate – petroleum ether); mp 102 °C. IR (KBr, cm^{-1}): 3358, 2952, 2875, 1723, 1598, 1505, 1343, 1235, 1114, 754. ^{1}H NMR (500 MHz, $CDCl_3$) δ: 8.34–8.36 (d, *J* = 9.2 Hz, 2H), 8.14 (s, 1H, pyrazole-CH), 7.92–7.94 (d, *J* = 9.2 Hz, 2H), 6.94–6.95 (d, J_1 = 2.9 Hz, 1H, *p*-methoxyphenyl), 6.74–6.76 (dd, J_1 = 2.9 and J_2 = 8.6 Hz, 1H, *p*-methoxyphenyl), 6.61–6.62 (d, J_2 = 8.6 Hz, 1H, *p*-methoxyphenyl), 4.66–4.67 (d, *J* = 5.75 Hz, 1H), 4.50–4.52 (d, *J* = 10.3 Hz, 1H), 4.02–4.07 (m, 1H), 3.96 (s, 3H), 3.84–3.89 (m, 1H), 3.76 (brs, 1H), 3.75 (s, 3H), 2.54–2.58 (m, 1H), 2.15–2.22 (m, 1H), 1.84–1.90 (m, 1H). ^{13}C NMR (125 MHz, $CDCl_3$, ppm) δ: 162.7, 153.1, 146.6, 143.9, 143.5, 138.8, 129.6, 127.9, 125.5, 121.6, 119.8, 116.7, 116.6, 114.5, 75.8, 65.8, 55.9, 52.7, 48.3, 43.9, 29.6. MS (*m*/*z*): 450 (M^+). Anal. calcd. for $C_{23}H_{22}N_4O_6$: C 61.33, H 4.92, N 12.44; found: C 61.38, H 4.90, N 12.38.

Ethyl 4-[(3aα,4β,9bα)-8-methoxy-2,3,3a,4,5,9b-hexahydrofuro[3,2-c]quinolin-4-yl]-1-(4-nitrophenyl)-1H-pyrazole-3-carboxylate (5e)

Yellow-coloured solid (first fraction in 15% ethyl acetate – petroleum ether); mp 192 °C. IR (KB, cm^{-1}): 3350, 2980, 2846, 1719, 1598, 1506, 1342, 1233, 1111, 754. ^{1}H NMR (500 MHz, $CDCl_3$) δ: 8.34–8.36 (d, *J* = 9.2 Hz, 2H), 8.25 (s, 1H, pyrazole-CH), 7.95–7.97 (d, *J* = 9.2 Hz, 2H), 6.92–6.93 (d, J_1 = 2.9 Hz, 1H, *p*-methoxyphenyl), 6.71–6.73 (dd, J_1 = 2.9 and J_2 = 8.6 Hz, 1H, *p*-methoxyphenyl), 6.56–6.57 (d, J_2 = 8.6 Hz, 1H, *p*-methoxyphenyl), 5.20–5.22 (d, *J* = 8.1 Hz, 1H), 5.14–5.15 (d, *J* = 2.9 Hz, 1H), 4.43–4.49 (m, 2H), 3.81 (brs, 1H), 3.73–3.80 (m, 2H), 3.76 (s, 3H), 3.05–3.11 (m, 1H), 2.07–2.15 (m, 1H), 1.60–1.66 (m, 1H), 1.43–1.45 (t, 3H). ^{13}C NMR (125 MHz, $CDCl_3$, ppm) δ: 162.1, 153.6, 146.5, 143.6, 142.9, 138.5, 130.0, 127.1, 125.5, 123.9, 119.7, 116.6, 116.0, 113.8, 75.8, 66.6, 61.7, 55.8, 49.4, 42.6, 25.3, 14.4. MS (*m*/*z*): 464 (M^+). Anal. calcd. for $C_{24}H_{24}N_4O_6$: C 62.06, H 5.21, N 12.06; found: C 62.12, H 5.23, N 12.10.

Ethyl 4-[(3aα,4α,9bα)-8-methoxy-2,3,3a,4,5,9b-hexahydrofuro[3,2-c]quinolin-4-yl]-1-(4-nitrophenyl)-1H-pyrazole-3-carboxylate (5e′)

Yellow-coloured solid (second fraction in 15% ethyl acetate – petroleum ether); mp 160 °C. IR (KBr, cm^{-1}): 3355, 2933, 2849, 1718, 1598, 1505, 1342, 1237, 1112, 752. ^{1}H NMR (500 MHz, $CDCl_3$) δ: 8.35–8.37 (d, *J* = 9.2 Hz, 2H), 8.12 (s, 1H, pyrazole-CH), 7.94–7.95 (d, *J* = 9.2 Hz, 2H), 6.96–6.97 (d, J_1 = 2.9 Hz, 1H, *p*-methoxyphenyl), 6.75–6.78 (dd, J_1 = 2.9 and J_2 = 8.6 Hz, 1H, *p*-methoxyphenyl), 6.61–6.63 (d, J_2 = 8.6 Hz, 1H, *p*-methoxyphenyl), 4.67–4.68 (d, *J* = 5.7 Hz, 1H), 4.48–4.50 (d, *J* = 10.3 Hz, 1H), 4.42–4.47 (m, 2H), 4.29 (brs, 1H), 4.03–4.07 (m, 1H), 3.84–3.89 (m, 1H), 3.77 (s, 3H), 2.56–2.61 (m, 1H), 2.16–2.23 (m, 1H), 1.85–1.91 (m, 1H), 1.39–1.42 (t, 3H). ^{13}C NMR (125 MHz, $CDCl_3$, ppm) δ: 162.2, 153.1, 146.6, 144.5, 143.6, 138.8, 129.5, 127.7, 125.5, 121.6, 119.8, 116.7, 116.5, 114.5, 75.9, 65.9, 61.8, 55.9, 48.3, 43.7, 29.5, 14.4. MS (*m*/*z*): 464 (M^+). Anal. calcd. for $C_{24}H_{24}N_4O_6$: C 62.06, H 5.21, N 12.06; found: C 62.10, H 5.28, N 11.98.

Ethyl 4-[(3aα,4β,9bα)-8-chloro-2,3,3a,4,5,9b-hexahydrofuro[3,2-c]quinolin-4-yl]-1-(2,4-dinitrophenyl)-1H-pyrazole-3-carboxylate (5f)

Yellow-coloured solid (first fraction in 15% ethyl acetate – petroleum ether); mp 152 °C. IR (KBr, cm^{-1}): 3356, 2943, 2846, 1721, 1605, 1539, 1343, 1225, 1110, 746. ^{1}H NMR (400 MHz, $CDCl_3$) δ: 8.81–8.82 (d, J_1 = 2.3 Hz, 1H), 8.56–8.59 (dd, J_1 = 2.3 and J_2 = 8.7 Hz, 1H), 7.93–7.95 (d, J_2 = 8.7 Hz, 1H), 7.92 (s, 1H, pyrazole-CH), 7.33–7.34 (d, J_3 = 2.3 Hz, 1H, *p*-chlorophenyl), 7.02–7.05 (dd, J_3 = 2.3 and J_4 = 8.6 Hz, 1H, *p*-chlorophenyl), 6.53–6.55 (d, J_4 = 8.6 Hz, 1H, *p*-chlorophenyl), 5.22–5.23 (d, *J* = 3.1 Hz, 1H), 5.13–5.15 (d, *J* = 7.7 Hz, 1H), 4.41–4.47 (q, *J* = 7.1 Hz, 2H), 4.01 (brs, 1H), 3.74–3.82 (m, 2H), 3.03–3.11 (doublet of quartet, J_5 = 3.1 and J_6 = 8.7 Hz, 1H), 1.99–2.08 (m, 1H), 1.68–1.76 (m, 1H), 1.41–1.45 (t, *J* = 7.1 Hz, 3H). ^{13}C NMR (100 MHz, $CDCl_3$, ppm) δ: 161.6, 146.8, 143.8, 142.8, 137.1, 130.3, 129.9, 129.4, 129.0, 128.5, 128.1, 127.9, 124.4, 121.2, 116.6, 116.5, 74.9, 66.5, 62.0, 48.5, 41.9, 25.3, 14.3. MS (*m*/z): 514 (M^+). Anal. calcd. for $C_{23}H_{20}ClN_5O_7$: C 53.76, H 3.92, N 13.63; found: C 53.85, H 3.96, N 13.55.

Ethyl 4-[(3aα,4α,9bα)-8-chloro-2,3,3a,4,5,9b-hexahydrofuro[3,2-c]quinolin-4-yl]-1-(2,4-dinitrophenyl)-1H-pyrazole-3-carboxylate (5f′)

Yellow-coloured solid (first fraction in 15% ethyl acetate – petroleum ether); mp 106 °C. IR (KBr, cm^{-1}): 3358, 2927, 2872, 1721, 1607, 1543, 1347, 1233, 1106, 752. ^{1}H NMR (400 MHz, $CDCl_3$) δ: 8.81–8.82 (d, J_1 = 2.3 Hz, 1H), 8.56–8.58 (dd, J_1 = 2.3 and J_2 = 8.7 Hz, 1H), 7.92–7.94 (d, J_2 = 8.7 Hz, 1H), 7.77 (s, 1H, pyrazole-CH), 7.34–7.35 (d, J_3 = 2.3 Hz, 1H, *p*-chlorophenyl), 7.06–7.08 (dd, J_3 = 2.3 and J_4 = 8.6 Hz, 1H, *p*-chlorophenyl), 6.58–6.60 (d, J_4 = 8.6 Hz, 1H, *p*-chlorophenyl), 4.63–4.64 (d, *J* = 5.7 Hz, 1H), 4.57 (brs, 1H), 4.52–4.54 (d, *J* = 9.8 Hz, 1H), 4.40–4.46 (q, *J* = 7.1 Hz, 2H), 4.00–4.04 (m, 1H), 3.84–3.88 (m, 1H), 2.55–2.60 (m, 1H), 2.19–2.26 (m, 1H), 1.87–1.92 (m, 1H), 1.38–1.41 (t, *J* = 7.1 Hz, 3H). ^{13}C NMR (100 MHz, $CDCl_3$, ppm) δ: 161.9, 146.4, 143.2, 142.0, 138.2, 131.2, 130.1, 129.2, 128.7, 128.5, 128.0, 127.3, 122.3, 121.5, 117.2, 116.2, 75.1, 66.7, 61.7, 49.4, 42.7, 29.2, 14.4. MS (*m*/z): 514 (M^+). Anal. calcd. for $C_{23}H_{20}ClN_5O_7$: C 53.76, H 3.92, N 13.63; found: C 53.79, H 3.98, N 13.67.

Methyl 4-[(4aα,5β,10bα)-9-methoxy-3,4,4a,5,6,10b-hexahydro-2H-pyrano[3,2-c]quinolin-5-yl]-1-(4-nitrophenyl)-1H-pyrazole-3-carboxylate (6g)

Yellow-coloured solid (first fraction in 15% ethyl acetate – petroleum ether); mp 218 °C. IR (KBr, cm^{-1}): 3357, 2949, 2857, 1722, 1598, 1507, 1342, 1234, 1114, 754. ^{1}H NMR (500 MHz, $CDCl_3$) δ: 8.35–8.37 (d, *J* = 9.2 Hz, 2H), 8.24 (s, 1H, pyrazole-CH), 7.96–7.98 (d, *J* = 9.2 Hz, 2H), 7.03–7.04 (d, J_1 = 2.9 Hz, 1H, *p*-methoxyphenyl), 6.71–6.73 (dd, J_1 =

© 2006 NRC Canada

2.9 and J_2 = 8.6 Hz, 1H, *p*-methoxyphenyl), 6.57–6.59 (d, J_2 = 8.6 Hz, 1H, *p*-methoxyphenyl), 5.30–5.31 (d, J = 5.75 Hz, 1H), 5.14–5.15 (d, J = 2.3 Hz, 1H), 4.01–4.03 (m, 1H), 4.00 (brs, 1H), 3.98 (s, 3H), 3.77 (s, 3H), 3.60–3.62 (m, 1H), 3.38–3.43 (m, 1H), 2.38–2.43 (m, 1H), 1.45–1.60 (m, 2H), 1.31–1.34 (m, 1H). ^{13}C NMR (125 MHz, $CDCl_3$, ppm) δ: 162.4, 153.6, 146.4, 143.6, 142.5, 138.7, 129.2, 127.9, 125.5, 122.2, 119.7, 116.3, 115.0, 111.9, 72.4, 60.9, 55.9, 52.5, 51.5, 36.0, 25.4, 18.4. MS (*m*/*z*): 464 (M^+). Anal. calcd. for $C_{24}H_{24}N_4O_6$: C 62.06, H 5.21, N 12.06; found: C 62.02, H 5.26, N 12.01.

Acknowledgement

One of the authors (RS) is grateful to the Council of Scientific and Industrial Research, New Delhi, India for financial support.

References

1. (*a*) R.W. Sidwell, J.H. Huffman, G.P Khare, L.B. Allen, J.T. Witkowski, and R.K. Robins. Science (Wasghington, D.C.), **177**, 705 (1972); (*b*) J.T. Witkowski, R.K. Robins, R.W. Sidwell, and L.N. Simon. J. Med. Chem. **15**, 1150 (1972).
2. S. Manfredini, R. Bazzanini, P.G. Baraldi, M. Guarneri, D. Simoni, M.E. Marongiu, A. Pani, E. Tramontano, and P.L. Colla. J. Med. Chem. **35**, 917 (1992).
3. S. Manfredini, R. Bazzanini, P.G. Baraldi, M. Bonora, M. Marangoni, D. Simoni, A. Pani, F. Scintu, E. Pinna, L. Pisano, and P.L.Colla. Anti–Cancer Drug Des. **11**, 193 (1996).
4. R. Sridhar, P.T. Perumal, S. Etti, G. Shanmugam, M.N. Ponnuswamy, V.R. Prabavathy, and N. Mathivanan. Bioorg. Med. Chem. Lett. **14**, 6035 (2004).
5. R. Sridhar and P.T. Perumal. Tetrahedron, **61**, 2465 (2005).
6. (*a*) M. Ramesh, P.S. Moham, and P. Shanmugam. Tetrahedron, **40**, 4041 (1984); (*b*) K.M. Witherup, R.W. Ransom, S.L. Varga, S.M. Pitzenberger, V.J. Lotti, and W.J. Lumma. US Patent 5 288 725, 1994; Chem. Abstr. **121**, 91779s (1994); (*c*) N.B. Perry, J.W. Blunt, J.D. McCombs, and M.H.G. Munro. J. Org. Chem. **51**, 5476 (1986); (*d*) N.M. Williamson, D.R. March, and A.D. Ward. Tetrahedron Lett. **36**, 7721 (1995); (*e*) J.V. Johnson, B.S. Rauckman, D.P. Baccanari, and B. Roth. J. Med. Chem. **32**, 1942 (1989); (*f*) S.A. Biller and R.N. Misra. US Patent 4 843 082, 1989; Chem. Abstr. **111**, 232600j (1989); (*g*) R.W. Carling, P.D. Leeson, A.M. Moseley, R. Baker, A.C. Foster, S. Grimwood, J.A. Kemp, and G.R. Marshall. J. Med. Chem. **35**, 1942 (1992); (*h*) R.W. Carling, P.D. Leeson, A.M. Moseley, J.D. Smith, K. Saywell, M.D. Tricklebank, J.A. Kemp, G.R. Marshall, A.C. Foster, and S. Grimwood. Bioorg. Med. Chem. Lett. **3**, 65 (1993); (*i*) G.D. Cuny, J.R. Hauske, M.Z. Hoemann, R.F. Rossi, and R.L. Xie. PCT Int. Appl. WO 9 967 238, 1999; Chem. Abstr. **132**, 64182 (1999); (*j*) K. Hanada, K. Furuya, K. Inoguchi, M. Miyakawa, and N. Nagata. PCT Int. Appl. WO 0 127 086, 2001; Chem. Abstr. **134**, 295752 (2001).
7. E.A. Mohamed. Chem. Pap. **48**, 261 (1994); Chem. Abstr. **123**, 9315 (1995).
8. C.J. Magesh, S.V. Makesh, and P.T. Perumal. Bioorg. Med. Chem. Lett. **14**, 2035 (2004).
9. (*a*) P.D. Leeson, R.W. Carling, K.W. Moore, A.M. Moseley, J.D. Smith, G. Stevenson, T. Chan, R. Baker, A.C. Foster, S. Grimwood, J.A. Kemp, G.R. Marshall, and K. Hoogsteen. J. Med. Chem. **35**, 1954 (1992); (*b*) R. Nagata, N. Tanno, T. Kodo, N. Ae, H. Yamaguchi, T. Nishimura, F. Antoku, T. Tatsuno, T. Kato, Y. Tanaka, and M. Nakamura. J. Med. Chem. **37**, 3956 (1994); (*c*) F. Guo, B.H. Chang, and C.J. Rizzo. Bioorg. Med. Chem. Lett. **12**, 151 (2002); (*d*) J.L. Stanton and M.H. Ackerman. J. Med. Chem. **26**, 986 (1983).
10. A.R. Katritzky, S. Rachwal, and B. Rachwal. Tetrahedron, **52**, 5031 (1996).
11. M.Z. Hoemann, R.L. Xie, R.F. Rossi, S. Meyer, A. Sidhu, G.D. Cuny, and J.R. Hauske. Bioorg. Med. Chem. Lett. **12**, 129 (2002).
12. G. Babu and P.T. Perumal. Tetrahedron Lett. **39**, 3225 (1998).
13. (*a*) J. Cabral and P. Laszlo. Tetrahedron Lett. **30**, 7237 (1989); (*b*) B. Crousse, J.P. Begue, and D.B. Delpon. Tetrahedron Lett. **39**, 5765 (1998); (*c*) J.S. Yadav, B.V.S. Reddy, R. Srinivas, C.R. Madhuri, and T. Ramalingam. Synlett, 240 (2001); (*d*) J.S. Yadav, B.V.S. Reddy, R. Srinivas, C.R. Madhuri, and G. Sabitha. Synthesis, 1065 (2001).
14. (*a*) D.F. Worth, S.C. Perricone, and E.F. Elslager. J. Heterocycl. Chem. **7**, 1353 1970; (*b*) G. Babu and P.T. Perumal. Tetrahedron Lett. **38**, 5025 (1997).
15. (*a*) Y. Ma, C.T. Qian, M. Xie, and J. Sun. J. Org. Chem. **64**, 6462 (1999); (*b*) Y. Ma, C.T. Qian, M. Xie, and J. Sun. Chin. J. Chem. **18**, 377 (2000); (*c*) S. Kobayashi, H. Ishitani, and S. Nagayama. Synthesis, 1195 (1995).
16. D. Passarella, G. Lesma, M. Martinelli, A. Silvani, M. Canto, and J. Hidalgo. Tetrahedron, **56**, 5205 (2000).
17. Y. Arai, T. Masuda, Y. Masaki, and M. Shiro. Tetrahedron: Asymmetry, **7**, 1199 (1996).
18. I.E. Markó and G.R. Evans. Tetrahedron Lett. **35**, 2767 (1994).
19. (*a*) I.E. Markó, G.R. Evans, and J.P. Declercq. Tetrahedron, **50**, 4557 (1994); (*b*) G. Desimoni, G. Faita, M. Guala, and C. Pratelli. J. Org. Chem. **68**, 7862 (2003).
20. G. Babu and P.T. Perumal. Tetrahedron, **55**, 4793 (1999).

© 2006 NRC Canada

Synthesis of pyrimidine annulated furothiopyrans — An efficient sequential and tandem catalyzed Claisen rearrangement – intramolecular hydroaryloxylation

K.C. Majumdar and S.K. Chattopadhyay

Abstract: Regioselective synthesis of a hitherto unreported furothiopyran moiety fused at the C-5 and C-6 positions of a pyrimidine heterocycle was achieved by the application of sequential Claisen rearrangement in which a second aromatic Claisen rearrangement and intramolecular hydroaryloxylation were catalyzed by aluminum chloride. The second aromatic Claisen rearrangement step was also studied under thermal conditions to give mostly isomerized exocyclic compounds. The precursor endocyclic compounds were synthesized by thermal [3,3] sigmatropic rearrangement of the corresponding sulfide.

Key words: aluminum chloride, sequential Claisen rearrangement, hydroaryloxylation, furothiopyran, pyrimidine.

Résumé : Faisant appel à une séquence des réarrangements de Claisen dans laquelle le deuxième réarrangement aromatique de Claisen et l'hydroaryloxylation sont catalysées par du chlorure d'aluminium, on a effectué la synthèse régiosélective qui n'avait pas été réalisée jusqu'à maintenant de la portion furothiopyrane condensée aux positions C-5 et C-6 de l'hétérocycle pyrimidine. On a aussi étudié le deuxième réarrangement de Claisen dans des conditions thermiques et il conduit principalement à des composés isomérisés exocycliques. On a réalisé la synthèse des composés endocycliques précurseurs en procédant à un réarrangement thermique [3,3] du sulfure correspondant.

Mots clés : chlorure d'aluminium, séquence de réarrangements de Claisen, hydroaryloxylation, furothiopyrane, pyrimidine.

[Traduit par la Rédaction]

Introduction

Claisen rearrangement, since its discovery in 1912, has been proven to be one of the preeminent methodologies for the construction of carbon–carbon bonds in synthetic organic chemistry (1). A high level of stereocontrol, securing its widespread use in the synthesis of natural products and medicinal agents, can be achieved by this concerted [3,3] sigmatropic rearrangement (1). The traditional methodologies for accomplishing the rearrangement are based on thermally controlled procedure; however, the development of new methodologies employing a catalyst in the Claisen rearrangement have been the focus of many recent investigations in organic synthesis (2). Over the past few years we embarked on the development of new synthetic methodologies for the synthesis of novel heterocycles based on sequential Claisen rearrangement (3). During the investigation of the synthetic perspectives of the aforementioned thermally controlled rearrangement, we observed interesting results in the second Claisen rearrangement (3*a*, 3*b*). We sought to extend this chemistry to encompass a new synthetic route leading to a [6,5]-furothiopyran moiety.

The incorporation of the pyrimidine moiety in the present investigation is due to its wide biological and pharmacological activities (4). Numerous pyrimidine- and uracil-based molecules, e.g., AZT, DDC, and BVDU, have been known to be active agents against cancer and the AIDS virus (5). Some pyrido-[2,3-*d*]-pyrimidines exhibit antibacterial activity and antitumor activities (6). Extensive investigations have been carried out with these heterocyclic systems (7). In contrast, a few examples dealing with the chemistry of an 8-sulfurisostere, thiopyrano-[2,3-*d*]-pyrimidine system, which may have potential biological activity, are reported in the literature (8). This has prompted us to undertake a study of sequential Claisen rearrangement with the development of broadly useful new routes to a [6,5]-furothiopyran system fused at the C-5 and C-6 positions of the pyrimidine moiety. Herein we report the results of our investigation.

Results and discussion

The requisite sulfides (**3a**–**3g**) for the present investigation were synthesized in 75%–92% yields by phase-transfer-catalyzed alkylation of 6-mercaptouracil (**2**) with different 1-chloro-4-aryloxybut-2-ynes. Compound **2** was in turn prepared by the reaction of 6-chlorouracil (**1**) with NaSH in dry ethanol at 0 °C. Compounds **3a**–**3g** were all solid and were

Received 28 November 2005. Published on the NRC Research Press Web site at http://canjchem.nrc.ca on 7 April 2006.

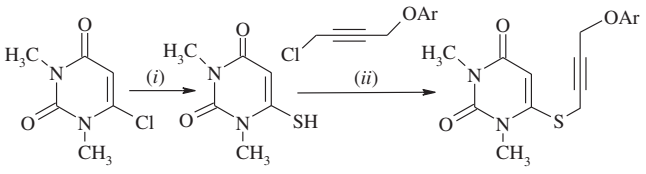
This paper is dedicated to Dr. J. William Lown, Professor Emeritus, University of Alberta, Edmonton.

K.C. Majumdar[1] and S.K. Chattopadhyay. Department of Chemistry, University of Kalyani, Kalyani 741235, WB, India.

[1]Corresponding author (e-mail: kcm_ku@yahoo.co.in).

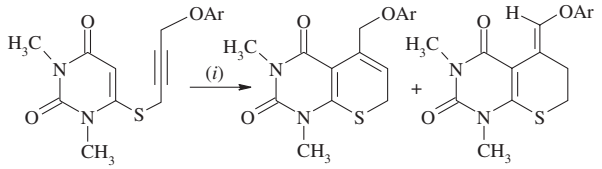
 doi:10.1139/V06-020 © 2006 NRC Canada

Scheme 1. Reagents and conditions: (*i*) NaSH, EtOH, 0 °C, stirring, 7 h; (*ii*) CH_2Cl_2, 1% aq. NaOH sol. BTEAC, rt, stirring, 12 h.



3a) Ar = 4-$MeOC_6H_4$ 3d) Ar = 2,3-$Me_2C_6H_4$ g) Ar = 2,4-$Me_2C_6H_3$
3b) Ar = 3,5-Me_2-4-ClC_6H_2 3e) Ar = 3,5-$Me_2C_6H_4$
3c) Ar = 2-ClC_6H_4 3f) Ar = 2,4-$Cl_2C_6H_3$

Scheme 2. Reagents and conditions: (*i*) chlorobenzene, reflux, 4 h.



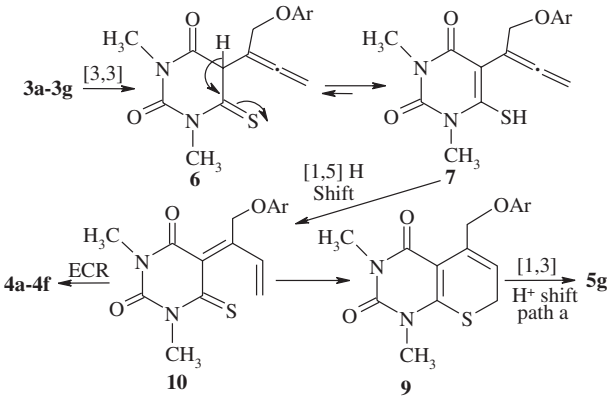
	Ar	Yield (%)
4a	4-$MeOC_6H_4$	94
4b	3,5Me_2-4-ClC_6H_2	88
4c	2-ClC_6H_4	92
4d	2,3-$Me_2C_6H_4$	88
4e	3,5-$Me_2C_6H_4$	85
4f	2,4-$Cl_2C_6H_3$	95
5g	2,4-$Me_2C_6H_3$	88

characterized from their elemental analyses and spectral data (Scheme 1).

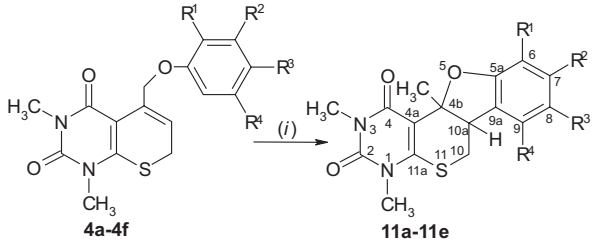
The substrates **3a**–**3g** possess two potential sites for [3,3] sigmatropic rearrangement: a vinyl propargyl sulfide moiety and an aryl propargyl ether moiety. Compounds with this structural feature offer an excellent scope for the study on the competition between oxy- and thio-Claisen rearrangement along with the synthesis of new heterocycles through [3,3] sigmatropic rearrangement. To accomplish the thio-Claisen rearrangement, the substrate **3a** was first subjected to thermal rearrangement by refluxing in the lower boiling solvent chlorobenzene (132 °C) for 4 h to give crystalline solid **4a** in 94% yield (Scheme 2). Elemental analysis and spectral data of compound **4a** established its endocyclic nature, which is necessary for further Claisen rearrangement. Encouraged by the initial accomplishment, the remaining substrates (**3b**–**3g**) were similarly treated to afford **4b**–**4f** (84%–95% yield) and **5g** (88% yield) (Scheme 2). The exocyclic nature of the product **5g** was established from the high field (300 MHz) ^{1}H NMR spectrum. The ^{13}C NMR chemical shift values of compound **5g** and multiplicities were assigned from the DEPT experiment. The DEPT spectrum obtained showed 10 protonated carbons, four -CH_3, two >CH_2, and four >CH-.

The mechanistic rationalization (Scheme 3) for the formation of compounds **4a**–**4f** and **5g** can be explained by assuming initial [3,3] sigmatropic rearrangement of **3a**–**3g**, followed by rapid enolization to form the allenylene–thiol intermediate **7**, which then undergoes a [1,5]-hydrogen shift, followed by 6π electrocyclic ring closure to give the products **4a**–**4f**. The product **5g** may also be formed because of the [1,3] protropic rearrangement of the thermally unstable endocyclic compound **9** to afford **5g** (Scheme 3). It is noteworthy that all the substrates **3a**–**3f**, except **3g**, regioselectively afforded exclusive products **4a**–**4f** in excellent yield. A lesser energy requirement for the sigmatropic rearrangement in vinyl propargyl sulfide systems (9) compared with that in aryl propargyl ether moieties (10) might be responsible for this excellent regioselectivity.

Scheme 3.



Scheme 4. Reagents and conditions: (*i*) $AlCl_3$, CH_2Cl_2, rt, 1 h.

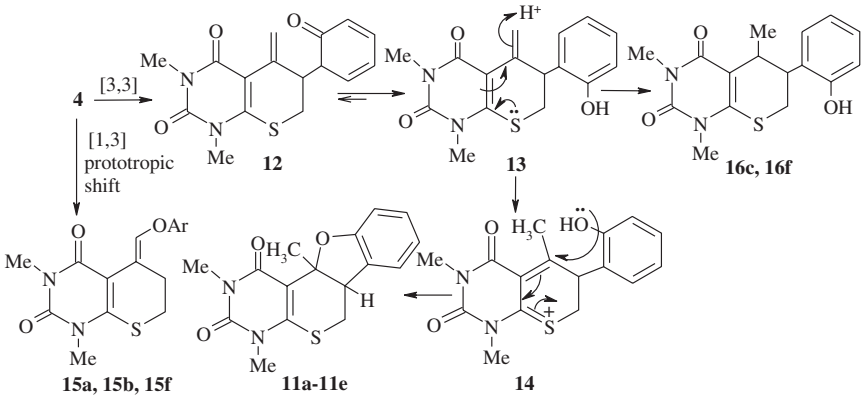


	R^1	R^2	R^3	R^4	Yield (%)
11a	H	H	OMe	H	96
11b	H	Me	Cl	Me	90
11c	Cl	H	H	H	92
11d	Me	Me	H	H	94
11e	H	Me	Me	H	90
11f	Cl	H	Cl	H	—

Compound **4** still posses an allyl aryl ether segment requisite for further study on the [3,3] sigmatropic rearrangement. In our earlier efforts, we found different regioselectivity with different substrates in the thermal second aromatic Claisen rearrangement (3). In some cases, [1,3] prototropic rearrangement was an important side reaction along with [3,3] sigmatropic rearrangement (11). To circumvent this unwanted problem in thermal second Claisen rearrangement, we turned our attention to the Lewis acid catalyzed Claisen rearrangement approach (2). Among the different Lewis acid catalysts available for the aromatic oxy-Claisen rearrangement, aluminum chloride and its different derivatives have received the most attention (1*d*, 2*a*). So we subjected compound **4a** to catalyzed Claisen rearrangement using aluminum chloride as the catalyst in dry dichloromethane at room temperature to afford the cyclized product **11a** (96% yield), which was characterized by its elemental analysis and spectral data. To test the generality of the reaction, other substrates (**4b**–**4f**) were similarly treated to afford the cyclized

© 2006 NRC Canada

Scheme 5.

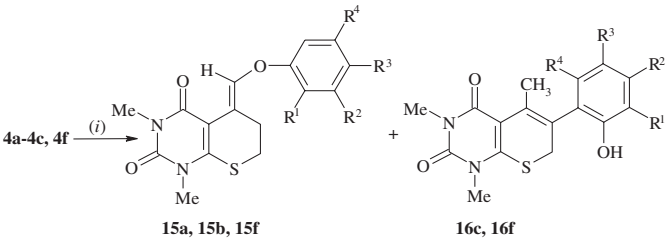


products **11b–11e** (90%–96% yield) (Scheme 4). No cyclized product corresponding to **11** was obtained in the case of compound **4f**, as several other unwanted products (TLC observation) were formed during the reaction that were not characterized. We have tried the reaction with other Lewis acids, e.g., $BF_3{\cdot}Et_2O$ and Cp_2TiCl_2. In the case of Cp_2TiCl_2, no reaction occurred. The reaction is quite sluggish with $BF_3{\cdot}Et_2O$ with the formation of undesired products, which were not characterized.

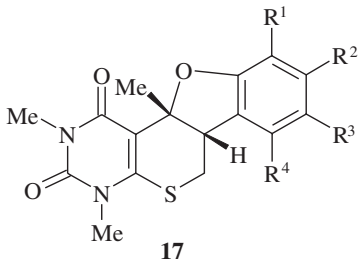
The conversion of **4** into **11** may take a pathway similar to that observed in thermal Claisen rearrangement via the 2-allylphenol intermediate **13** (Scheme 5). From the literature it may be assumed that this transformation may be a charge-induced Claisen rearrangement similar in mechanism to the process reported for BCl_3 by Schmid and co-workers (12). The reaction may be facilitated by the coordination of the oxygen atom, which itself is a strong Lewis base, to the hard Lewis acid, aluminum chloride. The hydroaryloxylation step leading to the formation of the benzofuran moiety may occur by the addition of H^+ to the position of the homothioenol ether followed by simultaneous conjugate addition of a phenolic OH group to the resulting thionium ion. To isolate the 2-allylphenol intermediate **13**, we tried the reaction in the presence of additives such as PPh_3 or amine base, e.g., morpholine and triethylamine. There too no reaction was observed. It is noteworthy that in the present investigation aluminium chloride promotes both Claisen rearrangement and hydroaryloxylation and the unusual ring contraction pertinent to the $AlCl_3$-catalyzed oxy-Claisen rearrangement (13) was unobserved, mainly owing to the soft basic character of sulfur being unable to form a complex with aluminum chloride. The overall regioselectivity of the catalyzed reaction leading to the formation of tetracyclic heterocycles **11** is excellent.

We have also examined the thermal second Claisen rearrangement of the same substrates. For compounds **4a**–**4c** and **4f**, when subjected to thermal rearrangement in refluxing dichlorobenzene in the presence of *N*,*N*-diethylaniline for 8 h (Scheme 6), the observed results were quite interesting as compounds **4a** and **4b** exclusively gave the exocyclic compounds **15a** and **15b** in 40% and 45% yield, respectively, and from compound **4c** the endocyclic phenolic compound **16c** was obtained in 10% yield. Both products **15f** and **16f** were isolated; in the case of substrate **4f**, in almost 38% and 25% yield, respectively. In each case, an appreciable amount of starting material was recovered. We have also attempted the reaction in dichlorobenzene and *N*,*N*-diethylaniline separately. There too the same products were obtained in very poor yield. All the compounds were solid and were characterized from their elemental analysis and spectral data.

Scheme 6. Reagents and conditions: (*i*) dichlorobenzene, *N*,*N*-diethylaniline, reflux, 8 h.



The formation of products **15a**, **15b**, **15f**, **16c**, and **16f** can be mechanistically interpreted as follows (Scheme 5). Compounds **15a**, **15b**, and **15f** can be obtained by [1,3] prototropic rearrangement in compounds **4a**, **4b**, and **4f**. Initial [3,3] sigmatropic rearrangement followed by rapid tautomerization may result in the formation of **16c** and **16f** from **4c** and **4f** via the 2-allyl phenol intermediate **13**. In the present investigation, the [1,3] prototropic rearrangement with the formation of an exocyclic compound as the major product is quite unusual. In two cases we were successful in isolating the endocyclic phenolic product, but in very poor yield. The presence of different substituents in the benzene nuclei of compounds **4a**, **4b**, and **4f** thus results in a change in the mode of rearrangement. However, the role of the substituent in the formation of products **15** and **16** is not clear. It may be conceivable that the thermal stability of the resulting compounds might be responsible for their formation.



© 2006 NRC Canada

From a molecular modelling (Dreiding model) study and comparison with the stereochemistry of natural pterocarpin (14), the stereochemistry of the ring fusion in the tetracyclic system may be assumed to be cis and is represented as **17**.

In conclusion, we have demonstrated a broadly useful new route based on a sequential thermal plus tandem-catalyzed Claisen rearrangement – intramolecular hydroaryloxylation approach that we expect to provide an expedient avenue for the synthesis of a furothiopyran system, quite similar to the petrocarpin system. This protocol is complementary to our preliminary thermal methodology. The mild reaction conditions and compatibility with various substituents on the aromatic ring make this route a significant addition to the existing methodologies for the synthesis of a synthetically challenging furothiopyran moiety fused with other heterocycles.

Experimental

General remarks

Melting points were determined in open capillaries and are uncorrected. IR spectra were recorded on a PerkinElmer L120-000A spectrometer (γ_{max} in cm^{-1}) using samples as neat liquids, solid samples were recorded in KBr disks, and UV absorption spectra were recorded in EtOH on a Shimadzu UV-2401PC spectrophotometer (λ_{max} in nm). ^1H NMR (300 MHz, 500 MHz) spectra were recorded on Bruker DPX-300 and Bruker DRX-500 spectrometers in $CDCl_3$ (chemical shifts in δ) with TMS as the internal standard. Elemental analyses and mass spectra were recorded on a JEOL JMS600 instrument. Silica gel (60–120 mesh, Spectrochem, India) was used for chromatographic separation. Silica gel G (E-Merck, India) was used for TLC. Petroleum ether refers to the fraction boiling between 60 and 80 °C.

The 1-aryloxy-4-chlorobut-2-ynes were prepared according to the published procedure (15).

General procedure for the preparation of 6-mercaptouracil (2)

To a magnetically stirred solution of NaSH (1.2 g, 20.8 mmol) in dry ethanol (50 mL), a solution of 6-chlorouracil (**1**) (1.5 g, 8.6 mmol) in dry ethanol (50 mL) was added dropwise for a period of 2 h. After the addition was complete, the stirring was continued for an additional 4 h. Ethanol was removed under vacuum at room temperature. The residue was acidified with concd. HCl (25 mL). This was then extracted with CH_2Cl_2 (4 × 20 mL). The dichloromethane solution was washed with water (2 × 10 mL) and dried (Na_2SO_4). Attempts to evaporate dichloromethane led to considerable decomposition of compound **2**. Therefore, this dichloromethane solution was directly used in the next phase-transfer-catalyzed alkylation step.

General procedure for the preparation of sulfides (3a–3g)

To a stirred solution of 6-mercaptouracil (**2**) (obtained from 1.5 g, 8.6 mmol of compound **1**) and 1-aryloxy-4-chlorobut-2-yne (8.6 mmol) in dichloromethane (100 mL), a solution of benzyltriethylammonium chloride (BTEAC) (0.5 g, 1.8 mmol) in 1% aq. NaOH solution (100 mL) was added, and the mixture was stirred for 12 h at room temperature. It was then diluted with water (25 mL). The dichloromethane layer was then separated and washed with 2 N HCl (25 mL), brine (25 mL), and water (25 mL), and dried (Na_2SO_4). The crude mass obtained upon evaporation of CH_2Cl_2 was subjected to column chromatography. Elution with petroleum ether – ethyl acetate (7:3) afforded the products **3a**–**3g**.

Compound 3a

Yield: 84%; brown solid, mp 70 °C. IR (KBr, cm^{-1}) ν_{max}: 1645, 1702, 2963. ^1H NMR ($CDCl_3$, 300 MHz) δ_H: 3.34 (s, 3H, -*N*CH_3), 3.45 (s, 3H, -*N*CH_3), 3.69 (s, 2H, -SCH_2), 3.77 (s, 2H, -OCH_3), 4.63 (s, 2H, -OCH_2), 5.66 (s, 1H, =CH), 6.81–6.88 (m, 4H, ArH). MS *m*/*z*: 346 (M^+). Anal. calcd. for $C_{17}H_{18}N_2O_4S$ (%): C 58.95, H 5.20, N 8.09; found: C 59.15, H 5.44, N 8.25.

Compound 3b

Yield: 78%; brown solid, mp 130 °C. IR (KBr, cm^{-1}) ν_{max}: 1644, 1706, 2930. ^1H NMR ($CDCl_3$, 300 MHz) δ_H: 2.33 (s, 6H, Ar$(CH_3)_2$), 3.33 (s, 3H, -*N*CH_3), 3.45 (s, 3H, -*N*CH_3), 3.70 (s, 2H, -SCH_2), 4.65 (s, 2H, -OCH_2), 5.65 (s, 1H, =CH), 6.66 (s, 2H, ArH). MS *m*/*z*: 378, 380 (M^+). Anal. calcd. for $C_{18}H_{19}N_2O_3SCl$ (%): C 56.99, H 5.01, N 7.38; found: C 57.23, H 5.18, N 7.59.

Compound 3c

Yield: 85%; brown solid, mp 116 °C. IR (KBr, cm^{-1}) ν_{max}: 1651, 1693, 2942. ^1H NMR ($CDCl_3$, 300 MHz) δ_H: 3.34 (s, 3H, -*N*CH_3), 3.44 (s, 3H, -*N*CH_3), 3.70 (s, 2H, -SCH_2), 4.79 (s, 2H, -OCH_2), 5.65 (s, 1H, =CH), 6.92–7.37 (m, 4H, ArH). MS *m*/*z*: 350, 352 (M^+). Anal. calcd. for $C_{16}H_{15}N_2O_3SCl$ (%): C 54.70, H 4.27, N 7.97; found: C 54.89, H 4.49, N 8.14.

Compound 3d

Yield: 78%; brown solid, mp 92 °C. IR (KBr, cm^{-1}) ν_{max}: 1630, 1691, 2949. ^1H NMR ($CDCl_3$, 300 MHz) δ_H: 2.14 (s, 3H, -ArCH_3), 2.26 (s, 3H, -ArCH_3), 3.34 (s, 3H, -*N*CH_3), 3.44 (s, 3H, -*N*CH_3), 3.70 (s, 2H, -SCH_2), 4.69 (s, 2H, -OCH_2), 5.66 (s, 1H, =CH), 6.74–7.04 (m, 4H, ArH). MS *m*/*z*: 344 (M^+). Anal. calcd. for $C_{18}H_{20}N_2O_3S$ (%): C 62.79, H 5.81, N 8.13; found: C 62.97, H 6.03, N 8.36.

Compound 3e

Yield: 82%; brown solid, mp 94 °C. IR (KBr, cm^{-1}) ν_{max}: 1634, 1697, 2953. ^1H NMR ($CDCl_3$, 300 MHz) δ_H: 2.28 (s, 6H, -Ar$(CH_3)_2$), 3.34 (s, 3H, -*N*CH_3), 3.45 (s, 3H, -*N*CH_3), 3.71 (s, 2H, -SCH_2), 4.66 (s, 2H, -OCH_2), 5.66 (s, 1H, =CH), 6.55 (s, 2H, ArH), 6.63 (s, 1H, ArH). MS *m*/*z*: 344 (M^+). Anal. calcd. for $C_{18}H_{20}N_2O_3S$ (%): C 62.79, H 5.81, N 8.13; found: C 63.01, H 5.97, N 8.30.

Compound 3f

Yield: 92%; brown solid, mp 126 °C. IR (KBr, cm^{-1}) ν_{max}: 1645, 1702, 2964. ^1H NMR ($CDCl_3$, 300 MHz) δ_H: 3.35 (s, 3H, -*N*CH_3), 3.45 (s, 3H, -*N*CH_3), 3.70 (s, 2H, -SCH_2), 4.77 (s, 2H, -OCH_2), 5.64 (s, 1H, =CH), 6.92–7.37 (m, 3H, ArH). MS *m*/*z*: 384, 386, 388 (M^+). Anal. calcd. for $C_{16}H_{14}N_2O_3SCl_2$ (%): C 49.87, H 3.63, N 7.27; found: C 50.09, H 3.81, N 7.46.

© 2006 NRC Canada

Compound 3g

Yield: 84%; brown solid, mp 92 °C. IR (KBr, cm^{-1}) ν_{max}: 1656, 1696, 2917. ^1H NMR ($CDCl_3$, 300 MHz) δ_H: 2.18 (s, 3H, -ArCH_3), 2.25 (s, 3H, -ArCH_3), 3.34 (s, 3H, -*N*CH_3), 3.44 (s, 3H, -*N*CH_3), 3.68 (s, 2H, -SCH_2), 4.67 (s, 2H, -OCH_2), 5.66 (s, 1H, =CH), 6.75–6.94 (m, 3H, ArH). MS *m/z*: 344 (M^+). Anal. calcd. for $C_{18}H_{20}N_2O_3S$ (%): C 62.79, H 5.81, N 8.13; found: C 62.99, H 6.01, N 8.32.

General procedure for the preparation of 4a–4f and 5g

Compounds **3a**–**3h** (250 mg, 0.72 mmol) were refluxed in chlorobenzene (10 mL) for 5 h. The reaction mixture was then cooled and directly subjected to column chromatography over silica gel. Chlorobenzene was eluted out with petroleum ether. On eluting the column with petroleum ether – ethyl acetate (4:1), compounds **4a**–**4g** and **5h** were obtained. All compounds were recrystalized from dichloromethane – petroleum ether.

Compound 4a

Yield: 94%; white solid, mp 102 °C. IR (KBr, cm^{-1}) ν_{max}: 1633, 1705, 2928. ^1H NMR ($CDCl_3$, 500 MHz) δ_H: 3.36 (s, 3H, -*N*CH_3), 3.39 (d, 2H, *J* = 6 Hz, -SCH_2), 3.56 (s, 3H, -*N*CH_3), 3.75 (s, 3H, -OCH_3), 5.04 (s, 2H, -OCH_2), 5.86 (t, 1H, *J* = 6 Hz, =CH), 6.78–6.88 (m, 4H, ArH). ^{13}C NMR ($CDCl_3$, 125 MHz) δ_C: 26.60, 28.62, 33.76, 56.11, 69.71, 107.74, 111.45, 114.45, 116.51, 136.53, 151.16, 153.18, 154.34, 155.19, 159.78. MS *m/z*: 346 (M^+). Anal. calcd. for $C_{17}H_{18}N_2O_4S$ (%): C 58.95, H 5.20, N 8.09; found: C 59.13, H 5.42, N 8.32.

Compound 4b

Yield: 88%; white solid, mp 148 °C. IR (KBr, cm^{-1}) ν_{max}: 1664, 1702, 2948. ^1H NMR ($CDCl_3$, 300 MHz) δ_H: 2.32 (s, 6H, -Ar(CH_3)$_2$), 3.36 (s, 3H, -*N*CH_3), 3.40 (d, 2H, *J* = 6 Hz, -SCH_2), 3.56 (s, 3H, -*N*CH_3), 5.03 (s, 2H, -OCH_2), 5.84 (t, 1H, *J* = 6 Hz, =CH), 6.66 (s, 2H, ArH). MS *m/z*: 378, 380 (M^+). Anal. calcd. for $C_{18}H_{19}N_2O_3SCl$ (%): C 56.99, H 5.01, N 7.38; found: C 57.17, H 5.23, N 7.62.

Compound 4c

Yield: 92%; white solid, mp 152 °C. IR (KBr, cm^{-1}) ν_{max}: 1647, 1696, 2892. ^1H NMR ($CDCl_3$, 300 MHz) δ_H: 3.37 (s, 3H, -*N*CH_3), 3.43 (d, 2H, *J* = 6 Hz, -SCH_2), 3.56 (s, 3H, -*N*CH_3), 5.16 (s, 2H, -OCH_2), 5.99 (t, 1H, *J* = 6 Hz, =CH), 6.88–7.35 (m, 4H, ArH). MS *m/z*: 350, 352 (M^+). Anal. calcd. for $C_{16}H_{15}N_2O_3SCl$ (%): C 54.70, H 4.27, N 7.97; found: C 54.92, H 4.45, N 8.18.

Compound 4d

Yield: 88%; white solid, mp 152 °C. IR (KBr, cm^{-1}) ν_{max}: 1646, 1696, 2917. ^1H NMR ($CDCl_3$, 300 MHz) δ_H: 2.15 (s, 3H, -ArCH_3), 2.26 (s, 3H, -ArCH_3), 3.37 (s, 3H, -*N*CH_3), 3.41 (d, 2H, *J* = 6 Hz, -SCH_2), 3.56 (s, 3H, -NCH_3), 5.07 (s, 2H, -OCH_2), 5.91 (t, 1H, *J* = 6 Hz, =CH), 6.73–7.03 (m, 3H, ArH). MS *m/z*: 344 (M^+). Anal. calcd. for $C_{18}H_{20}N_2O_3S$ (%): C 62.79, H 5.81, N 8.13; found: C 63.03, H 6.01, N 8.31.

Compound 4e

Yield: 85%; white solid, mp 134 °C. IR (KBr, cm^{-1}) ν_{max}: 1655, 1706, 2911. ^1H NMR ($CDCl_3$, 300 MHz) δ_H: 2.27 (s, 3H, -CH_3), 3.37 (s, 3H, -*N*CH_3), 3.40 (d, 2H, *J* = 6 Hz, -SCH_2), 3.56 (s, 3H, -*N*CH_3), 5.05 (s, 2H, -OCH_2), 5.88 (t, 1H, *J* = 6 Hz, =CH), 6.56 (s, 2H, ArH), 6.58 (s, 1H, ArH). MS *m/z*: 344 (M^+). Anal. calcd. for $C_{18}H_{20}N_2O_3S$ (%): C 62.79, H 5.81, N 8.13; found: C 62.95, H 6.05, N 8.32.

Compound 4f

Yield: 95%; white solid, mp 108 °C. IR (KBr, cm^{-1}) ν_{max}: 1647, 1702, 2944. ^1H NMR ($CDCl_3$, 300 MHz) δ_H: 3.36 (s, 3H, -*N*CH_3), 3.42 (d, 2H, *J* = 6 Hz, -SCH_2), 3.57 (s, 3H, -*N*CH_3), 5.13 (s, 2H, -OCH_2), 5.93 (t, 1H, *J* = 6 Hz, =CH), 6.89–7.35 (m, 3H, ArH). MS *m/z*: 384, 386, 388 (M^+). Anal. calcd. for $C_{16}H_{14}N_2O_3SCl_2$ (%): C 49.87, H 3.63, N 7.27; found: C 50.07, H 3.85, N 7.44.

Compound 5g

Yield: 88%; white solid, mp 128 °C. IR (KBr, cm^{-1}) ν_{max}: 1657, 1708, 2921. ^1H NMR ($CDCl_3$, 300 MHz) δ_H: 2.24 (s, 3H, -ArCH_3), 2.27 (s, 3H, -ArCH_3), 2.96–2.99 (m, 2H, =C-CH_2), 3.11–3.14 (m, 2H, -SCH_2), 3.37 (s, 3H, -*N*CH_3), 3.56 (s, 3H, -*N*CH_3), 6.94–6.97 (m, 3H, ArH), 8.03 (s, 1H, =CH). MS *m/z*: 344 (M^+). ^{13}C NMR ($CDCl_3$, 125 MHz) δ_C: 16.65, 20.84, 26.64, 33.77, 68.86, 107.87, 110.63, 112.37, 126.87, 127.37, 130.03, 131.78, 136.65, 151.76, 154.90, 155.13, 159.82. Anal. calcd. for $C_{18}H_{20}N_2O_3S$ (%): C 62.79, H 5.81, N 8.13; found: C 63.00, H 5.99, N 8.34.

General procedure for the aluminum chloride catalyzed reaction

To a stirred solution of the compounds **4a**–**4f** (0.28 mmol) in dry dichloromethane (10 mL), anhydrous aluminium chloride (36 mg, 0.28 mmol) was added at room temperature. The stirring was continued for about 1 h. After completion of the reaction, 1% HCl solution (5 mL) was added. The reaction mixture was then extracted with dichloromethane (2 × 10 mL). The organic layer was washed with water (2 × 10 mL) and brine (10 mL) and dried (Na_2SO_4). Dichloromethane was distilled off and the residue obtained was subjected to flash chromatography. On eluting the column with ethyl acetate – petroleum ether (1:10), compounds **11a**–**11e** were obtained as white solids. All compounds were recrystalized from dichloromethane.

Compound 11a

Yield: 96%; white solid, mp 132 °C. IR (KBr, cm^{-1}) ν_{max}: 1646, 1701, 2927. ^1H NMR ($CDCl_3$, 500 MHz) δ_H: 1.78 (s, 3H, C_{4b}-CH_3), 2.80 (dd, 1H, *J* = 11, 13 Hz, C_{10}-H), 3.02 (dd, 1H, *J* = 3, 13 Hz, C_{10}-H), 3.29 (dd, 1H, *J* = 3, 11 Hz, C_{10a}-H), 3.39 (s, 3H, -*N*CH_3), 3.51 (s, 3H, -*N*CH_3), 3.77 (s, 3H, -OCH_3), 6.72–6.86 (m, 3H, ArH). ^{13}C NMR ($CDCl_3$, 125 MHz) δ_C: 25.05, 28.57, 30.20, 32.89, 51.26, 56.41, 86.30, 108.54, 111.04, 111.69, 111.53, 129.13, 151.19, 151.77, 153.09, 154.67, 160.39. MS *m/z*: 346 (M^+). Anal. calcd. for $C_{17}H_{18}N_2O_4S$ (%): C 58.95, H 5.20, N 8.09; found: C 59.18, H 5.34, N 8.27.

Compound 11b

Yield: 90%; white solid, mp 102 °C. IR (KBr, cm^{-1}) ν_{max}: 1640, 1700, 2924, 2976. ^1H NMR ($CDCl_3$, 500 MHz) δ_H: 1.71 (s, 3H, C_{4b}-CH_3), 2.32 (s, 3H, Ar-CH_3), 2.37 (s, 3H, Ar-CH_3), 2.62 (dd, 1H, *J* = 11, 13 Hz, C_{10}-H), 2.93 (dd, 1H,

© 2006 NRC Canada

J = 3, 13 Hz, C_{10}-H), 3.22 (dd, 1H, J = 3, 11 Hz, C_{10a}-H), 3.40 (s, 3H, -NCH_3), 3.54 (s, 3H, -NCH_3), 6.71 (s, 1H, ArH). MS *m*/*z*: 378, 380 (M^+). Anal. calcd. for $C_{18}H_{19}N_2O_3SCl$ (%): C 56.99, H 5.01, N 7.38; found: C 57.19, H 5.29, N 7.62.

Compound 11c

Yield: 92%; white solid, mp 198 °C. IR (KBr, cm^{-1}) ν_{max}: 1629, 1692, 2895. ^{1}H NMR ($CDCl_3$, 500 MHz) δ_H: 1.83 (s, 3H, C_{4b}-CH_3), 2.82 (dd, 1H, J = 11, 13 Hz, C_{10}-H), 3.02 (dd, 1H, J = 3, 13 Hz, C_{10}-H), 3.39 (s, 3H, -NCH_3), 3.40 (dd, 1H, J = 3, 11 Hz, C_{10a}-H), 3.51 (s, 3H, -NCH_3), 6.83–6.86 (m, 1H, ArH), 7.12 (d, 1H, J = 7 Hz, Ar-H), 7.19 (d, 1H, J = 7 Hz, Ar-H). MS *m*/*z*: 350, 352 (M^+). Anal. calcd. for $C_{16}H_{15}N_2O_3SCl$ (%): C 54.70, H 4.27, N 7.97; found: C 54.92, H 4.46, N 8.21.

Compound 11d

Yield: 94%; white solid, mp 216 °C. IR (KBr, cm^{-1}) ν_{max}: 1651, 1702, 2926. ^{1}H NMR ($CDCl_3$, 300 MHz) δ_H: 1.76 (s, 3H, C_{4b}-CH_3), 2.16 (s, 3H, Ar-CH_3), 2.24 (s, 3H, Ar-CH_3), 2.76 (dd, 1H, J = 11, 13 Hz, C_{10}-H), 2.99 (dd, 1H, J = 3, 13 Hz, C_{10a}-H), 3.28 (dd, 1H, J = 3, 11 Hz, C_{10a}-H), 3.39 (s, 3H, -NCH_3), 3.51 (s, 3H, -NCH_3), 6.70 (d, 1H, J = 7 Hz, ArH), 6.95 (d, 1H, J = 7 Hz, ArH). ^{13}C NMR ($CDCl_3$, 125 MHz) δ_C: 12.35, 19.93, 25.18, 28.55, 30.29, 32.85, 51.16, 85.79, 108.72, 120.33, 121.07, 122.38, 125.15, 138.71, 151.31, 153.03, 156.46, 160.23. MS *m*/*z*: 344 (M^+). Anal. calcd. for $C_{18}H_{20}N_2O_3S$ (%): C 62.79, H 5.81, N 8.13; found: C 62.95, H 6.03, N 8.32.

Compound 11e

Yield: 90%; white solid, mp 188 °C. IR (KBr, cm^{-1}) ν_{max}: 1643, 1700, 2923. ^{1}H NMR ($CDCl_3$, 300 MHz) δ_H: 1.71 (s, 3H, C_{4b}-CH_3), 2.27 (s, 3H, Ar-CH_3), 2.31 (s, 3H, Ar-CH_3), 2.63 (dd, 1H, J = 11, 13 Hz, C_{10}-H), 2.96 (dd, 1H, J = 3, 13 Hz, C_{10}-H), 3.21 (dd, 1H, J = 3, 11 Hz, C_{10a}-H), 3.40 (s, 3H, -NCH_3), 3.53 (s, 3H, -NCH_3), 6.54 (s, 1H, Ar-H), 6.61 (s, 1H, Ar-H). MS *m*/*z*: 344 (M^+). Anal. calcd. for $C_{18}H_{20}N_2O_3S$ (%): C 62.79, H 5.81, N 8.13; found: C 63.00, H 5.98, N 8.33.

General procedure for the preparation of 15a, 15b, 15f, 16c, and 16f

Compounds **4a**–**4c** and **4f** (100 mg, 0.28 mmol) were refluxed in dichlorobenzene (10 mL) in the presence of *N*,*N*-diethylaniline (2 mL) for 8 h. The reaction mixture was then cooled and directly subjected to column chromatography over silica gel. Dichlorobenzene along with *N*,*N*-diethylaniline was eluted out with petroleum ether. On eluting the column with petroleum ether – ethyl acetate (4:1), compounds **15a**, **15b**, **15f**, **16c**, and **16f** were obtained. All compounds were solid and were recrystalized from dichloromethane – petroleum ether.

Compound 15a

Yield: 40%; white solid, mp 148 °C. IR (KBr, cm^{-1}) ν_{max}: 1647, 1707, 2932. ^{1}H NMR ($CDCl_3$, 500 MHz) δ_H: 2.93–2.96 (m, 2H, =C-CH_2), 3.11–3.13 (m, 2H, -SCH_2), 3.39 (s, 3H, -NCH_3), 3.55 (s, 3H, -NCH_3), 3.78 (s, 3H, -OCH_3), 6.83–7.25 (m, 4H, ArH), 8.02 (s, 1H, =CH). MS *m*/*z*: 346 (M^+). Anal. calcd. for $C_{17}H_{18}N_2O_4S$ (%): C 58.95, H 5.20, N 8.09; found: C 59.17, H 5.39, N 8.31.

Compound 15b

Yield: 45%; white solid, mp 168 °C. IR (KBr, cm^{-1}) ν_{max}: 1629, 1697, 2934. ^{1}H NMR ($CDCl_3$, 500 MHz) δ_H: 2.36 (s, 6H, -Ar$(CH_3)_2$), 2.91–2.95 (m, 2H, =C-CH_2), 3.09–3.11 (m, 2H, SCH_2), 3.40 (s, 3H, -NCH_3), 3.54 (s, 3H, -NCH_3), 6.81 (S, 2H, ArH), 8.05 (s, 1H, =CH). MS *m*/*z*: 378, 380 (M^+). Anal. calcd. for $C_{18}H_{19}N_2O_3SCl$ (%): C 56.99, H 5.01, N 7.38; found: C 57.17, H 5.22, N 7.64.

Compound 15f

Yield: 38%; white solid, mp 174 °C. IR (KBr, cm^{-1}) ν_{max}: 1632, 1699, 2917. ^{1}H NMR ($CDCl_3$, 300 MHz) δ_H: 2.97–3.01 (m, 2H, =C-CH_2), 3.13–3.16 (m, 2H, -SCH_2), 3.39 (s, 3H, -NCH_3), 3.55 (s, 3H, -NCH_3), 7.11–7.39 (m, 3H, ArH), 8.07 (s, 1H, =CH). MS *m*/*z*: 384, 386, 388 (M^+). Anal. calcd. for $C_{16}H_{14}N_2O_3SCl_2$ (%): C 49.87, H 3.64, N 7.27; found: C 50.11, H 3.83, N 7.48.

Compound 16c

Yield: 10%; white solid, mp 186 °C. IR (KBr, cm^{-1}) ν_{max}: 1648, 1698, 2927, 3322. ^{1}H NMR ($CDCl_3$, 300 MHz) δ_H: 2.06 (s, 3H, =C-CH_3), 3.40 (s, 3H, -NCH_3), 3.51 (s, 2H, -SCH_2), 3.57 (s, 3H, -NCH_3), 5.77 (s, 1H, -OH, D_2O exchangeable), 6.89–7.12 (m, 3H, ArH). MS *m*/*z*: 350, 352 (M^+). Anal. calcd. for $C_{16}H_{15}N_2O_3SCl$ (%): C 54.70, H 4.27, N 7.97; found: C 54.94, H 4.50, N 8.21.

Compound 16f

Yield: 25%; white solid, mp 208 °C. IR (KBr, cm^{-1}) ν_{max}: 1640, 1683, 2938, 3444. ^{1}H NMR ($CDCl_3$, 300 MHz) δ_H: 2.06 (s, 3H, =C-CH_3), 3.40 (s, 3H, -NCH_3), 3.48 (s, 2H, SCH_2), 3.57 (s, 3H, -NCH_3), 5.76 (s, 1H, -OH, D_2O exchangeable), 7.10 (d, 1H, J = 2 Hz, ArH), 7.31 (d, 1H, J = 2 Hz, ArH). MS *m*/*z*: 384, 386, 388 (M^+). Anal. calcd. for $C_{16}H_{14}N_2O_3SCl_2$ (%): C 49.87, H 3.64, N 7.27; found: C 50.03, H 3.87, N 7.49.

References

1. (*a*) F.E. Zieglar. Chem. Rev. **88**, 1423 (1988); (*b*) S. Blechert. Synthesis, **71**, 1989;. (*c*) P. Wipf. Comprehensive organic synthesis. Vol. 5. *Edited by* B.M. Trost. Pergamon, Oxford. 1991. p. 827; (*d*) A.M.M. Castro. Chem. Rev. **104**, 2939 (2004).
2. (*a*) R.P. Lutz. Chem. Rev. **84**, 205 (1984); (*b*) E.J. Corey and D.H. Lee. J. Am. Chem. Soc. **113**, 4026 (1991); (*c*) K. Maruoka, S. Saito, and H. Yamamoto. J. Am. Chem. Soc. **117**, 1165 (1995); (*d*) U. Kazmaier and A. Krebs. Angew. Chem. Int. Ed. Engl. **34**, 2012 (1995); (*e*) T.P. Yoon, V.M. Dong, and D.W.C. MacMillan. J. Am. Chem. Soc. **43**, 9726 (1999); (*f*) P. Wiff and S. Ribe. Org. Lett. **3**, 1503 (2001).
3. (*a*) K.C. Majumdar and U. Das. J. Org. Chem. **63**, 9997 (1998); (*b*) K.C. Majumdar, U.K. Kundu, and S.K. Ghosh. Org. Lett. **4**, 2629 (2002); (*c*) K.C. Majumdar, U.K. Kundu, and S. Ghosh. J. Chem. Soc. Perkin Trans. 1, 2139 (2002).
4. (*a*) T.K. Bradshow and D.W. Hutchison. Chem. Soc. Rev. **6**, 43 (1977); (*b*) T. Sasaki, K. Minamoto, T. Suzuki, and S. Yamashita. Tetrahedron, **36**, 865 (1980); (*c*) R. Marumoto and Y. Furukawa. Chem. Pharm. Bull. **25**, 2974 (1977); (*d*) A.S. Jones, J.R. Swgers, R.T. Walker, and E.D. Clercq. J. Med. Chem. **31**, 268 (1988); (*e*) H. Griengl, E. Wanck, W. Schwarz,

© 2006 NRC Canada

W. Streicher, B. Rosenwirth, and E.D. Clercq. J. Med. Chem. **262**, 14905 (1987).
5. (*a*) T. Miyasaka, H. Tanaka, M. Baba, H. Hayasaka, R.T. Walker, and M. Vandelpufe. Biochem. Biophys. Res. Commun. 1**42**, 128 (1987); (*b*) E.D. Clercq. J. Med. Chem. **29**, 1561 (1986).
6. (*a*) B.S. Hurlbert, R. Ferone, T.A. Herrmann, G.H. Hitchings, M. Barnett, and S.R.M. Busby. J. Med. Chem. **11**, 711 (1968); (*b*) G. Nam, C.M. Yoon, E. Kim, C.K. Rhee, J.H. Kim, J.H. Shin, and S.H. Kim. J. Bioorg. Med. Chem. Lett. **11**, 611 (2001); (*c*) E. Mounetou, J. Legault, J. Lacroix, and R. C-Gaudreault. J. Med. Chem. **44**, 694 (2001).
7. (*a*) W.G. Irwin and D.G. Wibberley. Adv. Heterocycl. Chem. **10**, 149 (1969); (*b*) R.A. Katritzky, W.J. Rogers, R.M. Witek, and S.K. Nair. ARKIVOC, **52** (2004); (*c*) R. Mamouni, M. Akssira, M. Aadil, A. Elhakmaoui, J. Lasri, E. Zaballos-Garcia. Synth. Commun. **33**, 4259 (2003).
8. (*a*) B.R. Baker, C.E. Morreal, and B.-T. Ho. J. Med. Chem. **6**, 658 (1963); (*b*) H. Ogura and M. Sakaguchi. Chem. Lett. 657 (1972) ; (*c*) T. Itoh, M. Honma, and H. Ogura. Chem. Pharm. Bull. **24**, 1390 (1976).
9. K.C. Majumdar, A.T. Khan, and R.N. De. Synth. Commun. **18**, 1589 (1988).
10. (*a*) J. Zsindely and H. Schmidt. Helv. Chim. Acta, **51**, 1510 (1968); (*b*) K.C. Majumdar, B.S. Thyagarajan, and K.K. Balasubramanian. J. Heterocycl. Chem. **10**, 159 (1973).
11. K.C. Majumdar, U.K. Kundu, P.P. Mukhopadhyay, and S. Ghosh. ARKIVOC, **9**, 47 (2003).
12. J. Borgulya, R. Madeja, P. Fahrni, H.-J. Hansen, H. Schmid, and R. Barner. Helv. Chim. Acta, **56**, 14 (1973).
13. D.K. Bates and M.C. Jones. J. Org. Chem. **43**, 3856 (1978).
14. B.S. Thyagarajan and K.C. Majumdar. J. Heterocycl. Chem. **10**, 159 (1973).
15. K.C. Majumdar and B.S. Thyagarajan. Int. J. Sulfur Chem. Part A, **2**, 67 (1972).

© 2006 NRC Canada

7-Azaindolyl- and indolyl-functionalized starburst molecules with a 1,3,5-triazine or a benzene core — Syntheses and luminescence[1]

Wei-Hua Huang, Wen-Li Jia, and Suning Wang

Abstract: The syntheses of several new 7-azaindolyl-, indolyl-, and 3-methylindolyl-functionalized starburst molecules that contain either a 1,3,5-triazine, a benzene, a 2,4,6-triphenyl-2,4,6-triazine, a 1,3,5-triphenylbenzene, a 2,4,6-tris(biphenyl)-1,3,5-triazine, or a 1,3,5-tris(biphenyl)benzene core have been achieved. The synthetic methods used for these new compounds involve mostly Ullmann condensation and Suzuki coupling reactions. The thermal properties of the new molecules have been found to be highly dependent on the molecular weight and the central core. Glass transition temperatures greater than 150 °C were observed for the large starburst molecules based on the 2,4,6-tris(biphenyl)-1,3,5-triazine or the 1,3,5-tris(biphenyl)benzene core. The new starburst molecules are luminescent in the violet-blue region in solution and in the solid state. The emission energy and the quantum efficiency were found to be highly dependent on the central core and the functional group. In general, the triazine-based molecules were found to have a smaller HOMO–LUMO energy gap than the benzene-based analogues. The triphenyltriazine- or triphenylbenzene-based molecules were found to display a higher emission quantum efficiency than the large tris(biphenyl)triazine- or tris(biphenyl)benzene-based molecules.

Key words: 7-azaindolyl, indolyl derivative, triazine and benzene cores, starburst molecule, blue luminescence.

Résumé : On a réalisé la synthèse de plusieurs nouvelles molécules à base d'indolyle, de 3-méthylindolye et de 7-azaindolyle fonctionnalisés qui donnent l'impression d'une explosion d'étoiles et qui contiennent comme partie centrale une 1,3,5-triazine, un benzène, un 2,4,6-triphényl-2,4,6-triazine, un 1,3,5-triphénylbenzène, un 2,4,6-tris(biphényl)-1,3,5-triazine ou un 1,3,5-tris(biphényl)benzène. Les méthodes de synthèse utilisées pour ces nouveaux produits impliquent principalement des réactions de condensation de Ullmann et de couplage de Suzuki. On a trouvé que les propriétés des nouvelles molécules dépendent fortement du poids moléculaire et de la nature de la partie centrale. On a observé des températures de transition de verre supérieures à 150 °C pour les grosses molécules qui donnent l'impression d'une explosion d'étoiles à base d'une partie centrale de 2,4,6-tris(biphényl)-1,3,5-triazine ou de 1,3,5-tris(biphényl)benzène. Tant en solution qu'à l'état solide, les nouvelles molécules qui donnent l'impression d'une explosion d'étoiles sont luminescentes dans la région du violet-bleu. On a trouvé que l'énergie d'émission et l'efficacité quantique dépendent fortement de la nature de la partie centrale et du groupe fonctionnel. On a trouvé que, en général, l'écart entre les énergies des orbitales moléculaires hautes occupées (HO) et basses vacantes (BV) des molécules à base de triazine sont plus faibles que celles de leurs analogues à base de benzène. On a observé que les efficacités quantiques d'émission des molécules à base de triphényltriazine ou de triphénylbenzène sont plus grandes que celles des molécules à base de tris(biphényl)triazine ou de tris(biphényl)benzène.

Mots clés : 7-azaindolyle, dérivé de l'indolyle, partie centrale à base de triazine et de benzène, molécule qui donne l'impression d'une explosion d'étoiles, luminescence bleue.

[Traduit par la Rédaction]

Introduction

Starburst or star-shaped molecules have been shown to have the tendency to form amorphous films with a relatively high T_g, a property that is highly desired for applications of organic materials in photonic and optoelectronic devices such as organic light emitting diodes (OLEDs) (1). Our group has recently demonstrated that 2,2′-dipyridylamino- or 7-azaindolyl-functionalized aromatic molecules can be used as effective blue emitters in OLEDs (2). In addition, the 2,2′-dipyridylamino and 7-azaindolyl functionalities allow the attachment of metal ions to the aromatic molecules for emission color tuning and supramolecular assembly (3). Several series of starburst molecules with a C_3 symmetry that are functionalized by 2,2′-dipyridylamino groups on a 1,3,5-triazine, benzene, triphenyltriazine, or triphenylbenzene core

Received 1 June 2005. Published on the NRC Research Press Web site at http://canjchem.nrc.ca on 31 March 2006.

W.-H. Huang, W.-L. Jia, and S. Wang.[2] Department of Chemistry, Queen University, Kingston, ON K7L 3N6, Canada.

[1]This article is part of a Special Issue dedicated to Professor Walter A. Szarek.
[2]Corresponding author (e-mail: wangs@chem.queensu.ca).

 doi:10.1139/V06-022 © 2006 NRC Canada

were reported previously by our group (3). These molecules indeed displayed good film-forming properties and were shown to be effective as emitters for blue OLEDs (2). Our current work focuses on the development of starburst molecules that are functionalized by the 7-azaindolyl group. In contrast to the 2,2′-dipyridylamino group, which can act as either a chelate ligand or a terminal ligand to metal ions, the 7-azaindolyl group can only bind to the metal center as a terminal ligand, which offers new binding modes for coordination compounds and supramolecular assembly (4). In our previous work, three starburst molecules containing the 7-azaindolyl group were investigated (1,3,5-tris(*N*-7-azaindolyl)benzene, 1,2,4,5-tetrakis(*N*-7-azaindolyl)benzene (4), and hexakis(*p*-*N*-7-azaindolylphenyl)benzene (3*e*)). Although these three compounds were found to form unusual complexes with a variety of metal ions and may be used as blue emitters in OLEDs (2*b*), they have the tendency to remain crystalline, which limits their applications in OLEDs. Our current efforts therefore focus on the synthesis of large starburst molecules containing the 7-azaindolyl or the indolyl group with the aim to enhance the T_g of the amorphous films. In this report, the syntheses, characterization, and thermal and luminescent properties of several new starburst molecules are presented.

Experimental

All reactions were carried out under a nitrogen atmosphere and monitored by thin layer chromatography (TLC). All starting materials were purchased from the Sigma-Aldrich Chemical Company and used without further purification. NMR spectra were recorded on Bruker 300, 400, or 600 MHz spectrometers. High-resolution mass spectra were recorded on an Applied Biosystems/MDS Sciex QSTAR XL instrument with an Agilent HP1100 Cap-LC system by electron spray ionization (ESI) and a Waters/Micromass GC–TOF instrument with an Agilent HP6890 GC system by electron impact (EI). Elemental analyses were performed by Canadian Microanalytical Service Ltd., Delta, British Columbia. TLC was carried out on SiO_2. Column chromatographic separation was carried out on silica (silica gel, 70–230 mesh 60). Melting points were measured on a Fisher-Johns melting point apparatus. Excitation and emission spectra were recorded on a Photon Technologies International QuantaMaster Model C-60 spectrometer at room temperature. DSCs were performed on a PerkinElmer Pyris DSC 6. Heating scans were performed at 10° min^{-1}. Cooling scans were performed at 20° min^{-1}. Cyclic voltammetry was performed on a BAS CV-50W analyzer with scan rates of 100 mV s^{-1}. The electrolytic cell used was a conventional three-compartment cell with a Pt working electrode, Pt auxiliary electrode, and Ag/AgCl reference electrode. All experiments were performed at room temperature in CH_2Cl_2 or THF with 0.10 mol/L tetrabutylammonium hexafluorophosphate as the supporting electrolyte. The ferrocenium/ferrocene couple was used as the internal standard. 1,3,5-Tris(*p*-bromophenyl)benzene and 2,4,6-tri(*p*-bromophenyl)-1,3,5-triazine were synthesized by a modified literature method (2*a*). Melting points were determined on a Fisher-Johns melting point apparatus (maximum temperature 330 °C) and were confirmed by DSC measurements.

Synthesis of 2,4,6-tris(1-*N*-7-azaindolyl)-1,3,5-triazine (1)

To a vigorously stirred solution of 7-azaindole (0.400 g, 3.4 mmol) in dry THF (15 mL), *n*-butyllithium solution in hexanes (1.6 mol/L, 2.2 mL, 3.5 mmol) was added slowly at –78 °C. After stirring for 30 min at –78 °C, a cyanuric chloride (0.186 g, 1.0 mmol) solution in THF (10 mL) was slowly added to the mixture. A yellow solid quickly appeared. After stirring for 1 h at –78 °C, the mixture was warmed to room temperature and stirred for 12 h. The mixture was then concentrated under vacuum. Water (40 mL) was added and the crude product was extracted with CH_2Cl_2 (3 × 40 mL). The organic layer was dried over $MgSO_4$ and then concentrated under vacuum to give a yellow solid. Recrystallization from CH_2Cl_2 and hexanes produced a white solid (0.350 g, yield 82%, mp 289 °C). ^{1}H NMR (400 MHz, $CDCl_3$, 298 K, ppm) δ: 8.70 (d, J = 4.8 Hz, 3H, 7-aza), 8.69 (d, J = 4.0 Hz, 3H, 7-aza), 8.00 (d, J = 7.8 Hz, 3H, 7-aza), 7.31 (dd, J_1 = 7.8 Hz, J_2 = 4.8 Hz, 3H, 7-aza), 6.80 (d, J = 4.0 Hz, 3H, 7-aza). ^{13}C NMR (400 MHz, $CDCl_3$, 298 K, ppm) δ: 163.5, 148.7, 145.1, 129.3, 127.1, 124.6, 118.9, 106.4. HRMS (ESI, *m*/*z*) calcd. for $C_{24}H_{16}N_9$: 430.1523; found: 430.1513.

Synthesis of 1,3,5-tris[*p*-(1-*N*-7-azaindolyl)phenyl]benzene (2)

A mixture of 1,3,5-tris(*p*-bromophenyl)benzene (1.100 g, 2.02 mmol), 7-azaindole (1.071 g, 9.08 mmol), CuI (0.115 g, 6.05 mmol), Cs_2CO_3 (4.160 g, 12.8 mmol), 1,10-phenanthroline (0.218 g, 1.21 mmol), and DMF (5 mL) was heated to 150 °C. After stirring for 48 h at 150 °C, the mixture was cooled to room temperature and was dissolved in CH_2Cl_2 (50 mL) and water (50 mL). The water layer was separated and was extracted with CH_2Cl_2 (2 × 50 mL). The combined organic layer was dried over $MgSO_4$, and the solvents were evaporated under reduced pressure to give a brown solid that was purified by a chromatographic column using THF–hexanes (1:2.5) as the eluent to obtain a white solid. Recrystallization from THF and hexanes yielded a colorless compound (0.842 g, yield 64%, mp 287 °C). ^{1}H NMR (300 MHz, $CDCl_3$, 298 K, ppm) δ: 8.45 (d, J = 4.7 Hz, 3H, 7-aza), 8.03 (d, J = 7.8 Hz, 3H, 7-aza), 7.96 (d, J = 8.8 Hz, 6H, ph), 7.92 (s, 3H, ph), 7.90 (d, J = 8.8 Hz, 6H, ph), 7.63 (d, J = 3.6 Hz, 3H, 7-aza), 7.20 (dd, J_1 = 7.8 Hz, J_2 = 4.7 Hz, 3H, 7-aza), 6.71 (d, J = 3.6 Hz, 3H, 7-aza). ^{13}C NMR (300 MHz, $CDCl_3$, 298 K, ppm) δ: 148.3, 144.4, 142.5, 139.6, 138.7, 129.8, 128.9, 128.4, 125.7, 125.0, 122.3, 117.5, 102.6. HRMS (ESI, *m*/*z*) calcd. for $C_{45}H_{31}N_6$: 655.2604; found: 655.2605.

Synthesis of 2,4,6-tris[*p*-(1-*N*-7-azaindolyl)phenyl]-1,3,5-triazine (3)

A mixture of 2,4,6-tri(*p*-bromophenyl)-1,3,5-triazine (0.789 g, 1.46 mmol), 7-azaindole (0.776 g, 6.58 mmol), CuI (0.083 g, 0.44 mmol), Cs_2CO_3 (3.00 g, 9.2 mmol), 1,10-phenanthroline (0.158 g, 0.87 mmol), and DMF (4 mL) was heated to 150 °C and stirred for 48 h at 150 °C. After cooling to room temperature, the mixture was dissolved in CH_2Cl_2 (100 mL) and water (100 mL). Two phases were separated and the water layer was extracted with CH_2Cl_2 (3 × 50 mL). All organic layers were combined and the solvents were evaporated to give a dry brown solid. The solid

© 2006 NRC Canada

was purified by column chromatography using THF–hexanes (2:5) first and then pure THF as the eluent to obtain a crude yellow product. The crude product was decolored with activated carbon in hot DMF and recrystallized in hot DMF three times. A pale yellow solid (0.464 g, yield 48%, mp 333 °C) was obtained. ^{1}H NMR (600 MHz, $CDCl_3$, 298 K, ppm) δ: 8.97 (d, J = 6.8 Hz, 6H, ph), 8.44 (d, J = 4.6 Hz, 3H, 7-aza), 8.10 (d, J = 6.8 Hz, 6H, ph), 8.01 (d, J = 7.8 Hz, 3H, 7-aza), 7.67 (d, J = 3.6 Hz, 3H, 7-aza), 7.19 (dd, J_1 = 7.8 Hz, J_2 = 4.6 Hz, 3H, 7-aza), 6.71 (d, J = 3.6 Hz, 3H, 7-aza). ^{13}C NMR (600 MHz, $CDCl_3$, 298 K, ppm) δ: 170.8, 147.5, 143.6, 142.0, 133.5, 130.1, 129.1, 122.9, 127.1, 122.0, 117.0, 102.5. Elemental anal. calcd. for $C_{42}H_{27}N_9$: C 76.71, H 4.10, N 19.18; found: C 76.64, H 4.04, N 19.21.

Synthesis of 1,3,5-tris{*p*-[*N*-(3-methyl-indolyl)]phenyl}-benzene (4)

A mixture of 1,3,5-tris(*p*-bromophenyl)benzene (1.00 g, 1.84 mmol), 3-methylindole (1.09 g, 8.29 mmol), CuI (0.11 g, 0.55 mmol), Cs_2CO_3 (3.78 g, 11.6 mmol), 1,10-phenanthroline (0.20 g, 1.10 mmol), and DMF (5 mL) was heated to 150 °C. After stirring for 48 h at 150 °C, the mixture was cooled to room temperature and dissolved in CH_2Cl_2 (20 mL) and water (20 mL). Two phases were separated and the water layer was extracted with CH_2Cl_2 (3 × 20 mL). All organic layers were combined, dried over $MgSO_4$, and concentrated to give a brown solid. The crude product was purified twice by a chromatographic column using chloroform–hexanes (at a 1:1.7 concentration initially and secondly, a 2:1 concentration) as the eluent to obtain a white solid. Recrystallization from CH_2Cl_2 and hexanes yielded the colorless compound **4** (0.65 g, yield 51%, mp 275 °C). ^{1}H NMR (400 MHz, $CDCl_3$, 298 K, ppm) δ: 7.93 (s, 3H, ph), 7.90 (d, J = 8.2 Hz, 6H, phenyl), 7.69 (d, J = 7.2 Hz, 3H, indolyl), 7.68 (d, J = 7.6 Hz, 3H, indolyl), 7.66 (d, J = 7.2 Hz, 6H, phenyl), 7.31 (dd, J_1 = 7.8 Hz, J_2 = 7.2 Hz, 3H, indolyl), 7.25 (s, 3H, indolyl), 7.24 (dd, J_1 = 7.8 Hz, J_2 = 7.6 Hz, 3H, indolyl), 2.46 (s, 9H, Me). ^{13}C NMR (400 MHz, $CDCl_3$, 298 K, ppm) δ: 141.79 (ph), 139.6 (ph), 138.4 (ph), 135.9, 129.9, 128.4, 125.3, 124.9, 124.2, 122.5, 119.9, 119.3, 113.2, 110.4, 9.6. HRMS (EI, *m*/*z*) calcd. for $C_{51}H_{39}N_3$: 693.3144; found: 693.3135.

Synthesis of intermediate 1-bromo-3,5-bis[*N*-(3-methyl-indolyl)]benzene (a)

A mixture of 1,3,5-tribromobenzene (2.160 g, 6.86 mmol), 3-methyl indole (1.807 g, 13.7 mmol), $CuSO_4{\cdot}5H_2O$ (0.086 g, 0.05 mmol), K_2CO_3 (1.89 g, 13.7 mmol), and dodecane (4 mL) was heated to 190 °C and stirred for 10 h at 195 °C. After cooling to room temperature, the mixture was dissolved in CH_2Cl_2 (50 mL) and water (50 mL). Two phases were separated and the water layer was extracted with CH_2Cl_2 (3 × 20 mL). All of the organic layers were combined, dried over $MgSO_4$, and concentrated to give a brown solid. The crude product was purified by a chromatographic column using CH_2Cl_2–hexanes (1:4) as the eluent to obtain a colorless solid (0.628 g, yield 22%, mp 184 to 185 °C). ^{1}H NMR (400 MHz, $CDCl_3$, 298 K, ppm) δ: 7.63 (d, J = 7.8 Hz, 2H, indolyl), 7.64 (d, J = 8.1 Hz, 2H, indolyl), 7.61 (s, 1H, ph), 7.59 (s, 2H, ph), 7.31 (dd, J_1 = 8.1 Hz, J_2 = 8.0 Hz, 2H, indolyl), 7.24 (dd, J_1 = 8.0 Hz, J_2 = 7.6 Hz, 2H, indolyl), 7.18 (s, 2H, indolyl), 2.41 (s, 6H, Me).

Synthesis of intermediate 1,3,5-tris[(*p*-boronic acid)phenyl]benzene (b)

To a vigorously stirred solution of 1,3,5-tris(*p*-bromophenyl)benzene (2.72 g, 4.98 mmol) in dry THF (100 mL), butyllithium solution in hexanes (1.6 mol/L, 15.6 mL, 24.9 mmol) was added slowly at –78 °C. After stirring for 1 h at –78 °C, triisopropyl borate (6.3 mL, 27.4 mmol) was added slowly. The solution was stirred for 1 h at –78 °C then warmed to room temperature and stirred for 12 h. The reaction was quenched by adding satd. aq. NH_4Cl (30 mL). The water phases were separated and extracted with CH_2Cl_2 (3 × 20 mL). All of the organic layers were combined and concentrated to give a white solid. Recrystallization from methanol and hexanes yielded a white compound (1.31 g, yield 64%, mp > 300 °C). ^{1}H NMR (400 MHz, acetone-d_6, 298 K, ppm) δ: 8.05 (d, J = 8.2 Hz, 6H, ph), 8.00 (s, 3H, ph), 7.88 (d, J = 8.2 Hz, 6H, ph), 7.27 (s, 6H, OH).

Synthesis of intermediate 1-bromo-3,5-bis(*N*-indolyl)benzene (c)

A mixture of 1,3,5-tribromobenzene (3.780 g, 12 mmol), indole (2.808 g, 24 mmol), $CuSO_4{\cdot}5H_2O$ (0.150 g, 0.6 mmol), and K_2CO_3 (3.312 g, 24 mmol) was heated to 195 °C and stirred for 16 h at 195 °C. After cooling to room temperature, the mixture was dissolved in CH_2Cl_2 (100 mL) and water (100 mL). Two phases were separated and the water layer was extracted with CH_2Cl_2 (3 × 30 mL). All of the organic layers were combined, dried over $MgSO_4$, and concentrated to give a brown solid. The crude product was purified by a chromatographic column using ethyl acetate – hexanes (1:20) as the eluent to obtain a colorless solid (0.580 g, yield 13%, mp 117 to 118 °C). ^{1}H NMR (400 MHz, $CDCl_3$, 298 K, ppm) δ: 7.65 (d, J = 7.8 Hz, 2H, indolyl), 7.64 (d, J = 8.1 Hz, 2H, indolyl), 7.61 (s, 1H, ph), 7.54 (s, 2H, ph), 7.29 (d, J = 3.3 Hz, 2H, indolyl), 7.21 (dd, J_1 = 8.1 Hz, J_2 = 7.2 Hz, 2H, indolyl), 7.14 (dd, J_1 = 8.0 Hz, J_2 = 7.8 Hz, 2H, indolyl), 6.66 (d, J = 3.3 Hz, 2H, indolyl).

Synthesis of intermediate 3,5-bis(1-*N*-indolyl)-1-phenylboronic acid (d)

A solution of *tert*-butyllithium (1.6 mol/L in hexanes, 4.85 mL, 7.76 mmol) was added slowly to a THF (50 mL) solution of 1-bromo-3,5-bis(1-*N*-indolyl)benzene (2.00 g, 5.17 mmol) at –78 °C. After stirring for 1 h at –78 °C, triisopropyl borate (2.02 mL, 8.79 mmol) was added slowly. The solution was stirred for 1 h at –78 °C then slowly warmed to room temperature and stirred for 12 h. The reaction was quenched by adding satd. aq. NH_4Cl solution (20 mL). The water phases were separated and extracted with CH_2Cl_2 (3 × 30 mL). All organic layers were combined and then concentrated to give a brown solid. The crude product was purified by a chromatographic column using THF–hexanes (2:5) as the eluent. Recrystallization from CH_2Cl_2 and hexanes yielded a colorless solid (1.15 g, yield 63%). ^{1}H NMR (400 MHz, actone-d_6, 298 K, ppm) δ: 8.10 (s, 2H, ph), 7.86 (s, 1H, ph), 7.75 (d, J = 7.7 Hz, 2H, indolyl), 7.73 (d, J = 3.3 Hz, 2H, indolyl), 7.70 (d, J = 7.8 Hz, 2H, indolyl), 7.54 (s, 2H, ph), 7.66 (s, 2H, OH), 7.26 (dd, J_1 = 8.0 Hz,

© 2006 NRC Canada

J_2 = 7.8 Hz, 2H, indolyl), 7.17 (dd, J_1 = 8.0 Hz, J_2 = 7.7 Hz, 2H, indolyl), 6.76 (d, J = 3.3 Hz, 2H, indolyl).

Synthesis of 1,3,5-tris[3,5-bis(*N*-indolyl)-4′-biphenyl]benzene (5)

A mixture of 1,3,5-tris[(*p*-boronic acid)phenyl]benzene (0.192 g, 0.439 mmol), 1-bromo-3,5-bis(*N*-indolyl)benzene (0.595 g, 1.537 mmol), $Pd(PPh_3)_4$ (0.020 g, 0.018 mmol), Na_2CO_3 solution (2 N, 30 mL), toluene (50 mL), and ethanol (20 mL) was refluxed for 40 h. A white precipitate formed. After cooling to room temperature, the mixture was extracted with CH_2Cl_2 (3 × 50 mL). All of the organic layers were combined and concentrated to give a colorless solid. The crude product was dried and purified by a chromatographic column using THF–hexanes (2:5) as the eluent to obtain a pale white solid. Recrystallization from CH_2Cl_2 and hexanes twice yielded compound **5** (0.47 g, yield 88%, mp > 330 °C). ^{1}H NMR (400 MHz, $CDCl_3$, 298 K, ppm) δ: 7.96 (s, 3H, ph), 7.91 (d, J = 8.2 Hz, 6H, ph), 7.85 (d, J = 8.2 Hz, 6H, ph), 7.84 (s, 6H, ph), 7.76 (d, J = 7.5 Hz, 6H, indolyl), 7.75 (d, J = 8.1 Hz, 6H, indolyl), 7.70 (s, 3H, ph) 7.50 (d, J = 3.2 Hz, 6H, indolyl), 7.32 (dd, J_1 = 8.1 Hz, J_2 = 7.2 Hz, 6H, indolyl), 7.22 (dd, J_1 = 7.5 Hz, J_2 = 7.2 Hz, 6H, indolyl), 6.80 (d, J = 3.2 Hz, 6H, indolyl). ^{13}C NMR (400 MHz, $CDCl_3$, 298 K, ppm) δ: 143.7, 141.8, 141.6, 141.0, 138.8, 135.7, 129.5, 128.1, 127.8, 127.7, 125.3, 122.8, 121.4, 120.8, 120.5, 118.6, 110.4, 104.4. Elemental anal. calcd. for $C_{90}H_{60}N_4$: C 88.24, H 4.90, N 6.86; found: C 87.87, H 4.96, N 6.78.

Synthesis of 1,3,5-tris{3,5-bis[*N*-(3-methyl-indolyl)]-4′-biphenyl}benzene (6)

A mixture of 1,3,5-tris[(*p*-boronic acid)phenyl]benzene (0.150 g, 0.343 mmol), 1-bromo-3,5-bis[*N*-(3-methyl-indolyl)]benzene (0.498 g, 1.20 mmol), $Pd(PPh_3)_4$ (0.016 g, 0.014 mmol), Na_2CO_3 solution (2 N, 30 mL), toluene (50 mL), and ethanol (20 mL) was refluxed for 40 h. A white precipitate formed. After cooling to room temperature, CH_2Cl_2 (50 mL) and water (50 mL) were added to the mixture. The water layer was separated and extracted with CH_2Cl_2 (2 × 50 mL). The combined organic layers were dried over $MgSO_4$, and the solvents were evaporated under reduced pressure. Purification of the crude product by column (THF–hexanes, 1:16) afforded a white solid. Recrystallization from CH_2Cl_2 and hexanes yielded compound **6** (0.254 g, yield 57%, mp 318 °C). ^{1}H NMR (600 MHz, $CDCl_3$, 298 K, ppm) δ: 7.93 (s, 3H, ph), 7.87 (d, J = 8.3 Hz, 6H, ph), 7.82 (d, J = 8.3 Hz, 6H, ph), 7.74 (s, 6H, ph), 7.71 (d, J = 8.2 Hz, 6H, indolyl), 7.66 (d, J = 7.7 Hz, 6H, indolyl), 7.61 (s, 3H, ph), 7.28 (dd, J_1 = 7.7 Hz, J_2 = 7.2 Hz, 6H, indolyl), 7.26 (s, 6H, indolyl), 7.22 (dd, J_1 = 8.0 Hz, J_2 = 7.2 Hz, 6H, indolyl), 2.42 (s, 18H, Me). ^{13}C NMR (600 MHz, $CDCl_3$, 298 K, ppm) δ: 143.5, 141.8, 141.7, 140.8, 139.1, 135.8, 130.0, 128.0, 127.7, 127.5, 125.2, 122.8, 120.2, 119.6, 119.4, 117.8, 113.6, 110.4, 9.6. Elemental anal. calcd. for $C_{96}H_{72}N_6$: C 88.07, H 5.50, N 6.42; found: C 88.26, H 5.21, N 6.18.

Synthesis of 2,4,6-tris[3,5-bis(1-*N*-indolyl)-4′-biphenyl]-1,3,5-triazine (7)

A mixture of 2,4,6-tris(*p*-bromophenyl)-1,3,5-triazine (0.412 g, 0.75 mmol), 3,5-bis(*N*-indolyl)-1-phenylboronic acid (0.930 g, 2.64 mmol), $Pd(PPh_3)_4$ (0.04 g, 0.03 mmol), Na_2CO_3 solution (2 N, 30 mL), toluene (50 mL), and ethanol (20 mL) was refluxed for 40 h. A white precipitate formed. After cooling to room temperature, CH_2Cl_2 (100 mL) and water (100 mL) were added to the mixture. The water layer was extracted with CH_2Cl_2 (3 × 30 mL). All of the organic layers were combined and concentrated to give a white solid. The crude product was dried and purified by a chromatographic column using THF–hexanes (2:5) as the eluent to obtain a yellow solid. Recrystallization from THF and hexanes initially, then from CH_2Cl_2 and hexanes three times yielded the colorless compound **7** (0.561 g, yield 61%, mp > 330 °C). ^{1}H NMR (600 MHz, $CDCl_3$, 298 K, ppm) δ: 8.94 (d, J = 8.5 Hz, 6H, ph), 7.92 (d, J = 8.5 Hz, 6H, ph), 7.85 (s, 6H, ph), 7.74 (d, J = 7.8 Hz, 6H, indolyl), 7.72 (d, J = 8.3 Hz, 6H, indolyl), 7.71 (s, 3H, ph), 7.30 (dd, J_1 = 8.3 Hz, J_2 = 8.0 Hz, 6H, indolyl), 7.48 (d, J = 3.2 Hz, 6H, indolyl), 7.22 (dd, J_1 = 8.0 Hz, J_2 = 7.8 Hz, 6H, indolyl), 6.78 (d, J = 3.2 Hz, 6H, indolyl). ^{13}C NMR (600 MHz, $CDCl_3$, 298 K, ppm) δ: 171.1, 143.4, 143.3, 141.7, 136.0, 135.5, 129.9, 129.6, 127.5, 127.3, 122.7, 121.2, 120.7, 120.5, 118.9, 110.2, 104.4. Elemental anal. calcd. for $C_{87}H_{57}N_9$: C 85.09, H 4.65, N 10.27; found: C 85.16, H 4.76, N 9.94.

Results and discussion

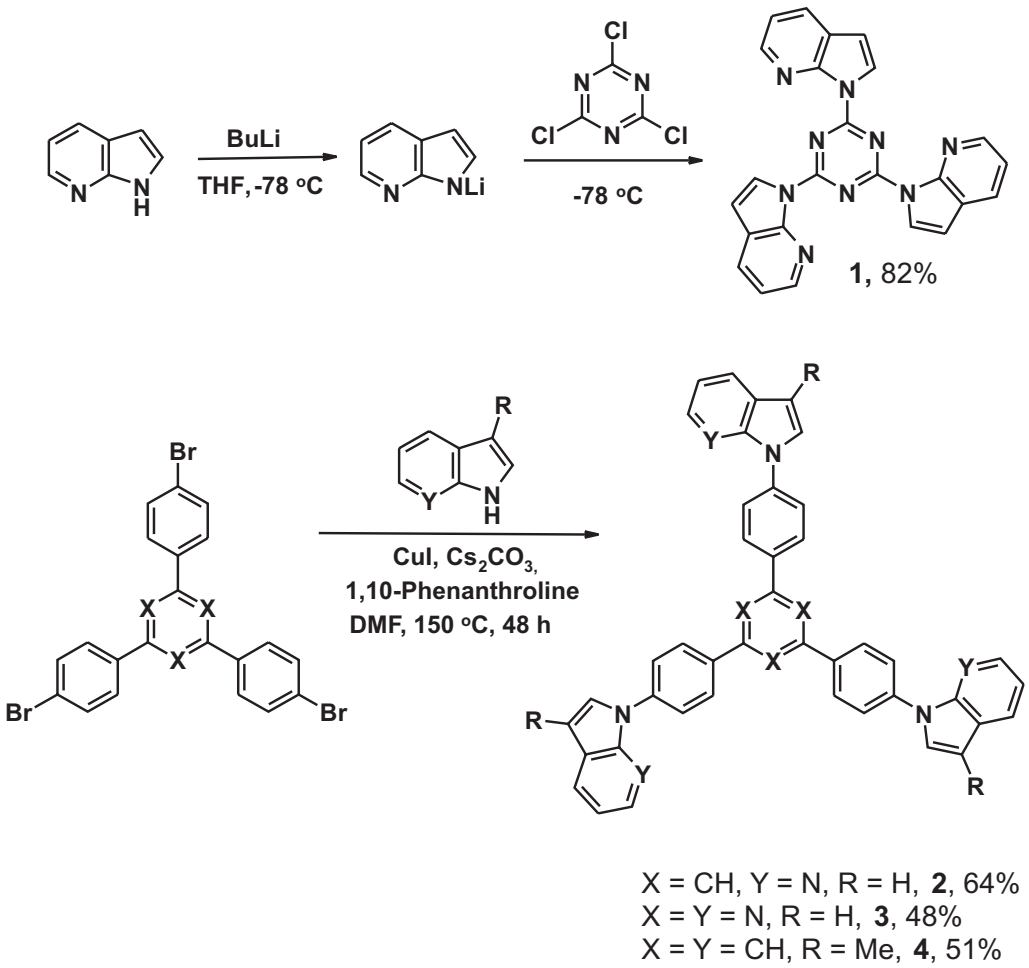
Synthesis and characterization

The new starburst molecules were obtained by using either the Ullmann condensation methods (5) or the Suzuki coupling methods (6) as depicted in Schemes 1–3.

Compound **1** was synthesized by the reaction of 7-azaindolyl lithium with cyanuric chloride in high yield (82%). Compounds **2**–**4** were prepared in moderate yields (48%–64%) from the reaction of 7-azaindole or 3-methylindole with 1,3,5-tris(*p*-bromophenyl)benzene or 2,4,6-tris(*p*-bromophenyl)-1,3,5-triazine using the modified Ullmann condensation procedure (5) where CuI and 1,10-phenanthroline acted as the catalysts and Cs_2CO_3 as the HBr scavenger. The intermediates, 1,3,5-tris(*p*-bromophenyl)benzene and 2,4,6-tris(*p*-bromophenyl)-1,3,5-triazine for compounds **2**–**4**, were synthesized by using modified literature methods (2). The syntheses of compounds **5** and **6** were achieved in good or moderate yields by Pd-catalyzed Suzuki–Miyaura cross couplings of 1,3,5-tris[(*p*-boronic acid)phenyl]benzene (intermediate **b**) with the corresponding disubstituted bromobenzene (intermediates **a** or **c**), as shown in Scheme 2. The intermediates **a** and **c** were synthesized by Ullmann condensation reactions between 2 equiv. of indole or 3-methylindole and 1,3,5-tribromobenzene (2). The intermediates 1,3,5-tris[(*p*-boronic acid)phenyl]benzene and 3,5-bis(1-*N*-indolyl)-1-phenylboronic acid were obtained by the reaction of B(O-*i*-Pr)$_3$ with 1,3,5-tris(4-lithium-phenyl]benzene and 3,5-bis(1-*N*-indolyl)phenyllithium, respectively. Compound **7** was obtained in good yield by Suzuki coupling between 2,4,6-tris(*p*-bromophenyl)-1,3,5-triazine and the intermediate **d** (Scheme 3). The switching from the boric acid triphenyltriazine core **c** as the one used in the syntheses of **5** and **6** to the brominated triphenyl-triazine core and the change of the bromo-substituted intermediate **a** to the boric acid intermediate **d** were necessary to ensure the successful synthesis of compound **7** (when the

© 2006 NRC Canada

Scheme 1.



bromide and the boronic acid starting materials were reversed as for **5** and **6**, no compound **7** was isolated).

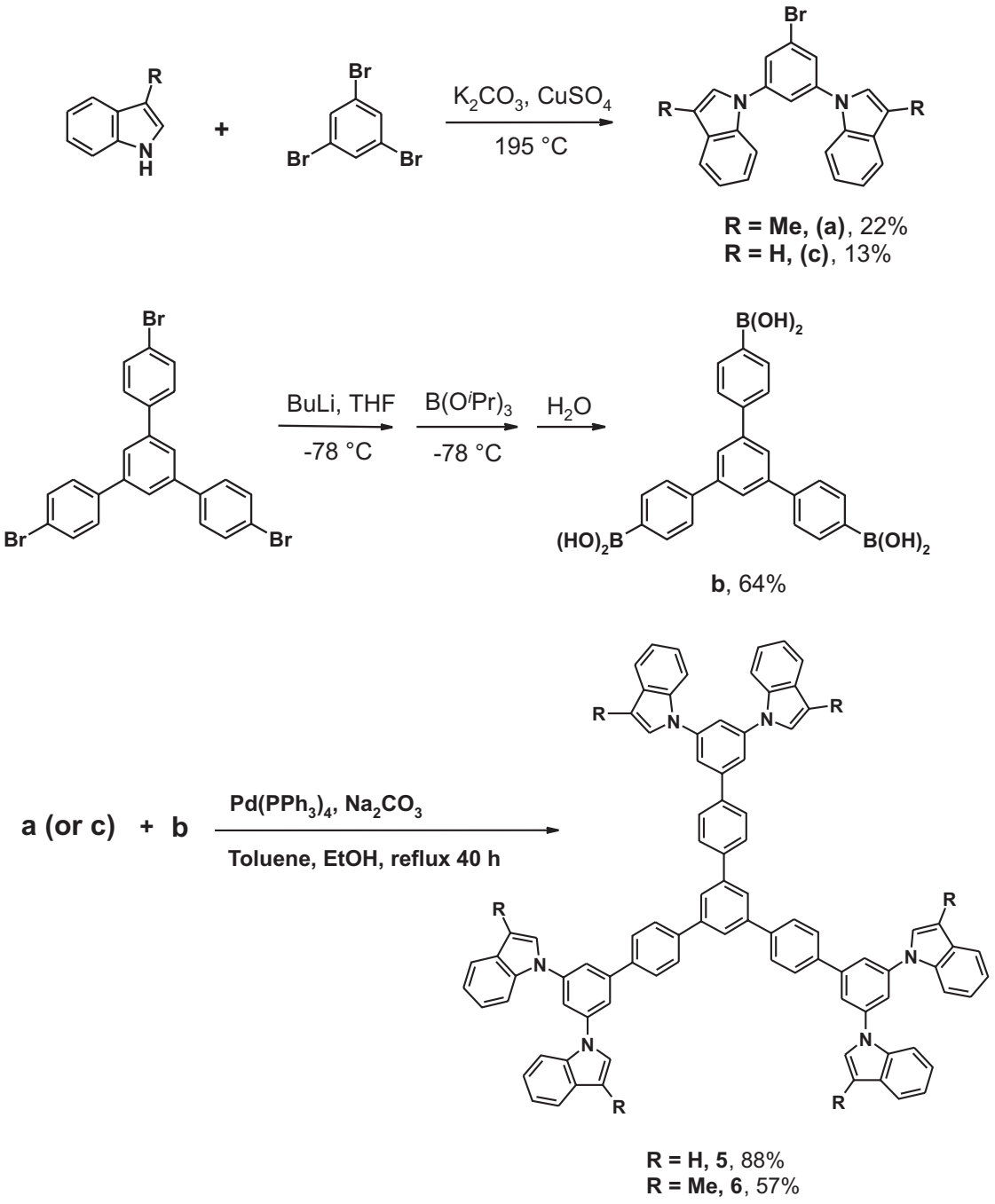
Based on the functional group, compounds **1**–**7** can be divided into three categories: 7-azaindolyl-substituted compounds (**1**–**3**), indolyl-substituted compounds (**5** and **7**), and 3-methyl-substituted compounds (**4** and **6**). Because of their potential use in coordination and supramolecular assembly, our initial synthetic effort focused on 7-azaindolyl derivatives with the triazine core (the benzene analogue of **1** was reported earlier by our group), the triphenyl triazine–triphenylbenzene core, and the tris(biphenyl)triazine–tris(biphenyl)benzene core. Although the smaller molecules (**1**–**3**) with 7-azaindolyl groups were obtained successfully, we were not able to isolate 7-azaindolyl products that contained the larger triphenyltriazine–triphenylbenzene or the tris(biphenyl)triazine–tris(biphenyl)benzene core. The problem appeared to be mostly caused by the poor solubility of the products in organic solvents (e.g., THF, CH_3CN, CH_2Cl_2, and DMF), which made the purification and (or) isolation and characterization difficult. The indolyl group is an analogue of 7-azaindolyl, but its derivatives are in general more soluble in organic solvents than the corresponding 7-azaindolyl derivatives. For the larger cores, we therefore attempted the syntheses of indolyl derivatives. The hexaindolyl-substituted compounds **5** and **7** were obtained successfully. To further enhance the solubility of the products, we also attempted the syntheses of 3-methylindolyl derivatives for the larger cores. Two 3-methylindolyl-substituted compounds (**4** and **6**) were obtained successfully. Compound **6** was found to be more soluble than the indolyl analogue **5** in organic solvents. Compounds **1**–**7** were characterized by ^1H, ^{13}C NMR, HRMS, or elemental analyses (for compounds whose HRMS data could not be obtained owing to either being too high in molecular weight or too insoluble in the solvent matrix).

Thermal properties

The glass-forming properties and phase transition of compounds **1**–**7** were studied by DSC experiments. All seven compounds were heated under argon with a heating rate of 10 °C min^{-1}. After heating, all compounds were cooled to 50 °C at a cooling rate of 20 °C min^{-1}. The second heating was carried out with a heating rate of 10 °C min^{-1}. Well-defined melting points were observed for all compounds except compounds **5** and **7** in the DSC diagrams. These melting point values are consistent with those obtained by using a melting point apparatus. The high melting points (275 to >330 °C, Table 1) displayed by compounds **1**–**7** support that they have a high thermal stability. Compounds **2** and **3** are 7-azaindolyl derivative molecules with similar structures, but a different central core (benzene for **2** and triazine for **3**). Interestingly, however, the melting point of compound **3** is

© 2006 NRC Canada

Scheme 2.



about 44 °C higher than that of **2**. The same trend was also observed previously in 2,2′-dipyridylamino-substituted triphenyltriazine–triphenylbenzene or tris(biphenyl)triazine–tris(biphenyl)benzene compounds, where the triazine-based compounds consistently have a much higher melting point than the corresponding benzene-based analogue (2, 7). This perhaps can be attributed to the fact that the electronegative nitrogen atoms in the triazine core makes the molecule more polar, hence the presence of stronger intermolecular interactions in the crystal lattice, compared with the benzene core analogue.

Glass transition temperatures were observed for compounds **5** (T_g ~ 168 °C), **6** (T_g ~ 188 °C), and **7** (T_g ~ 187 °C) in the second heating–cooling curve of the DSC experiments (Table 1). No glass transition temperatures were observed for compounds **1**–**4** in either the first or the second heating cycles, an indication that these smaller molecules have the tendency to remain crystalline. The DSC diagram (second and third heating and cooling cycles) of compound **6** is shown in Fig. 1 as a representative example. In addition to T_g and T_m, a well-defined crystallization temperature (T_c) was also observed for **6**. Compounds **5** and **7** are another pair of benzene core – triazine core analogues that contain six indolyl groups. Although no melting points were observed for either compound in the DSC experiments, the DSC data again support that triazine compound **7** has a

© 2006 NRC Canada

Scheme 3.

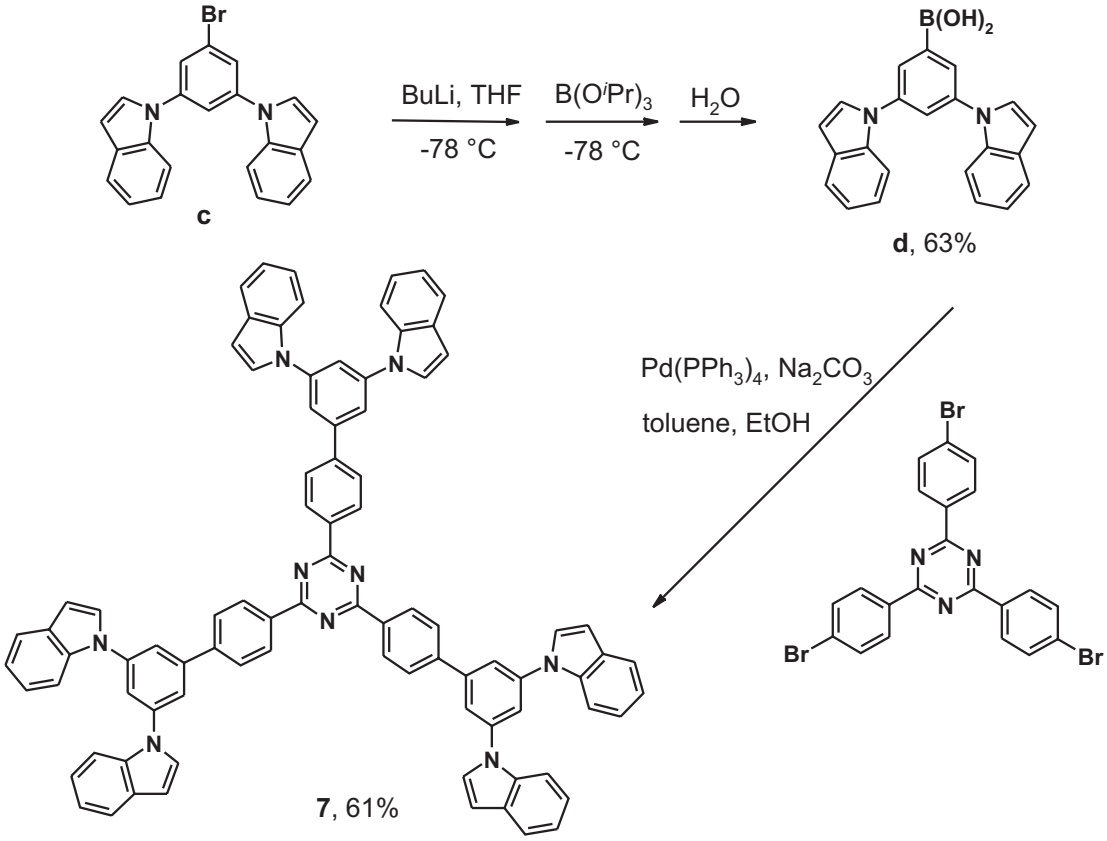


Table 1. Thermal properties of compounds **1**–**7**.

Compound	T_g (°C)	T_c (°C)	T_m (°C)[a]
1			289
2			287
3			333
4			275
5	160 (heating) / 168 (cooling)		>330
6	183 (heating) / 188 (cooling)	265	318
7	175 (heating) / 186 (cooling)		>330

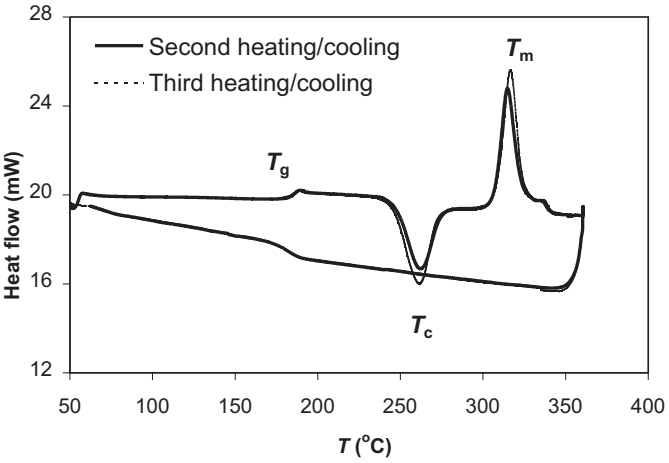
[a]Obtained by a melting point apparatus.

much higher T_g than its benzene analogue **5**. The inclusion of the methyl groups in **6** also appears to enhance the glass transition temperature of the molecule as shown by the higher T_g of **6**, compared with that of **5**. The exceptionally high T_g values of compounds **5**–**7** indicate that these large molecules are capable of forming stable amorphous phases, a property highly desired for applications in organic photonic devices such as organic light emitting diodes. The remarkable high thermal stability of compounds **5**–**7** can be attributed to their high molecular weights and their highly branched structures, in comparison with compounds **1**–**4**.

Electronic and luminescent properties

Compounds **1**–**7** have intense absorption bands in the UV–vis region that can be attributed to π–π* transitions. Attempts were made to measure the oxidation and reduction potentials of compounds **1**–**7** by using cyclic voltammetry.

Fig. 1. DSC diagrams of compound **6** (second and third) heating (10 °C min^{-1}) and cooling (20 °C min^{-1}) (the first heating and cooling diagram is identical to these).



For all seven compounds, no reliable reduction peaks were detected within the solvent limit (THF was used as the solvent for reduction potential measurements). For compounds **2** and **4**, well-defined oxidation peaks were observed in CH_2Cl_2. For the remaining compounds, no reliable oxidation peaks were detected in CH_2Cl_2. The failure to observe oxidation potentials for some of the compounds can be partially attributed to the poor solubility of the materials, especially the large molecules (**5**–**7**). The first oxidation potential of **2** and **4** were found to be 1.57 and 1.14 V (vs. Ag/AgCl), re-

© 2006 NRC Canada

Fig. 2. Cyclic voltammetry diagrams of **2** (top) and **4** (bottom) in CH_2Cl_2.

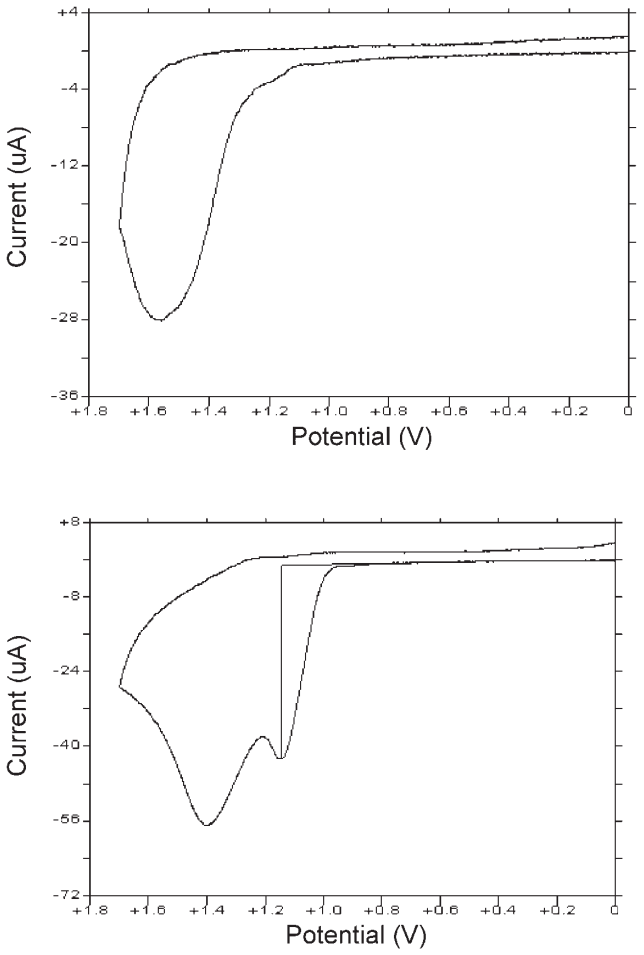
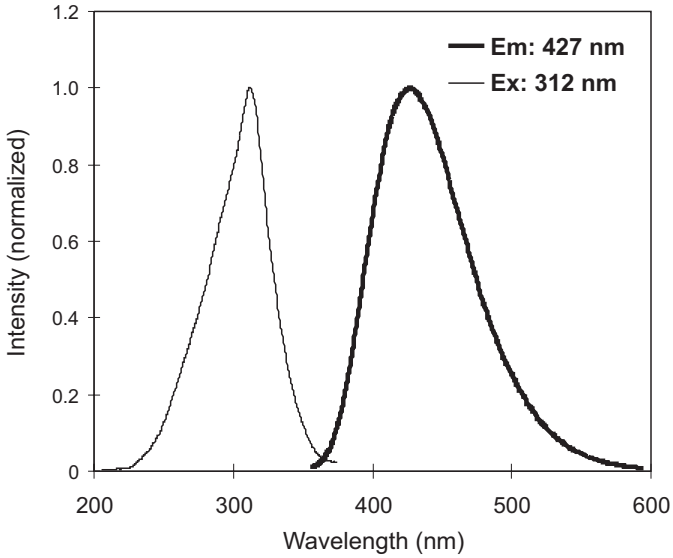


Fig. 3. The excitation and emission spectra of **6** in CH_2Cl_2.



spectively (Fig. 2). The HOMO energy levels for **2** and **4** were calculated to be –5.9 and –5.4 eV, respectively, by using the oxidation potential and the ferrocene HOMO energy level of –4.8 eV (relative to the vacuum level) as the standard (8). Clearly, the 7-azaindolyl derivative **2** has a much deeper HOMO level than that of the 3-methyl indolyl derivative **4**, which can be attributed to the extra electronegative nitrogen atom on the 7-azaindolyl ring that stabilizes the HOMO level, relative to that of the indolyl compound. By using the optical band gap obtained from the UV–vis absorption spectra (absorption edge), the LUMO energy levels of **2** and **4** were calculated to be –2.2 and –2.1 eV, respectively. The HOMO energy levels of **2** and **4** are considerably deeper than that of the well-known hole-transport material (9) NPB and the LUMO levels are much higher than those of the well-known electron-transport materials (Alq_3 and phenanthroline derivatives) (10). As a result, these compounds are not good candidates to act as hole- or electron-transport layers because of their relatively deep HOMO and high LUMO. However, they could be used as blue emitters or hosting materials in OLEDs.

Compounds **1**–**7** emit a blue or violet color in solution and the solid state when irradiated by UV light. The luminescent spectra of **1**–**7** are typical of fluorescence as shown by the spectra of **6** in Fig. 3. The absorption data and luminescent data are summarized in Table 2. Compared to the corresponding free 7-azaindole, indole, or 3-methylindole molecules, the absorption and emission spectra of compounds **1**–**7** are all red-shifted, which is clearly caused by the conjugation of the 7-azaindolyl, indolyl, or 3-methylindolyl chromophore with the aromatic central core. One obvious trend is the difference between the triazine and benzene core analogues (**2** and **3** and **5** and **7**). As shown by the data in Table 2, the triazine derivative consistently has smaller absorption–excitation and emission energies (i.e., the red shift of the absorption and emission band), compared with the corresponding benzene derivative. The same trend was also observed in 2,2′-dipyridylamino-functionalized triazine and benzene derivatives (2, 7). The methyl-substituted compound **6** has an emission energy that is about 25 nm red-shifted, compared with the nonsubstituted indolyl analogue **5**, which can be attributed to the electron-donating nature of the methyl group that effectively destablizes the HOMO level (π) and stablizes the LUMO level (π^*), hence decreasing the band gap. Similar emission energy red shift induced by electron-donating groups has been observed in BPh_2(2-Py-indolyl-X) compounds, where X is a substituent on the indolyl ring (11). The quantum efficiencies of compounds **1**–**7** vary considerably. Molecules (**2**–**4**) that have either a triphenyltriazine or triphenybenzene core display the highest emission quantum efficiencies. The quantum efficiencies of the large molecules (**5**–**7**) are substantially lower. For applications as emitters in organic light emitting diodes, it is required for the molecule to have both a high T_g and a high emission quantum efficiency. The high T_g is to ensure the morphological stability of the organic layer. Taking both factors into consideration, compounds **5** and **6** are the most promising as emitters in OLEDs, which are being examined by our group, and the results will be disclosed in due course. Although no T_g was detected, compound **2** has a fairly large band gap and a deep HOMO level, which makes it potentially useful as either a host material for phosphorescent dopants or as a hole-blocking layer.

© 2006 NRC Canada

Table 2. Absorption and luminescent properties of compounds **1**–**7**.

Compound	UV–vis absorption (solution)[a] λ (nm), ε ((mol/L)$^{-1}$ cm^{-1})	Solid λ (nm)		Solution[a] λ (nm)		Quantum yield[b] (%) (solution)[a]
		Ex.	Em.	Ex.	Em.	
1	270 (78 400), 294 (shoulder, 41 900)	314	361, 396	318	423	2
2	230 (46 800), 284 (97 600)	343	427	307	365	35
3	234 (10 700), 280 (82 400), 344 (79 600)	400	450	344	408	47
4	232 (79 400), 278 (67 900), 320 (94 300)	357	379	332	400	60
5	232 (89 400), 270 (167 000), 302 (208 000)	350	403	318	403	17
6	232 (129 000), 272 (175 000), 306 (221 000)	343	401	312	427	14
7	232 (89 100), 266 (127 000), 306 (169 000)	393	454	331	481	6

[a]All data were collected in CH_2Cl_2 solution at 298 K, except the data for S3 were collected in THF solution at 298 K. Concentration: [M] ≈ 10^{-5} mol/L.
[b]The quantum yields were obtained by using anthracene or 9,10-diphenylanthracene as a reference.

Acknowledgement

We thank the Natural Sciences and Engineering Research Council of Canada (NSERC) for financial support.

References

1. (*a*) Y. Shirota. J. Mater. Chem. **10**, 25 (2000); (*b*) E. Ueta, H. Nakano, and Y. Shirota. Chem. Lett. 2396 (1994); (*c*) I.Y. Wu, J.T. Lin, Y.T. Tao, and E. Balasubramaniam. Adv. Mater. **12**, 668 (2000); (*d*) S. Berleb, W. Brutting, M. Schwoerer, R. Wehrmann, and A. Elschner. Adv. Mater. **6**, 677 (1994).
2. (*a*) J. Pang, Y. Tao, S. Freiberg, X.P. Yang, M. D'Iorio, and S. Wang. J. Mater. Chem. **12**, 206 (2002); (*b*) Q. Wu, J.A. Lavigne, Y. Tao, M. D'Iorio, and S. Wang. Chem. Mater. **13**, 71 (2001).
3. (*a*) Q.G. Wu, A. Hook, and S. Wang. Angew. Chem. Int. Ed. **39**, 3933 (2000); (*b*) J. Pang, E.J.-P. Marcotte, C. Seward, R.S. Brown, and S. Wang. Angew. Chem. Int. Ed. **40**, 4042 (2001); (*c*) J. Pang, C. Seward, and S. Wang. Eur. J. Inorg. Chem. **6**, 1390 (2002); (*d*) C. Seward, W.L. Jia, R.Y. Wang, G.D. Enright, and S. Wang. Angew. Chem. Int. Ed. **43**, 2933 (2004); (*e*) W.L. Jia, R.Y. Wang, D.T. Song, S. Ball, A. McLean, and S. Wang. Chem. Eur. J. **11**, 832 (2005).
4. (*a*) D.T. Song and S. Wang. Comments Inorg. Chem. **25**, 1 (2004) and refs. therein; (*b*) D.T. Song and S. Wang. Eur. J. Inorg. Chem. 3773 (2003).
5. A. Klapars, J.C. Antilla, X. Huang, and S.L. Buchwald, J. Am. Chem. Soc. **123**, 7727 (2001).
6. (*a*). N. Muyaura. Adv. Met.–Org. Chem. **6**, 187 (1998), and refs. therein; (*b*) A. Suzuki. J. Organomet. Chem. **576**, 147 (1999), and refs. therein.
7. Q.D. Liu, W.L. Jia, G. Wu, and S. Wang. Organometallics, **22**, 3781 (2003).
8. J. Pommerehne, H. Vestweber, W. Guss, R.F. Mahrt, H. Bassler, M. Porsch, and J. Daub. Adv. Mater. **7**, 551 (1995).
9. (*a*) T. Tsutsui. Mater. Res. Soc. Bull. **22**, 39 (1997); (*b*) W.L. Jia, X.D. Feng, D.R. Bai, Z.H. Lu, and S. Wang. Chem. Mater. **17**, 164 (2005).
10. (*a*) C.W. Tang and S.A. VanSlyke. Appl. Phys. Lett. **51**, 913 (1987); (*b*) L.S. Hung and C.H. Chen. Mater. Sci. Eng. R. **39**, 143 (2002); (*c*) S. Naka, H. Okada, H. Onnagawa, and T. Tsutsui. Appl. Phys. Lett. **76**, 197 (2000).
11. Q.D. Liu, M.S. Mudadu, R. Thummel, Y. Tao, and S. Wang. Adv. Funct. Mater. **15**, 143 (2005).

© 2006 NRC Canada

Facile synthesis of α-D-Ara*f*-(1→5)-D-Gal*f*, the linker unit of the arabinan to the galactan in *Mycobacterium tuberculosis*[1]

Lucía Gandolfi-Donadío, Carola Gallo-Rodriguez, and Rosa M. de Lederkremer

Abstract: The arabinogalactan is a crucial constituent of the cell wall of mycobacteria. Both monosaccharides (arabinose and galactose) are found in the furanose configuration, absent in mammals. An efficient synthesis of α-D-Ara*f*-(1→5)-D-Gal*f*, the linker unit of the arabinan to the galactan, is described. The strategy relies on the use of a conveniently substituted D-galactono-1,4-lactone as a precursor of the reducing furanose ring. The glycosylation step was performed by the tin(IV) chloride promoted method using 1,2,3,5-tetra-*O*-benzoyl-α,β-D-arabinofuranose. The arabinose donor was obtained in a crystalline state in one step by benzoylation of arabinose in hot pyridine. Selective glycosylation of the exocyclic OH-5 was obtained in 75% yield to give 2,3,5-tri-*O*-benzoyl-α-D-arabinofuranosyl-(1→5)-2,6-di-*O*-pivaloyl-D-galactono-1,4-lactone. Reduction with disiamylborane gave the disaccharide synthon, useful for further glycosylations. Dec-9-enyl α-D-Ara*f*-(1→5)-β-D-Gal*f*, a convenient substrate for arabinofuranosyl transferases studies, was obtained by the trichloroacetimidate method of glycosylation.

Key words: arabinofuranose, galactofuranose, *Mycobacterium* arabinogalactan, trichloroacetimidate, tin(IV) chloride.

Résumé : L'arabinogalactane est un constituant crucial de la paroi de la cellule des mycobactéries. Les deux monosaccharides, arabinose et galactose, se retrouvent dans la configuration furanose qu'on ne retrouve pas chez les mammifères. On décrit une synthèse efficace du α-D-Ara*f*-(1→5)-D-Gal*f*, l'unité de liaison de l'arabinane au galactane. La stratégie repose sur l'utilisation d'une D-galactono-1,4-lactone substituée d'une façon appropriée comme précurseur du cycle réducteur du furanose. L'étape de glycosylation a été réalisée par la méthode de catalyse à l'aide de chlorure d'étain(IV) en utilisant le 1,2,3,5-tétra-*O*-benzoyl-α,β-D-arabinofuranose. Le donneur arabinose a été obtenu à l'état cristallin en une étape benzoylation de l'arabinose dans de la pyridine à chaud. La glycosylation sélective de OH-5 exocyclique a été réalisée avec un rendement de 75 % pour conduire à la formation de la 2,3,5-tri-*O*-benzoyl-α-D-arabinofuranosyl-(1→5)-2,6-di-*O*-pivaloyl-D-galactono-1,4-lactone. Sa réduction par du disiamylborane fournit le synthon disaccharide utile dans des glycosylations subséquentes. Par ailleurs, le dec-9-enyl α-D-Ara*f*-(1→5)-β-D-Gal*f*, un substrat approprié pour les études de transférases d'arabinofuranosyle a été préparé par la méthode de glycosylation au trichloroacétimidate.

Mots clés : arabinofuranose, galactofuranose, arabinogalactane *Mycobacterium*, trichloroacétimidate, chlorure d'étain(IV).

[Traduit par la Rédaction]

Introduction

Mycobacterial diseases have reemerged in the last years because of the appearance of multidrug-resistant strains of *Mycobacterium* and the relation of tuberculosis with AIDS (1). The integrity of the mycobacterial cell wall is essential for the viability of mycobacteria (2).

One of the components of this unique cell wall is arabinogalactan (AG) (3) in which both arabinose and galactose are found in the furanose form, which is absent in mammals. The galactan region consists of alternating β(1→5)- and β(1→6)-linked D-Gal*f* residues. This linear galactofuranose chain has branch points at OH-5 at which the arabinan chains are α-attached. Thus, an α-D-Ara*f*-(1→5)-D-Gal*f* linkage anchors the arabinan component to the galactan structure. The disaccharide has been previously synthesized as the *n*-octyl (4) and the ethyl glycosides (5*a*, 5*b*). These derivatives are not precursors for further elongation of the chain. In both procedures, the trichloroacetimidate method (6) was employed for the glycosylation step. The 2,3,5-tri-

Received 30 August 2005. Published on the NRC Research Press Web site at http://canjchem.nrc.ca on 6 April 2006.

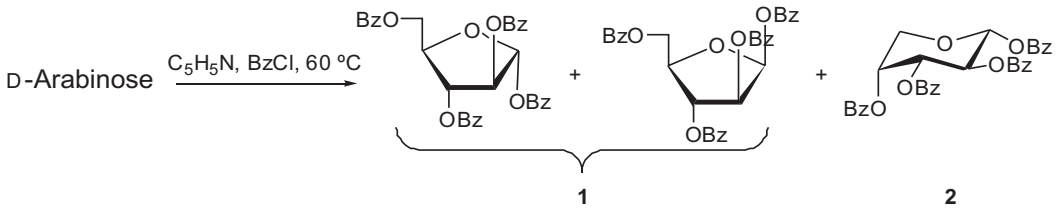
Dedicated to Professor Walter Szarek on the occasion of his 65th birthday.

L. Gandolfi-Donadío, C. Gallo-Rodriguez,[2] and R.M. de Lederkremer.[3] CIHIDECAR, Departamento de Química Orgánica, Facultad de Ciencias Exactas y Naturales, Universidad de Buenos Aires, Ciudad Universitaria, Pabellón II, 1428 Buenos Aires, Argentina.

[1]This article is part of a Special Issue dedicated to Professor Walter A. Szarek.
[2]Corresponding author (e-mail: cgallo@qo.fcen.uba.ar).
[3]Corresponding author (e-mail: lederk@qo.fcen.uba.ar).

 doi:10.1139/V06-025 © 2006 NRC Canada

Scheme 1.



O-acyl-α-D-arabinofuranosyl trichloroacetimidate donors were prepared from D-arabinose via the methyl arabinofuranoside in five steps.

The synthesis of a closely related trisaccharide fragment of the arabinogalactan was described by two groups (5). The procedures also employed the trichloroacetimidate method for the introduction of the Ara*f* unit.

The synthesis and conformation of D-arabinofuranosides from mycobacteria have been reviewed (7).

In the present work, we optimized the conditions for the one-step preparation of crystalline tetra-*O*-benzoyl-α,β-D-arabinofuranose (**1**) from D-arabinose. The D-arabinofuranose derivative **1** was used for tin(IV) chloride promoted glycosylation.

Results and discussion

The synthetic strategy relied on the use of a conveniently substituted D-galactono-1,4-lactone as the precursor of the reducing furanose ring (8, 9). Thus, after glycosylation, the disaccharide–lactone is reduced, acting as a virtually protected anomeric center. Activation of the anomeric center would allow further construction of different oligosaccharides.

We have extensively used the tin(IV) chloride promoted glycosylation method (10–12) for the activation of a peracylated galactofuranose. We employed α,β-perbenzoylgalactofuranose, which is obtained in the crystalline state in a one step-reaction from galactose (13). This is a very simple, direct, and convenient method for the construction of the β-D-galactofuranosyl linkage. Taking into account the stereochemical relationship between arabinose and galactose, we applied this glycosylation method to perbenzoyl arabinofuranose derivatives.

Tin(IV) chloride has been previously employed to achieve 1,2-*trans* α-arabinofuranosidic linkages. Tetra-*O*-acetyl-α-D-arabinofuranose, which was obtained in four steps as a syrup from arabinose, was used to give the expected 1,2-*trans* α-glycosidic linkage provided by the acetyl assistance in O-2 (14). On the other hand, it was described (15) that tetra-*O*-acetyl-α,β-D-arabinofuranose, obtained by ozonolysis of tri-*O*-acetyl-D-glucal, was employed as a glycosyl donor. However, the reaction gave low diastereoselectivity leading to a 2:1α:β ratio in the glycosylation of methyl 2,3,4-tri-*O*-benzyl-α-D-glucopyranoside (15). Similar results were obtained using the L-enantiomer (16).

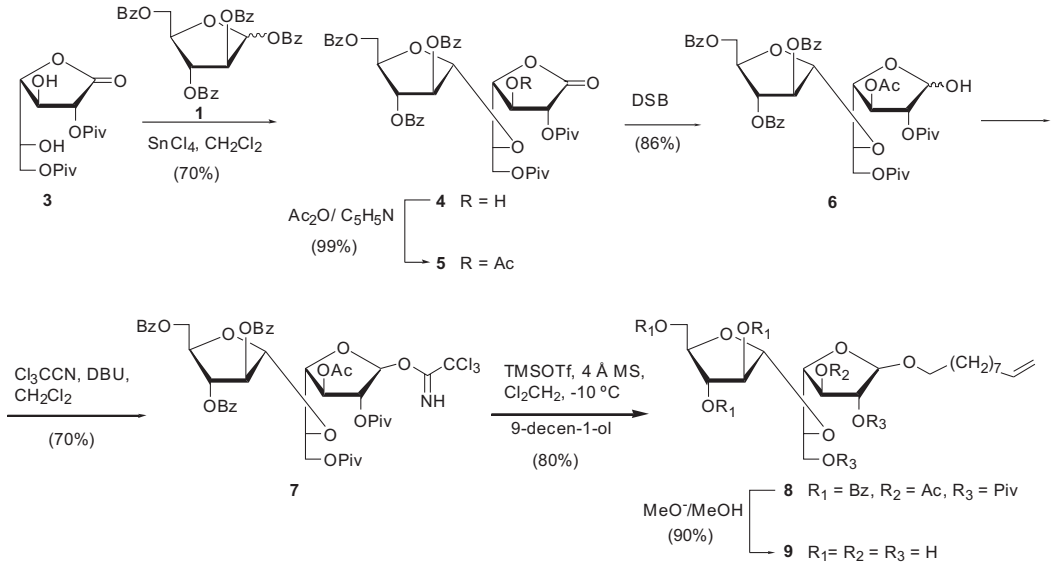
In the galactofuranose series, we have also noticed that glycosylation yields diminished when employing the peracetylated analog, which could be attributed to the lability of the acetyl compared with the benzoyl group in the presence of the strong Lewis acid tin(IV) chloride. Excellent yields were obtained when the benzoylated analog was employed (10–12). For that reason, we thought that 1,2,3,5-tetra-*O*-benzoyl-arabinofuranose (**1**) could be a good precursor for the tin(IV) chloride promoted glycosylation reaction. Compound **1** was synthesized, in one step, by the benzoylation of arabinose in hot pyridine (Scheme 1). The crude product was a mixture of β-furanose, α-furanose, and α-pyranose perbenzoates in a 30:27:43 ratio, respectively, as shown by the integration of the anomeric protons in the ^{1}H NMR spectrum: 6.88 (d, 0.30H, J = 4.4 Hz, H-1β furanose), 6.76 (s, 0.27H, H-1α furanose), 6.26 (d, 0.43H, J = 5.6 Hz, H-1α pyranose). No tetra-*O*-benzoyl-β-D-arabinopyranose was detected in the perbenzoylation reaction mixture. Crystallization of the crude product from ethanol gave a first crop of pure crystalline 1,2,3,4-tetra-*O*-benzoyl-α-D-arabinopyranose (**2**, 26%). Perbenzoyl arabinofuranose (**1**, 29%) crystallized from the mother liquors. On purification of a sample of the anomeric mixture by column chromatography, pure 1,2,3,5-tetra-*O*-benzoyl-α-D-arabinofuranose (**1α**) was obtained and fully characterized. Compound **1α** was previously obtained on reaction of 2,3,5-tri-*O*-benzoyl-α-D-arabinofuranosyl bromide with silver benzoate (17). The anomeric mixture was used for glycosylation. Although the furanose perbenzoate was isolated in a modest yield, its use as a donor in the route described in this paper has the advantage that it was obtained in a crystalline state in one step from D-arabinose.

With the arabinofuranosyl donor **1**, a tin(IV) chloride promoted glycosylation reaction could be performed with a Gal*f* template acceptor. Crystalline 2,6-di-*O*-pivaloyl-D-galactone-1,4-lactone (**3**) (9), obtained in one step from D-galactone-1,4-lactone, was employed as a precursor of the galactofuranose reducing end (Scheme 2). Compound **3** was previously used in our laboratory for the construction of β-D-Gal*f*-(1→5)-β-D-Gal*f*-(1→6)-D-Gal*f* (9). Thus, on treatment of 1.3 equiv. of acceptor **3** with 1 equiv. of arabinose donor **1**, and tin(IV) chloride as the promoter in CH_2Cl_2, selective glycosylation of the exocyclic OH-5 of **3** gave 2,3,5-tri-*O*-benzoyl-α-D-arabinofuranosyl-(1→5)-2,6-di-*O*-pivaloyl-D-galactono-1,4-lactone (**4**) in 70% yield. No product of condensation at the OH-3 of **3** was detected. The same regioselectivity was found when perbenzoyl galactofuranose or other galactofuranosyl derivatives were glycosylated with 2,6-di-*O*-substituted D-galactono-1,4-lactones (9, 11).

The diastereoselectivity of the glycosylation was determined from the coupling constants. In fact, the ^{1}H NMR spectrum of **4** showed a singlet at 5.44 ppm for the H-1′ and a doublet at 5.43 ppm (J = 1.7 Hz) for the H-2′, in agreement with an α-D-Ara*f* linkage. The ^{13}C NMR spectrum showed the resonance of the anomeric carbon at 107.6 ppm confirming the α-D-arabinofuranosyl linkage. The β linkage was not observed.

© 2006 NRC Canada

Scheme 2.



Previous to reducing the lactone function, acetylation of **4** was performed carefully to avoid β-elimination by-products. In this case, the ^{1}H NMR signal of H-3 in **5** was shifted 0.97 ppm downfield compared with H-3 in **4**, confirming that glycosylation had taken place regioselectively at OH-5. Further reduction of the lactone derivative **5** with disiamylborane gave 2,3,5-tri-*O*-benzoyl-α-D-arabinofuranosyl-(1→5)-3-*O*-acetyl-2,6-di-*O*-pivaloyl-D-galactofuranose (**6**); the target disaccharide showed both anomers in a 1:1 α:β ratio as indicated by the integration of the anomeric protons in the ^{1}H NMR spectrum at 5.53 ppm (d, J = 4.8 Hz, H-1α) and 5.33 (s, H-1β).

To synthesize the decenyl glycoside, the trichloroacetimidate method was chosen. This method has been successfully used for β-D-galactofuranosyl glycosylation (8, 9, 18–20). Thus, activation of the anomeric center of **6** with Cl_3CCN and DBU gave a mixture of β- and α-trichloroacetimidates (**7**) in 88% yield. Disaccharide imidate **7** was stable for 1 day at –20 °C. On reaction of **7** with 1.3 equiv. of 9-decen-1-ol in CH_2Cl_2 with TMSOTf as the catalyst, decenyl β-glycoside (**8**) was obtained diastereoselectively (80%). In the ^{1}H NMR spectrum, the galactofuranosyl anomeric proton of **8** gave a signal at 4.94 (s, H-1) indicating the β-configuration. This assignment was confirmed by the ^{13}C NMR spectrum, which showed the signal of C-1 at 106.5 ppm. Full assignments for compound **8** were supported by COSY and HETCOR experiments. Sodium methoxide deprotection of **8** afforded 1-decenyl α-D-Ara*f*-(1→5)-β-D-Gal*f* (**9**) in 90% yield. The ^{1}H NMR spectrum of **9** is shown in Fig. 1.

Conclusion

A facile synthesis of a synthon for the α-D-Ara*f*-(1→5)-D-Gal*f* (**4**) unit of *M. tuberculosis* arabinogalactan was achieved in 70% yield from **1** and **3**. The aldonolactone approach followed by DSB reduction produced the disaccharide **6**, conveniently protected for further coupling in the synthesis of oligosaccharide units, useful for studies on its biosynthesis. The decenyl glycoside was also synthesized allowing further functionalization of the double bond.

Experimental section

General

TLC was performed on 0.2 mm silica gel 60 F254 aluminium-supported plates. Detection was effected by exposure to UV light or by spraying with 5% (*v*/*v*) sulfuric acid in EtOH and charring. Column chromatography was performed on silica gel 60 (230–400 mesh). Melting points are uncorrected. Optical rotations were measured at 25 °C. High-resolution mass spectra (HRMS) were recorded on a VG ZAB2SE (1996) high-resolution mass spectrometer, with Opus V3.1 and DEC 3000 Alpha Station. NMR spectra were recorded at 500 MHz (^{1}H) and 125.8 MHz (^{13}C), or as indicated. Homo- and hetero-nuclear correlation spectroscopy experiments were performed when indicated.

1,2,3,5-Tetra-*O*-benzoyl-α,β-D-arabinofuranose (1αβ), 1,2,3,5-tetra-*O*-benzoyl-α-D-arabinofuranose (1α), and 1,2,3,4-tetra-*O*-benzoyl-α-D-arabinopyranose (2)

Arabinose (3.05 g, 20.3 mmol) in dry pyridine (63.9 mL) was heated in a boiling water bath for 45 min with the exclusion of moisture. The water bath was rapidly cooled to 60–65 °C and freshly distilled benzoyl chloride (11.3 mL, 97.4 mmol) was slowly added to the reaction mixture. After stirring at 60 °C for 1.3 h, water (6 mL) was added, and the stirring was continued for 30 min at room temperature. The solution was slowly poured into ice water (400 g) with vigorous stirring, affording an amorphous solid. After decantation, the remaining solid was washed five times with water. The ^{1}H NMR spectrum ($CDCl_3$) of the solid showed the anomeric signals with the following integrations: δ 6.88 (d, 0.30H, J = 4.4 Hz, H-1β furanosic), 6.76 (s, 0.27H, H-1α furanosic), 6.26 (d, 0.43H, J = 5.6 Hz, H-1α pyranosic). The

© 2006 NRC Canada

solid was dissolved in boiling EtOH (400 mL) and slow crystallization took place. After 1 day, crystals of 1,2,3,4-tetra-*O*-benzoyl-α-D-arabinopyranose (**2**, 3.02 g, 26%, R_f 0.46, hexane–EtOAc (3:1), twice developed) were obtained; mp 161 to 162 °C. $[\alpha]_D$ –113.8° (*c* 1, $CHCl_3$) (lit. value (21) mp 164 to 165 °C, MeOH–AcOH, 80:5.7; $[\alpha]_D$ –114.4° (*c* 0.848, $CHCl_3$)). ^{1}H NMR ($CDCl_3$) δ: 8.08–7.33 (m, 20H), 6.26 (d, 1H, *J* = 5.6 Hz, H-1), 5.95 (dd, 1H, *J* = 5.6, 7.3 Hz, H-2), 5.80 (ddd, 1H, *J* = 2.9, 3.6, 5.2 Hz, H-4), 5.78 (dd, 1H, *J* = 3.6, 7.3 Hz, H-3), 4.43 (dd, 1H, *J* = 5.2, 12.6 Hz, H-5a), 4.14 (dd, 1H, *J* = 2.9, 12.6 Hz, H-5b) (lit. value (22) ^{1}H NMR (acetone-d_6, 100 MHz)). ^{13}C NMR ($CDCl_3$) δ: 164.5–164.7 (*C*OPh), 133.7–128.5 (aromatic), 92.4 (C-1), 69.9 (C-3), 68.9 (C-2), 67.5 (C-4), 62.7 (C-5).

The mother liquors were kept at room temperature (20–23 °C) for 2 days and the second crop of crystals was filtered and characterized as 1,2,3,5-tetra-*O*-benzoyl-α,β-D-arabinofuranose (**1αβ**, 3.34 g, 29%, R_f 0.53 and 0.49, hexane–EtOAc (3:1), twice developed) in a 7:3 α:β ratio. ^{1}H NMR ($CDCl_3$) δ: 8.13–7.24 (m, 20H), 6.87 (d, 0.3H, *J* = 4.7 Hz, H-1 β anomer), 6.76 (s, 0.7H, H-1 α anomer), 6.11 (dd, 0.3H, *J* = 5.2, 7.0 Hz, H-3), 5.94 (dd, 0.3H, *J* = 4.7, 7.0 Hz, H-2), 5.82 (d, 0.7H, *J* = 0.8 Hz, H-2), 5.68 (dd, 0.7H, *J* = 3.7, 0.8 Hz, H-3), 4.83 (dd, 0.7H, *J* = 3.9, 12.7 Hz, H-5a), 4.82 (m, 0.7H, H-4), 4.81 (dd, 0.3H, *J* = 6.7, 14.1 Hz, H-5a), 4.73 (dd, 0.7H, *J* = 6.4, 12.7 Hz, H-5b), 4.67 (m, 0.3H, H-4), 4.66 (dd, 0.3H, *J* = 6.1, 14.1 Hz, H-5b). ^{13}C NMR ($CDCl_3$) δ: 166.2–164.6 (*C*OPh), 133.7–128.2 (aromatic), 99.8 (C-1 α anomer), 94.5 (C-1 β anomer), 83.9 (C-4 α anomer), 80.9 (C-2 α anomer), 79.8, 77.5, 76.2, 75.5, 64.7, 63.7.

A sample of **1αβ** was purified by column chromatography (toluene) to yield pure 1,2,3,5-tetra-*O*-benzoyl-α-D-arabinofuranose (**1α**). Crystallization from EtOH gave: mp 100 to 101 °C (EtOH). $[\alpha]_D$ +26.7° (*c* 1, $CHCl_3$) (lit. value (17) mp 117–121 °C (EtOH). $[\alpha]_D$ +27.9° (*c* 2.13, $CHCl_3$)). ^{1}H NMR ($CDCl_3$) δ: 8.14–7.26 (m, 20H), 6.76 (s, 1H, H-1), 5.82 (d, 1H, *J* = 0.8 Hz, H-2), 5.68 (dd, 1H, *J* = 3.7, 0.8 Hz, H-3), 4.83 (dd, 1H, *J* = 3.9, 12.7 Hz, H-5a), 4.82 (m, 1H, H-4), 4.73 (dd, 1H, *J* = 6.4, 12.7 Hz, H-5b). ^{13}C NMR ($CDCl_3$) δ: 166.2–164.6 (*C*OPh), 133.8–128.3 (aromatic), 99.8 (C-1), 83.9 (C-4), 80.9 (C-2), 77.5 (C-3), 63.7 (C-5). These assignments were supported by HETCOR experiments.

2,3,5-Tri-*O*-benzoyl-α-D-arabinofuranosyl-(1→5)-2,6-di-*O*-pivaloyl-D-galactono-1,4-lactone (4)

To an externally cooled (0 °C) solution of tetra-*O*-benzoyl-α,β-D-arabinofuranose (**1αβ**, 1.07 g, 1.9 mmol) in dry CH_2Cl_2 (50 mL) was added $SnCl_4$ (0.22 mL, 1.9 mmol) with stirring in an argon atmosphere. After 10 min, this solution was added to a solution of compound **3** (9) (0.86 g, 2.5 mmol) in CH_2Cl_2 (50 mL) over a 25 min period and then the mixture was stirred for 3 h at 0 °C. The solution was poured into aq. $NaHCO_3$ and extracted with CH_2Cl_2 (2 × 200 mL). The organic extract was washed with water (3 × 100 mL), dried (Na_2SO_4), filtered, and concentrated under reduced pressure. Purification of the residue by column chromatography (toluene–EtOAc, 20:1) gave 1.05 g of **4** (70% yield) as a foamy solid. R_f 0.45 (toluene–EtOAc, 3:1). $[\alpha]_D$ –28.1° (*c* 1, $CHCl_3$). ^{1}H NMR ($CDCl_3$) δ: 8.07–7.14 (m, 15H), 5.68 (dd, 1H, *J* = 1.7, 4.8 Hz, H-3′), 5.44 (bs, 1H, H-1′), 5.43 (d, 1H, *J* = 1.7 Hz, H-2′), 5.37 (d, 1H, *J* = 8.0 Hz, H-2), 4.80 (dd, 1H, *J* = 2.6, 11.2 Hz, H5a′), 4.79 (dt, 1H, *J* = 3.0, 8.0 Hz, H-3), 4.70 (m, 1H, H-4′), 4.67 (dd, 1H, *J* = 5.0, 11.2 Hz, H-5b′), 4.46 (dd, 1H, *J* = 5.5, 11.5 Hz, H-6a), 4.44 (dd, 1H, *J* = 3.5, 8.0 Hz, H-4), 4.34 (dd, 1H, *J* = 6.7, 11.5 Hz, H-6b), 4.20 (ddd, 1H, *J* = 3.5, 5.5, 6.7 Hz, H-5), 3.87 (d, 1H, *J* = 3.0, OH), 1.26, 1.19 (2s, 18H, $(CH_3)_3CCO$). ^{13}C NMR ($CDCl_3$) δ: 179.1, 177.0 ($(CH_3)_3C\mathit{C}O$), 168.7 (C-1), 166.1–165.8 (*C*OPh), 137.8–128.2 (aromatic), 107.6 (C-1′), 83.0 (C-2′), 81.2 (C-4′), 79.8 (C-4), 77.0 (C-3′), 76.4 (C-2), 74.8 (C-5), 72.4 (C-3), 63.4 (C-5′), 62.6 (C-6), 38.9, 38.7 ($(CH_3)_3\mathit{C}CO$), 27.1, 26.9 ($(\mathit{C}H_3)_3CCO$). These assignments were supported by COSY and HETCOR experiments. Anal. calcd. for $C_{42}H_{46}O_{15}$: C 63.79, H 5.86; found: C 63.72, H 6.13.

2,3,5-Tri-*O*-benzoyl-α-D-arabinofuranosyl-(1→5)-3-*O*-acetyl-2,6-di-*O*-pivaloyl-D-galactono-1,4-lactone (5)

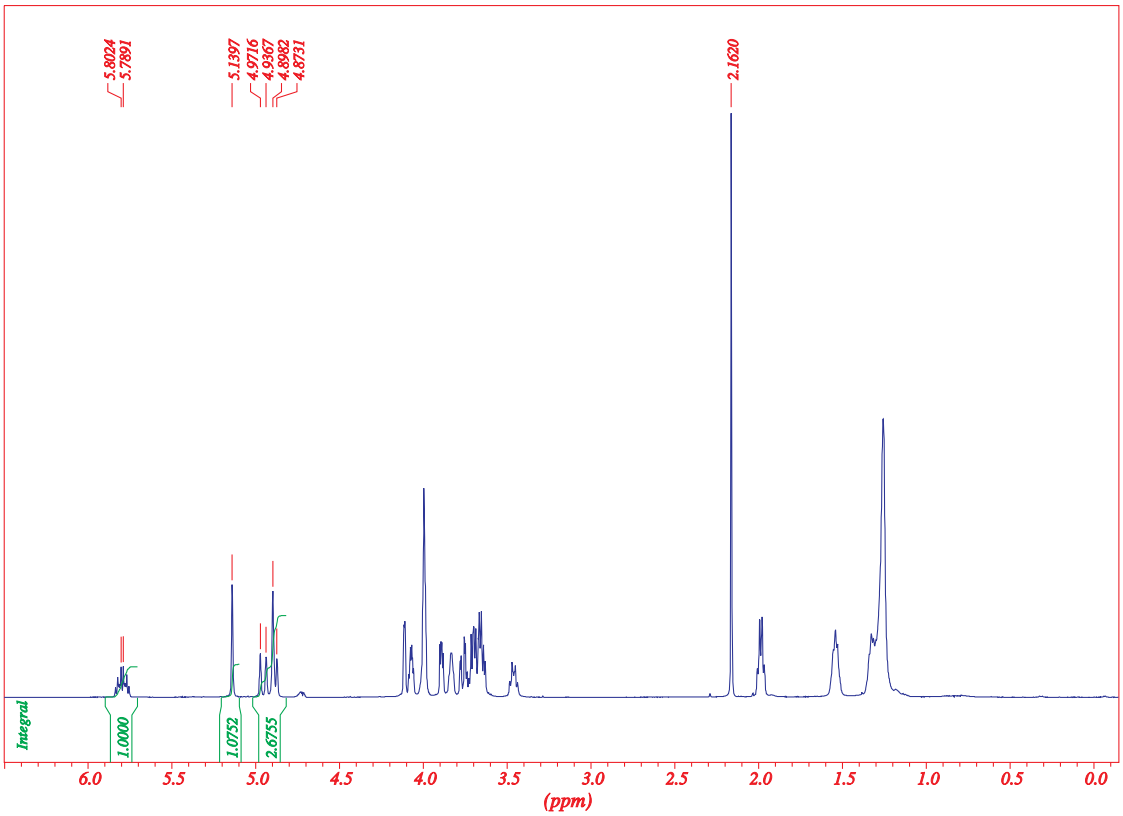
To a solution of **4** (1.29 g, 1.63 mmol) in dry pyridine (13 mL), cooled at 0 °C, was added acetic anhydride (13 mL, dropwise) and the mixture was stirred at room temperature for 30 min. After cooling to 0 °C, the reaction was quenched by a slow addition of MeOH (20 mL) and the stirring continued for 30 min at room temperature. The solution was diluted with CH_2Cl_2 (200 mL) and then sequentially washed with 10% HCl (2 × 200 mL), water (200 mL), satd. aq. $NaHCO_3$ (200 mL), water, dried (Na_2SO_4), and then concentrated to give **5** (1.34 g, 99%) as a chromatographically pure syrup. R_f 0.66 (toluene–EtOAc, 3:1). $[\alpha]_D$ –21.3° (*c* 1, $CHCl_3$). ^{1}H NMR ($CDCl_3$) δ: 8.04–7.16 (m, 15H, aromatic), 5.76 (t, 1H, *J* = 6.6 Hz, H-3), 5.66 (d, 1H, *J* = 6.9 Hz, H-2), 5.63 (dd, 1H, *J* = 1.4, 4.6 Hz, H-3′), 5.59 (bs, 1H, H-1′), 5.56 (d, 1H, *J* = 1.4 Hz, H-2′), 4.80 (dd, 1H, *J* = 5.3, 13.5 Hz, H-5a′), 4.67 (m, 2H, H-4′, H-5b′), 4.55 (dd, 1H, *J* = 3.0, 6.4 Hz, H-4), 4.48 (dd, 1H, *J* = 4.4, 11.0 Hz, H-6a), 4.29 (dd, 1H, *J* = 7.1, 11.0 Hz, H-6b), 4.25 (ddd, 1H, *J* = 3.0, 4.4, 7.1 Hz, H-5), 2.11 (s, 3H, CH_3), 1.20, 1.18 (2s, 18H, $(CH_3)_3CCO$)). ^{13}C NMR ($CDCl_3$) δ: 177.6, 177.1 ($(CH_3)_3C\mathit{C}O$), 169.9 (C-1), 168.4 ($\mathit{C}OCH_3$), 166.1–165.4 (*C*OPh), 133.5–128.3 (aromatic), 107.6 (C-1′), 82.4 (C-2′), 81.7 (C-4′), 79.1 (C-4), 77.2 (C-3′), 75.4 (C-5); 72.9, 72.0 (C-2, C-3), 63.6 (C-5′), 62.4 (C-6), 38.7, 38.6 ($(CH_3)_3\mathit{C}CO$), 27.1, 26.8 ($(\mathit{C}H_3)_3CCO$), 20.5 ($CO\mathit{C}H_3$). These assignments were supported by COSY and HETCOR experiments. Anal. calcd. for $C_{44}H_{48}O_{16}$: C 63.45, H 5.81; found: C 63.48, H 5.83.

2,3,5-Tri-*O*-benzoyl-α-D-arabinofuranosyl-(1→5)-3-*O*-acetyl-2,6-di-*O*-pivaloyl-D-galactofuranose (6)

A solution of bis(2-butyl-3methyl)borane (9.24 mmol) in anhydr. THF (2.6 mL), cooled to 0 °C and under an argon atmosphere, was added to a flask containing previously dried compound **5** (1.28 g, 1.54 mmol). The resulting solution was stirred for 22 h at room temperature and then processed as previously described (23). The organic layer was washed with water, dried (Na_2SO_4), and concentrated. Boric acid was eliminated by coevaporation with MeOH (5 × 20 mL) at room temperature. The residue was purified by column chromatography (toluene–EtOAc, 15:1) to give

© 2006 NRC Canada

Fig. 1. ^{1}H NMR spectrum of compound **9** (D_2O, 500 MHz, acetone was used as internal reference).



1.05 g (86%) of **6** (syrup) as a 2:3 α:β anomeric mixture. R_f 0.43 (toluene–EtOAc, 3:1). $[\alpha]_D$ –2.4° (*c* 1, $CHCl_3$). ^{1}H NMR ($CDCl_3$) anomeric protons δ: 5.67 (bs, 0.5H, H-1′ for β anomer), 5.63 (bs, 0.5H, H-1′ for α anomer), 5.53 (d, 0.5H, J = 4.7 Hz, H-1 α anomer), 5.33 (bs, 0.5H, H-1 β anomer). ^{13}C NMR ($CDCl_3$) δ: 178.0–177.4 (($CH_3)_3CCO$)), 170.6, 170.1 ($COCH_3$), 166.1–165.3 ($COPh$), 133.7–125.3 (aromatic), 107.6 (C-1′β anomer), 106.5 (C-1′α anomer), 100.6 (C-1 β anomer), 95.0 (C-1 α anomer), 82.8, 82.1, 82.0, 81.7, 81.2, 80.9, 80.3, 77.7, 77.2, 77.1, 76.9, 76.7, 75.5, 75.2, 63.7, 63.6, 63.5, 63.0, 38.7 (($CH_3)_3CCO$)), 27.1, 27.0, 26.9 (($CH_3)_3CCO$), 20.7, 20.6 (CH_3). These assignments were supported by COSY and HETCOR experiments. Anal. calcd. for $C_{44}H_{50}O_{16}$: C 63.30, H 6.04; found: C 63.65, H 6.44.

9-Decenyl 2,3,5-tri-*O*-benzoyl-α-D-arabinofuranosyl-(1→5)-3-*O*-acetyl-2,6-di-*O*-pivaloyl-D-galactofuranoside (8)

To a stirred solution of **6** (314 mg, 0.40 mmol) and trichloroacetonitrile (0.20 mL, 2.0 mmol) in dry CH_2Cl_2 (10 mL), cooled to 0 °C, DBU (28.4 µL, 0.18 mmol) was slowly added. After 1 h, the solution was concentrated under reduced pressure, and the residue was purified by column chromatography (toluene–EtOAc–TEA, 40:1:0.4) to give 342 mg (88%) of *O*-(2,3,5-tri-*O*-benzoyl-α-D-arabinofuranosyl-(1→5)-3-*O*-acetyl-2,6-di-*O*-pivaloyl-α,β-D-galactofuranosyl) trichloroacetimidate (**7**) as an amorphous solid (R_f 0.33 and 0.47 in toluene–EtOAc–TEA (9:1:0.09) for the α and β anomers, respectively). Compound **7** was stable for 1 day at –20 °C. ^{1}H NMR ($CDCl_3$, 200 MHz) δ: 8.61 (s, 0.8H, N*H*), 8.44 (s, 0.2H, N*H*), 6.55 (d, 0.2H, J = 4.6 Hz, H-1 α anomer), 6.30 (s, 0.8H, H-1 β anomer). ^{13} C NMR ($CDCl_3$, 25 MHz) for the β anomer δ: 177.8, 177.0 (($CH_3)_3CCO$), 170.0 (CH_3CO), 166.2–165.2 ($COPh$), 160.2 ($NHCOCl_3$), 133.5–125.3 (aromatic), 106.5 (C-1′), 102.8 (C-1), 97.9 (C-1 α anomer), 84.0, 82.1, 81.3, 80.4, 77.6, 75.8, 74.3, 63.6, 63.4, 38.6 (($CH_3)_3CCO$ × 2), 27.1, 26.9 (($CH_3)_3CCO$), 20.6 (CH_3CO).

A vigorously stirred suspension of the trichloroacetimidate **7** (241 mg, 0.25 mmol), 9-decen-1-ol (60.4 µL, 0.33 mmol), and powdered activated 4 Å molecular sieves (0.5 g) in anhydr. CH_2Cl_2 (9 mL) was cooled to –20 °C, and TMSOTf (13.3 µL, 0.073 mmol) was slowly added. After 30 min of stirring, the mixture was filtered into aq. $NaHCO_3$ (15 mL) and then extracted with CH_2Cl_2 (2 × 25 mL). The organic layer was washed with water (3 × 40 mL), dried (Na_2SO_4), filtered, and concentrated under reduced pressure. The residue was purified by column chromatography (toluene–EtOAc, 45:1) affording **8** (243 mg, 80%) as a syrup. R_f 0.60 (toluene–EtOAc, 9:1). $[\alpha]_D$ –23.9° (*c* 1, $CHCl_3$). ^{1}H NMR ($CDCl_3$) δ: 8.07–7.26 (m, 15H, aromatic), 5.80 (ddt, 1H, J = 6.7, 10.2, 17.2 Hz, C*H*=CH_2), 5.65 (s, 1H, H-1′), 5.61 (dd, 1H, J = 1.5, 5.0 Hz, H-3′), 5.57 (d, 1H, J = 1.5 Hz, H-2′), 5.23 (dd, 1H, J = 1.7, 5.5 Hz, H-3), 5.07 (d, 1H, J = 1.7 Hz, H-2), 4.98 (ddt, 1H, J = 1.2, 1.7, 17.2 Hz, HC=CH_aH), 4.94 (bs, 1H, H-1), 4.92 (ddt, 1H, J = 1.3, 2.5, 10.2 Hz, HC=CH_bH), 4.80 (dd, 1H, J = 3.2, 11.4 Hz, H-5a′), 4.71 (m, 1H, H-4′), 4.67 (dd, 1H, J = 4.8, 11.4 Hz, H-5b′), 4.36 (m, 1H, H-5), 4.24–4.30 (m, 3H, H-6a, H-6b, H-4), 3.67 (dt, 1H, J = 6.7, 9.7 Hz, CH_aHO), 3.40 (dt, 1H, J = 6.5, 9.7 Hz, CH_bHO), 2.07 (s, 3H, CH_3), 2.04 (m, 2H, CH_2), 1.58 (m, 2H, CH_2), 1.27 (m, 12H, CH_2), 1.17, 1.16 (2s, 18H,

© 2006 NRC Canada

((CH_3)$_3$CCO). ^{13}C NMR ($CDCl_3$) δ: 177.9, 177.4 ((CH_3)$_3$*C*CO), 170.2 (CH_3*C*O), 166.1–165.2 (*C*OPh), 139.1 (*C*H=CH_2), 133.5–128.3 (aromatic), 114.1 (CH=*C*H$_2$), 106.5 (C-1′), 105.3 (C-1), 82.2 (C-2′), 81.9 (C-2), 81.0 (C-4′), 80.9 (C-4), 77.7 (C-3′), 76.9 (C-3), 74.6 (C-5), 67.6 (CH_2O), 63.7 (C-5′), 63.6 (C-6), 38.7, 38.6, ((CH_3)$_3$*C*CO), 33.8, 29.4, 29.3, 29.0, 28.9, 27.1, 26.9, 26.0 (*C*H$_3$)$_3$CCO), 20.7 (CH_3). These assignments were supported by COSY and HETCOR experiments. Anal. calcd. for $C_{54}H_{68}O_{16}$: C 66.65, H 7.04; found: C 66.48, H 7.09.

9-Decenyl α-D-arabinofuranosyl-(1→5)-β-D-galactofuranoside (9)

Compound **8** (112 mg, 0.12 mmol) was suspended in 0.48 mol/L sodium methoxide in a methanol solution (1.7 mL) and cooled at 0 °C. After stirring for 1 h at 0 °C, the resulting solution was warmed to room temperature, stirred for 2 h, and water (0.5 mL) was added. The solution was passed through a column containing Amberlite IR-120 plus (H^+) resin (3 mL) and the column washed with MeOH–H_2O (9:1). The combined eluates were evaporated and the remaining methyl benzoate was eliminated by five successive coevaporations with water. The residue was dissolved in water, further purified through a C8-Maxi-Clean cartridge, and the solution lyophilized. Glycoside **9** (49 mg, 90%) was obtained as a hygroscopic syrup. R_f 0.86 (*n*-propanol–EtOH–H_2O, 7:1:1). $[\alpha]_D$ –4.4° (*c* 0.6, H_2O). ^{1}H NMR (D_2O) δ: 5.79 (ddt, 1H, *J* = 6.7, 10.4, 17.0 Hz, C*H*=CH$_2$), 5.14 (d, 1H, *J* = 1.9 Hz, H-1′), 4.95 (ddt, 1H, *J* = 1.5, 3.7, 17.0 Hz, HC=C*H*$_a$H), 4.90 (bs, 1H, H-1), 4.88 (ddt, 1H, *J* = 1.1, 2.2, 10.4 Hz, HC=C*H*$_b$H), 4.11 (dd, 1H, *J* = 1.9, 3.7 Hz, H-2′), 4.07 (ddd, 1H, *J* = 3.3, 5.9, 6.1 Hz, H-4′), 4.01–3.98 (m, 3H, H-2, H-3, H-4), 3.89 (dd, 1H, *J* = 3.7, 6.1 Hz, H-3′), 3.83 (m, 1H, H-5), 3.76 (dd, 1H, *J* = 3.3, 12.6 Hz, H-5a′), 3.74–3.63 (m, 3H, H-6a, H-6b, C*H*$_a$HO), 3.65 (dd, 1H, *J* = 5.9, 12.6 Hz, H-5b′), 3.46 (dt, 1H, *J* = 6.7, 10.0 Hz, C*H*$_b$HO), 1.98 (m, 2H, CH_2), 1.54 (m, 2H, CH_2), 1.36–1.22 (m, 10H, CH_2). ^{13}C NMR (D_2O) δ: 140.3 (*C*H=CH$_2$), 114.6 (CH=*C*H$_2$), 109.1 (C-1′), 107.6 (C-1), 84.4 (C-4′), 82.4 (C-2′), 81.9, 81.7 (C-4, C-2), 78.4 (C-5), 77.0, 76.9 (C-3′, C-3), 69.6 (CH_2O), 62.1 (C-6), 61.8 (C-5′), 34.0, 29.6, 29.5, 29.4, 29.2, 29.1, 26.1. HRMS (FAB+) *m*/*z* calcd. for $C_{21}H_{38}O_{10}Na$: 473.2363 (M + Na^+); found: 473.2356. Anal. calcd. for $C_{21}H_{38}O_{10}\cdot 0.5H_2O$: C 54.89, H 8.55; found: C 54.86, H 8.68.

Acknowledgments

This work was supported by grants from Agencia Nacional de Promoción Científica y Tecnológica, Universidad de Buenos Aires, and Fundación Antorchas. C. Gallo-Rodriguez and R.M. de Lederkremer are research members of Consejo Nacional de Investigaciones Científicas Técnicas (CONICET). L. Gandolfi-Donadio is a fellow from CONICET.

References

1. (*a*) World Health Organization (WHO). *In* Anti-tuberculosis drug resistance in the world. The WHO/IUATLD Global Project on Anti-tuberculosis Resistance Surveillance. WHO, Geneva, Switzerland. 1997. Publication WHO/TB/97.229; (*b*) D. Butler. Nature, **406**, 670 (2000).
2. F. Pan, M. Jackson, Y. Ma, and M. McNeil. J. Bacteriol. **183**, 3991 (2001).
3. D.C. Crick, S. Mahaprata, and P.J. Brennan. Glycobiology, **11**, 107 (2001).
4. A.K. Pathak, V. Pathak, W.J. Suling, S.S. Gurcha, C.B. Morehouse, G.S. Besra, J.A. Maddry, and R.C Reynolds. Bioorg. Med. Chem. **10**, 923 (2002).
5. (*a*) M.K. Gurjar, L.K. Reddy, and S. Hotha. Org. Lett. **3**, 321 (2001); (*b*) M.K. Gurjar, L.K. Reddy, and S. Hotha. J. Org. Chem. **66**, 4657 (2001); (*c*) H. Wang and J. Ning. J. Org. Chem. **68**, 2521 (2003).
6. R.R. Schmidt and K.-H. Jung. *In* Preparative carbohydrate chemistry. *Edited by* S. Hanessian. Marcel Dekker Inc., New York. 1997. pp. 283–312.
7. T.L Lowary. *In* Glycochemistry: Principles, synthesis, and applications. *Edited by* P.G Wang and C.R. Bertozzi. Marcel Dekker Inc., New York. 2001. pp. 133–162.
8. L. Gandolfi-Donadío, C. Gallo-Rodriguez, and R.M. de Lederkremer. J. Org. Chem. **67**, 4430 (2002).
9. L. Gandolfi-Donadío, C. Gallo-Rodriguez, and R.M. de Lederkremer. J. Org. Chem. **68**, 6928 (2003).
10. C. Marino, O. Varela, and R.M. de Lederkremer. Carbohydr. Res. **190**, 65 (1989).
11. R.M. de Lederkremer, C. Marino, and O. Varela. Carbohydr. Res. **200**, 227 (1990).
12. C. Gallo-Rodriguez, O. Varela, and R.M. de Lederkremer. J. Org. Chem. **61**, 1886 (1996).
13. (*a*) N.B. D'Accorso, I.M.E. Thiel, and M. Schüller. Carbohydr. Res. **124**, 177 (1983); (*b*) C. Gallo-Rodriguez, O. Varela, and R.M. de Lederkremer. Carbohydr. Res. **305**, 163 (1998).
14. A.K. Pathak, Y.A. El-Kattan, N. Bansal, J.A. Maddry, and R.C. Reynolds. Tetrahedron Lett. **39**, 1497 (1998).
15. F.W. D'Souza, P.E. Cheshev, J.D. Ayers, and T.L. Lowary. J. Org. Chem. **63**, 9037 (1998).
16. K. Mizutani, R. Kasai, M. Nakamura, O. Tanaka, and H. Matsuura. Carbohydr. Res. **185**, 27 (1989).
17. R.K. Ness and H.G. Fletcher. J. Am. Chem. Soc. **80**, 2007 (1958).
18. A.K. Choudhury and N. Roy. Carbohydr. Res. **308**, 207 (1998).
19. C. Gallo-Rodriguez, L. Gandolfi, and R.M. de Lederkremer. Org. Lett. **1**, 245 (1999).
20. C. Gallo-Rodriguez, M.A. Gil-Libarona, V.M. Mendoza, and R.M. de Lederkremer. Tetrahedron, **58**, 9373 (2002).
21. H.G. Fetcher, Jr. and C.S. Hudson. J. Am. Chem. Soc. **69**, 1145 (1947).
22. P.L. Durette and D. Horton. J. Org. Chem. **36**, 2658 (1971).
23. L.M. Lerner. Methods Carbohydr. Chem. **6**, 131 (1972).

© 2006 NRC Canada

Towards C-2 symmetrical macrocyles with an incorporated sucrose unit[1]

Sławomir Jarosz and Arkadiusz Listkowski

Abstract: The first C_2 symmetrical macrocyclic receptor containing two sucrose molecules has been prepared, albeit in low yield, by reaction of hexa-*O*-benzyl-6′-*O*-acroyl-6-*O*-allylsucrose in the presence of a second generation Grubbs catalyst (1,3-dimesityl-4,5-dihydroimidazol-2-ylidene ruthenium alkylidene complex). Highly selective protection of the 6′-OH group in 1′,2,3,3′,4,4′-hexa-*O*-benzylsucrose was a key step in the preparation of the precursor used under ring closing metathesis (RCM) conditions.

Key words: sucrose, macrocyclic receptors, metathesis, regioselective transformations.

Résumé : La réaction du hexa-*O*-benzyl-6′-*O*-acroyl-6-*O*-allylsucrose en présence du catalyseur de Grubbs de deuxième génération (complexe alkylidène 1,3-dimésityl-4,5-dihydroimidazol-2-ylidène ruthénium) nous a permis de préparer, avec un faible rendement, le premier récepteur macrocyclique de symétrie C_2 contenant deux molécules de sucrose. La protection hautement sélective du groupe OH en 6′ du 1′,2,3,3′,4,4′-hexa-*O*-benzylsucrose est l'étape clé dans la préparation du précurseur utilisé dans les conditions de fermeture de cycle par métathèse (RCM).

Mots clés : sucrose, récepteurs macrocycliques, métathèse, transformations régiosélectives.

[Traduit par la Rédaction]

Introduction

Sucrose, a cheap raw material, is available in more than 130 million tons per year; most of it is consumed on the food market. This chemical is very demanding to work with because of its very poor solubility in organic solvents (except DMF, pyridine, and DMSO), presence of eight hydroxyl groups that are difficult to differentiate, and the high sensitivity of the glycosidic bond in acidic media. However, this disaccharide is a subject of interest for several laboratories, which use it as a starting material for the preparation of fine chemicals (1–3), as well as biodegradable polymers or surfactants (4). Recently, a biocatalytic approach to sucrose analogs has been published (5).

As part of an on-going program, we elaborated a convenient route to 2,3,3′,4,4′-penta-*O*-benzylsucrose (6) (**1**), a useful starting material for the preparation of derivatives modified at the terminal (C1′, C6, C6′) positions. Differentiation of the primary hydroxyl groups in **1** is possible, which allows for the production of all three monoalcohols, as well as the 6,6′-diol **2**, in good yields (3, 7). Recently, we prepared another useful sucrose diol, compound **3** (8), and applied it in the preparation of a variety of crown ether analogs (**4**, Fig. 1) (9).

In this paper a methodology leading to complex sucrose macrocycles possessing higher symmetry will be described. Differentiation of the primary hydroxyl groups in **3** is required for regioselective introduction of the proper olefinic fragments needed for cyclization under ring closing metathesis (RCM) conditions.

Synthesis of selectively protected derivatives of hexa-*O*-benzylsucrose

Reaction of the free sucrose with 1 equiv. of silylating agent preferentially protects the 6′-OH group (10). Since the same feature applies for diol **2** (7), similar selective protection of **3** was also expected. Diol **3** was reacted with *tert*-butyldimethylsilyl chloride to afford alcohol **5** in 48% yield. Protection at the C-6′ position was confirmed by advanced NMR experiments performed on derivative **7** in which the COSY correlations between H-5 (glucose part) and both olefinic protons were visible. Since the yield of product **5** was not particularly impressive, we used the more bulky silyl reagent, *tert*-butyldiphenylsilyl chloride, and obtained alcohol **6** in 60% yield. Its structure was also confirmed by the NMR experiments performed on methyl uronate (**11**); the significant lowfield shift of the H-5 resonance (δ 4.56 ppm) proved that this proton is in close vicinity to the ester group, hence the 6-OH (and not 6′-OH) group in alcohol **7** was not protected (Scheme 1).

Synthesis of 6-*O*-allyl-6′-*O*-acroyl derivative **10**, the direct precursor of the C_2-symmetrical macrocycle, was achieved in 37% overall yield from **6** by allylation of the 6-

Received 30 August 2005. Published on the NRC Research Press Web site at http://canjchem.nrc.ca on 6 April 2006.

Dedicated to Professor Walter Szarek on the occasion of his 65th birthday.

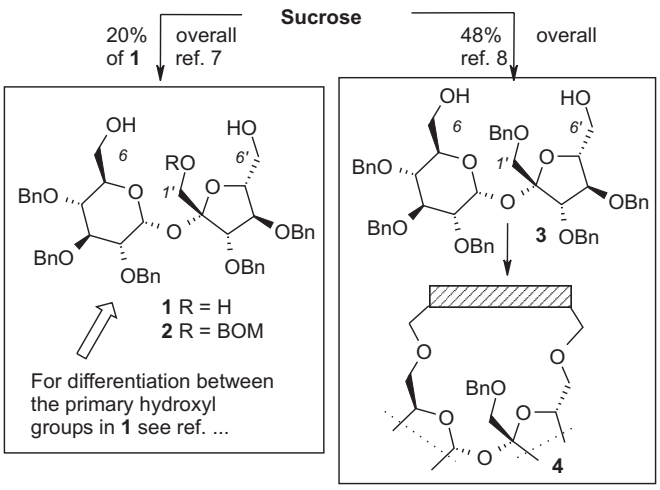
S. Jarosz[2] and A. Listkowski. Institute of Organic Chemistry, Academy of Sciences, 01-224 Kasprzaka 44/52, Warsaw, Poland.

[1]This article is part of a Special Issue dedicated to Professor Walter A. Szarek.

[2]Corresponding author (e-mail: sljar@icho.edu.pl).

 doi:10.1139/V06-035 © 2006 NRC Canada

Fig. 1. Preparation of partially protected sucrose derivatives and synthesis of the crown ether analogs containing sucrose.



OH group with allyl bromide,[3] followed by removal of the silyl protection from the 6′-OH and subsequent acroylation (Scheme 1).

Cyclization of sucrose derivative 11 to the C_2-symmetrical receptor

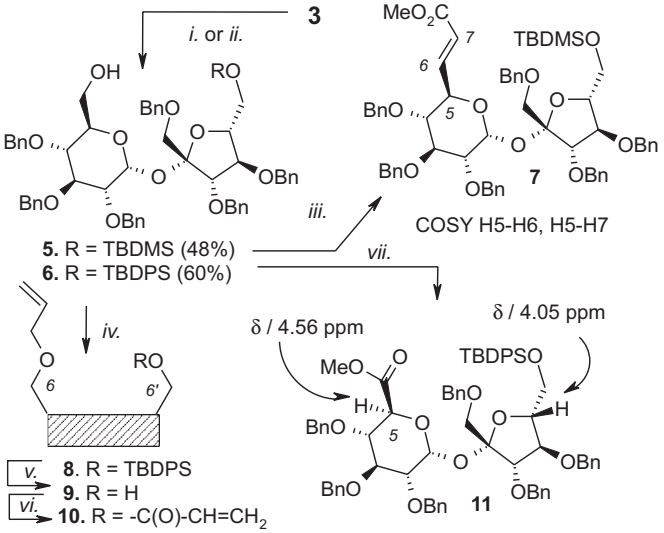
Reaction of **11** performed in the presence of a second generation Grubbs catalyst (1,3-dimesityl-4,5-dihydroimidazol-2-ylidene ruthenium alkylidene complex (11)) afforded a mixture of products in a total yield of about 35%. Four different compounds (**12**–**15**) were isolated by HPLC (Scheme 2).

Structures of all these products were established by MS and high-resolution NMR spectroscopy. The MS spectra of compounds **12** and **13** clearly pointed at the presence of only one molecule of sucrose (in both spectra, the signals *m*/*z* 971 [M($C_{58}H_{60}O_{12}$) + Na^+] and 987 [M($C_{58}H_{60}O_{12}$) + K^+] were seen). The geometry across the newly created double bonds was determined from the ^{1}H NMR spectra of these macrocycles. Thus, the large coupling constant (J = 16.1 Hz) pointed at the E geometry in **12**, while the smaller constant (J = 12.0 Hz) proved the Z geometry in **13**.

The MS data of one of the two remaining derivatives were in accordance with the dimeric structure; the signal at *m*/*z* 1919 [($C_{116}H_{120}O_{24}$) + Na^+] could be assigned to the expected cyclic derivative **14**. In the ^{13}C NMR spectrum of this compound, only one -CH=CH-C(O)- group was seen (δ 165.8, 145.6, and 120.0 ppm), which strongly supported the symmetrical structure. Further information was obtained from the ^{1}H NMR spectrum; the large coupling constant (J = 15.8 Hz) among two olefinic protons (at δ 6.83 and 5.96 ppm) clearly pointed at the E geometry across this double bond. This is consistent with the literature data reporting on a preferential synthesis of the E isomers under such conditions (12).

In the MS spectrum of the last identified product, the signal at *m*/*z* 1947 (differing by 28 Da (2 × CH_2 groups) from the dimer **14**) was detected. In the ^{13}C NMR spectrum, only

Scheme 1. (*i*) CH_2Cl_2, TBDMSCl (1 equiv.), DIPEA, DMAP, 48%; (*ii*) CH_2Cl_2, TBDPSCl (1 equiv.), DIPEA, DMAP, 60%; (*iii*) 1. Swern oxidation; 2. Ph_3P=CH-CO_2Me; (*iv*) CH_2Cl_2, 50% NaOH, AllBr, Bu_4NBr, rt, 66%; (*v*) Bu_4NF, THF, rt, 74%; (*vi*) CH_2Cl_2, Et_3N, DMAP, acroyl chloride, 75%; (*vii*) 1. Swern oxidation; 2. Jones oxidation; 3. CH_2N_2, 64% overall.



three olefinic carbon resonances (at δ 131.1 (=CH_2), 129.4, and ~128.2 ppm, respectively; assigned from the HETCOR correlations), one carbonyl resonance (at δ 165.9 ppm), and one set of signals connected with the sucrose skeleton (representative resonances at δ 104.7 (C-2′) and 90.3 (C-1)) were seen, which pointed at structure **15**. The geometry across the newly created double bond is most likely E (assumption based on the literature examples (12)), but because of the symmetry of **15**, it cannot be assigned by NMR.

We plan to assign this geometry by desymmetrization of the molecule; the results will be reported in a separate paper.

Conclusion

The first synthesis of a C_2-symmetrical macrocycle containing two sucrose units was realized by dimerization of the 6-*O*-allyl-6′-*O*-acroylsucrose monomer under RCM conditions with Grubbs II catalyst (1,3-dimesityl-4,5-dihydroimidazol-2-ylidene ruthenium alkylidene complex). Besides the expected receptor **14**, two compounds (with E and *Z* geometry, respectively, across the newly created double bond) resulting from the *intramolecular* cyclization and one dimeric open-chain product (from reaction among two allyl moieties) were produced. The overall yield of this process was low (ca. 35%).

Experimental

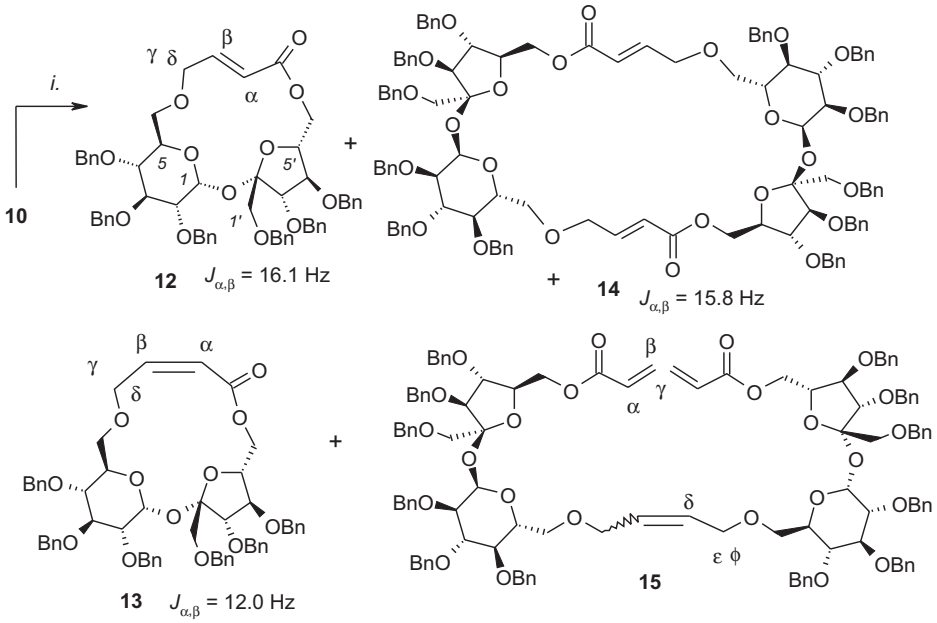
General

NMR spectra were recorded with a Bruker AM 500 spectrometer for solutions in $CDCl_3$ (internal Me_4Si) unless otherwise stated. Most of the resonances were assigned by COSY (^{1}H–^{1}H) and (or) HETCOR and DEPT correlations.

[3] Interestingly, the reaction with allyl chloride was not effective under PTC conditions; removal of the silyl block from the C-6′ end, followed by allylation of both 6-OH and 6′-OH groups, led to known 6,6′-di-*O*-allyl-1′2,3,3′,4,4′-hexa-*O*-benzylsucrose (ref. 3).

© 2006 NRC Canada

Scheme 2. (*i*) CH_2Cl_2, second generation Grubbs catalyst, reflux, 3.5 h.



The ^1H and ^{13}C aromatic resonances occurring at the typical δ values were omitted for simplicity. Mass spectra were recorded with an ESI/MS Mariner (PerSeptive Biosystem) mass spectrometer. Optical rotations were measured with a Jasco P-1020 polarimeter for solutions in $CHCl_3$ (*c* = 1) at room temperature (rt). IR spectra (film) were recorded with a PerkinElmer Spectrum 2000 apparatus. Column chromatography was performed on silica gel (Merck, 70–230 or 230–400 mesh). Methylene chloride was distilled from CaH_2 and THF from potassium prior to use. Organic solutions were dried over anhydrous sodium sulfate.

1′,2,3,3′,4,4′-Hexa-*O*-benzyl-6′-*O*-*tert*-butyldimethylsilylsucrose (5)

To a solution of diol **3** (1.25 g, 1.4 mmol), DMAP (0.12 g), and diisopropylethylamine (0.8 mL) in CH_2Cl_2 (50 mL), a solution of *tert*-butyldimethylsilyl chloride (0.27 mL, 1.4 mmol) in CH_2Cl_2 (5 mL) was added over 60 min and the mixture was stirred for 24 h at rt. Water (70 mL) was added, the organic phase was separated, and the aqueous one extracted with ether (70 mL). The combined organic solutions were dried, concentrated, and the crude product was isolated by column chromatography (hexane – ethyl acetate, 7:1 to 1:1) to give the title compound (**5**) (0.48 g, 0.48 mmol, 48% calcd. on consumed **3**) as a colorless oil and unreacted alcohol **3** (0.36 g, 0.41 mmol). Data for **6**: $[\alpha]_D$ +33.5°. ^1H NMR (200 MHz) δ: 5.97 (d, 1H, $J_{1,2}$ = 3.8 Hz, H-1), 0.88 (s, 9H, 3×CCH_3), 0.06, 0.05 (2×s, SiMe_2). ^{13}C NMR (50 MHz) δ: 104.3 (C-2′), 88.6 (C-1), 83.6, 81.9, 80.7, 80.6, 80.1, 77.8 and 71.2 (C-2,3,3′,4,4′,5,5′), 75.6, 74.9, 73.5, 73.1, 72.6, 72.0, 71.8, and 62.9, 62.0 (C-1′,6,6′, 6×OCH_2Ph), 25.9 (CMe_3), 18.3 (CMe$_3$), –5.0 (SiMe_2). MS *m*/*z*: 1019 [M($C_{60}H_{72}O_{11}Si$) + Na^+]. Anal. calcd. for $C_{60}H_{72}O_{11}Si$: C 72.26, H 7.28; found: C 72.0, H 7.4.

Determination of the structure of 5 — Synthesis of the α,β-unsaturated ester 7

Alcohol **5** (80 mg, 0.08 mmol) in CH_2Cl_2 (2 mL) was added at –78 °C within 5 min to a solution of a Swern reagent (generated from 0.1 mL of oxalyl chloride and 0.3 mL DMSO in 5 mL of CH_2Cl_2). After stirring for 15 min at –78 °C, triethylamine (0.3 mL) was added and the mixture was allowed to attain rt. Water (3 mL) was added, the organic layer was separated, dried, and concentrated. The residue was dissolved in dry benzene (5 mL) to which methoxycarbonyl methylenetriphenylphosphorane (50 mg) was added; the mixture was stirred for 2 h at rt, filtered, and concentrated. The crude product was purified by column chromatography (hexane – ethyl acetate, 8:1) to afford ester **7** (67 mg, 0.064 mmol, 80%). IR (film, cm^{-1}) υ: 2929, 2858, 1725, 1675, 1454, 1090, 1028, 736, 698. ^1H NMR δ: 6.93 (dd, 1H, $J_{5,6}$ = 4.4 Hz, $J_{6,7}$ = 15.8 Hz, H-6), 6,04 (dd, 1H, $J_{5,7}$ = 1.8 Hz, H-7), 5.95 (d, 1H, $J_{1,2}$ = 3.7 Hz, H-1), 4.46 (d, 1H, $J_{3',4'}$ = 7.5 Hz, H-3′), 4.33 (dd, 1H, $J_{4',5'}$ = 7.5 Hz, H-4′), 3.96 (dd, 1H, $J_{2,3}$ = 7.4 Hz, $J_{3,4}$ = 8.9 Hz), 3.75 (s, 3H, OCH_3), 3.69 (d, 1H, $J_{1'A,1'B}$ = 10.9 Hz, H-1′A), 3.22 (dd, 1H, $J_{1,2}$ = 10.1 Hz, H-4), 0,93 (s, 9H, CMe_3), 0.10, 0.08 (2×s, SiMe_2). ^{13}C NMR δ: 166.7 (CO), 145.1 (C-6), 120.8 (C-7), 104.2 (C-2′), 88.8 (C-1), 83.8 (C-3′), 81.8 (C-4′), 81.7 (C-5′), 81.6 (C-4′), 81.0 (C-3), 79.9 (C-2), 75.6, 75.1, 73.4, 73.0, 72.7, 72.1 (6×CH_2Ph), 71.7 (C-1′), 69.7 (C-5), 63.4 (C-6′), 51.4 (OCH_3), 25.9 (CMe_3), 18.3 (CMe$_3$), –5.42, –5.44 (SiMe_2). MS *m*/*z*: 1073 [M($C_{63}H_{74}O_{12}Si$) + Na^+].

1′,2,3,3′,4,4′-Hexa-*O*-benzyl-6′-*O*-*tert*-butyldiphenylsilylsucrose (6)

To a solution of diol **3** (1.23 g, 1.39 mmol), DMAP (78 mg, 0.64 mmol), and diisopropylethylamine (0.5 mL) in CH_2Cl_2 (50 mL), *tert*-butyldiphenylsilyl chloride (0.36 mL, 1.4 mmol) was added over 30 min and the mixture was stirred overnight at rt. Water (70 mL) was added, the organic phase was separated, and the aqueous one extracted with CH_2Cl_2 (30 mL). The combined organic solutions were dried, concentrated, and the crude product was isolated by column chromatography (hexane – ethyl acetate, 5:1) to give the title compound (**6**) (0.93 g, 0.829 mmol, 60%) as a col-

© 2006 NRC Canada

orless oil. $[\alpha]_D$ +26.2°. IR (film, cm^{-1}) υ: 2930, 2859, 1497, 1454, 1089, 1028, 737, 698. ^1H NMR δ: 5.90 (d, $J_{1,2}$ = 3.8 Hz, 1H, H-1), 1.06 (s, 9H, CMe_3). ^{13}C NMR δ: 104.2 (C-2′), 88.7 (C-1), 83.6, 81.9, 80.7, 80.5, 80.1, 77.7, 71.3 (C-2,3,3′,4,4′,5,5′), 75.5, 74.9, 73.4, 73.1, 72.7, 72.3, 72.1 (C-1′ and 6×CH$_2$Ph), 63.9, 61.8 (C-6 and C-6′), 26.9 (Me_3C-Si), 19.2 (Me$_3$$C$Si). MS *m/z*: 1143.6 [M($C_{70}H_{76}O_{11}Si$) + Na^+]. Anal. calcd. for $C_{70}H_{76}O_{11}Si$: C 74.97, H 6.83; found: C 74.6, H 6.9.

(5*S*)-2,3,4-Tri-*O*-benzyl-5-*C*-metoxycarbonyl-α-D-xylopiranosyl-(1↔2)-6-*O*-*tert*-butyldiphenylsilyl-1,3,4-tri-*O*-benzyl-β-D-fructofuranoside (11)

DMSO (1 mL) was added dropwise to a solution of oxalyl chloride (0.4 mL) in CH_2Cl_2 (25 mL) at –78 °C under an argon atmosphere. After 5 min, alcohol **6** (1.2 g, 1.1 mmol in 15 mL CH_2Cl_2) was added and the mixture was stirred at –78 °C for 30 min. Triethylamine (1 mL) was added, stirring was prolonged for an additional 15 min at –78 °C, and the mixture was allowed to reach rt. It was then partitioned between water (40 mL) and ether (150 mL), the organic phase was separated, washed with water (2 × 50 mL) and brine (50 mL), dried, and concentrated. The oily residue was dissolved in acetone (20 mL) and titrated with Jones reagent (3 mL) until TLC (hexane – ethyl acetate, 1:1) indicated the disappearance of the starting material (ca. 20 min). The excess of the Jones reagent was decomposed with isopropanol (5 mL), most of the acetone was removed by vacuum, and the residue was partitioned between water (50 mL) and ethyl acetate (100 mL). The organic phase was separated, washed with brine (50 mL), dried, concentrated, and the crude acid was methylated with diazometane under standard conditions. Evaporation of the solvent left an oily residue, which was purified by column chromatography (hexane – ethyl acetate, 5:1) to give the title methyl uronate (**11**) (0.80 g, 0.698 mmol, 64%) as a colorless oil. $[\alpha]_D$ +19.9°. IR (film, cm^{-1}) υ: 2930, 2859, 1750 (CO), 1454, 1089, 1028, 737, 698. ^1H NMR δ: 5.77 (d, $J_{1,2}$ = 3.6 Hz, 1H, H-1), 4.78–4.40 (m, 14H, 12×CH_2Ph, H-3′, H-5), 4.30 (dd, $J_{3'4'}$ = 6.9 Hz, $J_{4'5'}$ = 6.9 Hz, 1H, H-4′), 4.07–4.03 (m, 1H, H-5′), 3.97–3.91 (m, 2H, both H-6′), 3.87 (dd, $J_{2,3}$ = 9.3 Hz, $J_{3,4}$ = 9.3 Hz, 1H, H-3), 3.69 (dd, $J_{4,5}$ = 9.4 Hz, 1H, H-4), 3.68 (d, $J_{1'A,1'B}$ = 11.2 Hz, 1H, H-1′A) 3.48 (d, 1H, H-1′B) 3.47 (dd, 1H, H-2), 3.469 (s, 3H, OCH_3), 1.05 (s, 9H, Me_3CSi). ^{13}C NMR δ: 170 (CO), 104.8 (C-2′), 90.1 (C-1), 83.8 (C-3′), 82.7 (C-4′), 81.6 (C-5′), 81.3 (C-3), 79.6 (C-4), 79.4 (C-2), 75.6, 74.9, 73.4, 73.0, 72.6, 72.3 (6×CH$_2$Ph), 70.9 (C-1′), 70.5 (C-5), 64.9 (C-6′), 51.9 (OCH$_3$), 26.9 (Me_3CSi), 19.3 (Me$_3$$C$Si). MS *m/z*: 1071.8 [M($C_{71}H_{76}O_{12}Si$) + Na^+].

6-*O*-Allyl-1′,2,3,3′,4,4′-hexa-*O*-benzylsucrose (9)

To a solution of **6** (1.71 g, 1.52 mmol) and allyl bromide (6 mL) in CH_2Cl_2 (40 mL), 50% NaOH (40 mL) and Bu_4NBr (0.15 g, 0.47 mmol) were added. The mixture was stirred vigorously for 24 h at rt. A second portion of allyl bromide (4 mL) was added, the stirring was continued overnight, and the mixture was then partitioned between water (30 mL) and ether (70 mL). The organic layer was separated, washed with water (40 mL), dried, concentrated, and the product was isolated by column chromatography (hexane – ethyl acetate, 7:1 to 4:1) to give 6-*O*-allyl-1′,2,3,3′,4,4′-hexa-*O*-benzyl-6′-*O*-*tert*-butyl-diphenylsilylsucrose (**8**) (0.91 g, 0.782 mmol, 52%; 66% calcd. on consumed **6**) as a colorless oil and unreacted alcohol **6** (0.38 g, 0.339 mmol). $[\alpha]_D$ +24.8°. IR (film, cm^{-1}) υ: 2929, 2859, 1453, 1090, 1027, 737, 698. MS *m/z*: 1184.6 [M($C_{73}H_{80}O_{11}Si$) + Na^+].

When the allyl bromide was replaced with allyl chloride, removal of the silyl protection from the C-6′ position was noted and the diallylated product was isolated from the reaction mixture in good yield.

To a solution of **8** (0.91 g, 0.782 mmol) in THF (20 mL), $Bu_4NF{\cdot}3H_2O$ (0.32 g, 1.0 mmol) was added and the mixture was stirred overnight at rt. The solvent was removed under reduced pressure and the residue was partitioned between ethyl acetate (40 mL) and water (40 mL). The organic layer was separated, dried, concentrated, and the residue was purified by column chromatography (hexane – ethyl acetate, 3:1 to 2:1) to give alcohol **9** (0.54 g, 0.58 mmol, 74%) as a colorless oil. $[\alpha]_D$ +35.2°. IR (film, cm^{-1}) υ: 2917, 2867, 1496, 1454, 1088, 1073, 1028, 736, 697. ^1H NMR δ: 5.93–5.83 (m, 1H, CH=CH$_2$), 5.52 (d, $J_{1,2}$ = 3.5 Hz, 1H, H-1), 5.27–5.22 (m, 1H, -CH$_2$-CH=CH_2, J = 17.2 Hz), 5.15 (1H, -CH$_2$-CH=CH_2, J = 10.4 Hz). ^{13}C NMR δ: 134.5 (-CH$_2$-CH=CH$_2$), 117.3 (-CH$_2$-CH=CH$_2$), 103.9 (C-2′), 91.1 (C-1), 83.7, 81.7, 81.3, 79.6, 79.4, 77.4, 71.3 (C-2,3,3′,4,4′,5,5′), 75.5, 74.9, 73.4, 73.3, 72.9, 72.49, 72.47, 71.2 (6×CH$_2$Ph, C-1′ and -CH$_2$-CH=CH$_2$), 67.9, 61.2 (C-6 and C-6′). MS *m/z*: 945 [M($C_{57}H_{62}O_{11}$) + Na^+]. Anal. calcd. for $C_{57}H_{62}O_{11}$: C 74.17, H 6.77; found: C 74.0, H 6.8.

6-*O*-Allyl-6′-*O*-acroyl-1′,2,3,3′,4,4′-hexa-*O*-benzylsucrose (10)

Alcohol **9** (0.355 g, 0.385 mmol) was dissolved in CH_2Cl_2 (20 mL) containing triethylamine (1 mL) and DMAP (ca. ~20 mg). Acroyl chloride (0.13 mL, 1.5 mmol) was added, the mixture was stirred for 1 h at rt and then partitioned between ether (70 mL) and water (50 mL). The organic phase was separated, dried, concentrated, and the residue was purified by column chromatography (hexane – ethyl acetate, 3:1) to give **10** (0.268 g, 0.29 mmol, 75%) as a yellowish oil. $[\alpha]_D$ +41.2°. IR (film): 3070, 3031, 2930, 2857, 1727, 1636, 1497, 1454, 1428, 1361, 821, 739, 700. ^1H NMR δ: 6.39 (dd, J = 1.3, 17.4 Hz, 1H, COCH=CH_2), 6.11 (dd, J = 10.5 Hz, 1H, second COCH=CH_2), 5.90–5.80 (m, 1H, CH$_2$CH=CH$_2$), 5.75 (dd, 1H, COCH=CH$_2$), 5.64 (d, $J_{1,2}$ = 3.6 Hz, 1H, H-1), 5.22 (dd, J = 17.2, 1.6 Hz, 1H, CH$_2$CH=CH_2), 5.12 (dd, J = 10.4 Hz, 1H, second CH$_2$CH=CH_2). ^{13}C NMR δ: 165.8 (CO), 134.7 (-CO$_2$$C$H=CH$_2$), 131.0 (-CO$_2$CH=$CH_2$), 128.5–127 (-CH$_2$$C$H=CH$_2$), 117.1 (-CH$_2$CH=$CH_2$), 104.7 (C-2′), 90.2 (C-1), 83.8, 82.2, 81.9, 79.7, 78.2, 77.7 and 70.7 (C-2,3,3′,4,4′,5,5′), 75.5, 74.8, 73.4, 72.9, 72.6, 72.5, 72.3, 70.9, 68.5, 65.3 (C-1′, C-6, C-6′, -CH$_2$CH=CH$_2$, and 6×OCH$_2$Ph). MS *m/z*: 999 [M($C_{60}H_{64}O_{12}$) + Na^+].

Metathesis reaction of 6-*O*-allyl-6′-*O*-acroyl-1′,2,3,3′,4,4′-hexa-*O*-benzylsucrose (10) catalyzed by Grubbs II catalyst

Compound **10** (0.250 g, 0.256 mmol) was dissolved in CH_2Cl_2 (7 mL) to which Grubbs II catalyst (13.1 mg, 0.015 mmol) was added and the mixture was boiled under reflux for 3.5 h. The mixture was then partitioned between

© 2006 NRC Canada

CH_2Cl_2 (20 mL) and water (30 mL), the organic phase was separated, and the aqueous one extracted with ether (10 mL). The combined organic layers were dried, concentrated, and the products were partially purified by column chromatography (hexane – ethyl acetate, 5:1 to 3:1) to afford unreacted compound **10** (30 mg) and a mixture of four compounds (76 mg) from which the individual products were isolated by HPLC (hexane – ethyl acetate, 5:2).

E-Isomer **12** was the first to be isolated. IR (film, cm^{-1}) υ: 2923, 2856, 1726 (CO), 1454, 1091, 1073, 1028, 736, 697. ^1H NMR (for numbering see Scheme 2) δ: 7.13 (ddd, $J_{\alpha,\beta}$ = 16.1 Hz, $J_{\beta,\delta}$ = 7.0 Hz, $J_{\beta,\gamma}$ = 5.2 Hz, 1H, H-β), 5.81–5.76 (m, 1H, H-α), 5.67 (d, $J_{1,2}$ = 3.8 Hz, H-1). ^{13}C NMR δ: 165.7 (CO), 147.8 (-CH_2*C*H=CHCO-), 22.3 (-CH=*CH*-CO-), 102.8 (C-2′), 88.6 (C-1), 84.2, 81.6, 79.9, 78.31, 78.25, 78.18, 71.2 (C-2,3,3′,4,4′,5,5″), 75.19, 75.13, 74.6, 73.3, 73.1, 72.4, 72.2, 69.9, 67.6, 60.0 (C-1′,6,6′, -*C*H_2CH=CH_2 and 6×O*C*H_2Ph). MS *m*/*z*: 971 (main signal) [M($C_{58}H_{60}O_{12}$) + Na^+] and 987 [M($C_{58}H_{60}O_{12}$) + K^+] (minor).

Z-Isomer **13** was the second to be isolated (contaminated with ca. 30% of **12**). ^1H NMR δ: 6.21 (ddd, $J_{\beta,\gamma}$ = 12.0 Hz, $J_{\beta,\delta}$ = 12.0 Hz, $J_{\alpha,\beta}$ = 5.2 Hz, 1H, H-β), 5.77 (ddd, $J_{\alpha,\gamma}$ = 1.8 Hz, $J_{\alpha,\delta}$ = 1.8 Hz, 1H, H-α), 5.54 (d, $J_{1,2}$ = 3.6 Hz, H-1). ^{13}C NMR δ: 166.1 (CO), 144.8 (-*C*H=CHCO-), 121.5 (-*C*H=CH-CO_2), 103.7 (C-2′), 90.2 (C-1), 83.7, 81.7, 80.7, 79.7, 79.0, 77.8, 71.6 (C-2,3,3′,4,4′,5,5′), 75.4, 74.6, 73.3, 73.1, 72.4, 72.3 (2×), 70.5, 67.2, 61.9 (C-1′,6′,6, -*C*H_2CH=CH_2 and 6×O*C*H_2Ph). MS *m*/*z*: 971 (minor signal) [M($C_{58}H_{60}O_{12}$) + Na^+] and 987 [M($C_{58}H_{60}O_{12}$) + K^+] (main).

Macrocyclic dimer **14** was the third to be isolated (contaminated with **12**, **13**, and **15**; ca. 5%–10% each). ^1H NMR δ: 6.83 (ddd, $J_{\alpha,\beta}$ = 15.8 Hz, $J_{\beta,\gamma}$ = 4.0 Hz, $J_{\beta,\delta}$ = 4.0 Hz, 1H, H-β), 5.96 (ddd, $J_{\alpha,\gamma}$ = 2.0 Hz, $J_{\alpha,\delta}$ = 2.0 Hz, 1H, H-α), 5.66 (d, $J_{1,2}$ = 3.7 Hz, H-1). ^{13}C NMR δ: 165.8 (CO), 145.6 (-CH_2*C*H=CHCO-), 120.0 (-CH_2CH=*C*HCO-), 104.6 (C-2′), 89.4 (C-1), 89.4, 83.6, 82.1, 81.3, 80.0, 77.7, 70.9 (C-2,3,3′,4,4′,5,5′), 75.5, 74.9, 73.5, 72.9, 72.5, 72.3, 71.6, 70.1, 69.3, 64.1 (C-1′,6,6′, -*C*H_2CH=CH_2 and 6×*C*H_2Ph). MS *m*/*z*: 1919 [M($C_{116}H_{120}O_{24}$) + Na^+] (strongest signal: 1920 [M + 1 + Na^+]).

Open-chain dimer **15** was the fourth to be isolated. ^1H NMR δ: 6.36 (dd, $J_{\alpha,\beta}$ = 17.4 Hz, $J_{\beta,\gamma}$ = 1.4 Hz, 1H, H-β), 6.09 (dd, $J_{\alpha,\gamma}$ = 10.4 Hz, 1H, H-α), 5.72 (dd, 1H, H-γ), 5.70 (dd, $J_{\delta,\phi}$ = 3.0 Hz, $J_{\delta,\varepsilon}$ = 3.0 Hz, 1H, H-δ), 5.62 (d, $J_{1,2}$ = 3.6 Hz, H-1). ^{13}C NMR δ: 165.9 (CO), 131.1 (-CO_2CH=*C*H_2), 129.5 (-CO_2*C*H=CH_2), 104.7 (C-2′), 90.3 (C-1), 83.9, 82.3, 81.8, 79.8, 78.3, 77.6, 70.70 (C-2,3,3′,4,4′,5,5′), 75.5, 74.8, 73.4, 72.9, 72.59, 72.50, 71.4, 70.8, 68.6, 65.4 (C-1′,6,6′, -*C*H_2CH=CH_2 and 6×*C*H_2Ph). MS *m*/*z*: 1947 [M($C_{118}H_{124}O_{24}$) + Na^+] (strongest signal: 1948 [M + 1 + Na^+]).

References

1. (*a*) J.Y.C. Chan, L. Hough, and A.C. Richardson. J. Chem. Soc. Perkin Trans. 1, 1457 (1985); (*b*) A. de Raadt and A.E. Stütz. Tetrahedron Lett. **33**, 189 (1992); (*c*) G. Garndnig, G. Legler, and A.E. Stütz. Carbohydr. Res. **287**, 49 (1996); (*d*) F.W. Lichtenthaler. Acc. Chem. Res. **35**, 728 (2002).
2. Review: R. Khan. Pure Appl. Chem. **56**, 833 (1984), and refs. therein.
3. Review: S. Jarosz and M. Mach. Eur. J. Org. Chem. 769 (2002), and refs. therein.
4. (*a*) F.W. Lichtenthaler. Carbohydr. Res. **313**, 69 (1998); an overview of sucrose chemistry is included in: F.W. Lichtenthaler (*Editor*). Carbohydrates as organic raw materials. VCH Verlagsgesellschaft mbH, Weinheim, Germany. 1991; (*b*) F.W. Lichtenthaler and S. Mondel. Pure Appl. Chem. **69**, 1853 (1997); (*c*) G. Descotes, J. Gagnaire, A. Bouchu, S. Thevenet, N. Giry-Panaud, P. Salanski, S. Belniak, A. Wernicke, S. Porwanski, and Y. Queneau. Pol. J. Chem. **73**, 1069 (1999).
5. J. Seibel, R. Moraru, and S. Götze. Tetrahedron, **61**, 7081 (2005).
6. S. Jarosz. J. Carbohydr. Chem. **15**, 73 (1996).
7. S. Jarosz, M. Mach, and J. Frelek. J. Carbohydr. Chem. **19**, 693 (2000).
8. S. Jarosz and A. Listkowski. J. Carbohydr. Chem. **22**, 753 (2003).
9. S. Jarosz, A. Listkowski, B. Lewandowski, Z. Ciunik, and A. Brzuszkiewicz. Tetrahedron, **61**, 8485 (2005)
10. (*a*) F. Franke and R.D. Guthrie. Aust. J. Chem. **30**, 639 (1977); (*b*) F. Franke and R.D. Guthrie. Aust. J. Chem. **31**, 1285 (1978); (*c*) H. Karl, C.K. Lee, and R. Khan. Carbohydr. Res. **101**, 31 (1982).
11. (*a*) A.K. Chatterjee and R.H. Grubbs. Org. Lett. **1**, 1751 (1999); (*b*) T.M. Trnka and R.H. Grubbs. Acc. Chem. Res. **34**, 18 (2001); (*c*) S.B. Garber, J.S. Kingsbury, B.L. Gray, and A.H. Hoveyda. J. Am. Chem. Soc. **122**, 8168 (2000).
12. S.J. Connon and S. Blechert. Angew. Chem. Int. Ed. **42**, 1900 (2003).

© 2006 NRC Canada

Synthesis of zwitterionic selenonium and sulfonium sulfates from D-mannose as potential glycosidase inhibitors[1]

Hui Liu and B. Mario Pinto

Abstract: Four chain-extended analogues of the naturally occurring glycosidase inhibitor salacinol were synthesized for structure–activity studies with different glycosidase enzymes. The syntheses involved the reaction of isopropylidene-protected 1,4-thio- and 1,4-seleno-D-talitols and 1,5-thio- and 1,5-seleno-L-gulitols, derived from D-mannose, with a benzylidene- and isopropylidene-protected 1,3-cyclic sulfate, also derived from D-mannose. Deprotection of the products afforded the novel selenonium and sulfonium sulfates composed of heterocyclic five- and six-membered ring core structures with pendant polyhydroxylated, acyclic chains of six carbon atoms.

Key words: glycosidase inhibitors, zwitterionic selenonium and sulfonium sulfates, cyclic sulfate.

Résumé : Afin de pouvoir procéder à des études de structure–activité avec divers enzymes de glycosidase, on a synthétisé quatre analogues à chaîne allongée du salacinol, un inhibiteur de la glycosidase qu'on retrouve à l'état naturel. Ces synthèses ont impliquées les réactions de dérivés isopropylidènes de 1,4-thio et 1,4-séléno-D-talitols ainsi que de 1,5-thio- et 1,5-séléno-L-gulitols obtenus à partir du D-mannose avec des dérivés benzylidènes et isopropylidènes de sulfates cycliques-1,3 aussi obtenus à partir du D-mannose. La déprotection des produits a permis d'obtenir de nouveaux sulfates de sélénonium et de sulfonium formés structures à cycle central formé d'hétérocycles à cinq et à six chaînons portant des chaînes pendantes polyhydroxylées de six atomes de carbone.

Mots clés : inhibiteurs de glycosidase, sulfates de sélénonium et de sulfonium zwitterioniques, sulfate cyclique.

[Traduit par la Rédaction]

Introduction

The controlled inhibition of glycosidase enzymes plays important roles in the biochemical processing of biopolymers containing carbohydrates (1, 2). Recently, a new class of glycosidase inhibitors, namely salacinol (**1**) and kotalanol (**2**), with an intriguing inner-salt sulfonium sulfate structure was isolated from the roots and stems of the plant *Salacia reticulata*. These compounds have been found to be potent inhibitors of intestinal glucosidase enzymes (3, 4). Salacinol (**1**) and kotalanol (**2**) presumbly compete for substrate binding in the active site, thus preventing glucose oligosaccharides from being processed and thereby inhibiting a surge in blood glucose levels after a meal rich in carbohydrates (Chart 1). Hence, they have potential as therapeutics in the management of blood glucose levels for patients suffering from type II diabetes (5). The absolute configuration of the heptitol side chain of kotalanol has yet to be determined. However, kotalanol has shown more potent glucosidase inhibitory activity towards sucrase than salacinol (6). It is believed that the inhibitory activities of salacinol and kotalanol come from their ability to mimic both the shape and charge of the oxacarbenium-ion-like transition state involved in the enzymatic reactions (7–9). However, the details of the mechanism of action of these compounds are yet to be elucidated.

In our current research program, we have undertaken a limited structure–activity study of salacinol and related compounds. The synthesis of salacinol and its ammonium and selenonium analogues have been reported by us and others (10–14). We also have synthesized analogues containing six-membered heterocyclic rings and chain-extended analogues of salacinol, some of which have shown inhibitory activity in the micromolar range of recombinant human maltase glucoamylase, a key intestinal glucosidase (15–18). These studies have revealed an interesting variation in the inhibitory power of these compounds against glycosidase enzymes of different origin (11–14). The molecular basis for this selectivity is being investigated through structural studies of the enzyme-bound inhibitors using molecular modeling in conjunction with NMR techniques (19) and X-ray crystallography (20). To further understand this selectivity, additional examples of analogues of salacinol that differ in stereochemistry on both the heterocyclic ring and the side chain, in chain length of the acyclic chain, and in size of the heterocyclic ring are required.

Received 31 August 2005. Published on the NRC Research Press Web site at http://canjchem.nrc.ca on 6 April 2006.

This work is dedicated with respect and affection to Walter A. Szarek, an inspiring teacher and mentor, in celebration of his 65th birthday.

H. Liu and M. Pinto.[2] Department of Chemistry, Simon Fraser University, Burnaby, BC V5A 1S6, Canada.

[1]This article is part of a Special Issue dedicated to Professor Walter A. Szarek.

[2]Corresponding author (e-mail: bpinto@sfu.ca).

 doi:10.1139/V06-027 © 2006 NRC Canada

Scheme 1.

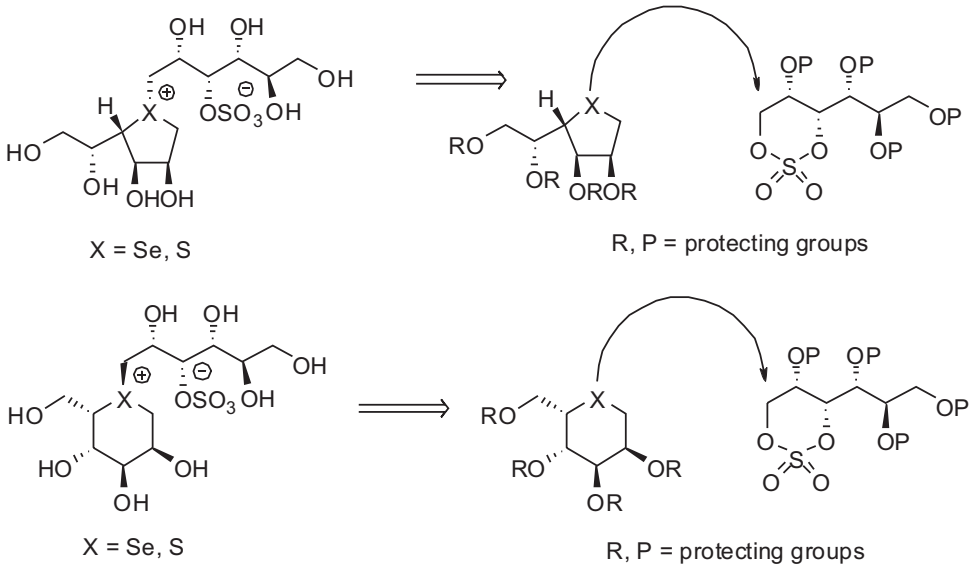


Chart 1.

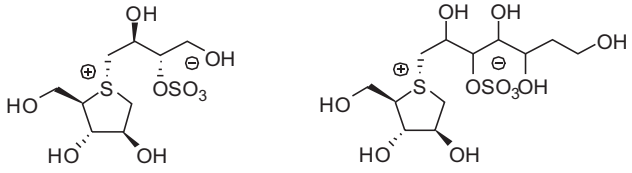
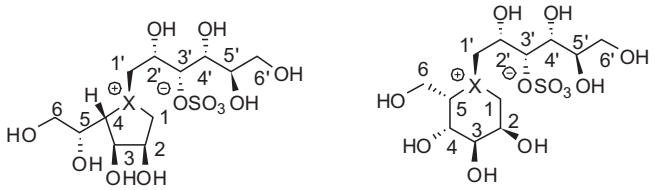


Chart 2.



Herein, we report the synthesis of two series of selenonium and sulfonium sulfates (**3**–**6**) based on seleno- and thio-anhydroalditols derived from D-mannose (Chart 2).

Results and discussion

Retrosynthetic analysis indicated that the analogues **3**–**6** could be synthesized by alkylation of the protected anhydroheteroalditols at the ring heteroatom with a terminal 1,3-cyclic sulfate derived from D-mannose (Scheme 1).

The choice of protecting groups for the seleno- and thio-anhydroalditols and the cyclic sulfate, however, merited careful consideration, especially in the case of the selenonium analogues. Our previous work suggested that hydrogenolysis and strongly basic conditions as deprotection steps were problematic for the selenonium analogues (12–14). Therefore, we envisioned the use of only isopropylidene and benzylidene acetals as the protecting groups for the seleno- and thio-anhydroalditols (**7**–**10**) and the cyclic sulfate (**11**), since these acetals would be subject to acidic hydrolysis (Chart 3).

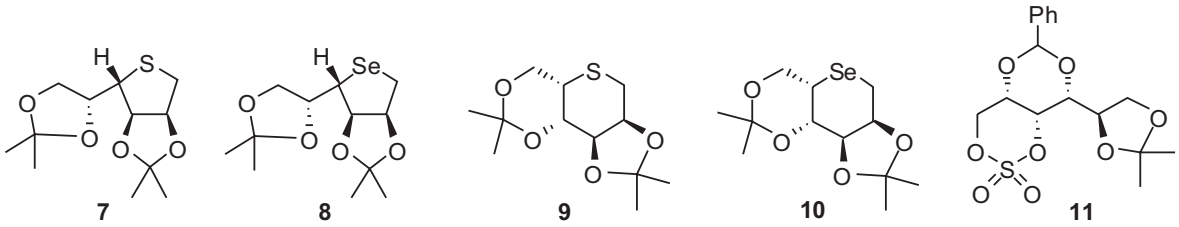
Our previous work also suggested that the release of ring strain in the opening of a cyclic sulfate was beneficial (11–14). Therefore, the benzylidene acetal at the 2,4-positions of the cyclic sulfate **11** played a dual role as both a protecting group and also as a facilitator of the coupling reactions with the heterocyclic ethers **7**–**10**. After the coupling reactions, the products could then be readily deprotected by simple treatment with trifluoroacetic acid.

The synthesis of the isopropylidene-protected 1,4-anhydro-1-thio-D-talitol (**7**) and 1,4-anhydro-1-seleno-D-talitol (**8**) started from D-mannose (**12**, Scheme 2). D-Mannose was first treated with 2,2-dimethoxypropane in dry acetone with *p*-toluenesulfonic acid as a catalyst to give 2,3,5,6-di-*O*-isopropylidene-D-mannose (**13**) (21). Compound **13** was subsequently subjected to reduction with sodium borohydride to afford the corresponding diol **14**. The diol was then converted to the corresponding dimesylate **15** in 80% yield by treatment with methanesulfonyl chloride and pyridine. The isopropylidene-protected 1,4-anhydro-1-thio-D-talitol (**7**) was prepared in 92% yield by treatment of the dimesylate **15** with sodium sulfide in DMF in 92% yield. When the dimesylate **15** was reacted with selenium and sodium borohydride in EtOH at 60–65 °C, the isopropylidene-protected 1,4-anhydro-1-seleno-D-talitol (**8**) was obtained in a 60% yield (Scheme 2).

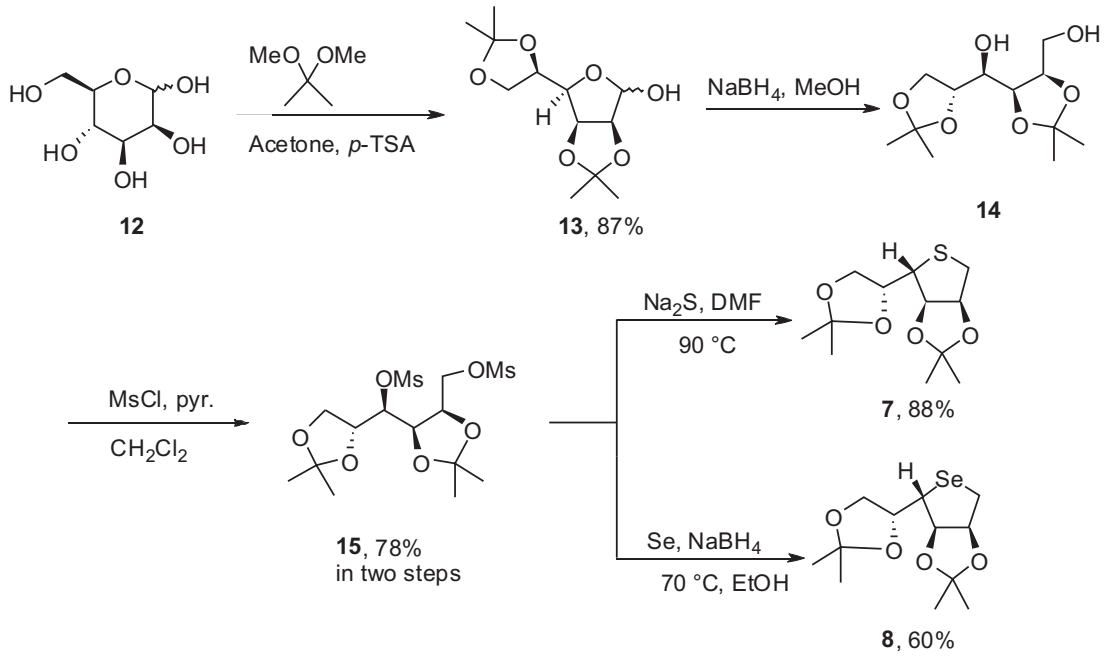
With D-mannose as a starting material, the isopropylidene-protected 1,5-anhydro-1-thio-L-gulitol (**9**) and 1,5-anhydro-1-seleno-L-gulitol (**10**) were also synthesized (Scheme 3). D-Mannose (**12**) was treated with 2-methoxypropene in dry DMF with *p*-toluenesulfonic acid as a catalyst to give the kinetically controlled product, 2,3,4,6-di-*O*-isopropylidene-D-mannose (**16**) (22). Compound **16** was subsequently subjected to sodium borohydride reduction to afford the corresponding diol **17**. The diol **17** was then converted to the corresponding dimesylate **18** in 90% yield by treatment with methanesulfonyl chloride and pyridine. The isopropylidene-protected 1,5-anhydro-1-thio-L-gulitol (**9**) was prepared in 85% yield by treatment of the dimesylate **18** with sodium sulfide in DMF. Reaction of dimesylate **18** with selenium

© 2006 NRC Canada

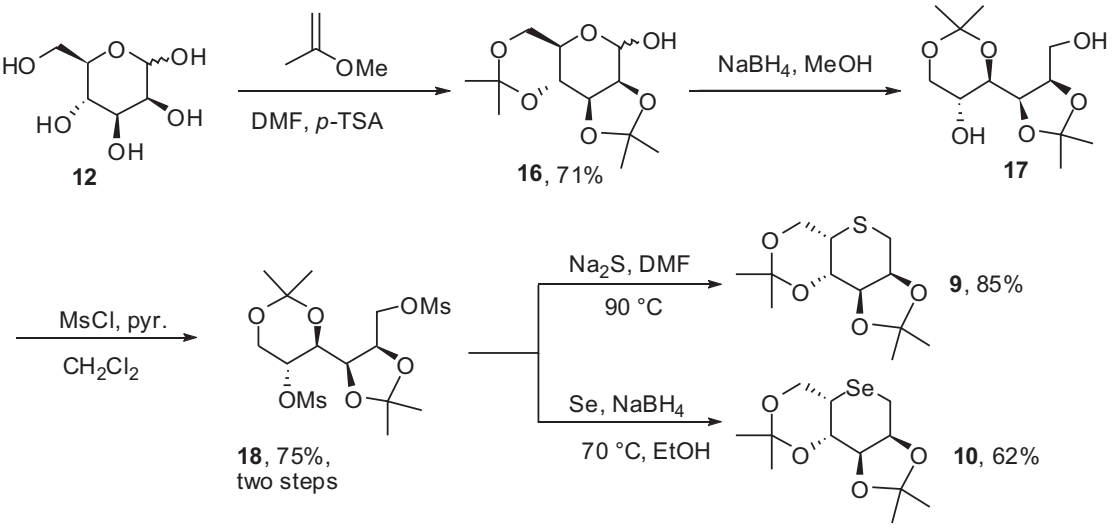
Chart 3.



Scheme 2.



Scheme 3.

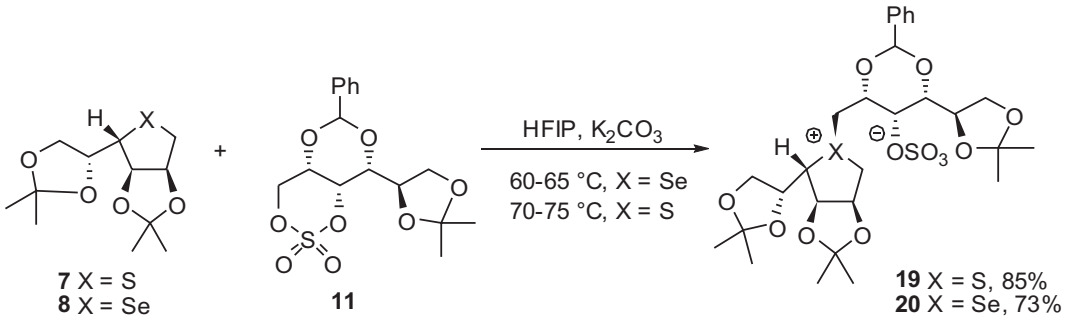


and sodium borohydride in EtOH at 60–65 °C gave isopropylidene-protected **10** in 62% yield (Scheme 3).

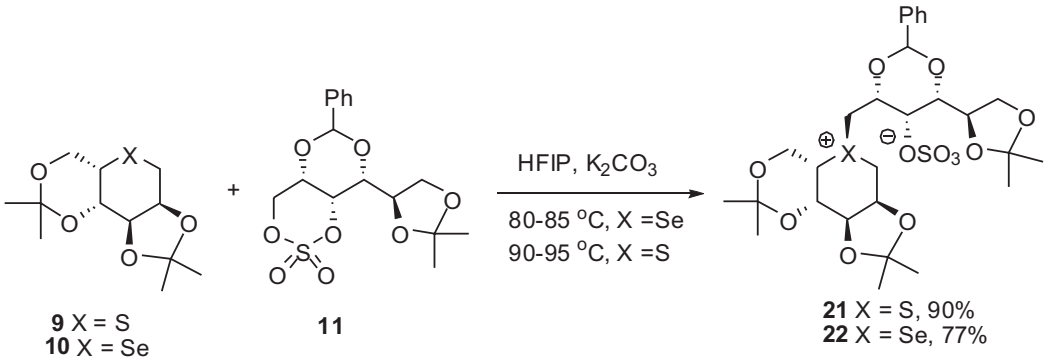
The coupling reactions of protected **7** and **8** were then investigated (Scheme 4). The solvent chosen for the coupling reactions was the unusual solvent 1,1,1,3,3,3-hexafluoroisopropanol (HFIP), which was demonstrated in our earlier work to offer significant advantage in analogous reactions. Cyclic sulfate (**11**), prepared by a method developed in our earlier work (16), was used as the coupling partner. **11** was reacted with isopropylidene-protected **7** and **8** to give the corresponding protected sulfonium and selenonium compounds **19** and **20**, respectively (Scheme 4).

© 2006 NRC Canada

Scheme 4.



Scheme 5.



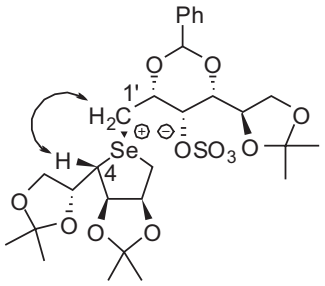
In analogous fashion, the coupling reactions of protected **9** and **10** with **11** afforded the protected sulfonium and selenonium compounds **21** and **22**, respectively (Scheme 5).

The reactivities of **7**, **8**, **9**, and **10** with **11** varied slightly. The five-membered-ring anhydroalditols **7** and **8** were more reactive than their six-membered-ring counterparts, **9** and **10**, as illustrated by the higher temperatures required for the coupling reactions in the latter cases. Compounds **7** and **8** reacted readily with **11** at 70–75 °C and 60–65 °C, respectively, while compounds **9** and **10** reacted very slowly and gave low yields of the coupling products at these temperatures. When the temperature was increased to 90–95 °C and 80–85 °C, respectively, compounds **9** and **10** reacted readily with **11**. Within the same series, the selenoalditols were found to be slightly more reactive than their sulfur counterparts. Selectivity for the attack at the primary center of **11** over possible alternative attack at the secondary center by compounds **7**–**10** was invariably excellent and in no case were isolable quantities of the regioisomers detected. In the case of the coupling reaction of **8** with **11**, there was a small amount (<10%) of the diastereomer formed resulting from electrophilic attack on the β-face of compound **8**. However, diastereoisomers at the stereogenic heteroatom centers were not detected in all other cases.

The absolute stereochemistry at the heteroatom centre of compounds **19**–**22** was established by 1D-NOE NMR spectroscopy (Fig. 1). Thus, for example, the 1D NOE spectra of compound **20** indicated an H-4 to H-1′b correlation, implying that these hydrogens are syn-facial, and consequently, C-1′ of the side chain must be anti to C-5 of the heterocyclic moiety.

Deprotection of the coupled products **19**–**22** was carried out by treatment with trifluoroacetic acid (Scheme 6). After rinsing away the cleaved protecting groups with dichloromethane, the resulting residues were purified by flash chromatography to yield compounds **3**–**6** as amorphous, hygroscopic solids. These compounds were characterized by spectroscopic methods.

Fig. 1. NOE correlations observed in the 1D-NOE spectrum of **20**.

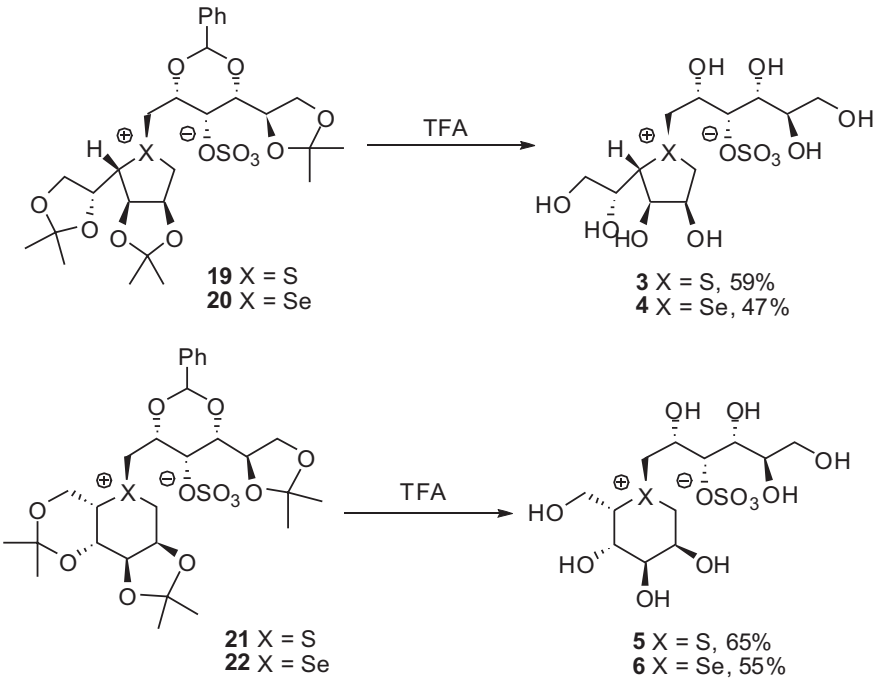


Conclusions

Two series of selenonium and sulfonium sulfates were synthesized from D-mannose. The analogues contained extended acyclic chains of six carbon atoms, as well as ring heteroatom substitution (S, Se) and five- and six-membered heterocyclic rings. These syntheses utilized a 1,3-cyclic sulfate, also derived from D-mannose, in four steps. The isopropylidene acetal and benzylidene acetal protecting groups on the coupled products ensured facile deprotection with TFA to yield the final compounds (**3**–**6**). These compounds are being tested for their enzymatic activities.

© 2006 NRC Canada

Scheme 6.



Experimental section

General

Optical rotations were measured at 23°. ^{1}H and ^{13}C NMR spectra were recorded at 500 and 125 MHz, respectively. All assignments were confirmed with the aid of two-dimensional ^{1}H, ^{1}H (COSYDFTP), or ^{1}H, ^{13}C (INVBTP) experiments using standard Bruker pulse programs. Column chromatography was performed with Merck Silica gel 60 (230–400 mesh). MALDI mass spectra were obtained on a PerSeptive Biosystems, Voyager DE time-of-flight spectrometer for samples dispersed in a 2,5-dihydroxybenzoic acid matrix. High-resolution mass spectra were obtained by the electrospray ionization (ESI) technique, using a ZabSpec oaTOF mass spectrometer at 10 000 RP.

2,3,5,6-Di-*O*-isopropylidene-1,4-di-*O*-methanesulfonyl-D-mannitol (15)

2,3,5,6-Di-*O*-isopropylidene-D-mannose (**13**) was prepared by the literature method (23). To a solution of **13** (20 g, 77 mmol) in MeOH (200 mL), $NaBH_4$ (5.8 g, 0.15 mol) was added portionwise at 0 °C. The progress of the reaction was followed by TLC analysis of the aliquots (developing solvent, hexane–EtOAc, 1:1). When starting material **13** had been essentially consumed, the solvent was evaporated under reduced pressure. The residue was redissolved in EtOAc (150 mL), washed with satd. NH_4Cl solution (200 mL) and brine (50 mL), and dried over Na_2SO_4. After evaporating the solvent, the crude diol (**14**) was used without further purification. Diol **14** was dissolved in CH_2Cl_2 (50 mL) and then added dropwise to a mixture of pyridine (100 mL) and methanesulfonyl chloride (26 mL, 0.34 mol) cooled to 0 °C. The reaction mixture was stirred at 0 °C for 30 min, then allowed to rise to room temperature for 6 h. When TLC analysis of the aliquots (developing solvent, hexane–EtOAc, 1:1) showed total consumption of the starting material, the reaction mixture was poured into ice water, extracted with CH_2Cl_2 (3 × 100 mL), washed with brine (50 mL), and dried over Na_2SO_4. Purification by column chromatography (hexane–EtOAc, 2:1) yielded compound **15** as a colorless syrup (25 g, 78%). $[\alpha]^{22}_D$ +18.0° (*c* 0.5, CH_2Cl_2). ^{1}H NMR ($(CD_3)_2O$) δ: 4.86 (1H, dd, $J_{3,4}$ = 6.8, $J_{4,5}$ = 6.5, H-4), 4.55–4.50 (3H, m, H-2, H-3, H-1b), 4.47 (1H, dd, $J_{1a,1b}$ = 11.1, $J_{1a,2}$ = 7.6, H-1a), 4.29 (1H, ddd, $J_{4,5}$ = 6.5, H-5), 4.16 (1H, dd, $J_{5,6b}$ = 6.4, $J_{6a,6b}$ = 8.5, H-6b), 3.99 (1H, dd, $J_{5,6a}$ = 7.5, $J_{6a,6b}$ = 8.5, H-6a), 3.22 and 3.16 (6H, 2 s, $2OSO_2CH_3$), 1.53, 1.43, 1.38, and 1.33 (12H, 4 s, 4 CH_3). ^{13}C NMR ($(CD_3)_2O$) δ: 109.97, 109.44 ($(CH_3)_2C(OR)_2$), 78.72 (C-4), 76.79 (C-3), 75.11 (C-5), 75.02 (C-2), 68.92 (C-1), 66.43 (C-6), 38.93, 36.75 (2 SO_2CH_3), 26.89, 25.68, 25.34, 24.82 ($4CH_3$). Anal. calcd. for $C_{14}H_{26}O_{10}S_2$: C 40.18, H 6.26; found: C 40.45, H 6.14.

2,3,4,6-Di-*O*-isopropylidene-1,5-di-*O*-methanesulfonyl-D-mannitol (18)

2,3,4,6-Di-*O*-isopropylidene-D-mannose (**16**) was prepared by the literature method (24). To a solution of **16** (20 g, 77 mmol) in MeOH (200 mL), $NaBH_4$ (5.8 g, 0.15 mol) was added portionwise at 0 °C. The progress of the reaction was followed by TLC analysis of the aliquots (developing solvent, hexane–EtOAc, 1:1). When starting material **13** had been essentially consumed, the solvent was evaporated under reduced pressure. The residue was redissolved in EtOAc (150 mL), washed with satd. NH_4Cl solution (200 mL) and brine (50 mL), and dried over Na_2SO_4. After evaporating the solvent, the crude diol (**17**) was used without further purification. Diol **17** was dissolved in CH_2Cl_2 (50 mL) and then added dropwise to a mixture of pyridine (100 mL) and methanesulfonyl chloride (26 mL, 0.34 mol) cooled to 0 °C. The reaction mixture was stirred at 0 °C for 30 min, then allowed to rise to room temperature

© 2006 NRC Canada

for 6 h. When TLC analysis of the aliquots (developing solvent, hexane–EtOAc, 1:1) showed total consumption of the starting material, the reaction mixture was poured into ice water, extracted with CH_2Cl_2 (3 × 100 mL), washed with brine (50 mL), and dried over Na_2SO_4. Purification by column chromatography (hexane–EtOAc, 2:1) yielded compound **18** as a colorless syrup (24 g, 75%). $[\alpha]^{22}_D$ +2.4° (*c* 0.5, CH_2Cl_2). ^{1}H NMR ($CDCl_3$) δ: 4.82 (1H, ddd, $J_{5,6a}$ = 7.3, $J_{5,6b}$ = 5.1, $J_{4,5}$ = 8.8, H-5), 4.54 (1H, ddd, $J_{1a,2}$ = 4.1, $J_{1b,2}$ = 7.5, $J_{2,3}$ = 6.3, H-2), 4.50 (1H, dd, $J_{1a,1b}$ = 10.3, $J_{1b,2}$ = 7.5, H-1b), 4.40 (1H, dd, $J_{3,4}$ = 1.1, H-3), 4.38 (1H, dd, H-1a), 4.14 (1H, dd, $J_{6a,6b}$ = 12.0, H-6b), 3.89 (1H, dd, H-6a), 3.82 (1H, dd, H-4), 3.09 and 3.08 (6H, 2 s, $2OSO_2CH_3$), 1.52, 1.49, 1.41, and 1.37 (12H, 4 s, $4CH_3$). ^{13}C NMR ($CDCl_3$) δ: 110.55, 100.03 ($(CH_3)_2C(OR)_2$), 74.94 (C-2), 73.85 (C-3), 72.22 (C-5), 69.58 (C-4), 68.13 (C-1), 62.64 (C-6), 38.11, 38.04 ($2SO_2CH_3$), 27.45, 26.83 25.82, 20.37 (four CH_3). Anal. calcd. for $C_{14}H_{26}O_{10}S_2$: C 40.18, H 6.26; found: C 39.99, H 6.02.

2,3,5,6-Di-*O*-isopropylidene-1,4-anhydro-1-thio-D-talitol (7)

To a solution of dimesylate **15** (4.0 g, 9.6 mmol) in DMF (80 mL), $Na_2S{\cdot}9H_2O$ (2.8 g, 11.5 mmol) was added and the reaction mixture was heated at 90 °C for 12 h. The reaction mixture was poured into water (100 mL), extracted with Et_2O (4 × 50 mL), washed with water (10 × 20 mL), and dried over Na_2SO_4. After evaporating the solvent, the crude product was purified by column chromatography (hexane–EtOAc, 3:1) to give **7** as a colorless oil (2.2 g, 88%). $[\alpha]^{22}_D$ –47° (*c* 0.5, CH_2Cl_2). ^{1}H NMR ($(CD_3)_2O$) δ: 4.93 (1H, ddd, $J_{2,3}$ = 5.7, $J_{1a,2}$ = 1.3, $J_{1b,2}$ = 5.1, H-2), 4.75 (1H, dd, $J_{3,4}$ = 1.6, $J_{2,3}$ = 5.7, H-3), 4.06 (1H, dd, $J_{6a,6b}$ = 7.7, $J_{5,6b}$ = 6.2, H-6b), 3.72 (1H, dd, $J_{5,6a}$ = 7.4, H-6a), 3.34 (1H, dd, H-4), 3.17 (1H, dd, $J_{1a,1b}$ = 12.2, H-1b), 2.74 (1H, dd, H-1a), 1.43, 1.38, 1.29, and 1.28 (12H, 4 s, $4CH_3$). ^{13}C NMR ($(CD_3)_2O$) δ: 110.85, 109.27 ($(CH_3)_2C(OR)_2$), 87.33 (C-3), 84.09 (C-2), 78.25 (C-5), 68.03 (C-6), 56.34 (C-4), 38.47 (C-1), 26.45, 25.93, 25.38, 24.24 ($4CH_3$). Anal. calcd. for $C_{12}H_{20}O_4S$: C 55.36, H 7.74; found: C 55.62, H 7.73.

2,3,5,6-Di-*O*-isopropylidene-1,4-andydro-1-seleno-D-talitol (8)

To a suspension of Se (1.6 g, 20.2 mmol) and 95% EtOH (100 mL), $NaBH_4$ (1.5 g, 40.4 mmol) was added portionwise until the black selenium color disappeared. To this mixture a solution of dimesylate **15** (6.0 g, 14.3 mmol) in THF (10 mL) was added and the reaction mixture was heated at 70 °C for 12 h. The solvent of the reaction mixture was evaporated under reduced pressure, redissolved in EtOAc, washed with water (20 mL) and brine (20 mL), and dried over Na_2SO_4. After evaporating the solvent, the crude product was purified by column chromatography (hexane–EtOAc, 3:1) to give **8** as a colorless oil (3.1 g, 71%). $[\alpha]^{22}_D$ –40° (*c* 1, CH_2Cl_2). ^{1}H NMR ($(CD_3)_2O$) δ: 4.97 (1H, ddd, $J_{2,3}$ = 5.7, $J_{1a,2}$ = 2.4, $J_{1b,2}$ = 5.5, H-2), 4.71 (1H, dd, $J_{3,4}$ = 2.9, $J_{2,3}$ = 5.7, H-3), 4.28 (1H, ddd, $J_{5,6a}$ = 7.4, $J_{5,6b}$ = 6.1, H-5), 4.09 (1H, dd, $J_{6a,6b}$ = 8.1, H-6b), 3.69 (1H, dd, $J_{5,6a}$ = 7.4, H-6a), 3.61 (1H, dd, $J_{4,5}$ = 5.1, H-4), 3.23 (1H, dd, $J_{1a,1b}$ = 11.3, H-1b), 2.87 (1H, dd, H-1a), 1.43, 1.38, 1.29, and 1.27 (12H, 4 s, $4CH_3$). ^{13}C NMR ($(CD_3)_2O$) δ: 110.59, 109.16 ($(CH_3)_2C(OR)_2$), 88.44 (C-3), 85.37 (C-2), 78.42 (C-5), 68.97 (C-6), 51.34 (C-4), 29.17 (C-1), 26.73, 26.06, 25.37, 24.31 (4 CH_3). Anal. calcd. for $C_{12}H_{20}O_4Se$: C 46.91, H 6.56; found: C 46.71, H 6.62.

2,3,4,6-Di-*O*-isopropylidene-1,5-anhydro-1-thio-L-gulitol (9)

To a solution of dimesylate **18** (6.0 g, 14.3 mmol) in DMF (100 mL), $Na_2S{\cdot}9H_2O$ (4.1 g, 18.2 mmol) was added and the reaction mixture was heated at 100 °C for 12 h. The reaction mixture was poured into water (100 mL), extracted with Et_2O (4 × 50 mL), washed with water (10 × 20 mL), and dried over Na_2SO_4. After evaporating the solvent, the crude product was purified by column chromatography (hexane–EtOAc, 3:1) to give **9** as a colorless oil (3.5 g, 93%). $[\alpha]^{22}_D$ –41° (*c* 0.5, CH_2Cl_2). ^{1}H NMR ($(CD_3)_2O$) δ: 4.51 (1H, ddd, $J_{2,3}$ = 2.9, $J_{1b,2}$ = 4.2, H-2), 4.30–4.24 (2H, m, H-4, H-6b), 4.06 (1H, dd, $J_{3,4}$ = 6.2, $J_{5,6b}$ = 6.2, H-3), 3.63 (1H, dd, $J_{5,6a}$ = 1.9, $J_{6a,6b}$ = 12.5, H-6a), 2.95 (1H, dd, $J_{1a,1b}$ = 13.5, H-1b), 2.92 (1H, m, H-5), 2.57 (1H, dd, $J_{1b,2}$ = 7.2, H-1a), 1.45, 1.39, 1.32, and 1.25 (12H, 4 s, $4CH_3$). ^{13}C NMR ($(CD_3)_2O$) δ: 112.52, 103.61 ($(CH_3)_2C(OR)_2$), 79.65 (C-3), 75.26 (C-4), 71.63 (C-2), 68.40 (C-6), 39.94 (C-5), 33.77 (C-1), 31.53, 29.55, 29.49, 23.22 ($4CH_3$). Anal. calcd. for $C_{12}H_{20}O_4S$: C 55.36, H 7.74; found: C 55.43, H 7.70.

2,3,4,6-Di-*O*-isopropylidene-1,5-anhydro-1-seleno-L-gulitol (10)

To a suspension of Se powder (1.6 g, 20.2 mmol) and 95% EtOH (100 mL), $NaBH_4$ was added portionwise until the black selenium color disappeared. To this mixture a solution of dimesylate **18** (6.0 g, 14.3 mmol) in THF (10 mL) was added and the reaction mixture was heated at 70 °C for 12 h. The solvent of the reaction mixture was evaporated under reduced pressure, redissolved in EtOAc, washed with water (20 mL) and brine (20 mL), and dried over Na_2SO_4. After evaporating the solvent, the crude product was purified by column chromatography (hexane–EtOAc, 3:1) to give **10** as a colorless oil (2.7 g, 62%). $[\alpha]^{22}_D$ –32° (*c* 0.5, CH_2Cl_2). ^{1}H NMR ($(CD_3)_2O$) δ: 4.97 (1H, ddd, $J_{2,3}$ = 5.8, $J_{1a,2}$ = 2.4, $J_{1b,2}$ = 5.4, H-2), 4.71 (1H, dd, $J_{3,4}$ = 2.9, H-3), 4.28 (1H, ddd, $J_{4,5}$ = 5.1, $J_{5,6a}$ = 7.9, $J_{5,6b}$ = 6.1, H-5), 4.09 (1H, dd, $J_{6a,6b}$ = 8.0, H-6b), 3.69 (1H, dd, H-6a), 3.61 (1H, dd, H-4), 3.23 (1H, dd, $J_{1a,1b}$ = 11.4, H-1b), 2.87 (1H, dd, H-1a), 1.45, 1.39, 1.28, and 1.26 (12H, 4 s, $4CH_3$). ^{13}C NMR ($(CD_3)_2O$) δ: 110.64, 109.13 ($(CH_3)_2C(OR)_2$), 88.46 (C-3), 85.42 (C-4), 78.46 (C-5), 68.93 (C-6), 51.34 (C-4), 26.71 (C-1), 26.06, 25.38, 25.23, 24.43 ($4CH_3$). Anal. calcd. for $C_{12}H_{20}O_4Se$: C 46.91, H 6.56; found: C 46.67, H 6.28.

General procedure for the preparation of sulfonium and selenium sulfates (19–22)

A mixture of 2,3,5,6-di-*O*-isopropylidene-1,4-anhydro-1-thio-D-talitol (**7**), 2,3,4,6-di-*O*-isopropylidene-1,5-anhydro-1-thio-L-gulitol (**9**), 2,3,5,6-di-*O*-isopropylidene-1,4-anhydro-1-seleno-D-talitol (**8**), or 2,3,4,6-di-*O*-isopropylidene-1,5-anhydro-1-seleno-L-gulitol (**10**) and cyclic sulfate **11** in HFIP were placed in a reaction vessel and K_2CO_3 (20 mg) was added. The stirred reaction mixture was heated in a sealed tube at the indicated temperature for the indicated time, as given in the following. The progress of the reaction

© 2006 NRC Canada

was followed by TLC analysis of the aliquots (developing solvent, EtOAc–MeOH, 10:1). When the limiting reagent had been essentially consumed, the mixture was cooled, then diluted with CH_2Cl_2 and evaporated to give a syrupy residue. Purification by column chromatography (EtOAc to EtOAc–MeOH, 10:1) gave the purified and sulfonium salts **19** and **21** and selenonium salts **20** and **22**.

*1,4-Anhydro-2,3,5,6-di-*O*-isopropylidene-1-[(S)-[(2′R,3′S,4′R,5′R)-2′,4′-benzylidenedioxy-5′,6′-isopropylidenedioxy-3′-(sulfooxy)hexyl]sulfonio]-D-talitol inner salt (19)*

Reaction of compound **7** (400 mg, 1.53 mmol) with **11** (740 mg, 1.99 mmol) in HFIP (2.0 mL) for 12 h at 70–75 °C gave compound **19** as a colorless, amorphous solid (820 mg, 85% based on **7**). $[\alpha]^{22}_D$ –40° (*c* 0.5, CH_2Cl_2). ^{1}H NMR (CD_2Cl_2) δ: 7.48–7.30 (5H, m, Ar), 5.68 (1H, s, C*H*Ph), 5.15 (1H, ddd, $J_{2,3}$ = 5.6, $J_{1a,2}$ = 1.9, $J_{1b,2}$ = 5.6, H-2), 4.98 (1H, dd, H-3), 4.55–4.51 (2H, m, H-4, H-2′), 4.46 (1H, ddd, $J_{4,5}$ = 4.1, $J_{5,6\ a}$ = 6.3, $J_{5,6b}$ = 6.3, H-5), 4.40 (1H, dd, $J_{1a,1b}$ = 13.4, $J_{1b,2}$ = 5.6, H-1b), 4.18 (2H, dd, H-6a, H-6b), 4.16–4.04 (4H, m, H-1a, H-3′, H-4′, H-5), 3.76 (2H, dd, H-1a, H-1b), 3.35 (1H, dd, $J_{6a,6b}$ = 9.5, $J_{5,6b}$ = 7.6, H-6b), 3.16 (1H, dd, $J_{5,6a}$ = 6.4, H-6a), 1.52, 1.33, 1.31, 1.28, 1.26, and 1.16 (18H, 6 s, 6C*H*$_3$). ^{13}C NMR (CD_2Cl_2) δ: 137.28, 129.65, 128.63, 126.37 (4C_{Ar}), 112.85, 111.37, 108.64 (three $(CH_3)_2C(OR)_2$), 100.87 (*C*HPh), 89.77 (C-3), 84.24 (C-2), 79.32 (C-3′), 75.48 (C-5′), 75.33 (C-5), 74.36 (C-4), 70.47 (C-2′), 67.92 (C-4′), 67.05 (C-6), 65.18 (C-6′), 50.12 (C-1), 44.42 (C-1′) 26.56, 26.15, 25.62, 25.57, 25.03, 22.86 (6*C*H$_3$). Anal. calcd. for $C_{28}H_{40}O_{12}S_2$: C 53.15, H 6.37; found: C 52.92, H 6.17.

*1,4-Anhydro-2,3,5,6-di-*O*-isopropylidene-1-[(S)-[(2′R,3′S,4′R,5′R)-2′,4′-benzylidenedioxy-5′,6′-isopropylidenedioxy-3′-(sulfooxy)hexyl]selenonio]-D-talitol inner salt (20)*

Reaction of compound **8** (500 mg, 1.63 mmol) with **11** (780 mg, 2.09 mmol) in HFIP (2.0 mL) for 12 h at 60–65 °C gave compound **20** and a minor product (<10%) as a colorless, amorphous solid (810 mg, 73% based on **8**). The major product (**20**): $[\alpha]^{22}_D$ –46° (*c* 0.5, CH_2Cl_2). ^{1}H NMR ($(CD_3)_2O$) δ: 7.62–7.38 (5H, m, Ar), 5.92 (1H, s, C*H*Ph), 5.47 (1H, ddd, $J_{2,3}$ = 5.6, $J_{1a,2}$ = 1.3, $J_{1b,2}$ = 5.9, H-2), 5.35 (1H, dd, H-3), 4.92 (1H, ddd, H-2′), 4.60 (1H, dd, $J_{1'b,2'}$ = 6.4, $J_{1'a,1'b}$ = 12.3, H-1′b), 4.57 (1H, m, H-4), 4.55 (1H, ddd, $J_{5,6b}$ = 6.9, $J_{5,6a}$ = 6.6, $J_{4,5}$ = 1.5, H-5), 4.48 (1H, ddd, $J_{5',6'b}$ = 6.7, $J_{5',6'a}$ = 7.4, $J_{4',5'}$ = 2.5, H-5′), 4.42–4.34 (3H, m, H-3′, H-6′b, H-4), 4.24 (1H, dd, $J_{6'a,6'b}$ = 8.1, H-6′a), 4.09 (1H, dd, $J_{1'a,2'}$ = 1.5, H-1′a), 3.89 (1H, dd, $J_{1a,1b}$ = 14.1, H-1b), 3.84 (1H, dd, H-1a), 3.70 (1H, dd, $J_{6a,6b}$ = 9.4, H-6b), 3.34 (1H, dd, H-6a),1.59, 1.38, 1.35, 1.30, 1.29, and 1.24 (18H, 6 s, 6C*H*$_3$). ^{13}C NMR ($(CD_3)_2O$) δ: 138.21, 129.24, 128.42, 126.48 (4C_{Ar}), 111.32, 107.67, 100.47 ($3(CH_3)_2C(OR)_2$), 100.41 (*C*HPh), 91.54 (C-3), 85.82 (C-2), 78.92 (C-3′), 76.67 (C-5), 75.54 (C-5), 74.18 (C-2), 70.82 (C-4′), 67.97 (C-6), 67.45 (C-4), 64.74 (C-6′), 46.24 (C-1), 41.78 (C-1) 26.02, 25.85, 25.67, 25.44, 24.02, 22.75 (6*C*H$_3$). Anal. calcd. for $C_{28}H_{40}O_{12}SSe$: C 49.48, H 5.93; found: C 49.16, H 6.09.

*1,5-Anhydro-2,3,4,6-di-*O*-isopropylidene-1-[(S)-[(2′R,3′S,4′R,5′R)-2′,4′-benzylidenedioxy-5′,6′-isopropylidenedioxy-3′-(sulfooxy)hexyl]sulfonio]-L-gulitol inner salt (21)*

Reaction of compound **9** (500 mg, 1.92 mmol) with **11** (860 mg, 2.30 mmol) in HFIP (2.0 mL) for 12 h at 90–95 °C gave compound **21** as a colorless, amorphous solid (1.12 g, 90% based on **9**). $[\alpha]^{22}_D$ –52 ° (*c* 0.5, CH_2Cl_2). ^{1}H NMR ($(CD_3)_2O$) δ: 7.62–7.38 (5H, m, Ar), 5.88 (1H, s, C*H*Ph), 4.94 (1H, ddd, $J_{2,3}$ = 3.0, $J_{1a,2}$ = 2.4, $J_{1b,2}$ = 3.0, H-2), 4.85 (1H, ddd, $J_{2',3'}$ = 1.8, $J_{1'a,2'}$ = 6.1, $J_{1'b,2'}$ = 3.1, H-2′), 4.60 (1H, dd, $J_{3,4}$ = 3.0, H-4), 4.55 (1H, ddd, $J_{4',5'}$ = 2.0, $J_{5',6'a}$ = 7.7, $J_{5',6'b}$ = 6.7, H-5′), 4.52 (1H, dd, $J_{3',4'}$ = 1.9, H-3′), 4.44 (1H, dd, $J_{1'a,1'b}$ = 14.2, H-1′b), 4.43 (1H, m, H-4′), 4.39 (1H, dd, $J_{6'a,6'b}$ = 8.5, H-6′b), 4.35 (1H, dd, H-3), 4.33 (1H, dd, H-1′a), 4.26 (1H, dd, H-6′a), 4.18 (1H, dd, $J_{1a,1b}$ = 13.6, H-1b), 4.14 (1H, m, H-6b), 3.93 (1H, dd, $J_{6a,6b}$ = 13.3, $J_{5,6a}$ = 1.6, H-6a), 3.80 (1H, dd, H-1a), 3.68 (1H, m, H-5), 1.62, 1.48, 1.40, 1.36, 1.35, and 1.29 (18H, 6 s, 6C*H*$_3$). ^{13}C NMR ($(CD_3)_2O$) δ: 138.12, 129.26, 128.46, 126.52 (4 C_{Ar}), 109.73, 107.42, 100.73 ($3(CH_3)_2C(OR)_2$), 100.46 (*C*HPh), 79.03 (C-4′), 76.84 (C-5′), 74.24 (C-2), 71.66 (C-3), 69.95 (C-3′), 67.16 (C-4), 65.71 (C-4), 64.66 (C-6′), 61.52 (C-6), 49.18 (C-1′), 48.93 (C-5), 33.77 (C-1), 28.73, 25.92, 25.74, 25.67, 22.72, 18.23 (6*C*H$_3$). Anal. calcd. for $C_{28}H_{40}O_{12}S_2$: C 53.15, H 6.37; found: C 52.95, H 6.14.

*1,5-Anhydro-2,3,4,6-di-*O*-isopropylidene-1-[(S)-[(2′R,3′S,4′R,5′R)-2′,4′-benzylidenedioxy-5′,6′-isopropylidenedioxy-3′-(sulfooxy)hexyl]selenonio]-L-gulitol inner salt (22)*

Reaction of compound **10** (500 mg, 1.63 mmol) with **11** (780 mg, 2.09 mmol) in HFIP (2.0 mL) for 12 h at 80–85 °C gave compound **22** as a colorless, amorphous solid (850 mg, 77% based on **10**). $[\alpha]^{22}_D$ –31° (*c* 0.5, CH_2Cl_2). ^{1}H NMR ($(CD_3)_2O$) δ: 7.62–7.40 (5H, m, Ar), 5.92 (1H, s, C*H*Ph), 5.46 (1H, ddd, $J_{2,3}$ = 5.6, $J_{1a,2}$ = 1.2, $J_{1b,2}$ = 5.9, H-2), 5.37 (1H, dd, H-3), 4.85 (1H, m, H-2′), 4.62 (1H, dd, $J_{1'b,2'}$ = 6.5, $J_{1'a,1'b}$ = 11.3, H-1′b), 4.60 (1H, m, H-3′), 4.55 (1H, ddd, $J_{4,5}$ = 1.3, $J_{5,6a}$ = 6.6, $J_{5,6b}$ = 6.8, H-5), 4.47 (1H, ddd, $J_{4',5'}$ = 2.4, $J_{5',6'a}$ = 7.4, $J_{5',6'b}$ = 6.6, H-5′), 4.39 (2H, m, H-4, H-4′)), 4.35 (1H, dd, $J_{6'a,6'b}$ = 8.5, H-6′b), 4.24 (1H, dd, H-6′a), 4.09 (1H, dd, $J_{1'a,2'}$ = 1.4, H-1 a), 3.90 (1H, dd, $J_{1a,1b}$ = 14.2, H-1b), 3.84 (1H, dd, H-1a), 3.70 (1H, dd, $J_{6a,6b}$ = 9.4, H-6b), 3.32 (1H, dd, H-6a), 1.59, 1.38, 1.35, 1.31, 1.30, and 1.24 (18H, 6 s, 6C*H*$_3$). ^{13}C NMR ($(CD_3)_2O$) δ: 138.23, 129.22, 128.47, 126.45 (4C_{Ar}), 110.43, 110.75, 107.67 ($3(CH_3)_2C(OR)_2$), 100.45 (*C*HPh), 91.58 (C-3), 85.89 (C-2), 78.93 (C-4), 76.55 (C-5′), 75.42 (C-5), 74.16 (C-2′), 70.95 (C-3′), 68.03 (C-6), 67.56 (C-4), 64.86 (C-6′), 46.23 (C-1), 41.60 (C-1′), 26.03, 25.85, 25.62, 25.34, 23.99, 22.72 (6*C*H$_3$). Anal. calcd. for $C_{28}H_{40}O_{12}SSe$: C 49.48, H 5.93; found: C 49.71, H 6.10.

General procedure for the deprotection of the coupling products to yield the final compounds (3–6)

The protected coupling products **19–22** were dissolved in CH_2Cl_2 (2 mL), TFA (10 mL) was then added, and the mixture was stirred for 6–8 h at room temperature. The progress of the reaction was followed by TLC analysis of the aliquots (developing solvent, EtOAc–MeOH–H_2O, 7:3:1). When the

© 2006 NRC Canada

starting material had been consumed, the TFA and CH_2Cl_2 were removed under reduced pressure. The residue was rinsed with CH_2Cl_2 (4 × 2 mL) and the CH_2Cl_2 was decanted to remove the cleaved protecting groups. The remaining gum was dissolved in MeOH and purified by column chromatography (EtOAc and EtOAc–MeOH, 2:1) to give the purified compounds **3**–**6** as colorless, amorphous, and hygroscopic solids.

1,4-Anhydro-1-[(S)-[(2′R,3′S,4′R,5′R)-2′,4′,5′,6′-tetrahydroxy-3′-(sulfooxy)hexyl]sulfonio]-D-talitol inner salt (3)

To a solution of **19** (400 mg, 0.63 mmol) in CH_2Cl_2 (2 mL) was added TFA (10 mL) to yield compound **3** as a colorless, amorphous, and hygroscopic solid (150 mg, 59%). $[\alpha]^{22}_D$ –29° (*c* 0.1, H_2O). ^{1}H NMR (D_2O) δ: 4.60 (1H, m, H-2), 4.56 (1H, dd, $J_{3',4'}$ = 1.1, $J_{2',3'}$ = 5.0, H-3′), 4.50 (1H, ddd, $J_{1'b,2'}$ = 10.5, $J_{1'a,2'}$ = 2.8, H-2′), 4.32 (1H, dd, $J_{2,3}$ = 9.6, $J_{3,4}$ = 2.8, H-3), 4.17 (1H, ddd, H-5), 4.00 (1H, dd, $J_{1'a,1'b}$ = 13.2, H-1′b), 3.92 (1H, dd, $J_{4,5}$ = 9.5, H-4), 3.91 (1H, dd, H-1′a), 3.80 (1H, dd, $J_{4',5'}$ = 9.0, H-4′), 3.78 (1H, dd, $J_{6a,6b}$ = 12.2, $J_{5,6b}$ = 3.5, H-6b), 3.73 (1H, dd, $J_{5',6'b}$ = 2.7, $J_{6'a,6'b}$ = 11.8, H-6′b), 3.69 (1H, ddd, $J_{5',6'a}$ = 6.1, H-5′), 3.66 (1H, dd, $J_{5,6a}$ = 4.1, H-6a), 3.56 (1H, dd, $J_{1b,2}$ = 7.6, $J_{1a,1b}$ = 11.4, H-1b), 3.55 (1H, dd, $J_{1a,2}$ = 5.8, H-1a), 3.54 (1H, m, H-6′a). ^{13}C NMR (D_2O) δ: 77.81 (C-3′), 76.26 (C-3), 72.93 (C-2), 70.52 (C-5′), 68.98 (C-4′), 67.91 (C-2′), 67.55 (C-5), 64.62 (C-6), 64.53 (C-4), 62.85 (C-6′), 49.41 (C-1′), 44.57 (C-1). HRMS calcd. for $C_{12}H_{24}O_{12}S_2Na$: 447.0601 (M + Na); found: 447.0604.

1,4-Anhydro-1-[(S)-[(2′R,3′S,4′R,5′R)-2′,4′,5′,6′-tetrahydroxy-3′-(sulfooxy)hexyl]selenonio]-D-talitol inner salt (4)

To a solution of **20** (400 mg, 0.59 mmol) in CH_2Cl_2 (2 mL) was added TFA (10 mL) to yield compound **4** as a colorless, amorphous, and hygroscopic solid (132 mg, 47%). $[\alpha]^{22}_D$ –50° (*c* 0.1, H_2O). ^{1}H NMR (D_2O) δ: 4.74 (1H, m, H-2), 4.54 (1H, dd, $J_{3',4'}$ = 1.1, $J_{2',3'}$ = 5.0, H-3′), 4.47 (1H, ddd, H-2), 4.22′ (1H, dd, $J_{2,3}$ = 10.0, $J_{3,4}$ = 2.9, H-3), 4.14 (1H, m, H-5), 3.96 (1H, dd, $J_{1'b,2'}$ = 10.3, H-1′b), 3.92 (1H, dd, $J_{1'a,2'}$ = 3.7, $J_{1'a,1'b}$ = 12.3, H-1′a), 3.85 (1H, dd, $J_{4,5}$ = 1.9, H-4), 3.77 (1H, dd, $J_{5,6b}$ = 2.6, $J_{6a,6b}$ = 12.2, H-6b), 3.71 (1H, dd, $J_{6'a,6'b}$ = 11.8, $J_{5',6'b}$ = 2.4, H-6′b), 3.70–3.63 (2H, m, H-4′, H-5′), 3.60 (1H, dd, $J_{5,6a}$ = 3.5, H-6a), 3.55 (1H, dd, $J_{5',6'a}$ = 9.1, H-6′a), 3.41 (1H, dd, $J_{1b,2}$ = 3.2, $J_{1a,1b}$ = 13.2, H-1b), 3.36 (1H, dd, H-1a). ^{13}C NMR (D_2O) δ: 78.44 (C-3′), 77.28 (C-3), 73.62 (C-2), 70.50 (C-5′), 69.13 (C-4′), 67.96 (C-2′), 67.22 (C-5), 65.06 (C-6), 63.69 (C-4), 62.73 (C-6), 46.84 (C-1′), 40.99 (C-1). HRMS calcd. for $C_{12}H_{24}O_{12}SSeNa$: 495.0046 (M + Na); found: 495.0044.

1,5-Anhydro-1-[(S)-[(2′R,3′S,4′R,5′R)-2′,4′,5′,6′-tetrahydroxy-3′-(sulfooxy)hexyl]sulfonio]-L-gulitol inner salt (5)

To a solution of **21** (400 mg, 0.63 mmol) in CH_2Cl_2 (2 mL) was added TFA (10 mL) to yield compound **5** as a colorless, amorphous, and hygroscopic solid (172 mg, 65%). $[\alpha]^{22}_D$ –54° (*c* 0.2, H_2O). ^{1}H NMR (D_2O) δ: 4.61 (1H, m, H-2), 4.57 (1H, dd, $J_{3',4'}$ = 3.0, $J_{2',3'}$ = 6.5, H-3′), 4.54 (1H, m, H-2′), 4.33 (1H, dd, $J_{2,3}$ = 5.5, $J_{3,4}$ = 2.4, H-3), 4.30 (1H, ddd, $J_{4,5}$ = 4.5, $J_{5,6b}$ = 6.3, H-5), 4.07 (1H, dd, $J_{1'b,2'}$ = 3.3, $J_{1'a,1'b}$ = 10.8, H-1′b), 4.06–4.02 (2H, m, H-4′, H-6′b), 3.98 (1H, dd, $J_{6'a,6'b}$ = 11.9, $J_{5',6'a}$ = 7.4, H-6′a), 3.94 (1H, dd, $J_{3,4}$ = 2.4, $J_{4,5}$ = 4.5, H-4), 3.86–3.83 (1H, m, H-5), 3.73 (1H, dd, $J_{5,6b}$ = 2.6, $J_{6a,6b}$ = 11.8, H-6b), 3.69 (1H, dd, $J_{1'a,2'}$ = 4.4, H-1′a), 3.58 (1H, dd, $J_{1b,2}$ = 5.5, $J_{1a,1b}$ = 11.4, H-1b), 3.56 (1H, dd, $J_{5,6a}$ = 5.8, H-6a), 3.46 (1H, dd, H-1a). ^{13}C NMR (D_2O) δ: 77.63 (C-2′), 70.53 (C-2), 69.57 (C-3), 69.04 (C-4), 68.84 (C-5′), 67.42 (C-3′), 63.55 (C-5), 62.73 (C-6), 59.60 (C-6′), 54.03 (C-4′), 45.56 (C-1′), 37.34 (C-1). HRMS calcd. for $C_{12}H_{24}O_{12}S_2Na$: 447.0601 (M + Na); found: 447.0601.

1,5-Anhydro-1-[(S)-[(2′R,3′S,4′R,5′R)-2′,4′,5′,6′-tetrahydroxy-3′-(sulfooxy)hexyl]selenonio]-L-gulitol inner salt (6)

To a solution of **22** (400 mg, 0.59 mmol) in CH_2Cl_2 (2 mL) was added TFA (10 mL) to yield compound **6** as a colorless, amorphous, and hygroscopic solid (150 mg, 55%). $[\alpha]^{22}_D$ –68° (*c* 0.1, H_2O). ^{1}H NMR (D_2O) δ: 4.74 (1H, m, H-2), 4.55 (1H, dd, $J_{3',4'}$ = 1.1, $J_{2',3'}$ = 5.0, H-3′), 4.49 (1H, ddd, $J_{1'b,2'}$ = 10.3, H-2′), 4.23 (1H, dd, $J_{2,3}$ = 3.1, $J_{3,4}$ = 10.2, H-3), 4.15 (1H, m, H-5), 3.98 (1H, dd, $J_{1'a,1'b}$ = 12.3, H-1′b), 3.94 (1H, dd, $J_{1'a,2'}$ = 3.7, H-1′a), 3.86 (1H, dd, $J_{4,5}$ = 1.7, H-4), 3.81–3.75 (2H, m, H-4′, H-6b), 3.73 (1H, dd, $J_{5',6'b}$ = 2.8, $J_{6'a,6'b}$ = 11.7, H-6′b), 3.69 (1H, ddd, H-5′), 3.61 (1H, dd, $J_{5,6a}$ = 3.3, $J_{6a,6b}$ = 8.7, H-6a), 3.55 (1H, dd, $J_{5',6'a}$ = 11.7, H-6′a), 3.41 (1H, dd, $J_{1b,2}$ = 3.2, $J_{1a,1b}$ = 13.4, H-1b), 3.37 (1H, dd, H-1a). ^{13}C NMR (D_2O) δ: 78.35 (C-3′), 77.22 (C-3), 73.54 (C-2), 70.54 (C-5′), 69.28 (C-4′), 67.92 (C-2′), 67.15 (C-5), 65.04 (C-6), 63.78 (C-4), 62.74 (C-6′), 46.63 (C-1′), 40.68 (C-1). HRMS calcd. for $C_{12}H_{24}O_{12}SSeNa$: 495.0046 (M + Na); found: 495.0045.

Acknowledgements

We are grateful to the Natural Sciences and Engineering Research Council of Canada (NSERC) for financial support and to B.D. Johnston for helpful discussions. We are also grateful to D.R. Bundle for the high-resolution mass spectra.

References

1. (*a*) F. Garcia-Olmeda, G. Salcedo, R. Sanchez-Monge, L. Gomez, L. Royo, and P. Carbonero. *In* Oxford surveys of plant molecular and cell biology. Vol. 4. *Edited by* B.J. Miflin. Oxford Univerity Press, New York. 1987. p. 275; (*b*) C. Bompard-Gilles, P. Rousseau, P. Rouge, and F. Payan. Structure, **4**, 1441 (1996); (*c*) F. Vallee, A. Kadziola, Y. Bourne, M. Juy, K.W. Rodenburg, B. Svensson, and R. Haser. Structure, **6**, 649 (1998); (*d*) S. Strobl, K. Maskos, G. Wiegand, R. Huber, F.-X. GomisRuth, and R. Glockshuber. Structure, **6**, 911 (1998).
2. (*a*) A. Varki, R. Cummings, J. Esko, H. Freeze, G. Hart, and J. Marth (*Editors*). Essentials of glycobiology. Cold Spring Harbor Laboratory Press, Cold Spring Harbor, New York. 1999; (*b*) D.H.R. Barton, K. Nakanishi, and O. Meth-Cohn (*Series editors*). A.D. Elbein, R.J. Molyneux, and B.M. Pinto (*editors*). Comprehensive natural products chemistry. Vol. 3. Elsevier, Oxford, UK. 1999. Chap. 7; (*c*) N. Asano, R.J. Nash, R.J. Molyneux, and G.W.J. Fleet. Tetrahedron: Asymmetry, **11**, 1645 (2000); (*d*) J.D. McCarter and S.G. Withers. Curr.

© 2006 NRC Canada

Opin. Struct. Biol. **4**, 885 (1994); (*e*) H.D. Ly and S.G. Withers. Annu. Rev. Biochem. **68**, 487 (1999).
3. M. Yoshikawa, T. Murakami, H. Shimada, H. Matsuda, J. Yamahara, G. Tanabe, and O. Muraoka. Tetrahedron Lett. **38**, 8367 (1997).
4. M. Yoshikawa, T. Murikawa, H. Matsuda, G. Tanabe, and O. Muraoka. Bioorg. Med. Chem. **10**, 1547 (2002).
5. B.M. Pinto, B.D. Johnston, A. Ghavami, M.G. Szczepina, H. Liu, and K. Sadalapure. US Patent Application No. 10/877490.
6. M. Yoshikawa, T. Murakami, K. Yashiro, and H. Matsuda. Chem. Pharm. Bull. **46**, 1339 (1998).
7. L. Svansson, B.D. Johnston, J.H. Gu, B. Patrick, and B.M. Pinto. J. Am. Chem. Soc. **122**, 10769 (2000).
8. H. Yuasa, J. Takada, and H. Hashimoto. Tetrahedron Lett. **41**, 6615 (2000).
9. A. Ghavami, B.D. Johnston, and B.M. Pinto. J. Org. Chem. **66**, 2312 (2001).
10. A. Ghavami, K.S. Sadalapure, B.D. Johnston, M. Lobera, B.B. Snider, and B.M. Pinto. Synlett, 1259 (2003).
11. A. Ghavami, B.D. Johnston, M.D. Maddess, S.M. Chinapoo, M.T. Jensen, B. Svensson, and B.M. Pinto. Can. J. Chem. **80**, 937 (2002).
12. B.D. Johnston, A. Ghavami, M.T. Jensen, B. Svensson, and B.M. Pinto. J. Am. Chem. Soc. **124**, 8245 (2002).
13. H. Liu and B.M. Pinto. J. Org. Chem. **70**, 753 (2005).
14. A. Ghavami, B.D. Johnston, M.T. Jensen, B. Svensson, and B.M. Pinto. J. Am. Chem. Soc. **123**, 6268 (2001).
15. B.D. Johnston, H.J. Hensen, and B.M. Pinto. J. Org. Chem. **71**, 1111 (2006).
16. H. Liu, L. Sim, D.R. Rose, and B.M. Pinto. J. Org. Chem. ASAP 10.1021/jo052539r.
17. M.G. Szczepina, B.D. Johnston, Y. Yuan, B. Svensson, and B.M. Pinto. J. Am. Chem. Soc. **126**, 12458 (2004).
18. Y. Li, C.R. Scott, N.A. Chamoles, A. Chavami, B.M. Pinto, T. Frantisek, and M.H. Gelb. Clin. Chem. (Washington, D.C.), **50**, 1785 (2004).
19. X. Wen, Y. Yuan, D.A. Kuntz, D.R. Rose, and B.M. Pinto. Biochemistry, **44**, 6729 (2005).
20. D. Kuntz, A. Ghavami, B.D. Johnston, B.M. Pinto, and D.R. Rose. Tetrahedron: Asymmetry, **16**, 25 (2005).
21. P.A.M. van der Klein, G.J.P.H. Boons, G.H. Veeneman, G.A. van der Marel, and J.H. van Boom. Tetrahedron Lett. **30**, 5477 (1989).
22. J. Gelas and D. Horton. Carbohydr. Res. **67**, 371 (1978).

© 2006 NRC Canada

Synthesis of the tetrasaccharide repeat unit of the O-antigen polysaccharide from *Escherichia coli* O77 employing the 2′-carboxybenzyl glycoside[1]

Bo Ram Lee, Joo Mi Jeon, Jae Hyuk Jung, Heung Bae Jeon, and Kwan Soo Kim

Abstract: The synthesis of the suitably protected form (**1**) of the tetrasaccharide repeat unit, →2)-α-D-Man*p*-(1→2)-β-D-Man*p*-(1→3)-α-D-Glc*p*NAc-(1→6)-α-D-Man*p*-(1→ (**A**), of the O-antigen polysaccharide of the lipopolysaccharide from *Escherichia coli* O77 has been accomplished by latent–active glycosylation employing the 2′-carboxybenzyl (CB) glycoside method. In addition to previously used latent glycosyl donors, 2′-(benzyloxycarbonyl)benzyl (BCB) glycosides, new latent glycosyl donors, 2′-(allyloxycarbonyl)benzyl (ACB) glycosides, have been introduced as a direct precursor for the active CB glycosides. We also demonstrate that 4,6-*O*-benzylidene-2-azido-2-deoxy-α-D-mannopyranoside (**7**) has been readily prepared from D-glucosamine in good yield.

Key words: Escherichia coli O77, glycosylation, 2′-carboxybenzyl (CB) glycosides, 2′-(allyloxycarbonyl)benzyl (ACB) glycosides, glycosyl donor.

Résumé : Faisant appel à une glycosilation latente active à l'aide de la méthode du glycoside de 2′-carboxybenzyle (CB), on a réalisé la synthèse de la forme adéquatement protégée du composé **1**, le tétrasaccharide →2)-α-D-Man*p*-(1→2)-β-D-Man*p*-(1→3)-α-D-Glc*p*NAc-(1→6)-α-D-Man*p*(1→ (**A**) qui est le motif constitutif du polysaccharide O-antigène du lipopolysaccharide du *Escherichia coli* O77. En plus des donneurs latents de glycosyle utilisés antérieurement, les glycosides de 2′-benzyloxycarbonyl)benzyle (BCB), on a introduit de nouveaux donneurs latents de glycosyle, les glycosides de 2′-(allylcarbonyl)benzyle (ACB), comme précurseurs directs de glycosides de CB actifs. On a aussi préparé facilement le 4,6-*O*-benzylidène-2-azido-2-désoxy-α-D-mannopyranoside (**7**) à partir de la D-glucosamine avec un bon rendement.

Mots clés : Escherichia coli O77, glycosylation, glycoside de 2′-carboxybenzle (CB), glycosides de 2′-(allyloxycarbonyl)benzyle (ACB), donneur de glycosyle.

[Traduit par la Rédaction]

Introduction

Escherichia coli is a facultative anaerobic Gram-negative rod and is a predominant specie of the human colonic flora. Normal nonpathogenic strains of *E. coli* usually remain harmlessly confined to the intestinal lumen. However, infections owing to inherently pathogenic *E. coli* strains result in clinical syndromes such as urinary tract infections, sepsis/meningitis, and enteric/diarrheal disease. The species is subdivided into different serotypes based on the immunogenicity of bacterial surface structures (1, 2). *E. coli* O77, which belongs to an O-serotype, causes diarrheal infections (3) and has been identified as producing a Shiga-like toxin in both humans and animals (4–7). Recently, Widmalm and coworkers (8) have reported that the lipopolysaccharide (LPS) from the *E. coli* O77 contains the O-antigen polysaccharide as its substructure. As shown in Fig. 1, this particular polysaccharide is composed of a series of the repeat unit of a tetrasaccharide with the following structure: →2)-α-D-Man*p*-(1→2)-β-D-Man*p*-(1→3)-α-D-Glc*p*NAc-(1→6)-α-D-Man*p*-(1→ (**A**).

One of the challenges in the synthesis of this tetrasaccharide repeat unit would be the elaboration of the β-mannopyranosyl linkage. Although several strategies for the β-mannopyranosylation have been developed (9), including Crich and co-workers' recent approach (10) employing 4,6-*O*-benzylidene-protected glycosyl sulfoxides or thioglycosides as glycosyl donors, the construction of β-mannopyranosyl linkages still poses a great challenge. Recently, we have developed an efficient glycosylation method that em-

Received 8 August 2005. Published on the NRC Research Press Web site at http://canjchem.nrc.ca on 11 April 2006.

Dedicated to Professor Walter A. Szarek, in recognition of his many achievements in carbohydrate chemistry, on the occasion of his 65th birthday.

B.R. Lee, J.M. Jeon, J.H. Jung, H.B. Jeon, and K.S. Kim.[2] Center for Bioactive Molecular Hybrids and Department of Chemistry, Yonsei University, Seoul 120-749, Korea.

[1]This article is part of a Special Issue dedicated to Professor Walter A. Szarek.
[2]Corresponding author (e-mail: kwan@yonsei.ac.kr).

 doi:10.1139/V06-030 © 2006 NRC Canada

Scheme 1. Retrosynthesis of tetrasaccharide **1**.

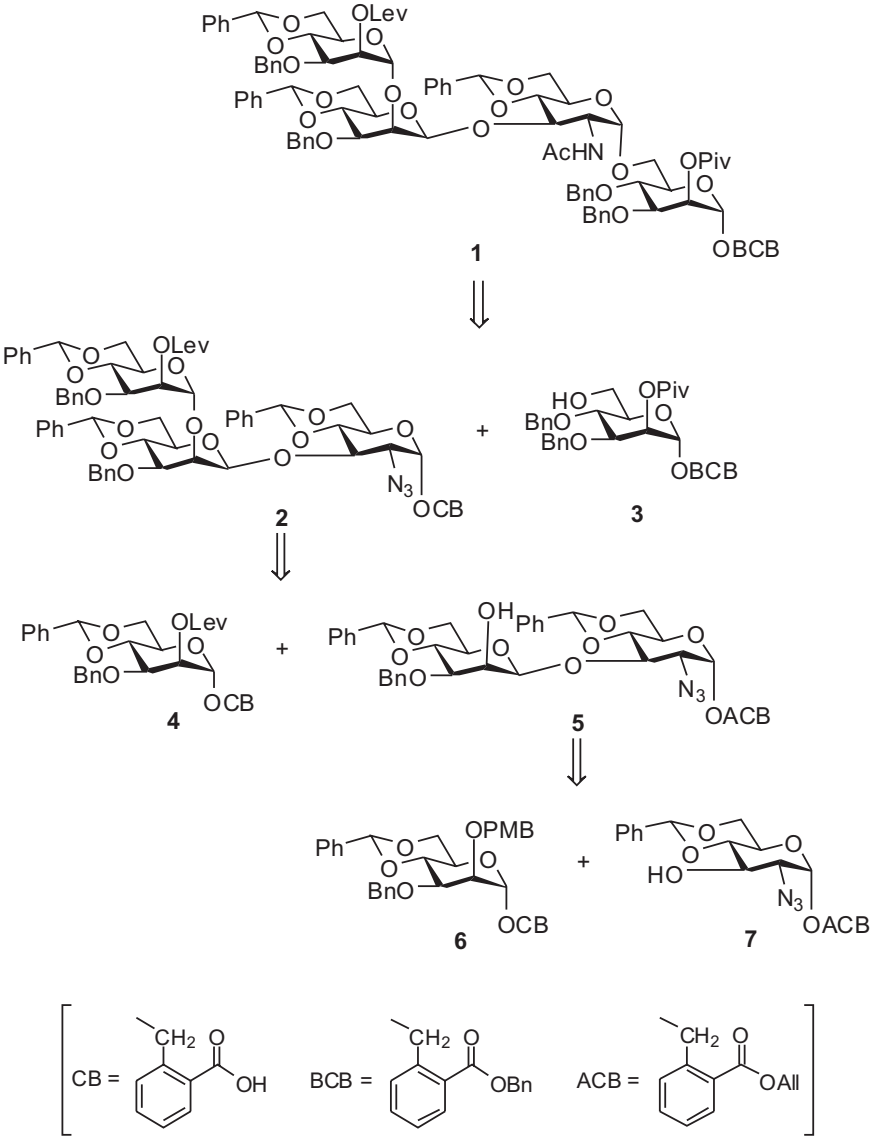
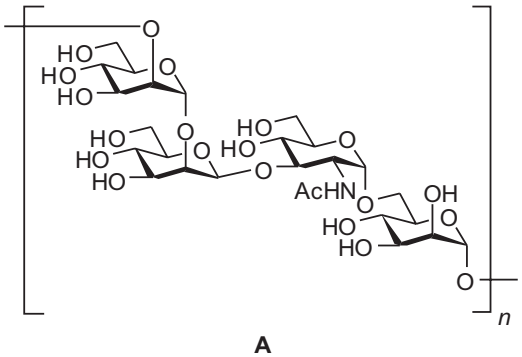


Fig. 1. The repeat unit of the O-antigen polysaccharide in *Escherichia coli* O77.



A

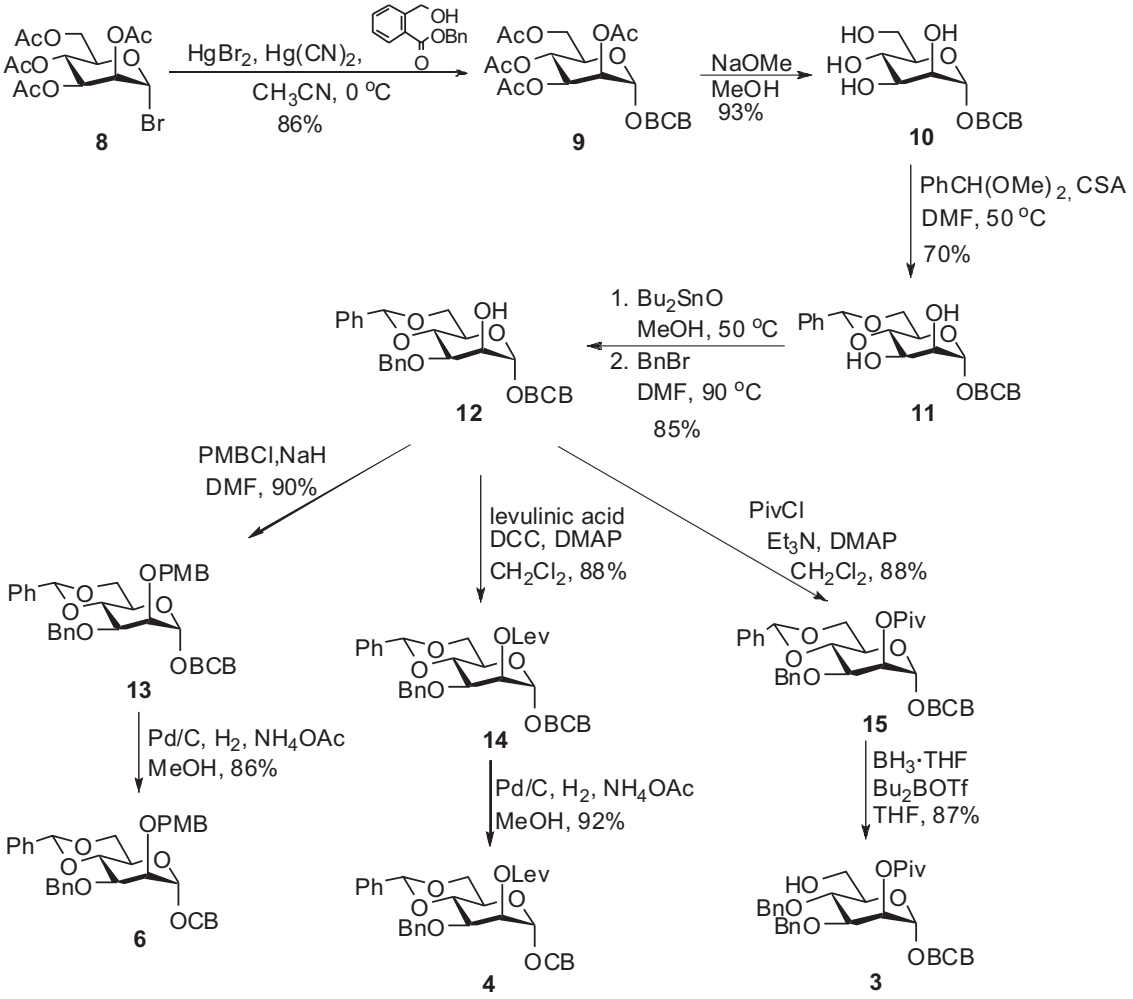
ploys a new type of glycosyl donor, 2′-carboxybenzyl (CB) glycoside. This methodology has been employed in the stereoselective β-mannopyranosylation and 2-deoxyglycosylation of various glycosyl acceptors (11–14). As an ongoing effort to explore the application and to understand the limitation of the CB-glycoside-mediated glycosylation, we disclose the synthesis of the protected tetrasaccharide **1**, which represents the elemental subunit of the O-antigen polysaccharide of the LPS from *E. coli* O77.

Results and discussion

The protective groups were carefully chosen in synthesizing the target tetrasaccharide **1**, since it was of importance to realize the selective deprotection during the future synthesis of an octasaccharide or a dodecasaccharide from **1** by dimerization or trimerization, respectively. Thus, the latent 2′-(benzyloxycarbonyl)benzyl (BCB) group at C-1 in the reducing end of the tetrasaccharide **1** would be readily converted into the active CB group to give a tetrasaccharide donor. The levulinyl (Lev) group at the C-2 in the nonreducing end of **1** would be selectively cleaved to provide a tetrasaccharide acceptor.

© 2006 NRC Canada

Scheme 2. Synthesis of monosaccharide building blocks **3**, **4**, and **6**.



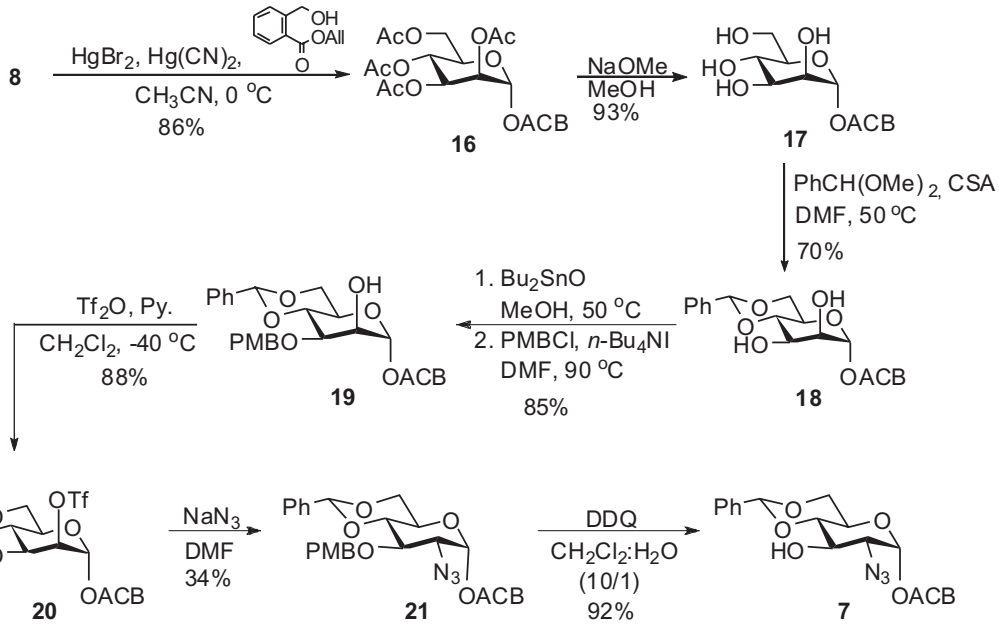
Retrosynthesis of **1** leads to trisaccharide donor **2** and pivaloyl (Piv)-protected mannosyl acceptor **3**, then further analysis of **2** provides levulinyl-protected mannosyl donor **4** and 2′-(allyloxycarbonyl)benzyl (ACB) glycoside **5** as an acceptor (Scheme 1). The acceptor **5** can be derived from *p*-methoxybenzyl(PMB)-protected mannosyl donor **6** and 2-azido-2-deoxy-glucospyranosyl acceptor **7**.

The monosaccharide building blocks **3**, **4**, and **6** were synthesized from a common intermediate **12**, which was prepared by the dibutyltinoxide-mediated selective benzylation of diol **11** (Scheme 2) (14). Diol **11** was efficiently prepared from tetraacetylmannosyl bromide (**8**) by the following sequence: (*i*) coupling of **8** and crystalline benzyl 2-(hydroxymethyl)benzoate, which was readily obtained in large quantities from inexpensive phthalide, in the presence of $HgBr_2$ and $Hg(CN)_2$ in acetonitrile; (*ii*) deacetylation of the resulting tetraacetylmannoside **9** under basic conditions; and (*iii*) subsequent benzylidenation of the resulting tetrol **10** (11). *P*-Methoxybenzylation of **12** followed by selective hydrogenolysis of the resulting BCB glycoside **13** in the presence of NH_4OAc gave the desired CB glycoside **6**. Pivaloylation of **12** and subsequent reductive cleavage of the resultant benzylidene acetal **15** with borane – dibutylboron triflate (15) provided C-6 alcohol **3**. Protection of **12** with levulinic acid in the presence of dicyclohexylcarbodiimide (DCC) and 4-(*N*,*N*-dimethylamino)pyridine (DMAP) followed by hydrogenolysis of the resulting levulinyl BCB glycoside **14** in the presence of NH_4OAc afforded the CB glycoside **4**.

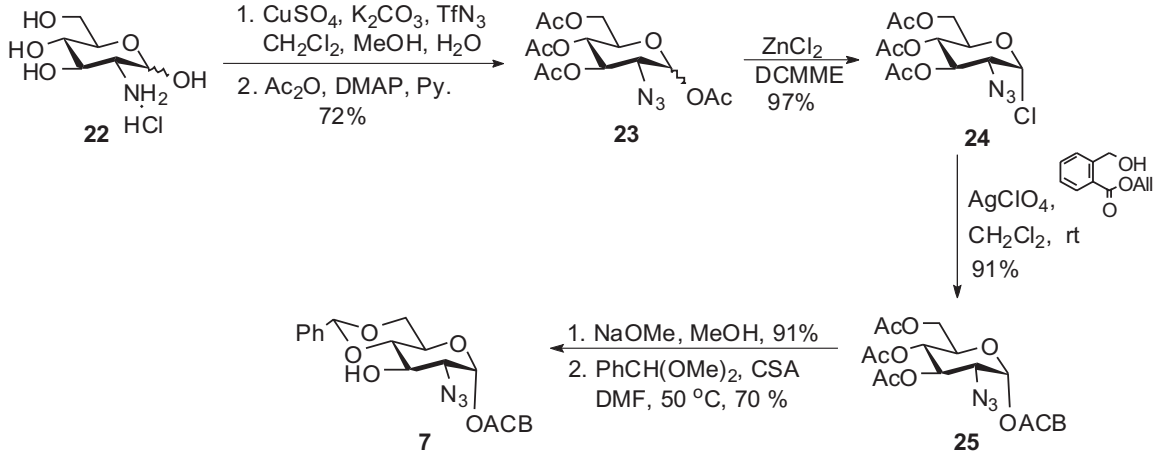
For the synthesis of the azidomonosaccharide building block **7**, **8** was used as a starting material (Scheme 3). The ACB mannoside **16** was prepared by coupling of **8** and allyl 2-(hydroxymethyl)benzoate in the presence of $HgBr_2$ and $Hg(CN)_2$. Introduction of the new ACB group in the place of the previously used BCB group was necessary because the azide functionality at C-2 was also reduced during the conversion of the BCB group into the CB group under the hydrogenolysis conditions. Deacetylation of **16** by NaOMe followed by benzylidenation of the resulting tetrol **17** afforded 4,6-*O*-benzylidene-protected ACB mannoside **18**. The hydroxy group at C-3 of diol **18** was selectively protected with the *p*-methoxybenzyl (PMB) group by using the dibutyltin oxide method to give PMB-protected alcohol **19**. Then, compound **19** was treated with triflic anhydride in the presence of pyridine to afford triflate **20**. Treating **20** with sodium azide in DMF gave the desired 2-azido-2-deoxy-glucospyranoside **21** in only 34% yield. The major by-product was the C-2,3 alkene, which was presumably to be

© 2006 NRC Canada

Scheme 3. Synthesis of monosaccharide building block **7** from **8**.



Scheme 4. Synthesis of monosaccharide building block **7** from glucosamine **22**.



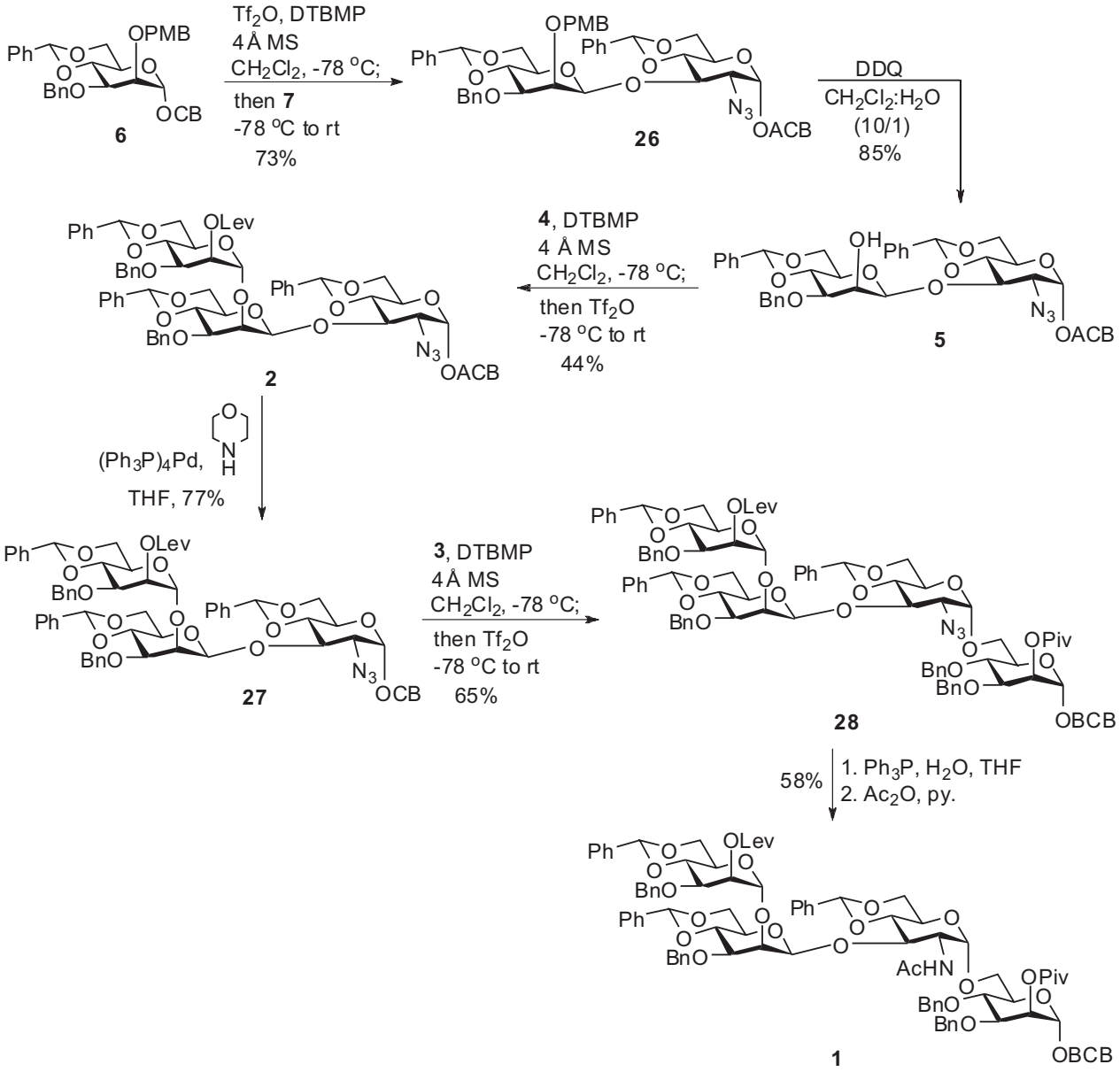
formed via the E_2 mechanism. To favor the nucleophilic substitution, a number of different reaction conditions were attempted. Unfortunately, there was no improvement.

A different route to compound **7** was realized using D-glucosamine hydrochloride (**22**) as a starting material (Scheme 4). Treating **22** with triflyl azide (TfN_3) in the presence of a catalytic amount of $CuSO_4$ in a cosolvent of CH_2Cl_2, MeOH, and H_2O to make a homogenous solution followed by acetylation provided tetraacetyl 2-azido-2-deoxyglucopyranoside (**23**) in 72% yield (16). Compound **23** was smoothly transformed into glucopyranosyl chloride **24** by using dichloromethyl methyl ether (DCMME) in the presence of a catalytic amount of zinc chloride (17). Reaction of **24** with allyl 2-(hydroxymethyl)benzoate using $AgClO_4$ as a promoter afforded α-ACB glycoside **25** as a single isomer in 91% yield, while the same reaction using AgOTf as a promoter gave **25** in 86% yield as a mixture of α and β anomers in a ratio of 4:1. Deacetylation of **25** with NaOMe followed by benzylidenation with benzaldehyde dimethyl acetal afforded the C-3 alcohol **7**.

The stage was set for the assembly of the properly protected monosaccharide building blocks **3**, **4**, **6**, and **7** to make tetrasaccharide **1**. The crucial stereoselective β-mannopyranosylation was achieved by activation of the glycosyl donor **6** with Tf_2O in the presence of 2,6-di-*tert*-butyl-4-methylpyridine (DTBMP) and 4 Å molecular sieves in CH_2Cl_2, followed by the addition of the acceptor **7** at –78 °C. The desired β-mannopyranosyl disaccharide **26** was obtained in 59% yield along with α-disaccharide as a by-product in 14% yield, as shown in Scheme 5. It was essential to activate the donor **6** with Tf_2O in the presence of DTBMP before the addition of the acceptor **7** to maximize the yield of **26**. The stereochemistry at the newly generated anomeric center of the disaccharide **26** was determined on the basis of its ^1H and ^{13}C NMR spectral data, especially the chemical shift in the ^{13}C NMR: δ 101.6 ppm for the β-

© 2006 NRC Canada

Scheme 5. Completion of the synthesis of tetrasaccharide **1**.



disaccharide in comparison with δ 100.1 ppm for the α-disaccharide. Removal of the PMB group in **26** with DDQ and the subsequent glycosylation of the resulting monohydroxy disaccharide acceptor **5** with the CB glycosyl donor **4** provided the desired α-trisaccharide **2** in 44% yield and the β-trisaccharide in 21% yield. Then, the ACB trisaccharide **2** was readily converted into the active CB trisaccharide **27** in 77% yield by deallylation with a catalytic amount of $Pd(Ph_3P)_4$ in the presence of morpholine (18). This result indicated that ACB glycosides were a useful precursor for CB glycosides, especially in the presence of the azide functionality, which could not survive during the conversion of the BCB glycosides into CB glycosides by hydrogenolysis. Finally, the coupling of the CB trisaccharide donor **27** and the BCB monosaccharide acceptor **3** in the presence of Tf_2O and DTBMP afforded α-tetrasaccharide **28** as a single isomer in 65% yield. Reduction of the azido group by treatment of **28** with triphenylphosphine (19), followed by acetylation of the resulting amine, furnished the desired target tetrasaccharide **1** in 58% yield.

Conclusion

We have described the synthesis of the suitably protected tetrasaccharide repeat unit **1** of the O-antigen polysaccharide of the LPS from *E. coli* O77. The 2′-carboxybenzyl (CB) glycoside method proved to be effective in the coupling of four monosaccharide components of the tetrasaccharide, **3**, **4**, **6**, and **7**. The newly introduced ACB glycoside was readily converted into the active CB glycosyl donors without affecting the azide functionality. Additionally, 4,6-*O*-benzylidene-2-azido-2-deoxy-α-D-mannopyranoside (**7**) was readily prepared from D-glucosamine hydrochloride in good yield.

© 2006 NRC Canada

Experimental

The known compounds **9** (11), **10** (11), **11** (11), **23** (16), and **24** (17) were prepared according to the procedures reported previously.

BCB 3-*O*-benzyl-4,6-*O*-benzylidene-α-D-mannopyranoside (12)

A solution of BCB 4,6-*O*-benzylidene-α-D-mannopyranoside (**11**) (450 mg, 0.9 mmol) and Bu_2SnO (228 mg, 0.9 mmol) in MeOH (40 mL) was stirred at 50 °C for 1 h. After removal of the solvent in vacuo, the residue was dissolved in DMF (10 mL) and then BnBr (0.19 mL, 1.6 mmol) was added to the reaction mixture. After stirring at 90 °C for 3 h, the reaction mixture was quenched with H_2O and then extracted with EtOAc. The combined organic layer was washed with satd. aq. NH_4Cl and brine, dried over $MgSO_4$, and concentrated in vacuo. The residue was purified by flash column chromatography (hexane–EtOAc, 2:1) to afford compound **12** (506 mg, 85%) as a colorless oil. R_f 0.36 (hexane–EtOAc, 2:1, *v*/*v*). $[\alpha]^{20}_D$ +42.9° (*c* 6.75, $CHCl_3$). IR ($CHCl_3$, film, cm^{-1}): 3447, 2921, 1637, 1460, 1381, 1098, 979. ^1H NMR (250 MHz, $CDCl_3$) δ: 2.79 (s, 1H), 3.83–3.89 (m, 2H), 3.97 (dd, *J* = 3.5, 9.5 Hz, 1H), 4.07–4.19 (m, 2H), 4.26 (dd, *J* = 2.7, 8.0 Hz, 1H), 4.71 (d, *J* = 11.7 Hz, 1H), 4.87 (d, *J* = 11.7 Hz, 1H), 4.93 (d, *J* = 14.0 Hz, 1H), 4.96 (s, 1H), 5.11 (d, *J* = 14.0 Hz, 1H), 5.31 (s, 2H), 5.61 (s, 1H) 7.25–7.54 (m, 18H), 8.00 (d, *J* = 7.5 Hz, 1H). ^{13}C NMR (63 MHz, $CDCl_3$) δ: 63.7, 66.9, 67.6, 68.9, 70.1, 73.2, 75.9, 79.0, 99.9, 101.6, 125.9, 127.3, 127.8, 127.8, 128.0, 128.1, 128.2, 128.3, 128.5, 128.7, 130.6, 132.5, 135.9, 137.7, 138.1, 139.5, 166.7.

BCB 3-*O*-benzyl-4,6-*O*-benzylidene-2-*O*-*p*-methoxybenzyl-α-D-mannopyranoside (13)

A solution of **12** (622 mg, 1.07 mmol), PMBCl (0.24 mL, 1.39 mmol), and NaH (51 mg, 2.14 mmol) in DMF (4 mL) was stirred at 0 °C for 10 min and at room temperature (rt) for 1 h. The reaction mixture was quenched with H_2O and then extracted with EtOAc. The combined organic layer was washed with satd. aq. NH_4Cl and brine, dried over $MgSO_4$, and concentrated in vacuo. The residue was purified by flash column chromatography (hexane–EtOAc, 2:1) to afford compound **13** (675 mg, 90%) as a colorless oil. R_f 0.47 (hexane–EtOAc, 2:1, *v*/*v*). $[\alpha]^{20}_D$ +52.9° (*c* 1.3, $CHCl_3$). IR ($CHCl_3$, film, cm^{-1}): 3420, 2920, 1720, 1624, 1430, 1381, 1088, 1021, 979. ^1H NMR (250 MHz, $CDCl_3$) δ: 3.78 (s, 3H), 3.79–3.91 (m, 3H), 4.02 (dd, *J* = 3.2, 10.0 Hz, 1H), 4.20–4.30 (m, 2H), 4.65 and 4.86 (ABq, *J* = 12.0 Hz, 2H), 4.67 and 4.74 (ABq, *J* = 12.0 Hz, 2H), 4.88 and 5.05 (ABq, *J* = 14.0 Hz, 2H), 4.89 (d, *J* = 1.2 Hz, 1H), 5.21 (s, 2H), 5.64 (s, 1H), 6.82–6.90 (m, 2H), 7.24–7.51 (m, 21H), 7.95 (d, *J* = 7.5 Hz, 1H). ^{13}C NMR (63 MHz, $CDCl_3$) δ: 55.3, 55.4, 64.6, 66.7, 67.4, 68.9, 73.1, 73.3, 75.8, 76.5, 79.3, 99.3, 101.5, 113.9, 114.1, 126.1, 127.3, 127.6, 127.7, 128.0, 128.2, 128.4, 128.8, 129.8, 130.2, 130.8, 132.4, 137.8, 139.6, 159.4, 159.8, 166.8. Anal. calcd. for $C_{43}H_{42}O_9$: C 73.49, H 6.02; found: C 73.47, H 6.03.

CB 3-*O*-benzyl-4,6-*O*-benzylidene-2-*O*-*p*-methoxybenzyl-α-D-mannopyranoside (6)

After compound **13** (416 mg, 0.59 mmol) was stirred under a hydrogen atmosphere using a balloon in the presence of Pd/C (10%, 63 mg) and ammonium acetate (46 mg, 0.59 mmol) in MeOH (10 mL) at rt for 1 h, the reaction mixture was filtered through Celite and the filtrate was concentrated in vacuo. The residue was purified by flash column chromatography (hexane–EtOAc, 1:1) to afford compound **6** (330 mg, 91%) as a white solid; mp 81 to 82. R_f 0.12 (hexane–EtOAc, 2:1, *v*/*v*). $[\alpha]^{20}_D$ +53.7° (*c* 1.3, $CHCl_3$). IR ($CHCl_3$, film, cm^{-1}): 2920, 1720, 1624, 1454, 1460, 1430, 1381, 1088, 1021, 979. ^1H NMR (250 MHz, $CDCl_3$) δ: 3.77 (s, 3H), 3.84–3.93 (m, 3H), 4.04 (dd, *J* = 3.2, 10.0 Hz, 1H), 4.25–4.32 (m, 2H), 4.65 and 4.86 (ABq, *J* = 12.0 Hz, 2H), 4.67 and 4.74 (ABq, *J* = 12.0 Hz, 2H), 4.88 and 5.05 (ABq, *J* = 14.0 Hz, 2H), 4.89 (d, *J* = 1.2 Hz, 1H), 5.64 (s, 1H) 6.84 (d, *J* = 8.5 Hz, 2H), 7.14–7.55 (m, 36H), 8.00 (d, *J* = 7.5 Hz, 1H). ^{13}C NMR (63 MHz, $CDCl_3$) δ: 55.3, 64.6, 66.9, 67.8, 71.6, 72.2, 74.2 78.5, 78.8, 100.0, 101.4, 101.7, 126.1, 126.2, 127.4, 127.6, 127.7, 128.2, 128.4, 128.5, 128.7, 128.9, 130.4, 130.6, 130.8, 132.6, 137.6, 138.4, 138.9, 139.5, 159.2, 171.9. Anal. calcd. for $C_{36}H_{36}O_9$: C 70.57, H 5.92; found: C 70.52, H 5.92.

BCB 3-*O*-benzyl-4,6-*O*-benzylidene-2-*O*-levulinyl-α-D-mannopyranoside (14)

After a solution of **12** (360 mg, 0.62 mmol), levulinic acid (107 mg, 0.93 mmol), DMAP (75 mg, 0.62 mmol), and DCC (191 mg, 0.93 mmol) in CH_2Cl_2 (10 mL) was stirred at rt for 1 h, the reaction mixture was filtered and the filtered solid was washed with further CH_2Cl_2. The filtrate was washed with satd. aq. $NaHCO_3$ and brine, dried over $MgSO_4$, and concentrated in vacuo. The residue was purified by flash column chromatography (hexane–EtOAc, 3:1) to afford compound **14** (371 mg, 88%) as a white solid. R_f 0.25 (hexane–EtOAc, 2:1, *v*/*v*). $[\alpha]^{20}_D$ +51.3° (*c* 1.5, $CHCl_3$). IR ($CHCl_3$, film, cm^{-1}): 3027, 2925, 2854, 1754, 713, 1617, 1499, 1372, 1275, 1036, 924, 751, 700. ^1H NMR (250 MHz, $CDCl_3$) δ: 2.16 (s, 3H), 2.65–2.80 (m, 4H), 3.78–3.94 (m, 2H), 4.02–4.12 (m, 2H), 4.24 (dd, *J* = 3.5, 9.0 Hz, 1H), 4.65 (s, 2H), 4.95 and 5.17 (ABq, *J* = 12.0 Hz, 2H), 4.93 (d, *J* = 1.5 Hz, 1H), 5.32 (s, 2H), 5.47 (br s, 1H), 5.63 (s, 1H), 7.23–7.53 (m, 18H), 8.02 (d, *J* = 7.7 Hz, 1H). ^{13}C NMR (63 MHz, $CDCl_3$) δ: 28.2, 29.9, 35.0, 38.1, 64.2, 66.9, 67.8, 68.9, 70.0, 72.3, 74.1, 78.5, 98.8, 101.7, 126.2, 127.6, 127.7, 127.9, 128.2, 128.3, 128.5, 129.0, 130.9, 132.7, 135.9, 137.6, 138.1, 139.4, 166.7, 172.1, 206.3. Anal. calcd. for $C_{40}H_{40}O_{10}$: C 70.57, H 5.92; found: C 70.58, H 5.93.

CB 3-*O*-benzyl-4,6-*O*-benzylidene-2-*O*-levulinyl-α-D-mannopyranoside (4)

Compound **14** was subjected to the same reaction conditions as that for the preparation of **6** from **13** to give the title compound **4** (92%) as a white solid. R_f 0.05 (hexane–EtOAc, 2:1, *v*/*v*). $[\alpha]^{20}_D$ +61.6° (*c* 3.7, $CHCl_3$). IR ($CHCl_3$, film, cm^{-1}): 3027, 2920, 1718, 1693, 1454, 1377, 1224, 1097, 914, 756, 695. ^1H NMR (250 MHz, $CDCl_3$) δ: 2.16 (s, 3H), 2.65–2.82 (m, 4H), 3.80–3.97 (m, 2H), 4.09 (dd, *J* = 1.2, 5.0 Hz, 1H), 4.26 (dd, *J* = 3.5, 9.0 Hz, 1H), 4.67 and 4.72 (ABq, *J* = 12.5 Hz, 2H), 4.95 and 5.16 (ABq, *J* = 12.0 Hz, 2H), 4.98 (d, *J* = 1.5 Hz, 1H), 5.48 (brs, 1H), 5.63 (s, 1H), 7.24–7.61 (m, 13H), 8.08 (d, *J* = 7.7 Hz, 1H). ^{13}C NMR (63 MHz, $CDCl_3$) δ: 28.2, 29.9, 38.1, 64.2, 67.8, 68.8, 70.1, 72.3, 73.9, 78.5, 98.8, 101.6, 126.1, 127.1, 127.5, 127.6, 127.7, 127.9,

© 2006 NRC Canada

128.2, 128.4, 128.9, 131.6, 133.4, 137.5, 138.0, 140.0, 171.8, 172.1, 206.6. Anal. calcd. for $C_{33}H_{34}O_{10}$: C 67.11, H 5.80; found: C 67.10, H 5.80.

BCB 3-*O*-benzyl-4,6-*O*-benzylidene-2-*O*-pivaloyl-α-D-mannopyranoside (15)

A solution of **12** (645 mg, 1.11 mmol), pivaloyl chloride (0.27 mL, 2.21 mmol), DMAP (67 mg, 0.55 mmol), and Et_3N (0.17 mL, 1.22 mmol) in CH_2Cl_2 (10 mL) was stirred at rt for 3 h. The reaction mixture was quenched with H_2O and then extracted with further CH_2Cl_2. The combined organic layer was washed with satd. aq. NH_4Cl and brine, dried over $MgSO_4$, and concentrated in vacuo. The residue was purified by flash column chromatography (hexane–EtOAc, 9:1) to afford compound **15** (650 mg, 88%) as a colorless oil. R_f 0.28 (hexane–EtOAc, 9:1, *v*/*v*). $[\alpha]^{20}_D$ +21.8° (*c* 3.0, $CHCl_3$). ^{1}H NMR (250 MHz, $CDCl_3$) δ: 1.26 (s, 9H), 3.78–4.12 (m, 4H), 4.24 (dd, *J* = 3.6, 9.1 Hz, 1H), 4.68 (s, 2H), 4.91 (d, *J* = 1.5 Hz, 1H), 4.96 (d, *J* = 14.0 Hz, 1H), 5.13 (d, *J* = 14.0 Hz, 1H), 5.33 (s, 2H), 5.46–5.48 (m, 1H), 5.63 (s, 1H), 7.23–7.56 (m, 18H), 8.00 (d, *J* = 7.7 Hz, 1H). ^{13}C NMR (63 MHz, $CDCl_3$) δ: 27.1, 27.3, 27.3, 64.2, 66.9, 67.8, 69.0, 69.4, 72.0, 74.2, 78.9, 99.0, 101.7, 126.3, 127.5, 127.6, 127.7, 127.8, 128.4, 128.4, 128.4, 128.7, 130.0, 130.9, 132.7, 136.0, 137.6, 138.3, 139.5, 166.7, 177.7.

BCB 3,4-di-*O*-benzyl-2-*O*-pivaloyl-α-D-mannopyranoside (3)

To a solution of **15** (61 mg, 0.09 mmol) in THF (2 mL) was added BH_3–THF (0.91 mL) and Bu_2BOTf (0.09 mL) at 0 °C. After stirring at 0 °C for 3 h, the reaction mixture was quenched with Et_3N (0.2 mL) and stirred at rt for another hour. The reaction mixture was diluted with MeOH and then concentrated in vacuo. The residue was purified by flash column chromatography (hexane–EtOAc, 3:1) to afford the compound **3** (53 mg, 87%) as a colorless oil. R_f 0.3 (hexane–EtOAc, 3:1, *v*/*v*). $[\alpha]^{20}_D$ +42.9° (*c* 6.75, $CHCl_3$). IR ($CHCl_3$, film, cm^{-1}): 3531, 3037, 2981, 2935, 2874, 1734, 1459, 1260, 1143, 1062, 746, 700. ^{1}H NMR (250 MHz, $CDCl_3$) δ: 1.23 (s, 9H), 3.70–3.87 (m, 4H), 4.06 (dd, *J* = 3.2, 10.1 Hz, 1H), 4.53 and 4.89 (ABq, *J* = 12.0 Hz, 2H), 4.63 and 4.72 (ABq, *J* = 12.0 Hz, 2H), 4.91 (s, 1H), 4.94 and 5.09 (ABq, *J* = 14.0 Hz, 2H), 5.32 (s, 2H), 5.42 (dd, *J* = 1.2, 1.3 Hz, 1H), 7.23–7.54 (m, 18H), 8.00 (d, *J* = 7.5 Hz, 1H). ^{13}C NMR (63 MHz, $CDCl_3$) δ: 27.3, 39.1, 62.1, 66.9, 67.6, 68.1, 71.5, 72.1, 73.9, 75.3, 78.3, 97.9, 127.4, 127.7, 127.8, 127.9, 128.1, 128.2, 128.3, 128.4, 128.5, 128.7, 130.8, 132.6, 135.9, 138.1, 138.2, 139.5, 166.7, 177.6. Anal. calcd. for $C_{40}H_{44}O_9$: C 71.84, H 6.63; found: C 71.80, H 6.65.

ACB 2,3,4,6-tetra-*O*-acetyl-α-D-mannopyranoside (16)

The title compound **16** was prepared from **8** according to the known procedure (11) in 86% yield. R_f 0.2 (hexane–EtOAc, 2:1, *v*/*v*). $[\alpha]^{20}_D$ +60.8° (*c* 0.2, $CHCl_3$). IR ($CHCl_3$, film, cm^{-1}): 3474, 3077, 2953, 1752, 1436, 1370, 1248, 1227, 1139, 1050, 978, 797, 744. ^{1}H NMR (250 MHz, $CDCl_3$) δ: 2.01 (s, 3H), 2.04 (s, 3H), 2.09 (s, 3H), 2.16 (s, 3H), 4.03–4.14 (m, 2H), 4.31 (dd, *J* = 5.1, 12.3 Hz, 1H), 4.96 (d, *J* = 1.5 Hz, 1H), 4.98 (d, *J* = 13.8 Hz, 1H), 5.18 (d, *J* = 13.8 Hz, 1H), 5.33 (s, 2H), 5.34 (t, *J* = 9.9 Hz, 1H), 5.38 (dd, *J* = 1.5, 3.3 Hz, 1H), 5.44 (dd, *J* = 3.3, 9.9 Hz, 1H), 7.30–7.46 (m, 6H), 7.56 (td, J_t = 8.1 Hz, J_d = 1.5 Hz, 1H), 7.63 (dd, *J* = 0.6, 8.1 Hz, 1H), 8.01 (dd, *J* = 1.5, 8.1 Hz, 1H). ^{13}C NMR (63 MHz, $CDCl_3$) δ: 20.7 (3), 20.9, 62.3, 66.1, 66.8, 67.8, 68.7, 69.3, 69.5, 97.5, 127.6, 127.8, 128.1, 128.2, 128.3, 128.6, 130.8, 132.7, 135.9, 139.0, 166.4, 169.7, 169.9, 170.0, 170.6. HRMS calcd. for $[M + Na]^+$: 545.1635; found: 545.1647.

ACB 4,6-*O*-benzylidene-α-D-mannopyranoside (18)

The title compound **18** was prepared from **17**, which was obtained from **16** in 93% yield, according to the known procedure (11) and in 70% yield. R_f 0.25 (hexane–EtOAc, 1:2, *v*/*v*). $[\alpha]^{20}_D$ +90.0° (*c* 0.1, $CHCl_3$). IR ($CHCl_3$, film, cm^{-1}): 3345, 3226, 2912, 1718, 1453, 1384, 1257, 1114, 1098, 1064, 1030, 1010, 740, 701. ^{1}H NMR (250 MHz, $CDCl_3$) δ: 3.04 (br s, 2H), 3.78–3.99 (m, 3H), 4.12 (s, 1H), 4.20–4.32 (m, 1H), 4.79–4.82 (dd, *J* = 1.1, 5.6 Hz, 2H), 4.92 and 5.12 (ABq, *J* = 14.0 Hz, 2H), 5.56 (s, 1H), 5.92–6.12 (m, 1H), 7.34–7.62 (m, 8H), 8.01 (dd, *J* = 1.0, 7.7 Hz, 1H). ^{13}C NMR (63 MHz, $CDCl_3$) δ: 63.5, 65.8, 67.8, 68.9, 71.1, 79.0, 100.2, 102.3, 118.7, 126.4, 127.6, 128.0, 128.4, 129.4, 130.8, 132.1, 132.6, 137.3, 139.5, 166.7. HRMS calcd. for $[M + Na]^+$: 465.1525; found: 465.1540.

ACB 4,6-*O*-benzylidene-3-*O*-*p*-methoxybenzyl-α-D-mannopyranoside (19)

A solution of **18** (523 mg, 1.18 mmol) and Bu_2SnO (324 mg, 1.30 mmol) in MeOH (40 mL) was stirred at 50 °C for 2 h. After removal of the solvent in vacuo, the residue was dissolved in DMF (10 mL) and then PMBCl (0.27 mL, 2.01 mmol) was added to the reaction mixture. After stirring at 90 °C for 1 h, the reaction mixture was quenched with H_2O and then extracted with EtOAc. The combined organic layer was washed with satd. aq. NH_4Cl and brine, dried over $MgSO_4$, and concentrated in vacuo. The residue was purified by flash column chromatography (hexane–EtOAc, 2:1) to afford compound **19** (565 mg, 85%) as a colorless oil. R_f 0.28 (hexane–EtOAc, 2:1, *v*/*v*). $[\alpha]^{20}_D$ +61.2° (*c* 0.1, $CHCl_3$). IR ($CHCl_3$, film, cm^{-1}): 3486, 2930, 2912, 1718, 1611, 1513, 1451, 1376, 1251, 1134, 1034, 916, 820, 747, 700. ^{1}H NMR (250 MHz, $CDCl_3$) δ: 3.04 (br s, 1H), 3.74 (s, 3H) 3.83–3.88 (m, 2H), 3.96 (dd, *J* = 3.3, 7.5 Hz, 1H), 4.05–4.16 (m, 2H), 4.26 (dd, *J* = 2.7, 8.0 Hz, 1H), 4.64 and 4.79 (ABq, *J* = 11.3 Hz, 2H) 4.77 (d, *J* = 5.5 Hz, 2H), 4.92 and 5.13 (ABq, *J* = 14.0 Hz, 2H), 4.97 (s, 1H), 5.23–5.29 (m, 1H), 5.35–5.43 (m, 1H), 5.59 (s, 1H), 5.93–6.09 (m, 1H), 6.85 (d, *J* = 8.5 Hz, 2H), 7.25–7.54 (m, 10H), 7.99 (d, *J* = 7.7 Hz, 1H). ^{13}C NMR (63 MHz, $CDCl_3$) δ: 55.2, 63.7, 65.6, 67.5, 68.8, 70.7, 72.8, 75.5, 78.8, 100.0, 101.5, 113.8 (2), 118.5, 126.0, 127.4, 127.9, 128.2 (2), 128.3, 128.5, 128.9, 129.6(2), 130.1, 130.7, 132.1, 132.4, 137.6, 139.5, 159.4, 166.5.

ACB 4,6-*O*-benzylidene-2-azido-2-deoxy-3-*O*-*p*-methoxybenzyl-α-D-glucopyranoside (21)

To a solution of **20** (310 mg, 0.45 mmol), which was prepared from **19** according to the known procedure (17), in DMF (10 mL) was added sodium azide (116 mg, 1.79 mmol). After stirring at 40 °C for 10 h, the reaction mixture was quenched with NH_4Cl and then extracted with EtOAc. The combined organic layer was washed with brine, dried over $MgSO_4$, and concentrated in vacuo. The residue was purified by flash column chromatography (hexane–

© 2006 NRC Canada

EtOAc, 3:1) to afford compound **21** (89 mg, 34%) as a colorless oil. R_f 0.53 (hexane–EtOAc, 2:1, *v*/*v*). $[\alpha]^{20}_D$ +81.0° (*c* 0.1, $CHCl_3$). IR ($CHCl_3$, film, cm^{-1}): 3704, 3580, 3411, 2921, 2865, 2553, 2392, 2106, 1716, 1613, 1514, 1452, 1371, 1257, 1139, 1086, 1036, 971, 738, 696. ^{1}H NMR (250 MHz, $CDCl_3$) δ: 3.46 (dd, *J* = 3.6, 9.9 Hz, 1H), 3.69–3.77 (m, 2H), 3.79 (s, 3H), 3.87–3.99 (m, 1H), 4.16 (t, *J* = 9.5 Hz, 1H), 4.28 (dd, *J* = 4.5, 5.5 Hz, 1H), 4.76 and 4.91 (ABq, *J* = 10.5 Hz, 2H), 4.81 (d, *J* = 5.7 Hz, 2H), 5.02 and 5.19 (ABq, *J* = 14.2 Hz, 2H), 5.05 (s, 1H), 5.27–5.32 (m, 1H), 5.38–5.45 (m, 1H), 5.59 (s, 1H), 5.96–6.12 (m, 1H), 6.86 (d, *J* = 8.6 Hz, 2H), 7.31–7.75 (m, 10H), 8.04 (d, *J* = 7.8 Hz, 1H). ^{13}C NMR (63 MHz, $CDCl_3$) δ: 29.8, 55.4, 63.1, 63.3, 65.8, 67.9, 69.0, 74.9, 76.2, 82.9, 98.3, 101.5, 113.9, 118.6, 126.1 (2), 127.5, 127.9, 128.4, 129.1, 130.0 (2), 130.1, 130.8, 132.2, 132.8, 137.3, 139.6, 159.5, 166.5. HRMS calcd. for $[M + Na]^+$: 610.2165; found: 610.2186.

ACB 4,6-*O*-benzylidene-2-azido-2-deoxy-α-D-glucopyranoside (7) (from 21)

To a solution of **21** (42 mg, 0.071 mmol) in CH_2Cl_2–H_2O (2.2 mL, 10:1, *v*/*v*) was added DDQ (32 mg, 0.14 mmol). After stirring at rt for 3 h, the reaction mixture was quenched with satd. aq. $NaHCO_3$ and then extracted with CH_2Cl_2. The combined organic layer was washed with satd. aq. $NaHCO_3$ and brine, dried over $MgSO_4$, and concentrated in vacuo. The residue was purified by flash column chromatography (hexane–EtOAc, 3:1) to afford compound **7** (31 mg, 92%) as a colorless oil. R_f 0.25 (hexane–EtOAc, 3:1, *v*/*v*). $[\alpha]^{20}_D$ +112.0° (*c* 0.1, $CHCl_3$). IR ($CHCl_3$, film, cm^{-1}): 3583, 3387, 2915, 2864, 2107, 1716, 1261, 1139, 1089, 1030, 739, 699. ^{1}H NMR (250 MHz, $CDCl_3$) δ: 2.96 (br s, 1H), 3.36 (dd, *J* = 3.6, 10.0 Hz, 1H), 3.54 (t, *J* = 9.2 Hz 1H), 3.72 (t, *J* = 10.2 Hz, 1H), 3.85–3.95 (m, 1H), 4.24–4.33 (m, 2H), 4.81 (d, *J* = 5.7 Hz, 2H), 5.02 and 5.20 (ABq, *J* = 14.2 Hz, 2H), 5.07 (d, *J* = 3.6 Hz, 1H), 5.27–5.32 (m, 1H), 5.38–5.45 (m, 1H), 5.53 (s, 1H), 5.96–6.12 (m, 1H), 7.35–7.75 (m, 8H), 8.04 (d, *J* = 6.9 Hz, 1H). ^{13}C NMR (63 MHz, $CDCl_3$) δ: 29.8, 62.7, 63.4, 65.8, 68.1, 69.1, 81.9, 98.3, 102.2, 118.6, 126.4 (2), 127.6, 127.9, 128.5 (2), 129.5, 130.9, 132.2 (2), 132.9, 137.0, 139.5, 166.5. Anal. calcd. for $C_{24}H_{25}N_3O_7$: C 61.66, H 5.39, N 8.99; found: C 61.87, H 5.58, N 9.16.

ACB 3,4,6-tri-*O*-acetyl-2-azido-2-deoxy-α-D-glucopyranoside (25)

A solution of **24** (650 mg, 1.85 mmol), allyl 2-(hydroxymethyl)benzoate (550 mg, 2.9 mmol), and DMAP (350 mg, 2.9 mmol) in CH_2Cl_2 (15 mL) was added to a solution of $AgClO_4$ (640 mg, 3.1 mmol) in CH_2Cl_2 (20 mL) at rt via cannula. After stirring at rt for 3 h, the reaction mixture was quenched with satd. aq. $Na_2S_2O_3$ and then filtered through Celite. The filtrate was washed with brine, dried over $MgSO_4$, and concentrated in vacuo. The residue was purified by flash column chromatography (hexane–EtOAc, 3:1) to afford compound **25** (900 mg, 91%) as a colorless oil. R_f 0.25 (hexane–EtOAc, 3:1, *v*/*v*). $[\alpha]^{20}_D$ +145.0° (*c* 0.1, $CHCl_3$). IR ($CHCl_3$, film, cm^{-1}): 3480, 3352, 3077, 2946, 2222, 2113, 1754, 1718, 1450, 1238, 1050, 742. ^{1}H NMR (250 MHz, $CDCl_3$) δ: 2.04 (s, 3H), 2.10 (s, 3H), 3.44 (dd, *J* = 3.5, 10.5 Hz, 1H), 3.85–3.95 (m, 1H), 4.02–4.15 (m, 2H), 4.27–4.34 (m, 1H), 4.24–4.33 (m, 2H), 4.80 (d, *J* = 5.6 Hz, 2H), 5.03 and 5.22 (ABq, *J* = 14.0 Hz, 2H), 5.08 (t, *J* = 10.0 Hz, 1H), 5.16 (t, *J* = 3.5 Hz, 1H), 5.28–5.33 (m, 1H), 5.38–5.45 (m, 1H), 5.93–6.12 (m, 1H), 7.37–7.73 (m, 3H), 8.05 (d, *J* = 6.9 Hz, 1H). ^{13}C NMR (63 MHz, $CDCl_3$) δ: 20.8, 20.9 (2), 61.3, 61.9, 65.8, 67.9, 68.3, 68.7, 70.8, 97.6, 118.7, 127.8, 128.1, 128.2, 130.9, 132.2, 132.9, 139.0, 166.4, 169.8, 170.2, 170.8. Anal. calcd. for $C_{23}H_{27}N_3O_{10}$: C 54.56, H 5.38, N 8.31; found: C 54.56, H 5.36, N 8.51.

ACB 4,6-*O*-benzylidene-2-azido-2-deoxy-α-D-glucopyranoside (7) (from 25)

To a solution of **25** (700 mg, 1.38 mmol) in MeOH (10 mL) was added NaOMe (8 mg, 0.15 mmol) at 0 °C. After stirring at 0 °C for 2 h, the reaction mixture was neutralized with DOWEX-MAC-3 (H^+ mode), filtered through Celite, and concentrated in vacuo. The residue was purified by flash column chromatography ($CHCl_3$–MeOH, 9:1) to afford the trihydroxy intermediate (478 mg, 91%) as a white solid.

The trihydroxy intermediate (300 mg, 0.79 mmol) was dissolved in DMF (5 mL) and then benzaldehyde dimethylacetal (0.14 mL, 0.87 mmol) and camphorsulfonic acid (10 mg, 0.04 mmol) were added to the solution. After stirring at 50 °C for 2 h, the reaction mixture was quenched with satd. aq. $NaHCO_3$ and then extracted with EtOAc. The combined organic layer was washed with satd. aq. NH_4Cl and brine, dried over $MgSO_4$, and concentrated in vacuo. The residue was purified by flash column chromatography (hexane–EtOAc, 3:1) to afford compound **7** (259 mg, 70%) as a colorless oil.

ACB (3-*O*-benzyl-4,6-*O*-benzylidene-2-*O*-*p*-methoxybenzyl-β-D-mannopyranosyl)-(1→3)-4,6-*O*-benzylidene-2-azido-2-deoxy-α-D-glucopyranoside (26)

A solution of donor **6** (55 mg, 0.089 mmol) and DTBMP (44 mg, 0.26 mmol) in CH_2Cl_2 (5 mL) in the presence of 4 Å molecular sieves was stirred for 30 min at rt and cooled to –78 °C, then Tf_2O (18 μL, 0.11 mmol) was added. After the resulting solution was stirred at –78 °C for 10 min, acceptor **7** (50 mg, 0.11 mmol) was added and stirred at –78 °C for 1 h and allowed to warm over 2 h to 0 °C. The reaction mixture was quenched with satd. aq. $NaHCO_3$ and then extracted with CH_2Cl_2. The combined organic layer was washed with satd. aq. $NaHCO_3$ and brine, dried over $MgSO_4$, and concentrated in vacuo. The residue was purified by flash column chromatography (hexane–EtOAc, 3:1) to afford compound **26** (61 mg, 73%, α:β = 1:4) as a colorless oil. R_f 0.20 (hexane–EtOAc, 3:1, *v*/*v*). $[\alpha]^{20}_D$ +37.0° (c 0.1, $CHCl_3$). IR ($CHCl_3$, film, cm^{-1}): 2922, 2855, 2105, 1717, 1513, 1454, 1373, 1251, 1095, 1037, 744, 698. ^{1}H NMR (250 MHz, $CDCl_3$) δ: 3.19 (m, 1H), 3.39 (dd, *J* = 3.7, 9.9 Hz, 1H), 3.57 (dd, *J* = 3.1, 9.8 Hz, 1H), 3.70 (d, *J* = 9.4 Hz, 1H), 3.76–3.82 (m, 2H), 3.77 (s, 3H), 3.86–3.94 (m, 2H), 4.03 (d, *J* = 2.9 Hz, 2H), 4.06–4.30 (m, 4H), 4.56 and 4.71 (ABq, *J* = 12.5 Hz, 2H), 4.75 (s, 1H), 4.80 and 4.90 (ABq, *J* = 11.7 Hz, 2H), 4.80 (t, *J* = 1.3 Hz, 1H), 4.83 (d, *J* = 0.9 Hz, 1H), 5.04 and 5.20 (ABq, *J* = 13.9 Hz, 2H), 5.13 (d, *J* = 3.7 Hz, 1H), 5.28–5.46 (m, 2H), 5.54 (s, 2H), 5.97–6.12 (m, 1H), 6.80 (d, *J* = 8.7 Hz, 2H), 7.28–7.72 (m, 20H), 8.05 (dd, *J* = 1.2, 7.8 Hz, 1H). ^{13}C NMR (63 MHz, $CDCl_3$) δ: 29.9, 55.3, 63.1, 63.3, 65.8, 67.6, 68.2, 68.7, 68.9, 72.5,

© 2006 NRC Canada

74.7, 77.0, 78.0, 78.5, 80.6, 98.3, 101.4, 101.6, 102.6, 113.5 (2), 118.6, 126.1 (2), 126.2 (2), 127.6 (3), 127.7, 128.1, 128.2 (3), 128.3 (2), 128.4 (2), 128.9, 129.3, 130.1 (2), 130.9 (2), 132.2, 132.8, 137.1, 137.7, 138.5, 139.2, 159.2, 166.4. Anal. calcd. for $C_{52}H_{53}N_3O_{13}$: C 67.30, H 5.76, N 4.53; found: C 67.41, H 5.73, N 4.26.

ACB (3-*O*-benzyl-4,6-*O*-benzylidene-β-D-mannopyranosyl)-(1→3)-4,6-*O*-benzylidene-2-azido-2-deoxy-α-D-glucopyranoside (5)

To a solution of **26** (85 mg, 0.09 mmol) in CH_2Cl_2–H_2O (4.4 mL, 10:1, *v*/*v*) was added DDQ (42 mg, 0.18 mmol). After stirring at rt for 1.5 h, the reaction mixture was quenched with satd. aq. $NaHCO_3$ and then extracted with CH_2Cl_2. The combined organic layer was washed with satd. aq. $NaHCO_3$ and brine, dried over $MgSO_4$, and concentrated in vacuo. The residue was purified by flash column chromatography (hexane–EtOAc, 2:1) to afford compound **5** (63 mg, 85%) as a colorless oil. R_f 0.18 (hexane–EtOAc, 2:1, *v*/*v*). $[\alpha]^{20}_D$ +81.8° (*c* 0.1, $CHCl_3$). IR ($CHCl_3$, film, cm^{-1}): 3498, 3064, 2921, 2106, 1717, 1453, 1378, 1258, 1094, 1039, 1010, 796, 745, 698. ^{1}H NMR (250 MHz, $CDCl_3$) δ: 2.76 (br s, 1H), 3.29 (m, 1H), 3.65 (dd, *J* = 3.3, 9.5 Hz, 1H), 3.68–3.85 (m, 2H), 3.91 (dd, *J* = 4.3, 9.7 Hz, 1H), 4.07–4.35 (m, 5H), 4.75 and 4.84 (ABq, *J* = 12.3 Hz, 2H), 4.79 (t, *J* = 12.3 Hz, 1H), 4.82 (s, 2H), 5.03 and 5.18 (ABq, *J* = 12.9 Hz, 2H), 5.12 (d, *J* = 3.6 Hz, 1H), 5.27–5.44 (m, 2H), 5.52 (s, 1H), 5.54 (s, 1H), 5.96–6.11 (m, 1H), 7.27–7.71 (m, 18H), 8.04 (d, *J* = 6.8 Hz, 1H). ^{13}C NMR (63 MHz, $CDCl_3$) δ: 60.47, 63.1, 63.3, 65.7, 67.0, 68.1, 68.6, 68.8, 70.0, 72.6, 76.6, 76.8, 78.2, 80.4, 98.1, 101.0, 101.4, 101.5, 118.6, 126.0, 126.1, 127.7, 127.9, 128.0, 128.2, 128.3, 128.5, 129.0, 129.2, 130.9, 132.1, 132.8, 132.8, 137.1, 137.5, 138.0, 139.1, 166.4. MALDI-TOF calcd. for $[M + Na]^+$: 846.2640; found: 846.2263.

ACB (3-*O*-benzyl-4,6-*O*-benzylidene-2-*O*-levulinyl-α-D-mannopyranosyl)-(1→2)-(3-*O*-benzyl-4,6-*O*-benzylidene-β-D-mannopyranosyl)-(1→3)-4,6-*O*-benzylidene-2-azido-2-deoxy-α-D-glucopyranoside (2)

A solution of donor **4** (53 mg, 0.089 mmol), acceptor **5** (60 mg, 0.065 mmol), and DTBMP (27 mg, 0.13 mmol) in CH_2Cl_2 (5 mL) in the presence of 4 Å molecular sieves was stirred for 30 min at rt and cooled to –78 °C. After addition of Tf_2O (18 μL, 0.11 mmol), the resulting solution was stirred at –78 °C for 1 h and allowed to warm over 3 h to 10 °C. The reaction mixture was quenched with satd. aq. $NaHCO_3$ and then extracted with CH_2Cl_2. The combined organic layer was washed with satd. aq. $NaHCO_3$ and brine, dried over $MgSO_4$, and concentrated in vacuo. The residue was purified by flash column chromatography (hexane–EtOAc–CH_2Cl_2, 5:2:1) to afford compound **2** (41 mg, 44%) as a colorless oil. R_f 0.8 (hexane–EtOAc, 1:1, *v*/*v*). $[\alpha]^{20}_D$ +37.3° (*c* 0.1, $CHCl_3$). IR ($CHCl_3$, film, cm^{-1}): 3372, 2923, 2853, 2397, 2104, 1743, 1718, 1454, 1262, 1138, 1095, 1028, 916, 748, 698. ^{1}H NMR (500 MHz, $CDCl_3$) δ: 2.12 (s, 3H), 2.64–2.69 (m, 4H), 3.32–3.36 (m, 2H), 3.41 (dd, *J* = 3.6, 9.8 Hz, 1H), 3.65–3.70 (m, 2H), 3.82–3.89 (m, 4H), 3.97 (t, *J* = 9.6 Hz, 1H), 4.04 (dd, *J* = 4.6, 10.0 Hz, 1H), 4.15 (d, *J* = 10.0 Hz, 2H), 4.26–4.31 (m, 4H), 4.36 (t, *J* = 9.8 Hz, 1H), 4.59 (m, 1H), 4.68 and 4.87 (ABq, *J* = 12.6 Hz, 2H), 4.79 (d, *J* = 5.6 Hz, 2H), 4.82 (s, 1H), 5.01 and 5.13 (ABq, *J* = 13.6 Hz, 2H), 5.09 (d, *J* = 3.0 Hz, 1H), 5.24 (s, 1H), 5.29 (d, *J* = 10.0 Hz, 1H), 5.38 (s, 1H), 5.39 (d, *J* = 17.5 Hz, 1H), 5.58 (s, 1H), 5.64 (s, 1H), 5.66 (s, 1H), 5.99–6.05 (m, 1H), 7.15–7.66 (m, 28H), 8.01 (d, *J* = 7.5 Hz, 1H). ^{13}C NMR (125 MHz, $CDCl_3$) δ: 28.3, 29.8, 38.3, 63.5, 64.0, 65.7, 67.5, 68.1, 68.4, 68.9, 70.1, 72.4, 73.1, 74.1, 74.3, 74.9, 78.0, 78.7, 79.1, 79.4, 98.3, 99.4, 99.7, 100.3, 101.2, 101.7, 118.6, 126.1, 126.2, 127.5, 127.6, 127.8, 128.1, 128.2, 128.3, 128.5, 128.8, 128.9, 129.0, 130.9, 132.2, 132.8, 137.6, 137.8, 138.4, 138.5, 139.1, 166.5, 171.8, 206.2. MALDI-TOF calcd. for $[M + Na]^+$: 1268.4579; found: 1268.4485.

CB (3-*O*-Benzyl-4,6-*O*-benzylidene-2-*O*-levulinyl-α-D-mannopyranosyl)-(1→2)-(3-*O*-benzyl-4,6-*O*-benzylidene-β-D-mannopyranosyl)-(1→3)-4,6-*O*-benzylidene-2-azido-2-deoxy-α-D-glucopyranoside (27)

To a solution of **2** (34 mg, 0.027 mmol) and $(Ph_3P)_4Pd$ (3 mg, 0.003 mmol) in THF (3 mL) was added morpholine (24 μL, 0.27 mmol). After stirring at rt for 1 h, the reaction mixture was diluted with EtOAc. The organic solution was washed with aq. 1 N HCl and brine, dried over $MgSO_4$, and concentrated in vacuo. The residue was purified by flash column chromatography (hexane–EtOAc, 1:1) to afford compound **27** (25 mg, 77%) as a white solid. R_f 0.05 (hexane–EtOAc, 2:1, *v*/*v*). $[\alpha]^{20}_D$ +4.0° (*c* 0.1, $CHCl_3$). IR ($CHCl_3$, film, cm^{-1}): 3350, 2923, 2854, 2393, 2105, 1718, 1602, 1454, 1371, 1095, 1028, 916, 750, 698. ^{1}H NMR (250 MHz, $CDCl_3$) δ: 2.14 (s, 3H), 2.57–2.75 (m, 4H), 3.31–3.46 (m, 3H), 3.65–3.72 (m, 2H), 3.86–3.98 (m, 5H), 4.02–4.15 (m, 4H), 4.25 (s, 2H), 4.30–4.42 (m, 2H), 4.55–4.62 (m, 1H), 4.67 and 4.88 (ABq, *J* = 12.4 Hz, 2H), 4.82 (s, 1H), 5.01 and 5.21 (ABq, *J* = 13.6 Hz, 2H), 5.12 (d, *J* = 3.8 Hz, 2H), 5.38 (s, 1H), 5.59 (br s, 1H), 5.66 (d, *J* = 6.3 Hz, 2H), 7.15–7.66 (m, 29H), 8.01 (d, *J* = 7.5 Hz, 1H). ^{13}C NMR (125 MHz, $CDCl_3$) δ: 28.3, 29.8, 30.0, 38.3, 30.0, 63.3, 64.0, 66.9, 67.4, 67.7, 68.3, 68.8, 70.0, 71.6, 72.4, 73.0, 73.9, 74.4, 75.4, 77.4, 77.9, 78.6, 79.1, 79.3, 97.9, 98.1, 99.4, 99.7, 100.3, 101.0, 101.6, 126.1, 126.2, 127.5, 127.6, 127.7, 128.0, 128.1, 128.2, 128.3, 128.4, 128.5, 128.8, 128.9, 129.1, 130.8, 132.7, 136.0, 137.6, 137.8, 138.1, 138.3, 138.4, 138.5, 139.5, 166.7, 171.8, 177.7, 206.4. MALDI-TOF calcd. for $[M + Na]^+$: 1228.4266; found: 1228.4352.

BCB (3-*O*-benzyl-4,6-*O*-benzylidene-2-*O*-levulinyl-α-D-mannopyranosyl)-(1→2)-(3-*O*-benzyl-4,6-*O*-benzylidene-β-D-mannopyranosyl)-(1→3)-(4,6-*O*-benzylidene-2-azido-2-deoxy-α-D-glucopyranosyl)-(1→6)-3,4-di-*O*-benzyl-2-*O*-pivaloyl-α-D-mannopyranoside (28)

A solution of donor **27** (18 mg, 0.015 mmol), acceptor **3** (12 mg, 0.018 mmol), and DTBMP (7 mg, 0.036 mmol) in CH_2Cl_2 (5 mL) in the presence of 4 Å molecular sieves was stirred for 30 min at rt and cooled to –78 °C. After addition of Tf_2O (3 μL, 0.018 mmol), the resulting solution was stirred at –78 °C for 1 h and allowed to warm over 3 h to 10 °C. The reaction mixture was quenched with satd. aq. $NaHCO_3$ and then extracted with CH_2Cl_2. The combined organic layer was washed with satd. aq. $NaHCO_3$ and brine,

© 2006 NRC Canada

dried over $MgSO_4$, and concentrated in vacuo. The residue was purified by flash column chromatography (hexane–EtOAc–CH_2Cl_2, 5:2:1) to afford compound **28** (17 mg, 65%) as a colorless oil. R_f 0.25 (hexane–EtOAc, 2:1, *v*/*v*). $[\alpha]^{20}_D$ –0.2° (*c* 0.1, $CHCl_3$). IR ($CHCl_3$, film, cm^{-1}): 3350, 2923, 2853, 2105, 1721, 1658, 1602, 1454, 1371, 1259, 1137, 1094, 748, 698. ^1H NMR (250 MHz, $CDCl_3$) δ: 1.25 (s, 9H), 2.14 (s, 3H), 2.59–2.68 (m, 4H), 3.24–3.37 (m, 3H), 3.63–3.71 (m, 2H), 3.77–3.87 (m, 7H), 3.96 (t, *J* = 9.5 Hz, 1H), 4.05–4.30 (m, 10H), 4.39 (t, *J* = 9.4 Hz, 1H), 4.50 and 4.70 (ABq, *J* = 11.0 Hz, 2H), 4.63 (q, *J* = 5.7 Hz, 3H), 4.80 (d, *J* = 15.1 Hz, 2H), 4.88–4.95 (m, 3H), 5.14 (d, *J* = 3.2 Hz, 1H), 5.21 (s, 1H), 5.31 (d, *J* = 1.6 Hz, 2H), 5.39 (s, 1H), 5.46–5.48 (m, 1H), 5.57–5.59 (m, 1H), 5.66 (s, 2H), 7.12–7.52 (m, 43H), 7.98 (d, *J* = 7.5 Hz, 1H). ^{13}C NMR (63 MHz, $CDCl_3$) δ: 28.3, 29.8, 38.3, 60.57, 63.5, 64.0, 67.4, 68.3, 68.8, 70.0, 72.4, 73.0, 74.1, 74.3, 74.9, 77.9, 78.7, 79.6, 79.1, 79.3, 98.3, 99.4, 99.7, 100.3, 101.2, 101.7, 118.6, 126.1, 126.2, 127.5, 127.6, 127.8, 128.1, 128.2, 128.3, 128.5, 128.8, 128.9, 129.0, 130.9, 132.2, 132.8, 137.6, 137.8, 138.4, 138.5, 139.1, 171.4, 171.8, 206.5. MALDI-TOF calcd. for $[M + Na]^+$: 1744.6778; found: 1744.6571.

BCB (3-*O*-benzyl-4,6-*O*-benzylidene-2-*O*-levulinyl-α-D-mannopyranosyl)-(1→2)-(3-*O*-benzyl-4,6-*O*-benzylidene-β-D-mannopyranosyl)-(1→3)-(4,6-*O*-benzylidene-2-acetamido-2-deoxy-α-D-glucopyranosyl)-(1→6)-3,4-di-*O*-benzyl-2-*O*-pivaloyl-α-D-mannopyranoside (1)

A solution of **28** (10 mg, 0.006 mmol) and triphenylphosphine (9 mg, 0.035 mmol) in THF (1.5 mL) and H_2O (0.15 mL) was stirred at rt for 3 h. The reaction mixture was diluted with EtOAc, and then washed with brine, dried over $MgSO_4$, and concentrated in vacuo. The residue was dissolved in pyridine (1 mL) and acetic anhydride (5 μL, 0.046 mmol) was added. After stirring at rt for 1 h, the reaction mixture was diluted with EtOAc. The resulting solution was washed with aq. 1 N HCl, H_2O, and brine, subsequently, then dried over $MgSO_4$, and concentrated in vacuo. The residue was purified by flash column chromatography (hexane–EtOAc, 1:1) to afford compound **1** (6 mg, 58%) as a colorless oil. R_f 0.25 (hexane–EtOAc, 1:1, *v*/*v*). $[\alpha]^{20}_D$ +0.1° (*c* 0.1, $CHCl_3$). IR ($CHCl_3$, film, cm^{-1}): 3350, 2923, 2853, 1721, 1658, 1602, 1454, 1371, 1259, 1137, 1094, 1036, 748, 698. ^1H NMR (500 MHz, $CDCl_3$) δ: 1.19 (s, 9H), 1.79 (s, 3H), 2.11 (s, 3H), 2.62–2.64 (m, 4H), 2.98–3.00 (m, 1H), 3.09–3.11 (m, 2H), 3.20 (t, *J* = 9.5 Hz, 2H), 3.59 (d, *J* = 8.0 Hz, 1H), 3.70–3.76 (m, 2H), 3.82–3.89 (m, 4H), 3.92–4.05 (m, 4H), 4.08–4.23 (m, 6H), 4.41 (m, 1H), 4.47 (d, *J* = 5.5 Hz, 1H), 4.53–4.63 (m, 4H), 4.72–4.80 (m, 2H), 4.83–4.90 (m, 3H), 5.16 (s, 2H), 5.26–5.35 (m, 3H), 5.44 (s, 1H), 5.52 (s, 1H), 5.63 (s, 2H), 5.71 (s, 3H), 6.12 (d, *J* = 9.5 Hz, 1H), 7.12–7.52 (m, 43H), 7.93 (d, *J* = 7.5 Hz, 1H). ^{13}C NMR (125 MHz, $CDCl_3$) δ: 27.4, 29.8, 38.3, 42.3, 46.0, 53.2, 63.4, 63.5, 63.7, 67.2, 67.4, 67.6, 68.0, 68.1, 68.3, 68.4, 68.4, 68.7, 68.9, 68.8, 70.2, 71.1, 71.7, 72.6, 72.8, 73.6, 74.2, 74.6, 75.3, 78.7, 79.4, 97.8, 99.0, 99.3, 99.7, 100.1, 100.7, 101.7, 126.2, 127.5, 127.8, 128.1, 128.4, 128.8, 130.0, 130.6, 131.0, 132.7, 135.6, 137.1, 138.0, 138.2, 138.4, 138.6, 138.8, 139.3, 167.3, 177.3, 171.8, 171.8, 206.1. MALDI-TOF calcd. for $[M + Na]^+$: 1760.6979; found: 1760.6322.

Acknowledgement

This work was supported by a grant from the Korea Science and Engineering Foundation through the Center for Bioactive Molecular Hybrids (CBMH).

References

1. F. Ørskov and I. Ørskov. Can. J. Microbiol. **38**, 699 (1992).
2. J.P. Nataro and J.B. Kaper. Clin. Microbiol. Rev. **11**, 142 (1998).
3. M.K. Wolf. Clin. Microbiol. Rev. **10**, 569 (1997).
4. N. Pradel, V. Livrelli, C. de Champs, J.-B. Palcoux, A. Reynaud, F. Scheutz, J. Sirot, B. Joly, and C. Forestier. J. Clin. Microbiol. **38**, 1023 (2000).
5. P. Boerlin, S.A. McEwen, F. Boerlin-Petzold, J.B. Wilson, R.P. Johnson, and C.L. Gyles. J. Clin. Microbiol. **37**, 497 (1999).
6. M. Blanco, J.E. Blanco, J. Blanco, A. Mora, C. Prado, M.P. Alonso, M. Mouriño, C. Madrid, C. Balsalobre, and A. Juárez. Vet. Microbiol. **54**, 309 (1997).
7. J. Blanco, D. Cid, J.E. Blanco, M. Blanco, J.A. Ruiz Santa Quiteira, and R. de la Fuente. Vet. Microbiol. **49**, 209 (1996).
8. H. Yildirim, A. Weintraub, and G. Widmalm. Carbohydr. Res. **333**, 179 (2001).
9. For reviews on β-mannopyranosylation, see: (*a*) F. Barresi and O. Hindsgaul. *In* Modern methods in carbohydrate synthesis. *Edited by* S.H. Khan and R.A. O'Neil. Harwood Academic Publishers, Amsterdam. 1996. p. 251; (*b*) J.J. Gridley and H.M.I. Osborn. J. Chem. Soc. Perkin Trans. 1, 1471 (2000); (*c*) A.V. Demchenko. Curr. Org. Chem. **7**, 35 (2003).
10. (*a*) D. Crich and S. Sun. J. Am. Chem. Soc. **119**, 11217 (1997); (*b*) D. Crich and S. Sun. J. Org. Chem. **61**, 4506 (1996); (*c*) D. Crich and S. Sun. J. Org. Chem. **62**, 1198 (1997); (*d*) D. Crich and S. Sun. J. Am. Chem. Soc. **120**, 435 (1998); (*e*) D. Crich and S. Sun. Tetrahedron, **54**, 8321 (1998); (*f*) D. Crich and M. Smith. Org. Lett. **2**, 4067 (2000); (*g*) D. Crich and M. Smith. J. Am. Chem. Soc. **123**, 9015 (2001); (*h*) D. Crich and Q. Yao. J. Am. Chem. Soc. **126**, 8232 (2004); (*i*) D. Crich, A. Banerjee, and Q. Yao. J. Am. Chem. Soc. **126**, 14930 (2004); (*j*) D. Crich, W. Li, and H. Li. J. Am. Chem. Soc. **126**, 15081 (2004).
11. K.S. Kim, J.H. Kim, Y. Joo Lee, Y. Jun Lee, and J. Park. J. Am. Chem. Soc. **123**, 8477 (2001).
12. K.S. Kim, J. Park, Y.J. Lee, and Y.S. Seo. Angew. Chem., Int. Ed. **42**, 459 (2003).
13. Y.T. Kwon, Y.J. Lee, K. Lee, and K.S. Kim. Org. Lett. **6**, 3901 (2004).
14. K.S. Kim, S.S. Kang, Y.S. Seo, H.J. Kim, Y.J. Lee, and K.-S. Jeong. Synlett, 1311 (2003).
15. L. Jiang and T.-H. Chan. Tetrahedron Lett. **39**, 355 (1998).
16. P.B. Alper, S.-C. Hung, and C.-H. Wong. Tetrahedron Lett. **37**, 6029 (1996).
17. V. Pavliak and P. Kovác. Carbohydr. Res. **210**, 333 (1991).
18. H. Kunz and H. Waldmann. Angew. Chem. Int. Ed. Engl. **23**, 71 (1984).
19. H. Staudinger and E. Hauser. Helv. Chim. Acta, **4**, 21 (1921).

© 2006 NRC Canada

Selective chemistry of tripentaerythritol — Synthesis of acetals and their derivatives[1]

Hussein Al-Mughaid and T. Bruce Grindley

Abstract: Tripentaerythritol was converted efficiently into 2′,2″:6′,6″:10′,10″-tri-*O*-cyclohexylidene-2,2,6,6,10,10-hexakis(hydroxymethyl)-4,8-dioxa-1,11-undecandiol (**4**) by the toluenesulfonic acid catalysed reaction with cyclohexanone in a mixture of *N*,*N*-dimethylformamide and benzene. Reaction of tripentaerythritol with benzaldehyde under similar conditions gave an easily separated mixture of the four possible stereoisomers. Structures of these stereoisomers were assigned based on ^{1}H and ^{13}C NMR chemical shifts using trends previously observed for the dibenzylidene acetals of dipentaerythritol, whose structures had been established unambiguously by X-ray crystallography. It was found that reduction of the mixture of benzylidene acetals to 2,6,10-tris(benzyloxymethyl)-4,8-dioxa-1,11-undecanediol could be accomplished using triethylsilane with ethylaluminium dichloride as the Lewis acid after a number of commonly used conditions for this transformation failed.

Key words: pentaerythritol, tripentaerythritol, dipentaerythritol, acetals, benzylidene acetals, reduction.

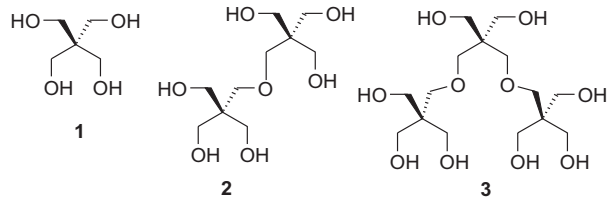
Résumé : La réaction du tripentaérythritol avec la cyclohexanone, en solution dans un mélange de *N*,*N*-diméthylformamide et de benzène et catalysée par l'acide toluènesulfonique, conduit à la formation de 2′,2″:6′,6″:10′,10″-tri-*O*-cyclohexylidène-2,2,6,6,10,10-hexakis(hydroxyméthyl)-4,8-dioxaundécane-1,11-diol (**4**). La réaction du tripentaérythritol avec le benzaldéhyde dans des conditions semblables conduit à un mélange des quatre stéréoisomères possibles qui ont pu être séparés facilement. Les structures de ces stéréoisomères ont été attribuées sur la base de déplacements chimiques dans les spectres RMN du ^{1}H et du ^{13}C et en faisant appel aux tendances observées antérieurement pour les acétals dibenzylidènes du pentaérythritol dont les structures avaient été déterminées sans ambiguïté par diffraction des rayons X. Après avoir essayé en vain de le faire en utilisant un certain nombre de conditions régulièrement à cette fin, on a trouvé qu'il est possible de réaliser la réduction du mélange d'acétals dibenzylidènes en 2,6,10-tris(benzoloxyméthyl)-4,8-dioxaundécane-1,11-diol en utilisant le triéthylsilane en présence de dichlorure d'éthylaluminium utilisé comme acide de Lewis.

Mots clés : pentaérythritol, tripentaérythritol, dipentaérytrhitol, acétals, acétals dibenzylidène, réduction.

[Traduit par la Rédaction]

Introduction

Dendrimers have become the subject of intense interest in the last few years (1–7). One of the molecules that has attracted the most attention as either the central core or a branching point of clusters and dendrimers is pentaerythritol (**1**) (8–20). The chemistry of pentaerythritol has been extensively investigated and there are now methods available to selectively prepare a wide range of derivatives (21–35). Dipentaerythritol (**2**), a commercially available compound with many of the favorable characteristics of pentaerythritol, had been comparatively neglected until we demonstrated that it was possible to make a variety of acetals regioselectively (36). Tripentaerythritol (**3**) also has many of the favourable characteristics of pentaerythritol and its chemistry also has been neglected. The only report of the selective chemistry of **3** deals with methylene acetals (37), derivatives that require vigorous conditions for removal.



Murguía et al. (38) recently used DMF–benzene mixtures to form acetals from diols and polyols that are very insoluble in benzene or toluene, particularly from pentaerythritol, and we have shown that these conditions also work efficiently with dipentaerythritol (36). In this publication, we demonstrate that these conditions also are very effective with

Received 29 August 2005. Published on the NRC Research Press Web site at http://canjchem.nrc.ca on 21 April 2006.

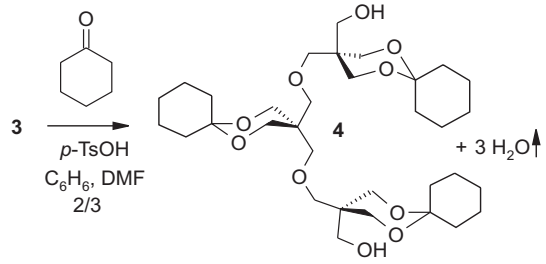
This paper is dedicated to Professor Walter Szarek in recognition of his many contributions to organic chemistry and for his friendship.

H. Al-Mughaid and T.B. Grindley.[2] Department of Chemistry, Dalhousie University, Halifax, NS B3H 4J3, Canada.

[1]This article is part of a Special Issue dedicated to Professor Walter A. Szarek.
[2]Corresponding author: (e-mail: bruce.grindley@dal.ca).

 doi:10.1139/V06-034 © 2006 NRC Canada

Scheme 1. Formation of the tricyclohexylidene acetal of tripentaerythritol.



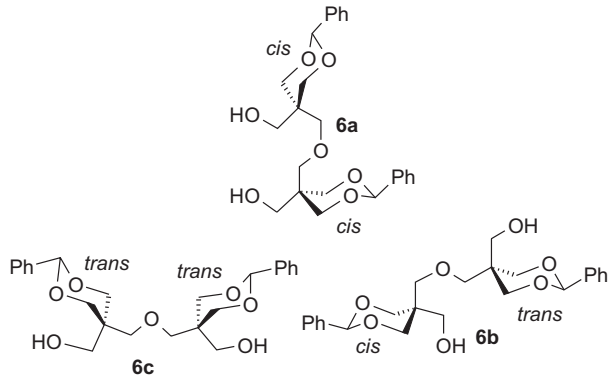
tripentaerythritol (**3**). We also show that these acetals can be transformed into other potentially useful compounds.

Results and discussion

Application of the conditions of Murguía et al. (38) to tripentaerythritol (**3**) using cyclohexanone as the carbonyl-containing component yielded 2′,2″:6′,6″:10′,10″-tri-*O*-cyclohexylidene-2,2,6,6,10,10-hexakis(hydroxymethyl)-4,8-dioxa-1,11-undecandiol (**4**), the tri-*O*-cyclohexylidene acetal of **3** in 96% yield (Scheme 1). This name is based on naming tripentaerythritol as having six hydroxymethyl substituents on the linear diether main chain, 4,8-dioxa-1,11-undecanediol. This product is the only possible fully acetalated product, if it is accepted that 10-membered ring acetals spanning hydroxyls from two different pentaerythritol units in **3** are too unstable to be formed. The chemical shifts of acetal carbons are strongly affected by ring size (39–41) and cyclohexylidene acetals also exhibit this trend (42). The chemical shifts observed for the acetal carbons of **4** (98.7 (2) and 98.8 ppm) fit what is expected for six-membered acetal rings, in agreement with the structure assigned.

The reaction of benzaldehyde with **3** under similar conditions yielded four compounds as the major products, which were shown to be isomeric tri-*O*-benzylidene acetals. Even although cis–trans isomerism can occur in each of the three benzylidene acetal rings derived from **3**, only four diastereomers are possible because of the C_{2v} symmetry of the parent compound (**3**). For the terminal rings, which bear CH_2OH and CH_2OR groups on the same carbon, the configuration is termed cis here and earlier (36) if the phenyl group is cis to the group with the higher Cahn–Ingold–Prelog priority. There is no stereoisomerism in the central benzylidene acetal ring if the two end rings have the same stereochemistry. If the terminal rings have different stereochemistries, the central benzylidene acetal ring is designated cis or trans if the phenyl group in that ring is cis or trans to the substituent bearing the cis-ring, respectively. These four products exhibited surprisingly different behaviour on TLC on silica gel, with R_fs of 0.77, 0.68, 0.60, and 0.49 in hexane – ethyl acetate (1:3) for **5a**, **5b**, **5c**, and **5d**, respectively, and were readily separated by flash column chromatography. The structures of these products are shown in Fig. 1.

Structures were assigned based on the NMR parameters of the three di-*O*-benzylidene acetals of dipentaerythritol (**6a**–**6c**), whose structures had been determined definitively by us previously using X-ray crystallography (36). Some of the observations about the NMR parameters of **6a**–**6c** were noted earlier (36); some are developed here.



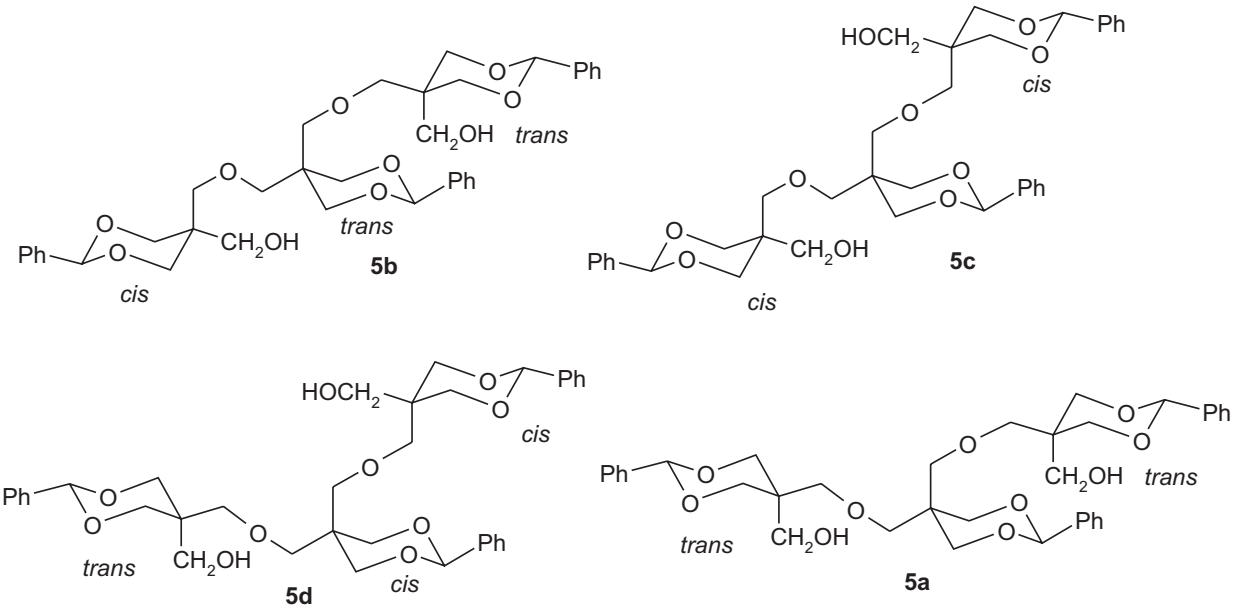
Each terminal benzylidene acetal ring of **5a**–**5d** has one hydroxymethyl group. It was previously noted that the chemical shifts of the carbon atoms of hydroxymethyl groups were 64 to 65 ppm if they were equatorially oriented in *cis*-benzylidene acetals, but 61–62.5 ppm if they were axially oriented in *trans*-benzylidene acetals (36). As noted above, a cis-configuration has the phenyl and CH_2OCH_2-groups on the same side of the ring with an equatorial CH_2OH group, while the trans-isomer has an axial CH_2OH group. On this basis, **5a** is the trans,trans-isomer (chemical shifts 61.3 and 61.8 ppm), while **5c** is the cis,cis-isomer (chemical shifts 64.3 and 65.0 ppm). Compounds **5b** (chemical shifts 62.8 and 64.3 ppm) and **5d** (chemical shifts 62.2 and 65.1 ppm) both have one terminal ring with the cis-configuration and one with the trans-configuration.

The ^{1}H NMR signals of isolated OCH_2 groups, where the oxygen atom is ethereal rather than hydroxylic, are easily identified because they can be correlated by HMQC or HSQC experiments to signals of carbon atoms with chemical shifts of 70.5–73.2 ppm. The values of these ^{1}H NMR chemical shifts can be used to make assignments. All of these CH_2OR groups are attached to C-5 of 2-phenyl-1,3-dioxane rings. The signals of the axial CH_2 groups appear between 3.75 and 4.05 ppm, while those of equatorially oriented CH_2 groups appear between 3.15 and 3.45 ppm. Weber (26) had previously assigned signals for analogous pentaerythritol signals in the same way, and it is well-known that ^{1}H NMR signals of axial substituents at C-5 of 1,3-dioxane derivatives are more deshielded than those of equatorial substituents (43–46).

All of these 5,5-disubstituted-2-phenyl-1,3-dioxane rings will be highly biased conformationally towards the chair conformation with the phenyl group equatorially oriented because the *A* value for a phenyl group at the 2-position in a 1,3-dioxane ring is >3 kcal/mol (1 cal = 4.184 J) (47), while those of the CH_2OR groups at the 5-position are small and almost identical (Fig. 1). To assign the structures of the two unassigned tri-*O*-benzylidenetripentaerythritols (**5b**, **5d**), the data for the di-*O*-benzylidenedipentaerythritols (**6a**–**6c**) will be reexamined and compared with that for the assigned tri-*O*-benzylidenetripentaerythritols (**5a**, **5c**). In the cis,cis-isomer **6a**, the ^{1}H NMR signal of the axial CH_2 attached to an axial CH_2 appears at 3.97 ppm. In the trans,trans-isomer **6c**, the ^{1}H NMR signal of the equatorial CH_2 attached to an

© 2006 NRC Canada

Fig. 1. The possible tribenzylidene acetals of tripentaerythritol.



equatorial CH_2 appears at 3.21 ppm. In the cis,trans-isomer **6b**, the ^{1}H NMR signal of the axial CH_2 attached to an equatorial CH_2 appears at 3.82 ppm and that of the equatorial CH_2 attached to an axial CH_2 appears at 3.32 ppm. In the next section, we determine whether similar values are observed for the same types of linkages in the spectra of the benzylidene acetals whose structures have already been assigned.

In the spectrum of the tri-*O*-benzylidene tripentaerythritol isomer **5a**, whose configuration has already been assigned as trans,trans- (see Fig. 1), there are four of these CH_2 signals at 3.21, 3.25, 3.36, and 3.79 ppm. This last signal can be assigned immediately to the axial CH_2 on the central ring attached to an equatorial CH_2 group. This structure contains two CH_2 groups that are equatorial and attached to each other; in accordance with the observations for **6c** made above, these can be assigned to the signals at 3.21 and 3.25 ppm. The remaining signal (at 3.36 ppm) fits that expected for an equatorial CH_2 attached to an axial CH_2. Thus, all the chemical shifts observed fit what was expected based on the di-*O*-benzylidene dipentaerythritol data.

In the spectrum of the cis,cis-isomer of the tri-*O*-benzylidene tripentaerythritol (isomer **5c**), the four signals of this type appear at 3.35, 3.83, 3.98, and 4.00 ppm. Clearly, the first signal is of an equatorial CH_2, and this structure only contains one (see Fig. 1) on the central ring attached to an axial CH_2 group. The two largest chemical shifts are the same size as those from **6a**, the cis,cis-isomer, and thus are assigned to the two axial CH_2s attached to each other. Finally, the 3.83 ppm value is assigned to the remaining axial CH_2, which is attached to the lone equatorial CH_2 group. The total agreement with the assignments made on the basis of the di-*O*-benzylidene dipentaerythritol data lends confidence to the use of this data for assigning the structures of the two unknown structures remaining.

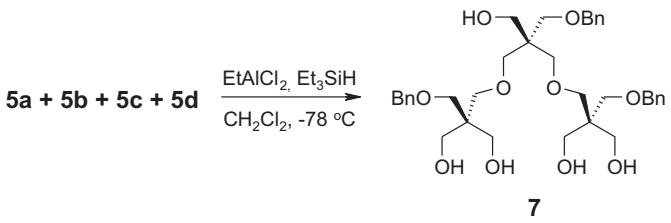
One of the remaining structures has two equatorial CH_2 groups linked to each other and two axial CH_2s linked to each other. Thus, its ^{1}H NMR spectrum is expected to exhibit two singlets in the range 3.20–3.25 ppm and two in the range 3.95–4.00 ppm. The ^{1}H NMR spectrum of **5d** fits these expectations exactly, with chemical shifts of 3.21, 3.23, 3.95, and 4.00 ppm. The other remaining structure has two equatorial CH_2s linked to axial CH_2s and two axial CH_2s linked to equatorial CH_2s. Hence, it would be expected to have two signals in the 3.30–3.35 ppm range and two in the 3.80–3.85 ppm range. The chemical shifts measured for **5b** were 3.34, 3.35, 3.82, and 3.86 ppm, again in near perfect agreement with expectation. Thus, the spectra of all four isomers fit the chemical shift relationships derived from the observations made for the di-*O*-benzylidene dipentaerythritols without exception.

A number of different reagents are commonly employed for the reduction of benzylidene acetals to hydroxy benzyl ethers, including $LiAlH_4$–$AlCl_3$ (48), $NaCNBH_3$–HCl (49), Et_3SiH–TFA (50), Et_3SiH–$BF_3{\cdot}Et_2O$ (51), and DIBAL (52). None of these methods was successful in the reduction of the tri-*O*-benzylidene acetals of tripentaerythritol. In a recent publication, Baskaran and co-workers (53) described a facile and efficient cleavage of benzylidene acetals using $EtAlCl_2$ and Et_3SiH in CH_2Cl_2. Application of the conditions of Baskaran and co-workers to the chromatographically purified mixture of the four possible tri-*O*-benzylidene acetals of tripentaerythritol resulted in the formation of the corresponding tri-*O*-benzyl ether of tripentaerythritol (**7**) in 65% yield (Scheme 2).

In summary, tripentaerythritol was efficiently converted into 2′,2″:6′,6″:10′,10″-tri-*O*-cyclohexylidene-2,2,6,6,10,10-hexakis(hydroxymethyl)-4,8-dioxa-1,11-undecandiol (**4**) by the toluenesulfonic acid catalysed reaction with cyclohexanone in a mixture of *N*,*N*-dimethylformamide and benzene. Reaction of tripentaerythritol with benzaldehyde under similar conditions gave an easily separated mixture of the four possible stereoisomers. Structures of these stereoisomers were assigned based on ^{1}H and ^{13}C NMR chemical shifts using trends previously observed for the dibenzylidene acetals of dipentaerythritol, whose structures had been established

© 2006 NRC Canada

Scheme 2. Reduction of the tribenzylidene acetals of tripentaerythritol.



7

unambiguously by X-ray crystallography. These acetals provide tripentaerythritol derivatives with two symmetrical hydroxyl groups unprotected, suitable for further elaboration into dendrimers or other larger derivatives.

The mixture of benzylidene acetals to 2,6,10-tris(benzyloxymethyl)-4,8-dioxa-1,11-undecanediol was accomplished using triethylsilane with ethylaluminium dichloride as the Lewis acid, after a number of commonly used conditions for this transformation failed. This product, two steps from inexpensive tripentaerythritol, is also well-positioned for further transformations, having five free hydroxyls, four of which could be protected by acetal formation. Results along these lines will be reported in due course.

Experimental section

The general methods and ^{1}H and ^{13}C NMR spectra of products described in the paper are given in the Supplemental material.[3]

2′,2″:6′,6″:10″,10″-Tri-*O*-cyclohexylidene-2,2,6,6,10,10-hexakis(hydroxymethyl)-4,8-dioxa-1,11-undecanediol (4)

A 250 mL round-bottomed flask containing a magnetic stir bar was charged with tripentaerythritol (**3**, 2.0 g, 0.0054 mol), freshly distilled cyclohexanone (0.019 mol, 3.5 eq), *p*-toluenesulfonic acid (0.45 g), dry benzene (60 mL), and dry dimethylformamide (90 mL), and the mixture was refluxed for 5 h with azeotropic removal of water. The stirred solution was cooled and then aqueous potassium carbonate (5%, 30 mL) was added. The reaction mixture was stirred for about 5 min, then extracted with dichloromethane (3 × 30 mL). The combined organic layers were dried over $MgSO_4$ and concentrated to give the title compound (3.2 g, 96%) as a pure colourless solid that was recrystallized from $CHCl_3$–hexane; mp 197 °C. ^{1}H NMR δ: 3.68, (s, 2 × H2′, H2″, H10′, H10″, 8H), 3.66, (s, H6′, H6″, 4H), 3.59 (s, C*H*$_2$OH, 4H), 3.44, 3.53 (2 × CC*H*$_2$OC*H*$_2$C, 8H), 1.42–1.73 (complex m, 3 × cyh H, 30H). ^{13}C NMR δ: 98.84, 98.72 (2 × acetal C), 72.51, 71.74 (2 × CCH_2OCH_2C), 64.12 (2 × CH_2OH), 62.25 (C2′, C2″, C10′, C10″), 62.46 (C6′, C6″), 39.63, 39.54 (3 × C quat), 33.56, 32.67, 31.79 (3 × cyh C2, C6), 25.80 (3 × cyh C4), 22.72 (3 × cyh C3, C5). HR ESI MS *m*/*z* calcd. for $C_{33}H_{56}O_{10}Na^+$: 635.3771; found: 635.3772.

Trans,*trans*-, *cis*,*trans*,*trans*-, *cis*,*cis*-, and *trans*,*cis*,*cis*-2′,2″:6′,6″:10′,10″-tri-*O*-benzylidene-2,2,6,6,10,10-hexakis(hydroxymethyl)-4,8-dioxa-1,11-undecanediol (5a, 5b, 5c, and 5d, respectively)

To a suspension of compound **3** (1.82 g, 4.90 mmol) in dry benzene and dry *N*,*N*-dimethylformamide (150 mL, 4:6 *v*/*v*) was added benzaldehyde (3.40 mL, 33.5 mmol) and *p*-toluenesulfonic acid (0.26 g). The reaction mixture was refluxed in a Dean–Stark trap with continous removal of water for 12 h, then cooled to room temperature, neutralized with solid $CaCO_3$ (1 g), filtered, and the filtrate was concentrated. The residue was separated by flash column chromatography on silica gel (hexane–EtOAc, 3:1 to 2:1 to 1:1). First to elute was *trans*,*trans*-2′,2″:6′,6″:10′,10″-tri-*O*-benzylidene-2,2,6,6,10,10-hexakis(hydroxymethyl)-4,8-dioxa-1,11-undecanediol (**5a**), an amorphous solid (0.23 g, 16%); mp 82–85 °C. R_f 0.77 (hexane–EtOAc, 1:3). ^{1}H NMR δ: 7.34–7.46 (complex m, phenyl protons, 15H), 5.44, 5.42 (2s, ratio 1:2, 3 × acetal H), 4.15, 4.14, 4.07 (3 overlapping d, 6H, *J* = 11.6 Hz, eq H2′, H2″, H6′, H6″, H10′, H10″), 4.03, 4.01 (2s, 2C*H*$_2$OH, 4H), 3.79 (s, ax CCH_2O, 2H), 3.77, 3.76, 3.76 (3 overlapping d, ax H2′, H2″, H6′, H6″, H10′, H10″, 6H), 3.36, 3.25, 3.21 (3s, eq CCH_2O, 6H). ^{13}C NMR δ: 126.00–138.10 (aromatic carbons), 102.21, 102.20 (ratio 2:1, 3 × acetal C), 72.80, 72.60, 71.90 (3 eq C*C*H$_2$O*C*H$_2$C), 70.40 (ax C*C*H$_2$O*C*H$_2$C), 70.50, 70.20, 70.00 (C2′, C2″, C6′, C6″, C10′, C10″), 62.70, 62.10 (2 × CH_2OH), 39.43, 39.38, 39.22 (3 × C quat.).

The second component was *cis*,*trans*,*trans*-2′,2″:6′,6″:10′,10″-tri-*O*-benzylidene-2,2,6,6,10,10-hexakis(hydroxymethyl)-4,8-dioxa-1,11-undecanediol (**5b**), an amorphous solid (0.39 g, 22%); mp 157–160 °C. R_f 0.68 (hexane–EtOAc, 1:3). ^{1}H NMR δ: 7.34–7.46 (complex m, phenyl protons, 15H), 5.42, 5.40, 5.39 (3 × acetal H), 4.15, 4.13, 4.10 (3 overlapping d, *J* = 11.8 Hz, eq H2′, H2″, H6′, H6″, H10′, H10″, 6H), 4.01 (s, C*H*$_2$OH in trans-ring, 2H), 3.86, 3.82 (2s, 2 ax CCH_2O, 4H), 3.75, 3.72, 3.70 (3 overlapping d, ax H2′, H2″, H6′, H6″, H10′, H10″, 6H), 3.45 (s, C*H*$_2$OH in cis-ring, 2H), 3.35, 3.26, (2s, 2 eq CCH_2O, 4H). ^{13}C NMR δ: 126.19–138.30 (aromatic carbons), 102.26, 102.23, 102.19 (3 × acetal C), 73.09, 72.25 (2 eq C*C*H$_2$O*C*H$_2$C), 71.45, 70.90 (2 ax C*C*H$_2$O*C*H$_2$C), 70.70, 70.57, 70.10 (C2′, C2″, C6′, C6″, C10′, C10″), 64.25, 62.84 (2 × CH_2OH), 39.35, 39.24, 39.14 (3 × *C* quat.).

The third component was *cis*,*cis*-2′,2″:6′,6″:10′,10″-tri-*O*-benzylidene-2,2,6,6,10,10-hexakis(hydroxymethyl)-4,8-dioxa-1,11-undecanediol (**5c**), an amorphous solid (0.27 g, 19%); mp 164–167 °C. R_f 0.60 (hexane–EtOAc, 1:3). ^{1}H NMR δ: 7.34–7.48 (complex m, phenyl protons, 15H), 5.42, 5.40 (2s, ratio 1:2, 3 acetal H), 4.17, 4.15, 4.10 (3d, *J* = 11.9 Hz, eq H2′, H2″, H6′, H6″, H10′, H10″, 6H), 3.44, 3.39 (2s, 2 C*H*$_2$OH, 4H), 3.99, 3.98, 3.82 (3s, ax CCH_2O, 6H), 3.75, 3.72, 3.70 (3d, ax H2′, H2″, H6′, H6″, H10′, H10″, 6H), 3.35 (s, eq CCH_2O, 2H). ^{13}C NMR δ: 126.23–138.23 (aromatic carbons), 102.40, 102.32, 102.28 (3 × acetal C), 73.09 (eq C*C*H$_2$O*C*H$_2$C), 72.16, 71.82, 71.72 (3 ax C*C*H$_2$O*C*H$_2$C), 70.65, 70.62, 70.59 (C2′, C2″, C6′, C6″,

[3] Supplementary data for this article are available on the journal Web site (http://canjchem.nrc.ca) or may be purchased from the Depository of Unpublished Data, Document Delivery, CISTI, National Research Council Canada, Ottawa, ON K1A 0R6, Canada. DUD 5018. For more information on obtaining material refer to http://cisti-icist.nrc-cnrc.gc.ca/irm/unpub_e.shtml.

© 2006 NRC Canada

C10′, C10″), 65.04, 64.31(2 × CH_2OH), 39.24, 39.08 (ratio 2:1, 3 × *C* quat.). HR ESI MS *m/z* calcd. for $C_{36}H_{44}O_{10}Na^+$: 659.2832; found: 659.2832.

The fourth component was *trans*,*cis*-2′,2″:6′,6″:10′,10″-tri-*O*-benzylidene-2,2,6,6,10,10-hexa(hydroxymethyl)-4,8-dioxa-1,11-undecanediol (**5d**), an amorphous solid (0.30 g, 21%); mp 165 to 166 °C. R_f 0.49 (hexane–EtOAc, 1:3). ^{1}H NMR δ: 7.34–7.50 (complex m, phenyl protons, 15H), 5.43, 5.37 (2s, ratio 2:1, 3 × acetal H), 4.17, 4.14, 4.10 (3d, *J* = 12 Hz, eq H2′, H2″, H6′, H6″, H10′, H10″, 6H), 4.00 (s, CH_2OH in trans-ring, 2H), 3.99, 3.95 (2s, ax CCH_2O, 4H), 3.76, 3.75, 3.70 (3d, ax H2′, H2″, H6′, H6″, H10′, H10″, 6H), 3.48 (s, CH_2OH in cis-ring, 2H), 3.25, 3.21 (2s, eq CCH_2O, 4H). ^{13}C NMR δ: 126.28–138.24 (aromatic carbon), 102.30, 102.11 (ratio 2:1, 3 × acetal C), 72.88, 72.46 (2 eq C*C*H_2O*C*H_2C), 72.21, 70.46 (2 ax C*C*H_2O*C*H_2C), 70.58, 70.46, 69.98 (C2′, C2″, C6′, C6″, C10′, C10″), 65.10, 62.22 (2 × CH_2OH), 39.31, 39.25 (ratio 2:1, 3 × *C* quat.). HR ESI MS *m/z* calcd. for $C_{36}H_{44}O_{10}Na^+$: 659.2832; found: 659.2832.

2,6,10-Tris(benzyloxymethyl)-4,8-dioxa-1,11-undecanediol (7)

To a chromatographically purified mixture of the tri-*O*-benzylidene acetals of tripentaerythritol (100 mg, 0.157 mmol, dried by coevaporation with dry toluene) in dry dichloromethane (20 mL) was added Et_3SiH (0.56 mmol, 3.6 equiv., 0.1 mL) and the solution was cooled to –78 °C under nitrogen. $EtAlCl_2$ (1.8 mol/L in toluene, 0.86 mmol, 5.5 equiv., 0.5 mL) was added dropwise and the reaction mixture was stirred at –78 °C for 40 min, then quenched with satd. $NaHCO_3$ (50 mL) and extracted with dichloromethane (5 × 40 mL). The combined organic layers were dried ($MgSO_4$) and concentrated to a residue that was purified by flash column chromatography (EtOAc–CH_3OH, 9:1, R_f 0.45) to afford the title compound as a colourless solid (65 mg, 65%); mp 91–93 °C. ^{1}H NMR δ: 7.24–7.34 (m, phenyl protons, 15H), 2 × 4.45, 4.43 (2s, 3 × $PhCH_2O$, 6H), 4 × 3.43, 3.42 (2s, 5 × CH_2OH, 10H), 3.40, 3.39 (2s, CCH_2O, 8H), 2 × 3.37, 3.34 (2s, 3 × CH_2OBn, 6H). ^{13}C NMR δ: 127.7–138.2 (aromatic carbons), 2 × 73.9, 73.8 (3 × OCH_2Ph), 71.9, 71.9 (4 × CCH_2O), 2 × 71.5, 71.0 (3 × CH_2OBn), 2 × 64.33, 2 × 64.28, 64.15 (5 × CH_2OH), 2 × 45.6, 45.5 (3 × C quat). HR ESI MS *m/z* calcd. for $C_{34}H_{50}O_{10}Na^+$: 665.3302; found: 665.3307; calcd. for $2(C_{34}H_{50}O_{10})Na^+$: 1307.6706; found: 1307.6715.

Acknowledgements

TBG thanks the Natural Sciences and Engineering Research Council of Canada (NSERC) for support. NMR spectra were recorded at the Atlantic Region Magnetic Resonance Centre, Dalhousie University, Halifax, Nova Scotia. We thank Dr. Yun Ling of the University of British Columbia, Vancouver, British Columbia, and Dr. Angelina Morales–Izquierdo of the University of Alberta, Edmonton, Alberta, for the high-resolution electrospray mass spectra.

References

1. M. Fischer and F. Vögtle. Angew. Chem. Int. Ed. **38**, 885 (1999).
2. O.A. Matthews, A.N. Shipway, and J.F. Stoddart. Prog. Polym. Sci. **23**, 1 (1998).
3. F.W. Zeng and S.C. Zimmerman. Chem. Rev. **97**, 1681 (1997).
4. N. Ardoin and D. Astruc. Bull. Soc. Chim. Fr. **132**, 875 (1995).
5. D.A. Tomalia, A.M. Naylor, and W.A. Goddard. Angew. Chem. Int. Ed. Engl. **29**, 138 (1990).
6. D.A. Tomalia and H.D. Durst. Top. Curr. Chem. **165**, 193 (1993).
7. S.K. Grayson and J.M.J. Fréchet. Chem. Rev. **101**, 3819 (2001).
8. A.B. Padias, H.K. Hall, D.A. Tomalia, and J.R. McConnell. J. Org. Chem. **52**, 5305 (1987).
9. S. Hanessian, D.X. Qiu, H. Prabhanjan, G.V. Reddy, and B.L. Lou. Can. J. Chem. **74**, 1738 (1996).
10. S. Hanessian, H.K. Huynh, G.V. Reddy, R.O. Duthaler, A. Katopodis, M.B. Streiff, W. Kinzy, and R. Oehrlein. Tetrahedron, **57**, 3281 (2001).
11. T.K. Lindhorst, M. Dubber, U. Krallmann-Wenzel, and S. Ehlers. Eur. J. Org. Chem. 2027 (2000).
12. E.C. Constable, C.E. Housecroft, M. Cattalini, and D. Phillips. New J. Chem. **22**, 193 (1998).
13. F. Dagron and A. Lubineau. J. Carbohydr. Chem. **22**, 481 (2003).
14. N.G. Lemcoff and B. Fuchs. Org. Lett. **4**, 731 (2002).
15. B. Liu and R. Roy. Tetrahedron, **57**, 6909 (2001).
16. T. Ivannikova, F. Bintein, A. Malleron, S. Juliant, M. Cerutti, A. Harduin-Lepers, P. Delannoy, C. Auge, and A. Lubineau. Carbohydr. Res. **338**, 1153 (2003).
17. A. Halabi and M.C. Strumia. J. Org. Chem. **65**, 9210 (2000).
18. M. Schmidt, B. Dobner, and P. Nuhn. Eur. J. Org. Chem. 669 (2002).
19. B.C. Liu and R. Roy. Tetrahedron, **57**, 6909 (2001).
20. J. Esnault, J.M. Mallet, Y.M. Zhang, P. Sinaÿ, T. Le Bouar, F. Pincet, and E. Perez. Eur. J. Org. Chem. 253 (2001).
21. S. David. Carbohydr. Res. **331**, 327 (2001).
22. T.J. Dunn, W.L. Neumann, M.M. Rogic, and S.R. Woulfe. J. Org. Chem. **55**, 6368 (1990).
23. A.-R. Abdun-Nur and C.H. Issidorides. J. Org. Chem. **27**, 67 (1962).
24. M. Apel and B. Tollens. Ann. **289**, 34 (1896).
25. E. Bograchov. J. Am. Chem. Soc. **72**, 2268 (1950).
26. E. Weber. J. Org. Chem. **47**, 3478 (1982).
27. C.H. Issidorides and R.C. Gulen. *In* Organic syntheses collected. Vol. IV. *Edited by* N. Rabjohn. John Wiley and Sons, New York. 1963. p. 679.
28. M. Schmidt, B. Dobner, and P. Nuhn. Synlett, 1157 (2000).
29. S. Hanessian, H. Prabhanjan, D.X. Qiu, and S. Nambiar. Can. J. Chem. **74**, 1731 (1996).
30. P. Westerduin, G.H. Veeneman, J.E. Marugg, G.A. van der Marel, and J.H. van Boom. Tetrahedron Lett. **27**, 1211 (1986).
31. J.M. Gardiner, P. Mather, R. Morjan, R.G. Pritchard, J.E. Warren, M.L. Cooper, A.E.S. Ferwanah, and O.S. Abu-Tiem. Tetrahedron Lett. **43**, 2091 (2002).
32. M.S. Shchepinov, I.A. Udalova, A.J. Bridgman, and E.M. Southern. Nucleic Acids Res. **25**, 4447 (1997).
33. C.J. Burns, P. Culshaw, L.D. Field, M. Islam, J. Morgan, B. Raguse, D.D. Ridley, L. Wieczorek, M. Wilkinson, and V. Vignevich. Aust. J. Chem. **52**, 1071 (1999).
34. M.E. Lizarzaburu, M.J. Kurth, and M.H. Nantz. Tetrahedron Lett. **40**, 8985 (1999).
35. S.J. Kim, E.K. Bang, and B.H. Kim. Synlett, 1838 (2003).
36. H. Al-Mughaid, T.B. Grindley, K.N. Robertson, and T.S. Cameron. Can. J. Chem. **81**, 505 (2003).
37. P. Werle and G. Nonnenmacher. Liebigs Ann. 150 (1983).
38. M.C. Murguía, S.E. Vaillard, and R.J. Grau. Synthesis, 1093 (2001).

© 2006 NRC Canada

39. J.G. Buchanan, M.E. Chacon-Fuertes, A.R. Edgar, S.J. Moorhouse, D.I. Rawson, and R.H. Wightman. Tetrahedron Lett. **21**, 1793 (1980).
40. T.B. Grindley and V. Gulasekharam. Carbohydr. Res. **74**, 7 (1979).
41. J.G. Buchanan, A.R. Edgar, D.I. Rawson, P. Shahidi, and R.H. Wightman. Carbohydr. Res. **100**, 75 (1982).
42. T.B. Grindley, C.J.P. Cote, and C. Wickramage. Carbohydr. Res. **140**, 215 (1985).
43. E.L. Eliel and R.J.L. Martin. J. Am. Chem. Soc. **90**, 682 (1968).
44. T.A. Crabb, M. Porssa, and N.F. Elmore. Magn. Reson. Chem. **29**, 613 (1991).
45. J.Q. Cai, A.G. Davies, and C.H. Schiesser. J. Chem. Soc. Perkin Trans. 2, 1151 (1994).
46. A.C. Coxon and J.F. Stoddart. J. Chem. Soc. Perkin Trans. 1, 767 (1977).
47. F.G. Riddell. The conformational analysis of heterocyclic compounds. Academic Press Inc., London. 1980.
48. A. Lipták, I. Jodál, and P. Nánási. Carbohydr. Res. **44**, 1 (1975).
49. P.J. Garegg, H. Hultberg, and S. Wallin. Carbohydr. Res. **108**, 97 (1982).
50. M.P. Deninno, J.B. Etienne, and K.C. Duplantier. Tetrahedron Lett. **36**, 669 (1995).
51. S.D. Debenham and E.J. Toone. Tetrahedron: Asymmetry, **11**, 385 (2000).
52. M.E. Lizarzaburu, R.M. Jones, M.H. Nantz, and M.J. Kurth. Org. Prep. Proced. Int. **31**, 440 (1999).
53. V. Balakumar, A. Aravind, and S. Baskaran. Synlett, 647 (2004).

© 2006 NRC Canada

Kinetics of the reaction catalyzed by inositol dehydrogenase from *Bacillus subtilis* and inhibition by fluorinated substrate analogs[1]

Richard Daniellou, Hongyan Zheng, and David R.J. Palmer

Abstract: Inositol dehydrogenase (EC 1.1.1.18) from *Bacillus subtilis* catalyzes the oxidation of *myo*-inositol to *scyllo*-inosose by transfer of the equatorial hydride of the substrate to NAD^+. This is a key enzyme in the metabolism of *myo*-inositol, a primary carbon source for soil bacteria. In light of our recent discovery that the enzyme has a broad substrate spectrum while maintaining high stereoselectivity, we seek a more thorough understanding of the enzyme and its active site. We have examined the kinetics of the recombinant enzyme, and synthesized fluorinated substrate analogues as competitive inhibitors. We have evaluated all rate constants in the ordered, sequential Bi Bi mechanism. No steady-state kinetic isotope effect is observed using *myo*-[2-^{2}H]-inositol, indicating that the chemical step of the reaction is not rate-limiting. We have synthesized the substrate analogs 2-deoxy-2-fluoro-*myo*-inositol, its equatorial analog 1-deoxy-1-fluoro-*scyllo*-inositol, the *gem*-difluorinated analog 1-deoxy-1,1-difluoro-*scyllo*-inositol, and the sugar analog α-D-glucosyl fluoride. Of these, 1-deoxy-1-fluoro-*scyllo*-inositol showed no inhibition, while all others tested had K_i values comparable to the K_m values of the analogous substrates *myo*-inositol and α-D-glucose.

Key words: inositol dehydrogenase, enzyme mechanism, kinetics, competitive inhibitor, substrate analogue.

Résumé : La déshydrogénase de l'inositol (EC 1.1.1.18) du *Bacillus subtilis* catalyse l'oxydation du *myo*-inositol en *scyllo*-inosose par le transfert d'un hydrure équatorial du substrat vers la NAD^+. C'est un enzyme clé dans le métabolisme du *myo*-inositol, une source de carbone primaire pour les bactéries du sol. Compte tenu de notre découverte récente à l'effet que l'enzyme peut agir sur un large éventail de substrats tout en maintenant une stéréosélectivité élevée, une étude plus approfondie a été entreprise pour mieux comprendre cet enzyme et son site actif. À cette fin, on a étudié la cinétique de l'enzyme recombinant et on a synthétisé des analogues fluorés de substrats comme inhibiteurs compétitifs. On a évalué toutes les constantes de vitesse dans le mécanisme Bi Bi, ordonné et séquentiel. On n'a pas observé d'effet isotopique cinétique à l'état stationnaire lorsqu'on a étudié le *myo*-[2-^{2}H]-inositol; cette observation indique que l'étape chimique n'est pas cinétiquement limitante. On a aussi synthétisé les analogues de substrats 2-désoxy-2-fluoro-*myo*-inositol, son analogue équatorial 1-désoxy-1-fluoro-*scyllo*-inositol, son analogue *gem*-difluoré 1-désoxy-1,1-difluoro-*scyllo*-inositol et le sucre analogue fluorure de α-D-glucosyle. De tous ces composés, le 1-désoxy-1-fluoro-*scyllo*-inositol ne présente pas d'inhibition alors que, avec tous les autres composés évalués, les valeurs de K_i sont comparables aux valeurs de K_m des substrats analogues du *myo*-inositol et du α-D-glucose.

Mots clés : inositol, déshydrogénase, mécanisme d'enzyme, cinétique, inhibition compétitive, analogue de substrat.

[Traduit par la Rédaction]

Introduction

Inositol is a ubiquitous natural product that is abundant in soil. Inositol derivatives are known to occupy key roles in the biology of bacteria, fungi, plants, and animals. It has been known for many years that environmental microorganisms perform regioselective oxidation reactions on inositols and related carbohydrate derivatives (1–3). The first step in the catabolism of inositol by soil bacteria is the NAD^+-dependent oxidation of *myo*-inositol to *scyllo*-inosose by inositol dehydrogenase (IDH, EC 1.1.1.18), shown in Scheme 1. Recently, interest in IDH has increased because of links between inositol catabolism, particularly IDH activity, and the competitiveness of certain beneficial soil bacteria that can form symbiotic relationships with important crops such as peas, beans, and other legumes (4–6).

The most detailed in vitro study of IDH catalysis has used the enzyme from *Bacillus subtilis*. The native enzyme was isolated and the kinetic mechanism described by Ramaley et al. (7) more than 25 years ago. This work revealed several aspects of IDH, including some tolerance of the active site to structural variations in the substrate: α-D-glucose and α-D-xylose were also observed to be substrates. Also demon-

Received 25 August 2005. Published on the NRC Research Press Web site at http://canjchem.nrc.ca on 21 April 2006.

This paper is dedicated to Professor Walter Szarek, whose knowledge of and enthusiasm for his science are inspirational.

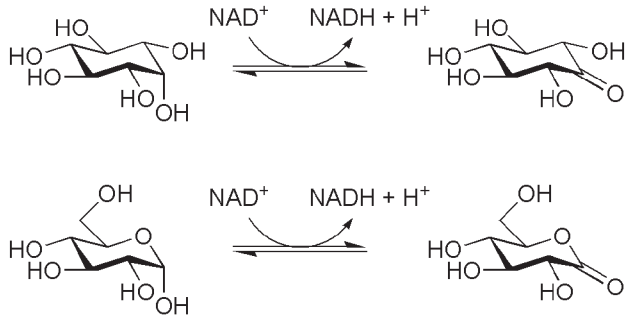
R. Daniellou, H. Zheng, and D.R.J. Palmer.[2] Department of Chemistry, University of Saskatchewan, 110 Science Place, Saskatoon, SK S7N 5C9, Canada.

[1]This article is part of a Special Issue dedicated to Professor Walter A. Szarek.

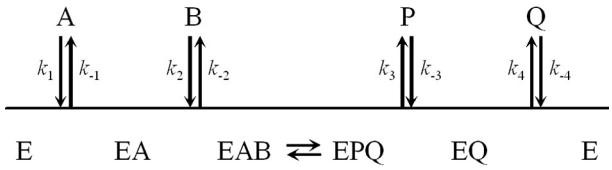
[2]Corresponding author (e-mail: palmer@sask.usask.ca).

 doi:10.1139/V06-033 © 2006 NRC Canada

Scheme 1. The IDH-catalyzed oxidation of *myo*-inositol to *scyllo*-inosose and α-D-glucose to D-glucono-1,5-lactone.



Scheme 2. Cleland diagram of an ordered, sequential Bi Bi mechanism. For IDH, A is NAD^+, B is *myo*-inositol, P is *scyllo*-inosose, and Q is NADH.



strated was a sequential, ordered Bi Bi mechanism in which NAD^+ binds first and NADH is released last, as indicated in Scheme 2. However, the authors reported only the apparent Michaelis constant for *myo*-inositol at 0.5 mmol/L NAD^+ (K_m^{App} = 18 mmol/L) rather than the true K_m. No specific insight into the active-site architecture was garnered.

Our laboratory has recently subcloned and expressed recombinant IDH from *B. subtilis*. We observed that IDH can oxidize 1L-4-*O*-subtituted derivatives of *myo*-inositol, and that the substituent can be as large as a camphorsulfonyl group (8). Disaccharides could also act as substrates, but the presence of a negative charge on the substituent decreased affinity for the enzyme. This suggests a large, nonpolar pocket adjacent to the active site, allowing stereoselective recognition of these alternative substrates.

We seek a thorough understanding of this enzyme, and to that end we have evaluated rate constants for each of the steps represented in Scheme 2. In addition, we have synthesized substrate mimics in which the axial hydroxyl group of the reaction centre has been replaced with an axial and (or) equatorial fluorine atom. Fluorine can act as a hydrogen bond acceptor, but not a donor, and the ability of these compounds to act as inhibitors will indicate the role of the hydroxyl group in binding to the active site. Development of a potent inhibitor could prove very useful in determining the roles of active-site residues if a high-resolution crystal structure of inhibitor-bound enzyme can be generated.

Experimental

General

Chemical reagents, including buffers, salts, *myo*-inositol, NAD^+, and NADH, were obtained from Sigma-Aldrich Canada, Ltd. (Oakville, Ontario), or VWR CanLab (Mississauga, Ontario), and were categorized as molecular biology grade or were the highest grade available. *scyllo*-Inosose was synthesized as previously described and its spectroscopic characteristics matched those reported before (9). Inositol dehydrogenase was purified as described previously (8). UV–vis absorbance was measured using a Beckman DU-640 spectrophotometer with a circulating-water-bath-controlled temperature block. Thin layer chromatography was performed on aluminium-backed plates of Silica gel $60F_{254}$ (EM Science, Gibbstown, New Jersey) using phosphomolybdic acid – ethanol reagent, or a 10% solution of sulfuric acid in ethanol, and (or) UV at 254 nm to visualize spots. Silica gel 60 (40–63 μm) was used for flash chromatography. NMR spectra were recorded on a Bruker 500 MHz spectrometer. Chemical shifts are reported in ppm downfield from tetramethylsilane. Mass spectra were recorded with a VG 70SE mass spectrometer. NMR, mass spectrometry, and elemental analysis facilities are part of the Saskatchewan Structural Sciences Centre, University of Saskatchewan, Saskatoon, Saskatchewan.

2-Deoxy-2-fluoro-*myo*-inositol (**1**), 1-deoxy-1-fluoro-*scyllo*-inositol (**2**), 1-deoxy-1,1-difluoro-*scyllo*-inositol (**3**) (10–13), and α-D-glucosyl fluoride (**4**) (14) were synthesized according to literature methods. All spectroscopic data matched that reported previously.

myo-[2-^{2}H]-Inositol

$NaBD_4$ was added to a solution of *scyllo*-inosose (0.53 g, 3 mmol) in water (27 mL). After stirring overnight at room temperature, the reaction was quenched by the addition of acetone (5 mL). The mixture was then concentrated and the residue was peracetylated by stirring in acetic anhydride (20 mL) and pyridine (10 mL) at 100 °C for 24 h (15). Flash chromatography of the residue (hexane – ethyl acetate, 1:1), followed by deacetylation using sodium methoxide in methanol at reflux for 10 min, neutralization with Dowex 50X8 (H^+ form), filtration and concentration, gave *myo*-[2-^{2}H]-inositol isolated in 41% yield as a white solid. No *scyllo*-inositol derivative was observed. ^{1}H NMR (500 MHz, D_2O) δ: 3.15 (t, J = 9.3 Hz, 1H, H-5), 3.42 (d, J = 10.0 Hz, 2H, H-1 and H-3), 3.51 (m, 2H, H-4 and H-6). ^{13}C NMR (125 MHz, D_2O) δ: 71.44, 72.13 (t, $J_{C\text{-}D}$ = 22 Hz), 72.78, 74.73. ESI-MS : 204.06 $[M + Na]^+$, 385.13 $[2M + Na]^+$. Anal. calcd. for $C_6H_{11}DO_6$: C 39.78, H 7.23; found: C 39.99, H 6.99.

Kinetics

Forward (oxidation of *myo*-inositol) and reverse (reduction of *scyllo*-inosose) reactions were measured by continuously monitoring the appearance or the disappearance of NADH at 340 nm (ε = 6.2 $(mmol/L)^{-1}$ cm^{-1}). Initial rates were determined using various concentrations of substrates in 100 mmol/L Tris-HCl pH 9.0 at 25 °C. Kinetic constants were determined using the program Leonora (16) by nonlinear least-squares fitting of the data to eq. [1], which describes an ordered sequential Bi Bi mechanism in the absence of products,

$$[1] \qquad v = \frac{V_{max}[A][B]}{K_{iA}K_{mB} + K_{mB}[A] + K_{mA}[B] + [A][B]}$$

where [A] is the concentration of the substrate that first binds (NAD^+ or NADH), [B] is the concentration of the second substrate (*myo*-inositol or *scyllo*-inosose), K_{iA} is the dis-

© 2006 NRC Canada

sociation constant for A, K_{mA} and K_{mB} are the respective limiting Michaelis constants for the substrates A and B, and V_{max} is the maximum velocity when both substrates are in saturating condition.

The concentration of each inhibitor needed to decrease the velocity by 50% (IC_{50}) was determined at [S] = 20 mmol/L by fitting the dependence of v/v_0 on [I], where v_0 is the rate in the absence of inhibitor. The inhibition constant (K_i) was calculated using the Cheng and Prusoff equation (17).

$$[2] \qquad K_i = \frac{IC_{50}}{1 + \frac{[S]}{K^{App}}}$$

To test the validity of this method in these conditions, the inhibition constant for 1-deoxy-1-fluoro-α-D-glucose (**4**) was determined by a Dixon plot, based on eq. [3],

$$[3] \qquad v = \frac{V^{App}[S]}{K^{App}\left(1 + \frac{[I]}{K_i}\right) + [S]}$$

where S is the varied substrate, V^{App} is the maximal velocity at the concentration of the fixed substrate, K^{App} is the substrate concentration necessary for half-maximal velocity under these conditions, and K_i is the inhibition constant. The result of this analysis (66 ± 5 mmol/L) was in good agreement with the value determined using eq. [2] (58 ± 8 mmol/L).

Results and discussion

Kinetics and mechanism

The work of Ramaley et al. (7) provided the basic facts regarding the IDH mechanism, including product inhibition studies consistent with an ordered Bi Bi mechanism and a pH–rate profile, which we have confirmed in our laboratory (data not shown). To examine the details of the kinetic mechanism, the initial velocities of the enzymatic reaction at pH 9.0 were recorded at several constant concentrations of one substrate (B) while varying the concentration of the other substrate (A). When data were plotted in the form $1/v$ against 1/A, a series of straight lines was obtained for the forward and reverse enzymatic reactions. The lines intersected to the left of the ordinate axis of the double-reciprocal plot, in agreement with the ordered Bi Bi mechanism depicted in Scheme 2 (18). The families of lines are shown in Fig. 1. Our results, shown in Table 1, provide a K_m = 1.1 mmol/L for *myo*-inositol for the first time, comparable to the value of 1 mmol/L for *scyllo*-inosose and consistent with a catabolic pathway.

Some other facts become apparent from the data of Table 1. First, although we are operating at the optimal pH for oxidation of *myo*-inositol, the reverse reaction, reduction of *scyllo*-inosose, is still faster. Second, the value of K_{iq}, representing the disassociation constant of NADH binding to free IDH, is notably lower than the Michaelis constant of the substrate inositol. Product inhibition thus limits the application of IDH as a catalyst for the synthesis of inosose derivatives, but this nonproductive ternary complex would yield a wealth of information if it could be crystallized.

Fig. 1. Double reciprocal plot of the variation of rate with: (A) NAD^+ concentration at constant *myo*-inositol concentrations (2 mmol/L (●), 4 mmol/L (□), 7 mmol/L (■), 10 mmol/L (▲), 20 mmol/L (○)); and (B) inositol concentration at constant inositol concentrations (0.1 mmol/L (●), 0.2 mmol/L (○), 0.4 mmol/L (■), 1.0 mmol/L (□)).

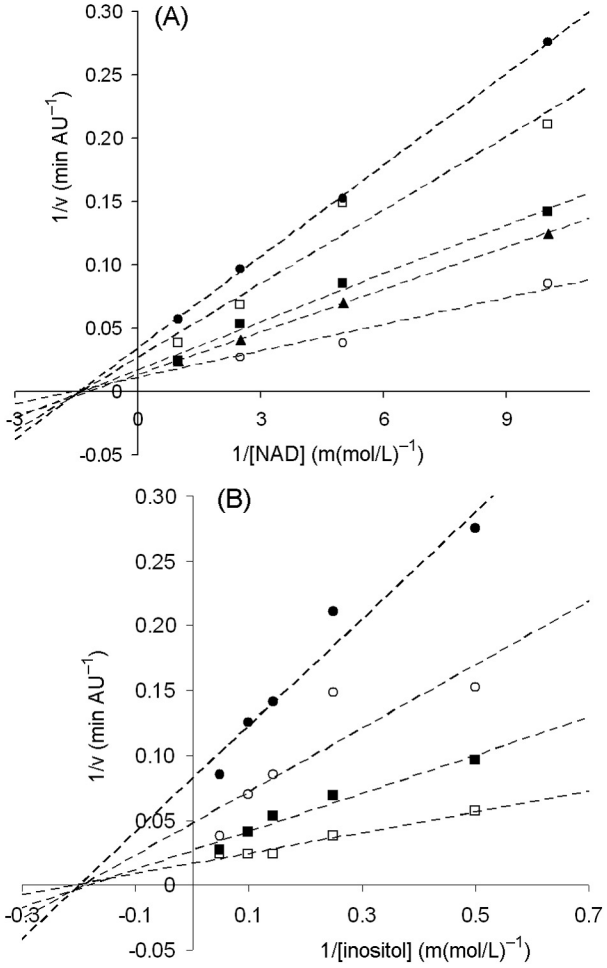


Table 1. Kinetic constants for the IDH-catalyzed reaction.

Constant	Value
K_{ia}	5±1 mmol/L
$K_{m(NAD^+)}$	0.26±0.05 mmol/L
$K_{m(inositol)}$	1.1±0.1 mmol/L
$V_{forward}$	13.5±2 μmol min^{-1} mg^{-1}
$k_{forward}$	9±1 s^{-1}
K_{iq}	50±5 μmol/L
$K_{m(NADH)}$	36±5 μmol/L
$K_{m(inosose)}$	1.0±0.1 mmol/L
$V_{reverse}$	19±2 μmol min^{-1} mg^{-1}
$k_{reverse}$	13±1 s^{-1}

Note: Conditions for the reaction were 100 mmol/L TRIS-HCl, pH 9.0, 25 °C.

© 2006 NRC Canada

Table 2. Calculated kinetic constants of IDH-catalyzed reactions.

Constant	Expression	Value
k_1	$\frac{V_{forward}}{K_{m(NAD^+)}[E_0]}$	(3.6±0.4) × 10^4 s^{-1} $(mol/L)^{-1}$
k_{-1}	$\frac{V_{forward}K_{ia}}{K_{m(NAD^+)}[E_0]}$	180±30 s^{-1}
k_2	$\frac{V_{forward}(k_{-2}+k_3)}{k_3K_{m\ (inositol)}[E_0]}$	(1.4±0.2) × 10^4 s^{-1} $(mol/L)^{-1}$
k_{-2}	$\frac{V_{forward}V_{reverse}\ K_{ia}}{[E_0](V_{forward}\ K_{ia}\ -\ V_{reverse}K_{m(NAD^+)})}$	14±1 s^{-1}
k_3	$\frac{V_{forward}V_{reverse}\ K_{iq}}{[E_0](V_{reverse}\ K_{iq}\ -\ V_{forward}K_{m(NADH)})}$	19± 1 s^{-1}
k_{-3}	$\frac{V_{reverse}(k_{-2}+k_3)}{k_{-2}K_{m\ (inositol)}[E_0]}$	(3.0±0.4) × 10^4 s^{-1} $(mol/L)^{-1}$
k_4	$\frac{V_{reverse}\ \frac{1}{K_{iq}}}{K_{m\ (NADH)}[E_0]}$	18±1 s^{-1}
k_{-4}	$\frac{V_{reverse}}{K_{m\ (NADH)}[E_0]}$	3.5±0.4 × 10^5 s^{-1} $(mol/L)^{-1}$
K_{ib}	$\frac{k_{-1}+k_{-2}}{k_2}$	14±2 mmol/L
K_{ip}	$\frac{k_{-1}+k_4}{k_1}$	5.5±0.9 mmol/L

Note: Conditions for the reactions were 100 mmol/L TRIS-HCl, pH 9.0, 25 °C.

The internal consistency of the kinetic constants in Table 1 was confirmed using the Haldane relationship for an ordered Bi Bi kinetic mechanism. A value of 5.7×10^{-3} was calculated for K_{eq}. This is in good agreement with the value of 2.5×10^{-3}, which was determined experimentally at pH 9.0 and at 25 °C for the thermodynamic equilibrium constant.

$$K_{eq} = \frac{[\text{NADH}][\textit{scyllo}\text{-inosose}]}{[\text{NAD}^+][\textit{myo}\text{-inositol}]}$$

The Theorell–Chance mechanism is a special case of the ordered Bi Bi mechanism in which the concentrations of the central EAB and EPQ complexes are essentially zero. To evaluate the kinetic importance of these species and discriminate between the two mechanisms, we have calculated the ratio R, as defined by Janson and Cleland (19).

$$R = \frac{\frac{1}{V_{forward}}\left(1 - \frac{K_{m(NAD^+)}}{K_{ia}}\right) + \frac{1}{V_{reverse}}\left(1 - \frac{K_{m(NADH)}}{K_{iq}}\right)}{\frac{1}{V_{forward}} + \frac{1}{V_{reverse}}}$$

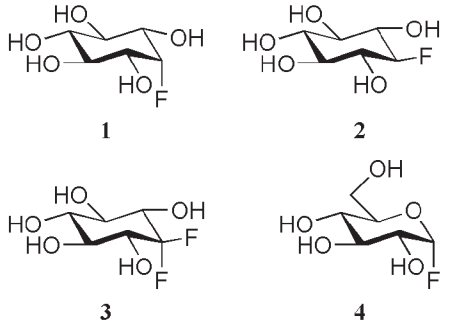
The value of R can vary between 0 and 1, where the limiting case $R = 0$ would indicate the canonical Theorell–Chance mechanism. Using our data, we calculated $R = 0.68$ for IDH under these conditions, indicating that the ternary complex has a lifetime.

By using the relationships of kinetic parameters to microscopic rate constants for an ordered Bi Bi mechanism (20), values for k_1–k_{-4} were calculated, and are summarized in Table 2. In both directions, the breakdown of the ternary complex (k_3 and k_{-2}) appears to constitute the rate-limiting step, although in the forward direction, liberation of the cofactor NADH is also slow and partially rate-limiting. This analysis does not distinguish between the chemical step, i.e., the hydride transfer, and the release of the first product.

To determine whether the chemical step or the liberation of the product is the limiting step, primary kinetic isotope effect experiments were performed. The synthesis of *myo*-[2-^{2}H]-inositol was easily effected by reaction of *scyllo*-inosose with sodium borodeuteride. One might expect a mixture of *myo*- and *scyllo*-inositol isomers, generated by hydride attack from either face of the ketone, however, only the *myo*-isomer is formed. The high stereoselectivity of this reaction, in agreement with results using related compounds (21, 22), is in accordance with the prevalence of the steric effects in reduction reactions with sodium borohydride; hydride attack occurs at the face anti to the substituents on the two adjacent carbons. A simple acetylation–deacetylation sequence was used to remove salts from the compound. For consistency, this process was also carried out using sodium borohydride to make *myo*-inositol, and this inositol was used for direct comparison with the deuterated analogue. *myo*-Inositol prepared in this manner showed no difference in behaviour from purchased *myo*-inositol. At [NAD$^+$] = 0.5 mmol/L, no kinetic isotope effect was observed on V_{max} ($V^H/V^D = 1.0$) and the isotope effect on V_{max}/K_m was only 1.1. These results lead us to the conclusion that the chemical reaction is rapid relative to liberation of product, the latter being the rate-limiting step of the enzymatic reaction.

© 2006 NRC Canada

Chart 1.



Fluorine-containing analogues

Replacement of the hydroxyl group of a substrate with a fluorine atom can help one understand the mechanism of an enzyme in a number of ways (23, 24). The carbon–fluorine bond length is close to that of the carbon–oxygen bond, but fluorine is a better leaving group than hydroxyl and cannot act as a hydrogen bond donor. A substrate bearing a fluorine atom might therefore behave as a pseudosubstrate, undergoing the "normal" enzymatic chemistry, but with altered reactivity; as an inhibitor, recognized by the enzyme but undergoing no reaction, or as an inactivator, alkylating the enzyme at the active site. However, a number of studies giving unexpected results has prompted Seebach to dub fluorinated substrates "flustrates" (25).

We chose to replace the reaction centre of *myo*-inositol with a carbon bearing a fluorine substituent since the resulting molecules are approximately isosteric with the substrate, but cannot undergo the dehydrogenation reaction. The inhibitors envisioned were all accessible by published procedures. 2-Deoxy-2-fluoro-*myo*-inositol (**1**) matches the configuration of the substrate, with an axial fluorine replacing the reactive hydroxyl. 1-Deoxy-1-fluoro-*scyllo*-inositol (**2**) has all non-hydrogen substituents in the equatorial position. The all-equatorial stereoisomer of *myo*-inositol (*scyllo*-inositol) is not a substrate nor an inhibitor of IDH (7). Therefore, if we understand the recognition behaviour of the active site, **2** should show little or no inhibition. While these two inhibitors test for the requirement of an axial substituent, the *gem*-difluoro analog, 1-deoxy-1,1-difluoro-*scyllo*-inositol (**3**), tests whether the presence of an equatorial substituent is deleterious. α-D-Glucosyl fluoride (**4**) is the isosteric analog of glucose, which is also a substrate for IDH (Chart 1).

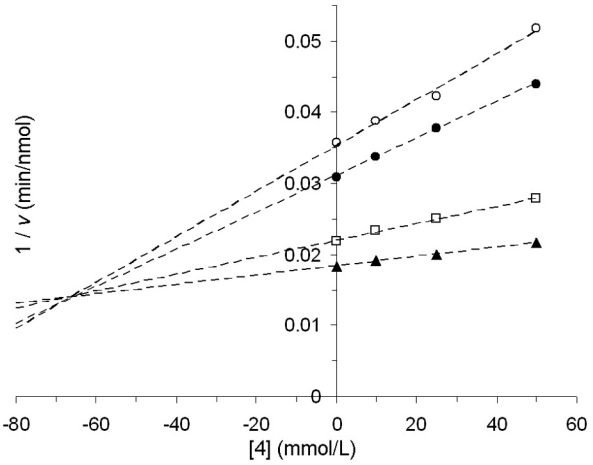
The results of the inhibition studies with **1–4** are shown in Table 3. None of these compounds could act as substrates, i.e., no reduction of NAD^+ was observed in the absence of *myo*-inositol. All experiments were performed under our standard assay conditions, where the K_m^{App} for *myo*-inositol is 18 mmol/L, and for α-D-glucose is 56 mmol/L. Solubility of the fluorinated compounds in aqueous buffer prevented very high concentrations of inhibitor from being used, but an IC_{50} value could be determined. Using the method of Cheng and Prusoff (17), a value for K_i was calculated from the IC_{50}. The Dixon plot generated for **4** shown in Fig. 2 is as expected for a competitive inhibitor. As predicted, the *myo*-inositol analog **1** inhibits IDH, while the *scyllo*-derivative **2** does not. The K_i value is about double the K_m value for *myo*-inositol under these conditions, suggesting that binding of the inhibitor to the active site is comparable, although not as favourable, as binding of substrate. Interestingly, The K_i value for **3** is very close to that for **1**, clearly indicating that the presence of an equatorial substituent is not intrinsically detrimental to binding in the active site. In this compound, a carbon–fluorine atom is taking the place of the scissile carbon–hydrogen bond (in addition to the carbon–oxygen bond), therefore, a fluorine atom can be accommodated between the carbon atom of the inositol derivative and carbon-4 of the nicotinamide ring of NAD^+. Inhibition by the glucose analog **4** suggests that binding is only slightly less favourable than substrate binding, suggesting that the fluorine atom can replace the hydroxyl group with only a small energetic penalty.

Table 3. Inhibition constants and IC_{50} values for inhibitors **1–4**.

Compound	IC_{50} (mmol/L)	K_i (mmol/L)
1	77±2	37±5
2	No inhibition	—
3	82±2	39±5
4	116±3	58±8

Note: Collected under the following conditions: 100 mmol/L TRIS-HCl, pH 9.0, 25 °C, 20 mmol/L *myo*-inositol, 0.5 mmol/L NAD^+.

Fig. 2. Dixon plot of variation of rate with varying concentrations of inhibitor **4** at constant *myo*-inositol concentrations: 10 mmol/L (○), 20 mmol/L (●), 40 mmol/L (□), 80 mmol/L (▲).



Conclusion

IDH is an enzyme that *B. subtilis* can use for catabolism of not only *myo*-inositol, but also for several monosaccharides and disaccharides (7, 8). Our results are in accord with the conclusions of Ramaley et al. (7) regarding the ordered mechanism of the enzyme, but we have now shown that the enzyme has evolved a fast hydride transfer mechanism, such that release of products limits the rate. The enzyme also regulates its production of inosose by product inhibition. The use of fluorinated analogs as inhibitors shows that an axial electronegative group is required for binding, and that fluorine can replace hydroxyl as this axial group. The presence of an equatorial carbon–fluorine bond at the reaction centre can be accommodated by the enzyme

© 2006 NRC Canada

if an axial substituent is also present. We hope that these or other inhibitors can be used to form crystals of IDH in a ternary complex, giving a clear picture of the active-site architecture during catalysis.

Acknowledgements

This work was supported by a Natural Sciences and Engineering Research Council of Canada (NSERC) Discovery grant and a New Opportunities grant from the Canadian Foundation for Innovation. The authors thank Ken Thoms for mass spectrometry and elemental analysis.

References

1. T. Posternak. Biochem. Prep. **2**, 52 (1952).
2. G.W. Schnarr and W.A. Szarek. Can. J. Chem. **56**, 1752 (1978).
3. K.-I. Yoshida, D. Aoyama, I. Ishio, T. Shibayama, and Y.J. Fujita. J. Bacteriol. **179**, 4591 (1997).
4. J. Fry, M. Wood, and P.S. Poole. Mol. Plant-Microbe Interac. **14**, 1016 (2001).
5. G. Jiang, A.H. Krishnan, Y.M. Kim, T.J. Wacek, and H.B. Krishnan. J. Bacteriol. **183**, 2594 (2001).
6. M.P. Galbraith, S.F. Feng, J. Borneman, E.W. Triplett, F.J. de Brujin, and S. Rossbach. Microbiology, **144**, 2915 (1998).
7. R. Ramaley, Y. Fujita, and E. Freese. J. Biol. Chem. **254**, 7684 (1979).
8. R. Daniellou, C.P. Phenix, P.H. Tam, M.C. Laliberte, and D.R.J. Palmer. Org. Biomol. Chem. **3**, 401 (2005).
9. C.A. Hansen, A.B. Dean, and J.W. Frost. J. Am. Chem. Soc. **121**, 3799 (1999)
10. S.K. Chung, Y.U. Kwon, Y.T. Chang, K.H. Sohn, J.H. Shin, K.H. Park, B.J. Hong, and I.H. Chung. Bioorg. Med. Chem. **7**, 2577 (1999).
11. G. Lowe and F. McPhee. J. Chem. Soc. Perkin Trans. 1, 1249 (1991).
12. D.A. Sawyer and B.V.L. Potter. J. Chem. Soc. Perkin Trans. 1, 923 (1992).
13. T. Desai, J. Gigg, R. Gigg, E. Martin-Zamora, and N. Schnetz. Carbohydr. Res. **258**, 135 (1994).
14. M. Hayashi, S.I. Hashimoto, and R. Noyori. Chem. Lett. 1747 (1984).
15. R. Mukherjee and E.M Axt. Phytochemistry, **23**, 2682 (1984).
16. A. Cornish-Bowden. Analysis of enzyme kinetic data. Oxford University Press, New York. 1995.
17. Y.C. Cheng and W.H. Prusoff. Biochemical Pharmacology, **22**, 3099 (1973).
18. I. Segel. Enzyme kinetics. Wiley Interscience, New York. Chap. 9. 1975.
19. C.A. Janson and W.W. Cleland. J. Biol. Chem. **249**, 2562 (1974).
20. A. Cornish-Bowden. Fundamentals of enzyme kinetics. Portland Press, Ltd., London. 1995.
21. G. Catelani, A. Corsaro, F. D'Andrea, M. Mariani, and V. Pistara. Bioorg. Med. Chem. Lett. **12**, 3313 (2002).
22. V. Pistara, P.L. Barili, G. Catelani, A. Corsaro, F. D'Andrea, and S. Fisichella. Tetrahedron Lett. **41**, 3523 (2000).
23. R. Pongdee and H.W. Liu. Bioorg. Chem. **32**, 393 (2004), and refs. therein.
24. S.J. Williams and S.G. Withers. Carbohydr. Res. **327**, 27 (2000).
25. D. Seebach. Angew. Chem. Int. Ed. Engl. **29**, 1320 (1990).

© 2006 NRC Canada

Pyrrolotriazine-5-carboxylate ester inhibitors of EGFR and HER2 protein tyrosine kinases and a novel one-pot synthesis of C-4 subsitituted pyrrole-2,3-dicarboxylate diesters[1]

Harold Mastalerz, Ashvinikumar V. Gavai, Brian Fink, Charles Struzynski, James Tarrant, Gregory D. Vite, Tai W. Wong, Guifen Zhang, and Dolatrai M. Vyas

Abstract: Pyrrolotriazines with an ester group at C-5 were prepared and evaluated as inhibitors of the EGFR and HER2 receptor tyrosine kinases, validated targets for cancer therapy. The C-5 ester (**15**) was at least as potent as its C-6 ester analogue (**17**), an example of a known series of pyrrolotriazine EGRF/HER2 kinase inhibitors that show good biochemical and cellular activity. The C-5 esters were synthesized from pyrrole 2,3-diesters that were made by a new, one-pot procedure. This involved reaction of readily available *N*-tosyl derivatives of α-amino acid esters or ketones with triphenylphosphine and diethyl acetylenedicarboxylate to form 3-pyrrolines via an intramolecular Wittig olefination. The 3-pyrroline intermediates were not isolated but treated directly with base to eliminate toluenesulfinic acid and generate the pyrrole 2,3-diesters in good yield.

Key words: pyrrolotriazine, EGFR, HER2, pyrrole, intramolecular Wittig reaction.

Résumé : On a préparé des pyrrolotriazines portant un groupe ester en position C-5 et on les a évalués comme inhibiteurs des kinases EGFR et HER2 du récepteur de tyrosine qui sont des cibles validées pour la thérapie du cancer. L'ester en C-5 (**15**) est au moins aussi puissant que son analogue **17**, l'ester en C-6, comme exemple d'une série connue de pyrrolotriazines qui peuvent agir comme inhibiteurs de la kinase EGRF/HER2 et qui présentent une bonne activité biochimique et cellulaire. Les esters en C-5 ont été synthétisés à partir de 2,3-diesters du pyrrole qui avaient été préparés par une nouvelle méthode monotope. Celle-ci implique la réaction des dérivés *N*-tosylés d'esters d'acides α-aminés ou de cétones avec de la triphénylphosphine et de l'acétylènedicarboxylate de diéthyle qui conduit à la formation de 3-pyrrolines par le biais d'une oléfination de Wittig intramoléculaire. Les intermédiaires 3-pyrrolines n'ont pas été isolés, mais traités directement avec une base pour éliminer l'acide toluènesulfinique et générer les 2,3-diesters du pyrrole avec de bons rendements.

Mots clés : pyrrolotriazine, EGFR, HER2, pyrrole, réaction de Wittig intramoléculaire.

[Traduit par la Rédaction]

Introduction

Receptor tyrosine kinases catalyze the phosphorylation of proteins that are involved in the signaling processes that control cell proliferation and differentiation. Since aberrant activation of this kinases results in uncontrolled cell growth, extensive drug discovery efforts have been made to find selective, small molecule inhibitors for the treatment of cancers (1). The epidermal growth factor receptor (EGFR) and HER2 are members of the ErbB family of receptor tyrosine kinases and they have been clinically validated as targets for cancer therapy (2). Their frequent coexpression in a variety of tumor types and their capacity to form heterodimers with other members of the ErbB family provides a strong rationale for simultaneous targeting of both receptors. The pyrrolo[2,1-*f*][1,2,4]triazine nucleus has been identified as a novel scaffold for ATP-competitive kinase inhibitors (3). BMS scientists have shown that pyrrolotriazine analogs (**1**) that carry an ester group at C-6 and a relatively large lipohilic amino group at C-4 can show potent inhibition of both the EGFR and the HER2 kinases (4). The C-6 ester group can be modified to further improve biochemical po-

Received 25 August 2005. Published on the NRC Research Press Web site at http://canjchem.nrc.ca on 21 April 2006.

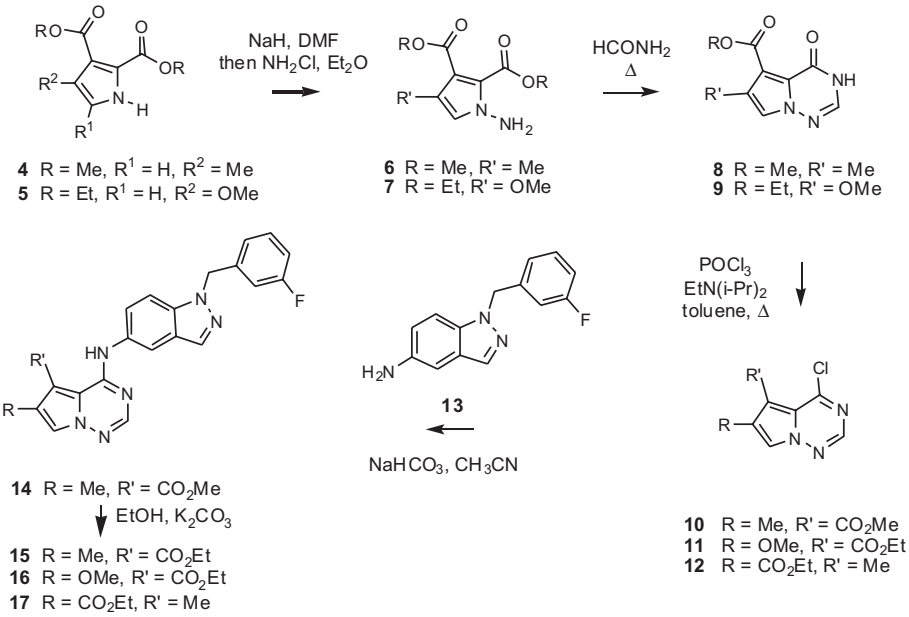
Dedicated to Professor Walter A. Szarek for his scientific contributions, and just as important, for his long-time friendship.

H. Mastalerz,[2] C. Struzynski, J. Tarrant, G. Zhang, and D.M. Vyas. Discovery Chemistry, Bristol-Myers Squibb Pharmaceutical Research Institute, 5 Research Parkway, Wallingford, CT 06492, USA.
A.V. Gavai, B. Fink, and G.D. Vite. Discovery Chemistry, Bristol-Myers Squibb PRI, P.O. Box 4000, Princeton, NJ 08543-4000, USA.
T.W. Wong. Oncology Drug Discovery, Bristol-Myers Squibb PRI, P.O. Box 4000, Princeton, NJ 08543-4000 USA.

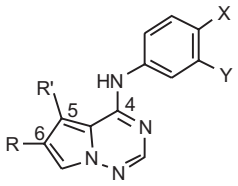
[1]This article is part of a Special Issue dedicated to Professor Walter A. Szarek.

 doi:10.1139/V06-037 © 2006 NRC Canada

Scheme 1.



tency and cellular activity. To explore the structure–activity relationships of these dual EGFR/HER2 pyrrolotriazine kinase inhibitors and expand the potential for further lead optimization, we prepared analogues of **1** where the C-6 ester function and the C-5 substitutent are transposed, e.g., **2** and **3**. This report describes the synthesis and the EGFR/HER2 kinase inhibition of some representative examples of these pyrrolotriazine 5-esters. It also details a convenient, one-pot synthesis of the pyrrole 2,3-diesters that are synthetic precursors of pyrrolotriazines **3**.

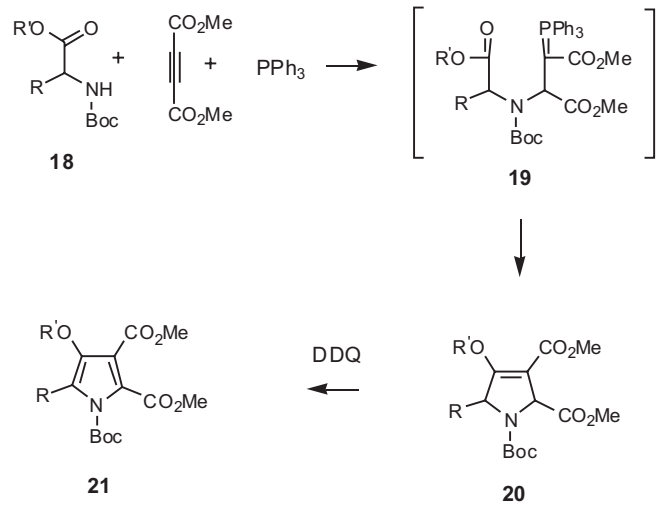


1 R = CO_2R'', R' = alkyl
2 R = alkyl, R' = CO_2R''
3 R = alkoxy, R = CO_2R''

Results and discussion

Preparation of the 6-methyl-5-ester **15** began with the known pyrrole **4** (5) and is outlined in Scheme 1. The pyrrole was converted to its *N*-amino derivative (**6**) by treatment with sodium hydride and monochloramine (6). Cyclization of **6** in hot formamide to the pyrrolotriazine-4-one (**8**) was followed by treatment with $POCl_3$ in refluxing toluene to give the 4-chloropyrrolotriazine (**10**). The 1-(3-fluorobenzyl)-1*H*-indazol-5-amino group was chosen as the lipohilic C-4 substituent and was introduced by reaction of **10** with **13** in the presence of base. The resulting methyl ester **14** was then converted to the ethyl ester **15** to enable a direct comparison of its biological activity with that of the transposed ethyl ester analogue (**17**).

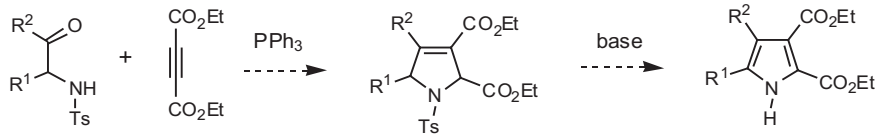
Scheme 2.



The preparation of 6-alkoxy pyrrolotriazine analogs **3** required access to pyrroles that have an alkoxy group at C-4, e.g., **5**. A novel synthesis of such pyrroles has been reported (7) and is outlined in Scheme 2. The readily available N-Boc derivatives of α-amino acid esters **18** were found to react with dimethyl acetylenedicarboxylate and triphenylphosphine to give 3-pyrrolines **20** by way of the stabilized ylide **19**. These pyrrolines were isolated and then could be oxidized to pyrroles **21** by heating with DDQ. We explored the potential one-pot version of this procedure that is outlined in Scheme 3. It was thought that the *N*-tosyl derivative of α-amino acid esters **22** would similarly react with triphenyl phosphine and an acetylenedicarboxylate to form pyrrolines **23** that could be treated directly with base to eliminate toluenesulfinic acid and give the desired pyrroles **24**. A similar base-promoted elimination of toluenesulfinic acid from a *N*-tosyl pyrroline intermediate has been reported (8) to generate the corresponding pyrrole.

© 2006 NRC Canada

Scheme 3.



22 **23** **24**

Table 1. Conversion of sulfonamides **22** to pyrroles.

Entry	22	R^1	R^2	Pyrrole (yield, %)
1	**a**	H	OCH_3	**5** (82)
2	**b**	H	$OCH_2CH_2OCH_3$	**24a** (76)
3	**c**	CH_3	OCH_3	**24b** (54)
4	**d**	Ph	OCH_3	**24c** (68)
5	**e**	CH_2CH_2O		**24d** (7)
6	**f**	H	4-$CH_3OC_6H_5$	**24e** (94)
7	**g**	H	CH_3	**24f** (80)
8	**h**	H	$CH_2CH_2CO_2CH_3$	**24g** (71)

Note: Reaction conditions: **22** (1 equiv.), PPh_3 (1.25 equiv.), diethyl acetylenedicarboxylate (1.2 equiv.), dioxane, 10 °C to room temperature, 1 h; reflux 16 h; DBU (2.0 equiv.), 90 °C, 2 h.

Table 2. EGFR and HER2 kinase inhibition.

	IC_{50} (μmol/L)[a,b]	
Compound	EGFR	HER2
15	0.31	0.20
16	>1	>1
17	0.47	0.63

[a]Recombinant HER2 cytoplasmic sequence is expressed in Sf9 insect cells as an untagged protein and purified by ion-exchange chromatography. HER2 kinase activity is measured under the same conditions as for EGFR. See refs. 3 and 9 for assay conditions.

[b]IC_{50} values are reported as the mean of at least three determinations. Variability around the mean value was <15%.

The proposed reaction was examined with toluenesulfonamide derivatives of α-amino acid esters of glycine, alanine, phenylglycine, and α-amino butyrolactone (**22a**–**22d**, Table 1, entries 1–5) that were prepared from commercially available material by the Fischer esterification of *N*-tosyl amino acids or by treatment of the α-amino acid esters or lactone with *p*-toluenesulfonyl chloride in the presence of base. The derivatives were indeed found to react with diethyl acetylenedicarboxylate and triphenyl phosphine in refluxing dioxane to give the *N*-tosyl pyrroline intermediates **23** (confirmed by LC–MS analysis of the reaction mixture). DBU was then added and the reaction was heating at 90 °C to effect the elimination of toluenesulfinic acid. Good yields (82% to 54%) of the pyrroles **5** and **24a** to **24c** were obtained. A low yield (7%) of the fused furopyrrole **24d** was obtained. LC–MS analysis of the initial cyclization reaction mixture indicated the presence of the desired furopyrroline **23e** together with other products that were not isolated or identified. In this case, competing side reactions are most likely seen because of the additional strain that is encountered in the transition state that leads to **23e**.

To further explore the scope of this reaction, the sulfonamide derivatives of some alkyl and aryl α-aminoketones (**22f**–**22h**) were prepared and examined as substrates (Table 1, entries 6–8). Good yields (94% to 71%) of the pyrroles **24e**–**24g** were obtained in all cases.

With a convenient synthesis of 4-alkoxy pyrrole-2,3-dicarboxylic acid diesters in hand, an example of a pyrrolotriazine 5-ester with an alkoxy group at C-6 was made. The 6-methoxy pyrrolotriazine (**16**) was prepared from **5** using the same sequence of reactions that were used to make **15** (Scheme 1): N-amination of pyrrole **5**; cyclization of **7** in formamide; formation of the chloroimidate **9**; and final attachment of the 1-(3-fluorobenzyl)-1*H*-indazol-5-amino side chain. The 6-ester analogue (**17**) was made for comparison purposes from the known (4) 4-chloropyrrolotriazine intermediate (**12**).

Data for the inhibition of the EGFR and HER2 kinases by **15**–**17** is show in Table 2. The directly transposed analogue (**15**) was found to be at least as potent a dual kinase inhibitor as **17**, while the 6-ether analogue (**16**) was less potent. Since the 5-ester group in **15** is well-suited for functional group modifications that could improve biochemical potency and cellular activity, **15** became the focus of further structure activity and lead optimization studies. These results will be reported in the future.

Experimental section

Methyl 6-methyl-4-oxo-3,4-dihydropyrrolo[1,2-*f*][1,2,4]-triazine-5-carboxylate (8)

A mixture of dimethyl 4-methyl-1*H*-pyrrole-2,3-dicarboxylate (5) (**4**, 1.0 g, 5.1 mmol) and NaH (236 mg, 60% dispersion in oil, 1.3 equiv.) in dry DMF (2 mL) was stirred at room temperature for 30 min. A solution of monochloramine (6) (66 mL, 0.1 mol/L in diethyl ether, 1.3 equiv.) was added with vigorous stirring. After 2 h, the reaction was cooled in an ice-water bath and an aqueous solution of $Na_2S_2O_3$ (20 mL, 1.0 N) was added with stirring. This was diluted with water (200 mL) and extracted with EtOAc (3 × 200 mL). The combined organic extracts were washed with brine and dried (Na_2SO_4). Removal of the solvent followed by silica gel column chromatography (gradient elution with mixtures of hexane containing 0%– 50% EtOAc) afforded dimethyl 1-amino-4-methyl-1*H*-pyrrole-2,3-dicarboxylate (**6**, 845 mg, 79% yield) as an oil. ^{1}H NMR (MeOH-d_4, 500 MHz, ppm) δ: 2.08 (s, 3H), 3.78 (s, 3H), 3.82 (s, 3H), 6.69 (s, 1H). A suspension of **6** (805 mg, 3.80 mmol) in formamide (8 mL) was heated at 170 °C for 2 h under a N_2 atmosphere. After cooling to room tempera-

© 2006 NRC Canada

ture, this was poured into water (20 mL) and left stirring overnight. The product was collect by filtration, washed with water and Et_2O, and then dried (590 mg, 75%). ^{1}H NMR (MeOH-d_4, 300 MHz, ppm) δ: 2.30 (s, 3H), 3.87 (s, 3H), 7.32 (s, 1H), 7.72 (s, 1H). HPLC purity: 93%. MS (ESI) *m*/*z*: 208 (M + H).

Methyl 4-(1-(3-fluorobenzyl)-1*H*-indazol-5-ylamino)-6-methylpyrrolo[1,2-*f*][1,2,4]triazine-5-carboxylate (14)

A mixture of methyl 6-methyl-4-oxo-3,4-dihydropyrrolo-[1,2-*f*][1,2,4]triazine-5-carboxylate (**8**, 1.00 g, 4.83 mmol), $POCl_3$ (0.54 mL, 1.2 equiv.) and diisopropylethylamine (0.67 mL, 0.8 equiv.) in dry toluene (15 mL) was heated at reflux for 5 h. After cooling to room temperature, the reaction was poured into a saturated aqueous solution of $NaHCO_3$ with vigorous stirring. The organic phase was separated, washed with additional satd. aq. $NaHCO_3$ solution and dried (Na_2SO_4). Removal of the solvent followed by silica gel chromatography (elution with dichloromethane) afforded methyl 4-chloro-6-methylpyrrolo[1,2-*f*][1,2,4]-triazine-5-carboxylate (**10**, 777 mg, 72%) as a solid. ^{1}H NMR ($CDCl_3$, 500 MHz, ppm) δ: 2.45 (s, 3H), 3.95 (s, 3H), 7.68 (s, 1H), 8.26 (s, 1H). MS (ESI) *m*/*z* 226 (M + H). A mixture of **10** (1.29 g, 5.06 mmol), 1-(3-fluorobenzyl)-1*H*-indazol-5-amine (**13**, 1.46 g, 1.2 equiv.) and $NaHCO_3$ (2.13 g, 5 equiv.) in dry CH_3CN (50 mL) was left stirring at room temperature for 4 h. The product was collected by filtration, washed with water, and dried (2.06 g, 95%). ^{1}H NMR ($CDCl_3$, 300 MHz, ppm) δ: 2.43 (s, 3H), 3.97 (s, 3H), 5.59 (s, 2H), 6.95 (m, 3H), 7.34 (m, 3H) 7.65 (m, 1H), 8.06 (s, 2H), 8.40 (s, 1H). MS (ESI) *m*/*z*: 431 (M + H). HRMS (ESI) calcd. for $C_{23}H_{20}N_6O_2F$: 431.1737; found: 461.1653.

Ethyl 4-(1-(3-fluorobenzyl)-1*H*-indazol-5-ylamino)-6-methylpyrrolo[1,2-*f*][1,2,4]triazine-5-carboxylate (15)

Transesterification (EtOH, K_2CO_3) of **14** gave the product: ^{1}H NMR ($CDCl_3$, 500 MHz) (ppm) δ: 1.44 (t, *J* = 7 Hz, 3H), 4.42 (q, *J* = 7 Hz, 2H), 5.58 (s, 2H), 6.85 (m, 1H), 6.94 (m, 2H), 7.27 (m, 3H), 7.63 (m, 1H), 8.05 (s, 2H), 8.39 (s, 1H). 7.65 (m, 1H), 8.06 (s, 2H), 8.40 (s, 1H). MS (ESI) *m*/*z*: 445 (M + H). HRMS (ESI) for $C_{24}H_{22}N_6O_2F$ calcd.: 445.1788; found: 445.1778.

2-Methoxyethyl 2-(4-methylphenylsulfonamido)acetate (22b)

A mixture of 2-(4-methylphenylsulfonamido)acetic acid (5.0 g, 21.8 mmol), 2-methoxyethanol (10.0 g, 6 equiv.), and *p*-toluenesulfonic acid (0.2 g, 0.05 equiv.) in xylene (50 mL) was heated at 150 °C for 10 h. After cooling to room temperature, this was washed with satd. aq. $NaHCO_3$ solution and dried (Na_2SO_4). Removal of the solvent followed by silica gel chromatography (step gradient elution with mixtures of hexane containing 5%–30% EtOAc) afforded the product as an oil (5.3 g, 84%). ^{1}H NMR ($CDCl_3$, 300 MHz, ppm) δ: 2.37 (s, 3H), 3.28 (s, 3H), 3.47 (t, *J* = 4.5 Hz, 2H), 3.76 (d, *J* = 5.4 Hz, 2H), 4.12 (t, *J* = 4.5 Hz, 2H), 5.38 (m, 1H), 7.26 (d, *J* = 8.1 Hz, 2H), 7.70 (d, *J* = 8.1 Hz, 2H). HPLC purity: 92%. MS (ESI) *m*/*z*: 320 (M + H).

Methyl 2-(4-methylphenylsulfonamido)propanoate (22c)

Triethylamine (1.53 mL, 2 equiv.) was added dropwise to an ice-cooled mixture of DL-alanine methyl ester hydrochloride (768 mg, 5.5 mmol) and toluenesulfonyl chloride (1.05 g, 1 equiv.) in dry dichloromethane (12 mL). After 1 h, the bath was removed and after a further 2 h, the reaction was filtered. The filtrate was washed with water, dried (Na_2SO_4), and the solvent removed. This left the crude product as an oil (1.26 g). ^{1}H NMR ($CDCl_3$, 500 MHz, ppm) δ: 1.35 (d, 3H, *J* = 7 Hz), 2.39 (s, 3H), 3.51 (s, 3H), 3.96 (m, 1H), 5.33 (d, *J* = 8.5 Hz, 1H), 7.27 (d, *J* = 8.0 Hz, 2H), 7.70 (d, *J* = 8.0 Hz, 2H). HPLC purity: 93%. MS (ESI) *m*/*z*: 228 (M + H).

(*S*)-Methyl 2-(4-methylphenylsulfonamido)-2-phenylacetate (22d)

Similarly, (*S*)-(+)-phenylglycine methyl ester hydrochloride was converted to the product. ^{1}H NMR ($CDCl_3$, 500 MHz, ppm) δ: 2.38 (s, 3H), 3.56 (s, 3H), 5.05 (d, *J* = 8 Hz, 1H), 5.63 (d, *J* = 8 Hz, 1H), 7.24 (m, 7H), 7.62 (d, *J* = 8.0 Hz, 2H). HPLC purity: 92%. MS (ESI) *m*/*z*: 320 (M + H).

4-Methyl-*N*-(2-oxo-tetrahydrofuran-3-yl)benzenesulfonamide (22e)

Similarly, 3-amino-dihydrofuran-2(3*H*)-one hydrobromide was converted to the product. ^{1}H NMR ($CDCl_3$, 500 MHz, ppm) δ: 2.29 (m, 1H), 2.43 (s, 3H), 2.70 (m, 1H), 3.89 (m, 1H), 4.18 (m, 1H), 4.20 (t, *J* = 9.0 Hz, 1H), 5.15 (m, 1H), 7.32 (d, *J* = 8.5 Hz, 2H), 7.78 (d, *J*= 8.5 Hz, 2H). HPLC purity: 90%. MS (ESI) *m*/*z*: 256 (M + H).

1-(4-Methoxyphenyl)-2-(4-methylphenylsulfonamido)-ethanone (22f)

Similarly, 2-amino-1-(4-methoxyphenyl)ethanone hydrochloride was converted to the product (solid). ^{1}H NMR ($CDCl_3$, 300 MHz, ppm) δ: 2.38 (s, 3H), 3.85 (s, 3H), 4.38 (d, 2H, (d, 1H, *J* = 4.5 Hz), 5.66 (m, 1H), 6.91 (d, 2H), 7.26 (d, 2H), 7.79 (m, 4H). HPLC purity: 90%. MS (ESI) *m*/*z*: 320 (M + H).

4-Methyl-*N*-(2-oxopropyl)benzenesulfonamide (22g)

Tetrapropylammonium perruthenate (70 mg, 0.1 equiv.) was added to a stirred suspension of *N*-(2-hydroxypropyl)-4-methylbenzenesulfonamide (458 mg, 2.0 mmol), *N*-methylmorpholine *N*-oxide (35 mg, 1.5 equiv.), and powdered, dry 4 Å molecular sieves (1.6 g) in dry CH_3CN. After 20 min, the CH_3CN was removed under vacuum and the residue was dissolved in dichloromethane and filtered through a short pad of silica gel. The solvent was removed from the filtrate and the product was isolated by radial silica gel chromatography (step gradient elution with mixtures of hexane containing 0%–30% ethyl acetate) as a solid (159 mg, 35%). ^{1}H NMR ($CDCl_3$, 500 MHz, ppm) δ: 2.09 (s, 3H), 2.39 (s, 3H), 3.83 (d, *J* = 5 Hz, 2H), 5.35 (m, 1H), 7.28 (d, *J* = 8.0 Hz, 2H), 7.71 (d, *J* = 8.0 Hz, 2H). HPLC purity: 84%. MS (ESI) *m*/*z*: 228 (M + H).

Methyl 5-(4-methylphenylsulfonamido)-4-oxopentanoate (22h)

Methyl 5-amino-4-oxopentanoate hydrochloride was converted to the product as described for **22c**. ^{1}H NMR ($CDCl_3$, 500 MHz, ppm) δ: 2.41 (s, 3H), 2.60 (m, 4H), 3.62 (s, 3H), 2.89 (d, *J* = 5 Hz, 2H), 5.30 (m, 1H), 7. 28 (d, *J* = 8.0 Hz,

© 2006 NRC Canada

2H), 7.71 (d, *J* = 8.0 Hz, 2H). HPLC purity: 93%. MS (ESI) *m*/*z*: 300 (M + H).

General procedure for the preparation of 5 and 24a–24g

A mixture of the sulfonamide (**22a**–**22h**) (1.0 equiv.) and triphenylphosphine (1.25 equiv.) in dry dioxane (0.5 mol/L) under a N_2 atmosphere was cooled in an ice-water bath. Diethyl acetylenedicarboxylate (1.2 equiv.) was added dropwise over 5 min and the bath was removed. After 1 h, the reaction was brought to reflux and left heating overnight. The temperature was reduced to 90 °C and DBU (2.0 equiv.) was added. After 2 h, the solvent was removed and the product was isolated by silica gel column chromatography eluting with mixtures of hexane containing 0%–25% ethyl acetate.

Diethyl 4-methoxy-1*H*-pyrrole-2,3-dicarboxylate (5)

^{1}H NMR (300 MHz, $CDCl_3$, ppm) δ: 1.28 (m, 6H), 3.71 (m, 3H), 4.28 (m, 4H), 6.43 (d, *J* = 2.93 Hz, 1H), 9.58 (s, 1H). ^{13}C NMR (125 MHz, $CDCl_3$, ppm) δ: 164.2, 160.4, 148.5, 119.4, 109.9, 104.1, 61.1, 61.0, 58.7, 14.3. HRMS (ESI) calcd. for $C_{11}H_{14}NO_5$: 240.0872; found: 240.0875.

Diethyl 4-(2-methoxyethoxy)-1*H*-pyrrole-2,3-dicarboxylate (24a)

^{1}H NMR (500 MHz, $CDCl_3$, ppm) δ: 1.24 (t, *J* = 7.2 Hz, 3H), 1.27 (t, *J* = 7.2 Hz, 3H), 3.34 (s, 3H), 3.61 (m, 2H), 3.95 (m, 2H), 4.24 (m, 4H), 6.45 (d, *J* = 3.1 Hz, 1H), 9.69 (s, 1 H). ^{13}C NMR (125 MHz, $CDCl_3$, ppm) δ: 164.3, 160.4, 146.9, 119.1, 110.9, 106.7, 71.7, 71.1, 60.9, 60.4, 59.5, 14.2, 14.0. HRMS (ESI) calcd. for $C_{13}H_{19}NO_6$: 285.1134; found: 284.1131.

Diethyl 4-methoxy-5-methyl-1*H*-pyrrole-2,3-dicarboxylate (24b)

^{1}H NMR (500 MHz, $CDCl_3$, ppm) δ: 1.31 (t, *J* = 7.2 Hz, 3H), 1.35 (t, *J* = 7.2 Hz, 3H), 2.20 (s, 3H), 3.77 (s, 3H), 4.28 (q, *J* = 7.1 Hz, 2H), 4.33 (q, *J* = 7.2 Hz, 2H), 9.42 (s, 1H). ^{13}C NMR (125 MHz, $CDCl_3$, ppm) δ: 164.9, 161.0, 143.5, 122.8, 115.4, 114.1, 62.7, 61.0, 60.8, 14.3, 14.2, 9.5. HRMS (ESI) calcd. for $C_{12}H_{16}NO_5$: 254.1028; found: 254.1021.

Diethyl 4-methoxy-5-phenyl-1*H*-pyrrole-2,3-dicarboxylate (24c)

^{1}H NMR (500 MHz, $CDCl_3$, ppm) δ: 1.33 (t, *J* = 7.2 Hz, 3H), 1.39 (t, *J* = 7.2 Hz, 3H), 3.79 (s, 3H), 4.32 (q, *J* = 7.1 Hz, 2H), 4.39 (q, *J* = 7.0 Hz, 2H), 7.31 (t, *J* = 7.3 Hz, 1H), 7.42 (t, *J* = 7.8 Hz, 2H), 7.69 (d, *J* = 7.7 Hz, 2H), 9.18 (s, 1 H). ^{13}C NMR (125 MHz, $CDCl_3$, ppm) δ: 164.7, 160.8, 143.8, 129.8, 128.9, 127.8, 125.9, 124.7, 117.4, 115.4, 62.2, 61.3, 61.2, 14.3, 14.2. HRMS (ESI) calcd. for $C_{17}H_{18}NO_5$: 316.1185; found: 316.1179.

Diethyl 3,4-dihydro-2*H*-*furo*[3,2-*b*]pyrrole-5,6-dicarboxylate (24d)

^{1}H NMR (500 MHz, $CDCl_3$, ppm) δ: 1.35 (m, 6H), 3.12 (t, *J* = 8.4 Hz, 2H), 4.32 (m, 4H), 4.96 (t, *J* = 8.2 Hz, 2H), 9.20 (s, 1H). ^{13}C NMR (125 MHz, $CDCl_3$, ppm) δ: 162.7, 160.3, 153.3, 122.3, 121.6, 103.9, 78.4, 61.0, 60.7, 26.2, 14.4, 14.3. HRMS (ESI) calcd. for $C_{12}H_{16}NO_5$: 254.1029; found: 254.1038.

Diethyl 4-(4-methoxyphenyl)-1*H*-pyrrole-2,3-dicarboxylate (24e)

^{1}H NMR (500 MHz, $CDCl_3$, ppm) δ: 1.28 (t, *J* = 7.2 Hz, 3H), 1.34 (t, *J* = 7.2 Hz, 3H), 3.80 (s, 3H), 4.32 (m, 4H), 6.88 (m, 2H), 6.94 (d, *J* = 3.1 Hz, 1H), 7.32 (m, 2H), 9.33 (s, 1H). ^{13}C NMR (125 MHz, $CDCl_3$, ppm) δ: 166.8, 160.4, 158.8, 128.8, 126.3, 125.8, 121.3, 120.4, 120.0, 114.1, 61.4, 61.0, 55.3, 14.3, 14.2. HRMS (ESI) calcd. for $C_{17}H_{19}NO_5$: 316.1185; found: 316.1178.

Diethyl 4-methyl-1*H*-pyrrole-2,3-dicarboxylate (24f)

^{1}H NMR (500 MHz, $CDCl_3$, ppm) δ: 1.29 (t, *J* = 7.2 Hz, 3H), 1.33 (t, *J* = 7.0 Hz, 3H), 2.12 (s, 3H), 4.27 (m, 2H), 4.31 (m, 2H), 6.63 (d, *J* = 2.8 Hz, 1H), 9.55 (s, 1H). ^{13}C NMR (125 MHz, $CDCl_3$, ppm) δ: 165.8, 160.5, 122.1, 121.9, 120.7, 120.5, 60.9, 60.7, 14.3, 14.2, 10.9. HRMS (ESI) calcd. for $C_{11}H_{15}NO_4$: 224.0922; found: 224.0913.

Diethyl 4-(3-methoxy-3-oxopropyl)-1*H*-pyrrole-2,3-dicarboxylate (24g)

^{1}H NMR (500 MHz, $CDCl_3$, ppm) δ: 1.25 (t, *J* = 7.0 Hz, 3H), 1.30 (t, *J* = 7.0 Hz, 3H), 2.53 (t, *J* = 7.5 Hz, 3H), 2.83 (t, *J* = 7.63 Hz, 2H), 3.58 (s, 3H), 4.26 (m, 4H), 9.83 (s, 1H). ^{13}C NMR (125 MHz, $CDCl_3$, ppm) δ: 173.6, 165.5, 160.4, 125.1, 122.1, 120.4, 119.9, 60.9, 60.8, 51.6, 35.1, 21.2, 14.3, 14.2. HRMS (ESI) calcd. for $C_{14}H_{19}NO_6$: 298.1291; found: 298.1277.

Ethyl 6-methoxy-4-oxo-3,4-dihydropyrrolo[1,2-*f*][1,2,4]-triazine-5-carboxylate (9)

A solution of diethyl 4-methoxy-1*H*-pyrrole-2,3-dicarboxylate (**5**, 2.48 g, 10.3 mmol) in dry CH_3CN (10 mL) was added to an ice-cooled suspension of NaH (535 mg, 60% dispersion in oil, 1.3 equiv.) in dry dimethyl formamide (20 mL) over 3 min. The bath was removed and the reaction was left stirring for 1 h after which it was cooled in an ice bath. A solution of monochloramine (135 mL, 0.1 mol/L in diethyl ether, 1.3 equiv.) was added with vigorous stirring. After 30 min, the bath was removed and the reaction was left stirring for 1.5 h. It was then cooled in an ice-water bath and worked up as described for **6**. Silica gel column chromatography (gradient elution with mixtures of hexane containing 0%–25% ethyl acetate) afforded diethyl 1-amino-4-methoxy-1*H*-pyrrole-2,3-dicarboxylate (**7**) as an oil (1.53 g, 58% yield). ^{1}H NMR ($CDCl_3$, 300 MHz, ppm) δ: 1.30 (m, 6H), 3.70 (s, 3H), 4.27 (m, 4H), 5.4 (br s, 2H), 6.47 (s, 1H). MS (ESI) *m*/*z*: 257 (M + H). A suspension of **7** (880 mg, 3.44 mmol) in formamide (5 mL) was heated at 170 °C for 4 h under a N_2 atmosphere. This was worked up as described for **8** to give the product (514 mg, 63%) as a solid. ^{1}H NMR (300 MHz, DMSO-d_6, ppm) δ: 1.25 (t, *J* = 7.2 Hz, 3H), 3.76 (s, 3H), 4.20 (q, *J* = 7.2 Hz, 2H), 7.44 (s, 1H), 7.91 (s, 1H). MS (ESI) *m*/*z*: 238 (M + H). HRMS (ESI) calcd. for $C_{10}H_{12}N_3O$: 238.0828; found: 238.0824.

Ethyl 4-(1-(3-fluorobenzyl)-1*H*-indazol-5-ylamino)-6-methoxypyrrolo[1,2-*f*][1,2,4]triazine-5-carboxylate (16)

A mixture of **9** (887 mg, 3.37 mmol), $POCl_3$ (0.79 mL, 1.5 equiv.), and diisopropylethylamine (0.59 mL, 1.0 equiv.) in dry toluene (12 mL) was heated at reflux for 5 h and then worked up as described for **10**. Silica gel radial chromatography (elution with DCM) afforded ethyl 4-chloro-6-

© 2006 NRC Canada

methoxypyrrolo[1,2-*f*][1,2,4]triazine-5-carboxylate (**11**, 458 mg, 53%) as a solid. MS (ESI) *m*/*z*: 256 (M + H). HRMS (ESI) calcd. for $C_{10}H_{11}N_3O_3Cl$: 256.0489; found: 256.0496. A mixture of **11** (1.30 g, 5.10 mmol), 1-(3-fluorobenzyl)-1*H*-indazol-5-amine (**13**, 1.25 g, 1.05 equiv.), and diisopropylethylamine (1.07 mL, 1.2 equiv.) in dry CH_3CN (45 mL) was heated at 70 °C overnight. The product was collected by filtration, washed with CH_3CN, and dried (2.15 g, 92%). ^{1}H NMR (300 MHz, $CDCl_3$, ppm) δ: 1.43 (t, *J* = 6.9 Hz, 3H), 3.89 (s, 3H), 4.42 (q, *J* = 6.9 Hz, 2H), 5.57 (s, 2H), 6.84 (m, 1H), 6.94 (m, 2H), 7.14 (s, 1H), 7.26 (m, 2H) 7.60 (m, 1H), 8.04 (s, 1H), 8.08 (s, 1H), 8.38 (m, 1H). MS (ESI) *m*/*z*: 461 (M + H). HRMS (ESI) calcd. for $C_{24}H_{22}N_6O_3F$: 461.1737; found: 461.1726.

Ethyl 4-[1-(3-fluoro-benzyl)-1*H*-indazol-5-ylamino]-5-methyl-pyrrolo[2,1-*f*][1,2,4]triazine-6-carboxylate (17)

A 2 L three-neck flask was charged with ethyl 4-chloro-5-methyl-pyrrolo[2,1-*f*][1,2,4]triazine-6-carboxylate (4) (**12**, 54.0 g, 226 mmol) and acetonitrile (500 mL). To the resulting suspension was added 1-(3-fluoro-benzyl)-1*H*-indazol-5-ylamine (**13**, 54.5 g, 226 mmol) and diisopropylethyl amine (21.7 g, 214.7 mmol). The reaction was heated to 55 °C and became homogeneous after 10 min. After 18 h, it was cooled to 10 °C and filtered. The filter cake was washed with cold acetonitrile (2 × 250 mL) and dried under vacuum to afford the product as a white crystalline solid (76.3 g, 76%). ^{1}H NMR (500 MHz, $CDCl_3$, ppm) δ: 1.39 (t, *J* = 7.2 Hz, 3H), 2.93 (s, 3H), 4.35 (q, *J* = 7.2 Hz, 2H), 5.59 (s, 2H), 6.86 (d, *J* = 9.3 Hz, 1H), 6.97 (m, 2H), 7.26 (ddd, *J* = 6.04, 8.24, 14.29 Hz, 1H), 7.35 (d, 1H, *J* = 8.80 Hz), 7.42 (br s, 1H), 7.49 (dd, 1H, *J* = 1.65, 8.80 Hz), 7.91 (s, 1H), 8.00 (s, 1H), 8.07 (s, 1H), 8.09 (s, 1H). ^{13}C NMR (125 MHz, $CDCl_3$, ppm) δ: 164.5, 163.0 (d, *J* = 246 Hz), 154.9, 148.5, 139.1 (d, *J* = 5 Hz), 137.6, 133.8, 130.3, 131.2 (d, *J* = 7 Hz), 124.6, 123.5, 122.7, 121.9 (2C), 115.4, 115.3, 114.8 (d, *J* = 20 Hz), 114.1 (d, *J* = 22 Hz), 113.4, 109.7, 60.2, 52.6, 14.4, 11.9. MS (ESI) *m*/*z*: 444 $(M + H)^+$. HRMS (ESI) calcd. for $C_{24}H_{22}FN_6O_2$: 445.171; found: 445.1805. Anal calcd. for $C_{24}H_{21}FN_6O_2$: C 64.85, H 4.76, N 18.90; found: C 64.62, H 4.73, N 18.85.

Conclusion

In summary, pyrrolotriazine analogs with an ester function at C-5 were made and evaluated as dual inhibitors of EGFR and HER2 kinases. The 5-ester 6-methyl analog (**15**) showed kinase inhibition that was at least comparable to that seen for the 6-ester 5-methyl analogue (**17**). It became the focus of further structure activity and lead optimization studies and these results will be reported in the future. In addition, a general, one-pot procedure for the synthesis of C-4 substituted pyrrole-2,3-diesters from readily available *N*-tosyl derivatives of α-amino acid esters and α-amino ketones was developed.

References

1. P. Traxler, G. Bold, E. Buchdunger, G. Caravatti, P. Furet, P. Manley, T. O'Reilly, J. Wood, and J. Zimmermann. Med. Res. Rev. **21**, 499 (2001).
2. J. Baselga and C.L. Arteaga. J. Clin. Oncol. **23**, 2445 (2005).
3. J.T. Hunt, T. Mitt, R. Borzilleri, J. Gullo-Brown, J. Fargnoli, B. Fink, W.-C. Han, S. Mortillo, G. Vite, B. Wautlet, T. Wong, C. Yu, X. Zheng, and R. Bhide. J. Med. Chem. **47**, 4054 (2004).
4. B.E. Fink, G.D. Vite, H. Mastalerz, J.F. Kadow, S.-H. Kim, K.J. Leavitt, K. Du, D. Crews, T. Mitt, T.W. Wong, J.T. Hunt, D.M. Vyas, and J.S. Tokarski. Bioorg. Med. Chem. Lett. **15**, 4774 (2005).
5. R. Grigg and V. Savic. Chem. Commun. (Cambridge), 873 (2000).
6. (*a*) J. Haynes, Jr., W.W. Doubleday, A.J. Dyckman, J.D. Godfrey, Jr., J.A. Grosso, S. Kiau, and K. Leftheris. J. Org. Chem. **69**, 1368 (2004); (*b*) G. A. Jaffari and A. J. Nunn. J. Chem. Soc. C, 823 (1971).
7. L.A. Evans, K.E. Griffiths, H. Guthmann, and P.J. Murphy. Tetrahedron Lett. **43**, 299 (2002).
8. K.M. Short, and C.B. Ziegler, Jr. Tetrahedron Lett. **36**, 355 (1995).
9. G.D. Vite, A.V. Gavai, B.E. Fink, H. Mastalerz, and J.F. Kadow. PCT Int. Appl. WO054514, 2004; Chem. Abstr. **141**, 89122 (2004).

© 2006 NRC Canada

Synthesis of 8-homocastanospermine[1]

Konrad Paśniczek, Dariusz Socha, Margarita Jurczak, Jolanta Solecka, and Marek Chmielewski

Abstract: The 1,3-dipolar cycloaddition of a five-membered cyclic nitrone derived from malic acid (**4**) and unsaturated D-*threo*-hexaldonolactone (**1**) leads to a single adduct **6**, which can be transformed into the 8-homocastanospermine (**13**) via a sequence involving rearrangement of the six-membered lactone ring into the five-membered one, removal of the terminal carbon atom from the sugar chain, cleavage of the N—O bond, and the intramolecular alkylation of the nitrogen atom. The iminosugar (**13**) does not show any interesting inhibitory activity towards α- and β-glucosidases.

Key words: iminosugars, homocastanospermine, nitrones, aldono-1,5-lactone, 1,3-dipolar cycloaddition, glucosidases.

Résumé : La cycloaddition 1,3-dipolaire d'une nitrone cyclique à cinq chaînons dérivée de l'acide malique (**4**) et de la D-*thréo*-hexaldonolactone insaturée (**1**) conduit à la formation d'un seul adduit qui peut être transformé en 8-homocastanospermine (**13**), par le biais d'une séquence impliquant le réarrangement de la lactone à six chaînons en une lactone à cinq chaînons, l'élimination de l'atome de carbone terminal de la chaîne du sucre, le clivage de la liaison N—O et d'une alkylation intramoléculaire de l'atome d'azote. L'iminosucre (**13**) ne présente pas d'activité inhibitrice intéressante vis-à-vis des α- et des β-glucosidases.

Mots clés : iminosucres, homocatanospermine, nitrones, aldono-1,5-lactone, cycloaddition 1,3-dipolaire, glucosidases.

[Traduit par la Rédaction]

Introduction

Recently, we have reported that the cycloaddition of 2,3-unsaturated aldono-1,5-lactones (**1** or **2**) and the five-membered cyclic nitrones (**3** or **4**) (Chart 1) proceeds exclusively in the exo mode and results in a high preference for the anti addition to both the acetoxymethyl group of the lactone and the 3-*tert*-butoxy group of the nitrone (1–3). In the case of mismatched pairs, the 4-acetoxy group of the lactone assumes a decisive role in the control of the stereochemical pathway of cycloaddition. The stereochemical preferences are the underlying reason that, in many cases, a single adduct or at least a high preponderance of a single adduct is observed. This observation has been well-illustrated by the exclusive formation of adducts **6** and **7** from D-*threo* 4-*O*-acetyl-lactone (**1**) and D-*erythro* 4-*O*-acetyl-lactone (**2**), respectively (Chart 2) (3).

We have shown that application of the known methodology (4) to cycloadduct **8** offers a convenient approach to the indolizidine alkaloids. This has been demonstrated by the synthesis of 7-hydroxylentiginosine (**9**) and the formal synthesis of lentiginosine (**10**) (5). The easy access to adducts **6** and **7** opens an entry to the corresponding indolizidines with an (*R*) or (*S*) configurations at the bridgehead carbon atom, which are closely related to the castanospermine (**11**) and swainsonine (**12**) (Chart 3) (6).

Both components of the cycloaddition, the nitrone and the unsaturated lactone, carry over their own substituents (protected hydroxyls) with their original configuration, whereas the configurations at C-1a, C-4a, and C-4b of the cycloadduct are established during the reaction. Adduct **6** is particularly interesting because it can be easily transformed into the compounds related to the castanospermine (**11**) and especially the 8-homocastanospermine (**13**). The castanospermine (**11**) (7) itself displays a range of interesting therapeutic properties (8), however, it is very toxic, therefore its use has a limited value. The present paper describes the synthesis of imino sugar **13** from adduct **6**.

Results and discussion

Adduct **6** (2, 3) was deacetylated with sodium methoxide in methanol to afford compound **14**. The reaction proceeds with rearrangement of the six-membered lactone ring into a five-membered one. The glycolic cleavage of the terminal diol group in **14** with $NaIO_4$ followed by the reduction of the aldehyde group with sodium triacetoxyborohydride gave compound **16** in 83% yield. The use of sodium borohydride resulted in the reduction of both carbonyl functions of the aldehyde **15**, whereas the sodium cyanoborohydride gave the desired product **16** in a low yield (Scheme 1).

The activation of the terminal hydroxymethyl group by the introduction of a halogen or sulfonyl as a leaving group, followed by the direct alkylation of the isoxazolidine nitrogen atom, led to an unattractive mixture of products. Therefore, we decided to form the indolizidine skeleton in a stepwise manner. First, the hydroxymethyl group was pro-

Received 30 August 2005. Published on the NRC Research Press Web site at http://canjchem.nrc.ca on 21 April 2006.

K. Paśniczek, D. Socha, M. Jurczak, and M. Chmielewski.[2] Institute of Organic Chemistry of the Polish Academy of Sciences, Kasprzaka 44/52, 01-224 Warsaw, Poland.
J. Solecka. National Institute of Hygiene, 00-791 Warsaw, Poland.

[1]This article is part of a Special Issue dedicated to Professor Walter A. Szarek.
[2]Corresponding author (e-mail: chmiel@icho.edu.pl).

 doi:10.1139/V06-032 © 2006 NRC Canada

Chart 1.

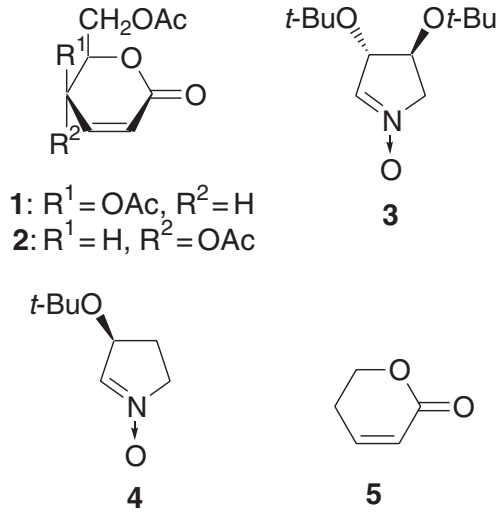
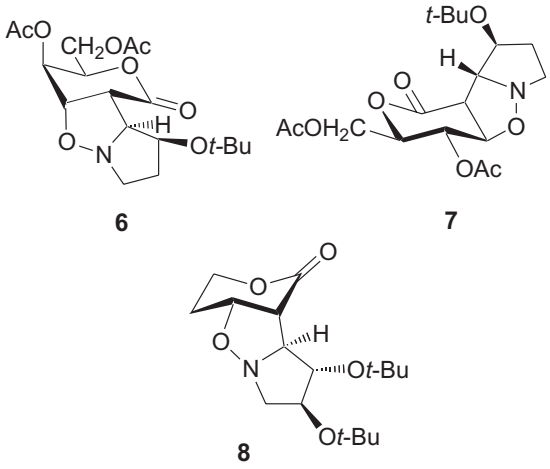
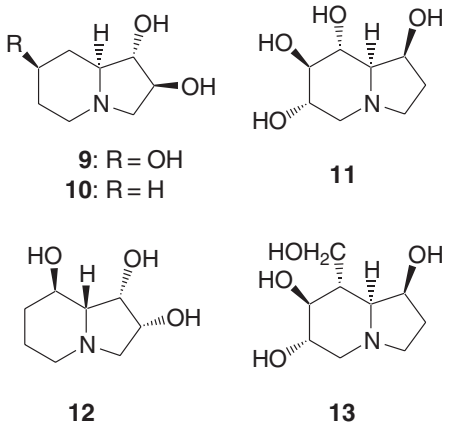


Chart 2.



tected as a *tert*-butyldiphenylsilyl derivative **17** and lactone was reduced with sodium borohydride to give diol **18**. Both hydroxy groups in **18** were masked by the formation of an isopropylidene moiety. The desilylation of **19** with tetrabutylammonium fluoride led to alcohol **20**. Due to the low stability of the isopropylidene fragment and the tendency of the terminal mesyloxymethyl group to undergo intramolecular alkylation, the next three steps were performed with only a partial purification of intermediary products. Alcohol **20** was mesylated to afford **21**, the isopropylidene protection was removed using 80% acetic acid, and the sequence was completed by the hydrogenolysis of the N—O bond over Pd/C and intramolecular alkylation of the nitrogen atom. The final product of this reaction sequence (indolizidine **22**) was acetylated and characterized as the triacetate **23**. The *tert*-butyl protection in **23** was subsequently removed with trifluoroacetic acid and the liberated hydroxy group was acetylated affording tetraacetate **24**. The complete deacetylation of **24** with ammonia in methanol furnished the **13**. Synthesis of a number of 8-hydroxymethylindolizidines using intramolecular 1,3-dipolar cycloaddition has been reported recently by Brandi's group (9).

Chart 3.



Note that the oxidation of the hydroxymethyl group in suitably protected **13** or **23** to the carboxylic function followed by an oxidative decarboxylation, for example, by the methodology recently reported by us for the other indolizidine (5), should provide **11**.

The biological activity of compound **13** toward commercially available α- and β-glucosidases was tested and compared with the corresponding data measured for commercially available **11**. Surprisingly, compound **13** showed only a trace inhibition of α-glucosidase activity in a concentration of 0.02 mol/L and no inhibition of β-glucosidase.

In summary, we have reported the simple synthesis of 8-homocastanospermine (**13**) in which a proper selection of readily available components of the 1,3-dipolar cycloaddition controls the absolute stereochemistry at all five stereogenic centers present in the target molecule. The reported synthesis demonstrated an exceptional effectiveness of the 1,3-dipolar cycloaddition of nitrones and sugar unsaturated δ-lactones, which led to formation of only one diastereomer with a fully defined configuration at all stereogenic centers.

Experimental

^{1}H NMR spectra were recorded on a Bruker DRX 500 Avance spectrometer. IR spectra were obtained on a PerkinElmer FT-IR 1600 spectrophotometer. The optical rotations were measured with a JASCO Dip-360 digital polarimeter. Mass spectra were recorded using an AMD-604 instrument and HPLC–MS were recorded with Mariner and API 356 detectors. Column chromatography was performed with E. Merck Kiesel Gel (230–400 mesh).

Adduct **6** was obtained according to the known procedure (2, 3).

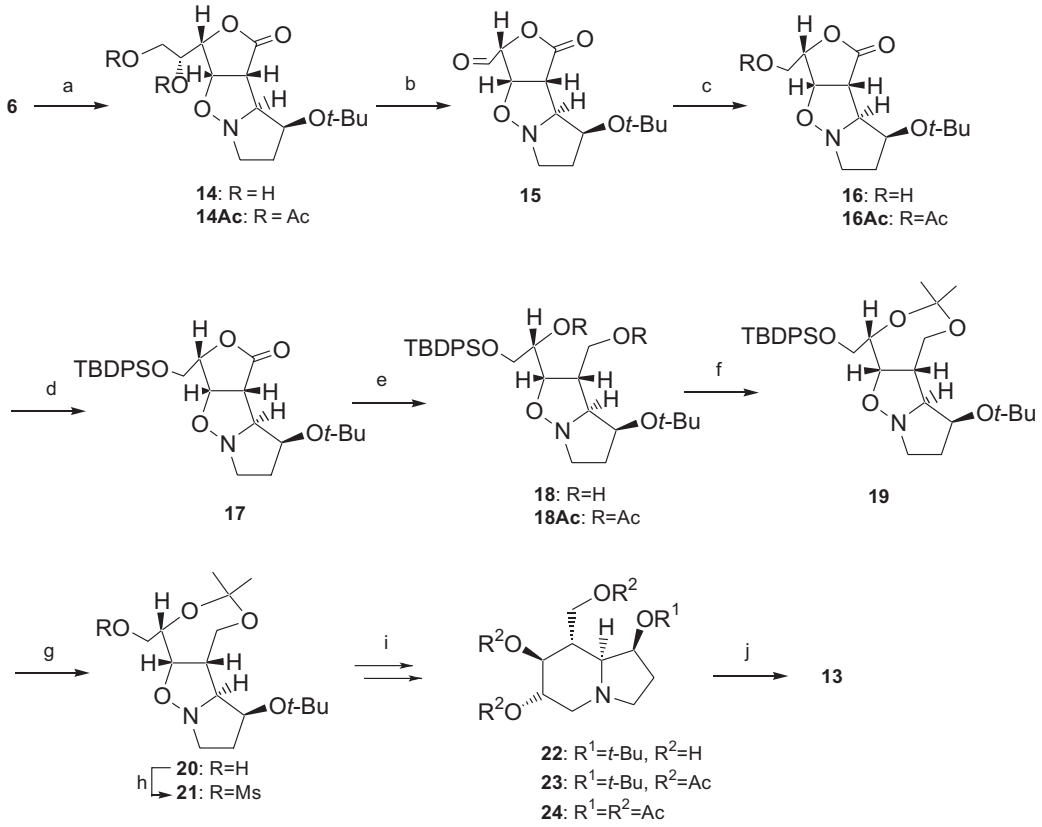
Enzymes and substrates were purchased from Sigma-Aldrich: α-glucosidase from rice, type V, 63.43 U/mg, 1.34 mg/mL; β-glucosidase from almonds, 25.8 U/mg, 95.4% protein.

(1a*S*,2*R*,4a*R*,4b*S*,5*S*,1′*R*)-5-*tert*-Butoxy-2-(1′,2′-dihydroxyethyl)-4-oxo-pyrrolidino[1,2-*b*]isoxazolidino[4,5-*c*]-tetrahydrofurane (14)

Adduct **6** was dissolved in methanol, treated with 1 molar equiv. of sodium carbonate, and stirred at room temperature

© 2006 NRC Canada

Scheme. 1. (*a*) Na_2CO_3, MeOH (88%); (*b*, *c*) $NaIO_4$, MeOH–H_2O; $NaBH(OAc)_3$, CH_2Cl_2 (74%); (*d*) *tert*-butyldiphenylchlorosilane, DMAP, CH_2Cl_2 (76%); (*e*) $NaBH_4$, MeOH (60%); (*f*) 2,2-dimethoxypropane, *p*-TsOH (87%); (*g*) Bu_4NF, THF (94%); (*h*) MsCl, Et_3N, CH_2Cl_2 (96%); (*i*) 80% AcOH; H_2, 10% Pd/C, MeOH; Ac_2O, Et_3N, DMAP (55%); (*j*) MeOH–NH_3 (91%).



until the disappearance of the substrate (1 h). Subsequently, the solution was neutralized with Amberlite IR-1200 [H^+], diluted with dichloromethane, filtered through Celite, and evaporated. The crude product was purified by chromatography using CH_2Cl_2–MeOH (20:1 *v*/*v*) as the eluent to afford **14** in 88% yield. $[\alpha]_D$ +5.3° (*c* 0.5, CH_2Cl_2). IR (film, cm^{-1}): 3392, 1773. ^1H NMR (500 MHz, $CDCl_3$) δ: 4.90 (dd, 1H, *J* = 6.3, 8.1 Hz, H-1a), 4.64 (dd, 1H, *J* = 2.8, 6.3 Hz, H-2), 4.23 (dt, 1H, *J* = 5.8, 7.3, 7.5 Hz, H-5), 4.20 (ddd, 1H, *J* = 2.8, 5.0, 6.4 Hz, C*H*OH), 3.93 (bd, 1H, *J* = 7.3 Hz, H-4b), 3.90 (dd, 1H, *J* = 0.9, 8.1 Hz, H-4a), 3.81 (dd, 1H, *J* = 6.4, 11.1 Hz, C*H*HOH), 3.72 (dd, 1H, *J* = 5.0, 11.1 Hz, CH*H*OH), 3.47 (ddd, 1H, *J* = 2.6, 7.8, 14.0 Hz, H-7), 2.90 (dddd, 1H, *J* = 0.6, 7.4, 10.8, 14.0 Hz, H-7′), 2.12 (ddt, 1H, *J* = 2.6, 7.4, 7.5, 13.1 Hz, H-6), 1.99 (dddd, 1H, *J* = 5.8, 7.8, 10.8, 13.1 Hz, H-6′), 1.21 (s, 9H, *t*-Bu). ^{13}C NMR (125 MHz, $CDCl_3$) δ: 176.4, 82.5, 78.5, 74.6, 73.5, 71.2, 69.4, 63.9, 53.1, 50.7, 34.0, 28.4. HRMS (ESI) *m*/*z* calcd. for $C_{14}H_{23}NO_6Na$: 324.1418 [M + Na]$^+$; found: 324.1430.

(1a*S*,2*R*,4a*R*,4b*S*,5*S*,1′*R*)-2-(1′,2′-Diacetoxyethyl)-5-*tert*-butoxy-4-oxo-pyrrolidino[1,2-*b*]isoxazolidino[4,5-*c*]-tetrahydrofurane (14Ac)

Melting point 81–83 °C. $[\alpha]_D$ –4.7° (*c* 0.3, CH_2Cl_2). IR (film, cm^{-1}): 1781, 1745. ^1H NMR (500 MHz, $CDCl_3$) δ: 5.49 (ddd, 1H, *J* = 2.9, 3.7, 8.8 Hz, CHOAc), 4.75 (dd, 1H, *J* = 4.6, 6.7 Hz, H-1a), 4.66 (dd, 1H, *J* = 4.6, 8.8 Hz, H-2), 4.54 (dd, 1H, *J* = 2.9, 12.6 Hz, C*H*HOAc), 4.31 (dd, 1H, *J* = 3.7, 12.6 Hz, CH*H*OAc), 4.21 (dt, 1H, *J* = 5.5, 7.2, 7.3 Hz, H-5), 3.94 (bd, 1H, *J* = 7.3 Hz, H-4b), 3.83 (dd, 1H, *J* = 0.8, 6.7 Hz, H-4a), 3.35 (ddd, 1H, *J* = 3.5, 7.7, 13.6 Hz, H-7). 2.92 (ddd, 1H, *J* = 7.2, 10.4, 13.6 Hz, H-7′), 2.10, 2.09 (2s, 6H, 2Ac), 2.06 (ddt, 1H, *J* = 3.5, 13.1, 7.2, 7.2 Hz, H-6), 1.90 (dddd, 1H, *J* = 5.5, 7.2, 10.4, 13.1 Hz, H-6″), 1.22 (s, 9H, *t*-Bu). ^{13}C NMR (125 MHz, $CDCl_3$) δ: 176.0, 170.5, 169.8, 80.1, 77.9, 74.6, 73.3, 71.1, 70.0, 62.7, 53.9, 52.0, 34.3, 28.4, 20.9, 20.7. HRMS (ESI) *m*/*z* calcd. for $C_{18}H_{28}NO_8$: 386.1809 [M + H]$^+$; found: 386.1827.

(1a*S*,2*S*,4a*R*,4b*S*,5*S*)-5-*tert*-Butoxy-2-hydroxymethyl-4-oxo-pyrrolidino[1,2-*b*]isoxazolidino[4,5-*c*]tetrahydrofurane (16)

Compound **14** (0.051 g, 0.17 mmol) was dissolved in methanol–water (6:1 *v*/*v*, 5 mL) and treated at room temperature with 2 molar equiv. of sodium metaperiodate (0.072 g). After 1 h the reaction was completed. The crude product (**15**) was passed through a short silica gel column using dichloromethane–methanol (20:1 *v*/*v*) as the eluent. After evaporation of the solvent, the product was dissolved in dry CH_2Cl_2 (15 mL) and reduced with 2 molar equiv. of $NaBH(OAc)_3$. Standard work up provided a product that was purified on a silica gel column (hexane – ethyl acetate, 1:2 *v*/*v*) to afford **16** (0.034 g, 74%). $[\alpha]_D$ +11.0° (*c* 0.4, CH_2Cl_2). IR (film, cm^{-1}): 3409, 1774. ^1H NMR (500 MHz, $CDCl_3$) δ: 4.90 (dd, 1H, *J* = 6.1, 7.9 Hz, H-1a), 4.66 (ddd, 1H, *J* = 3.7, 4.9, 6.0 Hz, H-2), 4.23 (dt, 1H, *J* = 5.7, 7.3, 7.5 Hz, H-5), 4.06 (dd, 1H, *J* = 3.7, 12.4 Hz, C*H*HOH), 3.96 (dd, 1H, *J* = 5.0, 12.4 Hz, CH*H*OH), 3.95 (d, 1H, *J* =

© 2006 NRC Canada

7.5 Hz, H-4b), 3.89 (d, 1H, *J* = 7.9 Hz, H-4a), 3.46 (ddd, 1H, *J* = 2.8, 7.8, 14.0 Hz, H-7), 2.93 (ddd, 1H, *J* = 7.4, 10.6 14.0 Hz, H-7′), 2.13 (ddt, 1H, *J* = 2.8, 13.2, 7.3, 7.4 Hz, H-6), 1.98 (dddd, 1H, *J* = 5.7, 7.8, 10.6, 13.2 Hz, H-6′), 1.22 (s, 9H, *t*-Bu). ^{13}C NMR (125 MHz, $CDCl_3$) δ: 176.5, 82.5, 78.4, 74.5, 73.6, 71.3, 60.3, 53.3, 51.1, 34.1, 28.3. HRMS (ESI) *m*/*z* calcd. for $C_{13}H_{22}NO_5$: 272.1492 $[M + H]^+$; found: 272.1486.

(1a*S*,2*S*,4a*R*,4b*S*,5*S*)-2-Acetoxymethyl-5-*tert*-butoxy-4-oxo-pyrrolidino[1,2-*b*]isoxazolidino[4,5-*c*]tetrahydrofurane (16Ac)

$[\alpha]_D$ –8.7° (*c* 0.4, CH_2Cl_2). IR (film, cm^{-1}): 1779, 1742. ^{1}H NMR (500 MHz, $CDCl_3$) δ: 4.81 (dd, 1H, *J* = 4.8, 6.8 Hz, H-1a), 4.72 (ddd, 1H, *J* = 3.8, 4.8, 8.3 Hz, H-2), 4.56 (dd, 1H, *J* = 3.8, 12.4 Hz, C*H*HOAc), 4.41 (dd, 1H, *J* = 8.3, 12.4 Hz, CH*H*OAc), 4.23 (dt, 1H, *J* = 5.3, 7.1, 7.3 Hz, H-5), 3.95 (d, 1H, *J* = 7.3 Hz, H-4b), 3.82 (d, 1H, *J* = 6.8 Hz, H-4a), 3.40 (ddd, 1H, *J* = 3.5, 7.7, 13.6 Hz, H-7), 2.94 (ddd, 1H, *J* = 7.3, 10.0, 13.6 Hz, H-7′), 2.13 (s, 3H, Ac), 2.10 (dddd, 1H, *J* = 3.5, 7.1, 7.3, 13.1 Hz, H-6), 1.95 (dddd, 1H, *J* = 5.3, 7.7, 10.0, 13.1 Hz, H-6′), 1.24 (s, 9H, *t*-Bu). ^{13}C NMR (125 MHz, C_6D_6) δ: 176.2, 169.9, 80.1, 77.6, 73.8, 73.7, 71.6, 63.0, 53.4, 51.6, 34.5, 28.2, 20.2. HRMS (ESI) *m*/*z* calcd. for $C_{15}H_{24}NO_6$: 314.15981 $[M + H]^+$; found: 314.1613.

(1a*S*,2*R*,4a*R*,4b*S*,5*S*)-5-*tert*-butoxy-2-formyl-4-oxo-pyrrolidino[1,2-*b*]isoxazolidino[4,5-*c*]tetrahydrofurane (15)

A small sample of **15** was partially purified by chromatography using hexane – ethyl acetate (1:2 *v*/*v*) as the eluent; mp 60.5–63.5 °C. $[\alpha]_D$ +29.1° (*c* 0.4, CH_2Cl_2). IR (film, cm^{-1}): 1773, 1728. ^{1}H NMR (500 MHz, C_6D_6) δ: 9.57 (d, 1H, *J* = 2.2 Hz, CHO), 4.29 (bt, 1H, *J* = 6.3, 7.4 Hz, H-1a), 3.94 (dd, 1H, *J* = 2.2, 6.3 Hz, H-2), 3.51 (bd, 1H, *J* = 7.6 Hz, H-4b), 3.42 (dt, 1H, *J* = 5.8, 7.2, 7.6 Hz, H-5), 3.23 (dd, 1H, *J* = 1.0, 7.4 Hz, H-4a), 3.04 (ddd, 1H, *J* = 2.2, 7.8, 13.9 Hz, H-7), 2.26 (dddd, 1H, *J* = 0.7, 7.4, 11.0, 13.9 Hz, H-7′), 1.60 (m, 1H, H-6), 1.35 (m, 1H, H-6′), 0.90 (s, 9H, *t*-Bu). HRMS (ESI) *m*/*z* calcd. for $C_{14}H_{23}NO_6Na$: 324.14176 [M + MeOH + Na]$^+$; found: 324.1408. HRMS (ESI) *m*/*z* calcd. for $C_{15}H_{25}NO_6Na$: 338.15741 [M + EtOH + Na]$^+$; found: 338.1590.

(1a*S*,2*S*,4a*R*,4b*S*,5*S*)-5-*tert*-Butoxy-2-*tert*-butyldiphenylsiloxymethyl-4-oxo-pyrrolidino[1,2-*b*]isoxazolidino[4,5-*c*]-tetrahydrofurane (17)

Alcohol **16** (0.043 g, 0.16 mmol) was dissolved in dichloromethane (15 mL), and treated with *tert*-butyldiphenylchlorosilane (0.057 g, 0.2 mmol) and DMAP (0.2 mmol). The solution was left under argon at room temperature for 24 h and then it was refluxed for 3 h. Subsequently, the mixture was cooled, washed with water, brine, and water again. The organic layer was dried and evaporated. The residue was purified on a silica gel column using hexane – ethyl acetate (4:1 *v*/*v*) as the eluent to afford **17** (0.062 g, 76% yield). $[\alpha]_D$ –0.9° (*c* 0.5, CH_2Cl_2). IR (film, cm^{-1}): 1779. ^{1}H NMR (500 MHz, $CDCl_3$) δ: 7.69 (m, 4H, Ph), 7.39 (m, 6H, Ph), 4.70 (dd, 1H, *J* = 4.2, 6.3 Hz, H-1a), 4.61 (ddd, 1H, *J* = 4.2, 5.8, 6.5 Hz, H-2), 4.17 (dt, 1H, *J* = 5.6, 7.0, 7.1 Hz, H-5), 4.04 (dd, 1H, *J* = 5.8, 11.2 Hz, C*H*HOH), 4.02 (dd, 1H, *J* = 6.5, 11.2 Hz, CH*H*OH), 3.94 (dd, 1H, *J* = 1.2, 7.1 Hz, H-4b), 3.76 (dd, 1H, *J* = 1.2, 6.3 Hz, H-4a), 3.22 (ddd, 1H, *J* = 4.5, 7.5, 13.0 Hz, H-7), 2.92 (ddd, 1H, *J* = 6.9, 9.3, 13.0 Hz, H-7′), 1.97 (dddd, 1H, *J* = 4.5, 6.9, 7.0, 13.0 Hz, H-6), 1.83 (dddd, 1H, *J* = 5.6, 7.5, 9.3, 13.0 Hz, H-6′), 1.20, 1.06 (2s, 18H, 2*t*-Bu). ^{13}C NMR (125 MHz, $CDCl_3$) δ: 177.1, 135.62, 135.61, 133.4, 133.2, 129.72, 129.70, 127.7, 127.6, 82.8, 77.8, 74.4, 72.9, 71.1, 61.7, 53.7, 52.0, 34.0, 28.4, 26.8, 19.2. HRMS (ESI) *m*/*z* calcd. for $C_{29}H_{39}NO_5NaSi$: 532.2490 $[M + H]^+$; found: 532.2516.

(1a*S*,2*S*,3*S*,3a*S*,4*S*)-2-(2′-*tert*-Butyldiphenylsiloxymethyl-1′-hydroxy)-4-*tert*-butoxy-3-hydroxymethyl-pyrrolidino-[1,2-*b*]isoxazolidine (18)

Lactone **17** (0.10 g, 0.2 mmol) was dissolved in methanol (25 mL), treated in portions with $NaBH_4$ (0.015 g, 0.4 mmol), and left for 4 h. Subsequently, 2 drops of water were added and the mixture was filtered through Celite. The solution was evaporated and the residue was purified on a silica gel column using hexane – ethyl acetate (1:3 *v*/*v*) as the eluent to afford **15** (0.062 g, 60%); mp 108.0–109.5 °C. $[\alpha]_D$ +38.2° (*c* 1.23, CH_2Cl_2). IR (film, cm^{-1}): 3392. ^{1}H NMR (500 MHz, C_6D_6) δ: 7.78 (m, 4H, Ph), 7.22 (m, 6H, Ph), 4.57 (d, 1H, *J* = 8.0 Hz, H-1a), 4.06 (dd, 1H, *J* = 8.6, 9.5 Hz, C*H*HOTBDPS), 4.01 (dd, 1H, *J* = 5.2, 9.5 Hz, CH*H*OTBDPS), 3.95 (dd, 1H, *J* = 5.2, 8.6 Hz, H-2), 3.89 (dd, 1H *J* = 5.3, 11.1 Hz, C*H*HOH), 3.83 (dd, 1H, *J* = 5.8, 11.1 Hz, CH*H*OH), 3.69 (q, 1H, *J* = 7.5, 7.5, 7.6 Hz, H-4), 3.57 (dd, 1H, *J* = 5.6, 7.6 Hz, H-3a), 3.26 (m, 1H, *J* = 5.3, 5.6, 5.8, 7.9 Hz, H-3), 3.09 (ddd, 1H, *J* = 2.9, 7.1, 13.3 Hz, H-6), 2.51 (ddd, 1H, *J* = 6.0, 11.0, 13.3 Hz, H-6′), 1.82 (m, 1H, H-5), 1.39 (m, 1H, H-5′), 1.15, 0.97 (2s, 18H, 2*t*-Bu). ^{13}C NMR (125 MHz, $CDCl_3$) δ: 135.5, 135.5, 133.3, 133.3, 129.7, 129.7, 127.7, 127.7, 78.8, 74.7, 71.4, 71.3, 70.4, 64.6, 60.6, 53.5, 47.6, 31.8, 28.2, 26.8, 19.2. HRMS (ESI) *m*/*z* calcd. for $C_{29}H_{44}NO_5Si$: 514.2983 $[M + H]^+$; found: 514.3003.

(1a*S*,2*S*,3*S*,3a*S*,4*S*)-2-(1′-Acetoxy-2′-*tert*-butyldiphenylsiloxymethyl)-3-acetoxymethyl-4-*tert*-butoxy-pyrrolidino[1,2-*b*]isoxazolidine (18Ac)

$[\alpha]_D$ +21.1° (*c* 1.8, CH_2Cl_2). IR (film, cm^{-1}): 1744. ^{1}H NMR (500 MHz, C_6D_6) δ: 7.82 (m, 4H, Ph), 7.23 (m, 6H, Ph), 5.61 (dt, 1H, *J* = 4.4, 6.1, 6.1 Hz, H-1a), 4.67 (dd, 1H, *J* = 4.4, 5.9 Hz, H-2), 4.35 (dd, 1H, *J* = 8.2, 10.9 Hz, C*H*HOAc), 4.32 (dd, 1H, *J* = 7.1, 10.9 Hz, CH*H*OAc), 4.07 (d, 2H, *J* = 6.1 Hz, CH_2OTBDPS), 3.68 (q, 1H, *J* = 6.0, 6.0, 6.0 Hz, H-4), 3.40 (dd, 1H, *J* = 2.8, 6.8 Hz, H-3a), 3.20 (dt, 1H, *J* = 11.7, 7.1, 7.1 Hz, H-6), 3.14 (m, 1H, *J* = 2.9, 5.9, 7.1, 8.2 Hz, H-3), 3.02 (dt, 1H, *J* = 11.7, 6.8, 6.8 Hz, H-6′), 1.76, 1.71 (2s, 6H, 2Ac), 1.64 (m, 1H, H-5), 1.50 (m, 1H, H-5′), 1.18, 0.97 (2s, 18H, 2*t*-Bu). ^{13}C NMR (125 MHz, $CDCl_3$) δ: 170.6, 170.1, 135.6, 135.5, 133.1, 133.0, 129.8, 129.8, 127.8, 127.7, 76.4, 73.7, 71.7, 71.6, 71.4, 63.6, 63.4, 54.1, 45.6, 33.5, 28.1, 27.0, 20.8, 20.4, 19.5. HRMS (ESI) *m*/*z* calcd. for $C_{33}H_{48}NO_7Si$: 598.31946 $[M + H]^+$; found: 598.3195.

(1a*S*,2*S*,6a*S*,6b*S*,7*S*)-2-(*tert*-Butyldiphenylsiloxymethyl)-7-*tert*-butoxy-4,4-dimethyl-3,5-dioxa-pyrrolidino[1,2-*b*]-isoxazolidino[4,5]cycloheptane (19)

Compound **15** (0.051 g, 0.1 mmol) was dissolved in 2,2-dimethoxypropane (25 mL), treated with a catalytic amount

© 2006 NRC Canada

of *p*-TsOH, and kept under reflux for 1 h. Subsequently, the solution was cooled, neutralized with triethylamine, and evaporated. The residue was purified by chromatography affording **19** (0.048 g) in 87% yield. $[\alpha]_D$ +4.3° (*c* 1.3, CH_2Cl_2). ^{1}H NMR (500 MHz, C_6D_6) δ: 7.81 (m, 4H, Ph), 7.20 (m, 6H, Ph), 4.43 (bd, 1H, *J* = 4.6 Hz, H-1a), 4.35 (t, 1H, *J* = 6.9, 7.2 Hz, H-2), 4.23 (t, 1H, *J* = 11.8, 12.3 Hz, H-6), 4.12 (dd, 1H, *J* = 6.9, 9.9 Hz, C*H*HOTBDPS), 4.07 (dd, 1H, *J* = 7.2, 9.9 Hz, CH*H*OTBDPS), 3.57 (dt, 1H, *J* = 6.5, 5.2, 5.2 Hz, H-7), 3.42 (dd, 1H, *J* = 4.9, 11.8 Hz, H-6′), 3.17 (m, 1H, H-9), 3.07 (m, 1H, H-9′), 3.00 (d, 1H, *J* = 6.5 Hz, H-6b), 2.89 (dt, 1H, *J* = 12.3, 4.6, 4.9 Hz, H-6a), 1.56 (m, 1H, H-8), 1.47 (m, 1H, H-8′), 1.36, 1.33 (2s, 6H, $C(CH_3)_2$), 1.20, 0.96 (2s, 18H, 2*t*-Bu). ^{13}C NMR (125 MHz, $CDCl_3$) δ: 135.6, 133.5, 129.6, 127.7, 101.5, 77.0, 74.2, 70.9, 70.1, 69.5, 64.0, 61.1, 54.4, 47.3, 33.9, 28.3, 26.8, 24.8, 23.9, 19.1. HRMS (ESI) *m*/*z* calcd. for $C_{32}H_{48}NO_5Si$: 554.32963 $[M + H]^+$; found: 554.3314.

(1a*S*,2*S*,6a*S*,6b*S*,7*S*)-7-*tert*-Butoxy-4,4-dimethyl-3,5-dioxa-2-hydroxymethylpyrrolidino[1,2-*b*]isoxazolidino-[4,5]cycloheptane (20)

Compound **19** (0.11 g, 0.2 mmol) was dissolved in THF (20 mL), treated with tetrabutylammonium fluoride (0.26 g, 1 mmol), and left overnight. Subsequently, the solvent was evaporated and the mixture was partially purified on a silica gel column to afford alcohol **20** (0.059 g, 94%). $[\alpha]_D$ +39.5° (*c* 0.7, CH_2Cl_2). IR (film, cm^{-1}): 3417. ^{1}H NMR (500 MHz, C_6D_6) δ: 4.17 (t, 1H, *J* = 11.8, 12.2 Hz, H-6), 4.12 (dd, 1H, *J* = 4.3, 8.6 Hz, H-2), 4.04 (d, 1H, *J* = 4.8 Hz, H-1a), 3.94 (dd, 1H, *J* = 8.6, 11.2 Hz, C*H*HOH), 3.62 (dd, 1H, *J* = 4.3, 11.2 Hz, CH*H*OH), 3.53 (q, 1H, H-7), 3.37 (dd, 1H, *J* = 5.1, 11.8 Hz, H-6′), 3.07 (m, 1H, H-9), 3.03 (m, 1H, H-9′), 2.94 (d, 1H, *J* = 6.7 Hz, H-6b), 2.84 (ddd, 1H, *J* = 4.8, 5.1, 12.2 Hz, H-6a), 1.50 (m, 1H, H-8), 1.44 (m, 1H, H-8′), 1.34, 1.32 (2s, 6H, $C(CH_3)_2$), 0.90 (s, 9H, *t*-Bu). ^{13}C NMR (125 MHz, C_6D_6) δ: 101.4, 78.4, 73.3, 71.4, 70.9, 69.3, 64.0, 61.6, 54.3, 48.5, 33.8, 27.9, 25.0, 24.2. HRMS (ESI) *m*/*z* calcd. for $C_{16}H_{29}NO_5Na$: 338.1938 $[M + Na]^+$; found: 338.1952.

(1a*S*,2*S*,6a*S*,6b*S*,7*S*)-7-*tert*-Butoxy-4,4-dimethyl-3,5-dioxa-2-mesyloxymethylpyrrolidino[1,2-*b*]isoxazolidino-[4,5]cycloheptane (21)

Alcohol **20** (0.063 g, 0.2 mmol) was dissolved in dry dichloromethane (20 mL), treated with triethylamine (0.040 g, 0.4 mmol), and cooled to –5 °C. Subsequently, mesyl chloride (0.027 g, 0.24 mmol) was added and the temperature of the mixture was allowed to rise to room temperature. After 2 h, the mixture was washed with brine (15 mL) and water (15 mL), dried and evaporated to get crude **21** (0.0755 g, 96%). $[\alpha]_D$ –2.0° (*c* 0.45, CH_2Cl_2). ^{1}H NMR (500 MHz, C_6D_6) δ: 4.35 (dd, 1H, *J* = 8.8, 10.5 Hz, C*H*HOMs), 4.22 (ddd, 1H, *J* = 1.0, 3.8, 8.8 Hz, H-2), 4.09 (t, 1H, *J* = 11.8, 12.3 Hz, H-6), 4.08 (dd, 1H, *J* = 3.9, 10.5 Hz, CH*H*OMs), 3.93 (d, 1H, *J* = 4.9 Hz, H-1a), 3.54 (q, 1H, H-7), 3.33 (dd, 1H, *J* = 5.3, 11.8 Hz, H-6′), 3.05 (m, 1H, H-9), 3.00 (m, 1H, H-9′), 2.91 (d, 1H, *J* = 6.7 Hz, H-6b), 2.82 (ddd, 1H, *J* = 4.9, 5.3, 12.3 Hz, H-6a), 2.19 (s, 3H, Ms), 1.49 (m, 2H, H-8,8′), 1.31, 1.27 (2s, 6H, $C(CH_3)_2$), 1.06 (s, 9H, *t*-Bu). ^{13}C NMR (125 MHz, C_6D_6) δ: 101.8, 77.9, 73.6, 71.6, 71.0, 69.6, 68.4, 61.7, 54.5, 48.5, 36.4, 34.0, 28.1, 25.0, 24.1. HRMS (ESI) *m*/*z* calcd. for $C_{17}H_{32}NO_7S$: 394.1894 $[M + H]^+$; found: 394.1913.

(1*S*,6*S*,7*S*,8*S*,9*S*)-6,7-Diacetoxy-8-acetoxymethyl-1-*tert*-butoxyindolizidine (23)

Compound **21** (0.04 g, 0.1 mmol) was dissolved in 80% acetic acid (15 mL) and kept at room temperature for 1 h. Subsequently, the solvent was evaporated, the residue was dissolved in methanol (20 mL) and treated with a catalytic amount of 10% Degussa Pd/C under hydrogen. After 24 h, the catalyst was filtered and the solvent was evaporated. The residue was dissolved in triethylamine (10 mL) and treated with acetic anhydride (10 mL) and DMAP (2 mg). After 2 h, the solvents were evaporated and a crude product was purified on a silicagel column using hexane – ethyl acetate (1:1 *v*/*v*) as the eluent to afford **23** (0.021 g, 55%). $[\alpha]_D$ +103° (*c* 0.1, $CHCl_3$). IR (film, cm^{-1}): 1746, 1231. ^{1}H NMR (500 MHz, $CDCl_3$) δ: 5.14 (t, 1H, *J* = 9.6, 10.5 Hz, H-7), 5.08 (dt, 1H, *J* = 5.0, 9.6, 10.0 Hz, H-6), 4.21 (dd, 1H, *J* = 2.7, 11.7 Hz, C*H*HOAc), 4.15 (ddd, 1H, *J* = 2.1, 5.3, 6.8 Hz, H-1), 4.12 (dd, 1H, *J* = 2.6, 11.7 Hz, CH*H*OAc), 3.35 (dd, 1H, *J* = 5.0, 10.3 Hz, H-5), 3.12 (dt, 1H, *J* = 1.6, 8.8, 9.0 Hz, H-3), 2.33 (m, 1H, H-8), 2.29 (dd, 1H, *J* = 5.3, 10.8 Hz, H-8a), 2.16 (dddd, 1H, *J* = 1.5, 6.8, 8.8, 13.4 Hz, H-2), 2.07, 2.05, 1.99 (3s, 9H, 3Ac), 2.04 (m, 1H, H-3′), 1.95 (m, 1H, H-5′), 1.90 (dddd, 1H, *J* = 2.0, 9.0, 9.1, 13.3 Hz, H-2′), 1.20 (s, 9H, *t*-Bu). ^{13}C NMR (125 MHz, $CDCl_3$) δ: 171.0, 170.5, 170.1, 74.1, 72.3, 71.9, 70.2, 66.8, 59.8, 53.7, 52.7, 38.3, 35.1, 28.8, 20.89, 20.85, 20.85. HRMS (ESI) *m*/*z* calcd. for $C_{19}H_{32}NO_7$: 386.2173 $[M + H]^+$; found: 386.2189.

(1*S*,6*S*,7*S*,8*S*,9*S*)-8-Acetoxymethyl-1,6,7-triacetoxy-indolizidine (24)

Compound **23** (0.02 g, 0.052 mmol) was dissolved in trifluoroacetic acid (5 mL) and stirred for 2 h. Subsequently, the solvent was carefully evaporated and the residue was dissolved in triethylamine (1 mL) and treated with acetic anhydride (1 mL) and DMAP (1 mg). After 1 h, the mixture was evaporated and the residue purified by chromatography using hexane – ethyl acetate (1:1 *v*/*v*) as the eluent to afford **24** (0.012 g, 62%). $[\alpha]_D$ +64.5° (*c* 0.18, $CHCl_3$). IR (film, cm^{-1}): 1745. ^{1}H NMR (500 MHz, C_6D_6) δ: 5.28 (dt, 1H, *J* = 5.1, 9.6, 10.0 Hz, H-6), 5.20 (dd, 1H, *J* = 9.6, 10.8 Hz, H-7), 5.12 (ddd, 1H, *J* = 1.3, 4.6, 7.2 Hz, H-1), 4.30 (dd, 1H, *J* = 4.8, 11.8 Hz, C*H*HOAc), 3.97 (dd, 1H, *J* = 3.1, 11.8 Hz, CH*H*OAc), 3.11 (dd, 1H, *J* = 5.1, 10.3 Hz, H-5), 2.63 (m, 1H, H-3), 2.36 (m, 1H, *J* = 3.1, 4.8, 10.4, 10.8 Hz, H-8), 1.92 (m, 1H, H-2), 1.77, 1.75, 1.70, 1.66 (4s, 12H, 4Ac), 1.74–1.70 (m, 2H, H-5′, H-8a), 1.60 (m, 1H, H-2′), 1.54 (m, 1H, H-3′). ^{13}C NMR (125 MHz, C_6D_6) δ: 169.9, 169.9, 169.7, 169.5, 73.2, 72.5, 71.9, 66.6, 61.0, 53.4, 51.6, 39.3, 32.6, 20.5, 20.42, 20.38, 20.36. HRMS (ESI) *m*/*z*, calcd. for $C_{17}H_{25}NO_8Na$: 394.1472 $[M + Na]^+$; found: 394.1486.

(1*S*,6*S*,7*S*,8*S*,9*S*)-8-Hydroxymethyl-1,6,7-trihydroxy-indolizidine (8-homocastanospermine, 13)

Compound **23** (0.013 g, 0.035 mmol) was dissolved in 1.3% of ammonia in methanol (5 mL) and left for 24 h at room temperature. Subsequently, the solvent was evaporated

© 2006 NRC Canada

and the residue was purified by chromatography using methanol – ethyl acetate (1:1 *v*/*v*) as the eluent to afford **24** (5.8 mg, 82%). $[\alpha]_D$ +35.8° (*c* 0.55, CH_3OH). IR (KBr, cm^{-1}): 3380. ^1H NMR (500 MHz, CD_3OD) δ: 4.32 (m, 1H, H-1), 3.90 (dd, 1H, *J* = 2.2, 10.9 Hz, C*H*HOH), 3.76 (ddd, 1H, *J* = 2.3, 5.1, 10.8 Hz, CH*H*OH), 3.58 (ddd, 1H, *J* = 5.0, 8.8, 10.4 Hz, H-6), 3.26 (dd, 1H, *J* = 8.8, 10.1 Hz, H-7), 3.18 (dd, 1H, *J* = 5.0, 10.6 Hz, H-5), 3.08 (ddd, 1H, *J* = 2.0, 9.0, 9.1 Hz, H-3), 2.25 (dddd, 1H, *J* = 2.0, 5.5, 9.0, 13.9 Hz, H-2), 2.08 (ddd, 1H, *J* = 9.1, 9.1, 9.1 Hz, H-3′), 1.91 (dd, 1H, *J* = 10.2, 10.9 Hz, H-5′), 1.86 (m, 2H, H-8,8a), 1.75 (dddd, 1H, *J* = 1.7, 9.0, 9.1, 13.8 Hz, H-2′). ^{13}C NMR (125 MHz, CD_3OD) δ: 75.8, 73.2, 71.8, 71.6, 61.1, 58.0, 53.5, 43.9, 34.2. HRMS (ESI) *m*/*z* calcd. for $C_9H_{18}NO_4$: 204.1230 $[M + H]^+$; found: 204.1227.

Biological tests

The β-glucosidase activity of **13** was measured by the modification of the procedures described previously (10, 11). The reaction mixture consisted of 100 μL of 0.014 mol/L *p*-nitrophenyl β-D-glucopyranoside, 250 μL of 0.2 mol/L acetate buffer (pH 4.6), 50 μL of inhibitor solution (either water or methanol), and 100 μL of enzyme solution (3 μg/mL). After incubation for 15 min at 30 °C, the reaction was terminated by the addition of 1 mL of 2% sodium carbonate. The absorbance of liberated *p*-nitrophenol was measured at 405 nm.

The α-glucosidase activity of **13** was measured by modification of the procedures described previously (12, 13). The reaction mixture consisted of 25 μL of 0.0165 mol/L *p*-nitrophenyl α-D-glucopyranoside, 403 μL of 0.1 mol/L acetate buffer (pH 4.0), 50 μL of inhibitor solution (either water or methanol), and 22 μL of enzyme solution (10 times diluted). After incubation for 15 min at 37 °C, the reaction was terminated by the addition of 1 mL of 2% sodium carbonate. The absorbance of liberated *p*-nitrophenol was measured at 405 nm.

Acknowledgements

This work was supported by the Ministry of Science and Information Grant No. 3 T09A 025 28.

References

1. M. Jurczak, J. Rabiczko, D. Socha, M. Chmielewski, F. Cardona, A. Goti, and A. Brandi. Tetrahedron: Asymmetry, **11**, 2015 (2000).
2. D. Socha, M. Jurczak, J. Frelek, A. Klimek, J. Rabiczko, Z. Urbańczyk-Lipkowska, K. Suwińska, M. Chmielewski, F. Cardona, A. Goti, and A. Brandi. Tetrahedron: Asymmetry, **12**, 3163 (2001).
3. K. Paśniczek, D. Socha, M. Jurczak, J. Frelek, A. Suszczyńska, Z. Urbańczyk-Lipkowska, and M. Chmielewski. J. Carbohydr. Chem. **22**, 613 (2003).
4. (*a*) A. Goti, V. Fedi, L. Nannelli, F. De Sarlo, and A. Brandi. Synlett, 577 (1997); (*b*) A. Goti, F. Cardona, and A. Brandi. Synlett, 761 (1996). (*c*) A. Goti, S. Cicchi, M. Cacciarini, F. Cardona, V. Fedi, and A. Brandi. Eur. J. Org. Chem. 3633 (2000); (*d*) A. Goti, M. Cacciarini, F. Cardona, F.M. Cordero, and A. Brandi. Org. Lett. **3**, 1367 (2001); (*e*) A. Goti, S. Cicchi, V. Fedi, L. Nannelli, and A. Brandi. J. Org. Chem. **62**, 3119 (1997); (*f*) A. Goti, M. Cacciarini, F. Cardona, F.M. Cordero, and A. Brandi. Org. Lett. **3**, 1367 (2001); (*g*) F. Pisaneschi, C.D. Monica, F.M. Cordero, and A. Brandi. Tetrahedron Lett. **43**, 5711 (2002); (*h*) A.E. McCaig, K.P. Meldrum, R.H. Wightman. Tetrahedron, **54**, 9429 (1998); (*i*) A.B. Holmes, B. Bourdin, I. Collins, E.C. Davison, A.J. Rudge, T.C. Stork, and J. Warner. Pure Appl. Chem. **69**, 531 (1997); (*j*) S.E. Denmark and A. Thorarensen. J. Am. Chem. Soc. **119**, 125 (1997); (*k*) S.E. Denmark and A.R. Hurd. J. Org. Chem. **65**, 2875 (2000); (*l*) S.E. Denmark and J.J. Cottell. J. Org. Chem. **66**, 4276 (2001); (*m*) J. Tufariello. Acc. Chem. Res. **12**, 396 (1979).
5. D. Socha, M. Jurczak, and M. Chmielewski. Carbohydr. Res. **336**, 315 (2001), and refs. cited therein.
6. (*a*) G.W.J. Fleet, L.E. Fellows, and B. Winchester. *In* Bioactive compounds from plants. *Edited by* P.J. Chadwick and J. March. Wiley and Sons, Chichester, UK. 1990. p. 112; (*b*) N. Asano, R.J. Nash, R.J. Molyneux, and G.W.J. Fleet. Tetrahedron: Asymmetry, **11**, 1645 (2000); (*c*) Y. Chapleur (*Editor*). Carbohydrate mimics. Wiley-VCH, Weinheim. 1998; (*d*) A.E. Stütz. Iminosugars as glycosidase inhibitors. Wiley-VCh, Weinheim. 1999; (*e*) O.R. Martin and Ph. Compain (*Editors*). Curr. Top. Med. Chem. **3**(5), (2003), and refs. cited therein; (*f*) A. El Nemr. Tetrahedron, **56**, 8579 (2000); (*g*) F.-X. Felpin and J. Lebreton. Eur. J. Org. Chem. 3693 (2003); (*h*) J. Cossy and P. Vogel. *In* Studies in natural products chemistry. *Edited by* Atta-ur-Rahman. Elsevier, Amsterdam. 1993. p. 275; (*i*) P. Herczegh, I. Kovacs, and F. Sztaricskai. Recent progress in chemical synthesis of antibiotics. *Edited by* G. Lukacs and M. Ohno. Springer-Verlag, Berlin. 1993. p. 751; (*j*) L. Cipolla, B. La Ferla, and F. Nicotra. Curr. Top. Med. Chem. **3**, 485 (2003).
7. (*a*) L.D. Hohenschutz, E.A. Bell, P.J. Jewess, D.P. Lewerothy, R.J. Pryce, E. Arnold, and J. Chardy. Phytochemistry, **20**, 811 (1981); (*b*) I. Pastuszak, R.J. Molyneux, L.F. James, and A.D. Elbien. Biochemistry, **29**, 1886 (1990).
8. (*a*) B.L. Reinhart, K.M. Robinson, A.J. Payne, M.E. Wheatley, J.L. Fisher, P.S. Liu, and W. Chang. Life Sci. **41**, 2325 (1987); (*b*) E. Truscheit, W. Frommer, L. Junge, L. Müller, D.D. Schmidt, and W. Wingender. Angew. Chem. Int. Ed. Engl. **20**, 744 (1981); (*c*) R. Pili, J. Chang, R.A. Partis, R.A. Mueller, F.J. Chrest, and A. Passaniti. Cancer Lett. **55**, 2995 (1995); (*d*) M.A. Spearman, B.C. Ballon, J.M. Gerrard, A.H. Greenberg, and J.A. Wright. Cancer Lett. **60**, 185 (1991); (*e*) E.J. Nichols, R. Manger, S. Hakomori, A. Herscovies, and L.R. Rohrschneider. Mol. Cell. Biol. **5**, 3467 (1985); (*f*) R.M. Ruprecht, S. Mullaney, J. Anderson, R. Bronson, and J. Acquired Immune Defic. Syndr. **2**, 149 (1989).
9. F.M. Cordero, F. Pisaneschi, M. Gensini, A. Goti, and A. Brandi. Eur. J. Org. Chem. 1941 (2002).
10. T. Niva, S. Inouye, T. Tsuruoka, Y. Koaze, and T. Niida. Agr. Biol. Chem. **34**, 966 (1970).
11. T. Tsuruoka, H. Fukuyasu, M. Ishii, T. Usui, S. Shibahara, and S. Inouye. J. Antibiot. **49**, 155 (1996).
12. G. Legler. Adv. Carbohydr. Chem. Biochem. **48**, 319 (1990).
13. H.U. Bergmeyer (*Editor*). Methods of enzymatic analysis. 3rd ed. 1984. p. 152.

© 2006 NRC Canada

Synthesis of mono- and di-sialophospholipids via the H-phosphonate approach[1]

Hongbin Yan and Harold J. Jennings

Abstract: To overcome their inherent instability, stable modified mono- and di-sialophospholipids of the group C meningococcal polysaccharide were synthesized. Stability was achieved by introducing a spacer between the sialic acid residue and the phospholipid component, and by replacing the native ester linkages to the lipid by ether linkages. Mono- and di-hydroxylethylenesialosides were coupled to phosphoglyceroldietherlipid using H-phosphonate chemistry to give the anomerically pure sialophospholipids in good yields.

Key words: polysialic acid, glycolipid, H-phosphonate, meningococcus.

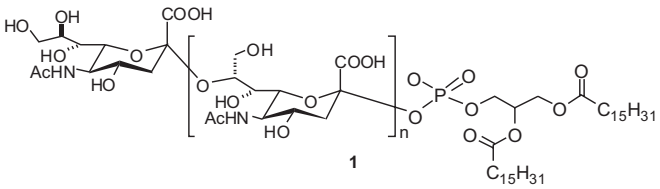
Résumé : Afin de circonvenir à leur instabilité inhérente, on a synthétisé des mono- et des di-sialophospholipides modifiés et stables du polysaccharide méningocoque du groupe C. On a atteint la stabilité en introduisant un groupe d'espacement entre le résidu d'acide sialique et le composant phospholipide et en remplaçant les liaisons esters naturelles vers le lipide par des liaisons éthers. On a réalisé le couplage des mono- et di-hydroxyéthylènesialosides au phosphoglycéroldiétherlipide en se basant sur la chimie des H-phosphonates afin d'obtenir des sialophospholipides anomériquement purs avec de bons rendements.

Mots clés : acide polysialique, glycolipide, H-phosphonate, méningocoque.

[Traduit par la Rédaction]

Introduction

Sialic acid (*N*-acetyl neuraminic acid) is a naturally occurring keto sugar that is involved in a wide range of biological processes. The capsular polysaccharides of various highly pathogenic bacteria, including those of *Escherichia coli* K1 and groups B and C *Neisseria meningitidis* are known to be homopolymers of sialic acid (1, 2), and both the group C polysaccharide and more recently, its improved protein conjugates (3, 4), have been shown to be effective human vaccines. Based on previous assays (5, 6), it was demonstrated that groups B and C *meningococcal* and *E. coli* K1 polysaccharides bear glycerol phospholipid anchors, and the proposed structure of the group C phospholipid anchor is as shown in **1** (5). Although small in size, this lipoidal group is responsible for the aggregation of the polysaccharides, and it has been proposed that it is the entity by which the polysaccharide is attached to the outer membrane of the above bacteria (5). While aggregation improves the immunogenicity of the group C *meningococcal* polysaccharide in humans (7), it has little or no effect on that of the group B *meningococcal* and *E. coli* K1 polysaccharides (8), because of the fact that their basic structure (α(2–8)-polysialic acid) mimics a human tissue antigen (9). However, highly aggregated forms of these lipidated polysaccharides do contain a protective epitope distinct from those of α(2–8) polysialic acid, but nevertheless having this latter molecule as a component (3, 10). This protective epitope is mimicked by the N-propionylated form of α(2–8) polysialic acid, which in its conjugated form is a potential human vaccine (3, 11, 12). To study the roles of α(2–8) polysialic acid and lipid anchor in the formation of this epitope, we proposed first to synthesize the truncated mono- and di-sialophospholipids, and then at a later date to use them as precursors to elongate the sialic acid chain at their nonreducing ends, using polysialyl transferases (13).



1

Results and discussion

Due to the miniscule content of phospholipid in the native lipidated polysaccharides (5) and its reported inherent instability (6), it has never been isolated. This latter property is probably also responsible for our inability to synthesize it using conventional synthetic methods (unpublished results). Therefore, we opted to synthesize more stable modified ver-

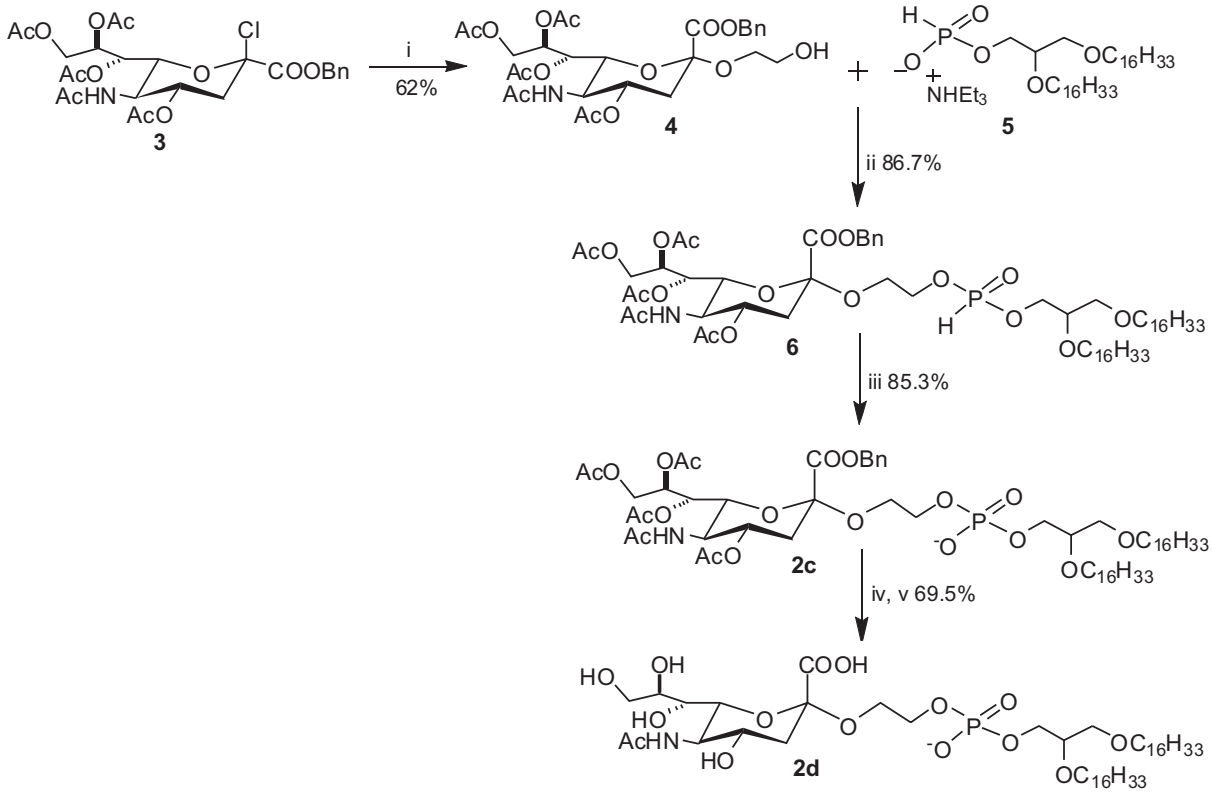
Received 8 August 2005. Published on the NRC Research Press Web site at http://canjchem.nrc.ca on 21 April 2006.

H. Yan and H.J. Jennings.[2] Institute for Biological Sciences, National Research Council of Canada, Ottawa, ON K1A OR6, Canada.

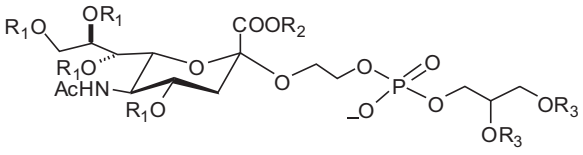
[1]This article is part of a Special Issue dedicated to Professor Walter A. Szarek.
[2]Corresponding author (e-mail: Harry.Jennings@nrc-cnrc.gc.ca).

 doi:10.1139/V06-031 © 2006 NRC Canada

Scheme 1. Reagents and conditions: (*i*) $HOCH_2CH_2OH$, AgOTf, 2,6-di-*tert*-butylpyridine, MeCN, $CaCO_3$, –20 °C to room temp.; (*ii*) **5**, $(CH_3)_3COCl$, C_5H_5N, 0 °C, 10 min; (*iii*) I_2, C_5H_5N–H_2O, room temp.; (*iv*) Pd/C, H_2, AcOEt–MeOH, 50 psi (1 psi = 6.894 757 kPa); (*v*) MeOH, CH_2Cl_2, NaOMe.



sions of the mono- and di-sialophospholipids as model compounds. In an attempt to stabilize the lipid anchor of the monosialophospholipid, we first introduced a spacer between the sialic acid and the phospholipid as shown in **2a**. Assembly of **2a** was effected by coupling **4** (14), previously prepared from chlorosugar **3** (15), to phospholipid **5**, using H-phosphonate chemistry (see the following). However, removal of the acetyl protecting groups from **2a** in the presence of the palmitoyl esters proved to be problematic, **2b** only being isolated in very poor yields. Having also had limited success in the synthesis of an alternate donor to **3**, the fully benzylated 1-chlorodeoxy derivative of sialic acid (16), which could have possibly avoided this problem, we decided to additionally replace the palmitoyl ester groups of the glycerol moiety with ether groups (as shown in **2c**). Because the long-chain ether groups are stable under the conditions under which *O*-acetates are removed by methoxide ion, the unblocking of the fully protected sialophospholipid **2c** should furnish **2d**.



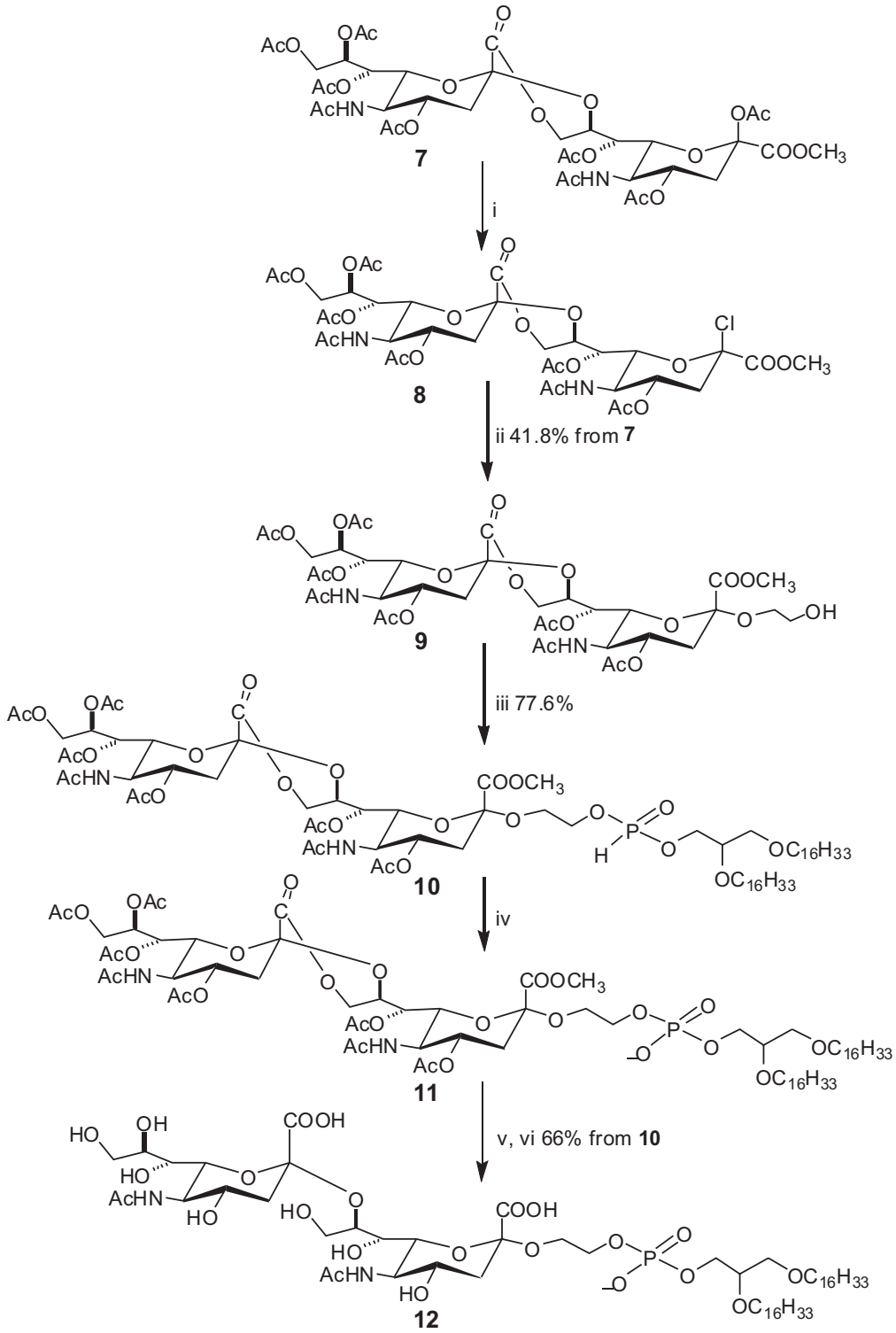
2a R_1 = Ac, R_2 = Bn, R_3 = $COC_{15}H_{31}$;
b R_1 =R_2 = H, R_3 = $COC_{15}H_{31}$;
c R_1 = Ac, R_2 = Bn, R_3 = $C_{16}H_{33}$;
d R_1 =R_2 = H, R_3 = $C_{16}H_{33}$;

To synthesize phosphoether lipid **2d** we found that H-phosphonate chemistry, which has been widely used in oligonucleotide synthesis (17), can be readily employed (Scheme 1). Thus, 1,2-dihexadecylglycerol (18) was readily phosphonylated by ammonium 4-methylphenyl H-phosphonate (19) to afford H-phosphonate **5**. Benzyl (glycolyl 5-acetamido-4,7,8,9-tetraacetyl-3,5-dideoxy-D-*glycero*-α-D-*galacto*-nonulpyranosid)onate **4** (14), which was obtained in an anomerically pure α form, was then coupled with **5** in the presence of pivaloyl chloride to yield the H-phosphonate diester **6** in good yield. Subsequent oxidation with iodine furnished phosphodiester **2c**, which on deesterification gave a good yield of the target compound (**2d**).

Synthesis of the disialophospholipid derivative (**12**), shown in Scheme 2, was achieved using similar methods to those employed in the synthesis of monosialophospholipid **2d**. The α-2,8-linked sialic acid dimer was obtained in a pure form by controlled acid hydrolysis of colominic acid, followed by fractionation of the hydrolysate on a Bio-gel P-10 column as previously described (20). More conveniently, the hydrolysate was transformed in situ (Scheme 2) to afford the peracetylated lactone disialoside methyl ester (**7**) in moderate yield (21). Thus, **7** was converted to its 2-chloro dervative (**8**) by treatment with a mixture of acetyl chloride, dichloromethane, and a trace amount of water. Glycosylation of chloride **8** with ethylene glycol was effected with silver triflate to afford α-anomer **9.** Coupling of **9** with H-phosphonate **5**, followed by oxidation of the H-phosphonate intermediate **10** gave the partially protected disialophosphate diester **11** in good yield. Subsequent deprotection of **11** with

© 2006 NRC Canada

Scheme 2. Reagents and conditions: (*i*) CH_2Cl_2, CH_3COCl, H_2O; (*ii*) $HOCH_2CH_2OH$, AgOTf, 2,6-di-*tert*-butylpyridine, MeCN, $CaCO_3$, –20 °C to room temp.; (*iii*) **5**, $(CH_3)_3COCl$, C_5H_5N, 0 °C, 10 min; (*iv*) I_2, C_5H_5N–H_2O, room temp.; (*v*) MeOH, NaOMe; (*vi*) MeOH, H_2O, NaOH.

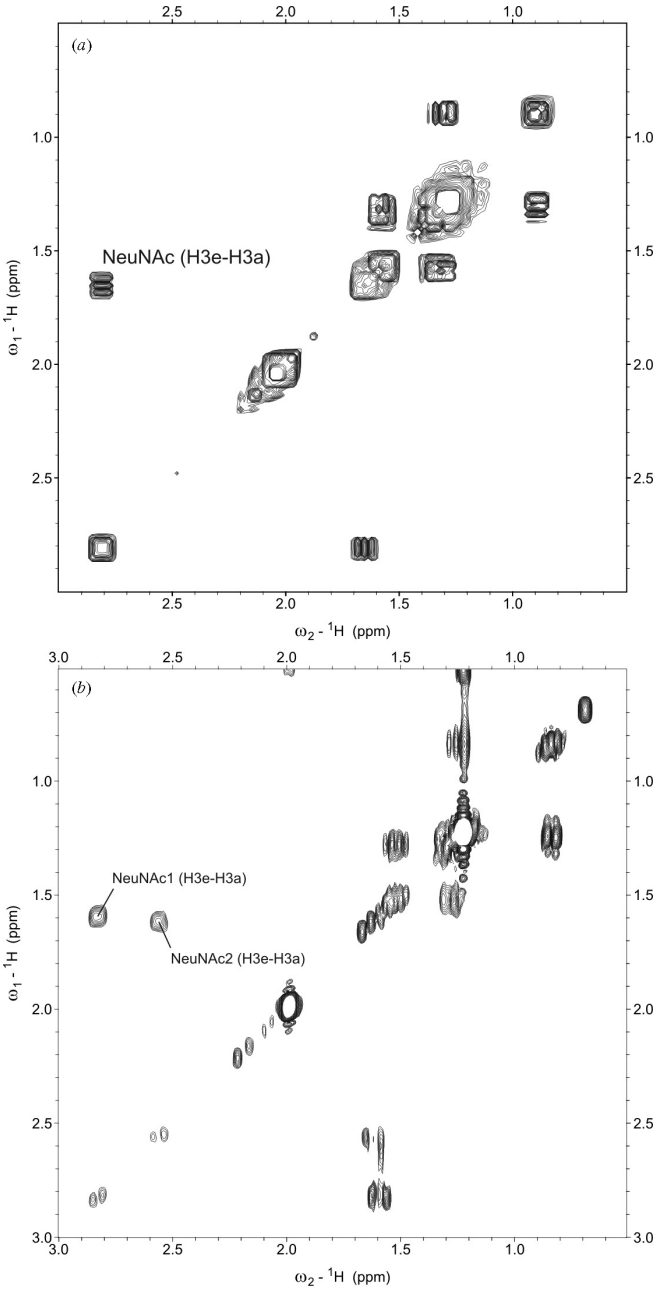


methoxide ion also gave a good yield of the target compound (**12**).

^{1}H NMR spectroscopic analysis of mono- (**2d**) and disialophospholipids (**12**) showed that they were both α-sialosides because the chemical shifts of the H_{3e} signals of their reducing end sialic acid residues were found to be 2.81 and 2.83 ppm, respectively (Fig. 1), which is indicative of α-sialosides (22). The presence of the disialic acid moiety in compound **12** is also clearly indicated by the resonances at 2.83 and 2.65 ppm, which represent the H_{3e} protons of both

© 2006 NRC Canada

Fig. 1. COSY spectra of (*a*) monosialophospholipid **2d** and (*b*) disialophospholipid **12**.



the reducing and nonreducing sialic acid residues of **12**, respectively.

Experimental

^{1}H and COSY NMR spectra were measured at 400 MHz with a Varian 400 spectrometer; tetramethylsilane was used as an internal standard and *J* values are given in Hz. ^{31}P NMR spectra were measured at 80.2 MHz with a Varian 200 spectrometer spectrometer; 85% orthophosphoric acid was used as an internal standard. The FAB and ESI mass spectra were measured with a Jeol AX 505H and an Applied Biosystems Q-Star quadrupole/time-of-flight (Qq-TOF) mass spectrometer, respectively. Merck silica gel 60 F254 TLC plates were developed in solvent systems A (dichloromethane–methanol (95:5 *v*/*v*)) and B (chloroform – methanol – water – acetic acid (50:50:7:0.2 *v*/*v*)). Merck silica gel 60 Art 7729 and Art 7734-3 were used for short column chromatography and flash column chromatography, respectively. Sialic acid was purchased from Rose Scientific (Edmonton, Alberta). Colominic acid was purchased from Nacalai Tesque (Kyoto, Japan). Anhydrous dichloromethane, methanol, pyridine, and tetrahydrafuran were purchased from Sigma-Aldrich. Ethylene glycol was distilled under reduced pressure. The other chemicals were purchased from Sigma-Aldrich and were used without further purification.

Triethylammonium 1,2-dihexadecyl-glycerol-3-H-phosphonate (5)

Ammonium 4-methylphenyl H-phosphonate (19) (3.16 g, 16.71 mmol), triethylamine (5.0 mL, 35.8 mmol), and methanol (5.0 mL) were coevaporated under reduced pressure. To the residue was added (±)-1,2-dihexadecyl glycerol (18) (3.00 g, 5.566 mmol) and the mixture was azeotroped with pyridine (2 × 5 mL). The residue was redissolved in pyridine (30 mL) and cooled to –10 °C. Pivotoyl chloride (2.0 mL, 16.2 mmol) was added over a period of 5 min. After 1 h, water (5 mL) was added and the reactants were allowed to warm up to room temperature over a period of 1 h. The products were then partitioned between dichloromethane (100 mL) and saturated aqueous sodium hydrogen carbonate (2 × 80 mL). The layers were separated and the combined aqueous layers were back extracted with dichloromethane (2 × 20 mL). The combined organic layers were further extracted with triethylammonium phosphate buffer (0.5 mol/L, pH 7.0, 50 mL). The layers were separated and the aqueous layer was back extracted with dichloromethane (15 mL). The combined dried ($MgSO_4$) organic layers were concentrated under reduced pressure. The residue was fractionated by short column chromatography on silica gel. The appropriate fractions, which were eluted with dichloromethane–methanol (9:1 *v*/*v*) were pooled and concentrated under reduced pressure to give the title compound (**5**) as a colourless froth (3.53 g, 89.9%). ^{1}H NMR($CDCl_3$–CD_3OD, 1:1 *v*/*v*) include the following peaks δ_H: 0.88 (6H, t, J = 6.6 Hz), 1.20–1.32 (52H, br), 1.50–1.58 (4H, br), 5.99 (0.5H, s), 7.56 (0.5H, s). ^{31}P NMR ($CDCl_3$–CD_3OD, 1:1 *v*/*v*) δ_P: 5.66 ($^1J_{P\text{-}H}$ = 628.3 Hz). FAB$^-$-HRMS calcd. for $C_{35}H_{72}O_5P^-$: 603.51174; found: 603.5117.

[Benzyl (glycolyl-5-acetamido-4,7,8,9-*O*-tetraacetyl-3,5-dideoxy-D-*glycero*-α-D-*galacto*-2-nonulopyranosyl)]-1,2-dihexadecyl-*glycero*-3-H-phosphonate (6)

Benzyl (glycolyl-5-acetamido-4,7,8,9-tetra-*O*-acetyl-3,5-dideoxy-β-*O*-manno-2-nonulopyranosid)onate (**4**) (0.500 g, 0.818 mmol) and triethylamonnium 1,2-dihexadecyl-glycerol-3-H-phosphonate (**5**) (0.693 g, 0.981 mmol) were evaporated with dry pyridine (2 × 5 mL) and the residue was redissolved in anhydrous pyridine (10 mL) and cooled (ice-water bath). Pivaloyl chloride (0.26 mL, 2.11 mmol) was added. After a period of 10 min, the reaction was quenched by addition of water (0.5 mL). After a further period of 10 min, the products were partitioned between dichloromethane (80 mL) and saturated aqueous sodium hydrogen carbonate (2 × 50 mL). The layers were separated and the

© 2006 NRC Canada

aqueous layer was back extracted with dichloromethane (2 × 10 mL). The combined organic layers were further washed with triethylammonium phosphate buffer (0.5 mol/L, pH 7.0, 50 mL). The layers were separated and the aqueous layer was back extracted with dichloromethane (10 mL). The combined dried ($MgSO_4$) organic layers were concentrated under reduced pressure. The residue was purified by flash column chromatography on silica gel. The appropriate fractions, which were eluted with ethyl acetate, were pooled and evaporated under reduced pressure to give the title compound (**6**) as a colourless froth (0.85 g, 86.7%). R_f (system A) 0.49. ^{1}H NMR ($CDCl_3$) include the following peaks $\delta_{H:}$ 0.88 (6H, t, J = 6.6 Hz), 1.22–1.32 (52H, br), 1.50–1.58 (4H, br), 1.87 (3H, s), 2.02 (3H, s), 2.03 (3H, s), 2.04 (3H, s), 2.12 (3H, s), 2.65 (1H, dt, J = 12.8, 4.0 Hz), 5.97 (0.5H), 7.37 (5H, m), 7.76 (0.5H). ^{31}P NMR ($CDCl_3$) δ_P: 10.50, 10.36, 10.33, 10.18 ($^1J_{P\text{-}H}$ = 713.2 Hz). ESI$^+$ calcd. for $C_{63}H_{108}NO_{18}PNa^+$: 1220.7; found: 1221.0.

[Benzyl (glycolyl-5-acetamido-4,7,8,9-*O*-tetraacetyl-3,5-dideoxy-D-*glycero*-α-D-*galacto*-2-nonulopyranosyl)]-1,2-dihexadecyl-*glycero*-3-phosphate (2c)

The H-phosphonate **6** (0.800 g, 0.668 mmol) was dissolved in pyridine–water (10 mL, 4:1 *v*/*v*) followed by addition of iodine (0.100 g, 0.394 mmol) at room temperature. After 30 min, the products were poured into aqueous sodium sulfite (10 mL, 0.1 mol/L) and extracted with dichloromethane (50 mL) and triethylammonium phosphate buffer (0.5 mol/L, pH 7.0, 50 mL). The layers were separated and the aqueous layer was back extracted with dichloromethane (2 × 20 mL). The combined dried ($MgSO_4$) organic layers were concentrated under reduced pressure. The residue was fractionated by short column chromatography on silica gel. The appropriate fractions, which were eluted with dichloromethane–methanol (85:15 *v*/*v*), were combined and concentrated under reduced pressure to give the title compound **2c** as a colourless waxy solid (0.75 g, 85.3%). ^{1}H NMR ($CDCl_3$–CD_3OD–D_2O, 1:1:0.04 *v*/*v*) include the following peaks δ_H: 0.89 (6H, t, J = 7.0 Hz), 1.24–1.32 (52H, br), 1.49–1.57 (4H, br), 1.86 (3H, s), 2.03 (3H, s), 2.04 (3H, s), 2.13 (6H, s), 2.69 (1H, dd, J = 12.8, 4.4 Hz), 5.83 (5H, m). ^{31}P NMR ($CDCl_3$–CD_3OD–D_2O, 1:1:0.04 *v*/*v*) δ_P: 1.39. FAB$^-$ calcd. for $C_{63}H_{107}NO_{19}P^-$: 1212.7; found: 1212.6.

(Glycolyl-5-acetamido-3,5-dideoxy-D-*glycero*-α-D-*galacto*-2-nonulopyranosyl)-1,2-dihexadecyl-*glycero*-3-phosphate (2d)

Phosphate **2c** (0.65 g, 0.494 mmol) was dissolved in a mixture of ethyl acetate (15 mL) and methanol (15 mL) and was hydrogenated in hydrogen at 50 psi (1 psi = 6.894 757 kPa) at room temperature in the presence of a catalytic amount of Pd/C. After 16 h, the products were filtered. The filtrate was concentrated under reduced pressure to give a colourless froth (0.60 g). A portion of this froth (50 mg) was dissolved in methanol–dichloromethane (2 mL, 1:1 *v*/*v*), and a solution of sodium methoxide in methanol (0.4 mL, 0.2% *w*/*v*) was added. After 80 min, the products were diluted with dichloromethane (5.0 mL) and purified by short column chromatography on silica gel. The appropriate fractions, which were eluted with dichloromethane–methanol (3:1 *v*/*v*), were combined and concentrated under reduced pressure to give the title compound **2d** as a colourless powder (30 mg, 69.5%). ^{1}H NMR ($CDCl_3$–CD_3OD–D_2O, 1:1:0.04 *v*/*v*) include the following peaks δ_H: 0.89 (6H), 1.28 (52H), 1.58 (4H), 2.04 (3H), 2.81 (1H). R_f (system B): 0.52. ^{31}P NMR ($CDCl_3$–CD_3OD–D_2O, 1:1:0.04 *v*/*v*) δ_P: 4.57. FAB$^-$ calcd. for $C_{48}H_{93}NO_{15}P^-$: 954.6; found: 954.6.

Methyl [glycolyl 5-acetamido-2,4,7-*O*-triacetyl-3,5-dideoxy-8-*O*-(5-acetamido-4,7,8,9-*O*-tetraacetyl-3,5-dideoxy-D-*glycero*-α-D-*galacto*-2-nonulopyranosylono-1′,9-lactone)-D-*glycero*-D-*galacto*-2-nonulopyranosid]onate (9)

The fully protected disialo-lacton peracetate **7** (0.600 g, 0.67 mmol) (R_f (system A) 0.32) was dissolved in dichloromethane (20.0 mL) and cooled to –20 °C. Acetyl chloride (8.0 mL) and water (0.1 mL) were then added. After 2 h, the reaction mixture was warmed up to room temperature, and stirring was continued for 16 h. The products were then concentrated under reduced pressure. The residue was dissolved in dichloromethane (40 mL) and washed with ice water (15 mL). The organic layer was separated and evaporated under reduced pressure. The residue was dissolved in acetonitrile (15 mL) and cooled to –20 °C. Calcium carbonate (0.48 g, 4.8 mmol), 2,6-di-*tert*-butylpyridine (0.30 mL, 1.34 mmol), ethylene glycol (2.0 mL, 35.86 mmol), and silver triflate (0.30 g, 1.17 mmol) were added. The reaction mixture was kept at –20 °C for 2 h and then allowed to warm up to room temperature. After 18 h, dichloromethane (10 mL) was added and the products were filtered. The filtrate was evaporated under reduced pressure, and the residue was dissolved in ethyl acetate (20 mL) and extracted with saturated aqueous sodium hydrogen carbonate (15 mL). The layers were separated and the dried ($MgSO_4$) organic layer was evaporated under reduced pressure. The residue was fractionated by short column chromatography on silica gel. The appropriate fractions, which were eluted with dichloromethane–methanol (96:4 *v*/*v*), were pooled and concentrated under reduced pressure to give the title compound **9** as a colourless froth (0.25 g, 41.8%). R_f (system A) 0.22. ^{1}H NMR ($CDCl_3$) include the following peaks δ_H: 1.90 (3H, s), 1.93 (3H, s), 2.02 (3H, s), 2.04 (6H, s), 2.09 (3H, s), 2.12 (3H, s), 2.23 (3H, s), 2.45 (1H, dd, J = 13.6, 5.6 Hz), 2.67 (1H, dd, J = 13.2, 4.8 Hz). FAB$^-$ calcd. for $C_{37}H_{51}N_2O_{23}^-$: 891.3; found: 891.3.

Methyl [glycolyl 5-acetamido-2,4,7-*O*-triacetyl-3,5-dideoxy-8-*O*-(5-acetamido-4,7,8,9-*O*-tetraacetyl-3,5-dideoxy-D-*glycero*-α-D-*galacto*-2-nonulopyranosylono-1′,9-lactone)-D-*glycero*-D-*galacto*-2-nonulopyranosyl]-1,2-dihexadecyl-*glycero*-3-H-phosphonate (10)

Methyl [glycolyl 5-acetamido-2,4,7-*O*-triacetyl-3,5-dideoxy-8-*O*-(5-acetamido-4,7,8,9-*O*-tetraacetyl-3,5-dideoxy-D-*glycero*-α-D-*galacto*-2-nonulopyranosylono-1′,9-lactone)-D-*glycero*-D-*galacto*-2-nonulopyranosid]onate (**9**) (0.100 g, 0.112 mmol) and triethylamonnium 1,2-dihexa-decyl-glycerol-3-H-phosphonate (**5**) (0.103 g, 0.146 mmol) were evaporated with dry pyridine (2 × 3 mL) and the residue was redissolved in anhydrous pyridine (3 mL) and cooled (ice-water bath). Pivaloyl chloride (50 μL, 0.406 mmol) was added. After a period of 10 min, the reaction was quenched by addition of water (0.5 mL). After a further period of

© 2006 NRC Canada

10 min, the products were partitioned between dichloromethane (15 mL) and saturated aqueous sodium hydrogen carbonate (2 × 15 mL). The layers were separated and the aqueous layer was back extracted with dichloromethane (2 × 5 mL). The combined organic layers were further washed with triethylammonium phosphate buffer (0.5 mol/L, pH 7.0, 10 mL). The layers were separated and the aqueous layer was back extracted with dichloromethane (5 mL). The combined dried ($MgSO_4$) organic layers were concentrated under reduced pressure. The residue was purified by flash column chromatography on silica gel. The appropriate fractions, which were eluted with dichloromethane–methanol (98:2 *v*/*v*), were pooled and evaporated under reduced pressure to give the title compound **11** as a colourless froth (0.130 g, 77.6%). R_f (system A) 0.32. ^{1}H NMR ($CDCl_3$) include the following peaks δ_H: 0.88 (6H, t, J = 6.6 Hz), 1.22–1.32 (52H, br), 1.52–1.59 (4H, br), 2.46 (1H, dd, J = 13.6, 5.6 Hz), 2.68 (1H, dd, J = 12.8, 5.2 Hz), 6.03 (0.5H), 7.82 (0.5H). ^{31}P NMR ($CDCl_3$) δ_P: 10.50, 10.41, 10.23, 10.13 ($^1J_{P\text{-}H}$ = 720 Hz). FAB$^-$ calcd. for $C_{72}H_{122}N_2O_{27}P^-$: 1477.8; found: 1477.9.

[Glycolyl 5-acetamido-3,5-dideoxy-8-*O*-(5-acetamido-3,5-dideoxy-D-*glycero*-α-D-*galacto*-2-nonulopyranosylono)-D-*glycero*-D-*galacto*-2-nonulopyranosyl]-1,2-dihexadecyl-*glycero*-3-phosphate (12)

The H-phosphonate diester **10** (65 mg, 43.9 μmol) was dissolved in a mixture of pyridine (3.0 mL) and water (0.5 mL), followed by addition of iodine (8.0 mg). After 30 min, the products were partitioned between dichloromethane (10 mL) and aqueous sodium sulfite (0.1 mol/L, 3.0 mL). The layers were separated and the aqueous layer was back extracted with dichloromethane (5 mL). The combined organic layers were further extracted with triethylammonium phosphate buffer (50 mol/L, pH 7.0, 5 mL). The aqueous layer was back extracted with dichloromethane (5 mL). The combined organic layers were dried ($MgSO_4$) and evaporated under reduced pressure. The residue was fractionated by short column chromatography on silica gel. The appropriate fractions, which were eluted with dichloromethane–methanol (85:15 *v*/*v*), were pooled and evaporated under reduced pressure to give phosphate **11** as a colourless froth (52 mg). A portion of this froth (40 mg, 27 μmol) was dissolved in anhydrous methanol (10.0 mL) followed by addition of a solution of sodium methoxide in methanol (1.5 mol/L, 0.1 mL). After 16 h, the products were evaporated under reduced pressure. The residue was taken up in methanol (8.0 mL) followed by the addition of water (0.16 mL). After 24 h, the products were concentrated under reduced pressure and the residue was dissolved in water (3.0 mL) and passed through a Sephadex G-25 column (1.6 cm × 35 cm), eluted with water. The appropriate fractions were pooled and lyophilized to give the title compound **12** as a colourless froth (30.0 mg, 66% over two steps). R_f (system B) 0.16. ^{1}H NMR ($CDCl_3$–CD_3OD–D_2O, 1:1:0.03 *v*/*v*) include the following peaks δ_H: 0.84 (6H), 1.23 (52H), 1.52 (4H), 1.99 (3H, s), 2.00 (3H, s), 2.56 (1H), 2.83 (1H). ^{31}P NMR ($CDCl_3$–CD_3OD–D_2O, 1:1:0.03 *v*/*v*) δ_P: 4.27. FAB$^-$ calcd. for $C_{59}H_{110}N_2O_{23}P^-$: 1245.7; found: 1245.6.

Acknowledgements

The authors thank Dr. Jianjun Li, Ms. Lisa Morrison, and Mr. Ken Chan at the Institute for Biological Sciences of the National Research Council of Canada, Ottawa Ontario, for mass spectrometry analysis.

References

1. A.K. Bhattacharjee, H.J. Jennings, C.P. Kenny, A. Martin, and I.C.P. Smith. J. Biol. Chem. **205**, 1926 (1975).
2. H.J. Jennings. Adv. Carbohydr. Chem. Biochem. **41**, 155 (1983).
3. H.J. Jennings and C. Lugowski. J. Immunol. **127**, 1011 (1981).
4. H.J. Jennings. *In* Carbohydrate-based drug discovery—Polysialic acid vaccines. *Edited by* C.-H. Wong. Wiley-VCH, Weinheim, Germany. 2003. pp. 357–380.
5. E.C. Gotschlich, B.A. Fraser, O. Nishimura, J.B. Robbins, and T.-Y. Liu. J. Biol. Chem. **256**, 8915 (1981).
6. M. Alexander Schmidt and K. Jann. FEMS Microbiol. Lett. **14**, 69 (1982).
7. E.C. Gotschlich, I.M. Goldschneider, M.L. Lepow, and R. Gold. Antibodies in human diagnosis and therapy. *Edited by* E. Huber and R.M Krause. Raven Press, New York. 1977. pp. 391–402.
8. F.A. Wyle, M.S. Artenstein, B.L. Brandt, E.C. Tramont, D.L. Kasper, P.L. Altieri, S.L. Berman, and J.P. Lowenthal. J. Infect. Dis. **126**, 514 (1972).
9. J. Finne. J. Biol. Chem. **257**, 11966 (1982).
10. R.A. Pon, M. Lussier, Q.-L. Yang, and H.J. Jennings. J. Exp. Med. **185**, 1929 (1997).
11. H.J. Jennings, A. Gamian, and F.E. Ashton. J. Exp. Med. **165**, 1207 (1987).
12. H.J. Jennings, A. Gamian, F. Michon, and F.E. Ashton. J. Immunol. **142**, 3585 (1989).
13. F.A. Troy. Glycobiology, **2**, 5 (1992).
14. J. Gervay, P.S. Ramamoorthy, and N.N. Mamuya. Tetrahedron, **53**, 11039 (1997).
15. P.V. Nikrad, M.A. Kashem, K.B. Wlasichuk, G. Alton, and A.P. Venot. Carbohydr. Res. **250**, 145 (1993).
16. Z.-G. Wang, X.-F. Zhang, Y. Ito, Y. Nakahara, and T. Ogawa. Bioorg. Med. Chem. **4**, 1901 (1996).
17. C.B. Reese and H. Yan. J. Chem. Soc. Perkin Trans. 1, 2619 (2002).
18. S. Osanai, M. Higami, Y. Ono, and E. Ohta. J. Mater. Chem. **7**, 1405 (1997).
19. V. Ozola, C.B. Reese, and Q. Song. Tetrahedron Lett. **37**, 8621 (1996).
20. R. Roy and R.A. Pon. Glycoconjugate J. **7**, 3 (1990).
21. S.M. Anderson, C.-C. Ling, P. Zhang, K. Townson, H.J. Willison, and D.R. Bundle. Org. Biomol. Chem. **2**, 1199 (2004).
22. U. Dabrowski, H. Friebolin, R. Brossmer, and M. Supp. Tetrahedron Lett. **20**, 4637 (1979).

© 2006 NRC Canada

Pyrolysis of 2-methoxy-5,5-dimethyl-2-methylthio-2,5-dihydro[1,3,4]oxadiazole studied with photoelectron spectroscopy and DFT calculations — He(I) photoelectron spectrum of methoxy(methylthio)carbene[1]

N.H. Werstiuk, A. Klys, and J. Warkentin

Abstract: Gas-phase pyrolysis of 2-methoxy-2-methylsulfanyl-5,5-dimethyl-2,5-dihydro[1,3,4]oxadiazole (**1**) (also known as 2-methoxy-5,5-dimethyl-2-methylthio-2,5-dihydro[1,3,4]oxadiazole and 2-methoxy-2-methylthio-5,5-dimethyl-Δ^3-l,3,4-oxadiazoline) in the source of an UV photoelectron spectrometer, by means of a CW CO_2 laser as directed heat source, gave a photoelectron (PE) spectrum that included ionization bands belonging to acetone and methoxy(methylthio)carbene (**3**). Photoelectron spectra of authentic samples of (*E*)-1,2-dimethoxy-1,2-dimethylthioethene (**4**), (*Z*)-1,2-dimethoxy-1,2-dimethylthioethene (**5**), *S*-methyl thioethanoate (**6**), and *O*-methyl ethanethioate (**7**), which can be derived by dimerization and rearrangement of the carbene, established that these compounds are not present in the pyrolysate. DFT calculations at the B3PW91/6-31+G(d,p) level and simulation of PE spectra at the B3LYP/6-31+G(d,p) level were instrumental in the interpretation of the experimental results. From the available experimental and calculated data, **3** is formed in a Sickle conformation upon pyrolysis of **1**. Transition states for the rearrangement of **3** were examined with QTAIM.

Key words: 2-methoxy-5,5-dimethyl-2-methylthio-2,5-dihydro[1,3,4]oxadiazole, pyrolysis, He(I) photoelectron spectroscopy, methoxy(methylthio)carbene, DFT calculations, QTAIM.

Résumé : La pyrolyse en phase gazeuse du 2-méthoxy-2-méthylsulfanyl-5,5-diméthyl-2,5-dihydro[1,3,4]oxadiazole (**1**) (aussi connu comme 2-méthoxy-5,5-diméthyl-2-méthylthio-2,5-dihydro[1,3,4]oxadiazole et comme 2-méthoxy-2-méthylthio-5,5-diméthyl-Δ^3-1,3,4-oxadiazoline) dans la source d'un spectromètre photoélectronique ultraviolet utilisant un laser au CO_2 à onde continue (OC) comme source focalisée de chaleur permet d'obtenir un spectre photoélectronique (PE) qui comprend des bandes d'ionisation appartenant à l'acétone ainsi qu'au méthoxy(méthylthio)carbène (**3**). Les spectres photoélectroniques d'échantillons authentiques de (*E*)-1,2-diméthoxy-1,2-diméthylthioéthène (**4**), de (*Z*)-1,2-diméthoxy-1,2-diméthylthioéthène (**5**), de thioéthanoate de *S*-méthyle et d'éthanethioate de *O*-méthyle (**7**) qui pourraient dériver d'une dimérisation et d'un réarrangement du carbène on permis d'établir que ces composés ne sont pas présents dans le produit de pyrolyse. Des calculs de la théorie de la densité fonctionnelle (TDF) au niveau B3PW91/6-31+G(d,p) et une simulation des spectres PE au niveau B3LYP/6-31+G(d,p) ont été utilisés en partie pour interpréter les résultats expérimentaux. Sur la base des données calculées et expérimentales, la pyrolyse du composé **1** conduit à la formation de l'intermédiaire **3** dans une conformation de Sickle. Les états de transition pour le réarrangement de l'intermédiaire **3** ont été étudiés par la méthode « QTAIM ».

Mots clés : 2-méthoxy-5,5,-diméthyl-2-méthylthio-2,5-dihydro[1,3,4]oxadiazole, pyrolyse, spectroscopie photoélectronique He(I), méthoxy(méthylthio)carbène, calculs selon la théorie de la densité fonctionnelle (TDF), QTAIM.

[Traduit par la Rédaction]

Introduction

Ultraviolet photoelectron (PE) spectroscopy, when combined with quantum chemical calculations of molecular orbital eigenvalues (energies) and eigenvectors (MOs), gives information about the electronic structure and bonding of stable as well as transient species that is provided by no other technique. PE spectra of transient carbenes are very rare (1) because of the high reactivity of these species. Special instrumentation is required. Reactive intermediates are

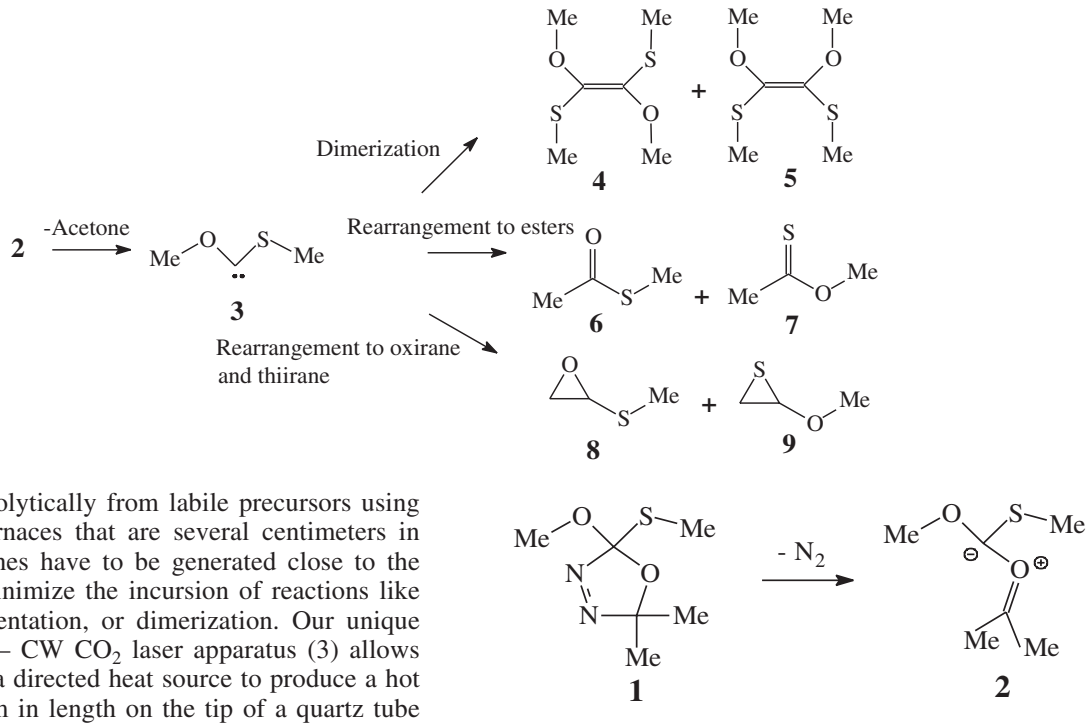
Received 20 July 2006. Published on the NRC Research Press Web site at http://canjchem.nrc.ca on 22 April 2006.

N.H. Werstiuk,[2] A. Klys, and J. Warkentin. Department of Chemistry, McMaster University, Hamilton, ON L8S 4M1, Canada.

[1]This article is part of a Special Issue dedicated to Professor Walter A. Szarek.
[2]Corresponding author (e-mail: werstiuk@mcmaster.ca).

 doi:10.1139/V06-026 © 2006 NRC Canada

Scheme 1.



usually generated pyrolytically from labile precursors using electrically heated furnaces that are several centimeters in length (2). Yet carbenes have to be generated close to the ionization beam to minimize the incursion of reactions like rearrangement, fragmentation, or dimerization. Our unique UV PE spectrometer – CW CO_2 laser apparatus (3) allows us to use the laser as a directed heat source to produce a hot zone as short as 1 mm in length on the tip of a quartz tube positioned at about 1 cm from the point of intersection with the ionization beam. We used this setup successfully to obtain PE spectra of short-lived, reactive species such as benzazete and *o*-benzyne (3), l-(2-thiaindane)ketene and benzocyclobutene-thione (4, 5), 1,2-cyclohexadiene (6), (dimethoxy)carbene (7), and p-substituted phenylketenes (8) through pyrolysis of suitable precursors. We have also observed cycloocta-2(*Z*),4(*E*)-dien-1-one (9) and bicyclo-[3.2.0]hepta-1,3,6-triene (10) and attempted to prepare and detect *N*,*N*-dimethylcyclohepta-1(*E*),3(*Z*),5(*Z*)-trien-1-amine (11).

We decided to study the gas-phase decomposition of a series of oxadiazolines because pyrolysis of these compounds in solution (12) yields products that indicate the formation of carbenes as intermediates. In benzene, 2-methoxy-2-methylsulfanyl-5,5-dimethyl-2,5-dihydro[1,3,4]oxadiazole (**1**) gave ethenes **4** and **5** in the absence of traps; esters **6** and **7** and the products of C-H insertion (**8** and **9**) were not observed (13). We earlier prepared and studied (dimethoxy)carbene generated by pyrolysis of 2,2-dimethoxy-5,5-dimethyl-Δ^3-l,3,4-oxadiazoline (7). The particular choice of oxadiazoline **1** for this study was made because (*a*) it is a convenient source of **3**, (*b*) it gave us the additional opportunity to confirm the mode of its decomposition because on a different path **1** can yield methyl(thiomethyl)carbonate and 2-diazopropane. The latter could decompose to nitrogen and (dimethyl)carbene that would yield propene; (*c*) Its pyrolysis has been studied in solution (13), and (*d*) it is the first member in a series of similar oxadiazolines that could be used as possible precursors of O,S- and O,N-substituted carbenes in the gas phase. Possible reactions of **3** derived from ylide **2** — the possible first-formed intermediate — are summarized in Scheme 1.

Our computational study on the first adiabatic and vertical ionization potentials of carbenes (14) provided us with a calculational method (B3LYP/6-31+G(*d*) for reliably predicting these values. By applying these calculations to methoxy(methylthio)carbene (**3**) and using the program PESPEC (15) to simulate PE spectra, we expected to identify **3** through its ionization potentials if it was present in the pyrolysis spectrum of **1** and possibly establish its preferred conformation. Four conformers of carbene **3**, **3-W**, **3-S1**(Sickle1), **3-S2**(Sickle2), and **3-U** (Fig. 1), excluding the methyl rotamers, are possible.

In this paper we report the results of a He(I) PE spectroscopic study of the pyrolysis of oxadiazoline **1** along with DFT (Gaussian 98 and 03 (16, 17)) calculational data on **1**, its decomposition into ylide **2**, decomposition of **2** into methoxy(methylthio)carbene (**3**), and rearrangement of the latter to *S*-methyl thioethanoate (**6**), *O*-methyl ethanethioate (**7**), (methylthio)oxirane (**8**), and (methoxy)thiirane (**9**).

Computational details

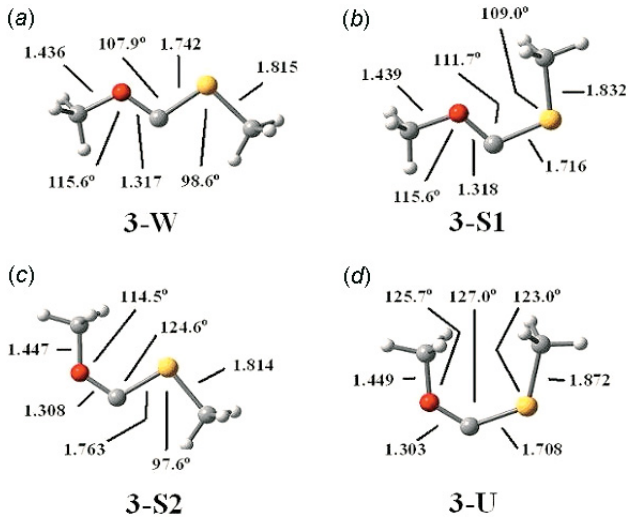
Equilibrium-optimized geometries and wave functions were obtained at the DFT level implemented in Gaussian 98 (16) and 03 (17) using the B3PW91 functional (18, 19) at the 6-31+G(d,p) level. All optimizations converged using the default convergence criteria, and vibration analyses were performed for all species to confirm that they were minima or transition states. PE spectra were simulated with the program PESPEC (15) based on calculations carried out at the B3LYP/6-31+G(d,p) level (14). Two recent publications document the procedure used to simulate spectra (9, 10). QTAIM (20) analyses were carried out with AIM 2000 (21).

Experimental details

Oxadiazoline **1** was prepared by the method described previously (13). Ethenes **4** and **5** were prepared by pyrolysis

© 2006 NRC Canada

Fig. 1. Optimized geometries of methoxy(methythio)carbene conformers and selected geometrical parameters. The red sphere is oxygen and the yellow sphere is sulfur.



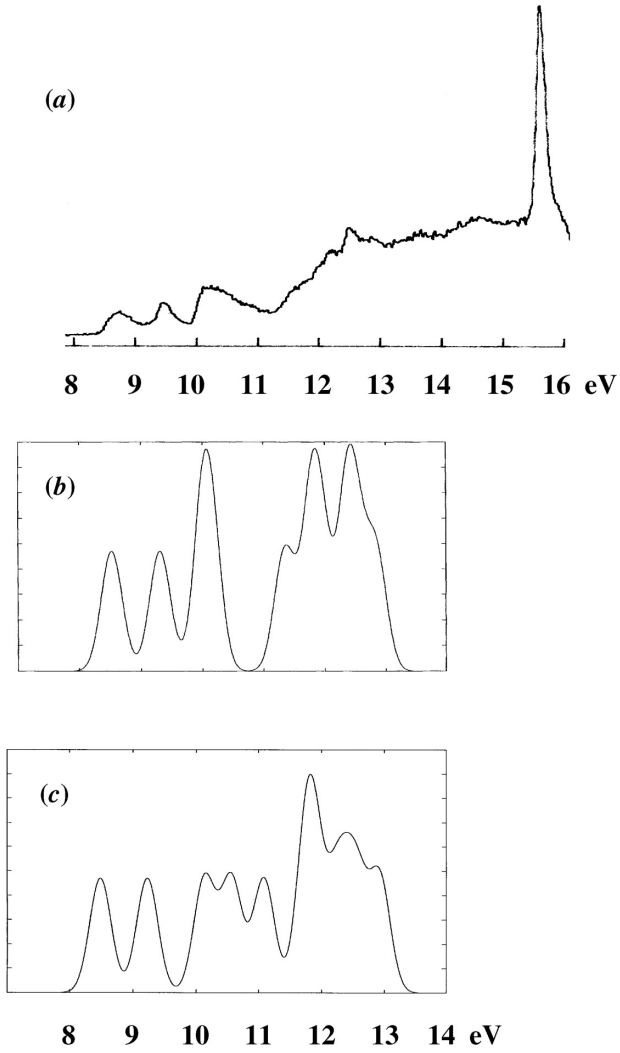
of **1** in benzene in the absence of traps as described previously (13). Esters **6** and **7** were prepared with the method described by Sah (22). PE spectra were recorded with our locally built UV PE spectrometer and calibrated with the 15.6 eV IP band of N_2 that is visible in all spectra (23). Linearity of the spectral scale was checked with the lowest IP bands of methyl iodide at 9.54 and 10.16 eV prior to the experiments. Our unique UV PE spectrometer – CW CO_2 laser apparatus (6) that is fitted with a heated probe, allows us to use the laser as a directed heat source to produce a hot zone as short as 1 mm in length at the tip of a quartz tube positioned about 1 cm from the point of intersection with the ionization beam. The oxadiazoline (20–30 mg) was placed in a 5 mL flask that was attached to a probe assembly through a ground glass joint. The sample was degassed with three freeze–pump–thaw cycles at roughing vacuum and the probe was inserted into the source of the PE spectrometer while the sample was maintained at –78 °C. The temperature of the dry ice bath was gradually increased until a pressure of ~3 × 10^{-3} Torr (1 Torr = 133.322 4 Pa) could be maintained with little fluctuation. A PE spectrum of **1** was obtained and the laser beam was focused on the tip of the quartz nozzle at the end of the probe assembly in the source. The laser was tuned to a line that yielded a temperature of <500 °C as determined by calibration studies and spectra of the pyrolysate obtained. Spectra of ethenes **4** and **5** as well as esters **6** and **7** were obtained using the method described for **1**. Collected spectra — usually 20–30 — were averaged to yield the spectra reported in this paper.

Results and discussion

Experimental and computational studies

The PE spectrum of **l** is displayed as Fig. 2*a* based on the relative areas of the bands at 8.8, 9.5, and 10.2 eV (ca. 1:1:3), these bands correspond to the first five IPs. The five conformers **1a**–**1e** (Figs. 3*a*–3*e*) were minima on the oxadiazoline potential energy surface at the B3PW91/6-31+G(d,p) level. The ZPE-corrected electronic energies (E_o)

Fig. 2. (*a*) PE spectrum of 2-methoxy-2-methylthio-5,5-dimethyl-Δ^3-l,3,4-oxadiazoline (**1**); (*b*) simulated PE spectrum of 2-methoxy-2-methylthio-5,5-dimethyl-Δ^3-l,3,4-oxadiazoline conformer **1a**; and (*c*) simulated PE spectrum of 2-methoxy-2-methylthio-5,5-dimethyl-Δ^3-l,3,4 oxadiazoline conformer **1b**.



of **1a**, **1b**, **1c**, **1d**, and **1e** are –893.564 302 (0.00 kcal mol^{-1}, 1 cal = 4.184 J), –893.562 989 (+0.82), –893.561 262 (+1.91), –893.560 307 (+2.44), and –893.558 525 (+3.56) hartrees, respectively. Noteworthy is the fact that the CH_3-O- and CH_3-S- groups of **1a** and **1c** have gauche–gauche orientations in which the anomeric effect is expected to be maximal as it is in the case of the gauche–gauche conformation of dimethoxymethane (24). The relative energies indicate that conformer **1a** should be populated preferentially in the gas phase followed by **1b**. At the B3LYP/6-31+G(d,p) level, **1b** is 1.06 kcal mol^{-1} higher in energy (ΔE_o) than **1a**. To a first approximation, a sum of the simulated spectrum of **1a** (Fig. 2*b*) and a minor contribution from **1b** (Fig. 2*c*) — in keeping with the shoulder on the band centered at 9.5 eV — correlates well with the experimental spectrum. That the first three bands of **1** correspond to five IPs is seen in the simulated spectra of conformers **1a** and **1b**, displayed as Figs. 2*b* and 2*c*. The MOs corresponding to the first two bands of **1a** are displayed as Figs. 4*a* and 4*b*. It is seen that the HOMO

© 2006 NRC Canada

Fig. 3. Optimized geometries of 2-methoxy-2-methylthio-5,5-dimethyl-Δ^3-l,3,4-oxadiazoline conformers **1a**–**1e**. The blue sphere is nitrogen, the red sphere is oxygen, and the yellow sphere is sulfur.

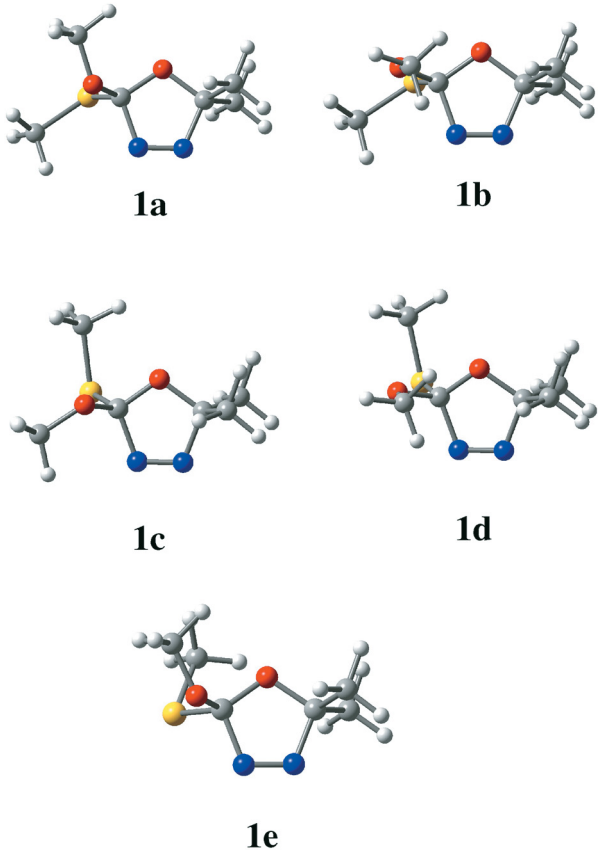
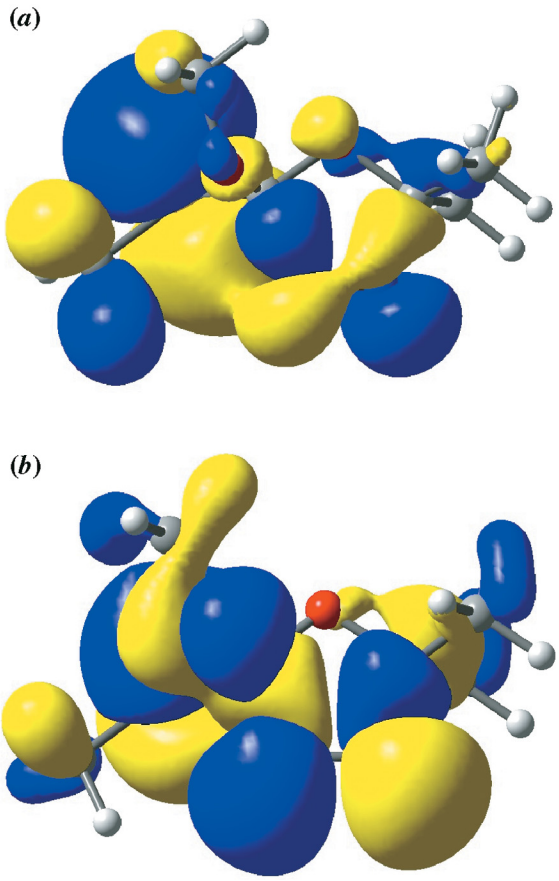


Fig. 4. Molecular orbitals of the 2-methoxy-2-methylthio-5,5-dimethyl-Δ^3-l,3,4-oxadiazoline conformer **1a** at the B3LYP/6-31+G(d,p) level. (*a*) HOMO and (*b*) HOMO–1 (contour value 0.02).



has considerable n_S character in keeping with the fact that it exhibits the lowest IP. On the other hand, HOMO–1 has significant n_N lone-pair character. The peak at 12.63 eV in Fig. 2*a* belongs to a trace of water.

The PE spectra of **1** and its pyrolysate are displayed as Figs. 5*a* and 5*b*, respectively. We take the absence of the band at 10.2 eV of **1** — labeled with a triangle (Fig. 5*a*) — in the spectrum of the pyrolysate from **1** (Fig. 5*b*) as an indication that the pyrolysis of **1** was complete. The relatively sharp feature at 9.7 eV in Fig. 5*b* is due to the lowest IP of acetone. Subtraction of a PE spectrum of acetone yielded the spectrum displayed as Fig. 5*c*.

The ZPE-corrected electronic energies and relative energies of the carbene conformers **3-W**, **3-S1**(Sickle1), **3-S2**(Sickle2), and **3-U** — the optimized structures and selected geometrical parameters are displayed in Fig. 1 — are collected in Table 1. Geometry optimizations were carried out with default convergence criteria without enforcing planarity. It is seen that **3-W** and **3-S1**(Sickle1) are close in energy and that **3-U**, the most sterically hindered conformer, is the least stable conformation of the four carbenes. It is seen that the C—O and C—S bonds to the carbenic carbon are ~0.1 Å shorter than the CH_3—O and CH_3—S bonds, a consequence of the n–π interaction between the lone pairs on the heteroatoms and the nominally vacant p orbital on the carbenic carbon. Also evident is a significant lengthening of the CH_3—O and CH_3—S bonds in the **3-S1**, **3-S2**, and **3-W** species, accountable on the basis of an anti-coplanar n–σ* interaction between the in-plane lone pair and a CH_3—X σ bond. The ZPE-corrected barrier for rearrangement of **3-W** to **3-S1** — the rotational barrier — is 18.42 kcal mol^{-1}; for the rearrangement of **3-S1** to **3-W**, it is 17.84 kcal mol^{-1}. In Fig. 6 are displayed the acetone-stripped spectrum (Fig. 6*a*) and the simulated spectra (Figs. 6*b*–6*d*) of the **3-S1**, **3-W**, and **3-S2** carbene conformers, respectively. The stripped spectrum correlates best with the simulated spectrum of carbene **3-S1**.

Transition states for extrusion of nitrogen from **1a** and **1c**, with computed barriers of 33.38 and 30.82 kcal mol^{-1}, respectively, and for the decomposition of ylide **2** are displayed in Fig. 7 along with selected geometrical parameters. Ylide **2** was derived from **TS-1c**, computed at the B3PW91/6-31+G(d,p) level (Table 2). Figure 7*a* displays **TS-1a**. There are two displays (Figs. 7*b* and 7*c*) of transition state **TS-1c**. Figure 7*c* displays **TS-1c** rotated in-plane clockwise by 90°. It is seen that the improper dihedral angle labeled as C1-C2-C3-S4 increases from 21.4° in **TS-1c** to 50.3° in ylide **2** (Fig. 2*d*) and 64.6° in **TS-2**, the transition state for the decomposition of **2** (Table 3). Ylide **2** is in a very shallow minimum (Table 2). Given the very small barrier for its decomposition to acetone and **3**, if **2** exists it must

© 2006 NRC Canada

Table 1. Thermochemical data for methoxy(methylthio)carbene conformers and the barrier for isomerization of **3-W** to **3-S1** at the B3PW91/6-31+G(d,p) level.

Carbene or transition state	E_{elec} [a]	E_o [a] (E_{elec}+ZPE)	Barrier (ΔE_o, kcal mol^{-1})
3-W	–591.150 788	–591.065 561	0.00
3-S1	–591.149 520	–591.064 637	0.59
3-S2	–591.145 321	–591.060 109	3.42
3-U	–591.131 638	–591.047 051	11.62
TS-3W→3-S1	–591.120 662	–591.036 202	18.42[b]

[a]In hartrees.
[b]Relative to **3-W**. For the isomerization of **3-S1** to **3-W**, the value is 17.84 kcal mol^{-1}.

Fig. 5. (*a*) PE spectrum of 2-methoxy-2-methylthio-5,5-dimethyl-Δ^3-l,3,4-oxadiazoline (**1**); (*b*) PE spectrum of 2-methoxy-2-methylthio-5,5-dimethyl-Δ^3-l,3,4-oxadiazoline pyrolysate; and (*c*) acetone-stripped PE spectrum of 2-methoxy-2-methylthio-5,5-dimethyl-Δ^3-l,3,4-oxadiazoline pyrolysate.

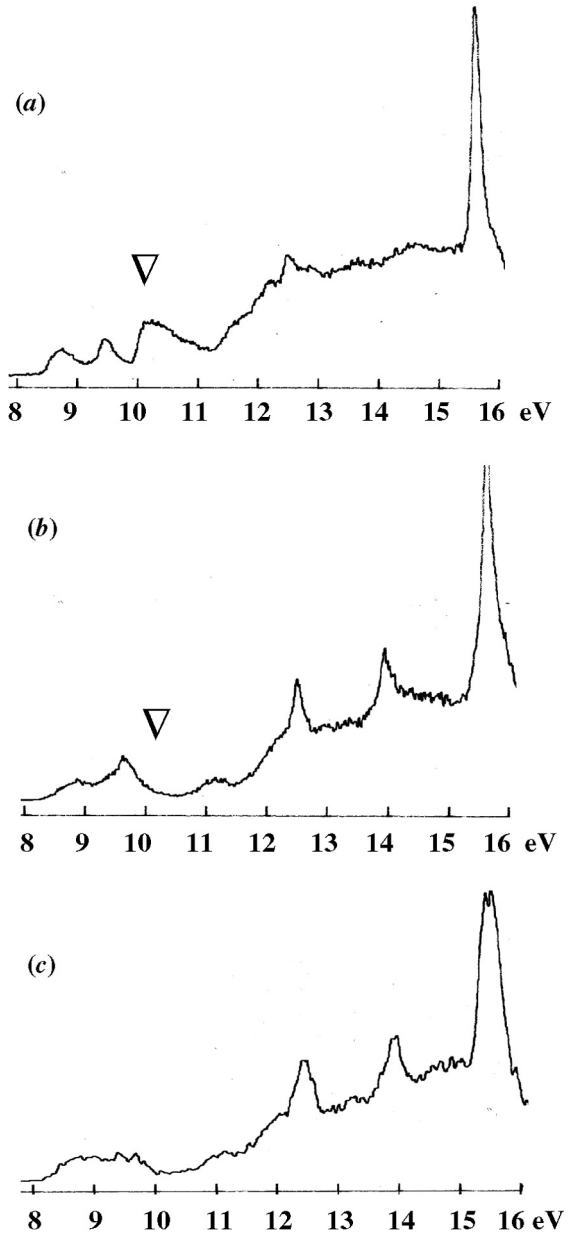
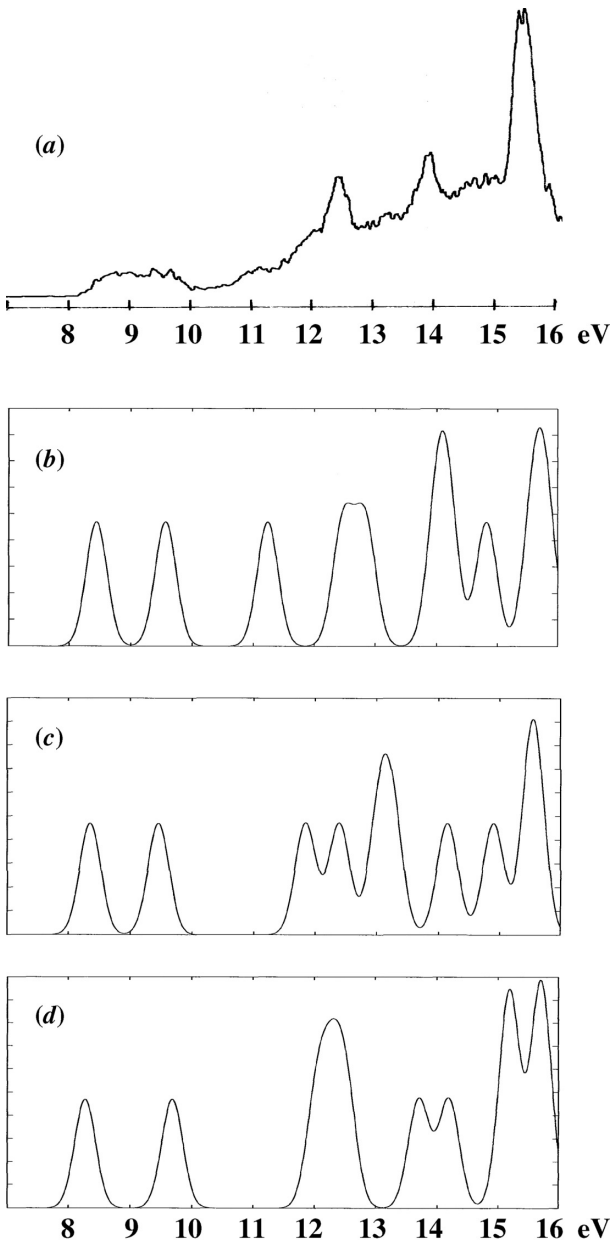


Fig. 6. (*a*) Acetone-stripped PE spectrum of 2-methoxy-2-methylthio-5,5-dimethyl-Δ^3-l,3,4-oxadiazoline pyrolysate; (*b*) simulated spectrum of methoxy(methythio)carbene conformer **3-S1**; (*c*) simulated spectrum of methoxy(methythio)carbene conformer **3-W**; and (*d*) simulated spectrum of methoxy(methythio)carbene conformer **3-S2**.



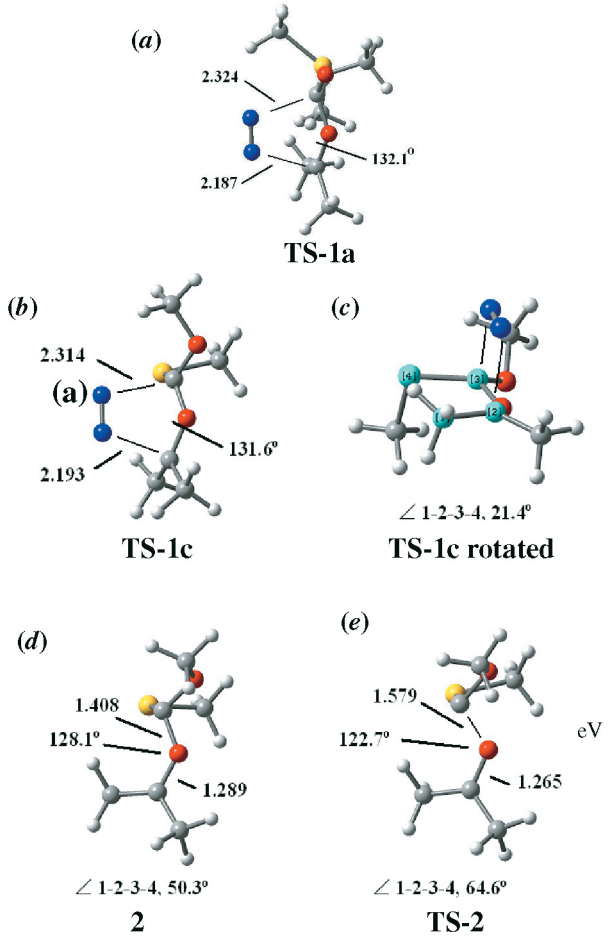
© 2006 NRC Canada

Table 2. Thermochemical data for the extrusion of N_2 from oxadiazoline conformers **1a** and **1c** at the B3PW91/6-31+G(d,p) level.

Oxadiazoline or transition state	E_{elec}[a]	E_o[a] (E_{elec}+ZPE)	Barrier (ΔE_o, kcal mol^{-1})
1a	–893.749 928	–893.564 302	
TS-1a	–893.691 376	–893.511 105 (–174.6)[b]	33.38[c]
1c	–893.746 683	–893.561 262	
TS-1c	–893.691 376	893.512 141 (–174.4)[b]	30.82[d]

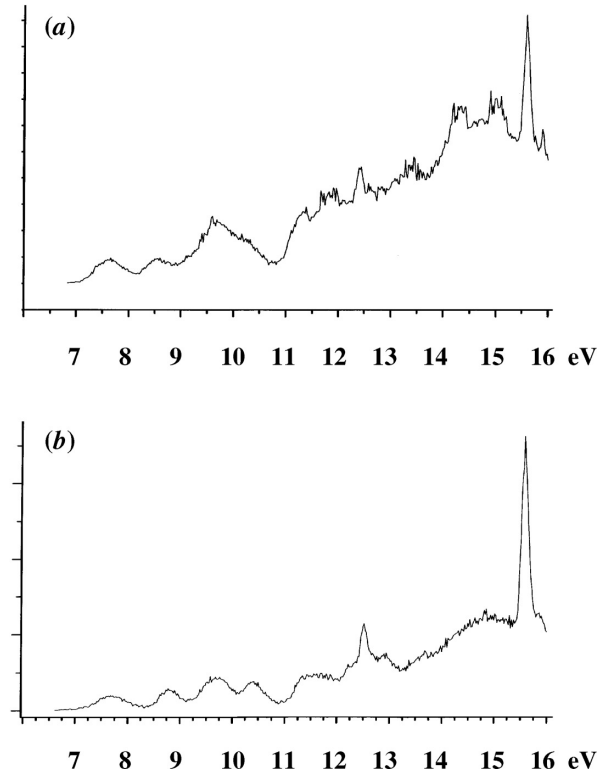
[a]In hartrees.
[b]The imaginary frequency in cm^{-1}.
[c]Relative to **1a**.
[d]Relative to **1c**.

Fig. 7. (*a*) Transition state for thermal cycloreversion of 2-methoxy-2-methylthio-5,5-dimethyl-Δ^3-l,3,4-oxadiazoline conformer **1a**; (*b*) transition state for thermal cycloreversion of 2-methoxy-2-methylthio-5,5-dimethyl-Δ^3-l,3,4-oxadiazoline conformer **1c**; (*c*) transition state for thermal cycloreversion of 2-methoxy-2-methylthio-5,5-dimethyl-Δ^3-l,3,4-oxadiazoline conformer **1c** rotated 90° in plane; (*d*) optimized geometry of ylide **2**; and (*e*) transition state **TS-2** for decomposition of **2** into acetone and carbene **3-S1**. The blue sphere is nitrogen, the red sphere is oxygen, and the yellow sphere is sulfur.



be a very short-lived species. Figure 7*e* (**TS2**) clearly shows the putative carbene in the upper portion of the structure being formed in the **3-S1** conformation. Even in **TS-c1** (Fig. 7*b*), the putative carbene fragment is approaching the

Fig. 8. (*a*) PE spectrum of tetrasubstituted (*E*)-ethene (**4**) and (*b*) PE spectrum of tetrasubstituted (*Z*)-ethene (**5**).



Sickle1 conformation, **3-S1**. We found that the same situation — not displayed — holds for conformer **1b**. This is also the case for **TS-1a**: in forming the ylide and then the carbene, the -OCH_3 is expected to rotate to yield **3-S1**, not the high-energy conformer, **3-U**.

We isolated (*E*)- and (*Z*)-ethenes **4** and **5** from a solution-phase pyrolysis (13) and recorded their PE spectra (Figs. 8*a* and 8*b*). Given that **4** and **5** exhibit their lowest IPs below 8 eV, it is clear that **4** and **5** are not present in the pyrolysate of **1**. We also recorded PE spectra of authentic samples of esters **6** (Fig. 9*b*) and **7** (Fig. 9*c*), the potential rearrangement products of **3**. While the spectrum of **7** (Fig. 9*c*) bears some resemblance to the stripped spectrum displayed again as Fig. 9*a*, the pyrolysate certainly does not contain significant quantities of **6**.

Transition states for the formation of esters **6** and **7** from **3-W**, **3-S1**, and **3-S2** were located; **TS-3W→6** and

© 2006 NRC Canada

Table 3. Thermochemical data for decomposition of ylide **2** at the B3PW91/6-31+G(d,p) level.

Compound	E_{elec}[a]	E_o[a] (E_{elec}+ZPE)	H[a,b] (E+RT)	G[a,c]
2	–784.215 044	–784.043 708	–784.030 238	–784.083 106
TS-2	–784.213 929 (–290.9)[d]	–784.043 781	–784.030 679	–784.030 679
Barrier (kcal mol^{-1})	0.73	–0.04	–0.028	0.53

[a]In hartrees.
[b]Corrected to 298.15 K ($E = E_o + E_{vib} + E_{rot} + E_{trans}$).
[c]Corrected to 298.15 K ($G = H - TS$).
[d]The imaginary frequency of the transition state.

Table 4. Thermochemical data (E_{elec}, E_o, and ZPE-corrected barriers) for the rearrangements of methoxy(methylthio)carbene conformers and at the Becke 3PW91/6-31+G(d,p) level.

Rearrangement	Transition state[a]	E_{elec}[a] transition state	E_o[a] (E_{elec}+ZPE) transition state	ZPE-corrected barriers (kcal mol^{-1})[b]
3-W→6	**TS-3W→6**	–591.074 694 (–909.9)[c]	–590.992 578	45.80
3-W→7	**TS-3W→7**	–591.067 067 (–802.9)[c]	–590.983 616	51.42
3-S1→6	**TS-3S1→6**	–591.074 872 (–913.1)[c]	–590.992 679	45.15
3-S2→7	**TS-3S2→7**	–591.064 403 (–815.0)[c]	–590.980 890	49.71
3-W→8	**TS-W→8**	–591.080 347 (–1176.1)[c]	–591.000 031	41.53
3-W→9	**TS-W→9**	–591.089 288 (–1176.7)[c]	–591.008 201	36.50
3-S1→8	**TS-S1→8**	–591.078 146 (–1185.3)[c]	–590.977 577	42.08
3-S2→9	**TS-S2→9**	–591.086 554 (–1199.5)[c]	–591.005 804	33.95

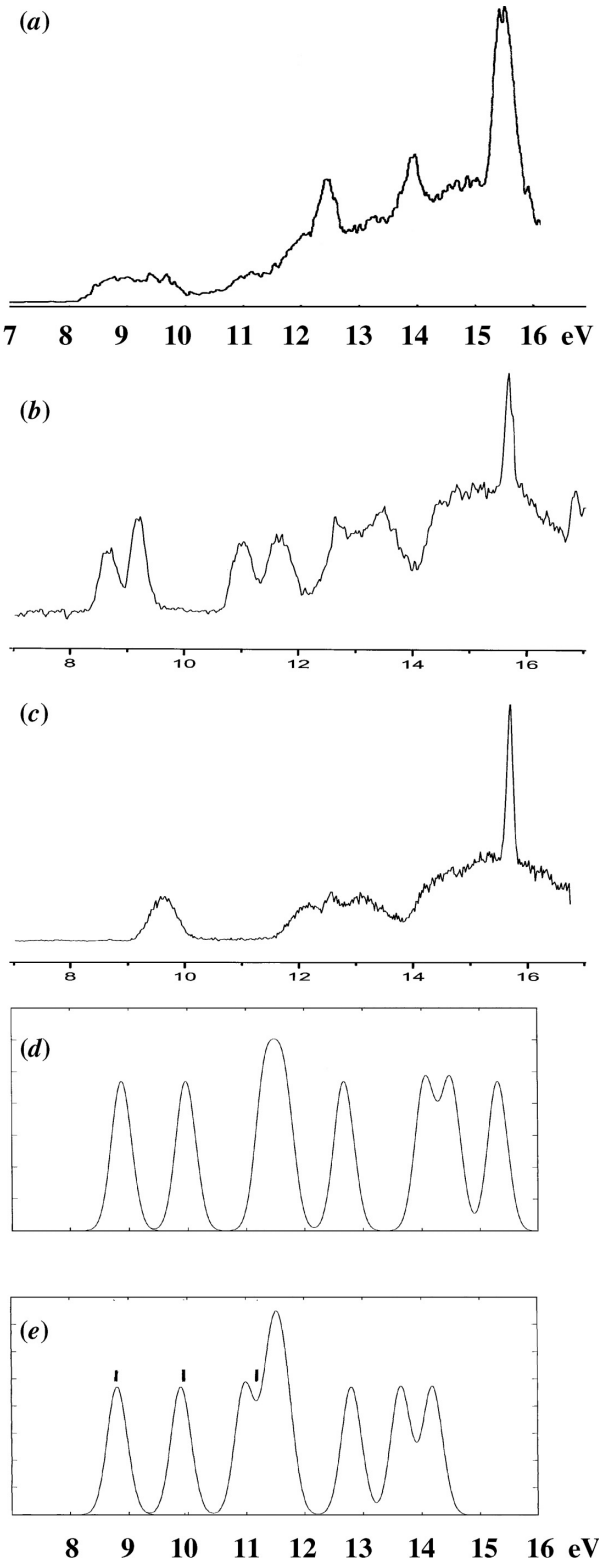
[a]See Figs. 10 and 11 (Supplementary information)[3] for displays of molecular graphs.
[b]The ZPE-corrected energies (E_o) of the methoxy(methylthio)carbene conformers are given in Table 3.
[c]The imaginary frequency in cm^{-1}.

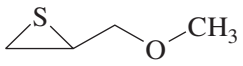
TS-3W→7 are the molecular graphs (Figs. 10*a* and 10*b*) of the transition structures for formation of **6** and **7** from **3-W**, while **TS-3S1→6** and **TS-3S2→7** are the molecular graphs (Figs. 10*c* and 10*d*) of the transition structures for the formation of **6** and **7** from **3-S1** and **3-S2**, respectively, are included as Supplementary information.[3] Only **TS-3S2→7** exhibits a penta-coordinate carbon. The molecular graphs (Figs. 11*a* and 11*b*) of the transition states for the formation of oxirane **8** and thiirane **9** from **3-W** are **TS-3W→8** and **TS-3W→9**, respectively (Table 4). **TS-3S1→8** and **TS-3S2→9** are the molecular graphs (Figs. 11*c* and 11*d*) of the formation of **8** and **9** from **3-S1** and **3-S2**, respectively, are also included as Supplementary information.[3] The migrating hydrogen is dicoordinate in all cases. Except for the rearrangement of **3-S2** to thiirane **9**, all barriers for the formation of esters **6** and **7** from **3-W**, **3-S1**, and **3-S2** exceed 40 kcal mol^{-1}, with the barriers for formation of *S*-methyl thioethanoate (**6**) being roughly 5 kcal mol^{-1} less than the barriers of formation of *O*-methyl ethanethioate (**7**). Given that the relative intensities of the bands at 9.3 and 11.9 eV of the stripped spectrum and the spectrum of **7** differ significantly, and more importantly, our computational studies show that the rearrangement of **3** to **6** would be preferred by 5 kcal mol^{-1} over the rearrangement to **7** in the gas phase, we conclude that **6** and **7** are also not present in the pyrolysate of **1**. As regards the formation of (methylthio)oxirane (**8**) and (methoxy)thiirane (**9**), they were not detected as products in the solution-phase pyrolysis of **1** (13). While the barrier for the rearrangement of **3** into **8** (40 kcal mol^{-1}) is in the range of the barriers of the formation of esters **6** and **7** that are not observed as products, the lower barrier of the formation of **9** from **3-W** and **3-S2** suggests that it may be a possible product. A search of the literature established that **9** is an unknown compound. Its simulated PE spectrum is displayed as Fig. 9*d*. On the other hand, (methoxymethylene)thiirane (**10**) is a known compound and its spectrum has been recorded (25). Consequently, we simulated the PE spectrum of **10** and compared it with the experimental one to validate the simulation of the spectrum of **9**. The simulated spectrum of **10** is displayed in Fig. 9*e* along with vertical bars that indicate the first three experimentally determined IPs. It is seen that there is excellent agreement between the important first two calculated IPs and the experimental vertical IPs. While the predicted value for the third IP is slightly higher than the experimental one, the assignment of the third experimental vertical IP may be inexact because the third experimental band is broad. In fact, it is clear from our simulated spectrum that the fourth band is due to two overlapping bands and not one as stated in the publication (25). We take the fact that the first three vertical IPs of **10** are reproduced with very good accuracy as an indication that the PE spectrum of **9** is also simulated with good accuracy. If this is the case, then the difference in the spectra displayed as Figs. 9*a* and 9*d* in the region of 11 to 12 eV, establishes that the experimental spectrum does not correspond to thiirane **9**.

[3] Supplementary data for this article are available on the journal Web site (http://canjchem.nrc.ca) or may be purchased from the Depository of Unpublished Data, Document Delivery, CISTI, National Research Council Canada, Ottawa, ON K1A 0R6, Canada. DUD 5014. For more information on obtaining material refer to http://cisti-icist.nrc-cnrc.gc.ca/irm/unpub_e.shtml.

© 2006 NRC Canada

Fig. 9. (*a*) Acetone-stripped PE spectrum of 2-methoxy-2-methylthio-5,5-dimethyl-Δ^3-l,3,4-oxadiazoline pyrolysate; (*b*) PE spectrum of *S*-methyl thioethanoate (**6**); (*c*) PE spectrum of *O*-methyl ethanethioate (**7**); (*d*) simulated PE spectrum of (methoxy)thiirane (**9**); and (*e*) simulated PE spectrum of (methoxymethylene)thiirane (**10**) and vertical bars indicating its three lowest experimental Ips.





10

Conclusions

This study nicely illustrates the versatility of our photoelectron spectrometer in studying organic reactions and transient species in the gas phase in combination with spectrum simulation and DFT calculations. Methoxy(methylthio)carbene has been prepared and detected and its IPs have been determined.

Acknowledgement

We gratefully acknowledge financial support by the Natural Sciences and Engineering Research Council of Canada (NSERC).

References

1. C. Wentrup, E. Wentrup-Byrne, and P. Müller. J. Chem. Soc. Chem. Commun. 210 (1977).
2. O.L. Chapman and C.J. Abelt. J. Org. Chem. **52**, 1218 (1987).
3. N.H. Werstiuk, J. Ma, and C.D. Roy. Can. J. Chem. **73**, 146 (1995).
4. N.H. Werstiuk, J. Ma, C.D. Roy, A.J. Kresge, and E.A. Jefferson. Can. J. Chem. **73**, 1738 (1995).
5. N.H. Werstiuk, J. Ma, C.D. Roy, A.J. Kresge, and E.A. Jefferson. Can. J. Chem. **73**, 2536 (1995).
6. N.H. Werstiuk, J. Ma, and C.D. Roy. Can. J. Chem. **74**, 1903 (1996).
7. H.M. Muchall, N.H. Werstiuk, B. Choudhury, J. Warkentin, and J. Pezacki. Can. J. Chem. **76**, 238 (1998).
8. N.H. Werstiuk, H.M. Muchall, J. Ma, and M.T.H. Liu. Can. J. Chem. **76**, 1162 (1996).
9. T. Bajorek and N.H. Werstiuk. Chem. Commun. (Cambridge), 648 (2002).
10. T. Bajorek and N.H. Werstiuk. Can. J. Chem. **83**, 1480 (2005).
11. T. Bajorek and N.H. Werstiuk. Can. J. Chem. **82**, 80 (2004).
12. J. Warkentin. J. Chem. Soc. Perkin Trans.1, 2161 (2000).
13. H.-T. Er, D.L. Pole, and J. Warkentin. Can. J. Chem. **74**, 1480 (1996).
14. H.M. Muchall, N.H. Werstiuk, and B. Choudhury. Can. J. Chem. **76**, 221 (1998).
15. N.H. Werstiuk, G. Timmins, J. Ma, and T.A. Wildman. Can. J. Chem. **70**, 1971 (1992).
16. M.J. Frisch, G.W. Trucks, H.B. Schlegel, G.E. Scuseria, M.A. Robb, J.R. Cheeseman, V.G. Zakrzewski, J.A. Montgomery, Jr., R.E. Stratmann, J.C. Burant, S. Dapprich, J.M. Millam, A.D. Daniels, K.N. Kudin, M.C. Strain, O. Farkas, J. Tomasi, V. Barone, M. Cossi, R. Cammi, B. Mennucci, C. Pomelli, C. Adamo, S. Clifford, J. Ochterski, G.A. Petersson, P.Y. Ayala, Q. Cui, K. Morokuma, D.K. Malick, A.D. Rabuck, K. Raghavachari, J.B. Foresman, J. Cioslowski, J.V. Ortiz, B.B. Stefanov, G. Liu, A. Liashenko, P. Piskorz, I. Komaromi, R. Gomperts, R.L. Martin, D.J. Fox, T. Keith, M.A. Al-Laham, C.Y. Peng, A. Nanayakkara, C. Gonzalez, M. Challacombe, P.M.W. Gill, B.G. Johnson, W. Chen, M.W. Wong, J.L. Andres, M. Head-Gordon, E.S. Replogle, and J.A. Pople. Gaussian 98. Revision A.9 [computer program]. Gaussian, Inc., Pittsburgh, Penn. 1998.

© 2006 NRC Canada

17. M.J. Frisch, G.W. Trucks, H.B. Schlegel, G.E. Scuseria, M.A. Robb, J.R. Cheeseman, J.A. Montgomery, Jr., T. Vreven, K.N. Kudin, J.C. Burant, J.M. Millam, S.S. Iyengar, J. Tomasi, V. Barone, B. Mennucci, M. Cossi, G. Scalmani, N. Rega, G.A. Petersson, H. Nakatsuji, M. Hada, M. Ehara, K. Toyota, R. Fukuda, J. Hasegawa, M. Ishida, T. Nakajima, Y. Honda, O. Kitao, H. Nakai, M. Klene, X. Li, J.E. Knox, H.P. Hratchian, J.B. Cross, C. Adamo, J. Jaramillo, R. Gomperts, R.E. Stratmann, O. Yazyev, A.J. Austin, R. Cammi, C. Pomelli, J.W. Ochterski, P.Y. Ayala, K. Morokuma, G.A. Voth, P. Salvador, J.J. Dannenberg, V.G. Zakrzewski, S. Dapprich, A.D. Daniels, M.C. Strain, O. Farkas, D.K. Malick, A.D. Rabuck, K. Raghavachari, J.B. Foresman, J.V. Ortiz, Q. Cui, A.G. Baboul, S. Clifford, J. Cioslowski, B.B. Stefanov, G. Liu, A. Liashenko, P. Piskorz, I. Komaromi, R.L. Martin, D.J. Fox, T. Keith, M.A. Al-Laham, C.Y. Peng, A. Nanayakkara, M. Challacombe, P.M.W. Gill, B. Johnson, W. Chen, M.W. Wong, C. Gonzalez, and J.A. Pople. Gaussian 03. Revision B.02 [computer program]. Gaussian, Inc., Pittsburgh, Penn. 2003.
18. J.P. Perdew and Y. Wang. Phys. Rev. B, **45**, 13244 (1992).
19. A.D. Becke. J. Chem. Phys. **98**, 5648 (1993).
20. R.F.W. Bader. Atoms in molecules. Oxford Science Publications, Oxford, UK. 1990.
21. F. Biegler-Konig. AIM 2000 [computer program]. University of Applied Science, Bielefeld, Germany.
22. P.P.T. Sah. J. Am. Chem. Soc. **50**, 516 (1928).
23. N.H. Werstiuk, D.N. Butler, and E. Shahid. Can. J. Chem. **65**, 760 (1986).
24. P. Deslongchamps. Stereoelectronic effects in organic chemistry. Wiley, New York. 1983.
25. E.J. McAlduff and K.N. Houk. Can. J. Chem. **55**, 319 (1977).

© 2006 NRC Canada

Convenient preparation of aryl-substituted nortropanes by Suzuki–Miyaura methodology[1]

Shyamali Ghosh, William A. Kinney, Diane A. Gauthier, Edward C. Lawson, Tomas Hudlicky, and Bruce E. Maryanoff

Abstract: The synthesis of a new bicyclic vinyl boronate (**5**) was accomplished from N-Boc-nortropinone (**6**) in two steps. The Suzuki–Miyaura coupling of **5** to a variety of aryl bromides and triflates afforded 3-aryl-8-azabicyclo[3.2.1]oct-2-enes in good yields by adjusting the substrate and (or) reaction conditions. Reduction to the 3-aryl-8-azabicyclo[3.2.1]octanes was achieved by hydrogenation. Interestingly, the coupling was also successful with benzyl bromides, providing entry into another group of intermediates.

Key words: nortropane, Suzuki–Miyaura, boronate, piperidine, GPCR, benzyl bromide.

Résumé : La synthèse d'un nouveau boronate de vinyle cyclique (**5**) a été réalisée en deux étapes à partir de la N-Boc-tropinone (**6**). Le couplage du composé **5** avec des bromures et des triflates d'aryles en faisant appel à la méthode de Suzuki–Miyaura et en ajustant le substrat et les conditions réactionnelles conduit à la formation de 3-aryl-8-azabicyclo[3.2.1]oct-2-ènes avec de bons rendements. La réduction des 3-aryl-8-azabicyclo[3.2.1]octanes a été réalisée par hydrogénation. Il est intéressant de noter que la réaction de couplage a été réalisée avec succès avec des bromures de benzyle, ce qui permet d'accéder à un autre groupe d'intermédiaires.

Mots clés : nortropane, Suzuki–Miyaura, boronate, pipéridine, GPCR, bromure de benzyle.

[Traduit par la Rédaction]

Introduction

Phenyl piperidines have proven to be valuable templates for the construction of modulators of G-protein coupled receptors (GPCRs), which are the target of the largest group of marketed drugs (~50%). Of the 38 GPCR-targeted drugs on the market, listed in a recent review (1), five are aryl piperidines (Allegra, Claritin, Duragesic, Risperdal) or aryl-substituted bicyclic piperidines (Atrovent, Combivent). Several others are aryl piperazines or morphine-related polycyclic aryl piperidines. To illustrate the structural diversity of piperidine-containing GPCR ligands, some examples are illustrated in the following: μ-opioid agonist loperamide (**1**) (2), selective δ-opioid agonist **2** (3), urotensin-II receptor antagonist palosuran (**3**) (4), and nonpeptidyl growth hormone secretagogue **4** (5). These compounds demonstrate the importance of aryl piperidines and how selectivity can be altered by making changes in the aryl piperidine architecture and pendant groups. We were interested in preparing aryl-substituted 8-azabicyclo[3.2.1]octane (nortropane) systems related to **2** and **4** in pursuit of novel GPCR ligands.

We envisioned accessing aryl nortropanes by a Suzuki–Miyaura (6) coupling of bicyclic vinyl boronate (**5**) with various aryl halides (Scheme 1). This approach was useful in the preparation of a variety of 4-phenyl tetrahydropyridines from an N-Boc-piperid-3-en-4-yl boronate (7*b*). The palladium/copper(I)-catalyzed Negishi coupling of 4-piperidinylzinc iodide with aryl halides and the piperid-3-en-4-ol phosphate coupling with aryl boronic acids are also noteworthy methods to prepare 4-arylpiperidines (8, 9). Recently, a Stille coupling of a bicyclic vinyl tin reagent provided access to phenyl-substituted 8-azabicyclo[3.2.1]oct-2-enes (nortropene) and nortropanes (5). The coupling of a bicyclic vinyl boronate with aryl halides might provide a less toxic alternative to a variety of interesting nortropenes and nortropanes. Besides investigating an alternative approach, we also wanted to determine whether a greater variety of aryl and benzyl halide coupling partners could be used in combination with **5** than had been demonstrated with the Suzuki couplings of the N-Boc-piperid-3-en-4-yl boronate (7*b*).

Results and discussion

The synthesis of **5** was accomplished by the methods outlined for the preparation of other pinacolato boronates (7).

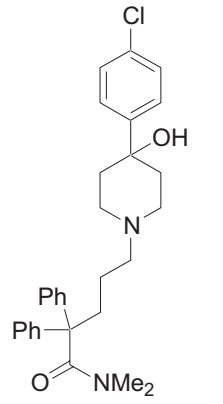
Received 16 September 2005. Published on the NRC Research Press Web site at http://canjchem.nrc.ca on 5 May 2006.

Dedicated to Professor Walter Szarek on the occasion of his 65th birthday.

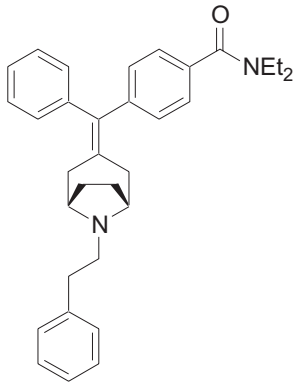
S. Ghosh, W.A. Kinney,[2] D.A. Gauthier, E.C. Lawson, and B.E. Maryanoff. Johnson & Johnson P.R.D., L.L.C., Spring House, PA 19477, USA.
T. Hudlicky. Brock University, St. Catharines, ON L2S 3A1, Canada.

[1]This article is part of a Special Issue dedicated to Professor Walter Szarek.
[2]Corresponding author (e-mail: wkinney1@prdus.jnj.com).

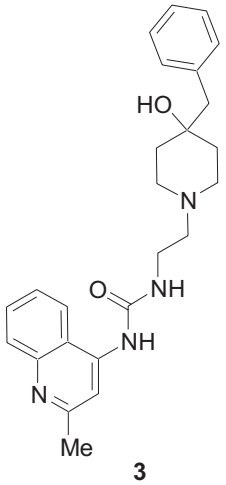
 doi:10.1139/V06-045 © 2006 NRC Canada



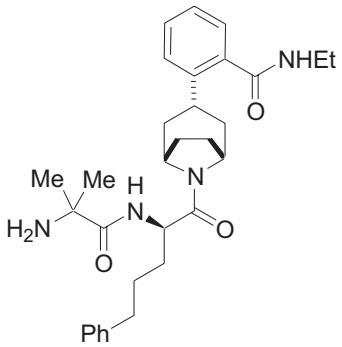
1



2



3

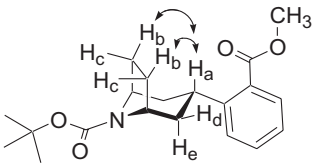


4

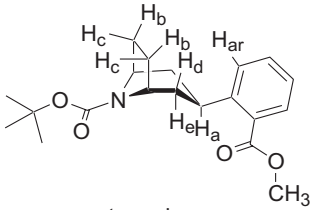
N-Boc-nortropinone (**6**) was deprotonated with potassium-hexamethyldisilazide at low temperature and reacted with Comins' reagent (2-(*N*,*N*-bistriflouromethanesulfonyl)amino-5-chloropyridine) to yield the vinyl triflate **7** in 92% yield. The triflate **7** was coupled with bis(pinacolato)diboron, using [1,1′-bis(diphenylphosphino)ferrocene]dichloropalladium(II) dichloromethane complex ($PdCl_2$-dppf, 2 mol%) as the catalyst, to afford bicyclic boronate (**5**) in good yield (77%–84%). This optimized yield was obtained by using only 1 equiv. of the diboron reagent and by carefully monitoring the reaction progress by ^{1}H NMR (vinyl proton of **5** vs. **7**).

The coupling of bicyclic boronate (**5**) with a variety of substituted benzene derivatives (**8**) was initially investigated (Table 1). Reaction of 1-bromo-4-methoxybenzene (**8a**) with **5** using $PdCl_2$-dppf as the catalyst (10 mol%) and potassium carbonate as the base (Method A) gave a low yield of the desired coupling. This poor result was overcome by instead utilizing triflate **8b**, which gave a quantitative yield of **9a**. In other cases the aryl bromides performed satisfactorily. For example, 1-bromo-4-methylbenzene (**8c**) and 2-bromobenzoic acid methyl ester (**8d**) gave a reasonable yield of the coupled products **9c** and **9d** (65% in each case). The example of 2-bromobenzoic acid ethyl ester (**8e**) was added to provide a direct comparison to the Stille approach, which gave a low yield (42%) of **9e** (5). In contrast, coupling of **8e** with **5** afforded **9e** more efficiently (72%). When an additional chlorine substituent was added to the aryl ring (**8f**, **8g**), the triflate (10) was a much better substrate than the bromo derivative, giving an excellent yield of **9f**. The nitro substituent in **8h** did not significantly affect the coupling yield with the arylbromide. The disubstituted nitro ester (**9h**) is a useful intermediate for adding a variety of groups at the 2- and 4-phenyl positions.

The fully reduced 3-aryl-8-azabicyclo[3.2.1]octanes (**10**, Scheme 1) could be achieved by reduction of the double bond in **9**. For example, **9d** was treated with hydrogen and 10% palladium on carbon to afford a quantitative yield of **10d** as a mixture of isomers. The same two isomers of **10d** were obtained when **9f** was reduced because of the additional reduction of the chlorine substituent. The isomers of **10d** (from **9f**) were separated by column chromatography and analyzed by 1D and 2D NMR to assign protons and distinguish the two isomers. For example, an expected NOE was observed between the H_a and H_b protons in the cis isomer (vide infra). The cis isomer is defined as having the aryl and the amine on the same side of the bicycle. Once the two isomers were distinguished, the ^{1}H NMR spectrum on the product **10d** derived from **9d** was analyzed to determine the ratio of isomers. There was a predominance of the cis isomer (cis:trans, 1.65:1), as determined by ratios of the H_a and CH_3O- integrations of the two isomers, which are clearly separated (e.g., H_a-cis δ 4.10 ppm, H_a-trans δ 3.29 ppm).



cis isomer
of **10d**



trans isomer
of **10d**

The nitrophenyl olefin (**9h**) was also efficiently (91%) reduced under the above conditions to yield the aminophenyl nortorpane (**10h**). In this case, the ratio of isomers was reversed (trans:cis, 1.27:1) based on the same comparison of H_a and CH_3O- integrations. Chlorophenyl tropane (**10f**) was available, albeit in low yield (29%, unoptimized), by a Sandmeyer reaction (11) with **10h**.

A variety of aryl and benzyl halides were evaluated as coupling partners for bicyclic boronate (**5**) (Table 1). The electron-deficient aryl bromide, 2-bromopyridine (**11**), coupled in good yield with **5** to give 2-pyridyl nortropene (**9i**). Electron-rich 3-bromoindole (**12**) did not couple efficiently under the usual conditions (Method A), but **9j** was obtained in good yield by using the same catalyst with aqueous sodium carbonate and dimethoxyethane (Method B) (12). While the reaction of benzyl bromides with aryl boronic acids has been seen in recent years (13), their reaction with vinyl boronic acids is less common (13*d*, 13*e*). Although the yield was only moderate (47%), boronate **5** coupled successfully with **13** using tetrakis(triphenylphoshine)palladium(0) as the catalyst (13*b*) to give benzyl-substituted 8-azabicyclo[3.2.1]oct-2-ene (**9k**). In the case of benzyl bromide (**14**), the coupling product **9l** and its isomer **15l** were isolated (**9l**:**15l**, 77:23) in similar yield to **9k**. The exocyclic

© 2006 NRC Canada

Scheme 1.

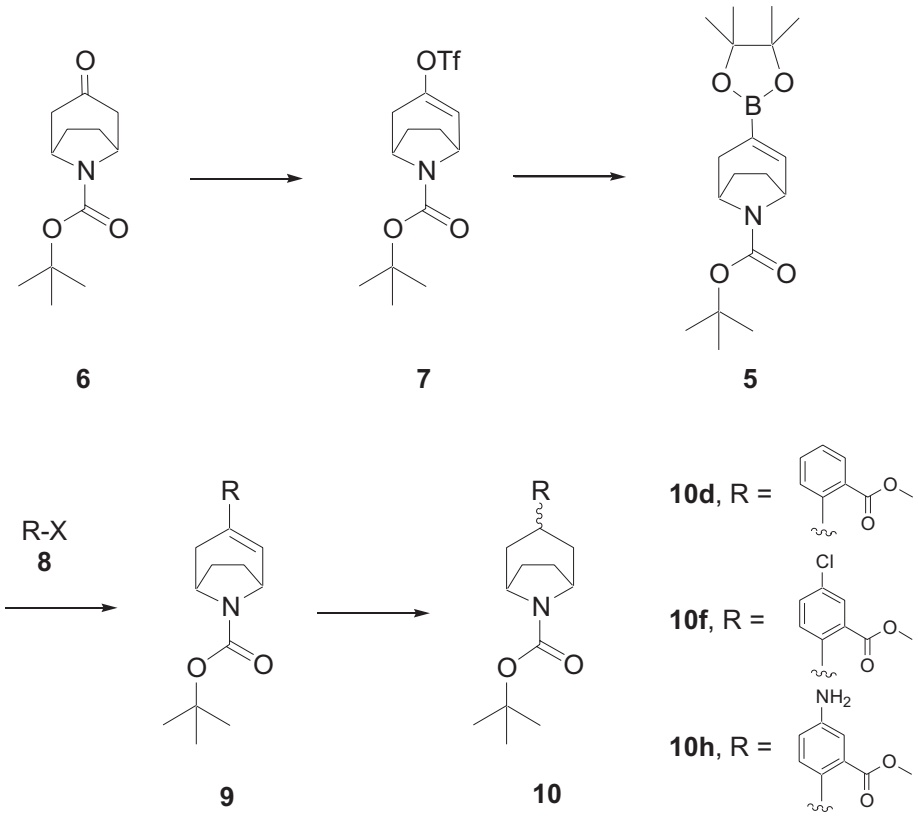
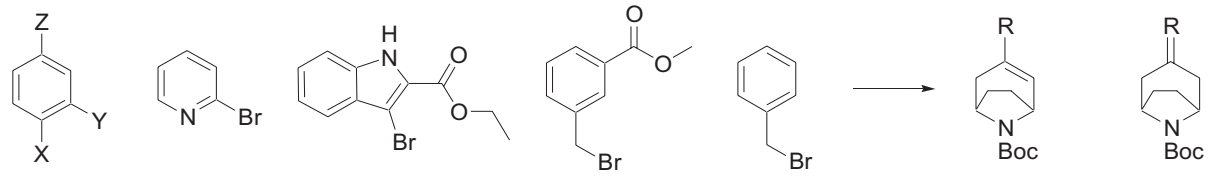


Table 1. Examples of coupling of **5** with aryl and benzyl groups.



8 **11** **12** **13** **14** **9** **15**

Ar-X	X, Y, Z	Isolated yield (%)	Product	Ar-X or Bz-X	X, Y, Z	Isolated yield (%)	Product
8a	Br, H, OMe	31[a]	**9a**	**8g**	OTf, CO_2Me, Cl	96[a]	**9f**
8b	OTf, H, OMe	100[a]	**9a**	**8h**	Br, CO_2Me, NO_2	63[a]	**9h**
8c	Br, H, Me	65[a]	**9c**	**11**		65[a]	**9i**
8d	Br, CO_2Me, H	65[a]	**9d**	**12**		16[a], 83[b]	**9j**
8e	Br, CO_2Et, H	72[a]	**9e**	**13**		47[c]	**9k**
8f	Br, CO_2Me, Cl	35[a]	**9f**	**14**		54[c]	**9l**, **15l** (77:23)

[a]Method A: Isolated yield using 0.1 equiv. $PdCl_2$-dppf, 3 equiv. K_2CO_3, DMF–EtOH (4:1), 100 °C, 3–16 h.
[b]Method B: Isolated yield using 0.1 equiv. $PdCl_2$-dppf, 4 equiv. 2 mol/L Na_2CO_3, DME, 100 °C, 10 h.
[c]Method C: Isolated yield using 0.1 equiv. $[Pd(PPh)_3]_4$, 2 equiv. 2 mol/L Na_2CO_3, DME, 100 °C, 16 h.

double bond product **15k** was also observed in the crude NMR spectrum of **9k** (**9k**:**15k**, 85:15), but it was not isolated.

In summary, the synthesis of new bicyclic boronate **5** was accomplished from N-Boc-nortropinone in two steps. The Suzuki–Miyaura coupling of **5** to a variety of aryl bromides and triflates afforded 3-aryl-8-azabicyclo[3.2.1]oct-2-enes in good yields by adjusting the substrate and (or) reaction conditions. Reduction to the 3-aryl-8-azabicyclo[3.2.1]octanes was achieved in good yields in cases in which the substrate had compatible functionality. Interestingly, the coupling of **5** also was successful with benzyl bromides, providing entry into another group of intermediates. The methodology described by Eastwood (7*b*) has been extended to an elaborated piperidine fragment, as well as to a greater variety of coupling partners. The chemistry demonstrated in this report should be applicable to other piperidine and bicyclic piperidine systems.

© 2006 NRC Canada

Experimental

^{1}H NMR spectra were acquired at 300 MHz on a Bruker Avance-300 spectrometer in $CDCl_3$ unless indicated otherwise, using Me_4Si as an internal standard. Normal-phase preparative chromatography was performed on an Isco Combiflash separation system Sg 100c equipped with a Redisep normal-phase disposable columns for flash chromatography containing 12 g of silica gel (optimal flow rate 30 mL/min, column volume 16.8 mL, normal-phase silica part no. 68-2203-026) with detection at 254 nm. Reverse-phase preparative chromatography was performed on a Gilson HPLC with a reversed-phase Kromasil column (10 μ, 100 Å, C18, column size 250 mm × 50 mm). Electrospray (ES) mass spectra were obtained on a Micromass platform LC single quadruple mass spectrometer in the positive mode. LC–MS analyses were performed on a Hewlett Packard series 1100 HPLC instrument eluting with a gradient of water/MeCN/CF_3COOH (10:90:0.2 to 90:10:0.2) over 6 min with a flow rate of 0.75mL/min on a Supelco ABZ + PLUS column (50 mm × 2.1 mm; 3.0 μ particle size) at 32 °C. Accurate mass measurements were performed using a Micromass (Manchester, UK) Autospec E OA-TOF high-resolution magnetic sector mass spectrometer tuned to a resolution of 6000 using the 10% valley definition. The ions were produced in a fast atom bombardment ion source at an accelerating voltage of 8 kV. Linear voltage scans at 33 Da/s were collected to include the protonated sample ion and two polyethylene glycol ions which were used as internal reference standards. The molecular mass was calculated using a linear extrapolation method. Reported mass values are averages over 100 s. Elemental analyses were determined by Quantitative Technologies, Inc., Whitehouse, New Jersey.

3-Trifluoromethanesulfonyloxy-8-azabicyclo[3.2.1]oct-2-ene-8-carboxylic acid *tert*-butyl ester (7)

A solution of N-Boc-nortropinone (**6**, 15.0 g, 67 mmol) in THF (80 mL) was added over 30 min to a cooled (–78 °C) 0.5 mol/L solution of potassium hexamethyldisilazide (162 mL, 81 mmol) in toluene under argon. More THF (20 mL) was added to the reaction mixture, which was stirred for 3.5 h and then treated with 2-(*N*,*N*-bistrifluoromethanesulfonyl)amino-5-chloropyridine (32.0 g, 81 mmol). The reaction mixture was stirred at –78 °C for 4 h and then allowed to warm to room temperature (rt) overnight (final temp: –30 °C). The reaction mixture was adsorbed onto silica gel (40 g) and purified by careful flash chromatography (elution with 10% ethyl acetate in pentane) to provide triflate **7** as a waxy solid (22 g, 92%). ^{1}H NMR ($CDCl_3$, 300 MHz) δ: 5.89 (br s, 1H), 4.25 (br m, 2H), 2.86 (br m, 1H), 2.15–1.59 (m, 5H), 1.30 (s, 9H).

3-(4,4,5,5-Tetramethyl[1,3,2]dioxaborolan-2-yl)-8-azabicyclo[3.2.1]oct-2-ene-8-carboxylic acid *tert*-butyl ester (5)

The triflate **7** (20.5 g, 57 mmol) was dissolved in dioxane (200 mL) and potassium acetate (16.8 g, 171 mmol), bis(pinacolato)diboron (15.0 g, 59 mmol), [1,1′-bis(diphenylphosphino)ferrocene]dichloropalladium(II) dichloromethane complex ($PdCl_2$-dppf, 1.0 g, 1.2 mmol), and 1,1′-bis(diphenylphosphino)ferrocene (0.7 g, mmol, 1.3 mmol) were added and the mixture was degassed with argon for 20 min. The reddish mixture was heated with stirring at 80 °C for 8–10 h, with the color turning a dark brown within the first 2 h. The product to starting material ratio was monitored by removing aliquots, evaporating the solvent, and examining the sample by ^{1}H NMR spectroscopy (ratio of vinyl H of the boronate **5** vs. the triflate **7**). The reaction mixture was cooled, filtered through Celite®, and adsorbed on silica gel (40 g). Chromatography (gradient elution with 5%–10% ethyl acetate in pentane) yielded the pure boronate **5** as a white solid (14.7 g, 77%, mp 98 °C). The fractions that showed an integration ratio of at least 10:14 (Boc-group : pinacol-group Hs) were combined to afford pure **5**. Crude boronate **5** of 41% purity (3.1 g, 7%), contaminated with diboron byproducts, was also obtained as a waxy solid. The purity of crude **5** was determined by coupling this crude material with **8b** affording a 41% yield of **9a** vs. 100% yield with pure **5** (1). ^{1}H NMR ($CDCl_3$, 300 MHz) δ: 6.71 (br s, 1H), 4.31–4.23 (m, 2H), 2.76–2.71 (m, 1H), 2.08 (m, 1H), 1.90–1.84 (m, 2H), 1.63–1.55 (m, 2H), 1.40 (s, 9H), 1.20 (s, 12H). HRMS (EI^+) *m*/*z* calcd. for $C_{18}H_{30}BNO_4$: 335.2268; found: 335.2278. Anal. calcd. for $C_{18}H_{30}BNO_4$: C 64.49, H 9.02; found: C 64.46, H 9.00.

Method A (ref. 7*b*): 3-(4-Methoxyphenyl)-8-azabicyclo-[3.2.1]oct-2-ene-8-carboxylic acid *tert*-butyl ester (9a)

To a mixture of 4-methoxy phenyl triflate (**8b**) (80 mg, 0.31 mmol), the bicyclic boronate **5** (100 mg, 0.30 mmol), [1,1′-bis(diphenylphosphino)ferrocene]dichloropalladium(II) dichloromethane complex ($PdCl_2$-dppf, 24 mg, 0.03 mmol), and K_2CO_3 (123 mg, 0.89 mmol) in a sealable tube (thick walled) was added DMF and EtOH (4:1, 2.5 mL). The mixture was stirred under argon at rt for 5–10 min and the tube was then sealed and heated at 100 °C for 3 h (3–16 h). The mixture was cooled to rt then filtered thru a pad of Celite®, washing with EtOAc. The combined organic layer was concentrated and purified by flash chromatography using a gradient system of 5%–50% ethyl acetate (0.1% TEA) in heptane. The desired product **9a** was isolated as a white solid (0.11 g, 100%). ^{1}H NMR ($CDCl_3$, 300 MHz) δ: 7.29 (d, *J* = 9 Hz, 2H), 6.85 (d, *J* = 9 Hz, 2H), 6.33 (br s, 1H), 4.6–4.4 (m, 2H), 3.80 (s, 3H), 3.1 (m, 1H), 2.3–1.6 (m, 5H), 1.45 (s, 9H). MS (ES^+, M – Boc + 1) *m*/*z*: 216.1. Anal. calcd. for $C_{19}H_{25}NO_3$: C 72.35, H 7.99, N 4.44; found: C 72.56, H 7.96, N 4.36.

3-*p*-Tolyl-8-azabicyclo[3.2.1]oct-2-ene-8-carboxylic acid *tert*-butyl ester (9c)

Aryl bromide **8c** was combined with **5** by Method A to yield **9c** as an oil (65%). ^{1}H NMR ($CDCl_3$, 300 MHz) δ: 7.25 (d, *J* = 8 Hz, 2H), 7.11 (d, *J* = 8 Hz, 2H), 6.39 (br s, 1H), 4.6–4.4 (m, 2H), 3.2–3.0 (m, 1H), 2.33 (s, 3H), 2.3–1.6 (m, 5H), 1.44 (s, 9H). MS (ES^+, M – Boc + 1) *m*/*z*: 200.1. HRMS (FAB^+) *m*/*z* calcd. for $C_{19}H_{25}NO_2$: 299.1885; found: 299.1893.

3-(2-Methoxycarbonylphenyl)-8-azabicyclo[3.2.1]oct-2-ene-8-carboxylic acid *tert*-butyl ester (9d)

Aryl bromide **8d** was combined with **5** by Method A to yield **9d** as an oil (65%). ^{1}H NMR ($CDCl_3$, 300 MHz) δ: 7.76 (d of d, *J* = 7.7, 1.3 Hz, 1H), 7.42 (m, 1H), 7.30 (m, 1H), 7.12 (d, *J* = 7.5 Hz, 1H), 5.83 (br s, 1H), 4.5–4.3 (m,

© 2006 NRC Canada

2H), 3.85 (s, 3H), 3.1–2.8 (m, 1H), 2.3–1.9 (m, 5H), 1.49 (s, 9H). MS (ES^+, M – Boc + 1) *m/z*: 244.2. HRMS (FAB^+) *m/z* calcd. for $C_{20}H_{25}NO_4$: 343.1784; found: 343.1788.

3-(2-Ethoxycarbonylphenyl)-8-azabicyclo[3.2.1]oct-2-ene-8-carboxylic acid *tert*-butyl ester (9e)

Aryl bromide **8e** was combined with **5** by Method A to yield **9e** as an oil (72%). ^1H NMR ($CDCl_3$, 300 MHz) δ: 7.74 (d, *J* = 7.6 Hz, 1H), 7.41 (m, 1H), 7.30 (m, 1H), 7.12 (d of d, *J* = 7.5, 0.8 Hz, 1H), 5.83 (br s, 1H), 4.6–4.2 (m, 4H), 3.1–2.8 (m, 1H), 2.3–1.9 (m, 5H), 1.49 (s, 9H), 1.36 (t, *J* = 7 Hz, 3H). MS (ES^+, M – Boc + 1) *m/z*: 258.1. HRMS (FAB^+) *m/z* calcd. for $C_{21}H_{27}NO_4$: 357.1940; found: 357.1935.

3-(4-Chloro-2-methoxycarbonylphenyl)-8-azabicyclo-[3.2.1]oct-2-ene-8-carboxylic acid *tert*-butyl ester (9f)

Aryl triflate **8g** (10), prepared from the corresponding phenol, was combined with **5** by Method A to yield **9f** as an oil (96%). ^1H NMR ($CDCl_3$, 300 MHz) δ: 7.75 (d, *J* = 2.2 Hz, 1H), 7.38 (d of d, *J* = 8.2, 2.2 Hz, 1H), 7.05 (d, *J* = 8.2 Hz, 1H), 5.83 (br s, 1H), 4.5–4.3 (m, 2H), 3.86 (s, 3H), 3.0–2.8 (m, 1H), 2.3–1.9 (m, 5H), 1.49 (s, 9H). MS (ES^+, M – Boc + 1) *m/z*: 278.1.

3-(2-Methoxycarbonyl-4-nitro-phenyl)-8-azabicyclo-[3.2.1]oct-2-ene-8-carboxylic acid *tert*-butyl ester (9h)

Aryl bromide **8h** was combined with **5** by Method A to yield **9h** as an oil (63%). ^1H NMR ($CDCl_3$, 300 MHz) δ: 8.63 (d, *J* = 2.4 Hz, 1H), 8.26 (d of d, *J* = 8.4, 2.4 Hz, 1H), 7.30 (d, *J* = 8.4 Hz, 1H), 5.91 (br s, 1H), 4.5–4.3 (m, 2H), 3.92 (s, 3H), 3.1–2.8 (m, 1H), 2.3–1.9 (m, 5H), 1.50 (s, 9H). MS (ES, M + Na) *m/z*: 411.1. HRMS (FAB^+) *m/z* calcd. for $C_{20}H_{24}N_2O_6$ + H: 389.1713; found: 389.1706.

3-Pyridin-2-yl-8-azabicyclo[3.2.1]oct-2-ene-8-carboxylic acid *tert*-butyl ester (9i)

2-Bromopyridine (**11**) was combined with **5** by Method A, but purified by reverse-phase HPLC (10%–90% MeCN–H_2O containing 0.2% TFA), to yield the TFA salt of **9i** as an oil (65%). ^1H NMR ($CDCl_3$, 300 MHz) δ: 8.9 (m, 1H), 8.1 (m, 1H), 7.6 (m, 2H), 7.04 (br m, 1H), 4.7–4.5 (m, 2H), 3.5–1.7 (m, 5H), 1.45 (s, 9H). MS (ES^+, M + 1) *m/z*: 287.3. HRMS (FAB^+) *m/z* calcd. for $C_{17}H_{22}N_2O_2$ + H: 287.1760; found: 287.1760.

Method B (ref. 12): 3-(8-*tert*-Butoxycarbonyl-8-azabicyclo[3.2.1]oct-2-en-3-yl)-1*H*-indole-2-carboxylic acid ethyl ester (9j)

To a mixture of the 3-bromoindole (**12**, 80 mg, 0.30 mmol), compound **5** (100 mg, 0.30 mmol), [1,1′-bis(diphenylphosphino)ferrocene]dichloropalladium(II) dichloromethane complex ($PdCl_2$-dppf, 30 mg, 0.04 mmol), and 2 mol/L aq. Na_2CO_3 (0.6 mL, 1.2 mmol) in a sealable tube (thick walled) was added DME (3 mL). After stirring under argon for 5 min, the tube was sealed and heated at 100 °C for 10 h. The reaction mixture was cooled to rt and then filtered through a pad of Celite®, washing with EtOAc. The organic layer was concentrated and purified by flash chromatography using a gradient system of 5%–50% ethyl acetate (0.1% TEA) in heptane. The desired product **9j** was isolated as a white solid (113 mg, 83%). ^1H NMR ($CDCl_3$, 300 MHz) δ: 8.78 (br s, NH), 7.61 (m, 1H), 7.4–7.2 (m, 2H), 7.13 (m, 1H), 6.09 (br s, 1H), 4.6–4.4 (m, 2H), 4.41 (q, *J* = 7 Hz, 2H), 3.6–3.4 (m, 1H), 3.2–2.9 (m, 1H), 2.4–2.0 (m, 4H), 1.50 (s, 9H), 1.42 (t, *J* = 7 Hz, 3H). MS (ES^+, M + Na) *m/z*: 419.2. Anal. calcd. for $C_{23}H_{28}N_2O_4$: C 69.67, H 7.12, N 7.07; found: C 69.86, H 7.25, N 6.90.

Method C (ref. 13*b*): 3-(3-Methoxycarbonyl-benzyl)-8-azabicyclo[3.2.1]oct-2-ene-8-carboxylic acid *tert*-butyl ester (9k)

To a mixture of benzyl bromide (**13**) (72 mg, 0.31 mmol), boronate **5** (100 mg, 0.30 mmol), tetrakis(triphenylphoshine)palladium(0) (34 mg, 0.03 mmol), and 2 mol/L Na_2CO_3 (0.30 mL, 0.60 mmol) in a sealable tube (thick walled) was added DME (3 mL). The mixture was stirred under argon for 5 min. The tube was then sealed and the reaction mixture was heated at 100 °C for 16 h. The reaction mixture was cooled to rt and then filtered through a pad of Celite®, washing with ethyl acetate. The filtrate was diluted with water and extracted with ethyl acetate. The organic layer was separated, dried (sodium sulfate), concentrated, and purified by flash chromatography using a gradient system of 5%–50% ethyl acetate (0.1% TEA) in heptane. Desired product **9k** was isolated as a white solid (53 mg, 47%). ^1H NMR ($CDCl_3$, 300 MHz) δ: 7.9–7.8 (m, 2H), 7.3 (m, 2H), 5.8 (br d, 1H), 4.4–4.1 (m, 2H), 3.91 (s, 3H), 3.24 (AB q, 2H), 2.8–1.8 (m, 4H), 1.6–1.3 (m, 2H), 1.4 (br s, 9H). MS (ES^+, M + Na) *m/z*: 380.1. HRMS (FAB^+) *m/z* calcd. for $C_{21}H_{27}NO_4$ + H: 358.2018; found: 358.2005.

3-Benzyl-8-azabicyclo[3.2.1]oct-2-ene-8-carboxylic acid *tert*-butyl ester (9l) and 3-benzylidene-8-azabicyclo-[3.2.1]octane-8-carboxylic acid *tert*-butyl ester (15l)

Benzyl bromide (**14**) was combined with **5** according to Method C to yield a mixture of **9l** and **15l** as a colorless oil (54%, **9l**:**15l**, 77:23, the exocyclic double bond isomer). ^1H NMR ($CDCl_3$, 300 MHz) δ: 7.39–7.15 (m, 5H), 6.45 (br s, 0.23H), 5.84 (br d, 0.77H), 4.4–4.1 (m, 2H), 3.5–2.5 (m, 4H), 2.2–1.5 (m, 4H), 1.40 (m, 9H). MS (ES^+, M + Na) *m/z*: 321.9. HRMS (FAB^+) *m/z* calcd. for $C_{19}H_{25}NO_2$ – H: 298.1807; found: 298.1799.

3-(2-Methoxycarbonylphenyl)-8-azabicyclo[3.2.1]octane-8-carboxylic acid *tert*-butyl ester (10d)

Compound **9d** (40 mg, 0.12 mmol), MeOH (15 mL), and 10% Pd-C (15 mg) were shaken in a Parr apparatus (40 psig of hydrogen, 3.7 atm) for 16 h. The reaction mixture was filtered through Celite® and concentrated to give **10d** as an oil (41 mg, mixture of two isomers, 100%). The ratio of isomers in the reaction mixture was determined to be 1.65:1 cis:trans. The isomers of **10d** were initially formed in the hydrogenation of **9f** and separated by flash chromatography using a gradient system of 5%–25% ethyl acetate (0.1% TEA) in heptane over 20 min (flow rate 40 mL/min) and their structures were determined. Analysis by ^1H, ^{13}C, and 2-D NMR determined that the faster eluting, major isomer was the cis isomer. Analysis of **10d** mixture from **9d**: ^1H NMR ($CDCl_3$, 300 MHz) δ: 7.78 (m, 0.62H), 7.65 (m, 0.38H), 7.44 (m, 1H), 7.34 (m, 1H), 7.24 (m, 1H), 4.4–4.2 (m, 2H), 4.10 (m, $0.62H_{a\text{-}cis}$), 3.91 (s, $1.9H_{cis}$), 3.87 (s, $1.1H_{trans}$), 3.29

© 2006 NRC Canada

(m, 0.38$H_{a\text{-}trans}$), 2.54 (m, 1H), 2.1–1.3 (m, 7H), 1.51 (s, 9H). MS (ES^+, M + Na) *m/z*: 368.0. HRMS (FAB+) *m/z* calcd. for $C_{20}H_{27}NO_4$: 345.1940; found: 345.1940.[3]

3-(4-Chloro-2-methoxycarbonylphenyl)-8-azabicyclo-[3.2.1]octane-8-carboxylic acid *tert*-butyl ester (10f)

To a stirred mixture (11) of copper(II) chloride (58 mg, 0.43 mmol) in dry acetonitrile (1.5 mL) was added *tert*-butyl nitrite (0.064 mL, 0.54 mmol) via syringe at rt under a nitrogen atmosphere. The resulting dark green suspension was then heated (65 °C) with vigorous stirring. To the warm reaction mixture was added a solution of **10h** (130 mg, 0.36 mmol) in dry acetonitrile (4 mL) via syringe (5 min). The resulting black solution was stirred at 65 °C for 1 h then allowed to cool to rt. The reaction was diluted with ether (10 mL), washed with aq. 1 N HCl (10 mL), washed with brine (10 mL), dried over anhydrous sodium sulfate, filtered, and concentrated in vacuo. The crude mixture was purified by flash chromatography using a gradient system of 5%–50% ethyl acetate (0.1% TEA) in heptane. The desired product **10f** was isolated as a clear colorless oil (40 mg, 29%) with the same mixture of isomers as **10h** (trans:cis, 1.3:1). ^{1}H NMR ($CDCl_3$, 300 MHz) δ: 7.77 (d, *J* = 2.3 Hz, 0.44H), 7.64 (d, *J* = 2.3 Hz, 0.56H), 7.38 (m, 1H), 7.3–7.2 (m, 1H), 4.4–4.2 (m, 2H), 4.09 (m, 0.44H), 3.91 (s, 1.3H), 3.88 (s, 1.7H), 3.26 (m, 0.56H), 2.5 (m, 1H), 2.1–1.3 (m, 7H), 1.51 (s, 9H), 1.36 (m, 2H). MS (ES^+, M + 1) *m/z*: 380.0.

3-(4-Amino-2-methoxycarbonylphenyl)-8-azabicyclo-[3.2.1]octane-8-carboxylic acid *tert*-butyl ester (10h)

Compound **9h** (180 mg, 0.46 mmol), MeOH (30 mL), and 10% Pd-C (60 mg) were shaken in a Parr apparatus (40 psig of hydrogen) for 16 h. The reaction mixture was filtered through Celite®, concentrated and purified by reverse-phase HPLC (20%–90% MeCN–H_2O containing 0.2% TFA). The TFA salt of compound **10h** was isolated as a white solid (200 mg, mixture of two isomers, 91%, ratio 1.27:1 of trans:cis by ^{1}H NMR) after lyophylization. ^{1}H NMR ($CDCl_3$, 300 MHz) δ: 7.39 (br s, 0.44H), 7.3–7.2 (m, 1.56H), 7.04 (m, 1H), 4.3–4.2 (m, 2H), 4.04 (m, 0.44H), 3.90 (s, 1.3H), 3.85 (s, 1.7H), 3.21 (m, 0.56H), 2.44 (m, 1H), 2.2–1.2 (m, 7H), 1.55 (s, 9H). MS (ES^+, M + 1) *m/z*: 361.2. HRMS (FAB^+) *m/z* calcd. for $C_{20}H_{29}N_2O_4$ + H: 361.2127; found: 361.2111.

Acknowledgements

This project was performed as a collaboration between Johnson & Johnson Pharmaceutical Research and Development, L.L.C. and TDC Research Inc., Department of Chemistry, Brock University, St. Catharines, Ontario. The authors thank William Jones for obtaining extensive accurate mass data, and Hank Breslin and Mark McDonnell for important scientific discussions.

References

1. P. Nambi and N. Aiyar. Assay Drug Dev. Technol. **1**, 305 (2003).
2. F. Awouters, A. Megens, M. Verlinden, J. Schuurkes, C. Niemegeers, and P.A. Janssen. Dig. Dis. Sci. **38**, 977 (1993).
3. J.R. Carson, S.J. Coats, E.E. Codd, S.L. Dax, J. Lee, R.P. Martinez, L.A. McKown, L.A. Neilson, P.M. Pitis, W.-N. Wu, and S.-P. Zhang. Bioorg. Med. Chem. Lett. **14**, 2113 (2004).
4. M. Clozel, C. Binkert, M. Birker-Robaczewska, C. Boukhadra, S.-S. Ding, W. Fischli, P. Hess, B. Mathys, K. Morrison, C. Mueller, C. Mueller, O. Nayler, C. Qiu, M. Rey, M.W. Scherz, J. Velker, T. Weller, J.-F. Xi, and P. Ziltener. J. Pharmacol. Exp. Ther. **311**, 204 (2004).
5. Z. Lu, J.R. Tata, K. Cheng, L. Wei, W.W.-S. Chan, B. Butler, K.D. Schleim, T.M. Jacks, G. Hickey, and A.A. Patchett. Bioorg. Med. Chem. Lett. **13**, 1817 (2003).
6. (*a*) N. Miyaura, T. Yanagi, and A. Suzuki. Synth. Commun. **11**, 513 (1981); (*b*) N. Miyaura and A. Suzuki. Chem. Rev. **95**, 2457 (1995).
7. (*a*) T. Ishiyama, Y. Itoh, T. Kitano, and N. Miyaura. Tetrahedron Lett. **38**, 3447 (1997); (*b*) P.R. Eastwood. Tetrahedron Lett. **41**, 3705 (2000).
8. E.G. Corley, K. Conrad, J.A. Murry, C. Savarin, J. Holko, and G. Boice. J. Org. Chem. **69**, 5120 (2004).
9. U.S. Larsen, L. Martiny, and M. Begtrup. Tetrahedron Lett. **46**, 4261 (2005).
10. D.E. Frantz, D.G. Weaver, J.P. Carey, M.H. Kress, and U.H. Dolling. Org. Lett. **4**, 4717 (2002).
11. L.E. Burgess. Synth. Commun. **27**, 2181 (1997).
12. W.W.K.R. Mederski, M. Lefort, M. Germann, and D. Kux. Tetrahedron, **55**, 12757 (1999).
13. (*a*) M.J. Sharp and V. Snieckus. Tetrahedron Lett. **26**, 5997 (1985); (*b*) G.J. Pernía, J.D. Kilburn, J.W. Essex, R.J. Mortishire-Smith, and M. Rowley. J. Am. Chem. Soc. **118**, 10220 (1996); (*c*) S. Chowdhury and P.E. Georghiou. Tetrahedron Lett. **40**, 7599 (1999); (*d*) C.H. Oh and Y.M. Lim. Bull. Korean Chem. Soc. **23**, 663 (2002); (*e*) S. Langle, M. Abarbri, and A. Duchêne. Tetrahedron Lett. **44**, 9255 (2003); (*f*) L. Chahen, H. Doucet, and M. Santelli. Synlett, 1668 (2003).

[3] Supplementary data (the ^{1}H NMR structural assignments and NOE data for the cis and trans isomers of **10d**) for this article are available on the journal Web site (http://canjchem.nrc.ca) or may be purchased from the Depository of Unpublished Data, Document Delivery, CISTI, National Research Council Canada, Ottawa, ON K1A 0R6, Canada. DUD 5023. For more information on obtaining material refer to http://cisti-icist.nrc-cnrc.gc.ca/irm/unpub_e.shtml.

© 2006 NRC Canada

Synthesis of 6-(alkoxymethyl)- and 6-(alkylsulfanylmethyl)furo[2,3-*d*]pyrimidin-2(3*H*)-one analogues[1,2]

Zlatko Janeba, Noha Maklad, and Morris J. Robins

Abstract: Treatment of 6-(hydroxymethyl)furo[2,3-*d*]pyrimidin-2(3*H*)-one (**2**) with 1-iodoalkanes and potassium carbonate resulted in predominant formation of N3 (and minor amounts of O2) alkylated regioisomers. Treatment of the 3-alkyl products (**3**) with thionyl chloride gave highly reactive 6-chloromethyl intermediates (**5**). Direct solvolysis of **5** in alcohol solutions (~50 °C) produced 3-alkyl-6-(alkoxymethyl)furopyrimidin-2(3*H*)-ones (**6**), whereas extensive decomposition of **5** occurred with added base promoters. Sonication of **5** with sodium thioacetate in acetonitrile gave the air-stable 6-(alkylsulfanylmethyl) intermediates (**7**), which were subjected to deacetylation (methanolic sodium methoxide) and in situ alkylation to give 3-alkyl-6-(alkylsulfanylmethyl)furo[2,3-*d*]pyrimidin-2(3*H*)-ones (**8**). Lipophilic derivatives of furo[2,3-*d*]pyrimidin-2(3*H*)-one are of interest as potential inhibitors of viral penetration of cells.

Key words: furo[2,3-*d*]pyrimidin-2(3*H*)-ones, alkyl, ether and thioether derivatives of furo[2,3-*d*]pyrimidin-2(3*H*)-one.

Résumé : La réaction de la 6-(hydroxyméthyl)furo[2,3-*d*]pyrimidin-2(3*H*)-one (**2**) avec des 1-iodoalcanes en présence de carbonate de potassium conduit à la formation prédominante des régioisomères alkylés en N3, avec des quantités mineures de produits alkylés en O2. Le traitement des produits 3-alkyles (**3**) avec du chlorure de thionyle fournit les intermédiaires 6-chlorométhyles (**5**) fortement réactifs. La solvolyse directe des intermédiaires **5** en solutions alcooliques, à environ ~50 °C, conduit à la production des 3-alkyl-6-(alkoxyméthyl)furopyrimidin-2(3*H*)-ones (**6**) alors qu'on observe des décompositions extensives des produits **5** lorsqu'on utilise des quantités supplémentaires de promoteurs basiques. La sonication des composés **5** avec du thioacétate de sodium dans de l'acétonitrile fournit les intermédiaires 6-(alkylsulfanylméthyl) (**7**) qui sont stables à l'air et qui ont été soumis à des désacétylation à l'aide de méthylate de sodium dans le méthanol ou d'alkylations in situ pour conduire à la formation de 3-alkyl-6-(alkylsulfanylméthyl)furo[2,3-*d*]pyrimidin-2(3*H*)-ones (**8**). Les dérivés lipophiles des furo[2,3-*d*]pyrimidin-2(3*H*)-one présentent de l'intérêt comme inhibiteurs potentiels de la pénétration virale des cellules.

Mots clés : furo[2,3-*d*]pyrimidin-2(3*H*)-ones, dérivés alkyles, éthers et thioéthers de la furo[2,3-*d*]pyrimidin-2(3*H*)-one.

[Traduit par la Rédaction]

Introduction

Certain derivatives of furo[2,3-*d*]pyrimidin-2(3*H*)-one (Fig. 1) exhibit potent antiviral activity. We have noted that Sonogashira coupling of terminal alkynes with 5-iodouracil derivatives gave the 5-(alkyn-1-yl)uracils plus variable quantities of furo[2,3-*d*]pyrimidine by-products (1). We also have reported that the latter bicyclic ring analogues could be produced in high yields by Cu(I)-catalyzed 5-endo-dig cyclization of the 5-alkynyluracil compounds (1, 2). Two decades later, Balzarini, De Clercq, McGuigan, and their co-workers described the remarkable selectivity and potency of longer-chain alkyl derivatives of such bicyclic 2′-deoxynucleosides against varicella-zoster virus (VZV) (3–5). Extensive structure–activity studies revealed that the presence of the long-chain alkyl substituents at C6 of the bicyclic ring (e.g., 6-octyl and 6-*p*-pentylphenyl) was essential for the potent anti-VZV activity. Other modifications including changing of the heteroatom at the 7 position, substituents at C6, and the sugar moiety at N3 (including acyclic analogues (6)) of the furo[2,3-*d*]pyrimidine ring did not produce compounds with more potent and selective anti-VZV activities (see refs. 7–9 for reviews).

Additional analogues that exhibited anti-human cytomegalovirus (HCMV) activity were discovered that did not require activation by nucleoside kinases. These included derivatives with an alkyl group (10) or a 2′,3′-dideoxyfuranosyl moiety at N3 (11). Interestingly, 2′-deoxynucleoside analogues with extended ether side chains at C6 showed dual anti-VZV and anti-HCMV activities (12), and interfer-

Received 5 August 2005. Published on the NRC Research Press Web site at http://canjchem.nrc.ca on 5 May 2006.

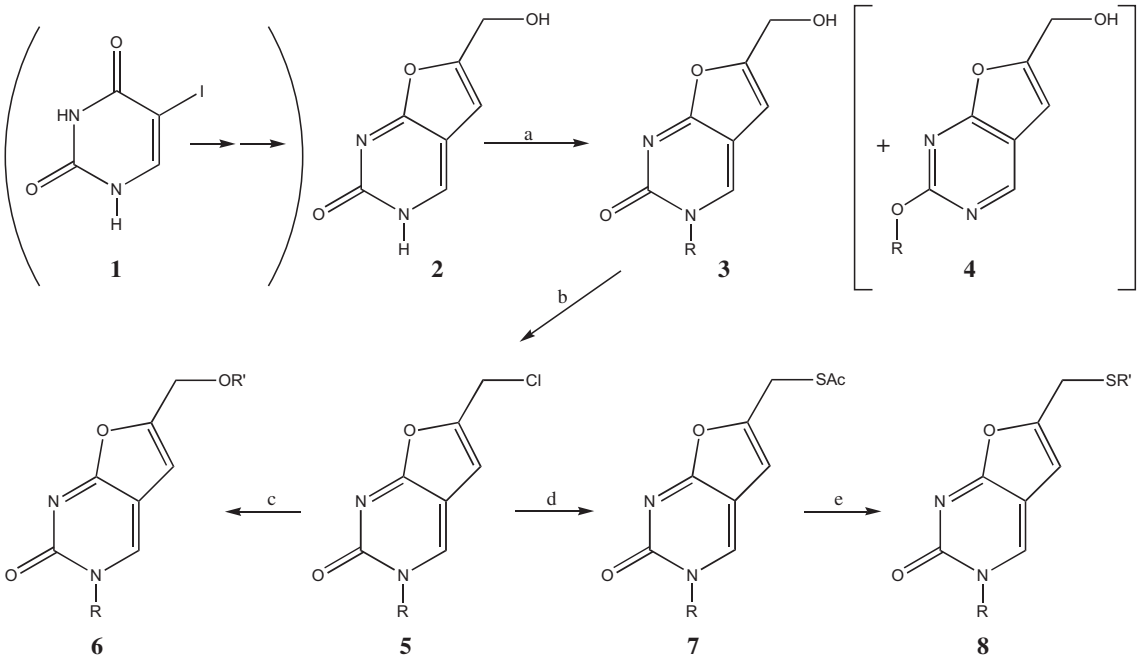
With congratulations and best wishes to Professor Walter Szarek.

Z. Janeba,[3] N. Maklad,[4] and M.J. Robins.[5] Department of Chemistry and Biochemistry, Brigham Young University, Provo, UT, 84602-5700. USA.

[1]This article is part of a Special Issue dedicated to Professor Walter A. Szarek.
[2]Nucleic acid related compounds Paper 133. Paper 132: Z. Janeba, J. Balzarini, G. Andrei, R. Snoeck, E. De Clercq, and M.J. Robins. Can. J. Chem. This issue.
[3]Present address: Moravek Biochemicals, Brea, California.
[4]Present address: Pfizer Inc., Groton, Connecticut.
[5]Corresponding author (e-mail: morris_robins@byu.edu).

 doi:10.1139/V06-042 © 2006 NRC Canada

Scheme 1. Reagents and conditions: (*a*) 1-iodoalkane/K_2CO_3/DMF; (*b*) $SOCl_2$/pyridine/CH_2Cl_2; (*c*) 1-alkanol; (*d*) KSAc/MeCN/sonication; (*e*) (*i*) NaOMe/MeOH, (*ii*) 1-iodoalkane.



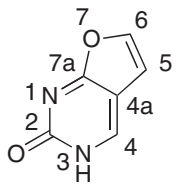
a R = butyl, R' = octyl
b R = hexyl, R' = octyl
c R = hexyl, R' = butyl
d R = hexyl, R' = hexyl
e R = octyl, R' = butyl
f R = octyl, R' = hexyl
g R = octyl, R' = octyl
h R = decyl, R' = butyl
i R = decyl, R' = hexyl
j R = decyl, R' = octyl
k R = dodecyl, R' = butyl
l R = dodecyl, R' = octyl

3, **4**, **5**, and **7**

a R = butyl
b R = hexyl
c R = octyl
d R = decyl
e R = dodecyl

a R = butyl, R' = hexyl
b R = butyl, R' = octyl
c R = hexyl, R' = octyl
d R = octyl, R' = hexyl
e R = octyl, R' = octyl
f R = decyl, R' = hexyl
g R = decyl, R' = octyl
h R = dodecyl, R' = butyl
i R = dodecyl, R' = hexyl
j R = dodecyl, R' = octyl

Fig. 1. Furo[2,3-*d*]pyrimidin-2(3*H*)-one.



ence with viral penetration at cell surfaces might be involved. Thus, empirical SAR examination of new derivatives of this ring system is warranted.

Alkyl analogues are more readily accessible than those whose synthesis begins with expensive 2′-deoxynucleosides. We have explored routes with the potential for divergent and efficient methods for production of new series of such analogues. We (13) and others (14) have recently developed syntheses of furo[2,3-*d*]pyrimidin-2(3*H*)-ones without substituents at N3 beginning with Sonogashira coupling of 5-iodouracil (13) and derivatives (14) with 3-hydroxy-substituted 1-alkynes. These hydroxyalkyne compounds undergo efficient Cu(I)-promoted cyclization, in contrast with other 5-(alkyn-1-yl)uracils without a substituent at N3. The 6-hydroxymethylfuro[2,3-*d*]pyrimidin-2(3*H*)-one (**2**) analogue was obtained in >50% overall yield from 5-iodouracil (13). Treatment of these 6-substituted furo[2,3-*d*]pyrimidin-2(3*H*)-ones with 1-iodoalkanes gives derivatives with an alkyl substituent at N3 (plus minor 2-*O*-alkyl regioisomers). Analogues with lipophilic alkyl groups at N3 and long-chain alkoxy or alkylthio substituents at C6 can be obtained readily.

Results and discussion

Alkylation of 6-(hydroxymethyl)furo[2,3-*d*]pyrimidin-2(3*H*)-one (**2**) (Scheme 1) with 1-iodoalkanes gave the 3-alkyl-6-(hydroxymethyl)furo[2,3-*d*]pyrimidin-2(3*H*)-ones (**3**) in 28%–72% yields. The minor 2-*O*-alkyl regioisomers (**4**) (13) were not isolated. Standard procedures for conversion of the side-chain hydroxyl group of **3** into a mesylate did not give a stable product, but chlorination with $SOCl_2$–pyridine–CH_2Cl_2 at 0 °C gave the corresponding 6-chloromethyl derivates (**5**) in good yields (62%–70%). The deoxychlorination reactions appeared quantitative (TLC), but isolated yields of **5** were lower because of the high reactivity and (or) instability of such benzylic-type chlorides. Careful handling

© 2006 NRC Canada

(including reaction time and temperature, flash evaporation of volatiles at ambient temperature, fast workup, and drying) was necessary to obtain good yields of **5**. Decomposition of these chloromethyl compounds was observed upon storage (TLC), and peaks for the molecular ions were present only in the mass spectra of **5a**, **5b**, and **5e**.

When solutions of compounds **5** were heated in alcohols at ~50 °C, solvolysis occurred to give the 3-alkyl-6-(alkyloxymethyl)furo[2,3-*d*]pyrimidin-2(3*H*)-ones (**6**) in 42%–87% yields. Serious decomposition of **5a** was observed when either sodium propoxide–THF or Et_3N–PrOH was added as a base promoter.

Thioether substituents were introduced at C6 indirectly. Acetylthio intermediates (**7**) were employed to avoid odors and potential oxidative problems with alkanethiols. Sonication of the chloromethyl derivatives (**5**) and potassium thioacetate in acetonitrile for ~5 min gave the air-stable 6-(acetylsulfanylmethyl)-3-alkylfuro[2,3-*d*]pyrimidin-2(3*H*)-ones (**7**) in good yields (53%–90%). Corresponding pairs of **5** and **7** had almost identical R_f values (TLC, MeOH–CH_2Cl_2, 8:92), but they showed slightly different fluorescence properties (UV lamp, 254 nm).

The thioacetates (**7**) were added to stirred solutions of deoxygenated NaOMe–MeOH at ambient temperature. Stirring was continued for a few minutes to remove the acetyl group, and then the 1-iodoalkanes were added. The resulting 3-alkyl-6-(alkylsulfanylmethyl)furo[2,3-*d*]pyrimidin-2(3*H*)-one products (**8**) were obtained in 42%–83% yields.

Conclusions

Two new series of furo[2,3-*d*]pyrimidin-2-one derivatives were prepared from the readily available 6-(hydroxymethyl)furo[2,3-*d*]pyrimidin-2(3*H*)-one (**2**). Alkylation of **2** with 1-iodoalkanes occurred predominantly at N3 to give **3**. Deoxychlorination of the 3-alkyl-6-(hydroxymethyl)furo-[2,3-*d*]pyrimidin-2(3*H*)-ones (**3**) gave the highly reactive chloromethyl intermediates (**5**). Direct solvolysis of **5** occurred in heated alcohol solutions to give the 3-alkyl-6-(alkyloxymethyl)furo[2,3-*d*]pyrimidin-2(3*H*)-one series (**6**). Sonication of **5** with potassium thioacetate gave the air-stable 6-acetylthiomethyl intermediates (**7**), which were deacetylated in deoxygenated methanolic sodium methoxide solution and then treated in situ with 1-iodoalkanes to give the 3-alkyl-6-(alkylsulfanylmethyl)furo[2,3-*d*]pyrimidin-2(3*H*)-ones (**8**). Preliminary cytotoxicity and anti-VZV and HCMV screening of the target compounds did not reveal significant activity.

Experimental

Uncorrected melting points were determined with a hot-stage apparatus. UV spectra were determined with solutions in MeOH. ^{1}H (500 MHz) and ^{13}C (125 MHz) NMR spectra were determined with solutions in $CDCl_3$ unless otherwise indicated. "Apparent" peak shapes are in quotation marks when the first-order splitting should be more complex or when peaks were poorly resolved. High-resolution mass spectra (HRMS) were determined with FAB (thioglycerol, NaOAc) unless otherwise indicated. All reactions were performed under an atmosphere of nitrogen or argon. EtOAc, CH_2Cl_2, DMF, and MeOH were HPLC grade. 1-Propanol, 1-butanol, 1-hexanol, and 1-octanol were reagent grade. Pyridine was purified by distillation. 1-Iodobutane, 1-iodohexane, 1-iodooctane, 1-iododecane, and 1-iodododecane were used as received from Aldrich. CuI (98%) was used as received from Aldrich for all coupling/cyclization reactions.

Method 1: (**2**/K_2CO_3/1-iodoalkane/DMF) is described for **2** → **3a**; method 2: (**3**/$SOCl_2$/pyridine/CH_2Cl_2) is described for **3a** → **5a**; method 3 (**5**/alcohol/Δ) is described for **5a** → **6a**; method 4: (**5**/$KSCOCH_3$/acetonitrile/sonication) is described for **5a** → **7a**; and method 5: (**7**/MeONa/MeOH/1-iodoalkane) is described for **7a** → **8a**.

3-Butyl-6-(hydroxymethyl)furo[2,3-*d*]pyrimidin-2(3*H*)-one (3a)

Method 1

A mixture of 6-(hydroxymethyl)furo[2,3-*d*]pyrimidin-2(3*H*)-one (**2**) (1.70 g, 10.2 mmol), K_2CO_3 (1.55 g, 11.2 mmol), and 1-iodobutane (1.3 mL, 2.06 g, 11.2 mmol) in DMF (17 mL) was stirred at 50 °C for 10 h. Volatiles were evaporated under vacuum, and toluene was added and evaporated (2×). The residue was purified by flash silica gel column chromatography and recrystallized from EtOAc to give **3a** (1.63 g, 72%); mp 179–180 °C. UV max: 245, 331 nm (ε 13 800, 7 500). ^{1}H NMR (DMSO-d_6) δ: 0.89 (t, J = 7.6 Hz, 3H), 1.28 ("hext", J = 7.6 Hz, 2H), 1.64 ("quint", J = 7.6 Hz, 2H), 3.92 (t, J = 7.3 Hz, 2H), 4.42 (d, J = 6.8 Hz, 2H), 5.50 (t, J = 5.9 Hz, 1H), 6.56 (s, 1H), 8.54 (s, 1H). ^{13}C NMR (DMSO-d_6) δ: 172.0, 157.7, 155.2, 143.8, 106.3, 101.4, 56.5, 51.3, 31.2, 19.8, 14.3. HRMS *m*/*z*: 223.1071 (MH^+ [$C_{11}H_{15}N_2O_3$] = 223.1083). Anal. calcd. for $C_{11}H_{14}N_2O_3$: C 59.45, H 6.35, N 12.60; found: C 59.35, H 6.15, N 12.80.

3-Decyl-6-(hydroxymethyl)furo[2,3-*d*]pyrimidin-2(3*H*)-one (3d)

Treatment of **2** (1.7 g, 10.2 mmol), K_2CO_3 (1.55 g, 11.2 mmol), and 1-iododecane (2.4 mL, 3.00 g, 11.2 mmol) by method 1 gave **3d** (1.26 g, 40%); mp 173–175 °C. UV max: 245, 331 nm (ε 15 800, 8 800). ^{1}H NMR (DMSO-d_6) δ: 0.84 (t, J = 6.8 Hz, 3H), 1.22–1.26 (m, 14H), 1.63–1.66 (m, 2H), 3.91 (t, J = 7.3 Hz, 2H), 4.42 (d, J = 5.9 Hz, 2H), 5.50 (t, J = 5.9 Hz, 1H), 6.56 (s, 1H), 8.53 (s, 1H). ^{13}C NMR (DMSO-d_6) δ: 172.0, 157.7, 155.2, 143.8, 106.3, 101.4, 56.5, 51.6, 32.0, 29.6, 29.35, 29.31, 29.1, 26.5, 22.8, 14.6. HRMS (EI) *m*/*z*: 306.1947 (M^+ [$C_{17}H_{26}N_2O_3$] = 306.1943). Anal. calcd. for $C_{17}H_{26}N_2O_3$: C 66.64, H 8.55, N 9.14; found: C 66.85, H 8.61, N 8.97.

3-Dodecyl-6-(hydroxymethyl)furo[2,3-*d*]pyrimidin-2(3*H*)-one (3e)

Treatment of **2** (1.7 g, 10.2 mmol), K_2CO_3 (1.55 g, 11.2 mmol), and 1-iodododecane (2.8 mL, 3.32 g, 11.2 mmol) by method 1 gave **3e** (0.95 g, 28%); mp 172–174 °C. UV max: 245, 331 nm (ε 15 600, 8 200). ^{1}H NMR (DMSO-d_6) δ: 0.84 (t, J = 6.8 Hz, 3H), 1.22–1.25 (m, 18H), 1.62–1.66 (m, 2H), 3.91 (t, J = 7.3 Hz, 2H), 4.42 (d, J = 5.9 Hz, 2H), 5.50 (t, J = 5.9 Hz, 1H), 6.56 (s, 1H), 8.53 (s, 1H). ^{13} C NMR (DMSO-d_6) δ: 172.0, 157.7, 155.1, 143.7, 106.3, 101.4, 56.5, 51.6, 32.0, 29.7, 29.63, 29.55, 29.4, 29.3,

© 2006 NRC Canada

29.1, 26.5, 22.8, 14.6. HRMS *m/z*: 335.2337 (MH^+ [$C_{19}H_{31}N_2O_3$] = 335.2335). Anal. calcd. for $C_{19}H_{30}N_2O_3$: C 68.23, H 9.04, N 8.38; found: C 68.17, H 8.89, N 8.30.

3-Butyl-6-(chloromethyl)furo[2,3-*d*]pyrimidin-2(3*H*)-one (5a)

Method 2

Dried CH_2Cl_2 (40 mL) was added to **3a** (1.11 g, 5.0 mmol) in a flame-dried flask. The solution (under N_2) was cooled to 0 °C, and pyridine (0.80 mL, 0.80 g, 10.0 mmol) followed by $SOCl_2$ (0.55 mL, 0.90 g, 7.5 mmol) were added. After 40 min, the reaction mixture was diluted with CH_2Cl_2 (40 mL), and ice was added. The solution was washed with 0.01 N HCl–H_2O (~5 mL), then $NaHCO_3$–H_2O (pH ~7), and water (2×). The organic layer was dried ($MgSO_4$), the solid was filtered and washed with CH_2Cl_2, and volatiles were evaporated at ambient temperature. The solid residue was dried under vacuum at ambient temperature to give **5a** (0.84 g, 70%). UV max: 251, 332 nm (ε 12 400, 6 800). ^{1}H NMR (DMSO-d_6) δ: 0.90 (t, *J* = 7.3 Hz, 3H), 1.29 ("quint", *J* = 7.6 Hz, 2H), 1.65 ("quint", *J* = 7.6 Hz, 2H), 3.94 (t, *J* = 7.6 Hz, 2H), 4.87 (s, 2H), 6.85 (s, 1H), 8.65 (s, 1H). ^{13}C NMR (DMSO-d_6) δ: 171.9, 155.1, 152.0, 145.4, 105.8, 105.3, 51.5, 38.3, 31.1, 19.8, 14.3. HRMS *m/z*: 241.0747 (MH^+ [$C_{11}H_{14}N_2{}^{35}ClO_2$] = 241.0744).

6-(Chloromethyl)-3-hexylfuro[2,3-*d*]pyrimidin-2(3*H*)-one (5b)

Treatment of 3-hexyl-6-(hydroxymethyl)furo[2,3-*d*]pyrimidin-2(3*H*)-one (**3b**) (13) (1.25 g, 5.0 mmol) by method 2 gave **5b** (0.83 g, 62%). UV max: 251, 332 nm (ε 14 500, 7 900). ^{1}H NMR δ: 0.84 (t, *J* = 6.6 Hz, 3H), 1.30–1.37 (m, 6H), 1.81 ("quint", *J* = 7.3 Hz, 2H), 4.04 (t, *J* = 7.3 Hz, 2H), 4.55 (s, 2H), 6.55 (s, 1H), 8.02 (s, 1H). ^{13}C NMR δ: 171.8, 155.5, 152.9, 141.4, 107.0, 103.2, 52.9, 37.2, 31.6, 29.3, 26.5, 22.7, 14.2. HRMS (EI) *m/z*: 268.0977 (M^+ [$C_{13}H_{17}N_2{}^{35}ClO_2$] = 268.0979).

6-(Chloromethyl)-3-octylfuro[2,3-*d*]pyrimidin-2(3*H*)-one (5c)

Treatment of 6-(hydroxymethyl)-3-octylfuro[2,3-*d*]pyrimidin-2(3*H*)-one (**3c**) (13) (1.39 g, 5 mmol) by method 2 gave **5c** (1.20 g, 81%). UV max: 252, 332 nm (ε 14 000, 7 400). ^{1}H NMR δ: 0.87–0.90 (m, 3H), 1.27–1.34 (m, 10H), 1.82–1.83 (m, 2H), 4.00–4.04 (m, 2H), 4.55 (s, 2H), 6.49 (s, 1H), 7.91 (s, 1H). ^{13}C NMR δ: 172.0, 155.3, 152.9, 141.1, 107.2, 103.0, 52.8, 37.1, 31.9, 29.4, 26.8, 22.8, 14.3.

6-(Chloromethyl)-3-decylfuro[2,3-*d*]pyrimidin-2(3*H*)-one (5d)

Treatment of **3d** (1.53 g, 5 mmol) by method 2 gave **5d** (1.05 g, 65%). UV max: 248, 331 nm (ε 14 300, 7 900). ^{1}H NMR δ: 0.87 (t, *J* = 6.8 Hz, 3H), 1.25–1.33 (m, 14H), 1.79–1.82 (m, 2H), 4.01 (t, *J* = 7.6 Hz, 2H), 4.54 (s, 2H), 6.50 (s, 1H), 7.94 (s, 1H). ^{13}C NMR δ: 171.9, 155.3, 152.8, 141.3, 106.7, 103.1, 52.8, 37.1, 32.0, 29.67, 29.65, 29.45, 29.38, 29.33, 26.8, 22.9, 14.3.

6-(Chloromethyl)-3-dodecylfuro[2,3-*d*]pyrimidin-2(3*H*)-one (5e)

Treatment of **3e** (1.67 g, 5 mmol) by method 2 gave **5e** (1.20 g, 68%). UV max: 253, 331 nm (ε 11 500, 9 500). ^{1}H NMR (DMSO-d_6) δ: 0.84 (t, *J* = 6.6 Hz, 3H), 1.20–1.24 (m, 18H), 1.63–1.65 (m, 2H), 3.92 (t, *J* = 6.9 Hz, 2H), 4.85 (s, 2H), 6.84 (s, 1H), 8.64 (s, 1H). ^{13}C NMR δ: 172.0, 155.3, 152.9, 141.1, 106.7, 103.0, 52.8, 37.1, 32.1, 29.83, 29.76, 29.70, 29.6, 29.43, 29.37, 26.8, 22.9, 14.4. HRMS (EI) *m/z*: 352.1921 (M^+ [$C_{19}H_{29}N_2{}^{35}ClO_2$] = 352.1918).

3-Butyl-6-(octyloxymethyl)furo[2,3-*d*]pyrimidin-2(3*H*)-one (6a)

Method 3

Compound **5a** (100 mg, 0.42 mmol) was added to 1-octanol (2 mL) and the reaction was stirred overnight at 50 °C. The solution was neutralized with Et_3N, and volatiles were evaporated under *high* vacuum. The residue was purified by flash silica gel column chromatography and recrystallized from MeOH to give **6a** (76 mg, 54%); mp 155 °C. UV max: 245, 331 nm (ε 16 500, 9 100). ^{1}H NMR δ: 0.88 (t, *J* = 6.8 Hz, 3H), 0.97 (t, *J* = 7.3 Hz, 3H), 1.27–1.42 (m, 12H), 1.60–1.63 (m, 2H), 1.79–1.82 (m, 2H), 3.55 (t, *J* = 6.6 Hz, 2H), 4.02 (t, *J* = 7.6 Hz, 2H), 4.47 (s, 2H), 6.39 (s, 1H), 7.84 (s, 1H). ^{13}C NMR δ: 172.2, 155.5, 140.3, 107.1, 101.6, 71.8, 65.2, 52.4, 32.0, 31.4, 29.9, 29.6, 29.5, 26.3, 22.9, 20.0, 14.3, 13.9. HRMS (EI) *m/z*: 334.2249 (M^+ [$C_{19}H_{30}N_2O_3$] = 334.2256). Anal. calcd. for $C_{19}H_{30}N_2O_3$: C 68.23, H 9.04, N 8.38; found: C 68.12, H 8.83, N 8.12.

3-Hexyl-6-(propyloxymethyl)furo[2,3-*d*]pyrimidin-2(3*H*)-one (6b)

Treatment of **5b** (100 mg, 0.37 mmol) with 1-propanol (2 mL) by method 3 gave **6b** (68 mg, 63%); mp 165 °C. UV max: 245, 331 nm (ε 14 500, 7900). ^{1}H NMR δ: 0.86–0.96 (m, 6H), 1.31–1.32 (m, 6H), 1.64 ("quint", *J* = 7.1 Hz, 2H), 1.79–1.82 (m, 2H), 3.50–3.54 (m, 2H), 4.02 (t, *J* = 7.1 Hz, 2H), 4.47 (s, 2H), 6.44 (s, 1H), 7.91 (s, 1H). ^{13}C NMR δ: 171.6, 155.5, 155.4, 140.3, 107.3, 101.7, 73.3, 65.1, 52.7, 31.5, 29.3, 26.4, 23.0, 22.7, 14.2, 10.7. HRMS *m/z*: 293.1869 (MH^+ [$C_{16}H_{25}N_2O_3$] = 293.1865). Anal. calcd. for $C_{16}H_{24}N_2O_3$: C 65.73, H 8.27, N 9.58; found: C 65.92, H 8.12, N 9.65.

6-(Butyloxymethyl)-3-hexylfuro[2,3-*d*]pyrimidin-2(3*H*)-one (6c)

Treatment of **5b** (100 mg, 0.37 mmol) with 1-butanol (2 mL) by method 3 gave **6c** (98 mg, 87%); mp 153–155 °C. UV max: 245, 331 nm (ε 12 500, 7 000). ^{1}H NMR δ: 0.89–0.95 (m, 6H), 1.33–1.42 (m, 8H), 1.57–1.62 (m, 2H), 1.80–1.81 (m, 2H), 3.57 (t, *J* = 6.6 Hz, 2H), 4.01 (t, *J* = 7.6 Hz, 2H), 4.47 (s, 2H), 6.38 (s, 1H), 7.83 (s, 1H). ^{13}C NMR δ: 172.1, 155.5, 140.2, 107.1, 101.6, 71.5, 65.2, 52.7, 31.9, 31.6, 29.3, 26.5, 22.7, 19.5, 14.2, 14.1. HRMS *m/z:* 329.1828 (MNa^+ [$C_{17}H_{26}N_2O_3Na$] = 329.1841). Anal. calcd. for $C_{17}H_{26}N_2O_3$: C 66.64, H 8.55, N 9.14; found: C 66.73, H 8.38, N 8.99.

© 2006 NRC Canada

3-Hexyl-6-(hexyloxymethyl)furo[2,3-*d*]pyrimidin-2(3*H*)-one (6d)

Treatment of **5b** (100 mg, 0.37 mmol) with 1-hexanol (2 mL) by method 3 gave **6d** (69 mg, 56%); mp 153–155 °C. UV max: 245, 331 nm (ε 14 200, 7 700). ^{1}H NMR δ: 0.89 (t, *J* = 6.6 Hz, 6H), 1.28–1.37 (m, 12H), 1.59–1.63 (m, 2H), 1.81 ("quint", *J* = 6.8 Hz, 2H), 3.56 (t, *J* = 6.6 Hz, 2H), 4.0 (t, *J* = 7.6 Hz, 2H), 4.47 (s, 2H), 6.39 (s, 1H), 7.84 (s, 1H). ^{13}C NMR δ: 172.1, 155.5, 140.2, 107.0, 101.6, 71.8, 65.2, 52.7, 31.8, 31.6, 29.8, 29.3, 26.5, 25.9, 22.8, 22.7, 14.2. HRMS *m*/*z*: 357.2148 (MNa^+ [$C_{19}H_{30}N_2O_3Na$] = 357.2154). Anal. calcd. for $C_{19}H_{30}N_2O_3$: C 68.23, H 9.04, N 8.38; found: C 68.50, H 8.96, N 8.14.

6-(Butyloxymethyl)-3-octylfuro[2,3-*d*]pyrimidin-2(3*H*)-one (6e)

Treatment of **5c** (100mg, 0.34 mmol) with 1-butanol (2 mL) by method 3 gave **6e** (97 mg, 85%): mp 149–151 °C. UV max: 245, 331 nm (ε 16 500, 8 900). ^{1}H NMR δ: 0.87–0.89 (m, 6H), 1.18–1.42 (m, 12H), 1.58–1.62 (m, 2H), 1.75–2.49 (m, 2H), 3.56 (t, *J* = 6.6 Hz, 2H), 4.0 (t, *J* = 7.6 Hz, 2H), 4.46 (s, 2H), 6.39 (s, 1H), 7.85 (s, 1H). ^{13}C NMR δ: 172.1, 155.50, 155.46, 140.3, 107.1, 101.7, 71.5, 65.2, 52.7, 32.0, 31.9, 29.9, 29.4, 26.8, 22.8, 19.5, 14.3, 14.1. HRMS *m*/*z*: 335.2325 (MH^+ [$C_{19}H_{31}N_2O_3$] = 335.2335). Anal. calcd. for $C_{19}H_{30}N_2O_3$: C 68.23, H 9.04, N 8.38; found: C 68.35, H 8.92, N 8.45.

6-(Hexyloxymethyl)-3-octylfuro[2,3-*d*]pyrimidin-2(3*H*)-one (6f)

Treatment of **5c** (100 mg, 0.34 mmol) with 1-hexanol (2 mL) by method 3 gave **6f** (67 mg, 54%); mp 141–143 °C. UV max: 245, 331 nm (ε 12 700, 6 800). ^{1}H NMR δ: 0.87–0.89 (m, 6H), 1.26–1.38 (m, 16H), 1.62 ("quint", *J* = 7.1 Hz, 2H), 1.81 ("quint", *J* = 6.8 Hz, 2H), 3.56 (t, *J* = 6.6 Hz, 2H), 4.01 (t, *J* = 7.3 Hz, 2H), 4.47 (s, 2H), 6.39 (s, 1H), 7.83 (s, 1H). ^{13}C NMR δ: 172.1, 155.5, 140.2, 107.0, 101.6, 71.8, 65.2, 52.7, 32.0, 31.8, 29.8, 29.4, 26.8, 26.0, 22.8, 14.3. HRMS *m*/*z*: 363.2662 (MH^+ [$C_{21}H_{35}N_2O_3$] = 363.2648. Anal. calcd. for $C_{21}H_{34}N_2O_3$: C 69.58, H 9.45, N 7.73; found: C 69.61, H 9.01, N 7.63.

3-Octyl-6-(octyloxymethyl)furo[2,3-*d*]pyrimidin-2(3*H*)-one (6g)

Treatment of **5c** (100 mg, 0.34 mmol) with 1-octanol (2 mL) by method 3 gave **6g** (0.1 g, 76%); mp 139–141 °C. UV max: 245, 331 nm (ε 13 600, 7 500). ^{1}H NMR δ: 0.87–0.89 (m, 6H), 1.27–1.33 (m, 18H), 1.59–1.68 (m, 4H), 1.79–1.81 (m, 2H), 3.55 (t, *J* = 6.8 Hz, 2H), 4.01 (t, *J* = 7.3 Hz, 2H), 4.47 (s, 2H), 6.39 (s, 1H), 7.85 (s, 1H). ^{13}C NMR δ: 172.1, 155.5, 140.2, 107.1, 101.6, 71.8, 65.2, 52.7, 32.04, 31.96, 29.9, 29.6, 29.5, 29.4, 26.8, 26.3, 22.9, 22.8, 14.34, 14.31. HRMS (EI) *m*/*z*: 390.2881 (M^+ [$C_{23}H_{38}N_2O_3$] = 390.2882). Anal. calcd. for $C_{23}H_{38}N_2O_3$: C 70.73, H 9.81, N 7.17; found: C 70.69, H 9.67, N 7.17.

6-(Butyloxymethyl)-3-decylfuro[2,3-*d*]pyrimidin-2(3*H*)-one (6h)

Treatment of **5d** (100 mg, 0.31 mmol) with 1-butanol (2 mL) by method 3 gave **6h** (76 mg, 68%); mp 150–152 °C. UV max: 245, 331 nm (ε 11 200, 6 400). ^{1}H NMR δ: 0.87–0.95 (m, 6H), 1.26–1.42 (m, 16H), 1.58–1.63 (m, 2H), 1.79–1.82 (m, 2H), 3.57 (t, *J* = 6.6 Hz, 2H), 4.01 (t, *J* = 7.3 Hz, 2H), 4.47 (s, 2H), 6.39 (s, 1H), 7.84 (s, 1H). ^{13}C NMR δ: 172.2, 155.5, 140.3, 107.1, 101.6, 71.5, 65.2, 52.7, 32.1, 31.9, 30.0, 29.7, 29.5, 29.44, 29.38, 26.8, 22.9, 19.5, 14.4, 14.1. HRMS *m*/*z* 385.2462 (MNa^+ [$C_{21}H_{34}N_2O_3Na$] = 385.2467). Anal. calcd. for $C_{21}H_{34}N_2O_3$: C 69.58, H 9.45, N 7.73; found: C 69.69, H 9.46, N, 7.86.

3-Decyl-6-(hexyloxymethyl)furo[2,3-*d*]pyrimidin-2(3*H*)-one (6i)

Treatment of **5d** (100 mg, 0.31 mmol) with 1-hexanol (2 mL) by method 3 gave **6i** (74 mg, 61%); mp 141–143 °C. UV max: 245, 331 nm (ε 14 100, 7 900). ^{1}H NMR δ: 0.87–0.90 (m, 6H), 1.26–1.37 (m, 18H), 1.59–1.62 (m, 4H), 1.79–1.82 (m, 2H), 3.56 (t, *J* = 6.6 Hz, 2H), 4.01 (t, *J* = 7.3 Hz, 2H), 4.47 (s, 2H), 6.40 (s, 1H), 7.85 (s, 1H). ^{13}C NMR δ: 172.1, 155.5, 140.3, 107.1, 101.6, 71.8, 65.2, 52.7, 32.1, 31.9, 30.0, 29.8, 29.7, 29.5, 29.44, 29.38, 26.8, 26.0, 22.9, 22.8, 14.4, 14.3. HRMS *m*/*z*: 413.2796 (MNa^+ [$C_{23}H_{38}N_2O_3Na$] = 413.2780). Anal. calcd. for $C_{23}H_{38}N_2O_3$: C 70.73, H 9.81, N 7.17; found: C 70.90, H 9.66, N 7.35.

3-Decyl-6-(octyloxymethyl)furo[2,3-*d*]pyrimidin-2(3*H*)-one (6j)

Treatment of **5d** (100 mg, 0.31 mmol) with 1-octanol (2 mL) by method 3 gave **6j** (71 mg, 55%); mp 139–141 °C. UV max: 245, 331 nm (ε 10 800, 6 100). ^{1}H NMR δ: 0.89 (t, *J* = 6.6 Hz, 6H), 1.26–1.34 (m, 22H), 1.59–1.62 (m, 4H), 1.80–1.82 (m, 2H), 3.56 (t, *J* = 6.6 Hz, 2H), 4.01 (t, *J* = 7.3 Hz, 2H), 4.47 (s, 2H), 6.38 (s, 1H), 7.83 (s, 1H). ^{13}C NMR δ: 172.2, 155.5, 140.2, 107.1, 101.6, 71.8, 65.2, 52.7, 32.1, 32.0, 29.9, 29.7, 29.6, 29.5, 29.44, 29.38, 26.8, 26.3, 22.9, 14.4. HRMS *m*/*z*: 441.3099 (MNa^+ [$C_{25}H_{42}N_2O_3Na$] = 441.3093). Elemental analyses were not obtained, but NMR spectra were equally clean.

6-(Butyloxymethyl)-3-dodecylfuro[2,3-*d*]pyrimidin-2(3*H*)-one (6k)

Treatment of **5e** (100 mg, 0.28 mmol) with 1-butanol (2 mL) by method 3 gave **6k** (72 mg, 65%); mp 147–149 °C. UV max: 245, 331 nm (ε 11 800, 6 400). ^{1}H NMR δ: 0.87–0.94 (m, 6H), 1.25–1.42 (m, 20H), 1.59–1.63 (m, 2H), 1.79–1.82 (m, 2H), 3.56 (t, *J* = 6.4 Hz, 2H), 4.0 (t, *J* = 7.6 Hz, 2H), 4.46 (s, 2H), 6.38 (s, 1H), 7.84 (s, 1H). ^{13}C NMR δ: 172.1, 155.49, 155.46, 140.2, 107.0, 101.6, 71.5, 65.2, 52.7, 32.1, 31.9, 29.8, 29.73, 29.67, 29.5, 29.41, 29.36, 26.8, 22.9, 19. 4, 14.3, 14.0. HRMS (EI) *m*/*z*: 391.2976 (MH^+ [$C_{23}H_{39}N_2O_3$] = 391.2961). Anal. calcd. for $C_{23}H_{38}N_2O_3$: C 70.73, H 9.81, N 7.17; found: C 70.90, H 9.60, N 7.31.

3-Dodecyl-6-(octyloxymethyl)furo[2,3-*d*]pyrimidin-2(3*H*)-one (6l)

Treatment of **5e** (100 mg, 0.28 mmol) with 1-octanol (2 mL) by method 3 gave **6l** (74 mg, 59%); mp 136–137 °C. UV max: 245, 331 nm (ε 12 000, 6 600). ^{1}H NMR δ: 0.88 (t, *J* = 6.8 Hz, 6H), 1.25–1.33 (m, 28H), 1.61 ("quint", *J* = 6.9 Hz, 2H), 1.80 ("quint", *J* = 6.9 Hz, 2H), 3.55 (t, *J* = 6.6 Hz, 2H), 4.00 (t, *J* = 7.3 Hz, 2H), 4.46 (s, 2H), 6.39 (s, 1H), 7.87 (s, 1H). ^{13}C NMR δ: 172.1, 155.4, 140.3, 107.1, 101.6, 71.8, 65.2, 52.6, 32.1, 32.0, 29.82, 29.79, 29.72,

© 2006 NRC Canada

29.65, 29.58, 29.52, 29.4, 29.3, 26.8, 26.2, 22.9, 22.8, 14.3. HRMS *m/z*: 469.3390 (MNa^+ [$C_{27}H_{46}N_2O_3Na$] = 469.3406). Anal. calcd. for $C_{27}H_{46}N_2O_3$: C 72.60, H 10.38, N 6.27; found: C 72.83, H 10.16, N 6.34.

6-(Acetylsulfanylmethyl)-3-butylfuro[2,3-*d*]pyrimidin-2(3*H*)-one (7a)

Method 4

Dried acetonitrile (10 mL) was added to **5a** (0.24 g, 1 mmol) in a flame-dried flask, and the solution was deoxygenated (Ar) for 30 min. Potassium thioacetate (0.23 g, 2 mmol) was added, and the reaction mixture (under Ar) was sonicated for 5 min. Volatiles were evaporated and the residue was purified by silica gel column chromatography and recrystallized from EtOAc to give **7a** (0.20 g, 76%). UV max: 249, 334 nm (ε 18 500, 8 900). ^{1}H NMR δ: 0.97 (t, *J* = 7.3 Hz, 3H), 1.39 ("hext", *J* = 7.6 Hz, 2H), 1.79 ("quint", *J* = 7.6 Hz, 2H), 2.39 (s, 3H), 4.0 (t, *J* = 7.3 Hz, 2H), 4.10 (s, 2H), 6.35 (s, 1H), 7.79 (s, 1H). ^{13}C NMR δ: 194.2, 172.0, 155.4, 154.0, 140.0, 107.3, 101.6, 52.4, 31.4, 30.6, 26.2, 20.0, 13.9. HRMS *m/z:* 303.0783 (MNa^+ [$C_{13}H_{16}N_2O_3SNa$] = 303.0779).

6-(Acetylsulfanylmethyl)-3-hexylfuro[2,3-*d*]pyrimidin-2(3*H*)-one (7b)

Treatment of **5b** (0.27 g, 1 mmol) by method 4 gave **7b** (0.20 g, 71%). UV max: 251, 333 nm (ε 16 900, 6 700). ^{1}H NMR δ: 0.87 (t, *J* = 6.6 Hz, 3H), 1.29–1.31 (m, 6H), 1.75–1.79 (m, 2H), 2.37 (s, 3H), 3.99 (t, *J* = 7.1 Hz, 2H), 4.10 (s, 2H), 6.35 (s, 1H), 7.83 (s, 1H). ^{13} C NMR δ: 194.2, 171.9, 155.4, 153.9, 140.2, 107.2, 101.6, 52.6, 31.6, 30.6, 29.3, 26.4, 26.2, 22.7, 14.2. HRMS *m/z*: 331.1096 (MNa^+ [$C_{15}H_{20}N_2O_3SNa$] = 331.1092).

6-(Acetylsulfanylmethyl)-3-octylfuro[2,3-*d*]pyrimidin-2(3*H*)-one (7c)

Treatment of **5c** (0.30 g, 1 mmol) by method 4 gave **7c** (0.28 g, 83%). UV max: 250, 333 nm (ε 18 600, 9 100). ^{1}H NMR δ: 0.88 (t, *J* = 6.6 Hz, 3H), 1.26–1.32 (m, 10H), 1.78–1.80 (m, 2H), 2.38 (s, 3H), 3.99 (t, *J* = 7.3 Hz, 2H), 4.01 (s, 2H), 6.35 (s, 1H), 7.79 (s, 1H). ^{13}C NMR δ: 194.2, 171.9, 155.4, 153.9, 140.0, 107.2, 101.6, 95.0, 52.6, 31.9, 30.6, 29.4, 26.8, 26.2, 22.8, 14.3. HRMS *m/z*: 337.1577 (MH^+ [$C_{17}H_{25}N_2O_3S$] = 337.1586).

6-(Acetylsulfanylmethyl)-3-decylfuro[2,3-*d*]pyrimidin-2(3*H*)-one (7d)

Treatment of **5d** (0.32 g, 1 mmol) by method 4 gave **7d** (0.19 g, 53%). UV max: 250, 333 nm (ε 16 200, 7 800). ^{1}H NMR δ: 0.86 (t, *J* = 7.3 Hz, 3H), 1.24–1.31 (m, 14H), 1.76–1.79 (m, 2H), 2.37 (s, 3H), 3.99 (t, *J* = 7.3 Hz, 2H), 4.09 (s, 2H), 6.35 (s, 1H), 7.84 (s, 1H). ^{13}C NMR δ: 194.2, 171.9, 155.5, 153.9, 140.3, 107.3, 101.7, 52.7, 32.1, 30.6, 29.71, 29.68, 29.5, 29.43, 29.38, 26.8, 26.2, 22.9, 14.3. HRMS *m/z*: 387.1707 (MNa^+ [$C_{19}H_{28}N_2O_3SNa$] = 387.1718).

6-(Acetylsulfanylmethyl)-3-dodecylfuro[2,3-*d*]pyrimidin-2(3*H*)-one (7e)

Treatment of **5e** (0.35 g, 1 mmol) by method 4 gave **7e** (0.35 g, 90%). UV max: 250, 333 nm (ε 15 000, 7 500). ^{1}H NMR δ: 0.89 (t, *J* = 6.8 Hz, 3H), 1.25–1.33 (m, 18H), 1.78–1.80 (m, 2H), 2.38 (s, 3H), 3.99 (t, *J* = 7.3 Hz, 2H), 4.10 (s, 2H), 6.35 (s, 1H), 7.79 (s, 1H). ^{13}C NMR δ: 194.3, 172.0, 155.4, 153.9, 140.1, 107.3, 101.6, 52.7, 32.1, 30.6, 29.83, 29.77, 29.70, 29.57, 29.44, 29.39, 26.8, 26.2, 22.9, 14.4. HRMS *m/z*: 415.2029 (MNa^+ [$C_{21}H_{32}N_2O_3SNa$] = 415.2031).

3-Butyl-6-(hexylsulfanylmethyl)furo[2,3-*d*]pyrimidin-2(3*H*)-one (8a)

Method 5

Compound **7a** (200 mg, 0.71 mmol) was added to a deoxygenated solution of MeOH (5 mL) and Na metal (23 mg, 1.0 mmol). The reaction mixture was stirred at ambient temperature for 10 min, and 1-iodohexane (0.15 mL, 212 mg, 1.0 mmol) was added. Stirring was continued for 2 h, and the solution was neutralized with acetic acid. Volatiles were evaporated, and the residue was purified by silica gel column chromatography and recrystallized from MeOH to give **8a** (110 mg, 48%); mp 162 °C. UV max: 249, 334 nm (ε 16 800, 8 700). ^{1}H NMR δ: 0.88 (t, *J* = 6.6 Hz, 3H), 0.96 (t, *J* = 7.3 Hz, 3H), 1.26–1.43 (m, 8H), 1.59 ("quint", *J* = 7.3 Hz, 2H), 1.79 ("quint", *J* = 7.3 Hz, 2H), 2.61 (t, *J* = 7.3 Hz, 2H), 3.67 (s, 2H), 4.02 (t, *J* = 7.3 Hz, 2H), 6.31 (s, 1H), 7.86 (s, 1H). ^{13}C NMR δ: 172.0, 156.2, 155.4, 139.9, 107.5, 100.4, 52.3, 32.7, 31.6, 31.3, 29.3, 28.7, 22.7, 20.0, 14.2, 13.8. HRMS *m/z*: 323.1793 (MH^+ [$C_{17}H_{27}N_2O_2S$] = 323.1793). Anal. calcd. for $C_{17}H_{26}N_2O_2S$: C 63.32, H 8.13, N 8.69; found: C 63.50, H 7.89, N 8.52.

3-Butyl-6-(octylsulfanylmethyl)furo[2,3-*d*]pyrimidin-2(3*H*)-one (8b)

Treatment of **7a** (100 mg, 0.36 mmol) with 1-iodooctane (91 μL, 121 mg, 0.50 mmol) by method 5 gave **8b** (92 mg, 73%); mp 162 °C. UV max: 249, 334 nm (ε 16 800, 8 700). ^{1}H NMR δ: 0.89 (t, *J* = 6.8 Hz, 3H), 0.97 (t, *J* = 7.3 Hz, 3H), 1.27–1.42 (m, 12H), 1.60 ("quint", *J* = 7.6 Hz, 2H), 1.79 ("quint", *J* = 7.6 Hz, 2H), 2.61 (t, *J* = 7.3 Hz, 2H), 3.67 (s, 2H), 4.01 (t, *J* = 7.3 Hz, 2H), 6.29 (s, 1H), 7.79 (s, 1H). ^{13}C NMR δ: 172.1, 156.2, 155.4, 139.6, 107.4, 100.3, 52.3, 32.8, 32.0, 31.4, 29.4, 29.0, 28.7, 22.9, 20.0, 14.3, 13.9. HRMS *m/z*: 373.1938 (MNa^+ [$C_{19}H_{30}N_2O_2SNa$] = 373.1926). Anal. calcd. for $C_{19}H_{30}N_2O_2S$: C 65.10, H 8.63, N 7.99; found: C 65.32, H 8.45, N 8.05.

3-Hexyl-6-(octylsulfanylmethyl)furo[2,3-*d*]pyrimidin-2(3*H*)-one (8c)

Treatment of **7b** (100 mg, 0.32 mmol) with 1-iodooctane (73 μL, 109 mg, 0.45 mmol) by method 5 gave **8c** (82 mg, 68%); mp 158–159 °C. UV max: 249, 334 nm (ε 13 900, 7 400). ^{1}H NMR δ: 0.87–0.89 (m, 6H), 1.27–1.37 (m, 16H), 1.57–1.63 (m, 2H), 1.80 ("quint", *J* = 7.1 Hz, 2H), 2.60–2.63 (m, 2H), 3.67 (s, 2H), 4.00 (t, *J* = 7.5 Hz, 2H), 6.29 (s, 1H), 7.79 (s, 1H). ^{13}C NMR δ: 172.1, 156.3, 155.5, 139.6, 107.4, 100.4, 52.7, 32.8, 32.0, 31.6, 29.4, 29.1, 28.7, 26.5, 22.9, 22.7, 14.4, 14.2. HRMS *m/z*: 401.2244 (MNa^+ [$C_{21}H_{34}N_2O_2SNa$] = 401.2239). Elemental analyses were not obtained, but NMR spectra were equally clean.

6-(Hexylsulfanylmethyl)-3-octylfuro[2,3-*d*]pyrimidin-2(3*H*)-one (8d)

Treatment of **7c** (100 mg, 0.30 mmol) with 1-iodohexane

© 2006 NRC Canada

(61 μL, 88 mg, 0.41 mmol) by method 5 gave **8d** (75 mg, 66%); mp 155–157 °C. UV max: 249, 334 nm (ε 11 900, 6 300). ^{1}H NMR δ: 0.88–0.90 (m, 6H), 1.26–1.41 (m, 16H), 1.57–1.62 (m, 2H), 1.79–1.81 (m, 2H), 2.62 (t, *J* = 7.4 Hz, 2H), 3.67 (s, 2H), 4.0 (t, *J* = 7.5 Hz, 2H), 6.30 (s, 1H), 7.80 (s, 1H). ^{13}C NMR δ: 172.1, 156.3, 155.5, 139.6, 107.4, 100.4, 52.7, 32.8, 32.0, 31.6, 29.9, 29.41, 29.37, 28.7, 26.8, 22.84, 22.77, 14.31, 14.27. HRMS (EI) *m*/*z*: 378.2357 (M^+ [$C_{21}H_{34}N_2O_2S$] = 378.2341). Anal. calcd. for $C_{21}H_{34}N_2O_2S$: C 66.63, H 9.05, N 7.40; found: C 66.80, H 8.87, N 7.22.

3-Octyl-6-(octylsulfanylmethyl)furo[2,3-*d*]pyrimidin-2-one (8e)

Treatment of **7c** (100 mg, 0.30 mmol) with 1-iodooctane (74 μL, 98 mg, 0.41 mmol) by method 5 gave **8e** (57 mg, 47%); mp 153–155 °C. UV max: 249, 334 nm (ε 12 700, 6 700). ^{1}H NMR δ: 0.88 (t, *J* = 7.1 Hz, 6H), 1.27–1.32 (m, 20H), 1.58–1.60 (m, 2H), 1.78–1.82 (m, 2H), 2.61 (t, *J* = 7.5 Hz, 2H), 3.67 (s, 2H), 4.00 (t, *J* = 7.4 Hz, 2H), 6.30 (s, 1H), 7.79 (s, 1H). ^{13}C NMR δ: 172.1, 156.2, 155.5, 139.6, 107.4, 100.4, 52.7, 32.8, 32.03, 31.97, 30.0, 29.4, 29.1, 28.7, 26.8, 22.9, 22.8, 14.34, 14.31. HRMS *m*/*z*: 429.2556 (MNa^+ [$C_{23}H_{38}N_2O_2SNa$] = 429.2552). Anal. calcd. for $C_{23}H_{38}N_2O_2S$: C 67.94, H 9.42, N 6.89; found: C 67.96, H 9.21, N 6.64.

3-Decyl-6-(hexylsulfanylmethyl)furo[2,3-*d*]pyrimidin-2(3*H*)-one (8f)

Treatment of **7d** (100 mg, 0.27 mmol) with 1-iodohexane (55 μL, 80 mg, 0.38 mmol) by method 5 gave **8f** (91 mg, 83%); mp 156–157 °C. UV max: 250, 334 nm (ε 15 100, 8 000). ^{1}H NMR δ: 0.86–0.89 (m, 6H), 1.25–1.41 (m, 20H), 1.57–1.63 (m, 2H), 1.77–1.83 (m, 2H), 2.61 (t, *J* = 7.3 Hz, 2H), 3.67 (s, 2H), 4.00 (t, *J* = 7.3 Hz, 2H), 6.29 (s, 1H), 7.79 (s, 1H). ^{13}C NMR δ: 172.1, 156.2, 155.5, 139.6, 107.4, 100.4, 52.7, 32.8, 32.1, 31.6, 29.7, 29.5, 29.44, 29.41, 29.35, 28.7, 26.8, 22.9, 22.8, 14.4, 14.3. HRMS *m*/*z*: 429.2544 (MNa^+ [$C_{23}H_{38}N_2O_2SNa$] = 429.2552). Elemental analyses were not obtained, but NMR spectra were equally clean.

3-Decyl-6-(octylsulfanylmethyl)furo[2,3-*d*]pyrimidin-2(3*H*)-one (8g)

Treatment of **7d** (100 mg, 0.27 mmol) with 1-iodooctane (68 μL, 91 mg, 0.38 mmol) by method 5 gave **8g** (81 mg, 69%). UV max: 249, 334 nm (ε 17 400, 9 300). ^{1}H NMR δ: 0.88 (t, *J* = 6.8 Hz, 6H), 1.26–1.38 (m, 24H), 1.58–1.63 (m, 2H), 1.81–2.60 (m, 2H), 2.63 (t, *J* = 7.6 Hz, 2H), 3.67 (s, 2H), 4.00 (t, *J* = 7.6 Hz, 2H), 6.29 (s, 1H), 7.79 (s, 1H). ^{13}C NMR δ: 172.1, 156.3, 155.5, 139.6, 107.4, 100.3, 52.7, 32.9, 32.1, 32.0, 29.7, 29.4, 29.1, 28.7, 26.9, 22.9, 14.3. MS (FAB) *m*/*z*: 457.2876 (MNa^+ [$C_{25}H_{42}N_2O_2SNa$] = 457.2865). Anal. calcd. for $C_{25}H_{42}N_2O_2S$: C 69.08, H 9.74, N 6.44; found: C 69.20, H 9.76, N 6.52.

6-(Butylsulfanylmethyl)-3-dodecylfuro[2,3-*d*]pyrimidin-2-one (8h)

Treatment of **7e** (100 mg, 0.25 mmol) with 1-iodobutane (40 μL, 64 mg, 0.35 mmol) by method 5 gave **8h** (49 mg, 48%); mp 160–161 °C. UV max: 250, 334 nm (ε 16 500, 8 500). ^{1}H NMR δ: 0.87–0.93 (m, 6H), 1.26–1.33 (m, 18H), 1.41 ("quint", *J* = 7.6 Hz, 2H), 1.62 ("quint", *J* = 7.6 Hz, 2H), 1.79–1.82 (m, 2H), 2.62 (t, *J* = 7.6 Hz, 2H), 3.67 (s, 2H), 3.99 (t, *J* = 7.3 Hz, 2H), 6.30 (s, 1H), 7.80 (s, 1H). ^{13}C NMR δ: 172.1, 156.2, 155.5, 139.7, 107.4, 100.4, 52.6, 32.5, 32.2, 31.5, 29.84, 29.78, 29.7, 29.6, 29.57, 29.47, 28.7, 26.8, 22.9, 22.2, 14.4, 13.9. MS (FAB) *m*/*z*: 429.2542 (MNa^+ [$C_{23}H_{38}N_2O_2SNa$] = 429.2552). Anal. calcd. for $C_{23}H_{38}N_2O_2S$: C 67.94, H 9.42, N 6.89; found: C 67.89, H 9.27, N 6.85.

3-Dodecyl-6-(hexylsulfanylmethyl)furo[2,3-*d*]pyrimidin-2(3*H*)-one (8i)

Treatment of **7e** (100 mg, 0.25 mmol) with 1-iodohexane (52 μL, 74 mg, 0.35 mmol) by method 5 gave **8i** (46 mg, 42%); mp 158–159 °C. UV max: 249, 334 nm (ε 16 400, 8 400). ^{1}H NMR δ: 0.87–0.90 (m, 6H), 1.26–1.29 (m, 24H), 1.59–1.61 (m, 2H), 1.79–1.81 (m, 2H), 2.61 (t, *J* = 7.6 Hz, 2H), 3.67 (s, 2H), 4.0 (t, *J* = 7.6 Hz, 2H), 6.29 (s, 1H), 7.79 (s, 1H). ^{13}C NMR δ: 172.1, 156.2, 155.5, 139.6, 107.4, 100.3, 52.6, 32.8, 32.1, 31.6, 29.82, 29.75, 29.69, 29.6, 29.43, 29.35, 28.7, 26.8, 22.9, 22.7, 14.3, 14.2. HRMS *m*/*z*: 457.2872 (MNa^+ [$C_{25}H_{42}N_2O_2SNa$] = 457.2865). Anal. calcd. for $C_{25}H_{42}N_2O_2S$: C 69.08, H 9.74, N 6.44; found: C 68.81, H 9.57, N 6.57.

3-Dodecyl-6-(octylsulfanylmethyl)furo[2,3-*d*]pyrimidin-2(3*H*)-one (8j)

Treatment of **7e** (100 mg, 0.25 mmol) with 1-iodooctane (63 μL, 84 mg, 0.35 mmol) by method 5 gave **8j** (49 mg, 42%); mp 152–153 °C. UV max: 250, 334 nm (ε 14 700, 7 300). ^{1}H NMR δ: 0.89 (t, *J* = 6.8 Hz, 6H), 1.26–1.39 (m, 28H), 1.59–1.63 (m, 2H), 1.82–1.79 (m, 2H), 2.62 (t, *J* = 7.3 Hz, 2H), 3.67 (s, 2H), 4.00 (t, *J* = 7.3 Hz, 2H), 6.29 (s, 1H), 7.79 (s, 1H). ^{13}C NMR δ: 172.1, 156.3, 155.5, 139.6, 107.4, 100.3, 52.6, 32.8, 32.1, 32.0, 29.82, 29.75, 29.69, 29.6, 29.4, 29.0, 28.7, 26.8, 22.90, 22.86, 14.3. HRMS *m*/*z*: 485.3172 (MNa^+ [$C_{27}H_{46}N_2O_2SNa$] = 485.3178). Anal. calcd. for $C_{27}H_{46}N_2O_2S$: C 70.08, H 10.02, N 6.05; found: C 70.25, H 9.89, N 5.96.

References

1. M.J. Robins and P.J. Barr. Tetrahedron Lett. **22**, 421 (1981).
2. M.J. Robins and P.J. Barr. J. Org. Chem. **48**, 1854 (1983).
3. C. McGuigan, C.J. Yarnold, G. Jones, S. Velázquez, H. Barucki, A. Brancale, G. Andrei, R. Snoeck, E. De Clercq, and J. Balzarini. J. Med. Chem. **42**, 4479 (1999).
4. C. McGuigan, H. Barucki, S. Blewett, A. Carangio, J.T. Erichsen, G. Andrei, R. Snoeck, E. De Clercq, and J. Balzarini. J. Med. Chem. **43**, 4993 (2000).
5. C. McGuigan, H. Barucki, A. Carangio, S. Blewett, S. Srinivasan, G. Andrei, R. Snoeck, E. De Clercq, and J. Balzarini. Nucleosides Nucleotides Nucleic Acids, **20**, 287 (2001).
6. Z. Janeba, J. Balzarini, G. Andrei, R. Snoeck, E. De Clercq, and M.J. Robins. J. Med. Chem. **48**, 4690 (2005).
7. C. McGuigan, A. Brancale, H. Barucki, S. Srinivasan, G. Jones, R. Pathirana, S. Blewett, R. Alvarez, C.J. Yarnold, A. Carangio, S. Velázquez, G. Andrei, R. Snoeck, E. De Clercq, and J. Balzarini. Drugs Future, **25**, 1151 (2000).
8. J. Balzarini and C. McGuigan. J. Antimicrob. Chemother. **50**, 5 (2002).
9. E. De Clercq. Med. Res. Rev. **23**, 253 (2003).
10. (*a*) K. Miranda. M.S. thesis, Brigham Young University, Provo, Utah, 2001; (*b*) M.J. Robins, K. Miranda, V.K.

© 2006 NRC Canada

Rajwanshi, M.A. Peterson, G. Andrei, R. Snoeck, E. De Clercq, and J. Balzarini. J. Med. Chem. **49**, 391 (2006).
11. C. McGuigan, R.N. Pathirana, R. Snoeck, G. Andrei, E. De Clercq, and J. Balzarini. J. Med. Chem. **47**, 1847 (2004).
12. C. McGuigan, A. Brancale, G. Andrei, R. Snoeck, E. De Clercq, and J. Balzarini. Bioorg. Med. Chem. Lett. **13**, 4511 (2003).
13. Z. Janeba, N. Maklad, and M.J. Robins. Nucleosides Nucleotides Nucleic Acids, **24**, 1729 (2005).
14. E. Petricci, M. Radi, F. Corelli, and M. Botta. Tetrahedron Lett. **44**, 9181 (2003).

© 2006 NRC Canada

Reconciling solvent effects on rotamer populations in carbohydrates — A joint MD and NMR analysis[1]

Jorge Gonzalez-Outeiriño, Karl N. Kirschner, Smita Thobhani, and Robert J. Woods

Abstract: The rotational preferences of the hydroxymethyl group in pyranosides is known to depend on the local environment, whether in solid, solution, or gas phase. By combining molecular dynamics (MD) simulations with NMR spectroscopy the rotational preferences for the ω angle in methyl 2,3-di-*O*-methyl-α-D-glucopyranoside (**3**) and methyl 2,3-di-*O*-methyl-α-D-galactopyranoside (**6**) in a variety of solvents, with polarities ranging from 80 to 2.3 D have been determined. The effects of solvent polarity on intramolecular hydrogen bonding have been identified and quantified. In water, the internal hydrogen bonding networks are disrupted by competition with hydrogen bonds to the solvent. When the internal hydrogen bonds are differentially disrupted, the rotamer populations associated with the ω angle may be altered. In the case of **3** in water, the preferential disruption of the interaction between HO6 and O4 destabilizes the *tg* rotamer, leading to the observed preference for gauche rotamers. Without the hydrogen bond enhancement offered by a low polarity environment, both **3** and **6** display rotamer populations that are consistent with expectations based on the minimization of repulsive intramolecular oxygen–oxygen interactions. In a low polarity environment, HO6 prefers to interact with O4, however, in water these interactions are markedly weakened, indicating that HO6 acts as a hydrogen bond donor to water.

Key words: carbohydrate, rotamer, molecular dynamics simulation, MD, NMR.

Résumé : Il est bien connu que les préférences rotationnelles des groupes hydroxyméthyles des pyranosides dépend de l'environnement local que ce soit à l'état solide, en solution ou en phase gazeuse. En combinant des simulations de dynamique moléculaire (DM) avec la spectroscopie RMN, on a pu déterminer les préférences rotationnelles pour l'angle ω du 2,3-di-*O*-méthyl-α-D-glucopyranoside de méthyle (**3**) 2,3-di-*O*-méthyl-α-D-galactopyranoside de méthyle (**6**), dans une variété de solvants dont les polarités s'étalent de 80 à 2,3 D. On a identifié et quantifié les effets de polarité du solvant sur la liaison hydrogène intramoléculaire. Dans l'eau, la liaison hydrogène interne est perturbée par la compétition avec les liaisons hydrogènes vers le solvant. Lorsque les liaisons hydrogènes internes sont perturbées de façons différentes, les populations de rotamères associées à l'angle ω peuvent être modifiées. Dans le cas du composé **3**, l'eau provoque une perturbation préférentielle de l'interaction entre le OH en position 6 et l'oxygène en 4 qui déstabilise le rotamère *tg*, ce qui conduit à une observation préférentielle des rotamères gauches. Lorsqu'ils ne présentent pas d'augmentation de la liaison hydrogène en raison d'un environnement de faible polarité, les populations de rotamères des composés **3** et **6** sont en accord avec ce qu'on pourrait attendre sur la base d'une minimisation des interactions répulsives oxygène–oxygène intramoléculaires. Dans une environnement de faible polarité, le OH en position 6 préfère l'interaction avec l'oxygène en 4; toutefois, dans l'eau, ces interactions sont de beaucoup affaiblies ce qui indique que le OH en position 6 agit comme donneur de liaison hydrogène pour l'eau.

Mots clés : hydrate de carbone, rotamère, simulation de dynamique moléculaire, DM, RMN.

[Traduit par la Rédaction]

Introduction

The importance of understanding the relationships between conformation and biological and chemical function in carbohydrates has come to the forefront of glycobiology as oligo- and poly-saccharides are increasingly implicated in both the healthy growth and functioning of organisms, as well as in a diverse range of disease states (1–3). Further, the covalent attachment of carbohydrates to proteins may affect both protein stability and structure (4–7), as well as,

Received 18 August 2005. Published on the NRC Research Press Web site at http://canjchem.nrc.ca on 5 May 2006.

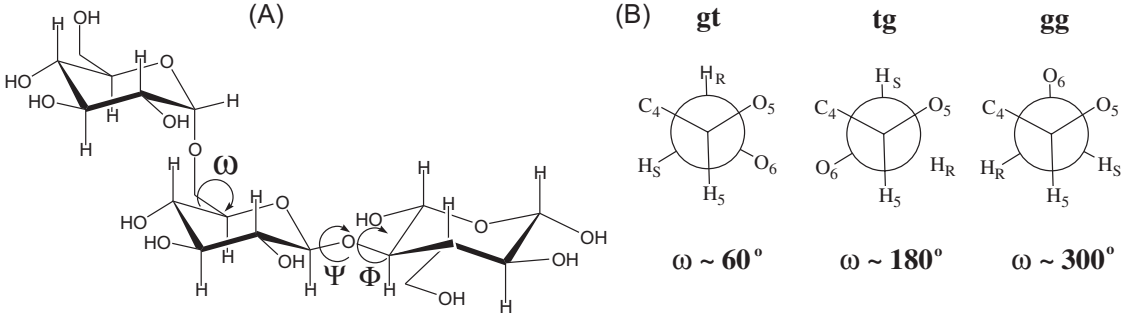
This manuscript is dedicated to Professor Walter A. Szarek.

J. Gonzalez-Outeiriño, K.N. Kirschner, S. Thobhani, and R.J. Woods.[2] Complex Carbohydrate Research Center, University of Georgia, 315 Riverbend Road, Athens, GA 30602, USA.

[1]This article is part of a Special Issue dedicated to Professor Walter A. Szarek.
[2]Corresponding author (e-mail: rwoods@ccrc.uga.edu).

 doi:10.1139/V06-036 © 2006 NRC Canada

Fig. 1. (A) Schematic diagram indicating glycosidic torsion angles in carbohydrates. (B) Nomenclature for the ω torsion angle (O6-C6-C5-O5). Qualitatively, the three staggered rotamers are commonly defined with respect to the O6-C6-C5-O5 and O6-C6-C5-C4 torsion angles as gauche-gauche (*gg*), gauche-trans (*gt*), and trans-gauche (*tg*).



conversely, function (8–10). The ability to correlate biological function with glycan structure can provide not only mechanistic insight (11), but is also of benefit in optimizing carbohydrate-based therapeutic agents (12).

X-ray crystallography, NMR spectroscopy, and theoretical calculations are the three techniques most commonly used in the conformational analysis of carbohydrates. X-ray crystallography has been very successful in characterizing protein–carbohydrate complexes, provided that the carbohydrate is limited in size (13, 14). However, single crystal X-ray diffraction structures of oligo- and poly-saccharides are extremely rare; a direct result of difficulties in crystallizing the generally flexible oligosaccharides (15). For solution conformational analysis, NMR spectroscopy is the preferred technique. However, the deconvolution of the observed NMR properties, such as chemical shifts, scalar *J* couplings, nuclear Overhauser effects (NOEs), and residual dipolar couplings, into the 3-D structures that are present in solution presents particular difficulties for these flexible molecules (16, 17). The challenge in deriving a mixture of physically real conformations from a spectroscopic signal that arises from the average of the conformational ensemble is generally met by introducing some aspect of theoretical modeling into the NMR data analysis. Unlike the situation with protein structure determinations by NMR, the use of NMR observables as restraints during the modeling of flexible carbohydrates can lead to the generation of nonphysical virtual conformations (18). To avoid this problem, theoretical calculations are generally employed in one of two ways, either to provide discrete models for the presumed conformations present in solution or to independently predict the conformational states. In the former application, a limited number of theoretical structures are generated, usually by some form of gas-phase energy minimization (quantum or classical mechanical energies) of initial conformations. Based on the computed NMR properties for each individual structure it may then be possible to establish the populations of the individual structures that give the best agreement with experiment. Perhaps the most significant limitation to the accuracy of this approach is the selection of the individual structures, which is often based on scientific intuition. In contrast, molecular dynamics (MD) simulations or Monte Carlo sampling may be employed to predict the ensemble of conformations that the carbohydrate populates at room temperature in the appropriate solvent, independent of investigator bias (19). The accuracy of this latter approach is limited by the choice of classical mechanical force field. Force field development remains an active research area; however, MD simulations are generally able to accurately identify the conformational states present in solution and can often predict their populations with reasonably accuracy (20–24, 19).

In solution, 3-D structures of oligosaccharides have been shown to exist as an equilibrium among several conformations, owing to the flexibility introduced in the structure by the glycosidic linkages, Φ, Ψ, and ω (see Fig. 1). The conformations of the first two torsion angles (Φ, Ψ) are dominated mainly by stereolectronic (anomeric effect) and steric effects (25, 26). As would be expected for an ether-type linkage, the ω torsion angle may adopt any of the three staggered rotamers, with populations depending heavily on the configuration at C4 and on the polarity of the local environment (27, 23).

In the solid state, an early report based on a statistical analysis of X-ray structures (28) revealed two remarkably different conformational behaviors for the ω torsion angle in carbohydrates. The glucopyranosides and mannopyranosides showed clear preferences for only the *gg* and *gt* conformations, with ratios of approximately 40:0:60 (*gt*:*tg*:*gg*), while galactopyranosides showed a significant population of the *tg* rotamer, with a ratio of approximately 58:34:8 (*gt*:*tg*:*gg*). Similar trends have been inferred from NMR data in aqueous solution for both the glucopyranosyl (50:0:53 (29), 38:4:58 (30), 44.7:3.5:51.8 (31), and 52:7:41 (32)) and galactopyranosyl series (56:32:12 (29), 61:21:18 (30), 71.6:13.9:14.5 (31), 65:21:14 (33), and 67:30:3(32)). A detailed review of the conformational properties of the ω angle has been provided by Bock and Duus (29).

In contrast to the condensed-phase experimental data, gas-phase quantum mechanical calculations fail to predict the correct rotamer populations unless the formation of internal hydrogen bonds among hydroxyl groups at C4 and C6 or between the hydroxyl group at C6 and the ring oxygen atom is prevented (34, 23, 31). A Boltzman analysis of the gas-phase quantum mechanical energies, computed at the B3LYP/6-31G(2d,2p) level has been performed for methyl α-D-glucopyranosides and galactopyranosides. A theoretical population ratio of 43:29:28 was obtained for the glucopyranoside when internal hydrogen bonding was allowed, whereas qualitative agreement with experiment (62:0:37) was only obtained when intramolecular hydrogen bonds were prevented from forming. Similarly for the galactopyranoside, ratios of 38:5:57 (with internal hydrogen bonds)

© 2006 NRC Canada

and 41:59:0 (without) were obtained (23). In neither derivative were the gas-phase calculations able to give quantitative agreement with experiment, although they suggested a role for internal hydrogen bonding. It should be noted that in all structures examined quantum mechanically, prevention of internal hydrogen bonding led to significantly higher energies relative to those of conformations in which intramolecular hydrogen bonds were present (23). Nonetheless, the observation that qualitative agreement with experiment was obtained only in the absence of intramolecular hydrogen bonds is consistent with an interpretation of rotamer populations as arising from the minimization of unfavorable 1,3-diaxial electrostatic interactions among O4, O5, and O6 (29, 23).

To obtain quantitative agreement between theoretical calculations and experiment, it was found necessary to include water explicitly in the MD simulations of the glucopyranosides and galactopyranosides (23). The mechanism whereby solvent influences ω population in methyl α-D-glucopyranoside has previously been examined experimentally in an NMR analysis of the 2,3,4,6-tetra- and 2,3,4-tri-*O*-methylated derivatives in several solvents (27). By examining the effect of solvent polarity on rotamer population of these methylated derivatives, Rockwell and Grindley (27) made two important observations, namely that permethylation removed any dependence of rotamer population on solvent polarity (maintaining approximately a ratio of 61:38:0), and, in contrast, that when O6 was unsubstituted there was a strong dependence on polarity. They inferred that polar solvents led to a decrease of intramolecular hydrogen bonding, but also that hydrogen bond donation from the hydroxymethyl group to water was not important in determining rotational preferences.

Here we extend the work of Rockwell and Grindley to derivatives of both glucopyranosides and galactopyranosides in which we elected to examine derivatives that, like the natural carbohydrates, have free hydroxyl groups at either O4 or O6. Thus, we have synthesized methyl 2,3-di-*O*-methyl-α-D-glucopyranoside (**3**) and methyl 2,3-di-*O*-methyl-α-D-galactopyranoside (**6**), and determined the rotational properties of each of their ω angles by NMR in a variety of solvents. By employing these simple models, an assessment of the importance of hydrogen bond donation from HO4 to O6 may be made, as well as of the effect of configuration at C4 on rotamer population as a function of solvent polarity. In addition, a detailed examination of the hydrogen bond properties for these glycosides and related disaccharides was undertaken by performing the longest explicitly solvated MD simulations reported to date in both water and dichloromethane. Data from the theoretical simulations is used to provide atomic level insight into the validity of the inferences made on the basis of the experimental data.

Experimental

General

^{1}H and ^{13}C NMR and 2-D correlation spectra were recorded on Varian 300 and 500 MHz spectrometers, each equipped with Sun off-line editing workstations. Chemical shifts were measured in parts per million (δ) relative to the appropriate solvent peaks and the scalar coupling constants (*J*) were measured in Hertz (Hz). Matrix assisted laser desorption ionization – time-of-flight (MALDI-TOF) mass spectra were recorded using a Hewlett Packard G2025A system with 2,5-dihydroxybenzoic acid (gentisic acid) (10 mg/mL in 50% acetonitrile) as the matrix. Melting points were recorded on a Kofler hot stage apparatus and are uncorrected.

Chemicals and reagents were purchased from Sigma-Aldrich, Fluka, or VWR and used without further purification unless otherwise stated. The reaction solvent (acetonitrile) was distilled from calcium hydride and stored over 4 Å molecular sieves prior to use. Ethanol was used without any further purification.

Synthesis

*Methyl 4,6-*O*-benzylidene-α-D-glucopyranoside (1)*

To a solution of methyl α-D-galactopyranoside (2.11 g, 10.87 mmol) in dry acetonitrile (60 mL) was added benzaldehyde dimethyl acetal (2.80 g, 18.40 mmol) and the solution acidified with camphorsulfonic acid (approx. 0.05 g, 0.22 mmol) to pH 3. After stirring at room temperature under an atmosphere of argon for 15 h, the mixture was neutralized with triethylamine and concentrated in vacuo to dryness using toluene as a cosolvent. The resulting residue was recrystallized from ethyl acetate – hexane to afford compound **1** as a white crystalline solid (2.22 g, 76%); mp 165–167 °C (lit. value (35) mp 166 to 167 °C). ^{1}H NMR (300 MHz, $CDCl_3$) δ: 7.53–7.45 (m, 2H, Ph), 7.41–7.33 (m, 3H, Ph), 5.53 (s, 1H, PhC*H*), 4.80 (d, 1H, H1), 4.30 (dd, 1H, H6a), 3.93 (t, 1H, H3), 3.85–3.77 (m, 1H, H5), 3.73 (t, 1H, H6b), 3.63 (dd, 1H, H2), 3.49 (t, 1H, H4), 3.46 (s, 3H, OCH_3). ^{13}C NMR (75 MHz, $CDCl_3$) δ: not observed (Cq, Ph), 129.2, 126.7 (5 × Ph), 101.7 (Ph*C*H), 99.2 (C1), 81.7 (C4), 72.9 (C2), 71.7 (C3), 69.2 (C6), 62.9 (C5), 55.4 (OCH_3). MALDI-TOF MS *m*/*z*: 305.2 $[M + Na]^+$.

*Methyl 4,6-*O*-benzylidene-2,3-di-*O*-methyl-α-D-glucopyranoside (2)*

Methyl 4,6-*O*-benzylidene-α-D-glucopyranoside (500 mg, 1.77 mmol) was dissolved in dry DMF (20 mL) under a nitrogen atmosphere. To this was added 60% NaH suspended in oil (260 mg, 6.50 mmol) followed by the dropwise addition of methyl iodide (340 μL, 5.46 mmol) and the reaction was left to stir for 16 h under a nitrogen atmosphere at room temperature. After this time, the reaction was quenched with water (40 mL) and the aqueous layer was washed with ethyl acetate (3 × 50 mL). The combined organic layers were then washed with satd. $NaHCO_3$ (3 × 50 mL) and water (3 × 50 mL). The combined organic layers were dried ($MgSO_4$), filtered, and the solvent removed in vacuo and the residue recrystallized from ethanol to furnish **2** as a white solid (270 mg, 49%); mp 121 to 122 °C (lit. value (36) mp 122 to 123 °C). ^{1}H NMR (300 MHz, $CDCl_3$) δ: 7.53–7.45 (m, 2H, Ph), 7.40–7.31 (m, 3H, Ph), 5.54 (s, 1H, PhC*H*), 4.85 (d, 1H, H1), 4.28 (dd, 1H, H6a), 3.88–3.78 (m, 1H, H5), 3.74 (dd, 1H, H6b), 3.69 (t, 1H, H3), 3.64 (s, 3H, OCH_3), 3.56 (s, 3H, OCH_3), 3.53 (t, 1H, H4), 3.45 (s, 3H, OCH_3), 3.30 (t, 1H, H2). ^{13}C NMR (75 MHz, $CDCl_3$) δ: not observed (Cq, Ph), 129.4, 126.9 (5 × Ph), 101.9 (Ph*C*H), 98.1 (C1), 81.9

© 2006 NRC Canada

(C2), 81.9 (C4), 80.6 (C3), 69.4 (C6), 61.9 (C5), 60.6, 59.4, 55.6 (3 × OCH_3). MALDI-TOF MS *m/z*: 332.8 $[M + Na]^+$.

*Methyl 2,3-di-*O*-methyl-α-D-glucopyranoside (3)*

To methyl 4,6-*O*-benzylidene-2,3-di-*O*-methyl-α-D-glucopyranoside (250 mg, 0.81 mmol) was added a solution of 80% acetic acid in water (15 mL) and the mixture was heated to 50 °C. After a period of 4 h, the reaction mixture was cooled, concentrated in vacuo, and then coevaporated with toluene (3 × 20 mL). The residue was recrystallized from ethyl acetate – hexane to give the desired compound **3** as a white solid (73 mg, 41%); mp 81–84 °C (lit. value (37) mp 84 °C). ^{1}H NMR (500 MHz, $CDCl_3$) δ: 4.84 (d, 1H, H1), 3.85 (dd, 1H, H6a), 3.80 (dd, 1H, H6b), 3.65–3.61 (m, 1H, H5), 3.63 (s, 3H, OCH_3), 3.49 (s, 3H, OCH_3), 3.50 (dd, 1H, H4), 3.43 (s, 3H, OCH_3), 3.46 (dd, 1H, H3), 3.21 (dd, 1H, H2). ^{13}C NMR (75 MHz, D_2O) δ: 97.3 (C1), 83.0 (C3), 80.6 (C2), 72.2 (C5) 69.8 (C4), 61.2 (C6), 60.6, 58.5, 55.4 (3 × OCH_3). MALDI TOF *m/z*: 245.2 $[M + Na]^+$.

*Methyl 4,6-*O*-benzylidene-α-D-galactopyranoside (4)*

The synthesis of methyl 4,6-*O*-benzylidene-α-D-galactopyranoside was carried out following the procedure described for the preparation of the methyl 4,6-*O*-benzylidene-α-D-glucopyranoside. Thus, methyl α-D-galactopyranoside (1.00 g, 5.15 mmol) in dry acetonitrile (160 mL) was reacted with benzaldehyde dimethyl acetal (2.20 g, 14.45 mmol) and camphorsulfonic acid (approx. 0.03 g, 0.13 mmol) to afford **4** as a white crystalline solid after recrystallization (0.73 g, 50%); mp 169–171 °C (lit. value (35) mp 168 to 169 °C). ^{1}H NMR (300 MHz, $CDCl_3$) δ: 7.52–7.35 (m, 5H, Ph), 5.55 (s, 1H, PhC*H*), 4.92 (d, 1H, H1), 4.28 (dd, 1H, H6a), 4.25 (dd, 1H, H4), 4.08 (dd, 1H, H6b), 3.93 (dd, 1H, H2), 3.89 (dd, 1H, H3), 3.69 (ddd, 1H, H5), 3.46 (s, 3H, OCH_3). ^{13}C NMR (75 MHz, $CDCl_3$) δ: not observed (Cq, Ph), 129.4, 128.2, 126.3 (5 × Ph), 101.3 (Ph*C*H), 100.0 (C1), 75.7 (C4), 70.0 (C2), 70.0 (C3), 69.4 (C6), 62.5 (C5), 55.7 (OCH_3). MALDI-TOF MS *m/z*: 305.1 $[M + Na]^+$.

*Methyl 4,6-*O*-benzylidene-2,3-di-*O*-methyl-α-D-galactopyranoside (5)*

The synthesis of methyl 4,6-*O*-benzylidene-2,3-di-*O*-methyl-α-D-galactopyranoside was carried out following the procedure described for the preparation of the methyl 4,6-*O*-benzylidene-2,3-di-*O*-methyl-α-D-glucopyranoside. Thus, methyl 4,6-*O*-benzylidene-α-D-galactopyranoside (700 mg, 2.48 mmol) was reacted with NaH (300 mg, 7.50 mmol) and methyl iodide (900 μL, 14.46 mmol) in dry DMF (20 mL) to give **5** as a white solid after recrystallization (230 mg, 40%); mp 126 to 127 °C (lit. value (38) mp 127 to 128 °C. ^{1}H NMR (300 MHz, $CDCl_3$) δ: 7.56–7.48 (m, 2H, Ph), 7.38–7.29 (m, 3H, Ph), 5.53 (s, 1H, PhC*H*), 4.97 (d, 1H, H1), 4.30 (d, 1H, H4), 4.22 (d, 1H, H6a), 4.03 (d, 1H, H6b), 3.77 (dd, 1H, H2), 3.66 (dd, 1H, H3), 3.57 (s, 1H, H5), 3.51 (s, 3H, OCH_3), 3.50 (s, 3H, OCH_3), 3.43 (s, 3H, OCH_3). ^{13}C NMR (75 MHz, $CDCl_3$) δ: 137.9 (Cq, Ph), 128.9, 128.1, 126.3 (5 × Ph), 101.1 (Ph*C*H), 98.5 (C1), 77.6 (C2), 77.6 (C3), 73.7 (C4), 69.4 (C6), 62.5 (C5), 59.0, 57.8, 55.4 (3 × OCH_3). MALDI-TOF MS *m/z*: 332.8 $[M + Na]^+$.

*Methyl 2,3-di-*O*-methyl-α-D-galactopyranoside (6)*

The synthesis of methyl 2,3-di-*O*-methyl-α-D-galactopyranoside was carried out following the procedure described for the preparation of the methyl 2,3-di-*O*-methyl-α-D-glucopyranoside. Thus, methyl 4,6-*O*-benzylidene-2,3-di-*O*-methyl-α-D-galacto-pyranoside (230 mg, 0.74 mmol) was treated with 80% acetic acid (15 mL) to give the desired product **6** as a white solid after recrystallization (49 mg, 30%). ^{1}H NMR (500 MHz, $CDCl_3$) δ: 4.90 (d, 1H, H1), 4.13 (dd, 1H, H4), 3.94 (dd, 1H, H6a), 3.81 (dd, 1H, H6b), 3.76 (t, 1H, H5), 3.56 (dd, 1H, H2), 3.52 (dd, 1H, H3), 3.49 (s, 3H, OCH_3), 3.48 (s, 3H, OCH_3), 3.41 (s, 3H, OCH_3), 2.01 (s, 3H, OCH_3). ^{13}C NMR (75 MHz, $CDCl_3$) δ: 97.7 (C1), 78.9 (C3), 77.2 (C2), 69.0 (C5), 67.4 (C4), 62.5 (C6), 58.7, 57.7, 55.1 (3 × OCH_3). MALDI-TOF MS *m/z*: 245.2 $[M + Na]^+$.

Molecular dynamics simulation

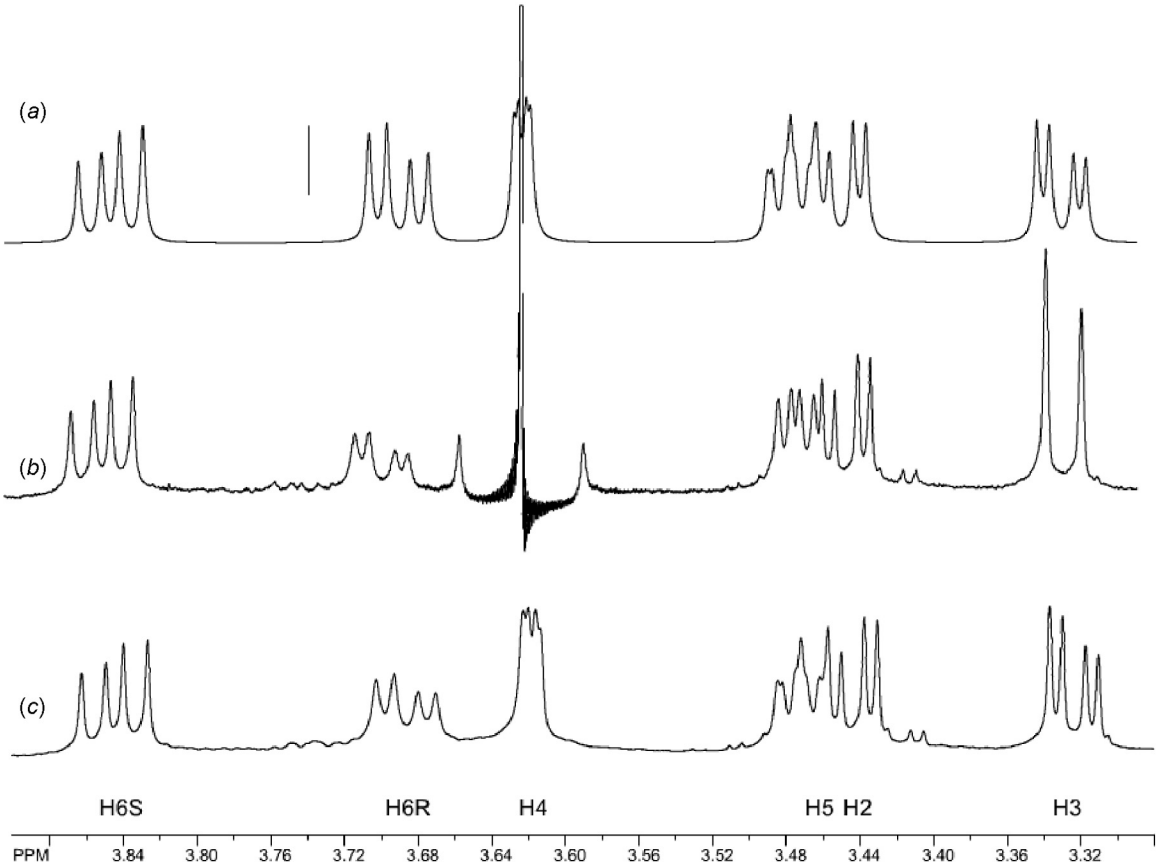
Molecular dynamics (MD) simulations were performed using the SANDER module in the AMBER5 program suite (39) with the GLYCAM (40) parameters for carbohydrates. The 1–4 electrostatic and van der Waals interactions were unscaled (SCEE = 1.0 and SCNB = 1.0), in contrast to the traditional AMBER formalism, but as demonstrated to be essential for carbohydrate simulations (23). The MD simulations were performed using an nPT ensemble with TIP3P water (41) and a dielectric constant set to unity. A long range cutoff of 8 Å was employed. For solvation in water, the carbohydrates were immersed in a theoretical box of 484 (**3**) and 473 (**6**) water molecules with approximate dimensions of 28 Å × 27 Å × 23 Å. For simulations employing dichloromethane, a cutoff of 12 Å was employed with a slightly larger theoretical box (34 Å × 32 Å × 29 Å) of 294 dichloromethane molecules (42) for both carbohydrates. The SHAKE algorithm was applied to all hydrogen-containing bonds, using the default settings. Initial conjugate-gradient energy minimization (20 000 cycles), with restrained solute coordinates, was performed on all systems studied, employing a 0.01 kcal mol^{-1} Å (1 cal = 4.184 J) convergence criterion in the energy gradient. Subsequently, energy minimization of the entire system was performed followed by a simulated annealing period for the solvent, during which the systems were heated from 5 to 300 K for a period of 50 ps, held at 300 K for 250 ps in the case of water, and 1350 ps in dichloromethane, and then the systems were cooled to 5 K over 50 ps. Lastly, the systems were heated from 5 to 300 K over 50 ps prior to the production run MD simulations. Between 100–120 ns of data were collected for each system at 300 K. In all simulations, a 2 fs time step was employed in the integration of the equations of motion. The extremely long MD simulation times were required to achieve adequate sampling of the rotational states. The post-simulation analyses were performed using the CARNAL module of the AMBER suite of programs.

NMR

Each carbohydrate (5–10 mg per sample) was dissolved in each of the different deuterated solvents (D_2O, DMSO-d_6, CD_3CN, CD_2Cl_2, $CDCl_3$, toluene-d_8, benzene-d_6) and introduced into a 5 mm NMR tube. The NMR experiments were performed on Varian 600 and 500 MHz spectrometers. One-

© 2006 NRC Canada

Fig. 2. Expansion of the experimental and simulated ^{1}H NMR spectra for **6** in toluene-d_8: (A) simulated spectrum; (B) homodecoupled experimental spectrum with irradiation of H4; (C) experimental spectrum.



dimensional ^{1}H spectra and homodecoupled experiments with irradiation of the H4 and hydroxyl proton, OH6, were performed to obtain the initial $^3J_{\text{H5-H6(R or S)}}$ couplings (Fig. 2). Final values for the scalar couplings were obtained by iterative spectral simulation using the SPINWORKS (43) and PERCH NMR software (44).

Results and discussion

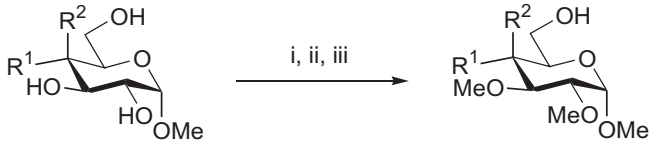
Synthesis of methyl 2,3-di-*O*-methyl-α-D-glucopyranoside and galactopyranoside

The desired 2,3-di-*O*-methylated α-D-glucopyranosides and galactopyranosides were prepared in three steps following established procedures (Scheme 1). Thus, regioselective benzylidenation of the commercially available methyl α-pyranosides at the O4 and O6 positions, followed by methylation of the hydroxyls at the C2 and C3 positions, resulted in the fully protected intermediates (**2** and **5**). The final step involved the acid-mediated cleavage of the benzylidene acetal to give the desired compounds (**3** and **6**) as white solids after recrystallization.

Calculation of $^3J_{HH}$ couplings

Due to the rapid rotational timescale for the ω angle (45, 46), the rotamer population from NMR spectroscopy may only be indirectly inferred. Any experimental measurement corresponding to a fast equilibrium with respect to the timescale of the technique can be interpreted as a weighted

Scheme 1. Synthesis of methyl 2,3-di-*O*-methyl-pyranosides. Reaction conditions: (*i*) $PhCH(OMe)_2$, CSA, MeCN; (*ii*) MeI, NaH, DMF, RT; (*iii*) 80% AcOH, H_2O, 50 °C.



R^1 = OH, R^2 = H
R^1 = H, R^2 = OH

3: R^1 = OH, R^2 = H
6: R^1 = H, R^2 = OH

average of contributions from the individual states involved in the process. In the case of ω-angle populations, at least three conformations should be considered as being in fast equilibrium on the NMR timescale (29, 27, 47). The NMR data for the $^3J_{HH}$ couplings related to the C5-C6 rotational equilibrium are generally deconvoluted into rotamer populations using eqs. [1]–[3]:

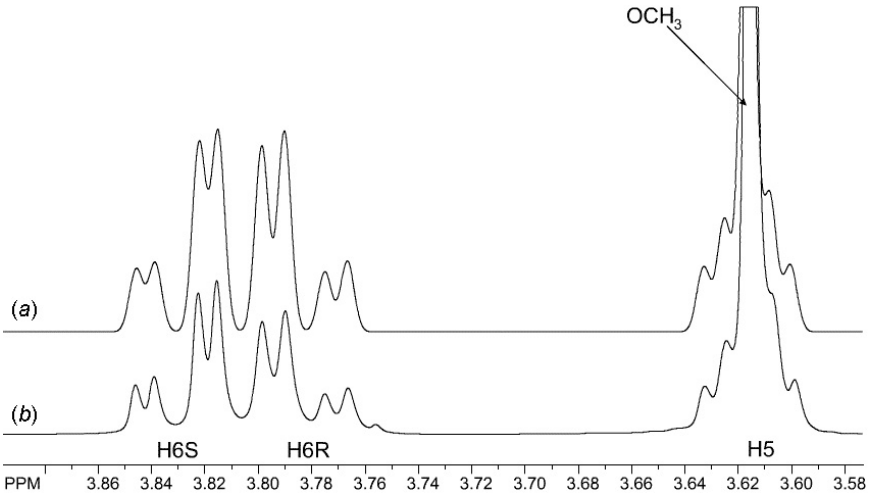
$$[1] \quad {}^3J_{\text{H5-H6R}} = n_{gt}{}^3J_{(\text{H5-H6R},\, gt)} + n_{tg}{}^3J_{(\text{H5-H6R},\, tg)} + n_{gg}{}^3J_{(\text{H5-H6R},\, gg)}$$

$$[2] \quad {}^3J_{\text{H5-H6S}} = n_{gt}{}^3J_{(\text{H5-H6S},\, gt)} + n_{tg}{}^3J_{(\text{H5-H6S},\, tg)} + n_{gg}{}^3J_{(\text{H5-H6S},\, gg)}$$

$$[3] \quad n_{gt} + n_{tg} + n_{gg} = 1$$

© 2006 NRC Canada

Fig. 3. Expansion of the experimental and simulated spectra for **3** in $CDCl_3$: (A) simulated spectrum; (B) experimental spectrum.



in which $^3J_{H5\text{-}H6R}$ and $^3J_{H5\text{-}H6S}$ are the experimentally measured couplings between protons H5 and each of the prochiral H6 protons, and $^3J_{(H5\text{-}H6,\ ii)}$ are the limiting values of the specific coupling constants in each conformational state *ii* with population n_{ii}.

There are numerous sources of uncertainty in this approach, both in terms of the experimental measurements and in the data interpretation. Second-order effects are commonly observed in this type of spectra (Fig. 3), making the use of directly measured ^3J values inappropriate. To remove the second-order effects, the spectra were simulated via an iterative procedure in which the first-order ^3J couplings were varied, until optimal agreement between the experimental and the predicted spectra was achieved (43).

There are two further significant limitations of this method, related to the calculation of the ^3J couplings. Firstly, ^3J couplings are generally computed using a Karplus-type equation that correlates coupling constants with dihedral angles and many approaches to the parameterization of these relationships have been proposed, including empirical methods based on experimental data (48) and theoretical methods based on quantum mechanical data (32). In the case of the empirical equation reported by Haasnoot et al. (48), the equation included the effects of electronegative substituents on the $^3J_{HH}$ values, but was parameterized using rigid model compounds. A single equation was developed for computing each of the $^3J_{H5\text{-}H6R}$ and $^3J_{H5\text{-}H6S}$ values. This approach can lead to the prediction of small negative rotamer populations, particularly for dynamic systems. The equation introduced by Stenutz et al. (32) was parameterized using ^3J couplings computed from density functional theory (DFT) for a set of model compounds. By considering variations in the ω conformations, as well as in the orientation of the hydroxyl groups, Stenutz et al. arrived at a separate equation for the couplings between H5 and each of the prochiral H6 protons, reflecting both geometric and electronic variations in the pro-R and pro-S environments. A promising alternative is to compute the ^3J couplings directly from quantum mechanical calculations, without employing an empirical Karplus-type equation (49). This method has many benefits; however, its computationally intensity makes it challenging to employ when analyzing the thousands of conformations typically generated during MD simulations.

Table 1. Limiting ^3J values employed in the present analysis.

	Empirically derived (48)			Quantum derived (32)		
Coupling constant	*gt*	*tg*	*gg*	*gt*	*tg*	*gg*
$^3J_{H5\text{-}H6R}$	10.7	5	0.9	9.9	4.5	0.8
$^3J_{H5\text{-}H6S}$	3.1	10.7	2.8	1.5	10.8	1.3

Note: *J* values are in Hertz.

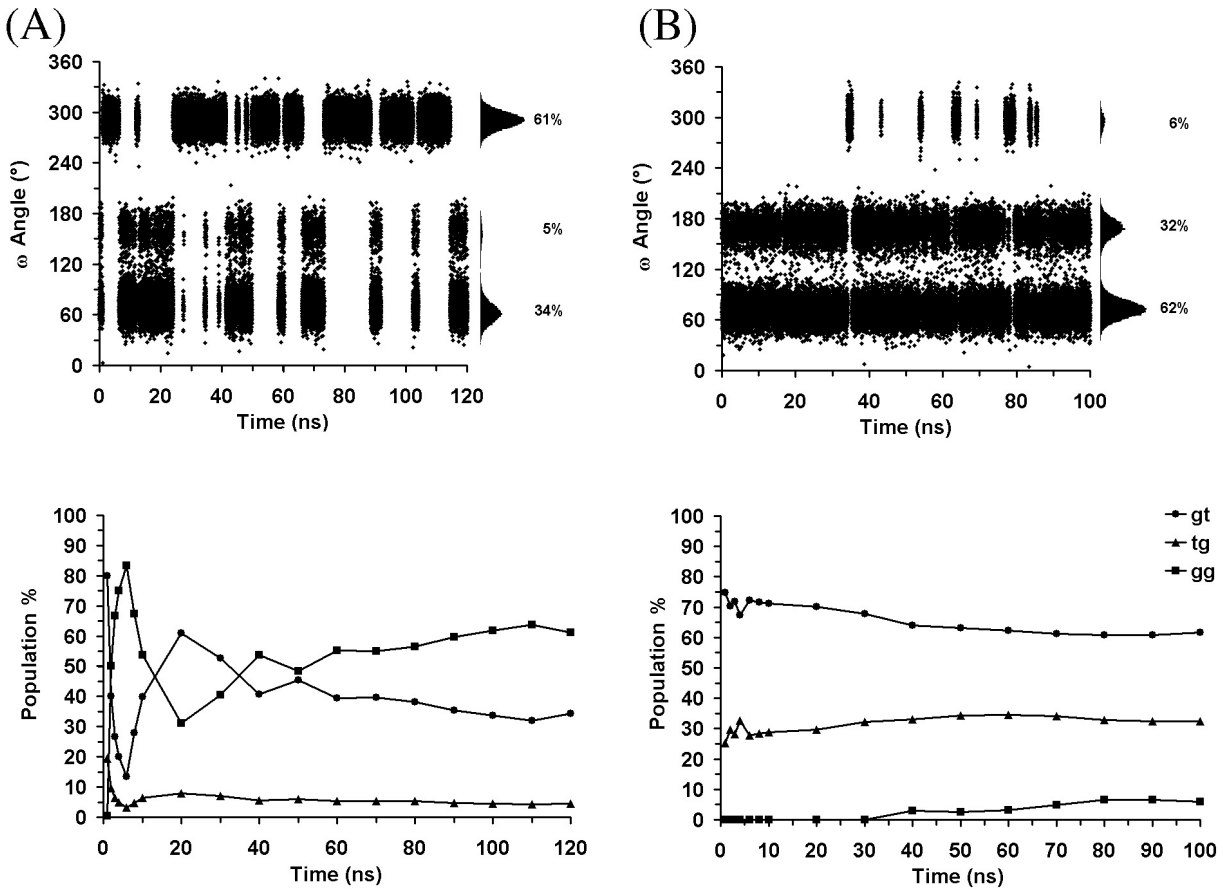
In the parameterization of the any given Karplus-type relationship, a set of limiting ^3J values must be derived for each rotamer. The accuracy of the limiting *J* values is critical when applying eqs. [1]–[3]. Previously, it was assumed that the ω angle would adopt idealized values of 60°, 180°, and –60° in each of the rotameric states; however, this approach often led to small unrealistic negative rotamer populations. More recently, gas-phase energy minimized geometries have been employed for each rotamer. Notably, these optimized geometries differed markedly from idealized values (29, 27). As part of this study, the extent to which the omission of solvent in the geometry optimizations biases the conformations away from those actually present in solution will be examined. Gas-phase energy minimization always leads to an excessive degree of internal hydrogen bonding (23), which is expected to introduce some level of distortion into the ω angle relative to its orientation in water. To assess the effect of the limiting *J* value on the derivation of the rotamer populations we have employed both the empirical and quantum-derived values (see Table 1).

MD simulations

The rotamer populations of the ω torsion angle were predicted (Fig. 4) from explicitly solvated simulations of **3** and **6** in both water and dichloromethane (see Fig. 4). It may be seen that conformational convergence for these systems was not reached until simulation times of between 40 and 80 ns. A reoccurring question when running MD simulations is, "When has a simulation been run long enough that conclu-

© 2006 NRC Canada

Fig. 4. MD trajectories (120 and 100 ns) of the ω angle in (A) methyl 2,3-di-*O*-methyl-α-D-glucopyranoside (**3**) and (B) methyl 2,3-di-*O*-methyl-α-D-galactopyranoside (**6**) in water, with resulting histograms and population % on the right-hand side of each figure. Conformational convergence is plotted below the respective trajectories.



sions about the dynamic properties of a system can be drawn?" The amount of simulation time required to reach conformational equilibration will vary depending on the lifetime of the possible conformations, which itself is directly related to the barrier heights among the states. A molecule that has long conformational lifetimes, exhibiting infrequent conformation transitions, will require a long simulation time period to reach dynamic convergence. Conversely, a molecule that possesses short conformational lifetimes and frequent conformation transitions, will require a shorter simulation to reach convergence. In terms of the rotational states of the ω angle in **3**, there are frequent transitions between the *gt* and *tg* rotamers, and infrequent transitions to the *gg* rotamer, as seen in Fig. 4. The infrequent transitions of the *gg* rotamer, coupled with the large populations of the *gt* and *gg* rotamers, resulted in the slow convergence of the *gt* and *gg* rotamers. A relatively low energy barrier between *gt* and *tg* would explain the rapid transitions, while a higher energy barrier between *tg* and *gg* is consistent with the long lifetime for each of these rotamers. These results are in qualitative agreement with the quantum mechanical rotational energy curves computed for the rotation of the ω angle in methyl α-D-glucopyranoside (23).

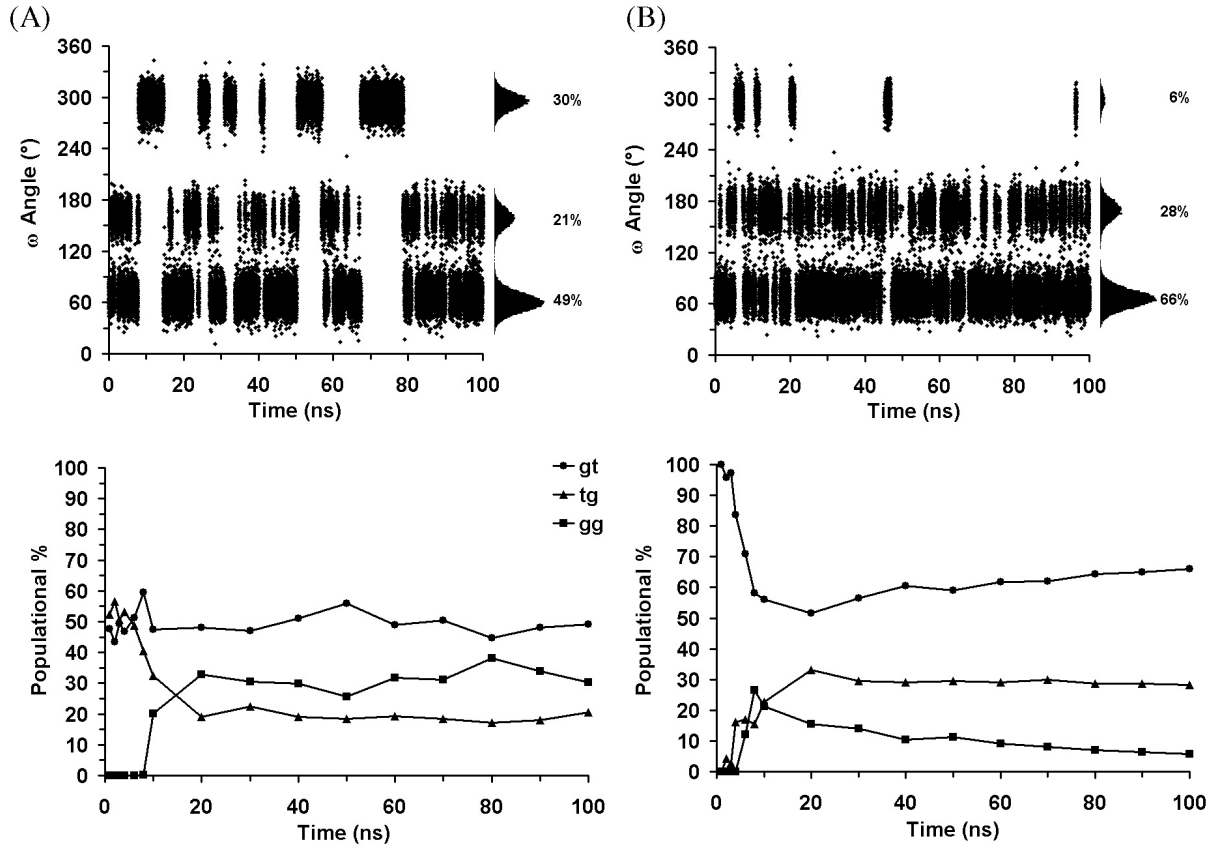
A very different behavior for rotamer interconversions was observed for **6**, displaying frequent transitions between the *gt* and *tg* rotamers, and only infrequent transitions to the *gg* rotamer. In contrast to the case of **3**, the rotamer distribution in **6** reached convergence in less than 50 ns, with a rotamer ratio of 62:27:11. Again, in terms of rotational barriers, the frequency of transitions between the *gt* and *tg* states indicates a low energy barrier between these rotamers and high energy barriers around the *gg*. The rotamer convergence was achieved more rapidly than in **3** because the two rotamers with higher populations are in frequent transition with each other.

In water, the rotamer distributions for methyl 2,3-di-*O*-methyl-α-D-glucopyranosides (**3**) and methyl 2,3-di-*O*-methyl-α–D–galactopyranoside (**6**) were predicted to be 34:6:61 and 62:32:6, respectively, which are in reasonable agreement with the previously reported experimental data for the underivatized methyl glycosides (41:1:58 and 61:18:21, respectively) (30). The results from the present MD simulations are also similar to those from the 50 ns fully solvated MD simulations previously reported (23) for methyl α-D-glucopyranoside (40:6:54) and methyl α-D-galactopyranoside (64:28:8). These observations confirm that methylation of oxygens O2 and O3 does not make a remarkable impact on the rotamer population of the ω torsion angle in either **3** or **6** in water.

In an attempt to examine the ability of MD simulations to predict the effect of solvent polarity on rotamer population, MD simulations of **3** and **6** in CH_2Cl_2 were performed. It

© 2006 NRC Canada

Fig. 5. MD trajectories (100 ns) of the ω angle in (A) methyl 2,3-di-*O*-methyl-α-D-glucopyranoside (**3**) and (B) methyl 2,3-di-*O*-methyl-α-D-galactopyranoside (**6**) in dichloromethane, with resulting histograms and population % on the right-hand side of each figure. Conformational convergence is plotted below the respective trajectories.



should be noted that there are at present no force field parameters available for deuterated solvents, and simulations in nonaqueous solvents are uncommon. Thus, the solvent model for CH_2Cl_2 is relatively untested; however, the initial results are encouraging, particularly in the case of **3** (Fig. 5).

The simulation produced a population conformation ratio of 49:21:30 for **3**, which indicates a significant increase in the population of the *tg* and *gt* rotamers at the expense of the *gg* rotamer, relative to the system in water (34:6:61, *gt*:*tg*:*gg*). A negligible effect was predicted for **6** (66:28:6 in CH_2Cl_2 vs. 64:28:8 in water); however, an examination of the convergence plots indicates that even after 100 ns the populations have not fully converged.

It is interesting to note that the ω torsion angle displayed sensitivity to the solvent, as determined from the values of the average O5-C5-C6-O6 torsion angles for each rotamer extracted from each simulation (Table 2). Clearly, idealized values of 60°, 180°, and 300° are in poor agreement with our averaged solution values. Solvation appears to significantly perturb the value of the ω angle in the *tg* rotamer away from the idealized value of 180°.

Table 2. Average ω torsion angles from the MD simulations of **3** and **6** in water, CH_2Cl_2, and vacuum.

	3			**6**		
Environment	*gt*	*tg*	*gg*	*gt*	*tg*	*gg*
H_2O	70.1	158.3	291.5	70.5	168.6	298.2
CH_2Cl_2	66.4	161.2	293.7	69.6	170.1	296.3
Vacuum[a]	72.6	171.3	289.4	—	—	—

[a]Calculated using MM3(94) with modified O-C-C-O torsion parameters (27).

NMR analysis

Presented in Tables 3 and 4 are the experimental ^3J values and the rotamer populations for **3** and **6**, respectively, predicted from these values using eqs. [1]–[3] and two sets of limiting ^3J values (32). Unlike the results from the empirically determined limiting *J* values (48), the results obtained with quantum-derived limiting *J* values (32) did not result in any nonphysical (negative) rotamer populations. In the case of **3**, regardless of the choice of the methodology, the population of the *tg* rotamer was shown to increase approximately linearly with the decreasing polarity of the small solvent molecules. This observation is consistent with expectations based on gas-phase quantum mechanical calculations of the rotational properties of the ω angle in methyl α-D-glucopyranoside (23), which implies that there would be a preferential enhancement of internal hydrogen bonding in low polarity environments, leading, in the limiting case (ε = 1), to a population ratio of approximately 43:28:28. In the larger aromatic solvents, the *tg* population is again high, but it does not follow a direct relationship with solvent polarity.

In contrast to **3**, little sensitivity to solvent polarity is displayed by **6**. This is an unexpected result in that quantum

© 2006 NRC Canada

Table 3. Experimental ^3J values and rotamer populations for **3**, listed in order of decreasing solvent polarity.

	Experimental $^3J_{HH}$[a]		Empirical fit (48)			Quantum mechanical fit (32)		
Solvent	$^3J_{H5\text{-}H6R}$	$^3J_{H5\text{-}H6S}$	*gt*	*tg*	*gg*	*gt*	*tg*	*gg*
D_2O	5.44	2.08	51 (49)	–11(0)[b]	60 (51)	48	7	45
DMSO-d_6	5.87	2.11	55 (53)	–11(0)[b]	56 (47)	53	7	40
CD_3CN	5.40	2.92	46	0	54	44	16	40
CD_2Cl_2	4.87	3.27	39	4	57	37	20	43
$CDCl_3$	4.34	3.47	32	7	61	30	22	48
Toluene-d_8	4.32	3.10	34	3	64	31	18	50
Benzene-d_6	3.74	2.91	29	0	71	26	16	58

Note: Dielectric constants (at 20°): D_2O (79.8), DMSO (48.9), CH_3CN (37.5), CH_2Cl_2 (9.1), $CHCl_3$ (4.8), toluene (2.4), benzene (2.3) (ref. 51).
[a] $^3J_{HH}$ from simulated spectra. The maximum error allowed between simulated and experimental spectra was 0.5 Hz.
[b] Values in parentheses were calculated by assuming a zero population for the *tg* rotamer.

Table 4. Experimental ^3J values and rotamer populations for **6**.

	Experimental $^3J_{HH}$[a]		Empirical equation (48)			DFT equation (32)		
Solvent	$^3J_{H5\text{-}H6R}$	$^3J_{H5\text{-}H6S}$	*gt*	*tg*	*gg*	*gt*	*tg*	*gg*
D_2O	7.13	4.30	57	17	27	57	30	12
CD_2Cl_2	5.99	5.19	40	29	31	41	40	19
$CDCl_3$	6.20	4.24	47	16	36	47	30	23
Toluene-d_8	6.37	4.88	46	25	30	46	37	17
Benzene-d_6	6.31	5.22	43	29	28	44	40	16

Note: Due to signal overlap, coupling constants could not be measured in DMSO-d_6 and CD_3CN.
[a] $^3J_{HH}$ from simulated spectra. The maximum error allowed between simulated and experimental spectra was 0.5 Hz.

calculations predict a decrease in polarity should lead to a significant decrease in the population of the *tg* rotamer with an increase in the *gg* (23). This change in population was predicted on the basis of the formation of strong internal hydrogen bonds in the limiting case of a purely apolar environment. However, based on the data in Table 4, it appears that an interpretation of rotamer behavior, based on the view that polar solvents disrupt the internal hydrogen bonds and therefore lead to the rotamer distribution being determined by repulsive 1,3-diaxial electrostatic interactions among O4, O5, and O6, may be correct (23). It should be noted that hydrogen bonds among conformationally restricted 1,3-diaxial hydroxyl groups appear to persist even in water (50).

Overall, the agreement with the predictions from the MD simulations both in terms of the response of the populations to polarity and in quantitative terms is notable. Thus, it is reasonable to probe the simulational results further to extract quantitative information pertaining to the level of intramolecular hydrogen bonding in each rotational state in both water and CH_2Cl_2. For each simulation the periods during which hydrogen bonds were present between O4, O5, and O6 were determined for **3** and **6** and are presented in Table 5.

Considerable insight into the sensitivity of internal hydrogen bonding to solvent polarity is provided by the MD data. Some overall trends are apparent; for example, the hydrogen bond between HO6 and O5 is consistently the most occupied (12.9%–18.0%) and the strongest, as indicated by the inter-oxygen distances. In contrast, hydroxyl group HO4 is consistently a very poor proton donor to HO6 (O4(H)···O6); displaying the lowest occupancies (2.9%–5.8%) and long internuclear distances is very weak. Similarly, the reverse interaction, that is, one in which HO6 donates a proton to HO4 (O6(H)···O4) is also weak; however, this hydrogen bond shows a strong sensitivity in both **3** and **6** to solvent polarity. In CH_2Cl_2, the O4(H)···O6 interaction was predicted to increase both in occupancy and strength. This may be understood given that as a primary alcohol, the proton at O6 is preferentially exposed to solvent and would generally be able to act as either a proton donor or acceptor with water molecules. In the low polarity environment, HO6 has little choice but to interact with either HO4 or HO5. In contrast, HO4 may continue to interact with HO3, regardless of the solvent. Similar arguments may be employed to explain the enhanced strength and occupancy in CH_2Cl_2 of the O6(H)···O5 hydrogen bond in **3** and **6**. It is notable that CH_2Cl_2 does not enhance all internal hydrogen bonding to an equal extent. When HO6 acts as a proton donor with O5, the occupancy time for this interaction is approximately doubled in both **3** and **6** in CH_2Cl_2. Notably, in the galacto-derivative **6**, the low polarity environment of the CH_2Cl_2 doubles the occupancy of the O6(H)···O4 hydrogen bond, relative to an aqueous environment, whereas for the gluco-derivative **3**, the occupancy of this hydrogen bond in CH_2Cl_2 increased nearly fourfold. Therefore, in **6**, although a low polarity environment increases the probability of interactions between O6(H) and O4 and O5, the relative strengths and occupancies of these interactions are unaffected by the solvent. On this basis, it would be predicted that the rotamer populations for **6** would not strongly influenced by solvent polarity, as confirmed by analysis of the NMR data. Since in **3** the O6(H)···O4 hydrogen bond is preferentially favored in

© 2006 NRC Canada

Table 5. Average hydrogen bond distances and occupancies for **3** and **6** from the MD data.

MD solvent	Total simulation time (ns)	Molecule	Hydrogen bond		
			O4(H)···O6	O6(H)···O4	O6(H)···O5
Water	122	**1**	3.41, 3.9	3.39, 4.8	2.98, 18.0
CH_2Cl_2	101	**1**	3.19, 2.9	3.14, 19.0	2.96, 31.4
Water	100	**2**	3.36, 5.8	3.34, 6.3	3.01, 12.9
CH_2Cl_2	114	**2**	3.36, 2.7	3.35, 12.3	3.00, 26.8

Note: Bond distances are between non-hydrogen atoms (in angstroms) and occupancies are presented as a % of total simulation time.

CH_2Cl_2, and as it can only form in the *tg* rotamer, a low polarity solvent should induce a shift in rotamer populations in favor of the *tg* state, as confirmed experimentally.

In water, the internal hydrogen bonding networks are disrupted by competition with hydrogen bonds to the solvent. When the internal hydrogen bonds are differentially disrupted, that is, when some become relatively weaker than others, the rotamer populations associated with the ω angle may be altered. In the case of **3**, in water the preferential disruption of the O6(H)···O4 interaction destabilized the *tg* rotamer, leading to the observed preference for gauche rotamers. In **6**, the O6(H)···O4 hydrogen bond forms most strongly in the *gg* orientation, an orientation in which the O6(H)···O5 hydrogen bond may also form. Thus, in the hydrogen bond strengthening environment of low polarity solvents, a higher ratio of *gg*:*gt* rotamers would be expected than in water. This trend was observed in the NMR data (see, for example, the ratios 27:57 in D_2O vs. 36:47 in $CDCl_3$). Unlike the case of **3**, the shift in rotamer populations in **6** is less profound, presumably reflecting the fact that the hydrogen bonds in **6** are approximately equally prone to disruption by water.

Conclusion

The joint NMR and MD analysis of **3** and **6** leads to the conclusion that the balance between inter- and intramolecular interactions involving HO6 plays a direct role in determining the rotational profiles for the ω angles. In a low polarity environment, internal hydrogen bonds are shown to be strengthened in both **3** and **6**, however, in **3**, such an environment disproportionately enhances the O6(H)···O4 interaction, leading to an increase in the population of the *tg* state. Without the hydrogen bond enhancement offered by a low polarity environment, both **3** and **6** display rotamer populations that are consistent with expectations based on the minimization of repulsive intramolecular oxygen–oxygen interactions. That is, when in an aqueous environment, the water disrupts stabilizing intramolecular hydrogen bonding and leads to a system whose bond rotational properties are dominated by internal electrostatic repulsions.

The results of this work are generally consistent with the conclusions reached by Rockwell and Grindley (27), to the extent that both studies illustrate that low polarity environments strengthen internal hydrogen bonds in carbohydrates. The data from the MD simulations confirm and quantify the strengthening of the intramolecular hydrogen bonds in CH_2Cl_2 inferred by the NMR analysis. A significant difference between the two studies pertains to the role of interactions between the solvent and HO6 in glucopyranosides. In this work, we find that in a low polarity environment HO6 prefers to interact with O4, but that in water these interactions are markedly weakened, indicating that HO6 acts as a hydrogen bond donor to water. That this conclusion was not supported by the studies on methyl 2,3,4-tri-*O*-methyl-α-D-glucopyranoside is perhaps related to the absence of a methyl group at O4 in the present work. It may be that the steric bulk of the methyl groups at the 2-, 3-, and 4-positions detracts from the ability of O4 to act as a hydrogen bond acceptor for HO6. The simulations performed in water have been shown to reproduce the rotamer populations to within experimental error; however, despite the long simulation times, the results from those in CH_2Cl_2 were less accurate. The MD simulations illustrate that not only are the rotamer populations sensitive to the configuration at C4 in hexopyranosides, but so are the lifetimes and pathways for transitions among the rotameric states. This latter observation indicates that MD simulations of flexible carbohydrates may require very long simulation times (>100 ns) to reach statistical convergence.

Acknowledgments

This paper is dedicated to Professor W.A. Szarek in honour of his innumerable contributions to carbohydrate chemistry and in recognition of his inspiration as a mentor. We thank the National Institutes of Health (RR05357 and GM55230) for financial support, and JG-O wishes to thank Dr. J. Glushka for helpful discussions regarding the optimization of the NMR experiments.

References

1. A. Varki. Glycobiology, **3**, 97 (1993).
2. R.A. Dwek. Chem. Rev. **96**, 683 (1996).
3. H. Lis and N. Sharon. Chem. Rev. **98**, 637 (1998).
4. H.C. Joao, I.G. Scragg, and R.A. Dwek. FEBS Lett. **307**, 343 (1992).
5. D.F. Wyss, J.S. Choi, J. Li, M.H. Knoppers, K.J. Willis, A.R.N. Arulanandam, A. Smoylar, E.L. Reinherz, and G. Wagner. Science (Washington, D.C.), **269**, 1273 (1995).
6. D.M. Coltart, R.A.K. Royyuru, L.J. Williams, P.W. Glunz, D. Sames, S.D. Kuduk, J.B. Schwarz, X.-T. Chen, S.J. Danishefsky, and D.H. Live. J. Am. Chem. Soc. **124**, 9833 (2002).
7. C.J. Bosques, S. Tschampel, R.J. Woods, and B. Imperiali. J. Am. Chem. Soc. **126**, 8421 (2004).
8. P.M. Rudd, H.C. Joao, E. Coghill, P. Fiten, M.R. Saunders, G. Opdenakker, and R.A. Dwek. Biochemistry, **33**, 17 (1994).

© 2006 NRC Canada

9. P.M. Rudd, M.R. Wormald, R.L. Stanfield, M. Huang, N. Mattsson, J.A. Speir, J.A. DiGennaro, J.S. Fetrow, R.A. Dwek, and I.A. Wilson. J. Mol. Biol. **293**, 351 (1999).
10. M. Tomana, J. Novak, B.A. Julian, K. Matousovic, K. Konecny, and J. Mestecky. J. Clinical Investigation, **104**, 73 (1999).
11. G.J. Davies, V.M.-A. Ducros, A. Varrot, and D.L. Zechel. Biochem. Soc. Trans. **31**, 523 (2003).
12. S. Sabesan, S. Neira, and Z. Wasserman. Carbohydr. Res. **267**, 239 (1995).
13. Y. Bourne, B. Bolgiano, D.-I. Liao, G. Strecker, P. Cantau, O. Herzberg, T. Feizi, and C. Cambillau. Nature Struct. Biol. **1**, 863 (1994).
14. A. Zdanov, Y. Li, D.R. Bundle, S.-J. Deng, C.R. MacKenzie, S.A. Narang, N.M. Young, and M. Cygler. Proc. Natl. Acad. Sci. U.S.A. **91**, 6423 (1994).
15. M.R. Wormald, A.J. Petrescu, Y.-L. Pao, A. Glithero, T. Elliot, and R.A. Dwek. Chem. Rev. **102**, 371 (2001).
16. J. Jiménez-Barbero and T. Peters. NMR of glycoconjugates. Wiley-VCH, Weinheim. 2002.
17. W.A. Bubb. Concept. Magn. Res. **19A**, 1 (2003).
18. D.A. Cumming and J.P. Carver. Biochemistry, **26**, 6664 (1987).
19. J. Gonzalez-Outeriño, R. Kadirvelraj, and R.J. Woods. Carbohydr. Res. **340**, 1007 (2005).
20. M. Martín-Pastor, J.L. Asensio, R. López, and J. Jiménez-Barbero. J. Chem. Soc. Perkin Trans. 2, 713 (1995).
21. M. Martin-Pastor and C.A. Bush. Biochemistry, **39**, 4674 (2000).
22. E.W. Sayers and J.H. Prestegard. Biophys. J. **79**, 3313 (2000).
23. K.N. Kirschner and R.J. Woods. Proc. Natl. Acad. Sci. U.S.A. **98**, 10541 (2001).
24. H.F. Azurmendi and C.A. Bush. Carbohydr. Res. **337**, 905 (2002).
25. R.U. Lemieux and S. Koto. Tetrahedron, **30**, 1933 (1974).
26. S. Wolfe, M.-H. Whangbo, and D.J. Mitchell. Carbohydr. Res. **69**, 1 (1979).
27. G.D. Rockwell and B.T. Grindley. J. Am. Chem. Soc. **120**, 10953 (1998).
28. R.H. Marchessault and S. Perez. Biopolymers, **18**, 2369 (1979).
29. K. Bock, and J.Ø. Duus. J. Carbohydr. Chem. **13**, 513 (1994).
30. Y. Nishida, H. Hori, H. Ohrui, and H. Meguro. J. Carbohydr. Chem. **7**, 239 (1988).
31. I. Tvaroska, F.R. Taravel, J.P. Utille, and J. Carver. Carbohydr. Res. **337**, 353 (2002).
32. R. Stenutz, I. Carmichael, G. Widmalm, and A.S. Serianni. J. Org. Chem. **67**, 949 (2002).
33. N.K. de Vries and H.M. Buck. Carbohydr. Res. **165**, 1 (1987).
34. D.A. Cumming and J.P. Carver. Biochemistry, **26**, 6676 (1987).
35. K. Yoza, N. Amanokura, Y. Ono, T. Akao, H. Shinmori, H. Takeuchi, S. Shinkai, and D.N. Reinhoudt. Chem. Eur. J. **5**, 2722 (1999).
36. R.A. Edington, E.L. Hirst, and E.E. Percival. J. Chem. Soc. 2281 (1955).
37. D. Trimnell, W.N. Doane, C.R. Russell, and C.E. Rist. Carbohydr. Res. **11**, 497 (1969).
38. D.J. Bell and G.D. Greville. J. Chem. Soc. 1136 (1955).
39. D.A. Case, D.A. Pearlman, J.W. Caldwell, T.E. Cheatham III, W.S. Ross, C.S. Simmerling, T.A. Darden, K.M. Merz, R.V. Stanton, A.L. Cheng, J.J. Vincent, M. Crowley, D.M. Ferguson, R.J. Radmer, G.L. Seibel, U.C. Singh, P.K. Weiner, and P.A. Kollman. AMBER 5.0 [computer program]. University of California San Francisco, San Francisco, California. 1997.
40. R.J. Woods, R.A. Dwek, C.J. Edge, and B. Fraser-Reid. J. Phys. Chem. **99**, 3832 (1995).
41. W.L. Jorgensen. J. Am. Chem. Soc. **103**, 341 (1981).
42. T. Fox and P.A. Kollman. J. Phys. Chem. B, **102**, 8070 (1998).
43. K. Marat. SPINWORKS 2.4 [computer program]. Department of Chemistry, University of Manitoba, Winnipeg, Manitoba. 2004
44. PERCH Solutions Ltd. PERCH NMR software [computer program]. PERCH Solutions Ltd., Kuopio, Finland. 2005
45. J.W. Brady. J. Am. Chem. Soc. **111**, 5155 (1989).
46. P.J. Hajduk, D.A. Horita, and L.E. Lerner. J. Am. Chem. Soc. **115**, 9196 (1993).
47. M. Kraszni, Z. Szakacs, and B. Noszal. Analyt. Bioanalyt. Chem. **378**, 1449 (2004).
48. C.A.G. Haasnoot, M. De Leeuw, and C. Altona. Tetrahedron, **36**, 2783 (1980).
49. J. Gonzalez-Outeriño, J. Glushka, A. Siriwardena, and R.J. Woods. J. Am. Chem. Soc. **126**, 6866 (2003).
50. J. Hawley, N. Bampos, N. Aboitiz, J. Jiménez-Barbero, M. López de la Paz, J.K.M. Sanders, P. Carmona, and C. Vicent. Eur. J. Org. Chem. 1925 (2002).
51. R.C. Weast (*Editor*). CRC handbook of chemistry and physics. 59th ed. CRC Press, Inc., Boca Raton, Florida. 1978.

© 2006 NRC Canada

Synthesis and biological evaluation of 5-(alkyn-1-yl)-1-(*p*-toluenesulfonyl)uracil derivatives[1,2]

Zlatko Janeba, Jan Balzarini, Graciela Andrei, Robert Snoeck, Erik De Clercq, and Morris J. Robins

Abstract: Sonogashira coupling of 5-iodouracil (**2**) and trimethylsilylacetylene gave 5-(trimethylsilylethynyl)uracil (**3**), which was deprotected to give 5-ethynyluracil (**4**). Copper(I)-catalyzed cyclization of **4** gave furo[2,3-*d*]pyrimidin-2(3*H*)-one (**5**). Tosylation of **2** and **4** gave the 1-(*p*-toluenesulfonyl) derivatives **6** and **7**, respectively. The tosylated compound **6** and trimethylsilylacetylene did not undergo Sonogashira coupling, and copper(I)-catalyzed cyclization of **7** did not occur. Coupling of **2** with several terminal alkynes gave 5-(alkyn-1-yl)uracil derivatives (**9**), which underwent tosylation to produce the targeted 5-(alkyn-1-yl)-1-(*p*-toluenesulfonyl)uracil compounds (**11**). Copper(I)-catalyzed cyclization of **9** gave the respective furopyrimidines (**10**) in low yields. Again, cyclization did not occur with the tosyl derivatives (**11**). Activity against varicella-zoster virus (VZV) was observed with longer-chain analogues of **9** and **11**, and compound **7** showed activity against human cytomegalovirus (HCMV) at near cytotoxic levels.

Key words: antiviral screening, furo[2,3-*d*]pyrimidin-2(3*H*)-one derivatives, Sonogashira coupling, 1-(*p*-toluenesulfonyl)pyrimidine derivatives.

Résumé : Un couplage selon la méthode de Sonogashira du 5-iodouracile (**2**) avec le triméthylsilylacétylène conduit à la formation de (triméthylsilyléthynyl)uracile (**3**) qui, par déprotection, conduit au 5-éthynyluracile (**4**). La cyclisation catalysée par le cuivre(I) du composé **4** fournit la furo[2,3-*d*]pyrimidin-2(3*H*)-one (**5**). La tosylation des composés **2** et **4** fournit respectivement les dérivés 1-(*p*-toluènesulfonyle) **6** et **7**. Le composé tosylé **6** et le triméthylsilyacétylène ne réagissent pas dans les conditions de couplage de Sonogashira alors que la cyclisation catalysée par le cuivre(I) du composé **7** ne se réalise pas. Le couplage du composé **2** avec plusieurs alcynes terminaux conduit aux 5-(alcyn-1-yl)uraciles (**9**) qui peut subir une tosylation pour conduire à la formation des composés cibles 5-(alcyn-1-yl)-1-(*p*-toluènesulfony)uraciles (**11**). La cyclisation catalysée par le cuivre(I) des composés **9** fournit les furopyrimidines (**10**) correspondantes avec de faibles rendements. Encore une fois, la cyclisation des dérivés tosylés **11** ne se produit pas. On a observé une activité contre le virus varicelle-zoster avec les analogues des composés **9** et **11** à longues chaînes alors que le composé **7** présente une activité contre le cytomégalovirus humain près des niveaux cytotoxiques.

Mots clés : évaluation antivirale, dérivés de la furo[2,3-*d*]pyrimidin-2(3*H*)-one, couplage de Sonogashira, dérivés 1-(*p*-toluènesulfonyl)pyrimidine.

[Traduit par la Rédaction]

Introduction

Furo[2,3-*d*]pyrimidin-2(3*H*)-ones (derivatives of compound **5**, Fig. 1) with methyl or sugar substituents at N3 and alkyl groups at C6 were reported in 1981 by Robins and Barr (1) as fluorescent by-products (~10%) of coupling reactions of 5-iodo-1-methyluracil and 5-iodo-3′,5′-di-*O*-acetyl-2′-deoxyuridine with terminal alkynes (1, 2). Inhibition of incorporation of thymidine and 2′-deoxyuridine into primary rabbit kidney DNA was observed, but no antiviral activity was found[5] with the 6-butylfuro[2,3-*d*]pyrimidin-2(3*H*)-one 2′-deoxynucleoside (prepared in 82% yield by cyclization of 2′-deoxy-5-(hexyn-1-yl)uridine with CuI–Et_3N–MeOH (2)). Two decades later, the remarkable anti-varicella-zoster virus (VZV) selectivity and potency of such bicyclic pyrimidine nucleoside analogues (BCNAs) with longer alkyl chains at

Received 5 August 2005. Published on the NRC Research Press Web site at http://canjchem.nrc.ca on 5 May 2006.

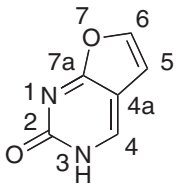
With congratulations and best wishes to Professor Walter Szarek.

Z. Janeba[3] and M.J. Robins.[4] Department of Chemistry and Biochemistry, Brigham Young University, Provo, Utah 84602-5700, USA.
J. Balzarini, G. Andrei, R. Snoeck, and E. De Clercq. Rega Institute for Medical Research, Katholieke Universiteit Leuven, Leuven B-3000, Belgium.

[1]This article is part of a Special Issue dedicated to Professor Walter A. Szarek.
[2]Nucleic acid related compounds Paper 132. Paper 131 is ref. 7*b*.
[3]Present address: Moravek Biochemicals, Brea, CA.
[4]Corresponding author (e-mail: morris_robins@byu.edu).
[5]M.J. Robins and E. De Clercq. Unpublished results.

 doi:10.1139/V06-041 © 2006 NRC Canada

Fig. 1. Furo[2,3-*d*]pyrimidin-2(3*H*)-one.



5

C6 were discovered (3). Extensive SAR studies have been pursued by McGuigan, Balzarini, De Clercq, and their coworkers (4–6).

In 2001, we observed that certain alkyl/alkynyl derivatives of **5** possess anti-human cytomegalovirus (HCMV) activity (7). It was recently reported that 2′,3′-dideoxynucleoside derivatives of **5** substituted at C6 with alkyl chains also inhibit HCMV by a "non-nucleoside" mechanism (i.e., activation by a nucleoside kinase is not required) (8). We have targeted the furo[2,3-*d*]pyrimidin-2(3*H*)-one ring system for other modifications at N3 and (or) C6 (9).

A prior synthetic approach to **5** employed cyclization of (*E*)-5-(2-bromovinyl)uracil (BVU) with potassium *tert*-butoxide (10, 11). However, the overall yield of **5** was very low for this five-stage route from uracil. The Cu(I)-promoted 5-endo-dig cyclization of 5-ethynyluracil (**4**) (Scheme 1) represented a plausible route to **5** because this type of cyclization had been shown to proceed in high yields with 1-methyl and 1-(2-deoxy-β-D-*erythro*-pentofuranosyl) derivatives of 5-(alkyn-1-yl)uracil (1, 2). However, such treatment of **4** produced **5** slowly and in limited yields (~15%). Introduction of a protecting group at N1 of **4** followed by cyclization and deprotection might provide an improved route to **5**.

Protection with a *p*-toluenesulfonyl group permits deprotection by transamidation (12). Tosylation of **4** gave 5-ethynyl-1-tosyluracil (**7**). However, **7** did not undergo cyclization with CuI–Et_3N–DMF under the usual conditions. Because **7** showed weak anti-HCMV activity, a new SAR study (13) with 5-(alkyn-1-yl)-1-tosyluracils was examined. We now describe the synthesis of such analogues with alkynyl chains of 6–10 and 12 carbon atoms and the results of evaluations against a number of viruses and tumor cell systems.

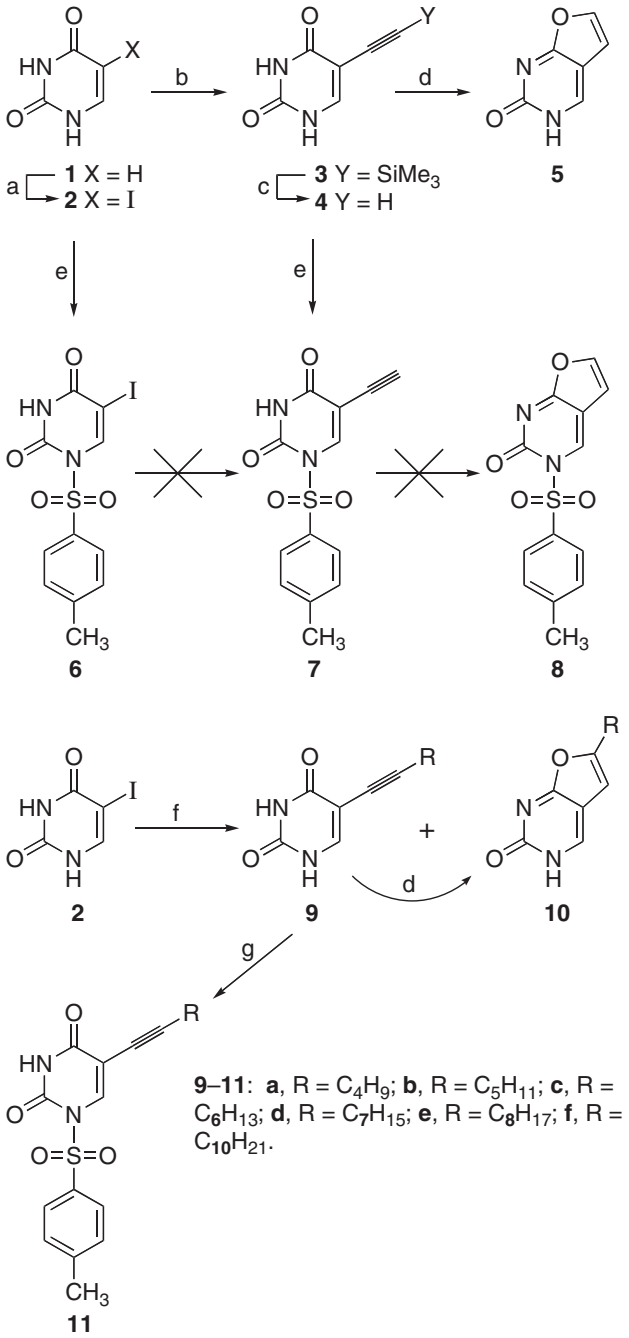
Results and discussion

Chemistry

The 5-iodouracil (**2**) starting material (Scheme 1) was conveniently prepared in >60 g scale by a modified cerium(IV)-mediated halogenation (14) of uracil (**1**). The use of acetonitrile rather than methanol as the solvent resulted in direct precipitation of the product **2**. Filtration of the reaction mixture and immediate recrystallization of the precipitated material from aqueous ethanol gave **2** (83%) of high purity.

Sonogashira coupling of **2** and trimethylsilylacetylene (TMSA) followed by removal of the TMS group from intermediate **3** with NaOH–H_2O (15) gave 5-ethynyluracil (**4**). Various reaction conditions (solvents, temperature, equivalents of CuI) were then examined. Treatment of **4** with CuI (1.1 equiv.) in DMF–Et_3N at 120 °C gave the best, although

Scheme 1. Synthesis of the test compounds. Reagents and conditions: (*a*) I_2–CAN–MeCN; (*b*) TMSA–$Pd(PPh_3)_4$–CuI–Et_3N–EtOAc; (*c*) NaOH–H_2O; (*d*) CuI–Et_3N–DMF, Δ; (*e*) TsCl–pyridine; (*f*) 1-alkyne–$Pd(PPh_3)_4$–CuI–Et_3N–DMF; (*g*) (*i*) HMDS, Δ, (*ii*) TsCl–MeCN, Δ.



limited, conversion to the cyclized ring system **5** (~15%). Tosylation of **4** under standard conditions (TsCl–pyridine) gave 5-ethynyl-1-tosyluracil (**7**) (25%). Treatment of **7** with Cu(I) did not give detected quantities of **8**. Thus, the N1-tosyl derivative **7** was more resistant to cyclization than **4** (which gave **5** slowly in ~15% yield). The strongly electron-withdrawing effect of the *p*-toluenesulfonyl group could significantly reduce electron donation from N1 into the 5,6-double bond. Such a diminished enamine contribution toward the triple bond of the alkyne substituent at C5 and (or)

© 2006 NRC Canada

the oxo group at C4 (enyne-amine and enamine-one conjugated systems, respectively) might result in sufficient retardation of complex formation with copper(I) to cause failure of the endo-dig cyclization process. Tosylation of **2** gave 5-iodo-1-tosyluracil (12) (**6**, 40%), but **6** failed to undergo Sonogashira coupling effectively with 1-hexyne or 1-octyne. Attempted coupling at ambient temperature with ethyl acetate as the solvent resulted in formation of more polar materials and recovery of starting **6** (TLC). Heating at 50 °C resulted in formation of both less and more polar materials and generation of dark coloration. Thus, withdrawal of electron density from N1 by the tosyl group apparently has significantly adverse effects on oxidative insertion of palladium into the C5–iodine bond and (or) subsequent steps in the Sonogishira cycle.

Because the Cu(I)-promoted cyclization of 5-ethynyluracil (**4**) was sluggish, we anticipated that Sonogashira couplings with 5-iodouracil (**2**) would give the desired 5-(alkyn-1-yl)uracil analogues (**9**) without significant formation of the cyclized furo[2,3-*d*]pyrimidin-2-one products (**10**). As expected, coupling of **2** with terminal alkynes–$Pd(PPh_3)_4$–CuI–Et_3N in DMF at ambient temperature gave the products **9** in moderate to good isolated yields (50%–80%), except for the highly lipophilic 1-dodecynyl derivative **9f** (~20%). Very minor amounts of the furanopyrimidine by-products (**10**) were detected as slower-migrating fluorescent spots (TLC) during these Sonogashira couplings. In several cases, we isolated the by-products in trace yields (~1%), and they were fully (**10a**, **10d**, and **10e**) or partially (**10b**) characterized. This corroborated our finding that cyclization of 5-ethynyluracil (**4**) without an N1 substituent was difficult, and is in harmony with another report of Sonogashira coupling of **2** with a terminal alkyne and cyclization to give the furanopyrimidine in low yield (16). Our treatment of purified **9d** and **9e** with CuI–Et_3N–DMF at 70 °C for 4 h resulted in complete disappearance of the starting materials, but the furanopyrimidines **10d** (34%) and **10e** (28%) were isolated in comparably low yields.

Treatment of pyrimidine bases with TsCl–pyridine and tosylation of trimethylsilylated pyrimidines have been recently employed for preparation of 1-tosylpyrimidine derivatives (12). Our treatment of 5-(decyn-1-yl)uracil (**9e**) with TsCl–pyridine at ambient temperature gave a poor yield (22%) of the 1-tosyl product **11e**, and no **11c** was detected (TLC) upon stirring 5-(octyn-1-yl)uracil (**9c**) with TsCl and K_2CO_3 in DMF for 2 days at ambient temperature. Fortunately, tosylation of the trimethylsilylated derivatives was successful. Hexamethyldisilazane (HMDS) and the 5-alkynyl compounds (**9**) were heated at reflux for 1 h, followed by evaporation of volatiles and in situ tosylation of the TMS derivatives (TsCl–MeCN, Δ). The 1-tosyl-5-(alkyn-1-yl)uracil products (**11**) (47%–75%) were isolated after ~24 h. Longer reaction times resulted in more complex reaction mixtures (TLC) with little improvement in the yields of **11**. The starting materials **9** were recovered after the 24 h treatment in 18%–28% yields by column chromatography.

Biological evaluations

Compound **6** showed weak activity against VZV (TK^+ (strain OKA) and TK^- (strain 07/1)), but no activity against HCMV or other DNA viruses such as herpes simplex viruses type 1 and type 2 and vaccinia virus (VV) (Table 1). No activity against RNA viruses such as vesicular stomatitis virus (VSV), Coxsackie B4 virus, respiratory syncytial virus (RSV), parainfluenza virus-3, reovirus-1, Sindbis virus, and Punta Toro virus, or HIV-1 and HIV-2 in cell cultures was observed (data not shown). The 5-alkynyl-substituted uracil derivatives (**9** series) and their corresponding 1-(*p*-toluenesulfonyl) derivatives (**11** series), as well as the bicyclic derivatives (**10** series), were devoid of antiviral activity at subtoxic concentrations, except for **9d**, **9e**, **11e**, and **11f** (for which weak anti-VZV activity (EC_{50}: 10–37 μmol/L) was found). The absence of significant biological activity with the **9** and **10** series compounds suggests that they do not function as substrates of thymidine phosphorylase or other cellular enzymes that convert pyrimidines to their corresponding nucleoside analogues. Attachment of the bulky tosyl group at N1 of the uracil base (for the **11** series) did not produce derivatives with significant intrinsic activity and precluded glycosyl transfer. No visible cytotoxic effects were found upon microscopic inspection of cells at compound concentrations as high as 80–400 μmol/L. These compounds were not markedly inhibitory (cytostatic) to human embryonic lung (HEL) cell proliferation (Table 1). Significant cytostatic effects were not observed with murine leukemia L1210, murine mammary carcinoma FM3A, human lymphocyte CEM, and human cervix carcinoma HeLa cells with these compounds (IC_{50}: 60 to >500 μmol/L, data not shown).

Conclusions

Sonogashira coupling of 5-iodouracil (**2**) with terminal alkynes afforded the 5-(alkyn-1-yl)uracil derivatives (**9**) in moderate to good yields. Certain 6-alkylfuro[2,3-*d*]pyrimidin-2-ones (**10**) were isolated as trace by-products. The Cu(I)-promoted cyclization of 5-ethynyluracil (**4**) gave the parent furo[2,3-*d*]pyrimidin-2(3*H*)-one (**5**) in ~15% yield, and the 6-alkyl derivatives (**10**) were obtained from the corresponding 5-(alkyn-1-yl)uracils (**9**) in yields of ~30%. In situ tosylation of trimethylsilylated derivatives of **9** gave the 5-(alkyn-1-yl)-1-tosyluracils (**11**) in moderate to good yields. Biological evaluations were performed with the 5-(alkyn-1-yl)uracils (**9**), their 1-tosyl analogues (**11**), and the 6-alkylfuro[2,3-*d*]pyrimidin-2-one derivatives (**10a**, **10d**, and **10e**). Weak anti-VZV activity was observed with **9d**, **9e**, **11e**, and **11f**, and anti-HCMV activity at near cytotoxic concentrations with **7**. No significant antiviral activity with other DNA and RNA viruses and no cytostatic activity of significance were found with other compounds in this study.

Experimental

Uncorrected melting points were determined with a hot-stage apparatus. UV spectra were measured with solutions in MeOH. ^1H (500 MHz) and ^{13}C (125 MHz) NMR spectra were determined with solutions in DMSO-d_6. "Apparent" peak shapes are in quotation marks when the first-order splitting should be more complex or when the peaks were poorly resolved. High-resolution mass spectra (HRMS) were determined by EI or FAB (thioglycerol, NaOAc). Chemicals and solvents were of reagent quality. Column chromatogra-

© 2006 NRC Canada

Table 1. Anti-DNA virus activity and cytotoxic activity of the test compounds in cell cultures.

	EC_{50}[a] (μmol/L)							MCC[b]	CC_{50}[c]
	HSV-1 (KOS)	HSV-2 (G)	VV	VZV (OKA)	VZV (07/1)	HCMV AD-169	HCMV Davis	(μmol/L)	(μmol/L)
Compd.	(HEL)	(HEL)	(HEL)	(HEL)	(HEL)	(HEL)	(HEL)	(HEL)	(HEL)
6	>200	>200	>200	45	80	>80	>80	400	131
7	>200	>200	>200	>16	>16	36	39	80	29
9a	>200	>200	>200	331	>400	>400	>400	>400	200
9b	>200	>200	>200	>80	>80	>400	>80	400	114
9c	>200	>200	>200	>80	>80	>400	>80	>400	132
9d	>40	>40	>40	37	34	>80	>80	>80	67
9e	>40	>40	>40	>16	16	>400	>400	>400	63
9f	>40	>40	>40	>80	>16	>80	>80	240	>200
10a	>200	>200	>200	213	171	>400	>400	>400	>200
10d	>200	>200	>200	>80	>80	>400	>400	400	>200
10e	>200	>200	>200	>80	>80	>400	>400	400	>200
11a	>40	>40	>40	>16	>16	>16	>16	80	61
11b	>40	>40	>40	>16	>16	>80	51	240	134
11c	>200	>200	>200	>16	>16	>16	>16	80	63
11d	>200	>200	>200	>16	>16	>80	>16	>80	98
11e	>200	>200	>200	16	10	>80	>16	48	31
11f	>200	>200	>200	>16	27	>80	>80	240	85
BVDU	0.032	300	60	0.012	198	>600	>600	>600	>600
GCV	0.032	0.096	>100	—	—	9.4	12	>1000	115

[a]50% Effective concentration (compound concentration required to inhibit virus-induced cytopathogenicity or plaque formation (VZV) by 50%).
[b]Minimum cytotoxic concentration (compound concentration required to cause a microscopically visible alteration of cell morphology).
[c]50% cytostatic concentration (compound concentration required to inhibit cell proliferation by 50%).

phy (silica gel, 230–400 mesh) was performed with solutions of CH_2Cl_2–MeOH.

Method 1: 5-substituted-uracil–TsCl–pyridine is described in detail for **2** → **6**. Method 2: 5-iodouracil–1-alkyne–$Pd(PPh_3)_4$–CuI–Et_3N–DMF for **2** → **9a**. Method 3: 5-(alkyn-1-yl)uracil–CuI–Et_3N–DMF for **9d** → **10d**. Method 4: (*a*) 5-(alkyn-1-yl)uracil–HMDS; (*b*) TsCl–MeCN, Δ for **9a** → **11a**.

5-Iodouracil (2) (ref. 14)

A mixture of uracil (**1**) (35.0 g, 0.31 mol), iodine (47.0 g, 0.19 mol), and CAN (85.5 g, 0.16 mol) in MeCN (750 mL) was stirred at reflux for 5 h, and precipitation of a white solid occurred. The reaction mixture was cooled to ~0 °C in a refrigerator, and the solid was filtered and washed with a small amount of cold MeCN. This material was recrystallized immediately (EtOH–H_2O, 1:1) to give **2** (61.6 g, 83%) as colorless needles; mp > 250 °C dec. (lit. value (14) mp 198 °C, 245 °C dec; lit. value (17) mp 272 °C). UV max: 280 nm (ε 7100). ^{1}H NMR δ: 7.88 (s, 1H), 11.15 (br s, 1H), 11.39 (br s, 1H). ^{13}C NMR δ: 161.5, 151.2, 146.9, 67.6. HRMS *m*/*z*: 237.9238 (M^+ $[C_4H_3IN_2O_2]$ = 237.9239).

5-Ethynyluracil (4) (ref. 15)

TMSA (14.5 mL, 10.1 g, 0.103 mol) and then Et_3N (60 mL) were added to a suspension of **2** (20.0 g, 84.0 mmol), $Pd(PPh_3)_4$ (4.9 g, 4.24 mmol), and CuI (1.3 g, 6.83 mmol) in deoxygenated EtOAc (220 mL). The reaction mixture was stirred at ambient temperature under N_2 for 3 h, and then cooled to ~0 °C. The solid TMS derivative **3** was filtered and then stirred in NaOH–H_2O (1 mol/L, 500 mL) at ambient temperature for 2 h. This mixture was diluted with H_2O (500 mL) and filtered, and the filtrate was concentrated in vacuo to half the volume (~500 mL). The pH of this solution was adjusted with AcOH (to pH ~ 5), and the suspension was cooled (~0 °C). The solid was filtered, washed (H_2O, acetone, Et_2O), and dried to give **4** (9.59 g, 83%) as a TLC-homogeneous orange powder with clean ^{1}H NMR spectra. An analytical sample was recrystallized (EtOH, 84% recovery) to give **4** as a slightly yellow powder; mp > 220 °C dec. UV max: 284, 224 nm (ε 10 000, 11 300). ^{1}H NMR δ: 4.04 (s, 1H), 7.81 (s, 1H), 11.32 (bs, 2H). ^{13}C NMR δ: 162.7, 150.5, 146.5, 96.3, 83.2, 76.6. HRMS *m*/*z*: 136.0270 (M^+ $[C_6H_4N_2O_2]$ = 136.0273). Anal. calcd. for $C_6H_4N_2O_2$: C 52.95, H 2.96, N 20.58; found: C 53.09, H 3.06, N 20.75.

Furo[2,3-*d*]pyrimidin-2(3*H*)-one (5) (refs. 10 and 11)

A suspension of **4** (680 mg, 5.0 mmol) and CuI (1 g, 5.25 mmol) in a deoxygenated mixture of Et_3N (3.5 mL) and DMF (30 mL) was heated at 120 °C for 23 h. Volatiles were evaporated in vacuo, and toluene was added to the residue and then evaporated (3 × 5 mL). The residue was chromatographed (5% MeOH – CH_2Cl_2 → 20% MeOH – CH_2Cl_2) and recrystallized (EtOH) to give slightly yellow crystals of **5** (102 mg, 14.7%); mp > 280 °C (lit. value (10) mp 260 °C; lit. value (11) mp 260–262 °C). UV max: 324, 242 nm (ε 4 800, 10 900). ^{1}H NMR δ: 6.74 (d, *J* = 2.8 Hz, 1H), 7.70 (d, *J* = 2.8 Hz, 1H), 8.34 (s, 1H), 12.15 (br s, 1H). ^{13}C NMR δ: 172.2, 156.0, 144.4, 141.3, 105.1, 104.5. HRMS *m*/*z*: 136.0279 (M^+ $[C_6H_4N_2O_2]$ = 136.0273). Anal. calcd. for $C_6H_4N_2O_2$: C 52.95, H 2.96, N 20.58; found: C 52.72, H 3.12, N 20.36.

© 2006 NRC Canada

5-Iodo-1-tosyluracil (6) (ref. 12)

Method 1

A mixture of **2** (1.0 g, 4.2 mmol) and TsCl (881 mg, 4.62 mmol) in pyridine (25 mL) was stirred at ambient temperature for 28 h. MeOH (3 mL) was added, the solution was stirred for 10 min, and volatiles were evaporated. The residue was dissolved in CH_2Cl_2 (60 mL), and the solution was washed (0.1 mol/L HCl–H_2O, satd. $NaHCO_3$–H_2O, and H_2O) and dried ($MgSO_4$). Volatiles were evaporated, and the residue was chromatographed and recrystallized (EtOAc) to give **6** (662 mg, 40%); mp 250–252 °C. UV max: 276, 231 nm (ε 9 500, 14 800). ^{1}H NMR δ: 2.43 (s, 3H), 7.49 (d, *J* = 8.3 Hz, 2H), 7.98 (d, *J* = 8.3 Hz, 2H), 8.39 (s, 1H), 12.03 (bs, 1H). ^{13}C NMR δ: 160.3, 147.0, 146.5, 141.0, 132.8, 129.8, 129.2, 73.3, 21.2. HRMS *m/z*: 391.9333 (M^+ [$C_{11}H_9N_2IO_4S$] = 391.9328). Anal. calcd. for $C_{11}H_9N_2IO_4S$: C 33.69, H 2.31, N 7.14; found: C 33.91, H 2.02, N 7.30.

5-Ethynyl-1-tosyluracil (7)

Treatment of **4** (500 mg, 3.67 mmol) by Method 1 gave **7** (263 mg, 25%); mp 206 °C. UV max: 277, 228 nm (ε 14 500, 17 100). ^{1}H NMR δ: 2.43 (s, 3H), 4.29 (s, 1H), 7.50 (d, *J* = 8.3 Hz, 2H), 7.98 (d, *J* = 8.3 Hz, 2H), 8.32 (s, 1H), 12.01 (bs, 1H). ^{13}C NMR δ: 161.2, 146.6, 146.4, 141.3, 132.7, 129.9, 129.3, 100.1, 85.2, 75.1, 21.2. HRMS *m/z*: 290.0364 (M^+ [$C_{13}H_{10}N_2O_4S$] = 290.0361). Anal. calcd. for $C_{13}H_{10}N_2O_4S$: C 53.79, H 3.47, N 9.65; found: C 53.83, H 3.60, N 9.66.

5-(Hexyn-1-yl)uracil (9a)

Method 2

A stirred suspension of **2** (2.0 g, 8.4 mmol), $(Ph_3P)_4Pd$ (490 mg, 0.42 mmol), and CuI (130 mg, 0.68 mmol) in DMF (25 mL) was purged with N_2 at room temperature. 1-Hexyne (1.26 mL, 898 mg, 10.9 mmol) was added, followed by dried Et_3N (8 mL). The reaction mixture was stirred under N_2 at ambient temperature for 40 h. Volatiles were evaporated, and toluene was added to the residue and then evaporated (2 × 8 mL). The residue was extracted with hot MeOH (100 mL), and the remaining solid was filtered and washed (MeOH). Volatiles were evaporated in vacuo from the combined MeOH extract and wash. Chromatography (5% MeOH – CH_2Cl_2) and recrystallization (MeOH) of the residue gave **9a** (980 mg, 61%); mp 248–251 °C. UV max: 289, 229 nm (ε 11 100, 13 100). ^{1}H NMR δ: 0.88 (t, *J* = 7.3 Hz, 3H), 1.37–1.44 (m, 2H), 1.46–1.48 (m, 2H), 2.34 (t, *J* = 6.8 Hz, 2H), 7.63 (s, 1H), 11.13 (s, 1H), 11.28 (s, 1H). ^{13}C NMR δ: 162.9, 150.5, 144.6, 97.7, 92.7, 73.0, 30.3, 21.4, 18.5, 13.5. HRMS *m/z*: 192.0892 (M^+ [$C_{10}H_{12}N_2O_2$] = 192.0899). Anal. calcd. for $C_{10}H_{12}N_2O_2$: C 62.49, H 6.29, N 14.57; found: C 62.56, H 6.23, N 14.72.

The fluorescent by-product was isolated from later fractions and recrystallized (EtOAc–EtOH) to give **10a** (25 mg, 1.5%); mp > 220 °C dec. UV max: 327, 244 nm (ε 4 900, 14 800). ^{1}H NMR δ: 0.90 (t, *J* = 7.6 Hz, 3H), 1.34 (dt, *J* = 7.3, 7.3 Hz, 2H), 1.59 ("quint", *J* = ~7.4 Hz, 2H), 2.63 (t, *J* = 7.3 Hz, 2H), 6.37 (s, 1H), 8.14 (s, 1H), 11.96 (bs, 1H). ^{13}C NMR (50 °C) δ: 171.9, 157.6, 155.7, 138.6, 105.9, 99.4, 28.3, 26.8, 21.3, 13.3. HRMS *m/z*: 192.0898 (M^+ [$C_{10}H_{12}N_2O_2$] = 192.0899). Anal. calcd. for $C_{10}H_{12}N_2O_2$: C 62.49, H 6.29, N 14.57; found: C 62.55, H 6.12, N 14.70.

5-(Heptyn-1-yl)uracil (9b)

Treatment of **2** (2.0 g, 8.4 mmol) by Method 2 gave **9b** (890 mg, 51%); mp 241–243 °C. UV max: 289, 230 nm (ε 11 400, 13 500). ^{1}H NMR δ: 0.86 (t, *J* = 7.3 Hz, 3H), 1.24–1.37 (m, 4H), 1.44–1.49 (m, 2H), 2.32 (t, *J* = 7.3 Hz, 2H), 7.62 (s, 1H), 11.11 (s, 1H), 11.26 (s, 1H). ^{13}C NMR δ: 162.9, 150.5, 144.6, 97.7, 92.8, 73.0, 30.5, 28.0, 21.7, 18.8, 13.9. HRMS *m/z*: 206.1052 (M^+ [$C_{11}H_{14}N_2O_2$] = 206.1055). Elemental analyses were not obtained for this compound, but NMR spectra were equally clean.

The fluorescent by-product was recrystallized to give **10b** (8 mg, 0.5%) as a white solid. ^{1}H NMR δ: 0.87 (t, *J* = 6.8 Hz, 3H), 0.88–1.32 (m, 4H), 1.59–1.62 (m, 2H), 2.62 (t, *J* = 7.3 Hz, 2H), 6.37 (s, 1H), 8.14 (s, 1H), 11.95 (bs, 1H). HRMS *m/z*: 206.1045 (M^+ [$C_{11}H_{14}N_2O_2$] = 206.1055).

5-(Octyn-1-yl)uracil (9c)

Treatment of **2** (1.0 g, 4.2 mmol) by Method 2 gave **9c** (490 mg, 53%); mp 231–235 °C. UV max: 289, 230 nm (ε 11 400, 13 500). ^{1}H NMR δ: 0.87 (t, *J* = 6.8 Hz, 3H), 1.25–1.31 (m, 4H), 1.32–1.41 (m, 2H), 1.48 ("quint", *J* = ~7.2 Hz, 2H), 2.34 (t, *J* = 6.8 Hz, 2H), 7.64 (s, 1H), 11.13 (s, 1H), 11.28 (s, 1H). ^{13}C NMR δ: 162.9, 150.5, 144.5, 97.7, 92.8, 73.0, 30.8, 28.2, 28.0, 22.1, 18.8, 13.9. HRMS *m/z*: 220.1205 (M^+ [$C_{12}H_{16}N_2O_2$] = 220.1212). Anal. calcd. for $C_{12}H_{16}N_2O_2$: C 65.43, H 7.32, N 12.72; found: C 65.27, H 7.18, N 12.58.

5-(Nonyn-1-yl)uracil (9d)

Treatment of **2** (2.0 g, 8.4 mmol) by Method 2 gave **9d** (1.19 g, 60%); mp 233–236 °C. UV max: 289, 230 nm (ε 12 500, 14 600). ^{1}H NMR δ: 0.86 (t, *J* = 6.6 Hz, 3H), 1.22–1.29 (m, 6H), 1.33–1.38 (m, 2H), 1.47 ("quint", *J* = 7.2 Hz, 2H), 2.33 (t, *J* = 7.1 Hz, 2H), 7.62 (s, 1H), 11.10 (s, 1H), 11.26 (s, 1H). ^{13}C NMR δ: 162.9, 150.5, 144.6, 97.7, 92.7, 72.9, 31.2, 28.2, 22.1, 18.8, 13.9. HRMS *m/z*: 234.1371 (M^+ [$C_{13}H_{18}N_2O_2$] = 234.1368). Anal. calcd. for $C_{13}H_{18}N_2O_2$: C 66.64, H 7.74, N 11.96; found: C 66.84, H 7.90, N 12.08.

The fluorescent by-product was recrystallized (EtOAc–EtOH) to give **10d** (19 mg, 1%), mp 265–266 °C; and identical spectral data with **10d** prepared by Method 3.

5-(Decyn-1-yl)uracil (9e)

Treatment of **2** (2.0 g, 8.4 mmol) by Method 2 gave **9e** (1.73 g, 81%); mp 210–215 °C. UV max: 289, 228 nm (ε 10 300, 12 700). ^{1}H NMR δ: 0.84 (t, *J* = 6.8 Hz, 3H), 1.22–1.26 (m, 8H), 1.35–1.37 (m, 2H), 1.46 ("quint", *J* = 7.2 Hz, 2H), 2.32 (t, *J* = 7.0 Hz, 2H), 7.61 (s, 1H), 11.11 (s, 1H), 11.27 (s, 1H). ^{13}C NMR δ: 162.9, 150.5, 144.5, 97.7, 92.8, 73.0, 31.3, 28.7, 28.6, 28.31, 28.26, 22.1, 18.8, 14.0. HRMS *m/z*: 248.1517 (M^+ [$C_{14}H_{20}N_2O_2$] = 248.1525). Anal. calcd. for $C_{14}H_{20}N_2O_2$: C 67.71, H 8.12, N 11.28; found: C 67.90, H 7.96, N 11.19.

The fluorescent by-product was recrystallized (EtOAc–EtOH) to give **10e** (15 mg, 0.7%), mp 255–256 °C; and identical spectral data with **10e** prepared by Method 3.

© 2006 NRC Canada

5-(Dodecyn-1-yl)uracil (9f)

Treatment of **2** (2.0 g, 8.4 mmol) by Method 2 gave **9f** (380 mg, 19%); mp 224–227 °C. UV max: 289, 229 nm (ε 12 500, 15 000). ^{1}H NMR δ: 0.85 (t, *J* = 6.8 Hz, 3H), 1.22–1.27 (m, 12H), 1.37–1.38 (m, 2H), 1.44–1.50 (m, 2H), 2.33 (t, *J* = 6.8 Hz, 2H), 7.61 (s, 1H), 11.10 (s, 1H), 11.25 (s, 1H). ^{13}C NMR δ: 162.8, 150.4, 144.4, 97.6, 92.7, 72.9, 31.3, 28.9, 28.7, 28.5, 28.22, 28.19, 22.1, 18.8, 13.9. HRMS *m*/*z*: 276.1838 (M^+ [$C_{16}H_{24}N_2O_2$] = 276.1838). Anal. calcd. for $C_{16}H_{24}N_2O_2$: C 69.53, H 8.75, N 10.14; found: C 69.60, H 8.59, N 10.00.

6-Heptylfuro[2,3-*d*]pyrimidin-2(3*H*)-one (10d)

Method 3

A mixture of **9d** (300 mg, 1.28 mmol), CuI (268 mg, 1.41 mmol), and Et_3N (5 mL) in deoxygenated DMF (25 mL) was stirred at 70 °C for 4 h. Volatiles were evaporated, and toluene was added and evaporated (2 × 5 mL). The residue was extracted with hot MeOH (50 mL), and the remaining solid was filtered. The filtrate was evaporated, and the residue was chromatographed (CH_2Cl_2 → 8% MeOH – CH_2Cl_2) and recrystallized (EtOAc–EtOH, 1:4) to give **10d** (103 mg, 34%); mp 267 °C. UV max: 327, 244 nm (ε 5 800, 17 000). ^{1}H NMR δ: 0.86 (t, *J* = 6.8 Hz, 3H), 1.26–1.31 (m, 8H), 1.59–1.62 (m, 2H), 2.62 (t, *J* = 7.3 Hz, 2H), 6.36 (s, 1H), 8.13 (s, 1H), 11.94 (bs, 1H). ^{13}C NMR (50 °C) δ: 171.9, 157.6, 155.7, 138.8, 105.9, 99.3, 30.9, 28.1, 28.0, 27.2, 26.2, 21.8, 13.6. HRMS (FAB) *m*/*z*: 257.1277 (MNa^+ [$C_{13}H_{18}N_2O_2Na$] = 257.1266). Anal. calcd. for $C_{13}H_{18}N_2O_2$: C 66.64, H 7.74, N 11.96; found: C 66.59, H 7.76, N 11.96.

6-Octylfuro[2,3-*d*]pyrimidin-2(3*H*)-one (10e)

Treatment of **9e** (249 mg, 1.0 mmol) by Method 3 gave **10e** (70 mg, 28%); mp 259 °C. UV max: 327, 244 nm (ε 5 500, 16 000). ^{1}H NMR δ: 0.85 (t, *J* = 6.8 Hz, 3H), 1.25–1.30 (m, 10H), 1.59–1.61 (m, 2H), 2.62 (t, *J* = 7.3 Hz, 2H), 6.36 (s, 1H), 8.13 (s, 1H), 11.92 (bs, 1H). ^{13}C NMR (50 °C) δ: 171.9, 157.6, 155.7, 138.5, 105.9, 99.3, 31.0, 28.3, 27.2, 26.2, 21.8, 13.6. HRMS *m*/*z*: 248.1535 (M^+ [$C_{14}H_{20}N_2O_2$] = 248.1525). Anal. calcd. for $C_{14}H_{20}N_2O_2$: C 67.71, H 8.12, N 11.28; found: C 67.88, H 8.15, N 11.24.

5-(Hexyn-1-yl)-1-tosyluracil (11a)

Method 4

A mixture of **9a** (500 mg, 2.60 mmol) and HMDS (15 mL) was refluxed under N_2 for 1 h. Volatiles were evaporated in vacuo with protection from moisture. The residual oil was dissolved in dried MeCN (20 mL) and TsCl (595 mg, 3.12 mmol) was added. The reaction mixture was refluxed under N_2 for 24 h. MeOH (1 mL) was added, and the mixture was stirred at ambient temperature for 10 min. Volatiles were evaporated, and the residue was chromatographed (3% MeOH in CH_2Cl_2) and recrystallized (EtOAc) to give **11a** (518 mg, 57%) as white needles; mp 196–197 °C. UV max: 284, 230 nm (ε 14 600, 22 300). ^{1}H NMR δ: 0.90 (t, *J* = 7.3 Hz, 3H), 1.40–1.44 (m, 2H), 1.50 ("quint", *J* = 7.0 Hz, 2H), 2.39–2.43 (m, 5H), 7.49 (d, *J* = 8.3 Hz, 2H), 7.98 (d, *J* = 8.3 Hz, 2H), 8.16 (s, 1H), 11.92 (s, 1H). ^{13}C NMR δ: 161.2, 146.5, 146.4, 139.2, 132.8, 129.8, 129.2, 101.3, 94.9, 71.7, 30.0, 21.3, 21.2, 18.4, 13.4. HRMS *m*/*z*: 346.0980 (M^+ [$C_{17}H_{18}N_2O_4S$] = 346.0987). Anal. calcd. for $C_{17}H_{18}N_2O_4S$: C 58.94, H 5.24, N 8.09; found: C 58.94, H 5.13, N 7.72.

Starting material **9a** (140 mg, 28%) was recovered from later chromatographic fractions.

5-(Heptyn-1-yl)-1-tosyluracil (11b)

Treatment of **9b** (250 mg, 1.21 mmol) by Method 4 gave **11b** (205 mg, 47%); mp 180 °C. UV max: 285, 230 nm (ε 13 500, 19 900). ^{1}H NMR δ: 0.88 (t, *J* = 7.3 Hz, 3H), 1.29–1.35 (m, 2H), 1.37–1.41 (m, 2H), 1.52 ("quint", *J* = 7.2 Hz, 2H), 2.40 (t, *J* = 7.1 Hz, 2H), 2.43 (s, 3H), 7.49 (d, *J* = 8.3 Hz, 2H), 7.98 (d, *J* = 8.3 Hz, 2H), 8.16 (s, 1H), 11.94 (s, 1H). ^{13}C NMR δ: 161.3, 146.5, 146.4, 139.3, 132.8, 129.8, 129.2, 101.3, 95.0, 71.7, 30.5, 27.7, 21.6, 21.2, 18.7, 13.9. HRMS (FAB) *m*/*z*: 383.1042 (M^+ [$C_{18}H_{20}N_2O_4SNa$] = 383.1041). Anal. calcd. for $C_{18}H_{20}N_2O_4S$: C 59.98, H 5.59, N 7.77; found: C 59.79, H 5.56, N 7.73.

Starting material **9b** (60 mg, 24%) was recovered from later chromatographic fractions.

5-(Octyn-1-yl)-1-tosyluracil (11c)

Treatment of **9c** (250 mg, 1.13 mmol) by Method 4 gave **11c** (320 mg, 75%); mp 168–169 °C. UV max: 284, 230 nm (ε 14 100, 21 300). ^{1}H NMR δ: 0.87 (t, *J* = 6.8 Hz, 3H), 1.27–1.28 (m, 4H), 1.39–1.40 (m, 2H), 1.51 ("quint", *J* = 7.2 Hz, 2H), 2.39 (t, *J* = 6.8 Hz, 2H), 2.42 (s, 3H), 7.48 (d, *J* = 8.3 Hz, 2H), 7.97 (d, *J* = 8.3 Hz, 2H), 8.16 (s, 1 H), 11.92 (s, 1H). ^{13}C NMR δ: 161.2, 146.5, 146.4, 139.2, 132.8, 129.8, 129.2, 101.3, 95.0, 71.7, 30.7, 27.9, 22.0, 21.2, 18.7, 13.9. HRMS (FAB) *m*/*z*: 397.1198 (MNa^+ [$C_{19}H_{22}N_2O_4SNa$] = 397.1198). Anal. calcd. for $C_{19}H_{22}N_2O_4S$: C 60.94, H 5.92, N 7.48; found: C 60.78, H 6.02, N 7.31.

Starting material **9c** (48 mg, 19%) was recovered from later chromatographic fractions.

5-(Nonyn-1-yl)-1-tosyluracil (11d)

Treatment of **9d** (250 mg, 1.07 mmol) by Method 4 gave **11d** (218 mg, 52%); mp 159 °C. UV max: 285, 230 nm (ε 13 800, 20 700). ^{1}H NMR δ: 0.86 (t, *J* = 6.8 Hz, 3H), 1.26–1.29 (m, 6H), 1.38–1.40 (m, 2H), 1.51 ("quint", *J* = 7.1 Hz, 2H), 2.39 (t, *J* = 7.0 Hz, 2H), 2.42 (s, 3H), 7.49 (d, *J* = 8.3 Hz, 2H), 7.97 (d, *J* = 8.3 Hz, 2H), 8.16 (s, 1H), 11.93 (s, 1H). ^{13}C NMR δ: 161.2, 146.5, 146.4, 139.2, 132.8, 129.8, 129.2, 101.3, 95.0, 71.7, 31.2, 28.2, 22.0, 21.2, 18.7, 13.9. HRMS (FAB) *m*/*z*: 411.1363 (MNa^+ [$C_{20}H_{24}N_2O_4SNa$] = 411.1354). Anal. calcd. for $C_{20}H_{24}N_2O_4S$: C 61.83, H 6.23, N 7.21; found: C 61.68, H 6.37, N 6.95.

Starting material **9d** (60 mg, 24%) was recovered from later chromatographic fractions.

5-(Decyn-1-yl)-1-tosyluracil (11e)

Treatment of **9e** (200 mg, 0.81 mmol) by Method 3 gave **11e** (70 mg, 22%) (as white crystals from MeOH); mp 153–154 °C. UV max: 285, 230 nm (ε 13 300, 20 000). ^{1}H NMR δ: 0.86 (t, *J* = 6.6 Hz, 3H), 1.26–1.29 (m, 8H), 1.38–1.40 (m, 2H), 1.51 ("quint", *J* = 7.1 Hz, 2H), 2.40 (t, *J* = 6.8 Hz, 2H), 2.43 (s, 3H), 7.49 (d, *J* = 8.3 Hz, 2H), 7.97 (d, *J* = 8.3 Hz, 2H), 8.16 (s, 1H), 11.93 (s, 1H). ^{13}C NMR δ: 161.2, 146.5, 146.4, 139.2, 132.8, 129.8, 129.2, 101.3, 95.0, 71.7,

© 2006 NRC Canada

31.2, 28.6, 28.5, 28.2, 27.9, 22.1, 21.2, 18.7, 13.9. HRMS (FAB) *m/z*: 425.1508 (MNa^+ $[C_{21}H_{26}N_2O_4SNa]$ = 425.1511). Anal. calcd. for $C_{21}H_{26}N_2O_4S$: C 62.66, H 6.51, N 6.96; found: C 62.80, H 6.70, N 7.04.

5-(Dodecyn-1-yl)-1-tosyluracil (11f)

Treatment of **9f** (177 mg, 0.64 mmol) by Method 4 gave **11f** (160 mg, 58%); mp 158–159 °C. UV max: 285, 229 nm (ε 12 900, 19 800). ^{1}H NMR δ: 0.85 (t, *J* = 6.6 Hz, 3H), 1.22–1.28 (m, 12H), 1.37–1.40 (m, 2H), 11.51 ("quint", *J* = 7.3 Hz, 2H), 2.39 (t, *J* = 7.1 Hz, 2H), 2.43 (s, 3H), 7.49 (d, *J* = 8.3 Hz, 2H), 7.97 (d, *J* = 8.3 Hz, 2H), 8.16 (s, 1H), 11.95 (s, 1H). ^{13}C NMR δ: 161.3, 146.5, 146.4, 139.2, 132.8, 129.8, 129.2, 101.3, 95.0, 71.7, 31.3, 28.9, 28.7, 28.5, 28.2, 27.9, 22.1, 21.2, 18.7, 14.0. HRMS (FAB) *m/z*: 453.1834 (MNa^+ $[C_{23}H_{30}N_2O_4SNa]$ = 453.1824). Anal. calcd. for $C_{23}H_{30}N_2O_4S$: C 64.16, H 7.02, N 6.51; found: C 63.96, H 7.02, N 6.36.

Starting material **9f** (32 mg, 18%) was recovered from later chromatographic fractions.

Antiviral assays

Antiviral assays, other than anti-HIV assays, were based on inhibition of virus-induced cytopathicity in either human embryonic lung (HEL) cells (herpes simplex virus type 1 (HSV-1) (KOS), HSV-2 (G), vaccinia virus, vesicular stomatitis virus, human cytomegalovirus (HCMV)), Vero (parainfluenza-3, reovirus-1, Sindbis, Coxsackie B4, Punta Toro virus), or HeLa (vesicular stomatitis virus, Coxsackie virus B4, respiratory syncytial virus) cell cultures or virus-induced plaque formation in HEL cells (varicella-zoster virus (VZV)). Confluent cell cultures in microtiter 96 well plates were inoculated with 100 $CCID_{50}$ of virus (1 $CCID_{50}$ is the virus dose required to infect 50% of the cell cultures). After a 1 h virus adsorption period, residual virus was removed and the cell cultures were incubated in the presence of varying concentrations (200, 40, 8, … μmol/L) of the test compounds. Viral cytopathicity was recorded as soon as it reached completion in the control virus-infected cell cultures that were not treated with the test compounds. The methodology for the anti-HIV assays was as follows: human CEM (~3 × 10^5 cells/cm^3) cells were infected with 100 $CCID_{50}$ HIV-1(III_B) or HIV-2(ROD)/mL and seeded in 200 μL wells of a microtiter plate containing appropriate dilutions of the test compounds. After 4 days of incubation at 37 °C, HIV-induced CEM giant cell formation was examined microscopically.

Acknowledgements

We gratefully acknowledge pharmaceutical company gift funds (MJR), Brigham Young University, and the Geconcerteerde Onderzoeksacties (GOA) – Vlaanderen for financial support. We thank Ann Absillis, Anita Camps, Steven Carmans, Frieda De Meyer, Lies Van den Heurck, and Anita Van Lierde for excellent technical assistance with the antiviral assays.

References

1. M.J. Robins and P.J. Barr. Tetrahedron Lett. **22**, 421 (1981).
2. M.J. Robins and P.J. Barr. J. Org. Chem. **48**, 1854 (1983).
3. C. McGuigan, C.J. Yarnold, G. Jones, S. Velázquez, H. Barucki, A. Brancale, G. Andrei, R. Snoeck, E. De Clercq, and J. Balzarini. J. Med. Chem. **42**, 4479 (1999).
4. C. McGuigan, A. Brancale, H. Barucki, S. Srinivasan, G. Jones, R. Pathirana, S. Blewett, R. Alvarez, C.J. Yarnold, A. Carangio, S. Velázquez, G. Andrei, R. Snoeck, E. De Clercq, and J. Balzarini. Drugs Fut. **25**, 1151 (2000).
5. J. Balzarini and C. McGuigan. J. Antimicrob. Chemother. **50**, 5 (2002).
6. E. De Clercq. Med. Res. Rev. **23**, 253 (2003).
7. (*a*) K. Miranda. M.S. thesis, Brigham Young University, Provo, Utah. 2001; (*b*) M.J. Robins, K. Miranda, V.K. Rajwanshi, M.A. Peterson, G. Andrei, R. Snoeck, E. De Clercq, and J. Balzarini. J. Med. Chem. **49**, 391 (2006).
8. C. McGuigan, R.N. Pathirana, R. Snoeck, G. Andrei, E. De Clercq, and J. Balzarini. J. Med. Chem. **47**, 1847 (2004).
9. Z. Janeba, J. Balzarini, G. Andrei, R. Snoeck, E. De Clercq, and M.J. Robins. J. Med. Chem. **48**, 4690 (2005).
10. R.C. Bleackley, A.S. Jones, and R.T. Walker. Tetrahedron, **32**, 2795 (1976).
11. K. Eger, M. Jalalian, and M. Schmidt. J. Heterocycl. Chem. **32**, 211 (1995).
12. B. Kasnar, I. Krizmanic, and M. Zinic. Nucleosides Nucleotides, **16**, 1067 (1997).
13. E. De Clercq, J. Descamps, J. Balzarini, J. Giziewicz, P.J. Barr, and M.J Robins. J. Med. Chem. **26**, 661 (1983), and refs. cited therein.
14. J.-I. Asakura and M.J. Robins. J. Org. Chem. **55**, 4928 (1990).
15. J.W.B. Cooke, R. Bright, M.J. Coleman, and K.P. Jenkins. Org. Process Res. Dev. **5**, 383 (2001).
16. J. Balzarini, R. Sienaert, S. Liekens, A. Van Kuilenburg, A. Carangio, R. Esnouf, E. De Clercq, and C. McGuigan. Mol. Pharmacol. **61**, 1140 (2002).
17. T.B. Johnson and C.O. Johns. J. Biol. Chem. **1**, 305 (1906).

© 2006 NRC Canada

Chemoenzymatic synthesis of thio-nod factor intermediates — Enzymatic transfer of glucosamine on thiochitobiose derivatives[1]

Latino Loureiro Morais, Hideya Yuasa, Khalil Bennis, Isabelle Ripoche, and France-Isabelle Auzanneau

Abstract: The chemoenzymatic syntheses of thioanalogues of nodulation factors in which the nonreducing end glucosamine residue is available for the introduction of the fatty acid moiety at the free NH_2 group are reported. We are describing the chemical synthesis of UDP-GlcNH_2 and its use in the enzymatic transfer of GlcNH_2 by the bovine galactosyltransferase (EC 2.4.1.90) onto O-4 of the nonreducing end *N*-acetylglucosamine residues of chitobiose, thiochitobiose, and allyl thiochitobioside. The enzymatic reactions on chitobiose and thiochitobiose were followed by TLC and MALDI MS and showed about 50% conversion of the disaccharides to the desired products. However, these reducing trisaccharides could not be obtained totally free of salts and degraded on ion exchange chromatography. Thus, we investigated the enzymatic transfer on the nonreducing allyl thiochitobioside analogue. We describe here the chemical synthesis of this thiodisaccharide and the enzymatic transfer of GlcNH_2 at O-4 of its nonreducing end glucosamine residue to give the desired allyl thiotrisaccharide. This thiotrisaccharide was obtained pure in 41% yield and was characterized by ^{1}H NMR (HSQC) and HRMS.

Key words: nodulation factors, synthesis, enzymatic transfer, thiooligosaccharides, UDP-glucosamine.

Résumé : On a réalisé la synthèse chimioenzymatique de thioanalogues de facteurs de nodulation dans lesquels le résidu glucosamine de l'extrémité non réductrice est disponible pour l'introduction de portions d'acides gras au niveau du groupe NH_2. On décrit la synthèse chimique de UDP-GlcNH_2 ainsi que son utilisation dans le transfert enzymatique du GlcNH_2 par la galactosyltransférase bovine (EC 2.4.1.90) sur le O-4 des résidus *N*-acétylglucosamine non réducteurs du chitobiose, du thiochitobiose et du thiochitobioside d'allyle. Les réactions enzymatiques sur le chitobiose et le thiochitobiose ont été suivies par chromatographie sur couche mince et par spectrométrie de masse MALDI et elles montrent qu'il se produit une conversion d'environ 50 % des disaccharides en produits désirés. Toutefois, on n'a pas pu éliminer complètement le sel de ces trisaccharides réducteurs et ils se dégradent lors de la chromatographie par échange d'ions. On a donc étudié le transfert enzymatique sur l'analogue thiochitobioside d'allyle non réducteur. On décrit les synthèses chimiques de ce thiodisaccharide et le transfert enzymatique du GlcNH_2 vers le O-4 du résidu glucosamine de l'extrémité non réductrice pour obtenir le thiotrisaccharide d'allyle désiré. Ce thiotrisaccharide a été obtenu à l'état pur avec un rendement de 41 % et on l'a caractérisé par RMN du ^{1}H (HSQC) et par spectrométrie de masse à haute résolution.

Mots clés : facteurs de nodulation, synthèse, transfert enzymatique, thiooligosaccharides, UDP-glucosamine.

[Traduit par la Rédaction]

Introduction

Symbiotic association (1) of leguminous plants with soil bacteria of the genera *Rhizobium*, *Bradyrhizobium*, and *Azorhizobium* leads to the formation of nodules on the plant roots. Within these nodules the bacteria can fix and metabolize atmospheric nitrogen into ammonia and alanine and release it for use by the host plant, which in turn supplies the

Received 6 September 2005. Published on the NRC Research Press Web site at http://canjchem.nrc.ca on 5 May 2006.

This paper is dedicated to Professor W. Szarek on his 65th birthday.

L. Loureiro Morais, K. Bennis, and I. Ripoche.[2] Laboratoire de Chimie des Hétérocycles et des Glucides, École Nationale Supérieure de Chimie de Clermont-Ferrand, BP 187, F-63174 Aubière, France.
H. Yuasa.[3] Department of Chemistry, University of Alberta, Edmonton, AB T6G 2G2, Canada.
F.-I. Auzanneau.[4] Department of Chemistry, University of Guelph, Guelph, ON N1G 2W1, Canada.

[1]This article is part of a Special Issue dedicated to Professor Walter A. Szarek.
[2]Corresponding author (e-mail: ripoche@chimie.univ-bpclermont.fr).
[3]Present address: Department of Life Science, Graduate School of Bioscience and Biotechnology, Tokyo Institute of Technology, 4259 Nagatsutacho, Midoriku, Yokohama 2268501, Japan.
[4]Corresponding author (e-mail: fauzanne@uoguelph.ca).

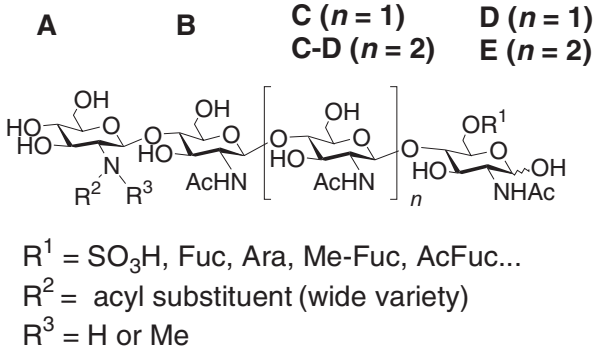
 doi:10.1139/V06-043 © 2006 NRC Canada

bacteria with various nutrients. Nodulation, the key step leading to this symbiotic association, is induced by the interaction with specific plant receptors of nodulation factors (Nod factors) produced by the bacteria (2). These lipooligosaccharides (3) are comprised of a tetra- or penta-oligomer of chitin with substitutions that determine the host specificity of the bacteria (Fig. 1, ref. 3). Although only very small concentrations (10^{-6} to 10^{-12} mol/L) of natural Nod factors are required to initiate nodulation, their activity is limited by the action of chitinases that cleave the glycosidic bond between the sugar units B and C (4). Therefore, we have developed a program (5) aimed at preparing thioanalogues of Nod factors in which a sulphur atom replaces one or more interglycosidic oxygen atoms, thus increasing the overall resistance of the lipooligosaccharide to chitinases (6). The synthesis of such oligosaccharide analogues with well-defined glycosidic linkages remains a challenge for carbohydrate chemists despite the advances made over the past decades. Therefore, we are investigating here the possibility of introducing a glucosamine unit at the nonreducing end of thioanalogues of Nod factors by enzymatic transfer (7). We report the use of the well-studied β-(1,4)-galactosyltransferase (7) isolated from bovine milk and involved in the biochemical synthesis of lactose and *N*-acetyllactosamine. The transfer of a glucosamine unit to the nonreducing end of chitotriose using the commercially available bovine galactosyltransferase (UDP-D-galactose:2-acetamido-2-deoxy-D-glucose 4-β-D-galactosyl tranferase; EC 2.4.1.90) has already been described (8). The work described here is, to our knowledge, the first enzymatic transfer to chitobiose derivatives that contain a sulphur atom in the glycosidic linkage and thus constitutes the first enzymatic synthesis of thiochitotriose derivatives. We describe herein the efficient chemical synthesis of UDP-glucosamine as well as the chemoenzymatic synthesis of new thiotrisaccharides precursors of thioanalogues of nodulation factors using this nucleotide donor and the bovine galactosyltranferase EC 2.4.1.90.

Results and discussion

As an alternative to the known (9) enzymatic preparation of UDP-$GlcNH_2$, the nucleotide donor **6** was synthesized chemically (Scheme 1) from the trifluoroacetamido derivative (**1**) obtained as described by Wolform and Conigliaro (10) from commercially available crystalline glucosamine hydrochloride. The synthetic strategy followed to prepare the key intermediate analogue (**5**) was similar to that employed by Sala et al. (11). Acetylation in pyridine – acetic anhydride gave the crude peracetate (**2**) as an anomeric mixture that contained the α anomer as the major compound. The crude peracetate was treated with hydrazine acetate to give the known (10, 11) α-hemiacetal (**3**) with an improved yield of 74% from **1** upon purification on silica gel. The hemiacetal **3** was treated with butyllithium to give the anomeric alkoxide that was reacted with dibenzyl phosphoryl chloride (12) in THF to give the anomeric dibenzylphosphate (**4**) in 54% yield, a yield similar to that described by Sala et al. (11) for the synthesis of the analogous anomeric diphenylphosphate (52%). The benzyl groups were removed by hydrogenolysis and the crude triacetylated anomeric phosphate (**5**) was activated with 1,1′-carbonyldiimidazole

Fig. 1. Schematic representation of nodulation factors.

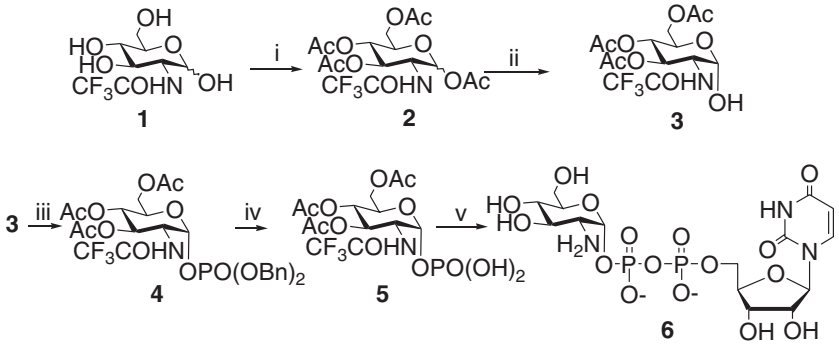


in acetone and coupled with the bistrioctylammonium salt of uridine 5′-monophophate dissolved in DMF. The crude adduct was in turn treated with ammonium hydroxide in methanol to remove the *O*-acetyl and *N*-trifluoroacetyl groups and the desired UDP-$GlcNH_2$ (**6**) was isolated pure in 51% yield (from **4**) following ion exchange chromatography.

The enzymatic transfer of glucosamine by the β-1,4-galactosyltransferase isolated from bovine milk (13) was first attempted on the reducing disaccharides chitobiose (**7**) and thiochitobiose (**8**) (Scheme 2) Although the products obtained in these reactions could not be purified (see the following), these reactions were used to determine the best reaction and purification conditions for the enzymatic transfer and more importantly to establish MALDI-MS conditions that can be used to follow such transfers. While chitobiose is commercially available, the known (14) thiodisaccharide (**8**) was prepared in one step through the deacetylation of the previously reported (5*b*) peracetylated thiochitobiose. The disaccharide (**8**) obtained as an anomeric mixture could not be totally purified by conventional chromatography. However, since ^{1}H NMR (Fig. 2C and ref. 14*b*) showed a purity superior than 90% and HRMS confirmed its structure, the α,β-thiochitobiose (**8**) was submitted to enzymatic transfer. The reducing chitobiose (**7**) and thiochitobiose (**8**) were incubated with UDP-$GlcNH_2$ (**6**, 1.2 equiv.) and galactosyltransferase (5.6 U) at ambient temperature with occasional gentle mixing. TLC analysis of the reaction mixture showed in both cases the formation of a new ninhydrin positive compound that was more polar than the starting material. The formation of the trisaccharides **9** and **10** was also assessed by MALDI-MS of the reaction mixtures (Fig. 3). As can be seen in Fig. 3A, we observed for the enzymatic transfer on **7** (+Na, *m*/*z* 448 ± 1) the appearance of a signal at *m*/*z* 608 ± 1 (+Na) corresponding to the desired adduct **9**. Similarly, both the starting thiochitobiose (**8**) and the adduct **10** were observed at *m*/*z* 464 ± 1 (+Na) and *m*/*z* 625 ± 1 (+Na), respectively, by MALDI-MS for the enzymatic transfer on disaccharide **8**. After 2 weeks of incubation, the conversion evaluated by TLC had reached ~50% in both cases, and the reaction mixtures were applied to a gel permeation chromatography column of Bio-Gel eluted with a 0.25 mol/L ammonium acetate solution. While this was an efficient way to separate the unreacted disaccharides **7** and **8** from the desired trisaccharides **9** and **10**, respectively, the products could not be isolated totally free of ammonium acetate even after repeated freeze drying from water. Additional attempts to remove the excess acetate ions

© 2006 NRC Canada

Scheme 1. Reagents: (*i*) Ac_2O–pyridine (crude, α/β = 94:6); (*ii*) NH_2NH_2-AcOH, DMF (74% pure α over *i* and *ii*); (*iii*) a. BuLi, THF; b. $ClPO(OBn)_2$, THF (59%); (*iv*) H_2-Pd/C, MeOH (not isolated); (*v*) a. **5**, 1,1′-carbonyldiimidazole, acetone; b. uridine 5′-monophosphate bistrioctylammonium salt, DMF; c. MeOH–NH_4OH (51% over *iv* and *v*).



Scheme 2.

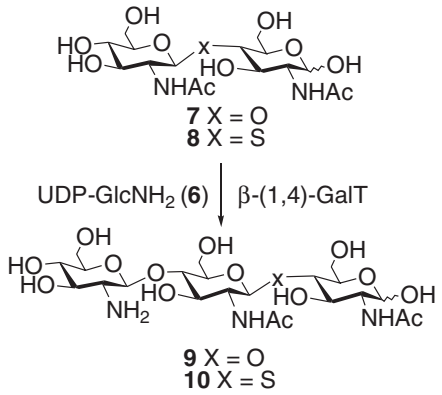
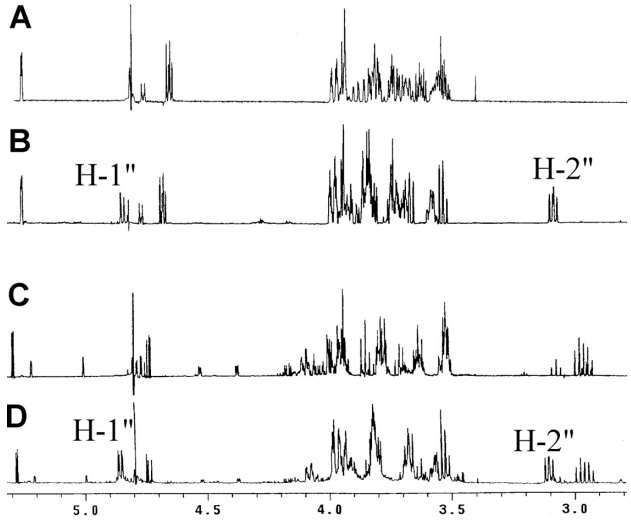


Fig. 2. ^1H NMR (600 MHz) of disaccharide acceptor (A) **7**, (B) semi-pure trisaccharide **9**, (C) disaccharide acceptor **8**, and (D) semi-pure trisaccharide **10**.

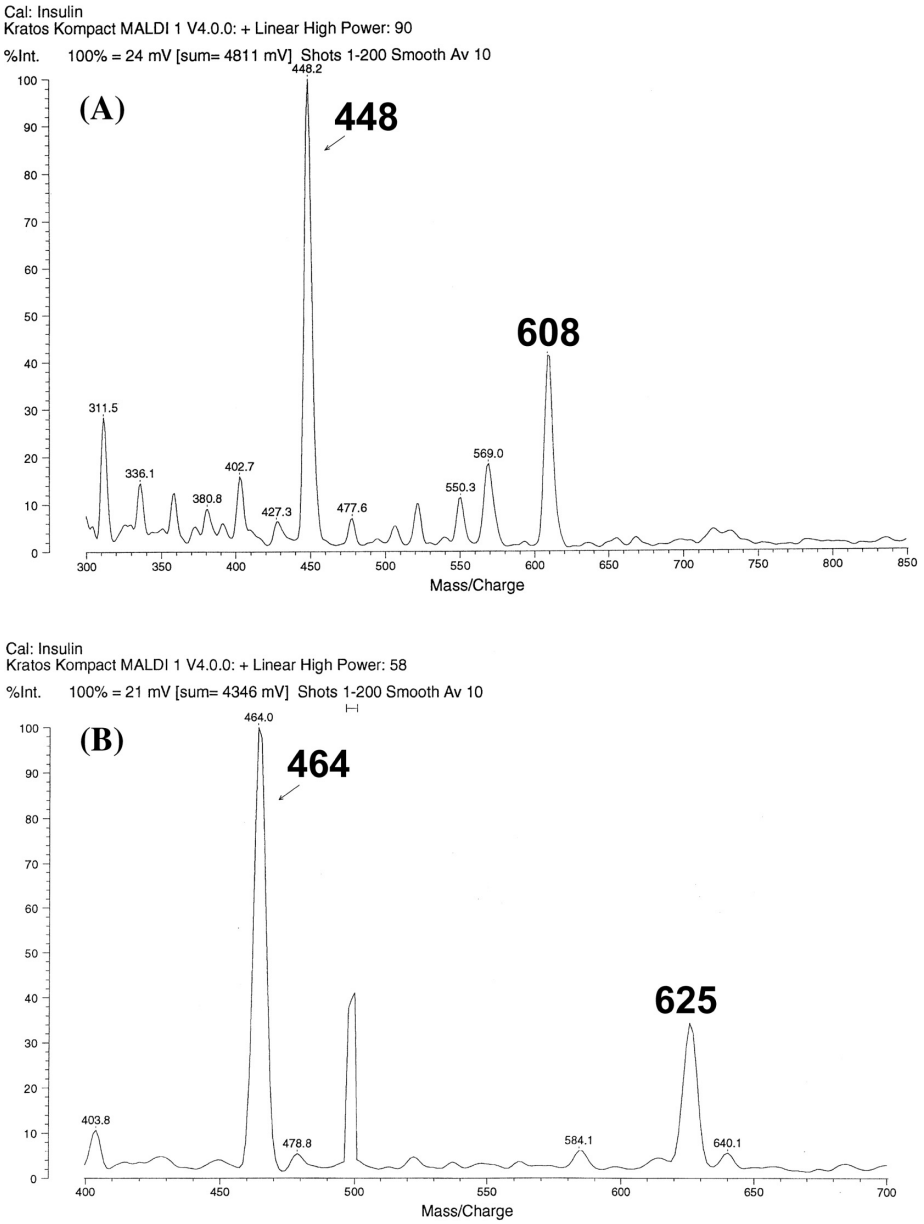


by applying the impure products to ion exchange columns (AG1X-8/OH^-) resulted in the degradation or adsorption and subsequent loss of the reducing sugars. Although the products could not be obtained free of salts, NMR confirmed that the products isolated were the desired trisaccharides. ^1H NMR of **9** (Fig. 2B) clearly showed signals that could be assigned to the newly introduced glucosamine residue at 4.82 ppm for the anomeric H-1″ and at 3.06 ppm for H-2″. The ^1H NMR spectrum obtained for **10** (Fig. 2D) showed the presence of the same contaminant already observed in **8**, which we concluded was also a substrate for the galactosyltransferase. However, it also clearly demonstrated that a glucosamine unit giving typical signals at 4.83 and 3.09 ppm for H-1″ and H-2″, respectively, had been transferred onto the thiochitobiose. Finally, the structures of **9** and **10** were unambiguously confirmed by HRMS that gave protonated molecular ions at *m/z* 586.2463 for **9** (calcd. [M + H] 586.2459) and *m/z* 602.2237 for **10** (calcd. [M + H] 602.2231). Thus, these results showed that the transfer of a glucosamine residue to thiochitobiose using UDP-$GlNH_2$ and bovine β-(1,4)-galactosyltransferase can be used for the preparation of thionodulation factor intermediate trisaccharides. However, because trisaccharide **10** could not be isolated pure and free of salt without degradation, we focused our synthetic effort on the preparation of the nonreducing allyl thiochitobioside derivative (**20**) (Scheme 3).

The allyl group was chosen as a versatile aglycon that is not only easily introduced and removed at the anomeric position, but can also be used to immobilize the oligosaccharides on solid support (15) to further attempt to isolate the specific plant receptor. Nucleophilic displacement of the known (5*c*) 1,6-anhydro triflate **12** with the anomeric thiolate obtained by treatment of the thiol **11** (5*b*) with sodium hydride, afforded the thiodisaccharide **13** in excellent yield (90%). The 1,6-anhydro ring in disaccharide **13** was opened with a mixture of Ac_2O and TFA to give the anomeric mixture of **14** (α/β, 65:35) in high yield (96%). Considering the low stability of the allyl group in debenzylation conditions, we replaced the benzyl group at the C-3 hydroxyl group of the reducing end glucosamine with an acetyl group prior to introducing the allyl aglycon. Thus, the benzyl group in compound **14** was removed using iron trichloride (16) in dichloromethane and the crude intermediate alcohol was acetylated to give the peracetate **15** as an anomeric mixture (Scheme 3). The thiodisaccharide **15** was subsequently converted to the hemiacetal **16** by selective deacetylation of the anomeric hydroxyl group and the hemiacetal **16** was treated with DBU and trichloroacetonitrile to give trichloroacetimidate **17** as an anomeric mixture in favor of the α anomer (α/β, 85:15). Glycosylation of allyl alcohol with the donor **17** was performed under $BF_3{\cdot}Et_2O$ catalysis in dichloromethane and gave the desired thiodisaccharide **18**

© 2006 NRC Canada

Fig. 3. MALDI-MS (accuracy *m*/*z*: ±1) of enzymatic transfer on (A) chitobiose (**7**) and (B) thiochitobiose (**8**).



in good yield (83%) and high selectivity in favor of the β anomer (α/β, 1:9). The β anomer **18**β was isolated anomerically pure by chromatography on alumina and converted to the *N*-acetate **19** in moderate yield through the reduction of the azido group (Zn-AcOH, ref. 17) followed by in situ N-acetylation. Finally, Zemplèn deacetylation of disaccharide **19** gave the acceptor **20** in good yield.

Enzymatic transfer of the glucosamine residue (Scheme 4) was accomplished using the same conditions as those described for the preparation of trisaccharides **9** and **10**. Thus, thiodisaccharide **20** was incubated for 2 weeks at ambient temperature with UDP-GlcNH$_2$ **6** (1.2 equiv.) and the bovine galactosyltransferase (5.6 U). The thiotrisaccharide **21** was obtained pure in 41% yield after chromatography on Bio-Gel P-2 ($AcONH_4$, 0.25 mol/L), followed by desalting on a small column of AG MP-1 (OH^-) eluted with water. The pure compound **21** was fully characterized by ^{1}H NMR spectroscopy, COSY, and HSQC, and its structure was confirmed by HR-ESI MS.

The results reported herein show that the transfer of a glucosamine unit to a thiochitobiose derivative by enzymatic catalysis using the well-known β-(1,4)-galactosyltransferase is applicable to the preparation of thiooligosaccharides. Further reactions on the thiotrisaccharide **21**, including the introduction of the fatty acid moiety, should provide access to a large series of thioanalogues of nodulation factors.

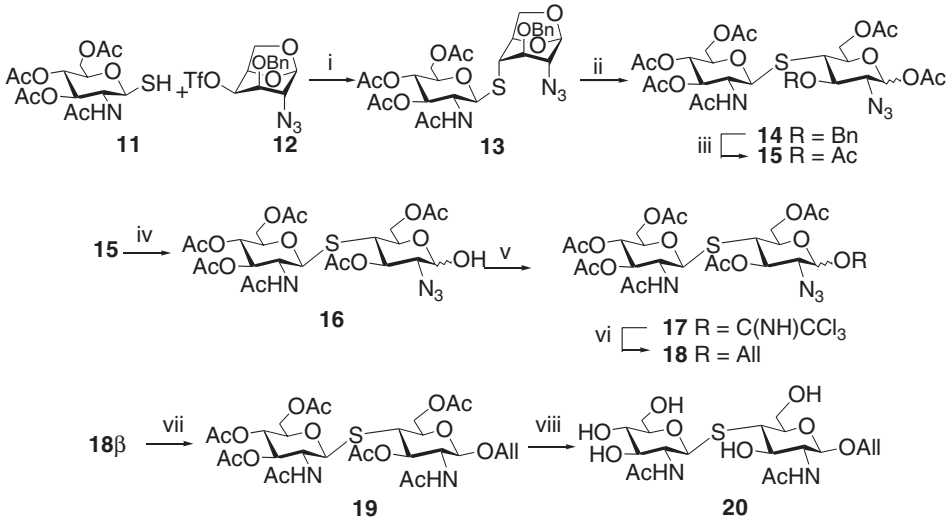
Experimental section

General procedure for the enzymatic reactions

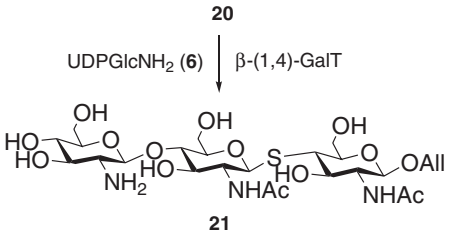
The acceptors **7**, **8**, and **20** (~5 mg, ~11 μmol) and UDP-glucosamine (~9 mg, 1.2 equiv.) were dissolved in 1 mL of a pH 7.4 buffer (80 mmol/L sodium cacodylate, 5 mmol/L $MgCl_2$, 0.1 mmol/L DTT) containing β-1,4-galactosyl-

© 2006 NRC Canada

Scheme 3. Reagents: (*i*) a. **11**, NaH, DMF, 0 °C; b. **12**, 20 °C (90%); (*ii*) 9:1 Ac_2O–TFA (96%, α/β = 65:35); (*iii*) a. $FeCl_3$, CH_2Cl_2; b. Ac_2O, pyridine (62%, α/β = 8:2); (*iv*) H_2NNH_2–AcOH, DMF (75%, α/β = 7:3); (*v*) Cl_3CCN, DBU, CH_2Cl_2 (95%, α/β = 85:15); (*vi*) AllOH, $BF_3{\cdot}Et_2O$, CH_2Cl_2 (83%, α/β = 1:9); (*vii*) a. Zn, AcOH, THF; b. Ac_2O (45% from **18**β); (*viii*) MeONa, MeOH (72%).



Scheme 4.



transferase (5.6 U). Solutions of $MnCl_2$ (1 mol/L, 25 μL, 5 mmol), α-lactalbumin (25 mg/mL, 45 μL), and alkaline phosphatase (1 U) were added to the mixture, which was then left at room temperature for 2 weeks. TLC monitoring of the reactions (*i*-PrOH–NH_4OH–H_2O, 7:2:1 or $CHCl_3$–MeOH–H_2O, 65:35:2) showed, in all three cases, the formation of new compounds more polar than the starting materials in ~50% yield estimated from the TLC. The reaction mixtures were then applied directly to a Bio-Gel P-2 column (100 cm × 1 cm) eluted with a 0.25 mol/L $NH_4^+AcO^-$ solution. The fractions containing the new compounds were combined and freeze dried repeatedly from MQ water. The allyl thiotrisaccharide **21** was additionally deionized on a column of AG MP-1(OH^-) eluted with H_2O.

3,4,6-Tri-*O*-acetyl-2-deoxy-2-trifluoroacetamido-α-D-glucopyranose (3)

2-Deoxy-2-trifluoroacetamido-D-glucopyranose (4.72 g, 17.1 mmol) was prepared as described by Wolform and Conigliaro (10) from commercially available crystalline D-glucosamine hydrochloride and was dissolved in pyridine (32 mL) and acetic anhydride (18 mL). The reaction mixture was kept at room temperature for 16 h and poured into ice water and stirred for 1 h. The mixture was extracted with dichloromethane and the organic layer was washed with aq. $NaHCO_3$ and dried on Na_2SO_4. The solution was concentrated to give a crude syrup (8.56 g) containing the peracetylated 2-deoxy-2-trifluoroacetamido-α/β-D-glucopyranose (**2**). ^{1}H NMR analysis showed that the α/β ratio was largely in favor of the desired α anomer (94:6). Therefore, the crude material was dissolved in DMF (50 mL) and the solution was warmed to 50 °C. Hydrazine acetate (1.74 g, 18.9 mmol, 1.05 equiv.) was added to the solution and stirring at 50 °C was maintained for 25 min. The reaction mixture was diluted with EtOAc and washed three times with brine. The organic layer was dried over $MgSO_4$ and concentrated to give a syrup (8.55 g). Chromatography on silica gel (hexane–EtOAc, 3:2) gave the title compound **3** (5.09 g, 74%) as a pure white powder. Compound **3** had characteristics in excellent agreement with those described (10, 11). $[\alpha]_D$ +21° (*c* 1.6, $CHCl_3$) (lit. value (10) +25° (*c* 1, $CHCl_3$), lit. value (11) +20° (*c* 0.5, $CHCl_3$)). ^{1}H NMR (360 MHz, $CDCl_3$) δ: 6.75 (d, 1H, $J_{NH,2}$ = 9.7 Hz, NH), 5.37 (dd, 1H, $J_{2,3}$ = 9.7 Hz, $J_{3,4}$ = 9.5 Hz, H-3), 5.37–5.34 (m, 1H, H-1), 5.27 (t, 1H, $J_{4,5}$ = 9.5 Hz, H-4), 4.32 (dt, 1H, $J_{1,2}$ = 3.5 Hz, H-2), 4.27–4.08 (m, 3H, H-5, H-6a, H-6b), 3.78 (bs, 1H, OH), 2.11, 2.06, and 2.04 (3 s, 9H, 3 × CH_3CO). ^{13}C NMR (75 MHz, $CDCl_3$) δ: 171.4, 171.0, 169.4 (*C*OCH_3), 157.3 (q, $J_{C,F}$ = 37.4 Hz, *C*OCF_3), 115.5 (q, $J_{C\text{-}F}$ = 290 Hz, *C*F_3), 91.0 (C-1), 70.5, 67.9 (C-3, C-4, C-5), 61.9 (C-6), 52.8 (C-2), 20.8, 20.6, 20.5 (*C*H_3CO).

3,4,6-Tri-*O*-acetyl-2-deoxy-2-trifluoroacetamido-α-D-glucopyranosyl dibenzyl phosphate (4)

A solution of butyllithium (1.6 mol/L, 8.4 mL, 13.4 mmol) in hexane was added to a solution of hemiacetal **3** (5.31 g, 13.2 mmol) in THF (160 mL) stirred at –70 °C. After 2 min, a solution of dibenzyl chlorophosphate (12) (5.5 mL, 29.3 mmol) in THF (200 mL) was added slowly at –70 °C under stirring and the mixture was stirred for a further 30 min while the temperature was kept between –60 and –50 °C. Triethylamine was added to pH 8 and the solvent was evaporated. The residue was partitioned between chloroform and aqueous sodium chloride. The organic layer was dried ($MgSO_4$), concentrated, and chromatography on silica gel (hexane–EtOAc, 3:2) gave the pure dibenzylphosphate **4** (5.17 g, 59%) as a colorless glass. $[\alpha]_D$ +55° (*c* 1.2, $CHCl_3$). ^{1}H NMR (360 MHz, $CDCl_3$) δ: 8.2 (d, 1H, $J_{NH,2}$ = 9.0 Hz,

© 2006 NRC Canada

NH), 7.40–7.20 (m, 10H, H-aromatics), 5.80 (dd, 1H, $J_{1,2}$ = 3.2 Hz, $J_{1,P}$ = 6.7 Hz, H-1), 5.35 (dd, 1H, $J_{2,3}$ = 10.5 Hz, $J_{3,4}$ = 10.0 Hz, H-3), 5.16 (t, 1H, $J_{4,5}$ = 10.0 Hz, H-4), 5.28–4.98 (m, 4H, 2 × CH_2Ph), 4.41 (ddd, 1H, $J_{2,P}$ = 3.2 Hz, H-2), 4.25–3.98 (m, 3H, H-5, H-6a, H-6b), 2.03, 2.02, 1.99 (3s, 9H, 3 × CH_3CO). ^{13}C NMR (75 MHz, $CDCl_3$) δ: 171.0, 170.5, 169.1 (*C*OCH_3), 157. 6 (q, $J_{C,F}$ = 37.7 Hz, *C*OCF_3), 135.2, 135.0, 129.0,128.8, 128.2 (C-aromatics), 115.5 (q, J_{C-F} = 286.8 Hz, *C*F_3), 95.1 (d, J_{C-P} = 5.7 Hz, C-1), 70.3, 70.2, 69.8, 67.2 (C-3, C-4, C-5, 2 × *C*H_2Ph), 61.1 (C-6), 52.6 (d, $J_{2,P}$ = 7.5 Hz, C-2), 20.6, 20.5, 20.4 (*C*H_3CO). Anal. calcd. for $C_{28}H_{31}NO_{12}PF_3$: C 50.84, H 4.72, N 2.12; found: C 50.90, H 4.67, N 1.97.

Uridine 5′-(2-amino-2-deoxy-α-D-glucopyranosyl)-diphosphate (6)

A solution of dibenzylphosphate **4** (5.17 g, 7.82 mmol) in MeOH (400 mL) containing 5% Pd/C (2.14 g) was stirred under hydrogen for 2.5 h. The catalyst was filtered off and the filtrate concentrated to dryness to give 3,4,6-tri-*O*-acetyl-2-deoxy-2-trifluoroacetamido-α-D-glucopyranosyl phosphate (**5**) as a white solid. R_f 0.28 (60:40:3, CH_2Cl_2–MeOH–H_2O). ^{1}H NMR (360 MHz, $CDCl_3$–CD_3OD, 2:1) δ: 5.64 (dd, 1H, $J_{1,2}$ = 3.0 Hz, $J_{1,P}$ = 6.0 Hz, H-1), 5.42 (dd, 1H, $J_{2,3}$ = 10.0 Hz, $J_{3,4}$ = 9.5 Hz, H-3), 5.17 (t, 1H, $J_{4,5}$ = 10.0 Hz, H-4), 4.42 (dt, 1H, $J_{2,P}$ = 3.0 Hz, H-2), 4.33–4.10 (m, 3H, H-5, H-6a, H-6b), 2.11, 2.06, 2.02 (3s, 9H, 3 × CH_3CO). Crude **5** was dissolved in acetone (130 mL) and 80% 1,1′-carbonyldiimidazole (3.3 g, 16.3 mmol) was added and the mixture was stirred for 15 h at room temperature. After completion of the reaction ($CHCl_3$–MeOH, 3:1, R_f 0.28), methanol (170 μL) was added and the mixture was stirred for another 0.5 h. The reaction mixture was concentrated and dried under reduced pressure over P_2O_5 for 6 h. While the crude imidazolate was drying, uridine 5′-monophosphate disodium salt (3.5 g, 9.51 mmol) was passed slowly through a column of Dowex 50-5X8 (H^+) resin and the column was thoroughly washed with water. The eluate was concentrated and trioctylamine (8.8 mL, 20 mmol) was added. The mixture was coevaporated three times with DMF and a solution of the aforementioned dry imidazolate in DMF (100 mL) was added. The mixture was stirred for 24 h at room temperature and the formation of the adduct was followed by TLC (CH_2Cl_2–MeOH–H_2O, 60:40:3, R_f 0.35). The solvent was evaporated and the dry residue was dissolved in methanol (150 mL) and ammonium hydroxide (60 mL). The solution was stirred at room temperature for 24 h and concentrated. The crude deacylated product was dissolved in 40 mmol/L aqueous ammonium bicarbonate and slowly passed through a Dowex 1X2-200 (HCO_2^-) column (3 cm × 30 cm). The column was kept at 23 °C and was first washed with 40 mmol/L aq. NH_4HCO_2, then it was eluted (1.6 mL/min) with a linear gradient of ammonium bicarbonate (mixing vessel 550 mL of 40 mmol/L NH_4HCO_2; reservoir 550 mL of 700 mmol/L NH_4HCO_2). The UV absorption of the eluate at 280 nm was monitored and 20 mL fractions were collected. Those fractions containing the product were pooled and concentrated and the residue dissolved in water was treated with Dowex 50-X8 (H^+) until the pH was below 7 and CO_2 gas had evolved. The resin was filtered off and the pH of the filtrate was adjusted to 8 by adding aqueous sodium hydroxide. The solution was passed through a Millex SR filter unit and the filtrate was lyophilized to give pure UDP-GlcNH_2 (**6**) as a white solid (2.43 g, 51%). ^{1}H NMR (400 MHz, D_2O) δ: 7.96 (d, 1H, $J_{5,6}$ = 8.0 Hz, H-6), 5.99 (d, 1H, $J_{1′,2′}$ = 4.4 Hz, H-1′), 5.96 (d, 1H, H-5), 5.75 (dd, 1H, $J_{1″,2″}$ = 3.3 Hz, $J_{1″\text{-}P}$ = 6.8 Hz, H-1″), 4.36 (m, 2H, H-5a′, H-5b′), 4.31–4.16 (m, 3H, H-2′, H-3′, H-4′), 3.78–3.96 (m, 4H, H-3″, H-5″, H-6a″, H-6b″), 3.53 (t, 1H, $J_{3″,4″}$ = $J_{4″,5″}$ = 9.6 Hz, H-4″), 3.16 (dd, 1H, $J_{2″,3″}$ = 10.4 Hz, $J_{2″,P}$ = 3.5 Hz, H-2″). ^{13}C NMR (75 MHz, D_2O) δ: 167.1 (C-4), 153.7 (C-2), 142.5 (C-6), 103.5 (C-5), 93.7 (d, $J_{C,P}$ = 5.3 Hz, C-1″), 89.5 (C-1′), 83.9 (d, $J_{C,P}$ = 8.7 Hz, C-4′), 74.6, 74.1, 70.8, 70.4, 69.9 (C-2′, C-3′, C-3″, C-4″, C-5″), 65.9 (d, $J_{C,P}$ = 5.3 Hz, C-5′), 60.9 (C-6″), 55.0 (d, $J_{C,P}$ = 9.3 Hz, C-2″). ^{31}P NMR (145 MHz, D_2O) δ: –10.9 (d, $J_{P,P}$ = 22.0 Hz, P-O-uridine), –13.5 (d, P-O-Glc). HRMS calcd. for $C_{15}H_{23}O_{16}N_3Na_2P_2S$ *m*/*z*: 632.0247 [M + Na]; found: 632.0245.

4-*S*-(2-Acetamido-2-deoxy-β-D-glucopyranosyl)-2-acetamido-2-deoxy-4-thio-α,β-D-glucopyranose (8)

The peracetylated thiochitobiose (5*b*) (37.2 mg, 0.040 mmol) was dissolved in anhydr. MeOH (4 mL) and a solution of sodium methoxide in MeOH (1 mol/L, 40 μL) was added. The reaction mixture was stirred for 3 days at room temperature and deionized with Amberlite® IR120 resin. The resin was filtered off, rinsed with MeOH, and the combined filtrate and washings were concentrated to dryness. The anomeric mixture of thiochitobiose (**8**) was obtained as a white precipitate (11.2 mg) from a mixture of MeOH and acetone. ^{1}H NMR was reported previously (14*b*) for the two anomers and showed the presence of less than 10% of an impurity (Fig. 2C) that could not be removed nor identified. Nevertheless, HRMS confirmed that the wanted anomeric mixture of thiochitobiose was the main product isolated. HRMS calcd. for $C_{16}H_{28}O_{10}N_2S$ *m*/*z*: 463.1362 [M + Na]; found: 463.1364.

Enzymatic transfer on chitobiose (7) and thiochitobiose (8)

MALDI-MS conditions (Kratos Kompact MALDI-TOF, external calibration on insulin): 10 μL of the reaction mixture were diluted with 90 μL of water or 0.25 mol/L $AcONH_4$ and 0.5 μL of these solutions were deposited on the target with 0.5 μL of THAP as the matrix. The trisaccharides **9** (5.7 mg) and **10** (10 mg) were isolated as amorphous white powders showing residual acetate salts by NMR (Supplementary material).[5] Compound **10** also showed the impurity seen in **8**. Nevertheless, HRMS and ^{1}H NMR showed that these compounds were the desired trisaccharides. HRMS for **9** calcd. for $C_{22}H_{39}O_{15}N_3$ *m*/*z*: 586.2459 [M + H]; found: 586.2463. HRMS for **10** calcd. for $C_{22}H_{39}O_{14}N_3S$ *m*/*z*: 602.2231 [M + H]; found: 602.2237.

[5] Supplementary data for this article are available on the journal Web site (http://canjchem.nrc.ca) or may be purchased from the Depository of Unpublished Data, Document Delivery, CISTI, National Research Council Canada, Ottawa, ON K1A 0R6, Canada. DUD 5022. For more information on obtaining material refer to http://cisti-icist.nrc-cnrc.gc.ca/irm/unpub_e.shtml.

© 2006 NRC Canada

4-*S*-(2-Acetamido-3,4,6-tri-*O*-acetyl-2-deoxy-β-D-glucopyranosyl)-1,6-anhydro-2-azido-3-*O*-benzyl-2-deoxy-4-thio-β-D-glucopyranose (13)

A solution of thiol **11** (5*b*) (17.6 g, 43 mmol) in DMF (300 mL) was added to a suspension of NaH (55% in oil, 2.33 g, 53 mmol, 1.2 equiv.) in DMF (10 mL) cooled to 0 °C. The mixture was stirred under Ar for 10 min at 0 °C, 10 min at 20 °C and was, in turn, added to triflate **12** (5*c*) (18.6 g, 51 mmol, 1.2 equiv.). The reaction mixture was stirred for 1 h at 20 °C and the reaction was quenched by addition of AcOH (20 mL), followed by stirring for a further 30 min at room temperature. The solvent was removed in vacuo and the residue was purified by chromatography on silica gel (1:0 to 1:4 toluene–EtOAc) to give thiodisaccharide **13** (24.5 g, 90%) as a white solid; mp 183 °C. ^{1}H NMR (400 MHz, $CDCl_3$) δ: 7.41–7.36 (m, 5H, H-aromatics), 5.54 (d, 1H, $J_{NH,2}$ = 9.1 Hz, NH), 5.44 (s, 1H, H-1), 5.26 (t, 1H, $J_{2,3} = J_{3,4}$ = 9.9 Hz, H-3′), 5.09 (t, 1H, $J_{3',4'} = J_{4',5'}$ = 9.8 Hz, H-4′), 4.93 (d, 1H, $J_{1',2'}$ = 10.4 Hz, H-1′), 4.76–4.70 (m, 2H, C*H*Ph, H-5), 4.67 (d, 1H, *J* = 11.9 Hz, C*H*Ph), 4.27 (d, 1H, $J_{6a,6b}$ = 7.4 Hz, H-6a), 4.19 (dd, 1H, $J_{6a',6b'}$ = 12.4 Hz, $J_{5',6a'}$ = 4.7 Hz, H-6a′), 4.14 (dd, 1H, $J_{5',6b'}$ = 2.3 Hz, H-6b′), 4.00 (td, 1H, $J_{2',3'}$ = 10.4 Hz, H-2′), 3.82 (m, 1H, H-4), 3.77 (dd, 1H, $J_{5,6b}$ = 5.6 Hz, H-6b), 3.68 (m, 1H, H-5′), 3.52 (s, 1H, H-3), 3.23 (s, 1H, H-2), 2.06, 2.05, 2.03, 1.95 (4s, 12H, 4 × CH_3CO). ^{13}C NMR (100 MHz, $CDCl_3$) δ: 170.9, 170.6, 170.2, 169.4 (*C*OCH_3), 137.5 (C-ipso), 128.6, 128.0, 127.7 (C-aromatics), 100.1 (C-1), 83.4 (C-1′), 78.6 (C-4), 76.1 (C-5′ and C-5), 73.3 (C-3′), 72.3 (*C*H_2Ph), 68.3 (C-4′), 67.8 (C-6), 62.0 (C-6′), 60.2 (C-3), 53.8 (C-2′), 44.0 (C-2), 23.3, 20.7, 20.6 (*C*H_3CO). HRMS calcd. for $C_{27}H_{34}N_4O_{11}S$ *m/z*: 645.1843 [M + Na]; found: 645.1845.

1,6-Di-*O*-acetyl-4-*S*-(2-acetamido-3,4,6-tri-*O*-acetyl-2-deoxy-β-D-glucopyranosyl)-2-azido-3-*O*-benzyl-2-deoxy-4-thio-α,β-D-glucopyranose (14)

Thiodisaccharide **13** (24.5 g, 39 mmol) was dissolved in Ac_2O–TFA (9:1, 166 mL), and the solution was stirred for 6.5 h at 40 °C. Solvents were evaporated under reduced pressure and residual Ac_2O was coevaporated with toluene. The residue was submitted to chromatography (3:2 to 0:1 toluene–EtOAc) to furnish compound **14** (23 g, 96%). ^{1}H NMR spectroscopy showed an α/β ratio of 65:35. ^{1}H NMR (400 MHz, $CDCl_3$) δ: 7.50–7.30 (m, 5Hα and 5Hβ, H-aromatics), 6.29 (d, 1Hα, $J_{1,2}$ = 3.2 Hz, H-1α), 5.58 (d, 1Hα, $J_{1',2'}$ = 8.6 Hz, H-1′α), 5.47 (m, 2Hβ, H-1β and H-1′β), 5.30 (t, 1Hα and 1Hβ, $J_{2',3'+3',4'}$ = 19.7 Hz, H-3′α and H-3′β), 5.08–4.95 (m, 2Hα and 2Hβ, C*H*Phα, C*H*Phβ, H-4′α and H-4′β), 4.95–4.85 (m, 2Hα and 2Hβ, C*H*Phα, C*H*Phβ, NHα and NHβ), 4.57–4.0 (m, 2Hα and 2Hβ, H-6aα, H-6aβ, H-6bα and H-6bβ), 4.19 (dd, 1Hα, $J_{6a',6b'}$ = 12.5 Hz, $J_{5',6a'}$ = 4.9 Hz, H-6a′α), 4.11–3.96 (m, 2Hα and 2Hβ, H-5α, H-6b′α, H-6b′β and H-6a′β), 3.89–3.77 (m, 1Hα and 2Hβ, H-2′α, H-2β and H-5β), 3.73 (t, 1Hα, *J* = 10.1 Hz, H-3α), 3.69–3.63 (m, 2Hα and 1Hβ, H-5′α, H-5′β and H-2α), 3.60 (t, 1Hβ, $J_{1,2} = J_{2,3}$ = 8.9 Hz, H-2β), 3.41 (t, 1Hβ, $J_{3,4}$ = 10.0 Hz, H-3β), 2.98 (t, 1Hα, $J_{3,4} = J_{4,5}$ = 10.5 Hz, H-4α), 2.93 (t, 1Hβ, $J_{4,5}$ = 10.5 Hz, H-4β), 2.20–2.17 (2s, 3Hα and 3Hβ, $CH_3COα$ and $CH_3COβ$), 2.12 (s, 3Hα, $CH_3COα$), 2.09 (s, 3Hα, $CH_3COα$), 2.05–2.00 (m, 6Hα and 12Hβ, 2 × $CH_3COα$ and 4 × $CH_3COβ$), 1.71 (s, 3Hα, C*H*$_3$CONHα), 1.68 (s, 3Hβ, $CH_3CONHβ$). ^{13}C NMR (100 MHz, $CDCl_3$) for the α anomer δ: 170.5, 168.7 (*C*OCH_3), 128.6, 128.2, 127.6, 127.5 (C-aromatics), 90.4 (C-1), 83.6 (C-1′), 77.0 (C-3), 75.6 (*C*H_2Ph), 75.2 (C-5′), 72.8 (C-3′), 72.5 (C-5), 68.2 (C-4′), 63.9 (C-2), 63.2 (C-6), 62.1 (C-6′), 54.5 (C-2′), 46.8 (C-4), 23.1, 21.0, 20.6 (*C*H_3CO). HRMS calcd. for $C_{31}H_{40}N_4O_{14}S$ *m/z*: 747.2159 [M + Na]; found: 747.2158.

1,3,6-Tri-*O*-acetyl-4-*S*-(2-acetamido-3,4,6-tri-*O*-acetyl-2-deoxy-β-D-glucopyranosyl)-2-azido-2-deoxy-4-thio-α,β-D-glucopyranose (15)

Anhydrous $FeCl_3$ (20.4 g, 126 mmol, 4 equiv.) was added to a solution of benzyl **14** (22.7 g, 31 mmol) in freshly distilled anhydr. CH_2Cl_2 (220 mL) and the mixture was stirred for 1.5 h under Ar at 20 °C. The solvent was evaporated then pyridine (210 mL) and Ac_2O (105 mL) were added. The reaction mixture was stirred for 1.5 h at 20 °C and concd. EtOAc (350 mL) was added to the residue and the resulting solution was washed successively with 1 mol/L HCl (250 mL), satd. $NaHCO_3$ (250 mL), and brine (250 mL). The aqueous layers were reextracted with EtOAc (2 × 250 mL) and the combined organic layers were dried and concentrated. The crude product was filtered off from EtOH and further purified by chromatography on silica gel (0:1 to 9:1 EtOAc–cyclohexane) to afford acetate **15** (13.1 g, 62%) as a white powder. ^{1}H NMR spectra gave an α/β ratio of 8:2. ^{1}H NMR (400 MHz, $CDCl_3$) δ: 6.33 (d, 1Hα, $J_{1,2}$ = 3.3 Hz, H-1α), 5.77 (d, 1Hα, $J_{NH,2}$ = 9.8 Hz, NHα), 5.69 (d, 1Hβ, $J_{NH,2}$ = 10.1 Hz, NHβ), 5.49 (d, 1Hβ, $J_{1,2}$ = 8.6 Hz, H-1β), 5.43 (t, 1Hα, $J_{2,3} = J_{3,4}$ = 10.5 Hz, H-3α), 5.11 (t, 1Hα, $J_{2',3'} = J_{3',4'}$ = 9.7 Hz, H-3′α), 5.08–4.91 (m, 1Hα and 3Hβ, H-4′α, H-4′β, H-3′β and H-3β), 4.74 (d, 1Hα and 1Hβ, $J_{1',2'}$ = 10.4 Hz, H-1′α and H-1′β), 4.60 (dd, 1Hα, $J_{6a,6b}$ = 12.5 Hz, $J_{5,6a}$ = 3.9 Hz, H-6aα), 4.55 (dd, 1Hβ, $J_{6a,6b}$ = 12.5 Hz, $J_{5,6a}$ = 4.6 Hz, H-6aβ), 4.46 (m, 1Hβ, H-6bβ), 4.40–4.29 (m, 2Hα, H-5α and H-6bα), 4.28–4.13 (m, 2Hα and 2Hβ, H-2′α, H-2′β, H-6a′α and H-6a′β), 4.10–4.00 (m, 1Hα and 1Hβ, H-6b′α and H-5β), 3.95 (dd, 1Hβ, $J_{6a',6b'}$ = 12.1 Hz, $J_{5',6b'}$ = 7.9 Hz, H-6b′β), 3.76–3.63 (m, 2Hα and 2Hβ, H-2α, H-2β, H-5′α and H-5′β), 2.95 (t, 1Hα, *J* = 11.2 Hz, H-4α), 2.86 (t, 1Hβ, $J_{3,4} = J_{4,5}$ = 10.5 Hz, H-4β), 2.22 (s, 3Hα, $CH_3COα$), 2.19 (s, 3Hα, $CH_3COα$), 2.19–2.18 (2s, 6Hβ, 2 × $CH_3COβ$), 2.13 (s, 3Hβ, $CH_3COβ$), 2.07 (s, 3Hα, $CH_3COα$), 2.06–2.01 (m, 9Hα and 9Hβ, 3 × $CH_3COα$ and 3 × $CH_3COβ$), 1.95 (s, 3Hα, $CH_3CONHα$) and 1.92 (s, 3Hβ, $CH_3CONHβ$). ^{13}C NMR (100 MHz, $CDCl_3$) for the α anomer δ: 171.3, 170.6, 170.3 (*C*OCH_3), 90.3 (C-1), 82.3 (C-1′), 75.9 (C-5′), 74.2 (C-3′), 71.1 (C-5), 68.5 (C-4′), 67.8 (C-3), 63.0, 62.9 (C-6 and C-6′), 61.8 (C-2), 51.9 (C-2′), 45.8 (C-4), 23.0, 20.9, 20.7, 20.6 (*C*H_3CO). HRMS calcd. for $C_{26}H_{36}N_4O_{15}S$ *m/z*: 699.1796 [M + Na]: found: 699.1796.

3,6-Di-*O*-acetyl-4-*S*-(2-acetamido-3,4,6-tri-*O*-acetyl-2-deoxy-β-D-glucopyranosyl)-2-azido-2-deoxy-4-thio-α,β-D-glucopyranose (16)

Hydrazine acetate (2.1 g, 23 mmol, 1.2 equiv.) was added to a solution of compound **15** (12.8 g, 19 mmol) in DMF (110 mL). The mixture was stirred for 1 h under Ar at room temperature and the solvent was removed under reduced

© 2006 NRC Canada

pressure. Residual traces of DMF were coevaporated with toluene and the residue was dissolved in EtOAc (200 mL) and washed with water (150 mL) and brine (150 mL). The aqueous layers were reextracted with EtOAc (2 × 250 mL) and the combined organic solvents were dried and concentrated. The crude product was purified by chromatography on silica gel (1:0 to 95:5 $CHCl_3$–MeOH) to yield hemiacetal **16** (8.9 g, 75%). The ^{1}H NMR spectra showed an α/β ratio of 7:3. ^{1}H NMR (400 MHz, $CDCl_3$) δ: 5.90 (d, 1Hα, $J_{1',2'}$ = 9.9 Hz, H-1′α), 5.81 (d, 1Hβ, $J_{1',2'}$ = 9.9 Hz, H-1′β), 5.55 (t, 1Hα, $J_{2,3}$ = $J_{3,4}$ = 10.5 Hz, H-3α), 5.40 (d, 1Hα, $J_{1,2}$ = 3.1 Hz, H-1α), 5.09 (t, 1Hα, $J_{2',3'}$ = $J_{3',4'}$ = 9.5 Hz, H-3′α), 5.08–4.97 (m, 1Hα, 3Hβ, H-3′β, H-3β, H-4′α and H-4′β), 4.82 (d, 1Hα, $J_{NH,2}$ = 10.4 Hz, NHα), 4.78 (d, 1Hβ, $J_{NH,2}$ = 10.5 Hz, NHβ), 4.69 (d, 1Hβ, $J_{1,2}$ = 7.9 Hz, H-1β), 4.57 (dd, 1Hα, $J_{6a,6b}$ = 11.8 Hz, $J_{5,6a}$ = 3.7 Hz, H-6aα), 4.55 (m, 1Hα and 2Hβ, H-5α, H-6aβ and H-6bβ), 4.44 (dd, 1Hα, $J_{5,6b}$ = 1.6 Hz, H-6bα), 4.26–4.16 (m, 2Hα and 2Hβ, H-2′α, H-2′β, H-6a′α and H-6a′β), 4.01 (dd, 1Hα and 1Hβ, $J_{6a',6b'}$ = 12.3 Hz, $J_{5',6b'}$ = 6.0 Hz, H-6b′α and H-6b′β), 3.92 (m, 1Hβ, H-5β), 3.73 (m, 1Hα and 1Hβ, H-5′α and H-5′β), 3.50 (m, 1Hα and 1Hβ, H-2α and H-2β), 2.91–2.82 (m, 1Hα and 1Hβ, H-4α and H-4β), 2.17 (s, 3Hα and 3Hβ, $CH_3COα$ and $CH_3COβ$), 2.10 (s, 3Hα, $CH_3COα$), 2.09 (s, 3Hβ, $CH_3COβ$), 2.07 (s, 3Hα, $CH_3COα$), 2.06 (s, 3Hβ, $CH_3COβ$), 2.03 (s, 3Hα and 3Hβ, $CH_3COα$ and $CH_3COβ$), 2.01 (s, 3Hα and 3Hβ, $CH_3COα$ and $CH_3COβ$), 1.94 (s, 3Hα, $CH_3COα$) and 1.92 (s, 3Hβ, $CH_3COβ$). ^{13}C NMR (100 MHz, $CDCl_3$) δ: 170.8, 170.7, 170.1, 169.4 (*C*OCH_3), 96.1 (C-1β), 91.8 (C-1α), 81.9 (C-1′α), 81.7 (C-1′β), 75.5 (C-5′α), 75.4 (C-5′β), 74.3 (C-3′α), 74.1 (C-3′β), 73.6 (C-5β), 70.1 (C-3β), 68.6 (C-5α), 68.4 (C-4′α), 68.3 (C-4′β), 67.9 (C-3α), 66.2 (C-2β), 63.5 (C-6α and C-6β), 63.2 (C-2α), 62.5 (C-6′α and C-6′β), 52.0 (C-2′α and C-2′β), 46.3 (C-4α), 46.1 (C-4β), 22.9, 21.1, 20.9, 20.7, 20.6 (*C*H_3CO). HRMS calcd. for $C_{24}H_{34}N_4O_{14}S$ *m/z*: 657.1690 [M + Na]; found: 657.1714.

3,6-Di-*O*-acetyl-4-*S*-(2-acetamido-3,4,6-tri-*O*-acetyl-2-deoxy-β-D-glucopyranosyl)-2-azido-3-*O*-benzyl-2-deoxy-4-thio-α,β-D-glucopyranosyl trichloroacetimidate (17)

Trichloroacetonitrile (27.5 mL, 275 mmol, 19 equiv.) and DBU (532 µL, 3.6 mmol, 0.26 equiv.) were added to a solution of hemiacetal **16** (8.74 g, 14 mmol) in anhydr. CH_2Cl_2 (130 mL). The reaction mixture was stirred under Ar at room temperature for 45 min. The reaction mixture was concentrated and the residue submitted to chromatography on silica gel (silica gel was previously washed with a 5% solution of Et_3N in EtOAc) (1:0 to 95:5 $CHCl_3$–MeOH) to give the unstable imidate **17** (10.2 g, 95%) as a glass. ^{1}H NMR spectra showed an α/β ratio of 85:15. ^{1}H NMR (400 MHz, $CDCl_3$) δ: 8.81 (s, 1Hα, $NHCCl_3α$), 8.73 (s, 1Hβ, $NHCCl_3β$), 6.52 (d, 1Hα, $J_{1,2}$ = 3.4 Hz, H-1α), 5.78 (d, 1Hα, $J_{NH,2}$ = 9.9 Hz, NHα), 5.70 (d, 1Hβ, $J_{NH,2}$ = 10.2 Hz, NHβ), 5.66 (d, 1Hβ, $J_{1,2}$ = 8.5 Hz, H-1β), 5.52 (t, 1Hα, $J_{2,3}$ = $J_{3,4}$ = 10.5 Hz, H-3α), 5.11–5.00 (m, 2Hα and 2Hβ, H-3′α, H-3′β, H-3β and H-4′α), 4.95 (t, 1Hβ, $J_{3',4'}$ = $J_{4',5'}$ = 9.6 Hz, H-4′β), 4.78–4.68 (m, 1Hα and 1Hβ, H-1′β and H-1′α), 4.66–4.55 (m, 1Hα and 1Hβ, H-6aα and H-6aβ), 4.50–4.38 (m, 2Hα and 1Hβ, H-5α, H-6bα and H-6bβ), 4.28–4.17 (m, 1Hα and 2Hβ, H-2′α, H-2′β and H-6a′β), 4.09 (dd, 1Hα, $J_{6a',6b'}$ = 12.4 Hz, $J_{5',6a'}$ = 2.8 Hz, H-6a′α), 4.06–3.98 (m, 1Hα and 1Hβ, H-6b′α and H-5β), 3.94 (dd, 1Hβ, $J_{6a',6b'}$ = 12.0 Hz, $J_{5',6b'}$ = 8.4 Hz, H-6b′β), 3.88–3.78 (m, 1Hα and 1Hβ, H-2α and H-2β), 3.74 (m, 1Hβ, H-5′β), 3.54 (m, 1Hα, H-5′α), 3.01 (t, 1Hα, $J_{4,5}$ = 11.0 Hz, H-4α), 2.93 (t, 1Hβ, $J_{3,4}$ = $J_{4,5}$ = 11.0 Hz, H-4β), 2.20 (s, 3Hβ, $CH_3COβ$), 2.19 (s, 3Hα, $CH_3COα$), 2.14 (s, 3Hβ, $CH_3COβ$), 2.06 (s, 3Hα, $CH_3COα$), 2.05–2.03 (m, 6Hα and 6Hβ, 2 × $CH_3COα$ and 2 × $CH_3COβ$), 2.02 (s, 3Hα and 3Hβ, $CH_3COα$ and $CH_3COβ$), 1.95 (s, 3Hα, $CH_3COα$), 1.93 (s, 3Hβ, $CH_3COβ$).

Allyl 3,6-di-*O*-acetyl-4-*S*-(2-acetamido-3,4,6-tri-*O*-acetyl-2-deoxy-β-D-glucopyranosyl)-2-azido-2-deoxy-4-thio-β-D-glucopyranoside (18β)

A suspension of imidate **17** (8.87 g, 11 mmol) in anhydr. CH_2Cl_2 (140 mL) containing 4 Å activated molecular sieves (8.0 g) was stirred under Ar at room temperature for 1 h and was then cooled down to – 45 °C. Allyl alcohol (1.55 mL, 23 mmol, 2 equiv.) and $BF_3·Et_2O$ (920 µL, 3.4 mmol, 3.2 equiv.) were added to the suspension and the mixture was allowed to reach –10 °C over 2 h. Triethylamine (200 µL) was added and after additional stirring (20 min) at room temperature, the molecular sieves were filtered off. The filtrate was diluted with CH_2Cl_2 (250 mL) and washed with brine (250 mL). The aqueous layer was reextracted with CH_2Cl_2 (3 × 100 mL) and the combined organic solutions were dried and concentrated. The residue was submitted to chromatography on neutral alumina (1:2, 1:1, 3:1, 5:1, then 1:0, EtOAc–cyclohexane) to give the thiodisaccharide **18**β (5.71 g, 74%) as a white powder; mp 187 °C. ^{1}H NMR (400 MHz, $CDCl_3$) δ: 5.94 (m, 1H, $OCH_2CH_cCH_2$), 5.70 (d, 1H, $J_{NH,2}$ = 9.7 Hz, NH), 5.34 (dd, 1H, $J_{c,e}$ = 17.2 Hz, $J_{d,e}$ = 1.5 Hz, $OCH_2CHCH_dH_e$), 5.26 (dd, 1H, $J_{c,d}$ = 10.4 Hz, $OCH_2CHCH_dH_e$), 5.08–4.96 (m, 2H, H-3′ and H-4′), 4.93 (dd, 1H, $J_{2,3}$ = 9.9 Hz, $J_{3,4}$ = 11.0 Hz, H-3), 4.72 (d, 1H, $J_{1',2'}$ = 10.7 Hz, H-1′), 4.54–4.49 (m, 2H, H-6a and H-6b), 4.43–4.35 (m, 2H, H-1 and $OCH_aH_bCHCH_2$), 4.25–4.09 (m, 3H, H-2′, H-6a′ and $OCH_aH_bCHCH_2$), 4.01 (dd, 1H, $J_{6a',6b'}$ = 12.3 Hz, $J_{5',6b'}$ = 6.4 Hz, H-6b′), 3.84 (m, 1H, H-5), 3.69 (m, 1H, H-5′), 3.52 (dd, 1H, $J_{1,2}$ = 8.1 Hz, $J_{2,3}$ = 9.7 Hz, H-2), 2.83 (t, 1H, $J_{4,5}$ = 10.9 Hz, H-4), 2.17, 2.09, 2.07, 2.04, 2.02, 1.92 (6s, 6 × CH_3CO). ^{13}C NMR (100 MHz, $CDCl_3$) δ: 171.3, 170.9, 170.5, 170.2, 169.7, 169.3 (*CO*CH_3), 133.0 ($OCH_2CH=CH_2$), 118.1 ($OCH_2CH=CH_2$), 100.8 (C-1), 81.7 (C-1′), 75.7 (C-5′), 74.1 (C-3′), 73.5 (C-5), 70.3 (C-6), 69.8 (C-3), 68.3 (C-4′), 65.0 (C-2), 63.5 ($OCH_2CH=CH_2$), 62.7 (C-6′), 51.9 (C-2′), 46.2 (C-4), 23.0, 21.1, 20.8, 20.6 (*C*H_3CO). HRMS calcd. for $C_{27}H_{38}N_4O_{14}S$ *m/z*: 697.2003 [M + Na]; found: 697.1996.

Allyl 3,6-di-*O*-acetyl-4-*S*-(2-acetamido-3,4,6-tri-*O*-acetyl-2-deoxy-β-D-gluco-pyranosyl)-2-acetamido-2-deoxy-4-thio-β-D-glucopyranoside (19)

Zinc (52.4 g) and AcOH (23 mL) were added to a solution of compound **18**β (5.4 g, 8 mmol) in anhydr. THF (260 mL). The mixture was stirred under Ar at room temperature for 1.5 h and Ac_2O (140 mL) was added. The reaction mixture was stirred for 1.5 h at room temperature and filtered through Celite. The filtrate was concentrated to dryness and the residue dissolved in EtOAc (300 mL), which was washed successively with water (200 mL), satd. $NaHCO_3$ (200 mL),

© 2006 NRC Canada

and brine (200 mL). The aqueous layers were reextracted with EtOAc (6 × 100 mL) and the combined organic solutions were dried and concentrated. The crude product was submitted to chromatography on silica gel (1:0 and 95:5 $CHCl_3$–MeOH) to give the title compound **19** (2.5 g, 45%) as a white powder; mp 238 °C. ^{1}H NMR (400 MHz, $CDCl_3$) δ: 5.87 (m, 1H, $OCH_2CH_cCH_2$), 5.78 (d, 1H, $J_{NH,2}$ = 9.4 Hz, NH′), 5.74–5.65 (m, 2H, H-3 and NH), 5.27 (dd, 1H, $J_{c,e}$ = 17.2 Hz, $J_{d,e}$ = 1.6 Hz, $OCH_2CHCH_dH_e$), 5.21 (dd, 1H, $J_{c,d}$ = 10.3 Hz, $OCH_2CHCH_dH_e$), 5.12–4.98 (m, 2H, H-3′ and H-4′), 4.91 (d, 1H, $J_{1,2}$ = 8.3 Hz, H-1), 4.74 (d, 1H, $J_{1',2'}$ = 10.5 Hz, H-1′), 4.53 (m, 2H, H-6a and H-6b), 4.32 (m, 1H, $OCH_aH_bCHCH_2$), 4.23–4.12 (m, 2H, H-2′ and H-6a′), 4.10–4.02 (m, 2H, H-6b′ and $OCH_aH_bCHCH_2$), 3.90 (m, 1H, H-5), 3.74 (m, 1H, H-5′), 3.46 (m, 1H, H-2), 2.83 (t, 1H, $J_{3,4}$ = $J_{4,5}$ = 10.8 Hz, H-4), 2.11, 2.10, 2.07, 2.04, 2.02, 1.99, 1.92 (7s, 7 × 3H, CH_3CO). ^{13}C NMR (100 MHz, $CDCl_3$) δ: 170.7, 169.8 ($COCH_3$), 133.6 ($OCH_2CH=CH_2$), 117.8 ($OCH_2CH=CH_2$), 98.8 (C-1), 82.2 (C-1′), 75.7 (C-5′), 74.3 (C-3′), 73.4 (C-5), 70.0 ($OCH_2CH=CH_2$), 68.9 (C-3), 68.2 (C-4′), 63.6 (C-6), 62.6 (C-6′), 57.3 (C-2), 52.2 (C-2′), 46.7 (C-4), 23.5, 23.0, 21.0, 20.9, 20.6 (CH_3CO). HRMS calcd. for $C_{27}H_{38}N_4O_{14}S$ *m/z*: 713.2204 [M + Na]; found: 713.2200.

Allyl 4-*S*-(2-acetamido-2-deoxy-β-D-glucopyranosyl)-2-acetamido-2-deoxy-4-thio-β-D-glucopyranoside (20)

MeONa (75 mg, 1.4 mmol) was added to a solution of allyl glycoside **19** (300 mg, 434 µmol) in anhydr. MeOH (3 mL). The mixture was stirred for 4 h under Ar at room temperature and then diluted with water. The pH was adjusted to 7 by adding Amberlite® IR120 resin, the resin was filtered off, and the filtrate was concentrated to dryness. The residue was precipitated from a mixture of acetone–MeOH (2:1) to afford the pure thiodisaccharide **20** (150 mg, 72%) as a white powder. ^{1}H NMR (400 MHz, D_2O) δ: 5.92 (m, 1H, $OCH_2CH_cCH_2$), 5.40–5.22 (m, 2H, $OCH_2CHCH_dH_e$ and $OCH_2CHCH_dH_e$), 4.74 (d, 1H, $J_{1',2'}$ = 10.4 Hz, H-1′), 4.55 (d, 1H, $J_{1,2}$ = 8.5 Hz, H-1), 4.35 (dd, 1H, $J_{a,b}$ = 12.9 Hz, $J_{a,c}$ = 4.5 Hz, $OCH_aH_bCHCH_2$), 4.17 (dd, 1H, $J_{b,c}$ = 6.0 Hz, $OCH_aH_bCHCH_2$), 4.09 (d, 1H, $J_{6a,6b}$ = 11.8 Hz, H-6a), 3.98–3.85 (m, 2H, H-6a′ and H-6b), 3.82–3.54 (m, 6H, H-2′, H-6b′, H-2, H-5, H-3, and H-3′), 3.54–3.40 (m, 2H, H-4′ and H-5′), 2.89 (t, 1H, $J_{3,4}$ = $J_{4,5}$ = 10.5 Hz, H-4), 2.04 (s, 6H, 2 × CH_3CO). ^{13}C NMR (100 MHz, D_2O) δ: 172.6, 172.5 ($COCH_3$), 131.3 ($OCH_2CH=CH_2$), 116.2 ($OCH_2CH=CH_2$), 97.7 (C-1), 81.8 (C-1′), 77.8 (C-4′ or C-5′), 74.4 (C-5), 72.9 (C-3′), 69.4 (C-3), 68.4 ($OCH_2CH=CH_2$), 67.6 (C-5′ or C-4′), 59.4 (C-6), 58.7 (C-6′), 54.8 (C-2), 52.9 (C-2′), 46.1 (C-4), 20.1 (CH_3CO). HRMS calcd. for $C_{19}H_{32}N_2O_{10}S$ *m/z*: 503.1675 [M + Na]; found: 503.1672.

Allyl 4-*S*-(2-acetamido-4-*O*-(2-amino-2-deoxy-β-D-glucopyranosyl)-2-deoxy-β-D-glucopyranosyl)-2-acetamido-2-deoxy-4-thio-β-D-glucopyranoside (21)

Thiodisaccharide **20** (5.45 mg, 11.35 µmol) was incubated for 14 days with UDP-$GlcNH_2$ (**6**) (8.9 mg, 13.7 µmol, 1.2 equiv.) and β-1,4-galactosyltransferase (5.6 U) as described in the general method for the enzymatic reactions. The pure trisaccharide **21** (3 mg, 41%) was isolated as a glass after freeze-drying from water. ^{1}H NMR (400 MHz, D_2O) δ: 5.88 (m, 1H, $OCH_2CH_cCH_2$), 5.35–5.19 (m, 2H, $OCH_2CHCH_dH_e$ and $OCH_2CHCH_dH_e$), 4.71 (d, 1H, $J_{1',2'}$ = 10.1 Hz, H-1′), 4.52 (d, 1H, $J_{1,2}$ = 8.4 Hz, H-1), 4.46 (d, 1H, $J_{1'',2''}$ = 8.0 Hz, H-1″), 4.30 (dd, 1H, $J_{a,b}$ = 13.1 Hz, $J_{a,c}$ = 6.3 Hz, $OCH_aH_bCHCH_2$), 4.12 (dd, 1H, $J_{b,c}$ = 6.4 Hz, $OCH_aH_bCHCH_2$), 4.05 (dd, 1H, $J_{6a,6b}$ = 12.0 Hz, $J_{6a,5}$ = 1.4 Hz, H-6a), 3.96–3.82 (m, 3H, H-6a′, H-6b and H-3′ or H-4′ or H-5′), 3.82–3.64 (m, 6H, H-2, H-2′, H-6b′, H-6a″, H-6b″ and H-3′ or H-4′ or H-5′), 3.63–3.52 (m, 3H, H-5, H-3 and H-3′ or H-4′ or H-5′), 3.46 (m, 1H, H-4″ or H-5″), 3.42–3.32 (m, 2H, H-3″ and H-4″ or H-5″), 2.85 (t, 1H, $J_{3,4}$ = $J_{4,5}$ = 10.8 Hz, H-4), 2.66 (m, 1H, H-2″), 2.03, 2.02 (2s, 2 × 3H, CH_3CO). ^{13}C NMR (D_2O, measured from HSQC at 400 MHz) δ: 132.0 ($CH_2CH=CH_2$), 117.0 ($CH_2CH=CH_2$), 102.0 (C-1″), 99.0 (C-1′), 83.0 (C-1), 78.0, 77.2, 76.1, 76.0, 75.5, 72.8, 71.0, 68.9 (not assigned), 69.0 ($CH_2CH=CH_2$), 61.0 (C-6), 59.7, 59.0, 56.5 (not assigned), 56.0 (C-2″), 54.0 (not assigned), 47.3 (C-4), 21.8 (CH_3CO). HRMS calcd.for $C_{25}H_{43}N_3O_{14}S$ *m/z*: 642.2544 [M + H]; found: 642.2563.

Acknowledgements

L. Loureiro Morais was supported by a grant from the French Ministry in charge of higher education. The authors are thankful for a grant from the France–Canada Research Foundation to support the collaborative exchange between the French and Canadian (F-IA) groups. LLM, KB, IR, and F-IA are thankful to Professor J. Gelas (École Nationale Supérieure de Chimie de Clermont-Ferrand (ENSCCF)) for his support of this work. UDP-$GlcNH_2$ was synthesized by HY in Professor O. Hindsgaul's group (University of Alberta, Edmonton, Alberta) and the isolation of the galactosyltransferase, as well as the transfers on **7** and **8,** were carried out by F-IA in Professor M. Palcic's group (University of Alberta). The authors are grateful to both O. Hindgsaul and M. Palcic (now at the Carlsberg Laboratories, Valby, Denmark) for their support of this work.

References

1. P. Van Rhin and J. Venderleyden. Microbiol. Rev. **59**, 124 (1995).
2. P. Lerouge, P. Roche, C. Faucher, F. Maillet, G. Truchet, J.-C. Promé, and J. Denarié. Nature, **344**, 781 (1990); G. Truchet, P. Roche, P. Lerouge, J. Vasse, S. Camut, F. de Billy, J.-C. Promé, and J. Dénarié. Nature, **351**, 670 (1991).
3. For reviews, see: J.-C. Promé and N. Demont. Plant-microbe interactions. *Edited by* G. Stacey and N.T. Keen. Chapman and Hally, New York. 1996. p. 272; J. Denarié, F. Debelle, and J.-C. Promé. Annu. Rev. Biochem. **65**, 503 (1996); W. D'Haeze and M. Holsters. Glycobiology, **12**, 79R (2002).
4. M. Schultze, B. Quiclet-Sire, E. Kondorosi, H. Virelizier, J.N. Glushka, G. Endre, S.D. Gero, and A. Kondorosi. Proc. Natl. Acad. Sci. U.S.A. **89**, 192 (1992); A.O. Ovtsyna, M. Schultze, I.A. Tikhonovich, H.P. Spaink, E. Kondorosi, A. Kondorosi, and C. Staehelin. Mol. Plant. Microbe Interact. **13**, 799 (2000); A.O. Ovtsyna, E.A. Dolgikh, A.S. Kilanova, V.E. Tsyganov, A.Y. Borisov, I.A. Tikhonovich, and C. Staehelin. Plant Physiol. **139**, 1051 (2005).
5. (*a*) F.-I. Auzanneau, M. Mialon, D. Promé, J.-C. Promé, and J. Gelas. J. Org. Chem. **63**, 6460 (1998); (*b*) F.-I. Auzanneau, K.

© 2006 NRC Canada

Bennis, E. Fanton, D. Promé, J. Defaye, and J. Gelas. J. Chem. Soc. Perkin Trans. 1, 3629 (1998); (*c*) L. Loureiro Morais, K. Bennis, I. Ripoche, L. Liao, F.-I. Auzanneau, and J. Gelas. Carbohydr. Res. **338**, 1369 (2003).
6. J. Defaye and J. Gelas. *In* Studies in natural products chemistry. Vol. 8. *Edited by* Atta-ur-Rhaman. Elsevier Science Publishers B.V., Amsterdam. 1991. p. 315.
7. X. Qian, K. Sujino, M.M. Palcic, and R.M. Ratcliffe. J. Carbohydr. Chem. **21**, 911 (2002).
8. M. Atkinson, M.M. Palcic, O. Hindsgaul, and S. Long. Proc. Natl. Acad. Sci. U.S.A. **91**, 8418 (1994).
9. (*a*) P.A. Ropp and P.-W. Cheng. Anal. Biochem. **187**, 104 (1990); (*b*) J.E. Heidlas, W.J. Lees, P. Pale, and G.M. Whitesides. J. Org. Chem. **57**, 146 (1992).
10. M.L. Wolform and P.J. Conigliaro. Carbohyd. Res. **11**, 63 (1969).
11. R.F. Sala, S. MacKinnon, M.M. Palcic, and M.E. Tanner. Carbohydr. Res. **306**, 127 (1998).
12. F.R. Atherton. Biochem. Prep. **5**, 1 (1957).
13. R. Barker, K.W. Olsen, J.H. Shaper, and R.L. Hill. J. Biol. Chem. **247**, 7135 (1972); T.A. Beyer, J.E. Sadler, J.I. Rearick, J.C. Paulson, and R.L. Hill. Adv. Enzymol. Relat. Areas Mol. Biol. **52**, 23 (1981).
14. (*a*) L.-X. Wang and Y.C. Lee. J. Chem. Soc. Perkin Tran. 1, 581 (1996); (*b*) J.L. Muñoz, A. Gracía-Herrero, J.L. Asensio, F.-I. Auzanneau, F.J. Cañada, and J. Jiménez-Barbero. J. Chem. Soc. Perkin Tran. 1, 867 (2001).
15. F.-I. Auzanneau, M.K. Christensen, S.L. Harris, M. Meldal, and B.M. Pinto. Can. J. Chem. **76**, 1109 (1998).
16. J.I. Padrón and J.T. Vásquez. Tetrahedron: Asymmetry, **6**, 857 (1995).
17. D. Qui and R.D. Koganty. Tetrahedron Lett. **38**, 45 (1997).

© 2006 NRC Canada

Stereoselective synthesis of dioxabicycles from 1-*C*-allyl-2-*O*-benzyl-glycosides — An intramolecular cyclization between 2-*O*-benzyl oxygen and the allyl double bond[1]

An-Tai Wu, Tian Yi, Huawu Shao, Shih-Hsiung Wu, and Wei Zou

Abstract: Addition of a proton to the double bond of 1-*C*-allyl-*O*-benzylglycosides gave a 2′-carbonium ion, which in turn reacted intramolecularly, in a regio- and diastereo-selective manner, with the nucleophilic oxygen of the 2-*O*-benzyl group to form an oxonium intermediate. Subsequent cleavage of the benzyl C—O bond led to dioxabicycles in moderate yields. Surprisingly, opposite diastereoselectivities were observed from 1-*C*-allylglycofuranosides and 1-*C*-allylglycopyranosides, which produced 2,2′-*trans*- and 2,2′-*cis*-dioxabicycles, respectively.

Key words: C-glycoside, olefin, cyclization, oxocarbonium, dioxabicycles.

Résumé : L'addition d'un proton sur la double liaison 1-*C*-allylglycosides de *O*-benzyle conduit à la formation d'un ion carbonium en 2′ qui réagit ensuite d'une façon intramoléculaire, régio- et diastéréosélective, avec l'oxygène nucléophile du groupe 2-*O*-benzyle pour conduire à la formation d'un intermédiaire oxonium. Un clivage subséquent de la liaison C—O du benzyle conduit à des dioxabicycles avec des rendements modérés. D'une façon surprenante, on a observé des diastéréosélectivités opposées les 1-*C*-allylglycofuranosides et les 1-*C*-allylglycopyranosides qui ont conduit respectivement aux 2,2′-*trans*- et 2,2′-*cis*-dioxabicycles.

Mots clés : C-glycoside, oléfine, cyclisation, oxocarbonium, dioxabicycles.

[Traduit par la Rédaction]

Introduction

The electrophile-promoted addition to an olefinic double bond is one of the most investigated reactions (1). The intermediate can be a carbonium ion or more often a bridged cation, which then reacts with a nucleophile, e.g., alcohol, acid, amine, and amide, to form an addition product. The stereoselectivity of the addition to a double bond can be achieved using selenium reagents (2), iodo complexes (3), mercury complexes (4), and Ru reagents (5). In certain cases, the stereochemistry may be guided by the asymmetric substrates (1).

Recently, during a large-scale preparation of 1-*C*-allyl-2,3,5-tri-*O*-benzyl-α-D-ribofuranoside (**2**) using ribofuranoside **1** and allyltrimethylsilane in the presence of TMSOTf, we also isolated 5-O-debenzylated **3** in 17% yield (Scheme 1), a useful intermediate obtained previously from **2** by regioselective 5-O-acetolysis followed by de-O-acetylation (6). This result prompted us to investigate if TMSOTf can selectively remove the 5-*O*-benzyl group from **2** (7). However, when compound **2** was treated with TMSOTf in acetonitrile, instead of the desired **3**, we obtained a dioxabicyclic compound as the only major product. Further studies using 1-*C*-allylglycofuranosides and 1-*C*-allylglycopyranosides as substrates revealed that the formation of dioxabicycles was both highly regioselective and diastereoselective. Here, we wish to describe this stereoselective intramolecular cyclization between 2-*O*-Bn and the allyl double bond.

Received 19 August 2005. Published on the NRC Research Press Web site at http://canjchem.nrc.ca on 5 May 2006.

A.-T. Wu and S.-H. Wu.[2] Institute of Biological Chemistry, Academia Sinica, Taipei 115, Taiwan, ROC.
T. Yi, H. Shao, and W. Zou.[3,4] Institute for Biological Sciences, National Research Council of Canada, Ottawa, ON K1A 0R6, Canada.

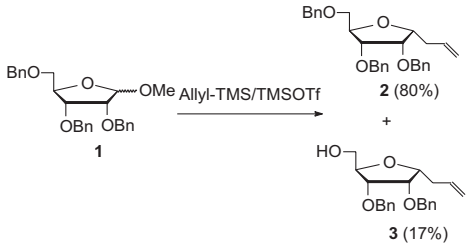
[1]This article is part of a Special Issue dedicated to Professor Walter A. Szarek.
[2]Corresponding author (e-mail: shwu@gate.sinica.edu.tw).
[3]Corresponding author (e-mail: wei.zou@nrc-cnrc.gc.ca).
[4]Dr. Wei Zou was a postdoctoral fellow with Professor Walter Szarek (1990–1993).

Results and discussion

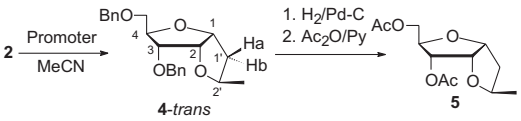
The dioxabicylic compound obtained by treatment of **2** with TMSOTf (1 equiv.) in acetonitrile was characterized as **4**-*trans* (Scheme 2). The newly formed ring and the stereochemistry at C2′ were established by NMR analysis. Because of the observation of NOE between H-1 and H-3, the cyclization must have occurred at the 2-O-position. In addition, the 2,2′-trans configuration was assigned on the basis of the NOE observed between H-2′ and H-4 and the lack of NOE between H-2′ and H-2/H-1. This stereochemistry was further confirmed by NMR analysis on acetylated derivative **5**, as we observed a downfield shift of the H-3 resonance from 3.85 to 4.87 ppm owing to acetylation, and the

 doi:10.1139/V06-046 © 2006 NRC Canada

Scheme 1. 1-C-Allylation promoted by TMSOTf.



Scheme 2. Regioselective cyclofunctionalization.



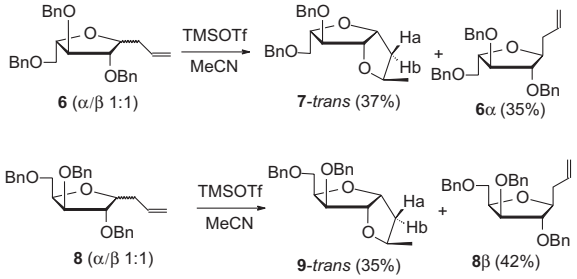
Promoter	*T/t*	*Isolated yield of* **4**-*trans*
TMSOTf (1equiv.)	0 °C-rt/16h	61%
TfOH (1equiv.)	0 °C/4h	41%
p-TsOH (1equiv.)	60 °C/24h	-
TfOH/p-TsOH (0.2/1 equiv.)	0 °C-rt/16h	53%

strong NOEs between H-1 and H-1′a and between H-2′ and H-1′b.

This regio- and diastereo-selective conversion of **2** to **4**-*trans* can also be promoted by TfOH (1 equiv.) at 0 °C, but with lower yield (see Scheme 2) because of the decomposition caused by nonselective de-O-benzylation. No significant transformation occurred when *p*-TsOH (1 equiv.) was used alone even at elevated temperature (60 °C, 24 h), but additional TfOH (0.2 equiv.) facilitated the formation of **4**-*trans*. Hence, this cyclization was likely acid-promoted. The proton source in the case of TMSOTf as a promoter might be the residual water from acetonitrile because when we performed the experiment under dry, but otherwise the same conditions, the reaction became very sluggish.[5] Additionally, acetonitrile as the proton source was excluded because when the reaction was performed in MeCN-d_3, no deuterium substitution on the methyl group of **4**-*trans* was detected by NMR and MS analyses.

The formation of a five-membered ring indicates that the reaction proceeded through a kinetic process. We were interested to know if six-membered ring products could also be formed under certain circumstances. For instance, using 1-*C*-allyl-L-arabinofuranoside (**6**), a mixture of two anomers (α/β, 1:1) as a substrate, we expected a similar cyclization occurred in **6β** because of its 1,2-cis configuration, but we were also interested to see if the 1-*C*-allyl group in the α anomer (**6α**) would react to the 3-*O*-Bn, which is sterically possible, to form a six-membered ring. Thus, a mixture of **6α/β** was treated with TMSOTf in acetonitrile under the aforementioned conditions. TLC analysis showed the formation of a new product, but a significant amount of starting material remained. After the separation, the newly formed product with a lower R_f was characterized as dioxabicyclic **7**-*trans* (37% yield based on total starting material), produced by the cyclization between the 2-*O*-Bn and the *cis*-1-*C*-β-allyl group (Scheme 3). Again, the 2,2′-trans configuration was assigned on the basis of NOE analysis. The remaining starting material (**6α**), contaminated only with very small amount of **6β**, was recovered, which did not produce a six-membered ring product.

Scheme 3.



Because of the close distance between C2′ and C4 as indicated by the observation of NOE between H-2′ and H-4 in **4**-*trans*, one might speculate that the 2,2′-trans selectivity in **4**-*trans* and **7**-*trans* may have resulted from the steric hindrance exerted by 3-*O*-Bn in **2** or 5-*O*-Bn in **6**, which could prevent the methyl group at C2′ from adopting a cis configuration in the transition state. However, this argument was proven not true because 1-*C*-allyl-D-xylofuranoside (**8**), which lacks such steric effect, under the above conditions produced **9**-*trans* as the only major product (35%) and the recovery of its 1,2-trans starting material (**8β**) (42%) (see Scheme 3).

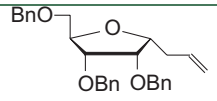
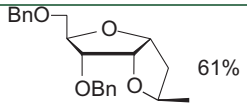
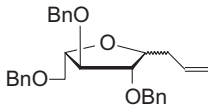
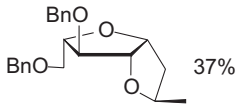
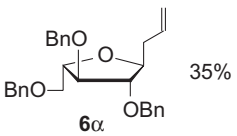
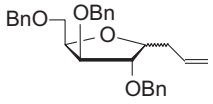
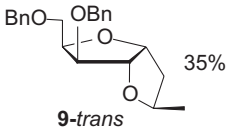
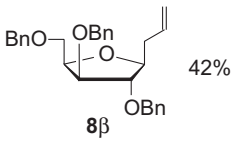
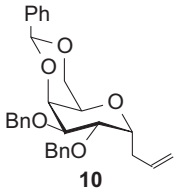
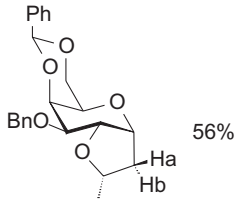
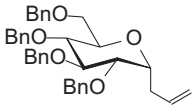
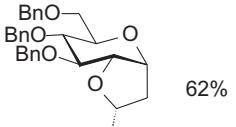
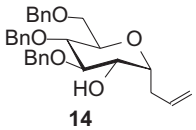
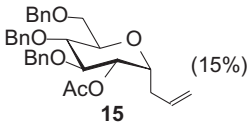
Besides the 1-*C*-allylglycofuranosides, the cyclization between the 1-*C*-allyl and the 2-*O*-Bn also occurred with 1-*C*-allylglycopyranosides under the above conditions. Remarkably, however, in contrast to the 2,2′-trans diastereoselectivity observed in 1-*C*-allylglycofuranosides, when 1-*C*-allylgalactoside (**10**) and 1-*C*-allylglucosides (**12**) were treated with TMSOTf in acetonitrile, we only obtained the respective products with the 2,2′-cis configurations, **11**-*cis* (56%) and **13**-*cis* (62%) (see Table 1). The cyclization also proceeded with 2-OH glucoside (**14**) to give **13**-*cis* (59%) as the major product and a 2-O-acetylated **15** (15%) as a minor one (8). The 2-O-acetylation resulted from the reaction between 2-OH and acetonitrile followed by hydrolysis. No cyclization occurred when **15** was used as a substrate because of the diminished 2-O-nucleophicility owing to the electron-withdrawing effect by 2-O-acetylation.

Although this acid-promoted cyclization was never reported, the iodonium-promoted cyclization between the olefin double bond and O-Bn are known. For example, Rychnovsky and Bartlett (9) prepared 2,5-cis disubstituted tetrahydrofurans by cyclizing olefinic ether in the presence of iodine and suggested that the 2,5-cis stereoselectivity was controlled by an oxonium ion intermediate with the 1,2-trans, 1,5-trans configurations. Nicotra and co-workers (10) also subjected 1-*C*-allyl-2-*O*-benzylglycoside to similar conditions to obtain a mixture of two diastereomers at C2′. The oxonium ion was also an intermediate in Fraser-Reid's glycosylation using *n*-pentenyl glycoside in which the formation of a bridged olefin halogenium ion was followed by

[5] Compound **2** and TMSOTf were separately dissolved in acetonitrile and dried over 3 Å molecular sieves. Equivalents of **2** and TMSOTf in acetonitrile were then mixed and kept at 0 °C overnight.

© 2006 NRC Canada

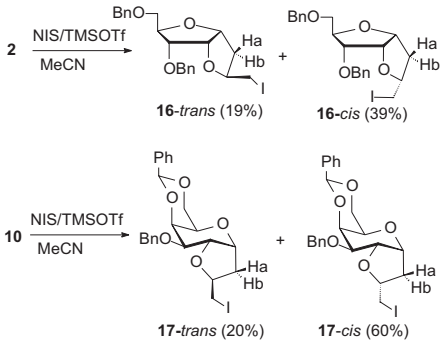
Table 1. Dioxabicycles from 1-*C*-allyl-*C*-glycosides.

Entry	Substrate	Product(s) (isolated yield)	
1	 **2**	 **4**-*trans* 61%	
2	 **6** (α/β 1:1)	 **7**-*trans* 37%	 **6**α 35%
3	 **8** (α/β 1:1)	 **9**-*trans* 35%	 **8**β 42%
4	 **10**	 **11**-*cis* 56%	
5	 **12**	 **13**-*cis* 62%	
6	 **14**	**13**-*cis* (59%)	 **15** (15%)
7	**15**	N/A	

nucleophilic attack from the glycosidic oxygen leading to a glycosyl oxocarbonium ion as a glycosyl donor and the concurrent formation of a tetrahydrofuran (11).

The poor stereoselection in the iodine-promoted cyclizations contrasts with those obtained from acid-promoted cyclization. Such a difference is not substrate dependent because when **2** and **10** were treated with NIS–TMSOTf in acetonitrile a mixture of diasteromers (**16**-*trans*/*cis* and **17**-*trans*/*cis*) were also obtained, respectively, in a 1:2 to 3 trans:cis ratio (Scheme 4). The NOE between H-2′ and H-4 in **16**-*trans*, similar to **4**-*trans*, was observed, but not between H-4 and CH_2I in **16**-*cis*.[6] The chemical shifts of H-1′a (cis to H-1) and H-1′b (trans to H-1) and the pattern of proton couplings were also similar to those observed in 2′-methyl dioxabicycles (**4**-*trans*, **7**-*trans*, **9**-*trans*, **11**-*cis*, and **13**-*cis*). The double doublet H-1′b resonance in the 2,2′-trans compounds always appears downfield (2.2–2.4 ppm) from that of the H-1′a resonance (1.5–2.0 ppm), and are reversed in the 2,2′-cis compounds likely because of the change of conformation from one envelope to another.

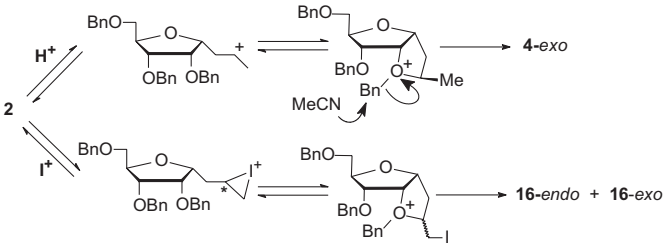
Scheme 4. Regioselective cyclization promoted by NIS–TMSOTf.



[6] Due to the overlap of the proton signals of H-2′ and H-4, this result was obtained from a TOCSY (H-5 to H-4) – NOESY (H-4) experiment.

© 2006 NRC Canada

Scheme 5. Stereoselective cyclization.



Unlike proton-promoted electrophilic addition, which follows Markovnikov's rule leading to a carbonium ion, the addition of an iodonium ion to a double bond can result in two bridged iodonium intermediates (Scheme 5). Consequently, the subsequent S_N2 displacement by 2-*O*-Bn produced two respective diastereoisomers (2,2′-cis and 2,2′-trans) (11) (see Scheme 4). Acetonitrile likely also plays a role by facilitating the cleavage of the O—Bn bond from the oxonium intermediate by forming a benzylacetonium ion (12) because the same reaction did not occur in dichloromethane.

The opposite stereochemistry obtained from 1-*C*-allyl-glycofuranosides and -glycopyranosides suggests two distinctive transition states. It is conceivable that the parent ring structure, the chair form in the pyranosides and the envelope form in the furanosides, may play a critical role in the stabilization of the respective oxonium ion transition states. It is also possible that the stereochemistry at C2′ may simply be predetermined by the orientation of the 2-*O*-Bn, which the 2′-carbonium ion must approach from the less-hindered side to form a 1,2-trans oxonium intermediate. Unfortunately, at this moment, we have no convincible explanation for those experimental results. Molecular modeling and calculation of the minimum energies of the possible oxonium transition states may provide the information on the most likely reaction pathway.

In summary, we described an intramolecular cyclization from 1-*C*-allyl-*O*-benzylglycosides in moderate to good yields. The allyl double bond was activated by electrophiles to generate a carbonium at C2′, which reacted with nucleophilic benzyl ether giving dioxabicyclic derivatives. The cyclization is highly regioselective in favor of five-membered products. The reaction is also highly diastereoselective to form 2,2′-cis and 2,2′-trans dioxabicycles from 1-*C*-pyranosides and 1-*C*-furanosides, respectively.[7]

Experimental section

General methods

^{1}H and ^{13}C NMR spectra were recorded at 400 and 100 MHz, respectively, with a Varian instrument at 293 K. Chemical shifts are given in ppm downfield from the signal of internal TMS and are assigned on the basis of 2D COSY, TOCSY, and ^{1}H–^{13}C chemical-shift correlated experiments. High-resolution fast atom bombardment mass spectrometry (HRFABMS) was carried out on a JEOL JMS-AX505H mass spectrometer using a 6 kV xenon beam at an accelerating voltage of 3 kV. *m*-Nitrobenzyl alcohol (*m*-NBA) was used as the matrix, and polyethylene glycol (PEG) was the internal calibrant. All chemicals were purchased from the Sigma-Aldrich Chemical Co. and used without further purification.

General procedure for cyclization

To a solution of substrate (50–100 mg) in CH_3CN (2 mL) was added dropwise TMSOTf (1 equiv.) at 0 °C. The mixture was stirred and allowed to warm to room temperature overnight. The reaction was quenched by the addition of Et_3N and the solvent was removed under reduced pressure. Product purification was performed by silica gel column chromatography (hexane–EtOAc, 3:1).

1-*C*-(*R*-Propan-2′-ol)-3,5-di-*O*-benzyl-2,2′-anhydro-α-D-ribofuranoside (4-*trans*)

This compound was obtained as an oil in 61% yield. $[\alpha]_D$ +79.4° (*c* 7.0, $CHCl_3$). ^{1}H NMR ($CDCl_3$) δ: 4.80 (d, *J* = 12 Hz, 1H, $PhCH_2$), 4.77 (dd, *J* = 4.8, 4.8 Hz, 1H, H-1), 4.60 (dd, *J* = 4.8, 4.8 Hz, 1H, H-2), 4.54–4.50 (m, 3H, $PhCH_2$), 4.29 (m, 1H, H-2′), 4.00 (ddd, *J* = 8.4, 5.2, 2.4 Hz, 1H, H-7), 3.83 (dd, *J* = 8.4, 5.2 Hz, 1H, H-3), 3.66 (dd, *J* = 10.8, 2.4 Hz, 1H, H-5a), 3.45 (dd, *J* = 10.8, 5.2 Hz, 1H, H-5b), 2.23 (dd, *J* = 13.2, 4.8 Hz, 1H, H-1′b), 1.58 (ddd, *J* = 13.2, 10.4, 4.8 Hz, 1H, H-1′a), 1.30 (d, *J* = 6.0 Hz, 3H, CH_3). ^{13}C NMR ($CDCl_3$) δ: 83.6 (C-2), 80.8 (C-3), 80.5 (C-4), 79.9 (C-1), 77.0 (C-2′), 73.4 ($PhCH_2$), 72.0 ($PhCH_2$), 70.1 (C-5), 43.2 (C-1′), 20.7 (CH_3). HRFABMS calcd. for $C_{22}H_{27}O_4$ *m/z*: 355.1831 (MH^+); found: 355.2230. Starting material **2** (10 mg, 10%) was also recovered.

1-*C*-(*R*-Propan-2′-ol)-3,5-di-*O*-acetyl-2,2′-anhydro-α-D-ribofuranoside (5)

A solution of compound **4**-*trans* (120 mg, 0.33 mmol) in methanol (15 mL) was hydrogenated with 10% Pd/C (50 mg) under 50 psi (1 psi = 6.894 757 kPa) overnight. The filtrate was concentrated to a residue. To a solution of this residue in CH_2Cl_2 (10 mL) was added TEA (1 mL) and acetic anhydride (210 mg, 2.11 mmol), and the mixture was stirred overnight. Work-up and purification by chromatography gave **5** (60 mg, 68%). $[\alpha]_D$ +113.9° (*c* 1.5, $CHCl_3$). ^{1}H NMR ($CDCl_3$) δ: 4.87 (dd, 1H, *J* = 4.8, 7.6 Hz), 4.81 (dd, 1H, *J* = 4.8 Hz), 4.76 (dd, 1H, *J* = 4.8 Hz), 4.28 (dd, 1H, *J* = 11.6, 2.8 Hz), 4.20 (m, 1H), 4.14 (m, 1H), 4.05 (dd, 1H, *J* = 11.6, 5.6 Hz), 2.23 (dd, 1H, *J* = 13.2, 4.8 Hz), 2.13 (s, 3H), 2.09 (s, 3H), 1.59 (m, 1H), 1.28 (d, 3H, *J* = 6.0 Hz). ^{13}C NMR ($CDCl_3$) δ: 170.8, 170.4, 84.0, 80.6, 78.7, 77.3, 75.2, 64.0, 42.9, 20.9, 20.8, 20.6. ESMS: 259.2 (MH^+).

1-*C*-(*R*-Propan-2′-ol)-3,5-di-*O*-benzyl-2,2′-anhydro-β-L-arabinofuranoside (7-*trans*)

Under the same conditions, **7**-*trans* (37%) and **6α** (35%) were obtained from **6** (α:β, 1:1).

For **7**-*trans*: $[\alpha]_D$ –44.0° (*c* 1.12, $CHCl_3$). ^{1}H NMR ($CDCl_3$) δ: 7.37–7.24 (m, 10H), 4.72 (m, 1H), 4.71 (d, 1H, *J* = 11.6 Hz), 4.63 (dd, 1H, *J* = 4.8, 1.6 Hz), 4.56 (s, 2H),

[7] Supplementary data for this article are available on the journal Web site (http://canjchem.nrc.ca) or may be purchased from the Depository of Unpublished Data, Document Delivery, CISTI, National Research Council Canada, Ottawa, ON K1A 0R6, Canada. DUD 5025. For more information on obtaining material refer to http://cisti-icist.nrc-cnrc.gc.ca/irm/unpub_e.shtml.

© 2006 NRC Canada

4.52 (d, 1H, *J* = 11.6 Hz), 4.15 (m, 1H), 3.95 (dt, 1H, *J* = 3.2, 6.4 Hz), 3.78 (dd, 1H, *J* = 7.2, 2.0 Hz), 3.65 (dd, 1H, *J* = 10.4, 3.2 Hz), 3.56 (dd, 1H, *J* = 10.8, 6.4 Hz), 2.17 (dd, 1H, *J* = 13.2, 4.4 Hz), 1.42 (m, 1H), 1.27 (d, 3H, *J* = 6.0 Hz). ^{13}C NMR ($CDCl_3$) δ: 138.2, 137.8, 128.5, 128.4, 127.9, 127.7, 88.5, 85.9, 83.8, 82.6, 74.7, 73.5, 72.1, 70.2, 41.0, 19.9. ESMS: 355.3 (MH^+).

For **6α**: $[\alpha]_D$ –19.5° (*c* 1.4, $CHCl_3$). ^{1}H NMR ($CDCl_3$) δ: 7.37–7.22 (m, 15H), 5.58 (m, 1H), 5.10 (m, 2H), 4.50 (m, 6H), 4.21 (m, 1H), 4.07 (m, 1H), 4.06 (dd, 1H, *J* = 3.2 Hz), 3.87 (dd, 1H, *J* = 4.4, 2.8 Hz), 3.57 (m, 2H). ^{13}C NMR ($CDCl_3$) δ: 138.4, 138.0, 134.4, 128.5, 128.4, 128.3, 127.8, 127.7, 87.0, 85.4, 82.0, 81.6, 73.4–71.9, 70.3, 37.7. ESMS: 445.2 (MH^+).

1-*C*-(*R*-Propan-2′-ol)-3,5-di-*O*-benzyl-2,2′-anhydro-α-D-xylofuranoside (9-*trans*)

Under the same conditions, **9**-*trans* (35%) and **8β** (42%) were obtained from **8** (α:β, 1:1).

For **9**-*trans*: $[\alpha]_D$ –44.0° (*c* 1.12, $CHCl_3$). ^{1}H NMR ($CDCl_3$) δ: 7.37–7.24 (m, 10H), 4.87 (dd, 1H, *J* = 4.4 Hz), 4.67 (d, 1H, *J* = 12.0 Hz), 4.63 (d, 1H, *J* = 11.6 Hz), 4.59 (m, 1H), 4.52 (d, 1H, *J* = 6.4 Hz), 4.49 (d, 1H, *J* = 6.4 Hz), 4.18 (m, 1H), 4.12 (m,1H), 3.97 (d, 1H, *J* = 4.0 Hz), 3.68 (d, 2H, *J* = 5.6 Hz), 2.25 (dd, 1H, *J* = 13.6 Hz, 5.2 Hz), 1.50 (m, 1H), 1.24 (d, 3H, *J* = 6.4 Hz). ^{13}C NMR ($CDCl_3$) δ: 128.5, 128.4, 127.9, 127.7, 85.9, 83.8, 83.5, 81.3, 75.9, 73.6, 72.2, 68.9, 42.5, 20.6. ESIMS: 355.3 (MH^+).

For **8β**: $[\alpha]_D$ –19.5° (*c* 1.4, $CHCl_3$). ^{1}H NMR ($CDCl_3$) δ: 7.37–7.22 (m, 15H), 5.80 (m, 1H), 5.08 (m, 2H), 4.63–4.44 (m, 6H), 4.20 (dt, 1H, *J* = 1.6, 4.4 Hz), 3.96 (d, 1H, *J* = 3.6 Hz), 3.90 (dt, 1H, *J* = 3.6, 6.8 Hz), 3.79 (dd, 1H, *J* = 9.6, 5.6 Hz), 3.76 (m, 1H), 3.73 (dd, 1H, *J* = 9.6, 6.0 Hz), 2.49–2.32 (m, 2H). ^{13}C NMR ($CDCl_3$) δ: 138.4, 138.0, 134.4, 128.5, 128.4, 127.9, 127.8, 127.7, 87.0, 85.4, 82.0, 81.6, 73.4–71.9, 70.3, 37.7. ESMS: 455.3 (MH^+).

1-*C*-(*S*-Propan-2′-ol)-3-*O*-benzyl-4,6-*O*-benzylidene-2,2′-anhydro-α-D-galactopyranoside (11-*cis*)

This compound was obtained from **10** as an oil in 56% yield. $[\alpha]_D$ +44.8° (*c* 0.67, $CHCl_3$). ^{1}H NMR ($CDCl_3$) δ: 5.47 (s, 1H, PhCH), 5.07 (m, 1H, H-1), 4.87 (d, *J* = 12.4 Hz, 1H, CH_2Ph), 4.73 (d, *J* = 12.4 Hz, 1H, CH_2Ph), 4.39 (bd, *J* = 2.4 Hz, 1H, H-4), 4.33 (d, *J* = 12.4 Hz, 1H, H-6a), 4.08–4.03 (m, 2H, H-6b, H-2), 3.92 (m, 1H, H-2, 3.71 (dd, *J* = 5.6, 2.0 Hz, 1H, H-3), 3.58 (bs, 1H, H-5), 2.38 (m, 1H, H-1), 1.82 (ddd, *J* = 13.6, 8.4, 3.2 Hz, 1H, H-1), 1.34 (d, *J* = 6 Hz, 3H, CH_3). ^{13}C NMR ($CDCl_3$) δ: 100.5 (PhCH), 82.8 (C-2), 79.5 (C-3), 78.0 (C-1), 74.2 (C-2′), 73.3 (C-4), 72.6 (C-6), 71.1 ($PhCH_2$), 67.5 (C-5), 40.8 (C-1′), 21.0 (CH_3). HRFABMS calcd. for $C_{23}H_{27}O_5$ *m/z*: 383.1780 (MH^+); found: 383.2146.

1-*C*-(*S*-Propan-2′-ol)-3,4,6-tri-*O*-benzyl-2,2′-anhydro-α-D-glucopyranoside (13-*cis*)

This compound was obtained from **12** as an oil in 62% yield. $[\alpha]_D$ +76° (*c* 0.1, $CHCl_3$). ^{1}H NMR ($CDCl_3$) δ: 7.18–7.40 (m, 15H, 3 × Ph), 4.90 (d, 1H, CH_2Ph, *J* = 11.6 Hz), 4.83 (d, 1H, CH_2Ph, *J* = 11.2 Hz), 4.73 (d, 1H, CH_2Ph, *J* = 11.6 Hz), 4.59 (d, 1H, H-1), 4.53 (d, 1H, CH_2Ph, *J* = 12.4 Hz), 4.46 (d, 1H, CH_2Ph, *J* = 11.2 Hz), 4.43 (d, 1H, CH_2Ph, *J* = 12.4 Hz), 3.95 (m, 1H, H-2′), 3.77–3.85 (m, 3H, H-2, H-3, H-5), 3.55–3.67 (m, 3H, H-4, H-6, 6′), 2.25 (m, 1H, H-1′a), 1.62 (m, 1H, H-1′b), 1.34 (d, 3H, H-3′, *J* = 6.0 Hz). ^{13}C NMR ($CDCl_3$) δ: 138.9, 138.7, 138.4 (Ph), 128.6, 128.4, 127.9, 127.8, 127.6 (Ph), 83.4 (C-3), 83.3 (C-2), 76.1 (C-1), 75.5 (C-4), 75.2 (C-5), 74.7 (C-2′), 74.6 (CH_2Ph), 73.5 (CH_2Ph), 73.0 (CH_2Ph), 70.1 (C-6), 39.4 (C-1′), 21.6 (C-3′). ESMS: 475.3 (MH^+).

1-*C*-(3′-Iodo-*R/S*-propan-2′-ol)-3,5-di-*O*-benzyl-2,2′-anhydro-α-D-ribofuranoside (16-*trans* and 16-*cis*)

Compounds **16**-*trans* (19%) and **16**-*cis* (39%) obtained from **2** were separated by chromatography.

For **16**-*trans*: oil. $[\alpha]_D$ +51.7° (*c* 0.12, $CHCl_3$). ^{1}H NMR ($CDCl_3$) δ: 4.79–4.76 (m, 2H, $PhCH_2$, H-1), 4.66 (dd, *J* = 4.0, 4.0 Hz, 1H, H-2), 4.57–4.49 (m, 3H, $PhCH_2$), 4.17 (m, 1H, H-2′), 4.02 (m, 1H, H-4), 3.86 (dd, *J* = 8.0, 4.4 Hz, 1H, H-3), 3.66 (dd, *J* = 10.4, 1.6 Hz, 1H, H-5a), 3.46 (dd, *J* = 10.4, 4.8 Hz, 1H, H-5b), 3.38–3.30 (m, 2H, CH_2I), 2.37 (dd, *J* = 13.6, 5.2 Hz, 1H, H-1′b), 1.79 (ddd, *J* = 13.6, 10.0, 5.2 Hz, 1H, H-1′a). ^{13}C NMR ($CDCl_3$) δ: 83.1 (C-2), 81.9 (C-3), 80.7 (C-4), 80.1 (C-1), 79.5 (C-2′), 73.5 ($PhCH_2$), 72.2 ($PhCH_2$), 70.0 (C-5), 41.9 (C-1′), 10.2 (CH_2-I). HRFABMS calcd. for $C_{22}H_{25}IO_4$ *m/z*: 480.0797 (M^+); found: 479.0749.

For **16**-*cis*: oil. $[\alpha]_D$ +79.5° (*c* 0.2, $CHCl_3$). ^{1}H NMR ($CDCl_3$) δ: 4.79–4.73 (m, 2H, $PhCH_2$, H-1), 4.57–4.49 (m, 3H, $PhCH_2$), 4.45 (dd, *J* = 4.4, 4.4 Hz, 1H, H-2), 4.20–4.15 (m, 2H, H-2 H-4), 3.89 (dd, *J* = 8.4, 4.4 Hz, 1H, H-3), 3.67 (dd, *J* = 10.8, 1.6 Hz, 1H, H-5a), 3.50 (dd, *J* = 10.8, 4.8 Hz, 1H, H-5b), 3.41 (dd, *J* = 10.0, 5.2 Hz, 1H, CH_2I), 3.32 (dd, *J* = 9.2, 8.4 Hz, 1H, CH_2I), 2.42 (dt, *J* = 14.0, 6.8 Hz, 1H, H-1), 1.99 (ddd, *J* = 14.0, 6.8, 2.4 Hz, 1H, H-1). ^{13}C NMR ($CDCl_3$) δ: 82.9 (C-1), 82.2 (C-2), 80.8 (C-2′), 79.2 (C-3), 79.0 (C-4), 73.4 ($PhCH_2$), 72.1 ($PhCH_2$), 69.6 (C-5), 40.2 (C-1′), 8.5 (CH_2I). HRFABMS calcd. for $C_{22}H_{25}IO_4$ *m/z*: 480.0797 (M^+); found: 479.0711.

1-*C*-(3′-Iodo-*R/S*-propan-2′-ol)-3-*O*-benzyl-4,6-*O*-benzylidene-2,2′-anhydro-α-D-galactopyranoside (17-*trans* and 17-*cis*)

Compounds **17**-*trans* (20%) and **17**-*cis* (60%) obtained from **10** were separated by chromatography.

For **17**-*trans*: oil. $[\alpha]_D$ –8° (*c* 5.8, $CHCl_3$). ^{1}H NMR ($CDCl_3$) δ: 5.48 (s, 1H, PhCH), 5.20 (dd, *J* = 8.8, 4.4 Hz, 1H, H-1), 4.86 (d, *J* = 12.4 Hz, 1H, CH_2Ph), 4.73 (d, *J* = 12.8 Hz, 1H, CH_2Ph), 4.48 (dd, *J* = 9.2, 4.4 Hz, 1H, H-2), 4.40 (bs, 1H, H-4), 4.33 (d, *J* = 12.4 Hz, 1H, H-6a), 4.23 (m, 1H, H-2, 4.05 (d, *J* = 12.8 Hz, 1H, H-6b), 3.63 (d, *J* = 5.2 Hz, 1H, H-3), 3.56 (bs, 1H, H-5), 3.34–3.25 (m, 2H, CH_2I), 2.23 (dd, *J* = 13.6, 5.6 Hz, 1H, H-1), 1.82 (ddd, *J* = 13.6, 9.2, 5.6 Hz, 1H, H-1). ^{13}C NMR ($CDCl_3$) δ: 100.5 (PhCH), 84.0 (C-2), 79.2 (C-3), 78.1 (C-1), 77.7 (C-2′), 73.5 (C-4), 72.6 (C-6), 70.8 ($PhCH_2$), 67.4 (C-5), 39.8 (C-1′), 10.1 (CH_2I). HRFABMS calcd. for $C_{23}H_{25}IO_5$ *m/z*: 508.0747 (M^+); found: 507.0730.

For **17**-*cis*: oil. $[\alpha]_D$ +6.8° (*c* 9.4, $CHCl_3$). ^{1}H NMR ($CDCl_3$) δ: 5.48 (s, 1H, PhCH), 5.15 (m, 1H, H-1), 4.86 (d, *J* = 12.4 Hz, 1H, CH_2Ph), 4.73 (d, *J* = 12.4 Hz, 1H, CH_2Ph), 4.39 (bs, 1H, H-4), 4.33 (d, *J* = 12.4 Hz, 1H, OCH_2), 4.25 (dd, *J* = 9.6, 4.8 Hz, 1H, H-2), 4.23 (m, 1H, H-2′), 4.05 (d, *J* = 12.4 Hz, 1H, H-6a), 3.66 (bd, *J* = 5.2 Hz, 1H, H-3), 3.57

© 2006 NRC Canada

(bs, 1H, H-5), 3.34–3.25 (m, 2H, CH_2I), 2.23 (m, 1H, H-1′a), 1.82 (dd, J = 14, 5.6 Hz, 1H, H-1′b). ^{13}C NMR ($CDCl_3$) δ: 100.5 (PhCH), 84.2 (C-2), 79.7 (C-3), 78.8 (C-2′), 77.6 (C-1), 73.4 (C-4), 72.5 (C-6), 70.9 ($PHCH_2$), 67.4 (C-5), 38.3 (C-1), 9.8 (CH_2I). HRFABMS calcd. for $C_{23}H_{25}IO_5$ *m/z*: 508.0747 (M^+); found: 507.0781.

Acknowledgments

This is NRCC publication No. 42508. The authors thank Ms. Milan Bhasin for technical assistance, Dr. Jean-Robert Brisson for assistance in NMR analysis, and Lisa Morrison and Dr. Jianjun Li for MS analysis.

References

1. (*a*) G. Cardillo and M. Orena. Tetrahedron, **46**, 3321 (1990); (*b*) G. Rousseau and S. Robin. Tetrahedron, **54**, 13681(1998); (*c*) M.B. Smith and J. March (*Editors*). March's advanced organic chemistry: Reactions, mechanisms, and structure. 5th ed. John Wiley and Sons, New York. 2001.
2. (*a*) M. Tiecco. Top. Curr. Chem. **208**, 7 (2000); (*b*) T. Wirth. Angew. Chem. Int. Ed. **39**, 3740 (2000); (*c*) T.G. Back, B.P. Dyck, and S. Nan. Tetrahedron, **55**, 3191 (1999); (*d*) Y. Nishibayashi, S.K. Srivastava, H. Takada, S.-I. Fukuzawa, and S. Uemura. J. Chem. Soc. Chem. Commun. 2321 (1995); (*e*) T. Wirth. Angew. Chem. Int. Ed. Engl. **34**, 1726 (1995); (*f*) R. Deziel, S. Goulet, L. Grenier, J. Bordeleau, and J. Nernier. J. Org. Chem. **58**, 3619 (1993).
3. (*a*) S.H. Kang, S.B. Lee, and C.M. Park. J. Am. Chem. Soc. **125**, 15748 (2003); (*b*) R.B. Grossman and R. Trupp. Can. J. Chem. **76**, 1233 (1998); (*c*) R.S. Brown and X.L. Cui. J. Org. Chem. **65**, 5653 (2000); (*d*) J. Hass, S. Piguel, and T. Wirth. Org. Lett. **4**, 297 (2002); (*e*) M. Wang, L.X. Gao, W.P. Mai, A.X. Xia, F. Wang, and S.B. Zhang. J. Org. Chem. **69**, 2874 (2004); (*f*) A.N. French, S. Bissmire, and T. Wirth. Chem. Soc. Rev. **33**, 354 (2004); (*g*) J. Hass, S. Bissmire, and T. Wirth. Chem. Eur. J. **11**, 5777 (2005).
4. (*a*) S.H. Kang, M. Kim, and S.Y. Kang. Angew. Chem. Int. Ed. **43**, 6177 (2004); (*b*) S.H. Kang and M. Kim. J. Am. Chem. Soc. **125**, 4684 (2003); (*c*) H.B. Vardhan and R.D. Bach. J. Org. Chem. **57**, 4948 (1992).
5. Y. Oe, T. Ohta, and Y. Ito. Synthesis, 179 (2005).
6. (*a*) W. Zou, E. Lacroix, Z. Wang, and S.-H. Wu. Tetrahedron Lett. **44**, 4431 (2003); (*b*) T. Yi, S.-H. Wu, and W. Zou. Carbohydr. Res. **340**, 235 (2005).
7. Lewis acid mediated removal of the *O*-benzyl group is known and the regioselectivity may also be achieved in some cases using TMSI, NIS, TIBAL, and BCl_3. See: (*a*) J. Stanek, Jr. Top. Curr. Chem. **154**, 211 (1990); (*b*) J. Madsen and M. Bols. Angew. Chem. Int. Ed. **37**, 3177 (1998); (*c*) J. Madsen, C. Viuf, and M. Bols. Chem. Eur. J. **6**, 1140 (2000); (*d*) B. Chevalier-du Roizel, E. Cabianca, P. Rollin, and P. Sinay. Tetrahedron, **58**, 9579 (2002); (*e*) T. Lecourt, A. Herault, A.J. Pearce, M. Sollogoub, and P. Sinay. Chem. Eur. J. **11**, 2960 (2004); (*f*) J. Xie, M. Menand, and J.-M. Valery. Carbohydr. Res. **340**, 481 (2005).
8. W. Zou, Z. Wang, E. Lacroix, S.-H. Wu, and H. Jennings. Carbohydr. Res. **334**, 223 (2001).
9. S.D. Rychnovsky and P.A. Bartlett. J. Am. Chem. Soc. **103**, 3963 (1981).
10. (*a*) F. Nicotra, L. Panza, and G. Russo. J. Org. Chem. **52**, 5627 (1987). (*b*) L. Cipolla, L. Lay, and F. Nicotra. J. Org. Chem. **62**, 6678 (1997).
11. (*a*) B. Fraser-Reid, P. Konradsson, D.R. Mootoo, and U.E. Udodong. J. Chem. Soc. Chem. Commun. 823 (1988); (*b*) B. Fraser-Reid and R. Madsen. *In* Preparative carbohydrate chemistry. *Edited by* S. Hanessian. Marcel Dekker, New York. 1997. pp. 339–359; (*c*) B. Fraser-Reid, G. Anilkumar, M.R. Gilbert, S. Joshi, and R. Kraehmer. *In* Carbohydrates in chemistry and biology. Vol. 1. *Edited by* B. Ernst, G.W. Hart, and P. Sinaÿ. Wiley-VCH, New York. 2000. pp. 135–154.
12. (*a*) A.J. Ratcliffe and B. Fraser-Reid. J. Chem. Soc. Perkin Trans 1, 747 (1990); (*b*) J.M. Concellon, E. Riego, J.R. Suarez, S. Garcia-Granda, and M.S. Diaz. Org. Lett. **6**, 4499 (2004).

© 2006 NRC Canada

Quantum mechanics studies of cellobiose conformations[1]

Alfred D. French and Glenn P. Johnson

Abstract: Three regions of the conformation space that describes the relative orientations of the two glucose residues of cellobiose were analyzed with quantum mechanics. A central region, in which most crystal structures are found, was covered by a 9 × 9 grid of 20° increments of the linkage torsion angles ϕ and ψ. Besides these 81 constrained minimizations, we studied two central subregions and two regions at the edges of our maps of complete ϕ,ψ space with unconstrained minimization, for a total of 85 target geometries. HF/6-31G(d) and single-point HF/6-311+G(d) calculations were used to find the lowest energies for each geometry. B3LYP/6-31G+G(d) and single point B3LYP/6-11+G(d) calculations were also used for all unconstrained minimizations. For each target, 181 starting geometries were tried (155 for the unconstrained targets). Numerous different starting geometries resulted in the lowest energies for the various target structures. The starting geometries came from five different sets that were based on molecular mechanics energies. Although all five sets contributed to the adiabatic map, use of any single set resulted in discrepancies of 3–7 kcal/mol (1 cal = 4.184 J) with the final map. For most of the targets, the starting geometry that gave the lowest energy depended on the basis set and whether the HF or B3LYP method was used. However, each of the above four calculations gave the same overall lowest energy structure that was found previously by Strati et al. This global minimum, stabilized by highly cooperative hydrogen bonds, is in a region that is essentially not populated by crystal structures. HF/6-31G(d) energy contours of the mapped central region were compatible with the observed crystal structures. Observed structures that lacked O3···O5′ hydrogen bonds were about 1 kcal/mol above the map's minimum, and observed structures that have a pseudo twofold screw axis ranged from about 0.4 to 1.0 kcal/mol. The HF/6-311+G(d) map accommodated the observed structures nearly as well.

Key words: cellulose, carbohydrate, conformation, energy, flexibility, folding, helix, shape.

Résumé : Faisant appel à des calculs de méanique quantique, on a étudié trois régions de l'espace conformationnel qui décrit les orientations relatives de deux résidus de glucose du cellobiose. La région centrale, dans laquelle on retrouve la plupart des structures cristallines a été couverte par une grille 9 × 9 avec des augmentations de 20° des angles de torsion ϕ et ψ de la liaison. En plus de ces 81 minimisations contraintes, on a aussi étudié deux sous régions centrales et deux régions aux limites extérieures de nos cartes de l'espace ϕ,ψ avec une minimisation sans contrainte, pour un total de 85 géométries cibles. On a utilisé des calculs HF/6-31G(d) et des calculs ponctuels HF/6-311+G(d) pour trouver les énergies minimales pour chaque géométrie. On a aussi utilisé des calculs B3LYP/6-31G+G(d) et des calculs ponctuels B3LYP/6-311+G(d) pour toutes les minimisations sans contrainte. Pour chaque cible, on a essayé 181 géométries de départ (155 pour les cibles sans contrainte). Plusieurs géométries de départ différentes on conduit à des énergies minimales pour diverses structures cibles. Les géométries de départ viennent de cinq différents ensembles qui étaient basés sur des énergies de mécanique moléculaire. Même si tous ces cinq ensembles ont contribué à la carte adiabatique, l'utilisation d'un seul ensemble conduit à des divergences allant de 3–7 kcal/mol (1 cal = 4,184 J) dans la carte finale. Pour la plupart des cibles, la géométrie de départ qui donne l'énergie la plus basse dépend de l'ensemble de base et de la méthode HF ou B3LYP qui est utilisée. Toutefois, chacun des quatre calculs mentionnés plus haut à conduit à la même structure d'énergie globale la plus basse et elle correspond à celle trouvée antérieurement par Strati et al. Ce minimum global, qui est stabilisé par des liaisons hydrogènes qui offrent beaucoup de coopération, se trouve dans une région des structures cristallines qui n'est pas peuplée. Des contours d'énergie au niveau HF/6-31G(d) de la région centrale cartographie sont compatibles avec les structures cristallines observées. Les niveaux d'énergie des structures observées qui ne comportent pas de liaisons hydrogènes O3···O5′ se trouvent à environ 1 kcal/mol au-dessus du minimum de la carte et pour les structures observées qui ont un axe d'hélice pseudo-binaire les valeurs vont de 0,4 à 1,0 kcal/mol. La carte obtenue au niveau HF/6-311+G(d) accommode les structures pratiquement aussi bien.

Mots clés : cellulose, hydrate de carbone, conformation, énergie, flexibilité, repli, hélice, forme.

[Traduit par la Rédaction]

Received 30 August 2005. Published on the NRC Research Press Web site at http://canjchem.nrc.ca on 13 May 2006.

A.D. French[2] and G.P. Johnson. Southern Regional Research Center, Agricultural Research Service, U.S. Department of Agriculture, 1100 Robert E. Lee Boulevard, New Orleans, LA 70124, USA.

[1]This article is part of a Special Issue dedicated to Professor Walter A. Szarek.

[2]Corresponding author (e-mail: afrench@srrc.ars.usda.gov).

 doi:10.1139/V06-050 © 2006 NRC Canada

Introduction

It has not been easy to reveal the structural secrets of cellulose, the most prevalent of all biological molecules. Despite studies that began more than 90 years ago (1), detailed structures of the main crystalline forms were reported only recently (2–5). Other structures are still controversial. For example, the helix chiralities of crystalline cellulose complexes and derivatives are not known for certain. In noncrystalline environments, the shape properties are even less well understood.

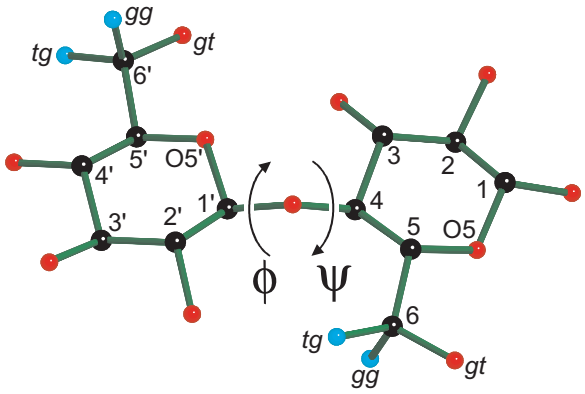
Computerized molecular modeling has often been called upon, with mixed success, to gain insight on such questions. Consider two recent studies aimed at determining the conformation of hydrated cellulose fragments. One study reported that the fragments were heavily hydrated and making tight turns in water (6). The other found them to be extended and more likely to hydrogen bond with each other rather than with water (7). Because of difficulties of modeling the stereoelectronic, hydrogen bonding and solvation characteristics of carbohydrates and water, various workers have not been able to agree on one method for energy calculations or other details such as atomic charges or assumed temperature. Currently, such contradictory results are to be expected.

As a simplification, investigators of cellulose structure have often studied cellobiose (β-D-glucopyranosyl-(1→4)-D-glucopyranose) (8–14), the disaccharide that can be described as the shortest cellulose chain. Lactose (β-D-galactopyranosyl-(1→4)-D-glucopyranose) should also be a good model for cellulose linkages. The intrinsic shapes of β-cellobiose and β-lactose are so similar that their crystal structures (15, 16) are isomorphous (17), as are crystals of their methyl glycosides (18, 19). Structural results from one sugar have strong implications for the other (20), and lactose conformations have been studied by modeling as well (21–23). Studies of other β-1,4-linked sugars, such as chitobiose (24, 25), are also relevant.

The primary variables of disaccharide shape are the linkage torsion angles ϕ and ψ (Fig. 1). Contemporary conformational analysis of cellobiose involves rotating each of the glucose rings about the glycosidic (ϕ) and aglycon (ψ) bonds and calculating a minimized relative energy at each increment of rotation. Most calculated energies for these molecules have been based on empirical force fields, also called molecular mechanics (MM). After the energies are calculated, a Ramachandran contour map of energies in ϕ,ψ space is created. The lowest energy regions indicate the most likely molecular shapes. Simulation of molecular dynamics (MD) trajectories is another approach that is usually carried out with energies calculated with MM force fields. The relatively rapid MM calculations permit, with today's computers, rather thorough treatments including large numbers of possible orientations of the exo-cyclic groups in mapping studies (26). In the case of MD, explicit solvent and multinanosecond simulations can now be considered. Because of the controversial results from these various studies, development of empirical energy functions for carbohydrates has continued (27).

Electronic structure theory or quantum mechanics (QM) methods inherently account for stereoelectronic effects that occur in carbohydrates. QM has been exploited for more than 30 years to quantify these effects (28, 29). Energy values for carbohydrates from QM are often different from those from MM studies (30–32) and differences in the degree of approximations of the electronic structure also cause different results (33, 34). So, even though QM results are based on the fundamentals of molecular structure, it is important to understand their limitations. In any event, ab initio QM methods take several orders of magnitude more computer time than MM, so they have typically been applied to molecules even smaller than disaccharides. For example, numerous studies of 2-methoxy-tetrahydropyran have been carried out. A fairly complete series was reported by Tvaroška and Carver (see ref. 35 and papers cited therein). Those studies were done with the idea of providing a basis for parameterization of empirical torsional parameters that would adequately mimic stereoelectronic effects around glycosidic linkages.

Fig. 1. Cellobiose with atom numbering, the linkage torsion angles ϕ and ψ, and the *gg*, *gt*, and *tg* O6 orientations. Hydrogen atoms are not shown. The O6 atoms shown shown in red are in the *gt* positions; and the other two staggered orientations (*gg* and *tg*) are cyan.



Additional insight on disaccharide conformations was gained with analogs of disaccharides that consisted of tetrahydropyran or cyclohexane rings standing in for glucopyranose, and tetrahydrofuran standing in for fructofuranose, linked by a "glycosidic" linkage. Semiempirical QM studies on an analog of trehalose were promising (36). With ab initio QM, only the ψ torsion was varied in initial studies (37, 38), but shortly afterwards, complete ϕ,ψ energy surfaces were published for analogs of a number of disaccharides (39). Despite the analogs' lack of hydroxyl and hydroxymethyl groups, those surfaces are remarkably predictive of linkage geometries observed in crystal structures of the disaccharides. Recently, we carried out QM studies with sterically more complete analogs of maltose and cellobiose in which all hydroxyl groups were replaced with fluorine atoms (40).

Several years ago, we devised a simple hybrid modeling method so that the electronic structure data at the glycosidic linkage could be combined with the MM results for the remainder of the molecule (41). That allowed a reasonably complete treatment of the exo-cyclic groups. Our hybrid method is better at predicting conformations of carbohydrates in crystal structures than the above QM-analog method, including the fluorinated analogs. However, even with our

© 2006 NRC Canada

hybrid method, we were not certain that we had provided an optimum rationalization for the observed structures. The experimental disaccharide conformations in the central region seemed to fall into three specific groups in ϕ,ψ space (17), but the energy surfaces suggested that there is only one central minimum. Of course, these groupings could just arise by chance or from external forces such as crystal packing effects. One way to explore whether these groups are based on intrinsic energy of the cellobiose molecule is to apply QM to the entire disaccharide. This paper conveys those results.

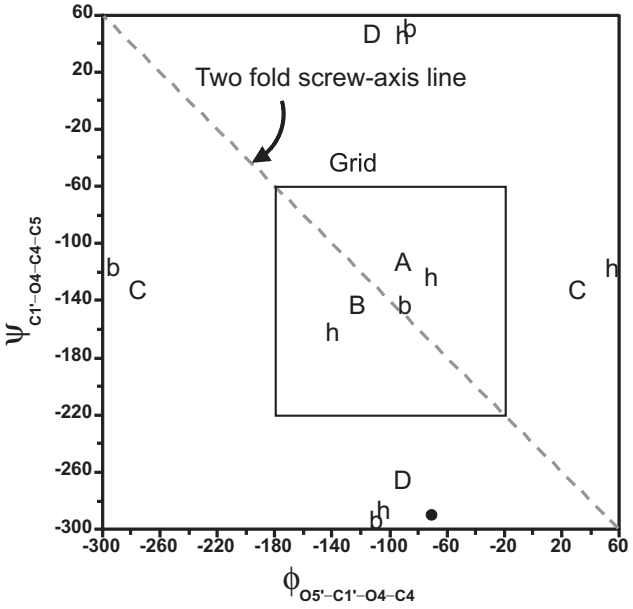
Besides the grouping of the crystal conformations, impetus to our efforts was provided by results from Momany and his group at our sister laboratory. That work identified 26 cellobiose structures that corresponded to local minima (42). Their structure with the lowest energy has a linkage conformation different from any of the 30 known conformations from small molecule crystal structures. With their computationally expensive B3LYP/6-311++G(d,p) calculations, this structure was 3.84 kcal/mol lower in electronic potential energy (before their zero point vibrational energy corrections) than any of the models in the region that corresponds to most experimentally observed structures. Their following work (43) showed that the low energy depended on an extensive, cooperative intramolecular hydrogen bonding system (O4′···O3′···O2′···O3···O2···O1). When the O4′ hydroxyl group was removed, the unusual ϕ,ψ conformation no longer had the lowest energy. Calculations with added water molecules have also indicated that the unusual shape is not likely in solution (F.A. Momany, private communication). Because QM energies of carbohydrates are rather dependent on the method and on the basis set, it is important to confirm their result with several types of calculation and with consideration of more possible structures. Also, a QM conformational energy surface for the isolated molecule should still be of interest.

Given the computer time required for such QM studies, it is not surprising that there are few such energy surfaces available for carbohydrates. Several types of QM calculation were used to make maps for trehalose (44), a symmetrical molecule that permitted substantial reduction in the size of the problem. QM maps for lactose have been constructed by da Silva and Nascimento (45), but the results differ somewhat from those of the present report. Preliminary results from the present study were published elsewhere (46).

Methods

To permit accurate comparison with crystal structures, we define the linkage torsion angles as ϕ = O5′-C1′-O4-C4 and ψ = C1′-O4-C4-C5 instead of the usual definitions based on H1′ and H4. To reduce the computer effort to a manageable level, we used a 9 × 9 grid of ϕ and ψ values that were spaced in increments of 20°. This grid, with ϕ = –180° to –20° and ψ = –220° to –60°, covers the central region of full ϕ,ψ maps (see Fig. 2). Some 97% of the conformations in crystal structures of molecules related to cellobiose are in this region, and polysaccharides having these ϕ,ψ conformations are extended helices (17). All variables except ϕ and ψ were optimized with HF/6-31G(d). Next, single point calculations, denoted HF/6-311+G(d)//HF/6-31G(d), were carried out on those geometries.

Fig. 2. ϕ,ψ Space with a diagonal line that represents structures having a twofold screw axis. The inset shows the restricted region of the QM energy surfaces, and the letters A–D indicate the important minimum energy regions. Lowercase letters b and h indicate the approximate locations of the minimized HF (h) and B3LYP (*b*) structures in Table 1. Also shown (●) is the location of the only small-molecule conformation (52) in the D region.



Besides the 81 target geometries and energies on the grid, four other targets were computed. Two targets were unconstrained minimizations in subregions of the central region, called A and B. The starting geometries were adjusted to have ϕ and ψ values that corresponded to minima found in our preliminary mapping studies (46). For the A region, ϕ and ψ values were –80°, –120°, and for the B region, –120°, –160°. The other two targets (C and D) correspond to the "flipped" conformations of Strati et al. (42) that are also called "folded" conformations (47) or "edge-of-the-map" structures (48). They had initial ϕ and ψ values of 60°, –120° (left and right edges) and –60°, 60° (top and bottom edges), for a total of 85 target structures for which the lowest energy was sought. Our map of the central region should allow an assessment of how predictive the vacuum electronic energies are for crystal structures, and the use of the unconstrained minimizations in the regions of the two other minima should address the relative energies of these structures.

The calculated energy of a disaccharide also depends on the orientations of the exo-cyclic groups. Because we are seeking the lowest possible energy for each target structure, it is necessary to try many combinations of the exo-cyclic group orientations (26). Because there are 10 bonds to exocyclic atoms in cellobiose about which rotation is possible, giving each group three staggered orientations would result in 3^{10} or 59 049 combinations. It is not feasible to evaluate all of these at each ϕ,ψ point, especially with QM. In this work we relied both on some structures in the literature and on our own work with MM methods to reduce the number of such combinations, or starting geometries, to a more manageable level. A conformational search procedure performed with Macromodel 7.1 (49) and its AMBER* all-atom poten-

© 2006 NRC Canada

Table 1. Minima and energies from unconstrained minimizations.

Entry name[a]	QM energy (a.u.)	QM method and basis	Φ	Ψ	Relative kcal/mol	Minimum
chem-x_40	–1298.284 874	B3LYP/6-311+G(d)	61.95	–120.04	0.000	C
momany_10A	–1298.278 296	B3LYP/6-311+G(d)	–91.22	–143.99	4.128	A/B
cluster_45	–1298.277 294	B3LYP/6-311+G(d)	–85.15	55.09	4.757	D
cluster_4	–1297.969 169	B3LYP/6-31+G(d)	61.95	–119.99	0.000	C
momany_10A	–1297.963 899	B3LYP/6-31+G(d)	–91.22	–143.99	3.307	A/B
momany_15A	–1297.962 668	B3LYP/6-31+G(d)	–108.72	66.54	4.079	D
cluster_36	–1290.994 716	HF/6-311+G(d)	58.22	–120.40	0.000	C
cluster_3	–1290.988 831	HF/6-311+G(d)	–139.45	–154.26	3.693	B
cluster_12	–1290.988 516	HF/6-311+G(d)	–70.79	–125.90	3.891	A
momany_8	–1290.987 416	HF/6-311+G(d)	–84.12	56.69	4.581	D
cluster_25	–1290.656 548	HF/6-31G(d)	58.21	–120.23	0.000	C
cluster_12	–1290.650 623	HF/6-31G(d)	–70.79	–125.90	3.718	A
cluster_34	–1290.649 253	HF/6-31G(d)	–141.08	–153.55	4.578	B
cluster_43	–1290.648 272	HF/6-31G(d)	–106.60	67.21	5.193	D

Note: The HF/6-311+G(d) and B3LYP/6-311+G(d) energies are for geometries optimized with HF/6-31G(d) and B3LYP/6-31+G(d), respectively.
[a]The names indicate the source of the structure, and the attached number, the particular variant. The momany structures were taken from the work of Strati et al. (42); the momany_10A and momany_15A structures were incorrect copies of the reported structures. The chem-x and cluster structures were created using Chem-X and MacroModel, respectively.

tial (50), followed by analysis with Xcluster 7.1, gave 45 conformers. Another set that we had developed earlier in an MM3 study of native and permethylated disaccharides (48) contained 58 structures. Those structures came from a rules-based conformational generator in Chem-X.[3] The 26 unique structures from the work of Strati et al. (42) were employed with three variations. As done for our cluster search and rules-based structures, all glycosidic bond angles were increased to 150°. This increase, which is quickly resolved during energy minimization, helps avoid interatomic conflicts that might otherwise arise during the rigid residue rotations to create the starting geometries for each ϕ,ψ point. Without the increase, such conflicts often cause the energy minimization to fail. Additionally, we started the grid-search minimizations (but not the unconstrained minimizations) for one set of the Strati et al. structures with the glycosidic bond angles at their as-reported angles. The third set involved alternative orientations of the hydroxyl groups based on a misinterpretation of their torsion angle descriptions for 15 of the structures. There was some redundancy within these 181 starting structures, depending on the criteria for determining a geometric difference, but the duplicates allowed internal checks on our process.

The energy of each starting geometry was minimized for all 85 target structures. Besides the HF methods mentioned above, we used B3LYP/6-31G+G(d) minimization and subsequent B3LYP/6-311+G(d) single point calculations for the unconstrained minimizations. Thus, more than 15 000 energy minimizations and an identical number of single point calculations with a larger basis set were carried out. Jaguar 5.5 (51) was used with the default convergence criteria utilizing 16 processors simultaneously on our compute farm. Because of the large number of structures evaluated, only the electronic potential energies are reported. No frequency calculations were undertaken that could have been used to determine the zero point vibrational energy or free energy.

Results and discussion

Unconstrained minimization

Figure 2 shows the complete ϕ,ψ space of cellobiose and the A–D regions. The ranges of the axes correspond to the approximate translation of ϕ,ψ if they were defined by H1′ and H4, ranging from –180° to +180°. There is an internal border for our 9 × 9 grid-point central region and the positions of the two HF minima and the B3LYP minimum within that boundary are indicated. The locations of the minimized edge-of-the-map, flipped, or folding structures are also shown. The only experimental small molecule structure (52) that does not fit into the central region is indicated in the D region. The dashed diagonal line corresponds to structures having internal twofold screw-axis (2_1) symmetry. This symmetry is reported for crystalline cellulose structures except for cellulose Iα (4), which has pseudo 2_1 symmetry. This symmetry is of interest because of controversy over potentially short contacts among the hydrogen atoms on C1′ and C4, as well as (possibly artifactual) evidence of odd-order meridional diffraction reflections that would rule out the symmetry (53). Cellobiose cannot possess actual intramolecular symmetry because the two glucose residues are chemically different, but cellulose molecules are long enough that its ends do not affect the apparent symmetry.

Table 1 shows the ϕ and ψ values and energies that were obtained during the studies of the A–D regions with the four combinations of QM method and basis set. Regarding the central region, its final minimized structures that were started with the A and B regional ϕ and ψ conformations had wide ranges of ϕ and ψ values. In the case of the HF calculations, the lowest energies were for structures that retained their regional conformations. For the B3LYP calculations, however, the lowest energy values were found for structures that were very close to the twofold symmetry line, where ϕ + ψ = –240°. This conformation is designated A/B, as it

[3]Chem-X is no longer available.

© 2006 NRC Canada

was the lowest energy structure in both the set of B3LYP minimizations started with the A conformation and the set started with the B conformation. There were minimized structures that retained the A and B regional conformations in their respective B3LYP/6-31+G(d) sets, but their energies were about 0.9 kcal/mol (1 cal = 4.184 J) higher than the nearly twofold A/B structure reported in Table 1.

The location of the D minimum depended more on the basis set than the method. Despite being single point calculations, $\phi \approx -85°$ and $\psi \approx +56°$ were preferred with the 6-311+G(d) basis set, whereas $\phi \approx -107°$ and $\psi \approx +67°$ with the smaller 6-31G(d) and 6-31+G(d) basis sets and full minimization. The (right- or left-hand edge) C minimum was essentially independent of the calculation. Five different starting geometries all minimized to give the same lowest-energy structure with both HF and B3LYP, confirmed by both single point calculations. For all combinations of method and basis set, that C-region structure has lower energy, by more than 3 kcal/mol, than structures in the other regions. This confirms the results of Strati et al. (42) with four more combinations of method and basis set, and is in agreement with da Silva and Nascimento's results (45) (minimized structure E in their Table 2). The HF/6-31G(d,p) results of Hardy et al. (47) on methyl α-cellobioside seem similar to those for our A and D regions. They found a structure in our D region (their C region) that was only 0.3 kcal/mol higher than the A region energy. Their slightly different level of theory, HF/6-31G(d,p), should give essentially the same results as our HF/6-31G(d) calculations. Their smaller energy difference may be because their A region structure (interchanged in their Fig. 1 with B) lacks an O3···O5′ hydrogen bond. They apparently did not consider structures in our C region.

Figure 3 shows the structures for each of the minima, with hydrogen bonds shown if the H···O distance is less than 2.8 Å and the O-H···O angle is greater than 90°. The HF/6-31G(d) and B3LYP/6-31+G(d) global minimum structures (C region) are both shown (Figs. 3*a* and 3*b*) to illustrate the effect of the particular calculation on the structures. Mostly, H···O distances are longer for HF/6-31G(d), but it should be said that both methods provide distances longer than seen in crystals. Their O6 atoms are in the *gg* position, allowing strong hydrogen bonds between O6 and O6′. The overall minimum is also stabilized by a strong inter-residue hydrogen bond from O2′ to O3. These hydroxyl–hydroxyl hydrogen bonds are considered to be stronger than hydroxyl donations to the ring oxygen found in the central region for the A and A/B structures, explaining in part the preference for the C structure.

The same A-region structure was preferred in both the HF/6-31G(d) and HF/6-311+G(d) calculations. That structure (Fig. 3*c*) is surprising in that two hydroxyl hydrogen atoms are almost in contact, separated by only 2.45 Å. The O6′ and O6 atoms are *gt*,*gg*, with counterclockwise hydroxyl orientations on the nonreducing ring and clockwise orientations on the reducing ring. This is a common arrangement of O6 positions in small molecule crystals, except that in crystals, *gt* O6′ hydroxyls are turned so that O6′ can accept a bifurcated donation from O3. The hydrogen bond between O3 and O5′ is somewhat long and all of the remaining interactions are likely to contribute very little to the low energy. The values of φ and ψ, however, are likely to be nearly optimal for stabilization by the exo-anomeric effect and the external anomeric torsional effect (54). They are very similar to those of crystalline β-cellobiose ($\phi = -76°$ and $\psi = -132°$ in the crystal (15), $\phi = -71°$ and $\psi = -126°$ in the model).

The lowest energy B3LYP structure from the central region (A/B, Fig. 3*d*) has a stronger hydrogen-bonding network. Not only is the O3···O5′ hydrogen bond shorter and straighter than the HF A-region structure, but there is an even shorter and straighter O2′···O6 hydrogen bond. The O6′ to O4′ hydrogen bond also has favorable geometry. The φ and ψ torsion angles place the structure very close to the twofold screw-axis line, and the *tg* O6 orientations on both residues complete the analogy with cellulose I crystal structures. This support for a low-energy twofold structure is even more compelling because it was selected by both B3LYP calculations. Interestingly, the reducing anomeric hydroxyl groups of this and the above HF A-region structures have orientations that would not be preferred by the exo-anomeric effect, but they participate in cooperative chains ending with O5′. With HF/6-31G(d), this structure is about 1 kcal/mol higher in energy than the structure in the preceding paragraph, while that structure is about 0.9 kcal/mol higher than the present structure at the B3LYP/6-31+G(d) level.

The HF/6-31G(d) and HF/6-311+G(d) B-region structures are almost identical (the HF/6-31G(d) structure is shown in Fig. 3*e*). No structure is shown to represent the B3LYP calculations for the A or B regions, since the A/B structure was preferred. The φ and ψ values for the B region do not permit an O3···O5′ hydrogen bond, but the geometry does allow a fairly strong hydrogen bond from O2′ to O6, with O6 in the *gg* position. O6′ is in the *gt* position. No small molecule crystal structures have φ,ψ conformations in this subregion, but carbohydrate moieties in the 1ct1[4] (55), 1se3 (56), 2chb (57), and 1fbw (58) complexes with crystalline proteins are within a few degrees. Our MM and hybrid energy surfaces (46) are typically 1 or more kcal/mol higher in this region.

The D region (top or bottom of the map) contains a surprise or two. The same structure is preferred with HF/6-31G(d) and B3LYP/6-31+G(d) (Fig. 3*f*), and a different structure is preferred by both the HF/6-311+G(d) and B3LYP/6-311+G(d) single point calculations (Fig. 3*g*). The main difference between the two structures is that the reducing ring has O6 in the *tg* position for the minimized structures and in the *gt* position for the structures preferred by the single point calculations. This causes a difference in the linkage conformation. The O6′ groups are in the *gt* position. Both of the structures that were preferred with the smaller basis sets have a short distance between the O6 and O6′ protons, similar, but even shorter at 2.36 and 2.22 Å, than found for the A-region HF structures.

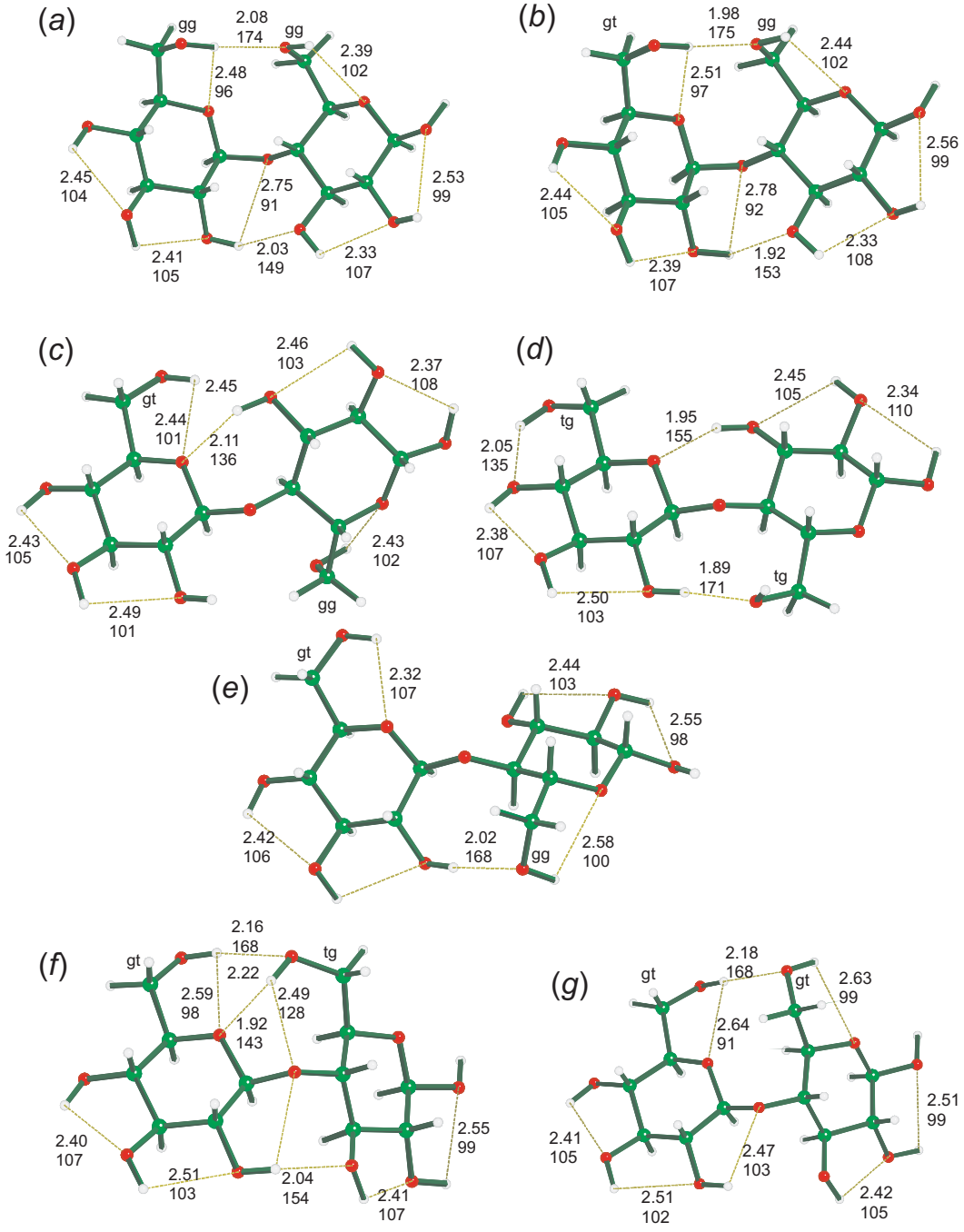
Energy surfaces

Figure 4 shows the HF/6-31G(d) contour map based on

[4] The four character codes correspond to the structure identifying codes that are used in the Protein Data Bank. H.M. Berman, J. Westbrook, Z. Feng, G. Gilliland, T.N. Bhat, H. Weissig, I.N. Shindyalov, and P.E. Bourne. Nucleic Acids Res. **28**, 235 (2000).

© 2006 NRC Canada

Fig. 3. Molecular drawings with hydrogen bonds of minimum energy structures. Their geometries are indicated by a pair of numbers with the upper being the length in angstroms and the lower being the O-H···O angle in degrees. The unpaired numbers 2.45 and 2.21 indicate an H···H short contact in angstroms. (*a*) The global minimum from the C region as optimized by HF/6-31G(d) theory. (*b*) The same structure as in (*a*) except optimized with B3LYP/6-31+G(d). Notice the differences in hydrogen bond geometries. (*c*) The best A region structure, optimized with HF/6-31G(d) theory. (*d*) The A/B structure, optimized with B3LYP/6-31+G(d) theory. (*e*) The best B region structure, optimized with HF/6-31G(d) theory. (*f*) The preferred D region structure, as determined with either HF/6-31G(d) or B3LYP/6-31+G(d) theory (details from the B3LYP structure). (*g*) The D region structure preferred by the HF/6-311+G(d) and B3LYP/6-311+G(d) calculations, with details from the B3LYP structure.



the lowest energy at each of the 81 grid points. Also shown are the conformations from small molecule crystal structures and from complexes of related carbohydrates with proteins. The lowest energy contour (0.25 kcal/mol) contains the structures from β-cellobiose itself (15), nitrated (59) and partially nitrated (60) cellobiose, methyl (2,3,4,6-tetra-*O*-acetyl-β-D-galactopyranosyl)-(1–4)-6-*O*-benzyl-2-deoxy-2-phthalimido-β-D-glucopyranoside (61), and β-lactose (16). There is a high density of the protein complex structures inside that small circle as well. All other small-molecule structures are

© 2006 NRC Canada

Fig. 4. HF/6-31G(d) contour map with crystal structures. The inner contour is 0.25 kcal/mol; all others are at intervals of 1.0 kcal/mol. Small-molecule structures are represented by (●). Carbohydrate conformations in complexes with proteins are shown as (▲).

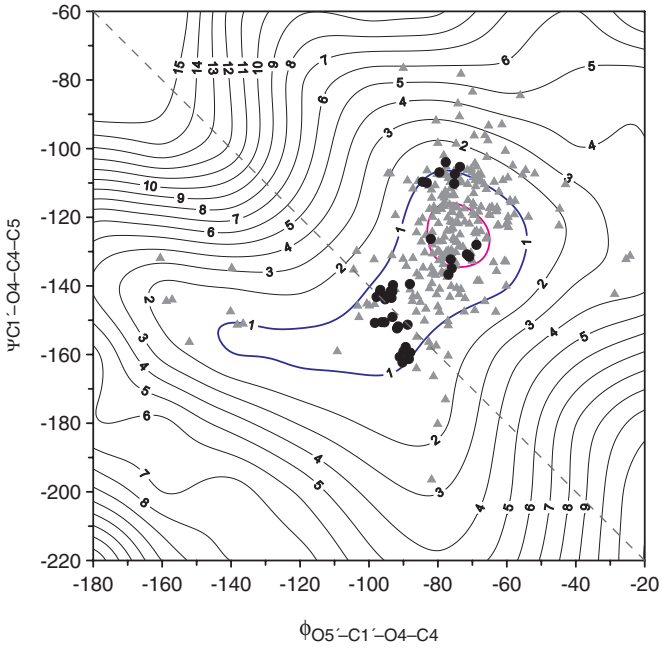
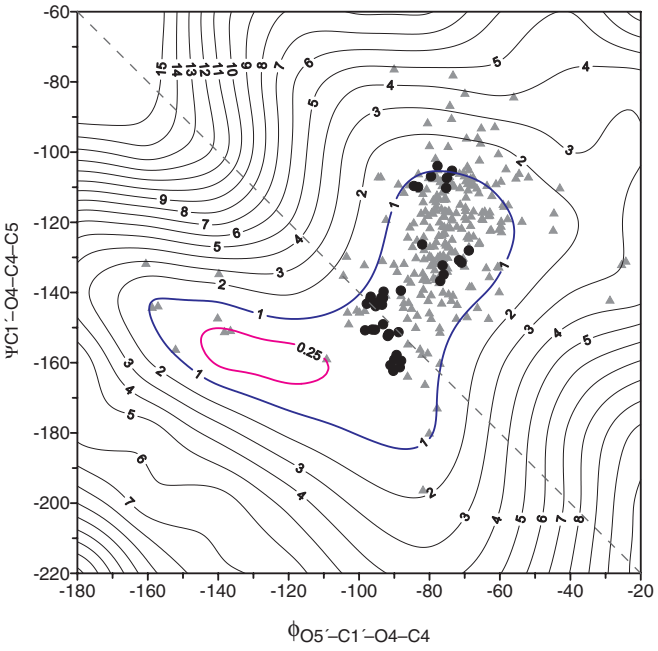


Fig. 5. HF/6-311+G(d) contour map with crystal structures, as in Fig. 4.



within, or just outside, the 1 kcal/mol contour, while a number of the protein complex structures are outside the 2 kcal/mol contour.

Figure 5 shows the corresponding surface for HF/6-311+G(d)//HF/6-31G(d) theory. Again, most of the experimental conformations are within the (somewhat larger) 1 kcal/mol contour. However, based on the dearth of observed structures within the 0.25 kcal/mol contour, we judge it to be less predictive than the HF/6-31G(d) surface (Fig. 4). In our study of trehalose, a seemingly similar single point calculation (HF/6-311++G(d,p)//B3LYP/6-31G(d)) yielded an energy surface that was more predictive of crystal structures than other surfaces in that work. That improved predictiveness was attributed to reduced stabilization of hydrogen-bonded structures, but the present single point calculations, based on HF/6-31G(d) geometries, do not reduce the energy of the hydrogen bonds to a similar extent. Instead, it is impressive to us that with full strength hydrogen bonding, Figs. 4 and 5 are as predictive as they are for cellobiose. This is curious because our hybrid and MM cellobiose maps demand reduction of hydrogen bond strength to be predictive (46). Fortuitous cancellation of errors may be important for these surfaces, and we cannot say that maps produced with the same approach for other disaccharides will accommodate the relevant crystal structures this well.

The biggest difference between these two QM surfaces and most of our other cellobiose energy surfaces is that structures with pseudo 2_1 symmetry now have lower relative energy. This is especially true for the preliminary HF/6-31G(d) and HF/6-311+G(d) single point surfaces, based on "only" 61 starting geometries (46). On those surfaces the diagonal symmetry line passed over a saddle point on the surface between two minima. On other surfaces in that paper, the symmetry line was tangential to the 1 kcal/mol contour. Similar, lower energies for the 2_1 structures were previously provided only by fluorinated cellobiose energy surfaces and a recent hybrid energy surface based on MM4 (40). Indication that the twofold structures may have even lower relative energy is given by the B3LYP/6-31+G(d) A/B structure that also had the lowest single point B3LYP/6-311+G(d) energy. It suggests that similar partial maps constructed with B3LYP and those basis sets might have their global minima bisected by the symmetry line.

One might have guessed that our preliminary surface based on 61 reasonably selected starting geometries would be essentially unchanged by the inclusion of more structures, but that was not the case. The individual energy surfaces provided by each of the different sets of starting geometries (see Methods) gave fairly different surfaces (not shown), except for the correct structures from the Strati et al. (42) paper, and the related set with the 150° glycosidic angle. Those two surfaces were quite similar, but the number of structures that failed to optimize (mostly because of interatomic conflicts in the starting structures) was much lower for the set with the 150° angle. Each of the sets contributed one or more points to the final map, but reliance on any single set of starting geometries resulted in discrepancies with the final composite maps of 3–7 kcal/mol.

These energy surfaces are completely different from the plot in Strati et al. (42), one that those authors had noted was not the same as conventional, grid-search plots like those prepared in the present work. Although our maps cover only the quarter of the ϕ,ψ territory where most crystal structures are found, the range of relative energies on our maps is greater than 18 kcal/mol, to which must be added the 3.7 kcal correction for the global minimum, as well as the

© 2006 NRC Canada

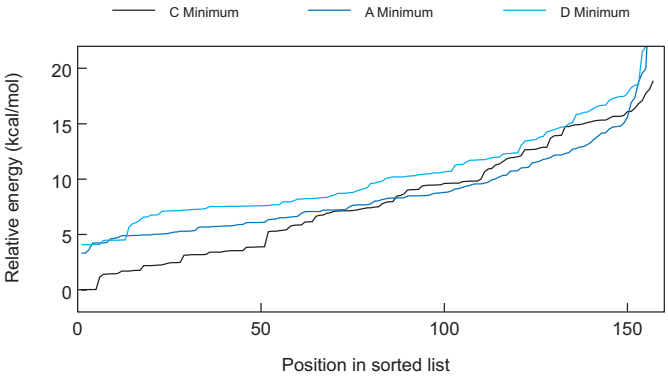
peaks that occur outside our central region. In the same portion of ϕ,ψ space as our limited surface covers, the Strati et al. energies have a range of about 2 kcal/mol. Unlike that flat surface, the da Silva and Nascimento surfaces (45), which were constructed with grid searches, have peaks of 85 kcal/mol and higher. Their tortuous surfaces may result, at least in part, from considering only a single starting structure for each linkage conformation. Our MM3 surfaces for cellobiose and permethylated cellobiose (48) have relative maxima of less than 30 kcal/mol, and our HF/6-31G(d) surfaces for the tetrahydropyran-based analog of cellobiose (39) have maxima of less than 20 kcal/mol.

Figure 6 shows the impact of exo-cyclic group orientation on the energies from the unconstrained minimizations. In each of the three regions of stable ϕ,ψ conformation, the energies based on exo-cyclic orientation variation have nearly continuous ranges that nearly equal the 18 kcal/mol range based on variation in ϕ and ψ. It should be kept in mind that the structures used in these calculations were preselected with the aim of providing the lowest energy, and the range based on exo-cyclic orientations would otherwise be even larger.

The conformations from the small-molecule crystals are well accounted for by Fig. 4, always bearing in mind, of course, that the global minimum is in region C, not included in the figure. The upper group of seven small-molecule structures is of interest because those crystal structures have no interresidue hydrogen bonding, yet their average energy is only about 1 kcal/mol above the map's lowest energy. There is considerably more scatter in the conformations from the protein complex structures. Those structures are not as reliably determined as the small-molecule structures, but are none-the-less interesting tests of energy surfaces. Some of these, mentioned previously when discussing the B region minimization, provide justification for the extension of the low-energy region to the lower values of the ϕ torsion angle, despite the absence of stabilization from the exo-anomeric effect. On the other hand, structures above ψ = –100° have remarkably high energies. Consider the observed point from the 1fv3 protein complex (62) with ϕ and ψ values of –72.3° and –78.2°. It lies between the 5 and 6 kcal/mol contours in Fig. 4. Rotation of the reducing ring in the 1fv3 structure to give a ψ value of –133°, a conformation essentially that of crystalline β-cellobiose, results in a O3···O5′ distance of only 2.13 Å. This indicates that the monosaccharide geometries in the 1fv3 structure are distorted considerably from those normally found, and that the structure is probably not accurately determined.

The three groups of experimental conformations from the small-molecule crystals that were mentioned in the Introduction are visible on Figs. 4 and 5. None of these surfaces have multiple minima that would account for three separated types of conformation. Instead, we can imagine that structures along the symmetry line are there because the molecules take the shape of a flat ribbon that can pack very efficiently. The remaining small-molecule structures are within a continuum of structures from the less accurately determined protein complexes. That continuum is consistent with the present energy calculations and together they imply that the groupings are not based on an intrinsic molecular energy.

Fig. 6. Sorted energies from structures started in the A, C, and D minima, calculated with B3LYP/6-31+G(d) minimization.



Conclusion

By restricting the range of ϕ and ψ to the most interesting region, we have been able to afford to construct energy surfaces for cellobiose at two levels of ab initio QM theory that involved an unusually large number of starting geometries. We also isolated the interesting minima by using the same starting geometries in unconstrained minimization. This work has confirmed that the global minimum structure for various affordable QM calculations is in a region that is not populated by any small-molecule crystal structures and is rather distant from any of the reported protein complex structures as well. The repeated finding that the same structure is the calculated global minimum, despite using several combinations of QM method and basis set, is unusual for a disaccharide. This rarity is exemplified by our finding of different structures for the other minima, or in the case of the central zone, finding a common structure with both B3LYP calculations despite starting from the A and B region conformations that had been identified with HF calculations. In support of the global minimum, its hydrogen-bonding system is arguably superior in that there are two hydroxyl–hydroxyl links between the two glucose residues instead of the weaker O3···O5′ hydrogen bonds found in the A region structures.

The large number of starting structures was important to the definition of the overall surface. Variations in energy from combinations of exo-cyclic group orientations are of a magnitude similar to those caused by variations in ϕ and ψ. The contours provided by both the HF calculations were quite predictive of the crystal structure conformations, bearing in mind that the global minimum was not included on our energy surfaces. Except for one structure that has a D conformation, the surfaces accommodated all of the experimental small-molecule structures within about 1.2 kcal of their respective minima, with the HF/6-31G(d) calculations being slightly more predictive than the single point energies that used a larger basis set. Even the experimental structure in the D region was not orphaned by these calculations. The unconstrained minimum for the D region is only 0.7 to 1.5 kcal higher than the A region, depending on the combination of method and basis set. Compared to many of our other surfaces, the experimental twofold structures corresponded to lower energy, suggesting that the strain of crystal

© 2006 NRC Canada

packing for cellulose and other small molecules near the twofold line is minimal.

Somewhat unusual structures appeared as local A and D region minima. These structures had distances between hydroxyl hydrogen atoms that are as short as 2.22 Å. That distance resulted from the better QM calculation used for minimization, B3LYP/6-31+G(d), which has been recommended for carbohydrates (63). Whether these are valid structures remains to be seen.

A great deal of progress has occurred in carbohydrate modeling. Even a decade ago, it would have been difficult to imagine that we would have been able to prepare energy surfaces such as presented herein. On the other hand, many of the problems are still present. In 1989, French and Brady (64) wrote "The biggest obstacle is the 'multiple minimum problem' which arises because energy surfaces for complex molecules have more than one local minimum." Even if this problem has been overcome in the present work by brute force, there was an important effect of the different starting geometries on the energy surface. That shows that it is important to make a thorough attempt to include all relevant structures and avoid making conclusions based on local minima. It is also clear that improved QM methods and basis sets will be useful in future calculations.

Acknowledgments

The authors dedicate this work to honor Walter Szarek, whose commitment, hard work, congeniality, and talent were inspiring during overlapping tenure with ADF on the Executive Committee of the Division of Carbohydrate Chemistry of the American Chemical Society. We thank Professors C.O. da Silva, Universidad Federal Rural do Rio de Janeiro, Brazil, and G.I. Csonka, Budapest University of Technology, Hungary, as well as Dr. K.Q. Robert of our research center for comments on a draft of this paper.

References

1. S. Nishikawa and S. Ono. Proc. Tokyo Math. Phys. Soc. **7**, 131 (1913).
2. P. Langan, Y. Nishiyama, and H. Chanzy. Biomacromolecules, **2**, 410 (2001).
3. Y. Nishiyama, P. Langan, and H. Chanzy. J. Am. Chem. Soc. **124**, 9074 (2002).
4. Y. Nishiyama, J. Sugiyama, H. Chanzy, and P. Langan. J. Am. Chem. Soc. **125**, 14300 (2003).
5. M. Wada, Y. Nishiyama, J. Sugiyama, H. Chanzy, and P. Langan. Macromolecules, **37**, 8548 (2004).
6. F. Tanaka and N. Fukui. Cellulose, **11**, 33 (2004).
7. M. Umemura, Y. Yuguchi, and T. Hirotsu. J. Phys. Chem. A, **108**, 7063 (2004).
8. D.A. Rees and R.J. Skerrett. Carbohydr. Res. **7**, 334 (1968).
9. S. Melberg and Kj. Rasmussen. Carbohydr. Res. **71**, 25 (1979).
10. G.M. Lipkind, V.E. Verovsky, and N.K. Kochetkov. Carbohydr. Res. **133**, 1 (1984).
11. I. Tvaroška and S. Perez. Carbohydr. Res. **149**, 389 (1986).
12. M.K. Dowd, A.D. French, and P.J. Reilly. Carbohydr. Res. **233**, 15 (1992).
13. E.A. Larsson, M. Staaf, P. Söderman, C. Höög, and G. Widmalm. J. Phys. Chem. A, **10**8 3932 (2004).
14. H. Yu, M. Amann, T. Hansson, J. Köhler, G. Wich, and W.F. van Gunsteren. Carbohydr. Res. **33**9 1697 (2004).
15. S.S.C. Chu and G.A. Jeffrey. Acta Crystallogr. Sect. B, **24**, 830 (1968).
16. K. Hirotsu and A. Shimada. Bull. Chem. Soc. Jpn. **47**, 1872 (1974).
17. A.D. French and G.P. Johnson. Cellulose, **11**, 5 (2004).
18. J.T. Ham and D.G. Williams. Acta Crystallogr. Sect. B, **26**, 1373 (1970).
19. R. Stenutz, M. Shang, and A.S. Serianni. Acta Crystallogr. Sect. C, **55**, 1719. (1999).
20. N.W.H. Cheetham, P. Dasgupta, and G.E. Ball. Carbohydr. Res. **338**, 955 (2003).
21. S. Engelsen and Kj. Rasmussen. J. Carbohydr. Chem. **16**, 773 (1997).
22. J.-F. Espinosa, F.J. Canada, J.L. Asensio, M. Martin-Pastor, H. Dietrich, M. Martin-Lomas, R.R. Schmidt, and J. Jimenez-Barberos. J. Am. Chem. Soc. **118**, 10862 (1996).
23. M. Martin-Pastor, A. Canales, F. Corzana, J. L. Asensio, and J. Jimenez-Barberos. J. Am. Chem. Soc. **127**, 3589 (2005).
24. K. Mazeau, S. Perez, and M. Rinaudo. J. Carbohydr. Chem. **19**, 1269 (2000).
25. K.J. Naidoo and J.W. Brady. J. Am. Chem. Soc. **121**, 2244 (1999).
26. C.A. Stortz. Carbohydr. Res. **322**, 77 (1999).
27. A.D. MacKerrel, Jr. J. Comput. Chem. **25**, 1595, (2004).
28. G.A. Jeffrey, J.A. Pople, and L. Radom. Carbohydr. Res. **25**, 117 (1972).
29. R.J. Woods, W.A. Szarek, and V.H. Smith, Jr. J. Chem. Soc. Chem. Commun. 334 (1991).
30. S.E. Barrows, F.J. Dulles, C.J. Cramer, A.D. French, and D.G. Truhlar. Carbohydr. Res. **276**, 219 (1995).
31. G.I. Csonka, K. Éliás, and I.G. Csizmadia. Chem. Phys. Lett. **49**, 257 (1996).
32. S.E. Barrows, J.W. Storer, C.J. Cramer, A.D. French, and D.G. Truhlar. J. Comput. Chem. **19**, 1111 (1998).
33. G.I. Csonka, K. Éliás, and I.G. Csizmadia. J. Comput. Chem. **18**, 330 (1997).
34. G.I. Csonka, K. Éliás, I. Kolossvá, C.P. Sosa, and I.G. Csizmadia. J. Phys. Chem. A, **102**, 1219 (1998).
35. I. Tvaroška and J. Carver. J. Mol. Struct: THEOCHEM, **395**–**396**, 1 (1997).
36. I. Tvaroška and L. Václavík. Carbohydr. Res. **160**, 137 (1987).
37. C. Van Alsenoy, A.D. French, M. Cao, S.Q. Newton, and L. Schafer. J. Am. Chem. Soc. **116**, 9590. (1994).
38. M. Odelius, A. Laaksonen, and G. Widmalm. J. Phys. Chem. **99**, 12686 (1999).
39. A.D. French, A.-M. Kelterer, G.P. Johnson, M.K. Dowd, and C.J. Cramer. J. Comput. Chem. **22**, 65 (2001).
40. A.D. French, G.P. Johnson, A.-M. Kelterer, and G.I. Csonka. Tetrahedron: Asymmetry, **16**, 577 (2005).
41. A.D. French, A.-M. Kelterer, G.P. Johnson, M.K. Dowd, and C.J. Cramer. J. Mol. Graphics Modell. **18**, 95 (2000).
42. G.L. Strati, J.L. Willett, and F.A. Momany. Carbohydr Res. **337**, 1833 (2002).
43. G.L. Strati, J.L. Willett, and F.A. Momany. Carbohydr Res. **337**. 1851 (2002).
44. A.D. French, G.P. Johnson, A.-M. Kelterer, M.K. Dowd, and C.J. Cramer. J. Phys. Chem. A, **106**, 4988 (2002).
45. C.O. da Silva and M.A.C. Nascimento. Carbohydr. Res. **339**, 113 (2004).
46. A.D. French and G.P. Johnson. Cellulose, **11**, 449 (2004).
47. B.J. Hardy, A. Gutierrez, K. Lesiak, E. Deidl, and G. Widmalm. J. Phys. Chem. **100**, 9187 (1996).

© 2006 NRC Canada

48. S. Mendonca, G.P. Johnson, A.D. French, and R.A. Laine. J. Phys. Chem. A, **106**, 4115 (2002).
49. Macromodel. Version 7.1 [computer program]. Schrodinger, LLC., Portland, Oregon.
50. H. Senderowitz and W.C. Still. J. Org. Chem. **62**, 1427 (1997).
51. Jaguar. Version 5.5 [computer program]. Schrodinger, LLC., Portland, Oregon.
52. A. Ernst and A. Vasella. Helv. Chim. Acta, **79**, 1279 (1996).
53. K.M. Paralikar and S.M. Betrabet. J. Appl. Crystallogr. **12**, 589 (1979).
54. J.-H. Lii, K.-H. Chen, G.P. Johnson, A.D. French, and N.L. Allinger. Carbohydr. Res. **340**, 853 (2005).
55. E.A. Merritt, S. Sarfaty, M.G. Jobling, T. Chang, R.K. Holmes, T.R. Hirst, and W.G. Hol. Protein Sci. **6**, 1516 (1997).
56. S. Swaminathan, W. Furey, J. Pletcher, and M. Sax. Nat. Struct. Biol. **2**, 680 (1995).
57. E.A. Merritt, S. Sarfaty, M.G. Jobling, T. Chang, R.K. Holmes, T.R. Hirst, and W.G. Hol. Protein Sci. **6**, 1516 (1997).
58. G. Parsiegla, C. Reverbel-Leroy, C. Tardif, J.P. Belaich, H. Driguez, and R. Haser. Biochemistry, **39**, 11238 (2000).
59. A.V. Nikitin, V.I. Andrianov, R.M. Myasnikova, S.I. Firgang, A.I. Usov, V.F. Sopin, and A.I. Pertsin. Kristallografiya, **31**, 676 (1986).
60. A.V. Nikitin, T.A. Shibanova, S.I. Firgang, A.I. Usov, V.F. Sopin, and R.M. Myasnikova. Kristallografiya, **32**, 896 (1987).
61. J. Xia, T. Srikrishnan, J.L. Alderfer, R.K. Jain, C.F. Piskorz, and K.L. Matta. Carbohydr. Res. **329**, 561 (2000).
62. C. Fotinou, P. Emsley, I. Black, H. Ando, H. Ishida, M. Kiso, K.A. Sinha, N.F. Fairweather, and N.W. Isaacs. J. Biol. Chem. **276**, 32274 (2001).
63. G.I. Csonka. J. Mol. Struct: THEOCHEM, **584**, 1 (2002).
64. A.D. French and J.W. Brady. ACS Symp. Ser. **340**, 1 (1990).

© 2006 NRC Canada

DNA and RNA enzymes with peroxidase activity — An investigation into the mechanism of action[1]

Paola Travascio, Dipankar Sen, and Andrew J. Bennet

Abstract: A DNA–hemin complex (PS2.M–hemin), and its RNA counterpart (rPS2.M–hemin), have previously been reported, in the presence of nitrogenous buffers such as HEPES, to show enhanced peroxidative activity relative to both uncomplexed hemin and a control DNA–hemin complex (Chem. Biol. **5**, 505, 1998). A kinetic analysis of these two hemin-utilizing nucleic acid enzymes provides key insights into the mechanisms for their catalyzed peroxidation reactions. First, control experiments indicate that charge on the added detergent, required for solubility reasons, has little effect on the efficiency of the nucleic-acid-catalyzed reactions. Second, the key functional impact of the two nucleic acid frameworks, either DNA or RNA, appears to be a reduction in the acidity of a water molecule coordinated to the iron atom of the hemin that is bound to the ribozyme and DNAzyme scaffolds. This effect could result from a polar environment and possibly hydrogen bond(s) at the axial position of the hemin, along with favourable hydrophobic interactions for the periphery of the porphyrin ring. Third, the basic component of the buffer enhances the activities; this likely results from a general-base-catalyzed process. Cumulatively, these data supply important clues as to how biopolymers other than a protein can complex with hemin to form productive peroxidase enzymes.

Key words: ribozyme, DNAzyme, hemin, peroxidase, mechanism, guanine quadruplex.

Résumé : Il a été rapporté antérieurement que, en présence de tampons azotés tel le HEPES, un complexe ADN–hémine (PS2.M–hémine) et sa contrepartie (rPS2.M–hémine) présentent une activité peroxydante plus élevée que celle tant de l'hémine ou un complexe ADN–hémine de contrôle (Chem. Biol. **5**, 505, 1998). Une analyse cinétique de ces deux enzymes d'acide nucléique utilisant de l'hémine fournit des éléments clés pour mieux comprendre les mécanismes de leurs réactions d'oxydation catalysées. Le premier provient des expériences de contrôle qui indiquent que la charge sur le détergent ajouté, requis pour des raisons de solubilité, n'a que peu d'effet sur l'efficacité des réactions catalysées par un acide nucléique. Le deuxième a trait au fait que l'impact fonctionnel des deux squelettes d'acides nucléiques, soit l'ADN ou l'ARN semble provenir d'une réduction de l'acidité d'une molécule d'eau liée à l'atome de fer de l'hémine qui est liée aux échafauds de ribozyme et ADNzyme. Cet effet pourrait provenir d'un environnement polaire et aussi de liaisons hydrogènes à la position axiale de l'hémine liée à des interactions hydrophobes favorables pour la périphérie du cycle porphyrine. Le troisième est lié au fait que la composante basique du tampon augmente les activités; ce qui résulte probablement d'un processus de catalyse basique générale. Dans leur ensemble, ces données fournissent des données importantes qui permettraient de comprendre comment des biopolymères autre qu'une protéine pourrait former un complexe avec l'hémine pour produire des enzymes peroxydases utiles.

Mots clés : ribozyme, ADNzyme, hémine, peroxydase, mécanisme, quadruplexe de guanine.

[Traduit par la Rédaction]

Introduction

The reaction of hydrogen peroxide with ferric porphyrins is of interest in relation to several classes of natural enzymes that use that metalloporphyrin as an essential cofactor. For instance, peroxidases catalyze the oxidation of a variety of substrates by hydrogen peroxide, whereas, catalases are enzymes that promote the disproportionation of hydrogen peroxide to give oxygen and water. Both classes of enzymes are highly efficient catalysts in which the formation of an outer-sphere porphyrin – hydrogen peroxide complex is generally the rate-determining step (1). Horseradish peroxidase (HRP), the most thoroughly studied and representative peroxidase enzyme, reacts with hydrogen peroxide, hydroperoxides, or peracids to form two distinct intermediates known as compounds I and II (2). Compound I is a green species (3) possessing two oxidizing equivalents above the Fe(III) state, and a variety of spectroscopic and kinetic studies have indicated that it is an oxo-ligated Fe(IV) porphyrin radical cation ($Fe^{IV}OP^{+\cdot}$) (4–9). Compound II is also a Fe(IV) species ($Fe^{IV}OP$), but possesses one fewer oxidizing equivalent (4–9). Extensive studies have established that the peroxidation

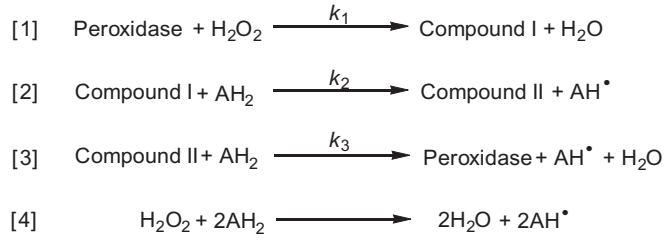
Received 20 September 2005. Published on the NRC Research Press Web site at http://canjchem.nrc.ca on 10 May 2006.

P. Travascio, D. Sen,[2] and A.J. Bennet.[3] Department of Molecular Biology and Biochemistry and Department of Chemistry, Simon Fraser University, Burnaby, BC V5A 1S6, Canada.

[1]This article is part of a Special Issue dedicated to Professor Walter A. Szarek.
[2]Corresponding author (e-mail: dipankar_sen@sfu.ca).
[3]Corresponding author (e-mail: bennet@sfu.ca).

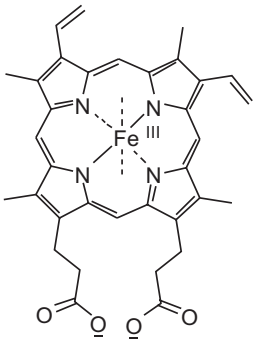
 doi:10.1139/V06-057 © 2006 NRC Canada

Scheme 1.

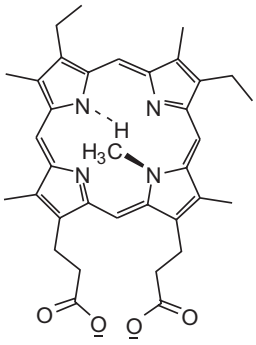


reaction catalyzed by HRP (and other peroxidases) proceeds according to the enzymatic cycle shown in Scheme 1 (4–9), where AH_2, a reducing substrate, is converted into a free radical species ($AH^{\bullet}$) by one-electron oxidation processes. A key mechanistic question concerning peroxidase catalysis is the means by which the high reaction rates for the generation of compound I are achieved. In this respect, a number of studies with peroxidase model systems have been carried out. For example, a series of articles from Traylor and coworkers (10–12) detail the oxidation reactions promoted by several ferric protoporphyrin derivatives, in methanol as solvent, using either hydrogen peroxide or a peracid as the oxidant. In comparison to hemin itself, it was reported that all derivatives possessing a covalently attached base were catalytically more active, and the observed rate accelerations upon attachment of a basic functionality were attributed to either a "proximal base effect", an intramolecular bonding interaction between the hemin and the base, or a "distal base effect", intramolecular general catalysis. Also of note, the addition of nitrogenous bases to the medium increased the reaction rate, an effect that presumably arises from intermolecular general catalysis. Other model studies on nonaggregating, water-soluble iron(III) porphyrins, which possessed meso-phenyl rings, yielded evidence for the occurrence of general catalysis by nitrogenous buffers, including 2,4,6-collidine (13).

In line with these studies on peroxidase model systems, a guanine-rich DNA oligomer and its corresponding RNA version ("PS2.M" and "rPS2.M", respectively) were found to bind hemin (**1**) with dissociation constants of 27 ± 2 nmol/L and 0.9 ± 0.2 μmol/L, respectively (14). Remarkably, PS2.M–hemin and rPS2.M–hemin complexes were found to possess high peroxidation activity, despite PS2.M being selected from a random sequence single-stranded DNA library for the specific binding of a different porphyrin, *N*-methyl mesoporphyrin IX (NMM, **2**) (14, 15).

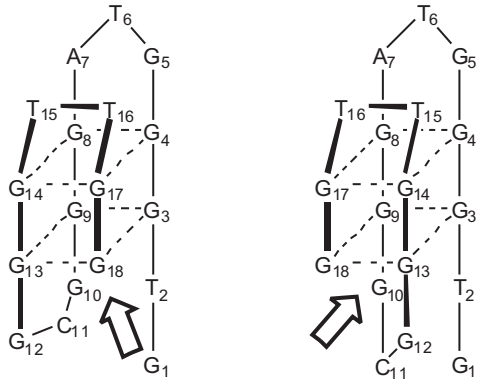


Fe(III) protoporphyrin IX (**1**)



N-Methylmesoporphyrin (**2**)

Fig. 1. Two possible models for the potassium-folded PS2.M. The postulated binding sites for the hemin are shown by the arrows. The hydrogen bonding in the two guanine quartets (G_4, G_8, G_{14}, and G_{17}, and G_3, G_9, G_{13}, and G_{18}) are shown by the dashed lines.



The PS2.M–hemin and rPS2.M–hemin complexes could therefore be regarded as a new category of deoxyribozyme (DNAzyme) and ribozyme, respectively. Recently, they have found practical applications (16, 17). UV–vis and electron paramagnetic resonance (EPR) spectroscopies (14, 18) indicated that the hemin iron changed the character of its coordination upon complexation to the folded nucleic acid oligomers. Thus, the observed spectra more closely resemble those of horseradish peroxidase (HRP) and other hemoproteins rather than those associated with uncomplexed hemin.

We have recently reported a pair of models for the actively folded structure of PS2.M and these two structures are shown in Fig. 1 (19). Two loop guanines (G_{10}, G_{12}) appear to be necessary for hemin binding and one of them may serve as an axial ligand (19).

This report addresses several key questions concerning the nature of the "active" species that participate in the DNA/RNA–hemin-catalyzed peroxidation reactions. Questions include: Are the nucleotides merely acting to stabilize dissociated hemin? What is the effect of pH on the peroxidation reaction rate? Finally, what catalytic role, nucleophilic or general base, does the added buffer perform?

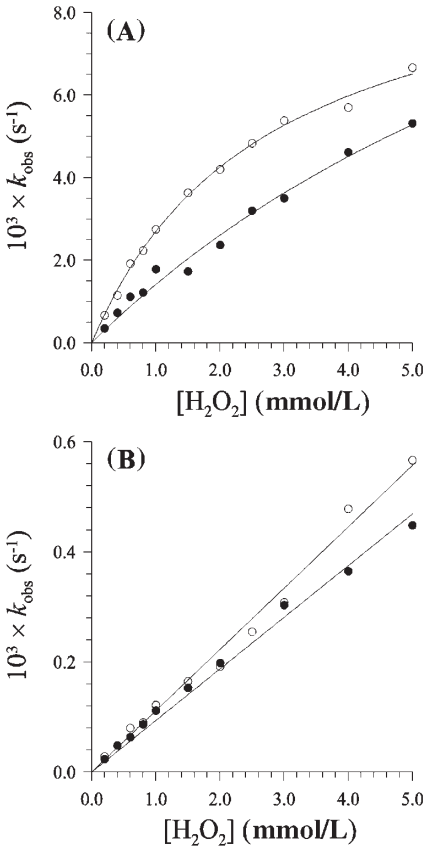
Results and discussion

Effect of detergents on the catalytic properties of hemin

To determine whether the contribution of the DNA moiety towards the catalytic properties of PS2.M–hemin results "trivially" from solubilization of the hemin (**1**) and surrounding it in a negatively charged environment, the catalytic activity of hemin was examined in positively, negatively, and neutrally charged micelles. Specifically, the properties of hemin solubilized by the charge neutral Triton X-100, negatively charged sodium dodecyl sulphate (SDS), and the positively charged cetyltrimethyl ammonium bromide ($CetMe_3N^+$) were studied. Hemin is solubilized by these three surfactants, however, while trying to measure the peroxidative activities of these complexes, it was observed in the case of $CetMe_3N^+$ that a precipitate formed during the peroxidation reactions, thus making it impossible to measure accurate rate constants in the positively charged micelles. Figure 2 shows the measured rate constants for hemin

© 2006 NRC Canada

Fig. 2. Plot of observed rate constant for Triton X-100–hemin-catalyzed (○) and SDS–hemin-catalyzed (●) peroxidation reactions as a function of H_2O_2 concentration. (A) HEPES buffer (200 mmol/L, pH 6.2); (B) buffer (5 mmol/L, pH 6.2).



solubilized in SDS and in Triton X-100 micelles, respectively, (in 4-(2-hydroxyethyl)piperazine–1-ethanesulfonic acid (HEPES) buffer (200 mmol/L and 5 mmol/L), and as a function of hydrogen peroxide concentration). The characteristics of the two plots are very similar, most notably under conditions of low buffer concentration.

Given that the peroxidative activity of hemin was not markedly different in neutral (Triton X-100) or anionic surfactant (SDS) micelles, it was possible to conclude that measured catalytic efficiency of the PS2.M– and rPS2.M–hemin complexes (14, 15) does not originate from solubilization of hemin in a negatively charged environment, thus suggesting that the polyanionic character of the phosphate backbone in the PS2.M– and rPS2.M–hemin complexes is not the primary reason for the observed peroxidation catalysis.

The "alkaline transition" of hemin complexes

It has been known for many years that acid–base transitions occur for many ferric hemoproteins, and that they are linked to the ionization of a water molecule coordinated to the sixth (axial) position of the hemin iron (20, 21). Therefore, the acid–base titrations for the nucleotide–hemin complexes were followed by monitoring the absorption curve at various pH values. The measured spectra showed sharp changes and clean isosbestic points, indicating that the

Fig. 3. Spectrophotometric titration to determine the pK_a of the water molecule ligated to the PS2.M–hemin complex from the ratio of absorptions at 404 and 360 nm. The symbols (○) are experimental values, and the curve is the best nonlinear fit to a standard titration equation.

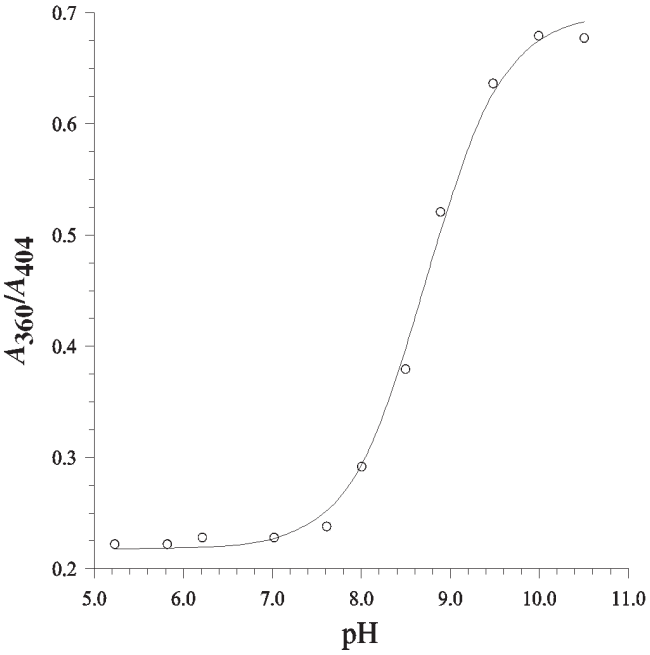


Table 1. Derived pK_a values for the acid–alkaline transitions of various hemin complexes.

Enzyme (hemin complex)	pK_a
PS2.M	8.70±0.03
rPS2.M	8.60±0.10
Triton X-100	3.4±0.2
$CetMe_3NBr$	3.0±0.1
SDS	4.0±0.5
OXY4	5.9±0.3
MetMyo[a]	8.93±0.03
MetHem[a]	8.33±0.02
HRP[b]	10.9±0.4

[a]Quoted values are from ref. 21.
[b]Quoted values are from ref. 36.

hemin complexes underwent a clean interconversion among two species. The pK_a values for these transitions were calculated from the ratio of the measured absorbances at 360 and 404 nm (Fig. 3 shows the data for PS2.M–hemin). The corresponding pK_a values were also calculated for the pH-dependent ionizations in the rPS2.M–hemin complex, the OXY4–hemin complex (OXY4 was a noncatalytic control guanine-rich DNA, 5′-d[T_4G_4]$_4$-3′), known to fold into a guanine quadruplex, but whose complex with hemin gave only a modest peroxidase activity (1), and the various hemin–detergent complexes. These measured pK_a values are compiled in Table 1.

By analogy to previous reports (20), it appears likely that the acidic species in the DNA–hemin complexes, such as PS2.M–hemin, rPS2.M–hemin, and OXY4–hemin, corre-

© 2006 NRC Canada

spond to a high-spin aquo iron(III) species, while the deprotonated form is likely a low-spin, hydroxide-coordinated iron moiety. Clearly, the pK_a values associated with the PS2.M–hemin and rPS2.M–hemin complexes are significantly different from that of the OXY4–hemin complex as well as of hemin in the presence of the three detergents. Of note, complexation of hemin to both PS2.M and rPS2.M considerably reduces the acidity of the iron-bound water molecule, and the pK_a values associated with these complexes are comparable to those of metmyoglobin and methemoglobin (ferric myoglobin and hemoglobin) (21–23), heme proteins with demonstrated peroxidase activities.

The large difference in pK_a values between Triton X-100 solubilized hemin and the PS2.M–hemin and rPS2.M–hemin complexes is almost certainly one of the major sources for the enhanced catalytic activity of the ribozyme– and DNAzyme–hemin complexes. That is, at pH values between 6.0 and 8.0, the transition-state structures for the respective HEPES-catalyzed peroxidations contain, in addition to the oxidant (H_2O_2) and the basic component of the buffer, either the acid form of the ribozyme– and DNAzyme–hemin complex or the conjugate base of a hemin molecule. In other words, the obligatory coordination of the peroxide to the iron centre by displacement of one of the axially bound ligands is likely to be a much slower process when a hydroxide group occupies one of these sites instead of a water molecule, with the concomitant result that, in the absence of the nucleotide, the hemin reactivity towards H_2O_2 is low. This notion is supported by data from studies on HRP, a hemin-containing enzyme that was shown to have a significantly reduced activity upon deprotonation in basic solutions (2, 24).

The pK_a of the hemin-bound water in the catalytically poorly active OXY4 aptamer is lower than for PS2.M (ca. 2.7 pH units), but higher than the values found for detergents. This suggests that, although the environment presented by OXY4 guanine quadruplex might be as polar as that for PS2.M, the distance and (or) the position of key functional group(s) with respect to the hemin (and vice versa) might be different between the folded PS2.M and OXY4 molecules. Likewise, the low pK_a values associated with hemin in the micellar systems suggested that a hydrophobic environment increases the acidity of one of the axial water protons (25). Finally, the high value for the pK_a of HRP compared with the other hemin complexes has been attributed to an acid–alkaline transition different from those found in the other complexes. It has been reported that HRP is converted from a high-spin five-coordinate species, with no water in the sixth position, to a six-coordinate low-spin heme at high alkaline pH (26).

The effect of HEPES buffer

Previous investigations on PS2.M–hemin-catalyzed peroxidations suggested that buffer catalysis was an important component to these biological reaction mimics (14). Indeed, HEPES was found to be a particularly good catalyst, and therefore the effect of HEPES concentration (between 0 and 200 mmol/L) on the rate of the peroxidation reactions catalyzed by both Triton-solubilized hemin and PS2.M–hemin were measured at four different pH values (6.2, 7.0, 7.7, and 8.0). Figure 4 shows the dependence of the observed rate constant (k_{obs}) of PS2.M–hemin- and hemin-catalyzed peroxidation reactions on HEPES concentrations (at pH values of 6.2 and 7.0).

Fig. 4. Plot of the measured pseudo-first-order rate constants for the PS2.M–hemin-cataylzed (pH 6.2, ■ and pH 7.0, ●) and hemin-catalyzed (pH 6.2, □ and pH 7.0, ○) peroxidation reactions as a function of the total HEPES concentration ([H_2O_2] = 600 μmol/L). The straight lines shown are the best linear fits of the rate constant data for [HEPES] ≤ 0.05 mol/L.

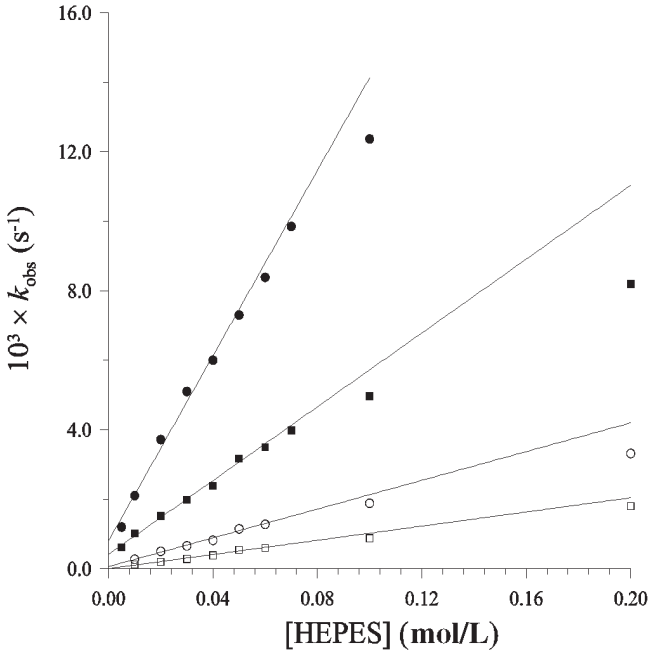


Table 2. Variation of k_3 ((mol/L)$^{-2}$ s^{-1}) with the mole fraction of free HEPES for the PS2.M–hemin-, rPS2.M–hemin-, and hemin-catalyzed peroxidation reactions.

f_B	PS2.M–hemin	rPS2.M–hemin	Hemin
0.043	0.53×10^6	0.53×10^6	0.089×10^6
0.220	1.54×10^6	1.71×10^6	0.157×10^6
0.585	4.34×10^6	4.00×10^6	0.073×10^6
0.738	3.90×10^6	3.90×10^6	0.070×10^6
0.081	—	—	0.105×10^6

Note: Estimated errors, 5%.

Linear fits of the above rate constant data, at the low buffer concentration yielded, after correction for the concentration of catalyst, pseudo-third-order rate constants. A listing of these calculated rate constants (k_3) as functions of the fraction of the basic component of the buffer (f_B) is given in Table 2.

A striking feature of the pseudo-third-order rate constants on oxidant concentration is a discontinuity in each dependence (Table 2). The decrease in activity for both nucleotide–hemin complexes at high pH likely results from the increasing concentration of the iron hydroxide form of the respective complexes. In contrast, in the hemin case the protonation state of the iron's ligands does not change at the pH values used in these experiment, and it is not clear as to the origin of the discontinuity evident in the rate constant data listed in Table 2.

© 2006 NRC Canada

Fig. 5. Plot of observed pseudo-first-order rate constants as functions of H_2O_2 at [HEPES] = 200 mmol/L (pH 6.2). The insert is the kinetic data at a HEPES concentration of 5 mmol/L (pH 6.2).

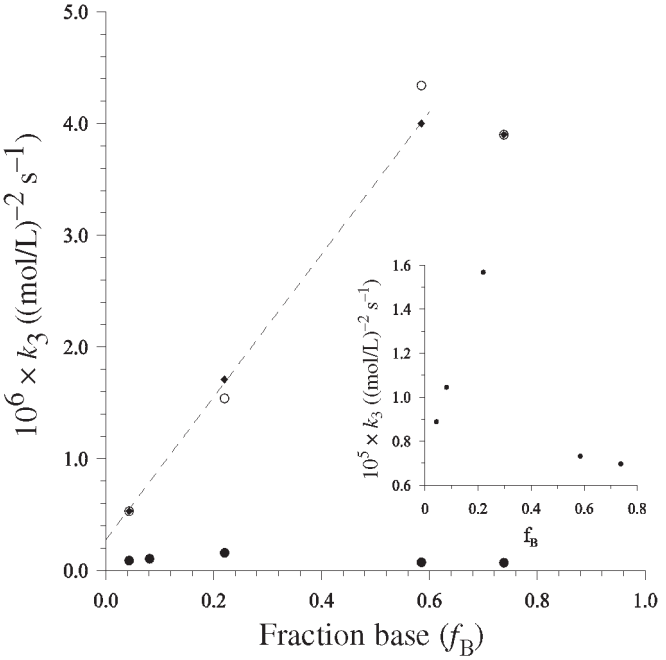
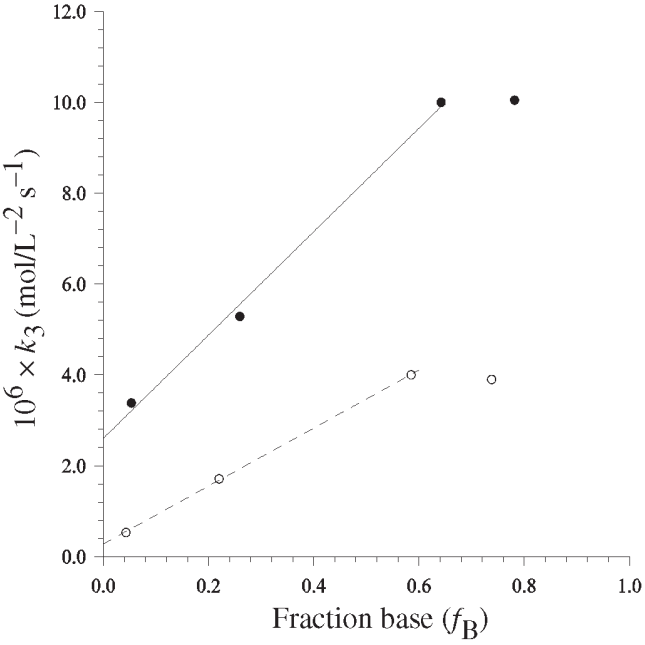


Fig. 6. Comparison of the variation of k_3 with the mole fraction of free base for collidine (●) and HEPES (○) buffers in the PS2.M–hemin-catalyzed peroxidation reactions.



In addition, to probe how the activity of the nucleotide–hemin complexes is affected by the concentration of oxidant, the pseudo-first-order rate constants (k_{obs}) for both PS2.M–hemin and rPS2.M–hemin-catalyzed peroxidations were measured as a function of the oxidant concentration ([H_2O_2]) at high and low HEPES concentrations (200 and 5 mmol/L, respectively). The so-derived rate constants are shown in Fig. 5.

It is clear that both PS2.M–hemin and rPS2.M–hemin display similar rate constants for their respective peroxidation reactions at high HEPES concentration, and that the rPS2.M–hemin complex is a much more active catalyst at low buffer concentrations. These observations are consistent with cleavage of the oxygen–oxygen bond not being rate-determining at high buffer concentration and that the RNA–hemin complex has a higher intrinsic activity than the DNA–hemin combination. PS2.M was isolated from a selection experiment designed to generate tight DNA binders of NMM (**2**), a nonplanar hemin analogue. Given that, it is remarkable that the corresponding RNA sequence (rPS2.M) also binds hemin and NMM, although this complexation is less strong and presumably less optimal. However, it is this complex (rPS2.M–hemin) that shows the greater catalytic efficiency.

Effect of collidine buffer

To investigate whether catalysis by the buffer results from coordination of the buffer to the ferric iron (27) or via a base-catalyzed pathway, the peroxidation reactions were monitored in a collidine/collidine-H^+ buffer, in place of the HEPES–NH_4OH buffer (14). Of note, the conjugate acid of collidine has a pK_a value similar to that of HEPES (p$K_a \approx$ 7.55); however, it is a sterically hindered base, which has been shown not to bind iron even at high concentrations (10). Figure 6 shows the results of peroxidation experiments with the PS2.M–hemin complex in collidine-buffered solutions. Of note, the observed rate constants in collidine-buffered solutions are higher than those measured in HEPES buffers. Also of note, it is evident that the conjugate acid of collidine also catalyzes the peroxidation by the PS2.M–hemin complex, albeit less efficiently than its basic form.

It can be concluded that the acceleration of the PS2.M–hemin- and rPS2.M–hemin-catalyzed peroxidations caused by both HEPES and collidine results from general base catalysis. Also, it is likely that the greater activity of collidine results from either its likely greater affinity for the Triton X-100 micelles or from a favourable π-stacking interaction with the nucleotide–hemin complex.

Conclusions

The PS2.M DNAzyme originally resulted from an in vitro selection for a reaction (porphyrin metallation) very different from peroxidation (28–30). In analyzing the mechanism of that quite distinct catalytic activity, it was found that the catalysis by PS2.M originated from its ability to enhance the basicity of the bound porphyrin substrate (30). Intriguingly, our conclusion in this paper is that PS2.M likewise reduces the acidity (or enhances the basicity) of the bound metalloporphyrin (hemin) cofactor in the incarnation of PS2.M as a peroxidase enzyme. The intial strangeness of a DNA enzyme selected for porphyrin metallation also proving capable of catalyzing peroxidation now appears both comprehensible and mechanistically reasonable.

The ribozyme (rPS2.M–hemin) is a better catalyst than the DNAzyme (PS2.M–hemin), in spite of hemin being bound approximately 10^3-fold more strongly to PS2.M than to rPS2.M (15). It is likely that the strongly bound PS2.M–hemin complex is structurally more rigid than rPS2.M–

© 2006 NRC Canada

hemin, which impacts negatively on its catalytic activity relative to that of rPS2.M–hemin.

The discovery of DNA– and RNA–hemin complexes capable of catalysis of peroxidation is of significant interest to the "RNA World" hypothesis for the origin of primordial life (31–34). According to this hypothesis, modern RNA-DNA-protein based life-forms were preceded by RNA molecules capable of self-replication and the catalysis of metabolic reactions. In modern primary metabolism, reduction–oxidation (redox) reactions comprise nearly one-quarter of the total number of classified enzymatic reactions (35). It is conceivable that in an RNA World, ribozymes (and DNAzymes) catalyzing metabolically important redox reactions might have recruited hemin or hemin-like molecules as cofactors.

Materials and methods

All chemicals were of the highest purity available and they were used without further purification. Sodium dodecyl sulfate (SDS), Triton X-100 (T X-100), cetyltrimethyl ammonium bromide ($CetMe_3N^+$), ammonium hydroxide (NH_4OH), nitric acid (HNO_3), cesium nitrate ($CsNO_3$), 2,2′-azinobis(3-ethylbenzothioazoline)-6-sulfonic acid (ABTS), 2,4,6-collidine, and HEPES buffer were purchased from Sigma-Aldrich. Hydrogen peroxide (3%, *w*/*v* stabilized form) was purchased from VWR Canlab.

PS2.M, a guanine-rich aptamer of DNA (deoxyribonucleic acid, 5′-GTG GGT AGG GCG GGT TGG-3′), PS2.M–hemin, DNA–aptamer–hemin complex, rPS2.M, the corresponding RNA (ribonucleic acid) version of PS2.M, were made using standard automated methods.

Titration and catalysis of hemin in the presence of various detergents

Standardized solutions of hemin were prepared as described previously (14, 15). All solutions used for spectral or kinetic measurements contained 0.2 mol/L caesium nitrate. 0.5–0.8 μmol/L hemin solutions (diluted from a 500 μmol/L stock solution in DMSO) were individually prepared in 2-[*N*-morpholino]ethanesulfonic acid (MES) – tris[hydroxymethyl]aminomethane (Tris) buffer (100 mmol/L MES, pH 6.2, 50 mmol/L Tris, DMSO 1%) containing different concentrations of either SDS, TX-100, or $CetMe_3N^+$. These solutions were scanned spectroscopically over the wavelength range of 300–700 nm to determine the detergent concentrations at which hemin aggregation became insignificant (yielding saturated absorption profiles). The so-derived saturating concentrations of each detergent obtained in this way were then used for the kinetic assays, which were carried out in *N*-[2-hydroxyethyl]piperazine-*N*-[2-ethanesulfonic acid] (HEPES)–NH_4OH buffer solutions with HEPES concentrations of 5 and 200 mmol/L and 0.1 μmol/L of hemin. Reactions were initiated by the addition of H_2O_2 and followed by monitoring the appearance of the ABTS radical cation ($ABTS^{+\cdot}$), which absorbs at 414 nm. Spectroscopic and kinetic data were measured using a dual-beam multicell holder Cary 3E spectrophotometer with thermostat controller, at 20 °C

Acid–alkaline transition for hemin complexes

The various buffers used were: pH 2.0–4.0 (glycine–HNO_3), pH 4.6–7.0 (MES–Tris), pH 5.8–8.0 (HPO_4^{2-}–$H_2PO_4^-$), pH 7.0–8.9 (Tris–HNO_3), and pH 8.5–10.5 (glycine–OH^-). The electronic absorption curves of various hemin complexes were found to be consistent at given pH values, although different buffers were used in regions of overlapping pH. All buffer solutions contained 0.1 mol/L caesium nitrate, and 20 mmol/L KCl to ensure proper DNA and RNA folding. KCl was omitted from the solutions containing SDS because even low potassium concentrations caused SDS precipitation. The concentrations of the various hemin complexes were made up to 0.5–0.8 μmol/L hemin with sufficient concentrations of the various detergents, RNA, or DNA oligomers to ensure saturation of the hemin binding.

Buffer catalysis by HEPES and collidine

The kinetics of the reaction of H_2O_2 with hemin and various hemin complexes were determined by following the increase in absorbance of $ABTS^{+\cdot}$ at 414 nm and 20 °C. Buffers were prepared by mixing appropriate amounts of the acid and base species at a fixed pH. Each individual sample was prepared by adding 500 μL of a 2× buffer (also containing 40 mmol/L KCl for proper DNA and RNA folding, and 0.2 mol/L caesium nitrate) to a 500 μL of 2× stock solution (final concentrations: 0.05% T X-100, 1% DMSO, 5 mmol/L ABTS). The final concentrations of hemin and of hemin complexes were ~0.1 μmol/L. Kinetic runs were typically carried out by mixing ~1.4 μL of a 0.44 mol/L solution of H_2O_2 (final 600 μL) to the previously prepared DNA or RNA solutions (1 mL), in a quartz cuvette with 10 mm path length. The experimental curves of A_{414} vs. time were digitized and computer-fitted (GraphPad Prism™ 2.0 software) to obtain pseudo-first-order rate constants (k_{obs}).

Acknowledgements

The authors gratefully acknowledge the Natural Sciences and Engineering Research Council of Canada (NSERC) for financial support of this work. DS is a senior scholar of the Michael Smith Foundation for Health Research, Vancouver, British Columbia. We also thank two anonymous referees for their many helpful comments concerning this manuscript.

References

1. H.B. Dunford and J.S. Stillman. Coord. Chem. Rev. **19**, 187 (1976).
2. H.B. Dunford. Heme peroxidases. John Wiley, New York. 1999. p. 507.
3. B. Chance, R.W. Estabrook, and T. Yonetani. Hemes and hemoproteins. Academic Press, New York. 1966. p. 624.
4. I. Morishima and S. Ogawa. Biochemistry, **17**, 4384 (1978).
5. C.E. Schulz, P.W. Devaney, H. Winkler, P.G. Debrunner, N. Doan, R. Chiang, R. Rutter, and L.P. Hager. FEBS Lett. **103**, 102 (1979).
6. J.E. Roberts, B.M. Hoffman, R. Rutter, and L.P. Hager. J. Biol. Chem. **256**, 2118 (1981).
7. C.E. Schulz, R. Rutter, J.T. Sage, P.G. Debrunner, and L.P. Hager. Biochemistry, **23**, 4743 (1984).

© 2006 NRC Canada

8. J.E. Penner-Hahn, K.S. Eble, T.J. Mcmurry, M. Renner, A.L. Balch, J.T. Groves, J.H. Dawson, and K.O. Hodgson. J. Am. Chem. Soc. **108**, 7819 (1986).
9. W.R. Browett, Z. Gasyna, and M.J. Stillman. J. Am. Chem. Soc. **110**, 3633 (1988).
10. T.G. Traylor, W.A. Lee, and D.V. Stynes. J. Am. Chem. Soc. **106**, 755 (1984).
11. T.G. Traylor, W.A. Lee, and D.V. Stynes. Tetrahedron, **40**, 553 (1984).
12. T.G. Traylor and R. Popovitz-Biro. J. Am. Chem. Soc. **110**, 239 (1988).
13. M.F. Zipplies, W.A. Lee, and T.C. Bruice. J. Am. Chem. Soc. **108**, 4433 (1986).
14. P. Travascio, Y. Li, and D. Sen. Chem. Biol. **5**, 505 (1998).
15. P. Travascio, A.J. Bennet, D.Y. Wang, and D. Sen. Chem. Biol. **6**, 779 (1999).
16. V. Pavlov, Y. Xiao, R. Gill, A. Dishon, M. Kotler, and I. Willner. Anal. Chem. **76**, 2152 (2004).
17. Y. Ito and H. Hasuda. Biotechnol. Bioeng. **86**, 72 (2004).
18. T.C. Bruice. *In* Mechanistic principles of enzyme activity. Vol. 9. *Edited by* J.F. Liebman and A. Greenberg. VCH Publishers, Deerfield Beach, Fla. 1988. pp. 227–277.
19. H.W. Lee, D.J.F. Chinnapen, and D. Sen. Pure Appl. Chem. **76**, 1537 (2004).
20. J.E. Falk. Haematin enzymes: A symposium of the International Union of Biochemistry, organized by the Australian Academy of Science. Symposium Publications Division, Pergamon Press, Oxford, New York. 1961. p. 666.
21. E. Antonini and M. Brunori. Hemoglobin and myoglobin in their reactions with ligands. Vol. 21. North-Holland Pub. Co., Amsterdam. 1971. p. 436.
22. P. George and G. Hanania. Biochem. J. **52**, 517 (1952).
23. P. George and G. Hanania. Biochem. J. **55**, 236 (1953).
24. J. Everse, K.E. Everse, and M.B. Grisham. Peroxidases in chemistry and biology. Vol. 1. CRC Press, Boca Raton, Fla. 1991.
25. J. Simplicio and K. Schwenze. Biochemistry, **12**, 1923 (1973).
26. A.J. Sitter, J.R. Shifflett, and J. Terner. J. Biol. Chem. **263**, 13032 (1988).
27. M.J. Beck, E. Gopinath, and T.C. Bruice. J. Am. Chem. Soc. **115**, 21 (1993).
28. Y. Li, C.R. Geyer, and D. Sen. Biochemistry, **35**, 6911 (1996).
29. Y. Li and D. Sen. Nat. Struct. Biol. **3**, 743 (1996).
30. Y. Li and D. Sen. Biochemistry, **36**, 5589 (1997).
31. W. Gilbert. Nature (London), **319**, 618 (1986).
32. R. Lewin. Science (Washington, D.C.), **231**, 545 (1986).
33. S.A. Benner, A.D. Ellington, and A. Tauer. Proc. Natl. Acad. Sci. U.S.A. **86**, 7054 (1989).
34. G.F. Joyce. Nature (London), **338**, 217 (1989).
35. J. Everse, B. Anderson, and K.-S. You. The pyridine nucleotide coenzymes. Academic Press, New York. 1982. p. 389.
36. B.C. Saunders, A.G. Holmes-Siedle, and B.P. Stark. Peroxidase: The properties and uses of a versatile enzyme and of some related catalysts. Butterworths, Washington. 1964. p. 271.

© 2006 NRC Canada

Lanthanum-catalyzed aqueous acylation of monosaccharides by benzoyl methyl phosphate[1]

Ian James Gray, Rui Ren, Bernhard Westermann, and Ronald Kluger

Abstract: It was previously reported that diols dissolved in water (pH 8, EPPS buffer) react with benzoyl methyl phosphate (BMP) in the presence of lanthanide ions to form monobenzoyl esters. We have investigated the possibility of extending this process to include formation of esters of monosaccharides in water from lanthanide-catalyzed reactions with BMP. The combination of methyl-α-D-glucopyranoside and BMP in the presence of lanthanum trichloride gave selective monoacylation of the 2- and 6-hydroxyl groups in a ratio of 2:1. The likely mechanism involves preferential bisbidentate coordination of BMP and the diol to lanthanide ion (which explains how an ester forms when water is in enormous excess) followed by base-catalyzed intramolecular acyl transfer. The method should be generally applicable where a selective acylation reaction in water as solvent is desirable.

Key words: benzoyl methyl phosphate, lanthanide, catalysis, water, monoacylation, selective.

Résumé : Il a été rapporté antérieurement que les diols dissous dans l'eau (pH de 8 et tampon « EPPS ») réagissent avec le phosphate de benzoyle et de méthyle (PBM), en présence d'ions de lanthanide, pour conduire à la formation d'esters monobenzoylés. On a examiné la possibilité d'étendre cette méthode de façon à inclure la formation d'esters de monosaccharides, par des réactions en milieu aqueux avec du PBM et catalysées par des lanthanides. La combinaison de l'α-D-glucopyranoside de méthyle et du PBM, en présence de trichlorure de lanthane, conduit à la monoacétylation sélective des groupes hydroxyles en positions 2 et 6, dans un rapport de 2 : 1. Le mécanisme probable implique la coordination bisbidentate préférentielle du PBM et du diol à l'ion lanthanide (qui explique comme un ester peut se former en présence d'un énorme excès d'eau), qui est suivie d'un transfert de groupe acyle intramoléculaire catalysé par la base. La méthode devrait être applicable d'une façon générale quand il est désirable d'effectuer une réaction d'acétylation sélective en utilisant l'eau comme solvant.

Mots clés : phosphate de benzoyle et de méthyle, lanthanide, catalyse, eau, monoacétylation, sélective.

[Traduit par la Rédaction]

Introduction

We are reporting our work in conjunction with the production of an issue of the *Canadian Journal of Chemistry* honoring Walter Szarek, whose work in the field of biological carbohydrate chemistry exemplifies his insight, perspective, and creativity. In addition, Walter's outstanding personal qualities match his science.

Reactions that accomplish selective monoacylation of carbohydrates take advantage of differences in the inherent reactivity of individual hydroxyl groups (1, 2). For example, monobenzoates result from reactions of *N*-benzoyl imidazole and benzoyl cyanide with protected monosaccharides, provided that the combination of regioselection and product stability is sufficient (3). Subtle differences in the reactivity of hydroxyls and the catalysis of group migration add to the complexity of possible outcomes (4).

Benzoyl methyl phosphate (BMP) is an acyl phosphate monoester, a class of materials that resists hydrolysis and is inherently unreactive toward alcohols (5). Yet, acyl phosphates are anhydrides that have a high chemical potential for acyl transfer and are utilized in diverse biochemical acylation, including the formation of aminoacyl tRNAs. It was recently reported that BMP can form monobenozyl esters from diols in water in the presence of lanthanide ions (6). It is likely that bidentate coordination is the key to the selective acylation reaction since under similar conditions there is only a modest acceleration of base-catalyzed hydrolysis and formation of methyl esters (in methanol–water mixtures) (7). The likely mechanism is consistent with Clarke et al.'s (8) observations of lanthanide-promoted monoacetylation of diols in nonhydroxylic solvents. They reported NMR data that characterized an intermediate bisbidentate-coordinated complex of the lanthanide with a diol and an anhydride. Ionization of a coordinated hydroxyl in such an intermediate leads to Lewis acid promoted intramolecular attack on the adjacent carbonyl of the coordinated anhydride to form the ester (7).

Based on this background, we have been interested in extending the utility of BMP as a water-stable benzoylating agent whose inherent specificity would be associated with

Received 8 September 2005. Published on the NRC Research Press Web site at http://canjchem.nrc.ca on 10 May 2006.

I.J. Gray, R. Ren, and R. Kluger.[2] Davenport Chemistry Laboratory, Department of Chemistry, University of Toronto, Toronto, ON M5S 3H6, Canada.
B. Westermann. Department of Bioorganic Chemistry, Leibniz Institute for Plant Biochemistry, Halle, Germany.

[1]This article is part of a Special Issue dedicated to Professor Walter A. Szarek.
[2]Corresponding author (e-mail: rkluger@chem.utoronto.ca).

 doi:10.1139/V06-047 © 2006 NRC Canada

the formation of lanthanide chelates from adjacent hydroxyls of the reactant, a description that could find useful applications in the carbohydrate field. Applications of lanthanide catalysis of reactions by acyl phosphate monoesters would be expected to provide for selection among hydroxyl groups based on the properties of their lanthanide chelates, rather than on the inherent differences of reactivity among the hydroxyl groups of the substrate. We have now investigated the reactions of typical monosaccharides with BMP and lanthanide ions and find that this combination can introduce chelation-based selectivity in monobenzoylation reactions conducted in water.

Experimental

Reagent grade chemicals were used as received. High-resolution mass spectrometry was performed at the QStar Chemistry Mass Spectral Facility, University of Toronto. HPLC analysis and preparation were performed with C18 reversed-phase analytical columns (Waters μBondapak™ C18 3.9 mm × 300 mm) and preparative columns (Waters μBondapak™ C18 7.8 mm × 300 mm). Samples were eluted with purified water and HPLC grade acetonitrile. Benzoyl methyl phosphate (BMP) was prepared by the previously reported procedure (6, 9). Acylation of the carbohydrates was followed by HPLC, detected at 230 nm on a C18 reverse-phase analytical column, and eluted with 75:25 (*v*/*v*) water–acetonitrile containing 0.1% trifluoroacetic acid (TFA). The flow rate was 1.5 mL/min. Solvents were filtered and degassed before use. The ratio of acylation and hydrolysis from BMP was determined from the relative molar amounts of reactants (carbohydrate:water) to their corresponding products (ester:acid), according to eq. [1]. The ratio of products was obtained from the areas of the HPLC peaks for the resulting esters and benzoic acid.

$$[1] \qquad k_{rel} = (\text{Area}_{ester}/\text{Area}_{acid}) \times ([H_2O]/[\text{carbohydrate}])$$

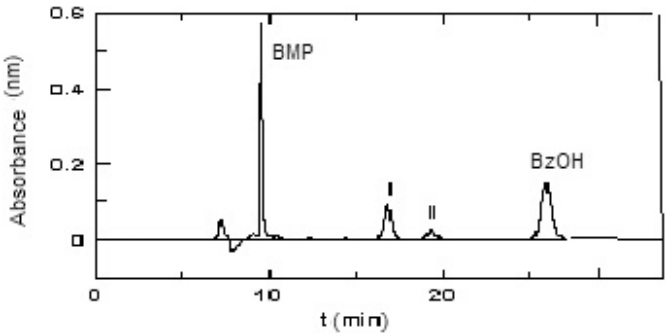
Separation of the ester products by was performed by HPLC. The effluent was continuously monitored at UV 230 nm on a C18 reverse-phase preparative column. The material in each product peak was freeze-dried and stored at –20 °C. The general structure was ascertained from the mass spectrum and refined by NMR analysis.

Methyl 4,6-*O*-benzylidene-α-D-glucopyranoside was obtained commercially. Methyl 4,6-*O*-benzylidene-α-D-mannopyranoside was prepared by the published method (10, 11).

Benzoylation of methyl-α-D-glucopyranoside (1) using BMP

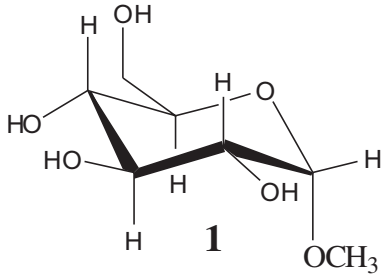
One equivalent of **1** and 2 equiv. of lanthanum trichloride were dissolved in 100 mmol/Lof EPPS buffer at pH 8. Freshly prepared BMP (1 equiv.) was added to this solution and stirred at room temperature. The reaction was monitored by HPLC (quenched with buffer (pH 8) containing EDTA at time points) and was complete within about 2 h. The disappearance of the BMP peak signified its conversion into benzoic acid and benzoyl ester products. Relative yields were calculated using internal standards.

Fig. 1. HPLC output for lanthanum-promoted reaction of BMP and **1**.



Results and discussion

Our initial studies focused on the monobenzoylation of methyl-α-D-glucopyranoside (**1**) with the intention of establishing a general procedure that extends to the monobenzoylation of other monosaccharides.



As expected, combining **1** with BMP in 100 mmol/L of EPPS (pH 8) without added lanthanum ion produces no reaction. Under the same conditions with added lanthanum, three new HPLC peaks are observed within 1 min (Fig. 1). We optimized reaction conditions by varying the concentration and found that 2 equiv. of lanthanum trichloride and 1 equiv. each of BMP and carbohydrate in 100 mmol/L of EPPS buffer at pH 8, produced a 33% conversion to the product esters within 2 h, while the remaining substrate could be recovered and BMP was hydrolyzed.

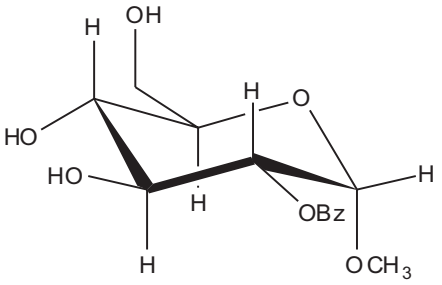
Each product was separated by preparative HPLC. ESI-MS analysis revealed two of the peaks to be monobenzoyl esters of **1**, while the third was that of benzoic acid from the hydrolysis of BMP.

The stability of the esters in the reaction solution was observed over several days in the reaction solution. Product ratios were invariant, indicating that the hydrolysis of the benzoate esters is not promoted by the metal ions in the solution under these conditions. We have noted that lanthanum ions promote formation of monoesters from cis-diols by BMP in water (6). In **1**, the geometry of adjacent diols is constrained by the ring and this will affect coordination as well as the reactions of the coordinated species. The primary hydroxyl (6-position) and equatorial hydroxyl groups at positions 2, 3, and 4 are all potential candidates for benzoylation. Each of the products peaks was isolated to determine the pattern of the reaction.

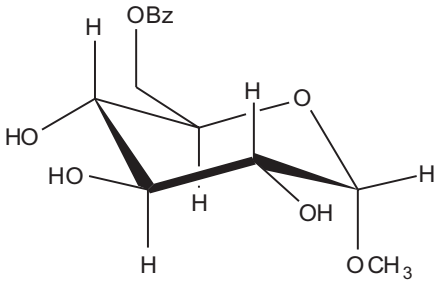
© 2006 NRC Canada

Table 1. ^{13}C NMR chemical shifts for the monobenzoyl esters of **1** in DMSO.

Carbohydrate	C-1	C-2	C-3	C-4	C-5	C-6
1	99.23	71.21	73.08	69.55	71.56	60.56
Ester A	96.81	**74.68**	71.01	70.63	73.18	61.05
Ester B	99.59	71.62	73.18	70.15	69.59	**64.33**



Ester A



Ester B

Table 2. Relative rates of acylation and hydrolysis in EPPS buffer (pH 8) with 50 mmol/L of lanthanum trichloride, 25 mmol/L of BMP, and 25 mmol/L of carbohydrate.

Carbohydrate	Time (min)	k_{rel} (25 °C)	k_{rel} (0 °C)
Methyl-α-D-mannopyranoside	60	50	100
Methyl-α-D-glucopyranoside	60	370	730
Methyl-β-D-galactopyranoside	60	800	1 310
D-Ribose	60	8800	11 330

Analysis of the ^{13}C NMR spectra of the products (Table 1) indicate that reaction occurs at 2-OH and 6-OH preferentially.

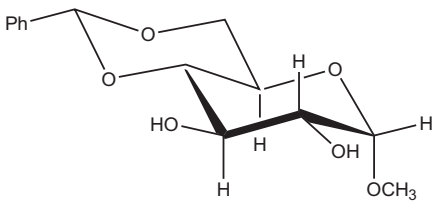
Due to competition with water, used as a solvent for the reaction, it is inevitable that BMP hydrolysis accompanies the monoacylation reaction. We found that hydrolysis was significantly less competitive at low temperatures (Table 2). The same carbohydrate reaction preferences hold at the lower temperatures, with ester formation being the major process.

In order for the reaction with BMP with the monosaccharide to compete with hydrolysis, the possibility of bidentate coordination must overwhelm the effect of overwhelmingly large excess of reaction sites in the water that serves as the solvent. To test this further, we proposed that no reaction would occur if the 6-hydroxyl is blocked, which would prevent the possibility of bidentate coordination. We used methyl-4,6-*O*-benzylidene-α-D-glucopyranoside and methyl-4,6-*O*-benzylidene-α-D-mannopyranoside. No ester formation occurs after 5 days with BMP and lanthanum trichloride under conditions where **1** reacts rapidly. This result supports the NMR-based analysis for reaction of **1**. More detailed product studies are in progress.

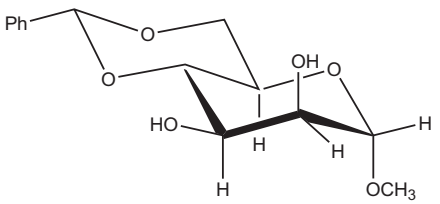
We have also done a preliminary survey of the reaction patterns of BMP and lanthanum trichloride with other monosaccharides (Table 3). From these results we see that the monobenzoylation process is applicable to a variety of species with varying efficacy: D-ribose > methyl-β-D-galactopyranoside > methyl-α-D-glucopyranoside > methyl-α-D-mannopyranoside.

For the reactants in Table 3, D-ribose gives the highest overall yield of ester products. However, we have not yet identified the individual monobenzoylated materials (there are three in all). The reaction of 2-deoxyribose leads to only two products, suggesting that one of the chelates involves the 2-OH. Two monobenzoylated esters were produced from uridine. There was no reaction with 2-deoxyuridine, as would be expected if 2,3-chelation is the major mode of reaction. The other aldohexose methyl pyranosides reacted similarly to the glucoside, giving two monobenzoylated products.

A probable mechanism, illustrated with methyl-α-D-glucopyranoside, is shown in Scheme 1. This involves internal addition from the conjugate base of the bisbidentate chelate of the lanthanide and the two reactants (7, 8), as has been shown in reactions of diol substrates.



Methyl-4,6-*O*-benzylidene-α-D-glucopyranoside



Methyl-4,6-*O*-benzylidene-α-D-mannopyranoside

© 2006 NRC Canada

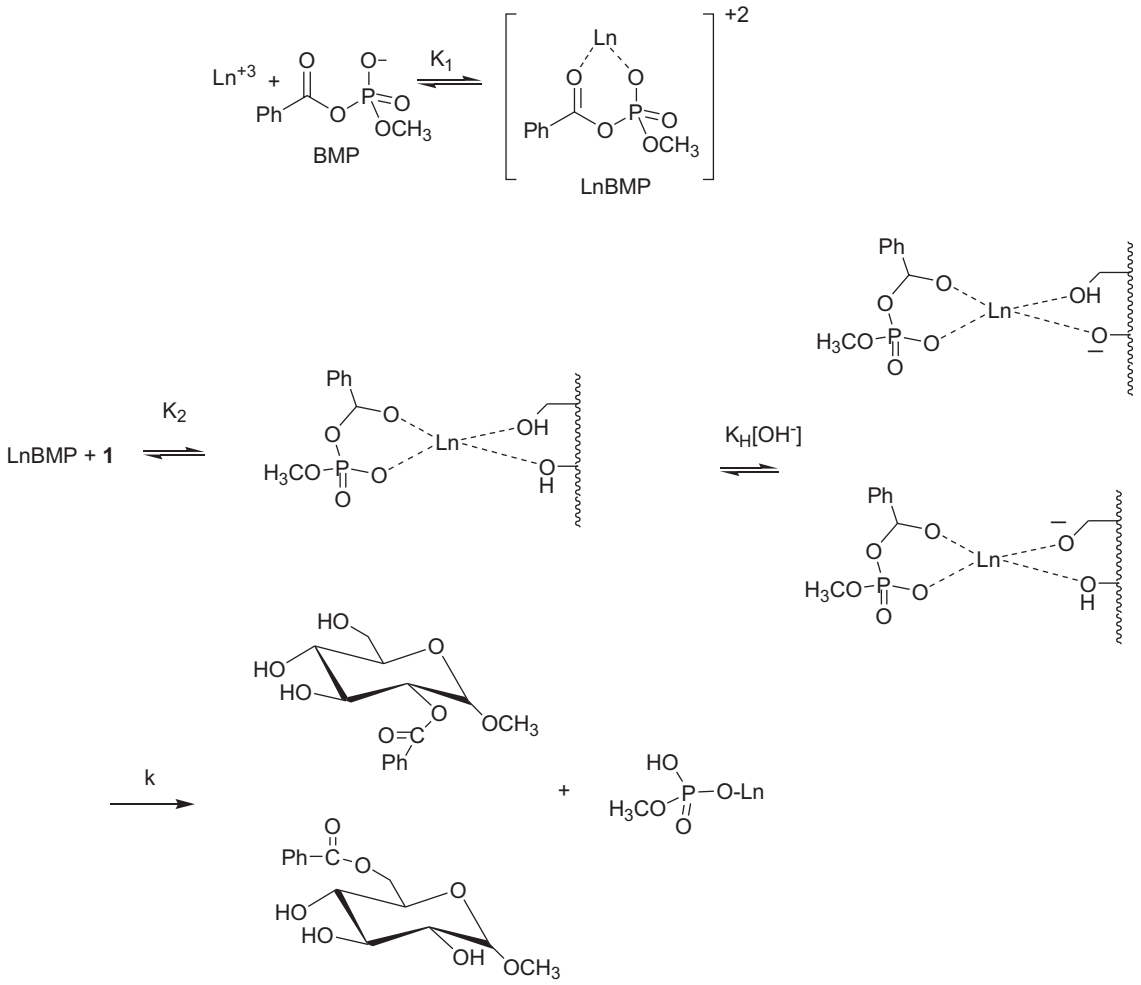
Table 3. Products of lanthanum-catalyzed monoacylation.

Carbohydrate	No. of ester products[a]	Ester ratios[a]	Total ester (%)[a]
Methyl-α-D-glucopyranoside	2	2.2:1	33.0
Methyl-β-D-galactopyranoside	2	1.1:1	41.0
Methyl-α-D-mannopyranoside	2	2.0:1	25.0
D-Ribose	3	5:1:3	91.0
2′-Deoxy-D-ribose	2	1:1.8	20.0
Uridine	2	1:1.8	76.0
2′-Deoxyuridine	0	0	0

Note: Reaction conditions: carbohydrate (1 equiv.), BMP (1 equiv.), $LaCl_3$ (2 equiv.), 100 mmol/L of EEPS buffer (pH 8) at room temperature.

[a]Relative yields were calculated from HPLC analysis.

Scheme 1. Proposed mechanism for the monobenzoylation of **1**.



Conclusions

We have for the first time shown that lanthanide-promoted monoesterification reactions of monosaccharides in water can be achieved by the reaction of an acyl phosphate monoester with lanthanum chloride. Products form from both hexoses and pentoses. NMR analysis indicated that the methyl-α-D-glucopyranoside (**1**) was benzoylated at the 2-oxygen and 6-oxygen in a ratio of 2:1. Since the 6-position is primary and the 2-position is secondary, it is clear that steric effects do not control the site of the reaction and that the geometry of the transition state is controlled by the coordination of the reacting complex. We intend to determine in further detail the scope, selectivity, and optimal conditions for this interesting new process. This approach should also be amenable to detection of species in complex mixtures and differential recognition, as well as for general synthetic applications.

Acknowledgements

We thank the Natural Sciences and Engineering Research

© 2006 NRC Canada

Council of Canada (NSERC) for support of this research through a Discovery Grant.

References

1. U.B. Gangadharmath and A.V. Demchenko. Synlett, **12**, 2191 (2004).
2. M. Nahmany and A. Melman. Org. Biomol. Chem. **2**, 1563 (2004).
3. S.A. Abbabs and A.H. Haines. Carbohydr. Res. **39**, 358 (1979).
4. G. Hu and A. Vasella. Helv. Chim. Acta, **86**, 4369 (2003).
5. R. Kluger, A.S.Grant, S.L. Bearne, and M.R. Trachsel. J. Org. Chem. **55**, 2864 (1990).
6. R. Kluger and L.L. Cameron. J. Am. Chem. Soc. **124**, 3033 (2002).
7. L.L Cameron, S.C.Wang, and R. Kluger. J. Am. Chem. Soc. **126**, 10721 (2004).
8. P.A. Clarke, P.L. Arnold, M.A. Smith, L.S. Natrajan, C. Wilson, and C. Chan. J. Chem. Soc. Chem. Commun. 2588 (2003)
9. L. Zervas and I. Dilaris. J. Am. Chem. Soc. **77**, 5354 (1955).
10. J.J. Patroni and R.V. Stick. Aust. J. Chem. **41**, 91 (1988).
11. O. Gronwald and K. Sakurai. Carbohydr. Res. **3**, 307 (2001).

© 2006 NRC Canada

Stereoselective synthesis of chiral piperidine derivatives employing arabinopyranosylamine as the carbohydrate auxiliary[1]

Birgit Kranke and Horst Kunz

Abstract: Stereoselective synthesis of 2-substituted dehydropiperidinones and their further transformation to variously disubstituted piperidine derivatives was achieved employing D-arabinopyranosylamine as the stereodifferentiating carbohydrate auxiliary. A domino Mannich–Michael reaction of 1-methoxy-3-(trimethylsiloxy)butadiene (Danishefsky's diene) with O-pivaloylated arbinosylaldimines furnished *N*-arabinosyl dehydropiperidinones in high diastereoselectivity. Subsequent conjugate cuprate addition gave 2,6-cis-substituted piperidinones, while enolate alkylation furnished 2,3-trans-substituted dehydropiperidinones. Electrophilic substitution at the enamine structure afforded 5-nitro- and 5-halogen dehydropiperidinones of which the latter were applied in palladium-catalyzed coupling reactions. The absolute configuration of the obtained products was proven by NMR and X-ray structure analysis as well as by syntheses of the alkaloids (+)-coniine and (+)-dihydropinidine.

Key words: piperidine alkaloids, carbohydrate auxiliary, domino Mannich–Michael reaction, conjugate cuprate and hydride addition, electrophilic substitution of enamines.

Résumé : On a réalisé la synthèse stéréosélective de déhydropipéridones substituées en position 2 et leur transformation subséquente en divers dérivés disubstitués de la pipéridine en utilisant de la D-arabinopyranosylamine comme hydrate de carbone auxiliaire permettant de faire une stéréodifférenciation. Une réaction de Mannich–Michael en domino du 1-méthoxy-3-(triméthylsiloxy)butadiène (réactif de Danishefsky) avec de *O*-pivaloyl-arbinosylaldimines conduit à la formation de *N*-arabinosyl déhydropipéridinones avec une grande diastéréosélectivité. Une addition subséquente conjuguée de cuprate fournit les pipéridinones 2,6-cis-substituées alors qu'une alkylation de l'énolate conduit déhydropipéridinones aux 2,3-trans-substituées. Une substitution électrophile de la structure énamine conduit aux 5-nitro- et 5-halogéno-déhydropipéridinones; ces dernières ont par la suite été utilisées dans des réactions de couplage catalysées par le palladiium. La configuration absolue des produits obtenus a été démontrée par RMN et par diffraction des rayons X ainsi que par synthèse des alcaloïdes (+)-coniine et (+)-dihydropinidine.

Mots clés : alcaloïde de la pipéridine, hydrate de carbone auxiliaire, réaction de Mannich–Michael en domino, addition conjuguée de cuprate et d'hydrure, substitution électrophile d'énamines.

[Traduit par la Rédaction]

Introduction

Due to their great diversity in biological and pharmacological activities (1), piperidine alkaloids and synthetic piperidines containing various substitution patterns are considered interesting target structures for drug development. Therefore, these heterocyclic structures are the subject of numerous synthetic, often stereoselective approaches (2).

During the past years, we have developed a strategy for the enantioselective synthesis of piperidine alkaloids using glycosylamines as chiral auxiliaries (3, 4). In this approach, steric, stereoelectronic, and complexing effects of carbohydrates are exploited for diastereofacial differentiation of nucleophilic additions to *N*-glycosyl aldimines. It is a special feature that this methodology offers the possibility of synthesizing both enantiomeric series of chiral piperidines by varying the carbohydrate auxiliary, e.g., employing the (pseudo-)enantiomeric carbohydrates, D-galactosylamine (3) and D-arabinosylamine (4), respectively. Herein, we report full experimental details for the application of D-arabinosylamine **1** in the stereoselective synthesis of 2-substituted *N*-arabinosyl dehydropiperidinones **4** and their subsequent regioselective and stereoselective modification in the preparation of variously substituted piperidines.

Received 7 September 2005. Published on the NRC Research Press Web site at http://canjchem.nrc.ca on 12 May 2006.

Dedicated to Professor Walter Szarek on the occasion of his 65th birthday.

B. Kranke and H. Kunz.[2] Institut für Organische Chemie, Johannes Gutenberg Universität Mainz, Duesbergweg 10-14, 55128 Mainz, Germany.

[1]This article is part of a Special Issue dedicated to Professor Walter A. Szarek.

[2]Corresponding author (e-mail: hokunz@uni-mainz.de).

Results and discussion

Formation of *N*-arabinosyl dehydropiperidinones

Condensation of 2,3,4-tri-*O*-pivaloyl-α-D-arabinopyranosylamine (**1**) (5) with aliphatic aldehydes in the presence of molecular sieves or with aromatic aldehydes under acidic ca-

 doi:10.1139/V06-060 © 2006 NRC Canada

Scheme 1. Stereoselectve synthesis of 2-substituted *N*-arabinosyl dehydropiperidinones.

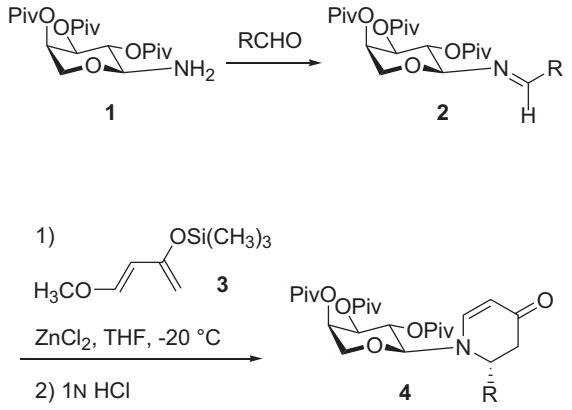


Table 1. Diastereoselective synthesis of 2-substituted *N*-arabinosyl dehydropiperidinones according to Scheme 1.

Product	R	Yield (%)	d.r.
4a	*p*-ClC_6H_4	96[a]	97:3[b]
4b	*p*-$NO_2C_6H_4$	74[a]	86:14,[c] 96:4[b]
4c	C_6H_4	84[a]	92:8[c]
4d	Methyl	49[d]	93:7[b]
4e	Ethyl	67[d]	96:4[c]
4f	Propyl	81[d]	87:13[c]
4g	Isopropyl	72[d]	95:5,[c] 99:1[b]
4h	$(CH_2)_3$OTBDPS	65[d]	90:10,[c] 96:4[b]

[a]Based on imine.
[b]Determined by HPLC after flash chromatography.
[c]Determined by HPLC of the crude product.
[d]Based on amine.

talysis furnished *N*-arabinopyranosylimines **2**. These aldimines reacted with 1-methoxy-3-(trimethylsiloxy)butadiene (Danishefsky's diene, **3**) in a domino Mannich–Michael reaction promoted by zinc chloride to give *N*-(2,3,4-tri-*O*-pivaloyl-α-D-arabinopyranosyl)-5,6-didehydropiperidin-4-ones (**4**) in high yields and high diastereoselectivity (Scheme 1, Table 1).

The stereochemical course of the reaction and hence the configuration of the nitrogen heterocycle in **4** was controlled by the sterically demanding pivaloyl group at C-2 of the carbohydrate auxiliary, which effectively shields the si side of aldimine **2**. Thus, the initial step in the domino Mannich–Michael reaction consists of the nucleophilic addition of Danishefsky's diene **3** at the re side of glycosyl imine **2**.

In contrast, in galactosyl imines **5** reported earlier (3) the re side is efficiently blocked by the C-2 pivaloyl group, leading to *N*-galactosyl dehydropiperidinones **6** bearing the opposite configuration at position 2 of the nitrogen heterocycle (Scheme 2). This is due to the fact that although arabinosylamine belongs to the D series of carbohydrates, it displays almost the mirror image of D-galactosylamine. Thus, by using either D-galactosylamine or its pseudoenantiomer, D-arabinosylamine, enantiomeric dehydropiperidinones are accessible offering the possibility of synthesizing both enantiomers of piperidines by choosing the appropriate auxiliary.

The absolute configuration of the *N*-arabinosyl dehydropiperidinones was proven by X-ray analysis showing **4f** to have (*S*)-configuration (Fig. 1). This compound preferably adopts a conformation in which the planes of the nitrogen heterocycle and the carbohydrate are almost perpendicular to each other allowing optimal overlap of the nonbonding orbital of the nitrogen and the σ* orbital of the C—O bond within the carbohydrate ring (exo-anomeric effect).

Conversion of *N*-arabinosyl dehydropiperidinone **4f** into the well-known alkaloid (*S*)-coniine **10** gave rise to further evidence of the absolute configuration of the nitrogen heterocycle in **4f**, and in addition, demonstrated the applicability of the shown reaction strategy for the stereoselective preparation of chiral 2-substituted piperidine alkaloids. Coniine is a highly toxic alkaloid leading to central respiratory paralysis and was the first alkaloid synthesized chemically (Ladenburg, 1886). In our auxiliary-mediated synthesis, the double bond of *N*-arabinosyl-2-propyl-5,6-

Scheme 2. A pair of (pseudo)-enantiomeric auxiliaries lead to enantiomeric piperidine derivatives.

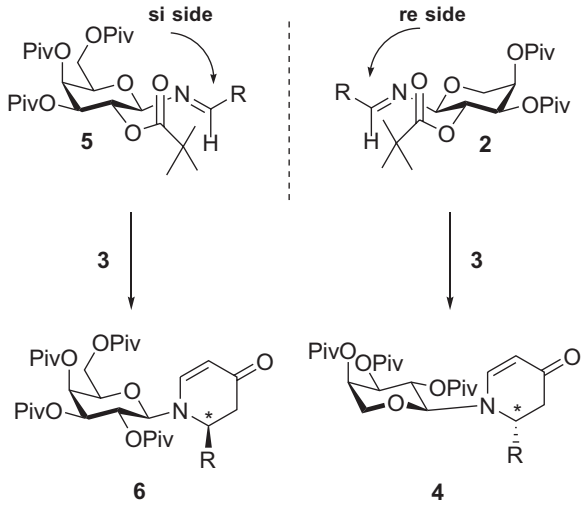
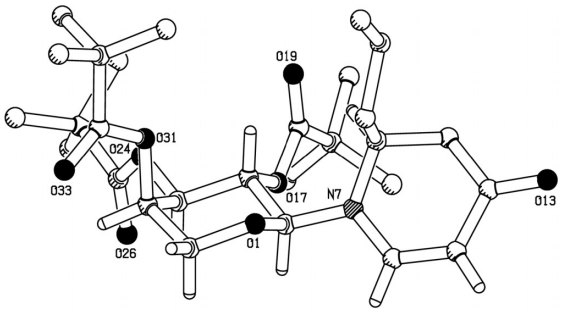


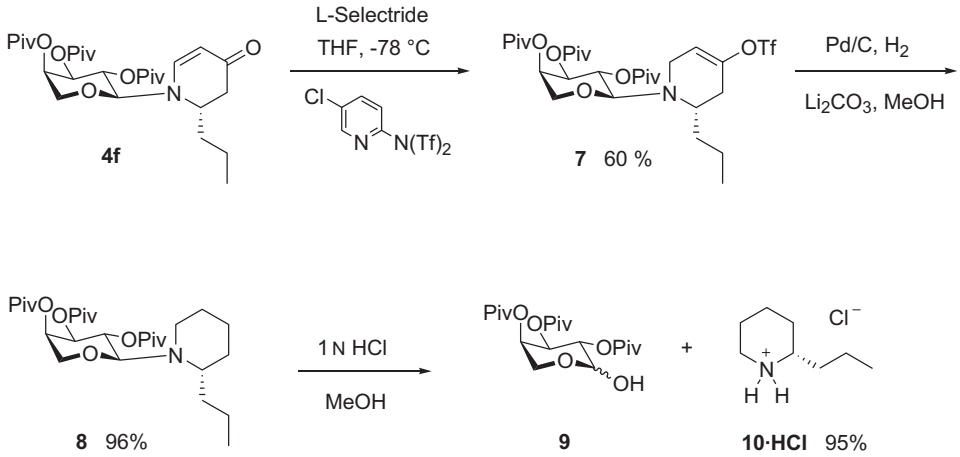
Fig. 1. X-ray structure of *N*-arabinosyl dehydropiperidinone **4f**.



dehydropiperidin-4-one (**4f**) was reduced with lithium tri-*sec*-butylborohydride (L-Selectride®) and the intermediate enolate was subsequently trapped as triflate **7**. Hydrogenation of the enol triflate afforded 2-propylpiperidine **8**. The enantiomerically pure alkaloid was released from the auxiliary by mild acidolysis using dilute HCl in methanol (Scheme 3). The optical rotation value of the formed coniine hydrochloride **10** was in agreement with literature data.

© 2006 NRC Canada

Scheme 3. Synthesis of enantiomerically pure (+)-(6*R*)-coniine hydrochloride.



Derivatization of *N*-arabinosyl dehydropiperidinones

N-Arabinosyl dehydropiperidinones **4** represent versatile precursors for the synthesis of variously substituted nitrogen heterocycles, e.g., the regioselective and stereoselective preparation of 2,6-, 2,5-, and 2,3-disubstituted piperidines.

2,6-cis-Disubstituted piperidines

N-Arabinosyl dehydropiperidinones **4** are α,β-unsaturated carbonyl compounds. Their reactivity as Michael acceptors is reduced because of the vinylogous amide structure. However, cuprate addition was accomplished by activation with hard electrophiles. For example, reaction of Yamamoto cuprates (6) activated by boron trifluoride diethyletherate ($RCu{\cdot}BF_3$) or of Gilman cuprates (8) (R_2CuLi) in combination with chlorotrimethylsilane (7) resulted in the formation of 2,6-cis-disubstituted piperidinones **11** with high diastereoselectivity (Scheme 4, Table 2).

The cis configuration was confirmed by X-ray analysis of **11a** (Fig. 2). The nitrogen heterocycle adopts a twisted conformation with the smaller substituent in axial position, the larger substituent in equatorial position, and a pyramidally configured nitrogen atom. The alignment of the two heterocycles is stabilized by the exo-anomeric effect (compare, Fig. 1).

The observed cis stereoselectivity of the 1,4-addition can be explained by stereoelectronic effects using the X-ray structure of **4f**. Two rotamers A and B, stabilized by the exo-anomeric effect, are expected for *N*-arabinosyl dehydropiperidinones **4** (Scheme 5). Compared with rotamer A, rotamer B benefits from a smaller steric hindrance between the substituent in position 2 of the nitrogen heterocycle and the pivaloyl group at C-2 of the carbohydrate. Thus, the backside of the nitrogen heterocycle is shielded by this pivaloyl group, and the front-side attack of the cuprate results in the favoured cis-substitution pattern.

Enantiomerically pure (+)-dihydropinidine was synthesized to demonstrate the applicability of *N*-arabinosyl dehydropiperidinones **4** in the stereoselective synthesis of cis-2,6-disubstituted piperidine alkaloids. For this purpose, piperidinone derivative **11e** was converted into dithiolane **13** and subsequently treated with Raney nickel to form *N*-arabinosyl piperidine **14**. The enantiomerically pure alkaloid

Scheme 4. Diastereoselective synthesis of 2,6-cis-substituted *N*-arabinosyl piperidinones.

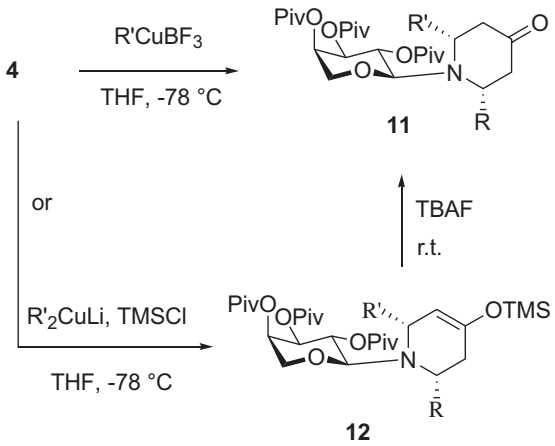
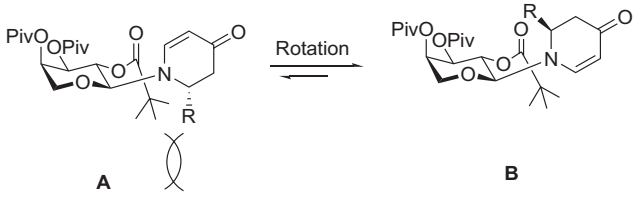


Table 2. Diastereoselective synthesis of 2,6-disubstituted *N*-arabinosyl piperidinones according to Scheme 4.

Product	R	R′	Yield (%)	d.r.
11a[a]	*p*Cl-C_6H_5	C_6H_5	72	99:1[b]
11b[a]	*p*Cl-C_6H_5	Allyl	51	98:2[b]
11c[a]	*n*-Propyl	C_6H_5	44	99:1[b]
11d[a]	*n*-Propyl	Allyl	75	94:6[c], 98:2[b]
11e[d]	*n*-Propyl	CH_3	88	91:9[c]

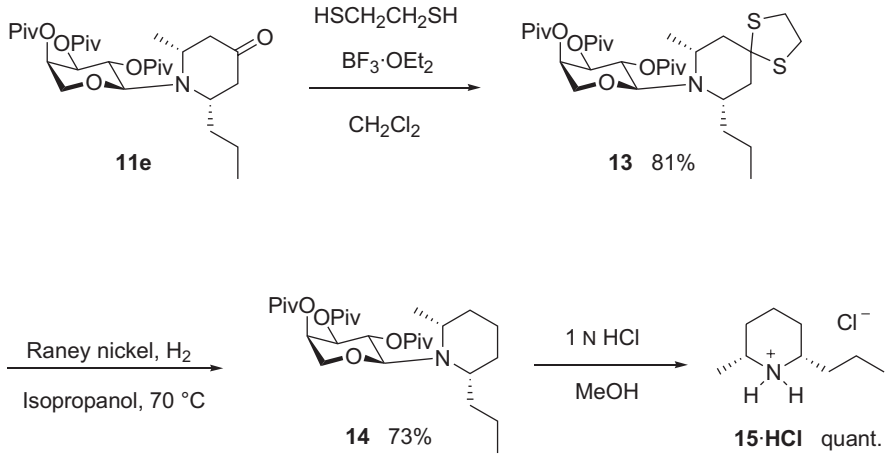
[a]Synthesized using Yamamoto cuprate.
[b]Determined by HPLC after chromatography.
[c]Determined by HPLC of the crude product.
[d]Synthesized using Gilman cuprate.

Scheme 5. Favored conformation of 2-substituted *N*-arabinosyl dehydropiperidinones according to Fig. 1.



© 2006 NRC Canada

Scheme 6. Synthesis of enantiomerically pure (+)-(2*S*,6*R*)-dihydropinidine hydrochloride.



Scheme 7. Electrophilic substitution at the enamine structure of dehydropiperidinones.

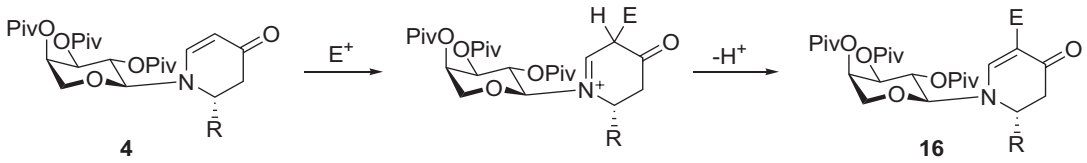
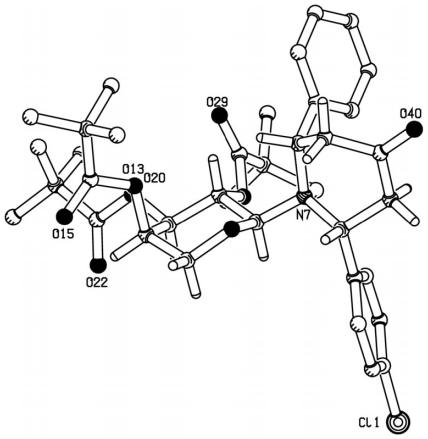


Fig. 2. X-ray structure of *N*-arabinosyl piperidinone **11a**.



hydrochloride **15** was released from the carbohydrate by mild acidolysis with dilute HCl in methanol (Scheme 6). The optical rotation value was in agreement with literature data (9) and confirmed the absolute configuration.

2,5-Disubstituted piperidines

Due to their enamine structure, *N*-arabinosyl dehydropiperidinones **4** are capable of adding electrophiles. Regeneration of the stable conjugated enaminone π system by abstraction of a proton subsequently leads to 2,5-disubstituted dehydropiperidinones **16** (Scheme 7).

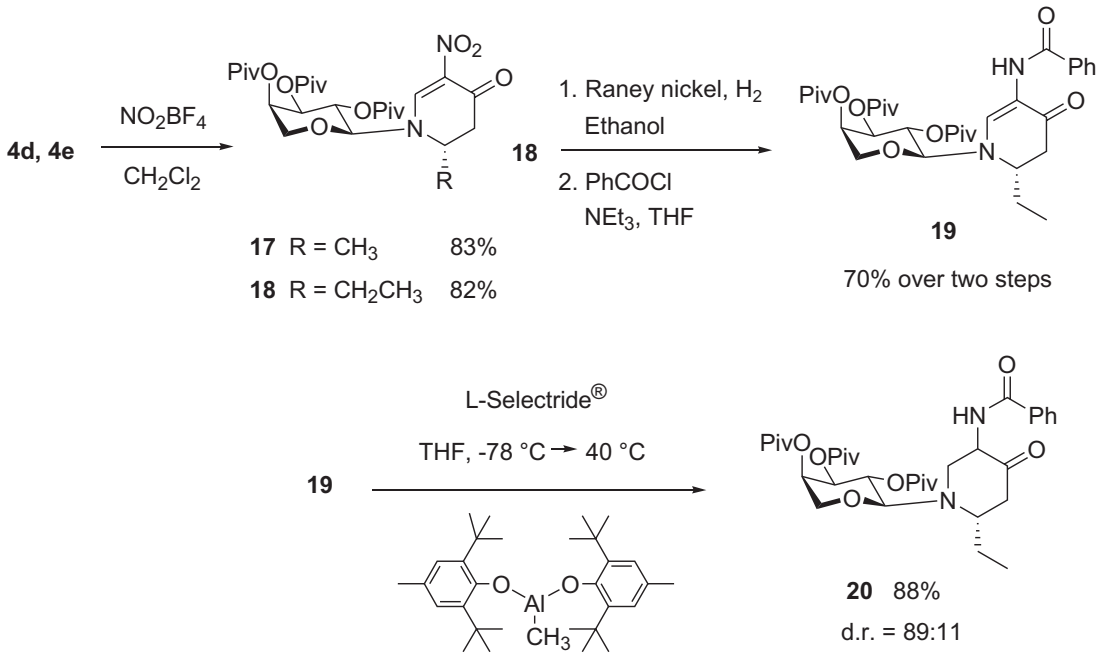
In terms of this electrophilic substitution, nitration of **4d** and **4e** was achieved in high yields using nitronium tetrafluoroborate applied as a solution in sulfolane allowing convenient handling of this air sensitive reagent (Scheme 8). Sulfolane can easily be separated from products **17** and **18**, respectively, by washing with water.

Reduction of the nitro group furnished an aminoketone, whose functionality is known to serve as precursor for syntheses of pharmacological important patterns like heterocycles, carbamates, or amides. Successful hydrogenation was achieved with Raney nickel, whereas reduction conditions such as zinc in hydrochloric acid or hydrogen and palladium on charcoal could not be applied. Immediate reaction of the sensitive amine with benzoyl chloride and triethylamine in ethanol gave the *N*-acyl compound **19** (Scheme 8).

N-Arabinosyl dehydropiperidinones that bear no substituent at C-5 of the nitrogen heterocycle, such as **4**, can be completely transformed into the corresponding piperidinones using L-Selectride®. This hydride reagent selectively reduces the double bond of the α,β-unsaturated carbonyl function in terms of a 1,4-addition without affecting the keto function in terms of a 1,2-addition. Using these reaction conditions for the hydrogenation of dehydropiperidinone **19**, a conversion of only 50% of the starting material was observed. Addition of further equivalents of L-Selectride® did not improve the conversion, but reduced already formed piperidin-4-one **20** to the 4-hydroxypiperidine. In contrast, complete chemoselective addition of the hydride was achieved applying an excess L-Selectride® in the presence of the sterically demanding Lewis acid methylaluminum bis(2,6-di-*tert*-butyl-4-methylphenoxide) (MAD). This reagent has been shown to induce 1,4-addition of organolithiums to α,β-unsaturated ketones (10) and to enable the chemoselective reduction of the double bond of polymer-bound galactosyl dehydropiperidinones (11). The oxygenophilic Lewis acid effectively shields the keto function and, thus, favours the selective hy-

© 2006 NRC Canada

Scheme 8. Nitration of *N*-arabinosyl dehydropiperidinones and subsequent reduction of the obtained products.



dride addition at the β-position even by application of an excess of L-Selectride® for complete conversion of the starting material (Scheme 8).

N-Bromo succinimide and *N*-iodo succinimide were used in electrophilic substitution reactions at the enamine structure of *N*-arabinosyl dehydropiperidinones **4** to furnish halogenated compounds **21** in high yields (Scheme 9, Table 3).

Halogenated dehydropiperidinones **21** constitute vinyl halides capable of reacting in metal-catalyzed coupling reactions. In this way, piperidine derivatives with functionalized aryl substituents at C-5 were accessible. It turned out that iododehydropiperidinones **21** were more suitable in palladium-catalyzed syntheses than the bromo-substituted derivatives. Thus, in Stille reactions (12) applying bromodehydropiperidinone **21g** and phenyltributyl tin, 68% conversion of the starting material was observed after 24 h, while iododehydropiperidinone **21a** reacted faster and was completely consumed under these conditions, although product **22** was isolated in only moderate yield (Scheme 9).

Since boronic acids benefit from a much lower toxicity and an insensitivity to water compared with the tin reagents used in Stille-type reactions, Suzuki–Miyaura coupling conditions (13) were also applied for the synthesis of 5-aryl piperidine derivatives. Reaction of dehydropiperidinone **21c** with *p*-methoxybenzene boronic acid under palladium catalysis resulted in the formation of **23**. The reaction conditions have not yet been optimized (Scheme 9).

Even though the reaction conditions require further optimization, it appears that palladium-catalyzed reactions at C-5 of *N*-arabinosyl dehydropiperidinones **21** suffer from the sterically demanding auxiliary hampering the palladium complex from reaching the reaction site. However, the presented method provides access to 2,5-disubstituted piperidine derivatives containing pharmacologically valuable functionalized aryl substituents.

2,3-trans-Disubstituted N-*arabinosyl dehydropiperidinones*

Functionalization of *N*-arabinosyl dehydropiperidinones **4** at C-3 was achieved by deprotonation with strong bases and subsequent reaction with electrophiles. For this purpose, **4** was treated with lithium bis(trimethylsilyl)amide (LiHMDS), and the intermediate enolate was reacted with alkylhalides to afford 2,3-trans-disubstituted *N*-arabinosyl dehydropiperidinones **24** in high yields (Scheme 10, Table 4).

The coupling constant of product **24a** ($J_{H\text{-}2,H\text{-}3}$ = 11.7 Hz) determined by ^{1}H NMR spectroscopy indicated that these two protons are positioned in an antiperiplanar alignment, while the methyl group, as well as the aryl substituent, are arranged trans to each other and in an equatorial position. The stereoselectivity of the reaction can be explained by assuming that deprotonation of **4** forms a 6π-electron system resulting in an additional flattening of the dehydropiperidinone. The axial position of the substituent at C-2 induces a diastereofacial differentiation of the enolate favouring an attack of the electrophile from the sterically less-hindered side, i.e., trans to the first substituent resulting in the formation of the 2,3-trans-disubstituted compounds **24**.

Conclusions

The described results show that chiral piperidine derivatives of varying substitution patterns, valuable as building blocks for the construction of drugs and natural products, can stereoselectively be synthesized using α-D-arabinopyranosylamine (**1**) as the chiral auxiliary. Imines **2** of **1** undergo domino Mannich–Michael reaction sequences to furnish 2-substituted 5,6-dihydropiperidinones **4** with excellent diastereoselectivity. These compounds are substrates to a versatile modification of the piperidine structure (*i*) by conjugate addition of cuprates to give 2,6-cis-disubstituted piperidinones **11** with high stereoselectivity, (*ii*) to 5-

© 2006 NRC Canada

Scheme 9. Halogenation of *N*-arabinosyl dehydropiperidinones and Stille or Suzuki coupling of the obtained products.

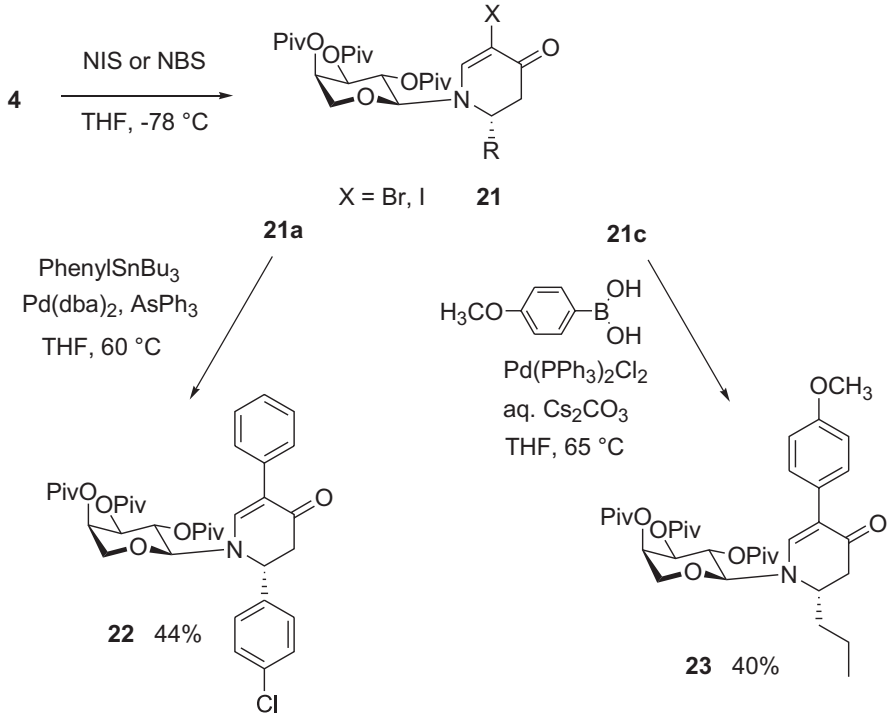
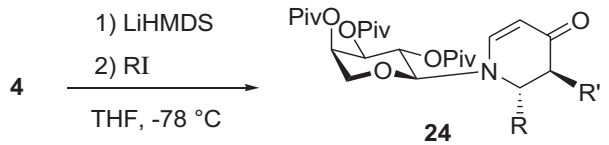


Table 3. Synthesis of halogen dehydropiperidinones according to Scheme 9.

Product	R	X	Yield (%)
21a	*p*-ClC_6H_4-	I	93
21b	Phenyl	I	67
21c	*n*-Propyl	I	69
21d	Isopropyl	I	87
21e	-$C_3H_6OTBDPS$	I	88
21f	*p*-ClC_6H_4-	Br	75
21g	Isopropyl	Br	83
21h	-$C_3H_6OTBDPS$	Br	79

Scheme 10. Stereoselective synthesis of 2,3-trans-substituted piperidine derivatives.



nitrogen-substituted derivatives, and (*iii*) to 5-halogen-substituted derivatives **21** of which the 5-iodo compounds are susceptible to Stille and Suzuku coupling reactions forming 5-aryl dehydropiperidinones. Enolates of the 2-substituted dehydropiperidinones **4** are alkylated to furnish 2,3-trans-disubstituted compounds **24** with excellent stereoselectivity. After reduction of the enaminone structure, the carbohydrate auxiliary can be cleaved off the enantiomerically pure substituted piperidine derivatives by a mild acidolysis.

Table 4. Synthesis of 2,3-disubstituted *N*-arabinosyl dehydropiperidinones according to Scheme 10.

Product	R	R′	Yield (%)	d.r.
24a	*p*-ClC_6H_4	Methyl	73	>95:5[a]
24b	$C_3H_6OTBDPS$	Methyl	87	75:25[a]
24c	$C_3H_6OTBDPS$	Ethyl	70	83:17[a]

[a]Determined by ^1H NMR.

Experimental

General methods

^1H NMR and ^{13}C NMR spectra were recorded on Bruker AC-200, AC-300, or AM-400 spectrometers. Mass spectra were recorded on a Navigator-1 ESI mass spectrometer (ThermoQuest) and a Finnigan MAT 95 spectrometer. Optical rotation values were measured on a PerkinElmer 241 polarimeter. Analytical HPLC were performed with a Phenomenex Luna C18 (2) column (5 μ, 250 mm × 4.6 mm).

Materials

THF was distilled over potassium benzophenone ketyl and CH_2Cl_2 over calcium hydride. 2,3,4-Tri-*O*-pivaloyl-α-D-arabinosylamine (**1**) was synthesized according to the literature procedure (5). Aldehydes used for imine formation were distilled prior to use. A solution of zinc chloride in THF was prepared by melting $ZnCl_2$ under high vacuum and dissolving it in dry THF after recooling. Diene **3** was prepared from 4-methoxybut-3-ene-2-one by the silylation procedure given by Danishefsky and Kitahara (14) followed by repeated careful distillation at moderate temperature (oil bath temperature has to be kept below 70 °C). TLC was performed on

© 2006 NRC Canada

Merck silica gel 60 F_{254} aluminum sheets. Flash chromatography was carried out with ICN Biomedicals silica gel (40–63 μm mesh).

General procedure for the synthesis of *N*-arabinosyl imines 2

Method A (aromatic aldehydes)

The aromatic aldehyde (12 mmol) and acetic acid (12 drops) were added to a solution of amine **1** (10 mmol) in isopropanol (20 mL) and heated to 80 °C for 3 h. The mixture was cooled and kept at 4 °C overnight. The crystallized product was filtered and washed with ice-cold isopropanol. Concentration of the mother liquor provided further amounts of product. The combined samples were, if necessary, recrystallized from *n*-heptane. Characterization was carried out upon the *N*-arabinosyl dehydropiperidinones **4**.

Method B (aliphatic aldehydes)

The aliphatic aldehyde (12 mmol) was added dropwise to a mixture of amine **1** (10 mmol), *n*-pentane (60 mL), and dried molecular sieves (6 g, 4 Å) and stirred for 36 h at room temperature. Filtration through Hyflo® and removal of the solvent in vacuo yielded an amorphous solid, which was used without further purification. Characterization was carried out upon the *N*-arabinosyl dehydropiperidinones **4**.

General procedure for the synthesis of *N*-arabinosyl dehydropiperidinones 4

A solution of $ZnCl_2$ in dry THF (1 mol/L, 11 mL) was added to a solution of imine **2** (10.0 mmol) in dry THF (50 mL) at –78 °C and stirred for 10 min. Danishefsky's diene **3** (2.5 mL, 12.5 mmol) was added. After stirring for 30 min, the solution was allowed to warm to –20 °C. After complete consumption of the starting material (1 to 2 days), the reaction was terminated by addition of 1 N aq. HCl (10 mL). THF was evaporated in vacuo, the residue was dissolved in diethyl ether, and the layers were separated. The organic layer was washed with satd. aq. $NaHCO_3$ (3 × 50 mL), 10% aq. Titriplex III® (2 × 50 mL) and brine, dried over $MgSO_4$, and concentrated.

*(2***R***)-***N***-(2′,3′,4′-Tri-***O***-pivaloyl-α-D-arabinopyranosyl)-2-(***p***-chlorophenyl)-5,6-dehydropiperidin-4-one (4a)*

Imine **2a** (5.10 g, 9.7 mmol) was treated according to the general procedure. Purification was achieved by flash chromatography (petroleum ether – ethyl acetate, 3:1). Yield: 5.49 g (9.0 mmol, 96%); colourless solid; mp 180 °C. R_f 0.18 (petroleum ether – ethyl acetate, 2:1). $[\alpha]^{25}_D$ –28.03° (*c* 1, $CHCl_3$); d.r.: 97:3 (HPLC: 80% CH_3CN, 20% H_2O → 100% CH_3CN, 20 min).^{1}H NMR (200 MHz, $CDCl_3$, ppm) δ: 7.32–7.19 (m, 5H, aryl, H-6), 5.60 (t, 1H, $J_{H\text{-}2',H\text{-}1'}$ = 9.8 Hz, $J_{H\text{-}2',H\text{-}3'}$ = 9.8 Hz, H-2′), 5.25–5.10 (m, 2H, H-4′, H-5), 4.99 (dd, 1H, $J_{H\text{-}3',H\text{-}2'}$ = 10.0 Hz, $J_{H\text{-}3',H\text{-}4'}$ = 3.2 Hz, H-3′), 4.81 (dd, 1H, $J_{H\text{-}2,H\text{-}3b}$ = 8.3 Hz, $J_{H\text{-}2,H\text{-}3a}$ = 5.9 Hz, H-2), 4.26 (d, 1H, $J_{H\text{-}1',H\text{-}2'}$ = 9.3 Hz, H-1′), 3.83 (dd, 1H, $J_{H\text{-}5'a,H\text{-}5'b}$ = 13.4 Hz, $J_{H\text{-}5'a,H\text{-}4'}$ = 2.2 Hz, H-5′a), 3.42 (d, 1H, $J_{H\text{-}5'b,H\text{-}5'a}$ = 12.7 Hz, H-5′b), 2.79 (dd, 1H, $J_{H\text{-}3a,H\text{-}3b}$ = 16.1 Hz, $J_{H\text{-}3a,H\text{-}2}$ = 5.9 Hz, H-3a), 2.60 (dd, 1H, $J_{H\text{-}3b,H\text{-}3a}$ = 16.1 Hz, $J_{H\text{-}3b,H\text{-}2}$ = 8.3 Hz, H-3b), 1.22, 1.56, 1.10 (3s, 27H, piv-CH_3). ^{13}C NMR (75.4 MHz, $CDCl_3$, ppm) δ: 191.1 (C-4), 177.1, 177.1, 177.0 (pivC=O), 149.9 (C-6), 137.2 (ipso-aryl), 134.2 (ipso-aryl), 129.0, 128.4 (aryl), 102.9 (C-5), 89.3 (C-1′), 71.1, 67.9, 65.6 (C-2′, C-3′, C-4′), 66.1 (C-5′), 58.6 (C-2), 43.5 (C-3), 38.9, 38.9, 38.7 ($piv_{quart.}$), 27.2, 27.1, 27.0 (piv-CH_3). ESI-MS for $C_{31}H_{42}ClNO_8$ *m/z*: 592.15 [M(^{35}Cl) + H]$^+$, 594.14 [M(^{37}Cl) + H]$^+$, 614.17 [M(^{35}Cl) + Na]$^+$, 616.17 [M(^{37}Cl) + Na]$^+$, 630.35 [M(^{35}Cl) + K]$^+$, 655.27 [M(^{35}Cl) + Na + CH_3CN]$^+$.

*(2***R***)-***N***-(2′,3′,4′-Tri-***O***-pivaloyl-α-D-arabinopyranosyl)-2-(***p***-nitrophenyl)-5,6-dehydropiperidin-4-one (4b)*

Imine **2b** (2.45 g, 4.6 mmol) was treated according to the general procedure. Purification was carried out by flash chromatography (petroleum ether – ethyl acetate, 5:1 → 3:1). Yield: 2.05 g (3.4 mmol, 74%); yellow solid; mp 179 °C. R_f 0.18 (petroleum ether – ethyl acetate, 2:1). $[\alpha]^{22}_D$ –15.1° (*c* 1, $CHCl_3$); d.r.: 86:14 (HPLC of the crude product), 96:4 (HPLC after flash chromatography), HPLC: 80% CH_3CN, 20% H_2O → 100% CH_3CN, 20 min. ^{1}H NMR (200 MHz, $CDCl_3$, ppm) δ: 8.13 (d, 2H, *J* = 8.8 Hz, aryl), 7.43 (d, 2H, *J* = 8.8 Hz, aryl), 7.22 (d, 1H, *J* = 7.8 Hz, H-6), 5.60 (t, 1H, $J_{H\text{-}2',H\text{-}1'}$ = 9.5 Hz, $J_{H\text{-}2',H\text{-}3'}$ = 9.5 Hz, H-2′), 5.20–5.05 (m, 2H, H-4′, H-5), 5.09 (dd, 1H, $J_{H\text{-}3',H\text{-}2'}$ = 6.6 Hz, $J_{H\text{-}3',H\text{-}4'}$ = 3.7 Hz, H-3′), 5.00 (dd, 1H, $J_{H\text{-}2,H\text{-}3a}$ = 6.8 Hz, $J_{H\text{-}2,H\text{-}3b}$ = 3.9 Hz, H-2), 4.47 (d, 1H, $J_{H\text{-}1',H\text{-}2'}$ = 9.3 Hz, H-1′), 3.79 (dd, 1H, $J_{H\text{-}5'b,H\text{-}5'a}$ = 13.2 Hz, $J_{H\text{-}5'b,H\text{-}4'}$ = 2.0 Hz, H-5′b), 3.53 (d, 1H, $J_{H\text{-}5'a,H\text{-}5'b}$ = 12.7 Hz, H-5′a), 3.01 (dd, 1H, $J_{H\text{-}3a,H\text{-}3b}$ = 16.4 Hz, $J_{H\text{-}3a,H\text{-}2}$ = 7.1 Hz, H-3a), 2.53 (dd, 1H, $J_{H\text{-}3b,H\text{-}3a}$ = 16.6 Hz, $J_{H\text{-}3b,H\text{-}2}$ = 3.9 Hz, H-3b), 1.89, 1.16, 1.11 (3s, 27H, piv-CH_3). ^{13}C NMR (50.3 MHz, $CDCl_3$, ppm) δ: 189.9 (C-4), 177.4, 177.1, 176.8 (pivC=O), 150.3 (C-6), 147.5, 147.1, 127.4, 123.8 (aryl), 102.0 (C-5), 91.4 (C-1′), 70.7, 67.7, 66.0, 66.3 (C-2′, C-3′, C-4′, C-5′), 56.6 (C-2), 42.8 (C-3), 39.0, 38.9, 38.8 ($pivC_{quart.}$), 27.2, 27.1, 27.0 (piv-CH_3). ESI-MS for $C_{31}H_{42}N_2O_{10}$ *m/z*: 666.4 [M + Na + MeCN]$^+$, 625.3 [M + Na]$^+$, 603.3 [M + H]$^+$, 501.3 [M – pivOH + H]$^+$.

*(2***R***)-***N***-(2′,3′,4′-Tri-***O***-pivaloyl-α-D-arabinopyranosyl)-2-phenyl-5,6-dehydropiperidin-4-one (4c)*

Imine **2c** (7.40 g, 15.0 mmol) was treated according to the general procedure. Purification was carried out by flash chromatography (petroleum ether – ethyl acetate, 3:1). Yield: 7.06 g (12.7 mmol, 84%); colourless amorpous solid; R_f 0.53 (petroleum ether – ethyl acetate, 4:1). $[\alpha]^{22}_D$ –27.3° (*c* 1, $CHCl_3$); d.r.: 92:8 (HPLC of the crude product: 80% CH_3CN, 20% H_2O → 100% CH_3CN, 20 min. ^{1}H NMR (200 MHz, $CDCl_3$, ppm) δ: 7.40–7.25 (m, 6H, aryl, H-6), 5.60 (t, 1H, $J_{H\text{-}2',H\text{-}1'}$ = 9.8 Hz, $J_{H\text{-}2',H\text{-}3'}$ = 9.8 Hz, H-2′), 5.23 (d, 1H, $J_{H\text{-}5,H\text{-}6}$ = 8.3 Hz, H-5), 5.15–5.09 (m, 1H, H-4′), 4.92 (dd, 1H, $J_{H\text{-}3',H\text{-}2'}$ = 10.0 Hz, $J_{H\text{-}3',H\text{-}4'}$ = 3.2 Hz, H-3′), 4.81 (t, 1H, $J_{H\text{-}2,H\text{-}3a}$ = 7.8 Hz, $J_{H\text{-}2,H\text{-}3b}$ = 7.8 Hz, H-2), 4.17 (d, 1H, $J_{H\text{-}1',H\text{-}2'}$ = 9.3 Hz, H-1′), 3.82 (dd, 1H, $J_{H\text{-}5'a,H\text{-}5'b}$ = 13.7 Hz, $J_{H\text{-}5'a,H\text{-}4'}$ = 1.9 Hz, H-5′a), 3.34 (d, 1H, $J_{H\text{-}5'b,H\text{-}5'a}$ = 13.2 Hz, H-5′b), 2.71 (d, 2H, *J* = 8.3 Hz, H-3a, H-3b), 1.23, 1.16, 1.09 (3s, 27H, piv-CH_3). ^{13}C NMR (50.3 MHz, $CDCl_3$, ppm) δ: 191.8 (C-4), 177.2, 177.1, 177.0 (pivC=O), 149.6 (C-6), 138.3 (ipso-aryl), 129.0, 128.7, 127.4 (aryl), 103.5 (H-5), 88.2 (C-1′), 71.4, 68.0, 65.4 (C-2′, C-3′, C-4′), 66.0

© 2006 NRC Canada

(C-5′), 60.6 (C-2), 43.9 (C-3), 39.0, 38.9, 38.8 (pivC$_{quart.}$), 27.2, 27.0 (piv-CH$_3$).

(2S)-N-*(2′,3′,4′-Tri*-O-*pivaloyl*-α-*D*-*arabinopyranosyl)*-2-*methyl*-5,6-*dehydropiperidin*-4-*one (4d)*

Crude imine **2d** (12.5 mmol) was treated according to the general procedure. Purification was achieved by flash chromatography (cyclohexane – ethyl acetate, 3:1 → 2:1). Yield: 3.02 g (6.09 mmol, 49%); colourless amorphous solid. R_f 0.12 (cyclohexane – ethyl acetate, 2:1). $[\alpha]^{22}_D$ +60.48° (*c* 1, $CHCl_3$); d.r.: 93:7 (HPLC after flash chromatography: 80% CH_3CH, 20% H_2O → 95% CH_3CN, 5% H_2O, 30 min). ^{1}H NMR (300 MHz, $CDCl_3$, ppm) δ: 6.91 (d, 1H, $J_{H\text{-}6,H\text{-}5}$ = 7.0 Hz, H-6), 5.55 (t, 1H, $J_{H\text{-}2',H\text{-}1'}$ = 9.6 Hz, $J_{H\text{-}2',H\text{-}3'}$ = 9.6 Hz, H-2′), 5.26–5.20 (m, 1H, H-4′), 5.13 (dd, 1H, $J_{H\text{-}3',H\text{-}2'}$ = 10.1 Hz, $J_{H\text{-}3',H\text{-}4'}$ = 3.1 Hz, H-3′), 5.01 (d, 1H, $J_{H\text{-}5,H\text{-}6}$ = 7.7 Hz, H-5), 4.44 (d, 1H, $J_{H\text{-}1',H\text{-}2'}$ = 8.8 Hz, H-1′), 4.02 (dd, 1H, $J_{H\text{-}5'a,H\text{-}5'b}$ = 13.2 Hz, $J_{H\text{-}5'a,H\text{-}4'}$ = 2.2 Hz, H-5′a), 3.98–3.89 (m, H-1, H-2), 3.67 (d, 1H, $J_{H\text{-}5'b,H\text{-}5'a}$ = 13.2 Hz, H-5′b), 2.68 (dd, 1H, $J_{H\text{-}3a,H\text{-}3b}$ = 16.6 Hz, $J_{H\text{-}3a,H\text{-}2}$ = 6.3 Hz, H-3a), 2.17 (dd, 1H, $J_{H\text{-}3b,H\text{-}3a}$ = 16.6 Hz, $J_{H\text{-}3b,H\text{-}2}$ = 1.9 Hz, H-3b), 1.30 (d, 3H, *J* = 6.6 Hz, CH_3), 1.26, 1.11, 1.10 (3s, 27H, piv-CH_3). ^{13}C NMR (100.6 MHz, $CDCl_3$, ppm) δ: 192.1 (C-4), 177.2, 177.1, 177.1 (pivC=O), 149.9 (C-6), 99.8 (C-5), 92.0 (C-1′), 71.0, 68.0, 65.9 (C-2′, C-3′, C-4′), 66.1 (C-5′), 49.4 (C-2), 42.6 (C-3), 38.9, 38.9, 38.8 (piv$_{quart}$), 27.1, 27.1, 27.0 (piv-CH_3), 17.7 (CH_3). ESI-MS for $C_{26}H_{41}NO_8$ *m/z*: 496.3 $[M + H]^+$, 518.3 $[M + Na]^+$, 534.3 $[M + K]^+$, 991.6 $[2M + H]^+$, 1013.6 $[2M + Na]^+$, 1029.6 $[2M + K]^+$.

(2S)-N-*(2′,3′,4′-Tri*-O-*pivaloyl*-α-*D*-*arabinopyranosyl)*-2-*ethyl*-5,6-*dehydropiperidin*-4-*one (4e)*

Crude imine **2e** (25 mmol) was treated according to the general procedure. Purification was achieved by flash chromatography (cyclohexane – ethyl acetate, 4:1). Yield: 8.49 g (16.7 mmol, 67%); colourless amorphous solid. R_f 0.19 (cyclohexane – ethyl acetate, 2:1). $[\alpha]^{22}_D$ +79.67° (*c* 1, $CHCl_3$); d.r.: 96:4 (HPLC of the crude product: 80% CH_3CH, 20% H_2O → 95% CH_3CN, 5% H_2O, 30 min). ^{1}H NMR (300 MHz, $CDCl_3$, ppm) δ: 6.90 (d, 1H, $J_{H\text{-}6,H\text{-}5}$ = 6.6 Hz, H-6), 5.56 (t, 1H, $J_{H\text{-}2',H\text{-}1'}$ = 9.4 Hz, $J_{H\text{-}2',H\text{-}3'}$ = 9.4 Hz, H-2′), 5.26–5.19 (m, 1H, H-4′), 5.12 (dd, 1H, $J_{H\text{-}3',H\text{-}2'}$ = 10.1 Hz, $J_{H\text{-}3',H\text{-}4'}$ = 3.1 Hz, H-3′), 4.93 (d, 1H, $J_{H\text{-}5,H\text{-}6}$ = 7.0 Hz, H-5), 4.44 (d, 1H, $J_{H\text{-}1',H\text{-}2'}$ = 9.2 Hz, H-1′), 4.01 (dd, 1H, $J_{H\text{-}5'a,H\text{-}5'b}$ = 13.2 Hz, $J_{H\text{-}5'a,H\text{-}4'}$ = 2.2 Hz, H-5′a), 3.66 (d, 1H, $J_{H\text{-}5'b,H\text{-}5'a}$ = 13.6 Hz, H-5′b), 3.67–3.56 (m, 1H, H-2), 2.59 (dd, 1H, $J_{H\text{-}3a,H\text{-}3b}$ = 16.7 Hz, $J_{H\text{-}3a,H\text{-}2}$ = 6.1 Hz, H-3a), 2.37 (d, 1H, $J_{H\text{-}3b,H\text{-}3a}$ = 16.9 Hz, H-3b), 1.98–1.79 (m, 1H, CH_2), 1.78–1.60 (m, 1H, CH_2), 1.25, 1.11, 1.10 (3s, 27H, piv-CH_3), 0.84 (t, 3H, *J* = 7.53 Hz, CH_3). ^{13}C NMR (75.4 MHz, $CDCl_3$, ppm) δ: 192.1 (C-4), 177.2, 177.1, 177.0 (pivC=O), 149.9 (C-6), 99.8 (C-5), 92.1 (C-1′), 71.1, 68.0, 66.0 (C-2′, C-3′, C-4′), 66.1 (C-5′), 55.2 (C-2), 39.0, 38.9, 38.7 (piv$_{quart}$), 38.4 (C-3), 27.1, 27.0 (piv-CH_3), 23.6 (CH_2), 10.1 (CH_3). ESI-MS for $C_{27}H_{43}NO_8$ *m/z*: 306.2 $[M - 2pivOH + H]^+$, 510.3 $[M + H]^+$, 532.3 $[M + Na]^+$, 573.3 $[M + Na + MeCN]^+$, 1041.3 $[2M + Na]^+$.

(2S)-N-*(2′,3′,4′-Tri*-O-*pivaloyl*-α-*D*-*arabinopyranosyl)*-2-*n-propyl*-5,6-*dehydropiperidin*-4-*one (4f)*

Crude imine **2f** (25 mmol) was treated according to the general procedure. Purification was achieved by flash chromatography (petroleum ether – ethyl acetate, 3:1). X-ray analysis: space group, $P2_12_12_1$ (orthorhombic); lattice parameters: *a* = 9.8895(13) Å, *b* = 10.1820(11) Å, *c* = 30.614(4) Å, *V* = 3082.7(6) Å^3, *Z* = 4, *F*(000) = 1136; diffractometer: CAD4 Enraf Nonius; irradiation: Cu K_α graphite monochromator.[3] Yield: 10.64 g (20.3 mmol, 81%); colourless solid; mp 192 °C. R_f 0.07 (petroleum ether – ethyl acetate, 3:1). $[\alpha]^{25}_D$ +66.64° (*c* 1, $CHCl_3$); d.r.: 87:13 (HPLC of the crude product: 80% CH_3CN, 20% H_2O → 100% CH_3CN, 20 min). ^{1}H NMR (200 MHz, $CDCl_3$, ppm) δ: 6.90 (d, 1H, $J_{H\text{-}6,H\text{-}5}$ = 7.3 Hz, H-6), 5.55 (t, 1H, $J_{H\text{-}2',H\text{-}1'}$ = 9.5 Hz, $J_{H\text{-}2',H\text{-}3'}$ = 9.5 Hz, H-2′), 5.30–5.20 (m, 1H, H-4′), 5.13 (dd, 1H, $J_{H\text{-}3',H\text{-}2'}$ = 10.0 Hz, $J_{H\text{-}3',H\text{-}4'}$ = 3.2 Hz, H-3′), 4.93 (d, 1H, $J_{H\text{-}5,H\text{-}6}$ = 7.3 Hz, H-5), 4.44 (d, 1H, $J_{H\text{-}1',H\text{-}2'}$ = 9.3 Hz, H-1′), 4.02 (dd, 1H, $J_{H\text{-}5'a,H\text{-}5'b}$ = 13.2 Hz, $J_{H\text{-}5'a,H\text{-}4'}$ = 2.0 Hz, H-5′a), 3.80–3.70 (m, 1H, H-2), 3.67 (d, 1H, $J_{H\text{-}5'b,H\text{-}5'a}$ = 13.2 Hz, H-5′b), 2.60 (dd, 1H, $J_{H\text{-}3a,\ H\text{-}3b}$ = 16.6 Hz, $J_{H\text{-}3a,H\text{-}2}$ = 6.3 Hz, H-3a), 2.34 (d, 1H, $J_{H\text{-}3b,H\text{-}3a}$ = 16.6 Hz, H-3b), 2.00–1.75 (m, 1H, CH_2), 1.65–1.50 (m, 1H, CH_2), 1.30–1.10 (m, 27H, piv-CH_3), 0.86 (t, 3H, *J* = 7.3 Hz, CH_3). ^{13}C NMR (50.3 MHz, $CDCl_3$, ppm) δ: 192.2 (C-4), 177.2, 176.8 (pivC=O), 149.9 (H-6), 99.8 (H-5), 92.1 (C-1′), 71.1, 68.0, 66.1 (C-2′, C-3′, C-4′), 66.2 (C-5′), 53.5 (C-2), 39.0 (C-3), 38.9, 38.8, 38.8 (pivC$_{quart.}$), 32.7 (CH_2), 27.2, 27.1, 27.0 (piv-CH_3), 18.9 (CH_2), 13.8 (CH_3). Anal. calcd. for $C_{28}H_{45}NO_8$: C 64.22, H 8.66, N 2.69; found: C 64.20, H 8.60, N 2.63.

(2R)-N-*(2′,3′,4′-Tri*-O-*pivaloyl*-α-*D*-*arabinopyranosyl)*-2-*isopropyl*-5,6-*dehydropiperidin*-4-*one (4g)*

Crude imine **2g** (25 mmol) was treated according to the general procedure. Purification was carried out by flash chromatography. Yield: 9.45 g (18 mmol, 73%); colourless amorphous solid. R_f 0.13 (cyclohexane – ethyl acetate, 3:1). $[\alpha]^{24}_D$ +70.14° (*c* 1, $CHCl_3$); d.r.: 95:5 (HPLC of the crude product), 99:1 (HPLC after flash chromatography), HPLC: 85% CH_3CH, 15% H_2O → 95% CH_3CN, 5% H_2O, 20 min). ^{1}H NMR (400 MHz, $CDCl_3$, ppm) δ: 7.01 (d, 1H, $J_{H\text{-}5,H\text{-}6}$ = 7.8 Hz, H-6), 5.58 (t, 1H, $J_{H\text{-}2',H\text{-}1'}$ = 9.6 Hz, $J_{H\text{-}2',H\text{-}4'}$ = 9.6 Hz, H-2′), 5.25–5.20 (m, 1H, H-4′), 5.12 (dd, 1H, $J_{H\text{-}3',H\text{-}2'}$ = 9.8 Hz, $J_{H\text{-}3',H\text{-}4'}$ = 3.1 Hz, H-3′), 4.93 (d, 1H, $J_{H\text{-}5,H\text{-}6}$ = 7.8 Hz, H-5), 4.49 (d, 1H, $J_{H\text{-}1',H\text{-}2'}$ = 9.0 Hz, H-1′), 3.99 (dd, 1H, $J_{H\text{-}5'a,H\text{-}5'b}$ = 13.3 Hz, $J_{H\text{-}5'a,H\text{-}4'}$ = 2.4 Hz, H-5′), 3.67 (dd, 1H, $J_{H\text{-}5'b,H\text{-}5'a}$ = 13.3 Hz, $J_{H\text{-}5'b,H\text{-}4'}$ = 0.8 Hz, H-5′b), 3.59–3.52 (m, 1H, H-2), 2.59 (dd, 1H, $J_{H\text{-}3a,H\text{-}3b}$ = 16.2 Hz, $J_{H\text{-}3a,H\text{-}2}$ = 7.8 Hz, H-3a), 2.40 (dd, 1H, $J_{H\text{-}3b,H\text{-}3a}$ = 16.8 Hz, $J_{H\text{-}3b,H\text{-}2}$ =

[3] Supplementary data for this article are available on the journal Web site (http://canjchem.nrc.ca) or may be purchased from the Depository of Unpublished Data, Document Delivery, CISTI, National Research Council Canada, Ottawa, ON K1A 0R6, Canada. DUD 5028. For more information on obtaining material refer to http://cisti-icist.nrc-cnrc.gc.ca/irm/unpub_e.shtml. CCDC 229785 and 229786 contain the crystallographic data for this manuscript. These data can be obtained, free of charge, via http://www.ccdc.cam.ac.uk/conts/retrieving.html (or from the Cambridge Crystallographic Data Centre, 12 Union Road, Cambridge CB2 1EZ, UK; fax +44 1223 336033; or deposit@ccdc.cam.ac.uk).

© 2006 NRC Canada

2.0 Hz, H-3a), 2.32–2.19 (m, 1H, C*H*(CH_3)$_2$), 1.25, 1.11, 1.10 (3s, 27H, piv-CH_3), 0.89 (d, 3H, J = 7.0 Hz, CH_3), 0.89 (d, 3H, J = 6.6 Hz, CH_3). ^{13}C NMR (50.3 MHz, $CDCl_3$, ppm) δ: 192.5 (C-4), 177.2, 177.1, 177.0 (pivC=O), 150.3 (C-6), 100.3 (C-5), 91.8 (C-1′), 71.4, 68.0, 65.8 (C-2′, C-3′, C-4′), 66.1 (C-5′), 58.9 (C-2), 38.9, 38.9, 38.8 (piv$_{quart}$), 35.5 (C-3), 32.2 (*C*H(CH_3)$_3$), 27.1, 27.0 (piv-CH_3), 19.5, 17.6 (CH_3). ESI-MS for $C_{28}H_{45}NO_8$ *m/z*: 524.4 [M + H]$^+$, 546.4 [M + Na]$^+$, 587.3 [M + CH_3CN + Na]$^+$, 1069.6 [2M + Na]$^+$.

(2S)-N-*(2′,3′,4′-Tri*-O-*pivaloyl*-α-*D-arabinopyranosyl)*-2-*(3-tert-butyldiphenylsiloxy)propyl*-5,6-*dehydropiperidin*-4-*one (4h)*

Crude imine **2h**, prepared from 4-(*tert*-butyldiphenylsiloxy)butanal (15) according to method B, was treated according to the general procedure. Purification was carried out by flash chromatography (cyclohexane – ethyl acetate, 4:1 → 3:1). Yield: 12.7 g (16.4 mmol, 65%); colourless amorphous solid. R_f 0.33 (petrolether – ethyl acetate, 2:1). $[\alpha]^{25}_D$ +32.84° (*c* 1, $CHCl_3$); d.r.: 90:10 (HPLC of the crude product), 96:4 (HPLC after chromatography), HPLC: 80% CH_3CN, 20% H_2O → 100% CH_3CN, 20 min). ^{1}H NMR (200 MHz, $CDCl_3$), δ: 7.70–7.50 (m, 4H, aryl), 7.46–7.27 (m, 6H, aryl), 6.92 (d, 1H, $J_{H\text{-}6,H\text{-}5}$ = 7.8 Hz, H-6), 5.55 (t, 1H, $J_{H\text{-}2',H\text{-}1'}$ = 9.5 Hz, $J_{H\text{-}2',H\text{-}3'}$ = 9.5 Hz, H-2′), 5.29–5.19 (m, 1H, H-4′), 5.12 (dd, 1H, $J_{H\text{-}3',H\text{-}2'}$ = 9.8 Hz, $J_{H\text{-}3',H\text{-}4'}$ = 2.9 Hz, H-3′), 4.98 (d, 1H, $J_{H\text{-}5,H\text{-}6}$ = 7.3 Hz, H-5), 4.44 (d, 1H, $J_{H\text{-}1',H\text{-}2'}$ = 8.8 Hz, H-1′), 4.04–3.90 (m, 1H, H-5′a), 3.81–3.50 (m, 4H, $J_{H\text{-}5'b,H\text{-}5'a}$ = 13.2 Hz, H-2, H-5′b, CH_2-O), 2.64 (dd, 1H, $J_{H\text{-}3a,H\text{-}3b}$ = 16.8 Hz, $J_{H\text{-}3a,H\text{-}2}$ = 6.1 Hz, H-3a), 2.34 (d, 1H, $J_{H\text{-}3b,H\text{-}3a}$ = 16.6 Hz, H-3b), 1.99–1.70 (m, 2H, CH_2), 1.69–1.38 (m, 2H, CH_2), 1.22, 1.11, 1.11, 0.99 (4s, 36H, C(CH_3)$_3$). ^{13}C NMR (50.3 MHz, $CDCl_3$, ppm) δ: 191.9 (C-4), 182.0, 177.2, 177.1 (pivC=O), 149.9 (C-6), 135.5, 133.8, 129.6, 127.7 (aryl), 99.8 (C-5), 91.8 (C-1′), 71.1, 68.0, 66.0 (C-2′, C-3′, C-4′), 66.2 (C-5′), 63.5 (CH_2-O), 53.9 (C-2), 39.1 (C-3), 39.0, 38.9, 38.8 (pivC$_{quart.}$), 28.9 (CH_2), 27.4 (CH_2), 27.2, 27.1 (pivCH$_3$), 26.8 (Si-C(*C*H$_3$)$_3$), 19.2 (Si-*C*(CH_3)$_3$). ESI-MS for $C_{44}H_{63}NO_9Si$ *m/z*: 472.1 [M – 3pivOH + H]$^+$, 574.2 [M – 2pivOH + H]$^+$, 700.3 [M – Phenyl], 778.3 [M + H]$^+$, 800.4 [M + Na]$^+$, 816.3 [M + K]$^+$, 841.3 [M + Na + CH_3CN]$^+$.

(2S)-N-*(2′,3′,4′-Tri*-O-*pivaloyl*-α-*D-arabinopyranosyl)*-2-n-*propyl*-4-*(trifluormethansulfonyloxy)*-4,5-*dehydropiperidine (7)*

To a solution of **4f** (1.31 g, 2.50 mmol) and 2-[*N*,*N*-bis(trifluoromethanesulfonyl)amino]-5-chloropyridine (1.18 g, 3.00 mmol) in dry THF (50 mL), L-Selectride® (1 mol/L in THF, 2.75 mL) was added at –78 °C and stirred for 1 h. The solution was allowed to warm slowly and stirred until the starting material was consumed. The reaction was terminated by addition of aq. $NaHCO_3$ (5 mL). THF was removed in vacuo, diethyl ether (100 mL) was added, and the layers were separated. The aqueous layer was extracted with ether, and the combined organic layers were washed with brine and dried over $MgSO_4$. The solvent was evaporated in vacuo. Flash chromatography (cyclohexane – ethyl acetate, 10:1) of the residue afforded **7** as a colourless amorphous solid (0.98 g, 1.49 mmol, 60%). R_f 0.67 (cyclohexane – ethyl acetate, 3:1). $[\alpha]^{22}_D$ –12.46° (*c* 1, $CHCl_3$). ^{1}H NMR (300 MHz, $CDCl_3$, ppm) δ: 5.72–5.64 (m, 1H, H-5), 5.40 (t, 1H, $J_{H\text{-}2',H\text{-}1'}$ = 9.6 Hz, $J_{H\text{-}2',H\text{-}3'}$ = 9.6 Hz, H-2′), 5.19–5.13 (m, 1H, H-4′), 5.07 (dd, 1H, $J_{H\text{-}3',H\text{-}2'}$ = 9.9 Hz, $J_{H\text{-}3',H\text{-}4'}$ = 3.3 Hz, H-3′), 4.13 (d, 1H, $J_{H\text{-}1',H\text{-}2'}$ = 9.2 Hz, H-1′), 3.90 (dd, 1H, $J_{H\text{-}5'a,H\text{-}5'b}$ = 13.1 Hz, $J_{H\text{-}5'a,H\text{-}4'}$ = 2.0 Hz, H-5′a), 3.62 (dd, 1H, $J_{H\text{-}6a,H\text{-}6b}$ = 17.6 Hz, $J_{H\text{-}6a,H\text{-}5}$ = 2.6 Hz, H-6a), 3.53 (d, 1H, $J_{H\text{-}5'b,H\text{-}5'a}$ = 13.2 Hz, H-5′b), 3.42 (d, 1H, $J_{H\text{-}6b,H\text{-}6a}$ = 17.3 Hz, H-6b), 3.24–3.11 (m, 1H, H-2), 2.55 (dd, 1H, $J_{H\text{-}3a,H\text{-}3b}$ = 16.4 Hz, $J_{H\text{-}3a,H\text{-}2}$ = 2.8 Hz, H-3a), 2.09 (d, 1H, $J_{H\text{-}3b,H\text{-}3a}$ = 16.6 Hz, H-3b), 1.68–1.53 (m, 1H, CH_2), 1.47–1.15 (m, 3H, CH_2), 1.23, 1.12, 1.10 (3s, 27H, pivCH$_3$), 0.89 (t, 3H, J = 7.2 Hz, CH_3). ^{13}C NMR (75.4 MHz, $CDCl_3$, ppm) δ: 177.3, 177.3, 177.1 (pivC=O), 146.6 (C-4), 116.1 (C-5), 92.8 (C-1′), 71.6, 68.6, 65.6 (C-2′, C-3′, C-4′), 65.1 (C-5′), 41.8 (C-6), 38.9, 38.7, 38.6 (piv$_{quart.}$), 33.6 (CH_2), 32.6 (CH_2), 27.1, 27.0, 27.0 (pivCH$_3$), 19.8 (CH_2), 14.1 (CH_3). ESI-MS for $C_{29}H_{46}F_3NO_{10}S$ *m/z*: 406.2 [M – pivOH – OTf]$^+$, 508.5 [M – OTf]$^+$, 556.3 [M – pivOH + H]$^+$, 658.3 [M + H]$^+$, 680.3 [M + Na]$^+$, 696.1 [M + K]$^+$, 721.4 [M + Na + CH_3CN]$^+$.

(2S)-N-*(2′,3′,4′-Tri*-O-*pivaloyl*-α-*D-arabinopyranosyl)*-2-n-*propylpiperidine (8)*

Li_2CO_3 (160 mg) and Pd/C (10%, 50 mg) were added to a solution of enol triflate **7** (888 mg, 1.35 mmol) in methanol (100 mL) and stirred for 20 h under a H_2 atmosphere. After filtration through Hyflo®, the solvent was removed in vacuo, and the remaining residue was dissolved in diethyl ether (100 mL). The solution was washed with water (40 mL) and brine (40 mL), dried over $MgSO_4$, and evaporated to dryness to yield pure **8** as a colourless amorphous solid (665 mg, 1.30 mmol, 96%). R_f 0.75 (cyclohexane – ethyl acetate, 4:1). $[\alpha]^{22}_D$ –28.12° (*c* 1, $CHCl_3$). ^{1}H NMR (300 MHz, $CDCl_3$, ppm) δ: 5.50 (t, 1H, $J_{H\text{-}2',H\text{-}1'}$ = 9.6 Hz, $J_{H\text{-}2',H\text{-}3'}$ = 9.6 Hz, H-2′), 5.20–5.11 (m, 1H, H-4′), 5.07 (dd, 1H, $J_{H\text{-}3',H\text{-}2'}$ = 9.7 Hz, $J_{H\text{-}3',H\text{-}4'}$ = 3.1 Hz, H-3′), 4.33–4.13 (m, 1H, H-1′), 3.90 (d, 1H, $J_{H\text{-}5'a,H\text{-}5'b}$ = 12.8 Hz, H-5′a), 3.51 (d, $J_{H\text{-}5'b,H\text{-}5'a}$ = 12.8 Hz, H-5′b), 3.27–3.06, 2.79–2.54, 2.51–2.27 (3m, 3H, H-2, H-6a, H-6b), 1.72–1.19 (m, 19H, 3CH_2, 2PropylCH_2, pivCH$_3$), 1.23, 1.14, 1.10 (3s, 27H, pivCH$_3$), 0.89 (t, 3H, J = 7.0 Hz, CH_3). ^{13}C NMR (75.4 MHz, $CDCl_3$, ppm) δ: 177.4 (pivC=O), 89.3 (C-1′), 72.1, 68.9, 65.1, 65.1 (C-2′, C-3′, C-4′, C-5′), 57.5 (C-2), 45.2 (C-6), 38.9, 38.7, 38.6 (piv$_{quart.}$), 34.8 (CH_2), 31.6 (CH_2), 27.3, 27.1, 27.0 (pivCH$_3$), 26.2 (CH_2), 24.1 (CH_2), 18.8 (CH_2), 14.5 (CH_3). ESI-MS for $C_{28}H_{49}NO_7$ *m/z*: 308.2 [M – 2pivOH + H]$^+$, 410.3 [M – pivOH + H]$^+$, 512.3 [M + H]$^+$, 534.3 [M + Na]$^+$, 550.3 [M + K]$^+$.

(2S)-2-n-*Propylpiperidine hydrochloride (coniine hydrochloride) (10·HCl)*

N-Arabinosyl piperidine **8** (563 mg, 1.1 mmol) in methanol (15 mL) was treated with 1 N HCl (2 mL) and stirred until completion of the reaction (48 h). The solvent was evaporated in vacuo, the residue was dissolved in diethyl ether (35 mL) and extracted with water (5 × 10 mL). Lyophilization of the aqueous layer gave coniine hydrochloride (**10·HCl**) as a colourless amorphous solid (171 mg, 1.0 mmol, 95%). $[\alpha]^{22}_D$ +5.33° (*c* = 1, ethanol); enantiomer (16): $[\alpha]^{22}_D$ –5.8° (*c* 1, methanol). ^{1}H NMR (300 MHz, DMSO, ppm) δ: 9.14 (br s, 1H, NH), 8.99 (br s, 1H, NH),

© 2006 NRC Canada

3.20–3.05 (m, 1H, NCH_2), 3.00–2.84 (m, 1H, H-2), 2.84–2.65 (m, 1H, NCH_2), 1.90–1.15 (m, 10H, CH_2), 0.86 (t, 3H, J = 7.2 Hz, CH_3). ^{13}C NMR (75.4 MHz, DMSO, ppm) δ: 55.5 (C-2), 43.8 (C-6), 35.0 (CH_2), 27.8 (CH_2), 21.9, (CH_2), 21.9 (CH_2), 17.9 (CH_2), 13.8 (CH_3). ESI-MS for $C_8H_{18}ClN$ *m/z*: 128.1 [M – Cl]$^+$, 291.2 [2M(^{35}Cl) – Cl]$^+$, 293.1 [M(^{37}Cl) – Cl]$^+$.

General procedure for the addition of R′Cu·BF_3 complexes to enaminones

The solution of the corresponding Grignard reagent in THF or diethyl ether was added to a suspension of copper salt (1 mmol) in dry THF (5–10 mL) at the temperature given for the corresponding cuprate (given in the following) and stirred until the cuprate was formed (time and change in colour for each compound is given in the following). Subsequently, the cuprate was cooled to –78 °C, $BF_3{\cdot}OEt_2$ (1 mmol) was added and the mixture stirred for 15 min. Dehydropiperidinone **4** in dry THF (20 mL per mmol piperidinone) was added dropwise, and the mixture was stirred for 15 h. In general, a slow increase of temperature was required for complete consumption of the starting material. The reaction was terminated by addition of concd. NH_4OH – satd. NH_4Cl (1:1 *v*/*v*). The mixture was warmed to room temperature (r.t.), diluted with diethyl ether (20 mL), and the layers were seperated. The organic layer was washed with concd. NH_4OH – satd. NH_4Cl (1:1 *v*/*v*), washed with brine and dried over $MgSO_4$. The solvent was removed in vacuo, and the residue was purified by flash chromatography.

*(2*R*,6*S*)*-*N*-*(2′,3′,4′-Tri*-O-*pivaloyl-*α*-*D*-*arabinopyranosyl)-2-(*p*-*chlorophenyl)-6-phenylpiperidin-4-one (11a)*

Piperidinone **11a** was prepared from **4a** (592 mg, 1.0 mmol) according to the general procedure. For the formation of the beige cuprate solution, CuI (952 mg, 5 mmol) and phenylmagnesium bromide (1 mol/L in THF, 5 mL) were treated in THF (30 mL) at –78 °C for 1 h. Purification of **11a** was achieved by flash chromatography (petroleum ether – ethyl acetate, 14:1 → 10:1). Yield: 484 mg (0.7 mmol, 72%); colourless solid; mp 179 °C. X-ray analysis: space group, *P*1 (triklin); lattice parameters: a = 10.1869(6) Å, b = 13.1017(12) Å, c = 15.5126(12) Å, V = 1901.1(3) Å^3, Z = 2, F(000) = 716; diffractometer, CAD4 Enraf Nonius; irradiation, Cu K_α graphite monochromator.[3] R_f 0.55 (petroleum ether – ethyl acetate, 3:1). $[\alpha]^{25}_D$ –35.44° (*c* 1, $CHCl_3$); d.r.: 99:1 (HPLC: 80% CH_3CN, 20% H_2O → 100% CH_3CN, 20 min). ^{1}H NMR (200 MHz, $CDCl_3$, ppm) δ: 7.50–7.15 (m, 9H, aryl), 5.36 (t, 1H, $J_{H\text{-}2',H\text{-}1'}$ = 9.5 Hz, $J_{H\text{-}2',H\text{-}3'}$ = 9.5 Hz, H-2′), 5.15–5.00 (m, 2H, H-4′, aryl-C*H*-N), 4.90–4.50 (m, 2H, H-3′, aryl-C*H*-N), 4.24 (d, 1H, $J_{H\text{-}1',H\text{-}2'}$ = 9.3 Hz, H-1′), 3.97 (dd, 1H, $J_{H\text{-}5'a,H\text{-}5'b}$ = 12.9 Hz, $J_{H\text{-}5'a,H\text{-}4'}$ = 2.2 Hz, H-5′a), 3.51–3.25 (m, 2H, H-5′, CH_2C=O), 2.86 (dd, 1H, $J_{gem.}$ = 16.1 Hz, $J_{vic.}$ = 2.4 Hz, CH_2C=O), 2.61 (dd, $J_{gem.}$ = 18.1 Hz, $J_{vic.}$ = 12.7 Hz, CH_2C=O), 2.41 (dd, 1H, $J_{gem.}$ = 18.3 Hz, $J_{vic.}$ = 3.7 Hz, CH_2C=O), 1.26, 1.08, 1.01 (3s, 27H, piv-CH_3). ^{13}C NMR (50.3 MHz, $CDCl_3$, ppm) δ: 208.0 (C-4), 177.5, 177.2, 175.3 (pivC=O), 144.1, 140.5, 133.8, 129.1, 128.6, 127.1, 126.3 (Aryl), 90.3 (C-1′), 72.9, 68.7, 66.3 (C-2′, C-3′, C-4′), 65.2 (C-5′), 58.3, 53.4 (C-2, C-6), 47.5, 46.4 (C-3, C-5), 39.0, 38.7, 38.6 (pivC$_{quart.}$), 27.2, 27.0 (piv-CH_3). ESI-MS for $C_{37}H_{48}NO_8$: 568.5 [M(^{35}Cl) – pivOH + H]$^+$, 570.6 [M(^{37}Cl) – pivOH + H]$^+$, 670.6 [M(^{35}Cl) + H]$^+$, 672.6 [M(^{37}Cl) + H]$^+$, 692.6 [M(^{35}Cl) + Na]$^+$, 694.6 [M(^{37}Cl) + Na]$^+$, 708.5 [M + K]$^+$.

*(2*R*,6*R*)*-*N*-*(2′,3′,4′-Tri*-O-*pivaloyl-*α*-*D*-*arabinopyranosyl)-2-allyl-6-(*p*-*chlorophenyl)-piperidin-4-one (11b)*

Piperidinone **11b** was prepared from **4a** (592 mg, 1.0 mmol) according to the general procedure. For the formation of the orange cuprate solution, CuCN (358 mg, 4 mmol) and allylmagnesium bromide (1 mol/L in ether, 4 mL) were treated in THF (30 mL) at –40 °C for 0.5 h. Purification of **11b** was performed by flash chromatography (petroleum ether – ethyl acetate, 13:1 → 10:1). Yield: 325 mg (0.5 mmol, 51%); colourless amorphous solid; mp 73 °C. R_f 0.64 (petroleum ether – ethyl acetate, 3:1). $[\alpha]^{25}_D$ +26.64° (*c* 1, $CHCl_3$); d.r.: 98:2 (HPLC: 80% CH_3CN, 20% H_2O → 100% CH_3CN, 20 min. ^{1}H NMR (400 MHz, $CDCl_3$, ppm) δ: 7.40–7.35 (m, 4H, aryl), 5.84–5.71 (m, 1H, C*H*=CH_2), 5.65 (t, 1H, $J_{H\text{-}2',H\text{-}1'}$ = 9.6 Hz, $J_{H\text{-}2',H\text{-}3'}$ = 9.6 Hz, H-2′), 5.22–5.12 (m, 3H, H-4′, CH=CH_2), 4.92 (dd, 1H, $J_{H\text{-}3',H\text{-}2'}$ = 9.8 Hz, $J_{H\text{-}3',H\text{-}4'}$ = 3.1 Hz, H-3′), 4.68 (dd, 1H, $J_{H\text{-}2,H\text{-}3a}$ = 12.1 Hz, $J_{H\text{-}2,H\text{-}3b}$ = 3.9 Hz, H-2), 4.12 (d, 1H, $J_{H\text{-}1',H\text{-}2'}$ = 9.4 Hz, H-1′), 4.00 (dd, 1H, $J_{H\text{-}5'a,H\text{-}5'b}$ = 13.3 Hz, $J_{H\text{-}5'a,H\text{-}4'}$ = 2.4 Hz, H-5′a), 3.80–3.70 (m, 1H, H-6), 3.53 (d, 1H, $J_{H\text{-}5'b,H\text{-}5'a}$ = 12.9 Hz, H-5′b), 2.93 (dd, 1H, $J_{gem.}$ = 16.4 Hz, $J_{vic.}$ = 5.7 Hz, H-5a), 2.71–2.61 (m, 2H, H-5b, H-3a), 2.57 (dd, 1H, $J_{gem.}$ = 18.2 Hz, $J_{vic.}$ = 4.1 Hz, H-3b), 2.47–2.37 (m, 1H, CH_2-CH=CH_2), 2.10–1.99 (m, 1H, CH_2-CH=CH_2), 1.34, 1.26, 1.18 (3s, 27H, piv-CH_3). ^{13}C NMR (50.3 MHz, $CDCl_3$, ppm) δ: 208.9 (C-4), 177.4, 177.2, 176.8 (pivC=O), 141.0 (ipso-aryl), 134.2 (*C*H=CH_2), 133.7 (ipso-aryl.), 129.0, 128.9 (aryl), 118.4 (CH=*C*H_2), 90.7 (C-1′), 72.7, 68.7, 66.2 (C-2′, C-3′, C-4′), 65.2 (C-5′), 58.4 (C-2), 50.7 (C-6), 47.4 (CH_2), 44.0 (CH_2), 42.0 (CH_2), 38.9, 38.8, 38.8 (pivC$_{quart.}$), 27.3, 27.2, 27.1 (piv-CH_3). ESI-MS for $C_{34}H_{48}ClNO_8$ *m/z*: 430.4 [M(^{35}Cl) – 2pivOH + H]$^+$, 532.5 [M(^{35}Cl) – pivOH + H]$^+$, 534.5 [M(^{37}Cl) – pivOH + H]$^+$, 634.5 [M(^{35}Cl) + H]$^+$, 636.5 [M(^{37}Cl) + H]$^+$, 656.5 [M(^{35}Cl) + Na]$^+$, 658.5 [M(^{37}Cl) + Na]$^+$, 672.6 [M(^{35}Cl) + K]$^+$. Anal. calcd. for $C_{34}H_{48}ClNO_8$ (634.20): C 64.39, H 7.63, N 2.21; found: C 64.42, H 7.83, N 2.13.

*(2S,6S)-*N*-(2′,3′,4′-Tri*-O-*pivaloyl-*α*-*D*-*arabinopyranosyl)-2-phenyl-6-*n*-*propylpiperidin-4-one (11c)*

Piperidinone **11c** was prepared from **4f** (524 mg, 1.0 mmol) according to the general procedure. For the formation of the beige cuprate solution, CuI (952 mg, 5 mmol) and phenylmagnesium bromide (1 mol/L in THF, 5 mL) were treated in THF (30 mL) at –78 °C for 1 h. Purification of **11c** was carried out by flash chromatography (petroleum ether – ethyl acetate, 10:1). Yield: 670 mg (0.4 mmol, 44%); colourless solid. R_f 0.55 (petroleum ether – ethyl acetate, 3:1). $[\alpha]^{26}_D$ –10.37° (*c* 1, $CHCl_3$); d.r.: 99:1 (HPLC: 80% CH_3CN, 20% H_2O → 100% CH_3CN, 20 min). ^{1}H NMR (200 MHz, $CDCl_3$, ppm) δ: 7.35–7.10 (m, 5H, aryl), 5.38 (t, 1H, $J_{H\text{-}2',H\text{-}1'}$ = 9.3 Hz, $J_{H\text{-}2',H\text{-}3'}$ = 9.3 Hz, H-2′), 5.20–5.12 (m, 1H, H-4′), 5.06 (dd, 1H, $J_{H\text{-}3',H\text{-}2'}$ = 9.5 Hz, $J_{H\text{-}3',H\text{-}4'}$ = 3.2 Hz, H-3′), 4.90–4.80 (m, 1H, H-6), 4.48 (d, 1H, $J_{H\text{-}1',H\text{-}2'}$ =

© 2006 NRC Canada

9.3 Hz, H-1′), 3.98 (dd, 1H, $J_{H\text{-}5'a,H\text{-}5'b}$ = 12.9 Hz, $J_{H\text{-}5'a,H\text{-}4'}$ = 2.2 Hz, H-5′a), 3.59 (d, 1H, $J_{H\text{-}5'b,H\text{-}5'a}$ = 13.2 Hz, H-5′b), 3.50–3.35 (m, 1H, H-2), 3.13 (dd, 1H, $J_{gem.}$ = 17.1 Hz, $J_{vic.}$ = 5.9 Hz, CH_2C=O), 2.93 (dd, 1H, $J_{gem.}$ = 17.1, $J_{vic.}$ = 3.4 Hz, CH_2C=O), 2.47 (dd, 1H, $J_{gem.}$ = 17.1 Hz, $J_{vic.}$ = 4.4 Hz, CH_2C=O), 2.14 (dd, 1H, $J_{gem.}$ = 17.1 Hz, $J_{vic.}$ = 10.8 Hz, CH_2C=O), 1.70–1.00 (m, 31H, piv-CH_3, CH_2), 0.88 (t, 3H, J = 6.8 Hz, propyl-CH_3). ^{13}C NMR (50.3 MHz, $CDCl_3$, ppm) δ: 209.8 (C-4), 177.5, 177.2, 176.0 (pivC=O), 143.8, 129.5, 128.2, 126.7 (aryl), 92.2 (C-1′), 72.7, 68.7, 66.7 (C-2′, C-3′, C-4′), 65.3 (C-5′), 55.7 (C-6), 53.9 (C-2), 46.2, 43.8 (C-3, C-5), 39.9 (propyl-CH_2), 38.9, 38.7 (pivC$_{quart.}$), 27.3, 27.2, 27.1 (piv-CH_3), 19.2 (propyl-CH_2), 14.0 (propyl-CH_3). ESI-MS for $C_{34}H_{51}NO_8$ *m/z*: 398.5 [M – piv – 2pivOH + H]$^+$, 500.5 [M – pivOH + H]$^+$, 602.5 [M + H]$^+$, 624.5 [M + Na]$^+$, 640.6 [M + K]$^+$.

*(2**R**,6**S**)-**N**-(2′,3′,4′-Tri-**O**-pivaloyl-α-D-arabinopyranosyl)-2-allyl-6-**n**-propylpiperidin-4-one (11d)*

Piperidinone **11d** was prepared from **4f** (1.05 g, 2.0 mmol) according to the general procedure. For the formation of the orange cuprate solution, CuCN (716 mg, 8 mmol) and allylmagnesium bromide (1 mol/L in ether, 8 mL) were treated in THF (60 mL) at –40 °C for 0.5 h. Purification of **11b** was accomplished by flash chromatography (cyclohexane – ethyl acetate, 10:1). Yield: 0.85 g (1.50 mmol, 75%); colourless crystalline solid; mp 176 °C. R_f 0.52 (cyclohexane – ethyl acetate, 3:1). $[\alpha]^{25}_D$ +7.21° (*c* 1, $CHCl_3$); d.r.: 98:2 (HPLC after flash chromatography), 94:6 (HPLC of the crude product), HPLC: 80% CH_3CN, 20% H_2O → 100% CH_3CN, 20 min). ^{1}H NMR (400 MHz, $CDCl_3$, ppm) δ: 5.72–5.60 (m, 1H, C*H*=CH_2), 5.49 (t, 1H, $J_{H\text{-}2',H\text{-}1'}$ = 9.6 Hz, $J_{H\text{-}2',H\text{-}3'}$ = 9.6 Hz, H-2′), 5.16 (br s, 1H, H-4′), 5.10–4.98 (m, 3H, H-3′, CH=C*H*$_2$), 4.26 (d, 1H, $J_{H\text{-}1',H\text{-}2'}$ = 9.4 Hz, H-1′), 3.92 (dd, 1H, $J_{H\text{-}5'a,H\text{-}5'b}$ = 13.1 Hz, $J_{H\text{-}5'a,H\text{-}4'}$ = 1.7 Hz, H-5′a), 3.56 (d, 1H, $J_{H\text{-}5'b,H\text{-}5'a}$ = 12.9 Hz, H-5′b), 3.60–3.50 (m, 1H, H-6), 3.40–3.30 (m, 1H, H-2), 2.67–2.57 (m, 2H, H-3a, H-5a), 2.39 (d, 1H, $J_{H\text{-}5b,H\text{-}5a}$ = 15.7 Hz, H-5b), 2.25 (m, 2H, $J_{H\text{-}3b,H\text{-}3a}$ = 15.5 Hz, $J_{H\text{-}3b,H\text{-}2}$ = 6.85 Hz, H-3b, C*H*$_2$-CH=CH_2), 2.06–1.95 (m, 1H, C*H*$_2$-CH=CH_2), 1.60–1.50 (m, 1H, C*H*$_2$-CH_2-CH_3), 1.40–1.25 (m, 2H, C*H*$_2$-C*H*$_2$-CH_3), 1.25–1.15 (m, 28H, piv-CH_3, CH_2-C*H*$_2$-CH_3), 0.86 (t, 3H, J = 7.2 Hz, propyl-CH_3). ^{13}C NMR (50.3 MHz, $CDCl_3$, ppm) δ: 210.5 (C-4), 177.4, 177.2, 176.9 (pivC=O), 135.4 (*C*H=CH_2), 117.6 (CH=*C*H$_2$), 94.6 (C-1′), 72.3, 68.7, 66.3 (C-2′, C-3′, C-4′), 65.1 (C-5′), 58.6 (alkyl-*C*H-N), 44.6 (CH_2), 43.4 (CH_2), 43.0 (CH_2), 40.1 (CH_2), 38.9, 38.8, 38.7 (pivC$_{quart.}$), 27.3, 27.1, 27.1 (piv-CH_3), 19.7 (propyl-CH_2), 14.0 (propyl-CH_3). ESI-MS for $C_{31}H_{51}NO_8$ *m/z*: 362.4 [M – 2pivOH + H]$^+$, 464.5 [M – pivOH + H]$^+$, 566.6 [M + H]$^+$, 588.5 [M + Na]$^+$, 604.5 [M + K]$^+$. Anal. calcd. for $C_{31}H_{51}NO_8$ (565.74): C 65.81, H 9.09, N 2.40; found: C 66.14, H 8.91, N 2.37.

*(2**R**,6**S**)-**N**-(2′,3′,4′-Tri-**O**-pivaloyl-α-D-arabinopyranosyl)-2-methyl-6-**n**-propylpiperidin-4-one (11e)*

A solution of methyllithium in diethyl ether (1.6 mol/L, 9.6 mL, 15.4 mmol) was added dropwise to a cold (–35 °C) suspension of CuI (1.50 g, 8.0 mmol) in dry THF (40 mL). The mixture was warmed to –25 °C in 2 h. During this time, the initially yellow solid was dissolved upon formation of a colourless solution, which was then cooled to –78 °C. Piperidinone **4f** (2.51 g, 4.8 mmol) and TMSCl (3 mL) in dry THF (80 mL) were added and the colour changed to yellow and finally to orange. The reaction mixture was allowed to warm to r.t. within 14 h. The reaction was terminated by addition of concd. NH_4OH – satd. NH_4Cl (1:1 *v/v*) (72 mL), and the mixture was diluted with diethyl ether (250 mL). The organic layer was washed with brine, dried over $MgSO_4$, and concentrated in vacuo to yield silylenol ether **12** as an amorphous solid. It was dissolved in THF (48 mL) and a solution of tetrabutylammonia fluoride in THF (1 mol/L, 7.2 mL, 7.2 mmol) was added and the mixture was stirred until **12** was consumed. The solvent was removed in vacuo, the residue was dissolved in diethyl ether (240 mL), washed with water (100 mL) and brine (100 mL), and dried over $MgSO_4$. The solvent was evaporated in vacuo and the residue was purified by flash chromatography (petroleum ether – ethyl acetate, 5:1) to yield **11e** as a colourless crystalline solid (2.28 g, 4.2 mmol, 88%); mp 162 °C. R_f 0.46 (petroleum ether – ethyl acetate, 3:1). $[\alpha]^{25}_D$ –6.11° (*c* 1, $CHCl_3$); d.r.: 91:9 (HPLC of the crude product), HPLC: 80% CH_3CN, 20% H_2O → 100% CH_3CN, 20 min). ^{1}H NMR (200 MHz, $CDCl_3$, ppm) δ: 5.48 (t, 1H, $J_{H\text{-}2',H\text{-}1'}$ = 9.5 Hz, $J_{H\text{-}2',H\text{-}3'}$ = 9.5 Hz, H-2′), 5.20–5.10 (m, 1H, H-4′), 5.06 (dd, 1H, $J_{H\text{-}3',H\text{-}2'}$ = 9.8 Hz, $J_{H\text{-}3',H\text{-}4'}$ = 3.4 Hz, H-3′), 4.23 (d, 1H, $J_{H\text{-}1',H\text{-}2'}$ = 9.3 Hz, H-1′), 3.93 (dd, $J_{H\text{-}5'b,H\text{-}5'a}$ = 13.2 Hz, $J_{H\text{-}5'b,H\text{-}4'}$ = 2.0 Hz, H-5′b), 3.85–3.70, 3.45–3.25 (2m, each 1H, H-2, H-6), 3.55 (d, 1H, $J_{H\text{-}5'a,H\text{-}5'b}$ = 12.7 Hz, H-5′a), 2.78 (dd, 1H, $J_{H\text{-}3a,H\text{-}3b}$ = 15.1 Hz, $J_{H\text{-}3a,H\text{-}2}$ = 6.8 Hz, H-3a), 2.62 (dd, 1H, $J_{H\text{-}3b,H\text{-}3a}$ = 15.1 Hz, $J_{H\text{-}3b,H\text{-}2}$ = 5.9 Hz, H-3b), 2.27 (dd, 1H, J_{gem} = 15.6 Hz, $J_{vic.}$ = 6.8 Hz, H-5a), 2.25–2.10 (m, 1H, H-5b), 1.70–1.50 (m, 1H, propyl-CH_2), 1.50–1.00 (m, 33H, piv-CH_3, CH_3, propyl-CH_2), 0.86 (t, 3H, J = 7.1 Hz, propyl-CH_3). ^{13}C NMR (50.3 MHz, $CDCl_3$, ppm) δ: 210.7 (C-4), 177.4, 177.2, 176.8 (pivC=O), 94.7 (C-1′), 72.2, 68.7, 66.4 (C-2′, C-3′, C-4′), 65.2 (C-5′), 58.7, 48.9 (C-2, C-6), 47.3, 44.3 (C-3, C-5), 40.3 (propyl-CH_2), 38.9, 38.7 (pivC$_{quart.}$), 27.2, 27.1, 27.1 (piv-CH_3), 24.5 (CH_3), 19.8 (propyl-CH_2), 14.0 (propyl-CH_3). Anal. calcd. for $C_{29}H_{49}NO_8$ (539.70): C 64.54, H 9.15, N 2.60; found: C 64.52, H 9.27, N 2.56.

*(2**S**,6**R**)-**N**-(2′,3′,4′-Tri-**O**-pivaloyl-α-D-arabinopyranosyl)-2-**n**-propyl-4-(1,3-dithiolan-2-yl)-6-methylpiperidine (13)*

To a solution of piperidinone **11e** (720 mg, 1.3 mmol) and ethanedithiol (0.22 mL, 2.6 mmol) in dry dichloromethane (9 mL) was added $BF_3{\cdot}OEt_2$ (0.78 mL, 6.7 mmol) at 0 °C. After 1 h the reaction mixture was warmed to r.t. and stirring was continued for 15 h. The mixture was diluted with dichloromethane (45 mL), washed with satd. aq. $NaHCO_3$ (2 × 20 mL) and water, dried over $MgSO_4$, and concentrated in vacuo. The crude product was purified by flash chromatography to yield **13** as colourless solid (662 mg, 1.1 mmol, 81%); mp 142 °C. R_f 0.29 (petroleum ether – ethyl acetate, 5:1). $[\alpha]^{26}_D$ –24.46° (*c* 1, $CHCl_3$). ^{1}H NMR (200 MHz, $CDCl_3$, ppm) δ: 5.57 (t, 1H, $J_{H\text{-}2',H\text{-}1'}$ = 9.8 Hz, $J_{H\text{-}2',H\text{-}3'}$ = 9.8 Hz, H-2′), 5.25 – 5.15 (m, 1H, H-4′), 4.94 (dd, 1H, $J_{H\text{-}3',H\text{-}2'}$ = 9.8 Hz, $J_{H\text{-}3',H\text{-}4'}$ = 2.9 Hz, H-3′), 4.31 (d, 1H, $J_{H\text{-}1',H\text{-}2'}$ = 9.3 Hz, H-1′), 3.92 (dd, 1H, $J_{H\text{-}5'b,H\text{-}5'a}$ = 13.2 Hz, $J_{H\text{-}5'b,H\text{-}4'}$ = 2.0 Hz, H-5′b), 3.53 (d, 1H, $J_{H\text{-}5'a,H\text{-}5'b}$ = 13.2 Hz,

© 2006 NRC Canada

H-5′a), 3.35–3.20 (m, 4H, SCH_2CH_2S), 3.15–3.00, 2.95–2.80 (2m, each 1H, H-2, H-6), 2.20–1.80 (m, 4H, $2CH_2$), 1.40–1.10 (m, 34 H, piv-CH_3, propyl-CH_2, CH_3), 0.91 (t, 3H, J = 6.8 Hz, propyl-CH_3). ^{13}C NMR (50.3 MHz, $CDCl_3$, ppm) δ: 177.5, 177.4, 176.8 (piv-CH_3), 88.6 (C-1′), 72.8, 68.8, 68.2 (C-2′, C-3′, C-4′), 65.9 (C-5′), 59.2, 53.6 (C-2, C-6), 50.0 (CH_2), 48.2 (CH_2), 38.9, 38.7, 38.7 (piv-$C_{quart.}$), 38.6 (CH_2), 38.5 (CH_2), 37.0 (CH_2), 27.3, 27.2, 27.1 (piv-CH_3), 21.8 (CH_3), 19.8 (propyl-CH_2), 14.3 (propyl-CH_3). Anal. calcd. for $C_{31}H_{35}NO_7S_2$ (615.89): C 60.45, H 8.67, N 2.27, S 10.41; found: C 60.09, H 8.68, N 2.17, S 10.68.

*(2**R**,6**S**)-**N**-(2′,3′,4′-Tri-**O**-pivaloyl-α-D-arabinopyranosyl)-2-methyl-6-**n**-propylpiperidine (14)*

Raney nickel (5 g) was added to a solution of dithioketal **13** (500 mg, 0.8 mmol) in isopropanol (50 mL) and vigorously stirred for 24 h at 70 °C under H_2 atmosphere. The mixture was filtered through Hyflo®, and the filtrate was concentrated in vacuo to afford pure **14** as a colourless amorphous solid (310 mg, 0.6 mmol, 73%). R_f 0.48 (petroleum ether – ethyl acetate, 5:1). ^{1}H NMR (200 MHz, $CDCl_3$, ppm) δ: 5.49 (t, 1H, $J_{H\text{-}2',H\text{-}1'}$ = 9.5 Hz, $J_{H\text{-}2',H\text{-}3'}$ = 9.5 Hz, H-2′), 5.20–5.07 (m, 1H, H-4′), 5.01 (dd, 1H, $J_{H\text{-}3',H\text{-}2'}$ = 9.8 Hz, $J_{H\text{-}3',H\text{-}4'}$ = 3.4 Hz, H-3′), 4.12 (d, 1H, $J_{H\text{-}1',H\text{-}2'}$ = 9.3 Hz, H-1′), 3.89 (dd, 1H, $J_{H\text{-}5'b,H\text{-}5'a}$ = 13.2 Hz, $J_{H\text{-}5'b,H\text{-}4'}$ = 2.0 Hz, H-5′b), 3.49 (d, 1H, $J_{H\text{-}5'a,H\text{-}5'b}$ = 13.2 Hz, H-5′a), 3.25–3.10, 3.00–2.85 (2m, each 1H, H-2, H-6), 1.80–1.05 (m, 40 H, piv-CH_3, CH_3, propyl-CH_2, CH_2), 0.86 (t, 3H, J = 7.1 Hz, propyl-CH_3). ^{13}C NMR (50.3 MHz, $CDCl_3$, ppm) δ: 177.5, 176.7 (pivC=O), 96.8 (C-1′), 72.7, 69.0, 66.0 (C-2′, C-3′, C-4′), 64.8 (C-5′), 38.9, 38.7, 38.7 (piv-$C_{quart.}$), 38.5 (CH_2), 31.7 (CH_2), 28.4 (CH_2), 27.3, 27.1, 27.1 (piv-CH_3), 22.4 (CH_3), 21.5 (CH_2), 15.4 (CH_2), 14.4 (propyl-CH_3).

*(+)-(2**R**,6**S**)-2-methyl-6-**n**-propylpiperidine hydrochloride (dihydropinidine) (15)*

Piperidine **14** (240 mg, 0.46 mmol) was dissolved in methanol (6 mL), treated with 1 N HCl (0.7 mL, 0.70 mmol) and stirred at r.t. for 48 h. The solvent was evaporated in vacuo the residue was dissolved in diethyl ether and extracted with water (3 × 10 mL). Lyophilization of the aqueous layers afforded **15** as colourless solid (quant.); mp 215–220 °C. $[\alpha]^{25}_D$ +11.05° (*c* 1, ethanol) (lit. value (9) $[\alpha]^{25}_D$ +11.6 to +14.2° (ethanol); enantiomer: lit. value (9) $[\alpha]^{25}_D$ –9.1 to –12.7° (ethanol); lit. value (3) $[\alpha]^{22}_D$ –11.1° (*c* 1, ethanol). ^{1}H NMR (200 MHz, $CDCl_3$, ppm) δ: 9.07 (br s, 1H, NH), 8.68 (br s, 1H, NH), 3.15–2.80 (m, 2H, H-2, H-6), 1.90–1.00 (m, 13H, $5CH_2$, CH_3), 0.87 (t, 3H, J = 7.1 Hz, propyl-CH_3). ^{13}C NMR (50.3 MHz, $CDCl_3$, ppm) δ: 56.0, 52.5 (C-2, C-6), 34.82, 29.78, 27.05, 22.01, 18.75, 17.86 ($5CH_2$, CH_3), 13.68 (propyl-CH_3).

*(2**S**)-**N**-(2′,3′,4′-Tri-**O**-pivaloyl-α-D-arabinopyranosyl)-2-methyl-5-nitro-5,6-dehydropiperidin-4-one (17)*

A solution of nitronium tetrafluoroborate in sulfolane (0.5 mol/L, 1.5 mL, 0.75 mmol) was added slowly to **4d** (198 mg, 0.4 mmol) in dichloromethane (4 mL) at –78 °C. The mixture was allowed to reach r.t. and was quenched with satd. aq. $NaHCO_3$. The solvent was removed in vacuo, the residue was dissolved in diethyl ether (20 mL), and extracted with satd. aq. $NaHCO_3$. The aqueous layer was extracted twice with diethyl ether, and the combined organic layers were concentrated in vacuo. For the removal of sulfolane, water was added to the oily residue and stirred until a solid was formed. This was filtered, washed with water, dissolved in diethyl ether, and dried over $MgSO_4$. After removal of the solvent, purification was carried out by flash chromatography (cyclohexane – ethyl acetate, 3:1) to give **17** as a colourless amorphous solid (178 mg, 0.3 mmol, 83%). R_f 0.53 (cyclohexane – ethyl acetate, 1:1). $[\alpha]^{22}_D$ +0.15° (*c* 1, $CHCl_3$). ^{1}H NMR (300 MHz, $CDCl_3$, ppm) δ: 8.57 (s, 1H, H-6), 5.51 (t, 1H, $J_{H\text{-}2',H\text{-}1'}$ = 9.6 Hz, $J_{H\text{-}2',H\text{-}3'}$ = 9.6 Hz, H-2′), 5.32–5.26 (m, 1H, H-4′), 5.20 (dd, 1H, $J_{H\text{-}3',H\text{-}2'}$ = 9.9 Hz, $J_{H\text{-}3',H\text{-}4'}$ = 3.3 Hz, H-3′), 4.76 (d, 1H, $J_{H\text{-}1',H\text{-}2'}$ = 8.8 Hz, H-1′), 4.11 (dd, 1H, $J_{H\text{-}5'a,H\text{-}5'b}$ = 13.2 Hz, $J_{H\text{-}5'a,H\text{-}4'}$ = 1.8 Hz, H-5′a), 4.16–4.03 (m, 1H, H-2), 3.81 (d, 1H, $J_{H\text{-}5'b,H\text{-}5'a}$ = 12.9 Hz, H-5′b), 2.82 (dd, 1H, $J_{H\text{-}3a,H\text{-}3b}$ = 16.2 Hz, $J_{H\text{-}3a,H\text{-}2}$ = 6.2 Hz, H-3a), 2.34 (dd, $J_{H\text{-}3b,H\text{-}3a}$ = 16.4, $J_{H\text{-}3b,H\text{-}2}$ = 1.7 Hz, H-3b), 1.35 (d, 3H, J = 7.0 Hz, CH_3), 1.26, 1.11, 1.08 (3s, each 9H, piv-CH_3). ESI-MS for $C_{26}H_{40}N_2O_{10}$ *m/z*: 541.7 $[M + H]^+$, 563.6 $[M + Na]^+$, 579.6 $[M + K]^+$, 604.6 $[M + MeCN + Na]^+$, 1104.2 $[2M + Na]^+$.

*(2**S**)-**N**-(2′,3′,4′-Tri-**O**-pivaloyl-α-D-arabinopyranosyl)-2-ethyl-5-nitro-5,6-dehydropiperidin-4-one (18)*

In a similar manner, dehydropiperidinone **4e** (3.02 g, 5.9 mmol) in dichloromethane (80 mL) was treated with a solution of nitronium tetrafluoroborate in sulfolane (0.5 mol/L, 18 mL, 9 mmol). Purification was carried out by flash chromatography (cyclohexane – ethyl acetate, 3:1) to give **18** as a colourless amorphous solid (2.68 g 4.8 mmol, 82%). R_f 0.57 (cyclohexane – ethyl acetate, 1:1). $[\alpha]^{22}_D$ +28.76° (*c* 1, $CHCl_3$). ^{1}H NMR (300 MHz, $CDCl_3$, ppm) δ: 8.58 (s, 1H, H-6), 5.52 (t, 1H, $J_{H\text{-}2',H\text{-}1'}$ = 9.4 Hz, $J_{H\text{-}2',H\text{-}3'}$ = 9.4 Hz, H-2′), 5.32–5.26 (m, 1H, H-4′), 5.19 (dd, 1H, $J_{H\text{-}3',H\text{-}2'}$ = 10.1 Hz, $J_{H\text{-}3',H\text{-}4'}$ = 3.1 Hz, H-3′), 4.78 (d, 1H, $J_{H\text{-}1',H\text{-}2'}$ = 8.8 Hz, H-1′), 4.12 (dd, 1H, $J_{H\text{-}5'a,H\text{-}5'b}$ = 13.2 Hz, $J_{H\text{-}5'a,H\text{-}4'}$ = 2.2 Hz, H-5′a), 3.87 – 3.71 (m, 1H, H-2), 3.81 (d, 1H, $J_{H\text{-}5'b,H\text{-}5'a}$ = 12.9 Hz, H-5′b), 2.74 (dd, 1H, $J_{H\text{-}3a,H\text{-}3b}$ = 16.5 Hz, $J_{H\text{-}3a,H\text{-}2}$ = 6.3 Hz, H-3a), 2.57 (dd, $J_{H\text{-}3b,H\text{-}3a}$ = 16.5, $J_{H\text{-}3b,H\text{-}2}$ = 1.1 Hz, H-3b), 1.87–1.72 (m, 2H, CH_2), 1.26, 1.11, 1.08 (3s, 27H, piv-CH_3), 0.88 (t, 3H, J = 7.5 Hz, CH_3). ^{13}C NMR (75.4 MHz, $CDCl_3$, ppm) δ: 180.1 (C-4), 177.3, 176.9, 176.8 (pivC=O), 153.2 (C-6), 123.5 (C-5), 93.0 (C-1′), 70.2, 67.5, 66.1 (C-2′, C-3′, C-4′), 66.7 (C-5′), 55.9 (C-2), 39.0, 39.0, 38.8 (piv$_{quart}$), 38.5 (C-3), 27.1, 27.0, 27.0 (piv-CH_3), 24.6 (CH_2), 9.9 (CH_3). ESI-MS for $C_{27}H_{42}N_2O_{10}$ (554.63) *m/z*: 555.2 $[M + H]^+$, 577.3 $[M + Na]^+$, 618.4 $[M + Na + MeCN]^+$, 1131.5 $[2M + Na]^+$.

*(2**S**)-**N**-(2′,3′,4′-Tri-**O**-pivaloyl-α-D-arabinopyranosyl)-5-benzamido-2-ethyl-5,6-dehydropiperidin-4-one (19)*

To a suspension of Raney nickel (3 g) in ethanol, saturated with H_2, was added a solution of **18** (4 g, 7.2 mmol) in ethanol (160 mL) and stirred for 22 h under a H_2 atmosphere. The mixture was filtered through Hyflo®, and the filtrate was concentrated in vacuo. The residue was dissolved in diethyl ether, dried over $MgSO_4$, and evaporated to dryness. The remaining solid was dissolved in dry THF. Triethylamine (4.5 mL, 32.4 mmol) and freshly distilled benzoyl chloride (2.5 mL, 21.6 mmol) were added, and the solution was stirred for 10 h at room temperature. After ad-

© 2006 NRC Canada

dition of satd. aq. NH_4Cl (200 mL), the mixture was extracted with diethyl ether (3 × 100 mL). The combined organic layers were washed with brine and dried over $MgSO_4$. The solvent was removed in vacuo and the crude product was purified by flash chromatography to yield **19** as a colourless amorphous solid (3.2 g, 5.1 mmol, 70%). R_f 0.35 (cyclohexane – ethyl acetate, 2:1). $[\alpha]^{22}_D$ +54.52° (*c* 1, $CHCl_3$). ^{1}H NMR (300 MHz, $CDCl_3$, ppm) δ: 8.73 (s, 1H, H-6), 8.40 (br s, 1H, NH), 8.12–8.04 (m, 1H, phenyl), 7.86–7.78 (m, 2H, phenyl), 7.47–7.39 (m, 2H, phenyl), 5.56 (t, 1H, $J_{H\text{-}2',H\text{-}1'}$ = 9.6 Hz, $J_{H\text{-}2',H\text{-}3'}$ = 9.6 Hz, H-2′), 5.28–5.22 (m, 1H, H-4′), 5.13 (dd, 1H, $J_{H\text{-}3',H\text{-}2'}$ = 10.1 Hz, $J_{H\text{-}3',H\text{-}4'}$ = 3.1 Hz, H-3′), 4.60 (d, 1H, $J_{H\text{-}1',H\text{-}2'}$ = 8.8 Hz, H-1′), 4.03 (dd, 1H, $J_{H\text{-}5'a,H\text{-}5'b}$ = 13.4 Hz, $J_{H\text{-}5'a,H\text{-}4'}$ = 2.0 Hz, H-5′a), 3.72–3.59 (m, 1H, H-2), 3.69 (d, 1H, $J_{H\text{-}5'b,H\text{-}5'a}$ = 13.2 Hz, H-5′b), 2.79 (dd, 1H, $J_{H\text{-}3a,H\text{-}3b}$ = 17.3 Hz, $J_{H\text{-}3a,H\text{-}2}$ = 6.6 Hz, H-3a), 2.55 (dd, $J_{H\text{-}3b,H\text{-}3a}$ = 17.3 Hz, $J_{H\text{-}3b,H\text{-}2}$ = 1.5 Hz, H-3b), 2.04–1.88 (m, 1H, CH_2), 1.87–1.71 (m, 1H, CH_2), 1.26, 1.11, 1.08 (3s, 27H, piv-CH_3), 0.86 (t, 3H, *J* = 7.4 Hz, CH_3). ^{13}C NMR (75.4 MHz, $CDCl_3$, ppm) δ: 184.5 (C-4), 177.4, 177.1, 177.0 (pivC=O), 164.4 (NH-C=O), 134.2 (ipso-aryl), 133.5, 131.5, 130.1, 128.6, 128.4, 126.9 (aryl, C-6), 112.4 (C-5), 92.6 (C-1′), 71.0, 68.0, 66.4 (C-2′, C-3′, C-4′), 66.1 (C-5′), 53.9 (C-2), 39.0, 38.9, 38.7 ($piv_{quart.}$), 36.8 (C-3), 27.1, 27.0 (piv-CH_3), 23.7 (CH_2), 10.2 (CH_3). ESI-MS *m/z*: 323.3 [M – 3pivOH + H]$^+$, 425.5 [M – 2pivOH + H]$^+$, 527.5 [M – pivOH + H]$^+$, 651.6 [M + Na]$^+$, 692.8 [M + Na + MeCN]$^+$. HRMS calcd. for $C_{34}H_{48}N_2O_9$: 629.3438; found: 629.3424.

N-*(2′,3′,4′-Tri*-O-*pivaloyl-*α-*D-arabinopyranosyl)-5-benzamido-2-ethylpiperidin-4-one (20)*

(a) Preparation of the aluminum complex MAD

At r.t., trimethylaluminium (2 mol/L in toluene, 0.1 mL) was added to a solution of 2,6-di-*tert*-butyl-4-methylphenol (86 mg, 0.39 mmol) in toluene (3 mL) and stirred until the methane evolution ceased (30 min).

(b) Conjugate hydride addition

The clear solution preapared under (*a*) was cooled to –78 °C and a solution of **19** (25 mg, 0.04 mmol) in THF (2 mL) was added dropwise. After 15 min, L-Selectride® (1 mol/L in THF, 0.08 mL) was added at the same temperature, and the mixture was then allowed to warm to –40 °C within 3 h. The reaction was terminated by addition of acetic acid (0.05 mL), and the solvent was evaporated in vacuo. The residue was dissolved in diethyl ether (50 mL), washed with 1 N HCl (20 mL) and water (20 mL), and dried over $MgSO_4$. Evaporation of the solvent in vacuo afforded the crude product, which was purified by flash chromatography (cyclohexane – ethyl acetate, 5:1) to yield **20** as a colourless amorphous solid (22 mg, 0.035 mmol, 88%). R_f 0.40 (toluene – ethyl acetate, 3:1). $[\alpha]^{22}_D$ +4.90° (*c* 1, $CHCl_3$); d.r.: 89:11 (HPLC: 80% CH_3CH, 20% H_2O → 100% CH_3CN, 30 min); recrystallization from ether afforded the pure major diastereomer. ^{1}H NMR (400 MHz, $CDCl_3$, ppm) δ: 7.80–7.75 (m, 2H, phenyl), 7.50–7.45 (m, 1H, phenyl), 7.44–7.37 (m, 2H, phenyl), 7.01 (d, 1H, $J_{NH,H\text{-}5}$ = 5.8 Hz, NH), 5.52 (t, 1H, $J_{H\text{-}2',H\text{-}1'}$ = 9.6 Hz, $J_{H\text{-}2',H\text{-}3'}$ = 9.6 Hz, H-2′), 5.26–5.22 (m, 1H, H-4′), 5.15 (dd, 1H, $J_{H\text{-}3',H\text{-}2'}$ = 9.8 Hz, $J_{H\text{-}3',H\text{-}4'}$ = 3.5 Hz, H-3′), 4.90–4.80 (m, 1H, H-5), 4.29 (d, 1H, $J_{H\text{-}1',H\text{-}2'}$ = 9.0 Hz, H-1′), 4.04 (dd, 1H, $J_{H\text{-}6a,H\text{-}6b}$ = 12.7 Hz, $J_{H\text{-}6a,H\text{-}5}$ = 7.6 Hz, H-6a), 3.98 (dd, 1H, $J_{H\text{-}5'a,H\text{-}5'b}$ = 13.1 Hz, $J_{H\text{-}5'a,H\text{-}4'}$ = 2.1 Hz, H-5′a), 3.61 (d, 1H, $J_{H\text{-}5'b,H\text{-}5'a}$ = 12.9 Hz, H-5′b), 3.44–3.35 (m, 1H, H-2), 2.87 (dd, 1H, $J_{H\text{-}3a,H\text{-}3b}$ = 12.9 Hz, $J_{H\text{-}3a,H\text{-}2}$ = 6.3 Hz, H-3a), 2.79 (dd, 1H, $J_{H\text{-}6b,H\text{-}6a}$ = 13.3 Hz, $J_{H\text{-}6b,H\text{-}5}$ = 10.2, H-6b), 2.47 (dd, $J_{H\text{-}3b,H\text{-}3a}$ = 12.9 Hz, $J_{H\text{-}3b,H\text{-}2}$ = 1.6 Hz, H-3b), 1.63–1.51 (m, 1H, CH_2), 1.43–1.31 (m, 1H, CH_2), 1.30, 1.15, 1.13 (3s, 27H, piv-CH_3), 0.85 (t, 3H, *J* = 7.4 Hz, CH_3). ^{13}C NMR (75.4 MHz, $CDCl_3$, ppm) δ: 206.6 (C-4), 177.7, 177.4, 177.1 (pivC=O), 166.6 (NH-C=O), 134.1 (ipso-aryl), 131.5, 128.5, 127.1 (aryl), 95.7 (C-1′), 71.9, 68.3, 66.2, 65.4 (C-2′, C-3′, C-4′, C-5′), 62.7 (C-5), 58.1 (C-2), 49.2 (C-6), 45.1 (C-3), 39.0, 38.8 ($piv_{quart.}$), 27.3, 27.2, 27.1 (piv-CH_3), 25.1 (CH_2), 11.3 (CH_3). ESI-MS for $C_{34}H_{50}N_2O_9$ *m/z*: 325.3 [M – 3pivOH + H]$^+$, 449.5 [M – 2pivOH + Na]$^+$, 551.6 [M – pivOH + Na]$^+$, 631.6 [M + H]$^+$, 653.6 [M + Na]$^+$.

General procedure for the halogenation of dehydropiperidinones 4

To a solution of *N*-arabinosyl dehydropiperidinone **4** (1 mmol) in dry THF (20 mL) were added several equivalents (see for each compound) of solid *N*-bromosuccinimide or *N*-iodosuccinimide at –78 °C and stirred until complete consumption of the starting material. The solution was diluted with diethyl ether (100 mL), washed with 10% aq. $Na_2S_2O_3$ (3 × 20 mL), and the resulting aqueous layers were extracted with diethyl ether (3 × 20 mL). The combined organic layers were washed with brine, dried over $MgSO_4$, and concentrated in vacuo. The crude product was purified by flash chromatography.

(2R)-N-*(2′,3′,4′-Tri*-O-*pivaloyl-*α-*D-arabinopyranosyl)-2-(*p*-chlorophenyl)-5-iodo-5,6-dehydropiperidin-4-one (21a)*

Iododehydropiperidinone **21a** was synthesized according to the general procedure using **4a** (1.18 g, 2 mmol) and *N*-iodosuccinimide (1.35, 6 mmol). Purification was carried out by flash chromatography (petroleum ether – ethyl acetate, 6:1) to yield **21a** (1.33 g, 1.9 mmol, 93%) as a colourless solid. R_f 0.65 (petroleum ether – ethyl acetate, 2:1); mp 205 °C under decomposition. $[\alpha]^{22}_D$ +3.77° (*c* 1, $CHCl_3$). ^{1}H NMR (400 MHz, $CDCl_3$, ppm) δ: 7.70 (s, 1H, H-6), 7.27 (d, 1H, *J* = 4.3 Hz, aryl), 7.17 (d, 1H, *J* = 8.6 Hz, aryl), 5.56 (t, 1H, $J_{H\text{-}2',H\text{-}1'}$ = 9.6 Hz, $J_{H\text{-}2',H\text{-}3'}$ = 9.6 Hz, H-2′), 5.18–5.13 (br s, 1H, H-4′), 5.05 (dd, 1H, $J_{H\text{-}3',H\text{-}2'}$ = 10.0 Hz, $J_{H\text{-}3',H\text{-}4'}$ = 3.3 Hz, H-3′), 4.91 (t, 1H, $J_{H\text{-}2,H\text{-}3a}$ = 6.3 Hz, $J_{H\text{-}2,H\text{-}3b}$ = 6.3 Hz, H-2), 4.37 (d, 1H, $J_{H\text{-}1',H\text{-}2'}$ = 9.0 Hz, H-1′), 3.85 (dd, 1H, $J_{H\text{-}5'a,H\text{-}5'b}$ = 13.3 Hz, $J_{H\text{-}5'a,H\text{-}4'}$ = 2.0 Hz, H-5′a), 3.49 (d, 1H, $J_{H\text{-}5'b,H\text{-}5'a}$ = 12.9 Hz, H-5′b), 3.05 (dd, 1H, $J_{H\text{-}3a,H\text{-}3b}$ = 16.4 Hz, $J_{H\text{-}3a,H\text{-}2}$ = 6.2 Hz, H-3a), 2.83 (dd, 1H, $J_{H\text{-}3b,H\text{-}3a}$ = 16.4 Hz, $J_{H\text{-}3b,H\text{-}2}$ = 6.3 Hz, H-3b), 1.23, 1.16, 1.10 (3s, 27H, $C(CH_3)_3$). ^{13}C NMR (75.4 MHz, $CDCl_3$, ppm) δ: 184.9 (C-4), 177.2, 177.1, 177.0 (pivC=O), 154.7 (C-6), 136.8 (ipso-aryl), 134.2 (ipso-aryl), 129.1, 128.0 (aryl), 89.8 (C-1′), 70.8, 67.7, 66.0 (C-2′, C-3′, C-4′), 66.1 (C-5′), 57.9 (C-2), 42.1 (C-3), 39.0, 38.9, 38.8 ($piv_{quart.}$), 27.2, 27.1, 27.0 (piv-CH_3). ESI-MS for $C_{31}H_{41}ClINO_8$ *m/z*: 718.2 [M(^{35}Cl) + H]$^+$, 720.2 [M(^{37}Cl) + H]$^+$, 740.2 [M(^{35}Cl) + Na]$^+$, 742.2 [M(^{37}Cl) + Na]$^+$.

© 2006 NRC Canada

(2R)-N-(2′,3′,4′-Tri-O-pivaloyl-α-D-arabinopyranosyl)-5-iodo-2-phenyl-5,6-dehydropiperidin-4-one (21b)

Iododehydropiperidinone **21b** was synthesized according to the general procedure using **4c** (1.40 g, 2.51 mmol) and *N*-iodosuccinimide (1.70 g, 7.53 mmol). Purification was achieved by flash chromatography (petroleum ether – ethyl acetate, 8:1) to yield **21b** (1.15 g, 1.68 mmol, 67%) as a pale yellow amorphous solid. R_f 0.58 (cyclohexane – ethyl acetate, 2:1). $[\alpha]^{22}_D$ –11.83° (*c* 1, $CHCl_3$). ^{1}H NMR (300 MHz, $CDCl_3$, ppm) δ: 7.76 (s, 1H, H-6), 7.36–7.28 (m, 3H, aryl), 7.27–7.19 (m, 2H, aryl), 5.58 (t, 1H, $J_{H\text{-}2',H\text{-}1'}$ = 9.6 Hz, $J_{H\text{-}2',H\text{-}3'}$ = 9.6 Hz, H-2′), 5.16–5.09 (m, 1H, H-4′), 4.99 (dd, 1H, $J_{H\text{-}3',H\text{-}2'}$ = 9.9 Hz, $J_{H\text{-}3',H\text{-}4'}$ = 2.9 Hz, H-3′), 4.91 (dd, 1H, $J_{H\text{-}2,H\text{-}3b}$ = 8.3 Hz, $J_{H\text{-}2,H\text{-}3a}$ = 6.1 Hz, H-2), 4.27 (d, 1H, $J_{H\text{-}1',H\text{-}2'}$ = 9.2 Hz, H-1′), 3.85 (dd, 1H, $J_{H\text{-}5'a,H\text{-}5'b}$ = 13.2 Hz, $J_{H\text{-}5'a,H\text{-}4'}$ = 2.2 Hz, H-5′a), 3.41 (d, 1H, $J_{H\text{-}5'b,H\text{-}5'a}$ = 13.2 Hz, H-5′b), 3.01 (dd, 1H, $J_{H\text{-}3a,H\text{-}3b}$ = 16.5 Hz, $J_{H\text{-}3a,H\text{-}2}$ = 5.9 Hz, H-3a), 2.88 (dd, 1H, $J_{H\text{-}3b,H\text{-}3a}$ = 16.2 Hz, $J_{H\text{-}3b,H\text{-}2}$ = 8.5 Hz, H-3b), 1.25, 1.17, 1.10 (3s, 27H, $C(CH_3)_3$). ^{13}C NMR (75.4 MHz, $CDCl_3$, ppm) δ: 185.5 (C-4), 177.2, 177.1, 177.1 (pivC=O), 154.8 (C-6), 137.8 (ipso-aryl), 129.0, 128.7, 126.9 (aryl), 88.7 (C-1′), 71.0, 67.8, 66.0, 65.8 (C-2′, C-3′, C-4′, C-5′), 59.7 (C-2), 42.4 (C-3), 39.0, 38.8, 38.8 ($piv_{quart.}$), 27.2, 27.2, 27.0 (piv-CH_3). ESI-MS for $C_{31}H_{42}I\,NO_8$ *m/z*: 322.0 [dehydropiperidinone + H + Na]$^+$, 706.0 [M + Na]$^+$, 747.1 [M + Na + MeCN]$^+$.

(2S)-N-(2′,3′,4′-Tri-O-pivaloyl-α-D-arabinopyranosyl)-5-iodo-2-n-propyl-5,6-dehydropiperidin-4-one (21c)

Iododehydropiperidinone **21c** was synthesized according to the general procedure using **4f** (524 mg, 1 mmol) and *N*-iodosuccinimide (900 mg, 4 mmol). Purification was carried out by flash chromatography (petroleum ether – ethyl acetate, 8:1) to yield **21c** (450 mg, 0.7 mmol, 69%) as a colourless amorphous solid. R_f 0.57 (petroleum ether – ethyl acetate, 2:1). $[\alpha]^{26}_D$ +123.19° (*c* 1, $CHCl_3$). ^{1}H NMR (400 MHz, $CDCl_3$, ppm) δ: 7.37 (s, 1H, H-6), 5.50 (t, $J_{H\text{-}2',H\text{-}1'}$ = 9.6 Hz, $J_{H\text{-}2',H\text{-}3'}$ = 9.6 Hz, H-2′), 5.27–5.23 (m, 1H, H-4′), 5.12 (dd, 1H, $J_{H\text{-}3',H\text{-}2'}$ = 10.0 Hz, $J_{H\text{-}3',H\text{-}4'}$ = 3.3 Hz, H-3′), 4.47 (d, 1H, $J_{H\text{-}1',H\text{-}2'}$ = 9.0 Hz, H-1′), 4.03 (dd, 1H, $J_{H\text{-}5'a,H\text{-}5'b}$ = 13.3 Hz, $J_{H\text{-}5'a,H\text{-}4'}$ = 2.3 Hz, H-5′a), 3.85–3.76 (m, 1H, H-2), 3.69 (d, 1H, $J_{H\text{-}5'b,H\text{-}5'a}$ = 13.3 Hz, H-5′b), 2.72 (dd, 1H, $J_{H\text{-}3a,H\text{-}3b}$ = 16.6 Hz, $J_{H\text{-}3a,H\text{-}2}$ = 5.7 Hz, H-3a), 2.67 (dd, 1H, $J_{H\text{-}3b,H\text{-}3a}$ = 16.64 Hz, $J_{H\text{-}3b,H\text{-}2}$ = 2.6 Hz, H-3b), 1.90–1.78 (m, 1H, CH_2), 1.67–1.55 (m, 2H, CH_2), 1.40–1.28 (m, 1H, CH_2), 1.25 (s, 9H, piv-CH_3), 1.11 (s, 18H, piv-CH_3), 0.86 (t, 3H, *J* = 7.2 Hz, CH_3). ^{13}C NMR (100.6 MHz, $CDCl_3$, ppm) δ: 185.8 (C-4), 177.2, 177.2, 177.0 (pivC=O), 154.4 (C-6), 91.7 (C-1′), 70.8, 67.8, 66.3 (C-2′, C-3′, C-4′), 66.4 (C-5′), 63.1 (C-5), 53.5 (C-2), 38.9, 38.9, 38.8 (piv_{quart}), 37.9, 32.8 (C-3, CH_2), 27.1, 27.1, 27.0 (piv-CH_3), 18.8 (CH_2), 13.7 (CH_3). ESI-MS for $C_{28}H_{44}INO_8$ *m/z*: 446.04 [M – 2pivOH + H]$^+$, 650.21 [M + H]$^+$, 672.19 [M + Na]$^+$, 713.08 [M + Na + CH_3CN]$^+$.

(2R)-N-(2′,3′,4′-Tri-O-pivaloyl-α-D-arabinopyranosyl)-5-iodo-2-isopropyl-5,6-dehydropiperidin-4-one (21d)

Iododehydropiperidinone **21d** was synthesized according to the general procedure using **4g** (4.0 g, 7.6 mmol) and *N*-iodosuccinimide (5.4 g, 24 mmol). Purification was accomplished by flash chromatography to yield **21d** (4.31 g, 6.6 mmol, 87%) as a colourless amorphous solid. R_f 0.49 (cyclohexane – ethyl acetate, 2:1). $[\alpha]^{22}_D$ +122.00° (*c* 1, $CHCl_3$). ^{1}H NMR (300 MHz, $CDCl_3$, ppm) δ: 7.45 (s, 1H, H-6), 5.53 (t, 1H, $J_{H\text{-}2',H\text{-}1'}$ = 9.6 Hz, $J_{H\text{-}2',H\text{-}3'}$ = 9.6 Hz, H-2′), 5.26–5.21 (m, 1H, H-4′), 5.12 (dd, 1H, $J_{H\text{-}3',H\text{-}2'}$ = 9.9 Hz, $J_{H\text{-}3',H\text{-}4'}$ = 3.3 Hz, H-3′), 4.51 (d, 1H, $J_{H\text{-}1',H\text{-}2'}$ = 9.2 Hz, H-1′), 4.03 (dd, 1H, $J_{H\text{-}5'a,H\text{-}5'b}$ = 13.2 Hz, $J_{H\text{-}5'a,H\text{-}4'}$ = 2.2 Hz, H-5′a), 3.68 (d, 1H, $J_{H\text{-}5'b,H\text{-}5'a}$ = 13.2 Hz, H-5′b), 3.68–3.60 (m, 1H, H-2), 2.77–2.70 (m, 2H, H-3a, H-3b), 2.34–2.17 (m, 1H, C*H*$(CH_3)_2$), 1.26, 1.12, 1.11 (3s, 27H, piv-CH_3), 0.88 (d, 3H, *J* = 7.0 Hz, CH_3), 0.87 (d, 3H, *J* = 6.6 Hz, CH_3). ^{13}C NMR (75.4 MHz, $CDCl_3$, ppm) δ: 186.2 (C-4), 177.2, 177.0, 177.0 (pivC=O), 154.8 (C-6), 91.6 (C-1′), 71.1, 67.8, 66.2 (C-2′, C-3′, C-4′), 66.2 (C-5′), 64.2 (C-5), 58.8 (C-2), 39.0, 39.0, 38.8 (piv_{quart}), 34.7 (C-3), 32.3 (*C*H$(CH_3)_3$), 27.2, 27.1, 27.0 (piv-CH_3), 19.6, 17.6 (CH_3). ESI-MS for $C_{28}H_{44}INO_8$ *m/z*: 650.3 [M + H]$^+$, 672.2 [M + Na]$^+$, 688.2 [M + K]$^+$.

(2S)-N-(2′,3′,4′-Tri-O-pivaloyl-α-D-arabinopyranosyl)-2-(3-tert-butyldiphenylsiloxy)propyl-5-iodo-5,6-dehydropiperidin-4-one (21e)

Iododehydropiperidinone **21e** was synthesized according to the general procedure using **4h** (1.56 g, 2 mmol) and *N*-iodosuccinimide (1.35 g, 6 mmol). Purification was performed by flash chromatography (petroleum ether – ethyl acetate, 8:1) to yield **21e** (1.57 g, 1.70 mmol, 87%) as a pale yellow amorphous solid. R_f 0.58 (petroleum ether – ethyl acetate, 2:1). $[\alpha]^{25}_D$ +71.63° (*c* 1, $CHCl_3$). ^{1}H NMR (400 MHz, $CDCl_3$, ppm) δ: 7.63–7.56 (m, 4H, aryl), 7.43–7.32 (m, 7H, aryl, H-6), 5.50 (t, $J_{H\text{-}2',H\text{-}1'}$ = 9.6 Hz, $J_{H\text{-}2',H\text{-}3'}$ = 9.6 Hz, H-2′), 5.26–5.21 (br s, 1H, H-4′), 5.12 (dd, 1H, $J_{H\text{-}3',H\text{-}2'}$ = 10.2 Hz, $J_{H\text{-}3',H\text{-}4'}$ = 3.1 Hz, H-3′), 4.45 (d, 1H, $J_{H\text{-}1',H\text{-}2'}$ = 9.0 Hz, H-1′), 3.99 (dd, 1H, $J_{H\text{-}5'a,H\text{-}5'b}$ = 13.3 Hz, $J_{H\text{-}5'a,H\text{-}4'}$ = 2.0 Hz, H-5′a), 3.83–3.73 (m, 1H, H-2), 3.69–3.50 (m, 3H, $J_{H\text{-}5'b,H\text{-}5'a}$ = 13.3 Hz, H-5′b, O-CH_2), 2.75 (dd, 1H, $J_{H\text{-}3a,H\text{-}3b}$ = 16.4 Hz, $J_{H\text{-}3a,H\text{-}2}$ = 6.3 Hz, H-3a), 2.65 (dd, 1H, $J_{H\text{-}3b,H\text{-}3a}$ = 16.6 Hz, $J_{H\text{-}3b,H\text{-}2}$ = 1.8 Hz, H-3b), 1.90–1.77 (m, 2H, CH_2), 1.63–1.36 (m, 2H, CH_2), 1.23 (s, 9H, $C(CH_3)_3$), 1.11 (s, 18H, $C(CH_3)_3$), 0.99 (s, 9H, $C(CH_3)_3$). ^{13}C NMR (75.4 MHz, $CDCl_3$, ppm) δ: 185.6 (C-4), 177.2, 177.0 (pivC=O), 154.0 (C-6), 135.5, 135.5 (aryl), 133.7, 133.7 (ipso-aryl), 129.6, 127.7 (aryl), 91.5 (C-1′), 70.8, 67.8, 66.3 (C-2′, C-3′, C-4′), 66.3 (C-5′), 63.2 (OCH_2), 53.9 (C-2), 39.0, 38.9, 38.8 ($piv_{quart.}$), 38.2 (C-3), 28.8, 27.6 (CH_2), 27.2, 27.2, 27.0, 26.8 (piv-CH_3, SiC(*C*$H_3)_3$), 19.2 (Si*C*$(CH_3)_3$). ESI-MS for $C_{44}H_{62}INO_9Si$ *m/z*: 826.3 [M – phenyl]$^+$, 904.2 [M + H]$^+$, 926.2 [M + Na]$^+$.

(2R)-N-(2′,3′,4′-Tri-O-pivaloyl-α-D-arabinopyranosyl)-5-bromo-2-(p-chlorophenyl)-5,6-dehydropiperidin-4-one (21f)

Bromodehydropiperidinone **21f** was synthesized according to the general procedure using **4a** (3.5 g, 5.9 mmol) and *N*-bromosuccinimide (2.1 g, 11.8 mmol). Purification was carried out by flash chromatography (cyclohexane – ethyl acetate, 8:1) to yield **21f** (3.0 g, 4.4 mmol, 75%) as a colourless amorphous solid. R_f 0.5 (cyclohexane – ethyl acetate, 2:1). $[\alpha]^{22}_D$ –11.57° (*c* 1, $CHCl_3$). ^{1}H NMR (200 MHz, $CDCl_3$, ppm) δ: 7.60 (s, 1H, H-6), 7.29 (d, 2H, *J* = 8.8 Hz, aryl), 7.18 (d, 2H, *J* = 8.8 Hz, aryl), 5.56 (t, 1H, $J_{H\text{-}2',H\text{-}1'}$ =

© 2006 NRC Canada

9.5 Hz, $J_{H\text{-}2',H\text{-}3'}$ = 9.5 Hz, H-2′), 5.22–5.13 (m, 1H, H-4′), 5.03 (dd, 1H, $J_{H\text{-}3',H\text{-}2'}$ = 10.0 Hz, $J_{H\text{-}3',H\text{-}4'}$ = 3.2 Hz, H-3′), 4.87 (t, 1H, $J_{H\text{-}2,H\text{-}3a}$ = 6.6 Hz, $J_{H\text{-}2,H\text{-}3b}$ = 6.6 Hz, H-2), 4.33 (d, 1H, $J_{H\text{-}1',H\text{-}2'}$ = 9.3, H-1′), 3.86 (dd, 1H, $J_{H\text{-}5'a,H\text{-}5'b}$ = 13.2 Hz, $J_{H\text{-}5'a,H\text{-}4'}$ = 2.0 Hz, H-5′a), 3.47 (d, 1H, $J_{H\text{-}5'b,H\text{-}5'a}$ = 13.2 Hz, H-5′b), 3.00 (dd, 1H, $J_{H\text{-}3a,H\text{-}3b}$ = 16.6 Hz, $J_{H\text{-}3a,H\text{-}2}$ = 5.9 Hz, H-3a), 2.78 (dd, 1H, $J_{H\text{-}3b,H\text{-}3a}$ = 16.6 Hz, $J_{H\text{-}3b,H\text{-}2}$ = 7.3 Hz, H-3b), 1.23, 1.16, 1.10 (3s, 27H, piv-CH_3). ^{13}C NMR (50.3 MHz, $CDCl_3$, ppm) δ: 183.7 (C-4), 177.2, 177.1, 177.0 (pivC=O), 150.2 (C-6), 136.5, 134.4 (ipso-aryl), 129.2, 128.2 (aryl), 94.5 (C-5), 89.6 (C-1′), 70.9 (C-3′), 67.8 (C-4′), 66.2 (C-5′), 65.9 (C-2′), 58.3 (C-2), 43.1 (C-3), 39.0, 38.9 ($piv_{quart.}$), 27.2, 27.2, 27.0 (piv-CH_3). ESI-MS for $C_{31}H_{41}BrClNO_8$ *m/z*: 672.5 [M(^{81}Br) + H]$^+$, 692.2 [M(^{79}Br) + Na]$^+$, 694.2 [M(^{81}Br) + Na]$^+$, 708.2 [M(^{79}Br) + K]$^+$, 710.2 [M(^{81}Br) + K]$^+$, 733.2 [M(^{79}Br) + Na + CH_3CN]$^+$, 735.2 [M(^{81}Br) + Na + CH_3CN]$^+$.

*(2***R***)-***N***-(2′,3′,4′-Tri-O-pivaloyl-α-D-arabinopyranosyl)-5-bromo-2-isopropyl-5,6-dehydropiperidin-4-one (21g)*

Bromodehydropiperidinone **21g** was synthesized according to the general procedure using **4g** (2.0 g, 3.8 mmol) and *N*-bromosuccinimide (3.4 g, 19 mmol). Purification was achieved by flash chromatography (cyclohexane – ethyl acetate, 5:1) to yield **21g** (1.7 g, 2.8 mmol, 73%) as a colourless amorphous solid. R_f 0.28 (cyclohexane – ethyl acetate, 3:1). $[\alpha]^{25}_D$ 108.56° (*c* 1, $CHCl_3$). ^{1}H NMR (300 MHz, $CDCl_3$, ppm) δ: 7.33 (s, 1H, H-6), 5.53 (t, 1H, $J_{H\text{-}2',H\text{-}1'}$ = 9.4 Hz, $J_{H\text{-}2',H\text{-}3'}$ = 9.6 Hz, H-2′), 5.26–5.20 (m, 1H, H-4′), 5.12 (dd, 1H, $J_{H\text{-}3',H\text{-}2'}$ = 9.9 Hz, $J_{H\text{-}3',H\text{-}4'}$ = 3.3 Hz, H-3′), 4.50 (d, 1H, $J_{H\text{-}1',H\text{-}2'}$ = 9.2 Hz, H-1′), 4.02 (dd, 1H, $J_{H\text{-}5'a,H\text{-}5'b}$ = 13.2 Hz, $J_{H\text{-}5'a,H\text{-}4'}$ = 2.2 Hz, H-5′), 3.69 (d, 1H, $J_{H\text{-}5'b,H\text{-}5'a}$ = 12.9 Hz, H-5′b), 3.63–3.55 (m, 1H, H-2), 2.76 (dd, 1H, $J_{H\text{-}3a,H\text{-}3b}$ = 16.9 Hz, $J_{H\text{-}3a,H\text{-}2}$ = 7.4 Hz, H-3a), 2.64 (dd, 1H, $J_{H\text{-}3b,H\text{-}3a}$ = 16.9 Hz, $J_{H\text{-}3b,H\text{-}2}$ = 2.6 Hz, H-3b), 2.34–2.13 (m, 1H, C*H*(CH_3)$_2$), 1.25, 1.11, 1.11 (3s, 27H, piv-CH_3), 0.89 (d, 6H, *J* = 7.0 Hz, CH_3). ^{13}C NMR (75.4 MHz, $CDCl_3$, ppm) δ: 184.9 (C-4), 177.2, 177.2, 177.0 (pivC=O), 150.2 (C-6), 91.7 (C-5), 91.7 (C-1′), 71.1, 67.8, 66.2 (C-2′, C-3′, C-4′), 66.3 (C-5′), 58.9 (C-2), 39.0, 38.8 (piv_{quart}), 35.6 (C-3), 32.0 (*C*H(CH_3)$_3$), 27.1, 27.0 (piv-CH_3), 19.6, 17.6 (CH_3). ESI-MS for $C_{28}H_{44}BrNO_8$ *m/z*: 602.2 [M(^{79}Br) + H]$^+$, 604.2 [M(^{81}Br) + H]$^+$, 624.2 [M(^{79}Br) + Na]$^+$, 626.2 [M(^{81}Br) + Na]$^+$, 665.3 [M(^{79}Br) + Na + CH_3CN]$^+$, 667.3 [M(^{81}Br) + Na + CH_3CN]$^+$.

*(2***S***)-***N***-(2′,3′,4′-Tri-O-pivaloyl-α-D-arabinopyranosyl)-5-bromo-2-(3′′-tert-butyldiphenylsiloxy)propyl-5,6-dehydropiperidin-4-one (21h)*

Bromodehydropiperidinone **21h** was synthesized according to the general procedure using **4h** (1.17 g, 1.5 mmol) and *N*-bromosuccinimide (0.53 g, 3.0 mmol). Purification was performed by flash chromatography (petroleum ether – ethyl acetate, 4:1) to yield **21h** (1.02 g, 1.2 mmol, 79%) as a colourless amorphous solid. R_f 0.45 (petroleum ether – ethyl acetate, 2:1). $[\alpha]^{24}_D$ +59.95° (*c* 1, $CHCl_3$). ^{1}H NMR (200 MHz, $CDCl_3$, ppm) δ: 7.65–7.55 (m, 4H, aryl), 7.45–7.30 (m, 6H, aryl), 7.26 (s, 1H, H-6), 5.50 (t, 1H, $J_{H\text{-}2',H\text{-}1'}$ = 9.3 Hz, $J_{H\text{-}2',H\text{-}3'}$ = 9.3 Hz, H-2′), 5.30–5.20 (m, 1H, H-4′), 5.12 (dd, 1H, $J_{H\text{-}3',H\text{-}2'}$ = 10.0 Hz, $J_{H\text{-}3',H\text{-}4'}$ = 3.2 Hz, H-3′), 4.44 (d, 1H, $J_{H\text{-}1',H\text{-}2'}$ = 8.8 Hz, H-1′), 3.99 (d, 1H, $J_{H\text{-}5'a,H\text{-}5'b}$ = 13.2 Hz, $J_{H\text{-}5'a,\ H\text{-}4'}$ = 2.0 Hz, H-5′a), 3.85–3.45 (m, 4H, $J_{H\text{-}5'b,\ H\text{-}5'a}$ = 13.2 Hz, H-5′b, CH_2-O, H-2), 2.76 (dd, 1H, $J_{H\text{-}3a,H\text{-}3b}$ = 16.6 Hz, $J_{H\text{-}3a,H\text{-}2}$ = 5.9 Hz, H-3a), 2.55 (dd, 1H, $J_{H\text{-}3b,H\text{-}3a}$ = 16.6 Hz, $J_{H\text{-}3b,H\text{-}2}$ = 2.0 Hz, H-3b), 1.95–1.70 (m, 2H, CH_2), 1.70–1.40 (m, 2H, CH_2), 1.23 (s, 9H, $C(CH_3)_3$), 1.11 (s, 18H, $C(CH_3)_3$), 0.99 (s, 9H, $C(CH_3)_3$). ^{13}C NMR (100.6 MHz, $CDCl_3$, ppm) δ: 184.3 (C-4), 177.2, 177.2, 177.0 (pivC=O), 149.6 (C-6), 135.5, 135.5 (aryl), 133.7, 133.6 (ipso-aryl), 129.6, 127.7 (aryl), 91.6, 91.0 (C-1′, C-5), 70.8, 67.8, 66.2 (C-2′, C-3′, C-4′), 66.3 (C-5′), 63.2 (OCH_2), 53.9 (C-2), 39.0 (C-3), 38.9, 38.9, 38.8 ($piv_{quart.}$), 28.8, 27.5 (CH_2), 27.2, 27.1, 27.0, 26.8 (pivCH_3, SiC(*C*H_3)$_3$), 19.2 (Si*C*(CH_3)$_3$). ESI-MS for $C_{44}H_{62}BrNO_9Si$ *m/z*: 778.2 [(M(^{79}Br) – phenyl]$^+$, 780.2 [M(^{81}Br) – phenyl]$^+$, 856.2 [M(^{79}Br) + H]$^+$, 858.2 [M(^{81}Br) + H]$^+$, 878.1 [M(^{79}Br) + Na]$^+$, 880.1 [M(^{81}Br) + Na]$^+$, 894.1 [M(^{79}Br) + K]$^+$, 896.1 [M(^{81}Br) + K]$^+$, 919.2 [M(^{79}Br) + Na + CH_3CN]$^+$, 921.2 [M(^{81}Br) + Na + CH_3CN]$^+$.

*(2***R***)-***N***-(2′,3′,4′-Tri-O-pivaloyl-α-D-arabinopyranosyl)-2-(p-chlorophenyl)-5-phenyl-5,6-dehydropiperidin-4-one (22)*

A two-necked round bottom flask equipped with a reflux condenser and a septum was charged with iodide **21a** (180 mg, 0.25 mmol), bis(dibenzylideneacetone)palladium (14 mg, 0.025 mmol), and triphenylarsine (31 mg, 0.10 mmol), and then evacuated and flushed with argon. Dry THF (10 mL) was added and the mixture was stirred for 5 min for the formation of the active catalyst (colour change from red to yellow). Phenyl tributyltin 0.16 mL (0.50 mmol) was then added and the solution was heated to 65 °C for 17 h. After cooling, the reaction mixture was treated with 1 mol/L aq. KF (1 mL) and stirred for 30 min. It was then diluted with diethyl ether (50 mL), washed with water, and dried over $MgSO_4$. The solvent was evaporated in vacuo and the product was purified by flash chromatography (cyclohexane – ethyl acetate, 7:1) affording **22** (74 mg, 0.11 mmol, 44%), as a pale yellow amorphous solid. R_f 0.46 (cyclohexane – ethyl acetate, 2:1). $[\alpha]^{22}_D$ –21.30° (*c* 1, $CHCl_3$). ^{1}H NMR (200 MHz, $CDCl_3$, ppm) δ: 7.54–7.10 (m, 10H, H-6, aryl), 5.68 (t, 1H, $J_{H\text{-}2',H\text{-}1'}$ = 9.5 Hz, $J_{H\text{-}2',\ H\text{-}3'}$ = 9.5 Hz, H-2′), 5.20–5.12 (m, 1H, H-4′), 5.03 (dd, 1H, $J_{H\text{-}3',H\text{-}2'}$ = 9.8 Hz, $J_{H\text{-}3',H\text{-}4'}$ = 2.9 Hz, H-3′), 4.88 (dd, 1H, $J_{H\text{-}2,H\text{-}3a}$ = 7.8 Hz, $J_{H\text{-}2,H\text{-}3b}$ = 5.9 Hz, H-2), 4.37 (d, 1H, $J_{H\text{-}1',H\text{-}2'}$ = 9.3 Hz, H-1′), 3.86 (dd, 1H, $J_{H\text{-}5'a,H\text{-}5'b}$ = 13.4 Hz, $J_{H\text{-}5'a,H\text{-}4'}$ = 1.7 Hz, H-5′a), 3.47 (d, 1H, $J_{H\text{-}5'b,H\text{-}5'a}$ = 13.2 Hz, H-5′b), 2.96 (dd, 1H, $J_{H\text{-}3a,H\text{-}3b}$ = 16.4 Hz, $J_{H\text{-}3a,H\text{-}2}$ = 5.6 Hz, H-3a), 2.75 (dd, 1H, $J_{H\text{-}3a,H\text{-}3b}$ = 16.3 Hz, $J_{H\text{-}3b,H\text{-}2}$ = 8.0 Hz, H-3b), 1.20, 1.14, 1.10 (3s, 27H, piv-CH_3). ^{13}C NMR (100.6 MHz, $CDCl_3$, ppm) δ: 188.8 (C-4), 177.1, 177.1, 177.0 (pivC=O), 148.7 (C-6), 137.1, 135.0, 134.2 (ipso-aryl), 129.1, 128.4, 128.2, 127.9, 126.5 (aryl), 115.4 (C-5), 89.6 (C-1′), 71.1, 67.9, 65.7 (C-2′, C-3′, C-4′), 66.1 (C-5′), 58.7 (C-2), 44.1 (C-3), 38.9, 38.9, 38.8 ($piv_{quart.}$), 27.2, 27.1, 27.0 (piv-CH_3). ESI-MS for $C_{37}H_{46}ClNO_8$ *m/z*: 668.5 [M(^{35}Cl) + H]$^+$, 690.5 [M(^{35}Cl) + Na]$^+$, 731.4 [M(^{35}Cl) + Na + CH_3CN]$^+$.

*(2***S***)-***N***-(2′,3′,4′-Tri-O-pivaloyl-α-D-arabinopyranosyl)-5-(p-methoxyphenyl)-2-n-propyl-5,6-dehydropiperidin-4-one (23)*

To a solution of **21c** (65 mg, 0.10 mmol), 4-methoxy-

© 2006 NRC Canada

benzene boronic acid (30 mg, 0.60 mmol), and $Pd(PPh_3)_2Cl_2$ (4 mg, 0.02 mmol) in THF (3 mL), aq. Cs_2CO_3 (2 mol/L, 0.25 mL) was added and the mixture was stirred at 65 °C for 20 h. The mixture was filtrated through Hyflo®, and the filtrate was concentrated in vacuo. The residue was diluted in diethyl ether (15 mL), washed with water (3 mL) and brine (1.5 mL), and dried over $MgSO_4$. The product was purified by flash chromatography (cyclohexane – ethyl acetate, 6:1) to yield **23** as a colourless amorphous solid (25 mg, 0.04 mmol, 40%, incomplete conversion). R_f 0.44 (cyclohexane – ethyl acetate, 2:1). $[\alpha]^{22}_D$ +55.18° (*c* 1, $CHCl_3$). ^{1}H NMR (300 MHz, $CDCl_3$, ppm) δ: 7.09 (s, 1H, H-6), 7.21 (d, 2H, *J* = 8.8 Hz, aryl), 6.83 (d, 2H, *J* = 8.8 Hz, aryl), 5.61 (t, $J_{H\text{-}2',H\text{-}1'}$ = 9.6 Hz, $J_{H\text{-}2',H\text{-}3'}$ = 9.6 Hz, H-2′), 5.30–5.22 (m, 1H, H-4′), 5.14 (dd, 1H, $J_{H\text{-}3',H\text{-}2'}$ = 9.9 Hz, $J_{H\text{-}3',H\text{-}4'}$ = 3.3 Hz, H-3′), 4.53 (d, 1H, $J_{H\text{-}1',H\text{-}2'}$ = 9.2 Hz, H-1′), 4.05 (dd, 1H, $J_{H\text{-}5'a,H\text{-}5'b}$ = 13.2 Hz, $J_{H\text{-}5'a,H\text{-}4'}$ = 2.2 Hz, H-5′a), 3.82–3.66 (m, 1H, H-2), 3.77 (s, 3H, OCH_3), 3.71 (d, 1H, $J_{H\text{-}5'b,H\text{-}5'a}$ = 12.8 Hz, H-5′b), 2.77 (dd, 1H, $J_{H\text{-}3a,H\text{-}3b}$ = 16.5 Hz, $J_{H\text{-}3a,H\text{-}2}$ = 6.2 Hz, H-3a), 2.54 (dd, 1H, $J_{H\text{-}3b,H\text{-}3a}$ = 16.5 Hz, $J_{H\text{-}3b,H\text{-}2}$ = 1.8 Hz, H-3b), 2.00–1.83 (m, 1H, CH_2), 1.73–1.55 (m, 1H, CH_2), 1.49–1.11 (m, 2H, CH_2), 1.26 (s, 9H, piv-CH_3), 1.12 (s, 9H, piv-CH_3), 1.08 (s, 9H, piv-CH_3), 0.87 (t, 3H, *J* = 7.2 Hz, CH_3). ^{13}C NMR (75.4 MHz, $CDCl_3$, ppm) δ: 189.7 (C-4), 177.2, 177.1, 177.1 (pivC=O), 158.1 (*C*-OCH_3), 148.5 (C-6), 129.0 (aryl), 127.8 (ipso-aryl), 113.7 (aryl), 112.0 (C-5), 92.3 (C-1′), 71.1, 67.9, 66.1 (C-2′, C-3′, C-4′), 66.3 (C-5′), 55.3, 53.6 (C-2, OCH_3), 39.4 (C-3), 39.0, 38.9, 38.8 ($piv_{quart.}$), 33.1 (CH_2), 27.1, 27.1, 27.0 (piv-CH_3), 18.9 (CH_2), 13.8 (CH_3). ESI-MS for $C_{35}H_{51}NO_9$ *m*/*z*: 630.4 $[M + H]^+$, 652.3 $[M + Na]^+$, 668.2 $[M + K]^+$.

(2R,3S)-N-(2′,3′,4′-Tri-O-pivaloyl-α-D-arabinopyranosyl)-2-(p-chlorophenyl)-3-methyl-5,6-dehydropiperidin-4-one (24a)

LiHMDS (1 mol/L in THF, 1.2 mL) was added slowly to a cold solution (–78 °C) of **4a** (592 mg, 1.0 mmol) in dry THF (30 mL) and stirred for 1 h. After addition of iodomethane (0.12 mL, 2 mmol), the reaction mixture was stirred for 15 h at the same temperature. The reaction was terminated by addition of satd. aq. NH_4Cl. After warming, the organic layer was washed with satd. aq. NH_4Cl (2 × 50 mL) and the resulting aqueous layer was extracted with diethyl ether (2 × 50 mL). The combined organic layers were dried over $MgSO_4$ and concentrated in vacuo. Flash chromatoraphy of the residue (petroleum ether – ethyl acetate, 5:1) furnished **24a** (444 mg, 0.73 mmol, 73%) as a colourless amorphous solid. R_f 0.38 (petroleum ether – ethyl acetate, 2:1); mp 162 °C. $[\alpha]^{25}_D$ –73.44° (*c* 1, $CHCl_3$). ^{1}H NMR (300 MHz, $CDCl_3$, ppm) δ: 7.37 (d, 2H, *J* = 8.8 Hz, aryl), 7.31 (d, 2H, *J* = 8.3 Hz, aryl), 7.24–7.20 (m, 1H, H-6), 5.57 (t, 1H, $J_{H\text{-}2',H\text{-}1'}$ = 9.8 Hz, $J_{H\text{-}2',H\text{-}3'}$ = 9.8 Hz, H-2′), 5.28 (d, 1H, $J_{H\text{-}5,H\text{-}6}$ = 8.3 Hz, H-5), 5.08–5.15 (m, 1H, H-4′), 4.87 (dd, 1H, $J_{H\text{-}3',H\text{-}2'}$ = 9.8 Hz, $J_{H\text{-}3',H\text{-}4'}$ = 3.4 Hz, H-3′), 4.35 (d, 1H, $J_{H\text{-}2,H\text{-}3}$ = 11.7 Hz, H-2), 4.02 (d, 1H, $J_{H\text{-}1',H\text{-}2'}$ = 9.3 Hz, H-1′), 3.82 (dd, 1H, $J_{H\text{-}5'a,H\text{-}5'b}$ = 13.7 Hz, $J_{H\text{-}5'a,H\text{-}4'}$ = 1.9 Hz, H-5′a), 3.28 (d, 1H, $J_{H\text{-}5'b,H\text{-}5'a}$ = 13.2 Hz, H-5′b), 2.57 (dq, 1H, $J_{H\text{-}3,H\text{-}2}$ = 12.0 Hz, $J_{H\text{-}3,methyl}$ = 6.8 Hz, H-3), 1.23, 1.16, 1.08 (3s, 27H, piv-CH_3), 0.89 (d, 3H, *J* = 6.8 Hz, CH_3). ^{13}C NMR (100.6 MHz, $CDCl_3$, ppm) δ: 194.3 (C-4), 177.2, 177.1, 176.7 (pivC=O), 148.18 (C-6), 136.18, 134.77 (ipso-aryl), 129.46 (aryl), 103.45 (C-5), 87.54 (C-1′), 71.66, 68.02, 67.52 (C-2′, C-3′, C-4′), 65.96 (C-5′), 65.10 (C-2), 46.03 (*C*HCH_3), 38.96, 38.85, 38.77 ($pivC_{quart.}$), 27.15, 27.04 (piv-CH_3), 13.46 (CH_3).

(2S,3S)-N-(2′,3′,4′-Tri-O-pivaloyl-α-D-arabinopyranosyl)-2-(3-tert-butyldiphenylsiloxy)propyl-3-methyl-5,6-dehydropiperidin-4-one (24b)

Disubstituted dehydropiperidinone **24b** was synthesized similarly to **24a** using **4h** (1.01 g, 1.30 mmol), dry THF (40 mL), LiHMDS (1 mol/L in THF, 3.90 mL, 3.90 mmol), and iodomethane (0.32 mL, 5.20 mmol). Purification by flash chromatography (cyclohexane – ethyl acetate, 5:1) yielded **24b** (0.89 g, 1.13 mmol, 87%) as a colourless amorphous solid. R_f 0.41 (cyclohexane – ethyl acetate, 2:1). $[\alpha]^{22}_D$ +0.81° (*c* 1, $CHCl_3$). ^{1}H NMR (300 MHz, $CDCl_3$, ppm) δ: 7.65–7.54 (m, 4H, aryl), 7.46–7.28 (m, 6H, aryl), 6.95 (d, 1H, $J_{H\text{-}6,H\text{-}5}$ = 7.7, H-6), 5.47 (t, $J_{H\text{-}2',H\text{-}1'}$ = 9.6 Hz, $J_{H\text{-}2',H\text{-}3'}$ = 9.6 Hz, H-2′), 5.24–5.16 (m, 1H, H-4′), 5.07 (dd, 1H, $J_{H\text{-}3',H\text{-}2'}$ = 9.7 Hz, $J_{H\text{-}3',H\text{-}4'}$ = 3.1 Hz, H-3′), 4.93 (dd, 1H, $J_{H\text{-}5,H\text{-}6}$ = 7.4 Hz, H-5), 4.44 (d, 1H, $J_{H\text{-}1',H\text{-}2'}$ = 9.2 Hz, H-1′), 3.92 (dd, 1H, $J_{H\text{-}5'a,H\text{-}5'b}$ = 13.2 Hz, $J_{H\text{-}5'a,H\text{-}4'}$ = 1.8 Hz, H-5′a), 3.72–3.40 (m, 3H, H-5′b, O-CH_2), 3.37–3.26 (m, 1H, H-2), 2.36–2.23 (m, 1H, H-3), 1.92–1.70 (m, 1H, CH_2), 1.70–1.40 (m, 2H, CH_2), 1.23 (s, 3H, $C(CH_3)_3$), 1.15–1.06 (m, 21H, $C(CH_3)_3$, CH_3), 1.02 ($C(CH_3)_3$). ^{13}C NMR (100.6 MHz, $CDCl_3$, ppm) δ: 196.4 (C-4), 177.3, 177.1, 176.6 (pivC=O), 146.6 (C-6), 135.5, 135.4 (aryl), 133.7, 133.6 (ipso-aryl), 129.7, 127.7 (aryl), 97.8 (C-5), 90.9 (C-1′), 72.0, 68.0, 65.5 (C-2′, C-3′, C-4′), 66.1 (C-5′), 63.3 (CH_2-O), 61.9 (C-2), 42.5 (C-3), 38.9, 38.8, 38.8 ($pivC_{quart.}$), 28.3 (CH_2), 27.1, 27.1, 27.1, 26.8 ($pivCH_3$, Si-C(*C*H_3)$_3$), 27.0 (CH_2), 19.2 (Si*C*$(CH_3)_3$), 17.7 (CH_3). ESI-MS for $C_{45}H_{65}NO_9Si$ *m*/*z*: 792.5 $[M + H]^+$, 814.5 $[M + Na]^+$, 830.5 $[M + K]^+$.

(2S,3S)-N-(2′,3′,4′-Tri-O-pivaloyl-α-D-arabinopyranosyl)-2-(3-tert-butyldiphenylsiloxy)propyl-3-ethyl-5,6-didehydropiperidin-4-one (24c)

Disubstituted dehydropiperidinone **24c** was synthesized similarly to **24a** using **4h** (1.01 g, 1.30 mmol), dry THF (40 mL), LiHMDS (1 mol/L in THF, 3.25 mL), and iodoethane (0.31 mL, 3.90 mmol). Purification by flash chromatography (cyclohexane – ethyl acetate, 6:1) yielded **24c** (0.74 mg, 0.91 mmol, 70%) as a colourless amorphous solid. R_f 0.50 (cyclohexane – ethyl acetate, 2:1). $[\alpha]^{22}_D$ +4.34° (*c* 1, $CHCl_3$). ^{1}H NMR (400 MHz, $CDCl_3$, ppm) δ: 7.63–7.57 (m, 4H, aryl), 7.43–7.32 (m, 6H, aryl), 6.93 (d, 1H, $J_{H\text{-}6,H\text{-}5}$ = 7.6, H-6), 5.47 (t, $J_{H\text{-}2',H\text{-}1'}$ = 9.4 Hz, $J_{H\text{-}2',H\text{-}3'}$ = 9.4 Hz, H-2′), 5.23–5.20 (m, 1H, H-4′), 5.06 (dd, 1H, $J_{H\text{-}3',H\text{-}2'}$ = 10.0 Hz, $J_{H\text{-}3',H\text{-}4'}$ = 3.3 Hz, H-3′), 4.95 (d, 1H, $J_{H\text{-}5,H\text{-}6}$ = 7.8 Hz, H-5), 4.45 (d, 1H, $J_{H\text{-}1',H\text{-}2'}$ = 9.4 Hz, H-1′), 3.94 (dd, 1H, $J_{H\text{-}5'a,H\text{-}5'b}$ = 13.3 Hz, $J_{H\text{-}5'a,H\text{-}4'}$ = 2.0 Hz, H-5′a), 3.63–3.54 (m, 3H, H-5′b, O-CH_2), 3.47–3.40 (m, 1H, H-2), 1.85–1.76 (m, 1H, H-3), 1.24, 1.12, 1.10, 1.01 (4s, 27H, $(CH_3)_3$), 0.91 (t, 3H, *J* = 7.42 Hz, CH_2CH_3). ^{13}C NMR (75.4 MHz, $CDCl_3$, ppm) δ: 195.6 (C-4), 177.3, 177.1, 176.6 (pivC=O), 146.3 (C-6), 135.5 (aryl), 133.7, 133.6 (ipso-aryl), 129.7, 127 7 (aryl), 97.7 (C-5), 91.1 (C-1′), 72.0, 68.0, 65.7 (C-2′, C-3′, C-4′), 66.2 (C-5′), 63.2 (CH_2-O), 59.6 (C-3), 49.7 (C-2), 38.9, 38.8, 38.8 ($pivC_{quart.}$), 28.4 (CH_2), 27.1, 27.1, 27.1

© 2006 NRC Canada

(pivCH$_3$), 26.8 (SiC(*C*H$_3$)$_3$), 24.7 (CH$_2$), 19.2 (*C*H$_2$CH$_3$), 11.6 (CH$_2$*C*H$_3$). ESI-MS for $C_{46}H_{67}NO_9Si$ *m/z*: 626.29 [M – phenyl – pivOH]$^+$, 728.24 [M – phenyl]$^+$, 806.34 [M + H]$^+$, 828.26 [M + Na]$^+$, 869.24 [M + Na + CH$_3$CN]$^+$.

Acknowledgements

This work was supported by the Deutsche Forschungsgemeinschaft and by the Fonds der Chemischen Industrie. We thank Dr. D. Schollmeyer, Institut für Organische Chemie, Universität Mainz, for the X-ray analyses. BK is grateful for being awarded the Adolf-Todt-Preis of the Adolf-Todt-Stiftung of the Universität Mainz.

References

1. (*a*) J.W. Daly, H.M. Garraffo, and T.F. Spande. *In* The alkaloids — Chemistry and pharmacology. Vol. 43. *Edited by* G.A Cordell. Academic Press, San Diego. 1993. p. 185; (*b*) J.W. Daly. Nat. Prod. **61**, 162 (1998); (*c*) J.W. Daly, H.M. Garraffo, and T.F. Spande. *In* Alkaloids — Chemical and biological perspectives. Vol. 13. *Edited by* S.W. Pelletier. Pergamon, New York. 1999. p. 1.
2. (*a*) P.D. Bailey, P.A. Millwood, and P.D. Smith. Chem. Commun. (Cambridge), 633 (1998); (*b*) S. Laschat and T. Dickner. Synthesis, 1781 (2000); (*c*) P.M. Weintraub, J.S. Sabol, J.M. Kane, and D.R. Borcherding. Tetrahedron, **59**, 2953 (2003); (*d*) S. Knauer, B. Kranke, L. Krause, and H. Kunz. Curr. Org. Chem. **8**, 1739 (2004).
3. (*a*) H. Kunz and W. Pfrengle. Angew. Chem. Int. Ed. Engl. **28**, 1067 (1989); (*b*) M. Weymann, W. Pfrengle, D. Schollmeyer, and H. Kunz. Synthesis, 1151 (1997).
4. B. Kranke, D. Hebrault, M. Schultz-Kukula, and H. Kunz. Synlett, 671 (2004).
5. H. Kunz, W. Pfrengle, K. Rück, and W. Sager. Synthesis, 1039 (1991).
6. Y. Yamamoto. Angew. Chem. Int. Ed. Engl. **25**, 947 (1986).
7. E.J. Corey and W. Boaz. Tetrahedron Lett. **26**, 6019 (1985).
8. H. Gilman, R.G. Jones, and L.A. Woods. J. Org. Chem. **17**, 1630 (1952).
9. S. Ciblat, P. Besse, V. Papastergiou, H. Veschambre, J.-L. Canet, and Y. Troin. Tetrahdron: Asymmetry, **11**, 2221 (2000), and refs. therein.
10. K. Maruoka, K. Nonoshita, and H. Yamamoto. Tetrahedron Lett. **28**, 5723 (1987).
11. (*a*) G. Zech and H. Kunz. Angew. Chem. Int. Ed. **42**, 787 (2003); (*b*) G. Zech and H. Kunz. Chem. Eur. J. **10**, 4136 (2004).
12. (*a*) J.K. Stille. Angew. Chem. Int. Ed. Engl. **25**, 508 (1986); (*b*) M.A.J. Duncton and G. Pattenden. J. Chem. Soc. Perkin Trans. 1, 1235 (1999).
13. N. Miyaura and A. Suzuki. Chem. Rev. **95**, 2457 (1995).
14. S. Danishefsky and T. Kitahara. J. Am. Chem. Soc. **96**, 7807 (1974).
15. J.A. Murphy, F. Rasheed, S.J. Roome, K.A. Scott, and N. Lewis. J. Chem. Soc. Perkin Trans. 1, 2331 (1998).
16. L. Guerrier, J. Royer, D.S. Grierson, and H.-P. Husson. J. Am. Chem. Soc. **105**, 7754 (1983).

© 2006 NRC Canada

Chemical and chemoenzymatic synthesis of a trisaccharide fragment of *Tsukamurella paurometabola* lipoarabinomannan[1]

Karen M. Ridgway, Wei Shi, Shuang-Jun Lin, Monica M. Palcic, and Todd L. Lowary

Abstract: The synthesis of a trisaccharide fragment (**1**) of the lipoarabinomannan from *Tsukamurella paurometabola* is reported. Two approaches were investigated for the synthesis of the target. One was purely chemical, while the other involved the addition of one of the monosaccharide residues via a mannosyltransferase-catalyzed reaction. Both approaches produced the target in good overall yields. Thus, this chemoenzymatic approach appears to be a useful addition to the arsenal of methods for the synthesis of lipoarabinomannan-derived oligosaccharides.

Key words: lipoarabinomannan, oligosaccharide, mannosyltransferase, enzymatic synthesis.

Résumé : On a réalisé la synthèse d'un fragment trisaccharide (**1**) du lipoarabinomannane extrait du *Tsukamurella paurometabola*. On a étudié deux approches pour la synthèse de ce produit cible. L'une est purement chimique alors que l'autre implique l'addition des résidus monosaccharides par le biais d'une réaction catalysée par la mannosyltransférase. Les deux approches ont permis d'arriver à la cible avec de bons rendements globaux. L'approche chimioenzymatique semble donc être une addition utile à l'arsenal des méthodes de synthèse des oligosaccharides dérivés du lipoarabinomannane.

Mots clés : lipoarabinomannane, oligosaccharide, mannosyltransférase, synthèse enzymatique.

[Traduit par la Rédaction]

Introduction

The human pathogen *Mycobacterium tuberculosis* produces an immunomodulatory lipidated polysaccharide, lipoarabinomannan (LAM), which plays a critical role in the progression of tuberculosis (1, 2). This disease, and those caused by other pathogenic mycobacteria (e.g., *M. leprae* and *M. avium*), are of increasing interest because of their resurgence in the industrialized world, the emergence of drug-resistant strains, and the susceptibility of immunocompromised individuals to these infections (3, 4). It is now well-appreciated that the immunomodulatory properties of mycobacterial LAM depend on structural motifs within the glycan (1, 2). For example, LAM from *M. tuberculosis* has been shown to inhibit the production of the proinflammatory cytokines including TNF-α (5). In contrast, LAM from the nonpathogenic *M. smegmatis*, which differs only slightly in structure from *M. tuberculosis* LAM, induces the release of these same cytokines (6). These observations have sparked interest in determining the structure of LAM molecules not only from mycobacterial strains, but also from other actinomycetes and a number of such investigations have been carried out, revealing an impressive range of structural diversity (7–17).

A general model for how LAMs influence the immune response has been proposed (10); however, there is relatively little detailed information on the role of various structural motifs within these glycans. A systematic structure function analysis of the activation or suppression of the immune response by fragments of LAM should open up new strategies for the treatment of mycobacterial disease. Among them are the design of biosynthetic inhibitors of the immunosuppressive glycans or the preparation of novel vaccines that generate antibodies capable of masking these epitopes. The fundamental biochemical studies that must precede achieving such a goal require access to discrete oligosaccharide fragments of a range of LAM motifs, which are most efficiently obtained via chemical synthesis. Previously, we synthesized fragments of LAM from *M. tuberculosis* (18, 19) and *Rhodococcus ruber* (20). Reported here is the synthesis of a fragment of LAM from *Tsukamurella paurometabola* (10) (TpaLAM). Human infections by this actinomycete,

Received 22 September 2005. Published on the NRC Research Press Web site at http://canjchem.nrc.ca on 12 May 2006.

Submitted in honor of the 65th birthday of Walter A. Szarek.

K.M. Ridgway, W. Shi, S.-J. Lin, and T.L. Lowary.[2] Department of Chemistry and Alberta Ingenuity Centre for Carbohydrate Science, Gunning–Lemieux Chemistry Centre, University of Alberta, Edmonton, AB T6G 2G2, Canada.
M.M. Palcic. The Carlsberg Laboratory, Gamle Carlsberg Vej 10, DK-2500 Valby, Denmark.

[1]This article is part of a Special Issue dedicated to Professor Walter A. Szarek.
[2]Corresponding author (e-mail: tlowary@ualberta.ca).

 doi:10.1139/V06-049 © 2006 NRC Canada

Fig. 1. Proposed structure of the LAM from *Tsukamurella pauroametabola* (TpaLAM) (10). Diacylglycerol (DAG). All monosaccharide residues are in the D-form.

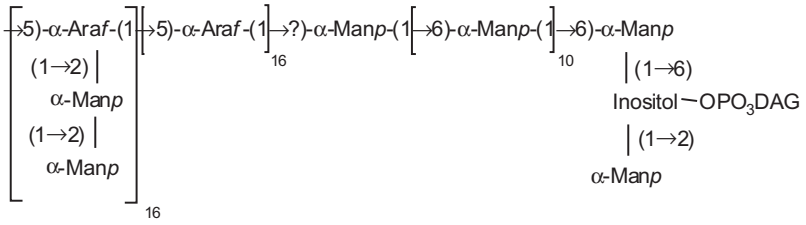
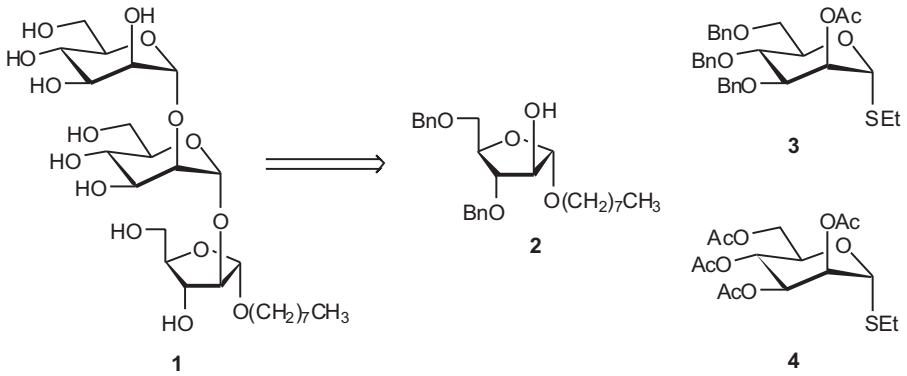


Fig. 2. Target oligosaccharide (**1**) and the building blocks chosen for its synthesis (**2**–**4**).



although rare, are occasionally found in immunocompromised patients (21).

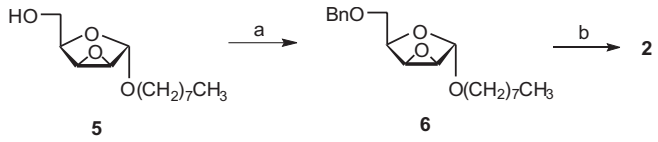
Results and discussion

The proposed structure of TpaLAM is shown in Fig. 1 (10). Similar to other glycoconjugates of this class, the glycan has at its core a mannosylated phosphatidylinositol moiety, to which is attached a chain of α-(1→6)-linked D-mannopyranose (Man*p*) residues. This mannan domain is devoid of branching Man*p* units, which is a common feature of all mycobacterial LAM structures reported to date (1, 2). The mannan is further elaborated by a linear arabinan, consisting of α-(1→5)-linked D-arabinofuranose (Ara*f*) residues. In contrast to the mycobacterial variant (1, 2), there is no branching within the arabinan; however, approximately half of the Ara*f* residues are further glycosylated on O-2 by an α-(1→2)-linked Man*p* disaccharide.

With this in mind, we chose to synthesize a trisaccharide fragment corresponding to the substituted Ara*f* residue present in the arabinan domain. The target thus chosen was **1** (Fig. 2), which we envisioned could be synthesized from three monosaccharide building blocks (**2**–**4**). Thioglycosides **3** and **4** were prepared as previously described (22, 23); the protected octyl glycoside **2** was straightforwardly synthesized as outlined in the following paragraph.

Access to **2** was achieved starting from the known epoxy glycoside **5** (24), first by benzylation of the hydroxyl group under standard conditions. The reaction proceeded to give **6** in 79% yield (Scheme 1). Octyl glycoside **2** was then obtained by heating **6** in a solution of benzyl alcohol and sodium benzylate at 100 °C overnight. The reaction proceeded with the expected high degree of regioselectivity (25), affording **2** in 88% yield. Given the relatively sluggish nature of this reaction, we also evaluated the use of microwave irradiation to effect the conversion of **6** into **2**. After optimization of the reaction conditions, we were able to carry out this reaction in only 30 min by microwave irradiation of a solution of **2** and sodium benzylate in benzyl alcohol at 170 °C. Under these conditions, an 82% yield of the product was obtained.

Scheme 1. (*a*) BnBr, NaH, THF, 0 °C → rt, 79%; (*b*) NaOBn, BnOH, 100 °C, 88%.

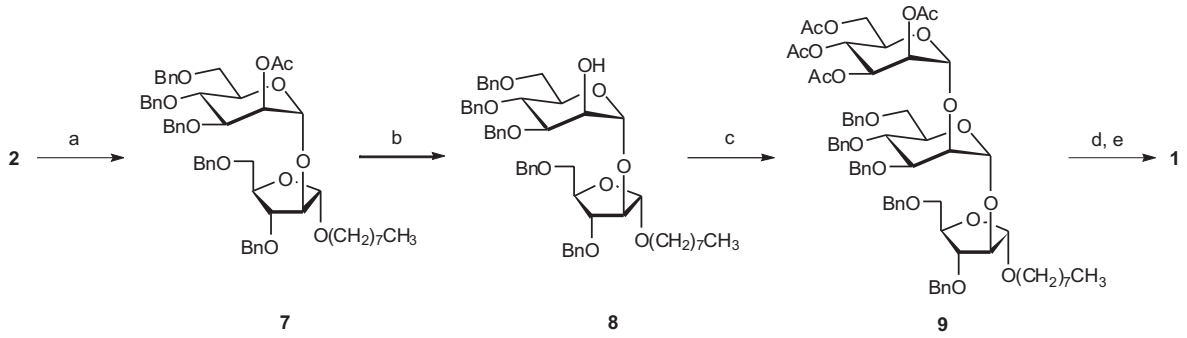


Once **2**–**4** were prepared, the target was synthesized without difficulty as illustrated in Scheme 2. Coupling of thioglycoside **3** with alcohol **2** was carried out under the promotion of *N*-iodosuccinimide and silver triflate (26), which afforded disaccharide **7** in 84% yield. The acetate protecting group in **7** was then cleaved giving a 97% yield of alcohol **8**. The final monosaccharide residue was introduced by reaction of **8** with **4**, again promoted by *N*-iodosuccinimde and silver triflate. The expected trisaccharide product (**9**) was obtained in 61% yield. Deprotection of **9** was achieved first by removal of the acetate esters by transesterification and then hydrogenation of the benzyl ethers, yielding a quantitative overall yield of **1**.

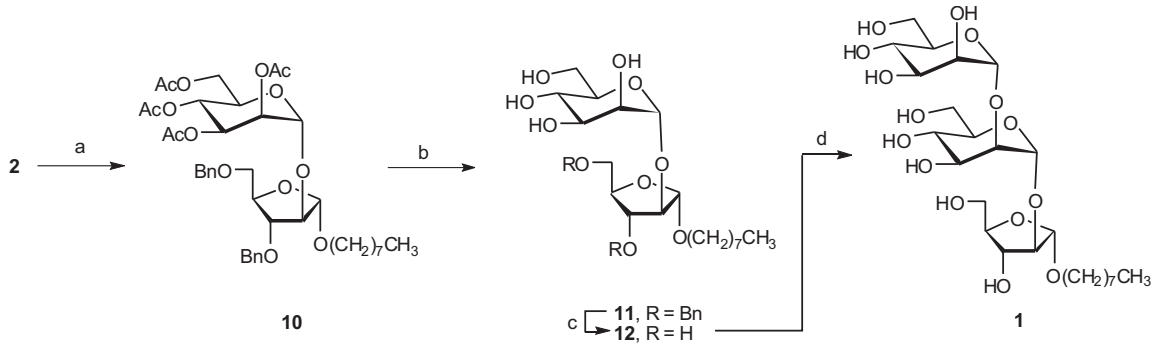
Having in place a route to **1** via a purely chemical approach, we explored an alternate method, which involved the introduction of the "nonreducing" mannopyranose unit via an enzymatic reaction. To test the feasibility of this route, we synthesized a fully deprotected disaccharide (**12**, Scheme 3), which is a potential substrate for an α-(1→2)-mannosyltransferase (α-(1→2)-ManT) from *Saccharomyces cerevisiae* that has been used in chemoenzymatic syntheses

© 2006 NRC Canada

Scheme 2. (*a*) **3**, NIS, AgOTf, CH_2Cl_2, –40 °C → rt, 84%; (*b*) $NaOCH_3$, CH_3OH, rt, 97%; (*c*) **4**, NIS, AgOTf, CH_2Cl_2, rt, 61%; (*d*) K_2CO_3, CH_3OH, rt, quantitative; (*e*) H_2, $Pd(OH)_2$/C, CH_3OH, rt, quantitative.



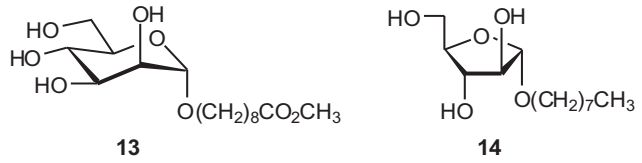
Scheme 3. (*a*) **4**, NIS, AgOTf, CH_2Cl_2, –50 °C → rt, 45%; (*b*) $NaOCH_3$, CH_3OH, rt, 83%; (*c*) H_2, $Pd(OH)_2$, CH_3OH, rt, 83%; (*d*) GDP-Man, ManT, rt, 90%.



of oligosaccharides (27–30). Thus, disaccharide **12** was synthesized by first reacting **2** with **4**, which gave **10** in 87% yield. Deprotection of **10** in two steps (transesterification and hydrogenation) gave **12** via **11**, in 69% overall yield.

With **12** in hand, we first tested its ability to serve as a substrate for this α-(1→2)-ManT by incubating it with radiolabelled guanosine diphosphate mannose ([^{3}H]-GDP-Man) in the presence of the enzyme and then quantitation by scintillation counting. Using this assay, the amount of radioactivity transferred to **12** was approximately 15% of that transferred to 8-methoxy(carbonyloctyl) α-D-mannopyranoside (**13**, Fig. 3), a substrate for this enzyme. Encouraged by this result, we then carried out a larger-scale incubation of **12** with GDP-Man and the α-(1→2)-ManT. After shaking the mixture for 25 h at room temperature (rt), the reaction was complete and purification of the product gave a 90% yield of **1**. The ^{1}H NMR spectrum for this trisaccharide was identical to that of **1** obtained from chemical synthesis (Fig. 4). In addition, the mass spectrum of the enzymatically formed product also showed a peak at *m/z* 609.6, which corresponds to the sodium adduct of the expected trisaccharide. Given the success in the synthesis of the trisaccharide by this chemoenzymatic approach, we also explored the synthesis of disaccharide **12** by the α-(1→2)-ManT catalyzed coupling of GDP-Man with octyl α-D-arabinofuranoside (**14**, Fig. 3). To explore this possibility, **14** was incubated with [^{3}H]-GDP-Man and the α-(1→2)-ManT. However, no transfer of radioactivity to the monosaccharide was observed,

Fig. 3. Positive and negative substrate controls for the α-(1→2)-ManT.



thus demonstrating that this simple furanoside is not a substrate for the enzyme, and therefore the synthesis of **12** from **14** via the action of this enzyme is not feasible.

In summary, a trisaccharide fragment of the LAM from *T. paurometabola*, has been synthesized using chemical and chemoenzymatic approaches. Both routes proceeded efficiently to give the target compound. To the best of our knowledge, this is the first example of a chemoenzymatic synthesis of an oligosaccharide substructure of LAM. The success of this approach suggests that similar strategies may facilitate the synthesis of more complicated fragments of these structurally diverse glycoconjugates.[3]

Experimental

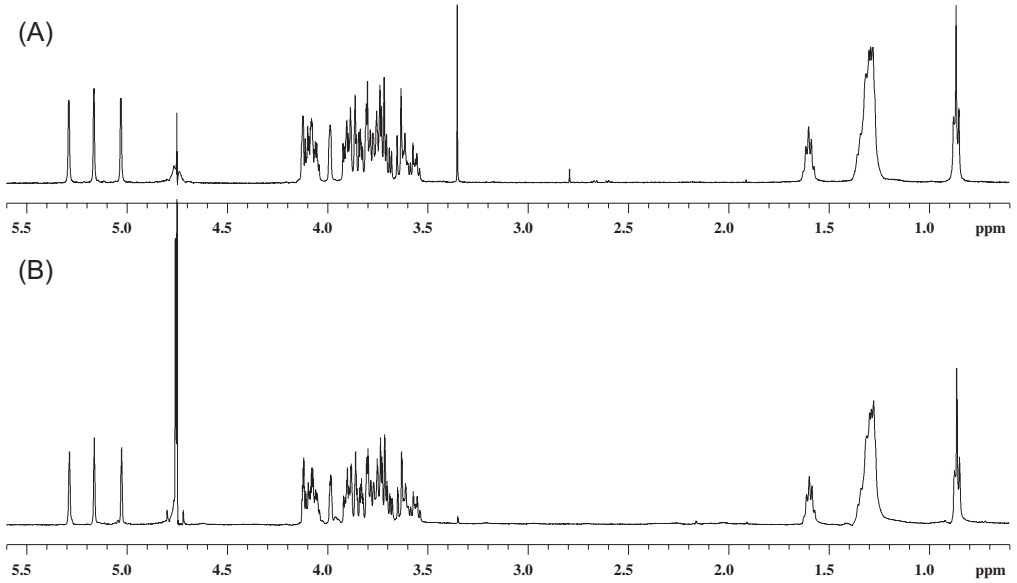
General methods

Reactions were carried out in oven-dried glassware. Reaction solvents were distilled from appropriate drying agents before use. Unless stated otherwise, all reactions were car-

[3] Supplementary data for this article are available on the journal Web site (http://canjchem.nrc.ca) or may be purchased from the Depository of Unpublished Data, Document Delivery, CISTI, National Research Council Canada, Ottawa, ON K1A 0R6, Canada. DUD 5026. For more information on obtaining material refer to http://cisti-icist.nrc-cnrc.gc.ca/irm/unpub_e.shtml.

© 2006 NRC Canada

Fig. 4. ^{1}H NMR spectra for trisaccharide **1** (recorded in D_2O). (A) Product obtained via chemical synthesis; (B) product obtained via chemoenzymatic synthesis. The peak at ~3.35 ppm is a methanol impurity.



ried out with stirring at rt under a positive pressure of argon and were monitored by TLC on silica gel 60 F_{254} (0.25 mm, E. Merck). Spots were detected under UV light or by charring with acidified *p*-anisaldehyde solution in EtOH. In the processing of reaction mixtures, solutions of organic solvents were washed with equal amounts of aqueous solutions. Organic solutions were concentrated under vacuum at <40 °C. All column chromatography was performed on silica gel (40–60 μmol/L) or Iatrobeads, which refers to a beaded silica gel 6RS-8060, manufactured by Iatron Laboratories (Tokyo). In all cases, the ratio between adsorbent and crude product ranged from 100 to 50:1 (*w*/*w*). Optical rotations were measured at 22 ± 2 °C and in units of degrees mL/g dm. ^{1}H NMR spectra were recorded at 400, 500, or 600 MHz, and chemical shifts were referenced to internal $CHCl_3$ (7.26 ppm, $CDCl_3$), CHD_2OD (3.30 ppm, CD_3OD), or external acetone (2.23 ppm, D_2O). ^{13}C NMR spectra were recorded at 100 or 125 MHz, and ^{13}C chemical shifts were referenced to internal $CDCl_3$ (77.23 ppm, $CDCl_3$) or CD_3OD (49.0 ppm, CD_3OD). ^{1}H NMR data are reported as though they were first order. Electrospray mass spectra were recorded on samples suspended in CH_3OH. The recombinant *S. cerevisiae* α-(1→2)-ManT used in the enzymatic reactions was produced as previously reported (31).

Octyl 2-*O*-[2-*O*-(α-D-mannopyranosyl)-α-D-mannopyranosyl]-α-D-arabinofuranoside (1)

Trisaccharide **9** (30.0 mg, 0.025 mmol) and K_2CO_3 (2.7 mg, 0.020 mmol) were stirred in CH_3OH (2.0 mL) at rt overnight. The solution was concentrated and the residue was purified by column chromatography (CH_2Cl_2–CH_3OH, 20:1) to give a partially deprotected intermediate (25.7 mg, 100%). To a solution of this intermediate (25.7 mg, 0.025 mmol) in methanol (5 mL) was added $Pd(OH)_2$/C (30 mg). The mixture was stirred overnight under an H_2 atmosphere and the catalyst was separated by filtration through Celite and then washed with CH_3OH (10 mL). Concentration of the filtrate gave **1** (14.5 mg, 100%) as a white solid. R_f 0.23 (CH_2Cl_2–CH_3OH, 2:1). $[\alpha]_D$ +93.9° (*c* 1.4, CH_3OH). ^{1}H NMR (500 MHz, CD_3OD) δ_H: 5.28 (d, 1H, $J_{1',2'}$ = 1.7 Hz, H-1′), 4.98 (d, 1H, $J_{1,2}$ = 1.6 Hz, H-1), 4.97 (d, 1H, $J_{1'',2''}$ = 1.7 Hz, H-1″), 4.08 (dd, 1H, $J_{1,2}$ = 1.6 Hz, $J_{2,3}$ = 3.8 Hz, H-2), 3.95–3.99 (m, 2H, H-3, H-2″), 3.88–3.91 (m, 1H, H-4), 3.78–3.88 (m, 4H, H-2′, H-6a′, H-6a″, H-6b″), 3.64–3.78 (m, 7H, H-5a, H-6b′, H-3′, H-3″, H-4′, H-5″, octyl OCH_2), 3.62 (dd, 1H, $J_{4,5b}$ = 5.6 Hz, $J_{5a,5b}$ = 12.2 Hz, H-5b), 3.57 (dd, 1H, $J_{3'',4''}$ = 9.5 Hz, $J_{4'',5''}$ = 9.5 Hz, H-4″), 3.53 (ddd, 1H, $J_{4',5'}$ = 9.6, $J_{5',6a'}$ = 2.4 Hz, $J_{5',6b'}$ = 5.3 Hz, H-5′), 3.42 (dt, 1H, *J* = 9.5, 6.6 Hz, octyl OCH_2), 1.53–1.61 (m, 2H, octyl CH_2), 1.26–1.38 (m, 10H, octyl CH_2), 0.87 (t, 3H, *J* = 6.9 Hz, octyl CH_3). ^{13}C NMR (125 MHz, CD_3OD) δ_C: 107.6 (C-1), 104.2 (C-1″, $^1J_{C\text{-}1'',H\text{-}1''}$ = 168.8 Hz), 99.5 (C-1′, $^1J_{C\text{-}1',H\text{-}1'}$ = 168.8 Hz), 88.9 (C-2), 84.5 (C-4), 80.3 (C-2′), 77.2 (C-2″), 75.1 (C-5), 75.0 (C-5″), 72.4 (C-3′), 71.9(2) (C-3″), 71.8(6) (C-3), 68.8(3) (C-4′), 68.8(2) (octyl OCH_2), 68.7(6) (C-4″), 63.2 (C-6′), 62.8 (C-6″), 62.7 (C-5), 33.0 (octyl CH_2), 30.8 (octyl CH_2), 30.5 (octyl CH_2), 30.4 (octyl CH_2), 27.3 (octyl CH_2), 23.7 (octyl CH_2), 14.4 (octyl CH_3). HRMS (ESI) calcd. for $C_{25}H_{46}O_{15}$: 609.2729 (M + Na); found: 609.2729.

Octyl 3,5-di-*O*-benzyl-α-D-arabinofuranoside (2)

Thermal method

Compound **6** (199 mg, 0.60 mmol) was dissolved in benzyl alcohol (10 mL). Sodium benzylate (1 mol/L, 7 mL, 7 mmol) was added and the reaction was stirred at 100 °C overnight. After cooling, a few drops of acetic acid were added to neutralize the reaction mixture. The solution was then concentrated to remove all but traces of the benzyl alcohol and the resulting residue was purified by column chromatography (hexanes–EtOAc, 6:1) to give **2** (231 mg, 88%) as a yellow syrup. R_f 0.19 (hexanes–EtOAc 6:1). $[\alpha]_D$ +81.1° (*c* 1.3, CH_2Cl_2). ^{1}H NMR (400 MHz, $CDCl_3$) δ_H: 7.27–7.38 (m, 10H, Ph), 5.01 (s, 1H, H-1), 4.68 (d, 1H, *J* = 12.1 Hz,

© 2006 NRC Canada

PhCH_2), 4.62 (d, 1H, J = 11.9 Hz, PhCH_2), 4.51 (d, 1H, J = 12.1 Hz, PhCH_2), 4.49 (d, 1H, J = 11.9 Hz, PhCH_2), 4.27 (ddd, 1H, $J_{4,5a}$ = 2.3 Hz, $J_{4,5b}$ = 2.4 Hz, $J_{3,4}$ = 3.1 Hz, H-4), 4.14 (s, 1H, H-2), 3.87 (d, 1H, $J_{3,4}$ = 3.1, H-3), 3.70 (dt, 1H, J = 9.7, 6.9 Hz, octyl OCH_2), 3.67 (dd, 1H, $J_{4,5a}$ = 2.3 Hz, $J_{5a,5b}$ = 10.4 Hz, H-5a), 3.50 (dd, 1H, $J_{4,5b}$ = 2.4 Hz, $J_{5a,5b}$ = 10.4 Hz, H-5b), 3.44 (dt, 1H, J = 9.7, 6.6 Hz, octyl OCH_2), 1.56–1.65 (m, 2H, octyl CH_2), 1.22–1.40 (m, 10H, octyl CH_2), 0.88 (t, 3H, J = 6.8 Hz, octyl CH_3). ^{13}C NMR (125 MHz, $CDCl_3$) δ_C: 138.0 (Ph), 137.1 (Ph), 128.6 (Ph, 2C), 128.4 (Ph, 2C), 128.0 (Ph), 127.9 (2C, Ph), 127.7(4) (2C, Ph), 127.7(0) (Ph), 109.1 (C-1), 85.4 (C-3), 83.2 (C-4), 78.1 (C-2), 73.8 (Ph*C*H_2), 71.9 (Ph*C*H_2), 69.9 (C-5), 67.7 (octyl OCH_2), 31.9 (octyl CH_2), 29.6 (octyl CH_2), 29.4 (octyl CH_2), 29.3 (octyl CH_2), 26.1 (octyl CH_2), 22.7 (octyl CH_2), 14.1 (octyl CH_3). HRMS (ESI) calcd. for $C_{27}H_{38}O_5$: 465.2617 (M + Na); found: 465.2612. Anal. calcd. for $C_{27}H_{38}O_5$: C 73.27, H 8.65; found: C 73.42, H 8.76.

Microwave method

Sodium benzylate (1 mol/L, 0.126 mL, 0.126 mmol) was added to **6** (21.2 mg, 0.063 mmol) in benzyl alcohol (0.37 mL). The mixture was heated, with stirring, in a CEM Discover/Explorer microwave system at 300 W and 170 °C for 0.5 h. After cooling, acetic acid was added dropwise until the mixture was neutralized. The solution was filtered through cotton, concentrated, and the resulting residue was purified by chromatography (hexanes–EtOAc, 6:1) to give **2** (22.9 mg, 82%) as a yellow syrup.

Octyl 2,3-anhydro-5-*O*-benzyl-α-D-lyxofuranoside (6)

To a solution of **5** (24) (2.71 g, 11.1 mmol) in THF (20 mL) at 0 °C, a mixture of NaH (60% in mineral oil, 0.89 g, 22.2 mmol) in THF (20 mL) was added dropwise. After 10 min, BnBr (1.7 mL, 14.3 mmol) was added dropwise. The reaction mixture was stirred for 2 h while warming to rt before water was added. The aqueous layer was extracted with CH_2Cl_2 and the organic extract was washed with brine, dried (Na_2SO_4), filtered, and concentrated. The crude product was purified by chromatography (hexanes–EtOAc (20:1) → hexanes–EtOAc (8:1)) to give **6** (2.94 g, 79%) as a pale yellow syrup. R_f 0.53 (hexanes–EtOAc, 8:1). $[\alpha]_D$ +13.5° (*c* 1.2, CH_2Cl_2). ^{1}H NMR (400 MHz, $CDCl_3$) δ_H: 7.27–7.38 (m, 5H, Ph), 5.05 (s, 1H, H-1), 4.63 (d, 1H, J = 12.0 Hz, PhCH_2), 4.58 (d, 1H, J = 12.0 Hz, PhCH_2), 4.21 (dd, 1H, $J_{4,5a}$ = $J_{4,5b}$ = 6.4 Hz, H-4), 3.77 (d, 1H, $J_{2,3}$ = 2.9 Hz, H-3), 3.75 (dt, 1H, J = 9.5, 6.7 Hz, octyl OCH_2), 3.66 (d, 2H, $J_{4,5}$ = 6.4 Hz, H-5), 3.65 (d, 1H, $J_{2,3}$ = 2.9 Hz, H-2), 3.46 (dt, 1H, J = 9.5, 6.7 Hz, octyl OCH_2), 1.53–1.62 (m, 2H, octyl CH_2), 1.23–1.38 (m, 10H, octyl CH_2), 0.89 (t, 3H, J = 6.8 Hz, octyl CH_3). ^{13}C NMR (125 MHz, $CDCl_3$) δ_C: 138.0 (Ph), 128.4 (Ph), 128.4 (Ph), 127.8 (Ph), 127.7 (Ph), 127.7 (Ph), 101.2 (C-1), 75.0 (C-4), 73.6 (Ph*C*H_2), 68.6 (C-5), 68.6 (octyl OCH_2), 56.3 (C-2), 54.5 (C-3), 31.8 (octyl CH_2), 29.6 (octyl CH_2), 29.3 (octyl CH_2), 29.2 (octyl CH_2), 26.1 (octyl CH_2), 22.6 (octyl CH_2), 14.1 (octyl CH_3). HRMS (ESI) calcd. for $C_{20}H_{30}O_4$: 357.2042 (M + Na); found: 357.2036. Anal. calcd. for $C_{20}H_{30}O_4$: C 71.82, H 9.04; found: C 71.58, H 8.92.

Octyl 2-*O*-(2-*O*-acetyl-3,4,6-tri-*O*-benzyl-α-D-mannopyranosyl)-3,5-di-*O*-benzyl-α-D-arabinofuranoside (7)

Alcohol **2** (42.9 mg, 0.097 mmol) and thioglycoside **3** (22) (106.5 mg, 0.18 mmol) were dissolved in CH_2Cl_2 (7.0 mL). To this solution were added 4 Å molecular sieves (500 mg). After stirring at rt for 15 min, the reaction mixture was cooled to –40 °C and stirred for another 15 min. NIS (43.6 mg, 0.19 mmol) was added, followed by AgOTf (7.5 mg, 0.03 mmol). After 3.5 h, a few drops of Et_3N were added until the pH was slightly basic. CH_2Cl_2 (20 mL) was added and the reaction mixture was filtered through Celite. The filtrate was concentrated and the resulting product was purified by column chromatography (hexanes–EtOAc, 8:1) to give **7** (75.0 mg, 84%) as a yellow syrup. R_f 0.18 (hexanes–EtOAc, 8:1). $[\alpha]_D$ +54.4° (*c* 6.2, CH_2Cl_2). ^{1}H NMR (400 MHz, $CDCl_3$) δ_H: 7.27–7.38 (m, 23H, Ph), 7.16–7.19 (m, 2H, Ph), 5.36 (dd, 1H, $J_{1',2'}$ = 1.8 Hz, $J_{2',3'}$ = 2.6 Hz, H-2′), 5.12 (s, 1H, H-1), 5.01 (d, 1H, $J_{1',2'}$ = 1.8 Hz, H-1′), 4.90 (d, 1H, J = 10.6 Hz, PhCH_2), 4.50–4.78 (m, 9H, PhCH_2), 4.22–4.28 (m, 2H, H-4, H-2), 3.96–4.01 (m, 2H, H-3′, H-4′), 3.84–3.91 (m, 3H, H-3, H-6a′, H-5′), 3.66–3.76 (m, 3H, H-5a, H-6b′, octyl OCH_2), 3.62 (dd, 1H, $J_{4,5a}$ = 5.3, $J_{5a,5b}$ = 10.8 Hz, H-5b), 3.37 (dt, 1H, J = 6.6, 9.7 Hz, octyl OCH_2), 2.22 (s, 3H, C(O)CH_3), 1.51–1.59 (m, 2H, octyl CH_2), 1.26–1.40 (m, 10H, octyl CH_2), 0.93 (t, 3H, J = 6.8 Hz, octyl CH_3). ^{13}C NMR (125 MHz, $CDCl_3$) δ_C: 170.4 (C=O), 138.3 (Ph), 138.1(3) (Ph), 138.1(0) (Ph), 137.9 (Ph), 137.8 (Ph), 128.4 (2C, Ph), 128.3(8) (3C, Ph), 128.3(5) (Ph, 2C), 128.3(2) (2C, Ph), 128.0 (2C, Ph), 127.9 (2C, Ph), 127.8(6) (2C, Ph), 127.7(8) (2C, Ph), 127.7(5) (2C, Ph), 127.6(8) (2C, Ph), 127.6(3) (2C, Ph), 127.6(2) (2C, Ph), 106.1 (C-1), 97.2 (C-1′), 86.4 (C-4), 83.6 (C-3), 80.8 (C-2), 78.0 (C-3′), 75.3 (Ph*C*H_2), 74.2 (C-4′), 73.5 (Ph*C*H_2), 73.4 (Ph*C*H_2), 72.2 (Ph*C*H_2), 72.0 (C-5′), 71.9 (Ph*C*H_2), 69.7 (C-5), 68.9 (C-2′), 68.7 (C-6′), 67.7 (octyl OCH_2), 31.9 (octyl CH_2), 29.6 (octyl CH_2), 29.4 (octyl CH_2), 29.3 (octyl CH_2), 26.1 (octyl CH_2), 22.7 (octyl CH_2), 21.1 (C(O)*C*H_3), 14.1 (octyl CH_3). HRMS (ESI) calcd. for $C_{56}H_{68}O_{11}$: 939.4654 (M + Na); found: 939.4655. Anal. calcd. for $C_{56}H_{68}O_{11}$: C 73.34, H 7.47; found: C 73.21, H 7.48.

Octyl 2-*O*-(3,4,6,-tri-*O*-benzyl-α-D-mannopyranosyl)-3,5-di-*O*-benzyl-α-D-arabinofuranoside (8)

Disaccharide **7** (64.4 mg, 0.070 mmol) and K_2CO_3 (6.9 mg, 0.050 mmol) were stirred together in CH_3OH (2.6 mL) at rt overnight. The solution was then concentrated and the residue was purified by chromatography (hexanes–EtOAc, 4:1) to give **8** (54.6 mg, 97%). R_f 0.30 (hexanes–EtOAc, 4:1). $[\alpha]_D$ +65.4° (*c* 3.9, CH_2Cl_2). ^{1}H NMR (500 MHz, $CDCl_3$) δ_H: 7.24–7.38 (m, 23H, Ph), 7.17–7.21 (m, 2H, Ph), 5.06 (s, 1H, H-1), 4.98 (d, 1H, $J_{1',2'}$ = 1.7 Hz, H-1′), 4.83 (d, 1H, J = 10.8 Hz, PhCH_2), 4.50–4.78 (m, 9H, PhCH_2), 4.20–4.23 (m, 2H, H-2, H-4), 3.87–3.95 (m, 2H, H-2′, H-4′), 3.77–3.86 (m, 4H, H-3, H-3′, H-5′, H-6a′), 3.57–3.71 (m, 4H, H-5a, H-5b, H-6b′, octyl OCH_2), 3.37 (dt, 1H, J = 6.6, 9.6 Hz, octyl OCH_2), 2.04 (br s, 1H, OH), 1.52–1.60 (m, 2H, octyl CH_2), 1.22–1.35 (m, 10H, octyl CH_2), 0.86–0.92 (m, 3H, octyl CH_3). ^{13}C NMR (125 MHz, $CDCl_3$) δ_C: 138.2 (Ph), 138.1(7) (Ph), 138.1(4) (Ph), 137.8(8) (Ph), 137.8(7) (Ph), 128.5 (2C, Ph), 128.4 (2C, Ph),

© 2006 NRC Canada

128.3(6) (2C, Ph), 128.3(2) (2C, Ph), 128.0 (2C, Ph), 127.9(6) (Ph), 127.8(7) (2C, Ph), 127.8(0) (2C, Ph), 127.7(7) (2C, Ph), 127.7(4) (2C, Ph), 127.6(8) (2C, Ph), 127.6(3) (2C, Ph), 127.5(7) (2C, Ph), 106.5 (C-1), 98.1 (C-1′), 85.2 (C-4), 83.1 (C-3), 81.1 (C-2), 80.0 (C-3′), 75.2 (Ph*C*H_2), 74.1 (C-4′), 73.5 (Ph*C*H_2), 73.4 (Ph*C*H_2), 72.1 (Ph*C*H_2), 72.0 (Ph*C*H_2), 71.7 (C-5′), 69.7 (C-5), 68.7 (C-6′), 68.5 (C-2′), 67.6 (octyl OCH_2), 31.9 (octyl CH_2), 29.6 (octyl CH_2), 29.4 (octyl CH_2), 29.3 (octyl CH_2), 26.1 (octyl CH_2), 22.7 (octyl CH_2), 14.1 (octyl CH_3). HRMS (ESI) calcd. for $C_{54}H_{66}O_{10}$: 897.4548 (M + Na); found: 897.4547.

Octyl 2-*O*-[2-*O*-(2,3,4,6-tetra-*O*-acetyl-α-D-mannopyranosyl)-3,4,6-tri-*O*-benzyl-α-D-mannopyranosyl]-3,5-di-*O*-benzyl-α-D-arabinofuranoside (9)

Disaccharide alcohol **8** (52.4 mg, 0.060 mmol) and thioglycoside **4** (23) (44.2 mg, 0.092 mmol) were dissolved in CH_2Cl_2 (8.0 mL). To this solution were added 4 Å molecular sieves (100 mg). After stirring at rt for 15 min, the reaction mixture was cooled to 0 °C and stirred for another 15 min. NIS (31.2 mg, 0.14 mmol) was added and the reaction was stirred for 20 min before the addition of AgOTf (4.6 mg, 0.02 mmol). After 4 h, a few drops of Et_3N were added until the pH was slightly basic and then CH_2Cl_2 (20 mL) was added and the reaction mixture was filtered through Celite. The filtrate was concentrated and the resulting product was purified by column chromatography (hexanes–EtOAc, 3:1) to give **9** (44.1 mg, 61%) as a yellow syrup. R_f 0.44 (hexanes–EtOAc 2:1). $[\alpha]_D$ +53.6° (*c* 4.5, CH_2Cl_2). ^{1}H NMR (400 MHz, $CDCl_3$) δ_H: 7.16–7.38 (m, 25H, Ph), 5.46 (dd, 1H, $J_{1'',2''}$ = 2.0 Hz, $J_{2'',3''}$ = 3.4 Hz, H-2′′), 5.40 (dd, 1H, $J_{2'',3''}$ = 3.4 Hz, $J_{3'',4''}$ = 10.0 Hz, H-3′′), 5.26 (dd, 1H, $J_{3'',4''}$ = $J_{4'',5''}$ = 10.0 Hz, H-4′′), 5.08 (d, 1H, $J_{1,2}$ = 0.9 Hz, H-1), 5.01 (d, 1H, $J_{1'',2''}$ = 2.0 Hz, H-1′′), 4.98 (d, 1H, $J_{1',2'}$ = 1.8 Hz, H-1′), 4.82 (d, 1H, *J* = 10.8 Hz, PhCH_2), 4.68 (d, 1H, *J* = 11.8 Hz, PhCH_2), 4.64 (d, 1H, *J* = 12.3 Hz, PhCH_2), 4.48–4.61 (m, 7H, PhCH_2), 4.21 (dd, 1H, $J_{5'',6a''}$ = 5.1 Hz, $J_{6a'',6b''}$ = 12.1 Hz, H-6a′′), 4.16–4.19 (m, 2H, H-4, H-5′′), 4.15 (dd, 1H, $J_{1,2}$ = 0.9 Hz, $J_{2,3}$ = 2.6 Hz, H-2), 4.03 (dd, 1H, $J_{5'',6b''}$ = 2.2 Hz, $J_{6a'',6b''}$ = 12.1 Hz, H-6b′′), 3.91 (dd, 1H, $J_{3',4'}$ = $J_{4',5'}$ = 9.5 Hz, H-4′), 3.84 (dd, 1H, $J_{2',3'}$ = 2.9 Hz, $J_{3',4'}$ = 9.5 Hz, H-3′), 3.78–3.82 (m, 3H, H-3, H-2′, H-5′), 3.73 (dd, 1H, $J_{5',6a'}$ = 5.1 Hz, $J_{6a',6b'}$ = 10.7 Hz, H-6a′), 3.73 (dd, 1H, $J_{5',6b'}$ = 2.1 Hz, $J_{6a',6b'}$ = 10.7 Hz, H-6b′), 3.56–3.64 (m, 3H, H-5a, H-5b, octyl OCH_2), 3.32 (dt, 1H, *J* = 9.5, 6.5 Hz, octyl OCH_2), 2.12 (s, 3H, C(O)CH_3), 2.03 (s, 3H, C(O)CH_3), 2.00 (s, 3H, C(O)CH_3), 1.98 (s, 3H, C(O)CH_3), 1.48–1.54 (m, 2H, octyl CH_2), 1.22–1.30 (m, 10H, octyl CH_2), 0.87 (t, 3H, *J* = 7.0 Hz, octyl CH_3). ^{13}C NMR (100 MHz, $CDCl_3$) δ_C: 170.6 (C=O), 169.8 (C=O), 169.7 (C=O), 169.6 (C=O), 138.3 (Ph), 138.2 (2C, Ph), 138.1 (Ph), 137.9 (Ph), 128.4 (2C, Ph), 128.3(7) (4C, Ph), 128.3(3) (2C, Ph), 128.2(9) (2C, Ph), 128.1 (Ph) 127.7 (3C, Ph), 127.7 (2C, Ph), 127.6(3) (Ph), 127.6(2) (Ph), 127.6(0) (2C, Ph), 127.5 (2C, Ph), 127.4 (Ph), 105.9 (C-1), 99.3 (C-1′), 98.5 (C-1′′), 87.2 (C-2), 83.8 (C-5′), 80.3 (C-4), 79.2 (C-3′), 77.8 (C-2′), 75.3 (Ph*C*H_2), 74.7 (C-4′), 73.4 (Ph*C*H_2), 73.2 (Ph*C*H_2), 72.5 (Ph*C*H_2), 72.4 (C-3), 72.1 (Ph*C*H_2), 69.8 (C-2′′), 69.5 (C-5), 69.1 (C-3′′), 69.0 (C-5′′), 68.9 (C-6′), 67.6 (octyl OCH_2), 66.1 (C-4′′), 62.5 (C-6′′), 31.8 (octyl CH_2), 29.6 (octyl CH_2), 29.4 (octyl CH_2), 29.3 (octyl CH_2), 26.1 (octyl CH_2), 22.6 (octyl CH_2), 20.9 (C(O)*C*H_3), 20.7(3) (C(O)*C*H_3), 20.7(0) (C, C(O)*C*H_3), 20.6(5) (C, C(O)*C*H_3), 14.1 (octyl CH_3). HRMS (ESI) calcd. for $C_{68}H_{84}O_{19}$: 1227.5499 (M + Na); found: 1227.5495.

Octyl 2-*O*-(2,3,4,6-tetra-*O*-acetyl-α-D-mannopyranosyl)-3,5-di-*O*-benzyl-α-D-arabinofuranoside (10)

Alcohol **2** (22.7 mg, 0.051 mmol) and thioglycoside **4** (23) (46.4 mg, 0.102 mmol) were dissolved in CH_2Cl_2 (5 mL). To this solution were added 4 Å molecular sieves (50 mg). After stirring at rt for 15 min, the reaction mixture was cooled to 0 °C and stirred for another 15 min. NIS (25.3 mg, 0.112 mmol) was added, followed by AgOTf (4.0 mg, 0.016 mmol). The reaction was monitored by TLC and after the disappearance of **4**, 3 drops of Et_3N were added. The reaction mixture was filtered through Celite. The filtrate was concentrated and the resulting crude product was purified by column chromatography (hexanes–EtOAc, 3:1) to give **11** (33.8 mg, 87%). R_f 0.27 (hexanes–EtOAc, 3:1). $[\alpha]_D$ +66.0° (*c* 3.4, CH_2Cl_2). ^{1}H NMR (400 MHz, $CDCl_3$) δ_H: 7.23–7.33 (m, 10H, Ph), 5.22–5.31 (m, 2H, H-4′, H-3′), 5.16 (dd, 1H, $J_{1,2}$ = 1.9 Hz, $J_{2,3}$ = 2.9 Hz, H-2′), 5.06 (s, 1H, H-1), 4.85 (d, 1H, $J_{1,2}$ = 1.8 Hz, H-1′), 4.46–4.60 (m, 4H, PhCH_2), 4.24 (dd, 1H, $J_{5,6a'}$ = 5.4 Hz, $J_{6a',6b'}$ = 12.2 Hz, H-6a′), 4.12–4.18 (m, 2H, H-2, H-4), 4.07 (dd, 1H, $J_{5,6b'}$ = 2.3, $J_{6a',6b'}$ = 12.2 Hz, H-6b′), 3.97–4.03 (m, 1H, H-5′), 3.88 (dd, 1H, *J* = 3.0 Hz, *J* = 6.7 Hz, H-3), 3.68 (dt, 1H, *J* = 9.5, 7.0 Hz, octyl OCH_2), 3.61 (dd, 1H, $J_{4,5a}$ = 3.7 Hz, $J_{5a,5b}$ = 10.8 Hz, H-5a), 3.56 (dd, 1H, $J_{4,5b}$ = 5.1 Hz, $J_{5a,5b}$ = 10.8 Hz, H-5b), 3.39 (dt, 1H, *J* = 9.5, 7.0 Hz, octyl OCH_2), 2.14 (s, 3H, C(O)CH_3), 2.06 (s, 3H, C(O)CH_3), 2.01 (s, 3H, C(O)CH_3), 1.97 (s, 3H, C(O)CH_3), 1.51–1.59 (m, 2H, octyl CH_2), 1.20–1.33 (m, 10H, octyl CH_2), 0.85 (t, 3H, *J* = 6.9 Hz, octyl CH_3). ^{13}C NMR (100 MHz, $CDCl_3$) δ_C: 170.5 (C=O), 169.9 (C=O), 169.8 (C=O), 169.7 (C=O), 138.0 (Ph), 137.6 (Ph), 128.3(9) (2C, Ph), 128.3(6) (2C, Ph), 127.8 (4C, Ph), 127.6 (2C, Ph), 105.6 (C-1), 97.2 (C-1′), 87.4 (C-4), 83.4 (C-3), 80.5 (C-2), 73.4 (Ph*C*H_2), 72.4 (Ph*C*H_2), 69.6 (C-3′), 69.5 (C-5), 69.1 (C-2′), 68.8 (C-5′), 67.8 (octyl OCH_2), 66.0 (C-4′), 62.3 (C-6′), 31.8 (octyl CH_2), 29.6 (octyl CH_2), 29.4 (octyl CH_2), 29.2 (octyl CH_2), 26.1 (octyl CH_2), 22.6 (octyl CH_2), 20.9 (C(O)*C*H_3), 20.6(9) (C(O)*C*H_3), 20.6(6) (2C, C(O)*C*H_3), 14.1 (octyl CH_3). HRMS (ESI) calcd. for $C_{41}H_{54}O_{14}$: 795.3568 (M + Na); found: 795.3562. Anal. calcd. for $C_{41}H_{54}O_{14}$: C 63.72, H 7.30; found: C 63.73, H 7.35.

Octyl 2-*O*-(α-D-mannopyranosyl)-α-D-arabinofuranoside (12)

Disaccharide **10** (41.1 mg, 0.054 mmol) and K_2CO_3 (4.1 mg, 0.030 mmol) were stirred together in CH_3OH (2 mL) at rt overnight. The solution was then concentrated and the residue purified by chromatography (CH_2Cl_2–CH_3OH, 10:1) to give **11** (26.8 mg, 83%). R_f 0.44 (CH_2Cl_2–CH_3OH, 10:1). ^{1}H NMR (500 MHz, CD_3OD) δ_H: 7.24–7.34 (m, 10H, Ph), 5.08 (s, 1H, H-1), 4.84 (d, 1H, *J* = 1.6 Hz, H-1′), 4.61 (d, 1H, *J* = 12.0 Hz, PhCH_2), 4.53 (s, 2H, PhCH_2), 4.51 (d, 1H, *J* = 12.0 Hz, PhCH_2), 4.17 (d, 1H, $J_{2,3}$ = 2.2 Hz, H-2), 4.14 (ddd 1H, $J_{3,4}$ = $J_{4,5a}$ = $J_{4,5b}$ = 5.4 Hz, H-4), 3.83

© 2006 NRC Canada

(dd, 1H, $J_{2,3}$ = 2.2 Hz, $J_{3,4}$ = 5.4 Hz, H-3), 3.81 (dd, 1H, $J_{5',6a'}$ = 2.2 Hz, $J_{6a',6b'}$ = 11.9 Hz, H-6a′), 3.54–3.73 (m, 7H, H-5a, H-5b, H-6b′, H-2′, H-3′, H-4′, octyl OCH_2), 3.50–3.54 (m, 1H, H-5′), 3.42 (dt, 1H, J = 9.5, 6.3 Hz, octyl OCH_2), 1.53–1.60 (m, 2H, octyl CH_2), 1.22–1.40 (m, 10H, octyl CH_2), 0.87 (t, 3H, J = 6.4 Hz, octyl CH_3). ^{13}C NMR (125 MHz, CD_3OD) δ_C: 139.5 (Ph), 139.3 (Ph), 129.4 (4C, Ph), 128.9(9) (2C, Ph), 128.9(5) (2C, Ph), 128.8(5) (Ph), 128.8 (Ph), 107.8 (C-1), 101.3 (C-1′), 87.1 (C-4), 85.0 (C-2), 82.5 (C-3), 75.3 (C-4′), 74.4 (Ph*C*H_2), 73.1 (Ph*C*H_2), 72.4 (C-2′), 72.3 (C-3′), 71.0 (C-5), 68.5 (octyl OCH_2), 68.4 (C-5′), 62.7 (C-6′), 33.0 (octyl CH_2), 30.7 (octyl CH_2), 30.5(2) (octyl CH_2), 30.4(6) (octyl CH_2), 27.3 (octyl CH_2), 23.7 (octyl CH_2), 14.5 (octyl CH_3).

Disaccharide **11** (26.8 mg, 0.045 mmol) was dissolved in CH_3OH (3 mL) and $Pd(OH)_2$/C (10.6 mg) was added. A balloon containing hydrogen was placed over the reaction flask. The solution stirred overnight at rt until the reaction was complete, as shown by TLC. The catalyst was removed by filtration through Celite. After washing the filtered catalyst with CH_3OH, the combined filtrates were concentrated, the residue dissolved in H_2O, and the resulting solution was then loaded onto a C18 Sep-Pak cartridge, which had been preequilibrated with CH_3OH (10 mL) and then water (10 mL). The cartridge was then washed with water (10 mL) and the product was eluted with CH_3OH (2 × 5 mL). The eluants were concentrated, the residue redissolved in water, and the solution filtered through a 0.22 μm Millex-GV filter. Freeze-drying of the filtered solution gave **12** (15.6 mg, 83%) as a white solid. R_f 0.55 (CH_2Cl_2–CH_3OH, 3:1. $[\alpha]_D$ +52.2° (*c* 1.1, CH_3OH). ^{1}H NMR (600 MHz, CD_3OD) δ_H: 4.99 (d, 1H, $J_{1',2'}$ = 1.2 Hz, H-1′), 4.98 (d, 1H, $J_{1,2}$ = 1.8 Hz, H-1), 4.08 (dd, 1H, $J_{1,2}$ = 1.8 Hz, $J_{2,3}$ = 4.2 Hz, H-2), 3.94 (dd, 1H, $J_{2,3}$ = 4.2 Hz, $J_{3,4}$ = 7.2 Hz, H-3), 3.88 (ddd, 1H, J = 3.0 Hz, J = 5.4 Hz, $J_{3,4}$ = 7.2 Hz, H-4), 3.77–3.81 (m, 2H, H-2′, H-6a′), 3.63–3.75 (m, 5H, H-5a, H-3′, H-4′, H-6b′, octyl OCH_2), 3.60 (dd, 1H, J = 4.8, 12.0 Hz, H-5b), 3.51–3.55 (m, 1H, H-5′), 3.40 (dt, 1H, J = 9.6, 6.6 Hz, octyl OCH_2), 1.53–1.59 (m, 2H, octyl CH_2), 1.26–1.37 (m, 10H, octyl CH_2), 0.87–0.92 (m, 3H, octyl CH_3). ^{13}C NMR (100 MHz, $CDCl_3$) δ_C: 107.4 (C-1), 101.2 (C-1′), 89.0 (C-2), 84.4 (C-4), 77.1 (C-3), 75.0 (C-5′), 72.4 (C-3′), 72.2 (C-2′), 68.4 (C-4′), 68.8 (octyl OCH_2), 62.7 (C-5), 62.6 (C-6′), 33.0 (octyl CH_2), 30.7 (octyl CH_2), 30.5 (octyl CH_2), 30.4 (octyl CH_2), 27.3 (octyl CH_2), 23.7 (octyl CH_2), 14.4 (octyl CH_3). HRMS (ESI) calcd. for $C_{19}H_{36}O_{10}$: 447.2206 (M + Na); found: 447.2201.

α-(1→2)-ManT assay for determining relative substrate activity of 12–14

Reaction mixtures for assessing the incorporation of [^{3}H]-Man into **12–14** consisted of 50 mmol/L MOPS (pH 7.5), 10 mmol/L $MgCl_2$, 0.5 mmol/L GDP-Man, 1.0 mmol/L potential acceptor substrate, the α-(1→2)-ManT (0.0134 mU for **12**, 0.0027 mU for **13**, 0.134 mU for **14**) (32), 0.1% Triton X-100, 1 mg/mL of BSA, guanosine diphosphate mannose (American Radiolabeled Chemicals, Inc., 8.9 Ci/mmol, 0.6 μL) in a total reaction volume of 30 μL. The mixture was incubated at 37 °C for 30 min. Control assays without acceptor were also performed. Radiolabeled products were isolated by reverse-phase chromatography on SepPak C18 cartridges (Waters) (32) and quantified by liquid scintillation counting on a Beckman LS6500 scintillation counter. Under these conditions, [^{3}H]-Man transfer to **12** was 15% of that of **13**, whereas the radioactivity transferred to **14** was at background levels. Modification of the assay with the use of 2.0 mmol/L GDP-Man, 4.0 mmol/L **14**, and increased α-(1→2)-ManT did not lead to greater levels of radioactivity transfer, thus demonstrating that this monosaccharide is not a substrate for the enzyme.

Enzymatic synthesis of 1 from 12

Disaccharide **12** (2.1 mg, 4.95 μmol) and GDP-mannose disodium salt (4.32 mg, μmol) were reacted with the α-(1→2)-ManT (200 mU) in 50 mmol/L MOPS buffer at pH 7.5, containing 0.1% Triton X-100, 10 mmol/L $MnCl_2$, 1 mg/mL BSA, 2 mmol/L DTT, and alkaline phosphatase (3 U). The total reaction volume was 600 μL. The reaction mixture was incubated on an end-to-end shaker at rt for 25 h and reaction progress was monitored by TLC ($CHCl_3$–CH_3OH–water, 70:35:2, R_f 0.5). When TLC showed the complete disappearance of **12**, cold water (~600 μL) was added and the incubation mixture was centrifuged to remove precipitates. The supernatent was loaded onto a C18 Sep-Pak cartridge, which had been preequilibrated with CH_3OH (50 mL) and then water (50 mL). The cartridge was then washed with water (50 mL) and the product was eluted with 50% CH_3OH–H_2O (2 × 20 mL). The eluants were concentrated to remove the CH_3OH and the resulting aqueous solution was filtered through a 0.22 μm Millex-GV filter. The filtrate was lyophilized to yield **1** as a white powder (2.6 mg, 90%). The ^{1}H NMR spectrum (500 MHz, D_2O) obtained on this product was identical to that obtained from **1** produced by chemical synthesis. Analysis of the product by ESI-MS showed a signal and *m/z* 609.6 corresponding to the $[M + Na]^+$ peak of the trisaccharide.

Acknowledgments

This work was supported by the University of Alberta, the Natural Sciences and Engineering Research Council of Canada (NSERC), and the Alberta Ingenuity Centre for Carbohydrate Science. KMR is the recipient of an Undergraduate Student Research Award from NSERC and a Summer Studentship from the Alberta Heritage Foundation for Medical Research. WS is the recipient of a Studentship from the Alberta Ingenuity Fund. We thank Professor Annette Herscovics (McGill University, Montreal, Quebec) for the clone of the recombinant mannosyltransferase used in the chemoenzymatic synthesis of **1**.

References

1. J. Nigou, M. Gilleron, and G. Puzo. Biochemie (Paris), **85**, 153 (2003).
2. V. Briken, S.A. Porcelli, G.S. Besra, and L. Kremer. Mol. Microbiol. **53**, 391 (2004).
3. L. Kremer and G.S. Besra. Expert Opin. Invest. Drugs, **11**, 1033 (2002).
4. W.J. Burman and B.E. Jones. Am. J. Resp. Crit. Care Med. **164**, 7 (2001).
5. J. Nigou, C. Zelle-Rieser, M. Gilleron, M. Thurnher, and G. Puzo. J. Immunol. **166**, 7477 (2001).

© 2006 NRC Canada

6. M. Gilleron, N. Himoudi, O. Adam, P. Constant, A. Venisse, M. Riviere, and G. Puzo. J. Biol. Chem. **272**, 117 (1997).
7. Y. Guérardel, E. Maes, E. Elass, Y. Leroy, P. Timmerman, G.S. Besra, C. Locht, G. Strecker, and L. Kremer. J. Biol. Chem. **277**, 30635 (2002).
8. J.B. Torrelles, K.-H. Khoo, P.A. Sieling, R.L. Modlin, N. Zhang, A.M. Marques, A. Treumann, C.D. Rithner, P.J. Brennan, and D. Chatterjee. J. Biol. Chem. **279**, 41227 (2004).
9. K.J.C. Gibson, M. Gilleron, P. Constant, G. Puzo, J. Nigou, and G.S. Besra. Biochem. J. **372**, 821 (2003).
10. K.J.C. Gibson, M. Gilleron, P. Constant, T. Brando, G. Puzo, G.S. Besra, and J. Nigou. J. Biol. Chem. **279**, 22973 (2004).
11. K.J.C. Gibson, M. Gilleron, P. Constant, G. Puzo, J. Nigou, and G.S. Besra. Microbiology, **149**, 1437 (2003).
12. N.J. Garton, M. Gilleron, T. Brando, H.-H. Dan, S. Giguère, G. Puzo, J.F. Prescott, and I.C. Sutcliffe. J. Biol. Chem. **277**, 31722 (2002).
13. M. Gilleron, N.J. Garton, J. Nigou, T. Brando, G. Puzo, and I.C. Sutcliffe. J. Bacteriol. **187**, 854 (2005).
14. I.C. Sutcliffe. Antonie Van Leeuwenhoek, **78**, 195 (2000).
15. C. Flaherty and I.C. Sutcliffe. Syst. Appl. Microbiol. **22**, 530 (1999).
16. C. Flaherty, D.E. Minnikin, and I.C. Sutcliffe. Zentralbl. Bakteriol. **285**,11 (1996).
17. K.J.C. Gibson, M. Gilleron, P. Constant, B. Sichi, G. Puzo, G.S. Besra, and J. Nigou. J. Biol. Chem. **280**, 28347 (2005).
18. V. Subramaniam and T.L. Lowary. Tetrahedron, **55**, 5965 (1999).
19. R.R. Gadikota, C.S. Callam, B.J. Appelmelk, and T.L. Lowary. J. Carbohydr. Chem. **22**, 459 (2003).
20. G.C. Completo, J.A. Ponto, and T.L. Lowary. J. Carbohydr. Chem. **24**, 517 (2005).
21. D. Rey, P. Fraisse, P. Riegel, Y. Piemont, and J.M. Lang. Pathol. Biol. **45**, 60 (1997).
22. C.S. Callam and T.L. Lowary. J. Org. Chem. **66**, 8961 (2001).
23. F. Dasgupta and P.J. Garegg. Acta Chem. Scand. **43**, 471 (1989).
24. C.S. Callam, R.R. Gadikota, and T.L. Lowary. J. Org. Chem. **66**, 4549 (2001).
25. N.R. Williams. Adv. Carbohydr. Chem. Biochem. **25**, 109 (1970).
26. P. Konradsson, U.E. Udodong, and B. Fraser-Reid. Tetrahedron Lett. **31**, 4313 (1990).
27. P. Wang, G.-J. Shen, Y.-F. Wang, Y. Ichikawa, and C.-H.Wong. J. Org. Chem. **58**, 3985 (1993).
28. G.F. Herrmann, P. Wang, G.-J. Shen, E. Garcia-Junceda, S.H. Khan, K.L. Matta, and C.-H. Wong. J. Org. Chem. **59**, 6356 (1994).
29. H.J.M. Gijsen, L. Qiao, W. Fitz, and C.-H.Wong. Chem. Rev. **96**, 443 (1996).
30. K.M. Koeller and C.-H. Wong. Chem. Rev. **100**, 4465 (2000).
31. P.A. Romero, M. Lussier, A.M. Sdicu, H. Bussey, and A. Herscovics. Biochem. J. **321**, 289 (1997).
32. M.M. Palcic, L.D. Heerze, M. Pierce, and O. Hindsgaul. Glycoconjugate J. **5**, 59 (1988).

© 2006 NRC Canada

Cyclodextrin derivatives with cyanohydrin and carboxylate groups as artificial glycosidases[1]

Fernando Ortega-Caballero and Mikael Bols

Abstract: Two cyclodextrin derivatives (**1** and **2**) were prepared in an attempt to create glycosidase mimics with a general acid catalyst and a nucleophilic carboxylate group. The catalysts **1** and **2** were found to catalyse the hydrolysis of 4-nitrophenyl β-D-glucopyranoside at pH 8.0, but rapidly underwent decomposition with loss of hydrogen cyanide to convert the cyanohydrin to the corresponding aldehyde. The initial rate of the catalysis shows that the cyanohydrin group in these molecules functions as a good catalyst, but that the carboxylate has no positive effect. The decomposition product aldehydes display little or no catalysis. A mechanism for the decomposition is suggested.

Key words: biomimicry, enzyme model, kinetics, intramolecular reaction.

Résumé : On a préparé deux dérivés de la cyclodextrine (**1** et **2**) dans le but de créer des imitations de glycosidase avec un catalyseur acide général et un groupe carboxylate nucléophile. On a trouvé que les catalyseurs **1** et **2** catalysent bien l'hydrolyse β-D-glucopyranoside de 4-nitrophényle, à un pH de 8,0, mais qu'ils subissent rapidement une décomposition avec perte de cyanure d'hydrogène qui transforme en aldéhyde correspondant. La vitesse initiale de la catalyse montre que le groupe cyanohydrine des ces molécules fonctionne comme un bon catalyseur, mais que le carboxylate n'a pas d'effet positif. Les aldéhydes obtenus comme produits de décomposition ne présentent pas, ou peu, d'activité catalytique. On propose un mécanisme pour la décomposition.

Mots clés : bio-imitation, modèle d'enzyme, cinétique, réaction intramoléculaire.

[Traduit par la Rédaction]

Introduction

Supramolecular chemistry is a science that attempts to understand and use chemistry beyond the molecule (1). A fascinating research area is aimed at using supramolecular chemistry to achieve catalysis thereby creating what is *de-facto* artificial enzymes (2).

We have recently reported some of the first examples of artificial glycosidases (3). The most effective type discovered was cyclodextrin derivatives, such as **A** (Fig. 1), containing a cyanohydrin group at the primary rim (4). For these catalysts, a k_{cat}/k_{uncat} of up to 8000 was obtained for the hydrolysis of aryl glycosides (5). Based on structure–activity analysis of a series of derivatives, it was found that both the cyano group and the cyanohydrin OH were essential for catalysis, indicating that the acidity of this group was essential. It is therefore suggested that **A** works by acid catalysis as shown in Fig. 1.

A second type of cyclodextrin, such as **B**, having two carboxylate or sulphate groups at the primary rim was also found to catalyse aryl glycoside cleavage. While these catalysts were found relatively inefficient (with k_{cat}/k_{uncat} of up to 10–50), at normal conditions (6), increasing the phosphate concentration led to k_{cat}/k_{uncat} values of up to 1000 (7). Since this type of artificial enzyme has both functional groups negatively charged, the catalysis was believed to be mainly electrostatic.

The observation, in this latter case, that increasing the phosphate concentration increased the catalytic rate, was taken as evidence for the involvement of nucleophilic substitution with phosphate and suggested that the catalysis could be increased by the presence of a nucleophile. Indeed, the catalysis by the better catalyst **A** is also boosted by phosphate, but not in a linear fashion. It was therefore proposed to incorporate a nucleophilic group into a cyanohydrin-containing cyclodextrin with the goal of achieving general acid catalysis and nucleophilic catalysis in the same molecule. It was decided to attempt to use a carboxylate as the nucleophile so that the desired catalyst essentially would become a hybrid on **A** and **B**. In this paper we report the synthesis of two such molecules (**1** and **2**), each having a cyanohydrin and a carboxylate group at the primary rim, only differing in the chain length between carboxylate and cyclodextrin (Fig. 1). Both compounds were found to be catalytic, but undergo rapid decomposition of the cyanohydrin group under the reaction conditions.

Received 14 September 2005. Published on the NRC Research Press Web site at http://canjchem.nrc.ca on 12 May 2006.

This paper is dedicated to Professor Szarek with thanks for his mentorship of one of us (MB), and for his contribution to science in general.

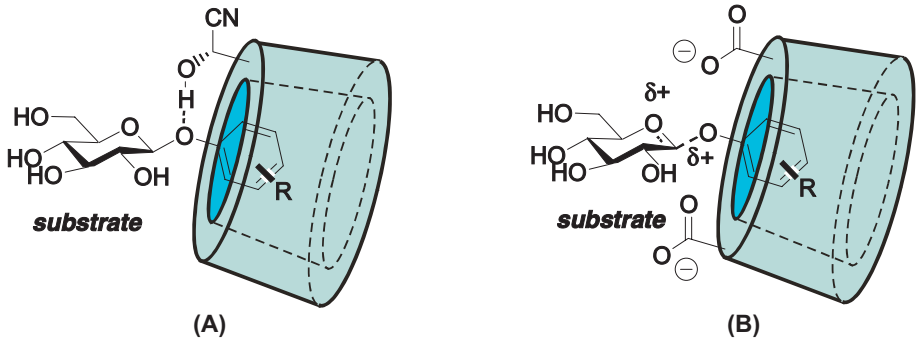
F. Ortega-Caballero and M. Bols.[2] Department of Chemistry, University of Aarhus, DK-8000 Aarhus, Denmark.

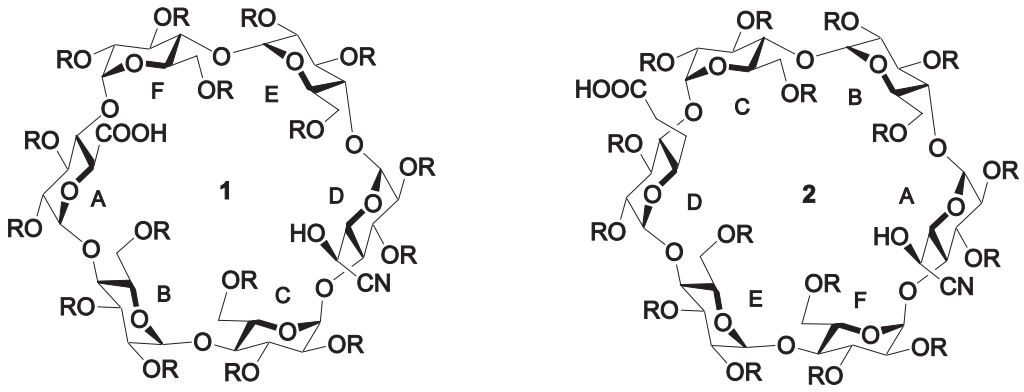
[1]This article is part of a Special Issue dedicated to Professor Walter A. Szarek.

[2]Corresponding author (e-mail: mb@chem.au.dk).

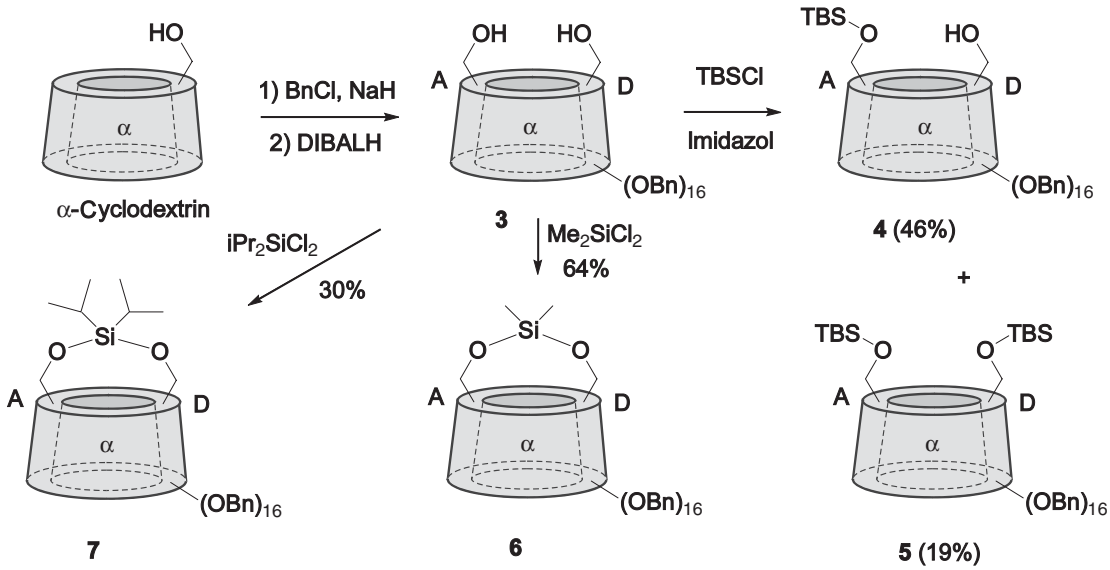
 doi:10.1139/V06-039 © 2006 NRC Canada

Fig. 1. Proposed mode of catalysis of cyclodextrin cyanohydrins (**A**) and cyclodextrin diacids (**B**).





Scheme 1. Synthesis of silylated derivatives **4**–**7**.



Results and discussion

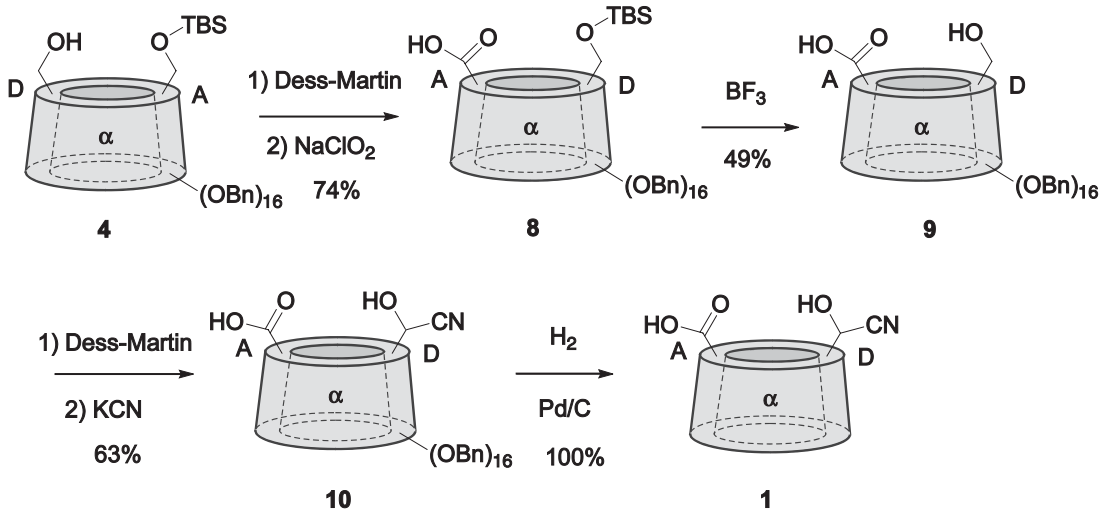
Synthesis

The synthesis of **1** and **2** was carried out from the hexadecabenzylated diol **3** readily available from α-cyclodextrin in two steps (Scheme 1) (8). Monosilylation of the diol **3** with TBSCl–imidazol was, however, not very selective, leading to a mixture of the mono- and di-silylated products (**4** and **5**), which could be separated by column chromatography to obtain them in 46% and 19% yield, respectively.

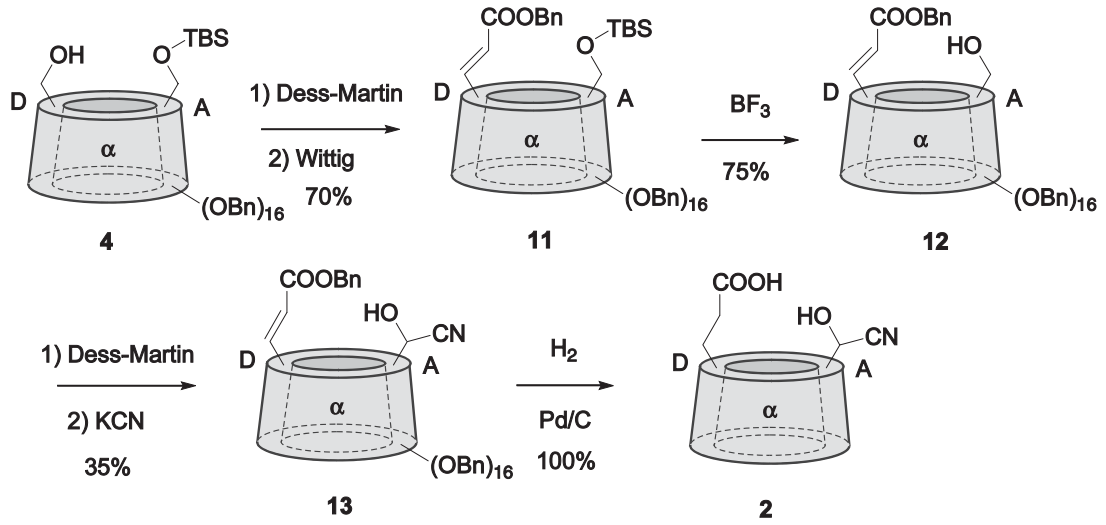
In an attempt to obtain **4** in a higher yield, a two-step synthesis procedure was attempted involving synthesis of silicon-bridged molecules **6** and **7** and subsequent attack on silicon with a *tert*-butyl organometalic reagent. The synthesis of the silicon diethers proceeded reasonably well; reaction of **3** with 1 equiv. of Me_2SiCl_2–pyridine gave **6** in 64% yield (Scheme 2). Similar reaction of **3** with *i*-Pr_2SiCl_2–

© 2006 NRC Canada

Scheme 2. Synthesis of **1**.



Scheme 3. Synthesis of **2**.



pyridine gave **7** in 30% yield. However, reaction of either **6** or **7** with a selection of organometalic reagents, such as methyl or *tert*-butyl magnesium chloride or butyllithium, gave neither a reaction nor loss of the protection group. Therefore, we had to satisfy ourselves with the relatively modest yield of **4**, obtained by direct silylation of **3**.

Oxidation of **4** to the aldehyde with Dess–Martin's periodinane, followed by subsequent oxidation to the carboxylic acid with $NaClO_2$, gave the acid **8** in 74% yield (Scheme 2). Removal of the TBS group with BF_3 afforded **9** in 49% yield. Oxidation of the remaining primary alcohol of **9** with Dess–Martin's periodinane and reaction of the resulting aldehyde with KCN then gave us **10** in 63% yield. Finally, hydrogenolysis of the benzyl groups gave target **1** in quantitative yield.

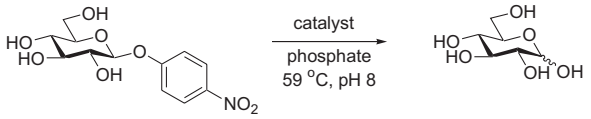
A related procedure was used to obtain **2**. Oxidation of **4** to the aldehyde was followed by Wittig reaction with benzyl 2-triphenylphosphonium acetate, which led to Wittig adduct **11** in 70% yield (Scheme 3). Deprotection of the silyl group with BF_3 gave structure **12**. As **12** was subjected to oxidation and reaction with KCN, the aldehyde was converted to the cyanohydrin **13**, albeit in a rather low yield of 35%. Hydrogenolysis eventually gave saturation of the double bond and removal of all protection groups affording a quantitative yield of target **2**.

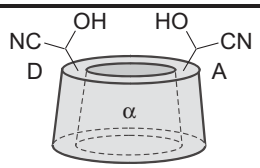
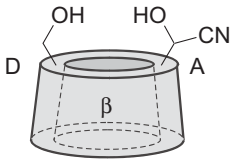
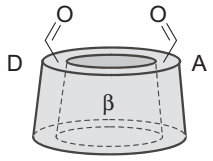
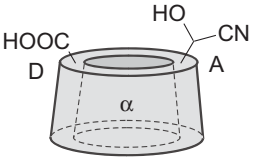
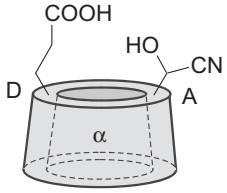
Catalysis

The glycosidase activity of **1** and **2** was investigated by monitoring their influence on the hydrolysis of 4-nitrophenyl-β-D-glucopyranoside at pH 8 and 59 °C (Table 1). These reactions were monitored by following the increase in absorption at 400 nm. Similarly to previously investigated cyclodextrin cyanohydrins (4, 5), both **1** and **2** were found to be catalytic. However, in contrast, the catalysis was found to decline rapidly as a function of time. As shown in Figs. 2 and 3, the progress curves were initiated by a boost of a rapid reaction, which in 1 to 2 h declined to become a steady-state rate that was identical or slightly higher than the background reaction rate. Since over the time period only a small amount of substrate was converted, the phenomenon cannot be caused by substrate depletion. Furthermore, since the change in rate, depending on the condi-

© 2006 NRC Canada

Table 1. Kinetic parameters for the **1** and **2** catalysed hydrolysis of β-glucoside at pH 8.0 and 59 °C.



Structure	Catalyst	k_{cat} ($x10^{-5}$ s^{-1})	K_m	k_{cat}/k_{uncat}
	Ref. 5	6.96±0.29	6.52±1.10	2688
	Ref. 5	1.47±0.12	30.6±4.9	1067
	Ref. 5	0.13±0.02	4.50±2.47	55
	**1**[a]	2.02±0.12	7.17±1.73	1102
	1[b]	0.07±0.02	11.98±6.99	43
	**2**[a]	1.07±0.06	9.25±1.59	563
	2[b]	—[c]	—[c]	—[c]

[a]Initial catalytic rate.
[b]End catalytic rate.
[c]No catalysis.

tions, was complete before even one turnover occurred, it is extremely unlikely that product inhibition or covalent reaction between substrate and catalyst is the reason for the decline in the hydrolysis rate. As a control, the catalyst (**1** or **2**) was incubated for 2 h in buffer at 59 °C before being added to the substrate, and under these conditions the rapid reaction onset disappears and the initial rate is identical to the end rate. It is therefore safe to conclude that the catalyst undergoes a chemical reaction – decomposition reaction under the reaction conditions.

By fitting a line either to the progress curve over the first 0.5 h or after 3 h, it was possible to determine an initial rate of reaction and an end reaction rate (Table 1). For **2**, the end rate is identical to the background rate, i.e., there is no catalysis. For the other cases, a catalytic rate is obtained by subtracting the background rates, giving catalysed rates. These catalysed rates follow, both for the initial rate and the end rate, Michaelis–Menten kinetics,giving the K_M and k_{cat} values as shown in Table 1. The k_{cat} is used together with the uncatalysed rate to calculate a k_{cat}/k_{uncat} value.

As demonstrated, the values for k_{cat}/k_{uncat} for the initial reaction is 1102 and 567 for **1** and **2**, respectively. This is very similar to the rate accelerations obtained with other cyclodextrin cyanohydrins. Thus, the α-cyclodextrin dicyanohydrin gave a k_{cat}/k_{uncat} of 2688 under these conditions, while β-cyclodextrin monocyanohydrin gave k_{cat}/k_{uncat} = 1067 (Table 1) (5). It is therefore probable that **1** and **2** are able to initially function with the cyanohydrin in-

© 2006 NRC Canada

Scheme 4. Two possible mechanisms for the decomposition of **1**.

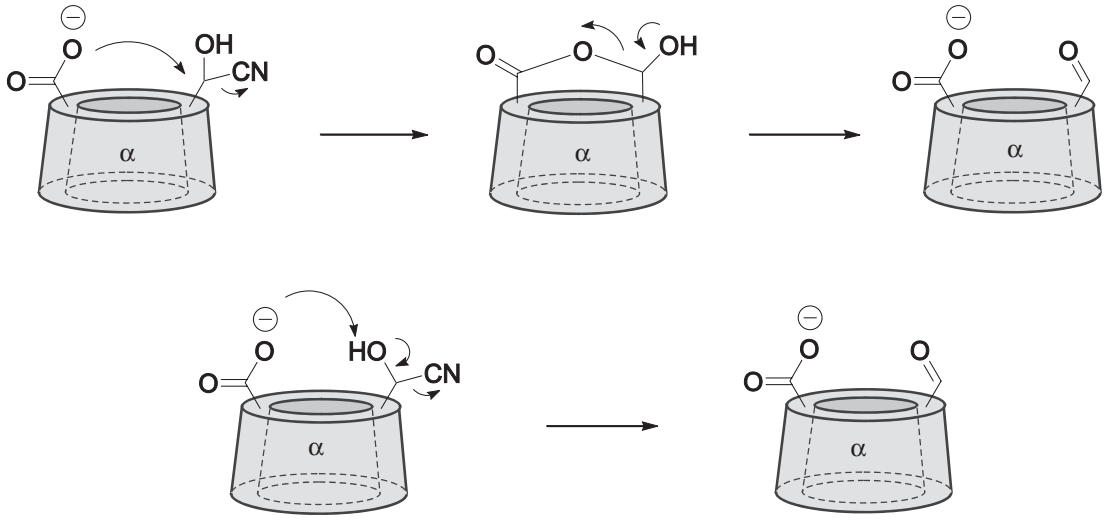


Fig. 2. Progress curve for the hydrolysis of 4-nitrophenyl β-D-glucopyranoside (pH 8, T = 59 °C, 50 mmol/L of phosphate buffer) in the presence of **1** or nothing (background).

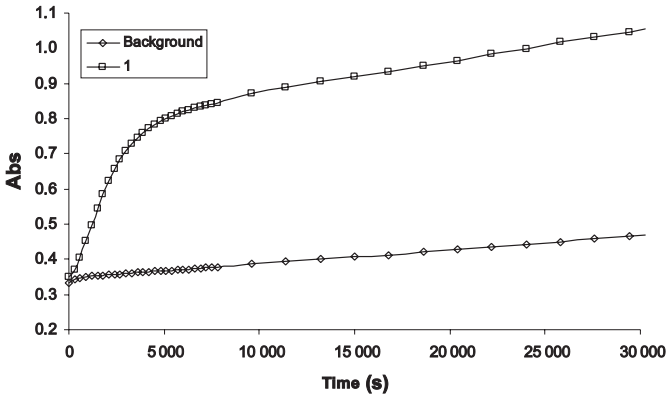
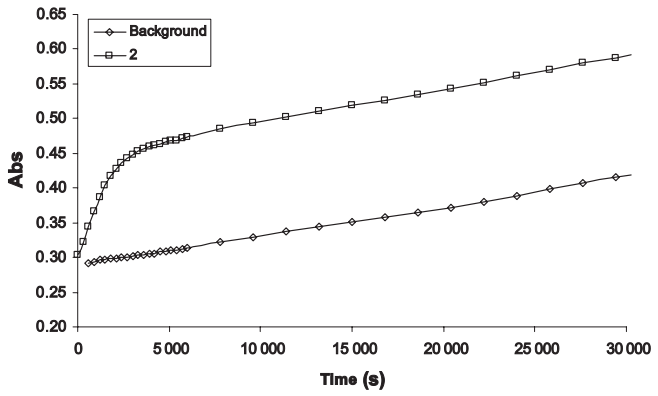


Fig. 3. Progress curve for the hydrolysis of 4-nitrophenyl β-D-glucopyranoside (pH 8, T = 59 °C, 50 mmol/L of phosphate buffer) in the presence of **2** or nothing (background).



tact and having the intended catalytic role. However, it was also observed that this initial catalysis was not higher than that of the previous catalysts, indicating that there is none of the intended cooperative catalysis between carboxylate and cyanohydrin.

The end k_{cat}/k_{uncat}, on the other hand, is 43 and no catalysis occurred for **1** and **2**, respectively (Table 1). This in likelihood means that the cyanohydrin has been blocked or destroyed. There are two reasonable possibilities of how this might occur. Either the free carboxylic acid might form an ester, a lactone, with the cyanohydrin hydroxyl group or another alcohol, which either blocks the catalytic group or the cavity to an extent that the substrate cannot enter. Alternatively, the carboxylate may function as an internal nucleophile and perform nucleophilic catalysis, not as intended on the substrate, but on the cyanohydrin, making it undergo hydrolysis to the aldehyde and cyanide. This latter explanation makes more chemical sense: lactonization of hydroxy acids is normally not thermodynamically favorable at pH 8, so it is not very plausible that a lactone would be the major form of **1** or **2** at pH 8. Further, the relatively weak catalysis obtained from decomposed **1** does indeed suggest that the compound has been converted to an aldehyde, since we have previously found that β-cyclodextrin dialdehyde is a weak catalyst (Table 1).

To support either hypothesis, the decomposition of **1** in buffer was followed by MS spectroscopy at different intervals, and the initial peak corresponding to M + Na of **1** was over time converted to new peak corresponding to M + Na of the corresponding cyclodextrin acidaldehyde. It is therefore clear that the rapidly declining catalytic activity of **1** and **2** is due to rapid decomposition of the cyanohydrin into the aldehyde, and we propose the intramolecular mechanisms outlined in Scheme 4 for this conversion. Thus, either attack of carboxylate ion on the cyanohydrin leads to substitution of this group and formation of a lactone hemiacetal that subsequently cleaves readily. Alternatively, the carboxylate acts as a general base catalyst, assisting the spontaneous decomposition of the cyanohydrin. At present these mechanisms are indistinguishable. It is remarkable that both **1** and **2** undergo this cleavage with ease despite the fact that the carboxylate is placed at rather different positions, though it is also clear that **2** undergoes decomposition faster. Nevertheless, the observation that **1** undergoes this reaction at all suggests that a considerable flexibility is present in the cyclodextrin.

© 2006 NRC Canada

In summary, we have prepared two new cyclodextrin derivatives that contain a cyanohydrin and a carboxylate group on the primary face of the cyclodextrin. Both compounds are able to catalyse the hydrolysis of glycosides with a rate that is equivalent to the rate previously seen with other cyclodextrin cyanohydrins, but rapidly lose activity. This decomposition was found to occur as the cyanohydrin cleaved into the corresponding aldehyde and cyanide, and the carboxylate group is believed to catalyse this process.

Experimental

All reagents were used as purchased without further purification. TLC was performed on Merck silica gel 60 F_{254} plates with detection by charring with cerium sulphate and ammonium heptamolybdat, and by UV light when applicable. Flash column chromatography was performed on Fluka silica gel (230–400 mesh) as the stationary phase. Optical rotations were recorded on a PerkinElmer 241 polarimeter at room temperature. IR spectra were recorded on a PerkinElmer FT-IR Paragon 1000. ^{1}H and ^{13}C NMR spectra were recorded on a Varian Mercury 400 MHz spectrometer. Chemical shifts are given in ppm and referenced to internal $SiMe_4$ (δ_H, δ_C 0.00). *J* values are given in Hz. MALDI-TOF mass spectra were recorded on a Bruker Daltonics mass spectrometer (Bruker) using an α-cyano-4-hydroxy-cinnamic acid (HCCA) matrix.

6^A-*O*-*tert*-Butyldimethylsilyl-2$^{A–F}$,3$^{A–F}$,6^B,6^C,6^E,6^F-hexadecakis-*O*-benzyl-α-cyclodextrin (4) and 6^A,6^D-di-*O*-*tert*-butyldimethylsilyl-2$^{A–F}$,3$^{A–F}$,6^B,6^C,6^E,6^F-hexadecakis-*O*-benzyl-α-cyclodextrin (5)

A solution of **3** (2.00 g, 0.83 mmol), imidazole (113 mg, 1.66 mmol), and TBDMSCl (150 mg, 0.99 mmol) in anhydr. DMF (20 mL) was stirred under a N_2 atmosphere at room temperature for 48 h. The reaction mixture was diluted with EtOAc and the organic phase was washed several times with water, dried ($MgSO_4$), filtered, and the organic solvent was removed in vacuo. The residue was purified by chromatography (eluent gradient, EtOAc–pentane, 1:4 → 2:7), to first afford **5** (19%) and then **4** (955 mg, 46%) as white foams. **4**: $[\alpha]_D$ +32.2° (*c* 1.0, CH_3Cl). IR (KBr, cm^{-1}): 3482, 3063, 3029, 2926, 2857, 1951, 1733, 1605, 1496, 1453, 1359, 1094, 1027. ^{1}H NMR (400 MHz, $CDCl_3$) δ: 7.33–7.08 (m, 80H, aromatic-H), 5.57 (d, 1H, $^3J_{1,2}$ = 3.2 Hz, H-1), 5.47 (d, 1H, $^3J_{1,2}$ = 3.2 Hz, H-1), 5.36 (d, 1H, ^2J = 10.8 Hz, C*H*Ph), 5.32 (d, 1H, ^2J = 10.8 Hz, C*H*Ph), 5.21 (t, 2H, ^2J = 10.8 Hz, CH_2Ph), 5.04 (d, 1H, $^3J_{1,2}$ = 3.2 Hz, H-1), 4.95–4.80 (m, 13H), 4.70 (t, 2H, ^2J = 12.4 Hz), 4.59–4.34 (m, 21H), 4.25–4.08 (m, 15H), 4.00–3.81 (m, 14H), 3.73–3.60 (m, 7H), 3.56 (dd, 1H, $^3J_{1,2}$ = 3.2 Hz, $^3J_{2,3}$ = 9.6 Hz, H-2), 3.50–3.43 (m, 3H), 3.41 (dd, 1H, $^3J_{1,2}$ = 3.0 Hz, $^3J_{2,3}$ = 9.8 Hz, H-2), 3.36 (dd, 1H, $^3J_{1,2}$ = 3.0 Hz, $^3J_{2,3}$ = 9.6 Hz, H-2), 2.56 (bs, 1H, OH), 0.87 (s, 9H, SiC(CH_3)$_3$), 0.00 (s, 6H, $SiCH_3$). ^{13}C NMR (100 MHz, $CDCl_3$) δ: 139.4–137.9 (C_{ipso}), 128.3–126.8 (CH aromatic), 98.7 (C-1), 98.1 (C-1), 98.0 (C-1), 97.9 (C-1), 97.8 (C-1), 97.7 (C-1), 81.4, 81.3, 81.0, 80.8, 80.5, 80.0, 79.8, 79.6, 79.4, 79.2, 79.1, 79.0, 78.6, 78.2, 76.1, 76.0, 75.9, 75.8, 75.7, 75.6, 74.8, 74.6, 73.3, 73.1, 73.0, 72.9, 72.6, 72.4, 72.2, 71.9, 71.8, 71.6, 71.4, 71.3, 69.3, 69.2, 68.8 (CH_2, CH), 62.5 (C-6), 61.4 (C-6), 60.3 (C-6), 26.0 (SiC(CH_3)$_3$), 18.3 (SiC), –4.7 ($SiCH_3$), –4.9 ($SiCH_3$). MALDI-TOF-MS *m*/*z* calcd. for $C_{154}H_{170}O_{30}SiNa$: 2550.144; found: 2550.526 [M]$^+$. **5**: ^{1}H NMR (400 MHz, $CDCl_3$) δ: 7.30–7.12 (m, 80H, aromatic-H), 5.31–5.20 (m, 8H), 5.14–5.11 (m, 4H), 4.91–4.86 (m, 6H), 4.62–4.41 (m, 19H), 4.33 (t, 4H, ^2J = 12.4 Hz), 4.23–3.94 (m, 21H), 3.80 (d, 1H, ^3J = 8.4 Hz), 3.66–3.50 (m, 10H), 3.42 (dd, 2H, $^3J_{1,2}$ = 3.4 Hz, $^3J_{2,3}$ = 9.4 Hz, H-2), 0.91 (s, 18H, SiC(CH_3)$_3$), 0.01 (s, 6H, $SiCH_3$), 0.00 (s, 6H, $SiCH_3$). ^{13}C NMR (100 MHz, $CDCl_3$) δ: 139.3–138.1 (C_{ipso}), 128.3–126.8 (CH aromatic), 98.3 (C-1), 98.1 (C-1), 98.0 (C-1), 81.3, 81.1, 80.7, 79.2, 79.1, 79.0, 78.1, 78.0, 75.8, 75.4, 75.3, 73.5, 73.4, 73.0, 72.8, 72.6, 72.4, 71.6, 71.4, 69.1, 69.0 (CH_2, CH), 62.3 (C-6), 26.0 (SiC(CH_3)$_3$), 18.2 (SiC), –4.9 ($SiCH_3$), –5.2 ($SiCH_3$).

6^A,6^D-Di-*O*-methylsilyl-2$^{A–F}$,3$^{A–F}$,6^B,6^C,6^E,6^F-hexadecakis-*O*-benzyl-α-cyclodextrin (6)

Dimethylsilyl chloride (60 μL, 0.50 mmol) was added to a solution of **3** (1.00 g, 0.41 mmol) in anhydrous pyridine (22 mL) and the reaction mixture was stirred at room temperature under a N_2 atmosphere for 48 h. The reaction mixture was concentrated under reduced pressure and toluene was added and pyridine was azeotroped. The residue was purified by chromatography (eluent gradient, EtOAc–pentane, 2:7) to afford **6** (650 mg, 64%) as white foam. ^{1}H NMR (400 MHz, $CDCl_3$) δ: 7.35–7.07 (m, 80H, aromatic-H), 5.85 (d, 2H, $^3J_{1,2}$ = 4.0 Hz, H-1), 5.64 (d, 2H, ^2J = 10.4 Hz, C*H*Ph), 5.25 (d, 2H, ^2J = 10.4 Hz, C*H*Ph), 5.01 (d, 2H, ^2J = 10.8 Hz, C*H*Ph), 5.93 (t, 4H, ^2J = 12.0 Hz, CH_2Ph), 4.83–4.75 (m, 8H), 4.64 (d, 2H, ^2J = 10.0 Hz), 4.57–4.41 (m, 19H), 4.30–4.09 (m, 16H), 4.02–3.98 (m, 4H), 3.85 (bd, 2H, *J* = 7.6 Hz), 3.75 (d, 2H, *J* = 10.4 Hz), 3.70 (dd, 2H, $^3J_{1,2}$ = 3.6 Hz, $^3J_{2,3}$ = 10.0 Hz, H-2), 3.59 (t, 2H, *J* = 9.2 Hz), 3.53–3.44 (m, 8H), 0.00 (s, 6H, $SiCH_3$). ^{13}C NMR (100 MHz, $CDCl_3$) δ: 139.5–137.8 (C_{ipso}), 128.3–126.1 (CH aromatic), 99.2 (C-1), 98.5 (C-1), 96.4 (C-1), 81.6, 81.5, 81.1, 80.8, 80.4, 80.3, 78.9, 77.8, 76.8, 76.5, 76.1, 73.6, 73.5, 73.3, 73.1, 72.8, 72.1, 71.9, 71.8, 69.8, 69.2, 68.9 (CH_2, CH), 63.1 (C-6), –4.1 ($SiCH_3$). MALDI-TOF-MS *m*/*z* calcd. for $C_{150}H_{160}O_{30}SiNa$: 2492.0661; found: 2492.306 [M]$^+$.

6^A,6^D-Di-*O*-isopropylsilyl-2$^{A–F}$,3$^{A–F}$,6^B,6^C,6^E,6^F-hexadecakis-*O*-benzyl-α-cyclodextrin (7)

Diisopropylsilyl chloride (27 μL, 0.15 mmol) was added to a solution of **3** (300 mg, 0.12 mmol) in anhydrous pyridine (7 mL) and the reaction mixture was stirred at room temperature under a N_2 atmosphere for 19 h. The reaction mixture was concentrated under reduced pressure and toluene was added and pyridine was azeotroped. The residue was purified by chromatography (eluent gradient, EtOAc–pentane, 2:7), to afford **7** (95 mg, 30%) as white foam. ^{1}H NMR (400 MHz, $CDCl_3$) δ: 7.26–6.86 (m, 80H, aromatic-H), 5.73 (d, 1H, $^3J_{1,2}$ = 4.4 Hz, H-1), 5.45 (d, 1H, ^2J = 10.8 Hz, C*H*Ph), 5.13–5.00 (m, 3H), 4.86–4.72 (m, 6H), 4.66–4.58 (m, 4H), 4.49–4.24 (m, 18H), 4.20–3.90 (m, 16H), 3.85–3.82 (m, 3H), 3.77–3.67 (m, 3H), 3.56 (dd, 1H, $^3J_{1,2}$ = 4.4 Hz, $^3J_{2,3}$ = 9.6 Hz, H-2), 3.52–3.40 (m, 6H), 3.36–3.30 (m, 5H), 1.17 (t, 2H, ^3J = 7.2 Hz, SiCH), 0.95 (d, 3H, ^3J = 7.6 Hz, SiCH(CH_3)$_2$), 0.90 (d, 3H, ^3J = 7.2 Hz,

© 2006 NRC Canada

SiCH(CH_3)$_2$), 0.88 (d, 3H, ^3J = 8.0 Hz, SiCH(CH_3)$_2$), 0.86 (d, 3H, ^3J = 7.2 Hz, SiCH(CH_3)$_2$). ^{13}C NMR (100 MHz, $CDCl_3$) δ: 139.5–137.8 (C_{ipso}), 129.0–126.0 (CH aromatic), 99.6 (C-1), 98.6 (C-1), 96.1 (C-1), 81.4, 81.2, 81.1, 80.9, 80.6, 79.9, 78.9, 77.9, 76.5, 75.9, 73.6, 73.4, 73.0, 72.8, 72.6, 72.0, 71.7, 70.2, 69.4, 68.3 (CH_2, CH), 63.3 (C-6), 18.1 (SiCH), 17.3–17.2 (SiCH(CH_3)$_2$). MALDI-TOF-MS *m/z* calcd. for $C_{154}H_{168}O_{30}SiNa$: 2548.1287; found: 2549.343 $[M]^+$.

6^D-*O*-*tert*-Butyldimethylsilyl-2$^{A–F}$,3$^{A–F}$,6^B,6^C,6^E,6^F-hexadecakis-*O*-benzyl-α-cyclodextrin-6^A-carboxylic acid (8)

To a solution of **4** (336 mg, 0.13 mmol) in CH_2Cl_2 (13 mL) was added Dess–Martin periodinane reagent (141 mg, 0.33 mmol) and the reaction mixture was stirred for 2 h and then quenched by addition of Et_2O (13 mL) and satd. aq. $NaHCO_3$ containing 3.0 g of $Na_2S_2O_3$ (13 mL). After stirring for an additional hour, the solution was diluted with Et_2O (50 mL) and washed successively with satd. aq. $NaHCO_3$ (30 mL) and water (30 mL). The organic phase was dried ($MgSO_4$), filtered, and the organic solvent was removed in vacuo. The residue was dissolved in a mixture of *t*-BuOH (9.5 mL), THF (4 mL), and 2-methyl-2-butene (4 mL), and $NaClO_2$ (240 mg, 2.66 mmol) and NaH_2PO_4 (266 mg) in water (4 mL) were added. The reaction mixture was stirred overnight and then quenched with 1 mol/L aq. HCl (10 mL) and extracted with EtOAc (3 × 50 mL). The organic phase was dried ($MgSO_4$), filtered, and the organic solvent was removed in vacuo. The residue was purified by chromatography (eluent, EtOAc–pentane, 2:7 → 2:5 and 2:5, containing 1% HCOOH) to afford **8** (251 mg, 74%) as white foam. $[\alpha]_D$ +28.6° (*c* 1.0, CH_3Cl). IR (KBr, cm^{-1}): 3442, 3063, 3030, 2927, 1724 (COOH), 1497, 1453, 1360, 1094, 1027. ^{1}H NMR (400 MHz, $CDCl_3$) δ: 7.38–7.10 (m, 80H, aromatic-H), 5.79 (d, 1H, ^3J = 3.6 Hz, H-1), 5.74 (d, 1H, ^3J = 3.6 Hz, H-1), 5.55 (d, 1H, ^2J = 10.4 Hz, C*H*Ph), 5.51 (d, 1H, ^2J = 10.4 Hz, C*H*Ph), 5.22 (d, 1H, ^2J = 12.0 Hz, C*H*Ph), 5.18 (d, 1H, ^2J = 11.2 Hz, C*H*Ph), 5.02–4.74 (m, 16H), 4.71–3.93 (m, 50H), 3.84–3.31 (m, 19H), 3.63 (dd, 1H, $^3J_{1,2}$ = 4.0 Hz, $^3J_{2,3}$ = 9.6 Hz, H-2), 0.88 (s, 9H, SiC(CH_3)$_3$), 0.00 (s, 6H, SiCH$_3$). ^{13}C NMR (100 MHz, $CDCl_3$) δ: 170.9 (CO), 139.3–136.4 (C_{ipso}), 128.7–126.3 (CH aromatic), 99.3 (C-1), 98.4 (C-1), 97.9 (C-1), 97.5 (C-1), 97.1 (C-1), 96.3 (C-1), 82.8, 81.3, 81.2, 80.8, 80.6, 80.5, 80.0, 79.9, 79.8, 79.2, 79.1, 78.9, 78.1, 77.9, 76.4, 76.2, 76.1, 75.8, 75.4, 74.1, 73.7, 73.5, 73.3, 73.2, 72.9, 72.7, 72.6, 72.2, 71.8, 71.6, 71.5, 71.2, 70.8, 70.3, 70.1, 69.5, 68.9, 68.8, 62.4 (CH_2, CH), 26.0 (SiC(*C*H$_3$)$_3$), 18.3 (SiC), –4.5 (SiCH$_3$), –4.6 (SiCH$_3$). MALDI-TOF-MS *m/z* calcd. for $C_{154}H_{168}O_{31}SiNa$: 2564.1237; found: 2565.203 $[M]^+$.

2$^{A–F}$,3$^{A–F}$,6^B,6^C,6^E,6^F-Hexadecakis-*O*-benzyl-α-cyclodextrin-6^A-carboxylic acid (9)

To a solution of **8** (463 mg, 0.18 mmol) in CH_2Cl_2 (5.5 mL) was added $BF_3{\cdot}Et_2O$ (0.2 mL). The reaction mixture was stirred for 1.5 h at room temperature, diluted with CH_2Cl_2, and poured in ice water. The mixture was basified with aq. NaOH (1 mol/L) and the phases were separated. The organic layer was acidified with aq. HCl (1 mol/L), dried ($MgSO_4$), filtered, and the organic solvent was removed in vacuo. The residue was purified by chromatography (eluent, EtOAc–pentane, 1:4 containing 1% HCOOH) to afford **9** (218 mg, 49%) as white foam. $[\alpha]_D$ +35.0° (*c* 0.5, CH_3Cl). IR (KBr, cm^{-1}): 3442 (OH), 3031, 2924, 1746 (COOH), 1496, 1454, 1354, 1095, 1045. ^{1}H NMR (400 MHz, $CDCl_3$) δ: 7.26–6.97 (m, 80H, aromatic-H), 5.66 (d, 1H, ^3J = 4.0 Hz, H-1), 5.64 (d, 1H, ^3J = 4.0 Hz, H-1), 5.42 (d, 1H, ^2J = 10.0 Hz, C*H*Ph), 5.36 (d, 1H, ^2J = 10.4 Hz, C*H*Ph), 5.07 (d, 2H, ^2J = 10.4 Hz, CH_2Ph), 4.85–4.76 (m, 5H), 4.73–3.89 (m, 60H), 3.79 (t, 3H, ^3J = 8.6 Hz), 3.74–3.46 (m, 14H), 3.42 (dd, 2H, $^3J_{1,2}$ = 3.2 Hz, $^3J_{2,3}$ = 9.6 Hz, H-2), 3.37 (d, 2H, $^3J_{1,2}$ = 3.2 Hz, $^3J_{2,3}$ = 9.6 Hz, H-2), 3.22–3.16 (m, 2H), 3.11 (t, 1H, ^3J = 9.0 Hz, OH). ^{13}C NMR (100 MHz, $CDCl_3$) δ: 171.1 (CO), 139.5–136.2 (C_{ipso}), 128.8–126.3 (CH aromatic), 99.3 (C-1), 99.0 (C-1), 98.1 (C-1), 97.9 (C-1), 97.8 (C-1), 96.5 (C-1), 83.4, 81.9, 81.6, 81.5, 81.3, 81.2, 80.9, 80.6, 80.5, 79.9, 79.5, 79.4, 79.2, 78.0, 76.6, 76.4, 76.2, 75.4, 74.1, 74.0, 73.8, 73.6, 73.5, 73.4, 73.3, 73.2, 72.8, 72.5, 72.2, 71.9, 71.8, 71.4, 71.0, 70.8, 70.2, 70.0, 69.3, 68.9, 68.1, 61.0 (CH_2, CH). MALDI-TOF-MS *m/z* calcd. for $C_{148}H_{154}O_{31}Na$: 2450.0372; found: 2450.447 $[M]^+$.

6^D-*C*-Cyano-2$^{A–F}$,3$^{A–F}$,6^B,6^C,6^E,6^F-hexadecakis-*O*-benzyl-α-cyclodextrin-6^A-carboxylic acid (10)

To a solution of **9** (217 mg, 0.09 mmol) in CH_2Cl_2 (9 mL) was added Dess–Martin periodinane reagent (95 mg, 0.22 mmol) and the reaction mixture was stirred 2 h and then quenched by addition of Et_2O (9 mL) and satd. aq. $NaHCO_3$ containing 0.36 g of $Na_2S_2O_3$ (9 mL). After stirring for an additional hour, the solution was diluted with Et_2O (30 mL) and washed successively with satd. aq. $NaHCO_3$ (25 mL) and water (25 mL). The organic phase was dried ($MgSO_4$), filtered, and the organic solvent was removed in vacuo. To a solution of the residue in Et_2O (3 mL) and MeOH (5 mL) were added KCN (164 mg, 2.52 mmol) and NH_4Cl (225 mg, 4.20 mmol) in water (10 mL). The reaction mixture was stirred for 20 h at room temperature. After that, the organic solvent was removed and the aqueous phase was extracted with CH_2Cl_2. The organic layer was washed with water, dried ($MgSO_4$), filtered, and the organic solvent was removed in vacuo. The residue was purified by chromatography (eluent gradient, EtOAc–pentane, 1:4 → 1:4 containing 1% HCOOH) to afford **10** (130 mg, 63%) as a white foam. $[\alpha]_D$ +38.6° (*c* 1.0, CH_3Cl). IR (KBr, cm^{-1}): 3031, 2927, 2247 (CN), 1741 (COOH), 1497, 1454, 1355, 1096, 1045. ^{1}H NMR (400 MHz, $CDCl_3$) δ: 7.25–6.96 (m, 80H, aromatic-H), 5.71 (d, 1H, ^3J = 3.2 Hz, H-1), 5.62 (d, 1H, ^3J = 4.0 Hz, H-1), 5.39 (d, 1H, ^2J = 10.4 Hz, C*H*Ph), 5.34 (d, 1H, ^3J = 3.6 Hz, H-1), 5.32–5.21 (m, 7H), 5.13 (d, 1H, ^2J = 15.6 Hz, C*H*Ph), 5.05 (m, 2H), 4.95–4.84 (m, 3H), 4.77–4.48 (m, 40H), 4.46–4.13 (m, 42H), 4.12–3.70 (m, 54H), 3.68–3.13 (m, 35H). ^{13}C NMR (100 MHz, $CDCl_3$) δ: 170.9 (CO), 169.9 (CO), 139.6–136.2 (C_{ipso}), 128.9–126.2 (CH aromatic), 118.4 (CN), 117.2 (CN), 100.4 (C-1), 99.6 (C-1), 99.4 (C-1), 98.5 (C-1), 98.1 (C-1), 97.9 (C-1), 97.6 (C-1), 97.1 (C-1), 97.0 (C-1), 96.3 (C-1), 84.4, 83.6, 81.5, 81.2, 81.1, 80.9, 80.5, 80.4, 80.3, 80.1, 80.0, 79.7, 79.6, 79.5, 79.4, 79.2, 79.1, 79.0, 78.6, 78.1, 76.5, 76.4, 76.2, 76.0, 75.7, 75.6, 75.4, 74.6, 74.3, 74.2, 74.0, 73.9, 73.7, 73.6, 73.5, 73.4, 73.3, 73.2, 73.1, 73.0, 72.9, 72.8, 72.7,

© 2006 NRC Canada

72.6, 72.5, 72.4, 72.3, 72.1, 72.0, 71.7, 71.6, 71.4, 71.3, 71.2, 71.0, 70.8, 70.6, 70.4, 70.2, 70.1, 69.9, 69.5, 69.2, 68.9, 68.8, 63.0 (CH_2, CH), 60.4 (*C*H(OH)CN). MALDI-TOF-MS *m/z* calcd. for $C_{149}H_{152}O_{31}NNa$: 2474.0246; found: 2474.316 $[M]^+$.

6^D-*C*-Cyano-α-cyclodextrin-6^A-carboxylic acid (1)

Compound **10** (130 mg, 0.05 mmol) was dissolved in a mixture of MeOH–EtOAc (1:1, 5 mL). Then Pd/C (13 mg) and TFA (cat) were added and the mixture was stirred overnight under a hydrogen atmosphere. Filtration over Celite and evaporation of the solvent gave **1** (54 mg, 100%) as a white solid. $[\alpha]_D$ +67.2° (*c* 0.5, H_2O). IR (KBr, cm^{-1}): 3423, 2942, 2246 (CN), 1679 (COOH), 1437, 1205, 1151, 1034. ^1H NMR (400 MHz, D_2O) δ: 5.14–5.07 (m, 6H, H-1), 4.02–3.63 (m, 40H), 3.32 (m, 1H). ^{13}C NMR (100 MHz, D_2O) δ: 163.3 (CO), 163.0 (CO), 119.0 (CN), 101.8 (C-1), 101.7 (C-1), 101.6 (C-1), 101.5 (C-1), 101.4 (C-1), 101.3 (C-1), 100.7 (C-1), 82.0, 81.7, 81.6, 81.5, 81.4, 81.3, 81.2, 80.9, 74.8, 73.1, 73.0, 72.9, 72.7, 72.4, 72.2, 72.1, 71.9, 71.7, 71.6, 71.5, 71.3, 65.4, 60.7, 60.3, 60.0, 59.7, 68.8, 63.0 (CH, CH_2, *C*H(OH)CN). MALDI-TOF-MS *m/z* calcd. for $C_{37}H_{57}O_{31}NNa$: 1034.2812; found: 1034.127 $[M]^+$.

Benzyl 6^A-*tert*-butyldimethylsilyl-$2^{A–F}$,$3^{A–F}$,6^B,6^C,6^E,6^F-hexadecakis-*O*-benzyl-α-cyclodextrin-6^D-propenoate (11)

To a solution of BnO_2CCH_2PPhBr (496 mg, 1.01 mmol) in anhydr. THF (13 mL) was added dropwise *n*-BuLi (0.6 mL, 0.96 mmol) and the mixture was stirred at room temperature for 1 h. The reaction mixture was cooled to –40 °C and a solution of **4** (850 mg, 0.34 mmol) in anhydr. THF (13 mL) was added. The mixture was stirred at –40 °C for 30 min and was then allowed to reach room temperature. Ether (200 mL) was added and the mixture was washed with aq. NH_4Cl (150 mL), water (2 × 100 mL), and brine (100 mL). The organic layer was dried ($MgSO_4$), filtered, and the organic solvent was removed in vacuo. The residue was purified by chromatography (eluent gradient, EtOAc–pentane, 2:11) to afford **11** (625 mg, 70%) as white foam. $[\alpha]_D$ +42.6° (*c* 1.0, CH_3Cl). IR (KBr, cm^{-1}): 3030 (C=C), 2926, 1720 (CO_2Bn), 1496, 1453, 1360, 1094, 1027. ^1H NMR (400 MHz, $CDCl_3$) δ: 7.50 (dd, 1H, $^3J_{4,5}$ = 4.0 Hz, $^3J_{trans}$ = 15.6 Hz, CH=), 7.44–7.16 (m, 85H, aromatic-H), 6.07 (d, 1H, $^3J_{trans}$ = 15.6 Hz, =$CHCO_2Bn$), 5.42 (d, 1H, $^3J_{1,2}$ = 3.2 Hz, H-1), 5.34 (d, 1H, ^2J = 10.8 Hz, C*H*Ph), 5.29–5.10 (m, 10H), 5.24 (d, 1H, $^3J_{1,2}$ = 3.2 Hz, H-1), 5.02 (d, 1H, $^3J_{1,2}$ = 3.2 Hz, H-1), 4.98–4.87 (m, 8H), 4.65–4.40 (m, 23H), 4.28–4.11 (m, 18H), 4.08–3.95 (m, 6H), 3.87 (bd, 2H,^3J = 8.0 Hz), 3.71–3.59 (m, 7H), 3.57–3.47 (m, 4H), 3.45–3.37 (m, 3H), 0.91 (s, 9H, $SiC(CH_3)_3$), 0.00 (s, 6H, $SiCH_3$). ^{13}C NMR (100 MHz, $CDCl_3$) δ: 165.9 (CO), 145.8 (CH=), 139.5–137.9 (C_{ipso}), 136.0 (C_{ipso}-CO_2Bn), 128.7–127.1 (CH aromatic), 122.0 (=*C*HCO_2Bn), 99.2 (C-1), 99.0 (C-1), 98.5 (C-1), 98.2 (2 × C-1), 98.1 (C-1), 84.5, 81.4, 81.3, 81.1, 80.9, 80.8, 80.1, 79.7, 79.6, 79.2, 78.7, 78.6, 78.4, 78.0, 76.0, 75.9, 75.5, 75.3, 73.7, 73.4, 73.2, 72.9, 72.8, 72.7, 72.6, 72.5, 72.1, 71.9, 71.5, 71.3, 69.5, 69.4, 68.9, 68.5, 66.3, 62.3, 60.5 (CH_2, CH). MALDI-TOF-MS *m/z* calcd. for $C_{163}H_{176}O_{31}SiNa$: 2680.1863; found: 2680.434 $[M]^+$.

Benzyl $2^{A–F}$,$3^{A–F}$,6^B,6^C,6^E,6^F-hexadecakis-*O*-benzyl-α-cyclodextrin-6^D-propenoate (12)

TBAF (0.12 mL, 0.12 mmol) was added to a solution of **11** (102 mg, 0.04 mmol) in anhydrous THF (1.2 mL) at 0 °C. The reaction mixture was stirred at 0 °C for 6 h. Aqueous NH_4Cl was added and the mixture was diluted with ether (50 mL) and washed successively with water (2 × 25 mL) and brine (25mL). The organic layer was dried ($MgSO_4$), filtered, and the organic solvent was removed in vacuo. The residue was purified by chromatography (eluent gradient, EtOAc–pentane, 2:7) to afford **12** (73 mg, 75%) as white foam. $[\alpha]_D$ +36.6° (*c* 1.0, CH_3Cl). IR (KBr, cm^{-1}): 3488 (OH), 3030 (C=C), 2924, 1722 (CO_2Bn), 1496, 1453, 1354, 1094, 1039. ^1H NMR (400 MHz, $CDCl_3$) δ: 7.25–6.98 (m, 86H, aromatic-H and CH=), 6.00 (d, 1H, $^3J_{trans}$ = 15.6 Hz, =$CHCO_2Bn$), 5.40 (d, 1H, $^3J_{1,2}$ = 3.6 Hz, H-1), 5.29 (d, 1H, ^2J = 10.4 Hz, C*H*Ph), 5.28 (d, 1H, $^3J_{1,2}$ = 4.0 Hz, H-1), 5.20–5.13 (m, 3H), 5.06 (d, 1H, ^2J = 10.8 Hz, C*H*Ph), 4.92 (s, 2H), 4.90 (d, 1H, $^3J_{1,2}$ = 3.0 Hz, H-1), 4.84–4.69 (m, 11H), 4.64 (d, 1H, $^3J_{1,2}$ = 3.2 Hz, H-1), 4.58 (t, 2H, ^2J = 11.2 Hz), 4.46 (d, 1H, $^3J_{1,2}$ = 4.0 Hz, H-1), 4.43 (d, 1H, $^3J_{1,2}$ = 4.0 Hz, H-1), 4.39–4.20 (m, 17H), 4.15–3.95 (m, 13H), 3.89–3.66 (m, 13H), 3.61–3.57 (m, 2H), 3.50–3.33 (m, 10H), 3.31 (dd, 1H, $^3J_{1,2}$ = 3.2 Hz, $^3J_{2,3}$ = 9.6 Hz, H-2), 3.25 (dd, 1H, $^3J_{1,2}$ = 3.2 Hz, $^3J_{2,3}$ = 9.6 Hz, H-2), 2.39 (bs, 1H, OH). ^{13}C NMR (100 MHz, $CDCl_3$) δ: 165.8 (CO), 145.8 (CH=), 139.6–137.9 (C_{ipso}), 135.9 (C_{ipso}-CO_2Bn), 128.7–126.5 (CH aromatic), 122.2 (=*C*HCO_2Bn), 99.3 (C-1), 99.0 (C-1), 98.7 (C-1), 98.3 (C-1), 98.2 (C-1), 97.5 (C-1), 82.5, 81.6, 81.4, 81.3, 81.2, 80.6, 80.1, 79.9, 79.6, 79.5, 79.0, 78.7, 78.3, 76.4, 76.2, 76.1, 75.9, 75.8, 74.8, 74.5, 73.5, 73.4, 73.3, 73.2, 73.1, 73.0, 72.9, 72.5, 72.4, 72.0, 71.9, 71.8, 71.6, 69.4, 69.0, 68.9, 66.3, 61.4 (CH_2, CH). MALDI-TOF-MS *m/z* calcd. for $C_{157}H_{162}O_{31}Na$: 2566.0998; found: 2566.760 $[M]^+$.

Benzyl 6^A-*C*-cyano-$2^{A–F}$,$3^{A–F}$,6^B,6^C,6^E,6^F-hexadecakis-*O*-benzyl-α-cyclodextrin-6^D-propenoate (13)

To a solution of **12** (246 mg, 0.10 mmol) in Et_2O (3.5 mL) and MeOH (6 mL) were added KCN (189 mg, 2.91 mmol) and NH_4Cl (259 mg, 4.85 mmol) in water (11.5 mL). The reaction mixture was stirred overnight at room temperature. After that, the organic solvent was removed and the aqueous phase was extracted with CH_2Cl_2. The organic layer was washed with water, dried ($MgSO_4$), filtered, and the organic solvent was removed in vacuo. The residue was purified by chromatography (eluent gradient, EtOAc–pentane, 1:4 → 2:7) to afford **13** (87 mg, 35%) as white foam. $[\alpha]_D$ +47.3° (*c* 0.8, CH_3Cl). IR (KBr, cm^{-1}): 3030 (C=C), 2924, 2246 (CN), 1721 (CO_2Bn), 1496, 1454, 1355, 1096, 1040. ^1H NMR (400 MHz, $CDCl_3$) δ: 7.38 (dd, 1H, $^3J_{4,5}$ = 4.8 Hz, $^3J_{trans}$ = 15.6 Hz, CH=), 7.33–7.09 (m, 85H, aromatic-H), 6.17 (d, 1H, $^3J_{trans}$ = 15.6 Hz, =$CHCO_2Bn$), 5.30 (bd, 1H, ^3J = 7.6 Hz), 5.24 (d, 1H, ^2J = 10.4 Hz, CH_2Ph), 5.22 (d, 1H, $^3J_{1,2}$ = 3.6 Hz, H-1), 5.18 (d, 1H, ^2J = 11.2 Hz, C*H*Ph), 5.16 (d, 1H, $^3J_{1,2}$ = 3.6 Hz, H-1), 5.11 (d, 1H, ^2J= 10.8 Hz, CHPh), 5.08–4.98 (m, 7H), 4.91–4.76 (m, 8H), 4.67–4.57 (m, 5H), 4.51–4.39 (m, 15H), 4.35 (d, 1H, ^2J = 12.0 Hz), 4.30 (d, 1H, ^2J = 12.4 Hz), 4.18–3.77 (m, 23H), 3.71 (t, 1H, ^3J = 9.0 Hz), 3.65 (d, 1H, ^2J = 10.8 Hz), 3.58–3.47 (m, 8H), 3.45 (dd, 1H, $^3J_{1,2}$ = 3.2 Hz, $^3J_{2,3}$ = 9.6 Hz, H-2), 3.41 (dd,

© 2006 NRC Canada

1H, $^3J_{1,2}$ = 3.2 Hz, $^3J_{2,3}$ = 9.6 Hz, H-2). ^{13}C NMR (100 MHz, $CDCl_3$) δ: 166.3 (CO), 146.2 (CH=), 139.5–137.8 (C_{ipso}), 135.7 (C_{ipso}-CO_2Bn), 128.7–126.8 (CH aromatic), 122.5 (=*C*HCO_2Bn), 117.5 (CN), 99.5 (C-1), 99.4 (C-1), 99.3 (C-1), 98.5 (C-1), 98.4 (C-1), 98.2 (C-1), 83.6, 80.9, 80.8, 80.4, 80.2, 80.1, 80.0, 79.6, 79.3, 79.2, 78.9, 78.7, 78.3, 77.9, 76.1, 75.5, 75.4, 74.9, 73.6, 73.5, 73.4, 73.3, 73.2, 73.1, 72.9, 72.8, 72.7, 72.0, 71.7, 71.6, 69.6, 69.5, 69.0, 68.8, 68.7, 66.4, 62.9 (CH_2, CH). MALDI-TOF-MS *m*/*z* calcd. for $C_{158}H_{161}O_{31}NNa$: 2591.0950; found: 2590.501 $[M]^+$.

6^A-*C*-Cyano-α-cyclodextrin-6^D-propanoic acid (2)

Compound **13** (113 mg, 0.04 mmol) was dissolved in a mixture of MeOH–EtOAc (1:1, 5 mL). Then Pd/C (12 mg) and TFA (cat) were added and the mixture was stirred overnight under a hydrogen atmosphere. Filtration over Celite and evaporation of the solvent gave **2** (46 mg, 100%) as a white solid. $[\alpha]_D$ +56.8° (*c* 1.0, H_2O). IR (KBr, cm^{-1}): 3431, 2247 (CN), 1685 (COOH), 1437, 1207, 1144, 1050. ^{1}H NMR (400 MHz, D_2O) δ: 4.94 (m, 6H, H-1), 3.89–3.77 (m, 20H), 3.49 (bs, 10H), 3.24–3.17 (m, 2H), 2.42 (bs, 1H), 2.29 (bs, 1H), 1.64 (bs, 2H). ^{13}C NMR (100 MHz, D_2O) δ: 163.3 (CO), 163.0 (CO), 118.0 (CN), 101.7 (C-1), 101.3 (C-1), 85.9, 81.6, 81.2, 73.3, 72.0, 71.8, 71.7, 70.6, 60.4, 39.5, 26.6 (CH, CH_2, *C*H(OH)CN). MALDI-TOF-MS *m*/*z* calcd. for $C_{39}H_{61}O_{31}NNa$: 1062.3125; found: 1062.284 $[M]^+$.

Procedure for determining the rate of hydrolysis

Each assay was performed on 2 mL samples prepared from 1 mL aqueous solutions of the appropriate aryl glycoside at different concentrations mixed with 1 mL of phosphate or other buffer containing either cyclodextrin derivative (0.5 mg/mL) or nothing as the control. The reactions were followed continuously at 59 °C using UV absorption at 400 nm. The reactions were monitored for 3–18 h. Velocities were determined as the slope of the progress curve of each reaction. Uncatalysed velocities were obtained directly from the control samples. Catalyzed velocities were calculated by subtracting the uncatalysed velocity from the velocity of the appropriate cyclodextrin-containing sample. The catalysed velocities were used to construct a Hanes plot ([S]/*V* vs. [S]) from which K_m and V_{max} were determined. k_{cat} was calculated as V_{max}/[cyclodextrin]. k_{uncat} was determined as the slope from a plot of V_{uncat} vs. [S].

Acknowledgements

We thank the Lundbeck Foundation and Forskningsrådet for Natur og Univers (FNU) for generous financial support.

References

1. J.W. Steed and J. Atwood. L. Supramolecular chemistry. John Wiley and Sons, Ltd., Chicester. 2001.
2. (*a*) A.J. Kirby. Angew. Chem. Int. Ed. Engl. **33**, 551 (1994); (*b*) Y. Murakami, J.I. Kikuchi, Y. Hisaeda, and O. Hayashida. Chem. Rev. **96**, 721 (1996); (*c*) W.B. Motherwell, M.J. Bingham, and Y. Six. Tetrahedron, **57**, 4663 (2001); (*d*) R. Breslow. Acc. Chem. Res. **28**, 146 (1995); (*e*) R. Breslow and C. Schmuck. J. Am. Chem. Soc. **118**, 6601 (1996); (*f*) R. Breslow and B. Zhang. J. Am. Chem. Soc. **114**, 5882 (1992); (*g*) T. Akiike, Y. Nagano, Y. Yamamoto, A. Nakamura, H. Ikeda, A. Veno, and F. Toda. Chem. Lett. 1089 (1994); (*h*) R. Breslow and B. Zhang. J. Am. Chem. Soc. **116**, 7893 (1994); (*i*) R. Breslow and S.D. Dong. Chem. Rev. **98**, 1997 (1998); (*j*) H. Ikeda, Y. Horimoto, M. Nakata, and A. Ueno. Tetrahedron Lett. **41**, 6483 (2000); (*k*) D.T.H. Chou, J. Zhu, X.C. Huang, and A.J. Bennet. J. Chem. Soc. Perkin Trans. 2, 83 (2001); (*l*) M. Kunishima, K. Yoshimura, H. Morigaki, R. Kawamata, K. Terao, and S. Tani. J. Am. Chem. Soc. **123**, 10760 (2001); (*m*) X.J. Ren, Y. Xue, K. Zhang, J.Q. Liu, G.M. Luo, J. Zheng, Y. Mu, and J.C. Shen. FEBS Lett. **507**, 377 (2001); (*n*) J.X. Yu, Y.Z. Zhao, M. Holterman, and D.L. Venton. Bioorg. Med. Chem. **10**, 3291 (2002); (*o*) X.J. Ren, Y. Xue, J.Q. Liu, K. Zhang, J. Zheng, G. Luo, C.H. Guo, Y. Mu, and J.C. Shen. ChemBioChem. **3**, 356 (2002); (*p*) Y. Liu, B. Li, L. Li, and H.Y. Zhang. Helv. Chim. Acta, **85**, 9 (2002); (*q*) J. Yang, B. Gabriele, S. Belvedere, Y. Huang, and R. Breslow. J. Org. Chem. **67**, 5057 (2002); (*r*) R. Kataky and E. Morgan. Biosens. Bioelectron. **18**, 1407 (2003); (*s*) W.K. Chan, W.Y. Yu, C.M. Che, and M.K. Wong. J. Org. Chem. **68**, 6576 (2003); (*t*) N.M. Milovic, J.D. Badjic, and N.M. Kostic. J. Am. Chem. Soc. **126**, 696 (2004); (*u*) C. Rousseau, B. Christensen, T.E. Pedersen, and M. Bols. Org. Biomol. Chem. **2**, 3476 (2004); (*v*) M. Fukudome, Y. Okabe, M. Sakaguchi, H. Morikawa, T. Fujioka, D.Q. Yuan, and K. Fujjta. Tetrahedron Lett. **45**, 9045 (2004); (*w*) Z.Y. Dong, J.Q. Liu, S.Z. Mao, X. Huang, B. Yang, X.J. Ren, G.M. Luo, and J.C. Shen. J. Am. Chem. Soc. **126**, 16395 (2004); (*x*) M. McNaughton, L. Engman, A. Birmingham, G. Powis, and I.A. Cotgreave. J. Med. Chem. **47**, 233 (2004); (*y*) C. Rousseau, B. Christensen, and M. Bols. Eur. J. Org. Chem. 2734 (2005); (*z*) S.H. Yoo, B.J. Lee, H. Kim, and J. Suh. J. Am. Chem. Soc. **127**, 9593 (2005).
3. For first research on artificial glycosidases, see: (*a*) T.H. Doug, J.Z. Chou, X. Huang, and A.J. Bennet. J. Chem. Soc. Perkin Trans. 2, 83 (2001); (*b*) T. Ohe, Y. Kajiwara, T. Kida, W. Zhang, Y. Nakatsuji, and I. Ikeda. Chem. Lett. 921 (1999).
4. F. Ortega-Caballero, C. Rousseau, B. Christensen, T.E. Petersen, and M. Bols. J. Am. Chem. Soc. **127**, 3238 (2005).
5. F. Ortega-Caballero, J. Bjerre, L.S. Laustsen, and M. Bols. J. Org. Chem. **70**, 7217 (2005).
6. C. Rousseau, N. Nielsen, and M. Bols. Tetrahedron Lett. **45**, 8709 (2004).
7. C. Rousseau, F. Ortega-Caballero, L.U. Nordstrøm, B. Christensen, T.E. Petersen, and M. Bols. Chem. Eur. J. **11**, 5094 (2005).
8. (*a*) A.J. Pearce and P. Sinaÿ. Angew. Chem. Int. Ed. **39**, 3610 (2000); (*b*) T. Lecourt, A. Herault, A.J. Pearce, M. Sollogoub, and P. Sinaÿ. Chem. Eur. J. **10**, 2960 (2004).

© 2006 NRC Canada

From enolates to anthraquinones[1]

David Bailey, Jeffrey N. Murphy, and Vance E. Williams

Abstract: A series of highly reactive cyclopentadienones were prepared in situ from the corresponding hydroxycyclopent-2-enones and trapped with a variety of quinones. Reaction of 1,4-naphthoquinone with 4-hydroxy-3,4-diphenyl-cyclopent-2-enone afforded 2,3-diphenylanthraquinone, whereas reaction of benzoquinone with this same cyclopentadienone precursor yielded a mixture of 6,7-diphenyl-1,4-naphthoquinone and 2,3,6,7-tetraphenylanthraquinone. A number of other 2,3-diarylanthraquinones were likewise prepared in moderate yields from the reaction of 1,4-naphthoquinone with the appropriate 4-hydroxy-3,4-diarylcyclopent-2-enones. This method appears to be generally applicable to the synthesis of anthraquinone derivatives substituted at the 2- and 3-positions from inexpensive starting materials.

Key words: anthraquinone, Diels–Alder, cyclopentadienone, in situ.

Résumé : On a préparé in situ une série de cyclopentadiénones très réactives à partir des hydroxycyclopent-2-énones correspondantes et on les a piégées à l'aide d'une variété de quinones. La réaction de la 1,4-naphtoquinone avec la 4-hydroxy-3,4-diphénylcyclopent-2-énone conduit à la formation de 2,3-diphénylanthraquinone alors que la réaction de la benzoquinone avec la même cyclopentadiénone conduit à un mélange de 6,7-diphényl-1,4-naphtoquinone et de 2,3,6,7-tétraphénylanthraquinone. On a préparé un certain nombre d'autres 2,3-diarylanthraquinones avec des rendements modérés par réaction de la 1,4-naphtoquinone avec des 4-hydroxy-3,4-diarylcyclopent-2-énones appropriées. Le domaine d'application de cette méthode semble général pour la synthèse de dérivés de l'anthraquinone substitués dans les positions 2 et 3, à partir de produits de départs peu coûteux.

Mots clés : anthraquinone, Diels–Alder, cyclopentadiénone, in situ.

[Traduit par la Rédaction]

Introduction

> *If you learn nothing else from this class, I want you to remember: "Enolates are nucleophiles."* — Walter Szarek, speaking to his 3rd year organic chemistry class in 1991.

Anthraquinones are a versatile class of compounds that have been exploited as dyes (1), chemical sensors (2), organogelators (3), liquid crystals (4–8), anticancer agents (9), DNA photooxidants (10), and as precursors to substituted anthracenes. Our own interest in the synthesis of anthraquinone derivatives arose out of investigations into the [4+4]-photocycloaddition reactions of peripherally substituted chromophores such as 2,3,6,7-tetraphenylanthracene (11), the logical precursor of which is the anthraquinone (**1**). This quinone could be prepared in a one-pot reaction between 3,4-diphenylthiophene-1,1-dioxide (**2**) and benzoquinone (Scheme 1). Likewise, treatment of compound **2** with 1,4-naphthoquinone afforded 2,3-diphenylanthraquinone (**3**) in 70% yield (12). Although these sulfones are relatively stable and can be prepared from readily accessible thiophenes, the large-scale synthesis of these molecules has, in our hands, proven unreliable. For this reason, we decided to investigate the use of in situ generated cyclopentadienones as synthetic equivalents of sulfones in the construction of anthraquinones.

Cyclopentadienones condense with alkynes to form Diels–Alder adducts, which, upon loss of carbon monoxide, afford highly substituted benzene derivatives (13–16). These cyclones therefore behave in a similar manner to thiophene-1,1-dioxides, although the former tend to be much more reactive than the latter. Unlike sulfones, cyclopentadienones are highly unstable unless substituted at the 2- and 5-positions, and derivatives that lack bulky groups at these sites generally must be generated in situ from precursors such as the corresponding hydroxycyclopent-2-enones (15, 17, 18). Perhaps for this reason, cyclopentadienones have rarely been employed in the synthesis of anthraquinones (15, 19, 20), and only relatively stable derivatives of this type have been used for this purpose. Indeed, while there is some precedent for in situ generated cyclones being used in Diels–Alder reactions with alkynes (15, 19), we are aware of no examples of these compounds being trapped with quinone dienophiles to afford either anthraquinones or naphthoquinones. We therefore wished to explore whether the use of

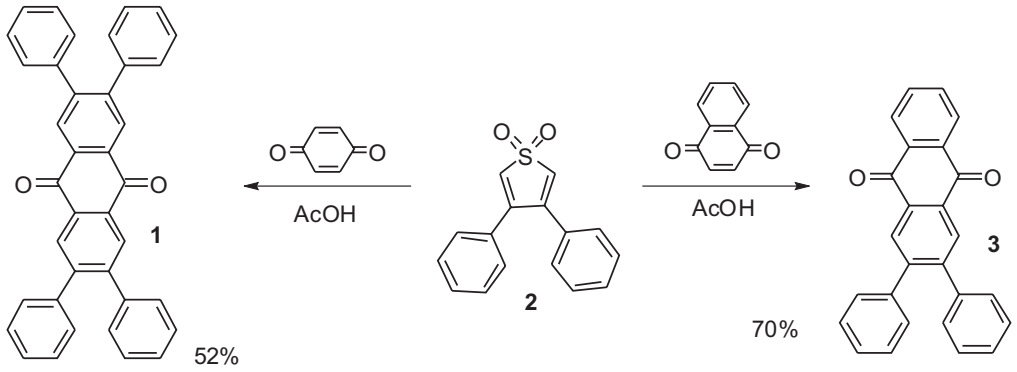
Received 31 August 2005. Published on the NRC Research Press Web site at http://canjchem.nrc.ca on 12 May 2006.

D. Bailey, J.N. Murphy, and V.E. Williams.[2] Department of Chemistry, Simon Fraser University, 8888 University Dr., Burnaby, BC V5A 1S6, Canada.

[1]This article is part of a Special Issue dedicated to Professor Walter A. Szarek.
[2]Corresponding author (e-mail: vancew@sfu.ca).

 doi:10.1139/V06-054 © 2006 NRC Canada

Scheme 1. Diels–Alder synthesis of compounds **1** and **3**. See ref. 12.



hydroxycyclopent-2-enones in the synthesis of anthraquinones was a viable strategy or would merely result in a fiasco.

Experimental

Materials and methods

^{1}H NMR (400 MHz) and ^{13}C NMR (100 MHz) were carried out on a Bruker AMX-400 400 MHz spectrometer; FT-IR spectroscopy was performed on a Thermo Nicolet Nexus 670 FT-IR ESP spectrometer, using KBr pellets. Microanalyses (C, H, N) were performed at Simon Fraser University, Burnaby, British Columbia, by Mr. Miki Yang. Low-resolution EI (70 eV) mass spectrometry was carried out on a Hewlett Packard 5985 mass spectrometer. Melting points were performed on either an Olympus BX50 polarizing microscope with a Linkam 94 heating stage or a MelTempII melting point apparatus and are uncorrected. MALDI-TOF mass spectra were obtained on a Perspective Voyager-DE STR from PE Applied Biosystems with a nitrogen laser (337 nm) and using 2,5-dihydroxybenzoic acid as the matrix.

1,4-Benzoquinone and *p*-toluenesulfonic acid were purchased from the Fisher Scientific Company. 1,4-Napthoquinone was obtained from Eastman Organic Chemicals. Copper sulfate, tetrakis(triphenylphosphine)palladium, copper(I) iodide, diisopropylamine, potassium iodide, benzaldehyde, *p*-anisaldehyde, 2-naphthaldehyde, 4-bromobenzaldehyde, 4-iodoanisole, and phenylacetylene were purchased from the Sigma-Aldrich Chemical Company Inc. The *o*-tolualdehyde was purchased from Matheson, Coleman, and Bell. Silica gel (230–400 mesh ASTM) was purchased from EMD Chemicals Inc. 1,4-Benzoquinone and 1,4-naphthoquinone were sublimed prior to use. Tetrahydrofuran was dried over sodium using benzophenone as an indicator. Benzaldehyde was distilled at reduced pressure. All other reagents were used as received.

Note that in the case of compounds **1**, **3**, **8**, **9**, **11**, **12**, and **24**, fewer peaks were observed in the ^{13}C NMR spectra than were predicted. This is probably due to inadequate peak resolution arising from the similarity in the chemical environments of many of the carbon nuclei. Attempts to resolve these peaks using d_6-benzene as the solvent were unsuccessful.

Synthesis

2,3,6,7-Tetraphenylanthraquinone (1) and 6,7-diphenyl-1,4-naphthaquinone (7)

To a solution of 1,4-benzoquinone (0.71 g, 6.6 mmol) in 180 mL acetic acid was added 0.84 g (3.3 mmol) of 4-hydroxy-3,4-diphenylcyclopent-2-enone (**4**) and 0.065 g (0.38 mmol) of *p*-toluenesulfonic acid. This mixture was refluxed for 49 h, then cooled to room temperature, poured over water (150 mL), and extracted with CH_2Cl_2 (3 × 100 mL). The combined organic extracts were dried over $MgSO_4$ and the solvent was removed in vacuo. The crude product was purified by column chromatography using silica gel with toluene as the eluent. 2,3,6,7-Tetraphenylanthraquinone (**1**) was eluted from the column first, followed by 6,7-diphenylnaphthoquinone (**7**).

*2,3,6,7-Tetraphenylanthraquinone (**1**)*

2,3,6,7-Tetraphenylanthraquinone (**1**) was recrystallized from ethanol to afford 0.22 g (0.46 mmol) of a yellow solid; mp: 323 to 324 °C. IR (cm^{-1}): 1672 (C=O stretch). ^{1}H NMR (ppm, acetone-d_6) δ: 8.39 (s, 4H), 7.22–7.29 (m, 20H). ^{13}C NMR (ppm, $CDCl_3$) δ: 182.8, 146.4, 139.6, 132.4, 129.7, 128.2, 127.7 (eight peaks predicted, seven observed). MS (EI) *m*/*z*: 512. HRMS calcd. for $C_{38}H_{24}O_2$: 512.1776; found: 512.1774.

*6,7-Diphenyl-1,4-naphthoquinone (**7**)*

6,7-Diphenyl-1,4-naphthoquinone (**7**) was recrystallized from ethanol to afford 150 mg (0.48 mmol) of a yellow solid; mp: 123–125 °C. IR (cm^{-1}): 1668 (C=O stretch). ^{1}H NMR (ppm, CD_2Cl_2) δ: 8.11 (s, 2H), 7.17–7.29 (m, 10H), 7.00 (s, 2H). ^{13}C NMR (ppm, $CDCl_3$) δ: 184.9, 146.2, 139.5, 138.8, 130.6, 129.6 128.8, 128.2, 127.7. MS (EI) *m*/*z*: 310 [M$^+$]. HRMS calcd. for $C_{22}H_{14}O_2$: 310.0994; found: 310.0996.

2,3-Diphenylanthraquinone (3)

To a solution of 1,4-naphthoquinone (0.81 g, 5.2 mmol) in 130 mL acetic acid was added 0.64 g (2.6 mmol) of 4-hydroxy-3,4-diphenylcyclopent-2-enone and 0.090 g (0.52 mmol) of *p*-toluenesulfonic acid. This mixture was then refluxed for 39 h. The solution was then cooled to room temperature, poured over water (150 mL), and then extracted with CH_2Cl_2 (3 × 100 mL). The combined organic extracts were dried over $MgSO_4$ and the solvent removed in vacuo. The crude product was purified by column chromatography on silica gel with toluene as the eluent and then recrystallized from ethanol to afford 0.39 g (1.1 mmol, 42%) of **3**; mp: 203–206 °C (lit. value (21) mp 211 to 212 °C). IR (cm^{-1}): 1676 (C=O stretch). ^{1}H NMR (ppm, $CDCl_3$) δ: 8.36 (s, 2H), 8.35 (dd, 2H, *J* = 3.36, 5.80 Hz), 7.82 (dd, 2H, *J* =

© 2006 NRC Canada

3.36, 5.80 Hz), 7.30–7.20 (m, 10H). ^{13}C NMR (ppm, $CDCl_3$) δ: 183.0, 146.4, 139.6, 134.1, 132.2, 129.7, 128.3, 127.7, 127.3 (11 peaks predicted, 9 observed). MS (EI) *m/z*: 360 [M^+].

2,3-Di(naphthalen-2-yl)anthraquinone (8)

2,3-Di(naphthalen-2-yl)anthraquinone (**8**) was prepared from 4-hydroxy-3,4-di(naphthalen-2-yl)cyclopent-2-enone (**16**) according to the method described previously. The crude product was eluted through silica gel with a 1:1 mixture of hexanes–toluene, and then recrystallized from ethanol to afford 0.055 g (0.13 mmol, 18%) of **8** as a yellow solid; mp: 238 °C. ^{1}H NMR (ppm, $CDCl_3$) δ: 8.53 (s, 2H), 8.38 (dd, 2H, *J* = 3.3, 5.8 Hz), 7.96 (s, 2H), 7.85 (dd, 2H, *J* = 3.3, 5.8 Hz), 7.81 (dd, 2H, *J* = 3.4, 6.0 Hz), 7.76 (dd, 2H, *J* = 3.4, 6.0 Hz), 7.59 (d, 2H, *J* = 8.6 Hz), 7.48 (dd, 4H, *J* = 3.2, 6.2 Hz), 7.17 (dd, 4H, *J* = 1.7, 8.5 Hz). ^{13}C NMR (ppm, $CDCl_3$) δ: 183.0, 146.4, 137.3, 134.2, 133.8, 133.3, 132.6, 132.4, 130.1, 128.9, 128.3, 127.7, 127.4, 127.3, 126.5, 126.3 (17 peaks predicted, 16 observed). MALDI-TOF *m/z*: 462 [M + 2, 100]. Elemental anal. calcd. for $C_{34}H_{20}O_2$: C 88.67, H 4.38; found: C 88.51, H 4.58.

2,3-Di(o-tolyl)anthraquinone (9)

2,3-Di(*o*-tolyl)anthraquinone (**9**) was prepared from 4-hydroxy-3,4-di(*o*-tolyl)cyclopent-2-enone (**17**) according to the method described previously. The crude product was eluted through silica gel with toluene and recrystallized from ethanol to yield 0.090 g (0.23 mmol, 17%) of **9** as an off-white solid; mp 247 °C. ^{1}H NMR (ppm, $CDCl_3$) δ: 8.34 (dd, 2H, *J* = 3.3, 5.7 Hz), 8.28 (s, 2H), 7.82 (dd, 2H, *J* = 3.3, 5.7 Hz), 7.13–6.91 (broad m, 8H), 2.11 (s, 6H). ^{13}C NMR (ppm, $CDCl_3$) δ: 183.1, 147.3 (broad), 139.1 (broad), 135.3, 134.1, 133.8, 131.9, 130.2, 129.8, 127.8, 127.2, 125.2, 20.2 (broad) (14 peaks predicted, 13 observed). MS (EI) *m/z*: 388.1 [M^+, 100]. Elemental anal. calcd. for $C_{28}H_{20}O_2$: C 86.57, H 5.19; found: C 86.38, H 5.27.

2,3-Bis(4-methoxyphenyl)anthraquinone (10)

2,3-Bis(4-methoxyphenyl)anthraquinone (**10**) was prepared from 4-hydroxy-3,4-bis(4-methoxyphenyl)cyclopent-2-enone (**18**) according to the method described previously. The crude product was eluted through silica gel with a 4:1 mixture of hexanes – ethyl acetate as the eluent. The resulting product was recrystallized from ethanol to afford 0.04 g (0.09 mmol, 7%) of **10** as a brown solid; mp 168 °C. ^{1}H NMR (ppm, $CDCl_3$) δ: 8.34 (dd, 2H, *J* = 3.3, 5.8 Hz), 8.31 (s, 2H), 7.81 (dd, 2H, *J* = 3.3, 5.8 Hz), 7.16 (d, 4H, *J* = 8.7 Hz), 6.82 (d, 4H, *J* = 8.7 Hz), 3.82 (s, 6H). ^{13}C NMR (ppm, $CDCl_3$) δ: 183.0, 159.2, 145.9, 134.0, 133.8, 132.1, 131.9, 130.9, 129.5, 127.2, 113.8, 55.2. MS (CI) *m/z*: 421.2, 422.1 [M + 1, 100] (29%). Elemental anal. calcd. for $C_{28}H_{20}O_4$: C 79.98, H 4.97; found: C 80.13, H 4.90.

2-(4-Methoxyphenyl)-3-phenylanthraquinone (11)

2-(4-Methoxyphenyl)-3-phenylanthraquinone (**11**) was prepared from a mixture of **21a** and **21b** according to the method described previously. The crude product was eluted through a silica gel column using toluene. Recrystallization from ethanol afforded 0.087 g (0.22 mmol, 18%) of **11** as a yellow solid; mp 89–91 °C. ^{1}H NMR (ppm, $CDCl_3$) δ: 8.36–8.34 (m, 4H), 7.82 (dd, 2H, *J* = 3.3, 5.8 Hz), 7.30–7.29 (m, 3H), 7.23 (dd, 2H, *J* = 3.0, 6.7 Hz), 7.14 (d, 2H, *J* = 8.7 Hz), 6.80 (d, 2H, *J* = 8.7 Hz), 3.80 (s, 3H). ^{13}C NMR (ppm, $CDCl_3$) δ: 183.3, 183.2, 159.5, 146.5, 146.3, 140.1, 134.3, 134.3, 134.0, 133.9, 132.5, 132.1, 131.1, 130.0, 129.8, 129.7, 128.5, 127.8, 127.5, 113.9, 55.5 (23 peaks predicted, 21 observed). MS (EI) *m/z*: 390.4 [$C_{27}H_{18}O_3^+$, 100]. Elemental anal. calcd. for $C_{27}H_{18}O_3$: C 83.06, H 4.65; found: C 82.80, H 4.89.

2-(4-Bromophenyl)-3-(4-methoxyphenyl)anthraquinone (12)

2-(4-Bromophenyl)-3-(4-methoxyphenyl)anthraquinone (**12**) was prepared from 3-(4-bromophenyl)-4-hydroxy-4-(4-methoxyphenyl)cyclopent-2-enone/4-(4-bromophenyl)-4-hydroxy-3-(4-methoxyphenyl)cyclopent-2-enone (**23**) according to the method described previously. The product was eluted through silica gel with toluene, then recrystallized from ethanol to afford 0.120 g (0.26 mmol, 21%) of **12** as an orange solid; mp 215 to 216 °C. ^{1}H NMR (ppm, $CDCl_3$) δ: 8.34 (dd, 2H, *J* = 3.1, 5.4 Hz), 8.33 (s, 1H), 8.30 (s, 1H), 7.83 (dd, 2H, *J* = 3.3, 5.8 Hz), 7.43 (d, 2H, *J* = 8.4 Hz), 7.14–7.09 (m, 4H), 6.83 (d, 2H, *J* = 8.7 Hz), 3.82 (s, 3H). ^{13}C NMR (ppm, $CDCl_3$) δ: 183.2, 183.1, 159.6, 146.3, 145.1, 139.0, 134.4, 134.4, 133.9, 132.7, 132.2, 131.8, 131.7, 131.4, 131.1, 129.8, 129.7, 127.5, 122.3, 114.1, 55.5 (23 peaks predicted, 21 observed). MS (CI) *m/z* (relative intensity): 468.2 (80%), 469.2 (60%), 470.2 (100%), 471.2 (58%), 472 (13%). Elemental anal. calcd. for $C_{27}H_{17}BrO_3$: C 69.10, H 3.65; found: C 69.27, H 3.72.

2-(4-Methoxyphenyl)-3,6,7-triphenylanthraquinone (24)

2-(4-Methoxyphenyl)-3,6,7-triphenylanthraquinone (**24**) was prepared from 6,7-diphenyl-1,4-naphthoquinone and a mixture of **21a** and **21b**. The crude product was purified through silica gel with toluene as the eluent. Recrystallization of this product from ethanol afforded 0.14 g (0.26 mmol, 26%) of **24** as an orange solid; mp 230 °C. ^{1}H NMR (ppm, $CDCl_3$) δ: 8.40 (s, 2H), 8.38 (d, 2H, *J* = 2.9 Hz), 7.31–7.23 (m, 15H), 7.17 (d, 2H, *J* = 8.8 Hz), 6.82 (d, 2H, *J* = 8.8 Hz), 3.81 (s, 3H). ^{13}C NMR (ppm, $CDCl_3$) δ: 183.1, 183.0, 159.5, 146.6, 146.6, 146.4, 146.3, 140.1, 139.9, 132.7, 136.7, 132.3, 132.1, 131.2, 130.0, 129.9, 129.8, 129.7, 128.5, 128.4, 127.9, 127.8, 113.9, 55.5 (31 peaks predicted, 24 observed). MALDI-TOF *m/z*: 543 [M^+, 100]. Elemental anal. calcd. for $C_{39}H_{26}O_3$: C 86.32, H 4.83; found: C 85.97, H 5.03.

2,3-Bis(4-methoxyphenyl)-6,7-diphenylanthraquinone (25)

2,3-Bis(4-methoxyphenyl)-6,7-diphenylanthraquinone (**25**) was prepared from 6,7-diphenyl-1,4-napthoquinone (**7**) and 4-hydroxy-3,4-bis(4-methoxyphenyl)cyclopent-2-enone (**18**) according to the method described previously. This mixture of products was then purified through silica gel with a 4:1 mixture of hexanes – ethyl acetate as the eluent. The resulting solid was recrystallized from ethanol to afford 0.050 g (0.09 mmol, 7%) of **25** as an orange solid; mp 235 °C. ^{1}H NMR (ppm, $CDCl_3$) δ: 8.39 (s, 2H), 8.35 (s, 2H), 7.30–7.22 (m, 10H), 7.18 (d, 4H, *J* = 8.8 Hz), 6.83 (d, 4H, *J* = 8.7 Hz), 3.82 (s, 6H). ^{13}C NMR (ppm, $CDCl_3$) δ: 183.1, 159.4, 146.6, 146.1, 139.9, 132.7, 132.4, 132.3, 131.1, 129.9, 129.9, 129.8, 128.4, 127.9, 114.0, 55.5. MALDI-TOF *m/z*: 584

© 2006 NRC Canada

[M + 2, 100]. Elemental anal. calcd. for $C_{40}H_{28}O_4$: C 83.90, H 4.93; found: C 84.20, H 5.16.

General method for the preparation of ethane diones

The aldehyde (32 mmol) and potassium cyanide (1.3 g, 20 mmol) were dissolved in 20 mL of ethanol and 10 mL of water. After refluxing for 24 h, the solution was poured over water and extracted with dichloromethane, yielding the coupled α-hydroxyketone. This product was then dissolved in 25 mL pyridine and 15 mL water, and 5.0 g $CuSO_4$ (35 mmol) was added. This solution was refluxed for 16 h, then cooled to room temperature and extracted with dichloromethane. The combined organic extracts were washed water and the solvent removed to afford the 1,2-dione.

1,2-Di(o-tolyl)ethane-1,2-dione (14)

1,2-Di(*o*-tolyl)ethane-1,2-dione (**14**) was prepared in the manner described in the previous paragraph and was isolated as a pale yellow solid (66% yield); mp 88 to 89 °C (lit. value (22) mp 92 °C). ^{1}H NMR (ppm, $CDCl_3$) δ: 7.66 (d, 2H, *J* = 7.8 Hz), 7.49 (t, 2H, *J* = 7.5 Hz), 7.35 (d, 2H, *J* = 7.6 Hz), 7.28 (m, 2H), 2.71 (s, 6H).

1,2-Bis(4-methoxyphenyl)ethane-1,2-dione (15)

1,2-Bis(4-methoxyphenyl)ethane-1,2-dione (**15**) was prepared in the manner described previously and was isolated as a yellow solid (32% yield); mp obs. 131 °C (lit. value (23) mp 133 °C). ^{1}H NMR (ppm, DCl_3) δ: 7.95 (d, 4H, *J* = 8.8 Hz), 6.97 (d, 4H, *J* = 8.9 Hz), 3.89 (s, 6H).

1,2-Di(naphthalen-2-yl)ethane-1,2-dione (16)

1,2-Di(naphthalen-2-yl)ethane-1,2-dione (**16**) was prepared in the manner described previously, except NaCN was used in place of KCN, and the benzoin condensation was only allowed to proceed for 1.5 h instead of 24 h. Compound **16** was isolated in 64% yield as an off-white solid; mp 155 °C (lit. value (24) mp 155 to 156 °C). ^{1}H NMR (ppm, $CDCl_3$) δ: 8.45 (s, 2H), 8.15 (dd, 2H, *J* = 1.6 8.6 Hz), 7.99 (d, 2H, *J* = 8.7 Hz), 7.90 (d, 4H, *J* = 8.8 Hz), 7.64 (t, 2H, *J* = 7.6 Hz), 7.55 (t, 2H, *J* = 7.6 Hz). ^{13}C NMR (ppm, $CDCl_3$) δ: 194.8, 136.4, 133.6, 132.4, 130.5, 130.0, 129.6, 129.2, 128.0, 127.2, 123.8.

1-(4-Methoxyphenyl)-2-phenylethane-1,2-dione (20)

1-(4-Methoxyphenyl)-2-phenylethane-1,2-dione (**20**) was prepared in the manner described previously and was purified by column chromatography (silica gel, toluene) as a pale yellow solid (22% yield); mp 58.5–60 °C (lit. value (25) mp 61 °C). ^{1}H NMR (ppm, $CDCl_3$) δ: 7.96 (m, 4H), 7.65 (t, 1H, *J* = 7.4 Hz), 7.51 (t, 2H, *J* = 7.8 Hz), 6.98 (d, 2H, *J* = 8.9 Hz), 3.89 (s, 1H).

1-(4-Bromophenyl)-2-(4-methoxyphenyl)ethane-1,2-dione (22)

1-(4-Bromophenyl)-2-(4-methoxyphenyl)ethane-1,2-dione (**22**) was prepared in the manner described previously and was isolated as a yellow solid (46% yield); mp 135 °C (lit. value (26) mp 136 to 137 °C). ^{1}H NMR (ppm, $CDCl_3$) δ: 7.93 (d, 2H, *J* = 8.9 Hz), 7.84 (d, 2H, *J* = 8.6 Hz), 7.65 (d, 2H, *J* = 8.6 Hz), 6.98 (d, 2H, *J* = 8.9 Hz), 3.89 (s, 3H).

Alternate synthesis of 1-(4-methoxyphenyl)-2-phenylethane-1,2-dione (20)

To a dried Schlenk flask was added 4-iodoanisole (3.2 g, 13.8 mmol), tetrakis(triphenylphosphine)palladium (0.059 g, 0.05 mmol), and copper(I) iodide (0.815 g, 4.3 mmol) under nitrogen. To this mixture was added via syringe phenylacetylene (1.75 mL, 16 mmol), 50 mL of dry tetrahydrofuran, and 10 mL of dry diisopropylamine. The resulting mixture was refluxed under nitrogen for 45 h, at which time it was cooled to room temperature and eluted through a short plug of silica gel with dichloromethane. After removing the solvent in vacuo, the crude product was oxidized by treating it with iodine (3.94 g, 15.6 mmol) in dimethylsulfoxide (50 mL) at 145 °C for 44 h. This solution was cooled to room temperature, poured into water, and the resulting mixture was extracted with dichloromethane. The combined organic extracts were washed with brine, then with a saturated aqueous potassium iodide solution, dried ($MgSO_4$), and the solvent removed under reduced pressure. The product was then recrystallized from a methanol–water mixture to **20** as a pale yellow solid (1.7 g, 8.2 mmol, 59% yield).

General method for the preparation of 4-hydroxy-3,4-diarylcyclopent-2-enones

Ethane-1,2-dione (10 mmol) was stirred for 1 week at room temperature in an ethanolic solution of potassium hydroxide (0.56 g, 10 mmol) and acetone (12 mL, 160 mmol). This solution was then poured over water and extracted with dichloromethane, yielding the desired product. Since these compounds proved difficult to purify, they were used directly in the condensation reactions with quinones.

4-Hydroxy-3,4-diphenylcyclopent-2-enone (4)

4-Hydroxy-3,4-diphenylcyclopent-2-enone (**4**) was prepared in the manner described in the previous paragraph as a pale yellow solid (96% yield). ^{1}H NMR (ppm, $CDCl_3$) δ: 7.52–7.50 (m, 2H), 7.47–7.44 (m, 2H), 7.37–7.27 (m, 6H), 6.71 (s, 1H), 3.02 (d, 1H, *J* = 18.5 Hz), 2.90 (d, 1H, *J* = 18.5 Hz).

4-Hydroxy-3,4-di(naphthalene-2-yl)cyclopent-2-enone (16)

4-Hydroxy-3,4-di(naphthalene-2-yl)cyclopent-2-enone **(16)** was prepared in the manner described previously as a brown solid. ^{1}H NMR (ppm, $CDCl_3$) δ: 8.19 (d, 2H, *J* = 11.5 Hz), 7.85–7.40 (m, 12H), 6.90 (s, 1H), 3.13 (d, 1H, *J* = 18.6 Hz), 3.02 (d, 1H, *J* = 18.6 Hz).

4-Hydroxy-3,4-di(o-tolyl)cyclopent-2-enone (17)

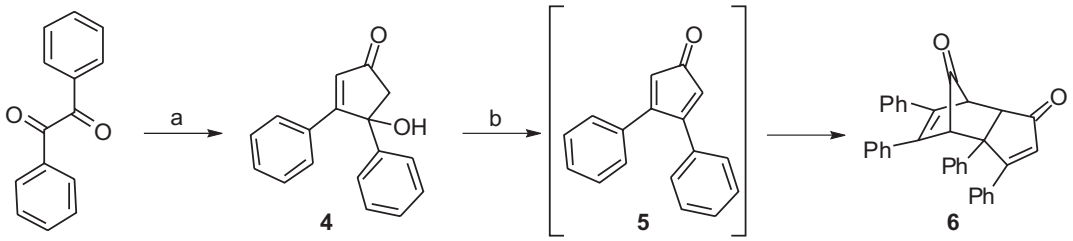
4-Hydroxy-3,4-di(*o*-tolyl)cyclopent-2-enone (**17**) was prepared in the manner described previously as a brown solid. ^{1}H NMR (ppm, $CDCl_3$) δ: 7.55–7.53 (m, 2H), 7.20–7.14 (m, 4H). 6.99–6.97 (m, 2H), 6.40 (s, 1H), 3.07 (d, 2H, *J* = 18.6 Hz), 2.98 (d, 2H, *J* = 18.6 Hz), 2.41 (s, 3H), 2.31 (s, 3H).

4-Hydroxy-3,4-bis(4-methoxyphenyl)cyclopent-2-enone (18)

4-Hydroxy-3,4-bis(4-methoxyphenyl)cyclopent-2-enone (**18**) was prepared in the manner described previously as a brown solid. ^{1}H NMR (ppm, $CDCl_3$) δ: 7.52 (d, 2H, *J* = 9.0 Hz), 7.34 (d, 2H, *J* = 8.8 Hz), 6.83 (dd, 4H, *J* = 8.9, 20.5 Hz),

© 2006 NRC Canada

Scheme 2. Reagents and conditions: (*a*) acetone, KOH, 1 week; (*b*) AcOH, TsOH, reflux 48 h.



6.60 (s, 1H), 3.79 (s, 3H), 3.78 (s, 3H), 2.98 (d, 2H, *J* = 18.5 Hz), 2.85 (d, 2H, *J* = 18.5 Hz).

4-Hydroxy-3-(4-methoxyphenyl)-4-phenylcyclopent-2-enone (21a)

4-Hydroxy-3-(4-methoxyphenyl)-4-phenylcyclopent-2-enone (**21a**) was prepared in the manner described previously and isolated via column chromatography (silica, toluene–EtOAc, 9:1 as eluent) as a white solid. ^{1}H NMR (ppm, $CDCl_3$) δ: 7.51 (dt, 2H, *J* = 9.0, 2.1 Hz), 7.45 (dt, 2H, *J* = 7.3, 1.6 Hz), 7.35 (td, 2H, *J* = 7.6, 1.8 Hz), 7.28–7.25 (m, 1H), 2.88 (d, 1H, *J* = 18.4 Hz), 2.53 (br, 1H).

4-Hydroxy-4-(p-methoxyphenyl)-3-phenylcyclopent-2-enone (21b)

4-Hydroxy-4-(*p*-methoxyphenyl)-3-phenylcyclopent-2-enone (**21b**) was prepared in the manner described previously and isolated via column chromatography (silica, toluene–EtOAc, 7:3 as eluent) as a yellow solid. ^{1}H NMR (ppm, $CDCl_3$) δ: 7.52 (dt, 2H, *J* = 7.1, 1.3 Hz), 7.37–7.35 (m, 3H), 7.30 (td, 2H, *J* = 7.4, 1.5 Hz), 6.87 (dt, 2H *J* = 8.8, 2.5 Hz), 6.66 (s, 1H), 3.79 (s, 3H), 3.00 (d, 1H, *J* = 18.5 Hz), 2.88 (d, 1H, *J* = 18.5 Hz), 2.65 (br, 1H).

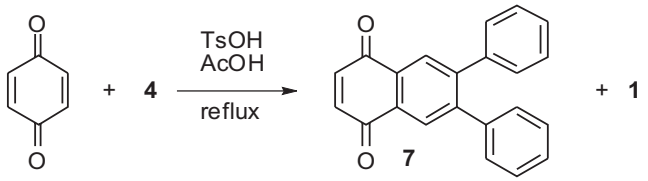
3-(4-Bromophenyl)-4-hydroxy-4-(4-methoxyphenyl)cyclopent-2-enone and 4-(4-bromophenyl)-4-hydroxy-3-(4-methoxyphenyl)cyclopent-2-enone (23)

3-(4-Bromophenyl)-4-hydroxy-4-(4-methoxyphenyl)cyclopent-2-enone and 4-(4-bromophenyl)-4-hydroxy-3-(4-methoxyphenyl)cyclopent-2-enone (**23**) were prepared in the manner described previously as a yellow solid. No attempt was made to separate these isomers. ^{1}H NMR (ppm, $CDCl_3$) δ: 7.52–7.43 (m, 4H), 7.34–7.32 (m, 2H), 6.86 (d, 2H, *J* = 9.0 Hz), 6.82 (d, 2H, *J* = 8.9 Hz), 6.66 (s, 1H), 6.64 (s, 1H), 3.79 (s, 3H), 2.97 (d, 1H, *J* = 18.6 Hz), 2.83 (d, 1H, *J* = 18.5 Hz).

Results and discussion

Our initial studies focused on the construction of 2,3-diphenylanthraquinone (**3**) starting from benzil, which has the advantage of being an inexpensive, commercially available starting material. 4-Hydroxy-3,4-diphenylcyclopent-2-enone (**4**) was synthesized in 96% yield by the condensation of benzil and acetone in the presence of catalytic potassium hydroxide (27). Heating **4** in refluxing acetic acid for 48 h caused no appreciable decomposition of this compound. When this reaction was carried out in the presence of catalytic *p*-toluenesulfonic acid, however, compound **6** was obtained almost quantitatively. The formation of this product, which arises from the dimerization of the highly reactive intermediate **5** (17, 18), demonstrates that this cyclone was indeed being generated under these conditions (Scheme 2).

Scheme 3. Condensation of compound **4** with benzoquinone.



We next turned our attention to trapping this in situ generated cyclone with 1,4-naphthoquinone. When cyclopentadienone **5** was generated in the presence of excess quinone, compound **3** was formed as the major product in 42% yield. Significantly, only trace quantities (<5%) of the dimer **6** were observed under these conditions. More generally, this side product did not arise to an appreciable extent in any subsequent reactions of **4** with quinones, indicating that the dimerization of **5** does not pose a significant problem in these syntheses.

The condensation of **4** with 1,4-benzoquinone was next investigated. This reaction affords two major products: the anthraquinone derivative **1** and the naphthoquinone **7** in an approximately 1:1 ratio (Scheme 3). That significant quantities of the anthraquinone were formed even in the presence of a twofold excess of benzoquinone — conditions that should strongly promote formation of the naphthoquinone **7** — suggests that compound **7** or one of its precursors is a much more reactive dienophile than benzoquinone itself, thus favouring the rapid reaction with a second equivalent of the cyclone. This tendency for benzoquinone to form bisadducts in acetic acid has previously been observed in its reaction with anthracene (28) and 1,1-thiophene dioxides (12).

Far from being an unwanted side product, the naphthoquinone **7** is desirable as a potential dienophile for the subsequent preparation of unsymmetrical anthraquinones. In an attempt to bias the reaction towards the formation of this compound, the condensation of **4** with benzoquinone was carried out in refluxing toluene, which has previously been found to favor formation of monoadducts (12, 28). Once again, catalytic *p*-toluenesulfonic acid was added to activate **4** towards dehydration. Under these conditions, the formation of the cyclopentadienone intermediate **5** is considerably slower than when the reaction was carried out in acetic acid. After 2 days, no appreciable reaction of the starting materials was observed. Allowing this reaction to proceed for 6 days led to only 25% of compound **4** being consumed, although it was gratifying to note that the ratio of naphthoquinone to anthraquinone obtained had increased to 20:1. Addition of a small amount of acetic acid to this reaction

© 2006 NRC Canada

Scheme 4. Reagents and conditions: (*a*) NaCN or KCN, EtOH–H_2O, reflux; (*b*) acetone, KOH, RT, 1 week; (*c*) 1,4-naphthoquinone, AcOH, TsOH, reflux 48 h.

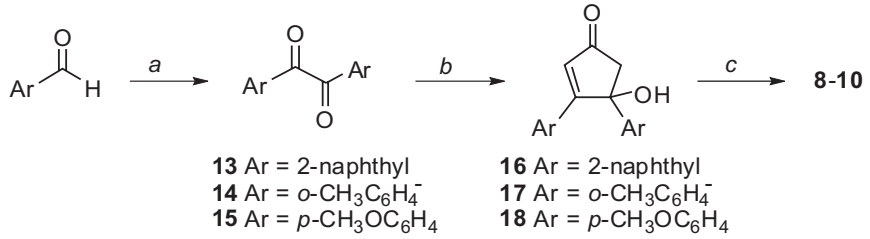
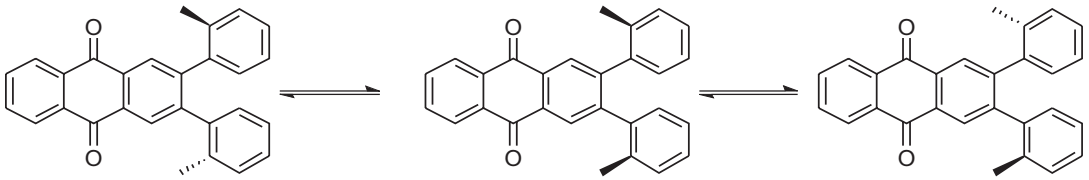


Fig. 1. syn–anti Isomerization of compound **10**.



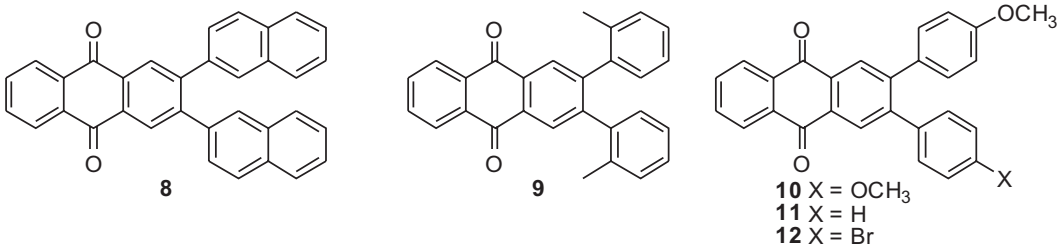
mixture greatly increased the rate; under these conditions, 40% of **4** had reacted after 2 days, but the ratio of naphthoquinone–anthraquinone dropped to 5:1.

The success of the approach described above prompted us to attempt the preparation of other 2,3-disubstituted anthraquinones. Since electronic and steric effects play important roles in the photochemistry of anthracene derivatives (11, 29), we were interested in synthesizing a range of anthraquinones with different pendant aromatic rings. The naphthyl- and *o*-tolyl-substituted derivatives **8** and **9** were therefore targeted as more sterically congested analogs of **3**. On the other hand, the introduction of para-substituents onto the peripheral aromatic rings in compounds **10**–**12** should not appreciably alter lateral bulk of the phenyl rings, but will change electronic properties of these groups. More specifically, methoxy- and bromo-substituents were chosen because they also provide useful points of attachment for the eventual incorporation of these compounds into polymers or other structures.

The symmetrical 1,2-diaryl-1,2-ethanediones (**13**–**15**) were synthesized from 2-naphthaldehyde, *o*-tolualdehyde, and *p*-anisaldehyde, respectively, using slightly modified literature procedures (22–24). Like benzil, these compounds are readily converted to the corresponding hydroxycyclopent-2-enones (**16**–**18**). These hydroxy compounds in general proved difficult to purify and were therefore used as obtained in subsequent reactions. Condensation of these compounds with 1,4-naphthoquinone afforded the desired products **8**–**10** in isolated yields that varied from 7%–18% (Scheme 4). It is unclear at this time why the reactions involving these substituted derivatives were much lower than for **4**, although both electronic and steric effects may have been in part responsible.

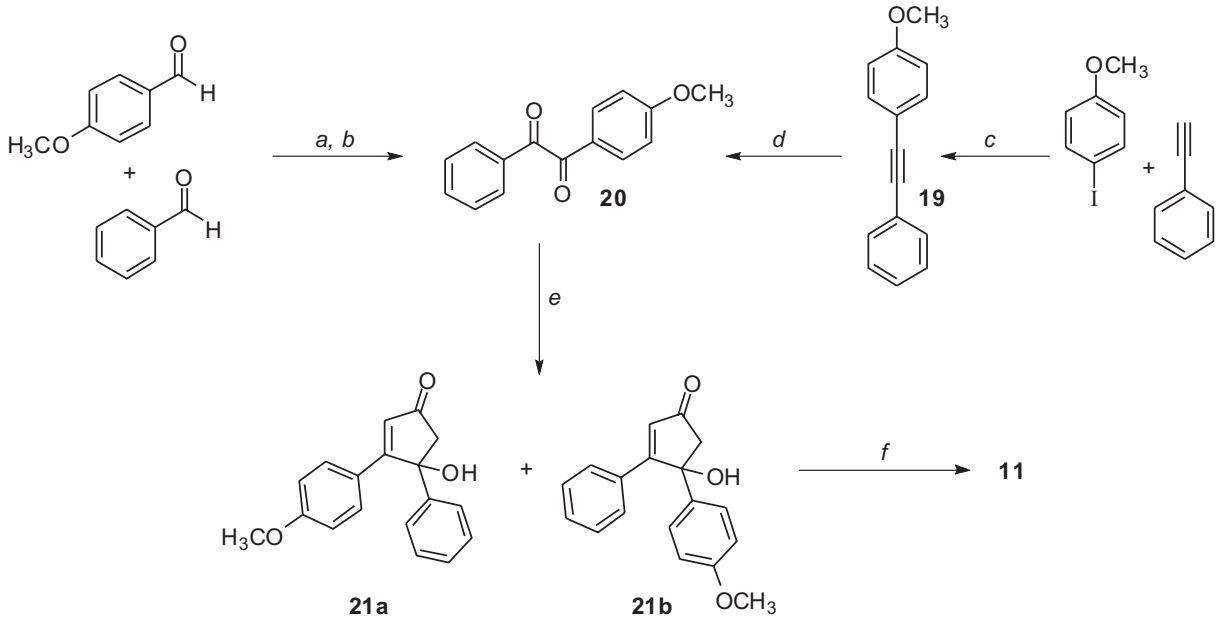
In the course of characterizing the tolyl derivative **9**, it was noted that several peaks in both the ^1H and ^{13}C NMR spectra of this compound were appreciably broadened. The affected peaks were identified as those associated with the pendant tolyl groups, suggesting that these rings are undergoing conformational syn-/anti-isomerism on the NMR timescale (Fig. 1). This is consistent with the observation that a similar molecule (2,2′-dimethyl-*o*-terphenyl) has a barrier to isomerization of 62 kJ/mol, with an NMR coalescence temperature of 9 °C (30). Although quantitative variable-temperature NMR experiments have not yet been carried out on **9**, the tolyl peaks were observed to sharpen at elevated temperatures, as expected.

This general synthetic approach can also be employed in the preparation of lower symmetry anthraquinones such as **11** and **12**, which were derived from the corresponding unsymmetrical benzils **20** and **22**, respectively (Schemes 5 and 6). Two routes were explored for the preparation of benzil **20**. This compound can be obtained via the cross-benzoin condensation of benzaldehyde and anisaldehyde (31). Although this synthesis has the advantage of employing relatively inexpensive starting materials, it does yield a mixture of benzil and compound **20** in an approximately 1:3 ratio, with **20** being isolated in only a 22% yield. A more systematic synthesis of this compound proceeds via the oxidation of the diphenylacetylene derivative (**19**), which is easily prepared from phenylacetylene and *p*-iodoanisole using standard Hagihara–Sonagashira conditions. Conversion of this compound to **20** has previously been reported using catalytic

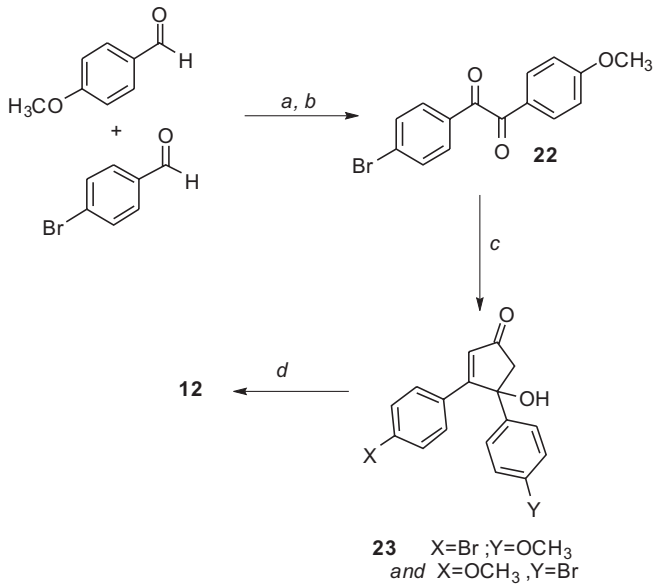


© 2006 NRC Canada

Scheme 5. Reagents and conditions: (*a*) NaCN or KCN, EtOH–H_2O, reflux; (*b*) $CuSO_4$, pyridine–H_2O; (*c*) $Pd(PPh_3)_4$, CuI, $(i\text{-}Pr)_2NH$, THF, reflux 48 h; (*d*) I_2, DMSO, 145 °C; (*e*) acetone, KOH, RT, 1 week; (*f*) 1,4-naphthoquinone, AcOH, TsOH, reflux 48 h.



Scheme 6. Reagents and conditions: (*a*) NaCN or KCN, EtOH–H_2O, reflux; (*b*) $CuSO_4$, pyridine–H_2O; (*c*) I_2, DMSO, 145 °C; (*d*) acetone, KOH, RT, 1 week; (*e*) 1,4-naphthoquinone, AcOH, TsOH, reflux 48 h.



palladium chloride in DMSO (32). We have found that, contrary to this previous report, **19** was also cleanly oxidized to **20** in the presence of I_2/DMSO. The overall yields for this alkyne route are considerably higher (59% vs. 22%) than for the cross-benzoin method, although the use of more costly reagents is required.

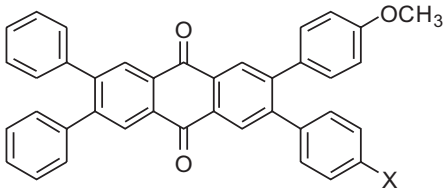
Condensation of the unsymmetrical benzil **20** with acetone yields two products that were formed in a 5:2 ratio. These products were readily separated by column chromatography and were identified as the two regioisomers of the hydroxycyclopent-2-enones **21a** and **21b**. To positively identify the two isomers, NOESY spectra were obtained for both compounds. The spectrum of the major product showed a strong NOE between the protons on the anisole ring and the vinylic proton on the cyclopentene ring, which led to the identification of this compound as **21a**. Conversely, a significant cross peak was observed between the phenyl ring and the vinylic proton in the NOESY spectrum of the minor product, confirming the identity of this compound as the second regioisomer **21b**. The formation of **21a** as the major product is consistent with the stabilization of the incipient positive charge on the cyclopentane ring by the electron-donating *p*-methoxy group during the elimination of water. From a practical standpoint, the formation of two isomers is not problematic, since both **21a** and **21b** yield the same cyclopentiadienone upon loss of water. These isomeric hydroxycyclopent-2-enones were therefore not separated prior to carrying out Diels–Alder reactions with naphthoquinone derivatives in subsequent experiments. Condensation of a mixture of these intermediates with 1,4-naphthoquinone afforded **11** in 18% yield.

In a similar manner, the brominated anthraquinone (**12**) was prepared from *p*-bromobenzaldehyde and anisaldehyde (Scheme 6). The two isomers of the cyclone precursor, collectively denoted as **23**, were not separated from one another prior to condensation with 1,4-naphthoquinone.

It is also possible to use these hydroxycyclopent-2-enone intermediates in the synthesis of 2,3,6,7-tetraarylanthraquinones bearing different aromatic rings at one or more of the sites. To demonstrate the feasibility of this approach, we condensed 6,7-diphenyl-1,4-naphthoquione (**7**) with both **21a**, **21b**, and **18**. In this manner, we were able to prepare compounds **24** and **25** in yields of 26% and 7%, respectively.

In conclusion, we have developed a new strategy for synthesizing highly substituted anthraquinone derivatives from in situ generated cyclopentadienones. This approach is complementary to other methods that have commonly been used to prepare anthraquinones, such as the Friedel–Crafts con-

© 2006 NRC Canada



24 X = H
25 X = OCH_3

densation of phthalic anhydrides with benzene derivatives, an approach that is incompatible with functional groups such as pendant aromatic rings. Although the yields of the condensation reactions reported herein were generally low, our approach nonetheless offers several advantages. These compounds were prepared in only four steps from inexpensive starting materials such as acetone, 1,4-naphthoquinone, and commercially available aldehydes. Significantly, these syntheses are also amenable to working at larger scales. The hydroxycyclopent-2-enone precursors reported herein are readily prepared in multigram quantities, and gram-scale reactions of naphthoquinone with these compounds have been routinely carried out in our laboratory. In contrast, the sulfone **2** is synthesized using much more expensive starting materials and catalysts and could not, in our hands, be prepared on large scales. Moreover, the use of cyclopentadienones lends itself to the formation of lower-symmetry derivatives, such as **10**–**12**, **24**, and **25**, which would be more difficult to prepare from the corresponding sulfones. This approach is also tolerant of functional groups such as aryl bromides, which are incompatible with the chemistry used to prepare diarylsulfone analogues of **2**. These cyclopentadienones are therefore viable precursors for the large-scale preparation of anthraquinones that are not otherwise readily accessible. Further work is being carried out in our laboratory in an ongoing attempt to optimize these reactions.

Acknowledgements

The authors gratefully acknowledge Simon Fraser University and the Natural Sciences and Engineering Research Council of Canada (NSERC) for funding, and Mr. Miki Yang for carrying out microanalyses.

References

1. R.M. Christie. Colour chemistry. RSC, Cambridge, UK. 2001.
2. B. Kampmann, Y. Lian, K.L. Klinkel, P.A. Vecchi, H.L. Quiring, C.C. Soh, and A.G. Sykes. J. Org. Chem. **67**, 3878 (2002).
3. P. Terech and R.G. Weiss. Chem. Rev. **97**, 3133 (1997).
4. V. Prasad, K. Krishnan, and V.S.K. Balagurusamy. Liq. Cryst. **27**, 1075 (2000).
5. S. Norvez, F.-G. Tournilhac, P. Bassoul, and P. Herson. Chem. Mater. **13**, 2552 (2001).
6. K.S. Raja, V.A. Raghunathan, and S. Ramakrishnan. Macromolecules, **31**, 3807 (1998).
7. K. Krishnan and V.S.K. Balagurusamy. Liq. Cryst. **27**, 991 (2000).
8. S. Kumar, J.J. Naidu, and S.K. Varshney. Liq. Cryst. **30**, 319 (2003).
9. M.A. Tius, J. Gomez-Galeno, X.Q. Gu, and J.H. Zaidi. J. Am. Chem. Soc. **113**, 5775 (1991).
10. B. Armitage, C. Yu, C. Devadoss, and G.B. Schuster. J. Am. Chem. Soc. **116**, 9847 (1994).
11. D. Bailey and V.E. Williams. Chem. Commun. (Cambridge, U.K.), 2569 (2005).
12. D. Bailey and V.E. Williams. Tetrahedron Lett. **45**, 2511 (2004).
13. J.S. Wu, Z. Tomovic, V. Enkelmann, and K. Mullen. J. Org. Chem. **69**, 8176 (2004).
14. A. Sygula, S.D. Karlen, R. Sygula, and P.W. Rabideau. Org. Lett. **4**, 3135 (2002).
15. M.A. Oglairus, M.G. Romanell, and E.I. Becker. Chem. Rev. **65**, 261 (1965).
16. V.S. Iyer, M. Wehmeier, J.D. Brand, M.A. Keegstra, and K. Mullen. Angew. Chem. Int. Ed. Engl. **36**, 1604 (1997).
17. C.F.H. Allen. Can. J. Chem. **45**, 1201 (1967).
18. C.F.H. Allen and E.W. Spanagel. J. Am. Chem. Soc. **55**, 3773 (1933).
19. A. Sygula, R. Sygula, A. Ellern, and P.W. Rabideau. Org. Lett. **5**, 2595 (2003).
20. J. Lu, J.J. Zhang, X.F. Shen, D.M. Ho, and R.A. Pascal. J. Am. Chem. Soc. **124**, 8035 (2002).
21. C.F.H. Allen, C.G. Eliot, and A. Bell. Can. J. Res. **17**, 75 (1939).
22. M.S. Kharasch, W. Nudenberg, and S. Archer. J. Am. Chem. Soc. **65**, 495 (1943).
23. Y. Ogata and M. Yamashita. Tetrahedron, **27**, 2725 (1971).
24. W. Tochtermann and R.G.H. Kirrstetter. Chem. Ber. **111**, 1228 (1978).
25. P. Girard and H.B. Kagan. Tetrahedron Lett. 4513 (1975).
26. A. McKillop, B.P. Swann, M.E. Ford, and E.C. Taylor. J. Am. Chem. Soc. **95**, 3641 (1973).
27. B.H. Freeman, J.M.F. Gagan, and D. Lloyd. Tetrahedron, **29**, 4307 (1973).
28. V.E. Williams and T.M. Swager. Macromolecules, **33**, 4069 (2000).
29. H. Bouas-Laurent, A. Castellan, J.P. Desvergne, and R. Lapouyade. Chem. Soc. Rev. **29**, 43 (2000).
30. R.H. Mitchell and J.S.H. Yan. Can. J. Chem. **58**, 2584 (1980).
31. N.J. Leonard, R.T. Rapala, H.L. Herzog, and E.R. Blout. J. Am. Chem. Soc. **71**, 2997 (1949).
32. M.S. Yusobov, K.W. Chi, E.A. Krasnokutskaya, V.P. Vasil'eva, and V.D. Filimonov. Zh. Org. Khim. **31**, 1675 (1995).

© 2006 NRC Canada

Iodosulfonation of alkenes with benzenesulfinic acid – *N*-iodosuccinimide — Facile preparation of α,β-unsaturated sulfones[1]

Russell R. Wolff, Vikram Basava, Robert M. Giuliano, Walter J. Boyko, and J. Herman Schauble

Abstract: Reaction of alkenes and alkenols with *N*-iodosuccinimide (NIS) and benzenesulfinic acid in dichloromethane at room temperature affords *vic*-iodophenylsulfonyl adducts in good to high yields. Treatment of the iodosulfones with neutral alumina in dichloromethane at room temperature results in dehydroiodination to give the corresponding vinyl sulfones in high yield and purity by this convenient two-step procedure. Application of the iodosulfonation–dehydroiodination sequence to allylic alcohols and silyl ethers gave γ-oxygenated, α,β-unsaturated phenylsulfones, while the attempted iodosulfonation of glycals, as intermediates to vinyl sulfones, resulted in addition of benzenesulfinic acid with double bond shift (Ferrier rearrangement).

Key words: iodosulfonation, vinyl sulfones, benzenesulfinic acid, *N*-iodosuccinimide, dehydroiodination.

Résumé : La réaction d'alcènes et d'alcénols avec du *N*-iodosuccinimide (NIS) et de l'acide benzènesulfinique dans le dichlorométhane à la température ambiante conduit à la formation d'adduits *vic*-iodophénylsulfonyles avec des rendements allant de bons à élevés. Le traitement des iodosulfones avec de l'alumine neutre dans le dichlorométhane à la température ambiante provoque une déshydroiodation qui fournit les vinylsulfones correspondantes avec un rendement et une pureté élevés et qui complète cette méthode de synthèse pratique en deux étapes. L'application de la séquence de réactions iodosulfonation–déshydroiodation à des alcools allyliques et à des éthers silylés conduit à la formation de phénylsulfones γ-oxygénées et α,β-insaturées alors que les essais d'iodosulfonation de glycals, pour conduire à des intermédiaires de vinyl sulfones, conduisent à une addition de l'acide benzènesulfinique avec un déplacement de la double liaison (réarrangement de Ferrier).

Mots clés : iodosulfonation, vinyl sulfones, acide benzènesulfinique, *N*-iodosuccinimide, déshydroiodation.

[Traduit par la Rédaction]

Introduction

The two-step halosulfonation–dehydrohalogenation sequence is a useful method for conversion of alkenes to α,β-unsaturated sulfones. The first step of this process has generally been carried out by the reaction of an alkene with an arylsulfonyl halide to give a *vic*-halo(arylsulfonyl)alkane (1). Such reactions with sulfonyl chlorides or bromides occur via a radical-chain process, and require initiators such Cu(I, II) (2–5) or Ru(II) (6) salts, peroxides (7–9), or UV irradiation (5, 8, 10, 11).

Arylsulfonyl iodides are considerably more susceptible to homolysis than the chlorides, typically undergoing slow addition to alkenes in the dark (12, 13), although being accelerated by ambient or applied visible light (12–16), Cu(II) salts (17), or other radical initiators (12). Arylsulfonyl iodides are unstable reagents that are prepared from iodine and sodium arylsulfinate. Direct iodosulfonation can also be carried out with iodine and sodium arylsulfinate; however, a catalyst, such as a Cu(II) or Hg(II) salt, is usually included (18–20).

Herein we describe an alternate synthesis of iodo(arylsulfonyl)alkanes by the reaction of alkenes with *N*-iodosuccinimide (NIS) and benzenesulfinic acid in dichloromethane at room temperature. The free sulfinic acid is soluble in organic solvents, and is stable for extended periods when stored at 0 °C. Iodophenylsulfonyl adducts are obtained regioselectively in good yields. We also report that treatment of the iodosulfones with neutral alumina at room temperature results in facile elimination of HI, to give synthetically useful vinyl sulfones in high yield and purity.

Results and discussion

Iodosulfonation products obtained from reaction of various alkenes and alkenols with NIS and benzenesulfinic acid are listed in Table 1. Reactions of cyclopentene, cyclohexene, 1-methylcyclohexene, and norbornylene all gave high

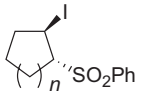
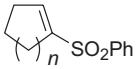
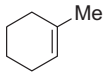
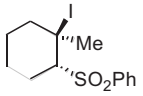
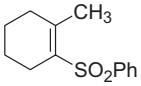
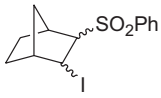
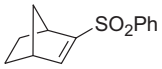
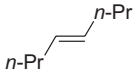
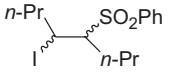
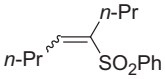
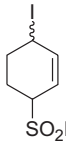
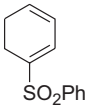
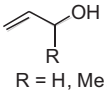
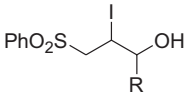
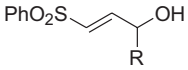
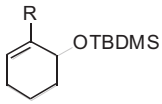
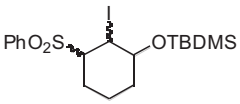
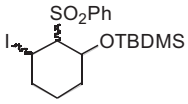
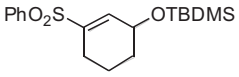
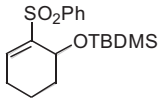
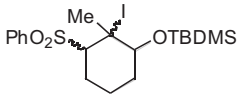
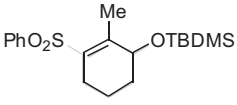
Received 30 August 2005. Published on the NRC Research Press Web site at http://canjchem.nrc.ca on 17 May 2006.

R.R. Wolff, V. Basava, R.M. Giuliano,[2] W.J. Boyko, and J.H. Schauble. Department of Chemistry, Villanova University, Villanova, PA 19085, USA.

[1]This article is part of a Special Issue dedicated to Professor Walter A. Szarek.
[2]Corresponding author (e-mail: robert.giuliano@villanova.edu).

 doi:10.1139/V06-051 © 2006 NRC Canada

Table 1. Iodophenylsulfonylation of alkenes using NIS – benzenesulfinic acid and dehydroiodination of iodo(henylsulfonyl) compounds on neutral alumina.

Alkene	Iodosulfonylation Product	Yield[a]	Dehydroiodination Product	Yield[b]
 *n* = 1, 2	 **1** *n* = 1 **3** *n* = 2	91% 86% (73%)[c]	 **2** *n* =1 **4** *n* = 2	92% 95% (83%)[c]
	 **5**	90%[d]	 **6**	10%[d, e]
	 **7a** 2-endo-3-exo **7b** 2-exo-3-endo	85%[f]	 **8**	89%
	 **9a** erythro, **9b** threo	83%[f]	 **10a** (Z), **10b** (E)	80%[f]
	 **11a, 11b** (cis, trans)	92%[f]	 **12**	92%
 R = H, Me, *n*-Pr	 **13** R = H **15** R = Me **17** R = *n*-Pr	60% 63% 83%	 **14** R = H **16** R = Me **18** R = *n*-Pr	95% 92% 85%
 R = H	 **19**  **20**	77%[f]	 **21**  **22**	92%[f, g]
R = Me	 **23**	57%	 **24**	38%[g]

[a]Literature yields are in parenthesis.
[b]Yields from the iodo(phenylsulfonyl) precursor.
[c]Iodosulfone **3** was accompanied by 5% of the cis isomer (17).
[d]Yield of side product from thermal elimination of **5**. Elimination on alumina was not investigated.
[e]Tosyl iodide gave 67% addition plus 10% thermal elimination product (17).
[f]Combined yield of isomers.
[g]Elimination did not occur on neutral alumina; carried out using DABCO.

© 2006 NRC Canada

yields of single *vic*-iodosulfones having the trans configuration. 1-Methylcyclohexene gave only *trans*-1-iodo-1-methyl-2-(phenylsulfonyl)cyclohexane, having the anti-Markovnikov regiochemistry, consistent with free radical, rather than ionic addition. The same regiochemistry, previously observed for reaction of alkenes with iodine and sodium arylsulfonates, was rationalized as being due to the steric bulk of the sulfinate anion, favoring rearside attack on the intermediate three-membered ring iodonium intermediates at the less-hindered position (18). However, an ionic pathway for such iodosulfonation reactions appears unlikely, since we observe that reaction of benzenesulfinic acid with NIS in dichloromethane-d_2 at room temperature gives benzenesulfonyl iodide at a rate similar to that for iodosulfonation of alkenes. A radical pathway is further supported by our observation that methyl vinyl ketone and the corresponding alcohol (3-buten-2-ol) undergo iodosulfonylation with NIS – benzenesulfinic acid at similar rates. Additionally, Yus and coworkers (21) have shown that reaction of α,β-unsaturated carbonyl compounds with sodium *p*-toluenesulfinate and iodine gives α-iodo-β-sulfonyl adducts, as expected for free radical addition.

Iodosulfonylation of *E*-4-octene gave a mixture of *threo*- and *erythro*-4-iodo-5-phenylsulfonyl octanes (**9a**, **9b**). This result is of interest in light of a report by Skell and McNamara (14) on reaction of phenylsulfonyl iodide with *cis*- or *trans*-2-butene, both of which gave identical mixtures of *threo*- and *erythro*-iodosulfones. The latter apparently formed via a 3-phenylsulfonyl-2-butyl radical, which undergoes conformational exchange at a rate competitive with that for iodine abstraction from phenylsulfonyl iodide to give the iodosulfonation product. No isomerization of starting butenes was observed (as occurred for chlorosulfonation with sulfonyl chlorides) (22), since iodine abstraction occurs faster than reversion of the phenylsulfonyl-2-butyl radical to alkene.

The mixture of *erythro*- and *threo*-4-iodo-5-(phenylsulfonyl)octanes (**9a**, **9b**) was inseparable by TLC. Although ^{1}H NMR revealed the isomers to be present in 71:29 molar ratio, their spectra were too similar to distinguish them. However, dehydroiodination on neutral alumina (vide infra) gave *E*- and *Z*-4-(phenylsulfonyl)octenes (**10a**, **10b**) in 67:32 molar ratio. Providing that elimination occurs by an E2 process, the major E isomer **10a** derives from the *erythro*-iodosulfone (**9a**) while the Z isomer **10b** forms via the *threo*-iodosulfone (**9b**).

Iodosulfonation of norbornylene gave a mixture of 2-*endo*-iodo-3-*exo*-(phenylsulfonyl)norbornane (**7a**) and a second compound, tentatively identified as the 2-*exo*-iodo-3-*endo*-phenylsulfonyl isomer **7b** in approximately equimolar ratio. Formation of **7a** is consistent with the intermediacy of the 3-*exo*-(phenylsulfonyl)-2-norbornyl radical, which would be trapped by iodine transfer from benzenesulfonyl iodide to the endo face. In contrast, **7b** apparently forms via the 2,3-*exo*-iodonium intermediate resulting from iodonium (I^+) transfer from NIS to norbornylene, followed by endo attack by the benzenesulfinate ion. It thus appears that iodosulfone formation via iodonium intermediates may be expected in cases involving more nucleophilic alkenes such as norbornylene.

1,3-Cyclohexadiene gave a mixture of *cis*/*trans*-3-iodo-6-(phenylsulfonyl)cyclohexene (**11a**, **11b**) in approximately equimolar ratio, determined from the integrated intensities for the CHI and $CHSO_2Ph$ peaks in the ^{1}H NMR spectrum. Vicinal coupling for H_6 indicated the sulfonyl group to be pseudoequatorial for the major isomer and pseudoaxial for the minor one; however, since J_{vic} values for H_3 could not be determined; it was not possible to distinguish the two isomers by NMR.

Dehydroiodination of α-iodo-β-alkylsulfonyl or arylsulfonyl compounds has previously been carried out using pyridine in benzene under reflux (14), or triethylamine in various solvents at room temperature, or with heating (12, 17–21, 23). In the present work, it was found that flash chromatography of *trans*-1-iodo-2-(phenylsulfonyl)cyclohexane (**3**) on neutral alumina resulted in partial conversion to 1-(phenylsulfonyl)cyclohexene (**4**). This led to the observation that dehydroiodination could be carried out preparatively, simply by stirring neutral alumina slurries of the iodosulfones in dichloromethane at room temperature to yield the corresponding α,β-unsaturated sulfones, generally in very good to excellent yields (Table 1). This procedure avoids the use of amine bases that may be incompatible with some functional groups. However, dehydroiodination of the iodosulfone TMBDS ethers **19**, **21**, and **23** (vide infra) did not occur on alumina. In these cases, we found that the elimination could be carried out using 1,4-diazabicyclo[2.2.2]octane (DABCO).

We were also interested in application of the iodophenylsulfonation–dehydroiodination sequence to the synthesis of γ-oxygenated, α,β-unsaturated phenylsulfones by using allylic alcohols or their derivatives as substrates. Products derived from allylic alcohols could thus serve as precursors to phenylsulfonyl-substituted, α,β-unsaturated ketones, which are established heterodienes in Diels–Alder reactions (24), as well as other synthetic applications involving conjugate additions (25). γ-Alkoxy-α,β-unsaturated phenylsulfones are useful as substrates in [3+2] cycloadditions, via π-allyl palladium complexes, as a method for cyclopentenone annulation (26), and also in six-membered ring annulations by a conjugate addition–alkylation sequence (27).

Examples of the allylic alcohols used as substrates in the iodophenylsulfonation–elimination sequence are shown in Table 1. Treatment of allyl alcohol with benzensulfinic acid and NIS in dry dichloromethane overnight gave a 54% yield of iodophenylsulfone **13**. The NMR spectrum indicated a single regioisomer, resulting from addition of the phenylsulfonyl group to the less-substituted carbon, consistent with our results for other unsymmetrically substituted alkenes. Treatment of the iodophenylsulfone with neutral alumina gave a nearly quantitative yield of the γ-hydroxy-α,β-unsaturated sulfone **14**, the structure of which was confirmed by comparison of physical data with reported values for this compound prepared by either microwave- or ultrasound-assisted alkylation of sodium benzenesulfinate by Villemin and Aloum (28).

Similarly, treatment of 3-butene-2-ol with benzenesulfinic acid and NIS gave iodophenylsulfone **15** as a mixture of diastereomers. Again, a single regiochemistry of addition was observed. Elimination w ith alumina occurred smoothly to give the known (29) γ-hydroxy-α,β-unsaturated sulfone **16**. An isomeric vinyl sulfone, 3-(phenylsulfonyl)-3-buten-2-ol, was previously prepared by the addition of phenyl vinyl

© 2006 NRC Canada

sulfone to acetaldehyde. Oxidation gave 3-(benzenesulfonyl)-3-buten-2-one, which was shown to undergo hetero-Diels–Alder reactions with vinyl ethers in high yield at or below room temperature (24). It is anticipated that the ketone derived by oxidation of **16** would also be useful as a heterodiene. Similarly, (*E*)-1-(phenylsulfonyl)-hex-1-en-3-ol (**18**) (30) was prepared from 1-hexen-3-ol in good overall yield by regioselective iodosulfonation–elimination.

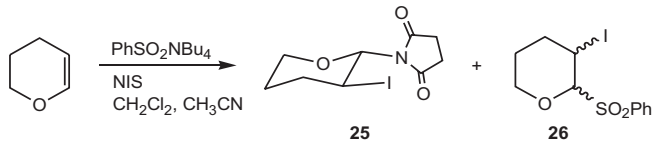
Both 2-cyclohexen-1-ol and 2-methyl-2-cyclohexen-1-ol were unsuitable as substrates for the synthesis of vinyl sulfones using the iodophenylsulfonation–elimination sequence because of side reactions. Better results were obtained using the *tert*-butyldimethylsilyl (TBDMS) ethers of these cyclic allylic alcohols. The attempted synthesis of 3-(*tert*-butyldimethylsiloxy)-1-(phenylsulfonyl)cyclohexene (**21**) from 2-cyclohexen-1-ol by this method resulted in a mixture of vinyl sulfones **21** and **22** because of a lack of regioselectivity in the initial addition step. Treatment of the TBDMS ether of 2-methyl-2-cyclohexen-1-ol gave diastereomeric 2-iodo-3-phenylsulfonyl derivatives (**23**), which were converted to vinyl sulfone **24**, albeit in lower overall yield than was observed for the other cases. Vinyl sulfone **21** was used in the synthesis of annulated cyclopentenones by Trost et al. (26).

Ley and co-workers (31) have developed synthetically useful alkylation reactions of anions derived from 2-benzensulfonyl tetrahydropyran. We decided to attempt the application of our iodophenylsulfonation reaction to dihydropyran and to glycals. The only products obtained from dihydropyran upon treatment with NIS – benzenesulfinic acid, were those resulting from addition of benzenesulfinic acid, suggesting that protonation of the double bond occurs faster than iodination, or alternatively, hydrogen atom abstraction by the adduct of DHP and benzenesulfonyl radical is again faster than iodination. We also attempted iodophenylsulfonation of dihydropyran using NIS and tetra-*N*-butylammonium benzenesulfinate and observed a significant amount of adduct **25** (apparently resulting from trapping of dihydropyran iodonium ion by succinimide), along with iodophenylsulfone **26** and other products that were not identified (Scheme 1).

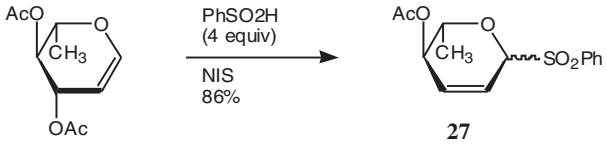
Iodophenylsulfonation of glycals was also attempted using NIS and benzenesulfinic acid in an effort to prepare carbohydrate vinyl sulfones. Ley and co-workers (31*a*) had observed that benzenesulfinic acid adds to tri-*O*-acetyl-L-glucal with double bond migration (Ferrier rearrangement). This same result was also observed in our study for the reaction of either tri-*O*-acetyl-D-glucal or di-*O*-acetyl-L-rhamnal, when treated with benzenesulfinic acid in the presence or absence of *N*-iodosuccinimide. In both cases, the Ferrier rearrangment product was obtained, with no evidence of iodophenylsulfone formation. Di-*O*-acetyl-L-rhamnal gave an 86% yield of the anomeric phenylsulfone adducts **27** when treated with excess benzenesulfinic acid at room temperature (Scheme 2).

In summary, a convenient two-step synthesis of α,β-unsaturated sulfones has been developed using iodophenylsulfonation of alkenes or alkenols with NIS – benzenesulfinic acid, followed by dehydroiodination on neutral alumina at room temperature. The overall process is highly regioselective for unsymmetrical alkenes, giving vinyl sulfones that can be used for a variety of synthetic applications.

Scheme 1.



Scheme 2.



Experimental

Preparation of benzenesulfinic acid

A stirred solution of sodium benzene sufinate (10.0 g, 61.0 mmol) in distilled water (25 mL) under nitrogen at 0 °C was slowly acidified to pH 1 by dropwise addition of 12 mol/L HCl. The white crystalline benzenesulfinic acid was filtered and air dried on a Büchner funnel, then stored at 0 °C (7.35 g, (85% yield); mp 82–86 °C (lit. value (32) mp 77 to 78 °C; (33) mp 82–84 °C).

General procedure for iodophenylsulfonation of alkenes using NIS – benzenesulfinic acid

To a stirred solution of NIS (225 mg, 1.0 mmol) in CH_2Cl_2 (50 mL) was added benzenesulfinic acid (142 mg, 1.0 mmol) and stirring continued for ~5 min to effect solution. The alkene (1.0 mmol) was added, and the reaction mixture was stirred for 30 min to 2 h at room temperature (monitored by TLC on silica gel using hexane – ethyl acetate, 1:1 *v*/*v* as eluent), then extracted with satd. aq. $NaHCO_3$ and $NaHSO_3$ (50 mL, each), dried ($MgSO_4$), and filtered. Flash chromatography on silica gel (60–200 mesh) using hexane – ethyl acetate (1:1) as eluent gave the oily liquid iodosulfones. No dehydroiodination products were detected, except in the case of iodosulfone **5**, which was accompanied by ~10% of 1-methyl-2-(phenylsulfonyl)cyclohexene (**6**).

trans-1-Iodo-2-(phenylsulfonyl)cyclopentane (1)

Yield: 322 mg (96%). ^{1}H NMR (300 MHz, $CDCl_3$) δ: 7.98 (m, 2H, Ph-H), 7.71 (m, 1H, Ph-H), 7.65 (m, 2H, Ph-H), 4.64 (ddd, 1H, H_1, $J_{1,2}$ = 4.2 Hz, $J_{1,5a}$ = 3.2 Hz, $J_{1,5b}$ = 3.0 Hz), 3.94 (ddd, 1H, H_2, $J_{1,2}$ = 4.2 Hz, $J_{2,3a}$ = 3.1 Hz, $J_{2,3b}$ = 3.0 Hz), 2.5–1.8 (cms, 6H, H_{3-5}) ^{13}C NMR (75.4 MHz, $CDCl_3$) δ: 138.8, 134.4, 129.8, 128.8 (Ph), 75.2 (C_2), 40.87 (C_5), 26.36, 25.41, 20.48 ($C_{1,3,4}$). The cyclopentane ring ^{1}H shifts are consistent with literature values for the corresponding 1-iodo-2-p-toluenesulfone (17).

trans-1-Iodo-2-(phenylsulfonyl)cyclohexane (3)

Yield: 238 mg (86%). ^{1}H NMR (300 MHz, $CDCl_3$) δ: 8.10–7.92 (m, 2H, Ph-H), 7.77–7.69 (m, 1H, Ph-H), 7.69–7.60 (m, 2H, Ph-H), 5.14 (bs, 1H, H_1), 3.41 (bs, 1H, H_2), 1.95–0.82 (cms, 8H, H_{3-6}). ^{13}C NMR (75.4 MHz, $CDCl_3$) δ: 138.2 (C_i), 134.3 (C_p), 129.7 (C_o), 128.8 (C_m), 67.86 (C_2),

© 2006 NRC Canada

34.0 (C_6); 25.9, 23.6, 22.6, 21.5 (C_1, $C_{3–5}$). The ^{1}H NMR shifts are consistent with published data (17).

***trans*-1-Iodo-1-methyl-2-(phenylsulfonyl)cyclohexane (5)**

Yield: 328 mg (90%). IR (KBr, cm^{-1}) ν_{max}: 1300 (SO_2, ν_{asym}), 1130 (SO_2, ν_{sym}). ^{1}H NMR (300 MHz, $CDCl_3$) δ: 7.92 (m, 2H, Ph-H), 7.64 (m, 1H, Ph-H), 7.55 (m, 1H, Ph-H), 3.70 (bs, 1H, H_2), 2.01 (s, 3H, CH_3), 2.2–1.1 (cms, 8H, $H_{3–6}$). The cyclohexyl ^{1}H shifts agree with those reported for *trans*-1-iodo-1-methyl-2-tosylcyclohexane (17). In addition to the iodosulfone **5**, column chromatography also gave 1-methyl-2-(phenylsulfonyl)cyclohexene (**6**, 24 mg, 10%) identified by comparison of the ^{1}H NMR spectrum with literature data (17).

2-Iodo-3-(phenylsulfonyl)norbornanes (7a, 7b)

Yield: 307 mg (85% combined yield; ~1:1 molar ratio by ^{1}H NMR). ^{1}H NMR (300 MHz, $CDCl_3$) for the 2-*endo*-iodo-3-*exo*-(phenylsulfonyl) isomer **7a** δ: 7.99 (m, 2H, Ph-H), 7.77 (m, 1H, Ph-H), 7.68 (m, 2H, Ph-H), 4.38 (cm, 1H, H_{2x}, $J_{2x,3n}$ = 5.9 Hz, $J_{1,2x}$= 3.7 Hz, $J_{2x,6x}$ = 1.7 Hz, $J_{2x,7s}$ = ~0 Hz; no COSY cross peak). A cross peak was observed for H_1-H_{2x}, aiding confirmation of H_{3n}, H_{2x}), 3.05 (dd, 1H, H_{3n}, $J_{2x,3n}$ = 5.9 Hz, $J_{3n,7a}$ = 1.7 Hz, $J_{3n,4}$ = ~0 Hz), 2.81 (m, 1H, H_4), 2.52 (m, 1H, H_1), 2.08 (m, 1H, H_{7s}), 1.67 (cms, 2H, H_{5x}, H_{6x}) 1.34 (m, 1H, H_{7a}), 1.27 (m,1H, H_{5n}), 1.08 (m, 1H, H_{6n}). ^{13}C NMR (75.4 MHz, $CDCl_3$) phenyl δ: 138.5 (C_i), 133.9 (C_p), 129.4 (C_m), 128.7 (C_o); norbornyl δ: 76.11 (C_3), 45.31 (C_1), 38.44 (C_4), 34.64 (C_7), 29.22 (C_5), 27.46 (C_6), 26.36 (C_1).

For 2-*exo*-iodo-3-*endo*-(phenylsulfonyl)norbornane (**7b**): ^{1}H NMR (300 MHz, $CDCl_3$) δ: 4.11 (dd, 1H, H_{2n}), 3.27 (dd, 1H, H_{3x}), 2.89 (bs, 1H, H_4), 2.50 (bs, 1H, H_1), 2.41 (d, 1H, H_{7s}), ~1.7–1.0 (ms, 5H, $H_{5,6}$, H_{7a}).

4-Iodo-5-(phenylsulfonyl)octane (9a, 9b)

Yield: 316 mg (83% combined yield); single component by TLC on silica gel (hexane – ethylacetate (1:1 *v*/*v* as eluent); however, ^{1}H NMR revealed the formation of **9a** and **9b** in 67:33 molar ratio. For the major isomer **9a**: ^{1}H NMR (300 MHz, $CDCl_3$) δ: 7.88 (m, 2H, Ph-H), 7.62 (m, 1H, Ph-H), 7.59 (m, 2H, Ph-H), 4.61 (ddd, 1H, H_4, $J_{3a,4}$ = 10.8 Hz, $J_{3b,4}$ = 3.3 Hz, $J_{4,5}$ = 2.4 Hz), 3.54 (ddd, 1H, H_5, $J_{5,6a}$ = 7.7 Hz, $J_{5,6b}$ = 3.7 Hz, $J_{4,5}$ = 2.4 Hz), 2.11, 1.99 (ms, 2H, $H_{6a,6b}$), 1.77, 1.67 (ms, 2H, $H_{3a,3b}$), 1.41 (m, 2H, H_7), 1.55, 1.25 (ms, 2H, $H_{2a,2b}$), 0.91 (t, 3H, H_1, $J_{1,2}$ = 7.3 Hz), 0.88 (t, 3H, H_8, $J_{7,8}$ = 7.3 Hz); $J_{2,3}$ and $J_{6,7}$ were not determined. ^{13}C NMR (75.4 MHz, $CDCl_3$) δ: 139.3 (s, C_i), 134.4 (d, C_p), 129.8 (d, C_m) 128.7 (d, C_o), 72.53 (d, C_5), 36.52 (t, C_3), 31.84 (d, C_4), 28.21 (t, C_6), 23.89 (t, C_2), 22.46 (t, C_7), 14.18 (q, C_8), 13.23 (q, C_1). Anal. calcd. for $C_{14}H_{21}SO_2I$ (%): C 44.08, H 5.55, S 8.41; found (mixture of **9a** and **9b**): C 44.24, H 5.29, S 8.01.

For the minor isomer **9b**: ^{1}H NMR δ: 7.94 (m, 2H, Ph), 7.62 (m, 1H, Ph), 7.59 (m, 2H, Ph), 4.51 (ddd, 1H, H_4, $J_{3a,4}$ = 9.2 Hz, $J_{3b,4}$ = 5.4 Hz, $J_{4,5}$ = 2.2 Hz), 2.70 (ddd, 1H, H_5, $J_{5,6a}$ = 5.9 Hz, $J_{5,6b}$ = 5.2 Hz, $J_{4,5}$ = 2.2 Hz), 2.02, 1.73 (ms, 2H $H_{6a,6b}$), 1.99, 1.70 (ms, 2H, $H_{3a,3b}$), 1.43 (m, 2H, H_7), 1.50, 1.39 (ms, 2H, $H_{2a,2b}$), 0.88 (t, 3H, H_1, $J_{1,2}$ = 7.1 Hz), 0.875 (t, 3H, H_8, $J_{7,8}$ = 7.3 Hz). ^{1}H shifts for **9a** and **9b** were determined using COSY, HETCOR, and 1D decoupling; $J_{2,3}$ and $J_{6,7}$ were not determined. ^{13}C NMR (75.4 MHz, $CDCl_3$) for **9b** δ: 138.47 (s, C_i), 134.33 (d, C_p), 129.53 (d, C_m and C_o), 68.66 (d, C_5), 42.34 (t, C_3), 33.27 (t, C_6), 30.62 (d, C_4), 23.04 (t, C_2), 21.63 (t, C_7), 14.30 (q, C_8), 13.16 (q, C_1).

***cis*/*trans*-3-Iodo-6-(phenylsulfonyl)cyclohexene (11a, 11b)**

Yield: 319 mg (92% combined yield); single component by TLC on silica gel; ~1:1 molar ratio determined by ^{1}H NMR. Configurations at C_3 could not be assigned since vicinal couplings for H_3 were unobtainable owing to peak overlap. For **11a**: ^{1}H NMR (300 MHz, $CDCl_3$) δ: 7.88 (m, 2H, Ph-H), 7.68 (m, 2H, Ph-H), 7.58 (m, 1H, Ph-H), 6.37 (dd, 1H, H_2, $J_{1,2}$ = 9.9 Hz, $J_{2,3}$ = 4.9 Hz), 5.61 (dd, 1H, H_1, $J_{1,2}$ = 9.9 Hz, $J_{1,6}$ = 4.4 Hz), 4.98 (m, 1H, H_3, $J_{2,3}$ = 4.9 Hz, $J_{3,6}$ = 1.0 Hz, $J_{1,3}$ = 1.0 Hz; $J_{3,4a}$ and $J_{3,4b}$ could not be determined), 3.95 (m, 1H, H_6, $J_{5,6a}$ = 5.6 Hz, $J_{5,6b}$ = 3.5 Hz, $J_{1,6}$ = 4.4 Hz, $J_{3,6}$ = 1.0 Hz), 2.17 (m, 2H, H_5), 2.08, 1.96 (ms, 2H, H_4). ^{13}C NMR (75.4 MHz, $CDCl_3$) δ: 138.04 (C_2), 118.32 (C_1), 59.06 (C_6), 26.14 (C_4), 24.22 (C_3), 19.39 (C_5); Ph absorptions for **11a** and **11b**: 136.87, 135.72 (C_i), 128.92, 128.78 (C_m), 128.8, 128.42 (C_o), 133.71 (C_p, both isomers). For **11b**: ^{1}H NMR δ: 6.19 (dd, 1H, H_2, $J_{1,2}$ = 10.0 Hz, $J_{2,3}$ = 5.1 Hz), 5.84 (dd, 1H, H_1, $J_{1,2}$ = 10.0 Hz, $J_{1,6}$ = 2.6 Hz, $J_{1,3}$ = 1.3 Hz), 4.87 (m, 1H, H_3, $J_{2,3}$ = 5.1 Hz, $J_{3,6}$ = 1.8 Hz, $J_{1,3}$ = 1.3 Hz; $J_{3,4a}$ and $J_{3,4b}$ could not be determined), 4.22 (m, 1H, H_6, $J_{5,6a}$ = 10.7 Hz, $J_{5,6b}$ = 6.2 Hz, $J_{1,6}$ = 2.6 Hz, $J_{3,6}$ = 1.8 Hz), 2.11, 2.02 (ms, 2H, H_5), 2.11, 1.69 (ms, 2H, H_4). Ph absorptions overlapped those for **11a**. ^{13}C NMR (75.4 MHz, $CDCl_3$) δ: 136.81 (C_2), 119.30 (C_1), 61.65 (C_6), 30.96 (C_4), 23.68 (C_3), 20.00 (C_5). Anal. calcd. for $C_{12}H_{13}SO_2I$ (%): C 41.25, H 3.75, S 9.18; found for **11a** and **11b**: C 40.83, H 3.68, S 8.66.

A mixture of *cis*/*trans*-3-iodo-6-*p*-tosylcyclohexenes was previously obtained from reaction of 1,3-cyclohexadiene wth iodine/sodium *p*-toluenesulfinate (20).

General procedure for dehydroiodination of iodo(phenylsulfonyl) compounds 1, 3, 5, 7, 9, and 11

To a solution of the iodosulfonyl compound (1.0 mmol) in CH_2Cl_2 (50 mL) under nitrogen, neutral alumina (60–200 mesh, 100 cc) was added, and the resulting slurry was stirred for 1 day at rt, filtered, and the alumina was extracted with CH_2Cl_2 (50 mL). The combined extract was evaporated to give the crude α,β-unsaturated sulfone, which was purified by flash column chromatography on silica gel (toluene eluent, unless noted otherwise). Products were oily liquids, unless noted otherwise.

1-(Phenylsulfonyl)cyclopentene (2)

Flash chromatography on silica gel with hexane – ethyl acetate (1:1 *v*/*v*) as eluent (192 mg, 92%); mp 20–25 °C. ^{1}H NMR (300 MHz, $CDCl_3$) δ: 7.9 (m, 2H, Ph), 7.6 (m, 3H, Ph), 6.81 (dd, 1H, H_2, $J_{2,3a}$ = 3.8 Hz, $J_{2,3b}$ = 3.1 Hz) 3.1 (m, 4H, H_3, H_5), 2.1 (m, 2H, H_4); the ^{1}H shifts are consistent with literature (34) data. ^{13}C NMR (75.4 MHz, $CDCl_3$) phenyl δ: 140.1 (C_i), 133.65 (C_p), 129.46 (C_m), 128.21 (C_o); cyclopentenyl δ: 145.52, 140.51, 33.29, 31.19, 23.97.

© 2006 NRC Canada

1-(Phenylsulfonyl)cyclohexene (4)

Yield: 198 mg (95%); mp 39–43 °C. IR (KBr, cm^{-1}) ν_{max}: 1620 (C=C), 1300 (SO_2, ν_{asym}), 1140, (SO_2, ν_{sym}). ^1H NMR (300 MHz, $CDCl_3$) δ: 7.11 (dd, 1H, H_2, $J_{2,3a}$ = 4.3 Hz, $J_{2,3b}$ = 3.1 Hz), 2.35 (m, 2H, H_3, H_6), 1.8–1.5 (m, 4H, H_4, H_5); the shifts and splitting pattern for Ph were similar to those for **2**. The ^1H shifts are consistent with published (17, 34) values.

2-(Phenylsulfonyl)norbornene (8) (ref. 34)

Yield: 209 mg (89%). ^1H NMR (300 MHz, $CDCl_3$) δ: 6.93 (d, 1H, H_3, $J_{3,4}$ = 3.8 Hz), 3.14 (cm, 1H, H_1), 3.01 (cm, 1H, H_4), 1.79 (cm, 1H, $H_{6\text{-exo}}$), 1.67 (cm, 1H, $H_{5\text{-exo}}$), 1.52 (m, 1H, $H_{7\text{-syn}}$), 1.24 (m, 1H, $H_{7\text{-anti}}$), 1.10 (cm, 1H, $H_{6\text{-endo}}$), 0.96 (cm, 1H, $H_{5\text{-endo}}$); the Ph shifts and splitting patterns were similar to those for **7**. ^{13}C NMR (75.4 MHz, $CDCl_3$) phenyl δ: 140.22 (C_i), 133,59 (C_p), 129.50 (C_m), 128.09 (C_o); norbornenyl δ: 147.80 (C_2), 146.39 (C_3), 49.73 (C_7), 44.03 (C_4), 43.38 (C_1), 25.18 (C_5), 25.07 (C_6). Anal. calcd. for $C_{13}H_{14}SO_2$ (%): C 66.63, H 6.02, S 13.68; found: C 66.50, H 6.29, S 13.58.

(*Z*,*E*)-4-(Phenylsulfonyl)-4-octene (10a, 10b)

Flash chromatography (hexane – ethyl acetate, 1:1 *v*/*v*), 187 mg (80% combined yield); E:Z = 67:33 determined by ^1H NMR. For the Z isomer (**10a**): ^1H NMR (300 MHz, $CDCl_3$) δ: 7.884 (m, 2H, C_o), 7.60 (m, 1H, H_p), 7.53 (m, 2H, H_m), 6.008 (dd, 1H, H_5, $J_{5,6}$ = 7.9 Hz, $J_{3,5}$ = 1.2 Hz), 2.604 (m, 2H, H_6, $J_{5,6}$ = 7.9 Hz, $J_{6,7}$ = 7.4 Hz, $J_{3,6}$ = 1.2 Hz), 2.284 (ddd, 2H, H_3, $J_{2,3}$ = 7.5 Hz, $J_{3,5}$ = 1.2 Hz, $J_{3,6}$ = 1.2 Hz), 1.522 (m, 2H, H_2, $J_{2,3}$ = 7.5 Hz, $J_{1,2}$ = 7.4 Hz), 1.393 (m, 2H, H_7, $J_{6,7}$ = 7.4 Hz, $J_{7,8}$ = 7.4 Hz), 0.889 (t, 3H, H_8, $J_{7,8}$ = 7.4 Hz) 0.877 (t, 3H, H_1, $J_{1,2}$ = 7.4 Hz); the ^1H shifts are consistent with literature (35) data. ^{13}C NMR (75.4 MHz, $CDCl_3$) phenyl δ: 141.53 (s, C_i), 132.82 (d, C_p), 128.78 (d, C_m), 126.90 (d, C_o); octene chain δ: 142.99 (d, C_5), 140.20 (s, C_4), 34.80 (t, C_3), 30.21 (t, C_6), 22.19 (t, C_7), 22.10 (t, C_2), 13.39 (q, C_1), 13.11 (q, C_8). For the E isomer (**10b**): ^1H NMR δ: 7.857 (m, 2H, C_o), 7.60 (m, 1H, H_p), 7.53 (m, 2H, H_m), 6.927 (dd, 1H, H_5, $J_{5,6}$ = 7.5 Hz, $J_{3,5}$ = 0.5 Hz), 2.185 (m, 2H, H_6, $J_{5,6}$ = 7.5 Hz, $J_{6,7}$ = 7.5 Hz; $J_{3,6}$ could not be determined), 2.189 (m, 2H, H_3, $J_{2,3}$ = 6.5 Hz, $J_{3,5}$ = 0.5 Hz), 1.522 (m, 2H, H_7, $J_{6,7}$ = 7.5 Hz, $J_{7,8}$ = 7.5 Hz), 1.359 (m, 2H, H_2, $J_{1,2}$ = 7.5 Hz, $J_{2,3}$ = 6.5 Hz), 0.947 (t, 3H, H_8, $J_{7,8}$ = 7.5 Hz) 0.826 (t, 3H, H_1, $J_{1,2}$ = 7.5 Hz); the ^1H shifts agree with published (35) data. ^{13}C NMR phenyl δ: 140.83 (s, C_i), 132.79 (d, C_p), 128.80 (d, C_m), 127.65 (d, C_o); octene chain δ: 142.06 (d, C_5), 139.89 (s, C_4), 30.08 (t, C_3), 28.22 (t, C_6), 21.54 (t, C_7), 22.10 (t, C_2), 13.71 (q, C_1), 13.51 (q, C_8). The chemical shift and coupling assignments for **10a** and **10b** were made using a combination of correlated COSY, HETCOR, and 1-D decoupling. Anal. calcd. for $C_{14}H_{20}SO_2$ (%): C 66.33, H 7.99, S 12.71; found (**10a** and **10b**): C 65.92, H 7.81, S 12.35.

1-(Phenylsulfonyl)-1,3-cyclohexadiene (12) (refs. 3*a*, 34)

Yield: 203 mg (92%). ^1H NMR (300 MHz, $CDCl_3$) δ: 7.9 (m, 2H, Ph-H), 7.5 (m, 2H, Ph-H), 7.04 (dd, 1H, H_2, $J_{2,3}$ = 4.5 Hz, $J_{2,4}$ = 2.0 Hz), 7.61 (m, 1H, Ph-H), 6.11 (dd, 1H, H_3, $J_{3,4}$ = 9.4 Hz, $J_{2,3}$ = 4.5 Hz) Hz, 6.07 (cm, 1H, H_4) 2.35 (cm, 2H, H_6), and 2.27 (cm, 2H, H_5). ^{13}C NMR (75.4 MHz, $CDCl_3$) phenyl δ: 139.50 (C_i), 133.08 (C_p), 129.01 (C_m), 127.67 (C_o); cyclohexadiene δ: 136.05 (C_1), 133.21 (C_4),131.59 (C_2),122.5 (C_3), 22.9 (C_5), 19.9 (C_6). The ^1H shifts are similar to published (34) data.

General procedure for the synthesis of γ-oxygenated, α,β-unsaturated sulfones

Allylic alcohols or their *tert*-butyldimethylsilyl ethers were treated with 1 equiv. each of benzensulfinic acid and *N*-iodosuccinimide in anhydrous dichloromethane at room termperature. Progress of reactions was monitored by TLC using mixtures of ethyl acetate – hexanes as noted with each example shown in the following. The reaction mixture was diluted with dichloromethane (10 mL), then washed with 5% aqueous sodium thiosulfate solution, water, and brine, dried (sodium sulfate), and concentrated. Crude iodophenylsulfones were redissolved in dichloromethane and stirred overnight at room temperature with neutral alumina (10× excess by weight). The reaction mixture was filtered, solids were washed with ethyl acetate, and the filtrate was concentrated to give the vinyl sulfones that were purified further in some cases as noted. In the case of iodophenylsulfones **19**, **20**, and **23**, elimination was carried out by stirring overnight in carbon tetrachloride containing 1.3 equiv. of DABCO.

(*E*)-3-Phenylsulfonyl-2-propen-1-ol (14)

Allyl alcohol was converted to the iodophenylsulfonyl derivative **13** in 60% yield as described in the previous paragraph. R_f 0.17 (40% ethyl acetate – hexanes). IR (ATR, cm^{-1}) ν_{max}: 3495 (OH), 3064, 2934, 1447, 1300 (S=O), 1142 (S=O), 1082. ^1H NMR ($CDCl_3$) δ: 7.9 (m, 2H, PhH), 7.7 (m, 3H, PhH), 4.57 (sextet, 1H, *J* = 4.5 Hz, CHI), 4.04 (dd, 1H, *J* = 4.5, 12.6 Hz, CHOH), 3.93 (dd, 1H, *J* = 4.5, 12.6 Hz, CHOH), 3.93 (dd, 1H, *J* = 9.6 Hz, $PhSO_2CH_2$), 3.67 (dd, 1H, *J* = 4.5 Hz, $PhSO_2CH_2$), 2.43 (bs, 1H, OH). ^{13}C NMR ($CDCl_3$) δ: 139.0, 134.6, 129.8, 128.2, 67.4 (CHOH), 62.3 (CH_2SO_2Ph), 22.0 (CHI). HRMS calcd. for $C_9H_{12}O_3SI$: 325.9552 (M + H); found: 325.9561.

Elimination as described in the general procedure gave crystalline vinyl sulfone **14** (202 mg, 95%); mp 134–136 °C (lit. value (27) mp 139 to 140 °C). R_f 0.18 (ethyl acetate – hexanes, 1:1). ^1H NMR ($CDCl_3$) δ: 7.9 (m, 2H, PhH), 7.6 (m, 3H, PhH), 7.06 (m, 1H, *J* = 18 Hz, C=CH), 6.66 (m, 1H, *J* = 18 Hz, C=CH), 4.42 (m, 2H, CH_2OH), 1.6, (bs, 1H, OH). The ^1H NMR spectrum of **14** reported in the literature lists the vinylic hydrogens as a multiplet at δ 7.1–6.6, the CH_2OH methylene hydrogens as a multiplet at δ 5.55–4.20, and the hydroxyl proton resonance as a broad singlet at δ 3.90 (28).

(*E*)-4-Phenylsulfonyl-3-buten-2-ol (16)

3-Butene-2-ol (72 mg, 1 mmol) was converted to diastereomeric 3-iodo-4-phenylsulfonyl-2-butanols (**15**). Yield: 216 mg (63%). R_f 0.23 (40% ethyl acetate – hexanes). IR (ATR, cm^{-1}) ν_{max}: 3531 (OH), 2960, 1447, 1280 (S=O), 1142 (S=O), 1082. ^1H NMR δ: 7.90 (m, 2H, PhH), 7.62 (m, 3H, PhH), 4.60 (ddd, 1H, *J* = 9.8, 4.2, 2.0 Hz, CHI), 4.53 (td, 1H, *J* = 6.6, 4.2 Hz, CHI), 4.06 (dd, 1H, *J* = 14.2, 9.8 Hz, $PhSO_2CH$), 3.74 (d, 2H, *J* = 6.6 Hz, $PhSO_2CH_2$), 3.70 (dd, 1H, *J* = 14.2, 4.4 Hz, $PhSO_2CH$), 3.62, (bs or dq if OH is decoupled, 1H, *J* = 4.2, 6.1 Hz, CHOH), 3.43 (bs or dq if OH is decoupled, 1H, *J* = 5.9, 2.0 Hz, CHOH), 2.20

© 2006 NRC Canada

(bs, OH), 1.29 (d, 3H, J = 6.1 Hz, CH_3), 1.27 (d, 3H, J = 5.9 Hz, CH_3). ^{13}C NMR ($CDCl_3$) δ: 134.1, 134.0, 128.4, 128.4, 128.0, 127.7, 69.7 (CHOH), 67.7 (CHOH), 62.5 ($PhSO_2CH_2$), 62.0 ($PhSO_2CH_2$), 32.6 (CHI), 30.7 (CHI), 25.0 (CH_3), 20.9 (CH_3). HRMS calcd. for $C_{10}H_{14}O_3SI$: 340.9708 (M + H); found: 340.9705.

Treatment with alumina (2.1 g) gave 122 mg (92%) of vinyl sulfone **16**; mp 74 to 75 °C (lit. value (29) mp 64–66 °C. R_f 0.19 (40% ethyl acetate – hexanes). The ^{1}H NMR spectrum of **16** matched that reported (29).

(*E*)-1-(Phenylsulfonyl)hex-1-en-3-ol (18)

1-Hexen-3-ol (100 mg, 1 mmol) was converted to diastereomeric 2-iodo-1-(phenylsulfonyl)hex-1-en-3-ols (**17**). Yield: 305 mg (83%). R_f 0.36 (40% ethyl acetate – hexanes). IR (ATR, cm^{-1}) ν_{max}: 3497, 2959, 2933, 1447, 1304 (S=O), 1142 (S=O) 1083. ^{1}H NMR δ: 7.90 (m, 2H, PhH), 7.60 (m, 3H, PhH), 4.62 (ddd, 1H, J = 10.0, 4.3, 2.0 Hz, CHI), 4.49 (td, 1H, J = 6.9, 6.3, 4.1 Hz, CHI), 4.09 (dd, 1H, J = 14.2, 10.0 Hz, $PhSO_2CH$), 3.79 (dd, 1H, J = 15.4, 6.3 Hz, $PhSO_2CH_2$), 3.71 (dd, 1, J = 15.4, 6.9 Hz, $PhSO_2CH$), 3.70 (dd, 1, J = 14.2, 4.3 Hz, $PhSO_2CH$), 3.54 (cm, 1H, J = 4.1 Hz, CHOH), 3.11 (cm, 1H, J = 2.0 Hz, CHOH), 2.10 (bs, OH), 1.64–1.32 (m, 2 × 4H, CH_2), 0.96 (m, 3H, J = 6.9 Hz, CH_3), 0.94 (m, 3H, J = 6.7 Hz, CH_3). ^{13}C NMR ($CDCl_3$) δ: 138.7, 138.5, 134.0, 134.0, 129.4, 129.3, 129.3, 128.0, 127.7, 74.3 (CHOH), 71.0 (CHOH), 62.6 ($PhSO_2CH_2$), 61.5 ($PhSO_2CH_2$), 41.3, 36.5, 31.6, 28.6, 18.7, 18.5, 13.9, 13.9. HRMS calcd. for $C_{12}H_{18}O_3SI$: 369.0021 (M + H); found: 369.0021.

Treatment with alumina (3 g) gave 211 mg (88%) of vinyl sulfone **18**; mp 54–57 °C (lit. value (30) mp 56–58 °C). R_f 0.25 (40% ethyl acetate – hexanes). The ^{1}H and ^{13}C NMR spectra of **18** matched those reported (30).

3-(*tert*-Butyldimethylsiloxy)-1-(phenylsulfonyl)cyclohexene (21) and 3-(*tert*-butyldimethylsiloxy)-2-(phenylsulfonyl)cyclohexene (22)

Iodophenylsulfonation of the TBDMS ether of cyclohexenol gave a mixture of regioisomeric 2-iodo-1-phenylsulfonyl and 1-iodo-2-phenylsulfonyl derivatives (**19**, **20**); from 214 mg (1 mmol) of alkene there was obtained 371 mg (77%) of iodophenylsulfonyl adducts as an oil. R_f 0.36 (10% ethyl acetate – hexanes). ^{1}H NMR δ: 7.90 (m, 2H, PhH), 7.60 (m, 3H, PhH), 5.15 (m, 1H), 4.90 (m, 1H), 4.40 (m, 1H), 3.61 (m, 1H), 3.51 (m, 1H), 3.19 (m, 1H), 2.14–1.90 (m, 4H), 1.66–1.48 (m, 2H), 0.90 (s, *t*-Bu), 0.82 (s, *t*-Bu), 0.06 (s, CH_3), 0.04 (s, CH_3).

The crude mixture was taken up in carbon tetrachloride (3 mL), DABCO was added (112 mg, 1.3 equiv.), and the mixture was stirred overnight at room temperature. The mixture was diluted with dichloromethane, extracted with water and brine, dried (Na_2SO_4), and concentrated to give 262 mg (92%) of a mixture of vinyl sulfone **21** and its regioisomer **22**, which were not separated. R_f 0.27 (10% ethyl acetate – hexanes). The ^{1}H NMR spectrum of the mixture of vinyl sulfones showed a 2.2:1 ratio of vinyl sulfone **21** (the resonances of which matched those reported in the literature, ref. 27) and another product, assigned as the regioisomeric vinyl sulfone **22**, which showed peaks at δ 7.17 (C=CH) and 4.66 (CHOSi). HRMS calcd. for $C_{18}H_{29}O_3SiS$: 353.1607 (M + H); found: 353.1612.

3-(*tert*-Butyldimethylsiloxy)-2-methyl-1-(phenylsulfonyl)-cyclohexene (24)

The TBDMS ether of 2-methylcyclohexenol gave diastereomeric 2-iodo-3-phenylsulfonyl derivatives (**23**) and a small amount of a side product that was not identified; from 266 mg (1.18 mmol) of alkene there was obtained 334 mg (57%) of iodophenylsulfonyl adducts as an oil. R_f 0.30 (10% ethyl acetate – hexanes). ^{1}H NMR δ: 7.89 (m, 2H, PhH), 7.51 (m, 3H, PhH), 3.83 (m, 1H), 3.12 (m, 1H), 2.75 (m, 1H), 2.47–1.41 (m, 6H), 1.29 (s, 3H, CH_3), 1.26 (s, 3H, CH_3), 0.85 (s, *t*-Bu), 0.83 (s, *t*-Bu), 0.06 (s, CH_3), 0.04 (s, CH_3).

The crude mixture was taken up in carbon tetrachloride (3 mL), DABCO was added (88 mg, 1.3 equiv.), and the mixture was stirred overnight at room temperature. The mixture was diluted with dichloromethane, extracted with water and brine, dried (Na_2SO_4), and concentrated to give 196 mg of a mixture of products that was purified using a Waters vacuum manifold with a 20 Sep-Pak silica gel cartridge and 5%–20% ethyl acetate – hexanes as eluant to give 95 mg (38%) of vinyl sulfone **24** as an oil. R_f 028 (10% ethyl acetate – hexanes). ^{1}H NMR δ: 7.86 (m, 2H, PhH), 7.60 (m, 3H, PhH), 3.87 (m, 1H, CHOSi), 3.12 (m, 1H), 2.45 (s, 3H, CH_3), 2.36–1.24 (m, 6H), 1.29 (s, CH_3), 0.93 (s, *t*-Bu), 0.13 (s, CH_3), 0.12 (s, CH_3). HRMS calcd. for $C_{19}H_{31}O_3SiS$: 366.1763 (M + H); found: 366.1772

Phenylsulfonyl 4-*O*-acetyl-2,3,6-trideoxy-α,β-L-*threo*-hex-2-enopyranoside (27)

Benzenesulfinic acid (560 mg, 4 equiv.) was added to a stirring solution of 3,4-di-*O*-acetyl-6-deoxy-L-glucal (214 mg, 1 mmol) in 5 mL of anhydrous dichloromethane at 0 °C. The reaction was allowed to warm to room temperature and stirred for 1 h, after which TLC (20% ethyl acetate – hexane) showed that starting material was consumed. The mixture was then diluted with 40 mL of dichloromethane and washed with 10% $NaHCO_3$ (40 mL) and brine (40 mL), dried (Na_2SO_4), and concentrated to an oil that was purified on a Waters vacuum manifold using a 20 cc Sep-Pak silica gel cartridge and 20% ethyl acetate – hexane as eluant to give a 3:1 mixture of α and β anomers that were not separated. Yield: 255 mg (86%). R_f 0.4 (40% ethyl acetate – hexanes). ^{1}H NMR (300 MHz, $CDCl_3$): see Table 2. ^{13}C NMR (75.4 MHz, $CDCl_3$) δ: 169.8, 169.4, 136.6, 134.0, 133.7 (C_2/C_3), 132.9 (C_2/C_3), 129.6, 128.7, 128.6, 128.1, 120.9 (C_2/C_3), 119.0 (C_2/C_3), 89.3 (C_1, α), 88.1 (C_1, β), 72.4, 68.7, 68.4, 20.7, 20.6, 17.8, 17.5. Analytical MW calcd. for $C_{14}H_{16}O_5S$: 296; found by ESIMS: 314.3 (38%) $(M + NH_4)^+$, 155.3 (100%). HRMS calcd. for $C_{14}H_{17}O_5S$: 296.0797 (M + H); found: 297.0787.

Iodophenylsulfonation of dihydropyran

Dihydropyran (252 mg, 3 mmol) was dissolved in a mixture of 3 mL each of anhydrous acetonitrile and anhydrous dichloromethane. Tetra-*N*-butylammonium benzenesulfinate (36) (3 mmol, 1.15 g) and 4 Å molecular sieves (100 mg) were added and the reaction mixture was stirred for 30 min, then *N*-iodosuccinimide (675 mg, 3 mmol) was added and

© 2006 NRC Canada

Table 2.

	α Anomer	β Anomer
δ_H, J	δ_H	δ_H
H_1	5.075	5.226
H_2	6.234	5.943[a,b]
H_3	6.234	6.120[a]
H_4	5.017	4.520
H_5	4.390	3.588
H_6	1.196	1.220
OAc	2.092	2.031
H_o	7.937	7.879
H_m	7.594	7.544
H_p	7.702[c]	7.693
$J_{1,2}$	[d]	2.1
$J_{1,3}$	[d]	2.2
$J_{1,4}$	2.5	2.7
$J_{1,5}$	0.7	~0
$J_{2,3}$	~10.5	10.5
$J_{2,4}$	[d]	1.7
$J_{3,4}$	[d]	2.2
$J_{4,5}$	8.4	8.4
$J_{5,6}$	6.3	6.1

[a]H_2 and H_3 shifts, including related coupling constants, may need to be exchanged.
[b]Broadened dt multiplet.
[c]Shifts determined with the help of COSY.
[d]The coupling constants could not be determined because of the small $\Delta\delta$ between H_2 and H_3, generating high order multiplets.

the reaction was allowed to stir for 8 h at –78 °C. The reaction was diluted with dichloromethane (50 mL), washed with 10% $NaHSO_3$ (50 mL), water (50 mL), and brine (50 mL), dried over Na_2SO_4, and concentrated to give a yellow oily product that was then purified by flash chromatography over silica gel using 40% ethyl acetate in hexanes as the eluant. One of the products separated as a waxy solid (101 mg, 11%) was determined to be the *trans*-3-iodo-2-succinimide adduct of dihydropyran. The other fractions contained a mixture (211 mg) of the 3-iodo-2-phenylsulfonyl adducts and other side products that were not identified. The *trans*-3-iodo-2-succinimide **26** adduct had: R_f 0.28 (40% ethyl acetate – hexane). IR (film, cm^{-1}) ν_{max}: 2950, 1716, 1371. ^1H NMR δ: 5.24 (d, 1H, J = 11.2 Hz, CHN), 5.16 (ddd, 1H, J = 2.8, 11.2 Hz, CHI), 4.15 (m, 1H), 3.68 (m, 1H), 2.74 (s, 4H, CH_2CH_2), 2.60 (m, 1H), 2.13 (m, 1H), 1.78 (m, 1H), 1.40 (m, 1H). ^{13}C NMR δ: 178.2, 86.2, 71.6, 39.9, 31.2, 30.4, 26.7. HRMS calcd. for $C_9H_{13}NO_3I$: 309.9940; found: 309.9942.

The 3-iodo-2-phenylsulfonyl adducts **27** had: R_f 0.5 (40% ethyl acetate – hexane). IR (film, (cm^{-1}) ν_{max}: 2950, 1625, 1439, 1320 (S=O), 1139 (S=O). ^1H NMR δ: 5.01 (d, 1H, J = 5.6 Hz, CHS) 4.86 (d, 1H, J = 6.7 Hz, CHS), 4.21–3.98 (m, 2H), 3.72 (m, 1H), 3.62 (m, 1H), 2.2–1.6 (m, 10H). HRMS calcd. for $C_{11}H_{12}O_3SI$: 350.9548 (M – H); found: 350.9582.

Acknowledgments

The authors thank Dr. John Wojcik for conducting experiments that revealed the formation of benzenesulfonyl iodide from benzenesulfinic acid and *N*-iodosuccinimide. We also thank Villanova University for financial support of this research.

References

1. Reviews: (*a*) T. Durst. *In* Comprehensive organic chemistry. Vol. 3. *Edited by* D.N. Jones. Pergamon Press, Oxford. 1979. p. 171; (*b*) M.P. Bertrand. Org. Prep. Proced. Int. **26**, 257 (1994); (*c*) C. Chatgilialoglu, M.P. Bertrand, and C. Ferreri. *In* S-Centered radicals. *Edited by* Z.B. Alfassi. John Wiley, New York. 1999. Chap. 11.
2. (*a*) M. Asscher and D. Vofsi. J. Chem. Soc. 4962 (1964); (*b*) A. Orochov, M. Asscher, and D. Vofsi. J. Chem. Soc. (B), 255 (1969); (*c*) J. Sinnreich and M. Asscher. J. Chem. Soc. Perkin Trans. 1, 1543 (1972).
3. (*a*) W.E. Truce, C.T. Goralski, L.W. Christensen, and R.H. Bavry. J. Org. Chem. **35**, 4217 (1970); (*b*) W.E. Truce and C.T. Goralski. J. Org. Chem. **35**, 4220, (1970); (*c*) W.E. Truce and C.T. Goralski. J. Org. Chem. **36**, 2536 (1971).
4. J.-P. Pillot, J. Dunoguès, and R. Calas. Synthesis, 469 (1977).
5. I. De Riggi, J.-M. Surzur, and M.P. Bertrand. Tetrahedron, **44**, 7119 (1988).
6. (*a*) N. Kamigata, H. Sawada, and M. Kobayashi. J. Org. Chem. **48**, 3793 (1983); (*b*) N. Kamigata, J. Ozaki, and M. Kobayashi. J. Org. Chem. **50**, 5045 (1985); (*c*) N. Kamigata, K. Udodaira, and T. Shimizu. J. Chem Soc. Perkin Trans. 1, 783 (1997).
7. M.S. Kharasch and A.F. Zavist. J. Am. Chem. Soc. **73**, 964 (1951).
8. (*a*) S.J. Cristol and J.A. Reeder. J. Org. Chem. **26**, 2182 (1961); (*b*) S.J. Cristol and D.I. Davies. J. Org. Chem. **29**, 1282 (1964).
9. W. Böll. Liebigs Ann. Chem. 1665 (1979).
10. H. Goldwhite, J.S. Gibson, and C. Harris. Tetrahedron, **21**, 2743 (1965).
11. A.S. Gozdz and P. Maslak. J. Org. Chem. **56**, 2179 (1991).
12. C.M.M. da Silva Corrêa and W.A. Waters. J. Chem. Soc. (C), 1874 (1968).
13. Y. Takahara, M. Iino, and M. Matsuda. Bull. Chem. Soc. Jpn. **49**, 2268 (1976).
14. P.S. Skell and J.H. McNamara. J. Am. Chem. Soc. **79**, 85 (1957).
15. W.E. Truce, D.L. Heuring, and G.C. Wolf. J. Org. Chem. **39**, 238 (1974).
16. C.M.M. da Silva Corrêa, M.D.C.M. Fleming, M.A.B.C.S. Oliveira, and E.M.J. Garrido. J. Chem. Soc. Perkin Trans 2, 1993 (1994).
17. L.K. Liu, Y. Chi, and K.-Y. Jen. J. Org. Chem. **45**, 406 (1980).
18. L.M. Harwood, M. Julia, and G. Le Thuillier. Tetrahedron, **36**, 2487 (1980).
19. (*a*) K. Inomata, T. Kobayashi, S.-i. Sasaoka, H. Kinoshita, and H. Kotake. Chem. Lett. 289 (1986); (*b*) K. Inomata, S-i. Sasaoka, T. Kobayashi, Y. Tanaka, S. Igarashi, T. Ohtani, H. Kinoshita, and H. Kotake. Bull. Chem. Soc. Jpn. **60**, 1767 (1987).
20. J. Barluenga, J.M. Martinez-Gallo, C. Nájera, F.J. Fañanás, and M. Yus. J. Chem. Soc. Perkin Trans. 1, 2605 (1987).
21. C. Nájera, B Baldó, and M. Yus. J. Chem. Soc. Perkin Trans. 1, 1029 (1988).
22. P.S. Skell, R.C. Woodworth, and J.H. McNamara. J. Am. Chem. Soc. **79**, 1253 (1957).
23. Synthesis of vinyl sulfones via iodosulfone intermediates has

© 2006 NRC Canada

also been carried out by Ce(IV)-mediated reaction of alkenes with aryl sulfinates and sodium iodide: V. Nair, A. Augustine, and T.D. Suja. Synthesis, 2259 (2002).
24. A. Weichert and H.M.R. Hoffmann. J. Org. Chem. **56**, 4098 (1991).
25. N.S. Simpkins. Sulphones in organic synthesis. Tetrahedron organic series Vol. 10. Pergamon Press, New York. 1993.
26. B.M. Trost, P. Seoane, S. Mignani, and M. Acemoglu. J. Am. Chem. Soc. **111**, 7487 (1989).
27. J. Ponton and P. Helquist. J. Org. Chem. **46**, 118 (1981).
28. D. Villemin and A.V. Aloum. Synth. Commun. **20**, 925 (1990).
29. E. Dominguez and J.C. Carretero. Tetrahedron, **46**, 7197 (1990).
30. A.D Westwell, M. Thornton-Pett, and C.M. Rayner. J. Chem. Soc. Perkin Trans. 1, 847 (1995).
31. (*a*) D.S. Brown, M. Bruno, R.J. Davenport, and S.V. Ley. Tetrahedron, **45**, 4293 (1989); (*b*) S.V. Ley, S.F. Lygo, and A. Wonnacott. Tetrahedron, **42**, 4333 (1986).
32. M. Uchino, K. Suzuki, and M. Sekiya. Chem. Pharm. Bull. **26**, 1837 (1978).
33. H.J. Shine, M. Rahman, H. Seeger, and G.-S. Wu. J. Org. Chem. **32**, 1901 (1967).
34. P.B. Hopkins and P.L. Fuchs. J. Org. Chem. **43**, 1208 (1978).
35. L. Benati, L. Capella, P.C. Montevecchi, and P. Spagnolo. J. Chem. Soc. Perkin Trans. 1, 1035 (1995).
36. G.E. Vennstra and B. Zwaneburg. Synthesis, 519 (1975).

© 2006 NRC Canada

HR-MAS NMR studies of ^{15}N-labeled cells confirm the structure of the *O*-methyl phosphoramidate CPS modification in *Campylobacter jejuni* and provide insight into its biosynthesis[1]

David J. McNally, Marc Lamoureux, Jianjun Li, John Kelly, Jean-Robert Brisson, Christine M. Szymanski, and Harold C. Jarrell

Abstract: Because *Campylobacter jejuni* is the leading cause of bacterial food-borne gastroenteritis throughout the world, there is intense effort to determine the mechanisms of infectivity associated with this bacterium. Capsular polysaccharide (CPS) has been shown to be an important virulence factor for *C. jejuni* and a recent study that examined the 11168V26 strain identified several phase-variable CPS modifications including an unusual *O*-methyl phosphoramidate (MeO*P*N) group on C-3 of the Gal*f*NAc residue. In this study, we examined the MeO*P*N group using homo- and hetero-nuclear high-resolution magic angle spinning (HR-MAS) NMR experiments of whole bacterial cells grown on $^{15}NH_4Cl$-enriched media. ^{1}H–^{31}P HSQC NMR experiments showed that the level of ^{15}N labeling within the MeO*P*N reached 80%, and a large $^{1}J(^{15}N$–$^{31}P)$ scalar coupling provided direct evidence that confirmed the structure of the MeO*P*N as $CH_3OP(O)(NH_2)(OR)$. Because ^{15}N was also detected within the major outer membrane protein as well as the NAc and NGro groups of CPS, ammonium was concluded to be an important building block used in the synthesis of amino acids and glycan structures in *C. jejuni*. HR-MAS NMR studies of ^{15}N-labeled cells revealed an unanticipated level of complexity as multiple MeO*P*N signals were observed within ^{1}H-^{31}P HSQC spectra for the 11168V26 and 11168H strains. While some signals originated from the MeO*P*N at C-3 of Gal*f*NAc, others were attributed to a novel MeO*P*N located on D-*glycero*-α-L-*gluco*-heptopyranose. Together, these HR-MAS NMR findings shed light on nitrogen metabolism in *C. jejuni*, confirm the chemical structure of the MeO*P*N, and demonstrate that the modification occurs on both furanose and pyranose CPS sugars for this bacterium.

Key words: Campylobacter jejuni, capsular polysaccharide, HR-MAS NMR, isotope labeling, phosphoramidate.

Résumé : Compte tenu du fait que le *Campylobacter jejuni* est la cause principale des gastroentérites reliées à l'alimentation dans le monde, un effort intense est développé pour déterminer les mécanismes d'infection associés à cette bactérie. Il a été démontré que le polysaccharide capsulaire (PSC) est un facteur important de virulence du *C. jejuni* et une étude récente qui a examiné la souche 11168V26 a permis d'identifier plusieurs modifications du PSC de phase variable, dont une comportant le groupement inhabituel phosphoramidate de *O*-méthyle (MeO*P*N) en position C-3 du résidu Gal*f*NAc. Dans cette étude, le groupe MeO*P*N a été examiné par des expériences de RMN homo- et hétéronucléaires à haute résolution, à l'angle magique de rotation (« HR-MAS ») sur des cellules complètes de bactéries cultivées dans un milieu enrichi en $^{15}NH_4Cl$. Des expériences de RMN « HSQC » ^{1}H–^{31}P ont permis de montrer que le niveau de marquage au ^{15}N dans le MeO*P*N atteint 80 % et le grand couplage scalaire $^{1}J(^{15}N$–$^{31}P)$ a fourni une preuve directe pour confirmer que la structure du MeO*P*N est $CH_3OP(O)(NH_2)(OR)$. Compte tenu du fait qu'on peut aussi détecter la présence de ^{15}N dans la protéine principale de la membrane extérieure de la cellule sous la forme de groupes NAc et NGro du PSC, on en conclut que l'ammonium est un produit important dans la synthèse des acides aminés et les structures des glycanes du *C. jejuni*. Les études de RMN à haute résolution, à l'angle magique de rotation, des cellules marquées au ^{15}N ont permis de montrer l'existence d'un degré inattendu de complexité alors qu'on a observé de multiples signaux de MeO*P*N dans les spectres HSQC ^{1}H–^{31}P des souches 11168V26 et 11168H. Alors que quelques signaux trouvent leur origine dans le MeO*P*N en position C-3 du Gal*f*NAc, d'autres peuvent être attribués à un nouveau MeO*P*N situé sur le D-*glycéro*-α-L-*gluco*-heptopyranose. Prises dans leur ensemble, ces données obtenues par des études RMN HR-MAS, permettent de jeter de la lumière sur le métabolisme de l'azote dans le *C. jejuni*,

Received 22 August 2005. Published on the NRC Research Press Web site at http://canjchem.nrc.ca on 17 May 2006.

Dedicated to Professor W.A. Szarek.

D.J. McNally, M. Lamoureux, J. Li, J. Kelly, J.-R. Brisson, C.M. Szymanski, and H.C. Jarrell.[2] Institute for Biological Sciences, National Research Council of Canada, Ottawa, ON K1A 0R6, Canada.

[1]This article is part of a Special Issue dedicated to Professor Walter A. Szarek.
[2]Corresponding author (e-mail: Harold.Jarrell@nrc-cnrc.gc.ca).

 doi:10.1139/V06-028 © 2006 NRC Canada

confirment la structure chimique du MeO*P*N et démontrent que la modification se produit tant sur les parties furanose et pyranose des sucres du PSC de cette bactérie.

Mots clés : Campylobacter jejuni, polysaccharide capsulaire, RMN HR-MAS, marquage isotopique, phosphoramidate.

[Traduit par la Rédaction]

Introduction

The Gram-negative, spiral-shaped bacterium *Campylobacter jejuni* is the leading cause of bacterial gastroenteritis worldwide and a significant cause of child morbidity in underdeveloped countries (1). In addition, there is convincing evidence linking *C. jejuni* infections to the development of Miller Fisher and Guillain-Barré neuropathies, the latter being the primary cause of neuroparalysis since the eradication of polio (1, 2). As a result, there is intense effort to elucidate the virulence factors and mechanisms of infectivity associated with this mucosal pathogen.

Capsular polysaccharides (CPSs) are found on the surface of a large number of bacterial species and play a key role in survival in the environment and often contribute to pathogenesis (3). By mimicking host cell antigens and through structural variation, CPSs also convey evasion from host immune responses and are therefore considered important virulence factors. Based on its role in ferret disease, chicken colonization, maintenance of cell surface hydrophilicity, diarrhoeal disease, adherence and invasion of human epithelial cells, and serum resistance, CPS has been established as an important virulence factor in *C. jejuni* (4, 5).

The CPSs produced by *C. jejuni* are structurally diverse and highly variable. For instance, there are presently more than 60 serostrains described for this bacterium, excluding nontypeable strains, representing different CPS structures (6). Genetic mechanisms for this structural variability were partially uncovered when examining the genome of *C. jejuni* NCTC11168 (HS:2) where hypervariable sequences were shown to be a prominent feature of genes encoding the biosynthesis or modification of glycan surface structures (7). By comparing the CPS biosynthetic regions for several strains of *C. jejuni* to the genome of NCTC11168, a recent study demonstrated multiple mechanisms of structural variation including exchange of CPS genes and entire clusters by horizontal transfer, gene duplication, deletion, and fusion, as well as gene variation (6). Direct evidence for structural mechanisms of variation was provided by a study that used high-resolution magic angle spinning (HR-MAS) NMR to examine CPS from growth of individual bacterial colonies of the 11168V26 strain (8). This study identified several phase-variable CPS modifications such as methyl, ethanolamine, and aminoglycerol groups and provided the first report of a variable *O*-methyl phosphoramidate, $CH_3OP(O)(NH_2)(OR)$ (MeO*P*N), on the CPS located at C-3 of the Gal*f*NAc residue (Fig. 1) (8). The structure of the MeO*P*N residue was deduced from mass spectrometric and NMR chemical shift data (8). Since these studies, the MeO*P*N CPS modification was detected on two other strains of *C. jejuni* including NCTC12517 (HS:19) and G1 (HS:1), suggesting it may be common to the species (6). Examination of CPS in the HS:1 serostrain (ATCC 43429, designation MK5-S7630) showed that it has a structurally heterogeneous, teichoic acidlike CPS with a [-4)-α-D-Gal*p*-(1-2)-(*R*)-Gro-(1-*P*]$_n$ repeating unit and two fructofuranose branches substituted at C-3 with MeO*P*N groups (9). By examining purified and cell-bound CPS on the surface of bacterial cells using HR-MAS NMR, this study demonstrated that structural heterogeneity was due to nonstoichiometric fructosylation of Gal and variable MeO*P*N groups. Based on these findings, it was postulated that structural heterogeneity of CPS may represent a mechanism of host evasion or increased fitness in the HS:1 strain (9).

Phosphoramidates are extremely labile structures with large standard free energies of hydrolysis (10, 11), likely explaining why the MeO*P*N was overlooked by previous studies examining CPSs in *C. jejuni*. Although there is little information available regarding the biochemistry or role of phosphoramidates in nature, there is convincing evidence for their involvement in two-component and phosphorelay signal transduction pathways in bacteria that mediate responses such as sporulation, chemotaxis, mucoidy, and flagellar movement (12–18). For *C. jejuni*, there is presently a lack of structural and biochemical information for this MeO*P*N CPS modification. Definitive evidence for the N—P bond would be provided by biosynthetically incorporating ^{15}N into the CPS MeO*P*N residues and demonstrating a $^1J(^{15}N–^{31}P)$ scalar coupling.

In this study, we have developed a method of labeling the MeO*P*N with ^{15}N by growing *C. jejuni* on $^{15}NH_4Cl$-enriched media. The amount of ^{15}N incorporation within the MeO*P*N and its structure were determined directly on the surface of bacterial cells using homo- and hetero-nuclear HR-MAS NMR experiments. Since nitrogen metabolism in campylobacters is largely uncharacterized, CE-ESI/MS and nanoLC–MS/MS were used to analyze the extent of ^{15}N labeling within select proteins and glycan structures. Herein, we show that ammonium is an important source of nitrogen for *C. jejuni*, provide conclusive NMR evidence confirming the structure of the MeO*P*N, and demonstrate the complexity of its distribution on the surface of *C. jejuni* cells.

Experimental

Solvents and reagents

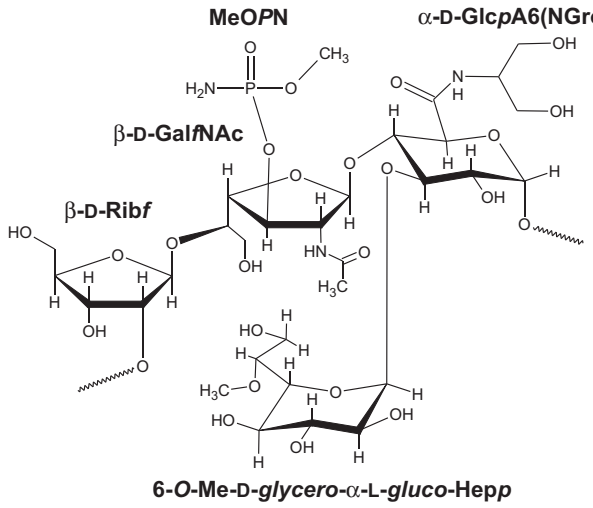
Unless otherwise stated, solvents and reagents were purchased from Sigma Biochemicals and Reagents (Oakville, Ontario).

Bacterial strains, media, and growth conditions

Both *C. jejuni* 11168 isolates, 11168V26 (HS:2) (8, 19) and 11168H (HS:2) (20), were routinely maintained on Mueller Hinton (MH) (Difco, Kansas City, Missouri) plates under microaerophilic conditions (10% CO_2, 5% O_2, and 85% N_2) at 37 °C. ^{14}N- and ^{15}N-labeled MH plates were prepared by combining filter sterilized (0.22 μm, Millipore,

© 2006 NRC Canada

Fig. 1. CPS structure for *Campylobactor jejuni* 11168V26 showing phase-variable modifications such as the 6-O-methyl group on D-*glycero*-α-L-*gluco*-heptopyranose, NGro on α-D-Glc*p*A, and the MeO*P*N on C-3 of β-D-Gal*f*NAc (8). Abbreviations: glycerol (Gro), *O*-methyl phosphoramidate (MeO*P*N).



Billerica, Massachusetts) aqueous solutions of $^{14}NH_4Cl$ (Sigma) or $^{15}NH_4Cl$ (Cambridge Isotopes Laboratories Inc., Andover, Maryland) with autoclaved MH agar to a final volume of 20 mL. To obtain ^{14}N- and ^{15}N-labeled bacterial cells, strains were grown for a total of 48 h under microaerophilic conditions on ^{14}N- or ^{15}N-labeled plates, with transfer onto fresh plates after 24 h.

HR-MAS NMR spectroscopy

For HR-MAS NMR analysis, bacterial cells were prepared as previously described before being loaded into a 40 μL nano-NMR tube (Varian, Palo Alto, California) (8, 9). HR-MAS experiments were performed using a Varian Inova 500 MHz spectrometer equipped with a Varian 4 mm indirect detection gradient nano-NMR probe with a broadband decoupling coil. Spectra from 40 μL cell samples were spun at 3 kHz and recorded at ambient temperature (23 °C), and all experiments were performed with suppression of the HOD signal by presaturation as previously described (8). ^1H NMR spectra of bacterial cells were acquired using the Carr–Purcell–Meiboom–Gill (CPMG) pulse sequence (90 – $(\tau - 180 - \tau)_n$ acquisition) to remove broad signals originating from lipids and solidlike materials (21). The total duration of the CPMG pulse ($n2\tau$) was 10 ms with τ set to (1/MAS spin rate). ^1H NMR spectra for cell-bound CPS on the surface of bacterial cells were typically obtained using 256 transients (11 min). 1D and 2D ^1H–^{31}P HSQC spectra were acquired with the standard Varian HSQC pulse sequence with 1D spectra representing the first increment of the standard HSQC experiment. Unless otherwise specified, 1D ^1H–^{31}P HSQC spectra were obtained with 600 scans and $^3J_{H,P}$ = 10 Hz (20 min), while 2D ^1H–^{31}P HSQC spectra were obtained using 128 scans, 64 increments, and $^3J_{H,P}$ = 10 Hz (8 h) with proton decoupling to remove $J_{H,P}$ scalar couplings. ^1H NMR spectra were referenced to an internal TSP (3-(trimethylsilyl)propionic-2,2,3,3-d_4 acid sodium salt, Sigma) standard (δ_H 0.00 ppm), and ^1H–^{31}P HSQC NMR spectra were referenced to the major MeO*P*N signal at δ_P 13.6 ppm (8).

Mass spectrometric analysis of ^{15}N labeling within CPS

For mass spectrometric analysis of ^{14}N- and ^{15}N-labeled CPS, *C. jejuni* 11168V26 cells were grown on four MH plates enriched with 100 mmol/L of $^{14}NH_4Cl$ or $^{15}NH_4Cl$ for 48 h as described in the previous section. Cells were harvested and blended in 90% phenol at 96 °C for 15 min to extract CPS, allowed to cool for 30 min, and then dialyzed (MWCO 12 kDa, Sigma) against running water for 72 h to eliminate traces of phenol. Cells were then ultracentrifuged (140 000 × *g*, 15 °C) for 2 h and the supernatant, which contained crude CPS, was lyophilized to dryness. Due to the high molecular weight of CPS, samples were mass-analyzed using in-source, collision-induced dissociation CE-ESI/MS (22) with a Crystal model 310 Capillary electrophoresis instrument (ATI Unicam, Boston, Massachusetts) coupled to an API 3000 mass spectrometer (Applied Biosystems/Sciex, Concord, Ontario) via a microion spray interface. A sheath solution (isopropanol–methanol, 2:1) was delivered at a flow rate of 1 μL min^{-1}. Separations were achieved on approximately 90 cm of bare fused-silica capillary (190 μm o.d. × 50 μm i.d., Polymicro Technologies, Phoenix, Arizona) using 15 mmol/L ammonium acetate – ammonium hydroxide in deionized water (pH 9.0) containing 5% MeOH as separation buffer. A voltage of 20 kV was typically applied during CE separation and +5 kV was used as the electrospray voltage. Mass spectra were acquired with dwell times of 3.0 ms per step of 0.1 m/z^{-1} unit in full-mass scan mode. Fragment ions formed by collision activation of selected precursor ions with nitrogen in the RF-only quadrupole collision cell were mass analyzed by scanning the third quadrupole. All samples were analyzed in positive ion mode using an orifice voltage of +200 V.

Mass spectrometric analysis of ^{15}N labeling within proteins

For mass spectrometric analysis of ^{14}N- and ^{15}N-labeling in proteins, *C. jejuni* 11168V26 cells were grown on two MH plates enriched with 100 mmol/L of $^{14}NH_4Cl$ or $^{15}NH_4Cl$ for 48 h as described in the previous section. Cells were harvested and proteins were extracted for 20 min with 500 μL of cold glycine (0.2 mol/L, pH 9.2). Extracts were then centrifuged (8900 × *g* for 2 min) to pellet cells and the supernatant was retained. A 2X SDS PAGE sample buffer (10 mL 1.5 mol/L Tris pH 6.8, 6 mL 20% SDS, 30 mL glycerol, 15 mL β-mercaptoethanol, 1.8 mg bromophenol blue, 40 mL H_2O) was then added to the extracts (buffer–supernatant, 3:1 *v/v* ratio) prior to heating at 100 °C for 15 min. To purify proteins, 20 μL of crude protein extract was loaded onto a 10% acrylamide gel (30% acrylamide–Bis solution, 37:1, BioRad, Mississauga, Ontario) and separation of proteins was achieved over 45 min (200 V, 0.04 A). Protein bands were visualized by staining with colloidal coomassie blue for 45 min (Biosafe Coomassie, G250 stain, BioRad) and pure protein bands were manually excised from the gel. Proteins were then destained with a 1:1 ratio of 30 mmol/L potassium ferricyanide and 100 mmol/L sodium thiosulphate, digested with Promega modified trypsin (Madison, Wisconsin) overnight in 50 mmol/L NH_4HCO_3 and peptides

© 2006 NRC Canada

were extracted with 5% HOAc – 50% aqueous MeOH as previously described (23). Peptide fragments were then analyzed by nanoLC–MS/MS using a Q-TOF2 mass spectrometer (Micromass, Waters, Milford, Massachusetts) in automated mode as previously reported (23).

Results

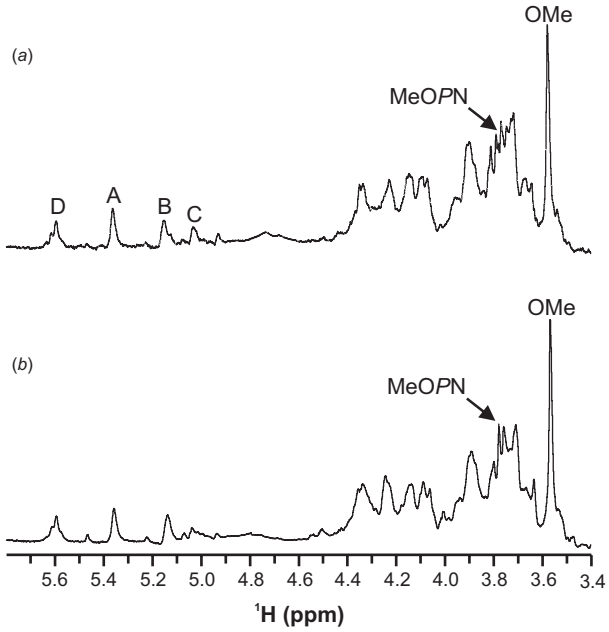
Bacterial growth on $^{15}NH_4Cl$-enriched media

To establish unambiguously the structure of the MeO*P*N residue, we sought to demonstrate a $^1J(^{15}N–^{31}P)$ scalar coupling in the $^1H–^{31}P$ HSQC spectra of CPS biosynthetically labeled with ^{15}N. To label the MeO*P*N with ^{15}N, *C. jejuni* 11168V26 cells were grown on six different concentrations of $^{15}NH_4Cl$ (0, 10, 25, 50, 75, and 100 mmol/L) for 48 h and then examined with HR-MAS NMR. Although bacteria exhibited moderately reduced growth at 75 and 100 mmol/L NH_4Cl (not shown), the HR-MAS ^1H NMR spectrum for cells grown on 100 mmol/L of $^{15}NH_4Cl$ had identical spectral features compared to control cells grown on unlabeled MH plates (Fig. 2*a* vs. 2*b*). Furthermore, the proton chemical shifts for the CPS anomeric resonances of cells grown on labeled and unlabelled media were nearly identical to those reported for this strain by our previous study (8). Because the expression of sensitive phase-variable CPS modifications such as OMe and MeO*P*N groups was not affected and since the chemical shifts of CPS anomeric resonances were not altered, it was concluded that growth on $^{15}NH_4Cl$-enriched media did not introduce obvious structural artifacts within the CPS.

HR-MAS NMR spectroscopy of ^{15}N labeling within the MeO*P*N

To quantify the levels of ^{15}N labeling within the MeO*P*N modification, *C. jejuni* 11168V26 cells grown on different concentrations of $^{15}NH_4Cl$ were examined using $^1H–^{31}P$ HSQC HR-MAS NMR (Fig. 3). Because of the low natural abundance of ^{15}N, $^1J(^{15}N–^{31}P)$ scalar couplings were not observed for the MeO*P*N residue in the spectra of control cells grown on unlabeled MH plates resulting in one phosphorous signal at 13.6 ppm, as expected (Fig. 3*a*). Upon the addition of 10 mmol/L $^{15}NH_4Cl$ to the media, however, additional phosphorous signals were observed as a result of a $^1J(^{15}N–^{31}P)$ scalar coupling (Fig. 3*b*). The magnitude of the $^1J(^{15}N–^{31}P)$ scalar coupling observed for the MeO*P*N at 39 (±2) Hz was consistent with values reported for $^1J(^{15}N–^{31}P)$ scalar couplings in the literature, where they were shown to range from approximately 28 to 43 Hz (24). Integration of these new signals revealed that the addition of 10 mmol/L of $^{15}NH_4Cl$ to the media resulted in approximately 35% ^{15}N labeling within the MeO*P*N. Increasing concentrations of $^{15}NH_4Cl$ within the media resulted in higher levels of ^{15}N incorporation within the MeO*P*N. For instance, bacteria grown on 25, 50, and 75 mmol/L of $^{15}NH_4Cl$ exhibited 50%, 65%, and 75% ^{15}N labeling, respectively, within their MeO*P*N modifications (Figs. 3*c*–3*e*). Bacteria grown on 100 mmol/L of $^{15}NH_4Cl$ exhibited the highest incorporation of ^{15}N within the MeO*P*N at 80% (Fig. 3*f*).

Fig. 2. HR-MAS NMR spectra showing the effects of adding $^{15}NH_4Cl$ to growth media in *Campylobactor jejuni*. (*a*) HR-MAS ^1H NMR spectrum of *C. jejuni* 11168V26 cells grown on media enriched with 100 mmol/L $^{15}NH_4Cl$. (*b*) HR-MAS ^1H NMR spectrum of *C. jejuni* 11168V26 cells grown on unlabelled media (control). Abbreviations: β-D-Rib*f* (A), α-D-Glc*p*A6(NGro) (B), β-D-Gal*f*NAc (C), D-*glycero*-α-L-*gluco*-heptopyranose (D), 6-*O*-methyl group of D-*glycero*-α-L-*gluco*-heptopyranose (OMe), *O*-methyl phosphoramidate (MeO*P*N).

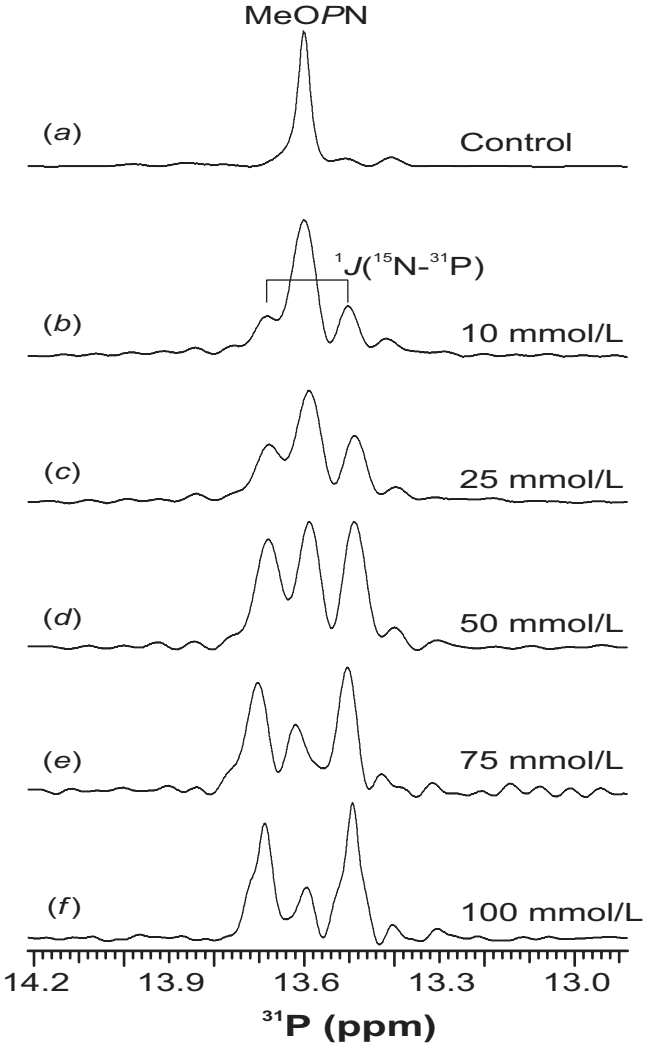


Mass spectrometric analysis of ^{15}N labeling within CPS

To confirm ^{15}N incorporation within the MeO*P*N and determine if the NGro and NAc CPS groups were being labeled, CPS was partially purified from 11168V26 cells grown on 100 mmol/L of $^{15}NH_4Cl$ or $^{14}NH_4Cl$ and analyzed with in-source, collision-induced dissociation CE-ESI/MS (22). Approximately 289 mg of cells (wet pellet mass) was harvested from four $^{15}NH_4Cl$ enriched plates that yielded 16 mg of crude CPS. A comparable amount of cells (281 mg) and crude CPS (12 mg) was recovered from four plates enriched with $^{14}NH_4Cl$. Due to the presence of contaminating ions originating from proteins, nucleic acids, and lipids, precursor ion scans for D-*glycero*-α-L-*gluco*-heptopyranose (*m*/*z* 250) were used to mass analyze both CPS samples (Figs. 4*a* and 4*b*). CE-ESI/MS analysis of CPS prepared from cells grown on $^{14}NH_4Cl$-labeled media showed the mass of one CPS repeat to be *m*/*z* 884.5 $[M + H]^+$, and was consistent with what has been reported for *C. jejuni* 11168V26 (8) (Fig. 4*a*). An intense ion at *m*/*z* 791.0, representing one CPS repeat minus the MeO*P*N $[M + H – 93]^+$, showed that the dominant isotope of nitrogen within the MeO*P*N for these cells was ^{14}N. Because only one sharp signal was observed for *m*/*z* 884.5, it was concluded that the amount of ^{15}N labeling for the NGro and NAc CPS groups was negligible, as expected. In contrast, three distinct ions at *m*/*z* 885.5, 886.5, and 887.5 observed for CPS prepared from cells grown on $^{15}NH_4Cl$ media confirmed that the MeO*P*N, NAc and NGro CPS groups were labeled with ^{15}N (Fig. 4*a*

© 2006 NRC Canada

Fig. 3. HR-MAS ^{1}H–^{31}P HSQC NMR spectra showing ^{15}N labeling within the MeO*P*N for *Campylobactor jejuni* 11168V26 cells. Spectra are shown as traces of the ^{31}P dimension centered on the same MeO*P*N modification. (*a*) Control cells grown on unlabelled media. (*b–f*) Cells grown on media enriched with 10, 25, 50, 75, and 100 mmol/L of $^{15}NH_4Cl$, respectively. For cells grown on $^{15}NH_4Cl$-labeled media, a doublet generated by a $^{1}J(^{15}N–^{31}P)$ of 39 (±2) Hz is evident. Abbreviations: *O*-methyl phosphoramidate (MeO*P*N).

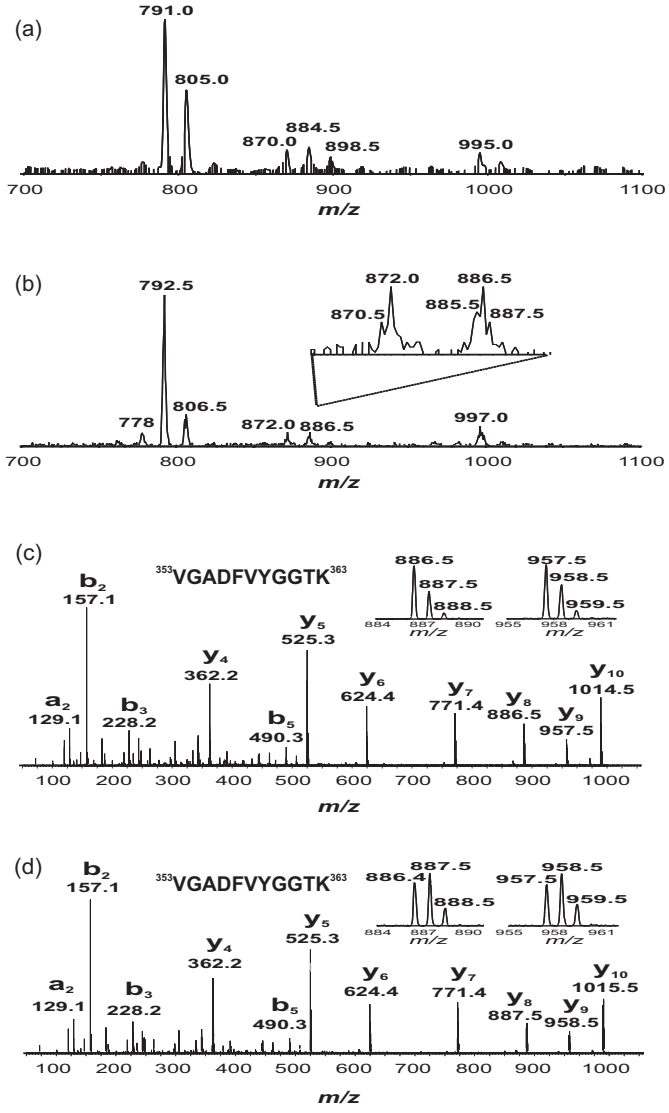


vs. 4*b*). Moreover, an ion at *m/z* 792.5, representing one CPS repeat minus the MeO*P*N $[M + H - 94]^{+}$, indicated that ^{15}N was the dominant isotope of nitrogen within the MeO*P*N for these cells.

Mass spectrometric analysis of ^{15}N labeling within proteins

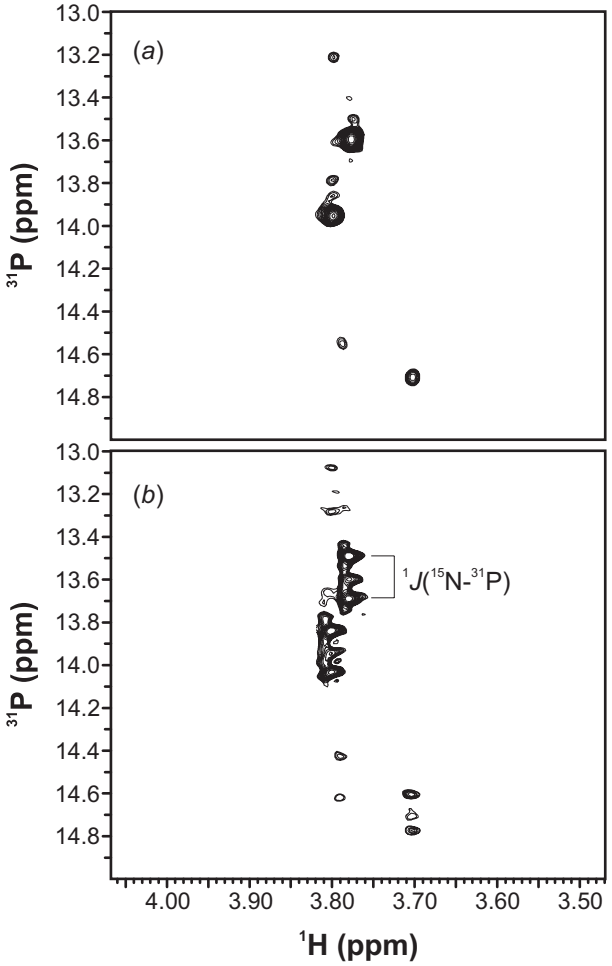
To characterize the amount of ^{15}N labeling within proteins, glycine extracts prepared from *C. jejuni* 11168V26 cells grown on MH plates enriched with 100 mmol/L of $^{14}NH_4Cl$ or $^{15}NH_4Cl$ were separated using SDS PAGE. A strong protein band at 47 kDa was identified as the major outer membrane protein (MOMP) using in-gel tryptic digestion and nanoLC–MS/MS. To analyze ^{15}N incorporation within this protein, the isotope profiles of the tryptic peptides from ^{14}N- and ^{15}N-labeled MOMP as well as their MS/MS fragment ions were compared. As an example, the MS/MS spectra obtained for the ^{14}N- and ^{15}N-labeled tryptic peptide, ^{353}VGADFVYGGTK^{363}, are presented in Figs. 4*c* and 4*d*, respectively. The y_8 (*m/z* 886.5) and y_9 (*m/z* 957.5)

Fig. 4. Mass spectrometry analysis of ^{15}N incorporation within the capsular polysaccharide (CPS) and major outer membrane protein (MOMP) isolated from *Campylobactor jejuni* 11168V26 cells. (*a*) CE-ESI/MS spectrum for a partially purified CPS sample from cells grown on media enriched with 100 mmol/L of $^{14}NH_4Cl$. (*b*) CE-ESI/MS spectrum for partially purified CPS prepared from cells grown on media enriched with 100 mmol/L of $^{15}NH_4Cl$ (precursor ion scans for *m/z* 250, orifice voltage +200 V). (*c*) NanoLC–MS/MS spectrum of the doubly protonated MOMP peptide fragment ion at *m/z* 557.3 (^{353}VGADFVYGGTK^{363}) prepared from cells grown on media enriched with 100 mmol/L of $^{14}NH_4Cl$. (*d*) The MS/MS spectrum obtained for the same peptide fragment ion prepared from cells grown on the 100 mmol/L $^{15}NH_4Cl$ media. The regions around the y8 (*m/z* 886.5) and the y9 (*m/z* 957.5) fragment ions are shown in the insets to demonstrate differences in the isotope profiles for the ^{14}N-only and ^{15}N-labeled samples.



© 2006 NRC Canada

Fig. 5. HR-MAS NMR analysis of the MeO*P*N CPS modification on the surface of *Campylobacter jejuni* 11168V26 cells. (*a*) Proton decoupled $^{1}H–^{31}P$ HSQC NMR spectrum showing five distinct signals originating from MeO*P*Ns on the surface of cells grown on media enriched with 100 mmol/L of $^{14}NH_4Cl$; and (*b*) the same NMR experiment for cells grown on media enriched with 100 mmol/L of $^{15}NH_4Cl$. For cells grown on $^{15}NH_4Cl$ media, $^{1}J(^{15}N–^{31}P)$ scalar couplings observed for MeO*P*Ns range from 32 to 40 (±2) Hz.

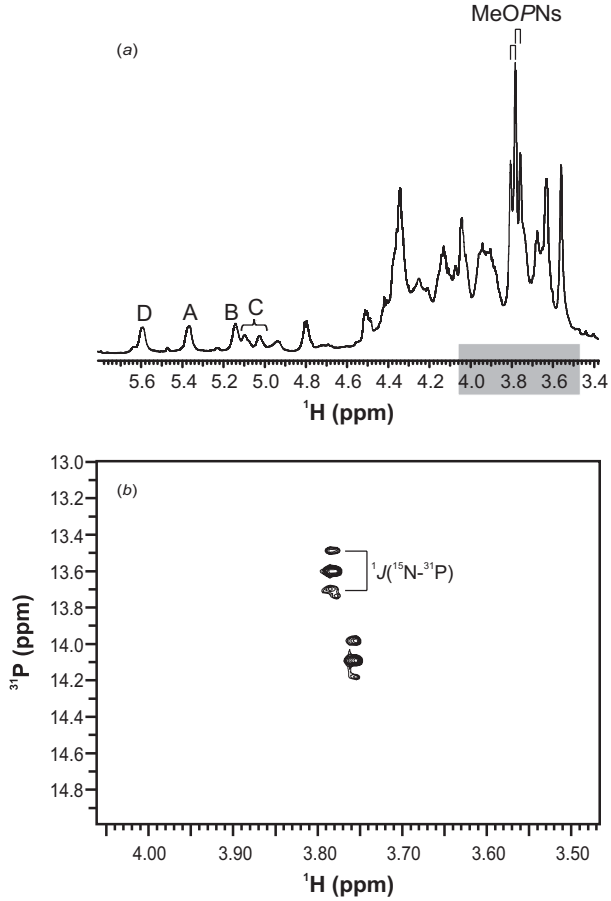


fragment ions are presented in the insets. Based on their isotope profiles, we calculated that approximately 40% of the nitrogen atoms in the ^{15}N-labeled ions have been substituted with ^{15}N. This result was in general agreement with the calculations performed for other peptides that were derived from proteins extracted from *C. jejuni* cells grown on the $^{15}NH_4Cl$ media.

HR-MAS NMR spectroscopy of ^{15}N-labeled 11168V26 and 11168H cells

To characterize the distribution of MeO*P*N on the surface of bacterial cells, *C. jejuni* 11168V26 and 11168H cells were grown on media enriched with 100 mmol/L $^{14}NH_4Cl$ or $^{15}NH_4Cl$ and examined with HR-MAS NMR (Figs. 5 and 6). The $^{1}H–^{31}P$ HSQC spectrum of ^{14}N-labeled 11168V26 cells revealed five distinct signals with chemical shifts characteristic of phosphoramidates between δ_P 13.2 and 13.8 ppm (25–27) (Fig. 5*a*). The $^{1}H–^{31}P$ HSQC spectrum of ^{15}N-

Fig. 6. HR-MAS NMR analysis of *Campylobacter jejuni* 11168H cells. (*a*) HR-MAS ^{1}H NMR spectrum for cells grown on unlabeled media showing two distinct MeO*P*Ns as overlapping doublets at 3.78 and 3.76 ppm ($^{3}J_{H,P}$ = 12 Hz). Two anomeric signals were observed for residue C (β-D-Gal*f*NAc) representing different forms of the sugar; one form where the MeO*P*N is present at C-3 of the sugar (5.10 ppm) and another where the MeO*P*N is absent (5.02 ppm). (*b*) Proton decoupled $^{1}H–^{31}P$ HSQC NMR spectrum for cells grown on media enriched with 100 mmol/L of $^{15}NH_4Cl$ showing an expanded view of the shaded region in (*a*). Two MeO*P*Ns are evident with $^{1}J(^{15}N–^{31}P)$ scalar couplings of approximately 40 (±2) Hz. Abbreviations: β-D-Rib*f* (A), α-D-Glc*p*A6(NGro) (B), B-D-Gal*f*NAc (C), 6-*O*-Me-D-*glycero*-α-L-*gluco*-heptopyranose (D), *O*-methyl phosphoramidate (MeO*P*N).

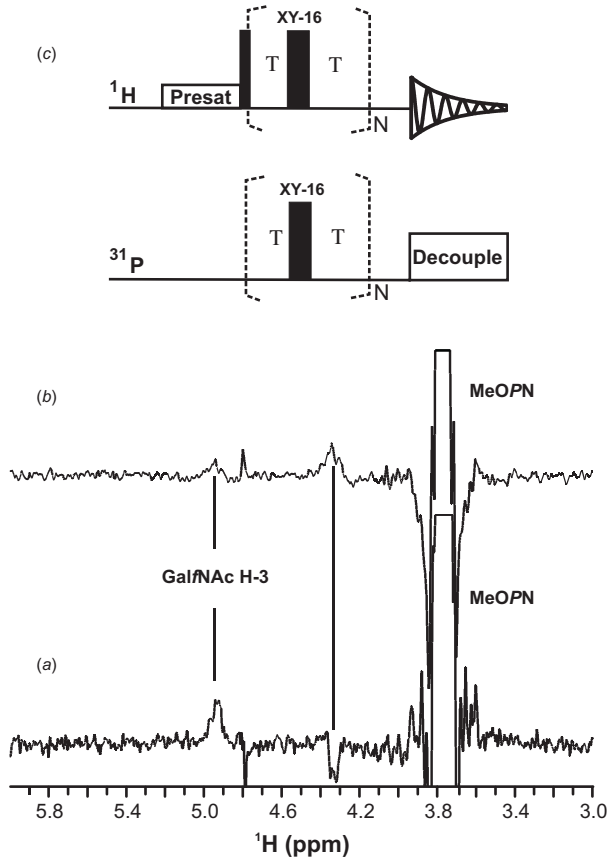


labeled cells confirmed that these signals originated from MeO*P*Ns as they exhibited $^{1}J(^{15}N–^{31}P)$ scalar couplings between 32 and 40 (±2) Hz (24) (Fig. 5*b*). Two MeO*P*N signals were observed within the HR-MAS ^{1}H NMR spectrum for *C. jejuni* 11168H cells as overlapping doublets at 3.78 and 3.76 ppm ($^{3}J_{P,H}$ = 12 Hz) (Fig. 6*a*). The $^{1}H–^{31}P$ HSQC spectrum of ^{15}N-labeled 11168H cells showed that these two signals at δ_P 13.6 and 14.1 ppm had $^{1}J(^{15}N–^{31}P)$ scalar couplings of approximately 40 (±2) Hz, and therefore confirmed that they originated from MeO*P*Ns (Fig. 6*b*).

That several MeO*P*N signals were detected for C. *jejuni* 11168V26 and 11168H cells is suggestive of environmental heterogeneity on the cell surface resulting in multiple signals

© 2006 NRC Canada

Fig. 7. (*a*) 1D ^{1}H–^{31}P HSQC HR-MAS spectrum of *Campylobactor jejuni* 11168H cells showing proton resonances for CPS carbohydrates linked to MeO*P*N residues. The peak at 4.94 ppm corresponds to the Gal*f*NAc H-3 MeO*P*N (2048 scans, $^{3}J_{H,P}$ = 15 Hz). (*b*) ^{1}H–^{31}P correlation difference spectrum showing proton resonances of CPS carbohydrates linked to MeO*P*N residues. The spectrum was acquired using the pulse sequence shown in (*c*) (4096 scans, $^{3}J_{H,P}$ = 12 Hz). (*c*) Pulse sequence used to obtain the ^{1}H–^{31}P correlation difference spectrum. Narrow and thick bars represent 90° and 180° RF pulses, respectively. The 90° pulse durations were 4.5 μs (^{1}H) and 23 μs (^{31}P). The 180° pulse durations for the CPMG pulse train were 27 μs (γB_1 = 9.26 kHz) and 102 μs (γB_1 = 2.45 kHz) for ^{1}H and ^{31}P, respectively. The ^{31}P pulses were on-resonance for the MeO*P*N residue during odd scans, and off-resonance (28 kHz) for even scans. The receiver phase was alternated between x and –x. Pulse phases in the XY-16 are: [x,y,x,y,y,x,y,x,–x,–y,–x,–y,–y,–x,–y,–x]. The number of cycles (*N*) and the *T* interval (~150 μs) were calculated so that the duration of *N* consecutive XY-16 cycles corresponded to 0.5 $J_{H,P}$ (12 Hz). Abbreviations: *O*-methyl phosphoramidate (MeO*P*N), presaturation (Presat).



for the MeO*P*N at C-3 of Gal*f*NAc, or that there are other MeO*P*N(s) substituted elsewhere. To investigate these possibilities, a 1D HR-MAS ^{1}H–^{31}P HSQC spectrum was acquired ($^{3}J_{H,P}$ = 15 Hz, Fig. 7), since MeO*P*N cross peaks to carbohydrate residues are not typically observed for the 2D ^{1}H–^{31}P HSQC experiment. In addition to the expected MeO*P*N methyl resonances and Gal*f*NAc H-3 resonance at 4.94 ppm, a novel signal at 4.34 ppm was detected for 11168H cells (Fig. 7*a*). Inversion of this novel resonance at 4.34 ppm relative to the one at 4.94 ppm was most likely the result of ^{1}H homonuclear couplings during the 1/2*J* period that had magnitudes approaching the heteronuclear coupling (6–8 Hz) (28), which suggested that the ^{31}P was scalar coupled to a geminal proton or a proton attached to a pyranose ring with a gluco configuration.

To establish that the signal at 4.34 ppm was not an artifact, a 1D difference spectrum was acquired using the pulse sequence shown in Fig. 7c. During odd acquisitions, a CPMG pulse train was simultaneously applied to ^{1}H and ^{31}P during the 1/2*J* coherence transfer step to maintain in-phase ^{1}H magnetization similar to the CPMG–INEPT transfer (28, 29). During even acquisitions, ^{31}P π pulses were applied off-resonance (28 kHz) and subtracted. After an evolution time of 1/2*J* (*J* = 12–15 Hz), the heteronuclear single quantum coherence (I_xS_z) is present, but does not evolve into a detectable signal during acquisition when ^{31}P is decoupled. Subtraction of the spectrum acquired without ^{31}P π pulses produces a difference spectrum in which only those protons scalar coupled to ^{31}P are visible. This is similar to a heteronuclear spin-echo difference spectrum, however; with this experiment, the evolution time is reduced by a factor of two, thereby reducing T_2 attenuation of the signal. The resulting spectrum for 11168H cells exhibited peaks at 4.94 and 4.34 ppm that were in-phase (Fig. 7*b*). Because both peaks were in phase, it was concluded that the resonance at 4.34 ppm was not an artifact since the ^{1}H CPMG-pulse train of this difference experiment selectively suppresses the evolution of homonuclear couplings ($J_{H,H}$).

Based on previous studies showing that substitution with the MeO*P*N causes a localized downfield shift of 0.6–0.8 ppm (8, 9), we propose that the signal at 4.34 ppm originates from a novel MeO*P*N located at the 3-O or 4-O position of the D-*glycero*-α-L-*gluco*-heptopyranose CPS residue. For example, addition of the MeO*P*N to the Gal*f*NAc 3-O position in 11168V26 was shown to cause a downfield shift of H-2 (0.2 ppm), H-3 (0.64 ppm), and H-4 (0.24 ppm) relative to that of the unsubstituted Gal*f*NAc (8). Similarly, addition of MeO*P*N to the 3-O position of Fru in the CPS of the HS:1 serostrain lead to a downfield shift of H-3 (0.74 ppm) and H-4 (0.7 ppm) compared with Fru without MeO*P*N (9). Inspection of the chemical shifts reported for the unsubstituted CPS of 11168V26 (30) reveals that the 3-O (3.72 ppm) and 4-O (3.52 ppm) positions of D-*glycero*-α-L-*gluco*-heptopyranose are both candidates for the MeO*P*N at 4.34 ppm, since this would correspond to downfield shifts of 0.62 and 0.82 ppm, respectively, at these locations.

Discussion

In this study, we used HR-MAS NMR of cells grown on $^{15}NH_4Cl$-enriched media to confirm the chemical structure of the MeO*P*N CPS modification. By doing so, we also present new findings on nitrogen metabolism in *C. jejuni*, the complexity of MeO*P*N distribution on the cell surface, and the biosynthetic pathway responsible for MeO*P*N production.

HR-MAS NMR is well-suited for the study of the MeO*P*N modification in *C. jejuni* since it is a highly labile surface structure that is readily hydrolyzed by chemical reagents used to purify CPS from bacteria (8, 9). By examin-

© 2006 NRC Canada

ing proton chemical shifts for the anomeric resonances of CPS sugars and the expression of phase-variable CPS modifications such as the OMe and MeO*P*N groups with ^{1}H HR-MAS NMR, we determined that the concentrations of NH_4Cl used during this study did not affect the structure of the CPS. These phase-variable CPS groups in *C. jejuni* are useful biomarkers since their expression is highly variable (8). A large $^{1}J(^{15}N–^{31}P)$ coupling of 39 (±2) Hz observed in the $^{1}H–^{31}P$ HSQC spectra for cells grown on $^{15}NH_4Cl$-enriched media provided, for the first time, direct evidence confirming the N—P bond for the MeO*P*N. This is an important result since phosphoramidates are rare in nature and prior to this study, the structure of the MeO*P*N in *C. jejuni* was proposed based on mass spectrometric and NMR chemical shift data (8, 9). That the amount of ^{15}N labeling within the MeO*P*N reached 80% and was directly correlated to the amount of $^{15}NH_4Cl$ in the media indicates that ammonium can be a primary source of nitrogen used for MeO*P*N biosynthesis in *C. jejuni*.

Because of phylogenetic similarities, it was previously thought that metabolism in *C. jejuni* closely resembled *Helicobacter pylori*, however, the genome sequence for *C. jejuni* NCTC11168 showed that only 55.4% of *C. jejuni* genes have orthologues in *H. pylori* (7). Consequently, the factors that contribute to the metabolic versatility of *C. jejuni* allowing it to adapt its metabolism to many environments within and outside its hosts are still poorly understood (31–46). That ^{15}N was detected within the major outer membrane protein, as well as the NAc and NGro groups of the CPS, shows that *C. jejuni* can exploit exogenous sources of inorganic nitrogen to make amino acids and glycan structures. This result suggests that growth on $^{15}NH_4Cl$-enriched media could potentially be used to label proteins, sugars, and phase-variable modifications in *C. jejuni* for NMR analysis.

It is interesting that two MeO*P*Ns were identified for the 11168H strain differing by $\Delta\delta_H$ 0.2 ppm; one at C-3 of Gal*f*NAc and a novel MeO*P*N most likely located at C-3 or C-4 of D-*glycero*-α-L-*gluco*-heptopyranose. Inspection of the ^{1}H-^{31}P HSQC spectra for 11168V26 cells shows that four of the five MeO*P*N signals can be grouped into two general populations that also differ by $\Delta\delta_H$ 0.2 ppm, suggesting that a novel heptose-associated MeO*P*N is present for this 11168 isolate as well (Fig. 5). Definitive location of the novel MeO*P*N in 11168 will require detailed NMR studies of the purified CPS. The diverse range of phosphorous chemical shifts exhibited by these different MeO*P*Ns is possibly due to structural heterogeneity for cell-bound CPS or moderately different pH environments, since the chemical shifts of phosphoramidates were shown to vary considerably with slight changes in pH (27). That a weak MeO*P*N signal at δ_H 3.70 ppm and δ_p 14.7 ppm was observed for 11168V26 cells is suggestive of another MeO*P*N at an unknown location. It is conceivable that MeO*P*N could be located on glycan structures other than CPS. For example, the harsh chemical treatments used to purify LOS would likely hydrolyze the MeO*P*N, resulting in it being overlooked by previous studies examining these structures in *C. jejuni*.

This is the first evidence suggesting that the MeO*P*N CPS modification in *C. jejuni* can be found on CPS sugars with a pyranose ring configuration, since it was shown to be substituted on furanose sugars for *C. jejuni* 11168V26 (C-3 of Gal*f*NAc) and the HS:1 serostrain (C-3 of Fru*f*) (8, 9). That MeO*P*Ns are found on both pyranose and furanose sugars in 11168 suggests that transfer of the MeO*P*N to CPS carbohydrates is possibly regulated by more than one gene. This hypothesis supports the genetic findings for the HS:23 serostrain, where *HS:23.07* and *HS:23.20* were speculated to be involved in adding MeO*P*N to CPS sugars (6). Interestingly, these genes were shown to have high sequence similarity with *cj1422c*, the putative glycosyltransferase from 11168 (6). Examination of the *cps* gene cluster from 11168 demonstrated that there exists a second gene (*cj1421c*) with similarity to *cj1422c*, which may also be involved in transferring MeO*P*N to CPS sugars (6).

In the case of 11168H, this study has shown that the phosphoramidate modification occurs at predominantly two sites in the CPS with approximately equal frequency. This raises the question as to whether each repeating unit in the CPS has two sites that are simultaneously decorated with the MeO*P*N modification, or only one MeO*P*N with equal frequency throughout the CPS. For the latter situation, two additional structures potentially exist, since repeats with only one MeO*P*N could be homogeneously or randomly distributed within the CPS. These structures present largely different CPS epitopes and have interesting implications regarding the details of CPS assembly from subunits containing the MeO*P*N modification. While the basic CPS structure of 11168 has been established (8, 30), it will be important to examine the structure of the purified CPS with respect to the topology of phosphoramidation.

Acknowledgements

The authors thank Dr. Brendan Wren for the 11168H strain, Nicolas Cadotte for technical assistance, Luc Tessier for nanoLC–MS/MS analysis, and the Natural Sciences and Engineering Research Council of Canada (NSERC) for funding.

References

1. J. Kelly, J.R. Brisson, N.M. Young, H.C. Jarrell, and C.M. Szymanski. *In* Bacterial genomes and infectious diseases. *Edited by* V.L. Chan, P.M. Sherman, and W. Burke. Humana Press, New Jersey. 2005.
2. B.C. Jacobs, P.H. Rothbarth, F.G. van der Meche, P. Herbrink, P.I. Schmitz, M.A. de Klerk, and P.A. van Doorn. Neurology, **51**, 1110 (1998).
3. I.S. Roberts. Annu. Rev. Microbiol. **50**, 285 (1996).
4. A.V. Karlyshev, D. Linton, N.A. Gregson, A.J. Lastovica, and B.W. Wren. Mol. Microbiol. **35**, 529 (2000).
5. D.J. Bacon, C.M. Szymanski, D.H. Burr, R.P. Silver, R.A. Alm, and P. Guerry. Mol. Microbiol. **40**, 769 (2001).
6. A.V. Karlyshev, O.L. Champion, C. Churcher, J.R. Brisson, H.C. Jarrell, M. Gilbert, D. Brochu, F. St. Michael, J. Li, W.W. Wakarchuk, I. Goodhead, M. Sanders, K. Stevens, B. White, J. Parkhill, B.W. Wren, and C.M. Szymanski. Mol. Microbiol. **55**, 90 (2005).
7. J. Parkhill, B.W. Wren, K. Mungall, J.M. Ketley, C. Churcher, D. Basham, T. Chillingworth, R.M. Davies, T. Feltwell, S. Holroyd, K. Jagels, A.V. Karlyshev, S. Moule, M.J. Pallen, C.W. Penn, M.A. Quail, M.A. Rajandream, K.M. Rutherford,

© 2006 NRC Canada

A.H. van Vliet, S. Whitehead, and B.G. Barrell. Nature, **403**, 665 (2000).
8. C.M. Szymanski, F. St. Michael, H.C. Jarrell, J. Li, M. Gilbert, S. Larocque, E. Vinogradov, and J.R. Brisson. J. Biol. Chem. **278**, 24509 (2003).
9. D.J. McNally, H.C. Jarrell, J. Li, N.H. Khieu, E. Vinogradov, C.M. Szymanski, and J.R. Brisson. Eur. J. Biochem. **272**, 4407 (2005).
10. R.E. Silversmith, J.L. Appleby, and R.B. Bourret. Biochemistry, **36**, 14965 (1997).
11. V.L. Robinson and A.M. Stock. Struct. Fold. Des. **7**, R47 (1999).
12. V. Deretic, J.H. Leveau, C.D. Mohr, and N.S. Hibler. Mol. Microbiol. **6**, 2761 (1992).
13. G.S. Lukat, W.R. McCleary, A.M. Stock, and J.B. Stock. Proc. Natl. Acad. Sci. U.S.A. **89**, 718 (1992).
14. M. Welch, K. Oosawa, S. Aizawa, and M. Eisenbach. Proc. Natl. Acad. Sci. U.S.A. **90**, 8787 (1993).
15. O. Amster-Choder and A.Wright. J. Bacteriol. **179**, 5621 (1997).
16. M.M. McEvoy and F.W. Dahlquist. Curr. Opin. Struct. Biol. **7**, 793 (1997).
17. T.L. Mayover, C.J. Halkides, and R.C. Stewart. Biochemistry, **38**, 2259 (1999).
18. J.A. Hoch. Curr. Opin. Microbiol. **3**, 165 (2000).
19. C.D. Carrillo, E. Taboada, J.H. Nash, P. Lanthier, J. Kelly, P.C. Lau, R. Verhulp, O. Mykytczuk, J. Sy, W.A. Findlay, K. Amoako, S. Gomis, P. Willson, J.W. Austin, A. Potter, L. Babiuk, B. Allan, and C.M. Szymanski. J. Biol. Chem. **279**, 20327 (2004).
20. A.V. Karlyshev, D. Linton, N.A. Gregson, and B.W. Wren. Microbiology, **148**, 473 (2002).
21. S. Meiboom and D. Gill. Rev. Sci. Instrum.. **29**, 688 (1958).
22. J. Li, Z. Wang, and E. Altman. Rapid Commun. Mass Spectrom. **19**, 1305 (2005).
23. N.M. Young, J.R. Brisson, J. Kelly, D.C. Watson, L. Tessier, P.H. Lanthier, H.C. Jarrell, N. Cadotte, F. St. Michael, E. Aberg, and C.M. Szymanski. J. Biol. Chem. **277**, 42530 (2002).
24. T. Viljanen, K.D. Klika, F. Fulop, and K. Pihlaja. J. Chem. Soc. Perkin Trans. 2, **6**, 1479 (1998).
25. J.R. van Wazer, C.F. Callis, J.N. Shoolery, and R.C. Jones. J. Am. Chem. Soc. **78**, 5715 (1956).
26. M.L. Nielsen, J.V. Pustinger, and J. Strobel. J. Chem. Eng. Data, **9**, 167 (1964).
27. J.I. Guijarro, J.E. Gonzalez-Pastor, F. Baleux, J.L. San Millan, M.A. Castilla, M. Rico, F. Moreno, and M. Delepierre. J. Biol. Chem. **270**, 23520 (1995).
28. H. Koskela, I. Kilpelainen, and S. Heikkinen. J. Magn. Reson. **164**, 228 (2003).
29. B. Luy and J.P. Marino. J. Am. Chem. Soc. **123**, 11306 (2001).
30. F. St. Michael, C.M. Szymanski, J. Li, K.H. Chan, N.H. Khieu, S. Larocque, W.W. Wakarchuk, J.R. Brisson, and M.A. Monteiro. Eur. J. Biochem. **269**, 5119 (2002).
31. M. Veron, A. Lenvoise-Furet, and P. Beaune. Curr. Microbiol. **6**, 349 (1981).
32. G.A. Hebert, D.G. Hollis, R.E. Weaver, M.A. Lambert, M.J. Blaser, and C.W. Moss. J. Clin. Microbiol. **15**, 1065 (1982).
33. P.S. Hoffman and T.G. Goodman. J. Bacteriol. **150**, 319 (1982).
34. G.K. Morris, M.R. El Sherbeeny, C.M. Patton, H. Kodaka, G.L. Lombard, P. Edmonds, D.G. Hollis, and D.J. Brenner. J. Clin. Microbiol. **22**, 714 (1985).
35. Z. Elharrif and F. Megraud. Curr. Microbiol. **22**, 714 (1986).
36. M.A. Karmali, M. Roscoe, and P.C. Fleming. J. Clin. Microbiol. **23**, 743 (1986).
37. H.N. Westfall, D.M. Rollins, and E. Weiss. Appl. Environ. Microbiol. **52**, 700 (1986).
38. P.A. Chalk, A.D. Roberts, and W.M. Blows. Microbiology, **140**, 2085 (1994).
39. T.E. Kearney, M.J. Larkin, and P.N. Levett. Appl. Environ. Microbiol. **60**, 3647 (1994).
40. J.M. Ketley. Microbiology, **143**, 5 (1997).
41. S. Leach, P. Harvey, and R. Wali. J. Appl. Microbiol. **82**, 631 (1997).
42. M.A. Smith, G.L. Mendz, M.A. Jorgensen, and S.L. Hazell. Int. J. Biochem. Cell Biol. **31**, 961 (1999).
43. M.J. Sellars, S.J. Hall, and D.J. Kelly. J. Bacteriol. **184**, 4187 (2002).
44. J. Velayudhan and D.J. Kelly. Microbiology, **148**, 685 (2002).
45. K.A. Mohammed, R.J. Miles, and M.A. Halablab. Lett. Appl. Microbiol. **39**, 261 (2004).
46. J. Velayudhan, M.A. Jones, P.A. Barrow, and D.J. Kelly. Infect. Immun. **72**, 260 (2004).

© 2006 NRC Canada

Ab initio DFT calculations of the configurational and conformational preferences of 2-phenylsulfinylcyclohexanones — Evidence for "exo-anomeric" interactions[1]

Melissa L. Trapp, John F. Wojcik, Walter W. Zajac, Jr., and B. Mario Pinto

Abstract: The conformational analysis of 2-phenylsulfinylcyclohexanone by ab initio density functional calculations is described. Six conformations corresponding to axial/equatorial isomers and rotation about the exocyclic C2—S bond in each of the RR or RS diastereomers were calculated and the results were examined in terms of relative energies, electrostatic interactions, orbital interactions, and geometrical variations. The global minimum conformation was the RS isomer that positioned the phenylsulfinyl moiety in an equatorial orientation and the sulfinyl oxygen in an anti orientation with respect to the carbonyl carbon atom. Of the other three low energy conformations, only one had a gauche arrangement of these atoms, and only in one of the four lower energy conformations was evidence found for a S-O(–)···C(+)-O electrostatic interaction. In contrast, the results were consistent with the operation of $n_S \rightarrow \pi^*_{C=O}$ stabilizing orbital interactions. Further support for this hypothesis was obtained from the increased C=O bond lengths in these four conformations relative to the other conformations, and by the torsional angle distortion away from ideal geometry, presumably to maximize the stabilizing orbital interaction. We propose that this conformational preference is a manifestation of a generalized exo-anomeric effect. The longer C2—S bond in the axial isomers was also interpreted in terms of a stabilizing $\pi_{C=O} \rightarrow \sigma^*_{C-S}$ interaction, analogous to an endo-anomeric interaction. Comparison of the computational results to available experimental data on the conformational equilibrium of each diastereomer in solution suggests which conformers are present in each of the equilibria. The available data for the solid state indicate that the RR and RS isomers both crystallize in high energy conformations, stabilized by intermolecular interactions.

Key words: 2-phenylsulfinylcyclohexanones, configurational isomers, conformational preferences, DFT calculations, exo-anomeric effect.

Résumé : On a fait appel à des calculs ab initio de densité fonctionnelle pour faire l'analyse conformationnelle de la 2-phénylsulfinylcyclohexanone. On a fait des calculs sur six conformations qui correspondent aux isomères axial/équatorial et de rotation autour de la liaison C2—S pour chacun des diastéréoisomères RR et RS et on a examiné les résultats en fonction des énergies relatives, des interactions électrostatiques, des interactions d'orbitales et des variations de géométrie. La conformation d'énergie globale minimale est celle de l'isomère RS portant le substituant phénylsulfinyle en position équatoriale avec l'oxygène du sulfinyle dans une orientation anti par rapport à l'atome de carbone du carbonyle. Des trois autres conformations de faible énergie, une seule comporte un arrangement gauche de ces atomes et on n'a trouvé des données suggérant l'existence d'une interaction électrostatique S-O(–)···C(+)-O que pour une seule des quatre conformations de basse énergie. Par ailleurs, les résultats sont en accord avec l'opération d'interactions d'orbitales stabilisantes $n_S \rightarrow \pi^*_{C=O}$. On a obtenu une confirmation supplémentaire pour cette hypothèse dans l'augmentation des longueurs de liaison C=O dans ces quatre conformations par rapport aux longueurs dans les autres conformations ainsi que dans la distorsion de l'angle de torsion par rapport à la géométrie idéale, probablement afin de maximiser l'interaction orbitalaire stabilisante. On propose que cette préférence conformationnelle est une manifestation d'un effet généralisé exo-anomère. On interprète aussi la longueur plus grande de la liaison C2—S des isomères axiaux par une interaction stabilisante $\pi_{C=O} \rightarrow \sigma^*_{C-S}$ semblable à celle d'une interaction endo-anomère. Une comparaison des résultats des calculs théoriques avec les résultats expérimentaux disponibles pour l'équilibre conformationnel de chaque diastéroisomère en solution suggère quels sont les conformères qui sont présents dans chacun des équilibres. Les

Received 14 August 2005. Published on the NRC Research Press Web site at http://canjchem.nrc.ca on 13 May 2006.

This work is dedicated, with respect and affection, to Walter A. Szarek, a friend, colleague, and mentor, in celebration of his 65th birthday.

M.L. Trapp and B.M. Pinto.[2] Department of Chemistry, Simon Fraser University, Burnaby, BC V5A 1S6, Canada.
J.F. Wojcik and W.W. Zajac Jr.[3] Department of Chemistry, Villanova University, Villanova, PA 19085 USA.

[1]This article is part of a Special Issue dedicated to Professor Walter A. Szarek.
[2]Corresponding author (e-mail: bpinto@sfu.ca).
[3]Deceased, after a valiant battle with an optimistic outlook, 3 March 2003.

 doi:10.1139/V06-040 © 2006 NRC Canada

données disponibles pour l'état solide indique que les isomères RR et RS cristallisent tous les deux dans des conformations d'énergie élevée, stabilisées par des interactions intramoléculaires.

Mots clés : 2-phénylsulfinylcyclohexanones, isomères de configuration, préférences conformationnelles, calculs selon la théorie de la densité de fonctionnelle, effet exo-anomère.

[Traduit par la Rédaction]

Scheme 1.

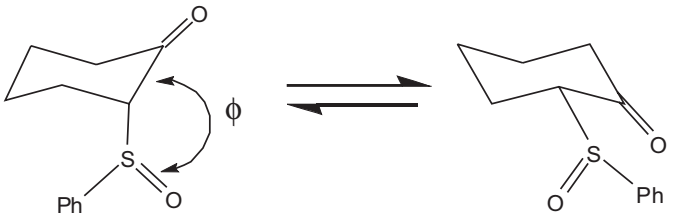
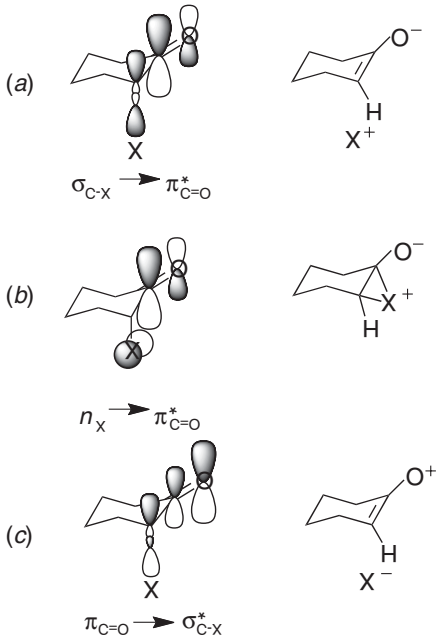


Fig. 1. Molecular orbital (left) and equivalent valence bond (right) descriptions of stabilizing orbital interactions in 2-substituted cyclohexanones.



Introduction

We have been intrigued by the conformational effects operating in 2-substituted cyclohexanones (e.g., Scheme 1), particularly when the substituents contain chalcogen atoms (1, 2). It had been suggested that the increased axial preference for the heavier chalcogen substituents was due to the increased nonbonded repulsion with the carbonyl group in the equatorial conformer (3, 4). However, the possibility of the role of $\sigma_{C\text{-}X} \rightarrow \pi^*_{C=O}$ and $n_X \rightarrow \pi^*_{C=O}$ stabilizing orbital interactions as contributors to the conformational preferences was also recognized (Fig. 1) (5, 6).

Recently, in a systematic study of 2-[4-R-substituted-phenyl)seleno]cyclohexanones, we provided evidence for the

Fig. 2. Stabilizing $n_{Se} \rightarrow \pi^*_{C=O}$ orbital interaction associated with the generalized exo-anomeric effect in 2-arylselenocyclohexanones.

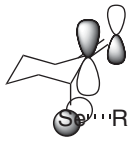
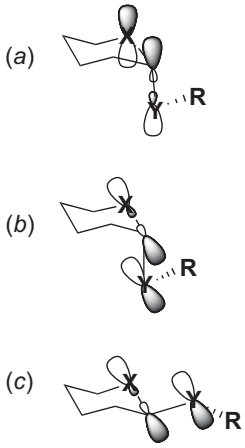


Fig. 3. Stabilizing $n \rightarrow \sigma^*$ orbital interactions associated with the (*a*) endo-anomeric effect and (*b*) and (*c*) exo-anomeric effect in 2-substituted heterocyclohexanes.



dominance of $n_{Se} \rightarrow \pi^*_{C=O}$ interactions in influencing the conformational equilibrium (2) by stabilizing the axial conformer (Fig. 2).

We further suggested that this interaction was akin to that proposed by R.U. Lemieux to account for the exo-anomeric effect in carbohydrates, which is the preference for the gauche conformation around the C_1-aglyconic carbon bond of glycopyranosides that permits expression of an $n_Y \rightarrow \sigma^*_{C\text{-}X}$ stabilizing orbital interaction (Fig. 3) (7), and that the $n_{Se} \rightarrow \pi^*_{C=O}$ interactions expressed in the 2-arylselenocyclohexanones are a manifestation of a generalized anomeric effect.

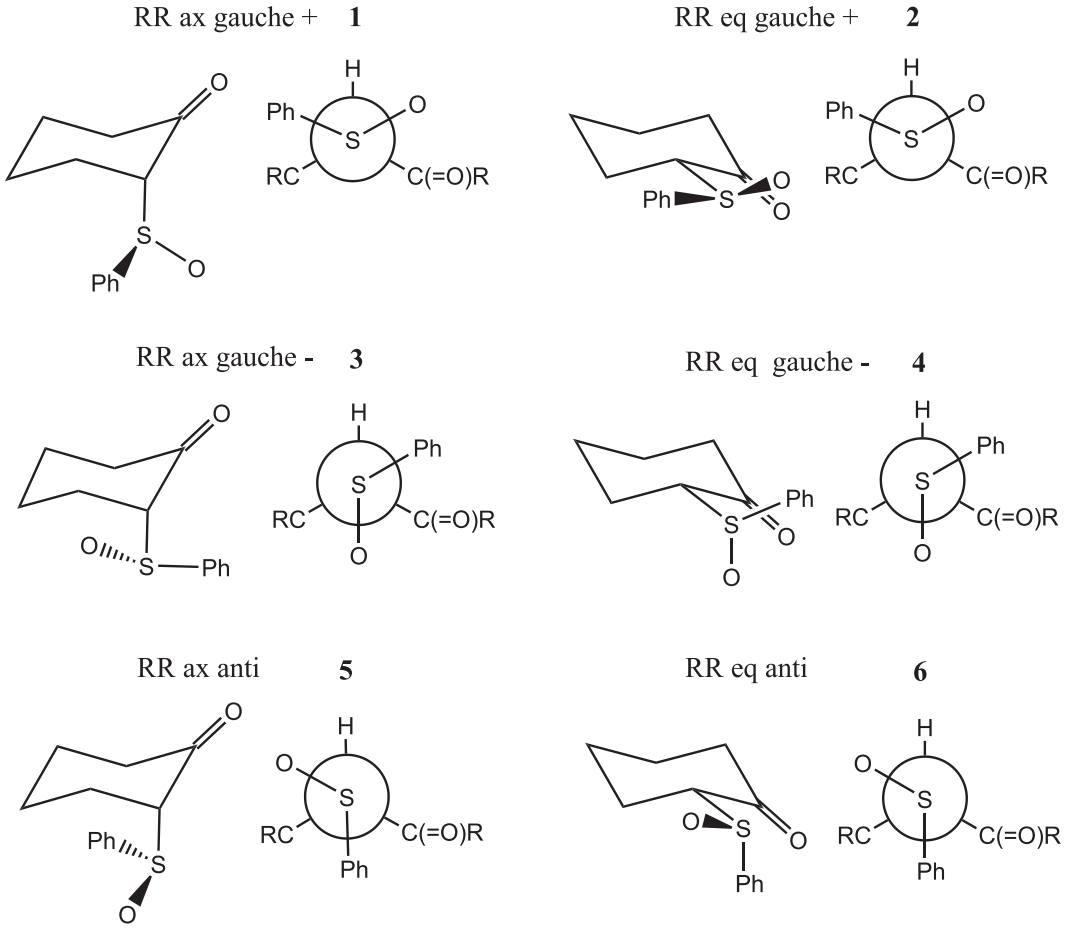
An additional possible interaction in these systems is a $\pi_{C=O} \rightarrow \sigma^*_{C\text{-}X}$ orbital interaction (Fig. 1*c*) that is only possible in the axial conformation, and is analogous to the $n_X \rightarrow \sigma^*_{C\text{-}Y}$ orbital interactions (Fig. 3) proposed to account for the endo-anomeric effect in carbohydrate derivatives (8–11).

Seemingly anomalous results obtained in the experimental evaluation of the conformational preferences of 2-phenylsulfinylcyclohexanone (1), (12)[4], (13)[5], prompted us to perform a detailed analysis of the configurational and

[4] M.A. Caglar and W.W. Zajac, Jr. Unpublished data.
[5] Y.C. Kwon and W.W. Zajac, Jr. Unpublished data.

© 2006 NRC Canada

Fig. 4. Conformations around the C2—S bond in the RR isomer of 2-phenylsulfinylcyclohexanone. Only the enantiomer ($2R,S_R$) is shown for convenience. Two different chair conformations for each pair are also shown to reflect the axial–equatorial interconversion.



conformational preferences of this compound by molecular orbital DFT calculations. The computations were intended to provide insight into the experimental observations. We note that Faria et al. (14) have recently reported a similar study at a lower level of computation, namely the PM3 semiempirical level. We report herein that the energy preferences and geometrical differences between configurational and conformational isomers can be rationalized in terms of a generalized "exo-anomeric" interaction between the sulfur lone pair and the $\pi^*_{C=O}$ fragment orbital. The conclusions differ somewhat from those of Faria et al. (14), who concluded that electrostatic interactions dominate.

Results and discussion

2-Phenylsulfinylcyclohexanone can exist as two enantiomeric pairs of diastereomers, dictated by the configuration at C2 of the cyclohexanone ring and at the stereogenic sulfur atom. For convenience, in this discussion only one enantiomer in each set will be shown. Thus, the diastereomers will be designated as RR or RS, where the first descriptor refers to the configuration at C2 and the second descriptor to the configuration at sulfur. The conformations of these compounds can be designated in terms of the axial or equatorial orientation of the phenylsulfinyl moiety, and the dihedral angle ϕ about the C—S bond, defined as +gauche, –gauche, or anti with respect to the C(carbonyl)-C2-S-O unit (Scheme 1). The conformations are shown in Figs. 4 and 5, but for simplicity, each conformer has been assigned a number to facilitate discussion. The structures were arranged in pairs as axial and equatorial conformers representing the two chair conformations.

To determine which basis set would be most appropriate for yielding accurate energy values within reasonable times for these twelve conformers, preliminary calculations were performed on conformers (**3**) and (**5**). The results are summarized in Table 1. It was found that the B3LYP/6-31+G* basis set was sufficient to obtain optimized energies for the purposes of this study. A summary of the ab initio energy values and dipole moments for the twelve conformers is given in Table 2. The optimized bond angles and bond lengths are listed in Table 3.

It is instructive to examine the orbital interactions and electrostatic interactions in the lower energy conformations (**3**, **6**, **11**, and **12**) of 2-phenylsulfinylcyclohexanone. Conformation **3**, with a relative energy of 0.21 kcal mol^{-1} (1 cal = 4.184 J), presents the S-O and C-O dipoles in a mutually perpendicular orientation and also aligns the sulfur lone pair for interaction with the $\pi^*_{C=O}$ fragment orbital, as indicated in Fig. 6*a*. This conformation also permits an attractive electrostatic interaction between the O of the sulfinyl moiety and the C of the CO moiety, an S-O (–)···C(+)-O interaction, as suggested by Faria et al. (14). In conformation **12**, the global minimum, the S-O and C-O dipoles are mutually perpendic-

© 2006 NRC Canada

Fig. 5. Conformations about the C—S bond in the RS isomer of 2-phenylsulfinylcyclohexanone. Only the enantiomer (2R,S_S) is shown for convenience. Two different chair conformations for each pair are also shown to reflect the axial–equatorial interconversion.

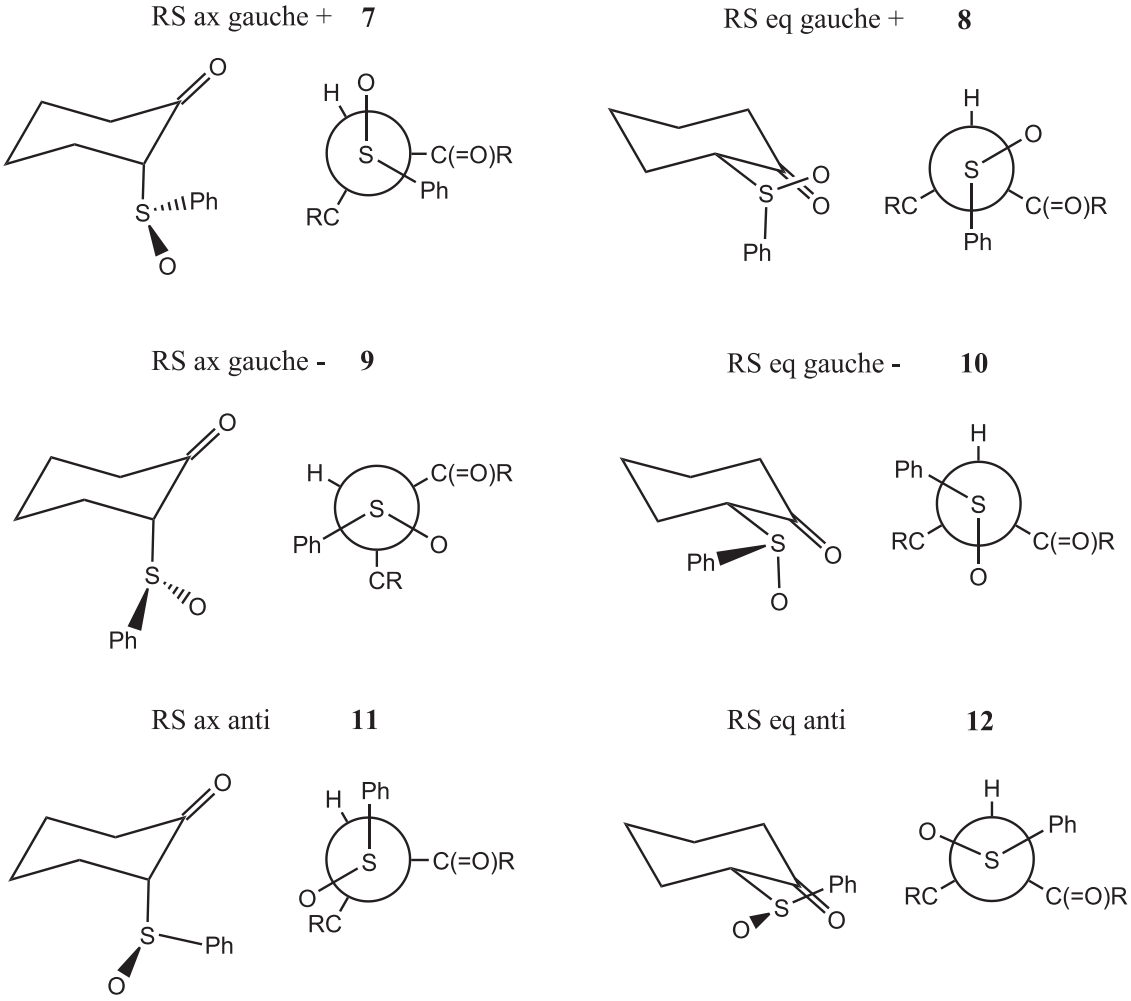


Table 1. Dependence on basis set of energies of the diastereomeric 2-phenylsulfinylcyclohexanones.

	Conformer **3**		Conformer **5**	
B3LYP basis set	Energy (a.u.)	Dipole moment (D)	Energy (a.u.)	Dipole moment (D)
6-31G*	–1014.299 387	1.7705	–1014.296 644	3.9054
6-31+G*	–1014.324 748	2.0108	–1014.321 723	4.0820
6-31+G**	–1014.344 949	1.8968	–1014.342 086	4.0912

ular, and the sulfur lone pair is in the same plane as the $\pi^*_{C=O}$ fragment orbital, and therefore, optimally aligned for interaction (Fig. 6*b*). The electrostatic interaction postulated by Faria et al. (14) is absent in this conformation. Conformation **11** (relative energy 0.57 kcal mol^{-1}) has anti-parallel dipoles and also has the orbitals suitably aligned for an $n_S \rightarrow \pi^*_{C=O}$ exo-anomeric interaction (Fig. 6*c*). Finally, in conformation **6** (relative energy 0.72 kcal mol^{-1}), the S-O and C-O dipoles are orthogonal, and an $n_S \rightarrow \pi^*_{C=O}$ exo-anomeric interaction is again possible (Fig. 6*d*). In the latter two cases, the electrostatic interaction postulated by Faria et al. (14) is again absent. We note that of the low energy conformations (**3**, **6**, **11**, and **12**), only **3** is in a gauche conformation, and the global minimum has the phenylsulfinyl group in an equatorial orientation, contrary to the earlier study (14).

As further evidence for the operation of exo-anomeric interactions, we note that the C—O bond lengths in **3**, **6**, **11**, and **12** are generally longer than in the other conformers, and that the C1-C2-S-O torsion angle (–50° in **3**, 172° in **6**, –157° in **11**, and –172° in **12**) is distorted from ideal geometry in these conformers relative to their counterparts, presumably to optimize the orbital interaction (Table 3). It is also of significance that the C—O bond lengths in **5**, **7**, and **9** are of similar magnitude to those in **3**, **6**, **11**, and **12**; we suggest that this feature results because an $n_S \rightarrow \pi^*_{C=O}$ exo-anomeric interaction is again possible in the former set of conformations. It should also be noted that **12** must be stabilized by some interaction that counteracts the high dipole moment in this conformation (Table 2). The dipole moments increase in the order **11** < **3** < **12** < **6**.

© 2006 NRC Canada

Table 2. Ab initio energies and dipole moments for the conformations of the diastereomeric 2-phenylsulfinylcyclohexanones using the B3LYP/6-31+G* basis set.

Conformation	Conformer	Energy (a.u.)	Relative energies (kcal/mol) overall	Relative energies (kcal/mol) per diastereomer	Dipole moment (D)	Relative dipole moment (D) per diastereomer
1	RR ax gauche+	–1014.320 355	2.97	2.76	6.098	4.088
2	RR eq gauche+	–1014.319 766	3.33	3.13	6.907	4.897
3	RR ax gauche–	–1014.324 748	0.21	0.00	2.011	0.000
4	RR eq gauche–	–1014.317 66	4.66	4.45	5.333	3.322
5	RR ax anti	–1014.321 723	2.11	1.90	4.082	2.071
6	RR eq anti	–1014.323 931	0.72	0.51	4.696	2.686
7	RS ax gauche+	–1014.316 192	5.58	5.58	5.957	4.818
8	RS eq gauche+	–1014.316 291	5.52	5.52	5.901	4.763
9	RS ax gauche–	–1014.324 046	0.65	0.65	4.101	2.962
10	RS eq gauche–	–1014.323 038	1.28	1.28	6.177	5.038
11	RS ax anti	–1014.324 167	0.57	0.57	1.139	0.000
12	RS eq anti	–1014.325 08	0.00	0.00	4.442	3.303

Further examination of the geometrical variations in Table 3 indicates that C2—S bond lengths in the axial isomers are consistently longer than in their equatorial counterparts, suggesting the operation of a $\pi_{C=O} \rightarrow \sigma^*_{C\text{-}S}$ interaction, analogous to an endo-anomeric interaction (11) (Figs. 1*c*, 3*a*). The simultaneous operation of endo- and exo-anomeric interactions and the resulting net stabilization is reminiscent of these effects in axially oriented carbohydrate acetals and hemiacetals (10, 11). Accompanying this geometrical change, the S—C (aryl) bond is shorter and the C6-C1-C2 bond angle is larger in the axial conformers.

As a final point of interest, we compare our computational results with the available experimental data. Analysis of the ^{1}H NMR data in $CDCl_3$ for a diastereomeric mixture of 2-phenylsulfinylcyclohexanone (**A** + **B**) had indicated the presence of two H-2 resonances at 3.31 and 3.55 ppm (12)[4]. Comparison of line widths with those of anancomeric, conformationally biased derivatives indicated that the isomer **A**, whose chemical shift was 3.31 ppm, existed as a 3:2 mixture of axial:equatorial conformers, whereas **B**, whose chemical shift was 3.55 ppm, existed as a 2:1 mixture of equatorial:axial conformers. Thus, energetically, there is no strong conformational bias in the equilibria of **A** and **B**. Fractional crystallization had also afforded separate diastereomers whose X-ray crystal structures were determined (13)[5]. It became clear that isomer **A** was the RS isomer and **B** was the RR isomer. Interestingly, both isomers adopted a conformation in which the phenylsulfinyl substituent was equatorially oriented. In addition, isomer **A** adopted a conformation about the C—S bond that corresponded to **10**, whose relative energy was calculated in the present work to be 1.28 kcal mol^{-1} higher than the global minimum. We suggest from our results that the RS isomer **A** exists predominantly as an equilibrium mixture of ax **11** and eq **12**, and that it crystallizes in the higher energy form **10**. Isomer **B** adopted a conformation about the C—S bond that corresponded to **2**, whose relative energy was calculated in the present work to be 3.33 kcal mol^{-1} higher than the global minimum. We suggest from our results that the RR isomer **B** exists as an equilibrium mixture of ax **3** and eq **6**, and that it too crystallizes in a high energy form.

The experimentally observed solvent effects on the axial–equatorial conformational equilibria for the RS (**A**) and RR (**B**) diastereomers are consistent with our interpretation. Thus, changing the solvent from $CDCl_3$ to CD_3CN results in a greater proportion of the equatorial isomer in the case of both **A** and **B** (12)[4], (13)[5]. One would predict from our data (Table 2) that in the equilibrium of ax **11** (dipole moment 1.139) with eq **12** (dipole moment 4.442), the isomer with the higher dipole moment, i.e., **12**, would be more favoured in the more polar solvent CD_3CN than in $CDCl_3$. Similarly, in the equilibrium of ax **3** (dipole moment 2.011) with eq **6** (dipole moment 4.696), the isomer with the higher dipole moment, i.e., **6**, would be more favoured in the polar solvent. Finally, we note that both **2** and **10** have high dipole moments and thus, the solid-state behaviour is not likely to reflect the behaviour in solution.

The conformational preferences in 2-phenylsulfinylcyclohexanone and its analogues are of interest in their own right but might also have implications in stereoselective aldol reactions such as those with lithium ester enolates (15).

Experimental section

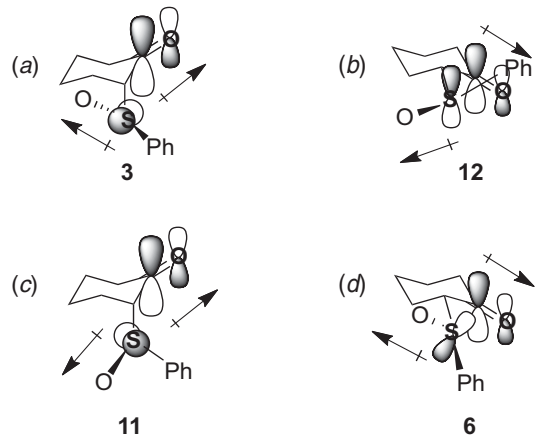
Ab initio calculations were performed with Gaussian 98 (16), using as input structures that were modeled on Insight II and initially optimized using force field calculations using Discover. The molecules were optimized in the gas phase with a full population analysis using the B3LYP version of density functional theory (17) and the Gaussian basis set 6-31G, 6-31+G*, or 6-31+G** (see text). Following optimization, a frequency calculation was performed, which provided the bending and stretching modes of the molecule and ensured that a stable minimum was found. With the exception of **7**, the frequencies found were real, and therefore, every structure is considered as a reliable geometrical minimum. Conformer **7**, which contained one nonreal frequency, represented a transition state in which the phenyl group was nearly eclipsed with the cyclohexanone ring. However, conformer **11** in which the sulfinyl moiety was eclipsed with C2 of the cyclohexanone ring was a stable minimum energy structure. The optimized output yielded the absolute ener-

© 2006 NRC Canada

Table 3. Ab initio optimized geometrical parameters for the conformations of the diastereomeric 2-phenylsulfinylcyclohexanones using the B3LYP/6-31+G* basis set.

			Bond lengths (Å)				Bond angles (°)			Torsion angles (°)		
Conformation	Conformer	Relative energies (kcal/mol) per diastereomer	C=O	S—C(Alk)	S—O	S—C(Ar)	C6-C1-C2	C2-S-C(Ar)	C1-C2-S	C1-C2-S-O	C2-S-C(Ar)-C(Ar)	O-C1-C2-S
1	RR ax gauche+	2.76	1.217	1.905	1.518	1.824	114.40	110.90	111.16	54.52	61.97	–111.67
2	RR eq gauche+	3.13	1.216	1.879	1.519	1.830	113.88	97.79	107.88	76.59	94.50	11.08
3	RR ax gauche-	0.00	1.221	1.902	1.522	1.823	115.96	98.94	112.00	–50.60	74.32	–101.05
4	RR eq gauche-	4.45	1.214	1.875	1.517	1.826	113.92	100.39	116.70	–57.38	75.01	–5.98
5	RR ax anti	1.90	1.224	1.950	1.518	1.828	118.78	103.02	109.76	–156.60	85.92	–70.18
6	RR eq anti	0.51	1.220	1.883	1.525	1.832	114.35	100.79	113.82	171.58	81.78	2.35
7	RS ax gauche+	5.58	1.221	1.937	1.515	1.824	117.86	103.59	114.59	94.83	85.20	–87.21
8	RS eq gauche+	5.52	1.213	1.876	1.517	1.827	113.07	102.23	117.58	55.64	100.82	8.26
9	RS ax gauche-	0.65	1.220	1.908	1.521	1.827	116.74	96.99	106.90	–84.14	110.71	–92.72
10	RS eq gauche-	1.28	1.217	1.887	1.519	1.833	115.07	96.12	108.87	–89.51	108.06	–9.74
11	RS ax anti	0.57	1.222	1.939	1.520	1.824	116.80	97.63	107.98	–156.71	105.05	–99.45
12	RS eq anti	0.00	1.220	1.884	1.524	1.833	114.40	98.12	112.67	–171.55	98.10	–1.69

Fig. 6. Proposed stabilizing orbital interactions and dipole–dipole interactions in lower-energy conformations of 2-phenylsulfinylcyclohexanone.



gies, bond lengths, bond angles, dihedral angles, dipole moments, and Mulliken atomic charges.

Acknowledgements

We are grateful to the Natural Sciences and Engineering Research Council of Canada (NSERC) for financial support.

References

1. (*a*) H. Özbal and W.W. Zajac, Jr. Tetrahedron Lett. **20**, 4821 (1979); (*b*) W.W. Zajac, Jr. and H. Özbal. J. Org. Chem. **45**, 4154 (1980).
2. R.G. McLeod, B.D. Johnston, and B.M. Pinto. Isr. J. Chem. **40**, 307 (2000).
3. E.A. Basso, C. Kaiser, R. Rittner, and J.B. Lambert. J. Org. Chem. **58**, 7865 (1993).
4. R.R. Fraser and N.C. Faibish. Can J. Chem. **73**, 88 (1995).
5. D. Cantacuzène and M. Tordeux. Can. J. Chem. **54**, 2759 (1976).
6. B. Wladislaw, H. Viertler, P.R. Olivato, I.C.C. Calegäo, V.L. Pardini, and R. Rittner. J. Chem. Soc. Perkin Trans 2, 453 (1980).
7. R.U. Lemieux and S. Koto. Tetrahedron, **30**, 1933 (1974).
8. J.T. Edward. Chem. Ind. (London), 1102 (1955).
9. R.U.Lemieux and N.J. Chü. Abstr. Papers Am. Chem. Soc. Meeting, **133**, 31N (1958).
10. For leading references: (*a*) W.A. Szarek and D. Horton (*Editors*). Anomeric effect: Origin and consequences. ACS Symp. Ser. 87. American Chemical Society, Washington, D.C. 1979; (*b*) G.R.J. Thatcher (*Editor*). The anomeric effect and associated stereoelectronic effects. ACS Symp. Ser. 539. American Chemical Society, Washington, D.C. 1993; (*c*) E. Juaristi and E.G. Cuevas (*Editors*). The anomeric effect. CRC Press, Boca Raton, Florida. 1995.
11. J.-P. Praly and R.U. Lemieux. Can. J. Chem. **65**, 213 (1987).
12. Y.C. Kwon. M.Sc. Thesis, Villanova University, Villanova, Pennsylvania. 1989.
13. M.A. Caglar. M.Sc. thesis, Villanova University, Villanova, Pennsylvania. 1993.
14. L.E. Faria, C.L. Donnici, and J.C. Dias Lopes. Int. J. Quant. Chem. **95**, 313 (2003).

© 2006 NRC Canada

15. J.L. García Ruano, D. Barros, M.C. Maestro, R. Araya-Maturana, and J. Fischer. J. Org. Chem. **61**, 9462 (1996).
16. M.J. Frisch, G.W. Trucks, H.B. Schlegel, G.E. Scuseria, M.A. Robb, J.R. Cheeseman, V.G. Zakrzewski, J.A. Montgomery, Jr., R.E. Stratmann, J.C. Burant, S. Dapprich, J.M. Millam, A.D. Daniels, K.N. Kudin, M.C. Strain, O. Farkas, J. Tomasi, V. Barone, M. Cossi, R. Cammi, B. Mennucci, C. Pomelli, C. Adamo, S. Clifford, J. Ochterski, G.A. Petersson, P.Y. Ayala, Q. Cui, K. Morokuma, D.K. Malick, A.D. Rabuck, K. Raghavachari, J.B. Foresman, J. Cioslowski, J.V. Ortiz, B.B. Stefanov, G. Liu, A. Liashenko, P. Piskorz, I. Komaromi, R. Gomperts, R.L. Martin, D.J. Fox, T. Keith, M.A. Al-Laham, C.Y. Peng, A. Nanayakkara, C. Gonzalez, M. Challacombe, P.M.W. Gill, B. Johnson, W. Chen, M.W. Wong, J.L. Andres, M. Head-Gordon, E.S. Replogle, and J.A. Pople. Gaussian 98. Revision A.11.3 [computer program]. Gaussian Inc., Pittsburgh, Penn. 2002.
17. (*a*) C. Lee, W. Yang, and R.G. Parr. Phys. Rev. B, **B37**, 785 (1988); (*b*) A.D. Becke. Phys Rev. A, **A38**, 3098 (1988); (*c*) A.D. Becke. J. Chem. Phys. **97**, 9173 (1992); (*d*) A.D. Becke. J. Chem. Phys. **98**, 5648 (1993); (*e*) P.J. Stephens, F.J. Devlin, C.F. Chabalowski, and M.J. Frisch. J. Phys. Chem. **98**, 11623 (1994).

© 2006 NRC Canada

Component analysis of the X-C-Y anomeric effect (X = O, S; Y = F, OMe, NHMe) by DFT molecular orbital calculations and natural bond orbital analysis[1]

Melissa L. Trapp, Jonathan K. Watts, Noham Weinberg, and B. Mario Pinto

Abstract: Six 2-Y-substituted oxacyclohexane and thiacyclohexane heterocycles (Y = F, OMe, NHMe) were examined using DFT molecular orbital calculations. Natural bond orbital (NBO) analysis of the total energy behaviour yielded the orbital-interaction factors contributing to the conformational equilibria. The dipole moments of the optimized systems were used to estimate the electrostatic contributions to the anomeric effect. The primary determinant of the X-C-Y anomeric effect was found to be the orbital interaction components associated with the combined endo- and exo-anomeric effects acting in concert in the axial conformers. Electrostatic interactions made a contribution to the observed conformer stabilization in all cases, but did not account for the relative magnitudes of the energy differences among conformers of homologous molecules. In the case of the methylamino substituent, accentuated steric interactions in the axial conformer precluded stabilization by the exo-anomeric interaction and consequently, the net endo/exo anomeric stabilization did not dominate the conformational equilibria.

Key words: anomeric effect, component analysis, natural bond orbital analysis, electrostatic, steric, and orbital interaction effects.

Résumé : Six oxacyclohexane et thiacyclohexane hétérocycles (substitués en position 2 par F, OMe, NHMe) ont été examinés par des calculs DFT des orbitales moléculaires. Des analyses des orbitales naturelles des liens (« NBO ») du comportement global de l'énergie a donné les contributions des interactions des orbitales aux équilibres conformationnels. Les moments dipolaires des systèmes optimizés ont été utilizés pour estimer les contributions électrostatiques à l'effet anomère. La cause déterminante primaire de l'effet anomère X-C-Y s'est montré les éléments d'interactions orbitalaires associés aux effets anomères endo et exo, qui agissent ensemble dans les conformères axiaux. Les interactions électrostatiques ont contribué à la stabilization du conformère observé dans tous les cas, mais n'ont pas pu expliquer les magnitudes relatives des différences de l'énergie entre les conformères des molécules homologues. Dans le cas du substituant methylamino, des interactions stériques accentuées dans le conformère axial ont interdit la stabilization par l'interaction anomère exo et par conséquent, la stabilization anomère endo/exo net n'a pas dominé les équilibres conformationnels.

Mots clés : effet anomère, analyse des composants, analyse des orbitales naturelles des liens, effets électrostatiques, effets stériques, effets des interactions orbitalaires.

Introduction

The anomeric effect (1, 2) has challenged the imagination and provoked the actions of both experimental and theoretical chemists alike (3). This effect, in its generalized form, refers to the gauche preferences of substituents about X—A and A—Y bonds in RX-A-YR′ or RX-A-Y structures (3, 4). With respect to substituted five- and six-membered heterocyclic rings, this effect is generally manifested as a preference of a 2-substituent for the axial orientation over and above that predicted on the basis of steric grounds. Several explanations have been advanced to account for the origin of this effect, including the favourable orientation of dipoles in the gauche conformations (1), stabilizing electrostatic inter-

Received 27 September 2005. Published on the NRC Research Press Web site at http://canjchem.nrc.ca on 13 May 2006.

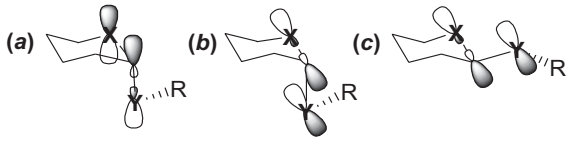
Dedicated, with much appreciation for the strong foundation, to Professor Walter A. Szarek, an inspiring mentor, on the occasion of his 65th birthday.

M.L. Trapp and B.M. Pinto.[2] Department of Chemistry, Simon Fraser University, Burnaby, BC V5A 1S6, Canada.
J.K. Watts. Department of Chemistry, McGill University, 801 Sherbrooke Street West, Montreal, QC H3A 2K6, Canada.
N. Weinberg. Department of Chemistry, University College of the Fraser Valley, Abbotsford, BC V2S 7M8, Canada.

[1]This article is part of a Special Issue dedicated to Professor Walter A. Szarek.
[2]Corresponding author (e-mail: bpinto@sfu.ca).

 doi:10.1139/V06-048 © 2006 NRC Canada

Fig. 1. Stabilizing $n \rightarrow \sigma^*$ orbital interactions associated with the (*a*) endo-anomeric effect and (*b*) and (*c*) exo-anomeric effect in 2-substituted heterocyclohexanes.

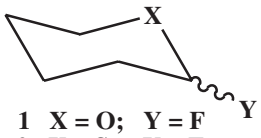


actions (2), and stabilizing molecular orbital interactions (5–7). The explanation for the axial preference in terms of electrostatic interactions derives from the observation that the favoured axial conformer has a lower dipole moment than the equatorial conformer, arising from fragment molecular dipoles whose directional Cartesian coordinates undergo vector subtraction. The orbital interaction component in carbohydrate derivatives has been further classified in terms of an endo-anomeric effect (8), or preference for an axial substituent that derives from an $n_X \rightarrow \sigma^*_{C\text{-}Y}$ stabilizing orbital interaction (Fig. 1), and an exo-anomeric effect (9), or preference for the gauche conformation around the C_1 – aglyconic carbon bond of glycopyranosides that permits expression of an $n_Y \rightarrow \sigma^*_{C\text{-}X}$ stabilizing orbital interaction (Fig. 1). What is still uncertain, however, is why the operation of both the endo- and exo-anomeric interactions, acting in concert in the axial conformers, and claimed to be in competition (8), should be net stabilizing.

Justification for the role of orbital interactions in influencing the conformational preferences in systems containing RX-A-YR′ fragments has been provided by the geometrical variations among the different conformations of these units (3, 10). The endo-anomeric interaction is predicted to lead to a lengthening of the C—Y bond and a shortening of the C—X bond (3, 10). Conversely, the exo-anomeric interaction would lead to the opposite trend in bond lengths, namely a shortening of the C—Y bond and a lengthening of the C—X bond. In the axial conformers, if both endo- and exo-anomeric interactions are active, a bond of intermediate length is observed; in the equatorial conformers, in which only the exo-anomeric effect can operate, the bond length changes described above ensue.

However, it is clear that electrostatic and steric effects do play a role, although their individual assessment is often problematic. We have previously attempted an evaluation of the individual components by estimation of the steric and electrostatic effects through molecular mechanics calculations, and by attribution of the orbital interaction component to the difference between the experimental conformational free energy and the calculated combined steric/electrostatic effects (11). This approximation, although informative at the time, is far from satisfactory. We now report the use of DFT molecular orbital calculations to determine the conformational preferences in three analogous pairs of 2-substituted heterocycles: 2-fluorooxacyclohexane (**1**) and 2-fluorothiacyclohexane (**2**), 2-methoxyoxacyclohexane (**3**) and 2-methoxythiacyclohexane (**4**), and 2-methylaminooxacyclohexane (**5**) and 2-methylaminothiacyclohexane (**6**) (Fig. 2). The magnitudes of the energy differences of axial and equatorial isomers in oxygen-containing and sulfur-containing rings were compared, and a quantitative analysis of the orbital interaction term was facilitated by means of a natural

Fig. 2. The 2-substituted heterocyclohexanes used in this study: 2-fluorooxacyclohexane (**1**), 2-fluorothiacyclohexane (**2**), 2-methoxyoxacyclohexane (**3**), 2-methoxythiacyclohexane (**4**), 2-methylaminooxacyclohexane (**5**), and 2-methylaminothiacyclohexane (**6**).



1 X = O; Y = F
2 X = S; Y = F
3 X = O; Y = OCH_3
4 X = S; Y = OCH_3
5 X = O; Y = $NHCH_3$
6 X = S; Y = $NHCH_3$

bond orbital (NBO) analysis of the total energy behaviour. The dipole moments of the optimized systems were used to estimate the electrostatic contributions to the anomeric effect. The results indicate that the orbital interaction component dominates the conformational equilibria, and can therefore be taken as the origin of the anomeric effect.

Computational

DFT calculations were carried out with Gaussian 98 (12), using as input unoptimized Cartesian coordinates from the WebLab program (Accelrys Inc.). The molecules were optimized in the gas phase in the $^4C_1$ chair conformation with a full population analysis using the B3LYP hybrid DFT method (13) at the 6-31++G** level. Following optimization, a frequency calculation was performed, which calculated the bending and stretching modes of the molecule and ensured that a stable minimum was found. In every calculation, the frequencies found were of the real number system, and therefore, every structure is considered as a reliable geometrical minimum.

A NBO analysis was performed on the optimized geometry, using NBO version 3.1 (14) in Gaussian 98. NBOs arise from an occupancy-weighted symmetric orthogonalization (OWSO) procedure in which delocalized molecular orbitals are mathematically transformed into a minimal basis set to represent localized electron pairs (15). The categorized NBOs correspond to the natural Lewis structure of core orbitals, bonding orbitals, and lone-pair orbitals, as well as the antibonding and Rydberg orbitals that do not correspond to Lewis representations (15). Rydberg orbitals are weakly occupied, extra valence shell functions that arise from the extended basis set used for the calculation (16).

A second-order perturbation theory analysis was performed on the NBOs to estimate the stabilization energy of donor–acceptor orbital interactions. In this way, the perturbative origin of the anomeric effect was analyzed and a quantitative measure of the energy associated with orbital interactions was estimated. The perturbative surface is approximated by a quadratic function and therefore contains some uncertainty, but the technique is nonetheless useful for understanding the relative magnitudes of orbital interactions.

Destabilizing interactions were calculated as the orthogonalization energy of the NBOs. The Pauli exclusion principle requires that spatially overlapping orbitals be mutually

© 2006 NRC Canada

Table 1. Bond lengths, bond angles, energies (*E*) and dipole moments (μ) of the axial and equatorial conformers of compounds **1**–**6**, optimized at the B3LYP/6-31++G** level (if applicable, the values for the most stable rotamers are given).

Compound	X/Y	X—C bond length (Å)	C—Y bond length (Å)	X-C-Y bond angle (°)	*E* (a.u.)	μ (D)
1ax	O/F	1.385	1.423	109.36	–371.047 450 2	2.406
1eq	O/F	1.403	1.386	105.77	–371.042 837 4	3.531
2ax	S/F	1.818	1.416	110.48	–694.014 474 5	2.454
2eq	S/F	1.843	1.399	106.60	–694.010 396 7	3.627
3ax	O/OCH_3	1.421	1.414	112.16	–386.329 788 4	0.433
3eq	O/OCH_3	1.430	1.392	108.63	–386.328 538 5	1.855
4ax	S/OCH_3	1.860	1.412	113.60	–709.299 617	0.807
4eq	S/OCH_3	1.875	1.402	110.03	–709.296 438 4	2.106
5ax	O/$NHCH_3$	1.429	1.455	110.20	–366.461 877 5	1.654
5eq	O/$NHCH_3$	1.449	1.430	110.25	–366.466 626 8	1.025
6ax	S/$NHCH_3$	1.857	1.456	111.45	–689.434 129 2	2.071
6eq	S/$NHCH_3$	1.895	1.437	111.94	–689.437 049 9	1.194

orthogonal. The resulting compression and formation of orthogonalization tails is often considered to be the source of destabilizing "steric" interactions (17). In the context of NBO analysis, this destabilization can be calculated as the difference in energy between preorthogonal NBOs and their orthogonal counterparts (18, 19). To quantitate the energy of steric interactions in a pairwise fashion, all orbitals were first orthogonalized and the orbitals of interest were subsequently partially reconverted to their preorthogonal forms with respect to each other; this allowed the calculation to take place in the context of the nodal and electronic structure corresponding as closely as possible to the real system, making this approximation reasonably accurate in the weak overlap limit (18). A further improvement was obtained by using natural localized molecular orbitals (NLMOs) and their preorthogonal counterparts instead of NBOs because of the associated incorporation of the delocalization tails of the NLMOs (20). The calculations were carried out using the Steric feature of the GENNBO 5.0 program (21). We focused our attention on the large $n \rightarrow \sigma$ interactions that parallel the endo- and exo-anomeric orbital interactions.

Molecular orbital diagrams were prepared with the NBOView program (22), using plot files prepared with GENNBO 5.0 (21). The overlap matrix element in the preorthogonal NBO (PNBO) basis is proportional to the NBO orbital overlap (23), and is, therefore, ideally suited to visualize orbital overlap in interactions such as the anomeric effect. PNBOs also have the most intuitive orbital shapes; thus, all diagrams were constructed using the PNBO basis. The apparent orbital size was reduced from the default setting by increasing the first contour value to 0.06 and the contour step size to 0.10 (approximately doubled from their default values). This process allowed the most meaningful visualization of the structure of the PNBO orbitals.

To investigate the contribution of dipole–dipole interactions to the anomeric effect, we sought to represent the cyclic molecules by a series of fragments with their individual dipole moments and polarizabilities. For example, 2-fluorothiacyclohexane was represented by three fragments: propane, 2-fluoropropane, and dimethylsulfide. However, after optimization of the acyclic fragments, it was determined that the methyl groups in the fragments did not accurately represent the electrostatic environment in the cyclic molecule. Therefore, the dipole moment of the propane, 2-fluoropropane, and dimethylsulfide fragments could not be used to mimic the fragment dipoles of the cyclic system. Thus, the dipole moments of the optimized cyclic systems themselves were used to estimate the electrostatic contributions to the anomeric effect.

Results

Table 1 summarizes the optimized parameters found for the 2-substituted oxacyclohexanes and thiacyclohexanes. Table 2 compares the energies, dipole moments, bond lengths, and valence bond angles for the axial and equatorial conformers. NBO perturbation theory analysis was used to identify specific orbital interactions corresponding to the endo- and exo-anomeric effects (Table 3). The values of the interactions were determined independently of each other, so the numbers associated with each particular interaction cannot be compared directly to the overall energies, nor to the energy differences between axial and equatorial conformers. Orbital interactions are favoured by a low energy difference between the donor (d) and acceptor (a) orbitals and (or) a high off-diagonal NBO Fock matrix element, F(d,a), which is proportional to orbital overlap, as shown in eq. [1] (24). These two elements were examined as part of the perturbation theory analysis, and the resulting energy differences and Fock matrix elements are given in Table 3.

$$[1] \qquad E = \frac{F(\mathrm{d},\mathrm{a})^2}{e_\mathrm{a} - e_\mathrm{d}}$$

The salient features of each system are discussed in the following section.

Dipolar interactions

In every case in which a particular conformer was energetically preferred, that structure also had a lower dipole moment. However, in comparison of the 2-fluoro- and 2-methoxy-oxacyclohexanes with the corresponding thiacyclohexanes, the analogue that showed the greatest differ-

© 2006 NRC Canada

Table 2. Comparison of the differences in energies, dipole moments, and geometrical parameters in axial and equatorial conformers, where Δ = (ax) – (eq) (a negative energy value reflects an axial preference).

Compound	ΔX—C (Å)	ΔC—Y (Å)	ΔX-C-Y (°)	Δ*E* (kcal mol^{-1})	Δμ (D)
1	–0.018	0.037	3.59	–2.89	–1.125
2	–0.025	0.017	3.89	–2.56	–1.173
3	–0.009	0.022	3.53	–0.78	–1.422
4	–0.015	0.010	3.57	–1.99	–1.299
5	–0.020	0.026	–0.05	2.98	0.629
6	–0.038	0.019	–0.49	1.83	0.877

Table 3. Individual orbital interactions from the NBO perturbation theory analysis.

		Endo-anomeric ($n_X \rightarrow \sigma_{C\text{-}Y}$)			Exo-anomeric ($n_Y \rightarrow \sigma_{C\text{-}X}$)				
Compound	X/Y	Stabilization *E* (kcal mol^{-1})	Orbital Δ (a.u.)[a]	*F*(a,d) (a.u.)[b]	Stabilization *E* (kcal mol^{-1})	Orbital Δ (a.u.)[a]	*F*(a,d) (a.u.)[b]	$n_X \rightarrow \sigma_{C\text{-}Y}$ Destabilization (kcal mol^{-1})	$n_Y \rightarrow \sigma_{C\text{-}X}$ Destabilization (kcal mol^{-1})
1ax	O/F	20.90	0.50	0.092	10.51	0.72	0.077	9.57	6.91
1eq	O/F	5.08[c]	0.81	0.057	11.61	0.70	0.08	2.44[c]	9.14
2ax	S/F	12.96	0.42	0.066	8.54	0.56	0.0062	5.29	8.90
2eq	S/F	0.68	0.84	0.021	8.14	0.54	0.059	0.66[c]	10.88
3ax	O/OCH_3	13.57	0.60	0.081	13.89	0.59	0.082	8.10	7.51
3eq	O/OCH_3	3.76[c]	0.90	0.052	14.54	0.58	0.083	2.10[c]	9.73
4ax	S/OCH_3	8.38	0.52	0.059	13.22	0.44	0.068	4.44	10.22
4eq	S/OCH_3	*n/o*[d]	—	—	12.84	0.43	0.067	*n/o*[d]	11.91
5ax	O/$NHCH_3$	9.13	0.65	0.069	5.36	0.59	0.051	8.92	1.90
5eq	O/$NHCH_3$	2.19[c]	0.97	0.041	16.15	0.55	0.085	2.87[c]	13.41
6ax	S/$NHCH_3$	5.72	0.58	0.052	3.26	0.43	0.034	5.29	2.77
6eq	S/$NHCH_3$	*n/o*[d]	—	—	15.49	0.40	0.071	0.77[c]	13.75

[a]Energy difference between interacting fragment orbitals.
[b]Fock matrix element indicating extent of overlap between interacting fragment orbitals.
[c]Interactions observed from the sp-type (n_{sp}) lone-pair orbital on the ring heteroatom. In all other cases, the interaction is via the p-type (n_p) orbital.
[d]Not observed; interactions below 0.5 kcal mol^{-1} are not listed.

ence in energy between axial and equatorial conformers also had the smallest change in dipole moment. Thus, 2-methoxythiacyclohexane (**4**) had a greater Δ*E* value among conformers than 2-methoxy-oxacyclohexane (**3**), but the latter (**3**) had a greater Δμ value among conformers. A similar relationship was observed for the 2-fluoro derivatives **1** and **2**, although in this case, it was the oxygen congener **1** that had a smaller Δ*E* value and a higher Δμ value. Since a larger difference in dipole moment among axial/equatorial pairs was not manifested in a greater energy difference among conformers, it follows that dipole–dipole interactions are not the primary determinants of the net stabilization.

Orbital interactions

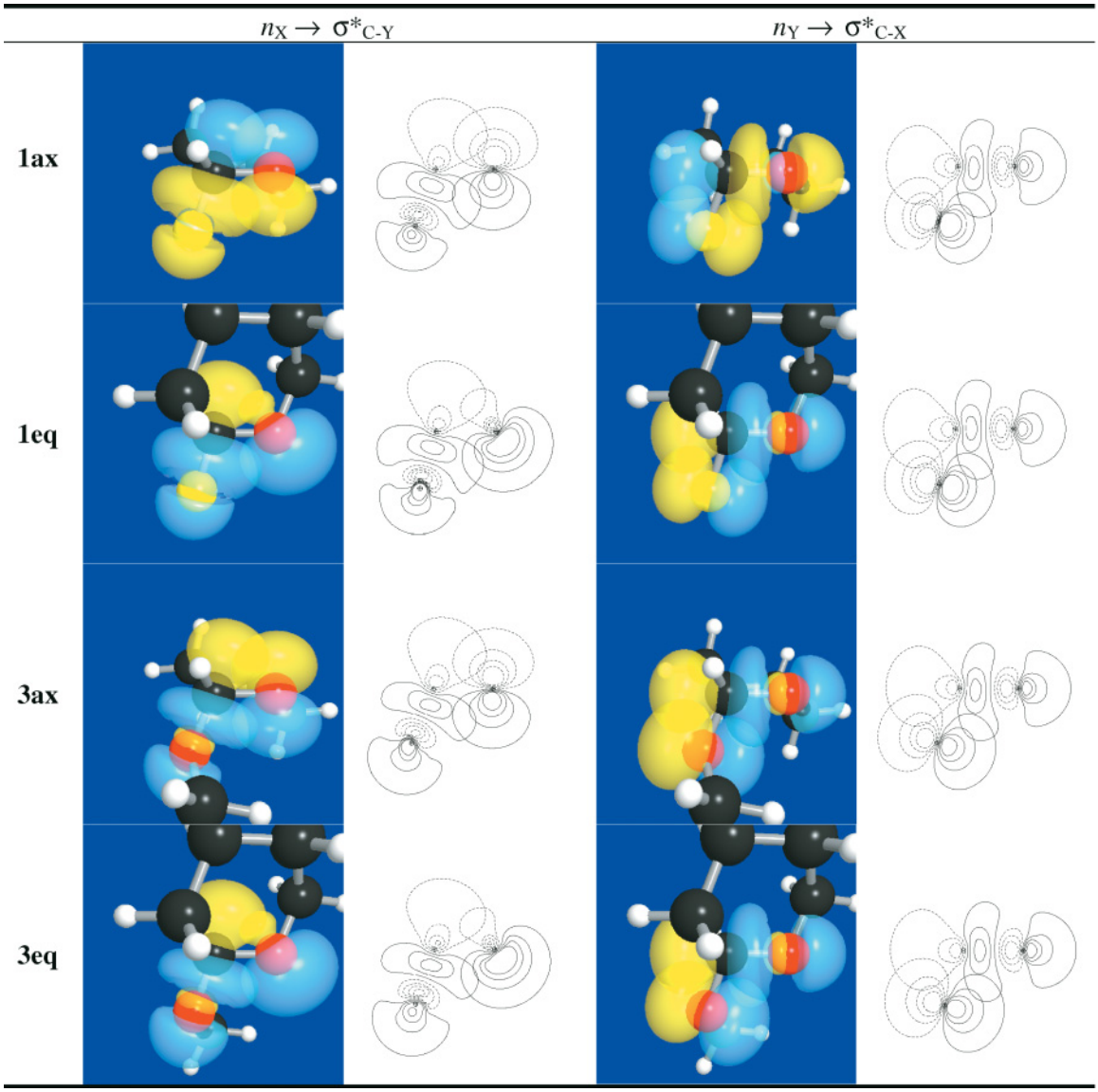
2-Fluorooxacyclohexane (1) and 2-fluorothiacyclohexane (2)

In 2-fluorooxacyclohexane (**1**), the axial conformer is preferred over the equatorial by 2.89 kcal mol^{-1} (1 cal = 4.184 J). NBO analysis (Table 3) indicated that in the axial conformer, the orbital interactions with the highest stabilization energy were the endo-anomeric ($n_O \rightarrow \sigma^*_{C\text{-}F}$) interaction of 20.9 kcal mol^{-1} and the exo-anomeric ($n_F \rightarrow \sigma^*_{C\text{-}O}$) interaction of 10.5 kcal mol^{-1}. In the equatorial conformer, the greatest orbital interaction is the exo-anomeric ($n_F \rightarrow \sigma^*_{C\text{-}O}$) interaction of 11.6 kcal mol^{-1}. In addition, there is an endo-anomeric orbital interaction of 5.1 kcal mol^{-1} that derives from interaction of the subjacent sp lone-pair fragment orbital on oxygen with the $\sigma^*_{C\text{-}F}$ fragment orbital. These interactions are shown in Fig. 3. It is clear that the large difference in the endo-anomeric interactions leads to the strong preference for the axial conformer. The consequences of these orbital interactions are reflected in the bond lengths and valence bond angles shown in Table 2: the C—O bond was shorter, the C—F bond was longer, and the O-C-F angle was greater in the axial conformer than in the equatorial conformer (10). The magnitudes of the axial vs. equatorial stabilizing interactions shown in Table 3 do not correspond directly to the energy difference between the conformers (Table 1) because of the steric effects that destabilize the axial isomer.

In 2-fluorothiacyclohexane (**2**), the axial conformer was preferred over the equatorial by 2.56 kcal mol^{-1}). From the NBO perturbation theory analysis, in the axial conformer, the two greatest orbital interactions were the $n_S \rightarrow \sigma^*_{C\text{-}F}$ endo-anomeric effect of 13.0 kcal mol^{-1} and the $n_F \rightarrow \sigma^*_{C\text{-}S}$ exo-anomeric effect of 8.5 kcal mol^{-1}. These interactions result in a shortened C—S bond length of 1.818 Å and lengthened C—F bond of 1.416 Å in the axial structure. In the equatorial conformer, the greatest interaction was the $n_F \rightarrow \sigma^*_{C\text{-}S}$ exo-anomeric effect of 8.1 kcal mol^{-1}, of similar magnitude to the exo-anomeric orbital interaction in the axial conformer. It can be concluded that the appreciable endo-

© 2006 NRC Canada

Fig. 3. Fragment molecular orbital interactions in the axial and equatorial conformers of **1** and **3**, illustrating the endo- and exo-anomeric orbital interactions. In the equatorial conformers, the $n_X \rightarrow \sigma^*_{C\text{-}Y}$ interaction is from the subjacent sp-type orbital on the ring oxygen atom. The preorthogonalized NBOs were generated with the NBOView program (21). Figures showing the orbital interactions of compounds **2**, **4**, **5**, and **6** are given in the Supplementary data.[3]



anomeric orbital interaction in the axial conformer controls its energetic preference. The interactions are shown in the Supplementary information.[3] In this case, the endo-anomeric orbital interaction that derives from interaction of the subjacent sp lone-pair fragment orbital on sulfur with the $\sigma^*_{C\text{-}F}$ fragment orbital is small (0.68 kcal mol^{-1}), in contrast to the oxygen congener.

Further comparison of the results for 2-fluorooxacyclohexane (**1**) and 2-fluorothiacyclohexane (**2**) indicated that the energy difference between axial and equatorial conformers was only slightly greater for the oxygen congener (**1**). This result is due to the much lesser steric effect in the axial isomer of the thiacyclohexane derivative, but still correlates with the sum of the exo and endo interactions for the two conformers, which gave a smaller energy difference for the 2-fluorothiacyclohexane (**2**). It is noteworthy that the difference in the combined destabilizing $n_X \rightarrow \sigma_{C\text{-}F}$ and $n_F \rightarrow \sigma_{C\text{-}X}$ interactions between axial and equatorial conformers is of much lesser magnitude than the stabilizing endo and exo interactions in the axial conformers (Table 3).

2-Methoxyoxacyclohexane (3) and 2-methoxythiacyclohexane (4)

In 2-methoxyoxacyclohexane (**3**), the axial conformer was

[3] Figures showing the endo- and exo-orbital interactions from NBO analysis in the axial and equatorial conformers of **2**, **4**, **5**, and **6**. Supplementary data for this article are available on the journal Web site (http://canjchem.nrc.ca) or may be purchased from the Depository of Unpublished Data, Document Delivery, CISTI, National Research Council Canada, Ottawa, ON K1A 0R6, Canada. DUD 5020. For more information on obtaining material refer to http://cisti-icist.nrc-cnrc.gc.ca/irm/unpub_e.shtml.

© 2006 NRC Canada

preferred by 0.78 kcal mol^{-1}. NBO perturbation analysis indicated that the orbital interactions with the largest stabilization energies in the axial conformer were the exo-anomeric orbital interaction of 13.9 kcal mol^{-1} and the endo-anomeric orbital interaction of 13.6 kcal mol^{-1}. These values were similar due to the approximate equivalence of the $n_O \rightarrow \sigma^*_{C\text{-}O}$ interactions. In the equatorial conformer, the largest stabilizing orbital interaction was the exo-anomeric orbital interaction of 14.5 kcal mol^{-1}. The interactions are shown in Fig. 3. In addition, an endo-anomeric orbital interaction of the subjacent sp lone-pair fragment orbital on the ring oxygen atom with the $\sigma^*_{C\text{-}O}$ orbital of energy 3.8 kcal mol^{-1} was present. Thus, the presence of the endo-anomeric orbital interaction dictates the axial preference.

In 2-methoxythiacyclohexane (**4**), the axial conformer was favoured by 1.99 kcal mol^{-1}. In the axial conformation, NBO perturbation theory analysis indicated that the greatest stabilizing orbital interactions were the exo-anomeric ($n_O \rightarrow \sigma^*_{C\text{-}S}$) interaction of 13.2 kcal mol^{-1} and the endo-anomeric ($n_S \rightarrow \sigma^*_{C\text{-}O}$) interaction of 8.4 kcal mol^{-1}. It is noteworthy that the exo-anomeric orbital interaction was greater than the endo-anomeric orbital interaction in the axial conformer, although the C—O (1.412 Å) and C—S (1.860 Å) bond lengths relative to the equatorial conformer reflect the balance of the endo- and exo-anomeric effects. The interactions are shown in the Supplementary information.[3]

It is of direct relevance to the present work that Wolfe and Shi (25), in an examination of methyl thiomethyl ether by electron momentum spectroscopy and photoelectron spectroscopy, have shown that although the p-type lone pair on sulfur is the HOMO of the molecule, the dominant orbital interactions are of the $n_O \rightarrow \sigma^*_{C\text{-}S}$ type, with some contribution from the destabilizing $n_O \rightarrow \sigma_{C\text{-}S}$ interaction. Thus, the lone pair on oxygen dominates the anomeric interactions in an RS-CH_2-OR′ fragment.

NBO perturbation theory analysis of the equatorial conformer of 2-methoxythiacyclohexane (**4**) indicated that the greatest stabilizing orbital interaction was the exo-anomeric ($n_O \rightarrow \sigma^*_{C\text{-}S}$) interaction of 12.8 kcal mol^{-1}. This result was consistent with the optimized parameters in which the C—S bond was lengthened (1.875 Å) and the C—O bond was shortened (1.402 Å) when compared with the axial conformer. In this case, the endo-anomeric orbital interaction of the subjacent sp lone-pair fragment orbital on the ring sulfur atom with the $\sigma^*_{C\text{-}O}$ orbital was negligible.

Comparison of the results of 2-methoxyoxacyclohexane (**3**) and 2-methoxythiacyclohexane (**4**) indicated that the energy difference between axial and equatorial conformers was greater in the sulfur congener. This trend is in contrast to compounds **1** and **2** where the energy difference was greater for the oxygen congener. The discrepancy may be attributed to the dominant role of the combined endo and exo interactions in stabilizing the axial conformer. This result verifies the conclusions from our previous work (11) that showed the preferential stabilization of the axial conformers in 2-alkoxythiacyclohexanes relative to their oxygen counterparts. If dipole–dipole interactions had dominated, one would have predicted the opposite trend. As was the case for **1** and **2**, the difference in the combined destabilizing $n_X \rightarrow \sigma_{C\text{-}O}$ and $n_O \rightarrow \sigma_{C\text{-}X}$ interactions between axial and equatorial conformers is of much lesser magnitude than the stabilizing endo and exo interactions in the axial conformers (Table 3).

2-Methylaminooxacyclohexane (5) and 2-methylaminothiacyclohexane (6)

Both 2-methylaminooxacyclohexane **(5)** and 2-methylaminothiacyclohexane **(6)** preferred the equatorial conformers despite the fact that the C—X and C—Y bond length differences (Table 2) and perturbation analysis (Table 3) showed evidence of increased endo-anomeric orbital interactions in the axial conformers. We turn, therefore, to a detailed discussion of the rotamers shown in Tables 4 and 5.

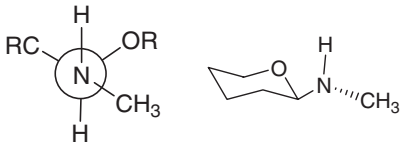
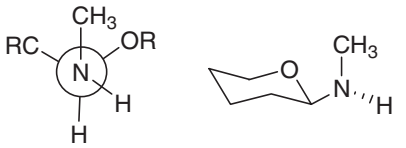
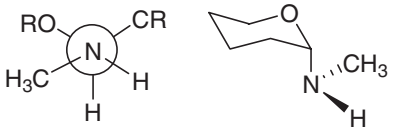
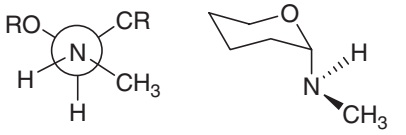
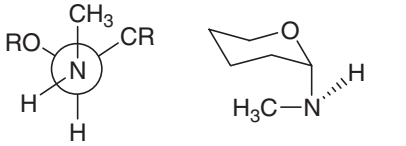
In 2-methylaminooxacyclohexane (**5**) (Table 4), the most stable equatorial conformer was favoured over the most stable axial conformer by 2.98 kcal mol^{-1}. In fact, two equatorial conformers of 2-methylaminooxacyclohexane (**5**) were more stable than the axial conformers. As argued previously (11, 26), the axial conformers cannot enjoy the stabilization by the exo-anomeric effect because the required rotamer would necessarily place one of the substituents on nitrogen under the six-membered ring, resulting in a dramatic steric destabilization. The contention is supported by the observation that of the axial structures, those with the nitrogen lone pair projected under the ring were more stable, in spite of their less favourable orbital interactions. The steric penalty of placing a methyl group under the ring (structure **E**) overwhelms the $n_N \rightarrow \sigma^*_{C\text{-}O}$ orbital interaction. In contrast, the equatorial conformer features a large exo-anomeric orbital interaction (>16 kcal mol^{-1}), and the stabilizing endo-anomeric orbital interaction of 9 to 10 kcal mol^{-1}, available in the axial conformer, is not sufficient to outweigh the former interaction (see Supplementary information).[3] Thus, as predicted previously (7*c*, 25), the $n_N \rightarrow \sigma^*_{C\text{-}O}$ orbital interaction outweighs the $n_O \rightarrow \sigma^*_{C\text{-}N}$ orbital interaction. Both of the low-energy equatorial structures (**A** and **B**), shown in Table 3, were stabilized by exo-anomeric interactions. Steric effects determine which of the two is more stable, as structure **A** features only one gauche interaction and structure **B** has two (see Newman projections, Fig. 3). In this case, the endo-anomeric orbital interaction of the subjacent sp lone-pair fragment orbital on the ring sulfur atom with the $\sigma^*_{C\text{-}N}$ orbital was 2.2 kcal mol^{-1}.

It is of interest to also comment on the dominant destabilizing interactions in the rotamers of **5** (Table 4). In rotamers **5A**, **5B**, and **5E**, the nitrogen lone-pair orbital is properly aligned to interact with the $\sigma_{C\text{-}O}$ orbital. This $n_N \rightarrow \sigma_{C\text{-}O}$ interaction is worth 13.41, 13.29, and 10.56 kcal mol^{-1} in **5A**, **5B**, and **5E**, respectively. In rotamers **5C** and **5D**, the dominant destabilizing interaction is the $n_O \rightarrow \sigma_{C\text{-}N}$ interaction, worth 8.92 and 10.17 kcal mol^{-1}, respectively. These interactions are significant, but it is the stabilizing exo interaction in the equatorial conformer **5A** that dictates its stabilization relative to the most stable axial conformer, **5C**.

In 2-methylaminothiacyclohexane **6** (Table 5), the most stable equatorial conformer was energetically preferred by 1.83 kcal mol^{-1} over the axial conformer. Once again, structure **A** was favoured over structure **B** because of the fewer number of gauche interactions. Of the four axial structures, those with the nitrogen lone pair beneath the ring (structures **C** and **D**) were more stable than those with a substituent beneath the ring (structures **E** and **F**). In this case, the endo-

© 2006 NRC Canada

Table 4. Newman projections and structures of the rotamers and conformers of 2-methylaminooxacyclohexane and the values of the orbital interactions taken from the second-order perturbation theory NBO analysis.

Rotamer of **5**		Relative E (kcal mol^{-1})	$n_O \rightarrow \sigma^*_{C\text{-}N}$ (kcal mol^{-1})	$n_N \rightarrow \sigma^*_{C\text{-}O}$ (kcal mol^{-1})	$n_O/\sigma_{C\text{-}N}$ (kcal mol^{-1})	$n_N/\sigma_{C\text{-}O}$ (kcal mol^{-1})
A		0.00	2.2	16.2	2.87[a]	13.41
B		1.73	2.2	16.1	2.92[a]	13.29
C		2.98	9.1	5.4	8.92[b]	1.90
D		4.11	9.1	1.3	10.17[b]	*n/o*[c]
E		7.29	10.6	17.8	8.42	10.56

[a]Interaction was with the sp-type (n_{sp}) orbital.
[b]A small destabilizing interaction with n_{sp} (not shown) was also observed.
[c]Not observed; interactions below 0.5 kcal mol^{-1} are not listed.

anomeric orbital interaction of the subjacent sp lone-pair fragment orbital on the ring sulfur atom with the $\sigma^*_{C\text{-}N}$ orbital was negligible.

The axial structures all displayed an endo-anomeric orbital interaction, while differing in the extent of an exo-anomeric orbital interaction. Once again, as predicted (7*c*, 25), the $n_N \rightarrow \sigma^*_{C\text{-}S}$ orbital interaction outweighs the $n_S \rightarrow \sigma^*_{C\text{-}N}$ orbital interaction. Structure **C**, a stereoisomer of **D**, was found to be the most stable axial structure overall. The appropriate orientation of the methyl group allowed an exo-anomeric orbital interaction of 3.26 kcal mol^{-1} in addition to an endo-anomeric orbital interaction of 5.72 kcal mol^{-1}. Increasing the exo-anomeric interaction would necessitate placing one of the nitrogen substituents under the ring. The most stable rotamers **(C** and **D)** thus lacked the exo-anomeric orbital interaction, but also the accentuated steric interaction (see Supplementary information)[3] (11, 26).

A comparison of rotamers **E** and **F** illustrates the influence of orbital interactions in overcoming a significant steric penalty. Thus, rotamer **E** is destabilized by the placement of a methyl group directly under the ring, but features a highly stabilizing exo-anomeric interaction of nearly 17 kcal mol^{-1}. In contrast, structure **F** does not have an exo-anomeric interaction and only places the smaller substituent (H) under the ring; yet rotamer **E** is favoured over **F** by 0.75 kcal mol^{-1}.

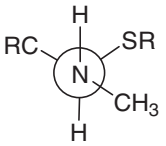
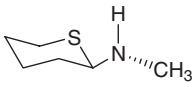
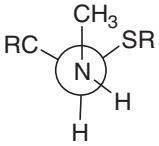
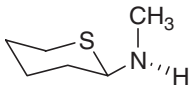
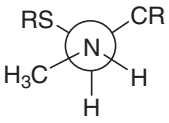
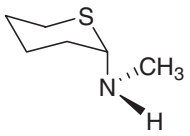
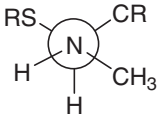
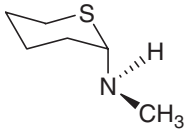
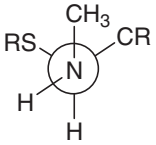
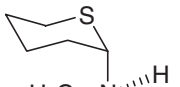
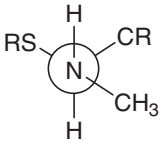
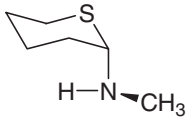
Once again, we also comment on the dominant destabilizing interactions in the rotamers of **6** (Table 4). In each of rotamers **6A, 6B**, and **6E**, the nitrogen lone-pair orbital is properly aligned to interact with the $\sigma_{C\text{-}S}$ orbital. This $n_N \rightarrow \sigma_{C\text{-}S}$ interaction is worth 13.75, 13.68, and 12.29 kcal mol^{-1} in **6A**, **6B**, and **6E**, respectively. In rotamer **6C**, the $n_S \rightarrow \sigma_{C\text{-}N}$ and $n_N \rightarrow \sigma_{C\text{-}S}$ destabilizing interactions of 5.29 and 2.77 kcal mol^{-1}, respectively, were observed. These interactions are significant, but are smaller than the stabilizing exo interaction in the equatorial conformer **6A** that dictates its stabilization relative to the most stable axial conformer, **6C**.

Discussion

Comparison of the endo-anomeric orbital interactions in

© 2006 NRC Canada

Table 5. Newman projections and structures of the rotamers and conformers of 2-methylaminothiacyclohexane and the values of the orbital interactions taken from the second-order perturbation theory NBO analysis.

Rotamer of **6**			Relative E (kcal mol^{-1})	$n_S \rightarrow \sigma^*_{C\text{-}N}$ (kcal mol^{-1})	$n_N \rightarrow \sigma^*_{C\text{-}S}$ (kcal mol^{-1})	$n_S/\sigma_{C\text{-}N}$ (kcal mol^{-1})	$n_N/\sigma_{C\text{-}S}$ (kcal mol^{-1})
A			0.00	*n/o*[a]	15.5	0.77[b]	13.75
B			1.57	*n/o*[a]	15.7	0.65[b]	13.68
C			1.83	5.7	3.3	5.29	2.77
D			2.11	5.7	*n/o*[a]	6.42	*n/o*[a]
E			4.53	6.6	16.9	4.47	12.29
F			5.28	6.3	1.8	5.70	2.76

[a]Not observed; interactions below 0.5 kcal mol^{-1} are not listed.
[b]Interaction was via the sp-type (n_{sp}) orbital.

the oxygen vs. the sulfur series (Table 3) indicates that they are greater in the former series than in the latter, as previously suggested for first-row vs. second-row anomeric interactions (27). In the thiacyclohexane compounds, the energy difference between orbitals (ΔE) was less than that of the corresponding oxacyclohexane compounds for the endo interactions. However, the F(d,a) term was consistently greater in the substituted oxacyclohexanes, indicating that the orbital overlap is greater in the oxygen series because of the shorter C—O vs. C—S bond, and dominates the orbital interaction, as suggested by Wolfe and Shi (25). Thus, irrespective of the exocyclic substituent and the exo-anomeric contribution, the endo-anomeric effect is greater for O vs. S. Interestingly, for the exo-anomeric interaction, one also observes a greater interaction in the oxygen series, irrespective of the exocyclic substituent, because of a lesser energy difference between interacting orbitals and greater overlap between the interacting orbitals. Presumably, the greater overall overlap is due to the greater electronegativity of oxygen, which leads, in turn, to the increased size of the σ* orbital lobe on C and thus, to better overlap with the exocyclic donor orbital. A noticeable $n_X \rightarrow \sigma^*_{C\text{-}Y}$ interaction (endo-anomeric interaction) from the subjacent sp lone pair orbital on the ring heteroatom was observed in the *equatorial* conformers of the substituted oxacyclohexanes, but this was small (Y = F) or negligible (Y = OCH_3, $NHCH_3$) for the thiacyclohexanes. Again, this difference is related to the larger Fock matrix element (better orbital overlap) in the oxygen series, and not the relative energy levels.

It would appear that although dipolar interactions play

© 2006 NRC Canada

some role in the stabilization of the axial conformers in this series of compounds, they are not the dominant force in controlling the conformational preferences. It is the combined endo- and exo-anomeric orbital interactions that dominate.

It is important to note that the exo- and endo-anomeric orbital interactions do not compete energetically, as the sets of orbitals involved are orthogonal to each other. A valence bond interpretation might suggest otherwise (8). By way of example, in 2-fluorothiacyclohexane (**2**), the axial conformer has an endo-anomeric interaction of 13.0 kcal mol^{-1} and an exo-anomeric interaction of 8.5 kcal mol^{-1}. If these were in competition, a net endo-anomeric interaction of 4.5 kcal mol^{-1} would result and would be disfavoured relative to the net exo-anomeric interaction of 8.1 kcal mol^{-1} available in the equatorial conformer. That the axial conformer is preferred suggests that the endo- and exo-anomeric orbital interactions do not compete energetically.

Finally, we reiterate (11, 26) that in 2-methylaminoheterocyclohexanes, the stabilization provided by the exo-anomeric interaction in the axial conformers does not ensue because it would force an accentuated steric interaction. Consequently, the equatorial conformer, which does exhibit an exo-anomeric effect, is favoured since, as predicted previously (7*c*, 25), the $n_N \rightarrow \sigma^*_{C\text{-}X}$ exo-orbital interaction outweighs the $n_X \rightarrow \sigma^*_{C\text{-}N}$ endo-orbital interaction.

Acknowledgements

We are grateful to the Natural Sciences and Engineering Research Council of Canada (NSERC) for financial support in the form of grants (to BMP and NW), and a Canada Research Scholarship (to JKW). JKW is also grateful to the Tomlinson Foundation for a postgraduate fellowship. We thank F. Weinhold for helpful discussion.

References

1. J.T. Edward. Chem. Ind. (London), 1102 (1955).
2. R.U. Lemieux and N.J. Chü. Abstr. Papers 133rd Am. Chem. Soc. Meeting, 31N (1958).
3. For leading references: (*a*) W.A. Szarek and D. Horton (*Editors*). Anomeric effect: Origin and consequences. ACS Symposium Series 87. American Chemical Society, Washington, D.C. 1979; (*b*) A.J. Kirby. The anomeric effect and related stereoelectronic effects at oxygen. Springer-Verlag, Berlin. 1983; (*c*) G.R.J. Thatcher (*Editor*). The anomeric effect and associated stereoelectronic effects. ACS Symposium Series 539. American Chemical Society, Washington, D.C. 1993; (*d*) E. Juaristi and G. Cuevas (*Editors*). The anomeric effect. CRC Press, Boca Raton, Florida. 1995.
4. R.U. Lemieux. Pure Appl. Chem. **25**, 527 (1971).
5. E.A.C. Lücken. J. Chem. Soc. **111**, 2954 (1959).
6. C. Romers, C. Altona, H.R. Buys, and E. Havinga. Top. Stereochem. **4**, 39 (1969).
7. (*a*) R. Hoffmann, L. Radom, J.A. Pople, P.v.R. Schleyer, W.J. Hehre, and L. Salem. J. Am. Chem. Soc. **94**, 6221 (1972); (*b*) O. Eisenstein, N.T. Anh, Y. Jean, A. Devaquet, J. Cantacuzene, and L. Salem. Tetrahedron, **30**, 1717 (1974); (*c*) S. Wolfe, M.-H. Whangbo, and D.J. Mitchell. Carbohydr. Res. **69**, 1 (1979).
8. J.-P. Praly and R.U. Lemieux. Can. J. Chem. **65**, 213 (1987).
9. R.U. Lemieux and S. Koto. Tetrahedron, **30**, 1933 (1974).
10. (*a*) B.M. Pinto, H.B. Schlegel, and S. Wolfe. Can. J. Chem. **65**, 1658 (1987); (*b*) S. Wolfe, B. M. Pinto, V. Varma, and R.Y.N. Leung. Can. J. Chem. **68**, 1051 (1990).
11. B.M. Pinto and R.Y.N. Leung. *In* The anomeric effect and associated stereoelectronic effects. ACS Symposium Series 539. *Edited by* G.R.J. Thatcher. American Chemical Society, Washington, D.C. 1993.
12. M.J. Frisch, G.W. Trucks, H.B. Schlegel, G.E. Scuseria, M.A. Robb, J.R. Cheeseman, V.G. Zakrzewski, J.A. Montgomery, Jr., R.E. Stratmann, J.C. Burant, S. Dapprich, J.M. Millam, A.D. Daniels, K.N. Kudin, M.C. Strain, O. Farkas, J. Tomasi, V. Barone, M. Cossi, R. Cammi, B. Mennucci, C. Pomelli, C. Adamo, S. Clifford, J. Ochterski, G.A. Petersson, P.Y. Ayala, Q. Cui, K. Morokuma, P. Salvador, J.J. Dannenberg, D.K. Malick, A.D. Rabuck, K. Raghavachari, J.B. Foresman, J. Cioslowski, J.V. Ortiz, A.G. Baboul, B.B. Stefanov, G. Liu, A. Liashenko, P. Piskorz, I. Komaromi, R. Gomperts, R.L. Martin, D.J. Fox, T. Keith, M.A. Al-Laham, C.Y. Peng, A. Nanayakkara, M. Challacombe, P.M.W. Gill, B. Johnson, W. Chen, M.W. Wong, J.L. Andres, C. Gonzalez, M. Head-Gordon, E.S. Replogle, and J.A. Pople. Gaussian 98. Revision A.11.3 [computer program]. Gaussian, Inc., Pittsburgh, Penn. 2002.
13. (*a*) C. Lee, W. Yang, and R.G. Parr. Phys.l Rev. B **37**, 785 (1988); (*b*) A.D. Becke. Phys. Rev. A, **38**, 3098 (1988); (*c*) A.D. Becke. J. Chem. Phys. **97**, 9173 (1992); (*d*) A.D. Becke. J. Chem. Phys. **98**, 5648 (1993); (*e*) P.J. Stephens, F.J. Devlin, C.F. Chabalowski, and M.J. Frisch. J. Phys. Chem. **98**, 11623 (1994).
14. E.D. Glendening, A.E. Reed, J.E. Carpenter, and F. Weinhold. NBO Version 3.1 [computer program]. Theoretical Chemistry Institute, University of Wisconsin, Madison, Wisconsin.
15. (*a*) J.E. Carpenter and F. Weinhold. THEOCHEM. **46**, 41 (1988); (*b*) J.E. Carpenter. Ph.D thesis, University of Wisconsin, Madison, Wisconsin. 1987; (*c*) F. Weinhold and J.E. Carpenter. *In* The structure of small molecules and ions. *Edited by* R. Naaman and V. Vager. Plenum, New York. 1988. p. 227; (*d*) A.E. Reed, R.B. Weinstock, and F. Weinhold. J. Chem. Phys. **83**, 735 (1985); (*e*) A.E. Reed and F. Weinhold. J. Chem. Phys. **78**, 4066 (1983); (*f*) J.P. Foster and F. Weinhold. J. Am. Chem. Soc. **102**, 7211 (1980); (*g*) A.E. Reed and F. Weinhold. J. Chem. Phys. **83**, 1736 (1985); (*h*) A.E. Reed, L.A. Curtiss, and F. Weinhold. Chem. Rev. **88**, 899 (1988).
16. E.D. Glendening, A.E. Reed, J.E. Carpenter, and F. Weinhold. NBO 3.0 Program Manual, Theoretical Chemistry Institute, University of Wisconsin, Madison, Wisconsin.
17. (*a*) V.F. Weisskopf. Science (Washington, D.C.), **187**, 605 (1975); (*b*) P.A. Christiansen and W.E. Palke. J. Chem. Phys. **67**, 57 (1977).
18. J.K. Badenhoop and F. Weinhold. J. Chem. Phys. **107**, 5406 (1997).
19. J.K. Badenhoop and F. Weinhold. Int. J. Quantum Chem. **72**, 269 (1999).
20. NBO 5.0 program manual. *Edited by* F. Weinhold. Theoretical Chemistry Insitute, University of Wisconsin, Madison, Wisconsin. 2001
21. E.D. Glendening, J. Badenhoop, K.A.E. Reed, J.E. Carpenter, J.A. Bohmann, C.M. Morales, and F. Weinhold. GenNBO 5.0 [computer program]. Theoretical Chemistry Institute, University of Wisconsin, Madison, Wisconsin. 2001.
22. M. Wendt and F. Weinhold. NBOView 1.1 [computer program]. Theoretical Chemistry Institute, Madison, Wisconsin. 2001.
23. A.E. Reed and P.v.R. Schleyer. J. Am. Chem. Soc. **109**, 7362 (1987).

© 2006 NRC Canada

24. T.A. Albright, J.K. Burdett, and M.-H. Whangbo. Orbital interactions in chemistry. John Wiley and Sons, New York. 1985.
25. S. Wolfe and Z. Shi. Isr. J. Chem. **40**, 343 (2000).
26. (*a*) M.C. Krole, J.M.C. Huige, and C.J. Altona. J. Comput. Chem. **10**, 265 (1990); (*b*) C.J. Cramer. J. Org. Chem. **57**, 7034 (1992); (*c*) R.J. Batchelor, D.F. Green, B.D. Johnston, B.O. Patrick, and B.M. Pinto. Carbohydr. Res. 330, 421 (2001).
27. (*a*) U. Salzner, and P.v.R. Schleyer. J. Am. Chem. Soc. **115**, 10231 (1993); (*b*) S.D. Kahn, J. Korppi-Tommola, R.Y.N. Leung, and B.M. Pinto. J. Mol. Struct: THEOCHEM, **303**, 163 (1994).

© 2006 NRC Canada

Complexation of diazinon, an organophosphorus pesticide, with α-, β-, and γ-cyclodextrin — NMR and computational studies[1,2]

Doreen Churchill, Jason Chiu Fung Cheung, Yong Sung Park, Vedene H. Smith, Gary vanLoon, and Erwin Buncel

Abstract: Complexation of the organophosphorus pesticide, diazinon, with α-, β- and γ- cyclodextrin has been investigated through NMR and computational methodologies. Binding constants (K_b) determined by ^{1}H and ^{31}P NMR follow the order γ-CD > α-CD = β-CD, in contrast with reported K_b data for other pesticides and thus indicative of steric encumbrance by the isopropyl group in diazinon being an important factor influencing binding constants. The interaction of diazinon with the CDs has also been investigated through computational studies via molecular dynamics – molecular mechanics (MD–MM2) and density functional theory (DFT), B3LYP/6-31G*. It is shown that the most favorable orientation in binding corresponds to the hydrophobic heterocyclic residue of diazinon being pulled deepest into the CD cavity, in agreement with the experimentally determined order of binding constants. Moreover, the computations show that it is only with γ-CD that the heterocyclic residue of diazinon and the phosphoryl residue are both largely encrypted in the CD cavity, marking a clear differentiation with α-CD and β-CD where the phosphoryl residue is located largely outside the cavity. Thus, the computational results are in essential agreement with the experimental binding constants where γ-CD stands out with the highest K_b value. Our work could point to the potential usefulness of computational studies to be undertaken in tandem with experimental work in environmental situations such as soil remediation.

Key words: organophosphorus pesticides, diazinon complexation, cyclodextrins, computational studies, molecular mechanics.

Résumé : Faisant appel à la RMN et à des calculs théoriques, on a étudié la complexation du diazinon, un pesticide organophosphoré, avec les α-, β- et γ-cyclodextrines. Faisant appel à la RMN du ^{1}H et du ^{31}P, on a déterminé que les constantes de fixation (K_b) sont dans l'ordre γ-CD > α-CD = β-CD, ce qui contraste avec les valeurs de K_b rapportées pour d'autres pesticides; ces différences pourraient suggérer que l'encombrement stérique provoqué par le groupe isopropyle du diazinon est un facteur qui présente une influence importante dans les constantes de fixation. L'interaction du diazinon avec les cyclodextrines a été examinée d'une façon théorique en faisant appel à la théorie de la dynamique moléculaire – mécanique moléculaire (DM–MM2) et à la théorie de la densité fonctionnelle (TDF), B3LYP/6-31G*. On a montré que l'orientation la plus favorable lors de la fixation correspond à celle où le résidu hétérocyclique hydrophobe du diazinon est inséré au point le plus profond de la cavité de la cyclodextrine, ce qui correspond à l'ordre déterminé d'une façon expérimentale par les constantes de fixation. De plus, les calculs montrent le résidu hétérocyclique du diazinon et le résidu phosphoryle ne sont bien insérés que dans la cavité de la γ-CD, ce qui la différencie clairement de l'α-CD et de la β-CD avec lesquelles le résidu phosphoryle se trouve largement à l'extérieur de la cavité. Les résultats théoriques sont donc, pour l'essentiel, en accord avec les constantes de fixations expérimentales alors que la valeur pour la γ-CD est la plus élevée. Ce travail pourrait démontrer l'utilité potentielle d'études théoriques pour étudier, en tandem, avec des expérimentales, des situations environnementales, telles que la récupération des sols.

Mots clés : pesticides organophosphorés, complexation du diazinon, cyclodextrines, études théoriques, mécanique moléculaire.

[Traduit par la Rédaction]

Received 6 December 2005. Published on the NRC Research Press Web site at http://canjchem.nrc.ca on 13 May 2006. Reposted on the Web site with correction on 16 May 2006.

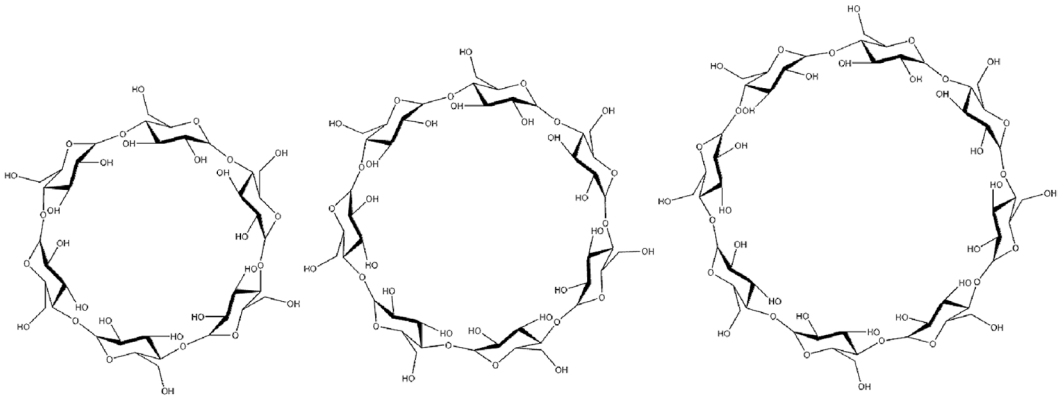
This paper is dedicated to Professor Walter Szarek in recognition of his contributions to chemistry.

D. Churchill. Centre of Environmental Excellence, c/o Sir Wilfred Grenfell College, Corner Brook, NF A2H 6P9, Canada.
J.C.F. Cheung, Y.S. Park, V.H. Smith,[3] G. vanLoon, and E. Buncel.[4] Department of Chemistry, Queen's University, Kingston, ON K7L 3N6, Canada.

[1]This article is part of a Special Issue dedicated to Professor Walter A. Szarek.
[2]Part 9 in a series titled "Mechanisms of abiotic degradation and soil–water interactions of pesticides and other hydrophobic organic compounds". For part 8, see ref. 1.
[3]Deceased.

 doi:10.1139/V06-053 © 2006 NRC Canada

Fig. 1. Chemical structure of α-CD, β-CD, and γ-CD consisting of six, seven, and eight glucose units, respectively.

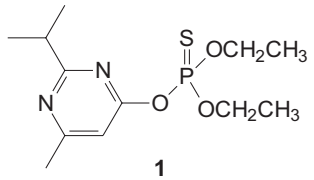


α-cyclodextrin β-cyclodextrin γ-cyclodextrin

Introduction

The wide usage of pesticides in modern agriculture, coupled with the known toxicity of pesticide residues to humans and other nontarget organisms, calls for fresh research into methods for the facile degradation of such residues under environmentally benign conditions and without generating further toxic materials (metabolites) in the process. Our own approach toward that goal is through the tools of structure–reactivity relationships in physical organic chemistry and environmental science. Several papers have been published from our laboratories concerning the degradation of various pesticides and other hydrophobic organic compounds (1–7).

In the present work we have explored, through computational and NMR methodology, the interaction of the organophosphorus pesticide, diazinon (**1**), with several cyclodextrin (CD) molecules.



1

The CDs being investigated are α-, β-, and γ-CD, containing six, seven, and eight glucose moieties, respectively, in the cyclic structure (Fig. 1). The CDs may be shown by the torus ("bucket") representation in which the secondary hydroxyls are situated on the upper, wider rim, and the primary hydroxyls on the lower rim (see figures in the Computational studies section).

The important characteristic of the CD-type glucose oligosaccharide structure is a hydrophilic exterior imparted by the CD hydroxyl groups and an interior lined by H-C-O linkages that impart hydrophobic character (8, 9). The hydrophobic interior is then capable of encapsulating a hydrophobic or low polarity molecule, for example, a typical pesticide containing an aromatic or heteroaromatic moiety, resulting in the formation of a host–guest complex. The driving force for CD host–guest complex formation is presumed to have as its origin the combination of the following factors: (1) release of "high-energy" H_2O molecules from the CD cavity; (2) relief of strain in the CD molecule upon complexation of the guest (important for the small α-CD); (3) hydrophobic and van der Waals interactions; (4) hydrogen bonding between host and guest; (5) compatability between guest size and dimensions of the host cavity; (6) orientation of the guest molecule in the cavity. The computer modeling and NMR studies reported in this paper bring insight into some of these factors.

CDs have a potentially uniquely important role in the removal of pesticide residues from contaminated soils, for example, from localized industrial sites. In such a situation, the leaching of the pesticide through rainwater, along with other hydrophobic compounds, causes these to localize below the ground water table where they accumulate as DNPLs (dense nonaqueous phase liquids); there they remain virtually immune to degradation through bacterial action over several decades or longer (10). Now, if a CD solution is pumped from the surface into the DNPL, it complexes the hydrophobic material, which once solubilized, can be carried downstream. From there it can be pumped up to the surface where it is separated into its constituents and degraded, while the CD solution is recycled upstream. This process is similar to the traditional "pump-and-treat" procedure using surfactants (11).

Measurement of binding constants between a given pesticide and available CDs enables one to quantify and optimize this methodology. Different methods for the determination of binding constants have been developed (8, 9, 12), including NMR spectroscopy (13, 14). In the case of diazinon, both ^1H and ^{31}P NMR become particularly convenient.

Experimental

Materials

Diazinon was synthesized based on the method of Gysin and Margot (15). The dried sodium salt of 2-isopropyl-6-methylpyrimidin-4-ol was heated for 2 days under nitrogen with diethyl chlorothiophosphate in dry acetone at 35 °C. After cooling and filtering to remove KCl, then removal of solvent under vacuo, the residue was chromatographed with methylene chloride as eluent. Further purification was effected by dissolving in hexanes and extracting with water. The hexane layer was dried ($MgSO_4$), and after filtering was first concentrated and then dried in vacuo to yield pure diazinon. Purity was checked by ^1H, ^{13}C (proton-decoupled),

© 2006 NRC Canada

and ^{31}P (proton-decoupled) NMR. Spectra were run on a 300 MHz Bruker Avance spectrophotometer using $CDCl_3$ as solvent. All spectra were consistent with diazinon and contained no impurity peaks. ^{1}H NMR (ppm) δ: 6.64 (s, 1H), 4.33 (d of q, $J_{H\text{-}H}$ = 7.1 Hz, $J_{H\text{-}P}$ = 11.2 Hz, 4H), 3.10 (sept, $J_{H\text{-}H}$ = 6.9 Hz, 1H), 2.47 (s, 3H), 1.37 (t, $J_{H\text{-}H}$ = 7.1 Hz, 6H), 1.30 (d, $J_{H\text{-}H}$ = 6.9 Hz, 6H). ^{13}C NMR (ppm) δ: 176 (s), 170(s), 165 (d, $J_{C\text{-}P}$ = 4.6 Hz), 107 (d, $J_{C\text{-}P}$ = 6.4 Hz), 65.6 (d, $J_{C\text{-}P}$ = 5.1 Hz), 37.7 (s), 24.5 (s), 21.8 (s), 16.2 (d, $J_{C\text{-}P}$ = 8.0 Hz). ^{31}P NMR (ppm) δ: 61 (s).

α-, β-, and γ-CDs were a generous gift from Cerestar USA and were used without further treatment. DMSO-d_6 and D_2O were purchased from Cambridge Isotopes and used as received.

NMR determination of binding constants

Sample preparation

To determine each binding constant, 10 samples were prepared in NMR tubes; the first with diazinon (plus DMSO cosolvent, 0.2% *v*/*v*) in D_2O, and the following containing successively more CD. First, a 0.99 mol/L stock solution of diazinon was prepared in DMSO-d_6, then a 0.006–0.06 mol/L stock solution of CD in 2.5 mL D_2O. Ten NMR tubes were filled with various amounts of the CD solution and D_2O to give a range of CD concentrations from zero (D_2O only) to that of the pure CD stock solution (no added D_2O). To each tube was added 2.5 μL of the diazinon stock solution, giving a final diazinon concentration of 4.93×10^{-3} mol/L in each. The NMR spectra were recorded using a 400 or 500 MHz Bruker Avance spectrophotometer.

K_b *determination by* ^{1}*H NMR*

^{1}H NMR spectra were run on all 10 tubes using a water presat to remove the HOD peak from the spectra. Two proton signals were examined, the aromatic proton (Ar-H) on the pyrimidinol ring and the CH_3 protons (Ar-Me) located on the pyrimidinol ring, as illustrated in Fig. 2. Both singlets appear in an area of the spectrum with no interference from CD signals. The change in chemical shift (Δδ) for the Ar-Me and Ar-H peaks of diazinon with increasing CD concentration, when plotted against [CD], yielded a curved binding isotherm. The curve-fitting program GraphPad Prism® was used to determine K_b according to eq. [1]

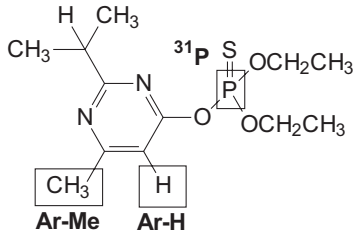
$$[1] \qquad \Delta = \frac{\Delta_b K_b [CD]}{1 + [CD] K_b}$$

where Δ is the observed change in chemical shift, Δ_b is the maximum change in chemical shift for 100% bound substrate, and K_b is the binding constant. K_b values were also obtained by the Benesi–Hildebrand eq. [2], the linear double reciprocal plot of the binding isotherm equation.

$$[2] \qquad \frac{1}{\Delta} = \frac{1}{\Delta_b K_b [CD]} + \frac{1}{\Delta_b}$$

On plotting 1/Δ vs. 1/[CD], K_b was found by dividing the intercept by the slope, as determined by linear regression using Microsoft Excel®. Each determination was made at least twice by each method, and all of the values acquired were averaged to obtain the reported K_b value.

Fig. 2. Structure of diazinon illustrating the portions studied by NMR to determine the binding constant (K_b) with cyclodextrins.



K_b *determination by* ^{31}*P NMR*

Proton-decoupled ^{31}P NMR spectra were recorded for each tube (see the general Sample preparation section), as singlets, no other peaks being observed. The change in chemical shift (Δδ) with increasing CD concentration gave a curved binding isotherm. Plotting Δδ vs. [CD] and using the curve-fitting program GraphPad Prism® yielded K_b according to eq. [1]. K_b was again evaluated using the Benesi–Hildebrand eq. [2]. Each determination was made at least twice by each method, and all of the acquired values were averaged to obtain the reported K_b value.

Results and discussion

CD–diazinon binding constants

K_b *from* ^{1}*H NMR*

The change in chemical shift of the Ar-H and Ar-Me peaks in the NMR spectra of diazinon on increasing the CD concentration was followed for α-, β-, and γ-CD. The change in chemical shift was downfield, except for the Ar-H peak in γ-CD, where it shifted upfield with increasing [CD]. The data were used to produce binding isotherms that fit a 1:1 binding model for all three CDs. Figure 3 shows results for α-CD. Figure 3*a* gives the binding isotherm generated for the Ar-H peak, which yields K_b = 183 $(mol/L)^{-1}$, while Fig. 3*b* provides the plot according to the Benesi–Hildebrand treatment, yielding K_b = 221 $(mol/L)^{-1}$. Plots for β-CD and γ-CD are qualitatively similar.

K_b *from* ^{31}*P NMR*

Downfield changes in the ^{31}P NMR chemical shift for diazinon were observed on increasing the CD concentration for α-, β-, and γ-CD. Figure 4*a* shows the binding isotherm for α-CD, while Fig. 4*b* gives the Benesi–Hildebrand plot of the data. β-CD and γ-CD yield similar plots.

Structure–stability relationships

The overall average K_b values obtained from the ^{1}H (Ar-H and Ar-Me) and ^{31}P NMR data are given in Table 1. Clearly, the largest K_b value is found for γ-CD, around 400 $(mol/L)^{-1}$, while the values for α-CD and β-CD are not significantly different, at around 200 $(mol/L)^{-1}$.

A partial summary of existing literature K_b data for pesticides is given in Table 2. The values generally vary from 100 to 600 $(mol/L)^{-1}$. Thus, the present results for diazinon (Table 1) fall within the range of existing data for other pesticides (Table 2). Data for all three CDs are available for parathion (**2**), methyl parathion (**3**), and paraoxon (**4**), all three organophosphorus pesticides with an aromatic moiety

© 2006 NRC Canada

Fig. 3. (A) Binding isotherm and (B) Benesi–Hildebrand plots for the binding of diazinon with α-CD generated from ^{1}H NMR data for the Ar-H peak.

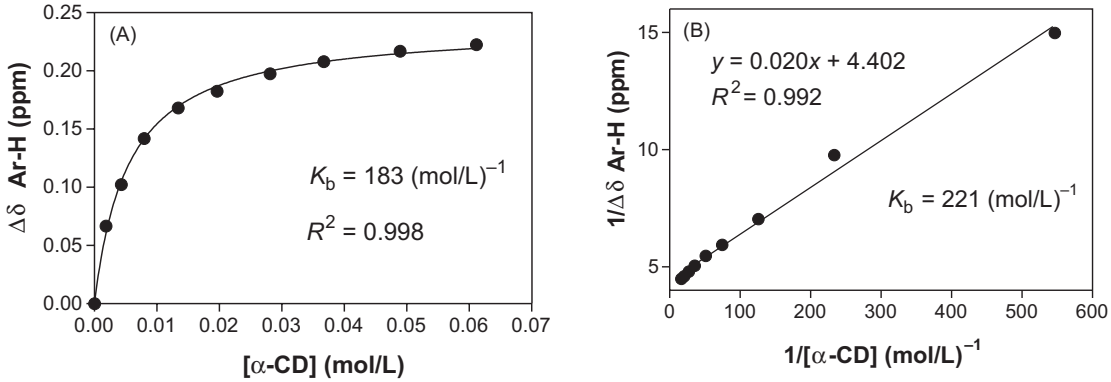
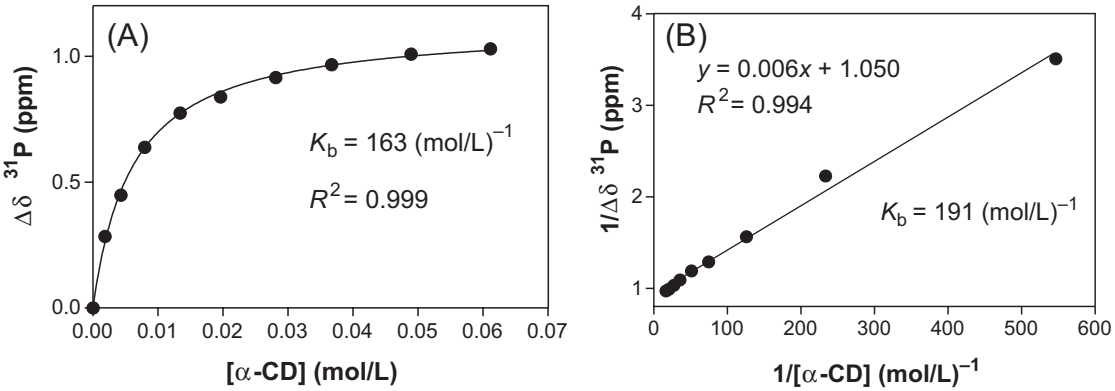
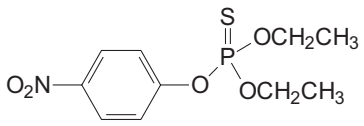


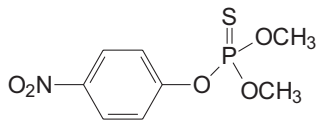
Fig. 4. (A) Binding isotherm and (B) Benesi–Hildebrand plots for the binding of diazinon with α-CD generated from ^{31}P NMR data.



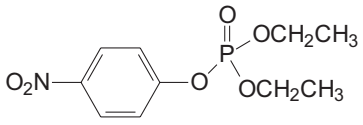
in place of the heteroaromatic moiety in diazinon, but otherwise similar structures.



2



3



4

A major difference between our results and earlier ones now becomes apparent in that K_b values in Table 2 are lowest for γ-CD, while in our study (Table 1), γ-CD has the highest K_b. A plausible explanation for this variance lies with the sterically demanding isopropyl group in diazinon, which together with the Ar-methyl cannot easily be accommodated in the α-CD or β-CD cavity, but can be readily accommodated in the γ-CD cavity. The computational study that follows sheds further light on this aspect.

Computational studies

The manifold applications of computational chemistry have made enormous impact in the field of cyclodextrin chemistry, including modeling studies of the host–guest type. The article by Kenny Lipkowitz on this subject, which appeared in 1998 in a special issue of *Chemical Reviews* featuring cyclodextrin chemistry, provides an excellent overview of this area up to that time; it lists 214 references (24), while many have appeared since then. In this study we present results of two approaches in computational chemistry as applicable to the present system: molecular mechanics (MM) and ab initio, density functional theory (DFT).

B3LYP energy optimized structures

Figure 5 presents the B3LYP/6-31G** minimized structure of diazinon in the form of the space-filling model and as ball-and-stick representation. These are used in visualizing the orientations of diazinon bound in the α-, β-, and γ-CD cavities presented in the following.

Binding orientations of diazinon into α-, β-, and γ-CDs

The dimensions of the diazinon – CD bound complex have been evaluated using MD–MM2 and the results are

© 2006 NRC Canada

Table 1. Diazinon–CD binding constants (K_b, $(mol/L)^{-1}$) determined by ^1H and ^{31}P NMR.

CD	Average K_b $((mol/L)^{-1})^a$ determined by Ar-H ^1H NMR		Average K_b $((mol/L)^{-1})^a$ determined by Ar-Me ^1H NMR		Average K_b $((mol/L)^{-1})^a$ determined by ^{31}P NMR		Average K_b from all methods
	Binding isotherm	Benesi–Hildebrand	Binding isotherm	Benesi–Hildebrand	Binding isotherm	Benesi–Hildebrand	
α-CD	181±3	220±1	200±0	283±54	157±8	179±18	203±46
β-CD	200±0	156±14	200±0	215±45	134±35	121±31	170±45
γ-CD	422±32	368±41	456±16	335±30	454±33	328±38	390±63

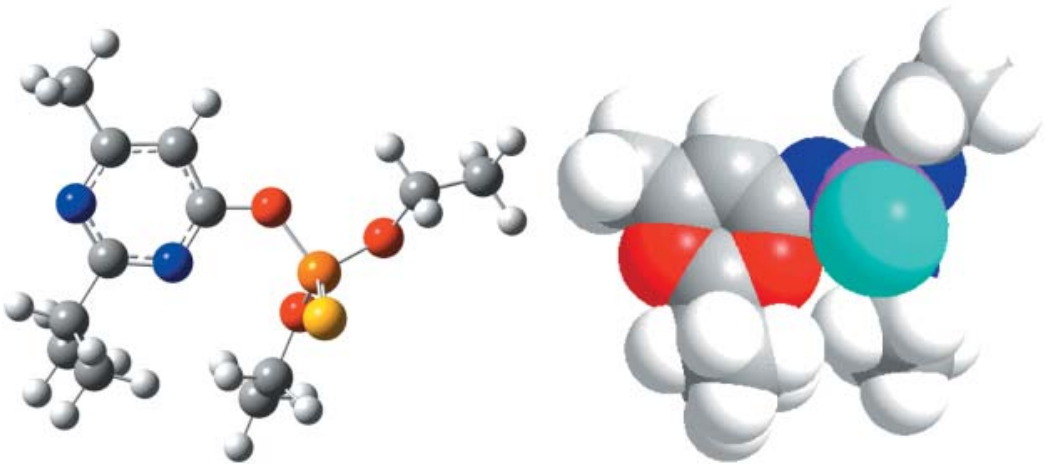
[a]Error limits in the K_b value were taken as the standard deviation (three or more values) or the average deviation (only two values).

Table 2. Binding constants of different pesticides with α-CD, β-CD, and γ-CD.

Pesticide	α-CD[a] K_b $((mol/L)^{-1})$	β-CD[a] K_b $((mol/L)^{-1})$	γ-CD[a] K_b $((mol/L)^{-1})$	Ref.
Diazinon	203±46	170±45	390±63	This work
Parathion	—	526	—	16
	—	286	—	17
	588	192	83	18
Paraoxon	123	182	110	18
Methyl parathion	285	526	119	18
	—	625	—	16
	—	526	—	17
Fenitrothion	—	417	—	16
	—	227	—	17
Pirimiphos-methyl	—	171±34	—	19
Chlorpyriphos	—	90±28	—	19
DCPE[b]	—	555	—	20
(S)-(+)-Sarin	167±25	—	—	21
(S)-(–)-Sarin	25±2	—	—	21
Warfarin	—	160	—	22
Coumatetraly	—	565±42	—	19
Carbaryl	—	289±21	—	23
Deltamethrin	—	627±104	—	19
Fenvalerate	—	316±46	—	19

[a]K_b error limits listed as available in the referenced paper.
[b]α-(Diethoxyphosphinoximino)dicyclopropylmethane (DCPE).

Fig. 5. Ball-and-stick (left) and space-filling model (right) of diazinon optimized with B3LYP/6-31G**.



© 2006 NRC Canada

Fig. 6. α-CD–, β-CD–, and γ-CD–diazinon binding orientation, energy optimized with MD–MM2. Top row shows the diazinon in the ball-and-stick model and the α-CD, β-CD, and γ-CD in the wire-frame model; bottom row shows the torus representation of α-CD, β-CD, and γ-CD.

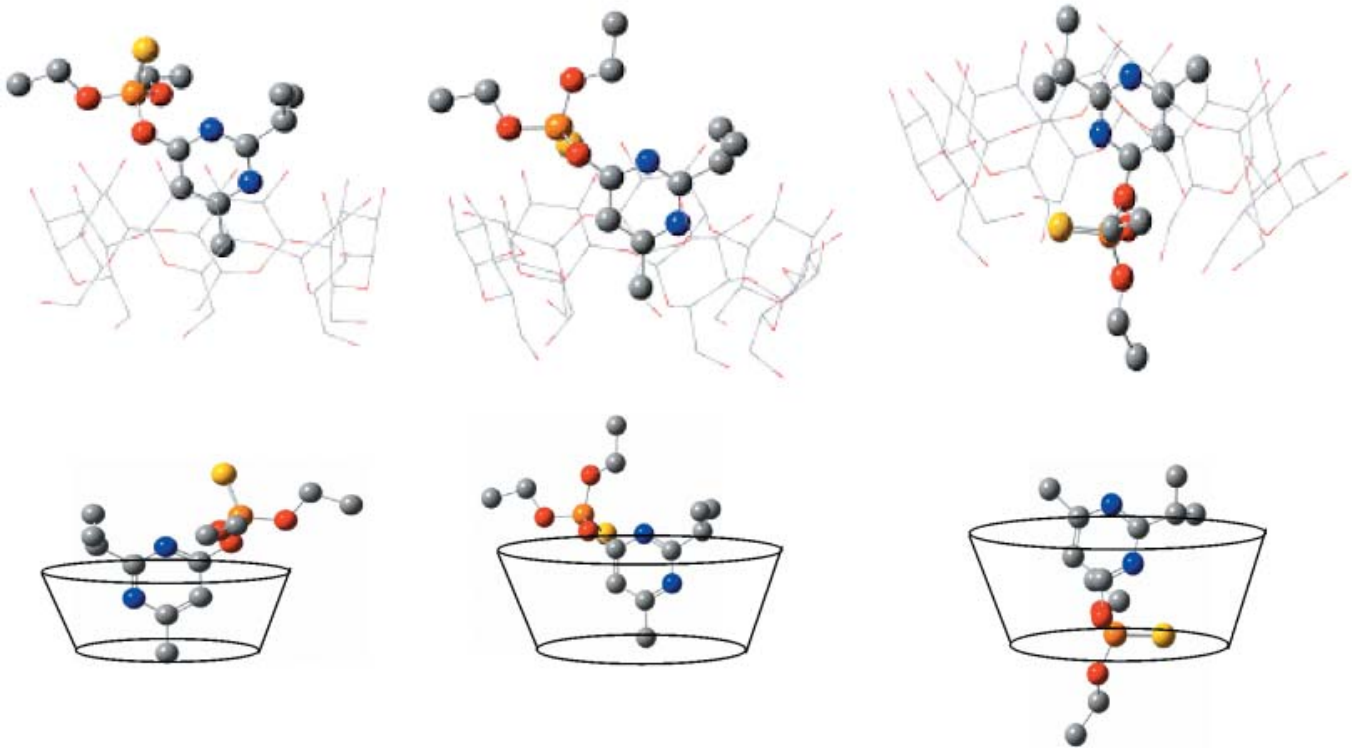


Table 3. Primary OH rim radius, secondary OH rim radius, and height of the diazinon–CD complexes, with errors, optimized with MD–MM2.

	Primary OH rim radius (Å)	Error in primary rim radius (Å)	Secondary OH rim radius (Å)	Error in secondary radius (Å)	Height (Å)	Error in height (Å)
α-CD + diazinon	4.97	1.25	5.13	1.00	5.24	0.41
β-CD + diazinon	5.77	1.62	6.25	0.85	5.40	0.47
γ-CD + diazinon	5.57	1.45	6.76	1.31	5.86	0.39

given in Table 3 as the primary OH rim and secondary OH rim radii, and the height of the complexed CDs. The diazinon-complexed γ-CD is found to have the largest secondary OH rim radius, as expected. Interestingly however, the primary OH rim radius in the complexed CD is about equal for β- and γ-CD.

We have also calculated (using MM2) the distance from the phosphorus atom of diazinon to the secondary OH rim, as the average distance to the three nearest secondary oxygen neighbours. This gives a measure of the depth of the diazinon molecule inside the CD cavity. The results given in Table 4 clearly show that this distance is greatest with γ-CD, i.e., diazinon is found deepest in the CD cavity with γ-CD.

Figure 6 shows the different orientations for the binding of diazinon in α-, β-, and γ-CD optimized with MD–MM2. The illustrations given are for both ball-and-stick models showing diazinon inside the wire-frame CD and the corresponding CD torus representation (Fig. 6), and also space-filling models (Fig. 7).

Table 4. Calculation of average distance from the phosphorus atom to the secondary oxygen plane optimized with MM2 with three nearest oxygen neighbours.

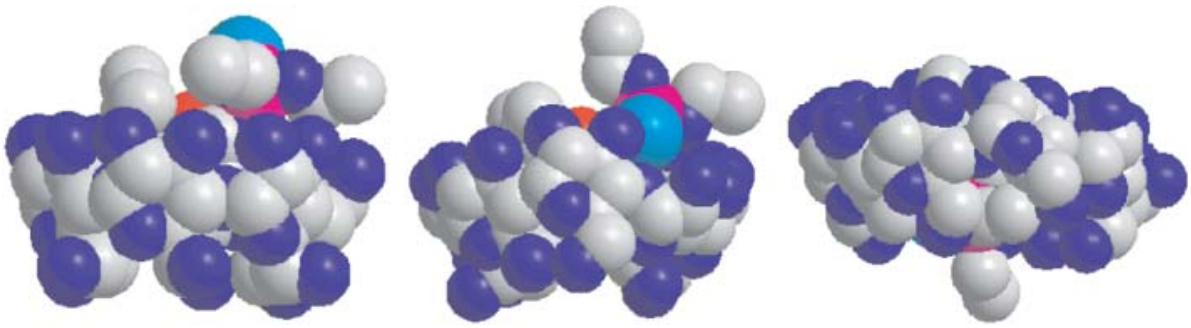
	Distance (Å)
α-CD + diazinon	2.52
β-CD + diazinon	0.55
γ-CD + diazinon	6.37

Note: Alternatively one can indicate distance measurements above the rim as + and below the rim as –, giving the values for α-CD (+2.52), β-CD (+0.55), γ-CD (–6.37).

Several important observations follow on visual examination of these models. (1) The heterocyclic residue of diazinon appears inside the cavity for all three CDs. (2) The methyl substituent is inside the cavity and points downwards for α- and β-CD, while for γ-CD it is situated largely out-

© 2006 NRC Canada

Fig. 7. Space-filling model of diazinon with α-, β-, and γ-cyclodextrins complex optimized with MD–MM2.



side, pointing upwards. (3) The isopropyl substituent is largely outside pointing upwards for α- and β-CD, while being situated on the secondary rim with γ-CD (4). The main contrast comes with the phosphoryl residue that is essentially outside the cavity for α- and β-CD, while with γ-CD it is inside the cavity, with the exception of one ethoxy substituent that protrudes from the lower rim.

Thus, the computations reveal a clear contrast in the three computed orientations. In the case of γ-CD, the bulk of the hydrophobic diazinon molecule, i.e., both the heterocyclic residue and the phosphoryl residue, are situated inside the CD cavity, whereas with α- and β-CD only the heterocyclic residue is present inside the cavity. This, then, provides a rationale for the experimental observation of γ-CD having the greatest binding constant compared with α-CD and β-CD, which possess much smaller and virtually equal K_b values. Any attempts at environmental remediation of pesticides, e.g., from soils, must be cognizant of these findings.

Concluding comments

Binding of the organophosphorus pesticide, diazinon, to α-, β-, and γ-cyclodextrin has been investigated through NMR and computational methodologies. The largest K_b value (400 $(mol/L)^{-1}$) was observed for γ-CD (^1H and ^{31}P NMR). This was corroborated computationally (MD–MM2 and B3LYP/6-31**), which have revealed the deepest location for the hydrophobic diazinon molecule within γ-CD. The direct correspondence and mutually supporting nature of the experimental and computational results, suggests a promising role for computational methodology in environmental remediation of pesticides.

References

1. V.K. Balakrishnan, E. Buncel, and G.W. vanLoon. Environ. Sci. Technol. **39**, 5824 (2005).
2. V.K. Balakrishnan, X. Han, G.W. vanLoon, J.M. Dust, J. Toullec, and E. Buncel. Langmuir, **20**, 6586 (2004).
3. S. Shirin, E. Buncel, and G.W. vanLoon. Can. J. Chem. **81**, 45 (2003).
4. V.K. Balakrishnan, J.M. Dust, G.W. vanLoon, and E. Buncel. Can. J. Chem. **79**, 157 (2001).
5. J.E. Omakor, I. Onyido, G.W. vanLoon, and E. Buncel. J. Chem. Soc. Perkin Trans. 2, 324 (2001).
6. G.W. vanLoon and S. Duffy. Environmental chemistry: A global perspective. Oxford University Press, New York. 2000.
7. M.T. Annandale, G.W. VanLoon, and E. Buncel. Can. J. Chem. **76**, 873 (1998).
8. M.L. Bender and M. Komiyama. Cyclodextrin chemistry. Springer-Verlag, Berlin, Heidelberg, New York. 1978.
9. J. Szejtli and T. Osa (*Editors*). Comprehensive supramolecular chemistry. Vol. 3. Cyclodextrins. Elsevier Science, Ltd., New York. 1996.
10. (*a*) T.B. Boving, X. Wang, and M.L. Brusseau. Environ. Sci. Technol. **33**, 764 (1999); (*b*) M.L. Brusseau, X. Wang, and W. Wang. Environ. Sci. Technol. **31**, 1087 (1997); (*c*) J.E. McCray and M.L. Brusseau. Environ. Sci. Technol. **33**, 89 (1999); (*d*) J.EE. Morillo, J.I. Pérez-Martinez, and J.M. Ginés. Chemosphere, **44**, 1065 (2001).
11. (*a*) D.A. Sabatini, R.C. Knox, and J.H. Harwell (*Editors*). Surfactant-enhanced subsurface remediation-emerging technologies. ACS Symposium Series 594. American Chemical Society, Washington, D.C. 1995; (*b*) D.F. Lowe, C.L. Oubre, and C.H. Ward. Surfactants and cosolvents for NAPL remediation — A technology practices manual. Lewis Publishers, Boca Raton, Florida. 1999.
12. (*a*). K.A. Connors. Chem. Rev. **97**, 1325 (1997); (*b*). K.A. Connors. Binding constants. John Wiley and Sons Inc., Toronto. 1987.
13. L. Fielding. Tetrahedron, **56**, 6151 (2000).
14. H.-J. Schneider, F. Hacket, and V. Rüdiger. Chem. Rev. **98**, 1755 (1998).
15. H. Gysin and A. Margot. J. Agric. Food Chem. **6**, 900 (1958).
16. M. Kamiya and K. Nakamura. Pestic. Sci. **41**, 305 (1994).
17. M. Kamiya, K. Nakamura, and C. Sasaki. Chemosphere, **30**, 653 (1995).
18. M. Kamiya, S. Mitsuhashi, and M. Makino. Chemosphere, **25**, 1783 (1992).
19. A. Coly and J.-J. Aaron. Anal. Chim. Acta, **360**, 129 (1998).
20. Y.L. Loukas, E.A. Vyza, and A.P. Valiraki. Analyst (Cambridge, U.K.), **120**, 533 (1995).
21. C. Van Hooidonk and J.C.A.E. Breebaart-Hansen. Recl. Trav. Chim. Pays–Bas, **89**, 289 (1970).
22. J.C. Marquez, M. Hernandez, and F. Garcia Sanchez. Analyst (Cambridge, U.K.), **115**, 1003 (1990).
23. F. Barbato, M.I. La Rotonda, A. Miro, P. Morrica, and F. Quaglia. J. Inclusion Phenom. Macrocyclic Chem. **38**, 423 (2000).
24. K.B. Lipkowitz. Chem. Rev. **98**, 1829 (1998).

© 2006 NRC Canada

Photochemical reactions of thiols with organic nitrates — Oxygen atom transfer via a thionitrate[1]

Jennifer L. Clarke, Irida Kastrati, Linda J. Johnston, and Gregory R.J. Thatcher

Abstract: Nitroglycerin is an organic nitrate that has been used in the clinical treatment of angina for 130 years, yet important details of its mechanism of action remain unanswered. The biological activity of nitrates suggests that they are bioactivated to NO via a three-electron reduction. The involvement of free or bound protein thiols in this reduction has often been proposed. To examine the involvement of thiyl radicals in such a process, the photochemical generation of benzenethiyl radical from thiol and disulfide precursors was studied in the presence of isopropyl nitrate. Analysis of reaction products and kinetics led to the conclusion that photolysis of the nitrate to NO_2 dominated the observed photochemistry. Formation of sulfonothioate and NO as products, and trapping of NO_2 by 4-chlorophenol, indicated a mechanism involving oxygen atom transfer from N to S via a thionitrate intermediate. The results of the study did not indicate a rapid reaction between thiyl radical and organic nitrate. Despite weak nitrate absorption of light >300 nm and a relatively high BDE for homolysis to give NO_2, the photochemistry under thiyl-generating conditions was driven by nitrate photolysis to NO_2. A novel nitrate, containing a phenyl disulfanyl group linked to nitrate groups, did not undergo photolysis to NO_2 or generate sulfonothioate, but did yield NO. These observations suggest that reaction between thiyl radicals and nitrates leading to NO release is a viable pathway, but it is subservient to other competing reactions, such as photolysis, in the case of IPN, and reaction with thiolate, in the case of the novel nitrate.

Key words: nitrate, photolysis, thiyl radical, nitrogen dioxide, nitric oxide.

Résumé : Même si la nitroglycérine est un nitrate organique qui a été utilisé depuis 130 ans dans le traitement de l'angine, beaucoup de détails importants de son mode d'action restent sans réponse. L'activité biologique des nitrates suggère qu'ils sont biologiquement activés en NO par le biais d'une réduction à trois électrons. L'implication de groupes thiols de protéines libres ou liées dans cette réduction a été souvent proposée. Afin d'examiner l'implication des radicaux thiyles dans ce processus, on a étudié la génération photochimique du radical benzènethiyle à partir de précurseurs thiols et disulfures, en présence de nitrate d'isopropyle. L'analyse de la cinétique et des produits de la réaction conduit à la conclusion que la photolyse du nitrate en NO_2 domine la photochimie observée. La formation de sulfonothioate et de NO comme produits et le piégeage du NO_2 par du 4-chlorophénol suggèrent un mécanisme impliquant le transfert d'un atome d'oxygène du N vers le S par le biais d'un intermédiaire thionitrate. Les résultats de cette étude indiquent qu'il n'y a pas de réaction rapide entre le radical thiyle et le nitrate organique. Malgré la faible absorption de la lumière par le nitrate à des valeurs supérieures à 300 nm et une valeur relativement élevée du « BDE » pour l'homolyse conduisant au NO_2, la photochimie dans les conditions conduisant à la formation de thiyle est dominée par la photolyse du nitrate en NO_2. Un nouveau nitrate contenant du groupe phényl disulfanyle lié à des groupes nitrates conduit à du NO, mais ne donne pas lieu à une photolyse conduisant au NO_2 ou à la génération d'un sulfonothionate. Ces observations suggèrent que la réaction entre les radicaux thiyles et les nitrates est une voie viable pour la production de NO, mais elle est soumise à d'autres réactions de compétition, dont la photolyse dans le cas du nitrate d'isopropyle et d'une réaction avec le thiolate dans le cas du nouveau nitrate.

Mots clés : nitrate, photolyse, radical thiyl, bioxyde d'azote, oxyde nitrique.

[Traduit par la Rédaction]

Received 3 October 2005. Published on the NRC Research Press Web site at http://canjchem.nrc.ca on 17 May 2006.

This work is dedicated to Walter A. Szarek in celebration of his 65th birthday and his continuing contributions to medicinal and carbohydrate chemistry.

J.L. Clarke and L.J. Johnston. Steacie Institute for Molecular Sciences, National Research Council, Ottawa, ON K1A OR6, Canada.
I. Kastrati and G.R.J. Thatcher.[2] Department of Medicinal Chemistry and Pharmacognosy, College of Pharmacy, University of Illinois at Chicago, 833 S. Wood St. Chicago, IL 60612-7231, USA.

[1]This article is part of a Special Issue dedicated to Professor Walter A. Szarek.
[2]Corresponding author (e-mail: thatcher@uic.edu).

 doi:10.1139/V06-056 © 2006 NRC Canada

Introduction

The synthesis of nitroglycerin (glyceryl trinitrate, GTN) was first reported in 1846. In 1878, it was demonstrated that small doses of GTN taken sublingually provided rapid and remarkable relief from the pain of angina. This led to clinical use of GTN in the treatment of angina pectoris that has continued to this day (1, 2). GTN is now applied in controlled hypotension during cardiac surgery and in congestive heart failure, whereas other organic nitrate vasodilators, including isosorbide dinitrate (ISDN), are used in the treatment of angina pectoris. ISDN, in a combination therapy, is entering the clinic for prevention of heart failure (3). Hybrid nitrates that conjugate a nitrate group to an established drug via a labile linker have been the subject of numerous preclinical and clinical studies (4), and novel nitrates are being explored beyond traditional cardiovascular applications (5). However, despite the historical and growing importance of nitrates in disease therapy, their mechanism of action is not well understood. One prevailing theory is that nitrates function as NO prodrugs, requiring bioactivation (or mechanism-based biotransformation) of the nitrate moiety ($RONO_2$) to NO (6, 7).

Nitrate esters (or organic nitrates) contain the nitrooxy functional group (-ONO_2); conversion of the nitrooxy group to NO is a three-electron reduction that must involve oxygen atom transfer. To date, no purified protein system has been demonstrated to mediate the direct reduction of nitrates to yield relevant quantities of NO, although this is widely held to be the biologically active product of nitrate bioactivation (8, 9). The biotransformation of GTN yields the dinitrate metabolites, glyceryl-1,2-dinitrate (1,2-GDN) and glyceryl-1,3-dinitrate (1,3-GDN), as products. Several proteins have been identified that are capable of mediating the denitration of GTN, yielding GDN and NO_2^- as products, including hemoglobin, myoglobin, xanthine oxidoreductase, old yellow enzyme, glutathione *S*-transferase (GST), cytochrome P450 oxidase, and cytochrome P450 reductase (10–17). More recently, it was confirmed that ALDH2 (aldehyde dehydrogenase) was capable of mediating denitration of classical nitrates (18–20).

The vascular effects of nitrates are believed to be mediated primarily via activation of soluble guanylyl cyclase (sGC), which converts GTP to the secondary messenger, cGMP. sGC is activated by binding of NO to its ferrous-heme centre, inducing a conformational change that triggers activation (21, 22). However, in the context of nitrates and GTN, there is a disparity between sGC activity in intact tissue vs. both broken cell preparations and purified protein: only in intact tissue is GTN a potent sGC activator. In contrast, GTN and simple organic nitrates are incapable of activating sGC above basal levels, in vitro, in the absence of thiol adjuvants (23–25). GTN does react with cysteine in simple aqueous buffer to release NO, but the reaction is slow and does not yield a large flux of NO (26). Nevertheless, the reaction of an organic nitrate with a thiol, whether a free thiol or protein thiol such as in GST or ALDH2, does provide the simplest reaction leading to nitrate bioactivation. Study of the reaction of nitrates with thiols, and their oxidation and reduction products, is therefore important for understanding the mechanism of nitrate biotransformation and bioactivation.

The putative bioactivation of organic nitrate to NO is a three-electron reduction. If bioactivation is mediated by a thiol, of the three potential reducing agents, thiol, thiolate, and disulfide radical anion, the latter is clearly the best candidate simply based on reduction potentials (27).

$$[1a] \quad RS^{\cdot} + e^- \rightarrow RS^- \qquad E^\circ = 0.78 \text{ V}$$

$$[1b] \quad RS^{\cdot} + e^- + H^+ \rightarrow RSH \qquad E^\circ = 1.35 \text{ V}$$

$$[1c] \quad RSSR + e^- \rightarrow (RSSR)^{\cdot -} \qquad E^\circ = -1.42 \text{ V}$$

The reactions of nitrates with disulfide radical anions are worthy of study in this respect. Disulfide radical anions can be formed by the reversible combination of thiyl radical with thiolate (eq. [2]) and by reduction of disulfides (eq. [1*c*]).

$$[2] \quad RS^{\cdot} + RS^- \underset{k_{-f}}{\overset{k_f}{\rightleftharpoons}} (RSSR)^{\cdot -}$$

It is apparent that thiyl radicals are likely to be present in any system designed to generate a disulfide radical anion. It is also possible to draw a mechanism of reaction for nitrate with thiyl leading to NO.

$$[3] \quad R'S^{\cdot} + RONO_2 \rightarrow [RON(O)OSR']^{\cdot} \rightarrow R'SO^{\cdot} + RONO$$

$$[4] \quad RONO + 1e^- + H^+ \rightarrow ROH + NO$$

Therefore, it is essential to explore the reactivity of thiyl radicals themselves with nitrates. However, the clean generation of thiyl radicals (and disulfide radical anions) presents a challenge since there is no ready thermal source as has been described for other biological radicals, such as superoxide (28). Conversely, a number of photochemical systems for thiyl radical generation have been described. In this paper, thiyl radicals generated from disulfide and thiol photochemical precursors are studied in the presence of nitrates.

Experimental section

All reagents were supplied by Sigma-Aldrich (Oakville, Ontario), with the exception of GTN and GT-130 that were synthesized by literature methods (29). All solvents used were HPLC grade. NO was supplied by Praxair Products Inc. (Mississauga, Ontario) and was used with a NO specific regulator. Phosphate buffer (PB) (0.1 mol/L, pH 7.4) was adjusted to pH and microfiltered before use.

All ^{1}H NMR analyses were done on a Bruker Avance-400 (400 MHz) spectrometer. A Varian Cary 3 UV–vis diode array spectrometer was used, with 1 cm × 1 cm quartz cells. Kinetic measurements were performed on a HP 8452A diode array spectrophotometer at 40 °C. Chemiluminescence measurements were made using a SIEVERS 270B NO chemiluminescence analyzer and a SIEVERS 207B nitric oxide analyzer (Boulder, Colorado). The UV light sources used were 300, 350, and mixed 300/350 nm Rayonet reactors equipped with lamps from the Southern New England Ultraviolet Company (Brantford, Connecticut).

The lasers used in the laser flash photolysis experiments were an EX-530 Excimer-500 (Lumonics, Inc.), an UV-24 N_2 laser (Laser Photonics), and a HY 750 ytrium–aluminum–garnet (YAG) laser (Lumonics, Inc.). The detec-

© 2006 NRC Canada

tor consisted of a Digikrom 240 monochromator (CVI Instruments) with a six dynode photomultiplier tube. The oscilloscope used was a Tektronix 7912 AD programmable digitizer and the delay generator was a DG535 four-channel digital delay/pulse generator (Stanford Research Systems).

All gas chromatography (GC) work was done on a Hewlett Packard 5890 series II gas chromatograph with flame ionization detection. The column used was a HP-1 with dimensions 25 m × 0.2 mm × 0.33 μm, column pressure 20 psi He (1 psi = 6.894 757 kPa), and splitflow 30 cc/min. One microliter injection volumes were made by an autoinjector using a 10 μL syringe that was cleaned with acetonitrile (MeCN). The GC–MS used was a HP 5890 gas chromatograph with a HP 5970 series mass selective detector. The MS library used was the Wiley138 database. One microliter manual injections were made. The column used was a HP-5 with dimensions 25 m × 0.2 mm × 0.33 μm, column pressure 10 psi He, and splitflow 30 cc/min. The optimal GC method for analyzing the thiol-nitrate samples used an injection port temperature of 200 °C, a detector temperature of 300 °C, and an initial oven temperature of 50 °C with a gradient of 10 °C/min to a final temperature of 250 °C. This temperature was maintained for an additional 9 min.

All high-pressure liquid chromatography (HPLC) analyses were done at room temperature on Hewlett Packard series II 1090 liquid chromatographs using diode array spectrophotometers (HPIB 15). An autosampler was used with 25 μL injections. Both C8 and C18 reverse-phase columns were used. The C8 column was a Waters Nova-Pak HPLC column, with a 4 μm diameter and dimensions of 3.9 mm × 150 mm. The C18 column was a Waters Spherisorb ODS2 column with a diameter of 5 μm and dimensions of 4.6 mm × 250 mm. For all experiments, the eluant was a mixture of methanol (MeOH) and Millipore-filtered water, with a flow rate of 1 mL/min. Three HPLC methods were used, where A is H_2O and B is MeOH. Method 1 used a gradient from 35% to 95% B over 16 min, followed by a plateau at 95% B for 6 min and gradient to 35% B over 2 min. Method 2 used a gradient from 35% to 95% B over 30 min, followed by a 5 min plateau. Products from the PhSH/IPN photoreaction were detected using HPLC Method 2 and the C18 column. HPLC Method 2 and the C8 column were used for the GT-130 photochemical and thermal product analysis. Detection of GDNs from GTN electron capture was done using Method 1 with the C18 column.

Benzenethiyl radical was generated by irradiation of benzenethiol (1) (PhSH, 10 mmol/L), diphenyl disulfide (PhSSPh, 4 or 1 mmol/L), or GT-130 (1 mmol/L) in the presence of 100 mmol/L 2,3-dimethyl-1,3-butadiene in oxygen- or nitrogen-saturated acetonitrile (MeCN/N_2) using either a 300 nm Rayonet reactor (arrangement of UV lamps) or a laser flash photolysis setup, respectively. Decane (3 mmol/L, anhydr.) was used as a standard for GC-FID analysis of the Rayonet reactions. GC–MS was first used to identify the 1,4- and 1,2-addition products, the identity of which was further confirmed by ^{1}H NMR analysis and quantified by GC-FID.

Benzenethiyl radical was also generated in the presence of isopropyl nitrate (IPN, 100 mmol/L or 1.0 mol/L) by irradiating PhSH (10 mmol/L or 100 mmol/L) or PhSSPh (5 mmol/L) in nitrogen-saturated acetonitrile (MeCN–N_2) using 300 and 350 nm Rayonets, respectively. All experiments were done in duplicate. Reactions were analyzed by GC-FID using 3 mmol/L anhydrous decane as standard. Relative peak areas from the GC traces were calibrated and converted to concentration plots using GC calibration curves. These calibration curves were obtained using authentic PhSH, PhSSPh, and $PhSO_2SPh$. For $PhSO_2SPh$, a photodegradation calibration was necessary because it is photolabile and breaks down during the course of the experiment. The use of a photodegradation calibration run under identical conditions to the experiment provided an estimated correction. The calibrated concentrations were transformed to molar "% conversion" relative to the starting concentration of PhSH.

IPN (0.5 mol/L) with and without PhSH (10 mmol/L) in MeCN–N_2, GTN (5 mmol/L), and GT-130 (5 mmol/L) in MeCN–PB–N_2 (40:60), were each irradiated using Rayonets with 300 and (or) 350 nm lamps, and NO release was quantified using a NO chemiluminescence (CL) detector. CL was calibrated by the use of the diazeniumdiolate NO donor, SPE–NO: initial rates data were collected for NO release over 10 min and calibrated by comparison to the first-order rate constant obtained by spectrophotometric analysis of SPE–NO decay.

Solutions of 10 mmol/L PhSH, 1.0 mol/L IPN, and varying concentrations of 0–100 mmol/L 4-chlorophenol in MeCN–N_2 were irradiated for 0 and 10 min in a 300 nm Rayonet reactor. To determine the extent of photolysis at longer wavelength, solutions of 5 mmol/L PhSSPh, 1.0 mol/L IPN, and 0–100 mmol/L *p*-chlorophenol were deoxygenated with nitrogen and irradiated for 0 and 45 min in a 350 nm Rayonet reactor. Anhydrous decane was used as a standard in both experiments and product analysis was done by GC-FID.

Nitric oxide gas was purified according to the method of Bostrup et al. (30). Using this purification setup, three 25 mL portions of MeCN were each saturated with argon. One was flushed with purified NO for 25 min (until saturated) and another with unpurified NO. A stock solution was made with 20 mmol/L PhSH and 20 mmol/L decane standard. One milliliter of this solution was saturated with nitrogen and diluted with 1 mL of either (*i*) argon-saturated, (*ii*) purified NO-saturated, or (*iii*) unpurified NO-saturated MeCN, giving final concentrations of 10 mmol/L PhSH and 10 mmol/L decane. Another stock solution was made with 60 mmol/L *p*-chlorophenol and 20 mmol/L decane. This solution was deoxygenated with nitrogen and diluted with the satd. MeCN solutions similar to the above method. The resulting concentrations were 30 mmol/L and 10 mmol/L *p*-chlorophenol and decane, respectively. All samples were analyzed by GC-FID with decane as a standard.

Theoretical methods

Geometry optimizations were performed with density functional theory using the (U)B3LYP function (31) with the 6-311++G(d,p) basis set implemented in the Gaussian 03 suite of programs (32). Calculation of structure and energy of the excited state of IPN was carried out in Spartan 04 (Wavefunction, Inc.) using TDDFT at the B3LYP/6-31G* level. For calculation of the thermodynamics of homolysis, minima were fully optimized and characterized by harmonic

© 2006 NRC Canada

vibrational frequency analysis, followed by further optimization and energy evaluation using the complete basis set (CBS-QB3) methodology, known to provide thermochemical estimates approaching experimental accuracy. Energy minimum structures were confirmed to have adequate convergence and zero imaginary vibrational frequencies. For the radical species, spin determinant calculations were evaluated to check for spin contamination.

Results

The photochemical sources of thiyl radicals used were photolysis of the RS—H bond (eq. [5]) and photolysis of the S—S bond (eq. [6]) of the corresponding disulfide (33). Hydrogen abstraction from RSH by photochemically generated *tert*-butoxyl radicals (*t*-BuO$^{\cdot}$) is an alternative route (eq. [7]) that is complicated by the potential side reactions of the alkoxyl radical in solutions containing nitrates.

[5] $$RSH \xrightarrow{h\nu} RS^{\cdot} + {}^{\cdot}H$$

[6] $$RSSR \xrightarrow{h\nu} 2RS^{\cdot}$$

[7] $$t\text{-BuO–O-}t\text{-Bu} \xrightarrow{h\nu} t\text{-BuO}^{\cdot} \xrightarrow{RSH} RS^{\cdot} + t\text{-BuOH}$$

A restriction to these methods is the chromophore of the source, which is often weak. Alkyl thiyl radicals typically absorb at 330 nm, which is similar to the optical spectra of their sources, and have low extinction coefficients ($\varepsilon \sim 500$ (mol/L)$^{-1}$ cm^{-1}) (27). They are therefore difficult to detect and monitor using photochemical techniques (27, 34). Generation of aryl thiyl radicals is more facile owing to higher wavelength chromophores with higher extinction coefficients ($\varepsilon \sim 2500$ at 460 nm and 10 000 (mol/L)$^{-1}$ cm^{-1} at 295 nm) (27). Consequently, aryl thiols and aryl disulfides are preferred as thiyl radical sources. A relatively clean method of generating thiyl radicals was found by irradiation in MeCN using a YAG laser ($\lambda = 355$ nm). Benzenethiyl radical (PhS$^{\cdot}$) was generated from the disulfide or thiol precursor and characterized by laser flash photolysis (LFP). The PhS$^{\cdot}$ spectrum obtained displayed the well-characterized absorbance maxima at 490 and 450 nm.

The thiyl radical was further characterized by measuring the kinetics of conjugate addition to 2,3-dimethyl-1,3-butadiene (DMB). Under anaerobic conditions, thiyl is known to add to olefinic bonds in anti-Markovnikov fashion (27), where the 1,4-adduct is expected to be the major product in the case of DMB (35). LFP was used to measure the addition rates of PhS$^{\cdot}$ to DMB in the presence and absence of oxygen. The rate constants thus derived for the addition of PhS$^{\cdot}$ to DMB under aerobic and anaerobic conditions were found to be 1.3×10^8 and 0.83×10^8 (mol/L)$^{-1}$ s^{-1}, respectively. These experiments validate and quantify the formation of thiyl radical, the rate of addition to the diene, and the utility of the diene trap in measuring thiyl formation.

Generation of PhS$^{\cdot}$ in the presence of IPN — An intermolecular model

To facilitate product monitoring, photolysis of PhSH in the presence of DMB was carried out using a Rayonet photoreactor fitted with 300 nm lamps. In the absence of DMB, the only product observed by GC-FID analysis was disulfide. However, with excess quantities of DMB present, the yield of disulfide was reduced and both the 1,4- and 1,2-adducts were observed by GC-FID and ^{1}H NMR analysis, with the major product being that of conjugate addition. Thermal generation of benzenethiyl at 95 °C and subsequent addition to DMB has previously been investigated, where the yield of the 1,4-adduct was found to be 98% (35). DMB is therefore an effective thiyl trap as predicted by the rate constants determined by LFP analysis. Addition of IPN to this reaction system led to a decrease in the yield of addition product in a concentration dependent manner (data not shown), suggesting that IPN inhibited reaction of thiyl radical with the conjugated diene.

To examine whether a reaction between benzenethiyl and IPN was responsible for the observed reduction in formation of the 1,4-DMB adduct, PhSH (10 mmol/L) was irradiated in the presence of IPN (1.0 mol/L) alone. A new product was observed in the GC-FID chromatogram, which was identified as a sulfonothioate (*S*-phenyl benzenesulfonothioate; $RS(O)_2SR$, R = Ph) by GC–MS and by comparison to an authentic sample. Formation of this product increased with irradiation time (Fig. 1); however, the sulfonothioate is a photolabile compound and its quantity is therefore underestimated by this assessment, especially at longer irradiation times. As a result, the sulfonothioate product stability was measured by GC-FID analysis as a function of irradiation time under the reaction conditions. This enabled construction of a corrected calibration curve that was used to more accurately estimate sulfonothioate formation (Fig. 1).

It is evident from Fig. 1 that in addition to a decrease in PhSH with irradiation time, a decrease in the disulfide product is also observed. The disulfide absorbs light at 300 nm and is cleaved into thiyl radicals, though requiring longer irradiation times than the corresponding thiol. This is compatible with the increase in sulfonothioate product observed at irradiation times where the PhSH source has been depleted. The sulfonate product therefore results from reaction of PhS$^{\cdot}$ formed from photolysis of both the thiol and the disulfide.

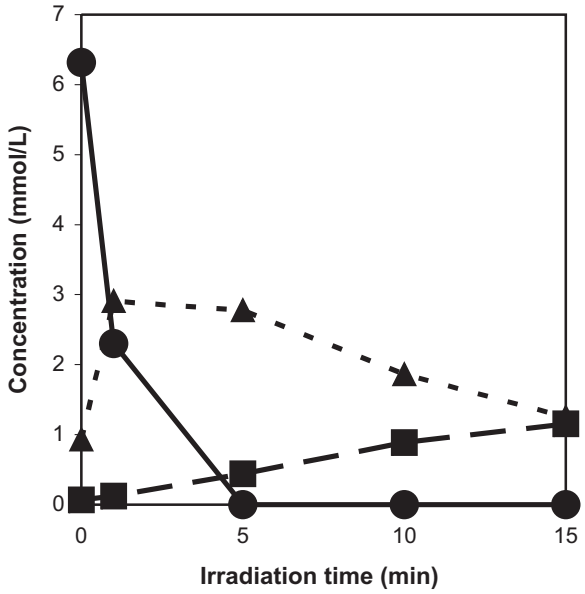
PhS$^{\cdot}$ was also generated from 5 mmol/L PhSSPh using LFP. A second-order fit to the decay trace (monitored at 460 nm) gave a rate constant for radical recombination of 2×10^7 (mol/L)$^{-1}$ s^{-1}. Addition of IPN had no effect on the decay rate of the radical, even when 80% IPN – 20% MeCN was used as the solvent, indicating that any reaction with IPN cannot compete with radical recombination. This effect was consistent under aerobic and anaerobic conditions, and questions the viability of a direct and rapid reaction between thiyl radical and nitrate.

Sulfonothioate as a product of NO_2 reaction

The sulfonothioate product could potentially result from direct reaction between benzenethiyl radical and NO_2, since NO_2 is the expected product of IPN photolysis. Smaller amounts of sulfonothioate were observed in photochemical experiments where longer wavelength irradiation was used: reaction of PhS$^{\cdot}$ with IPN was performed using a 350 nm lamp and PhSSPh as the thiyl precursor. As shown in Fig. 2, much smaller amounts of sulfonothioate were detected, in comparison to the irradiation of PhSH and IPN at 300 nm. It should be noted that at $\lambda = 300$ nm, the relative molar

© 2006 NRC Canada

Fig. 1. Left: Decay of reactant (●) and growth of products (thiosulfonate (■) and disulfide (▲)) from irradiation of PhSH (10 mmol/L) in the presence of IPN (1.0 mol/L) in MeCN–N_2 using a 300 nm lamp, as assayed by GC-FID calibrated using authentic samples (average of two trials). Right: Identical reactant and product data incorporating a correction for the photochemical decomposition of the products under the reaction conditions.



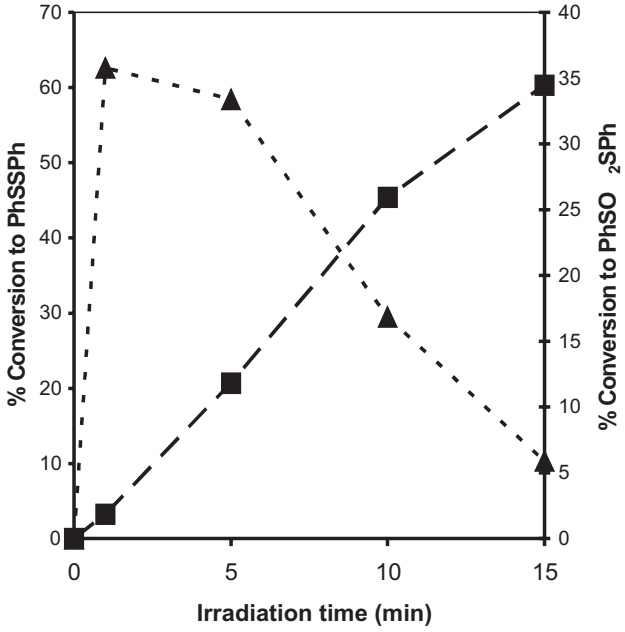
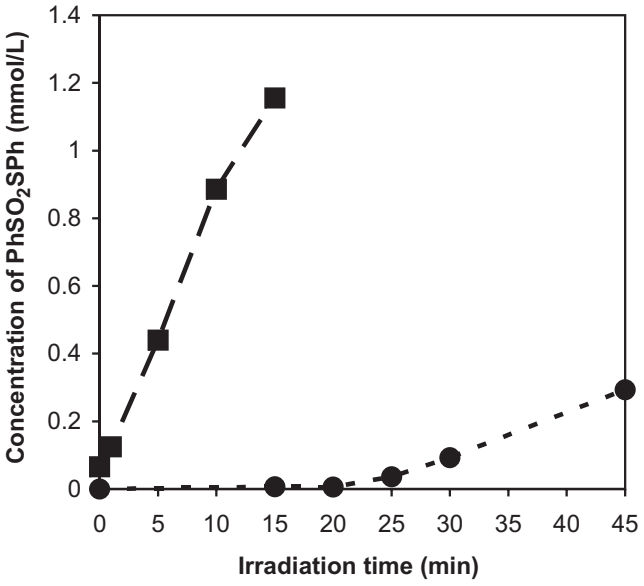


Fig. 2. Comparison of $PhS(O)_2SPh$ yield from IPN (1.0 mol/L) in MeCN–N_2. Irradiation of PhSH (10 mmol/L) at 300 nm (■); irradiation of PhSSPh (5 mmol/L) at 350 nm (●). Average of two trials.



absorbance of PhSH to IPN is approximately 10:1, whereas at 350 nm, the absorbance of IPN is lower by a factor of 40. Thus, it is expected that less NO_2, and consequently less sulfonate, would be generated at 350 nm as a result of decreased light absorption and photolysis of the nitrate. Evidence for thermal decomposition of IPN to NO_2 was seen in careful inspection of Fig. 1, which shows sulfonothioate product present at time zero. Sulfonothioate was formed owing to thermolysis in the high-temperature GC injection port (200 °C). To examine the photolysis of IPN, a NO_2 trapping experiment was designed using 4-chlorophenol. Photonitration of arenes has been known for many years and recent work has been published reporting the formation of 2- and 4-nitrophenol resulting from irradiation of nitrate or nitrite ion in the presence of phenol in aqueous solution (36, 37). The ortho-nitration of tyrosine is a well-known reaction (38), and the use of 4-chlorophenol has the advantage of limiting nitration to one isomeric product. Generation of 4-chloro-2-nitrophenol was shown to result from irradiation of 1.0 mol/L IPN in the presence of 10 mmol/L *p*-chlorophenol, where the product identity was confirmed by GC–MS analysis.

Increasing concentrations of 4-chlorophenol were added to irradiated solutions of IPN with PhSH or PhSSPh to compete with $PhS^{\cdot}$ for any NO_2 generated by nitrate photolysis (Fig. 3). The decrease in relative peak area of 4-chlorophenol was the same as the increase observed in the relative peak area of 4-chloro-2-nitrophenol (data not shown), indicating that nitration was efficient and was the only reaction occurring with 4-chlorophenol. The observation of 4-chloro-2-nitrophenol formation confirmed the generation of NO_2 on irradiation, while nonirradiated solutions gave no nitration products. Clearly, NO_2 is generated by irradiation of 1.0 mol/L IPN at 300 nm and to a lesser extent at 350 nm. It also appears from Fig. 3 that the amount of 4-chloro-2-nitrophenol formed reaches a plateau. A simple rationale would be the lower yield of $PhS^{\cdot}$ and of NO_2 owing to competitive absorbance by 4-chlorophenol and 2-nitro-4-chlorophenol in the reaction solution. At 100 mmol/L 4-chlorophenol, A(300 nm) = 2.4 and A(350 nm) = 0.079; whereas for PhSH (10 mmol/L), A(300 nm) = 0.85; for PhSSPh (5 mmol/L), A(350 nm) = 0.75; and for IPN (1.0 mmol/L), A(300 nm) = 3.4 and A(350 nm) = 0.087.

Both the nitration of 4-chlorophenol and the formation of sulfonothioate appeared to result from the photolysis of IPN to NO_2. Commercial gaseous NO provides a further means

© 2006 NRC Canada

Fig. 3. Formation of 4-chloro-2-nitrophenol from irradiation of IPN (1.0 mol/L) in the presence of (top) 10 mmol/L PhSH and *p*-chlorophenol using a 300 nm lamp and (bottom) 5 mmol/L PhSSPh and *p*-chlorophenol using a 350 nm lamp. Averages of two trials.

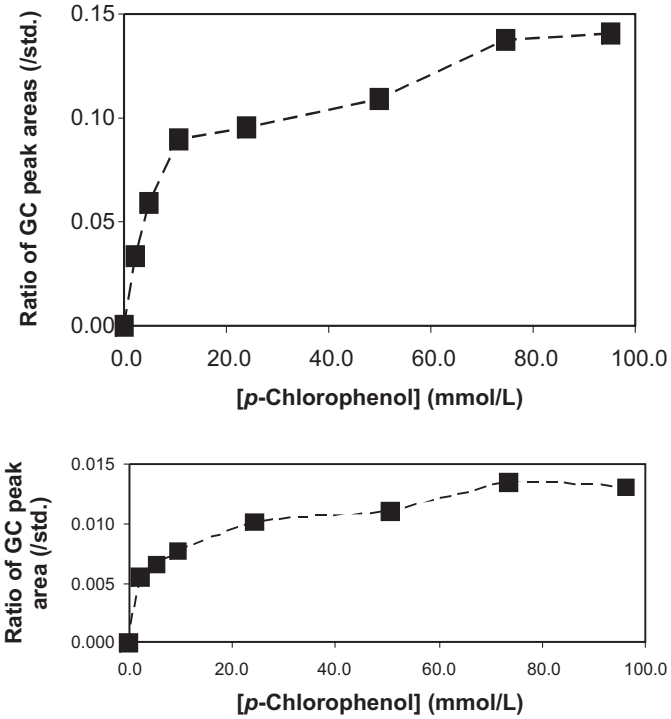
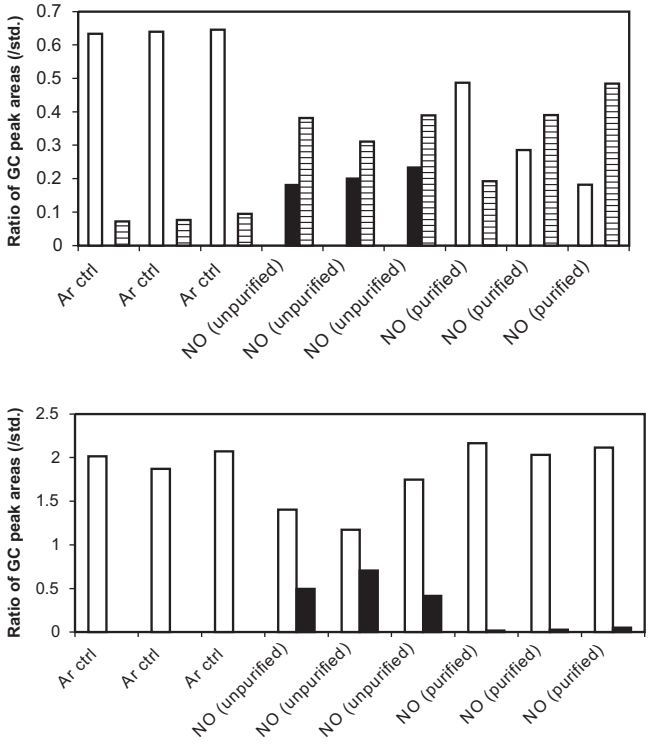


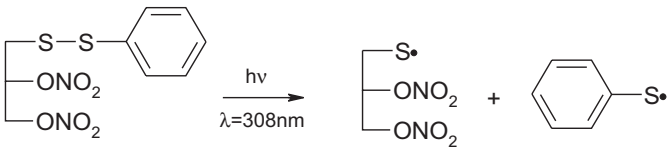
Fig. 4. Quantitation of products from reaction of NO gas with PhSH (10 mmol/L) in MeCN–N_2 by GC-FID. Argon, unpurified NO–NO_2 gas, or purified NO gas passed through alkaline scrubbers was bubbled through the reaction solution at comparable rates. Top: reactant PhSH (open bar), $PhS(O)_2SPh$ (solid bar), and PhSSPh (hashed bar) were measured. Bottom: the same reactions were carried out in the presence of 4-chlorophenol (open bar) and product 4-chloro-2-nitrophenol (solid bar) was measured. Triplicate reactions shown.



to test this hypothesis because the unscrubbed gas contains NO_2 as the major impurity. Nitration of 4-chlorophenol was measured in solutions of PhSH in MeCN–N_2 treated with gas streams of either argon, the unpurified NO–NO_2, or NO purified by passage through alkaline scrubbers (Fig. 4, bottom). Only in the samples treated with NO–NO_2 was significant nitration observed, indicating that this system is useful for studying reactions of NO_2 in the presence of other nitrogen oxide species and that 4-chlorophenol is an effective NO_2 trap. In parallel experiments, unreacted thiol, disulfide, and sulfonothioate were measured by GC-FID analysis in solutions of PhSH in MeCN–N_2 treated with gas streams of either argon, unpurified NO–NO_2, or purified NO. Treatment with purified NO resulted in significant oxidation of thiol to disulfide, but no sulfonothioate formation. In contrast, treatment with NO–NO_2 gas led to complete depletion of thiol, yielding both disulfide and sulfonothioate (Fig. 4, top). The nitration of 4-chlorophenol in PhSH solution flushed with NO–NO_2 was also monitored in a UV–vis spectrometer at 350 nm in which 4-chloro-2-nitrophenol was observed to form immediately upon flushing with the gas (data not shown).

An intramolecular model for thiyl-nitrate interactions — GT-130

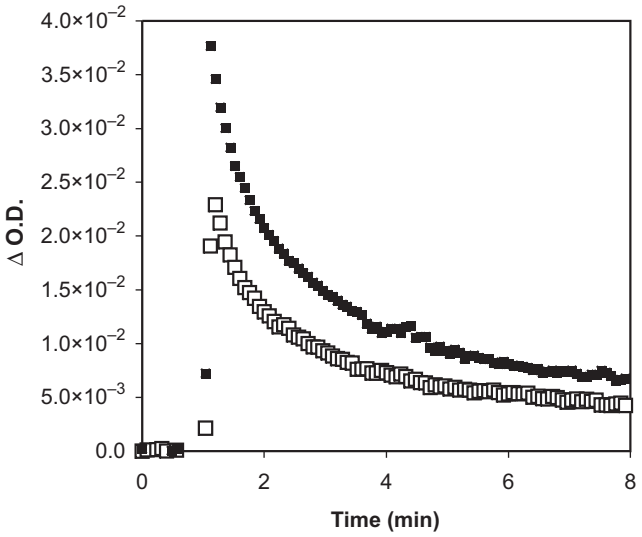
The phenyldisulfanyl dinitrate (GT-130) contains both disulfide and nitrate moieties, and is therefore a suitable candidate for studying the likelihood of thiyl radical reactivity with nitrates owing to the proximity of the two reactive groups. In the presence of DMB and under identical conditions to those used for the study of PhSH–IPN, irradiation of GT-130 resulted in formation of the same 1,4-thiyl-DMB adduct, verifying that $PhS^{\bullet}$ was produced and therefore confirming photolysis of the S—S bond.



Using an Excimer laser (308 nm) to excite GT-130, $PhS^{\bullet}$ was again identified by LFP analysis of its characteristic spectrum and shown to be a product of GT-130 photolysis. The decay curves of $PhS^{\bullet}$ generated by photolysis of GT-130 and Ph_2S_2 at equal concentrations are shown in Fig. 5. As expected, the change in optical density from Ph_2S_2 photolysis was approximately twice that from GT-130 photolysis, since twice as many $PhS^{\bullet}$ radicals would result from photolysis of the S—S bond. The decay rate constants measured for each curve were second order and were found to be similar, indicating that the recombination pathway for the GT-130 radicals has similar kinetics to the radical–radi-

© 2006 NRC Canada

Fig. 5. Decay curves of $PhS^{\cdot}$ monitored at 450 nm by LFP. Formed by irradiation of 1 mmol/L GT-130 (□) or 1 mmol/L PhSSPh (■) in MeCN–N_2 using an Excimer laser (308 nm).



cal recombination of $PhS^{\cdot}$ forming PhSSPh. This suggests that the $PhS^{\cdot}$ radical formed via photolysis undergoes recombination to GT-130 with a rate similar to that of self-combination to PhSSPh.

To explore possible nitrate photolysis of GT-130, irradiation was performed at 300 nm in the presence of the 4-chlorophenol trap. Nitration was not observed (data not shown), indicating that NO_2 either was not formed or was trapped more rapidly by another species. A reasonable explanation is the low absorbance associated with the nitrate groups in GT-130 (5 mmol/L), which is substantially less than in experiments with IPN (1.0 mol/L). Disulfide cleavage is therefore the dominant route of photolysis upon irradiation of GT-130 at 5 mmol/L.

NO release from reaction of GT-130

The thermal reaction of GT-130 with thiols has been reported to result in production of NO (29). The photolysis of GT-130 was compared with that of GTN by chemiluminescence detection of NO in headspace gas of the reaction mixtures (Fig. 6). Small, submicromolar quantities of NO were observed from GTN photolysis, but GT-130 photolysis generated more than 20 μmol/L NO after 20 min irradiation. However, comparison of NO release from thermal reaction of GT-130 with cysteine vs. photochemical reaction of GT-130 showed that the thermal reaction is more efficient in generating NO (29). Irradiation of GT-130 under aerobic or anaerobic conditions exhibited no change in the NO response (data not shown).

Interestingly, irradiated solutions of PhSH–IPN in MeCN–N_2 also generated NO, with a linear rate of NO release for at least the first 20 min of reaction (Fig. 7). As shown, photolysis of IPN alone did not produce NO within the detection limits.

Once it was established that irradiation of GT-130 resulted in efficient S—S bond cleavage, the nature of the resulting organic products was investigated. The products resulting from thermal reaction of GT-130 with PhSH in neutral aqueous solution were analyzed by HPLC with UV detection and

Fig. 6. Comparison of cumulative NO response. Irradiation of 5 mmol/L GTN (○) and 5 mmol/L GT-130 (■) in MeCN–PB–N_2 (40:60) using mixed 300 and 350 nm lamps (average of three trials).

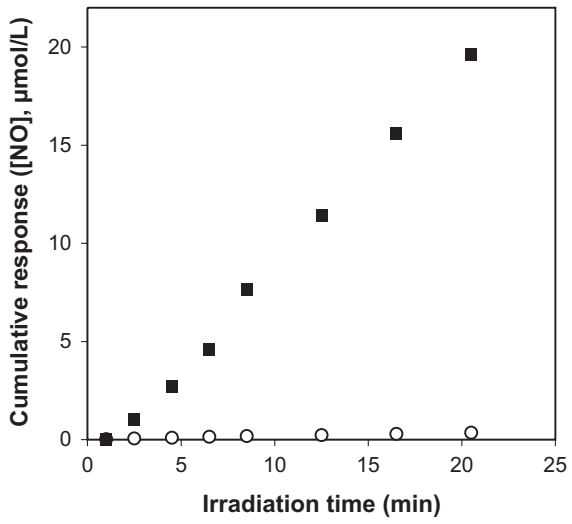
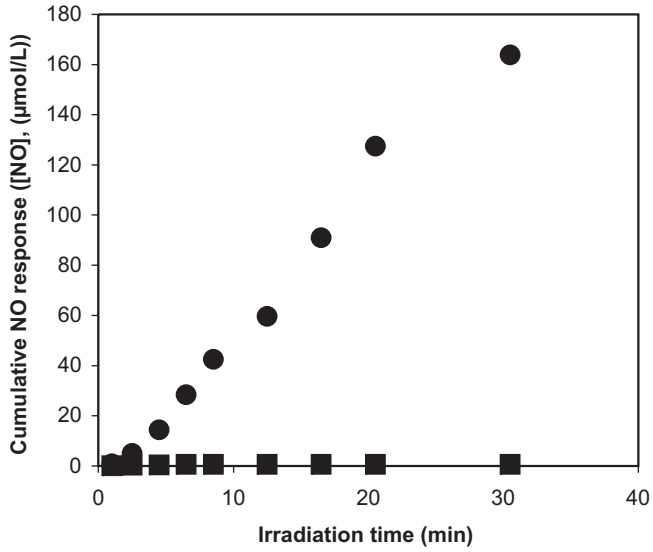


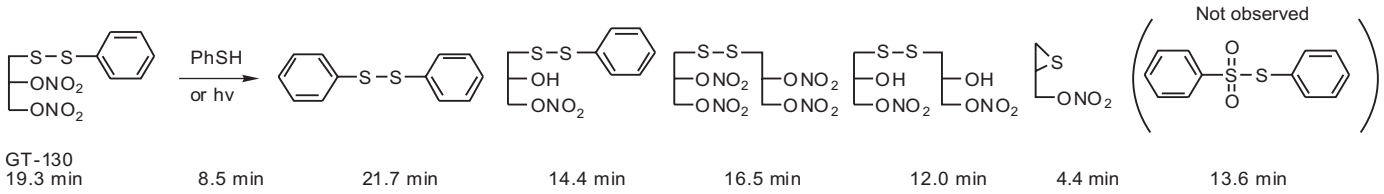
Fig. 7. Comparison of NO response. Irradiation of 10 mmol/L PhSH + 0.5 mol/L IPN (●) vs. irradiation of 0.5 mol/L IPN (■) in MeCN–N_2 (average of three trials).



have been reported previously (29). The major products were identified by comparison of HPLC chromatograms with authentic samples, and were found to be PhSSPh and 2-denitro-GT-130, with an equal amount of unreacted GT-130 present (Scheme 1). Of numerous minor products, the cyclic thiirane was the most abundant and the symmetrical disulfide 1,2-di(3-nitrooxy-2-hydroxypropyl)disulfane was also identified (Scheme 1). The products identified in the photolysis of GT-130 (excluding the starting material) were, in order of abundance, diphenyldisulfide > 2-denitro-GT-130 > 1,2-di(2,3-dinitrooxypropyl)disulfane > 3-nitrooxypropylthiirane > 1,2-di(3-nitrooxy-2-hydroxypropyl)disulfane (Scheme 1). In the context of this work, it is important to note that no $PhS(O)_2SPh$ was detected in either the thermochemical or photochemical reactions of GT-130. In

© 2006 NRC Canada

Scheme 1. HPLC retention times are annotated under the conditions described in the text.



contrast, HPLC analysis of reaction mixtures of PhSH and IPN did reveal sulfonothioate after irradiation.

Irradiation of GT-130 for 20 min at 300 nm was sufficient to identify the photoproducts. Further experiments revealed no change in photochemical products from nitrogen-deoxygenated to air-equilibrated solutions. It can therefore be confirmed that oxygen has no effect on the photochemical reaction of GT-130 leading to the products shown.

Discussion

The release of NO from organic nitrates in complex biological systems can often be observed using a variety of different methods. In human plasma, NO release was observed from solutions of nitrates and thiosalicylic acid using amperometric detection (39). In plasma, the series of 1,2-dinitrooxy propane derivatives including GTN were all observed to release NO in the presence of TSA with an initial rate of ~4–80 nmol/L s^{-1} at 0.25–0.5 mmol/L nitrate concentration. At physiological pH, the reactivity of free thiols towards nitrates is dependent on thiol pK_a and is too slow to account for the rapid bioactivation of GTN; for example, only 10% reaction of GTN (1 mmol/L) with cysteine (2 mmol/L) is observed in aqueous solution at pH 7.4, 37 °C, after 1 h (26). Using earlier electrochemical devices, this reaction was not found to produce NO within the detection limits, while chemiluminescence was able to detect the low levels of NO produced in these mixtures (26, 40). Nevertheless, catalysis of the reaction between cysteine thiol and nitrate at an enzyme active site or at other protein sites containing reactive thiols, such as thioredoxin folds, may lead to acceleration of reaction and an increased flux of NO (6). The most popular, contemporary theory for GTN bioactivation invokes ALDH2, which contains three cysteines at the active site (41, 42). ALDH2 and several other proteins are capable of accelerating reductive denitration of nitrates to inorganic nitrite (eq. [8]), however, conversion to NO requires further reduction.

[8] $RONO_2 + 2e^- + 2H^+ \rightarrow ROH + NO_2^-$

[9] $NO_2^- + e^- + H^+ \rightarrow HO^- + NO$

A chemical mechanism that identified an organic thionitrate ($RSNO_2$) as the common intermediate in a mechanism leading to either NO_2^- or NO from the reaction of thiol with nitrate was first described by Yeates (43). Later computational and experimental approaches to this reaction yielded a cohesive thionitrate rearrangement pathway for a thiol-nitrate reaction leading to NO release (eqs. [10]–[13]) (44, 45). In an investigation of the aqueous decomposition of *tert*-butyl thionitrate, the only organic products observed were sulfonothioate and sulfinothioate, which were proposed to result from radical combination based on computational studies (eqs. [14] and [15]). The lack of disulfide product formed from reaction of pure samples of thionitrate indicated that rxns. [16]–[18] (and thiyl radical recombination) were not competitive under the reaction conditions.

[10] $RSH + R'ONO_2 \rightarrow RSNO_2 + R'OH$

[11] $RSNO_2 \rightarrow [RS^{\cdot}NO_2^{\cdot}]$

[12] $[RS^{\cdot}NO_2^{\cdot}] \rightarrow RSONO$ or $RS(O)NO$

[13] $RSONO \rightarrow RSO^{\cdot} + NO$

[14] $2RSO^{\cdot} \rightarrow RS(O)_2SR$

[15] $RSO^{\cdot} + RS^{\cdot} \rightarrow RS(O)SR$

[16] $[RS^{\cdot}NO_2^{\cdot}] \rightarrow RS^{\cdot} + NO_2^{\cdot}$

[17] $RS^- + NO_2^{\cdot} \rightarrow RS^{\cdot} + NO_2^-$

[18] $RS^- + RSNO_2 \rightarrow RSSR + NO_2^-$

GT-150 (2,3-dinitrooxypropane-1-thiol) contains a thiol group *vicinal* to a nitrate group. This compound was shown to spontaneously generate NO in neutral aqueous solution, as was the related disulfanyl nitrate GT-130 on addition of thiol (Scheme 1) (29), with no evidence being obtained for sulfonyl or sulfinyl products (S=O containing). Reaction of the disulfanylnitrates was unaffected by O_2, and other reductants studied did not facilitate NO release. The simplest mechanism, compatible with these observations was proposed to be a thiol-disulfide exchange.

[19] $RSSCH_2CHRONO_2 + R'S^- \rightarrow RSSR' + {}^-SCH_2CHRONO_2$

[20] ${}^-SCH_2CHRONO_2 \rightarrow \rightarrow NO$

A sequence of reactions postulated to account for NO production in the absence of S=O containing products proceeds via a sulfenate (RSO^-) and a nitrosothiol (RSNO) intermediate (eqs. [21]–[24]). The spontaneous release of NO from nitrosothiols in the presence of thiol is a well-studied phenomenon (46, 47).

[21] $RS^- + R'ONO_2 \rightarrow RSO^- + R'ONO$

[22] $RSO^- + RSH + H^+ \rightarrow RSSR + H_2O$

[23] $R'ONO + RSH \rightarrow RSNO + R'OH$

[24] $RSNO \rightarrow RS^{\cdot} + NO$

Alternative mechanisms were considered, including an inner-sphere electron-transfer process via an intermediate in thiol-disulfide exchange or a disulfide radical anion. Since

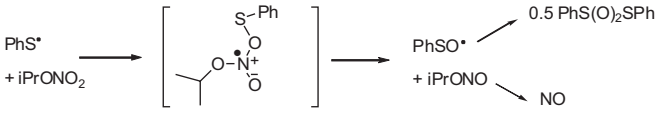
© 2006 NRC Canada

the overall reaction is a $3e^-$ reduction, radicals in addition to NO must be involved or released at some stage of the reaction. In many such reaction mechanisms a thiyl radical is a by-product.

To initiate studies into the reactivity of S-centred radicals with nitrates, thiyl radical, the simplest of such radicals, was studied using photochemical systems to generate the radical in the presence of a simple aliphatic nitrate (IPN). The $PhS^{\bullet}$ radical was generated by photolysis of benzene thiol or the disulfide and characterized by LFP analysis of its characteristic spectrum and decay rates in the presence of DMB. The conjugate addition of the thiyl radical to the DMB diene was also used as a measure of the ability of the nitrate to react with thiyl radical and inhibit the addition reaction. Significant inhibition of the formation of addition product from reaction of $PhS^{\bullet}$ with DMB was only observed at high concentrations of the nitrate ([IPN] = 1.0 mol/L). The reaction of the benzene thiyl radical with IPN at this high concentration was studied by identifying the reaction products and quantifying formation as a function of irradiation time. In addition to the expected disulfide product of thiyl radical combination, the sulfonothioate ($PhS(O)_2SPh$), was observed. The observation of this product under the anaerobic reaction conditions demonstrated that the photochemical reaction of thiyl with nitrate involved O atom transfer from nitrogen to sulfur.

Direct reaction of the electrophilic thiyl radical with the HOMO of the nitrate (localized on the nonbonding orbitals of the terminal oxygens) would yield a radical intermediate leading to O atom transfer (eq. [25]). Homolysis of this intermediate yields sulfinyl radical and organic nitrite, with subsequent sulfinyl radical combination leading to the observed sulfonothioate product. An important feature of this mechanism is that the organic nitrite product is a known source of NO (48).

[25]



However, a sulfonothioate is also the major product of the thermal decomposition of *tert*-butyl thionitrate (*t*-$BuSNO_2$) in neutral aqueous solution at room temperature (44), hinting at the formation of $PhSNO_2$ as an intermediate in the photochemical reaction of $PhS^{\bullet}$ with IPN. The simplest route to thionitrate is by the rapid radical combination of NO_2 with thiyl radical.

[26] $PhS^{\bullet} + NO_2^{\bullet} \rightarrow PhSNO_2$

[27] $PhSNO_2 \rightarrow PhSONO \rightarrow PhSO + NO$

[28] $2PhSO \rightarrow 0.5PhS(O)_2SPh$

Evidence against the direct reaction of thiyl with nitrate was seen in the photochemical generation of $PhS^{\bullet}$ from irradiation of PhSSPh at 350 nm in which sulfonothioate formation was greatly reduced from the 35% yield observed on irradiation of PhSH at 300 nm. This observation is compatible with thionitrate formation from NO_2 formed by the initial photolysis of IPN, which would be greatly reduced owing to the negligible absorbance of organic nitrates at 350 nm compared with 300 nm.

Nitration of 4-chlorophenol was used to confirm the nitrate photolysis pathway. The nitration of phenols by NO_2, involving oxidation and radical addition, is a well-known reaction that leads to tyrosine nitration in vivo. 4-Chlorophenol was used as a NO_2 trap, where formation of 4-chloro-2-nitrophenol revealed release of NO_2 upon irradiation of PhSH–IPN at 300 nm. In contrast, significantly less NO_2 was observed from irradiation of PhSSPh–IPN at 350 nm, compatible with the very weak absorbance of nitrates at higher wavelength.

The use of the 4-chlorophenol trap was validated by observation of nitration by unpurified NO gas containing NO_2 impurity, whereas purified NO gave almost no nitration product. Treatment of a PhSH solution with NO–NO_2 gave substantial formation of $PhS(O)_2SPh$, which was not observed with purified NO gas, supporting photolysis of IPN to NO_2 as the source of sulfonothioate. The thermal experiments with the gaseous NO–NO_2 source confirm that reaction of NO_2 with thiyl radical (eq. [26]) competes both with thiol oxidation and with radical combination with NO (eqs. [29]–[31]), which is in accord with literature rate data.

[29] $RSH + NO_2 \rightarrow RS^{\bullet} + HNO_2$

[30] $RS^{\bullet} + NO_2 \rightarrow RSNO_2$

[31] $NO + NO_2 \rightarrow N_2O_3$

In addition to photolysis to NO_2, the irradiation of PhSH–IPN solutions generated a reasonable flux of NO, with the presence of thiol being a requirement. This novel observation is entirely compatible with the rearrangement of the thionitrate intermediate to yield NO (eq. [27]), which we have previously reported in the context of the thermal decomposition of a thionitrate (44).

A large part of the early work on organic nitrate reactivity, including photochemistry, is part of the impressive ouevre of Canadian carbohydrate chemists, and published in this journal (49, 50). From these and other studies, it is seen that various benzyl nitrates are photolabile, whereas simple aliphatic nitrates require extended reaction times to observe photolysis products (51, 52). Work by Csizmadia and Hayward investigating the photolysis of hydrobenzoin and acenaphthenediol dinitrates in benzene found the predominant process to be photolysis to NO_2 (49, 50). This was validated by the detection of NO_2 as a reaction product using ESR spectroscopy (49). There is no evidence for direct photolysis leading to NO.

Calculation of the thermodynamics for homolysis of IPN reveals the BDE and ΔG of reaction to be 43.7 and 31.6 kcal/mol, respectively, (1 cal = 4.184 J) employing CBS-QB3//B3LYP methodology. The structure of the first excited state was calculated and the energy shown to be 54 kcal/mol above the ground state (Table 1). The calculated BDE for a nitrate is substantially larger than that for homolysis of the S—N bond of a nitrosothiol as shown by comparison of the thermochemical data calculated for $MeONO_2$ and MeSNO, which reveals a BDE for the nitrate greater by 11 kcal/mol. Nitrosothiols are well-known to be labile to photolysis to NO. Nitrosothiol photolysis is facili-

© 2006 NRC Canada

Table 1. Calculated homolysis thermodynamics for IPN compared with methyl nitrate and thionitrite.

	Energy (kcal/mol)		
Isodesmic reaction	$E^{o a}$	BDE	ΔG
i-$PrONO_2$ → *i*-PrO + NO_2	44.0	43.7	31.6
$MeONO_2$ → MeO + NO_2	42.0	43.2	30.6
MeSNO → MeS + NO	31.0	31.9	20.9

Note: Calculated using CBS-QB3//B3LYP/6-311++G**.
[a]Total energy including scaled zero-point energy.

tated by significant absorbance and a λ_{max} above 300 nm, in contrast to nitrates.

The disulfanyl dinitrate (GT-130) might be anticipated to undergo competitive photolysis to yield either PhS$^{\cdot}$ or NO_2. Good evidence for efficient thiyl radical formation was obtained, but no evidence for formation of NO_2 was found. This novel nitrate, containing a phenyl disulfanyl group linked to an organic nitrate, introduces the possibility of an intramolecular reaction between thiyl radical and the nitrate functionality. Photolysis of GT-130 (5 mmol/L) was observed to give a reasonable rate of NO flux, but the rate was lower than from the thermal reaction of GT-130 with thiol.

Taken together, the results of this study provide no support for a rapid reaction between thiyl radical and organic nitrate. Despite weak absorption of light >300 nm and a relatively high BDE for homolysis, the dominant photochemistry under conditions required to generate thiyl radical was driven by nitrate photolysis to NO_2. The observation of both sulfonothioate and NO as products of reaction is readily explained by the formation of a thionitrate intermediate and provides further evidence that thionitrates are a source of NO. A novel nitrate containing a phenyl disulfanyl group did not undergo photolysis to NO_2, nor generate sulfonothioate, but did yield NO. The observations with the novel nitrate suggest that reaction between thiyl radicals and nitrates leading to NO release is a viable pathway, but is subservient to other competing reactions, such as photolysis in the case of IPN and reaction with thiolate in the case of the novel nitrate.

Acknowledgements

This work was supported in part by a Natural Sciences and Engineering Research Council of Canada (NSERC) grant (245617-01) and a National Institutes of Health (NIH) grant (CA 102590).

References

1. T.L. Brunton. Lancet, **2**, 97 (1867).
2. W. Murrell. Lancet, **1**, 80 (1879).
3. J.A. Franciosa, A.L. Taylor, J.N. Cohn, C.W. Yancy, S. Ziesche, A. Olukotun, E. Ofili, K. Ferdinand, J. Loscalzo, and M. Worcel. J. Card. Failure, **8**, 128 (2002).
4. G.R.J. Thatcher. Curr. Top. Med. Chem. **5**, 597 (2005).
5. G.R.J. Thatcher, B.M. Bennett, and J.N. Reynolds. Curr. Alzheimer Res. **2**, 171 (2005).
6. G.R.J. Thatcher, A.C. Nicolescu, B.M. Bennett, and V. Toader. Free Radicals Chem. Biol. Med. **37**, 1122 (2004).
7. H.L. Fung. Annu. Rev. Pharmacol. Toxicol. **44**, 67 (2004).
8. B.M. Bennett and G.S. Marks. Trends Pharmacol. Sci. **5**, 329 (1984).
9. G.R.J. Thatcher and H. Weldon. Chem. Soc. Rev. **27**, 331 (1998).
10. J.J. Doel, B.L. Godber, R. Eisenthal, and R. Harrison. Biochim. Biophys. Acta, **1527**, 81 (2001).
11. B.M. Bennett, S.M. Kobus, J.F. Brien, K. Nakatsu, and G.S. Marks. J. Pharmacol. Exp. Ther. **237**, 629 (1986).
12. J.D. Ratz, J.J. McGuire, D.J. Anderson, and B.M. Bennett. J. Pharmacol. Exp. Ther. **293**, 569 (2000).
13. Y. Meah, B.J. Brown, S. Chakraborty, and V. Massey. Proc. Natl. Acad. Sci. U.S.A. **98**, 8560 (2001).
14. B.J. McDonald and B.M. Bennett. Can. J. Physiol. Pharmacol. **68**, 1552 (1990).
15. J.J. McGuire, D.J. Anderson, B.J. McDonald, R. Narayanasami, and B.M. Bennett. Biochem. Pharmacol. **56**, 881 (1998).
16. R. Nigam, T. Whiting, and B.M. Bennett. Can. J. Physiol. Pharmacol. **71**, 179 (1993).
17. R. Nigam, D.J. Anderson, S.F. Lee, and B.M. Bennett. J. Pharmacol. Exp. Ther. **279**, 1527 (1996).
18. Z. Chen, J. Zhang, and J.S. Stamler. Proc. Natl. Acad. Sci. U.S.A. **99**, 8306 (2002).
19. J. Towell, T. Garthwaite, and R. Wang. Alcohol Clin. Exp. Res. **9**, 438 (1985).
20. N. Mukerjee and R. Pietruszko. J. Biol. Chem. **269**, 21664 (1994).
21. K. Schmidt, A. Schrammel, D. Koesling, and B. Mayer. Mol. Pharmacol. **59**, 220 (2001).
22. Y. Zhao, P.E. Brandish, D.P. Ballou, and M.A. Marletta. Proc. Natl. Acad. Sci. U.S.A. **96**, 14753 (1999).
23. S. Chong and H.L. Fung. Biochem. Pharmacol. **42**, 1433 (1991).
24. L.J. Ignarro and C.A. Gruetter. Biochim. Biophys. Acta, **631**, 221 (1980).
25. R.A. Yeates, H. Laufen, and M. Leitold. Mol. Pharmacol. **28**, 555 (1985).
26. J.D. Artz, V. Toader, S.I. Zavorin, B.M. Bennett, and G.R.J. Thatcher. Biochemistry, **40**, 9256 (2001).
27. Z.B. Alfassi. S-Centered radicals. John Wiley and Sons, Chichester, UK. 1999.
28. K.U. Ingold, T. Paul, M.J. Young, and L. Doiron. J. Am. Chem. Soc. **119**, 12364 (1997).
29. S.I. Zavorin, J.D. Artz, A. Dumitrascu, A. Nicolescu, D. Scutaru, S.V. Smith, and G.R.J. Thatcher. Org. Lett. **3**, 1113 (2001).
30. O. Bostrup, R.S. Tobias, S.S. Hutcheson, and W.H. Engelmann. *In* Inorganic syntheses. *Edited by* H.F.J. Holtzclaw. McGraw-Hill, New York. p. 191. 1966.
31. A.D. Becke. J. Chem. Phys. **98**, 5648 (1993).
32. M.J. Frisch, G.W. Trucks, H.B. Schlegel, G.E. Scuseria, M.A. Robb, J.R. Cheeseman, J.A. Montgomery, Jr., T. Vreven, K.N. Kudin, J.C. Burant, J.M. Millam, S.S. Iyengar, J. Tomasi, V. Barone, B. Mennucci, M. Cossi, G. Scalmani, N. Rega, G.A. Petersson, H. Nakatsuji, M. Hada, M. Ehara, K. Toyota, R. Fukuda, J. Hasegawa, M. Ishida, T. Nakajima, Y. Honda, O. Kitao, H. Nakai, M. Klene, X. Li, J.E. Knox, H.P. Hratchian, J.B. Cross, V. Bakken, C. Adamo, J. Jaramillo, R. Gomperts, R.E. Stratmann, O. Yazyev, A.J. Austin, R. Cammi, C. Pomelli, J.W. Ochterxki, P.Y. Ayala, K. Morokuma, G.A. Voth, P. Salvador, J.J. Dannenberg, V.G. Zakrzewski, S. Dapprich, A.D. Daniels, M.C. Strain, O. Farkas, D.K. Malick, A.D. Rabuck, K. Raghavachari, J.B. Foresman, J.V. Ortiz, Q. Cui, A.G. Baboul, S. Clifford, J. Cioslowski, B.B. Stefanov, G. Liu,

© 2006 NRC Canada

A. Liashenkko, P. Piskorz, I. Komaromi, R.L. Martin, D.J. Fox, T. Keith, M.A. Al-Laham, C.Y. Peng, A. Nanayakkara, M. Challacombe, P.M.W. Gill, B. Johnson, W. Chen, M.W. Wong, C. Gonzalez, and J.A. Pople. Gaussian 03. Revision C.02 [computer program]. Gaussian, Inc., Wallingford, Connecticut. 2004.
33. C. Chatgillialoglu and K.-D. Asmus. Life Sci. **197**, 451 (1990).
34. D.J. McPhee, M. Campredon, M. Lesage, and D. Griller. J. Am. Chem. Soc. **111**, 7563 (1989).
35. A.A. Oswald, K. Griesbaum, W.A. Thaler, and B.E. Hudson, Jr. J. Am. Chem. Soc. **84**, 3897 (1964).
36. D.L. Bunbury. Can. J. Chem. **43**, 1714 (1965).
37. D. Vione, V. Maurino, C. Minero, and E. Pelizzetti. Chemosphere, **45**, 893 (2001).
38. T.B. Johnson and E.F. Kohmann. J. Am. Chem. Soc. **37**, 1863 (1915).
39. J.D. Artz and G.R.J. Thatcher. Chem. Res. Toxicol. **11**, 1393 (1998).
40. D. Jourd'heuil, F.S. Laroux, A.M. Miles, D.A. Wink, and M.B. Grisham. Arch. Biochem. Biophys. **361**, 323 (1999).
41. Z. Chen, M.W. Foster, J. Zhang, L. Mao, H.A. Rockman, T. Kawamoto, K. Kitagawa, K.I. Nakayama, D.T. Hess, and J.S. Stamler. Proc. Natl. Acad. Sci. U.S.A. **102**, 12159 (2005).
42. J. DiFabio, Y. Ji, V. Vasiliou, G.R. Thatcher, and B.M. Bennett. Mol. Pharmacol. **64**, 1109 (2003).
43. R.A. Yeates. Arzneim.-Forsch./Drug Res. **42**, 1314 (1992).
44. J.D. Artz, K. Yang, J. Lock, C. Sanchez, B.M. Bennett, and G.R.J. Thatcher. J. Chem. Soc. Chem. Commun. 927 (1996).
45. D.R. Cameron, A.M.P. Borrajo, B.M. Bennett, and G.R.J. Thatcher. Can. J. Chem. **73**, 1627 (1995).
46. D.L.H. Williams. J. Chem. Soc. Chem. Commun. 1085 (1996).
47. M.D. Bartberger, J.D. Mannion, S.C. Powell, J.S. Stamler, K.N. Houk, and E.J. Toone. J. Am. Chem. Soc. **123**, 8868 (2001).
48. A.C. Nicolescu, J.N. Reynolds, L.R. Barclay, and G.R.J. Thatcher. Chem. Res. Toxicol. **17**, 185 (2004).
49. I.G. Csizmadia and L.D. Hayward. Photochem. Photobiol. **4**, 657 (1965).
50. L.D. Hayward, R.A. Kitchen, and D.J. Livingstone. Can. J. Chem. **40**, 434 (1962).
51. J.G. Batelaan, H.J. Hageman, and J. Verbeek. Tetrahedron Lett. **28**, 2163 (1987).
52. M.P. Turberg, D.M. Giolando, C. Tilt, T. Soper, S. Mason, M. Davies, P. Klingensmith, and G.A. Takacs. J. Photochem. Photobiol. A, **51**, 281 (1990).

© 2006 NRC Canada

Sulfonated-polydimethylsiloxane (PDMS) microdevices with enhanced electroosmotic pumping and stability[1]

Bin Wang, J. Hugh Horton, and Richard D. Oleschuk

Abstract: Polydimethylsiloxane (PDMS) microfluidic devices offer several advantages in terms of cost and ease of fabrication compared with those fabricated from both glass and silicon materials. PDMS, however, has some potential disadvantages compared with other materials including high hydrophobicity, which makes filling the micron-sized channels difficult, and minimal surface charge resulting in reduced electroosmotic flow (EOF). Here, we describe the oxidation of the PDMS surface to form silanol groups using both air plasma and a discharge from a Tesla coil, and subsequent modification to form sulfonated-PDMS surfaces. The flow performance of freshly prepared and aged sulfonated-PDMS chips was determined at pH 5 and compared with those of unmodified and oxidized PDMS chips. The electroosmotic mobility (μ_{eo}) for a sulfonated-PDMS microdevice was determined at various pH values (pH 3~8) and compared with that for an oxidized PDMS chip. The lower pK_a of a sulfonic acid modified surface compared with a silanol modified surface generated a stronger EOF over the entire pH range studied. Chemical force titrations were used to characterize the changes in functional groups present on the surface of freshly prepared and aged sulfonated-PDMS surfaces. These experiments show that the sulfonated-PDMS is a superior material for use in microfluidic applications because (*i*) it supports EOF over a much wider range of pH than similar polymer materials and (*ii*) is less susceptible to degradation of its EOF rate owing to air aging effects and surface reorganization.

Key words: polydimethylsiloxane (PDMS), sulfonated surface modification, electroosmotic flow (EOF), aging effect, chemical force titrations.

Résumé : Les dispositifs en polydiméthylsiloxane (PDMS) microfluide offrent de nombreux avantages en termes de coût et de facilité de fabrication par comparaison à ceux fabriqués de matériaux tant en verre qu'en silicone. Toutefois le PDMS possèdent quelques désavantages par rapport aux autres matériaux, dont son caractère hydrophobe élevé qui rend difficile le remplissage de canaux de la taille du micron et une charge superficielle minimale qui réduit l'écoulement électroosmotique (EEO). On a effectué une oxydation de la surface du PDMS en faisant appel à un plasma d'air ainsi qu'une décharge à partir d'une bobine de Tesla qui a conduit à la formation de groupes silanols qui ont été par la suite modifiés pour former des surfaces de PDMS sulfoné. Opérant à un pH de 5, on a déterminé la performance d'écoulement de copeaux de PDMS sulfoné fraîchement préparé et vieilli et on l'a comparée à celles de copeaux de PDMS non modifié et de copeaux de PDMS oxydé. On a déterminé la mobilité électroosmotique (μ_{eo}) d'un microdispositif en PDMS sulfoné sur une plage de pH allant de 3~8 et on l'a comparée à celle d'un copeau de PDMS oxydé. Le fait que le pK_a est plus bas pour une surface modifié avec de l'acide sulfonique que celui d'une surface modifiée en silanol fait que le EEO est plus élevé sur toute la plage de pH étudiés. On a utilisé des titrages de la force chimique pour caractériser les changements dans les groupes fonctionnels présents sur les surfaces de PDMS sulfoné fraîchement préparé et vieilli. Ces expériences montrent que le PDMS sulfoné est un matériau dont l'usage est avantageux dans les applications microfluides en raison (*i*) du fait qu'il supporte un EEO sur une plage plus grande de pH que les matériaux polymères similaires et (*ii*) du fait qu'il est moins susceptible de subir une réorganisation de sa surface ou de voir son taux de EEO dégradé en raison d'effets de vieillissement par l'air.

Mots clés : polydiméthylsiloxane (PDMS), modification de la surface par sulfonation, écoulement électroosmotique, EEO, effet de vieillissement, titrages de la force chimique.

[Traduit par la Rédaction]

Received 6 September 2005. Published on the NRC Research Press Web site at http://canjchem.nrc.ca on 17 May 2006.

Submitted for and in dedication to the special issue for Walter Szarek.

B. Wang, J.H. Horton, and R.D. Oleschuk.[2] Department of Chemistry, Queen's University, Kingston, ON K7L 3N6, Canada.

[1]This article is part of a Special Issue dedicated to Professor Walter A. Szarek.

[2]Corresponding author (e-mail: oleschuk@chem.queensu.ca).

 doi:10.1139/V06-044 © 2006 NRC Canada

Introduction

Recently, polymeric micro-total analysis system (μ-TAS) devices have been developed as an alternative to expensive glass- and silicon-based devices. Many polymer types have been investigated for their use as substrate materials including polydimethylsiloxane (PDMS) (1–4), polymethylmethacrylate (PMMA)(5, 6), polycarbonate (PC) (6), polyethylene (PE) (4), and polystyrene (4), amongst others. The composition of polymer materials can be readily adapted to suit a particular application or the polymer can be surface modified to alter its characteristics. Different surface functionalities, such as carboxyl groups and amine groups, can be generated during the modification process to appropriately alter the surface chemistry and may also be used to further functionalize the surface with biochemical reagents such as proteins and antibodies (4, 7–9). PDMS has been widely investigated as a material for constructing microfluidic devices because of the relative ease with which devices can be fabricated using micromolding (1, 2). PDMS, however, has some potential disadvantages compared with other materials, including high hydrophobicity, which makes filling the micron-sized channels difficult, and minimal surface charge resulting in reduced electroosmotic flow (EOF). A plasma oxidation method has been used to form silanol groups on PDMS surfaces to increase the surface charge and make the surface hydrophilic (10, 11). As a result, the Si-CH_3 groups on the PDMS surface can be modified through oxidation to Si-OH, which increases the microchannel EOF rate owing to an increase in the surface ζ potential arising from deprotonation to form SiO^- sites. One significant drawback of this surface modification is that it is only temporary. Following oxidation, the PDMS begins to revert back to its original surface properties, which has been ascribed to the diffusion of low molecular weight polymer from the bulk to cover SiO_x sites on the surface (12–14). Other groups have covalently attached a variety of functional groups to PDMS surfaces to augment microfluidic device performance (15–18). In particular, Hu et al. (16) have used UV light to graft a series of acrylate monomers onto PDMS surfaces and measured the electroosmotic flow characteristics of resulting devices. Slentz et al. (18) have utilized a metal-catalyzed radical polymerization reaction to graft sulfonic acid containing moieties on the surface of PDMS microdevices. Although these coupling strategies yielded PDMS surfaces with different functionalization, the grafting process is more complicated than that described here. Chemical derivatization methods have also been used to extend the effective lifetime of the surface-modified PDMS (16, 18–20). In our previous work, we described a facile two-stage surface modification process for PDMS, consisting of an oxidation step followed by chemical derivatization with aminopropyltriethoxysilane (APTES) to form amine groups on the PDMS surface (19, 20). The APTES group enhanced the stability of the surface modification considerably. However, the surface ζ potential also changed sign: at low pH values (≈3.0), the flow within the microfluidic device could be reversed (anodic EOF) compared with native PDMS (cathodic EOF) through the protonation of the amino group on the PDMS surface.

Oxidized PDMS microchips show excellent flow performance at high pH values. However, the EOF rate in oxidized microchannels is reduced at pH values near the pK_a of the SiOH (≈4 to 5) because of protonation of the SiO^- sites and a consequent decrease in ζ potential. To increase the pH range over which strong cathodic EOF can be maintained, a chemical derivatization method was employed using 2-(4-chlorosulfonylphenyl)ethyltrimethoxysilane (SUFTMS) as the surface modification reagent. This compound has been previously used to terminate oxidized silicon wafers with sulfonic acid groups (21). In this paper, we describe the oxidation of the PDMS surface to form silanol groups using both air plasma and a discharge from a Tesla coil, with subsequent modification to form sulfonated-PDMS surfaces that have a lower surface pK_a than the unmodified silanol. The flow performance of freshly prepared and aged sulfonated-PDMS microchips is compared with that of unmodified and oxidized PDMS chips. Chemical force titrations (22, 23) are used to characterize changes in functional groups present on the surface of freshly prepared and aged sulfonated-PDMS surfaces. AFM imaging is also used to follow changes in surface morphology and patterning effects on the PDMS and showed that the stability of sulfonated-PDMS surfaces is significantly improved (in other words, the aging effect is reduced) and is comparable to that of the amine-modified PDMS surfaces. This report discusses devices that have been aged in air. This represents a worst-case scenario for aging as others have shown that contacting a modified PDMS surface with a solvent of higher surface free energy results in a greatly reduced aging effect (13, 14). The surface modification protocol described in this paper is facile, extends the application of polymer-based materials in microfluidic devices to lower pH, and aids in maintaining the surface and electrokinetic pumping characteristics of PDMS devices.

Experimental section

Chemical reagents

Sylgard 184 silicone elastomer and curing agent were purchased from Dow Corning Corporation (Midland, Michigan). Cy5™ monocarboxyl dye was purchased from Amersham Pharmacia Biotech UK (Amersham, UK). 2-(4-Chlorosulfonylphenyl)ethyltrimethoxysilane (SUFTMS), acetic acid, sodium salt (anhydrous reagent ACS), and pyridine (reagent ACS) were obtained from ACROS Organics (New Jersey). Potassium phosphate, sodium hydroxide, and methylene chloride (dichloromethane) were purchased from Fisher Scientific (Fair Lawn, New Jersey), while acetic acid (glacial), phosphoric acid, and hydrochloric acid were acquired from Fisher Scientific (Nepean, Ontario). Toluene was obtained from Anachemia Canada (Montréal, Quebec).

Fabrication of PDMS microchips and surface modification

Fabrication protocols for PDMS microchips based on a Sylgard 184 PDMS formulation have been described in detail elsewhere (19) and will only be briefly outlined here. Sylgard 184 PDMS prepolymer was mixed thoroughly in a 10:1 mass ratio of silicone elastomer to curing agent and poured onto a glass substrate (Twin-T, Micralyne, Edmonton, Alberta) containing six identical electrophoretic devices (as shown in Table 1) that acted as a negative master. The PDMS was polymerized at 65 °C for 4 h and peeled from

© 2006 NRC Canada

Table 1. The high-voltage switching programs used for migration time measurements and electroosmotic mobility measurements.

(*a*) 5 mmol/L Acetate buffer at pH 5.0 (*E* = 400 V/cm).					
	Reservoir/potential				
Step	Sample	Sample waste	Buffer	Buffer waste	Duration (s)
Injection	1 kV	Gnd	Float	Float	20
Migration	3 kV	3 kV	4 kV	Gnd	30–150
(*b*) μ_{eo} Measurement (*E* = 400 V/cm).					
	Reservoir/potential				
Step	Sample	Sample waste	Buffer	Buffer waste	Duration (s)
Migration	Float	Float	3.45 kV	Gnd	180

Note: The reservoirs noted in the table correspond to those indicated on the accompanying microchip schematic.



(Channels 50 μm wide, 20 μm deep)

the substrate and then used in a second PDMS molding step to yield the microfluidic substrate. Following this, one of two surface oxidation methods was used. A Tesla coil was used to oxidize the resulting PDMS substrate and an unpatterned cover plate for about 10 min. Alternatively, the PDMS substrate and the unpatterned cover were placed in an air plasma (Harrick Scientific Corporation, Ossining, New York) for 2 min (10 MHz RF level at 70 mTorr, 1 Torr = 133.322 4 Pa). The sulfonated-PDMS devices were produced by immersing the freshly oxidized PDMS substrate and cover into a 20 mmol/L SUFTMS in pyridine solution for approximately 4 h. The PDMS substrate and cover were then immersed in Milli-Q deionized water (resistivity 18.2 MΩ cm at 25 °C) for about 0.5 h to hydrolyze the chlorosulfonate groups. After modification was completed, the PDMS substrate and cover were dried in a stream of dry nitrogen gas. They were then laid on top of one another, forming a reversible air- and water-tight seal.

The SUFTMS compound is commercially available as a 50% solution in dichloromethane. Initial attempts to prepare sulfonic acid terminated PDMS surfaces used this solution diluted to a 20 mmol/L concentration in either dichloromethane or toluene. Immersion in such solutions, even for short times, resulted in a cloudy, etched polymer. This was ascribed to acid etching of the PDMS by sulfonic acid produced by hydrolysis of SUFTMS from trace amounts of water in solution. Using the weakly basic pyridine as a solvent eliminated this problem.

Migration time measurements and electroosmotic mobility (μ_{eo}) measurements

A microfluidic tool kit (Micralyne, Edmonton, Alberta) was used to determine the migration rates of fluorescent samples of Cy5™ (1.4 μmol/L) in the different substrate materials. The kit consists of a high-voltage (HV) power supply coupled with a laser-induced fluorescence (LIF) detection system (635 nm diode laser with a 670 nm band pass filter for detection of Cy5™ fluorescence). The detector was moved manually from the intersection of the injection channel and separation channel along the length of the separation channel to measure the migration time at each detector distance for each substrate material. An identical voltage program for injection and separation was used for all migration time experiments at pH 5.0, as shown in Table 1*a*. These two-step programs were repeated six times for replicate injection and migration measurements.

The measurement of electroosmotic mobility (μ_{eo}) in the microchannels was performed using current monitoring (3). The microchannels were first filled with a low ionic strength buffer (5 mmol/L). Subsequently, the buffer reservoir (as shown in Table 1) was emptied and filled with a higher ionic strength buffer (10 mmol/L). The electrodes were then placed in the two wells (buffer reservoir and buffer waste reservoir) and the current monitored as a function of time. The current increases owing to filling of the microchannel with the higher ionic strength buffer. The EOF was measured at various pH values using either phosphate (pH 3, 6.2, 7, and 8) or acetate (pH 4 and 5) buffer solutions.

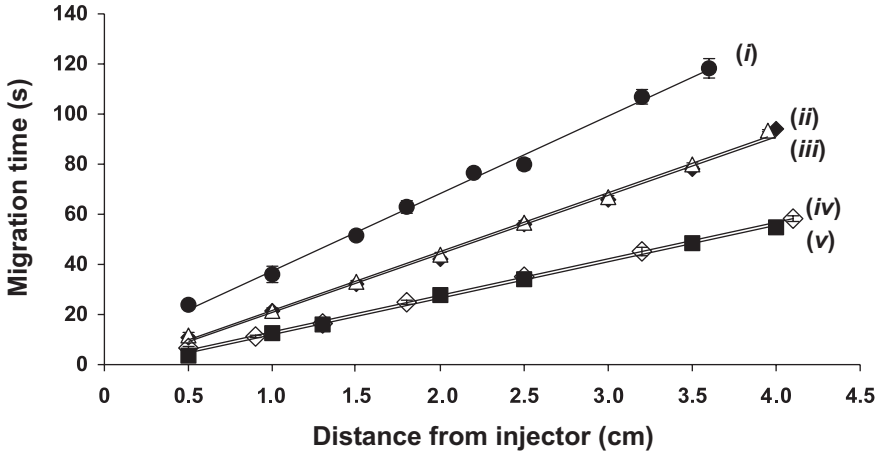
As a result of using two methods to determine the flow performance of PDMS devices, we need to compare the consistency of these two methods. In the EOF rate measurements, the rate of migration (apparent mobility, μ_{app}) for the charged fluorescent marker is a combination of the electrophoretic mobility (μ_{ep}) of negatively charged Cy5™ dye and electroosmotic mobility (μ_{eo}) where:

$$[1] \qquad \mu_{app} = \mu_{ep} + \mu_{eo}$$

Using the data for oxidized PDMS at a pH of 8, the migration rate of oxidized PDMS (20) is (10.4 ± 0.2) × 10^{-2} cm/s, which is (2.6 ± 0.2) × 10^{-4} cm^2/V s (μ_{app}).

© 2006 NRC Canada

Fig. 1. Migration times of a Cy5™ marker in a PDMS microfluidic device, whose flow channels had undergone various surface modifications. All flow measurements were performed at a pH of 5.0, immediately following surface modification. (*i*) Unmodified PDMS (●); (*ii*) PDMS oxidized using the Tesla coil method (Δ); (*iii*) PDMS oxidized using the air plasma method (◆); (*iv*) PDMS oxidized using the Tesla coil and subsequently modified with sulfonic acid (◇); (*v*) PDMS oxidized using the air plasma method and subsequently modified with sulfonic acid (■).



The μ_{ep} of negatively charged Cy5™ is $(-1.7 \pm 0.2) \times 10^{-4}$ cm^2/V s (20). Therefore, μ_{eo} for oxidized PDMS is $(4.3 \pm 0.2) \times 10^{-4}$ cm^2/V s. In comparison, current monitoring showed the EOF of oxidized PDMS at pH 8 to be $(4.5 \pm 0.2) \times 10^{-4}$ cm^2/V s. The results show that these two flow performance measurement methods are comparable and can be used interchangably.

Surface characterization using AFM

All AFM image data shown were acquired using a PicoSPM (Molecular Imaging, Tempe, Arizona) and a Nanoscope IIE controller (Digital Instruments, Santa Barbara, California). Images were acquired in air, using intermittent contact mode, while chemical force measurements were carried out in solution. All CFM data was acquired on a PDMS film cast in a similar manner to the cover plates used in microfluidic chip manufacture. The PDMS film underwent exactly the same synthesis and surface modification procedures as cover plates used in the manufacture of the microfluidic chips. The cantilevers used for image acquisition were terminated with standard Si_3N_4 tips (40–100 nm) and had a resonance frequency of ~100 kHz. Height and phase shift data were recorded simultaneously, although only the height mode images are shown here. Images were recorded at scan rates of 1 to 2 Hz using a 30 μm × 30 μm scanner.

Chemical force titration data were obtained using the same apparatus (23, 24). Force–distance curves were acquired using freshly prepared unbuffered NaOH or HCl solutions of pH ranging from 2–12. Unbuffered solutions were chosen to avoid potential interference of buffer ions in solution on the probe–substrate interactions. Solutions were checked after each experiment to ensure that their pH had not changed significantly. Experiments were carried out at low ionic strength conditions (0.01 mol/L), i.e., the only ions in solution were those introduced by pH adjustment with NaOH and HCl. Some 300–500 force–distance curves were obtained for each sample. The reported values of the adhesive interaction are an average of all the force curves obtained, while the reported errors reflect the standard deviation of the data. The AFM tips used in the chemical force titration measurements were silicon oxide sharpened silicon nitride tips. The tips were functionalized with sulfonic acid end groups by immersion in a 20 mmol/L pyridine solution of SUFTMS for 24 h, then immersed in Milli-Q deionized water for about 0.5 h, finally drying in a stream of nitrogen gas. The force constants of the cantilevers ranged from 0.08 to 0.4 N m^{-1} as determined by the method of Hutter and Bechhoefer (25).

Results

The flow characteristics of devices constructed from unmodified PDMS and PDMS, which had undergone various oxidation and sulfonic acid modification treatments, are shown in Fig. 1. Migration rates were determined at different distances from the injector to enhance measurement accuracy. The graph shows the time taken for the fluorescent Cy5™ marker to migrate down the channel, as a function of the distance from the injector at which the detector is placed. In Fig. 1, a steep slope corresponds to a long migration time and thus a low electroosmotic flow velocity (v_{EOF}), while a shallow slope corresponds to a high v_{EOF}. All flow measurements shown in Fig. 1 were performed at a pH of 5.0. From the graph we may observe that devices constructed from oxidized PDMS exhibit similar flow rates regardless of whether the Tesla coil (curve *ii*) or plasma method (curve *iii*) is used. Devices constructed from sulfonated-PDMS (curve *iv* and *v*) exhibit larger v_{EOF}, but again the initial oxidation method seems to have little effect.

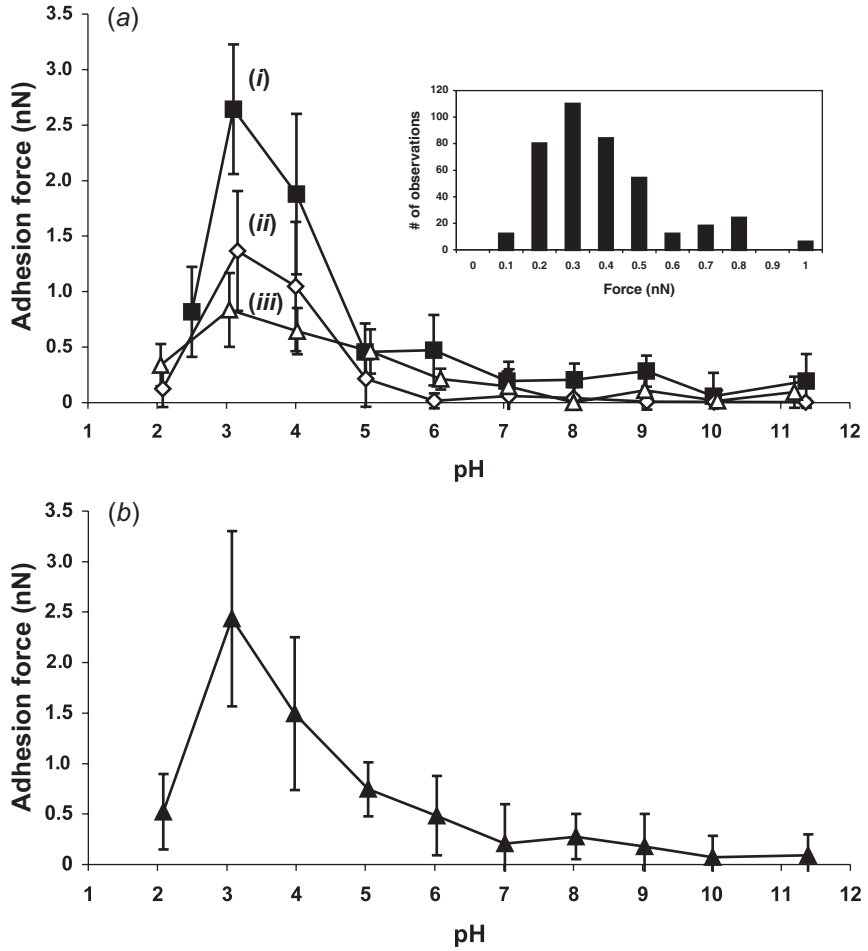
The migration rates, determined using the data in Fig. 1, for modified PDMS surfaces are summarized in Table 2. These measurements were carried out within 1 h of the sample treatment process ("freshly prepared"). We may note that devices from freshly prepared oxidized PDMS exhibit a migration rate that is 35% faster than that of unmodified PDMS at pH 5. Devices made from freshly prepared

© 2006 NRC Canada

Table 2. Migration rates for modified PDMS surfaces.

Chip surface treatment	Aging time	Migration rate ($\times 10^{-2}$ cm/s)
Unmodified PDMS	Freshly prepared	3.2±0.1
Oxidized PDMS (Tesla coil)	Freshly prepared	4.2±0.1
Oxidized PDMS (air plasma)	Freshly prepared	4.3±0.1
Sulfonic acid modified PDMS (Tesla coil oxidized)	Freshly prepared	6.8±0.1
Sulfonic acid modified PDMS (air plasma oxidized)	Freshly prepared	6.8±0.1
	24 h	6.5±0.1
	10 Days	5.1±0.1

Fig. 2. Chemical force titration curves showing the adhesive force between an AFM tip terminated with sulfonic acid and various substrates as a function of solution pH. The error bars represent the standard deviation in the adhesion force as measured from the average of 300–500 force-distance curves. (*a*): (*i*) PDMS substrate oxidized using the air plasma method and subsequently modified with sulfonic acid, freshly prepared (■); (*ii*) a 24 h aged PDMS substrate oxidized using the air plasma method and subsequently modified with sulfonic acid (◇); (*iii*) a 10 day aged PDMS substrate oxidized using the air plasma method and subsequently modified with sulfonic acid (Δ). The inset shows a typical adhesion force histogram, in this case obtained for the 10 day aged PDMS sample oxidized using air plasma and subsequently modified with sulfonic acid at pH 2.05. (*b*) A PDMS substrate oxidized using the Tesla coil and subsequently modified with sulfonic acid, freshly prepared (▲).



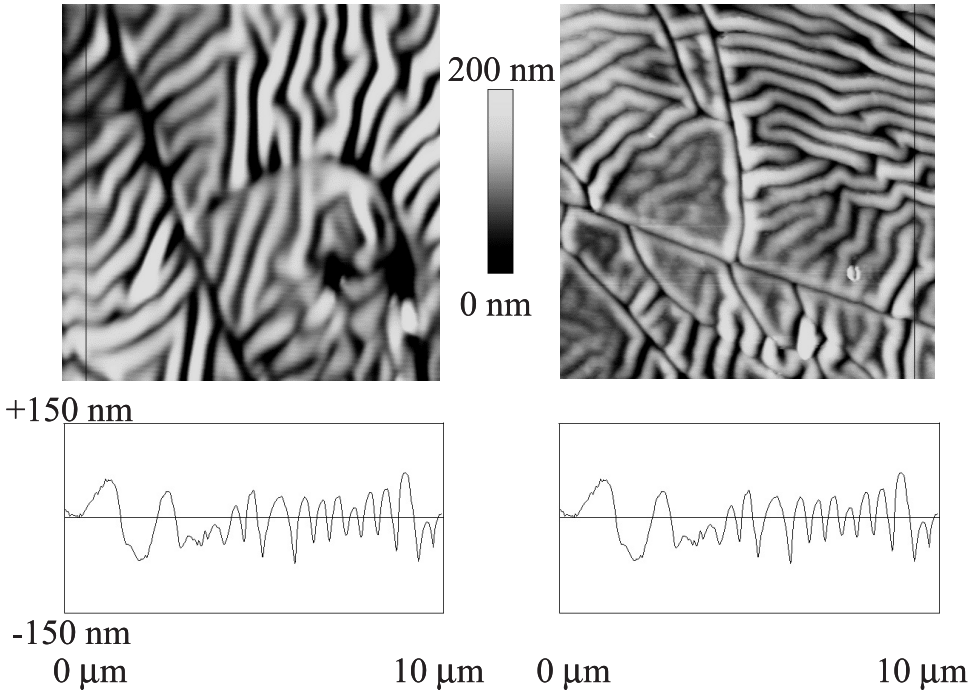
sulfonated-PDMS exhibit a migration rate that is 112% faster than that of unmodified PDMS. Migration times are about 60% faster than those PDMS devices that had only undergone the oxidation step.

Flow rate experiments were also carried out on sulfonic acid modified PDMS 24 h and 10 days after the surface modification process had been carried out ("aged" samples). They are also shown in Table 2. From the table we may observe that the freshly prepared sulfonated-PDMS exhibits the fastest v_{EOF}, while the 24 h aged sulfonated-PDMS exhibits a similar but somewhat slower (4%) migration rate in comparison. The 10 day aged sulfonated-PDMS is 25% slower than that of freshly prepared sulfonated-PDMS.

The aging flow results should be considered in conjunction with Fig. 2*a*, which shows the results of the chemical force measurements for freshly prepared, 24 h aged and

© 2006 NRC Canada

Fig. 3. AFM images (scale 10 μm) of sulfonic acid modified PDMS formed by exposure of air plasma oxidized PDMS to a solution of SUFTMS. The left image shows the surface within 2 h of forming the sulfonic acid modified surface, while the right one shows the same sample 10 days later. Image scales are noted in the figure. Cross sections of the images appear directly below the relevant image, and the cross section is indicated with a black line on the image.



10 day aged sulfonic acid modified air plasma oxidized PDMS surfaces. In all cases, measurements were carried out using a silicon oxide sharpened Si_3N_4 tip derivatized with SUFTMS and then rinsed with Milli-Q deionized water, to form a sulfonic acid terminated layer on the tip. The same tip was used to acquire all three curves. In Fig. 2*a*, the adhesive force observed between the AFM tip and the sample surface is plotted as a function of the solution pH. This is referred to as a force titration curve. The freshly prepared sulfonic acid modified PDMS (curve *i*) has an adhesive interaction of 2.7 nN, with a maximum peak near a pH of 3. The 24 h aged sulfonic acid modified PDMS (curve *ii*) also exhibits a maximum at a pH of 3 but which has been reduced in magnitude to 1.4 nN. The 10 days aged sulfonic acid-modified PDMS (curve iii) shows weaker force interaction of 0.8 nN, but the maximum still remains at pH 3. The inset depicted in Fig. 2*a* represents a typical force histogram comprised of 300–500 individual measurements that are translated into an average tip/sample adhesive force.

Figure 2*b* shows the result of the chemical force measurements for freshly prepared sulfonic acid modified Tesla coil oxidized PDMS surfaces. We may observe that the adhesive force between the sulfonic acid terminated Si_3N_4 tip and the sample surface is about 2.5 nN, with a maximum peak near a pH of 3. The magnitude and position of the peak are all similar with that of freshly prepared sulfonic acid modified air plasma oxidized PDMS surfaces, as shown in Fig. 2*a*.

In Fig. 3, we show two AFM images of a PDMS substrate, which had been oxidized by air plasma and subsequently exposed to the 20 mmol/L pyridine solution of SUFTMS to form a sulfonic acid terminated surface. The left image, at the 10 μm scale, taken within 2 h following the sulfonation process, shows undulating surface features. Such features are not observed on the original unmodified or solvent exposed (blank) PDMS samples (19). The right image, taken at the same scale as the left one, shows that after 10 days the structures remain essentially intact on the surface. Cross sections of the freshly prepared and aged surfaces shown in the figure demonstrate that the height and width of the features remain essentially unchanged after 10 days.

The EOF profiles of freshly prepared sulfonic acid modified air plasma oxidized PDMS and freshly prepared air plasma oxidized PDMS as a function of pH are shown in Fig. 4. Electroosmotic mobility measured in sulfonated-PDMS microchannels (curve *ii*) showed significantly higher values at all pH values studied when compared with the oxidized PDMS (curve *i*). Figure 5 and Table 3 show the electrophorograms and corresponding efficiencies obtained by injection and separation of a Cy5™ sample plug with differently modified substrate materials.

Discussion

The results of the flow experiments shown in Table 2 may be interpreted by considering that during electroosmosis in the microfluidic device, the flow velocity is directly proportional to the potential gradient (E) along the microchannel (26):

$$[2] \qquad \nu_{EOF} = \frac{\varepsilon_0 \varepsilon_r \zeta E}{\eta}$$

© 2006 NRC Canada

Fig. 4. EOF at different pH for modified PDMS devices. (*i*) PDMS oxidized using the air plasma, freshly prepared (◆). (*ii*) PDMS oxidized using the air plasma method and subsequently modified with sulfonic acid, freshly prepared (■).

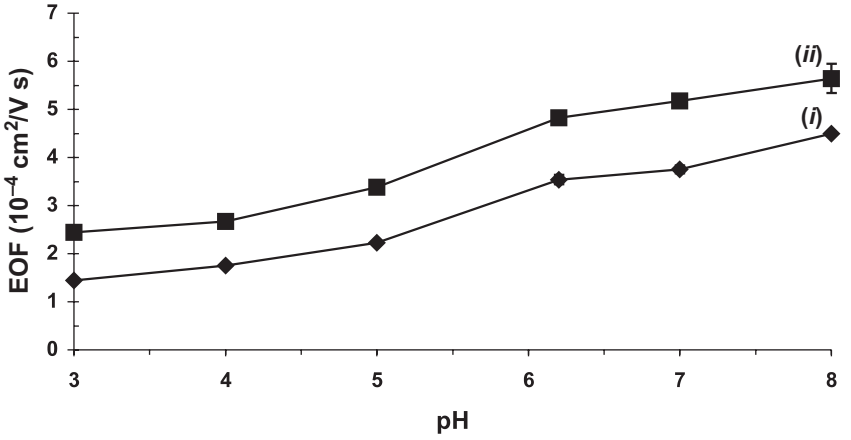


Fig. 5. The electrophorograms obtained by injection and separation of a Cy5™ sample plug with differently modified substrate materials.

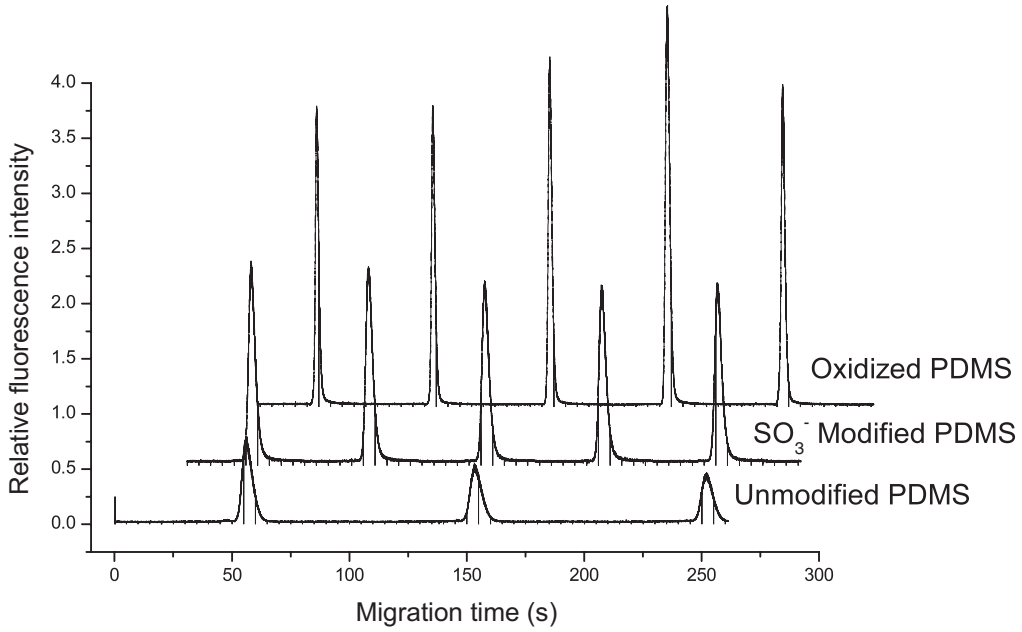


Table 3. The efficiencies obtained by injection and separation of a Cy5™ sample plug with differently modified substrate materials.

PDMS surface modification	Efficiency (plates/m)	t_R (RSD %) n = 50
Unmodified	58 000	3.1
Oxidized	108 000	2.3
Sulfonic acid	83 000	1.4

where ζ is the potential of the surface (i.e., the potential at the boundary between bound and free solvent and (or) electrolyte at the surface), ε_0 is the vacuum permittivity, ε_r is the relative permittivity of the solution, and η is the dynamic viscosity of the solution. Since both the buffer and potential gradient used in each case are identical within the set of experiments, the relative values of the measured ν_{EOF} are a direct measure of the relative ζ potential, and hence the fixed charge density on the surface of the PDMS.

The results in Fig. 1 demonstrate that the unmodified PDMS surface shows the slowest flow rate, and hence the smallest ζ potential. This might be initially considered surprising, as native PDMS should contain no surface ionizable sites under these conditions, and we would hence expect no EOF at all. Using X-ray photoelectron spectroscopy (XPS), it has been shown that the surface elemental composition of the Sylgard 184 PDMS formulation used here is enriched in oxygen and depleted in carbon by about 5% relative to the expected stoichiometric ratio (27, 28). The higher content of oxygen was attributed to the contribution from the silica filler, even though previous studies suggested that silica filler is rarely observed in the depth range probed by XPS (~7–10 nm) (29, 30). This may explain the small EOF observed in native PDMS microchannels as being due to residual SiOH sites being exposed on the surface.

Following oxidation using either the Tesla coil or air plasma method, the flow rate and hence the ζ potential increases, demonstrating that sites have been formed on the

© 2006 NRC Canada

surface that are ionizable under the pH 5 conditions of the flow experiments. Previously published (19, 20) chemical force titration measurements showed that the average surface pK_a of oxidized PDMS (Si-OH) is between 4 and 5. Therefore, there are ionizable Si-O$^-$ sites on the oxidized PDMS surface at pH 5.

We and others (12, 14, 16, 20) have observed that oxidized PDMS surfaces rapidly lose their efficacy in supporting electroosmotic flow through an "aging effect". This effect has been attributed to the rapid diffusion of surface hydroxyl sites into the bulk (surface reorganization), reducing the availability of ionizable groups at the surface. Such diffusion is aided by the fact that the oxidation process results in breaking of the polymer chain in the surface region, with the concomitant production of shorter chain oligomers that can undergo much more rapid diffusion. While the oxidized surfaces indeed effectively support electroosmotic flow, the aging effect means that they are not useful as a means of permanently augmenting flow in PDMS microfluidic devices. Instead, we considered the possibility of further surface modification to form ionizable groups that are more stable. In this study, we terminate the PDMS surface with sulfonic acid functional groups by means of SUFTMS treatment of the oxidized PDMS.

We may observe from Fig. 1 that sulfonated-PDMS microchips exhibit a ν_{EOF} that is double that of unmodified PDMS. The higher flow rate demonstrates that the surface negative charge density is increased dramatically. Chemical force titration measurements (Fig. 2*a*, curve *i*) on freshly prepared sulfonated-PDMS surfaces oxidized using the air plasma shows a maximum peak at a pH of 3. Previous workers have shown that, under low ionic strength conditions, the maxima in chemical force titration plots occur at pH values that are at the surface pK_a of the ionizable group (23, 31). At the surface pK_a, exactly half of the sites are ionized on both the tip and the sample. This allows for maximum ionic hydrogen bonding taking place, leading to a maximum adhesive interaction. Since the tip and sample site in this study contain the same functional group, the maximum should appear at the average surface pK_a of sulfonic acid. Figure 2 indicates that the pK_a of the sulfonated-PDMS surface is about 3.0. This value is higher than the typical pK_a of a sulfonic acid group in solution. Such a result is typically observed and may be attributed to two effects: intermolecular H-bonding taking place among neighboring SO_3H groups on the surface and the absence of charge screening among neighboring SO_3^- sites on the sample surface.

With the lower surface pK_a, there are many ionized SO_3^- sites on the sulfonated-PDMS surface at the pH 5 conditions under which the flow measurements were carried out. The ν_{EOF} in sulfonated-PDMS microchannels is 60% faster than that of oxidized PDMS.

In this study, we compared two surface oxidation methods: Tesla coil and air plasma oxidation. According to the migration rates shown in Fig. 1 and Table 2, it is apparent that these two methods can achieve the same oxidizing effects. Sulfonating derivatization following either oxidation method results in modified PDMS devices that exhibit the same flow performance ($(6.8 \pm 0.1) \times 10^{-2}$ cm/s). Chemical force titration results (Figs. 2*a* and 2*b*) show that freshly prepared sulfonated-PDMS substrates that have undergone oxidation with either air plasma or Tesla coil exhibit a maximum peak at the same position (pH 3) and similar magnitude (2.5~2.7 nN). Chemical force titration results confirm the conclusion that Tesla coil and air plasma oxidation are comparable oxidizing methods and can be used interchangably.

The flow characteristics of freshly prepared, 24 h and 10 day aged sulfonated-PDMS devices at pH 5 are also shown in Table 2. From the table, we observe that the freshly prepared sulfonic acid modified PDMS exhibits the fastest ν_{EOF}, while the 24 h aged sulfonic acid modified PDMS exhibits similar but somewhat slower (4%) ν_{EOF} in comparison. After 10 days, the migration rate is $(5.1 \pm 0.1) \times 10^{-2}$ cm/s, which is 75% of that of freshly prepared sulfonated-PDMS. We may observe that after exposure in air for 10 days, the ν_{EOF} of aged sulfonated-PDMS is still higher than that of freshly prepared oxidized and unmodified PDMS under the pH 5 conditions. The sulfonated PDMS surface shows similar stability to mixed monomer grafted PDMS over a 24 h period (16), however, comparing stability beyond 24 h is not possible as the previous study did not monitor aging effects for longer than 24 h in air. Also, a long term stability experiment was performed by Slentz et al. (18) that showed the sulfonic acid coating was stable for greater than 1 month. However, the details of device storage were not given so a direct comparison of the relative stabilities of the grafting and derivatization methodologies is not possible.

In previously published work, we found the changes in ν_{EOF} owing to aging of PDMS modified with an amine group was of effectively the same magnitude (20), although we cannot compare the absolute ν_{EOF} values of amine modified and sulfonic acid modified PDMS since they have opposite surface charges. In effect then, whatever the mechanism of the aging process, it results in a loss of a similar relative number of ionizable sites on the surface, regardless of which species — amine or sulfonic acid — has been grafted onto it.

The force titration curves shown in Fig. 2*a* are consistent with the flow performance results. As the sulfonic acid terminated surface ages over a period of 24 h and then 10 days, we can see from curves *ii* and *iii* that the extent of the force interaction between tip and sample diminishes. This indicates that the SO_3H sites are diffusing away or being covered up from the surface layer. Unlike the oxidized case (20), however, even after 10 days enough sulfonic acid sites remain on the surface to produce a recognizable force titration curve. This is consistent with the SUFTMS forming a denser cross-linked surface layer that would inhibit oligomer migration into the surface region. The AFM images of the aged surface in Fig. 3 are also consistent with this: the undulations remain intact and the surface morphology does not change dramatically after 10 days of aging. Only some finer structures disappear suggesting that the surface layer undergoes a slow reorganization, leading to fewer sulfonic acid sites exposed on the surface.

Finally, we used the current monitoring method to measure EOF mobility in modified PDMS microchannels at various pH values. The electroosmotic mobility (μ_{eo}) is obtained by eq. [3]:

$$[3] \qquad \mu_{eo} = L/(tE)$$

© 2006 NRC Canada

where L is the effective length from buffer reservoir to buffer waster reservoir, t the time to reach the current plateau, and E the applied field strength (3, 32).

With a lower surface pK_a of 3, the sulfonic acid terminated PDMS should be more appropriate for use in microfluidic devices operating under low pH conditions owing to its ability to support higher negative charge density below pH 5. We compared the EOF in sulfonated-PDMS and oxidized PDMS microchannels at various pH values from 3 to 8, as shown in Fig. 4. Under the pH 3 conditions, according to the definition of pK_a, half of the sulfonic acid groups present on the surface should be deprotonated to form -SO_3^-. The experimentally measured EOF is $(2.44 \pm 0.04) \times 10^{-4}$ cm^2/V s, higher than the measured EOF of oxidized PDMS at pH 5 ($(2.22 \pm 0.02) \times 10^{-4}$ cm^2/V s), which is above the surface pK_a value of Si-OH. Indeed, we observe from Fig. 4 that sulfonated-PDMS shows higher EOF at all pH values when compared with that of oxidized PDMS.

Previous workers (6) have compared the EOFs for sulfonated-polycarbonate and unmodified polycarbonate at pH values from 4 to 10. They found that EOFs measured in sulfonated-PC microchannels showed significantly higher values at pH below 8 when compared with the unmodified PC. However, the EOFs of both PC surfaces were similar from pH 8 to 10, thus indicating that the surface charge density was comparable at those pH (6). In our case, under the pH 8 condition, the EOFs of two modified PDMS surfaces were not comparable. From Fig. 4, we may also observe that curve *i* and curve *ii* show similar shapes. This may be related to the property of PDMS from which the devices are constructed and the inflection point (pH ≈5.5) has been interpreted to correspond to acidic groups in the PDMS support (3). These results demonstrate that sulfonated-PDMS is a superior material for generating improved EOF and stability at all pH values, compared with oxidized PDMS.

The relative separation efficiencies produced by the unmodified and modified PDMS substrates are quite different (Fig. 5 and Table 3). The oxidized PDMS substrate produced the highest efficiencies (≈108 000 plates/m), followed by the sulfonic acid modified (≈83 000 plates/m), and unmodified (≈58 000 plates/m). These efficiencies are similar to those reported for grafting of mixed monomer (17) onto PDMS, but are generally lower than those shown for PDMS grafted with sulfonic acid moieties (18). Slentz et al. (18) have, however, proposed that the separation involved both electrophoretic and chromatographic separation mechanisms, which may explain the increased efficiencies.

Conclusions

The surface modification of sulfonic acid terminated PDMS and the subsequent aging effects on this modified surface have been studied using EOF measurements in microfluidic devices in addition to atomic force and chemical force microscopy.

The sulfonic acid modified PDMS microdevices showed excellent flow performance at various pH values from 3 to 8, compared with oxidized PDMS devices. The sulfonic acid modified surface also showed aging effects; however, the change in EOF was significantly reduced compared with the oxidized surface where flow enhancements resulting from the surface modification disappear in a matter of hours. After 24 h of aging, the migration rate (under pH 5 conditions) in a sulfonic acid modified PDMS chip had dropped by only 4%; after 10 days it was still at 75% of its initial value. Chemical force titrations and AFM imaging demonstrated that there were still reasonable concentrations of sulfonic acid groups present on these aged surfaces. The aging experiment conditions were chosen to represent a worst case scenario, and when modified surfaces are contacted with a higher energy medium, it is expected that the stability of the surface modification will be considerably enhanced.

The results demonstrate that facile sulfonic acid modification can significantly decrease the rate of the surface aging effect and generate a surface with significant ζ potential. Therefore, a sulfonic acid based chemical derivatization is an effective means of improving the flow performance and durability of surface modifications for microfluidic devices made from PDMS. As a result, sulfonated-PDMS is a superior material for use in microfluidic applications because it can support high EOF over a wide range of pH and is less susceptible to degradation of its EOF rate owing to aging effects.

Acknowledgements

We acknowledge the Natural Sciences and Engineering Research Council of Canada (NSERC), the Canadian Foundation of Innovation, the Ontario Innovation Trust, and Queen's University for financial support.

References

1. J.C. McDonald, D.C. Duffy, J.R. Anderson, D.T. Chiu, H. Wu, O.J.A. Schueller, and G.M. Whitesides. Electrophoresis, **21**, 27 (2000).
2. D.C. Duffy, J.C. McDonald, O.J.A. Schueller, and G.M. Whitesides. Anal. Chem. **70**, 4974 (1998).
3. G. Ocvirk, M. Munroe, T. Tang, R. Oleschuk, K. Westra, and D.J. Harrison. Electrophoresis, **21**, 107 (2000).
4. J. Rossier, F. Reymond, and P.E. Michel. Electrophoresis, **23**, 858 (2002).
5. L.J. Kricka, P. Fortina, N.J. Panaro, P. Wilding, G. Alonso-Amigo, and H. Becker. Lab Chip, **2**, 1 (2002).
6. S.A. Soper, A.C. Henry, B. Vaidya, M. Galloway, M. Wabuyele, and R.L. McCarley. Anal. Chim. Acta, **470**, 87 (2002).
7. Y.H. Chen, W.C. Wang, K.C. Young, T.T. Chang, and S.H. Chen. Clin. Chem. **45**, 1938 (1999).
8. L.A. Chrisey, G.U. Lee, and C.E. O'Ferrall. Nucleic Acids Res. **24**, 3031 (1996).
9. G.A. Korbel, G. Lalic, and M.D. Shair. J. Am. Chem. Soc. **123**, 361 (2001).
10. Y. Xia and G.M. Whitesides. Angew. Chem. Int. Ed. **37**, 550 (1998).
11. T. Murakami, S. Kuroda, and Z. Osawa, J. Colloid Interface Sci. **202**, 37 (1998).
12. J. Kim, M.K. Chaudhury, and M.J. Owen. J. Colloid Interface Sci. **226**, 231 (2000).
13. M. Morra, E. Occhiello, R. Marola, F. Garbassi, P. Humphrey, and D. Johnson. J. Colloid Interface Sci. **137**, 11 (1990).
14. X. Ren, M. Bachman, C. Sims, G.P. Li, N. Allbritton. J. Chromatogr. B, **762**, 117 (2001).
15. M.K. Chaudhury and G.M. Whitesides. Langmuir, **7**, 1013 (1991).

© 2006 NRC Canada

16. S. Hu, X. Ren, M. Bachman, C.E. Sims, G.P. Li, N. Allbritton. Anal. Chem. **74**, 4117 (2002).
17. S. Hu, X. Ren, M. Bachman, C.E. Sims, and G.P. Li, and N. Allbritton. Electrophoresis, **24**, 3679 (2003).
18. B.E. Slentz, N.A. Penner, F.E. Regnier. J. Chromatogr. A, **948**, 225 (2002).
19. B. Wang, Z. Abdulali-Kanji, E. Dodwell, J.H. Horton, and R.D. Oleschuk. Electrophoresis, **24**, 1442 (2003).
20. B. Wang, L. Chen, Z. Abdulali-Kanji, J.H. Horton, and R.D. Oleschuk. Langmuir, **19**, 9792 (2003).
21. V.V. Tsukruk and V.N. Bliznyuk. Langmuir, **14**, 446 (1998).
22. E.W. van der Vegte and G. Hadziioannou. Langmuir, **13**, 4357 (1997).
23. A. Noy, D.V. Vezenov, and C.M. Lieber. Annu. Rev. Mater. Sci. **27**, 381 (1997).
24. W. Han, S.M. Lindsay, and T. Jing. Appl. Phys. Lett. **69**, 4111 (1996).
25. J.L. Hutter and J. Bechhoefer. Rev. Sci. Instrum. **64**, 1868 (1993).
26. M. Riekkola, J.Å. Jönsson, and R.M. Smith. Pure Appl. Chem. **76**, 443 (2004).
27. K. Fateh-Alavi, M.E. Núñez, S. Karlsson, and U.W. Gedde. Polym. Degrad. Stab. **78**, 17 (2002).
28. H. Hillborg, N. Tomczak, A. Olàh, H. Schönherr, and G.J. Vancso. Langmuir, **20**, 785 (2004).
29. K. Efimenko, W.E. Wallace, and J. Genzer. J. Colloid Interface Sci. **254**, 306 (2002).
30. M.J. Owen and P.J. Smith. J. Adhes. Sci. Technol. **8**, 1063 (1994).
31. E.W. van der Vegte and G. Hadziioannou. J. Phys. Chem. B, **101**, 9563 (1997).
32. X. Huang, M.J. Gordon, and R.N. Zare. Anal. Chem. **60**, 1837 (1988).

© 2006 NRC Canada

Conformational analysis in aqueous solution and estimation of the persistence length of exopolysaccharides produced by *Lactobacillus helveticus* Lh59 and *Streptococcus macedonicus* Sc136[1]

J. Albert van Kuik, Sébastien J.F. Vincent, Bas R. Leeflang, Loes M.J. Kroon-Batenburg, and Johannis P. Kamerling

Abstract: The conformations of two exopolysaccharides, one produced by *Lactobacillus helveticus* Lh59 and one by *Streptococcus macedonicus* Sc136, were investigated by molecular modelling to get insight into their physical properties. In particular, the influence of side chains and glycosidic linkage types on the overall shapes and persistence lengths of the polysaccharides were studied. It appeared that the side chains had only minor effects on the persistence lengths of the polysaccharides, with the exception of the monosaccharide residue directly attached to the backbone. The extensiveness of the backbone is enhanced by β-D-Hex*p*-(1→4) structural elements, whereas α-D-Hex*p*-(1→3) and α-D-Hex*p*-(1→4) elements create structural variability by introducing bends. The occurrence of either (1→5)- or (1→6)-linked monosaccharides, resulting in one extra bond between monosaccharide units, causes the overall flexibility of the polysaccharide chain to be enhanced and extensiveness to be reduced. The presence of such flexible linkages in the backbone leads to a shorter persistence length than when present in the side chain: a value of only 4.5 nm was found for the *L. helveticus* Lh59 EPS with a (1→5) linkage in the backbone, and a value of 8.5 nm for the *S. macedonicus* Sc136 EPS with two (1→6) linkages in the side chain.

Key words: conformational analysis, exopolysaccharide, *Lactobacillus helveticus*, molecular modelling, persistence length, *Streptococcus macedonicus*.

Résumé : Faisant appel à la modélisation moléculaire, on a étudié les conformations de deux exopolysaccharides, l'un produit par *Lactobacillus helveticus* Lh59 et l'autre par le *Streptococcus macedonicus* Sc136, dans le but de mieux comprendre leurs propriétés physiques. On a étudié particulièrement l'influence des chaînes latérales et les types de liaisons glycosidiques sur les formes globales et sur la longuer de persistance des polysaccharides. Il semble que les chaînes latérales n'ont que des effets mineurs sur la longuer de persistance des chaînes des polysaccharides, à l'exception du résidu monosaccharide attaché directement au squelette. L'étendue du squelette est augmentée par les éléments structuraux β-D-Hex*p*-(1→4) alors que les éléments α-D-Hex*p*(1→3) et α-D-Hex*p*(1→4) créent de la variabilité structurale en introduisant des courbures. La présence de monosaccharides liés soit en (1→5)- ou (1→6)-, qui conduit à la présence d'une liaison supplémentaire entre les unités de monosaccharides, provoque une augmentation de la flexibilité globale de la chaîne polysaccharide et à une diminution de l'étendue du squelette. La présence de telles liaisons flexibles dans le squelette conduit à une longuer de persistance moins longue que celle observée lorsqu'on les retrouve dans les chaînes latérales. La valeur de l'« EPS » pour le *L. helveticus* Lh59 comportant une liaison (1→5) dans le squelette n'est que de 4,5 nm alors que pour le *S. macedonicus* Sc136 comportant deux liaisons (1→6) dans la chaîne latérale, cette valeur est de 8,5 nm.

Mots clés : analyse conformationnelle, exopolysaccharide, *Lactobacillus helveticus*, modélisation moléculaire, longueur de persistance, *Streptococcus macedonicus*.

[Traduit par la Rédaction]

Received 19 August 2005. Published on the NRC Research Press Web site at http://canjchem.nrc.ca on 17 May 2006.

J.A. van Kuik,[2] B.R. Leeflang,[3] and J.P. Kamerling. Bijvoet Center, Department of Bio-Organic Chemistry, Utrecht University, Padualaan 8, NL-3584 CH Utrecht, The Netherlands.
S.J.F. Vincent. Nestlé Research Center, PO Box 44, Vers-chez-les-Blanc, CH-1000 Lausanne 26, Switzerland.
L.M.J. Kroon-Batenburg. Bijvoet Center, Department of Crystal and Structural Chemistry, Utrecht University, Padualaan 8, NL-3584 CH Utrecht, The Netherlands.

[1]This article is part of a Special Issue dedicated to Professor Walter A. Szarek.
[2]Deceased.
[3]Corresponding author (e-mail: b.r.leeflang@chem.uu.nl).

 doi:10.1139/V06-055 © 2006 NRC Canada

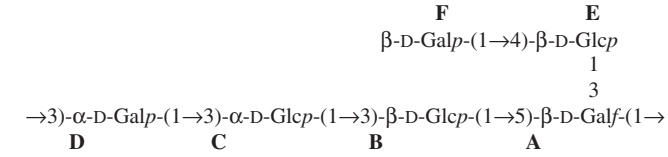
Introduction

In recent years, the interest in exopolysaccharides (EPSs) from lactic acid bacteria (LAB) has increased remarkably in the food industry, mainly because of the thickening capacities of EPSs in dairy products and the GRAS (Generally Recognized As Safe) status of the associated microorganisms (1–3). In the context of getting insight into the physical and (or) rheological properties of EPSs, conformational analysis of these biopolymers in aqueous solution is of the utmost importance. To explore this area, in an earlier investigation we have presented a method for constructing conformational models in water of heteropolysaccharides built up from repeating units, and applied this methodology to the exopolysaccharide produced by *Lactobacillus helveticus* 766 (4). Polysaccharide models were formed from oligosaccharide fragment models that were obtained from molecular dynamics (MD) simulations. The fragments were incorporated in the backbone in a ratio dictated by the population distribution of the glycosidic linkages. These were determined by the method of adaptive umbrella sampling (AUS) of the potential of mean force (PMF) (5).

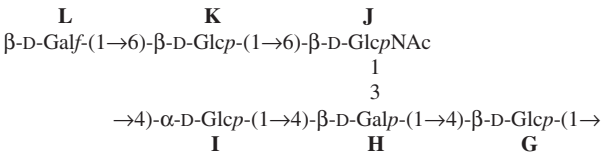
When cultured in skimmed milk, *L. helveticus* Lh59, one of the attractive alternatives to replace currently used thickeners, produces a high-molecular-mass EPS ($\geq 2 \times 10^6$ Da) with a branched hexasaccharide repeating unit (Scheme 1A) (6). *Streptococcus macedonicus* Sc136, being part of the starter flora present in Greek sheep and used in goat cheese production, produces an EPS with a different branched hexasaccharide repeating unit (Scheme 1B) (7), having a large molecular-mass distribution ranging from 1×10^5 to $\geq 2 \times 10^6$ Da and highly texturizing properties. The viscosity of the growth medium was shown to be significantly reduced by alteration of the EPS side chain (7).

In the present study, the conformational properties of the EPSs of the *L. helveticus* Lh59 and *S. macedonicus* Sc136 strains were investigated. Because the presence and structure of a side chain within the repeating unit of a polysaccharide is a key element for its texturizing properties, specific attention was paid to the relation between the polysaccharide conformation in solution and the side-chain structure as well as to the persistence length of the EPSs.

Scheme 1.



(A) *Lactobacillus helveticus* Lh59 EPS



(B) *Streptococcus macedonicus* Sc136 EPS

Experimental

Nomenclature

For the three staggered conformations of the C5—C6 bonds in hexopyranoses and the C4—C5 bonds in hexofuranoses, the notation *tg*, *gt*, and *gg* was used. In this nomenclature, *g* and *t* are abbreviations of gauche (±60°) and trans (180°), respectively, indicating qualitatively the value of a dihedral angle. The angle of the O_n-C_n-C_{n-1}-O_{n-1} moiety is indicated by the first character and the angle of the O_n-C_n-C_{n-1}-C_{n-2} moiety by the second.

Isoenergy (φ, ψ) maps

Minimum energy calculations were performed using the TINKER modelling package (8). TINKER has the ability to use various common force fields such as AMBER or CHARMm. In this study we provided TINKER with the force field parameters of CHEAT (9, 10), a CHARMm-based force field where special atom types and related parameters are introduced for hydroxyl groups. In CHEAT, hydroxyl groups are represented by extended atoms to prevent the formation of intramolecular hydrogen bonds, and whereby energies are independent of the hydroxyl group orientation. Isoenergy contour maps were generated by incrementing the interglycosidic torsion angles of disaccharides in steps of 10°, producing a 36 × 36 grid. For the (1→5) and (1→6) linkage, a three-dimensional energy map was generated at a 20 × 20 × 20 resolution. Three dihedral angles per sugar ring and both interglycosidic angles were kept fixed by setting constraints during a first minimization at each grid point. For a second minimization, all constraints inside the ring were removed and the molecule was minimized again. Contour levels were plotted in steps of 1 kcal/mol (1 cal = 4.184 J), starting at the global minimum.

Molecular dynamics calculations

Molecular dynamics simulations were performed using the GROMOS-87 program package (11) and the improved force field for carbohydrates (12), on Linux computers. Each molecule was surrounded by SPC/E water molecules (13) and placed in a truncated octahedral periodic box. All bond lengths were kept fixed using the SHAKE procedure (14). Nonbonded interactions were calculated using a cutoff radius of 0.8 nm, and a time step of 2 fs. Simulations were performed with loose coupling to a pressure bath at 1 atm (1 atm = 101.325 kPa) and a temperature bath at 300 K (15) with time constants of 0.5 and 0.1 ps, respectively. A hydrogen bond is considered to be present if O-H···O < 2.5 Å, and if O-H···O angle >120°. Interglycosidic torsion angles are defined as φ (O_{ring}-$C_{1'}$-O_n-C_n), ψ ($C_{1'}$-O_n-C_n-C_{n-1}), and ω (O_n-C_n-C_{n-1}-C_{n-2}) according to IUPAC convention (16).

PMF calculations

To calculate the free energy differences of the disaccharide conformers in relation to one dihedral angle of the glycosidic linkage, PMF calculations were performed with the AUS method (5) and the GROMOS force field. All simulations were divided into jobs of 10 ps. Dihedral angle values were partitioned into 72 classes, each having a width of 5°. The derivatives of the PMF were fitted to a 12 term Fourier series. The first 0.2 ps of each job were discarded. Each system was simulated between 5 and 10 ns for

© 2006 NRC Canada

disaccharides, and up to 35 ns for the tetrasaccharide, and the final PMF was used to obtain the rotamer population distribution of the sampled dihedral angle.

Persistence length calculations

The persistence lengths of the polysaccharides were calculated similarly as has been done for cellulose (17). For cellulose, disaccharide conformational data have been used that had been selected from appropriate conformational regions of the MD simulations. For the exopolysaccharides, extended repeating units were used instead of disaccharides. For each persistence length calculation, extended repeating unit frames were selected at regular intervals from suitable MD runs, and used to randomly create 1000 polymer chains consisting of 100 repeating units each. For these compact molecules, steric hindrance can not be neglected, as could be done for cellulose. Interaction among nonbonded segments is taken into account by putting together polysaccharide models that still contain all atoms, instead of using a simplified model with vectors derived from the disaccharide building blocks. During the construction of the polysaccharide a new unit is added only after it has been checked for occupied space violations with the already existing part of the polysaccharide. The persistence length was determined by fitting the angular correlation function

$$C(j) = < \cos \vartheta_{i,i+j} >_i = \frac{< \vec{r}_i \cdot \vec{r}_{i+j} >_i}{|\vec{r}_i| \cdot |\vec{r}_{i+j}|}$$

Results and discussion

General

The *L. helveticus* Lh59 EPS is composed of a hexasaccharide repeating unit built up from a four-residue backbone, including a galactofuranose branching point, and a lactosyl side chain (Scheme 1A) (6). For this EPS the influence of the (**F**→**E**→) lactosyl side chain on the polysaccharide conformation has been evaluated through constructing polysaccharide models from MD simulations. The *S. macedonicus* Sc136 EPS is composed of a hexasaccharide repeating unit built up from three backbone residues and a trimeric side chain (Scheme 1B) (7). For this EPS separate MD simulations have been performed for repeating units with different numbers of side-chain residues attached. In fact, the influence of the (**L**→**K**→**J**→) side chain was evaluated through a conformational analysis performed on polysaccharide models consisting of (*i*) only the backbone (**I**→**H**→**G**), (*ii*) the backbone with a side chain composed of one residue attached to the branching **H** unit (**I**→[**J**→]**H**→**G**), (*iii*) the backbone with a side chain composed of two residues attached to the branching **H** unit (**I**→[**K**→**J**→]**H**→**G**), or (*iv*) the backbone with the complete side chain of three residues attached to the branching **H** unit (**I**→[**L**→**K**→**J**→]**H**→**G**). For both EPSs, specific attention has been paid to linkages with three bonds, the (1→6) linkages for hexopyranoses and the (1→5) linkages for hexofuranoses, since these linkages, when present in the backbone, induce flexibility in the polysaccharide.

Minimum energy calculations

To explore the conformational space of both EPSs, first the global and local energy minima of the glycosidic dihedral angles of the constituting disaccharide fragments in vacuo were investigated. Relaxed energy contour maps for the φ and ψ glycosidic dihedral angles were created by means of the CHEAT force field at 10° resolution. For each map generated for the (1→3) and (1→4) linkages, the energy minima differed only in ψ and have φ essentially at one position, either 60° or –60° (Fig. 1, Lh59 EPS and Fig. 2, Sc136 EPS). The (1→5) linkages for internal furanoses and the (1→6) linkages for internal pyranoses involve one extra dihedral angle (ω) and therefore three-dimensional (3D) maps were created at 18° resolution. It appeared from the 3D maps that the low energy conformations have φ essentially at –60°, with ψ either near –60° or 120° for (1→5) linkages, or near 180°, 60°, or –60° for (1→6) linkages. The angles ω were found to be near 180°, 60°, or –60°. Hence, for all (1→5) and (1→6) linkages, three (φ, ψ) maps were generated at 10° resolution, with ω at 180°, 60°, and –60°, respectively, reflecting the gauche–trans (*gt*), gauche–gauche (*gg*), and trans–gauche (*tg*) orientations of the ω angle. Moreover, one (ψ, ω) map with φ set at –60° was calculated. The results are depicted in Fig. 1 (Lh59 EPS) and Fig. 2 (Sc136 EPS). For all minimum energy positions in the maps, conformations were minimized without constraints. For each map, the obtained glycosidic dihedral angles and the relative energies of the minima are listed in Table 1.

Adaptive umbrella sampling of the PMF

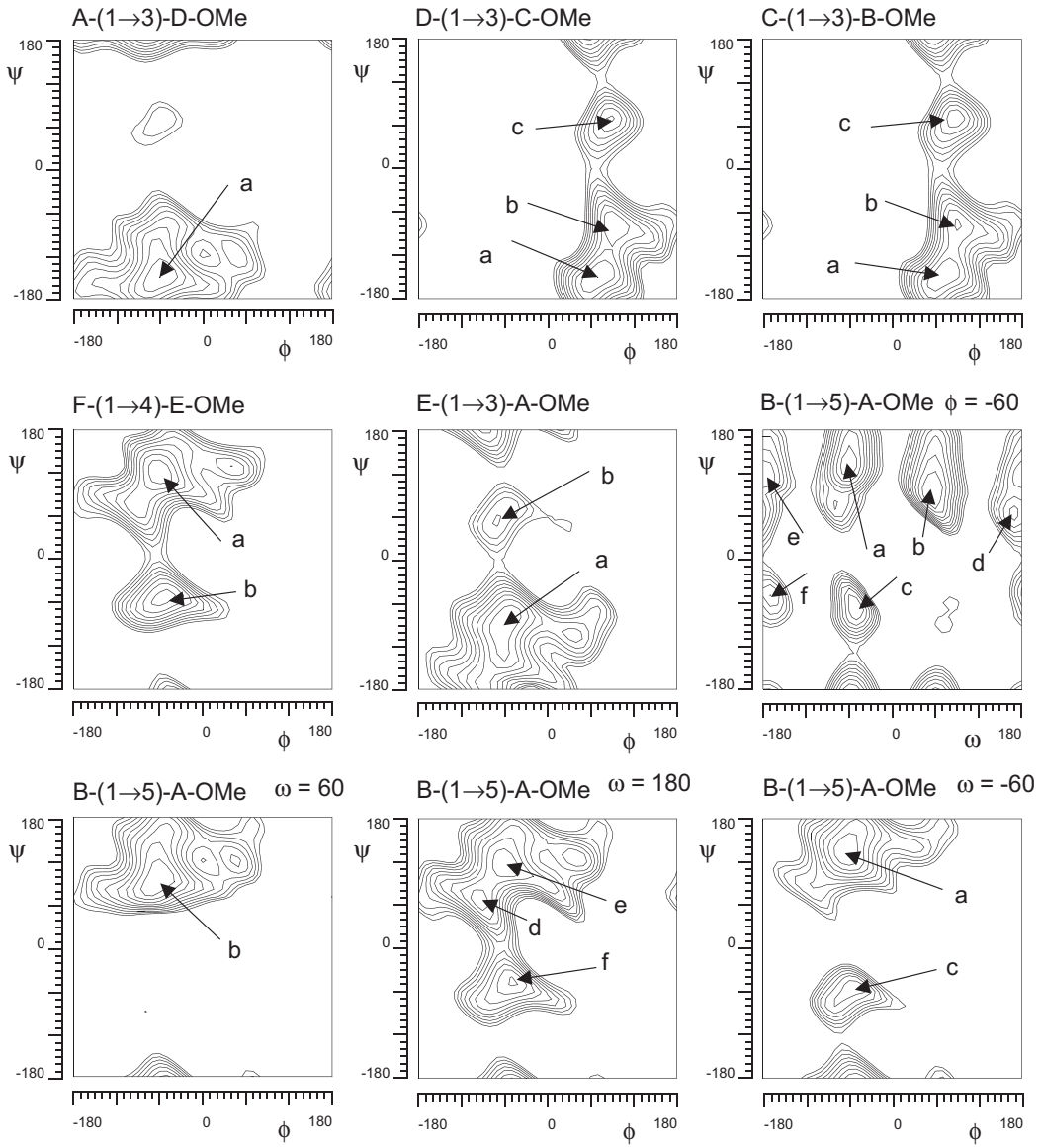
The low-energy conformations in vacuo were obtained from the calculation of energy minima. Then, the population distributions of these energy minima in aqueous solution were obtained from the PMF calculated for each low energy conformer (5). Hydrogen bonds are known to play a key role in carbohydrates (18). By explicitly including water, the influence of hydrogen bonds is modelled properly. For each set of (1→3) and (1→4) linkages, only the ψ angle spanned multiple conformational regions, while the φ angle was found to be essentially constant. Therefore, the PMF was only calculated for the ψ angles. For all AUS simulations, disaccharides were used with simulation times from 5 to 10 ns.

Lactobacillus helveticus Lh59 EPS

From the PMF calculations, the population distribution can be calculated. It turned out that the (1→3) and (1→4) linkages each adopt one single dominant conformation (Table 2). From the energy maps of the (1→5) linkage, it emerged that low energy conformations have a φ angle at –60°, and a ψ angle of 140° and sometimes –60°, whereas ω takes values of 180°, –60°, or 60°. To get the population distribution for ω, an AUS run was performed for ω with φ and ψ initially set to –60° and 140°, respectively. The calculations were performed on the tetrasaccharide fragment **B**→[**E**→]**A**→**D** to incorporate the influence of long range interactions as much as possible. The result is a population distribution for the ω angle of 180°/–60°/60° = 31/67/2 (Fig. 3A). The φ and ψ dihedral angles remained close to –70° and 140°, respectively, during a 17 ns calculation. Subsequently, a 35 ns AUS run for the ψ dihedral angle was performed, again with φ initially set at –60°. This demonstrated

© 2006 NRC Canada

Fig. 1. Energy contour plots of glycosidic dihedral angles for *L. helveticus* Lh59 EPS disaccharide fragments. For the coding system, see Scheme 1A. Contours are plotted at regular intervals of 1 kcal/mol (1 cal = 4.184 J) with respect to the global energy minimum. (*a*) Global minima; (*b*)–(*f*) Local minima.



that the ψ dihedral angle has a marked preference for values around 140° (Fig. 3B). During this run, ω visited all low-energy positions that were discovered in the energy contour maps (Fig. 4B). This was in accordance with the results of the AUS run for ω, and indicates that ψ has been adequately sampled. Note that during the AUS run of dihedral ω, the ψ dihedral angle varied between 180° and 60°, and did not sample all low-energy positions that were discovered in the energy contour maps (Fig. 4A). However, this is in agreement with the population distribution of the ψ dihedral angle.

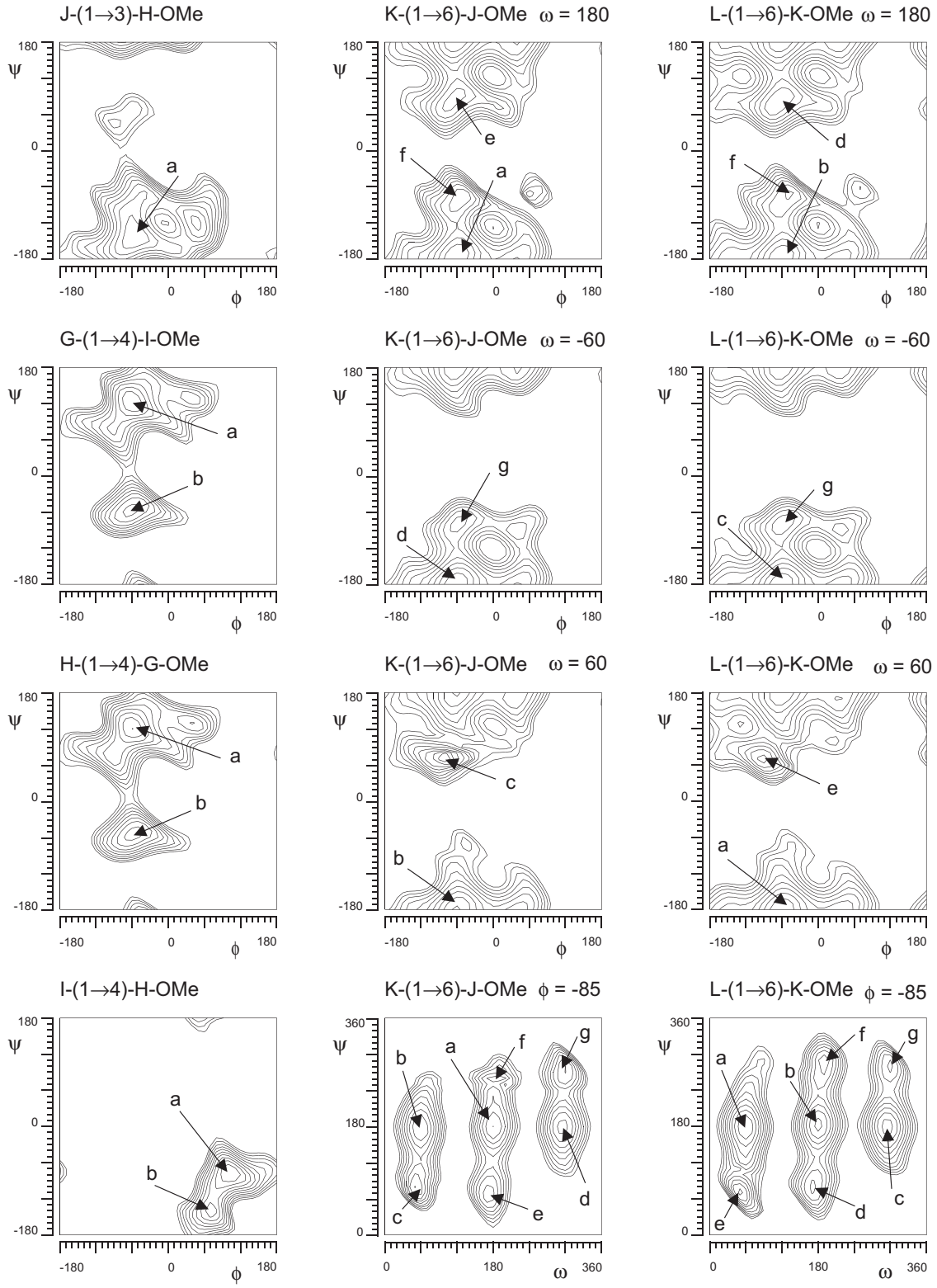
Streptococcus macedonicus Sc136 EPS

The population distributions of the (1→4) and (1→3) linkages (**G→I**, **I→H**, **H→G**, and **J→H**) showed essentially one conformational region (Table 2). From the energy maps of the (1→6) linkages, it emerged that low-energy conformations have a φ angle at –85°, a ψ angle predominantly at 180°, and ω with values of 180°, –60°, or 60°. The population distribution for ω was again obtained from AUS runs performed for the ω angle with φ and ψ initially set to –85° and 180°, respectively. The (1→6) linkages (**K→J** and **L→K**) both displayed two main conformational regions for ω of 180° and 60° (Table 2, Figs. 3C and 3D). Similarly to the (1→5) linkage in the EPS of *L. helveticus* Lh59, the ψ dihedral angle has a preference for values around 180°. Figures 4C and 4D show that ψ visited all low-energy positions during the sampling of the ω dihedral angles. The population distribution of both ω dihedral angles (Table 2) reveals that the flexibility of this polysaccharide is located mainly in the side chains.

Note that the low-energy positions and the relative energies obtained from the energy maps might deviate slightly from those resulting from the AUS method. For **B→A** (Lh59 EPS) and **L→K** (Sc136 EPS), this resulted even in different global minima.

© 2006 NRC Canada

Fig. 2. Energy contour plots of glycosidic dihedral angles for *S. macedonicus* Sc136 EPS disaccharide fragments. For the coding system, see Scheme 1B. Contours are plotted at regular intervals of 1 kcal/mol (1 cal = 4.184 J) with respect to the global energy minimum. (*a*) Global minima; (*b*)–(*g*) Local minima.



Molecular dynamics calculations

MD simulations were performed on polysaccharide fragments. The results of the AUS simulations were used to identify the most probable conformations for each fragment, which would then be used to start the MD simulations. The ω dihedral angle of the (1→5) and (1→6) linkages spanned

© 2006 NRC Canada

Table 1. Minimal energy conformations of the six constituting disaccharide fragments of *L. helveticus* Lh59 EPS and of *S. macedonicus* Sc136 EPS.

Disaccharide fragment	Minima	Dihedral angles φ	ψ	ω	ΔE^a
***L. helveticus* Lh59 EPS**					
D-(1→3)-**C**	a	59.5	–165.7		0.0
	b	87.2	–70.1		1.4
	c	84.3	68.2		3.1
C-(1→3)-**B**	a	59.8	–165.8		0.0
	b	85.5	–69.4		0.8
	c	84.3	68.8		2.3
B-(1→5)-**A**	a	–50.0	170.6	–56.8	0.0
	b	–63.6	79.1	56.4	0.6
	c	–59.4	–63.0	–53.2	1.0
	d	–83.3	60.7	173.7	3.2
	e	–53.3	103.2	179.6	5.3
	f	–52.6	–54.6	–169.2	5.8
A-(1→3)-**D**	a	–62.7	–164.8		0.0
E-(1→3)-**A**	a	–52.3	–74.2		0.0
	b	–63.6	53.2		7.4
F-(1→4)-**E**	a	–54.0	107.1		0.0
	b	–56.3	–56.0		0.2
***S. macedonicus* Sc136 EPS**					
L-(1→6)-**K**	a	–61.0	179.2	59.1	0.0
	b	–62.2	179.5	–65.5	0.3
	c	–61.8	–176.7	–179.7	1.1
	d	–72.6	73.2	169.8	1.5
	e	–86.4	73.0	52.0	2.1
	f	–47.7	–69.8	–167.0	2.7
	g	–58.0	–78.4	–60.6	3.4
K-(1→6)-**J**	a	–61.6	–175.9	–179.5	0.0
	b	–88.7	73.8	52.7	0.1
	c	–62.9	179.4	–65.8	0.5
	d	–61.1	179.8	59.0	0.7
	e	–73.2	76.5	171.8	2.1
	f	–52.0	–77.2	–168.9	2.3
	g	–56.0	–77.1	–61.0	4.1
J-(1→3)-**H**	a	–54.2	–142.0		0.0
H-(1→4)-**G**	a	–60.6	121.4		0.0
	b	–54.8	–52.3		1.6
G-(1→4)-**I**	a	–60.4	122.3		0.0
	b	–63.8	–56.5		1.6
I-(1→4)-**H**	a	102.5	–76.9		0.0
	b	71.6	–140.3		1.5

[a]Relative energy (kcal/mol).

multiple low-energy regions, making an adequate sampling during the MD calculations unlikely. Therefore, three separate simulations were started for these linkages with the most stable conformations taking ω initially set to 180°, –60°, and 60°.

Lactobacillus helveticus Lh59 EPS

All glycosidic φ and ψ dihedral angles were set at their global energy minima. The polysaccharide fragment was composed of a repeating unit (six monosaccharides) and three supplementary backbone monosaccharides (**D′→C′→B′**). These extra monosaccharides were connected to galactofuranose residue **A**, thus resulting in fragment **D→C→B→[F→E→]A→D′→C′→B′**. This was done to ensure that the branching residue **A**, likely to be a very flexible position in the backbone, might allow the sampling of conformations with long-range interactions between the side chain and the backbone of the polysaccharide. Three starting conformations were established with varying **B**-(1→5)-**A** ω angles of 180°, –60°, and 60°, respectively. For each of the starting conformations of this fragment, a 5 ns MD simulation was performed (data not shown). The MD trajectories were inspected to determine the transitions of the various dihedral angles, the formation of hydrogen bonds, and the general shape of the molecule. Trajectory-averaged dihedral angles of the MD simulations are given in Table 3. During the 5 ns

© 2006 NRC Canada

Table 2. Minimum energy values and probability distributions of the ψ and ω dihedral angles of the six constituting disaccharide fragments of *L. helveticus* Lh59 EPS and of *S. macedonicus* Sc136 EPS, as calculated by the AUS runs.

Dihedral angle		Minimum energy value (°) and population distribution (%)											
Lh59		**D**-(1→3)-**C**		**C**-(1→3)-**B**		**B**-(1→5)-**A**		**A**-(1→3)-**D**		**E**-(1→3)-**A**		**F**-(1→4)-**E**	
ψ													
		–115	(>99)	–125	(>98)	150	(>99)	–120	(>99)	–90	(>99)	110	(>99)
ω													
	(*gt*)					–170	(31)						
	(*tg*)					–75	(67)						
	(*gg*)					660	(2)						
Sc136		**L**-(1→6)-**K**		**K**-(1→6)-**J**		**J**-(1→3)-**H**		**H**-(1→4)-**G**		**G**-(1→4)-**I**		**I**-(1→4)-**H**	
ψ													
						–140	(100)	120	(>97)	120	(>97)	–120	(100)
ω													
	(*gt*)	–170	(56)	–175	(76)								
	(*tg*)	–80	(2)	–85	(2)								
	(*gg*)	60	(42)	60	(22)								

Note: Probability distributions are given in parentheses in %.

Table 3. Trajectory-averaged dihedral angles of the MD simulations of *L. helveticus* Lh59 EPS.

	Repeating unit		
	D→**C**→**B**→[**F**→**E**→]**A**→**D′**→**C′**→**B′**		
Dihedral angle	ω_{BA} = 180°	ω_{BA} = –60°	ω_{BA} = 60°
D-(1→3)-**C**			
φ	89	93	93
ψ	–135	–130	–130
C-(1→3)-**B**			
φ	95	92	94
ψ	–127	–132	–131
B-(1→5)-**A**			
φ	–77	–80	–78
ψ	142	148	135
ω	–166/–84[a]	–75/–157[b]	58
F-(1→4)-**E**			
φ	–85	–85	–86
ψ	109	109	108
E-(1→3)-**A**			
φ	–77	–78	–80
ψ	–94	–101	–98/59[c]
A-(1→3)-**D′**			
φ	–83	–86	–94
ψ	–125	–125	–132
D′-(1→3)-**C′**			
φ	92	91	91
ψ	–131	–132	–130
C′-(1→3)-**B′**			
φ	99	91	95
ψ	–123	–133	–129

[a]Transition: 180° → –60° after 2.7 ns, –60° → 180° after 2.9 ns.
[b]Transition: –60° → 180° after 2.5 ns, 180° → –60° after 2.8 ns.
[c]Transition: –100° → 60° after 4.5 ns.

simulation time, transitions observed for the ω angle were in the simulations started from conformations with ω either at 180° or –60°. For a short period of 200 ps, ω changed from 180° to –60° before returning to 180° again in the first MD simulation. Similarly, in the second MD simulation, ω changed from –60° to 180° for a short period of 300 ps and then switched back to –60°. In the third MD simulation, the glycosidic ψ angle of the disaccharide **E**→**A** showed a transition from –100° to 60° after 4.5 ns. Otherwise, it was found that the other trajectory-averaged dihedral angles were essentially the same for all MD simulations. The trajectory-averaged dihedral angles of the polysaccharide fragment were found to be similar to those calculated during the AUS simulations of the disaccharides or of the tetrasaccharide **B**→[**E**→]**A**→**D**. No major long-range hydrogen bond formation was detected in any of the MD runs. The hydrogen bonds detected for more than 7% of the simulation time were usually between neighbouring monosaccharide residues. The only exception was a hydrogen bond between **E** OH-6 and **B** OH-2 for the simulation with ω = 60°, which was observed for 50% of the simulation time. This hydrogen bond might be a stabilizing factor for this conformation. Because the conformation with ω = 60° only contributes at a level of 2% to the conformation of the polysaccharide, this was not further investigated. Conformations with ω = 180° or –60° induced a curved backbone, while ω = 60° yielded an almost straight backbone (Figs. 5A–5C).

Streptococcus macedonicus Sc136 EPS

To study the influence of the side chains on the conformational behaviour of the polysaccharide, 5 ns MD simulations were performed on polysaccharide units containing zero to three side-chain residues. The simulated molecules were relatively large fragments consisting of three repeating units. A first MD simulation was performed with a polysaccharide fragment representing the bare backbone and only consists of three times the **I**→**H**→**G** backbone unit (*i*), resulting in a fragment of nine monosaccharide residues. As expected from the energy contour maps and the AUS calculations of the PMF, all linkages were found almost exclusively in one conformational region (Table 4). This clearly showed that the backbone of the Sc136 EPS is more rigid than that of the Lh59 EPS. The second MD simulation (*ii*) was made with the fragment in (*i*) extended with one

© 2006 NRC Canada

Fig. 3. Population distributions of the (1→5) glycosidic (A) ω dihedral angle and (B) ψ dihedral angle of *L. helveticus* Lh59 EPS. Population distributions of the (1→6) glycosidic ω dihedral angles of (C) K→**J** and (D) **L**→**K** of *S. macedonicus* Sc136 EPS.

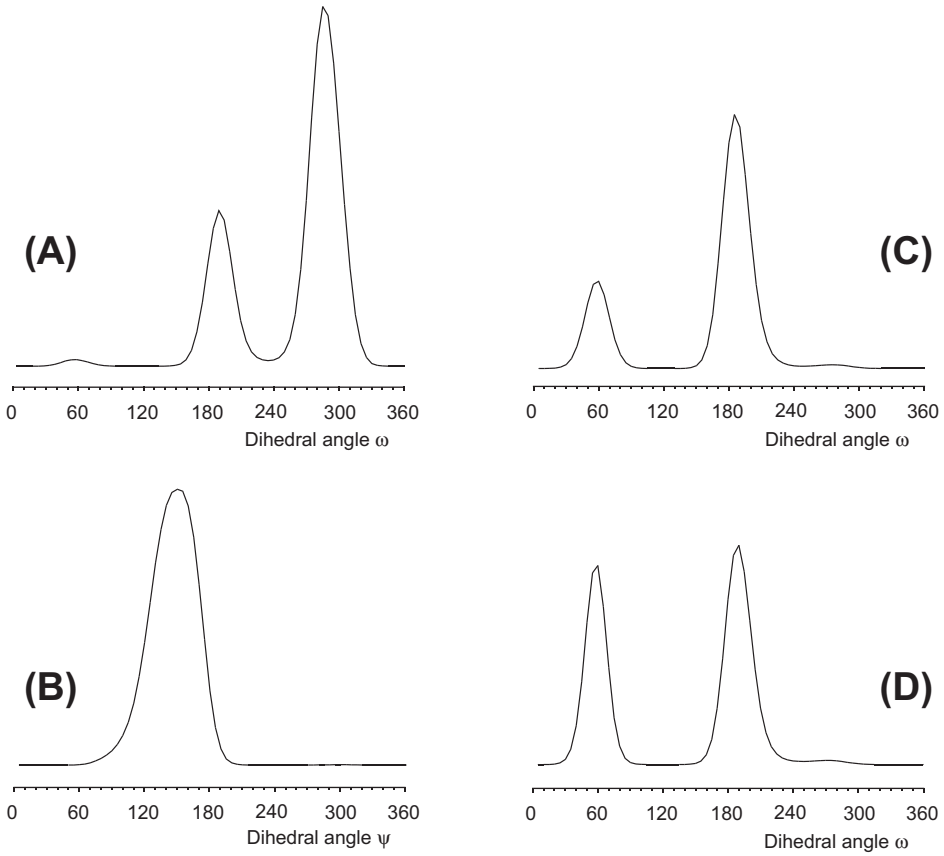
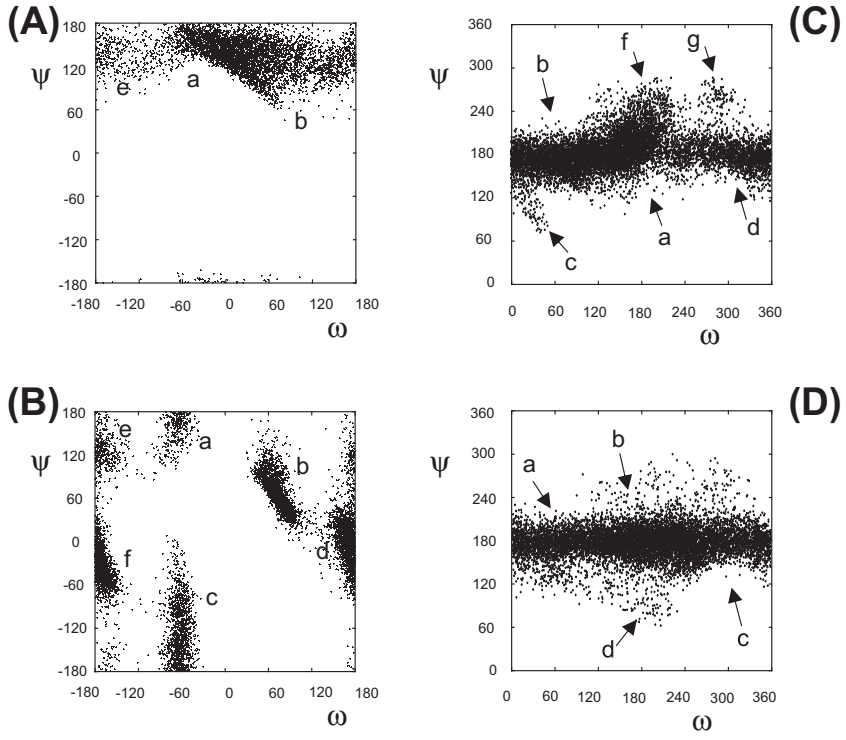
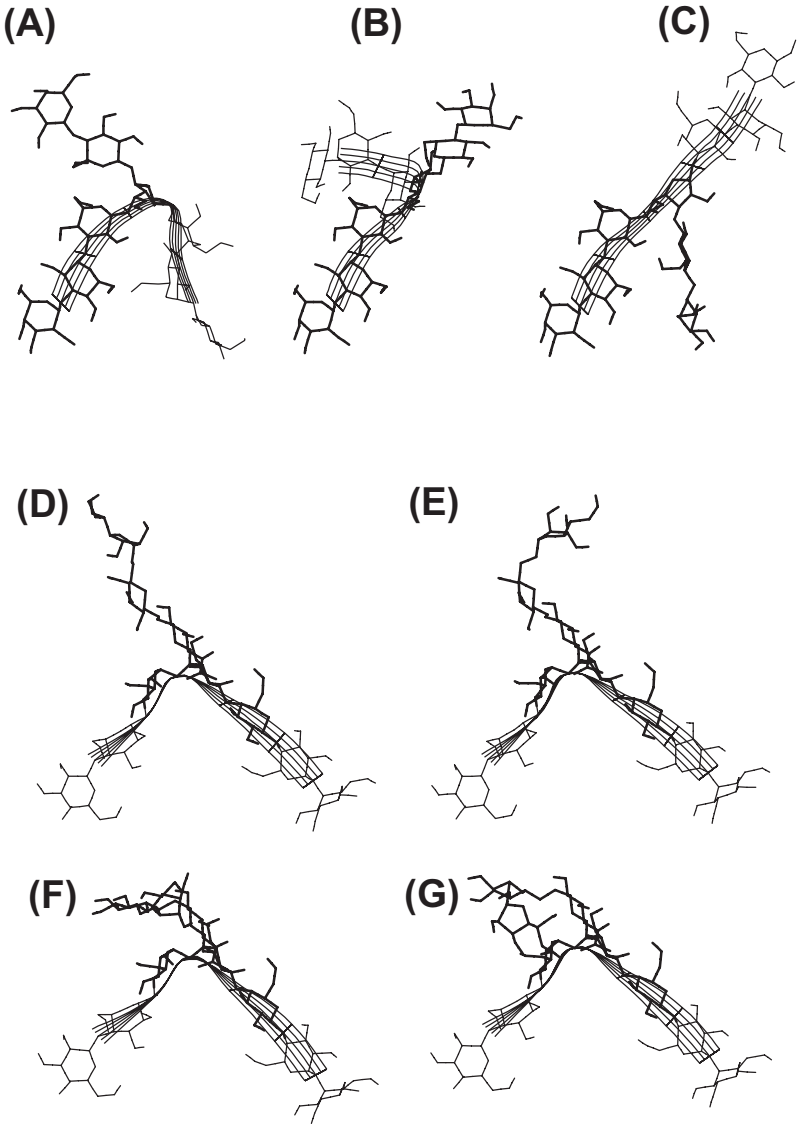


Fig. 4. Scatter plots of the (1→5) glycosidic ψ and ω dihedral angles of the AUS run of (A) the ω angle and (B) the ψ angle of *L. helveticus* Lh59 EPS. Scatter plots of the (1→6) glycosidic ω dihedral angles of the AUS runs of ω of (C) **K**→**J** and (D) **L**→**K** of *S. macedonicus* Sc136 EPS. For the coding system of the minima, see Figs. 1 and 2.



© 2006 NRC Canada

Fig. 5. The three most probable conformations of a repeating unit of *L. helveticus* Lh59 EPS, (A) $B_{180}\rightarrow$**A**, (B) $\mathbf{B}_{-60}\rightarrow$**A**, and (C) $\mathbf{B}_{60}\rightarrow$**A**. The four most probable conformations of a repeating unit of *S. macedonicus* Sc136 EPS, (D) $\mathbf{L}_{180}\rightarrow\mathbf{K}_{180}\rightarrow$**J**, (E) $\mathbf{L}_{60}\rightarrow\mathbf{K}_{180}\rightarrow$**J**, (F) $\mathbf{L}_{180}\rightarrow\mathbf{K}_{60}\rightarrow$**J**, and (G) $\mathbf{L}_{60}\rightarrow\mathbf{K}_{60}\rightarrow$**J**. A ribbon is drawn to visualize the backbone of the polysaccharides. Monosaccharide residues belonging to one repeating unit are drawn in bold.



side chain monosaccharide **J** for each repeating unit, resulting in a fragment composed of three **I**→[**J**→]**H**→**G** units. Again, each linkage was confined to its most stable conformation. For the following two MD simulations, the fragment in (*ii*) was further extended with monosaccharide **K** on each repeating unit, defining a fragment consisting of three **I**→[**K**→**J**→]**H**→**G** units. The MD simulations were performed with (*iii*) $\mathbf{I}\rightarrow[\mathbf{K}_{180}\rightarrow\mathbf{J}\rightarrow]\mathbf{H}\rightarrow\mathbf{G}$ (ω_{KJ} = 180°) and (*iv*) $\mathbf{I}\rightarrow[\mathbf{K}_{60}\rightarrow\mathbf{J}\rightarrow]\mathbf{H}\rightarrow\mathbf{G}$ (ω_{KJ} = 60°). A simulation with ω_{KJ} = –60° was not considered because of the low probability (2%) of the associated conformation. The conformations of the two "external" repeating units (numbered 1 and 3) were chosen to be the same as the central unit (numbered 2). Only during the first MD simulation (*iii*) a transition did occur. The ω_{KJ} angle (middle unit) switched from 180° to –60° and back to 180° after 400 ps. In the last series of MD simulations monosaccharide **L** was added, completing the repeating unit **I**→[**L**→**K**→**J**→]**H**→**G**. Four different MD simulations were performed with (*v*) $\mathbf{I}\rightarrow[\mathbf{L}_{180}\rightarrow\mathbf{K}_{180}\rightarrow\mathbf{J}\rightarrow]\mathbf{H}\rightarrow\mathbf{G}$ (ω_{LK} = 180°, ω_{KJ} = 180°), (*vi*) $\mathbf{I}\rightarrow[\mathbf{L}_{60}\rightarrow\mathbf{K}_{180}\rightarrow\mathbf{J}\rightarrow]\mathbf{H}\rightarrow\mathbf{G}$ (ω_{LK} = 60°, ω_{KJ} = 180°), (*vii*) $\mathbf{I}\rightarrow[\mathbf{L}_{180}\rightarrow\mathbf{K}_{60}\rightarrow\mathbf{J}\rightarrow]\mathbf{H}\rightarrow\mathbf{G}$ (ω_{LK} = 180°, ω_{KJ} = 60°), and (*viii*) $\mathbf{I}\rightarrow[\mathbf{L}_{60}\rightarrow\mathbf{K}_{60}\rightarrow\mathbf{J}\rightarrow]\mathbf{H}\rightarrow\mathbf{G}$ (ω_{LK} = 60°, ω_{KJ} = 60°). The four different conformations for each repeating unit are shown in Figs. 5D–5G. In MD simulation (*v*), the ω_{KJ} angle (middle unit) went from 180° to –100° and back to 180° after 3 ns. In the same simulation, the ω_{LK} (first unit) went from 180° to 60° after 2 ns, while ω_{LK} (middle unit) went from 180° to 60° after 3 ns. During MD simulation (*vi*), all ω dihedral angles kept the initial conformation during the simulation. In MD simulation (*vii*), the ω_{KJ} angle (first unit) went from 60° to 180° after 500 ps. A simulation (*viii*) with ω_{LK} = 60° and ω_{KJ} = 60° was started three times, but within a few ps, ω_{LK} or ω_{KJ} (in the middle unit) jumped from 60° to 180°. It seems that ω = 60° for

© 2006 NRC Canada

Table 4. Trajectory-averaged dihedral angles of the 5 ns MD simulations of the central repeating unit in fragments comprising three repeating units of *S. macedonicus* Sc136 EPS.

	Repeating unit Simulation						
	I→H→G	**I→[J→]H→G**	**I→[K→J→]H→G**		**I→[L→K→J→]H→G**		
Dihedral angle	(*i*)	(*ii*)	(*iii*)	(*iv*)	(*v*)	(*vi*)	(*vii*)
I-(1→4)-**H**							
φ	106	99	100	113	94	99	118
ψ	–99	–108	–109	–96	–116	–111	–96
H-(1→4)-**G**							
φ	–78	–82	–79	–81	–84	–85	–79
ψ	109	111	112	110	110	108	113
G-(1→4)-**I**							
φ	–87	–81	–86	–91	–82	–86	–83
ψ	110	109	108	108	114	107	108
J-(1→3)-**H**							
φ		–91	–92	–91	–98	–98	–92
ψ		–127	–131	–134	–138	–138	–134
K-(1→6)-**J**							
φ			–84	–85	–84	–84	–83
ψ			–167	174	–173/–109[a]	–159	176
ω			–164[b]	59	–170	–172	60
L-(1→6)-**K**							
φ					–88	–87	–85
ψ					171	172	180
ω					–168/58[c]	58	–168

[a]Transition: 180° → –100° after 10 ps, –100° → 180° after 3 ns.
[b]Transition: 180° → –60° after 3.2 ns, –60° → 180° after 3.6 ns.
[c]Transition: 180° → 60° after 3 ns.

both (1→6) linkages does not result in a stable conformation. Therefore, this conformation is not used in the rest of the work. Figure 5 shows that the **H→G** and **G→I** segments have a linear conformation, while the **I→H** segment introduces a turn in the backbone. The **J→H** segment points away from the backbone into the solution.

Constructing polysaccharide models

The data generated by the MD simulations were used to construct a number of polysaccharide models with lengths between 10 and 500 repeating units. To this end, configurations were selected randomly from the MD runs choosing suitable conformations based on their statistical representation in the runs. The chosen repeating unit was then attached to the "growing" chain by a homemade polysaccharide-building program, which checked for space-filling constraints and prevented van der Waals clashes. Although the polysaccharide models themselves are grown in vacuo, the models do represent polysaccharides in aqueous solution because the applied building blocks are directly transferred from MD simulations in the presence of water. Since the interaction between water and the saccharides is very dynamic — no "sticky" water molecules have been observed during the MD simulations — no persistent influence is expected on the spatial arrangement of the building blocks.

Lactobacillus helveticus Lh59 EPS

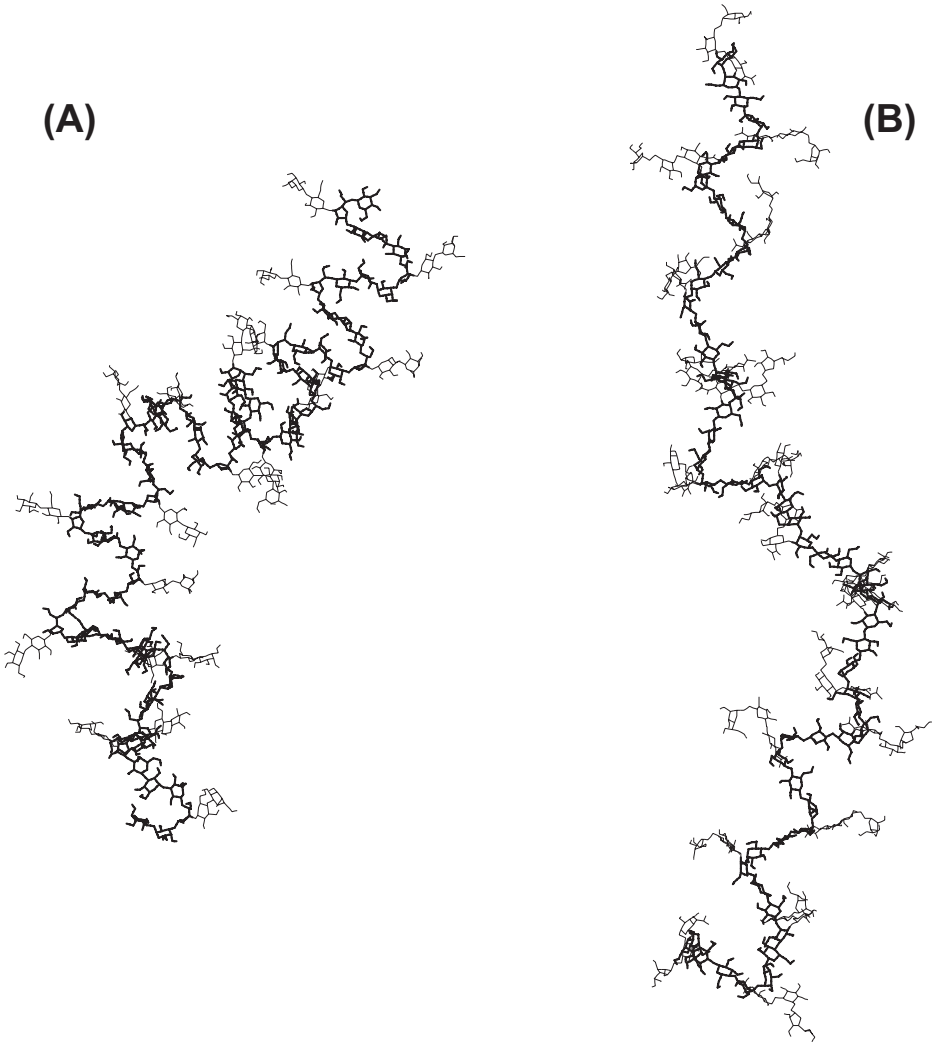
Configurations were selected randomly from the MD runs of **D→C→B→[F→E→]A→D′→C′→B′** with ω = 180°/–60°/60° in a ratio of 31:67:2. Connections were made by the attachment of residue **C′** of one configuration to residue **B** of the next configuration, in addition to the removal of redundant residues (**B′**, **D**, and **C**). The newly attached fragments were checked for steric overlap with the already present part of the polysaccharide and, if needed, replaced with other fragments until no overlap occurred. Visual inspection showed a flexible structure with a secondary conformation presenting zigzags and a random coil tertiary conformation for *L. helveticus* Lh59 EPS. The galactofuranose units induced a twist in the backbone and all lactosyl side chains were extended into the solvent. A model that demonstrates the general shape of the polysaccharide is depicted in Fig. 6A.

Streptococcus macedonicus Sc136 EPS

Configurations were again selected randomly from appropriate MD runs. Connections were made by attaching residue **G** of one configuration to residue **I** of the next configuration, and removing the redundant first and last repeating units. Again, newly attached fragments were checked for steric overlap with the already present part of the polysaccharide and, if needed, replaced with other fragments until no overlap occurred. Visual inspection shows a secondary conformation that consisted of a stretched β-D-Gal*p*-(1→4)-β-D-Glc*p*-(1→4)-α-D-Glc*p* part, and then a curve where α-D-Glc*p* connects to β-D-Gal*p*. This leads to an overall "random coil" spatial conformation. The side chains were found to be very flexible, but did not seem to influence the secondary conformation. Therefore, the shape of *S. mace-*

© 2006 NRC Canada

Fig. 6. Polysaccharide models consisting of 20 repeating units. The monosaccharide residues that comprise the backbone of the polysaccharide are drawn in bold. (A) Model of *L. helveticus* Lh59 EPS. (B) Model of *S. macedonicus* Sc136 EPS.



donicus EPS is mainly determined by the rigid backbone. A model that demonstrates the general shape of the polysaccharide is depicted in Fig. 6B.

Persistence length calculations

Finally, the stiffness of the polysaccharides was estimated by calculating the persistence length L_p (17), which was statistically derived from 1000 generated polysaccharide structures with a length of 100 repeating units each. The results are compiled in Table 5.

The persistence length is a measure for the "extensiveness" of a polysaccharide. The occurrence of disaccharide linkages with multiple (and populated) glycosidic conformations has enormous lowering effects on the L_p. This almost always applies to (1–6) linkages. Similar effects are observable for variations in the carbohydrate ring structure as is most prominent for furanose rings. Smaller effects are caused by the natural variation between snapshots of a "single" conformation. Here the width of the glycosidic potential energy wells plays a role. The presence of steric effects (e.g., induced by side chains) will narrow these potential energy wells resulting in an increased persistence length.

Lactobacillus helveticus Lh59 EPS

Calculation of the L_p yielded a value of 4.5 nm. The EPS turned out to be flexible and compact. By comparison, the L_p of the very stiff polysaccharide cellulose was estimated to be 14 nm (17). Steric interactions were also shown to have a considerable influence on the L_p value as demonstrated by calculations of the L_p without checking for steric overlap: a value of 2.2 nm was found, being a reduction of the L_p value by a factor of two. In addition, L_p calculations were performed on polysaccharides where the side chain had been either shortened or removed. Note that this was done with configurations from the MD simulations of the intact side chain. The side chain was only been trimmed prior to the building process. Thus, the effect on the L_p only reflects the steric hindrance during the construction of the polysaccharides. Nevertheless, as the side chains did not show many interactions with the backbone during the MD simulations, even for "long" side chains, the assumption was made that this approximation was in essence valid.

Streptococcus macedonicus Sc136 EPS

All models, except for the bare backbone (**I→H→G**),

© 2006 NRC Canada

Table 5. Persistence length (L_p) and average length of the repeating unit (l) of *L. helveticus* Lh59 EPS and *S. macedonicus* Sc139 EPS that were built from tri-, tetra-, penta-, and hexa-meric repeating units from MD simulations in water.

Repeating unit	L_p (nm)	l (nm)
Lh59		
D→C→B→[F→E→]A	4.5	1.05
D→C→B→[E→]A	4.2	1.05
D→C→B→A	3.7	1.05
D→C→B→[F→E→]A[a]	2.2	1.04
Sc136		
I→H→G	6.5	1.00
I→[J→]H→G	8.9	1.13
I→[K_{180}→J→]H→G	10.5	1.08
I→[K_{60}→J→]H→G	9.5	0.97
I→[K→J→]H→G	8.7	1.06
I→[L_{180}→K_{180}→J]H→G	10.1	1.19
I→[L_{60}→K_{180}→J→]H→G	8.1	1.12
I→[L_{180}→K_{60}→J→]H→G	9.3	1.07
I→[L→K→J→]H→G	8.5	1.14

Note: When an exclusive conformational region is used for the **K**-(1→6)-**J** and **L**-(1→6)-**K** glycosidic linkages, this is indicated by 180 or 60.

[a]No excluded volume effects were taken into account.

showed a similar L_p of ~8.7 nm. For **I→[J→]H→G**, **I→[K→J→]H→G**, and **I→[L→K→J→]H→G**, the persistence lengths were found to be 8.9, 8.7, and 8.5 nm, respectively. The bare backbone (**I→H→G**) yielded an L_p of 6.5 nm, thereby indicating a higher flexibility. From these results it can be deduced that only the first side-chain residue (**J**) influences the L_p of the polysaccharide in such a way as to strech the polysaccharide, a finding that can be explained by the position of **J** in close contact with the **I→H→G** backbone.

Conclusions

The conformational analysis method used in this paper allowed one to explicitly include the key influence of water solvation. The secondary structures of both polysaccharides studied showed a twisted backbone with side chains extending in the solvent. The main flexibility was found to be located in the intrinsically flexible (1→5) or (1→6) linkages, as well as in the furanose ring form. For *L. helveticus* Lh59 EPS, this flexibility is located in the backbone, resulting in a more compact overall shape. Analysis of the polysaccharide models showed no interactions between side chains and backbone except for the linkage point, and generally no long-range interaction among backbone units. Therefore, for the polysaccharides studied, the conclusion is that the extrapolation of small oligosaccharide fragments to polysaccharides was well-justified.

The general shape of the polysaccharides was found to be compact. This was expressed by the values obtained for the calculated persistence length. In this study, we have taken into account only the most probable conformations of the glycosidic linkages. Neglecting the less-occurring conformations may have had some influence on the calculated persistence length, since some of those minor conformations could introduce sharp bends in the backbone of the polysaccharide. Nevertheless, the dominant conformations used for the construction of the polysaccharide models and the sizes of the fragments used were large enough to include all intermonomer interactions.

The conformation of the side chains was shown to have only a small influence on the flexibility and the persistence length of the polysaccharide. Only the first residue of the side chain, linked directly to the backbone, had a clear influence. It reduced the flexibility of the backbone and made the chain stiffer. The backbone glycosidic linkages largely determined the overall shapes of the polysaccharides. The fully stretched parts were stemming from the β-D-Hex*p*-(1→4) elements, similarly as is the case for the β-D-Glc*p*-(1→4) elements in cellulose. The structural elements, α-D-Hex*p*-(1→4) and α-D-Hex*p*-(1→3), introduced bends in the backbone, thereby reducing the calculated persistence length. As the distance O4—O1 in a 4-substituted monosaccharide is longer than the distance O3—O1 in a 3-substituted monosaccharide, (1→4) linkages usually produce a longer residue length (l) than (1→3) linkages. Backbone three-bond linkages (φ, ψ, and ω) gave rise to a large variation in conformations, enhancing the flexibility and giving shorter persistence lengths.

Acknowledgments

SJFV acknowledges the constant support of Dr. J.-R. Neeser (Nestlé Switzerland).

References

1. L. De Vuyst, F. De Vin, F. Vaningelgem, and B. Degeest. Int. Dairy J. **11**, 687 (2001).
2. A.P. Laws and V.M. Marshall. Int. Dairy J. **11**, 709 (2001).
3. P. Duboc and B. Mollet. Int. Dairy J. **11**, 759 (2001).
4. E.J. Faber, J.A. van Kuik, J.P. Kamerling, and J.F.G. Vliegenthart. Biopolymers, **63**, 66 (2002).
5. R.W.W. Hooft, B.P. van Eijck, and J. Kroon. J. Chem. Phys. **97**, 6690 (1992).
6. F. Stingele, J. Lemoine, and J.-R. Neeser. Carbohydr. Res. **302**, 197 (1997).
7. S.J.F. Vincent, E.J. Faber, J.-R. Neeser, F. Stingele, and J.P. Kamerling. Glycobiology, **11**, 131 (2001).
8. J.W. Ponder. TINKER: Software tools for molecular design. Washington University School of Medicine, St. Louis, Missouri. 2000.
9. P.D.J. Grootenhuis and C.A.G. Haasnoot. Mol. Simul. **10**, 75 (1993).
10. M.L.C.E. Kouwijzer and P.D.J. Grootenhuis. J. Phys. Chem. **99**, 13426 (1995).
11. W.F. van Gunsteren and H.J.C. Berendsen. GROMOS-87: Groningen molecular simulation program package. University of Groningen, The Netherlands. 1987.
12. S.A.H. Spieser, J.A. van Kuik, L.M.J. Kroon-Batenburg, and J. Kroon. Carbohydr. Res. **322**, 264 (1999).
13. H.J.C. Berendsen, J.R. Grigera, and T.P.J. Straatsma. Phys. Chem. **91**, 6269 (1987).
14. J.-P. Ryckaert, G. Giccotti, and H.J.C. Berendsen. Comput. Phys. **23**, 327 (1977).
15. H.J.C. Berendsen, J.P.M. Postma, W.F. van Gunsteren, A. DiNola, and J.R. Haak. J. Chem. Phys. **81**, 3684 (1984).

© 2006 NRC Canada

16. IUPAC-IUB Joint Commission on Biochemical Nomenclature. Eur. J. Biochem. **131**, 5 (1983).
17. L.M.J. Kroon-Batenburg, P.H. Kruiskamp, J.F.G. Vliegenthart, and J. Kroon. J. Phys. Chem. **B101**, 8454 (1997).
18. K.N. Kirschner and R.J. Woods. Proc. Natl. Acad. Sci. U.S.A. **98**, 10541 (2001).

© 2006 NRC Canada

A concise synthesis of α-D-ribofuranosyl alkylphosphonates — Putative substrate intermediates for the carbon–phosphorous lyase system[1]

Yan Luo and David L. Zechel

Abstract: Carbon–phosphorous lyase is a multienzyme system found in many species of bacteria that is distinguished by its ability to hydrolyze a broad array of unactivated alkylphosphonates. α-D-Ribofuranosyl alkylphosphonates are potential metabolic intermediates generated by the carbon–phosphorous lyase pathway. Here we describe a facile synthesis of α-D-ribofuranosyl alkylphosphonates using β-D-ribofuranosyl trichloracetimidate as a glycosyl donor.

Key words: carbon–phosphorous lyase, *phn* operon, phnN, phosphonates, glycosyl trichloroacetimidate donor, α-D-ribofuranosyl ethylphosphonate.

Résumé : La lyase carbone–phosphore est un système multienzyme qu'on retrouve dans plusieurs espèces et qui se distingue par sa facilité à hydrolyser une grande variété d'alkylphosphonates qui ne sont pas activés. Les alkylphosphonates de α-D-ribofuranosyle sont des intermédiaires métaboliques potentiels générés par la voie réactionnelle de la lyase carbone–phosphore. Dans ce travail, on décrit une méthode facile de synthèse d'alkylphosphonates de α-D-ribofuranosyle utilizant le trichloroacétimidate de β-D-ribofuranosyle comme donneur de glycosyle.

Mots clés : lyase carbone–phosphore, *phn* opéron, phnN, phosphonates, trichloroacétimidate de glycosyle comme donneur, éthylphosphonate de α-D-ribofuranosyle.

Introduction

Phosphate is a fundamental functional group in biology as exemplified by its many structural, signalling, and energy storage roles. Organophosphonates are characterized by a highly stable carbon–phosphorous (CP) bond that is comparable in energy to a carbon–carbon bond (1). In addition to other reduced forms of phosphate such as phosphite and hypophosphite, organophosphonates are significant contributors to the global phosphate pool. They may well have served as the original source of water soluble phosphorous for the assembly of biological precursors on prebiotic earth, as inorganic phosphate would have been largely inaccessible as the mineral apatite (2). Although anthropogenic generation of organophosphonates is considerable (1), natural production is also substantial. The biosynthesis of the majority of organophosphonate natural products begins with the rearrangement of phosphenolpyruvate to phosphonopyruvate by phosphoenolpyruvate mutase (3). From this precursor, *Streptomyces* species biosynthesize a number of bioactive phosphonates, including the antibiotic fosfomycin and the herbicide bialaphos (4). 2-Amino-3-phosphonopropionic acid and 2-aminoethylphosphonic acid are the most widely distributed biogenic organophosphonates, occurring as constituents of lipids, proteins, and polysaccharides in virtually all organisms, including man (5). Due to the global abundance of organophosphonates, bacteria have also evolved a number of strategies to cleave the CP bond to produce inorganic phosphate when the latter is scarce in the environment (1, 6). At present, four distinct CP bond-cleaving activities are known. Three of these activities, comprised of phosphonoacetaldehyde hydrolase (7), phosphonopyruvate hydrolase, (8) and phosphonoacetate hydrolase (9), share a β-carbonyl group as a feature of their respective substrates (**1** in Scheme 1). A mechanism for the cleavage of the CP bond in these substrates can be envisioned as direct nucleophilic attack by water or an enzyme residue on phosphorous, displacing a carbanion to form an enzyme stabilized enolate. In the case of phosphonoacetaldehyde hydrolase, the substrate β-carbonyl is activated as a Schiff base (**2**) followed by attack of a carboxylate nucleophile to form an acyl phosphate intermediate (**3**); hydrolysis forms acetaldehyde (**4**) and inorganic phosphate (7).

Unlike phosphonoacetaldehyde hydrolase, CP-lyase is a multienzyme system that is distinguished by its ability to cleave a broad array of "unactivated" alkylphosphonates (**5**) yielding alkanes (**7**) and inorganic phosphate as products (Scheme 2) (10). In *Escherichia coli*, the *phn* operon encoding CP-lyase consists of 14 genes (*phnCDEFGHIJKLMNOP*) (11, 12); mutational and sequence analysis of the *phn* operon in whole cell metabolic studies has shown that *phnCDE* encodes a phosphonate transport system and *phnG–phnP* en-

Received 1 September 2005. Published on the NRC Research Press Web site at http://canjchem.nrc.ca on 17 May 2006.

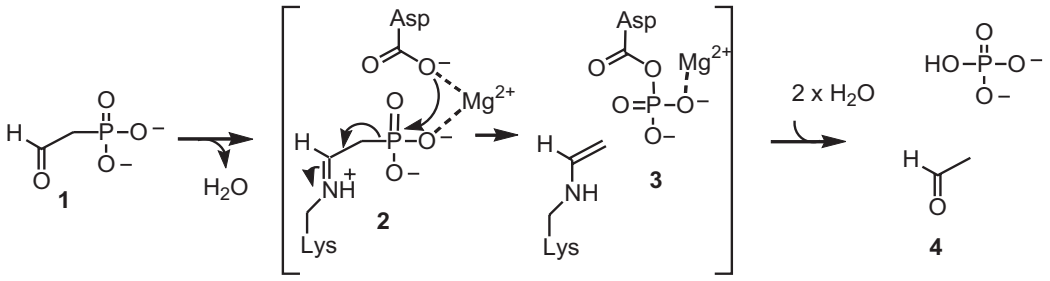
Y. Luo and D.L. Zechel.[2] Department of Chemistry, Chernoff Hall, Queen's University, Kingston, ON K7L 3N6, Canada.

[1]This article is part of a Special Issue dedicated to Professor Walter A. Szarek.

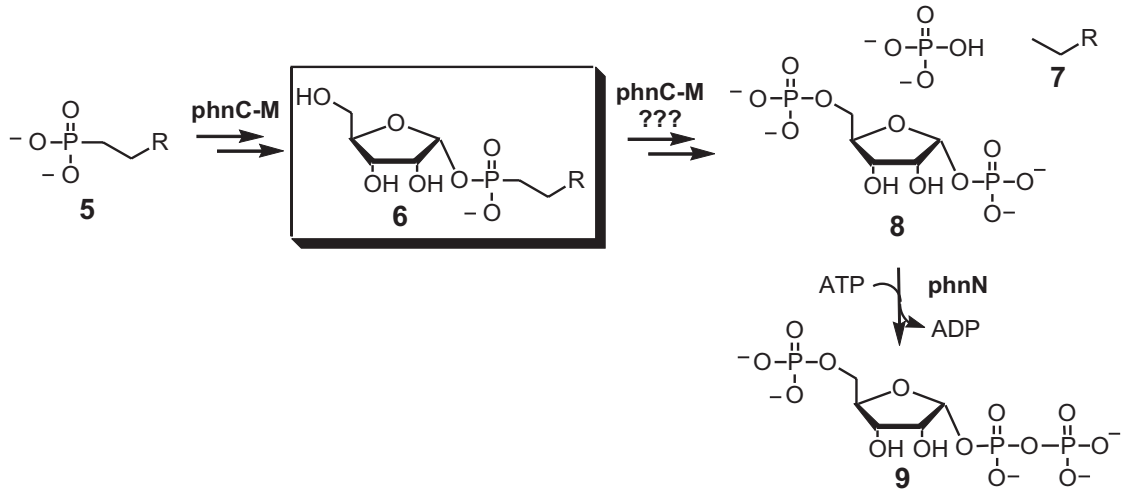
[2]Corresponding author (e-mail: dlzechel@chem.queensu.ca).

 doi:10.1139/V06-038 © 2006 NRC Canada

Scheme 1. Cleavage of an "activated" carbon–phosphorous bond by phosphonoacetaldehyde hydrolase (7).



Scheme 2. A hypothetical reaction pathway depicting the cleavage of "unactivated" alkylphosphonates by CP-lyase utilizing **6** as an intermediate. The subsequent phosphorylation reaction by phnN produces a precursor (**9**) for NADH biosynthesis (14).



codes enzymes that are required for CP bond cleavage and transcription regulation (13). The sequences of several of these enzymes are unique, yielding no insight via homology into their possible function. An in vitro reconstruction of CP-lyase activity has not yet been achieved, further hampering functional assignments. This is primarily due to the difficulty in expressing several of these enzymes, some of which appear to be associated with the membrane of bacterial cells (13). The only in vitro reaction assigned to a *phn* protein is that of phnN, which was recently shown to be an ATP-dependent kinase, phosphorylating 5-phospho-α-D-ribofuranosyl phosphate (**8**) to yield 5-phospho-α-D-ribofuranosyl diphosphate (PRPP, **9**), a precursor in the biosynthesis of the essential cofactor NAD (14). Intriguingly, α-D-ribofuranosyl ethylphosphonate (**6**) was observed to reach significant concentrations in the culture medium when *E. coli* with a mutated, yet partly functional *phn* operon subsisted on ethylphosphonate. Free phosphate was not produced. By contrast, a mutant strain of *E. coli* with an inoperative *phn* operon did not produce **6** when fed ethylphosphonate, indicating that the some of the CP-lyase enzymes were likely involved in its biosynthesis (15). The substrate specificity of phnN and the biosynthesis of **6** by CP-lyase enzymes strongly suggest that a *phn* enzyme can cleave the CP bond of **6** (or a derivative) and in doing so support NAD biosynthesis. The chemical mechanism of CP-lyase is of great interest, not only for its ability to cleave the remarkably stable carbon–phosphorous bond, but also for the development of environmental remediation catalysts that will degrade phosphonates, such as nerve agents and herbicides. As part of our current program in characterizing the functions and reactions of individual CP-lyase enzymes, we have synthesized **6** and other phosphonate analogues as putative CP-lyase substrate intermediates.

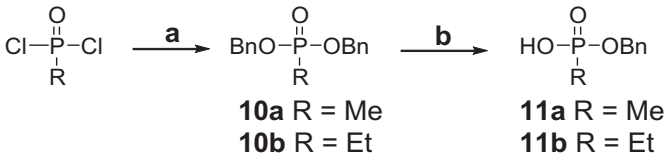
Results and discussion

A major challenge facing the stereoselective synthesis of α-D-ribofuranosyl phosphates is the reactivity and 1,2-cis arrangement of the glycosidic linkage (the product itself is a glycosyl donor (16)). The diphosphate **8** has been synthesized enzymatically (17) by direct condensation of the per-O-acetylated sugar with phosphoric acid (18, 19) or by reaction of the ribofuranosyl bromide with dibenzyl phosphate (20, 21). A synthetically useful enzymatic route to **6** is not yet possible, and the current synthetic methods suffer from low yields or the use of toxic and difficult to handle reagents (e.g., HBr gas). We report that β-D-ribofuranosyl trichloroacetimidate serves as a high yielding and stereoselective donor for the synthesis of **6**.

The required glycosyl acceptors (**11a** and **11b**) were conveniently prepared in two steps (Scheme 3). The corresponding phosphonochloridates were reacted with benzyl alcohol to yield dibenzyl methylphosphonate (**10a**) and dibenzyl ethylphosphonate (**10b**) (22). Refluxing with DABCO in anhydrous toluene afforded mono-protected **11a** and **11b** quan-

© 2006 NRC Canada

Scheme 3. Reagents and conditions: (*a*) BnOH, toluene–pyridine, 0 °C to RT, 5 h; (*b*) DABCO, toluene, reflux, 3 h.



titatively (23). The trichloroacetimidate glycosyl donor **12** was prepared from methyl 2,3,5-tri-*O*-benzyl-α-D-ribofuranoside after solvolysis in 5% aq. HCl – dioxane and treatment of the free anomeric hydroxyl with trichloroacetonitrile and potassium carbonate in dry dichloromethane (Scheme 4). Phosphonic acids **11a** and **11b** were reacted with the donor **12** in dry dichloromethane in the presence of 4 Å molecular sieves to produce a 2:1 α/β mixture of the ribofuranosyl alkylphosphonates **14** and **15** in 60% yield. Reaction with dibenzyl phosphoric acid produced a similar mixture of the corresponding ribofuranosyl phosphate (**13**). An attempt to increase the α/β ratio by reducing the reaction temperature to –20 °C was unsuccessful. However, the β anomers readily isomerized to the thermodynamically stable α anomer in the presence of $BF_3{\cdot}Et_2O$ and 2-chloropyridine. The β anomer was notably unstable, as we observed that **13**β decomposed overnight at room temperature. The stereochemistry of the α anomer was assigned based on NOESY experiments: the signal corresponding to H-1 (δ 6.09) exhibits an NOE with both H-2 and H-3, indicating that H-1, H-2, and H-3 are on the same side of the ribofuranose ring. Compounds **13**α, **14**α, and **15**α were deprotected by catalytic hydrogenolysis to afford the desired α-D-ribofuranosyl phosphate (**16**) and alkylphosphonates (**17** and **18**) in quantitative yield. These were subsequently converted to the triethylammonium salts.

The putative substrate intermediates (**17** and **18**) are very likely to be crucial for assigning the functions of CP-lyase proteins as they are all, or in part, produced in a soluble form suitable for in vitro studies. The stereoselective and high yielding synthetic route described here is considerably more facile than previously reported methods. We can now readily synthesize a wide array of putative CP-lyase intermediates that can also include radiolabels, chromaphores, or fluorophores. Of particular interest is the substrate specificity of the CP-lyase enzyme that ultimately cleaves the CP bond: Does this enzyme cleave simple alkylphosphonates or only glycosylated derivatives like **6** or both? Likewise, which CP-lyase enzyme is responsible for forming **6**? As the ultimate CP bond cleaving mechanism is suspected to be radical based (10), we can also readily incorporate radical stabilizing functionalities (thio, allyl, etc.) into **17** and **18** to serve as radical probes. Our current success in producing soluble CP-lyase proteins will benefit from access to these substrates and will be the topic of future reports.

Experimental

General

Solvents were distilled under dry nitrogen by standard methods (THF from Na/benzophenone and CH_2Cl_2 from CaH_2) prior to use. All commercially available reagents were used without further purification. All reactions were performed under a dry nitrogen atmosphere. ^{1}H NMR spectra was recorded on a 400 MHz Bruker spectrometer using $CDCl_3$ (δ 7.26 ppm), MeOD (δ 3.35 ppm), and D_2O (δ 4.81 ppm) as internal references. ^{13}C NMR and ^{31}P NMR spectra were recorded at 100.6 and 162.0 MHz, respectively. ^{31}P NMR spectra are reported relative to phosphate. Mass spectra were determined by electrospray ionization (ESI) or fast atom bombardment (FAB) mass spectroscopy. Analytical TLC was perfomed on Silicycle F_{254} silica gel plates. Visualization was performed under UV light or by staining with ceric ammonium molybdate. Flash chromatography was performed using Silicycle (40–63 μm) silica gel.

Synthesis

Dibenzyl ethylphosphonate (10b)

A suspension of ethylphosphonylchloridate (1 mL, 9.4 mmol) was stirred rapidly in dry toluene (5 mL) at 0 °C. A mixture of dry benzyl alcohol (2 mL, 18.8 mmol) and dry pyridine (1.5 mL, 18.8 mmol) was added over 90 min while the temperature was maintained. After the addition was complete, the reaction was allowed to reach room temperature and stirred for a further 3 h. The solid product, dibenzyl ethylphosphonate (**10b**), was removed by filtration and washed with toluene, 2 mol/L NaOH, water, then dried over Na_2SO_4 and concentrated in vacuo. Crude **10b** was used in the next reaction without further purification. Data for **10b**: ^{1}H NMR (400 MHz, $CDCl_3$) δ: 7.4–7.3 (m, 10H, aromatic), 5.08 (m, 2H, OCH_2Ph), 4.98 (m, 2H, OCH_2Ph), 1.76 (m, 2H, CH_2), 1.22 (m, 3H, CH_3). ^{31}P NMR ($CDCl_3$) δ: 35, 37.

Benzyl ethylphosphonic acid (11b)

To a stirred solution of crude **10b** (3.0 g, 10 mmol) in dry toluene (20 mL) was added DABCO (1.12 g, 10 mmol) under a nitrogen atmosphere. The reaction mixture was refluxed for 3 h before the solvent was removed in vacuo and the residue was redissolved in 5% aq. HCl. The aqueous layer was extracted with ethyl acetate, dried over Na_2SO_4, then evaporated under reduced pressure to yield benzyl ethylphosphonic acid (**11b**) (1.87 g, 99% calcd. from ethylphosphonylchloridate). Data for **11b**: ^{1}H NMR (400 MHz, $CDCl_3$) δ: 5.07 (m, 2H, OCH_2Ph), 1.8 (m, 2H, CH_2), 1.2 (m, 3H, CH_3). ^{31}P NMR ($CDCl_3$) δ: 36.

Dibenzyl methylphosphonate (10a)

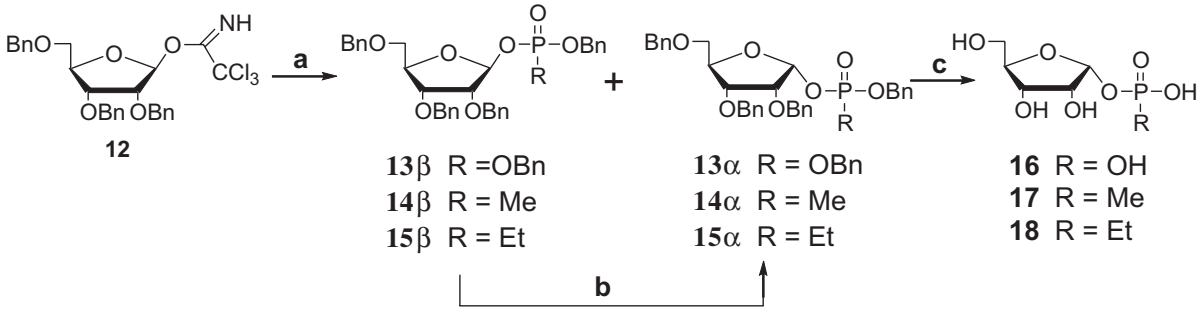
The procedure for the preparation of **10b** was followed. Data for **10a**: ^{1}H NMR (400 MHz, $CDCl_3$) δ: 7.4–7.3 (m, 10H, aromatic), 5.08 (m, 2H, OCH_2Ph), 4.98 (m, 2H, OCH_2Ph), 1.5 (d, J = 17.6 Hz, 3H, CH_3). ^{13}C NMR ($CDCl_3$) δ: 67.16 (OCH_2Ph), 67.09 (OCH_2Ph), 12.42, 10.99 (CH_3). ^{31}P NMR ($CDCl_3$) δ: 31.

Benzyl methylphosphonic acid (11a)

The procedure for the preparation of **11b** was followed. Data for **11a**: ^{1}H NMR (400 MHz, $CDCl_3$) δ: 7.3–7.4 (m, 5H, aromatic), 5.07 (m, 2H, OCH_2Ph), 1.55 (d, J = 17.9 Hz, 3H, CH_3). ^{13}C NMR ($CDCl_3$) δ: 66.59 (OCH_2Ph), 12.39, 11.14 (CH_3).

© 2006 NRC Canada

Scheme 4. Reagents and conditions: (*a*) phosphonic acid, dichloromethane, 0 °C to RT, 3 h; (*b*) $BF_3{\cdot}Et_2O$, 2-chloropyridine, RT, 2 h; (*c*) Pd/C (10%), H_2, 12 h.



*2,3,5-Tri-*O*-benzyl-*D*-ribofuranosyl benzyl ethylphosphonate (15)*

A solution of 2,3,5-tri-*O*-benzyl-D-ribofuranose (1 g, 2.5 mmol), potassium carbonate (396 mg, 2.87 mmol), and trichloroacetonitrile (4 mL, 40 mmol) in anhydrous dichloromethane (20 mL) was stirred overnight at room temperature. The mixture was filtered through Celite and concentrated in vacuo. Flash chromatography using ethyl acetate – hexanes (1:2) yielded pure 2,3,5-tri-*O*-benzyl-β-D-ribofuranosyl trichloracetimidate (**12**). Data for **12**: ^{1}H NMR (400 MHz, $CDCl_3$) δ: 8.5 (s, 1H, NH), 7.4–7.3 (m, 15H, aromatic), 6.35 (s, 1H, H1), 4.8–4.4 (m, 7H, OCH_2Ph, H2), 4.15 (m, 2H, H3, H4), 3.7 (dd, 2H, H5a, H5b). ^{13}C NMR ($CDCl_3$) δ: 160.77 (C=NH), 103.43 (C1), 82.15 (C4), 78.48 (C2), 77.22 (C3), 73.25, 72.54, 72.18 (CH_2Ph), 70.19 (C5). To an ice-cold solution of **12** (698 mg, 1.24 mmol) in anhydrous dichloromethane was added **11b** (527 mg, 2.6 mmol) in the presence of 4 Å molecular sieves. The mixture was stirred for 3 h whereupon TLC indicated complete conversion of **12**. The mixture was filtered through Celite and concentrated in vacuo to yield an anomeric mixture of **15** (450 mg, 60%, α/β = 2:1). The anomers were resolved by flash chromatography (ethyl acetate – hexanes, 1:3 to 1:1). The β anomer **15**β (100 mg, 0.17 mmol) was subsequently dissolved in anhydrous dichloromethane (5 mL) followed by $BF_3{\cdot}Et_2O$ (10 μL, 0.087 mmol) and 2-chloropyridine (16 μL, 0.174 mmol). The mixture was stirred at room temperature for 1.5 h then neutralized with triethylamine and evaporated in vacuo. The crude product was purified by flash chromatography (ethyl acetate – hexane, 1:1) to yield the α anomer **15**α (75 mg, 75%). Data for **15**α: ^{1}H NMR (400 MHz, $CDCl_3$) δ: 7.1–7.4 (m, 20H, aromatic), 6.09 (dd, $J_{1,2}$ = 4.4 Hz, $J_{1,P}$ = 4.6 Hz, 1H, H1), 5.0–5.1 (m, 2H, $POCH_2Ph$), 4.8–4.4 (m, 6H, OCH_2Ph), 4.38 (m, 1H, H4), 3.9 (d, 2H, H2, H3), 3.5 (dd, 2H, H5), 1.9 (m, 2H, CH_2), 1.2 (m, 3H, CH_3). ^{13}C NMR ($CDCl_3$) δ: 97 (C1), 84.3 (C4), 78.97 (C2), 75.54 (C3), 73.53, 72.56, 72.63 (OCH_2Ph), 69.92 (C5), 66.20 ($POCH_2Ph$), 18.89 (CH_2), 6.44 (CH_3). ^{31}P NMR ($CDCl_3$) δ: 34. ESI-MS *m*/*z*: 603.22 (50%, $[M + H]^+$), 295.12 (100%, $[M - C_{16}H_{20}O_4P - H]^+$). HR-MS *m*/*z* calcd. for $C_{35}H_{40}O_7P$ $[M + H]^+$: 603.25116; found: 603.21992. Data for **15**β: ^{1}H NMR (400 MHz, $CDCl_3$) δ: 7.1–7.4 (m, 20H, aromatic), 5.88 (dd, $J_{1,2}$ = 5.9 Hz, $J_{1,P}$ = 6.1 Hz, 1H, H1), 4.9–5.1 (m, 2H, $POCH_2Ph$), 4.5–4.7 (m, 6H, OCH_2Ph), 4.4 (m, 1H, H4), 4.15 (m, 1H, H3), 3.9 (m, 1H, H2), 3.7 (dd, 1H, H5a), 3.55 (dd, 1H, H5b), 1.9 (m, 2H, CH_2), 1.2 (m, 3H, CH_3). ^{13}C NMR ($CDCl_3$) δ: 100.63 (C1), 81.54 (C4), 80.01 (C2), 77.03 (C3), 73.16, 72.54, 72.27 (OCH_2Ph), 72.19 (C5), 66.8 ($POCH_2Ph$). ^{31}P NMR ($CDCl_3$) δ: 34.

*2,3,5-Tri-*O*-benzyl-*D*-ribofuranosyl dibenzylphosphate (13)*

The procedure for **15** was followed. Data for **13**α: ^{1}H NMR (400 MHz, $CDCl_3$) δ: 7.34–7.2 (m, 25H, aromatic), 6.1 (t, $J_{1,2}$ = 1.5 Hz, $J_{1,P}$ = 2.1 Hz, 1H, H1), 5.08 (m, 4H, $P(OCH_2Ph)_2$), 4.7 (m, 2H, OCH_2Ph), 4.5–4.6 (m, 4H, OCH_2Ph), 4.4 (m, 1H, H4), 4.02 (d, 2H, H2,H3), 3.5 (d, 2H, H5). ^{13}C NMR ($CDCl_3$) δ: 99.1, 99.06 (C1), 8.4.64 (C4), 79.05 (C2), 75.44 (C3), 73.55, 72.68, 72.63 (OCH_2Ph), 69.79 (C5), 69.31, 69.25 ($P(OCH_2Ph)_2$). ^{31}P NMR ($CDCl_3$) δ: –2.51. Data for **13**β: ^{1}H NMR (400 MHz, $CDCl_3$) δ: 7.34–7.2 (m, 25H, aromatic), 5.86 (d, *J* = 4.9 Hz, 1H, H1), 5.0–5.1 (m, 4H, $P(OCH_2Ph)_2$), 4.7–4.5 (m, 6H, OCH_2Ph), 4.4 (m, 1H, H4), 4.1 (m, 1H, H3), 3.9 (m, 1H, H2), 3.6–3.7 (dd, 2H, H5). ^{13}C NMR ($CDCl_3$) δ: 102.65 (C1), 81.08 (C4), 79.13 (C2), 77.71 (C3), 73.18, 72.58, 72.32 (OCH_2Ph), 70.4 (C5), 69.33, 69.29 ($P(OCH_2Ph)_2$). ^{31}P NMR ($CDCl_3$) δ: –3.1.

*2,3,5-Tri-*O*-benzyl-*D*-ribofuranosyl benzyl methylphosphonate (14)*

The procedure for **15** was followed. Data for **14**α: ^{1}H NMR (400 MHz, $CDCl_3$) δ: 7.4–7.3 (m, 20H, aromatic), 6.09 (dd, 1H, $J_{1,2}$ = 1.6 Hz, $J_{1,P}$ = 3.8 Hz, H1), 4.9–5.1 (m, 2H, $POCH_2Ph$), 4.7 (d, 2H, OCH_2Ph), 4.6 (m, 2H, OCH_2Ph), 4.5 (d, 2H, OCH_2Ph), 4.3 (m, 1H, H4), 3.9 (m, 2H, H2, H3), 3.4 (m, 2H, H5). ^{13}C NMR ($CDCl_3$) δ: 97.37 (C1), 84.13 (C4), 78.63 (C2), 75.27 (C3), 73.52 (OCH_2Ph), 72.73 (OCH_2Ph), 72.49 (OCH_2Ph), 69.81 (C5), 67.15 ($POCH_2Ph$). ^{31}P NMR ($CDCl_3$) δ: 32, 31. Data for **14**β: ^{1}H NMR (400 MHz, $CDCl_3$) δ: 7.4–7.3 (m, 20H, aromatic), 5.87 (d, 1H, *J* = 5.8 Hz, H1), 5.0 (m, 2H, $POCH_2Ph$), 4.7 (d, 2H, OCH_2Ph), 4.6 (d, 2H, OCH_2Ph), 4.5 (m, 2H, OCH_2Ph), 4.1 (m, 1H, H4), 3.9 (m, 2H, H2, H3), 3.59 (m, 2H, H5). ^{13}C NMR ($CDCl_3$) δ: 100.75 (C1), 80.07 (C4), 79.99 (C2), 76.65 (C3), 73.17 (OCH_2Ph), 72.58 (OCH_2Ph), 72.26 (OCH_2Ph), 69.84 (C5), 66.95 ($POCH_2Ph$). ^{31}P NMR ($CDCl_3$) δ: 30, 31.

α-D-Ribofuranosyl ethylphosphonate (18)

To a solution of compound **15**α (200 mg, 0.33 mmol) in MeOH (10 mL) was added 10% Pd/C. The reaction mixture was stirred under H_2 overnight, filtered through Celite, and concentrated to afford **18** (82 mg, 100%). The crude product was purified through an Amberlite IR-120 ion exchange column, titrated with triethylamine, then dried in vacuo to obtain the triethylammonium salt. Data for **18**: ^{1}H NMR

© 2006 NRC Canada

(400 MHz, D_2O) δ: 4.78 (s, 1H, H1), 4.03 (m, 1H, H3), 3.9–3.8 (m, 2H, H2, H4), 3.7 (dd, 1H, H5a), 3.5 (dd, 1H, H5b), 1.3 (m, 2H, CH_2), 0.9 (m, 3H, CH_3). ^{13}C NMR (D_2O) δ: 107.82 (C1), 82.69 (C2), 74.07 (C4), 70.64 (C3), 62.62 (C5), 21 (CH_2), 7 (CH_3). ^{31}P NMR (D_2O) δ: 25.89.

α-D-Ribofuranosyl phosphate (16)

The procedure for **18** was followed. Data for **16**: ^1H NMR (400 MHz, D_2O) δ: 4.77 (s, 1H, H1), 4.02 (m, 1H, H2), 3.8–3.9 (m, 2H, H3, H4), 3.67 (dd, 1H, H5a), 3.5 (m, 1H, H5b). ^{13}C NMR ($CDCl_3$) δ: 107.82 (C1), 82.7 (C2), 74.08 (C4), 69.57 (C3), 61.40 (C5). ^{31}P NMR ($CDCl_3$) δ: 0.11.

α-D-Ribofuranosyl methylphosphonate (17)

The procedure for **18** was followed. Data for **17**: ^1H NMR (400 MHz, MeOD) δ: 4.76 (s, 1H, H1), 4.04 (m, 1H, H3), 3.96 (m, 1H, H2), 3.89 (d, 1H, H4), 3.74 (dd, 1H, H5a), 3.55 (dd, 1H, H5b), 1.3 (s, 3H, CH_3). ^{13}C NMR (MeOD) δ: 108.44 (C1), 83.44 (C2), 74.77 (C4), 71.27 (C3), 63.61 (C5), 15 (CH_3). ^{31}P NMR (MeOD) δ: 30.24.

Acknowledgements

This paper is dedicated to Professor Walter Szarek, not only for his inspirational contributions to the fields of carbohydrate chemistry and Alzheimer's research, but also for his infallible warmth and good humor as a colleague. We also thank the Natural Sciences and Engineering Research Council of Canada (NSERC) and the Canadian Foundation for Innovation (CFI) for financial support.

References

1. N.G. Ternan, J.W. McGrath, G. McMullan, and J.P. Quinn. World J. Microbiol. Biotechnol. **14**, 635 (1998).
2. R.M. de Graaf, J. Visscher, and A.W. Schwartz. Nature (London), **378**, 474 (1995).
3. J. Kim and D. Dunaway-Mariano. Biochemistry, **35**, 4628 (1996).
4. H. Seto and T. Kuzuyama. Nat. Prod. Rep. **16**, 589 (1999).
5. S.A. Tan and L.G. Tan. Clin. Physiol. Biochem. **7**, 303 (1989).
6. S.V. Kononova and M.A. Nesmeyanova. Biochemistry (Moscow), **67**, 184 (2002).
7. M.C. Morais, G. Zhang, W. Zhang, D.B. Olsen, D. Dunaway-Mariano, and K.N. Allen. J. Biol. Chem. **279**, 9353 (2004).
8. A.N. Kulakova, G.B. Wisdom, L.A. Kulakov, and J.P. Quinn. J. Biol. Chem. **278**, 23426 (2003).
9. M.Y. Galperin and M.J. Jedrzejas. Proteins, **45**, 318 (2001).
10. J.W. Frost. J. Am. Chem. Soc. **109**, 2166 (1987).
11. A.K. White and W.W. Metcalf. J. Bacteriol. **186**, 4730 (2004).
12. C.M. Chen, Q.Z. Ye, Z.M. Zhu, B.L. Wanner, and C.T. Walsh. J. Biol. Chem. **265**, 4461 (1990).
13. G.M. Yakovleva, S.K. Kim, and B.L. Wanner. Appl. Microbiol. Biotechnol. **49**, 573 (1998).
14. B. Hove-Jensen, T.J. Rosenkrantz, A. Haldimann, and B.L. Wanner. J. Bacteriol. **185**, 2793 (2003).
15. L.Z. Avila, K.M. Draths, and J.W. Frost. Biorg. Med. Chem. Lett. **1**, 51 (1991).
16. O.J. Plante, E.R. Palmacci, R.B. Andrade, and P.H. Seeberger. J. Am. Chem. Soc. **123**, 9545 (2001).
17. H. Klenow and R. Emberland. Arch. Biochem. Biophys. **58**, 276 (1955).
18. R. Hanna and J. Mendicino. J. Biol. Chem. **245**, 4031 (1970).
19. D.L. MacDonald. J. Org. Chem. **27**, 1107 (1961).
20. B.E. Maryanoff, A.B. Reitz, and S.O. Nortey. Tetrahedron, **44**, 3093 (1988).
21. G.M. Tener and H.G. Khorana. J. Am. Chem. Soc. **80**, 1999 (1958).
22. P.C. Bulman Page, M.J. McKenzie, and J.A. Gallagher. Synth. Commun. **32**, 211 (2002).
23. M. Saady, L. Lebeau, and C. Mioskowski. J. Org. Chem. **60**, 2946 (1995).

© 2006 NRC Canada

Enantiomeric synthesis of carbocyclic analogs of D- and L-6-azapyrimidine ribonucleosides[1]

Peng Liu and Chung K. Chu

Abstract: An effective and practical synthesis of carbocyclic D- and L-6-azapyrimidine nucleosides (**3**–**8**) was described. Starting from D-ribose, a new efficient methodology for the synthesis of L-2,3-*O*-cyclohexylidene-4-cyclopentenone (**23**) was developed via a ring-closing metathesis, which was applied for the synthesis of L-cyclopentyl-6-azapyrimidine nucleosides (**6**–**8**). The regiospecific introduction of 6-azauracil on the carbocyclic moiety (**9** and **25**) was also achieved by masking its N_3 position with a 4-methylthio group.

Key words: carbocyclic nucleosides, 6-azapyrimidine nucleosides, enantiomeric synthesis.

Résumé : On décrit une méthode efficace et pratique de synthèse des nucléosides des D- et L-6-azapyrimidines carbocycliques (**3**–**8**). Utilisant le D-ribose comme produit de départ, on a développé une nouvelle méthodologie efficace pour la synthèse de la L-2,3-*O*-cyclohexylidène-4-cyclopenténone (**23**) qui fait appel à une réaction de métathèse conduisant à une fermeture de cycle et on l'a appliquée à la synthèse de nucléosides de la L-cyclopentyl-6-azapyrimidine (**6**–**8**). L'introduction régiospécifique du 6-azauracile sur la portion carbocyclique (**9** et **25**) a été réalisée en masquant sa position N_3 à l'aide d'un groupe 4-méthylthio.

Mots clés : nucléosides carbocycliques, nucléosides de 6-azapyrimidine, synthèse énantiomérique.

[Traduit par la Rédaction]

Introduction

Nucleosides are the building blocks of nucleic acids and therefore of fundamental importance in all living systems (1, 2). They have been playing a major role in fighting tumors and viruses, either as selective inhibitors of certain necessary enzymes for cancer or viral reproduction (3) or as nucleic acid chain terminators that interrupt the replication of cancer cells or a virus (4, 5). Currently, 8 out of 21 FDA approved anti-HIV agents are nucleoside analogues, and more than 10 other nucleosides are available for the treatment of other viral infections (2, 6). However, the toxicities (7), enzymatic degradation (8), as well as the emergence of resistant viral strains (9), prompted the search for novel nucleoside analogues. Consequently, extensive modifications on both the sugar and the heterocyclic moiety of the nucleosides have been carried out. Carbocyclic nucleosides, where the furanose ring is replaced with a cyclopentyl ring, have attracted much attention because of their increased metabolic stability as well as interesting biological activities (10, 11). Two milestones in carbocyclic nucleosides are the approval of abacavir (12) and entecavir (13) by the FDA as anti-HIV and anti-HBV agents, respectively (Fig. 1).

Azapyrimidine nucleosides are an interesting class of nucleosides, which are derived from the replacement of the carbon atom of a pyrimidine ring by a nitrogen. For example, D-6-azacytidine (**1**) is an antimetabolite with a wide spectrum of therapeutic activities (14). D-6-Azauridine (**2**) exhibited antitumor activity both experimentally and clinically (15). More recently, 6-azauridine **2** was identified to be significantly effective against West Nile Virus (WNV) in vitro (16). Therefore, as a part of our ongoing antiviral drug discovery program, herein we report an enantiomeric synthesis of carbocyclic analogues of D- and L-6-azapyrimidine ribonucleoside (**3**–**8**) as analogues of 6-azauridine.

Received 15 September 2005. Published on the NRC Research Press Web site at http://canjchem.nrc.ca on 18 May 2006

P. Liu and C.K. Chu.[2] The University of Georgia College of Pharmacy, Athens, GA 30602, USA.

[1]This article is part of a Special Issue dedicated to Professor Walter A. Szarek.

[2]Corresponding author (e-mail: dchu@rx.uga.edu).

Results and discussion

In preliminary studies, we have reported the synthesis of carbocyclic D-6-azauridine **4** and found that the 6-azauracil moiety is a more reactive base in comparison to uracil for Mitsunobu reaction with cyclopentanol **9** because of the introduction of the third nitrogen atom (17). However, the competition among N_1-, N_3-, and O-substitutions caused difficulties in separating the desired N_1 product and gave a poor yield of **10** (Table 1), thus limiting the application of this methodology for the preparation of other carbocyclic 6-azapyrimidine nucleosides. Therefore, finding the suitable N_3-blocked 6-azapyrimidines, which can be condensed with D-cyclopentanol **9** under the standard Mitsunobu conditions, was crucial for the current project.

4-Methylthiotriazinone (**14**) (18) can be regarded as a precursor of 6-azacytosine or 6-azauracil as it can be readily converted to 6-azacytosine upon treatment with saturated methanolic ammonia (19) or to 6-azauracil by hydrolysis (20, 21). In addition, it possesses the structural feature of a N_3-blocked analog, which makes it a N_1-regioselective building block to couple with the sugar moiety **9**. To our sur-

 doi:10.1139/V06-052 © 2006 NRC Canada

Fig. 1. Structures of abacavir, entecavir, and 6-azanucleosides.

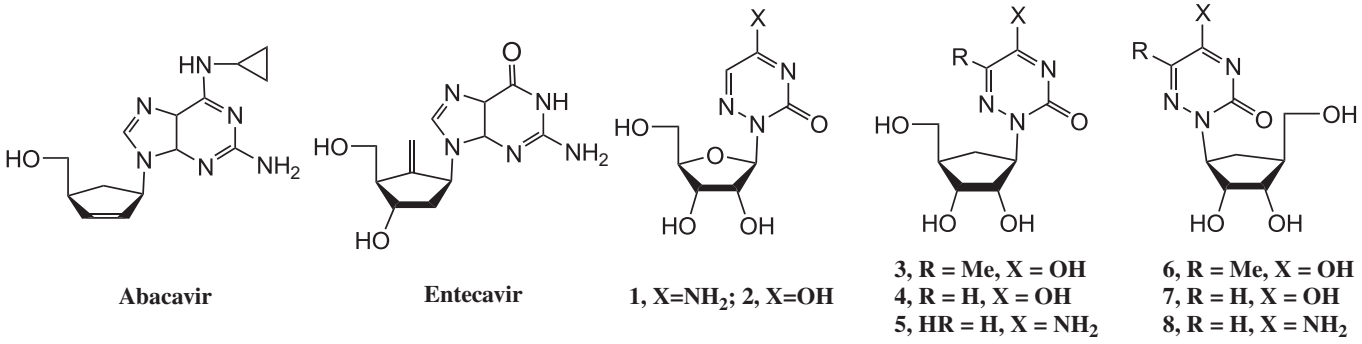
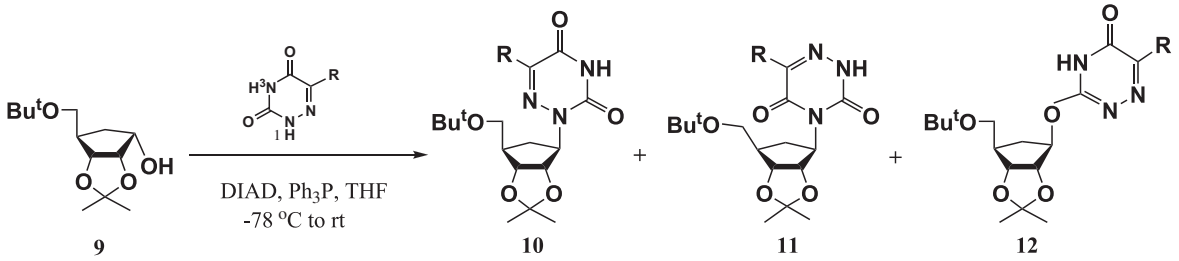


Table 1. Direct coupling of free 6-azauracil and 6-azathymine with D-α-cyclopentanol (**9**).



			Regioisomer ratio			
R	Reaction time	Temperature	**10**	**11**	**12**	Overall yield (%)
H	5 Days	rt	4	1.7	1	83
H	5 h	50–60 °C	Trace	Trace	1	—
Me	11 Days	rt	2	1	2	75

prise, the coupling reaction between **14** and D-cyclopentanol (**9**) took place in a regiospecific manner under the standard Mitsunobu conditions (Scheme 1). Using **14** is the convenient way to avoid the undesired N_3 isomer. The coupled product (**16**) was isolated as a mixture of the desired nucleoside along with reduced DIAD as a by-product. After amination of crude **16** with saturated methanolic ammonia at room temperature for 24 h, compound **17** was obtained in two steps in 89% overall yield. Preparation of the final carbocyclic D-6-azacytidine (**5**) was accomplished by deprotection of **17** with HCl–MeOH (1:3) in quantitative yield. Carbocyclic D-6-azauridine (**4**) was also obtained by hydrolysis of **16** in 3 N HCl in methanol in 92% yield.

For the synthesis of L-6-azapyrimidine analogues **6**–**8**, we utilized the intermediate, 2,3-*O*-cyclohexylidene protected L-cyclopentenone (**23**, Scheme 2) owing to reasons described below.

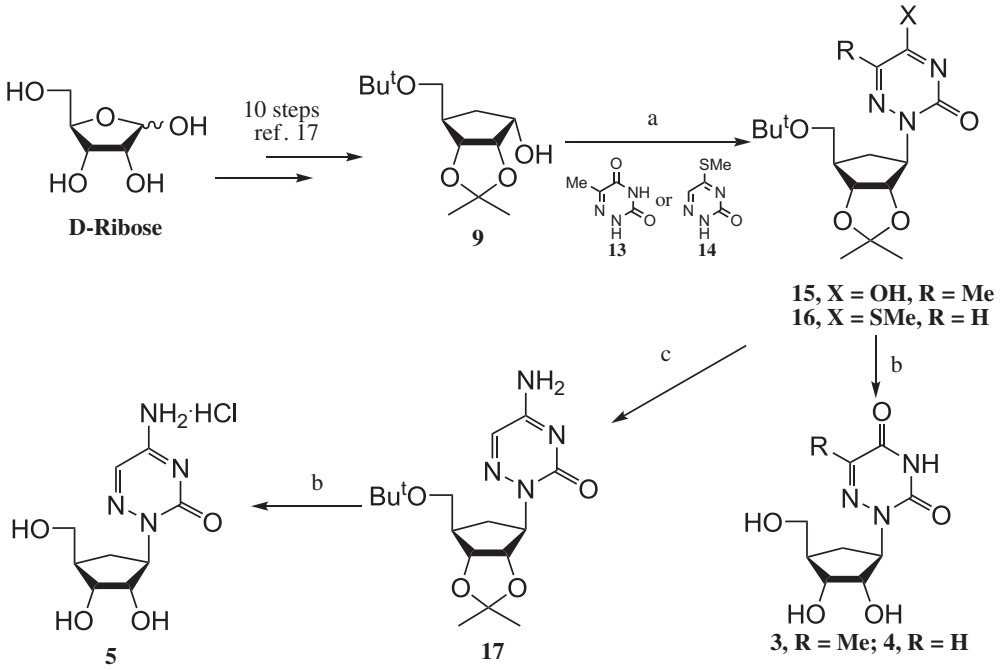
Jeong and co-workers (22) have reported a short route to isopropylidene-protected L-cyclopentenone (**30**) from intermediate **29** (Scheme 3). However, it was found that the handling of vinyl aldehyde **29** was quite inconvenient and often lead to irreproducible yield because of its high volatility (22, 23). This difficulty prompted us to seek an alternative and practical method for the synthesis of L-enone (**23**). Starting from D-ribose, the cyclohexylidene-protected product **18** was prepared with cyclohexanone in the presence of *p*-toluenesulfonic acid as the catalyst in 92% yield (Scheme 2). By using triphenylphosphonium methylidene in THF, a Wittig reaction of **18** was carried out to give the diol **19**, which underwent an oxidative cleavage with sodium periodate to furnish the vinyl aldehyde **20** in two steps in 65% yield. The aldehyde **20** is a nonvolatile oil that can be conveniently purified by column chromatography and thoroughly dried in vacuum. Treatment of **20** with vinylmagnesium bromide in anhydr. THF gave the diene **21** as a mixture of two diastereoisomers in 85% yield. The metathesis ring-closing reaction of **21** was carried out in the presence of 1 mol% of Grubbs catalyst in CH_2Cl_2 at room temperature for 24 h, followed by PDC oxidation in one pot gave the cyclopentenone **23** in two steps in 80% yield. The key intermediate L-α-cyclopentanol (**25**) was prepared in two steps from **23** using the same procedure as for **9**. The Mitsunobu reaction was used to couple the alcohol **25** with 6-azathymine (**13**) and 4-methylthiotriazinone (**14**) to yield compounds **26** and **27**, respectively. The final compounds, L-6-azapyrimidine carbanucleosides (**6**–**8**), were prepared using the same procedure for carbocyclic D-6-azapyrimidine nucleosides (**3**–**5**) (Scheme 1).

The antiviral activities of **3**–**8** were evaluated against SARS, Yellow Fever, West Nile, VEE, and Punta Toro A viruses; however, no significant antiviral activity against these viruses was detected.

In summary, we have developed an efficient and practical synthetic methodology for D- and L-cyclopentenones as the key intermediates in the preparation of various carbocyclic nucleosides. By choosing 4-methylthiotriazinone (**14**) as the N_3-blocked base, we achieved the N_1-regiospecific coupling

© 2006 NRC Canada

Scheme 1. Synthesis of D-cyclopentyl-6-azapyrimidine analogues. Reagents and conditions: (*a*) DIAD, Ph_3P, base **13** or **14**, THF, –78 °C to rt, 3–11 days; (*b*) 3 N HCl–MeOH, rt, 6–8 h; (*c*) NH_3–MeOH, rt, 24 h.



of 6-azapyrimidine base with D- and L-α-cyclopentanols (**9** and **25**) under Mitsunobu conditions.

Experimental section

Melting points were determined on a Mel-Temp II laboratory device and are uncorrected. NMR spectra were recorded on a Varian 500 spectrometer at 500 MHz (^{1}H) and 100 MHz (^{13}C) in the indicated solvents with TMS as the internal standard. UV spectra were obtained on a Beckman DU-650 spectrophotometer. Optical rotations were measured on a JASCO DIP-370 digital polarimeter. Mass spectra were recorded on a Micromass Autospec high-resolution mass spectrometer in ESI mode. Elementary analyses were performed by Atlantic Microlab, Inc., (Atlanta, Georgia).

(1′*R*,2′*S*,3′*R*,4′*R*)-1-[2,3-Dihydroxy-4-(hydroxymethyl)cyclopent-1-yl]-6-azathymine (3)

Diisopropyl azodicarboxylate (DIAD, 0.41 mL, 2.1 mmol) was added dropwise to the solution of triphenylphosphine (550 mg, 2.1 mmol) in THF (15 mL) at 0 °C. After the formation of DIAD–Ph_3P complex, the slurry was stirred for 10 min and transferred to a solution of 6-azathymine (200 mg, 1.57 mmol) and **9** (17) (245 mg, 1.05 mmol) in anhydr. THF (10 mL) at –78 °C. The reaction mixture was stirred for additional 1 h at –78 °C and then warmed up to room temperature (rt). After the suspension was kept stirring at rt for 11 days, the resulting clear amber solution was concentrated and the residue was purified by flash column chromatography on silica gel (hexanes–EtOAc, 10:1) to yield **15**. Compound **15** was contaminated with reduced DIAD and was used for the next reaction without further purification.

The crude product (**15**) was dissolved in a 3:1 mixture of MeOH with 37% hydrochloric acid (15 mL), and the mixture was stirred at rt for 6 h. The solvent was removed under reduced pressure and the residue was purified by flash column chromatography on silica gel (CH_2Cl_2–MeOH, 20:1 to 10:1) to yield compound **3** (82 mg, 31%) as a white solid; mp 186–188 °C. $[\alpha]^{26}_D$ 1.46° (*c* 0.64, CH_3OH). UV (H_2O, nm) λ_{max}: 259.0 (4934, pH 2), 259.0 (4909, pH 7), 300.0 (5538, pH 11). ^{1}H NMR (CD_3OD) δ: 5.15–5.11 (m, 1H), 4.58 (t, *J* = 6.0 Hz, 1H), 4.05 (t, *J* = 6.0 Hz, 1H), 3.75–3.72 (m, 1H), 3.58–3.54 (m, 1H), 2.15–2.14 (m, 1H), 2.14 (s, 3H), 2.04 1.98 (m, 1H), 1.89 1.84 (m, 1H). ^{13}C NMR (CD_3OD) δ: 157.50, 150.45, 143.13, 72.59, 72.20, 63.66, 57.55, 45.95, 25.71, 15.70. MS (ESI) *m*/*z*: 258 (M^+ + H), 280 (M^+ + Na). Anal. calcd. for $C_{10}H_{15}N_3O_5 \cdot 0.6H_2O$: C 44.81, H 6.09, N 15.68; found: C 44.96, H 6.10, N 15.48.

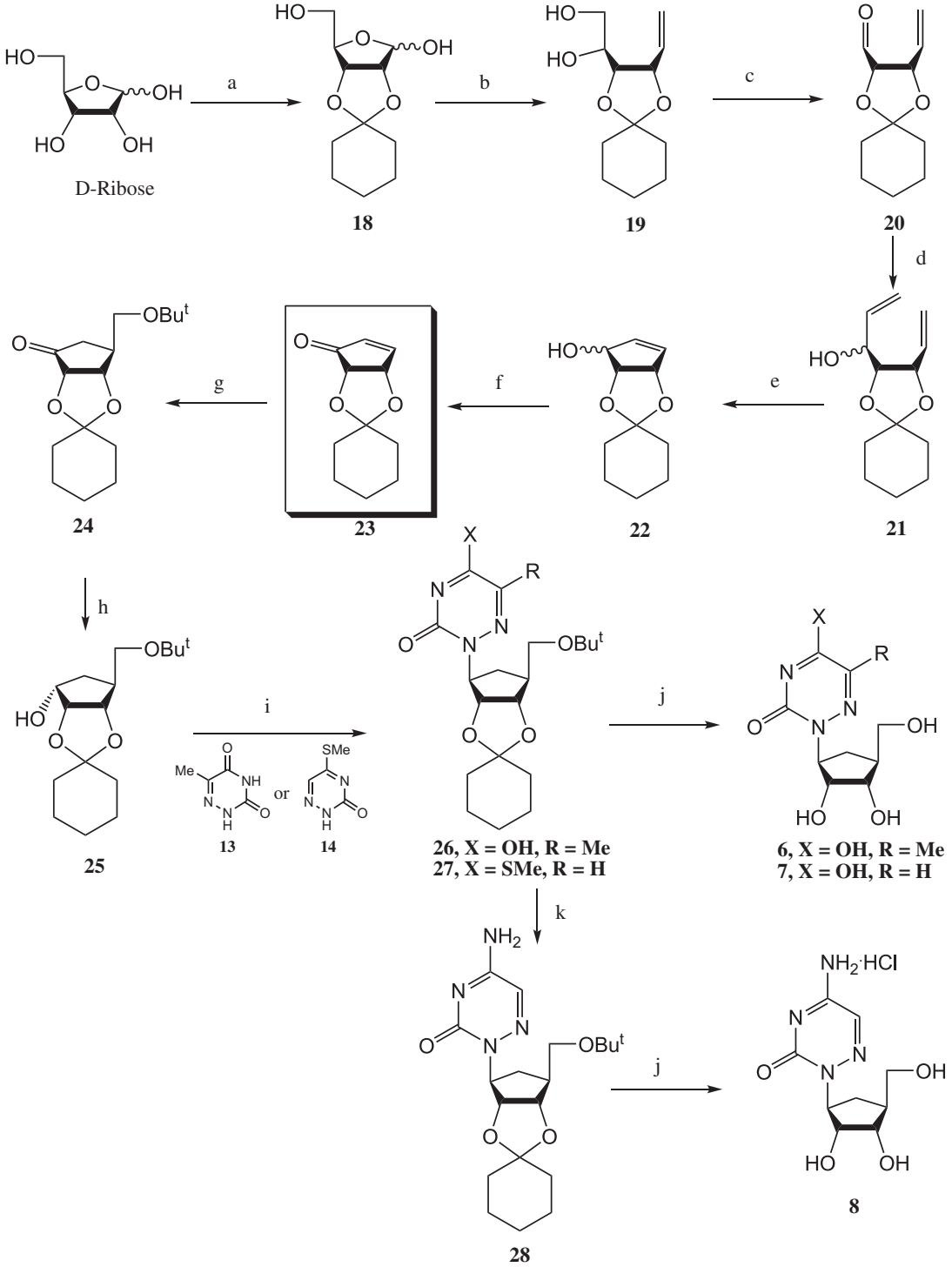
(1′*R*,2′*S*,3′*R*,4′*R*)-1-[4-(*tert*-Butoxymethyl)-2,3-(isopropylidenedioxy)cyclopent-1-yl]-6-azacytosine (17)

DIAD (0.58 mL, 2.92 mmol) was added dropwise to a solution of Ph_3P (840 mg, 3.2 mmol) in THF (30 mL) at 0 °C. The resulting slurry was stirred for 10 min and added to a solution of **14** (313 mg, 2.19 mmol) and **9** (16) (360 mg, 1.46 mmol) in THF (15 mL) at –78 °C. The reaction mixture was stirred for an additional hour at –78 °C and allowed to warm up to rt. After the suspension had been stirred for 4 days, the clear amber solution was evaporated and the residue was purified by column chromatography on silica gel (hexanes–EtOAc, 10:1) to yield **16** and used for the next reaction without further purification.

The crude product (**16**) was dissolved in saturated methanolic ammonia (20 mL) and stirred at rt for 24 h. The mixture was concentrated under reduced pressure, and the residue was purified by flash column chromatography on silica gel (CH_2Cl_2–MeOH, 50:1 to 20:1) to give compound **17** (362 mg, 89%) as a white solid; mp 236 to 237 °C. $[\alpha]^{27}_D$ –95.45° (*c* 1.31, $CHCl_3$). UV ($CHCl_3$, nm) λ_{max}: 261, 289.

© 2006 NRC Canada

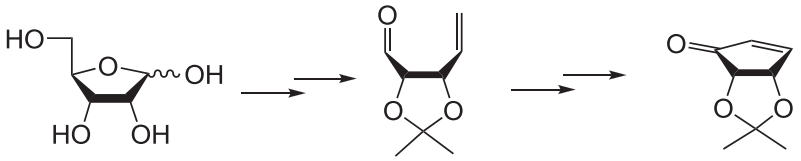
Scheme 2. Synthesis of L-cyclopentyl-6-azapyrimidine analogues. Reagents and conditions: (*a*) cyclohexanone, *p*-toluenesulfonic acid, rt, 10 h; (*b*) methyltriphenylphosphonium bromide, KO-*t*-Bu, THF, rt, 10 h; (*c*) $NaIO_4$, CH_2Cl_2–H_2O, rt, 1 h; (*d*) vinylmagnesium bromide, THF, –78 °C to rt, 1 h; (*e*) Grubbs catalyst, CH_2Cl_2, rt, 24 h; (*f*) PDC, 4 Å molecular sieves, CH_2Cl_2, rt, 4 h; (*g*) $(t\text{-}BuOCH_2)_2CuLi$, *t*-$BuOCH_3$, THF, –30 °C, 30 min; (*h*) $NaBH_4$, $CeCl_2{\cdot}7H_2O$, MeOH, –30 °C to rt, 1 h; (*i*) DIAD, Ph_3P, base **13** or **14**, THF, –78 °C to rt, 3–11 days; (*j*) 3 N HCl–MeOH, rt, 6–8 h; (*k*) NH_3–MeOH, rt, 24 h.



^{1}H NMR ($CDCl_3$) δ: 8.72 (s, br, 1H), 7.67 (s, 1H), 7.11 (s, br, 1H), 5.21–5.17 (m, 1H), 4.81 (t, *J* = 6.0 Hz, 1H), 4.45 (t, *J* = 6.0 Hz, 1H), 3.50–3.47 (m, 1H), 3.36–3.33 (m, 1H), 2.32–2.20 (m, 1H), 1.90–1.86 (m, 1H), 1.72–1.70 (m, 1H), 1.53 (s, 3H), 1.30 (s, 3H), 1.17 (s, 9H). ^{13}C NMR ($CDCl_3$) δ: 159.45, 154.83, 127.43, 113.24, 83.55, 81.43, 72.91, 63.68, 62.71, 44.90, 33.85, 27.85, 27.74, 25.52. MS (ESI) *m/z*: 339 (M^+ + H), 361 (M^+ + Na), 699 (M_2^+ + Na). Anal. calcd. for $C_{16}H_{26}N_4O_4$: C 56.79, H 7.74, N 16.56; found: C 56.68, H 7.85, N 16.59.

© 2006 NRC Canada

Scheme 3.



D-Ribose **29** **30**

(1′*R*,2′*S*,3′*R*,4′*R*)-1-[2,3-Dihydroxy-4-(hydroxymethyl)cyclopent-1-yl]-6-azauracil (4)

The crude product (**16**) (195 mg, 0.48 mmol) was dissolved in a 3:1 mixture of methanol with 37% hydrochloric acid (15 mL), and the mixture was stirred at rt for 12 h. The solvent was evaporated under vacuum and the residue was chromatographed on silica gel (CH_2Cl_2–MeOH, 20:1 to 10:1) to obtain compound **4** (98 mg, 84%) as a white solid; mp 278 to 279 °C. $[\alpha]^{25}_D$ –3.26° (*c* 0.61, CH_3OH). UV (H_2O, nm) λ_{max}: 257.5 (3459, pH 2), 257.5 (4548, pH 7), 300 (3110, pH 11). ^{1}H NMR (CD_3OD) δ: 7.34 (s, 1H), 5.14–5.09 (m, 1H), 4.58 (t, *J* = 6.0 Hz, 1H), 4.04 (t, *J* = 6.0 Hz, 1H), 3.74–3.71 (m, 1H), 3.76–3.54 (m, 1H), 2.15–2.12 (m, 1H), 2.04–1.99 (m, 1H), 1.89–1.82 (m, 1H). ^{13}C NMR (CD_3OD) δ: 157.40, 149.83, 135.11, 72.54, 72.14, 63.62, 57.39, 45.92, 25.62. MS (ESI) *m*/*z*: 242 (M^+ + H), 266 (M^+ + Na), 282 (M^+ + K). Anal. calcd. for $C_9H_{13}N_3O_5$: C 44.44, H 5.39, N 17.28; found: C 44.56, H 5.54, N 17.18.

(1′*R*,2′*S*,3′*R*,4′*R*)-1-[2,3-Dihydroxy-4-(hydroxymethyl)cyclopent-1-yl]-6-azacytosine hydrochloride (5)

Compound **17** (630mg, 1.86 mmol) was dissolved in a 1:3 mixture of 37% hydrochloric acid with methanol (15 mL), and the mixture was stirred at rt for 6 h. The solvent was evaporated under vacuum and the residue was dissolved in distilled water (5 mL). The resulting aqueous solution was extracted with IPA–$CHCl_3$ (1:4, 3 × 10 mL). The aqueous phase was freeze-dried, and the crude product (**5**) was recrystalized from methanol – ethyl ether to obtain **5** as a white solid in quantitative yield; mp > 300 °C (dec.). $[\alpha]^{26}_D$ –72.85° (*c* 0.82, CH_3OH). UV (H_2O, nm) λ_{max}: 281.5 (7689, pH 2), 284 (7760, pH 7), 280 (7728, pH 11). ^{1}H NMR (CD_3OD) δ: 7.65 (s, 1H), 5.11–5.08 (m, 1H), 4.21 (dd, J_1 = 9.0 Hz, J_2 = 5.5 Hz, 1H), 3.93–3.91 (m, 1H), 3.63–3.54 (m, 2H), 2.13–2.15 (m, 2H), 1.53–1.48 (m, 1H). ^{13}C NMR (CD_3OD) δ: 159.19, 156.11, 127.87, 74.90, 72.60, 63.53, 63.00, 45.41, 28.13. MS (ESI) *m*/*z*: 243 (M^+ + H), 485 (M_2H^+). Anal. calcd. for $C_9H_{15}ClN_4O_4{\cdot}0.5H_2O$: C 37.57, H 5.61, N 19.47; found: C 37.56, H 5.77, N 19.57.

(1*R*)-1-((2*R*,3*S*)-3-Vinyl-1,4-dioxaspiro[4.5]dec-2-yl)-ethane-1,2-diol (19)

To a suspension of methyltriphenylphosphonium bromide (45.1 g, 125 mmol) in THF (350 mL) was added potassium *tert*-butoxide (18.5 g, 143.4 mmol) at 0 °C. The reaction mixture was stirred at 0 °C for 15 min and then at room temperature for 1 h. The reaction mixture was cooled to 0 °C again, compound **18** (24) (10.32 g, 44.8 mmol) dissolved in THF (100 mL) was added, and the resulting mixture was stirred at rt overnight. The reaction was quenched carefully by adding water (200 mL) at 0 °C, and extracted with ethyl acetate (3 × 300 mL). The combined organic phases were washed with brine (2 × 100 mL), dried (Na_2SO_4), filtered, and concentrated. The resulting yellow syrup was purified by vacuum chromatography (hexanes–EtOAc, 2:1) to give crude compound **19** (14.5 g) along with triphenylphosphine oxide. ^{1}H NMR ($CDCl_3$) δ: 5.97–6.01 (m, 1H), 5.47 (dd, J_1 = 18 Hz, J_2 = 1.5 Hz, 1H), 5.32 (dd, J_1 = 11.5 Hz, J_2 = 1.5 Hz, 1H), 4.70 (t, *J* = 6 Hz, 1H), 4.07 (t, *J* = 7.5 Hz, 1H), 3.81–3.83 (m, 1H), 3.71–3.74 (m, 1H), 1.54–1.69 (m, 8H), 1.38–1.42 (m, 2H). ^{13}C NMR ($CDCl_3$) δ: 134.02, 118.53, 109.73, 78.22, 77.84, 69.91, 64.49, 37.64, 34.77, 25.10, 24.08, 23.75. HR-ESI MS calcd. for $C_{12}H_{20}O_4$: 229.1362 (M^+ + H); found: 229.1402.

(2*S*,3*S*)-3-Vinyl-1,4-dioxaspiro[4.5]decane-2-carbaldehyde (20)

To a solution of crude product **19** (14.5 g) in CH_2Cl_2 (200 mL) was added a solution of $NaIO_4$ (14.24 g, 66 mmol) in water (100 mL) at rt and the reaction mixture was stirred for 30 min. The mixture was filtered through a short pad of Celite and the aqueous filtrate was separated and extracted with CH_2Cl_2 (2 × 200 mL). The combined organic layers were dried (Na_2SO_4) and concentrated. The residue was chromatographed on silica gel (hexanes–EtOAc, 10:1) to give **20** as a colorless oil. ^{1}H NMR ($CDCl_3$) δ: 9.56 (d, *J* = 3.0 Hz, 1H), 5.72–5.79 (m, 1H), 5.47 (dd, J_1 = 17.5 Hz, J_2 = 1.5 Hz, 1H), 5.32 (dd, J_1 = 9.0 Hz, J_2 = 1.5 Hz, 1H), 4.85 (t, *J* = 7.5 Hz, 1H), 4.40–4.42 (m, 1H), 1.59–1.84 (m, 8H), 1.42–1.47 (m, 2H). ^{13}C NMR ($CDCl_3$) δ: 201.08, 131.53, 119.64, 112.09, 81.94, 78.74, 37.20, 34.81, 25.01, 24.01, 23.73.

(1*R*)- and (1*S*)-1-((2*R*,3*S*)-3-Vinyl-1,4-dioxaspiro[4.5]dec-2-yl)prop-2-en-1-ol (21)

To a solution of **20** (400 mg, 2.04 mmol) in THF (5 mL) was added vinylmagnesium bromide solution (1 mol/L, 3 mL, 3 mmol) at 0 °C over 10 min. The mixture was stirred at rt for 1 h and satd. aq. NH_4Cl (5 mL) was added to quench the reaction. The aqueous layer was extracted with ethyl acetate (3 × 10 mL). The combined organic layers were dried (Na_2SO_4), filtered, and concentrated in vacuo. The residue was purified by column chromatography on silica gel (hexanes–EtOAc, 30:1) to give **21** as two diastereoisomers (**21a** and **21b**, dr 1:1) in 85% overall yield. **21a**: $[\alpha]^{26}_D$ 4.81° (*c* 0.85, $CHCl_3$). ^{1}H NMR ($CDCl_3$) δ: 5.96–6.03 (m, 1H), 5.81–5.88 (m, 1H), 5.21–5.40 (m, 4H), 4.58–4.63 (m, 1H), 4.05–4.13 (m, 2H), 2.47 (d, *J* = 13 Hz, 1H), 1.58–1.76 (m, 8H), 1.39–1.44 (m, 2H). ^{13}C NMR ($CDCl_3$) δ: 136.68, 134.17, 119.29, 117.15, 109.47, 80.29, 78.55, 70.70, 37.30, 34.50, 25.13, 24.07, 23.70. **21b**: $[\alpha]^{26}_D$ 24.15 (*c* 0.9, $CHCl_3$). ^{1}H NMR ($CDCl_3$) δ: 6.01–6.09 (m, 2H), 5.22–5.46 (m, 4H), 4.68 (t, *J* = 7.0 Hz, 1H), 4.18 (s, 1H), 4.00–4.03 (m, 1H), 2.04 (s, 1H), 1.56–1.70 (m, 8H), 1.38–1.41 (m, 2H). ^{13}C NMR ($CDCl_3$) δ: 137.80, 134.38, 118.24, 116.17, 109.51,

© 2006 NRC Canada

80.16, 78.38, 71.02, 37.53, 34.79, 25.15, 24.05, 23.73. Anal. calcd. for $C_{13}H_{20}O_3$: C 69.61, H 8.99; found: C 69.85, H 9.08.

(2*S*,3*S*)-2,3-(Cyclohexylidenedioxy)-4-cyclopentenone (23)

Grubbs catalyst (13 mg, 0.01 mmol) was added to a solution of **21** (153 mg, 0.68 mmol) in anhydr. CH_2Cl_2 (5 mL) and the resulting dark brown solution was stirred at rt for 24 h. PDC (293 mg, 1.36 mmol) and 4 Å molecular sieves (150 mg) were added to the reaction mixture, and the suspension was stirred at rt for 4 h. The reaction mixture was filtered through a short pad of silica gel and thoroughly washed with acetone. The filtrate was concentrated under reduced pressure and the residue was purified by column chromatography (hexanes–EtOAc, 10:1) to yield **23** (105 mg, 80%) as a white solid; mp 86–88 °C (lit. value (25) mp 87 °C). $[\alpha]^{27}_D$ 74.33° (*c* 1.11, $CHCl_3$). ^{1}H NMR ($CDCl_3$) δ: 7.61–7.62 (m, 1H), 6.20 (d, *J* = 6 Hz, 1H), 5.26–5.27 (m, 1H), 4.46 (d, *J* = 5.5 Hz, 1H), 1.54–1.67 (m, 8H), 1.38–1.39 (m, 2H).

(2*S*,3*S*,4*S*)-4-(*tert*-Butoxymethyl)-2,3-(cyclohexylidenedioxy)-1-cyclopentanone (24)

Compound **23** (1.57g, 8.1 mmol) was converted to **24** (1.97 g, 86%) according to the reported procedure (26). $[\alpha]^{25}_D$ 139.45° (*c* 0.61, $CHCl_3$). The melting point and ^{1}H NMR data were identical to that described in ref. 26.

(1*R*,2*R*,3*S*,4*S*)-4-(*tert*-Butoxymethyl)-2,3-(cyclohexylidenedioxy)-1-cyclopentanol (25)

To a solution of **24** (1.97 g, 7.0 mmol) in methanol (30 mL) was added cerium(III) chloride heptahydrate (1.82 g, 4.9 mmol) at –30 °C. After stirring at this temperature for 15 min, sodium borohydride (532 mg, 14.0 mmol) was added portionwise. The reaction mixture was gradually warmed up to rt and stirred for 30 min. Hexane – ethyl acetate (1:1, 30 mL) was added, and the resulting precipitated mixture was filtered through a pad of silica gel. The filtrate was concentrated and the residue was chromatographed on silica gel (hexanes–EtOAc, 50:1) to afford **25** as a colorless oil (1.87 g, 94%). $[\alpha]^{27}_D$ 0.04 (*c* 0.67, $CHCl_3$). ^{1}H NMR ($CDCl_3$) δ: 4.43–4.45 (m, 2H), 4.22–4.25 (m, 1H), 3.31–3.33 (m, 1H), 3.19–3.22 (m, 1H), 2.52 (d, *J* = 9.0 Hz, 1H), 2.21 (s, br, 1H), 1.82–1.85 (m, 2H), 1.55–1.68 (m, 8H), 1.40 (s, 2H), 1.13 (s, 9H). ^{13}C NMR ($CDCl_3$) δ: 111.34, 83.18, 79.18, 72.59, 72.10, 63.10, 42.21, 36.16, 36.00, 33.79, 27.42, 25.21, 24.09, 23.65. Anal. calcd. for $C_{16}H_{19}O_4$: C 67.57, H 9.92; found: C 67.59, H 10.03.

(1′*S*,2′*R*,3′*S*,4′*S*)-1-[2,3-Dihydroxy-4-(hydroxymethyl)cyclopent-1-yl]-6-azathymine (6)

Compound **6** was prepared from **25** on a 1.72 mmol scale following the same procedure used for compound **3**. Purification on silica gel using 5% MeOH in CH_2Cl_2 as eluent gave 154 mg of **6** (35%) as a white solid. $[\alpha]^{26}_D$ –1.13° (*c* 0.79, CH_3OH). ^{1}H NMR (CD_3OD) δ: 5.15–5.20 (m, 1H), 4.63 (t, *J* = 6.0 Hz, 1H), 4.10 (t, *J* = 6.0 Hz, 1H), 3.77 (q, J_1 = 10.5 Hz, J_2 = 6.5 Hz, 1H), 3.60 (q, J_1 = 10.5 Hz, J_2 = 6.5 Hz, 1H), 3.34–3.35 (m, 1H), 2.19 (s, 3H), 2.04–2.08 (m, 1H), 1.87–1.93 (m, 1H). ^{13}C NMR (CD_3OD) δ: 157.30, 150.27, 142.98, 72.49, 72.06, 63.42, 57.39, 45.73, 25.49, 15.51. MS (ESI) *m*/*z*: 258 (M^+ + H), 280 (M^+ + Na). Anal. calcd. for $C_{10}H_{15}N_3O_5$·0.3MeOH: C 46.36, H 6.12, N 15.75; found: C 46.50, H 6.05, N 15.51.

(1′*S*,2′*R*,3′*S*,4′*S*)-1-[4-(*tert*-Butoxymethyl)-2,3-(cyclohexylidenedioxy)cyclopent-1-yl]-6-azacytosine (28)

Using the same procedure as described for compound **17**, compound **25** (330 mg, 1.17 mmol) was coupled with **14** under Mitsunobu conditions to give **27**. The crude product (**27**) was treated with saturated methanolic ammonia at rt to afford compound **28** (400 mg, 90%) as a white solid after flash column chromatography on silica gel (CH_2Cl_2–MeOH, 50: 1 to 20:1); mp 258 to 259 °C. $[\alpha]^{27}_D$ 78.91° (*c* 0.60, $CHCl_3$). UV (CH_3OH, nm) λ_{max}: 277. ^{1}H NMR ($CDCl_3$) δ: 8.20 (s, br, 1H), 7.60 (s, 1H), 6.60 (s, br, 1H), 5.15–5.18 (m, 1H), 4.82–4.84 (m, 1H), 4.41–4.43 (m, 1H), 3.48–3.51 (m, 1H), 3.32–3.36 (m, 1H), 2.29–2.33 (m, 2H), 1.50–1.82 (m, 9H), 1.35–1.36 (m, 2H), 1.17 (s, 9H). ^{13}C NMR ($CDCl_3$) δ: 158.98, 154.41, 127.37, 113.53, 82.68, 81.07, 72.68, 64.11, 62.75, 44.76, 37.52, 34.84, 33.70, 27.56, 25.17, 24.07, 23.60. HR-ESI MS calcd. for $C_{19}H_{30}N_4O_4$: 379.2267 (M^+ + H); found: 379.2297.

(1′*S*,2′*R*,3′*S*,4′*S*)-1-[2,3-Dihydroxy-4-(hydroxymethyl)cyclopent-1-yl]-6-azauracil (7)

Compound **27** (105 mg, 0.26 mmol) was converted to **7** (57 mg, 92%) according to the same procedure for **4**; mp 278–280 °C. $[\alpha]^{27}_D$ 2.96 (*c* 0.68, MeOH). ^{1}H NMR (CD_3OD) δ: 7.37 (s, 1H), 5.14–5.16 (m, 1H), 4.61 (t, *J* = 6.0 Hz, 1H), 4.07 (t, *J* = 6.0 Hz, 1H), 3.74–3.78 (m, 1H), 3.58–3.62 (m, 1H), 2.08–2.18 (m, 1H), 2.02–2.08 (m, 1H), 1.88–1.93 (m, 1H). ^{13}C NMR (CD_3OD) δ: 157.20, 149.67, 135.02, 73.03, 72.38, 63.16, 57.32, 45.71, 25.39. MS (ESI) *m*/*z*: 242 (M^+ – 1), 266 (M^+ + Na). Anal. calcd. for $C_9H_{13}N_3O_5$·0.5CH_3OH: C 44.01, H 5.83, N 16.21; found: C 44.04, H 5.66, N 16.04.

(1′*S*,2′*R*,3′*S*,4′*S*)-1-[2,3-Dihydroxy-4-(hydroxymethyl)-cyclopent-1-yl]-6-azacytosine hydrochloride (8)

Compound **28** (630 mg, 1.66 mmol) was converted to **8** (448 mg, 97%) according to the same procedure as for **5**; mp 235–238 °C (dec.). $[\alpha]^{26}_D$ 74.37 (*c* 0.91, CH_3OH). ^{1}H NMR (CD_3OD) δ: 7.79 (s, 1H), 5.17–5.13 (m, 1H), 4.23 (dd, J_1 = 9.0 Hz, J_2 = 5.5 Hz, 1H), 3.95 (dd, J_1 = 5.5 Hz, J_2 = 4.0 Hz, 1H), 3.66–3.58 (m, 2H), 2.28–2.19 (m, 2H), 1.61–1.55 (m, 1H). ^{13}C NMR (CD_3OD) δ: 153.68, 147.03, 135.38, 127.78, 74.52, 72.11, 63.14, 45.14, 27.46. MS (ESI) *m*/*z*: 243 (M^+ + H), 485 (M_2^+ + H). Anal. calcd. for $C_9H_{15}ClN_4O_4$·0.5H_2O: C 37.57, H 5.61, N 19.47; found: C 37.56, H 5.77, N 19.57.

Acknowledgment

This research was supported by grants from the National Institute of Allergy and Infectious Diseases.

References

1. D. Voet and J.G. Voet. Biochemistry. 2nd ed. John Wiley and Sons, New York. 1995.
2. G. Gumina, Y. Chong, H. Choo, G. Song, and C.K. Chu. Curr. Top. Med. Chem. **2**, 1065 (2002).
3. D.C. Orr, H.T. Figueiredo, C.L. Mo, C.R. Penn, and J.M. Cameron. J. Bio. Chem. **267**, 4177 (1992).

© 2006 NRC Canada

4. (*a*) M.A. Turner, X. Yang, D. Yin, K. Kuczera, R.T. Borchardt, and P.L. Howell. Cell Biochem. Biophys. **33**, 101 (2000); (*b*) Y. Kitade, C. Kozaki, T. Miwa, and M. Nakanishi. Tetrahedron, **58**, 1271 (2002)
5. (*a*) K.S. Anderson. Biochim. Biophys. Acta, **1587**, 296 (2002); (*b*) G. Maga and S. Spadari. Curr. Drug Metab. **3**, 73 (2002).
6. (*a*) M.J. Otto. Curr. Opin. Pharm. **4**, 431 (2004); (*b*) P.J. Ruane and E. DeJesus. J. Acquired Immune Defic. Syndr. **37**, S21 (2004).
7. R. Fleischer, D. Boxwell, and K.E. Sherman. Clin. Infect. Dis. **38**, 79 (2004).
8. X. Tan, C.K. Chu, and F.D. Boudinot. Adv. Drug Delivery Rev. **39**, 117 (1999).
9. T. Shirasaka, M.F. Kavlick, T. Ueno, W.Y. Gao, E. Kojima, M.L. Alcaide, S. Chokekijchai, B.M. Roy, E. Arnald, R. Yarchoan, and H. Mitsuya. Proc. Natl. Acad. Sci. U.S.A. **92**, 2398 (1995).
10. M.T. Crimmins. Tetrahedron, **54**, 9229 (1998).
11. R.J. Ferrier. Carbohydr. Chem. **34**, 248 (2003).
12. S.M. Douglas, S.S. Good, M.B. Faletto, W.H. Miller, M.H. St Clair, L.R. Boone, M. Tisdale, N.R. Parry, J.E. Reardon, R.E. Dornsife, D.R. Averett, and T.A. Krenitsky. Antimicrob. Agents Chemother. **41**, 1082 (1997).
13. S. Levine, D. Hernandez, G. Yamanaka, S. Zhang, R. Rose, S. Weinheimer, and R.J. Colonno. Antimicrob. Agents Chemother. **46**, 2525 (2002).
14. S.P. Samijlenko, I.V. Alexeeva, L.H. Palchykivs'ka, I.V. Kondratyuk, A.V. Stepanyuin, A.S. Shalamay, and D.M. Hovorun. J. Mol. Struct. **484**, 31 (1999).
15. L.L. Wotring and L.B. Townsend. Cancer Res. **49**, 289 (1989).
16. J.D. Morrey, D.F. Smee, R.W. Sidwell, and C. Tseng. Antiviral Res. **55**, 107 (2002).
17. Y.H. Jin, P. Liu, J. Wang, R. Baker, J. Huggins, and C.K. Chu. J. Org. Chem. **68**, 9012 (2003).
18. W.W. Zorbach and R.S. Tipson. Synthetic procedures in nucleic acid chemistry. John Wiley and Sons, New York. 1973. p. 102.
19. C.C. Tzeng, N.C. Motola, and R.P. Panzica. J. Org. Chem. **48**, 1271 (1983).
20. J. Daunis and M. Follet. J. Heterocycl. Chem. **14**, 729 (1977).
21. (*a*) C. Cristescu. Rev. Roum. Chim. **31**, 881 (1986); (*b*) C. Cristescu and S. Tomas. Rev. Roum. Chim. **34**, 1321 (1989).
22. H.R. Moon, W.J. Choi, H.O. Kim, and L.S. Jeong. Tetrahedron: Asymmetry, **13**, 1189 (2002).
23. T.V. RajanBabu, W.A. Nugent, D.F. Taber, and P.J. Fagan. J. Am. Chem. Soc. **110**, 7128 (1988).
24. K. Mori and H. Kikuchi. Liebigs Ann. Chem. 1267 (1989).
25. B. Sundermann and H. Scharf. Tetrahedron: Asymmetry, **7**, 1995 (1996).
26. M.S. Wolfe, B.L. Anderson, D.R. Borcherding, and R.T. Borchardt. J. Org. Chem. **55**, 4712 (1990).

© 2006 NRC Canada

TRIBUTE / HOMMAGE

"How bittersweet it is"

Walter Szarek was born on 19 April 1938 in St. Catharines, Ontario. He received his B.Sc. in Honours Chemistry in 1960 from McMaster University, Hamilton, Ontario. During the summer months of 1956–1958 he was employed at the Ontario Paper Co. in Thorold, Ontario where he studied the alkaline oxidation of lignin, an experience that first exposed him to industrial chemistry and research. Walter received a M.Sc. degree in 1962 from McMaster University, having studied with Professor David B. MacLean in the area of alkaloid chemistry. His thesis research was concerned with the structural elucidation of annotine, a member of the *Lycopodium* alkaloids. This class of alkaloids had attracted the attention of several of the internationally renowned stars of natural products chemistry in Canada. For example, annotine itself was first isolated from *L. annotinium* of Canadian origin by the legendary Canadian alkaloid duo, R.H.F. Manske and L. Marion. In addition to Dave MacLean and Ian Spenser at McMaster, other Canadian researchers in the field who studied the elucidation and subsequent synthesis of the fascinating *Lycopodium* structures included K. Wiesner, Z. Valenta, W.A. Ayer, and F.A.L. Anet. Walter was well-advanced towards the completion of his Ph.D. program at McMaster when a certain restlessness had set in and he began contemplating a change of venue and a change of research interests. Thus, in 1962 he began studies towards the Ph.D. degree with Professor J.K.N. Jones at Queen's University in Kingston, Ontario. He completed his studies in 1964 in the area of carbohydrate chemistry.

Having worked with both alkaloids and carbohydrates, Walter has been tempted to say that his career has been "bittersweet". His thesis research at Queen's was concerned with the replacement of the ring oxygen of sugars by nitrogen. Among the accomplishments, the first example of a sugar having nitrogen in a five-membered ring (methyl 4-acetamido-4-deoxy-L-erythrofuranoside) was synthesized, and the hindered internal rotation of such sugars was demonstrated by NMR spectroscopy. This area of the replacement of the ring oxygen by other hetero atoms remained dormant for several years, but the discovery of the so-called azasugars in Nature and the recognition that some of them are inhibitors of glycosidases and possess other biological activities of potential therapeutic value stimulated tremendous chemical and biological interest in this class of compounds and in related analogs in which the ring oxygen has been replaced by sulfur or selenium. Thus, originating with some of Walter's work, this activity continues to this day.

Carbohydrate chemistry was to become the field to which Walter would make the greatest contributions. Upon completion of his Ph.D. studies in 1964, he went on to do postdoctoral work with Professor Melville L. Wolfrom at The Ohio State University, Columbus, Ohio. Professor Wolfrom had developed the outstanding School of Carbohydrate Chemistry that attracted hundreds of students and postdoctoral fellows from many countries; in the Canadian context, Professor Raymond Lemieux had been a postdoctoral fellow and Professor Steve Hanessian had been a graduate student with Professor Wolfrom. Professor Wolfrom had a very large group and Walter, during his time at Ohio State, served as a cosupervisor in the old laboratories known as "Sugar Alley". This experience was truly excellent training for his own future career in academia. Within a year he was offered the position of Assistant Professor of Biochemistry in the Department of Physiology and Biochemistry at Rutgers University in New Jersey. Walter was successfully developing his research programs, but he yearned to be back in a chemistry department. In 1967 he returned to Queen's as Assistant Professor of Chemistry where he remains to this day. He was promoted to Associate Professor in 1971 and to Full Professor in 1976. During the period 1976–1985 he was also Director of the Carbohydrate Research Institute at Queen's. In 2003 he became Professor Emeritus, and continues to be very active in research.

In addition to serving on many committees, both at Queen's and outside of Queen's, he has had a distinguished teaching career at both the undergraduate and graduate levels, having won four teaching awards including the Queen's University Arts and Science Undergraduate Teaching Excellence Award in 1989, as well as a distinguished research career. To date 18 M.Sc. (degree conferred), 29 Ph.D. (degree conferred) students, and ~85 Postdoctoral Fellows have studied under his supervision. His caring mentorship both in chemistry and in the trials and tribulations of life are much appreciated by his students and postdoctoral fellows. To date, Walter is the author of over 250 peer-reviewed papers, over 30 issued patents, 11 book chapters, and is the editor of 2 books. His research accomplishments in carbohydrate chemistry have been recognized by the receipt of the American Chemical Society Claude S. Hudson Award in Carbohydrate Chemistry in 1989 and the Melville L. Wolfrom Award of the Division of Carbohydrate Chemistry of the American Chemical Society in 1992.

Walter's interest in carbohydrates has been truly comprehensive. His publications cover almost every aspect of carbohydrates. He has published on the structure and synthesis of carbohydrates and carbohydrate-containing antibiotics, design of biologically active nucleosides, including carbocyclic analogs, biochemical aspects, conformational and mechanistic studies of carbohydrate reactions, photochemistry of carbohydrates, heterocyclic conformational analysis, synthesis of radiopharmaceuticals for use in positron emission reconstruction tomography, chemistry and novel applications of vitamin C, microbiological oxidation of sugars and their derivatives, chemical modification of polysaccharides, design and synthesis of carbohydrate sweeteners, theory of sweetness, carbohydrate derivatives in the enantioselective synthesis of biologically active compounds, targeted delivery of drugs, studies on *Pseudomonas aeruginosa* A-Band lipopolysaccharide: a common antigen, vaccine development, oligomeric carbohydrates in parenteral nutrition, and inhibitors of glycosidases and glycosyltransferases.

Throughout his career, Walter has had great interest in medicinal chemistry and in drug development, and it is in these areas that his potentially longest-lasting and most significant contributions reside. In the mid-1980s, Walter began collaborating with Dr. Bob Kisilevsky of the Department of Pathology at Queen's University. Bob had developed an interest in amyloid as a result of an association with Dr. Michael Axelrad of the Department of Pathology. Dr. Axelrad began the work on amyloid at Queen's because he was suffering from and eventually succumbed to a form of amyloid disease himself. When Bob Kisilevsky and Walter started collaborating, there was growing interest that a carbohydrate polymer, known generally as a glycosaminoglycan, was implicated in amyloid deposition.

© 2006 NRC Canada

The research collaboration was highly successful, and in late 1993, Neurochem, Inc. was founded at Queen's, together with Dr. Don Weaver, who is now at Dalhousie University. Neurochem is now a public biopharmaceutical company currently located in Laval, Quebec. Its clinical milestones include Fibrillex™ for the treatment of amyloid A (AA) amyloidosis, Alzhemed™ for the treatment of Alzheimer's Disease, and Cerebril™ for the treatment of hemorrhagic stroke owing to cerebral amyloid angiopathy. The drug candidates for all of these indications were synthesized in Walter's laboratory in old Gordon Hall at Queen's University. In addition to these developments in the amyloid area, Walter and his collaborators have discovered some new exciting lead candidates showing high potency against malaria, a program that Walter characteristically continues to pursue. His current interests are focused on the applications of chemistry to problems of medical interest.

Walter has always been known as the Godfather of the carbohydrate family and the Prince of hospitality. He has served as a mentor to many young scientists, giving freely of his time to provide valuable advice in his unassuming way. He is truly a "great colleague next door" to many in the chemistry department at Queen's. This issue is dedicated to Walter for his many contributions to Canadian Chemistry. It is evidence of his profound influence on the next generations of chemists, and clearly demonstrates that the situation is not always "a fiasco", one of his favorite expressions. Indeed, one might venture to describe Walter's achievements with the expression, "How sweet it is".

B. Mario Pinto

© 2006 NRC Canada

TRIBUTE / HOMMAGE

« Une carrière aigre-douce »

Walter Szarek est né le 19 avril 1938 à St. Catharines (Ontario). En 1960, il obtient un baccalauréat spécialisé en chimie de l'Université McMaster, à Hamilton (Ontario). Au cours des étés de 1956 à 1958, il fait ses premières armes en chimie industrielle et en recherche à la société Ontario Paper, de Thorold (Ontario), où il examine l'oxydation alcaline de la lignine. Il étudie la chimie des alcaloïdes auprès du professeur David B. MacLean et obtient une maîtrise ès sciences de l'Université McMaster en 1962. Son mémoire de maîtrise porte alors sur l'élucidation des structures de l'annotine, de la famille des alcaloïdes du Lycopodium, catégorie d'alcaloïdes qui capte alors l'attention de bon nombre de sommités mondiales dans le domaine de la chimie des produits naturels au Canada. Ainsi, le célèbre « tandem des alcaloïdes », soit R.H.F. Manske et L. Marion, isolait pour la première fois l'annotine proprement dite à partir du Lycopodium annotinum du Canada. Outre Dave MacLean et Ian Spenser de l'Université McMaster, d'autres chercheurs ont étudié l'élucidation et la synthèse des étonnantes structures du Lycopodium, notamment K. Wiesner, Z. Valenta, W.A. Ayer et F.A.L. Anet. Walter Szarek, progressant pourtant à pas de géant dans son programme de doctorat, est soudain pris d'une certaine inquiétude qui le conduit à envisager une nouvelle orientation et d'autres sujets de recherche. C'est ainsi qu'en 1962, il entreprend un doctorat en chimie des glucides avec le professeur J.K.N. Jones, à l'Université Queen's de Kingston, en Ontario, qu'il achève en 1964.

Comme il a travaillé à la fois sur les alcaloïdes et sur les glucides, Walter Szarek se plaît à dire qu'il a connu une carrière « aigre-douce ». Sa thèse de doctorat à Queen's portait sur le remplacement de l'oxygène du cycle des glucides par l'azote. Parmi ses réalisations, notons le premier exemple de synthèse des glucides contenant un cycle à cinq atomes (4-acétamide-4-déoxy-L-erythrofuranoside de méthyle) et la rotation interne empêchée de tels glucides, démontrée par spectroscopie RMN. Ce domaine du remplacement de l'oxygène du cycle par d'autres structures hétérocycliques est demeuré dans l'ombre pendant de nombreuses années. Toutefois, la découverte de ce qu'il convient d'appeler des aza-sucres naturels – et le fait que certains de ces aza-sucres sont inhibiteurs de glycosidase et exercent d'autres activités biologiques d'intérêt thérapeutique potentiel – a suscité un immense intérêt, tant sur le plan chimique que biologique, pour ce type de composé chimique et pour d'autres analogues issus du remplacement de l'oxygène du cycle par du soufre ou du sélénium. C'est donc dire que certaines recherches stimulées par Walter Szarek se poursuivent encore aujourd'hui.

Walter Szarek allait devenir un acteur de premier plan dans le domaine de la glycobiologie. Aussitôt son doctorat terminé en 1964, il entreprend des travaux postdoctoraux auprès du professeur Melville L. Wolfrom, à l'Université d'État d'Ohio, à Columbus. Le professeur Wolfrom a mis sur pied la célèbre School of Carbohydrate Chemistry qui a accueilli des centaines d'étudiants et de détenteurs d'une bourse de perfectionnement postdoctoral provenant de nombreux pays. Le Canada n'étant pas en reste, les professeurs Raymond Lemieux, détenteur d'une bourse de perfectionnement postdoctoral, et Steve Hanessian, étudiant de troisième cycle, ont étudié avec le professeur Wolfrom. Eu égard à la taille importante du groupe d'étudiants du professeur Wolfrom, Walter Szarek a assumé la codirection des vieux laboratoires appelés « Sugar Alley » lors de son séjour en Ohio. Cette expérience s'est avérée des plus bénéfiques pour sa future carrière universitaire. En effet, moins d'un an plus tard, on lui offre le poste de chargé d'enseignement en biochimie au département de physiologie et de biochimie de l'Université Rutgers, au New Jersey. Bien qu'élaborant avec brio ses programmes de recherche, Walter Szarek aspire à un retour dans un département de chimie. En 1967, il retourne assumer une charge d'enseignement de la chimie à l'Université Queen's, où il enseigne toujours aujourd'hui. Il est promu professeur agrégé en 1971, puis professeur titulaire en 1976. De 1976 à 1985, il dirige également le Carbohydrate Research Institute de l'Université Queen's. Il est nommé professeur émérite en 2003 et demeure très actif dans le domaine de la recherche.

Non content de siéger auprès de maints comités, tant à l'Université Queen's qu'ailleurs, il mène une prestigieuse carrière d'enseignant au premier cycle comme aux cycles supérieurs. Lauréat de quatre prix en enseignement, dont le prix d'excellence de l'Université Queen's pour l'enseignement des arts et des sciences au premier cycle, en 1989, il mène parallèlement une brillante carrière de chercheur. À ce jour, 18 étudiants à la maîtrise ès science (diplôme obtenu), 29 étudiants au doctorat (diplôme obtenu) et quelque 85 détenteurs d'une bourse de perfectionnement postdoctoral ont étudié sous sa gouverne. Ses étudiants et les détenteurs de bourse de perfectionnement ne tarissent pas d'éloges pour son encadrement attentionné, tant dans le domaine de la chimie que devant les épreuves et tribulations de la vie quotidienne. À ce jour, on doit à Walter Szarek plus de 250 publications avérées, plus de 30 brevets délivrés et 11 chapitres de livre. Il a en outre dirigé la rédaction de deux ouvrages. En reconnaissance de ses réalisations dans le domaine de la recherche en glycobiologie, la Division of Carbohydrate Chemistry de l'American Chemical Society lui a décerné le prix Claude S. Hudson, en 1989, et le prix Melville L. Wolfrom, en 1992.

Walter Szarek affiche un intérêt des plus vastes pour les glucides. Ses publications en touchent pratiquement tous les aspects, dont la structure et la synthèse des glucides et des antibiotiques contenant des glucides, la conception des nucléosides biologiquement actifs, notamment les analogues carbocycliques, les aspects biochimiques, l'étude conformationnelle et mécaniste des réactions des glucides, la photochimie des glucides, l'analyse conformationnelle hétérocyclique, la synthèse des produits radiopharmaceutiques utilisés en tomographie par émission de positons, la chimie et les nouvelles applications de la vitamine C, l'oxydation microbiologique des glucides et de leurs produits dérivés, la transformation chimique des polysaccharides, la conception et la synthèse des glucides utilisés comme édulcorants, la théorie du goût sucré, les produits dérivés des glucides dans la synthèse énantiosélective de composés chimiques biologiquement actifs, la libération ciblée de médicaments, l'étude du lipopolysaccharide de bande A du Pseudomonas aeruginosa (un antigène commun), la mise au point de vaccins, les glucides oligomériques dans la nutrition parentérale et les inhibiteurs des glycosidases et des glycosyltransférases.

Tout au long de sa carrière, Walter Szarek s'est intéressé de près à la chimie médicale et à la mise au point de médicaments, des domaines auxquels il a apporté une contribution

© 2006 NRC Canada

d'envergure et durable. Au milieu des années 1980, il entreprend une collaboration avec Bob Kisilevsky, du département d'anatomie pathologique de l'Université Queen's, qui s'était intéressé aux produits amyloïdes dans la foulée d'une collaboration avec Michael Axelrad, du même département. M. Axelrad, lui-même atteint d'une amylose qui finit par l'emporter, avait entrepris des travaux sur les produits amyloïdes. Messieurs Kisilevsky et Szarek commencent à collaborer à un moment où le polymère glucidique glycosaminoglycan suscite de plus en plus d'intérêt du fait qu'il serait lié au dépôt d'amyloïde. À la fin de 1993, au terme d'une collaboration fructueuse, les deux collègues fondent Neurochem inc. à l'Université Queen's, en compagnie de Don Weaver, qui œuvre aujourd'hui à l'Université Dalhousie. Neurochem, société biopharmaceutique ouverte, a actuellement pignon sur rue à Laval (Québec). Ses jalons cliniques importants comprennent la mise au point de Fibrillex™ pour le traitement de l'amylose amyloïde, Alzhemed™ pour le traitement de la maladie d'Alzheimer et Cerebril™ pour le traitement des accidents vasculaires cérébraux hémorragiques causés par l'angiopathie amyloïde cérébrale. Dans tous les cas, les candidats-médicaments à l'essai ont été synthétisés dans le laboratoire de Walter Szarek, à l'immeuble Gordon Hall de l'Université Queen's. Parallèlement à leurs percées dans le domaine des produits amyloïdes, Walter Szarek et ses collaborateurs ont découvert de puissants candidats-médicaments très prometteurs contre la malaria, et ce, dans le cadre d'un programme que Szarek poursuit toujours, faut-il s'en étonner. Aujourd'hui, Walter Szarek s'intéresse plus particulièrement aux applications de la chimie à des problèmes qui présentent un intérêt sur le plan médical.

Walter Szarek a toujours été le parrain de la famille des glucides et le prince de l'hospitalité. Il a été pour bon nombre de jeunes scientifiques un mentor, donnant généreusement de son temps et prodiguant de précieux conseils, sans prétention aucune. Il représente pour de nombreux spécialistes du département de l'Université Queen's le collègue idéal. Nous rendons hommage à Walter Szarek pour son importante contribution à l'avancement de la chimie au pays. Les prochaines générations de chimistes pourront lui être grandement reconnaissantes, ce qui démontre hors de tout doute que tout ne se termine pas toujours en « fiasco », pour emprunter une expression qui lui est chère. S'il faut qualifier ses réalisations, oserons-nous affirmer qu'il a mené une carrière beaucoup moins « aigre » que « douce »!

B. Mario Pinto

© 2006 NRC Canada

Titanium pyridyl-phosphinimide complexes — Synthesis, structure, and ethylene polymerization catalysis

Chad Beddie, Pingrong Wei, and Douglas W. Stephan

Abstract: A series of Ti–pyridyl-phosphinimide complexes of the form $Cp'TiX_2[NPR_2(2\text{-}CH_2Py)]$ (Cp' = Cp, Cp*, R = *i*-Pr, *t*-Bu, X = Cl, Me) have been prepared and characterized. These complexes generate ethylene polymerization catalysts upon activation with MAO or $B(C_6F_5)_3$. The resulting polymers exhibit broad molecular weight distributions. The role of the pyridyl group is discussed in light of stoichiometric reactions of $CpTiCl_2[NPR_2(2\text{-}CH_2Py)]$ with $B(C_6F_5)_3$.

Key words: phosphinimide complexes, pyridyl-phosphinimides, olefin polymerization.

Résumé : On a préparé et caractérisé une série de complexes Ti–pyridyl-phosphinimide de la forme $Cp'TiX_2[NPR_2(2\text{-}CH_2Py)]$ (Cp' = Cp, Cp*, R = *i*-Pr, *t*-Bu, X = Cl, Me). Par activation avec du MAO ou du $B(C_6F_5)_3$, ces complexes peuvent générer des catalyseurs pour la polymérisation de l'éthylène. Les polymères ainsi obtenus présentent de larges distributions de poids moléculaires. On discute du rôle du groupe pyridyle à la lumière des réactions stoechiométriques du $CpTiCl_2[NPR_2(2\text{-}CH_2Py)]$ avec le $B(C_6F_5)_3$.

Mots clés : complexe du phosphimide, pyridyl-phosphimides, polymérisation d'oléfines.

[Traduit par la Rédaction]

Introduction

The quest for new and effective homogeneous olefin polymerization catalysts have prompted much interest in early transition metal chemistry over the last two decades. Studies of non-metallocene systems have probed a wide variety of novel ancillary ligands (1–3). In our own work we have described titanium catalysts that contain bulky-phosphinimide ligands. This family of compounds of the form $CpTi(NPR_3)Cl_2$ yield active ethylene polymerization catalysts upon activation by MAO (4–10), while activation of the species $Ti(t\text{-}Bu_3PN)_2Me_2$ by $B(C_6F_5)_3$ or $Ph_3C[B(C_6F_5)_4]$ provides a remarkably active catalyst, producing polyethylene of narrow polydispersity and relatively high molecular weight (7). Single-site or living polymerization catalysts typically afford narrow polydispersities (1.0–2.0), however, in practical terms such resins prove difficult to process (11, 12). Thus, while single-site polymerization offers access to unique polymers, such materials prompt other problems. A number of methods can be employed to alter both the molecular weight and the molecular weight distributions of resulting polymers. In some cases, controlled hydrogenolysis (13, 14) can be utilitzed to broaden the molecular weight distributions. Alternatively, sequential catalysts can be employed to produce bimodal resins (15–29). In attempting to address this issue, we are examining potential single-site catalyst precursors that offer the possibility of generating several single-site catalysts upon activation. To this end, we report the synthesis and evaluation of Ti–phosphinimide complexes that incorporate pendant pyridyl substituents. The notion here is that these substituents may interact with the Lewis acid activators in a reversible manner and thus afford the possibility of two or more catalysts in solution. In this, our first report employing this strategy, we describe the synthesis and characterization of such compounds and evaluate such species in ethylene polymerization catalysis. The effect of the pyridyl group on the polymer molecular weight distributions is considered and discussed.

Received 16 January 2006. Published on the NRC Research Press Web site at http://canjchem.nrc.ca on 12 May 2006.

C. Beddie, P. Wei, and D.W. Stephan.[1] Department of Chemistry and Biochemistry, University of Windsor, Windsor, ON N9B 3P4, Canada.

[1]Corresponding author (e-mail: stephan@uwindsor.ca).

Experimental

General data

All preparations were done under an atmosphere of dry, O_2-free N_2 employing both Schlenk line techniques and a MBraun inert atmosphere glovebox. Solvents were purified employing a Grubbs' type solvent purification system manufactured by Innovative Technology. All organic reagents were purified by conventional methods. ^1H, $^{31}P\{^1H\}$, and $^{13}C\{^1H\}$ NMR spectra were recorded on Bruker Avance-300 and -500 spectrometers. All spectra were recorded in C_6D_6 at 25 °C unless otherwise noted. All chemical shifts are reported in ppm. Trace amounts of protonated solvents were used as references and chemical shifts are reported relative to $SiMe_4$. $^{31}P\{^1H\}$ NMR spectra were referenced to external 85% H_3PO_4. Combustion analyses were done in-house employing a PerkinElmer CHN analyzer. The compounds $PR_2(2\text{-}CH_2Py)$ (R = *i*-Pr (**1**), *t*-Bu (**2**)) (30, 31), and $Me_3SiNP(i\text{-}Pr)_2(2\text{-}CH_2Py)$ (**3**) (32)) were prepared by literature methods. $CpTiCl_3$, Cp^*TiCl_3 ($Cp^* = Me_5Cp$), and

 doi:10.1139/V06-071 © 2006 NRC Canada

Me_3SiN_3 were purchased from Strem Chemical Co. and Sigma-Aldrich Chemical Co., respectively, and employed without further purification. MAO and Al(*i*-Bu)$_3$, as well as GPC analysis service, were generously provided by NOVA Chemicals Corp.

Synthesis of Me_3SiNP-*t*-Bu_2(2-CH_2Py) (4)

To a solution of **2** (1.99 g, 8.38 mmol) in toluene (30 mL) was added Me_3SiN_3 (2.24 mL, 16.9 mmol). The resulting solution was heated at refluxing temperature for 48 h. The volume of the solution was reduced to ca. 5 mL, and the solution was filtered through Celite. The remaining solvent and excess Me_3SiN_3 were removed under vacuum, resulting in a pale yellow oil. Yield: 2.06 g, 6.36 mmol, 76%. ^{1}H NMR δ: 8.41 (d, 1H, $^3J_{H-H}$ = 4 Hz, Py), 7.44 (m, 1H, Py), 7.17 (m, 1H, Py), 6.65 (m, 1H, Py), 3.14 (d, 2H, $^2J_{P-H}$ = 11 Hz, CH_2), 1.04 (d, 18H, $^3J_{P-H}$ = 14 Hz, *t*-Bu), 0.30 (s, 9H, $SiMe_3$). ^{13}C{^{1}H} NMR δ: 157.0 (d, $^2J_{P-C}$ = 7 Hz, Py, (ipso-C)), 149.4 (s, Py), 135.3 (s, Py), 126.1 (s, Py), 121.6 (s, Py), 37.5 (d, $^1J_{P-C}$ = 61 Hz, *t*-Bu), 34.8 (d, $^1J_{P-C}$ = 53 Hz, CH_2), 27.8 (s, *t*-Bu), 5.3 (s, $SiMe_3$). ^{31}P{^{1}H} NMR δ: 25.9 (s).

Syntheses of Cp′$TiCl_2$[NPR_2(2-CH_2Py)] (Cp′ = Cp, *i*-Pr (5), *t*-Bu (6), Cp′ = Cp*, R = *i*-Pr (7), *t*-Bu (8))

These complexes were prepared in similar fashions and thus only one preparation is detailed. To a yellow slurry of $CpTiCl_3$ (0.370 g, 1.69 mmol) in toluene (40 mL) was added a solution of **3** (0.501 g, 1.69 mmol) in toluene (10 mL). The resulting solution was stirred for 12 h at room temperature. The solvent and volatile products were removed under vacuum to cause the formation of a yellow crystalline solid, which was washed with hexanes and dried under vacuum. Yield: 0.641 g, 1.57 mmol, 93%. **5**: ^{1}H NMR δ: 8.25 (br, 1H, Py), 7.40 (m, 1H, Py), 7.15 (m, 1H, Py), 6.58 (m, 1H, Py), 6.34 (s, 5H, Cp), 2.97 (d, 2H, $^2J_{P-H}$ = 13 Hz, CH_2), 1.68 (d(sept), 2H, $^3J_{P-H}$ = 10 Hz, $^3J_{H-H}$ = 7 Hz, CH), 0.94 (dd, 6H, $^3J_{P-H}$ = 16 Hz, $^3J_{H-H}$ = 7 Hz, Me) 0.86 (dd, 6H, $^3J_{P-H}$ = 17 Hz, $^3J_{H-H}$ = 7 Hz, Me). ^{13}C{^{1}H} NMR δ: 153.1 (d, $^2J_{P-C}$ = 7 Hz, Py (ipso-C)), 149.7 (s, Py), 135.6 (s, Py), 126.6 (s, Py), 122.6 (s, Py), 115.5 (s, Cp), 33.8 (d, $^1J_{P-C}$ = 51 Hz, CH_2), 27.3 (d, $^1J_{P-C}$ = 59 Hz, CH), 16.1 (d, $^2J_{P-C}$ = 6 Hz, Me). ^{31}P{^{1}H} NMR δ: 31.7 (s). Elemental anal. calcd.: C 50.15, H 6.19, N 6.88; found: C 49.95, H 6.41, N 6.76. X-ray quality crystals were obtained via slow evaporation of a toluene solution. **6**: Yield: 0.320 g, 0.735 mmol, 75%. ^{1}H NMR δ: 8.32 (d, 1H, $^3J_{H-H}$ = 5 Hz, Py), 7.65 (d, 1H, $^3J_{H-H}$ = 8 Hz, Py), 7.26 (m, 1H, Py), 6.63 (dd, 1H, $^3J_{H-H}$ = 6 Hz, $^3J_{H-H}$ = 6 Hz, Py), 6.26 (s, 5H, Cp), 3.06 (d, 2H, $^2J_{P-H}$ = 11 Hz, CH_2), 1.07 (d, 18H, $^3J_{P-H}$ = 15 Hz, *t*-Bu). ^{13}C{^{1}H} NMR δ: 153.7 (d, $^2J_{P-C}$ = 8 Hz, Py, (ipso-C)), 149.6 (s, Py), 136.7 (s, Py), 127.7 (d, $^3J_{P-C}$ = 3 Hz, Py), 122.6 (s, Py), 115.7 (s, Cp), 39.5 (d, $^1J_{P-C}$ = 51 Hz, *t*-Bu), 33.0 (d, $^1J_{P-C}$ = 46 Hz, CH_2), 27.4 (s, *t*-Bu). ^{31}P{^{1}H} NMR δ: 36.6 (s). Elemental anal. calcd.: C 52.44, H 6.72, N 6.44; found: C 52.34, H 6.69, N 6.33. X-ray quality crystals were obtained via slow evaporation of a toluene solution. **7**: Yield: 0.748 g, 1.57 mmol, 92%. ^{1}H NMR δ: 8.24 (d, 1H, $^3J_{H-H}$ = 4 Hz, Py), 7.18 (d, 1H, $^3J_{H-H}$ = 6 Hz, Py), 7.06 (m, 1H, Py), 6.55 (dd, 1H, $^3J_{H-H}$ = 6 Hz, $^3J_{H-H}$ = 6 Hz, Py), 3.39 (d, 2H, $^2J_{P-H}$ = 15 Hz, CH_2), 2.18 (s, 15H, Cp*), 1.93 (d(sept), 2H, $^3J_{P-H}$ = 10 Hz, $^3J_{H-H}$ = 7 Hz, CH), 1.07 (dd, 6H, $^3J_{P-H}$ = 16 Hz, $^3J_{H-H}$ = 7 Hz, Me), 0.94 (dd, 6H, $^3J_{P-H}$ = 16 Hz, $^3J_{H-H}$ = 7 Hz, Me). ^{13}C{^{1}H} NMR δ: 154.2 (d, $^2J_{P-C}$ = 7 Hz, Py, (ipso-C)), 149.7 (s, Py), 135.8 (s, Py), 126.3 (s, Cp*), 126.2 (s, Py), 122.1 (s, Py), 35.1 (d, $^1J_{P-C}$ = 51 Hz, CH_2), 27.6 (d, $^1J_{P-C}$ = 59 Hz, CH), 16.6 (d, $^2J_{P-C}$ = 2 Hz, Me), 16.3 (d, δ: $^2J_{P-C}$ = 2 Hz, Me), 13.5 (s, Cp*). Elemental anal. calcd.: C 55.36, H 7.39, N 5.87; found: C 55.13, H 7.49, N 5.58. ^{31}P{^{1}H} NMR δ: 30.6 (s). X-ray quality crystals were obtained via slow evaporation of a toluene solution. **8**: Yield: 0.561 g, 1.11 mmol, 72%. ^{1}H NMR δ: 8.28 (d, 1H, $^3J_{H-H}$ = 4 Hz, Py), 7.61 (d, 1H, $^3J_{H-H}$ = 6 Hz, Py), 7.16 (m, 1H, Py), 6.59 (dd, 1H, $^3J_{H-H}$ = 6 Hz, $^3J_{H-H}$ = 6 Hz, Py), 3.59 (d, 2H, $^2J_{P-H}$ = 14 Hz, CH_2), 2.19 (s, 15H, Cp*), 1.17 (d, 18H, $^3J_{P-H}$ = 15 Hz, *t*-Bu). ^{13}C{^{1}H} NMR δ: 154.9 (d, $^2J_{P-C}$ = 7 Hz, Py, (ipso-C)), 149.4 (s, Py), 136.7 (s, Py), 127.1 (d, $^3J_{P-C}$ = 4 Hz, Py), 126.2 (s, Cp*), 122.3 (s, Py), 39.5 (d, $^1J_{P-C}$ = 52 Hz, *t*-Bu), 35.7 (d, $^1J_{P-C}$ = 45 Hz, CH_2), 28.1 (s, *t*-Bu), 13.5 (s, Cp*). ^{31}P{^{1}H} NMR δ: 38.0 (s). Elemental anal. calcd.: C 56.23, H 7.59, N 5.70; found: C 56.52, H 7.75, N 5.65. X-ray quality crystals were obtained via slow evaporation of a toluene solution.

Syntheses of $CpTiCl_2$[NPR_2(2-CH_2Py)]·$B(C_6F_5)_3$ (R = *i*-Pr (9), *t*-Bu (10))

These complexes were prepared in similar fashions and thus only one preparation is detailed. To a yellow solution of $CpTiCl_2$[NP(*i*-Pr)$_2$(2-CH_2Py)] (**5**) (0.020 g, 0.49 mmol) in benzene (2 mL) was added a solution of $B(C_6F_5)_3$ (0.025 g, 0.049 mmol) in benzene (2 mL). The resulting clear yellow solution was stirred for 5 min. The solvent was removed under vacuum to produce a yellow solid. Yield: 0.044 g, 0.48 mmol, 98%. **9**: ^{1}H NMR δ: 9.46 (d, 1H, $^3J_{H-H}$ = 8 Hz, Py), 8.35 (m, 1H, Py), 7.53 (m, 1H, Py), 6.35 (m, 1H, Py), 6.24 (s, 5H, Cp), 3.43 (dd, 1H, $^2J_{P-H}$ = 12 Hz, $^3J_{H-H}$ = 16 Hz, CH_2), 3.13 (dd, 1H, $^2J_{P-H}$ = 12 Hz, $^3J_{H-H}$ = 16 Hz, CH_2), 1.69 (d(sept), 1H, $^2J_{P-H}$ = 9 Hz, $^3J_{H-H}$ = 7 Hz, CH), 0.94 (m, 1H, CH), 0.76 (dd, 3H, $^3J_{P-H}$ = 17 Hz, $^3J_{H-H}$ = 7 Hz, Me), 0.74 (dd, 3H, $^3J_{P-H}$ = 17 Hz, $^3J_{H-H}$ = 7 Hz, Me), 0.69 (dd, 3H, $^3J_{P-H}$ = 17 Hz, $^3J_{H-H}$ = 7 Hz, Me), 0.29 (dd, 3H, $^3J_{P-H}$ = 17 Hz, $^3J_{H-H}$ = 7 Hz, Me). ^{13}C{^{1}H} NMR (partial, some resonances in the C_6F_5 rings could not be observed) δ: 153.4 (s, Py (ipso-C)), 148.9 (s, Py), 148.2 (br d, $^1J_{C-F}$ ~ 240 Hz, C_6F_5), 143.8 (s, Py), 138.1 (br d, $^1J_{C-F}$ ~ 230 Hz, C_6F_5), 131.6 (s, Py), 124.2 (s, Py), 116.3 (s, Cp), 28.3 (d, $^1J_{P-C}$ = 51 Hz, CH_2), 28.2 (d, $^1J_{P-C}$ = 60 Hz, CH), 28.1 (d, $^1J_{P-C}$ = 59 Hz, CH), 16.2 (s, Me), 15.8 (d, $^2J_{P-C}$ = 3 Hz, Me), 15.3 (s, Me), 15.2 (d, $^2J_{P-C}$ = 3 Hz, Me). ^{11}B{^{1}H} NMR δ: –3.4 (s). ^{19}F NMR δ: –126.4 (dd, 1F, $^3J_{F-F}$ = 25 Hz, $^3J_{F-F}$ = 25 Hz), –127.0 (br, 1F), –130.4 (d, 1F, $^3J_{F-F}$ = 23 Hz), –132.6 (br, 2F), –135.2 (dd, 1F, $^3J_{F-F}$ = 25 Hz, $^3J_{F-F}$ = 25 Hz), –153.7 (dd, 1F, $^3J_{F-F}$ = 21 Hz, $^3J_{F-F}$ = 21 Hz), –154.1 (dd, 1F, $^3J_{F-F}$ = 21 Hz, $^3J_{F-F}$ = 21 Hz), –155.8 (dd, 1F, $^3J_{F-F}$ = 21 Hz, $^3J_{F-F}$ = 21 Hz), –160.8 (m, 1F), –162.0 (m, 1F), –162.1 (m, 1F), –162.6 (m, 1F), –163.3 (m, 1F), –164.0 (m, 1F). ^{31}P{^{1}H} NMR δ: 30.2 (s). Elemental anal. calcd.: C 45.74, H 2.74, N 3.05; found: C 45.33, H 3.04, N 2.93. **10**: Yield: 0.037 g, 0.39 mmol, 85%. ^{1}H NMR δ: 9.63 (d, 1H, $^3J_{H-H}$ = 8 Hz, Py), 8.42 (m, 1H, Py), 7.52 (m, 1H, Py), 6.37 (m, 1H, Py), 6.30 (s, 5H, Cp), 3.59 (dd, 1H, $^2J_{P-H}$ = 13 Hz, $^3J_{H-H}$ = 18 Hz, CH_2), 2.88 (dd, 1H, $^2J_{P-H}$ = 9 Hz, $^3J_{H-H}$ = 18 Hz, CH_2), 0.85 (d, 9H, $^3J_{P-H}$ = 15 Hz, *t*-Bu), 0.68

© 2006 NRC Canada

(d, 9H, $^3J_{P-H}$ = 16 Hz, *t*-Bu). $^{13}C\{^1H\}$ NMR (partial): 153.8 (s, Py, (ipso-C)), 149.4 (s, Py), 143.6 (s, Py), 137.8 (br d, $^1J_{C-F}$ ~ 260 Hz, C_6F_5), 131.8 (s, Py), 124.1 (s, Py), 116.5 (s, Cp), 40.3 (d, $^1J_{P-C}$ = 53 Hz, $C(CH_3)_3$), 39.6 (d, $^1J_{P-C}$ = 53 Hz, *t*-Bu), 26.9 (s, *t*-Bu), 26.6 (s, *t*-Bu), 26.1 (d, $^1J_{P-C}$ = 41 Hz, CH_2). $^{11}B\{^1H\}$ NMR δ: –3.4 (s). ^{19}F NMR δ: –125.8 (dd, 1F, $^3J_{F-F}$ = 25 Hz, $^3J_{F-F}$ = 25 Hz), –126.6 (br, 1F), –130.9 (d, 1F, $^3J_{F-F}$ = 25 Hz), –131.7 (br, 1F), –132.8 (m, 1F), –135.5 (m, 1F), –153.6 (dd, 1F, $^3J_{F-F}$ = 20 Hz, $^3J_{F-F}$ = 20 Hz), –154.6 (dd, 1F, $^3J_{F-F}$ = 20 Hz, $^3J_{F-F}$ = 20 Hz), –155.8 (dd, 1F, $^3J_{F-F}$ = 20 Hz, $^3J_{F-F}$ = 20 Hz), –160.8 (m, 1F), –160.8 (m, 1F), –161.7 (m, 1F), –162.4 (m, 2F), –162.8 (m, 1F), –163.6 (m, 1F). $^{31}P\{^1H\}$ NMR δ: 36.3 (s). Elemental anal. calcd.: C 46.92, H 3.09, N 2.96; found: C 47.33, H 2.94, N 2.70.

Synthesis of $Cp^*TiMe_2[NP\text{-}t\text{-}Bu_2(2\text{-}CH_2Py)]$ (11)

To a yellow suspension of **8** (0.306 g, 0.605 mmol) in a mixture of diethyl ether (30 mL) and toluene (50 mL) cooled to –78 °C was added 3.0 mol/L MeMgCl in THF (0.38 mL, 1.14 mmol). The resulting yellow suspension was stirred at –78 °C for ~20 min and then was slowly warmed to room temperature over a period of 1.5 h. The solvent was removed under vacuum, and the crude residue was extracted with hexanes. The suspension was filtered through Celite and the solvent was removed under vacuum to yield a crude brown solid. Subsequent recrystallization attempts from hexanes produced a yellow solid that was 95% pure by NMR analysis. Yield: 0.155 g, 0.336 mmol, 59%. ^1H NMR δ: 8.39 (d, 1H, $^3J_{H-H}$ = 4 Hz, Py), 7.61 (d, 1H, $^3J_{H-H}$ = 6 Hz, Py), 7.16 (m, 1H, Py), 6.63 (m, 1H, Py), 3.35 (d, 2H, $^2J_{P-H}$ = 12 Hz, CH_2), 2.04 (s, 15H, Cp*), 1.21 (d, 18H, $^3J_{P-H}$ = 14 Hz, *t*-Bu), 0.41 (s, 6H, $TiMe_2$). $^{13}C\{^1H\}$ NMR δ: 156.2 (d, $^2J_{P-C}$ = 6 Hz, Py, (ipso-C)), 149.6 (s, Py), 135.9 (s, Py), 127.1 (s, Py), 122.0 (s, Py), 118.8 (s, Cp*), 44.5 (s, $TiMe_2$, 39.4 (d, $^1J_{P-C}$ = 54 Hz, *t*-Bu), 36.1 (d, $^1J_{P-C}$ = 45 Hz, CH_2), 28.2 (s, *t*-Bu), 12.6 (s, Cp*). $^{31}P\{^1H\}$ NMR δ: 22.9 (s). Elemental anal. calcd.: C 67.23, H 9.76, N 6.03; found: C 66.16, H 9.97, N 6.25.

Polymerization protocol

Polymerization experiments were performed using a glass Büchi polymerization reactor. Toluene (600 mL) was transferred into the reactor, heated to 30 °C ± 2 °C, and presaturated with ethylene prior to injection of catalyst and cocatalyst. The solution was stirred at 1000 rpm for the duration of the polymerization experiment. At the end of the experiments, the polymer was collected and treated as previously described (9). For the catalyst precursors (**5**–**10**), polymerization experiments were conducted for 30 min employing MAO as the cocatalyst. In these polymerizations, 500 equiv. of MAO was injected into the reactor and the solution was stirred for 5 min prior to injecting a toluene solution of the precatalyst. Catalyst concentrations of 100 μmol/L were employed, thus 0.060 mmol of catalyst in 8 mL of toluene was injected. In the case of **11**, 1, 2, and 10 equiv. of $B(C_6F_5)_3$ were used as the cocatalyst, while 20 equiv. of $Al(i\text{-}Bu)_3$ was used as a scavenger. Catalyst concentrations of 20 μmol/L were employed, thus 0.012 mmol of catalyst in 4 mL of toluene was injected. These polymerization experiments were conducted for 10 min.

X-ray data collection and reduction

Crystals were manipulated and mounted in capillaries in a glovebox, thus maintaining a dry, O_2-free environment for each crystal. Diffraction experiments were performed on a Siemens SMART System CCD diffractometer. The data were collected in a hemisphere of data in 1329 frames with 10 s exposure times. The observed extinctions were consistent with the space groups in each case. The data sets were collected ($4.5° < 2\theta < 45–50.0°$). A measure of decay was obtained by recollecting the first 50 frames of each data set. The intensities of reflections within these frames showed no statistically significant change over the duration of the data collections. The data were processed using the SAINT and XPREP processing packages. An empirical absorption correction based on redundant data was applied to each data set. Subsequent solution and refinement was performed using the SHELXTL solution package operating on a Pentium computer.

Structure solution and refinement

Non-hydrogen atomic scattering factors were taken from the literature tabulations (33). The heavy atom positions were determined using direct methods employing the SHELXTL direct-methods routine. The remaining non-hydrogen atoms were located from successive difference Fourier map calculations. The refinements were carried out by using full-matrix least-squares techniques on *F*, minimizing the function $\omega(|F_o| - |F_c|)^2$, where the weight (ω) is defined as $4F_o^2/2\sigma(F_o^2)$ and F_o and F_c are the observed and calculated structure factor amplitudes, respectively. In the final cycles of each refinement, all non-hydrogen atoms were assigned anisotropic temperature factors in the absence of disorder or insufficient data. In the latter cases, atoms were treated isotropically. C-H atom positions were calculated and allowed to ride on the carbon to which they are bonded, assuming a C—H bond length of 0.95 Å. H-atom temperature factors were fixed at 1.10 times the isotropic temperature factor of the C-atom to which they are bonded. The H-atom contributions were calculated, but not refined. The locations of the largest peaks in the final difference Fourier map calculation, as well as the magnitude of the residual electron densities in each case, were of no chemical significance. Additional details are provided in the supplementary data.[2]

Results and discussion

The phosphinimine ligands, $Me_3SiNPR_2(2\text{-}CH_2Py)$ (R = *i*-Pr (**3**) (32), *t*-Bu (**4**)), were prepared in conventional fashion

[2] Supplementary data for this article are available on the journal Web site (http://canjchem.nrc.ca) or may be purchased from the Depository of Unpublished Data, Document Delivery, CISTI, National Research Council Canada, Ottawa, ON K1A 0R6, Canada. DUD 5031. For more information on obtaining material refer to http://cisti-icist.nrc-cnrc.gc.ca/irm/unpub_e.shtml. CCDC 233404–233407 contain the crystallographic data for this manuscript. These data can be obtained, free of charge, via http://www.ccdc.cam.ac.uk/conts/retrieving.html (Or from the Cambridge Crystallographic Data Centre, 12 Union Road, Cambridge CB2 1EZ, UK; fax +44 1223 336033; or deposit@ccdc.cam.ac.uk).

© 2006 NRC Canada

Scheme 1.

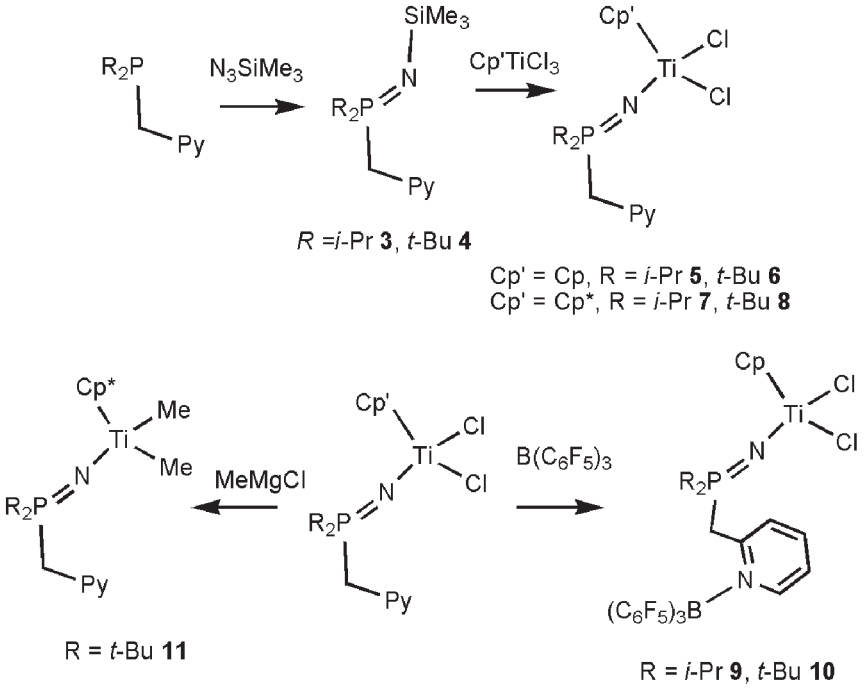


Table 1. Crystallographic data for **5**–**8**.

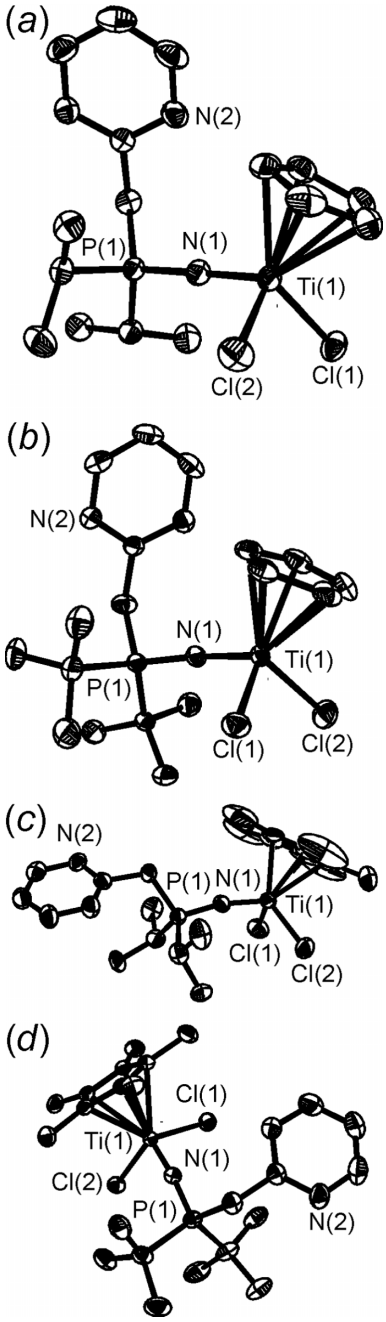
	5	**6**	**7**	**8**
Formula	$C_{17}H_{25}Cl_2N_2PTi$	$C_{19}H_{29}Cl_2N_2PTi$	$C_{22}H_{35}Cl_2N_2PTi$	$C_{24}H_{39}Cl_2N_2PTi$
Formula weight	407.16	435.21	477.29	505.34
a (Å)	26.51(1)	9.745(6)	20.41(1)	9.773(5)
b (Å)	8.170(4)	12.713(8)	7.769(4)	17.010(9)
c (Å)	18.58(1)	17.94(1)	16.455(9)	16.414(9)
β (°)	97.87(1)	98.34(1)	102.29(1)	99.04(1)
Crystal system	Monoclinic	Monoclinic	Monoclinic	Monoclinic
Space group	*C*2/*c*	$P2_1/n$	$P2_1/c$	$P2_1/c$
Volume (Å^3)	3987(4)	2199(2)	2549(2)	2695(3)
D_{calcd} (g cm^{-3})	1.357	1.314	1.244	1.246
Z	8	4	4	4
Abs. coeff. (μ, mm^{-1})	0.778	0.710	0.618	0.589
θ Range (°)	2.21–23.29	1.97–23.24	2.04–23.38	1.74–23.23
Total reflections	8193	9012	10 674	11 234
Data $F_o^2 > 3\sigma(F_o^2)$	2839	3138	3676	3839
Parameters	208	226	253	271
R (%)	0.0312	0.0351	0.0554	0.0349
R_w (%)	0.0849	0.0909	0.1270	0.0895
Goodness-of-fit	1.010	1.026	0.859	1.031

Note: Data collected at 20 °C; Mo Kα radiation (λ = 0.710 69 Å); $R = \Sigma||F_o| - |F_c||/\Sigma|F_o|$; $R_w = [\Sigma(|F_o| - |F_c|)^2/\Sigma|F_o|^2]^{1/2}$.

from reaction of the precursor phosphines (30) with Me_3SiN_3 in toluene at refluxing temperatures. These products were characterized by ^1H, $^{31}P\{^1H\}$, and $^{13}C\{^1H\}$ NMR spectroscopy, and all data were consistent with the proposed formulation. The corresponding Ti complexes, Cp′$TiCl_2[NPR_2(2\text{-}CH_2Py)]$ (Cp′ = Cp, R = *i*-Pr (**5**), *t*-Bu (**6**); Cp′ = Cp*, R = *i*-Pr (**7**), *t*-Bu (**8**)), were prepared via reaction of the phosphinimine ligands, $Me_3SiNPR_2(2\text{-}CH_2Py)$ (R = *i*-Pr (**3**) (32), R = *t*-Bu (**4**)), with the precursors $CpTiCl_3$ and Cp*$TiCl_3$, respectively (Scheme 1). Similar preparative methods for species of the form Cp′$Ti(NPR_3)Cl_2$ have been previously described (9). Spectroscopic data for **5**–**8** were as expected and elemental analyses were consistent with the formulations. Single crystal X-ray data were also obtained for these complexes (Table 1) (Fig. 1). All of these complexes are monomeric as expected, with pseudo-tetrahedral geometries at Ti with the coordination sphere comprised of a η^5-bound Cp or Cp* ligand, an N-bound phosphinimide, and

© 2006 NRC Canada

Fig. 1. ORTEP diagrams (30% probability ellipsoids) of (*a*) **5**, (*b*) **6**, (*c*) **7**, (*d*) **8**. Hydrogen atoms have been omitted for clarity.



two chloride ligands. Metric parameters (Table 2) are similar to those reported for related compounds (4, 9, 34–37). The P-N-Ti bond angles for complexes **5**–**8** are approximately linear at 173.8(1)°, 170.9(2)°, 165.0(3)°, and 166.5(2)°, respectively, and are within the range of 158.7(1)° to 178.38(11)° for related titanium phosphinimide compounds (34, 37). The smaller P-N-Ti angles for **7** and **8** are attributable to the greater electron donation and steric demand of the Cp* ligand. This view is also consistent with the longer Ti—N distances for complexes **7** and **8** (1.775(4) and 1.792(2) Å) compared with those in **5** and **6** (1.768(2) and 1.761(2) Å). Similarly, the P—N bond lengths for compounds **5** and **6** (1.607(2) and 1.609(2) Å) are longer than those for **7** and **8** (1.600(4) and 1.597(2) Å). The orientation of the pyridyl substituent of the phosphinimide ligands varies. In **5** and **6**, this substituent is oriented in the general direction of the Cp ligand, while in **7** and **8**, it projects away from the Cp* ligand. This is presumably a steric effect. No preferred orientation of the nitrogen atom of the pyridyl group is observed and there is no intra- or inter-molecular interactions of this donor atom with the Lewis acidic Ti center.

Table 2. Metric parameters (bond lengths and angles) for **5**–**8**.

	5	**6**	**7**	**8**
Bond lengths (Å)				
Ti1—N1	1.768(2)	1.761(2)	1.775(4)	1.792(2)
N1—P1	1.607(2)	1.609(2)	1.599(4)	1.597(2)
Ti1—Cl1	2.337(1)	2.315(1)	2.307(2)	2.330(1)
Ti1—Cl2	2.320(1)	2.331(1)	2.319(2)	2.323(1)
Bond angles (°)				
Ti1-N1-P1	173.8(1)	170.9(2)	165.2(3)	166.5(2)
N1-Ti1-Cl1	103.12(8)	103.24(8)	102.8(1)	104.18(9)
N1-Ti1-Cl2	102.70(7)	104.23(8)	103.0(2)	101.47(8)
Cl1-Ti1-Cl2	101.48(3)	99.54(6)	101.31(9)	100.70(4)

Table 3. Ethylene polymerization data and MAO activation.

Precat.	M_n	M_w	PDI	Activity (g mmol^{-1} h^{-1} atm^{-1})
5	23 700	635 400	26.8	19
6	37 700	417 300	11.1	5.6
7	22 500	229 300	10.2	3
8	81 400	323 000	4	0.89
9	112 400	556 900	5	7.7
10	67 000	534 800	8	2

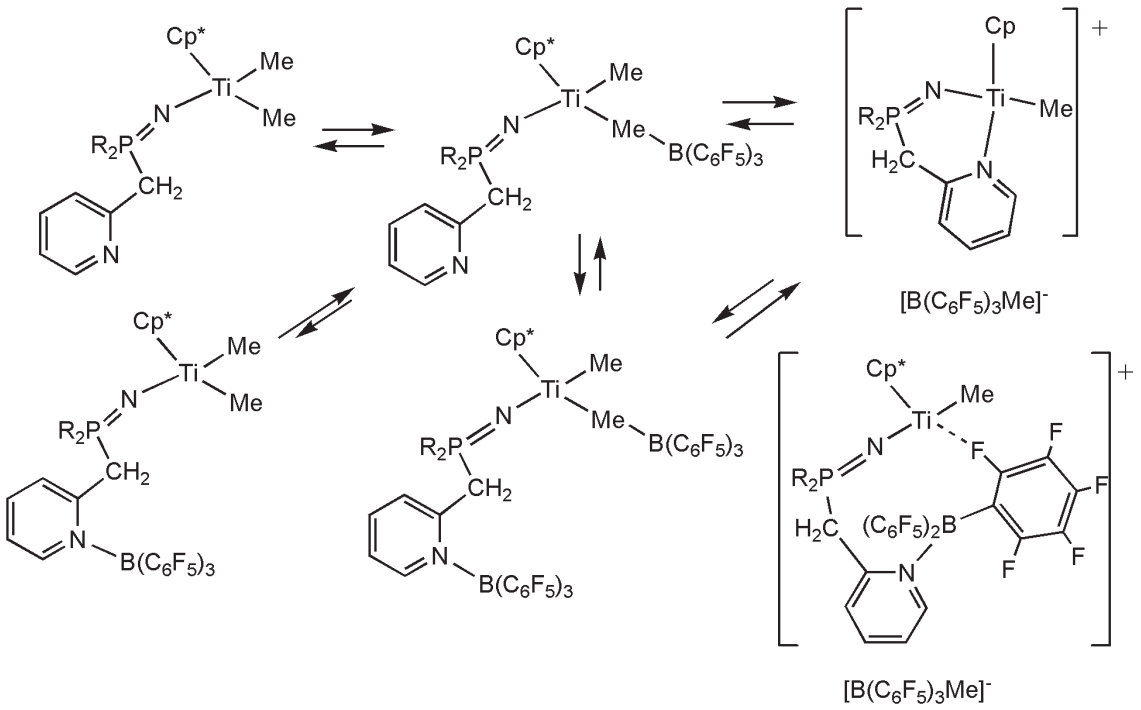
Note: Conditions for polymerization: ethylene pressure = 2 atm, T = 30 °C, toluene, [catalyst] = 100 µmol/L, 500 equiv. MAO.

Polymerization

The complexes **5**–**8** were tested as ethylene polymerization precatalysts using a Büchi polymerization reactor at 30 °C for 30 min in toluene, under an atmosphere of 2 atm of ethylene (1 atm = 101.325 kPa). A precatalyst concentration of 100 µmol/L was used and 500 equiv. of MAO was used as cocatalyst (Table 3). The resulting polymers have molecular weight (M_w) ranges from approximately 200 000 to 600 000 g/mol with polydispersity indices (PDI) varying from 4 to 26. These relatively high molecular weights together with high PDIs suggest that there may be several active catalyst species generated in solution. Certainly, these species do not behave as single site catalysts, nonetheless, such systems are of interest as they may provide polymers with desirable processability. In terms of activities, complex **5** displayed moderate activity (18 g mmol^{-1} h^{-1} atm^{-1}), while complexes **6**–**8** showed low activity. These results stand in contrast to previous results that demonstrated a high activity catalyst was derived from $CpTiCl_2(NP\text{-}t\text{-}Bu_3)$ under similar conditions (4, 9). These data also contrast the polymerization activity observed for $Cp^*TiCl_2[NP(t\text{-}Bu)_2(CH_2Ph)]$ under similar conditions (142 g mmol^{-1} h^{-1} atm^{-1}) (38). Clearly,

© 2006 NRC Canada

Scheme 2.



the only structural difference between **8** and $Cp^*TiCl_2[NP(t\text{-}Bu)_2(CH_2Ph)]$ is the N atom of the pyridine ring, and thus efforts to query the role of this atom were undertaken.

$B(C_6F_5)_3$ adducts

In an attempt to sequester any potential interference of the pyridyl group in the polymerization process, the complexes **5** and **6** were treated with $B(C_6F_5)_3$ producing donor–acceptor complexes of the general formula, $CpTiCl_2[NPR_2(2\text{-}CH_2Py)]\cdot B(C_6F_5)_3$ (R = *i*-Pr (**9**), *t*-Bu (**10**) (Scheme 1). $^{31}P\{^1H\}$, ^1H, ^{19}F, and $^{13}C\{^1H\}$ NMR data were consistent with the formulation. In particular, the $^{19}F\{^1H\}$ NMR spectra revealed 15 resonances for both **9** and **10**, indicating complexation and the inequivalence of all F atoms in the $B(C_6F_5)_3$ fragment. The downfield ^1H NMR shifts of the protons ortho to N in **5** and **6** upon reaction with the borane were greater than 1 ppm, consistent with B—N donor–acceptor bond formation. It is a noteworthy comparison that no reaction is observed between $CpTiCl_2(NP\text{-}t\text{-}Bu_3)$ and $B(C_6F_5)_3$ at 25 °C (39). The proposed structures of **9** and **10** were not confirmed crystallographically, despite numerous attempts to acquire suitable crystals.

The species **9** and **10** were evaluated as precatalysts for ethylene polymerization activity. Aliquots of the freshly prepared solutions were employed. The polymerization experiments were conducted in an identical fashion to those described previously (Table 3). The resulting activities of the catalysts derived from **9** and **10** were significantly lower than those derived from **5** and **6**, respectively. However, the causes of these observations remain unclear. It is likely that MAO competes with $B(C_6F_5)_3$ for coordination to the pyridyl N. Thus, the notion that one might use of coordination of borane to the pyridyl group to provide a sterically crowded phosphinimide ligand in situ is clearly simplistic.

Table 4. Ethylene polymerization data and $B(C_6F_5)_3$ activation.

Precat.	$B(C_6F_5)_3$ (equiv.)	Activity (g $mmol^{-1}$ h^{-1} atm^{-1})
11	1	47
11	2	120
11	10	75

Note: Conditions for polymerization: ethylene pressure = 2 atm, T = 30 °C, toluene, [catalyst] = 20 μmol/L, [TiBAl] = 400 μmol/L, 10 min.

Reaction of MeMgX with **5**–**7** resulted in mixtures of products that could not be separated despite exhaustive attempts to effect extraction, selective precipitation, or crystallization. These difficulties are thought to arise from the known acidity of the methylene protons of the pyridyl-phosphinimide ligand. For example, it is known that reaction of *n*-BuLi with **3** results in the formation of $Li(THF)_2[Me_3SiNP(i\text{-}Pr)_2(2\text{-}CHPy)]$ (32). Nonetheless, the species $Cp^*TiMe_2[NP(t\text{-}Bu)_2(2\text{-}CH_2Py)]$ (**11**) (Scheme 1) was successfully produced from reaction of MeMgCl with **8**, although multiple extractions with hexanes and subsequent reprecipitations were required to effect adequate purification.

Ethylene polymerization catalysis were examined using **11** and 1, 2, and 10 equiv. of $B(C_6F_5)_3$ as a cocatalyst (Table 4). These data reveal that **11**–$B(C_6F_5)_3$ is a much more active catalyst system than those derived from **8**–MAO. Interestingly, increasing the amount of borane from 1 to 2 equiv. prompted an increase in the polymerization activity from 47 to 120 g $mmol^{-1}$ h^{-1} atm^{-1}. In the presence of a larger excess of $B(C_6F_5)_3$, i.e., 10 equiv., a polymerization activity of 75 g $mmol^{-1}$ h^{-1} atm^{-1} was observed. Molecular weight distributions (GPC analysis) in these polymerizations were precluded by solubility problems, presumably a result of polymer molecular weights exceeding the limit of the instrumentation (i.e., >1 000 000 g mol^{-1}). It is noteworthy

© 2006 NRC Canada

that use of $B(C_6F_5)_3$ to activate Ti–phosphinimide catalysts has previously been shown to give rise to high molecular weight polymers in comparison to the similar systems in which MAO was employed as the activator (4–10).

The above polymerization data show that increasing from 1 to 2 equiv. of borane appears to increase the concentration of the active catalyst, while further increases in cocatalyst concentration reduce the observed activity. This suggests the involvement of several equilibria governing the concentration of the active catalyst(s). While the precise nature of these species involved remains unclear, it is tempting to speculate that such species could involve interaction of $B(C_6F_5)_3$ with the Ti-bound alkyl groups or the pyridyl group, chelation of the pyridyl fragment to Ti, or interaction of the Ti center with the pyridyl-bound $B(C_6F_5)_3$ (Scheme 2).

In conclusion, a series of Ti–pyridyl-phosphinimide complexes generate ethylene polymerization catalysts upon activation with MAO or $B(C_6F_5)_3$. While these catalysts do not exhibit the exceptional activity of previously reported Ti–phosphinimides, the presence of the pyridyl substituents appears to result in polymers with broadened molecular weight distributions. While the cause of this effect is the subject of speculation, the potential of a substituent modification approach to the alteration of the polydispersity remains a subject of on-going study.

Acknowledgements

Financial support from the Natural Sciences and Engineering Research Council of Canada (NSERC), NOVA Chemicals Corporation, and the Ontario Research and Development Challenge Fund (ORDCF) is gratefully acknowledged.

References

1. G.G. Hlatky. Coord. Chem. Rev. **181**, 243 (1999).
2. G.G. Hlatky. Coord. Chem. Rev. **199**, 235 (2000).
3. G.J.P. Britovsek, V.C. Gibson, and D.F. Wass. Angew. Chem. Int. Ed. **38**, 428 (1999).
4. D.W. Stephan, J.C. Stewart, F. Guerin, R.E.v.H. Spence, W. Xu, and D.G. Harrison. Organometallics, **18**, 1116 (1999).
5. D.W. Stephan. Macromol. Symp. **173**, 105 (2001).
6. D.W. Stephan. Can. J. Chem. **80**, 125 (2002).
7. D.W. Stephan, F. Guerin, R.E.v.H. Spence, L. Koch, X. Gao, S.J. Brown, J.W. Swabey, Q. Wang, W. Xu, P. Zoricak, and D.G. Harrison. Organometallics, **18**, 2046 (1999).
8. D.W. Stephan, J.C. Stewart, S.J. Brown, J. Swabey, J. William, and Q. Wang. US Patent 6 342 463, 2002.
9. D.W. Stephan, J.C. Stewart, F. Guerin, S. Courtenay, J. Kickham, E. Hollink, C. Beddie, A. Hoskin, T. Graham, P. Wei, R.E.v.H. Spence, W. Xu, L. Koch, X. Gao, and D.G. Harrison. Organometallics, **22**, 1937 (2003).
10. D.W. Stephan. Organometallics, **23**, 5240 (2004).
11. H.H. Zabusky and R.F. Heitmiller. SPE Trans. **4**, 17 (1964).
12. R.B. Wilson, Jr. PCT Int. Application, WO 5892079, 1999.
13. M.S.A. Kunzel, F.-Q. Liu, H.W. Roesky, M. Noltemeyer, H.-G. Schmidt, and I. Uson. J. Chem. Soc. Dalton Trans. 913 (1996).
14. R. Blom and I.M. Dahl. Macromol. Chem. Phys. **202**, 719 (2001).
15. Z.J.A. Komon and G.C. Bazan. Macromol. Rapid Commun. **22**, 467 (2001).
16. J.D. Kim and J.B.P. Soares. J. Polym. Sci. Part A: Polym. Chem. **38**, 1427 (2000).
17. L. Li, M.V. Metz, H. Li, M.-C. Chen, T.J. Marks, L. Liable-Sands, and A.L. Rheingold. J. Am. Chem. Soc. **124**, 12725 (2002).
18. I. Jaber and S.J. Brown. PCT Int. Application, WO 200001724, 2000.
19. P. Marechal. Eur. Patent Application, EP1195388, 2002.
20. E. Van Praet, P. Lehmus, and K. Kallio. Polyolefins 2001: International Conference on Polyolefins, Houston, Texas, 25–28 February 2001. p. 236.
21. M. Vaehaelae, H. Salminen, and A. Lehtinen. PCT Int. Application, WO 2001062847, 2001.
22. J.B.P. Soares and J.D. Kim. J. Polym. Sci. Part A: Polym. Chem. **38**, 1408 (2000).
23. R.I. Mink, T.E. Nowlin, S.D. Schregenberger, P.P. Shirodkar, and G.O. Tsien. PCT Int. Application, WO 9702294, 1997.
24. D.H. McConville, D.R. Loveday, M.W. Holtcamp, J.F. Szul, K.A. Erickson, S. Mawson, T.H. Kwack, F.J. Karol, D.J. Schreck, M.G. Goode, P.T. Daniell, M.G. McKee, and C.C. Williams. *In* PCT Int. Application, WO 2001030861, 2001.
25. W. Michalke, S. Kreitmeier, M. Lang, A. Buchner, and D. Goritz. Comp. Theoret. Polym. Sci. **11**, 459 (2001).
26. P.J. Maddox, D. Pratt, and J.P. McNally. Eur. Patent Application, EP676421, 1995.
27. A.K. Lindahl, H. Oysaed, and R. Goris. Eur. Patent Application, EP1146077, 2001.
28. A.K. Kulshreshtha and S.K. Awasthi. Pop. Plast. Packag. **45**, 53 (2000).
29. A. Follestad, V. Almquist, U. Palmqvist, and H. Hokkanen. *In* PCT Int. Application, WO 994016, 1999.
30. A. Jansen and S. Pitter. Monatsh. Chem. **130**, 783 (1999).
31. P.G. Edwards, I.A. Fallis, and B.S. Yong. British Patent Application, GB2378182, 2003.
32. W.-P. Leung, Z.-X. Wang, H.-W. Li, Q.-C. Yang, and T.C.W. Mak. J. Am. Chem. Soc. **123**, 8123 (2001).
33. D.T. Cromer and J.B. Mann. Acta Crystallogr. Sect. A, **A24**, 321 (1968).
34. K. Dehnicke, M. Krieger, and W. Massa. Coord. Chem. Rev. **182**, 19 (1999).
35. M.D. Mikoluk, R. McDonald, and R.G. Cavell. Inorg. Chem. **38**, 2791 (1999).
36. C.-A. Carraz and D.W. Stephan. Organometallics, **19**, 3791 (2000).
37. F. Guerin, C.L. Beddie, D.W. Stephan, R.E.v.H. Spence, and R. Wurz. Organometallics, **20**, 3466 (2001).
38. E. Hollink, P. Wei, and D.W. Stephan. Can. J. Chem. **82**, 1304 (2004).
39. E. Hollink. Ph.D. dissertation, University of Windsor, Windsor, Ontario. 2004.

© 2006 NRC Canada

Indium(I) iodide promoted cleavage of dialkyl disulfides — Application of the Michael addition of thiolate anions to conjugated carbonyl compounds and regioselective ring opening of epoxides

Brindaban C. Ranu and Tanmay Mandal

Abstract: Indium(I) iodide promotes cleavage of dialkyl disulfides generating thiolate anions that then undergo facile addition to α,β-unsaturated ketones, aldehydes, carboxylic esters, and nitriles under neutral conditions producing corresponding β-ketosulfides or β-cyanosulfides. This strategy has also been used for the regioselective nucleophilic ring opening of epoxides by thiolate anions in presence of indium(III) chloride producing corresponding β-hydroxyphenyl sulfides. The reactions are in general, very clean, high yielding, and reasonably fast. Thus, simple and convenient procedures for the synthesis of β-ketosulfides or β-cyanosulfides and β-hydroxyalkyl sulfides have been developed using this cleavage reaction.

Key words: indium(I) iodide, Michael addition, β-ketosulfide, β-cyanosulfide, epoxide, β-hydroxy sulfide.

Résumé : L'iodure d'indium(I) facilite le clivage des disulfures d'alkyles et génère la formation d'anions thiolates qui peuvent ensuite s'additionner facilement sur des cétones, des aldéhydes, des esters carboxyliques et des nitriles α,β-insaturés, dans des conditions neutres, pour conduire à la formation des β-céto ou β-cyanosulfures correspondants. On a aussi utilisé cette stratégie pour l'ouverture de cycle nucléophile et régiosélective d'époxydes par des anions thiolates en présence de chlorure d'indium(III) qui conduisent à la formation des sulfures de β-hydroxyphényle. Les réactions sont, en général, très propres et elles donnent des rendements élevés rapidement. Des méthodes simples et faciles utilisant cette réaction de clivage permettent donc de synthétiser des β-cétosulfures ou des β-cyanosulfures ainsi que des sulfures de β-hydroxyalkyles.

Mots clés : iodure d'indium(I), addition de Michael, β-cétosulfure, β-cyanosulfure, époxyde, β-hydroxysulfure.

[Traduit par la Rédaction]

Introduction

The importance of indium reagents in organic synthesis has been well-demonstrated through novel protocols for carbon–carbon bond formation, rearrangements, and a variety of other useful transformations over past few years (1) and increasing interest in this area is continuing (2). As a part of our activities in indium-mediated reactions (3), we are constantly looking for new indium reagents and we reported the application of indium(I) iodide (4) for the cleavage of diphenyl diselenide and disulfide followed by in situ condensation with alkyl halide (4*a*, 4*b*). We also communicated the cleavage of dialkyl disulfides promoted by InI followed by subsequent Michael addition of thiolate anions to conjugated carbonyl compounds (4*c*). We have now discovered another application of this protocol for regioselective ring opening of epoxides by thiolate anions in presence of indium(III) chloride to provide β-hydroxy sulfides. We wish to report here the results of our earlier communication (4*c*) in detail together with this new observation (Scheme 1).

The β-oxy- and β-hydroxy-sulfides are very useful molecules as they constitute a common structural component in a vast group of natural products (5). Some of the synthetic molecules are found to have biological and pharmaceutical activities (6). These molecules are also very useful intermediates in organic synthesis (7). Many methods are available in the literature for the synthesis of β-oxy- (8) and β-hydroxy-sulfides (9) and these are primarily based on reaction with thiols under base or acid catalysis. However, many of them suffer from disadvantages of harsh reaction conditions, poor regioselectivity, unsatisfactory yields, long reaction times, and are associated with undesirable side reactions owing to the oxidation of thiol or rearrangement of epoxides. Since β-oxy- and β-hydroxy-sulfides have become increasingly useful and important in organic synthesis, development of simple, efficient, and mild procedures for their

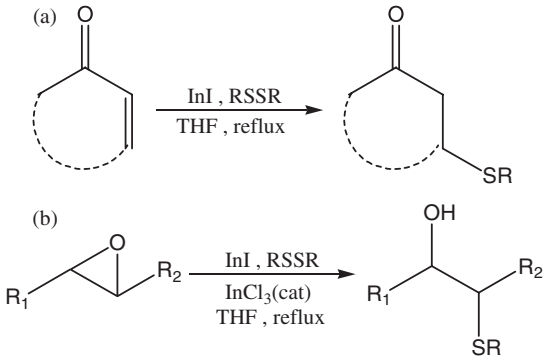
Received 21 December 2005. Published on the NRC Research Press Web site at http://canjchem.nrc.ca on 17 May 2006.

B.C. Ranu[1] and T. Mandal. Department of Organic Chemistry, Indian Association for the Cultivation of Science, Jadavpur, Kolkata – 700 032, India.

[1]Corresponding author (e-mail: ocbcr@iacs.res.in).

 doi:10.1139/V06-065 © 2006 NRC Canada

Scheme 1.



synthesis are highly desirable. Thus, we sought an alternative approach replacing thiol by a more stable sulphur reagent and we found that dialkyl disulfide can do this job more efficiently (Scheme 1).

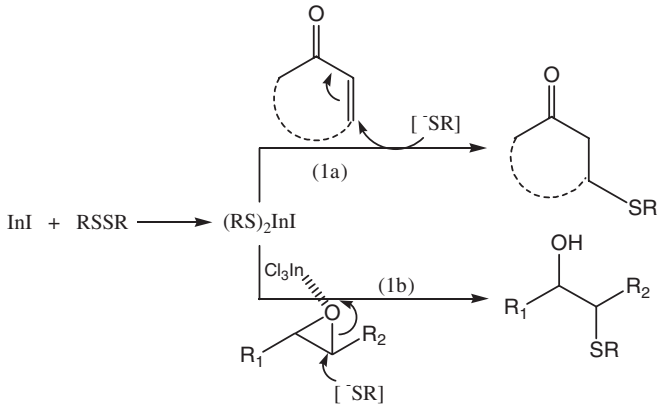
Results and discussion

The experimental procedures for both of these reactions are very simple and convenient. A solution of dialkyl disulfide and activated alkene in THF was heated under reflux in the presence of indium(I) iodide and the Michael adduct was isolated by the usual workup. On the other hand, a stirred solution of indium(I) iodide, dialkyl disulfide, and epoxide in dry THF was heated under reflux in the presence of a catalytic amount of indium trichloride (5 mol%) (TLC) and quenched with a few drops of water. Extraction with ether and the usual workup produced a pure product.

Several α,β-unsaturated ketones, aldehydes, and carboxylic esters underwent facile Michael additions to dithiolate anions generated by the cleavage of disulfides by this procedure to provide the corresponding adducts in high yields. Conjugated nitriles were also found to react with the thiolate anions, although the yields are relatively low compared with those with carbonyl compounds. The results are summarized in Table 1. Aliphatic as well as aromatic disulfides are found to undergo cleavage and subsequent reaction. On the other hand, both cyclic and acyclic conjugated carbonyl compounds participate in this reaction as Michael acceptors.

A wide range of structurally diverse epoxides underwent cleavages by reaction with dialkyl or diaryl disulfides by this procedure to provide the corresponding β-hydroxysulfides in high yields. The results are summarized in Table 2. The cleavages are highly regio- and stereo-selective. As expected, attack of thiolate anion occurred at the less-hindered carbon atom of the terminal alkyl-substituted epoxides (Table 2, entries 1–5). However, an aryl-substituted epoxide (Table 2, entry 6) attack occurs at the benzylic carbon atom. The cyclic epoxides (Table 2, entries 7–12) produced stereospecifically trans-diequatorial β-hydroxysulfides. In case of open-chain, α-keto aryl epoxides (Table 2, entries 13–15) thiolate anion also stitched at the benzylic carbon producing the corresponding γ-keto-β-hydroxysulfides. In all cases, the syn orientation of hydroxy and thiophenyl were observed as revealed by their coupling constants in ^{1}H NMR. The nonaromatic cyclic α-keto epoxides (Table 2, entries 16–18) underwent the attack of thiolate anion to the epoxycarbon atom α to the carbonyl group and simultaneous dehydration

Scheme 2.



occurred under the reaction process to produce the corresponding α-thiophenyl α,β-unsaturated ketones, although in β-methyl epoxyketone (Table 2, entry 18), a minor product (20%) from the β attack was isolated. However, in the case of α-methyl-α,β-epoxyketone (Table 2, entry 19) α-methyl-α-thiophenyl-β-hydroxyketone was obtained, as dehydration is not feasible.

In general, the reactions are considerably fast, clean, and high yielding. Presumably, these reactions are going through the intermediacy of bis(phenylthiophenyl)iodoindium(III), formed readily by the oxidative insertion of equimolar quantities of InI to diphenyl disulfide, which then releases thiolate anion to trigger the Michael addition and epoxide cleavage under the catalysis of $InCl_3$ (Scheme 2). It has also been observed that the epoxide cleavage reactions did not proceed at all without the presence of $InCl_3$.

In conclusion, this one-pot procedure for the synthesis of β-oxy- and β-hydroxyalkyl sulfides has been developed involving indium(I) iodide mediated cleavage of diorganyl disulfides and subsequent reaction with conjugated carbonyl compounds and epoxides. The significant advantages offered by this method are operational simplicity, relatively fast reaction, neutral and mild reaction conditions, general applicability, high regio- and stereo-selectivity, and good yields. Thus, it provides a better and practical alternative to the existing procedures (8, 9). Moreover, this constitutes a novel approach demonstrating the synthetic potential of indium(I) iodide, and further useful applications of this reagent are in progress.

Experimental

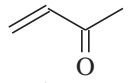
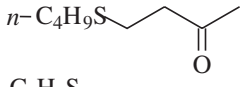
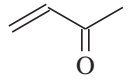
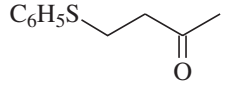
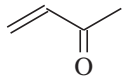
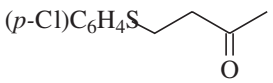
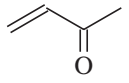
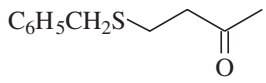
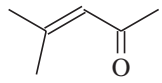
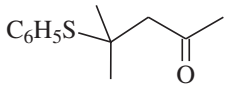
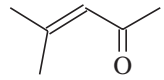
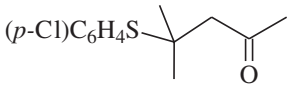
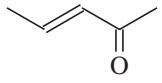
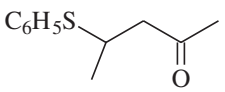
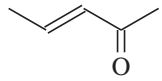
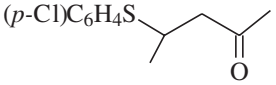
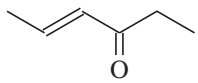
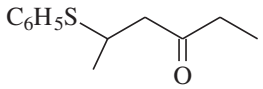
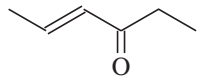
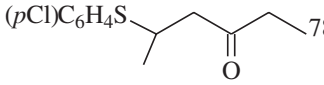
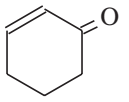
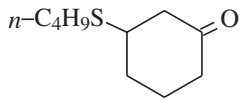
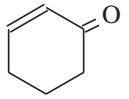
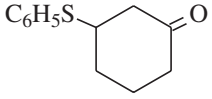
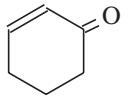
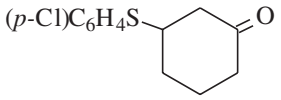
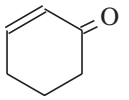
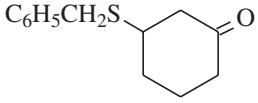
General experimental procedure

Representative procedure for the cleavage of diphenyl disulfide and subsequent reaction with methyl vinyl ketone (Table 1, entry 2)

Indium(I) iodide (121 mg, 0.5 mmol) was added to a solution of diphenyl disulfide (109 mg, 0.5 mmol) in freshly distilled tetrahydrofuran (2.5 mL) under an argon atmosphere followed by the addition of methyl vinyl ketone (70 mg, 1 mmol). The reaction mixture was heated under reflux for 2.5 h (TLC). THF was then evaporated off and the residue was quenched with water and extracted with diethyl ether (3 × 10 mL). The ether extract was washed with water and

© 2006 NRC Canada

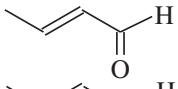
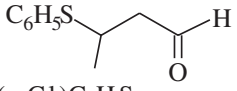
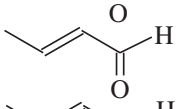
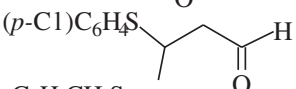
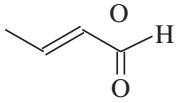
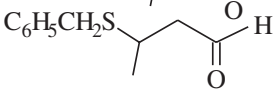
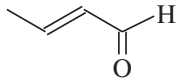
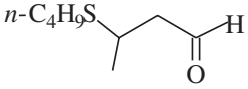
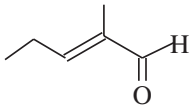
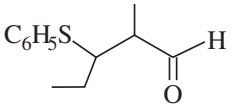
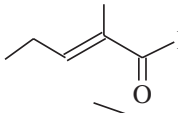
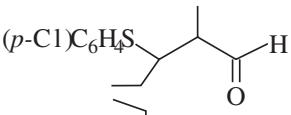
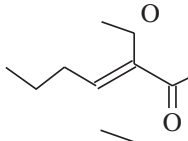
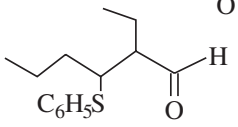
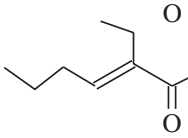
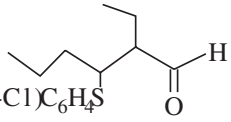
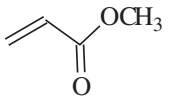
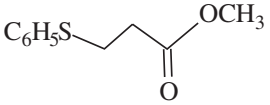
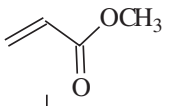
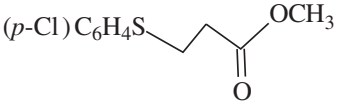
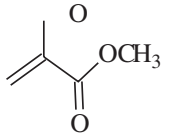
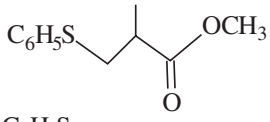
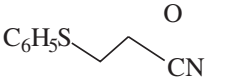
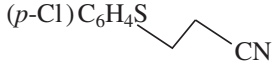
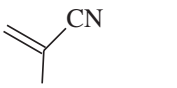
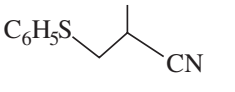
Table 1. InI-mediated cleavage of disulfides followed by Michael addition.

Entry	Disulfide	Substrate	Time (h)	Product	Yield (%)[a]	Ref.
1	n-C_4H_9S-S-n-C_4H_9		3.0		85	8*a*
2	C_6H_5S-SC_6H_5		2.5		86	10
3	(*p*-Cl)C_6H_4S-SC_6H_4(*p*-Cl)		2.5		85	
4	$C_6H_5CH_2$S-S$CH_2C_6H_5$		3.0		82	11
5	C_6H_5S-SC_6H_5		2.5		85	8*e*
6	(*p*-Cl)C_6H_4S-SC_6H_4(*p*-Cl)		3.0		81	
7	C_6H_5S-SC_6H_5		2.5		82	
8	(*p*-Cl)C_6H_4S-SC_6H_4(*p*-Cl)		3.0		80	
9	C_6H_5S-SC_6H_5		2.25		80	
10	(*p*-Cl)C_6H_4S-SC_6H_4(*p*-Cl)		3.0		78	
11	n-C_4H_9S-S-n-C_4H_9		2.5		90	8*e*
12	C_6H_5S-SC_6H_5		1.5		95	11
13	(*p*-Cl)C_6H_4S-SC_6H_4(*p*-Cl)		2.0		92	8*f*
14	$C_6H_5CH_2$S-S$CH_2C_6H_5$		2.5		89	11

dried (Na_2SO_4). The aqueous extract containing indium derivatives was discarded, although in relatively large-scale reactions indium salts may be recovered. Evaporation of the solvent left the crude product, which was purified by column chromatography over silica gel (hexane–ether, 95:5) to provide the pure addition product, 4-phenylsulfanylbutan-2-one (155 mg, 86%) as a colourless liquid. IR (neat, cm^{-1}) ν: 1716, 1477. ^{1}H NMR (300 MHz, $CDCl_3$) δ: 2.14 (s, 3H), 2.76 (t, J = 7.26 Hz, 2H), 3.13 (t, J = 7.26 Hz, 2H), 7.20–7.22 (m, 2H), 7.26–7.35 (m, 3H). ^{13}C NMR (75 MHz, $CDCl_3$) δ: 27.9, 30.5, 43.5, 126.7, 127.9, 129.4 (2C), 130.0 (2C). These values are in good agreement with those reported for this compound (10). Several Michael adducts are known and are identified by comparison of their spectroscopic data with those reported. The new compounds are characterized by their spectroscopic data and elemental analysis. The data for a few selective representative compounds are provided here.

© 2006 NRC Canada

Table 1 (*concluded*).

Entry	Disulfide	Substrate	Time (h)	Product	Yield (%)[a]	Ref.
15	C_6H_5S-SC_6H_5		2.5		92	8*e*
16	(*p*-Cl)C_6H_4S-SC_6H_4(*p*-Cl)		3.0		90	
17	$C_6H_5CH_2S$-$SCH_2C_6H_5$		3.5		82	
18	n-C_4H_9S-S-n-C_4H_9		4.0		80	8*e*
19	C_6H_5S-SC_6H_5		3.0		80 (61:39)[b]	
20	(*p*-Cl)C_6H_4S-SC_6H_4(*p*-Cl)		3.5		78 (59:41)[b]	
21	C_6H_5S-SC_6H_5		3.0		80 (53:47)[b]	
22	(*p*-Cl)C_6H_4S-SC_6H_4(*p*-Cl)		3.5		76 (51:49)[b]	
23	C_6H_5S-SC_6H_5		4.0		73	8*e*
24	(*p*-Cl)C_6H_4S-SC_6H_4(*p*-Cl)		4.25		70	
25	C_6H_5S-SC_6H_5		5.0		60	8*e*
26	C_6H_5S-SC_6H_5		4.0		72	8*e*
27	(*p*-Cl)C_6H_4S-SC_6H_4(*p*-Cl)		4.5		65	
28	C_6H_5S-SC_6H_5		5.0		55	

[a]Yields refer to those of pure isolated products characterized by spectroscopic data (IR and ^{1}H and ^{13}C NMR).
[b]Ratio of diastereoisomers as determined by ^{1}H NMR.

4-(4-Chlorophenylsulfanylbutan-2-one (Table 1, entry 3)

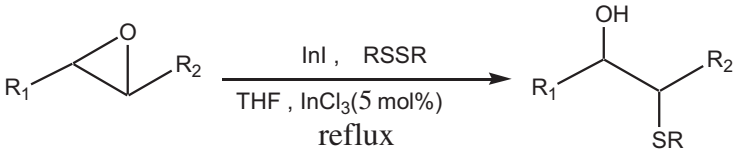
Colourless liquid. IR (neat, cm^{-1}) ν: 1438, 1477, 1578, 1716. ^{1}H NMR (300 MHz, $CDCl_3$) δ: 2.14 (s, 3H), 2.73 (t, *J* = 7.2 Hz, 2H), 3.10 (t, *J* = 7.2 Hz, 2H), 7.25 (s, 4H). ^{13}C NMR (75 MHz, $CDCl_3$) δ: 28.1, 30.5, 43.3, 129.5 (2C), 131.2 (2C), 132.8, 134.7, 206.7. Anal. calcd. for $C_{10}H_{11}ClOS$: C 55.94, H 5.16; found: C 55.81, H 5.09.

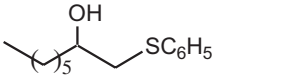
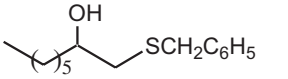
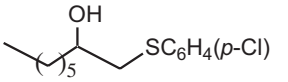
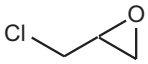
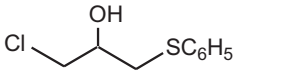
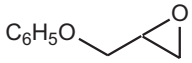
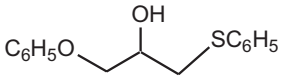
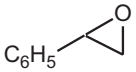
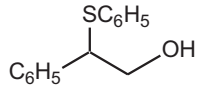
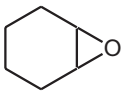
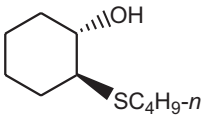
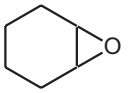
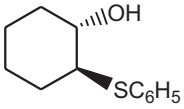
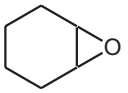
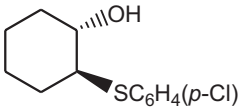
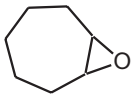
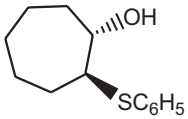
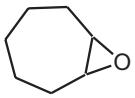
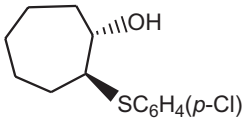
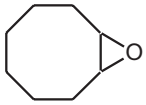
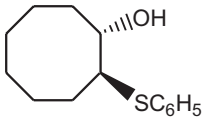
4-(4-Chlorophenylsulfanyl)-4-methyl-pentan-2-one (Table 1, entry 6)

Colourless liquid. IR (neat, cm^{-1}) ν: 1438, 1473, 1573, 1715. ^{1}H NMR (300 MHz, $CDCl_3$) δ: 1.36 (s, 6H), 2.11 (s, 3H), 2.62 (s, 2H), 7.28 (d, *J* = 8.4 Hz, 2H), 7.41 (d, *J* = 8.4 Hz, 2H). ^{13}C NMR (75 MHz, $CDCl_3$) δ: 28.1 (2C), 32.0, 47.2, 54.2, 128.8 (2C), 129.8, 136.9, 138.7 (2C), 206.2.

© 2006 NRC Canada

Table 2. Cleavages of epoxides by dialkyl and diaryl disulfides.



Entry	Epoxide	R	Time (h)	Product	Yield (%)[a]	Ref.
1		C_6H_5	3.0		98	9*g*
2		$C_6H_5CH_2$	4.0		78	9*b*
3		C_6H_4(*p*-Cl)	4.5		80	
4		C_6H_5	2.5		76	9*g*
5		C_6H_5	3.0		80	9*g*
6		C_6H_5	2.75		60	9*b*
7		*n*-C_4H_9	4.5		69	9*b*
8		C_6H_5	3.0		82	9*e*
9		C_6H_4(*p*-Cl)	3.0		80	
10		C_6H_5	3.5		82	9*g*
11		C_6H_4(*p*-Cl)	3.5		72	
12		C_6H_5	3.5		78	9*g*

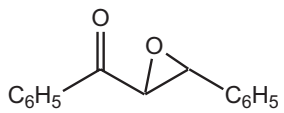
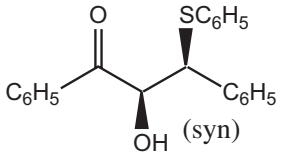
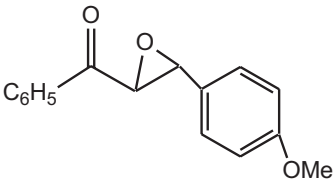
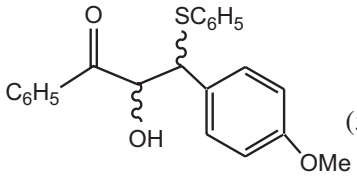
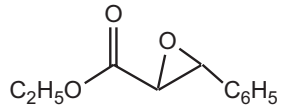
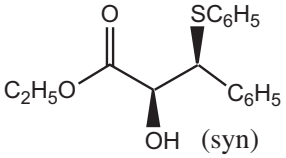
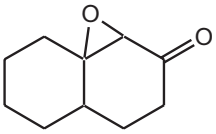
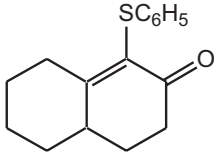
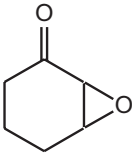
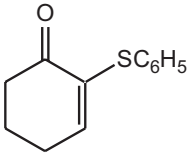
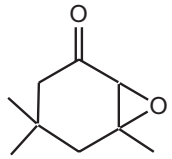
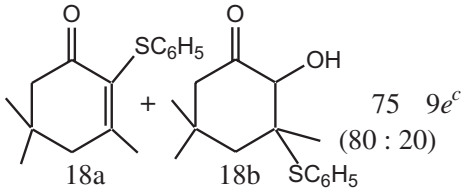
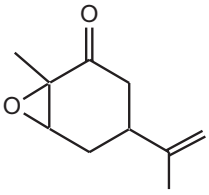
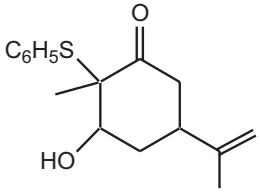
Anal. calcd. for $C_{12}H_{15}ClOS$: C 59.37, H 6.23; found: C 59.22, H 6.09.

4-Phenylsulfanylpentan-2-one (Table 1, entry 7)

Colourless liquid. IR (neat, cm^{-1}) ν: 1438, 1477, 1583, 1714. ^1H NMR (300 MHz, $CDCl_3$) δ: 1.28 (d, J = 6.6 Hz, 3H), 2.12 (s, 3H), 2.55 (dd, J_1 = 8.5 Hz, J_2 = 17.0 Hz, 1H), 2.75 (dd, J_1 = 5.3 Hz, J_2 = 17.0 Hz, 1H), 3.63–3.72 (m, 1H), 7.22–7.35 (m, 3H), 7.39–7.49 (m, 2H). ^{13}C NMR (75 MHz, $CDCl_3$) δ: 20.9, 30.5, 38.1, 50.2, 127.1, 128.8 (2C), 132.3 (2C), 134.1, 206.4. Anal. calcd. for $C_{11}H_{14}OS$: C 68.00, H 7.26; found: C 67.73, H 7.11.

© 2006 NRC Canada

Table 2 (*concluded*).

Entry	Epoxide	R	Time (h)	Product	Yield (%)[a]	Ref.
13		C_6H_5	2.25	 (syn)	81	
14		C_6H_5	2.5		80 (52:48)[b]	
15		C_6H_5	5.5	 (syn)	85	
16		C_6H_5	3.25		70	
17		C_6H_5	3.0		75	9*e*
18		C_6H_5	2.75	 18a 18b	75 (80 : 20)	9*e*[c]
19		C_6H_5	3.0		76	9*e*

[a]Yields refer to pure isolated products characterized by spectroscopic data (IR and ^{1}H and ^{13}C NMR).
[b]The ratio was determined by ^{1}H NMR spectroscopic data.
[c]Corresponds to compound 18a.

4-(4-Chlorophenylsulfanyl)pentan-2-one (Table 1, entry 8)

Colourless liquid. IR (neat, cm^{-1}) ν: 1475, 1716. ^{1}H NMR (300 MHz, $CDCl_3$) δ: 1.27 (d, J = 6.5 Hz, 3H), 2.12 (s, 3H), 2.55 (dd, J_1 = 8.3 Hz, J_2 = 17.2 Hz, 1H), 2.72 (dd, J_1 = 5.3 Hz, J_2 = 17.2 Hz, 1H), 3.65 (m, 1H), 7.26 (d, J = 8.6 Hz, 2H), 7.33 (d, J = 8.6 Hz, 2H). ^{13}C NMR (75 MHz, $CDCl_3$) δ: 20.9, 30.5, 38.4, 50.0, 129.0 (2C), 132.5, 133.4, 133.6 (2C), 206.2. Anal. calcd. for $C_{11}H_{13}ClOS$: C 57.76, H 5.73; found: C 57.84, H 5.81.

5-Phenylsulfanyl-hexan-3-one (Table 1, entry 9)

Colourless liquid. IR (neat, cm^{-1}) ν: 1477, 1712. ^{1}H NMR (300 MHz, $CDCl_3$) δ: 1.03 (t, J = 7.3 Hz, 3H), 1.27 (d, J = 6.7 Hz, 3H), 2.39 (q, J = 14.8 Hz, 2H), 2.53 (dd, J = 8.5 Hz, 16.9 Hz, 1H), 2.73 (dd, J = 5.3 Hz, 16.9 Hz, 1H), 3.71 (m, 1H), 7.23–7.32 (m, 3H), 7.38–7.42 (m, 2H). ^{13}C NMR (75 MHz, $CDCl_3$) δ: 7.5, 20.9, 36.6, 38.2, 48.9, 124.5, 127.1 (2C), 132.2 (2C), 134.2, 209.2. Anal. calcd. for $C_{12}H_{16}OS$: C 69.19, H 7.74; found: C 68.93, H 7.60.

© 2006 NRC Canada

5-(4-Chlorophenylsulfanyl)hexan-3-one (Table 1, entry 10)

Colourless liquid. IR (neat, cm^{-1}) ν: 1475, 1714. ^1H NMR (300 MHz, $CDCl_3$) δ: 1.03 (t, *J* = 7.3 Hz, 3H), 1.26 (d, *J* = 6.7 Hz, 3H), 2.39 (q, *J* = 14.3 Hz, 2H), 2.52 (dd, *J* = 8.3 Hz, 16.4 Hz, 1H), 2.69 (dd, *J* = 5.5 Hz, 16.3 Hz, 1H), 3.68 (m, 1H), 7.25 (d, *J* = 8.5 Hz, 2H), 7.33 (d, *J* = 8.5 Hz, 2H). ^{13}C NMR (75 MHz, $CDCl_3$) δ: 7.5, 20.9, 36.6, 38.5, 48.8, 128.9 (2C), 132.8, 132.9, 133.3 (2C), 208.9. Anal. calcd. for $C_{12}H_{15}ClOS$: C 59.37, H 6.23; found: C 59.21, H 6.07.

3-(4-Chlorophenylsulfanyl)butanal (Table 1, entry 16)

Colourless liquid. IR (neat, cm^{-1}) ν: 1437, 1475, 1724. ^1H NMR (300 MHz, $CDCl_3$) δ: 1.34 (d, *J* = 6.6 Hz, 3H), 2.54–2.73 (m, 2H), 3.63–3.69 (m, 1H), 7.23–7.37 (m, 4H), 9.74 (t, *J* = 1.5 Hz, 1H). ^{13}C NMR (75 MHz, $CDCl_3$) δ: 21.5, 38.2, 50.4, 128.1, 129.6 (2C), 132.3, 134.7 (2C), 200.5. Anal. calcd. for $C_{10}H_{11}ClOS$: C 55.94, H 5.16; found: C 55.73, H 5.07.

3-Benzylsulfanyl-butanal (Table 1, entry 17)

IR (neat, cm^{-1}) ν: 1477, 1724. ^1H NMR (300 MHz, $CDCl_3$) δ: 1.33 (d, *J* = 6.8 Hz, 3H), 2.55–2.61 (m, 2H), 3.13–3.19 (m, 1H), 3.78 (s, 2H), 7.24–7.33 (m, 5H), 9.66 (s, 1H). ^{13}C NMR (75 MHz, $CDCl_3$) δ: 21.3, 33.6, 35.2, 50.1, 127.1, 128.5 (2C), 128.7 (2C), 137.9, 200.5. Anal. calcd. for $C_{11}H_{14}OS$: C 68.0, H 7.26; found: C 68.09, H 7.17.

2-Methyl-3-phenylsulfanyl-pentanal (Table 1, entry 19)

Obtained as a mixture of diastereoisomers (61:39). IR (neat, cm^{-1}) ν: 1447, 1722, 2721. ^1H NMR (300 MHz, $CDCl_3$) δ: 1.08 (t, *J* = 7.2 Hz, 3H), 1.20 (d, *J* = 7.2 Hz, 3H), 1.54–1.67 (m, 2H), 2.55–2.59 (m, 1H), 3.39–3.45 (m, 1H), 7.22–7.33 (m, 3H), 7.41–7.44 (m, 2H), 9.68 (d, *J* = 1.6 Hz, 1H major), 9.69 (d, *J* = 1.0 Hz, 1H, minor). ^{13}C NMR (75 MHz, $CDCl_3$) δ: 9.7 (minor), 10.1 (major), 11.8 (major), 12.1 (minor), 24.2 (major), 26.2 (minor), 49.1 (minor), 49.7 (major), 51.3 (major), 52.7 (minor), 127.2, 128.9 (2C), 132.3 (2C), 133.2, 203.5. Anal. calcd. for $C_{12}H_{16}OS$: C 69.19, H 7.74; found: C 69.03, H 7.60.

3-(4-Chlorophenylsulfanyl)-2-methyl-pentanal (Table 1, entry 20)

Colourless liquid obtained as a mixture of diastereoisomers (59:41). IR (neat, cm^{-1}) ν: 1475, 1724, 2721. ^1H NMR (300 MHz, $CDCl_3$) δ: 1.04 (t, *J* = 7.2 Hz, 3H), 1.20 (d, *J* = 7.21 Hz, 3H), 1.62–1.73 (m, 2H), 2.63–2.67 (m, 1H), 3.34–3.40 (m, 1H), 7.26 (d, *J* = 8.3 Hz, 2H), 7.37 (d, *J* = 8.3 Hz, 2H), 9.67 (d, *J* = 1.6 Hz, 1H, minor), 9.68 (d, *J* = 1.0 Hz, 1H, major). ^{13}C NMR (75 MHz, $CDCl_3$) δ: 9.7 (major), 10.2 (minor), 11.8 (minor), 12.1 (major), 24.2 (minor), 26.2 (major), 48.9 (major), 49.6 (minor), 51.7 (minor), 52.9 (major), 129.1 (2C), 133.4, 133.5 (2C), 133.6, 203.2. Anal. calcd. for $C_{12}H_{15}ClOS$: C 59.37, H 6.23; found: C 59.41, H 6.17.

2-Ethyl-3-phenylsulfanyl-hexanal (Table 1, entry 21)

Colourless liquid obtained as a mixture of diastereoisomers (53:47). IR (neat, cm^{-1}) ν: 1479, 1720, 2715. ^1H NMR (300 MHz, $CDCl_3$) δ: 0.88–0.96 (m, 6H), 1.51–1.71 (m, 6H), 2.33–2.37 (m, 1H), 3.35–3.43 (m, 1H), 7.21–7.32 (m, 3H), 7.38–7.43 (m, 2H), 9.66 (d, *J* = 2.7 Hz, 1H, major), 9.75 (d, *J* = 2.3 Hz, 1H, minor). ^{13}C NMR (75 MHz, $CDCl_3$) δ: 11.9 (major), 12.0 (minor), 13.6 (major), 13.7 (minor), 19.3 (major), 19.3 (minor), 20.2 (major), 20.5 (minor), 34.1 (minor), 34.6 (major), 49.2 (major), 49.8 (minor), 56.5 (minor), 56.9 (major), 127.2, 128.9 (2C), 132.3 (2C), 134.8, 203.5 (major), 204.1 (minor). Anal. calcd. for $C_{14}H_{20}OS$: C 71.14, H 8.53; found: C 70.93, H 8.39.

3-(4-Chlorophenylsulfanyl)-2-ethyl-hexanal (Table 1, entry 22)

Colourless liquid obtained as a mixture of diastereoisomers (51:49). IR (neat, cm^{-1}) ν: 1475, 1722, 2719. ^1H NMR (300 MHz, $CDCl_3$) δ: 0.88, 0.94 (m, 6H), 1.49–1.84 (m, 6H), 2.32–2.36 (m, 1H), 3.31–3.37 (m, 1H), 7.28 (d, *J* = 7.8 Hz, 2H), 7.34 (d, *J* = 7.8 Hz, 2H), 9.66 (d, *J* = 2.7 Hz, 1H, minor), 9.73 (d, *J* = 2.2 Hz, 1H, major). ^{13}C NMR (75 MHz, $CDCl_3$) δ: 11.9 (major), 12.0 (minor), 13.6 (major), 13.6 (minor), 19.2 (major), 19.3 (minor), 20.2 (major), 20.5 (minor), 34.0 (major), 34.6 (minor), 49.6 (major), 50.2 (minor), 56.8 (major), 56.4 (minor), 129.1 (2C), 133.3, 133.4, 133.6 (2C), 203.3 (major), 203.6 (minor). Anal. calcd. for $C_{14}H_{19}ClOS$: C 62.09, H 7.07; found: C 61.89, H 6.94.

3-(4-Chlorophenylsulfanyl)propionic acid methyl ester (Table 1, entry 24)

Colourless liquid. IR (neat, cm^{-1}) ν: 1477, 1737. ^1H NMR (300 MHz, $CDCl_3$) δ: 2.59 (t, *J* = 7.5 Hz, 2H), 3.13 (t, *J* = 7.5 Hz, 2H), 3.67 (s, 3H), 7.19–7.29 (m, 4H). ^{13}C NMR (75 MHz, $CDCl_3$) δ: 29.7, 34.4, 52.3, 129.5 (2C), 131.8 (2C), 134.1, 134.2, 172.4. Anal. calcd. for $C_{10}H_{11}ClO_2S$: C 52.06, H 4.77; found: C 52.11, H 4.71.

3-(4-Chlorophenylsulfanyl)propionitrile (Table 1, entry 27)

Pale yellow gummy liquid. IR (neat, cm^{-1}) ν: 1431, 1477, 2243. ^1H NMR (300 MHz, $CDCl_3$) δ: 2.55–2.61 (m, 2H), 3.07–3.13 (m, 2H), 7.25–7.37 (m, 4H). ^{13}C NMR (75 MHz, $CDCl_3$) δ: 18.1, 30.4, 117.6, 129.5 (2C), 131.6, 132.7 (2C), 133.9. Anal. calcd. for C_9H_8ClNS: C 54.68, H 4.08, N 7.09; found: C 54.49, H 4.01, N 7.02.

2-Methyl-3-phenylsulfanyl-propionitrile (Table 1, entry 28)

Pale yellow liquid. IR (neat, cm^{-1}) ν: 1438, 1481, 1583, 2241. ^1H NMR (300 MHz, $CDCl_3$) δ: 1.40 (d, *J* = 6.9 Hz, 3H), 2.71–2.78 (m, 1H), 2.93–3.02 (m, 1H), 3.12–3.28 (m, 1H), 7.23–7.35 (m, 3H), 7.38–7.43 (m, 2H). ^{13}C NMR (75 MHz, $CDCl_3$) δ: 17.1, 26.0, 38.2, 121.4, 127.4, 129.3 (2C), 131.1 (2C), 137.0. Anal. calcd. for $C_{10}H_{11}NS$: C 67.75, H 6.25, N 7.90; found: C 75.43, H 6.16, N 7.81.

General procedure for the synthesis of β-hydroxyalkyl/aryl sulfides

Representative procedure for 1-phenylsulfanyloctan-2-ol (Table 2, entry 1)

To a stirred solution of indium(I) iodide (121 mg, 0.5 mmol) and diphenyldisulphide (109 mg, 0.5 mmol) in dry THF (2.5 mL) was added 1-octene oxide (128 mg, 1 mmol) and indium trichloride (11.05 mg, 5 mol%) under nitrogen. The reaction mixture was heated under reflux for 3 h (TLC) and quenched with a few drops of water. THF was then evaporated off and the residual mixture was then extracted with ether (3 × 20 mL). The combined ether ex-

© 2006 NRC Canada

tract was washed with brine and dried (Na_2SO_4). Evaporation of the solvent left the crude product, which was purified by column chromatography over silica gel (hexane–ether, 85:15) to furnish the pure product, 1-thiophenyloctan-2-ol as a colourless oil (233 mg, 98%). The product was identified by comparison of its spectroscopic data (IR and ^{1}H and ^{13}C NMR) with the reported values (8*g*).

This procedure was followed for all the reactions listed in Table 2. All the products are adequately characterized by their spectroscopic data (IR and ^{1}H and ^{13}C NMR). The values for the known compounds are in good agreement with those reported (Table 2). The spectroscopic data and elemental analysis for new compounds that are not available in the literature are provided here.

1-(4-Chlorophenylsulfanyl)octan-2-ol (Table 2, entry 3)

Colourless liquid. IR (neat, cm^{-1}) ν: 1439, 1479, 1580, 3467. ^{1}H NMR (300 MHz, $CDCl_3$) δ: 0.87 (t, *J* = 6.36 Hz, 3H), 1.26–1.41 (m, 7H), 1.42–1.53 (m, 3H), 2.36 (bs, 1H), 2.84 (dd, *J* = 8.49, 13.56 Hz, 1H), 3.08 (dd, *J* = 3.39 Hz, 13.56 Hz, 1H), 3.62–3.70 (m, 1H), 7.23–7.32 (m, 4H). ^{13}C NMR (75 MHz, $CDCl_3$) δ: 14.4, 22.9, 25.9, 29.6, 32.1, 36.5, 42.7, 69.9, 129.5 (2C), 131.6 (2C), 132.9, 134.5. Anal. calcd. for $C_{14}H_{21}ClOS$: C 61.63, H 7.76; found: C 61.50, H 7.61.

2-(4-Chlorophenylsulfanyl)cyclohexanal (Table 2, entry 9)

Colourless liquid. IR (neat, cm^{-1}) ν: 1446, 1477, 1581, 3398. ^{1}H NMR (300 MHz, $CDCl_3$) δ: 1.17–1.38 (m, 4H), 1.67–1.79 (m, 2H), 2.03–2.12 (m, 2H), 2.70–2.77 (m, 1H), 2.80 (s, 1H), 3.30 (ddd, *J* = 4.20, 9.86, 10.01 Hz, 1H), 7.23–7.26 (m, 2H), 7.35–7.39 (m, 2H). ^{13}C NMR (75 MHz, $CDCl_3$) δ: 24.6, 26.4, 32.9, 34.3, 56.9, 72.4, 129.4 (2C), 131.7, 134.3, 135.3 (2C). Anal. calcd. for $C_{12}H_{15}ClOS$: C 59.37, H 6.23; found: C 59.21, H 6.11.

2-(4-Chlorophenylsulfanyl)cycloheptanol (Table 2, entry 11)

Colourless liquid. IR (neat, cm^{-1}) ν: 1438, 1478, 1582, 3473. ^{1}H NMR (300 MHz, $CDCl_3$) δ: 1.46–1.61 (m, 4H), 1.69–1.77 (m, 2H), 1.99–2.25 (m, 2H), 2.27–2.40 (m, 2H), 2.41 (s, 1H), 3.64 (ddd, *J* = 3.21, 8.73, 9.87 Hz, 1H), 4.02–4.09 (m, 1H), 7.24–7.38 (m, 4H). ^{13}C NMR (75 MHz, $CDCl_3$) δ: 22.0, 25.0, 26.9, 32.6, 35.3, 66.1, 79.2, 126.4, 127.7, 129.5 (2C), 133.5 (2C). Anal. calcd. for $C_{13}H_{17}ClOS$: C 60.80, H 6.67; found: C 60.62, H 6.51.

3-Hydroxy-1,3-diphenyl-2-phenylsulfanyl-propan-1-one (Table 2, entry 13)

Yellow oil. IR (neat, cm^{-1}) ν: 1438, 1477, 1597, 1683, 3460. ^{1}H NMR (300 MHz, $CDCl_3$) δ: 2.94 (bs, 1H), 4.64 (d, *J* = 2.58 Hz, 1H), 5.48 (d, *J* = 2.58 Hz, 1H), 7.10–7.13 (m, 2H), 7.20–7.24 (m, 6H), 7.45–7.62 (m, 4H), 7.62–7.68 (m, 3H). ^{13}C NMR (75 MHz, $CDCl_3$) δ: 58.0, 75.1, 128.2, 128.5 (2C), 128.6, 128.7 (2C), 129.0 (2C), 129.2 (2C), 129.3 (2C), 129.4, 129.5, 133.3 (2C), 134.5, 135.9, 198.9. Anal. calcd. for $C_{21}H_{18}O_2S$: C 75.42, H 5.42; found: C 75.31, H 5.33.

2-Hydroxy-3-(4-methoxy-phenyl)-1-phenyl-3-phenylsulfanyl-propan-1-one (as a mixture of diastereomers, 52:48) (Table 2, entry 14)

Yellowish, low-melting solid; mp 40–43 °C. IR (neat, cm^{-1}) ν: 1438, 1477, 1581, 1682, 3465. ^{1}H NMR (300 MHz, $CDCl_3$) δ: 3.74 (s, 3H, major), 3.78 (s, 3H, minor), 4.57 (d, *J* = 2.64 Hz, 1H, minor), 4.64 (d, *J* = 2.58 Hz, 1H, major), 5.42 (d, *J* = 2.64 Hz, 1H, minor), 5.45 (d, *J* = 2.58 Hz, 1H, major), 6.74 (d, *J* = 7.32 Hz, 2H, minor), 6.86 (d, *J* = 8.70 Hz, 2H, major), 7.04–7.07 (m, 4H, (2H for major and 2H for minor)), 7.29–7.32 (m, 4H (2H for major and 2H for minor)), 7.41–7.50 (m, 8H (4H for major and 4H for minor)), 7.62–7.64 (m, 4H (2H for major and 2H for minor)), 7.66 (d, *J* = 8.70 Hz, 2H, major), 7.84 (d, *J* = 7.32 Hz, 2H, minor). ^{13}C NMR (75 MHz, $CDCl_3$) δ: 55.5 (major), 55.6 (minor), 57.3 (minor), 58.4 (major), 75.2 (minor), 77.1 (major), 113.9 (minor, 2C), 114.3 (major, 2C), 127.6 (minor), 127.8 (major), 128.1 (minor), 128.2 (major), 128.8 (major, 2C), 128.9 (minor, 2C), 129.1 (major, 2C), 129.2 (minor, 2C), 129.4 (major, 2C), 129.5 (minor, 2C), 129.9 (minor, 2C), 130.1 (minor), 130.4 (major, 2C), 130.5 (major), 132.8 (minor, 2C), 133.3 (major, 2C), 134.2 (minor), 134.5 (major), 134.7 (minor), 135.1 (major), 159.5 (minor), 159.7 (major), 199.1 (minor), 199.7 (major). Anal. calcd. for $C_{22}H_{20}O_3S$: C 72.50, H 5.53; found: C 72.41, H 5.43.

2-Hydroxy-3-phenyl-3-phenylsulfanyl propionic acid ethyl ester (Table 2, entry 15)

Colourless liquid. IR (neat, cm^{-1}) ν: 1439, 1479, 1583, 1732, 3484. ^{1}H NMR (300 MHz, $CDCl_3$) δ: 1.07 (t, *J* = 7.20 Hz, 3H), 2.88 (bs, 1H), 3.99 (q, *J* = 7.20 Hz, 2H), 4.49 (d, *J* = 3.69 Hz, 1H), 4.52 (d, *J* = 3.69 Hz, 1H), 7.11–7.18 (m, 6H), 7.28–7.33 (m, 4H). ^{13}C NMR (75 MHz, $CDCl_3$) δ: 13.9, 56.5, 61.8, 72.6, 127.4, 127.9, 128.2 (2C), 128.3 (2C), 128.7 (2C), 132.1 (2C), 134.2, 136.4, 171.8. Anal. calcd. for $C_{17}H_{18}O_3S$: C 67.52, H 6.00; found: C 67.45, H 5.91.

1-Phenylsulfanyl-4,4a,5,6,7,8-hexahydro-3*H*-naphthalen-2-one (Table 2, entry 16)

Yellowish liquid. IR (neat, cm^{-1}) ν: 1439, 1477, 1582, 1674, 3477. ^{1}H NMR (300 MHz, $CDCl_3$) δ: 0.97–1.51 (m, 4H), 1.52–2.13 (m, 5H), 2.44–2.83 (m, 3H), 3.59–3.69 (m, 1H), 7.07–7.44 (m, 5H). ^{13}C NMR (75 MHz, $CDCl_3$) δ: 25.3, 27.2, 28.2, 34.6, 35.2, 37.0, 41.0, 125.3, 127.2 (2C), 128.9 (2C), 137.2, 137.4, 174.0, 195.1. Anal. calcd. for $C_{16}H_{18}OS$: C 74.38, H 7.02; found: C 74.25, H 6.92.

2-Hydroxy-3,5,5-trimethyl-3-phenylsufanyl-cyclohexanone (Table 2, entry 18b)

Colourless liquid. IR (neat, cm^{-1}) ν: 1439, 1477, 1582, 1740. ^{1}H NMR (300 MHz, $CDCl_3$) δ: 1.15 (s, 3H), 1.27 (s, 3H), 1.42 (s, 3H), 1.81–1.86 (m, 1H), 2.25–2.34 (m, 2H), 2.53–2.59 (m, 1H), 4.44 (s, 1H), 7.15–7.26 (m, 5H). ^{13}C NMR (75 MHz, $CDCl_3$) δ: 26.3, 30.7, 31.1, 32.9, 47.1, 54.7, 56.8, 71.3, 128.0, 129.0 (2C), 133.2, 133.8, 134.2, 220.7. Anal. calcd. for $C_{15}H_{20}O_2S$: C 68.14, H 7.62; found: C 67.95, H 7.48.

3-Hydroxy-5-isopropenyl-2-methyl-2-phenylsulfanyl-cyclohexanone (Table 2, entry 19)

Colourless liquid. IR (neat, cm^{-1}) ν: 1439, 1474, 1646, 1696, 3464. ^{1}H NMR (300 MHz, $CDCl_3$) δ: 1.18 (s, 3H), 1.76 (s, 3H), 1.89–1.97 (m, 1H), 2.32–2.42 (m, 2H), 2.57 (bs, 1H), 2.84–2.94 (m, 1H), 3.30–3.41 (m, 1H), 4.18–4.20 (m, 1H), 4.79 (d, *J* = 0.75 Hz, 2H), 7.24–7.35 (m, 5H). ^{13}C NMR (75 MHz, $CDCl_3$) δ: 18.8, 20.4, 33.4, 39.2, 41.7, 59.9,

© 2006 NRC Canada

76.0, 110.3, 129.0 (2C), 129.6, 129.7, 136.5 (2C), 147.0, 208.5. Anal. calcd. for $C_{16}H_{20}O_2S$: C 69.53, H 7.29; found: C 69.43, H 7.13.

Acknowledgements

We are pleased to acknowledge the financial support from the Council of Scientific and Industrial Research (CSIR), New Delhi (Grant No. 01(1936)/04) for this investigation. TM is also thankful to CSIR for his fellowship.

References

1. (*a*) P. Cintas. Synlett, 1087 (1995); (*b*) C.-J. Li. Tetrahedron, **52**, 5643 (1996); (*c*) C.-J. Li and T.H. Chan. Tetrahedron, **55**, 11149 (1999); (*d*) K.K. Chauhan and C.G. Frost. J. Chem. Soc. Perkin Trans. 1, 3015 (2000); (*e*) B.C. Ranu. Eur. J. Org. Chem. 2347 (2000); (*f*) J. Podlech and T.C. Maier. Synthesis, 633 (2003); (*g*) V. Nair, S. Ros, C.N. Jayan, and B.S. Pillai. Tetrahedron, **68**, 1959 (2004).
2. (*a*) S. Juan, Z.-H. Hua, S. Qi, S.-J. Ji, and T.-P. Loh. Synlett, 829 (2004); (*b*) H. Miyabe, Y. Yamaoka, T. Naito, and Y. Takemoto. J. Org. Chem. **69**, 1415 (2004); (*c*) R. Yanada, Y. Koh, N. Nishimori, A. Matsumara, S. Obika, H. Mitsuya, N. Fujii, and Y. Takemoto. J. Org. Chem. **69**, 2417 (2004); (*d*) K. Miura, N. Fujisawa, and A. Hosomi. J. Org. Chem. **69**, 2427 (2004); (*e*) C. Peppe and R. Pavão das Chagas. Synlett, 1187 (2004); (*f*) T. Hirashita, S. Kambe, H. Tsuji, H. Omori, and S. Araki. J. Org. Chem. **69**, 5054 (2004); (*g*) N. Sakai, K. Annaka, and T. Konakahara. Org. Lett. **6**, 1527 (2004); (*h*) G.R. Cook, B.C. Maity, and R. Kargbo. Org. Lett. **6**, 1741 (2004).
3. (*a*) B.C. Ranu, A. Hajra, and U. Jana. J. Org. Chem. **65**, 6270 (2000); (*b*) B.C. Ranu, A. Hajra, and U. Jana. Tetrahedron Lett. **41**, 531 (2000); (*c*) B.C. Ranu, S. Samanta, and A. Hajra. Synlett, 987 (2002); (*d*) B.C. Ranu, A. Das, and S. Samanta. Synlett, 727 (2002); (*e*) B.C. Ranu, S.S. Dey, and A. Hajra. Tetrahedron, **58**, 2529 (2002); (*f*) B.C. Ranu, A. Hajra, S.S. Dey, and U. Jana. Tetrahedron, **59**, 813 (2003); (*g*) B.C. Ranu and S. Samanta. J. Org. Chem. **68**, 7130 (2003); (*h*) B.C. Ranu, A. Das, and A. Hajra. Synthesis, 1012 (2003); (*i*) B.C. Ranu and S. Samanta. Tetrahedron, **59**, 7901 (2003); (*j*) B.C. Ranu, R. Jana, and S. Samanta. Adv. Synth. Catal. **346**, 446 (2004); (*k*) B.C. Ranu and A. Das. Adv. Synth. Catal. **347**, 712 (2005).
4. (*a*) B.C. Ranu, T. Mandal, and S. Samanta. Org. Lett. **5**, 1439 (2003); (*b*) B.C. Ranu and T. Mandal. J. Org. Chem. **69**, 5793 (2004); (*c*) B.C. Ranu and T. Mandal. Synlett, 1239 (2004); (*d*) B.C. Ranu and A. Das. Tetrahedron Lett. **45**, 6875 (2004).
5. (*a*) E.J. Corey, D.A. Clark, G. Goto, A. Marfat, C. Mioskowski, C. Samuelsson, and S. Hammarstrom. J. Am. Chem. Soc. **102**, 3663 (1980); (*b*) E.J. Corey, D.A. Clark, and G. Goto. Tetrahedron Lett. **21**, 3143 (1980).
6. J.R. Luly, N. Yi, J. Soderquist, H. Stein, J. Cohen, T.J. Perun, and J.J. Plattner. J. Med. Chem. **30**, 1609 (1987).
7. R.J. Cremlyn. An introduction to organo-sulfur chemistry. Wiley and Sons, New York. 1996.
8. (*a*) N. Srivastava and B.K. Banik. J. Org. Chem. **68**, 2109 (2003); (*b*) M. Zahouily, Y. Abrouki, A. Rayadh, S. Sebti, H. Dhimane, and M. David. Tetrahedron Lett. **44**, 2463 (2003); (*c*) M. Zahouily, Y. Abrouki, and A. Rayadh. Tetrahedron Lett. **43**, 7729 (2002); (*d*) Y. Abrouki, M. Zahouily, A. Rayadh, B. Bahlaouan, and S. Sebti. Tetrahedron Lett. **43**, 8951 (2002); (*e*) B.C. Ranu, S.S. Dey, and A. Hajra. Tetrahedron, **59**, 2417 (2003); (*f*) J.S. Yadav, B.V.S. Reddy, and G. Baishya. J. Org. Chem. **68**, 7098 (2003); (*g*) T.C. Wabnitz and J.B. Spencer. Org. Lett. **5**, 2141 (2003).
9. (*a*) A.E. Vogioukas and H.B. Kagan. Tetrahedron Lett. **28**, 6065 (1987); (*b*) H. Yamashita. Bull. Chem. Soc. Jpn. **61**, 1213 (1988); (*c*) J. Iqbal, A. Pandey, A. Shukla, R. Srivastava, and S. Tripathi. Tetrahedron, **46**, 6423 (1990); (*d*) J. Cossy, V. Bellosta, C. Hamoir, and J.R. Desmurs. Tetrahedron Lett. **43**, 7083 (2002); (*e*) F. Fringuelli, F. Pizzo, and L. Vaccaro. J. Org. Chem. **69**, 2315 (2004); (*f*) A.R. Khosropour, M.M. Khodaei, and K. Ghozati. Chem. Lett. **33**, 1379 (2004).
10. J.P. Cherkquaskas and T. Cohen. J. Org. Chem. **57**, 6 (1992).
11. M.M. Alam, R. Varala, and S.R. Adapa. Tetrahedron Lett. **44**, 5115 (2003).

© 2006 NRC Canada

Ab initio charge density analysis of $(B_6C)^{2-}$ and B_4C_3 species — How to describe the bonding pattern?

Cina Foroutan-Nejad, Gholam Hossein Shafiee, Abdolreza Sadjadi, and Shant Shahbazian

Abstract: In this study, a detailed topological charge density analysis based on the quantum theory of atoms in molecules (QTAIM) developed by Bader and co-workers, has been accomplished (using the B3LYP method) on the CB_6^{2-} anion and three planar isomers of the C_3B_4 species, which had been first proposed by Exner and Schleyer as examples of molecules containing hexacoordinate carbon atoms. The analysis uncovers the strong (covalent) interactions of boron atoms as well as the "nondirectional" interaction of central carbon atom with those peripheral atoms. On the other hand, instabilities have been found in the topological networks of $(B_6C)^{2-}$ and B_4C_3(para) species. A detailed investigation of these instabilities demonstrates that the topology of charge density has a floppy nature near the equilibrium geometries of the species under study. Thus, these species seems to be best described as complexes of a relatively concrete ring containing boron or carbon atoms and a central carbon atom that is confined in the plane of the molecule, but with nondirectional interactions with the surrounding atoms.

Key words: hypervalency, hexacoordinate carbon, quantum theory of atoms in molecules, charge density analysis, ab initio methods.

Résumé : Faisant appel à la méthode B3LYP et en se basant sur la théorie quantique des atomes dans les molécules développée par Bader et ses collaborateurs, on a fait une analyse détaillée de la densité de charge topologique de l'anion CB_6^{2-} et de trois isomères plans de l'espèce C_3B_4 qui ont été originalement proposées par Exner et Schleyer comme exemples de molécules contenant des atomes de carbone hexacoordinés. L'analyse met en évidence les fortes interactions covalentes des atomes de bore ainsi que l'interaction sans direction de l'atome centre de carbone avec les atomes périphériques. On a par ailleurs mis en évidence des instabilités dans les réseaux topologiques des espèces $(B_6C)^{2-}$ et B_4C_3(para). Une étude détaillée de ces instabilités démontre que la topologie de la densité de charge est de nature souple près des géométries d'équilibre des espèces étudiées. Il semble donc que la meilleure façon de décrire ces espèces soit de les assimiler à des complexes d'un noyau relativement concret contenant du bore ou des atomes de carbone et un atome de carbone central qui est confiné dans le plan de la molécule mais qui a des interactions non directionnelles avec les atomes qui l'entourent.

Mots clés : hypervalence, carbone hexacoordiné, théorie quantique des atomes dans les molécules, analyse de la densité de charge, méthodes ab initio.

[Traduit par la Rédaction]

Introduction

During the last two decades of the previous millennium, a real revolution took place in theoretical chemistry. Due to advances in both computational implementation (software) of reliable quantum chemical methods and hardware facilities, the role of theoretical chemistry has been changed from an almost descriptive tool to a powerful predictive mean. Nowadays, it is a routine procedure to investigate the properties of molecules prior to synthesis by employing high level ab initio quantum chemical methods. So, this unprecedented opportunity in combination with a chemist's imagination makes it possible to designate novel molecules before any experiments. On the other hand, by modeling a single molecule in a computer, it is possible to investigate species that in usual laboratory conditions have no thermodynamic stability. Therefore intermediates, transient and unstable species, and even transition states could be studied with much less effort (rather than using experimental procedures) using current theoretical methods.

In this regard, strange carbon compounds (strange in comparison to traditional ideas in classical organic chemistry) have always been the central attention of predators of odd

Received 9 October 2005. Published on the NRC Research Press Web site at http://canjchem.nrc.ca on 17 May 2006.

C. Foroutan-Nejad. Department of Chemistry, Faculty of Science, University of Tehran, Tehran, Iran.
G.H. Shafiee and A. Sadjadi.[1] Department of Chemistry, Islamic Azad University of Kazeroon, P.O. Box 73135-168, Kazeroon, Fars, Iran.
Sh. Shahbazian. Department of Chemistry, Faculty of Science, Shahid Beheshti University, P.O. Box 19395-4716, Evin, Tehran, Iran.

[1]Corresponding author (e-mail: abdi_1374@kau.ac.ir or abdi_1374@yahoo.com).

 doi:10.1139/V06-059 © 2006 NRC Canada

molecules. Historically, the pioneering work done by Schleyer and co-workers (1–3) almost 20 years ago may be viewed as the first systematic research (using ab initio quantum chemical methods) in this field. Since then, a wealth of studies has been conducted to investigate novel, unprecedented hypervalent carbon compounds. In 1997, Olah and Rasul (4) reviewed different previous calculations on penta- to hepta-coordinate carbon-containing species. In the same period, reports on new experimental data confirmed that odd carbon compounds are not hypothetical entities imagined by theoretical chemists, but real molecules, some even with bulk stability (5–7).

In such an atmosphere, Exner and Schleyer (8) proposed a new class of boron–carbon compounds, which they believed to be the first examples of planar hexacoordinate carbon compounds. Since that pioneering work, new theoretical studies have been conducted to dig more into the nature of these and related similar compounds (9–11). Not only in these studies has a special attention been paid on the bonding pattern of cited compounds, but the bonding mode of these species is also the main concern of our study.

Although these and related studies (for an up-to-date review of the relevant literature, see ref. 11) confirm the great power of theoretical approaches that are unprecedented during the whole history of chemistry, but such an approach brings delicate technical problems regarding the connection of the theoretical quantum chemical calculations with the usual chemical concepts. Questions regarding the mode of bonding in these odd molecules can be used as the best examples of these approaches. How can we propose or classify the bonding patterns in these molecules? How is it possible to make a relationship with the experimentally known species? And more importantly: Could traditional approaches in common bonding models (based and developed on well-known species) be successfully extended to embed these odd species?

Traditionally, and indeed in the great part of the history of chemistry, chemists have developed the bonding patterns for experimentally known compounds to construct a model that connects the different aspects of the chemical and physical properties of the molecule under study in a logical manner. So, in most cases (but not all), bonding models have been developed to "describe" experimental facts. Consequently, it seems that the bonding models have been employed more for "classification" of the known facts rather than predictive tools in chemistry. In a more detailed view, it is reasonable to claim that the "molecular structure hypothesis" along with the "bonding scheme" of the constituent atoms or functional groups of the target molecule, "coded" the chemical and even some physical information in a compact form. So, a question naturally arises: What does one really ask of a theory of bonding model using only the facts that are obtained from the computed expectation values of quantum mechanical operators? It seems to us that this and similar related questions are crucial in the extension of chemical bonding models to extreme domains as exemplified above.

Therefore, our concern in this paper is the role of the rigorous quantum theory of atoms in molecules (QTAIM) developed by Bader and co-workers (12) in the description of the bonding pattern of the species under study. Since charge density and related functions are the main inputs of QTAIM, in this study we will concentrate on charge densities and relevant topological features of the four species described in the original study (8), namely CB_6^{2-} and three isomers of C_3B_4 (see Fig. 1), and leave other aspects of QTAIM study to another paper. Although these species are intrinsically interesting, our main motivation in this study is not solely confined to these species and they serve as prototypes for applying the general strategy of QTAIM to give answers to some of methodological questions mentioned previously.

Computational details

Density functional calculations have been performed on $(B_6C)^{2-}$, *ortho*-B_4C3, *meta*-B_4C_3, and *para*-B_4C_3 species (see Fig. 1) at the B3LYP/6-311+G(d) level (the same computational level was used in the original study (8)), without any spatial symmetry constraints. In the first step, the equilibrium geometries were located and then frequency calculations were done to establish the local minima. To compare the C—C, B—B, and B—C bonded interactions in the cited species with those in the known chemical species, the molecules C_2H_6, C_2H_4, B_2H_4 (D_{2d}), B_2H_2 (linear), BH_2CH_3 (bisected), and $BHCH_2$ were chosen and their local minimum geometries were obtained at the same level of calculations. Then QTAIM's 3D partitioning scheme of charge densities was performed using the wave function of each molecule. All DFT calculations were carried out using PC GAMESS (version 6.4) (13, 14) and QTAIM calculations with MORPHY99 (15–20). The useful utilities implemented in the ChemCraft (version 1.4 beta) program (21) were optimized for handling the outputs of GAMESS.

Results and discussion

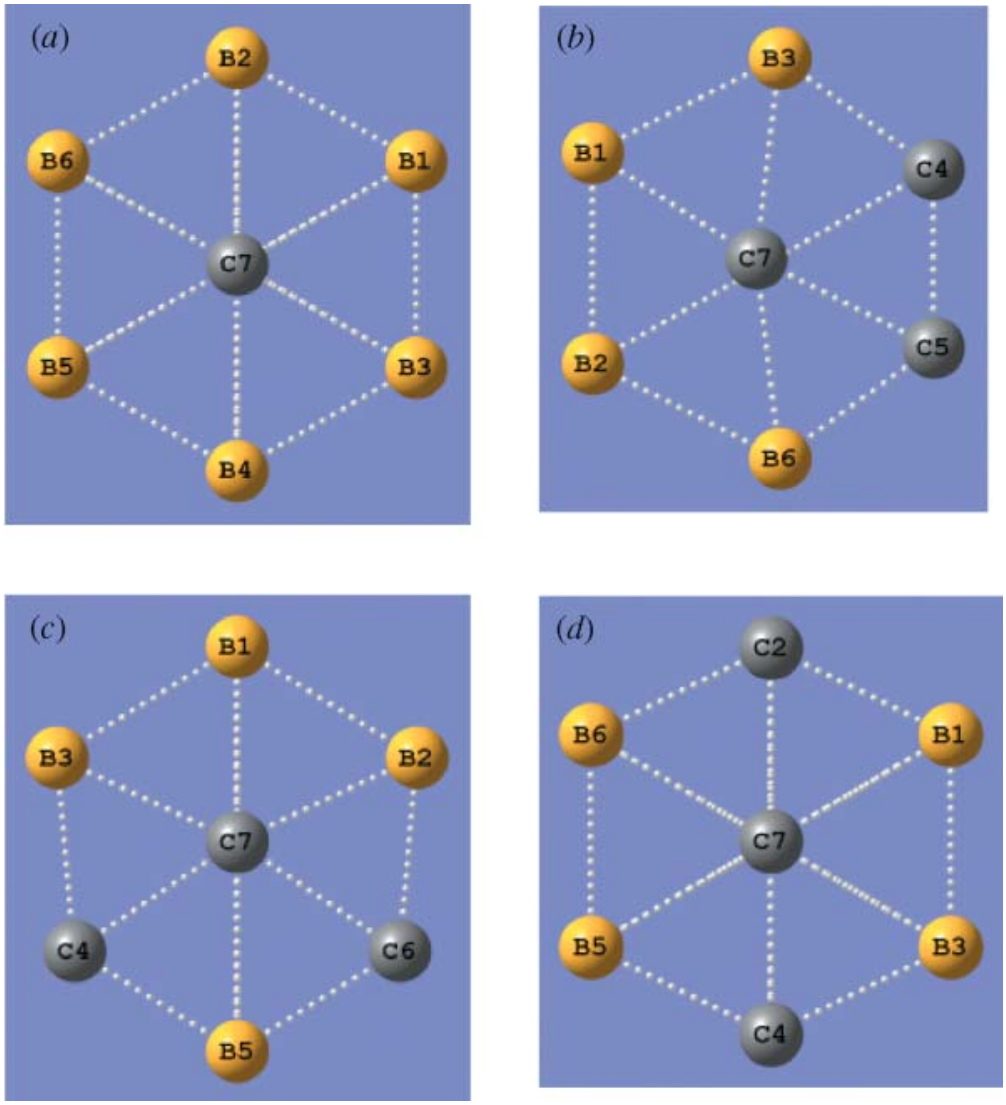
Although the optimized geometries of the species under study were reported in the original account (8) using another computational package a reoptimization was carried out to check the consistency. The results of the geometry optimizations are offered in Table 1 (the numbering scheme from Fig. 1 is used). With no exceptions, the internuclear distances of all the species under study coincide with the original study within 0.001 Å. The internuclear distances are important since they are usually employed to decide whether certain atoms are "bonded" or not (8). As will be discussed (vide infra), this is not the approach followed in this study.

The corresponding state functions of the optimized geometries have been used to construct electronic charge densities. The results of the topological analysis of charge densities are qualitatively depicted in Fig. 2, with the usual emphasis on general topological characters and the corresponding quantitative results are in Table 2. The standard topological analysis and nomenclature were employed in this study, therefore, the details of the analysis have not been discussed in this paper and only some primary descriptions are made in following paragraphs (for details and a comprehensive discussion of relevant analysis, see ref. 12).

According to QTAIM, the bonded atoms are determined by duo-gradient paths of charge density function, which originate from a bond critical point (a point where the gradient of charge density vanishes and the Hessian matrix of charge density has two negative and one positive eigenvalues) and terminate on corresponding atomic nuclei. As

© 2006 NRC Canada

Fig. 1. Spatial orientation of nuclei and their labels for optimized geometries at B3LYP/6-311+G* level. (*a*) $(B_6C)^{2-}$; (*b*) *o*-B_4C_3; (*c*) *m*-B_4C_3; (*d*) *p*-B_4C_3.



has been discussed by Bader in detail (12, 22), these gradient paths, which at equilibrium geometry are called "bond paths", must be regarded as the "universal indicators of bonded interactions" even when this contradicts descriptions based on classical physics or chemical intuition. The details of methodological problems and controversies regarding this choice have been discussed elsewhere (23). So, in this paper we follow the standard QTAIM proposal and admit the bond paths as a necessary and sufficient condition for the two atoms so-linked to be bonded to one another (22).

Even a brief look at Figs. 1 and 2 clearly denotes that there are differences in the overall bond path networks in the four species under study. Particularly, the number of bonded atoms to the central carbon atom vary. On the other hand, a detailed inspection of Fig. 2 demonstrates that, in the case of $(B_6C)^{-2}$ and *para*-B_4C_3 species, we are faced with unusual molecular graphs (we will use the phrase "molecular graph" to distinguish the topological networks (graphs) at equilibrium geometry with those corresponding to nonequilibrium geometries). Before discussing the detailed topological analysis of the individual members of the molecular set selected in this paper, this point necessitates special attention and further elaboration.

Stable vs. unstable molecular graphs

As has been discussed fully elsewhere (12), the stable topological networks are invariant under some finite geometrical changes of nuclei (the nuclear excursions). So, for a finite domain of nuclear geometrical changes, the "equivalent" topological network is retained. The word equivalent means that in the two topological networks corresponding to two neighboring nuclear geometries, the number and type of critical points and also the gradient paths that originate or terminate from these critical points remains the same. In the technical literature, this topological equivalence is termed homomorphism. On the other hand, under sufficiently steep deformations of nuclear geometry, new topological networks will appear. According to catastrophe theory, as implemented in the dynamical theory of charge density evolution relative to nuclear geometrical variations, the two networks interconverted abruptly (for details and a comprehensive discussion see ref. 12). Accordingly, there is a certain nuclear

© 2006 NRC Canada

Table 1. The internuclear distances (Å) between C—C, B—C, and B—B nuclei at the B3LYP/6-311+G* level.

C—C nuclei	Internuclear distance	B—C nuclei	Internuclear distance	B—B nuclei	Internuclear distance
$(B_6C)^{2-}$					
—	—	B1—C7	1.5928	B1—B2	1.5928
—	—	B2—C7	1.5928	B1—B3	1.5928
—	—	B3—C7	1.5928	B2—B6	1.5928
—	—	B4—C7	1.5928	B3—B4	1.5928
—	—	B5—C7	1.5928	B4—B5	1.5928
—	—	B6—C7	1.5928	B5—B6	1.5928
o-B_4C_3					
C4—C5	1.3747	B1—C7	1.4984	B1—B2	1.6235
C4—C7	1.5266	B2—C7	1.4984	B1—B3	1.6171
C5—C7	1.5266	B3—C4	1.4591	B2—B6	1.6171
		B3—C7	1.5550		
		B6—C5	1.4591		
		B6—C7	1.5550		
m-B_4C_3					
C4—C7	1.4968	B1—C7	1.4940	B1—B2	1.6152
C6—C7	1.4968	B2—C7	1.5178	B1—B3	1.6152
		B2—C6	1.4869		
		B3—C7	1.5178		
		B3—C4	1.4869		
		B5—C4	1.4601		
		B5—C6	1.4601		
		B5—C7	1.6044		
p-B_4C_3					
C2—C7	1.4430	B1—C2	1.4882	B1—B3	1.5834
C4—C7	1.4430	B1—C7	1.5548	B5—B6	1.5834
		B3—C4	1.4882		
		B3—C7	1.5548		
		B5—C4	1.4882		
		B5—C7	1.5548		
		B6—C2	1.4882		
		B6—C7	1.5548		

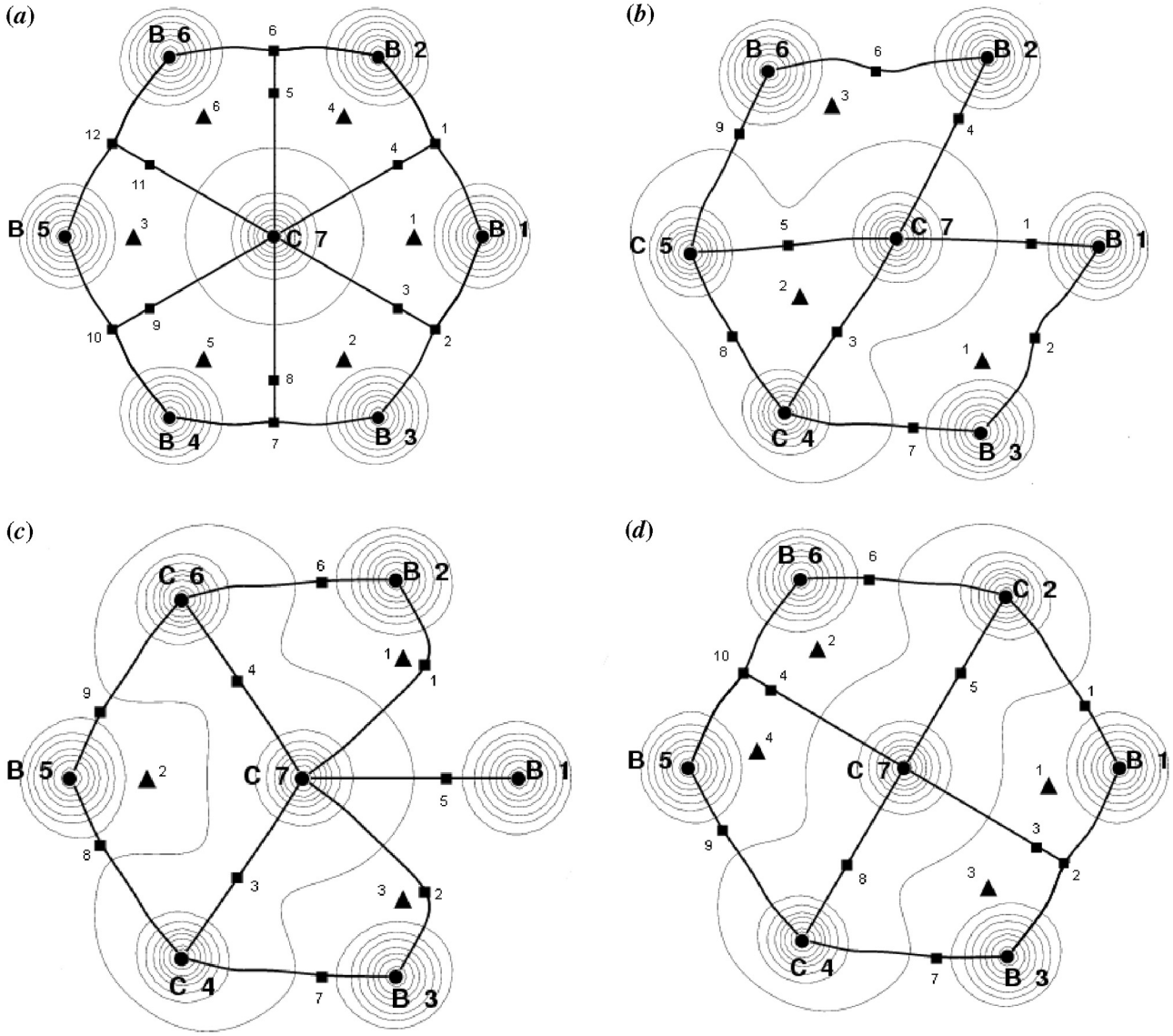
geometry for which the topological network does not belong to either of the two networks mentioned previously. This topological network may be imagined as a borderline between the two stable topological domains. By implementation of a mathematical theorem on structural stability as first derived by Palis and Smale (24) (and then implemented on the topological evolution of charge density relative to changes of nuclear geometry (12)), the borderline unstable topological networks may be classified systematically. Without going into detail, this classification leads to two distinct groups of unstable topological networks. In the first class, one encounters topological networks with degenerate critical points (critical points with ranks lower than three) and the other class contains networks with critical points whose connection causes the "nontransverse" intersect of stable and unstable manifolds (for details, see ref. 12). The first type of unstable topological network (with degenerate critical points) has been named bifurcation points, whereas the second type has been named conflict structures. The nuclear geometries corresponding to these two types of topological networks may be viewed as a natural borderline between the two topologically stable domains. So, with a small perturbation of nuclear geometry corresponds to an unstable topological network, this network will disappear and a new topological structure with a finite domain of stability will appear. In this regard, Fig. 2 vividly depicts the conflict topological networks at equilibrium geometries of the $(B_6C)^{2-}$ and *para*-B_4C_3 species. In the case of the molecular graph of $(B_6C)^{2-}$, the bond paths that originated from bond critical points (3,4,5,8,9,11), from one end have been terminated (normally) in the nucleus of central carbon atom, but from the other end have been terminated in another group of bond critical points (2,1,6,7,10,12), respectively. Similarly, in the case of the topological network of *para*-B_4C_3, the bond paths that originated from the bond critical points (3,4), from one end have been terminated in the nucleus of the central carbon atom, but from the other end have been terminated to another group of bond critical points (2,10), respectively. Both cases exemplify conflict structures. These topological instabilities have delicate effects on the bonding description of associated species and will be considered in detail in this paper.

Topological analysis

Table 2 offers the quantitative information regarding the

© 2006 NRC Canada

Fig. 2. The complete molecular graphs (MG) for (*a*) $(B_6C)^{2-}$, (*b*) *o*-B_4C_3, (*c*) *m*-B_4C_3, and (*d*) *p*-B_4C_3 at B3LYP/6-311+G* optimized geometries. Small black squares are BCPs and small black triangles are RCPs.



amount of charge density, the values of the Laplacian of charge density ($\nabla^2\rho$), the ellipticities ($\varepsilon = (\lambda_1/\lambda_2) - 1$), and the corresponding λ_1 and λ_2 values at bond critical points (BCPs) of all four species (λ_1 and λ_2 are the two negative eigenvalues of the Hessian matrix of charge density. By convention, λ_2 is the smaller curvature. Ellipticity provides a measure of the extent to which charge is preferentially accumulated in a given plane. For details, see ref. 12 and refs. cited therein). Table 3 has also been constructed to compare the results of Table 2 with a standard set. Table 3 contains some geometrical as well as topological characters (like those offered in Table 2) for the set of molecules C_2H_6, C_2H_4, B_2H_4 (D_{2d}), B_2H_2 (linear), BH_2CH_3 (bisected), and $BHCH_2$. This set has been selected as a prototype standard reference for C—C, B—C, and B—B single and double bonds (of course, single and double bonds in a classical context). Although such selection and corresponding comparison is inevitably arbitrary and since this is a common strategy in similar considerations, we also adapted this strategy in our study. Accordingly, with this standard set and the information available from Table 2 and Fig. 2, it is now possible to make a detailed analysis of the charge density of the species under study.

The $(B_6C)^{2-}$ anion

A detailed inspection of Tables 2 and 3, as well as Fig. 2, demonstrates some interesting patterns regarding the bonding mode of $(B_6C)^{2-}$. The amount of charge density in BCPs connecting boron atoms to each other is only 0.150 au, which is a bit lower than those in the B_2H_4 and B_2H_2 species. On the other hand, the ellipticity is 0.583, which is between the ellipticity of the B—B bonded interaction in the B_2H_4 and B_2H_2 species. Also, the sign of the Laplacian of electronic charge density is negative like those for the B_2H_4 and B_2H_2 molecules. These negative values are indicator of a "shared" interaction, which is usually interpreted as presence of a "covalent" bond (12). As is evident from Fig. 2, there are no direct bonded interactions between boron atoms and

© 2006 NRC Canada

Table 2. The topological characters of the BCPs and RCPs of charge density distributions at the B3LYP/6-311+G* level.

CP numbering scheme	Type of CP	ρ_b (au)	$\nabla^2\rho_b$ (au)	ε	λ_1 (au)	λ_2 (au)
$(B_6C)^{2-}$						
1,2,6,7,10,12	BCP	0.150	–0.234	0.583	–0.167	–0.105
3,4,5,8,9,11	BCP	0.143	–0.048	188.730	–0.155	–0.001
1,2,3,4,5,6	RCP	0.140	0.356		–0.160	0.005
12 BCPs	**6 RCPs**					
***o*-B_4C_3**						
1,4	BCP	0.157	0.526	3.099	–0.222	–0.054
2,6	BCP	0.147	–0.154	5.842	–0.160	–0.023
3,5	BCP	0.214	–0.099	2.486	–0.317	–0.091
7,9	BCP	0.181	0.248	0.123	–0.269	–0.240
8	BCP	0.292	–0.626	0.019	–0.456	–0.447
1,3	RCP	0.145	0.249		–0.146	0.035
2	RCP	0.205	0.088		–0.306	0.082
9 BCPs	**3 RCPs**					
***m*-B_4C_3**						
1,2	BCP	0.150	–0.088	5.736	–0.159	–0.024
3,4	BCP	0.229	–0.202	0.919	–0.325	–0.169
5	BCP	0.162	0.536	1.723	–0.218	–0.080
6,7	BCP	0.179	0.130	0.335	–0.288	–0.215
8,9	BCP	0.187	0.136	0.047	–0.280	–0.267
1,3	RCP	0.150	0.174		–0.169	0.019
2	RCP	0.139	0.415		–0.138	0.132
9 BCPs	**3 RCPs**					
***p*-B_4C_3**						
1,6,7,9	BCP	0.175	0.199	0.193	–0.259	–0.217
2,10	BCP	0.153	–0.208	0.939	–0.155	–0.080
3,4	BCP	0.150	–0.079	14.657	–0.152	–0.010
5,8	BCP	0.248	–0.283	0.808	–0.349	–0.193
1,2,3,4	RCP	0.146	0.392		–0.154	0.027
10 BCPs	**4 RCPs**					

Table 3. Internuclear distances (Å) and topological characters of the BCPs between C—C, B—B, and B—C nuclei in a standard set of molecules at the B3LYP/6-311+G** level (only singlet ground states have been considered).

Molecule	Type of bonded atoms	Internuclear distance	CP type	ρ_b (au)	$\nabla^2\rho_b$ (au)	ε
H_3CCH_3	C—C	1.531	BCP	0.238	–0.531	0.000
H_2CCH_2	C—C	1.329	BCP	0.344	–1.028	0.332
H_2BBH_2[a]	B—B	1.629	BCP	0.179	–0.476	0.000
HBBH[b]	B—B	1.523	BCP	0.195	–0.517	0.835
H_2BCH_3[c]	B—C	1.554	BCP	0.189	–0.285	0.298
$HBCH_2$	B—C	1.376	BCP	0.248	–0.107	0.550

[a]The point group of the optimized geometry is D_{2d}.
[b]The optimized geometry is linear.
[c]The optimized geometry is bisected.

the central carbon atom. The topological characters of other BCPs, as well as ring critical points (RCPs), may be used to investigate the instability of the topological network of $(B_6C)^{2-}$.

In the case of the topological network of $(B_6C)^{2-}$ at equilibrium geometry, we encountered a conflict structure as discussed previously. The data in Table 2, also confirm the unstable nature of this topological network. The comparison of the amounts of charge density of BCPs (3,4,5,8,9,11) and RCPs reveals small differences (less than 0.01 au), so the overall charge density is relatively flat in a hypothetical ring imagined around the central carbon nucleus. This flatness of charge density may be interpreted as an indication of the ease of change in topological structure (12). On the other hand, the large ellipticities that are associated with BCPs (3,4,5,8,9,11) also confirm this conclusion. The large ellipti-

© 2006 NRC Canada

cities are another indicator of the readiness of topological changes (12). Indeed, a more detailed inspection of the corresponding negative eigenvalues of the Hessian matrix of charge density (λ_1 and λ_2) from Table 2 demonstrates the near vanishing of the negative curvature of the BCPs (λ_2 = –0.001) along an axes in the plane of the ring and perpendicular to the bond path, and the same near vanishing of the correspondingly directed positive curvature at the RCPs (λ_2 = 0.005). To establish these changes unequivocally, small arbitrary perturbations of geometrical parameters have been made to demonstrate the abrupt onset of topological changes in the molecular graph of $(B_6C)^{2-}$.

Figure 3 depicts the topological networks of this molecule after some small, arbitrary shifting in nuclear geometrical parameters. In the first step, with a small 0.02 Å shift of the central carbon (C7) nucleus toward a line bisecting a hypothetical line going through B—B (X direction), the molecular graph of $(B_6C)^{2-}$ has been changed dramatically and a new topological network has emerged. Accordingly, from this new graph (shown in Fig. 3*a*), it is evident that there are two BCPs, which are connected from one side to the nucleus of the central carbon and from the other side to another BCP, so, this molecular graph is also a new conflict structure (must be distinguished from the original conflict structure). In a second step, a 0.2 Å shift of the central carbon nucleus in the same direction was performed and as is evident from Fig. 3*b*, this new topological structure is now a stable topological network. The same procedure (shifting of central carbon nucleus) was accomplished for two other directions, namely one directly toward one of the boron nuclei of the peripheral ring (Y direction) and the other in a perpendicular, out-of-plane shifting (Z direction). Figures 3*c*–3*f* depict the resultant topological networks. In all cases, dramatic changes of molecular graphs have taken place following the applied geometrical changes. Except for Fig. 3*c*, all other topological networks are conflict structures (with the same criterion described previously). What is more interesting in considering these graphs, is that there are two or even three "distinct gradient paths" connecting the central carbon nucleus and one of the boron nuclei of the peripheral ring, as is evident from Fig. 3. This is an unusual and possibly a novel trait regarding the common topological networks considered previously (12). Although these are only a selected set of possible graphs (with a constraint search in selected directions of geometrical parameters space), even with this set and taking into account the nuclear excursion during the vibrations, it is evident that $(B_6C)^{2-}$ does not have a "unique" topological structure around its equilibrium geometry.

On the other hand, with external energy pumping into the vibrational degrees of freedom (vibrationally "hot" molecules), not only the low-lying vibrational states, but also the higher (excited) vibrational levels, may also gain considerable population. So, the high amplitude vibrations may take place and as previous analysis has demonstrated (with controlled shifting of the central carbon from 0.02 to 0.2 Å) new topological regimes will be available to the molecule (since explicit consideration of nuclear motion has not yet been incorporated in QTAIM, this is an ad hoc, but reasonable assumption). The other interesting feature of the topological networks of Fig. 3 is the bonded pattern of corresponding atoms. By changing the mode of geometrical perturbations of the central carbon, bonded interactions have been created and annihilated according to the amount and also the direction of the corresponding geometrical shift. For instance, whereas B5—B6 internuclear distances are the same in Figs. 3*a* and 3*b*, in Fig. 3*a* there is a bonded interaction between them, whereas the same bonded interaction has been ruptured in the topological network that is depicted in Fig. 3*b*. The same feature may be traced in the other topological networks, which are depicted in Fig. 3. Since the molecular vibrations are usually considered using normal mode analysis (25) (from nuclear dynamics analysis in the context of Born–Oppenheimer approximation) and this implies complex relative motions of nuclei, therefore, with the mixture of different normal modes and possible contributions of excited vibrational states with corresponding normal modes, it seems hard (if not impossible) to attribute a single or even a well-defined set of molecular graphs to the $(B_6C)^{2-}$ anion. So, it seems that $(B_6C)^{2-}$ anion must be viewed topologically as a "floppy" molecule.

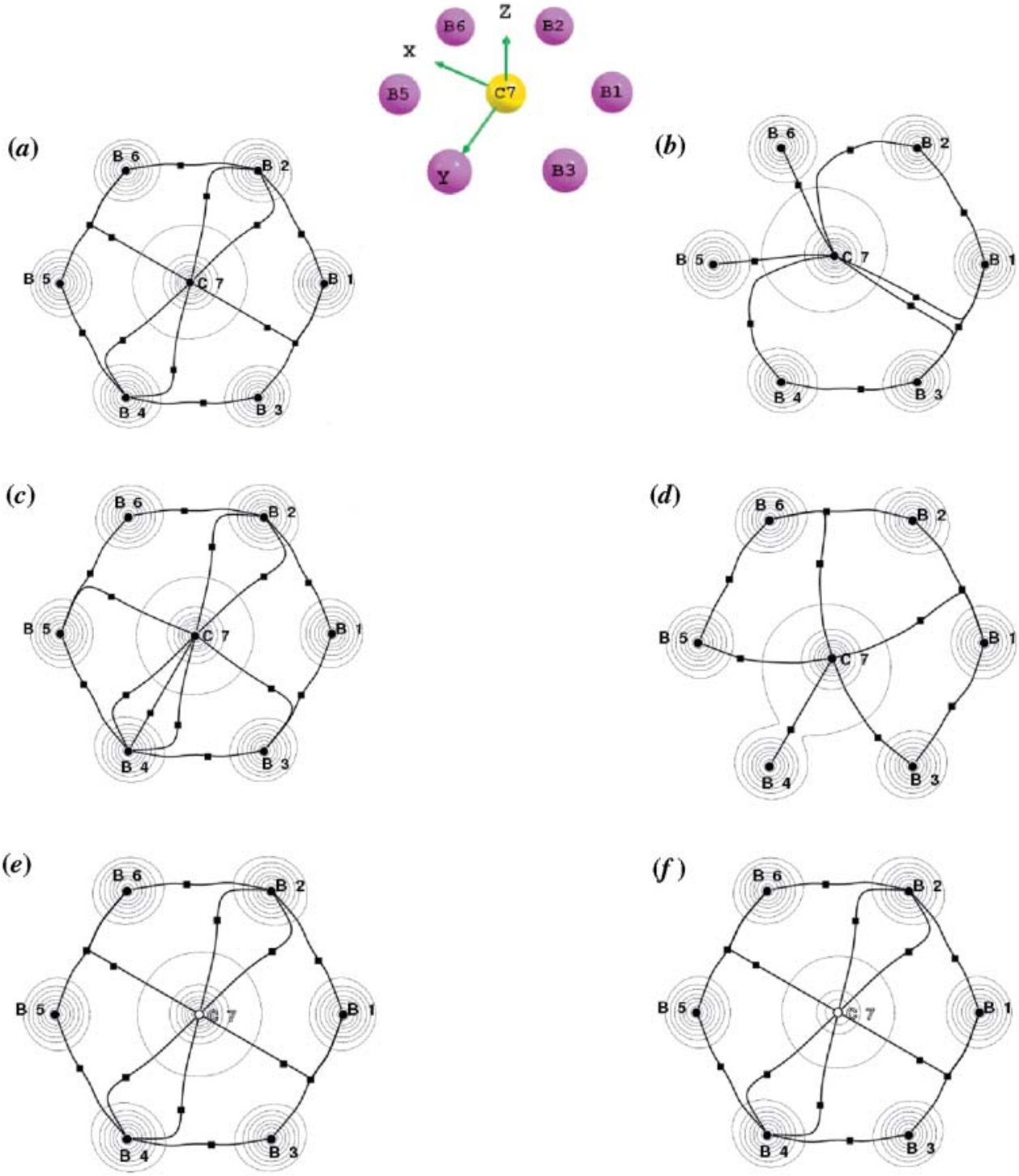
The three isomers of B_4C_3

In the case of B_4C_3, we are faced with numerous possible isomers, but this study is confined to the three isomers that were considered in the original study (8) and are depicted in Fig. 1. They have been named according to the relative position of the two carbon atoms in the peripheral ring of atoms around the central carbon atom, applying the usual classical nomenclature, namely *ortho*-B_4C_3, *meta*-B_4C_3, and *para*-B_4C_3. As noted previously and as is evident from Fig. 2, the molecular graphs of these three species differ remarkably. These differences, as well as the similarities, will be considered separately.

In the case of the *ortho*-B_4C_3 molecule, we are faced with a stable molecular graph. The central carbon atom is bonded from one side to the two carbon atoms, whereas from the other side, there are two other bonded interactions with boron atoms. So, all three types of bonding couples, namely B—B, C—C, and B—C, coexist in this molecule. The comparison of topological characters from Tables 2 and 3 reveals some interesting patterns. In all cases, except the C4—C5 bonded interaction, the amount of charge density at BCPs are smaller than those in reference double and even single bond BCPs, although, with no exception, they are all in the range of shared interactions. On the other hand, the Laplacians of charge density at BCPs of C—C and B—B bonded interactions are negative, also indicating shared interactions, whereas the same quantity is positive at BCPs of B—C bonded interactions. This positive value of the Laplacian of charge density seems to be in contradiction with the shared interaction proposed according to the charge density of corresponding BCPs. But, it must keep in mind that the internuclear distance of B—C (1.46 and 1.50 Å) in this molecule is shorter than the internuclear distance of B—C in BH_2CH_3 (1.55 Å), and so it is probable that the shortening of B—C bonds in the *ortho*-B_4C_3 molecule causes a transition to the "internal" regime of the positive Laplacian of charge density (see ref. 26 and refs. cited therein). As considered in detail by Costales et al. (26), the lengthening and shortening of internuclear distances will motivate some universal changes of charge density distributions. One of these characteristics is the appearance of a positive

© 2006 NRC Canada

Fig. 3. The molecular graphs of the $(B_6C)^{2-}$ ion when the C7 nucleus is moved in the X, Y, and Z directions of the molecular axis (shown at the top). (*a*, *b*) 0.02 and 0.2 Å displacements in the X direction. (*c*, *d*) 0.02 and 0.2 Å displacements in the Y direction. (*e*, *f*) 0.02 and 0.2 Å displacements in the Z direction. The hollow circle shows the out-of-plane nucleus.



Laplacian of charge density at BCPs (indicator of closed shared interactions) in molecules, where there is no doubt on their shared interaction (like the N_2 molecule). These positive values appear at large and small internuclear distances (usually out of the range of normal equilibrium internuclear distances), whereas at intermediate distances the usual negative value is retained. So, it is reasonable to assume that if the equilibrium internuclear distance of certain nuclei decreases considerably (like the B—C in *ortho*-B_4C_3 molecule), then a positive value of the Laplacian of charge density at BCP is not unexpected. The values of ellipticities are also worth mentioning in this analysis. In spite of small ellipticities in C4—C5 and B—C bonded interactions, large, unusual ellipticites (in comparison to those in Table 3) were

© 2006 NRC Canada

observed at other BCPs. As mentioned in the case of the $(B_6C)^{2-}$ anion, the large unusual value of ellipticity is an indicator of the proximity of a topological instability. Also, in this case one may find the near vanishing of the negative curvature of the BCPs ($\lambda_2 < -0.09$) along an axes in the plane of the ring and perpendicular to the bond path and the same near vanishing of the correspondingly directed positive curvature at the RCPs ($\lambda_2 < 0.08$). Accordingly, the comparison of the charge density values at BCPs, which possess the large of ellipticity values, with the charge density values at RCPs, confirms the proximity of topological instability. The difference between the amounts of charge density at BCPs (1,4,2,6,3,5) with neighboring RCPs (1,3,2) is between 0.002 and 0.012 au, which reveals the relative flatness of charge density around the central carbon nucleus. This feature is reminiscent of the charge density distribution of the $(B_6C)^{2-}$ anion as discussed previously. So, the presence of a multiple of topological networks regarding the nuclear excursion in a vibrational normal mode analysis is not unexpected.

Some of these topological characteristics of *ortho*-B_4C_3 seem to be shared with the two other isomers. In the case of the *meta*-B_4C_3 isomer, the amounts of charge density at BCPs are comparable with those in the *ortho*-B_4C_3 isomer. The sign of the Laplacian of charge density is also like those in the *ortho*-B_4C_3 isomer, although the sign of this function at the two BCPs of the B—C bonded interactions (B2—C7 and B3—C7) are slightly negative. As is evident from Fig. 2*c*, this may be due to a large deformation of corresponding bond paths from a straight line. On the other hand, large ellipticities have been observed again, particularly at the BCPs of the B2—C7 and B3—C7 bonded interactions. The proximity of the RCPs (1, 3) to the BCPs (1, 2) reveals the origin of these large ellipticities. One may also observe the near vanishing of the negative curvature of the BCPs ($\lambda_2 = -0.024$) along an axes in the plane of the ring and perpendicular to the bond path and the same near vanishing of the correspondingly directed positive curvature at the RCPs ($\lambda_2 = 0.019$). Comparison of the amounts of charge density at these RCPs and BCPs confirms that the difference is even smaller than 0.001 au, and so we are near to an unstable topological network with a "degenerate critical point", which may be created from the coalescence of a RCP and a BCP (see ref. 12 and refs. cited therein). So, this topological graph is also on the edge of the stability–instability regime. In the case of *para*-B_4C_3, in contrast to the two other isomers, a conflict structure exists at equilibrium geometry like those in the $(B_6C)^-$ anion. However, in the case of bonded interactions, namely B—B, B—C, and C—C, the amounts of charge density at the corresponding critical points is almost similar to those found in *ortho*-B_4C_3, *meta*-B_4C_3, and $(B_6C)^{2-}$ species. In all species considered, with the minor exception of B2—C7 and B3–C7 in *meta*-B_4C_3, the sign of the Laplacian of charge density at BCPs corresponding to all C—C and B—B bonded interactions are negative and those belonging to B—C bonded interactions are positive. The large ellipticity values of the BCPs (3,4) also confirm the topological instability of the molecular graph. Again, the difference between the amounts of the charge density of BCPs (3,4) and neighboring RCPs (1,2,3,4) is only 0.004 au, and combined with the near vanishing of the negative curvature of the BCPs ($\lambda_2 = -0.010$) along an axes in the plane of the ring and perpendicular to the bond path and the same near vanishing of the correspondingly directed positive curvature at the RCPs ($\lambda_2 = 0.027$), may be interpreted as the possibility of coalescence of BCPs and RCPs and creation of degenerate critical points is probable. Like the $(B_6C)^{2-}$ anion, some selected deformations have been applied to the equilibrium geometry of this molecule and the corresponding topological networks are depicted in Fig. 4. Again, dramatic changes have taken place in the topological networks. Some of these structures, such as Figs. 4*a*, 4*b*, 4*e*, and 4*f*, are also unstable conflict structures. So, according to the reasoning that has been offered in the case of the $(B_6C)^{2-}$ anion, the vibrational dynamics of nuclei prevent the attribution of a single definite molecular graph to the *para*-B_4C_3 molecule around equilibrium geometry, another example of a topologically floppy molecule.

Conclusion and remarks

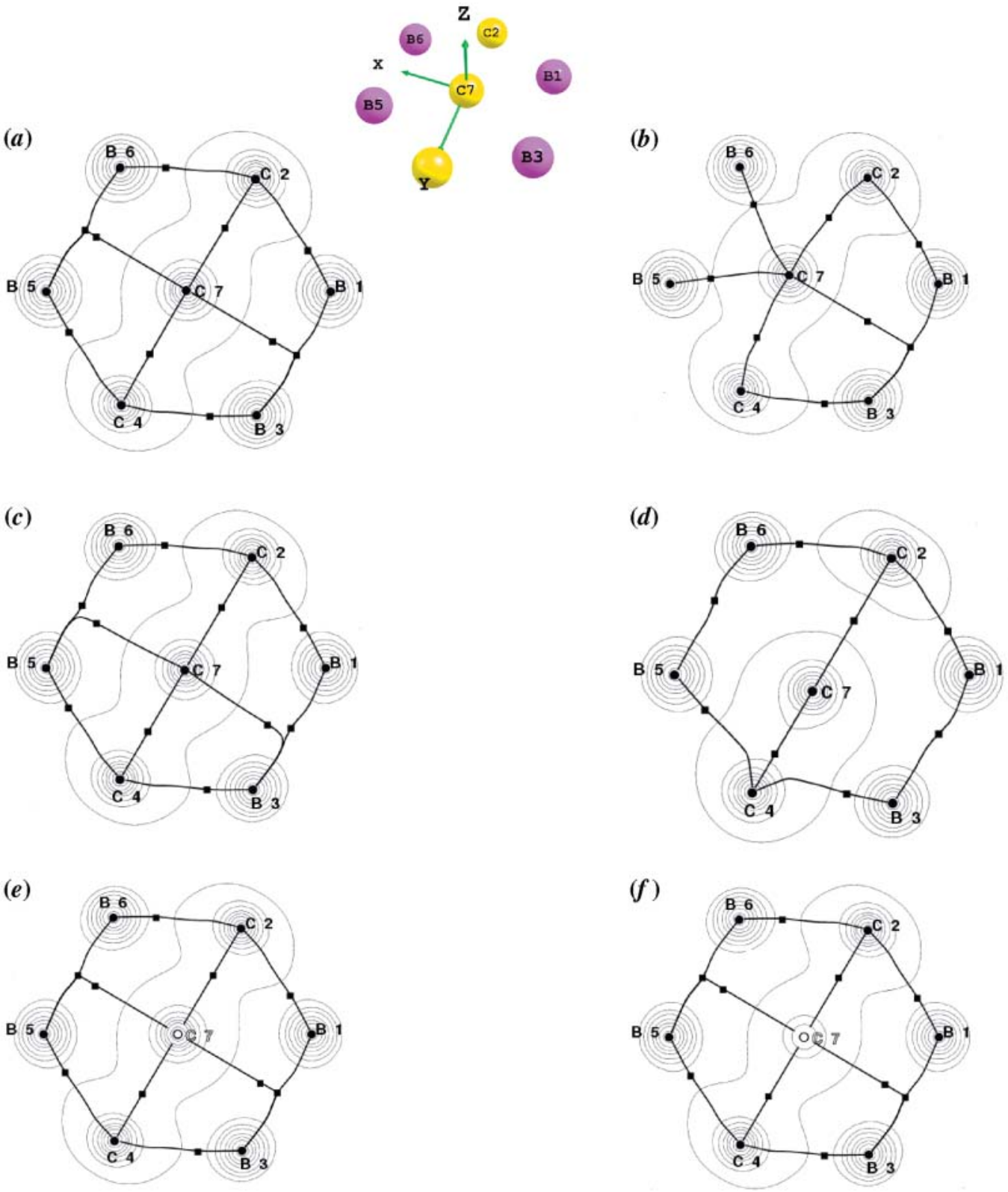
This study reveals some of the interesting features of the topological characters of the charge density in the species under consideration and clearly indicates that a nontrivial, possibly floppy topological pattern exists in this series of molecules because of the extraordinary sensitivity of the topological characters of these species relative to the small changes in their geometries. In this regard, it is worth mentioning that such a topological floppiness is not unique and has been reported previously in other sets of molecules (27–29). So, what can be said about their bonding pattern?

In a recent paper entitled "Where to draw the line in defining a molecular structure", Bader et al. (30) discussed in detail an interesting case, namely bonding between Mn, Si, and H atoms in the adduct resulting from the reaction between $HSiCl_3$ and $Cp(CO)_2Mn$ molecules. Since there were conflicting opinions regarding the most appropriate bonding pattern of this adduct (31, 32), the QTAIM clear-cut answer regarding the associated bonding pattern based solely on quantum mechanics of proper open systems seems a remarkable achievement. So, at least if one may neglect (with or without reasonable physical justification) the nuclear motion and hence just describe the topology of the charge density of a certain point in geometrical space or corresponding PES, QTAIM could offer unambiguous results. Unfortunately, this study did not encounter such a well-defined case. Left alone, the conflict structures of $(B_6C)^{2-}$ and *para*-B_4C_3 molecules, which are inherently topologically unstable structures, and even in the case of *ortho*-B_4C_3 and *meta*-B_4C_3 molecules with stable topological structure, there are clues that nuclear excursions may cause geometrical deformations that make available new topological domains different from those corresponding to the equilibrium geometry. So, it seems to us that explicit consideration of the nuclear motion in the framework of QTAIM could be helpful for a better understanding of the bonding pattern of these molecules. Although this possibility for a general extension of QTAIM is under study,[2] even the analysis accomplished in this paper reveals certain points that are worth mentioning.

[2] Sh. Shahbazian. Manuscript under preparation.

© 2006 NRC Canada

Fig. 4. The complete molecular graphs of p-B_4C_3 when the C7 nucleus is moved in the X, Y, and Z directions of the molecular axis (shown at the top). (*a*, b) 0.02 and 0.2 Å in the X direction. (*c*, *d*) 0.02 and 0.2 Å in the Y direction.



Intuitionally, one expects that in such hexacoordinate species, the nucleus of the central carbon atom should be connected to the nuclei of peripheral atoms with six distinct bond paths, but Figs. 2–4 clearly demonstrate that none of the topological networks corresponding to the species under study have a central carbon atom with six or more bond

© 2006 NRC Canada

paths connecting them to all six atoms in the peripheral ring. It is interesting to note that the same topological analysis that has been done on the other celebrated hexacoordinate molecule, namely CLi_6, came to another conclusion and confirmed that the central carbon atom, which is confined in an octahedral structure, has indeed six bond paths connecting the carbon atom to six lithium atoms (33). (The same molecular graph was retained using more extended basis sets and even taking into account the correlation effects by employing sophisticated DFT methods).[3] So, it seems to us that we are faced with unusual, "possibly" hexacoordinate species in this study.

On the other hand, the topological characteristics of the BCPs of the $(B_6C)^{2-}$ anion unequivocally established the shared interaction between boron atoms and also the flat charge density around the nucleus of the central carbon. This seems to indicate that no firm "directional interaction" takes place between the central carbon and the boron atoms. Although the free rotation of a single atom is not of physical significance, if the charge density distribution of the other extended planar boron rings encompassing the small molecular clusters resembles the $(B_6C)^{2-}$ anion, then a nearly free rotation of the central cluster must be expected. Although according to the best of our knowledge no study of the topological characters of charge density distributions have been yet performed on such extended boron–carbon clusters, the ab initio calculations (11) have been conducted on such species and indeed have been estimated to have a very low barrier for the rotation of the central carbon clusters encompassing the ring of boron atoms. The future direct examination of the topological features of the charge density of these species will establish the possible common trait among them. This study has been restricted only to the detailed analysis of charge density distributions and corresponding topological networks. The evaluation of atomic expectation values, as well as analysis of localization/delocalization indices, will be done in a subsequent paper.

Acknowledgments

Special thanks to Professor Kirk A. Peterson from Washington State University for his very useful comments and Dr. Paul Lode Albert Popelier from the University of Manchester Institute of Science and Technology, Manchester, UK (UMIST) for helping us to access the MORPHY99 software and sending the related materials. We are also grateful to Professor R.F.W Bader and two other reviewers for their useful technical comments and to the respected editor, since his final comments on the linguistic aspects of this paper helped us to improve the manuscript.

References

1. E.D. Jemmis, J. Chandeasekhar, E.U. Würthwein, and P.v.R. Schleyer. J. Am. Chem. Soc. **104**, 4275 (1982).
2. P.v.R. Schleyer, E.U. Würthwein, E. Kaufmann, and T. Clark. J. Am. Chem. Soc. **105**, 5930 (1983).
3. E.U. Würthwein, K.D. Sen, J.A. Pople, and P.v.R. Schleyer. Inorg. Chem. **22**, 496 (1983).
4. G.A. Olah and G. Rasul. Acc. Chem. Res. **30**, 245 (1997).
5. W. Siebert and A. Gunale. Chem. Soc. Rev. **28**, 367 (1999).
6. D. Rottger and G. Erker. Angew. Chem. Int. Ed. Engl. **36**, 812 (1997).
7. V.I. Minikin, R.M. Minyaev, and R. Hoffman. Russ. Chem. Rev. **71**, 869 (2002).
8. K. Exner and P.v.R. Schleyer. Science, **290**, 1937 (2000).
9. Z.-X. Wang and P.v.R. Schleyer. Science, **292**, 2465 (2001).
10. Z.-X. Wang and P.v.R. Schleyer. Angew. Chem. Int. Ed. **41**, 4082 (2002).
11. S. Erhardt, G. Frenking, Z. Chen, and P.v.R. Schleyer. Angew. Chem. Int. Ed. **44**, 2 (2005).
12. R.F.W. Bader. Atoms in Molecules: A quantum theory. Oxford University Press, Oxford. 1990.
13. A.A. Granovsky. PC GAMESS [online]. Version 6.4 [computer program]. Laboratory of Chemical Cybernetics, Moscow State University, Moscow. Available from http://classic.chem.msu.su/gran/gamess/index.html. 1999.
14. M.W. Schmidt, K.K. Baldridge, J.A. Boatz, S.T. Elbert, M.S. Gordon, J.H. Jensen, S. Koseki, N. Matsunaga, K.A. Nguyen, S.J. Su, T.L. Windus, M. Dupuis, and J.A. Montgomery. J. Comput. Chem. **14**, 1347 (1993).
15. P.L.A. Popelier and R.G.A. Bone. MORPHY99 [computer program]. University of Manchester Institute of Science and Technology, Manchester, UK. 1999.
16. P.L.A. Popelier. Comput. Phys. Commun. **93**, 212 (1996).
17. P.L.A. Popelier. Theor. Chim. Acta, **87**, 465 (1994).
18. P.L.A. Popelier. Mol. Phys. **87**, 169 (1996).
19. P.L.A. Popelier. Comput. Phys. Commun. **108**, 180 (1998).
20. P.L.A. Popelier. Can. J. Chem. **74**, 829 (1996).
21. G.A. Zhurko and D.A. Zhurko. ChemCraft. Version 1.4 beta [computer program]. Available from http://www.chemcraftprog.com. 2005.
22. R.F.W. Bader. J. Phys. Chem. A, **102**, 7314 (1998).
23. Sh. Shahbazian and M. Zahedi. Found. Chem. [online], (2006). doi: 10.1007/s10698-005-8247-4.
24. J. Palis and S. Smale. Pure Math. **14**, 223 (1970).
25. I.N. Levine. Molecular spectroscopy. John Wiley and Sons, New York. 1975.
26. A. Costales, M.A. Blanco, A. Martin Pendas, P. Mori-Sanchez, and V. Luana. J. Phys. Chem. A, **108**, 2794 (2004).
27. R.F.W. Bader and D. Legare. Can. J. Chem. **70**, 657 (1992).
28. R.F.W. Bader and C.F. Matta. Inorg. Chem. **40**, 5603 (2001).
29. F. Cortés-Guzmán and R.F.W. Bader. Coord. Chem. Rev. **249**, 633 (2005).
30. R.F.W. Bader, C.F. Matta, and F. Cortés-Guzmán. Organometallics, **23**, 6253 (2004).
31. D.L. Lichtenberger. Organometallics, **22**, 1599 (2003).
32. G.I. Nikonov. Organometallics, **22**, 1597 (2003).
33. J.P. Ritchie and S.M. Bachrach. J. Am. Chem. Soc. **109**, 5909 (1987).

[3] Sh. Shahbazian. Unpublished results on some carbon–lithium (CLi_x) clusters (details of calculations and original files are all available upon request from the authors).

© 2006 NRC Canada

Living biomembrane bitemplate route for simultaneous synthesis of different morphologies of CdSe and ZnSe nanomaterials

Li Li, Qing-Sheng Wu, and Ya-Ping Ding

Abstract: In this paper, CdSe (nanotubes, nanorods) and ZnSe (nanorods, nanoslats) were simultaneously synthesized through a biomineralization process through biomembrane bitemplates of mungbean sprouts at room temperature. The XRD patterns indicated that these nanocrystals were crystallized in the hexagonal structure and cubic structure with lattice constants a = 0.423 and c = 0.701 nm (CdSe) and a = 0.567 nm (ZnSe), respectively. The possible formation mechanism was investigated in the paper.

Key words: CdSe, ZnSe, nanotubes, nanorods, nanoslats, living biomembrane, bitemplates.

Résumé : On a synthétisé simultanément du CdSe (nanotubes, nanotiges) et du ZnSe (nanotiges, nanolamelles) dans le cadre d'un processus de biominéralisation à la température ambiante, à travers une biomembrane à double gabarit de germe de haricot mungo. Les patrons de diffraction des rayons X indiquent que ces nanocristaux appartiennent respectivement à des structures hexagonale et cubique avec des constantes a = 0,423 et c = 0,701 nm (CdSe) et a = 0,567 nm (ZnSe) respectivement. On a étudié le mécanisme possible de formation.

Mots clés : CdSe, ZnSe, nanotubes, nanotiges, nanolamelles, biomembrane vivante, double gabarit.

[Traduit par la Rédaction]

Teeth, bones, and shells are known as the products of biological mineralization by cells (1, 2). They are nanodimensional materials synthesized by organism itself. Biomembranes, formed by orderly arrangements of cells, are highly regular and controllable. Some difficult functions such as high penetrability and selectivity that haven't been achieved can be obtained by biomembranes with powerful transmission capacities and ideal separation efficiencies. Recently, monomolecular membranes (3) and multimolecular membranes (LB membranes) (4, 5) have been utilized as a simplified model for biomembranes that are used to simulate the transportation of ions and the transfer of information and energy in the biomembranes. Now membrane research is at the molecule level. In recent years, it has attracted many researchers' interest in using biomembranes as templates for the synthesis of nanomaterials (6–8). But no one has been trying to utilize bitemplates, and only a few 1-D nanomaterials have been produced. No reports about the method of manipulating the nucleation and the growth of the molecule to simultaneously synthesize different morphologies of nanomaterials by means of biomembrane bitemplates with dense structure, orderly arrangement, and different inner and outer structures have been made.

The nanoscale II–VI semiconductor compounds, such as the direct band gap materials ZnSe and CdSe, have been thoroughly investigated and widely used (9–13). These wide-gap II–VI semiconductors are efficient emitters in the blue to ultraviolet spectral region, and excitons in these compounds are much more stable than those in conventional III–V semiconductors that are widely used in optoelectronic applications such as blue laser diodes, light-emitting diodes, and photodetectors (14, 15).

The mung bean radicle is a kind of simple and available living biomembrane material that is able to live in solution. There are many well-distributed grooves on its stem surface and many conduits in the stem (Fig. 1). The structures of the inner and outer membranes of the stem are very different. Because the membrane controls the entrance and exit of inorganic ions and affects mineralization, therefore, the mung bean radicle is an ideal material for use as a living biomembrane bitemplate for the synthesis of allomorphic nanomaterials. By using biological mineralization, 1-D selenides, such as ZnSe and CdSe semiconductor nanomaterials, were simultaneously synthesized by induction of these living biological bitemplates.

Experimental section

Materials

Selenium (99.95%), KBH_4 (94%), $CdCl_2$, $ZnSO_4$, and absolute ethanol (A.R.) were all purchased from the Shanghai

Received 16 April 2005. Published on the NRC Research Press Web site at http://canjchem.nrc.ca on 17 May 2006.

L. Li and Q.-S. Wu.[1] Department of Chemistry, Tongji University, Shanghai, P. R. China 200092.
Y.-P. Ding. Department of Chemistry, Shanghai University, Shanghai, P. R. China 200436.

[1]Corresponding author (e-mail: qswu@mail.tongji.edu.cn).

 doi:10.1139/V06-064 © 2006 NRC Canada

Fig. 1. ESEM pattern of the mung bean sprout. (*a*) The interior of the mung bean sprout. (*b*) The surface of the mung bean sprout.

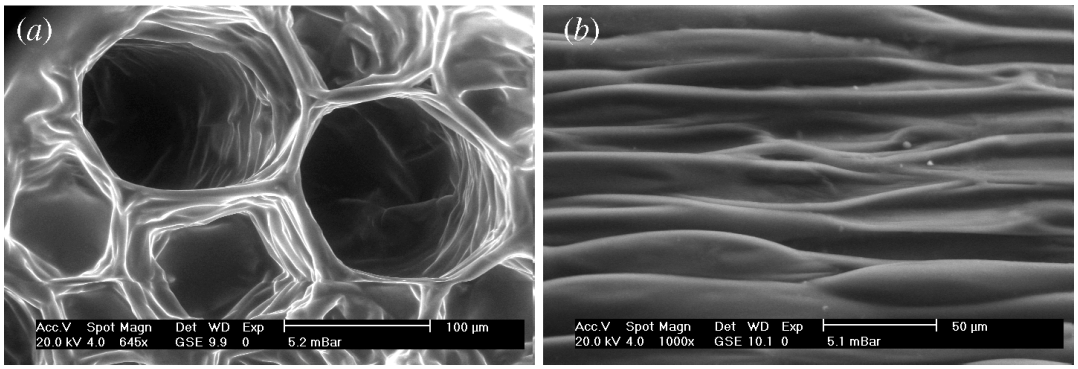
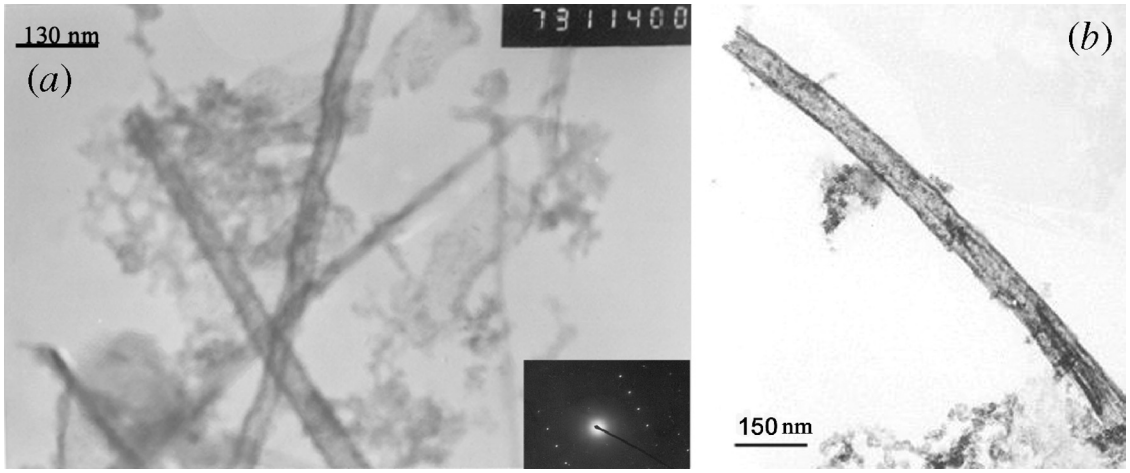


Fig. 2. (*a*) TEM image of as-prepared CdSe nanotubes (external products) and SAED. (*b*) TEM image of a single CdSe nanotube.



Chemical Reagent Factory, China. Mung bean sprouts were fresh and purchased from the market.

Instrumentation

TEM images and electron diffraction spectra were generated on a Hitachi model-800 transmission electron microscope. Powder X-ray diffraction (XRD) patterns of the samples were measured on a Phillips 1710 X-ray diffractometer with Cu Kα radiation (λ = 1.5406 Å). ESEM images were obtained on a Phillips XL-30E environmental scanning electron microscope. Absorption spectra were recorded on an Aligent 8453 UV–vis spectrophotometer. Photoluminescence (PL) spectra were obtained on a PerkinElmer LS-55 luminescence spectrophotometer (Boston, Massachusetts).

Procedure

One-dimensional semiconductor ZnSe nanomaterials were prepared according to the following procedure: mung bean sprouts (except for laminae) were immersed in a solution of 0.1 mol/L aq. $ZnSO_4$ at room temperature for 6 h before they were taken out and rinsed under deionized water. After immersion in a solution of 0.1 mol/L aq. KHSe (KBH_4–Se in 20 mL deionized water) for 3 h (10), the mung bean sprouts were rinsed under deionized water and anhydrous ethanol successively. The brown solid on the surface of the mung bean sprouts was scraped off with a glass rod and transferred into a beaker. Then these mung bean sprouts were silted, and the inner product was scraped off with a glass rod and transferred into another beaker. Ten milliliters of carbon tetrachloride was added to the beakers, and the suspensions were agitated with an ultrasonator for 30 min followed by centrifugalization. The solids were kept in absolute ethanol.

When $CdCl_2$ was used in this procedure in place of $ZnSO_4$, ZnSe nanomaterials were prepared.

Characterization method

The crystal structures of the products were examined by XRD. The morphology and size of the synthesized products were observed by TEM. The PL spectra of the products were obtained using a PerkinElmer luminescence spectrophotometer (LS-55). The UV spectra of the products were obtained using an UV–vis spectrophotometer (Aligent 8453).

Results

Morphology and structure

Figure 2*a* and the inset display a CdSe TEM image of the external products and their selected area electron diffraction (SAED) patterns, suggesting that they are nanotubes and

© 2006 NRC Canada

Fig. 3. (*a*) TEM image of as-prepared CdSe nanorods (internal products) and SAED. (*b*) TEM image of CdSe nanorods.

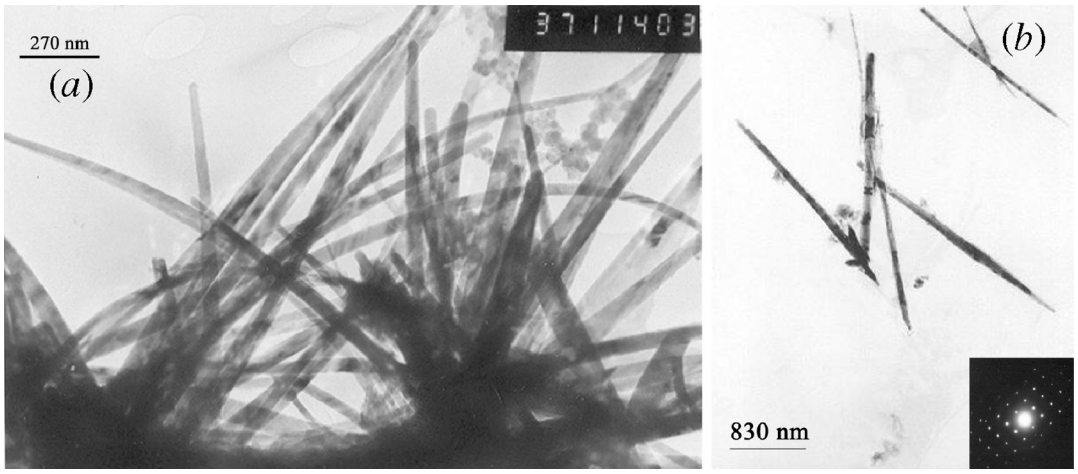
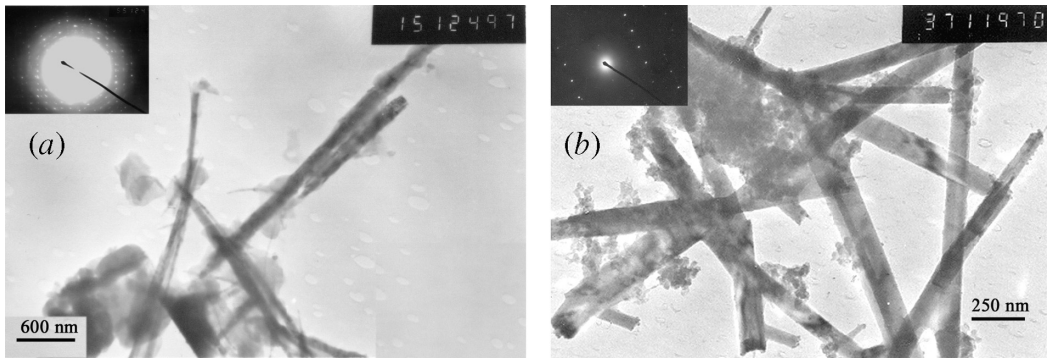


Fig. 4. (*a*) TEM image of as-prepared ZnSe nanorods (external products) and SAED. (*b*) TEM image of as-prepared ZnSe nanoslats (internal products) and SAED.



single crystals. The outside diameter of these nanotubes is 65–70 nm, the inner diameter is 60–65 nm, and the lengths are up to 800–1000 nm. Observation (Figs. 3*a* and 3*b*) of the inside products shows that they are nanorods with a diameter of about 50 nm and a length longer than 3000 nm. The nanorods are smooth and straight. Figure 3*b* shows the typical electron diffraction pattern of nanorods, which indicates that they are single crystals.

Figure 4*a* shows the ZnSe TEM micrographs and SAED patterns of the external products. The diameter of the nanorod is about 80 nm, and the average length is about 3.5 μm. The SAED pattern inserted in Fig. 4*a* shows that the nanorods synthesized in the experiment are single crystals. Figure 4*b* and the inset display a TEM image of the interior products and their SAED pattern, suggesting that they are regular nanoslats and they are single crystals. Their diameter is in the range of 150 nm, their length about 1100–1250 nm, and their thickness in the range of about 50 nm.

Figures 5*a* and 5*b* show the XRD patterns of the ZnSe and CdSe samples prepared using the living biomembrane. In Fig. 5*a*, the peaks can be indexed as cubic zinc-blende phase ZnSe with a lattice parameter of $a = 0.567$ nm, which is consistent with The Joint Committee on Powder Diffraction Standards (JCPDS) card No. 5-0522. The XRD pattern of CdSe is shown in Fig. 5*b* and all of the peaks were indexed as the hexagonal phase of CdSe (JCPDS card No. 8-459). The broadness of the XRD peaks corresponded to their small grain size.

Experimental conditions

We have tried the synthesis of CdSe or ZnSe materials without the templates of the mung bean sprouts. The morphologies and structures of these materials are quite different from the products produced using the templates. The TEM images of the CdSe or ZnSe material (Fig. 6), which were synthesized without the templates of the mung bean sprouts, suggest that they were all amorphous crystals.

When the concentration was at 0.1–0.2 mol/L, a range of 1-D nanomaterials were commonly observed. When the concentration was less than 0.1 mol/L, the nanoparticles gradually increased. When the concentration was more than 0.2 mol/L, it was not a suitable environment for mung bean sprouts to live. There were two reasons for our selection of KBH_4 as the reductant: one was the possible existence of active H^- in KBH_4, which activated the reaction between Se and $Cd^{2+}(Zn^{2+})$ (16); another was the existence of K^+ ions in KBH_4, which "eliminated the toxicity of the single salt" caused by the $Cd^{2+}(Zn^{2+})$ ions.

© 2006 NRC Canada

Fig. 5. (*a*) XRD pattern of ZnSe nanomaterials. (*b*) XRD pattern of CdSe nanomaterials.

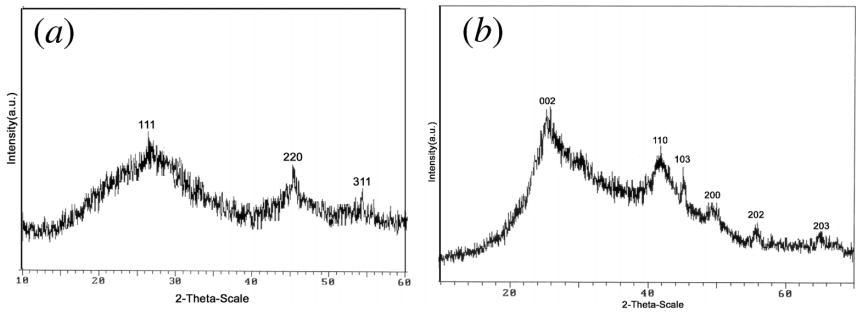
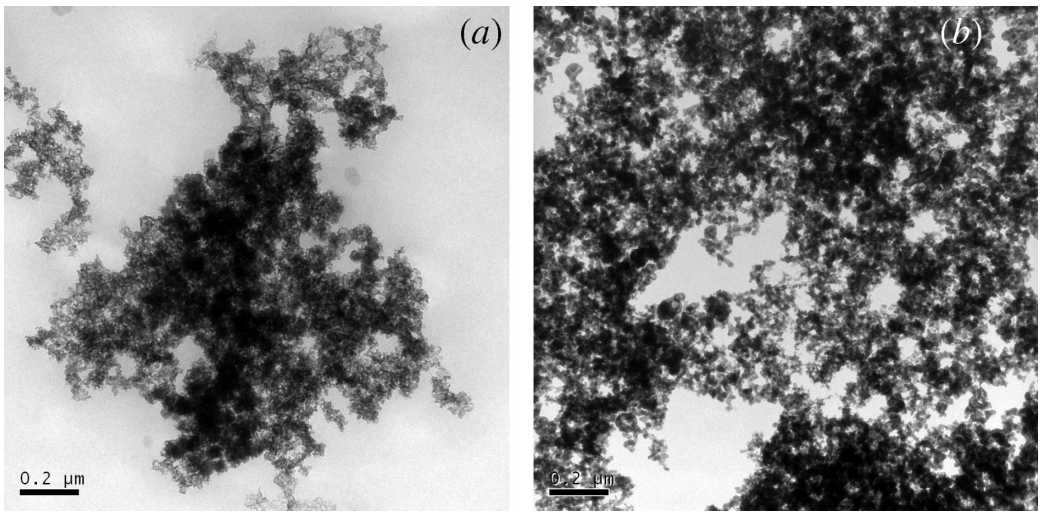


Fig. 6. (*a*) TEM image of as-prepared ZnSe materials (*without* using the mung bean sprout). (*b*) TEM image of as-prepared CdSe materials (*without* using the mung bean sprout).



Optical properties

Until now, a few reports of ZnSe or CdSe preparation referred to the luminescence properties, largely for their unique semiconductor properties. Here, we examined the UV spectra and PL spectra of the as-prepared nanomaterials at room temperature and our result shows it as a potential application in optical devices. Figure 7*a* shows the UV–vis absorption spectrum at 327 nm for the CdSe nanomaterials and an obvious blue shift was observed when compared with the bulk CdSe at 712 nm (1.74 eV) owing to quantum confinement. The PL of the CdSe nanostructure was characterized with an excitation wavelength of 230 nm. As compared with the PL spectrum acquired from the source CdSe powders, whose luminescence peak is located at 735 nm, the CdSe nanomaterials showed a peak at 394 nm (nanotubes) and 410 nm (nanorods) (Figs. 7*c* and 7*d*), shifted toward blue, possibly because of the small diameters of the CdSe nanomaterials.

UV–vis absorption spectra (Fig. 7*b*) of ZnSe quasi-nanospheres showed a strong absorption peak at about 320 nm (4.84 eV) and an obvious blue shift was observed when compared with bulk ZnSe at 480 nm (2.6 eV) owing to quantum confinement. The absorption peak for the products shifted about 160 nm, which is consistent with those ZnSe nanomaterials synthesized by other methods (17, 18). Figures 7*e* and 7*f* show the PL spectrra of an ethanol solution containing ZnSe nanomaterials. The PL spectrum of the ZnSe shows a broad emission band peaked at ca. 340 nm (nanoslats) and 485 nm (nanorods), using a 230 nm excitation wavelength. The characteristic blue shift of the PL spectrum of nanomaterials is attributed to their small diameter and larger aspect ratio.

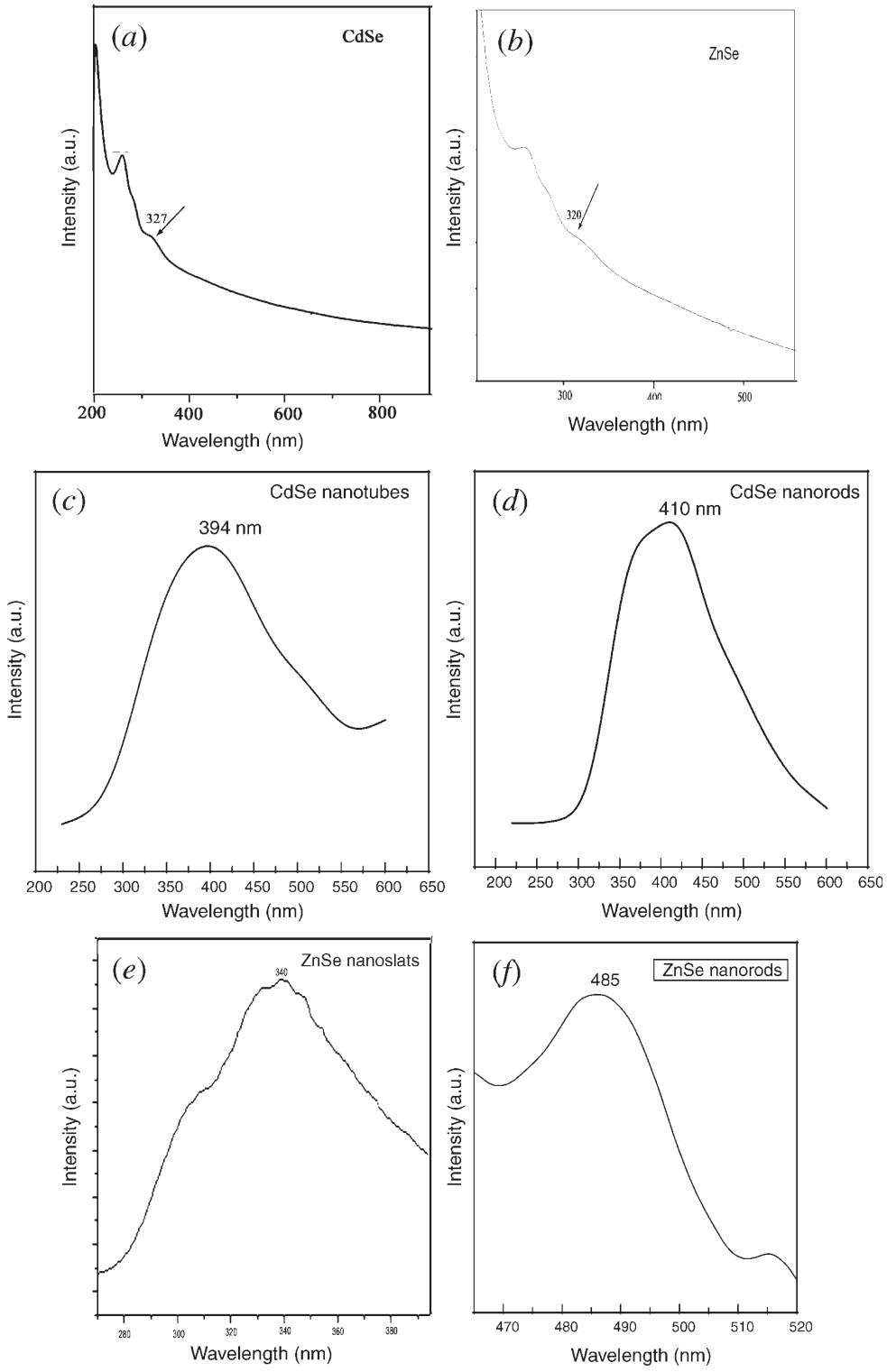
Conclusions

In summary, different morphologies of CdSe and ZnSe 1-D nanomaterials have been synthesized under the control of living bitemplates using fresh mung bean sprouts.[2] This method is mild, convenient, and "green" because of the absence of surfactant and organic solvent (19, 20). This approach can be extended to synthesize other nanostructured materials. We could use other living biomembranes instead of mung bean sprouts. The synthesis mechanism, especially the organism changes, the process of action, and the trans-

[2] Supplementary data for this article are available on the journal Web site (http://canjchem.nrc.ca) or may be purchased from the Depository of Unpublished Data, Document Delivery, CISTI, National Research Council Canada, Ottawa, ON K1A 0R6, Canada. DUD 5030. For more information on obtaining material refer to http://cisti-icist.nrc-cnrc.gc.ca/irm/unpub_e.shtml.

© 2006 NRC Canada

Fig. 7. (*a*) UV–vis spectrum of as-prepared CdSe nanomaterials. (*b*) UV–vis spectrum of as-prepared ZnSe nanomaterials. (*c*) PL spectrum of an ethanol solution containing CdSe as-prepared nanotubes. (*d*) PL spectrum of an ethanol solution containing CdSe as-prepared nanorods. (*e*) PL spectrum of an ethanol solution containing ZnSe as-prepared nanoslats. (*f*) PL spectrum of an ethanol solution containing ZnSe as-prepared nanorods.



© 2006 NRC Canada

portation of the biological system in the high-salt solution maybe very complicated and further research is needed.

Acknowledgements

The authors are grateful for the financial support of the National Natural Science Foundation of China (grant Nos. 20471042 and 20571051), the Doctoral Program Foundation of the Ministry of Education (No. 20040247045), and the NanoFoundation of Shanghai in China (grant Nos. 0452nm075 and 0552nm048).

References

1. M. Li, H. Schnablegger, and S. Mann. Nature (London), **402**, 393 (1999).
2. E. Baeuerlein. Angew. Chem. Int. Ed. **42**, 614 (2003).
3. V.L. Colvin, A.P. Alivisatos, A.N. Goldstein, et al. J. Am. Chem. Soc. **114**, 5221 (1992).
4. K. Frankin, K. Serena, and P.D. Yang. J. Am. Chem. Soc. **123**, 4360 (2001).
5. H.F. Gong and M.H. Liu. Chem. Mater. **14**, 4933 (2002).
6. S. Behrens, K. Rahn, W. Habicht, K.-J. Böhm, H. Rösner, E. Dinjus, and E. Unger. Adv. Mater. **14**, 1621 (2002).
7. P. Mukherjee, S. Senapati, D. Mandal, A. Ahmad, M.I. Khan, R. Kumar, and M. Sastry. Angew. Chem. Int. Ed. **40**, 3585 (2001).
8. A. Li, S.-W. Chung, J.-M. Nam, D.S. Ginger, and C.A. Mirkin. Angew. Chem. Int. Ed. **42**, 2306 (2003).
9. Q. Peng, Y. Dong, Z. Deng, and Y. Li. Inorg. Chem. **41**, 5249 (2002).
10. C.N.R. Rao, A. Govindaraj, F. Leonard Deepak, N.A. Gunari, and M. Nath. Appl. Phys. Lett. **78**, 1853 (2001).
11. C. Ma, Y. Ding, D. Moore, X. Wang, and Z.L. Wang. J. Am. Chem. Soc. **126**, 708 (2004).
12. Q. Peng, Y.J. Dong, and Y.D. Li. Angew. Chem. Int. Ed. **42**, 3027 (2003).
13. Y. Jiang, X.M. Meng, and S.-T. Lee. J. Phys. Chem. B, **108**, 2784 (2004).
14. S.H. Tolbert and A.P. Alivisatos. Science (Washington, D.C.), **265**, 373 (1994).
15. B.Q. Sun, E. Marx, and N.C. Greenham. Nano Lett. **3**, 961 (2003).
16. W.Z. Wang, Y. Geng, and Y.T. Qian. Adv. Mater. **10**, 1479 (1998).
17. M.A. Hines and P. Guyot-Sionnest. J. Phys. Chem. B, **102**, 3655 (1998).
18. F.T. Quinlan, J. Kuther, and P. Stroeve. Langmuir, **16**, 4049 (2000).
19. L. Li, Q.S. Wu, and Y.P. Ding. Nanotechnology, **15**, 1877 (2004).
20. Y. Xia, P. Yang, Y. Sun, Y. Wu, B. Mayers, B. Gates, Y. Yin, F. Kim, and H. Yan. Adv. Mater. **15**, 353 (2003).

© 2006 NRC Canada

Interaction of peroxynitrite with myoglobin and hemoglobin

Shivashankar Kalinga

Abstract: Peroxynitrite, a biological toxin produced in vivo by the nearly diffusion-controlled reaction of nitrogen monoxide with superoxide, can nitrate and oxidize various biomolecules. Modifications caused by peroxynitrite have been linked to many human diseases, in particular, increased levels of free or protein-bound 3-nitrotyrosine, a biomarker for peroxynitrite in vivo, have been detected in a variety of pulmonary and cardiovascular diseases as well as in neurodegenerative and chronic inflammatory disorders. These observations have led to the search for a drug that can scavenge this powerful nitrating and oxidizing agent. Heme proteins, in particular myoglobin and hemoglobin, present in large amounts in muscles and red blood cells, respectively, have been proposed to serve as sinks for peroxynitrite in these cells. This report reviews the current knowledge of the reactions of different forms of myoglobin and hemoglobin with peroxynitrite and discusses their physiological role on the basis of measured rate constants.

Key words: myoglobin, hemoglobin, peroxynitrite, tyrosine nitration, iron(III) peroxynitrite complex.

Résumé : Le peroxynitrite est une toxine biologique qui est produite in vivo par la réaction dont la vitesse est pratiquement contrôlée par la diffusion du monoxyde d'azote avec le superoxyde et qui peut conduire à la nitration et à l'oxydation de diverses biomolécules. Des modifications provoquées par le peroxynitrite ont été liées à diverses pathologies humaines, en particulier, des niveaux accrus de 3-nitrotyrosine libre ou liée à une protéine, un biomarqueur du peroxynitrite in vivo, ont été détectés dans une variété de maladies pulmonaires ou cardiovasculaires ainsi que dans des désordres neurodégénératifs et des inflammations chroniques. Ces observations ont orienté des recherches vers le développement d'un médicament qui pourrait capter ce puissant agent de nitration et d'oxydation. Les héme protéines, en particulier la myoglobine et l'hémoglobine, qui sont présentes en grandes quantités respectivement dans les muscles et les cellules rouges du sang ont été proposées pour servir de piège pour le peroxynitrite présent dans ces cellules. Le présent travail passe en revue les connaissances actuelles des réactions des diverses formes de la myoglobine et de l'hémoglobine avec le peroxynitrite et discute de leur rôle physiologique sur la base de constantes de vitesse mesurées.

Mots clés : myoglobine, hémoglobine, peroxynitrite, nitration de la tyrosine, complexe du fer(III) et du peroxynitrite.

[Traduit par la Rédaction]

Introduction

In humans, the endothelial, neuronal, and inducible nitric oxide synthases produce nitrogen monoxide in nanomolar concentration from arginine with the aid of dioxygen and nicotinamide adenine dinucleotide phosphate (reduced form, NADPH) (1). Under physiological levels, nitrogen monoxide plays an important role in regulating blood pressure, as a defensive cytotoxin of the immune system, and as a neurotransmitter (1). However, overproduction of nitrogen monoxide is known to be involved in the pathogenesis of several inflammatory diseases (2). For example, overproduction of nitrogen monoxide in blood vessels of a septic organism leads to sustained, often lethal hypotension (3). Importantly, the extravascular half-life of nitrogen monoxide ranges from 0.09 to ~2 s; it can readily diffuse across cellular membranes and react with molecules such as dioxygen and superoxide radicals (4). Nitrogen monoxide reacts with dioxygen to give nitrogen dioxide and the rate constant for this ternary reaction in aqueous solution is 2×10^6 $(mol/L)^{-2}$ s^{-1} at 25 °C (5). However, this reaction proceeds slowly under physiological conditions. Nitrogen monoxide reacts rapidly with superoxide to form peroxynitrite, which is a far more reactive molecule than its precursors (eqs. [1] and [2]) (6).

$$[1] \quad NO^{\cdot} + O_2^{\cdot -} \xrightarrow{1.6 \times 10^{10}\ (mol/L)^{-1}\ s^{-1}} ONOO^- \overset{H^+}{\rightleftharpoons} ONOOH$$

$$[2] \quad 2O_2^{\cdot -} + 2H^+ \xrightarrow[SOD]{2 \times 10^9\ (mol/L)^{-1}\ s^{-1}} O_2 + H_2O_2$$

Peroxynitrite, a reactive transient species with a biological half-life of 10–20 ms, is a potent oxidant with the ability to destroy critical cellular components (6, 7). It may oxidize thiols (8) and (or) nitrates of all major types of biomolecules including DNA (9, 10), proteins (11, 12), and lipids (13). Koppenol and co-workers (14, 15) pointed out that the second-order rate constant for the reaction of nitrogen monoxide with superoxide is $(1.6 \pm 0.3) \times 10^{10}$ $(mol/L)^{-1}$ s^{-1} (eq. [1]), a value that is larger than that for the reaction of

Received 16 December 2005. Published on the NRC Research Press Web site at http://canjchem.nrc.ca on 17 May 2006.

S. Kalinga. Department of Chemistry and Applied Biosciences, ETH Hönggerberg, Zürich 8093, Switzerland. (e-mail: kss@mit.edu).

 doi:10.1139/V06-067 © 2006 NRC Canada

superoxide with superoxide dismutase (2×10^9 (mol/L)$^{-1}$ s^{-1}, ref. 16) (eq. [2]). Thus, peroxynitrite may be formed even in the presence of physiological concentrations of superoxide dismutase, especially if the nitrogen monoxide concentration is in the micromolar range. The normal intracellular concentration of nitrogen monoxide is ca. 10 nmol/L and that of superoxide dismutase is 10 μmol/L (17). However, during inflammation, the extracellular concentration of nitrogen monoxide is expected to rise to ~2 μmol/L (17). Under these conditions, nitrogen monoxide can out compete superoxide dismutase and react with superoxide to form peroxynitrite.

The reactivity of peroxynitrite is complex and highly pH-dependent (18). Kissner et al. (14) reported that the pK_a of peroxynitrous acid is about 6.8 in 50 mmol/L phosphate buffer, but can increase up to 8, depending on the buffer composition and concentration. The term peroxynitrite refers to the sum of peroxynitrite anion ($ONOO^-$) and its conjugate acid, peroxynitrous acid (ONOOH). Peroxynitrite can directly perform one- or two-electron oxidation reactions with electrode potentials (E″ (ONOOH, $H^+/NO_2^{\cdot}$, H_2O) = 1.6 ± 0.1 V) or (E″ (ONOOH, H^+/NO_2^-, H_2O) = 1.3 ± 0.1 V), respectively (19). The peroxynitrite anion is rather stable in alkaline solutions, slowly decomposing to nitrite and dioxygen (20). However, peroxynitrous acid is unstable and isomerizes to give nitrate or decomposes into a reactive intermediate, though the final outcome is still under debate.

The first proposed pathway is the decomposition of peroxynitrous acid to give nitrogen dioxide and hydroxyl radicals (18). This proposed homolytic cleavage leads to a pair of radicals formed in a cage surrounded by water molecules. These caged radicals can recombine to reform peroxynitrous acid, diffuse apart to give nitrogen dioxide and hydroxyl radicals, or recombine to form nitrate (eq. [3]). The yield of nitrogen dioxide and hydroxyl radicals was estimated to be 30% (21, 22). However, the rate of homolysis (0.6 to 10^{-4} s^{-1}) of peroxynitrous acid is slower than the rate of isomerization (1.2 s^{-1}), and thus homolysis is highly unlikely (23).

$$[3]\quad ONOOH \underset{\text{Cage}}{\overset{\text{Homolysis}}{\rightleftharpoons}} [NO_2^{\cdot}\bullet\bullet\bullet OH^{\cdot}] \begin{cases} \xrightarrow{70\%} NO_3^- + H^+ \\ \xrightarrow{30\%} NO_2^{\cdot} + OH^{\cdot} \end{cases}$$

Koppenol et al. (23) proposed an alternative pathway for the decomposition of ONOOH that involves an as yet undefined metastable species of peroxynitrous acid, HOONO* (eq. [4]). This intermediate can rapidly isomerize to nitrate (eq. [4]). As the half-life of peroxynitrous acid is less than a second, it is difficult to directly study this metastable intermediate. However, theoretical studies support the existence of such a metastable species (24).

$$[4]\quad ONOOH \rightleftharpoons [ONOOH^*] \xrightarrow{\text{Isomerization}} NO_3^- + H^+$$

$$[5]\quad ONOOH + ONOO^- \rightleftharpoons \underset{\text{adduct}}{ONOOHONOO^-} \longrightarrow 2NO_2^- + O_2 + H^+$$

In recent work, no direct evidence was found for the formation of hydroxyl radicals (14, 18, 19, 23). In contrast, several studies reported results that are not in agreement with the following hypothesis: (*i*) when the concentration of peroxynitrite exceeds 100 μmol/L, its disappearance is delayed because of the formation of an adduct between peroxynitrite anion and peroxynitrous acid (14). This adduct ($ONOOHONOO^-$) decomposes to give nitrite and dioxygen (eq. [5]). Thus, the yields of nitrite and nitrate depend on the peroxynitrite concentration and the pH. For instance, at pH 7.0, 2.5 mmol/L peroxynitrite gives less than 10% nitrite, whereas at pH 10, up to 80% nitrite is formed (25). (*ii*) The decay of peroxynitrous acid in the presence of [^{15}N]nitrite involves initial formation of an adduct between nitrite and peroxynitrite to give [^{15}N]nitrate. However, according to the homolysis hypothesis, the yields of [^{15}N]nitrate predicted for low [^{15}N]nitrite concentrations are much larger than those obtained experimentally (26). (*iii*) The reaction of peroxynitrous acid with monohydroascorbate gives nitrate via an intermediate adduct without formation of ascorbyl radicals (27). (*iv*) The isomerization of peroxynitrite has a small entropy of activation of 3 ± 2 eu (24) and a volume of activation of 6.9 ± 0.9 cm^3 mol^{-1} (28), two values that are not fully compatible with homolysis. In general, activation volumes for homolysis reactions are close to 10 cm^3 mol^{-1}, however, values found for the isomerization of peroxynitrous acid (6–10 cm^3 mol^{-1}) do not reveal a mechanism of conversion. In conclusion, the above results support the notion put forth by Kissner and Koppenol (25) for the isomerization of peroxynitrite: "a radical-free mechanism rather than a free-radical mechanism."

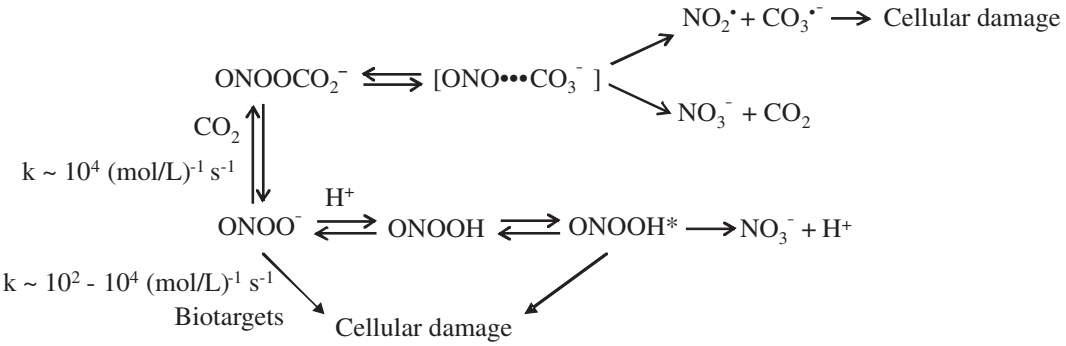
In all peroxynitrite study, it is important to minimize the contamination of nitrite and nitrate in the peroxynitrite salt and to accurately measure these nitrogen oxo anion products formed during the decomposition of peroxynitrite. Equally important is to test the degree of dioxygen retention during the isomerization of peroxynitrite. By using isotopic labeling studies, it has been demonstrated that only a small fraction of the product nitrate contained isotopic dioxygen when peroxynitrous acid was allowed to decompose in dioxygen-labeled water ($^{18}OH_2$) (29). The amount of peroxynitrous acid that isomerizes does so with exchange of the dioxygen with the solvent. However, a major fraction (83%) of the nitrate product had complete retention of its dioxygen atoms from the isomerization of peroxynitrite (29).

Numerous studies have been reported on the cytotoxicity of peroxynitrite (6–13), however, one of the main targets of peroxynitrite in human tissues is carbon dioxide, present at mmol/L concentration. Peroxynitrite reacts rapidly with carbon dioxide to form the adduct 1-carboxylato-2-nitrosodioxidane ($ONOOCO_2^-$), which rapidly produces carbon dioxide and nitrate, possibly via the formation of nitrogen dioxide and trioxidocarbonate (·1–). At 37 °C, the second-order rate constant for the reaction is 5.7×10^4 (mol/L)$^{-1}$ s^{-1} (30) (eq. [6]). Since the intracellular and extracellular carbon dioxide concentrations are about 1 to 2 mmol/L, this reaction

$$[6]\quad ONOO^- + CO_2 \underset{}{\overset{5.7\times10^4\ (\text{mol/L})^{-1}\ \text{s}^{-1}}{\rightleftharpoons}} ONOOCO_2^- \longrightarrow \text{Products}$$

© 2006 NRC Canada

[7]



represents one of the major routes for peroxynitrite reactivity in vivo (30). Therefore, reactions of peroxynitrite in vivo are more likely to be mediated by $ONOOCO_2^-$ and by the products derived from its decomposition than by peroxynitrite itself (31, 32). While the adduct $ONOOCO_2^-$ has not yet been directly detected, an observed delay before the combined carbon dioxide – peroxynitrite begins to decay is consistent with the formation of $ONOOCO_2^-$ (31–35). The amount of radicals generated from the decay of $ONOOCO_2^-$ is still under investigation. It is assumed that 70% of the radicals formed recombine inside the solvent cage to give nitrate and carbon dioxide, while the remaining 30% are able to react with target molecules (33, 34). In contrast, it has been shown that upon mixing peroxynitrite with carbon dioxide in the presence of nitrogen monoxide, the extent of nitrogen dioxide and trioxidocarbonate (·1–) formed is less than 4% (35). Nitrogen monoxide is known to react with nitrogen dioxide and trioxidocarbonate (·1–) to give carbon dioxide and nitrite, but does not react with peroxynitrite anion. Trioxidocarbonate (·1–) is a strong oxidant, and nitrogen dioxide is both an oxidizing and a nitrating agent. The electrode potential of the couple $CO_3^{\bullet-}/CO_3^{2-}$ is 1.58 V (35) and that of $NO_2^{\bullet}/NO_2^-$ pair is 0.99 V (19).

Although, peroxynitrite can oxidize many substrates in biological systems either directly or by producing secondary oxidants (eq. [7]), most of the peroxynitrite in vivo will be consumed by direct reactions, mainly with thiols, ascorbate, uric acid, transition metal centers, and carbon dioxide.

Myoglobin and hemoglobin

The idea that myoglobin and hemoglobin, apart from dioxygen storage and transport, may function as scavengers of nitrogen monoxide and (or) peroxynitrite in the blood vessels and in the cardiac and skeletal muscles is currently a subject of great interest. It has been shown that myoglobin efficiently scavenges nitrogen monoxide generated by induced nitric oxide synthase (iNOS), leading to an attenuation of heart disease, especially cardiac arrest (36). This study used double transgenic mice with high levels of cardiac specific over expression of iNOS (tg-$iNOS^+$) combined with myoglobin deficiency (myo^-) that ultimately developed signs of heart disease (37). However, mice with tg-$iNOS^+$ and functional myoglobin (myo^+) demonstrated normal cardiac function (37). Thus, it is reasonable to propose globin proteins like myoglobin and hemoglobin, present in high concentrations in cardiac and skeletal muscle and in blood vessels, respectively, may act as scavengers of nitrogen monoxide and (or) peroxynitrite.

Despite the presence of 1.2 mmol/L carbon dioxide in the blood (30), peroxynitrite is able to diffuse across the red blood cell membrane and react with oxyhemoglobin. Thus, the reaction of peroxynitrite with oxyhemoglobin (and oxymyoglobin) to yield methemoglobin (and metmyoglobin) has been considered pathophysiologically relevant. This reaction proceeds in two steps via a ferryl intermediate. The second-order rate constants for the peroxynitrite-mediated oxidation of oxymyoglobin and oxyhemoglobin are on the order of 10^4 $(mol/L)^{-1}$ s^{-1} at pH 7.0 and 20 °C (eq. [8]) (38). However, in the presence of physiological amounts of carbon dioxide (1.2 mmol/L), the first reaction step proceeds faster with a second-order rate constant of 10^5 $(mol/L)^{-1}$ s^{-1} (39).

[8] $$HbFe^{II}O_2 \xrightarrow[ONOOH]{5.4\times10^4\ (mol/L)^{-1}\ s^{-1}} HbFeI^{V}{=}O$$

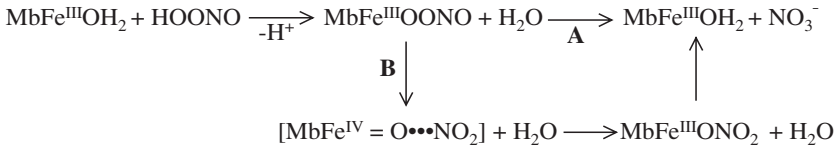
$$HbFeI^{V}{=}O \xrightarrow[ONOOH]{2.2\times10^4\ (mol/L)^{-1}\ s^{-1}} HbFe^{III}OH_2$$

[9] $$MbFe^{III}OH_2 \xrightarrow[ONOOH]{2.9\times10^4\ (mol/L)^{-1}\ s^{-1}} MbFe^{III}OH_2 + NO_3^- + H^+$$

The met forms of horse heart myoglobin and human hemoglobin have been shown to catalyze the isomerization of peroxynitrite to nitrate (40). The catalytic rate constants determined at pH 7.0 and 20 °C are $(1.2 \pm 0.1) \times 10^4$ and $(2.9 \pm 0.1) \times 10^4$ $(mol/L)^{-1}$ s^{-1}, for methemoglobin and metmyoglobin, respectively, at pH 7.5 and 20 °C (eq. [9]) (40). In contrast to the oxyhemoglobin and oxymyoglobin, no intermediate ferryl species could be detected when the met forms of hemoglobin and myoglobin were allowed to react with peroxynitrite in the absence or presence of 1.2 mmol/L carbon dioxide. However, to explain the catalytic isomerization of peroxynitrite to nitrate, it has been proposed that this reaction proceeds as shown in Scheme 1. In the first step, the coordinated water is replaced by peroxynitrite, and thus an intermediate iron(III) peroxynitrite complex ($MbFe^{III}OONO$) is generated. Since this complex could not be detected, it probably decays to nitrate and metmyoglobin at a very fast rate (40). Hence, binding of peroxynitrite to metmyoglobin must be the rate-determining step. The decay of the intermediate $MbFe^{III}OONO$ can proceed according to two possible mechanisms (pathways A and B) as shown in Scheme 1. The same $MbFe^{III}OONO$ or $HbFe^{III}OONO$ complexes have been characterized by UV–

© 2006 NRC Canada

Scheme 1. Possible mechanisms for the metMb-catalyzed isomerization of peroxynitrite.



vis and EPR spectroscopies as intermediates of the reaction of nitrogen monoxide with oxymyoglobin or with oxyhemoglobin at alkaline pH (41–43). The $MbFe^{III}OONO$ decays to give nitrate and metmyoglobin, and the rate constant reported is 205 ± 5 s^{-1} at pH 9.5 and 20 °C (eq. [10]) (42).

[10] $MbFe^{II}O_2 + NO^{\cdot} \longrightarrow MbFe^{III}ONOO \xrightarrow{k \sim 205\ s^{-1}} MbFe^{III}OH_2 + NO_3^-$

[11] $MbFe^{IV}{=}O + NO_2^{\cdot} \longrightarrow [MbFe^{IV}{=}O\cdots NO_2] \longrightarrow MbFe^{III}ONO_2 \xrightarrow{k \sim 35\ s^{-1}} MbFe^{III}OH_2 + NO_3^-$

In another experiment, $MbFe^{III}ONO_2$, generated by pulse radiolysis from the reaction between ferrylmyoglobin and nitrogen dioxide, has been reported to decay to give nitrate and metmyoglobin at a rate of 35 s^{-1} (eq. [11]) (42). Recent reinvestigation of this reaction showed that this value is probably incorrect and indeed, the values of the nitrate dissociation rate constants measured by Herold et al. (42) in a series of preliminary experiments were not reproducible, but they were always significantly lower than 205 s^{-1}. Taken together, these dissociation constants suggest that the decay of $MbFe^{III}OONO$ to nitrate and metmyoglobin cannot occur via the formation of the corresponding nitrato complex (pathway B in Scheme 1). Thus, based on these observations, it is proposed that the intermediate formed from the reaction between peroxynitrite and metmyoglobin decays to give nitrate and metmyoglobin via pathway A (Scheme 1).

Very recently, Goldstein et al. (44) remeasured the rate of dissociation of nitrate from $MbFe^{III}ONO_2$ (also generated by pulse radiolysis from the reaction between ferrylmyoglobin and nitrogen dioxide) and obtained a value of 190 ± 20 s^{-1} (at pH 9.7 and 20 °C). Under slightly different experimental conditions, the value obtained for the observed rate constant was reproducible. Additionally, by considering the calculated lifetime of alkyl peroxynitrites to nearly 1 μs, they suggested that the $MbFe^{III}OONO$ complex should rapidly convert to $MbFe^{III}ONO_2$ via ferryl myoglobin and nitrogen dioxide (44). Thus, they concluded that $MbFe^{III}OONO$ cannot be detected and that the intermediate characterized under alkaline conditions is $MbFe^{III}ONO_2$. However, the UV–vis spectrum of the hemoglobin peroxynitrite complex ($HbFe^{III}OONO$) is different from that of the nitrato complex ($HbFe^{III}ONO_2$) (42). In conclusion, based on the new value reported for the rate constant of the decay of $MbFe^{III}ONO_2$, which is essentially identical to that of the decay of $MbFe^{III}OONO$, it is reasonable to suggest that both pathways (Scheme 1) are possible for the metmyoglobin-catalyzed isomerization of peroxynitrite.

Groves and co-workers (45) also studied the metmyoglobin-catalyzed isomerization of peroxynitrite and proposed a mechanism similar to pathway B in Scheme 1. They suggested that part of the nitrogen dioxide eludes the reaction with ferrylmyoglobin and undergoes hydrolysis to nitrite and nitrate. Their conclusion is based on the observation that a constant level of approximately 10% nitrite was produced from the decay of peroxynitrite in the presence of 100–200 μmol/L of metmyoglobin (45). However, it is reported that in the presence of higher concentrations of metmyoglobin (750 μmol/L) peroxynitrite is converted quantitatively to nitrate (40). If large amounts of nitrogen dioxide escape recombination, one might expect ferrylmyoglobin to be observed, but no intermediate was detected (45). Thus, if the decomposition of peroxynitrite to nitrate proceeds via pathway B (Scheme 1), nitrogen dioxide and ferryl myoglobin react quantitatively to $MbFe^{III}ONO_2$.

Furthermore, studies with distal histidine sperm whale myoglobin mutants have shown that when His64 is replaced with alanine or aspartic acid, very low concentrations (5 μmol/L) of these proteins were needed to achieve 100% isomerization of peroxynitrite to nitrate (46). The efficiency of these proteins to catalyze the isomerization of peroxynitrite is consistent with the larger value of k_{cat} (see the following). These data indicate that, in contrast to the hypothesis of Groves and co-workers (45), in the presence of efficient catalysts (H64A or H64D), the decomposition of peroxynitrite does not lead to nitrite formation. This supports the above-mentioned mechanism for the decay of the $MbFe^{III}OONO$ complex: if the reaction proceeds via pathway B (Scheme 1), the reaction between ferryl myoglobin and nitrogen dioxide must be quantitative.

The catalytic rate constants reported for the decay of peroxynitrite in the presence of the iron(III) forms of myoglobin and hemoglobin is lower compared with that of water-soluble iron(III)-porphyrin complexes such as iron(III) 5,10,15,20-tetrakis(*N*-methyl-4′-pyridyl) porphyrin (Fe(III)-TM-2-PyP) and iron(III) 5,10,15,20-tetrakis(2,4,6-trimethyl-3,5-sulfonatophenyl) porphyrin (Fe(III)-TMPS) (47). These complexes react rapidly with peroxynitrite and therefore, are proposed to be promising drug candidates against peroxynitrite toxicity. However, to explain the difference in catalytic rate constants, we hypothesized that the reactivity of peroxynitrite with the iron(III) center of the proteins is most likely regulated by the distal histidine, which is strongly hydrogen bonded to the water molecule coordinated to the iron(III) center (40). Indeed, mechanistic studies by using mutants of sperm whale metmyoglobin in which the distal histidine was substituted with amino acid residues that cannot undergo a hydrogen bond with the coordinated water, react faster with peroxynitrite and catalyze its isomerization to nitrate more efficiently (46). The catalytic rate constants for the decay of peroxynitrite are (5.8 ± 0.1) × 10^6 and (4.8 ± 0.1) × 10^6 $(mol/L)^{-1}$ s^{-1}, (at pH 7.5 and 20 °C) for H64A-metMb and H64D-metMb, respectively (46). These values are comparable to those of the most efficient iron(III)-porphyrin catalysts such as Fe(III)-TM-2-PyP (k_{cat} = 2.2 ×

© 2006 NRC Canada

10^6 (mol/L)$^{-1}$ s^{-1}, at pH 7.4 and 37 °C) and Fe(III)-TMPS (k_{cat} = 6.4 × 10^5 (mol/L)$^{-1}$ s^{-1}, at pH 7.4 and 37 °C) (47).

Apart from its reaction with the heme center, in principle peroxynitrite could induce nitration of aromatic residues in these proteins (1). However, to be an efficient scavenger, myoglobin or hemoglobin should not be damaged in the course of its reaction with peroxynitrite. The tyrosine residues of the oxy- and met-forms of hemoglobin and myoglobin are nitrated to less than 1% upon addition of 1 equiv. of peroxynitrite (48). These nitration yields are physiologically irrelevant since the concentration of peroxynitrite in vivo will never be as high as that of myoglobin and hemoglobin. Indeed, no nitrated tyrosine residues were found in the hemoglobin of aged red blood cells (49). The mechanistic studies showed relatively larger nitration yields of tyrosine and tryptophan residues in apomyoglobin or in the cyanide-bound form of iron(III) myoglobin (metMbCN) treated with peroxynitrite (48). This suggests that the iron center in the oxy- and met-forms of the proteins plays a role in inhibiting peroxynitrite-mediated nitrotyrosine formation. Furthermore, experiments with different forms of myoglobin and hemoglobin showed that oxymyoglobin is the species that most efficiently prevents peroxynitrite-mediated nitration of added free tyrosine (40, 48). Significantly larger nitration yields of free tyrosine were observed by addition of peroxynitrite in the presence of apomyoglobin or metMbCN. Taken together, these results strongly indicate that the heme center in the oxy- and met-forms of myoglobin and hemoglobin acts as an efficient scavenger of peroxynitrite and thus may prevent peroxynitrite-mediated nitration, not only of the tyrosine and tryptophan residues of the globins, but also those of other proteins.

Under physiological conditions, hemoglobin and myoglobin are mostly found in the oxygenated form with only 1%–5% present in the oxidized iron(III) form of the corresponding proteins. Since the second-order rate constants of the reactions of peroxynitrite with oxymyoglobin and oxyhemoglobin (10^4 (mol/L)$^{-1}$ s^{-1}) are on the same order of magnitude as the catalytic rate constants for the metmyoglobin- and methemoglobin-catalyzed isomerization of peroxynitrite, oxyhemoglobin and oxymyoglobin are primarily involved in the scavenging of peroxynitrite in vivo (38). Moreover, the deoxygenated forms of myoglobin and hemoglobin have been shown to react with peroxynitrite at a rate of 2 orders of magnitude larger (10^6 (mol/L)$^{-1}$ s^{-1}) than that for the reaction with the corresponding oxygenated proteins (38). Thus, under hypoxic conditions, the reaction of the deoxygenated forms of the protein with peroxynitrite may be biologically relevant.

Under ischemic conditions such as low dioxygen tension, one can argue whether or not there is formation of nitrogen monoxide and (or) peroxynitrite in venous blood. Two different enzymes may produce nitrogen monoxide or superoxide under different conditions (50). When there is sufficient supply of L-arginine and dioxygen, nitric oxide synthase makes nitrogen monoxide (1), whereas the same enzyme may generate considerable amounts of superoxide when the concentrations of arginine and cofactors are limited (50). Xanthine oxidase generates superoxide, for example, during reperfusion after ischemia (51), whereas nitrite reduction to nitrogen monoxide occurs preferentially during hypoxia (52). Moreover, nitrite can react with deoxyhemoglobin to generate nitrosylated hemoglobin ($HbFe^{II}NO$) (53–55). Cosby et al. (56) have shown that intra-arterial infusion of nitrite at physiological levels caused vasodilation in healthy humans, thus demonstrating that nitrogen monoxide can be liberated from nitrosylated hemoglobin in vivo. Thus, there is an efficient pathway to also make nitrogen monoxide and peroxynitrite under hypoxic conditions. Deoxymyoglobin and deoxyhemoglobin may play a role as peroxynitrite scavengers. Indeed, these proteins are present in high concentrations and are among the species that react with the highest rate constants with peroxynitrite (38, 39).

Conclusion

In conclusion, the concentrations of myoglobin and hemoglobin in cardiac and skeletal muscle and in the blood vessels, respectively, are significantly larger than that of peroxynitrite (which is often generated continuously in nmol/L range). Under physiological conditions, these proteins may trap most peroxynitrite by its reaction with the heme center and prevent damage to the surrounding biomolecules.

References

1. S. Moncada, R.M. Palmer, and E.A. Higgs. Pharmacol. Rev. **43**, 109 (1991).
2. D.A. Wink and J.B. Mitchell. Free Radical Biol. Med. **25**, 434 (1998).
3. J.B. Laursen, M. Somers, S. Kurz, L. McCann, A. Warnholtz, B.A. Freeman, M. Tarpey, T. Fukai, and D.G. Harrison. Circulation, **103**, 1282 (2001).
4. D.D. Thomas, X. Liu, S.P. Kantrow, and J.R. Lancaster, Jr. Proc. Natl. Acad. Sci. U.S.A. **98**, 355 (2001).
5. P.C. Ford, D.A. Wink, and D.M. Stanbury. FEBS Lett. **326**, 1 (1993).
6. J.S. Beckman, T.W. Beckman, J. Chen, P.A. Marshall, and B.A. Freeman. Proc. Natl. Acad. Sci. U.S.A. **87**, 1620 (1990).
7. A. Denicola, J.M. Souza, and R. Radi. Proc. Natl. Acad. Sci. U.S.A. **95**, 3566 (1998).
8. S. Inoue and S. Kawanishi. FEBS Lett. **371**, 86 (1995).
9. M.G. Salgo, K. Stone, G.L. Squadrito, J.R. Battista, and W.A. Pryor. Biochem. Biophys. Res. Commun. **210**, 1025 (1995).
10. H. Ischiropoulos and A.B. Al-Mehdi. FEBS Lett. **364**, 279 (1995).
11. T. Grune, L.O. Klotz, J. Gieche, M. Rudeck, and H. Sies. Free. Radical Biol. Med. **30**, 1243 (2001).
12. R. Radi, J.S. Beckman, K.M. Bush, and B.A. Freeman. J. Biol. Chem. **266**, 4244 (1991).
13. R. Radi, J.S. Beckman, K.M. Bush, and B.A. Freeman. Arch. Biochem. Biophys. **288**, 481 (1991).
14. R. Kissner, T. Nauser, P. Bugnon, P.G. Lye, and W.H. Koppenol. Chem. Res. Toxicol. **10**, 1285 (1997).
15. T. Nauser and W.H. Koppenol. J. Phys. Chem. A, **106**, 4084 (2002).
16. J.M. McCord and I. Fridovich. Free. Radical Biol. Med. **5**, 363 (1998).
17. R. Kissner, T. Nauser, C. Kurz, and W.H. Koppenol. IUBMB Life, **55**, 567 (2003).
18. W.A. Pryor and G.L. Squadrito. Am. J. Physiol. **268**, L699 (1995).

© 2006 NRC Canada

19. W.H. Koppenol and R. Kissner. Chem. Res. Toxicol. **11**, 87 (1998).
20. W.H. Koppenol. Redox Rep. **6**, 339 (2001).
21. G. Merényi, J. Lind, S. Goldstein, and G. Czapski. J. Phys. Chem. A, **103**, 5685 (1999).
22. J.W. Coddington, J.K. Hurst, and S.V. Lymar. J. Am. Chem. Soc. **121**, 2438 (1999).
23. W.H. Koppenol, J.J. Moreno, W.A. Pryor, H. Ischiropoulos, and J.S. Beckman. Chem. Res. Toxicol. **5**, 834 (1992).
24. H. Tsai, T.P. Hamilton, J.M. Tsai, M. van der Woerd, J.G. Harrison, M.J. Jablonsky, J.S. Beckman, and W.H. Koppenol. J. Phys. Chem. **100**, 15087 (1996).
25. R. Kissner and W.H. Koppenol. J. Am. Chem. Soc. **124**, 234 (2001).
26. P. Maurer, C.F. Thomas, R. Kissner, H. Rüegger, O. Greter, U. Röthlisberger, and W.H. Koppenol. J. Phys. Chem. A, **107**, 1763 (2003).
27. C.R. Kurz, R. Kissner, T. Nauser, D. Perrin, and W.H. Koppenol. Free. Radical Biol. Med. **35**, 1529 (2003).
28. R. Kissner, C. Thomas, M.S.A. Hamsa, R. van Eldik, and W.H. Koppenol. J. Phys. Chem. A, **107**, 11261 (2003).
29. D.S. Bohle and B. Hansert. Nitric Oxide, **1**, 502 (1997).
30. A. Denicola, B.A. Freeman, M. Trujillo, and R. Radi. Arch. Biochem. Biophys. **333**, 49 (1996).
31. G.L. Squadrito and W.A. Pryor. Free. Radical Biol. Med. **25**, 392 (1998).
32. R.M. Uppu, G.L. Squadrito, and W.A. Pryor. Arch. Biochem. Biophys. **327**, 335 (1996).
33. S. Goldstein and G. Czapski. Inorg. Chem. **36**, 5113 (1997).
34. S.V. Lymar and J.K. Hurst. Inorg. Chem. **37**, 294 (1998).
35. R. Meli, T. Nauser, P. Latal, and W.H. Koppenol. J. Biol. Inorg. Chem. **7**, 31 (2002).
36. D.S. Bohle, P.A. Glassbrenner, and B. Hansert. Methods Enzymol. **269**, 302 (1996).
37. A. Gödecke, A. Molojavyi, J. Heger, U. Flögel, Z. Ding, C. Jacoby, and J. Schrader. J. Biol. Chem. **278**, 21761 (2003).
38. M. Exner and S. Herold. Chem. Res. Toxicol. **13**, 287 (2000).
39. F. Boccini and S. Herold. Biochemistry, **43**, 16393 (2004).
40. S. Herold and K. Shivashankar. Biochemistry, **42**, 14036 (2003).
41. S. Herold. FEBS Lett. **443**, 81 (1999).
42. S. Herold, M. Exner, and T. Nauser. Biochemistry, **40**, 3385 (2001).
43. J.S. Olson, E.W. Foley, C. Rogge, A.L Tsai, M.P. Doyle, and D.D. Lemon. Free. Radical Biol. Med. **15**, 685 (2004).
44. S. Goldstein, G. Mérenyi, and A. Samuni. J. Am. Chem. Soc. **126**, 15694 (2004).
45. J.L. Bourassa, E.P. Ives, A.L. Marqueling, R. Shimanovich, and J.T. Groves. J. Am. Chem. Soc. **123**, 5142 (2001).
46. S. Herold, S. Kalinga, T. Matsui, and Y. Watanabe. J. Am. Chem. Soc. **126**, 6945 (2004).
47. M.P. Jensen and D.P. Riley. Inorg. Chem. **41**, 4788 (2002).
48. S. Herold, K. Shivashankar, and M. Mehl. Biochemistry, **41**, 13460 (2002).
49. K. Kikugawa, K. Nakauchi, M. Beppu, K. Hiramoto, K. Ando, and M. Hayakawa. Biol. Pharm. Bull. **23**, 379 (2000).
50. Y. Xia, V.L. Dawson, T.M. Dawson, S.H. Snyder, and J.L. Zweier. Proc. Natl. Acad. Sci. U.S.A. **93**, 6770 (1996).
51. A. Meneshian and G.B. Bulkley. Microcirculation (Philadelphia, PA, U.S.), **9**, 161 (2002).
52. B.L. Godber, J.J. Doel, G.P. Sapkota, D.R. Blake, C.R. Stevens, R. Eisenthal, and R. Harrison. J. Biol. Chem. **275**, 7757 (2000).
53. M.P. Doyle, R.A. Pickering, T.M. DeWeert, J.W. Hoekstra, and D. Pater. J. Biol. Chem. **256**, 12393 (1981).
54. S. Herold. Inorg. Chem. **43**, 3783 (2004).
55. E. Nagababu, S. Ramaswamy, D.R. Abernethy, and J.M. Rifkind. J. Biol. Chem. **278**, 46349 (2003).
56. K. Cosby, K.S. Partovi, J.H. Crawford, R.P. Patel, C.D. Reiter, S. Martyr, B.K. Yang, M.A. Waclawiw, G. Zalos, X. Xu, K.T. Huang, H. Shields, D.B. Kim-Shapiro, A.N. Schechter, R.O. Cannon, and M.T. Gladwin. Nat. Med. **9**, 1498 (2003).

© 2006 NRC Canada

A novel and green version of the Passerini reaction in an ionic liquid ([bmim][BF_4])

Xuesen Fan, Yanzhen Li, Xinying Zhang, Guirong Qu, and Jianji Wang

Abstract: The Passerini three-component condensation among a carboxylic acid (**1**), an aldehyde or ketone (**2**), and an isocyanide (**3**) was carried out for the first time in an ionic liquid, [bmim][BF_4], and a series of acyloxycarboxamides were obtained through this reaction. The method presented herein has the advantages of high efficiency, a greener nature, and a simple operational procedure. Moreover, the ionic liquid can be easily recovered and reused for several runs without obvious loss of efficiency.

Key words: Passerini reaction, acyloxycarboxamides, ionic liquid, green synthesis.

Résumé : La condensation de Passerini à trois composants d'un acide carboxylique (**1**), d'un aldéhyde ou d'une cétone (**2**) et d'un isocyanure (**3**) a été réalisée pour la première fois dans un liquide ionique [bmim][BF_4] et on a en obtenu une série d'acyloxycarboxamides. La méthode décrite présente les avantages d'une grande efficacité, de sa nature écologique et de la simplicité d'opération. De plus, le liquide ionique peut facilement être récupéré et réutilisé plusieurs fois sans perte apparente de son efficacité.

Mots clés : réaction de Passerini, acyloxycarboxamides, liquide ionique, synthèse écologique.

[Traduit par la Rédaction]

Introduction

Multicomponent reactions (MCRs) are special types of synthetically useful organic reactions in which three or more reactants come together in a single reaction vessel to form a new product containing portions of all the components. They hold a privileged position among the synthetic strategies in terms of efficiency, particularly regarding the preparation of a library of molecules or in diversity-oriented synthesis (1). Among the MCRs, those with isocyanides, such as the Passerini and Ugi reactions, have developed into popular organic reactions in the pharmaceutical industry for the preparation of compound libraries of low-molecular druglike compounds (2). The Passerini reaction, also called the 3-CC reaction, which consists of the reaction of a carboxylic acid, a carbonyl compound, and an isocyanide providing an α-acyloxycarboxamide in a single step, was first discovered by Passerini more than 80 years ago (3). This reaction was often used as a key step in the total synthesis of natural products (4) and the α-acyloxycarboxamide group is also a frequently recurring motif in biologically active compounds, for example, in the pharmacologically interesting depsipeptides (5).

Usually, the Passerini reaction was carried out in volatile organic solvents, such as CH_2Cl_2. Reaction times from 12 h to several days are often prescribed and the yields of the products still have room to be improved (6). Therefore, developing a more efficient and environmentally friendly methodology for the Passerini reaction is highly desirable. In recent years, room-temperature ionic liquids have attracted considerable interest as greener reaction media in organic synthesis because of their unique properties such as nonvolatility, nonflammability, excellent chemical and thermal stability, and recyclability (7). Many chemical transformations have been carried out successfully by employing ionic liquids as "green" substitutes for traditional organic solvents (8). In view of the rapidly increasing importance of imidazolium-based ionic liquids as novel reaction media, we have been exploring the use of 1-butyl-3-methylimidazolium tetrafluoroborate ([bmim][BF_4]) as a recyclable solvent and promoter for greener organic synthesis (9). As a continuation of our research in this area, herein we would like to report the results of our investigation of the Passerini reaction in [bmim][BF_4] for the first time (Scheme 1).

Received 3 February 2006. Published on the NRC Research Press Web site at http://canjchem.nrc.ca on 17 May 2006.

X. Fan,[1] Y. Li, X. Zhang, G. Qu, and J. Wang. School of Chemical and Environmental Sciences, Henan Key Laboratory for Environmental Pollution Control, Henan Normal University, Xinxiang, Henan 453007, P. R. China.

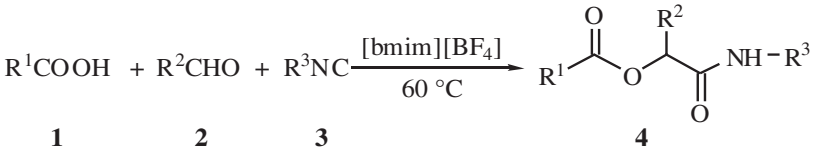
[1]Corresponding author (e-mail: xuesen.fan@yahoo.com).

Results and discussion

Initially, the reaction among benzoic acid (**1a**, 0.55 mmol), *m*-nitrobenzaldehyde (**2a**, 0.50 mmol), and cyclohexyl isocyanide (**3a**, 0.50 mmol) in 1 mL of [bmim][BF_4] was studied under various conditions (Scheme 2, Table 1). It turned out that this three-component reaction can be carried out smoothly in [bmim][BF_4]. The results listed in Table 1 also show that the process of this reaction is significantly subject to the reaction temperature. While this process needs as long as 2 days to be completed at ambient temperature (Table 1, entry 2), it results in full conversion of the starting material and good yield of the product in only several hours at 60 °C (Table 1, entry 4). It

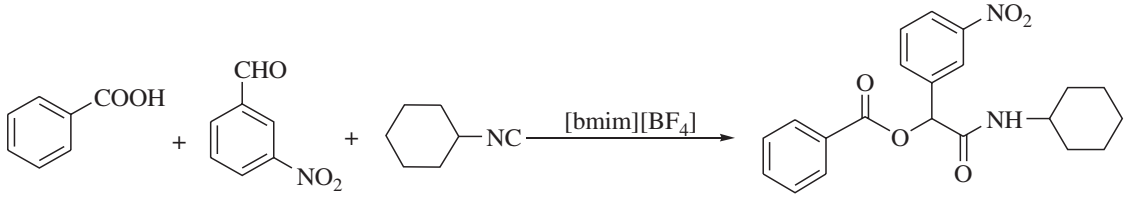
 doi:10.1139/V06-070 © 2006 NRC Canada

Scheme 1.



1 **2** **3** **4**

Scheme 2.



1a **2a** **3a** **4a**

Table 1. Studies of the effect of reaction temperature on the preparation of **4a**.

Entry	Reaction temperature (°C)	Reaction time	Yield[a] (%)
1	0	3 days	79
2	25	2 days	82
3	40	18 h	85
4	60	7 h	91
5	80	6 h	88

Note: Reagents: **1a** (0.55 mmol), **2a** (0.5 mmol), and **3a** (0.5 mmol), [bmim][BF_4] (1 mL).

[a]Isolated yields.

was also observed that as the reaction proceeded, the initially clear solution became heterogeneous because the product formed was poorly soluble in [bmim][BF_4]. At completion, the product was readily collected with high purity upon suction, featuring an easy isolation process of the final product.

The mild reaction conditions, good yield, and simple operational process encouraged us to examine the scope and generality of the present method. In this regard, structurally diversified carbonyl compounds, various carboxylic acids, and two isocyanides were screened and the results are listed in Table 2.

Firstly, it turned out that a variety of substituted aromatic (Table 2, entries 1–13) and aliphatic (Table 2, entries 14–16) carboxylic acids underwent the reaction and produced the corresponding products in high purity with good yield. For the carbonyl component, aromatic aldehydes bearing either electron-donating or electron-withdrawing substituents on the aromatic ring could be introduced effectively. Two aliphatic aldehydes were also tried (Table 2, entries 17 and 18). Unlike their aromatic counterparts, reactions involving aliphatic aldehydes seemed to be complicated and several unidentified substances were formed together with the desired α-(acyloxy)carboxamide products according to TLC analysis. Furthermore, the α-(acyloxy)carboxamides could only be obtained with high purity through column chromatography separation, in contrast with the simple suction collection as experienced with the aromatic aldehydes. In the case of ketones, cyclohexanone (**2k**) was found to be successfully included into this 3-CC process and gave the corresponding product in reasonable yield (Scheme 3, Table 2, entry 19). However, attempts to use acetophenone as the carbonyl substrate failed and acetophenone was found intact after being stirred with benzoic acid and isocyanocyclohexane at 60 °C for 8 h. Though no mechanistic studies were made on this result, it may be reasonable to attribute the inactivity of acetophenone in this reaction to the steric effect of the relatively bulky phenyl group. Actually, a steric congestion effect was also manifested with other substrates. For example, with aromatic carboxylic acids or aldehydes substituted on the *o*-position of the aromatic ring, the reactions gave lower yields compared with those unsubstituted or substituted on the *p*- or *m*-position (Table 2, entries 1–3, entries 4–6, respectively). Finally, in terms of isocyanides, both cyclohexyl isocyanide (**3a**) and *tert*-butyl (**3b**) isocyanide have proved to be good components. Therefore, variations in all three components have been accommodated comfortably.

On the other hand, the recovery and reuse of solvent and (or) catalyst are highly preferable in terms of a green synthetic process. We continued our research in this regard by studying the reusage of [bmim][BF_4], and **1a**, **2a**, and **3a** were used as model substrates. Upon completion of the condensation process, precipitated products were collected by suction and rinsed with water and cold ethanol. The filtrate was concentrated under reduced pressure, washed with ethyl ether (2 × 5 mL) and then dried at 100 °C for several hours. The recovered [bmim][BF_4] was then checked by ^{1}H NMR and no obvious difference in the NMR spectrum was observed compared to that of the original ionic liquid. Further studies also showed that the recovered [bmim][BF_4] could be successively recycled in subsequent reactions without obvious loss in its efficiency (Table 3). It should also be noted that even in the fifth round, reuse of [bmim][BF_4] recovered from the fourth round still produced the corresponding product with good yield (Table 3, entry 5).

It has been reported that, in many cases, compared with classical organic solvents, ionic liquids not only possess a green nature, but also demonstrate the advantages of offering

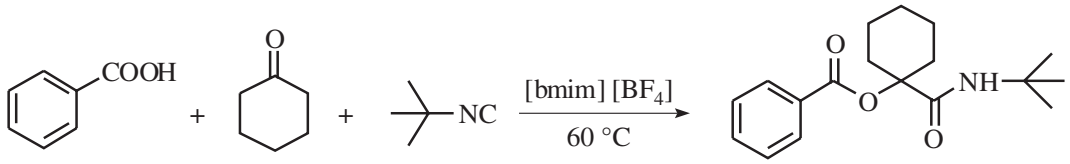
© 2006 NRC Canada

Table 2. Preparation of acyloxycarboxamide **4** in an ionic liquid ([bmim][BF_4]).

Entry	R^1 (**1**)	R^2 (**2**)	R^3 (**3**)	Product (**4**)[a]	Reaction time (h)	Yield (%)[b,c]
1	C_6H_5 (**1a**)	*m*-$NO_2C_6H_4$ (**2a**)	Cyclohexyl (**3a**)	**4a**	7	91
2	C_6H_5 (**1a**)	*p*-$NO_2C_6H_4$ (**2b**)	Cyclohexyl (**3a**)	**4b**	5	88
3	C_6H_5 (**1a**)	*o*-$NO_2C_6H_4$ (**2c**)	Cyclohexyl (**3a**)	**4c**	7	71
4	*p*-ClC_6H_4 (**1b**)	*m*-$NO_2C_6H_4$ (**2a**)	Cyclohexyl (**3a**)	**4d**	4	92
5	*m*-ClC_6H_4 (**1c**)	*m*-$NO_2C_6H_4$ (**2a**)	Cyclohexyl (**3a**)	**4e**	5	80
6	*o*-ClC_6H_4 (**1d**)	*m*-$NO_2C_6H_4$ (**2a**)	Cyclohexyl (**3a**)	**4f**	5	75
7	C_6H_5 (**1a**)	C_6H_5 (**2d**)	*tert*-Butyl (**3b**)	**4g**	9	88
8	C_6H_5 (**1a**)	*p*-$CH_3C_6H_4$ (**2e**)	*tert*-Butyl (**3b**)	**4h**	7	72
9	C_6H_5 (**1a**)	*p*-BrC_6H_4 (**2f**)	*tert*-Butyl (**3b**)	**4i**	7	73
10	C_6H_5 (**1a**)	*o*-BrC_6H_4 (**2g**)	*tert*-Butyl (**3b**)	**4j**	6	78
11	C_6H_5 (**1a**)	*m*-$NO_2C_6H_4$ (**2a**)	*tert*-Butyl (**3b**)	**4k**	7	87
12	*p*-$OCH_3C_6H_4$ (**1e**)	*p*-ClC_6H_4 (**2h**)	Cyclohexyl (**3a**)	**4l**	9	75
13	*p*-$OCH_3C_6H_4$ (**1e**)	*p*-$NO_2C_6H_4$ (**2b**)	Cyclohexyl (**3a**)	**4m**	7	88
14	$C_6H_5OCH_2$ (**1f**)	*m*-$NO_2C_6H_4$ (**2a**)	Cyclohexyl (**3a**)	**4n**	5	91
15	CH_3 (**1g**)	*m*-$NO_2C_6H_4$ (**2a**)	Cyclohexyl (**3a**)	**4o**	8	80
16	*n*-C_3H_7 (**1h**)	*m*-$NO_2C_6H_4$ (**2a**)	*tert*-Butyl (**3b**)	**4p**	9	78
17	C_6H_5 (**1a**)	*n*-C_3H_7 (**2i**)	tert-Butyl (**3b**)	**4q**	8	58
18	C_6H_5 (**1a**)	*n*-C_6H_{13} (**2j**)	tert-Butyl (**3b**)	**4r**	9	45
19	C_6H_5 (**1a**)	-$(CH_2)_5$- (**2k**)	*tert*-Butyl (**3b**)	**4s**	8	40

Note: Reagents: **1** (0.55 mmol), **2** (0.5 mmol), **3** (0.5 mmol), and [bmim][BF_4] (1 to 2 mL).
[a]All products were fully characterized by IR, ^{1}H NMR, MS, and elemental analysis.
[b]Isolated yields based on aldehyde.
[c]All the reactions were carried out at 60°C.

Scheme 3.



1a **2k** **3b** **4s**

Table 3. Studies on the recovery and reuse of [bmim][BF_4].

Round	Reaction time (h)	Temperature (°C)	Yield (%)	Ionic liquid recovered (*w*/*w* %)
1	5	60	91	99
2	5	60	92	98
3	5	60	90	99
4	5	60	90	98
5	5	60	88	97

Note: Reagents: **1a** (0.55 mmol), **2a** (0.5 mmol), **3a** (0.5 mmol), and [bmim][BF_4] (1 mL).

a simple operational process and (or) actually accelerating the reaction rate and increasing the yields. To compare [bmim][BF_4] with conventional organic solvents with regard to their efficiency and practicality, four conventional organic solvents (dichloromethane, methanol, THF, and toluene) were also studied as reaction media. The results of this investigation using **1a**, **2a**, and **3b** as the model substrates are listed in Table 4 and we conclude that the reaction run in [bmim][BF_4] is more efficient over dichloromethane, toluene, and methanol in terms of yield and reaction time. Though a higher yield can be obtained with THF, the product is dissolved in solution, as in the cases of dichloromethane, toluene, and methanol, and it has to be separated from the impurities by column chromatography instead of suction collection, as experienced with [bmim][BF_4].

In conclusion, a greener procedure for the synthesis of acyloxycarboxamides through a Passerini three-component condensation reaction was described in this paper. The work demonstrated the scope and limitations of this reaction by using an ionic liquid ([bmim][BF_4]) as a greener reaction medium and resulted in a library of 19 numbered α-(acyloxy)carboxamides. To the best of our knowledge, this is the first example in which an ionic liquid was used as a greener reaction medium for the Passerini reaction. The method presented here has the advantages of high efficiency, a green nature, a simple operation, and ease of recovery and reuse of the reaction medium. Moreover, the insolubility of the products in ionic liquid makes the isolation procedure especially convenient. Further studies on other MCRs in ionic liquids are currently in progress.

© 2006 NRC Canada

Table 4. Studies of the effect of various solvents on the Passerini reaction.

Entry	Solvent	Temperature (°C)	Time (h)	Yield (%)
1	[bmim][BF_4]	60	7	87
2	CH_2Cl_2	Reflux	15	78
3	MeOH	Reflux	18	32
4	THF	60	7	92
5	Toluene	60	10	77

Note: Reagents: **1a** (0.55 mmol), **2a** (0.50 mmol), **3b** (0.50 mmol), and solvent (1 to 2 mL).

Experimental

Melting points were measured by a Kofler micromelting point apparatus and are uncorrected. Infrared spectra were recorded on a FTS-40G spectrometer in KBr with absorption in cm^{-1}. ^1H NMR spectra were determined on a Bruker AC 400 spectrometer as $CDCl_3$ solutions. Chemical shifts (δ) are expressed in ppm downfield from the internal standard tetramethylsilane and coupling constants (*J*) are given in Hz. Mass spectra were obtained by a HP-5989B mass spectrometer. Elemental analyses were performed on an EA-1110 instrument.

The ionic liquid, [bmim][BF_4], was prepared and purified according to literature procedure (10). Other reagents were of reagent grade and were used without further purification.

General procedure for the Passerini reaction in ionic liquid

A mixture of a carboxylic acid (**1**, 0.55 mmol), an aromatic aldehyde (**2**, 0.50 mmol), and an isocyanide (**3**, 0.50 mmol) in 1 mL of [bmim][BF_4] was stirred at 60 °C for a certain period of time (shown in Table 2). Upon completion, the reaction mixture was allowed to cool to room temperature and 2 mL of water was then added. The precipitate was collected by suction, subsequently rinsed with water and cyclohexane, and then dried to give product **4** with high purity. The filtrate was concentrated under reduced pressure and dried at 100 °C for several hours to recover the ionic liquid for subsequent reuse.

(Cyclohexylcarbamoyl)(3-nitrophenyl)methyl benzoate (4a)

Melting point: 201 to 202 °C. IR (KBr, cm^{-1}) ν: 3282, 1728, 1660, 1531, 1345, 1250. ^1H NMR ($CDCl_3$, 400 MHz) δ: 1.16–1.96 (m, 10H, $5CH_2$), 3.81–3.88 (m, 1H, N-CH), 6.23 (br, 1H, NH), 6.41 (s, 1H, CH), 7.55 (t, 2H, *J* = 8.0 Hz, ArH), 7.61 (t, 1H, *J* = 8.0 Hz, ArH), 7.69 (t, 1H, *J* = 8.0 Hz, ArH), 7.94 (d, 1H, *J* = 8.0 Hz, ArH), 8.13 (d, 2H, *J* = 8.0 Hz, ArH), 8.25 (d, 1H, *J* = 8.0 Hz, ArH), 8.41 (s, 1H, ArH). MS *m/z*: 382 (M^+), 256, 207, 135, 105 (100%), 83, 77, 55, 28. Anal. calcd. for $C_{21}H_{22}N_2O_5$: C 65.96, H 5.80, N 7.33; found: C 65.80, H 5.92, N 7.42.

(Cyclohexylcarbamoyl)(4-nitrophenyl)methyl benzoate (4b)

Melting point: 210–212 °C. IR (KBr, cm^{-1}) ν: 3290, 1730, 1658, 1535, 1341, 1240. ^1H NMR ($CDCl_3$, 400 MHz) δ: 1.12–1.94 (m, 10H, $5CH_2$), 3.77–3.86 (m, 1H, N-CH), 6.16 (br, 1H, NH), 7.26 (s, 1H, CH), 7.53 (t, 2H, *J* = 8.0 Hz, ArH), 7.67 (t, 1H, *J* = 8.0 Hz, ArH), 7.72 (d, 2H, *J* = 8.0 Hz, ArH), 8.10 (d, 2H, *J* = 8.0 Hz, ArH), 8.24 (d, 2H, *J* = 8.0 Hz, ArH). MS *m/z*: 382 (M^+), 207, 161, 135, 105 (100%), 77, 55, 28. Anal. calcd. for $C_{21}H_{22}N_2O_5$: C 65.96, H 5.80, N 7.33; found: C 65.83, H 5.66, N 7.44.

(Cyclohexylcarbamoyl)(2-nitrophenyl)methyl benzoate (4c)

Melting point: 116–118 °C. IR (KBr, cm^{-1}) ν: 3315, 1732, 1661, 1523, 1350, 1267. ^1H NMR ($CDCl_3$, 400 MHz) δ: 1.15–1.99 (m, 10H, $5CH_2$), 3.76–3.85 (m, 1H, N-CH), 6.33 (br, 1H, NH), 6.84 (s, 1H, CH), 7.48 (t, 2H, *J* = 8.0 Hz, ArH), 7.53 (t, 1H, *J* = 8.0 Hz, ArH), 7.62 (t, 1H, *J* = 8.0 Hz, ArH), 7.69 (t, 1H, *J* = 8.0 Hz, ArH), 7.89 (d, 1H, *J* = 8.0 Hz, ArH), 8.03 (d, 1H, *J* = 8.0 Hz, ArH), 8.09 (d, 2H, *J* = 8.0 Hz, ArH). MS *m/z*: 382 (M^+), 207, 135, 105 (100%), 77, 55, 28. Anal. calcd. for $C_{21}H_{22}N_2O_5$: C 65.96, H 5.80, N 7.33; found: C 65.88, H 5.63, N 7.48.

(Cyclohexylcarbamoyl)(3-nitrophenyl)methyl 4-chlorobenzoate (4d)

Melting point: 199–201 °C. IR (KBr, cm^{-1}) ν: 3282, 1720, 1662, 1530, 1349, 1241. ^1H NMR ($CDCl_3$, 400 MHz) δ: 1.12–1.97 (m, 10H, $5CH_2$), 3.77–3.86 (m, 1H, N-CH), 6.11 (br, 1H, NH), 6.35 (s, 1H, CH), 7.50 (d, 2H, *J* = 8.0 Hz, ArH), 7.59 (t, 1H, *J* = 8.0 Hz, ArH), 7.90 (d, 1H, *J* = 8.0 Hz, ArH), 8.03 (d, 2H, *J* = 8.0 Hz, ArH), 8.23 (d, 1H, *J* = 8.0 Hz, ArH), 8.36 (s, 1H, ArH). MS *m/z*: 416 (M^+), 207, 139 (100%), 135, 104, 83, 55, 28. Anal. calcd. for $C_{21}H_{21}ClN_2O_5$: C 60.51, H 5.08, N 6.72; found: C 60.66, H 4.93, N 6.60.

(Cyclohexylcarbamoyl)(3-nitrophenyl)methyl 3-chlorobenzoate (4e)

Melting point: 166–168 °C. IR (KBr, cm^{-1}) ν: 3286, 1722, 1661, 1531, 1350, 1262. ^1H NMR ($CDCl_3$, 400 MHz) δ: 1.14–1.97 (m, 10H, $5CH_2$), 3.78–3.87 (m, 1H, N-CH), 6.11 (br, 1H, NH), 6.35 (s, 1H, CH), 7.47 (t, 1H, *J* = 8.0 Hz, ArH), 7.60 (t, 1H, *J* = 8.0 Hz, ArH), 7.63 (d, 1H, *J* = 8.0 Hz, ArH), 7.90 (d, 1H, *J* = 8.0 Hz, ArH), 7.98 (d, 1H, *J* = 8.0 Hz, ArH), 8.05 (s, 1H, ArH), 8.24 (d, 1H, *J* = 8.0 Hz, ArH), 8.37 (s, 1H, ArH). MS *m/z*: 416 (M^+), 291, 207, 139 (100%), 135, 111, 83, 76, 55, 28. Anal. calcd. for $C_{21}H_{21}ClN_2O_5$: C 60.51, H 5.08, N 6.72; found: C 60.68, H 5.03, N 6.80.

(Cyclohexylcarbamoyl)(3-nitrophenyl)methyl 2-chlorobenzoate (4f)

Melting point: 176–178 °C. IR (KBr, cm^{-1}) ν: 3301, 1736, 1670, 1531, 1349, 1275. ^1H NMR ($CDCl_3$, 400 MHz) δ: 1.15–1.98 (m, 10H, $5CH_2$), 3.78–3.85 (m, 1H, N-CH), 6.38 (s, 1H, CH), 6.71 (br, 1H, NH), 7.40 (m, 1H, ArH), 7.53 (m, 2H, ArH), 7.58 (t, 1H, *J* = 8.0 Hz, ArH), 7.89 (d, 1H, *J* = 8.0 Hz, ArH), 7.91 (d, 1H, *J* = 8.0 Hz, ArH), 8.22

© 2006 NRC Canada

(d, 1H, *J* = 8.0 Hz, ArH), 8.37 (s, 1H, ArH). MS *m/z*: 416 (M^+), 291, 207, 139 (100%), 135, 111, 83, 55, 28. Anal. calcd. for $C_{21}H_{21}ClN_2O_5$: C 60.51, H 5.08, N 6.72; found: C 60.44, H 5.22, N 6.86.

(*tert*-Butylcarbamoyl)(phenyl)methyl benzoate (4g)

Melting point: 148–150 °C. IR (KBr, cm^{-1}) ν: 3296, 1721, 1660, 1542, 1260. ^1H NMR ($CDCl_3$, 400 MHz) δ: 1.37 (s, 9H, $3CH_3$), 5.98 (br s, 1H, NH), 6.22 (s, 1H, CH), 7.40 (m, 3H, ArH), 7.48 (t, 2H, *J* = 8.0 Hz, ArH), 7.52 (d, 2H, *J* = 8.0 Hz, ArH), 7.61 (t, 1H, *J* = 8.0 Hz, ArH), 8.09 (d, 2H, *J* = 8.0 Hz, ArH). MS *m/z*: 311 (M^+), 212, 105 (100%), 77, 57. Anal. calcd. for $C_{19}H_{21}NO_3$: C 73.29, H 6.80, N 4.50; found: C 73.21, H 6.62, N 4.36.

(*tert*-Butylcarbamoyl)(4-methylphenyl)methyl benzoate (4h)

Melting point: 151–153 °C. IR (KBr, cm^{-1}) ν: 3280, 1718, 1664, 1531, 1257. ^1H NMR ($CDCl_3$, 400 MHz) δ: 1.36 (s, 9H, $3CH_3$), 2.35 (s, 3H, CH_3), 5.95 (br s, 1H, NH), 6.18 (s, 1H, CH), 7.20 (d, 2H, *J* = 8.0 Hz, ArH), 7.40 (d, 2H, *J* = 8.0 Hz, ArH), 7.47 (t, 2H, *J* = 8.0 Hz, ArH), 7.60 (t, 1H, *J* = 8.0 Hz, ArH), 8.08 (d, 2H, *J* = 8.0 Hz, ArH). MS *m/z*: 325 (M^+), 226, 105 (100%), 77, 57, 15. Anal. calcd. for $C_{20}H_{23}NO_3$: C 73.82, H 7.12, N 4.30; found: C 73.72, H 7.33, N 4.22.

(*tert*-Butylcarbamoyl)(4-bromophenyl)methyl benzoate (4i)

Melting point: 194–196 °C. IR (KBr, cm^{-1}) ν: 3313, 1738, 1665, 1548, 1260. ^1H NMR ($CDCl_3$, 400 MHz) δ: 1.37 (s, 9H, $3CH_3$), 6.03 (br s, 1H, NH), 6.16 (s, 1H, CH), 7.40 (d, 2H, *J* = 8.0 Hz, ArH), 7.48 (d, 2H, *J* = 8.0 Hz, ArH), 7.51 (t, 2H, *J* = 8.0 Hz, ArH), 7.62 (t, 1H, *J* = 8.0 Hz, ArH), 8.07 (d, 2H, *J* = 8.0 Hz, ArH). MS *m/z*: 389 (M^+), 211, 131, 105 (100%), 77, 57. Anal. calcd. for $C_{19}H_{20}BrNO_3$: C 58.47, H 5.17, N 3.59; found: C 58.61, H 5.01, N 3.66.

(*tert*-Butylcarbamoyl)(2-bromophenyl)methyl benzoate (4j)

Melting point: 158–160 °C. IR (KBr, cm^{-1}) ν: 3302, 1726, 1667, 1559, 1262. ^1H NMR ($CDCl_3$, 400 MHz) δ: 1.37 (s, 9H, $3CH_3$), 6.03 (br s, 1H, NH), 6.50 (s, 1H, CH), 7.23 (t, 1H, *J* = 8.0 Hz, ArH), 7.37 (t, 1H, *J* = 8.0 Hz, ArH), 7.47 (t, 2H, *J* = 8.0 Hz, ArH), 7.60 (t, 1H, *J* = 8.0 Hz, ArH), 7.65 (d, 2H, *J* = 8.0 Hz, ArH), 8.11 (d, 2H, *J* = 8.0 Hz, ArH). MS *m/z*: 389 (M^+), 211, 105 (100%), 77, 57. Anal. calcd. for $C_{19}H_{20}BrNO_3$: C 58.47, H 5.17, N 3.59; found: C 58.43, H 5.03, N 3.70.

(*tert*-Butylcarbamoyl)(3-nitrophenyl)methyl benzoate (4k)

Melting point: 163–165 °C. IR (KBr, cm^{-1}) ν: 3298, 1728, 1661, 1542, 1350, 1258. ^1H NMR ($CDCl_3$, 400 MHz) δ: 1.39 (s, 9H, $3CH_3$), 6.20 (br s, 1H, NH), 6.31 (s, 1H, CH), 7.52 (t, 2H, *J* = 8.0 Hz, ArH), 7.58 (t, 1H, *J* = 8.0 Hz, ArH), 7.66 (t, 1H, *J* = 8.0 Hz, ArH), 7.90 (d, 1H, *J* = 8.0 Hz, ArH), 8.10 (d, 2H, *J* = 8.0 Hz, ArH), 8.22 (d, 1H, *J* = 8.0 Hz, ArH), 8.37 (s, 1H, ArH). MS *m/z*: 356 (M^+), 257, 105 (100%), 77, 57. Anal. calcd. for $C_{19}H_{20}N_2O_5$: C 64.04, H 5.66, N 7.86; found: C 64.21, H 5.41, N 7.82.

(Cyclohexylcarbamoyl)(4-chlorophenyl)methyl 4-methoxybenzoate (4l)

Melting point: 184–186 °C. IR (KBr, cm^{-1}) ν: 3280, 1732, 1664, 1532, 1262. ^1H NMR ($CDCl_3$, 400 MHz) δ: 1.09–1.94 (m, 10H, $5CH_2$), 3.78–3.85 (m, 1H, N-CH), 3.88 (s, 3H, OCH_3), 6.06 (br, 1H, NH), 6.25 (s, 1H, CH), 6.96 (d, 2H, *J* = 8.8 Hz, ArH), 7.35 (d, 2H, *J* = 8.4 Hz, ArH), 7.46 (d, 2H, *J* = 8.4 Hz, ArH), 8.03 (d, 2H, *J* = 8.8 Hz, ArH). MS *m/z*: 401 (M^+), 370, 124, 104 (100%), 55. Anal. calcd. for $C_{22}H_{24}ClNO_4$: C 65.75, H 6.02, N 3.49; found: C 65.61, H 5.89, N 3.42.

(Cyclohexylcarbamoyl)(4-nitrophenyl)methyl 4-methoxybenzoate (4m)

Melting point: 199–201 °C. IR (KBr, cm^{-1}) ν: 3301, 1745, 1661, 1531, 1350, 1255. ^1H NMR ($CDCl_3$, 400 MHz) δ: 1.12–1.93 (m, 10H, $5CH_2$), 3.77–3.84 (m, 1H, N-CH), 3.90 (s, 3H, OCH_3), 6.17 (br, 1H, NH), 6.36 (s, 1H, CH), 6.99 (d, 2H, *J* = 8.8 Hz, ArH), 7.71 (d, 2H, *J* = 8.8 Hz, ArH), 8.05 (d, 2H, *J* = 8.8 Hz, ArH), 8.23 (d, 2H, *J* = 8.8 Hz, ArH). MS *m/z*: 412 (M^+), 381, 135, 104 (100%), 55. Anal. calcd. for $C_{22}H_{24}N_2O_6$: C 64.07, H 5.87, N 6.79; found: C 64.21, H 5.68, N 6.91.

(Cyclohexylcarbamoyl)(3-nitrophenyl)methyl 2-phenoxyacetate (4n)

Melting point: 137–139 °C. IR (KBr, cm^{-1}) ν: 3281, 2926, 1766, 1656, 1533, 1352, 1194. ^1H NMR ($CDCl_3$, 400 MHz) δ: 0.93–1.80 (m, 10H, $5CH_2$), 3.64–3.73 (m, 1H, N-CH), 4.80 (s, 2H, OCH_2), 6.02 (br, 1H, NH), 6.17 (s, 1H, CH), 6.93 (d, 2H, *J* = 8.0 Hz, ArH), 7.06 (t, 1H, *J* = 8.0 Hz, ArH), 7.34 (t, 2H, *J* = 8.0 Hz, ArH), 7.53 (t, 1H, *J* = 8.0 Hz, ArH), 7.74 (d, 1H, *J* = 8.0 Hz, ArH), 8.20 (d, 1H, *J* = 8.0 Hz, ArH), 8.22 (s, 1H, ArH). MS *m/z*: 412 (M^+), 135 (100%), 94, 55, 42, 28. Anal. calcd. for $C_{22}H_{24}N_2O_6$: C 64.07, H 5.87, N 6.79; found: C 64.12, H 5.70, N 6.88.

(Cyclohexylcarbamoyl)(3-nitrophenyl)methyl acetate (4o)

Melting point: 146–148 °C. IR (KBr, cm^{-1}) ν: 3288, 2939, 1748, 1656, 1533, 1349, 1232. ^1H NMR ($CDCl_3$, 400 MHz) δ: 1.19–1.94 (m, 10H, $5CH_2$), 2.24 (s, 3H, CH_3), 3.74–3.83 (m, 1H, N-CH), 6.11 (s, 1H, CH), 6.16 (br, 1H, NH), 7.56 (t, 1H, *J* = 8.0 Hz, ArH), 7.82 (d, 1H, *J* = 8.0 Hz, ArH), 8.20 (d, 1H, *J* = 8.0 Hz, ArH), 8.26 (s, 1H, ArH). MS *m/z*: 320 (M^+), 207, 135 (100%), 105, 83, 55, 43, 28. Anal. calcd. for $C_{16}H_{20}N_2O_5$: C 59.99, H 6.29, N 8.74; found: C 60.12, H 6.43, N 8.68.

(*tert*-Butylcarbamoyl)(3-nitrophenyl)methyl butyrate (4p)

Melting point: 96–98 °C. IR (KBr, cm^{-1}) ν: 3331, 1754, 1666, 1529, 1350, 1166. ^1H NMR ($CDCl_3$, 400 MHz) δ: 0.98 (t, 3H, *J* = 8.0 Hz, CH_3), 1.37 (s, 9H, $3CH_3$), 1.72 (m, 2H, CH_2), 2.46 (t, 2H, *J* = 8.0 Hz, CH_2), 6.05 (s, 1H, CH), 6.12 (br, 1H, NH), 7.55 (t, 1H, *J* = 8.0 Hz, ArH), 7.81 (d, 1H, *J* = 8.0 Hz, ArH), 8.20 (d, 1H, *J* = 8.0 Hz, ArH), 8.25 (s, 1H, ArH). MS *m/z*: 322 (M^+), 135 (100%), 105, 71, 57, 43, 28. Anal. calcd. for $C_{16}H_{22}N_2O_5$: C 59.61, H 6.88, N 8.69; found: C 59.52, H 6.66, N 8.85.

© 2006 NRC Canada

1-(*tert*-Butylcarbamoyl)butyl benzoate (4q)

Melting point: 84–86 °C. IR (KBr, cm^{-1}) ν: 3296, 1751, 1663, 1538, 1342, 1165. ^1H NMR ($CDCl_3$, 400 MHz) δ: 0.93 (t, 3H, *J* = 7.6 Hz, CH_3), 1.33 (s, 9H, $3CH_3$), 1.44 (m, 2H, CH_2), 1.94 (m, 2H, CH_2), 5.30 (t, 1H, *J* = 6.0 Hz, CH), 5.88 (br, 1H, NH), 7.47 (t, 2H, *J* = 8.0 Hz, ArH), 7.60 (t, 1H, *J* = 8.0 Hz, ArH), 8.04 (d, 2H, *J* = 8.0 Hz, ArH). MS *m/z*: 277 (M^+), 105 (100%), 77, 57. Anal. calcd. for $C_{16}H_{23}NO_3$: C 69.29, H 8.36, N 5.05; found: C 69.43, H 8.12, N 5.10.

1-(*tert*-Butylcarbamoyl)heptyl benzoate (4r)

Melting point: 93–95 °C. IR (KBr, cm^{-1}) ν: 3301, 1755, 1665, 1541, 1341, 1162. ^1H NMR ($CDCl_3$, 400 MHz) δ: 0.86 (t, 3H, *J* = 7.6 Hz, CH_3), 1.24–1.41 (m, 17H, $3CH_3$, $4CH_2$), 1.94 (m, 2H, CH_2), 5.29 (t, 1H, *J* = 6.0 Hz, CH), 5.87 (br, 1H, NH), 7.47 (t, 2H, *J* = 8.0 Hz, ArH), 7.58 (t, 1H, *J* = 8.0 Hz, ArH), 8.04 (d, 2H, *J* = 8.0 Hz, ArH). MS *m/z*: 319 (M^+), 105 (100%), 57. Anal. calcd. for $C_{19}H_{29}NO_3$: C 71.44, H 9.15, N 4.38; found: C 71.38, H 9.30, N 4.21.

1-(*tert*-Butylcarbamoyl)cyclohexyl benzoate (4s)

Melting point: 132–134 °C. IR (KBr, cm^{-1}) ν: 3300, 1758, 1666, 1538, 1340, 1158. ^1H NMR ($CDCl_3$, 400 MHz) δ: 1.29 (s, 9H, $3CH_3$), 1.51–1.68 (m, 6H, $3CH_2$), 1.83–1.90 (m, 2H, CH_2), 2.29–2.32 (m, CH_2), 5.56 (br, 1H, NH), 7.44 (t, 2H, *J* = 8.0 Hz, ArH), 7.58 (t, 1H, *J* = 8.0 Hz, ArH), 8.05 (d, 2H, *J* = 8.0 Hz, ArH). MS *m/z*: 303 (M^+), 105 (100%), 77, 57. Anal. calcd. for $C_{18}H_{25}NO_3$: C 71.26, H 8.31, N 4.62; found: C 71.12, H 8.08, N 4.81.

Acknowledgements

We are grateful to the National Natural Science Foundation of China (Project No. 20273019) and the Science Foundation of Henan Normal University for Young Scholars (No. 0307032) for financial support.

References

1. (*a*) H. Bienayme, C. Hulme, G. Oddon, and P. Schmitt. Chem. Eur. J. **6**, 3321 (2000); (*b*) R.V.A. Orru and M. de Greef. Synthesis, 1471 (2003); (*c*) M.D. Burke and S.L. Schreiber. Angew. Chem. Int. Ed. **43**, 46 (2004).
2. A. Domling and I. Ugi. Angew. Chem. Int. Ed. **39**, 3168 (2000).
3. M. Passerini. Gazz. Chim. Ital. **51**, 126 (1921).
4. (*a*) J.R. Falck and S. Manna. Tetrahedron Lett. **22**, 619 (1981); (*b*) U. Schmidt and S. Weinbrenner. J. Chem. Soc. Chem. Commun. 1003 (1994).
5. (*a*) U. Fetzer and I. Ugi. Justus Liebigs Ann. Chem. **659**, 184 (1962); (*b*) J. Rachon. Chimia, **37**, 299 (1983).
6. (*a*) S.W. Kim, S.M. Bauer, and R.W. Armstrong. Tetrahedron Lett. **39**, 7031 (1998); (*b*) T. Ziegler, H. Kaisers, R. Schlomer, and C. Koch. Tetrahedron, **55**, 8397 (1999).
7. (*a*) T. Welton. Chem. Rev. **99**, 2071 (1999); (*b*) M.J. Earle and K.R. Seddon. Pure Appl. Chem. **72**, 1391 (2000); (*c*) R.A. Sheldon. Chem. Commun. (Cambridge), 2399 (2001); (*d*) J.S. Wilkes. Green Chem. **4**, 73 (2002); (*e*) J. Dupont, R.F. De Souza, and P.A.Z. Suarez. Chem. Rev. **102**, 3667 (2002).
8. For some recent examples, see: (*a*) C.M. Gordon. Appl. Catal. A, **222**, 101 (2001); (*b*) Q. Yao. Org. Lett. **4**, 2197 (2002); (*c*) H.M. Zerth, N.M. Leonard, and R.S. Mohan. Org. Lett. **5**, 55 (2003); (*d*) G. Rai, J.M. Jeong, Y. Lee, H.W. Kim, D.S. Lee, J. Chung, and M.C. Lee. Tetrahedron Lett. **46**, 3987 (2005); (*e*) B.C. Ranu and S. Banerjee. J. Org. Chem. **70**, 4517 (2005); (*f*) Z. Yang and W. Pan. Enzyme Microb. Technol. **37**, 19 (2005).
9. (*a*) X.Y. Zhang, X.S. Fan, H.Y. Niu, and J.J. Wang. Green Chem. **5**, 267 (2003); (*b*) X.S. Fan, X.Y. Hu, X.Y. Zhang, and J.J. Wang. Can. J. Chem. **83**, 16 (2005); (*c*) J.J. Wang, X.S. Fan, X.Y. Zhang, and L.J. Han. Can. J. Chem. **82**, 1192 (2004); (*d*) X.S. Fan, X.Y. Hu, X.Y. Zhang, and J.J. Wang. Aust. J. Chem. **57**, 1067 (2004).
10. J.D. Holbrey and K.R. Seddon. J. Chem. Soc. Dalton Trans. 2133 (1999).

© 2006 NRC Canada

A simple, highly regioselective and efficient reaction of indole with epoxides under solvent-free conditions

Najmedin Azizi, Shokopheh Mehrazma, and Mohammad R. Saidi

Abstract: Lithium perchlorate has been found to be an inexpensive and efficient catalyst for the ring opening of epoxides by indole and *N*-methylindole, which provides an environmentally friendly method for the synthesis of substituted indoles. A complete regioselectivity in favor of nucleophilic attack at the benzylic carbon atom of aromatic epoxides, such as styrene oxide, is observed. However, aliphatic unsymmetrical alkene oxides undergo selective nucleophilic attack at the sterically less-hindered carbon atom. This catalyst offers several advantages, such as short reaction time, high yields, lower catalytic loading, simple experimental procedure, and easy isolation of the products, under solvent-free conditions.

Key words: indole, epoxide, regioselectivity, solvent-free.

Résumé : On a observé que le perchlorate de lithium est un catalyseur peu dispendieux et efficace pour l'ouverture des cycles époxydes par l'indole et le *N*-méthylindole et la synthèse dans un environnement écologique d'indoles substitués. Les réactions sont complètement régiosélectives en faveur d'une attaque nucléophile au niveau de l'atome de carbone benzylique d'époxydes aromatiques tels que l'oxyde de styrène. Toutefois, avec les oxydes d'alcènes aliphatiques non symétriques, l'attaque nucléophile se fait sélectivement au niveau de l'atome de carbone le moins encombré. Ce catalyseur présente plusieurs avantages, tel son court temps de réaction, des rendements élevés, une quantité plus faible de catalyseur, une procédure expérimentale simple et une méthode facile d'isoler les produits dans des conditions sans solvant.

Mots clés : indole, époxyde, régiosélectivité, sans solvant.

[Traduit par la Rédaction]

Introduction

Epoxides have been recognized as important and versatile synthetic intermediates in organic synthesis (1) because they are susceptible to attack by several nucleophiles and readily accessible in pure form (2). Therefore, there is a significant current interest in the ring opening of epoxides with a large variety of reagents such as electrophiles, nucleophiles, acids, bases, reducing agents, and some oxidizing agents. However, the epoxide ring-opening reaction with certain nucleophiles is generally performed with acid or base catalysis, with a large excess of nucleophiles at elevated temperature, and often fails when poor nucleophiles such as indole and hindered epoxides are used. Few procedures for the ring-opening reaction of epoxides with indole are reported in the literature by using high pressure or SiO_2 (3), $InCl_3$ (4), and $InBr_3$ (5) as catalysts. While the employment of high pressure requires the use of special equipment, for a catalyst such as SiO_2, although simple, several days were necessary to obtain good yields of products. Indium salts are expensive and indoles were only reactive toward vinyl epoxides. Furthermore, all of these reactions have been extensively investigated in toxic organic solvents, and to the best of our knowledge, reactions of indole with epoxides under solvent-free conditions have not been reported. Thus, there is a need to develop a convenient and efficient protocol for the regioselective ring opening of epoxides with indole to produce 3-alkylindole derivatives of biological importance.

Received 9 October 2005. Published on the NRC Research Press Web site at http://canjchem.nrc.ca on 17 May 2006.

N. Azizi, S. Mehrazma, and M.R. Saidi.[1] Department of Chemistry, Sharif University of Technology, P.O. Box 11465-9516, Tehran, Iran.

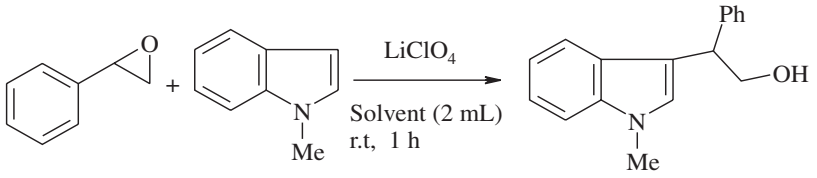
[1]Corresponding author (email: saidi@sharif.edu).

Results and discussion

As part of our research on organic synthesis under solvent-free conditions (6), in this paper we describe a simple and practical method for the synthesis of indole derivatives using a catalytic amount of lithium perchlorate. To find out the best reaction conditions for the ring opening of epoxide with indole in the presence of $LiClO_4$, styrene oxide was reacted with 1-methylindole in a common organic solvent and under solvent-free conditions with a different amount of solid lithium perchlorate. A series of experiments carried out on epoxide and indole indicated that the best yields were obtained in the presence of 20 mol% anhydr. $LiClO_4$ and 1.0 equiv. of epoxide at 60 °C under neat conditions (Table 1). In the absence of lithium perchlorate, only the starting material was obtained after prolonged reaction times. As was expected, conducting the same reaction with 20 mol% of anhydrous lithium perchlorate in common organic solvents such as THF, diethyl ether, petroleum ether, dichloro-

 doi:10.1139/V06-063 © 2006 NRC Canada

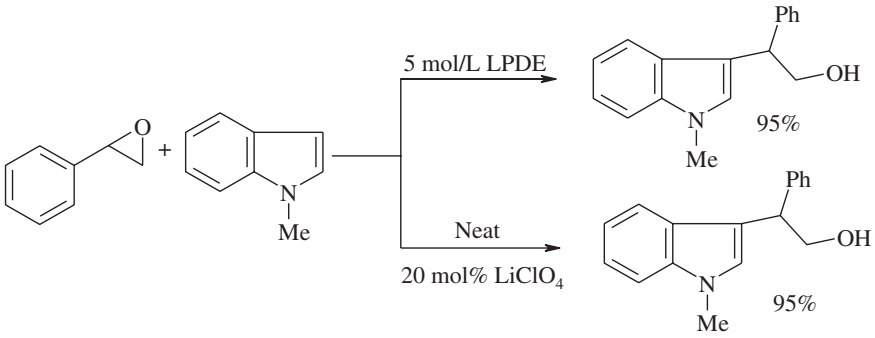
Table 1. Reactions of 1-methylindole and styrene oxide under different conditions.



Entry	Solvent	$LiClO_4$ (g)	Yield (%)
1	CH_2Cl_2	0.2	15
2	CH_2Cl_2	0.5	32
3	THF	0.2	23
4	Diethyl ether	1	95
5	CH_3CN	0.2	35
6	Petroleum ether	0.2	20
7	Methanol	0.2	0
8	Water	0.2	0
9[a]	—	0.1	95

[a]Reaction run at 60 °C.

Scheme 1. Reactions of indole and styrene oxide in 5 mol/L LPDE and neat conditions.

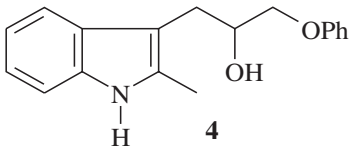


methane, acetonitrile, methanol, and water resulted, for the most part, in the recovery of the starting materials.

This shows that the solvent-free conditions play an essential role in facilitating the desired epoxide ring-opening reaction in the presence of anhydr. $LiClO_4$. On the other hand, our study shows that by increasing the amount of lithium perchlorate to 200 mol% in diethyl ether (5 mol/L solution of lithium perchlorate in diethyl ether, LPDE), the direct nucleophilic addition of indole to styrene oxide is faster than the rearrangement of the epoxide to the corresponding carbonyl compounds (Scheme 1). It also indicates that the solvent-free condition is a superior method owing to low loading of catalyst.

Lithium perchlorate is an extraordinarily efficient catalyst for the highly regioselective ring-opening reaction of epoxides. To show the generality and scope of the $LiClO_4$-promoted ring opening of epoxide with indole, the reaction was examined with various structurally diverse epoxides. The data in Table 2 clearly show that all reactions proceed smoothly under these reaction conditions to afford the desired indolyl alcohols in good yields with high regioselectivity. This method is also effective with aliphatic oxiranes. No precaution is needed to exclude moisture from the reaction media. The regioselectivity in the reaction for unsymmetrical epoxides is governed by both steric and electronic effects. The regioselectivity was determined by ^1H NMR and by comparison with the known samples. Aliphatic oxiranes underwent cleavage by indole and *N*-methylindole with the preferential attack at the less-substituted carbon atom. On the other hand, in the case of styrene oxide and other aromatic oxiranes, the reaction likely proceeds partly through an attack by the indole on the more stabilized "carbocation" with participation of phenyl groups. The role of $LiClO_4$ in catalyzing the opening of epoxide rings with indole may be realized through the coordination of Li^+ with epoxide oxygen and rendering the epoxide more susceptible to nucleophilic attack by indole, followed by hydrogen transfer to form the indolyl alcohols. The comparison of the present methods with respect to the amount of the catalyst used, reaction time and requirement of solvent, products yield and regioselectivity with those reported in the literature, reveals that this newly developed method is superior to the previous procedures.

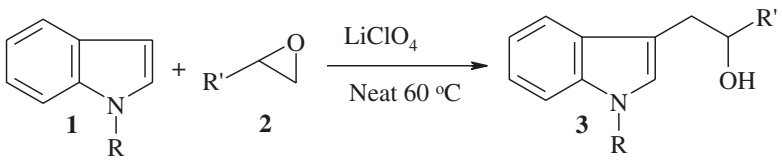
Reaction of 2-methylindole with 2,3-epoxypropyl phenyl ether proceeds efficiently at 60 °C in the presence of 20 mol% of anhydr. $LiClO_4$ under neat conditions and gave the corresponding 3-substituted 2-methylindole (**4**) in 60% yield after 1.5 h.

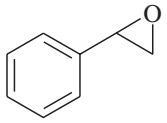
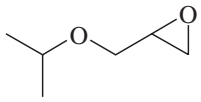
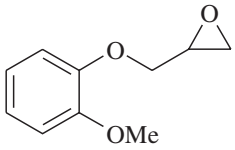
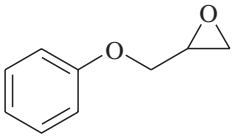
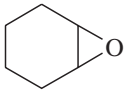


4

© 2006 NRC Canada

Table 2. Reactions of indoles with epoxide under solvent-free conditions.



Entry	Epoxides		Time (min)	Yield (%)
1		**3a** R = H	45	95
2		**3b** R = Me	120	95
3		**3c** R = H	120	66
4		**3d** R = Me	60	78
5		**3e** R = H	120	64
6		**3f** R = Me	60	80
7		**3g** R = H	60	64
8		**3h** R = Me	90	79
9				
10		**3i** R = H	180	45
11		**3j** R = Me	180	62

In summary, we have described a new direct protocol for the preparation of indolyl alcohol derivatives by ring-opening reactions of epoxides with indole and *N*-methylindole in the presence of 20 mol% of anhydr. $LiClO_4$. The notable features of this procedure are the mild reaction conditions, high conversions, short reaction times, economic viability of the reagents, simple experimental procedure, and product isolation. Although lithium perchlorate is normally responsible for the rearrangement of aromatic epoxides to the corresponding carbonyls, the mild reaction conditions allowed the isolation of the desired compounds in high yields and without rearrangement, when a 5 mol/L solution of LPDE was used.

Experimental

General procedure for the preparation of tryptophol derivatives

To a mixture of indole (4 mmol) and epoxide (4 mmol), anhydrous lithium perchlorate (0.1 mmol) was added and stirred at 60 °C for 1–4 h. When the reaction was completed, as indicated by TLC or GC, the reaction mixture was diluted with diethyl ether or ethyl acetate and purified by flash column chromatography (Et_2O–hexanes, 30:70) to give the desired products. All compounds were characterized on the basis of NMR spectroscopic data.

Selected spectroscopic data

3a

^{1}H NMR ($CDCl_3$, 500 MHz) δ_H: 2.28 (br s, 1 H, OH), 4.03–4.41 (m, 3H), 6.73–7.63 (m, 10H), 8.34 (br s, 1H, NH). ^{13}C NMR ($CDCl_3$, 500 MHz) δ_C: 45.7, 66.4, 111.2, 116.2, 119.4, 119.6, 121.9, 122.3, 126.7, 127.1, 128.3, 128.6, 136.6, 141.8.

3b

^{1}H NMR ($CDCl_3$, 500 MHz) δ_H: 1.80 (br s, 1H, OH), 3.82 (s, 3H), 4.23–4.53 (m, 3H), 7.02 (s, 1H), 7.11–7.53 (m, 9H). ^{13}C NMR ($CDCl_3$, 500 MHz) δ_C: 33.1, 46.0, 66.9, 109.7, 114.9, 119.5, 119.9, 122.3, 126.6, 127.1, 127.9, 28.7, 128.8, 137.6, 142.3.

3c

^{1}H NMR ($CDCl_3$, 500 MHz) δ_H: 1.17 (d, 3H, J = 6.3 Hz), 1.24 (d, 3H, J = 6 Hz), 2.19 (br s, 1H, OH), 3.01 (m, 2H), 3.43 (m, 1H), 3.53 (m, 1H), 3.65 (m, 1H), 4.18 (m, 1H), 6.57 (s, 1H), 6.87–7.71 (m, 4H), 8.56 (br s, 1H, NH).

© 2006 NRC Canada

3d

^{1}H NMR ($CDCl_3$, 500 MHz) δ_H: 1.28 (d, 3H, J = 6.3 Hz), 1.30 (d, 3H, J = 6.3 Hz), 2.69 (br s, 1H, OH), 3.07 (d, 2H, J = 6.5 Hz), 3.47 (m, 1H), 3.59 (m, 1H), 3.70 (m, 1H), 3.83 (s, 3H), 4.22 (m, 1H), 6.60 (s, 1H), 7.03–7.76 (m, 4H).

3g

^{1}H NMR ($CDCl_3$, 500 MHz) δ_H: 2.14 (br s, 1H, OH), 3.13–3.22 (m, 2H), 3.99–4.08 (m, 2H), 4.29 (m, 1H), 6.63 (s, 1H), 6.99–7.75 (m, 9H), 8.37 (br s, 1H, NH). ^{13}C NMR ($CDCl_3$, 500 MHz) δ_C: 29.1, 71.1, 71.9, 111.1, 111.5, 114.7, 118.1, 119.9, 121.6, 122.8, 123.1, 127.9, 129.9, 136.5, 158.8.

3h

^{1}H NMR ($CDCl_3$, 500 MHz) δ_H: 2.27 (br s, 1H, OH), 3.08–3.15 (m, 2H), 3.86 (s, 3H), 4.13–4.15 (m, 2H), 4.45 (m, 1H), 6.74 (s, 1H), 6.75–7.93 (m, 9H).

Acknowledgments

We are grateful to the Research Council of Sharif University of Technology for financial support. We also thank Volkswagen Stiftung, Germany, for financial support towards the purchase of chemicals.

References

1. (*a*) R.E. Parker and N.S. Isaacs. Chem. Rev. **59**, 737 (1959); (*b*) J.G. Buchanan and H.Z. Sable. *In* Selective organic transformations. Vol. 2. *Edited by* B.S. Thyagarajan. Wiley, New York. 1972. p. 1; (*c*) J.G. Smith. Synthesis, 629 (1984).
2. (*a*) A. Pfenninger. Synthesis, 89 (1986); (*b*) R.M. Hanson. Chem. Rev. **91**, 437 (1991); (*c*) V. Schurig and F. Betschinger. Chem. Rev. **92**, 873 (1992); (*d*) P. Besse and H. Veschambre. Tetrahedron, **50**, 8885 (1994).
3. (*a*) H. Kotsuki, K. Hayashida, T. Shimanouchi, and H. Nishizawa. J. Org. Chem. **61**, 984 (1996); (*b*) H. Kotsuki, M. Nishiuchi, S. Kobayashi, and H. Nishizawa. J. Org. Chem. **55**, 2969 (1990); (*c*) H. Kotsuki, M. Teraguchi, N. Shimomoto, and M. Ochi. Tetrahedron Lett. **37**, 3727 (1996).
4. J.S. Yadav, B.V.S. Reddy, S. Abraham, and G. Sabitha. Synlett, 1550 (2002).
5. M. Bandini, P.G. Cozzi, P. Melchiorre, and A. Umani-Ronchi. J. Org. Chem. **67**, 5386 (2002).
6. (*a*) N. Azizi and M.R. Saidi. Synth. Commun. **34**, 1207 (2004); (*b*) N. Azizi and M.R. Saidi. Organometallics, **23**, 1457 (2004); (*c*) N. Azizi and M.R. Saidi. Tetrahedron, **60**, 383 (2004); (*d*) N. Azizi and M.R. Saidi. Eur. J. Org. Chem. 630 2003); (*e*) N. Azizi and M.R. Saidi. J. Organomet. Chem. **688**, 283 (2003).

© 2006 NRC Canada

A topological analysis of the interion interactions of tetraphenylphosphonium squarate

David Wolstenholme, Manuel A.S. Aquino, T. Stanley Cameron, Joseph D. Ferrara, and Katherine N. Robertson

Abstract: The tetraphenylphosphonium squarate salt crystallizes with a number of diverse interactions, which all have the potential to be classified as hydrogen bonds. The squarate anions are found as dimers linked by O-H···O interactions. The multipole refinement of the tetraphenylphosphonium squarate was performed using the Hansen–Coppens model followed by topological analysis of its intermolecular interactions. A total of 28 interactions were found among the symmetry related molecules, which include a number of C-H···C_π, C-H···O, and C-H···H-C interactions, along with the O-H···O interaction. With the criteria for hydrogen bonding proposed by Popelier and Koch, it is possible to determine which of these interactions are hydrogen bonds and which are van der Waals interactions. Both linear and exponentially dependent correlations can be seen for the properties of the bond critical points involving the intermolecular interactions that fulfill these criteria. All this leads to a better understanding of the role that hydrogen bonds play in the formation of small organic compounds.

Key words: electron density, multiple refinement, hydrogen bonds.

Résumé : Le squarate de tétraphénylphosphonium cristallise avec un certain nombre d'interactions qui pourraient éventuellement toutes être considérées comme des liaisons hydrogènes. On retrouve les anions squarate sous la forme de dimères liés par des interactions O-H···O. On a effectué un affinement multipôle du squarate de tétraphénylphosphonium en utilisant le modèle Hansen–Coppens suivi d'une analyse topologique de ses interactions intermoléculaires. On a trouvé un total de 28 interactions entre les molécules reliées par de la symétrie, y compris un certain nombre d'interactions C-H···C_π, C-H···O et C-H···H-C en plus de l'interaction O-H···O. Avec le critère d'une liaison hydrogène proposé par Popelier et Koch, il est possible de déterminer lesquelles de ces interactions sont des liaisons hydrogènes et lesquelles sont des interactions de van der Waals. On peut déceler des corrélations qui dépendent tant linéairement qu'exponentiellement pour les propriétés des points critiques de liaison impliquant les interactions intermoléculaires qui répondent à ces critères. Toutes ces observations conduisent à une meilleure compréhension du rôle que les liaisons hydrogènes jouent dans la formation de petits composés organiques.

Mots clés : densité électronique, affinement multiple, liaisons hydrogènes.

[Traduit par la Rédaction]

Introduction

The experimental measurement and analysis of the charge density in a variety of molecular crystals has been achieved through the use of high-resolution X-ray diffraction data at low temperatures (1, 2). The charge density of a compound is evaluated through the interpretation of its electron density. There are several different ways of obtaining the electron density, but the most common method is the multipole expansion, which incorporates the Hansen–Coppens (3) model, and can be expressed by the following equation:

$$[1]\quad \rho(r) = P_c\rho_{core}(r) + P_v\kappa^3\rho_{valence}(\kappa r) + \sum_{l=0}^{l_{max}}\kappa'^3 R_l(\kappa' r)\sum_{m=0}^{1} P_{lm\pm} d_{lm\pm}(\theta,\phi)$$

where ρ_{core} and $\rho_{valence}$ are spherically averaged Hartree–Fock core and valence densities, $d_{lm\pm}$ represents spherical harmonic angular functions, R_l is the radial function, κ and κ' are the expansion–contraction parameters, and P_v and $P_{lm\pm}$ represent the population parameters.

The theory of atoms in molecules (AIM) can then be used to evaluate the experimental electron density as determined from the above model through topological means. It is this methodology that allows for the identification of a bond between any two atoms in a molecule (2). This involves locating critical points obtained from the Hessian matrix of the electron density and in particular {3,–1} critical points, also referred to as bond critical points. The bond critical point is not the only topological component of importance; the line of maximum electron density (the bond path) is also essential for identifying a bond from its topology. Another important AIM property obtained from the electron density is the

Received 5 January 2006. Published on the NRC Research Press Web site at http://canjchem.nrc.ca on 17 May 2006.

D. Wolstenholme,[1] T.S. Cameron, and K.N. Robertson. Department of Chemistry, Dalhousie University, Halifax, NS B3H 4J3, Canada.
J.D. Ferrara. Rigaku MSC, 9009 New Trails Drive, The Woodlands, TX 77381-5209.
M.A.S. Aquino. St. Francis Xavier University, PO Box 5000, Antigonish, NS B2G 2W5, Canada.

[1]Corresponding author (e-mail: dwolsten@Dal.ca).

 doi:10.1139/V06-058 © 2006 NRC Canada

Laplacian, which can be defined as the sum of the eigenvalues of the Hessian matrix ($\nabla^2\rho(r) = \lambda_1 + \lambda_2 + \lambda_3$). A wealth of knowledge can be obtained from interpreting the Laplacian; when $\nabla^2\rho(r) < 0$, the density is locally concentrated, which is typical of a shared interaction, and when $\nabla^2\rho(r) > 0$, the density is locally depleted, such as a closed shell interaction. Another topological component of the charge density distribution is the interaction length (R_{ij}). This is the length of the bond path between a pair of noncovalently bonded atoms.

It is simply not enough to specify that a bond is occurring between two atoms. What is of greater importance is to determine the type of bonding that is involved in the molecule, in particular, hydrogen bonding. This can be achieved both experimentally and theoretically by evaluating the properties of the bond critical points. Koch and Popelier (4, 5) have proposed eight criteria to distinguish a hydrogen bond from a van der Waals interaction. All eight criteria must be fulfilled in order for the bond to be classified as a hydrogen bond and not a van der Waals interaction. The first four criteria involve the properties of the bond critical points, such as the presence of charge density at the critical point and a positive value of the Laplacian. The fourth criterion, considered necessary and sufficient for hydrogen bonding, involves the mutual penetration of the hydrogen and acceptor atoms (2, 4). The last four criteria involve the integration over the atomic basin of the hydrogen atoms of interest. This will result in the loss of charge, energetic destabilization, decrease of dipolar polarization, and a decrease in volume of the hydrogen atoms (4, 5).

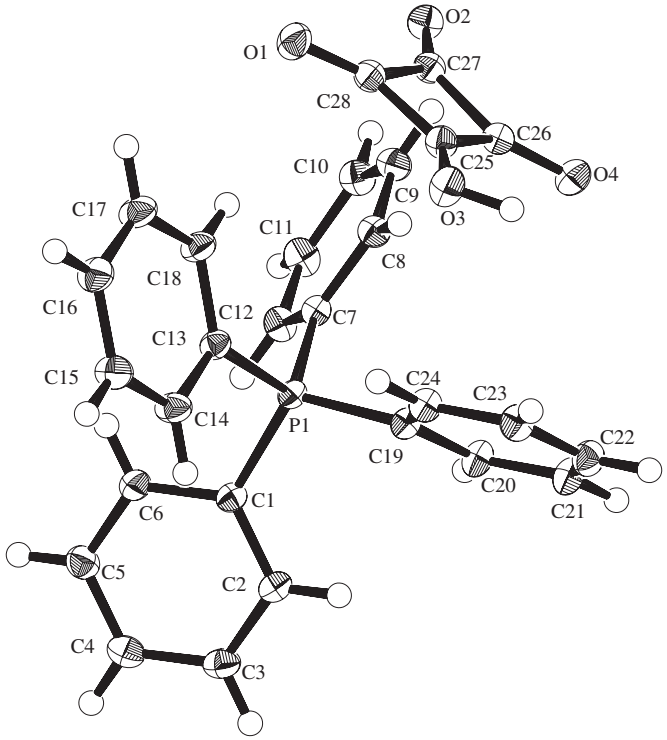
Espinosa et al. (6–11) have shown that there are many correlations between the topological and energetic properties of the electron density distributions in hydrogen-bonded systems. In closed shell interactions, they found a linear fit between the local kinetic and potential energy densities and the Hessian eigenvalues (7). Mallinson et al. (12) have also evaluated both intra- and inter-molecular interactions in terms of the first four criteria (2). For example, they demonstrated that the length of the interaction line is correlated to many of the topological properties, showing a general trend on going from weak hydrogen bonds to strong hydrogen bonds (12). These types of analyses will be applied to the tetraphenylphosphonium squarate compound.

We chose the tetraphenylphosphonium squarate (Fig. 1) compound to analyze because of the number and variety of interactions that were possible in its crystalline state. Evaluation of the experimental charge density resulted in the following four types of interactions being found: C-H···H-C, C-H···Cπ, C-H···O, and O-H···O. These types of interactions are important because they have been shown to influence the packing motif of this type of molecule (13, 14). This article will focus on the characterization of all four of these types of interactions according to the first four criteria proposed by Koch and Popelier (5).

Experimental

The synthesis of the compound tetraphenylphosphonium squarate involved squaric acid (0.074 g, 0.65 mmol) being dissolved in 10 mL of triply deionized water. The solution was then adjusted to pH 4 using NaOH. Tetraphenylphosphonium bromide (0.271 g, 0.65 mmol) was then dissolved in 15 mL of triply deionized water, gravity filtered and added, with stirring, to the squaric acid solution. The reaction mixture was stirred in a sealed Erlenmeyer flask for 2 h at room temperature, filtered, placed into a beaker, and allowed to slowly evaporate at room temperature. After about 2 weeks, large colourless crystals had formed with a yield of 90%.

Fig. 1. ORTEP diagram with labels for atoms of tetraphenylphosphonium squarate at 93 K with 50% ellipsoid probability.



A colorless prism crystal of $C_{28}H_{21}O_4P$ having approximate dimensions of 0.20 mm × 0.20 mm × 0.20 mm was mounted on a glass fiber. All measurements were made on a Rigaku Raxis rapid imaging plate area detector with graphite-monochromated Mo Kα radiation. The crystal data of the X-ray diffraction experiment can be found in Table 1. The data were collected with eight scans, each containing 36 images with an exposure time of 36 s/°, and slices of ω between 20 and 200 in increments of 5° (χ = 0° and 45° and ϕ = 0°, 90°, 180°, and 270°). The data collection was monitored and reduced with the HKL2000 (15) software, while the sorting, scaling, and merging of the intensities were performed with Sortav (16) as included in the WinGX (17) package. The structure was solved by direct methods and expanded using Fourier techniques through the CrystalStructure™ software (18). The non-hydrogen atoms were refined anisotropically and the hydrogen atoms were refined isotropically. The final cycle of full-matrix least-squares refinement on F^2 was based on 12 107 observed reflections and 303 variable parameters. All calculations were performed using the CrystalStructure™ (18) crystallographic software package except for the refinement, which was per-

© 2006 NRC Canada

Table 1. Experimental X-ray data.

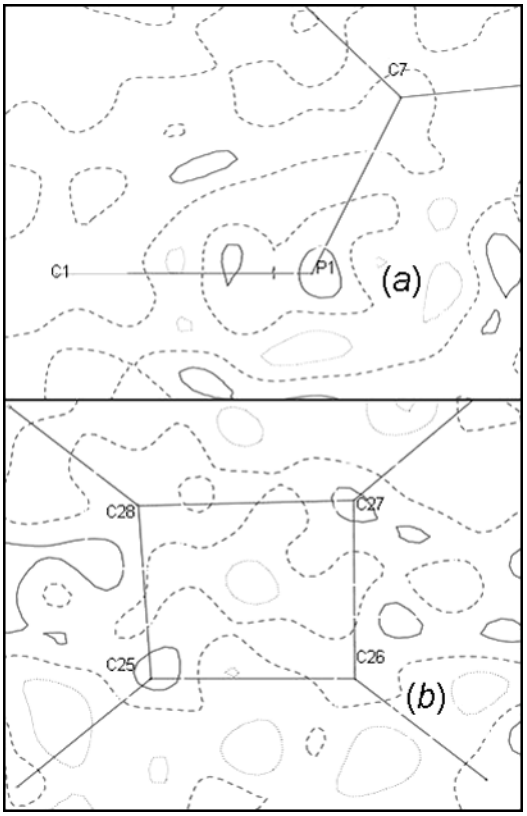
Compound formula	$C_{28}H_{21}O_4P$
Crystal size (mm)	0.2×0.2×0.2
Formula weight (g/mol)	452.45
Space group	*P*21/*n* (No. 14)
Temperature (°C)	–180
a (Å)	13.2849(3)
b (Å)	12.1411(2)
c (Å)	14.6423(3)
β (°)	109.7180(12)
V (Å^3)	2223.23(8)
Z	4
μ (cm^{-1})	1.57
D_c (g/cm^3)	1.352
F(000)	944.00
Reflections collected	180 813
Reflections (multipole)	12 107
R(*F*)	1.94%
No. of parameters (multipole)	936
Collection ranges	$23 \le h \le 21$, $0 \le k \le 21$, $0 \le l \le 25$
Maximum resolution (θ)	73.8

formed using a SHELXL-97 interface (19). All of the molecular thermal ellipsoid plots were generated using the ORTEP-3 program (20). The CIF has been deposited.[2]

Multipole refinement

The refinements were carried out with the module XDLSM incorporated in the software package XD (21). The residual bonding density not modeled in the conventional spherical refinement was taken into account in the multipole refinement (2). The scattering factors used in the multipole refinement were those derived by Su, Macchi, and Coppens' wave functions for all atoms (22, 23). The function minimized in the least-squares refinement is $\Sigma w(|F_0|^2 - K|F_c|^2)^2$ for all reflections with $I > 3\sigma(I)$ (2). For the carbon and oxygen atoms, the multipole expansion was applied up to the octapole level (l_{max} = 3), for the phosphorus up to the hexadecapole (l_{max} = 4), and for the hydrogen atoms up to the dipole level (l_{max} = 1). Separate κ and κ′ parameters were employed for each oxygen atom, as well as each type of carbon (squarate, tetraphenylphosphonium), and for the phosphorus atom. The expansion–contraction parameters of the hydrogen atoms were left fixed at the default XDLSM value of 1.2. It has been shown on several occasions that the default values of n_l and ξ used by XDLSM are not sufficient for multipole refinement of four-coordinate phosphorus atoms (13, 24). The n_l and ξ parameters were therefore chosen based on previous work on triphenylphosphonium benzylide (n_l = 6,6,6,7,7 and ξ = 3.6 b^{-1} (13)). To determine accurate positional and thermal parameters for the non-hydrogen atoms, a high-order (sin θ/λ ≥ 0.6 Å) refinement was performed. A low-order (sin θ/λ ≤ 0.6 Å) refinement was then performed to obtain accurate positional and thermal parameters of all the hydrogen atoms. The positions of the hydrogen atoms were then set to the reported neutron diffraction distance for the rest of the multipole refinement ($C_{ar/sq}$-H = 1.083, O-H = 1.03) (2, 25, 26). The charge neutrality constraint was applied throughout the multiple refinement to achieve an overall neutral molecule. The multipole refinement strategy used was as follows: (*a*) scale factor, (*b*) P_v and κ, (*c*) P_v and P_{lm}, (*d*) P_{lm} and κ, (*e*) P_{lm} and the thermal and positional parameters of all non-hydrogen atoms, and finally, (*f*) κ′. A secondary extinction of type 1 was also applied throughout all the steps and the procedure was cycled through until convergence. Difference mean square displacement amplitudes (DMSDA) for all the bonds where within the Hirshfeld limits. The good quality of the final model is also indicated by Fig. 2, which shows the residual density of the squarate and the C-P-C plane of the tetraphenylphosphonium. The accumulation of residual charge density in the vicinity of the phosphorus atom is most likely due to the

Fig. 2. Residual density map with positive contours as solid lines, negative contours as dotted lines, and the zero contour line as dashes. (*a*) C1-P1-C7 plane with contour intervals of 0.1 e Å^{-3}. (*b*) Squarate plane with contour intervals of 0.05 e Å^{-3}.



[2] Supplementary data for this article are available on the journal Web site (http://canjchem.nrc.ca) or may be purchased from the Depository of Unpublished Data, Document Delivery, CISTI, National Research Council Canada, Ottawa, ON K1A 0R6, Canada. DUD 5032. For more information on obtaining material refer to http://cisti-icist.nrc-cnrc.gc.ca/irm/unpub_e.shtml. CCDC 296857 contains the crystallographic data for this manuscript. These data can be obtained, free of charge, via http://www.ccdc.cam.ac.uk/conts/retrieving.html (Or from the Cambridge Crystallographic Data Centre, 12 Union Road, Cambridge CB2 1EZ, UK; fax +44 1223 336033; or deposit@ccdc.cam.ac.uk).

© 2006 NRC Canada

possible nature of polarization and the deficiencies in the multipole model to account for the overall density at that particular site (2). The XDPROP program incorporated into the XD (21) package was used to determine the total electron density, $\rho(r)$, the Laplacian, and the ellipticity at all the bond critical points that were observed for the tetraphenylphosphonium squarate compound. All static, residual, dynamic, and deformation maps were produced using the XDGRAPH option in the XD (21) package. The final atomic coordinates, thermal parameters, and bond lengths of the tetraphenylphosphonium squarate are provided as Supporting information.[2]

Results and discussion

The asymmetric unit of the compound of interest contains one squarate anion and one tetraphenylphosphonium cation. The squarate anions exist as symmetric dimers bonded by hydrogen bonds around a centre of symmetry in the crystalline state. Thus, five atoms (O4-C25-C26-O3-H25) from one squarate ion form a 10-membered ring involving two hydrogen bonds with the equivalent atoms from another squarate ion. The four oxygen atoms and the two hydrogen atoms are very close to planar; the hydrogen atom, H(25), is +0.036(18) Å from the least-squares best plane through the O(3)-H(25)···O(4)/O(4)′···H(25)′-O(3)′ system. The two carbon atoms at each end of the ring are puckered in opposite directions; C(25) and C(26) are –0.250(1) and –0.260(1) Å, respectively, from this plane. With the least-squares best plane through all 10 atoms, the largest deviation from planarity occurs at O(4) (0.1132(5) Å), with C(25) and C(26) –0.0774(6) Å and –0.0813(5) Å, respectively from this 10-atom plane. The squarate dimer and its interactions with different tetraphenylphosphonium cations in the unit cell play a significant role in how the crystal is formed. The carbonyl oxygens each form several interactions to the tetraphenylphosphonium phenyl hydrogens with varying interaction lengths (Table 2). The most significant of these interactions are those of O(1) to X2_H(11) and $X4^1$_H(20), as well as O(2) to X1_H(5), X2_H(6), and H(9), all of which have short interaction lengths ranging from 2.13 to 2.54 Å. The anionic squarate oxygen, O(4), also forms several strong interactions with other phenyl hydrogens, in particular X1_H(4) and X4_H(16), which have interaction lengths of 2.54 and 2.61 Å, respectively. The *xyz* and translations of the symmetry related molecules used throughout the text can be found at the end of Table 2. Some of the tetraphenylphosphonium carbons and hydrogens also play significant roles in the way the crystal is formed. The most significant of these are the interactions between C(3) with X3_H(11) and $X3^1$_H(23), C(9) with X2_H(6), C(21) with $X3^1$_H(15), C(22) with $X3^1$_H(14), and H(3) with $X2^2$_H(21). Their interaction lengths are all short (2.91, 2.75, 2.97, 2.89, 3.00, and 2.17 Å, respectively) and are characteristic of hydrogen bonds; this will be investigated in more detail in the following paragraphs.

The main objectives of the present study are to characterize the intermolecular interactions involving C-H···O, C-H···C_π, C-H···H-C, and O-H···O for the tetraphenylphosphonium squarate molecule and to evaluate them based on the first four criteria proposed by Koch and Popelier (5).

Criteria 1–4

Consistent bond paths (BP) and bond critical points (BCP) were found for 28 intermolecular interactions; these can be divided into 13 C-H···O, 11 C-H···C_π, 3 C-H···H-C, and 1 O-H···O interactions (Fig. 3). The electron density (ρ_{cp}) at the BCPs for hydrogen bonds generally falls within a certain range of values, typically between 0.013 and 0.5 e Å^{-3}, as determined by a number of independent studies (2, 5). The experimental electron density for the BCPs of the C-H···O interactions in tetraphenylphosphonium squarate lie within the range 0.01 to 0.1 e Å^{-3}. The C-H···C interactions are within the range 0.01 to 0.05 e Å^{-3}. The C-H···H-C interactions are within the range 0.01 to 0.05 e Å^{-3}, and the O-H···O interaction has a ρ_{cp} value of 0.493 e Å^{-3}. This means that all 28 interactions have ρ_{cp} values consistent with hydrogen bonding. The experimental topological parameters used to characterize these interactions are given in Table 2. All of the tetraphenylphosphonium squarate interactions follow an exponential dependence for ρ_{cp} vs. R_{ij}, although different types of interactions tend to occupy particular subranges of R_{ij}. This dependence is analogous to Pauling's relation between bond order and internuclear distances (12). If we now look at the correlations between the electron density at the BCP and R_{ij}, which generally has values ranging from 1.5 to 3.6 Å, several regions of separation are observed and can be used to help classify the strengths of the hydrogen bonds (Fig. 4). It can be seen that as the values of the electron density at the BCPs increase, the interaction lengths decrease, and this is directly proportional to the strength of the hydrogen bonds. A region of overlap has previously been determined to offer a possible distance limit for hydrogen bonding (2). This region has been used here to separate the C-H···C_π interactions (classically referred to as van der Waals interactions) and C-H···O interactions.

The local potential energy density, $V(r_{cp})$, at the BCPs represents a quantity proportional to the hydrogen bond energy (4). It generally ranges from –4 to –300 KJ mol^{-1} b^{-3} for hydrogen bonds. Again, a region of separation and overlap can be distinguished through the correlation of the interaction lengths and the local potential energy densities (Fig. 5). As in the case of the correlation between the electron density and interaction lengths, the local potential energy density decreases as the interaction length decreases allowing for a separation of the hydrogen bond strengths into one of two categories: strong and weak hydrogen bonds. The region of overlap can again be used to determine which C-H···C and C-H···O interactions are hydrogen bonds.

The characteristic hydrogen bond values of the Laplacian ($\nabla^2\rho$) generally fall within the range of 0.35 to 4.0 e Å^{-5} as proposed by Koch and Popelier (5). The experimental values of the Laplacian for the C-H···O interactions of tetraphenylphosphonium squarate lie within the range 0.18 to 1.85 e Å^{-5}; the C-H···C interactions are within the range 0.185–0.64 e Å^{-5}; the C-H···H-C interactions are within the range 0.16 to 0.74 e Å^{-5} and the O-H···O interaction has a value of 5.4 e Å^{-5}. This means that 25 of the observed interactions in tetraphenylphosphonium squarate satisfy the Laplacian criterion. The correlation of the Laplacian and the interaction

© 2006 NRC Canada

Table 2. Properties of the bond critical points.

Bond (A—B)	ρ (e Å^{-3})	$\nabla^2\rho$ (e Å^{-5})	R_{ij} (Å)	$d1$ (A—CP) (Å)	$d2$ (CP—B) (Å)	λ_1 (e Å^{-5})	λ_2 (e Å^{-5})	λ_3 (e Å^{-5})	$\Delta r_H + \Delta r_B$ (Å)	$\Delta r_H - \Delta r_B$ (Å)	$V(r)$ (KJ mol^{-1} b^{-3})	$G(r)$ (KJ mol^{-1} b^{-3})
C(3)—X3_H(11)	0.035	0.468	2.91	1.72	1.19	–0.06	–0.03	0.56	0.136	–0.119	–6.59	9.67
C(3)—X3^1_H(23)	0.039	0.636	2.79	1.75	1.04	–0.09	–0.05	0.77	0.258	0.054	–8.58	12.95
C(4)—X3_H(10)	0.040	0.459	3.02	1.70	1.33	–0.08	–0.05	0.59	0.028	–0.281	–7.09	9.80
C(8)—X4_H(16)	0.036	0.434	3.01	1.74	1.27	–0.07	–0.03	0.54	0.043	–0.186	–6.40	9.11
C(9)—X2_H(6)	0.020	0.351	2.97	1.79	1.18	–0.03	–0.02	0.41	0.084	–0.044	–4.11	6.83
C(9)—X4_H(17)	0.038	0.470	2.97	1.75	1.22	–0.08	–0.04	0.59	0.080	–0.125	–6.95	9.88
C(15)—X2^1_H(10)	0.010	0.185	3.32	2.03	1.29	–0.02	–0.01	0.22	–0.266	0.086	–1.97	3.50
C(21)—X3^1_H(15)	0.029	0.412	2.89	1.73	1.15	–0.06	–0.05	0.52	0.162	–0.070	–5.45	8.34
C(22)—X3^1_H(14)	0.027	0.430	3.00	1.88	1.12	–0.04	–0.02	0.49	0.046	0.102	–5.42	8.57
C(25)—X3^2_H(22)	0.034	0.399	3.08	1.72	1.36	–0.05	–0.04	0.49	–0.025	–0.286	–5.86	8.36
C(26)—X3^2_H(23)	0.044	0.545	2.84	1.62	1.22	–0.11	–0.04	0.70	0.211	–0.257	–8.38	11.61
C(3)—H(3)-X2^2_H(21)	0.047	0.724	2.17	1.04	1.14	–0.20	–0.15	1.08	0.229	0.101	–10.40	15.07
C(5)—H(5)-X2^1_H(18)	0.035	0.530	2.35	1.24	1.11	–0.12	–0.10	0.75	0.050	–0.136	–7.15	10.80
C(12)—H(12)-X3_H(12)	0.013	0.166	3.07	1.54	1.54	–0.03	–0.01	0.20	–0.673	0.000	–1.96	3.24
O(1)—X2_H(11)	0.069	0.967	2.53	1.42	1.11	–0.21	–0.19	1.37	0.210	–0.026	–16.04	21.19
O(1)—H(17)	0.036	0.527	2.88	1.54	1.33	–0.09	–0.07	0.69	–0.136	–0.134	–7.24	10.80
O(1)—X4^1_H(20)	0.106	1.843	2.14	1.32	0.82	–0.49	–0.46	2.79	0.603	0.162	–31.59	40.89
O(2)—X1_H(4)	0.035	0.483	2.97	1.63	1.31	–0.06	–0.01	0.56	–0.234	–0.058	–6.73	9.94
O(2)—X1_H(5)	0.040	0.703	2.62	1.51	1.1	–0.12	–0.10	0.92	0.122	0.065	–9.31	14.23
O(2)—X2_H(6)	0.059	0.936	2.47	1.44	1.04	–0.23	–0.21	1.37	0.266	0.0642	–14.09	19.79
O(2)—H(8)	0.044	0.715	2.79	1.73	1.06	–0.10	–0.02	0.83	–0.049	0.329	–9.92	14.70
O(2)—H(9)	0.075	1.080	2.43	1.38	1.04	–0.27	–0.23	1.58	0.315	0.001	–18.15	23.78
O(3)—X3^1_H(3)	0.013	0.191	3.28	1.79	1.49	–0.03	–0.02	0.24	–0.541	–0.047	–2.18	3.69
O(3)—X2^3_H(15)	0.023	0.390	2.80	1.60	1.20	–0.08	–0.06	0.53	–0.063	0.064	–4.70	7.66
O(3)—X4^1_H(21)	0.037	0.566	2.74	1.54	1.20	–0.12	–0.11	0.80	0.0017	–0.002	–7.71	11.56
O(4)—X1_H(4)	0.075	1.013	2.54	1.42	1.12	–0.24	–0.23	1.48	0.202	–0.038	–17.54	22.57
O(4)—X4_H(16)	0.026	0.598	2.61	1.57	1.05	–0.09	–0.08	0.76	0.128	0.178	–6.86	11.57
O(4)—X3^2_H(25)-X3^2_O(3)	0.493	5.400	1.55	1.01	0.54	–3.56	–3.27	12.2	1.187	0.134	–241.52	194.30

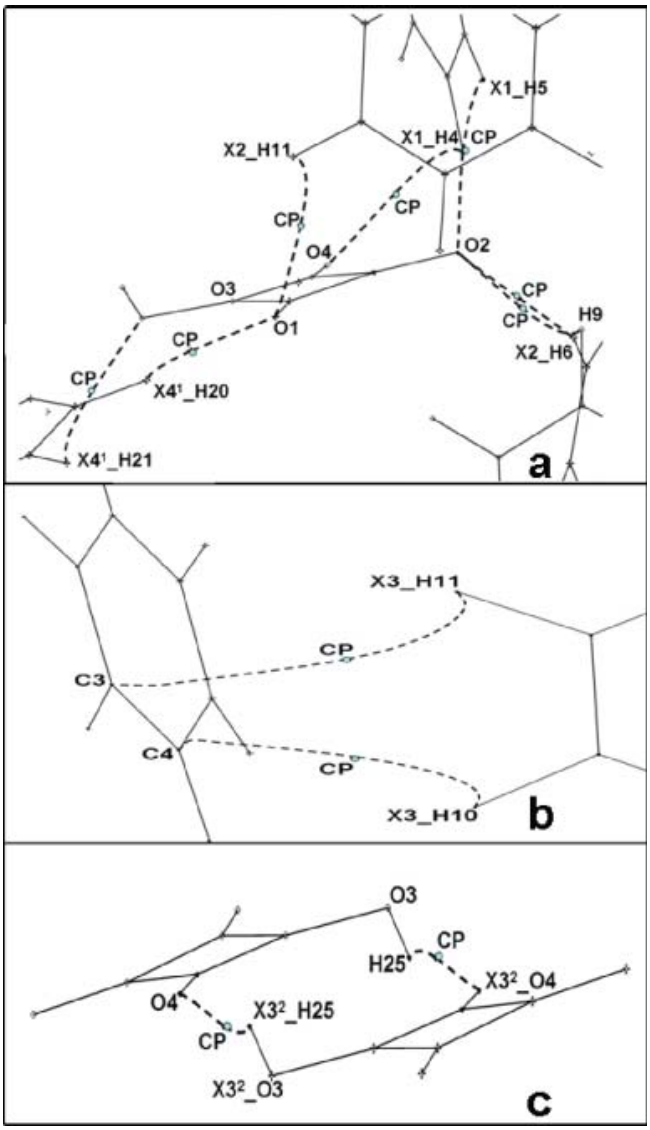
Note:

Symmetry

	x, y, z	TA	TB	TC		x, y, z	TA	TB	TC
X1		0	1	0	X2	$1/2 - x, 1/2 + y, 1/2 - z$	0	0	0
X2^1	$1/2 - x, 1/2 + y, 1/2 - z$	0	–1	0	X2^2	$1/2 - x, 1/2 + y, 1/2 - z$	0	–1	1
X2^3	$1/2 - x, 1/2 + y, 1/2 - z$	–1	0	0	X3	$-x, -y, -z$	1	0	1
X3^1	$-x, -y, -z$	0	0	1	X3^2	$-x, -y, -z$	0	1	1
X4	$1/2 + x, 1/2 - y, 1/2 + z$	0	0	0	X4^1	$1/2 + x, 1/2 - y, 1/2 + z$	–1	0	–1

© 2006 NRC Canada

Fig. 3. (*a*) Bond path character in tetraphenylphosphonium squarate showing the critical point locations along the C-H···O interactions shown in blue. (*b*) Bond path character showing the critical point locations along the C-H···C interactions shown in blue. (*c*) Bond path character showing the critical point locations along the O-H···O interactions shown in blue.



length shows that as the Laplacian decreases, the interaction length increases (Fig. 6). Again the region of overlap shows a range of R_{ij} values that includes both C-H···C_π and C-H···O interactions that can be classified as hydrogen bonds.

The most important of the four Popelier criteria involves the mutual penetration of the hydrogen and the acceptor atoms. This is measured by looking at the $\Delta r_H + \Delta r_B$ values, where Δr_X is simply the non-bonding radius of the acceptor or donor atom minus its bonding radius. The nonbonding radius is taken to be equivalent to the gas-phase van der Waals radius for any particular atom. In this work, the nonbonding radius for carbon is taken as 1.85 Å, oxygen as 1.54 Å, and hydrogen as 1.2 Å (21, 27, 28). The bonding radius is taken as the distance from the nucleus to the BCP. For an interaction to be classified as a hydrogen bond, the penetration

Fig. 4. Exponential dependence of ρ_{cp} (e Å^{-3}) on the interaction lengths (R_{ij}, Å) for all the hydrogen bonds in tetraphenylphosphonium squarate (R^2 = 0.9808).

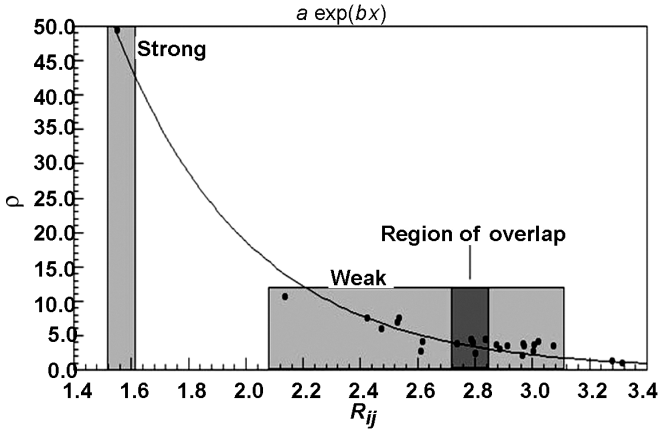


Fig. 5. Exponential dependence of $V(r_{cp})$ (KJ mol^{-1} b^{-3}) on the interaction lengths (R_{ij}, Å) for all the hydrogen bonds in tetraphenylphosphonium squarate (R^2 = 0.9948).

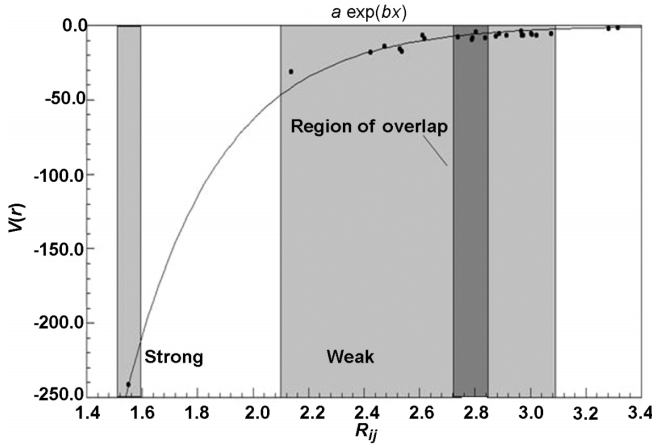
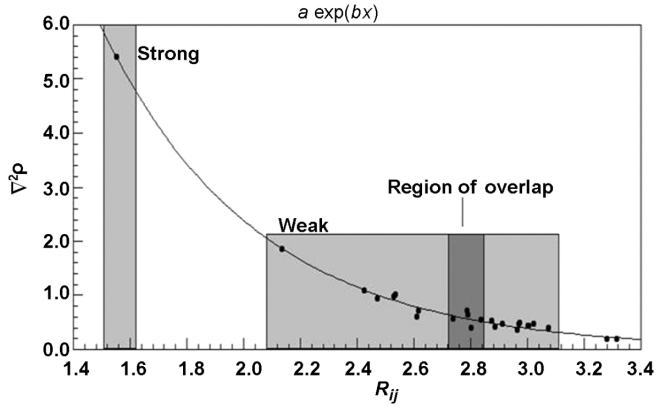


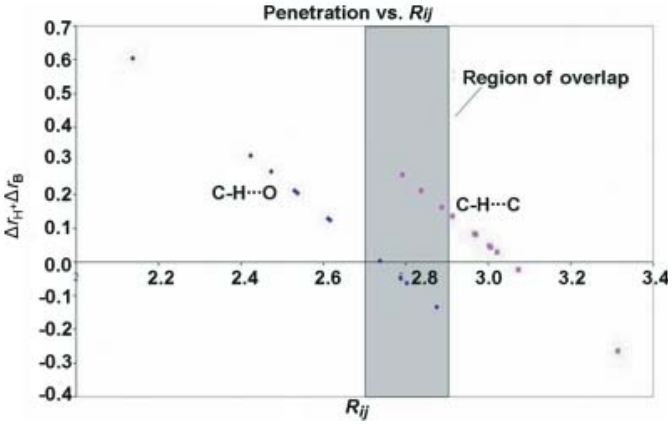
Fig. 6. Exponential dependence of the Laplacian ($\nabla^2\rho$, e Å^{-5}) on the interaction lengths (R_{ij}, Å) for all the hydrogen bonds of tetraphenylphosphonium squarate (R^2 = 0.9936).



value ($\Delta r_H + \Delta r_B$) must be positive, which indicates that the van der Waals spheres of the two atoms are overlapping. Investigation of the tetraphenylphosphonium squarate interac-

© 2006 NRC Canada

Fig. 7. Linear dependence of $\Delta r_H + \Delta r_B$ (Å) on the interaction lengths (R_{ij}, Å) for all the hydrogen bonds for tetraphenylphosphonium squarate ($R^2 = 0.9999$).



tions resulted in eight C-H···O, nine C-H···C, two C-H···H-C, and one O-H···O interactions that satisfy this criterion. Another important factor in the mutual penetration of the hydrogen and acceptor atoms is the amount by which the critical point penetrates the donor's van der Waals sphere in comparison to that of the acceptor atom. This is measured by looking at $\Delta r_H - \Delta r_B$, where Δr_X is the same as in the above example, and should still be positive. The tetraphenylphosphonium squarate possesses five C-H···O, two C-H···C, one C-H···H-C, and the O-H···O interactions that completely satisfy this portion of the fourth criterion. Of the 28 interactions found in this compound, only nine show full penetration of both the hydrogen atom and the acceptor atom and thus fully satisfy this criterion. Full penetration implies that both the acceptor and donor atoms have Δr values that are positive, meaning that both atoms are being penetrated along the bond axis. It is also apparent that there is a strong linear correlation between $\Delta r_H + \Delta r_B$ and R_{ij} (Fig. 7). As expected, this shows that the penetrations of the two atoms are quite dependent on the distance between them (12).

The C-H···H-C interactions observed for the tetraphenylphosphonium squarate, unlike the other three types of interactions, can be classified as either simple van der Waals interactions or as hydrogen–hydrogen bonds, but not as hydrogen bonds. This means that of the nine interactions mentioned previously, all of which satisfy the first four criteria of hydrogen bonding proposed by Popelier, only eight of them can in fact be considered as hydrogen bonds. The final interaction involves a C-H···H-C type interaction and is better classified as a hydrogen–hydrogen bond. This is due to the fact that both hydrogen atoms carry a small positive charge, whereas dihydrogen bonds possess both a positively charged (donor) and a negatively charged (acceptor) hydrogen (29). Supplementary data tables that summarize the refinement are available.[2]

Conclusion

Experimental charge density calculations on the tetraphenylphosphonium squarate molecule have shown that 8 of the 28 intermolecular interactions can be classified as hydrogen bonds according to the first four criteria proposed by Koch and Popelier. One of the C-H···H-C interactions can be classified as a hydrogen–hydrogen bond even though it seems to fulfill all of the first four criteria for hydrogen bonding, and the remainder of the interactions can be classified as weak van der Waals interactions. Using the correlations between the properties of the bond critical point and the interaction lengths can lead to several subsets of hydrogen bonding according to their relative bond strengths (12). The correlations also show a region of overlap, which can be used as a good approximation for a borderline between hydrogen bonding and van der Waals interactions (2). This region of overlap must be carefully interpreted because of the fact that not all interactions, at least, of the tetraphenylphosphonium squarate will fall within the hydrogen bond region even though they completely fulfill all of the first four criteria. These interactions are of importance because they are clearly used to hold the crystalline form of the molecule together.

Acknowledgements

We are grateful to the Natural Sciences and Engineering Research Council of Canada (NSERC) for financial support. We would also like to thank the Department of Chemistry at Dalhousie University, Halifax, Nova Scotia, for financial support. We also thank Dr. Parthapratin Munshi for helpful discussions.

References

1. P. Coppens. Acta Crystallogr. Sect. A, **A54**, 779 (1998).
2. P. Munshi and T.N.G. Row. J. Phys. Chem. A, **109**, 659 (2005).
3. P. Coppens. X-ray charge densities and chemical bonding. Oxford University Press, Oxford. 1997. p. 106.
4. P. Popelier. Atoms in molecules. An introduction. Prentice Hall, Manchester. 2000. Chap. 10.
5. U. Koch and P. Popelier. J. Phys. Chem. **99**, 9747 (1995).
6. E. Espinosa, E. Molins, and C. Lecomte. Chem. Phys. Lett. **285**, 170 (1998).
7. E. Espinosa, C. Lecomte, and E. Molins. Chem. Phys. Lett. **300**, 745 (1999)
8. E. Espinosa, M. Souhassou, H. Lachekar, and C. Lecomte. Acta Crystallogr. Sect. B, **B55**, 563 (1999).
9. E. Espinosa and E. Molins. J. Chem. Phys. **113**, 5686 (2000).
10. E. Espinosa, I. Alkorta, I. Rozas, J. Elguero, and E. Molins. Chem. Phys. Lett. **336**, 457 (2001)
11. E. Espinosa, I. Alkorta, J. Elguero, and E. Molins. J. Chem. Phys. **117**, 5529 (2002).
12. P.R. Mallinson, G.T. Smith, C.C. Wilson, E. Grech, and K. Wozniak. J. Am. Chem. Soc. **125**, 4259 (2003).
13. D.S. Yufit, J.A.K. Howard, and M.G. Davidson. J. Chem. Soc. Perkins Trans. 2, 249 (2000).
14. G. Desiraju, S. Kashino, M.M. Coombs, and J. Glusker. Acta Crystallogr. Sect. B, **B49**, 880 (1993).
15. Z. Otwinowski and W. Minor. *In* Methods in enzymology. Vol. 276. Macromolecular crystallography, Part A. Academic Press, London. 1997. pp. 307–326.
16. R.H. Blessing. Crystallogr. Rev. **1**, 3 (1987).
17. WinGX (Version 1.64.05): L.J. Farrugia. J. Appl. Crystallogr. **32**, 837 (1999).
18. Rigaku and Rigaku/MSC. CrystalStructure. Version 3.6.0 [computer program]. Rigaku and Rigaku/MSC, The Woodlands, Texas. 2000–2004.

© 2006 NRC Canada

19. G.M. Sheldrick. SHELXS97 and SHELXL97 [computer programs]. University of Göttingen, Göttingen, Germany. 1997.
20. ORTEP-3: L.J. Farrugia. J. Appl. Crystallogr. **30**, 565 (1997).
21. T.S. Koitsanszky, S. Howard, P. Macchi, C. Gatti, L.J. Farrugia, P.R. Mallinson, A. Volkov, Z. Su, T. Richter, and N.K. Hansen. XD. Version 4.10, July [computer program]. Free University of Berlin, Germany, University of Wales, Cardiff, UK, Universita di Milano, CNR-ISTM, Milan, Italy, University of Glasgow, UK, State University of New York, Buffalo, and University of Nancy, France. 2003.
22. Z. Su and P. Coppens. Acta Crystallogr. Sect. A, **A54**, 646 (1998).
23. P. Macchi and P. Coppens. Acta Crystallogr. Sect. A, **A57**, 656 (2001).
24. N. Peres, A. Boukhris, M. Souhassou, G. Gavoille, and C. Lecomte. Acta Crystallogr. Sect. A, **A55**, 1038 (1999).
25. J. Semmingsen. J. Chem. Phys. **66**, 4405 (1977).
26. F.H. Allen. Acta Crystallogr. Sect. B, **B42**, 512 (1986)
27. A. Bondi. J. Phys. Chem. **68**, 441 (1964).
28. S.C. Nyburg and C.H. Faerman. Acta Crystallogr. Sect. B, **B41**, 274 (1985).
29. C.F. Matta. *In* Hydrogen bonding — New insight (Challenges and advances in computational chemistry and physics series). *Edited by* S. Grabowski. Kluwer, Dordrecht, The Netherlands. 2006.

© 2006 NRC Canada

Solvent-free and selective tosylation of alcohols and phenols with *p*-toluenesulfonyl chloride by heteropolyacids as highly efficient catalysts

Razieh Fazaeli, Shahram Tangestaninejad, and Hamid Aliyan

Abstract: Tosylation of some alcohols and phenols has been directly carried out with *p*-toluenesulfonyl chloride using heterodoxy acids ($H_3PW_{12}O_{40}$, $H_3PMo_{12}O_{40}$, $AlPW_{12}O_{40}$, and $AlPMo_{12}O_{40}$) as catalysts in the absence of solvent. We found that heteropoly acids $AlPW_{12}O_{40}$ and $AlPMo_{12}O_{40}$ were effective catalysts for the tosylation of alcohols and phenols. In the case of aliphatic alcohols, secondary alcohols undergo tosylation chemoselectively in the presence of primary hydroxyl groups. This new method consistently has the advantage of excellent yields and short reaction time.

Key words: tosylation, *p*-TsCl, Keggin-type polyoxometalate, solvent-free reaction.

Résumé : La réaction de tosylation de quelques alcools et phénols a été réalisée directement par réaction avec du chlorure de *p*-toluènesulfonyle en utilisant des acides hétérodoxes ($H_3PW_{12}O_{40}$, $H_3PMo_{12}O_{40}$, $AlPW_{12}O_{40}$ et $AlPMo_{12}O_{40}$) comme catalyseurs, en l'absence de solvants. On a trouvé que les hétéropolyacides $AlPW_{12}O_{40}$ et $AlPMo_{12}O_{40}$ sont des catalyseurs efficaces pour la tosylation des alcools et des phénols. Dans le cas des alcools aliphatiques, les alcools secondaires subissent une tosylation chimiosélective lorsqu'ils sont en présence de groupes hydroxyles primaires. Cette nouvelle méthode présente les avantages d'excellents rendements et de temps de réaction courts.

Mots clés : tosylation, chlorure de *p*-tosyle, polyoxométallate de type Keggin, réaction sans solvant.

[Traduit par la Rédaction]

Introduction

Tosylation of alcohols is an important transformation in organic synthesis (1, 2). The most widely used reagents, *p*-toluenesulfonyl chloride (*p*-TsCl) or anhydride, are reactive in comparison with *p*-toluenesulfonic acid (3). Preparation of sulfonates generally relies on the use of the corresponding sulfonyl chloride or anhydride in the presence of pyridine (3*b*, 4), triethylamine (3*a*, 3*c*), 1,4-diazabicyclo[2.2.2]octane (DABCO) (3*d*), or an aqueous base.

p-Toluenesulfonic acid (*p*-TsOH) has also been used (5) as a tosylating agent, but in this case, expensive reagents such as trialkyl orthoformates, alkylethers, esters, or 2-alkoxybenzothiazolium salt are also necessary. Organic base adducts of sulfonyls such as aryl sulfonyl methylimidazolium salts, 1-phenylsulfonyl benzotriazole, and 1-(benzenesulfonyl)- and 1-(*p*-toluenesulfonyl)-3-methylimidazolium triflates have also been employed for sulfonate synthesis (6). The formation of the side products using these reagents in the presence of a base is also a problem (1, 3*b*, 5).

Fe^{3+}-montmorillonite clay has been reported to catalyze the tosylation of alcohols with *p*-TsOH (7). This catalyst is effective for tosylation of aliphatic alcohols, but aromatic alcohols give rearranged or polymeric products. Also, in this case, primary and secondary alcohols behaved very similarly. $CoCl_2 \cdot 6H_2O$ (8), silica chloride (9), and $ZrCl_4$ (10) have also been used to catalyze the tosylation of both aliphatic and aromatic alcohols with *p*-TsOH. In these methods, tosylation of long-chain alcohols required longer reaction times and the yields were poor.

Selective tosylation of a primary hydroxyl group in a molecule containing primary and secondary hydroxyl groups is often required. The resulting sulfonates are the precursors for epoxides enroute to the synthesis of a number of natural products and drugs (11). It is important to realize a high regioselectivity in the initial sulfonylation step to obtain epoxides with high purity via cyclization of the product hydroxyl sulfonates. Thus, there are a limited number of suitable direct tosylation methods for alcohols with *p*-TsOH and there is still a need to develop efficient protocols for this purpose.

Herein, we wish to report a suitable method for direct tosylation of alcohols with *p*-TsCl catalyzed by polyoxometalates as Lewis acid catalysts (Scheme 1).

Polyoxometalates belong to a large class of nanosized metal–oxygen cluster anions. The chemistry of polyoxometalates (heteropolyacids and heteropolysalts), started by Berzelius back in 1826, has now reached maturity. But it is still a rapidly developing field interconnected with many disciplines (12).

The applications of polyoxometalates (POMs, especially polyoxotungstates) for environmental protection and remediation have attracted much attention in recent years (13–19). The majority of POMs have structures composed of molyb-

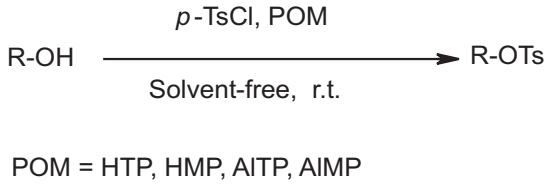
Received 7 November 2005. Published on the NRC Research Press Web site at http://canjchem.nrc.ca on 17 May 2006.

R. Fazaeli and S. Tangestaninejad.[1] Department of Chemistry, Isfahan University, Isfahan, 81746-73441, Iran.
H. Aliyan. Department of Chemistry, Shahreza Islamic Azad University 31186145, Shahreza, Isfahan, Iran.

[1]Corresponding author (e-mail: stanges@sci.ui.ac.ir).

 doi:10.1139/V06-066 © 2006 NRC Canada

Scheme 1.



denum and tungsten polyhedrons. Other elements occur in small amounts in these structures. Polyoxotungstates and polyoxomolybdates decompose in alkaline media to form simple tungstate and molybdate ions, and therefore, they can be determined in these forms (20).

The relative activity of Keggin heteropolyacids primarily depends on their acid strength. Other properties, such as the oxidation potential as well as the thermal and hydrolytic stability, are also important.

Tungsten heteropolyacids are usually the catalysts of choice because of their stronger acidity, higher thermal stability, and lower oxidation potential compared with molybdenum acids. Generally, if the reaction rate is controlled by the catalyst acid strength, $H_3PW_{12}O_{40}$ shows the highest catalytic activity in the Keggin series. The acids $H_3PW_{12}O_{40}$, (HTP) and $H_3PMo_{12}O_{40}$, (HMP) are readily available and most frequently used as catalysts. These acids have relatively high thermal stabilities and decompose at 465 and 375 °C, respectively (12).

Preparation of aluminum dodecatungstophosphate ($AlPW_{12}O_{40}$) was reported in 1982 by Ono (21) from the reaction of aluminum nitrate and dodecatungstophosphoric acid in a quantitative yield. We have also prepared aluminum dodecatungstophosphate ($AlPW_{12}O_{40}$ or AlTP) and aluminum dodecamolybdophosphate ($AlPMo_{12}O_{40}$ or AlMP) by the addition of aluminum nitrate or aluminum carbonate to the aqueous solution of tungstophosphoric acid or molybdatophosphoric acid, respectively, which on complete evaporation of water gave the desired compound as white (AlTP) and yellow (AlMP) powders in quantitative yield. AlTP prepared by both protocols gave satisfactory analytical results within the range of the experimental error. This salt is a water stable and nonhygroscopic compound (21–23).

Experimental

Tungstophosphoric acid and dodecamolybdophosphoric acid (HTP and HMP), which are cheap, reusable, heterogeneous, and easily available catalysts, were purchased from Merck and were purified by extraction with Et_2O from the aqueous solution of the acids. After evacuation at 150–300 °C for 1 to 2 h under reduced pressure, pure HTP and HMP were obtained (24). AlTP can be prepared from cheap and commercially available chemicals in a quantitative yield in aqueous media. In contrast to many other Lewis acids, storage of this compound does not need special precautions, e.g., it can be stored on a bench top for months without losing its catalytic activity. In addition, as a nonhygroscopic, noncorrosive, and water stable compound, handling of AlTP is easy, which makes it a suitable catalyst for large-scale operations.

All solvents were reagent grade. All reaction mixtures were stirred magnetically and were monitored by TLC. IR spectra were recorded on a PerkinElmer FT-IR Impact 400D spectrophotometer with KBr. ^{1}H and ^{13}C NMR spectra were recorded on a Bruker AW 500 MHz spectrometer.

General procedure for tosylation

The solvent-free method has an operationally simple procedure. An alcohol or phenol (1 mmol) and POM ($AlPW_{12}O_{40}$, $AlPMo_{12}O_{40}$, $H_3PW_{12}O_{40}$, or $H_3PMo_{12}O_{40}$, 0.03 mmol) and *p*-TsCl (1.2 mmol) were ground together in a mortar and pestle at room temperature for several minutes to form the tosylates. In cases when the mixture stuck to the walls of the mortar, it was taken off the walls with a spatula and grounding was redone. The progress of the reaction was monitored by GC and TLC. After complete disappearance of the starting material, the mixture was poured into a satd. $NaHCO_3$ solution, extracted with CH_2Cl_2 (3 × 20 mL), and the organic phase was dried over Na_2SO_4. The residue was subjected to column chromatography over silica gel using EtOAc–hexane (1:4) as eluent to produce pure tosylate. The structures of the products were established from their spectral (^{1}H and ^{13}C NMR, IR, and MS) data.

Selected spectroscopic data

Cyclopentyl* p-*toluenesulfonate (Table 1, n)

Thick oil. IR (film, cm^{-1}): 1172, 1354. ^{1}H NMR (200 MHz, $CDCl_3$) δ: 1.54–1.78 (8H, m, -$[CH_2]_4$-), 2.43 (3H, s, CH_3), 4.49 (1H, m, CHO-), 7.32 (2H, d, *m*-H, J = 8.1 Hz), 7.78 (2H, d, *o*-H, J = 8.1Hz). MS (EI) *m/z*: 240 (M^+, 2), 172 (61), 107 (33), 91 (100), 65 (34).

Cyclohexyl* p-*toluenesulfonate (Table 1, m)

Thick oil. IR (film, cm^{-1}): 1170, 1351. ^{1}H NMR (200 MHz, $CDCl_3$) δ: 1.30–1.78 (10H, m, -$[CH_2]_5$-), 2.44 (3H, s, CH_3), 4.49 (1H, m, CHO-), 7.32 (2H, d, *m*-H, J = 8.8 Hz), 7.79 (2H, d, *o*-H, J = 8.8 Hz). ^{13}C NMR (200 MHz, $CDCl_3$) δ: 143.99, 134.32, 129.38, 127.11 (Ar carbons), 81.12 (CHO), 31.90, 24.46, 22.92, 21.11 (alkane). MS (EI) *m/z*: 254 (M^+, 2), 173 (100), 155 (46), 91 (31), 82 (31), 67 (22), 65 (7).

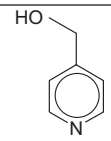
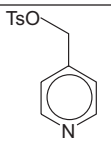
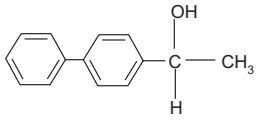
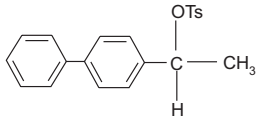
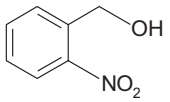
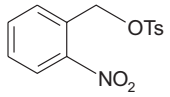
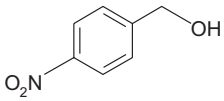
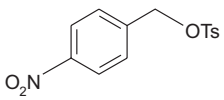
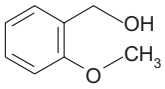
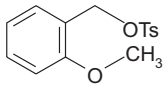
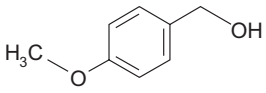
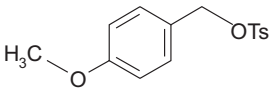
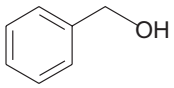
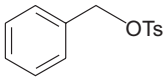
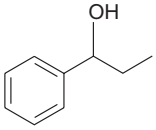
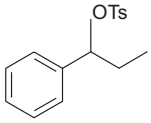
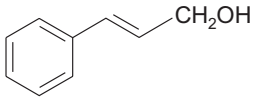
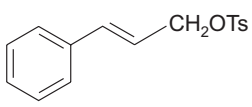
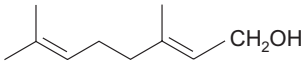
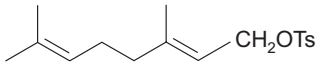
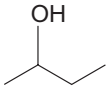
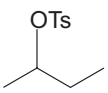
Results and discussion

At first, to investigate the catalytic ability of heteropolyacids ($H_3PW_{12}O_{40}$, $H_3PMo_{12}O_{40}$, $AlPW_{12}O_{40}$, $AlPMo_{12}O_{40}$) to act as catalysts on the tosylation of alcohols and phenols, different alcohols and phenols were mixed with *p*-TsCl in the presence of POMs to form the tosylates under solvent-free conditions. The results showed that $AlPW_{12}O_{40}$ and $AlPMo_{12}O_{40}$ show higher catalytic activity than the acid forms in our experimental conditions (Tables 1 and 2). The catalytic activities are as follows: $AlPW_{12}O_{40}$ ~ $AlPMo_{12}O_{40}$ ≥ $H_3PW_{12}O_{40}$ > $H_3PMo_{12}O_{40}$. The blank experiments, in the absence of catalysts, showed that *p*-TsCl is much less efficient in producing the tosylated products.

As shown in Tables 1 and 2, by using $AlPW_{12}O_{40}$ or $AlPMo_{12}O_{40}$ as catalyst, primary, secondary, benzylic, and allylic alcohols gave tosylated products in good yields. Benzylic alcohols, such as benzyl, 2-nitrobenzyl, 4-

© 2006 NRC Canada

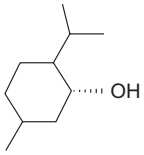
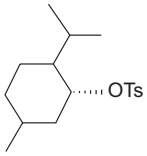
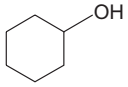
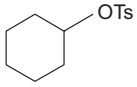
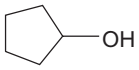
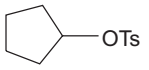
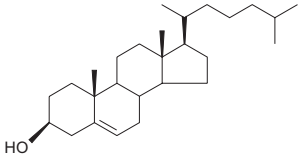
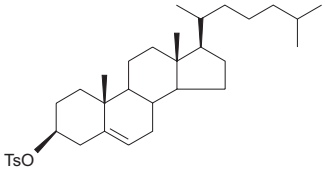
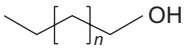
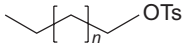
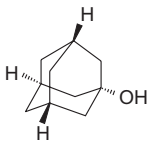
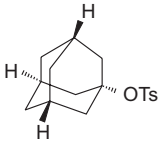
Table 1. Results on the tosylation of different alcohols using some heteropoly acids.

Entry	Substrate	Product	Type of POM	Time (min)	Yield (%)[a,b,c]
a			HTP	20	45
			HMP	27	50
			AlTP	7	100
			AlMP	9	95
b			HTP	25	50
			HMP	31	55
			AlTP	8	100
			AlMP	8	98
c			HTP	20	60
			HMP	25	45
			AlTP	15	98
			AlMP	18	78
d			HTP	20	50
			HMP	25	55
			AlTP	10	90
			AlMP	14	95
e			HTP	21	60
			HMP	28	60
			AlTP	5	92
			AlMP	7	95
f			HTP	20	55
			HMP	35	60
			AlTP	7	98
			AlMP	7	92
g			HTP	20	60
			HMP	30	55
			AlTP	10	98
			AlMP	10	98
h			HTP	20	60
			HMP	20	55
			AlTP	10	98
			AlMP	11	93
i			HTP	20	60
			HMP	30	55
			AlTP	14	98
			AlMP	17	98
j			HTP	20	65
			HMP	25	65
			AlTP	10	90
			AlMP	10	95
k			HTP	25	60
			HMP	25	50
			AlTP	7	98
			AlMP	13	89

nitrobenzyl, 3-methoxybenzyl, 4-methoxybenzyl, and 1-phenylpropyl alcohol, were converted to the corresponding tosylates in 78%–100% yields (Table 1, entries b–h). Similarly, allylic alcohols, such as cinnamyl and geraniol alcohol, underwent tosylation to afford the corresponding tosylates in 90%–98% yields (Table 1, entries i and j). Aliphatic alcohols were more easily tosylated than aromatic alcohols. However, long-chain alcohols, in the presence of $AlPW_{12}O_{40}$ or $AlPW_{12}O_{40}$ as catalyst, were converted to the desired products in moderate yields (Table 1, entries q–t, 73%–80%). Cholesterol (Table 1, entry o), which is a more complex secondary alcohol, produced the tosylated product

© 2006 NRC Canada

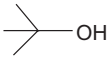
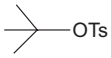
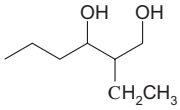
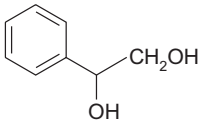
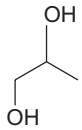
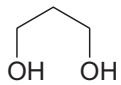
Table 1. (*continued*).

Entry	Substrate	Product	Type of POM	Time (min)	Yield (%)[a,b,c]
l			HTP	15	75
			HMP	16	60
			AlTP	9	96
			AlMP	9	90
m			HTP	20	65
			HMP	20	50
			AlTP	6	96
			AlMP	9	90
n			HTP	20	65
			HMP	25	65
			AlTP	11	96
			AlMP	17	90
o			HTP	20	65
			HMP	20	50
			AlTP	6	96
			AlMP	9	90
					
p	$n = 2$	$n = 2$	HTP	55	60
			HMP	55	45
			AlTP	30	80
			AlMP	38	75
q	$n = 7$	$n = 7$	HTP	60	55
			HMP	55	50
			AlTP	30	80
			AlMP	35	75
r	$n = 11$	$n = 11$	HTP	50	50
			HMP	50	50
			AlTP	40	80
			AlMP	48	75
s	$n = 13$	$n = 13$	HTP	20	40
			HMP	20	40
			AlTP	11	75
			AlMP	13	73
t	$n = 15$	$n = 15$	HTP	55	45
			HMP	60	40
			AlTP	29	83
			AlMP	48	75
u			HTP	60	65
			HMP	20	55
			AlTP	7	95
			AlMP	9	95

in high yield (90%–96%). Some phenols (Table 2) and tertiary alcohols (Table 1, entries u and v) undergo tosylation under the same experimental conditions. For aromatic alcohols, no rearranged or polymeric products were observed. In the case of diols, under the same reaction conditions, no tosylate product was detected in the reaction mixture and both hydroxyl groups remained intact in the presence of *p*-TsCl (Table 1, entries w–z).

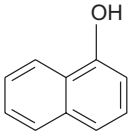
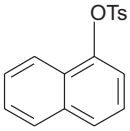
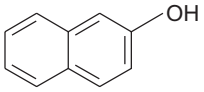
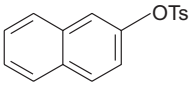
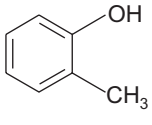
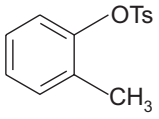
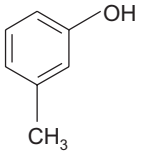
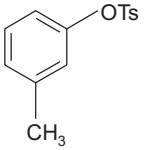
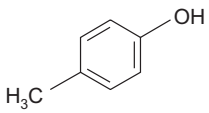
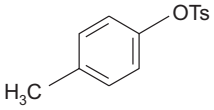
© 2006 NRC Canada

Table 1 (*concluded*).

Entry	Substrate	Product	Type of POM	Time (min)	Yield (%)[a,b,c]
v			HTP	40	60
			HMP	55	30
			AlTP	15	80
			AlMP	23	75
w		No product	HTP	120	0
			HMP	120	0
			AlTP	120	0
			AlMP	120	0
x		No product	HTP	120	0
			HMP	120	0
			AlTP	120	0
			AlMP	120	0
y		No product	HTP	120	0
			HMP	120	0
			AlTP	120	0
			AlMP	120	0
z		No product	HTP	120	0
			HMP	120	0
			AlTP	120	0
			AlMP	120	0

[a]Substrate (1 mmol), *p*-TsCl (1.2 mmol), and POM (3 mol%) were ground together in a mortar with a pestle at room temperature for the appropriate time to form the tosylates.
[b]Isolated yield.
[c]Identification of the products was ascertained by NMR, IR, and mass spectrometric analysis.

Table 2. Results of the tosylation of different phenols using some heteropolyacids (polyoxometalates).

Entry	Substrate	Product	Type of POM	Time (min)	Yield (%)[a,b,c]
a			HTP	20	50
			HMP	35	50
			AlTP	10	85
			AlMP	10	85
b			HTP	38	51
			HMP	40	44
			AlTP	5	90
			AlMP	8	85
c			HTP	25	50
			HMP	30	35
			AlTP	5	98
			AlMP	8	91
d			HTP	25	30
			HMP	25	30
			AlTP	8	95
			AlMP	9	91
e			HTP	22	50
			HMP	40	45
			AlTP	10	90
			AlMP	10	83

[a]Substrate (1 mmol), *p*-TsCl (1.2 mmol), and POM (3 mol%) were ground together in a mortar with a pestle at room temperature for the appropriate time to form the tosylates.
[b]Isolated yield.
[c]Identification of the products was ascertained by NMR, IR, and mass spectrometric analysis.

© 2006 NRC Canada

Scheme 2.

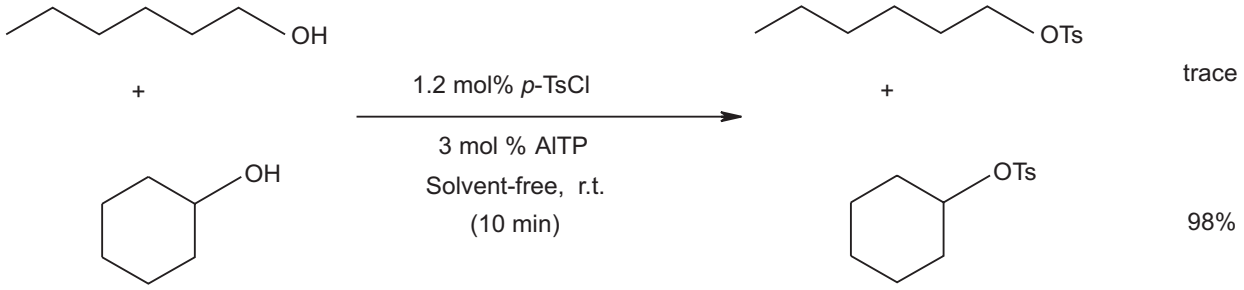
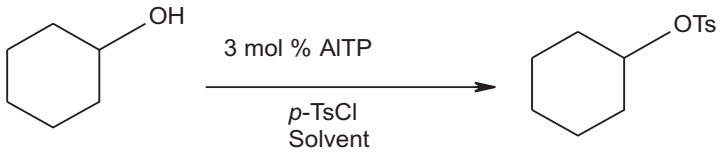


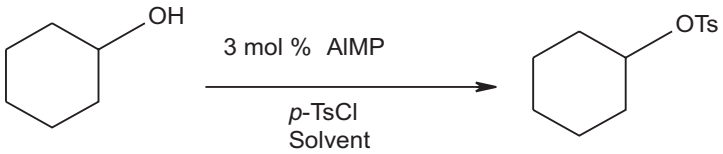
Table 3. Tosylation of cyclohexanol with *p*-TsCl in the presence of $AlPW_{12}O_{40}$ in various solvents.



Entry	Solvent	GC yield (%) after 6 min	GC yield (%) after 30 min
1	$CHCl_3$	20	50
2	CH_3CN	35	65
3	CH_2Cl_2	10	35
4	Acetone	25	50
5	EtOH	15	35

Note: Reaction conditions: cyclohexanol (1 mmol), *p*-TsCl (1.2 mmol), $AlPW_{12}O_{40}$ (3 mol%), and reflux.

Table 4. Tosylation of cyclohexanol with *p*-TsCl in the presence of $AlPMo_{12}O_{40}$ in various solvents.



Entry	Solvent	GC yield (%) after 9 min	GC yield (%) after 30 min
1	$CHCl_3$	20	30
2	CH_3CN	35	50
3	CH_2Cl_2	10	35
4	Acetone	15	35
5	EtOH	20	35

Note: Reaction conditions: cyclohexanol (1 mmol), *p*-TsCl (1.2 mmol), $AlPMo_{12}O_{40}$ (3 mol%), and reflux.

In the case of the aliphatic alcohols, secondary alcohols were tosylated much faster compared with primary hydroxyl groups (Table 1, entries k–t). Thus, a secondary alcohol can be tosylated chemoselectively in the presence of a primary alcohol, as previously reported in the case of $CoCl_2{\cdot}6H_2O$ (8) and silica chloride (9).

The difference in reaction rates between primary and secondary alcohols, which is observed in Table 1, prompted us to examine the chemoselective tosylation of alcohols. For example, when a mixture of *n*-hexanol and cyclohexanol was allowed to react with 0.5 equiv. *p*-TsCl in the presence of these catalysts for 10 min, cyclohexanol underwent tosylation chemoselectively in 98% yield and only a trace amount of *n*-hexyl tosylate was detected (Scheme 2). These studies clearly reveal that this methodology can be applied for the chemoselective direct tosylation of aliphatic secondary alcohols in the presence of primary hydroxyl groups.

Effect of solvent

The tosylation of cyclohexanol was also conducted in different solvents (chloroform, acetonitrile, dichloromethane, acetone, and ethanol). The results show that the yield of the reaction in solutions is much less than those observed under solvent-free conditions (Tables 3 and 4).

Effect of the catalyst

Amongst the catalysts used ($H_3PW_{12}O_{40}$, $H_3PMo_{12}O_{40}$, $AlPW_{12}O_{40}$, and $AlPMo_{12}O_{40}$) in the tosylation of alcohols

© 2006 NRC Canada

and phenols, it was found that both $AlPW_{12}O_{40}$ and $AlPMo_{12}O_{40}$ were effective catalysts for the tosylation of alcohols and phenols. The results showed that in the absence of the catalysts, the tosylation reaction did not proceed after 30 min at room temperature, but in the presence of two heteropolyacids ($AlPW_{12}O_{40}$ and $AlPMo_{12}O_{40}$), the conversion proceeded efficiently in a few minutes under similar reaction conditions (Tables 1 and 2). Therefore, we chose $AlPW_{12}O_{40}$ and $AlPMo_{12}O_{40}$ which are heterogeneous and environmentally benign compounds, as catalysts for further tosylation studies. Furthermore, the use of just 3 mol% POM is sufficient to promote the reaction and no other additives are required for this conversion. No improvements were observed in the reaction yields by increasing the amount of POM from 3 to 5 mol%.

Conclusions

In this study, we have introduced aluminum dodecatungstophosphate ($AlPW_{12}O_{40}$) and aluminium dodecamolybdophosphate ($AlPMo_{12}O_{40}$) as new, highly effective, nonhygroscopic, noncorrosive, heterogeneous, and environmentally benign catalysts for the efficient tosylation of a variety of alcohols and phenols in high yields. Phenols and primary, secondary, benzylic, and allylic alcohols gave tosylated products in good yields. In the case of aliphatic alcohols, secondary alcohols are transformed to the corresponding tosylates chemoselectively in the presence of the primaryhydroxy groups. The advantages of the present methods may be summarized as: high stereoselectivities, good yields of the desired products, short reaction times, mild and solvent-free conditions, and simple experimental procedure and product isolation. The only disadvantage of this system is the release of HCl as a by-product. We feel our protocol is an attractive alternative to the existing procedures for tosylation of alcohols and phenols.

Acknowledgment

We gratefully thank Isfahan University, Isfahan, Iran, for financial support.

References

1. T.W. Green and P.G.M. Wuts. Protective groups in organic synthesis. 3rd ed. Wiley, New York. 1999.
2. (*a*) R.A. Adlington, A.G.M. Barrett, P. Quayle, and A. Walker. J. Chem. Commun. 404 (1981); (*b*) S. Holand, and R. Epsztein. Synthesis, 706 (1977); (*c*) H. Kotsuki, T. Oshisi, and M. Inoue. Synlett, 255 (1988).
3. (*a*) K. Kurita. Chem. Ind. (London), 345 (1974); (*b*) G.W. Kabalka, M. Varma, R.S. Varma, P.C. Srivastava, and F.F. Knapp, Jr. J. Org. Chem. **51**, 2386 (1986); (*c*) Y. Yoshida, Y. Sakakura, N. Aso, S. Okada, and Y. Tanabe. Tetrahedron, **55**, 2183 (1999); (*d*) J. Hartung, S. Hunig, R. Kueuer, M. Schwarz, and H. Wenner, Synthesis, 1433 (1997).
4. (*a*) V.C. Sekera and C.S. Marvel. J. Am. Chem. Soc. **55**, 345 (1933); (*b*) R.S. Tipson. J. Org. Chem. **9**, 235 (1944).
5. (*a*) Y. Nitta and Y. Arakawa. Chem. Pharm. Bull. **33**, 1380 (1985); (*b*) R. Karaman, H. Leader, A. Goldblum, and E. Breuer. Chem. Ind. (London), 857 (1987); (*c*) D. Klamann, and P. Weyerstahl. Chem. Ber. **98**, 2070 (1965); (*d*) T. Mukaiyama and K. Hojo. Chem. Lett. 893 (1976).
6. (*a*) J.F. O'Connell and H.J. Rapoport. J. Org. Chem. **57**, 4775 (1992); (*b*) A.R. Katritzky, G. Zhang, and J. Wu. Synth. Commun. **24**, 205 (1994).
7. B.M. Choudary, N.S. Chowdari, and M.L. Kantam. Tetrahedron, **56**, 7291 (2000).
8. S. Velusamy, J.S.K. Kumar, and T. Punniyamurthy. Tetrahedron Lett. **45**, 203 (2004).
9. B. Das, V.S. Reddy, and R. Reddy. Tetrahedron Lett. **45**, 6717 (2004).
10. B. Das and V.S. Reddy. Chem. Lett. **33**, 11 (2004).
11. (*a*) J.G. Smith. Synthesis, 629 (1984); (*b*) R. Oi and K.B. Sharpless. Tetrahedron Lett. **33**, 2095 (1992).
12. I. Kozhevnikov. Catalysts for fine chemical synthesis. Catalysis by polyoxometalates. Vol. 2. Wiley, NewYork. 2002.
13. C.S.Turchi and D.F. Ollis. J. Catal. **122**, 178 (1990).
14. A. Mylonas and E. Papaconstantantinou. J. Mol. Catal. **92**, 261 (1994).
15. U. Stafford, K.A. Gray, and P.V. Kamat. J. Catal. **167**, 25 (1997).
16. C. Hu, B. Yue, and T. Yamase. Appl. Catal. A, **194**, 99 (2000).
17. T. Okuhara, H. Watanabe, T. Nishimura, K. Lnumaru, and M. Misono. Chem. Mater. **12**, 2230 (2000).
18. M. Misono. Chem. Commun. (Cambridge), **13**, 1141 (2001).
19. T. Okuhara. Chem. Rev. **102**, 3641 (2002).
20. H. Hayashi and J.B. Moffat. Talanta, **29**, 943 (1982).
21. (*a*) T. Baba, J. Sakai, and Y. Ono. Bull. Chem. Soc. Jpn. **55**, 2657 (1982); (*b*) T. Baba, H. Watanabe, and Y. Ono. J. Phys. Chem. **87**, 2406 (1983).
22. (*a*) H. Firouzabadi, N. Iranpoor, and K. Amani. Green Chem. **3**, 131 (2000); (*b*) H. Firouzabadi, N. Iranpoor, and K. Amani. Synthesis, 59 (2002); (*c*) H. Firouzabadi, N. Iranpoor, K. Amani, and F. Nowrouzi. J. Chem. Soc. Perkin Trans. 1, 2601 (2002); (*d*) H. Firouzabadi, N. Iranpoor, and K. Amani. Synthesis, 408 (2003).
23. H. Firouzabadi, N. Iranpoor, F. Nowrouzi, and K. Amani. Chem. Commun. (Cambridge), 764 (2003).
24. T.H. Chang. J. Chem. Soc. Faraday Trans. **91**, 375 (1995).

© 2006 NRC Canada

Microwave-assisted regioselective synthesis of acyclic nucleosides through an alkylating reaction with 2-oxa-1,4-butanediol diacetate

Guirong Qu, Suhui Han, Zhiguang Zhang, Mingwei Geng, and Feng Xue

Abstract: An efficient and green procedure for the synthesis of purine acyclic nucleosides through microwave-assisted alkylation of various purine nucleobases with 2-oxa-1,4-butanediol diacetate in the absence of solvent and catalyst is described. The advantages of using this method include its environmental friendliness, simple manipulation, short reaction time, high regioselectivity, and good yields.

Key words: acyclic nucleosides, microwave irradiation, regioselectivity, alkylation, 2-oxa-1,4-butanediol diacetate.

Résumé : On a mis au point une méthode efficace et verte pour la synthèse de nucléosides acyclique de l'acide qui fait appel à une alkylation à l'aide de micro-onde de nucléobases purines avec le diacétate du 2-oxa-1,4-butanediol en absence de solvant et de catalyseur. Les avantages de cette méthode reposent sur son caractère écologique, sa facilité de manipulation, sa faible durée de réaction, sur sa grande régiosélectivité et sur ses bons rendements.

Mots clés : nucléosides acycliques, irradiation micro-onde, régiosélectivité, alkylation, diacétate du 2-oxa-1,4-butanediol.

[Traduit par la Rédaction]

Introduction

In the past two decades, considerable efforts have been invested to develop an efficient treatment against human immunodeficiency virus (HIV) infection. The use of acyclic nucleosides as therapeutic agents, such as acyclovir (**1**), ganciclovir (**2**), and penciclovir (**3**) (Fig. 1), leads to promising results in the treatment of patients with devastating infections by viruses such as varicella zoster virus (VZV), human cytomegalovirus (HCMV), Epstein–Barr virus (EBV), and herpes viruses (1). While versatile methods for the synthesis of acyclic nucleosides have been developed (2), many of them suffer from harsh reaction conditions, the use of expensive alkylating reagents and catalysts, long reaction time, and low selectivity and yields. Thus, simple and efficient protocols for the synthesis of acyclic nucleosides with excellent bioactivities are still in demand.

As one of the most frequently used pathways to prepare purine acyclic nucleosides, the alkylating reaction involves the condensation of purine nucleobases with a haloalkyl ether, trimethylsilyalkyl ether, or polyfunctional open-chain riboside analogues having a reactive α-methylene group (3). This classical process is usually carried out by freezing a DMF solution of reactants at temperatures ranging from –78 to –50 °C in the presence of strong bases or Lewis acids to produce corresponding functionalized 9-(2-acetoxyethoxymethyl) derivatives of purines with moderate yields. Unfortunately, the obtained acyclic nucleosides often were N^9/N^7 isomeric mixtures that were difficult to separate (4). Subsequent studies showed the problems resulting from the classical alkylating procedures can be overcome either by heating the mixture of N^2,N^9-diacetylguanine and 2-oxa-1,4-butanediol diacetate at 105 °C for 80 h to generate the desired N^2-acetyl-9-(2-acetoxyethoxymethyl)guanine in high yield (5). However, these methods still have some drawbacks, notably requiring the use of an oil bath that can maintain the reaction mixture at 105 °C for 80 h, thus making these methods unsuitable for scale up in an environmentally benign and economical way.

Microwave irradiation as a nonconventional energy source has been a very popular and useful technique in organic chemistry (6). The combination of microwave irradiation and solvent-free reaction conditions leads to significantly reduced reaction time, enhanced conversions, and sometimes, higher selectivity, with several advantages for the eco-friendly approach, termed green chemistry. The synthesis of acyclic nucleosides accelerated by this technique is scarce (7). In line with our research program of using microwave irradiation to synthesize a series of nucleoside compounds (8), we wish to report here a facile and efficient procedure for the synthesis of 9-(2-acetoxyethoxymethyl) derivatives of purines through a solvent-free alkylating reaction of purine

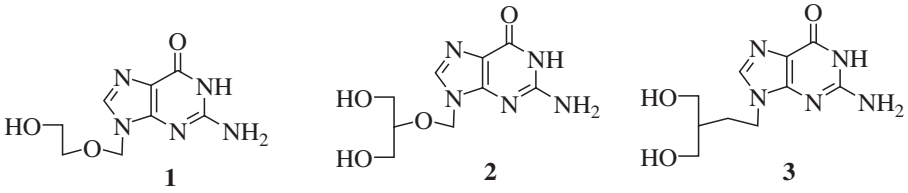
Received 31 October 2005. Published on the NRC Research Press Web site at http://canjchem.nrc.ca on 19 May 2006.

G. Qu,[1] S. Han, Z. Zhang, M. Geng, and F. Xue. College of Chemistry and Environmental Science, Key Laboratory of Environmental Science and Engineering for Colleges and Universities of Henan Province, Henan Normal University, Xinxiang 453007, Henan, P.R. China.

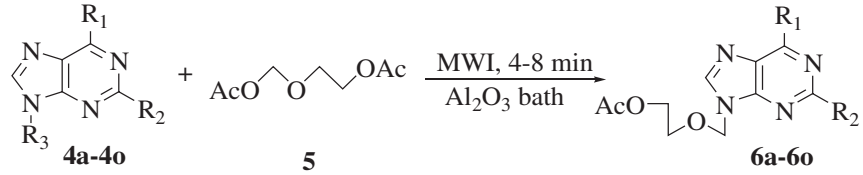
[1]Corresponding author (e-mail: quguir@163.com).

 doi:10.1139/V06-061 © 2006 NRC Canada

Fig. 1. Structures of acyclovir (**1**), ganciclovir (**2**), and penciclovir (**3**).



Scheme 1. Microwave-assisted regioselective synthesis of purine acyclic nucleosides **6a**–**6o**.



Scheme 2. Microwave-assisted synthesis of **6a** under solvent-free conditions.

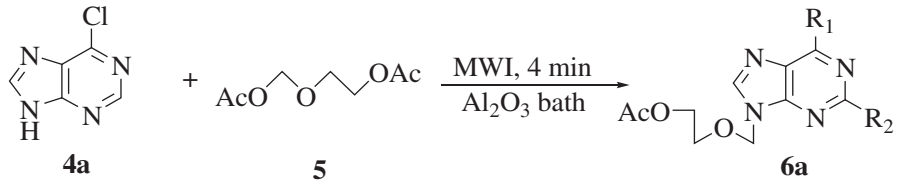


Table 1. Alkylating reaction of 6-chloropurine (**4a**) and 2-oxa-1,4-butanediol diacetate (**5**) in different conditions under microwave irradiation.

Entry	Equivalents of **5**	Catalyst	Microwave power (W)	Reaction time (min)	Yield (%)[a]
1	10	None	400	10	34
2[b]	3	None	400	5	31
3[c]	3	None	400	5	0
4[d]	3	None	400	4	93
5	3	PTSA	400	8	36
6	3	NP–$ZnBr_2$	400	8	12
7	3	K10 mont.	400	9	58
8	3	None	400	6	85
9	3	None	500	4	78
10	3	None	600	4	65
11[e]	3	None	400	4	52

[a]Isolated yields for **6a** purified by silica gel column chromatography ($CHCl_3$–CH_3OH, 95:5 *v*/*v*).
[b]Neutral alumina was used as the supporting agent.
[c]Silica gel was used as the supporting agent.
[d]Neutral alumina as the bath and silica gel as the supporting material were used. This condition is applied for entries 4–10.
[e]Silica gel as the bath and neutral alumina as the supporting material were used.

nucleobases with 2-oxa-1,4-butanediol diacetate in a neutral alumina bath using silica gel as the supporting material under microwave irradiation (Scheme 1).

Results and discussion

We set out to optimize the alkylating reaction conditions under microwave irradiation, using 6-chloropurine (Scheme 2, **4a**) and 2-oxa-1,4-butanediol diacetate (**5**) as the starting materials.

Firstly, the mixture of **4a** and **5** (10 equiv.) in a 25 mL round-bottomed flask was irradiated directly at 400 W for 10 min, two obvious new spots both showing higher R_f than **4a** on TLC. After purification by column chromatography, the compound with the higher R_f was proved to be the N^9 isomer by HMBC with 34% isolated yield, and the one with the lower R_f was the N^7 isomer with a similar yield, which showed the regioselectivity was very low (Table 1, entry 1). To reduce the ratio of the N^7 isomer, we shortened the equivalents of **5** to 3 and added an appropriate amount of neutral alumina as the supporting material to overcome the possible agglomeration because of the decrease of the fluid **5**. After being crushed vigorously with neutral alumina, the mixture was irradiated in a small beaker at 400 W for 5 min. To our delight, the desired N^9 isomer was predominant for the part facing the irradiation source, which was almost

© 2006 NRC Canada

Table 2. Regioselective synthesis of 9-(2-acetoxyethoxymethyl) derivatives of purines through microwave-assisted alkylation of various purine nucleobases with 2-oxa-1,4-butanediol diacetate (**5**).

Entry	R_1	R_2	R_3	Microwave power (W)	Reaction time (min)	Product	Yield (%)[a]
1	Cl	H	H	400	4	**6a**	93
2	Cl	Cl	H	300	6	**6b**	91
3	$NHCH_2C_6H_5$	H	H	600	4	**6c**	95
4	OH	AcNH	Ac	500	5	**6d**	48
5	OH	H	H	500	5	**6e**	53
6	NHC_6H_{11}	H	H	500	8	**6f**	82
7	NHC_6H_5	H	H	500	8	**6g**	85
8	$NHC_6H_4CH_3$-*p*	H	H	550	8	**6h**	80
9	$NHC_6H_4OCH_3$-*p*	H	H	500	8	**6i**	80
10	$NHC_6H_4OC_2H_5$-*p*	H	H	550	8	**6j**	79
11	NHC_6H_{11}	Cl	H	550	8	**6k**	81
12	NHC_6H_5	Cl	H	500	8	**6l**	83
13	$NHC_6H_4CH_3$-*p*	Cl	H	500	8	**6m**	78
14	$NHC_6H_4OCH_3$-*p*	Cl	H	500	8	**6n**	76
15	$NHC_6H_4CH_3$-*p*	NH_2	H	550	8	**6o**	62

[a]Isolated yields for **6a–6o** purified by silica gel column chromatography.

molted to yellow; the part opposite of the irradiation source remained white and no obvious reaction took place as indicated by TLC. The integrated yield of this method is low (Table 1, entry 2). Under the same conditions, no new spot was observed using silica gel instead of neutral alumina as the supporting material (Table 1, entry 3). Considering the different absorption capacities of neutral alumina and silica gel to microwave, we chose neutral alumina as the bath and silica gel as the supporting material. Fortunately, the expected product **6a** was obtained with high yield when the bath system was irradiated at 400 W for 4 min (Table 1, entry 4). Further studies showed that the yields could not be improved when *p*-toluenesulfonic acid (PTSA), $ZnBr_2$-doped natural phosphate (NP–$ZnBr_2$) (9), or K10 montmorillonite (K10 mont.) were used as catalysts (Table 1, entries 5–7), or when the microwave irradiation time and power were increased (Table 1, entries 8–10). So we chose 400 W and 4 min as irradiation conditions and no catalyst was used.

As for the possible mechanism of this reaction, we believe that the microwave energy was accumulated quickly by the alumina bath and dramatically accelerated the molecule activity of the mixture in a very short time and made the reaction easily occur at position 9 and not 7 because of the electronic origin (10–12).

Based on the above results, this process was then extended to other purine substrates to investigate its scope and generality (Table 2). It can be seen that under microwave irradiation, a wide range of purine nucleobases can be alkylated easily with **5** to give 9-(2-acetoxyethoxymethyl) purine analogs in a short time and with very high yields (Table 2, entries 1–3). When 6-substituted aminopurines (**4f–4n**) were used as the substrates, the desired N^9 products (**6f–6n**) can be obtained with good yields (Table 2, entries 6–14). In the structures of **4f–4n**, the unmatched electrons on the nitrogen atom can spread effectively to the aromatic ring, which decreased the possibility of an electron density increase at position 7. In addition, the use of silica gel acting as the supporting agent also eases the work-up manipulation, which can permit direct purification by silica gel column chromatography.

Table 3. A comparative synthesis of compounds **6a** and **6b** using the conventional protocol of Robins and Hatfield (2*b*) vs. the solvent-free, microwave-assisted method.

Product	Time (h)[a]	Yield (%)[a]	Time (min)[b]	Yield (%)[b]
6a	6	81	4	93
6b	6	87	4	91

[a]Conventional protocol of Robins and Hatfield (2*b*).
[b]Solvent-free, microwave-assisted method.

To demonstrate the advantage of our method, we synthesized compounds **6a** and **6b** following the conventional protocol of Robins and Hatfield (2*b*) and compared the results with the microwave irradiation method (Table 3). As Table 3 indicates, an acceleration of the reaction rate on the order of a 90-fold increase is observed when the microwave was used. Higher yields of **6a** and **6b** were reached at 4–6 min with microwave heating than those obtained at 6 h using the classical method.

In conclusion, the solvent-free, microwave-assisted alkylating reaction was proved to be a useful and facile protocol to synthesize a series of 9-(2-acetoxyethoxymethyl) derivatives of purines with high regioselectivity. The system of alumina as bath and silica gel as supporting agent was found to be efficient for the quick absorption of microwave energy and for the dramatic and homogeneous acceleration of the reactions. The simple experimental and product isolation procedures are expected to contribute to the development of greener and waste-free chemical processes for the preparation of other acyclic nucleosides. Further studies to develop other new uses for microwave irradiation in the synthesis of nucleoside compounds are now in progress in our laboratory.

© 2006 NRC Canada

Experimental

Melting points were determined with an XRC-1 micro melting point apparatus and are uncorrected. ^{1}H and ^{13}C NMR spectra were recorded in $CDCl_3$ and DMSO-d_6 solutions on a Bruker DPX-400 spectrometer (at 400 and 100 MHz, respectively) using TMS as internal standard. Chemical shifts (δ) are expressed in ppm and coupling constants (*J*) are given in Hz. IR spectra were recorded for KBr tablets on a Bruker Vector 22 spectrometer with absorptions expressed in cm^{-1}. Mass spectra (ESI) were recorded on an Agilent 1100 (LC–MSD-Tarp-SL) mass spectrometer. Elemental analyses were performed on an EA-1110 (CE Instruments) instrument.

The starting substrates **4a**–**4e** and **5** were achieved from Xinxiang Tuoxin Biochemical Technology and Science Co. Ltd, P.R. China. **4f**–**4o** were synthesized by the amination of **4a**, **4b**, and 2-amino-6-chloropurine with the corresponding amines (our unpublished work). All reagents were reagent grade and used without any further purification. The progress of reaction was followed by TLC analysis using silica gel plates (Merck, silica gel 60F$_{254}$). Column chromatography was performed on silica gel (Merck, 200–300 mesh). All the reactions were carried out in a SANYO EM-202MSI microwave oven.

General procedure for the synthesis of 9-[(2-acetoxyethoxy)methyl]-6-chloropurine (6a)

In a mortar, a mixture of 6-chloropurine **4a** (0.308 g, 2 mmol) and 2-oxa-1,4-butanediol diacetate (**5**) (0.94 mL, 6 mmol) was crushed vigorously to give a homogeneous mass, an appropriate amount of silica gel (Merck, 200–300 mesh) was added as supporting agent and mixed carefully with a small spatula to give a fluent mixture. Subsequently, the mixture was transferred to a small beaker (5 mL), which was placed in an alumina bath (60 g neutral alumina (>70 mesh) was placed in a big beaker (100 mL)). The system was irradiated at 400 W for 4 min at several time intervals. At each irradiation time interval (1 min), the microwave was stopped and then the reaction mixture was stirred with a small spatula to homogenize the reaction mixture. After the reaction was completed (monitored by TLC), the reaction mixture was purified directly by silica gel column chromatography ($CHCl_3$–CH_3OH, 95:5 *v*/*v*) to give **6a** (0.503 g, 93% yield). Compounds **6b**–**6o** were synthesized from the corresponding starting materials **4b**–**4o** under similar procedure. The spectra data of **6a**–**6e** were identified by using the available literature (2*b*, 3*d*, 13, 14). The melting point of **6e** was not available and compounds **6f**–**6o** were unknown. All new compounds were fully characterized by IR, ^{1}H NMR, ^{13}C NMR, MS, and elemental analysis.

9-[(2-Acetoxyethoxy)methyl]hypoxanthine (6e)

Melting point 170–172 °C. ^{1}H NMR (400 MHz, DMSO-d_6) δ: 1.94 (s, 3H, CH_3CO), 3.70 (t, *J* = 4.4 Hz, 2H, $AcOCH_2CH_2$), 4.07 (t, *J* = 4.4 Hz, 2H, $AcOCH_2CH_2$), 5.56 (s, 2H, NCH_2O), 8.08 (s, 1H, H-2), 8.23 (s, 1H, H-8).

9-[(2-Acetoxyethoxy)methyl]-6-cyclohexylaminopurine (6f)

Melting point 118–120 °C. IR *v* (cm^{-1}): 3218, 2935, 1744, 1598, 1243, 1048, 761. ^{1}H NMR (400 MHz, DMSO-d_6) δ: 1.12–1.90 (m, 10H, H cyclohexyl), 1.94 (s, 3H, $COCH_3$), 3.71 (t, 2H, *J* = 4.8 Hz, OCH_2CH_2OAc), 4.08 (t, 2H, *J* = 4.8 Hz, OCH_2CH_2OAc), 4.13 (br, 1H, H cyclohexyl), 5.57 (s, 2H, NCH_2O), 7.56 (d, 1H, *J* = 8.0 Hz, NH), 8.23 (s, 1H, H-2), 8.27 (s, 1H, H-8). ^{13}C NMR (100 MHz, DMSO-d_6) δ: 20.95 ($COCH_3$), 25.43, 25.68, 32.78, 49.12 (C cyclohexyl), 63.21 (OCH_2CH_2OAc), 67.34 (OCH_2CH_2OAc), 72.42 (NCH_2O), 119.09 (5-C), 141.18 (8-C), 149.56 (4-C), 153.37 (2-C), 154.28 (6-C), 170.64 ($COCH_3$). MS (ESI) *m*/*z* + Na$^+$ – 1: 355.8, 333.8, 247.9, 229.9, 217.8, 165.9, 147.7. Anal. calcd. for $C_{16}H_{23}N_5O_3$ (%): C 57.64, H 6.95, N 21.01; found: C 57.53, H 6.99, N 21.12.

9-[(2-Acetoxyethoxy)methyl]-6-phenylaminopurine (6g)

Melting point 84 to 85 °C. IR *v* (cm^{-1}): 3354, 1727, 1627, 1582, 1500, 1050, 759. ^{1}H NMR (400 MHz, DMSO-d_6) δ: 1.95 (s, 3H, CH_3CO), 3.76 (t, *J* = 4.8 Hz, 2H, $AcOCH_2CH_2$), 4.10 (t, *J* = 4.8 Hz, 2H, $AcOCH_2CH_2$), 5.66 (s, 2H, NCH_2O), 7.05 (t, 1H, *J* = 7.2 Hz, H_{Ar}), 7.34 (t, 2H, *J* = 8.0 Hz, H_{Ar}), 7.96 (d, 2H, *J* = 8.0 Hz, H_{Ar}), 8.45 (s, 1H, H-2), 8.48(s, 1H, H-8). ^{13}C NMR (100 MHz, DMSO-d_6) δ: 20.97 ($COCH_3$), 63.21 ($AcOCH_2CH_2O$), 67.49 ($AcOCH_2CH_2O$), 72.65 (NCH_2O), 120.04 (5-C), 121.31, 123.10, 128.82, 140.04 (C_{Ar}), 142.52 (8-C), 150.38 (6-C), 152.54 (4-C), 152.85 (2-C), 170.65 ($COCH_3$). MS (ESI) *m*/*z* + Na$^+$ – 1: 349.8, 327.6. Anal. calcd. for $C_{16}H_{17}N_5O_3$ (%): C 58.71, H 5.23, N 21.39; found: C 58.62, H 5.28, N 21.47.

9-[(2-Acetoxyethoxy)methyl]-6-(*p*-tolylamino)purine (6h)

Melting point 69–71 °C. IR *v* (cm^{-1}): 3321, 1726, 1642, 1585, 1237, 1054, 766. ^{1}H NMR (400 MHz, DMSO-d_6) δ: 1.94 (s, 3H, CH_3CO), 2.28 (s, 3H, CH_3C_{Ar}), 3.75 (t, *J* = 4.8 Hz, 2H, $AcOCH_2CH_2$), 4.09 (t, *J* = 4.8 Hz, 2H, $AcOCH_2CH_2$), 5.65 (s, 2H, NCH_2O), 7.14 (d, 2H, *J* = 8.4 Hz, H_{Ar}), 7.81 (d, 2H, *J* = 8.4 Hz, H_{Ar}), 8.42 (s, 1H, H-2), 8.45 (s, 1H, H-8), 9.82 (s, 1H, NH). ^{13}C NMR (100 MHz, DMSO-d_6) δ: 20.96 ($COCH_3$), 26.68 (CH_3C_{Ar}), 63.21 ($AcOCH_2CH_2O$), 67.47 ($AcOCH_2CH_2O$), 72.63 (NCH_2O), 119.93 (5-C), 121.43, 129.23, 132.08, 137.45 (C_{Ar}), 142.34 (8-C), 150.26 (6-C), 152.60 (4-C), 152.90 (2-C), 170.65 ($COCH_3$). MS (ESI) *m*/*z* + Na$^+$ – 1: 363.8, 300.0, 281.8, 251.8, 125.3. Anal. calcd. for $C_{17}H_{19}N_5O_3$ (%): C 59.81, H 5.61, N 20.52; found: C 59.64, H 5.67, N 20.65.

9-[(2-Acetoxyethoxy)methyl]-6-(*p*-methoxyphenylamino)purine (6i)

Colorless oil. ^{1}H NMR (400 MHz, DMSO-d_6) δ: 1.95 (s, 3H, CH_3CO), 3.75 (s, 3H, CH_3O), 3.75 (t, *J* = 4.8 Hz, 2H, $AcOCH_2CH_2$), 4.10 (t, *J* = 4.8 Hz, 2H, $AcOCH_2CH_2$), 5.64 (s, 2H, NCH_2O), 6.93 (d, 2H, *J* = 9.2 Hz, H_{Ar}), 7.80 (d, 2H, *J* = 9.2 Hz, H_{Ar}), 8.38(s, 1H, H-2), 8.43(s, 1H, H-8), 9.77 (s, 1H, NH). ^{13}C NMR (100 MHz, DMSO-d_6) δ: 20.94 ($COCH_3$), 55.62 (CH_3O), 63.21 ($AcOCH_2CH_2O$), 67.46 ($AcOCH_2CH_2O$), 72.61 (NCH_2O), 119.76 (5-C), 114.04, 123.21, 132.95 (C_{Ar}), 142.16 (8-C), 150.16 (6-C), 152.96 (4-C), 155.62 (2-C), 170.66 ($COCH_3$). MS (ESI) *m*/*z* + Na$^+$ – 1: 377.0, 357.8, 241.7, 226.7, 198.7, 113.6. Anal. calcd. for $C_{17}H_{19}N_5O_4$ (%): C 57.14, H 5.36, N 19.60; found: C 57.04, H 5.42, N 19.68.

© 2006 NRC Canada

9-[(2-Acetoxyethoxy)methyl]-6-(p-ethoxyphenylamino)-purine (6j)

Melting point 117–119 °C. IR ν (cm^{-1}): 3415, 1739, 1619, 1512, 1232, 1043, 760. ^1H NMR (400 MHz, DMSO-d_6) δ: 1.94 (s, 3H, CH_3CO), 2.28 (s, 3H, CH_3C_{Ar}), 3.75 (t, J = 4.8 Hz, 2H, $AcOCH_2CH_2$), 4.09 (t, J = 4.8 Hz, 2H, $AcOCH_2CH_2$), 5.65 (s, 2H, NCH_2O), 7.14 (d, 2H, J = 8.4 Hz, H_{Ar}), 7.81 (d, 2H, J = 8.4 Hz, H_{Ar}), 8.42 (s, 1H, H-2), 8.45 (s, 1H, H-8), 9.82 (s, 1H, NH). ^{13}C NMR (100 MHz, DMSO-d_6) δ: 15.16 (OCH_2CH_3), 20.97 ($COCH_3$), 63.21 ($AcOCH_2CH_2O$), 63.56 (OCH_2CH_3), 67.46 ($AcOCH_2CH_2O$), 72.60 (NCH_2O), 119.75 (5-C), 114.60, 123.16, 132.87 (C_{Ar}), 142.18 (8-C), 150.15 (6-C), 152.96 (4-C), 154.85 (2-C), 170.65 ($COCH_3$). MS (ESI) m/z + Na^+ – 1: 393.8, 371.8, 255.8, 227.8, 198.8, 158.8, 119.7. Anal. calcd. for $C_{18}H_{21}N_5O_4$ (%): C 58.21, H 5.70, N 18.86; found: C 58.07, H 5.79, N 18.95.

9-[(2-Acetoxyethoxy)methyl]-2-chloro-6-cyclohexylamino-purine (6k)

Colorless oil. ^1H NMR (400 MHz, DMSO-d_6) δ: 1.11–1.86 (m, 10H, H cyclohexyl), 1.94 (s, 3H, $COCH_3$), 3.69 (t, 2H, J = 4.8 Hz, OCH_2CH_2OAc), 4.01 (br, 1H, H cyclohexyl), 4.08 (t, 2H, J = 4.8 Hz, OCH_2CH_2OAc), 5.53 (s, 2H, NCH_2O), 8.17 (d, 1H, J = 8.0 Hz, NH), 8.31 (s, 1H, H-8). ^{13}C NMR (100 MHz, DMSO-d_6) δ: 20.95 ($COCH_3$), 25.14, 25.36, 25.56, 32.46, 33.48, 49.45 (C cyclohexyl), 63.19 (OCH_2CH_2OAc), 67.30 (OCH_2CH_2OAc), 72.68 (NCH_2O), 118.33 (5-C), 141.73 (8-C), 150.41 (4-C), 154.13 (2-C), 154.69 (6-C), 170.62 ($COCH_3$). MS (ESI) m/z + Na^+ – 1: 389.8, 307.8, 271.7, 212.8. Anal. calcd. for $C_{16}H_{22}ClN_5O_3$ (%): C 52.24, H 6.03, N 19.04; found: C 52.10, H 6.11, N 19.12.

9-[(2-Acetoxyethoxy)methyl]-2-chloro-6-phenylamino-purine (6l)

Melting point 102–104 °C. ^1H NMR (400 MHz, DMSO-d_6) δ: 1.96 (s, 3H, CH_3CO), 3.74 (t, J = 4.8 Hz, 2H, $AcOCH_2CH_2$), 4.10 (t, J = 4.8 Hz, 2H, $AcOCH_2CH_2$), 5.61 (s, 2H, NCH_2O), 7.11 (t, 1H, J = 8.0 Hz, H_{Ar}), 7.38 (t, 2H, J = 8.0 Hz, H_{Ar}), 7.84 (d, 2H, J = 8.0 Hz, H_{Ar}), 8.48 (s, 1H, H-8). ^{13}C NMR (100 MHz, DMSO-d_6) δ: 20.98 ($COCH_3$), 63.19 ($AcOCH_2CH_2O$), 67.44 ($AcOCH_2CH_2O$), 72.90 (NCH_2O), 119.19 (5-C), 121.82, 124.05, 128.98, 139.13 (C_{Ar}), 143.03 (8-C), 151.42 (6-C), 152.96 (4-C), 153.28 (2-C), 170.64 ($COCH_3$). MS (ESI) m/z + Na^+ – 1: 383.7, 361.9, 300.0, 245.7, 145.9, 86.0. Anal. calcd. for $C_{16}H_{16}ClN_5O_3$ (%): C 53.12, H 4.46, N 19.36; found: C 53.02, H 4.52, N 19.43.

9-[(2-Acetoxyethoxy)methyl]-2-chloro-6-(p-tolylamino)-purine (6m)

Yellow oil. ^1H NMR (400 MHz, DMSO-d_6) δ: 1.96 (s, 3H, CH_3CO), 2.30 (s, 3H, CH_3C_{Ar}), 3.74 (t, J = 4.8 Hz, 2H, $AcOCH_2CH_2$), 4.10 (t, J = 4.8 Hz, 2H, $AcOCH_2CH_2$), 5.60 (s, 2H, NCH_2O), 7.17 (d, 2H, J = 8.4 Hz, H_{Ar}), 7.69 (d, 2H, J = 8.4 Hz, H_{Ar}), 8.45(s, 1H, H-8), 10.26 (s, 1H, NH). ^{13}C NMR (100 MHz, DMSO-d_6) δ: 20.94 ($COCH_3$), 25.21 (CH_3C_{Ar}), 63.59 ($AcOCH_2CH_2O$), 67.97 ($AcOCH_2CH_2O$), 72.86 (NCH_2O), 119.07 (5-C), 121.97, 129.37, 133.18, 136.50 (C_{Ar}), 142.82 (8-C), 151.31 (6-C), 153.02 (4-C), 153.36 (2-C), 170.74 ($COCH_3$). MS (ESI) m/z + Na^+ + 1: 400.6, 242.8, 156.7, 103.0. Anal. calcd. for $C_{17}H_{18}ClN_5O_3$ (%): C 54.33, H 4.83, N 18.64; found: C 54.13, H 4.89, N 18.82.

9-[(2-Acetoxyethoxy)methyl]-2-chloro-6-(p-methoxy-phenylamino)purine (6n)

Melting point 140–142 °C. IR ν (cm^{-1}): 3375, 1720, 1627, 1510, 1257, 1045. ^1H NMR (400 MHz, DMSO-d_6) δ: 1.95 (s, 3H, CH_3CO), 3.76 (s, 3H, CH_3O), 3.74 (t, J = 4.8 Hz, 2H, $AcOCH_2CH_2$), 4.10 (t, J = 4.8 Hz, 2H, $AcOCH_2CH_2$), 5.59 (s, 2H, NCH_2O), 6.95 (d, 2H, J = 8.8 Hz, H_{Ar}), 7.69 (d, 2H, J = 8.8 Hz, H_{Ar}), 8.43 (s, 1H, H-8), 10.21 (s, 1H, NH). ^{13}C NMR (100 MHz, DMSO-d_6) δ: 20.95 ($COCH_3$), 55.66 (CH_3O), 63.19 ($AcOCH_2CH_2O$), 67.40 ($AcOCH_2CH_2O$), 72.84 (NCH_2O), 118.92 (5-C), 114.18, 123.70, 131.95 (C_{Ar}), 142.66 (8-C), 151.18 (6-C), 153.10 (4-C), 156.24 (2-C), 170.64 ($COCH_3$). MS (ESI) m/z + Na^+ – 1: 413.8, 391.7. Anal. calcd. for $C_{17}H_{18}ClN_5O_4$ (%): C 52.11, H 4.63, N 17.87; found: C 51.99, H 4.72, N 17.94.

9-[(2-Acetoxyethoxy)methyl]-2-amino-6-(p-tolylamino)-purine (6o)

Melting point 76–78 °C. IR ν (cm^{-1}): 3327, 1733, 1624, 1598, 1513, 1243, 1051, 765. ^1H NMR (400 MHz, DMSO-d_6) δ: 1.94 (s, 3H, CH_3CO), 2.28 (s, 3H, CH_3C_{Ar}), 3.76 (t, J = 4.8 Hz, 2H, $AcOCH_2CH_2$), 4.10 (t, J = 4.8 Hz, 2H, $AcOCH_2CH_2$), 5.56 (s, 2H, NCH_2O), 7.10 (d, 2H, J = 8.4 Hz, H_{Ar}), 8.04 (d, 2H, J = 8.4 Hz, H_{Ar}), 8.31 (s, 1H, H-8), 9.78 (s, 1H, NH). ^{13}C NMR (100 MHz, DMSO-d_6) δ: 20.91 ($COCH_3$), 25.12 (CH_3C_{Ar}), 63.21 ($AcOCH_2CH_2O$), 67.40 ($AcOCH_2CH_2O$), 72.52 (NCH_2O), 116.75 (5-C), 121.06, 129.21, 131.68, 137.59 (C_{Ar}), 141.42 (8-C), 151.00 (6-C), 152.32 (4-C), 153.18 (2-C), 170.67 ($COCH_3$). MS (ESI) m/z + Na^+ – 1: 378.8, 330.6, 204.7, 262.8. Anal. calcd. for $C_{17}H_{20}N_6O_3$ (%): C 57.29, H 5.66, N 23.58; found: C 57.18, H 5.72, N 23.66.

Acknowledgment

We thank the National Natural Science Foundation of China (Grant No. 20372018) for financial support.

References

1. (*a*) R. Dalpozzo, A. De Nino, L. Maiuolo, A. Procopio, G. De Munno, and S. Giovanni. Tetrahedron, **57**, 4035 (2001); (*b*) R. Kumar, N. Sharma, M. Nath, H.A. Saffran, and D.L.J. Tyrrell. J. Med. Chem. **44**, 4225 (2001); (*c*) R. Kumar, M. Nath, and D.L.J. Tyrrell. J. Med. Chem. **45**, 2032 (2002); (*d*) G.Y. Minuk, G.B. German, C. Bernstein, A. Benarroch, T. Gauthiar, and L. Sekla. Clin. Invest. Med. **15**, 506 (1992); (*e*) H.J. Schaeffer, L. Beauchamp, P. de Miranda, G.B. Elion, D.J. Bauer, and P. Collins. Nature (London), **272**, 583 (1978); (*f*) K.K. Oglive, U.O. Cheriyan, B.K. Radatus, K.O. Smith, K.S. Galloway, and W.L. Kennell. Can. J. Chem. **60**, 3005 (1982); (*g*) W.T. Ashton, L.F. Caning, G.F. Reynolds, R.L. Tolman, J.D. Karkas, R. Liou, M.E. Davies, C.M. DeWitt, H.C. Perry, and A.K. Field. J. Med. Chem. **28**, 926 (1985).
2. (*a*) H.J. Schaeffer, S. Gurwara, R. Vince, and S. Bittner. J. Med. Chem. **14**, 367 (1971); (*b*) M.J. Robins and P.W. Hatfield. Can. J. Chem. **60**, 547 (1982); (*c*) D.R. Haines, C.K.H. Tseng, and V.E. Marquez. J. Med. Chem. **30**, 943 (1987);

© 2006 NRC Canada

(*d*) G. Stéphane, L. Stéphane, A. Anne-Marie, O. Cécile, B. Nathalie, and H. François. Tetrahedron, **59**, 2177 (2003); (*e*) H.-W. Gao and A.K. Mitra. Synth. Commun. **31**, 1399 (2001).
3. (*a*) G.E. Keyser, J.D. Bryant, and J.R. Barrio. Tetrahedron Lett. **20**, 3263 (1979); (*b*) D.L. Anton, B.D. Korant, and C.L.J. Wang. US Patent 4 803 272, 1989; Chem. Abstr. **111**, 97692 (1989); (*c*) J.R. Barrio, J.D. Bryant, and G.E. Keyser. J. Med. Chem. **23**, 572 (1980); (*d*) M.L. Taha and H.B. Lazrek. Bull. Soc. Chim. Belg. **104**, 591 (1995).
4. (*a*) G.H. Hakimelahi, T.W. Ly, A.A. Moosavi-Movahedi, M.L. Jain, M. Zakerinia, H. Davari, H.-C. Mei, T.Sambaiah, A.A. Moshfegh, and S. Hakimelahi. J. Med. Chem. **44**, 3710 (2001); (*b*) J. Boryski and A. Manikowski. Nucleosides Nucleotides, **14**, 287 (1995); (*c*) H. Matsumoto, C. Kaneko, K. Yamada, T. Takeuchi, T. Mori, and Y. Mizuno. Chem. Pharm. Bull. **36**, 1153 (1988).
5. D. Singh, M.J. Wani, and A. Kumar. J. Org. Chem. **64**, 4665 (1999).
6. (*a*) A. Khalafi-Nezhad, M.N. Soltani Rad, and G.H. Hakimelahi. Helv. Chim. Acta, **86**, 2396 (2003); (*b*) C.O. Kappe. Angew. Chem. Int. Ed. **43**, 6250 (2004); (*c*) R.S. Varma. Green Chem. **1**, 43 (1999).
7. A. Khalafi-Nezhad, M.N. Soltani Rad, and A. Khoshood. Synthesis, **4**, 583 (2004).
8. (*a*) G.-R. Qu, Y. Li, and H.-S. Han. J. Chem. Res. 167 (2005); (*b*) G.-R. Qu and Q.-B. Liu. Indian. J. Chem. B, **44**, 196 (2005).
9. A. Alahiane, A. Rochdi, M. Taourirte, N. Redwane, S. Sebti, and H.B. Lazrek. Tetrahedron Lett. **42**, 3579 (2001).
10. A.A. Gevorkyan, A.S. Arakelyan, and K.A. Petrosyan. Russ. J. Gen. Chem. **72**, 767 (2002).
11. A.A. Gevorkyan, A.S. Arakelyan, K.A. Petrosyan, and A.Kh. Margaryan. Russ. J. Gen. Chem. **71**, 729 (2001).
12. A.A. Gevorkyan, A.S. Arakelyan, Zh.L. Dzhandzhulyan, A.R. Mikaelyan, K.A. Petrosyan, and G.A. Panosyan. Russ. J. Org. Chem. **41**, 134 (2005).
13. H. Matsumoto, C. Kaneko, K. Yamada, T. Takeuchi, T. Mori, and Y. Mizuno. Chem. Pharm. Bull. **36**, 1153 (1988).
14. M.J. Robins, P.W. Hatfield, J. Balzarini, and E. De Clercq. J. Med. Chem. **27**, 1486 (1984).

© 2006 NRC Canada

Organosulfur oxoacids. Part 1. Synthesis, structure, and reactivity of dimethylaminoiminomethanesulfinic acid (DMAIMSA)

Jonathan F. Ojo, Jeffrey L. Petersen, Adenike Otoikhian, and Reuben H. Simoyi

Abstract: One of the major metabolites of dimethylthiourea, dimethylaminoiminomethanesulfinic acid (DMAIMSA), was synthesized by controlled oxidation of dimethylthiourea using hydrogen peroxide. The crystal structure was determined by X-ray crystallography. It is a zwitterionic species in its solid form, with a positive charge delocalized around an sp^2-hybridized carbon center and two nitrogen atoms. It crystallizes in the triclinic $P\bar{1}$ space group. The C—S bond, at 1.880(2) Å, is much longer than a typical C—S single bond length of 1.79 Å. It is also longer than the one observed in thiourea trioxide, a comparable sulfonic acid. This C—S bond is stable in acidic conditions and is easily cleaved in basic conditions or in the presence of suitable nucleophiles that can attack the positively disposed carbon center. DMAIMSA is highly reactive and easily decomposes in basic conditions to yield dithionite in the presence of oxygen, whereas in strictly anaerobic conditions it gives a mixture of sulfite and sulfide. The precursor to dithionite, $SO_2^{\cdot-}$, is formed from the one-electron oxidation of the sulfoxylate anion, SO_2^{2-}, which results from an initial heterolytic cleavage of the C—S bond in DMAIMSA. The sulfur center is oxidized, even by mild oxidants such as aqueous iodine, to sulfate.

Key words: thiourea metabolites, synthesis, structure, reactivity.

Résumé : On a réalisé la synthèse de l'acide diméthylaminoiminométhanesulfinique (ADMAIMS), un des métabolites principaux de la diméthylthiourée, en procédant à l'oxydation contrôlée de la diméthylthiourée à l'aide de peroxyde d'hydrogène. On en a déterminé la structure cristalline par diffraction des rayons X. Dans sa forme solide, il s'agit d'une espèce zwitterionique comportant une charge positive délocalisée autour d'un atome de carbone à hybridisation sp^2 et de deux atomes d'azote. Cet acide cristallise dans le groupe d'espace triclinique $P\bar{1}$. La longueur de la liaison C—S, à 1,880(2) Å, est beaucoup plus longue qu'une liaison C—S simple de longueur typique 1,79 Å. Elle est aussi beaucoup plus longue que celle observée dans le trioxyde de thiourée, un acide sulfonique comparable. Cette liaison C—S est stable dans des conditions acides et elle peut facilement être clivée dans des conditions basiques ou en présence de nucléophiles appropriés qui peuvent attaquer le centre carboné à disposition positive. L'ADMAIMS est fortement réactif et se décompose facilement dans des conditions basiques pour fournir du dithionite en présence d'oxygène alors que, dans des conditions strictement aérobiques, il conduit à la formation du sulfite et du sulfure. Le précurseur dans la formation du dithionite, le $SO_2^{\cdot-}$, se forme à partir d'une oxydation impliquant un électron qui conduit à l'anion sulfoxylate, SO_2^{2-}, qui résulte d'un clivage hétérolytique initial de la liaison C—S de l'acide ADMAIMS. Le centre sulfuré est oxydé en sulfate sous l'influence d'oxydants, même doux, tel que l'iode aqueux.

Mots clés : métabolites de la thiourée, synthèse, structure, réactivité.

[Traduit par la Rédaction]

Introduction

N,*N*′-Dimethylthiourea (DMTU), a thiocarbamide, is a small diffusive molecule that efficiently scavenges toxic oxygen metabolites in vitro and reduces oxidative injury in many biological systems (1). DMTU is one of the most efficient scavengers known for hydrogen peroxide, hydroxyl radical, and hypochlorous acid (2). In this respect, DMTU should act as a powerful antioxidant in vivo. The known effects of DMTU on human health, however, have been contradictory (3). For example, the DMTU treatment resulted in decreases in blood glutathione (GSH) levels in humans (4). GSH can limit damage caused by toxic oxygen metabolites, and the loss of GSH might partially offset some of the

Received 20 June 2005. Published on the NRC Research Press Web site at http://canjchem.nrc.ca on 19 May 2006.

J.F. Ojo. Department of Chemistry, Obafemi Awolowo University, Ile-Ife, Osun State, Nigeria.
J.L. Petersen. C. Eugene Bennett Department of Chemistry, West Virginia University, Morgantown, WV 26506-6045, USA.
A. Otoikhian and R.H. Simoyi.[1] Department of Chemistry, Portland State University, Portland, OR 97207-0751, USA.

[1]Corresponding author (e-mail: rsimoyi@pdx.edu).

 doi:10.1139/V06-023 © 2006 NRC Canada

oxygen-metabolite-scavenging benefits of DMTU. Ultimately, the occurrence of increased stomach size, lethargy, and other behavioral changes in rats provides support to the premise that DMTU is toxic (4). This formally unrecognized toxicity of DMTU provides a possible explanation for the apparently conflicting reports regarding the efficacy of DMTU in cytoprotectivity.

Closely related thiocarbamides cause severe pulmonary edema and large pleural effusions that appear to reflect highly specific damage to the pulmonary capillary endothelium (5, 6). This creates a seemingly intractable problem: while lung injury from thioureas can be reduced by OH scavengers like DMTU, this therapy brings its own toxicity. A pertinent question is whether DMTU toxicity is mediated by intact DMTU molecules or by metabolic products of DMTU. The answer lies in a mechanistic evaluation of the metabolic pathways of ingested organosulfur compounds. The nucleophilic nature of the sulfur center and its low oxidation state of –2 would suggest that the pathway to metabolic activation of nearly all organosulfur atoms is oxidative (7). The use of labeled sulfur atoms in phenylthiourea fed to rats showed that all the sulfur atoms in phenylthiourea ended up as sulfate in the urine. Several studies, including ours, have suggested that the active forms of organosulfur compounds in the physiological environment must be the reactive sulfur oxoacids generated in the S-oxidation of thiocarbamides, such as thiourea and thioacetamide (8).

While these oxoacids have been postulated, few have been isolated and studied to examine their possible role in the physiological environment. Not much is known about the structure and reactivities of these possible metabolic intermediates. One major reason for this lack of knowledge is the instability of the first metabolite that is formed in the stepwise oxidation of thiocarbamides: the sulfenic acid (9). Very few sulfenic acids have been isolated as free acids, and those that have been isolated, such as 1-anthraquinonesulfenic acid, are stabilized by extensive hydrogen bonding and steric hindrance (10).

We report on the synthesis, characterization, and structure of the sulfinic acid of DMTU, dimethylaminoiminomethanesulfinic acid (DMAIMSA). The isolation of the intermediate of a bioactive thiocarbamide is essential in deriving a possible mechanism for the observed physiological effects of this thiocarbamide.

Experimental

DMTU, hydrogen peroxide, and acetonitrile (Sigma-Aldrich) were purchased and used without any further purification. Some batches of DMTU were damp and oily and could not form DMAIMSA according to the following method. Instead, the product formed slowly, and turned yellow upon exposure to the atmosphere and at ambient temperatures. The consistency of the DMTU batches was extremely important for the generation of high and consistent yields of DMAIMSA. Aqueous iodine solutions were prepared by dissolving iodine crystals (Sigma-Aldrich) in distilled water, followed by filtration and storage in the dark. Standard solutions of sodium hydroxide were purchased from Fisher Scientific.

Synthesis of DMAIMSA

N,*N*′-Dimethylaminoiminomethanesulfinic acid was prepared according to the synthetic procedure given in the literature (11), which was followed with some modification. DMTU (10.42 g, 0.10 mol) was dissolved in 80 mL of a 50% acetonitrile solution, which was chilled in an acetone–CO_2 ice bath at –59 °C. To this ice-cold solution, 2 equiv. (0.2 mol) of hydrogen peroxide, which were measured as a 20.41 mL aliquot of a 30% concentrated solution, were added dropwise with the rate of addition maintained such that temperature of the reaction mixture did not exceed –39 °C. The 2:1 ratio of hydrogen peroxide to DMTU had to be strictly maintained to avoid the production of mixtures of oxoacids. The frozen mixture was allowed to sit until it melted out and was then stirred at room temperature for 2 h. The resulting long, colorless needlelike crystals were filtered and washed twice with 50% acetonitrile solution and deionized water and then dried in a dessicator. Typical yields were approximately 80%. Further recrystallization and purification was still performed using the same strength acetonitrile solution. Thus, most of the product was lost during the washing, giving much lower yields.

Methods

UV–vis spectra were taken on a PerkinElmer Lambda 2S spectrophotometer equipped with a thermostatable compartment. Most experiments were performed at 25 ± 0.5 °C. Distilled and deionized water were utilized to prepare all standard solutions used in these experiments. The reaction between DMAIMSA and iodine was followed by the use of the iodine–triiodide isosbestic point, which had been experimentally determined as 465 nm in this work and other previous studies from our laboratory using the same spectrophotometer (12). Only freshly prepared iodine solutions were utilized. A Hi-Tech Scientific SF-DX2 (Wiltshire, UK) stopped-flow spectrophotometer was used to follow the oxidation of DMAIMSA by aqueous iodine. KinetAsyst 2.1 software (Hi-Tech, 1998) was used for data acquisition and analysis. Temperature control was maintained with a NesLab RTE-101 thermostat bath. Some reaction solutions were degassed with argon and tightly capped to reduce the effects of dissolved oxygen.

Structure determination

Well-defined needlelike crystals used for X-ray analysis were first recrystallized from a trifluoroacetic acid – water solution and vacuum dried overnight. A colorless crystal of $SO_2C(NHMe)_2$ was covered in the perfluoropolyether PFO-XR75 (Lancaster, UK), and sealed under nitrogen in a glass capillary. The crystal was optically aligned on the four-circle of a Siemens P4 diffractometer equipped with a graphite monochromatic crystal, a MoKα radiation source (λ = 0.710 73 Å), and a SMART CCD detector held at 5.084 cm from the crystal.

Structure solution and refinement

The crystal structure was solved by a combination of direct methods and Fourier methods with the use of SHELXTL6.1 (13). Idealized positions for the hydrogen atoms were included as fixed contributions using a riding model with isotropic temperature factors set at 1.2 (amine

© 2006 NRC Canada

Table 1. Crystal data and structure refinement for DMAIMSA ($SO_2C(NHMe)_2$).

Empirical formula	$C_3H_8N_2O_2S$
Formula weight	136.16
Temperature (K)	295(2)
Wavelength (Å)	0.710 73
Crystal system	Triclinic
Space group	$P\bar{1}$
Unit cell dimensions	
a (Å)	6.080 0(7)
b (Å)	6.968 7(8)
c (Å)	7.947 3(9)
α (°)	73.917(2)
β (°)	88.507(2)
γ (°)	69.565(2)
Volume (Å^3), Z	302.25(6), 2
Density (calculated) (g/cm^3)	1.496
Absorption coefficient (cm^{-1})	4.47
F(000)	144
Crystal size (mm^3)	0.36 × 0.40 × 0.42
θ Range for data collection (°)	2.68–27.48
Limiting indices	$-7 \le h \le 7$
	$-9 \le k \le 9$
	$-9 \le l \le 10$
Reflections collected	2114
Independent reflections	1335 (R_{int} = 0.031 0)
Refinement method	Full-matrix least-squares on F^2
Data/restraints/parameters	1335/0/75
Goodness-of-fit on F^2	1.056
Final R indices [$I > 2\sigma(I)$]	$R1$ = 0.046 6, $wR2$ = 0.133 1
R indices (all data)	$R1$ = 0.050 2, $wR2$ = 0.136 2
Largest diff. peak and hole (e Å^{-3})	0.489 and –0.259

protons) or 1.5 (methyl protons) times that of the adjacent carbon. The positions of the methyl hydrogen atoms were optimized by a rigid rotating group refinement with idealized tetrahedral angles. Full-matrix least-squares refinement, based upon the minimization of $\Sigma w_i|F_o^2 - F_c^2|^2$, with $w_i^{-1} = [\sigma^2(F_o^2) + (0.0811P)^2 + 0.09P]$, where $P = (\max(F_o^2, 0) + 2F_c^2)/3$, converged to give final discrepancy indices of R_1 = 0.0466, wR_2 = 0.1331 for 1209 reflections with $I > 2\sigma(I)$. The goodness-of-fit (GOF) value was 1.056.

A correction for secondary extinction was not applied. The maximum and minimum residual electron density peaks in the final difference Fourier map were 0.489 and –0.259 e/Å^3, respectively. The linear absorption coefficient, atomic scattering factors, and anomalous dispersion corrections were calculated from values from the *International Tables for X-ray Crystallography* (14).

The refined lattice parameters and other relevant crystallographic information are summarized in Table 1 and the bond angles and bond lengths are given in Table 2.

Table 2. Bond lengths (Å) and bond angles (°) for DMAIMSA ($SO_2C(NHMe)_2$).

Bond lengths (Å)	
S(1)—O(2)	1.4761(16)
S(1)—O(1)	1.4786(19)
S(1)—C(1)	1.880(2)
N(1)—C(1)	1.303(3)
N(1)—C(2)	1.457(3)
N(2)—C(1)	1.304(3)
N(2)—C(3)	1.457(3)
Bond angles (°)	
O(2)-S(1)-O(1)	112.27(12)
O(2)-S(1)-C(1)	99.25(9)
O(1)-S(1)-C(1)	99.78(9)
C(1)-N(1)-C(2)	125.03(19)
C(1)-N(2)-C(3)	124.44(18)
N(1)-C(1)-N(2)	123.63(19)
N(1)-C(1)-S(1)	120.94(15)
N(2)-C(1)-S(1)	115.43(14)

Results and discussion

Description of the molecular structure of DMAIMSA ($SO_2C(NHMe)_2$)

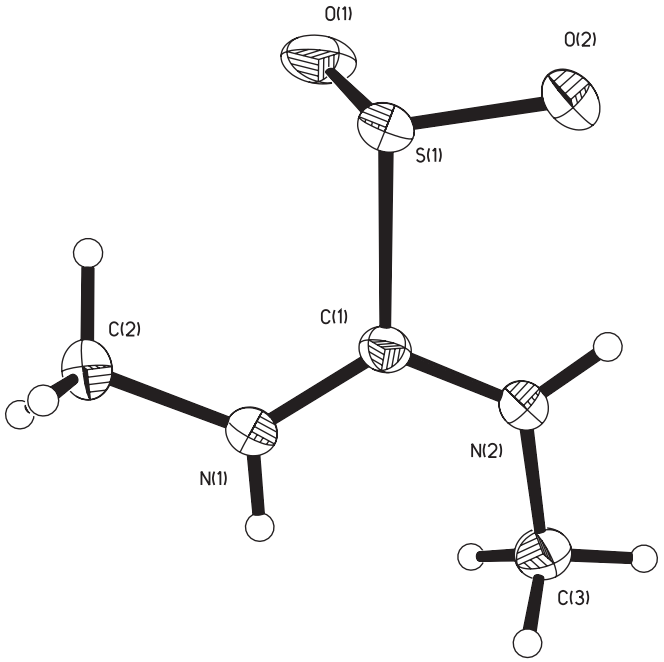
The molecular structure of DMAIMSA was determined by X-ray crystallography.[2] The perspective view is shown in Fig. 1. It is a zwitterionic species with a delocalized negative charge over the O(1)-S-O(2) framework. Whereas the geometry about the S atom is pyramidal, the geometry about the carbon is strictly planar with the sum of angles about C(1) being exactly 360°. The molecular structure of DMAIMSA is highlighted by a three-center four-electron π-interaction of two filled nitrogen p_π orbitals and a vacant carbon p_π orbital at the formally cationic carbon center. This helps to account for the very short C—N bonds observed for C(1)—N(1) (1.303(3) Å) and C(1)—N(2) (1.304(3) Å). In contrast, the corresponding N—C(methyl) bond lengths of 1.457(3) Å are typical of a single C—N bond. The orientation of the methyl groups with respect to the sulfinic acid group does not conform to either a "U" or "W" configuration. The methyl groups, however, are oriented to minimize intramolecular repulsion.

The C—S bond length of 1.880(2) Å is nearly 0.1 Å longer than a typical C—S bond length of 1.79 Å (15) based upon the sum of the covalent radii. This can be compared with the values observed for the unsubstituted thiourea dioxide ($(NH_2)_2CSO_2$) with 1.867(7) Å (16), thiourea trioxide ($(NH_2)_2CSO_3$) with 1.815(2) Å, and the sulfonic acid analogue of DMAIMSA ($(MeHN)_2CSO_3$) with a bond length of 1.820(3) Å (17). The bond lengthening is likely due to antibonding interaction between the sulfur lone pair and the filled π orbitals in the CN_2 central unit.

[2] Supplementary data for this article are available on the journal Web site (http://canjchem.nrc.ca) or may be purchased from the Depository of Unpublished Data, Document Delivery, CISTI, National Research Council Canada, Ottawa, ON K1A 0R6, Canada. DUD 5012. For more information on obtaining material refer to http://cisti-icist.nrc-cnrc.gc.ca/irm/unpub_e.shtml. CCDC 284131 contain the crystallographic data for this manuscript. These data can be obtained, free of charge, via www.ccdc.cam.ac.uk/conts/retrieving.html (or from the Cambridge Crystallographic Data Centre, 12 Union Road, Cambridge CB2 1EZ, UK; fax +44 1223 336033; or deposit@ccdc.cam.ac.uk).

© 2006 NRC Canada

Fig. 1. The perspective view of the molecular structure of DMAIMSA ($SO_2C(NHMe)_2$) with the atom labeling scheme. Thermal ellipsoids are scaled to enclose 30% probability.



Recent experimental results from this laboratory have shown that thiourea dioxides are much more reactive than their trioxides (18). The longer C—S bonds in the dioxides clearly suggests that this reactivity is based on the cleavage of the C—S bond to yield the highly reducing sulfoxylate anion (HSO_2^-) (19). This theory was tested by stability analysis experiments (pH stability and reaction with mild oxidants). The two S—O bonds are nearly equivalent at 1.479(2) and 1.476(2) Å. They are shorter than the unique S—O bonds in unsubstituted thiourea dioxide (1.496(3) Å) and are much longer than those that range from 1.431 to 1.446 Å in thiourea trioxide. The density of DMAIMSA (1.496 g cm^{-3}) is much lower than that recorded for thiourea trioxide (1.948 g cm^{-3}) (17), which is probably a consequence of the absence of extensive H-bonding in DMAIMSA (17).

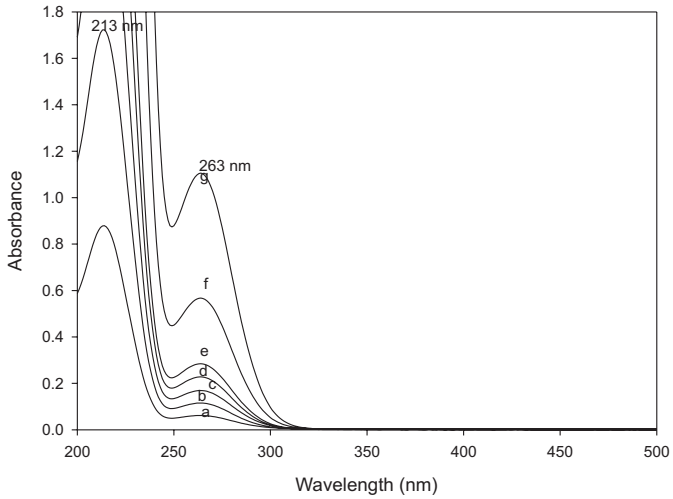
The UV–vis spectrum of DMAIMSA in aqueous solutions is shown in Fig. 2. It shows two peaks in the UV region centered at 213 and 263 nm. No other peaks are visible after the 263 nm peak. The absorptivity coefficient of DMAIMSA at 213 nm is 8695 $(mol/L)^{-1}$ cm^{-1} and at 263 nm is 573 $(mol/L)^{-1}$ cm^{-1}.

Reactivity and stability of DMAIMSA in aqueous solutions

Effect of pH

Figure 3*a* shows a series of experiments carried out at varying pH conditions to evaluate the stability of DMAIMSA. Carefully weighed out samples of DMAIMSA were dissolved in aqueous solutions at specific pH conditions. These solutions were capped in a spectrophotometric cuvette and the rate of disappearance of the 263 nm peak was observed. DMAIMSA is very stable in acidic and slightly basic conditions as traces a to e in Fig. 3*a* show. Although unstable in slightly basic conditions, the decomposition is very slow in pH conditions lower than pH 11.0. Full decomposition of DMAIMSA at pH 11.0 could be effected after an incubation of several days. At pH 12.0 (NaOH, 0.01 mol/L), the decomposition was very fast and could be complete in less than 5 min.

Fig. 2. The UV–vis spectrum of DMAIMSA in aqueous solutions and neutral pH. Only two peaks are visible at 213 and 263 nm. The peak at 263 nm was used to monitor the rate of decomposition of DMAIMSA. The concentrations of DMAIMSA were: (a) 0.0001, (b) 0.0002, (c) 0.0003, (d) 0.0004, (e) 0.0005, (f) 0.001, (g) 0.002 mol/L.



Decomposition products

A decomposing solution of DMAIMSA (see Fig. 3*b*) was subjected to several periodic spectral scans between 200 and 400 nm. These spectral scans showed the decay of peaks at 213 and 263 nm with a concomitant increase in a peak at 315 nm after some time delay (induction period). From an examination of spectrum k (Fig. 3*b*), which is the final product spectrum obtained, one of the products of this decomposition was deduced to be dithionite ($S_2O_4^{2-}$). Dimethylurea, which would be the product organic moiety, does not have any absorption peaks at $\lambda > 280$ nm. Figure 4*a* shows the formation of dithionite in solutions of varying DMAIMSA concentrations. These traces, as expected (20), are characterized by an induction period followed by a slow formation of dithionite. The induction period is virtually eliminated in high concentrations of DMAIMSA. Some solutions were first degassed with argon, immediately capped, and absorbance at 315 nm monitored (see Fig. 4*b*). Degassing greatly reduced the induction period and also decreased the amount of dithionite formed.

The precursor to the formation of dithionite is the sulfoxyl anion radical ($SO_2^{\cdot-}$) (21):

$$[1] \qquad 2SO_2^{\cdot-} \rightleftharpoons S_2O_4^{2-}$$

This would suggest that the cleavage of the C—S bond could occur in DMAIMSA by the nucleophilic attack of the hydroxyl ion on the carbon atom, followed by the elimination of the sulfoxylate anion (SO_2^{2-}):

© 2006 NRC Canada

Fig. 3. (*a*) The decomposition of DMAIMSA at various pH conditions monitored at 263 nm. Its decomposition is slow to negligible in acidic conditions. Decomposition products include dithionite, bisulfite, sulfide, and a urea residue. For all experiments, the concentration of DMAMSA used was 0.0052 mol/L. The pH conditions used were: (a) 0.0, (b) 2.0, (c) 3.0, (d) 8.0, (e) 9.0, (f) 11.0, (g) 12.0, (h) 13.0. (*b*) Spectral scans taken every 60 s between wavelengths of 200 and 400 nm, showing all the active regions during the decomposition of DMAIMSA. Initially, the peak at 263 nm goes down without any activity at 315 nm. The absorbance at 315 nm next grows to a maximum value that is determined by the amount of oxygen present in solution. $[DMAIMSA]_0$ = 0.0004 mol/L, $[NaOH]_0$ = 0.50 mol/L.

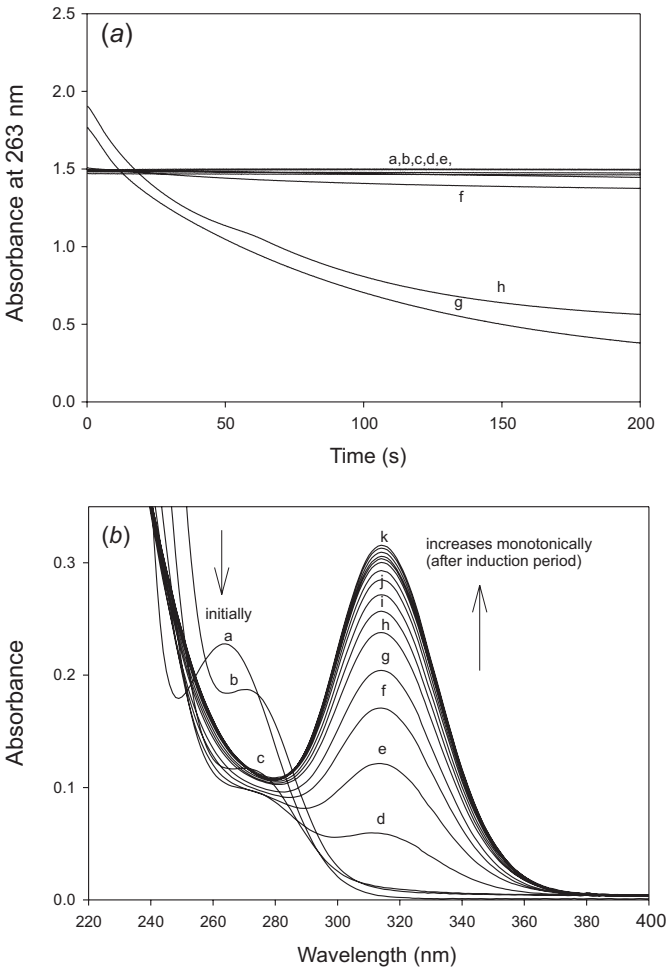
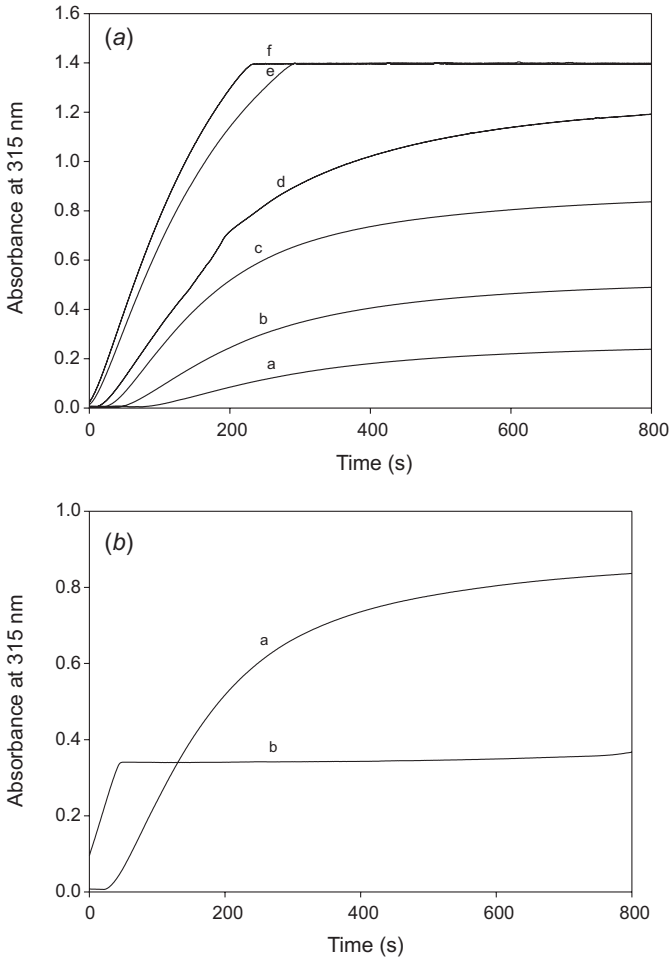


Fig. 4. (*a*) The decomposition of DMAIMSA in high pH conditions and in aerobic environments showing the formation of dithionite after a short induction period. The presence of oxygen is a prerequisite for the formation of dithionite. $[NaOH]_0$ = 0.50 mol/L; $[DMAIMSA]_0$ = (a) 0.0004, (b) 0.0005, (c) 0.0006, (d) 0.0007, (e) 0.00095, (f) 0.001 mol/L. (*b*) Comparison of the traces obtained from an air-saturated solution and an argon-purged solution. The induction period and amount of dithionite formed is greatly reduced in reduced-oxygen environments. Trace a is obtained from air-saturated solutions and trace b is from solutions degassed by bubbling argon into the reaction mixture for 7 min. $[NaOH]_0$ = 0.50 mol/L, $[DMAIMSA]_0$ = 0.0006 mol/L.



[2] $MeHN(MeN=)C\text{-}SO_2^- + OH^- \rightarrow (MeHN)_2C{=}O + SO_2^{2-}$

The hydroxide ion can be regenerated:

[3] $SO_2^{2-} + H_2O \rightarrow HSO_2^- + OH^-$

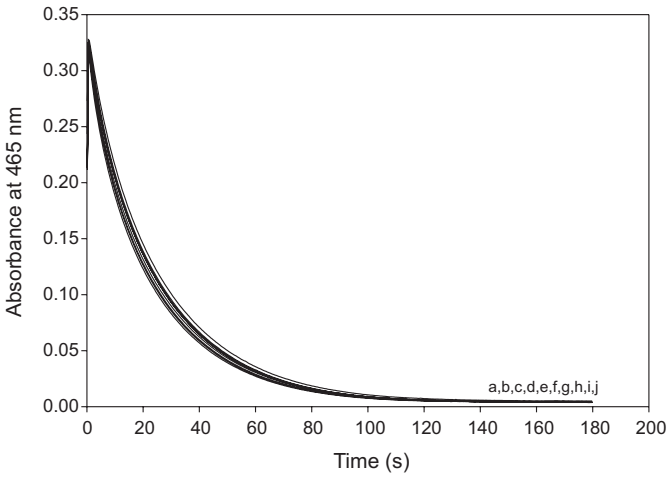
The sulfoxylate anion is known to have a strong affinity for oxygen, with which it reacts at a diffusion-controlled rate to produce the sulfoxyl anion radical (22):

[4] $SO_2^{2-} + O_2(aq) \rightarrow SO_2^{\cdot -} + O_2^-$

The sulfoxyl anion radical can react according to rxn. [1] to produce dithionite. The superoxide ion can then subsequently decompose into oxygen and hydrogen peroxide (23). The reaction solutions that were not degassed had the standard concentrations of 2.0×10^{-4} mol/L in dissolved oxygen, while degassed solutions, though not completely depleted in oxygen, had concentrations that were much lower than 2.0×10^{-4} mol/L. Previous experiments from this laboratory on the decomposition of thiourea dioxide did not form dithionite in strictly anaerobic conditions (20). The induction period is the time taken for reactions of type [4] to mop up all the oxygen in the solution. This explains why higher DMAIMSA concentrations delivered shorter induction periods. The final amount of dithionite is also controlled by the

© 2006 NRC Canada

Fig. 5. The direct oxidation of DMAIMSA by aqueous iodine under pseudo-first-order kinetics. The age of the DMAIMSA solutions does not have any effect on the rate of reaction. $[I_2]_0 = 5.1 \times 10^{-4}$ mol/L, $[DMAIMSA]_0 = 0.00679$ mol/L. The solutions were aged for: (a) 3, (b) 10, (c) 20, (d) 38, (e) 60, (f) 90, (g) 116, (h) 165, (i) 186, (j) 214 min.



amount of oxygen initially present in solution. Figure 4*a* also shows that higher DMAIMSA concentrations quickly attain saturation with respect to the amount of dithionite formed.

Reaction with iodine

The ease of oxidation of any organosulfur compound can be tested by the use of the mild oxidant, iodine. Figure 5 shows a series of experiments in which the DMAIMSA aqueous solutions were first allowed to age before being used to reduce iodine. The reaction of iodine and DMAIMSA is moderately fast, but not as fast as the reaction between thiourea dioxide and iodine (18). The reaction also does not display the classic autoinhibition that characterizes most iodine oxidations. Previous experiments with other sulfinic and sulfonic acids have suggested that in aqueous solutions these oxoacids slowly degenerate (see Figs. 3*a* and 3*b*) until there is mixture of urea, bisulfite, and sulfide (19):

[5] $$MeHN(MeN=)C\text{-}SO_2H + H_2O \rightarrow (MeHN)_2C=O + HSO_2^- + H^+$$

[6] $$3HSO_2^- \rightleftharpoons 2HSO_3^- + HS^-$$

The bisulfite and sulfide formed in rxn. [6] are much easier to oxidize, so if rxn. [5] is rate-determining in the oxidation of the sulfinic acid, then aged solutions should react much faster. Data in Fig. 5 shows that there is no real distinction in the reaction rates of aged and unaged solutions. This would suggest that rxn. [5] is rapid enough to not influence the rate of oxidation of DMAIMSA.

Conclusion

We have managed to synthesize, isolate, and characterize the most important metabolite of the physiologically active radical scavenger, DMTU. DMAIMSA is also extremely reactive, much more reactive than either the parent compound (DMTU) or the sulfonic acid analogue. This reactivity could be attributed to the very long C—S bond, which is easily cleaved to yield the highly reducing sulfoxylate anion and which upon oxidation by molecular oxygen, should yield a dithionite precursor.

Acknowledgement

This work was supported by research grant numbers CHE 0137435, CHE 0341769 (Bio-inorganic Chemistry), and CHE 0315808 (International Programs) from the National Science Foundation.

References

1. C.P. Lewis, D. Dinsdale, and B. Nemery. Free Radical Biol. Med. **16**, 561 (1994).
2. R.B. Fox. J. Clin. Invest. **74**, 1456 (1984).
3. C.J. Beehler, M.L. Simchuk, J.M. McCord, and J.E. Repine. J. Lab. Clin. Med. **119**, 508 (1992).
4. C.J. Beehler, M.E. Ely, K.S. Rutledge, M.L. Simchuk, O.K. Reiss, P.F. Shanley, and J.E. Repine. J. Lab. Clin. Med. **123**, 73 (1994).
5. A.M. Scott, G.M. Powell, D.G. Upshall, and C.G. Curtis. Environ. Health Perspect. **85**, 43 (1990).
6. J.B. Mackenzie and C.G. Mackenzie. Proc. Soc. Exp. Biol. Med. **54**, 43 (1943).
7. A. Del Corso, M. Cappiello, and U. Mura. Int. J. Biochem. **26**, 745 (1994).
8. H.V. Vadi and R.A. Neal. Chem. Biol. Interact. **35**, 25 (1981).
9. R. Okazaki and K. Goto. Heteroat. Chem. **13**, 414 (2002).
10. T.C. Bruice and A.B. Sayigh. J. Am. Chem. Soc. **81**, 3416 (1959).
11. W.E. Curtis, M.E. Muldrow, N.B. Parker, R. Barkley, S.L. Linas, and J.E. Repine. Proc. Natl. Acad. Sci. U.S.A. **85**, 3422 (1988).
12. C. Mundoma and R.H. Simoyi. Int. J. Chem. Kin. **32**, 193 (2000).
13. G.M. Sheldrick. SHELXTL6.1 [computer program]. Bruker AXS, Inc. Madison, Wisconsin. 2000.
14. J.A. Ibers and W.C. Hamilton (*Editors*). International Tables for X-ray Crystallography. Kynoch Press, Birmingham. 1974.
15. J. Huheey, E.A. Keiter, and R.L. Keiter. Inorganic chemistry of structure and reactivity. Harper Collins College Publishing, New York. 1993.
16. J.S. Song, E.H. Kim, S.K. Kang, S.S. Yun, I.-H. Suh, S.S. Choi, and S. Lee. Bull. Korean Chem. Soc. **17**, 201 (1996).
17. S.V. Makarov, C. Mundoma, J.H. Penn, J.L. Petersen, S.A. Svarovsky, and R.H. Simoyi. Inorg. Chim. Acta, **286**, 149 (1999).
18. S.V. Makarov, C. Mundoma, J.H. Penn, S.A. Svarovsky, and R.H. Simoyi. J. Phys. Chem. A, **102**, 6786 (1998).
19. S.A. Svarovsky, R.H. Simoyi, and S.V. Makarov. J. Chem. Soc. Dalton Trans. 511 (2000).
20. S.A. Svarovsky, R.H. Simoyi, and S.V. Makarov. J. Phys. Chem. B, **105**, 12634 (2001).
21. S.V. Makarov, C. Mundoma, S.A. Svarovsky, X. Shi, P.M. Gannett, and R.H. Simoyi. Arch. Biochem. Biophys. **367**, 289 (1999).
22. J.Z. Zhang and F.J. Millero. Environmental geochemistry of sulfide oxidation. American Chemical Society, Washington, D.C. 1992.
23. B. Halliwell and J.M. Gutteridge. Arch. Biochem. Biophys. **246**, 501 (1986).

© 2006 NRC Canada

Synthesis and characterization of a series of 3-methyl-3-{3-[1-methyl-3-aryl-2-triazenyl]propyl}-1-aryl-1-triazenes and related compounds

Jeff D. Clarke, Shasta L. Moser, and Keith Vaughan

Abstract: A series of diazonium salts has been coupled to both secondary nitrogen atoms of the bis-secondary amine, *N*,*N*′-dimethyl-1,3-propanediamine ($MeNHCH_2CH_2CH_2NHMe$), to afford the new bistriazene series, the 3-methyl-3-{3-[1-methyl-3-aryl-2-triazenyl]propyl}-1-aryl-1-triazenes (**9**). These compounds have been fully characterized by IR and NMR spectroscopy, with supporting data from elemental analysis and high-resolution mass spectrometry. A limited number of model compounds in the *N*,*N*-dimethyl-*N*-{3-[1-methyl-3-aryl-2-triazenyl]propyl}amine series (**10**) have been synthesized to aid in the interpretation of the NMR spectra of the bistriazenes (**9**). A series of related compounds, the 3-ethyl-3-{(*E*)-4-[1-ethyl-3-aryl-2-triazenyl]-2-butenyl}-1-aryl-1-triazenes (**11**), have been synthesized by diazonium coupling with the bis-secondary amine *N*,*N*′-diethyl-2-butene-1,4-diamine (**15**), and the diazonium coupling reaction with *trans-N*,*N*′-dimethycyclohexane-1,2-diamine (**19**) has been used to prepare another related series of bistriazenes, the 3-methyl-3-{2-[1-methyl-3-aryl-2-triazenyl]cyclohexyl}-1-aryl-1-triazenes (**12**). The ^{1}H NMR spectra of these compounds are complex because of the presence of two chiral centres in the cyclohexanediamine moiety; the diastereotopic protons of the methylene groups in the cyclohexane ring are clearly distinguished in the 500 MHz spectra of these compounds.

Key words: triazene, bistriazene, synthesis, nuclear magnetic resonance, propanediamine, 1,4-diamino-2-butene, cyclohexanediamine.

Résumé : Le couplage d'une série de sels de diazonium à chacun des deux atomes d'azote secondaire de l'amine bis-secondaire, *N*,*N*′-diméthyl-1,3-propanediamine ($MeNHCH_2CH_2CH_2NHMe$), conduit à la formation d'une série de nouveaux bistriazène, les 3-méthyl-3-{3-[1-méthyl-3-aryl-2-triazényl]propyl}-1-aryl-1-triazènes (**9**). On a effectué une caractérisation complète de ces composés par analyse élémentaire, spectroscopies IR et RMN et spectrométrie de masse. Afin de pouvoir faire une interprétation des spectres RMN des bistriazènes (**9**), on a synthétisé un nombre limité de composés modèles de la série *N*,*N*-diméthyl-*N*-{3-[1-méthyl-3-aryl-2-triazényl]propyl}amine (**10**). On a aussi synthétisé une série de composés apparentés, les 3-éthyl-3-{(*E*)-4-[1-éthyl-3-aryl-2-triazényl]-2-buténYl}-1-aryl-1-triazènes (**11**), par couplage de sels de diazonium avec l'amine bis-secondaire *N*,*N*′-diéthyl-2-butène-1,4-diamine (**15**) alors qu'on a fait appel à une réaction de couplage de diazonium avec le *trans-N*,*N*′-diméthylcyclohexane-1,2-diamine (**19**) pour préparer une autre série de bistriazènes apparentés, les 3-méthyl-3-{2-[1-méthyl-3-aryl-2-triazényl]cyclohexyl}-1-aryl-1-triazènes (**12**). Les spectres RMN de ces composés sont complexes en raison de la présence de deux centres chiraux dans la portion cyclohexanediamine; les protons diastéréotopes des groupes méthylènes du noyau cyclohexane peuvent facilement être distingués dans les spectres à 500 MHz de ces composés.

Mots clés : triazène, bistriazène, synthèse, résonance magnétique nucléaire, propanediamine, 1,4-diamino-2-butène, cyclohexanediamine.

[Traduit par la Rédaction]

Introduction

The term "bistriazene" has been coined to describe any molecule that contains two triazene units in the same molecule, with a link or spacer between the triazene moieties. Recent progress in the synthesis of bistriazenes has been reviewed (1) and the variety of known bistriazenes can be described by the general structures **1** and **2**. In bistriazenes of type **1** the triazenes are linked at N-3 of each triazene unit through the spacer (2, 3) whereas in bistriazenes of type **2** the spacer is attached at N-1 of each triazene unit (4). Mixed bistriazenes of type **3**, where a triazene is linked at N-1 via a spacer to N-3 of a second triazene, are at present unknown.

Bistriazenes have been investigated for their chemical and biological properties by several groups. The antitumor properties of certain bistriazenes of type **1** have been investigated, with the conclusion that these triazenes may be potential prodrugs for the cytotoxic monomethyltriazene (5). This was followed up with a study of bistriazenes of type **4** as multifunctional alkylating agents (6); triazenes of type **5** were found to interact with DNA forming a highly reactive species capable of multistrand breaks and interstrand cross

Received 12 January 2006. Published on the NRC Research Press Web site at http://canjchem.nrc.ca on 26 May 2006.

J.D. Clarke, S.L. Moser, and K. Vaughan.[1] Department of Chemistry, Saint Mary's University, Halifax, NS B3M 3X6, Canada.

[1]Corresponding author (e-mail: keith.vaughan@smu.ca).

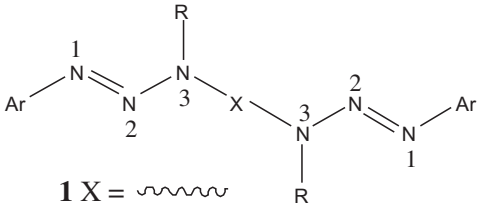
 doi:10.1139/V06-074 © 2006 NRC Canada

links (7). A synthetic application of bistriazenes is the reported (8) thermal cleavage reaction of a series of *N*,*N*′-bis(arylazo)piperazines to afford the related substituted biphenyl derivatives. Indeed, triazenes have been recognised as being versatile tools in organic synthesis (9) and multifunctional triazene linkers have found application in the efficient solid-phase synthesis of heterocyclic libraries (10). Bistriazenes have been used as one of many functional groups required for characterization of polyarylene compositions with enhanced modulus profiles (11). A recent report (12) describes a neutral 1,2-bis(phenyltriazenido)benzene complex of platinum(II), the first example of a π fragment of platinum(II) stabilized by two symmetrical triazenido chains.

An earlier documented molecule of the bistriazene type is bis(3-phenyltriazen-1-yl)ethane (**5**), obtained by Pochinok et al. (13) by the addition of phenylmagnesium bromide to 1,2-diazidoethane. A similar method was used more recently by Blumenstein and Michejda (6) to prepare the series of 1,2-bis(alkyltriazeno)ethanes (**4**). A serendipitous development in bistriazene chemistry came about during studies of the diazonium coupling reaction with formaldehyde–methylamine mixtures (14). The by-product of these reactions was found to be the *N*,*N*′-bis(1-aryl-3-methyltriazen-3-ylmethyl)methylamine (**6**) (15, 16). A further development in this area of research was the study of the reaction of diazonium salts with ammonia–formaldehyde mixtures, which affords the cagelike bistriazenes, the 3,7-bis(arylazo)-1,3,5,7-tetraazabicyclo[3.3.1]nonanes (**7**) (17). The molecule of type **7** is structurally derived from **6** by the insertion of an extra nitrogen atom to link the carbon atoms of the three *N*-methyl groups.

A more predictable reaction was observed when the diazonium salt was coupled with a *N*,*N*′-dialkylethylenediamine, which affords the 1,2-bis(1-aryl-3-alkyltriazen-3-yl)ethanes (**8**) (2). These bistriazenes were studied extensively by NMR spectroscopy and the bistriazene connectivity was established by X-ray crystallography (18). More recently (19), this work was extended to include the bis(3-pyridyl) derivative (**8**, Ar = 3-pyridyl). In this paper, we wish to report a logical extension of the previous work (2), in which the diazonium salt has been coupled to both secondary nitrogen atoms of the bis-secondary amine, *N*,*N*′-dimethyl-1,3-propanediamine ($MeNHCH_2CH_2CH_2NHMe$), to afford the new bistriazene series, the 3-methyl-3-{3-[1-methyl-3-aryl-2-triazenyl]propyl}-1-aryl-1-triazenes (**9**).

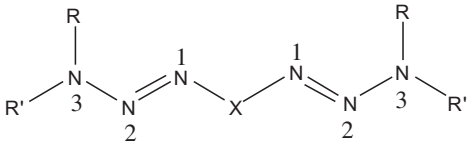
These compounds have been fully characterized by IR and NMR spectroscopy, with supporting data from elemental analysis or high-resolution mass spectrometry. A limited number of model compounds in the *N*,*N*-dimethyl-*N*-{3-[1-methyl-3-aryl-2-triazenyl]propyl}amine series (**10**) have



1 X = ~~~

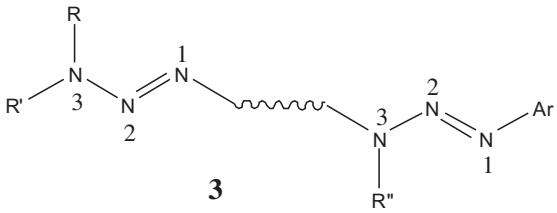
5 X = CH_2CH_2 ; R=H

8 X = CH_2CH_2; R=Me

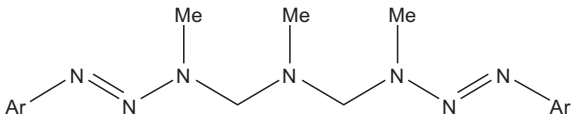


2 X = ~~~

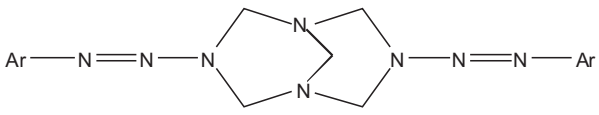
4 X = CH_2CH_2; R'=H



3

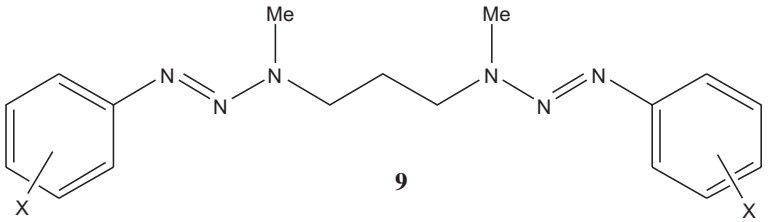


6

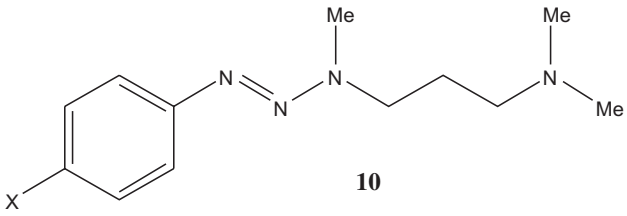


7

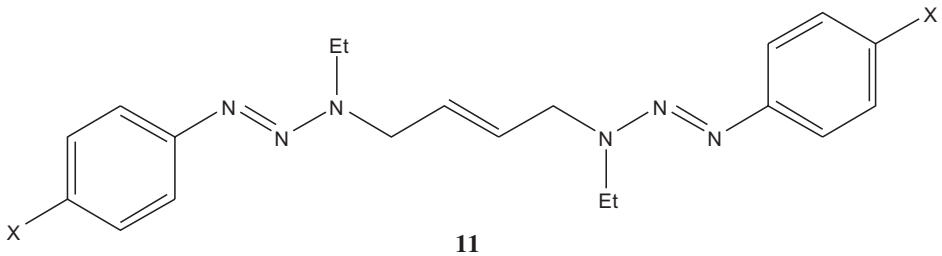
© 2006 NRC Canada



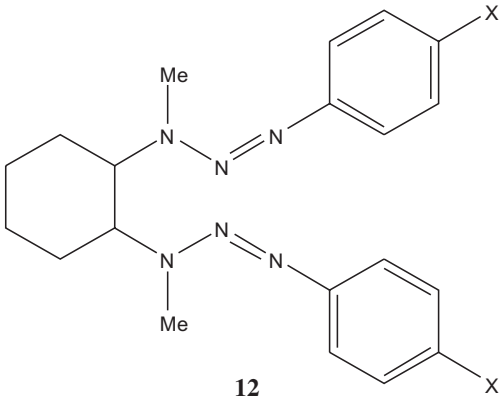
9



10



11



12

been synthesized to aid in the interpretation of the NMR spectra of the bistriazenes (**9**). A series of related compounds, the 3-ethyl-3-{(*E*)-4-[1-ethyl-3-aryl-2-triazenyl]-2-butenyl}-1-aryl-1-triazenes (**11**), have been synthesized by diazonium coupling with the bis-secondary amine *N*,*N*′-diethyl-2-butene-1,4-diamine, and the diazonium coupling reaction with *trans*-*N*,*N*′-dimethycyclohexane-1,2-diamine has been used to prepare another related series of bistriazenes, the 3-methyl-3-{2-[1-methyl-3-aryl-2-triazenyl]cyclohexyl}-1-aryl-1-triazenes (**12**). The structural connection between these seemingly different series (**8**, **9**, **11** and **12**) is that these molecules are composed of two (1-aryl-3-alkyltriazen-3-yl-)methyl groups linked by different spacers. It is noteworthy that the compounds of series **11** and **12** are isomeric.

Experimental

All reagents were reagent grade materials purchased from Sigma-Aldrich Canada Ltd., Oakville, Ontario, and were used without further purification. Melting points were determined on a Fisher-Johns melting point apparatus and are uncorrected. Infrared spectra were obtained using Nujol mulls on a Bruker Vector 22 spectrometer. ^{1}H and ^{13}C NMR spectra were obtained with either (*i*) the Bruker 500 MHz spectrometer at the Atlantic Regional Magnetic Resonance Center at Dalhousie University or (*ii*) the ANASAZI 60 MHz EFT spectrometer at St. Mary's University (SMU). Chemical shifts were recorded in $CDCl_3$ solutions at 300 K (unless specified otherwise) and are relative to TMS as internal standard. Elemental analyses were performed by the Canadian Microanalytical Service Ltd., Delta, British Columbia. Accurate mass measurements were made on a CEC 21-110B mass spectrometer operated at a mass resolution of 8000 (10% valley) by computer-controlled peak matching to appropriate PFK reference ions. Spectra were obtained using electron ionization at 70 V and a source temperature of 175 °C, with samples being introduced by means of a heatable quartz probe. The standard deviation of mass measurement is ±0.0008 amu, which is an average of 3.6 ppm over the mass range 100 to 300 amu.

© 2006 NRC Canada

Table 1. Physical data for the 3-methyl-3-{3-[1-methyl-3-aryl-2-triazenyl]propyl}-1-aryl-1-triazenes (**9**).

Cpd	X	Yield (%)	mp (°C)	Recrystn. Solvent	Crystal appearance	IR (cm^{-1})
9a	*p*-CN	86	153 to 154	EtOH–EtOAc	Small off-white needles	2217 (CN), 839 (OOP)
9b	*p*-NO_2	57	202 to 203	DMSO	Small yellow prisms	1505, 1309 (NO_2)
9c	*p*-CO_2Me	92	81–83	Hexanes–EtOAc	Pale yellow needles	1709 (C=O), 858 (OOP)
9d	*p*-CO_2Et	88	57 to 58	Hexanes	Yellow clusters	1698 (C=O), 777 (OOP)
9e	*p*-$COCH_3$	84	119 to 120	Ethanol	Lustrous pale brown needles	1661 (C=O) 849, 834 (OOP)
9f	*p*-$CONH_2$	44	210–212	Ethanol	White powder	1646 (C=O), 857 (OOP)
9g	*p*-Cl	27	59 to 60	Petroleum ether	Pale yellow prisms	829 (OOP)
9h	*p*-Br	74	68–70	Hexanes–EtOAc	Small white needles	827 (OOP)
9i	p-CH_3	73	40 to 41	Petroleum ether	Pale cream needles	822 (OOP)
9j	*p*-OCH_3	63	—	—	Oil	836 (OOP)
9k	*m*-CF_3	57	—	—	Oil	799 (OOP)
9l	*o*-CN	54	105–108	Hexanes–EtOAc	Red prisms	2209 (CN), 749 (OOP)
9m	H	75	—	—	Oil	694, 764 (OOP)
9n	3-Pyridyl	65	—	—	Oil	808, 709 (OOP)

3-Methyl-3-{3-[1-methyl-3-aryl-2-triazenyl]propyl}-1-aryl-1-triazenes (9a–9n)

General procedure

The aromatic primary amine (0.01 mol) was dissolved in 10 mL of 3 mol/L hydrochloric acid, with the aid of heat if necessary, and the resulting solution was cooled in an ice–salt bath to 0 °C. The solution was diazotized with a solution of sodium nitrite (0.76 g) in deionized water (3.0 mL) while maintaining the temperature below 5 °C, and then stirred for a further 0.5 h in the cold. The resulting diazonium salt solution was cold-filtered if necessary. A separate solution of *N*,*N*′-dimethy-1,3-propanediamine (0.005 mol) in deionized water (5 mL) was prepared and this solution was added slowly to the diazonium salt solution. After stirring in the cold for 0.5 h, the resulting mixture was then neutralized with saturated sodium bicarbonate solution. The mixture was then left to stir until precipitation was deemed to be complete (0.5–3 h). The solid product was filtered under suction, dried, and recrystallized from an appropriate solvent. Products that separated as oils were extracted into dichloromethane, dried over anhydrous magnesium sulfate, and isolated by evaporation under vacuum. Physical data of the products, i.e., yield, mp, recrystallization solvent, and IR data, are listed in Table 1. Table 2 is a list of ^{1}H NMR chemical shift data, with appropriate assignments, and selected ^{13}C NMR data are listed in Table 3. The elemental analysis and high-resolution mass spectral data of selected compounds of series **9** are reported in Tables 4 and 5, respectively.

N,*N*-Dimethyl-*N*-{3-[1-methyl-3-aryl-2-triazenyl]propyl}amines (10)

4-Aminobenzonitrile (0.311 g) was dissolved in 3.0 mL of 3 mol/L hydrochloric acid, with the aid of heat if necessary, and the resulting solution was cooled in an ice–salt bath to 0 °C. The solution was diazotized with sodium nitrite (0.21 g) in water (2.0 mL) while maintaining the temperature below 5 °C, and then stirred for a further 0.5 h in the cold. A solution of *N*,*N*,*N*′-trimethyl-1,3-propanediamine (0.32 g) in water (2.0 mL) was added to the cold diazonium salt solution and the resulting mixture stirred in the cold for a further 0.5 h. The mixture was then neutralized with saturated aqueous sodium bicarbonate, and the product was either filtered and dried under suction or extracted into dichloromethane, dried with anhydrous magnesium sulfate, and isolated by evaporation under vacuum to give the following products.

4-{3-[3-(Dimethylamino)propyl]-3-methyl-1-triazenyl}benzonitrile (10a)

X = *p*-CN; 21% yield, metastable solid, mp 52 °C. IR (cm^{-1}) ν_{max}: 2221 (CN), 841 (OOP). ^{1}H NMR (500 MHz, $CDCl_3$, ppm) δ: 1.90 (2H, quintet, J = 6.8 Hz, CH_2), 2.26 (6H, s, NMe_2), 3.25 (2H, br, N-CH_2), 3.40 (3H, s, N-Me), 3.86 (2H, t, J = 6.5 Hz, N-CH_2), 7.58 (2H, d, J = 8.5 Hz, arom.), 7.58 (2H, d, J = 8.5Hz, arom.). ^{13}C NMR (125.77 MHz, $CDCl_3$, ppm) δ: 26.8, 35.1, 45.4, 51.8, 56.5, 107.6, 121.0, 133.0, 149.9, 154.4. MS (EI) *m*/*z* calcd. for $C_{13}H_{19}N_5$: 245.1640; found: 245.1627.

Methyl 4-{3-[3-(dimethylamino)propyl]-3-methyl-1-triazenyl}benzoate (10b)

X = *p*-CO_2CH_3; 51% yield, oil. IR (cm^{-1}) ν_{max}: 1721 (C=O), 1265 (C O), 860 (OOP). ^{1}H NMR (60 MHz, $CDCl_3$, ppm) δ: 1.69 (2H, br quintet, J = 7.8 Hz, CH_2), 2.21 (6H, s, NMe_2), 3.00 (2H, br, N-CH_2), 3.24 (3H, s, N-Me), 3.68 (2H, t, J = 7.2Hz, N-CH_2), 3.85 (3H, s, O-Me), 7.44 (2H, d, J = 8.7 Hz, arom.), 8.00 (2H, d, J = 8.3 Hz, arom.).

4-{3-[3-(Dimethylamino)propyl]-3-methyl-1-triazenyl}acetophenone (10c)

X = *p*-$COCH_3$; 37% yield, red powder, mp 147 °C (hexanes – ethyl acetate). IR (cm^{-1}) ν_{max}: 1676 (C=O), 840 (OOP). ^{1}H NMR (60 MHz, $CDCl_3$, ppm) δ: 1.60 (2H, br, CH_2), 2.24 (6H, s, NMe_2), 2.61 (3H, s, acetyl Me), 3.05 (2H, br, N-CH_2), 3.27 (3H, s, N-Me), 3.82 (2H, br, N-CH_2), 7.60 (2H, d, J = 8.0 Hz, arom.), 7.90 (2H, d, J = 7.7 Hz, arom.).

1-Bromo-4-{3-[3-(dimethylamino)propyl]-3-methyl-1-triazenyl}benzene (10d)

X = *p*-Br; 58% yield, oil. IR (cm^{-1}) ν_{max}: 830 (OOP). ^{1}H NMR (60 MHz, $CDCl_3$, ppm) δ: 1.62 (2H, quintet, J = 6.6 Hz, CH_2), 2.02 (6H, s, NMe_2), 3.02 (3H, s, N-Me), 3.02

© 2006 NRC Canada

Table 2. ^{1}H NMR data for the 3-methyl-3-{3-[1-methyl-3-aryl-2-triazenyl]propyl}-1-aryl-1-triazenes (**9**).

Cpd	X	Solvent	Spectrometer[a]	Aromatic (8H)	N-Me (6H)	N-CH_2 ($4H_a$)[b]	C-CH_2-C ($2H_b$)[b]	J_{ab} (Hz)	X
9a	*p*-CN	$CDCl_3$	A	7.41 (d, *J* = 9.0 Hz), 7.60 (d, *J* = 9.0 Hz)	3.31 (s)	3.77 (t)	1.75 (p)	7.0	—
9b	*p*-NO_2	d_6-DMSO	A	7.43 (d, *J* = 9.0 Hz), 8.08 (d, *J* = 9.0 Hz)	3.26 (s)	3.94 (t)	Not observed	6.75	—
9c	*p*-CO_2Me	$CDCl_3$	A	7.43 (d, *J* = 8.8 Hz), 8.00 (d, *J* = 8.9 Hz)	3.29 (s)	3.86 (t)	1.79 (p)	6.8	3.90 (6H, s, O-Me)
9d	*p*-CO_2Et	$CDCl_3$	B	7.42 (d, *J* = 8.7 Hz), 8.01 (d, *J* = 8.7 Hz)	3.28 (s)	3.83 (t)	2.12 (p)	6.8	1.38 (6H, t, *J* = 7.2 Hz), 4.36 (4H, q, *J* = 7.1 Hz)
9	*p*-$COCH_3$	$CDCl_3$	A	7.45 (d, *J* = 8.6 Hz), 7.93 (d, *J* = 8.6 Hz)	3.31 (s)	3.56 (t)	1.73 (p)	6.8	2.58 (6H, s, acetyl Me)
9f	*p*-$CONH_2$	d_6-DMSO	A	7.36 (d, *J* = 8.5 Hz), 7.84 (d, *J* = 8.5 Hz)	3.20 (s)	3.86 (br)	2.09 (br)	—	7.22 (2H, br, NH), 7.86 (2H, br, NH)
9g	*p*-Cl	$CDCl_3$	A	7.23 (d, *J* = 8.0 Hz), 7.36 (d, *J* = 8.0 Hz)	3.23 (s)	3.78 (t)	2.07 (p)	6.8	—
9h	*p*-Br	$CDCl_3$	A	7.26 (d, *J* 6.1 Hz), 7.40 (d, *J* = 6.2 Hz)	2.94 (s)	3.48 (t)	1.76 (p)	6.8	—
9i	*p*-CH_3	$CDCl_3$	A	7.10 (d, *J* = 8.5 Hz), 7.34 (d, *J* = 8.5 Hz)	3.21 (s)	3.77 (t)	2.22 (p)	6.9	2.32 (6H, s, tolyl Me)
9j	*p*-OCH_3	$CDCl_3$	A	6.83 (d, *J* = 8.9 Hz), 7.39 (d, *J* = 9.1 Hz)	3.17 (s)	3.72 (t)	2.01 (p)	6.7	3.75 (6H, s, O-Me)
9k	*m*-CF_3	$CDCl_3$	A	7.35 (dd, *J* = 1.5, 3.0 Hz), 7.4 (br s), 7.69 (br s), 7.56 (dd, *J* = 1.5, 4.7 Hz)	3.25 (s)	3.81 (t)	2.08 (p)	7.0	—
9l	*o*-CN	$CDCl_3$	A	7.26–7.72 (m)	3.32 (s)	3.44 (t)	1.75 (p)	6.6	—
9m	H	$CDCl_3$	A	7.07–7.30 (10H, m)	3.20 (s)	3.73 (t)	2.02 (p)	6.9	—
9n	3-Pyridyl	$CDCl_3$	A	7.21 (ddd, *J* = 0.7, 4.6, 8.2 Hz), 7.70 (ddd, *J* = 1.6, 2.3, 8.3 Hz), 8.36 (dd, *J* = 1.5, 4.6 Hz), 8.67 (dd, *J* = 0.7, 2.5 Hz)	3.28 (s)	3.85 (t)	2.15 (p)	6.8	—

[a]Anasazi 60 MHz spectrometer (A); Bruker 500 MHz spectrometer (B).
[b]Singlet (s); triplet (t); quartet (q); pentuplet (p); broad (br).

© 2006 NRC Canada

Table 3. ^{13}C NMR data for the 3-methyl-3-{3-[1-methyl-3-aryl-2-triazenyl]propyl}-1-aryl-1-triazenes (**9**) recorded in deuteriochloroform solution at 300 K with TMS as internal standard.

Cpd	X	Aromatic	N-Me	N-CH_2	C-CH_2-C	X
9d	*p*-CO_2Et	120.5, 127.2, 130.7, 154.5	35.3 (br)	53.2 (br)	26.1 (br)	14.6 (CH_3)
						60.8 (O-CH_2)
9k	*m*-CF_3	115.2, 117.2, 121.5, 123.6, 129.2, 151.1	36.0 (br)	52.0 (br)	27.0 (br)	—
9j	*p*-OCH_3	114.9, 121.1, 127.6, 157.9	36.2	52.0	26.7	56.6 (O-CH_3)
9m	H	120.3, 125.7, 129.7, 149.0	36.5	52.7	27.0	—

Table 4. Elemental analysis data for selected compounds from series **9**.

Cpd	Substituent	Formula	Calculated (%)	Found (%)
9a	*p*-CN	$C_{19}H_{20}N_8$	C 63.3, H 5.55, N 31.11	C 63.27, H 5.51, N 31.22
9b	*p*-NO_2	$C_{17}H_{20}N_8O_4$	C 51.00, H 5.00, N 28.00	C 51.02, H 5.03, N 27.65
9c	*p*-CO_2Me	$C_{21}H_{26}N_6O_4$	C 59.15, H 5.34, N 19.71	C 59.23, H 5.41, N 19.27
9d	*p*-CO_2Et	$C_{23}H_{30}N_6O_4$	C 60.79, H 6.61, N 18.50	C 60.80, H 6.64, N 18.46
9f	*p*-$CONH_2$	$C_{19}H_{24}N_8O_2$	C 57.57, H 6.06, N 28.28	C 57.39, H 6.10, N 27.61
9j	*p*-OCH_3	$C_{19}H_{26}N_6O_2$	C 61.62, H 7.03, N 22.70	C 61.64, H 7.09, N 22.57
9k	*m*-CF_3	$C_{19}H_{20}N_6F_6$	C 51.12, H 4.48, N 18.83	C 51.17, H 4.55, N 18.66
9m	H	$C_{17}H_{22}N_6$	C 65.81, H 7.10, N 27.10	C 66.18, H 7.26, N 27.15

Table 5. High-resolution mass spectral data for selected compounds from series **9**.

Cpd	Substituent	Formula	Calculated mass	Found mass
9d	*p*-CO_2Et	$C_{23}H_{30}N_6O_4$	454.2328	454.2322
9e	*p*-$COCH_3$	$C_{21}H_{26}N_6O_2$	394.2117	394.2100
9g	*p*-Cl	$C_{17}H_{20}N_6Cl_2$	378.1126	378.1125
9h	*p*-Br	$C_{17}H_{20}N_6Br_2$	466.0116	466.0104
9i	*p*-CH_3	$C_{19}H_{26}N_6$	338.2219	338.2224

(2H, t, J = 5.8 Hz, N-CH_2), 3.58 (2H, t, J = 6.8 Hz, N-CH_2), 7.33 (2H, d, J = 12.5 Hz, arom.), 7.36 (2H, d, J = 12.5 Hz, arom.).

3-Ethyl-3-{(*E*)-4-[1-ethyl-3-aryl-2-triazenyl]-2-butenyl}-1-aryl-1-triazenes (11)

General procedure

The aromatic primary amine (0.00 703 mol) was dissolved in 7.1 mL of 3 mol/L hydrochloric acid, with the aid of heat if necessary, and the resulting solution was cooled in an ice–salt bath to 0 °C. The solution was diazotized with a solution of sodium nitrite (0.518 g) in deionized water (2.0 mL) while maintaining the temperature below 5 °C, and then stirred for a further 0.5 h in the cold. The resulting diazonium salt solution was cold-filtered if necessary. A separate solution of *N*,*N*′-diethyl-2-butene-1,4-diamine (0.0035 mol, 0.505 g) in deionized water (2.0 mL) was prepared and this solution was added slowly to the diazonium salt solution. After stirring in the cold for 0.5 h, the resulting mixture was then neutralized with saturated sodium bicarbonate solution. The mixture was then left to stir for 1 h. The solid product was filtered under suction, dried, and recrystallized from an appropriate solvent. The following products were obtained.

*3-Ethyl-3-{(***E***)-4-[1-ethyl-3-(***p***-cyanophenyl)-2-triazenyl]-2-butenyl}-1-(***p***-cyanophenyl)-1-triazene (11a)*

X = *p*-CN; 88% yield, tan-colored powder, mp 115.5–117.5 °C (hexanes). IR (cm^{-1}) ν_{max}: 2221 (CN), 842 (OOP). ^1H NMR (500 MHz, $CDCl_3$, ppm) δ: 1.30 (6H, br, 2 × CH_3), 3.79 (4H, br, 2 × N-CH_2), 4.39 (4H, br, 2 × N-CH_2 allylic), 5.74 (2H, br, =CH-), 7.46 (4H, d, J = 8.6 Hz, arom.), 7.59 (4H, d, J = 8.5 Hz, arom.). MS (EI) *m*/*z* calcd. for $C_{22}H_{24}N_8$: 400.2124; found: 400.2128.

*3-Ethyl-3-{(***E***)-4-[1-ethyl-3-(***p***-nitrophenyl)-2-triazenyl]-2-butenyl}-1-(***p***-nitrophenyl)-1-triazene (11b)*

X = *p*-NO_2; 76% yield, ochre powder, mp 155–156.5 °C (ethanol). IR (cm^{-1}) ν_{max}: 1507, 1341 (NO_2), 852 (OOP). ^1H NMR (500 MHz, $CDCl_3$, ppm) δ: 1.34 (6H, br, 2 × CH_3), 3.83 (4H, br, 2 × N-CH_2), 4.42 (4H, br, 2 × N-CH_2 allylic), 5.75 (2H, br, =CH-), 7.48 (4H, d, J = 8.8 Hz, arom.), 8.18 (4H, d, J = 8.8 Hz, arom.). MS (EI) *m*/*z* calcd. for $C_{20}H_{24}N_8O_4$: 440.1920; found: 440.1933.

*3-Ethyl-3-{(***E***)-4-[1-ethyl-3-(***p***-methoxycarbonylphenyl)-2-triazenyl]-2-butenyl}-1-(***p***-methoxycarbonylphenyl)-1-triazene (11c)*

X = *p*-CO_2Me; 90% yield, red-brown chunky prisms, mp 63 °C (hexanes by trituration). IR (cm^{-1}) ν_{max}: 1705 (C=O), 1267.5 (C O), 860 (OOP). ^1H NMR (500 MHz, $CDCl_3$,

© 2006 NRC Canada

ppm): 1.26 (6H, br, 2 × CH_3), 3.78 (4H, br q, J = 6.5 Hz, 2 × N-CH_2), 3.90 (6H, s, 2 × O-Me), 4.375 (4H, br, 2 × N-CH_2 allylic), 5.77 (2H, br, =CH-), 7.44 (4H, d, J = 8.5 Hz, arom.), 8.00 (4H, d, J = 8.65 Hz, arom.). MS (EI) m/z calcd. for $C_{24}H_{30}N_6O_4$: 466.2328; found: 466.2327.

3-Ethyl-3-{(*E*)-4-[1-ethyl-3-(p-tolyl)-2-triazenyl]-2-butenyl}-1-(p-tolyl)-1-triazene (11d)

X = *p*-Me; 32% yield, fine khaki needles, mp 50 to 51 °C (aqueous ethanol). IR (cm^{-1}) ν_{max}: 825 (OOP). ^{1}H NMR (500 MHz, $CDCl_3$, ppm) δ: 1.22 (6H, t, J = 7.2 Hz, 2 × CH_3), 2.33 (6H, s, tolyl Me), 3.72 (4H, q, J = 7.2 Hz, 2 × N-CH_2), 4.31 (4H, d, J = 4.6 Hz, 2 × N-CH_2 allylic), 5.74 (2H, t, J = 3.1 Hz, =CH-), 7.12 (4H, d, J = 7.9 Hz, arom.), 7.30 (4H, d, J = 8.2 Hz, arom.). MS (EI) m/z calcd. for $C_{22}H_{30}N_6$: 378.2532; found: 378.2535.

3-Ethyl-3-{(*E*)-4-[1-ethyl-3-(p-bromophenyl)-2-triazenyl]-2-butenyl}-1-(p-bromophenyl)-1-triazene (11e)

X = Br; 86% yield, off-white chunky needles, mp 76 to 77 °C (methanol). IR (cm^{-1}) ν_{max}: 834.5 (OOP). ^{1}H NMR (500 MHz, $CDCl_3$, ppm) δ: 1.23 (6H, br t, 2 × CH_3), 3.73 (4H, q, J = 7.1 Hz, 2 × N-CH_2), 4.32 (4H, d, J = 4.4 Hz, 2 × N-CH_2 allylic), 5.73 (2H, br, =CH-), 7.28 (4H, d, J = 8.7 Hz, arom.), 7.42 (4H, d, J = 8.8 Hz, arom.). MS (EI) m/z calcd. for $C_{20}H_{24}N_6Br_2$: 506.0429; found: 506.0429.

3-Ethyl-3-{(*E*)-4-[1-ethyl-3-(p-chlorophenyl)-2-triazenyl]-2-butenyl}-1-(p-chlorophenyl)-1-triazene (11f)

X = *p*-Cl; 85% yield, beige powder, mp 74 to 75 °C (aqueous ethanol). IR (cm^{-1}) ν_{max}: 835 (OOP). ^{1}H NMR (500 MHz, $CDCl_3$, ppm) δ: 1.23 (6H, br t, J = 6.1 Hz, 2 × CH_3), 3.73 (4H, q, J = 7.0Hz, 2 × N-CH_2), 4.32 (4H, d, J = 4.1 Hz, 2 × N-CH_2 allylic), 5.74 (2H, br, =CH-), 7.27 (4H, d, J = 8.8 Hz, arom.), 7.33 (4H, d, J = 8.8 Hz, arom.). MS (EI) m/z calcd. for $C_{20}H_{24}N_6Cl_2$: 418.1439; found: 418.1442.

3-Methyl-3-{2-[1-methyl-3-aryl-2-triazenyl]cyclohexyl}-1-aryl-1-triazenes (12)

General procedure

The aromatic primary amine (0.015 mol) was dissolved in 15 mL of 3 mol/L hydrochloric acid, with the aid of heat if necessary, and the resulting solution was cooled in an ice–salt bath to 0 °C. The solution was diazotized with a solution of sodium nitrite (1.1 g, 0.016 mol) in deionized water (3.0 mL) while maintaining the temperature below 5 °C, and then stirred for a further 0.5 h in the cold. The resulting diazonium salt solution was cold-filtered if necessary. A separate solution of *trans-N,N′*-dimethycyclohexane-1,2-diamine (0.005 mol, 0.715 g) in deionized water (2.0 mL) was prepared and this solution was added slowly to the diazonium salt solution. After stirring in the cold for 0.5 h, the resulting mixture was then neutralized with saturated sodium bicarbonate solution. The mixture was then left to stir until precipitation was deemed to be complete (~1.75 h). The solid product was filtered under suction, dried, and recrystallized from an appropriate solvent. Products that separated as oils were extracted into dichloromethane, dried over anhydrous magnesium sulfate, and isolated by evaporation under vacuum. The following products were obtained.

3-Methyl-3-{2-[1-methyl-3-(p-cyanophenyl)-2-triazenyl]cyclohexyl}-1-(p-cyanophenyl)-1-triazene (12a)

X = *p*-CN; 96% yield, fine pale yellow plates, mp 147 to 148 °C (aqueous ethanol). IR (cm^{-1}) ν_{max}: 2220 (CN), 840 (OOP). ^{1}H NMR(500 MHz, $CDCl_3$, ppm) δ: 1.48 (2H, quintet, J = 9.8 Hz, H_e or H_d), 1.83 (2H, dq, J = 2.8, 9.2 Hz, H_e or H_d), 1.97 (2H, br d, J = 8.1 Hz, H_b or H_c), 2.18 (2H, d, J = 13.5 Hz, H_b or H_c), 3.13 (6H, s, 2 × N-CH_3), 4.16 (2H, d (J = 9.6 Hz) + dt (J = 3.7, 13.6 Hz), H_a), 7.37 (4H, d, J = 8.5 Hz, arom.), 7.55 (4H, d, J = 8.4 Hz, arom.). MS (EI) m/z calcd. for $C_{22}H_{24}N_8$: 400.2124; found: 400.2137.

3-Methyl-3-{2-[1-methyl-3-(p-acetylphenyl)-2-triazenyl]cyclohexyl}-1-(p-acetylphenyl)-1-triazene (12b)

X = *p*-COMe; 98% yield, red-brown prisms, mp 114–119 °C (water). IR (cm^{-1}) ν_{max}: 1677 (C=O), 842 (OOP). ^{1}H NMR (500 MHz, $CDCl_3$, ppm) δ: 1.48 (2H, quintet, J = 9.7 Hz, H_e or H_d), 1.83 (2H, br q, J = 9.2 Hz, H_e or H_d), 1.96 (2H, br d, J = 8.2 Hz, H_b or H_c), 2.18 (2H, br d, J = 13.2 Hz, H_b or H_c), 2.57 (6H, s, 2 × acetyl Me), 3.13 (6H, s, 2 × N-CH_3), 4.18 (2H, d (J = 9.6 Hz) + dt (J = 2.3, 13.1 Hz), H_a), 7.38 (4H, d, J = 8.5 Hz, arom.), 7.89 (4H, d, J = 8.65 Hz, arom.). MS (EI) m/z calcd. for $C_{24}H_{30}N_6O_2$: 434.2430; found: 434.2420.

3-Methyl-3-{2-[1-methyl-3-(p-methoxycarbonylphenyl)-2-triazenyl]cyclohexyl}-1-(p-methoxycarbonylphenyl)-1-triazene (12c)

X = *p*-COOMe; 98% yield, pale yellow prisms, mp 106–108 °C (hexanes). IR (cm^{-1}) ν_{max}: 1724 (C=O), 1283 (C-O), 858 (OOP). ^{1}H NMR (500 MHz, $CDCl_3$, ppm) δ: 1.47 (2H, quintet, J = 9.9 Hz, H_e or H_d), 1.82 (2H, br q, J = 9.2 Hz, H_e or H_d), 1.95 (2H, br d, J = 8.3 Hz, H_b or H_c), 2.17 (2H, d, J = 13.2 Hz, H_b or H_c), 3.12 (6H, s, 2 × N-CH_3), 3.90 (6H, s, 2 × OMe), 4.17 (2H, d (J = 9.7 Hz) + dt (J = 2.2, 12.5 Hz), H_a), 7.36 (4H, d, J = 8.4 Hz, arom.), 7.96 (4H, d, J = 8.4 Hz, arom.). MS (EI) m/z calcd. for $C_{24}H_{30}N_6O_4$: 466.2328; found: 466.2340.

3-Methyl-3-{2-[1-methyl-3-(p-tolyl)-2-triazenyl]cyclohexyl}-1-(p-tolyl)-1-triazene (12d)

X = *p*-CH_3; 82% yield, oil. IR (cm^{-1}) ν_{max}: 823 (OOP). ^{1}H NMR (500 MHz, 273 K, $CDCl_3$, ppm) δ: 1.40 (2H, quintet, J = 9.7 Hz, H_e or H_d), 1.76 (2H, br q, J = 9.3 Hz, H_e or H_d), 1.87 (2H, br d, J = 8.0 Hz, H_b or H_c), 2.08 (2H, d, J = 13.0 Hz, H_b or H_c), 2.32 (6H, s, 2 × tolyl Me), 3.06 (6H, s, 2 × N-CH_3), 4.08 (2H, d (J = 9.7 Hz) + dt (J = 2.4, 12.9 Hz), H_a), 7.10 (4H, d, J = 8.1 Hz, arom.), 7.26 (4H, d, J = 8.3 Hz, arom.). ^{13}C NMR (125.77 MHz, 273 K, $CDCl_3$, ppm) δ: 21.0 (tolyl Me), 25.0 (C-1), 31.25 (C-2), 32.75 (N-Me), 66.32 (C-3), 120.3, 129.3, 134.8, 148.6 (aromatic). MS (EI) m/z calcd. for $C_{22}H_{30}N_6$: 378.2532; found: 378.2544.

3-Methyl-3-{2-[1-methyl-3-(p-bromophenyl)-2-triazenyl]cyclohexyl}-1-(p-bromophenyl)-1-triazene (12e)

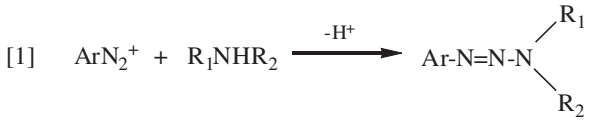
X = Br; 92% yield, fine white needles, mp 98 to 99 °C (aqueous ethanol). IR (cm^{-1}) ν_{max}: 830 (OOP). ^{1}H NMR (500 MHz, $CDCl_3$, ppm) δ: 1.45 (2H, quintet, J = 9.7 Hz, H_e or H_d), 1.79 (2H, br q, J = 8.7 Hz, H_e or H_d), 1.93 (2H, br d, J = 7.8 Hz, H_b or H_c), 2.13 (2H, d, J = 12.6 Hz, H_b or H_c), 3.07 (6H, s, 2 × N-CH_3), 4.09 (2H, d (J = 9.5 Hz) + br m,

© 2006 NRC Canada

H_a), 7.19 (4H, d, J = 8.5 Hz, arom.), 7.38 (4H, d, J = 8.5 Hz, arom.). MS (EI) *m/z* calcd. for $C_{20}H_{24}N_6Br_2$: 506.0429; found: 506.0405.

Results and discussion

The reaction of a diazonium salt with a secondary alkylamine is the traditional way of synthesizing a simple triazene (20) (eq.[1]).



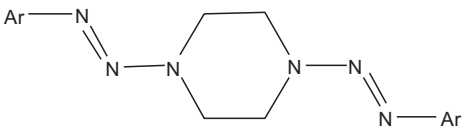
A logical extension of this approach is to couple the diazonium salt with an alkanediamine to afford a bistriazene (1) and this approach was used successfully to prepare the bistriazene series **8** (2). More recent work in this laboratory has developed this approach to the synthesis of a series of *N*,*N*′-bis(aryldiazenyl)piperazines (**13**) (21) by diazonium coupling with piperazine. Further development with the heterocyclic homologue, homopiperazine (*diazepane*), led to the synthesis of the novel bistriazene series **14** (22). The main thrust of the present work is to investigate the synthesis of the new bistriazenes series, the 3-methyl-3-{3-[1-methyl-3-aryl-2-triazenyl]propyl}-1-aryl-1-triazenes (**9**), which are the homolgues of series **8**, and are also of interest as being the acyclic analogues of the known bis(aryldiazenyl)diazepines (**14**).

The synthesis of the new series **9** was undertaken by reaction of 2 equiv. of the diazonium salt (ArN_2^+) with 1 equiv. of *N*,*N*′-dimethyl-1,3-propanediamine ($MeNHCH_2CH_2CH_2NHMe$). The yields and physical data of the products are reported in Table 1. The yields are mostly moderate to excellent. The compounds of type **9** with electron-withdrawing aryl substituents are crystalline solids, whereas others are oils. The IR spectra of the series **9a**–**9n** are consistent with the nature of the aryl substituent and with the position of substitution in the aromatic ring. The elemental composition of all but two of the compounds in this series has been determined by either high-resolution mass spectrometry (EI) or by elemental analysis. Further structure elucidation of series **9** is supported by the results of ^{1}H NMR analysis, which is reported in Table 2.

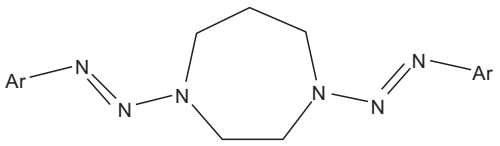
In the ^{1}H NMR spectra, the *N*-methyl proton resonance is observed as a six-proton singlet in the range 2.9–3.3 ppm. The protons of the methylene groups in the propane spacer appear as a four-proton triplet at ca. 3.4–3.9 ppm and a two-proton quintet at ca. 1.7–2.2 ppm. The coupling constant between the methylene groups is in the range 6.6–6.9 Hz. The protons present in the aryl substituent (X) are observed as expected, as are the AA′BB′ signal patterns in the p-substituted derivatives **9a**–**9j**. The results of ^{13}C NMR analysis of some of the compounds in series **9** are reported in Table 3. ^{13}C NMR analysis of the compounds in this series was limited by the severe broadening of the signals of the *N*-alkyl carbon atoms owing to the restricted rotation about the N—N bond of the triazene moiety (23), which results in weak carbon signals being undetectable at ambient temperature. The results reported in Table 3 are those for which a complete set of ^{13}C signals is observed. The *N*-methyl carbon resonates at ca. 36 ppm; the central methylene carbon of the spacer is observed at ca. 27 ppm and the *N*-methylene carbon of the spacer resonates at ca. 52 ppm.

Comparison of these observations with previous NMR studies with compounds of series **8** (2) is very favourable. The N-Me resonance in **8** is ca. 3.2–3.3 ppm, compared to 2.9–3.3 ppm in series **9**. The *N*-methylene signal in **8** occurs at ca. 4.0–4.1 ppm, compared to 3.4–3.9 ppm in **9**. The *N*-methyl carbon signal in series **8** arises at ca. 35 ppm, compared to 35 to 36 ppm in **9**, and the *N*-methylene carbon in **8** resonates at ca. 54 ppm, compared to 52 to 53 ppm in **9**.

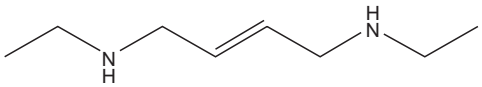
The synthesis of the model compounds (**10**) was achieved by diazonium coupling with *N*,*N*,*N*′-trimethyl-1,3-propanediamine ($Me_2NCH_2CH_2CH_2NHMe$). The triazenes of series **10** proved to be somewhat troublesome; many of the prod-



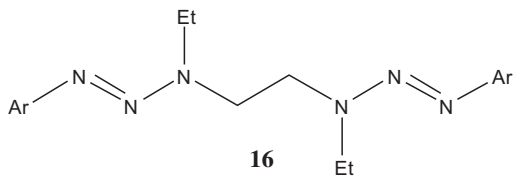
13



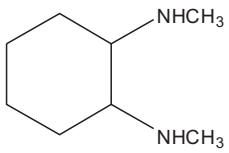
14



15



16



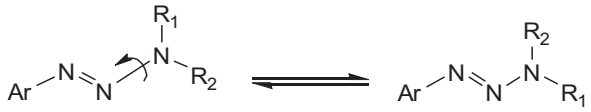
19

© 2006 NRC Canada

ucts were found to be intractable solids or viscous oils. Successful characterization was achieved with triazenes of type **10** with electron-withdrawing aryl substituents (i.e., X = CN, CO_2Me, COMe, and Br). Comparison of the NMR spectra of compounds of series **9** and **10** shows that the *N*-methyl resonance occurs at ca. 3.2–3.4 ppm in the model compounds **10**, compared with 2.9–3.3 ppm in **9**. The *N*-methylene protons adjacent to the triazene moiety in **10** resonates at ca. 3.6–3.8 ppm compared with 3.4–3.9 ppm in **9**. The *N*-methyl carbon signals occur at ca. 35 ppm in both series and the *N*-methylene carbons are found at ca. 52 ppm in both.

The bistriazenes of series **9** have a three-carbon spacer connecting the N-3 nitrogen atoms, compared with the two-carbon spacer in series **8** previously reported (2). The target molecules of structure **11** are relevant to this study because of the natural extension to the four-carbon spacer. The compounds of series **11** were prepared by reaction of 2 equiv. of the diazonium salt with 1 equiv. of *N*,*N*′-diethyl-2-butene-1,4-diamine (**15**), which is a commercially available starting material. The products are crystalline solids and are obtained in excellent yields (76%–90%), with the exception of the *p*-tolyl derivative (**11d**). The bistriazenes of series **11** have been characterized by IR and NMR spectroscopy and the elemental composition has been verified by high-resolution mass sapectrometry (EI) in all cases.

Although the ^{1}H NMR spectra of products **11a**–**11f** are fully consistent with the assigned structures, the complete interpretation of the splitting patterns in the spectra proved difficult owing to extreme broadening of the NMR signals. Line broadening in the NMR spectra of triazenes is a common occurrence owing to the restricted rotation around the N2—N3 single bond alluded to earlier in this paper (23) (eq. [2]).

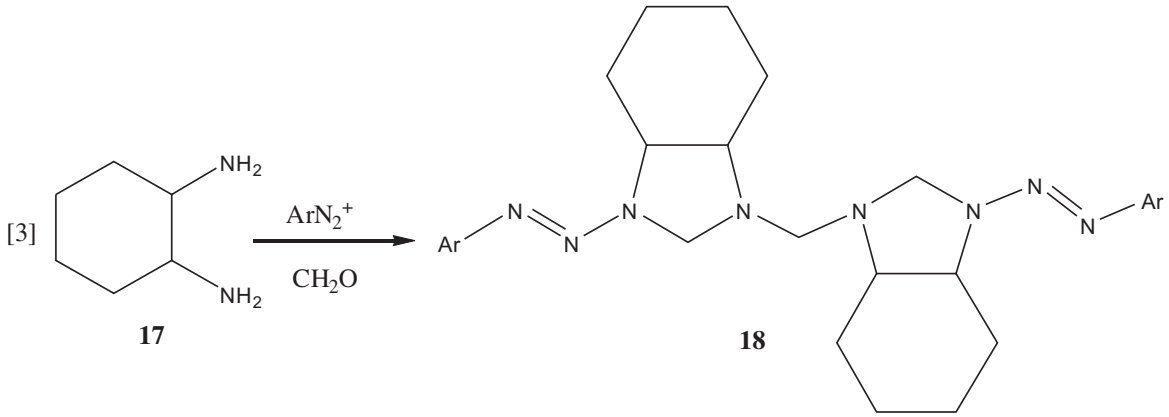
[2] 

The restriction to the rotation around N2—N3 is enhanced by the ubiquitous resonance phenomenon present in triazenes. Such resonance is enhanced by the presence of electron-withdrawing groups in the aryl substituent (X); significantly, most of the compounds of series **11** have an electron-withdrawing substituent (X = CN, NO_2, CO_2Me, Br, or Cl), and equally significantly, the NMR spectrum of the tolyl derivative (**11d**) is the one that provides the most information about the splitting patterns.

Thus, the ^{1}H NMR spectrum of **11d** shows the predicted resonances of the AA′BB′ aromatic system at 7.12 and 7.30 ppm, and also displays the tolyl Me groups as a six-proton singlet at 2.33 ppm. The *N*-ethyl protons show up as a six-proton triplet methyl signal at 1.22 ppm and a four-proton methylene quartet at 3.72 ppm. The *N*-methylene group of the butenyl spacer is a four-proton doublet at 4.31 ppm and the vinylic proton resonates at 5.74 ppm with the expected triplet multiplicity. The chemical shifts observed in the other bistriazenes of series **11** are analogous to those assigned in the spectrum of **11d**. The *N*-ethyl protons are in the range 1.22–1.34 ppm and 3.72–3.83 ppm; the allylic *N*-methylene protons resonate in the range 4.31–4.42 ppm and the vinylic protons are observed at 5.73–5.77 ppm. The resonances of the *N*-ethyl protons compare favourably with the published data (2) for the bistriazene series (**16**), which display signals in the range 1.24–1.36 ppm and 3.74–3.84 ppm.

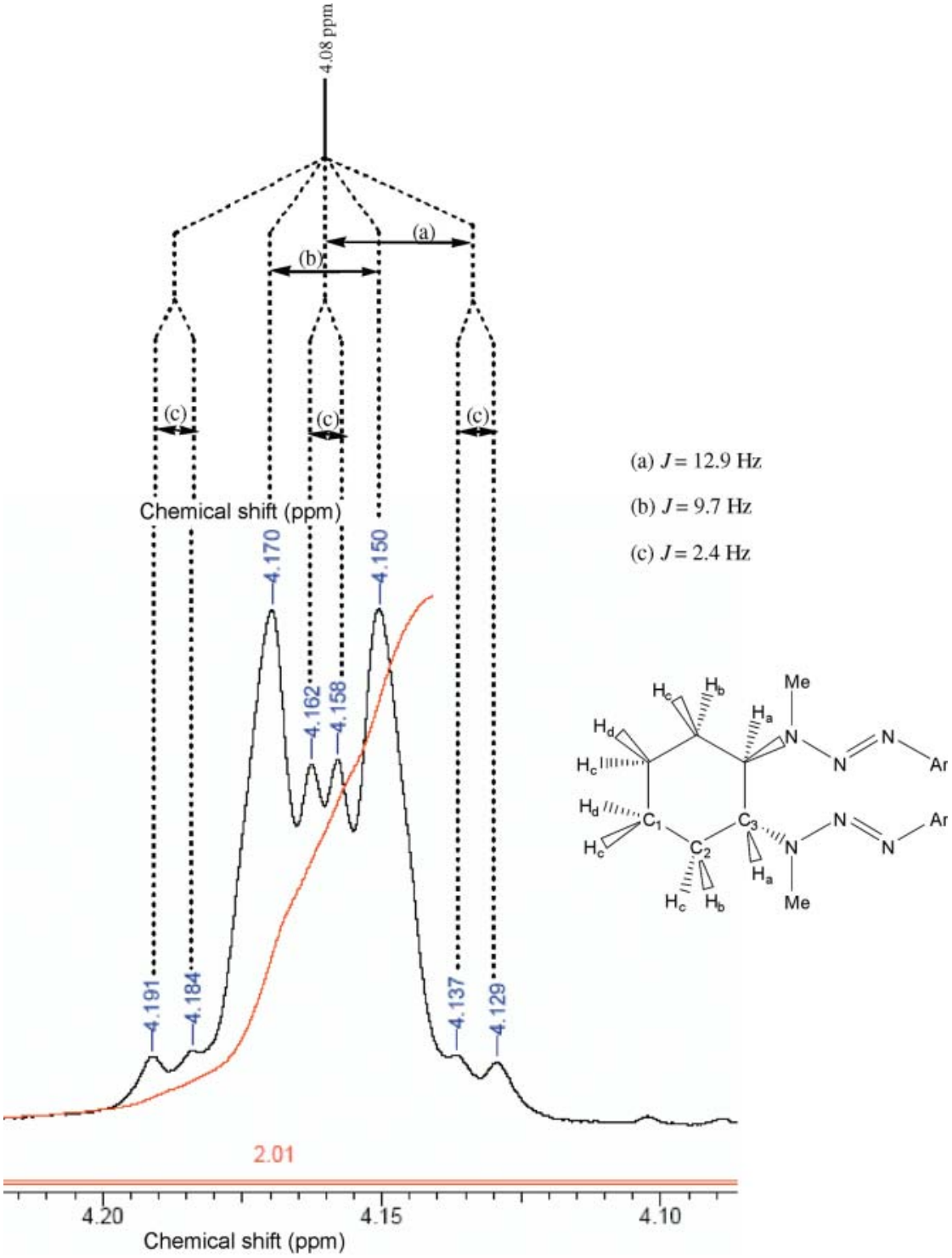
The final variation on the bistriazene theme in this paper is series **12**, which have a cyclohexane moiety as the spacer group between the N-3 nitrogens of the triazene units. Cyclohexanediamine chemistry has a rather oblique but significant connection to another aspect of the research being pursued in this laboratory, which is the general study of diazonium coupling reactions with primary alkanediamines mixed with formaldehyde (3, 24). When 1,2-diaminocyclohexane (**17**) is mixed with formaldehyde and the mixture is treated with a diazonium salt solution, the resulting product is the 1-[2-aryl-1-diazenyl]-3-({3-[2-aryl-1-diazenyl]perhydrobenzo[*d*]imidazol-1-yl}methyl)perhydrobenzo[*d*]imidazole (**18**) (25, 26).

Thus, we undertook the study of the diazonium coupling reaction with *trans*-*N*,*N*′-dimethylcyclohexane-1,2-diamine (**19**), a commercially available bis-secondary amine, which affords the series of 3-methyl-3-{2-[1-methyl-3-aryl-2-triazenyl]cyclohexyl}-1-aryl-1-triazenes (**12**). The yields of these products are excellent and, with one exception, they are crystalline solids. The IR spectra of the bistriazenes of series **12** are consistent with the functional groups present and the elemental composition was verified by high-resolution mass spectrometry (EI). The ^{1}H NMR spectra of these compounds are complex because of the presence of two chiral centres in the cyclohexanediamine moiety. The diastereotopic protons of the methylene groups (H_b/H_c and

[3] 

© 2006 NRC Canada

Fig. 1. Detail of the ^{1}H NMR spectrum of 3-methyl-3-{2-[1-methyl-3-(*p*-tolyl)-2-triazenyl]cyclohexyl}-1-(*p*-tolyl)-1-triazene (**12d**) at 273 K in $CDCl_3$ showing the H_a proton signals.



H_d/H_e, see Fig. 1 for the proton key), are clearly distinguished in the 500 MHz spectra of these compounds.

The protons furthest away from the triazene units in **12** give rise to the high field signals at 1.40–1.48 ppm and 1.76–1.83 ppm, which are assigned to protons H_d and H_e. The multiplicity of these two signals is different; one signal is a quintet, the other is a doublet of quartets (when resolved). Either of these multiplicities is consistent with a given proton, e.g., H_e, having four nonequivalent neighbours, i.e., geminal H_d, vicinal H_d, and vicinal H_b/H_c. The reason why H_d and H_e are slightly different in this respect is not clear. However, H_b and H_c are also observed as diastereotopic protons at 1.87–1.97 ppm and 2.08–2.18 ppm. These signals are unequivocally broad doublets and we

© 2006 NRC Canada

Fig. 2. Stack plot of the variable temperature ^{1}H NMR spectrum of compound **12d** in $CDCl_3$ in the region 3.95–4.20 ppm showing the H_a proton signals.

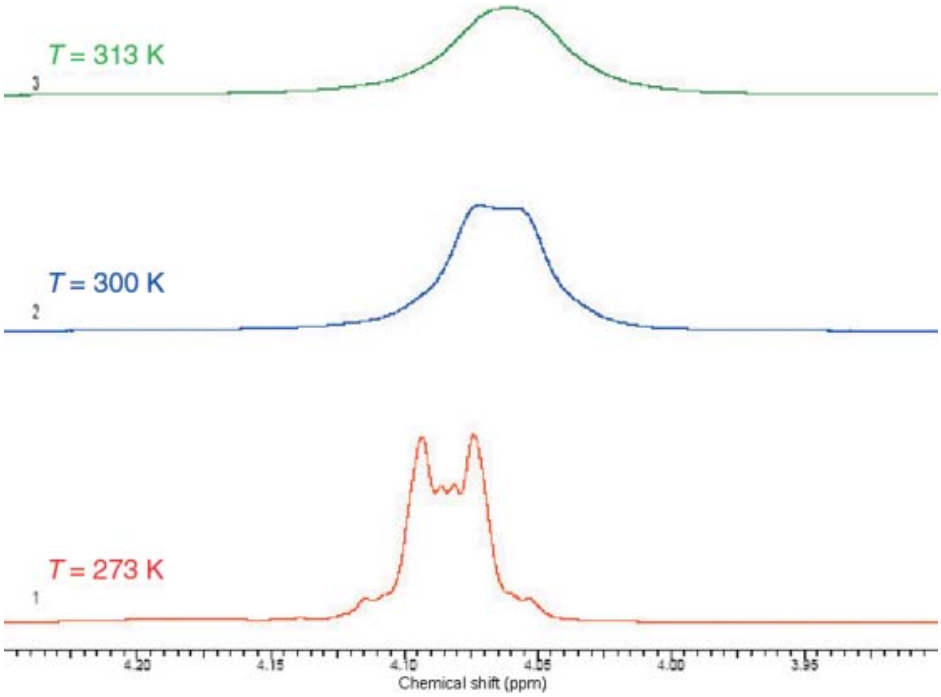


Table 6. Comparison of the ^{1}H and ^{13}C NMR chemical shifts (ppm) in the spectra of the new bistriazenes **9**, **10**, **11**, and **12** compared with previously reported data for various bistriazenes.

	Protons			Carbon		
Cpd series	Triazene N-Me	Triazene N-CH_2	C-CH_2-C in spacer	Triazene N-Me	Triazene N-CH_2	Ref. no.
6	3.23–3.37	4.63–4.80	—	37.5	74.2	27
8	3.22–3.32	4.00–4.35	—	35–36.5	ca. 54	2
9	3.20–3.32 (2.94)	3.44–3.94	1.75–2.20	ca. 36	52 to 53	This paper
10	3.02–3.40	3.58–3.86	1.6–1.9	35.1	51.8	This paper
11	—	3.73–3.83	—	—	—	This paper
12	3.06–3.07	—	1.9–2.2	32.75	—	This paper
13	—	3.9–4.2	—	—	46.48	21
14	—	3.76–4.25	1.75–2.41	—	44–54	22
16	—	3.94–4.05	—	—	ca. 51	2

attribute the doublet splitting to coupling with the vicinal methane proton (H_a). The signal of the methine proton itself (H_a) is found in the range 4.08–4.18 ppm, but the multiplicity of this two-proton signal is a very intriguing combination of a broad doublet and a doublet of triplets, both centered at the same frequency. This pattern is consistent for all substituents; Fig. 1 shows a detail of this multiplet taken from the spectrum of the *p*-tolyl derivative (**12d**). The precise origin of this doublet – doublet of triplets combination is not immediately clear, but the most likely explanation is that it is connected to the dynamic equilibrium of the N2—N3 rotamers. This hypothesis is supported by the result of a VT NMR experiment with **12d**, illustrated in Fig. 2. The H_a signal becomes a broad hump when the temperature of a solution of **12d** is raised to 313 K. The triazene *N*-methyl signal at 3.06 ppm also shows significant broadening at higher temperature, whereas the signal of the tolyl methyl group, which is far removed from the rotameric center in the triazene moiety, does not appear to change. Likewise, the signals in the range 1.3–2.1 ppm, those from the cyclohexane methylene groups (H_b, H_c, H_d, and H_e), change little with an increase in temperature.

Conclusion

A fitting conclusion to this paper is to take a broad view of the NMR characteristics of the new compounds reported here in comparison to the known NMR data of previously reported compounds. This comparison is shown in Table 6. There is consistency in the ^{1}H chemical shift data of *N*-methyl groups attached to N-3 of the triazene and also of the spacer *N*-methylene groups linking the N-3 atoms of two triazene units. The ^{13}C NMR data are also consistent. One final point of comparison is to take up the suggestion made earlier that the new compounds of series **9** are the acyclic analogues of the diazepane series (**14**). Since there are no *N*-

© 2006 NRC Canada

methyl groups in **14**, the valid comparison is to compare the NMR characteristics of the propane spacer, which is common to both. In series **9**, the *N*-methylene proton signal is observed in the range 3.44–3.94 ppm compared with 3.76–4.25 ppm in **14**; the central methylene of the three-carbon spacer is observed at 1.75–2.20 ppm in **9**, compared to 1.75–2.41 ppm in **14**.

Acknowledgements

The authors are grateful to the Natural Sciences and Engineering Research Council of Canada (NSERC) for a Discovery Grant to the principal author (KV) and to the Faculty of Graduate Studies and Research at Saint Mary's University for Summer Research Awards to Shasta Moser (2003) and Jeff Clarke (2005). We are also grateful to the Atlantic Region Magnetic Resonance Centre at Dalhousie University for providing NMR spectra and to Dalhousie University for providing mass spectral data. In particular, we would like to thank Dr. Bob Berno for assistance with interpretation of the NMR spectral data and Mr. Xiao Feng for assistance with mass spectra.

References

1. K. Vaughan. Org. Prep. Proced. Int. **33**, 59 (2001).
2. D.L. Hooper, I.R. Pottie, M. Vacheresse, and K. Vaughan. Can. J. Chem. **76**, 125 (1998).
3. M.B. Peori, K. Vaughan, and D.L. Hooper. J. Org. Chem. **63**, 7437 (1998).
4. D.S. Brown, M.P. Merrin, and K. Vaughan. Proc. N. S. Inst. Sci. **40**, 67 (1995).
5. H.W. Manning, L.M. Cameron, R.J. LaFrance, K. Vaughan, and R. Rajaraman. Anti-Cancer Drug Des. **1**, 37 (1985).
6. J.J. Blumenstein and C.J. Michejda. Tetrahedron Lett. **32**, 183 (1991).
7. J.J. Blumenstein and C.J. Michejda. US Patent 5 731 301, 24 March 1998.
8. E. Yanarates, A. Disli, and Y. Yildirin. Org. Prep. Proc. Int. **31**, 429 (1999).
9. D.B. Kimball and M.M. Haley. Angew. Chem. Int. Ed. **41**, 3338 (2002).
10. S. Brase. Acc. Chem. Res. **37**, 805 (2004).
11. J.P. Godschalx, Q.S.J. Niu, K.J. Bruza, C.H. Cummins, and P.H. Townsend. US Patent 6 646 081 B2, 11 November 2003.
12. M. Horner, G.M. de Oliviera, J.S. de Oliviera, W.M. Teles, C.A.L. Filgueiras, and J. Beck. J. Organometal. Chem. **691**, 251 (2006).
13. A.V. Pochinok, M.Y. Kornilov, and L.I. Savranski. Ukr. Khim. Zh. (Russ. Ed.), **43**, 180 (1977); Chem. Abstr. **86**, 188927j (1977).
14. A. Gescher, J.A. Hickman, R.J. Simmonds, M.F.G. Stevens, and K. Vaughan. Tetrahedron Lett. 5041 (1978).
15. R.J. LaFrance, Y. Tang, K. Vaughan, and D.L. Hooper. J. Chem. Soc. Chem. Commun. 721 (1983).
16. S.C. Cheng, L. Fernandez, J. Iley, and E. Rosa. J. Chem. Res. (S), 108 (1983).
17. R.D. Singer, K. Vaughan, and D.L. Hooper. Can. J. Chem. **64**, 1567 (1986).
18. I.R. Pottie, C.V.K. Sharma, K. Vaughan, and M.J. Zaworotko. J. Chem. Crystallogr. **28**, 5 (1998).
19. K. Vaughan, E. Turner, and H. Jenkins. Can. J. Chem. **82**, 448 (2004).
20. J. Elks and D.H. Hey. J. Chem. Soc. 441 (1943).
21. V.R. Little, R. Tingley, and K. Vaughan. Can. J. Chem. **83**, 471 (2005).
22. S.L. Moser and K. Vaughan. Can. J. Chem. **82**, 1725 (2004).
23. M. Barra, S. Srivastava, and E. Brockman. J. Phys. Org. Chem. **17**, 1057 (2004), and refs. cited therein.
24. S.L. Moser and K. Vaughan. Can. J. Chem. **83**, 1071 (2005).
25. J.F. Glister and K. Vaughan. J. Heterocycl. Chem. **43**, 217 (2006).
26. J.F. Glister, H. Jenkins, and K. Vaughan. J. Chem. Crystallogr. Online First. Available from http://www.springerlink.com. 2006.
27. H.W. Manning, C.M. Hemens, R.J. LaFrance, Y. Tang, and K. Vaughan. Can. J. Chem. **62**, 749 (1984).

© 2006 NRC Canada

Novel synthesis of 2-naphthol Mannich bases and their NMR behaviour

Amitabh Jha, Nawal K. Paul, Smriti Trikha, and T. Stanley Cameron

Abstract: A novel two-step procedure involving the formation of 1-arylidene-2-tetralones from 2-tetralone and subsequent Michael addition of a cyclic secondary amine on the alkenone followed by in situ aerial oxidation was developed to produce 2-naphthol Mannich bases. A simple microwave-assisted one-pot synthesis of 2-naphthol Mannich bases was also carried out under solvent-free conditions from 2-naphthol and corresponding aldehydes and amines in the presence of *p*-toluenesulfonic acid. The compounds of this series displayed interesting NMR behaviour. Extensive variable-temperature NMR investigations, including HSQC experiments, are herein reported. NMR results on the conformation in solution phase were found to be consistent with the X-ray crystal structure in the solid state.

Key words: Mannich bases, microwave-assisted Mannich reaction, temperature-variable NMR spectroscopy, NMR dynamics, X-ray crystallography.

Résumé : On a mis au point une nouvelle méthode en deux étapes qui permet de produire des bases de Mannich du 2-naphtol et qui implique la formation de 1-arylidène-2-tétralones à partir de la 2-tétralone, puis une addition subséquente de Michael d'une amine secondaire cyclique sur l'alcénone, suivie d'une oxydation in situ par de l'air. On a aussi réalisé une synthèse des bases de Mannich du 2-naphtol par une simple réaction monotope du 2-naphtol, des aldéhydes et des amines correspondants en présence d'acide *p*-toluènesulfonique, sous l'effet de micro-ondes, dans des conditions sans solvant. Les composés de cette série présentent des comportements RMN intéressants. On a effectué de nombreuses études RMN à température variable, y compris des expériences de « HSQC ». On a trouvé que les résultats de la RMN sur la conformation en solution sont en accord avec la structure cristalline déterminée par diffraction des rayons X, à l'état solide.

Mots clés : bases de Mannich, réaction de Mannich assistée par les micro-ondes, spectroscopie RMN à température variable, dynamique RMN, cristallographie par diffraction des rayons X.

[Traduit par la Rédaction]

Introduction

Numerous chiral aminomethyl phenols have been reported as excellent chelating agents in metal-catalyzed asymmetric induction in a variety of reactions (1–10). Chiral Mannich bases of 2-naphthol are particularly popular in metal-mediated and ligand-accelerated catalysis of enantioselective carbon–carbon bond formation (11–17). Many of these carbon–carbon bond formation reactions involve the use of organozinc compounds as alkylating agents, which are relatively unreactive if uncoordinated (11). These ligands may be used in catalytic amounts. The first synthesis of racemic Mannich bases of 2-naphthol was achieved by Betti (18–22) at the turn of the 20th century. Thereafter, numerous modifications of this reaction surfaced (23–27) and optically pure Betti base analogs were prepared either by resolution or by the induction of chirality by the use of optically active amines (11–17, 28, 29).

In addition, potent oxytocic activity of compounds of this type is reported in the literature (30). Since these compounds have multiple centres for chelation with metal ions, they are likely to be potent inhibitors of metalloenzymes containing Fe, Cu, Zn, Co, etc., ions as cofactors (31–34). Also, these compounds have the potential to be used as scavengers in cases of heavy metal (Pd, Hg, Cd, As, Sb, etc.) poisoning (35, 36).

We herein report a novel synthetic route to this class of compounds (**1**–**4**, Fig. 1) involving two steps starting from 2-tetralones. Also, additional analogs (**5**–**11**, Fig. 1) were obtained in moderate to excellent yields with improved reaction time by modifying a reported microwave-assisted procedure (26). While characterizing the compounds using the usual spectroscopic means, we observed anomalous and interesting NMR behaviour of heterocyclic rings. NMR experiments to study the solution phase dynamics as well as

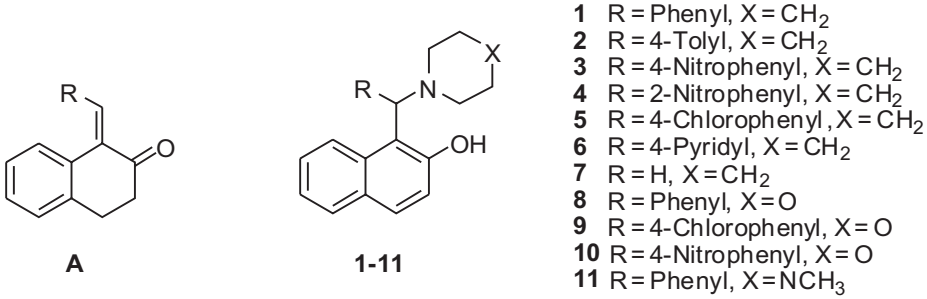
Received 4 October 2005. Published on the NRC Research Press Web site at http://canjchem.nrc.ca on 7 June 2006.

A. Jha,[1] **N.K. Paul, and S. Trikha.** Department of Chemistry, Acadia University, Wolfville, NS B4P 2R6, Canada.
T.S. Cameron.[2] Department of Chemistry, Dalhousie University, Halifax, NS B3H 4J3, Canada.

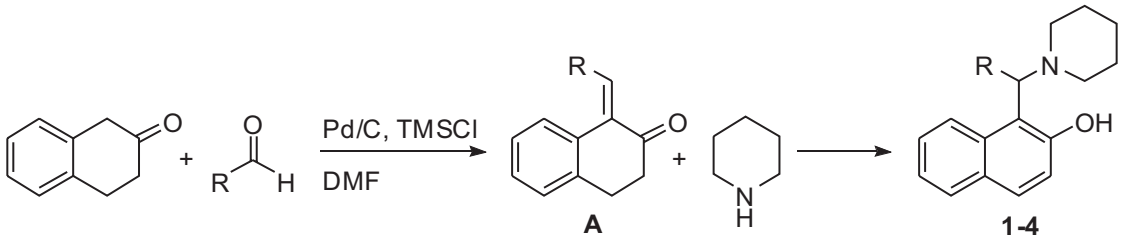
[1]Corresponding author (email: amitabh.jha@acadiau.ca).
[2]Corresponding author regarding X-ray crystallography (e-mail: cameron@dal.ca).

 doi:10.1139/V06-081 © 2006 NRC Canada

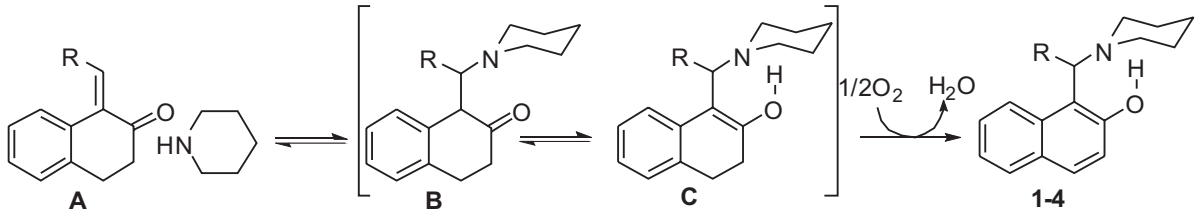
Fig. 1. Molecular structure of the compounds investigated.



Scheme 1. Novel synthethic route to 2-naphthol Mannich bases (**1**–**4**).



Scheme 2. Proposed mechanism for conversion of 1-arylidene-2-tetralone to 2-naphthol Mannich bases following Scheme 1.



solid-state X-ray crystal structure of representative compounds are also reported here.

Experimental

General

All chemicals were obtained from the Sigma-Aldrich Chemical Company, Inc. Column chromatographic purifications were undertaken using silica gel (230–400 mesh) obtained from Silicycle. ^{1}H and ^{13}C NMR were recorded on Bruker AV500 and AV300 NMR spectrometers. HSQC spectra were obtained on a Bruker AV500 spectrometer using 256 increments and a sweep width of 20 kHz in the indirect (carbon) dimension. Coherence selection was achieved using gradients and phase-sensitive HSQC data were obtained using the echo-antiecho method. All 180° pulses in the sequence were replaced with adiabatic shapes for improved broadband inversion and refocussing over the entire carbon frequency range. EI-MS and HR-MS spectra were obtained on a CEC 21-110B Sector instrument. Melting points were recorded on an electrothermal apparatus and are uncorrected. UV–vis and IR spectra were recorded on LKB Biochrom Ultraspec Plus 4054 and Nicolet Avatar 330 FT-IR spectrophotometers, respectively. A domestic microwave oven manufactured by Kenmore was used for the microwave-assisted reactions at highest power (900 W) and 2450 MHz operating frequency.

Synthesis of substituted 1-arylidene-2-tetralones (A)

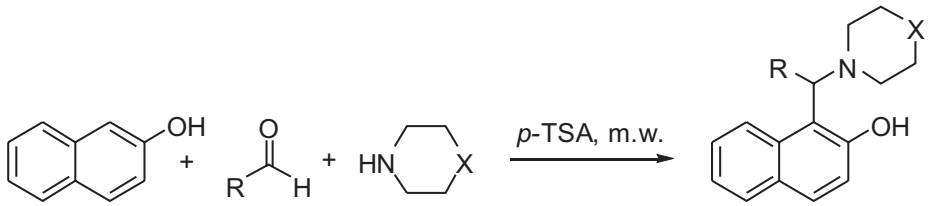
Palladium-catalyzed Knoevenagel-type condensation (37) from 2-tetralone and appropriate aldehydes resulted in 1-arylidene-2-tetralones. To a mixture of 2-tetralone (20 mmol), appropriate aromatic aldehyde (22 mmol), 10% Pd/C (2 mol %), and DMF (30 mL) was added TMSCl (22 mmol) in dropwise fashion at room temperature. After 30 min, the reaction was warmed to 75 °C and stirred for 5 h. DMF was rotary evaporated and the residue was chromatographed with 2% EtOAc in hexanes. The resulting products were characterized as 1-arylidene-2-tetralones (**A**) by comparison of their physical and spectral data with those reported in the literature (38). The melting points (°C) and percentage yields of the compounds in this series were as follows: **A** (R = phenyl): 116 to 117, 76; **A** (R = 4-tolyl): 103 to 104, 73; **A** (R = 4-NO_2-phenyl): 153 to 154, 82; **A** (R = 2-NO_2-phenyl): 122 to 123, 71.

Synthesis of 1-(arylpiperidin-1-yl methyl)naphthalen-2-ols (1–11)

Procedure A (Schemes 1 and 2): Appropriate 1-arylidene-2-tetralones (**A**, 10 mmol) reacted with excess piperidine at room temperature to produce the compounds (**1**–**4**) over a period of 7 days. No reaction progress was observed by TLC after 24 h. The resulting compounds were purified using silica gel column chromatography with 3% ethyl acetate in hexanes as the eluent. Unreacted starting materials (**A**) were also recovered.

© 2006 NRC Canada

Scheme 3. Synthethic route for the microwave-assisted reactions of compounds **1**–**12**.



1-12

Procedure B (Scheme 3): A mixture of 2-naphthol (10 mmol), appropriate aromatic aldehyde (12 mmol), *p*-TSA (50 mg, cat.), and appropriate secondary amine (12 mmol) was irradiated using the microwave for 1 min (30 s × 2, to avoid overheating). The reaction mixture was cooled and methanol was added to it. Several products, viz. compounds **1**, **3**, **5**, **6**, and **8**, were purified by digestion in methanol as follows. The reaction mixture was stirred in hot methanol (20 mL) for 1 h and kept at room temperature overnight for crystallization and precipitation. The solid product was filtered, washed with cold methanol (2 × 5 mL), and dried under vacuum. The rest of the derivatives were purified by column chromatography using silica gel. The desired product eluted with 2% ethyl acetate in hexanes. The products thus obtained were further purified by crystallization.

1-(Phenylpiperidin-1-ylmethyl)naphthalen-2-ol (1)

^{1}H and ^{13}C NMR were identical to those reported in the literature (27). UV–vis (MeOH, nm) λ_{max}: 244, 280, 336. IR (KBr disc, cm^{-1}) ν: 3443, 3050, 2971, 1621, 1599, 1455, 1268, 1238, 702. EI-MS (70 eV) *m*/*z* (% int.): 317 (M$^+$, 11), 231 (100), 200 (2), 84 (41). HR-MS calcd. for $C_{22}H_{23}NO$: 317.1780; found: 317.1785.

1-(4-Methylphenyl)piperidin-1-ylmethyl)naphthalen-2-ol (2)

UV–vis (MeOH, nm) λ_{max}: 244, 291, 336. IR (KBr disc, cm^{-1}) ν: 3439, 3060, 2963, 1621, 1595, 1384, 1359, 1261, 1231, 821. ^{1}H NMR (300 MHz, 273 K, $CDCl_3$) δ: 1.41 (1H, bs, CH), 1.50–1.91 (5H, m, 5 × CH), 2.27–2.46 (4H, m, Ar-CH_3, NCH), 2.92 (1H, bs, NCH), 3.23 (1H, bs, NCH), 3.53 (1H, bs, NCH), 5.23 (1H, s, Ar-CH-Ar′), 7.01–7.08 (1H, m, Ar-H), 7.22–7.28 (2H, m, Ar-H), 7.37–7.42 (3H, m, Ar-H), 7.49–7.52 (2H, m, Ar-H), 7.68–7.73 (1H, m, Ar-H), 7.81–7.84 (1H, m, Ar-H), 13.32 (1H, bs, OH). ^{13}C NMR (75 MHz, 273 K, $CDCl_3$) δ: 21.63, 24.03, 25.72, 26.00, 52.10, 55.20, 64.90, 109.00, 117.82, 120.33, 121.24, 123.06, 126.22, 127.10, 129.11, 129.47, 130.25, 130.87, 134.88, 155.36. EI-MS (70 eV) *m*/*z* (% int.): 331 (M$^+$, 14), 247 (10), 231 (100). HR-MS calcd. for $C_{23}H_{25}NO$: 331.1936; found: 331.1930.

1-(4-Nitrophenyl)piperidin-1-ylmethyl)naphthalen-2-ol (3)

UV–vis (MeOH, nm) λ_{max}: 244, 295, 335. IR (KBr disc, cm^{-1}) ν: 3439, 3080, 3060, 2926, 1621, 1514, 1441, 1414, 1346, 1265, 1231, 830. ^{1}H NMR (300 MHz, 273 K, $CDCl_3$) δ: 1.28 (1H, bs, CH), 1.58–1.73 (5H, m, 5 × CH), 2.02 (1H, bs, -NCH), 2.15 (1H, bs, -NCH), 2.65 (1H, bs, -NCH), 3.37 (1H, bs, -NCH), 5.23 (1H, s, Ar-CH-Ar′), 7.18–7.31 (2H, m, Ar-H), 7.42 (1H, t, *J*= 7.5 Hz, Ar-H), 7.70–7.81 (5H, m, Ar-H), 8.13–8.16 (2H, m, Ar-H), 13.78 (1H, bs, OH). ^{13}C NMR (75 MHz, 273 K, $CDCl_3$) δ: 24.32, 26.10, 26.40, 52.78, 55.03, 71.45, 115.26, 120.48, 120.83, 123.22, 124.61, 127.26, 129.06, 129.61, 130.21, 130.62, 132.33, 147.61, 147.73, 155.74. EI-MS (70 eV) *m*/*z* (% int.): 362 (M$^+$, 14), 279 (9), 260 (61), 231 (39), 230 (100), 85 (54), 58 (14). HR-MS calcd. for $C_{22}H_{22}N_2O_3$: 362.1630; found: 362.1634.

1-(2-Nitrophenyl)piperidin-1-ylmethyl)naphthalen-2-ol (4)

UV–vis (MeOH, nm) λ_{max}: 241, 335. IR (KBr disc, cm^{-1}) ν: 3439, 3052, 2926, 1621, 1595, 1514, 1316, 1265, 1231, 830. ^{1}H NMR (500 MHz, 273 K, $CDCl_3$) δ: 1.25–1.32 (1H, m, CH), 1.67–1.77 (5H, m, 5 × CH), 2.35–2.38 (2H, m, 2 × NCH), 2.58 (1H, d, *J* = 9.5 Hz, NCH), 3.30 (1H, d, *J* = 11.5 Hz, NCH), 6.08 (1H, s, Ar-CH-Ar′), 7.15 (1H, d, *J* = 9.0 Hz, Ar-H), 7.21–7.26 (1H, m, Ar-H), 7.31–7.45 (3H, m, Ar-H), 7.65–7.71 (3H, m, Ar-H), 7.81–7.85 (2H, m, Ar-H), 14.54 (1H, bs, OH). ^{13}C NMR (125 MHz, 273 K, $CDCl_3$) δ: 23.90, 25.93, 26.52, 49.92, 54.62, 64.02, 115.07, 120.20, 120.64, 122.69, 124.29, 126.97, 128.58, 128.86, 128.93, 130.09, 131.55, 132.61, 133.65, 133.70, 150.22, 156.94. EI-MS (70 eV) *m*/*z* (% int.): 362 (M$^+$, 2), 231 (100), 232 (47), 85 (3). HR-MS calcd. for $C_{23}H_{23}NO_3$: 362.1630; found: 362.1633.

1-(4-Chlorophenyl)piperidin-1-ylmethyl)naphthalen-2-ol (5)

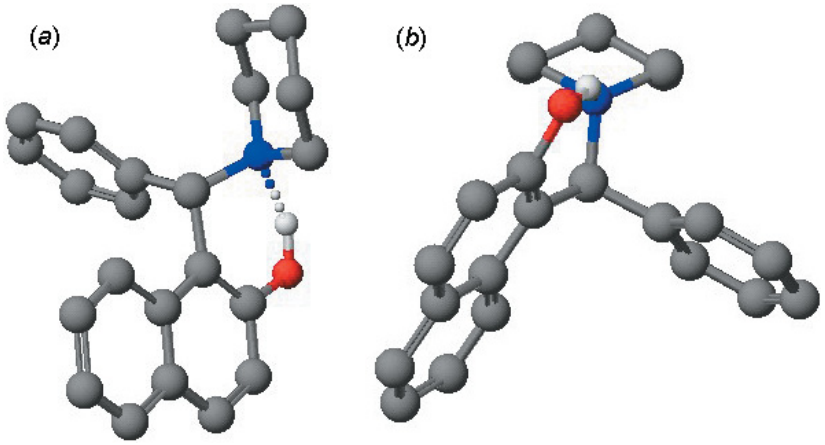
UV–vis (MeOH, nm) λ_{max}: 242, 291, 336. IR (KBr disc, cm^{-1}) ν: 3440, 3080, 2951, 1620, 1519, 1474, 1384, 1104, 742, 515. ^{1}H NMR (300 MHz, 273 K, $CDCl_3$) δ: 1.27 (1H, bs, CH), 1.62–1.70 (5H, bs, 5 × CH), 1.97 (1H, bs, NCH), 2.03 (1H, bs, NCH), 2.73 (1H, bs, NCH), 3.36 (1H, bs, NCH), 5.07 (1H, s, Ar-CH-Ar′), 7.19–7.41 (4H, m, Ar-H), 7.43–7.46 (1H, m, Ar-H), 7.54–7.68 (2H, m, Ar-H), 7.71–7.81 (3H, m, Ar-H), 3.12 (1H, bs, OH). ^{13}C NMR (75 MHz, 273 K, $CDCl_3$) δ: 24.35, 26.10, 26.30, 52.41, 55.14, 71.49, 117.13, 120.45, 121.20, 123.06, 127.08, 129.51, 129.77, 130.22 130.94, 131.16, 132.50, 134.21, 138.33, 156.12. EI-MS (70 eV) *m*/*z* (% int.): 353 (M + 2, 0.7), 350 (M$^+$, 2), 266 (2), 264 (2), 231 (6), 84 (100). HR-MS calcd. for $C_{22}H_{22}ClNO$: 351.1390; found: 351.1387.

1-(Piperidin-1-yl-pyridin-4-ylmethyl)naphthalen-2-ol (6)

UV–vis (MeOH, nm) λ_{max}: 241, 298. IR (KBr disc, cm^{-1}) ν: 3442, 3044, 2944, 1621, 1598, 1451, 1384, 1267, 1236, 816. ^{1}H NMR (300 MHz, 273 K, $CDCl_3$) δ: 1.61 (1H, bs, CH), 1.72–1.88 (5H, bs, 5 × CH), 2.10 (1H, bs, -NCH), 2.71 (1H, bs, -NCH), 3.16 (1H, bs, -NCH), 3.35 (1H, bs, -NCH),

© 2006 NRC Canada

Fig. 2. Energy minimized molecular model of compound **1** in two orientations. Hydrogen atoms are omitted for clarity.



5.07 (1H, s, Ar-CH-Ar′), 7.15–7.82 (8H, m, Ar-H), 8.50–8.52 (2H, d, J = 8 Hz, Ar-H), 13.75 (1H, bs, OH). ^{13}C NMR (75 MHz, 273 K, $CDCl_3$) δ: 24.40, 26.42, 26.44, 52.71, 54.94, 71.26, 115.17, 120.41, 120.94, 123.15, 124.12, 127.17, 129.01, 129.55, 130.48, 132.39, 149.11, 150.67, 155.87. EI-MS (70 eV) *m/z* (% int.): 318 (M^+, 5), 235 (4), 233 (100), 232 (51). HR-MS calcd. for $C_{21}H_{22}N_2O$: 318.1732; found: 318.1727.

1-Piperidin-1-ylmethylnaphthalen-2-ol (7)

UV–vis (MeOH, nm) λ_{max}: 245, 288, 334. IR (KBr disc, cm^{-1}) ν: 3448, 3051, 2935, 1621, 1599, 1474, 1384, 1271, 786. ^{1}H NMR (300 MHz, 273K, $CDCl_3$) δ: 1.23 (1H, bs, CH), 1.77 (5H, m, CH_2, -NCH_2), 2.37 (2H, bs, 2 × NCH), 3.36 (2H, bs, 2 × NCH), 4.37 (2H, s, -NCH_2Ar), 7.28–7.35 (2H, m, Ar-H), 7.46–7.51 (1H, m, Ar-H), 7.73–7.84 (3H, m, Ar-H), 13.2 (1H, bs, OH). ^{13}C NMR (75 MHz, 273K, $CDCl_3$) δ: 24.38, 26.25, 54.60, 57.68, 111.39, 119.67, 121.34, 122.68, 126.59, 128.79, 129.26, 129.36, 133.09, 157.17. EI-MS (70 eV) *m/z* (% int.): 241 (M^+, 5), 157 (5), 84 (100). HR-MS calcd. for $C_{16}H_{19}NO$: 241.1467; found: 241.1474.

1-(Morpholin-4-ylphenylmethyl)naphthalen-2-ol (8)

^{1}H and ^{13}C NMR were identical to those reported in literature (27). UV–vis (MeOH, nm) λ_{max}: 242, 291, 325. IR (KBr disc, cm^{-1}) ν: 3443, 3058, 2971, 2842, 1619, 1598, 1454, 1384, 1236, 1116. EI-MS (70 eV) *m/z* (% int.): 319 (M^+, 7), 233 (4), 231 (100), 86 (1). HR-MS calcd. for $C_{21}H_{21}NO_2$: 319.1572; found: 319.1566.

1-[(4-Chlorophenyl)morpholin-4-ylmethyl]naphthalen-2-ol (9)

UV–vis (MeOH, nm) λ_{max}: 242, 293, 319. IR (KBr disc, cm^{-1}) ν: 3438, 3062, 2958, 1619, 1597, 1450, 1411, 1384, 1238, 1117. ^{1}H NMR (300 MHz, 273 K, $CDCl_3$) δ: 2.32–2.54 (3H, m, 3 × NCH), 3.14–3.18 (1H, m, NCH), 3.51–3.71 (4H, m, 4 × OCH), 5.14 (1H, s, Ar-CH-Ar′), 7.17–7.31 (4H, m, Ar-H), 7.40–7.45 (1H, m, Ar-H), 7.53–7.56 (2H, m, Ar-H), 7.71–7.76 (3H, m, Ar-H), 13.15 (1H, bs, OH). ^{13}C NMR (75 MHz, 273 K, $CDCl_3$) δ: 51.95, 54.28, 67.10, 67.30, 71.59, 115.03, 120.27, 121.19, 123.33, 127.23, 129.22, 129.50, 129.91, 130.55, 131.10, 132.44, 134.55, 137.37, 154.95. EI-MS (70 eV) *m/z* (% int.): 355 (M+2, 4) 353 (M^+, 12), 268 (12), 265 (38), 231 (100), 202 (23), 86 (15). HR-MS calcd. for $C_{21}H_{20}ClNO_2$: 353.1183; found: 353.1193.

1-[(4-Nitrophenyl)morpholin-4-ylmethyl]naphthalen-2-ol (10)

^{1}H and ^{13}C NMR were identical to those reported in literature (27). UV–vis (MeOH, nm) λ_{max}: 242, 298. IR (KBr disc, cm^{-1}) ν: 3448, 3051, 2935, 1621, 1599, 1519, 1466, 1384, 1364, 786, 739. EI-MS (70 eV) *m/z* (% int.): 364 (M^+, 1), 231 (2), 221 (100). HR-MS calcd. for $C_{21}H_{20}N_2O_4$: 364.1423; found: 364.1429.

1-[(4-Methylpiperazin-1-yl)phenylmethyl)]naphthalen-2-ol (11)

UV–vis (MeOH, nm) λ_{max}: 241, 293, 320. IR (KBr disc, cm^{-1}) ν: 3448, 3056, 1621, 1581, 1450, 1310, 1240, 1137. ^{1}H NMR (300 MHz, 273 K, $CDCl_3$) δ: 2.40–2.57 (8H, m, 5 × NCH, NCH_3), 2.95 (2H, bs, 2 × NCH), 3.25 (1H, bs, NCH), 5.17 (1H, s, Ar-CH-Ar′), 7.14–7.29 (4H, m, Ar-H), 7.39–7.44 (1H, m, Ar-H), 7.53–757 (2H, m, Ar-H), 7.68–7.71 (3H, m, Ar-H), 7.83–7.87 (1H, m, Ar-H), 13.37 (1H, bs, OH). ^{13}C NMR (75 MHz, 273 K, $CDCl_3$) δ: 46.16, 51.20, 53.74, 55.31, 55.62, 71.94, 115.98, 120.27, 121.54, 123.03, 127.01, 128.12, 128.60, 128.81, 129.08, 129.34, 130.11, 132.61, 139.51, 155.31. EI-MS (70 eV) *m/z* (% int.): 332 (M^+, 13), 233 (3), 232 (16), 231 (100). HR-MS calcd. for $C_{23}H_{24}NO_3$: 332.1889; found: 332.1882.

Molecular modeling

The molecular modeling on compound **1** was performed using CaChe WorkSystem Pro Version 5. After having set a weak bond between the hydroxyl hydrogen and the N of the piperidine ring, an energy minimization experiment was performed in two steps. First, the "fastest procedure" (augmented MM3 parameters) was used, followed by the "standard procedure" (PM3 parameters). The energy-minimized conformation indicated strong H-bonding in the molecule (Fig. 2).

X-ray crystallography

Crystals of compound **9** were grown from a saturated dichloromethane–methanol (1:1) solution, while crystals of compound **11** were grown from saturated diethyl ether solu-

© 2006 NRC Canada

Table 1. Crystallographic data collection parameters for **9** and **11**.

Parameter	Compound **9**	Compound **11**
Empirical formula	$C_{21}H_{20}ClNO_2$	$C_{22}H_{24}N_2O$
Formula weight	353.85	332.44
Crystal color, habit	Colorless, needle	Colorless, block
Crystal dimensions (mm^3)	0.17 × 0.22 × 0.30	0.24 × 0.27 × 0.38
$F(000)$	744	712
Crystal system	Monoclinic	Orthorhombic
Space group	Cc (No. 9)[a]	$Pna2_1$ (No. 33)
Z	4	4
a (Å)	9.782(5)	10.723(6)
b (Å)	18.645(5)	13.483(8)
c (Å)	10.240(4)	12.849(8)
β (°)	91.42(3)	
V ($Å^3$)	1867(1)	1857(2)
d_{calcd} (g cm^{-3})	1.259	1.189
Temperature (K)	213	213
Radiation	Mo Kα (λ = 0.710 69 Å)	Mo Kα (λ = 0.710 69 Å)
μ (mm^{-1})	0.217	0.073
Total reflections	2975	3090
Observed reflections ($F_o > 4\sigma(F_o)$)	2893	2836
No. of variables	231	227
R_{int}	0.067	0.000
θ range (°)	0–30	0–30
S (GoF) on F^2	0.950	0.942
R_1 ($I > 4\sigma(I)$)[b]	0.039	0.039
wR_2 (all data)[c]	0.138	0.202
Largest diff. peak and hole (e $Å^{-3}$)	0.19 and –0.17	0.20 and –0.17

[a]Flack parameter 0.0 (1).
[b]$R_1 = \Sigma||F_o| - |F_c||/\Sigma|F_o|$.
[c]$wR_2 = [\Sigma(w(F_o^2 - F_c^2)^2)/\Sigma w(F_o^2)^2]^{1/2}$, where $w = 1/[\sigma^2(F_o^2) + (0.0664P)^2 + (0.0000P)]$ (**9**) and $w = 1/[\sigma^2(F_o^2) + (0.1000P)^2 + (0.0000P)]$ (**11**), where $P = (\max(F_o^2, 0) + 2F_c^2)/3$.

tion. Crystals were mounted using a glass fiber. All measurements were made on a Rigaku AFC5R diffractometer with graphite monochromated Mo Kα radiation.

The data were collected at a temperature of –60 ± 1 °C to a maximum 2θ value of 60.2°. The structure was solved by direct methods (39) and expanded using Fourier techniques (40). The non-hydrogen atoms were refined anisotropically. Hydrogen atoms were refined using the riding model. The neutral atom scattering factors were taken from Cromer and Weber (41). Anomalous dispersion effects were included in F_{calcd} (42); the values for $\Delta f'$ and $\Delta f''$ were those of Creagh and McAuley (43). The values for the mass attenuation coefficients are those of Creagh and Hubbell (44). All calculations were performed using the CrystalStructure crystallographic software package (45, 46) except for refinement, which was performed using SHELXL-97 (47).

The crystallographic data collection parameters, bond lengths, and bond angles for **9** and **11** are presented in Tables 1–3. The full details of the structure have been deposited.[3]

Results and discussion

One of the interests of this laboratory lies in the use of 2-tetralone–2-naphthol skeletons as versatile building blocks (48–50). Substituted 1-arylidene-2-tetralones (**A**) were prepared from 2-tetralone and appropriate aldehydes by palladium-catalyzed Knoevenagel-type condensation (37). Subsequently, 1-arylidene-2-tetralones reacted with piperidine to produce the compounds **1**–**4** instead of the expected aza-Michael adducts (**B** or **C**). Based on this observation, it appears highly probable that aza-Michael adducts (**B** or **C**) are unstable and that they collapse back to the starting materials if they are not trapped by aerial oxidation of the dihydronaphthalene ring to form stable and aromatic 1-(aryl-piperidin-1-ylmethyl)naphthalen-2-ols (**1**–**4**), as shown in Scheme 2. This rather unusual conversion, driven by the aromatization, was found to be slow and the best yield after a reaction time of 7 days was ~30%. Although the reactions suffer from rather long reaction times and low yields, this is a novel conversion.

[3] Supplementary data for this article are available on the journal Web site (http://canjchem.nrc.ca) or may be purchased from the Depository of Unpublished Data, Document Delivery, CISTI, National Research Council Canada, Ottawa, ON K1A 0R6, Canada. DUD 5046. For more information on obtaining material refer to http://cisti-icist.nrc-cnrc.gc.ca/irm/unpub_e.shtml. CCDC 606518 and 606519 contain the crystallographic data for this manuscript. These data can be obtained, free of charge, via http://www.ccdc.cam.ac.uk/conts/retrieving.html (Or from the Cambridge Crystallographic Data Centre, 12 Union Road, Cambridge CB2 1EZ, UK; fax +44 1223 336033; or deposit@ccdc.cam.ac.uk).

© 2006 NRC Canada

Table 2. Bond lengths and angles for **9**.

Bond lengths (Å)		Bond angles (°)	
Cl(1)—C(5)	1.745(4)	Cl(1)-C(5)-C(4)	119.5(4)
O(1)—C(19)	1.413(6)	Cl(1)-C(5)-C(6)	120.4(3)
O(1)—C(20)	1.414(6)	**O(1)-C(19)-C(18)**	112.2(4)
O(2)—C(9)	1.351(5)	C(20)-O(1)-C(19)	110.5(4)
N(1)—C(1)	1.492(5)	**O(1)-C(20)-C(21)**	111.0(4)
N(1)—C(18)	1.470(6)	O(2)-C(9)-C(8)	123.6(4)
N(1)—C(21)	1.483(6)	O(2)-C(9)-C(10)	116.1(4)
C(1)—C(2)	1.516(6)	C(18)-N(1)-C(1)	113.5(3)
C(1)—C(8)	1.530(5)	C(21)-N(1)-C(1)	108.9(3)
C(2)—C(3)	1.385(6)	N(1)-C(1)-C(8)	111.1(3)
C(2)—C(7)	1.391(6)	N(1)-C(1)-C(2)	113.2(3)
C(3)—C(4)	1.365(7)	**N(1)-C(18)-C(19)**	109.3(4)
C(4)—C(5)	1.372(7)	C(21)-N(1)-C(18)	108.5(3)
C(5)—C(6)	1.366(6)	**N(1)-C(21)-C(20)**	109.3(4)
C(6)—C(7)	1.362(6)	C(1)-C(2)-C(3)	122.4(4)
C(8)—C(9)	1.378(6)	C(8)-C(1)-C(2)	109.6(3)
C(8)—C(17)	1.432(6)	C(1)-C(2)-C(7)	121.3(3)
C(9)—C(10)	1.425(6)	C(1)-C(8)-C(9)	121.0(4)
C(10)—C(11)	1.347(7)	C(1)-C(8)-C(17)	119.5(4)
C(11)—C(12)	1.402(7)	C(2)-C(3)-C(4)	122.3(5)
C(12)—C(13)	1.409(7)	C(7)-C(2)-C(3)	116.2(4)
C(12)—C(17)	1.436(6)	C(2)-C(7)-C(6)	122.2(4)
C(13)—C(14)	1.344(8)	C(3)-C(4)-C(5)	119.4(5)
C(14)—C(15)	1.408(8)	C(4)-C(5)-C(6)	120.1(4)
C(15)—C(16)	1.361(7)	C(5)-C(6)-C(7)	119.6(4)
C(16)—C(17)	1.398(6)	C(8)-C(9)-C(10)	120.2(4)
C(18)—C(19)	1.508(7)	C(17)-C(8)-C(9)	119.5(4)
C(20)—C(21)	1.511(7)	C(8)-C(17)-C(16)	123.9(4)
		C(8)-C(17)-C(12)	119.2(4)
		C(9)-C(10)-C(11)	120.8(4)
		C(10)-C(11)-C(12)	121.6(4)
		C(11)-C(12)-C(17)	118.7(4)
		C(11)-C(12)-C(13)	122.0(4)
		C(17)-C(12)-C(13)	119.3(4)
		C(12)-C(13)-C(14)	121.1(5)
		C(12)-C(17)-C(16)	116.9(4)
		C(13)-C(14)-C(15)	120.6(5)
		C(14)-C(15)-C(16)	119.2(5)
		C(15)-C(16)-C(17)	122.8(5)

Table 3. Bond lengths and angles for **11**.

Bond lengths (Å)		Bond angles (°)	
O(1)—C(9)	1.361(7)	O(1)-C(9)-C(8)	123.1(4)
N(1)—C(1)	1.499(6)	O(1)-C(9)-C(10)	116.2(5)
N(1)—C(18)	1.470(7)	N(1)-C(1)-C(2)	113.4(4)
N(1)—C(21)	1.452(8)	N(1)-C(1)-C(8)	109.0(4)
N(2)—C(19)	1.413(9)	C(21)-N(1)-C(1)	110.3(4)
N(2)—C(20)	1.454(7)	C(18)-N(1)-C(1)	114.5(4)
N(2)—C(22)	1.481(8)	C(21)-N(1)-C(18)	108.4(4)
C(1)—C(2)	1.507(7)	**N(1)-C(18)-C(19)**	108.5(4)
C(1)—C(8)	1.529(7)	**N(1)-C(21)-C(20)**	111.4(5)
C(2)—C(3)	1.389(8)	**N(2)-C(19)-C(18)**	112.3(6)
C(2)—C(7)	1.386(8)	C(20)-N(2)-C(19)	109.8(4)
C(3)—C(4)	1.39(1)	C(22)-N(2)-C(19)	111.7(5)
C(4)—C(5)	1.36(1)	**N(2)-C(20)-C(21)**	110.1(5)
C(5)—C(6)	1.36(1)	C(22)-N(2)-C(20)	109.6(5)
C(6)—C(7)	1.38(1)	C(1)-C(2)-C(7)	122.6(5)
C(8)—C(9)	1.371(7)	C(8)-C(1)-C(2)	111.3(4)
C(8)—C(17)	1.428(7)	C(1)-C(2)-C(3)	120.5(5)
C(9)—C(10)	1.423(7)	C(1)-C(8)-C(9)	121.0(4)
C(10)—C(11)	1.341(9)	C(1)-C(8)-C(17)	119.3(4)
C(11)—C(12)	1.406(9)	C(7)-C(2)-C(3)	116.9(5)
C(12)—C(13)	1.426(9)	C(2)-C(3)-C(4)	121.1(6)
C(12)—C(17)	1.442(7)	C(2)-C(7)-C(6)	121.1(6)
C(13)—C(14)	1.34(1)	C(3)-C(4)-C(5)	120.8(6)
C(14)—C(15)	1.41(1)	C(4)-C(5)-C(6)	118.9(7)
C(15)—C(16)	1.365(9)	C(5)-C(6)-C(7)	121.2(7)
C(16)—C(17)	1.395(8)	C(8)-C(9)-C(10)	120.7(5)
C(18)—C(19)	1.514(8)	C(17)-C(8)-C(9)	119.5(4)
C(20)—C(21)	1.513(9)	C(8)-C(17)-C(16)	123.5(4)
		C(8)-C(17)-C(12)	118.6(5)
		C(9)-C(10)-C(11)	121.0(5)
		C(10)-C(11)-C(12)	120.9(5)
		C(11)-C(12)-C(17)	119.3(5)
		C(11)-C(12)-C(13)	122.3(5)
		C(17)-C(12)-C(13)	118.3(5)
		C(12)-C(13)-C(14)	120.8(6)
		C(12)-C(17)-C(16)	117.9(5)
		C(13)-C(14)-C(15)	121.3(7)
		C(14)-C(15)-C(16)	119.0(7)
		C(15)-C(16)-C(17)	122.6(5)

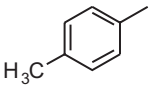
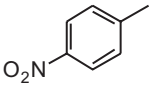
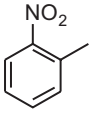
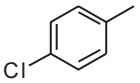
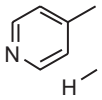
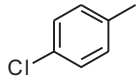
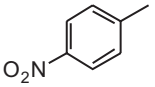
Several attempts were made to expedite the reaction course by addition of oxidizing agents (viz., H_2O_2, MnO_2, DDQ, and O_2). No decline in the reaction time could be achieved; rather, undesired products and complex mixtures were obtained. No attempts were made to identify the undesired products. The results suggest that the first elementary step (formation of **B** or **C**, Scheme 2) is rate-limiting and the presence of oxidizing agents lead to undesired reactions with the starting materials. We are in the process of optimizing the conditions.

We prepared additional analogs (**1**–**11**, Table 4) by modifying a reported microwave-assisted procedure (26) for which we achieved an appreciable improvement in yields and reaction time (Scheme 3). Sharifi et al. (26) have reported the synthesis of related compounds on acidic alumina support under solvent-free conditions and microwave irradiation with an average yield of 64% in the reaction time range of 4–8 min, compared to an average yield of 75.1% and a reaction time of 1 min under our conditions. The irradiation time was split into two 30 s pulses with a nearly 30 s intervening gap to avoid superheating and charring the reaction contents. Our procedure involved solvent-free conditions and the use of only catalytic amounts of *p*-TSA, thus avoiding the use of excessive acidic alumina. Numerous trials of microwave-assisted reaction under solvent-free conditions using 2-nitrobenzaldehyde (for compound **4**) were not successful and violent splashing of the contents was noticed within the irradiation period of ~10 s; TLC did not indicate the formation of any product even after continued irradiation for up to 2 min. The use of solvent (DMF) and solid support (silica gel) under microwave irradiation did not change the outcome.

Although the Mannich bases of 2-naphthols with heterocyclic amines were reported in the past (24, 26, 27, 51), their

© 2006 NRC Canada

Table 4. Comparative reaction data for compounds synthesized by two different procedures.

No.	R	X	Scheme 1 Time: 7 days		Scheme 2 Time 1 min		
			Yield (%)	mp (°C)	Yield (%)	mp (°C)	Lit. mp (°C)
1		CH_2	22.0	194 to 195	79.7	192–194	198 to 199 (27)
2		CH_2	17.5	145–147	82.7	144–146	—
3		CH_2	29.5	187–190	83.3	186–188	—
4		CH_2	18.5	194 to 195	Ns[a]	—	—
5		CH_2	Nd[b]	—	72.0	165 to 166	—
6		CH_2	Nd	—	82.4	185–187	—
7		CH_2	Nd	—	43.1	88–90	95 to 96 (51)
8		O	Nd	—	85.8	177–179	181–183 (27)
9		O	Nd	—	71.7	132–134	—
10		O	Nd	—	72.0	178 to 179	177–179 (27)
11		NCH_3	Nd	—	78.1	138–140	—

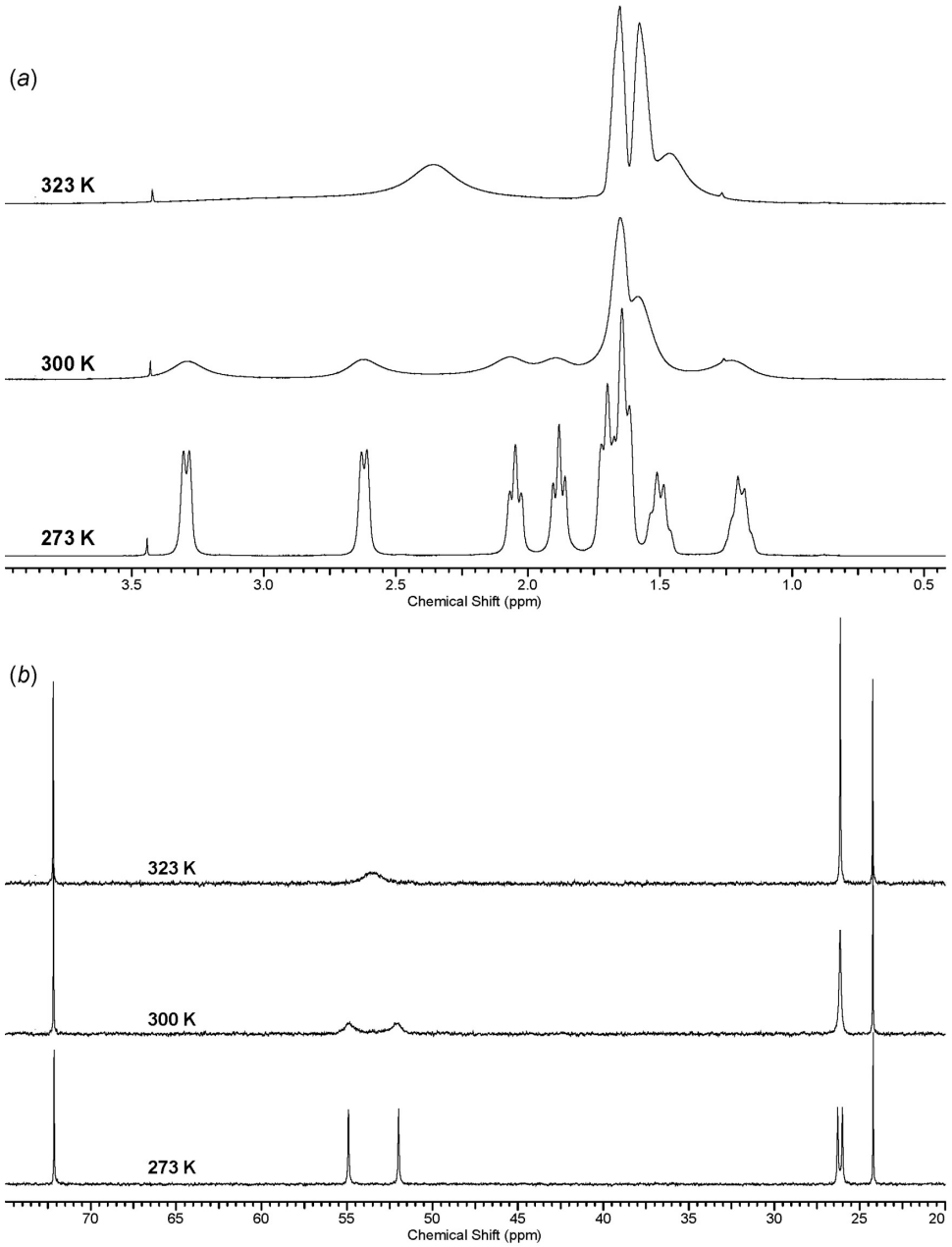
[a]Ns (Not successful).
[b]Nd (Not done).

detailed NMR behavior has not been examined, to the best of our knowledge; some NMR peaks are reported in broad range (27). We consistently noted interesting NMR activities of the compounds under investigation, as they often gave poorly resolved heterocyclic proton and carbon peaks in their respective spectra at ambient temperature. We decided to systematically investigate this behaviour. Besides the indispensable use of NMR spectroscopy in structure elucidation, it remains a powerful technique for stereochemical analysis of organic molecules. From the point of view of conformational analysis, six-membered saturated carbocycles and heterocycles have been studied (52–55). A recent study on 1-(2-hydroxy-2,2-diarylethyl)piperidin-4-ones describes a new mechanism of N-inversion — a concerted H-bond dissociation – N inversion process (56). The piperidine ring is a common structural fragment of many alkaloids and, therefore, conformational analysis of these biologically active amines is necessary for the comprehension of the molecular mechanisms of their action.

The ^{1}H and ^{13}C NMR spectra obtained at ambient temperature (300 K) suffered from the broadening of several peaks suggesting dynamism in the piperidine conformation, making the interpretation ambiguous. Thus, we resorted to recording the NMR experiments at lower temperatures. As expected, the ^{1}H NMR spectrum of compound **1** at 273 K gave better resolved peaks. The peak at δ 14.1, integrating for one proton of -OH group at position 2 of the naphthalene ring, clearly indicated strong H-bonding with the N of the piperidine ring. In addition, most of the protons on the piperidine ring gave discrete peaks, making it obvious that the symmetry of the piperidine ring was lost. This observation was also supported by the ^{13}C NMR spectrum of compound **1** at 273 K, which not only resulted in better resolved peaks but also showed distinct peaks for each CH_2 of the piperidene ring. This was another indication that the magnetic equivalence of the two pairs of methylene carbons is destroyed by restricted rotation of the piperidine ring with two flanking aromatic rings and the H bond. The NMR experiments that were recorded in a temperature span of 50 °C (three each for ^{1}H and ^{13}C) clearly demonstrated an increase in molecular dynamics with the rise in temperature. The portion of NMR plots of compound **1** that were most affected by the temperature change is shown in Fig. 3. The five C peaks of nonsymmetric piperidine at 273 K converge into

© 2006 NRC Canada

Fig. 3. Stack plot of (*a*) a portion of ^{1}H NMR and (*b*) ^{13}C NMR of compound **1** at various temperatures.



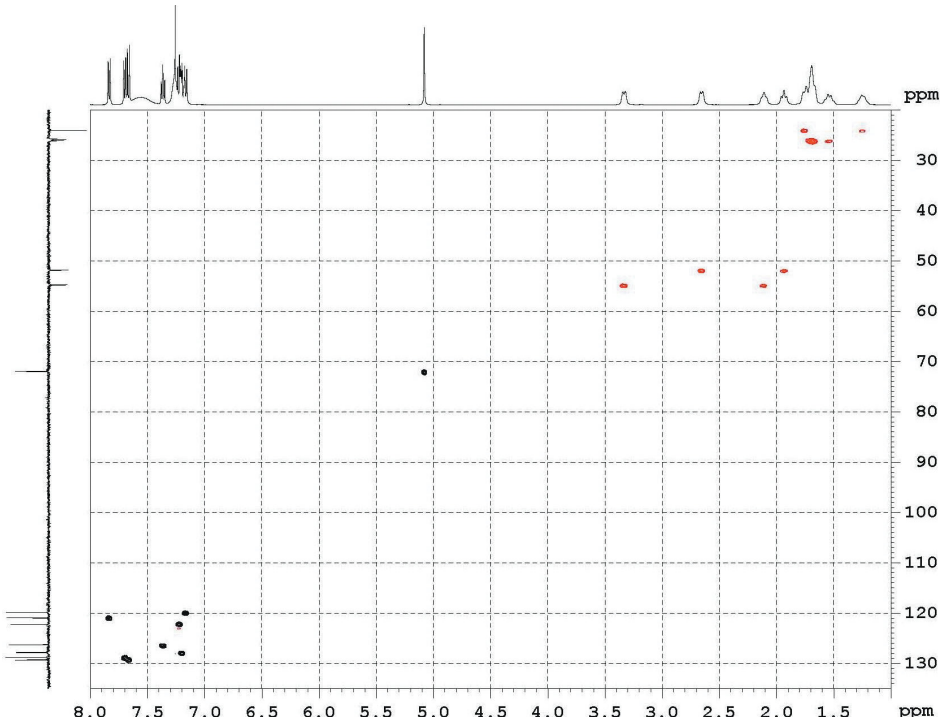
three C peaks of symmetric piperidine at 323 K. A similar observation was made in the H spectrum at corresponding temperatures, albeit at the cost of resolution.

The molecular model shown in Fig. 2 also demonstrates the existence of a very strong H bond (calculated distance = 1.83 Å) and a consequent loss of symmetry. This is more evident in Fig. 3*b,* where methylene Cs on the right side of N are magnetically nonequivalent to those on the left side because of restricted rotation. At lower temperature, this system may be regarded as a hindered spirocyclic system. As the temperature is increased, the H bond is disrupted allowing rotation of the piperidine ring along the benzylic C—N axis with concurrent ring flipping and (or) N-inversion. Being rather fast for the NMR timescale, the convergence of a pair of piperidine methylene takes place with loss of resolution in the ^{13}C NMR. As seen in Fig. 3, as the two discrete piperidine -NCH_2, appearing at 51.83 and 54.77 ppm, observed at 273 K coalesce to a broad peak at ~53.30 ppm when recorded at 323 K, it can be qualitatively said that a temperature increase of 50 °C leads to approximately 800 conformational interchanges per second (based on the expression for the rotational rate constant at the coalescence point (57) ($k_{coal} = \pi\ (\Delta\nu)/\sqrt{2}$). Thus, at the coalescence temperature, the interchanging conformations have a lifetime of about 1.25 ms ($1/k_{coal}$). Contrary to this, for the C-3 and C-5 carbons of piperidine that are away from the crowded centre, a similar effect is achieved with a temperature increase of ~27 °C (k_{coal} ~ 75 s^{-1}). The ^{1}H NMR also shows this behaviour where peak broadening is more severe.

The HSQC experiment with shaped pulse recorded at 273 K resulted in the expected correlations (Fig. 4). In addition to the presence of piperidine methylenes (inverted

© 2006 NRC Canada

Fig. 4. HSQC with shaped pulse for inversion of compound **1** recorded at 273 K.



peaks), the HSQC experiment also showed the presence of at least eight magnetically nonequivalent protons on the piperidine ring. A pronounced disparity in the appearance of seemingly similar diastereotopic methylene (C2, C6 pair) protons was observed. The more deshielded protons on the two carbons are 0.65 ppm apart, while the more shielded ones are 0.20 ppm apart. Also, the amount of shielding and deshielding on the protons on these carbons is considerably disparate (1.23 vs. 0.78 ppm).

Similar NMR behaviour was consistently noticed for all the compounds (except compound **7**) irrespective of the heterocycle substituents. At 273 K, piperidinyl, morpholinyl, and *N*-methylpiperzinyl groups showed magnetic nonequivalence of all constituent carbons and hydrogens. Compound **7**, being devoid of an aryl group compared to others in the series, has significantly reduced crowding near the heterocyclic nitrogen atom and, therefore, the heterocyclic ring retains the symmetry even at 273 K.

Finally, X-ray crystal structures of compounds **9** and **11** were solved to compare the NMR solution- and solid-phase crystal conformations. The prominent feature of both compounds **9** and **11** is an internal hydrogen bond from the hydrogen atom of the OH group to N(1), the nitrogen of the piperidine or morpholine ring, which are bonded to C(1). It can be seen in Fig. 5 that the O—H bond approaches the piperidine or morpholine ring obliquely so that the C(18) and C(21) carbon atoms of this ring are not equivalent. This is a strong hydrogen bond; the observed H(20)—N(1) and H(24)—N(1) distances in **9** and **11** are 1.78 and 1.75 Å, respectively. This H-bonding also persists in solution as evidenced by the appearance of the hydrogen-bonded -OH peak at values >13 ppm in ^{1}H NMR. This H bond forms a six-membered cycle and restricts the free rotation of the heterocyclic ring along the benzylic C—N bond. A close inspection of the bond lengths and angles of the heterocyclic ring (shown in bold face in Tables 2 and 3) reveal that the ring is slightly distorted, compounding the magnetic nonequivalence of Hs and Cs on seemingly symmetric heterocyclic rings.

Conclusion

2-Naphthol Mannich bases with heterocyclic amines were synthesized using two different approaches. Variable-temperature NMR investigations proved helpful in resolving complicated NMR spectra of these rather simple molecules. Molecular modeling and X-ray crystallography supported the NMR results. These results can be explained by the loss of magnetic equivalence of certain heterocyclic Cs and Hs caused by restricted rotation of the heterocyclic ring when N is involved in strong H-bonding with phenolic -OH.

Acknowledgements

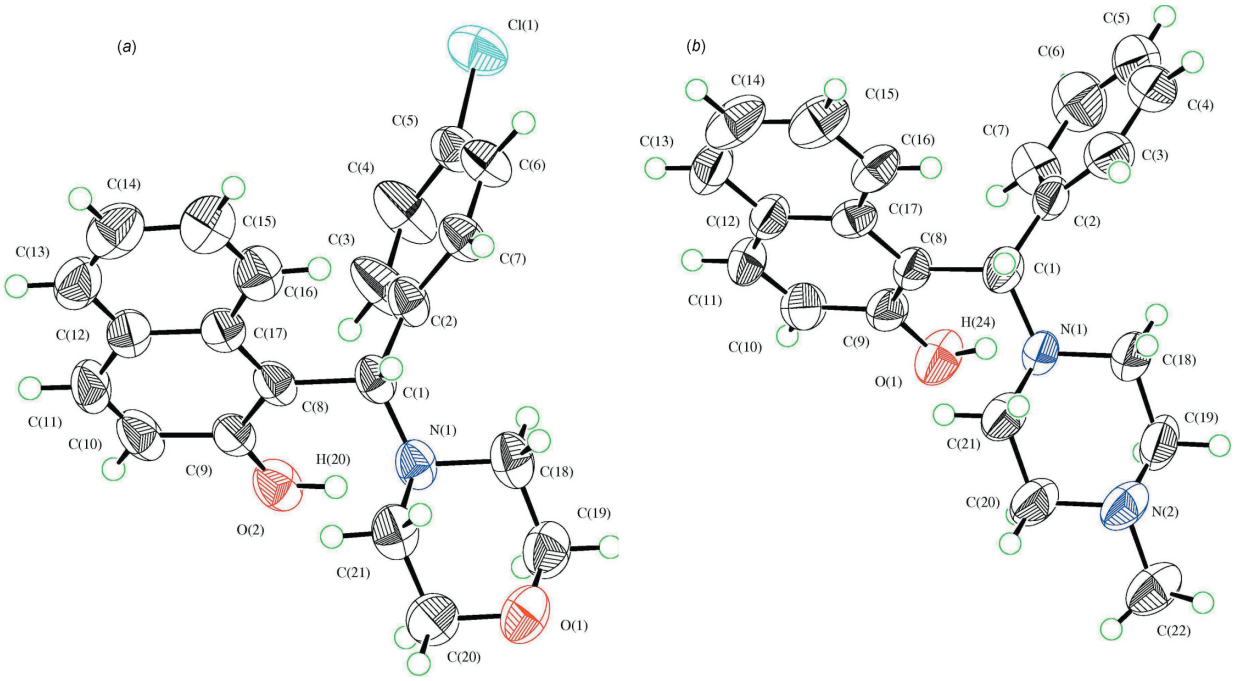
We are grateful to the Natural Sciences and Engineering Research Council of Canada (NSERC) and the Nova Scotia Health Research Foundation (NSHRF) for their financial support. Ms. J. Beal is thanked for preliminary investigations. The Atlantic Region Magnetic Resonance Centre (ARMRC) and the Maritime Mass Spectrometry Laboratory (MMSL) at Dalhousie University are acknowledged for providing NMR and MS support, respectively. Dr. Michael Lumsden of ARMRC is thanked for technical suggestions.

References

1. P. Kocovsky, S. Vyskocil, and M. Smrcina. Chem. Rev. **103**, 3213 (2003).

© 2006 NRC Canada

Fig. 5. ORTEP diagrams of compounds (*a*) **9** and (*b*) **11**.



2. S. Vyskocil, S. Jaracz, M. Smrcina, M. Sticha, V. Hanus, M. Polasek, and P. Kocovsky. J. Org. Chem. **63**, 7727 (1998).
3. M. Smrcina, S. Vyskocil, B. Maca, M. Polasek, T.A. Claxton, A.P. Abbott, and P. Kocovsky. J. Org. Chem. **59**, 2156 (1994).
4. M. Smrcina, M. Lorenc, V. Hanus, P. Sedmera, and P. Kocovsky. J. Org. Chem. **57**, 1917 (1992).
5. Y. Kim, R.A. Singer, and E.M. Carreira. Angew. Chem. Int. Ed. **37**, 1261 (1998).
6. E.M. Carreira, W. Lee, and R.A. Singer. J. Am. Chem. Soc. **117**, 3649 (1995).
7. R.A. Singer and E.M. Carreira. J. Am. Chem. Soc. **117**, 12360 (1995).
8. Y.N. Belokon, K.A. Kochetkov, T.D. Churkina, N.S. Ikonnikov, O.V. Larionov, S.R. Harutyunyan, S. Vyskocil, M. North, and H.B. Kagan. Angew. Chem. Int. Ed. **40**, 1948 (2001).
9. Y. Yuan, X. Li, I. Sun, and K.L. Ding. J. Am. Chem. Soc. **124**, 14866 (2002).
10. G. Bernardinelli, D. Fernandez, R. Gosmini, P. Meier, A. Ripa, P. Schupfer, B. Treptow, and E.P. Kundig. Chirality, **12**, 529 (2000).
11. C. Cardellicchio, G. Ciccarella, F. Naso, F. Perna, and P. Tortorella. Tetrahedron, **55**, 14685 (1999).
12. C. Cardellicchio, G. Ciccarella, F. Naso, E. Schingaro, and F. Scordari. Tetrahedron: Asymmetry, **9**, 3667 (1998).
13. G. Palmieri. Tetrahedron: Asymmetry, **11**, 3361 (2000).
14. D.-X. Liu, L.-C. Zhang, Q. Wang, C.-S. Da, Z.-Q. Xin, R. Wang, M.C.K. Choi, and A.S.C. Chan. Org. Lett. **3**, 2733 (2001).
15. C. Cimarelli, G. Palmieri, and E. Volpini. Tetrahedron: Asymmetry. **13**, 2417 (2002).
16. C. Cimarelli, A. Mazzanti, G. Palmieri, and E. Volpini. J. Org. Chem. **66**, 4759 (2001).
17. J.X. Ji, L.Q. Qiu, C.W. Yip, and A.S.C. Chan. J. Org. Chem. **68**, 1589 (2002).
18. M. Betti. Gazz. Chim. Ital. **30 II**, 310 (1900).
19. M. Betti. Gazz. Chim. Ital. **31 I**, 377 (1901).
20. M. Betti. Gazz. Chim. Ital. **31 II**, 170 (1901).
21. M. Betti. Gazz. Chim. Ital. **33 I**, 1 (1903).
22. M. Betti. Org. Syn. Coll. Vol. **1**, 381 (1941).
23. K.-W. Chi, Y.S. Ahn, K.T. Shim, T.H. Park, and J.S. Ahn. Bull. Korean Chem. Soc. **20**, 973 (1999).
24. M.R. Saidi, N. Azizi, and M.R. Naimi-Jamal. Tetrahedron Lett. **42**, 8111 (2001).
25. M. Saidi and H.R. Khalaji. J. Chem. Res. Synop. 340 (1997).
26. A. Sharifi, M. Mirzaei, and M.R. Naimi-Jamal. Monatsh. Chem. **132**, 875 (2001).
27. A.R. Katritzky, A.A.A. Abdel-Fattah, D.O. Tymoshenko, S.A. Belyakov, I. Ghiviriga, and P.J. Steel. J. Org. Chem. **64**, 6071 (1999).
28. Y. Dong, J. Sun, X. Wang, L. Cao, and Y. Hu. Tetrahedron: Asymmetry, **15**, 1667 (2004).
29. M.R. Saidi and N. Azizi. Tetrahedron: Asymmetry, **14**, 389 (2003).
30. A. Cohen, R.A. Hall, B. Heath-Brown, M.W. Parkes, and A.H. Rees. Br. J. Pharmacol. Chemother. **12**, 194 (1957).
31. P.D. Brown. Med. Oncol. **14**, 1 (1997).
32. K.W. Johnson, D. Lofland, and H.E. Moser. Curr. Drug Targets: Infect. Disord. **5**, 39 (2005).
33. W.T. Lowther and B.W. Matthews. Biochim. Biophys. Acta, **1477**, 157 (2000).
34. A.S. Waller and J.M. Clements. Curr. Opin. Drug Discovery Dev. **5**, 685 (2002).
35. L.T. Chappell. Altern. Med. Rev. **3**, 426 (1998).
36. M.D. Ford. Heavy metals. 4th ed. McGraw Hill, New York. 1996.
37. Y. Zhu and Y. Pan. Chem. Lett. **33**, 668 (2004).
38. J.R. Dimmock, M.P. Padmanilyam, G.A. Zello, J. Wilson Quail, E.O. Oloo, J.S. Prisciak, H.-B. Kraatz, A. Cherkasov, J.S. Lee, and T.M. Allen. Eur. J. Med. Chem. **37**, 813 (2002).
39. A. Altomare, G. Cascarano, C. Giacovazzo, A. Guagliardi, M. Burla, G. Polidori, and M. Camalli. J. Appl. Crystallogr. **27**, 435 (1994).
40. P.T. Beurskens, G. Admiraal, G. Beurskens, W.P. Bosman, R. de Gelder, R. Israel, and J.M. M. Smits. The DIRDIFF-99 program system: technical report of the crystallography labora-

© 2006 NRC Canada

tory. University of Nijmegem, Nijmegem, The Netherlands, 1999.
41. D.T. Cromer and D.J. Weber. *In* International tables of X-ray crystallography. Vol. IV. The Kynoch Press, Birmingham, UK. 1974. Table 2.2. A.
42. J.A. Ibers and W.C. Hamilton. Acta Crystallogr. **17**, 781 (1964).
43. D.C. Creagh and W.J. McAuley. *In* International tables of crystallography. Vol. C. Kluwer Academic Publishers, Boston, 1992. Table 4.2.6.8. pp. 219–222.
44. D.C. Creagh and J.H. Hubbell. *In* International tables of crystallography. Vol. C. Kluwer Academic Publishers, Boston, 1992. Table 4.2.4.3. pp. 200–206.
45. Rigaku and Rigaku/MSC. CrystalStructure 3.6.0 [computer program]. Rigaku and Rigaku/MSC, The Woodlands, Tex. 2000–2004.
46. D.J. Watkin, C.K. Prout, J.R. Carruthers, and P.W. Betteridge. Crystals issue 10 [computer program]. Chemical Crystallography Laboratory, Oxford, UK. 1996.
47. G.M. Sheldrick. SHELXL97 [computer program]. University of Göttingen, Göttingen, Germany. 1997.
48. A. Jha and J. Beal. Tetrahedron Lett. **45**, 8999 (2004).
49. A. Jha and J.R. Dimmock. Can. J. Chem. **81**, 293 (2003).
50. A. Jha, M.P. Padmanilayam, and J.R. Dimmock. Synthesis, 463 (2002).
51. J.R. Feldman and E.C. Wagner. J. Org. Chem. **7**, 31 (1942).
52. R.J. Abraham, N. Aboitiz, J. Merrett, B. Sherborne, and I. Whitecombe. J. Chem. Soc. Perkin Trans. 2, 2382 (2000).
53. R.J. Abraham and D.S. Ribeiro. J. Chem. Soc. Perkin Trans. 2, 302 (2001).
54. A.M. Belostoskii, H.E. Gottlieb, P. Aped, and A. Hassner. Chem. Eur. J. **5**, 449 (1999).
55. Y. Fu, Z. Zhou, P. Hazendonk, A.D. Bain, F.R. Fronczek, J. Escobedo, M.L. McLaughlin, and R.P. Hammer. J. Mol. Struct. **687**, 65 (2004).
56. A.M. Belostoskii, H.E. Gottlieb, and P. Aped. Chem. Eur. J. **8**, 3016 (2002).
57. M. Oki. Applications of dynamic NMR spectroscopy to organic chemistry. VCH Publishers, Deerfields Beach, Fla, 1985.

© 2006 NRC Canada

Efficient stabilization of oligonucleotide duplexes through terpyridine metal complexes

Fabrice Freville, Nathalie Pierre, and Serge Moreau

Abstract: A large increase in the melting temperature of complementary oligonucleotides was obtained through the conjugation of terpyridine ligands at their nearby 5′ or 3′ ends and the addition of stoichiometric amounts of various transition metals. We describe here a short efficient synthetic route for the conjugation of terpyridine moieties and report new data on the stabilizing contribution of metal-assisted hybridization of oligonucleotides through UV-monitored melting temperature experiments.

Key words: oligonucleotides, metal complexes, terpyridine.

Résumé : Une augmentation importante de la température de fusion d'oligonucléotides complémentaires peut être obtenue par la conjugaison des ligands terpyridine à leurs extrémités adjacentes (5′ ou 3′) et l'addition de quantités stœchiométriques de divers métaux de transition. On décrit ici une courte voie de synthèse efficace pour la conjugaison des groupes terpyridine. On présente également de nouvelles données expérimentales sur l'effet stabilisant des métaux dans l'hybridation des oligonucléotides par des mesures de température de fusion soumises en spectroscopie UV.

Mots clés : oligonucléotides, complexes métalliques, terpyridine.

Introduction

We previously reported a high stabilization of complementary DNA strands association through the addition of a coordination link between the oligomers (1). Such a link was obtained using terpyridine moieties as chelating agents and serinol as a deoxyribose mimic to allow easy conjugation of the chelator to oligonucleotides at nearby 3′ and 5′ ends.

We report here a new way to access the efficient conjugation of terpyridine moieties on both 3′ and 5′ ends of oligonucleotides. To allow structural studies, we chose to use a pantolactone-based ribose mimic developed by Dioubankova et al. (2). This synthetic route was used to extend our studies on metal-assisted hybridization of oligonucleotides, providing an easy way to increase nucleic acid duplex stability.

Results

We chose to use two short complementary DNA sequences to evaluate the contribution of the metallic bridge on duplex stability. This data was obtained by UV-thermal denaturation experiments. The introduction of the terpyridine chelators at nearby 5′ and 3′ ends required the synthesis of a phosphoramidite monomer bearing the terpyridine moiety and a specific solid-supported reagent for 3′ conjugation.

Chemical synthesis

Taking into account the strategy develop by Dioubankova et al., we designed a new synthetic route involving pantolactone as a precursor for a nonnucleosidic monomer. The new monomer was derivatized as a phosphoramidite unit and used in a solid-supported terpyridine linker. The whole synthetic scheme is depicted in Fig. 1.

Pantolactone **1** was treated with an excess of 1,3 diaminopropane. The side chain aminogroup was transiently protected through trifluoroacetylation. The primary hydroxyl group was then selectively tritylated using 4,4′-dimethoxytrityl chloride, yielding compound **3**. **3** was purified by silica gel flash chromatography using a dichloromethane – ethyl acetate gradient. The overall yield from **1** was 68%. The N-protecting group was then removed by sodium carbonate treatment leading to **4** (yield of 74%). The terpyridine monomer **5** was obtained by the reaction with the *N*-hydroxysuccinimide ester **9** in high yield (82%), after chromatography over aluminum oxide using an ethyl acetate – hexane gradient. This monomer **5** was used either to synthesize the phosphoramidite **6** through phosphitylation with 2-cyanoethyl-*N*,*N*-diisopropylchloro phosphoramidite or to yield a solid-supported reagent **7** by reaction with succinylated LCAA-CPG. **6** was purified by reverse-phase chromatography and elution with neat acetonitrile (yield 43%). The overall yield from **1** was 17%. The solid-supported reagent **7** was obtained by known procedure (3). The loading range of the CPG reagent was found to be 25–35 μmol/g. The terpyridine moiety **8** was synthesized according to published procedures (4) and the *N*-hydroxysucciimide ester **9** was obtained in high yield (93%).

Duplex formation

To evaluate the stability of various metallic bridges be-

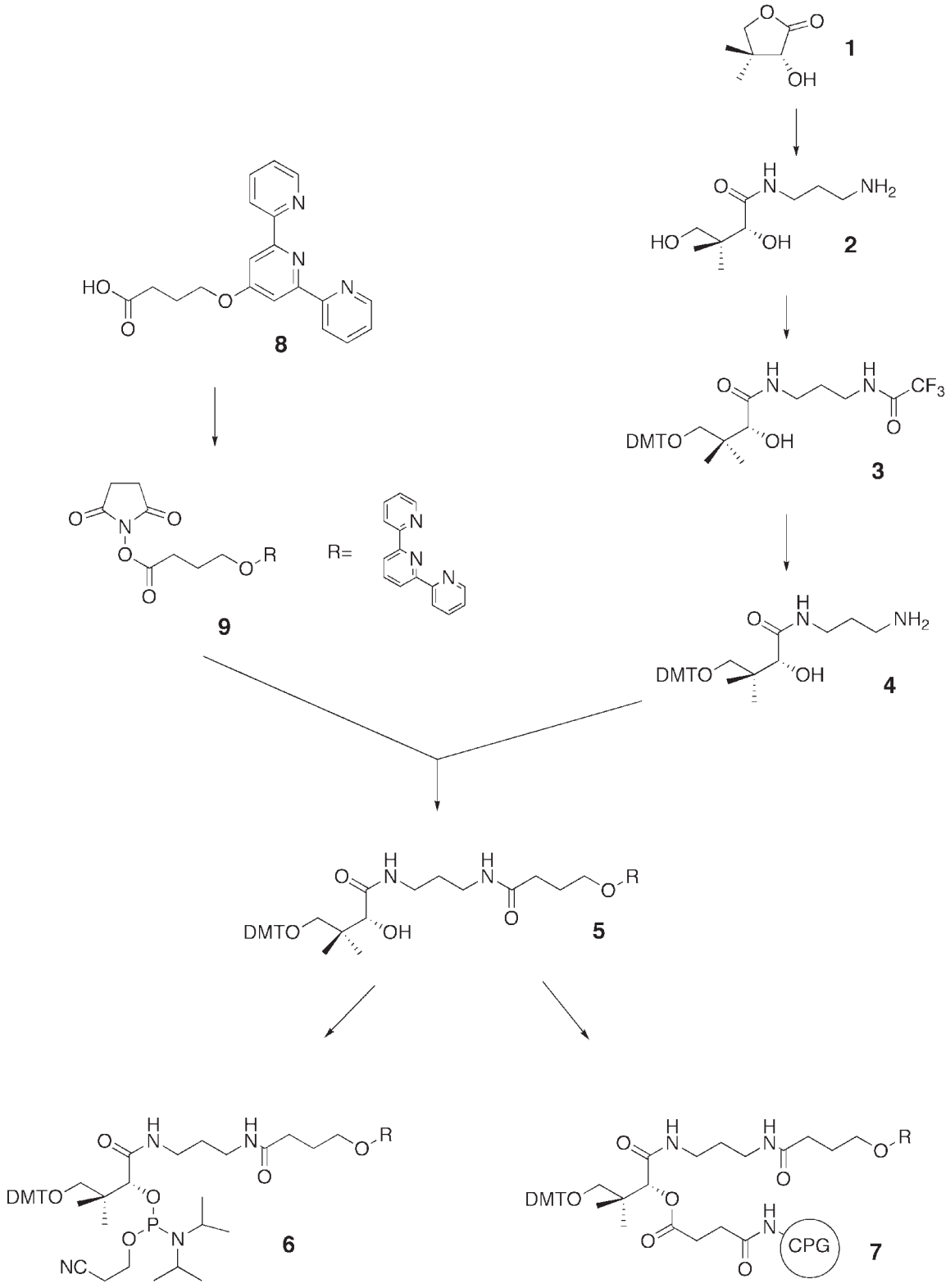
Received 30 November 2005. Published on the NRC Research Press Web site at http://canjchem.nrc.ca on 7 June 2006.

F. Freville, N. Pierre, and S. Moreau.[1] INSERM U386, Université Victor Segalen Bordeaux 2, 146 rue Léo Saignat, F33076 Bordeaux, CEDEX, France.

[1]Corresponding author (email: serge.moreau@bordeaux.inserm.fr).

 doi:10.1139/V06-080 © 2006 NRC Canada

Fig. 1. Chemical synthetic pathway for the various monomer units.



tween complementary oligomers, we designed specific strand combinations. Oligonucleotide sequences are gathered in Table 1, together with the MS analysis of TPY-conjugated strands by MALDI-Q-TOF in negative mode. We thus confirmed the chemical structure of modified oligomers with the monoisotopic peaks in the MS analysis. Using the previously mentioned linkers, the terpyridine chelator was introduced into the 3′ or 5′ ends of complementary

© 2006 NRC Canada

Table 1. Sequences of the duplexes used in the melting temperature experiments.

No.	Duplex sequences	Calcd. (*m*/*z*)	Expt. $(M - H)^-$ (*m*/*z*)
I	5′ CCTTTCTTG 3′		
	3′ GGAAAGAAC 5′		
II	5′ CCTTTCTTG-TPY 3′	3237.68	3236.68
	3′ GGAAAGAAC 5′		
III	5′ CCTTTCTTG 3′		
	3′ GGAAAGAAC-TPY 5′	3362.76	3361.75
IV	5′ CCTTTCTTG-TPY 3′		
	3′ GGAAAGAAC-TPY 5′		
V	5′ CCTTTCTTG-TPY 3′		
	3′ TPY-GGAAAGAAC 5′	3362.76	3361.75

Note: TPY accounts for the terpyridine ligand. Columns 3 and 4 show the results of MS analysis (MALDI-Q-TOF, negative mode) of TPY-conjugated strands, calculated and experimental data, respectively.

Table 2. Effect of terpyridine ligands on values of Tm of oligonucleotide duplexes.

	Tm[a] (ΔTm)[b]					
Duplexes	EDTA	Zn^{2+}	Fe^{2+}	Co^{2+}	Ni^{2+}	Cu^{2+}
I	26.5	26.4	26.4	Nd[c]	Nd	Nd
II	30.6	30.0	32.3	Nd	Nd	Nd
III	32.0	33.0	32.6	Nd	Nd	Nd
IV	37.0	61.8 (35.3)	63.5 (37)	63.6 (37.1)	65.2 (38.7)	57.5 (31)
V	34.5	34.0	34.4	Nd	Nd	Nd

Note: Oligomers concentrations are 1 μmol/L.
[a]Melting temperature (Tm, °C, ±1 °C) (mean values from at least three experiments).
[b]ΔTm: Tm duplex IV – Tm duplex I (ΔTm indicated inside parentheses).
[c]Nd: not determined.

strands. Five different duplexes were studied, allowing comparisons between unmodified double-stranded oligomers and either mono- or bis-terpyridine conjugated oligonucleotides.

Thermal denaturation experiments were conducted in two different buffers. Data from nonmetalated species were obtained in a buffer containing EDTA to avoid contamination from traces of metal ions. As can be deduced from Table 2, the addition of at least 1 equiv. of Zn^{2+} ions (relative to duplex concentration) to the terpyridine-containing duplex IV resulted in a large increase in Tm (ΔTm = + 35.3 °C) in comparison with that of the unmodified duplex I. All other combinations of terpyridines moieties did not produce this stabilizing contribution. Duplexes II and III, although revealing some slight stabilization compared with I, did not reveal any stabilizing effect when compared with the data obtained from an unmetallated incubation medium (see column 2, Table 2). The presence of the two nearby terpyridine ligands is a prerequisite for the stabilization through added metal ions; duplex V, which exhibits noncontiguous terpyridine ligands, was not stabilized. The expected stoichiometry of the ligation reaction was obtained from a titration experiment with Zn^{2+} ions using the specific absorption band (320 nm) of the metalated terpyridine determined in a previous study (1) (Fig. 2).

Data from the nonmetalated buffer revealed a slight contribution from the terminal terpyridine in the stabilization of the duplexes (see column 2, Table 2). This stabilizing effect might arise from the formation of stacked aromatic pyridines on double-stranded oligonucleotide ends. The intercalation abilities of the terpyridine nucleus was discarded from previously observed data.

Fig. 2. Titration experiment showing the variation of the absorbance at 320 nm as a function of added $ZnCl_2$ (equiv. refers to the duplex concentration (1 μmol/L)).

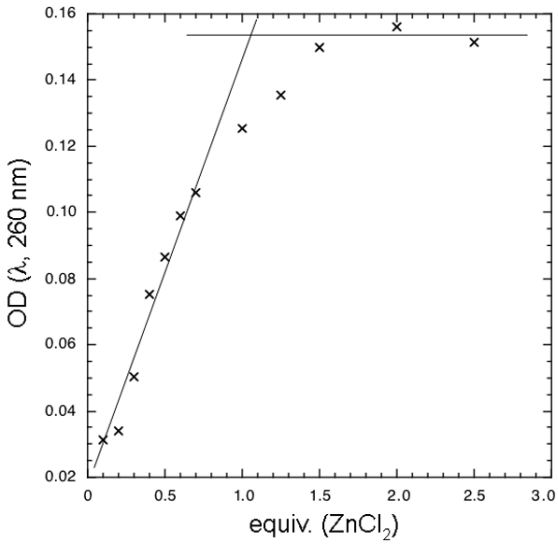


Table 2 also showed data from various chelating metals. All produced large increases in the Tm values of metalated duplexes; ΔTm from the unmodified duplex I ranged from 31 to 38.7 °C. The observed variations in the stabilizing contributions of the various chelated metals might arise from the coordination properties of the metals. All are known to form octahedral terpyridine complexes (5), however, other coordination numbers of 4 and 5 are also observed for copper (6,

© 2006 NRC Canada

7) and zinc–nickel complexes (8, 9). We cannot, therefore, exclude the occurrence of different coordination patterns in the metal-assisted hybridization of the oligonucleotides with coordination links between the nearby terpyridines varying from one to three.

Experimental section

General

Thin layer chromatography was performed on Merck silica gel 60F254 aluminum-backed plates. Flash chromatography refers to column chromatography performed with a Biotage system. NMR spectra were recorded with a Bruker Avance 300 spectrometer working at 300 MHz for ^{1}H, 75.45 for ^{13}C, and 121.49 for ^{31}P. The chemical shifts are expressed in ppm using TMS as internal standard (for ^{1}H and ^{13}C NMR data) and 85% H_3PO_4 as external standard for ^{31}P NMR data. Mass spectra (MALDI-Q-TOF, negative mode) were recorded on a Waters Ultima spectrometer. A special preparation technique was designed to analyse the TPY-modified oligonucleotides. The stainless steel target was first covered with a thin layer of matrix (0.5 μL of 2,4,6-trihydroxyacetophenone (THAP), 10 mg/mL in acetone) and this layer was washed with a saturated EDTA solution (2 × 1 μL) and water (2 × 1 μL). The oligonucleotides (0.5 μL of a 20 μmol/L solution in water) were then deposited on this matrix layer and allowed to dry. The final preparation step was the application of a second layer of matrix (0.5 μL of a 1:1 solution of THAP (30 mg/mL in ethanol) and 100 mmol/L aqueous ammonium citrate) that was allowed to dry at room temperature.

Chemical synthesis

Compound 3

A solution of (*R*)-(–)-pantolactone (1 g, 7.68 mmol) and 1,3-diaminopropan (1.67 mL, 38.42 mmol) in 6 mL EtOH was kept at 55 °C for 48 h, to which was added 13.7 mL (115.3 mmol) of ethyl trifluoroacetate. The mixture was kept at room temperature overnight, evaporated, then co-evaporated with toluene and dry pyridine. The residue was dissolved in dry pyridine (40 mL), cooled in an ice bath, and 4,4′-dimethoxytrityl chloride (2.86 g, 8.45 mmol) was slowly added. The reaction was stopped after 2 h by the addition of 0.5 mL of water and then diluted with 200 mL of $CHCl_3$. The organic phase was washed with 2.5% $NaHCO_3$ (3 × 60 mL), water (2 × 60 mL), and 20% NaCl (60 mL), then dried ($MgSO_4$). The residue was purified by flash chromatography using a stepwise gradient of EtOAC (0%–15%) in CH_2Cl_2–Et_3N (0.25%) to yield **3** as a colorless oil (3.14 g, 68%). ^{1}H NMR (300 MHz, $CDCl_3$, ppm) δ: 8.03 (t, 1H, N*H*COCF$_3$), 7.36–6.82 (m, 13H, H_{DMTr}), 6.66 (t, 1H, NHCOCH(OH), $^{3}J_{NH-CH_2}$ = 6 Hz), 4.07 (s, 1H, C*H*OH), 3.77 (s, 6H, OCH_3), 3.27 (m, 2H, C*H*$_2$NHCOCF$_3$), 3.16 (m, 3H, C*H*$_2$NHCO and CH_{2a}ODMTr), 3.01 (d, 1H, CH_{2b}ODMTr), 1.57 (m, 2H, $CH_2CH_2CH_2$), 1.12 (s, 3H, CH_{3a}), 1.02 (s, 3H, CH_{3b}). ^{13}C NMR (75.45 MHz, $CDCl_3$, ppm) δ: 173.8 (*C*ONH), 158.7 (*C*OCH$_3$), 157.5 (q, *C*OCF$_3$, $^{2}J_{C-F}$ = 36.5 Hz), 144.1–113.4 (7C, DMTr), 116.0 (q, CO*C*F$_3$, $^{1}J_{C-F}$ = 285.9 Hz), 86.8 (O*C*$_{DMTr}$), 77.8 (*C*HOH), 71.2 (*C*H$_2$ODMTr), 55.3 (OCH_3), 38.9 (*C*(CH$_3$)$_2$), 36.0 (*C*H$_2$NHCOCF$_3$) 35.4 (*C*H$_2$NHCO), 29.0 ($CH_2CH_2CH_2$), 22.0 (CH_{3a}), 20.9 (CH_{3b}).

Compound 4

Compound **3** (3 g, 5.9 mmol) was dissolved in MeOH (40 mL), then an aqueous solution of Na_2CO_3 (10%, 11 mL) was added. The reaction mixture was stirred overnight at 65 °C, evaporated, diluted with 200 mL of EtOAc, washed with 1.5% $NaHCO_3$ (3 × 150 mL), then dried (Na_2SO_4), evaporated, and co-evaporated with toluene (3 × 30 mL) and CH_2Cl_2 (2 × 30 mL) to yield 2.2 g of **4** (74% yield). This compound was used without further purification. ^{1}H NMR (300 MHz, $CDCl_3$, ppm) δ: 7.36–6.82 (m, 14H, H_{DMTr} and NHCO), $^{3}J_{NH-CH_2}$ = 6 Hz), 4.08 (s, 1H, C*H*OH), 3.78 (s, 6H, OCH_3), 3.16 (m, 3H, C*H*$_2$NHCO and CH_{2a}ODMTr), 3.01 (d, 1H, CH_{2b}ODMTr), 2.62 (t, 2H, C*H*$_2$NH$_2$, $^{3}J_{H-H}$ = 6.6 Hz), 1.57 (m, 2H, $CH_2CH_2CH_2$), 1.12 (s, 3H, CH_{3a}), 1.02 (s, 3H, CH_{3b}). ^{13}C NMR (75.45 MHz, $CDCl_3$, ppm) δ: 172.4 (*C*ONH), 158.6 (*C*OCH$_3$), 144.1–113.4 (7C, DMTr), 86.4 (O*C*$_{DMTr}$), 77.1 (*C*HOH), 70.8 (*C*H$_2$ODMTr), 55.2 (OCH_3), 39.3 (CH_2NH_2), 39.0 (*C*(CH$_3$)$_2$), 36.4 (*C*H$_2$NHCO), 33.0 ($CH_2CH_2CH_2$), 22.0 (CH_{3a}), 20.9 (CH_{3b}).

Compound 5

4 was carefully dried by three co-evaporations with pyridine and then dissolved in anhydrous pyridine. The NHS ester **9** was added and the solution stirred at RT and monitored by TLC. The reaction medium was evaporated and purified by chromatography over aluminum oxide with a gradient of ethyl acetate in hexane (50%–80%) in the presence of 0.25% triethylamine (1.35 g, yield 82%). ^{1}H NMR (300 MHz, $CDCl_3$, ppm) δ: 8.68 (ddd, 2H, $^{3}J_{ortho}$ = 4.8 Hz, $^{4}J_{meta}$ = 1.8 Hz, and $^{5}J_{para}$ = 0.9 Hz, H6 and H6″), 8.62 (ddd, 2H, $^{3}J_{ortho}$ = 7.5 Hz, $^{4}J_{meta}$ = 1.0 Hz and $^{5}J_{para}$ = 0.9 Hz, H3 and H3″), 8.02 (s, 2H, H3′ and H5′), 7.85 (ddd, 2H, $^{3}J_{ortho}$ = 7.8 Hz, $^{3}J_{ortho}$ = 7.5 Hz, and $^{4}J_{meta}$ = 1.5 Hz, H4 and H4″), 7.41–6.85 (m, 15H, H_{DMTr}, H5 and H5′), 6.64 (t, 1H, $^{3}J_{H-H}$ = 6 Hz, NHCO), 6.52 (t, 1H, $^{3}J_{H-H}$ = 5.7 Hz, NHCO), 4.29 (t, 2H, $^{3}J_{H-H}$ = 5.9 Hz, CH_2CH_2O), 4.09 (s, 1H, C*H*OH), 3.80 (s, 6H, CH_3O), 3.19 (m, 5H, C*H*$_2$NHCO and CH_{2a}ODMTr), 3.02 (d, 1H, CH_{2b}ODMTr), 2.45 (t, 2H, $^{3}J_{H-H}$ = 7.2 Hz, CH_2CO), 2.22 (m, 2H, NHCH$_2$C*H*$_2$CH$_2$NH), 1.50 (m, 2H, CH$_2$C*H*$_2$CH$_2$), 1.07 (s, 3H, CH_{3a}), 1.00 (s, 3H, CH_{3b}). ^{13}C NMR (75.45 MHz, $CDCl_3$, ppm) δ: 172.8 (CONH), 172.2 (CONH), 166.9 (C4′), 158.5 (*C*OCH$_3$), 156.9 (C2′, C6′), 155.9 (C2,C2″), 148.9 (C6, C6″), 144.3–113.2 (12C, DMTr), 136.6 (C4, C4″), 123.7 (C5, C5″), 121.2 (C3, C3″), 107.4 (C3′, C5′), 86.4 (O*C*$_{DMTr}$), 77.3 (*C*HOH), 70.8 (*C*H$_2$ODMTr), 66.2 (O*C*H$_2$), 55.2 (OCH_3), 38.8 (*C*(CH$_3$)$_2$), 35.8 (*C*H$_2$NHCO) 35.6 (*C*H$_2$NHCO), 32.8 ($OCH_2CH_2CH_2CONH$), 29.6 (NHCH$_2$*C*H$_2$CH$_2$NH), 25.1 (NHCH$_2$*C*H$_2$CH$_2$O), 22.0 (CH_{3a}), 20.9 (CH_{3b}). MS (FAB$^-$) calcd.: 823.97; found: 822 (M – H)$^-$.

Compound 6

5 (1 g, 1.2 mmol) was dissolved in anhydr. CH_2Cl_2 (10 mL). Diisopropylethylamine (520 μL, 3 mmol) and 2-cyanoethyl diisopropylchlorophosphoramidite (1.8 mmol, 430 mg) were then added to the previous solution. The reaction was stopped after 1 h at RT with 500 mL of CH_3OH and diluted with 100 mL of EtOAc, washed with 2.5%

© 2006 NRC Canada

$NaHCO_3$ (200 mL), and then dried over Na_2SO_4. The residue was purified over reverse phase silica gel (Lichroprep RP-18 (40–63 μmol/L)) and eluted with CH_3CN–Et_3N (0.25%) to yield 534 mg of solid **5** (43%). ^{1}H NMR (300 MHz, $CDCl_3$, ppm) δ: 8.67 (d, 2H, $^3J_{ortho}$ = 4.2 Hz, H6 and H6″), 8.60 (d, 2H, $^3J_{ortho}$ = 7.8 Hz, H3 and H3″), 8.01 (s, 2H, H3′ and H5′), 7.85 (td, 2H, $^3J_{ortho}$ = 7.5 Hz, and $^4J_{meta}$ = 0.9 Hz, H4 and H4″), 7.41–6.85 (m, 15H, H_{DMTr}, H5 and H5″), 6.56 (t, 1H, $^3J_{H–H}$ = 6.0 Hz, NHCO), 6.43 (t, 1H, $^3J_{H–H}$ = 5.7 Hz, NHCO), 4.28 (t, 2H, $^3J_{H–H}$ = 6.0 Hz, $COCH_2CH_2CH_2O$), 4.09 (d, 1H, $^2J_{H–P}$ = 12.6 Hz, C*H*OP), 3.78 (s, 6H, CH_3O), 3.70–3.4 (m, 4H, CH_2NHCO), 3.4–2.9 (m, 6H, CH_2ODMTr, CH_2CH_2OP, NC*H*), 2.43 (m, 4H, $OCH_2CH_2CH_2CO$, $POCH_2CH_2CN$), 2.21 (m, 2H, $NHCH_2CH_2CH_2NH$), 1.55 (m, 2H, $OCH_2CH_2CH_2CO$), 1.11 (m, 15H, CH_3), 1.00 (s, 3H, CH_{3b}). ^{13}C NMR (75 MHz, $CDCl_3$, ppm) δ: 171.4 (CONH), 170.0 (CONH), 167.0 (C4′), 158.6 ($COCH_3$), 157.1 (C2′, C6′), 156.1 (C2, C2″), 149.0 (C6, C6″), 145.2–112.9 (7C, DMTr), 136.7 (C4, C4″), 123.8 (C5, C5″), 121.3 (C3, C3″), 117.9 (CH_2CN), 107.4 (C3′, C5′), 85.8 (OC_{DMTr}), 77.3 (CHOP), 70.8 (CH_2ODMTr), 67.3 ($OCH_2CH_2CH_2CO$), 58.2 ($NCCH_2CH_2OP$), 55.2 (OCH_3), 43.4 (NCH), 38.8 ($C(CH_3)_2$), 35.9 (CH_2NHCO) 35.7 (CH_2NHCO), 32.8 ($OCH_2CH_2CH_2CONH$), 29.6 ($NHCH_2CH_2CH_2NH$), 25.1 ($COCH_2CH_2CH_2O$), 24.6 ($NCH(CH_3)_2$), 22.7 and 22.3 ($C(CH_3)_2$), 20.4 (CH_2CN). ^{31}P NMR (120 MHz, $CDCl_3$, ppm) δ: 156.0, 152.5. MS (FAB^-) calcd.: 1023.19 $(M – H)^-$; found: 1022 $(M – H)^-$.

Compound 7

A solution of succinic anhydride (300 mg, 3 mmol) and DMAP (80 mg, 0.66 mmol) in 10 mL of dry pyridine was added to 3000 mg of LCAA-CPG (500 Å) and the mixture was left at RT for 24 h with occasional swirling. After filtration, successive washes with 10 mL portions of pyridine, CH_2Cl_2, Et_2O, and drying, the succinylated LCAA-CPG was suspended in 4 mL of DMF pyridine (1:1 *v*/*v*); compound **5** (206 mg, 0.25 mmol), 1,3-diisopropylcarbodiimide (0.28 mL, 1.8 mmol)), and DMAP (20 mg) were added. The suspension was left for 48 h at RT. To block the remaining carboxylic groups, a solution of pentachlorophenol (100 mg) was added and the mixture was kept at RT for further 12 h. The support was filtered, resuspended in 5% *v*/*v* solution of piperidine (3 mL), reacted for 10 min, filtered again and washed successively with 10 mL portions of $CHCl_3$, CH_3OH, CH_3CN, and dried in vacuo. Loading was determined by treating a portion (5 mg) of **7** with 1 mL of 3% *w*/*v* CCl_3CO_2H in 1,2-dichloroethane and measuring the absorbance of DMTr cation at 504 nm (ε = 75 000 L mol^{-1} cm^{-1}). Loading found: 25–35 μmol/g.

Compound 9

Compound **8** (5.36 mmol, 2 g), obtained according to previously published procedures (4), was dissolved in dimethylformamide (40 mL), and *N*,*N*-diisopropylcarbodiimide (1.1 equiv., 5.9 mmol, 923 mL) and *N*-hydroxysuccinimide (1.1 equiv., 5.9 mmol, 678 mg) were added. The reaction was stirred at 40 °C overnight. The crude mixture was concentrated and crystallization from methanol yielded **9** (2.17 g, 93%).

Oligonucleotide synthesis

All oligonucleotides were synthesized on a 0.2 μmol scale with a Millipore Expedite 9809 synthesizer using conventional β-cyanoethyl phosphoramidite chemistry. The standard bases were dissolved in anhydrous acetonitrile (0.1 mol/L final concentrations). The modified phosphoramidites were dissolved in anhydrous acetonitrile and coupled manually with a coupling time of 15 min. The coupling efficiency was the same as that of unmodified amidites. All oligomers were synthesized "trityl off". The solid support was treated overnight at 55 °C with fresh concd. NH_4OH (1 mL). The crude oligomers were purified by electrophoresis on denaturated polyacrylamide gels (20%) and visualized by UV shadowing. The pure samples were desalted through reverse-phase set-pak cartridges (C18, Waters)

UV-monitored melting experiments

Purified oligonucleotides (each strand was 1 μmol/L) were diluted in 200 mL of the appropriate buffer. The mixture was boiled for 2 min and the hybridization was assured by low-temperature cooling of the sample. Melting experiments were performed with a Cary 1E UV–vis spectrophotometer with a temperature controller unit. Samples were kept at 5 °C for at least 30 min and then heated from 4 to 90 °C at a rate of 0.4 °C/min. The absorbance (λ = 260 nm) was measured every minute. The melting temperature was determined from the maxima of the first derivative. Two different buffers were used. The studies on the metalated species were performed in a buffer containing 10 mmol/L sodium phosphate (10 mmol/L, pH 7) and sodium chloride (150 mmol/L). The metal-free experiments were measured in an EDTA-containing buffer: EDTA (200 mmol/L), sodium phosphate (10 mmol/L, pH 7), and sodium chloride (150 mmol/L).

References

1. L. Zapata, K. Bathany, J.M. Schmitter, and S. Moreau. Eur. J. Org. Chem. **6**, 1022 (2003).
2. N.N. Dioubankova, A.D. Malakhov, D.A. Stetsenko, V.A. Korshun, and M. Gait. Org. Lett. **4**, 4607 (2002).
3. R.T. Pon. *In* Methods in molecular biology-protocols for oligonucleotides and analogs. Vol 20. *Edited by* S. Agrawal. Humana Press, Totowa, New Jersey. 1993. pp. 465–496.
4. G.R. Newkome, F. Cardullo, E.C. Constable, C.N. Moorefield, and A.M.W. Cargil Thompson. J. Chem. Soc. Chem. Commun. 925 (1993).
5. E.C. Constable and M.D. Ward. J. Chem. Soc. Dalton Trans. 1405 (1990).
6. E. Meggers, P.L. Holland, W.B. Tolman, F.E. Romesberg, and P.G. Schultz. J. Am. Chem. Soc. **122**, 10714 (2000).
7. H. Weizman and Y. Tor. J. Am. Chem. Soc. **123**, 3375 (2001).
8. J.M. Berg and Y. Shi. Science (Washington, D.C.), **271**, 1081 (1996).
9. C. Harford and B. Sarkar. Acc. Chem. Res. **30**, 123 (1997).

© 2006 NRC Canada

The synthesis of butene glycol ethers with aluminium triflate

Yvette M. Terblans, Michelle Huyser, Desmond A. Young, and Michael J. Green

Abstract: The use of aluminium triflate as a ring-opening catalyst for butene oxide (BuO) was evaluated in the presence of different alcohols such as methanol, ethanol, *n*-propanol, *n*-butanol, 2-propanol, 2-methyl-1-propanol, and 2-methyl-2-propanol. The reaction with methanol was studied kinetically by varying the temperature, catalyst concentration, and methanol – butene oxide molar ratio. These reactions yielded two major products (2-methoxy-1-butanol and 1-methoxy-2-butanol) in a approximate ratio of 1:1. It was noted that at low catalyst concentrations (<5 ppm), low temperatures (<90 °C), and a MeOH–BuO molar ratio of 8:1, the selectivity of the reaction could be kinetically manipulated to shift the product ratio towards 1-methoxy-2-butanol, the α-alkoxyalcohol. This result was confirmed by an experimental design program. Statistical calculations using the data from the experimental design identified a feasible region in which reactions with methanol could be carried out, which would lead to slightly higher selectivities to 1-methoxy-2-butanol. This region shows that the methanol – butene oxide ratio should be 8:1, the temperature between 80 and 85 °C, and the catalyst concentration between 3.9 and 5 ppm. These reaction conditions were used to carry out a test reaction with methanol and an extended series of alcohols. All the alcohols, except for 2-methyl-2-propanol, reacted with butene oxide under these conditions, with the selectivity to the α-alkoxyalcohol higher than to the β-alkoxyalcohol. To obtain a ring-opening reaction with 2-methyl-2-propanol, it was found that a higher catalyst concentration (approximately 10 ppm) and a lower alcohol – butene oxide ratio (6:1) at a temperature of 80 °C were necessary. This reaction led to a mixture of 1-*tert*-butoxy-2-butanol and 2-*tert*-butoxy-1-butanol with the selectivity to the α-alkoxyalcohol being somewhat higher because of the steric influence of the bulky *tert*-butoxy group.

Key words: aluminium triflate, alcohols, butene oxide, ring opening, α-alkoxyalcohol, β-alkoxyalcohol.

Résumé : On a évalué l'utilité du triflate d'aluminium comme catalyseur pour effectuer l'ouverture du cycle de l'oxyde de butène (BuO) en présence de divers alcools, dont le méthanol, l'éthanol, le *n*-propanol, le *n*-butanol, le 2-propanol, le 2-methyl-1-propanol et le 2-methyl-2-propanol. On a étudié la cinétique de la réaction avec le méthanol en faisant varier la température, la concentration de catalyseur et le rapport molaire méthanol – oxyde de butène. Ces réactions conduisent à la formation de deux produits principaux (le 2-méthoxybutan-1-ol et le 1-méthoxy-2-butanol) dans un rapport approximatif de 1 : 1. On a noté que, à de faibles concentrations de catalyseurs (<5 ppm), de faibles températures (<90 °C) et un rapport molaire MeOH–BuO de 8 : 1, la sélectivité de la réaction peut être manipulée d'une façon cinétique pour déplacer le rapport des produits en faveur du le 1-méthoxy-2-butanol, le α-alkoxyalcool. Ce résultat a été confirmé par un programme de modélisation expérimental. Des calculs statistiques à l'aide de données de modélisations expérimentales ont permis d'identifier une région appropriée dans laquelle les réactions avec le méthanol pourraient se produire pour conduire à des sélectivités légèrement supérieures en le 1-méthoxy-2-butanol. Ces calculs montrent que le rapport méthanol – oxyde de butène devrait être de 8 : 1, la température entre 80 et 85 °C et la concentration en catalyseur entre 3,9 et 5 ppm. On a utilisé ces conditions pour évaluer la réaction avec le méthanol et une série importante d'alcools. Dans ces conditions, tous les alcools réagissent avec l'oxyde de butène, à l'exception de l'alcool *tert*-butylique, et dans tous les cas la sélectivité favorise le α-alkoxyalcool par rapport au β-alkoxyalcool. Pour obtenir une réaction d'ouverture de cycle avec le 2-methyl-2-propanol, il est nécessaire d'utiliser une concentration en catalyseur plus élevée (environ 10 ppm) et un rapport alcool – oxyde de butène plus faible (6 : 1), à une température de 80 °C. Cette réaction conduit à un mélange de 1-*tert*-butoxy-2-butanol et de 2-*tert*-butoxy-1-butanol dans lequel la sélectivité en faveur du α-alkoxyalcool est légèrement supérieure en raison de l'influence stérique du groupe *tert*-butoxy.

Mots clés : triflate d'aluminium, oxyde de butène, ouverture de cycle, α-alkoxyalcool, β-alkoxyalcool.

[Traduit par la Rédaction]

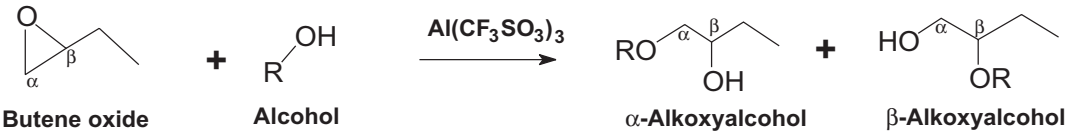
Received 14 February 2006. Published on the NRC Research Press Web site at http://canjchem.nrc.ca on 9 June 2006.

Y.M. Terblans,[1] M. Huyser, D.A. Young, and M.J. Green. Homogeneous Catalysis and Organic Synthesis, SASOL Technology (Pty) Ltd., Research and Development Division, SASOL, 1 Klasie Havenga Road, Sasolburg, 1947, South Africa.

[1]Corresponding author (e-mail: yvette.terblans@sasol.com).

 doi:10.1139/V06-086 © 2006 NRC Canada

Scheme 1. Ring opening of butene oxide with an alcohol.



Introduction

Ring-opening reactions of epoxides with alcohols, which have been successfully carried out for many decades, can be either base- or acid-catalyzed (1). In recent years the use of triflate salts (also known as trifluoromethane sulfonate salts) has become increasingly popular as catalysts for these reactions. The catalytic acitivity of rare earth triflates (e.g., $Eu(CF_3SO_3)_3$, $La(CF_3SO_3)_3$, $Lu(CF_3SO_3)_3$, $Nd(CF_3SO_3)_3$, $Sm(CF_3SO_3)_3$, $Sc(CF_3SO_3)_3$, $Y(CF_3SO_3)_3$, and $Ce(CF_3SO_3)_4$) has been investigated for the ring opening of epoxides by alcohols (2). Scandium triflate was found to be an exceptionally active catalyst for the ring opening of epoxides. $Yb(CF_3SO_3)_3$ has also been reported as a catalyst for intermolecular ring-opening reactions of epoxides with alcohols to give β-alkoxyalcohols in good to high yields with high regio- and stereo-selectivity (3).

Aluminium triflate is a Lewis acid that has been used as a catalyst in organic synthesis, for reactions including Friedel–Crafts acylation and alkylation (4, 5), the epoxidation of olefins with iodosylbenzene (6), the preparation of esters and lactones (7), as initiators for cationic polymerization (8), and as co-catalysts in the polymerization of olefins (9). Aluminium triflate has also been used as a catalyst for the ring-opening reactions of epoxides in the presence of alcohols and amines (10–12). Some work has also been carried out in which different epoxides and alcohols have been employed (13). In a recent study, we described the reaction of butene oxide with methanol, catalyzed by aluminium triflate (14). We now report on a kinetic study in which the effect of reaction variables (i.e., catalyst concentration, temperature, and reagent molar ratio) on the rate of conversion of butene oxide and selectivity to the major products (the α- and β-alkoxyalcohols) was investigated. The study was further expanded to include reactions with ethanol, *n*-propanol, *n*-butanol, 2-propanol, 2-methyl-1-propanol, and 2-methyl-2-propanol, with the aim of comparing the activity of $Al(CF_3SO_3)_3$ as a ring-opening catalyst of butene oxide in the presence of different alcohols (Scheme 1).

Due to the fact that $Al(CF_3SO_3)_3$ is a Lewis acid, its use as a ring-opening catalyst for butene oxide leads to the formation of both isomers of the corresponding butene glycol ether, i.e., α- and β-alkoxyalcohols. Previous studies have shown that the two isomers form in a molar ratio of close to one with the β-alkoxyalcohol in a slight excess compared with the α-alkoxyalcohol (10–12, 14). In a recent communication, three examples were provided in which the selectivity to the α-alkoxyalcohol is higher when using butene oxide and several others in the case of styrene oxide (13). In this study we show that it is possible to slightly increase the selectivity to the α-alkoxyalcohol with a simultaneous decrease in selectivity to the β-alkoxyalcohol by choosing the correct reaction conditions. Lower temperatures and catalyst concentrations were found to increase the selectivity to the α-alkoxyalcohol, whereas the opposite was observed for higher temperatures and increased catalyst concentrations. These results were verified by statistical calculations on data obtained from an experimental design program.

Experimental

Unless otherwise stated, all chemicals used in this study were purchased from Sigma-Aldrich and used without further purification. Aluminium triflate was prepared as described in the literature (12). Stock solutions of $Al(CF_3SO_3)_3$ (500 ppm) were prepared in each alcohol and the desired quantity thereof was weighed for every reaction. Kinetic reactions were carried out in a Parr autoclave. Gas chromatography was carried out using a Shimadzu GC-17A equipped with a flame ionization detector and a PONA capillary column (50 m × 0.21 mm × 0.5 μm). Each sample was weighed into a GC vial and *n*-heptane was used as an internal standard.

Typical experimental procedure for the ring opening of butene oxide

Methanol (192.25 g, 6 mol) and butene oxide (72.11 g, 1 mol) were combined in a 300 mL Parr reactor. On closing the reactor, it was flushed with nitrogen and evacuated to remove all air present. This flushing procedure was repeated three times.

A catalyst bomb was placed under vacuum prior to the run. The desired amount of the stock solution (2.644 g, 5 ppm) was weighed and transferred via a syringe to the bomb, which was then connected to the inlet of the autoclave. Next, a high-pressure nitrogen line was connected to the opposite side of the catalyst bomb after which stirring in the reactor commenced. The reactor was subsequently heated to 100 °C after which the catalyst solution was discharged into the reactor and a sample taken immediately (0 min) and weighed. The sample was weighed to determine the mass removed from the reactor. Further sampling from the reactor was carried out at the following intervals: 5, 10, 15, 20, 30, 60, and 120 min and each sample was weighed. Saturated NaOH–water solution (0.5 mL) was added to all samples to quench the reaction.

Results and discussion

Butoxylation of methanol

Catalyst concentration

In the first part of this study, the influence of catalyst concentration on the conversion of butene oxide and the selectivity to the major products (the α- and β-alkoxyalcohols) was studied over a range of catalyst concentrations. Included in this was the uncatalyzed reaction. The conversion of butene oxide is shown in Table 1. The data showed that the rate of conversion of the uncatalyzed reaction (0 ppm) was

© 2006 NRC Canada

Table 1. Conversion of butene oxide at different $Al(CF_3SO_3)_3$ catalyst concentrations.

	Conversion (mol%) of butene oxide			
Time (min)	$Al(CF_3SO_3)_3$ (0 ppm)	$Al(CF_3SO_3)_3$ (1 ppm)	$Al(CF_3SO_3)_3$ (5 ppm)	$Al(CF_3SO_3)_3$ (10 ppm)
5	3.00	16.00	74.00	85.00
10	6.00	36.00	97.00	100.00
15	11.00	46.00	100.00	100.00
20	16.00	50.00	100.00	100.00
30	21.00	61.00	100.00	100.00
60	29.00	77.00	100.00	100.00
120	41.00	88.00	100.00	100.00

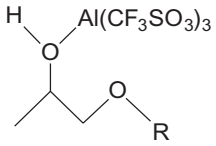
Note: T = 100 °C; MeOH–BuO = 6:1.

Table 2. Selectivity to products at different $Al(CF_3SO_3)_3$ catalyst concentrations.

	1-Methoxy-2-butanol		2-Methoxy-1-butanol	
Catalyst concentration (ppm)	Selectivity (%)	Yield (%)	Selectivity (%)	Yield (%)
0	49.60	10.42	42.94	9.02
1	49.75	30.35	42.25	25.77
5	43.39	43.39	48.61	48.61
10	42.98	42.98	49.02	49.02

Note: T = 100 °C; MeOH–BuO = 6:1.

Fig. 1. Ring-opened intermediate.



significantly slower than those of the catalyzed reactions. The increase in the rates from 0 to 1 ppm and to 5 ppm can clearly be seen; thus, as the catalyst concentration was increased, the rate of conversion also increased. However, hardly any difference was observed in the rate of conversion when the catalyst concentration was increased from 5 to 10 ppm. At these two catalyst concentrations, the rate of the reaction was very fast and the reactions were completed after approximately 10 min. The low catalyst concentration needed for a fast reaction is due to the fact that the Lewis acid ($Al(OCF_3SO_3)_3$) coordinates to the epoxide, which leads to further activation of the already active electrophile. It was also further demonstrated that the transfer of the $Al(OCF_3SO_3)_3$ from the ring-opened intermediate (Fig. 1) to the next butene oxide molecule is energetically favourable (14).

In these reactions two major products (the α- and β-alkoxyalcohols, 1-methoxy-2-butanol and 2-methoxy-1-butanol) were formed. By-products such as dimers, diols, and in some instances, trimers, were also formed during these reactions with a total yield of dimers, diols, and trimers of approximately 8%, selectivity to dimers of approximately 4%, selectivity to diols of approximately 1%, and selectivity to the trimers of approximately 3%. All products were identified using GC–MS. It was noticed that the higher the catalyst concentration, the higher the concentration of by-products.

The selectivities to the α- and β-alkoxyalcohols and yields of these products were calculated after 30 min of reaction time and are tabulated in Table 2. Upon considering the influence of the catalyst concentration on the selectivity to the products, it is observed that the selectivity to 1-methoxy-2-butanol was slightly higher than to 2-methoxy-1-butanol. However, as the catalyst concentration was increased above 2.5 ppm, the selectivity to the 2-methoxy-1-butanol was slightly higher than to 1-methoxy-2-butanol. This observation shows that as the catalyst concentration is increased, the formation of the sterically more hindered isomer becomes more facile.

Temperature

The second part of the study with methanol focused on the influence of reaction temperature on the rates of conversion, as well as the selectivity to the products. The conversion data are shown in Table 3.

The temperature data display a similar trend as the catalyst concentration data, i.e., the rate of conversion, increased as the reaction temperature was increased. The data also showed that the increase in the rate of conversion was not as significant when the temperature was increased from 100 to 120 °C, as was the case when it was increased from 60 to 80 °C and to 100 °C. This is due to the fact that the rates become very fast at the higher temperatures. It was also seen that the higher the temperature, the higher the concentration of by-products, i.e., dimers and trimers (total yield approximately 10%, selectivity to dimers approximately 7% and to trimers approximately 3%).

The selectivities to the alkoxyalcohols and the yields of these products were calculated after 30 min of reaction time. The data are shown in Table 4. It was observed that, although the ratio of the major products is approximately 1, at temperatures below 80 °C, the selectivity to 1-methoxy-2-butanol is slightly higher than to 2-methoxy-1-butanol, whereas the opposite is observed at temperatures above 80 °C. At 90 °C, the selectivity to 1-methoxy-2-butanol is

© 2006 NRC Canada

Table 3. Conversion of butene oxide at different temperatures.

	Conversion (mol%) of butene oxide				
Time (min)	60 °C	80 °C	90 °C	100 °C	120 °C
5	16.05	16.68	31.67	59.18	88.80
10	36.43	54.31	73.62	94.39	100.00
15	53.47	79.95	97.22	99.55	100.00
20	69.64	81.95	100.00	100.00	100.00
30	74.33	89.17	100.00	100.00	100.00
60	88.50	93.32	100.00	100.00	100.00
120	95.86	97.15	100.00	100.00	100.00

Note: $Al(CF_3SO_3)_3$ catalyst concentration = 5 ppm; MeOH–BuO = 6:1.

Table 4. Selectivity to products at different temperatures.

	1-Methoxy-2-butanol		2-Methoxy-1-butanol	
Temperature (°C)	Selectivity (%)	Yield (%)	Selectivity (%)	Yield (%)
60	56.01	41.63	43.99	32.70
80	55.17	49.20	44.83	39.97
90	46.00	46.00	45.94	45.94
100	43.39	43.39	48.61	48.61
120	43.33	43.33	50.67	50.67

Note: $Al(CF_3SO_3)_3$ catalyst concentration = 5 ppm; MeOH–BuO = 6:1.

Table 5. Conversion of butene oxide with $Al(CF_3SO_3)_3$ at different methanol – butene oxide ratios.

	Conversion (mol%) of butene oxide					
Time (min)	MeOH–BuO (4:1)	MeOH–BuO (6:1)	MeOH–BuO (8:1)	MeOH–BuO (10:1)	MeOH–BuO (12:1)	Me–BuO (14:1)
5	76.69	59.18	57.44	55.53	56.75	57.03
10	100.00	94.39	96.57	96.37	96.20	92.55
15	100.00	100.00	100.00	100.00	100.00	100.00

Note: T = 100 °C; catalyst concentration = 5 ppm.

virtually equal to the selectivity to 2-methoxy-1-butanol. These observations correlate well with those already observed for the catalyst concentration. It was observed that as the temperature is increased, the formation of the sterically more hindered isomer becomes more facile; the same trend is observed for the catalyst concentration.

Reactant molar ratio

The last part of the study with methanol focused on the influence of the molar ratio of the reagents on the rates of conversion, as well as the selectivity to the alkoxyalcohol products. The conversion data are shown in Table 5. In this study the ratio of MeOH–BuO was varied from 4:1 to 14:1.

It was observed that as the ratio of MeOH–BuO is increased, the rate of the reaction decreases, since the transfer of the $Al(CF_3SO_3)_3$ from the ring-opened intermediate (Fig. 1) to butene oxide depends on the concentration of butene oxide in the reaction mixture. Since the increase in the MeOH–BuO ratio will lead to a lowering in butene oxide concentration, a drop in rate was observed as expected. It was observed that the lower the MeOH–BuO ratio, the higher the concentration of by-products such as dimers and trimers (total yield approximately 10%, selectivity to dimers approximately 7% and to trimers approximately 3%).

The selectivities to the alkoxy alcohols and the yields of these products were calculated after 30 min and the data are shown in Table 6.

The data show that at lower MeOH–BuO ratios, the selectivity to 2-methoxy-1-butanol is slightly higher, however, this slight excess decreases and the selectivity to 1-methoxy-2-butanol starts to increase. At a 14:1 ratio of MeOH–BuO, the selectivity to the two products is virtually the same. This is due to the fact that at lower MeOH–BuO ratios, the formation of the sterically hindered product 2-methoxy-1-butanol is more facile than at higher MeOH–BuO ratios.

Experimental design

All the results obtained from this kinetic study led us to formulate an experimental design program in which to optimize conditions that would lead to shifting the selectivity to the formation of more 1-methoxy-2-butanol and less 2-methoxy-1-butanol. All work done in the experimental design program can be found in the Supplementary material[2] to the publication. After all the data had been accumulated

[2] Supplementary data for this article are available on the journal Web site (http://canjchem.nrc.ca) or may be purchased from the Depository of Unpublished Data, Document Delivery, CISTI, National Research Council Canada, Ottawa, ON K1A 0R6, Canada. DUD 5044. For more information on obtaining material refer to http://cisti-icist.nrc-cnrc.gc.ca/irm/unpub_e.shtml.

© 2006 NRC Canada

Table 6. Selectivity to products at different methanol – butene oxide ratios.

	1-Methoxy-2-butanol		2-Methoxy-1-butanol	
MeOH–BuO molar ratio	Selectivity (%)	Yield (%)	Selectivity (%)	Yield (%)
4:1	41.48	41.48	48.52	48.52
6:1	42.54	42.54	47.46	47.46
8:1	43.10	43.1	46.90	46.9
10:1	44.12	44.12	45.88	45.88
12:1	43.83	43.83	46.17	46.17
14:1	44.93	44.93	45.07	45.07

Note: T = 100 °C; catalyst concentration = 5 ppm.

Table 7. Conversion of butene oxide with $Al(CF_3SO_3)_3$ in the presence of different alcohols.

	Conversion (mol%) of butene oxide						
Time (min)	MeOH	EtOH	*n*-PrOH	*n*-BuOH	*i*-PrOH	*i*-BuOH	*t*-BuOH
5	31.73	20.94	17.00	13.87	11.63	5.63	0.80
10	47.09	37.5	28.03	21.36	17.36	8.71	0.12
15	59.00	46.27	38.03	29.47	21.10	9.57	0.03
20	69.85	53.69	43.81	33.15	25.89	10.58	1.13
30	80.13	64.77	49.53	39.04	28.45	3.24	0.07
60	88.50	73.74	60.46	47.12	34.50	15.91	0.46

and the relevant calculations had been carried out to determine the selectivities to 1-methoxy-2-butanol and 2-methoxy-1-butanol, the data were statistically evaluated by fitting response surface models. A response surface model describes the response as a function of the influential variables and yields a regression model. The significance of the regression model is evaluated through an analysis of variance table. This was done for each time interval. As a similar result was obtained for each time interval, only the results obtained for the 5 min interval are discussed here; the rest of the statistical calculations can be found in the Supplementary material[2] to the publication.

The results obtained for the 5 min interval were evaluated to determine the simultaneous effect of the variables on the responses. An overlay plot (a three-point design plot) of the predicted trends from the models in Fig. 2 was used to determine this effect.

Figure 2 depicts the feasible region (white area demarcated by three blue lines) for temperature and catalyst concentration where the 1-methoxy-2-butanol – butene oxide ratio is greater than 0.45, the 2-methoxy-1-butanol – butene oxide ratio is smaller than 0.35, and the mass of butene oxide reacted is greater than 0.18 mol simultaneously. This feasible region is shown for a methanol – butene oxide ratio at its centre value (8:1). It is clear that the criteria are satisfied simultaneously for temperatures between 80 and 85 °C and catalyst concentrations between 3.9 and 5 ppm.

The statistical interpretation of the data indicates that for slightly higher selectivities to 1-methoxy-2-butanol and lower selectivities to 2-methoxy-1-butanol, lower temperatures and catalyst concentrations should be used. This would represent the feasible region as indicated by the overlay plot (T = 80–85 °C, catalyst concentration = 3.9–5 ppm, and MeOH–BuO ratio = 8:1).

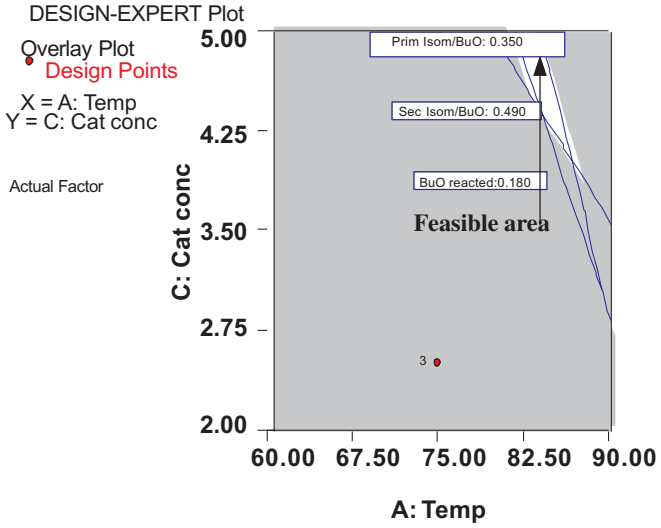
Butoxylations of various alcohols

The results obtained from the methanol butoxylation reactions led to the expansion of the study to include other alcohols. The conditions identified for methanol were used to carry out reactions with ethanol, *n*-propanol, 2-propanol, *n*-butanol, 2-methyl-1-propanol, and 2-methyl-2-propanol, to test the activity of $Al(OCF_3SO_3)_3$ as an epoxide ring-opening catalyst in the presence of these alcohols. A reaction was also carried out with methanol at these reaction conditions, to verify that these were indeed suitable for slightly higher selectivities to 1-methoxy-2-butanol. The reaction conditions chosen were T = 80 °C, catalyst concentration = 4 ppm, and ROH–BuO = 8:1.

The conversion data obtained for the different alcohols are shown in Table 7.

The results show that an increase in the carbon chain length of the alcohol has an influence on the rate of the reaction: the longer the carbon chain, the lower the reaction rate. This was evident when the alcohol was changed from

Fig. 2. Overlay contour plot presenting a feasible area.



© 2006 NRC Canada

Table 8. Selectivity to major products with different alcohols.

	α-Alkoxyalcohol		β-Alkoxyalcohol		
Alcohol	Selectivity (%)	Yield (%)	Selectivity (%)	Yield (%)	Sel α : Sel β
MeOH	51.17	41.002 52	40.83	32.72	1.3:1
EtOH	59.90	38.797 23	32.10	20.79	1.9:1
PrOH	62.27	30.842 33	26.73	13.24	2:1
n-BuOH	66.21	25.848 38	24.79	9.68	2.7:1
i-PrOH	59.37	16.890 77	16.63	4.73	3.5:1
i-BuOH	39.00	1.263 6	0	0	—
t-BuOH	0	0	0	0	—

$C_1 \rightarrow C_2 \rightarrow C_3 \rightarrow C_4$ *n*-alcohols. When the sterically more hindered alcohols (2-propanol, 2-methyl-1-propanol, and 2-methyl-2-propanol) were used, the rate decreased even further, up to the point where negligible reaction was observed when 2-methyl-2-propanol was used.

The selectivities to the alkoxyalcohols were calculated after 30 min of reaction time and are shown in Table 8. The yields of these products were also calculated at this time, as well as the ratio of the selectivity of the α-alkoxyalcohol to the the selectivity of the β-alkoxyalcohol (ratio Sel α : Sel β); these values are also shown in Table 8.

The nature of the alcohol plays a role on the product selectivity, clearly demonstrationg a greater selectivity for the α-alkoxyalcohol with increasing chain length and (or) steric bulk of the alcohol. No products were formed when using *tert*-butanol.

At these conditions, irrespective of the alcohol used, the reactions favoured the formation of the α-alkoxyalcohol above that of the β-alkoxyalcohol, in that more of the former and less of the latter were formed. The longer the carbon chain of the alcohol, the slower the rate of formation of the β-alkoxyalcohol. Results showed that even with methanol as the alcohol, 2-methoxy-1-butanol was only detected after 5 min. The ratio of 1-methoxy-2-butanol (the α-alkoxyalcohol) to 2-methoxy-1-butanol (the β-alkoxyalcohol) was, on average, 1.3. With an increase of one carbon atom in the chain length of the alcohol to ethanol, 2-ethoxy-1-butanol, the β-alkoxyalcohol was only detected after 10 min. The ratio of the two monomeric products (1-ethoxy-2-butanol to 2-ethoxy-1-butanol; α-alkoxyalcohol to β-alkoxyalcohol) was, on average, 1.9.

It should be noted that the reaction conditions used here were optimized for methanol as the alcohol and are not necessarily the optimum conditions when using the other alcohols. It was therefore decided to further investigate the reaction conditions for reaction with 2-methyl-2-propanol to determine whether any reaction will take place when $Al(CF_3SO_3)_3$ is used as the catalyst. If any reaction was observed, these conditions would also be used to carry out reactions with 2-propanol and 2-methyl-1-propanol.

The reaction conditions chosen were T = 80, 100, and 120 °C, catalyst concentration = 10 ppm, and *t*-BuOH–BuO = 6:1. The butene oxide conversion data are shown in Table 9. As expected, it was observed that as the temperature was increased, the reaction rate increased. Interestingly, at the higher catalyst concentration of 10 ppm and a lower *t*-BuOH–BO ratio of 6:1, a reaction between *t*-BuOH and BO was observed at 80 °C. Previously, the butoxylation reaction attempted at T = 80 °C, *t*-BuOH–BO = 8:1, and a catalyst concentration of 4 ppm showed no activity. Although the possibility of impurities in the feedstock acting as catalyst poisons cannot be ruled out at this stage, it has previously been indicated that higher catalyst concentrations are required with longer chain and bulkier alcohols (13).

Table 9. Conversion of BuO with *t*-BuOH at different temperatures.

	Conversion (mol%) of butene oxide		
Time (min)	80 °C	100 °C	120 °C
5	9.04	15.10	24.62
10	13.60	28.05	45.32
15	17.06	39.62	64.60
20	22.14	45.17	78.29
30	30.75	54.43	90.07
60	44.33	71.72	98.64
120	65.31	85.48	99.45

Note: $Al(CF_3SO_3)_3$ catalyst concentration = 10 ppm; *t*-BuOH–BuO = 6:1.

The selectivities to the major products, as well as their yields, were calculated after 30 min of reaction time. These results are shown in Table 10.

As the temperature was increased, the selectivity to the major products decreased. The ratio of the α-alkoxyalcohol to the β-alkoxyalcohol was approximately 2:1 at all three temperatures. This is expected as the sterically hindered alcohol (*t*-BuOH) would prefer to attach to the primary carbon (α-C) of butene oxide, rather than to the secondary carbon (β-C). This ratio is lower than expected (*n*-BuOH, 8:1) and can be rationalized as follows. The formed β-alkoxyalcohol is a primary alcohol and would react faster with the next molecule of BuO to produce dimers. Experimentally this is verified by large concentrations of the by-products such as dimers and trimers that are formed (yields between 15% and 20%). It can thus be concluded that an increase in the temperature leads to an increase in the conversion of the β-alkoxyalcohol to dimers and trimers.

As reactions with *t*-BuOH are generally known to be difficult because of the steric hinderance of the *tert*-butyl group, and as reaction conditions for the ring opening of butene oxide with *t*-BuOH were identified, it was decided to employ these reaction conditions in reactions with *i*-PrOH and *i*-BuOH, which have previously shown low activity. The influence of the different branched alcohols at the same set of reaction conditions on the rate of conversion of the butoxylation reaction is shown in Table 11.

© 2006 NRC Canada

Table 10. Selectivities to products at different temperatures with *t*-BuOH.

	1-*tert*-Butoxy-2-butanol		2-*tert*-Butoxy-1-butanol	
Temperature (°C)	Selectivity (%)	Yield (%)	Selectivity (%)	Yield (%)
80	62.20	19.13	26.80	8.24
100	59.50	32.39	27.50	14.97
120	51.00	45.94	29.90	26.93

Note: $Al(CF_3SO_3)_3$ catalyst concentration = 10 ppm; *t*-BuOH–BuO = 6:1.

Table 11. Conversion of BuO with different branched alcohols.

	Conversion (mol%) of butene oxide		
Time (min)	*t*-BuOH	*i*-BuOH	*i*-PrOH
5	15.10	33.89	35.67
10	28.05	53.06	49.96
15	39.62	70.50	71.80
20	45.17	77.91	82.47
30	54.43	86.42	88.02
60	71.72	95.84	96.53
120	85.48	99.09	99.65

Table 12. Selectivity to products with different branched alcohols.

	α-Alkoxyalcohol		β-Alkoxyalcohol	
Alcohol	Selectivity (%)	Yield (%)	Selectivity (%)	Yield (%)
t-BuOH	45.10	24.56	5.90	14.10
i-BuOH	52.1	45.026	33.90	29.30
i-PrOH	49.10	43.22	34.30	30.19

With *t*-BuOH, which is sterically more hindered than *i*-BuOH and *i*-PrOH, the rate of the butoxylation reaction with *t*-BuOH was slower. It was also observed that the rate with *i*-BuOH (a primary alcohol with branching) was similar to that with *i*-PrOH (a shorter chain secondary alcohol).

The selectivities to the major product and their yields were calculated at 30 min. These results are shown in Table 12.

For each of the three alcohols, the selectivity to the α-alkoxyalcohol (secondary alcohol) is higher than to the β-alkoxyalcohol (primary alcohol). This was also previously observed when the chain length of the alcohol was increased. The selectivity with *t*-BuOH was lower than for the other two alcohols, which correlates with the slower reaction rate, as the sterically more hindered alcohol will react slower. The selectivity for *i*-BuOH is higher than for *i*-PrOH, as the former alcohol is a primary alcohol and the latter a secondary alcohol. In all of these reactions, by-products were formed that are dimers and trimers.

Conclusion

The ring-opening reaction of butene oxide with different alcohols (methanol, ethanol, propanol, *n*-butanol, 2-propanol, 2-methyl-1-propanol, and 2-methyl-2-propanol) can easily be achieved in the presence of low concentrations of $Al(CF_3SO_3)_3$ as the catalyst. For short chain primary alcohols, e.g., methanol, ethanol, propanol, and *n*-butanol, very low catalyst concentrations (<5 ppm) and temperatures (<80 °C) are required to achieve this ring-opening reaction. For branched alcohols such as 2-propanol, 2-methyl-1-propanol, and 2-methyl-2-propanol, either slightly higher catalyst concentrations (approximately 10 ppm) or temperatures (approximately 120 °C) are required because of increased steric bulk and (or) hinderance.

It was also observed that the regioselectivity to the two major products (α- and β-alkoxyalcohols) can be kinetically manipulated to slightly favour either the one or the other, by changing the reaction conditions. For the reaction with methanol, it was observed that by choosing the correct reaction conditions, i.e., low catalyst concentrations and temperatures, the selectivity is slightly shifted to the α-alkoxyalcohol and vice versa. By using these conditions for the other alcohols, it was observed that the regioselectivity is shifted towards the α-alkoxyalcohol, except for 2-methyl-2-propanol where no reactivity was observed. However, by choosing the correct set of reaction conditions for 2-methyl-2-propanol to obtain activity (catalyst concentration of approximately 10 ppm and an alcohol–BuO molar ratio of 6), it was observed that the α-alkoxyalcohol is the preferred product. The same result is obtained when using 2-propanol and 2-methyl-1-propanol at the reaction conditions employed for 2-methyl-2-propanol.

Acknowledgements

The authors would like to thank SASOL Technology (Pty) Ltd. for the opportunity to publish this work. We would also

© 2006 NRC Canada

like to acknowledge our colleague, Mr. R. Coetzer, for performing all the statistical calculations in the experimental design program.

References

1. T.W. Graham Solomons. Organic chemistry. 5th ed. John Wiley and Sons Inc., New York. 1992. p. 778.
2. A. Berkessel, E. Ashkenazi, and M.R.M. Andreae. Appl. Catal. A, **254**, 27 (2003).
3. S. Kobayashi, M. Sugiura, H. Kitagawa, and W.W.-L. Lam. Chem. Rev. **102**, 2227 (2002).
4. G.A. Olah, O. Farroq, S.M.F. Farina, and J.A. Olah. J. Am. Chem. Soc. **110**, 2560 (1988).
5. S. Kobayashi and I. Komoto. Tetrahedron, **56**, 6463 (2000).
6. Y. Yang, Y.F. Diederich, and J.S. Valentine. J. Am. Chem. Soc. **112**, 7826 (1990).
7. Y. Ishii and T. Nakano. EP 1078922 A1. Daiceil Chemical Company Industries Ltd. 2001.
8. O. Farooq and W. Minn. US Patent 5 084 586. Minnesota Mining and Manufacturing Company. 1992.
9. S.J. Mclain. WO 98/03559. Du Pont. 1997.
10. M.J. Green. US Patent 4 605 769. BP Chemicals Limited. 1986.
11. M.J. Green. US Patent 4 762 952. BP Chemicals Limited. 1987.
12. D. Falgoux, D. Simoulin, and M. Pascal-Mousselard. US Patent 4 543 430. BP Chemicals Ltd. 1983.
13. D.B.G. Williams and M. Lawton. Org. Biomol. Chem. **3**, 3269 (2005).
14. Y.M. Terblans, J.J. Huyser, M. Huyser, M.J. Green, D.A. Young, and M.S. Sibiya. Can. J. Chem. **83**, 854 (2005).

© 2006 NRC Canada

Synthesis, characterization, and the molecular structures of two new kinds of stilbene

Yan-Hong Liu, Tong-Lai Zhang, Jian-Guo Zhang, Li Yang, Jin-Yu Guo, Wei Yu, Rui-Feng Wu, and Kai-Bei Yu

Abstract: We report in this study the synthesis, crystal culture, and single-crystal X-ray crystallography of two new kinds of double stilbene, which were readily prepared from trinitro-*p*-xylene and *p*-tolualdehyde in the presence of piperidine. We found that these triclinic crystals belong to the space group *P*-1. These compounds were also investigated using FT-IR, ^{1}H NMR, ^{13}C NMR, and MS spectroscopy techniques. The thermal decomposition processes of the compounds were tested by DSC and TG-DTG at a heating rate of 10 °C/min. These results indicate that the compounds have high heat-resistant stability.

Key words: polynitrostilbene, molecular structure, thermal decomposition.

Résumé : Dans ce travail, on rapporte la synthèse, la culture des cristaux, et la cristallographie par diffusion des rayons X de deux nouveaux types de double stilbène qui ont été facilement préparés par réaction du trinitro-*p*-xylène avec le *p*-tolualdéhyde en présence de pipéridine. On a trouvé que les cristaux tricliniques appartiennent au groupe d'espace *P*-1. On a aussi examiné ces produits par les techniques de spectroscopie infrarouge à transformée de Fourier, de RMN du^{1}H et du ^{13}C et par spectroscopie de masse. On a évalué les processus de décomposition thermique des composés par les techniques d'analyse calorimétrique différentielle (ACD) et de thermogravimétrie (TG) et de thermogravimétrie différentielle (TGD), à des taux de chauffage de 10 °C/min. Ces résultats indiquent que ces composés sont dotés d'une grande stabilité et d'une grande résistance à la chaleur.

Mots clés : polynitrostilbène, structure moléculaire, décomposition thermique.

[Traduit par la Rédaction]

Introduction

Nitro aromatic compounds, such as 2,4,6-trinitrotoluene (TNT), are well-known explosives that can be applied as energetic materials. These compounds have relatively high energy and good thermal stability and thus have been extensively studied (1–7). In previous papers, we reported the synthesis and properties of several new compounds of this kind, e.g., trinitro-*p*-xylene (TPX) and trinitro-trimethylbenzene (TNTM) (8, 9), which are more stable but less energetic than TNT. In this study, we present two other new kinds of stilbene that were synthesized by using TPX, *p*-tolualdehyde (PTD), and piperidine.

Stilbene is a type of compound whose structure contains C=C between phenyl rings (10–12), such as hexanitrostilbene (HNS), and is widely used in the medical and energetic materials industries. HNS is a heat-resistant explosive that has very low vapor pressure and high vacuum stability (13, 14). It is relatively insensitive to heat, spark, impact, and friction, yet it can be used widely as a heat-resistant booster charge for military applications.

During crude oil extraction, explosives are utilized for perforating the source rocks. As the average depths of the wells increase, as a consequence, the ambient temperatures in the wells increase. For these wells and for other applications requiring the explosive to withstand significant temperatures before initiation, heat-resistant explosives are of growing interest for the petroleum industry. Modern explosives have to withstand temperatures up to 260 °C for several hours without noticeable thermal decomposition (15).

We are interested in exploring some new heat-resistant explosives that have a similar structure to HNS, in which there exists a double stilbene bond and a piperidine ring that contains an aromatic nitrogen atom. To the best of our knowledge, this kind of structure has not been reported in the literature.

In this work, we cultured single crystals of the two compounds. The molecular and crystal structures were determined by X-ray single-crystal diffraction analysis. The thermal decomposition processes of the compounds were investigated to examine their thermal stability.

Received 18 October 2005. Published on the NRC Research Press Web site at http://canjchem.nrc.ca on 16 June 2006.

Y.-H. Liu, T.-L. Zhang[1], J.-G. Zhang, L. Yang, J.-Y. Guo, W. Yu, and R.-F. Wu, State Key Laboratory of Explosion Science and Technology, Beijing Institute of Technology, Beijing, P. R. China 100081.
K.-B. Yu. Center of Analysis and Test of Chengdu Branch, Chinese Academy of Sciences, Chengdu, P. R. China 610041.

[1]Corresponding author (e-mail: ztlbit@bit.edu.cn na).

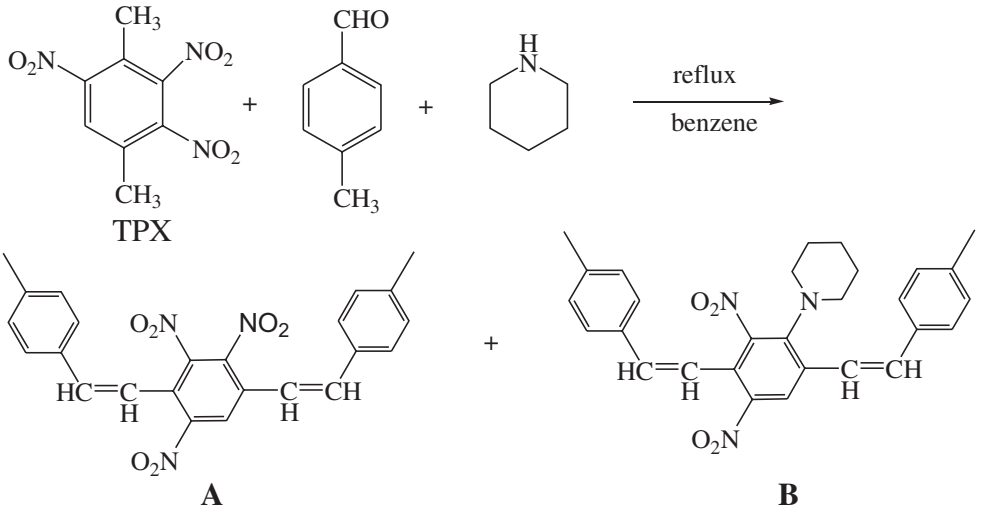
Results and discussion

Synthesis

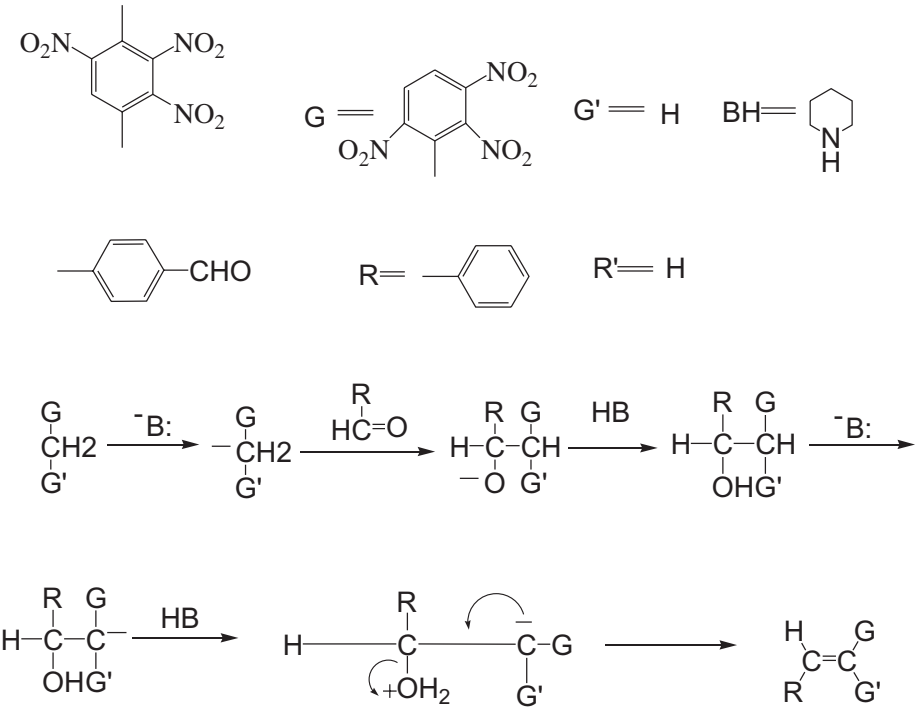
Scheme 1 shows the equation of the synthesis of 1,4-di(*p*-methyl-styryl)2,3,6-trinitrobenzene (**A**) and 1,4-di(*p*-methyl-styryl)-2-piperidine-3,6-dinitrobenzene (**B**).

 doi:10.1139/V06-083 © 2006 NRC Canada

Scheme 1. The equation of the synthesis of **A** and **B**.



Scheme 2. The mechanism of reaction **A**.



The reactant TPX (CCDC number 25641) was synthesized and studied in a previous work (8).

The mechanism of the reaction is shown in Scheme 2. In this reaction the piperidine is used as the catalyst. When the proportion of the piperidine and TPX is more than 4:1, piperidine will react with the product as a nucleophilic reagent attached to C11 in the middle benzene ring, as shown in Scheme 3.

Crystal structure of the compounds

The X-ray single crystal structures of **A** and **B** were determined. The select bond lengths and bond angles are summarized in Tables 1 and 2. The unit structures of the molecules in the crystal lattice are illustrated in Fig. 1.

The data from Table 1 show that in structure **A** the left benzene ring is coplanar with the middle ring. The C8=C9 bond is in the same plane with the two phenyl rings, while the torsion angles of the C16=C17 bond between the middle benzene ring and the right benzene ring are 47.0° and 23.7°, respectively. The C=C bond (1.32 Å) is the shortest in this structure. Affected by the methyl and C=C bond, the endocyclic angles in the side benzene rings, C7-C2-C3 (117.3°), C6-C5-C4 (117.0°), C19-C18-C23 (117.7°), and C22-C21-C20 (116.7°) are smaller than the others (121°). The largest deviation between the inner angles and the stable benzene ring (120°) is 3.3°, which indicates that the two side benzene rings are stable. The C10—C11 and C13—C14 bonds are of normal length in the middle benzene ring; the C10—C15 and C12—C13 bonds (average length 1.40 Å) are found to be longer; and the C11—C12 (1.39 Å) bond is shorter. The C14—C15 (1.36 Å) is found to be the shortest among the benzene ring bonds because there is no

© 2006 NRC Canada

Scheme 3. The mechanism of reaction **B**.

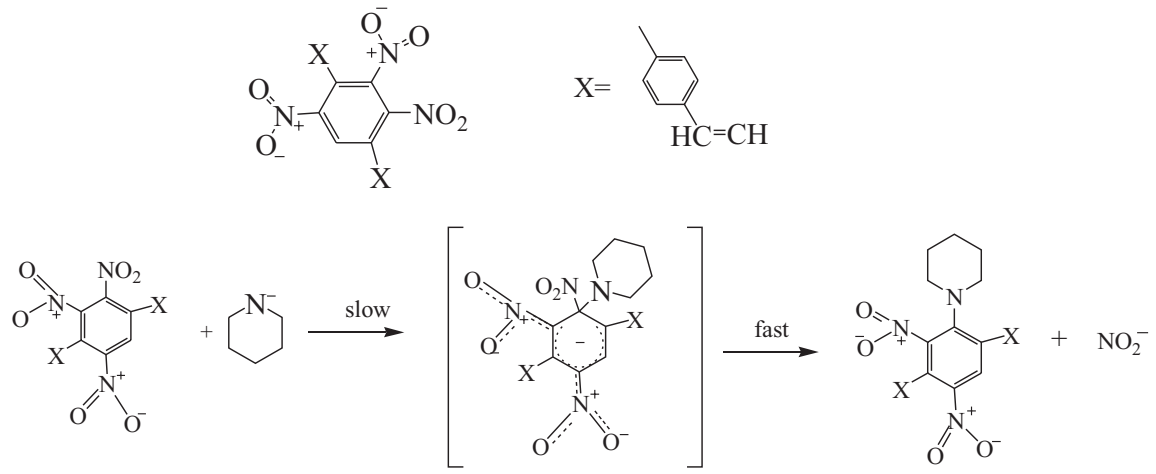


Table 1. Select bond lengths, bond angles, and dihedral angles for **A**.

Bond lengths (Å)		Bond angles (°)		Dihedral angles (°)	
O1—N1	1.215(2)	O2-N1-O1	125.3 (2)	C1-C2-C3-C4	–176.4(2)
O2—N1	1.215(2)	O2-N1-C11	117.4(2)	C8-C5-C6-C7	–177.3(2)
O3—N2	1.220(2)	O1-N1-C11	117.3(2)	C1-C2-C7-C6	176.3(2)
O4—N2	1.209(2)	O4-N2-O3	125.6(2)	C4-C5-C8-C9	–1.6(4)
O5—N3	1.212(2)	O4-N2-C12	117.7(2)	C6-C5-C8-C9	177.5(2)
O6—N3	1.205(2)	O3-N2-C12	116.7(2)	C5-C8-C9-C10	–178.4(2)
N1—C11	1.473(2)	O6-N3-O5	124.9(2)	C8-C9-C10-C11	178.1(2)
N2—C12	1.480(3)	O6-N3-C14	118.0(2)	C8-C9-C10-C15	–2.0(3)
N3—C14	1.484(3)	O5-N3-C14	117.0(2)	C16-C17-C13-C14	–47.0(3)
C1—C2	1.511(3)	C7-C2-C3	117.3(2)	O1-N1-C11-C12	120.0(2)
C5—C8	1.460(3)	C3-C2-C1	121.6(2)	C16-C17-C18-C23	–23.7(4)
C8—C9	1.318(3)	C16-C17-C18	126.7(2)	O2-N1-C11-C10	116.4(2)
C9—C10	1.464(3)	C22-C21-C20	116.7(3)	N1-C11-C12-C13	179.2(2)
C13—C16	1.473(3)	C4-C5-C8	124.3(2)	N1-C11-C12-N2	–0.7(3)
C14—C15	1.360(3)	C6-C5-C8	118.6(2)	O4-N2-C12-C11	128.6(2)
C16—C17	1.333(3)	C9-C8-C5	129.3(2)	O3-N2-C12-C13	129.4(2)
		C8-C9-C10	124.6(2)	N2-C12-C13-C16	1.5(3)
		C11-C10-C15	114.8(2)	C16-C13-C14-N3	–6.6(3)
		C11-C10-C9	123.7(2)	O6-N3-C14-C15	116.7(2)
		C12-C11-N1	118.8(2)	O5-N3-C14-C13	121.1(2)
		C10-C11-N1	118.5(2)	N3-C14-C15-C10	–173.9(2)
		C11-C12-C13	122.8(2)	C16-C17-C18-C19	157.0(2)
		C11-C12-N2	118.3(2)		
		C15-C14-C13	125.3(2)		
		C15-C14-N3	114.9(2)		
		C13-C14-N3	119.8(2)		

substituent at C15. The inner angles in the middle phenyl ring are about 123°, except for C15-C10-C11 (114.8°). The smaller bond angle of C15-C10-C11 may be caused by the conjugation of the C=C bond connected to C10. The other inner angles are larger than 120°, which indicates that there is some tension in the benzene and that the stability of the phenyl plane is weakened. The torsion angles about the C—N bonds are 60.9°, 50.7°, and 60.7° at C11, C12, and C14, respectively. N1 and N3 nitro groups have similar dihedral angles to the phenyl ring and rotate to the same face of the phenyl ring. The C—N bond length (N1—C11, 1.47 Å; N2—C12, 1.48 Å; N3—C14, 1.48 Å) is the largest and similar to the C—N length in TNT (14). The angles O-N-O and the two C-N-O average angle values are 125°, 118°, and 117°, respectively, so we can conclude that the N is sp^2 hybridized. The lengths and angles that contain the N are larger so we can predict that the C—N bond is easier to split than others. These results are similar to those for TPX (8) and TNT (16).

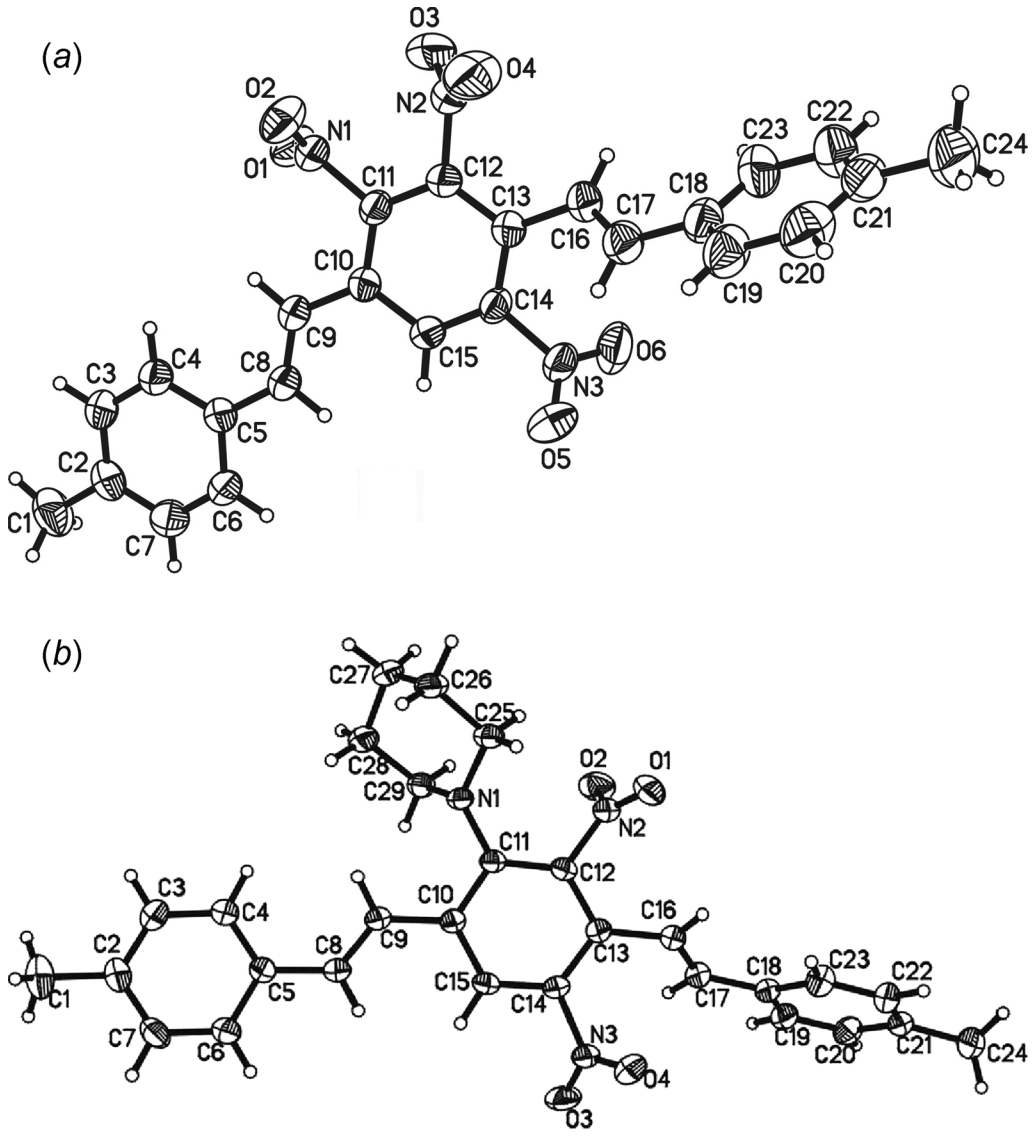
In structure **A**, there are two nitro groups in the ortho and para of the N1-nitro group, respectively, which make the density of the electric charge dispersal and the nucleophilic substitution easier for C11. Structure **B**, which results from the substitution of the nitro group at the N1 position of

© 2006 NRC Canada

Table 2. Select bond lengths, bond angles, and dihedral angles for **B**.

Bond lengths (Å)		Bond angles (°)		Dihedral angles (°)	
O1—N2	1.214(2)	O1-N2-O2	125.1(2)	O1-N2-C12-C13	–66.1(2)
O2—N2	1.222(2)	O1-N2-C1	118.4(2)	O2-N2-C12-C11	–59.8(3)
O3—N3	1.227(2)	O2-N2-C1	116.4(2)	C14-C13-C16-C17	51.7(3)
O4—N3	1.218(2)	O4-N3-O3	123.7(2)	C16-C17-C18-C23	15.0(3)
N2—C12	1.484(2)	O4-N3-C5	119.7(2)	C10-C15-C9-C8	17.4(2)
N3—C14	1.471(2)	O3-N3-C5	116.5(2)	C9-C8-C5-C4	22.0(4)
N1—C11	1.399(2)	C2-N1-C25	122.1(2)		
C25—C26	1.516(3)	C2-N1-C29	118.4(2)		
N1—C25	1.460(2)	C25-N1-C29	112.1(2)		
N1—C29	1.461(2)	C13-C12-C11	125.5(2		
C13—C16	1.476(3)	C12-C11-C10	117.4(2)		
C16—C17	1.323(3)	C15-C10-C11	118.2(2)		
C17—C18	1.460(3)	C15-C14-C13	123.6(2)		
C21—C24	1.512(3)	C14-C13-C12	113.9(2)		
C9—C8	1.326(2)	C19-C18-C23	116.9(2)		
C8—C5	1.461(3)	C4-C4-C6	116.6(2)		

Fig. 1. (*a*) The unit structures of the molecule for **A**. (*b*) The unit structures of the molecule for **B**.



© 2006 NRC Canada

Fig. 2. (*a*) The DSC curve for **A**. (*b*) The DSC curve for **B**.

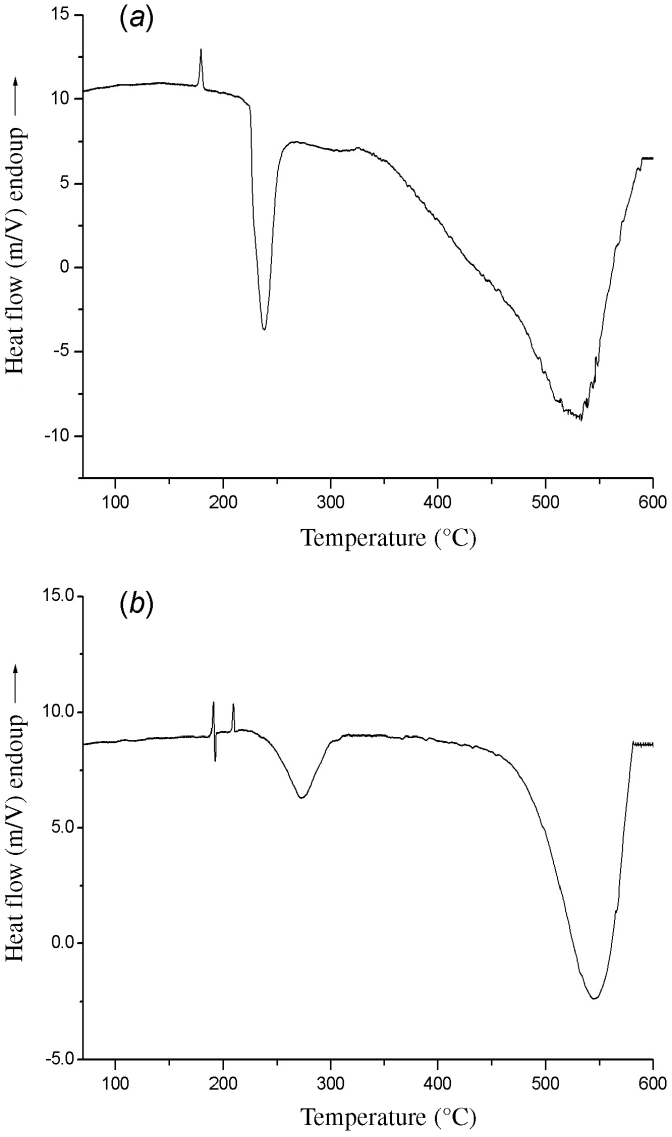
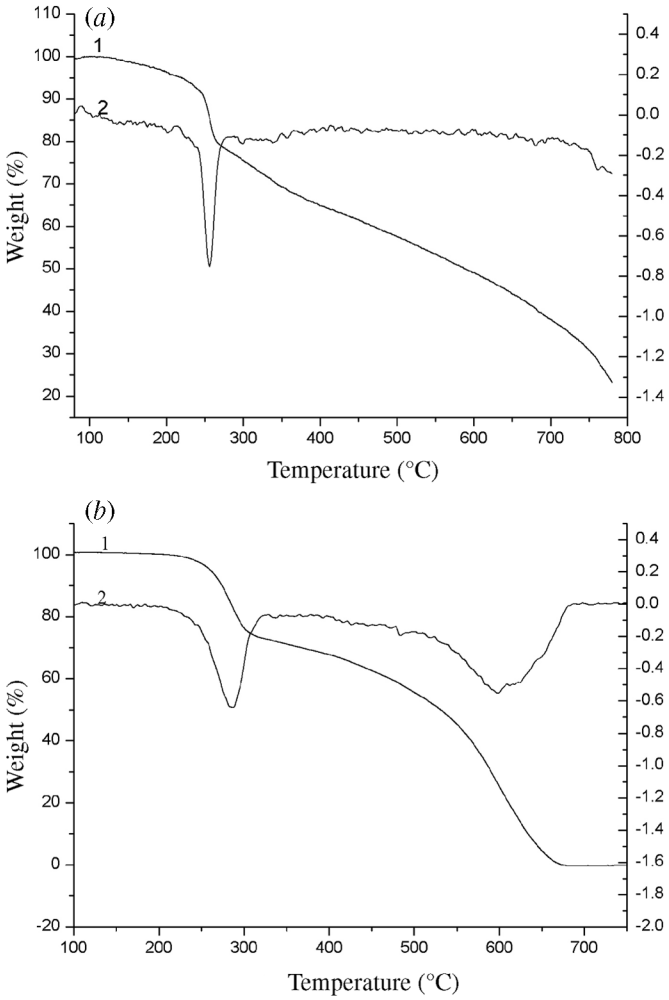


Fig. 3. (*a*) The TG-DTG curve for **A**. (*b*) The TG-DTG curve for **B**.



structure **A** by a piperidine group, has a similar structure to **A**. From the data, we find that the results for the side benzene rings of structure **B** are basically the same as those of structure **A**. But there are some larger differences owing to the effect of the piperidine. Both C=C bonds are not coplanar to the benzene rings and the torsion angles C16-C17-C18-C23, C14-C13-C16-C17, C8-C9-C10-C15, and C4-C5-C8-C9 are 15.0°, 51.7°, 17.4°, and 22.0°.

Thermal behaviour

The results of DSC and TG-DTG analyses are shown in Figs. 2 and 3, which show TG and DTG curves, respectively. In the DSC curve, there is one aculeate endothermic peak and two exothermic peaks (see Fig. 2*a*). The temperatures at the peaks are 179, 238, and 530 °C. The second endothermic peak is wider than the first and corresponds to the second decomposition process. Correspondingly, the TG-DTG curve in Fig. 3*a* shows two processes of weight loss. The initial degradation temperature is 238 °C. In the first decomposition process, the largest mass loss rate is 9.0% per min at 252 °C. At 780 °C, the compound has not decomposed completely, with 30% residual mass. In Fig. 2*b*, there are two aculeate intense endothermic peaks, one sequential exothermic peak, and two exothermic peaks. The temperatures at the peaks are 191.6, 192.7, 209.5, and 272.6 °C. Compound **B** begins degrading at 253 °C and undergoes two obvious mass-losing processes. In the first decomposition process, the largest mass loss rate is 6.1% per min at 286 °C, with a total mass loss of 29.2% occurring in the range from 253 to 325 °C. During the second decomposition process, the largest mass rate is 5.5% per min at 599 °C, and at 683 °C the compound is completely decomposed. When the nitro group is substituted by piperidine, the initial degradation temperature becomes higher, probably because **B** has a larger formula weight than **A**. From the results, we find that the compounds have higher initial decomposition temperatures and higher heat resistances. The melting points of **A** and **B** are 179 and 192.7 °C, higher than TNT (80.9 °C), 1,3,5-trinitrobenzen (TNB, 121.2 °C), and TPX (141 °C). But the thermal abilities of these compounds do not compare with HNS, which has higher symmetry and more nitro groups. In the future, we will introduce more nitro groups to these compounds to improve their thermal abilities.

© 2006 NRC Canada

Table 3. Crystal data and structure refinement for **A** and **B**.

Compound	**A**	**B**
Chemical formula	$C_{24}H_{19}N_3O_6$	$C_{29}H_{29}N_3O_4$
Molecular weight	445.42	483.55
Crystal system	Triclinic	Triclinic
a (Å)	8.312(2)	8.226(1)
α (°)	89.12(2)	91.89(1)
b (Å)	8.537(2)	10.613(1)
β (°)	87.11(2)	102.42(1)
c (Å)	16.733(2)	14.889(2)
γ (°)	66.10(2)	94.58(1)
Volume (Å^3)	1084.2(5)	1263.7(3)
Z	2	2
Temperature (K)	296(2)	288(2)
Space group	*P*-1	*P*-1
Wavelength (nm)	0.071 073	0.071 073
$D_{calcd.}$ (g/cm^3)	1.364	1.271
Absorption coefficient (mm^{-1})	0.100	0.086
F(000)	464	512
Crystal size (mm)	0.46 × 0.38 × 0.28	0.48 × 0.38 × 0.26
θ range for data collection (°)	1.22–25.50	1.40–25.50
Limiting indices	$0 \le h \le 9$,	$0 \le h \le 9$,
	$-9 \le k \le 10$,	$-12 \le k \le 12$,
	$-20 \le l \le 20$	$-18 \le l \le 17$
Reflections collected	4459	5212
Independent reflections	4015 [*R*(int) = 0.0176]	4697 [*R*(int) = 0.0167]
Data / restraints / parameters	4015 / 0 / 299	4697 / 0 / 328
Goodness-of-fit on F^2	0.840	0.856
Final *R* indices [$I > 2\sigma(I)$]	$R_1 = 0.0426$	$R_1 = 0.0437$
	$wR_2 = 0.1008$	$wR_2 = 0.0947$
R indices (all data)	$R_1 = 0.0892$	$R_1 = 0.0908$
	$wR = 0.1133$	$wR = 0.1078$
Extinction coefficient	0.010(2)	0.036(7)
Largest diff. peak and hole (e nm^{-3})	184 and –138	160 and –127

Conclusion

Polynitro dimethyldoublestilbene and piperidine substitutes have been prepared and characterized. In both crystal structures, there are two C=C bonds, three benzene rings, and two methyl-substituted groups. The difference between **A** and **B** is at the N1 position (at which **A** has a nitro group and **B** has a piperidine group). The two compounds have higher initial decomposition temperatures and higher heat-resisting abilities. But their thermal abilities do not compare to HNS. In the side benzene rings, there are eight unoccupied positions that could be substituted by other groups and that may produce some desired properties. So we expect that they could be used as heat-resistant explosives similar to HNS.

Experimental

General

The NMR spectra were determined using a Bruker AV400 MHz 400 spectrometer. ^{1}H NMR and ^{13}C NMR spectra were recorded for identification purposes in deuteriochloroform solutions at room temperature. All chemical shifts are reported in ppm downfield with tetramethylsilane as the internal marker. Infrared spectra were performed using a Bruker Equinox 55 FT-IR spectrometer (KBr pellet) in the range of 4000–400 cm^{-1}. Elemental analyses were carried out with a Flash EA 1112 fully automatic microanalyser. Mass spectra (MS) of the electronic impact positive ions were obtained using a GCT–MS Micromass spectrometer. Thermal properties of the compounds were measured using a differential scanning calorimeter (DSC), PerkinElmer Pyris-1 DSC, under a nitrogen atmosphere at a heating rate of 10 °C per min. A PerkinElmer Pyris-1 TG analyzer was used for thermogravimetric analysis. About 0.5 mg of the sample was held in a platinum pan, in a flow of dry oxygen-free nitrogen at 20 mL/min, and at a heating rate of 10 °C per min. The structures of the compounds were determined by single-crystal X-ray diffraction.

X-ray crystallography

The structure was solved by direct methods. Anisotropic displacement parameters were applied to all non-hydrogen atoms in full-matrix least-squares refinements based on F^2. The hydrogen atoms were set in calculated positions and refined as riding atoms with a common fixed isotropic thermal parameter.

© 2006 NRC Canada

All calculations were carried out using SHELXLS-98 (17). The conjugated and derivational effects of the nitro groups reduce the density of the electrons of the benzene ring. Crystallographic and refinement parameters are given in Table 3.[2]

Synthesis

1,4-Di(*p*-methyl-styryl)2,3,6-trinitrobenzene (A)

The general procedure for preparing **A** is as follows. 2,3,5-Trinitro-*p*-xylene (TPX) (0.02 mol), *p*-tolualdehyde (PTD) (0.042 mol), piperidine (3 mL), and benzene (100 mL) were placed in a dry 100 mL flask, equipped with a separate vessel of water and oil and a condenser. The reaction mixture was heated to reflux for 20 h. The mixture was cooled and ethanol was then added to the flask. The product was cooled in a refrigerator for 12 h. The mixture was filtrated and purified with acetone. The crystal was cultured in DMF, becoming pale yellow. Yield: 54%. IR (KBr, cm^{-1}): 3036, 2966, 2923, 1679, 1636, 1531, 1461, 1399, 1347, 1294, 1260, 1171, 1120, 1093, 1041, 979, 900, 804, 760, 725, 638, 550, 506. ^{1}H NMR ($CHCl_3$–TMS, *J* (Hz)) δ: 2.44–2.46 (d, 6H), 6.78–6.82 (d, 1H), 7.03–7.07 (d, 1H), 7.10–7.14 (d, 1H), 7.24–7.26 (d, 2H), 7.29–7.31 (d, 2H), 7.34–7.42 (t, 3H), 7.49–7.51 (d, 2H), 8.43 (s, 1H). ^{13}C NMR ($CDCl_3$–TMS, *J* (Hz), ppm) δ: 0.068, 21.33, 21.42, 114.32, 115.99, 123.38, 125.33, 126.04, 127.30, 127.65, 129.57, 129.82, 131.92, 132.08, 132.22, 138.75, 138.88, 140.14, 140.84, 142.71. EI-MS *m*/*z* 445 (M+, 33). Anal. calcd. for $C_{24}H_{19}N_3O_6$: C 64.78, H 4.64, N 9.22; found: C 64.71, H 4.31, N 9.43.

1,4-Di(*p*-methyl-styryl)-2-piperidine-3,6-dinitrobenzene (B)

The procedure followed is that described for **A** except that more piperidine (9 mL) is added. Yield: 62%. IR (KBr, cm^{-1}): 3036, 2940, 2844, 1627, 1592, 1531, 1443, 1347, 1241, 1084, 979, 804, 743, 506. ^{1}H NMR ($CDCl_3$–TMS, *J* (Hz)) δ: 1.68–1.69 (s, 6H), 2.36 (s, 3H), 2.39 (s, 3H), 3.07 (s, 4H), 6.59–6.63 (d, 1H), 7.11–7.18 (d, 1H), 7.17–7.15 (d, 3H), 7.22–7.24 (d, 1H), 7.26–7.28 (d, 2H), 7.32–7.36 (d, 2H), 7.45–7.47 (d, 2H), 8.26 (s, 1H). ^{13}C NMR ($CDCl_3$–TMS, *J* (Hz), ppm) δ: 0.014, 21.35, 23.81, 26.53, 51.57, 117.17, 121.42, 123.72, 126.78, 126.87, 127.03, 129.39, 129.73, 132.65, 133.21, 133.62, 135.76, 136.85, 138.96, 143.56, 146.11, 148.25. EI-MS *m*/*z* 483 (M+, 27). Anal. calcd. for $C_{29}H_{29}N_3O_4$: C 71.25, H 6.02, N 8.72; found: C 72.02, H 6.06, N 8.69.

Acknowledgement

We are grateful to the National Natural Science Foundation of China (No. 20471008).

References

1. P.S. Makashir and E.M. Kurian. J. Therm. Anal. Calorim. **55**, 173 (1999).
2. T.B. Brill and K.J. James. J. Phys. Chem. **97**, 8759 (1993).
3. J.C. Oxley, J.L. Smith, H. Ye, R.L. Mckenney, and P.R. Bolduc. J. Phys. Chem. **99**, 9593 (1995).
4. J. Janni, B.D. Gilbert, R.W. Field, and J.I. Steinfeld. Spectrochim. Acta Part A, **53**, 1375 (1997).
5. J.J.P. Stewart, S.R. Bosco, and W.R. Carper. Spectrochim. Acta Part A, **42**, 13 (1986).
6. W.R. Carper and J.J.P. Stewart. Spectrochim. Acta Part A, **43**, 1249 (1987).
7. C.P. Nash, T.E. Nelson, J.J.P. Stewart, and W.R. Carper. Spectrochim. Acta Part A, **45**, 585 (1989).
8. Y.-H. Liu, T.-L. Zhang, J.-G. Zhang, J.-Y. Guo, and K.-B. Yu. Struct. Chem. **16**, 475 (2005).
9. Y.-.H Liu, T.-L. Zhang, J.-G. Zhang, J.-Y. Guo, and K.-B. Yu. Struct. Chem. Accepted for publication.
10. X.C. Li and D. Ferreira. Tetrahedron, **59**, 1501 (2003).
11. N.F. Thomas, K.C. Lee, T. Paraidathathu, J.F.F. Weber, K. Awang, D. Rondeau, and P. Richomme. Tetrahedron, **58**, 7201 (2002).
12. M. Lehmann, B. Schartel, M. Hennecke, and H. Meler. Tetrahedron, **55**, 13377 (1999).
13. K.G. Shipp. J. Org. Chem, **29**, 2620 (1964).
14. G.P. Sollott, M. Warman, and E.E. Gilbert. J. Org. Chem. **44**, 3328, (1979)
15. Th. Rieckman and S. Volker. Chem. Eng. Sci. **56**, 1327 (2001).
16. J. Clarkson and W.E. Smith. J. Mol. Struct. **648**, 203 (2003).
17. G.M. Sheldrick. SHELXLS-98 [computer program]. University of Göttingen, Göttingen, Germany 1998.

[2] Supplementary data for this article are available on the journal Web site (http://canjchem.nrc.ca) or may be purchased from the Depository of Unpublished Data, Document Delivery, CISTI, National Research Council Canada, Ottawa, ON K1A 0R6, Canada. DUD 5047. For more information on obtaining material refer to http://cisti-icist.nrc-cnrc.gc.ca/irm/unpub_e.shtml. CCDC 274768 (**A**) and 274767 (**B**) contain the crystallographic data for this manuscript. These data can be obtained, free of charge, via http://www.ccdc.cam.ac.uk/conts/retrieving.html (Or from the Cambridge Crystallographic Data Centre, 12 Union Road, Cambridge CB2 1EZ, UK; fax +44 1223 336033; or deposit@ccdc.cam.ac.uk).

© 2006 NRC Canada

Solubility prediction of anthracene in nonaqueous solvent mixtures using a combination of Jouyban–Acree and Abraham models

Abolghasem Jouyban, Maryam Khoubnasabjafari, and William E. Acree, Jr.

Abstract: The applicability of previously developed quantitative structure–property relationships was extended to predict the solubility of anthracene in nonaqueous binary and ternary solvent mixtures. The accuracy of the proposed methods was evaluated using 81 solubility data sets collected from the literature. The individual and mean percentage deviation (IPD and MPD) of experimental and computed solubilities were calculated as accuracy criteria. The computations were carried out using experimental and predicted mole fraction solubility of anthracene in monosolvent systems for binary and ternary solvent systems. The overall MPD of solubility prediction using experimental values in monosolvents varied from 5.2% to 4.2% and from 16.5% to 10.7% for binary and ternary solvents, using water to solvent and gas to solvent solvational parameters, respectively. The IPD distribution was better for the gas to solvent model. The corresponding ranges for the predicted solubility of anthracene in monosolvents were 47.9% to 28.1% and 23.9% to 22.5% for binary and ternary solvents, respectively, and IPD distribution was more favourable for the gas to solvent model. In general, the models derived from gas to solvent coefficients provided more accurate predictions and are recommended for practical applications.

Key words: solubility, prediction, cosolvency, anthracene, Abraham model, Jouyban–Acree model.

Résumé : On a étendu le domaine d'applicabilité des relations quantitatives structure–propriété développées antérieurement de façon à pouvoir prédire la solubilité de l'anthracène dans des mélanges de solvants non aqueux binaires et ternaires. On a évalué l'exactitude des méthodes proposées en faisant appel à 81 ensembles de données de solubilité tirés de la littérature. On a calculé le pourcentage de déviations individuelles (PDI) et moyennes (PDM) des solubilités expérimentales et calculées comme critère de l'exactitude. On a effectué les calculs en utilisant les fractions molaires expérimentales et calculées de solubilité de l'anthracène dans des systèmes à solvant unique pour les systèmes de solvant binaires et ternaires. Lorsqu'on utilise des paramètres de solvatation de l'eau au solvant et du gaz au solvant, les PDM globaux des valeurs prédites pour la solubilité en utilisant des valeurs expérimentales dans des solvants uniques varient respectivement de 5,2 % à 4,2 % et de 16,5 % à 10,7 % pour les solvants binaires et ternaires. La distribution des PDI est meilleure pour le modèle de gaz au solvant. Les plages correspondantes des valeurs prédites à partir de la solubilité de l'anthracène dans des solvants uniques varient respectivement de 47,9 % à 28,1 % et de 23,9 % à 22,5 % pour les solvants binaires et ternaires alors que la distribution PDI est plus favorable pour le modèle gaz à solvant. En général, les modèles dérivés de coefficients gaz à solvant conduisent à des prédictions plus exactes et on les recommande pour les applications pratiques.

Mots clés : solubilité, prédiction, cosolvant, anthracène, modèle d'Abraham, modèle de Jouyban–Acree.

[Traduit par la Rédaction]

Introduction

Anthracene is a low molecular weight polycyclic aromatic hydrocarbon (PAH), formerly known as a carcinogenic agent used for modelling purposes. However, later reports have stated that anthracene is not classifiable for its carcinogenicity to humans. Studies conclude that the toxicity of an oil appears to be a function of its diaromatic and triaromatic hydrocarbons, which include three-ring hydrocarbons. Acute toxicity of PAHs is rarely reported in humans, fish, or wildlife as a result of exposure to low levels of a single PAH compound. PAHs, in general, are more frequently associated with chronic risks. These risks include cancer and often are the result of exposures to complex mixtures of chronic-risk aromatics (such as PAHs, alkyl PAHs, benzenes, and alkyl benzenes), rather than exposures to low levels of a single compound. Anthracene is a very phototoxic compound, therefore, any of the water criteria that have been developed

Received 5 March 2006. Published on the NRC Research Press Web site at http://canjchem.nrc.ca on 16 June 2006.

A. Jouyban.[1] Faculty of Pharmacy and Drug Applied Research Centre, Tabriz University of Medical Sciences, Tabriz 51664, Iran.
M. Khoubnasabjafari. Kimia Research Institute, Tabriz, P.O. Box 51665-171, Iran.
W.E. Acree, Jr. Department of Chemistry, University of North Texas, Denton, TX 76203-5070, USA.

[1]Corresponding author (e-mail: ajouyban@hotmail.com).

 doi:10.1139/V06-082 © 2006 NRC Canada

for it using bioassays performed in the absence of UV light may be underestimating its true toxicity. The phototoxicity of PAHs was discovered when organisms that had survived laboratory exposures to PAHs died quickly after being moved into sunlight. Anthracene is ubiquitous in the aquatic environment. It has been detected in industrial effluents, in run-off waters, in surface water and sediments, in groundwater, and in drinking water. The industrial effluents that are most likely to contain PAHs, including anthracene, are wastewaters from the synthetic fuel industry. PAHs could be degraded using enzymatic reactions as has been reported in a recent paper (1), however, their poor solubility is a limiting factor and to overcome this limitation, researchers used mixed-solvent systems (1).

Solubility data of PAHs in mixed solvents is required for designing many industrial processes. In addition to experimental determinations, a number of mathematical models were developed for computation of the solubility. These include a quantitative structure–property relationship (QSPR) model recently proposed by our group to predict the solubility in binary and ternary solvent mixtures (2). Except for our study, we are not aware of any published work employing QSPRs or linear free energy relationships (LFERs) for describing the solubility of crystalline solutes in binary (or even higher-order multicomponent) solvent mixtures. QSPR and LFER correlations have been limited to single solvent systems. Katritzky et al. (3, 4) derived correlations that allow solubility predictions of about 500 substances in up to 69 diverse organic solvents using theoretical CODESSA-PRO descriptors. Each solute or solvent correlation employed a different set of molecular descriptors. Such correlations, while quite useful for solubility predictions in a single solvent, are not easily extendible to binary solvent mixtures as there is no convenient way to incorporate the binary solvent compositional dependence. Each individual solvent correlation uses a different set of solute descriptors. Acree, Abraham, and co-workers (5–8) have correlated the solubility behaviour of numerous crystalline nonelectrolyte solutes in a wide range of neat organic solvents, based on the Abraham solvation parameter model. The Abraham model uses a single set of solute descriptors for all partition and solubility processes. The additive terms in each derived Abraham correlation describe the various types of solute–solvent interactions, such as the interaction between the hydrogen bond acidity site(s) on the solute with the hydrogen bond basicity site(s) on the solvent.

The solubility of anthracene in nonaqueous mixed solvents has been extensively studied by our group (9–23). Details of previously published anthracene solubility data in binary and ternary solvent mixtures are listed in Tables 1 and 4, respectively. The experimentally determined data have been correlated using a solution model, i.e., the Jouyban–Acree model, which is proposed for correlating the solubility of PAHs in nonaqueous solvent mixtures (24, 25). The general form of the model is

$$[1] \qquad \ln X_m = f_1 \ln X_1 + f_2 \ln X_2 + f_1 f_2 \sum_{j=0}^{2} B_i (f_1 - f_2)^j$$

where X is the mole fraction solubility of the solute, f denotes the mole fraction of solvents 1 and 2 in the solvent mixture, subscripts m, 1, and 2 denote the mixed solvent and solvents 1 and 2, respectively, and B_i are the model constants, which are calculated using a no intercept least-squares analysis (26). The model can be readily extended to ternary solvent systems as follows

$$[2] \qquad \ln X_m = f_1 \ln X_1 + f_2 \ln X_2 + f_3 \ln X_3 + f_1 f_2 \sum_{i=0}^{2} B_i' (f_1 - f_2)^i + f_1 f_3 \sum_{i=0}^{2} B_i' (f_1 - f_3)^i + f_2 f_3 \sum_{i=0}^{2} B_i'' (f_2 - f_3)^i$$

where f_3 stands for the mole fraction of solvent 3 in the mixed solvent and B_i, B_i', and B_i'' are the sub-binary interaction terms. The main drawback of the Jouyban–Acree model is that it possesses a number of curve-fitting parameters and needs at least a number of experimental data points for training of the model. In a previous work, a QSPR model was proposed to estimate the numerical values of these model constants using Abraham's solvational parameters (27).

The Abraham solvational parameter model provides a convenient solubility prediction method for a wide variety of neat organic solvents. The basic models proposed for processes within condensed phases (water to solvent) and processes involving gas to condensed phase (gas to solvent) transfer are

$$[3] \qquad \log\left(\frac{C_S}{C_W}\right) = c + rR_2 + s\pi_2^H + a\sum \alpha_2^H + b\sum \beta_2^H + vV_X$$

$$[4] \qquad \log\left(\frac{C_S}{C_G}\right) = c + rR_2 + s\pi_2^H + a\sum \alpha_2^H + b\sum \beta_2^H + l \log L^{16}$$

where C_S and C_W are the solute solubilities in the organic solvent and water (in mol/L), respectively, C_G is the gas-phase concentration of the solute, R_2 is the excess molar refraction, π_2^H is dipolarity–polarizability of solute, $\sum \alpha_2^H$ denotes the solute's hydrogen bond acidity, $\sum \beta_2^H$ stands for the solute's hydrogen bond basicity, V_X is the McGowan volume of the solute, $\log L^{16}$ is the logarithm of the solute gas – hexadecane partition coefficent at 298.15 K, and c, r, s, a, b, v, and l are the model constants, which depend on the solvent system under consideration. The numerical values of the Abraham model constants were reported in previous works (5–8).

The solubilities of anthracene in 56 different binary solvent mixtures were used to compute the B_i terms of each binary solvent and the B_i terms were employed to build up a QSPR model using coefficients of the Abraham models of the solvents. The reported (27) QSPR models using water to solvent coefficients of the Abraham model for calculating B_i terms are

© 2006 NRC Canada

Table 1. Details of the binary solvent systems studied and mean percentage deviations (MPDs) of eq. [1] for various numerical methods.

				MPD (water to solvent)		MPD (gas to solvent)	
No.	Solvent 1	Solvent 2	Ref. No.	Experimental[a]	Predicted[b]	Experimental[a]	Predicted[c]
1	1-Butanol	1-Propanol	9	1.2	34.9	0.6	21.3
2	1-Butanol	2-Propanol	9	2.0	56.9	2.5	40.8
3	1-Butanol	Acetonitrile	10	14.2	11.0	4.4	4.3
4	1-Butanol	Methyl *tert*-butyl ether	11	6.1	16.6	11.5	22.5
5	1-Octanol	1-Butanol	12	7.3	13.1	7.6	17.7
6	1-Octanol	1-Propanol	9	13.3	121.1	12.2	73.7
7	1-Octanol	2-Propanol	9	8.8	113.4	9.9	72.7
8	1-Octanol	Methyl *tert*-butyl ether	11	13.4	14.0	13.4	34.4
9	1-Pentanol	Acetonitrile	13	13.6	12.2	4.0	12.1
10	1-Pentanol	Methyl *tert*-butyl ether	11	4.9	22.4	7.7	29.1
11	1-Propanol	Acetonitrile	10	13.0	9.9	1.9	10.6
12	1-Propanol	Methyl *tert*-butyl ether	11	9.8	16.3	14.5	31.0
13	2,2,4-Trimethylpentane	2-Propanol	14	1.8	29.8	4.1	36.9
14	2,2,4-Trimethylpentane	1-Octanol	14	3.0	59.0	3.7	42.8
15	2,2,4-Trimethylpentane	Carbon tetrachloride	15	10.4	29.4	9.3	12.5
16	2,2,4-Trimethylpentane	Methyl *tert*-butyl ether	16	7.8	16.7	5.5	26.4
17	2-Butanol	1-Butanol	12	2.5	26.6	0.7	12.2
18	2-Butanol	1-Propanol	9	1.5	29.2	2.4	21.6
19	2-Butanol	2-Propanol	9	0.9	33.3	1.8	16.8
20	2-Butanol	Acetonitrile	10	19.2	17.1	7.3	20.3
21	2-Butanol	Methyl *tert*-butyl ether	11	8.9	11.2	11.0	32.5
22	2-Methyl-1-Propanol	1-Butanol	12	1.6	33.0	1.0	7.5
23	2-Methyl-1-propanol	Acetonitrile	10	16.7	11.7	1.6	10.0
24	2-Methyl-1-propanol	Methyl *tert*-butyl ether	11	0.5	30.4	6.1	22.9
25	2-Propanol	1-Propanol	9	1.1	38.4	1.4	18.2
26	2-Propanol	Acetonitrile	10	16.1	16.1	2.3	5.4
27	2-Propanol	Methyl *tert*-butyl ether	11	15.9	11.6	18.0	29.7
28	Cyclohexane	1-Octanol	14	1.5	72.2	1.0	15.0
29	Cyclohexane	2-Propanol	14	5.1	263.5	5.8	88.3
30	Cyclohexane	Carbon tetrachloride	15	1.4	97.3	1.0	6.4
31	Cyclohexane	Methyl *tert*-butyl ether	16	8.5	65.4	8.0	22.9
32	Ethanol	Acetonitrile	13	6.3	33.1	12.7	17.5
33	Heptane	1-Octanol	14	4.5	33.0	3.6	27.2
34	Heptane	2-Propanol	14	8.3	77.5	9.1	67.0
35	Heptane	Carbon tetrachloride	15	12.6	32.5	7.7	9.6
36	Heptane	Methyl *tert*-butyl ether	16	11.1	17.8	0.8	25.9
37	Hexane	1-Octanol	14	10.8	45.0	7.0	32.3
38	Hexane	2-Propanol	14	11.4	62.0	7.2	55.1
39	Hexane	Carbon tetrachloride	15	6.1	26.3	4.4	11.2
40	Hexane	Methyl *tert*-butyl ether	16	3.3	11.5	1.5	26.2
41	Methanol	Acetonitrile	13	1.7	10.3	7.4	6.6
42	Methylcyclohexane	Carbon tetrachloride	15	8.2	70.6	4.2	7.5
43	Methylcyclohexane	1-Octanol	14	3.5	35.8	4.7	22.6
44	Methylcyclohexane	2-Propanol	14	14.4	172.2	10.1	81.5
45	Methylcyclohexane	Methyl *tert*-butyl ether	16	3.9	48.7	4.5	25.1
46	Octane	1-Octanol	14	3.7	35.9	1.5	21.9
47	Octane	2-Propanol	14	5.9	198.8	12.9	92.2
48	Octane	Carbon tetrachloride	15	11.7	65.1	7.2	6.4
49	Octane	Methyl *tert*-butyl ether	16	1.7	35.4	2.5	23.7
			Overall MPD	7.9	47.9	6.5	28.1

[a] X_1 and X_2 determined experimentally.
[b] X_1 and X_2 determined using eq. [11].
[c] X_1 and X_2 determined using eq. [12].

© 2006 NRC Canada

Table 2. The water to solvent coefficients derived using Abraham's model (eq. [3]) for the binary solvent systems studied in this work.

No.[a]	c_1	r_1	s_1	b_1	v_1	c_2	r_2	s_2	b_2	v_2
1	0.152	0.437	–1.175	–3.914	4.119	0.148	0.436	–1.098	–3.893	4.036
2	0.152	0.437	–1.175	–3.914	4.119	0.063	0.320	–1.024	–3.824	4.067
3	0.152	0.437	–1.175	–3.914	4.119	0.413	0.077	0.326	–4.391	3.364
4	0.152	0.437	–1.175	–3.914	4.119	0.376	0.264	–0.788	–5.030	4.410
5	–0.034	0.490	–1.048	–4.229	4.219	0.152	0.437	–1.175	–3.914	4.119
6	–0.034	0.490	–1.048	–4.229	4.219	0.148	0.436	–1.098	–3.893	4.036
7	–0.034	0.490	–1.048	–4.229	4.219	0.063	0.320	–1.024	–3.824	4.067
8	–0.034	0.490	–1.048	–4.229	4.219	0.376	0.264	–0.788	–5.030	4.410
9	0.080	0.521	–1.294	–3.908	4.208	0.413	0.077	0.326	–4.391	3.364
10	0.080	0.521	–1.294	–3.908	4.208	0.376	0.264	–0.788	–5.030	4.410
11	0.148	0.436	–1.098	–3.893	4.036	0.413	0.077	0.326	–4.391	3.364
12	0.148	0.436	–1.098	–3.893	4.036	0.376	0.264	–0.788	–5.030	4.410
13	0.288	0.382	–1.668	–5.000	4.461	0.063	0.320	–1.024	–3.824	4.067
14	0.288	0.382	–1.668	–5.000	4.461	–0.034	0.490	–1.048	–4.229	4.219
15	0.288	0.382	–1.668	–5.000	4.461	0.260	0.573	–1.254	–4.558	4.589
16	0.288	0.382	–1.668	–5.000	4.461	0.376	0.264	–0.788	–5.030	4.410
17	0.106	0.272	–0.988	–3.805	4.110	0.152	0.437	–1.175	–3.914	4.119
18	0.106	0.272	–0.988	–3.805	4.110	0.148	0.436	–1.098	–3.893	4.036
19	0.106	0.272	–0.988	–3.805	4.110	0.063	0.320	–1.024	–3.824	4.067
20	0.106	0.272	–0.988	–3.805	4.110	0.413	0.077	0.326	–4.391	3.364
21	0.106	0.272	–0.988	–3.805	4.110	0.376	0.264	–0.788	–5.030	4.410
22	0.177	0.335	–1.099	–3.570	3.990	0.152	0.437	–1.175	–3.914	4.119
23	0.177	0.335	–1.099	–3.570	3.990	0.413	0.077	0.326	–4.391	3.364
24	0.177	0.335	–1.099	–3.570	3.990	0.376	0.264	–0.788	–5.030	4.410
25	0.063	0.320	–1.024	–3.824	4.067	0.148	0.436	–1.098	–3.893	4.036
26	0.063	0.320	–1.024	–3.824	4.067	0.413	0.077	0.326	–4.391	3.364
27	0.063	0.320	–1.024	–3.824	4.067	0.376	0.264	–0.788	–5.030	4.410
28	0.159	0.784	–1.678	–4.929	4.577	–0.034	0.490	–1.048	–4.229	4.219
29	0.159	0.784	–1.678	–4.929	4.577	0.063	0.320	–1.024	–3.824	4.067
30	0.159	0.784	–1.678	–4.929	4.577	0.260	0.573	–1.254	–4.558	4.589
31	0.159	0.784	–1.678	–4.929	4.577	0.376	0.264	–0.788	–5.030	4.410
32	0.208	0.409	–0.959	–3.645	3.928	0.413	0.077	0.326	–4.391	3.364
33	0.325	0.670	–2.061	–4.733	4.543	–0.034	0.490	–1.048	–4.229	4.219
34	0.325	0.670	–2.061	–4.733	4.543	0.063	0.320	–1.024	–3.824	4.067
35	0.325	0.670	–2.061	–4.733	4.543	0.260	0.573	–1.254	–4.558	4.589
36	0.325	0.670	–2.061	–4.733	4.543	0.376	0.264	–0.788	–5.030	4.410
37	0.361	0.579	–1.723	–4.764	4.344	–0.034	0.490	–1.048	–4.229	4.219
38	0.361	0.579	–1.723	–4.764	4.344	0.063	0.320	–1.024	–3.824	4.067
39	0.361	0.579	–1.723	–4.764	4.344	0.260	0.573	–1.254	–4.558	4.589
40	0.361	0.579	–1.723	–4.764	4.344	0.376	0.264	–0.788	–5.030	4.410
41	0.329	0.299	–0.671	–3.389	3.512	0.413	0.077	0.326	–4.391	3.364
42	0.246	0.782	–1.982	–4.293	4.528	0.260	0.573	–1.254	–4.558	4.589
43	0.246	0.782	–1.982	–4.293	4.528	–0.034	0.490	–1.048	–4.229	4.219
44	0.246	0.782	–1.982	–4.293	4.528	0.063	0.320	–1.024	–3.824	4.067
45	0.246	0.782	–1.982	–4.293	4.528	0.376	0.264	–0.788	–5.030	4.410
46	0.223	0.642	–1.647	–5.067	4.526	–0.034	0.490	–1.048	–4.229	4.219
47	0.223	0.642	–1.647	–5.067	4.526	0.063	0.320	–1.024	–3.824	4.067
48	0.223	0.642	–1.647	–5.067	4.526	0.260	0.573	–1.254	–4.558	4.589
49	0.223	0.642	–1.647	–5.067	4.526	0.376	0.264	–0.788	–5.030	4.410

[a]Details of the numbers are the same as in Table 1.

[5] $$B_0 = 0.128 - 4.772(c_1 - c_2)^2 - 1.123(r_1 - r_2)^2 + 0.546(s_1 - s_2)^2 + 0.670(b_1 - b_2)^2 + 1.262(v_1 - v_2)^2$$

[6] $$B_1 = 0.194 - 10.404(c_1 - c_2)^2 - 1.746(r_1 - r_2)^2 + 0.133(s_1 - s_2)^2 + 0.372(b_1 - b_2)^2 - 1.402(v_1 - v_2)^2$$

© 2006 NRC Canada

$$[7]\quad B_2 = -0.047 - 1.340(c_1 - c_2)^2 - 0.934(r_1 - r_2)^2 + 0.140(s_1 - s_2)^2 + 0.178(b_1 - b_2)^2 + 0.876(v_1 - v_2)^2$$

The corresponding equations for gas to solvent coefficients are

$$[8]\quad B_0 = 0.022 - 2.918(c_1 - c_2)^2 - 2.677(r_1 - r_2)^2 + 0.749(s_1 - s_2)^2 + 0.756(b_1 - b_2)^2 + 15.191(l_1 - l_2)^2$$

$$[9]\quad B_1 = 0.160 - 5.975(c_1 - c_2)^2 - 4.944(r_1 - r_2)^2 + 0.192(s_1 - s_2)^2 + 0.404(b_1 - b_2)^2 - 6.965(l_1 - l_2)^2$$

$$[10]\quad B_2 = -0.089 - 0.476(c_1 - c_2)^2 - 1.023(r_1 - r_2)^2 + 0.178(s_1 - s_2)^2 + 0.222(b_1 - b_2)^2 + 6.895(l_1 - l_2)^2$$

In eqs. [5]–[10], subscripts 1 and 2 denote solvents 1 and 2, respectively. The B_i terms, computed using eqs. [5]–[7] and [8]–[10], were used in eq. [1] and the solubility of anthracene in nonaqueous binary solvents was predicted employing experimental values of X_1 and X_2. The sub-binary interaction terms of the Jouyban–Acree model for ternary solvents, i.e., B_i, B_i', and B_i'', were computed using eqs. [5]–[7] and [8]–[10] and the Abraham's solvational coefficients of the corresponding solvents. To further reduce the required experimental data for solubility prediction, the numerical values of X_1 and X_2 were predicted using eqs. [11] and [12], then a full predictive version of the Jouyban–Acree model was proposed. By replacing numerical values of the descriptors, i.e., R_2, π_2^H, $\sum \beta_2^H$, V_X, and L^{16}, of anthracene taken from a previous paper (5), in eqs. [3] and [4], the solubilities (in mol/L) of anthracene in various organic solvents were calculated using

$$[11]\quad \log\left(\frac{C_S}{3.715\times10^{-7}}\right) = c + 2.290r + 1.340s + 0.280b + 1.454v$$

$$[12]\quad \log\left(\frac{C_S}{3.467\times10^{-10}}\right) = c + 2.290r + 1.340s + 0.280b + 7.568l$$

and converted to mole fraction solubilities using the density of neat solvents.

The aim of the present work is to check the applicability of the proposed QSPR model in predicting the solubility of anthracene in binary and ternary solvents. Anthracene data was choosen as the model system because of the vast amount of published experimental data. It is obvious that this approach could be employed for other solutes in mixed solvents.

Computational methods

The model constants of the Jouyban–Acree model were computed using eqs. [5]–[7] and [8]–[10] and the solubility of anthracene in binary and ternary solvents was predicted using eqs. [1] and [2], respectively. Using B_i values computed by the developed models, the only remaining unknown parameters needed to predict the solubility of a solute in binary and ternary solvent systems are the numerical values of the solute solubility in pure solvents, i.e., X_1, X_2, and X_3. To provide a predictive model (without any experimentally determined parameters), C_S values of anthracene in the solvents under consideration, computed using Abraham's models, were converted to the mole fraction solubilities using the density of the pure organic solvent. The computed X_1, X_2, and X_3 values were then used to predict the solubility in binary and ternary solvents using the Jouyban–Acree model. It is obvious that to convert C_S to mole fraction solubilities, we should use the density of saturated solutions, however, since that would require more experimental effort, we have used the density of pure organic solvents and ignored the effect of solute on the density of the solution.

The predicted B_i values were used to compute the solubility of anthracene in binary and ternary solvent mixtures and the mean percentage deviation (MPD) of observed and calculated solubilities were computed using

$$\mathrm{MPD} = \frac{100}{N}\sum \frac{|(X_m)_{cal.} - (X_m)_{obs.}|}{(X_m)_{obs.}}$$

where N is the number of data points. To check the variability of each solubility data point with the corresponding experimental value, individual percentage deviation (IPD) was also calculated using

$$\mathrm{IPD} = 100\,\frac{|(X_m)_{cal.} - (X_m)_{obs.}|}{(X_m)_{obs.}}$$

Computational results and discussion

Solubility prediction in binary solvents using experimental values of X_1 and X_2

The B_i terms, calculated using eqs. [5]–[7] and [8]–[10], and the experimental values of X_1 and X_2 were used to predict the solubility of anthracene in binary solvent mixtures and the MPD values are listed in Table 1. In this analysis, the only required information for predicting the solubility of anthracene in binary solvents are the numerical values of X_1 and X_2, i.e., two points for each binary solvent system, and there is no need to employ any experimental data from mixed-solvent systems. For B_i terms calculated using the water to solvent coefficients of Abraham's model (for details of the coefficients see Table 2), the minimum MPD (0.5%) was for 2-methyl-1-propanol + methyl *tert*-butyl ether, whereas the maximum MPD (19.2%) was for 2-butanol + acetonitrile solvent systems. The overall MPD (±SD) was 7.4 ± 5.2. In the next set of computations, B_i terms calculated using the gas to solvent coefficients of Abraham's model, i.e., eqs. [8]–[10] using the coefficients listed in Table 3, the minimum MPD (0.6%) was for 1-butanol + 1-propanol, whereas the maximum MPD (18.0%) was for 2-propanol + methyl *tert*-butyl ether solvent systems. The overall MPD (±SD) was 5.9 ± 4.3. The mean differences between the two numerical methods were not statistically significant (paired *t*-test, $p > 0.057$).

© 2006 NRC Canada

Table 3. The gas to solvent coefficients derived using Abraham's model (eq. [4]) for the binary solvent systems studied in this work.

No.[a]	c_1	r_1	s_1	b_1	l_1	c_2	r_2	s_2	b_2	l_2
1	–0.039	–0.276	0.539	0.995	0.934	–0.028	–0.185	0.648	1.043	0.869
2	–0.039	–0.276	0.539	0.995	0.934	–0.060	–0.335	0.702	1.040	0.893
3	–0.039	–0.276	0.539	0.995	0.934	–0.007	–0.595	2.461	0.418	0.738
4	–0.039	–0.276	0.539	0.995	0.934	0.278	–0.489	0.801	0.000	0.993
5	–0.119	–0.203	0.560	0.702	0.940	–0.039	–0.276	0.539	0.995	0.934
6	–0.119	–0.203	0.560	0.702	0.940	–0.028	–0.185	0.648	1.043	0.869
7	–0.119	–0.203	0.560	0.702	0.940	–0.060	–0.335	0.702	1.040	0.893
8	–0.119	–0.203	0.560	0.702	0.940	0.278	–0.489	0.801	0.000	0.993
9	–0.042	–0.277	0.526	0.983	0.932	–0.007	–0.595	2.461	0.418	0.738
10	–0.042	–0.277	0.526	0.983	0.932	0.278	–0.489	0.801	0.000	0.993
11	–0.028	–0.185	0.648	1.043	0.869	–0.007	–0.595	2.461	0.418	0.738
12	–0.028	–0.185	0.648	1.043	0.869	0.278	–0.489	0.801	0.000	0.993
13	0.275	–0.244	0.000	0.000	0.972	–0.060	–0.335	0.702	1.040	0.893
14	0.275	–0.244	0.000	0.000	0.972	–0.119	–0.203	0.560	0.702	0.940
15	0.275	–0.244	0.000	0.000	0.972	0.282	–0.303	0.460	0.000	1.047
16	0.275	–0.244	0.000	0.000	0.972	0.278	–0.489	0.801	0.000	0.993
17	–0.013	–0.456	0.780	1.064	0.906	–0.039	–0.276	0.539	0.995	0.934
18	–0.013	–0.456	0.780	1.064	0.906	–0.028	–0.185	0.648	1.043	0.869
19	–0.013	–0.456	0.780	1.064	0.906	–0.060	–0.335	0.702	1.040	0.893
20	–0.013	–0.456	0.780	1.064	0.906	–0.007	–0.595	2.461	0.418	0.738
21	–0.013	–0.456	0.780	1.064	0.906	0.278	–0.489	0.801	0.000	0.993
22	0.012	–0.407	0.670	1.283	0.895	–0.039	–0.276	0.539	0.995	0.934
23	0.012	–0.407	0.670	1.283	0.895	–0.007	–0.595	2.461	0.418	0.738
24	0.012	–0.407	0.670	1.283	0.895	0.278	–0.489	0.801	0.000	0.993
25	–0.060	–0.335	0.702	1.040	0.893	–0.028	–0.185	0.648	1.043	0.869
26	–0.060	–0.335	0.702	1.040	0.893	–0.007	–0.595	2.461	0.418	0.738
27	–0.060	–0.335	0.702	1.040	0.893	0.278	–0.489	0.801	0.000	0.993
28	0.163	–0.110	0.000	0.000	1.013	–0.119	–0.203	0.560	0.702	0.940
29	0.163	–0.110	0.000	0.000	1.013	–0.060	–0.335	0.702	1.040	0.893
30	0.163	–0.110	0.000	0.000	1.013	0.282	–0.303	0.460	0.000	1.047
31	0.163	–0.110	0.000	0.000	1.013	0.278	–0.489	0.801	0.000	0.993
32	0.012	–0.206	0.789	1.311	0.853	–0.007	–0.595	2.461	0.418	0.738
33	0.275	–0.162	0.000	0.000	0.983	–0.119	–0.203	0.560	0.702	0.940
34	0.275	–0.162	0.000	0.000	0.983	–0.060	–0.335	0.702	1.040	0.893
35	0.275	–0.162	0.000	0.000	0.983	0.282	–0.303	0.460	0.000	1.047
36	0.275	–0.162	0.000	0.000	0.983	0.278	–0.489	0.801	0.000	0.993
37	0.292	–0.169	0.000	0.000	0.979	–0.119	–0.203	0.560	0.702	0.940
38	0.292	–0.169	0.000	0.000	0.979	–0.060	–0.335	0.702	1.040	0.893
39	0.292	–0.169	0.000	0.000	0.979	0.282	–0.303	0.460	0.000	1.047
40	0.292	–0.169	0.000	0.000	0.979	0.278	–0.489	0.801	0.000	0.993
41	–0.004	–0.215	1.173	1.432	0.769	–0.007	–0.595	2.461	0.418	0.738
42	0.318	–0.215	0.000	0.000	1.012	0.282	–0.303	0.460	0.000	1.047
43	0.318	–0.215	0.000	0.000	1.012	–0.119	–0.203	0.560	0.702	0.940
44	0.318	–0.215	0.000	0.000	1.012	–0.060	–0.335	0.702	1.040	0.893
45	0.318	–0.215	0.000	0.000	1.012	0.278	–0.489	0.801	0.000	0.993
46	0.215	–0.049	0.000	0.000	0.967	–0.119	–0.203	0.560	0.702	0.940
47	0.215	–0.049	0.000	0.000	0.967	–0.060	–0.335	0.702	1.040	0.893
48	0.215	–0.049	0.000	0.000	0.967	0.282	–0.303	0.460	0.000	1.047
49	0.215	–0.049	0.000	0.000	0.967	0.278	–0.489	0.801	0.000	0.993

[a]Details of the numbers are the same as in Table 1.

In addition to the MPD criterion, we used the relative frequency of the IPDs of the predicted solubilities. The IPDs were sorted in three error ranges, i.e., ≤4% (comparable with experimental uncertainty (28)), 4%–30% (acceptable error range in pharmaceutical and chemical areas (29–31)), and >30% (unacceptable error range). These frequencies are shown in Fig. 1 for two solvational models using experimental X_1 and X_2 values. Using eq. [4], the probability of solubility prediction with error less than 30% was 0.994, whereas the corresponding probability for eq. [3] was 0.931. This finding reveals that despite the insignificant difference between MPDs of the two equations, the IPD distribution of

© 2006 NRC Canada

Fig. 1. Relative frequencies of the IPDs for predicted solubilities in binary solvents using two sets of solvational parameters of the Abraham model (experimental and predicted X_1 and X_2 values).

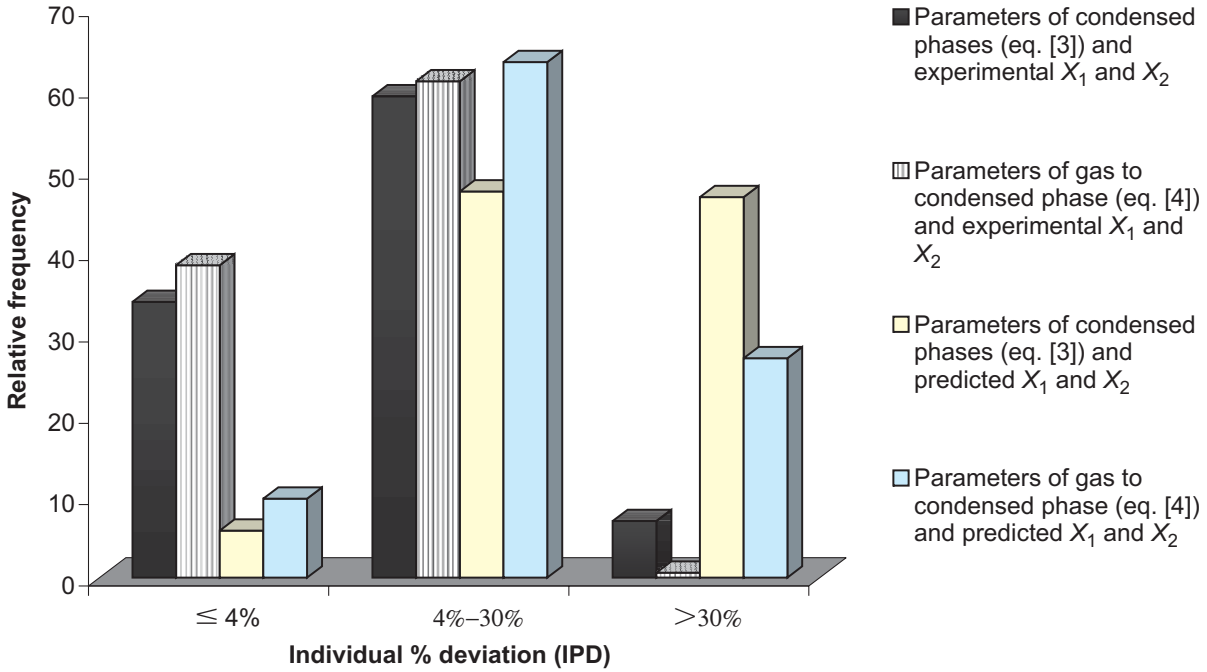
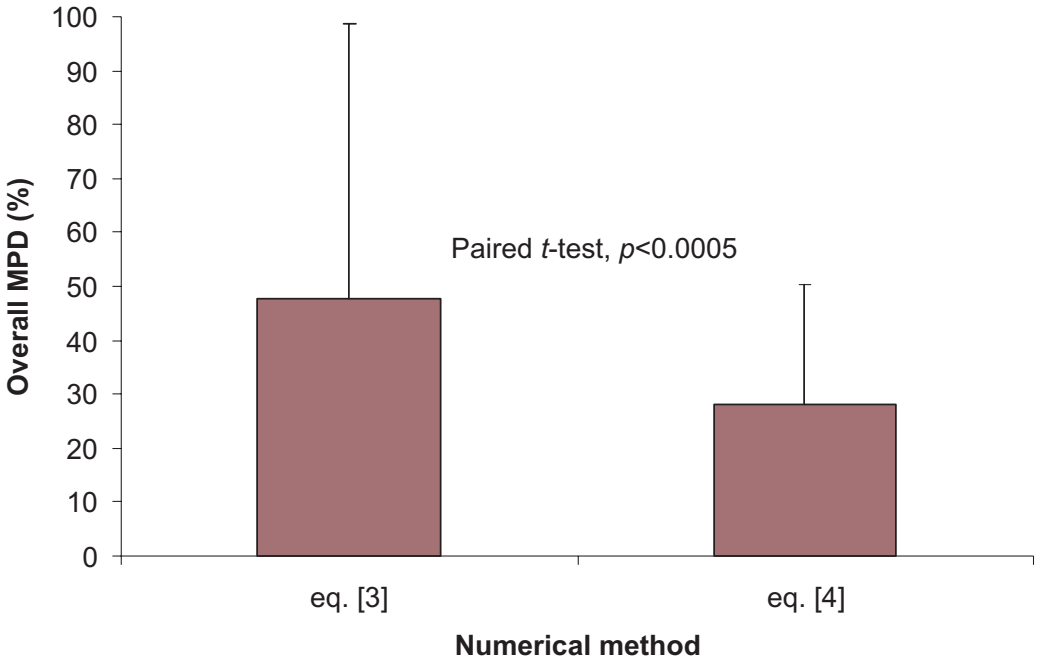


Fig. 2. Overall MPDs for fully predictive methods for the binary solvent systems studied



eq. [4] is better than that of eq. [3], and eq. [4] promises more accurate predictions and is recommended for predictive purposes.

Solubility prediction in binary solvents using predicted values of X_1 and X_2

The B_i terms, calculated using eqs. [5]–[7] and [8]–[10], and the predicted values of X_1 and X_2 were employed to predict the solubility of anthracene in binary solvent mixtures and the corresponding MPDs. This analysis was fully predictive and no experimental data was used in the prediction procedure. The results were also listed in Table 1. For B_i terms calculated using the water to solvent coefficients of Abraham's model, i.e., eqs. [5]–[7], and X_1 and X_2 calculated using eq. [11], the minimum MPD (9.9%) was for 1-propanol + acetonitrile, whereas the maximum MPD (263.5%) was for cyclohexane + 2-propanol solvent system. The overall MPD (±SD) was 47.9 ± 50.7. For B_i terms cal-

© 2006 NRC Canada

Table 4. Details of the ternary solvent systems studied and mean percentage deviations (MPDs) of eq. [2] for various numerical methods.

					MPD (water to solvent)		MPD (gas to solvent)	
No.	Solvent 1	Solvent 2	Solvent 3	Ref. No.	Experimental[a]	Predicted[b]	Experimental[a]	Predicted[c]
1	1,4-Dioxane	1-Butanol	2,2,4-Trimethylpentane	17	6.0	8.8	7.1	17.7
2	1,4-Dioxane	1-Butanol	Cyclohexane	18	13.4	32.2	8.1	16.7
3	1,4-Dioxane	1-Butanol	Heptane	19	7.5	10.0	7.1	17.2
4	1,4-Dioxane	1-Propanol	2,2,4-Trimethylpentane	17	11.9	9.0	10.0	27.9
5	1,4-Dioxane	1-Propanol	Cyclohexane	18	19.7	24.6	12.7	25.8
6	1,4-Dioxane	1-Propanol	Heptane	19	12.1	6.4	11.4	28.7
7	1,4-Dioxane	2-Butanol	2,2,4-Trimethylpentane	17	12.5	12.5	10.7	33.0
8	1,4-Dioxane	2-Butanol	Cyclohexane	18	19.7	22.6	15.2	30.5
9	1,4-Dioxane	2-Butanol	Heptane	19	12.0	10.2	12.1	32.3
10	1,4-Dioxane	2-Methyl-1-propanol	2,2,4-Trimethylpentane	17	6.4	11.1	8.6	19.9
11	1,4-Dioxane	2-Methyl-1-propanol	Cyclohexane	18	11.4	32.6	8.9	23.3
12	1,4-Dioxane	2-Methyl-1-propanol	Heptane	19	9.2	13.0	8.5	22.3
13	1,4-Dioxane	2-Propanol	2,2,4-Trimethylpentane	17	19.5	16.6	16.2	32.1
14	1,4-Dioxane	2-Propanol	Cyclohexane	18	25.5	19.1	20.5	29.9
15	1,4-Dioxane	2-Propanol	Heptane	19	19.0	13.6	19.0	32.7
16	1-Butanol	2-Butanol	Cyclohexane	20	4.2	60.6	1.8	11.2
17	1-Propanol	2-Propanol	Cyclohexane	20	3.3	53.6	4.3	12.8
18	Dibutyl ether	1-Butanol	2,2,4-Trimethylpentane	21	8.2	13.8	7.0	14.7
19	Dibutyl ether	1-Butanol	Cyclohexane	22	3.1	58.7	3.9	10.7
20	Dibutyl ether	1-Butanol	Heptane	23	8.0	15.6	5.3	16.6
21	Dibutyl ether	1-Propanol	2,2,4-Trimethylpentane	21	4.8	11.0	5.5	24.6
22	Dibutyl ether	1-Propanol	Cyclohexane	22	4.4	53.0	3.2	16.7
23	Dibutyl ether	1-Propanol	Heptane	23	8.4	14.1	5.9	22.4
24	Dibutyl ether	2-Butanol	2,2,4-Trimethylpentane	21	5.4	8.4	7.4	28.1
25	Dibutyl ether	2-Butanol	Cyclohexane	22	5.7	48.3	5.7	22.7
26	Dibutyl ether	2-Butanol	Heptane	23	9.7	8.6	8.3	27.4
27	Dibutyl ether	2-Methyl-1-propanol	2,2,4-Trimethylpentane	21	15.2	22.2	12.8	15.9
28	Dibutyl ether	2-Methyl-1-propanol	Cyclohexane	22	7.9	74.8	8.0	9.9
29	Dibutyl ether	2-Methyl-1-propanol	Heptane	23	13.7	26.2	9.8	16.8
30	Dibutyl ether	2-Propanol	2,2,4-Trimethylpentane	21	8.4	8.8	10.0	28.3
31	Dibutyl ether	2-Propanol	Cyclohexane	22	12.7	36.7	11.0	22.9
32	Dibutyl ether	2-Propanol	Heptane	23	12.6	6.8	11.8	28.4
				Overall MPD	10.7	23.9	9.3	22.5

[a] X_1, X_2, and X_3 determined experimentally.
[b] X_1, X_2, and X_3 determined using eq. [11].
[c] X_1, X_2, and X_3 determined using eq. [12].

culated using the gas to solvent coefficients of Abraham's model, i.e., eqs. [8]–[10], and X_1 and X_2 calculated using eq. [12], the minimum MPD (4.3%) was for 1-butanol + acetonitrile, whereas the maximum MPD (92.2%) was for octane + 2-propanol solvent systems. The overall MPD (±SD) was 28.1 ± 22.3. The mean differences between the two numerical methods was statistically significant (paired *t*-test, $p < 0.0005$) as is shown in Fig. 2. The main reason for the relatively high MPD values for these analyses is the high prediction error for the predicted solubility of anthracene in monosolvent systems where the reported errors were 37.1% and 23.0%, respectively, for eqs. [11] and [12] (5). The next possible reason could be an error in solubility unit conversion from mol/L to mole fraction for which we used the density of pure solvent instead of the density of saturated solutions. The MPD differences for predicted solubilities in binary solvents were similar to those reported in a previous paper (5) for the solubility of anthracene in select organic solvents. The IPD distribution is shown in Fig. 1, in which the probability of solubility prediction using eq. [3] and its coefficients for IPD greater than 30% was 0.468 and the corresponding probability of eq. [4] was 0.270, revealing that eq. [4] is more accurate in comparison with eq. [3]. This finding was in agreement from earlier results using experimental X_1 and X_2 values.

Solubility prediction in ternary solvents using experimental values of X_1, X_2, and X_3

The B_i terms, calculated using eqs. [5]–[7] and [8]–[10], and experimental values of X_1, X_2, and X_3 were used to predict the solubility of anthracene in ternary solvent mixtures. The MPD values are listed in Table 4. In this analysis, the only required information for predicting the solubility of anthracene in ternary solvents is the numerical values of X_1, X_2, and X_3, i.e., three points for each ternary solvent system, and there is no need to employ any experimental data from mixed-solvent systems. For B_i terms calculated using the water to solvent coefficients of Abraham's model, i.e.,

© 2006 NRC Canada

Table 5. The water to solvent coefficients derived using Abraham's model (eq. [3]) for the ternary solvent systems studied in this work.

No.[a]	c_1	r_1	s_1	b_1	v_1	c_2	r_2	s_2	b_2	v_2	c_3	r_3	s_3	b_3	v_3
1	0.098	0.350	–0.083	–4.826	4.172	0.152	0.437	–1.175	–3.914	4.119	0.288	0.382	–1.668	–5.000	4.461
2	0.098	0.350	–0.083	–4.826	4.172	0.152	0.437	–1.175	–3.914	4.119	0.159	0.784	–1.678	–4.929	4.577
3	0.098	0.350	–0.083	–4.826	4.172	0.152	0.437	–1.175	–3.914	4.119	0.325	0.670	–2.061	–4.733	4.543
4	0.098	0.350	–0.083	–4.826	4.172	0.148	0.436	–1.098	–3.893	4.036	0.288	0.382	–1.668	–5.000	4.461
5	0.098	0.350	–0.083	–4.826	4.172	0.148	0.436	–1.098	–3.893	4.036	0.159	0.784	–1.678	–4.929	4.577
6	0.098	0.350	–0.083	–4.826	4.172	0.148	0.436	–1.098	–3.893	4.036	0.325	0.670	–2.061	–4.733	4.543
7	0.098	0.350	–0.083	–4.826	4.172	0.106	0.272	–0.988	–3.805	4.110	0.288	0.382	–1.668	–5.000	4.461
8	0.098	0.350	–0.083	–4.826	4.172	0.106	0.272	–0.988	–3.805	4.110	0.159	0.784	–1.678	–4.929	4.577
9	0.098	0.350	–0.083	–4.826	4.172	0.106	0.272	–0.988	–3.805	4.110	0.325	0.670	–2.061	–4.733	4.543
10	0.098	0.350	–0.083	–4.826	4.172	0.177	0.335	–1.099	–3.570	3.990	0.288	0.382	–1.668	–5.000	4.461
11	0.098	0.350	–0.083	–4.826	4.172	0.177	0.335	–1.099	–3.570	3.990	0.159	0.784	–1.678	–4.929	4.577
12	0.098	0.350	–0.083	–4.826	4.172	0.177	0.335	–1.099	–3.570	3.990	0.325	0.670	–2.061	–4.733	4.543
13	0.098	0.350	–0.083	–4.826	4.172	0.063	0.320	–1.024	–3.824	4.067	0.288	0.382	–1.668	–5.000	4.461
14	0.098	0.350	–0.083	–4.826	4.172	0.063	0.320	–1.024	–3.824	4.067	0.159	0.784	–1.678	–4.929	4.577
15	0.098	0.350	–0.083	–4.826	4.172	0.063	0.320	–1.024	–3.824	4.067	0.325	0.670	–2.061	–4.733	4.543
16	0.152	0.437	–1.175	–3.914	4.119	0.106	0.272	–0.988	–3.805	4.110	0.159	0.784	–1.678	–4.929	4.577
17	0.148	0.436	–1.098	–3.893	4.036	0.063	0.320	–1.024	–3.824	4.067	0.159	0.784	–1.678	–4.929	4.577
18	0.203	0.369	–0.954	–5.426	4.508	0.152	0.437	–1.175	–3.914	4.119	0.288	0.382	–1.668	–5.000	4.461
19	0.203	0.369	–0.954	–5.426	4.508	0.152	0.437	–1.175	–3.914	4.119	0.159	0.784	–1.678	–4.929	4.577
20	0.203	0.369	–0.954	–5.426	4.508	0.152	0.437	–1.175	–3.914	4.119	0.325	0.670	–2.061	–4.733	4.543
21	0.203	0.369	–0.954	–5.426	4.508	0.148	0.436	–1.098	–3.893	4.036	0.288	0.382	–1.668	–5.000	4.461
22	0.203	0.369	–0.954	–5.426	4.508	0.148	0.436	–1.098	–3.893	4.036	0.159	0.784	–1.678	–4.929	4.577
23	0.203	0.369	–0.954	–5.426	4.508	0.148	0.436	–1.098	–3.893	4.036	0.325	0.670	–2.061	–4.733	4.543
24	0.203	0.369	–0.954	–5.426	4.508	0.106	0.272	–0.988	–3.805	4.110	0.288	0.382	–1.668	–5.000	4.461
25	0.203	0.369	–0.954	–5.426	4.508	0.106	0.272	–0.988	–3.805	4.110	0.159	0.784	–1.678	–4.929	4.577
26	0.203	0.369	–0.954	–5.426	4.508	0.106	0.272	–0.988	–3.805	4.110	0.325	0.670	–2.061	–4.733	4.543
27	0.203	0.369	–0.954	–5.426	4.508	0.177	0.335	–1.099	–3.570	3.990	0.288	0.382	–1.668	–5.000	4.461
28	0.203	0.369	–0.954	–5.426	4.508	0.177	0.335	–1.099	–3.570	3.990	0.159	0.784	–1.678	–4.929	4.577
29	0.203	0.369	–0.954	–5.426	4.508	0.177	0.335	–1.099	–3.570	3.990	0.325	0.670	–2.061	–4.733	4.543
30	0.203	0.369	–0.954	–5.426	4.508	0.063	0.320	–1.024	–3.824	4.067	0.288	0.382	–1.668	–5.000	4.461
31	0.203	0.369	–0.954	–5.426	4.508	0.063	0.320	–1.024	–3.824	4.067	0.159	0.784	–1.678	–4.929	4.577
32	0.203	0.369	–0.954	–5.426	4.508	0.063	0.320	–1.024	–3.824	4.067	0.325	0.670	–2.061	–4.733	4.543

[a]Details of the numbers are the same as in Table 4.

© 2006 NRC Canada

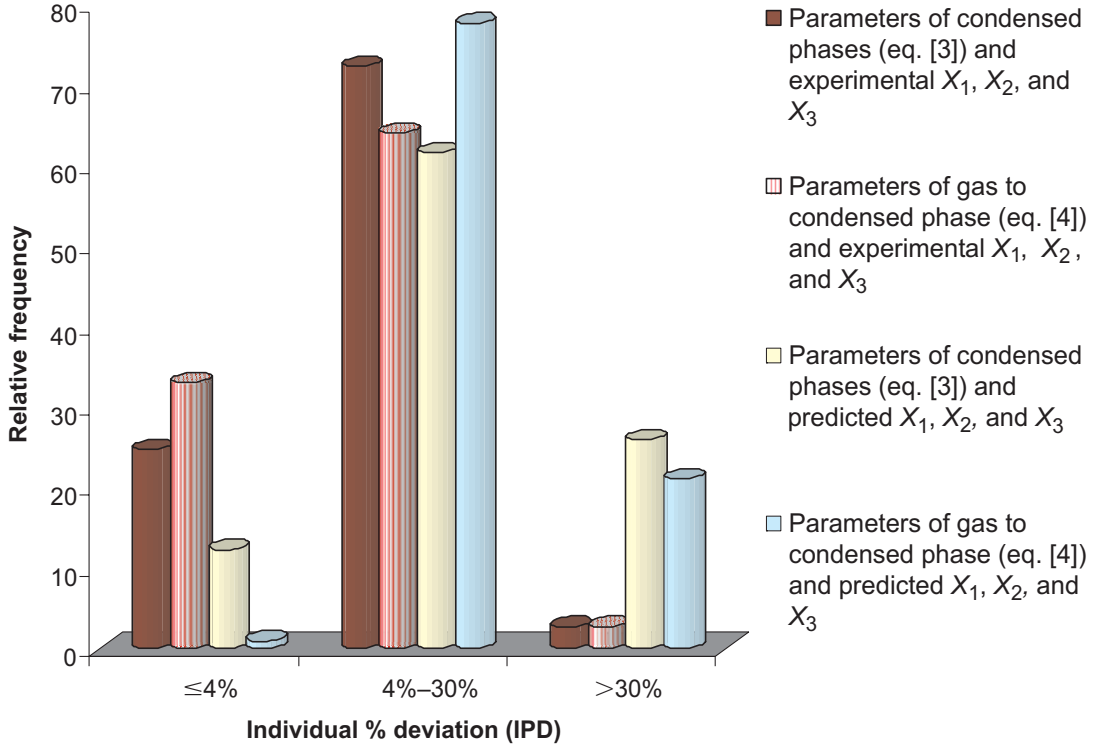
Table 6. The gas to solvent coefficients derived using Abraham's model (eq. [4]) for the ternary solvent systems studied in this work.

No.[a]	c_1	r_1	s_1	b_1	l_1	c_2	r_2	s_2	b_2	l_2	c_3	r_3	s_3	b_3	l_3
1	–0.034	–0.354	1.674	0.000	0.919	–0.039	–0.276	0.539	0.995	0.934	0.275	–0.244	0.000	0.000	0.972
2	–0.034	–0.354	1.674	0.000	0.919	–0.039	–0.276	0.539	0.995	0.934	0.163	–0.110	0.000	0.000	1.013
3	–0.034	–0.354	1.674	0.000	0.919	–0.039	–0.276	0.539	0.995	0.934	0.275	–0.162	0.000	0.000	0.983
4	–0.034	–0.354	1.674	0.000	0.919	–0.028	–0.185	0.648	1.043	0.869	0.275	–0.244	0.000	0.000	0.972
5	–0.034	–0.354	1.674	0.000	0.919	–0.028	–0.185	0.648	1.043	0.869	0.163	–0.110	0.000	0.000	1.013
6	–0.034	–0.354	1.674	0.000	0.919	–0.028	–0.185	0.648	1.043	0.869	0.275	–0.162	0.000	0.000	0.983
7	–0.034	–0.354	1.674	0.000	0.919	–0.013	–0.456	0.780	1.064	0.906	0.275	–0.244	0.000	0.000	0.972
8	–0.034	–0.354	1.674	0.000	0.919	–0.013	–0.456	0.780	1.064	0.906	0.163	–0.110	0.000	0.000	1.013
9	–0.034	–0.354	1.674	0.000	0.919	–0.013	–0.456	0.780	1.064	0.906	0.275	–0.162	0.000	0.000	0.983
10	–0.034	–0.354	1.674	0.000	0.919	0.012	–0.407	0.670	1.283	0.895	0.275	–0.244	0.000	0.000	0.972
11	–0.034	–0.354	1.674	0.000	0.919	0.012	–0.407	0.670	1.283	0.895	0.163	–0.110	0.000	0.000	1.013
12	–0.034	–0.354	1.674	0.000	0.919	0.012	–0.407	0.670	1.283	0.895	0.275	–0.162	0.000	0.000	0.983
13	–0.034	–0.354	1.674	0.000	0.919	–0.060	–0.335	0.702	1.040	0.893	0.275	–0.244	0.000	0.000	0.972
14	–0.034	–0.354	1.674	0.000	0.919	–0.060	–0.335	0.702	1.040	0.893	0.163	–0.110	0.000	0.000	1.013
15	–0.034	–0.354	1.674	0.000	0.919	–0.060	–0.335	0.702	1.040	0.893	0.275	–0.162	0.000	0.000	0.983
16	–0.039	–0.276	0.539	0.995	0.934	–0.013	–0.456	0.780	1.064	0.906	0.163	–0.110	0.000	0.000	1.013
17	–0.028	–0.185	0.648	1.043	0.869	–0.060	–0.335	0.702	1.040	0.893	0.163	–0.110	0.000	0.000	1.013
18	0.165	–0.421	0.760	–0.664	1.002	–0.039	–0.276	0.539	0.995	0.934	0.275	–0.244	0.000	0.000	0.972
19	0.165	–0.421	0.760	–0.664	1.002	–0.039	–0.276	0.539	0.995	0.934	0.163	–0.110	0.000	0.000	1.013
20	0.165	–0.421	0.760	–0.664	1.002	–0.039	–0.276	0.539	0.995	0.934	0.275	–0.162	0.000	0.000	0.983
21	0.165	–0.421	0.760	–0.664	1.002	–0.028	–0.185	0.648	1.043	0.869	0.275	–0.244	0.000	0.000	0.972
22	0.165	–0.421	0.760	–0.664	1.002	–0.028	–0.185	0.648	1.043	0.869	0.163	–0.110	0.000	0.000	1.013
23	0.165	–0.421	0.760	–0.664	1.002	–0.028	–0.185	0.648	1.043	0.869	0.275	–0.162	0.000	0.000	0.983
24	0.165	–0.421	0.760	–0.664	1.002	–0.013	–0.456	0.780	1.064	0.906	0.275	–0.244	0.000	0.000	0.972
25	0.165	–0.421	0.760	–0.664	1.002	–0.013	–0.456	0.780	1.064	0.906	0.163	–0.110	0.000	0.000	1.013
26	0.165	–0.421	0.760	–0.664	1.002	–0.013	–0.456	0.780	1.064	0.906	0.275	–0.162	0.000	0.000	0.983
27	0.165	–0.421	0.760	–0.664	1.002	0.012	–0.407	0.670	1.283	0.895	0.275	–0.244	0.000	0.000	0.972
28	0.165	–0.421	0.760	–0.664	1.002	0.012	–0.407	0.670	1.283	0.895	0.163	–0.110	0.000	0.000	1.013
29	0.165	–0.421	0.760	–0.664	1.002	0.012	–0.407	0.670	1.283	0.895	0.275	–0.162	0.000	0.000	0.983
30	0.165	–0.421	0.760	–0.664	1.002	–0.060	–0.335	0.702	1.040	0.893	0.275	–0.244	0.000	0.000	0.972
31	0.165	–0.421	0.760	–0.664	1.002	–0.060	–0.335	0.702	1.040	0.893	0.163	–0.110	0.000	0.000	1.013
32	0.165	–0.421	0.760	–0.664	1.002	–0.060	–0.335	0.702	1.040	0.893	0.275	–0.162	0.000	0.000	0.983

[a]Details of the numbers are the same as in Table 4.

© 2006 NRC Canada

Fig. 3. Relative frequencies of the IPDs for predicted solubilities in ternary solvents using two sets of solvational parameters of the Abraham model (experimental and predicted X_1, X_2, and X_3 values).



eqs. [5]–[7] (details of the coefficients are listed in Table 5), the minimum MPD (3.1%) was for dibutyl ether + 1-butanol + cyclohexane, whereas the maximum MPD (25.5%) was for 1,4-dioxane + 2-propanol + cyclohexane solvent systems. The overall MPD (±SD) was 10.7 ± 5.5. For B_i terms calculated using the gas to solvent coefficients of Abraham's model, i.e., eqs. [8]–[10] (details of the coefficients are listed in Table 6), the minimum MPD (1.8%) was for 1-butanol + 2-butanol + cyclohexane, whereas the maximum MPD (20.5%) was for 1,4-dioxane + 2-propanol + cyclohexane solvent systems and the overall MPD (±SD) was 9.3 ± 4.3. The mean differences between the two numerical methods were statistically significant (paired *t*-test, $p < 0.001$). The probability of solubility prediction within acceptable error range (<30%) using eqs. [3] and [4] was 0.972 and both equations showed similar IPD distributions, as shown in Fig. 3. However, it should be kept in mind that eq. [4] produced less MPD and also better results for IPD (≤4%).

Solubility prediction in ternary solvents using predicted values of X_1, X_2, and X_3

The B_i terms, calculated using eqs. [5]–[7] and [8]–[10], and predicted values of X_1, X_2, and X_3 using eqs. [11] and [12] were employed to predict the solubility of anthracene in ternary solvent mixtures and the corresponding MPDs. This analysis was fully predictive and no experimental data was used in the prediction procedure. The computed MPD values are listed in Table 4. For B_i terms calculated using the water to solvent coefficients of Abraham's model, i.e., eqs. [5]–[7] and X_1, X_2, and X_3 calculated using eq. [11], the minimum MPD (6.4%) was for 1,4-dioxane + 1-propanol + heptane, whereas the maximum MPD (74.8%) was for dibutyl ether + 2-methyl-1-propanol + cyclohexane solvent systems. The overall MPD (±SD) was 23.9 ± 18.8. For B_i terms calculated using the gas to solvent coefficients of Abraham's model, i.e., eqs. [8]–[10] and X_1, X_2, and X_3 calculated using eq. [12], the minimum MPD (9.9%) was for dibutyl ether + 2-methyl-1-propanol + cyclohexane, whereas the maximum MPD (33.0%) was for 1,4-dioxane + 2-butanol + 2,2,4-trimethylpentane solvent systems. The overall MPD (±SD) was 22.5 ± 7.1. The mean differences between the two numerical methods were not statistically significant (paired *t*-test, $p > 0.75$). Figure 3 shows that the probability of solubility prediction in ternary solvents within acceptable error range using fully predictive models with model constants derived from eqs. [3] and [4] were 0.740 and 0.788, respectively.

Conclusion

The QSPR models proposed in an earlier work provided accurate solubility predictions for anthracene dissolved in binary solvents using X_1 and X_2 values (and without these values) and the MPD values were within acceptable error range. The applicability of the methods was extended for predicting the solubility of anthracene in ternary solvents, which provided reasonably accurate predictions and could be used in solubility estimation methods that are widely required in the chemical and pharmaceutical industries. In the comparison between two solvational models and their coefficients for the solvents, the QSPR method derived from eq. [4] provided more accurate computations and is recommended for practical uses. We suspect that the superiority of the correlations derived from eq. [4] vs. those derived from

© 2006 NRC Canada

eq. [3] results from the fact that when the log P (e.g., eq. [3]) and log L (e.g., eq. [4]) correlations for the various organic solvents were developed, the log L equations generally had lower standard deviations and higher correlation coefficients. Often, different data sets were used in developing the two sets of correlations. In the case of highly water-insoluble organic compounds, the experimental uncertainty in the compound's aqueous solubility, needed in the indirect determination of the experimental log P value, undoubtedly contributed to a larger standard deviation for the Abraham eq. [3] correlations. It also should be added that the models discussed in this work were trained for mole fraction of solvents in the mixtures and that users should consider this point, since using volume and (or) weight fractions for expressing solvent composition will result in different model constants for eqs. [5]–[10]. As the results show, when employing solubility of anthracene in monosolvent systems, the proposed method provided accurate predictions. If solubility estimation with less accuracy is required, it is possible to use the fully predictive method proposed in this work.

References

1. G. Eibes, T. Lú-Chau, G. Feijoo, M.T. Moreira, and J.M. Lema. Enzyme Microb. Technol. **37**, 365 (2005).
2. A. Jouyban, M. Khoubnasabjafari, H.K. Chan, B.J. Clark, and W.E. Acree, Jr. Chem. Pharm. Bull. **50**, 21 (2002).
3. A.R. Katritzky, A.A. Oliferenko, P.V. Oliferenko, R. Petrukhin, D.B. Tatham, U. Maran, A. Lomaka, and W. E. Acree, Jr. J. Chem. Inf. Comput. Sci. 43, 1794 (2003).
4. A.R. Katritzky, A.A. Oliferenko, P.V. Oliferenko, R. Petrukhin, D.B. Tatham, U. Maran, A. Lomaka, and W.E. Acree, Jr. J. Chem. Inf. Comput. Sci. **43**, 1806 (2003).
5. W.E. Acree, Jr. and M.H. Abraham. Can. J. Chem. **79**, 1466 (2001).
6. D.M. Stovall, W.E. Acree, Jr., and M.H. Abraham. Fluid Phase Equilib. **232**, 113 (2005).
7. D.M. Stovall, C. Givens, S. Keown, K.R. Hoover, R. Barnes, C. Harris, J. Lozano, M. Nguyen, E. Rodriguez, W.E. Acree, Jr., and M.H. Abraham. Phys. Chem. Liq. **43**, 351 (2005).
8. W.E. Acree, Jr. and M.H. Abraham. Fluid Phase Equilib. **201**, 245 (2002).
9. W.E. Acree, Jr. and A.I. Zvaigzne. Fluid Phase Equilib. **99**, 167 (1994).
10. K.M. De Fina, S. Abernathy, K. Alexander, C. Olugbuyi, A. Vance, and W.E. Acree, Jr. J. Chem. Eng. Data, **48**, 402 (2003).
11. J.R. Powell, M.E.R. McHale, A.-S.M. Kauppila, and W.E. Acree, Jr. J. Chem. Thermodyn. **28**, 1215 (1996).
12. A.I. Zvaigzne, M.E.R. McHale, J.R. Powell, A.-S.M. Kauppila, and W.E. Acree, Jr. J. Chem. Eng. Data, **40**, 1273 (1995).
13. C.I. Monarrez, J.H. Woo, P.G. Taylor, A.M. Tran, and W.E. Acree, Jr. J. Chem. Eng. Data, **48**, 720 (2003).
14. W.E. Acree, Jr., A.I. Zvaigzne, and S.A. Tucker. Fluid Phase Equilib. **92**, 233 (1994).
15. S.A. Tucker and W.E. Acree, Jr. Phys. Chem. Liq. **19**, 73 (1989).
16. M.E.R. McHale, A.-S.M. Kauppila, and W.E. Acree, Jr. J. Chem. Eng. Data, **41**, 1203 (1996).
17. K.J. Pribyla, T.T. Van, C. Ezell, and W.E. Acree, Jr. J. Chem. Eng. Data, **45**, 968 (2000).
18, K.J. Pribyla, M.A. Spurgin, I. Chuca, and W.E. Acree, Jr. J. Chem. Eng. Data, **45**, 971 (2000).
19. K.J. Pribyla, M.A. Spurgin, I. Chuca, and W.E. Acree, Jr. J. Chem. Eng. Data, **45**, 965 (2000).
20. T. Deng, S. Horiuchi, K.M. De Fina, C.E Hernandez, and W.E. Acree, Jr. J. Chem. Eng. Data, **44**, 798 (1999).
21. K.J. Pribyla, M.A. Spurgin, I. Chuca, and W.E. Acree, Jr. J. Chem. Eng. Data, **44**, 1265 (1999).
22. K.J. Pribyla and W.E. Acree, Jr. J. Chem. Eng. Data, **44**, 1020 (1999).
23. K.J. Pribyla and W.E. Acree, Jr. J. Chem. Eng. Data, **44**, 1259 (1999).
24. W.E. Acree, Jr. and A.I. Zvaigzne. Thermochim. Acta, **178**, 151 (1991).
25. W.E. Acree, Jr. Int. J. Pharm. **127**, 27 (1996).
26. A. Jouyban-Gharamaleki and J. Hanaee. Int. J. Pharm. **154**, 243 (1997).
27. A. Jouyban, M. Khoubnasabjafari, and W.E. Acree, Jr., Chem. Pharm. Bull. Accepted for publication.
28. A. Jouyban, H.K. Chan, N.Y.K. Chew, M. Khoubnasabjafari, and W.E. Acree, Jr. Chem. Pharm. Bull. **54**, 428 (2006).
29. A. Beerbower, P.L. Wu, and A. Martin. J. Pharm. Sci. **73**, 179 (1984).
30. R.M. Dickhut, D.E. Armstrong, and A.E. Andren. Environ. Toxicol. Chem. **10**, 881 (1991).
31. A. Reillo, M. Cordoba, B. Escalera, E. Selles, and M. Cordoba, Jr. Pharmazie, **50**, 472 (1995).

© 2006 NRC Canada

NMR study of hydrogen bonding in methanol – carbon tetrachloride solutions

J.Q. Deng and R.H. Lipson

Abstract: The nuclear magnetic resonance (NMR) frequencies of the hydroxyl protons of methanol clusters in carbon tetrachloride were measured as a function of concentration between 245.4 and 320.2 K. The size of the methanol cluster (n) and the enthalpy and entropy of methanol self-association were obtained from nonlinear least-squares fittings to a model that assumed that only one dominant cluster was in equilibrium with the monomer at each temperature. The chemical shift measurements at 273 and 299.1 K fit best to theoretical curves calculated for a monomer–tetramer equilibrium. However, at higher and lower temperatures, the analyses indicate that the most dominant clusters are smaller and larger, respectively.

Key words: alcohol liquid solutions, structure, hydrogen bonding, thermodynamics of self-association, nuclear magnetic resonance.

Résumé : Opérant entre 245,4 et 320,2 K, on a mesuré les fréquences en résonance magnétique nucléaire (RMN) des protons hydroxyles d'agrégats de méthanol en fonction de sa concentration dans le tétrachlorure de carbone. On a évalué la taille (n) de l'agrégat de méthanol ainsi que ses enthalpie et entropie d'autoassociation sur la base d'ajustements non linéaires par la méthode des moindres carrés avec un modèle qui fait l'hypothèse que, pour chaque température, il n'existe qu'un seul agrégat dominant dans l'équilibre avec le monomère. Les valeurs expérimentales obtenues pour les mesures de déplacements chimiques à 273 et à 299,1 K s'ajustent bien aux courbes théoriques calculées pour un équilibre monomère–tétramère. Toutefois, à des températures plus élevées ou moins élevées, les analyses indiquent que les agrégats dominants sont respectivement plus petits et plus gros.

Mots clés : solutions liquides d'alcool, structure, liaison hydrogène, thermodynamique de l'autoassociation, résonance magnétique nucléaire.

[Traduit par la Rédaction]

Introduction

Liquid alcohols have been widely studied since the 1930s as model systems to understand the influence of hydrogen bonding and the alkyl chain on their physical properties. Despite a significant experimental effort to understand both neat liquid methanol (CH_3OH) and its solutions with relatively unreactive solvents such as carbon tetrachloride (CCl_4), the results have often been contradictory, particularly regarding the dominant cluster species at the microscopic level. This can be attributed primarily to the fact that most experimental techniques cannot directly image liquid structure at the molecular scale. An overview of previous studies on the structure of neat CH_3OH and CH_3OH–CCl_4 solutions (vide infra) reveals many uncertainties regarding the dominant cluster size in solution and at different temperatures. Therefore, CH_3OH–CCl_4 solutions were reexamined in this work by high-resolution NMR spectroscopy over a wide range of concentrations. In addition, measurements were carried out at four different temperatures (T = 245.4, 273, 299.1, and 320.2 K) to extract thermodynamic enthalpy and entropy of methanol self-association. This study was also undertaken to complement our recent work on the VUV laser – mass spectra of gas-phase methanol clusters (1).

Received 23 February 2006. Published on the NRC Research Press Web site at http://canjchem.nrc.ca on 16 June 2006.

J.Q. Deng and R.H. Lipson.[1] Department of Chemistry, University of Western Ontario, London, ON N6A 5B7, Canada.

[1]Corresponding author (e-mail: rlipson@uwo.ca).

Neat methanol

The role of hydrogen bonding in neat liquid methanol was first recognized by Zachariasen (2), who invoked this interaction to interpret his X-ray diffraction data. More recently, Magini et al. (3) provided X-ray diffraction data as evidence for extensive hydrogen-bonded chains, similar to that proposed in solid methanol (4). This conclusion agrees with that reached by Durov (5), who modeled methanol's thermodynamic, dielectric, and optical properties. His model indicates that methanol does not form small clusters, but instead, aggregates into long chains where the mean number of association at T = 293 K is n = 42. Tanaka et al. (6), however, using both X-ray and neutron diffraction data, concluded that the dominant species in neat methanol are clusters consisting of three or four hydrogen-bonded monomers. Yamaguchi et al. (7) revisited this problem using neutron diffraction and found the cluster size to be $n = 6.27 \pm 0.7$ at T = 193 K and $n = 5.5 \pm 1.0$ at T = 298 K. Sarkar and Joarder (8) argued that their X-ray diffraction data is strongly consistent with the presence of cyclic hexamers (n = 6). More recently, Saykally and co-workers (9) measured the room-temperature X-ray absorption spectrum of liquid methanol expanded in a

 doi:10.1139/V06-085 © 2006 NRC Canada

microjet, and using DFT calculations concluded that the bulk liquid is comprised of long chains ($n > 6$) and rings of hydrogen-bonded monomers.

The OH-stretching frequency of liquid methanol, monitored by IR (10) and Raman spectroscopy (11, 12), exhibits a structure that can be attributed to hydrogen bonding. Neat methanol exhibits three OH features, which in order of decreasing frequency are attributed to moieties that are nonbonded, those that interact weakly, and those that interact strongly, respectively. In essence, the last two bands arise essentially from weakly and strongly induced collective dipole moments; that is, from different degrees of clustering (13). The earlier Raman results (11) were interpreted in the framework of an electrostatic model, where it was concluded that the structure of liquid methanol is not chainlike but is instead a three-dimensional network featuring a mix of linear hydrogen bonds between two monomers, bifurcated hydrogen bonds among three monomers, and trifurcated hydrogen bonds among four monomers. The latter work (12) attributed the lowest frequency OH stretch to tetramers and higher aggregates.

A detailed statistical mechanical simulation of neat methanol at $T = 298$ K by Jorgensen (14) indicates that the liquid consists of long, winding hydrogen-bonded chains, where linear ($n = 2$) hydrogen bonding dominates. In contrast, semiempirical quantum calculations undertaken to understand the observed heat of vaporization indicate that methanol self-associates in pure liquids to form tetramers ($n = 4$) (15).

Methanol – carbon tetrachloride solutions

The physicochemical properties and supramolecular structure of MeOH–CCl_4 solutions have been reviewed and have been shown to be strong functions of solution concentration, temperature, and pressure (16). For example, methanol diffusion constants are inversely proportional to the degree of association and therefore, strongly concentration-dependent (17). Huyskens et al. (18) interpreted the dielectric studies of dilute methanol – carbon tetrachloride solutions in terms of cyclic alcoholic trimers ($n = 3$). Using similar techniques, Ibbitson and Moore (19) argued that linear dimers and trimers should be present when the mole fraction of methanol is ≤0.02. Light scattering, on the other hand, indicates cluster sizes between $n = 5$ and 6 (20). The methanol OH-stretching frequency in solution has also been investigated by vibrational spectroscopy (21–23). The IR spectra recorded by Bellamy and Pace (22) suggested that alcohols form open chain structures rather than cyclic compounds, and the hydrogen bonds linking trimers and higher polymers are significantly stronger than those for dimers. Fletcher and Heller (23) have presented evidence from IR spectra to support that the tetramer is the predominant polymeric species in solution.

NMR spectroscopy is well-suited to the study of alcohol solutions because hydrogen bonding decreases the electron cloud density around the H atom in the OH moiety. As a result, the nucleus becomes less screened from the applied magnetic field, which causes a shift to higher frequency in the observed resonance. The position of the OH proton resonance relative to those for the protons on the alkyl chain can therefore be taken as a measure of the extent of hydrogen bonding. Increases in temperature or dilution are expected to break the hydrogen-bonding network, causing the OH proton to become more shielded. In the limit of infinite dilution, the alcoholic proton chemical shift should approach that for a single uncomplexed monomer in the gas phase.

One of the earliest NMR studies of methanol in carbon tetrachloride was published by Saunders and Hyne (24) who covered concentrations down to 0.01 mol/L at a fixed temperature ($T = 294$ K). In their study, a model was developed to fit their data that assumed only one hydrogen-bonded species is in equilibrium with the monomer and a monomer–tetramer combination fit their data best. Symons and Thomas (25) compared IR and NMR spectra of CH_3OH in CCl_4 to show that hydrogen bonding remains complete down to below 0.1 mol fraction methanol, and that tetramers dominate at low temperature ($T = 183$ K). However, they also concluded that this model does not explain the room temperature data. Davis et al. (26) also reported an NMR study of MeOH in CCl_4, but their data covered a concentration range that excludes a large region (<0.04 mol/L) where the OH resonance frequency is still expected to change. They recognized that methanol polymers will exist at higher concentrations, but assignments were not provided. They also suggested that cyclic ring structures were expected to be particularly stable for clusters with $n \geq 4$. A recent NMR study (27) simply assumed that the most important equilibrium exists between monomers and tetramers in solution at room temperature. However, the emphasis in that study was the effect of high pressure on the NMR spectra. Specifically, chemical shifts were measured indicating the formation of new hydrogen bonds and (or) the strengthening of the existing interactions by bond length reduction.

Experimental

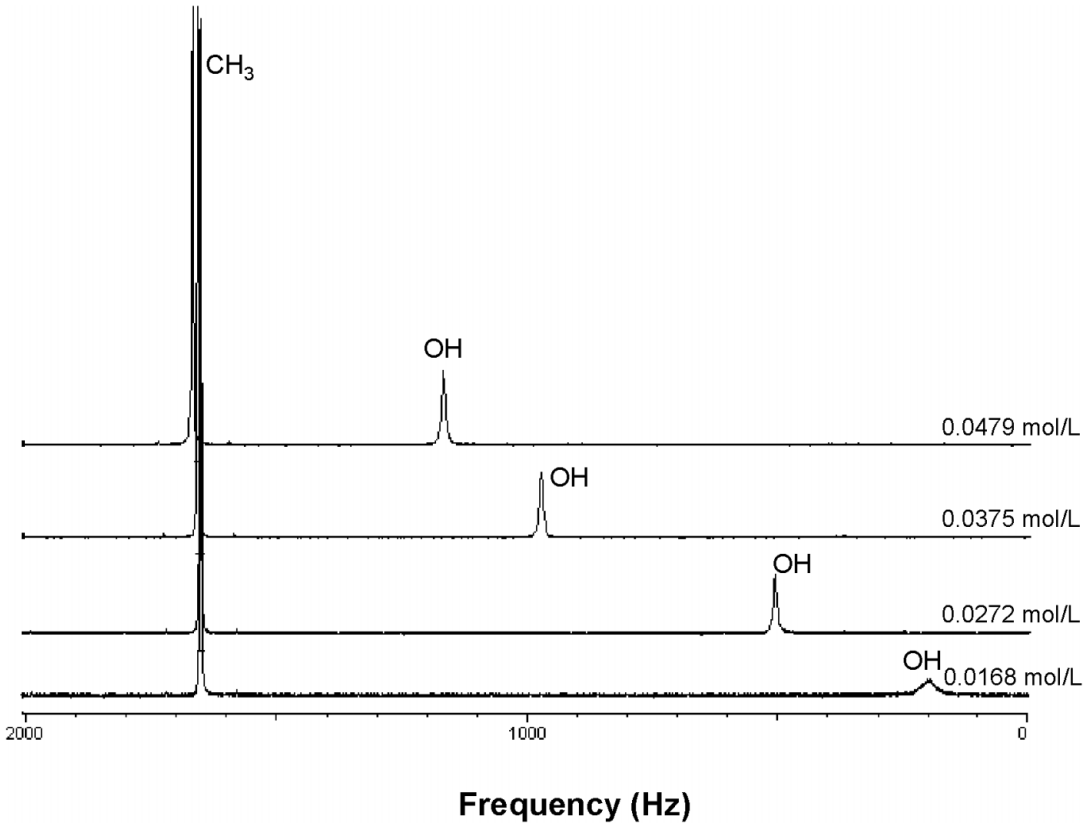
^{1}H NMR spectra were acquired on a Varian Inova 600 MHz spectrometer. Sigma-Aldrich HPLC grade methanol was distilled and placed under argon immediately prior to use. HPLC grade anhydrous carbon tetrachloride from Sigma-Aldrich was used without further purification. Working with neat methanol and solutions with molarities as low as ~0.0168 mol/L by volumetric dilution of liquid methanol, it was found that a concentration of 0.0168 mol/L was the lowest concentration that could still yield a spectrum with a good signal-to-noise ratio. Each sample was run in a NMR tube filled to the top with the solution to minimize contamination by moisture and to limit the amount of magnetic field shimming required. Prior to sample introduction, each NMR tube was cleaned with methanol and dried in a vacuum desiccator. Each tube was purged with Ar before filling. Once filled, the sample tubes were closed at the top and sealed with Parafilm.

The temperature of the sample was varied and calibrated to ~± 0.1 K using neat methanol NMR signals as a thermometer (28). Each sample was allowed to equilibrate for a minimum of 15 min to reach a stable temperature. At the lowest temperature ($T = 245.4$ K), at least 30 min were taken for stabilization to avoid a temperature gradient in the NMR tube, which might cause line broadening.

In this work, the peak center was taken as the resonance frequency for that signal. Each OH proton chemical shift

© 2006 NRC Canada

Fig. 1. Resonance frequency of the OH proton as a function of solution concentration at 245.4 K.



was measured relative to the methyl group resonance. A negative sign indicates that the hydroxyl resonance occurs at a lower frequency than the reference peak. Each reported shift is the average of at least three separate measurements. The precision of each chemical shift measurement lies within ±50 Hz and reflects the uncertainty in making solutions of identical concentration.

Results and discussion

Observations

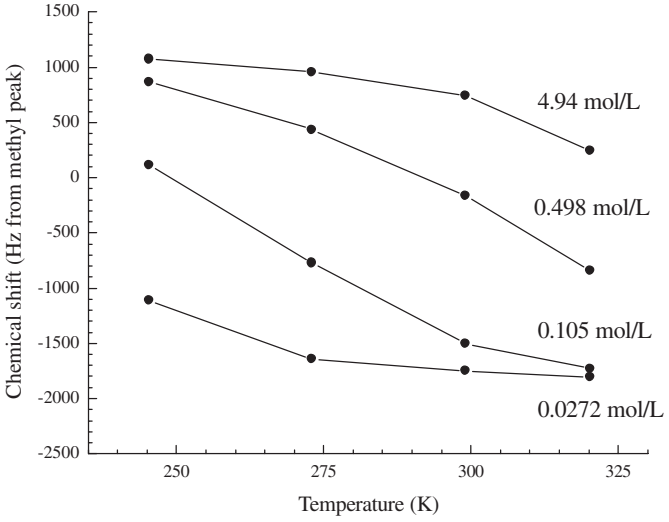
The NMR spectra in Fig. 1 show the variation of the methanol OH signal frequency as a function of methanol – carbon tetrachloride mixture composition at 245.4 K. Increasing the methanol concentration increases the probability of hydrogen bonding, and as a result shifts the OH proton signal to higher frequencies. At low concentrations, when the probability of intermolecular hydrogen bond formation is greatly reduced, the resonance frequency of the OH proton should shift to lower values. The OH proton resonance for the lowest concentration mixture (0.0168 mol/L) studied in this work came at –1815.2 Hz or –3.02 ppm relative to the CH_3 peak at T = 320.2 K. This is consistent with the work of Chauvel and True (29), who reported an OH chemical shift in gaseous methanol of –3.39 ppm relative to CH_3 at T = 422 K. Therefore, it can be inferred that if the concentration of the methanol was sufficiently low, the measured chemical shift would correspond to a single methanol molecule.

Under the experimental conditions used to record the NMR spectra of methanol in Fig. 1, no coupling was observed between the hydroxyl hydrogen and the hydrogens belonging to the methyl group. Whether spin-spin splitting involving the hydroxyl hydrogen is observed or not depends on several factors including the resolution of the NMR spectrometer, the temperature, the purity of the sample, and the solvent used. Typically, spin coupling can only be observed in neat methanol at temperatures <223 K (30). Fine structure has been observed in ~0.068 mol/L methanol–benzene-d_6 solutions when the samples were very dry (30). The loss of spin coupling fine structure is a consequence of exchange of the methanol hydroxyl proton. At low concentrations in dry solvents, methanol can only exchange its proton with other methanol molecules. Thus, a loss of spin structure indicates that the hydrogen bonding is becoming important. As we do not see fine structure with solution concentrations <0.026 mol/L in this work, we conclude that despite precautions, our samples simply were not dry enough. Still, it is also evident in Fig. 1 that, at the lowest concentrations, the line width of the hydroxyl proton resonance is greater than that at higher concentrations. This is attributed to a decreasing exchange rate. At low concentrations, the methanol monomers and the hydrogen-bonded clusters experience different chemical environments, leading to the observed broadening.

The effect of increasing temperature is similar to lowering the solution concentration. An increased temperature causes hydrogen bonds to break shift the OH proton signal to lower frequencies (Fig. 2).

© 2006 NRC Canada

Fig. 2. Effect of temperature on the OH chemical shifts as a function of concentration.



Analysis of self-association to determine dominant cluster size at T = 298 K

Different approaches to the analyses of hydrogen-bonding and association equilibria by NMR have been reviewed previously (31). Our analysis follows the procedure outlined below, which was first described by Saunders and Hyne (24) and Feeney and Walker (32). In their model, it is assumed that the solution is predominantly one cluster composed of n monomers, which obeys the following equilibrium.

$$[1] \qquad n(CH_3OH) \rightleftharpoons (CH_3OH)_n$$

Let $[CH_3\ OH] = C_1$ and $[(CH_3OH)_n] = C_n$. The equilibrium constant (K_n) associated with rxn. [1] can then be written as

$$[2] \qquad K_n = \frac{C_n}{C_1^n}$$

In this analysis it is assumed that all hydroxyl groups in the same cluster contribute to the absorption at the same frequency. The model also assumes only one type of n-mer exists in solution, when in fact there could be a number of different geometric isomers. For an n-mer with n hydroxyl protons, the concentration of hydroxyl groups that absorb at the same frequency is given by nC_n or $nK_nC_1^n$. On the timescale of the experiment, the observed OH chemical shift is a weighted average of the chemical shifts of all the associated forms of the alcoholic compound.

The weighting factors are the fraction of the total number of hydrogen-bonded protons present in a given state at equilibrium. Thus, the transition frequency (ν) can be written as

$$[3] \qquad \nu = \frac{\nu_1 C_1 + 2\nu_2 K_2 C_1^2 + 3\nu_3 K_3 C_1^3 + \cdots}{C}$$

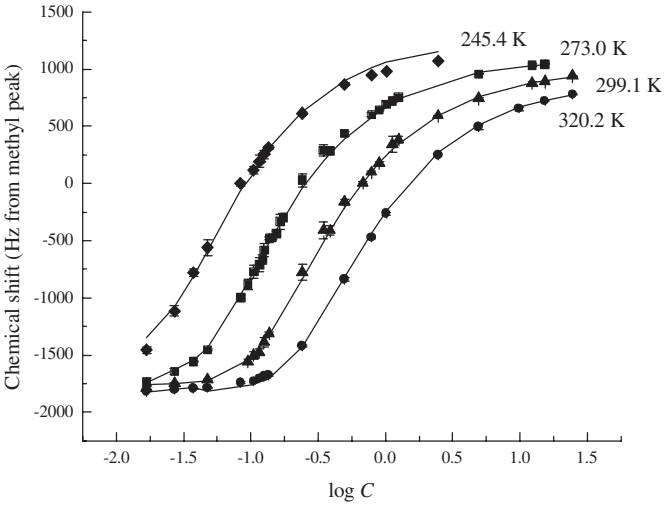
C is the total concentration of hydroxyl group in all clusters, which must equal the solution concentration; that is

$$[4] \qquad C = C_1 + C_2 + C_3 + ... = C_1 + 2K_2C_1^2 + 3K_3C_1^3 + ...$$

Table 1. Best-fit results for different n and K_n values at 299.1 K.

n	K_n (L^{n-1}/mol^{n-1})	ν_1 (Hz)	ν_n (Hz)	χ^2
2	4.0	–24691±5	1243±3	176.9
3	9.0	–1855±4	1063±2	21.0
4	30.7	–1757±4	1001±2	1.8
5	120.0	–1730±4	969±2	13.3

Fig. 3. Nonlinear least-squares fit of chemical shift (Hz) vs. log C, assuming a monomer–tetramer equilibrium at four different temperatures.



If only a single hydrogen-bonding equilibrium is significant and ν_n constant throughout the entire concentration range probed, then eqs. [3] and [4] simplify to

$$[5] \qquad \nu = \frac{\nu_1 C_1 + n\nu_n K_n C_1^n}{C}$$

where

$$[6] \qquad C = C_1 + nK_nC_1^n$$

Equation [5] was used as a fitting model with K_n set to an arbitrary value for a particular integer n at a given temperature to determine the characteristic chemical shifts of the monomer (ν_1) and n-mer (ν_n) by nonlinear least-squares fitting. Our experimental data were fit using four models: monomer–dimer, monomer–trimer, monomer–tetramer, and monomer–pentamer (n = 2, 3, 4, and 5 in eq. [5], respectively). In each case, K_n was varied until the χ^2 value of the fit was minimized.

Of all the fits done for the data at T = 299.1 K, the analysis obtained for n = 4 proved to be the best, inferring that tetramers are the predominant hydrogen-bonded species in solution. This agrees with the conclusion reached by Saunders and Hyne (24). The best-fit parameters for different values of n at 299.1 K are listed in Table 1.

Temperature studies

Figure 3 shows the fitted curves of chemical shift vs. log C as a function of temperature, assuming that the tetramer is the predominant hydrogen-bonded cluster in solution. The best-fit parameters are listed in Table 2. At very high dilu-

© 2006 NRC Canada

Table 2. Best-fit parameters assuming a monomer–tetramer equilibrium at different temperatures.

Temperature (K)	K_4 (L^3 mol^{-3})	ν_1 (Hz)	ν_4 (Hz)	χ^2
245.4	3550±150	–1494±21	1307±12	3.8
273.0	380±80	–1730±3	1102±1	1.8
299.1	31±3	–1757±4	1001±2	1.8
320.2	4.5±0.5	–1809±1	893.743±0.821	9.5

tion, the solution is assumed to be composed of only isolated methanol monomers surrounded by carbon tetrachloride. Although CCl_4 is expected to be relatively inert because it has no permanent dipole moment, the lone pairs of the chlorine atoms can interact weakly with the methanol hydroxyl proton. At each temperature except T = 245.4 K, the chemical shifts at high dilution are small and relatively unaffected by temperature as expected since they reflect an unchanging environment around the monomer. The change in ν_1 at the lowest temperature to higher frequencies suggests that the interaction between MeOH and CCl_4 is becoming more important. This low-temperature behavior is not unexpected given the small binding energy of MeOH and CCl_4 (2.6 kJ mol^{-1} at an uncorrelated Hartree–Fock level; 2.85 kJ mol^{-1} using B3LYP/6-31+G* density functional theory (30)). This binding energy, however, is considerably less than the interaction between two methanol monomers (22.7 kJ mol^{-1} at an uncorrelated Hartree–Fock level; 26.2 kJ mol^{-1} using B3LYP/6-31+G* density functional theory (30)), and illustrates the preference methanol has to self-associate.

As the concentration of methanol increases, the chemical shifts increase rapidly until they reach a plateau. The sharp increase in chemical shift is attributed to the strong preference of methanol monomers to hydrogen bond to other methanol molecules rather than to solvent molecules. In can be seen that the chemical shift of the tetramer (ν_4, listed in Table 2) is not a constant but decreases with increasing temperature. This change may be due in part to changes in the relative populations of linear and cyclic polymers in solution. A linear species has a free hydroxyl group. Since the average electronic shielding of a linear form is greater than a cyclic one, the chemical shift of a linear tetramer will be smaller than that for the cyclic isomer. In addition, the temperature variation of the tetramer proton might result from changes in the effective length of the H···O bond, which is influenced by low-frequency hydrogen-bond stretching vibrations and anharmonicity effects.

However, another important reason for a changing ν_4 chemical shift with temperature is the limitation of the analysis model itself. Based on the χ^2 values in Table 2, the monomer–tetramer model reproduces the shifts measured at 273.0 and 299.1 K well, but is less successful at higher and lower temperatures. At each temperature, a distribution of clusters is expected in solution. Thus, species other than the tetramer are expected to exist to a larger extent at higher and lower temperatures, which could affect the analyses. Since methanol – carbon tetrachloride solutions are composed of clusters of various sizes, then the average cluster size (n) may not necessarily correspond to an integer. Thus, the nonlinear least-squares fits were redone, but now allowing n to be a real number >1. In this way, better fits with smaller χ^2 values were obtained than those achieved using the monomer–tetramer model.

Table 3. Estimated ΔH values using ν_1 and ν_4 values obtained at different temperatures (C = 0.126 mol L^{-1}).

Temperature (K)	ν_1 (Hz)	ν_4 (Hz)	ΔH (kJ mol^{-1})
245.4	–1494	1307	–92.5±8.3
273.0	–1730	1102	–86.4±0.9
299.1	–1757	1001	–86.0±1.8
320.2	–1809	894	–86.7±4.9

At the lower temperature, the n value that gave the best fits was n = 4.3 (a change in χ^2 from 3.8 to 1.6), which implies that species larger than the tetramer are present in solution. Conversely, at higher temperatures, the best fit was obtained for n = 3.5 (a change in χ^2 from 9.4 to 3.2), indicating that smaller clusters are becoming the dominant species. It should be noted that the least-squares fits were not strongly sensitive to small changes in n, so it would be difficult to read more into the actual noninteger values of n other than the trends, which are the expected ones.

Thermodynamics of methanol association

Having equilibrium constants at different temperatures allows the enthalpy of association (ΔH) and the entropy of association (ΔS) to be determined since the Gibbs free energy change at a given temperature ($\Delta G = \Delta H - T\Delta S$) is related to K_n by

$$[7] \qquad \Delta G = RT \ln K_n$$

where R is the gas constant. Assuming that ΔH and ΔS are independent of temperature over the range of measurements, it is straightforward to show that

$$[8] \qquad \ln K_n = -\frac{\Delta H}{RT} + \frac{\Delta S}{R}$$

A van't Hoff plot of $\ln K_n$ vs. T^{-1} should then be linear with a slope of $-\Delta H/R$ and an intercept of $\Delta S/R$. Using the two equilibrium constants for T = 273.0 and 299.1 K yields a ΔH for tetramer association of –68.2 ± 8.4 kJ mol^{-1} and tetramer entropy of association of –200.2 ± 28.8 J mol^{-1} K^{-1}.

In the second approach (32), eqs. [5] and [6] were combined to yield

$$[9] \qquad K_n = \frac{(\nu - \nu_1)(\nu_n - \nu_1)^{n-1}}{nC^{n-1}(\nu_n - \nu)^n}$$

Assuming that ν_1 and ν_n are independent of temperature, then $(\nu_n - \nu_1)^{n-1}$ will also be a constant. It follows therefore that

© 2006 NRC Canada

Table 4. Summary of results obtained for methanol self-association in inert solvents.

Reference	Technique	Solvent	Temperature (K)	n	ΔH (kJ mol^{-1})	ΔS (J mol^{-1})
This work	NMR	CCl_4	245.4	>4	–86.2±1.4	–200±29
			273.0	4		
			299.1	4		
			320.2	<4		
32	NMR	CCl_4	—	4	–47.7	—
24	NMR	CCl_4	294	4	—	—
	NMR	$CHCl_3$	302	3, 4	—	—
25	NMR, IR	CH_2Cl_2	183	4	—	—
23	IR	CCl_4	293	4	—	—
16	DS[a]	CCl_4	298	4	–59±1	—
18	DS	CCl_4	—	3	—	—
19	DS, near-IR	CCl_4, C_6H_{12}	298	2, 3	—	—

[a]Dielectric study (see ref. 36).

$$[10] \quad \log K_n = \log \frac{(\nu - \nu_1)}{(\nu_n - \nu)^n} + B$$

where B is a constant. It is straightforward, using eqs. [10] and [8], to derive

$$[11] \quad \frac{1}{T} = -\frac{2.303R}{\Delta H} \log \frac{(\nu - \nu_1)}{(\nu_n - \nu)^n} + B''$$

where B'' is another constant. For a fixed total methanol concentration C, a plot of $1/T$ vs. $\log(\nu - \nu_1)/(\nu_n - \nu)^n$ should be linear with a slope of $-2.303R/\Delta H$. Using the frequencies ν_1 and ν_4 derived from chemical shifts measured at T = 273.0 K and C = 0.126 mol/L, such a plot yields a value of $\Delta H = -86.4 \pm 0.9$ kJ mol^{-1}. Table 3 gives the ΔH values obtained from similar plots using ν_1 and ν_4 values obtained at different temperatures. The values are quite consistent except when T = 245.4 K. The larger enthalpy change in this case is again attributed to the increased importance of methanol – CCl_4 interactions. Since we have shown that a monomer–tetramer model may not be completely valid at the highest and lowest temperatures considered in this work, an average ΔH of tetramer association of –86.2 ± 1.4 kJ mol^{-1} was calculated from the mid-temperature results alone.

Conclusion

A comparison of the thermodynamic data derived in this work with other experiments and solvents is presented in Table 4. Not surprisingly, the value of ΔS, corresponding to the entropy change for the formation of tetramers from monomers, is negative, indicating a more ordered solution. The sign of ΔH indicates that methanol self-association is an exothermic process.

The binding energy of the linear methanol dimer has been calculated using density functional theory to be –15.5 kJ mol^{-1} (33). If the methanol tetramer is linear and the three internal hydrogen-bond energies are additive, the resultant total binding energy would be –46.5 kJ mol^{-1}. Similarly, a cyclic structure with four hydrogen bonds would have a minimum binding energy of –62.0 kJ mol^{-1}. The enthalpy derived in this work is closer to the cyclic structure prediction.

Large differences between higher level calculations and the values above are attributed in part to cooperativity effects (34, 35). While the increase in binding energies for clusters above n = 4 follows an asymptotic approach to linear H bonds in larger systems, the particularly large cyclic tetramer binding energy of –113.84 kJ mol^{-1} (33) is attributed to cooperativity effects coupled with minimum ring strain (34). Still, this value is higher than experimental values determined for the gas-phase cluster from IR intensities (–75.3 kJ mol^{-1}) (34) and by heat capacity, vapor density, and thermal conductivity measurements (92.5–100.9 kJ mol^{-1}) (34), and the enthalpy obtained in this work. Interestingly, calculations place the binding energy of the linear chain configuration at –80.9 kJ mol^{-1}, the unequal branched chain at –61.4 kJ mol^{-1}, the equal branch chain at –69.8 kJ mol^{-1}, and the branch cycle at –83.5 kJ mol^{-1} (33). The enthalpy of association derived in this work lays closer to that expected for the linear chain and the branch cycle configurations. It must therefore be concluded that the actual dominant tetramer geometry in solution remains an open question, but it is most likely that the cluster adopts several forms.

Acknowledgments

This work was supported by the Natural Sciences and Engineering Research Council of Canada (NSERC). The authors thank Diane Lacey and Chris Kirby for their assistance with the experiments.

References

1. Y.J. Shi, S. Consta, A.K. Das, B. Mallik, D. Lacey, and R.H. Lipson. J. Chem. Phys. **116**, 6990 (2002).
2. W.H. Zachariasen. J. Chem. Phys. **3**, 158 (1935).
3. M. Magini, G. Paschina, and C. Piccaluga. J. Chem. Phys. **77**, 2051 (1982).
4. B.H. Torrie. S.-X. Weng, and B. Powell. Mol. Phys. **67**, 575 (1989).
5. V.A. Durov. J. Mol. Liq. **78**, 51 (1998).
6. Y. Tanaka, N. Ohtomo, and K. Arakawa. Bull. Chem. Soc. Jpn. **58**, 270 (1985).

© 2006 NRC Canada

7. T. Yamaguchi, K. Hidaka, and A.K. Soper. Mol. Phys. **97**, 603 (1999).
8. S. Sarkar and R.N. Joarder. J. Chem. Phys. **99**, 2032 (1993).
9. K.R. Wilson, M. Cavalleri, B.S. Rude, R.D. Schaller, T. Catalano, A. Nilsson, R.J. Saykally, and L.G.M. Pettersson. J. Phys. Chem. B, **109**, 10194 (2005).
10. W.A.P. Luck and M. Fritzsche. Z. Phys. Chem. (Muenchen, Ger.), **191**, 71 (1995).
11. P.A. Giguère and M. Pigeon-Gosselin. J. Sol. Chem. **17**, 1007 (1988).
12. A. Arencibia, M. Taravillo, F.J. Pérez, J. Núñez, and V.G. Boanza. Phys. Rev. Lett. **89**, 195504-1 (2002).
13. M.S. Skaf, T. Fonseca, and B.M. Ladanyi. J. Chem. Phys. **98**, 8929 (1993).
14. W.L. Jorgensen. J. Am. Chem. Soc. **102**, 543 (1980).
15. S.W. Benson. J. Am. Chem. Soc. **118**, 10645 (1996).
16. V.A. Durov and I.Yu. Shilov. J. Mol. Liq. **92**, 165 (2001).
17. D.K Anderson and A.L.Babb. J. Phys. Chem. **67**, 1362 (1963); Y. Oishi, Y. Kamei, and H. Sumie. J. Chem. Phys. **61**, 2227 (1974); Y. Oishi and M. Nanba. J. Chem. Phys. **70**, 2205 (1979); N.-Y.R. Ma, D. Stanford, and A.L. Beyerlein. J. Phys. Chem. **87**, 5464 (1983); S. Prabhakar and H. Weingärtner. Z. Phys. Chem. N. F. **137**, 1 (1983).
18. P. Huyskens, G. Gillerot, and Th. Zeegers-Huyskens. Bull. Soc. Chim. Belg. **72**, 666 (1963).
19. D.A. Ibbitson and L.F. Moore. J. Chem. Soc. B, 76 (1967).
20. T. Kato, T. Nakanishi, and T. Fujiyama. Bull. Chem. Soc. Jpn. **53**, 2173 (1980).
21. U. Liddel and E.D. Becker. Spectrochimica Acta, **10**, 70 (1957).
22. L.J. Bellamy and R.J. Pace. Spectrochimica Acta, **22**, 525 (1966).
23. A.N. Fletcher and C.A. Heller. J. Phys. Chem. **72**, 1839 (1968).
24. M. Saunders and J.B. Hyne. J. Chem. Phys. **29**, 1319 (1958).
25. M.C.R. Symons and V.K. Thomas. J. Chem. Soc. Faraday Trans. 1, **77**, 1883 (1981).
26. J.C. Davis, Jr., K.S. Pitzer, and C.N.R. Rao. J. Phys. Chem. **64**, 1744 (1960).
27. C. Czeslik and J. Jonas. Chem. Phys. Lett. **302**, 633 (1999).
28. C. Ammann, P. Meier, and A.E. Merbach. J. Magn. Reson. **46**, 319 (1982).
29. J.P. Chauvel, Jr. and N.S. True. Chem. Phys. **95**, 435 (1985).
30. M.A. Wendt, J. Meiler, F. Weinhold, and T.C. Farrar. Mol. Phys. **93**, 145 (1998).
31. J.C. Davis, Jr. and K.K. Deb. Adv. Magn. Reson. **4**, 201 (1970).
32. J. Feeney and S.M. Walker. J. Chem. Soc. A, 1148 (1966).
33. F.C. Hagemeister, C.J. Gruenloh, and T.S. Zwier. J. Phys. Chem. A, **102**, 82 (1998).
34. L.A. Curtiss and M. Blander. Chem. Rev. **88**, 827 (1988).
35. U. Buck, J.-G. Siebers, and R.J. Wheatley. J. Chem. Phys. **108**, 20 (1998).
36. A.D. Cohen and C. Reid. J. Chem. Phys. **25**, 790 (1956).

© 2006 NRC Canada

One-electron oxidation of methionine peptides — Stability of the three-electron S—N(amide) bond

Patrick Brunelle, Christian Schöneich, and Arvi Rauk

Abstract: The possibility of sulfur–nitrogen (S—N) three-electron bond formation in a one-electron oxidized methionine peptide model was investigated computationally following the detection of such species in pulse radiolysis experiments (C. Schöneich, D. Pogocki, G.L. Hug, and K. Bobrowski. J. Am. Chem. Soc. **125**, 13700 (2003)). Geometry optimizations were carried out at the B3LYP/6-31G(d) level of theory. Relative free energies in aqueous solution at pH 7 were predicted for all intermediates with enthalpy evaluations at the CCSD(T)/6-31+G(d′) level and free energies of solvation predicted using a continuum model (CPCM). Both the initial oxidation product and the intermediate formed at higher pH were identified as cyclic S—N bonded species in which the intramolecular three-electron interaction is between the S atom and the π orbital of the amide group. TD-B3LYP calculations of the UV spectra support the assignments. A mechanism for the conversion to the most stable α-C-centered radical is proposed. The mechanism involves a novel deprotonation–reprotonation via an intermediate backbone-delocalized radical anion.

Key words: methionine oxidation, three-electron bonding, S—N bonding, B3LYP.

Résumé : À la suite de la détection d'espèces comportant des liaisons à trois électrons entre le soufre et l'azote (S—N) dans des expériences de radiolyse pulsée (C. Schöneich, D. Pogocki, G.L. Hug, and K. Bobrowski. J. Am. Chem. Soc. **125**, 13700 (2003)), on a fait appel à des calculs théoriques pour examiner la possibilité de formation d'un tel type de liaison lors de l'oxydation par un électron d'un peptide modèle de la méthionine. On a effectué les optimisations de la géométrie au niveau B3LYP/6-31G(d) de la théorie. On a pu faire des prédictions pour les énergies libres relatives en solution aqueuse, à un pH de 7, pour tous les intermédiaires avec des évaluations d'enthalpie au niveau CCSD(T)/6-31+G(d′) et les énergies libres de solvatation ont été faites utilisant un modèle continu, CPCM. On a établi que le produit d'oxydation initial ainsi que l'intermédiaire qui se forme à des pH plus élevés sont des espèces cycliques comportant des liaisons S—N dans lesquelles l'interaction intramoléculaire à trois électrons se situe entre l'atome de soufre et l'orbitale π du groupe amide. Des calculs de spectre UV faits au niveau TD-B3LYP sont en accord avec ces attributions. On propose un mécanisme pour la conversion vers le radical le plus stable centré sur le carbone-α. Le mécanisme implique une nouvelle réaction de déprotonation–reprotonation qui se fait par le biais d'un intermédiaire anion radical délocalisé sur le squelette.

Mots clés : oxydation de la méthionine, liaison à trois électrons, liaison S—N, B3LYP.

[Traduit par la Rédaction]

Introduction

Oxidation of methionine sulfur is an important feature of "oxidative stress" in biological systems (1–7), and may be a key step in the neurotoxicity of the β-amyloid peptide (Aβ) in Alzheimer's disease (8–10). The reduction potential of dimethyl sulfide radical cation is typical of a dialkyl sulfide, E° = 1.66 V vs. SHE (11, 12). Oxidation of aqueous methionine is an irreversible process. The reduction potential of 1 e oxidized zwitterionic methionine (Met) (exptl. at pH 7, $E^{\circ\prime} < 1.48$ V (13); calcd. $E^{\circ\prime} = 1.25$ V, $E^\circ = 1.66$ V (14)) is about the same as that of a typical dialkyl sulfide radical cation, and that of oxidized MetGly is modestly lower (1.42 ± 0.3 V) (15). It was confirmed by a recent ab initio investigation that intermediates with three-electron bonds between S and the -NH_2 group (S∴N) or -CO_2^- group (S∴O) of the Met amino acid are formed but do not result in a substantial lowering of the reduction potential (14). Both S∴O and S∴N bonds in Met derivatives and small organic sulfides have been proposed (15) and observed spectroscopically (16, 17) in pulse-radiolysis and flash photolysis experiments in aqueous solutions.

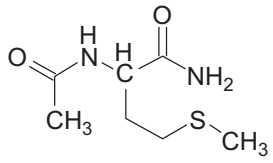
In a recent publication on the hydroxyl-radical-induced oxidation of *N*-acetylmethioninamide **2** (18), one of us presented experimental spectroscopic and kinetic evidence for the formation of a new sulfur–nitrogen 3 e bonded species, most likely **5a/5b**, in which an intramolecular 3 e bond (S∴N) was transiently formed between the S atom of a Met peptide and the N of a deprotonated amide group upon one-electron oxidation by hydroxyl radical after pulse radiolysis.

Received 7 March 2006. Published on the NRC Research Press Web site at http://canjchem.nrc.ca on 23 June 2006.

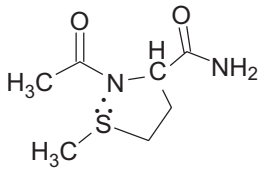
P. Brunelle and A. Rauk.[1] Department of Chemistry, University of Calgary, Calgary, AB T2N 1N4, Canada.
C. Schöneich. Department of Pharmaceutical Chemistry, University of Kansas, Lawrence, KS 66047, USA.

[1]Corresponding author (e-mail: rauk@ucalgary.ca).

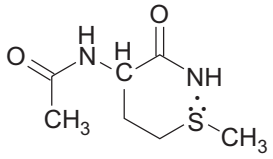
 doi:10.1139/V06-079 © 2006 NRC Canada



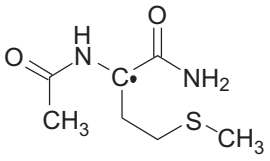
2



5a



5b



8

The putative structures **5a/5b** are the only asymmetric sulfide radical species detected 10 μs after the pulse at pH 5.4. The observed UV absorption was best fit with a broad band peaking at 390 nm, attributed to **5a/5b**. It was not possible at the time to distinguish **5a** from **5b**, or to characterize in more detail the nature of the S∴N bonding. As part of the present study, we provide an estimate of the S∴N bond strength in aqueous solution and in the gaseous phase and characterize it by the predicted UV spectrum in water.

Furthermore, some of the initially formed **5a/5b** are transformed into the α-C-centered radical **8**. This transformation is expected to be highly exothermic and can be formulated as a simple intramolecular hydrogen atom transfer (1,2- in the case of **5a**, or 1,3- for **5b**). However, such H-atom transfers typically encounter high activation barriers, and alternative routes involving elimination and addition of protons or H-atoms may be formulated. A secondary part of this study is to propose a mechanism for the transformation of **5a/5b** into **8**.

Methods

Ab initio calculations were performed with the Gaussian 98 (19) or Gaussian 03 (20) suites of quantum chemistry programs. Geometry optimization and frequencies for all species were carried out at the B3LYP/SB level of theory. Henceforth, we will use SB to represent the small basis set (6-31G(d)) and LB for the larger basis set (6-311+G(3df,2p)). All other basis sets will be given explicitly. A thorough investigation of the geometries of the related three electron bonded species in the gaseous phase and in solution found only minor differences in the two geometries (21). Zero point energies were obtained from the frequencies scaled by a factor of 0.9806 (22), while no scaling was applied for the calculation of entropies or the temperature dependence of the enthalpy ($H^{\circ}_{298K} - H^{\circ}_{0K}$). No attempts were made to locate all conformers for all species. The contribution to the entropy from the flexibility of the species was approximated as $R \ln(n)$, where n is an estimate of the number of significantly populated conformers (23). Values of n are given in Table S1 of the Supporting information.[2] To improve relative values of the enthalpy, energies were calculated at the B3LYP/LB, CCSD(T)/6-31+G(d′),[3] or CBS-RAD level (24) on the B3LYP/SB geometries. CBS-RAD is a high-level theoretical method for obtaining accurate thermochemical values for radicals to experimental accuracy. The CBS-RAD//B3LYP/SB method employed here was found to yield good reaction enthalpies and barriers for the addition of C-centered radicals to alkenes (25–27) and the β-scission reactions of alkoxy radicals (28). However, for reasons described in the following, relative energies of species involving 3 e S∴N bonds are more appropriately described at the CCSD(T) level. For consistency, all relative energies are cited at the CCSD(T) level.

Time-dependent density functional theory, with the B3LYP/6-311+G(d,p) description of the Hamiltonian (TD-B3LYP) (29) and the CPCM reaction field (30), is used to calculate the lowest UV transitions of selected species (20). In the case of cyclic structures containing a 3 e S∴N bond, spectra are very sensitive to the S—N separation. We show in the following that the CCSD(T)/6-31+(d′) level of theory yields the most reliable S—N separation. The CPCM procedure, as implemented in Gaussian, requires atom-centered spheres to describe the cavity in the solvent. The radii of atom-centered spheres were chosen so as to fill the volume defined by the gaseous-phase 0.001 e bohr^{-3} isodensity surface derived for a B3LYP/SB wave function (31, 32).

Orbitals were obtained from B3LYP/SB wave functions and shown at the contour level encompassing 60% of the electron.

Aqueous solvation

Solvation effects are modeled according to the conductor-like polarizable continuum model, as implemented in Gaussian 98 or Gaussian 03 as SCRF=CPCM with the cavity defined by an isodensity surface of the molecule, as described above. It is anticipated that calculation of the Gibbs free energy of solvation (ΔG_{SOLV}) in this manner will render inevitable errors to be more systematic and hence amenable to cancellation or to correction by reference to experiments. For entropy and free energy calculations in the gaseous and aqueous phases, a standard state of 1 mol L^{-1} is required. At 298.15 K, the change in volume from 24.6 L at 1 atm (1 atm = 101.325 kPa) to 1 L at 1 mol L^{-1} yields a change in the Gibbs free energy of +7.98 kJ mol^{-1}.

To reduce the errors in the calculated changes in Gibbs free energy of solvation for all the species involved in a reaction, values derived from experiment were adopted for the free energy of solvation of water ($G_{SOLV}(H_2O)$[4] = –26.4 kJ mol^{-1} and of the proton ($G_{SOLV}(H^+)$ =

[2] Supplementary data for this article are available on the journal Web site (http://canjchem.nrc.ca) or may be purchased from the Depository of Unpublished Data, Document Delivery, CISTI, National Research Council Canada, Ottawa, ON K1A 0R6, Canada. DUD 5035. For more information on obtaining material refer to http://cisti-icist.nrc-cnrc.gc.ca/irm/unpub_e.shtml.

[3] The 6-31+G(d′) basis set is the 6-31G† basis set of: G.A. Petersson and M.A. Al-Laham. J. Chem. Phys. **94**, 6081 (1991).

[4] Calculated as the difference between ${}_fG_g(H_2O)$ and ${}_fG_l(H_2O)$, both corrected to a standard state of 1 mol/L. The CPCM procedure yields a very similar value, $G_{SOLV}(H_2O)$ = –28.1 kJ mol

© 2006 NRC Canada

–1107 kJ mol^{-1} (33)). Values of pK_a are calculated from free energy changes for reactions involving loss of a proton.

Results and discussion

The present study aims to examine the thermodynamics of deprotonation–protonation equilibria of the Met dipeptide, *N*-acetylmethioninamide **2**, after one-electron oxidation to the sulfide radical cation (**2**$^{+\cdot}$) in aqueous solution. The nature of the bonding is of special interest. We begin by examining the simpler system comprised of dimethyl sulfide (DMS) and *N*-methylacetamide (NMA).

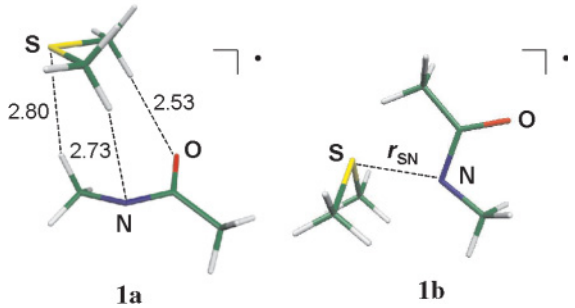
Dimethyl sulfide-*N*-methylacetamide (1, DMS-NMA)

The present methodology relies on structures determined at the B3LYP/SB level of theory. While this is the method of choice for many applications, it may suffer in the description of 3 e bonds (34). In previous work it was concluded that 3 e bonds between sulfur and oxygen (S.∴O) appear to be adequately described (14). For instance, the S.∴O bond between dimethylsulfide radical cation (DMS$^{+\cdot}$) and a water molecule was calculated to be too short by 0.1 Å at the B3LYP/SB level, compared with the CCSD(T)/6-31+G(d′) level. This may not be the case for S.∴N to divalent N as in amidyl radicals because of a larger disparity of sulfide and amide ionization potentials. A (σ,σ*) 3 e S.∴N bond may be described by resonance structures **a**–**c**.

$$\underset{\mathbf{a}}{S^{\bullet+}:N^{-}} \longleftrightarrow \underset{\mathbf{b}}{S.\therefore N} \longleftrightarrow \underset{\mathbf{c}}{S:\bullet N}$$

Such a bond between an oxidized DMS and deprotonated amide would ideally involve the nonbonding 3p orbital of the S and the in-plane sp^2-like orbital of the amide. Several unsuccessful computational attempts were made to obtain this type of bond between DMS$^{+\cdot}$ and the deprotonated amide, *N*-methylacetamide (NMA$^-$). Part of the problem arises from consideration of the wide disparity in the gaseous-phase ionization energies (IE) of a dialkyl sulfide compared with an anionic deprotonated amide. For example, IE(DMS) (calcd. CBS-RAD = 839 kJ mol^{-1}, expt. = 838 kJ mol^{-1} (35)) and IE(NMA$^-$) (calcd. CBS-RAD = 224 kJ mol^{-1}). Thus, the amidyl radical (NMA·) is predicted to be more stable than a DMS$^{+\cdot}$ by more than 600 kJ mol^{-1}. At least in the gaseous phase, a S.∴N bond will have most of the radical character on the nitrogen moiety (resonance structure **c**) and structure **a** should be a minor component. Aqueous solvation may alter this situation, since it will reduce IE(DMS) and raise IE(deprotonated amide). Description **c** requires that the amidyl radical be in the ^{2}A′ state, an electronically excited state of the amidyl radical whose ground state is ^{2}A″. Indeed, unconstrained optimization yields the structure **1a** shown in Fig. 1, which does not have a (σ,σ*) 3 e S.∴N bond, but rather a loose association of the parent DMS making three points of contact with the amidyl radical as shown. The amidyl radical does not optimize to a planar geometry; rather, the dihedral angle (CNCO) is 18°. However, since the planar C_s geometry is calculated to be only 0.4 kJ mol^{-1} higher at the CBS-RAD level, we will use symmetry designations a′ and a″ to denote σ and π radicals, respectively. To enforce a (σ,σ*) 3 e description of the S.∴N bond, we imposed C_s symmetry on the DMS amidyl radical complex (**1b** in Fig. 1) and varied the S—N separation (r_{SN}) over the range 2.2 to 3.7 Å in 10 steps, while optimizing all other variables at the B3LYP/SB level.

Fig. 1. Structures of complexes between dimethyl sulfide and *N*-methylacetamidyl radical. Optimized at the B3LYP/SB level (**1a**); structure with enforced C_S symmetry (**1b**).



At each of the distances, the energy was reevaluated at several higher levels: B3LYP/LB, MP2/CBSB3, CCSD(T)/6-31+G(d′), and CBS-RAD (no ZPE). MP2/CBSB3 and CCSD(T)/6-31+G(d′) are components of the CBS-RAD prescription. The results are shown in Fig. 2, plotted relative to the lowest energy points. At each point, at each level, the electronic state is ^{2}A′, i.e., the complex possesses a 3 e (σ,σ*) S.∴N bond.

The results displayed in Fig. 2 do not lend confidence in the ability of the various methods to describe the (σ,σ*) 3 e S.∴N(amide) bond. The MP2 and HF (not shown) procedures clearly favour unrealistically short bonds as was also found previously in the case of DMS$^{+\cdot}$/O$_2$ (36) and these results bias the CBS-RAD energies toward a shorter distance (2.35 Å). On the other hand, the B3LYP/SB-predicted S.∴N separation (2.95 Å) is too long compared to CCSD(T). This is corrected to a large extent with the larger 6-311+(G3df,2p) basis set (2.65 Å). We judge the CCSD(T) results to be the most reliable. The predicted S.∴N bond length is about 2.5 Å.

The energy of the ^{2}A′ complex at the CCSD(T) minimum is 49 kJ mol^{-1} higher than the CCSD(T)/6-31+G(d′) energy of **1a** (Fig. 1) at the B3LYP/SB-optimized geometry. Since the energy difference between σ and π radicals (i.e., ^{2}A′ and ^{2}A″ states) is greater than 70 kJ mol^{-1} based on a TD-B3LYP/6-311+G(d,p) calculation on the planar amidyl radical, the stabilization owing to the (σ,σ*) 3 e S.∴N bond in the gaseous phase must be approximately 20 kJ mol^{-1}. The most stable complex between DMS$^{+\cdot}$ and NMA$^-$, namely **1a**, is 11 kJ mol^{-1} more stable than the separated products but is predicted to dissociate to DMS and NMA· exergonically at 298 K (ΔG_g = –28 kJ mol^{-1} in the gaseous phase). The reaction is even more exergonic in solution (ΔG_{aq} = –44 kJ mol^{-1}).

The results for the DMS-NMA system (**1b**) indicate that the 3 e bond lengths of the complexes discussed in the following for oxidized **2** (optimized at B3LYP/SB) are likely to be too long. However, the S and N moieties are tethered together and cannot dissociate as in the case of **1a** or **1b**. We note also that the B3LYP bond-stretching potential for **1b** is very flat, and that the error in relative energy evaluations is likely to be less than 5 kJ mol^{-1} (the difference between the

© 2006 NRC Canada

Fig. 2. Potential energy (kJ mol^{-1}) as a function of r_{SN} (Å) in **1b** at various levels of theory. B3LYP/SB (○), B3LYP/LB (●), CBS-RAD (□), MP2/6-31G(d′) (◇), and CCSD(T)/6-31+G(d′) (Δ).

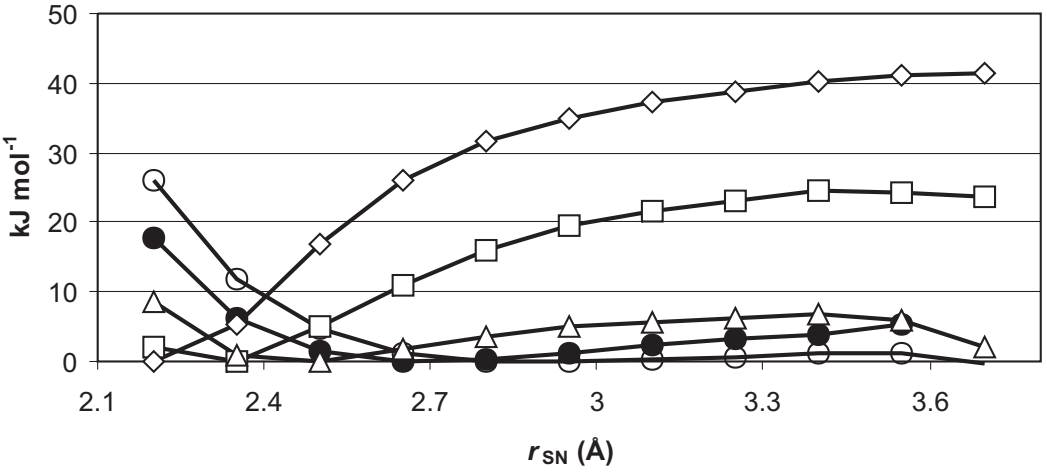
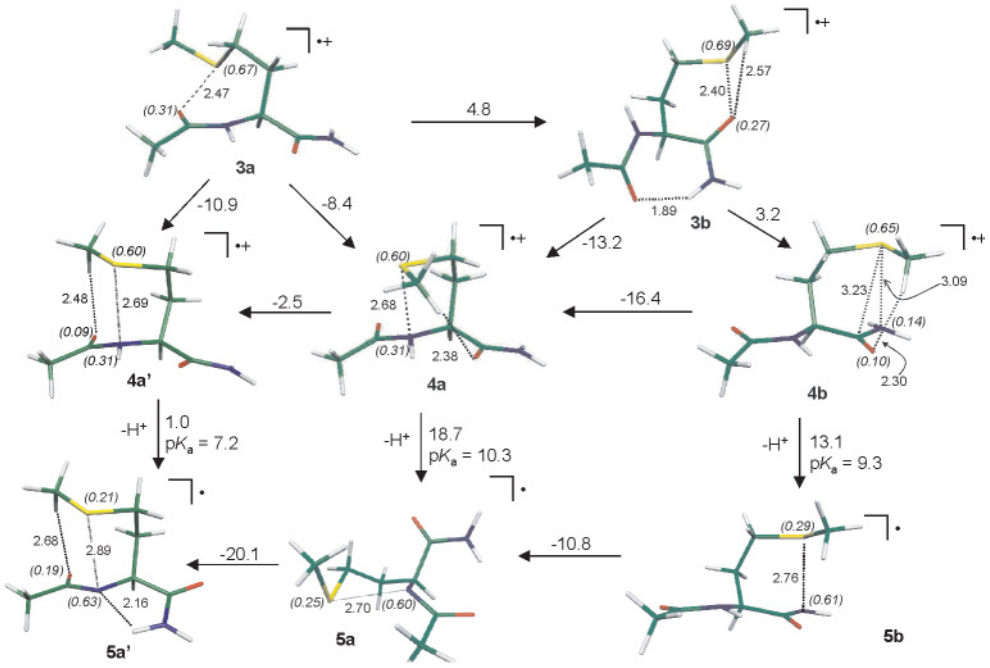


Fig. 3. Structures **3a**, **3b**, **4a′**, **4a**, and **4b** are primary species formed after one-electron oxidation of *N*-acetylmethioninamide **2**. Structures **5a′**, **5a**, and **5b** are primary N-H deprotonation products. Numbers on the arrows indicate the aqueous free energy change at pH 7 in the direction indicated by the arrow. Predicted pK_a values are also shown. Distances are in Å; numbers in italics and parentheses are spin populations.



B3LYP/LB and CCSD(T) energies even at the long distance of the B3LYP/SB minimum in Fig. 2).

Initial intermediates of one-electron oxidation of *N*-acetylmethioninamide (2)

N-Acetylmethioninamide (**2**) serves as a model of a midchain Met residue. One-electron oxidation of **2** yields four types of 3 e bonded intermediates as reported previously (14). The side chain is long enough to permit the S radical to make intramolecular three-electron bonds to the amide group on either side. Coordination may be either to the pro-R or pro-S face of the -CH_2-S-CH_3 plane. Each amide may be either a σ donor through the carbonyl O atom or a π donor, principally through the amide N atom. The oxygen-coordinated structures are similar in stability to the N-coordinated amide ones.

Of the structures previously examined (14), structure **3a** (Fig. 3) was found to be the most stable. Structure **3a** has a three-electron bond between the S and the carbonyl oxygen atom of the preceding (*i*–1) residue, forming a seven-membered ring. The S∴O distance is r_{SO} = 2.47 Å. Extensive spin delocalization is evident with 67% of the spin on S and 31% of the spin on O. The other S∴O structure (**3b**, Fig. 3) is 5 kJ mol^{-1} higher in energy than **3a**. The six-membered

© 2006 NRC Canada

ring of **3a** permits a shorter S∴O bond (r_{SO} = 2.40 Å). Structures analogous to **3a** and **3b** have been discussed previously by Pogocki et al. (21) who had found structures that were diastereomeric to, and less stable than, either **3a** or **3b**.

The energies of all structures were reevaluated at the CCSD(T)/6-31+G(d′) level. While **3a** and **3b** are unaffected, the S∴N bonded species are lower in energy at this level by about 10 kJ mol^{-1}. One of the S∴N coordinated structures (**4a**, Fig. 3) is 8 kJ mol^{-1} more stable than **3a**. The other (**4b**) is the least stable of the four (8 kJ mol^{-1} higher in energy than **3a**). The amide-coordinated S∴N distance is r_{SN} = 2.68 Å. Previously, we had not examined **4a′**, the diastereomeric form of **4a** in which the 3 e S∴N bond is to the opposite face of the C-S-C moiety. Structure **4a′**, shown in Fig. 3, is *more* stable than **4a** by 2.5 kJ mol^{-1} in aqueous solution. Deprotonation of the amide group from each of **4a** or **4a′** yields two distinctly different structures (see the following).

Deprotonation of midchain-oxidized methionine

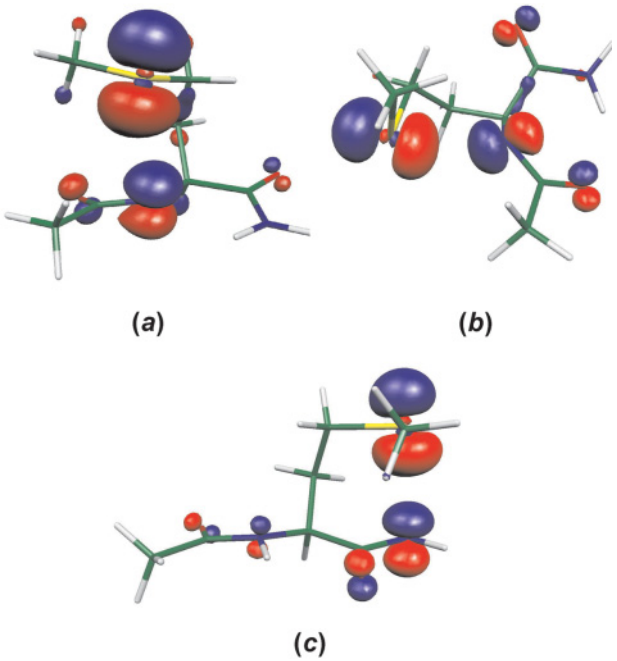
Deprotonation of **4a**, **4a′**, and **4b** yields the S∴N three-electron-bonded complexes **5a**, **5a′**, and **5b**, respectively (Fig. 3). Neither structure **5a′** nor **5b** has a bonding configuration that is entirely analogous to the model system (**1a**, Fig. 1) that was discussed previously as the most stable complex between an amidyl radical and a dialkylsulfide. The amidyl moiety in **5a′** or **5b** is the more stable π radical and makes two points of contact with the S-CH_3 moiety, but unlike **1a**, both **5a′** and **5b** have a loose 3 e S∴N bond (r_{SN} = 2.89 and 2.76 Å, respectively). Structure **5a** is conceptually different, having a 3 e (σ,σ*)-like S∴N bond entirely analogous to **1b** (Fig. 1). In the case of **5a**, the amidyl group is prevented from rotating into the more stable π-type 3 e interaction by the presence of a H-bond between N-H of the NH_2 group and the O of the acetyl group ($r_{O\cdots H}$ = 2.40 Å). A plot of the SOMO of **5a** is shown in Fig. 4*b*.

Structure **5a** is 11 kJ mol^{-1} less stable than **5a′** in the gaseous phase and less favourable solvation raises its aqueous free energy further to 19 kJ mol^{-1} above **5a′**. About 25% of the spin is on S, while 60% resides on N. The S—N distance is 2.70 Å, significantly shorter than the distance at the B3LYP/SB minimum of **1a** (Fig. 1), but quite similar to the B3LYP/LB potential curve for **1b** (Fig. 2).

In the case of the **5a′** and **5b** complexes, the three-electron bond is between the sulfur radical cation and the π system of the amidyl radical. This is clearly visible in the plots of the SOMO of **5a′** and **5b** shown in Figs. 4*a* and 4*c*. Different optimizations of **5b** were attempted to yield a 3 e (σ,σ*)-like S∴N bond with the lone pair on N^{i+1}, analogous to that in **5a**. However, they all reverted to structure **5b**. The S—N and S—O distances are 2.76 and 3.68 Å, respectively, in structure **5b**. Only 29% of the spin stays on S, while 61% of the spin is on N, indicating extensive oxidation of the negatively charged amido group.

The most stable amide deprotonation product of 1 e oxidized **2** is **5a′**. The direct precursor (**4a′**) has a calculated pK_a of 7.2. This value is higher than the pH range implied from spectroscopic observations (18). Reoptimization of the two species with a single water initially H-bonded to the carbonyl group lowers the energy of the cationic parent amide **4a′** relative to the neutral **5a′** by 7 kJ mol^{-1} at the B3LYP/LB level. However, continuum solvation favours the products by a small amount with the result that the calculated pK_a is lowered by one unit of pK_a at this level. If the effect of the explicit water of hydration is reflected at the CCSD(T)/6-1+G(d′) level, one might anticipate pK_a(**4a′**) ≈ 6. While we have not tested them explicitly, we expect similar results for the effect of explicit solvation on the acidity of **4a** and **4b** (Fig. 3). Thus, on the basis of calculated acidities of the initially formed products of the 1 e oxidation of **2**, only **4a′** has a pK_a sufficiently low to be a likely precursor to the species responsible for the 390 nm absorption required to fit the observed spectrum at pH 5.4 (18), and **5a′** is likely to be that species. We return to this point in the following when we compare computed UV spectra with that observed.

Fig. 4. SOMOs of (*a*) **5a′**, (*b*) **5a**, and (*c*) **5b**. The contour accounts for 0.6 e in each case.



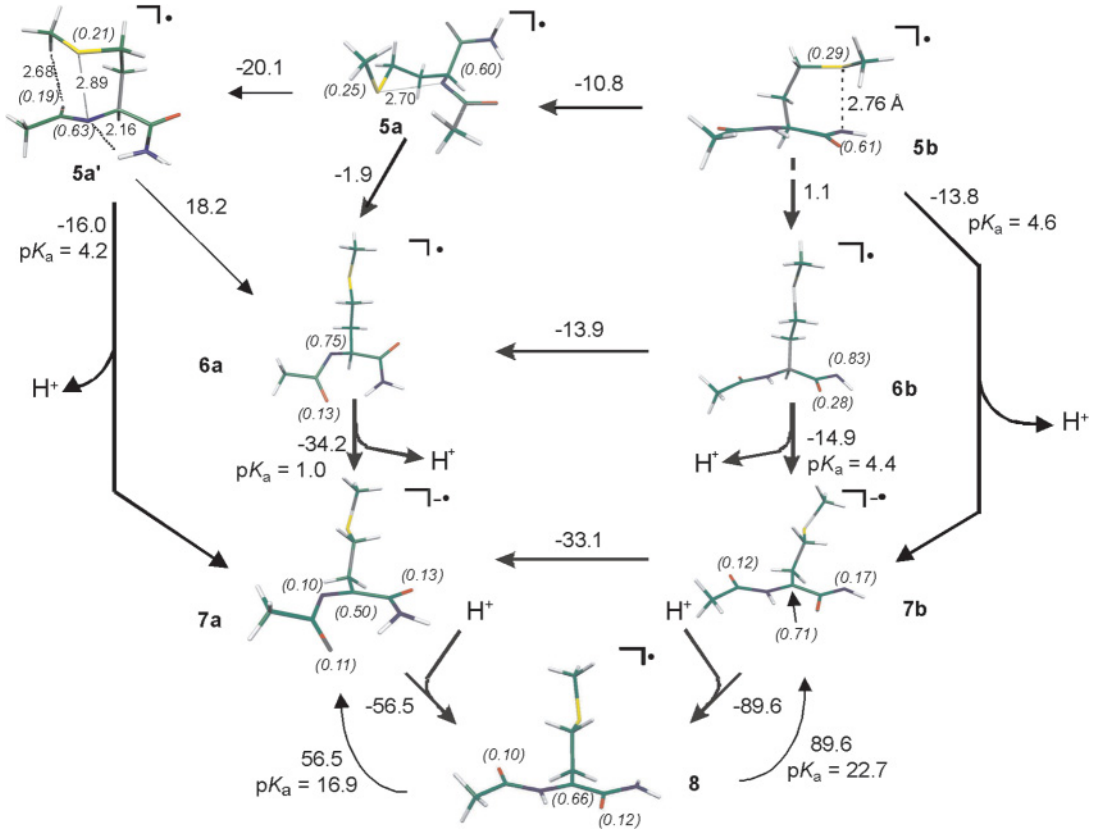
Formation of the α-C-centered radical (8)

Several plausible intermediates in a sequence terminating in the most stable radical (**8**) are shown in Fig. 5. Opening up of the 3 e bonded ring of **5a** or **5a′** yields the extended amidyl π radical, **6a**, while **5b** leads to **6b**. Both processes are endergonic from **5a′** and **5b**, by 18 kJ mol^{-1} and 1 kJ mol^{-1}, respectively, but slightly exergonic from **5a**. The primary amidyl radical **6b** is 14 kJ mol^{-1} less stable than the secondary radical **6a**.

Perhaps surprisingly, loss of a proton from the α-C position of either **6a** or **6b** is an exergonic process, by 34 kJ mol^{-1} (pK_a = 1.0) and 15 kJ mol^{-1} (pK_a = 4.4), respectively, at pH 7. The stability of the product anionic π radicals (**7a** and **7b**) ensues from extensive π delocalization over seven heavy atoms, as well as increased solvation of the ionic products. This deprotonation has the effect of moving the radical from the amido group to the α-C position, where the radical is more stable. We note that **6a** and **6b** are not necessary intermediates. Deprotonation of **5a′** directly to **7a** is exergonic by 16 kJ mol^{-1} at pH 7, corresponding to pK_a =

© 2006 NRC Canada

Fig. 5. Mechanism to form the α-C radical from the S∴N three-electron bond. Numbers on the arrows indicate the aqueous free energy change at pH 7 in the direction indicated by the arrow. Predicted pK_a values are also shown. Distances are in Å; numbers in italics and parentheses are spin populations.



4.2 for the α-C-H proton of **5a′**. Likewise, deprotonation of **5b** directly to **7b** is exergonic by 14 kJ mol^{-1} at pH 7, corresponding to pK_a = 4.6 for the α-C-H proton of **5b**. Thus, **5a′**, **5a**, or **5b** should undergo loss of a proton from the α-C site to yield **7a** or **7b**.

Reprotonation at the amide N atom of **7a** and **7b** is even more exergonic (ΔG = –56 kJ mol^{-1} and –90 kJ mol^{-1}, respectively), yielding the neutral α-C radical (**8**) in both cases. A direct 1,2-hydrogen shift in **5a′** or **6a** was deemed impossible because of the orientation of the α-C—H bond. The 1,3-hydrogen shift enthalpic barrier in **6b** was calculated to be ~135 kJ mol^{-1}, which would make this 1,3-shift very unlikely on energetic grounds. This proposed mechanism explains the observation of a captodatively stabilized α-C radical after the one-electron oxidation of acetylmethioninamide **2** (18).

UV spectra of intermediates

The spectra of intermediates used to fit the UV spectrum measured 10 μs after the initial formation of **2**$^{+\cdot}$ are shown in Fig. 6. Of special interest is the origin of the broad absorption peaking at 390 nm, attributed to **5a/5b** (18).

Time-dependant DFT calculations of the seven lowest excited states, in the presence of the CPCM solvation field, were determined for all of the species discussed previously. We begin by a discussion of the nature of the electronic transitions expected of a 3 e (σ,σ*)-type S∴N(amide) bonded system, using **1b** as the prototypical example.

UV spectra of the 3 e (σ,σ)-type S∴N(amide) bond*

The electronic structure of the 3 e (σ,σ*)-type S∴N(amide) bond may be understood in terms of the orbital interaction diagram shown in Fig. 7. Two orbitals of each moiety are involved, the two lone pairs of the dialkyl sulfide (n_S and $3p_S$), the amidyl lone pair (n_N), and the second π orbital, shown as singly occupied in the amidyl radical. Only $3p_S$ and n_N interact significantly in C_s symmetry to give the σ_{SN} and σ^*_{SN} orbitals of the 3 e bond. As it happens, the first three electronic transitions shown on the right-hand side of Fig. 6 are as expected on the basis of orbital interaction theory (37).

A graphical depiction of the predicted UV spectrum of **1b** as a function of S—N distance is presented in Fig. 8. The lowest energy transition of **1b** at the CCSD(T) equilibrium distance (r_{SN} = 2.5 Å) is of a″ symmetry and corresponds to excitation of a β electron from the HOMO of the amidyl moiety (a π MO) into the β equivalent of the SOMO (σ^*_{SN}). The energy of the amidyl π MO is insensitive to the S—N separation, but the SOMO varies strongly, decreasing monotonically as the S—N distance increases. At r_{SN} = 2.5 Å, the lowest energy excitation occurs at 840 nm (1.48 eV) but is predicted to have zero oscillator strength.

The transition to the second excited state is of a′ symmetry and originates from excitation of a β electron from n_S, the nonbonded MO of the sulfide moiety not involved in 3 e bonding, to σ^*_{SN}. The n_S MO is also not very sensitive to r_{SN}, and the excitation energy parallels that of the first tran-

© 2006 NRC Canada

Fig. 6. Resolution of the spectral components in the transient absorption spectrum following HO· induced oxidation of **2** (2×10^{-4} mol/L) in N_2O saturated aqueous solutions at pH 5.4 taken 10 μs after the pulse (adapted from Fig. 3C of ref. 18). Components (**A**) and (**B**) were identified as [-S.∴S$^+$-] and [-C·HSCH$_3$/-CH$_2$SC·H$_2$] radicals, respectively.

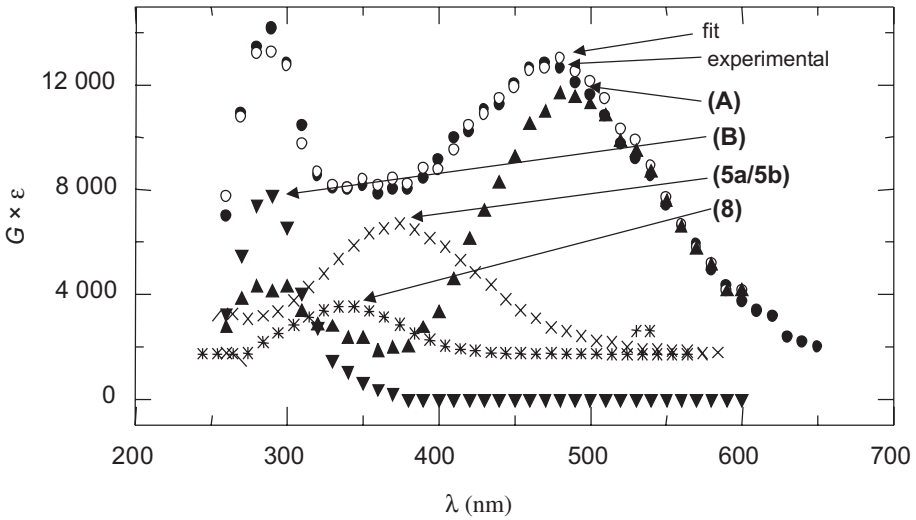
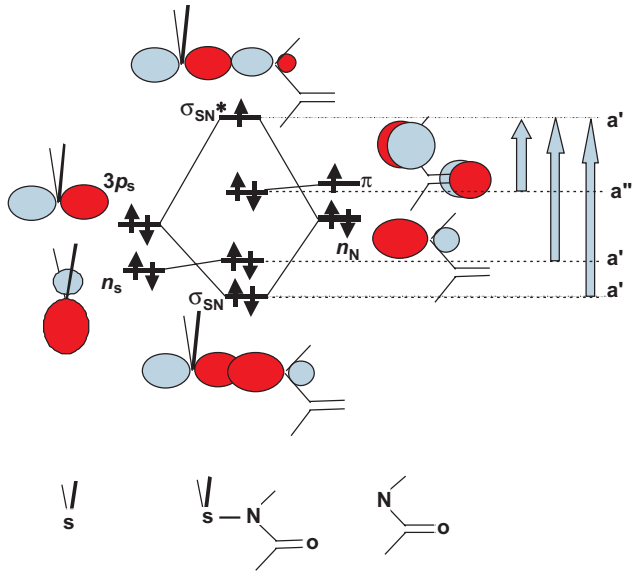


Fig. 7. Orbital interaction diagram of the bonding between DMS and NMA·, oriented so as to have C_S symmetry as in **1b**. The three lowest energy transitions are identified by the vertical arrows. MOs are labeled as a′ (σ type) or a″ (π type).



sition as r_{SN} increases. At r_{SN} = 2.5 Å, the second lowest excitation occurs at 440 nm (2.84 eV) and is predicted to have substantial oscillator strength (f = 0.13).

The transition to the third excited state is also of a′ symmetry and originates from excitation of a β electron from σ_{SN} to σ^*_{SN}. The σ_{SN} MO increases in energy as r_{SN} increases. As a consequence, the third excitation energy is very sensitive to r_{SN}. At r_{SN} = 2.5 Å, the third excitation occurs at 340 nm (3.62 eV) and is predicted to have even higher oscillator strength (f = 0.24).

As the next few higher energy transitions are predicted to have very low oscillator strength, the appearance of the longer wavelength UV spectrum of **1b** is dominated by the positions and intensities of the second and third transitions. The two transitions mix and exchange intensity as r_{SN} increases. The intensities are the same at r_{SN} = 2.65 and at 3.1 Å, the first band peaks at 700 nm and has almost all of the intensity.

The spectrum corresponding to the predicted minimum S—N distance (r_{SN} = 2.5 Å), if broadened, would correspond very well to the band with λ_{max} = 390 nm, attributed to **5a/5b** (Fig. 6) (18).

The predicted UV spectra of **5a**, **5a′**, and **5b** are shown in Fig. 9. Structure **5a** has a 3 e (σ,σ*)-type S.∴N bond (with optimized r_{SN} = 2.70 Å). Its predicted UV spectrum is entirely analogous to that expected from the model system **1b** at the same separation (Fig. 8). Assuming that the B3LYP procedure may yield too large a value for r_{SN}, structure **5a** was optimized with the constraint, r_{SN} = 2.5 Å. Such a structure is actually lower than the B3LYP/SB-optimized geometry by 3.0 kJ mol^{-1} at the CCSD(T)/6-31+G(d′)//B3LYP/SB level (by 0.3 kJ mol^{-1} at the B3LYP/LB//B3LYP/SB level). In the lower-symmetry environment, the first excitation at 680 nm has gained some intensity, compared with **1b** at the same 2.5 Å separation. However, the spectrum in the region 300–500 nm is entirely analogous to that of **1b**, and is an excellent match for the observed spectrum (Fig. 8). However, **5a** is predicted to be 20 kJ mol^{-1} less stable than **5a′**.

The most stable structure (**5a′**), which has a 3 e bond between the S and the amidyl π radical, is not modeled by **1a**. It is calculated to have a very long S—N separation (r_{SN} = 2.89 Å). The predicted spectrum for **5a′** at the B3LYP/SB geometry has its strongest absorption at 600 nm and virtually no absorbance at 390 nm. As in the case of **5a**, the r_{SN} of **5a′** was contracted in 0.1 Å steps to 2.5 Å. The total deformation energy between the optimized structure and that with r_{SN} = 2.5 Å is only 5 kJ mol^{-1}, indicating a very soft potential at the B3LYP level. The CCSD(T) energies of the r_{SN} = 2.5, 2.6, and 2.7 Å structures relative to the B3LYP-optimized structure are +4.4, +1.6, and +0.3 kJ mol^{-1}, respectively. Thus, a substantial shortening of the S—N separation at a higher level is not found in this case and the S—N separation is probably greater than 2.7 Å. The spectra

© 2006 NRC Canada

Fig. 8. TD-B3LYP predicted UV spectrum of **1b** as a function of r_{SN}. The spectra are simulated with a Gaussian line shape and bandwidth at half height = 100 nm. The integrated area under each band is its total oscillator strength.

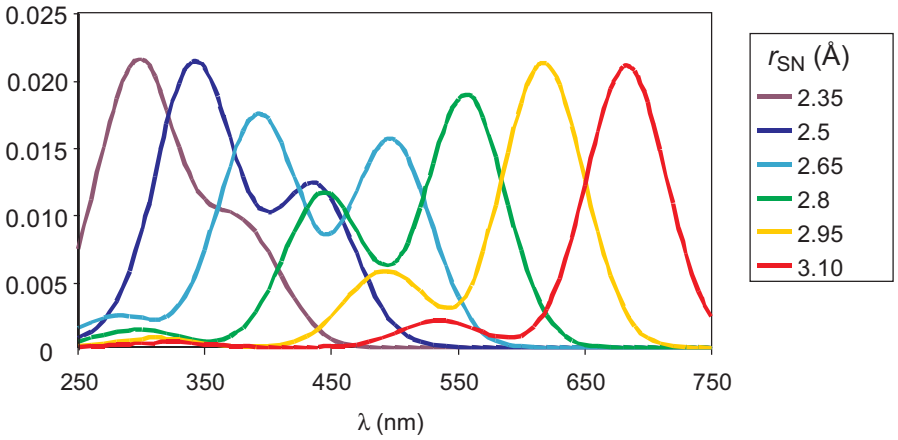
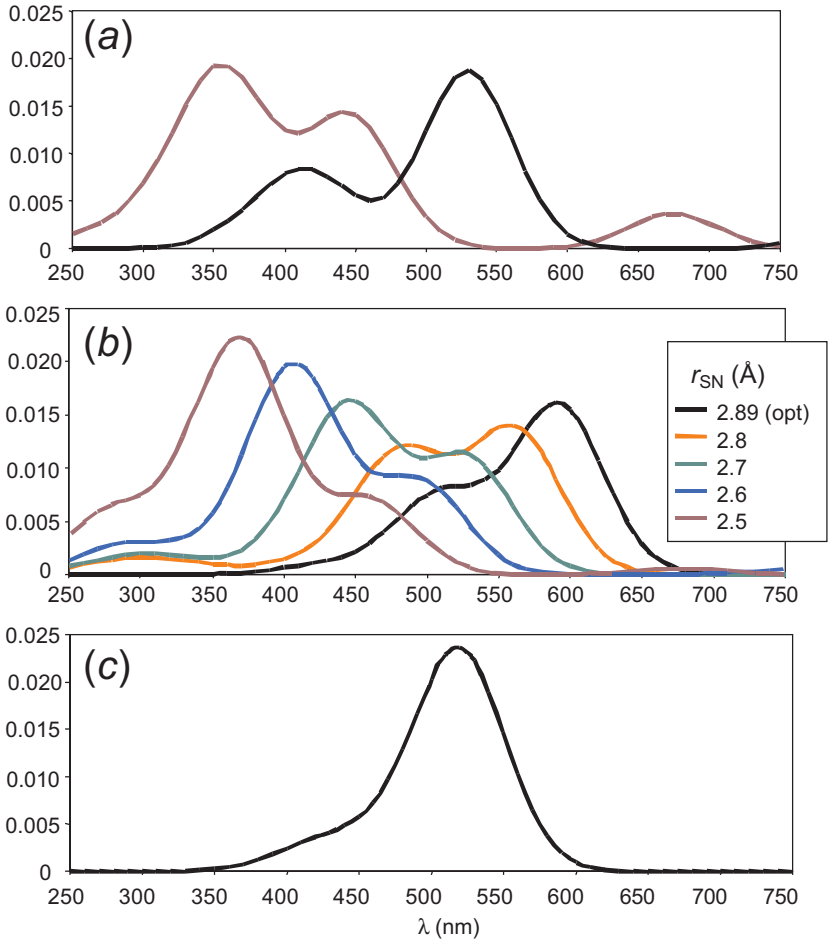


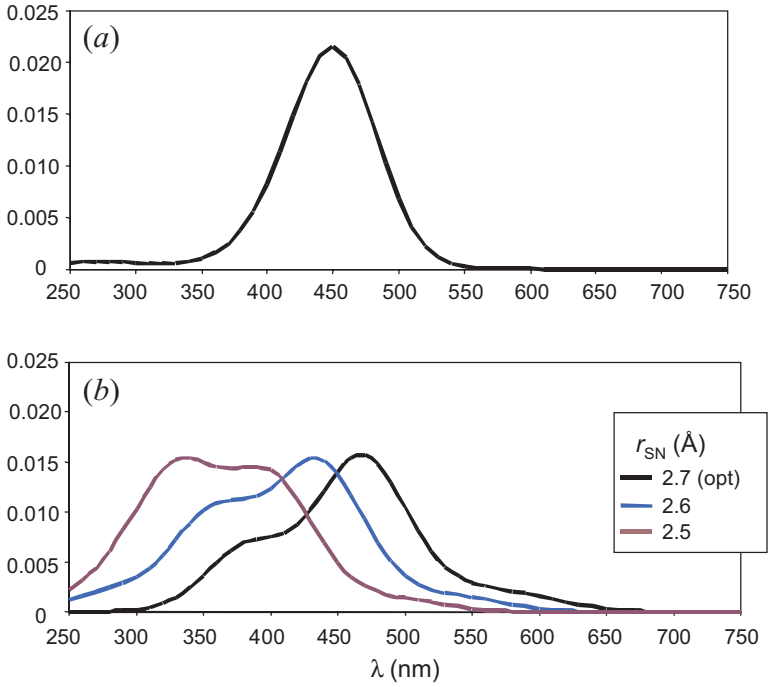
Fig. 9. TD-B3LYP predicted UV spectrum of (*a*) **5a**, (*b*) **5a′**, and (*c*) **5b**. Optimized structure (black line); r_{SN} = 2.5 Å (purple line). The spectra are simulated with a Gaussian line shape and bandwidth at half height = 100 nm. The integrated area under each band is its total oscillator strength.



at each S—N separation are shown in Fig. 9*b*. The predicted spectrum varies strongly with r_{SN} in the same manner as was found for **1b**, and the origin of the transitions parallel those shown by the orbital interaction diagram in Fig. 7 and spectra in Fig. 8. The spectra corresponding to r_{SN} = 2.5 and 2.6 Å are both a very good match to the 390 nm band used in fitting the experimental spectrum (Fig. 6), but that at the lowest energy point (r_{SN} = 2.7 Å) has a maximum closer to 450 nm. As **5a′** is the most stable species from the kinetically favourable N-H deprotonation of the most stable

© 2006 NRC Canada

Fig. 10. TD-B3LYP predicted UV spectrum of (*a*) **3a** and (*b*) **4a′**. Optimized structure (black line); r_{SN} = 2.5 Å (purple line). The spectra are simulated with a Gaussian line shape and bandwidth at half height = 100 nm. The integrated area under each band is its total oscillator strength.



primary oxidation product (**4a′**), we conclude that it is not a likely candidate for the 390 nm UV band, unless vibronic averaging or explicit solvation can lower the S—N separation into the range 2.5 Å < r_{SN} < 2.6 Å. In support of the latter possibility, we note that the single water of solvation mentioned previously in connection with the pK_a calculations of **5a′** lowers r_{SN} from 2.89 (no water) to 2.74 Å (one water) after optimization at the B3LYP/SB level.

Simulated UV absorption spectra of **3a** and **4a′**, the two most stable primary oxidation products, are shown in Fig. 10. In the original radiolysis study, the observed spectrum at 2 and 4 μs after the pulse and at low pH (pH 4) was fitted with a band peaking at 390 nm and attributed to a S∴O species, presumably **3a** (r_{SO} = 2.47 Å). Since the S∴O bond is already short, and since previous work has shown that S∴O bonds are satisfactorily described at the B3LYP/SB level, we have not computed the spectroscopic properties at distances other than r_{SO} = 2.47 Å. The simulated UV spectrum of **3a** is a composite of three transitions but dominated by a σ → σ* (second highest occupied MO to SOMO) excitation of a β electron, and peaking at 450 nm. On the basis of the computed spectrum of **3a**, and the fact that it is not the most stable primary oxidation product (see Fig. 3), it is unlikely that the 390 nm band required to fit the experimental spectrum is due to **3a**.

The UV spectrum of the most stable primary product (**4a′**), at three different values of r_{SN}, is shown in Fig. 10. The S—N stretching potential is very flat. The CCSD(T) energy of the structure at the shortest distance (r_{SN} = 2.5 Å) is 0.4 kJ mol^{-1} lower than at the B3LYP-optimized distance (r_{SN} = 2.7 Å). The UV spectrum at r_{SN} = 2.5 Å is a composite of two bands of similar intensity peaking at 330 and 400 nm, while that at r_{SN} = 2.6 Å is composed of two bands peaking at 350 and 440 nm. The summed spectrum is a very good match to the 390 nm band used to fit the observed spectrum at pH 4 (18) if the S—N separation of **4a′** were between 2.5 and 2.6 Å.

For completeness, the simulated aqueous spectra of the radical anions **6a** and **7a** are shown in Fig. 11. The presence of the amidyl radical anions (**6a** and **6b**) in the radiolysis experiment is unlikely for reasons discussed previously. Both species have significantly lower absorbance than the other species discussed, so that their detection would be unlikely in any case.

For the α-C-deprotonated radical anions (**7a** and **7b**, not shown), strong absorptions are calculated at 334 and 315 nm, respectively. However, these species are most likely not observable over the course of an experimental time frame because of the expected fast reprotonation step to form **8**.

Lastly, we show the simulated UV spectrum of the α-C-centered radical (**8**) in Fig. 12. As expected from the extended π system of this species, several long wavelength absorptions at 450, 370, 354, and 333 nm are predicted for this radical. However, all have low intensities, the largest being *f* = 0.015 for the 333 nm absorption. The first strong UV absorptions were calculated at 312 nm (*f* = 0.115) and 268 nm (*f* = 0.285). The spectroscopic properties of α-C-centered radicals have been well-characterized experimentally. For example, α-C-centered alanyl dipeptide radicals have an experimentally measured absorption with a maximum at ~350 nm (18). In the present case, the calculated UV absorption of **8** is to shorter wavelength than the experimentally assigned peak maximum, the discrepancy corresponding to an error of 0.9 eV in the excitation energy. We also carried out CIS calculations for the UV spectrum of

© 2006 NRC Canada

Fig. 11. TD-B3LYP predicted UV spectrum of (***a***) **6a** and (***b***) **7a**. Dashed lines are individual transitions. The spectra are simulated with a Gaussian line shape and bandwidth at half height = 100 nm. The integrated area under each band is its total oscillator strength.

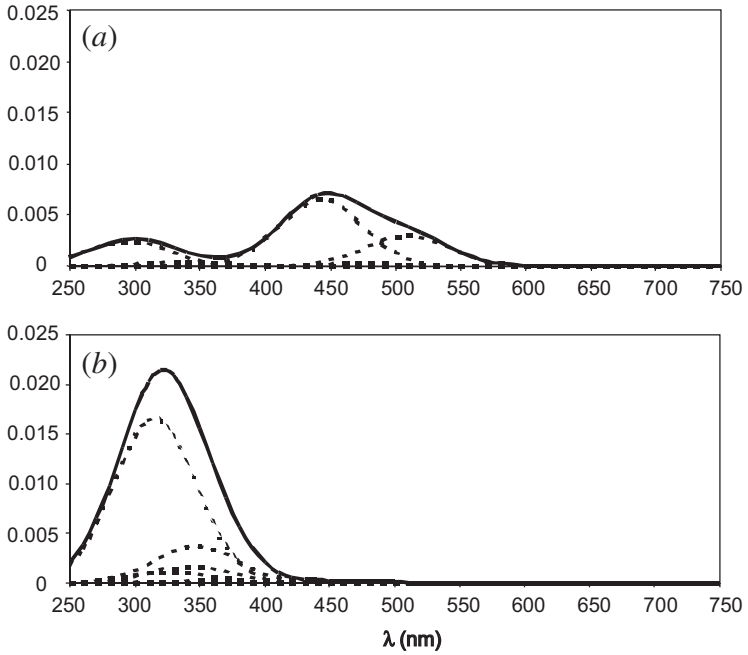
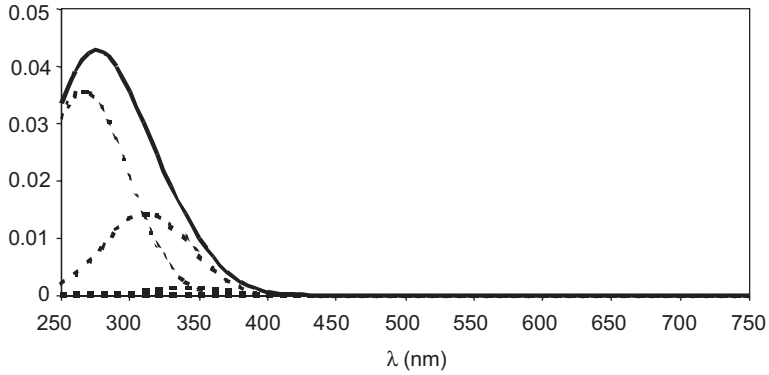


Fig. 12. TD-B3LYP predicted UV spectrum of **8**. Dashed lines are individual transitions. The spectra are simulated with a Gaussian line shape and bandwidth at half height = 100 nm. The integrated area under each band is its total oscillator strength. The vertical scale is two times that of Figs. 9–11.



8 with the same basis set. The predicted strong absorptions were at even shorter wavelength and further from the experiment. We conclude that the excitations of the extended π radical system are not adequately described with a single determinantal starting point.

Conclusions

In a conformationally unconstrained system, a S∴N (3 e, σ,σ*) bond between a dialkylsulfide radical cation and a deprotonated amide is unstable. Extensive electron transfer takes place and the system adopts a loose π complex between an amidyl radical and a neutral dialkyl sulfide (Fig. 1). With geometric constraints that keep the S and N atoms in the proper orientation for a S∴N (3 e, σ,σ*) bond, a bond length (r_{SN} = 2.5 Å) is predicted at the CCSD(T)/6-31+G(d′) level. B3LYP/SB optimization yields a much longer value (r_{SN} = 2.9 Å). The UV spectrum is strongly dependent on the S—N separation.

The spectroscopic and pH-dependent behaviour of one-electron oxidized methionine dipeptide **2** was examined. The radical cation $\mathbf{2}^{+\cdot}$ preferentially adopts structure **4a′** (Fig. 3), with an intramolecular S∴N bond between the sulfide radical cation and the highest occupied π orbital of the first amide group. The acidity of the amide N-H of **4a′** is calculated to have a pK_a of 7, a value that may be too high by two units on the basis of the experiment. The length of the S∴N bond is predicted to be in the range 2.5 Å < r_{SN} < 2.6 Å based on CCSD(T) energies, and the match between the predicted UV spectrum and the absorbance at 390 nm used to fit the observed experimental spectrum (18) at low pH (pH 4). At pH > 5, after 10 μs, a new species generated by proton loss and also absorbing at 390 nm was invoked.

Species **5a′**, generated directly by deprotonation of **4a′**, is predicted to be the most stable deprotonated structure.

© 2006 NRC Canada

5a′ has an intramolecular S—N bond formed by interaction of the singly occupied π MO of the amidyl radical and the S atom. B3LYP optimization yields a long 3 e bond (r_{SN} = 2.89 Å). This value is reduced to 2.70 Å by inclusion of a single explicit water molecule. CCSD(T) calculation yields a similar value without explicit inclusion of the water molecule. With the additional water, it was not computationally feasible to scan shorter r_{SN} values at the CCSD(T) level. However, the results should be cumulative to bring the predicted UV transition into the vicinity of 390 nm, if **5a′** is responsible for the 390 nm absorption required to fit the observed spectrum (18). Structure **5a** (r_{SN} = 2.5 Å) is also predicted to absorb near 390 nm, but **5a** is calculated to be 20 kJ mol^{-1} less stable than **5a′** (Fig. 5).

The α-C-centered radical **8** of the Met dipeptide can be generated from **5a′** via two intermediate structures **6a** and **7a**, or directly via **7a**. The α-C—H bond of **5a′** is predicted to be moderately acidic: pK_a = 4.2 for loss of the α-C-H proton to yield **7a**. However, to achieve the skeletal geometry of **7a** from **5a′** requires rotation about the α-C—N bond (the Ramachandran angle, ϕ). This is more readily accomplished prior to loss of the proton from the α-C, while the α-C—N bond is a single bond. Rupture of the S∴N bond and rotation about the α-C—N bond of **5a′** yield **6a**, which is 18 kJ mol^{-1} less stable. The acidity of the α-C—H bond of **6a** is even higher (pK_a = 1). Loss of the α-C proton from **6a** directly yields **7a**. Reprotonation of **7a** at the N atom yields **8** in an exergonic process (ΔG_{aq} = –56 kJ mol^{-1} at pH 7).

Acknowledgements

We are grateful for financial support of this work from the Natural Sciences and Engineering Research Council of Canada (NSERC) and the National Institutes of Health (NIH, AG 12993). PB is grateful to the Alberta Ingenuity Fund for a Graduate Studentship Award. We thank Professor Emeritus David A. Armstrong for many fruitful discussions.

References

1. W. Vogt. Free Radical Biol. Med. **18**, 93 (1995).
2. R.L. Levine, L. Mosoni, B.S. Berett, and E.R. Stadtman. Proc. Natl. Acad. Sci. U.S.A. **93**, 15036 (1996).
3. C.C. Chao, Y.S. Ma, and E.R. Stadtman. Proc. Natl. Acad. Sci. U.S.A. **94**, 2969 (1997).
4. J. Moskovitz, B.S. Berett, J.M. Poston, and E.R. Stadtman. Proc. Natl. Acad. Sci. U.S.A. **94**, 9585 (1997).
5. J. Moskovitz, E. Flescher, B.S. Berett, J. Azare, J.M. Poston, and E.R. Stadtman. Proc. Natl. Acad. Sci. U.S.A. **95**, 14071 (1998).
6. T. Hoshi and S.H. Heinemann. J. Physiol. (Oxford, U.K.), **531.1**, 1 (2001).
7. E.R. Stadtman, J. Moskovitz, B.S. Berlett, and R.L. Levine. Mol. Cell. Biochem. **234/235**, 3 (2002).
8. D.A. Butterfield. Chem. Res. Toxicol. **10**, 495 (1997).
9. L.M. Sayre, M.G. Zagorski, W.K. Surewicz, G.A. Krafft, and G. Perry. Chem. Res. Toxicol. **10**, 518 (1997).
10. (*a*) C. Schöneich. Arch. Biochem. Biophys. **397**, 370 (2002); (*b*) C. Schöneich and T.D. Williams. Chem. Res. Toxicol. **5**, 717 (2002).
11. G. Merényi, J. Lind, and L. Engman. J. Phys. Chem. **100**, 8875 (1996).
12. D.A. Armstrong. *In* S-centered radicals. *Edited by* Z.B. Alfassi. John Wiley and Sons, New York. 1999. pp. 27–61.
13. Sanaullah, G.S. Wilson, and R.S. Glass. J. Inorg. Biochem. **55**, 87 (1994).
14. P. Brunelle and A. Rauk. J. Phys. Chem. A, **108**, 11032 (2004).
15. W.A. Prütz, J. Butler, E.J. Land, and A.J. Swallow. Int. J. Radiat. Biol. **55**, 539 (1989).
16. K.-O. Hiller, B. Masloch, M. Göbl, and K.-D. Asmus. J. Am. Chem. Soc. **103**, 2734 (1981).
17. K. Bobrowski, G.L. Hug, B. Marciniak, B. Miller, and C. Schöneich. J. Am. Chem. Soc. **119**, 8000 (1997).
18. C. Schöneich, D. Pogocki, G.L. Hug, and K. Bobrowski. J. Am. Chem. Soc. **125**, 13700 (2003).
19. M.J. Frisch, G.W. Trucks, H.B. Schlegel, G.E. Scuseria, M.A. Robb, J.R. Cheeseman, V.G. Zakrzewski, J.A. Montgomery, Jr., R.E. Stratmann, J.C. Burant, S. Dapprich, J.M. Millam, A.D. Daniels, K.N. Kudin, M.C. Strain, O. Farkas, J. Tomasi, V. Barone, M. Cossi, R. Cammi, B. Mennucci, C. Pomelli, C. Adamo, S. Clifford, J. Ochterski, G.A. Petersson, P.Y. Ayala, Q. Cui, K. Morokuma, P. Salvador, J.J. Dannenberg, D.K. Malick, A.D. Rabuck, K. Raghavachari, J.B. Foresman, J. Cioslowski, J.V. Ortiz, A.G. Baboul, B.B. Stefanov, G. Liu, A. Liashenko, P. Piskorz, I. Komaromi, R. Gomperts, R.L. Martin, D.J. Fox, T. Keith, M.A. Al-Laham, C.Y. Peng, A. Nanayakkara, M. Challacombe, P.M.W. Gill, B. Johnson, W. Chen, M.W. Wong, J.L. Andres, C. Gonzalez, M. Head-Gordon, E.S. Replogle, and J.A. Pople. Gaussian 98. Revision A.11 [computer program]. Gaussian, Inc., Pittsburgh Penn. 2001.
20. M.J. Frisch, G.W. Trucks, H.B. Schlegel, G.E. Scuseria, M.A. Robb, J.R. Cheeseman, J.A. Montgomery, Jr., T. Vreven, K.N. Kudin, J.C. Burant, J.M. Millam, S.S. Iyengar, J. Tomasi, V. Barone, B. Mennucci, M. Cossi, G. Scalmani, N. Rega, G.A. Petersson, H. Nakatsuji, M. Hada, M. Ehara, K. Toyota, R. Fukuda, J. Hasegawa, M. Ishida, T. Nakajima, Y. Honda, O. Kitao, H. Nakai, M. Klene, X. Li, J.E. Knox, H.P. Hratchian, J.B. Cross, C. Adamo, J. Jaramillo, R. Gomperts, R.E. Stratmann, O. Yazyev, A.J. Austin, R. Cammi, C. Pomelli, J.W. Ochterski, P.Y. Ayala, K. Morokuma, G.A. Voth, P. Salvador, J.J. Dannenberg, V.G. Zakrzewski, S. Dapprich, A.D. Daniels, M.C. Strain, O. Farkas, D.K. Malick, A.D. Rabuck, K. Raghavachari, J.B. Foresman, J.V. Ortiz, Q. Cui, A.G. Baboul, S. Clifford, J. Cioslowski, B.B. Stefanov, G. Liu, A. Liashenko, P. Piskorz, I. Komaromi, R.L. Martin, D.J. Fox, T. Keith, M.A. Al-Laham, C.Y. Peng, A. Nanayakkara, M. Challacombe, P.M.W. Gill, B. Johnson, W. Chen, M.W. Wong, C. Gonzalez, and J.A. Pople. Gaussian 03. Revision C.02 [computer program]. Gaussian, Inc., Wallingford, Conn. 2004.
21. D. Pogocki, K. Serdiuk, and C. Schöneich. J. Phys. Chem. A, **107**, 7032 (2003).
22. A.P. Scott and L. Radom. J. Phys. Chem. **100**, 16502 (1996).
23. J.P. Guthrie. J. Phys. Chem. A, **105**, 8495 (2001).
24. P.M. Mayer, C.J. Parkinson, D.M. Smith, and L. Radom. J. Chem. Phys. **108**, 604 (1998).
25. H. Fischer and L. Radom. Angew. Chem. Int. Ed. **40**, 1340 (2001).
26. M.W. Wong and L. Radom. J. Phys. Chem. **99**, 8582 (1995).
27. M.W. Wong and L. Radom. J. Phys. Chem. A, **102**, 2237 (1998).
28. A. Rauk, R.J. Boyd, S.L. Boyd, D.J. Henry, and L. Radom. Can. J. Chem. **81**, 431 (2003).
29. (*a*) R.E. Stratmann, G.E. Scuseria, and M.J. Frisch. J. Chem. Phys. **109**, 8218 (1998); (*b*) R. Bauernschmitt and R. Ahlrichs. Chem. Phys. Lett. **256**, 454 (1996); (*c*) M.E. Casida, C.

© 2006 NRC Canada

Jamorski, K.C. Casida, and D.R. Salahub. J. Chem. Phys. **108**, 4439 (1998).
30. (*a*) V. Barone and M. Cossi. J. Phys. Chem. A, **102**, 1995 (1998); (*b*) M. Cossi, N. Rega, G. Scalmani, and V. Barone. J. Comput. Chem. **24**, 669 (2003).
31. B.O. Leung, D.L. Reid, D.A. Armstrong, and A. Rauk. J. Phys. Chem. A, **108**, 2720 (2004).
32. C. Zhan, J. Bentley, and D.M. Chipman. J. Chem. Phys. **108**, 177 (1998).
33. M.D. Liptak, K.C. Gross, P.G. Seybold, S. Feldgus, and G.C. Shields. J. Am. Chem. Soc. **124**, 6421 (2002).
34. B. Braïda, P.C. Hiberty, and A. Savin. J. Phys. Chem. A, **102**, 7872 (1998).
35. Industrial Scientific Corporation. Ionization potentials for common industrial gases [online]. Industrial Scientific Corporation, Oakdale, Penn. Available from http://www.indsci.com/docs/manuals/VX500_IP.pdf.
36. M.L. Huang and A. Rauk. J. Chem. Phys. A, **108**, 6222 (2004).
37. A. Rauk. Orbital interaction theory of organic chemistry. 2nd ed. Wiley-Interscience, New York. 2000.

© 2006 NRC Canada

Cucurbit[7]uril host–guest complexes with cationic bis(4,5-dihydro-1*H*-imidazol-2-yl) guests in aqueous solution

D. Saroja N. Hettiarachchi and Donal H. Macartney

Abstract: The host–guest interactions between cucurbit[7]uril and a series of novel cationic bis(4,5-dihydro-1*H*-imidazol-2-yl)arene and 1-(4,5-dihydro-1*H*-imidazol-2-yl)- and 1,3-bis(4,5-dihydro-1*H*-imidazol-2-yl)-adamantane guests have been investigated in aqueous solution using UV–vis and NMR spectroscopy, and electrospray mass spectrometry. With the exception of the 1,3-bis(4,5-dihydro-1*H*-imidazol-2-yl)adamantane (which binds externally to the CB[7]), these guests form very stable inclusion complexes with slow exchange on the ^{1}H NMR timescale. The direction and magnitude of the complexation-induced shifts (CIS) in the proton resonances of the guests are indicative of the residence of the hydrophobic core of the guest within the CB[7] cavity and the charged 4,5-dihydro-1*H*-imidazol-2-yl units outside the cavity adjacent to the carbonyl-lined portals of the host. The CIS values and the inclusion stability constants have been correlated with the nature of the guest core and with the distance between the charges on the terminal 4,5-dihydro-1*H*-imidazol-2-yl rings.

Key words: cucurbit[7]uril, host–guest complex, dihydroimidazolyl, inclusion stability constants.

Résumé : Faisant appel aux spectroscopies UV–vis et RMN ainsi qu'à la spectrométrie de masse par électronébulisation, on a étudié les interactions hôte–invité entre le cucurbit[7]urile {CB[7]} et une série de nouveaux invités cationiques bis(4,5-dihydro-1*H*-imidazoly-2-yl)arènes et 1-(4,5-dihydro-1*H*-imidazol-2-yl)- et 1,3-bis(4,5-dihydro-1*H*-imidazol-2-yl)-adamantanes. À l'exception du 1,3-bis(4,5-dihydro-1*H*-imidazol-2-yl)adamantane qui se lie d'une façon externe avec le CB[7], ces invités forment des complexes d'inclusion très stables qui ne présentent que des échanges lents à l'échelle de temps de la RMN du ^{1}H. La direction et l'amplitude des déplacements induits par la complexation (DIC) dans les résonances des protons des invités indiquent que la portion hydrophobe de l'invité réside à l'intérieur de la cavité du CB[7] et que les unités 4,5-dihydro-1*H*-imidazol-2-yles se trouvent à l'extérieur de la cavité, adjacentes aux portails de l'hôte alignés de groupes carbonyles. On a établi une corrélation entre les valeurs des DIC ou les constantes de stabilité et la nature de la portion hydrophobe de l'invité ou la distance entre les charges qui se trouvent sur les noyaux terminaux 4,5-dihydro-1*H*-imidazol-2-yles.

Mots clés : cucurbit[7]urile, complexe hôte–invité, dihydroimidazolyle, constantes de stabilité d'inclusion.

[Traduit par la Rédaction]

Introduction

The cucurbit[*n*]urils (CB[*n*], *n* = 5–10) are a family of macrocyclic host molecules (1–5) formed in the acid-catalyzed condensation reactions of glycoluril with paraformaldehyde. While this reaction, which yields primarily CB[6], was first reported in 1905 by Behrend et al. (6), the utility of these host molecules was not fully recognized until the work of Mock and co-workers on cucurbit[6]uril in the 1980s (7–10). More recently, improvements in the synthetic yields of the other members of the cucurbituril family, primarily CB[7] and CB[8] were independently reported by the research groups of Kim et al. (11) and Day et al. (12). Since these reports, there has been considerable interest in the guest–host chemistry of CB[7] and CB[8], and the use of these host molecules as reaction vessels for photochemical isomerizations and dimerizations (13–16), stabilizers for dyes (17, 18) and other molecules (19, 20), for solubilizing ferrocene (21, 22), and in the development of molecular shuttles, switches, and sensors (23–25).

The cucurbiturils CB[6], CB[7], and CB[8] have similarly sized hydrophobic cavities as the more well-studied α-, β-, and γ-cyclodextrins (CD), respectively, but differ in the nature and size of the portals to the cavities (4, 5). Nevertheless, a number of studies have dealt with the comparisons between the binding of guests to cucurbiturils and cyclodextrins and their respective effects on the chemistries of the guest molecules (22, 26, 27). The portals of the CB[*n*] cavities are lined with ureido carbonyl groups and provide a more restrictive entry to guest molecules than the corresponding CD hosts. The polar nature of the carbonyls, however, makes them attractive to cationic guest molecules, from simple metal ions (3) to protonated α,ω-diaminoalkanes (8). The CB[7] host (Scheme 1) has been shown to form very

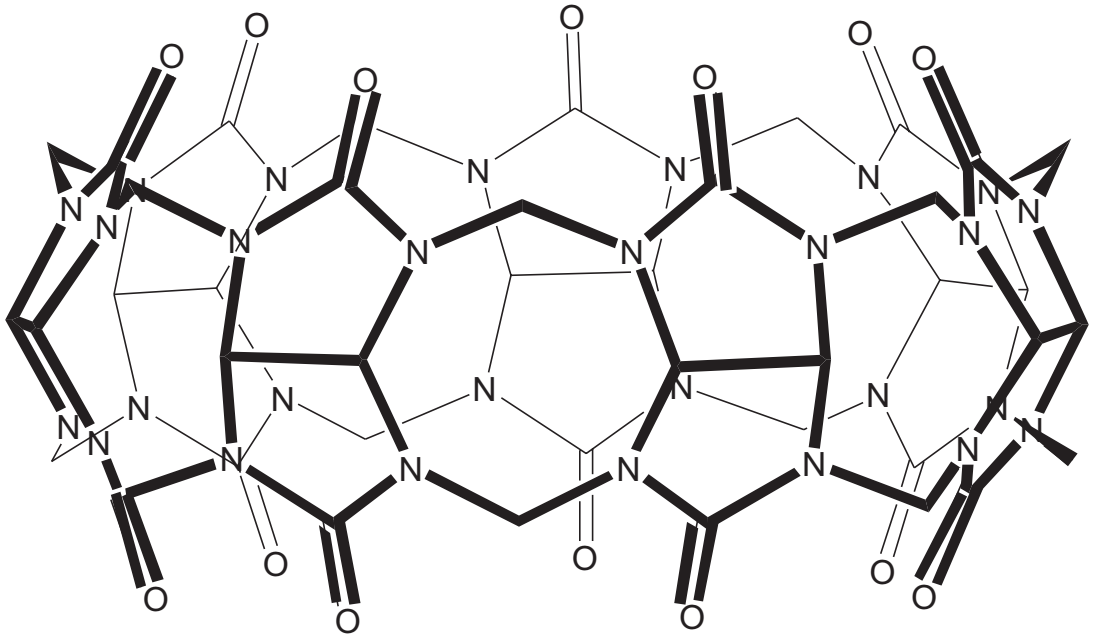
Received 2 May 2006. Published on the NRC Research Press Web site at http://canjchem.nrc.ca on 6 July 2006.

D.S.N. Hettiarachchi and D.H. Macartney.[1] Department of Chemistry, Queen's University, Kingston, ON K7L 3N6, Canada.

[1]Corresponding author (e-mail: donal@chem.queensu.ca).

 doi:10.1139/V06-099 © 2006 NRC Canada

Scheme 1. Structure of cucurbit[7]uril (CB[7]).



stable inclusion complexes with guests containing a diverse set of central units, including metalloferrocenes (21, 22), carboranes (28), aromatic rings (29–32), and adamantanes (32), particularly if these groups contain cationic substituents that can be aligned with the carbonyl-lined portals upon guest inclusion.

The CDs have two sets of protons on the internal surface of the cavity and changes in the chemical shifts of these provide evidence of inclusions of the guest molecules. The complexation-induced shifts (CISs) of the guest proton resonances, however, tend to be relatively small (33). While the cucurbiturils lack any protons inside the cavity, the CIS values for the guest protons located in the cavity tend to be quite large (upfield) and opposite in sign to those for protons located near the carbonyl portals. Mock and Shih (8) carried out a systematic study of the CISs of the methylene proton resonances of $H_3N(CH_2)_nNH_3^{2+}$ (n = 4–8) guests upon inclusion in CB[6]. There has not, however, been a similar study conducted on a series of related guests in complexes with CB[7]. In connection with their improved synthesis of CB[7], Kim's group (11) used the dicationic 2,6-bis(4,5-dihydro-1*H*-imidazol-2-yl)naphthalene guest to demonstrate the formation of guest–host inclusion complexes between aromatic guests and the larger CB[7], but did not report an inclusion stability constant. This guest has subsequently been employed in ab initio calculations of the energy-minimized structures of the 1:1 and 2:1 guest–host complexes with CB[7] (34) and CB[8] (35), respectively. These studies have indicated that the guest–host complexes are stabilized by hydrophobic interactions between the naphthalene group and the inside of the CB[*n*] cavity, and by ion–dipole and hydrogen bonding interactions between the dihydroimidazolyl rings and the carbonyl-rimmed portals of the CB[*n*] host molecule.

As the CB[7] cavity has a strong affinity for aromatic and adamantyl guests (32), we synthesized and characterized a series of novel cationic aromatic (Scheme 2) and adamantyl (Scheme 3) guests using the protonated (4,5-dihydro-1*H*-imidazol-2-yl) end groups. The advantage of these terminal groups is that the ethylene portion of the imidazole ring affords four equivalent protons to probe the environment of the ends of the guest molecule, in addition to the aromatic core. The guest–host inclusion stability constants with CB[7] were determined by using ^{1}H NMR chemical shift titrations and competitive binding experiments. The stability constants and CISs in the ^{1}H NMR resonances of the guests were correlated with the length of the guest (distance between positive charges) and the nature of the aromatic or aliphatic core.

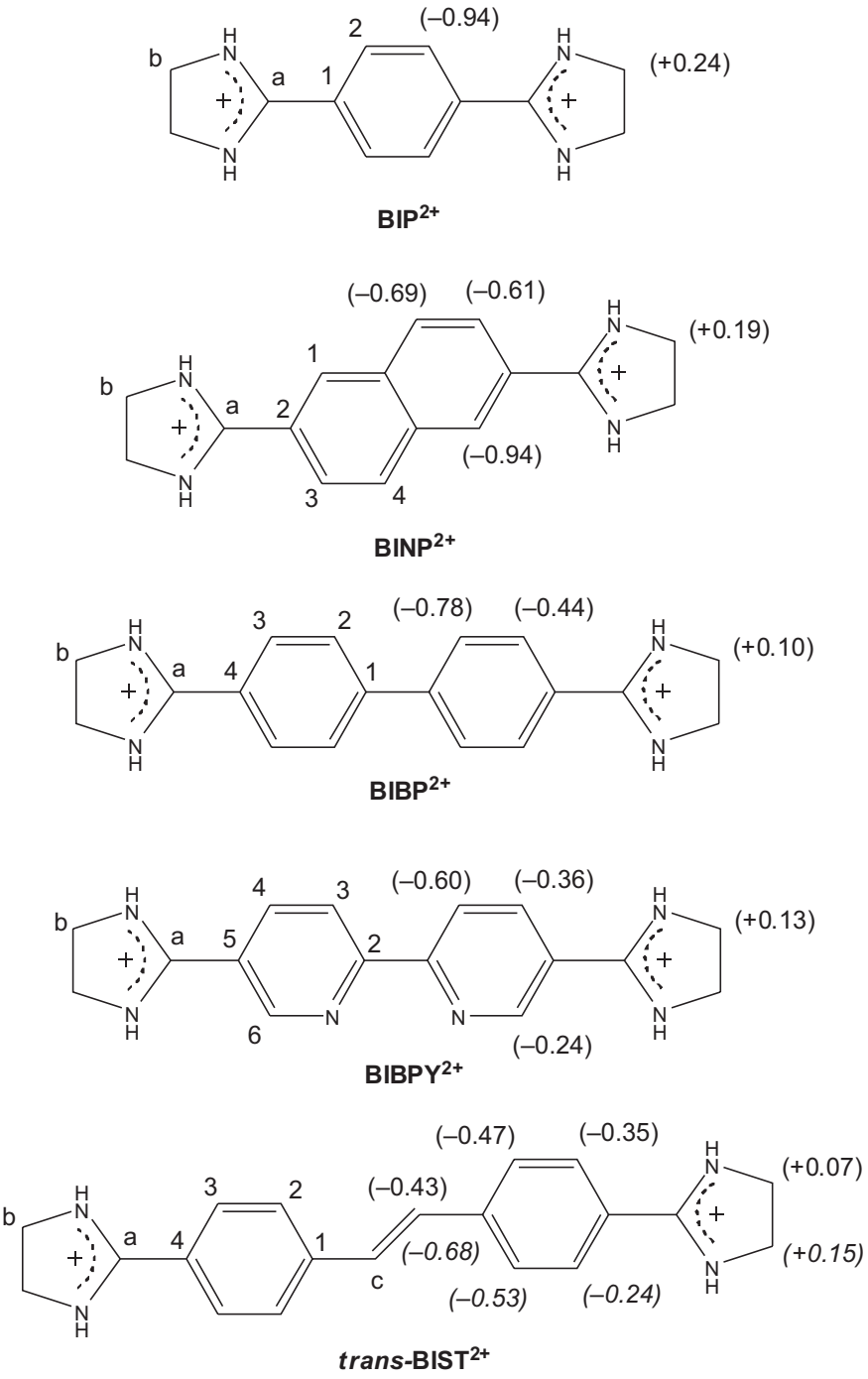
Experimental section

Materials

CB[7] was prepared by a reported method (12). CB[8] (Sigma-Aldrich) and the α-, β-, and γ-cyclodextrins (Sigma-Aldrich, Cyclolab) were used as received. The guest compounds were prepared in accordance with the literature method of Kim et al. (11) by reacting the appropriate mono- or dicarboxyclic acids (Sigma-Aldrich) with a mixture of ethylenediamine and ethylenediamine dihydrochloride under argon gas. The ethylenediamine dihydrochloride was prepared prior to the experiment by adding ice-cold concd. HCl into an ethylenediamine solution until a white precipitate formed that was filtered and oven-dried for 12 h. The monocarboxylic acid (20 mmol) or dicarboxylic acid (10 mmol), ethylenediamine (20 mmol), ethylenediamine dihydrochloride (20 mmol), *p*-toluenesulfonic acid monohydrate (0.75 mmol), and ethylene glycerol (15 mL) were placed in a 50 mL round bottom flask and heated at reflux (190 °C) for 1–10 h (depending on the carboxylic acid used) under argon gas. The precipitates, which formed on cooling and from the removal of the solvent from the filtrate, were dissolved in 50 mL of distilled water (containing

© 2006 NRC Canada

Scheme 2. Structures of the dicationic bis(4,5-dihydro-1*H*-imidazol-2-yl)arene guests with the proton labeling and the complexation induced chemical shifts changes (Δδ (ppm) in parantheses) of the ^{1}H NMR proton resonances of the guest upon formation of the 1:1 guest–host complex with cucurbit[7]uril. The Δδ values in italics for *trans*-BIST^{2+} refer to the corresponding *cis*-BIST^{2+} guest.



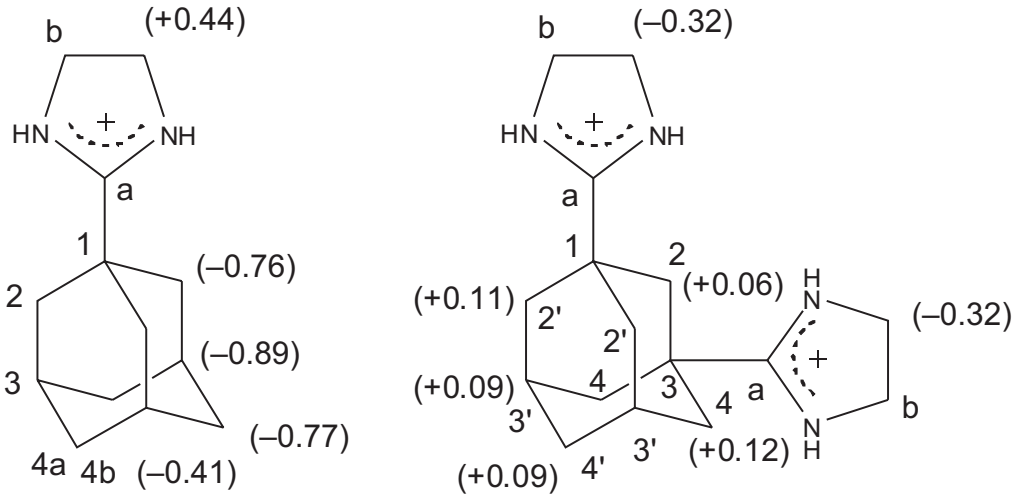
1.5 mL concd. HCl). The addition of 20 mL of 50% aq. NaOH into the mixture produced white or yellow precipitates, which were filtered, washed several times with distilled water, and dried under reduced pressure for several hours. Yields in the range of 68%–94% were obtained for the neutral guest compounds. The hydrochloride salts of the bis(dihydroimidazolyl) compounds were obtained as white or yellow solids by slowly adding a 10% HCl solution into a suspension of the product in methanol. The deposited precipitate was filtered and dried under vacuum.

*2,6-Bis(4,5-dihydro-1*H*-imidazol-2-yl)naphthalene dihydrochloride ([BINP]Cl$_2$)*

^{1}H NMR (D_2O, ppm) δ: 4.06 (s, 8H, N-CH_2), 7.83 (d, 2H, H_4, $J_{3,4}$ = 8.6 Hz), 8.18 (d, 2H, H_3), 8.45 (s, 2H, H_1 and H_5). Lit. (11) (D_2O, ppm) δ: 4.20 (s, 8H, N-CH_2), 7.94 (d, 2H,

© 2006 NRC Canada

Scheme 3. Structures of the cationic 1-(4,5-dihydro-1*H*-imidazol-2-yl)adamantane and 1,3-bis(4,5-dihydro-1*H*-imidazol-2-yl)adamantane guests with the proton labeling and the complexation-induced chemical shift changes (Δδ (ppm) in parentheses) of the ^{1}H NMR proton resonances of the guest upon formation of the inclusion complexes with CB[7].



IAD$^+$ **BIAD^{2+}**

J = 8.6 Hz), 8.31 (d, 2H, J = 8.6 Hz), 8.55 (s, 2H). ^{13}C NMR (D_2O, ppm) δ: 44.73 (C_b), 122.32 (C_1), 124.46 (C_3), 129.65 (C_4), 130.74 (C_2), 134.23 (C_c), 165.92 (C_a). Lit. (11) (D_2O, ppm) δ: 47.6, 125.3, 132.5, 133.5, 137.2, 169.0. ES-MS *m*/*z*: 266.5 $[M - H]^+$.

4,4′-Bis(4,5-dihydro-1*H*-imidazol-2-yl)biphenyl dihydrochloride ([BIBP]Cl_2·H_2O)

Melting point > 300 °C (dec). ^{1}H NMR (D_2O, ppm) δ: 4.04 (s, 8H, N-CH_2), 7.85 (d, 4H, H_2, $J_{2,3}$ = 8.6 Hz), 7.89 (d, 4H, H_3, $J_{2,3}$ = 8.6 Hz). ^{13}C NMR (D_2O, ppm) δ: 44.56 (C_b), 122.03 (C_4), 128.05 (C_2), 128.70 (C_3), 144.55 (C_1), 166.05 (C_a). ES-MS *m*/*z*: 146.0 $[M]^{2+}$. Anal. calcd. for $C_{18}H_{20}N_4Cl_2$·H_2O: C 56.70, H 5.82, N 14.69; found: C 56.31, H 5.60, N 14.32.

1,4-Bis(4,5-dihydro-1*H*-imidazol-2-yl)benzene dihydrochloride ([BIP]Cl_2·H_2O)

Melting point > 235 °C. ^{1}H NMR (D_2O, ppm) δ: 4.04 (s, 8H, N-CH_2), 7.93 (s, 4H, H_2 and H_3). ^{13}C NMR (D_2O, ppm) δ: 44.93 (C_b), 45.30 (C_2), 127.94 (C_1), 128.79 (C_3), 165.69 (C_a). ES-MS *m*/*z*: 215.7 $[M - H]^+$. Anal. calcd. for $C_{12}H_{16}N_4Cl_2$·H_2O: C 48.04, H 5.73, N 18.53; found: C 47.22, H 5.24, N 18.36.

4,4′-Bis(4,5-dihydro-1*H*-imidazol-2-yl)stilbene dihydrochloride ([BIST]Cl_2·3H_2O)

Melting point > 280 °C (dec). ^{1}H NMR (D_2O, ppm) δ: 4.02 (s, 8H, NH-CH_2), 7.39 (s, 2H, HC=CH), 7.77 (s, 8H, H_2 and H_3). ^{13}C NMR (D_2O, ppm) δ: 44.46 (C_b), 127.2 (C_c), 127.5 (C_2), 128.51 (C_3), 129.6 (C_4), 139.8(C_1), 157.4 (C_a). ES-MS *m*/*z*: 159.5 $[M]^{2+}$. Anal. calcd. for $C_{20}H_{22}N_4Cl_2$·H_2O: C 54.18, H 6.37, N 12.64; found: C 54.77, H 6.04, N 12.67.

5,5′-Bis(4,5-dihydro-1*H*-imidazol-2-yl)-2,2′-bipyridine tetrahydrochloride ([BIBPY]Cl_4)

Melting point > 250 °C (dec). ^{1}H NMR (D_2O, ppm) δ: 4.05 (s, 8H, NH-CH_2), 8.38 (d, 2H, H_3, $J_{3,4}$ = 8 Hz), 8.42 (d, 2H, H_4, $J_{3,4}$ = 8 Hz), 9.04 (s, 2H, H_6). ^{13}C NMR (D_2O, ppm) δ: 44.9 (C_b), 120.3 (C_5), 123.0 (C_3), 138.2 (C_4), 148.5 (C_6), 158.4 (C_2), 164.2 (C_a). ES-MS *m*/*z*: 293.1 $[M - 3H]^+$. Anal. calcd. for $C_{16}H_{20}N_6Cl_4$: C 43.86, H 4.60, N 19.18; found: C 43.80, H 4.25, N 19.13.

1-(4,5-Dihydro-1*H*-imidazol-2-yl)adamantane hydrochloride ([IAD]Cl)

Melting point 152–154 °C (dec). ^{1}H NMR (D_2O, ppm) δ: 1.65 (d, 3H, H_{4b}, $J_{4a,4b}$ = 12.7 Hz), 1.71 (d, 3H, H_{4a}), 1.78 (d, 6H, H_2, $J_{2,3}$ < 0.5 Hz), 1.97 (s, 3H, H_3), 3.53 (s, 4H, NH-CH_2). ^{13}C NMR (D_2O, ppm) δ: 27.7 (C_3), 35.1 (C_1), 35.8 (C_2), 39.0 (C_4), 46.5 (C_b), 170.4 (C_a). ES-MS *m*/*z*: 205.4 $[M]^+$. Anal. calcd. for $C_{13}H_{21}N_2Cl$: C 64.85, H 8.79, N 11.63; found: C 64.46, H 7.75, N 11.53.

1,3-Bis(4,5-dihydro-1*H*-imidazol-2-yl)adamantane dihydrochloride ([BIAD]Cl_2·3H_2O)

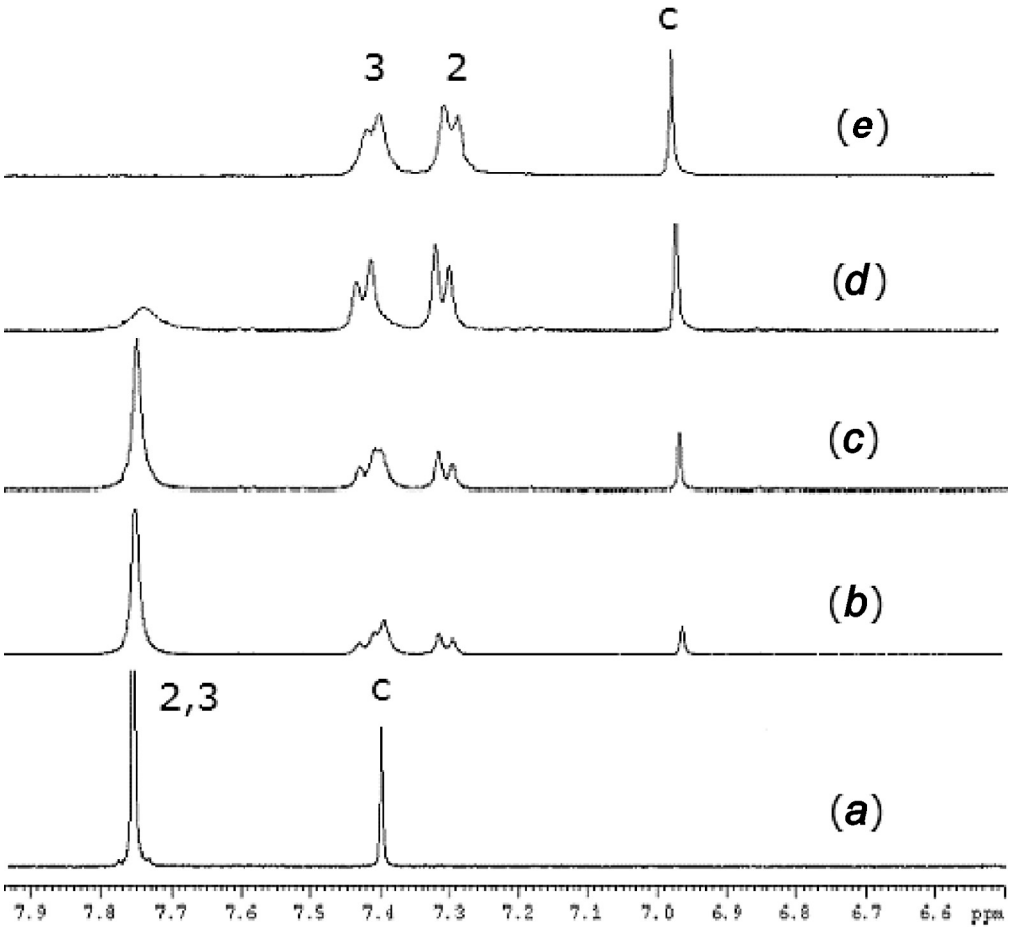
Melting point > 280 °C (dec). ^{1}H NMR (D_2O, ppm) δ: 1.72 (s, 2H, $H_{4'}$), 1.87 (m, 8H, $H_{2'}$ and H_4), 2.01 (s, 2H, H_2), 2.25 (s, 2H, $H_{3'}$), 3.85 (s, 8H, NH-CH_2). ^{13}C NMR (D_2O, ppm) δ: 26.96 (C_4), 33.46 (C_5), 34.96 (C_1), 36.81 (C_3), 38.91 (C_2), 44.02 (C_b), 175.55 (C_a). ES-MS *m*/*z*: 273.4 $[M - H]^+$. Anal. calcd. for $C_{16}H_{26}N_4Cl_2$·3H_2O: C 48.12, H 8.08, N14.03; found: C 47.39, H 7.56, N 13.64.

Physical measurements

The NMR spectra were recorded on a Bruker Avance-400 instrument in D_2O (the residual solvent proton signal at 4.75 ppm served as the internal reference). Electrospray mass spectrometry measurements were obtained on a VG Quattro quadrupole mass spectrometer with an atmospheric pressure electrospray ionization source and a mass range for single-charged ions of 4000. Samples were prepared as solutions in distilled water containing the guest (2.5×10^{-3} mol/L) and CB[7] (0.015 mol/L). UV–vis spectra were recorded on a Hewlett-Packard 8452 diode array spectrome-

© 2006 NRC Canada

Fig. 1. The aromatic portion of the ^{1}H NMR spectra of *trans*-[BIST]$^{2+}$ with (*a*) 0.0, (*b*) 0.25, (*c*) 0.50, (*d*) 0.85, and (*e*) 2.0 equiv. of CB[7] in D_2O.



ter. Elemental analyses were preformed by Canadian Microanalytical Services Ltd., Delta, British Columbia.

The inclusion stability constants were determined from competitive binding studies monitored by ^{1}H NMR spectroscopy in D_2O at 25 °C, using the procedure of Isaacs and coworkers (32). The competitor primarily employed with the guests was sodium 3-(trimethylsilyl)propionate-2,2,3,3-d_4 (Sigma-Aldrich, $K_{CB[7]}$ = (1.82 ± 0.22) × 10^7 (mol/L)$^{-1}$ (32)), except for the BINP^{2+} guest, in which case (trimethylammonio)methylferrocene iodide (Sigma-Aldrich, $K_{CB[7]}$ = (3.31 ± 0.62) × 10^{11} (mol/L)$^{-1}$ (22, 32)) was used. For the weaker external binding of BIAD^{2+} to CB[7], a ^{1}H NMR chemical shift titration of the guest with CB[7] was performed in D_2O at 25 °C, with the data fit to a 1:1 binding model as described previously (33). Molecular modelling of the structures of the guest–host complexes was performed using Chem3D software (CambridgeSoft) with MM2 energy minimizations.

Results and discussion

The macrocyclic host molecule CB[7] forms very stable host–guest complexes with cationic guest molecules in aqueous solution. For organic guests, especially strong binding has been observed when the guest is comprised of a hydrophobic central core with positively charged substituents, which can be placed near the polar carbonyl groups that line the portals of the host. The dication guests formed by protonations of α,α′-diamino-*p*-xylene and 1,3-diaminoadamantane, for example, bind to CB[7] with stability constants of (1.84 ± 0.34) × 10^9 and (2.06 ± 0.33) × 10^8 (mol/L)$^{-1}$, respectively (32). The cationic guests synthesized in this study, as shown in Schemes 2 and 3, have variable hydrophobic aryl or adamantyl cores with 4,5-dihydroimidazol-2-yl end groups and would be expected to likewise form very stable inclusion complexes with CB[7].

The inclusion of the guests in the cavity of CB[7] is clearly seen by ^{1}H NMR spectroscopy (Fig. 1). The guest protons that reside within the hydrophobic cavity experience shielding and, therefore, upfield CISs in their resonances. The guest protons that are located near the ureido carbonyl groups rimming the portals are deshielded and the resonances move downfield, compared with the chemical shifts observed in the free guest. The ^{1}H NMR chemical shifts of the free guest and CB[7]-included guest protons are summarized in Table 1. The formation of 1:1 host–guest complexes is also supported by electrospray mass spectrometry. All of the complexes formed with the dicationic aromatic guests (M) exhibit peaks for the {M·CB[7]}$^{2+}$ species, while the adamantyl guests IAD$^+$ and BIAD^{2+} exhibit peaks for {M·CB[7]}$^+$ and {M·CB[7]-H}$^+$, respectively.

While Mock and Shih (8) carried out a systematic study

© 2006 NRC Canada

Table 1. ^{1}H NMR chemical shifts (in ppm) of the guest protons before and after (*in italics*) the formation of the guest–host complexes with CB[7] in D_2O (HOD at 4.75 ppm) at 25 °C, and the guest–host stability constants ($K_{CB[7]}$).

Guest	H_1	H_2	H_3	H_4	H_6	H_b	H_c	$K_{CB[7]}$ ((mol/L)$^{-1}$)
$BINP^{2+}$	8.45		8.18	7.83		4.06		$(6.0 \pm 1.0) \times 10^{10}$
	7.51		*7.57*	*7.14*		*4.25*		
$BIBP^{2+}$		7.85	7.89			4.04		$(1.7 \pm 0.2) \times 10^{8}$
		7.07	*7.45*			*4.14*		
BIP^{2+}		7.93				4.04		$(5.2 \pm 0.6) \times 10^{9}$
		6.99				*4.28*		
$BIBPY^{2+}$			8.38	8.42	9.04	4.05		$(8.9 \pm 1.1) \times 10^{7}$
			7.78	*8.06*	*8.80*	*4.18*		
trans-$BIST^{2+}$		7.77				4.02	7.39	$(5.6 \pm 0.7) \times 10^{8}$
		7.30	*7.42*			*4.09*	*6.96*	
cis-$BIST^{2+}$		7.39	7.59			3.96	6.85	
		6.86	*7.35*			*4.11*	*6.17*	
IAD^{+}		1.78	1.97	1.71, 1.65		3.53		$(1.4 \pm 0.7) \times 10^{8}$
		1.30	*1.09*	*0.94*, *1.24*		*3.97*		
$BIAD^{2+}$		1.87, 2.01	2.25	1.72, 1.87		3.85		$(1.0 \pm 0.5) \times 10^{4}$
		1.98, *2.07*	*2.34*	*1.80*, *1.98*		*3.53*		

of the complexation-induced chemical shifts of the methylene protons of $H_3N(CH_2)_nNH_3^{2+}$ guests upon inclusion in CB[6], there had not been a similar study conducted on a series of related guests in inclusion complexes with CB[7]. The upfield chemical shift changes for the ^{1}H NMR resonances of the core aryl and adamantyl protons of the guests range from –0.24 to –0.94 ppm, a similar range of shifts as observed by Mock and Shih (8) for the methylene protons (up to –1.08 ppm) of the α,ω-alkyldiammonium guests included in the cavity of CB[6]. The CISs of highest magnitude for the ligands in this study are found for the protons near the centers of the aromatic cores of the guests. Even with the guests shuttling back and forth between orientations that place one of the positively charged dihydroimidazoyl rings near one of the portals, these central protons remain in the cavity. The lower magnitude shifts in the range are observed for the protons near the ends of the aromatic cores of the longer and (or) more weakly bound guests ($BIBPY^{2+}$ and *trans*-$BIST^{2+}$), which may spend proportionately more time near the portals or outside the cavity as the guests move back and forth along the axis of the cavity.

The further away that the cationic dihydroimidazolyl rings are from the portal carbonyl groups, on average, the less deshielding will be felt by the ethylene H_b protons on the ring. The largest CIS values for the H_b protons are observed for the shorter BIP^{2+} and $BINP^{2+}$ guests, while a much smaller value is exhibited by the more extended *trans*-$BIST^{2+}$. Using the distances between the C_a carbons on the rings as a measure of the extension of the guests (determined using Chem3D MM2 energy minimizations, see Fig. 2), a good correlation between the lengths of the guests (distances between the positive charges) and the CIS values for the H_b protons is established (see Fig. 3).

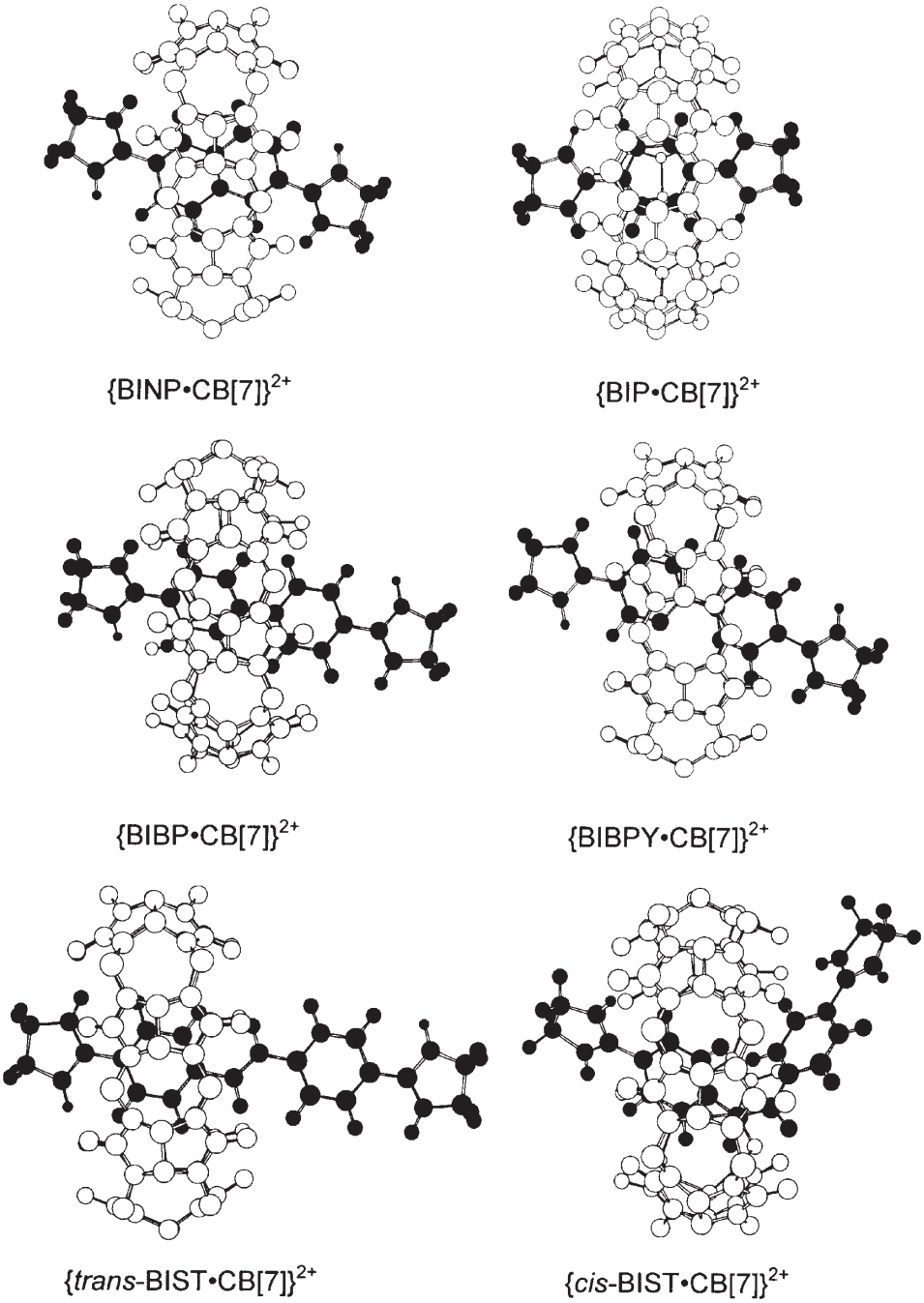
The inclusion of the dicationic guests in the cavity of CB[7] resulted in bathochromic shifts in the λ_{max}, with a lowering of the molar absorptivity coefficient for the π–π* transitions in the UV–vis spectra compared with the free guests (Table 2). This behaviour has also been observed with other dicationic guest molecules, such as methyl viologen (29, 30), 2,7-dimethyldiazapyrenium (31), and protonated 2-aminoanthracene (24). The bathochromic shifts are consistent with the solvatochromic behaviour of the aromatic guests within the CB[7] cavity, which has a less polar environment than the bulk aqueous solution (18, 36).

The stability constants for the host–guest inclusion complexes formed between CB[7] and the dicationic guests in this study (with the exception of the external binding of $BIAD^{2+}$, discussed later) are too large (>10^7 (mol/L)$^{-1}$) to be measured by conventional UV–vis spectrophotometric or ^{1}H NMR chemical shift titrations. The stability constants for the host–guest complexes formed between CB[7] and the cationic guests were thus determined by performing competitive binding studies, monitored by ^{1}H NMR spectroscopy, using guests whose stability constants with CB[7] had been reported previously (32). The 3-(trimethylsilyl)propionic acid-2,2,3,3-d_4 ($K_{CB[7]} = (1.82 \pm 0.22) \times 10^7$ (mol/L)$^{-1}$ (32)) was employed as the competitor for the BIP^{2+}, $BIBP^{2+}$, $BIBPY^{2+}$, *trans*-$BIST^{2+}$, and IAD^+ guests, while (trimethylammonio)methylferrocene iodide ($K_{CB[7]} = (3.31 \pm 0.62) \times 10^{11}$ (mol/L)$^{-1}$ (22, 32)) was used for the $BINP^{2+}$ guest.

The stability constants (Table 1) for the aromatic guests decrease in the order $BINP^{2+}$ > BIP^{2+} > *trans*-$BIST^{2+}$ > $BIBP^{2+}$ > $BIBPY^{2+}$. The trend is likely the result of several factors, including (*i*) the length of the aromatic core (distance between the positive charges), (*ii*) the fit of the aromatic core to the interior of the CB[7] cavity, and (*iii*) the hydrophobicity of the aromatic core. The highest stability constant is observed for the guest with the naphthyl core, suggesting that this guest optimizes the fit of the aromatic core with the CB[7] cavity and the cation–dipole and hydrogen bonding interactions between the dihydroimidazoyl groups and the portal carbonyl groups. The lowest stability constant among this set of guests is observed for $BIBPY^{2+}$. This is not unexpected as the introduction of the N hetero-

© 2006 NRC Canada

Fig. 2. Energy-minimized structures of the CB[7] host–guest complexes with $BINP^{2+}$, BIP^{2+}, $BIBP^{2+}$, $BIBPY^{2+}$, and *trans*- and *cis*-$BIST^{2+}$. The hydrogen atoms on CB[7] have been removed for clarity.



atoms into the bipyridine rings would reduce the hydrophobicity of the aromatic core and the stability constant compared with the biphenyl core of the $BIBP^{2+}$ guest.

The mono(IAD^{+}) and bis(dihydroimidazolyl) ($BIAD^{2+}$) substituted adamantane cations exhibit different modes of binding to CB[7] and CB[8]. For the monocation, the adamantyl portion binds tightly to the interior of CB[7] (Fig. 4), as reported previously for the protonated 1-aminoadamantane (32), with upfield shifts in the adamantyl proton resonances and a large downfield shift for the H_b protons on the dihydroimidazolyl ring. Contrary to the observation of binding of the 1,3-diaminoadamantane in the cavity of CB[7] (32), we observe that only external binding occurs with the $BIAD^{2+}$ dication. The 1,3-bis(4,5-dihydro-1*H*-imidazol-2-yl)adamantane ($BIAD^{2+}$) guest is too large to form a guest–host complex with CB[7], in which the adamantyl core is located in the cavity of the host. The H_b protons on the ring shift upfield (–0.32 ppm), while the adamantyl protons shift downfield (+0.06 to +0.12 ppm). These changes in the chemical shifts of the guest protons, upon the addition of CB[7], reveal that it is one of the dihydroimidazolyl rings that is located in the cavity, while

© 2006 NRC Canada

Fig. 3. Plot of the downfield chemical shift change ($\Delta\delta$) for the H_b protons upon inclusion of the dicationic guests in cucurbit[7]uril as a function of the distance between the C_a carbon atoms of the two dihydroimidazolyl rings. BIP^{2+} (■), $BINP^{2+}$ (●), *cis*-$BIST^{2+}$ (Δ), $BIBP^{2+}$ (▼), $BIBPY^{2+}$ (◆), and *trans*-$BIST^{2+}$ (▲).

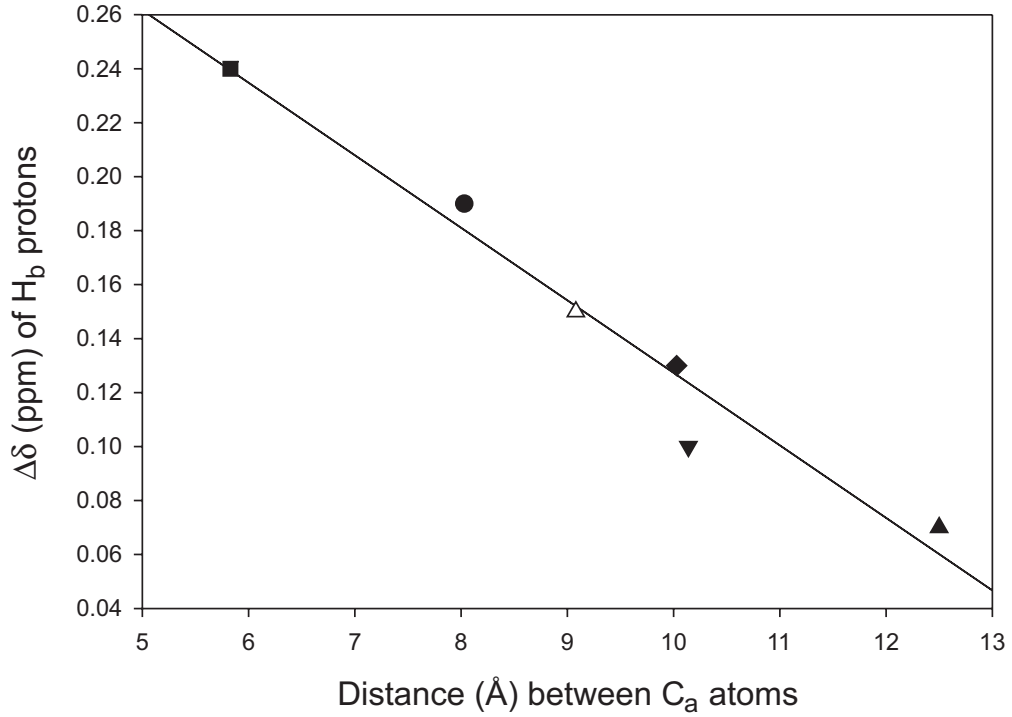


Table 2. Wavelength maxima and molar absorptivity coefficients of the bis(4,5-dihydroimidazol-2-yl) dicationic guests and the guest–host complexes with CB[7] in aqueous solution.

Guest	λ_{max} (nm)	ε ($(mol/L)^{-1}$ cm^{-1})
$[BINP]^{2+}$	246	6.41×10^4
$\{BINP\cdot CB[7]\}^{2+}$	250	4.53×10^4
$[BIP]^{2+}$	246	3.76×10^4
$\{BIP\cdot CB[7]\}^{2+}$	244	2.11×10^4
$[BIBP]^{2+}$	288	3.96×10^4
$\{BIBP\cdot CB[7]\}^{2+}$	290	2.98×10^4
$[BIBPY]^{2+}$	252	1.04×10^4
	300	1.67×10^4
$\{BIBPY\cdot CB[7]\}^{2+}$	258	8.40×10^3
	308	1.56×10^4
$[trans\text{-}BIST]^{2+}$	336	6.44×10^4
$\{trans\text{-}BIST\cdot CB[7]\}^{2+}$	344	4.29×10^4

the remainder of the guest is outside. The presence of only average resonances for the guest in the presence of a stoichiometric deficiency of CB[7] indicates that the guest is exchanging between the bound and unbound states rapidly on the NMR timescale.

A chemical shift titration and Job's plot of the $BIAD^{2+}$ with CB[7], as depicted in Fig. 5, confirms a 1:1 stoichiometry (maximum at $\chi^{BIAD} \approx 0.5$) and yields a stability constant of $(1.0 \pm 0.5) \times 10^4$ $(mol/L)^{-1}$. As indicated earlier, the protonated 1,3-diaminoadamantane guest forms a very stable complex with CB[7], in which the adamantyl core is located in the cavity. The smaller size of the ammonium group compared with the 4,5-dihydroimidazol-2-yl ring may account for the difference in the accessibility of the guest to the cavity. The addition of the larger CB[8] host to a solution of $BIAD^{2+}$, however, does result in the formation of an internal inclusion complex (Fig. 4), and the expected upfield shifts in the adamanyl proton resonances with downfield shifts in the H_b protons of the 4,5-dihydroimidazol-2-yl rings are observed.

A comparison of the binding behaviours of CB[7] with the CDs was undertaken in which the $[BIBP]^{2+}$ guest was mixed with slight stoichiometric excesses of α-, β-, and γ-CD and the ^1H NMR spectra compared to the inclusion complex formed with CB[7]. The $[BIBP]^{2+}$ guest undergoes inclusion complex formation with β- and γ-CD (but not the smaller α-CD cavity), exhibiting fast guest exchange on the NMR timescale. The larger ^1H NMR CIS values for the $[BIBP]^{2+}$ guest are observed for inclusion by β-CD, with its similar cavity size to CB[7].

The *trans*-$BIST^{2+}$ dication undergoes a photochemical isomerization to *cis*-$BIST^{2+}$ under UV irradiation in aqueous solution.[2] Inclusion of the *trans*-$BIST^{2+}$ guest in CB[7] also facilitates photoisomerization and eliminates photohydration side products. The resulting $\{cis\text{-}BIST\ B[7]\}^{2+}$ complex exhibits similar, but somewhat larger, chemical shifts of the guest protons upon inclusion in the CB[7] cavity. This is most likely the result of a more compact guest core within the CB[7] cavity.

We are currently investigating the CB[7] inclusion of other dicationic guest molecules with 4,5-dihydroimidazol-

[2] R. Wang, L. Yuan, D.S.N. Hettiarachchi, and D.H. Macartney. Manuscript in preparation.

© 2006 NRC Canada

Fig. 4. Energy-minimized structures of the CB[7] host–guest complex with IAD^+ and the CB[8] host–guest complex with $BIAD^{2+}$. The hydrogen atoms on CB[7] have been removed for clarity.

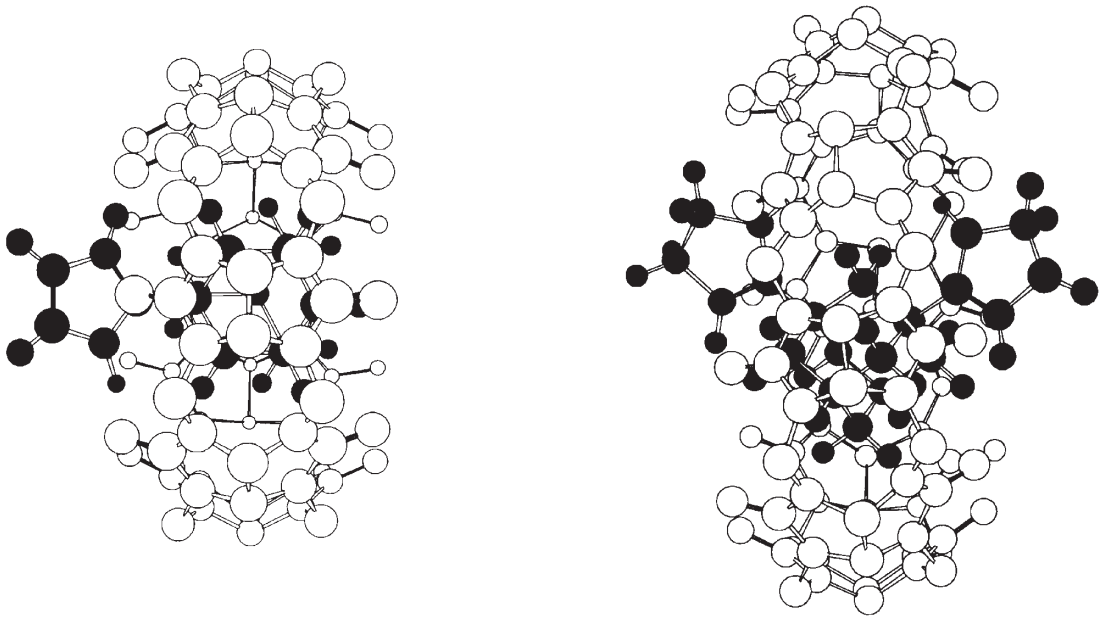
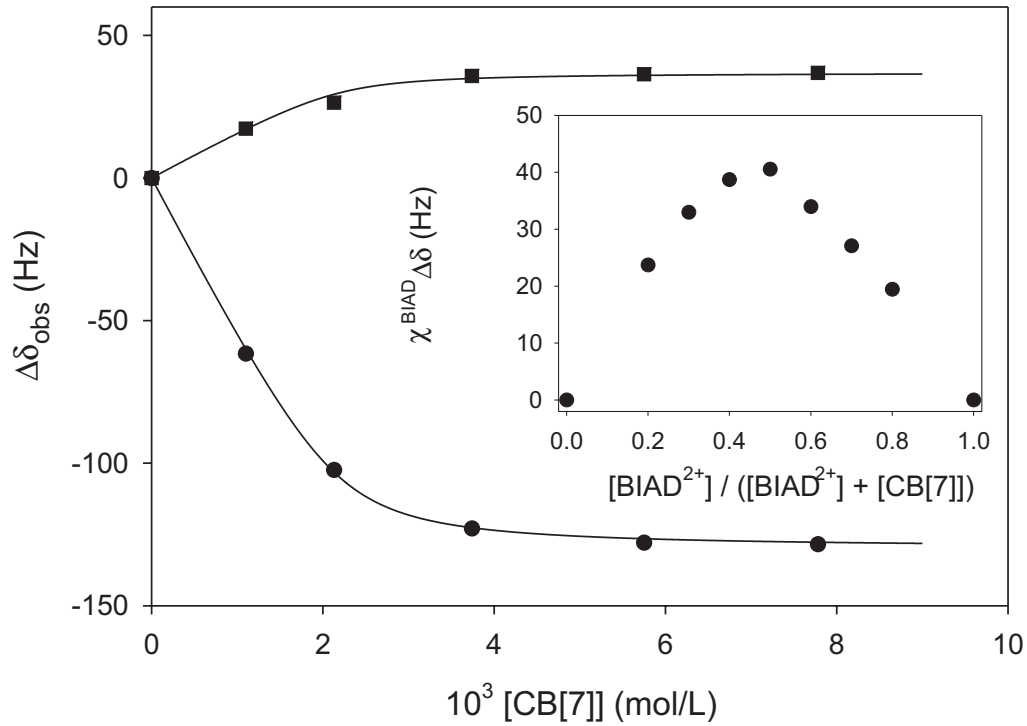


Fig. 5. A ^1H NMR chemical shift titration of $[BIAD]^{2+}$ (2.2×10^{-3} mol/L) with CB[7] in D_2O at 25 °C. The solid lines represent the fits of the H_b (●) and H_4 (■) resonances to a 1:1 binding model with a guest–host stability constant of 1.0×10^4 $(mol/L)^{-1}$. Inset: Job's plot of $\chi^{BIAD}\Delta\delta$ against $[BIAD^{2+}]$ / ($[BIAD^{2+}]$ + [CB[7]]) for the guest H_b resonance.



2-yl and related cationic end groups, including the protonated forms of the water-soluble azo radical initiators azobis[2-(4,5-dihydro-1*H*-imidazol-2-yl)propane] and azobis(2-amidinopropane). Preliminary studies indicate that these initiators bind to CB[7] with comparable strength to the guests in the present study and that inclusion in the CB[7] cavity significantly stabilizes them with respect to unimolecular decomposition to carbon-centered radicals.

Acknowledgements

We thank the Natural Sciences and Engineering Research

© 2006 NRC Canada

Council of Canada (NSERC) and Queen's University for their financial support of this research. Dr. F. Sauriol is thanked for technical assistance with the NMR spectroscopy and helpful discussions.

References

1. W.L. Mock. Top. Curr. Chem. **175**, 1 (1995).
2. K. Kim. Chem. Soc. Rev. **31**, 96 (2002).
3. O.A. Gerasko, D.G. Samsonenko, and V.P. Fedin. Russ. Chem. Rev. **71**, 741 (2002).
4. J.W. Lee, S. Samal, N. Selvapalam, H.-J. Kim, and K. Kim. Acc. Chem. Res. **36**, 621 (2003).
5. J. Lagona, P. Mukhopadhyay, S. Chakrabarti, and L. Isaacs. Angew. Chem. Int. Ed. **44**, 4844 (2005).
6. R. Behrend, E. Meyer, and F. Rusche. Liebigs Ann. Chem. **339**, 1 (1905).
7. W.A. Freeman, W.L. Mock, and N.Y. Shih. J. Am. Chem. Soc. **103**, 7367 (1981).
8. W.L. Mock and N.Y. Shin. J. Org. Chem. **51**, 4440 (1986).
9. W.L. Mock and N.Y. Shih. J. Am. Chem. Soc. **110**, 4706 1988).
10. W.L. Mock and N.Y. Shih. J. Am. Chem. Soc. **111**, 2697 (1989).
11. J. Kim, I.-S. Jung, S.-Y. Kim, E. Lee, J.-K. Kang, S. Sakamoto, K. Yamaguchi, and K. Kim. J. Am. Chem. Soc. **122**, 540 (2000).
12. A. Day, A.P. Arnold, R.J. Blanch, and B. Snushall. J. Org. Chem. **66**, 8094 (2001).
13. S.Y. Jon, Y.H. Ko, S.H. Park, H.-J. Kim, and K. Kim. Chem. Commun. (Cambridge), 1938 (2001).
14. S. Choi, S.H. Park, A.Y. Ziganshina, Y.H. Ko, J.W. Lee, and K. Kim. Chem. Commun. (Cambridge), 2176 (2003).
15. M. Pattabiraman, A. Natarajan, R. Kaliappan, J. T. Mague, and V. Ramamurthy. Chem. Commun. (Cambridge, U.K.), 4542 (2005).
16. R. Wang, L. Yuan, and D.H. Macartney. J. Org. Chem. **71**, 1237 (2006).
17. J. Mohanty and W.M. Nau. Angew. Chem. Int. Ed. **44**, 3750 (2005).
18. W.M. Nau and J. Mohanty. Int. J. Photoenergy, **7**, 133 (2005).
19. R. Wang, L. Yuan, and D.H. Macartney. Organometallics, **25**, 1820 (2006).
20. N.J. Wheate, D.P. Buck, A.I. Day, and J. Collins. J. Chem. Soc. Dalton Trans. 451 (2006).
21. W. Ong and A.E. Kaifer. Organometallics, **22**, 4181 (2003).
22. W.S. Jeon, K. Moon, S.H. Park, H. Chun, Y.K. Ho, J.Y. Lee, S.E. Lee, S. Samal, N. Selvapalam, M.V. Rekharsky, V. Sindelar, D. Sobransingh, Y. Inoue, A.E. Kaifer and K. Kim. J. Am. Chem. Soc. **127**, 12984 (2005).
23. V. Sindelar, S. Silvi, and A.E. Kaifer. Chem. Commun. (Cambridge, U.K.), 2185 (2006).
24. R. Wang, L. Yuan, and D.H. Macartney. Chem. Commun. (Cambridge, U.K.), 5867 (2005).
25. V. Sindelar, M.A. Cejas, F.M. Raymo, W. Chen, S.E. Parker, and A.E. Kaifer. Chem. Eur. J. **11**, 7054 (2005).
26. H.-J. Buschmann and E. Schollmeyer. J. Inclusion Phenom. **29**, 167 (1997).
27. M.V. Rekharsky, Y. Hatsuo, M. Kawai, I. Osaka, R. Arakawa, A. Sato, Y.H. Ko, N. Selvapalam, K. Kim, and Y. Inoue. Org. Lett. **8**, 815 (2006).
28. R.J. Blanch, A.J. Sleeman, T.J. White, A.P. Arnold, and A.I. Day. Nano Lett. **2**, 147 (2002).
29. W. Ong, M. Gomez-Kaifer, and A.E. Kaifer. Org. Lett. **4**, 1791 (2002).
30. H.-J. Kim, W.S. Keon, Y.H. Ko, and K. Kim. Proc. Nat. Acad. Sci. U.S.A. **99**, 507 (2002).
31. V. Sindelar, M.A. Cejas, F.M. Raymo, and A.E. Kaifer. New J. Chem. **29**, 280 (2005).
32. S. Liu, C. Ruspic, P. Mukhopadhyay, S. Chakrabarti, P.Y. Zavalij, and L. Isaacs. J. Am. Chem. Soc. **127**, 15959 (2005).
33. R.S. Wylie and D.H. Macartney. Inorg. Chem. **32**, 1830 (1993).
34. K.-C. Zhang, T.-W. Mu, L. Liu, and Q.-X. Guo. Chin. J. Chem. **19**, 558 (2001).
35. T.W. Mu, L. Liu, K. Ch. Zhang, and Q.X. Guo. Chin. Chem. Lett. **12**, 783 (2001).
36. M.A. Rankin and B.D. Wagner. Supramol. Chem. **16**, 513 (2004).

© 2006 NRC Canada

The volatilities and conductivities of ionic liquids — GC–MS methodology and preliminary studies of acetic acid – base systems

Ronald G. Treble, Keith E. Johnson, and Evangeline Tosh

Abstract: Gas chromatography – mass spectrometry studies of the headspaces above the binary systems pyridine (bp 115 °C) – acetic acid (bp 116 °C), 1-methylimidazole (bp 198 °C) – acetic acid, and triethylamine (bp 89 °C) – acetic acid show both components in the first case, acetic acid only in the second, and triethylamine only in the third. Negative deviations from Raoult's law are confirmed and proton transfer is evidenced by the downfield shift of the acidic proton as the addition of base proceeds. Specific conductances >2 mS cm^{-1} are found over wide composition ranges for all three systems with values >8 mS cm^{-1} at high (>2) mole ratios of acetic acid, suggesting the formation of acetatohydrogenate ionic liquids.

Key words: GC–MS, air, vapor pressure, conductivity, ionic liquids, acetic acid.

Résumé : Des études de spectrométrie de masse combinées à la chromatographie gazeuse des espaces de tête se trouvant au-dessus de systèmes binaires pyridine (p.é. 115 °C) – acide acétique (p.é. 116 °C), 1-méthylimidazole (p.é. 198 °C) – acide acétique et triéthylamine (p.é. 89 °C) – acide acétique montrent la présence des deux composants dans le premier cas, alors qu'on n'observe que la présence de l'acide acétique dans le second et que la triéthylamine dans le dernier. Des déviations négatives par rapport à la loi de Raoult ont été confirmées et on a mis en évidence un transfert de proton par le déplacement chimique vers les bas champs du proton acide au fur et à mesure de l'addition de la base. Pour les trois systèmes, on a observé des conductances spécifiques supérieures à 2 mS cm^{-1} sur un large spectre de composition, avec des valeurs supérieures à 8 mS cm^{-1} à des rapports molaires supérieurs à 2 d'acide acétique, ce qui suggère la formation de liquides ioniques acétatohydrogénates.

Mots clés : chromatographie gazeuse – spectrométrie de masse, air, tension de vapeur, liquides ioniques, acide acétique.

[Traduit par la Rédaction]

Introduction

Ionic liquids (ILs) consisting of organic cations and anions or organic cations and inorganic anions have presented chemists, particularly organic chemists, with a whole new range of solvents, catalysts, and reagents that can be used at ambient temperatures (RTILs) and upwards of 200–300 °C (1). These liquids are modest conductors of electricity (σ values in the mS cm^{-1} range) (2), have manageable fluidities, can have wide electrochemical windows, have modest dielectric constants (<30) (3, 4), and in many cases exhibit negligible vapor pressure (5) (reversibly decomposing anions are the exception and such behavior also applies to totally inorganic ILs such as alkali carbonates and heptachloroaluminates).

Deliberate measurements of the vapor pressures of ionic liquids are scant, but a foray into history is intriguing. Gardner in 1890 (6) observed that certain liquid mixtures of the bases pyridine, picoline, and triethylamine with the acids formic, acetic, and propionic, were maximum boiling azeotropes. Zawidzki in 1900 (7) presented measurements for the binary systems of pyridine with the above acids: large negative deviations from Raoult's law occurred, but both components were found in the vapor over a wide composition range. Gardner, Zawidzki, and later Dolezalek (8) suggested that compound formation took place and assigned molecular formulae or provided routines to evaluate stoichiometry. There seems to be no suggestion that the compounds were ionic. More recently, vapor pressure measurements were made on a chloroaluminate system (9), the distillation under reduced pressure of several dialkylimidazolium salts was reported (10), and the withstanding of UHV by an IL noted (5).

We reported recently on the use of gas chromatography – mass spectrometry (GC–MS) to study liquids and vapors in equilibrium with time intervals between gas and liquid sampling as low as 2.5 min (11). Among the applications of this technique we were able to (*i*) reproduce the classical vapor pressure data for the chloroform–acetone system (11),

Received 14 February 2006. Published on the NRC Research Press Web site at http://canjchem.nrc.ca on 7 July 2006.

R.G. Treble.[1] Department of Chemistry and Biochemistry, University of Regina, Regina, SK S4S 0A2 and Saskatchewan Department of Health, 3475 Albert Street, Regina, SK S4S 6X6, Canada.
K.E. Johnson. Department of Chemistry and Biochemistry and Centre for Studies in Energy and Environment, University of Regina, Regina, SK S4S 0A2, Canada.
E. Tosh. Department of Chemistry and Biochemistry, University of Regina, Regina, SK S4S 0A2, Canada.

[1]Corresponding author (e-mail: treblero@uregina.ca).

 doi:10.1139/V06-098 © 2006 NRC Canada

(*ii*) determine the products of reaction of hydrocarbons with nonvolatile ionic liquids (12), and (*iii*) investigate the electroreduction of organic cations (13). The question arises as to *the temperatures at which various ionic liquids possess significant vapor pressure*. In this paper we discuss some preliminary results for acid–base systems. First, we describe the methodology for obtaining high-quality data on ambient-temperature air samples and then present a preliminary study of several ionic liquid systems. We also include some NMR data to establish whether or not proton transfer occurs to make salts in the liquid and some conductance data to evaluate any ionicity in the systems.

Experimental

Prior to sampling ionic liquid headspace fractions, ambient and fresh air samples were repeatedly analyzed. Data were correlated employing both full scan and selected ion monitoring modes to determine if any differences would dictate a preferred methodology.

All liquids employed in the binary mixtures that were used for the vapor pressure studies were first distilled and then run individually using GC–MS to determine purity. Preliminary full scan liquid fractions were also run to (*i*) first determine the relative retention times for the subsequent vapor phase studies and (*ii*) to produce the entire mass spectra, which then would allow for selection of "unique ions", if necessary, for employment of the selected ion monitoring mode. All GC–MS analyses were performed using a Finnigan Mat Incos 50 mass spectrometer system. The instrument consisted of a Hewlett-Packard 5890 gas chromatograph directly interfaced to an Incos 50 quadrupole mass spectrometer via a heated transfer line – capillary interface. The GC was configured with a splitless injection port and a DB-5MS fused-silica capillary column coated with a 0.25 μm film of stationary phase (15 m, 0.25 mm i.d., J & W Scientific, Folsom, California). As little as 0.05 mL of the headspace could be conveniently sampled and injected employing a latex-free 1 mL tuberculin disposable syringe (Becton Dickinson and Co., Franklin Lakes, New Jersey). An attempt was made to compare results of sampling precision using a gas-tight syringe. The additional sampling was performed employing a 0–500 μL 81256 Hamilton Samplelock™ syringe (Sigma-Aldrich Canada Ltd., Oakville Ontario).

The mass spectrometer was operated in the electron impact ionization mode with an electron energy of 70 eV. The ion source temperature was maintained at 180 °C for all analyses and the capillary interface transfer line was held at 250 °C. The headspace studies for the air samples were carried out with the gas chromatograph run at varied temperatures (isothermal), while the splitless injection port was held at 210 °C. Imperative to the headspace analyses was the requirement to acquire data while continuously making injections without having to reprogram the instrumentation. Prior to each run, the mass spectrometer was calibrated with perfluorotributylamine.

Headspace correlation studies of ionic liquids included the systems pyridine – acetic acid (sampling at 80 °C), 1-methylimidazole – acetic acid (sampling at 80 °C), and triethylamine – acetic acid (sampling at 23 °C). The gas chromatograph column was set at 60 °C isothermal for the triethylamine – acetic acid and the pyridine – acetic acid systems, producing satisfactory component resolution, while a 125 °C isothermal column temperature was required for the headspace analysis of the methylimidazole – acetic acid mixture. Our methodology employed 5 mL borosilicate vials with Teflon® septa in open cap screw tops (Chromatographic Specialties Inc., Brockville, Ontario). It is important to note that for all samples other than "air" employed for the precision studies, once the headspace was sampled, the syringe tip was not pulled out immediately from the sample vial septa; instead, it was allowed to remain with the plunger withdrawn for about 60–90 s in an attempt to approach a reasonable equilibrium. The vials containing the ionic liquid mixtures were kept in a continuously stirred hot water bath and supported by a Styrofoam collar.

^{1}H NMR spectra were obtained with a Bruker AC-200 MHz NMR with DMSO–d_6 as an external locking solvent.

Specific conductivities were measured by means of an Orion conductivity meter model 160 across a cell with platinum electrodes calibrated with 0.01 mol/L KCl solution. Approximate densities were obtained by weighing 1 mL portions in a volumetric flask.

Results and discussion

Reproducibility studies for ambient and fresh air components

Two separate modes of scanning were employed to monitor the relative amounts of nitrogen, oxygen, and argon. Both ambient (within the laboratory) and fresh air (outside the building) samples were subjected to full scan (5–50 amu) and selected ion monitoring (SIM). When the quadrapole mass filter was operated in the SIM mode, five ions were monitored for total relative amounts of nitrogen, oxygen, and argon (m/z for $z = +1$ were 28, 32, and 40; m/z for $z = +2$ were 14 and 16). For the full scan mode, these ions were also selected for the calculation of total relative amounts and results compared with those found in the SIM mode. The ability of the system to reliably identify the resolved total and selected ion chromatograms using electron impact ionization for any species is subject to certain criteria:

(*i*) peaks (all fragments) for identical species must appear at the same relative retention times (±0.02 min); (*ii*) the reconstructed ion chromatogram peaks of all ions monitored must have signal-to-noise ratios that are greater than 3:1.

Using the aforementioned criteria, carbon dioxide did not contribute to the envelope sampling.

Over 100 air samples were analyzed for the purpose of choosing (*i*) whether full scan or selected ion monitoring (SIM) should be employed and (*ii*) whether the technique could produce the required precision for relative proportions, regardless of volumes injected. It was found that although the SIM mode most certainly produces results with a magnitude greater sensitivity, the full scan mode worked extremely well with the required sensitivity with less noise for the required dynode voltage.

Table 1 depicts the precision afforded for 14 consecutively run random air samples at the indicated retention times (RT). All 14 samples were analyzed with full resolution in less

© 2006 NRC Canada

Table 1. Air composition reproducibility study in full scan mode (5–50 amu monitored).

Retention time (min)	Intensity at 28 amu	Intensity at 14 amu	Intensity at 32 amu	Intensity at 16 amu	Intensity at 40 amu	Total counts
0.98	79 993	5532	19 125	1 888	1326	107 864
1.87	73 071	4890	16 955	1 692	1167	97 776.9
2.57	122 733	8341	29 709	2 715	2184	165 682
8.06	99 045	6644	23 940	2 197	1757	133 583
8.45	149 345	9735	36 170	3 190	2644	201 084
10.53	118 847	7896	28 569	2 575	2076	159 963
11.05	112 689	7506	26 958	2 430	2003	151 586
11.64	97 258	6535	23 389	2 213	1704	131 099
13.08	121 358	7919	29 182	2 565	2152	163 176
16.89	75 168	4887	17 614	1 741	1246	100 656
17.37	95 223	6229	22 775	2 097	1670	127 994
18.14	103 710	6812	24 939	2 246	1832	139 539
18.54	78 673	5112	18 775	1 762	1334	105 656
18.94	107 492	7039	26 024	2 234	1875	144 664
0.98	0.792 9	0.194 8	0.012 29	108 124	0.997 6	0.245 7
1.87	0.797 3	0.190 7	0.011 94	96 104	1.017 41	0.239 2
2.57	0.791 1	0.195 7	0.013 18	164 299	1.008 418	0.247 4
8.06	0.791 2	0.195 7	0.013 15	133 651	0.999 5	0.247 3
8.45	0.791 1	0.195 7	0.013 15	201 606	0.997 4	0.247 4
10.53	0.792 3	0.194 7	0.012 98	159 289	1.004 231	0.245 7
11.05	0.792 9	0.193 9	0.013 21	150 838	1.004 959	0.244 5
11.64	0.791 7	0.195 3	0.013 00	131 239	0.998 9	0.246 7
13.08	0.792 3	0.194 6	0.013 19	163 244	0.999 6	0.245 6
16.89	0.795 3	0.192 3	0.012 38	100 400	1.002 550	0.241 8
17.37	0.792 6	0.194 3	0.013 05	129 250	0.990 3	0.245 2
18.14	0.792 1	0.194 8	0.013 13	139 136	1.002 896	0.246 0
18.54	0.793 0	0.194 4	0.012 63	106 081	0.996 0	0.245 1
18.94	0.791 7	0.195 3	0.012 96	145 438	0.994 7	0.246 7
Standard deviation	0.001 724	0.001 401	0.000 403 5			0.000 403 45

than 20 min. As can be seen in Table 1 for the total ion chromatograms (TIC), full scan mode, it is imperative that the 2+ ions for nitrogen and oxygen be included for the calculation of total relative amounts (14). Figure 1 shows the completely resolved, total ion chromatograms for random volumes of air sampled (volumes injected, 0.05–0.2 mL air). It can be clearly seen that although total peak areas are purposely quite varied (deliberate varied injection volumes), the respective standard deviations for all components monitored are very low. *The reproducibility studies for air were found to more than satisfy the requirements necessary for the subsequent partial-pressure studies on the selected ionic liquid mixtures.*

Ionic liquid systems

Analysis of 1-methylimidazole – acetic acid (mim–aa) mixtures

Five liquids containing mim–aa with varied mole fractions were analyzed employing the above technique. Because enhanced sensitivity was required for identification and integration of the respective species in the vapor phase, SIM was necessary. Initial studies on these systems included preliminary runs sampling every 2° or 3° from room temperature to 95 °C, in full scan and SIM modes. It was evident that the appearance of constituents (acetic acid) in the vapor phase could be seen at least 7 to 8 °C lower when employing the SIM mode. Also, in the initial studies of the mim–aa system as in the air composition analyses, the gas chromatograph was held at 60 °C. Selected subsequent samples were run at elevated, isothermal temperatures (125, 150, and 200 °C) to attain better chromatography only for the ionic liquid samples. Again, it was imperative in the integration of all peaks that the individual signals scanned qualify for a 3:1 signal-to-noise requirement.

Table 2 lists the various concentrations when the liquid was maintained at 80 °C for the mim–aa mixtures analyzed. It was discovered that for all five cases, the acetic acid was present in all headspace volumes (recorded in Table 2), whereas the 1-methylimidazole could not be detected even at the highest mole ratios for the mim constituent when the vials were heated as high as 95 °C and monitored in the single ion mode. Figure 2 includes the chromatograms and full scan mode for these mixtures. All five peaks observed (retention times, 2.5–12.5 min) are due to acetic acid in the headspace. Figure 3 is the mass spectrum (upper) and library search (lower) for the peak sampled between 3.01 and 3.03 min. Figure 4 shows the resulting respective chromatograms of headspace and liquid samples for the same mim–aa mixture where the mim concentration is the highest and the temperature was taken to 90 °C. It can be noted that the isolated single peak to the left is a result of the acetic acid in

© 2006 NRC Canada

Fig. 1. Total ion chromatograms for random samples of air.

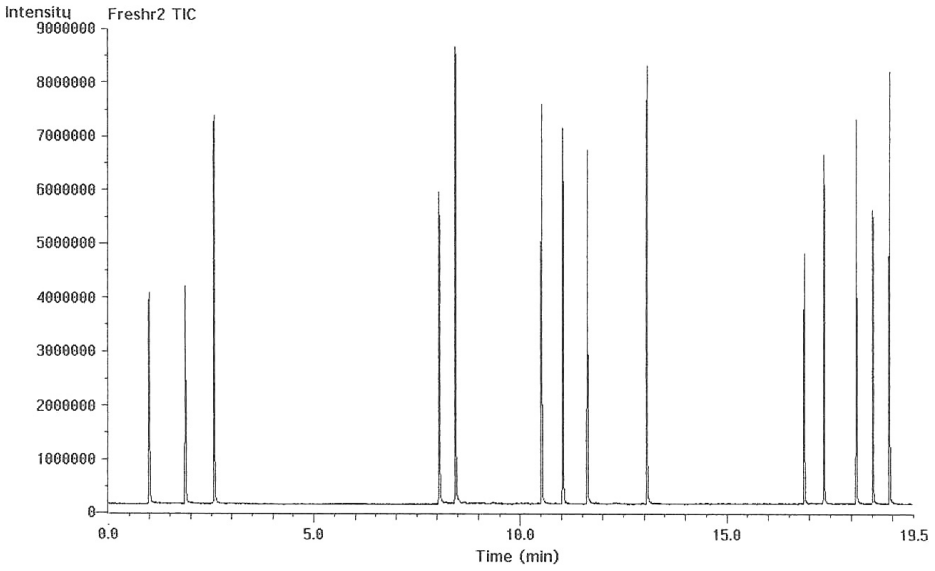


Fig. 2. Total ion chromatograms (full scan model) for mixtures of 1-methylimidazole and acetic acid. Peaks correspond to vials 1–5, Table 2.

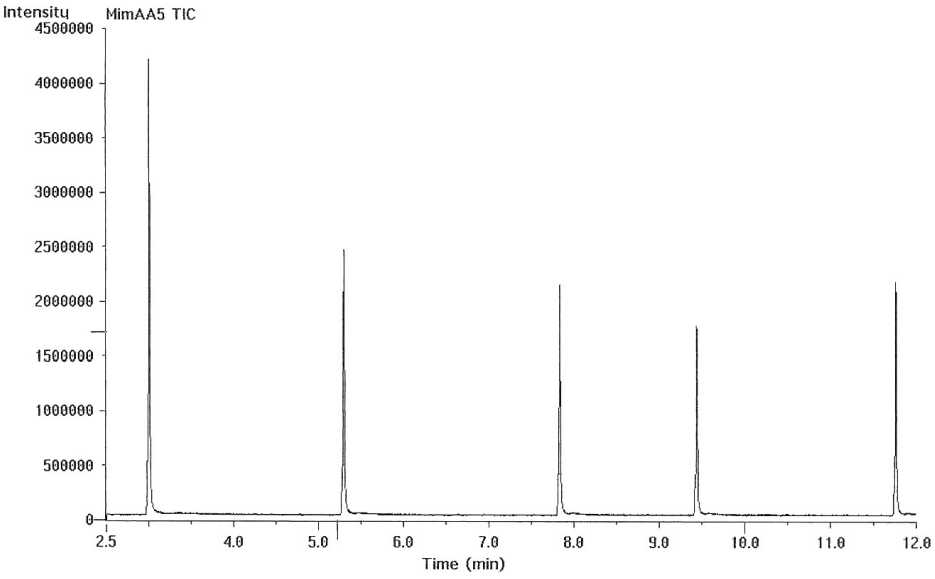


Table 2. Analysis of 1-methylimidazole – acetic acid (mim–aa) liquids at 80 °C.

Vial	Acetic acid (mol)	1-Methylimidazole (mol)	Headspace acetic acid peak area (au)
1	0.0116	0.0226	378
2	0.0140	0.0213	330
3	0.0173	0.0188	403
4	0.0192	0.0180	461
5	0.0227	0.0149	737

the headspace volume and the two peaks to the right are a result of the acetic acid and the methylimidazole (extreme right) in the respective liquid portions (both sampled at 90 °C). The ratio of the acetic acid liquid to vapor was calculated for this concentration and was found to be 32.5:1.

The NMR signal of the carboxylic acid proton is shifted from 11.73 ppm vs. TMS to 13.92 and 14.42 ppm in 2:1 and 1:2 aa–mim mixtures, respectively. Conductivities across the system are shown in Fig. 5.

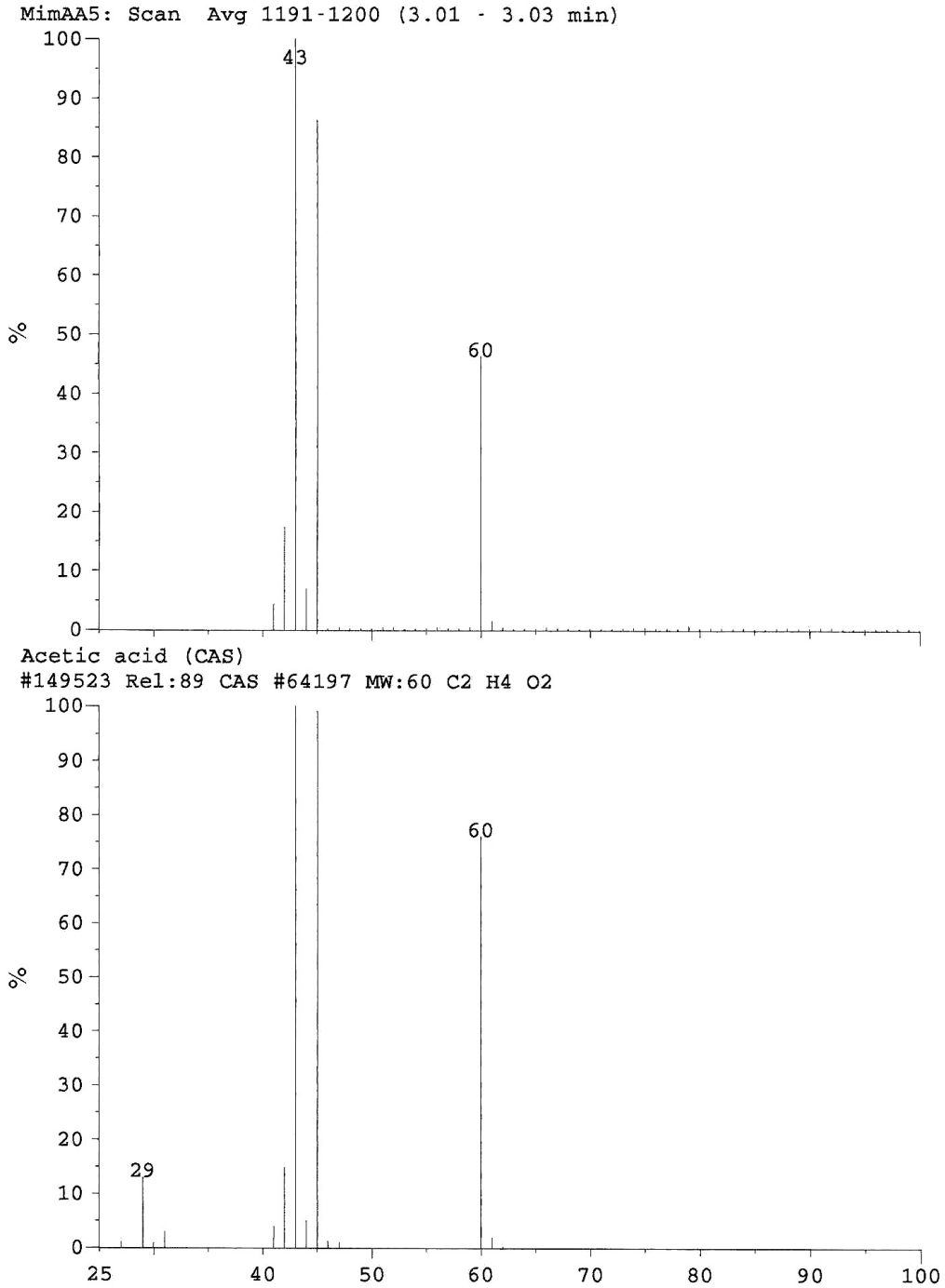
Correlation of the partial pressures of a pyridine – acetic acid (py–aa) mixture at 80 °C

An attempt was made to employ data received from headspace analyses of pyridine – acetic acid mixtures to correlate previously reported partial pressures of this binary mixture (7).

Table 3 is a tabulation of the integrated areas attained from the total ion chromatograms of seven separate 0.3 mL

© 2006 NRC Canada

Fig. 3. Mass spectrum (upper) and library search (lower) for the 3 min peak of Fig. 2.



headspace pyridine – acetic acid mixtures sampled at 80 °C using full scan monitoring.

A plot of the respective areas from Table 3 vs. the mole ratios yields a trend that is very similar to the previous work reported (7). Previous work indicated that for this system the partial pressures were exactly equivalent when the mole ratio was 0.50 for the respective species. Figure 6 shows the respective separate plots of headspace intensities vs. mole ratio acetic acid – pyridine.

The NMR signal for the carboxylic acid proton in the 1:5 aa–py system appears at 12.21 ppm. Conductivity data are shown in Fig. 5.

Examination of the triethylamine – acetic acid system

Headspace analyses of two separate mixtures of triethylamine – acetic acid were performed at room temperature. The impetus in the development of a method for analyzing this system was based upon a need to compare data received with that of the previously studied system, where the boiling point of the base (1-methylimidazole) was much higher. Ambient-temperature headspace samples of 0.3 mL were run on the GC–MS system for the 40% and 60% triethylamine mixtures. Gas chromatograph column temperatures were set at 60 and 125 °C isothermal and the mass spectrometer was operated using the full scan mode monitoring

© 2006 NRC Canada

Fig. 4. Chromatograms of headspace and liquid at 90 °C for the mixture of acetic acid (0.0115 mol) and 1-methylimidazole (0.0226 mol).

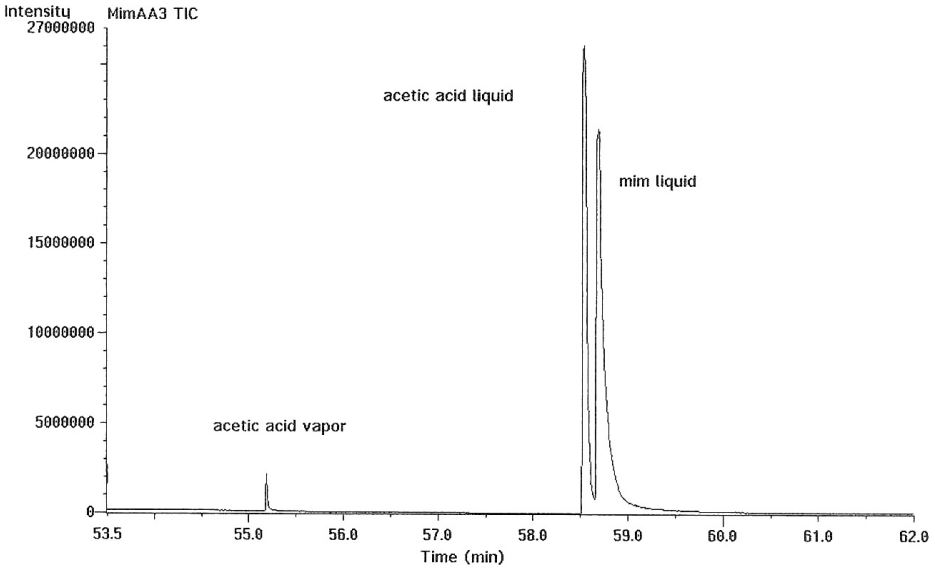
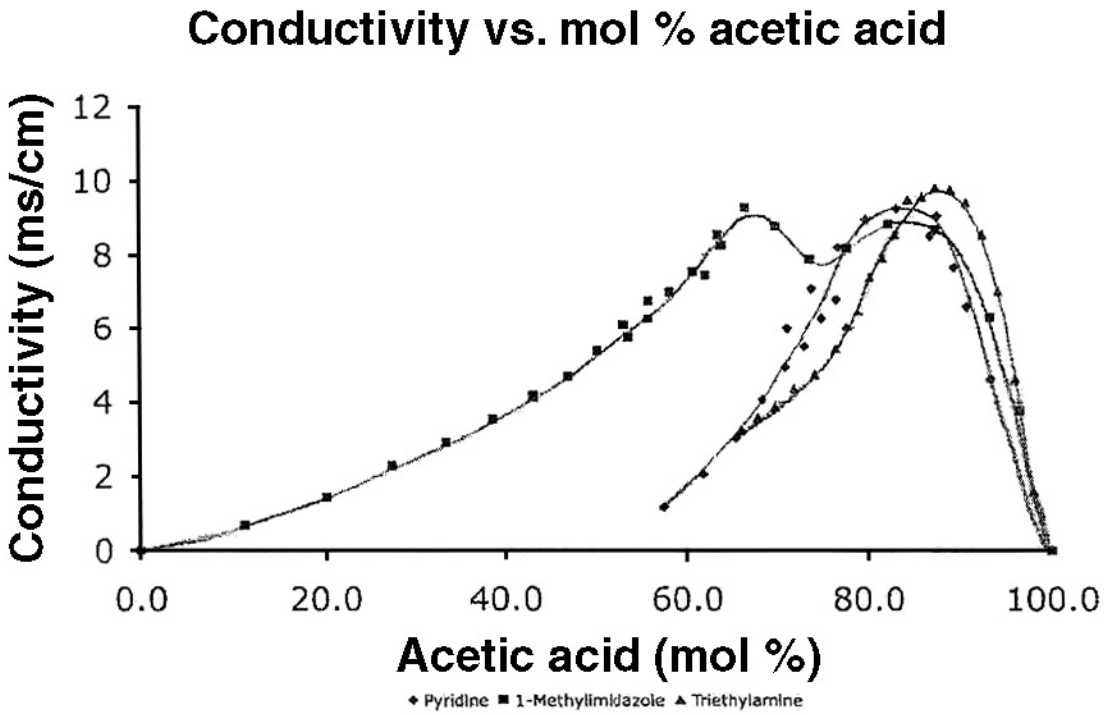


Fig. 5. Specific conductivity vs. mol % acetic acid for mixtures with three bases.



from 41 to 125 amu. Both headspace fractions were found to be entirely triethylamine, with barely traceable amounts of acetic acid present, using SIM (monitoring the molecular ion, 60 amu and the respective base peak, 43 amu). A completely miscible liquid was evident for the mixture containing 40% triethylamine. Following the headspace analysis, 0.05 μL of this 40% liquid mixture was sampled at room temperature and then injected and analyzed using the GC–MS system with full scan monitoring (last peak Fig. 7; retention times, 8.75–9 min). It was discovered that although we have a coeluting system, two distinct peaks could be seen emerging and confirmed and (or) attributed, respectively, to acetic acid (eluting first) and triethylamine. Matches confirmed with the library database (15) for the coeluting triethylamine (Fig. 8) were found to be in 97% agreement. The 60% triethylamine mixture visibly produced two distinct layers of about equal volumes with the top layer clear while the bottom layer was slightly discolored. Careful sampling (0.05 μL) and analysis of the bottom layer (same GC–MS conditions) resulted in the first peak in Fig. 7

© 2006 NRC Canada

Table 3. Headspace intensities (sampled at 80 °C) for pyridine – acetic acid mixtures using full scan monitoring (headspace volume sampled, 0.3 mL).

Concentration of acetic acid (mol, mole fraction)	Concentration of pyridine (mol)	Integrated intensity of area for acetic acid	Integrated intensity of area for pyridine
0.0344, 0.85	0.0062	2 015 785	None detected
0.0304, 0.76	0.0097	1 061 621	83 215
0.0258, 0.66	0.0130	731 880	367 483
0.0210, 0.57	0.0158	386 749	780 000
0.0155, 0.44	0.0199	85 485	2 908 276
0.0105, 0.31	0.0235	None detected	4 290 437
0.0052, 0.16	0.0277	None detected	5 665 703

Fig. 6. Relative vapour pressure of pyridine (●) and acetic acid (▲) as a function of acetic acid mole fraction.

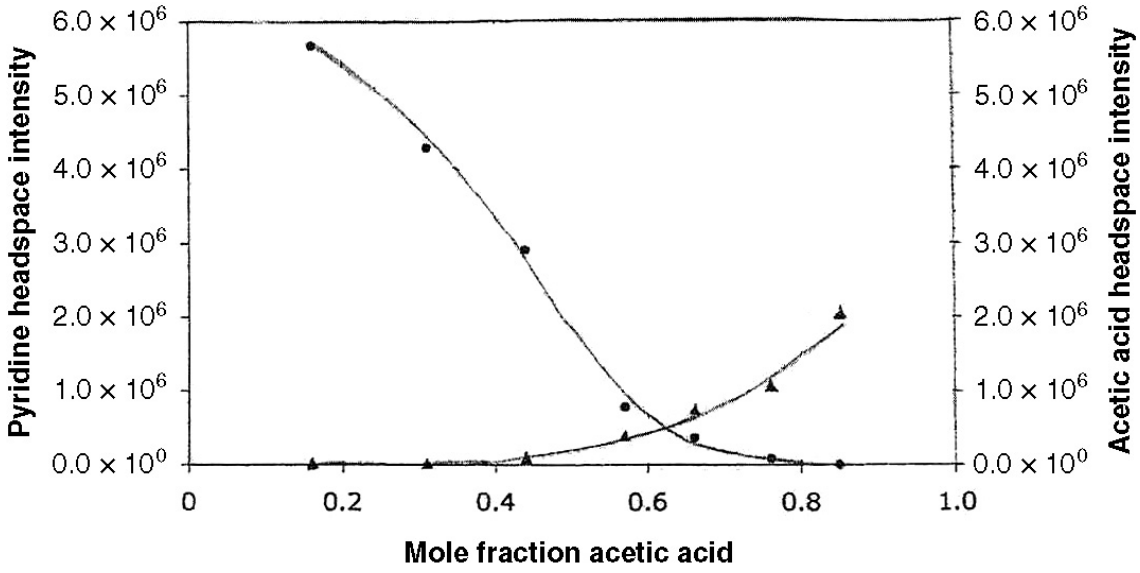
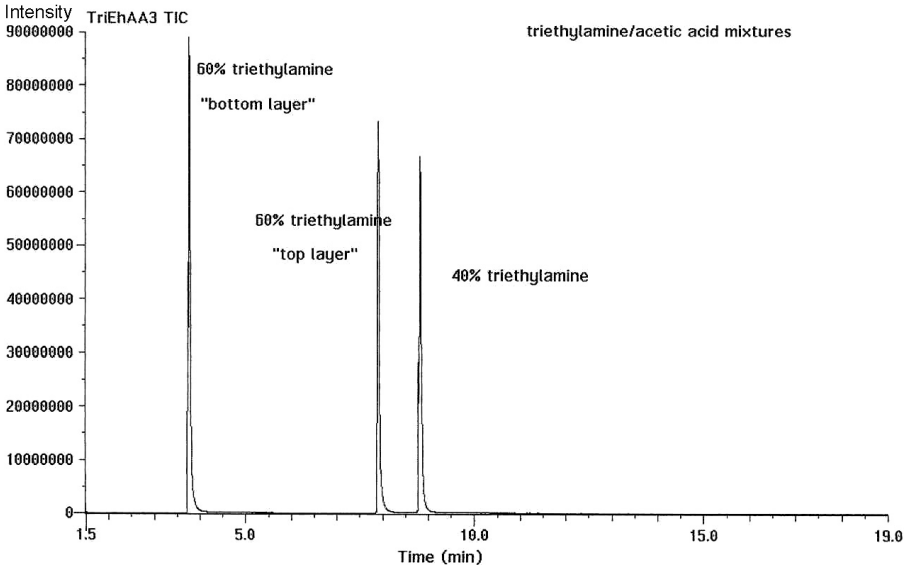
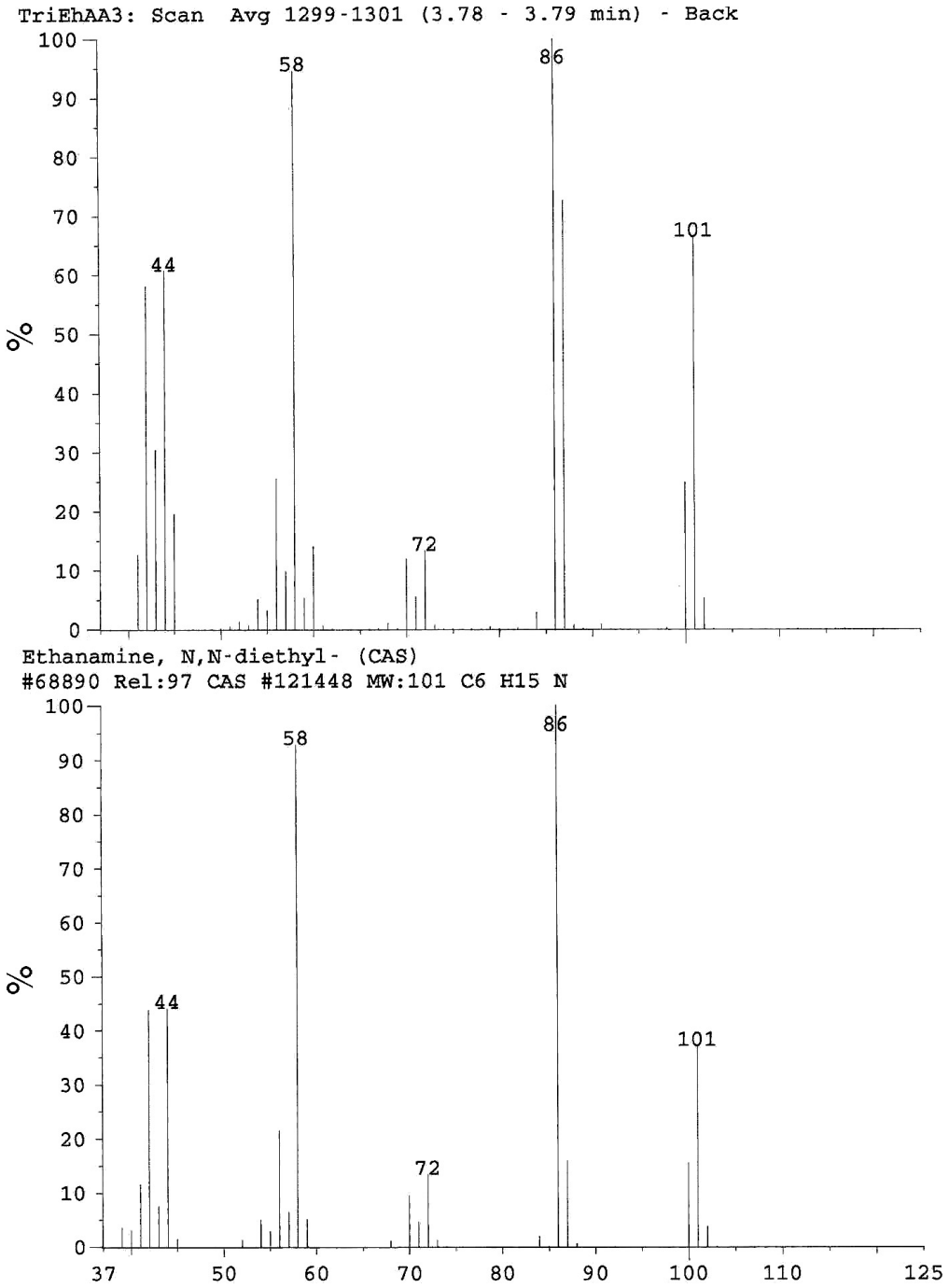


Fig. 7. Total ion chromatograms for triethylamine – acetic acid mixtures.



© 2006 NRC Canada

Fig. 8. Mass spectrum obtained for triethylamine (top) compared with the database.



(retention time, 3.75–4 min), producing exactly the same results as found for the 40% triethylamine mixture. Sampling of the clear top layer (second peak in Fig. 7, retention time, 7.9–8.1 min) showed triethylamine with a traceable amount of acetic acid. An additional species, which upon close examination of the chromatograms eluted, just prior to each headspace peak in Fig. 7, was found to be CO_2. Its origin was not apparent.[2]

The NMR signal of the carboxylic acid proton was shifted to 12.97 ppm for a 1:1 mixture.

[2] Pure acetic acid was repeatedly analyzed employing the aforementioned instrumental parameters to determine whether or not it contained dissolved carbon dioxide, which was detected in the previous acid–base headspace fractions. There was no evidence of residual carbon dioxide over and above that level associated with normal ambient air samples in the same acetic acid used in the headspace experiments. The headspace for all three pure bases was also analyzed in an attempt to determine where the residual CO_2 may be. It was found that for all three bases, residual CO_2 could not be detected. Additional attempts were made to analyze for residual methane that may also be present in the reported headspace fractions. No evidence of methane could be found in the samples analyzed.

© 2006 NRC Canada

Conclusions and prospects

For the 1-methylimidazole – acetic acid system, only the more volatile acetic acid was detectable in the headspace above the liquids even at 95 °C, while for the triethylamine – acetic acid system, only the more volatile triethylamine was observed. However, for the system derived from components with almost the same boiling points, pyridine (bp 115 °C) and acetic acid (bp 116 °C), *both* compounds were observed in the vapor except at the extremes of composition. Moreover, in the latter system, both compounds were obtained from mixtures in which their mole fractions were <0.5. If the 1:l compound is stable and has zero vapor pressure, then we would expect a v-shaped vapor pressure diagram.

The ^{1}H NMR data indicate that proton transfer does indeed occur from acetic acid to the different bases in the liquids, i.e., the compounds are ionized (16). It does not follow that the ion pairs are dissociated; that this occurs to a considerable extent is confirmed by the conductivity data. Values of specific conductivity in the mS cm^{-1} range are common for organic or semiorganic ionic liquids at ambient temperatures (2). Somewhat more surprising are the maxima in the conductivity–composition curves at high acetic acid mole ratios, although maximum boiling azeotropes have been observed for several carboxylic acid – base systems in the excess acid region (17). It appears that conjugate anions of the type H_nA_{n+1} are formed, similar to the halohydrogenates HCl_2^- and $H_2Br_3^-$, which we have described in pyridinium and 1-methylimidazolium ionic liquids (18, 19).

Do ionic liquids have a vapor pressure? The evidence, particularly from the pyridine – acetic acid system, is that they do. As the temperature is raised, we would expect the GC–MS technique to detect both components of the three systems we examined. No evidence of compound formation in the vapors was obtained, but this is in accord with the proton affinities (20) of acetate and the bases; the gas-phase equilibria should favor acetic acid.

$$\begin{array}{l} \mathrm{HA(l) + B(l) \rightarrow [BH^+][A^-](l) \rightarrow HA(g) + B(g)} \\ \qquad \downarrow\uparrow \\ \mathrm{\{[BH^+] + [A^-]\}(l)} \\ \mathrm{[A^-](l) + HA(l) \rightarrow [HA_2^-](l),\ etc.} \end{array}$$

Where the proton in the cation is replaced by an alkyl group, as in the familiar alkylpyridinium and dialkylimidazolium salts, vaporization of ion pairs (10) would be the only alternative to irreversible decomposition; lower conductivities, within this compound class, should then correspond to greater volatility.

$$\begin{array}{l} \mathrm{\{[RB^+] + [A^-]\}(l)\ \grave{A}\ \{[RB^+][A^-]\}(l)} \\ \qquad\qquad\qquad\qquad \mathrm{\grave{A}\ \{[RB^+][A^-]\}(g)} \\ \mathrm{[A^-](l) + HA(l)\ \grave{A}\ [HA_2^-](l),\ etc.} \end{array}$$

The product distribution in both of these situations is, of course, characterized by several equilibrium constants and disproportionations, such as $2[H_nA_{n+1}^-] \leftrightarrow [H_{n-1}A^-] + [H_{n+1}A_{n+2}^-]$, may be involved. In the cases of the aromatic bases, homoconjugate cation formation (21) may account for their miscibility at low base compositions, while the excess aliphatic base triethylamine appears as a separate phase (containing traces of acetic acid) from the primary salt phase.

One of the obstacles encountered in the GC–MS study was attempting to overcome and avoid contamination of the sampling syringe when in contact with any condensation on the underside of the vial septa, when the solution mixtures were taken somewhat above ambient temperatures. Future attempts at upgrading and refining this technique will eliminate condensation problems while incorporating a completely *closed temperature programmable sampling, vapor transfer, and gas-tight injection system*. The present methodology lends itself to a scope much larger and not confined to correlating vapor pressures. The present method without refinement is amenable to (1) rapid identification of any volatile species regardless of whether or not the chromatograms are completely resolved or what phase they are in, (2) possible isolation and identification of intermediates in the vapor phase for those reactions requiring time/temperature monitoring, (3) greatly enhanced sensitivity if necessary while employing SIM and (or) collective sampling techniques, and (4) immediate determination of relative proportions of constituents present in liquid and vapor phases.

Future work will include not only a more advanced study of vapor pressures associated with various ionic liquid mixtures at various temperatures *above and below ambient*, but also a study of (*i*) gas *saturation or storage capacities* and *ability to release* systems and (*ii*) analysis of various types of exhaust emissions (internal combustion engines, industrial gas plants, etc.).

Acknowledgements

Partial support of this work by the Petroleum Technology Research Centre (Regina, Saskatchewan) is sincerely appreciated.

References

1. See, for example: (*a*) P. Wasserscheid and T. Welton (*Editors*). Ionic liquids in synthesis. Wiley-VCH, Weinheim, Germany. 2003; (*b*) R.D. Rogers and K.R. Seddon (*Editors*). ACS Symposium series 818. American Chemical Society, Washington, D.C. 2002; (*c*) R.D. Rogers, K.R. Seddon, and S. Volkov (*Editors*). Green industrial applications of ionic liquids. *Edited by* Kluwer, Dordrecht, The Netherlands. 2002; (*d*) International symposia on molten salts I–XIV. Electrochemical Society, Pennington, New Jersey. 1976–2005.
2. P.C. Trulove and R.A. Mantz. *In* Ionic liquids in synthesis. *Edited by* P. Wasserscheid and T. Welton. Wiley-VCH, Weinheim, Germany. 2003. p. 103.
3. G. Charlot and B. Tremillon. Chemical reactions in solvents and melts. Pergamon Press, Oxford. 1969.
4. H. Weingartner, A. Knocks, W. Schrader, and U. Kaetze. J. Phys. Chem. A, **105**, 8646 (2001).
5. E.F. Smith, E.J. VillarGarcia, D. Briggs, and P. Licence. Chem. Commun. (Cambridge), **45**, 5633 (2005).
6. J.A. Gardner. Ber. Dtsch. Chem. Ges. **23**, 1587 (1890).
7. J. von Zawidski. Z. Phys. Chem. **35**, 129 (1900).
8. F. Dolezalek. Z. Phys. Chem. **64**, 727 (1908).
9. H.A. Oye, M. Jagtoyen, T. Oksefjell, and J.S. Wilkes. Mater. Sci. Forum, **73**, 183 (1991).

© 2006 NRC Canada

10. L.P.N. Rebelo, J.N. Conongia Lopes, J.M.S.S. Esperança, and E. Filipe. J. Phys. Chem. B, **109**, 6040 (2005); M.J. Earle, J.M.S.S. Esperança, M.A. Gilea, J.N. Canongia Lopes, L.P.N. Rebelo, J.W. Magee, K.R. Seddon, and J.A. Widegren. Nature, **439**, 831 (2006).
11. R.G. Treble, K.E. Johnson, L. Xiao, and T.S. Thompson. Anal. Chem. **74**, 3247(2002).
12. L. Xiao, K.E. Johnson, and R.G. Treble. J. Mol. Cat. A: Chem. **214**, 121 (2004).
13. L. Xiao and K.E. Johnson. J. Electrochem. Soc. **150**, E307 (2003).
14. F.W. McLaffery. Interpretation of mass spectra. University Science Books, Mill Valley, California. 1980.
15. W.G. Mallard (*Editor*). NIST Chemistry Webbook [online]. National Institute of Standards and Technology, Gaithersburg, Maryland. Available from http://webbook.nist.gov. 2005.
16. I.M. Kolthoff and S. Bruckenstein. J. Am. Chem. Soc. **78**, 1 (1956).
17. M. Yoshizawa, W. Xu, and C.A. Angell. J. Am. Chem. Soc. **125**, 15411 (2003).
18. K.E. Johnson and P. Driver. *In* Proceedings of the international symposium on ionic liquids in honour of Marcelle Gaune-Escard, Carry le Rouet, France, 26–28 June 2003. *Edited by* H.A. Oye and A. Jagtoyen. Norwegian University of Science and Technology, Trondheim, Norway. 2003. p. 233.
19. G. Driver and K.E. Johnson. Green Chem. **5**, 163 (2003).
20. G. Lias, J.F. Liebman, and R.D. Levin. J. Phys. Chem. Ref. Data, **13**, 718 (1984).
21. O. Popovych and R.P.T. Tomkins. Nonaqueous solution chemistry. Wiley, New York. 1981. p. 41.

© 2006 NRC Canada

ERRATUM / ERRATUM

Erratum: Valence bond calculations on the transition state for the E2 reaction of fluoride ion with ethyl fluoride — Implications for the More O'Ferrall – Jencks diagram

Wei Wu, Sason Shaik, and William H. Saunders, Jr.

Ref.: Can. J. Chem. **83**: 1649–1653 (2005).

In the above paper on page 1652, Table 4 has two incorrect values in the third line (data for β-CH_2) in columns two and three. Table 4 is reproduced below with the corrected values in bold.

Table 4. Group charges in the F···H···CH_2==CH_2F transition state.

Group	VB (HF/6-31+G)	Mulliken (MP2/6-31+G*)	NPA (MP2/6-31+G*)
F	–0.703	–0.654	–0.697
H	0.639	0.535	0.584
β-CH_2[a]	–0.454	**–0.388**	**–0.389**
α-CH_2[a]	0.444	0.267	0.350
F	–0.927	–0.780	–0.849

Note: VB = valence bond; NPA = natural population analysis.
[a]α refers to the carbon bearing the fluorine and β refers to the carbon bearing the hydrogen in transit.

NRC Research Press apologizes for any inconvenience to the reader.

Received 7 March 2006. Published on the NRC Research Press Web site at http://canjchem.nrc.ca on 10 June 2006.

W. Wu. The State Key Laboratory for Physical Chemistry of Solid Surfaces and Institute of Physical Chemistry, Xiamen University, Xiamen 361005, P.R. China.
S. Shaik. Department of Organic Chemistry and the Lise Meitner-Minerva Center for Computational Quantum Chemistry, The Hebrew University, Jerusalem 91904, Israel.
W.H. Saunders, Jr.[1] Department of Chemistry, University of Rochester, Rochester, NY 14627, USA.

[1]Corresponding author (e-mail: saunders@chem.rochester.edu).

 doi:10.1139/V06-101 © 2006 NRC Canada

ADDITIONS AND CORRECTIONS / AJOUTS ET CORRECTIONS

Additions and corrections: Complexation of diazinon, an organophosphorus pesticide, with α-, β-, and γ-cyclodextrin — NMR and computational studies

Doreen Churchill, Jason Chiu Fung Cheung, Yong Sung Park, Vedene H. Smith, Gary vanLoon, and Erwin Buncel

Ref.: Can. J. Chem. **84**: 702–708 (2006).

In the above paper on page 702, footnote 4 was inadvertently left out. Please find footnote 4 below.

[4]Corresponding author (e-mail: erwin.buncel@chem.queensu.ca).

NRC Research Press apologizes for any inconvenience to the reader.

Received 7 June 2006. Published on the NRC Research Press Web site at http://canjchem.nrc.ca on 24 June 2006.

D. Churchill. Centre of Environmental Excellence, c/o Sir Wilfred Grenfell College, Corner Brook, NL A2H 6P9, Canada.
J.C.F. Cheung, Y.S. Park, V.H. Smith, G. vanLoon, and E. Buncel.[1] Department of Chemistry, Queen's University, Kingston, ON K7L 3N6, Canada.

[1]Corresponding author (e-mail: erwin.buncel@chem.queensu.ca).

 doi:10.1139/V06-106 © 2006 NRC Canada

Synthesis and thermolysis rate constants of diastereomeric oxadiazoline sources of acetoxy(methoxy)carbene — Reaction of acetoxy(methoxy)carbene with isocyanates

Wojciech Sokol and John Warkentin

Abstract: Oxidation of the methoxycarbonylhydrazone of *p*-methoxyacetophenone affords both the *cis*- and *trans*-2-acetoxy-2-methoxy-5-(*p*-methoxyphenyl)-5-methyl-Δ^3-1,3,4-oxadiazolines (also known as corresponding 2,5-dihydro-1,3,4-oxadiazoles) as well as methyl 1-acetoxy-1-(*p*-methoxyphenylethyl)diazenecarboxylate. The three isomers were separated and identified by spectroscopic means. Methyl 1-acetoxy-1-(*p*-methoxyphenylethyl)diazenecarboxylate is the major product from oxidation in dichloromethane. Oxidation in acetic acid did not afford the oxadiazolines but gave the diazenecarboxylate and, in addition, 1-(*p*-methoxyphenyl)ethyl acetate. Attempts to isomerize the diazenecarboxylate to the oxadiazolines by acid catalysis were not successful. Thermolysis of the oxadiazolines at 50.4 °C occurred with approximately the same rate constant (ca. 3.6×10^{-5} s^{-1}) to afford acetoxy(methoxy)carbene, which rearranges to methyl pyruvate by acetyl transfer. The carbene, which reacts with relatively unhindered isocyanates to transfer the methoxycarbonyl group to carbon and the acetyl group to nitrogen, can be considered an acyl anion equivalent in that reaction.

Key words: acetoxy(methoxy)carbene, diazene, oxadiazoline, isocyanate, (acetylamino)oxoacetate.

Résumé : L'oxydation de la méthoxycarbonylhydrazone de la *p*-méthoxyacétophénone conduit à la formation d'un mélange des 2-acétoxy-2-méthoxy-5-(*p*-méthoxyphényl)-5-méthyl-Δ^3-1,3,4-oxadiazolines *cis* et *trans* (aussi connues sous le nom des 2,5-dihydro-1,3,4-oxadiazoles correspondantes) accompagné de 1-acétoxy-1-(*p*-méthoxyphényléthyl)diazènecarboxylate de méthyle. On a séparé les trois isomères et on les a identifiés par des méthodes spectroscopiques. Le 1-acétoxy-1-(*p*-méthoxyphényléthyl)diazènecarboxylate de méthyle est le produit majeur de l'oxydation dans le dichlorométhane. L'oxydation dans l'acide acétique ne fournit pas d'oxadiazolines, mais conduit à la formation du diazènecarboxylate ainsi qu'à de l'acétate de 1-(*p*-méthoxyphényl)éthyle. On n'a pas réussi dans nos tentatives d'isomériser le diazènecarboxylate en oxadiazolines par catalyse acide. Les constantes de vitesse des thermolyses de chacune des oxadiazolines effectuées à 50,4 °C sont approximativement les mêmes, soit environ $3,6 \times 10^{-5}$ s^{-1}, et elles conduisent toutes les deux à la formation d'acétoxy(méthoxy)carbène qui se réarrange en pyruvate de méthyle par transfert d'un groupe acétyle. Le carbène, qui réagit avec les isocyanates non encombrées pour conduire à un transfert du groupe méthoxycarbonyle vers le carbone et du groupe acétyle vers l'azote, peut être considéré comme équivalent à un anion acyle dans cette réaction.

Mots clés : acétoxy(méthoxy)carbène, diazène, oxadiazoline, isocyanate, (acétylamino)oxoacétate.

[Traduit par la Rédaction]

Introduction

Generation of dimethoxycarbene from 2,2-dimethoxy-5-(*p*-methoxyphenyl)-5-methyl-Δ^3-1,3,4-oxadiazoline was reported recently (1). The *p*-methoxyphenyl substituent provided an extra methoxy signal in the ^{1}H NMR spectrum and it lowered the temperature for generation of the carbene from about 110 °C (for the 5,5-dimethyl analogue) to about 50 °C. We decided to make the isomeric 2-acetoxy-2-methoxy-5-(*p*-methoxyphenyl)oxadiazolines because acetoxy(methoxy)carbene (also known as (acetyloxy)methoxymethylene), which had been generated earlier at 110 °C (2), might have interesting properties, similar to those of acetoxy(methylthio)carbene that were reported in 2005, Scheme 1 (2). The diastereomers were separated and identified. We now report their spectra and rate constants for their thermolysis to carbonyl ylides that, in turn, fragment rapidly to acetoxy(methoxy)carbene. The carbene was intercepted with various isocyanates to afford methyl (acetylamino)oxoacetates.

Received 27 February 2006. Accepted 9 June 2006. Published on the NRC Research Press Web site at http://canjchem.nrc.ca on 27 July 2006.

W. Sokol and J. Warkentin.[1] Department of Chemistry, McMaster University, Hamilton, ON L8S 4M1, Canada.

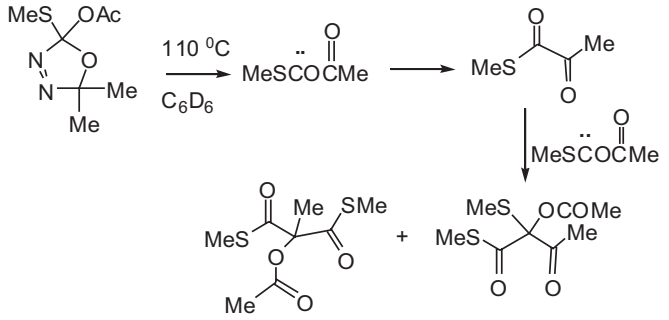
[1]Corresponding author (e-mail: warkent@mcmaster.ca).

Results and discussion

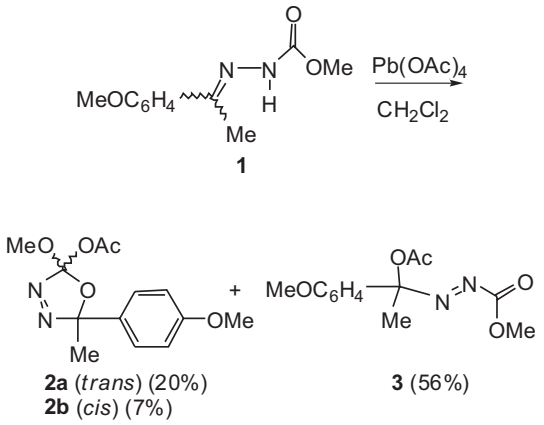
The isomeric oxadiazolines, **2a** and **2b** (also known as corresponding 2,5-dihydro-1,3,4-oxadiazoles), were prepared by oxidative cyclization (3) of a mixture of the (*E*)- and (*Z*)-methoxycarbonylhydrazones (**1**) of *p*-methoxy-

 doi:10.1139/V06-109 © 2006 NRC Canada

Scheme 1.



Scheme 2.



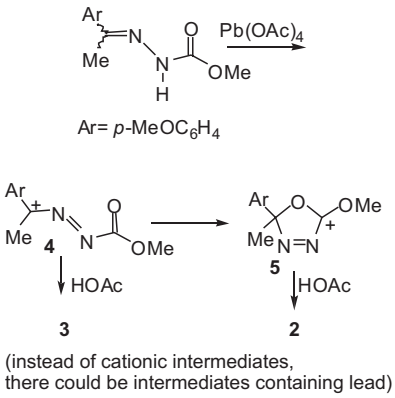
acetophenone with lead tetraacetate in dichloromethane. The products isolated were **2a** (20%), **2b** (7%), and a surprisingly large amount of an acyclic isomer **3** (ca. 56%) (Scheme 2). Oxidation in dry acetic acid did not produce **2** but gave **3** (28%) as well as 1-(*p*-methoxyphenyl)ethyl acetate (22%).

The formation of **3** as a major oxidation product (Scheme 2) suggests that there are cationlike precursors of the type **4** and **5** (Scheme 3). Exchange of acetoxy for methoxy, allyloxy (4), or other hydroxyl-containing groups under conditions of acid catalysis supports the intermediacy of ions such as **4** under exchange conditions. Probably, ion **4** does not cyclize easily to **5** because the stabilization afforded by the *p*-methoxyphenyl group is lost if the species cyclizes.

Cyclization in acetic acid was explored in the expectation that better solvation of cationlike intermediates would lessen the energy difference between **4** and **5**. Oxidation in acetic acid did not result in any oxadiazolines **2**. Attempts to isomerize **3** into a mixture of the diastereomers **2** by means of acid catalysis (CF_3CO_2H–CH_3CO_2H in CH_2Cl_2) did not succeed either. In the latter case, equal amounts of *p*-methoxyacetophenone and 1-(*p*-methoxyphenyl)ethyl acetate (**6**) (22%) were obtained. We suggest that those arise through the reactions shown in Scheme 4.

The ratio in which oxadiazolines **2a** and **2b** were formed by oxidation of **1** (Scheme 2) suggested that **2b** is more hindered and that it was expected to thermolyse more rapidly than **2a**. Oxadiazolines **2a** and **2b** are expected to undergo thermolysis by concerted 1,3-dipolar cycloreversion, to afford carbonyl ylides **7a**–**7d** (Scheme 5). The cycloreversion

Scheme 3.



of an oxadiazoline is a disrotatory process, requiring that cis substituents at C-2 and C-5 rotate either both inward (endo) or both outward (exo) (5). Substituents in a trans relationship place one group endo and the other exo. Assuming that the aryl group has the largest steric requirement at C-5 and that polar effects are less important, one would predict that oxadiazoline **2a** would form ylide **7b** in preference to **7a**. Similarly, **2b** should form **7c** in preference to **7d** (Scheme 5). There was little hope of trapping those ylides, whose lifetimes are probably very short (6, 7), with barriers to fragmentation to carbene and ketone of only a few kcal mol^{-1} (1 cal = 4.184 J), but rate constants for thermolysis of the isomeric precursors could be measured. Those rate constants are a measure of the difference between ground-state and transition-state energies.

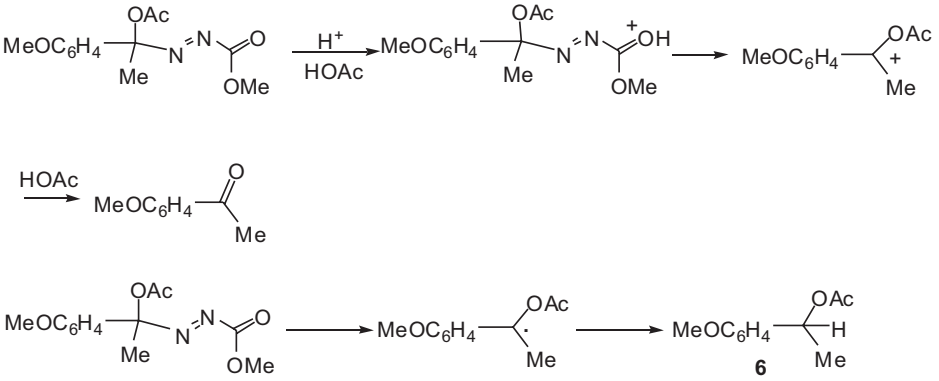
It turned out that **2b** does thermolyse faster than **2a** (3.74×10^{-5} s^{-1} vs. 3.49×10^{-5} s^{-1} in benzene at 50.4 °C). Isomer **2b** should have a higher ground-state energy than isomer **2a**, while the transition states for thermolysis of the isomers could be more nearly isoenergetic. Of course, the fact that **2b** could place both larger substituents exo (**7c**, Scheme 5) should favour its thermolysis additionally, but there would be a statistical penalty (a factor ≤ 2) involved in a restriction that favours outward rotation of the larger groups. The result suggests that the difference between the steric factors that operate in **2a** and **2b** is relatively small and probably partly compensated for by the statistical factor.

The putative carbonyl ylide intermediate shown in Scheme 5 has never been observed. Computations (7) on the dimethyl analog (rather than aryl methyl as in Scheme 2) indicate that the ylide is a real intermediate with a barrier to fragmentation to acetoxy(methoxy)carbene and ketone of about 2 to 3 kcal mol^{-1}. Although the aryl group of **7** could change that barrier, a change large enough to make the ylide trappable by conventional 1,3-dipolarophiles is hard to imagine. In an attempt to trap the ylide, thermolysis was carried out in neat phenyl isothiocyanate, which has been shown to trap carbonyl ylides (8). The ^1H NMR spectrum of the crude product showed *p*-methoxyacetophenone as the major product (>85%) with the characteristic pair of doublets at low field.

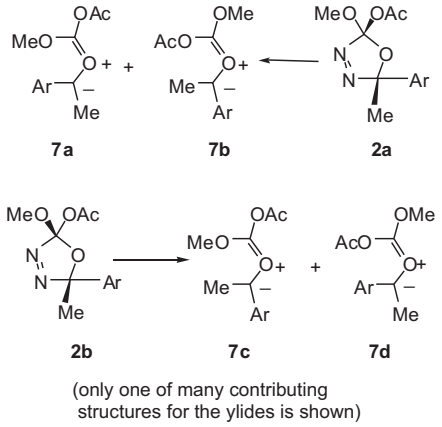
Evidence of the intermediacy of acetoxy(methoxy)carbene (**9**) (also known as (acetyloxy)methoxymethylene) came from two sources. First, it is known from both experiment (9) and theory (6) that the carbene rearranges to methyl

© 2006 NRC Canada

Scheme 4.



Scheme 5.



pyruvate (**10**). That product could be detected by ^{1}H NMR spectroscopy during kinetic runs in C_6D_6, but amounted to only 5% of the signal from *p*-methoxyacetophenone at 30% reaction and only about 2% when essentially all of the oxadiazoline had fragmented (Scheme 6). The reason for the low yield lies in the fact that methyl pyruvate is very self-reactive and does not survive the reaction conditions (10).

Rearrangement of acetoxy(methoxy)carbene to methyl pyruvate could be suppressed, but not eliminated, by an isocyanate (**11**) at high concentration. The pyruvate could always be detected (≤2%) among the crude reaction products. Eight isocyanates, with a variety of functional groups ranging from unhindered alkyl to hindered alkyl and from phenyl to variously substituted phenyls (Scheme 7) at nitrogen were treated with **2** at 50.4 °C. A liquid isocyanate (1 equiv. or more) was mixed with the liquid oxadiazolines **2** prior to degassing and heating. Homogeneous solutions resulted. A solid isocyanate, melting near 50 °C, and **2** gave a homogeneous solution immediately after the mixture had been heated to 50.4 °C. In the cases of aryl or alkyl isocyanates, except for *tert*-butyl isocyanate, reaction occurred to yield methyl (acetylamino)oxoacetates **12** (Scheme 7). Yields, not optimized, ranged from 48% for isopropyl isocyanate to 76% for phenyl isocyanate, after flash chromatography on silica. Product **12c** was obtained simply by washing the crude with ethyl acetate – hexane. Compound **12c** and other solid products from column chromatography were recrystallized from a benzene–hexane mixture. *tert*-Butyl isocyanate afforded many products (many OMe signals in the ^{1}H NMR spectrum), suggestive of extensive rearrangement of the carbene and subsequent reactions of methyl pyruvate. Although the isocyanate appeared to be unchanged (only one *tert*-butyl signal in the ^{1}H NMR spectrum), a low yield of the appropriate **12** (<5%) could not be excluded. Neat phenyl isothiocyanate mixed 1:1 with **2** also did not afford any of the expected product.

A possible mechanism for the reaction of **9** with isocyanates is shown in Scheme 7. Acetoxy(methoxy)carbene must be nucleophilic toward isocyanates. Although that carbene has not been placed on a nucleophilicity scale (11), it is probably ambiphilic toward alkenes. Trifluoroethoxy(methoxy)carbene is ambiphilic toward alkenes (12) and the acetoxy is only a little poorer than trifluoroethoxy as an electron donor (13). However, philicity depends on the partner; for example, acetic acid is acidic towards water and basic towards sulfuric acid.

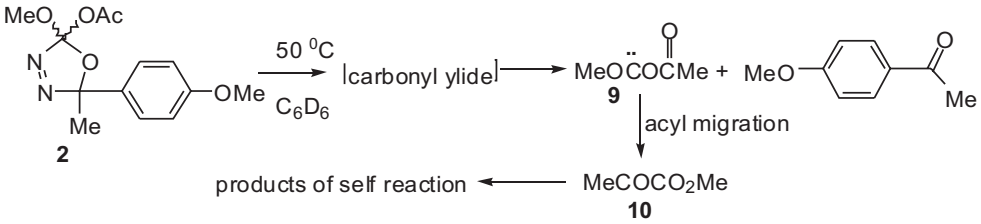
A nucleophilic singlet carbene is expected to attack an isocyanate at the carbonyl carbon atom to generate zwitterion **12** or it could add to either double bond in a concerted process. However, the three-membered rings resulting from the latter process would have to undergo ring opening and acetyl transfer (2) to arrive at the product. Model α-lactams or iminooxiranes with *gem*-dialkoxy and carboxylate functions at the ring carbons, which could help to resolve the latter aspect, are unknown and there was no evidence for ring formation in the present case. On the other hand, there are many precedents for formation of zwitterionic intermediates in nonpolar solvents (14).

α-Lactams and iminooxiranes that could form by ring closure of **12** may well be unstable at 50 °C. Lengyel et al. (15) reported that α-lactams that are thermally unstable and chemically reactive afford 3-benzylamino products upon reaction with benzyl amine (Scheme 8). A possible explanation of that result is that such lactams open easily to zwitterions of the type **12**. Such an open form of an α-lactam was invoked by Ohshiro et al. (16) to account for the product from a reaction with a vinyl isocyanate (Scheme 9). There is also good evidence that *gem*-dialkoxycyclopropanes undergo thermal ring opening at moderate temperatures (17–20). In the present case, the negative charge of an intermediate is dispersed by conjugation, making it more likely that a three-membered-ring system (not shown in Scheme 7) would either not be formed or would open easily to **12**.

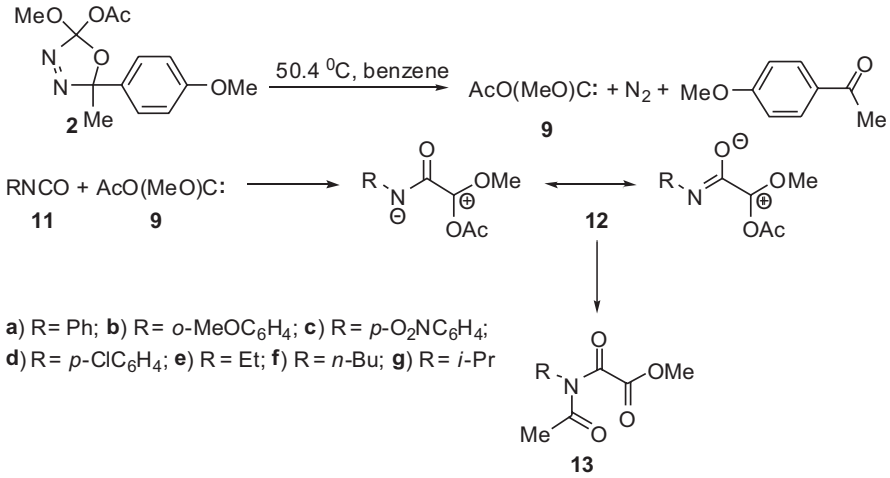
Phenyl isothiocyanate is known to be less reactive, by a

© 2006 NRC Canada

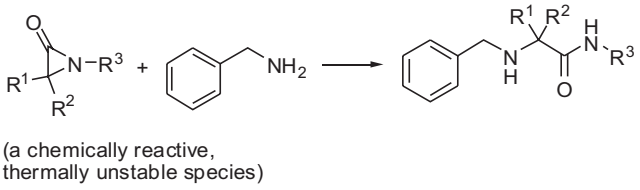
Scheme 6.



Scheme 7.



Scheme 8.



factor of 11, than phenyl isocyanate toward dimethoxycarbene at 140 °C (21). With a less nucleophilic carbene (acetoxy(methoxy)carbene) and a lower temperature (50.4 rather than 140 °C), the difference in reactivity between phenyl isocyanate and phenyl isothiocyanate could well be larger than 11. A product analogous to **12** (Scheme 7) was not obtained with phenyl isothiocyanate.

Summary

Diastereomeric oxadiazoline sources of acetoxy(methoxy)carbene were synthesized, separated, and fully characterized. Their thermolyses in benzene at 50.4 °C occurred with roughly equal rate constants (ca. 3.6×10^{-5} s^{-1}) and they afforded acetoxy(methoxy)carbene. The carbene reacted with various isocyanates to add the methoxycarbonyl group at carbon and the acetyl group at nitrogen. In its addition at carbon, the carbene behaved as an acyl anion equivalent.

Experimental

NMR spectra were taken with Bruker Avance 600 MHz and Bruker Avance 200 MHz instruments operating at frequencies given in each section. IR spectra came from a Bio Rad FTS 40 spectrometer and mass spectra were run with a Waters Micromass GCT instrument. Melting points were measured with a Uni-Melt Thomas Hoover capillary melting point apparatus. Yields were not optimized.

2-Acetoxy-2-methoxy-5-(*p*-methoxyphenyl)-5-methyl-Δ^3-1,3,4-oxadiazoline (2)

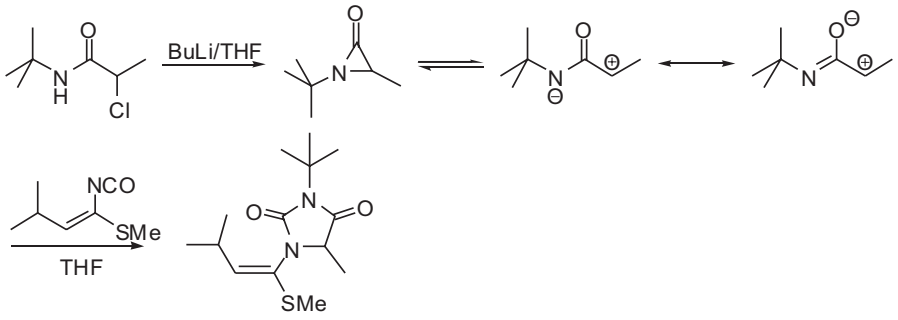
Lead tetraacetate (7.49 g, 16.05 mmol, 95% purity) was dissolved in dichloromethane (50 mL), the solution was cooled to about 0 °C, and the methoxycarbonylhydrazones of *p*-methoxyacetophenone (3.61 g, 16.24 mmol) were added in the solid state. After 0.5 h the temperature had risen to 25 °C and the mixture was stirred for an additional 4 h. It was filtered through a bed of Celite to afford a clear solution. The Celite cake was extracted with dichloromethane (2 × 25 mL) and the combined organic solution was washed twice with aqueous sodium bicarbonate (2 × 25 mL) and dried over $MgSO_4$. Evaporation of the solvent at room temperature left 4.84 g of crude product. The ^{1}H NMR spectrum of the mixture revealed the ratios of isomers **3**:**2a**:**2b** as 67.1:24.4:8.5. The products were purified by flash-chromatography on silica with diethyl ether – hexane (25:75) as eluent. Isolated were **3** (2.53 g, 9.02 mmol, 56%) and the diastereomers **2a** and **2b** (1.10 g, 3.91 mmol, 24.4%). Separation of the oxadiazolines was carried out by centrifugal chromatography with a Chromatotron® apparatus.

trans-2-Acetoxy-2-methoxy-5-(*p*-methoxyphenyl)-5-methyl-Δ^3-1,3,4-oxadiazoline (2a, major diastereomer)

Pale pink oil. IR (neat, cm^{-1}): 3000, 2955, 2843, 1774, 1612, 1514, 1446, 1372, 1306, 1253, 1032, 834. ^{1}H NMR

© 2006 NRC Canada

Scheme 9.



(200.2 MHz, $CDCl_3$, ppm) δ: 1.88 (s, 3H, CH_3), 2.15 (s, 3H, $COCH_3$), 3.47 (s, 3H, OCH_3), 3.78 (s, 3H, $C_6H_4OCH_3$), 6.87 (d, J = 8.9 Hz, 2H, CH_{Ar}), 7.44 (d, J = 8.9 Hz, 2H, CH_{Ar}). ^{1}H NMR (200.2 MHz, C_6D_6, ppm) δ: 1.53 (s, 3H, CH_3), 1.95 (s, 3H, CH_3), 3.24 (s, 3H, OCH_3), 3.29 (s, 3H, OCH_3), 6.70 (d, J = 8.9 Hz, 2H, CH_{Ar}), 7.49 (d, J = 8.9 Hz, 2H, CH_{Ar}). ^{13}C NMR (50.3 MHz, $CDCl_3$, ppm) δ: 21.43 ($COCH_3$), 24.95 (CH_3), 52.87 (OCH_3), 55.23 ($C_6H_4OCH_3$), 113.87 (CH_{Ar}), 124.10 (C_{benzyl}), 126.41 (CH_{Ar}), 130.41 (C_{Ar}), 135.11 (C_{ring}), 159.77 (C_{Ar}—O), 166.36 (CO). ^{13}C NMR (50.3 MHz, C_6D_6, ppm) δ: 20.69 (CH_3), 24.85 (CH_3), 52.57 (OCH_3), 54.74 (OCH_3), 114.16 (CH_{Ar}), 124.45 (C_{benzyl}), 126.87 (CH_{Ar}), 131.34 (C_{Ar}), 135.86 (C_{ring}), 160.21 (C_{Ar}—O), 166.23 (CO). HRMS (CI, NH_3) m/z calcd. for $C_{13}H_{17}N_2O_5$: 281.1137 $(MH)^+$; found: 281.1159.

Assignments of the NMR signals are based on 2D correlation spectra. Gradient HMBC and gradient HSQC spectra were run in $CDCl_3$ with a Bruker AV 600 instrument. The relative configurations of substituents at C-2 and C-5 was established at the same time on the basis of a selective 1D NOESY experiment with a pulsed field gradient, with the pulse delay set at 5.0 s and the NOESY mixing time set at 0.6 s. Irradiation of the signal at 1.88 ppm caused enhancement of the signal at 7.44 ppm. Similarly, irradiation at 3.47 ppm caused strong enhancement at 2.15 and 7.44 ppm and weak enhancement at 6.87 ppm, while irradiation at 3.78 ppm caused signal enhancement at 6.87 ppm.

cis-2-Acetoxy-2-methoxy-5-(*p*-methoxyphenyl)-5-methyl-Δ^3-1,3,4-oxadiazoline (2b, minor diastereomer)

Pale yellow oil. IR (neat, cm^{-1}): 2993, 2955, 2843, 1776, 1612, 1515, 1445, 1372, 1306, 1253, 1080, 1031, 834. ^{1}H NMR (200.2 MHz, $CDCl_3$, ppm) δ: 1.82 (s, 3H, CH_3), 2.00 (s, 3H, $COCH_3$), 3.62 (s, 3H, OCH_3), 3.78 (s, 3H, $C_6H_4OCH_3$), 6.87 (d, J = 8.9 Hz, 2H, CH_{Ar}), 7.40 (d, J = 8.9 Hz, 2H, CH_{Ar}). ^{1}H NMR (200.2 MHz, C_6D_6, ppm) δ: 1.41 (s, 3H, CH_3), 1.62 (s, 3H, CH_3), 3.22 (s, 3H, OCH_3), 3.35 (s, 3H, OCH_3), 6.70 (d, J = 8.9 Hz, 2H, CH_{Ar}), 7.52 (d, J = 8.9 Hz, 2H, CH_{Ar}). ^{13}C NMR (50.3 MHz, $CDCl_3$, ppm) δ: 21.28 ($COCH_3$), 26.53 (CH_3), 52.95 (OCH_3), 55.23 ($C_6H_4OCH_3$), 113.81 ($2CH_{Ar}$), 123.83 (C_{benzyl}), 126.32 ($2CH_{Ar}$), 129.67 (C_{Ar}), 134.98 (C_{ring}), 159.77 (C_{Ar}—O), 166.06 (CO). ^{13}C NMR (50.3 MHz, C_6D_6, ppm) δ: 20.62 (CH_3), 26.68 (CH_3), 52.53 (OCH_3), 54.7 (OCH_3), 114.10 ($2CH_{Ar}$), 123.86 (C_{benzyl}), 126.83 ($2CH_{Ar}$), 130.58 (C_{Ar}), 135.83 (C_{ring}), 160.21 (C_{Ar}—O), 165.42 (CO).

The relative configurations of substituents at C-2 and C-5 were established on the basis of selective 1D NOESY experiments with a pulsed field gradient, as described previously. Selective irradiation at 1.82 ppm caused signal enhancements at 3.62 and 7.44 ppm, while irradiation at 2.00 ppm caused strong enhancement at 7.40 ppm and medium enhancement at 3.62 ppm. Irradiation at 3.62 and 3.78 ppm caused enhancements of signals at 1.82 and 6.87 ppm, respectively.

Acyclic isomer 3

Lemon yellow oil. IR (neat, cm^{-1}): 2960, 2842, 1770, 1611, 1514, 1439, 1371, 1305, 1252, 1110, 1029, 835. ^{1}H NMR (200.2 MHz, $CDCl_3$, ppm) δ: 2.00 (s, 3H), 2.13 (s, 3H), 3.76 (s, 3H), 3.94 (s, 3H), 6.88 (d, J = 8.9 Hz, 2H), 7.42 (d, J = 8.9 Hz, 2H). ^{1}H NMR (200.2 MHz, C_6D_6, ppm) δ: 1.73 (s, 3H), 2.00 (s, 3H), 3.218 (s, 3H), 3.222 (s, 3H) (these signals not resolved), 6.72 (d, J = 8.9 Hz, 2H), 7.46 (d, J = 8.9 Hz, 2H). ^{13}C NMR (50.3 MHz, $CDCl_3$, ppm) δ: 21.53, 23.87, 54.75, 55.07, 102.07, 113.84, 126.98, 130.43, 159.59, 161.75, 168.31. ^{13}C NMR (50.3 MHz, C_6D_6, ppm) δ: 21.17, 24.29, 54.04, 54.71, 102.28, 114.23, 127.53, 131.42, 160.17, 162.50, 167.81. HRMS (CI, NH_3) m/z calcd. for $C_{13}H_{17}N_2O_5$: 281.1137 $(MH)^+$; found: 281.1130.

Thermolysis of oxadiazolines

A solution of **2b** (0.1837 mmol) and *tert*-butylbenzene (0.1021 mmol) in C_6D_6 (1 mL), in an NMR tube fitted with a ground glass joint, was degassed by means of three freeze–pump–thaw cycles before the tube was sealed and heated at 50.4 °C. Oxadiazoline **2a** (0.2498 mmol) and *tert*-butylbenzene (0.1512 mmol) were treated analogously. Every 3 h, ^{1}H NMR spectra were acquired with the tubes still sealed and with a pulse delay of 6 s to ensure complete relaxation. For **2b**, the signal at 1.41 ppm was integrated and compared with the signal of *tert*-butylbenzene at 1.20 ppm. For **2a**, the signal at 1.95 ppm was integrated and compared with the signal of *tert*-butylbenzene. Standard first-order treatment of the data gave $k_{\mathbf{2b}} = 3.74 \times 10^{-5}$ s^{-1} (seven points, $R2$ = 0.9914) and $k_{\mathbf{2a}} = 3.49 \times 10^{-5}$ s^{-1} (seven points, $R2$ = 0.9920).

Attempt to cyclize 3

A solution of **3** (0.32 g, 1.14 mmol) and trifluoroacetic acid (0.012 g, 0.105 mmol, 10 mol%) in acetic acid (25 mL) was stirred at room temperature for 9 days. The mixture was diluted with water (25 mL) and extracted with dichloromethane (3 × 15 mL). The solution in dichloromethane was then washed with aqueous sodium bicarbonate to remove acids and dried over $MgSO_4$. After flash chromatography on

© 2006 NRC Canada

silica with diethyl ether – hexane (25:75), *p*-methoxyacetophenone (0.038 g, 0.25 mmol, 22%), 1-(*p*-methoxyphenyl)ethyl acetate (0.049 g, 0.25 mmol, 22%), and unreacted **3** (0.178 g, 0.634 mmol, 55%) were obtained.

1-(*p*-Methoxyphenyl)ethyl acetate

Colourless oil. IR (neat, cm^{-1}): 2983, 2938, 2839, 1735, 1614, 1516, 1372, 1242, 1063, 1035, 832. ^1H NMR (200.2 MHz, $CDCl_3$, ppm) δ: 1.50 (d, J = 6.5 Hz, 3H), 2.03 (s, 3H), 3.78 (s, 3H), 5.83 (q, J = 6.5 Hz, 1H), 6.86 (d, J = 8.7 Hz, 2H), 7.28 (d, J = 8.7 Hz, 2H). ^{13}C NMR (50.3 MHz, $CDCl_3$, ppm) δ: 21.33, 21.87, 55.17, 71.93, 113.74, 127.53, 133.64, 159.18, 170.32.

Thermolysis of oxadiazolines in the presence of isocyanates

All isocyanates except **11c** and **11d** are liquids at room temperature. The liquids except isopropyl isocyanate were freshly distilled before use. The isopropyl compound was used as received from Sigma-Aldrich. *p*-Chlorophenyl isocyanate and *p*-nitrophenyl isocyanate melted at 28–30.5 and 56–60 °C, respectively.

A mixture of **2** (1.00 mmol) and isocyanate (0.96–1.63 mmol), placed in an ampoule, was degassed by means of three freeze–pump–thaw cycles before the ampoule was sealed and heated at 50.4 °C for 41 h. A large excess of isocyanate was avoided after initial experiments with a two-fold excess indicated that a considerable amount of residual isocyanate hindered isolation of **12**. The crude reaction mixture was analysed by ^1H NMR spectroscopy before pure products were isolated as described.

Reaction of 2 with phenyl isocyanate

Heating **2** with 1.28 equiv. of *p*-chlorophenyl isocyanate gave **12a**, which was isolated by means of flash chromatography on silica with ethyl acetate – hexane (20:80) as eluent. Yield of colourless oil: 76%. IR (neat, cm^{-1}): 3064, 3018, 2958, 1750, 1729, 1706, 1597, 1439, 1370, 1343, 1273, 1235, 1140, 1046, 756, 733, 698. ^1H NMR (200.2 MHz, $CDCl_3$, ppm) δ: 2.01 (s, 3H), 3.90 (s, 3H), 7.19–7.25 (m, 2H), 7.44–7.52 (m, 3H). ^{13}C NMR (50.3 MHz, $CDCl_3$, ppm) δ: 24.37, 52.90, 128.38, 129.84, 130.08, 135.67, 161.72, 162.52, 172.45. HRMS (CI, NH_3) m/z calcd. for $C_{11}H_{12}NO_4$: 222.0766 $(MH)^+$; found: 222.0760.

Reaction of 2 with *o*-methoxyphenyl isocyanate

Heating **2** with 1.63 equiv. of the isocyanate and flash chromatography of the crude products on silica with ethyl acetate – hexane (32:68) gave **12b** in 74% yield as pale yellow crystals, mp 115.5–118.5 °C. IR (NaCl, cm^{-1}): 3018, 2960, 2946, 1755, 1729, 1705, 1600, 1436, 1346, 1283, 1253, 1146, 1023, 754. ^1H NMR (200.2 MHz, $CDCl_3$, ppm) δ: 1.99 (s, 3H), 3.84 (s, 3H), 3.91 (s, 3H), 7.00–7.09 (m, 2H), 7.16–7.21 (m, 1H), 7.39–7.48 (m, 1H). ^{13}C NMR (50.3 MHz, $CDCl_3$, ppm) δ: 23.48, 52.81, 55.86, 112.25, 121.36, 124.27, 129.68, 131.44, 155.01, 161.88, 162.34, 172.95. HRMS (CI, NH_3) m/z calcd. for $C_{12}H_{14}NO_5$: 252.0872 $(MH)^+$; found: 252.0875.

Reaction of 2 with *p*-nitrophenyl isocyanate

Heating **2** with 1.50 equiv. of *p*-nitrophenyl isocyanate gave a crude product that was not chromatographed, but was washed with ethyl acetate – hexane (35:65) to afford yellow crystals of **12c** (mp 107.0–110.0 °C) in 72% yield. IR (NaCl, cm^{-1}): 3118, 3082, 2955, 1752, 1732, 1710, 1597, 1530, 1352, 1271, 1236, 1141, 855, 750, 699. ^1H NMR (200.2 MHz, $CDCl_3$, ppm) δ: 2.08 (s, 3H), 3.90 (s, 3H), 7.45 (d, J = 9.08 Hz, 2H), 8.37 (d, J = 9.08 Hz, 2H). ^{13}C NMR (50.3 MHz, $CDCl_3$, ppm) δ: 24.54, 53.18, 125.36, 129.93, 141.22, 148.42, 161.04, 162.11, 170.97. HRMS (CI, NH_3) m/z calcd. for $C_{11}H_{11}N_2O_6$: 267.0617 $(MH)^+$; found: 267.0609.

Reaction of 2 with *p*-chlorophenyl isocyanate

Heating **2** with 1.08 equiv. of the isocyanate gave, after flash chromatography and recrystallization from benzene–hexane (50:50), 57% of **12d** as white crystals melting at 115.5–117.5 °C. IR (NaCl, cm^{-1}): 3098, 3076, 2956, 1752, 1727, 1706, 1341, 1275, 1237, 1145, 1095, 1041, 832, 770, 720, 675, 635. ^1H NMR (200.2 MHz, $CDCl_3$, ppm) δ: 2.03 (s, 3H), 3.90 (s, 3H), 7.17 (d, J = 8.75 Hz, 2H), 7.47 (d, J = 8.75 Hz, 2H). ^{13}C NMR (50.3 MHz, $CDCl_3$, ppm) δ: 24.44, 53.03, 129.86, 130.41, 134.17, 136.09, 161.49, 162.41, 171.98. HRMS (CI, NH_3) m/z calcd. for $C_{11}H_{11}NO_4Cl$: 256.0377 $(MH)^+$; found: 256.0339.

Reaction of 2 with ethyl isocyanate

Heating **2** with 1.37 equiv. of the isocyanate gave, after flash chromatography on silica with ethyl acetate – hexane (35:65) as eluent, product **12e** as a pale yellow oil in 55% yield. IR (neat, cm^{-1}): 2986, 2960, 1752, 1720, 1695, 1438, 1380, 1350, 1260, 1217, 1142, 1071, 1009, 781, 735, 635. ^1H NMR (200.2 MHz, $CDCl_3$, ppm) δ: 1.20 (t, J = 7.1 Hz, 3H), 2.30 (s, 3H), 3.69 (q, J = 7.1 Hz, 2H), 3.81 (s, 3H). ^{13}C NMR (50.3 MHz, $CDCl_3$, ppm) δ: 13.66, 23.16, 39.02, 52.63, 161.93, 162.60, 172.47. HRMS (CI, NH_3) m/z calcd. for $C_7H_{12}NO_4$: 174.0766 $(MH)^+$; found: 174.0768.

Reaction of 2 with *n*-butyl isocyanate

Flash chromatography on silica with ethyl acetate – hexane (20:80) gave, after heating **2** with 0.96 equiv. of **11f** and 55% of **12f** as a colourless oil. IR (neat, cm^{-1}): 2963, 2877, 1754, 1724, 1701, 1464, 1437, 1379, 1349, 1282, 1233, 1202, 1145, 1078, 1019, 735, 638. ^1H NMR (200.2 MHz, $CDCl_3$, ppm) δ: 0.89 (t, J = 7.2 Hz, 3H), 1.22–1.41 (m, 2H), 1.47–1.62 (m, 2H), 2.29 (s, 3H), 3.57–3.64 (m, 2H), 3.81 (s, 3H). ^{13}C NMR (50.3 MHz, $CDCl_3$, ppm) δ: 13.49, 19.84, 23.16, 30.65, 43.73, 52.60, 161.94, 162.81, 172.65. HRMS (CI, NH_3) m/z calcd. for $C_9H_{16}NO_4$: 202.1079 $(MH)^+$; found: 202.1040.

Reaction of 2 with isopropyl isocyanate

Heating **2** with 1.08 equiv. of **11g** gave **12g** by means of flash chromatography on silica, with ethyl acetate – hexane (28:72) as eluent. The product was obtained as a pale yellow oil in 48% yield. IR (neat, cm^{-1}): 3012, 2980, 2957, 1750, 1718, 1696, 1438, 1403, 1368, 1331, 1283, 1212, 1183, 1110, 1055, 1009, 770, 728, 638. ^1H NMR (200.2 MHz, $CDCl_3$, ppm) δ: 1.42 (d, J = 6.9 Hz, 6H), 2.29 (s, 3H), 3.79 (s, 3H), 4.16 (sept, J = 6.9 Hz, 1H). ^{13}C NMR (50.3 MHz,

© 2006 NRC Canada

$CDCl_3$, ppm) δ: 19.65, 23.96, 50.19, 52.55, 161.48, 163.53, 173.41. HRMS (CI, NH_3) *m/z* calcd. for $C_8H_{14}NO_4$: 188.0923 $(MH)^+$; found: 188.0922.

Acknowledgements

The authors thank the Natural Sciences and Engineering Research Council of Canada (NSERC) for continued financial support and the Department of Chemistry of McMaster University for office and laboratory space as well as access to spectroscopy facilities.

References

1. H. Zhou, G. Mloston, and J. Warkentin. Org. Lett. **7**, 487 (2005).
2. A. Klys, W. Czardybon, J. Warkentin, and N.H. Werstiuk. Can. J. Chem. **83**, 1360 (2005).
3. For example: X. Lu, D.L. Reid, and J. Warkentin. Can. J. Chem. **79**, 319 (2001).
4. D. Plazuk, J. Warkentin, and N.H. Werstiuk. Tetrahedron, **61**, 5788 (2005).
5. (*a*) T.L. Gilchrist and R.L. Storr. Organic reactions and orbital symmetry. 2nd ed. Cambridge University Press, Cambridge, UK. 1979; (*b*) M.W. Majchrzak and J. Warkentin. Can. J. Chem. **67**, 1753 (1989); Erratum: Can. J. Chem. **68**, 795 (1990).
6. W. Czardybon, J. Warkentin, and N.H. Werstiuk. J. Phys. Org. Chem. **18**, 486 (2005).
7. W. Czardybon, J. Warkentin, and N.H. Werstiuk. J. Org. Chem. **70**, 8431 (2005).
8. T. Ibata, H. Nakano, and H. Tamura. Bull. Chem. Soc. Jpn. **65**, 1362 (1992).
9. W. Czardybon, A. Klys, J. Warkentin, and N.H. Werstiuk. Can. J. Chem. **81**, 1438 (2003).
10. S. Sugiyama, A. Ohkawa, M. Fujiwara, and H. Hayashi. Chem. Express, **5**, 57 (1990).
11. (*a*) R.A. Moss. Acc. Chem. Res. **13**, 58 (1980); (*b*) R.A. Moss. Acc. Chem. Res. **22**, 15 (1989).
12. C.-S. Ge, E.A. Jefferson, and R.A. Moss. Tetrahedron Lett. **34**, 7549 (1993).
13. R.A. Moss, X. Song, and W. Liu. J. Am. Chem. Soc. **116**, 1583 (1994).
14. (*a*) V. Nair, A. Deepthi, M. Poonoth, B. Santhamma, S. Vellalath, B.P. Babu, R. Mohan, and E. Suresh. J. Org. Chem. **71**, 2313 (2006); (*b*) V. Nair, B.P. Beneesh, V. Sreekumar, S. Bindu, R.S. Menon, and A. Deepthi. Tetrahedron Lett. **46**, 201 (2005); (*c*) A.A. Ismaeili and H. Zendegani. Tetrahedron, **61**, 4031 (2005); (*d*) H. Zhou, G. Mloston, and J. Warkentin. Org. Lett. **7**. 487 (2005); (*e*) H. Giera, R. Huisgen, E. Langhals, and K. Polborn. Helv. Chim. Acta, **85**, 1523 (2002).
15. I. Lengyel, V. Cesare, S. Chen, and T. Taldone. Heterocycles, **57**, 677 (2002).
16. Y. Ohshiro, M. Komatsu, A. Okamura, and T. Agawa. Bull. Chem. Soc. Jpn. **57**, 901 (1984).
17. (*a*) M.L. Graziano and M.R. Iesce. J. Chem. Res. Synop. 362 (1987); (*b*) M.L. Graziano and G. Cimminiello. J. Chem. Res. Synop. 42 (1989); (*c*) M.L. Graziano and S. Chiosi. J. Chem. Res. Synop. 44 (1989); (*d*) M.L. Graziano, M.R. Iesce, F. Cermola, and G. Cimminiello. J. Chem. Res. Synop. 4 (1992); (*e*) M.L. Graziano, M.R. Iesce, and F. Cermola. J. Chem. Res. Synop. 82 (1996); (*f*) M.L. Graziano, M.R. Iesce, and F. Cermola. Synthesis, 1994 (1999); (*g*) M.L. Graziano, M.R. Iesce, F. Cermola, G. Caputo, and F. De Lorenzo. J. Chem. Soc. Perkin Trans. 1, 664 (2002); (*h*) M.L. Graziano and V. Piccialli. Tetrahedron Lett. **40**, 8469 (2004); (*i*) F. Cermola, L. Di Gioia, M.L. Graziano, and M.R. Iesce. J. Chem. Res. 677 (2005).
18. H.-U. Reissig and R. Zimmer. Chem. Rev. **103**, 1151 (2003).
19. S. Shimada, Y. Hashimoto, A. Sudo, M. Hasegawa, and K. Saigo. J. Org. Chem. **57**, 7126 (1992).
20. T. Tsuji and S. Nishida. Acc. Chem. Res. **17**, 56 (1984).
21. R.W. Hoffmann, K. Steinbach, and B. Dittrich. Chem. Ber. **76**, 2174 (1976).

© 2006 NRC Canada

Direct detection of methylphenylgermylene and 1,2-dimethyl-1,2-diphenyldigermene — Kinetic studies of their reactivities in solution

William J. Leigh, Ileana G. Dumbrava, and Farahnaz Lollmahomed

Abstract: Photolysis of 1,3,4-trimethyl-1-phenylgermacyclopent-3-ene (**5**) in hydrocarbon solvents containing isoprene, methanol, or acetic acid affords 2,3-dimethyl-1,3-butadiene (DMB) and the expected trapping products of methylphenylgermylene (GeMePh) in chemical yields exceeding 90%. The germylene has been detected in hexane solution by laser flash photolysis as a short-lived species (τ ~ 2 μs) exhibiting a UV–vis absorption spectrum centered at λ_{max} = 490 nm. It decays with second-order kinetics and a rate constant close to the diffusion-controlled limit, with the concomitant growth of a second longer-lived transient (λ_{max} = 420 nm) that is assigned to a mixture of (*E*)- and (*Z*)-1,2-dimethyl-1,2-diphenyldigermene (**4**). Absolute rate constants have been determined for the reactions of the germylene with primary and tertiary amines (*n*-$BuNH_2$ and Et_3N, respectively), acetic acid (AcOH), a terminal alkyne and alkene, isoprene, DMB, CCl_4, and the group 14 hydrides Et_3SiH and Bu_3SnH. GeMePh is slightly more reactive than $GePh_2$ towards all the reagents studied in this work; both are significantly less reactive than $GeMe_2$ toward the same substrates. Absolute rate constants for the reactions of **4** have also been measured or assigned upper limits in every case and are compared to previously reported values for tetraphenyl- and tetramethyl-digermene with the same reagents.

Key words: germylene, digermene, kinetics, laser flash photolysis, germirane, germirene, vinylgermirane, complex, UV–vis spectrum, insertion, addition.

Résumé : La photolyse du 1,3,4-triméthyl-1-phénylgermacyclopent-3-ène (**5**) dans des solvants hydrocarbonés contenant de l'isoprène, du méthanol ou de l'acide acétique conduit à la formation de 2,3-diméthylbuta-1,3-diène (DMB) et aux produits de piégeage attendus du méthylphénylgermylène (GeMePh) avec des rendements supérieurs à 90%. Faisant appel à la photolyse éclair au laser et opérant dans une solution d'hexane, on a détecté la présence du germylène sous la forme d'une espèce transitoire (τ d'environ 2μs) qui présente un spectre d'absorption UV–visible centré autour d'un λ_{max} de 490 nm. Sa décroissance présente une cinétique du second ordre et une constante de vitesse qui se rapproche de la limite d'un contrôle par la diffusion et qui est accompagnée de la croissance d'une deuxième espèce transitoire (λ_{max} = 420 nm) qui est attribuée à un mélange (*E*)- et (*Z*)-1,2-diméthyl-1,2-diphényldigermène (**4**). On a déterminé les constantes de vitesse absolues de la réaction du germylène avec des amines primaires et tertiaires (respectivement $BuNH_2$ et Et_3N), l'acide acétique (AcOH), un alcyne terminal, un alcène terminal, l'isoprène, le DMB, le CCl_4 et les hydrures du groupes 14, Et_3SiH et Bu_3SnH. Le GeMePh est légèrement plus réactif que le $GePh_2$ vis-à-vis tous les réactifs examinés dans ce travail; les deux sont toutefois beaucoup moins réactifs que le $GeMe_2$ par rapport aux même réactifs. Dans tous les cas, on a aussi mesuré ou attribué des valeurs limites supérieures pour les constantes de vitesses absolues de la réaction avec le composé (**4**) et on les a comparées aux valeurs rapportées antérieurement pour les réactions du tétraphényl- et du tétraméthyl-digermène avec les mêmes réactifs.

Mots clés : germylène, digermène, cinétique, photolyse éclair au laser, germirane, germirène, vinylgermirane, complexe, spectre UV–visible, insertion, addition.

[Traduit par la Rédaction]

Introduction

Germylenes are important intermediates in the thermal and photochemical reactions of germanium compounds (1), and the study of their synthesis and chemistry continues to be of considerable interest (2–6). Of particular fundamental and practical importance is the parent molecule, GeH_2, whose chemistry has been extensively studied in the gas phase by time-resolved kinetic methods.[2] Studies of several simple substituted derivatives by time-resolved spectroscopic methods in matrices and in solution have been reported,[3] but the solution-phase studies have been characterized by a particular lack of consistency in the spectroscopic properties and reactivities of these species (5). We have speculated that the problem is due to two main factors — the characteristic weakness of the lowest energy ($S_0 \rightarrow S_1$) electronic transition in divalent group 14 compounds and the pronounced complexity of the photochemistry of the particular organo-

Received 12 March 2005. Accepted 23 May 2006. Published on the NRC Research Press Web site at http://canjchem.nrc.ca on 9 August 2006.

W.J. Leigh,[1] I.G. Dumbrava, and F. Lollmahomed. Department of Chemistry, McMaster University, 1280 Main Street West, Hamilton, ON L8S 4M1, Canada.

[1]Corresponding author (e-mail: leigh@mcmaster.ca).

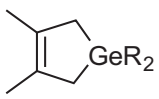
[2]See refs. 5 and 6 and the refs. cited therein.

[3]See ref. 5 for a complete bibliography.

 doi:10.1139/V06-107 © 2006 NRC Canada

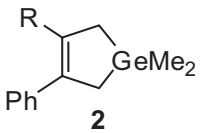
germanium compounds (typically oligogermanes and oligosilagermanes) that have been employed as germylene precursors (7). As we have recently demonstrated (8), the combination of these factors can make transient germylenes relatively difficult to detect, even when they are the major products of photolysis.

We recently reported the first comprehensive kinetic studies of the reactivities of diphenyl- and dimethyl-germylene ($GePh_2$ and $GeMe_2$, respectively) in hydrocarbon solution, generating and monitoring them directly by laser flash photolysis of the 1,1-disubstituted germacyclopent-3-ene derivatives **1** and **2** (9–11). Trapping experiments showed that photolysis of these molecules proceeds very cleanly and with remarkably high efficiency in every case, producing the expected trapping products of the germylenes along with the corresponding conjugated dienes in chemical yields exceeding 90% and quantum yields on the order of 0.5. Absolute rate constants were reported for dimerization of the two species, which yields the transient digermene derivatives **3**, and for their reaction with a variety of representative substrates such as aliphatic amines, halocarbons (RX), aliphatic alkynes, dienes and alkenes, oxygen, acetic acid, and the group 14 hydrides R_3MH (M = Si, Ge, Sn; R = ethyl or *n*-butyl). Several of the reactions of these species were found to be reversible, such as the [2+1]-cycloaddition reactions with alkenes and dienes, and Lewis acid–base complexation with tertiary amines; they are nonetheless very fast, with forward rate constants on the order of 10^9–10^{10} $(mol/L)^{-1}$ s^{-1} in hexane at room temperature. The absolute rate constants measured for the reactions of $GeMe_2$ with the C—C unsaturated compounds and oxygen in solution (11) were found to agree quite well with earlier data reported by Walsh and coworkers (6, 12) for reactions with the same or similar substrates in the gas phase. The solution-phase data for the two germylenes showed $GeMe_2$ to be significantly more reactive than its phenylated counterpart in every reaction that was studied. Rate constants were also reported for the reactions of the digermenes **3a** and **3b** in several cases, providing the first indications of the effects of methyl vs. phenyl substitution on the reactivity of digermene derivatives toward various nucleophilic and electrophilic reagents.



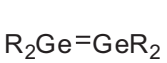
1

a: R = Ph
b: R = Me



2

a: R = H
b: R = Me

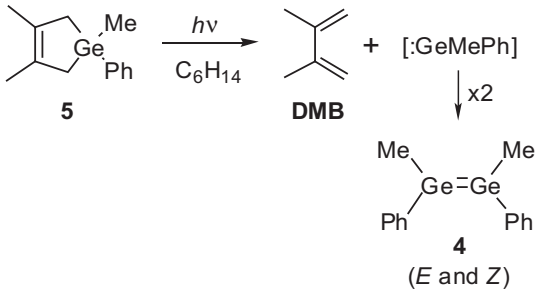


3

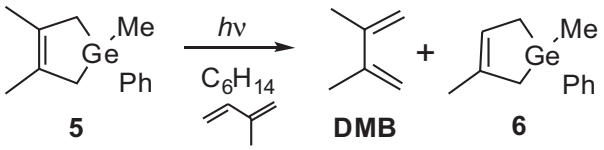
a: R = Ph
b: R = Me

Reasonably precise determination of equilibrium constants for the (reversible) reactions with C=C bonds was possible only with $GePh_2$, which has a significantly higher extinction coefficient than $GeMe_2$ (thus affording stronger transient absorptions) and exhibits equilibrium constants that are in an ideal range to be measured under the conditions of our experiments. Furthermore, the (transient) products of these reactions could also be detected. We were less successful in characterizing the reactions of $GeMe_2$ with the same substrates; there were clear indications of reversibility, but the equilibrium constants are evidently significantly higher than those for $GePh_2$ and close to the upper limit measurable under the conditions of our experiments. While absolute rate constants for these reactions could be determined in a straightforward fashion, the weaker transient absorptions of the dialkylgermylene made it possible only to derive estimates of the equilibrium constants. The products also could not be detected, presumably because they do not absorb at sufficiently long wavelengths to enable detection with our methods.

Scheme 1.



Scheme 2.



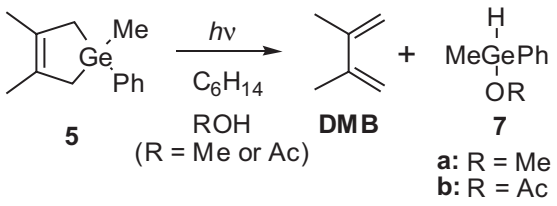
In the present paper, we report the results of a time-resolved spectroscopic study of methylphenylgermylene (GeMePh) and (*E*)- and (*Z*)-1,2-dimethyl-1,2-diphenyldigermene (**4**, as a mixture of isomers) in hydrocarbon solution, generated by laser flash photolysis of 1,3,4-trimethyl-1-phenylgermacyclopent-3-ene (**5**, Scheme 1). This work represents the first step in a more extensive study of the effects of substituents (directly attached to germanium) on germylene and digermene reactivity, as well as an attempt to confirm and elaborate on some of the differences in the reactivity of $GeMe_2$ and $GePh_2$ towards the various substrates that have been examined so far. Our previous results for the other two germylenes lead to the expectation that the presence of a single phenyl group should provide a chromophore that would lead to stronger transient absorptions (thus enabling more precise kinetic measurements), facilitate the detection of transient products, and provide some moderation of reactivity (compared with $GeMe_2$) so that meaningful structure–reactivity relationships might eventually be derived.

Results

Steady state photolysis (254 nm) of a deoxygenated hexane solution of **5** (0.025 mol/L) containing isoprene (0.1 mol/L) led to the formation of 1,3-dimethyl-1-phenylgermacyclopent-3-ene (**6**) as the only detectable germanium-containing product at conversions below ca. 15% and an equal yield of 2,3-dimethyl-1,3-butadiene (DMB) (Scheme 2). The identity of **6** was established by GC coinjection of the crude photolysate with an authentic, independently synthesized sample of the compound. Similarly, photolysis of a cyclohexane-d_{12} solution of **5** (0.05 mol/L) containing methanol (MeOH, 0.5 mol/L) or acetic acid (AcOH, 0.095 mol/L), with periodic monitoring of the

© 2006 NRC Canada

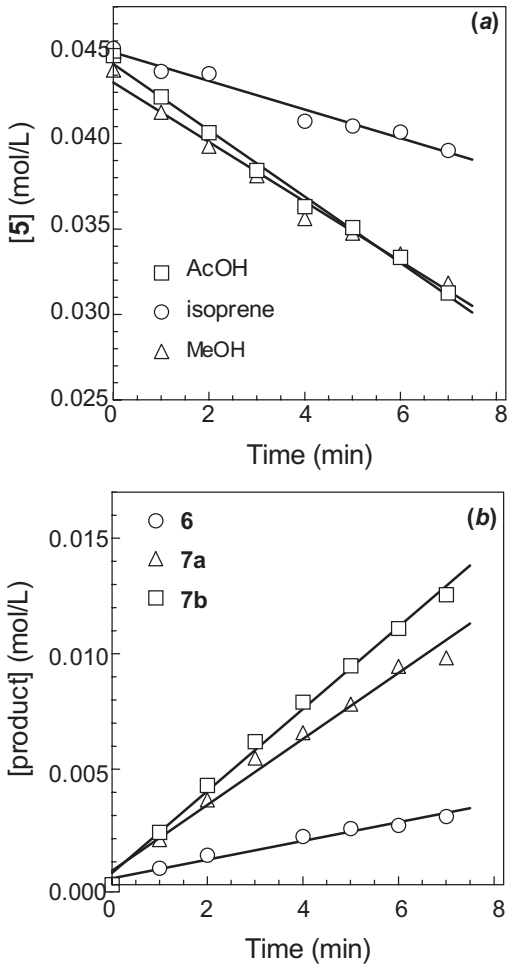
Scheme 3.



photolysates by ^{1}H NMR spectroscopy between 0% and ca. 25% conversion, afforded DMB and a single other product in each case. These were tentatively identified as methoxymethylphenylgermane and acetoxymethylphenylgermane (**7a** and **7b**, respectively, Scheme 3) on the basis of their ^{1}H NMR spectra. The results are consistent with formal [4+1]-cycloreversion to yield GeMePh and DMB as the predominant photochemical reaction pathway of **5**. The quantum yield was not rigorously determined, but qualitative comparisons of the rate of product formation in the MeOH-trapping experiment with those for **1a** (9) and **2a** (11) under the same conditions suggest that it is similar to the value of 0.55 that had been previously reported by us (9, 11) for the quantum yields for formation of $GePh_2$ and $GeMe_2$, respectively, from these compounds. A merry-go-round experiment was carried out, in which 0.045 mol/L solutions of **5** in cyclohexane-d_{12} containing MeOH (0.25 mol/L), AcOH (0.095 mol/L), and isoprene (0.094 mol/L) were irradiated in parallel, to assess any possible differences in reaction quantum yield with trapping agent. Concentration vs. time plots, showing the consumption of **5** and the formation of the products (**6**, **7a**, and **7b**), measured by ^{1}H NMR spectroscopy over the 0%–20% conversion range, are shown in Fig. 1. Correction of the isoprene concentration vs. time data for primary inner filter effects (because of coabsorption of the excitation light by the substrate) leads to the conclusion that product formation using the diene as trap (at ca. 0.1 mol/L) proceeds with roughly half the efficiency as in the experiments employing MeOH or AcOH as germylene scavengers. This corresponds to a $k_Q\tau$ value of ca. 10 $(mol/L)^{-1}$ for quenching of the reactive excited state of **5** by the diene, consistent with a lifetime of 10 ns or less assuming a quenching rate constant in excess of 10^9 $(mol/L)^{-1}$ s^{-1}.

Laser flash photolysis of continuously flowing deoxygenated solutions of **5** (ca. 0.0015 mol/L) in anhydrous hexane with the pulses from a KrF excimer laser (248 nm, ~25 ns, ~100 mJ) led to the formation of two transient species, one that appeared to be formed within ca. 50 ns of the onset of the laser pulse (λ_{max} = 490 nm) and another (λ_{max} = 415 nm) that grew to a maximum in concentration over the first ca. 4 μs after the pulse and then decayed to baseline over the next ca. 100 μs. Figure 2 shows transient absorption spectra recorded 95–200 ns and 3.4–3.6 μs after excitation, along with typical transient decay–growth profiles recorded at 510 and 410 nm, to the red and blue, respectively, of the absorption maxima of the two species, to isolate the transient decays as completely as possible without sacrificing appreciably in signal intensity. The decay of the first-formed species fits well to second-order kinetics (eq. [1]), affording

Fig. 1. Plots of concentration vs. time showing (*a*) the consumption of **5** and (*b*) the formation of trapping products from photolysis of **5** in cyclohexane-d_{12} containing AcOH (0.095 mol/L, □), MeOH (0.5 mol/L, Δ), and isoprene (0.094 mol/L, ○). The data from the latter have not been corrected for inner filter effects.



a decay constant of $k/\varepsilon_{510} = (1.6 \pm 0.1) \times 10^7$ cm s^{-1}. The behaviour is exactly analogous to that previously reported for **1a** and **1b** (9) and **2a** and **2b** (11) under similar conditions. We thus assign the two transients to GeMePh and its dimerization products, (*E*)- and (*Z*)-1,2-dimethyl-1,2-diphenyldigermene (**4**), respectively, (Scheme 1), which we assume are formed as a mixture of isomers.

$$[1] \qquad \Delta A_t = \Delta A_0 \,/\, (1 + 2k_{dim}(\Delta A_0/\varepsilon_\lambda l)t)$$

where ΔA_0 and ΔA_t are the transient absorbances at time = 0 and time = t after the laser pulse, ε_λ is the extinction coefficient at the monitoring wavelength, and l is the path length.

We next investigated the reactivities of the two species with various germylene scavengers (see Chart 1). Addition of AcOH, Bu_3SnH, CCl_4, or *tert*-butylacetylene (TBE) resulted in effects consistent with irreversible[4] scavenging of the germylene (9–11); the (germylene) absorption at 510 nm

[4] Any reaction with a (forward) rate constant of 10^9–10^{10} $(mol/L)^{-1}$ s^{-1} and an equilibrium constant greater than ca. 25 000 $(mol/L)^{-1}$ appears to be irreversible under the conditions of our experiments, to the extent that the reacting species decay completely to baseline with pseudo-first-order kinetics.

© 2006 NRC Canada

Fig. 2. Transient absorption spectra recorded 95–220 ns (○) and 3.4–3.6 μs (●) after the laser pulse from flash photolysis of a ca. 0.0015 mol/L solution of **5** in deoxygenated, anhydrous hexane. The inset shows representative transient decay and growth profiles recorded at 410 nm and 510 nm; the solid line in the latter is the fit of the data to second order decay kinetics

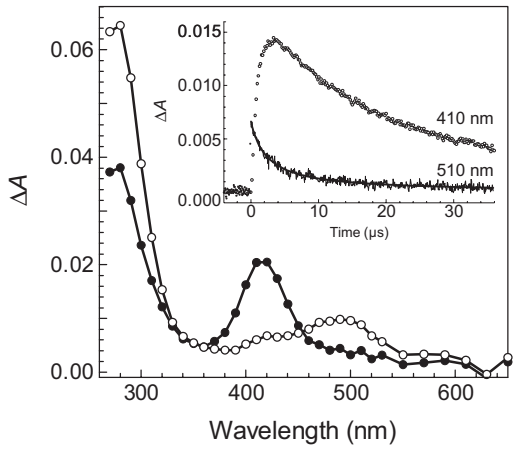
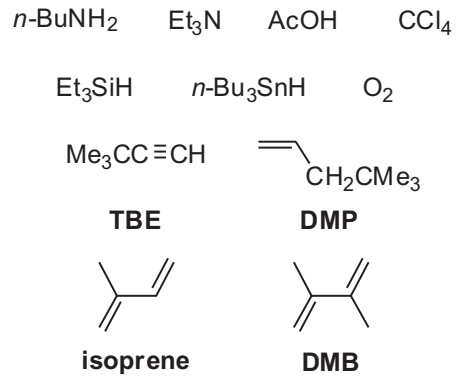


Chart 1.



decayed at increased rates, completely to baseline, with clean first-order kinetics at concentrations above those required to reduce the peak digermene signal intensities to less than ca. 50% of their values in the absence of added reagent. As well, both the peak intensities and growth time of the absorptions because of **4** (measured at 410 nm) were reduced in proportion to the concentration of added scavenger. Plots of the pseudo-first-order rate constants for germylene decay (k_{decay}) vs. concentration were linear, consistent with the relationship of eq. [2],

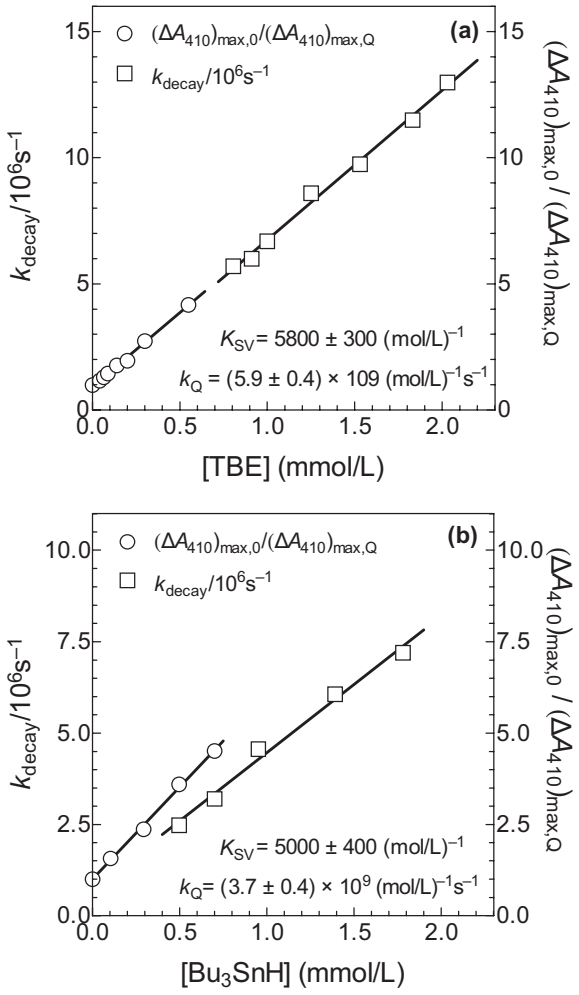
$$[2] \qquad k_{decay} = k_0 + k_Q[Q]$$

where k_Q is the second-order rate constant for reaction of the species with the added reagent (Q) and k_0 is the (hypothetical) pseudo-first-order rate constant for decay in the absence of Q. Plots of the ratios of the peak transient absorbances due to **4**, in the absence and presence of scavenger at concentration [Q] ($\Delta A_{410,0}/\Delta A_{410,Q}$), were also linear in every case and were analyzed according to eq. [3],

$$[3] \qquad (\Delta A_{410})_{max,0}/(\Delta A_{410})_{max,Q} = 1 + K_{SV}[Q]$$

where K_{SV} is a proportionality factor reflecting the efficiency of the germylene scavenging reaction relative to

Fig. 3. Plots of k_{decay} (□) and $(\Delta A_{410})_{max,0}/(\Delta A_{410})_{max,Q}$ (○) vs. [Q] for scavenging of GeMePh by (*a*) 3,3-dimethyl-1-butyne (TBE) and (*b*) tri-*n*-butylstannane (Bu_3SnH). The solid lines are the linear least-squares fits of the data to eqs. [2] and [3], respectively. Decay and growth profiles for MePhGe and **4** were measured at 510 and 410 nm, respectively.



dimerization. Typical plots are shown in Fig. 3, from the experiments employing TBE and Bu_3SnH as scavengers. The absolute rate constants and K_{SV} values for reaction of GeMePh with the various reagents studied in this work are collected in Table 1. Also included in the table are the K_{SV}/k_Q ratios, calculated for each of the scavengers studied from the K_{SV} and k_Q values. Similar effects on the germylene and digermene absorptions to those noted above were observed in the presence of $BuNH_2$, even though its reaction with GeMePh is most likely reversible (vide infra).

In several cases, the reagent also had the effect of accelerating the decay of the digermene (**4**) signal over the concentration range where it could be detected, consistent with reaction of the scavenger with the digermene as well. The digermene decays followed reasonably good first-order kinetics in the presence of the scavenger, and plots of k_{decay} vs. [Q], according to eq. [2], were linear; the absolute rate constants obtained are also listed in Table 1. For those scavengers that did not exhibit distinctive effects on the digermene decay kinetics, upper limits of the rate constants were esti-

© 2006 NRC Canada

Table 1. Absolute rate constants (k_Q) and K_{SV} values for reactions of GeMePh and 1,2-dimethyl-1,2-diphenyldigermene (**4**) with various substrates in dry deoxygenated hexane solution at 23 °C.

	GeMePh[a]			PhMeGe=GeMePh (**4**)[b]
Reagent (Q)	k_Q ($\times 10^9$ (mol/L)$^{-1}$ s^{-1})[c]	K_{SV} (mol/L)$^{-1}$[d]	K_{SV}/k_Q (μs)	k_Q ($\times 10^6$ (mol/L)$^{-1}$ s^{-1})[b]
AcOH	5.6±0.5	4 900±300	0.88	140±10
Et_3SiH	≤0.000 44	Nd[e]	—	—
Bu_3SnH	3.7±0.4	5 000±300	1.35	≤390[f]
CCl_4	0.017±0.002[g]	29±2	1.72	6±1
O_2	<0.06[f]	50±12	>0.85	24±3
TBE	5.9±0.4	5 800±300	0.98	24±4
$BuNH_2$	11.7±1.4	14 200±900	1.21	5200±600
Et_3N	3.9±0.4	1 120±130	0.29	—
Isoprene	8.0±09	3 800±100	0.48	≤4[e]
DMB	4±2	175±25[h]	0.044	≤12[e]
DMP	5.1±0.7	110±100	0.21	≤32[e]

[a]Measured by laser flash photolysis of deoxygenated solutions of **5** (~0.0015 mol/L) in hexane. Errors are listed as ±2σ from linear least-squares analyses of the data.
[b]Determined from plots of k_{decay} (for **4**, monitored at 410 nm) vs. [Q].
[c]From plots of k_{decay} (for GeMePh, monitored at 510 nm) vs. [Q] according to eq. [2], over concentration ranges corresponding to >50% quenching of the peak ΔA_{410} value ($(\Delta A_{410})_{max,0}$) because of **4**.
[d]From plots of $[(\Delta A_{410})_{max,0}/(\Delta A_{410})_{max,Q}]$ vs. [Q] according to eq. [3].
[e]Nd (not determined).
[f]Calculated from k_{decay} at the highest concentration of scavenger studied.
[g]The slope of the low concentration range of (nonlinear) plots of k_{decay} vs. [Q].
[h]Corrected for primary inner filter effects.

mated from the rate constant for decay of the signal at the highest scavenger concentration investigated, obtained by fitting the transient decay profiles to single exponential decay kinetics. These data are also listed in Table 1.

Addition of Et_3N, 4,4-dimethyl-1-pentene (DMP), isoprene, and DMB resulted in behaviour consistent with reversible scavenging of GeMePh, the main indication of which is a significantly less efficient reduction in the peak intensity of digermene absorption with increasing scavenger concentration; formation of the digermene could still be readily observed even at high enough substrate concentrations to reduce the lifetime of the germylene to the point where it could no longer be detected. This effect was common to all four substrates. Other anticipated effects varied with the substrate according to the magnitudes of the forward rate constant and equilibrium constant for the particular reaction. For example, addition of Et_3N caused the germylene signals to decay with clean first-order kinetics completely to the prepulse level at all concentrations throughout the 0.3–2 mmol/L range in added substrate, similar to the behaviour observed with the irreversible substrates; this is consistent with an equilibrium constant significantly in excess of ca. 25 000 (mol/L)$^{-1}$ (10), the approximate upper limit of the value measurable under the conditions of our experiment given a forward rate constant in the 10^9–10^{10} (mol/L)$^{-1}$ s^{-1} range. On the other hand, addition of DMP and isoprene caused the germylene signal to decay with bimodal kinetics within certain concentration ranges, consisting of a fast, approximately first-order decay followed by a much longer-lived residual absorption; the decay rate of the initial component increased while the residual absorption level and its decay rate both decreased with increasing substrate concentration. To illustrate this behaviour, Fig. 4*a* shows a series of germylene decay traces obtained in the presence of DMP. We associate the fast initial decay with the approach to equilibrium with the scavenging product and the residual absorption as being due to residual free germylene present at equilibrium and undergoing slow dimerization. This behaviour was evident over the full concentration range in which the germylene could be detected in the case of DMP (0.35–2.1 mmol/L), but only over the 0.1–0.5 mmol/L concentration range in the case of isoprene, with the decays proceeding completely to the prepulse level (within detection limits) at higher concentrations. This is consistent with a larger equilibrium constant for reaction with isoprene compared with that for DMP.

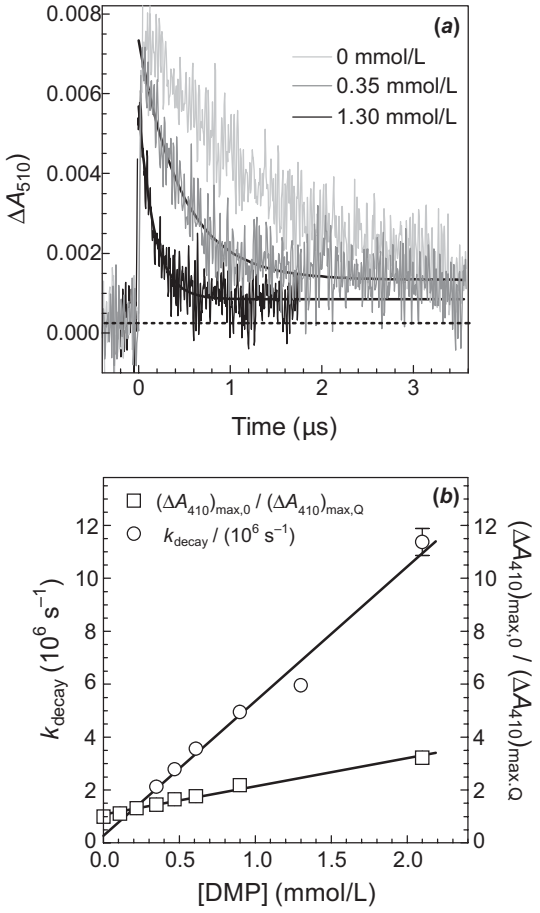
The germylene decay profiles in the experiments with DMP and isoprene were analyzed as single exponential decays to a nonzero residual absorption, as in our earlier study (10). Plots of the decay rate constants vs. scavenger concentration exhibited excellent linearity (see Fig. 4*b*), and analysis of the data according to eq. [4] afforded k_Q values of $(5.1 \pm 0.7) \times 10^9$ and $(8.0 \pm 0.4) \times 10^9$ (mol/L)$^{-1}$ s^{-1} for DMP and isoprene, respectively. The corresponding values of K_{SV}, obtained from analysis of the peak ΔA_{410} values due to digermene **4**, according to eq. [3], were 1060 ± 100 and 3800 ± 100 (mol/L)$^{-1}$. Plots of the ratios of the initial and residual germylene ΔA values, according to eq. [5], exhibited considerable scatter, mainly because of the rather low signal-to-noise that characterized the present series of experiments. It was thus not possible to determine the equilibrium constants with reasonable precision and reproducibility. Nevertheless, qualitative comparisons of the data to those previously published for $GePh_2$ (10) with the same substrates suggest the K_{eq} values to be in the range of 4000–8000 (mol/L)$^{-1}$ for DMP and 12 000–15 000 (mol/L)$^{-1}$ for isoprene.

$$[4] \qquad k_{decay} = k_{-Q} + k_Q[Q]$$

$$[5] \qquad (\Delta A_{510,0}/\Delta A_{510,res})_Q = 1 + K_{eq}[Q]$$

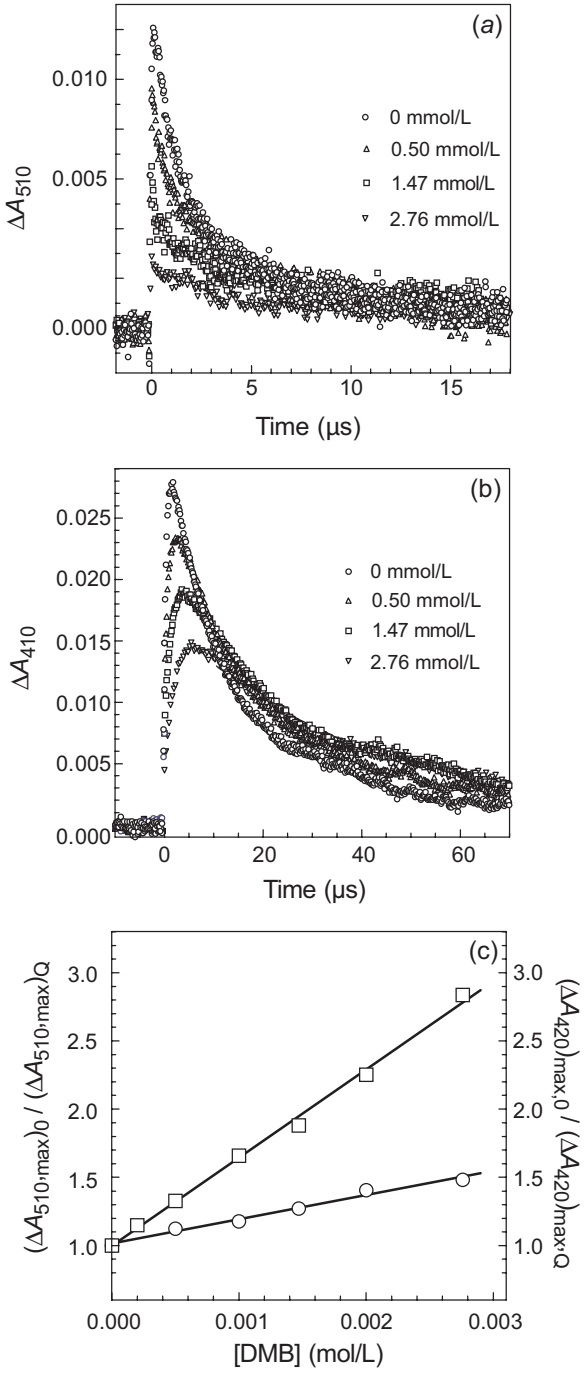
© 2006 NRC Canada

Fig. 4. (*a*) Absorbance vs. time profiles for GeMePh in deoxygenated hexane containing DMP (0, 0.35, and 1.30 mmol/L), monitored at 510 nm. The solid lines are the best fits of the data to single exponential decays. (*b*) Plots of k_{decay} and $(\Delta A_{410})_{max,0}/(\Delta A_{410})_{max,Q}$ vs. [DMP], showing the fits of the data to eqs. [4] and [3], respectively.



The data obtained with DMB as scavenger were very difficult to analyze accurately. Marked reductions in the strength of the germylene signals accompanied addition of the diene over the 0.5–3 mmol/L concentration range, yet effected only minor reductions in the strength of the digermene signals and consistent lengthening of their growth times with increasing concentrations. Typical data, corrected for inner filter effects because of coabsorption of the excitation light by the diene, are shown in Fig. 5. An initial fast component to the predominantly second-order germylene decay appeared to develop over the 0–0.8 mmol/L concentration range in added diene; it became distinctive enough to allow analysis between 1.0 and 2.0 mmol/L, but was too short-lived above 2.0 mmol/L to analyze accurately, leaving behind a much weaker residual second-order decay. This behaviour is again consistent with rapid reversible reaction, but with an equilibrium constant of less than ca. 1000 $(mol/L)^{-1}$ (13). A rate constant of $k_Q = (4 \pm 2) \times 10^9$ $(mol/L)^{-1}$ s^{-1} was estimated from the decay rate constants for the fast initial component of the bimodal decay profiles from several determinations (at shorter timescales) in the presence of 1.0–2.0 mmol/L DMB, analyzed in the same way as the data obtained with DMP, while a value of $K_{SV} = 175 \pm 25$ $(mol/L)^{-1}$ was obtained from analysis of the digermene peak signal strengths according to eq. [3].

Fig. 5. Growth and decay profiles for the signals due to (*a*) GeMePh and (*b*) **4** in the presence of DMB (0–2.76 mmol/L), and (*c*) plots of the relative peak signal intensities for the germylene (□) and digermene (○) absorptions vs. DMB concentration according to eq. [3].



As is evident from the raw data shown in Figs. 4 and 5, the strength of the germylene signals decreased noticeably with addition of reactive substrate in increasing concentrations; this was generally observed with all of the substrates studied, to an extent comparable to that shown in Fig. 4 with DMP as scavenger. It may be the result of the fact that

© 2006 NRC Canada

germylene formation appears to lag slightly behind the laser pulse; this is evident from the [DMP] = 0 trace of Fig. 4*a*, which suggests that the signal grows with a rise time of ca. 50 ns, significantly longer than the ca. 25 ns width of the laser pulse. This behaviour suggests that germylene formation is not a direct excited (singlet) state process, but rather ensues from a secondary intermediate. If this is true, then a reduction in germylene signal strength with increasing scavenger concentration would be expected, as reaction of the germylene with the scavenger becomes increasingly competitive with its formation. The effect on signal strength was much more pronounced in the experiments with isoprene and DMB as scavengers, suggesting an additional mechanism for quenching of the signals beyond that exhibited by the other scavengers. Plots of the relative peak transient absorbances at 510 nm vs. concentration (cf. eq. [3]) afforded Stern–Volmer constants of 1000 ± 150 $(mol/L)^{-1}$ and 650 ± 40 $(mol/L)^{-1}$ for isoprene and DMB (see Fig. 5*c*), respectively.

On the other hand, significant increases in the strength of the transient absorptions at 260–300 nm occurred with increasing DMB concentration; these absorptions, which are centered at ca. 285 nm and are superimposed on those formed in the absence of the scavenger (vide supra), decayed over a similar timescale as the weak germylene absorption at 510 nm at low diene concentrations. Figure 6 shows a series of transient absorption spectra recorded at various time intervals after the laser pulse for the solution containing 2.76 mmol/L DMB. Higher diene concentrations could not be investigated in this case because of coabsorption at the excitation wavelength by the diene.

New long-lived transient absorptions in the 270–350 nm range were also observed in the presence of the amines and the other C—C unsaturated compounds. The absorption maximum of the species that was formed in the presence of Et_3N (λ_{max} = 330 nm, Fig. 7*a*) was red-shifted sufficiently from the absorptions due to the free germylene and its oligomerization products to enable a growth in the signal to be detected at the upper end of the amine concentration range studied; the growth rate constant was found to be in reasonable agreement with that for decay of the germylene at the same amine concentration, consistent with the new species being formed by reaction of GeMePh with the amine. For example, a trace recorded at 350 nm with a solution of **5** containing 1.5 mmol/L Et_3N exhibited a growth rate constant of (10.5 ± 1.8) × 10^6 s^{-1}, which agrees reasonably well with the decay rate constant of k_{decay} = (6.5 ± 0.5) × 10^6 s^{-1}, measured for the germylene signal at 510 nm at the same amine concentration. We assign the species formed in the reaction to the Lewis acid–base complex **8a**. The analogous product (**8b**) is formed in the presence of $BuNH_2$ and exhibits its λ_{max} = 310 nm; however, the expected growth of its absorption could not be resolved because of overlap with other transient absorptions that are present in the short wavelength region at scavenger concentrations at which the germylene signal could still be detected. The same was true of the products formed in the presence of isoprene, DMP, and TBE, which absorb in the 270–285 nm range.

Transient decay profiles and spectra of the new products formed in the presence of isoprene, DMP, and TBE were re-

Fig. 6. Transient absorption spectra recorded at selected time intervals after the laser pulse for a solution of **5** (0.0015 mol/L) in deoxygenated hexane containing DMB (2.76 mmol/L). The inset shows a decay trace recorded at a monitoring wavelength of 280 nm.

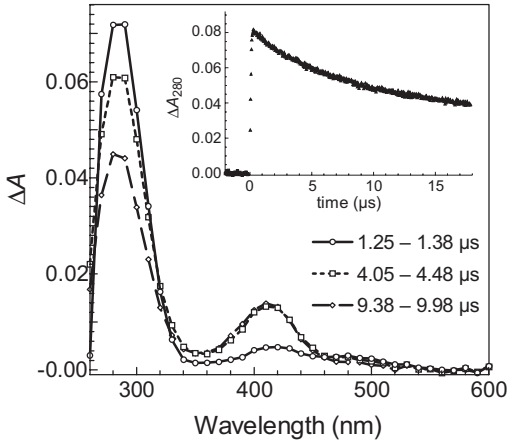
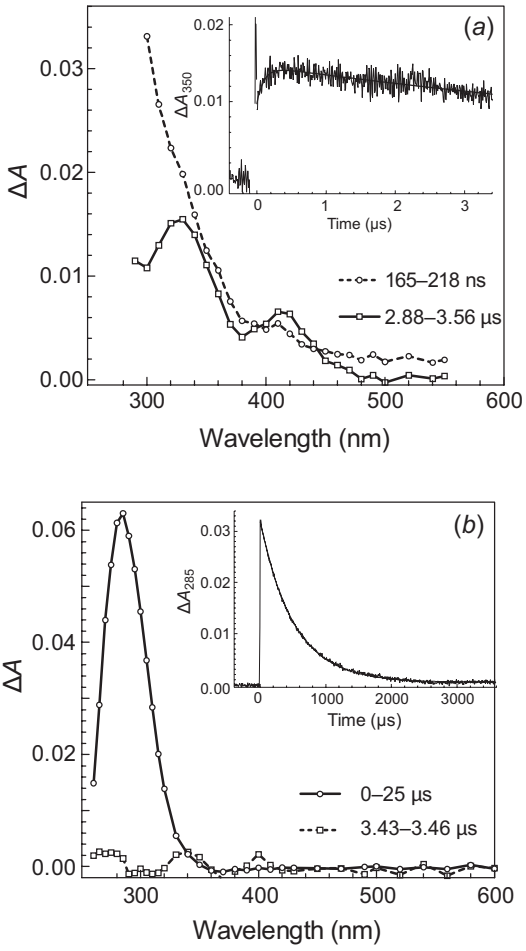
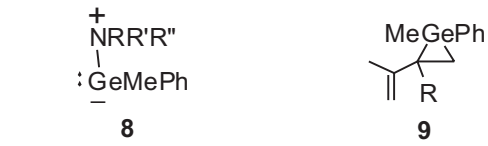


Fig. 7. Transient absorption spectra recorded by flash photolysis of a solution of **5** (ca. 0.0015 mol/L) in deoxygenated, anhydrous hexane containing (*a*) Et_3N (2.0 mmol/L) and (*b*) isoprene (20 mmol/L). The insets show growth and decay profiles recorded at 350 nm and 285 nm, respectively.



© 2006 NRC Canada

corded at relatively high (3.3–200 mmol/L) substrate concentrations to minimize contributions to the lifetimes from germylene dimerization or from overlapping transient absorptions because of GeMePh or its oligomerization products. It was possible to employ reasonably high substrate concentrations in the experiments with DMP, and the lifetime of the species formed from the alkene was found to be approximately independent of concentration over the 0.1–0.35 mol/L range. The species formed from isoprene absorbs with λ_{max} = 285 nm and decays with clean pseudo-first-order kinetics in the presence of 0.02 mmol/L diene (τ ~ 670 μs). The spectra and lifetimes of these species are similar to those observed previously from $GePh_2$ with the same substrates (10) and we tentatively assign them to the three-membered germanocycles **9a**–**11**. The species absorbing with λ_{max} ~ 285 nm in the transient spectra of Fig. 6 is similarly assigned to vinylgermirane **9b**. Table 2 contains a summary of the absorption maxima and lifetimes of the primary transient products formed from reaction of GeMePh with these compounds, while Fig. 7 shows examples of the spectra and decays obtained in the presence of Et_3N and isoprene.

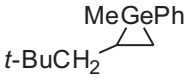


8

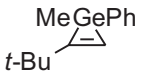
a. R = R' = R" = Et
b. R = *n*-Bu; R' = R" = H

9

a. R = H
b. R = Me



10



11

Saturation of a hexane solution of **5** with oxygen caused a ca. 40% drop in the peak absorbance due to digermene **4** compared with its value in deoxygenated solution, but had no discernible effect on the decay characteristics of the germylene signal. An upper limit of $k_{O_2} < 6 \times 10^7$ (mol/L)$^{-1}$ s^{-1} for quenching of GeMePh was thus obtained from the pseudo-first-order rate constant for decay of the germylene in O_2-saturated hexane (k_{decay} ~ 1×10^6 s^{-1}), using a value of 0.015 mol/L for the concentration of O_2 (14) and with the assumption that the decay of the germylene is dominated by its reaction with oxygen under these conditions. Modest reductions in the lifetime of the digermene were observed with increasing O_2 concentration, affording a value of k_{O_2} = (2.4 ± 0.3) × 10^7 (mol/L)$^{-1}$ s^{-1} from analysis of the digermene decays according to eq. [2].

Discussion

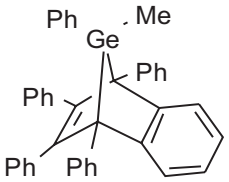
As we found previously for the related compounds **1** and **2** (9), steady state photolysis of **5** in the presence of MeOH (0.5 mol/L), AcOH (0.095 mol/L), or isoprene (0.1 mol/L) affords the expected trapping products of GeMePh in high yields, along with 2,3-dimethyl-1,3-butadiene (DMB). Qualitative comparisons of the rate of product formation in the MeOH-trapping experiment to those obtained in our earlier studies of **1a** and **2a**, which were carried out under the same conditions of lamp intensity and concentration, indicate similar quantum yields for germylene extrusion (Φ ~ 0.5) from the three compounds.

Table 2. UV absorption maxima and lifetimes of transient products from the reaction of GeMePh with amines and C—C unsaturated compounds in hexane at 23 °C.

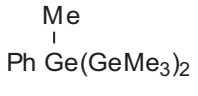
Scavenger	Tentative assignment	λ_{max} (nm)	τ (ms) (conc. in mmol/L)
$BuNH_2$	**8b**	310	0.015 (0.3)
Et_3N	**8a**	330	0.014 (1.5)
Isoprene	**9a**	285	0.670 (20)
DMB	**9b**	285	Nd[a]
DMP	**10**	275	2.6 (350)
TBE	**11**	270	>2000 (3.3)

[a]Nd (not determined).

The UV–vis spectrum of GeMePh in a 3-methylpentane (3-MP) matrix at 77 K was reported in the late 1980s by two different groups; Ando et al. (15) generated the species by photolysis of the 1,4-germanonaphthalene derivative **12** and reported a UV spectrum exhibiting λ_{max} = 440 nm, while Mochida and co-workers (16) employed the photolysis of trigermane **13** and reported λ_{max} = 456 nm in 3-MP at 77 K and λ_{max} = 440 nm in cyclohexane solution at room temperature. The latter group also reported rate constants for reaction of the species in cyclohexane solution with DMB (k = 2.2×10^6 (mol/L)$^{-1}$ s^{-1}), Et_3SiH (k = 4.1×10^6 (mol/L)$^{-1}$ s^{-1}), and CCl_4 (k = 6.5×10^7 (mol/L)$^{-1}$ s^{-1}) (16). A transient exhibiting a similar UV absorption spectrum but much different reactivity toward DMB and CCl_4, from flash photolysis of poly(methylphenylgermylene) (**14**), was later assigned to GeMePh by the same group (17). The results reported in the present work using **5** as precursor differ significantly from those of the earlier studies, but are fully consistent with the spectroscopic and kinetic data reported by us recently for $GePh_2$ and $GeMe_2$ under similar conditions (9–11).



12



13

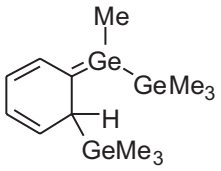


14
(*n* ~ 28)

For example, the long wavelength absorption maximum of the initially formed transient from laser photolysis of **5** (λ_{max} = 490 nm) lies between those of $GePh_2$ (λ_{max} = 500 nm, ε_{500} = 1850 dm^3 mol^{-1} cm^{-1} (9)) and $GeMe_2$ (λ_{max} = 470–480 nm (9, 11, 12), ε_{475} = 730 dm^3 mol^{-1} cm^{-1} (11)). The spectrum also shows a somewhat stronger absorption band centered at λ_{max} ~ 290 nm due to the $S_0 \rightarrow S_2$ transition, which is shifted ca. 10 nm to the blue of the corresponding band in the spectrum of $GePh_2$ (9). We note that the long wavelength absorption maximum of GeMePh is the same as that reported for the silicon homologue (SiMePh) in

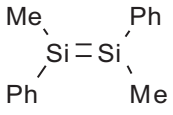
© 2006 NRC Canada

a hydrocarbon matrix at 77 K (λ_{max} = 490 nm (18)). Such similarities are also evident in the UV–vis spectra of $GeMe_2$ and $SiMe_2$ (λ_{max} = 453–465 nm (18, 19)), as well as those of $GePh_2$ and $SiPh_2$ (λ_{max} = 495 nm (18)). It thus seems clear that the transient absorptions assigned to GeMePh in the earlier time-resolved studies in solution, using **13** and **14** as precursors, must be due to other more strongly absorbing transient products; as we have shown previously for related systems (8), the likely candidates are conjugated germene derivatives and (or) germanium-centered radicals. For example, the conjugated germene derivative (**15**) that might be anticipated from photolysis of **13** can be predicted to exhibit an absorption maximum in the 430–450 nm range and exhibit moderate reactivity toward CCl_4 and DMB, based on analogies taken from related systems (7, 8, 20).

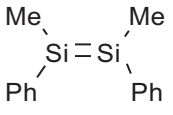


15

Similarly, the absorption maximum of the second-formed species (λ_{max} = 415 nm) falls between those of Ge_2Ph_4 (**3a**, λ_{max} = 440 nm (9)) and Ge_2Me_4 (**3b**, λ_{max} = 370 nm (9, 11, 21, 22)) and can thus be assigned with confidence to (*E*)- and (or) (*Z*)-1,2-dimethyl-1,2-diphenyldigermene (**4**, Scheme 1), formed most likely as a mixture of isomers. The spectra of (*E*)- and (*Z*)-**4** are also quite similar to those reported by Sekiguchi et al. (23) for the silicon homologues, (*E*)- and (*Z*)-1,2-dimethyl-1,2-diphenyldisilene [(*E*)- and (*Z*)-**16**, λ_{max} = 417 and 423 nm, respectively] in cyclohexane solution. An absorption maximum of λ_{max} = 420 nm was reported earlier for **16** in a 3-MP glass at 77 K, formed (presumably as a mixture of isomers) by dimerization of SiMePh (18).



***E*-16**

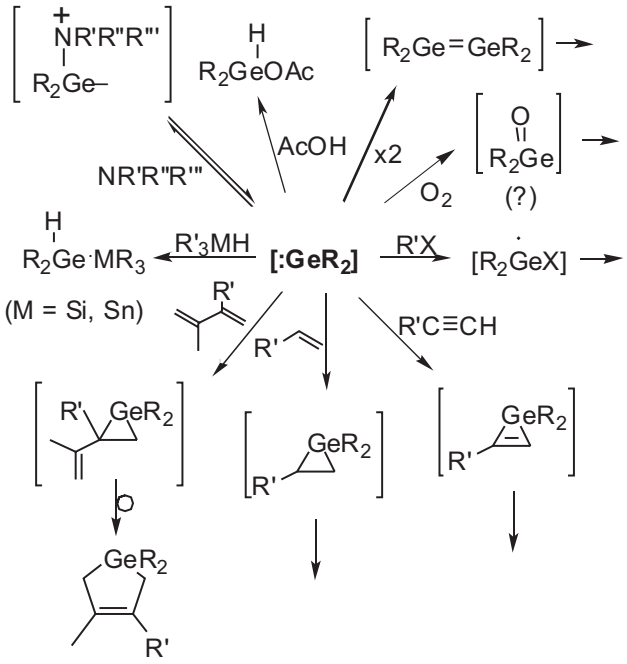


***Z*-16**

Absolute rate constants have been determined in this work for the reaction of GeMePh with a selection of representative germylene scavengers in hexane solution. The reactions studied include O-H insertion with AcOH, Lewis acid–base complexation with primary and tertiary amines, M-H insertions with trialkylhydridosilanes and -stannanes, reaction with terminal alkenes, alkynes, and conjugated dienes, chlorine atom abstraction from CCl_4, reaction with oxygen, and dimerization, as summarized in Scheme 4. While product studies specific to GeMePh have not been carried out in most instances, the course of these reactions are well established for $GeMe_2$ and other reactive germylenes (1, 10, 11, 24, 25) and all of them have direct analogies in silylene chemistry (26).

As we found in our earlier studies of $GePh_2$ and $GeMe_2$ (10, 11), two distinct types of kinetic behaviour are observed in the signals due to GeMePh and **4**, depending on whether

Scheme 4.



scavenging of the germylene is reversible or not. A reasonably reliable indicator of reversibility in the data is the K_{SV}/k_Q ratio, which (within certain limitations (11)) provides a normalized measure of the efficiency with which a given scavenger suppresses germylene dimerization as a result of its competing reaction with the digermene precursor (i.e., the germylene). The K_{SV}/k_Q ratio tends toward significantly smaller values (indicating lower scavenging efficiencies) for those substrates that react with the germylene reversibly compared with those for irreversible scavengers. Because K_{SV} is measured from the relative peak intensities of the signal due to digermene **4**, its magnitude is also affected by the reactivity of the digermene with the scavenger. This leads to artificially high values of the efficiency parameter, which become particularly significant when the reactivity of the digermene toward the scavenger is within a factor of ca. 5 of that of the germylene; the smaller the differential reactivity, the greater the distortion in the magnitude of K_{SV}, and K_{SV}/k_Q, from their true values. Thus, the K_{SV}/k_Q ratios for those reagents for which this differential reactivity is relatively small (e.g., $BuNH_2$, CCl_4, and O_2) can be expected to overestimate the efficiency (i.e., the rate relative to that of dimerization) of the scavenging reaction. For this reason, we have not attached an absolute value to the rate constant for scavenging of GeMePh by O_2 based on the K_{SV} value and report only the upper limit of the rate constant as defined by the lifetime of the germylene in O_2-saturated solution; similarly, the value estimated previously for the reaction of $GePh_2$ with O_2 ($k_{O_2} \sim 3 \times 10^7$ (mol/L)$^{-1}$ s^{-1}) (10) should also be considered an upper limit. In any event, it is clear from the data of Table 1 that those scavengers that react at least ca. three times faster with GeMePh than with **4** fall into two groups, those with $K_{SV}/k_Q \geq 0.9$ (AcOH, Bu_3SnH, O_2, CCl_4, and TBE) and those with $K_{SV}/k_Q < 0.5$ (Et_3N, isoprene, DMB, and DMP). The first group is comprised of those reagents that react with GeMePh irreversibly, while the second

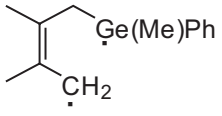
© 2006 NRC Canada

consists of the reversible scavengers. The K_{SV}/k_Q value for $BuNH_2$ would seem to suggest that it belongs in the group of irreversible scavengers, but as it reacts with digermene **4** only twice slower than it does with GeMePh, the K_{SV} value (and hence K_{SV}/k_Q) is likely to be significantly overestimated. This reaction is most likely reversible, like that with Et_3N (vide infra).

The absolute rate constants for the various reactions of GeMePh that have been studied in the present work are in most cases the same, within experimental error, as the corresponding values for $GePh_2$ (9, 10) and are consistently a factor of two to eight times smaller than those for reaction of $GeMe_2$ with the same substrates (11). The smallest variations throughout the series are exhibited by the rate constants for dimerization and Lewis acid–base complexation with the primary amine, which proceed within a factor of ca. 2 of the diffusional rate constant in hexane at 25 °C in all three cases (11). An estimate of $k_{dim} \sim 2 \times 10^{10}$ $(mol/L)^{-1}$ s^{-1} for the rate constant for dimerization of GeMePh can be obtained from the measured second-order decay coefficient ($k/\varepsilon_{510} = (1.6 \pm 0.1) \times 10^7$ cm s^{-1}), assuming an extinction coefficient intermediate between those of $GePh_2$ ($\varepsilon_{max} \sim 1850$ dm^3 mol^{-1} cm^{-1}) (9) and $GeMe_2$ ($\varepsilon_{max} \sim 730$ dm^3 mol^{-1} cm^{-1}) (11). The results suggest that phenyl for methyl substitution has relatively small effects on the reactivity of simple germylenes toward this diverse set of reagents, but confirm the earlier conclusion that phenyl substitution has a distinct moderating effect on germylene reactivity (11). The present results indicate that most of the effect on the rate constant arises with substitution of the first alkyl substituent in $GeMe_2$ and replacing the second has much smaller consequences.

As might be expected, the equilibrium constants for the reversible reactions of GeMePh also appear to lie between those for $GeMe_2$ and $GePh_2$, although we have not been able to measure them with reasonable precision owing to the low signal-to-noise ratios that characterize the present experiments. Nevertheless, the equilibrium constants appear to be more sensitive to germylene substitution than the absolute rate constants for the forward component of the reaction. For example, the rate constants for reaction of the three germylenes with the alkene DMP vary by less than a factor of 2, while the equilibrium constants vary between $K_{eq} \sim 2500$ $(mol/L)^{-1}$ for $GePh_2$ (10) and $K_{eq} \sim 20\,000$ $(mol/L)^{-1}$ for $GeMe_2$ (11); these should be compared with the qualitative estimate of 4000–8000 $(mol/L)^{-1}$ for reaction of GeMePh with the same substrate. The estimated equilibrium constant for reaction of GeMePh with isoprene ($K_{eq} \sim 15\,000$ $(mol/L)^{-1}$) also falls within the range defined by $GePh_2$ and $GeMe_2$. The total range in K_{eq} exhibited by the reactions of DMP with the three germylenes corresponds to a range of ca. 1.3 kcal/mol (1 cal = 4.184 J) in standard free energy.

The two dienes have remarkably different effects on the germylene and digermene growth–decay profiles, which can be attributed primarily to a substantial difference in the equilibrium constants for the reactions of these substrates coupled with similar absolute rate constants for formation of the primary products. Interestingly, they also appear to quench the formation of the free germylene, to the extent that they cause significant reductions in the initial (peak) signal strengths of the GeMePh absorptions in laser flash photolysis experiments with these substrates. Apparent Stern–Volmer constants on the order of 1000 $(mol/L)^{-1}$ have been determined from analysis of the peak germylene absorbances as a function of diene concentration over the 0–3 mmol/L concentration range, which is consistent with diffusion-controlled quenching ($k \sim 2 \times 10^{10}$ $(mol/L)^{-1}$ s^{-1}) of an intermediate possessing a lifetime of $\tau \sim 50$ ns. However, product studies indicate that product formation remains efficient in the presence of isoprene in concentrations as high as ca. 0.1 mol/L; compound **6**, the expected product of trapping of GeMePh by the diene, is formed in only modestly (ca. 2×) lower quantum yield than the corresponding products of trapping of the germylene by MeOH or AcOH. This indicates that whatever phenomenon is primarily responsible for the loss in signal strength in the flash photolysis experiments, it does not lead to a reduction in the yield of germylene-derived products; this effectively rules out energy-transfer quenching of an excited state of **5** as the process responsible for the effect. In this regard, it is noteworthy that in the absence of added scavengers the germylene signals appear to be characterized by a ca. 50 ns growth, which is discrete from the temporal characteristics of the laser pulse. This could be indicative of the involvement of an additional intermediate such as 1,5-biradical **17**, formed via Ge—C bond cleavage in the reactive excited state of **5**, which undergoes further fragmentation to yield GeMePh and DMB. Such a species would also be expected to undergo ring closure to yield **5** and **9b** competitively with fragmentation. The same temporal feature was also evident in our earlier studies of $GePh_2$ (generated from **1b**) (9) and $GeMe_2$ (generated from **2a**) (11), although the effects of added diene on the signal strengths were much less pronounced than in the present case. It is reasonable to expect that such a species might be reactive toward dienes, though again, the product studies demand that it must do so reversibly. Neumann and co-workers (27, 28) isolated products corresponding to the addition of two molecules of diene to $GeMe_2$ in their early studies of the reactions of $GeMe_2$ with aliphatic dienes; we have found no evidence for the formation of such products in the present instance, although the highest diene concentration we have employed in product studies is only 0.1 mol/L. Further work will be required to address the possible involvement of such intermediates in the photochemistry of 1-germacyclopent-3-ene derivatives and the reaction of the corresponding germylenes with dienes in a more conclusive way.

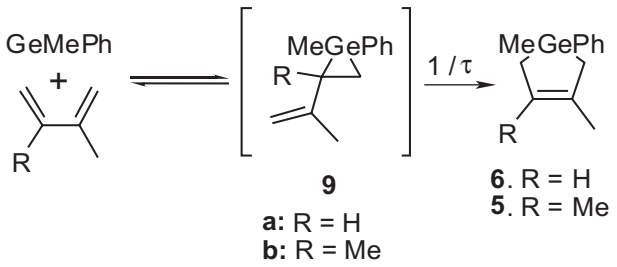


17

Addition of the dienes leads to the formation of new strongly absorbing transients exhibiting $\lambda_{max} = 285$ nm in both cases, which are assigned to the corresponding vinylgermirane derivatives **9a** and **9b**. The absorption spectrum and lifetime of the species formed from reaction of GeMePh with isoprene (**9a**, $\tau \sim 670$ μs, Fig. 7*b*) are quite close to those of the analogous product from reaction of

© 2006 NRC Canada

Scheme 5.



$GePh_2$ with the same diene (λ_{max} = 285 nm, τ ~ 500 μs) (10). It should be noted that the lifetime of the isoprene-derived product has been determined in the presence of sufficiently high diene concentrations to suppress digermene formation more or less completely, and where the decay of the species follows clean first-order kinetics. We thus tentatively associate the decay rate constant with that for further (unimolecular) rearrangement to yield the stable final product of the reaction (1, 27, 29), the corresponding germacyclopent-3-ene derivative **6** (Scheme 5). Unfortunately, the greater absorptivity of DMB at the laser excitation wavelength precluded experiments at sufficiently high diene concentrations to determine a lifetime for **9b** under comparable conditions. It is interesting to note that the relative equilibrium constants for formation of **9a** and **9b** from GeMePh indicate that **9b** is ca. 1.5 kcal/mol less thermodynamically stable than **9a**, with respect to cycloreversion back to the free germylene and the diene.

The intermediates formed in the reactions of GeMePh with the alkene (DMP) and alkyne (TBE) are also relatively long-lived and have been detected as discrete species with absorption maxima in the 270–285 nm range and lifetimes of ca. 2.6 ms or greater (see Table 2). The corresponding intermediates formed in the reactions of these substrates with $GePh_2$ exhibit similar absorption maxima (λ_{max} = 275 nm in both cases), but somewhat shorter lifetimes (τ ~ 1.2 and 600 ms, respectively) (10); the analogous products could not be detected from $GeMe_2$ under similar conditions, presumably because they absorb too far to the blue to be detectable under the conditions of our experiments (11). We similarly assign these products to the three-membered germanocycles **10** and **11**.

The significantly longer lifetimes of **9a**–**11** compared to those of the corresponding adducts from $GePh_2$ indicate that the greater degree of stabilization of the GeMePh adducts (as measured by the equilibrium constants for their formation) is also reflected in the rate constants for their further reaction. The processes responsible for the decay of the germirane (**10**) and germirene (**11**) at high substrate concentrations are unfortunately not clear; our earlier study of the reaction of DMP with $GePh_2$ indicated that it led to the formation of germanium-containing polymers, while the reaction with TBE produced a primary product that underwent further thermal or photochemical reaction under the conditions employed for its generation (10). Indeed, very few stable examples of such compounds are known (30–36), unlike the situation with the corresponding silicon analogues, which enjoy much greater thermodynamic stability (36–38). As mentioned previously, the reactions of $GeMe_2$ with alkenes, dienes, and alkynes are known to yield five-membered ring compounds derived from reaction of the germylene with two molecules of substrate, most likely via the intermediacy of the corresponding three-membered germanocycle (1, 27). We thus suspect that the relatively slow decay of these species is due to these secondary reactions, perhaps involving biradical intermediates formed by (single) Ge—C bond cleavage processes. In the case of **10** this process occurs with a rate constant of k ~ 500 s^{-1} in the presence of 0.1–0.35 mol/L alkene, roughly half that observed for the analogous species formed from reaction of $GePh_2$ with DMP under similar conditions (11). The process occurs roughly 10^3 times more slowly than cycloreversion to regenerate GeMePh and the alkene, based on an estimate derived from the estimated K_{eq} value and measured rate constant for the (forward) reaction of GeMePh with the alkene. The somewhat shorter lifetime observed for vinylgermirane **9a** is consistent with an additional contribution to its decay due to unimolecular isomerization, yielding **6**.

The reactions of GeMePh with $BuNH_2$ and Et_3N also result in the formation of detectable transient products, which can be identified as the Lewis acid–base complexes **8a** and **8b**, respectively. The equilibrium constants for formation of these complexes are in considerable excess of ca. 25 000 $(mol/L)^{-1}$, the approximate upper limit of K_{eq} for which residual germylene absorptions can be detected under the present experimental conditions. This was also found for the corresponding amine complexes with $GePh_2$ and $GeMe_2$ (10, 11), so it is not possible to comment on the relative stabilities of the amine complexes of this series of germylenes. Again, however, the rate constants for their formation are very similar. The only hint of a difference between the three germylenes in their reaction with amines is in the absorption spectra of the complexes, which are in both cases shifted significantly to the blue of those formed from $GePh_2$ (10), and significantly red-shifted compared with the complexes from $GeMe_2$ (11). Ando et al. (15) suggested that the positions of the absorption maxima of the complexes of amines, sulfides, phosphines, and ethers with a given germylene reflects their relative stabilities, in that they correlate broadly with Lewis base strength, shifting to the blue as the strength of the complex increases. This suggests that with a given amine, GeMePh forms the somewhat stronger Lewis acid–base complex and hence possesses somewhat higher Lewis acid strength than $GePh_2$. The opposite is true in regards to $GeMe_2$. For a given amine, the absorption maxima of the three germylene complexes vary to a much greater extent than those of the free germylenes. It is interesting to note that since the complex with $BuNH_2$ can be detected as a discrete, relatively long-lived intermediate, the formal H-migration process required to convert it to the putative N-H insertion product must be relatively slow. We previously reported that the reaction of $GePh_2$ with primary and secondary amines affords mainly polymeric material, and the germylamines derived from formal N-H insertion are formed in very low yields (10).

The effects of methyl vs. phenyl substitution on the reactivity of digermenes **3a**, **3b**, and **4** are somewhat greater and more varied than is the case with the corresponding germylenes. We have been successful in determining absolute rate constants for the reactions of **4** with four of the substrates studied ($BuNH_2$, AcOH, CCl_4, and O_2) and have determined

© 2006 NRC Canada

upper limits for the rate constants in the other cases. As mentioned earlier, we make the assumption that dimerization of GeMePh proceeds nonstereospecifically to yield a mixture of the (*E*)- and (*Z*)-isomers of the digermene, which seems reasonable enough considering that the reaction is fully diffusion-controlled. In most cases, the rate constants again fall between those of Ge_2Me_4 (**3b**) and Ge_2Ph_4 (**3a**), and since the mechanistic implications of these results have been discussed in some detail (11), they will not be elaborated on further here. The exception is the value for reaction with $BuNH_2$, which indicates somewhat greater reactivity for **4** compared with the tetraphenyl derivative. This is perhaps suggestive of a small steric effect on the rate of nucleophilic attack at the Ge=Ge bond in Ge_2Ph_4 (**3a**), which is thought to be the rate-determining step of the reaction (11).[5] It is also interesting to note that the rate constant for reaction with O_2 is ca. 30× lower than that reported (39) for the homologous disilenes, (*E*)- and *(Z)*-**16**, providing the first quantitative indication of the differences in reactivity of digermenes and disilenes of otherwise identical substitution. The reaction of disilenes and digermenes with oxygen has been reasonably well-studied and is known to yield the corresponding 1,2-dimetallaoxetane in both cases (40–42), presumably via the intermediacy of a triplet 1,4-(metalla-oxa)-biradical intermediate (43). Comparison of the rate constants for reaction of oxygen with the series of digermenes Ge_2Me_4 (**3b**, $k_{O_2} = 5.0 \times 10^7$ $(mol/L)^{-1}$ s^{-1}) (11), $Ge_2Me_2Ph_2$ (**4**, $k_{O_2} = 2.4 \times 10^7 (mol/L)^{-1}$ s^{-1}), and Ge_2Ph_4 (**3a**, $k_{O_2} = 4.8 \times 10^6$ $(mol/L)^{-1}$ s^{-1}) (10) indicates that phenyl for methyl substitution results in a consistent decrease in reactivity, spanning a factor of about 10 throughout the series. To our knowledge, there is little information available on the sensitivity of the rate constant to substituent for the reaction of O_2 with disilenes.

Similar trends in reactivity are evident in the rate constants for the reactions of **3a**, **4**, and **3b** with CCl_4 and AcOH (10, 11); the former is thought to proceed via initial chlorine atom abstraction to yield a (singlet) radical pair (44–46), while the latter most likely proceeds via 1,2-addition (of H-OAc) across the Ge=Ge bond, as is known for the reaction of alcohols with digermenes (9, 21) and disilenes (39, 47, 48). Interestingly, the opposite trend in reactivity is observed with the strong nucleophile, $BuNH_2$, for which the rate constants for the reactions with both **4** and Ge_2Ph_4 (**3a**) are ca. two orders of magnitude greater than that reported for Ge_2Me_4 (**3b**) (11). The difference in the reactivities of **3a** and **3b** toward this substrate is consistent with frontier molecular orbital control of the reaction, as the rate constants correlate with the relative LUMO energies of the two compounds (11).

Summary and conclusions

The direct detection and characterization of the reactivities of methylphenylgermylene (GeMePh) and (*E*)- and (*Z*)-1,2-dimethyl-1,2-diphenyldigermene (**4**), formed as a mixture by dimerization of the germylene, have been accomplished for the first time. The two species have been produced by photoextrusion of GeMePh from germacyclopent-3-ene derivative **5**, which affords GeMePh in >90% chemical yield and high quantum efficiency, based on the results of steady-state trapping experiments with methanol, acetic acid, and isoprene. The germylene is detectable as a weakly absorbing transient species with λ_{max} = 490 nm by laser flash photolysis of **5** in hexane solution, where it decays by diffusion-controlled dimerization to yield **4** (λ_{max} = 415 nm). The trends in the experimental UV–vis absorption spectra of $GeMe_2$, GeMePh, and $GePh_2$ mirror those in the spectra of the corresponding silylenes and similar correlations are found in the spectra of the corresponding digermenes and disilenes.

Absolute rate constants for reaction of GeMePh with several representative germylene scavengers have been measured, including primary and tertiary amines, acetic acid, triethylsilane, tri-*n*-butylstannane, O_2, CCl_4, two aliphatic dienes, and a terminal alkene and alkyne. With every reagent studied, GeMePh reacts with a similar absolute rate constant to that previously reported for $GePh_2$ under similar conditions and both germylenes are significantly less reactive than $GeMe_2$ toward the same substrates. Equilibrium constants falling between those determined earlier for $GeMe_2$ and $GePh_2$ have been estimated for the reversible reactions of GeMePh with amines, the alkene, and the dienes; the primary products of these reactions have also been detected as long-lived transient intermediates exhibiting similar UV–vis absorption spectra to the analogous products from $GePh_2$.

More detailed mechanistic studies of the photochemistry of arylgermacyclopent-3-ene derivatives and the reactions of transient germylenes and digermenes, including those with oxygenated substrates, are currently in progress in our laboratory.

Experimental

^1H and ^{13}C NMR spectra were recorded on Bruker AV 200 or AV 600 spectrometers in deuteriochloroform or cyclohexane-d_{12} solution and were referenced to the residual solvent proton and ^{13}C signals, respectively. Gas chromatographic analyses were carried out using a Hewlett-Packard 5890 gas chromatograph equipped with a conventional heated injector, a flame ionization detector, a Hewlett-Packard 3396A integrator, and a SPB-5 capillary column (25 m, 0.25 μm, Supelco, Inc.). Gas chromatographic – mass spectrometric (GC–MS) separations employed a Hewlett-Packard 5890 Series II gas chromatograph equipped with a HP-5971A mass selective detector and a SPB-5 capillary column (25 m, 0.25 μm, Supelco, Inc.). High-resolution electron impact mass spectra and exact masses were determined on a Micromass TofSpec 2E mass spectrometer. Exact masses were determined for the molecular ion (M^+), employing a mass of 12.000 000 for carbon-12. Column chromatography employed a 30 mm × 800 mm column using silica gel (120 g, acid-washed, 230–400 mesh ASTM, particle size 0.040–0.063 mm, Silicycle) and pentane as the eluant. Steady state photolyses employed a Rayonet® photochemical reactor (Southern New England Ultraviolet Co.,

[5] W.J. Leigh and L.A. Huck. To be published.

© 2006 NRC Canada

Branford, Connecticut) equipped with a merry-go-round apparatus and six RPR-2537 lamps (254 nm).

2,3-Dimethyl-1,3-butadiene, isoprene, phenylmagnesium bromide (3.0 mol/L solution in diethyl ether), methylmagnesium bromide (3.0 mol/L solution in diethyl ether), and magnesium were used as received from Sigma-Aldrich. Hexanes (Caledon Reagent) was dried by refluxing for several days under nitrogen with sodium–potassium amalgam followed by distillation, or by passage through activated alumina under nitrogen using a Solv-Tek solvent purification system (Solv-Tek, Inc., Berryville, Virginia). Diethyl ether (Caledon Reagent) and tetrahydrofuran (Caledon Reagent) were dried by the latter method. Each of the scavengers investigated in this work were obtained from commercial sources in the highest purity available. The amines were refluxed over solid KOH for 12 h and distilled, while triethylsilane (Et_3SiH) and tri-*n*-butylstannane (Bu_3SnH) were stirred at room temperature for 18 h over lithium aluminum hydride and distilled at atmospheric pressure (Et_3SiH) or under mild vacuum (Bu_3SnH). CCl_4 was refluxed over phosphorus pentoxide and distilled. 4,4-Dimethyl-1-pentene (DMP) was dried by passage through a silica gel column, while isoprene, DMB, and 3,3-dimethyl-1-butyne (TBE) were distilled at atmospheric pressure. 1,1-Dichloro-3,4-dimethylgermacyclopent-3-ene and 1,1-dichloro-3-methylgermacyclopent-3-ene were prepared as previously described (9, 49, 50). Deuterated solvents were used as received from Cambridge Isotopes Laboratories.

1,3,4-Trimethyl-1-phenyl-1-germacyclopent-3-ene (**5**) was synthesized by a procedure similar to that of Mazerolles and Manuel (51). In a flame-dried apparatus consisting of a 250 mL two-necked round-bottomed flask, reflux condenser, nitrogen inlet, addition funnel, and magnetic stirrer was prepared a solution of 1,1-dichloro-3,4-dimethyl-1-germacyclopent-3-ene (3.7 g, 0.016 mol) in anhydrous diethyl ether (80 mL) under nitrogen. The solution was cooled to 0 °C using an ice bath, and then a stirred solution of phenylmagnesium bromide (5.7 mL of a 3.0 mol/L solution in diethyl ether, 0.0171 mol) in dry diethyl ether (20 mL) was added dropwise over 1 h. The cooling bath was removed after 2 h and the white suspension was allowed to stir at room temperature for another 20 h. A solution of methylmagnesium bromide (6.3 mL of a 3.0 mol/L solution in diethyl ether, 0.019 mol) in anhydrous diethyl ether (20 mL) was then added dropwise over 1 h, and the reaction mixture was then stirred under reflux for a further 3 h. After cooling, the resulting yellow suspension was hydrolyzed with saturated aqueous ammonium chloride (40 mL) over 20 min, transferred to a separatory funnel, and the aqueous and organic fractions were separated. The aqueous fraction was extracted with diethyl ether (3 × 60 mL), and then the combined ether fractions were washed with distilled water (2 × 30 mL), 5% aqueous sodium bicarbonate (2 × 30 mL), dried with anhydrous magnesium sulfate (30 min), and filtered. The solvent was removed on a rotary evaporator to yield a yellow-green liquid (4.4 g). Distillation under vacuum (bp = 103–105 °C at 0.3 mm Hg, 1 mm Hg = 133.322 Pa) afforded **5** (3.78 g, 0.015 mol, 86%) as a colorless liquid. Further purification by column chromatography, using pentane as eluant, was performed until the purity of the compound was at least 99% according to GC analysis. The compound exhibited the following spectroscopic data: ^{1}H NMR ($CDCl_3$, 200 MHz) (52) δ: 0.56 (s, 3H), 1.74 (m, 10 H), 7.31–7.51 (m, 5H). ^{13}C NMR ($CDCl_3$) δ: –4.5, 19.4, 26.4, 128.0, 128.5, 130.9, 133.3, 143.9. MS *m/z*: 248 (65), 246 (45), 244 (35), 233 (38), 231 (28), 229 (20), 166 (70), 164 (43), 151 (100), 149 (85), 147 (80). Exact mass calcd. for $C_{13}H_{18}{}^{74}Ge$: 248.0620; found: 248.0617.

1,3-Dimethyl-1-phenyl-1-germacyclopent-3-ene (**6**) was prepared in similar fashion. A solution of 1,1-dichloro-3-methyl-1-germacyclopent-3-ene (2.0 g, 0.009 mol) in anhydrous diethyl ether (40 mL) was introduced into a flame-dried apparatus consisting of a two-necked round-bottomed flask (100 mL), reflux condenser, nitrogen inlet, addition funnel, and magnetic stirrer. After cooling to 0 °C, a solution of phenylmagnesium bromide (3.3 mL of a 3.0 mol/L solution in diethyl ether, 0.010 mol) in dry diethyl ether (20 mL) was added dropwise over 1.5 h with stirring. The cooling bath was removed after 2 h and the suspension was stirred at room temperature for another 15 h. A solution of methylmagnesium bromide (4.1 mL of a 3.0 mol/L solution in diethyl ether, 0.012 mol) in anhydrous diethyl ether (20 mL) was then added dropwise over 1.5 h, and the resulting mixture was stirred under reflux for a further 4 h. After cooling, the resulting yellow suspension was hydrolyzed with saturated aqueous ammonium chloride (40 mL) over 20 min and transferred to a separatory funnel, where the aqueous and organic fractions were separated. The aqueous fraction was extracted with diethyl ether (3 × 60 mL) and then the combined ether fractions were washed with distilled water (2 × 30 mL), 5% aqueous sodium bicarbonate (2 × 30 mL), dried with anhydrous magnesium sulfate (30 min), and filtered. The solvent was removed on a rotary evaporator to yield a yellow oil (2.3 g), which was purified by silica gel column chromatography with pentane as the eluting solvent. This afforded a colorless oil (1,9 g, 0.008 mol, 89%) in >99% purity, according to GC analysis, which was identified as **6** on the basis of the following spectroscopic data. ^{1}H NMR ($CDCl_3$, 200 MHz) δ: 0.58 (s, 3H), 1.23–1.80 (m, 7 H), 5.64 (s, 1H), 7.24–7.50 (m, 5H). ^{13}C NMR ($CDCl_3$) δ: –4.2, 14.2, 22.7, 31.7, 125.4, 128.1, 128.6, 130.9, 133.2, 140.3. MS *m/z*: 234 (35), 232 (25), 230 (18), 220 (67), 219 (36), 217 (15), 214 (10), 166 (40), 151 (100), 149 (85), 147 (50), 122 (20). Exact mass calcd. for $C_{12}H_{16}{}^{74}Ge$: 234.0464; found: 234.0446.

Steady state photochemical trapping experiments were carried out in quartz NMR tubes using 0.045 mol/L solutions of **5** in cyclohexane-d_{12} containing methanol (0.5 mol/L), acetic acid (0.095 mol/L), or isoprene (0.094 mol/L), monitoring the course of the reactions over the 0%–40% conversion range by ^{1}H NMR spectroscopy. The tubes were sealed with rubber septa and deoxygenated with a stream of dry argon for ca. 20 min prior to photolysis. The photolyses afforded equal yields of 2,3-dimethyl-1,3-butadiene (DMB; δ: 1.96, 4.88, 4.97) and a single additional major (>90%) product in each case. The identity of the isoprene adduct (**6**) was established by ^{1}H NMR spectroscopy, GC–MS, and GC coinjection of the crude photolysate with the authentic sample described above. The MeOH and AcOH adducts **7a** and **7b**, respectively, were identified on

© 2006 NRC Canada

the basis of comparisons of their ^{1}H NMR spectra to those of closely related compounds (9, 11, 53). Neither compound survived attempted GC separation without significant decomposition. Methoxymethylphenylgermane (**7a**): ^{1}H NMR (C_6D_{12}, 600 MHz) δ: 0.59 (d, 3H, J = 2.3 Hz), 3.45 (s, 3H), 5.68 (q, 1H, J = 2.3 Hz), 7.28 (m, 3H), 7.48 (m, 2H). Acetoxymethylphenylgermane (**7b**): ^{1}H NMR (C_6D_{12}, 600 MHz) δ: 0.79 (d, 3H, J = 2.3 Hz), 1.88 (s, 3H), 6.01 (q, 1H, J = 2.3 Hz), 7.28 (m, 3H), 7.58 (d, 2H).

Laser flash photolysis experiments employed the pulses from a Lambda Physik Compex 120 excimer laser, filled with F_2–Kr–Ne (248 nm, ~25 ns, 100 ± 5 mJ) mixtures and a Luzchem Research mLFP-111 laser flash photolysis system, modified as described previously (9). Solutions were prepared at concentrations such that the absorbance at the excitation wavelength (248 nm) was between ca. 0.7 and 0.9 and were flowed continuously through a thermostatted 7 × 7 mm Suprasil flow cell connected to a calibrated 100 mL reservoir, fitted with a glass frit to allow bubbling of nitrogen or argon gas through the solution for at least 30 min prior to and throughout the duration of each experiment. The glassware, sample cells, and transfer lines used for these experiments were stored in a 85 °C vacuum oven when not in use, and the oven was vented with dry nitrogen just prior to assembling the sample-handling system at the beginning of an experiment. Solution temperatures were measured with a Teflon-coated copper–constantan thermocouple inserted directly into the flow cell. Transient decay and growth rate constants were calculated by nonlinear least-squares analysis of the absorbance–time profiles using the Prism 3.0 software package (GraphPad Software, Inc., San Diego, California) and the appropriate user-defined fitting equations, after importing the raw data from the Luzchem mLFP software. Reagents were added directly to the reservoir by microliter syringe as aliquots of standard solutions. Rate constants were calculated by linear least-squares analysis of decay rate concentration data (five to seven points) that spanned as large a range in transient decay rate as possible. Errors are quoted as twice the standard deviation obtained from the least-squares analyses.

Acknowledgement

We thank the Natural Sciences and Engineering Research Council of Canada (NSERC) for financial support, the McMaster Regional Centre for Mass Spectrometry (Hamilton, Ontario) for mass spectrometric analyses, and Teck-Cominco Metals Ltd. (Vancouver, British Columbia) for a generous gift of germanium tetrachloride.

References

1. W.P. Neumann. Chem. Rev. **91**, 311 (1991).
2. J. Barrau and G. Rima. Coord. Chem. Rev. **180**, 593 (1998).
3. M. Weidenbruch. Eur. J. Inorg. Chem. **1999**, 373 (1999).
4. N. Tokitoh and R. Okazaki. Coord. Chem. Rev. **210**, 251 (2000).
5. S.E. Boganov, M.P. Egorov, V.I. Faustov, and O.M. Nefedov. *In* The chemistry of organic germanium, tin, and lead compounds. Vol. 2. *Edited by* Z. Rappoport. John Wiley and Sons, New York. 2002. p. 749.
6. S.E. Boganov, M.P. Egorov, V.I. Faustov, I.V. Krylova, O.M. Nefedov, R. Becerra, and R. Walsh. Russ. Chem. Bull. **54**, 483 (2005).
7. W.J. Leigh, N.P. Toltl, P. Apodeca, M. Castruita, and K.H. Pannell. Organometallics, **19**, 3232 (2000).
8. C.R. Harrington, W.J. Leigh, B.K. Chan, P.P. Gaspar, and D. Zhou. Can. J. Chem. **83**, 1324 (2005).
9. W.J. Leigh, C.R. Harrington, and I. Vargas-Baca. J. Am. Chem. Soc. **126**, 16105 (2004); Erratum, **128**, 1394 (2006).
10. W.J. Leigh and C.R. Harrington. J. Am. Chem. Soc. **127**, 5084 (2005).
11. W.J. Leigh, F. Lollmahomed, and C.R. Harrington. Organometallics, **25**, 2055 (2006).
12. R. Becerra, S.E. Boganov, M.P. Egorov, V.Ya. Lee, O.M. Nefedov, and R. Walsh. Chem. Phys. Lett. **250,** 111 (1996).
13. R. Becerra, C.R. Harrington, P.P. Gaspar, W.J. Leigh, I. Vargas-Baca, R. Walsh, and D. Zhou. J. Am. Chem. Soc. **127**, 17469 (2005).
14. R. Battino, T.R. Rettich, and T. Tominaga. J. Phys. Chem. Ref. Data, **12**, 163 (1983).
15. W. Ando, H. Itoh, and T. Tsumuraya. Organometallics, **8**, 2759 (1989).
16. M. Wakasa, I. Yoneda, and K. Mochida. J. Organomet. Chem. **366**, C1 (1989).
17. K. Mochida, K. Kimijima, and H. Chiba. Organometallics, **13**, 404 (1994).
18. M.J. Michalczyk, M.J. Fink, D.J. De Young, C.W. Carlson, K.M. Welsh, R. West, and J. Michl. Silicon Germanium Tin Lead Compds. **9**, 75 (1986).
19. G. Levin, P.K. Das, C. Bilgrien, and C.L. Lee. Organometallics, **8**, 1206 (1989).
20. W.J. Leigh and G.W. Sluggett. Organometallics, **13**, 269 (1994).
21. K. Mochida, T. Kayamori, M. Wakasa, H. Hayashi, and M.P. Egorov. Organometallics, **19**, 3379 (2000).
22. M.B. Taraban, O.S. Volkova, V.F. Plyusnin, Y.V. Ivanov, T.V. Leshina, M.P. Egorov, O.M. Nefedov, T. Kayamori, and K. Mochida. J. Organomet. Chem. **601**, 324 (2000).
23. A. Sekiguchi, I. Maruki, and H. Sakurai. J. Am. Chem. Soc. **115**, 11460 (1993).
24. B. Klein, W.P. Neumann, M.P. Weisbeck, and S. Wienken. J. Organomet. Chem. **446**, 149 (1993).
25. W.P. Neumann, M.P. Weisbeck, and S. Wienken. Main Group Met. Chem. **17**, 151 (1994).
26. P.P. Gaspar and R. West. *In* The chemistry of organic silicon compounds. Vol. 2. *Edited by* Z. Rappoport and Y. Apeloig. John Wiley and Sons, New York. 1998. p. 2463.
27. W.P. Neumann, E. Michels, and J. Kocher. Tetrahedron Lett. **28**, 3783 (1987).
28. M. Schriewer and W.P. Neumann. J. Am. Chem. Soc. **105**, 897 (1983).
29. E.C.L. Ma, K. Kobayashi, M.W. Barzilai, and P.P. Gaspar. J. Organomet. Chem. **224**, C13 (1982).
30. W. Ando, H. Ohgaki, and Y. Kabe. Angew. Chem. Int. Ed. Engl. **33**, 659 (1994).
31. H. Ohgaki, Y. Kabe, and W. Ando. Organometallics, **14**, 2139 (1995).
32. M.P. Egorov, S.P. Kolesnikov, Y.T. Struchkov, M.Y. Antipin, S.V. Sereda, and O.M. Nefedov. J. Organomet. Chem. **290**, C27 (1985).
33. A. Krebs and J. Berndt. Tetrahedron Lett. **24**, 4083 (1983).
34. F. Meiners, W. Saak, and M. Weidenbruch. Z. Anorg. Allg. Chem. **628**, 2821 (2002).
35. N. Tokitoh, K. Kishikawa, T. Matsumoto, and R. Okazaki. Chem. Lett. 827 (1995).

© 2006 NRC Canada

36. M. Driess and H. Grutzmacher. Angew. Chem. Int. Ed. Engl. **35**, 828 (1996).
37. J.A. Boatz, M.S. Gordon, and L.R. Sita. J. Phys. Chem. **94**, 5488 (1990).
38. D.A. Horner, R.S. Grev, and H.F. Schaefer, III. J. Am. Chem. Soc. **114**, 2093 (1992).
39. T.L. Morkin, T.R. Owens, and W.J. Leigh. *In* The chemistry of organic silicon compounds. Vol. 3. *Edited by* Z. Rappoport and Y. Apeloig. John Wiley and Sons, New York. 2001. p. 949.
40. S. Masamune, S.A. Batcheller, J. Park, W.M. Davis, O. Yamashita, Y. Ohta, and Y. Kabe. J. Am. Chem. Soc. **111**, 1888 (1989).
41. M.S. Samuel, M.C. Jennings, and K.M. Baines. J. Organomet. Chem. **636**, 130 (2001).
42. R. Okazaki and R. West. Adv. Organomet. Chem. **39**, 231 (1996).
43. K. McKillop, R. West, T. Clark, and H. Hofmann. Z. Naturforsch. B: Chem. Sci. **49**, 1737 (1994).
44. M.S. Samuel, M.C. Jennings, and K.M. Baines. Organometallics, **20**, 590 (2004).
45. M.-D. Su. Inorg. Chem. **43,** 4846 (2004).
46. M.-D. Su. J. Phys. Chem. A, **108**, 823 (2004).
47. H. Sakurai. *In* The chemistry of organic silicon compounds. *Edited by* Z. Rappoport and Y. Apeloig. John Wiley and Sons, New York. 1998. p. 827.
48. T. Veszpremi, M. Takahashi, B. Hajgato, and M. Kira. J. Am. Chem. Soc. **123**, 6629 (2001).
49. S.P. Kolesnikov, I.S. Rogozhin, and O.M. Nefedov. Izv. Akad. Nauk SSSR, Ser. Khim. 2297 (1974).
50. O.M. Nefedov, S.P. Kolesnikov, and A.I. Ioffe. Izv. Akad. Nauk SSSR, Ser. Khim. 602 (1976).
51. P. Mazerolles and G. Manuel. Bull. Soc. Chim. Fr. **56**, 327 (1965).
52. K.L. Bobbitt, V.M. Maloney, and P.P. Gaspar. Organometallics, **10**, 2772 (1991).
53. M. Massol, J. Satge, P. Riviere, and J. Barrau. J. Organomet. Chem. **22**, 599 (1970).

© 2006 NRC Canada

Tris(biimidazolato)chromium(III) as a building block for hydrogen-bonded supramolecular assemblies

Letitia M. Gruia, Fernande D. Rochon, and André L. Beauchamp

Abstract: The trischelate $[Cr(H_2biim)_3](NO_3)_3$ complex of 2,2′-biimidazole (H_2biim) was obtained by reacting $CrCl_3 \cdot 3THF$ with $[Ag(H_2biim)](NO_3)$ in methanol. In the solvent-free material, each ligand forms two N-H···O bonds to a nitrate ion and generates locally neutral $[Cr(H_2biim)_3](NO_3)_3$ units. A methanol solvate was also obtained in which intermolecular interactions involve optimal use of the hydrogen-bonding ability of the $[Cr(H_2biim)_3]^{3+}$ cations, NO_3^- anions, and methanol molecules. In both cases, there is no long-range regular organization of the complex units. Deprotonation of $[Cr(H_2biim)_3](NO_3)_3$ with $NaOCH_3$ yielded neutral $Cr(Hbiim)_3$. Its powder pattern is similar to that of $Ru(Hbiim)_3$, suggesting that it also consists of mutually perpendicular interlocked honeycomb sheets. Recrystallization by slow diffusion of diisopropyl ether into a methanol solution yielded a porous material of composition $Cr(Hbiim)_3 \cdot 2.6C_6H_{14}O$ in which superposed honeycomb sheets create infinite channels (~13 Å diameter) filled with disordered solvent molecules. A totally different structure is adopted by the solvate $Cr(Hbiim)_3 \cdot C_6H_6 \cdot 2H_2O$, where the benzene molecule is encapsulated in a cavity created by five complex molecules.

Key words: chromium, biimidazole, supramolecular, crystal structure, hydrogen bonding.

Résumé : Le complexe trischélate $[Cr(H_2biim)_3](NO_3)_3$ du 2,2′-biimidazole (H_2biim) a été obtenu par réaction de $CrCl_3 \cdot 3THF$ avec $[Ag(H_2biim)](NO_3)$ dans le méthanol. Dans les cristaux sans solvant, chaque ligand forme deux liaisons N-H···O avec un ion nitrate, ce qui crée localement des motifs neutres $[Cr(H_2biim)_3](NO_3)_3$. Un solvate méthanolique a également été isolé, dans lequel les interactions intermoléculaires font intervenir une utilisation optimale des liaisons hydrogène possibles entre les cations $[Cr(H_2biim)_3]^{3+}$, les anions NO_3^- et le méthanol. Dans les deux cas, il n'y a pas d'organisation régulière à grande échelle des motifs complexes. La déprotonation de $[Cr(H_2biim)_3](NO_3)_3$ avec $NaOCH_3$ a conduit au composé neutre $Cr(Hbiim)_3$. Son diagramme de poudre est semblable à celui de $Ru(Hbiim)_3$, ce qui laisse supposer qu'il est également constitué de feuillets hexagonaux mutuellement perpendiculaires, qui s'emboîtent les uns dans les autres. La recristallisation par diffusion lente d'éther diisopropylique dans une solution méthanolique a produit un matériau microporeux de composition $Cr(Hbiim)_3 \cdot 2.6C_6H_{14}O$, où des couches hexagonales superposées engendrent des canaux infinis (diamètre ~13 Å) occupés par des molécules de solvant désordonnées. Le solvate $Cr(Hbiim)_3 \cdot C_6H_6 \cdot 2H_2O$ adopte une structure complètement différente, dans laquelle le benzène est encapsulé dans une cavité créée par cinq molécules de complexe.

Mots clés : chrome, biimidazole, supramoléculaire, structure cristalline, liaison hydrogène.

Introduction

The assembly of molecular units by self-organization is one of the most important methods of developing new molecular materials with built-in features like porosity (1) or magnetism (2). One way to exert some control over the structure of the assembled product is to rely on hydrogen bonds. The strength and directionality of hydrogen bonding account for its significance and make it an extremely important interaction in supramolecular synthesis. The use of building blocks with such carefully positioned functionality can increase the odds of producing ensembles where the individual subunits are arranged in an expected way. This strategy has been used to produce a variety of architectures (3–6).

A particular organic target for the construction of such materials is the 2,2′-biimidazolate monoanion ($Hbiim^-$). This ligand can coordinate in a bidentate manner to metal centers (**1a**) and form a complementary hydrogen-bonding system using two sets of N-H donors and N acceptors (**1b**). A variety of inorganic molecular architectures in the solid state were obtained via these interactions. The resulting structural

Received 11 April 2006. Accepted 13 June 2006. Published on the NRC Research Press Web site at http://canjchem.nrc.ca on 9 August 2006.

L.M. Gruia and A.L. Beauchamp.[1] Département de Chimie, Université de Montréal, C. P. 6128, Succ. Centre-Ville, Montréal, QC H3C 3J7, Canada.
F.D. Rochon. Département de Chimie, Université du Québec à Montréal, C. P. 8888, Succ. Centre-Ville, Montréal, QC H3C 3P8, Canada.

[1]Corresponding author (e-mail: andre.beauchamp@umontreal.ca).

 doi:10.1139/V06-110 © 2006 NRC Canada

units can be simple dimeric or oligomeric species without complementary interunit hydrogen bonds (zero-dimensional structure), 1-D hydrogen-bonded ribbons, 2-D hydrogen-bonded sheets, or 3-D cross-catenated networks (7–11).

The systematic study of Tadokoro and Nakasuji (8) on salts of the $[Ni(Hbiim)_3]^-$ unit revealed that the complex anion can either remain isolated or form extended multidimensional assemblies, depending on the countercations present. To cast some light on the intrinsic potential of trisbiimidazolate metal units for the development of controlled architectures, we turned to the uncharged $Cr(Hbiim)_3$ compound. The only Cr(III)-biimidazole complex structurally characterized so far is the mixed $[Cr(Hbiim)(H_2biim)_2]SO_4$ compound (11).

Experimental

Reactants and methods

The starting material ($CrCl_3$·3THF) was prepared following the procedure of Boudjouk and So (12). Biimidazole was prepared according to Fieselmann et al. (13) and recrystallized in boiling aq. NaOH (0.025 mol/L). $[Ag(H_2biim)](NO_3)$ was obtained by the published procedure (14). Solvents and all other chemicals were used as received.

FT-IR spectra (4000 and 250 cm^{-1}) were recorded as CsI pellets on a Nicolet Avatar 370 CsI spectrophotometer. Elemental analyses were run by the Laboratoire d'Analyse Élémentaire de l'Université de Montréal. Mass spectra were recorded in the FAB^+ mode from nitrobenzylic alcohol solutions at the Centre Régional de Spectrométrie de Masse de l'Université de Montréal. The X-ray powder diffraction study was carried out with a D500 Siemens diffractometer (Co Kα radiation, λ = 1.7902 Å) at the Laboratoire de Radiocristallographie de l'Université du Québec à Montréal. Magnetic susceptibility data on powdered samples were measured with a Faraday balance at the Université du Québec à Montréal. The diamagnetic corrections were estimated from Lewis and Wilkins (15).

Preparative work

$[Cr(H_2biim)_3](NO_3)_3$ (1)

$CrCl_3$·3THF (37.4 mg, 0.10 mmol) and $[Ag(H_2biim)](NO_3)$ (91.2 mg, 0.30 mmol) in methanol (20 mL) were refluxed in the dark for 3 h. The cooled mixture was filtered to remove precipitated AgCl. The filtrate was then evaporated under reduced pressure to a volume of 10 mL and kept in a refrigerator. Dark-red crystals were deposited after 48 h. μ_{eff} = 3.82 BM. FAB^+-MS *m/z:* 452 $[Cr(Hbiim)_3 + H]^+$. Anal. calcd. for $[Cr(H_2biim)_3](NO_3)_3$·(1/8)CH_3OH·(1/4)H_2O: C 33.55, H 2.95, N 32.38; found: C 33.48, H 2.77, N 32.26.

$Cr(Hbiim)_3$ (2)

$[Cr(H_2biim)_3](NO_3)_3$ (64.0 mg, 0.10 mmol) was suspended in methanol (5 mL). $NaOCH_3$ (3.27 mL of a 0.50% *w/v* methanol solution) was added slowly, and the orange suspension was stirred for 15 min. The mixture was concentrated under reduced pressure and filtered. The orange solid was washed with diethyl ether and dried in vacuo. μ_{eff} = 3.93 BM. FAB^+-MS *m/z*: 452 $[Cr(Hbiim)_3 + H]^+$. Anal. calcd. for $Cr(Hbiim)_3$·H_2O·(1/2)CH_3OH: C 45.77, H 3.95, N 34.62; found: C 45.83, H 3.69, N 34.67.

Once precipitated, the solid is difficult to redissolve. Vapor diffusion of benzene into the (wet) methanol filtrate gave a small amount of dark-orange crystals, which were identified by X-ray diffraction (see later) as the $Cr(Hbiim)_3$·C_6H_6·$2H_2O$ solvate (**2a**). Vapor diffusion of diisopropyl ether into the filtrate produced dark-orange crystals of the $Cr(Hbiim)_3$·$2.6C_6H_{14}O$ solvate (**2b**).

X-ray powder diffraction on $Cr(Hbiim)_3$

The pattern of a dried sample was indexed using the 16 strongest reflections with the dichotomy method implemented in DICVOL (16, 17). This procedure gave a unique solution, consisting of a monoclinic cell similar to that of $Ru(Hbiim)_3$ (9), with satisfactory figures of merit, $F(16)$ = 22.4 and $M(16)$ = 22.8 (18, 19). Further refinement of the unit cell parameters using the Le Bail method with FULLPROF (20) yielded the following values: a = 12.283(3) Å, b = 12.722(7) Å, c = 13.231(7) Å, and β = 95.77(3)°. Analysis via an alternate refinement method using the PowderCell program (21) led to similar conclusions. The structural data of $Ru(Hbiim)_3$ (replacing Ru by Cr) were first used and the model was refined by comparison with the experimental values. The cell parameters, the zero shift, the scale factor, the background (modeled by a ninth-order polynomial), and the coefficients of the reflection profiles (using the Pseudo-Voigt2 function) were refined. The final parameters were a = 12.225 Å, b = 12.720 Å, c = 13.288 Å, and β = 95.80°, with satisfactory agreement factors R_p = 23.7, R_{wp} = 32.9, and R_{exp} = 6.8.

Crystallographic measurements and structure determination

The single-crystal X-ray data of **1** and **2b** were obtained with a Bruker SMART diffractometer, equipped with a 2K CCD area detector, using Cu Kα radiation. They were collected in the 512 pixel × 512 pixel mode under the control of the SMART software (22). Narrow frames with ω scan widths of 0.30° were recorded, exposure time being 15 s per frame for **1** and 9 s for **2b**. The first 101 frames were remeasured at the end of data collection to monitor instrument and crystal stability. The data were integrated using the SAINT program (23) and the intensities were corrected for the Lorentz factor, polarization, air absorption, and absorption due to variation in the path length through the detector faceplate. SADABS (24) was used to calculate the absorption correction.

Crystals **1a** and **2a** were studied with an Enraf-Nonius CAD-4 diffractometer operating with Cu Kα radiation under the control of the CAD-4 software (25). The reduced cell was initially determined from 20–25 spots located on a preliminary rotation photograph and centered in the detector aperture. Accurate cell parameters were then determined from the positions of 25 high-angle reflections centered by the SETANG and DETTH procedures. A whole sphere of data was collected by the ω/2θ scan technique. Possible crystal decomposition was monitored by measuring five standard reflections every hour. The data were corrected for the effect of Lorentz and polarization and an absorption correction based on the crystal geometry was applied (26).

© 2006 NRC Canada

Table 1. Crystal data.

Crystal	**1**	**1a**	**2a**	**2b**
Empirical formula	$C_{18}H_{18}CrN_{15}O_9$	$C_{19}H_{22}CrN_{15}O_{10}$	$C_{24}H_{25}CrN_{12}O_2$	$C_{33.6}H_{51.4}CrN_{12}O_{2.6}$
Formula mass	640.47	672.52	565.56	717.05
Color, habit	Red, block	Red-orange, block	Orange-brown, block	Orange, block
Crystal system	Trigonal	Tetragonal	Trigonal	Monoclinic
Space group	$R\bar{3}c$ (No. 167)	$P4_2/n$ (No. 86)	$P\bar{3}1c$ (No. 163)	$C2/m$ (No. 12)
a (Å)	17.1741(1)	11.895(3)	11.132(3)	16.877(3)
b (Å)	17.1741(1)	11.895(3)	11.132(3)	32.105(5)
c (Å)	15.9696(1)	19.421(5)	12.200(5)	15.983(2)
α (°)	90	90	90	90
β (°)	90	90	90	108.181(6)
γ (°)	120	90	120	90
Volume (Å^3)	4079.18(4)	2747.9(12)	1309.3(6)	8228(2)
Z	6	4	2	8
$D_{calcd.}$ (g cm^{-3})	1.564	1.626	1.435	1.158
Crystal size (mm)	0.60 × 0.32 × 0.26	0.48 × 0.42 × 0.16	0.38 × 0.28 × 0.16	0.26 × 0.13 × 0.10
μ (mm^{-1})	4.157	4.172	3.996	2.672
λ (Å)	1.541 78	1.541 78	1.541 78	1.541 78
Temperature (°C)	20	–50	20	–50
Measured reflections	15 493	10 405	1578	51 271
Independent reflections	900 ($R_{int.}$ = 0.036)	2618 ($R_{int.}$ = 0.076)	822 ($R_{int.}$ = 0.022)	5280 ($R_{int.}$ = 0.094)
Reflections with $I > 2\sigma(I)$	810	2147	760	1 884
Ranges of h, k, l	$-21 \le h \le 21$, $-21 \le k \le 21$, $-19 \le l \le 17$	$-14 \le h \le 14$, $-14 \le k \le 14$, $-23 \le l \le 23$	$-13 \le h \le 13$, $-13 \le k \le 13$, $-14 \le l \le 14$	$-17 \le h \le 17$, $-34 \le k \le 34$, $-16 \le l \le 16$
$R_1{}^a(I > 2\sigma(I))$	0.0436	0.0461	0.0350	0.0822
$WR_2{}^a(I > 2\sigma(I))$	0.1209	0.1129	0.0979	0.1460
$S^a(I > 2\sigma(I))$	1.030	1.078	1.038	1.005

$^a R_1 = \Sigma(||F_o| - |F_c||)/\Sigma|F_o|$, $wR_2 = \{\Sigma[w(F_o^2 - F_c^2)^2]/\Sigma[w(F_o^2)^2]\}^{1/2}$, S = GoF = $\{\Sigma[w(F_o^2 - F_c^2)^2]/(N_{reflns.} - N_{params.})\}^{1/2}$.

The SHELXTL package (27) was used for all calculations. The structures were solved by direct methods and ΔF map calculations. Non-hydrogen atoms were refined anisotropically using F^2 by full-matrix least-squares analysis. Hydrogens were fixed at idealized coordinates and allowed to ride on the supporting atoms during the refinement. They were assigned fixed isotropic thermal parameters U_{iso} = 1.2–1.5 × U_{eq} of the supporting atom. The final model was analyzed by means of the VOID routine of PLATON software (28) to check that no appreciable empty space remained in the structure. Crystal data are listed in Table 1 and CIF files are provided as Supplementary material.[2]

For **1**, the $\bar{3}m$ Laue symmetry and the systematic absences (hkl, $-h + k + l \ne 3n$; $h\bar{h}l$, $l \ne 2n$) were consistent with space groups $R3c$ and $R\bar{3}c$. The structure solved and refined normally in the centric $R\bar{3}c$ group. Positions were first found for the Cr atoms on equipoint 6a (32 local symmetry), surrounded by six "half-biimidazole" units in general position. The nitrate ions, in which one N—O bond lied on a twofold axis (18e), were then located from a ΔF map.

The $P4_2/n$ space group of **1a** was determined unambiguously from the 4/m Laue symmetry and systematic absences ($hk0$, $h + k \ne 2n$; $00l$, $l \ne 2n$). The Cr atom was found to lie on a crystallographic twofold axis (equipoint 4f) and the biimidazole ligands were readily identified. One of the nitrates (centered on N2) was located on a twofold axis (4e). The remaining nitrates and a lattice methanol molecule showed disorder. The latter nitrate adopted two slightly displaced orientations, but resolved positions could be defined for only one of the oxygens (O21/O21′, half occupancies). The C atom of the methanol molecule occupied a twofold axis (4e), whereas the OH group was disordered over two symmetry-equivalent sites about the axis (half occupancy imposed by symmetry).

For **2a**, space groups $P31c$ and $P\bar{3}1c$ were consistent with the observed $\bar{3}m$ Laue symmetry and systematic absences (hhl, $l \ne 2n$). The structure solved and refined normally in the centric $P\bar{3}1c$ group. The Cr(Hbiim)$_3$ unit was readily found, consisting of a Cr atom on equipoint 2c (32 local symmetry) surrounded by six "half-biimidazolate" units in

[2] Supplementary data for this article are available on the journal Web site (http://canjchem.nrc.ca) or may be purchased from the Depository of Unpublished Data, Document Delivery, CISTI, National Research Council Canada, Ottawa, ON K1A 0R6, Canada. DUD 5064. For more information on obtaining material refer to http://cisti-icist.nrc-cnrc.gc.ca/irm/unpub_e.shtml. CCDC 603707 (**1**), 603729 (**1a**), 603730 (**2a**), and 603731 (**2b**) contain the crystallographic data for this manuscript. These data can be obtained, free of charge, via http://www.ccdc.cam.ac.uk/conts/retrieving.html (Or from the Cambridge Crystallographic Data Centre, 12 Union Road, Cambridge CB2 1EZ, UK; fax +44 1223 336033; or deposit@ccdc.cam.ac.uk).

© 2006 NRC Canada

general position. A ΔF map then revealed the presence of lattice benzene molecules (one per complex) centered on equipoint 2d (32 symmetry), with the C (and H) atoms lying on crystallographic twofold axes (6h). Also, oxygens for lattice water molecules (two per complex) were aligned on the threefold axis (4e). In this high-symmetry environment, the N-H and O-H hydrogens had to be disordered. Since there was only one proton on each biimidazolate ligand, this proton had to be distributed statistically over the two uncoordinated N atoms. It was fixed at the idealized positions with half occupancy. For the water molecule, some electron density was found on the threefold axis (4e) at a reasonable position for hydrogen atom H1A, which was assigned only half occupancy, since another position generated by space group symmetry would be too close to be occupied simultaneously. Another small residual was detected in the ΔF map, near the line joining the water oxygen O1 and an uncoordinated biimidazolate N atom. This was considered as the position of the missing hydrogen (H1B), since the O1—H1B bond would make an angle of ~105° with O—H1A and ~121° with the two other symmetry-equivalent O—H1B bonds. An H1B atom was thus introduced along this direction at an idealized distance with half occupancy. This model provides the four water O1 atoms in the unit cell with eight hydrogens altogether, namely two H1A (half occupancy of fourfold equipoint 4c) and six H1B (half occupancy of 12-fold general equipoint). As will be discussed in the next section, this allowed full complementary hydrogen bonding to take place about the water molecule and uncoordinated biimidazolate N atoms.

Compound **2b** was found to be monoclinic (2/*m* Laue symmetry) and since only the centering systematic absence was noted ($hk0$, $h + l \neq 2n$), the space group could be *C*2, *Cm* or *C*2/*m*. The crystals did not diffract very well, especially at high angles, so these data were collected only up to $\theta = 55°$. Direct methods yielded a reasonable solution in the centric *C*2/*m* group. The eight Cr atoms were found to occupy two fourfold special positions (4g and 4h, respectively) on crystallographic twofold axes. They were each surrounded by biimidazolate units defining $Cr(Hbiim)_3$ molecules. Anisotropic refinement of these positions converged to $R = 0.16$. The ΔF map showed many weak peaks (<3 e/Å^3) in two large channels parallel to the *c* axis at (x, y) = (0, 1/2) and (1/2, 0), respectively. They were assumed to correspond to trapped solvent molecules. Extensive efforts were made to assemble these peaks into methanol or diisopropyl ether molecules, but without success. At this stage, the lower-symmetry space groups *C*2 and *Cm* were considered, but they did not solve the problem: the same structure was obtained for the complex, described by a greater number of parameters, and the very high correlations made refinement extremely unstable. Furthermore, no reasonable model could be unraveled for the solvent region in either case. Therefore, the *C*2/*m* model was retained. Since the solvent region could not be modelled with discrete fractional molecules, it was described via the SQUEEZE procedure implemented in the PLATON software (28). Analysis of the ordered model with the VOID routine of PLATON indicated that a volume of 4920 Å^3 occupied by 1205 electrons was available in the unit cell. Considering that a diisopropyl ether molecule contains 58 electrons and its volume is 235.5 Å^3 (based on a density of 0.720 g cm^{-3}), the presence of 20.8 molecules per cell would correspond to 1206 electrons and 4894 Å^3, which is very close to the above result. Methanol – diisopropyl ether mixtures were also considered, but they invariably led to poorer agreement. The contribution of the disordered solvent calculated by SQUEEZE was used to generate an adjusted set of intensity data bypassing the solvent contribution (29) and the ordered part of the structure was refined in space group *C*2/*m*. Two N-H protons with half occupancies were introduced at idealized positions to account for the fact that only one uncoordinated N atom of each biimidazolate ligand was protonated. Anisotropic refinement of the non-hydrogen atoms in the nonsolvent part of the structure converged normally to $R = 0.082$. Although this *R* factor is higher, it is considered to be quite satisfactory, considering the severe disorder present. The solvent composition deduced above was used to calculate the derived quantities in Table 1 and the Supplementary material.[2]

Results and discussion

Characterization of the cationic complex

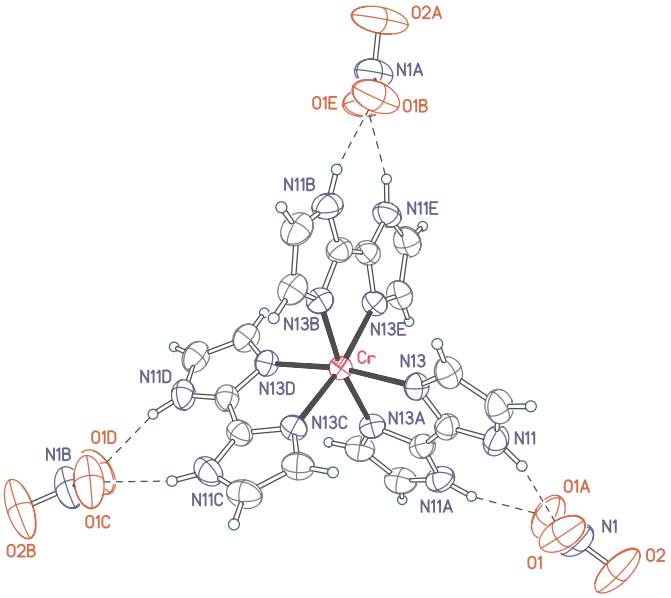
The $[Cr(H_2biim)_3]^{3+}$ complex was obtained as the nitrate salt by reacting $CrCl_3 \cdot 3THF$ with 3 equiv. of $[Ag(H_2biim)](NO_3)$ in methanol. After filtering AgCl and reducing the volume of the solution, the compound was isolated in good yields. Upon cooling the methanol solution, two types of crystals were visible. Both were examined by X-ray diffraction, which confirmed the presence of the octahedral trischelate cation. The two types of crystals are actually the monomethanol solvate (**1a**) and the solvent-free material (**1**). The magnetic moment ($\mu = 3.82$ BM) is typical of discrete Cr(III) species. The FAB$^+$ mass spectrum shows a peak for the $[Cr(Hbiim)_3+H]^+$ species.

The IR data (4000–250 cm^{-1}) for H_2biim and the chromium complexes are provided in Table S-1.[2] The tentative assignments proposed for H_2biim are based on the detailed work of Bonsor et al. (30) on imidazole. Their assignments, which are largely supported by a normal coordinate analysis by Tatara et al. (31), were transferred to H_2biim. In principle, band splitting should occur throughout the spectrum since each imidazole ring should produce its own series of vibrations. However, splitting is observed only in a few cases. The ν, δ, and γ modes of the imidazole C2—H2 bond are replaced here by motions centered on the C2-C2′ junction, most of which are expected to occur at low frequency, except for the ν(C2-C2′) mode, which likely contributes significantly to the strong band observed at 1217 cm^{-1} in H_2biim.

In the spectrum of $[Cr(H_2biim)_3](NO_3)_3$, the nitrate ion gives a very strong and broad band at 1383 cm^{-1}. A small feature at 1036 cm^{-1} originates from lattice methanol. The most obvious perturbation for the ligand involves the very strong ν(N-H) band, which shifts from 2900 to ~3 000 cm^{-1} and loses most of its combination and (or) overtone fine structure. The easily detectable slightly broadened feature, observed at 1634 cm^{-1} in the complex, is probably due to a combination or overtone involving γ(N-H) and γ(C-H) modes observed between 700 and 900 cm^{-1}. Various other changes in position and (or) intensity are noted throughout

© 2006 NRC Canada

Fig. 1. The $[Cr(H_2biim)_3]^{3+}$ cation and the hydrogen-bonded nitrate ions (**1**). Ellipsoids correspond to 30% probability. In the numbering scheme, the first digit corresponds to ring number and the second digit to the position in the ring. Symmetry operations are (A) $-y, x - y, z$; (B) $-x + y, -x, z$; (C) $y, x, 1/2 - z$; (D) $x - y, -y, 1/2 - z$; (E) $-x, -x + y, 1/2 - z$.



the spectrum, the most characteristic being the replacement of the 1217 cm^{-1} band, believed to involve the C2-C2′ stretching, by a strong feature at 1177 cm^{-1}. A ring mode at 1143 cm^{-1} and a δ(C, N-H) band at 1072 cm^{-1} shift to 1134 and 1083 cm^{-1}, respectively, with substantially increased intensity. Two low-frequency bands at 505 and 449 cm^{-1}, respectively, where free H_2biim shows no absorption, are assigned to chelate ring deformation. Bands at 393 and 365 cm^{-1} are likely due to Cr-N stretching, these modes occurring at these same positions for $[Cr(bipy)_3]^{3+}$ (32) and other Cr^{3+}–bipyridine chelates (33).

Crystal structures of 1 and 1a

Both compounds are nitrate salts of the trischelate $[Cr(H_2biim)_3]^{3+}$, where the metal center has an octahedral coordination distorted by the small bite angle of H_2biim. In the solvent-free crystals **1**, the $[Cr(H_2biim)_3]^{3+}$ cation (Fig. 1) retains maximum symmetry (32 or D_3). Selected distances and angles are listed in Table 2. The Cr atom lies on a crystallographic threefold axis, whereas three twofold axes in a perpendicular plane bisect the C2—C2′ bond of each H_2biim ligand. The nitrate N1—O2 bonds also lie on these twofold axes. The remaining oxygens O1 form two symmetry-equivalent N-H···O1 hydrogen bonds with the ligand N-H groups. This crystal has the same structure as the Co(III) analogue (10).

The two five-membered rings of biimidazole are almost coplanar (N3-C2-C2′-N3′, torsion angle of –4.6°). Hydrogen bonding would be optimized if the nitrate anion and the biimidazole unit were coplanar, but the twist of the nitrate ion by 32.7(2)° about the twofold axis, because of molecular packing, does not appreciably weaken the hydrogen bonds, since the N···O1 separation is small (2.75 Å). The structural

Table 2. Selected bond lengths, bond angles, and torsion angles for $[Cr(H_2biim)_3](NO_3)_3$ (**1**).

Bond lengths (Å)	
Cr—N13	2.029(2)
Bond angles (°)	
N13-Cr-N13[a]	80.47(10)
N13-Cr-N13[b]	171.13(9)
N13-Cr-N13[c]	93.36(9)
N13-Cr-N13[d]	93.41(7)
N13-Cr-N13[e]	93.41(7)
C12-N13-Cr	113.5(1)
C14-N13-Cr	139.9(2)
C12[a]-C12-N11	133.6(1)
C12[a]-C12-N13	116.1(1)
Torsion angles (°)	
N11-C12-C12[a]-N11[a]	–6.5(6)
N13-C12-C12[a]-N13[a]	–4.6(4)

[a]Symmetry operation: $y, x, -z + 1/2$.
[b]Symmetry operation: $x - y, -y, -z + 1/2$.
[c]Symmetry operation: $-x, -x + y, -z + 1/2$.
[d]Symmetry operation: $-x + y, -x, z$.
[e]Symmetry operation: $-y, x - y, z$.

units of Fig. 1 form columns parallel to the *c* axis at $(x, y) = (0,0)$, (1/3, 2/3), and (2/3, 1/3) (Fig. S-1).[2] The only particular interunit interaction involves the nitrate oxygen O2, nested between the H5 atoms of two adjacent molecules in different columns, with which it forms rather strong dipolar interactions (H5···O2 = 2.356 Å, C5-H5-O2 = 158°). Thus, in this compound, there is no long-range effect of hydrogen bonding on molecular packing.

In the methanol solvate $[Cr(H_2biim)_3](NO_3)_3{\cdot}CH_3OH$ (**1a**), the Cr^{3+} center retains the distorted octahedral coordination of **1** (Fig. 1). According to the geometrical data in Table 3, the only significant difference in the complex cation is a slightly greater twist about the central ligand bond, the N3-C2-C2′-N3′ torsion angles being –7.9° and –13.6° compared with –4.6° in **1**. The lattice contains methanol molecules, which can participate in hydrogen bonding without imposing strict directional constraints, and this lead to a totally different packing pattern (Fig. 2, stereoview S-2 available in the Supplementary material).[2] The complex cations form layers parallel to the *ab* plane at (z = 0 and 1/2) in which the methanol molecule is embedded. The interlayer region is occupied by the NO_3^- ions. In contrast with the solvent-free phase (**1**), the nitrates do not form a pair of hydrogen bonds to the same ligand but they tend to connect several adjacent molecules. All ligand N—H bonds participate in relatively strong N-H···O(nitrate) hydrogen bonds (N···O separation = 2.69–2.84 Å). The methanol molecule is disordered over two orientations about a crystallographic twofold axis and it forms an O-H···O bond (O···O = 2.84 Å) with O11 in one of the two adjacent nitrate ions.

Characterization of the neutral complexes

Neutralizing a suspension of the nitrate with 3 equiv. $NaOCH_3$ in methanol yields the deprotonated compound $Cr(Hbiim)_3$ as a poorly soluble orange solid. The compound has to be dried thoroughly to remove traces of solvent. Its

© 2006 NRC Canada

Table 3. Selected bond lengths, bond angles, and torsion angles for $[Cr(H_2biim)_3](NO_3)_3 \cdot CH_3OH$ (**1a**).

Bond lengths (Å)	
Cr—N13	2.031(2)
Cr—N23	2.025(2)
Cr—N33	2.042(2)
Bond angles (°)	
N13-Cr-N33[a]	170.23(9)
N23-Cr-N23[a]	172.83(12)
N13-Cr-N23	80.24(9)
N33-Cr-N33[a]	79.97(14)
N13-Cr-N13[a]	96.96(12)
N13-Cr-N23[a]	94.97(9)
N13-Cr-N33	91.74(9)
N23-Cr-N33	90.88(9)
N23-Cr-N33[a]	94.61(9)
C12-N13-Cr	113.5(2)
C14-N13-Cr	139.2(2)
C22-N23-Cr	113.7(2)
C24-N23-Cr	139.0(2)
C32-N33-Cr	113.4(2)
C34-N33-Cr	139.1(2)
C22-C12-N11	133.9(3)
C22-C12-N13	116.0(2)
C12-C22-N21	133.8(3)
C12-C22-N23	116.1(2)
C32[a]-C32-N31	133.9(2)
C32[a]-C32-N33	116.4(2)
Torsion angles (°)	
N11-C12-C22-N21	0.0(5)
N13-C12-C22-N23	–0.7(4)
N31-C32-C32[a]-N31[a]	–13.6(8)
N33-C32-C32[a]-N33[a]	–7.9(5)

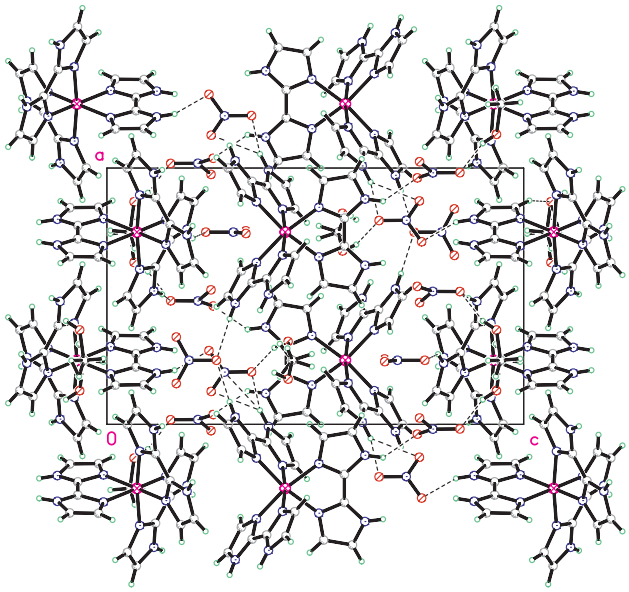
[a]Symmetry operation: 3/2 – *x*, 3/2 – *y*, *z*.

magnetic moment (μ_{eff} = 3.93 BM) is normal. The FAB^+ mass spectrum shows a peak for $[Cr(Hbiim)_3 + H]^+$.

Infrared data for $Cr(Hbiim)_3$ are compared with those of $[Cr(H_2biim)_3](NO_3)_3$ in Table S-1.[2] As expected, the strong nitrate band at ~1380 cm^{-1} has disappeared. The most characteristic spectral feature of the complex is a broad band at 1909 cm^{-1} in a featureless region for both the free ligand and $[Cr(H_2biim)_3](NO_3)_3$. Similar bands in the same region were reported for complexes of other metals containing biimidazole as the monoanion (8, 9, 34, 35) and were attributed to the 2γ(N-H) overtone on the basis of a study by Malarski and Sobczyk on imidazole (36). This assignment would imply that the fundamental γ(N-H) mode is near 950 cm^{-1}, and there is indeed a broad feature underlying other ligand vibrations in this region. The ν(N-H) vibration is shifted from 2900 to 2520 cm^{-1} in the complex. Several other differences are noted with respect to the above $[Cr(H_2biim)_3]^{3+}$ complex. In the sensitive 1000–1200 cm^{-1} region, the ν(C2-C2′) band is found at 1198 cm^{-1} and various shifts are noted. The chelate ring vibrations undergo small shifts to 523 and 460 cm^{-1}, whereas the ν(Cr-N) bands are not greatly affected (390 and 355 cm^{-1}).

In an attempt to replace all the N-H protons by Ag^+ ions, $[Cr(H_2biim)_3](NO_3)_3$ was reacted with Tollen's reagent (ammoniacal silver nitrate). Although the basic character of this concentrated ammonia solution neutralized one of the ligand protons, substitution of the second proton did not take place and $Cr(Hbiim)_3$ was isolated.

Fig. 2. View of the unit cell of $[Cr(H_2biim)_3](NO_3)_3 \cdot MeOH$ (**1a**) along the *b* axis.



Crystal structures of solvent-free Cr(Hbiim)$_3$ (2) and solvates 2a and 2b

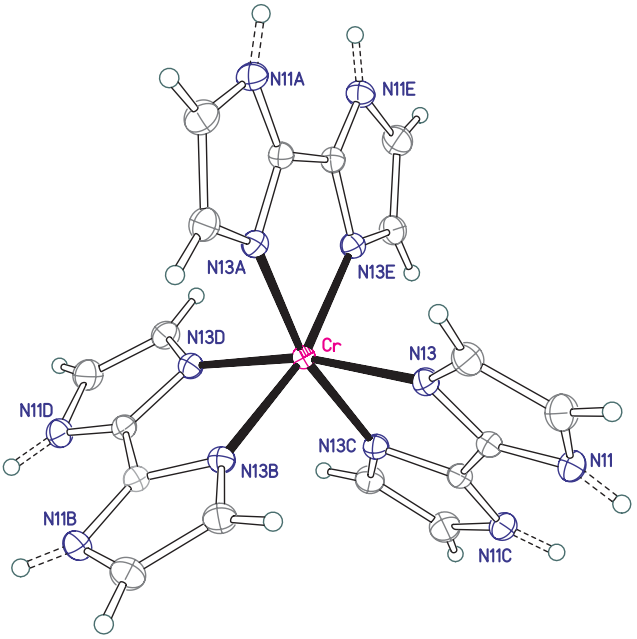
Single crystals of $Cr(Hbiim)_3$ for X-ray work could not be grown, but a powder pattern was recorded on a thoroughly dried sample. Indexation based on the 16 strongest peaks yielded a monoclinic unit cell very similar to that reported by Tadokoro et al. (9) for $Ru(Hbiim)_3$. The experimental pattern for $Cr(Hbiim)_3$ is very similar to the one calculated by PLATON (28) from the unit cell and atom coordinates of $Ru(Hbiim)_3$ ($P2_1$, a = 12.243 Å, b = 12.643 Å, c = 13.207 Å, β = 92.74°, V = 2042 $Å^3$), suggesting that the Cr and Ru compounds are isostructural. Refinement of the cell parameters with FULLPROF (20) yielded the following values: a = 12.283(3) Å, b = 12.722(7) Å, c = 13.231(7) Å, β = 95.77(3)°, V = 2 057 $Å^3$. The unit cell of $Cr(Hbiim)_3$ is found to be slightly larger than that of $Ru(Hbiim)_3$, despite the fact that the six-coordinate radii of Cr^{3+} (0.76 Å) and Ru^{3+} (0.82 Å) are in the reverse order (37). Subtle packing effects could lead to this tiny difference, which lies, at any rate, near the limit of discrimination of the present study.

The crystal of **2a** contains neutral $Cr(Hbiim)_3$ molecules, together with one benzene and two water molecules per complex. The molecular unit (Fig. 3) has a distorted octahedral structure similar to that of the above $[Cr(H_2biim)_3]^{3+}$ cation, with the difference that there remains only one N-H proton per $Hbiim^-$ ligand, which is disordered statistically over the two rings. Distances and angles are given in Table 4. Any small geometrical differences between the protonated and the deprotonated rings are averaged, each uncoordinated N atom bears a half-proton, and the species exhibits an averaged structure with 32 (D_3) symmetry.

A view of the unit cell is provided in Fig. 4. Benzene and

© 2006 NRC Canada

Fig. 3. The $Cr(Hbiim)_3$ molecule in **2a**. Ellipsoids correspond to 30% probability. Numbering scheme as in Fig. 1. The N-H proton (dashed bond) of each ligand is disordered statistically over two sites. Symmetry operations are (A) $1 - y, 1 + x - y, z$; (B) $-x + y, 1 - x, z$; (C) $1 - y, 1 - x, 1/2 - z$; (D) $-x + y, y, 1/2 - z$; (E) $x, 1 + x - y, 1/2 - z$.



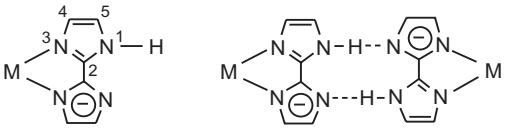
complex molecules centered on a crystallographic threefold axis are repeated in alternance along this axis, which is parallel to the unit cell *c* direction. Although $Hbiim^-$ ligands are good candidates for complementary hydrogen bonding (Scheme 1*b*), the complexes are not directly hydrogen bonded to one another in the present structure, since all hydrogen bonds involve a participation of the lattice water molecules sitting on the *c* axis. The environment of the *c* axis, which is a crystallographic threefold axis, is depicted in Fig. 5. All N-H and O-H protons are disordered, but four hydrogen-bonding interactions take place around each water molecule and all imidazole rings are efficiently used. In one of the possible "snapshot" arrangements given in the figure, pairs of water molecules along the *c* axis form an O1-H1···O1 bond (O1···O1 = 2.76 Å). For the O1 atom acting as a donor, an O1-H1B···N11 bond is established with the deprotonated ring of a complex (O1···N11 = 2.75 Å). The corresponding rings in the two other threefold related complexes are protonated and act as donors in N11-H11···O1 interactions (N11···O1 = 2.75 Å). The D-H···A systems are all nearly linear and the angles around O1 are close to 110°. When O1 is an acceptor in the O1-H1A···O1 bond, its two hydrogens are of the H1B type and they participate in donor interactions to deprotonated imidazole rings in two complex molecules, while the ring in the third (threefold related) complex molecule is protonated and forms an N11-H11···O1 bond. A number of other instantaneous patterns can be generated by rotating the hydrogen-bonding pattern of either (or both) of the O1 atoms about the threefold axis or by allowing the O1-H1A···O1 bond to be directed up instead of down (inversion via the center of symmetry included in the $\bar{3}$ operation on *c*). In all cases, optimal use is made of the donor–acceptor abilities of the groups that are available to form efficient hydrogen bonds.

Table 4. Selected bond lengths, bond angles, and torsion angles for $Cr(Hbiim)_3 \cdot C_6H_6 \cdot 2H_2O$ (**2a**).

Bond lengths (Å)	
Cr—N13	2.039(2)
Bond angles (°)	
N13-Cr-N13[a]	91.90(7)
N13-Cr-N13[b]	167.23(8)
N13-Cr-N13[c]	79.67(7)
N13-Cr-N13[d]	97.93(6)
C12-N13-Cr	114.43(12)
C14-N13-Cr	139.87(13)
C12[c]-C12-N11	131.56(10)
C12[c]-C12-N13	115.80(10)
Torsion angles (°)	
N11-C12-C12[c]-N11[c]	–6.0(4)
N13-C12-C12[c]-N13[c]	–3.5(3)

[a]Symmetry operation: $1 - y, 1 + x - y, z$.
[b]Symmetry operation: $-x + y, y, 1/2 - z$.
[c]Symmetry operation: $1 - y, 1 - x, 1/2 - z$.
[d]Symmetry operation: $x, 1 + x - y, 1/2 - z$.

Scheme 1.



1a **1b**

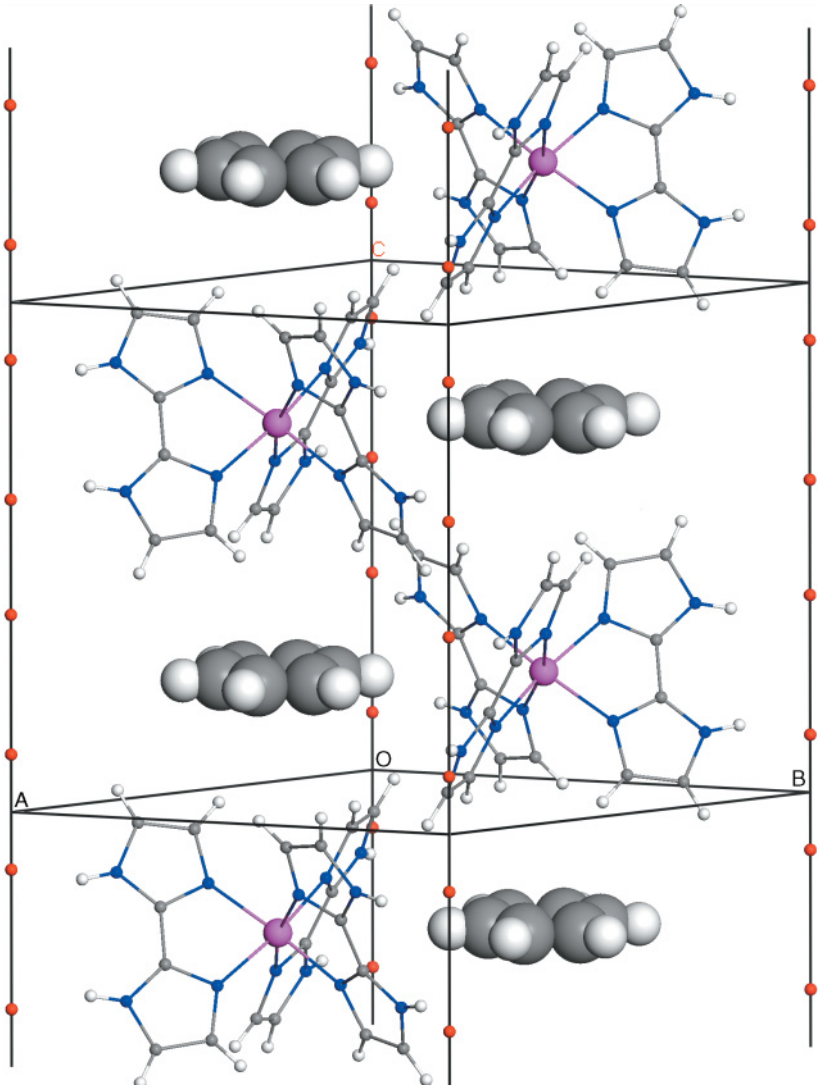
The benzene molecule occupies a crystallographic site of 32 symmetry and the C—H bonds all lie on crystallographic twofold axes (Fig. 6). It sits in a cavity produced by three coplanar complex molecules repeated by the threefold axis through the middle of the benzene ring, together with two more complexes lying on this threefold axis, above and below. Local 32 symmetry implies that the benzene ring is perfectly planar with angles of 120° and identical C—C bond lengths. The observed C—C distance, 1.360(4) Å, is somewhat below the typical aromatic bond length (1.380 Å) (38), but this is probably an artefact of the relatively large thermal motion.

The crystal structure of **2b** also consists of discrete neutral $Cr(Hbiim)_3$ molecules. The asymmetric unit includes two independent molecules, but their structures are not significantly different. Distances and angles are provided in Table S-2.[2]

In this case, the molecules are associated via hydrogen bonding taking place directly between the ligands. The N—H bond and the free N atom are oriented so that a pair of complementary N-H···N bonds can be formed between any pair of ligands facing each other in different molecules; these interactions are strong (N···N separation of 2.67–2.80 Å) and the N-H···N angles (158°–167°) are favourable. In this racemic compound, each Δ enantiomer is surrounded by three Λ enantiomers and vice versa. This alternating sequence of Δ and Λ molecules allows the hydrogen bond pairs formed by a given molecule to take place roughly in

© 2006 NRC Canada

Fig. 4. Unit cell of $Cr(H_2biim)_3 \cdot C_6H_6 \cdot 2H_2O$ (**2a**). Benzene and complex molecules are stacked in alternance along the *c* axis (vertical in the figure). The spheres on the *c* axis represent the oxygen atoms of the water molecules (hydrogens not shown).



the same plane with its three neighbours, generating six-membered rings that propagate into a two-dimensional honeycomb sheet, parallel to the *ab* plane and superposed in the *c* direction (Fig. 7; perpendicular and parallel views of the sheet are provided in Figs. S-3 and S-4).[2] Intersheet contact involves only normal van der Waals interactions. The sheets do not lie exactly above one another, since the repetition by the *c* axis shifts the sheets in the *a* direction (monoclinic β angle of 108°). The fairly large hole in the middle of each hexagon in the honeycomb sheet is also displaced similarly. However, this does not create significant obstruction between the free regions of successive sheets, so that the lattice contains infinite channels parallel to *c* (Fig. 7), each of whose diameter is ~13 Å. The channels are filled with disordered diisopropyl ether molecules.

Geometry of chelated biimidazole

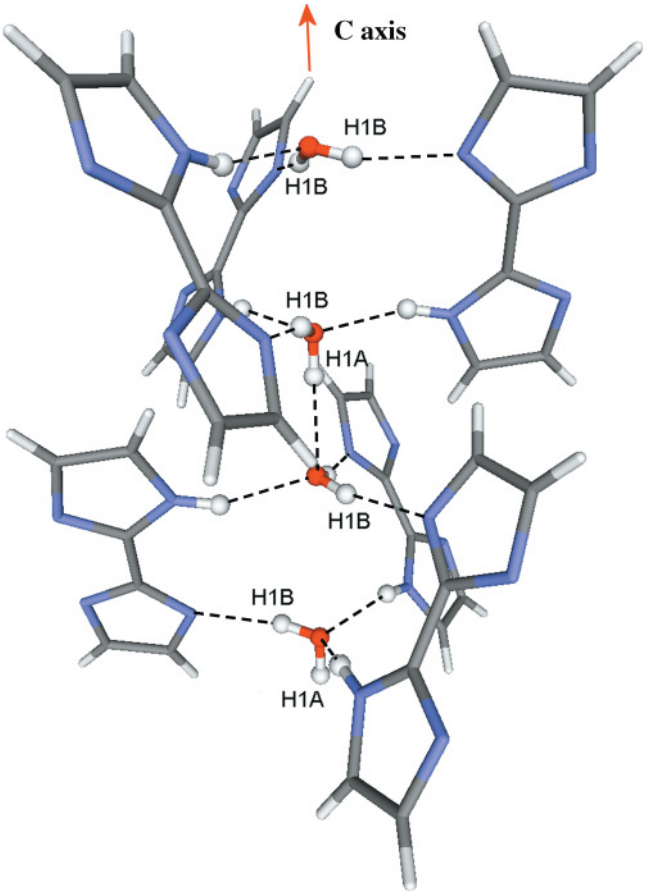
Despite the fact that the ligand is differently protonated in $[Cr(H_2biim)_3]^{3+}$ and $Cr(Hbiim)_3$, no drastic geometrical variations are detected (Tables 2–4 and S-2[2]). It should be mentioned that because the N-H proton is statistically disordered over the two rings in the neutral compound, ring geometry is averaged and any effect of deprotonation is obscured. The only substantial effect of deprotonation is detected on the internal angle C2-N1-C5 at the uncoordinated N atom, which is 108.0° for $[Cr(H_2biim)_3]^{3+}$ and 104.7° for $Cr(Hbiim)_3$. Reduction of ~3°–5° of C-N-C ring angles upon deprotonation is well-documented for related systems (39–41).

The mean Cr—N distance of 2.023 Å (range = 1.98–2.06 Å) is shorter than the values found in structures with various imidazole units (mean = 2.050 Å, range = 2.035–2.068 Å).[3] It is not clear why relatively large distances of 2.154(5)–2.216(5) Å have been observed for the sulphate salt of $[Cr(Hbiim)(H_2biim)_2]^{2+}$ (11). The N-Cr-N bite angle of ~80° is normal for metal ions of this size. No appreciable changes are noted on bond lengths or angles with respect to free 2,2′-biimidazole (43) or 1,1′-dimethyl-2,2′-biimidazole (44). As usually found for chelate formation, the internal

[3] Based on 19 values for 11 compounds found in the Cambridge Structural Database (42).

© 2006 NRC Canada

Fig. 5. Possible "instantaneous" hydrogen bonding around the *c* axis (crystallographic threefold axis) of **2a**. H1A and H1B are disordered as a result of the presence of other instantaneous patterns generated by the space group operations.

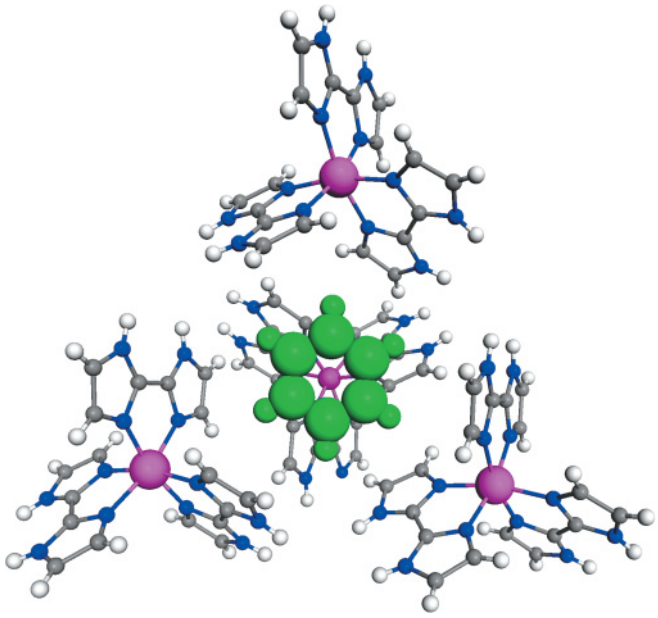


N3-C2-C2′ angles (mean = 116.2°) are much smaller than the external N1-C2-C2′ angles (mean = 133.8°). The metal atom does not lie exactly about the expected lone pair direction (mean values for Cr-N3-C2 and Cr-N3-C4 of 113.9° and 139.0°, respectively) and it is displaced significantly from the plane of the five-membered ring (mean Cr-to-plane distance = 0.15 Å). All these distortions, together with small relative twists of the rings about the C2—C2′ bond (mean = 5°, maximum = 14°), help chelate formation and contribute to absorbing the stress imposed by molecular packing.

Discussion

The structures of the octahedral trischelates $[Co(H_2biim)_3]^{3+}$ (10, 45) and $[M(H_2biim)_3]^{2+}$ (M = Fe, Co, and Ni) (46, 47) have been described. The solvent-free $[Cr(H_2biim)_3](NO_3)_3$ compound (**1**) reported here adopts the same structure as $[Co(H_2biim)_3](NO_3)_3$. Since both nitrogens are protonated on all ligands, these species can only act as hydrogen bond donors, and crystal organization in these materials depends on the counteranions. Each ligand in $[Cr(H_2biim)_3]^{3+}$ forms two N-H···O(nitrate) interactions and the complex cation is surrounded by nitrate anions, making full use of the hydrogen-bonding capability of the complex. No readily controlled long-range architecture develops, however. Since there is no partner for the third nitrate oxygen to form H-bonds, it participates in dipolar intermolecular interactions of low directionality with C-H protons. When precipitated in methanol, this solvent-free compact phase (**1**) cocrystallizes with a monomethanol solvate crystal (**1a**). Methanol is a good hydrogen bonding partner, but it does not impose strict directional constraints on molecule packing. Thus, although efficient use is made of the available donor and acceptor capabilities of the partners, no structural constraints are built in the methanol molecule and packing is controlled mainly by local packing efficiency.

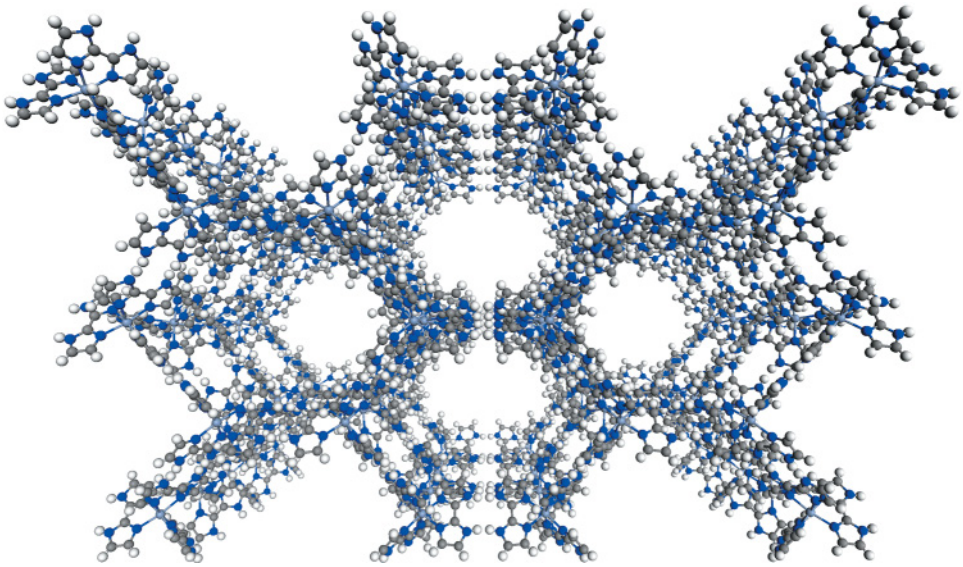
Fig. 6. Pocket containing the benzene molecule in $Cr(Hbiim)_3 \cdot C_6H_6 \cdot 2H_2O$ (**2a**) as viewed down the *c* axis. The pocket consists of three complex molecules related by a threefold axis and coplanar with the benzene molecule, with one molecule behind and an extra molecule in front (not shown).



The neutral $Cr(Hbiim)_3$ unit is a promising building block to create controlled superstructures. Kinetic inertness imparts to the Cr^{3+} centre a relatively long lifetime for architecture generation. The presence of one protonated and one deprotonated ring provides optimal hydrogen-bonding complementarity for each $Hbiim^-$ ligand. The formation of pairs of complementary N-H···N bonds has been observed in a number of cases (8). A series of $A[Ni(Hbiim)_3]$ salts were prepared, and depending on the A^+ cations present, the complex either remained isolated or formed extended uni- or multi-dimensional assemblies. A pattern encountered in these structures is the honeycomb sheet, based on rings of six $M(Hbiim)_3$ units connected via pairs of complementary N-H···N interactions. This pattern, which requires an alternance of Δ and Λ configurations around the ring, can be obtained only with racemic materials. When these honeycomb sheets are stacked with ring centers roughly above one another, they generate infinite channels, as observed for $[Ni(Hbiim)_3]^-$ salts with cations of the type $(K\text{-cryptate})^+$. A related framework has been obtained with $Co(Hbiim)_3$, the channels being filled in this case by methanol and methyl acetate molecules (48). On the other hand, for $Ru(Hbiim)_3$ (9), mutually perpendicular honeycomb sheets are inter-

© 2006 NRC Canada

Fig. 7. View of the solvent-filled channels parallel to the *c* axis of **2b**, running through the middle of the hexagons in the honeycomb sheets



locked to form a compact, solvent-free, three-dimensional framework.

With the present racemic $Cr(Hbiim)_3$ compound, both the compact solvent-free and the porous honeycomb-sheet solvated materials were isolated. The X-ray powder pattern shows that solvent-free $Cr(Hbiim)_3$ is structurally very close to the $Ru(Hbiim)_3$ solid described by Tadokoro et al. (9). Our $Cr(Hbiim)_3$·2.6diisopropyl ether solvate exhibits a structure similar to that of the the ethyl acetate – methanol solvate of $Co(Hbiim)_3$ (48). An unexpected material was obtained when crystallization of $Cr(Hbiim)_3$ took place in a wet atmosphere containing benzene. In this case, both the water and the benzene molecules play a determining role. The hydrogen-bonding ability of $Cr(Hbiim)_3$ was not expressed by direct intercomplex hydrogen bonding, but via properly positioned water molecules. Again, hydrogen bonding is optimized, since the number of hydrogen bond donors and acceptors in the three complex molecules surrounding any given pair of water molecules are perfectly complementary. The resulting layers leave exactly the amount of space necessary to host the benzene molecule.

In summary, $Cr(Hbiim)_3$ appears to be a robust building block and this Cr(III) centre is particularly attractive for the development of tailored magnetic compounds that have many applications in the field of materials science. The metal centre with its d^3 configuration could be coupled with other paramagnetic metal ions to produce molecular-based magnets of great interest. Compounds of Cr(III) with biimidazole ligands might be interesting building blocks for the design of homometallic, heterometallic, or other mixed-valent magnetic compounds. Although protonated and monodeprotonated biimidazole can form bridges between metal ions, the imidazole dianion ($biim^{2-}$) should be much more efficient. The complete deprotonation of H_2biim does not seem to take place very easily, but compounds of the types $[Cr(Hbiim)_2(biim)]^-$, $[Cr(Hbiim)(biim)_2]^{2-}$, or $[Cr(biim)_3]^{3-}$ seem to be very promising building blocks for the assembly of tailored designed uni- or multi-dimensional architectures.

Acknowledgement

We wish to thank the Natural Sciences and Engineering Research Council (NSERC) of Canada for financial support, Dr. M. Simard and Ms. F. Bélanger-Gariépy for assistance in the interpretation of the X-ray diffraction data and Drs. T. Maris and M. Fakhfakh for their help with the X-ray powder patterns.

References

1. P.J. Langley and J. Hulliger. Chem. Soc. Rev. **28**, 279 (1999).
2. J.S. Miller. Inorg. Chem. **39**, 4392 (2000).
3. B. Moulton and M.J. Zaworotko. Chem. Rev. **101**, 1629 (2001).
4. C.B. Aakeroy and A.M. Beatty. Aust. J. Chem. **54**, 409 (2001).
5. M.D. Ward. Chem. Commun. (Cambridge, U.K.), 5838 (2005).
6. J.D. Wuest. Chem. Commun. (Cambridge, U.K.), 5830 (2005).
7. M. Tadokoro, K. Isobe, H. Uekusa, Y. Ohashi, J. Toyoda, K. Tashiro, and K. Nakasuji. Angew. Chem. Int. Ed. **38**, 95 (1999).
8. M. Tadokoro and K. Nakasuji. Coord. Chem. Rev. **198**, 205 (2000).
9. M. Tadokoro, H. Kanno, T. Kitajima, H. Shimada-Umemoto, N. Nakanishi, K. Isobe, and K. Nakasuji. Proc. Natl. Acad. Sci. U.S.A. **99**, 4950 (2002).
10. L. Öhrström, K. Larsson, S. Borg, and S.T. Norberg. Chem. Eur. J. **7**, 4805 (2001).
11. K. Larsson and L. Öhrström. CrystEngComm. **5**, 222 (2003).
12. P. Boudjouk and J.-H. So. Inorg. Synth. **29**, 108 (1992).
13. B.F. Fieselmann, D.N. Hendrickson, and G.D. Stucki. Inorg. Chem. **17**, 2078 (1978).
14. P. Majumdar, S.-M. Peng, and S. Goswami. J. Chem. Soc. Dalton Trans. 1569 (1998).

© 2006 NRC Canada

15. J. Lewis and R.G. Wilkins. *In* Modern coordination chemistry: principles and methods. Interscience Publishers, New York. 1960.
16. A. Boultif and D. Louër. J. Appl. Crystallogr. **24**, 987 (1991).
17. A. Boultif and D. Louër. J. Appl. Crystallogr. **37**, 724 (2004).
18. G.S. Smith and R.L. Snyder. J. Appl. Crystallogr. **12**, 60 (1979).
19. P.M. De Wolff. J. Appl. Crystallogr. **1**, 108 (1968).
20. J. Rodriguez-Carvajal. FULLPROF [computer program]. 1990.
21. W. Kraus and G. Nolze. PowderCell for Windows [computer program]. Version 2.4. Federal Institute for Materials Research and Testing, Berlin, Germany. 2000.
22. Bruker AXS Inc. SMART [computer program]. Release 5.059. Bruker AXS Inc., Madison, Wis. 1999.
23. Bruker AXS Inc. SAINT [computer program]. Release 6.06. Bruker AXS Inc., Madison, Wis. 1999.
24. G.M. Sheldrick. SADABS [computer program]. Bruker AXS Inc., Madison, Wis. 1996.
25. Enraf-Nonius. CAD-4 [computer program]. Version 5.0. Enraf-Nonius, Delft, The Netherlands. 1989.
26. E.J. Gabe, Y. LePage, J.P. Charland, F.L. Lee, and P.S. White. J. Appl. Crystallogr. **22**, 384 (1989).
27. Bruker AXS Inc. SHELXTL. Release 5.10 [computer program]. Bruker AXS Inc., Madison, Wis. 1997.
28. A.L. Spek. PLATON [computer program]. University of Utrecht, Utrecht, The Netherlands. 2000.
29. P. van der Sluis and A.L. Spek. Acta Crystallogr. Sect. A: Fundam. Crystallogr. **46**, 194 (1990).
30. D.H. Bonsor, B. Borah, R.L. Dean, and J.L. Wood. Can. J. Chem. **54**, 2458 (1976).
31. W. Tatara, M.J. Wojcik, J. Lindgren, and M. Probst. J. Phys. Chem. **107**, 7827 (2003).
32. J. Takemoto, B. Hutchinson, and K. Nakamoto. J. Chem. Soc. Chem. Commun. 1007 (1971).
33. J.R. Ferraro, R. Driver, W.R. Walker, and W. Wozniak. Inorg. Chem. **6**, 1586 (1967).
34. M. Tadokoro, J. Toyoda, K. Isobe, T. Itoh, A. Miyazaki, T. Enoki, and K. Nakasuji. Chem. Lett. 613 (1995).
35. M. Tadokoro, K. Isobe, and K. Nakasuji. Mol. Cryst. Liq. Cryst. **278**, 209 (1996).
36. Z. Malarski and L. Sobczyk. Spectrochim. Acta Part A, **48**, 519 (1992).
37. J.E. Huheey, E.A. Keiter, and R.L. Keiter. Chimie inorganique. De Boeck and Larcier, Bruxelles, Belgique. 1996.
38. A.G. Orpen, L. Brammer, F.H. Allen, O. Kennard, D.G. Watson, and R. Taylor (*Editors*). International tables for crystallography. Vol. C. Kluwer Academic Press, Dordrecht, The Netherlands. 1995.
39. S. Bélanger and A.L. Beauchamp. Acta Crystallogr. Sect. C: Cryst. Struct. Commun. **52**, 2588 (1996).
40. M. Leduc and A.L. Beauchamp. Acta Crystallogr. Sect. C: Cryst. Struct. Commun. **50**, 1683 (1994).
41. R. Taylor and O. Kennard. J. Am. Chem. Soc. **104**, 3209 (1982).
42. F.H. Allen. Acta Crystallogr. Sect. B: Struct. Sci. **58**, 380 (2002).
43. D.T. Cromer, R.R. Ryan, and C.B. Storm. Acta Crystallogr. Sect. C: Cryst. Struct. Commun. **43**, 1435 (1987).
44. B. Therrien and A.L. Beauchamp. Acta Crystallogr. Sect. C: Cryst. Struct. Commun. **55**(Suppl. IUC9900054), (1999).
45. K. Larsson and L. Öhrström. CrystEngComm. **6**, 354 (2004).
46. B.-B. Ding, Y.-Q. Weng, Z.-W. Mao, C.-K. Lam, X.-M. Chen, and B.-H. Ye. Inorg. Chem. **24**, 8836 (2005).
47. M.A.M. Lorente, F. Dahan, Y. Sanakis, V. Petrouleas, A. Bousseksou, and J.-P. Tuchagues. Inorg. Chem. **34**, 5346 (1995).
48. M. Tadokoro, T. Shiomi, T. Shiromizu, K. Isobe, K. Matsumoto, and K. Nakasuji. Mol. Cryst. Liq. Cryst. **306**, 235 (1997).

© 2006 NRC Canada

Chemicals and energy from biomass

Lucian A. Lucia, Dimitris S. Argyropoulos, Lambrini Adamopoulos, and Armindo R. Gaspar

Abstract: Approximately 89 million metric tonnes of organic chemicals and lubricants are produced annually in the United States (T.M. Carole, J. Pellegrino, and M.D. Paster. Appl. Biochem. Biotechnol. **115**, 871 (2004)). The majority of these materials are fossil fuel based and may load the environment during use and at the end of their life cycle. Issues, such as disposal, pollution, and degradation, must be considered and weighed. As a result, the need to decrease pollution caused by petrochemical usage is currently impelling the development of green technologies. It is virtually inarguable that the dwindling hydrocarbon economy will eventually become unsustainable. The cost of crude oil continues to increase, while agricultural products see dramatic decreases in world market prices. These trends provide sufficient basis for renewed interest in the use of biomass as a feedstock and for the development of a carbohydrate-based economy as the logical alternative to fossil fuel resources.

Key words: biomass, biochemicals, natural products, bioenergy.

Résumé : Au cours d'une année, aux États-Unis d'Amérique, il se produit environ 89 millions de tonnes métriques de produits chimiques et de lubrifiants organiques. La majorité de ces produits sont obtenus à partir de combustibles fossiles et ils peuvent encrasser l'environnement durant leur cycle d'utilisation et de fin de vie. On doit donc considérer et pondérer des sujets tels que l'élimination, la pollution et la dégradation. En conséquence, la nécessité de diminuer la pollution qui est causée par l'usage des produits de l'industrie pétrochimique propulse le développement de technologies vertes. Il est pratiquement impossible de nier que l'économie basée sur les hydrocarbures ne pourra pas continuer. Le coût du brut continue d'augmenter alors que les prix des produits agricoles sur les marchés mondiaux font face à des réductions dramatiques. Ces tendances sont les bases du nouvel intérêt dans l'utilisation de la biomasse comme matière première ainsi que pour le développement d'une économie basée sur les hydrates de carbone comme alternative logique pour les ressources à base de combustibles fossiles.

Mots clés : biomasse, produits biochimiques, produits naturels, bioénergie.

[Traduit par la Rédaction]

Petroleum — The current resource

Petroleum is the most chemically versatile and important of the fossil fuels, the so-called "biomass of earlier eras" (1). Petroleum is an indispensable resource, whose availability is integral to the functioning of our modern society. However, since the energy crises of the 1970s, the world realizes all too well that petroleum is a finite resource and its availability is limited. Taking into account production and existing reserves, Hubbert (see graph in Campbell (2)) has predicted a maximum peak for oil production (Fig. 1*a*, and see ref. 2) whose timing ominously coincides with current increasing petroleum prices. Yet, the price of petroleum tends to fluctuate, but is very intimately related to world events (Fig. 1*b* and see ref. 3).

In the United States, 40% of the total energy consumption is petroleum-based. This makes it perhaps the world's most important commodity, and obtaining it has been a factor in several military conflicts. Petroleum is primarily used as fuel oil (90% by volume), such as gasoline and diesel fuel. Nonfuel uses include chemical solvents, lubricating oils, and raw feedstock (naphtha and various refinery gases) for many sundry chemicals.

Biomass — The alternative resource

The National Renewable Energy Laboratory (Golden, Colorado) defines biomass as organic matter available on a renewable basis (4). Biomass includes forest and mill residues, agricultural crops and wastes, wood and wood wastes, animal wastes, livestock operation residues, aquatic plants, fast-growing trees and plants, and municipal and industrial wastes. In general, biomass can include anything that is not a fossil fuel that is bioorganic-based.

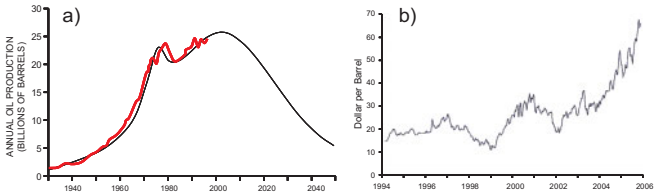
Biomass provides a naturally abundant resource that is not only cheap but also sustainable. The bioindustry presents an environmentally friendly alternative to the petroleum industry. The productive use of waste residues allows for lower emissions to the atmosphere, since CO_2 from biomass is considered neutral and could have ancillary benefits, such as providing a new source of economic growth for rural communities. Presently, the available biomass resources could provide as much as $6–10 \times 10^{15}$ Btu (1 Btu = 1.055 056 kJ)

Received 15 March 2006. Accepted 23 May 2006. Published on the NRC Research Press Web site at http://canjchem.nrc.ca on 1 September 2006.

L.A. Lucia,[1] D.S. Argyropoulos, L. Adamopoulos, and A.R. Gaspar. Department of Forest Biomaterial Science and Engineering, College of Natural Resources, North Carolina State University, Raleigh, NC 27695-8005, USA.
[1]Corresponding author (e-mail: lucian.lucia@ncsu.edu).

 doi:10.1139/V06-117 © 2006 NRC Canada

Fig. 1. (*a*) Hubbert's peak oil production. (*b*) Ten day moving average of prices (nominal, not adjustable for inflation) of NYMEX Light Sweet Crude.



of feedstock energy. This corresponds to the energy required to manufacture over 300×10^9 lb (1 lb = 0.453 592 37 kg) of organic chemicals (4).

There exists a real opportunity to discover new ways to produce novel and quality products within the context of sustainability issues that are beginning to permeate recent industrial thinking. In this context, issues such as producing biomaterials from renewable natural resources, are at the forefront. As fossil fuel feedstocks are irreversibly diminishing, environmental pressures are escalating, and the availability of inexpensive crude oil is coming to an end (5–7); thus, the evolution to renewable feedstocks for energy and chemicals seems inevitable (7, 8). The biomass technologies, therefore, have an opportunity to become competitive.

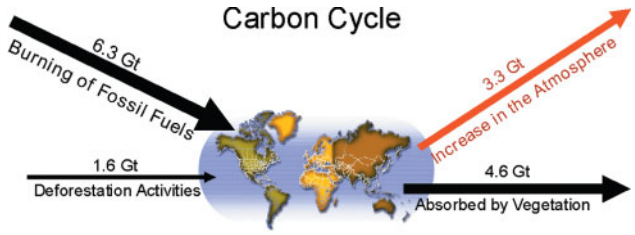
The combustion of fossil fuels contributes to carbon dioxide accumulation in the atmosphere. Its accumulation and deforestation activities are the main culprits behind radical climactic changes in the global environment (9). During the 1990s, annual greenhouse gas emissions to the atmosphere from the burning of fossil fuels was 6.3 Gt (in carbon units) (1 t = 1000 kg) and emissions from deforestation activities was an additional 1.6 Gt (10, 11). Furthermore, it has been estimated that the annual increase of CO_2 to the atmosphere is 3.3 Gt as carbon (12). The remaining 4.6 Gt is absorbed annually by the world's oceans and terrestrial vegetation (11). Figure 2 (see refs. 10–12) is a representation of the carbon cycle mass balance.

Bioproducts are industrial and consumer goods manufactured wholly or in part from renewable biomass. They are mainly created from primary resources, which are corn, wood, soybeans, and plant oils. The tremendous diversity of bioproducts, ranging from paper to solvents to pharmaceuticals, makes them an integral part of our lives.

Variations in the definition of what should be considered a bioproduct are responsible for disparities in the estimates of the annual usage of biomass in the manufacture of industrial and consumer products. The National Renewable Energy Laboratory estimated that about 21×10^9 lb of biomass were used in 2001 (4). On the other hand, the estimate by Energetics Inc. (Columbia, Maryland) was much more conservative, approximately 12.4×10^9 lb for 2001 (4).

The thousands of different industrial bioproducts produced today can be considered as stemming from sugar and starch, oils and lipids, gum, wood, and finally cellulose (4, 13–16). Annual production of industrial corn starch products is estimated to be 6500×10^6 lb, which corresponds to an estimated value of $2200 million US. Industrial ethanol production is estimated at 3.41×10^9 lb, with an estimated value of $961 million US. Oil- and lipid-based bioproducts include fatty acids and oils derived from soybeans, rapeseed,

Fig. 2. Mass balance of the carbon cycle during the 1990s.



or other oilseeds. Four hundred million pounds of glycerine, equivalent to $320 million US, are produced annually. Over 1200×10^6 lb of soy oil, peppermint, spearmint, and other plant oils produced annually have an estimated value of $550 million US. Gum and wood chemicals include tall oil, alkyd resins, rosins, pitch, fatty acids, turpentine, and other chemicals derived from trees. The annual production of these is approximately 3200×10^6 lb. The value of these is estimated at $890 million US. Cellulose derivatives, fibers and plastics, include products such as cellulose acetate (cellophane) and triacetate, cellulose nitrate, alkali cellulose, and regenerated cellulose. The primary sources of cellulose are bleached wood pulp and cotton linters. Cellulose derivatives have an annual production of 2140×10^6 lb. Their estimated value is $1400 million US.

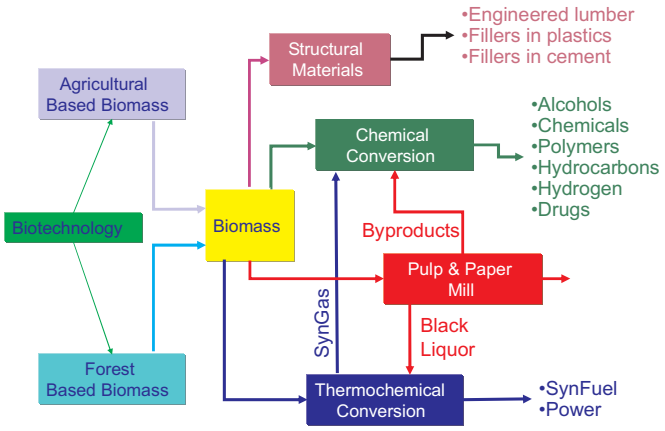
The use of biomass for energy, materials, and chemicals parallels the concept of the biorefinery, as well as that of sustainability. A biorefinery is a facility that integrates biomass conversion processes and equipment to produce fuels, power, heat, and high-value chemicals from biomass. By-products, residues, and a portion of the produced fuels would be used to fuel the biorefinery itself. A biorefinery might produce transportation fuels (low-value product) in high volumes, high-value chemicals in low volumes, while generating electricity and process heat for its own use, and perhaps produce surplus electricity for sale into the power grid. The high-value products enhance profitability, the high-volume fuel helps meet national energy needs, and the power production reduces costs and avoids greenhouse gas emissions.

The pulp and paper industry has been practicing aspects of the biorefinery philosophy almost since its inception. Indeed, wood is converted into pulp for papermaking and black liquor (liquid phase containing the organic material from wood and the chemicals after the pulping process) is used in the recovery furnace for power and steam generation, while the tall oil is sold for conversion into high-value chemicals. However, one of the unifying themes in all of their biomaterials efforts is the redefinition of the pulp mill as a biorefinery, i.e., a conceptualized site that provides biobased resources and energy that are usually outside the scope of traditional functions. Figure 3 illustrates this concept using a flow diagram. The pulp and paper mill participates in the biorefinery concept by providing raw feedstock (by-products, such as hemicellulose, extractives) that may be chemically converted into a variety of fine chemicals, polymers, and other materials.

For example, Archer Daniels Midland Co. is a chemical company that has an expanded biorefinery in Decatur, Illinois. Their large corn wet-milling plant produces industrial enzymes, lactic acid, citric acid, amino acids, and ethanol.

© 2006 NRC Canada

Fig. 3. Flow diagram that represents the biorefinery concept in pulp, paper, agricultural residues, and related biomass.



Electricity and steam are obtained through an on-site cogeneration system.

Another company that has received a lot of attention for its biorefinery is Cargill Dow (17, 18). Their polylactide facility in Blair, Nebraska, currently relies on corn grain for glucose, which it converts to lactic acid. The plant capacity is 300×10^6 lb, and they project a possible market of 8×10^9 lb by 2020.

With the right technology, abundant biomass resources may be converted into valuable bioproducts and energy. Also, the development of low-cost enzymes and recombinant technologies allows for the engineering of exemplary microbes. These should also be examined in conjunction with chemicals derived from biomass, as they are an essential part of the biorefinery.

Biobased chemicals vs. parallel petrochemicals

Cellulosic biomass or lignocellulosics from plants can be a raw source of sugars for industrial processes. The use of this biomaterial presents several advantages. Theoretically, cellulose and lignin are a less expensive feedstock than petroleum. Moreover, its use would not affect food supplies and chemicals derived from lignocellulosics would have a lower impact on the environment than petrochemicals. Additionally, cellulosic biomass is considered carbon dioxide neutral since its burning does not add any carbon to the atmosphere, beyond what was required for the plant to grow. This makes it a very green, environmentally friendly alternative to fossil fuels.

Presently, only 5% of all global chemical sales are made up of green products derived from natural resources. Nevertheless, this market share has the potential to rise as high as 20% by 2010 and may reach two-third of the total global economy, if technological advances, low-cost enzymes, and new recombinant technologies are made available on a large scale. Consequently, the potential benefits of a bioindustry are enormous and alternate biobased routes for the synthesis of traditionally petrochemically derived products should be carefully examined.

The Pacific Northwest National Laboratory, North Richland, Washington, took part in a collaborative study with the National Renewable Energy Laboratory in an effort to identify the top-tier building block chemicals for biorefineries (19). The top twelve chemicals (Fig. 4) were selected based on their compatibility with existing petrochemical processing as well as their ease of synthesis. The compounds are 1,4 diacids (succinic, fumaric, and malice), 2,5-furandicarboxylic acid, 3-hydroxypropionic acid, aspartic acid, glucaric acid, glutamic acid, itaconic acid, levulinic acid, 3-hydroxybutyrolactone, glycerol, sorbitol, and xylitol–arabinitol. These molecules have six to twelve carbon atoms and multiple functional groups. Examining some of these is worthwhile in the effort to show different synthesis pathways for the same product, as well as product derivatives.

Different synthesis pathways for succinic acid

Succinic acid ($C_4H_6O_4$) occurs frequently in nature in animal tissues, vegetables and fruits, and in amber (20). Succinic acid and its salts may serve as building blocks for numerous chemical intermediates and end products (Fig. 5 and see ref. 21) in industries producing food and pharmaceutical products, surfactants, detergents, green solvents, and biodegradable plastics. Reaction with glycols gives polyesters, and specifically, esters formed by reaction with monoalcohols are important plasticizers and lubricants (22).

The total market for succinic acid is more than $400 million US per year (21). Currently, the food market is the only one using succinic acid produced by fermentation. For other uses, succinic acid is, to a large extent, produced petrochemically from butane through maleic anhydride. Succinic acid can be produced by hydrogenation of maleic acid, maleic anhydride, or fumaric acid with standard catalysts, such as Raney nickel, Cu, NiO, or CuZnCr, Pd-Al_2O_3, Pd-$CaCO_3$, or Ni-diatomite (22).

Succinic acid is a common metabolite for plants and microorganisms. It is derived through the fermentation of glucose and is a very green technology because it is CO_2 fixing. Succinate is formed from sugars or amino acids by propionate-producing bacteria, such as the genus *Propionibacterium*, gastrointestinal bacteria such as *Escherichia coli*, and rumen bacteria such as *Ruminococcus flavefaciens*.

For the rumen ecosystem, succinate is an important precursor for propionate, which after oxidation, provides energy and biosynthetic precursors to the animal. Rumen microorganisms are major cellulose-digesting anaerobes that produce acetic and succinic acids in the rumen (23). *Actinobacillus succinogenes* 130 Z is a ruminal anaerobic bacterium that is capable of producing very high concentrations of succinate from many different substrates, such as glucose, maltose, mannose, sucrose, cellobiose, and D-xylose (24).

Actinobacillus succinogenes uses the phosphoenolpyruviate (PEP) carboxykinase pathway to produce succinic acid (see Fig. 6 and ref. 25). Four key enzymes come into play, PEP carboxykinase, malate dehydrogenase, funarase, and fumarate dehydrogenase. The pathway used for succinic acid production, in which PEP carboxykinase fixes CO_2 and synthesizes oxaloacetate from phosphoenolpyruvate, is regulated by CO_2 levels. At low CO_2 levels (10 mol of CO_2 per 100 mol of glucose), *A. succinogens* produces mostly ethanol. At high CO_2 levels (100 mol of CO_2 per 100 mol of glu-

© 2006 NRC Canada

Fig. 4. Chemical building blocks from biomass compatible with existing petrochemicals.

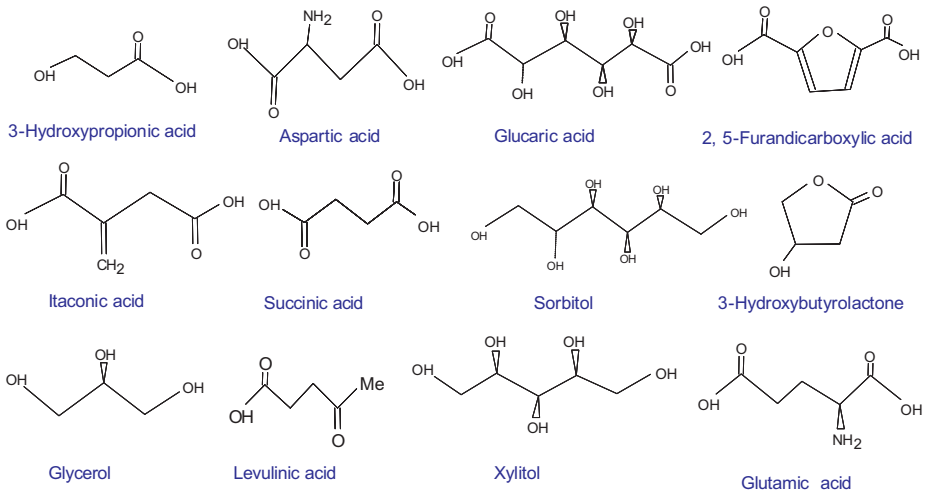


Fig. 5. Map of routes to succinic acid based products.

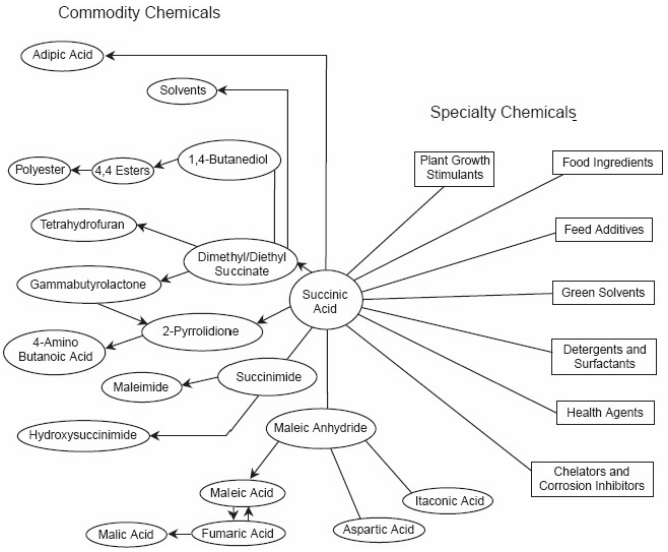
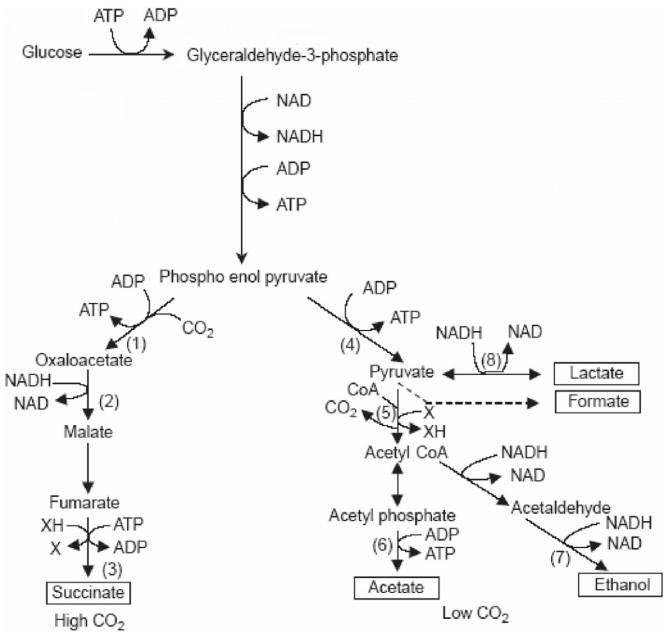


Fig. 6. Proposed catabolic pathway for glucose fermentation in *Actinobacillus succiniciproducens* and *A. succinogens.* Steps: (1) phosphoenolpyruviate carboxykinase, (2) malate dehydrogenase, (3) fumarate reductase, (4) pyruvate kinase, (5) pyruvate ferredoxin oxidoreductase, (6) acetate kinase, (7) alcohol dehydrogenase, (8) lactate dehydrogenase.



cose), succinate is the major product with only trace amounts of lactic acid or ethanol.

In actuality, the CO_2 concentration regulates the levels of the key enzymes in the pathway, thus determining what the majority product will be. At high CO_2 levels, phosphoenolpyruvate carboxykinase levels rise and alcohol dehydrogenase and lactate dehydrogenase are imperceptible. The CO_2 functions as an electron acceptor and PEP flows to succinate at high levels.

Most fermentation organisms are not tolerant of acidic conditions and the fermentation is usually neutralized to obtain a salt of succinic acid. This must then be separated, recovered, and reacidified to form free succinic acid. Significant research in microbial production of succinic acid has resulted in the development of a strain of *E. coli*, AFP111, which shows greatly improved productivity, and fermentation using this microorganism has been successfully tested at a commercial scale (4). Moreover, the development of a two-stage desalting and water-splitting electrodialysis system has facilitated the seperation, concentration, purification, and acidification of the product (26).

In 1992, fermentation production costs for succinic acid ranged from $1.50US to $2.00US per lb (4). Advances in fermentation and especially separation technology for the biobased route have reduced the potential production costs to about $0.50US per pound (21). Further improvements in separation and fermentation technologies could drop the production costs even more, enabling commodity scale production. This would allow for the expansion of current markets and for opportunities in new markets.

Different synthesis pathways for itaconic acid

Itaconic acid (2-methylenebutanedioic acid) is an unsaturated dicarbonic acid. It can be regarded as an α-substituted

© 2006 NRC Canada

acrylic of methacrylic acid and may serve as a substitute for these petrochemical-based chemicals. On account of its two carboxyl groups, itaconic acid may easily be incorporated into polymers.

Currently, polymerized methyl, ethyl, or vinyl esters of itaconic acid are used as plastics, adhesives, and coatings. Also, it is used as a comonomer in rubberlike resins and in the manufacture of emulsion paints, where it improves the adhesion of the polymer. Acrylic lattices are supplemented with itaconic acid and used as nonwoven fabric binders. Furthermore, itaconic acid may have agricultural, pharmaceutical, and medicinal applications. It is used as a hardening agent in organosiloxanes for use in contact lenses. In addition, mono- and di-esters of partly substituted itaconic acid possess analgesic properties and some also present plant growth related activities.

The first synthesis of itaconic acid was by pyrolysis of citric acid and anhydride hydrolysis (S. Baup. Ann. Chim. Phys. **19**, 29 (1837)) (Fig. 7 and ref. 27). Similarly, chemical synthesis is mainly carried out by dry distillation of citric acid and treatment of the anhydride with water. However, use of itaconic acid has been limited because the petroleum route is still expensive. It cannot compete with the fermentation of carbohydrates by fungi as a source of itaconic acid. In fact, approximately 15 000 t of itaconic acid are produced annually by fermentation. Production rates do not exceed 1 g L^{-1} h^{-1} and production concentrations of 80 g L^{-1} (28). This makes itaconic acid an expensive product, whose use is therefore limited.

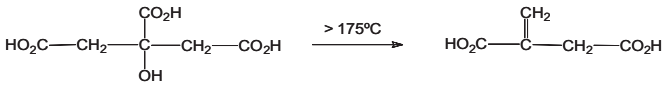
The biosynthesis of itaconic acid most probably happens through glycolysis, followed by the tricarboxylic acid cycle. Citric acid and aconitic acid are intermediates. Enzymatic decarboxylation of the latter allows for the formation of itaconic acid (Fig. 8 and ref. 28).

The most frequently used commercial application of itaconic acid is the cultivation of *Aspergillus terreus* with molasses. Molasses products are less expensive than other kinds of carbohydrates, but the cost of itaconic acid is still high because molasses contain many impurities that are not consumed by microorganisms. So, downstream processing and waste treatment therefore become expensive. Thus, alternate carbon sources are being examined. The best yields of itaconic acid are achieved with glucose or sucrose, but these are expensive raw materials. Raw starch materials show particular potential as a substitute to molasses. Itaconic acid was produced by *A. terreus* TN-484 in a medium containing raw corn starch (140 g L^{-1}) at pH 2.0, hydrolyzed with nitric acid at a concentration of more than 60 g L^{-1} in a 2.5 L air lift bioreactor (29).

Efforts are also being made in the selection of different microorganisms, such as various *Ustalgo* and *Candida* species. Furthermore, mutant microorganisms are also being produced and used to increase yields and biomass immobilization is being considered.

Finally, fermentation conditions are important and must be optimized. The itaconic acid fermentation is most favorable under phosphate-limited growth conditions at sugar concentrations between 100 and 150 g L^{-1}. During fermentation, the pH drops to 2.0 and itaconic acid becomes the main product. The temperature is normally kept at 37 °C, but certain mutated microorganisms may perform better at higher temperatures. Also, aerobic conditions are required and culture medium components, such as Fe, Mn, Mg, Cu, Zn, P, and N, must be carefully monitored.

Fig. 7. Thermal decomposition of citric acid.



The market for itaconic acid is still growing because of the possibilities of substituting it for acrylic and methacrylic acid in polymers. Moreover, its potential production from agricultural plant biomass makes it an attractive biofriendly alternative. It also provides a source of inexpensive raw feedstock. Efforts in effectively utilizing such waste, as well as the introduction of new technologies, are required for reducing itaconic acid production costs and market expansion.

Synthetic pathways for levulinic acid

Levulinic acid ($H_8C_5O_3$), also known as γ-ketovaleric acid, β-acetylpropionic acid, or 4-oxopentanoic acid, is a short chain fatty acid with a ketone carbonyl group and an acidic carboxyl group. These two highly reactive functional groups make it a highly versatile chemical capable of serving as a building block for other chemicals (Fig. 9 and ref. 30). Levulinic acid is the starting compound for many heterocycles. It can be used as a raw material for resins, plasticizers, textiles, animal feed, coatings, and antifreeze. It is an auxiliary in electroplating and levulinic acid esters are used in cosmetics.

Industrially, levulinic acid is prepared from wood processing and agricultural wastes. It basically hails from the transformation of hexose sugars in acidic media. The hexoses are obtained by the hydrolysis of cellulose at atmospheric pressure with strong acids, such as HCl and H_2SO_4, at 100 °C. The hydrolysate is then heated to 110 °C with 20% HCl and kept at this temperature for 1 day. Free halogens, as well as transition metals and anion-exchange resins, accelerate the process.

Initially, the intermediate compound 5-hydroxymethyl furfural is formed from the hexoses. This happens through a series of reactions (Fig. 10 and ref. 31). The first step is the enolization of D-glucose, D-mannose, or D-fructose in acidic media to give the enediol. Next, this compound is dehydrated to the enol form of 3-deoxyhexosulose. This substance then produces 3,4-dideoxyglycosulosene-3, which is converted to the dienediol that results in 5-hydroxymethylfurfural (31).

5-Hydroxymethylfurfural can then be converted to levulinic acid by addition of a molecule of water to the C2—C3 bond of the furan ring. The ring opens and an unstable tricarbonyl intermediate is formed, which is finally decomposed to formic and levulinic acids (Fig. 11 and ref. 31). Levulinic acid is isolated from the mixture with a yield of approximately 40% with respect to the hexose content (31). Furthermore, for each levulinic acid molecule generated, a formic acid molecule is also created and insoluble residues, including humics, are produced.

Furthermore, levulinic acid can be synthesized starting from furfuryl alcohol (Fig. 12 and ref. 31). Heating furfuryl alcohol in aqueous organic acids in the presence of hydrochloric acid allows an 80% yield of levulinic acid. The yield

© 2006 NRC Canada

Fig. 8. Biosynthesis of itaconic acid.

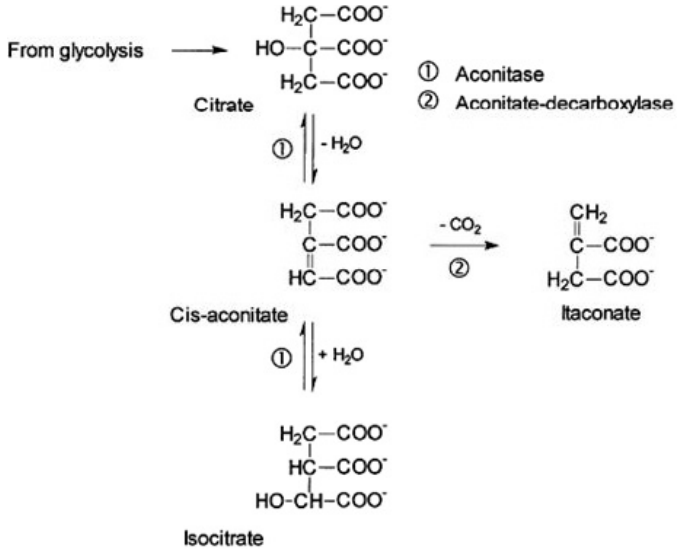
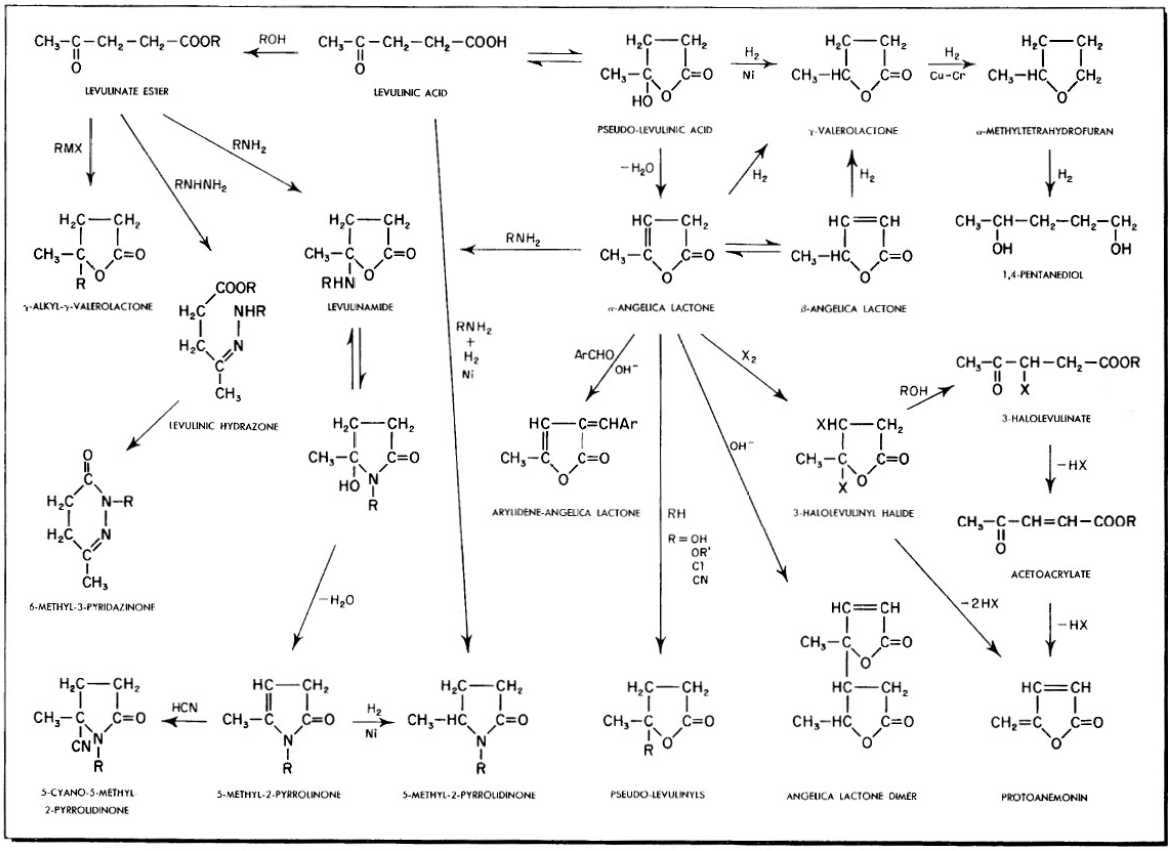


Fig. 9. Principal reactions of levulinic acid and relationships among its derivatives.



can be increased to approximately 90% when the reaction is performed in boiling ethyl methyl ketone.

Moreover, the oxidation of 5-methylfurfural with 28% H_2O_2 at 60 °C in the presence of HCOOH produces levulinic acid, as well as 4-oxopent-2-enoic acids (Fig. 13 and ref. 31). Levulinic acid can also be formed in high yields from the reaction of 4-(diphenylmethylsilyl)butyrolactone with MeMgI.

Levulinic acid can also be prepared from biomass, such as rice, straw, paper, and cotton (32). In this case, biomass is reacted at 40–240 °C for 1–96 h in the presence of 5%–90% sulfuric acid. Another substrate that can be used for levulinic acid production is sorghum grain. It has low cash value when sold as a feed grain and is a major source of carbohydrates. Pentosans, starch, and cellulose make up 80%–85% of the sorghum grain. Flour made from this grain at a 10%

© 2006 NRC Canada

Fig. 10. 5-Hydroxymethylfurfural (**8**) obtained from D-glucose (**9**), D-mannose (**10**), or D-fructose (**11**).

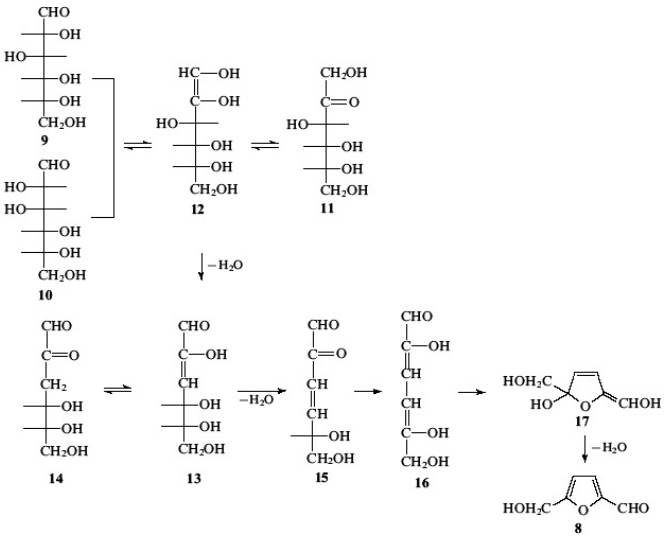
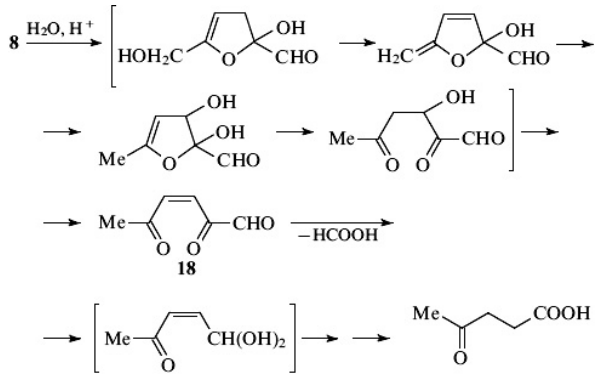


Fig. 11. 5-Hydroxymethylfurfural to levulinic acid.



loading and blended with 8% sulfuric acid gives a yield of approximately 33% levulinic acid at 200 °C (33).

Finally, a two-step dilute mineral acid hydrolysis is available, the Biofine process (34), to break down biomass containing lignocellulose into intermediate chemicals. It was developed by BioMetics Inc. (Camarillo, California), with funding from the US Department of Energy. This high-temperature, dilute acid hydrolysis process fractionates lignocellulosic biomass into platform chemicals. The primary fractions of the process are levulinic acid, formic acid, furfural, and a bone dry char. The char residue contains approximately 11 000 Btu per lb and is a suitable feedstock for gasification.

BioMetics has operated a small commercial demonstration unit in New York State for four years and has just completed the first large-scale commercial facility in Italy. This large-scale facility will produce levulinic acid for monomer use, oxygenated diesel esters, and formic acid based solvents. The char residue will be converted to synthesis gas that will be burned in a gas engine to generate electricity. Approximately 0.5 lb of levulinic acid is produced per lb of cellulose processed (4). Currently, levulinic acid has a worldwide market of about 1.0×10^6 lb per year at a price of

Fig. 12. Levulinic acid from furfuryl alcohol (**19**).

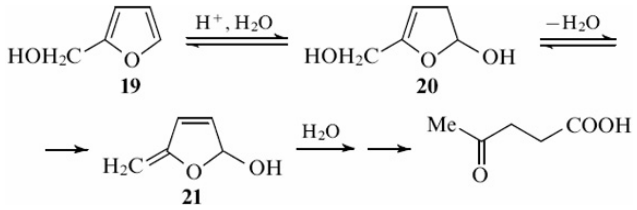
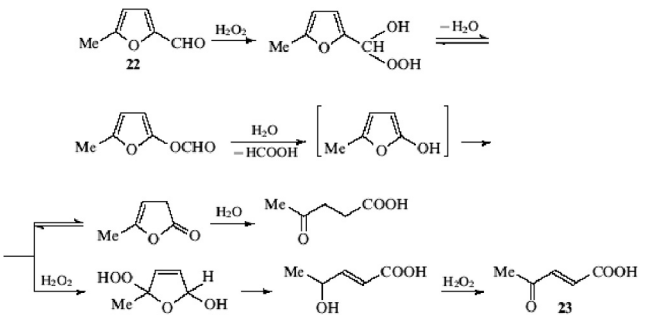


Fig. 13. Oxidation of 5-methylfurfural (**22**) to levulinic acid.



$4US–$6US per lb (35). Large-scale commercialization of the Biofine process could produce levulinic acid for as little as $0.32 per lb (35), spurring increased demand.

In parallel with the process development program, BioMetics has an ongoing program aimed at expanding commercial markets for the chemical derivatives of levulinic acid in cooperation with New York State, Rensselaer Polytechnic Institute (Troy, New York), the National Renewable Energy Laboratory, the Pacific Northwest National Laboratory, and major chemical companies.

This effort has allowed for the development of a one-step catalytic process facilitating the conversion of levulinic acid to methyl tetrahydrofuran (MTHF) approved for P-series alternative fuel formulations (36). Also, it has provided a low cost route to the herbicide and plant growth regulator, δ-aminolevulinic acid. New polycarbonate resin formulations using diphenolic acid are being examined and a new oxygenated diesel additive (ethyl levulinate) that reduces particulate matter emission has been developed.

The Biofine process allows for the manufacture of many high-value chemical and fuel products from cheap lignocellulosic biomass. This process is fast and continuous and is capable of utilizing a wide range of biomass feedstocks. Moreover, the gasification of the char covers the entire energy needs of the plant, making it self-sufficient. Finally, the process can be retrofitted into existing plants.

Levulinic acid is a compound that has many industrial applications. Its efficient preparation from biomass has many avenues. Its efficient extraction from decomposition products of natural materials would prove to be worthwhile for both industry and the environment.

Sample reactions for high-value chemicals

As opposed to many synthetic chemicals, forest-based and agricultural biomaterials are readily renewable, inexpensive, and environmentally benign. Despite a significant amount of recent research for augmenting the industrial use of readily

© 2006 NRC Canada

Fig. 14. Shown in the top structure is the natural product extract, tulapilin A (A–α-methylenebutyrolactone), found in tulips, and in the lower structure is its synthetic analogue, methyl methacrylate. Notice the strong chemical structural similarity in both the monomer and polymer.

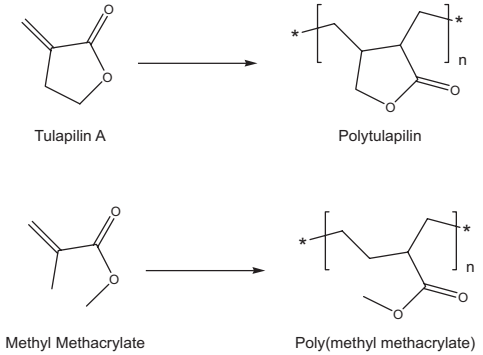
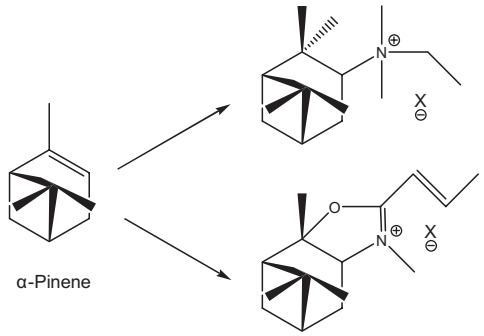


Fig. 15. Structure of α-pinene, a natural extractive from pine trees, which can be converted to two distinct chiral ionic liquids.



available carbohydrates as raw materials (37–42) (e.g., car moldings, cosmetics, food, and additives), the systematic exploitation of this vast resource, as already indicated, is still in its infancy. Since clean air pressures are mounting and while the availability of cheap and abundant fossil fuel becomes increasingly questionable, as seen in the current climate, it is likely that any economic advantages for a petrochemical-based economy will literally evaporate within the next 50 years.

For example, DuPont has determined that once the price point at which an extract from plants, tulipalin A (A–α-methylenebutyrolactone) shown in Fig. 14, becomes competitive with its commercial analogue, methyl methacrylate (MM), the natural material will be used commercially for polymer applications (43). MM is a feedstock that is used for polymerization to manufacture a number of plastics, moldings, and related materials. Its natural analogue (tulapilin A) produces a polymer whose durability and refractive index rival that of MM (43). Remarkably, DuPont has also found that limonene, a citrus tree extractive, mimics the chemistry of 4-vinyl-1-cyclohexene in that it can be used as an anchoring point for the introduction of alkoxylsilanes for exterior coatings (43).

An early example of a biobased green solvent is a new class of chiral ionic liquids that can be derived from α-pinene, an extract from pine trees, as shown in Fig. 15. Ionic liquids are salts that are liquid at or near room temperature. As such, they are composed of an anion and a cation, like any salt, but they do not have the high melting points typical of such species. Since the combination of organic cations and anions is virtually limitless, several classes of ionic liquids have actually been reported, with more and more such systems being continually discovered.

Energy derived from biomass

Since antiquity, biomass has been used by humanity as a source of energy, mainly for heating. Nowadays, new developing energy technologies are broadening the use of biomass well beyond simple combustion for heating. The conversion processes used on biomass feedstock allow the generation of steam and electric power, as well as a wide range of energy products, such as ethanol, biodiesel, fuel gas, and chemical intermediates and products. The conversion of biomass feedstock into energy products are well-established technologies, with enhanced improvements in the last decades. This subject was reviewed by Paisley (44).

Steam and electric power

Biomass has been used for simple heating by direct combustion, which by nature is a very low efficient operation (~7% for an open fireplace and ~15% for a fireplace with convective tubes) (45). Efficiency improvements are realized by larger scale combustion processes in boilers or furnaces, thus improving heat recovery, and therefore, overall efficiency.

Boiler applications further provide the opportunity to generate electrical power from the incoming biomass. The biomass is burned to generate steam, which is then used to turn a turbine to generate electric power. The majority of the biomass-based power plants are found in the pulp and paper industry. Woody residues from the wood raw material and the black liquor, a by-product from the pulping process, are consumed to generate the necessary power for plant operations. When black liquor is burned for energy recovery, the pulping chemicals are recovered and recycled, thus further reducing the costs.

Biomass-based combined heat and power (CHP) systems provide the primary energy for large segments of the population in many European countries, mainly Scandinavian and northern countries. These systems typically combust biomass to produce high-pressure steam for further electric power generation. Lower-pressure steam is then extracted from the turbine system and used for district heating.

Ethanol

Ethanol production is known historically from the manufacture of alcoholic beverages, such as wines and beers. It is produced through natural fermentation of the starch and sugars present in different forms of biomass by biological organisms. Nowadays, grains of wheat or corn (biomass materials) are typically the primary source for the production of ethanol as fuel, which can be blended with other fuels such as gasoline (46, 47). Other sources for ethanol

© 2006 NRC Canada

production that are also in use are straw, sugar cane, sugar beet, and wood (48).

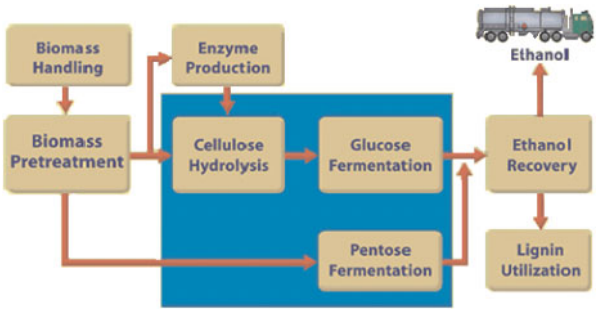
Large-scale production of ethanol makes use of the fermentation process as well. In a first stage, biomass material, such as corn kernel or other starchy grain, is milled through a dry or wet milling mode. The fermentation then takes place by mixing the resulting flour (biomass polysaccharides) in water with yeast. The mixture is heated at ~30 °C to initiate the fermentation reactions under an anaerobic environment, and the process takes ~1 to 2 days for completion. After fermentation, the ethanol is filtered and then distilled to increase its concentration from 10% to 95%. The concentrated ethanol is then blended with petroleum-based fuels to the desired concentration.

Ethanol can also be produced from cellulosic biomass such as agricultural residues, forestry residues, waste paper, yard wastes, portions of municipal residues, and industrial residues (49). The long-chain polysaccharide materials are initially treated with acid or enzymes to cleave the glycosidic bonds. The acid recovery system can be a complex process. Research is being performed to find ways to reduce the acid levels while maintaining high conversion levels. The resulting small fractions can then readily be fermented to ethanol. In parallel, small fractions of biomass can be used to grow fungi and other organisms to produce enzymes (cellulase), which hydrolyze cellulose (in pretreated biomass) to glucose. Figure 16 (see ref. 49) presents a scheme for the production of ethanol from cellulosic biomass (49). There are a variety of technologies that combine two or all three of the hydrolysis and fermentation steps within the shaded box.

US ethanol production has grown significantly in recent years. In 2004, a record 3.41×10^9 gal (1 gal Am. = 3.79 L) of ethanol were produced — an incredible 109% increase from 2000 (50). But ethanol plants also produce other products. Depending on the type of facility, a number of other coproducts result from ethanol production, adding even more value to corn feedstocks and to the economy. Dry mill facilities also produce distillers dried grain with solubles (DDGS) and carbon dioxide. Ethanol wet mills can also produce corn gluten meal feed, sweeteners, and corn oil. These coproducts and by-products from cellulosic biomass ethanol production can be used to produce value-added chemicals, contributing to the economy of fuel production from biomass. On the other hand, ethanol can also be used as a chemical intermediate in the production of other organic chemicals.

Oxygenated transportation fuels, such as the ethanol–gasoline blends, can benefit environmental conditions. Mixtures of up to 10% ethanol, referred to as E10, can be utilized in most gasoline engines with no modification. More concentrated blends, namely the E85 and E95 blends (85% and 95% ethanol, respectively) require specifically designed engines, referred to as "flexible fuel" engines, to perform properly. These flexible fuel engines can run on either gasoline or high-concentration ethanol blends. Automobile manufacturers are producing more vehicles that can use these high ethanol blends each year, thus increasing demand. The spark-ignition Otto-cycle engines used in today's automobiles, even in their early stages of development, were designed to operate with ethanol-containing fuels. Henry Ford designed the early Model T to use ethanol as a major fuel source. Such plans were subsequently changed when storage and transportation difficulties, combined with high corn prices at the time caused the supply of ethanol-containing blends to be reduced.

Fig. 16. Basic steps in production of ethanol from cellulosic biomass.



Biodiesel

Biodiesel is a fuel that can be made from renewable resources such as vegetable oils or animal fats. It is usually produced from soy or canola oil. Other possible resources are recycled fryer oils. Through a transesterification process, the oils are converted into biodiesel. The latter can be used as pure fuel or blended at any level with petrodiesel for use by diesel engines. Biodiesel is designated B100 and meets the requirements of ASTM D6751 (51).

Biodiesel comprises of a mix of monoalkyl esters of long-chain fatty acids. A lipid transesterification reaction is used to convert the base oil to the desired biodiesel. The most common process uses methanol to produce methyl esters, although ethanol can also be used to produce an ethyl ester biodiesel. In the production of biodiesel, the triglicerides in the oils and fats are reacted with methanol (or ethanol) to make methyl esters (or ethyl esters) and glycerol as a by-product. The process uses a catalyst, typically NaOH or KOH, to enhance the reaction rates. Some oils may have to undergo some pretreatment before reaction with methanol to avoid the formation of high concentrations of free fatty acids. The reactions take place at low temperatures (~65 °C) and at modest pressures (2 atm, 1 atm = 101.325 kPa). Biodiesel is further purified by washing and evaporation to remove any remaining methanol. The oil (87%), alcohol (9%), and catalyst (1%) are the inputs in the production of biodiesel (86%), the main output. Other by-products include glycerine (9%), alcohol (4%), and fertilizer (1%). Nothing is wasted in biodiesel production (52).

Biodiesel can be a direct substitute for petrodiesel, either as neat fuel (B100 or BD100) or as an oxygenate additive at any concentration, blended with diesel. Typically, the biodiesel that is primarily utilized is the B20 blend (20% biodiesel and 80% petrodiesel). Pure biodiesel or blends can be used in any compression-ignition (diesel) engine. B20 earns credits for alternative fuel under the US Energy Policy Act of 1992. Ranges as low as 2% (BD2 or B2), have shown lubricity benefits (53). In 2004, almost 30×10^6 gal of commercially produced biodiesel were sold in the US, up from less than 0.5×10^6 gal in 1999 (54). Because of increasing pollution control requirements and tax relief, the US market is expected to grow to 1 or 2×10^9 gal by 2010.

© 2006 NRC Canada

Looking back, Rudolf Diesel had successfully presented his engine powered by peanut oil (biofuel) at the World's Fair in Paris, France, in 1900, where he received the "Grand Prix" (highest prize). He believed that the utilization of biomass fuel was the real future of this engine. In a prophetic 1912 speech, Rudolf Diesel said, "the use of vegetable oils for engine fuels may seem insignificant today, but such oils may become, in the course of time, as important as petroleum and the coal–tar products of the present time" (55).

Conclusions

In retrospect, the petroleum age has served the growth of civilization quite well. However, it has also become an albatross to further growth, given its intrinsic deficiencies for environmental compatibility, sustainability, and micro- and macro-economics. As Rudolph Diesel so astutely intimated, we are now at the nexus of a major crossroads in the future of humanity with respect to the production of chemicals, materials, and energy. The only real solution that is viable and necessary is the efficient and intelligent use of biomass as derived from plant and animal residues. Capturing the chemical and material value of bioderived succinic, itaconic, and levulinic acids, as indicated in this review, will provide the world with freedom from the economic and geopolitical uncertainties associated with petroleum dependency. In addition, tapping into biobased fuel sources, such as ethanol and biodiesel, expands that horizon considerably by supporting environmental stewardship by their renewable nature and carbon neutrality. North Carolina State University realizes the importance of achieving this biomass age and is therefore poised by virtue of its faculty, research mission, and resources to promote it and thereby improve the world.

References

1. J.T. Boepple. Petrochemicals, feedstocks. Kirk-Othmer encyclopedia of chemical technology [online]. John Wiley and Sons, Inc. Hoboken, N.J. Available from http://www.mrw.interscience.wiley.com/kirk/articles/petraubr.a01/frame.html. 2005.
2. C.J. Campbell. The end of cheap oil [online]. Available from http://dieoff.org/page140.htm. 1999.
3. Anonymous. Oil prices medium term [online]. Wikipedia. Available from http://en.wikipedia.org/wiki/Image:Oil_Prices_Medium_Term.png. 2006.
4. M. Paster, J.L. Pellegrino, and T.M. Carole. Industrial bioproducts: today and tomorrow. Prepared by Energetics, Inc., Columbia, Maryland for the US Department of Energy, Office of Energy Efficiency and Renewable Energy, Office of the Biomass Program, Washington, D.C. 2003.
5. C.J. Campbell and J.H. Laherrère. The end of cheap oil. Sci. Am. March, 60–65 (1998).
6. D.H. Klass. Biomass for renewable energy, fuels, and chemicals. Acad. Press, San Diego, Calif. 1998. pp. 10–19.
7. C. Okkerse and H. van Bekkum. Green Chem. **1**, 107 (1999).
8. Committee on Biobased Industrial Products, National Research Council, USA. Biobased industrial products: Priorities for research and commercialization. Natl. Acad. Press, Washington, D.C. 2000.
9. Biomass Energy Research Association [online]. Biomass Energy Research Association, Washington, D.C. Available from www.bera1.org. 2006
10. FAO. Global forest resources assessment 2000. Summary report [online]. Food and Agriculture Organisation, Rome, Italy. Available from www.fao.org/docrep/meeting/003/x9835e/x9835e00.htm. 2001.
11. R. Matthews and K. Robertson. Answers to ten frequently answered questions about bioenergy, carbon sinks, and their role in global climate change [online]. International Energy Agency Bioenergy Task 38. Available from www.joanneum.at/iea-bioenergy-task38/publications/faq. 2001.
12. R.T. Watson, I.R. Noble, B. Bolin, N.H. Ravindranath, D.J. Verardo, and D.J. Dokken. (*Editors*). Intergovernmental Panel on Climate Change. Special report on land use, land-use change, and forestry. Intergovernmental Panel on Climate Change, Cambridge University Press, Cambridge, UK. 2000.
13. J. Chang. Vertec biosolvents on verge of breaking out with new replacement applications. Chem. Mark. Rep. **267**, 4 2002.
14. US Department of Commerce. 1999 Annual survey of manufactures. US Census Bureau, Washington, D.C. 1999.
15. Chemical Market Report. Chemical profiles, ChemExpo [online]. Chem. Mark. Rep. Available from www.chemexpo.com. 2002.
16. Energetics, Inc. Biomass use for power, fuels, and products: Current use and trends. Energetics, Inc., Columbia, Md. April 2002.
17. M.A. Verespej. Winning technologies: polylactide polymers. Industry Week, Cleveland, Ohio. Dec. 2000.
18. Nature Works® LLC [online]. Nature Works® LLC, Minneapolis, Minn. Available from http://www.natureworksllc.com/corporate/news.asp.
19. S.K. Ritter. Chem. Eng. News **82**, 22 (2004).
20. C. Fumagalli. Succinic acid and succinic anhydride. Kirk-Othmer encyclopedia of chemical technology. 4th Ed. Vol 22. John Wiley and Sons, Inc. Hoboken, N.J. 1997. pp. 1074–1088.
21. J.G. Zeikus, M.K. Jain, and P. Elankovan. Appl. Microbiol. Biotechnol. **52**, 545 (1999).
22. B. Cornils and P. Lappe. Dicarboxylic acids. Ullmann's encyclopedia of industrial chemistry. 6th Ed. Vol. 10. 2003. pp. 525–526.
23. P.J. Weimer. Arch. Microbiol. **160**, 288 (1993).
24. M.V. Guettler, D. Rumler, and M.K. Jain. Int. J. Syst. Bacteriol. **49**, 207 (1999).
25. N.S. Samuelov, R. Lamed, S. Lowe, and J.G. Zeikus. Appl. Environ. Microbiol. **57**, 3013 (1991).
26. Oak Ridge National Laboratory, Argonne National Laboratory, Pacific Northwest National Laboratory, National Renewable Energy Laboratory, and Applied Carbochemicals, Inc. Production of chemical derivatives from renewables: CRADA final report for CRADA ORNL 96-0407. November 1999.
27. Kirk-Othmer encyclopedia of chemical technology. 4th Ed. Vol. 6. John Wiley and Sons, Inc. Hoboken, N.J. 1997. pp. 353–359.
28. Th. Wilke and K.-D. Vorlop. Appl. Microbiol. Biotechnol. **56**, 289 (2001).
29. K. Yahiro, S. Shibata, S.-R. Jia, Y. Park, and M. Okabe. J. Ferment. Bioeng. **84**, 375 (1997).
30. H.L. Reid. Ind. Eng. Chem. **48**, 1331 (1956).
31. B.V. Timokhin, V.A. Baransky, and G.D. Eliseeva. Russ. Chem. Rev. **68**, 73 (1999).
32. W.A. Farone and J. Cuzens. US Patent 6/054/611, 24 April 2000.

© 2006 NRC Canada

33. Q. Fang and M.A.Hanna. Bioresour. Technol. **81**, 187 (2002).
34. P. Anastas, M. Kirchchoff, and T. Williamson. Green Chem. **1**, G124 (1999).
35. US Environmental Protection Agency. Green chemistry [online]. US EPA, Washington, D.C. Available from http://www.epa.gov/greenchemistry.
36. Institute for the Analysis of Global Security. P-Series fuels [online]. IAGS, Washington, D.C. Available from http://www.iags.org/biofine.htm. 2004.
37. F.W. Lichtenthaler (*Editor*). Carbohydrates as organic raw materials. VCH Publishers, Weinheim, Germany. 1991.
38. G. Descotes (*Editor*). Carbohydrates as organic raw materials II. VCH Publishers, Weinheim, N.Y. 1993.
39. H. van Bekkum, H. Roper, and A.G.J. Voragen (*Editors*). Carbohydrates as organic raw Materials III. VCH Publishers, Weinheim, Germany. 1996.
40. H. Eierdanz (*Editor*). Perspektiven Nachwachsender Rohstofe in der Chemie. VCH Publishers, Weinheim, Germany. 1996.
41. F.W. Lichtenthaler and S. Mondel. Pure Appl. Chem. **69**, 1853 (1997).
42. Introductory dedicational metaphor in: A. Hugill. Sugar and all that. A history of Tate and Lyle. Gentry Books, London. 1978.
43. R. Mullin. Chem. Eng. News, **82**, 29 (2004).
44. M.A. Paisley. Biomass energy. Kirk-Othmer encyclopedia of chemical technology [online]. John Wiley and Sons, Inc. Hoboken, N.J. http://www.mrw.interscience.wiley.com/kirk/articles/fuelklas.a01/frame.html. 2003.
45. J.E. Houck and P.E. Tiegs. Residential wood combustion review. Vol. 1. Technical Report. US Environmental Protection Agency, Office of Research and Development, Washington, D.C. 1998.
46. General Biomass Company [online]. Biomass, renewable energy. General Biomass Company, Evanston, Ill. Available from www.generalbiomass.com/renew2.htm.
47. US Department of Energy. History of biofuels. US Department of Energy, Office of Transportation Technologies,Washington, D.C. 2002.
48. Department for Transport, UK. International resource costs of biodiesel and bioethanol [online]. Department of Transport, London, UK. Available from www.dft.gov.uk/stellent/groups/dft_roads/documents/page/dft_roads_024054.hcsp [updated 29 June 2004]. 2003.
49. Renewable Fuels Association. How ethanol is made [online]. Renewable Fuels Association, Washington, D.C. Available from http://www.ethanolrfa.org/resource/made. 2005.
50. National Corn Growers Association [online]. National Corn Growers Association, Washington, D.C. Available from http://www.ncga.com/ethanol/main/production.htm. 2005.
51. ASTM. D6751 standard specification for biodiesel fuel (B100) blend [online]. American Society for Testing and Materials, West Conshohocken, Penn. Available from http://www.astm.org.
52. National Biodiesel Board [online]. National Biodiesel Board, Jefferson City, Mo. Available from http://www.biodiesel.org. 2005.
53. US Department of Energy. Biomass program, renewable diesel fuel [online]. US Department of Energy, Energy Efficiancy and Renewable Energy, Washington, D.C. Available from http://www.eere.energy.gov/biomass/renewable_diesel.html. 2005.
54. Soy Stats™. A reference guide to important soybean facts and figures [online]. American Soybean Association, Saint Louis, Mo. Available from http://www.soystats.com/2005/Default-frames.htm. 2005.
55. Yokayo Biofuels. A history of biofuels [online]. Yokayo Biofuels, Ukiah, Calif. Available from www.ybiofuels.org. 2006.

© 2006 NRC Canada

Synthesis and characterization of [M^{II}(bqb)] (M = Co, Ni, Cu), [N(*n*-Bu)$_4$][Co^{III}(bqb)(CN)$_2$], and [N(*n*-Bu)$_4$][Co^{III}(bqb)(N_3)$_2$] containing deprotonated *N*,*N*′-bis(2-quinolinecarboxamide)-1,2-benzene (bqb) — X-ray crystal structures of [Ni^{II}(bqb)] and [N(*n*-Bu)$_4$][Co^{III}(bqb)(N_3)$_2$]

Soria Meghdadi, Mehdi Amirnasr, Vratislav Langer, and Alison Zamanpoor

Abstract: Cobalt(II), nickel(II), copper(II), and two cobalt(III) complexes of a new dianionic ligand, bqb, [H_2bqb = *N*,*N*′-bis(2-quinolinecarboxamide)-1,2-benzene] have been synthesized and characterized by elemental analyses, IR, and ^{1}H NMR spectroscopy. The crystal and molecular structures of the [Ni(bqb)] (**2**) and [N(*n*-Bu)$_4$][Co^{III}(bqb)(N_3)$_2$] (**5**) complexes were determined by X-ray crystallography. Complex **2** crystallizes in the monoclinic space group *C*2/*c* with a distorted square-planar structure including two short Ni—N (1.848 Å) and two long Ni—N (1.958 Å) bonds. The structure consists of sheets formed in the plane parallel to the *b* axis and diagonal to vectors ***a*** and ***c*** by intermolecular hydrogen bonds. Complex **5** crystallizes in the monoclinic space group *C*2 with a distorted octahedral structure. The [N(*n*-Bu)$_4$]$^+$ ion is disordered at the C3A and C4A atoms of one Bu. The IR and ^{1}H NMR spectra of the complexes are also discussed.

Key words: N_4-dianionic amido ligand (bqb), (bqb) complexes of Co(II), Ni(II), Cu(II), and Co(III), azide, cyanide, X-ray crystal structures.

Résumé : On a réalisé la synthèse de complexes du cobalt(II), du nickel(II), du cuivre(II) et de deux complexes du cobalt(III) avec un nouveau ligand dianionique, bqb, [H_2bqb = *N*,*N*‘-bis(quinoléine-2-carboxamide)-1,2-benzène] et on les a caractérisés par analyses élémentaires, spectroscopies IR et RMN du ^{1}H. Faisant appel à la diffraction des rayons X, on a déterminé les structures cristallines et moléculaires des complexes [Ni(bqb)] (**2**) et [N(*n*-Bu)$_4$][[Co^{III}(bqb)(N_3)$_2$] (**5**). Le complexe **2** cristallise dans le groupe d'espace monoclinique *C*2/*c* avec une structure plan carré déformée comportant deux liaisons Ni—N courtes (1,848 Å) et deux liaisons Ni—N longues (1,958 Å). La structure est formée de feuillets alignés dans un plan parallèle à l'axe b et à la diagonale des vecteurs ***a*** et ***c*** par des liaisons hydrogènes intermoléculaires. Le complexe **5** cristallise dans le groupe d'espace monoclinique *C*2 avec une structure octaédrique déformée. L'ion [N(*n*-Bu)$_4$]$^+$ est désordonné au niveau des atomes C3A et C4A d'un des Bu. On discute aussi des spectres IR et RMN du ^{1}H des complexes.

Mots clés : ligand amido N_4-diatomique (bqb), complexes (bqb) du Co(II), du Ni(II), du Cu(II) et du Co(III), azide, cyanure, structures cristallines par diffraction des rayons X.

[Traduit par la Rédaction]

Introduction

The coordination chemistry of the dianionic organic amide ligands has been of great interest because of their role in biologically important coordination compounds (1–5). Structural modification of these ligands by altering the diamine backbone or by the introduction of suitable substituents in the pyridine nuclei makes the ligands attractive for stabilizing metals in high formal oxidation states (6–10), influencing the reactivity of metal centers (5, 8, 11), designing

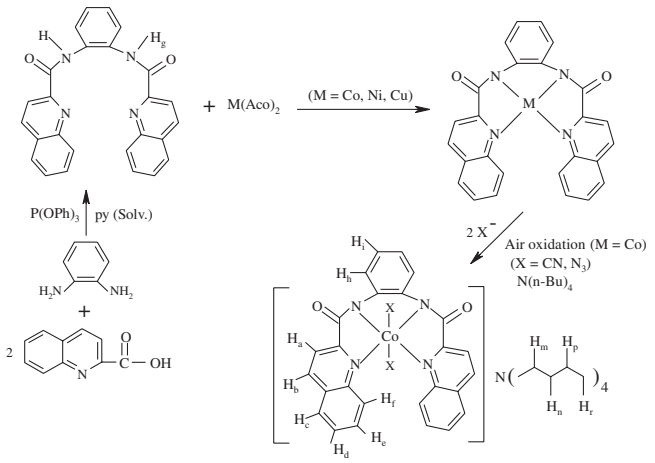
Received 16 March 2006. Accepted 14 June 2006. Published on the NRC Research Press Web site at http://canjchem.nrc.ca on 26 August 2006.

S. Meghdadi, M. Amirnasr,[1] and A. Zamanpoor. Department of Chemistry, Isfahan University of Technology, Isfahan 84156-83111, Iran.
V. Langer. Environmental Inorganic Chemistry, Department of Chemical and Biological Engineering, Chalmers University of Technology, SE-412 96 Gothenburg, Sweden.

[1]Corresponding author (e-mail: amirnasr@cc.iut.ac.ir).

 doi:10.1139/V06-118 © 2006 NRC Canada

Scheme 1.



sensitive and selective tools for specific analytical applications (12, 13),[2] and for providing catalysts with significant catalytic activity (8, 14).

Vagg and co-workers (15, 16) developed a series of acyclic tetradentate ligands with two central amide groups and two terminal pyridine groups. These and other related ligands act as chelating agents to form monomeric, dimeric, and polymeric complexes with transition-metal ions (17–19). The deprotonated anionic ligand is a strong σ donor that usually acts as a planar tetradentate N_4 ligand in the structure of square planar, square pyramidal, or octahedral complexes.

As part of our continued interest (17) in the transition-metal chemistry of dianionic bis(amide) in-plane ligands, we herein describe the synthesis and spectroscopic characterization of Co(II), Ni(II), Cu(II), and Co(III) complexes with the new bis(amide) ligand bqb(2-) [H_2bqb = *N*,*N*-bis(2-quinolinecarboxamide)-1,2-benzene] (Scheme 1). We have recently used the ligand for the construction of a Ho(III)-selective electrode (13), and we have obtained promising results using the [Co^{II}(bqb)] complex as a sensor for the potentiometric determination of cyanide.[2]

Contrary to [Co^{II}(bpb)], H_2bpb = *N*,*N*-bis(2-pyridinecarboxamide)-1,2-benzene, which is fairly reactive towards oxidative addition of σ donor amines like pyrrolidine (17), the reactivity of [Co^{II}(bqb)] towards addition of σ donor amines under oxidative conditions to produce *trans*-[Co^{III}(bqb)(amine)$_2$]$^+$ is substantially reduced. However, *trans*-[Co^{III}(bqb)(X)$_2$]$^-$ complexes are prepared in high yields in the presence of π acceptor ligands such as CN^- and N_3^-, under a vigorous stream of air. The X-ray crystal structures of [Ni(bqb)] (**2**) and [N(*n*-Bu)$_4$][Co^{III}(bqb)(N_3)$_2$] (**5**) complexes are also reported.

Experimental

All chemicals were used as supplied by Merck and Fluka without further purification. Solvents were either of reagent or spectroscopic grade and were dried by conventional procedures. 1,2-Phenylenediamine was recrystallized from hot ethanol prior to use.

Physical measurements

Elemental analyses were performed using a Heraeus CHN-O-RAPID elemental analyzer. IR spectra (KBr pellet) were obtained on a Shimadzu 435 spectrophotometer. ^{1}H NMR spectra were obtained on a BRUKER ACP-500 spectrometer at 500 MHz. Proton chemical shifts δ are reported in parts per million (ppm) relative to an internal standard of Me_4Si.

Synthesis

N,N′-*Bis[(2-quinolinecarboxamide)-1,2-benzene] (H_2bqb)*

To a solution of 1.038 g (0.006 mol) quinaldic acid in 5 mL pyridine was added a solution of 0.324 g (0.003 mol) of 1,2-diaminobenzene in 5 mL pyridine and the resulting yellow solution was stirred at 40–45 °C for 10 min. Triphenyl phosphite (1.57 mL, 0.006 mol) was then added dropwise and the reaction mixture was stirred at 90–100 °C for 4 h. The resulting dark red solution was left undisturbed at room temperature for 24 h until needlelike red crystals appeared. To this was then added 20 mL of ethanol resulting in a bulk of crystalline product that was filtered and washed with cold ethanol. The ligand was recrystallized from methanol. Yield: 1.193 g, 95%. IR (KBr, cm^{-1}) ν_{max}: 3320 (m, N-H), 1690 (s, C=O), 1590 (s, C=C), 1530 (s, C-N). ^{1}H NMR (500 MHz, $CDCl_3$, assignment as in Scheme 1) δ 10.61 (br s, 2H, H_{amidic}), 8.45 (d, 2H, H_a), 8.37 (d, 2H, H_b), 8.03 (2H, AA′XX′, J_m = 3.5 Hz, J_o = 9.5 Hz, H_h), 7.89 (dd, 2H, H_f), 7.85 (dd, 2H, H_c), 7.60 (m, 4H, $H_{d,e}$), 7.37 (2H, AA′XX′, J_m = 3.5 Hz, J_o = 9.5 Hz, H_i). Anal. calcd. for $C_{26}H_{18}N_4O_2$ (418.45): C 74.63, H 4.34, N 13.39; found: C 74.45, H 4.34, N 13.37.

[Co(bqb)(DMF)] (1)

A solution of 1.250 g (0.003 mol) of H_2bqb in 5 mL DMF was added dropwise to a solution of 0.747 g (0.003 mol) of cobalt(II) acetate tetrahydrate in 5 mL DMF. The resulting orange-brown solution was left undisturbed to give needlelike crystals. The crystals were isolated by filtration, washed with cold DMF, and dried in vacuo. Yield: 1.580 g, 96%. IR (KBr, cm^{-1}) ν_{max}: 1665 (s, C=O), 1590 (s, C=C), 1540 (s, C-N). Anal. calcd. for $C_{29}H_{23}N_5O_3Co$ (548.46): C 63.51, H 4.23, N 12.77; found: C 62.20, H 4.19, N 12.39.

[Ni(bqb)] (2)

A solution of 1.250 g (0.003 mol) of H_2bqb in 5 mL DMF was added dropwise to a solution of 0.747 g (0.003 mol) of nickel(II) acetate tetrahydrate in 5 mL DMF. The resulting deep green solution was left undisturbed to give dark green crystals, suitable for X-ray crystallography. The crystals were isolated by filtration, washed with cold DMF, and dried in vacuo. Yield: 1.383 g, 97%. IR (KBr, cm^{-1}) ν_{max}: 1630 (s, C=O), 1590 (s, C=C), 1575 (s, C-N). Anal. calcd. for $C_{26}H_{16}N_4O_2Ni$ (475.12): C 65.73, H 3.39, N 11.79; found: C 64.76, H 3.52, N 11.76.

[Cu(bqb)] (3)

A solution of 1.250 g (0.003 mol) of H_2bqb in 5 mL DMF was added dropwise to a solution of 0.599 g (0.003 mol) of copper(II) acetate monohydrate in 5 mL DMF. The resulting

[2] H. Teymourian, M. Aghamohammadi, S. Meghdadi, M. Amirnasr, N. Alizadeh. Manuscript in preparation.

© 2006 NRC Canada

brown solution was left undisturbed to give dark brown crystals. The crystals were isolated by filtration, washed with cold DMF, and dried in vacuo. Yield: 1.368 g, 95%. IR (KBr, cm^{-1}) ν_{max}: 1610 (s, C=O), 1590 (s, C=C), 1560 (s, C-N). Anal. calcd. for $C_{26}H_{16}N_4O_2Cu$ (479.98): C 65.03, H 3.36, N 11.67; found: C 64.60, H 3.52, N 11.73.

[N(n-Bu)$_4$][Co^{III}(bqb)(CN)$_2$ (4)

To a solution of 0.250 g (0.001 mol) of cobalt(II) acetate tetrahydrate in 10 mL of DMF was added dropwise a solution of 0.420 g (0.001 mol) H_2bqb in 10 mL DMF. The resulting orange-brown solution was stirred for 2 h to give a microcrystalline red-brown precipitate. A solution of 0.260 g (0.004 mol) KCN in 10 mL DMF was then added to the reaction mixture and air was bubbled through it for 12 h. The reddish-brown suspension gradually dissolved, generating a cherry-red clear solution. The final solution was filtered and a solution of 0.640 g (0.002 mol) [N(*n*-Bu)$_4$]Br in 5 mL DMF was added to the filtrate. The resulting solution was stirred for 5 min and the solvent removed under vacuum. The cherry-red solid was redissolved in acetone and filtered. Cherry red crystals of the complex were obtained by diffusion of Et_2O vapour into the filtrate. Yield: 0.732 g, 78%. IR (KBr, cm^{-1}) ν_{max}: 1610 (s, C=O), 1590 (s, C=C), 1560 (s, C-N), 2120 (m, C≡N). ^{1}H NMR (500 MHz, $(CD_3)_2CO$, assignment as in Scheme 1) δ 8.75 (2H, AA′XX′, J_m = 3.5 Hz, J_o = 9.5 Hz, H_h), 8.71 (d, 2H, H_a), 8.16 (d, 2H, H_b), 8.10 (dd, 2H, H_f), 7.88 (dd, 2H, H_c), 7.57 (m, 2H, H_e), 7.09 (m, 2H, H_d), 6.91 (2H, AA′XX′, J_m = 3.5 Hz, J_o = 9.5 Hz, H_i), 3.34 (m, 8H, H_m), 1.73 (m, 8H, H_n), 1.36 (m, 8H, H_p), 0.91 (m, 8H, H_r)]. Anal. calcd. for $C_{44}H_{52}N_7O_2Co$ (769.86): C 68.65, H 6.81, N 12.74; found: C 67.00, H 6.75, N 12.70.

[N(n-Bu)$_4$][Co^{III}(bqb)(N$_3$)$_2$ (5)

This complex was prepared by a procedure similar to that for **4**, except that NaN_3 (0.260 g, 0.004 mol) was used as the source of N_3^- ligand. The final dark red solid was redissolved in acetone and filtered. Dark red crystals of the complex, suitable for X-ray crystallography, were obtained by slow diffusion of ethyl acetate vapour into the filtrate at 0 °C. These crystals were isolated by filtration, washed with a mixture of cold ethyl acetate – acetone (9:1, *v*/*v*), and dried in vacuo. Yield: 0.706 g, 88%. IR (KBr, cm^{-1}) ν_{max}: 1610 (s, C=O), 1590 (s, C=C), 1560 (s, C-N), 2000 (m, N_3). ^{1}H NMR (500 MHz, $(CD_3)_2CO$, assignment as in Scheme 1) δ 8.88 (2H, AA′XX′, J_m = 3.5 Hz, J_o = 9.5 Hz, H_h), 8.70 (d, 2H, H_a), 8.28 (d, 2H, H_b), 8.09 (dd, 2H, H_f), 7.99 (dd, 2H, H_c), 7.55 (m, 2H, H_e), 7.05 (m, 2H, H_d), 6.92 (2H, AA′XX′, J_m = 3.5 Hz, J_o = 9.5 Hz, H_i), 3.37 (m, 8H, H_m), 1.75 (m, 8H, H_n), 1.38 (m, 8H, H_p), 0.91 (m, 8H, H_r)]. Anal. calcd. for $C_{42}H_{52}N_{11}O_2Co$ (801.87): C 62.91, H 6.54, N 19.21; found: C 61.90, H 6.71, N 19.56.

X-ray crystallography

Data were collected on a Siemens SMART CCD diffractometer, equipped with a LT-2A low-temperature device, using graphite-monochromated Mo Kα (λ = 0.710 73 Å) radiation. A full sphere of reciprocal lattice was scanned by 0.3° steps in ω with a crystal to detector distance of 3.97 cm. Preliminary orientation matrices were obtained from the first frames using SMART (20). The frames were integrated using the preliminary orientation matrices that were updated every 100 frames. Final cell parameters were obtained by the refinement of the positions of 8192 (for both **2** and **5**) reflections with $I > 2\sigma(I)$, after integration of all the frames using SAINT (20). The data were empirically corrected for absorption and other effects using SADABS (21). The structures were solved by direct methods and refined by the full-matrix least-squares method on F^2 data using SHELXTL (22). All non-H atoms were refined anisotropically. The structure of **5** is a racemic twin. One of the Bu chains of tetrabutyl ammonium ion was found to be disordered with occupancy factors of 0.530(9) and 0.470(9), respectively. The H atoms were constrained to idealized geometries and refined isotropically. The crystallographic and refinement data are summarized in Table 1.

Results and discussion

Synthesis

H_2bqb was prepared by the condensation of quinaldic acid and 1,2-diaminobenzene in pyridine in the presence of triphenyl phosphite. The product, as a red crystalline material, was characterized by CHN analysis, IR, UV–vis, and ^{1}H NMR spectroscopy.

The syntheses of mononuclear Co(II), Ni(II), Cu(II), and two Co(III) complexes (**1**–**5**) of the new dianionic ligand bqb(2-) are outlined in Scheme 1. The [M(bqb)] complexes (**1**–**3**) were prepared by the reaction of equimolar quantities of the ligand and the corresponding metal acetate in DMF. The [N(*n*-Bu)$_4$][Co(bqb)(X)$_2$] complexes (**4** and **5**) were synthesized by the air oxidation of [Co(bqb)], prepared in situ, in the presence of the corresponding X ligand in DMF. A vigorous stream of air was passed through the reaction mixture for a period of 12 h, during which the reddish-brown suspension dissolved. Cherry-red crystals of **4** and dark red crystals of **5** were obtained in good yields (78%–88%).

The [Co^{II}(bqb)] complex is sparingly soluble in any solvent and contrary to [Co^{II}(bpb)] (17), its reactivity towards the addition of σ donor amines like piperidine, pyrrolidine, and morpholine under oxidative conditions to produce *trans*-[Co^{III}(bqb)(amine)$_2$]$^+$ is substantially reduced. Preliminary electrochemical results indicate that [Co^{II}(bqb)] is less readily oxidized than [Co^{II}(bpb)], which is in accord with the stronger π accepting character of bqb, with two extra fused phenyl rings, as compared with bpb.[2]

Structure of [Ni(bqb)] (2)

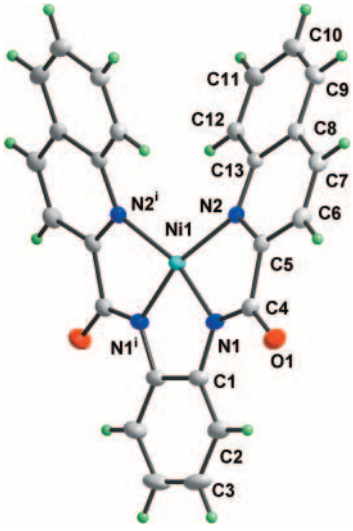
Complex **2**, as illustrated in Fig. 1, crystallizes with the Ni atom placed at a twofold axis with a square-planar structure slightly distorted towards a tetrahedron as evidenced by the N1-Ni1-N2^i and N1^i-Ni1-N2 bond angles of 163.63(6)°. The Ni atom is on the mean plane defined by the amido and pyridine nitrogen atoms, which deviate alternatively above and below the mean plane as follows: N1, –0.185(2) Å; N1^i, +0.185(2) Å; N2^i, +0.142(2) Å; and N2, –0.142(2) Å. Ni atoms are apically attacked by symmetry related O1 atoms at a distance of 3.210(2) Å. The chelate molecules stack with their molecular plane parallel to the *b* axis and diagonal to vectors ***a*** and ***c*** (Fig. 2) and are stabilized in this plane by weak intermolecular hydrogen bonds. The shortest Ni···Ni separation of 5.4869(2) Å (perpendicular to the stack) is

© 2006 NRC Canada

Table 1. Crystal data and structure refinement data for **2** and **5**.

Compound	**2**	**5**
Empirical formula	$C_{26}H_{16}N_4NiO_2$	$C_{42}H_{52}CoN_{11}O_2$
Formula weight	475.14	801.88
Temperature (K)	183(2)	173(2)
Wavelength (Å)	0.710 73	0.710 73
Crystal system	Monoclinic	Monoclinic
Space group	*C*2/*c*	*C*2
a (Å)	17.4253(2)	19.7721(1)
b (Å)	12.9676(1)	12.8034(1)
c (Å)	9.7265(1)	19.6625(1)
β (°)	115.275(1)	117.684(1)
V (Å^3)	1987.44(3)	4407.75(5)
Z	4	4
$D_{calcd.}$ (mg/m^3)	1.588	1.208
μ (mm^{-1})	1.011	0.436
F(000)	976	1696
Crystal size (mm^3)	0.25 × 0.08 × 0.08	0.81 × 0.48 × 0.19
θ range for data collection (°)	2.59–32.85	2.33–31.60
Index ranges	$-25 \le h \le 26$, $-19 \le k \le 19$, $-14 \le l \le 14$	$-29 \le h \le 29$, $-18 \le k \le 18$, $-28 \le l \le 28$
Reflections collected	16 782	36 559
Independent reflections	3541	14 584
R_{int}	0.0471	0.0381
Completeness to θ (°)	30.00, 99.9%	30.00, 99.9%
Max. and min. transmission	0.9235, 0.7862	0.9217, 0.7189
Refinement method	Full-matrix least-squares on F^2	Full-matrix least-squares on F^2
Data, restraints, parameters	3541, 0, 158	14 584, 1, 533
Goodness-of-fit on F^2	1.012	1.043
Final *R* indices [$I > 2\sigma(I)$]	$R_1 = 0.0436$, $wR_2 = 0.1243$	$R_1 = 0.0522$, $wR_2 = 0.1286$
R indices (all data)	$R_1 = 0.0579$, $wR_2 = 0.1358$	$R_1 = 0.0707$, $wR_2 = 0.1425$
Largest diff. peak and hole (e Å^{-3})	0.690 and –1.635	0.498 and –0.320

Fig. 1. Numbering scheme and temperature ellipsoids at 50% probability level. The Ni atom is placed at the twofold axis, which is vertical in the picture. Symmetry code: (*i*) –*x*, *y*, 3/2 – *z*.



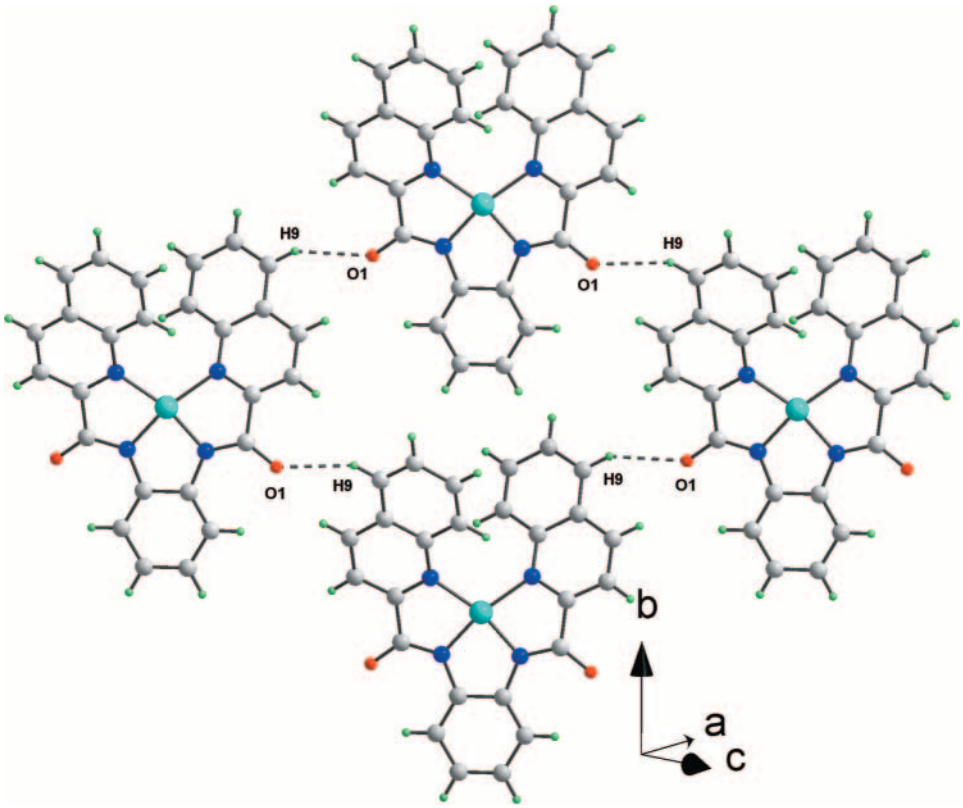
significantly larger than the sum of the van der Waals radii of the Ni atoms (3.20 Å) (23). Selected bond lengths and angles are listed in Table 2. The Ni—N(amide) bond length of 1.848(1) Å agrees well with those reported (1.82–2.02 Å) for other deprotonated Ni—N(amide) bonds (17, 24–26) and is significantly shorter than the Ni—N(py) bond length of 1.958(1) Å. It is also shorter than the Ni—N(amine) bond length of 1.930(6) Å in $[Ni(C_9H_{24}N_4)](ClO_4)_2$ (27). This is in accord with the fact that the deprotonated amide nitrogen is a very strong σ donor. The Ni—N(py) bond length of 1.958(1) Å is also typical (1.952–2.004 Å) (17, 24, 28).

Structure of $[N(n\text{-}Bu)_4][Co(bqb)(N_3)_2]$ (5)

Complex **5**, as illustrated in Fig. 3, crystallizes with an octahedral structure. There are two crystallographically independent Co complexes, both located at the twofold axis. The octahedral polyhedron around Co(III) is slightly distorted, with the bqb ligand ($N_2N'_2$) occupying the equatorial positions and the two azides occupying the axial sites. Selected bond lengths and angles are listed in Table 3. The Co (amide) bond lengths of 1.871(2) Å for the first complex and 1.876(2) Å for the second, and the bond lengths of Co—N(py), 2.001(2) and 1.988(2) Å, are symmetric and compare well with the corresponding bond lengths reported for other deprotonated Co—N(amide) and Co—N(py) bonds (17, 28, 29). The deprotonated mode of coordination of the amide nitrogens is also evident from the absence of the amidic proton

© 2006 NRC Canada

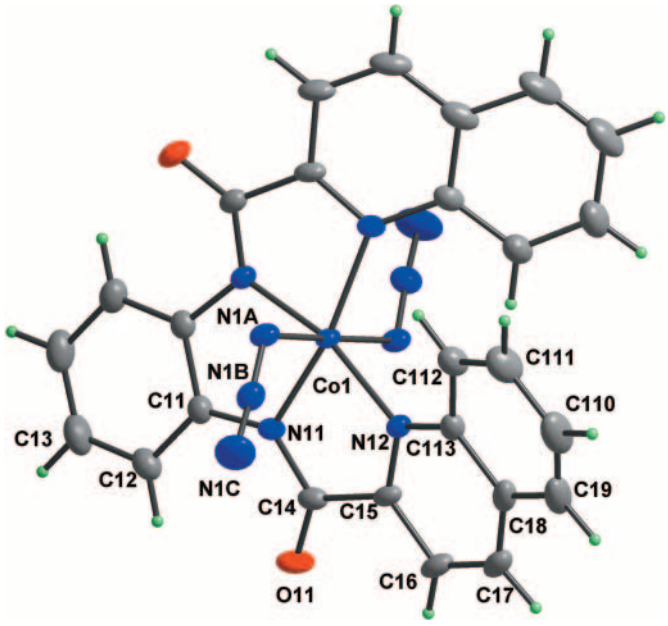
Fig. 2. The molecules form sheets in the plane, parallel with the *b* axis and diagonal to vectors ***a*** and ***c***, by weak intermolecular hydrogen bonds.



signal from the ^{1}H NMR spectrum of complex **5** (vide infra). The Co—N_3 bond length is 1.969(2) Å for both complexes, which is in good agreement with the Co—N_3 bond length of 1.959(3) Å in *trans*-[Co(3,2,3-tet)$(N_3)_2$]ClO_4, where 3,2,3-tet = 1,10-diamino-4,7-diazadecane (30).

All angles around the Co centers deviate significantly from 90°, indicating a rectangular distortion. The ligand–cobalt–ligand bond angles in the equatorial planes consist of one angle that is larger than 90 (N12^i-Co1-N12 = 111.9(1)°, N22-Co2-N22^{ii} = 110.0(1)°) and three that are smaller than 90° (N11^i-Co1-N11 = 84.5(1)°, N11^i-Co1-N12^i = N11-Co1-N12 = 81.96(8)° for the first complex and N21-Co2-N21^{ii} = 85.6(1)°, N21-Co2-N22 = N21^{ii}-Co2-N22^{ii} = 82.5(1)° for the second complex). This indicates that there might be some strain in the coordination sphere due to the rigid geometry of the ligand. The trans N1A-Co1-N1A^i unit with a bond angle of 177.2(1)° is almost linear, as is N2A^{ii}-Co2-N2A at 178.8(1)°. The four equatorial N-donor atoms deviate alternatively above and below the mean plane (N11^i +0.070(2) Å, N11 –0.070(2) Å, N12^i –0.053(1) Å, N12 +0.053(1) Å) for the first complex and (N21 +0.109(2) Å, N21^{ii} –0.109(2) Å, N22 –0.085(1) Å, and N22^{ii} +0.085 Å) for the second complex. The internal coordinates of the azide anions are 1.191(3) Å, 1.149(3) Å, and 175.9(3)° for the first complex and 1.205(3) Å, 1.153(3) Å, and 177.0(3)° for the second complex, as compared to 1.192(4) Å, 1.150(4) Å, and 175.4(4)° and 1.173(4) Å, 1.147(5) Å, and 176.7(5)° reported for *trans*-[Co(3,2,3-tet)$(N_3)_2$]ClO_4 (30). The so-called covalent azides are linear and asymmetric, possessing unequal N—N bond lengths (31). In ionic azides

Fig. 3. Atom-numbering scheme for the first complex $[Co(bqb)(N_3)_2]^-$ anion. Displacement ellipsoids are drawn at the 30% probability level.



both N—N bonds are of equal length and close to 1.17 Å (32). The variation of the long N—N bond is an indication of the degree of covalent character of the coordinate bond, being 1.24 Å in highly covalent structures. In the present

© 2006 NRC Canada

Table 2. Selected bond lengths and angles for [Ni(bqb)] (**2**).

Bond lengths (Å)	
Ni1—N1	1.848(1)
Ni1—N1^{i}	1.848(1)
Ni1—N2^{i}	1.958(1)
Ni1—N2	1.958(1)
O1—C4	1.243(2)
N1—C4	1.345(2)
N1—C1	1.410(2)
N2—C5	1.347(2)
N2—C13	1.381(2)
Bond angles (°)	
N1-Ni1-N1^{i}	84.6(1)
N1-Ni1-N2^{i}	163.6 (1)
N1^{i}-Ni1-N2^{i}	83.5(1)
N1-Ni1-N2	83.5(1)
N1^{i}-Ni1-N2	163.6(1)
N2^{i}-Ni1-N2	110.3(1)
C4-N1-C1	126.1(1)
C4-N1-Ni1	117.7(1)
C1-N1-Ni1	115.8(1)
C5-N2-C13	118.1(1)
C5-N2-Ni1	110.5(1)
C13-N2-Ni1	131.4(1)
N1-C1-C1^{i}	111.9(1)
O1-C4-N1	129.1(2)
O1-C4-C5	121.4(2)
N1-C4-C5	109.4(1)
N2-C5-C4	115.2(1)

Note: Symmetry code (i) $-x$, y, 3/2 $-$ z.

Table 3. Selected bond lengths and angles for [N(*n*-Bu)$_4$][Co(bqb)(N$_3$)$_2$] (**5**).

Bond lengths (Å)	
Co1—N11^{i}	1.871(2)
Co1—N11	1.871(2)
Co1—N1A	1.969(2)
Co1—N1A^{i}	1.969(2)
Co1—N12^{i}	2.001(2)
Co1—N12	2.001(2)
O11—C14	1.240(3)
Co2—N21^{ii}	1.876(2)
Co2—N21	1.876(2)
Co2—N2A	1.969(2)
Co2—N2A^{ii}	1.969(2)
Co2—N22^{ii}	1.988(2)
Co2—N22	1.988(2)
O21—C24	1.243(3)
Bond angles (°)	
N11^{i}-Co1-N11	84.5(1)
N11^{i}-Co1-N1A	94.4(1)
N11-Co1-N1A	87.7(1)
N11^{i}-Co1-N1A^{i}	87.7(1)
N11-Co1-N1A^{i}	94.4(1)
N1A-Co1-N1A^{i}	177.2(1)
N11^{i}-Co1-N12^{i}	82.0(1)
N11-Co1-N12^{i}	165.9(1)
N1A-Co1-N12^{i}	89.2(1)
N1A^{i}-Co1-N12^{i}	89.2(1)
N11^{i}-Co1-N12	165.9(1)
N11-Co1-N12	82.0(1)
N1A-Co1-N12	89.2(1)
N1A^{i}-Co1-N12	89.2(1)
N12^{i}-Co1-N12	111.8(1)
C14-N11-C11	125.2(2)
C14-N11-Co1	117.0(2)
C11-N11-Co1	114.6(2)
C15-N12-Co1	109.2(2)
C113-N12-Co1	132.3(2)
N1B-N1A-Co1	120.9(2)
N1C-N1B-N1A	175.9(3)
C12-C11-N11	127.1(2)
C11^{i}-C11-N11	113.1(1)
O11-C14-N11	129.2(3)
O11-C14-C15	120.7(2)
N11-C14-C15	109.9(2)
N12-C15-C14	116.0(2)
C16-C15-C14	120.3(2)
N21^{ii}-Co2-N21	85.6(1)
N21^{ii}-Co2-N2A	94.7(1)
N21-Co2-N2A	86.2(1)
N21^{ii}-Co2-N2A^{ii}	86.2(1)
N21-Co2-N2A^{ii}	94.7(1)
N2A-Co2-N2A^{ii}	178.8(1)
N21^{ii}-Co2-N22^{ii}	82.5(1)
N21-Co2-N22^{ii}	166.4(1)
N2A-Co2-N22^{ii}	88.4(1)
N2A^{ii}-Co2-N22^{ii}	91.0(1)
N21^{ii}-Co2-N22	166.5(1)
N21-Co2-N22	82.5(1)

case, the long N—N bond length of 1.191(3) Å signifies some covalent character in the Co—N$_3$ bonds. The shortest distance between Co atoms is 10.205(1) Å.

Spectral characterization

The main features of the IR spectrum of the H$_2$bqb ligand are (*i*) the vibration due to the amidic NH that appears as a sharp band at 3320 cm^{-1}, (*ii*) the strong band at 1690 cm^{-1} owing to amidic C=O stretching vibration, and (*iii*) the C—N stretching vibration of medium intensity appearing at 1530 cm^{-1}. The absence of ν(N-H) (3320 cm^{-1} band) in the IR spectra of the complexes confirms that the bqb ligand is coordinated in its deprotonated form. The ν(C-N) is shifted to higher frequencies relative to the free H$_2$bqb (1530 cm^{-1}), ranging from 1540 cm^{-1} in **1** to 1560 cm^{-1} in **5**. Correspondingly, the ν(C=O) is shifted to lower frequencies relative to the free H$_2$bqb (1690 cm^{-1}), ranging from 1665 cm^{-1} in **1** to 1610 cm^{-1} in **5**, which is in agreement with the data reported for related complexes (33). A planar conformation involving maximum delocalization would be achieved on deprotonation, leading to an increase in the double-bond character of the amidic C—N bond and a simultaneous decrease in the double-bond character of the C—O bond in this mode of coordination. This is also evident from the amidic C—N bond lengths in **2** (1.345(2) Å) and **5** (1.325(3) and 1.341(3) Å), which are close to the C=N bond lengths of the py ring of the coordinated bqb (1.347 Å in **2** and 1.333 Å in **5**) given in

© 2006 NRC Canada

Fig. 4. ^{1}H NMR spectrum (500 MHz) of [N(*n*-Bu)$_4$][Co(bqb)(CN)$_2$] (**4**) in $(CD_3)_2CO$ solution. The spectrum is labeled with peak assignments as discussed in the text.

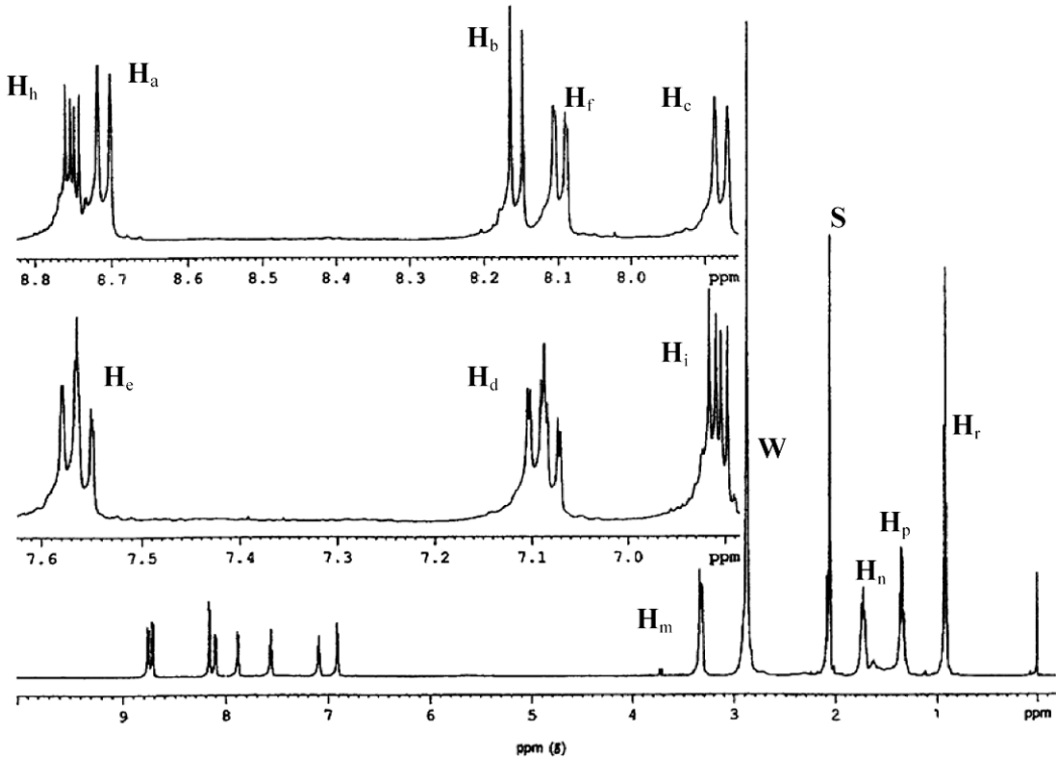


Table 3 (*concluded*).

N2A-Co2-N22	91.0(1)
N2A^{ii}-Co2-N22	88.4(1)
N22^{ii}-Co2-N22	110.0(1)
C24-N21-C21	128.3(2)
C24-N21-Co2	116.1(2)
C21-N21-Co2	113.2(2)
C25-N22-Co2	109.8(2)
C213-N22-Co2	130.8(2)
N2B-N2A-Co2	119.9(2)
N2C-N2B-N2A	177.0(3)
C22-C21-N21	126.2(3)
C21^{ii}-C21-N21	113.9(1)
O21-C24-N21	128.4(3)
O21-C24-C25	121.4(3)
N21-C24-C25	110.0(2)
N22-C25-C24	116.3(2)
C26-C25-C24	122.1(2)

Note: Symmetry codes (i) –*x*, *y*, 1 –*z*, (ii) 1 – *x*, *y*, – *z*.

Tables 2 and 3. The C—O bond lengths of 1.243(2) Å in **2** and of 1.240(3) and 1.243(3) Å in **5** are also longer than the isolated C=O bonds. A comparison of the C—N and C=O bond lengths of 1.475(11) and 1.196(5) Å, respectively, reported for 1-aza-2-adamantanone (34), with 1.545(11) and 1.124(12) Å, respectively, reported for the amides (35), would be convincing.

The hexacoordinate geometry of **5** is evident from the X-ray structure analysis (Fig. 3). A hexacoordinate trans structure for complex **4** can be inferred based on the similarity of the ^{1}H NMR spectra of this complex with that of **5**. There are three main features in the ^{1}H NMR spectra of the complexes. (*i*) The absence of the amidic (δ 10.61 ppm) proton signal confirms that the equatorial amide ligand is coordinated in its deprotonated form. (*ii*) The expansion, toward downfield chemical shifts, of the aromatic proton signals range. These signals in the spectrum of the free H_2bqb ligand are located between 7.37 and 8.45 (Δδ 1.08 ppm), while in the spectra of the complexes they lie between 6.91 and 8.88 (Δδ 1.87 ppm), showing a common pattern in the two complexes (Fig. 4). These signals have been assigned by comparison with the spectra of closely related complexes [18]. The appearance of one signal set for each type of proton in $(CD_3)_2CO$ solution conform with the symmetric conformation of the equatorial ligand. (*iii*) The aliphatic protons of the [N(*n*-Bu)$_4$]$^+$ appear in the 3.37–0.91 ppm range. The NMR data are in agreement with the existence of a diamagnetic *trans*-[Co(bqb)X$_2$]$^-$ anion in both complexes, confirmed by the X-ray crystal structure of [N(*n*-Bu)$_4$][Co(bqb)(N$_3$)$_2$] (**5**).

Conclusion

We have reported the synthesis and characterization of two series of complexes, [M^{II}(bqb)] and [N(*n*-Bu)$_4$][Co^{III}(bqb)X$_2$], with the new bqb ligand. The substitution level in the pyridyl rings has a significant effect on the structure of the complexes and on the reactivity of the central metal ion towards other ligands. The fused phenyl rings in the structure of bqb, as compared with that of bpb, increases the π accepting character of bqb. Consequently, the reactivity of Co^{II} in [Co^{II}(bqb)] towards σ donor ligands

© 2006 NRC Canada

(such as amines) is lowered and only σ donor and π acceptor ligands such as CN^- and N_3^- with strong π accepting character are suitable for addition to the axial positions in an oxidative process.[3]

Acknowledgements

Partial support of this work by the Isfahan University of Technology Research Council is gratefully acknowledged by MA. The authors would also like to thank Mr. H.R. Bijanzadeh of Tarbiat Modarres University (Tehran, Iran) for obtaining the NMR spectra. Thanks are also due to Professor H. Hadadzadeh, Sistan and Bluchestan University (Zahedan, Iran), for helpful discussions and assistance with the electrochemical studies.

References

1. P.J.M.W.L. Birker. Inorg. Chem. **16**, 2478 (1977).
2. J.P. Barbier, A.E. Biyyadh, C. Kappenstein, N. Mabiala, and R.P. Hugel. Inorg. Chem. **24**, 3615 (1985).
3. S.T. Mak, W.T. Wong, V.W.W. Yam, T.F. Lai, and C.M. Che. J. Chem. Soc. Dalton Trans. 1915 (1991).
4. F.A. Chavez, M.M. Olmstead, and P.K. Mascharak. Inorg. Chem. **35**, 1410 (1996).
5. S.M. Rodmore, C.E.F. Rickard, S.J. Webb, and L.J. Wright. Inorg. Chem. **36**, 4743 (1997).
6. M. Ray, D. Ghosh, Z. Shirin, and R. Mukherjee. Inorg. Chem. **36**, 3568 (1997).
7. A.K. Singh and R. Mukherjee. J. Chem. Soc. Dalton Trans. 2886 (2005).
8. T.J. Collins. Acc. Chem. Res. **27**, 279 (1994).
9. C.-M. Che, W.K. Cheng, and T.C.W. Mak. J. Chem. Soc. Chem. Commun. 200 (1986).
10. C.-M. Che and W.-K. Cheng. J. Chem. Soc. Chem. Commun. 1443 (1986).
11. N. Niklas, H. Hampel, O. Walter, G. Liehr, and R. Alsfasser. Eur. J. Inorg. Chem. 1839 (2002).
12. A.K. Singh, P. Saxena, S. Mehtab, and B. Gupta. Talanta, **69**, 521 (2006).
13. M.R. Ganjali, S. Rasoolipour, M. Rezapour, P. Norouzi, M. Amirnasr, and S. Meghdadi. Sens. Actuators B. In press.
14. O. Belda and C. Moberg. Coord. Chem. Rev. **249**, 727 (2005).
15. D.J. Barnes, R.L. Chapman, R.S. Vagg, and E.C. Watton. J. Chem. Eng. Data, **23**, 349 (1978).
16. R.R. Fenton, F.S. Stephens, R.S. Vagg, and P.A. Williams. J. Coord. Chem. **23**, 291 (1991).
17. M. Amirnasr, K.J. Schenk, and S. Meghdadi. Inorg. Chim. Acta, **338**, 19 (2002).
18. F.S. Stephens and R.S. Vagg. Inorg. Chim. Acta, **142**, 43 (1988).
19. F. Lloret, M. Julve, J. Faus, Y. Journaux, M. Philoche-Levisalles, and Y. Jeannin. Inorg. Chem. **28**, 3702 (1989).
20. Siemens Analytical X-ray Instruments Inc. SMART and SAINT [computer programs]. Siemens Analytical X-ray Instruments Inc., Madison, Wis. 1995.
21. G.M. Sheldrick. SADABS. Version 2.03 [computer program]. University of Göttingen, Göttingen, Germany. 2002.
22. Bruker Analytical X-ray Systems. SHELXTL. Version 6.10 [computer program]. Bruker Analytical X-ray Systems, Madison, Wis. 2001.
23. A. Bondi. J. Phys. Chem. **68**, 441 (1964).
24. F.S. Stephens and R.S. Vagg. Inorg. Chim. Acta, **57**, 9 (1982).
25. F.S. Stephens and R.S. Vagg. Inorg. Chim. Acta, **120**, 165 (1986).
26. C.L. Weeks, P. Turner, R.R. Fenton, and P.A. Lay. J. Chem. Soc. Dalton Trans. 93 (2002).
27. T.-H. Lu, T.H. Tahirov, K. Shu, and C.-S. Chung. Acta Crystallogr. Sect. C: Cryst. Struct. Commun. **53**, 204 (1997).
28. U. Beckmann, E. Bill, T. Weyhermuller, and K. Weighardt. Inorg. Chem. **42**, 1045 (2003).
29. C. Jubert, A. Mohamadou, C. Gérard, S. Brandes, A. Tabard, and J.P. Barbier. J. Chem. Soc. Dalton Trans. 2660 (2002).
30. S.S. Massoud, F.A. Mautner, M. Abu-Youssef, and N.M. Shuaib. Polyhedron, **18**, 2287 (1999).
31. N.Z. Muller. Z. Anorg. Allg. Chem. **382**, 110 (1971).
32. N.Z. Muller. Z. Anorg. Allg. Chem. **392**, 159 (1972).
33 O. Rotthaus, S. LeRoy, A. Tomas, K.M. Barkigia, and I. Artaud. Eur. J. Inorg. Chem. 1545 (2004).
34. D. Quiñonero, A. Frontera, M. Capó, P. Ballester, G.A. Suñer, C. Garau, P.M. Deyà. New J. Chem. **25**, 259 (2001).
35. F.H. Allen, O. Kennard, D.G. Watson, L. Brammer, A.G. Orpen, and R. Taylor. J. Chem. Soc. Perkin Trans. 2, 1 (1987).

[3] Supplementary data for this article are available on the journal Web site (http://canjchem.nrc.ca) or may be purchased from the Depository of Unpublished Data, Document Delivery, CISTI, National Research Council Canada, Ottawa, ON K1A 0R6, Canada. DUD 5073. For more information on obtaining material refer to http://cisti-icist.nrc-cnrc.gc.ca/irm/unpub_e.shtml. CCDC 288088 for **2** and 288089 for **5** contain the crystallographic data for this manuscript. These data can be obtained, free of charge, via http://www.ccdc.cam.ac.uk/conts/retrieving.html (Or from the Cambridge Crystallographic Data Centre, 12 Union Road, Cambridge CB2 1EZ, UK; fax +44 1223 336033; or deposit@ccdc.cam.ac.uk).

© 2006 NRC Canada

Microwave-assisted N-nitroarylation of some pyrimidine and purine nucleobases

Ali Khalafi-Nezhad, Abdolkarim Zare, Abolfath Parhami, Mohammad Navid Soltani Rad, and Gholam Reza Nejabat

Abstract: An efficient procedure for the synthesis of some *N*-nitroaryl derivatives of nucleobases via microwave-assisted N-nitroarylation of nucleobases in the presence of SiO_2 and Cs_2CO_3 in DMSO, as the homogenizing solvent, is described. In this method, some pyrimidine and purine nucleobases are nitroarylated regioselectively in moderate to high yields and short reaction times.

Key words: microwave, N-nitroarylation, pyrimidine, purine, SN_{Ar}.

Résumé : On a mis au point une méthode efficace de synthèse de quelques dérivés *N*-nitroaryles de nucléobase en procédant à la N-nitroarylation des nucléobases, assistée par les micro-ondes, en présence de SiO_2 et de Cs_2CO_3 dans le DMSO comme solvant homogénéisant. Dans cette méthode, on a pu réaliser la nitroarylation régiosélective de nucléobases de la pyrimidine et de la purine avec des rendements allant de moyens à élevés et de faibles temps de réaction.

Mots clés : microonde; N-nitroarylation; pyrimidine; purine; SN_{Ar}.

[Traduit par la Rédaction]

Introduction

In recent years, there has been a growing interest in the synthesis of bioactive compounds in organic chemistry (1). One important class of these compounds is modified N-substituted nucleobases (nucleoside analogues) including acyclic (2), carboacyclic (3), carbocyclic (4), aza (5), and thionucleosides (6). The majority of nucleosides are known because of their nucleobase linkages with acyclic or cyclic side chains; however, there are a few reports of chemical synthesis as well as chemotherapeutic characterization for *N*-aryl derivatives of pyrimidines and purines (7–16). The *N*-aryl nucleobases have been found to be of particular interest in a variety of biological studies. Several N9-arylpurines are agonists or antagonists for various receptors such as adenosine receptors (7) and corticotropin-releasing hormone receptors (8) and for enzymes like xanthine oxidase (9), adenosine deaminase (10), and guanosine deaminase (11). Other bioactivities are reported, including antitumor activity (12), antimicrobial activity (13), and plant growth stimulating effects (14). These compounds are usually prepared by multistep reactions (15). Moreover, there are a few reports of the synthesis of these compounds via N-arylation of nucleobases with arylboronic acids or diaryliodonium salts in the presence of coupling agents (16). These methods are associated with one or more of the following drawbacks: long reaction time, low reaction yield, and reaction difficulty. Indeed, to the best of our knowledge, there are no reports of N1-nitroarylation of pyrimidines or N9-nitroarylation of purines via nucleophilic aromatic substitution (SN_{Ar}).

Microwave-assisted organic reactions have been used as an useful technique in organic synthesis (17). Microwave irradiation often leads to large reduction in reaction times, increased yields, easier workups, and may enhance the regio- and stereo-selectivity of reactions (17).

In an extension of our previous studies on the synthesis of nucleoside derivatives (18), we describe here an efficient, rapid, and operationally simple method for regioselective N-nitroarylation of nucleobases via SN_{Ar}. In this method, various pyrimidine and purine nucleobases were nitroarylated with activated nitroaryl halides in the presence of SiO_2 and Cs_2CO_3 in DMSO, as the homogenizing solvent, under microwave irradiation (Schemes 1 and 2).

Results and discussion

To initially optimize reaction conditions, the synthesis of compound **1a** was selected as a model reaction (Scheme 1); thus, a well-ground mixture of uracil (1 mmol), 1-chloro-2,4-dinitrobenzene (1.3 mmol), and Cs_2CO_3 (1 mmol) in DMSO (1 mL) was irradiated in a microwave oven (200 W, max. 160 °C) for 8 min; however, a low yield of product was obtained, even with increased reaction time and microwave power (Table 1). Yields improved remarkably when support was added to the reaction mixture. By testing different supports in the reaction, silica gel showed the best results (Table 1).

To select the appropriate base for the N-nitroarylation reaction, the influence of various bases was investigated on the

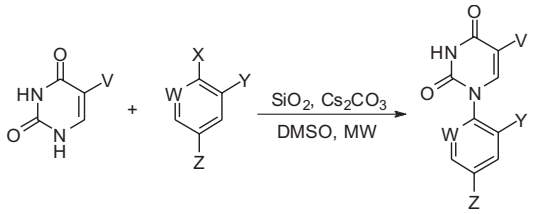
Received 26 April 2006. Accepted 26 June 2006. Published on the NRC Research Press Web site at http://canjchem.nrc.ca on 1 September 2006.

A. Khalafi-Nezhad,[1] A. Zare, A. Parhami, and G.R. Nejabat. Department of Chemistry, College of Sciences, Shiraz University, Shiraz 71454, Iran.
M.N. Soltani Rad. Department of Chemistry, College of Basic Sciences, Shiraz University of Technology, Shiraz 71555-313, Iran.

[1]Corresponding author (e-mail: khalafi@chem.susc.ac.ir).

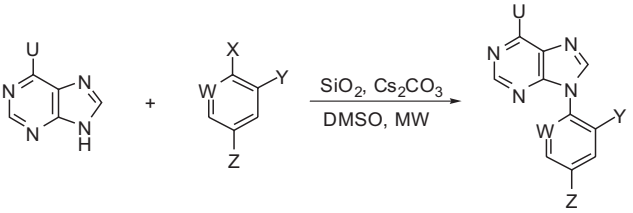
 doi:10.1139/V06-119 © 2006 NRC Canada

Scheme 1. N-Nitroarylation of pyrimidine derivatives.



1	a	b	c	d	e	f	g	h
V	H	Me	F	H	Me	H	H	H
W	CH	CH	CH	CH	CH	CH	CH	N
Y	NO_2	NO_2	NO_2	NO_2	NO_2	H	NO_2	NO_2
Z	NO_2	NO_2	NO_2	H	H	NO_2	Cl	H

Scheme 2. N-Nitroarylation of purine derivatives.



2	a	b	c	d
U	NH_2	NH_2	OH	Cl
W	CH	CH	N	CH
Y	NO_2	NO_2	NO_2	NO_2
Z	NO_2	H	H	NO_2

Table 1. The effect of supports on the N-nitroarylation of uracil with 1-chloro-2,4-dinitrobenzene in the presence of Cs_2CO_3 in DMSO under microwave irradiation (200 W, max. 160 °C).

Entry	Support	Time (min)	Yield[a] (%)
1[b]	—	8	52
2	Silica gel	2	84
3	Neutral alumina	4	64
4	Basic alumina	4	70
5	Molecular sieve	6	63
6	Montmorillonite K-10	6	65

[a]Isolated yield.
[b]Without support.

Table 2. The influence of bases on the N-nitroarylation of uracil with 1-chloro-2,4-dinitrobenzene in the presence of SiO_2 in DMSO under microwave irradiation (200 W, max. 160 °C).

Entry	Base	Time (min)	Yield[a] (%)
1	Cs_2CO_3	2	84
2	K_2CO_3	3	62
3	CaO	6	15
4	MgO	6	10
5	NaOH	3	26
6	DABCO	4	19
7	NBu_3	4	18

[a]Isolated yield.

described model reaction. The results are summarized in Table 2. As shown in Table 2, higher yields and shorter reaction times were observed when Cs_2CO_3 was applied. Therefore, Cs_2CO_3 was the base of choice for all reactions.

In another study, the effect of different solvents in the presence of SiO_2 and Cs_2CO_3 was examined (Table 3). As is clear from Table 3, the use of DMSO gave the best results. Thus, DMSO was applied as an homogenizing solvent in our reaction.

Interestingly, in our method, pyrimidine and purine nucleobases were regioselectively nitroarylated at the N-1 and N-9 positions, respectively. The sites of N-nitroarylation in both pyrimidine and purine nucleobases were indicated by ^1H and ^{13}C NMR spectral analysis. Several reports from the literature also confirmed this site of N-substitution (18*a*, 18*b*, 19).

Table 3. The influence of various solvents on the reaction of uracil with 1-chloro-2,4-dinitrobenzene in the presence of SiO_2 and Cs_2CO_3 under microwave irradiation (200 W, max. 160 °C).

Entry	Solvent	Time (min)	Yield[a] (%)
1	DMSO	2	84
2	DMF	3	66
3	HMPTA	6	55
4	*o*-Xylene	8	20

[a]Isolated yield.

Table 4. Comparative synthesis of compounds **1f** and **1g** using conventional heating (Δ, 160 °C) vs. the microwave method (400 W, max. 160 °C).

	Time (min)		Yield[a] (%)	
Compound	Δ	MW	Δ	MW
1f	200	3.5	49	62
1g	180	3	68	77

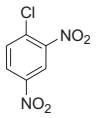
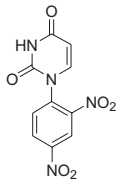
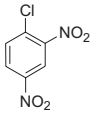
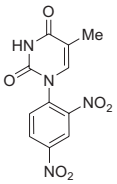
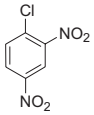
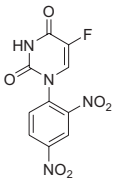
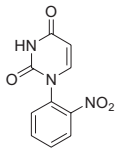
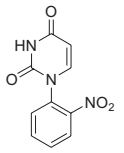
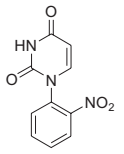
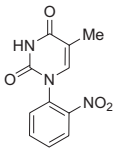
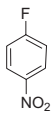
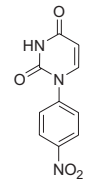
[a]Isolated yield.

To realize the capability and efficiency of microwave heating compared with conventional heating in our reaction, we also synthesized compounds **1g** and **1f** via N-nitroarylation of uracil with nitroaryl halides in the presence of SiO_2 and Cs_2CO_3 in DMSO under thermal conditions (160 °C) (Table 4). As Table 4 indicates, the microwave method is more efficient. Furthermore, the syntheses of compounds **1g** and **1f** were examined in solvent-free conditions (microwave and thermal); lower yields and longer reaction times were obtained in comparison with in-solution conditions.

To investigate the versatility and scope of our method, the reaction was examined with various nucleobases and

© 2006 NRC Canada

Table 5. N-Nitroarylation of some pyrimidine and purine nucleobases in the presence of SiO_2 and Cs_2CO_3 in DMSO under microwave irradiation.

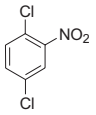
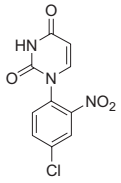
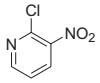
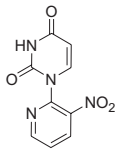
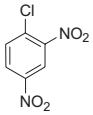
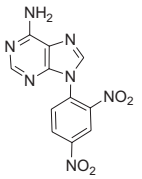
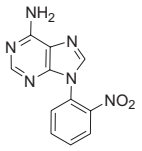
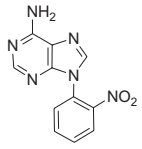
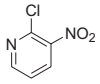
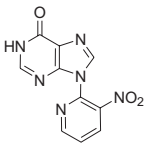
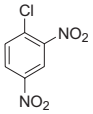
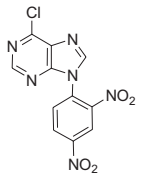
Entry	ArX	Product	MW Power (W)	Time (min)	Yield[a] (%)
1			200	2	84
2			200	2.5	81
3			200	2	82
4			400	3	74
5			400	3.5	66
6			400	5	11
7			400	3.5	72
8			400	3.5	62

nitroaryl halides (Table 5). As is depicted in Table 5, the reactions proceeded efficiently and the desired *N*-nitroaryl nucleobases were obtained in moderate to high yields.

The presence of substituents (Me and F) on the 5 position of pyrimidine nucleobases had no significant effect on results of the reaction (Table 5, entries 2, 3, and 7). To investi-

© 2006 NRC Canada

Table 5 (*concluded*).

Entry	ArX	Product	MW Power (W)	Time (min)	Yield[a] (%)
9			400	3	77
10			200	3	82
11			200	1.5	85
12			400	2	76
13			400	2.5	65
14			300	2.5	75
15			200	1.5	86

[a]Isolated yield.

gate the effect of leaving groups (halogens) at nitroaryl halides on the reaction, we examined the reaction of nucleobases with 2-nitroaryl fluoride, chloride, and bromide. As was expected, the reaction of nucleobases with 2-nitroaryl fluoride is the most efficient (Table 5, entries 4–6, 12, and 13). The higher reactivity of 2-nitroaryl fluoride is attributed to the higher electronegativity of the fluorine atom that increases positive charge on the ipso carbon. In this method, purine nucleobases were also nitroarylated regioselectively at the N-9 position in good to high yields (Table 5, entries 11–15). The presence of -NH_2 or -Cl substituents on C-6 of the purines gave similar results (Table 5, entries 11 and 15). Moreover, hypoxanthine was N-nitroarylated at N-9 in good yield (Table 5, entry 14). The biological evaluations of the named compounds are under investigation.

In summary, we have developed an efficient, clean, and rapid method for N-nitroarylation of different nucleobases via nucleophilic aromatic substitution. This new method afforded N1-nitroaryl pyrimidines and N9-nitroaryl purines as

© 2006 NRC Canada

biologically interesting compounds in short reaction times and reasonable yields.

Experimental

All chemicals were supplied by either Merck or Fluka. Solvents were purified and dried according to the reported methods and stored over molecular sieves (20). The progress of the reactions was followed with TLC, using silica gel SILG-UV 254 plates. Silica gel 60 (0.063–0.200 mm, 70–230 mesh ASTM) was used for column chromatography and support. All reactions were carried out using a CEM MARS 5™ microwave oven. IR spectra were run on a Shimadzu FT-IR-8300 spectrophotometer (ν_{max} in cm^{-1}). The ^1H NMR (250 MHz) and ^{13}C NMR (62.5 MHz) were run on a Bruker Avance DPX-250 FT-NMR spectrometer. Mass spectra were recorded on a Shimadzu GC–MS QP 1000 EX apparatus. Microanalyses were performed on a PerkinElmer 240-B microanalyzer. Melting points were recorded on a Büchi B-545 apparatus in open capillary tubes and are uncorrected.

General procedures for the preparation of compound 1a

A well-ground mixture of compounds consisting of nucleobase (2 mmol), 1-chloro-2,4-dinitrobenzene (0.52 g, 2.6 mmol), Cs_2CO_3 (0.65 g, 2 mmol), and SiO_2 (0.70 g) in anhydr. DMSO (2 mL) was poured into a microwave vessel and irradiated in a microwave oven for an appropriate time and at an appropriate power level (Table 5). The microwave was programmed to give a maximum internal temperature of 160 °C. Afterward, the reaction mixture was cooled to room temperature and poured into ice water (20 mL), the solids were filtered, and the filtrate was extracted with ethyl acetate. The solvent was evaporated and the the residue was combined with solids. This mixture was purified by column chromatography on silica gel with EtOAc–*n*-hexane (1:1) to give **1a** as a pale yellow solid, mp 225–227 °C. IR (KBr, cm^{-1}): 3435, 3042, 1688, 1657, 1608, 1283. ^1H NMR (DMSO-d_6, ppm) δ: 5.87 (d, 1H, J = 7.9 Hz, H_5 of uracil), 7.89 (d, 1H, J = 7.9 Hz, H_6 of uracil), 8.02 (d, 1H, J = 8.7 Hz, H_6 of aromatic ring), 8.71 (d, 1H, J = 8.7 Hz, H_5 of aromatic ring), 8.83 (s, 1H, H_3 of aromatic ring), 11.78 (s, 1H, NH, exchangeable with D_2O). ^{13}C NMR (DMSO-d_6) δ: 103.1, 120.6, 129.2, 131.4, 136.0, 143.6, 144.9, 146.9, 149.5, 163.3. MS *m*/*z*: 278 (M^+). Anal. calcd. for $C_{10}H_6N_4O_6$: C 43.18, H 2.17, N 20.14; found: C 42.99, H 2.36, N 20.26.

1-(2,4-Dinitrophenyl)-5-methyl-1*H*-pyrimidine-2,4-dione (1b)

Column chromatography on silica gel and eluting with EtOAc–*n*-hexane (1:1) gave a pale yellow solid, mp 228–230 °C. IR (KBr, cm^{-1}): 3437, 3056, 1694, 1652, 1591, 1289. ^1H NMR (DMSO-d_6, ppm) δ: 2.00 (s, 3H, CH_3), 7.98 (s, 1H, H_6 of thymine), 8.15 (d, 1H, J = 8.8 Hz, H_6 of aromatic ring), 8.83 (d, 1H, J = 8.8 Hz, H_5 of aromatic ring), 8.97 (s, 1H, H_3 of aromatic ring), 11.93 (s, 1H, NH, exchangeable with D_2O). ^{13}C NMR (DMSO-d_6) δ: 11.8, 110.9, 120.6, 129.1, 131.1, 136.1, 139.1, 144.9, 146.7, 149.5, 163.9. MS *m*/*z*: 292 (M^+). Anal. calcd. for $C_{11}H_8N_4O_6$: C 45.21, H 2.76, N 19.17; found: C 45.40, H 2.87. N 19.29.

1-(2,4-Dinitrophenyl)-5-fluoro-1*H*-pyrimidine-2,4-dione (1c)

Column chromatography on silica gel and eluting with EtOAc–*n*-hexane (1:1) gave a pale yellow solid, mp 246–248 °C. IR (KBr, cm^{-1}): 3441, 3061, 1718, 1670, 1608, 1285. ^1H NMR (DMSO-d_6, ppm) δ: 8.03 (d, 1H, J = 8.7 Hz, H_6 of aromatic ring), 8.47 (d, 1H, J = 6.6 Hz, H_6 of 5-fluorouracil), 8.74 (d, 1H, J = 8.7 Hz, H_5 of aromatic ring), 8.84 (s, 1H, H_3 of aromatic ring), 12.34 (s, 1H, NH). ^{13}C NMR (DMSO-d_6) δ: 120.7, 129.2, 131.6, 135.4, 138.9, 142.6, 145.1, 146.9, 148.3, 157.0. MS *m*/*z*: 296 (M^+). Anal. calcd. for $C_{10}H_5FN_4O_6$: C 40.55, H 1.70, N 18.92; found: C 40.41, H 1.49, N 18.79.

1-(2-Nitrophenyl)-1*H*-pyrimidine-2,4-dione (1d)

Column chromatography on silica gel and eluting with EtOAc–*n*-hexane (1:1) gave a pale yellow solid, mp 234–236 °C. IR (KBr, cm^{-1}): 3439, 3055, 1694, 1647, 1607, 1290. ^1H NMR (DMSO-d_6, ppm) δ: 5.79 (d, 1H, J = 7.9 Hz, H_5 of uracil), 7.69–7.77 (complex, 2H, H_4 and H_6 of aromatic ring), 7.82–7.94 (complex, 2H, H_3 and H_5 of aromatic ring), 8.01 (d, 1H, J = 7.9 Hz, H_6 of uracil), 11.62 (s, 1H, NH). ^{13}C NMR (DMSO-d_6) δ: 103.7, 123.4, 128.8, 131.6, 133.9, 136.5, 143.1, 146.1, 149.9, 163.6. MS *m*/*z*: 233 (M^+). Anal. calcd. for $C_{10}H_7N_3O_4$: C 51.51, H 3.03, N 18.02; found: C 51.67, H 2.88, N 18.26.

1-(2-Nitrophenyl)-5-methyl-1*H*-pyrimidine-2,4-dione (1e)

Column chromatography on silica gel and eluting with EtOAc–*n*-hexane (1:1) gave a pale yellow solid, mp 278–280 °C. IR (KBr, cm^{-1}): 3438, 3051, 1701, 1657, 1608, 1284. ^1H NMR (DMSO-d_6, ppm) δ: 1.82 (s, 3H, CH_3), 7.67–7.75 (complex, 3H, H_4 and H_6 of aromatic ring as well as H_6 of thymine), 7.94 (dd, 1H, J = 4.3, 8.2 Hz, H_5 of aromatic ring), 8.13 (d, 1H, J = 8.6 Hz, H_3 of aromatic ring), 11.61 (s, 1H, NH). ^{13}C NMR (DMSO-d_6) δ: 12.8, 103.5, 123.9, 126.4, 128.6, 133.6, 136.4, 138.6, 141.7, 149.9, 164.1. MS *m*/*z*: 247 (M^+). Anal. calcd. for $C_{11}H_9N_3O_4$: C 53.44, H 3.67, N 17.00; found: C 53.59, H 3.79, N 16.89.

1-(4-Nitrophenyl)-1*H*-pyrimidine-2,4-dione (1f)

Column chromatography on silica gel and eluting with EtOAc–*n*-hexane (1:1) gave a yellow solid, mp 186–189 °C. IR (KBr, cm^{-1}): 3431, 3062, 1691, 1661, 1598, 1288. ^1H NMR (DMSO-d_6, ppm) δ: 5.77 (d, 1H, J = 7.9 Hz, H_5 of uracil), 7.72–7.85 (complex, 3H, H_2 and H_6 of aromatic ring as well as H_6 of uracil), 8.21 (d, 2H, H_3 J = 7.8 Hz, and H_6 of aromatic ring), 11.56 (s, 1H, NH). ^{13}C NMR (DMSO-d_6) δ: 102.5, 124.2, 127.9, 144.0, 144.4, 145.6, 150.8, 163.7. MS *m*/*z*: 233 (M^+). Anal. calcd. for $C_{10}H_7N_3O_4$: C 51.51, H 3.03, N 18.02; found: C 51.38, H 2.89, N 18.17.

1-(4-Chloro-2-nitrophenyl)-1*H*-pyrimidine-2,4-dione (1g)

Column chromatography on silica gel and eluting with EtOAc–*n*-hexane (2:1) gave a pale yellow solid, mp 245–247 °C. IR (KBr, cm^{-1}): 3432, 3071, 1692, 1648, 1605, 1303. ^1H NMR (DMSO-d_6, ppm) δ: 5.80 (d, 1H, J = 7.9 Hz, H_5 of uracil), 7.74–7.82 (complex, 2H, H_5 and H_6 of aromatic ring), 7.99 (d, 1H, J = 7.9 Hz, H_6 of uracil), 8.28 (s, 1H, H_3 of aromatic ring), 11.68 (s, 1H, NH). ^{13}C NMR (DMSO-d_6) δ: 102.5, 125.1, 130.3, 131.6, 134.1, 134.8,

© 2006 NRC Canada

144.3, 145.6, 149.9, 163.4. MS *m/z*: 267 (M^+). Anal. calcd. for $C_{10}H_6ClN_3O_4$: C 44.88, H 2.26, N 13.25; found: C 44.71, H 2.08, N 13.14.

1-(3-Nitropyridin-2-yl)-1*H*-pyrimidine-2,4-dione (1h)

Column chromatography on silica gel and eluting with EtOAc–*n*-hexane (2:1) gave a pale yellow solid, mp 223–225 °C. IR (KBr, cm^{-1}): 3438, 3049, 1687, 1655, 1592, 1296. ^1H NMR (DMSO-*d*6, ppm) δ: 5.88 (d, 1H, J = 8.0 Hz, H_5 of uracil), 7.81 (dd, 1H, J = 4.8, 8.0 Hz, H_5 of pyridine), 8.06 (d, 1H, J = 8.0 Hz, H_6 of uracil), 8.63 (d, 1H, J = 8.0 Hz, H_4 of pyridine), 8.86 (d, 1H, J = 4.8 Hz, H_6 of pyridine), 11.78 (s, 1H, NH). ^{13}C NMR (DMSO-d_6) δ: 103.1, 125.3, 134.8, 141.3, 141.9, 142.7, 149.6, 153.0, 163.1. MS *m/z*: 234 (M^+). Anal. calcd. for $C_9H_6N_4O_4$: C 46.16, H 2.58, N 23.93; found: C 46.05, H 2.40, N 24.05.

9-(2,4-Dinitrophenyl)-9*H*-purin-6-ylamine (2a)

Column chromatography on silica gel and eluting with EtOAc–*n*-hexane (3:1) gave a yellowish brown solid, mp 286–288 °C. IR (KBr, cm^{-1}): 3311, 3092, 1689, 1607, 1296. ^1H NMR (DMSO-d_6, ppm) δ: 7.55 (s, 2H, NH_2, exchangeable with D_2O), 8.08 (s, 1H, H_2 of adenine), 8.19 (d, 1H, J = 8.7 Hz, H_6 of aromatic ring), 8.57 (s, 1H, H_8 of adenine), 8.74 (d, 1H, J = 8.7 Hz, H_5 of aromatic ring), 8.93 (s, 1H, H_3 of aromatic ring). ^{13}C NMR (DMSO-d_6) δ: 120.1, 127.9, 129.3, 132.0, 137.5, 141.0, 143.2, 145.1, 151.8, 154.9, 156.4. MS *m/z*: 301 (M^+). Anal. calcd. for $C_{11}H_7N_7O_4$: C 43.86, H 2.34, N 32.55; found: C 43.76, H 2.52, N 32.42.

9-(2-Nitrophenyl)-9*H*-purin-6-ylamine (2b)

Column chromatography on silica gel and eluting with EtOAc–*n*-hexane (3:1) gave a yellow solid, mp 268–270 °C. IR (KBr, cm^{-1}): 3318, 3141, 1658, 1585, 1293. ^1H NMR (DMSO-d_6, ppm) δ: 7.52 (s, 2H, NH_2, exchangeable with D_2O), 7.75–7.86 (complex, 2H, H_4 and H_6 of aromatic ring), 7.92 (dd, 1H, J = 4.5, 7.8 Hz, H_5 of aromatic ring), 8.09 (s, 1H, H_2 of adenine), 8.23 (d, 1H, J = 8.3 Hz, H_3 of aromatic ring), 8.48 (s, 1H, H_8 of adenine). ^{13}C NMR (DMSO-d_6) δ: 118.4, 125.7, 127.4, 129.6, 130.2, 134.8, 139.7, 144.4, 149.8, 153.2, 156.2. MS *m/z*: 256 (M^+). Anal. calcd. for $C_{11}H_8N_6O_2$: C 51.56, H 3.15, N 32.80; found: C 51.43, H 3.01, N 32.91.

9-(3-Nitropyridin-2-yl)-9*H*-purin-6-one (2c)

Column chromatography on silica gel and eluting with EtOAc gave a yellow solid, mp 253–255 °C. IR (KBr, cm^{-1}): 3173, 3077, 1686, 1289. ^1H NMR (DMSO-d_6, ppm) δ: 7.88 (dd, 1H, J = 4.8, 8.1 Hz, H_5 of pyridine), 8.06 (s, 1H, H_2 of hypoxanthin), 8.59 (s, 1H, H_8 of hypoxanthin), 8.71 (d, 1H, J = 8.2 Hz, H_4 of pyridine), 8.95 (d, 1H, J = 4.8 Hz, H_6 of pyridine), 12.76 (br, 1H, NH, exchangeable with D_2O). ^{13}C NMR (DMSO-d_6) δ: 124.3, 126.1, 134.7, 138.6, 145.7, 148.1, 153.1, 153.5, 153.8, 156.4. MS *m/z*: 258 (M^+). Anal. calcd. for $C_{10}H_6N_6O_3$: C 46.52, H 2.34, N 32.55; found: C 46.64, H 2.23, N 32.42.

6-Chloro-9-(2,4-dinitrophenyl)-9*H*-purine (2d)

Column chromatography on silica gel and eluting with EtOAc–*n*-hexane (1:3) gave a pale red solid, mp 167–169 °C. IR (KBr, cm^{-1}): 3094, 1607, 1291. ^1H NMR (DMSO-d_6, ppm) δ: 8.21 (d, 1H, J = 8.7 Hz, H_6 of aromatic ring), 8.62 (s, 1H, H_8 of 6-chloropurine), 8.73 (d, 1H, J = 8.7 Hz, H_5 of aromatic ring), 8.92 (s, 1H, H_3 of aromatic ring), 9.01 (s, 1H, H_2 of 6-chloropurine). ^{13}C NMR (DMSO-d_6) δ: 121.7, 129.4, 131.1, 141.1, 142.8, 143.6, 145.9, 147.5, 150.0, 151.7, 152.5. MS *m/z*: 320 (M^+). Anal. calcd. for $C_{11}H_5ClN_6O_4$: C 41.20, H 1.57, N 26.21; found: C 41.33, H 1.39, N 26.05.

Acknowledgements

We thank the Shiraz University and Shiraz University of Technology research councils for their financial support of this work. We are also grateful to Professor H. Sharghi for helpful discussions and to Mr. H. Sajedian Fard for running the NMR spectra.

References

1. (*a*) M. Negwer and H.-G. Scharnow. Organic-chemical drugs and their synonyms. 8th ed. Wiley-VCH, Weinheim, Germany. 2001; (*b*) G. Thomas. Medicinal chemisty. John Wiley and Sons Ltd., New York. 2000; (*c*) A.R. Gennaro. Remington: the science and practice of pharmacy. 19th ed. Vol. 2. Mack Publishing Company, Easton, Penn. 1995; (*d*) B.G. Katzung. Basic clinical pharmacology. 8th ed. McGraw-Hill, New York. 2001; (*e*) A. Kleeman, J. Engel, B. Kutscher, and D. Reichert. Pharmaceutical substances. 3rd ed. Thieme, Stuttgart and New York. 1999; (*f*) E. De Clercq. Advance in antiviral drug design. Vol. 1. *Edited by* N.G. Johnsson. Jai Press Inc., Greenwich, Conn. 1993; (*g*) C. Heidelberger. Cancer medicine. *Edited by* J.F. Holland and E. Frei. Lea and Febiger, Philadelphia, Penn. 1973.
2. (*a*) G. Qu, S. Han, Z. Zhang, M. Geng, and F. Xue. Can. J. Chem. **84**, 819 (2006); (*b*) H. Gao and A.K. Mitra. Synthesis, **329** (2000); (*c*) S. Guillarme, S. Legoupy, N. Bourgougnon, A.-M. Aubertin, and F. Huet. Tetrahedron, **59**, 9635 (2003); (*d*) S. Guillarme, S. Legoupy, A.-M. Aubertin, C. Olicard, N. Bourgougnon, and F. François Huet, Tetrahedron, **59**, 2177 (2003); (*e*) A.-I. Hernandez, J. Balzarini, A. Karlsson, M.-J. Camarasa, and M.-J. Perez-Perez. J. Med. Chem. **45**, 4254 (2002); (*f*) I.M. Buck, A. Eleuteri, and C.B. Reese. Tetrahedron, **50**, 9195 (1994).
3. (*a*) C.K. Chu and D.C. Baker (*Editors*). Nucleosides and nucleotides as antitumor and antiviral agents. Plenum Press, New York. 1993; (*b*) L. Naesens, J. Balzarini, and E. De Clercq. Rev. Med. Virol. **4**, 147 (1994); (*c*) M.R. Harnden, A. Parkin, M.J. Parratt, and R.M. Perkins. J. Med. Chem. **36**, 1343 (1993); (*d*) E. De Clercq, A. Holy, I. Rosenberg, T. Sakuma, J. Balzarini, and P.C. Maudgal. Nature, **323**, 464 (1986).
4. (*a*) G. Gosselin, L. Griffe, J.-C. Meillon, and R. Storer. Tetrahedron, **62**, 906 (2006); (*b*) A.D. Borthwick and K. Biggadike. Tetrahedron, **48**, 571 (1992); (*c*) Y.H. Jin, P. Liu, J. Wang, U. Das, R. Baker, J. Huggins, and C.K. Chu. J. Org. Chem. **70**, 394 (2005); (*d*) Y.-Y. Yang, W.-D. Meng, and F.-L. Qing. Org. Lett. 4257 (2004); (*e*) M.J. Comin, J.B. Rodriguez, P. Russ, and V.E. Marquez. Tetrahedron, **59**, 295 (2003).
5. (*a*) M. Yokoyama and A. Momotake. Synthesis, 1541 (1999); (*b*) M. Koszytkowska-Stawinska and W. Sas. Tetrahedron Lett. **45**, 5437 (2004).
6. (*a*) M. Yokoyama. Synthesis, 1637 (2000); (*b*) N.A. Van Draanen, G.A. Freeman, S.A. Short, R. Harvey, R. Jansen, and G.W. Szczech. J. Med. Chem. **39**, 538 (1996).

© 2006 NRC Canada

7. (*a*) R.D. Thompson, S. Secunda, J.W. Daly, and R.A. Olsson. J. Med. Chem. **34**, 2877 (1991); (*b*) H. Harada, O. Asano, T. Kawara, T. Inoue, T. Horizoe, N. Yasuda, K. Nagata, M. Murakami, J. Nagaoka, S. Kobayashi, I. Tanaka, and S. Abe. Bioorg. Med. Chem. **9**, 2709 (2001).
8. R.J. Chorvat, R. Bakthavatchalam, J.P. Beck, P.J. Gilligan, R.G. Wilde, A.J. Cocuzza, F.W. Hobbs, R.S. Cheeseman, M. Curry, J.P. Rescinito, P. Krenitsky, D. Chidester, J.A. Yarem, J.D. Klaczkiewicz, C.H. Fernandez, R. Zaczek, L.W. Fitzgerald, S.-M. Huang, H.L. Shen, Y.N. Wong, B.M. Chien, C.Y. Quon, and A. Arvanitis. J. Med. Chem. **42**, 833 (1999).
9. (*a*) R.K. Robine and G.R. Revankar. J. Heterocycl. Chem. **22**, 601 (1985); (*b*) C. Silipo and C. Hansch. J. Med. Chem. **19**, 62 (1976); (*c*) I. Moriguchi and Y. Kanada. Chem. Pharm. Bull. **25**, 926 (1977).
10. M. Brakta, D. Murthy, L. Ellis, and S. Phadtare. Bioorg. Med. Chem. Lett. **12**, 1489 (2002).
11. (*a*) B.R. Baker and W.F. Wood. J. Med. Chem. **12**, 216 (1969); (*b*) B.R. Baker and H.U. Siebeneick. J. Med. Chem. **14**, 802 (1971).
12. (*a*) H.C. Koppel and R.K. Robins. J. Am. Chem. Soc. **80**, 2751 (1958); (*b*) H.C. Koppel, D.E. O'Brien, and R.K. Robins. J. Am. Chem. Soc. **81**, 3046 (1959).
13. (*a*) D. Sen, A. Dasgupta, and P. Sengupta. Indian J. Chem. Sect. B: Org. Chem. **24**, 952 (1985); (*b*) W.M. Basyouni, H.M. Hosni, and S.M. Helmy. Egypt. J. Chem. **42**, 587 (1999).
14. K.A.M. El-Bayouki, B. Haggag, and W.M. Basyouni. Egypt. J. Chem. **33**, 243 (1990).
15. (*a*) B.R. Baker, W.F. Wood, and J.A. Kozma. J. Med. Chem. **11**, 661 (1968); (*b*) I. Chu and B.M. Lynch. J. Med. Chem. **18**, 161 (1975); (*c*) C.C. Cheng and R.K. Robins. J. Org. Chem. **21**, 1240 (1956); (*d*) S.M. Greenberg, L.O. Ross, and R.K. Robins. J. Org. Chem. **24**, 1314 (1959); (*e*) C.C. Cheng and R.K. Robins. J. Org. Chem. **23**, 852 (1958); (*f*) J.P. Beck, A.G. Arvanitis, M.A. Curry, J.T. Rescinito, L.W. Fitzgerald, P.J. Gilligan, R. Zaczek, and G.L. Trainor. Bioorg. Med. Chem. Lett. **9**, 967 (1999); (*g*) T. Kumagai, T. Okubo, H. Kataoka-Okubo, S. Chaki, S. Okuyama, and A. Nakazato. Bioorg. Med. Chem. **9**, 1357 (2001).
16. (*a*) S. Ding, N.S. Gray, Q. Ding, and P.G. Schultz. Tetrahedron Lett. **42**, 8751 (2001); (*b*) A.K. Bakkestuen and L.-L. Gundersen. Tetrahedron Lett. **44**, 3359 (2003); (*c*) M. Tokumi, F. Keiichi, and F. Mitsutoshi. J. Chem. Soc. Perkin Trans. 1, 733 (1995); (*d*) Y. Yue, Z.-G. Zheng, B. Wu, C.-Q. Xia, and X.-Q. Yu. Eur. J. Org. Chem. 5154 (2005); (*e*) T. Zhou, T.-C. Li, and Z.-C. Chen. Helv. Chim. Acta, **88**, 290 (2005).
17. (*a*) A. Loupy. Microwave in organic synthesis. Wiley-VCH, Weinheim, Germany. 2004; (*b*) R.S. Varma. Advances in green chemistry: chemical synthesis using microwave irradiation. Astra Zeneca Research Foundation, Kavitha Printers, Bangalore, India. 2002; (*c*) H.M. Kingston and S.J. Haswell. Microwave-enhanced chemistry. Fundamentals, sample preparation, and applications. American Chemical Society, Washington, D.C. 1997; (*d*) J. Yin, X. Li, X. Wu, B. Chen, Z. Liu, and Q. Song. Can. J. Chem. **83**, 2140 (2005); (*e*) B.P. Joshi, A. Sharma, and A.K. Sinha. Can. J. Chem. **83**, 1826 (2005).
18. (*a*) A. Khalafi-Nezhad, A. Zarea, M.N. Soltani Rad, B. Mokhtari, and A. Parhami. Synthesis, 419 (2005); (*b*) A. Khalafi-Nezhad, M.N. Soltani Rad, and A. Khoshnood. Synthesis, 583 (2004); (*c*) A. Khalafi-Nezhad, M.N. Soltani Rad, G.H. Hakimelahi, and B. Mokhtari. Tetrahedron, **58**, 10341 (2002); (*d*) A. Khalafi-Nezhad and B. Mokhtari. Tetrahedron Lett. **45**, 6737 (2004).
19. (*a*) D. Singh, M.J. Wani, and A. Kumar. J. Org. Chem. **64**, 4665 (1999); (*b*) L.W. Dudycz and G.E. Wright. Nucleosides Nucleotides, 33 (1984); (*c*) G.E. Wright and L.W. Dudycz. J. Med. Chem. **27**, 175 (1984); (*d*) K.C. Schneider and S.A. Benner. Tetrahedron Lett. **31**, 335 (1990); (*e*) M.-T. Chenon, R.J. Pugmire, D.M. Grant, R.P. Panzica, and L.B. Townsend. J. Am. Chem. Soc. **97**, 4628 (1975); (*f*) M.T. Crimmins, B.W. King, W.J. Zuercher, and A.L. Choy. J. Org. Chem. **65**, 8499 (2000); (*g*) J. Kjellberg and N.G. Johansson. Tetrahedron, **42**, 6541 (1986); (*h*) P. Gamer and S. Ramakanth. J. Org. Chem. **53**, 1294 (1988).
20. A.I. Vogel. Textbook of practical organic chemistry. 4th ed. Longman Inc., London and New York. 1978.

© 2006 NRC Canada

Protein mass measurement combined with mass spectrometric sequencing of protein digests for detection and characterization of protein modifications[1]

Chengjie Ji, Zhengping Wang, and Liang Li

Abstract: A method for the characterization of modifications of low molecular weight proteins (<20 kDa) extracted from a microorganism based on the use of multiple separation tools and mass spectrometric techniques is described. In this method, intact proteins from cell extracts are first separated and fractionated by liquid chromatography (LC). Individual fractions are then analyzed by matrix-assisted laser desorption ionization (MALDI) mass spectrometry (MS) to provide intact protein mass information. The fractions are further characterized by using trypsin digestion and LC electrospray ionization (ESI) MS/MS analysis of the resultant peptides to identify the proteins. Gel electrophoresis of a fraction is also carried out to estimate the molecular masses of the proteins. The gel bands are identified by in-gel digestion and peptide mass mapping and sequencing using MALDI-MS and MALDI-MS/MS. The combined information generated from these experiments is interpreted for detecting and characterizing modified proteins. This method has been developed and applied to the analysis of posttranslational modifications (PTMs) of low-mass proteins (5–20 kDa) extracted from a relatively well-characterized microorganism, *Escherichia coli*. Using this method, not only previously reported PTMs involving acetylation, methylation, oxidation, and the removal of signal peptides, but also two novel PTMs, namely loss of N-terminal Met-Thr-Met (MTM) and hydroxylation of arginine, were identified. It is envisaged that this method should be applicable to other relatively simple microorganisms for the discovery of new PTMs.

Key words: top-down proteomics, protein modification, HPLC, gel electrophoresis, tandem mass spectrometry.

Résumé : On a mis au point une méthode de caractérisation des modifications des protéines de faible poids moléculaire (< 20 kDa) extraites d'un microorganisme; elle est basée sur l'utilisation de multiples techniques de séparation et de spectrométrie de masse. Dans cette méthode, les cellules intactes telles qu'extraites des cellules sont d'abord soumises à une séparation, puis elles sont soumises à un fractionnement par chromatographie liquide (CL). Afin d'obtenir des informations relatives à la masse des protéines intactes, les fractions individuelles sont alors analysées par spectrométrie de masse avec ionisation par désorption laser assistée par la matrice. Les fractions sont ensuite caractérisées d'une façon plus poussée en faisant appel à une digestion à l'aide de trypsine et à de la SM/SM avec ionisation par électronébulisation des peptides qui en résultent pour identifier les protéines. On a aussi effectué une électrophorèse sur gel d'une fraction pour évaluer les masses moléculaires des protéines. On a identifié les bandes du gel en procédant à une digestion dans le gel et à une cartographie de masse des peptides et une détermination de la séquence à l'aide de SM-MALDI et de SM/SM. On a interprété les informations combinées générées à l'aide de ces expériences pour détecter et caractériser les protéines modifiées. On a développé cette méthode et on l'a appliquée à l'analyse de modifications post-translationnellle (MPT) de protéines de faibles masses moléculaires (5–20 kDa) extraites d'un microorganisme relativement bien caractérisé, *Escherichia coli*. Utilisant cette méthode, on a pu identifier des MPT qui avaient été rapportée antérieurement, telles l'acétylation, la méthylation, l'oxydation et l'enlèvement des peptides signaux, ainsi que deux nouvelles MPT, à savoir la perte du groupe Met-Thr-Met (MTM) N-terminal et l'hydroxylation de l'arginine. On croit que cette méthode devrait pouvoir être appliquée à d'autres microorganismes relativement simples pour découvrir de nouvelles MPT.

Mots clés : protéomiques descendantes, modification de protéine, chromatographie liquide à haute performance (CLHP), électrophorèse sur gel, spectrométrie de masse en tandem.

[Traduit par la Rédaction]

Received 13 December 2005. Accepted 28 June 2006. Published on the NRC Research Press Web site at http://canjchem.nrc.ca on 8 September 2006.

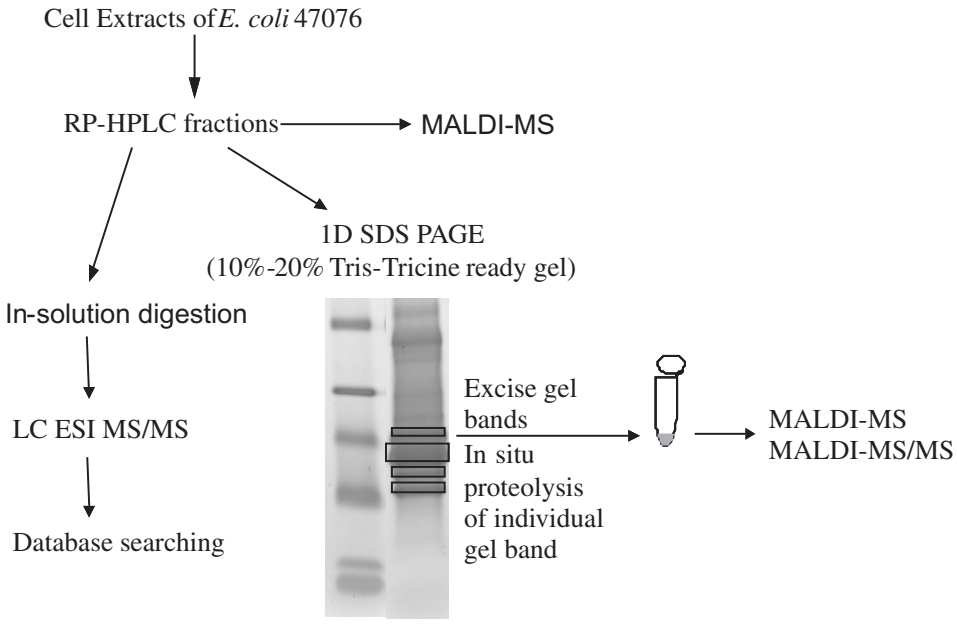
This paper is dedicated to Professor Paul Kebarle in recognition of his outstanding and pioneering research in mass spectrometry and ion chemistry.

C. Ji, Z. Wang, and L. Li.[2] Department of Chemistry, University of Alberta, Edmonton, AB T6G 2G2, Canada.

[1]This article is part of a Special Issue dedicated to Professor P. Kebarle.
[2]Corresponding author (e-mail: Liang.Li@ualberta.ca).

 doi:10.1139/V06-114 © 2006 NRC Canada

Fig. 1. Schematic representation of the strategy used for the detection and characterization of protein modifications. Proteins identified by tandem MS/MS in each HPLC fraction were assigned to those apparent masses observed in the MALDI-MS spectrum of the same fraction.



Introduction

Posttranslational modifications (PTMs) of proteins are chemical processing events by proteolytic cleavage or addition of a modifying group to one or more amino acid residues that alter a protein's properties after its translation. PTMs include phosphorylation, glycosylation, acetylation, methylation, sulfation, disulfide bond formation, deamidation, ubiquitination, and nitration of tyrosine (1). Most proteins undergo co- and (or) post-translational modifications. Knowledge of these modifications is extremely important because they may alter the proteins' physical and chemical properties, such as folding, conformational distribution, stability and activity, and consequently change the function of the proteins and their interaction with other proteins. Moreover, the modification itself can act as an added functional group. Examples of the biological effects of protein modifications include phosphorylation for signal transduction, ubiquitination for proteolysis, and attachment of fatty acids for membrane anchoring and association. Consequently, the analysis of proteins and their posttranslational modifications is particularly important for the study of many different types of diseases including cancer, neurodegenerative diseases, and diabetes.

Despite the major role of PTMs in biological functions, large-scale study still remains a great challenge because of a lack of suitable analytical methods (1). Mass spectrometry (MS) plays an increasingly important role in characterizing protein PTMs. Recent applications of MS to the identification of PTMs have ranged in scale from the study of single purified proteins (2–4) to the search for one type of modification on all the proteins or proteome in a sample (5–8), and to scanning for all modifications on a proteome-wide scale (9). Considering the complexities involved in identifying all the modifications on a single protein, proteome-wide scanning is, at present, not comprehensive. Nevertheless, large amounts of biologically useful information can be generated. To determine the sites of modification, maximum protein sequence coverage is desirable. For this purpose, in the bottom-up proteomic approach, peptide mass mapping using two or more different enzymes, such as trypsin, Asp-N, or Glu-C, can be employed. Protein modifications are then identified from the measured masses and fragmentation spectra using manual or computer-assisted interpretation (10). In the top-down proteomic approach, intact protein mass is accurately measured and compared to that calculated from the database sequence of the identified protein. Some amino acid sequence information of the intact protein can also be deduced. For example, multiple-charged intact protein ions generated by electrospray ionization (ESI) can be dissociated and the resulting product ion spectra are interpreted for the characterization of protein modifications (11–14).

While using the bottom-up or top-down approach alone can generate useful information on protein modifications, recent studies have indicated that these two approaches are complementary to each other and the combination of the two techniques can provide more detailed characterization of modified proteins (15–19). In this study, we present a method for the characterization of PTMs of low-mass proteins (5–20 kDa) extracted from a relatively simple microorganism by combining separation tools with intact protein mass measurement and protein digest analysis based on ESI and matrix-assisted laser desorption ionization (MALDI) MS. This method is applied for the analysis of a number of low-mass proteins from an *Escherichia coli* cell extract.

Results and discussion

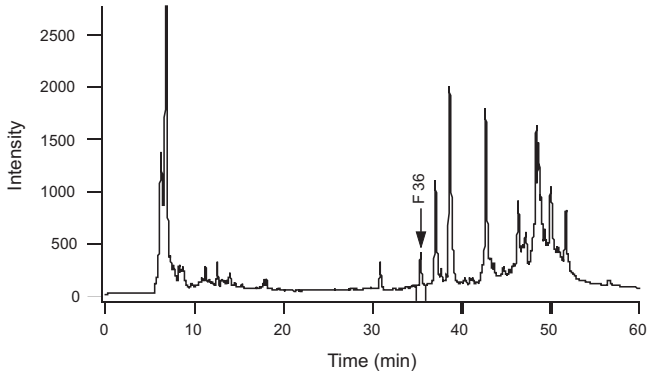
Figure 1 shows the work flow developed for the characterization of PTMs of low-mass proteins observed in MALDI-MS spectra. The proteins in the cell extracts of *E. coli* were

© 2006 NRC Canada

separated by HPLC. For this relatively simple microorganism, one-dimensional HPLC separation was used, while for more complex organisms with large sizes of proteome, multidimensional HPLC is likely needed to simplify the protein mixture. The apparent molecular masses of low-mass proteins in each HPLC fraction were detected using MALDI-MS. Then, the proteins in each selected HPLC fraction were identified using two different tandem MS experiments. First, proteins in the selected fraction were digested in solution by trypsin. The resulting peptide mixture was separated by capillary column HPLC using a gradient of acetic acid – acetonitrile. Individual peptide ions were automatically selected for collision-induced dissociation (CID) MS/MS followed by database searching using the SEQUEST (20) software. Second, proteins in each selected HPLC fraction were separated by one-dimensional SDS polyacrylamide gel electrophoresis (PAGE). Following electrophoretic separation, individual low-mass gel bands were digested in situ by trypsin. Peptides were then extracted from the gel and each peptide mixture was analyzed by MALDI-MS and MALDI-MS/MS, followed by database searching using the MASCOT (21) software. Finally, the identified proteins in each selected fraction were assigned to the apparent masses observed in the MALDI mass spectrum and any possible PTMs were assigned by comparing the theoretical mass of the identified protein in the public database with the observed mass in the MALDI-MS analysis.

Figure 2 shows the chromatogram of cell extracts of *E. coli* 47076. Since the major components eluted between 35 and 52 min, efforts were concentrated on those fractions. The apparent molecular masses observed in MALDI-MS spectra of HPLC fractions collected between 35 and 52 min, which had signal-to-noise ratios over 5, are listed in Table 1. Some proteins appeared in two consecutive fractions because we collected the fractions based on time intervals instead of the UV absorbance peak. For example, the proteins with *m/z* 8327 and 9080 were observed in fractions 36 and 37 and the molecular weights for those proteins are the same in the consecutive fractions. For proteins that appeared in several consecutive fractions, Table 1 only lists their initial fraction. The possible matched proteins in the SWISS-PROT and TrEMBL databases, searched using the sequence retrieval system (SRS), are listed in the third column in Table 1. It should be noted that the technique described here is not suitable for detecting deamidation, which only generates 1 Da mass difference, not readily differentiated by low-resolution intact mass measurement. Most of the apparent molecular masses observed in MALDI-MS spectra have more than one match in the public proteome database. Accession numbers and names of proteins identified by combining the LC–ESI-MS/MS and MALDI-MS/MS experiments, which correspond to those observed in MALDI mass spectra, are listed in the fifth and sixth columns in Table 1. Each of these proteins was identified by at least two peptides with significant matches. In the ESI-MS/MS experiments, peptides are considered to be identified only when they pass the following criteria: for the 1+ charge state, $X_{corr} \geq 2.0$ for fully tryptic peptides and $X_{corr} \geq 3.0$ for partially tryptic peptides; for the 2+ charge state, $X_{corr} \geq 2.4$ for fully tryptic peptides and $X_{corr} \geq 3.5$ for partially tryptic peptides; for the 3+ charge state, $X_{corr} \geq 3.7$ for fully tryptic peptides and $X_{corr} \geq 4.5$ for partially tryptic peptides. All criteria have a ΔC_n value of ≥ 0.1. In the MALDI-MS/MS experiments, peptides are considered to be identified only when the first assigned peptide with score is above the identity threshold score. Table 1 shows that nine of the identified proteins have masses that are different from those in the public proteome database. This is because some of the proteins in the public proteome database are posttranslationally modified in vivo or processed in vitro during the sample preparation process.

Fig. 2. Chromatogram of cell extracts of *E. coli*. Note that F36 indicates the fraction collected between 36 min and 37 min.



Protein truncation is one of the PTMs. Protein fragments have been identified by Edman sequencing of gel-separated *E. coli* proteins (22, 23). The N-terminal sequence tags of these fragments matched the predicted internal region of the genes in the *E. coli* preparation, in vivo events, or translation products initiated at the internal sites of the genes. None of these putative cleavage sites matches with any known *E. coli* protease recognition sequences, although little is known of the target specificity of *E. coli* proteases (24–26). In this work, efforts toward the identification of protein fragments by MS/MS will be discussed. Using a program called Paws (27), mass searching was attempted to correlate the identified proteins in Table 1 with the unidentified low-mass species in the MALDI mass spectrum. By entering a peptide mass, Paws will search over an entire protein sequence to determine if any stretch of the sequence has a mass that matches with the input mass. If the observed mass in MALDI-MS matched with a part of the sequence covered by the identified peptide sequences, the low-mass species observed in MALDI was considered as a fragment of the specific protein. Mass information from one-dimensional gel electrophoresis was used to achieve a conclusive identification.

As an example, in fraction 36, the observed molecular mass of 10 386 Da ($M + H^+$) is a fragment of outer membrane protein A (OMPA, accession number P02934) instead of those matched by SRS. Figure 3(*A*) shows the MALDI spectrum of the tryptic digests of the indicated gel band as shown in Fig. 4. Peptides matched with OMPA are labeled with an asterisk in Fig. 3(*B*). OMPA was identified based on the fragmentation patterns of four peptides. Figure 3(*C*) shows one representative MS/MS spectrum. This protein has the following amino acid sequence:
MKKTAIAIAVALAGFATVAQAAPKDNTWYTGAKLGWS
QYHDTGFINNNGPTHENQLGAGAFGGYQVNPYVGFE
MGYDWLGRMPYKGSVENGAYKAQGVQLTAKLGYPIT

© 2006 NRC Canada

Table 1. Protein masses of protonated species observed in the MALDI-MS spectra of HPLC fractions of *E. coli* cell extracts and tentative protein assignments based on the molecular mass and matched proteins and possible PTMs identified by combining LC–MS/MS and MALDI-MS/MS.

		Possible match		Identified protein		
Fraction No.	$M + H^+$ in MALDI-MS	Accession No.	Mass (Da)	Accession No.	Name	PTM
35	8370	P05702	8 372	P02379	30S Ribosomal protein S21	
		P33649	8 371			
		P02379, Q8ZI69	8 369			
		P52038	8 372			
		Q8X4G7	8 366			
36	8876	P02428	8 875	P02428	50S Ribosomal protein L28	
		P76521	8 874			
		Q8X9N0	8 876			
		Q8X8R3	8 876			
		Q8X720	8 873			
36	8327	P05794	8 328	P32691	Protein yjbJ	
		P02937	8 323			
		P32691	8 325			
		Q9L6J8	8 325			
		Q8X675	8 328			
		Q8X498	8 327			
36	9080	Q9X5P1	9 083	P26605	Protein hdeB	Loss of signal peptide and oxidation
36	10386	P05380	10 387	P02934	OMPA	fragment
		P97104	10 388			
		Q8XBH5	10 391			
36	11453	P02370	11 449	P02370	30S Ribosomal protein S14	
		Q9RPJ4	11 455			
		Q46693	11 454			
		Q8VV17	11 453			
		Q8X9V3	11 454			
37	7273	P15277, P37410	7 272	P36996	Cold shocklike protein cspC	
		P36996, O68636	7 271			
		P02429	7 273			
		P58096	7 273			
		Q46774	7 275			
		P76136	7 272			
		Q9EYC3	7 268			
37	9064	Q8RTD2	9 064	P26605	Protein hdeB	Loss of signal peptide
		Q8XBG7	9 059			
		Q8X4J7	9 058			
		P76358	9 065			
38	9756	P41039	9 756	P26604	Protein hdeA	Loss of signal peptide and oxidation
		Q47641	9 753			
39	9584	P13479	9 582			
		Q9R602	9 580			
		P77387, P77204	9 580			
39	9740	Q47037	9 737	P26604	Protein hdeA	Loss of signal peptide
		Q8XAC1	9 742			
		Q8X4M7	9 743			
		Q9R605	9 734			
39	10300	P75877, Q9R7Q1	10 300	P02375	30S Ribosomal protein S19	
		P02375	10 299			
		P32700	10 303			
		Q8RTC2	10 299			
		Q8XB54	10 294			
		Q8X9M2	10 297			

© 2006 NRC Canada

Table 1 (*continued*).

Fraction No.	$M + H^+$ in MALDI-MS	Possible match		Identified protein		PTM
		Accession No.	Mass (Da)	Accession No.	Name	
39	10695	P77618, O54336	10 689	P02426	50S Ribosomal protein L25	
		P02426	10 693			
		Q8VQR3	10 692			
		Q8VNS4	10 693			
40	7334	P36997, P80434, P77103	7 332	P36997	Cold shocklike protein cspE	
		P77098	7 332			
		Q03535	7 333			
		Q8X3H6	7 334			
		Q8X378	7 329			
40	8898	Q8XDS8	8 899	P02374	30S Ribosomal protein S18	Acetylation
41	6242	P02436	6 240			
		Q9AGQ2	6 242			
		P77224	6 241			
		Q8XCC4	6 241			
		Q8X479	6 238			
41	6412	P02430	6 411	P02430	50S Ribosomal protein L30	
43	5458	Q47654	5 457			
		Q51953	5 457			
43	6600	Q9RM53	6 600			
		P37770	6 599			
43	11978	Q8X7A6	11 973	P52083	Protein ygiW	Loss of signal peptide
		P71284	11 982			
		Q8X6M6	11 976			
		Q8X549	11 980			
		Q8X3N1	11 982			
44	7865	P33230, P77683	7 863			
		P58033	7 861			
44	12775	P04737, P14517	12 768	P02419	50S Ribosomal protein L18	
		P02419	12 770			
		P22539	12 780			
		P76367, O07995, O07992	12 778			
		P31445	12 779			
		O32571	12 777			
		Q8X6T4	12 771			
		Q8X4F0	12 774			
		O88118	12 771			
45	6699	P77370	6 694			
		Q8X2R5	6 701			
		Q8X2C4	6 697			
45	9192	Q52277	9 195	P02372	30S Ribosomal protein S16	
		P02372, P77006	9 190			
		P76575	9 193			
		Q9AJD9	9 190			
		P97155	9 188			
		Q47583	9 191			
		Q46853	9 189			
45	11037	P25521, Q47383	11 035	P25521	Hfq protein	
		P37668	11 033			
		O82887	11 030			
		Q8RTD5	11 038			
		Q8X741	11 039			
46	6509	P22986, P77441	6 507			
		Q9EYC5	6 504			

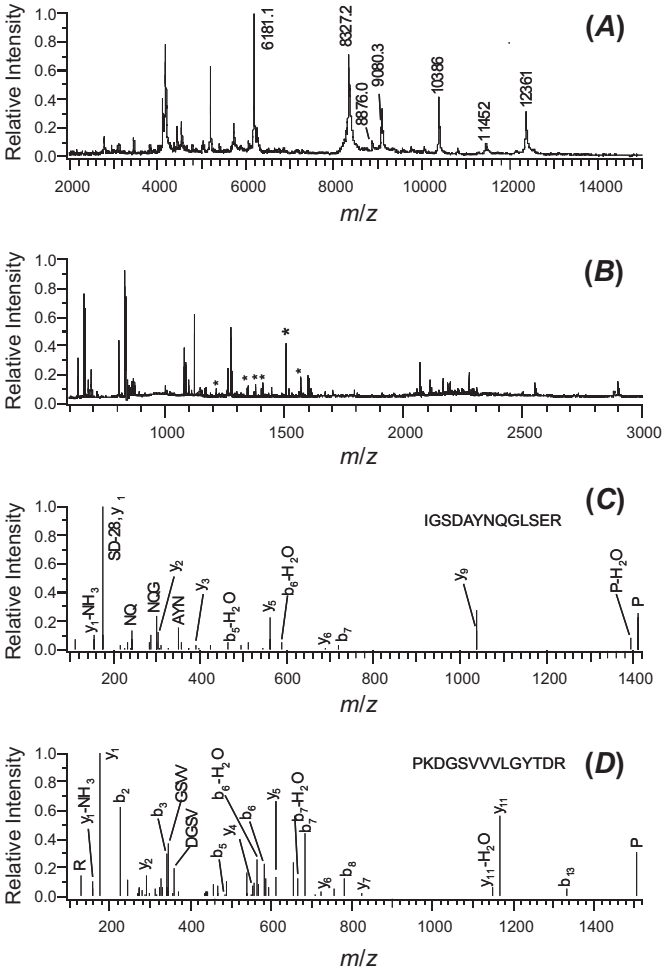
© 2006 NRC Canada

Table 1 (*concluded*).

Fraction No.	$M + H^+$ in MALDI-MS	Possible match		Identified protein		PTM
		Accession No.	Mass (Da)	Accession No.	Name	
		Q8X3Y8	6 507			
		Q9KXD1	6 509			
46	9191	P02372, P77006	9 190	P02372	30S Ribosomal protein S16	
		P76575	9 193			
		Q9AJD9	9 190			
		P97155	9 188			
		Q8VR95	9 185			
		Q47583	9 191			
		Q46853	9 189			
46	12010	P08338	12 009			
		P08372	12 004			
		P17577, P09994	12 015			
		O52669	12 012			
		Q9F573	12 015			
		Q8VR73	12 015			
		Q8X9R5	12 004			
		Q8X894	12 008			
46	12654	P77326	12 658	P11285	Protein yfiA	
		P11285	12 653			
		Q9X730	12 659			
		P71177	12 655			
		P75729	12 658			
47	9536	P02342	9 535	P02342	DNA-binding protein HU-α	
		Q9R601	9 537			
		Q8X3G5	9 533			
48	9385	P46132, P77447	9 386			
		P22847	9 381			
		Q93CH7	9 388			
		Q9Z9I6	9 383			
		Q8X8C1	9 382			
48	10651	P08756	10 651	P08756	Integration host factor beta-subunit	
49	11223	P07008	11 225	P06984	Histone H1A, sperm	Loss of N-terminal methionine
		Q8X3Y6	11 226			
		Q8X5G9	11 218			
		Q8X2D0	11 224			
49	15327	P24233	15 332	P02414	50S Ribosomal protein L16	Methylation and hydroxylation
		P03852	15 322			
		O06959	15 332			
		Q46764	15 325			
		Q8XBH1	15 324			
49	15409	P08936	15 408	P08936	DNA-binding protein H-NS	
		P75684	15 411			
50	9226	P02341	9 225	P02341	DNA-binding protein HU-β	
		P13966, Q52770	9 227			
		Q8X8Q7	9 226			
50	9271	P08365, P76803	9 272	P32164	Hypothetical protein yiiU	Loss of N-terminal MTM
		Q9JMS6	9 271			

© 2006 NRC Canada

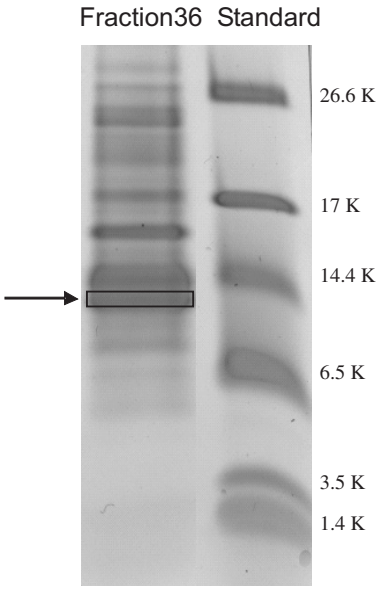
Fig. 3. Fragmentation of OMPA observed in MALDI-MS. (*A*) MALDI-MS spectrum of HPLC fraction 36 of *E. coli* cell extracts. (*B*) Peptide map of tryptic digest of the band indicated in Fig. 2. Peptides matched with that of OMPA are labeled with an asterisk (*). (*C*) LC–MS/MS spectrum of the peptide sequence NNSLSQEVQNAQHQR. (*D*) LC–MS/MS spectrum of the peptide sequence SLEVFEK.



DDLDIYTRLGGMVWRADTKSNVYGKNHDTGVSPVFA
GGVEYAITPEIATRLEYQWTNNIGDAHTIGTRPDNGM
LSLGVSYRFGQGEAAPVVAPAPAPAPEVQTKHFTLKS
DVLFNFNKATLKPEGQAALDQLYSQLSNLD*PKDGSVV*
*VLGYTDR*IGSDAYNQGLSERRAQSVVDYLISKGIPADKI
SARGMGESNPVTGNT*C*DNVKQR**AALID*C*LAPDRR**VE
IEVK**GIKDVVTQPQA.**

The bold characters show the sequence coverage of the MS/MS results. The molecular mass of this protein is 37 292 Da, which was not found in the MALDI spectrum (Fig. 3(*A*)). Simple calculation shows that the underlined protein sequence has the molecular mass of 10 386.7 Da, matching a major component in Fig. 3(*A*). This molecular mass information matches the molecular mass estimate of the gel. There is also a disulfide bond formed between two cysteines inside the underlined sequence. Therefore, the final molecular mass ($M + H^+$) of the underlined sequence is 10 385.7 Da, which is very close to that observed in the MALDI mass spectrum. This was confirmed by the identification of an unexpected tryptic peptide PKDGSVVVLGYTDR (Fig. 3(*D*)). Thus, the apparent molecular mass of 10 386 Da corresponds to the fragment from OMPA. This was done by MASCOT searching without any enzyme type constraint. Seven y ions and seven b ions matched with the in silico fragmentation pattern, showing a strong correlation between the MS/MS spectrum and the identified peptide sequence. The fragmentation of this protein most likely occurred during protein extraction and isolation because of acid-labile cleavage of an amino acid bond between Asp (D) and Pro (P). It is found that in dilute acidic conditions, aspartyl peptide bonds tend to be more rapidly hydrolyzed than other aminoacyl peptide bonds, particularly for aspartyl proline bonds (28). This is due to the neighbouring group effects caused by the proximity of the side-chain carboxyl group of the amino acid residue Asp to the α-carboxyl peptide bond. On the basis of this notion, the fragmentation of this protein most likely occurred during protein extraction and isolation, since dilute TFA aqueous solution was used in both steps.

Fig. 4. Proteome map of HPLC fraction 36 of *E. coli* cell extracts.



The most common PTM of the proteins in *E. coli* involves loss of the N-terminal methionine. For cytoplasmic proteins, the amino-terminal processing model (29, 30) predicts that the truncation of N-terminal Met residue by methionine aminopeptidase depends on the side-chain length of the second amino acid. This modification occurs most often in cases where the amino acid next to this methionine has a short side chain. Sterically large side chains are believed to prevent proteins from docking in the methionine aminopeptidase active site. When the second amino acid is Ala, Cys, Gly, Pro, Ser, Thr, or Val, the initiator Met is excised. Violations of the model were observed by Edman sequencing of the gel-separated *E. coli* proteins (23) and it was believed that protein structures other than the second amino acid residue were involved in the excision specificity. It has been shown (23) that all initial Met residues are removed when the second residue is Ala or Ser, and none of the Met

© 2006 NRC Canada

Fig. 5. Hydroxylation of arginine in 50S ribosomal protein L16 observed in MALDI-MS. (*A*) MALDI-MS spectrum of HPLC fraction 50 of *E. coli* cell extracts. (*B*) LC–MS/MS spectrum of the peptide sequence NNSLSQEVQNAQHQR. (*C*) LC–MS/MS spectrum the peptide sequence SLEVFEK.

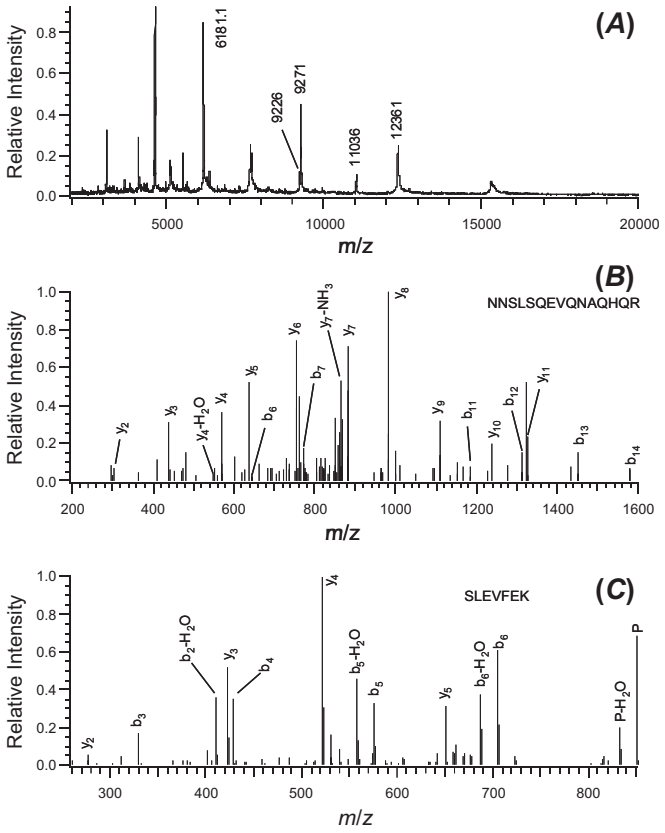
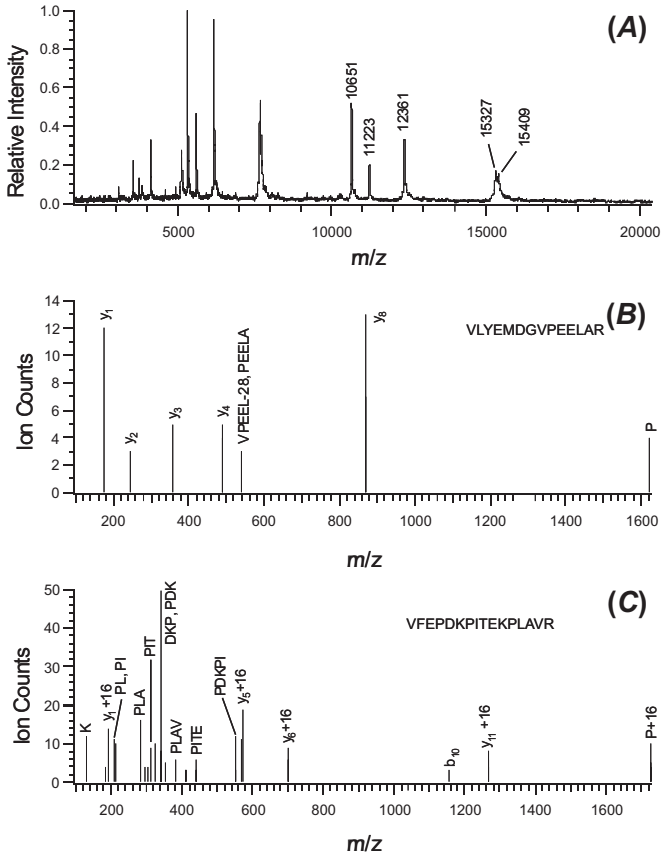


Fig. 6. Loss of MTM in hypothetical protein YIIU_ECOLI observed in MALDI-MS. (*A*) MALDI-MS spectrum of HPLC fraction 49 of *E. coli* cell extracts. (*B*) MALDI-MS/MS spectrum of the peptide sequence VLYEMDGVPEELAR. (*C*) MALDI-MS/MS spectrum of the peptide sequence VFEPDKPITEKPLAVR.



is removed when Val is in the second position. The excision of Met is variable when the second residue is Thr, Gly, or Pro. It is very easy for the integration host factor α-subunit protein precursor (accession number P06984), observed in the MALDI spectrum of fraction 49, to lose the first methionine in its sequence because the amino acid in the second position is alanine, which has a small side chain.

The removal of signal peptides from protein precursors is another common PTM of the proteins in *E. coli*. Proteins located in the periplasm and outer membrane region are expected to have a signal sequence that helps direct their transport across the inner membrane (29, 31). The signal peptide generally has a positively charged amino-terminal region, a central hydrophobic region, and a carboxy-terminal region. *Escherichia coli* signal peptides are 15–30 amino acids long and they are removed from the protein precursors (i.e., the gene expression products) by the signal peptidase (Lep) after transport through the membrane (29). Therefore, the mature protein has a molecular mass 1500–3000 Da lower than predicted from the genome. The proteins with masses of 9740, 9064, and 11 978 Da listed in Table 1 were identified to correspond to HDEA (accession number P26604), HDEB (accession number P26605), and YGIW (accession number P52083) with the removal of their signal peptides. Additionally, the removal of the signal peptides from HDEA, HDEB, and YGIW was confirmed previously by Link et al. (23) via N-terminal Edman degradation following separation of these proteins by 2D gel electrophoresis.

Loss of MTM (methionine, threonine, methionine) from an amino terminus is a novel PTM observed in this study. In fraction 50, none of the proteins identified by LC–ESI-MS/MS matched with the molecular mass of 9271 Da observed in the MALDI mass spectrum (Fig. 5(*A*)). One possible reason was that this molecular mass corresponded to a posttranslationally modified protein. Thus, SEQUEST database searching was done on LC–ESI-MS/MS spectra without an enzyme type constraint. Four y ions and four b ions matched with the in silico fragmentation pattern of the peptide SLEVSEK (Fig. 5(*C*)). This peptide sequence is a partial sequence of hypothetical protein YIIU (accession number P32164). YIIU was identified based on the fragmentation patterns of three peptides. Figure 5(*B*) shows one representative MS/MS spectrum. YIIU_ECOLI has the following sequence: MTM**SLEVFEK**LEAK**VQQAIDTITL-LQMEIEELKEKNNSLSQEVQNAQHQR**EELERENNH LKEQQNGWQER**LQALLGR**MEEV.

The bold sequence represents coverage by the MS/MS results. Using the Paws program, it was found that the underlined protein sequence has an average molecular mass of

© 2006 NRC Canada

9271 Da, matching one major component in the MALDI-MS spectrum of HPLC fraction 50. This means that the apparent mass of 9271 Da observed in MALDI MS is YIIU_ECOLI with the loss of MTM at the N-terminus.

Several other PTMs, including methylation, oxidation, and acetylation, are also detected and listed in Table 1. In fraction 49, none of the proteins identified by LC–ESI-MS/MS and MALDI-MS/MS matched with the molecular mass of 15 327 Da observed in the MALDI mass spectrum (Fig. 6(*A*)). It was reported that 50S ribosomal protein L16, which has a nominal molecular mass of 15 281 Da based on the genome sequence, was seen to have an apparent mass of 15 326 Da, 45 Da higher, in its MALDI mass spectrum (32). 50S Ribosomal protein L16 was identified based on the fragmentation patterns of four peptides. Figure 6(*B*) shows one representative MS/MS spectrum. The N-terminal methionine of this protein has been reported as being methylated (33). The original sequencing of this subunit also indicated that the arginine residue at position 81 was modified in some way. Subsequent work by Brosius and Chen (33) suggested it was hydroxylated. This is confirmed by MALDI-MS/MS on the selected parent peptide ion of 1726.01 Da (VFPDKPITEKPLAVR, Fig. 6(*C*)), which correlates to 1710.00 Da and the addition of 16 Da because of hydroxylation of an arginine residue at position 81 of the sequence of 50S ribosomal protein L16. When the MS/MS spectrum of the parent ion of 1726.0 Da was searched on MASCOT, there were no significant matches. After 16 Da was added to arginine, the spectrum matched with the product ion of peptide VFPDKPITEKPLAVR. These two modifications still yield a protein that is 15 Da lighter than the observed mass, suggesting that another methylation or hydroxylation is present. Efforts to confirm this were unsuccessful because another peptide that had a molecular mass 16 or 14 Da higher than the theoretical mass could not be found. This example illustrates that only partial information on the modification of this protein can be produced using the method described. Other complementary techniques are needed to generate the additional information required for the complete characterization of this protein. These techniques may include intact protein sequencing by mass analysis of polypeptide ladders (MAP) after controlled hydrolysis of the modified protein (34) and top-down sequence analysis from the product ion spectra of the intact protein generated in ESI Fourier transform (FT) MS. Work in these directions is underway.

Finally, the sensitivity of the method was evaluated using a protein standard, cytochrome *c*. It was found that the lowest total amount used for intact protein mass measurement, LC fractionation, gel electrophoresis, and subsequent in-gel digest analysis was about 6.5 ng (525 fmol) of cytochrome *c*.

Conclusions

We have presented a method for characterizing protein modifications of low-mass proteins extracted from a microorganism using a combination of HPLC protein fractionation, intact protein mass measurement, LC–ESI-MS/MS of peptides produced from trypsin digestion of individual protein fractions, and gel electrophoresis of protein fractions followed by MALDI-MS and MALDI-MS/MS. Using the described method, not only previously reported PTMs involving acetylation, methylation, oxidation, and the removal of signal peptides, but also two novel PTMs, namely loss of N-terminal Met-Thr-Met (MTM) and hydroxylation of arginine, were observed. In this study, 37 low-mass proteins were observed in the MALDI mass spectra of HPLC fractions of *E. coli* cell extracts and 28 of them were identified. Among the identified proteins, nine were modified, resulting in mass shifts between the theoretical masses and the apparent masses in MALDI-MS. While the current method was developed and applied to the analysis of PTMs of proteins extracted from a relatively well-characterized microorganism, it is envisaged that this method should be applicable to other microorganisms for the discovery of new PTMs of low-mass proteins (<20 kDa). For higher mass proteins, mass resolution and mass measurement accuracy of intact proteins need to be improved, which can be done by using ESI-MS. For more complex organisms with large sizes of proteome, multidimensional HPLC separation of intact proteins, instead of the one-dimensional separation used in this work, is likely required.

Experimental section

Chemicals and reagents

HPLC grade acetone, methanol, acetonitrile (ACN), 2-propanol, and glacial acetic acid were from Fisher Scientific Canada (Edmonton, Alberta). Water used in all experiments was obtained from a Milli-Q Plus purification system (Millipore Corp., Bedford, Massachusetts). Bovine trypsin, cytochrome *c*, trifluoroacetic acid (TFA), and α-cyano-4-hydroxycinnamic acid (HCCA) were from Sigma-Aldrich-Fluka (Oakville, Ontario). HCCA was purified by recrystallization from ethanol (95%) at 50 °C prior to use. Tris(hydroxymethyl)aminomethane (electrophoresis purity grade) and Coomassie Blue G250 staining solution were purchased from Bio-Rad Laboratories (Hercules, California).

Cell growth and protein extraction

Escherichia coli (ATCC 47076) cells were ordered from the American Type Culture Collection (ATCC). Cells were grown in Luria Broth (LB) (BBL, Becton Dickinson, Franklin Lakes, New Jersey) at 37 °C with constant shaking and harvested at 72 h. The cells were then washed with sterile water, lyophilized, and stored at –20 °C before extraction. *Escherichia coli* extracts were prepared by a solvent suspension method as described previously (35). In brief, proteins were extracted by probe tip sonication using 0.1% TFA as extraction solvent. About 100 mg of lyophilized *E. coli* sample was suspended in 5 mL of 0.1% TFA solution in a 15 mL centrifuge tube. For sonication, a Branson Sonifier 450 (VWR Scientific, Bridgeport, New Jersey), with the duty cycle set to 75% and the output control set to 5, was used. The *E. coli* cell suspension was sonicated for 1 min with the tube on ice and then centrifuged at 13 000 g. Supernatant (i.e., the clear solution above the cell debris) was then transferred into fresh 1.5 mL vials. The extracts were filtered using a Microcon-3 (Millipore Corporation, Billerica, Massachusetts) with 3000 Da molecular mass cutoff and then concentrated to ~0.5 mL by SpeedVac (Thermo Electron Corporation, Waltham, Massachusetts).

© 2006 NRC Canada

Fractionation of proteins from the soluble *E. coli* whole cell lysates by RP-HPLC

Solvent delivery and separations were performed on an Agilent (Palo Alto, California) HP1100 HPLC system. The solvents used for reversed-phase HPLC were water (**A**) and acetonitrile (**B**) with 0.1% (*v*/*v*) TFA in both phases. The gradients were 2%–20% **B** in 10 min, 20%–40% **B** in 30 min, 40%–55% **B** in 5 min, 55%–65% **B** in 10 min, and 65%–90% **B** in 10 min. After the column was equilibrated for 30 min with 100% mobile phase **A**, 70 μL of bacterial extract was separated on a 250 mm × 4.6 mm i.d. C_8 column (5 μm particles with 300 Å pore size, Grace Vydac, Hesperia, California) at a flow rate of 500 μL/min. One minute fractions were collected with a Gilson FC 203B fraction collector (Gilson, Middleton, Wisconsin) and then concentrated to about 10 μL by SpeedVac.

In-solution digestion

Each of the selected HPLC fractions was adjusted to pH 8.5 with 1 mol/L NH_4HCO_3 and ~0.8 μg of trypsin was then added to each. Digestion was performed at 37 °C for ~2 h.

LC–ESI-MS/MS

Peptides in the in-solution protein digest of each HPLC fraction were desalted using commercial C18 μZiptips from Millipore prior to LC–ESI tandem mass spectrometry analysis. LC–ESI-MS/MS was performed on an LCQ Deca quadrupole ion trap mass spectrometer equipped with a dynamic nanospray source (ThermoFinnigan, San Jose, California). The dynamic nanospray source was coupled to a Surveyor HPLC system (ThermoFinnigan, San Jose, California). The flow from the pump was reduced from 300 to 1 μL/min by using a splitting tee and a length of restriction tubing made from fused silica. All separations were performed on a 150 μm × 15 cm i.d. capillary column, packed with 5 μm 218MS (C_{18}) beads (Grace Vydac). A 2 μL sample solution was injected for each run. The HPLC gradient was 5%–10% **B** in 2 min, 10%–45% **B** in 38 min, 45%–65% **B** in 10 min, and followed by 65%–85% **B** in 5 min (solvent **A**, 0.5% acetic acid in water; **B**, 0.5% acetic acid in acetonitrile, *v*/*v*). The nanospray tip used was a 50 μm i.d. tip from New Objective (Woburn, Massachusetts). During the HPLC separation, the ion trap repetitively surveyed the full scan MS over the *m*/*z* range of 400–1800 and executed data-dependent MS/MS scans. MS/MS spectra were acquired using a relative collision energy of 30% (LCQ instrumental settings). An isolation width of 2 *m*/*z* units was used and recurring ions were dynamically excluded after two MS/MS spectra were obtained. Interpretation of the resulting MS/MS spectra was performed by the SEQUEST software. The *E. coli* proteome database created from a nonredundant protein database, which was downloaded from NCBI (36), was used for database searching.

1D SDS PAGE

Proteins in each of the selected HPLC fractions were also separated using Tris-Tricine 10%–20% gradient Ready Gels (Bio-Rad Laboratories, Hercules, California). The premixed running buffer composition of the Tris–Tricine–SDS was as follows: 100 mmol/L Tris, 100 mmol/L Tricine, and 0.1% SDS. The sample buffer was composed of 200 mmol/L Tris-HCl, 2% SDS, 40% glycerol, and 0.04% Coomassie G-250. Gel electrophoresis was performed at a constant voltage of 100 V. For some fractions, to increase the sample quantity, the same fractions from two separate runs were combined for 1D SDS-PAGE mini-gel separation. Proteins in the gel bands were visualized by staining with Coomassie Blue G-250.

In-gel digestion

Low-mass gel bands of interest were excised and subjected to tryptic digestion according to the published digestion protocol (37). Reduction was performed at 56 °C for at least 30 min in 10 mmol/L DTT in 100 mmol/L NH_4HCO_3. Alkylation was performed in the dark at room temperature for 30 min in 55 mmol/L iodoacetamide in 100 mmol/L NH_4HCO_3. Sufficient 12.5 ng/μL trypsin in 50 mmol/L NH_4HCO_3 was added to cover the gel piece. Trypsin digestion was performed overnight (~12 h) at 30 °C. Sequential extraction of peptides from the gel was done twice with 0.25% TFA – 20% ACN, twice with 0.25% TFA – 50% ACN, and once with 0.25% TFA – 80% ACN. The extracts were pooled and the organic solvent removed by SpeedVac.

MALDI-MS

MALDI-MS results were obtained using a Bruker Reflex III MALDI time-of-flight (TOF) mass spectrometer (Bremen, Leipzig, Germany) equipped with a SCOUT 384 multiprobe inlet and a 337 nm nitrogen laser operated with a 3 ns pulse. Spectra were acquired in positive ion mode with delayed extraction using reflectron mode. The sample spot was scanned with the laser beam under video observation and spectra were acquired by averaging 300–500 individual laser shots and processed with the Bruker supporting software. The spectra were then reprocessed using the Igor Pro software package (WaveMetrics, Lake Oswego, Oregon). Each spectrum was normalized to the most intense signal in the mass range displayed.

For LC off-line MALDI analysis, each HPLC fraction was concentrated by a factor of 50 times to ~10 μL before mixing with matrix for analysis. A two-layer method was used for MALDI sample preparation (38). HCCA was used as a matrix. About 1 μL of 100 mmol/L HCCA in acetone–methanol (130:45, *v*/*v*) was applied to the MALDI plate to quickly form the first layer. For the second layer, the sample solution was mixed at a volume ratio of 1:2 with saturated HCCA in formic acid–2-propanol–water (1:2:3, *v*/*v*/*v*). About 1 μL of the second layer solution was then applied onto the first layer and allowed to dry. On-spot washing of the MALDI sample with water was performed to remove any salts. Quasi-internal mass calibration was done as follows to improve the accuracy. Once the sample spot was dried, about 0.5 μL of a mixture of standard protein solution with second layer HCCA matrix solution was spotted adjacent to the sample spot. The spectrum was collected from the sample spot first. After the intensity of the signal reached a certain level, the plate was moved and the laser beam was aimed at the standard. Finally, a spectrum, including peaks from both sample and standard, was recorded. Singly, doubly, and triply charged peaks from cytochrome *c* were used to make this quasi-internal calibration. For MALDI-MS on digests from in-gel tryptic digestions, the

© 2006 NRC Canada

spectra were internally calibrated with trypsin autolysis peptide peaks and matrix peaks.

MALDI-MS/MS

MALDI-MS/MS spectra of the selected peptide peaks from the MALDI-MS spectra of in-gel tryptic digests were acquired on an Applied Biosystems/MDS-Sciex QSTAR Pulsar QqTOF instrument equipped with an orthogonal MALDI source employing a 337 nm nitrogen laser (Concord, Ontario). The instrument was operated in positive ion mode and collisional-induced dissociation (CID) of peptides was achieved with argon as the collision gas. Spectra were acquired and processed using Sciex supplied software and reprocessed with Igor Pro software for presentation.

Database search

Possible matches in the public proteome database with the apparent masses observed in MALDI-MS were searched as previously described (39). The SWISS-PROT and TrEMBL (40) databases were searched using the SRS. The molecular mass measured by MALDI-MS was entered into the information field, along with the organism *E. coli*. Proteins were accepted as possible matches only if the database molecular masses matched with the experimental masses to within ±0.05%.

Mass spectral data interpretation

Known contaminant peak masses were eliminated from each MALDI-MS spectrum. The sample peaks were determined by comparing the peaks from a sample to the peaks from a blank piece of gel. Only sample peaks were considered for database searching. Artificial modifications of peptides by electrophoresis, such as acrylamide adducts to cysteine or oxidation of methionine, were also considered for the database search. Both peptide mass figure printing (PMF) and the peptide sequencing results were searched for protein identification using the MASCOT search program and the UCSF Protein Prospector Database (41). The obtained partial sequence information for each peptide was used to confirm, discard, or correct the previously obtained results from PMF.

Acknowledgements

We are grateful to the Natural Sciences and Engineering Research Council of Canada (NSERC), the Canada Foundation for Innovation, the Canada Research Chairs Program, the Alberta Science and Research Investments Program, and the Genome Canada Program through the Genome Prairie's Enabling Technology project for financial support. CJ was supported by a Graduate Studentship from the Alberta Heritage Foundation for Medical Research (AHFMR).

References

1. M. Mann and O.N. Jensen. Nat. Biotechnol. **21**, 255 (2003).
2. T. Exner, O.N. Jensen, M. Mann, C. Kleuss, and B. Nurnberg. Proc. Natl. Acad. Sci. U.S.A. **96**, 1327 (1999).
3. K.F. Medzihradszky, X. Zhang, R.J. Chalkley, S. Guan, M.A. McFarland, M.J. Chalmers, A.G. Marshall, R.L. Diaz, C.D. Allis, and A.L. Burlingame. Mol. Cell. Proteomics, **3**, 872 (2004).
4. I. Michaud-Soret, A. Adrait, M. Jaquinod, E. Forest, D. Touati, and J.M. Latour. FEBS Lett. **413**, 473 (1997).
5. S.B. Ficarro, M.L. McCleland, P.T. Stukenberg, D.J. Burke, M.M. Ross, J. Shabanowitz, D.F. Hunt, and F.M. White. Nat. Biotechnol. **20**, 301 (2002).
6. B.A. Ballif, J. Villen, S.A. Beausoleil, D. Schwartz, and S.P. Gygi. Mol. Cell. Proteomics, **3**, 1093 (2004).
7. J. Vasilescu, J.C. Smith, M. Ethier, and D. Figeys. J. Proteome Res. **4**, 2192 (2005).
8. J. Peng, D. Schwartz, J.E. Elias, C.C. Thoreen, D. Cheng, G. Marsischky, J. Roelofs, D. Finley, and S.P. Gygi. Nat. Biotechnol. **21**, 921 (2003).
9. M.J. MacCoss, W.H. McDonald, A. Saraf, R. Sadygov, J.M. Clark, J.J. Tasto, K.L. Gould, D. Wolters, M. Washburn, A. Weiss, J.I. Clark, and J.R. Yates, III. Proc. Natl. Acad. Sci. U.S.A. **99**, 7900 (2002).
10. R. Aebersold and M. Mann. Nature (London), **422**, 198 (2003).
11. G.E. Reid and S.A. McLuckey. J. Mass Spectrom. **37**, 663 (2002).
12. N.L. Kelleher, R.A. Zubarev, K. Bush, B. Furie, B.C. Furie, F.W. McLafferty, and C.T. Walsh. Anal. Chem. **71**, 4250 (1999).
13. F. Meng, A.J. Forbes, L.M. Miller, and N.L. Kelleher. Mass Spectrom. Rev. **24**, 126 (2005).
14. S.M. Patrie, J.P. Charlebois, D. Whipple, N.L. Kelleher, C.L. Hendrickson, J.P. Quinn, A.G. Marshall, and B. Mukhopadhyay. J. Am. Soc. Mass Spectrom. **15**, 1099 (2004).
15. K.M. Millea, I.S. Krull, S.A. Cohen, J.C. Gebler, and S.J. Berger. J. Proteome Res. **5**, 135 (2006).
16. B. Bogdanov and R.D. Smith. Mass Spectrom. Rev. **24**, 168 (2005).
17. O. Loo, R. Rachel, R. Hayes, Y. Yang, F. Hung, P. Ramachandran, N. Kim, R. Gunsalus, and J.A. Loo. Int. J. Mass Spectrom. **240**, 317 (2005).
18. M.B. Strader, N.C. VerBerkmoes, D.L. Tabb, H.M. Connelly, J.W. Barton, B.D. Bruce, D.A. Pelletier, B.H. Davison, R.L. Hettich, F.W. Larimer, and G.B. Hurst. J. Proteome Res. **3**, 965 (2004).
19. N.C. VerBerkmoes, J.L. Bundy, L. Hauser, K.G. Asano, J. Razumovskaya, F.W. Larimer, R.L. Hettich, and J.L. Stephenson, Jr. J. Proteome Res. **1**, 239 (2002).
20. Thermo Electron Corporation. SEQUEST [computer program]. Thermo Electron Corporation, Waltham, Mass. Available from http://www.thermo.com.
21. D.N. Perkins, D.J. Pappin, D.M. Creasy, and J.S. Cottrell. Electrophoresis, **20**, 3551 (1999); Matrix Science Inc. MASCOT [computer program]. Matrix Science Inc., Boston, Mass. Available from http://www.matrixscience.com.
22. V.C. Wasinger and I. Humphery-Smith. FEMS Microbiol. Lett. **169**, 375 (1998).
23. A.J. Link, K. Robison, and G.M. Church. Electrophoresis, **18**, 1259 (1997).
24. M.R. Maurizi. Experientia, **48**, 178 (1992).
25. A.M. Lazdunski. FEMS Microbiol. Rev. **5**, 265 (1989).
26. C.G. Miller. *In Escherichia coli* and salmonella: Cellular and molecular biology. Vol. 1. *Edited by* F.C. Neidhardt, R. Curtiss, J.L. Ingraham, E.C. Lin, K.B. Low, B. Magasanik, W.S. Reznikoff, M. Riley, M. Schaechter, and H.E. Umbarger. ASM Press, Washington, D.C. 1996. p. 938.
27. ProteoMetrics LLC. Paws [computer program]. ProteoMetrics LLC., New York, N.Y. Available from http://prowl.rockefeller.edu/prowl/prowl-description_.html. 1997.

© 2006 NRC Canada

28. D. Piszkiewicz, M. Landon, and E.L. Smith. Biochem. Biophys. Res. Commun. **40**, 1173 (1970).
29. C.K. Murphy and J. Beckwith. *In Escherichia coli* and salmonella: Cellular and molecular biology. Vol. 1. *Edited by* F.C. Neidhardt, R. Curtiss, J.L. Ingraham, E.C. Lin, K.B. Low, B. Magasanik, W.S. Reznikoff, M. Riley, M. Schaechter, and H.E. Umbarger. ASM Press, Washington, D.C. 1996. p. 967.
30. A. Ben-Bassat, K. Bauer, S.Y. Chang, K. Myambo, A. Boosman, and S. Chang. J. Bacteriol. **169**, 751 (1987).
31. P.H. Hirel, M.J. Schmitter, P. Dessen, G. Fayat, and S. Blanquet. Proc. Natl. Acad. Sci. U.S.A. **86**, 8247 (1989).
32. R.J. Arnold and J.P. Reilly. Anal. Biochem. **269**, 105 (1999).
33. J. Brosius and R. Chen. FEBS Lett. **68**, 105 (1976).
34. H. Zhong, Y. Zhang, Z. Wen, and L. Li. Nat. Biotechnol. **22**, 1291 (2004).
35. Z. Wang, L. Russon, L. Li, D.C. Roser, and S.R. Long. Rapid Commun. Mass Spectrom. **12**, 456 (1998).
36. NCBI. *E. coli* database [online]. National Center for Biotechnology Information, Bethesda, Md. Available from http://www.ncbi.nlm.nih.gov.
37. A. Shevchenko, M. Wilm, O. Vorm, and M. Mann. Anal. Chem. **68**, 850 (1996).
38. Y. Dai, R.M. Whittal, and L. Li. Anal. Chem. **71**, 1087 (1999).
39. K.Y. Dunlop and L. Li. J. Chromatogr. A, **925**, 123 (2001).
40. European Bioinformatics Institute. SWISS-PROT and TrEMBL databases [online]. European Bioinformatics Institute, Cambridge, UK. Available from http://www.ebi.ac.uk/swissprot.
41. K.R. Clauser, P.R. Baker, and A.L. Burlingame. Anal. Chem. **71**, 2871 (1999); USCF Mass Spectrometry Facility. Protein prospector database [online]. USCF Mass Spectrometry Facility, San Francisco, Calif. Available from http://prospector.ucsf.edu.

© 2006 NRC Canada

Characterization of Au and Pd nanoparticles by high-temperature TGA–MS

Weijuan Jia, Jessica McLachlan, Jiayan Xu, Seyed M. Tadayyon, Peter R. Norton, and S. Holger Eichhorn

Abstract: Noble metal nanoparticles (NPs) prepared by a surfactant-free single-phase solution method have been proposed to contain fewer ionic contaminants than similar NPs prepared by a two-phase method. Reported herein is the possible contamination of Au and Pd NPs, prepared by a surfactant-free single-phase method, with Li_2CO_3 and other Li salts. High-temperature thermal gravimetric analysis measurements coupled with mass spectrometry (TGA–MS) up to 1100 °C were employed to determine the relative amounts of ionic contaminants since protecting thiolate groups and inorganic contaminants were removed in separate weight loss events. Assignment of the different weight loss events was supported by MS analysis of the evolved gases. TGA–MS also revealed the presence of larger amounts of oxidized sulfur species in the Pd NPs. High-resolution transmission electron microscopy (HRTEM), UV–vis, IR, elemental analysis (EA), and X-ray photoelectron spectroscopy (XPS) measurements complemented the characterization of the NPs. The amount of ionic contaminants crucially depended on the workup conditions, and quenching of the reaction mixture with ethanol was found to be essential for the formation of Li_2CO_3. Workup procedures that avoid the formation of TGA–MS detectable ionic contaminants are proposed along with purification steps for contaminated NPs.

Key words: gold, palladium, nanoparticles, TGA, mass spectrometry, ionic contamination.

Résumé : Il a été suggéré que les nanoparticules de métaux nobles (NP) préparées par une méthode impliquant une solution en une phase sans agent de surface contiennent moins de contaminants ioniques que des particules semblables préparées par une méthode en deux phases. Dans ce travail, on rapporte des résultats qui suggèrent que les nanoparticules d'or ou de palladium préparées par une méthode en une seule phase sans agent de surface pourraient avoir été contaminées par du Li_2CO_3 ou d'autres sels de lithium. On a fait appel à des mesures d'analyse gravimétrique thermique à haute température couplées à la spectrométrie de masse (ATG–SM) jusqu'à 1100 °C pour déterminer les quantités relatives de contaminants ioniques puisque les groupes protecteurs thiolates et les contaminants inorganiques avaient été enlevés dans des manipulations séparées de pertes de poids. Les attributions de pertes de poids aux différentes manipulations sont en accord avec l'analyse par spectrométrie de masse des gaz qui se dégagent. La méthode ATG–SM a aussi révélé la présence de plus grandes quantités d'espèces de soufre oxydé dans les nanoparticules de Pd. La microscopie électronique par transmission à haute résolution, les spectroscopies UV–vis et IR, les analyses élémentaires et les mesures de spectroscopie photoélectronique des rayons X ont permis d'ajouter un complément à la caractérisation des nanoparticules. La quantité de contaminants ioniques dépend d'une façon cruciale sur les conditions du traitement conclusif et on a trouvé que la désactivation du mélange réactionnel avec de l'éthanol est essentielle pour la formation du carbonate de lithium. On propose des méthodes pour le traitement conclusif qui évitent la formation de contaminants ioniques détectables par ATG–SM ainsi que des étapes de purification pour les nanoparticules contaminées.

Mots clés : or, palladium, nanoparticules, analyse thermogravimétrique, spectrométrie de masse, contamination ionique.

[Traduit par la Rédaction]

Introduction

Noble metal nanoparticles (NPs) have become important building blocks in nanoscience (1) They can be prepared by a wide range of different physical and chemical methods, of which the preparations by wet chemistry have proved versatile and straightforward. Stable and soluble thiolate-protected metal NPs have been prepared by convenient two- (2) and single-phase (3) solution methods. Their average sizes and size distributions crucially depend on the reaction conditions (4).

Thiolates are usually considered to be the only molecules attached to the surface of noble metal NPs because of their relatively strong interactions. Other molecules and ions,

Received 30 November 2005. Accepted 25 May 2006. Published on the NRC Research Press Web site at http://canjchem.nrc.ca on 13 September 2006.

W. Jia, J. McLachlan, J. Xu, and S. Holger Eichhorn.[1] Department of Chemistry and Biochemistry, University of Windsor, Windsor, ON N9B 3P4, Canada.
S.M. Tadayyon and P.R. Norton. Department of Chemistry, University of Western Ontario, London, ON N6A 5B7, Canada.

[1]Corresponding author (e-mail: eichhorn@uwindsor.ca).

 doi:10.1139/V06-108 © 2006 NRC Canada

however, may compete for a place at the high-energy and large-area surface during the synthesis and workup or may be trapped in the organic layer of the protecting groups. The presence of such contaminants has seldom been reported as their detection is difficult, especially at low concentrations. NMR studies of long-chain alkyl thiol protected Au NPs prepared by the two-phase method revealed contamination by ionic phase transfer agents, such as tetraalkylammonium bromide (5). Soxhlet extraction has been shown to successfully remove the phase transfer agent but it is the experience of both our and other groups (5*a*) that excessive extraction of the NP powders with organic solvents also removes thiolate groups and that the yields of soluble particles decrease drastically.

Rowe et al. (6) proposed that metal NPs prepared by a surfactant-free single-phase method contain smaller amounts of ionic contaminants than similar Au NPs prepared by a two-phase method. This assumption, however, was based solely on the differences in the ionic conduction of these NPs. No spectroscopic or other analytical evidence was provided.

The identification and quantification of ionic impurities is essential as they might affect the solubility (5) and stability of the NPs, as well as their optical and electronic properties (7). It is expected that the type and quantity of contaminants crucially depend on the reaction and workup conditions as well as the type of thiol ligand. Large dendritic ligands, for example, have been shown to effectively entrap solvent molecules and phase transfer agents (8).

The methods that are typically applied in the characterization of metal NPs are restricted in their ability to detect contaminants. Standard solution NMR (9) only monitors hydrogen- and carbon-containing molecules and may be limited by the relatively low solubility of many NPs (often <1 mg/mL) as well as line-broadening of groups that are close to the metal surface. IR spectroscopy (10) is a convenient and sensitive method if the contaminants give rise to strong and characteristic absorptions that do not overlap with the absorptions of the NPs, but a quantification of the contaminants by IR is difficult. XPS (11) is the most straightforward method for the detection of unexpected elements and elements in unexpected chemical environments but, again, quantification is complicated by a limited penetration depth (approximately 1 to 2 nm, depending on the element and the electron energy channel) and the increasing attenuation of the photoelectron yield with increasing size of the organic ligands. XRD (12) and TEM (13) only detect contaminants that are present as particles, preferentially crystalline, of about 1 nm in diameter or larger. Low-temperature TGA (<700 °C) (4*a*, 14) has been routinely employed for the quantification of organic vs. metal content, but weight losses above 500 °C have not been discussed, though are occasionally observed (3*b*).

Herein, we introduce high-temperature TGA–MS as a convenient method for the identification and possible quantification of contaminants that also ensures a more accurate determination of the thiolate to gold ratios. Au and Pd NPs protected by octane-1-thiol (Au-C8), dodecane-1-thiol (Au-C12 and Pd-C12), octadecane-1-thiol (Au-C18), and 2-phenylethanethiol (Au-C2Ph and Pd-C2Ph) were prepared by a surfactant-free one-phase method in THF first described by Ulman and co-workers (3*b*, 3*c*). All NPs were characterized by TEM, UV–vis, TGA–MS, and XRD. Some particles were also examined by IR, XPS, and elemental analysis.

Experimental

The following compounds were used, 1-Octanethiol (Sigma-Aldrich, 98.5+%), 1-dodecanethiol (Sigma-Aldrich, 98+%), 1-octadecanethiol (Sigma-Aldrich, 98%), 2-phenylethanethiol (Sigma-Aldrich, 98%), lithium triethylborohydride (Super-Hydride® Sigma-Aldrich, 1.0 mol/L in THF), hydrogen tetrachloroaurate(III) hydrate (Strem Chemicals Inc., Newburyport, Massachsetts, 99.9%), and palladium(II) acetate (Sigma-Aldrich, 99.9%). THF was freshly distilled from sodium under nitrogen or run through activated Al_2O_3 columns using an Innovative Technology Inc. (Newburyport, Massachsetts) solvent purification system. Ethanol was first dried over $MgSO_4$ and then over a molecular sieve (4 Å). All other solvents were of ACS grade and used as received.

Transmission electron microscopy (HRTEM) was performed by Fred Pearson at McMaster University (Hamilton, Ontario) on a JEOL 2010F FEG TEM/STEM at 200 kV. Dilute solutions of NPs in THF were filtered through a 0.02 μm filter, dropped onto a carbon-coated copper grid, and the solvent was allowed to evaporate. Reported size distributions are based on the measurements of at least 200 particles per sample. Thermal gravimetric analysis with mass spectrometric detection of evolved gases was conducted on a Mettler Toledo TGA SDTA 851e that was attached to a Pfeiffer Vacuum Thermostar™ mass spectrometer (1–300 amu) via a thin glass capillary. Helium (99.99%) was used to purge the system at a flow rate of 60 mL/min. Samples were held at 25 or 30 °C for 20 or 30 min before being heated to 1000 °C at rates of 5 or 10 °C/min. A mass range from 16–240 *m*/*z* was constantly scanned for low-resolution measurements. High-resolution scans were conducted at a scan rate of 2 °C/min and specific *m*/*z* values were monitored at a high frequency. UV–vis spectra of solutions in THF (spectroscopic grade) were recorded on a Varian Cary 50. Powder XRD measurements were run on a Bruker D8 Discover diffractometer, equipped with a GADDS 2D detector, and operated at 40 kV and 40 mA. Cu Kα1 radiation (λ = 1.541 87 Å) was used and the initial beam diameter was 0.5 mm. All samples were sealed in Charles Supper Company (Natick, Massachusetts) 1.0 mm glass capillaries and run at θ angles of 18°, 50°, and 80°, each for 120 min. Spectra were combined and evaluated in EVA and plotted with Origin.

Crude and acid-washed samples of Au-C8 and Au-C12 were cast from DCM solution onto silicon wafers for FTIR and XPS investigations. One set of wafers with crude NPs was also heated to 500 °C in a stream of He for 30 min. FT-IR measurements were performed on a Bruker Vector 22. XPS measurements were conducted on a self-built system that consisted of an Al Kα X-ray source (1486.6 eV, unmonochromated) and a VG Scientific CLAM2 concentric hemispherical electron analyzer in a vacuum chamber (base pressure 2×10^{-10} torr, 1 torr = 133.322 4 Pa). The Au($4f_{7/2}$) peak of clean gold metal served as the energy standard (84.0 eV) and photoelectrons were analyzed at 50 eV pass energy with a resolution of about 1 eV for survey scans over

© 2006 NRC Canada

the entire binding energy range. An energy increment of 0.1 eV was used for regional scans over the photoelectron peaks of interest. Ten to fifteen scans were collected for each region, depending on the signal-to-noise ratio.

Synthesis and purification

Hydrogen tetrachloroaurate(III) hydrate (0.306 g, 1 mmol) or palladium(II) acetate (0.224 g, 1 mmol) were dissolved in 15 mL of dry THF and stirred under Ar for 15 min. Thiol (2.53 equiv.) was added and the mixture was stirred for another 30 min. Super-Hydride® (15 equiv., 1 mol/L solution in 15 mL of THF, 15 mmol of Super-Hydride®) was added within 30 min (0.75 mL/min) via a syringe pump and the mixture was stirred for another 2 h before being quenched by the addition of dry ethanol (30 mL). The sample was refrigerated for 12 h to fully precipitate all NPs, which were collected on a 0.2 μm PTFE membrane filter and washed with ethanol (95%). THF (10 mL) was used to wash the NPs through the filter and they were again precipitated from the filtrate by the addition of ethanol (60 mL). The final precipitate was collected on a PTFE membrane filter and dried in vacuum (4 mbar, 1 bar = 100 kPa) for 24 h.

The following yields of crude NPs, based on the initial amount of metal salt and the average composition of the NPs derived from TGA and TEM, were obtained: Au-C8 (81%), Au-C12 (72%), Au-C18 (89%), Au-C2Ph (72%), Pd-C12 (86%), Pd-C2Ph (72%).

Alternative workup procedures

A fraction of the Au-C8 reaction mixture was transferred into 10 mL Beckman polyallomer centrifuge tubes and run in a Beckman Coulter (Fullerton, California) Optima™ MAX E ultracentrifuge at 45 000 r/min (140 000*g*) at 12 °C for 20 min. The solvent was decanted off and the pellet was again dissolved in dry THF and centrifuged. This procedure was repeated two more times before the pellet was washed with deionized water and ethanol (95%) and dried in vacuum (4 mbar) for 24 h.

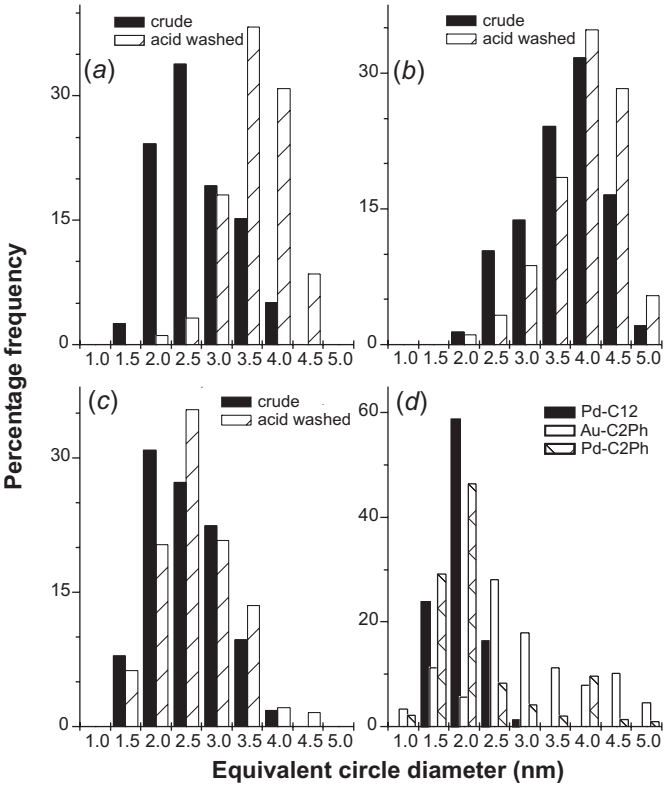
Quenching under Ar

One fraction of Pd-C2Ph was precipitated from the THF reaction mixture by the addition of dry ethanol under Ar. The precipitate was then filtered off under air (0.45 μm PTFE membrane filter) and the NPs were washed with 95% ethanol as described previously.

Acid-wash

Fractions of crude NPs that were isolated by precipitation from ethanol were dissolved in THF (10 mL) and precipitated by the addition of a 1:1 mixture of ethanol and aqueous hydrochloric acid (0.1 mol/L). This procedure was repeated until the filtrate reached a pH of 6 or lower (usually after the second precipitation). Acetic acid and 1 mol/L NH_4Cl (aq) were also tested for 0.1 mol/L HCl (aq) but the carbonate salts were not removed.

Fig. 1. Size distributions of (*a*) Au-C8, (*b*) Au-C12, (*c*) Au-C18, and (*d*) Au-C2Ph and Pd NPs derived from TEM measurements (TEM images are provided in the Supplementary information, Figs. S1–S5).[2]



Results and discussion

TEM and XRD characterization

The average sizes and size distributions of the NP cores were determined by TEM analysis (Fig. 1 and Supplementary information (SI), Figs. S1–S5).[2] Pd-C12 consisted of the smallest NPs (2.0 nm) with the narrowest size distribution (1.5–3.0 nm) (15). Au-C8 and Au-C18 both had an average size of 2.5 nm (1.5–4.0 nm), while the largest NPs were obtained for Au-C12 with an average size of 3.5 nm (2.0–5.0 nm). Au-C2Ph and Pd-C2Ph showed broader size distributions than those of alkyl thiolate protected NPs with average sizes of 2.9 nm (1.0–5.0 nm) and 2.3 nm (1.0–5.0 nm), respectively. All observed sizes and size distributions are in a typical range for nonfractionated NPs prepared by single- or two-phase solution methods in the presence of thiols (3*b*, 3*c*, 4*a*).

Acid wash treatment with 0.1 mol/L HCl (aq) for the removal of basic impurities caused a minor increase in average sizes (<0.5 nm) of Au-C12 and Au-C18, whereas a considerable increase in average size (>1.0 nm) was observed for Au-C8 (Fig. 1). No TEM pictures were taken of acid-washed Au-C2Ph as it quickly increased in size according to UV–vis

[2] Supplementary data for this article are available on the journal Web site (http://canjchem.nrc.ca) or may be purchased from the Depository of Unpublished Data, Document Delivery, CISTI, National Research Council Canada, Ottawa, ON K1A 0R6, Canada. DUD 5077. For more information on obtaining material refer to http://cisti-icist.nrc-cnrc.gc.ca/irm/unpub_e.shtml.

© 2006 NRC Canada

Table 1. Comparison of thiolate, Li_2CO_3, and metal contents based on TGA–MS, as well as the calculated average compositions of the NPs based on TGA and TEM.

Metal NPs	TGA event	Loss (*wt %*)	Temp. range (°C)	Org. loss (*wt %*)[a]	EAbased (C, H) content	TGA based (C, H, S) content[b]	N_{metal}[c] (No.)	$N_{thiolates}$[d] (No.)	$Au_{surface}$/ thiolate[e]
Au-C8, crude	Org. loss	5.7	100–370	7.2	10.6	11.3	466	49	4.5
	Inorg. loss	20.8	660–930	—	—	—	—	—	—
Au-C8, acid-washed	Org. loss	7.2	100–410	7.2	5.9	7.2	—	—	—
	Inorg. loss	<0.1	—	—	—	—	—	—	—
Au-C12, crude	Org. loss	10.6	170–480	11.6	11.4	12.9	1280	164	2.7
	Inorg. loss	8.7	510–950	—	—	—	—	—	—
Au-C12, acid-washed	Org. loss	11.5	160–380	11.5	9.9	11.5	—	—	—
	Inorg. loss	<0.1	—	—	—	—	—	—	—
Au-C18, crude	Org. loss	28.6	205–460	30	31.2	29.9	466	138	1.6
	Inorg. loss	4.7	570–890	—	—	—	—	—	—
Au-C18, acid-washed	Org. loss	36.8[f]	200–450	36.8[f]	34.4[f]	36.8[f]	—	—	—
	Inorg. loss	<0.1	—	—	—	—	—	—	—
Au-C2Ph, crude	Org. loss	5.7	80–380	9.7	—	16.9	728	112	2.7
	Inorg.loss	41.2	610–950	—	—	—	—	—	—
Au-C2Ph, acid-washed	Org. loss	10	110–470	10	—	10	—	—	—
	Inorg. loss	<0.1	—	—	—	—	—	—	—
Pd-C12	Org. loss	24.3	90–450	25.2	—	25.2	281	95	1.6
	Inorg. loss	3.5	500–920	—	—	—	—	—	—
Pd-C2Ph[g]	Org. loss	27.9	120–450	31.5	—	31.5	427	152	1.4
	Inorg. loss	13.4	550–850	—	—	—	—	—	—

[a]These values represent the organic loss corrected for the inorganic contamination by subtracting the inorganic weight losses from the total weight.
[b]These calculated values, based on the assumption that only CO_2 contributes to the inorganic second losses, are multiplied by 0.273 to give the C contribution in *wt %*, which was added to the value of the first loss.
[c]The average number of gold atoms per NP based on the TEM derived average size and a *FCC* packing.
[d]The average number of thiolate groups attached to a NP based on N_{metal} and organic loss values.
[e]The ratio between the average number of surface gold atoms per NP, based on the TEM derived radii, N_{metal}, and $N_{thiolates}$.
[f]This sample still contained excess octadecane thiol. It was removed from the crude sample by extraction with acetone–ethanol (1:1).
[g]The third loss of 8.5 *wt %*, observed above 900 °C in high-resolution TGA, was disregarded.

and the Pd NPs were even less stable in these conditions and coagulated to bulk material.

Assuming an *FCC*-like crystal structure for Au and Pd NPs as suggested by XRD, the average number of metal atoms per NP might be calculated from the average diameters of the NPs determined by TEM (15). Average diameters of 2.0 nm (Pd-C12), 2.3 nm (Pd-C2Ph), 2.5 nm (Au-C8,-C18), 2.9 nm (Au-C2Ph), and 3.5 nm (Au-C12) are equivalent to about 281, 427, 466, 728, and 1280 gold atoms per NP, respectively. Similarly, the average percentage of gold atoms at the surfaces of the NPs was calculated to be 54%, 48%, 47%, 42%, and 35%, respectively. These numbers, together with the average contents of metal and organic groups as determined by TGA, were used for the calculation of the average compositions of the NPs (Table 1, part 5).

Wide-angle XRD of the Au NPs revealed the typical peaks of an *FCC*-like gold core (12), while the Pd NPs appeared to be predominantly amorphous as no diffraction peaks of the Pd cores were observed (SI, Figs. S13–S15)[2] (16). The diffraction pattern of crude Au-C2Ph showed an unusual set of sharp peaks between $2\theta = 20°$ to 35°, which were identified as diffractions of Li_2CO_3 crystallites. The same peaks, but of much lower intensity, were found in the pattern of crude Au-C8. The small sharp peaks between $2\theta = 20°$ to 25° in the diffraction pattern of Au-C18 did not match the pattern of Li_2CO_3 and were likely caused by partial crystallization of the aliphatic side chains. No diffraction peaks of Li_2CO_3 were observed in the crude samples of Au-C12, AuC18, or the Pd NPs, although they contained Li_2CO_3 as confirmed by TGA–MS and IR analyses. It is assumed that Li_2CO_3 was present as too small a crystallite to give sufficiently intense diffraction peaks. All acid-washed NPs were free of Li_2CO_3 based on XRD, TGA–MS, and IR.

TGA–MS analysis

Two distinct weight losses were observed by TGA (Fig. 2). The first loss, between 100 and 400 °C, was caused mainly by the desorption and decomposition of the thiolate monolayer (3*b*, 4*a*, 4*c*), while the previously unreported second weight loss, between 650 and 900 °C, was mainly caused by the decomposition of the contaminant Li_2CO_3. TGA–MS measurements on a reference sample of Li_2CO_3 gave identical results (SI, Fig. S11)[2], and Li_2CO_3 was also identified by XRD and IR in the samples with high content (Au-C8 and Au-C2Ph). LiCl would have been completely removed in the same temperature range as Li_2CO_3 but no chlorine related ion peaks (*m*/*e* = 35 and 37) were observed by MS in any of the NPs, nor was Cl detected by XPS. Li_2O, another possible contaminant, is stable up to 1100 °C and consequently not detectable by TGA–MS.

All weight loss curves of the Au NPs levelled out at temperatures above 900 °C and bulk gold was left in the crucibles, based on visual inspection. Pd NPs that were heated to 1000 °C did not generate bulk palladium with a shiny metal-

© 2006 NRC Canada

Fig. 2. TGA curves of crude NPs.

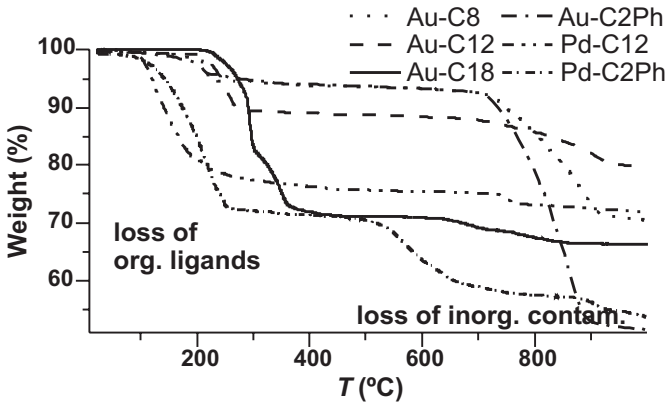
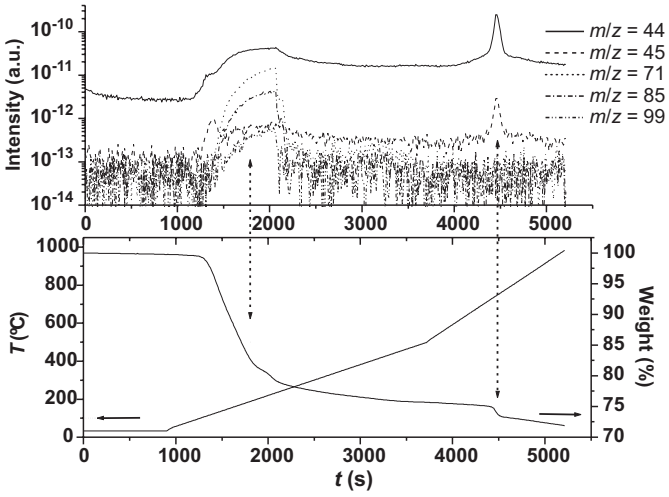


Fig. 3. TGA–MS measurement of Pd-C12. MS curves of only a small number of significant *m/e* values are shown for clarity.



lic surface but rather with a dull black appearance. High-resolution measurements on Pd NPs discussed later confirmed another weight loss above 900 °C that originated from the removal of oxidized sulfur species.

The thermal stability of the thiol monolayer, based on the onset temperatures of the first weight loss, decreased in the order Au-C18 > Au-C12 > Au-C8 > Au-C2Ph > Pd-C2Ph > Pd-C12. This suggests a decrease in thermal stability with decreasing chain lengths, which has also been observed by others (6, 9*b*), and a generally lower thermal stability of the Pd NPs. The amount of Li_2CO_3 in the Au NPs, based on the second weight loss in TGA, increased with decreasing thermal stability of the thiol monolayer. Thiols with longer alkyl chains seem to exclude ionic contaminants more effectively, which might be explained by the formation of more dense, partially crystalline, monolayers (10*a*, 17). Pd NPs, on the other hand, contained the least thermally stable thiolate monolayers and the lowest weight % of Li_2CO_3.

MS analysis of the TGA exhaust gas confirmed the loss of the organic ligands between 100 and 400 °C as increased intensities for masses of typical aliphatic fragment ions (e.g., 71, 85, and 99) were observed (Fig. 3 and SI, Figs. S8–S10).[2] The second weight loss, between 600 and 900 °C, coincided with the loss of other fragments than those from the thiol ligands, according to MS. Large increases in intensities were observed for *m/e* values of 28 (CO), 44 (CO_2), and 45 (CO_2H), which are typical decomposition products of carbonate salts. Temperature range and fragment ions in MS matched the reference spectrum of Li_2CO_3.

No second weight loss was observed in the TGA graphs of the acid-washed Au NPs, indicating a complete removal of Li_2CO_3 and possibly other contaminants (SI, Fig. S6)[2] (18). A comparison of the first weight losses between acid-washed and crude samples shows that the *wt %* losses of organic ligands were very similar when the *wt %* of the second losses were subtracted from the total weights of the crude samples (Table 1). Thermally, however, only CO_2 is assumed to be removed, leaving Li_2O (38% of the weight) behind. This discrepancy may be explained by other contaminants in the crude samples that were removed in the first weight loss below 500 °C and also by the acid wash procedure. This assumption is supported by the observation that intensities of ions, such as 28 (CO) and 44 (CO_2), also peaked at about 150 °C in the TGA–MS spectra of the crude samples, but no such peaks were observed for the acid-washed samples. The absence of oxidized carbon species in the acid-washed samples was also verified by XPS, as discussed later.

MS analysis of the evolved gases also revealed a considerable contribution from SO_2 (*m/e* = 64) and SO for Pd NPs, while it was small for the Au NPs and did not contribute to a significant weight loss (<0.5 *wt %*). The loss of SO_2 peaked twice in a high-resolution measurement of Pd-C2Ph up to 1100 °C (Fig. 4). One portion was removed with the aliphatic side chains between 100 and 300 °C, according to MS; the second loss occurred well after the loss of CO_2 at temperatures above 900 °C. Thiols have been shown to more easily oxidize on palladium than on gold surfaces (19), which would explain the loss of larger amounts of SO_2 in the MS of Pd NPs. This additional high-temperature loss of about 8 *wt %* complicates the calculation of the organic content based on TGA as a third weight loss process must be considered. Interesting, however, is the observation that considerable amounts of oxidized sulfur species remain on the metal surface at temperatures up to 900 °C. In contrast, the sulfur of the alkyl thiolates is fully removed with the organic groups at a temperature of 500 °C, according to the TGA–MS and XPS measurements discussed later.

UV–vis spectroscopy

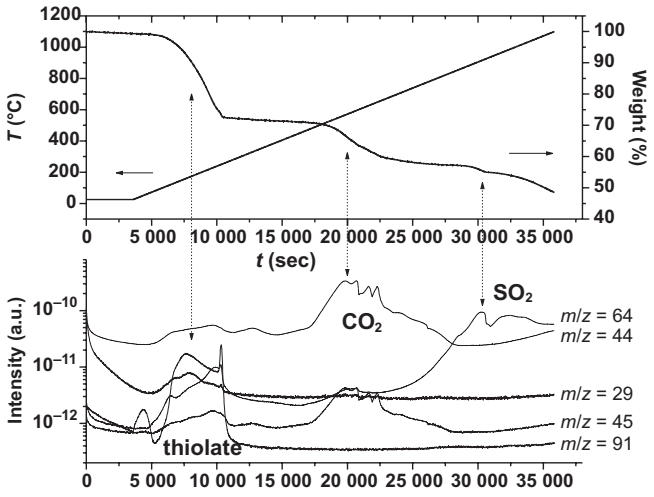
All crude Au-NPs showed surface plasmon absorption peaks between 518 and 533 nm (SI, Fig. S12).[2] These are typical values for particles with gold cores in the 2–6 nm diameter range (18). The absorption maxima for the crude and acid-washed samples were almost identical for Au-C8 (520 and 518 nm, respectively), Au-C12 (524 and 523 nm, respectively), and Au-C18 (both at 530 nm). A large shift was observed for Au-C2Ph (518–533 nm), which suggested a significant increase in average particle size. No distinct maxima were observed for the surface plasmon bands of the Pd NPs in THF and chloroform solutions. Values between 225 and 302 nm have been reported in the literature for Pd NPs of average sizes between 3 and 4 nm (3*b*, 3*c*).

IR and XPS measurements

Crude and acid-washed samples of Au-C8 and Au-C12 were cast from DCM solution onto silicon wafers and one

© 2006 NRC Canada

Fig. 4. High-resolution TGA–MS data for Pd-C2Ph (run at 2 °C/min).



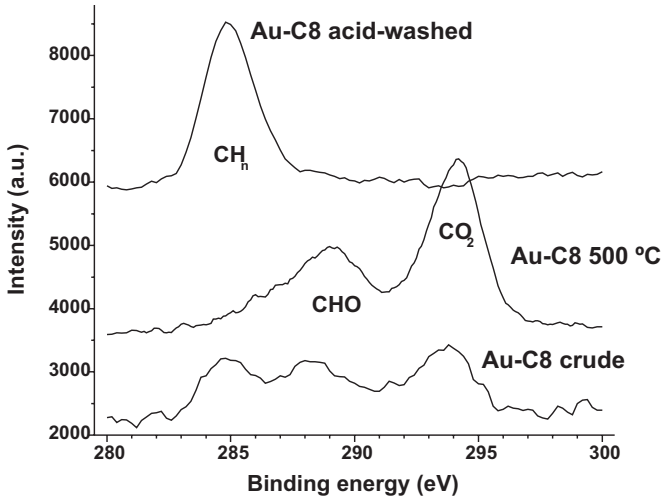
set of wafers with crude NPs was also heated to 500 °C in a stream of He for 30 min. The IR spectra of the crude and heated samples were dominated by strong absorptions at 1500, 1435, and 880 cm^{-1}, but these peaks were absent in the acid-washed samples (SI, Fig. S16).[2] These three absorptions were also found in the reference IR spectrum of Li_2CO_3. The C-H stretching bands of the aliphatic side chains at around 2900 cm^{-1} were present in the crude and acid-washed samples, while they were missing in the heated samples. These results independently verified the presence of Li_2CO_3 in the crude samples, the selective removal of the aliphatic side chains below 500 °C, and the complete removal of Li_2CO_3 by the acid wash procedure.

XPS measurements on the same six samples revealed the presence of Au, C, S, O, and Li, whereas no other elements such as N, Cl, or B were detected. The relative intensities of the elements changed depending on the treatment. A drastic decrease in the relative content of O was observed for the acid-washed samples, but the O content increased in the crude samples that were heated to 500 °C. This finding was surprising as the samples were first purged with He for 30 min and then heated under a flow of He. Possible explanations include the reaction of the organic material with the silicon oxide surface (e.g., reduction by sulfur species) or, less likely, remaining small amounts of molecular oxygen in the sample or purge gas. A detection of the silicon oxide surface owing to incomplete coverage by the decomposed NPs can be excluded since no increase in the intensity of the Si (2p) signal was observed.

The intensities of the S (2p) signals between 163 and 164 eV drastically decreased in the heated samples and the maxima were shifted to much higher binding energies between 168 and 170 eV, which could be explained by the formation of small amounts of oxidized sulfur. The lithium signal was very weak because of its small atomic sensitivity factor, which made quantitative comparisons difficult, but the lithium content was about the same in the crude and heated samples and lower in the acid-washed samples.

Detailed studies of the carbon signal identified at least four different species in the crude samples of which three matched the values for CH, CHO/CHOH, and CO_2 (Fig. 5).

Fig. 5. XPS of the C (1s) binding energies in Au-C8 samples on silicon wafers. Three samples are compared, a crude sample, an acid-washed sample, and a crude sample that was heated at 500 °C in a stream of He.



The acid-washed samples only contained CH species while the heated crude samples only contained oxidized carbon. Two single peaks were observed for Au $4f_{7/2}$ and Au $4f_{5/2}$ with maxima at 83.85 and 87.35 eV, and agree with values reported by others (11).

Elemental analysis and calculation of average compositions

The compositions of Au-C8, -C12, and -C18 were also studied by EA (C, H, N) for comparison. Crude samples gave carbon–hydrogen contents of 9.86:0.70 *wt %*, 10.24:1.18 *wt %*, and 26.55:4.64 *wt %*, respectively. The calculated H:C ratios for pure alkyl chains are 0.18 (C_8), 0.17 (C_{12}), and 0.17 (C_{18}) and the values found for the crude samples were lower with 0.07 (Au-C8), 0.12 (Au-C12), and 0.14 (Au-C18). These values are comparable to the TGA results if the inorganic loss is considered to be predominantly CO_2 (see Table 1) and suggest a high content of carbon bond to other elements than hydrogen. EA also confirms an increase in the content of non-hydrocarbon carbon with decreasing chain lengths that was observed by TGA. The acid-washed samples gave decreased carbon and increased hydrogen contents for Au-C8, -C12, and -C18 of 5.07:0.81 *wt %*, 8.55:1.36 *wt %*, and 29.31:5.06 *wt %*, respectively. Calculated H:C ratios of 0.16, 0.16, and 0.17, respectively, were now close to the theoretical values for alkyl chains given earlier. This confirms a close to complete removal of non-hydrocarbon carbon and is consistent with XPS and TGA–MS results.

A comparison of the C, H content based on EA with the C, H, S content based on TGA also gave comparable values. The TGA values are approximate numbers based on two simplifications: the first weight loss is solely caused by the removal of the thiolate ligands and the second weight loss is exclusively due to the loss of CO_2 (Table 1). TGA values were 4%–20% larger than the EA-derived values, which is in the range of the expected sulfur contribution depending on the length of the alkyl chains. Only the crude sample of Au-

© 2006 NRC Canada

C18 gave a slightly higher C, H content by EA than by TGA.

TGA and EA data, in combination with structural information obtained by HRTEM and XRD, were used for the calculation of the average compositions of NP samples (Table 1). Estimated surface gold to thiolate ratios were in the typical range of 1.5–2.6 for Au-C18 and Au-C12, respectively. The lower ratio for Au-C18 could be explained by a previously reported decrease in the ratio with decreasing particle size (4*a*), but may also reflect a larger number of surface sites being occupied by inorganic contaminants in Au-C12. Au-C8 gave an unusually large value of 4.5, which suggests a considerable replacement of thiolates by inorganic contaminants, such as Li_2CO_3, at the metal surface. Au-C8 of gold core sizes of 300–400 gold atoms prepared by the two-phase method was reported to lose 19.7% of its weight below 500 °C, which would account for a surface gold to thiolate ratio of about 2.0 (9*b*).

Removal of the lithium salts by the acid wash treatment gave stable, although not very soluble, Au-C8 NPs of even larger surface gold to thiolate ratios and slightly increased ratios were also calculated for the acid-washed samples of Au-C12 and Au-C18. Based on these results, it may be concluded that the lithium salts are capable of replacing thiolates at the metal surface but the majority are incorporated as smaller or larger crystallites into the organic layers of individual NPs as well as into larger aggregates of NPs. However, the surface gold to thiolate ratios of neither crude nor acid-washed gold NPs were lowered significantly by their treatments with thiols at room temperature.

Alternative workup procedures

One fraction of the Au-C8 reaction mixture was not quenched with ethanol but the NPs were separated by ultracentrifugation and then washed with water and ethanol. TGA measurements of these NPs revealed an increase of the first weight loss to 27 *wt %* in comparison with the crude Au-C8 sample, possibly because of an incomplete removal of excess thiols and disulfides, but no second weight loss (SI, Fig. S7).[2] This sample did not contain any Li_2CO_3 or LiCl, but the presence of lithium ions cannot be excluded based on TGA–MS.

In a different experiment, a fraction of the Pd-C2Ph reaction mixture was quenched with dry ethanol under argon, which may have avoided the initial carbonate formation, but filtration of the NPs in air generated the same amount of carbonate as in the crude sample discussed earlier. Workup and handling of the NPs strictly under CO_2 and water-free conditions was not tested as it was assumed that LiOEt would still be trapped in the particles and eventually converted to Li_2CO_3 upon exposure to air.

These experiments suggest that the formation of Li_2CO_3 requires the quenching of the reaction mixture with ethanol–alcohol and subsequent exposure to air. It is likely that excess $LiB(Et)_3H$ reacts with dry ethanol to form LiOEt that is subsequently converted to LiOH when exposed to water. LiOH eventually reacts with CO_2 to form Li_2CO_3. Separation by ultracentrifugation is a possible but tedious alternative workup that avoids the contamination with Li_2CO_3.

Hydrophobic NPs appear to be best purified by liquid–liquid extraction methods and precipitated with polar aprotic solvents (5*a*, 6). Much lower Li_2CO_3 contents were observed in NPs that were dissolved in toluene and extracted with 0.01 mol/L HCl (aq) before precipitation by the addition of acetonitrile. Both Au and Pd NPs were stable in these conditions, and a small amount of thiol may be added to the toluene phase to compensate for ligand loss because of excessive extractions. However, treatment of contaminated NPs with an excess of thiol in the THF and toluene solutions did not result in any removal of Li_2CO_3 at room temperature.

Additional Comments

Previously, only the content of organic ligands and the thermal stability of Au and Pd NPs were determined by TGA measurements up to 500–700 °C. Measurements up to 1100 °C, collected herein, provide valuable additional information on the composition of NPs as inorganic contaminants, as well as the fact that oxidized sulfur and carbon species may be detected in separate weight loss events. Parallel MS analysis of the evolved gasses was essential for determining the structures of removed fragments and for concluding what structures contributed to each of the observed weigh losses.

High-temperature TGA–MS analysis revealed a complex composition of the NPs presented herein. They contained inorganic salts, such as Li_2CO_3, in addition to the expected thiolate ligands and their relative contents could be quantified by TGA as the organic ligands were removed below 500 °C, while the CO_2 loss of Li_2CO_3 occurred above 600 °C. TGA–MS could also distinguish between the evaporation of the original thiolate ligands and their oxidized species. All this information may be collected from a 2 mg sample in one measurement.

TGA–MS also has its limitations since nonvolatile contaminants, such as Li_2O, cannot be detected by this method and other techniques are required for their detection. XPS, IR, and XRD were used here to detect nonvolatile components and to verify the conclusions drawn from the TGA–MS analysis. Quantifications of the content of certain groups and (or) compounds based on TGA are only accurate if their weight losses occur at different temperatures. Events that occur at similar temperatures may be further separated by optimizing the heating program. Still, overlapping events may be recognized by MS, but unfortunately, quantification of the intensities observed in the MS data is not straightforward.

The second significant outcome of this study is the possible contamination of metal NPs with inorganic salts. This is likely to be a specific problem of surfactant-free single-phase methods as any generated inorganic salts have low solubility in the organic solvent. Once contaminated, only aggressive acidic conditions may remove the inorganic contaminants, but two-phase workup conditions have been demonstrated to prevent the contamination right from the beginning.

It is unlikely that Li_2CO_3 played a significant role in controlling the growth of the NPs as they were not detected in the sample purified by ultracentrifugation that otherwise produced NPs of similar size but higher organic content. However, the lower solubility and larger calculated surface gold to thiolate ratios of the contaminated NPs suggested that the lithium salts are capable of replacing thiolate ligands at the

© 2006 NRC Canada

gold surface, although most of these contaminants must have been incorporated in the organic layer of the thiolates. It is assumed that the surface bond Li salts are not fully removed by the acid treatment and account for the remaining Li ion content observed by XPS. This may also explain why their thiolate content cannot be increased by exposure to excess thiol and a replacement of larger amounts of Li_2CO_3 in the crude NPs by excess thiol in solution at room temperature was also unsuccessful.

Conclusions

TGA–MS has been demonstrated to be a powerful tool for the characterization of Au and Pd NPs. Measurements up to 1100 °C revealed complex weight loss patterns and identified oxidized sulfur and carbon species that must be considered for calculations of organic ligand to gold ratios. NPs prepared by a surfactant-free single-phase method contained Li_2CO_3 as a major contaminant when the reaction mixture was quenched with alcohols. The content of Li_2CO_3 was quantified by TGA–MS, which also appeared to be more sensitive than XRD and IR. Contaminated Au-NPs, passivated with thiolates of C_{12} or longer alkyl chains, remained mostly unaffected when purified by extractions with dilute acids, but Au-NPs with shorter alkyl groups and Pd-NPs increased in size or even coagulated to bulk metal. Incorporation of Li_2CO_3 was avoided by precipitating them in an ultracentrifuge or by liquid–liquid extraction and the initial application of aprotic solvents for precipitation.

Acknowledgments

The authors thank Fred Pearson (McMaster University) for TEM measurements as well as the Natural Sciences and Engineering Research Council (NSERC) of Canada, Canada Foundation for Innovation (CFI), Materials and Manufacturing Ontario (MMO), and Ontario Innovation Trust (OIT) for funding.

References

1. (*a*) J.D. Aiken and R.G. Finke. J. Mol. Catal. A: Chem. **145**, 1 (1999); (*b*) M. Brust and C.J. Kiely. Colloids Surf. A, **202**, 175 (2002); (*c*) M.C. Daniel and D. Astruc. Chem. Rev. **104**, 293 (2004); (*d*) G. Schmid, M. Baumle, M. Geerkens, I. Helm, C. Osemann, and T. Sawitowski. Chem. Soc. Rev. **28**, 179 (1999); (*e*) G. Schmid and B. Corain. Eur. J. Inorg. Chem. **17**, 3081 (2003).
2. M. Brust, M. Walker, D. Bethell, D.J. Schiffrin, and R. Whyman. J. Chem. Soc. Chem. Commun. **7**, 801 (1994).
3. (*a*) N.R. Jana and X.G. Peng. J. Am. Chem. Soc. **125**, 14280 (2003); (*b*) C. Yee, M. Scotti, A. Ulman, H. White, M. Rafailovich, and J. Sokolov. Langmuir, **15**, 4314 (1999); (*c*) C.K. Yee, R. Jordan, A. Ulman, H. White, A. King, M. Rafailovich, and J. Sokolov. Langmuir, **15**, 3486 (1999).
4. (*a*) M.J. Hostetler, J.E. Wingate, C.J. Zhong, J.E. Harris, R.W. Vachet, M.R. Clark, J.D. Londono, S.J. Green, J.J. Stokes, G.D. Wignall, G.L. Glish, M.D. Porter, N.D. Evans, and R.W. Murray. Langmuir, **14**, 17 (1998); (*b*) R.L. Whetten, M.N. Shafigullin, J.T. Khoury, T.G. Schaaf, I. Vezmar, M.M. Alvarez, and A. Wilkinson. Acc. Chem. Res. **32**, 397 (1999); (*c*) F.P. Zamborini, S.M. Gross, and R.W. Murray. Langmuir, **17**, 481 (2001).
5. (*a*) J.E. Martin, J.P. Wilcoxon, J. Odinek, and P.J. Provencio. J. Phys. Chem. B, **104**, 9475 (2000); (*b*) C.A. Waters, A.J. Mills, K.A. Johnson, and D.J. Schiffrin. Chem. Commun. (Cambridge), **4**, 540 (2003).
6. M.P. Rowe, K.E. Plass, K. Kim, C. Kurdak, E.T. Zellers, and A.J. Matzger. Chem. Mater. **16**, 3513 (2004).
7. V. Torma, G. Schmid, and U. Simon. Chem. Phys. Chem. **2**, 321 (2001).
8. K.R. Gopidas, J.K. Whitesell, and M.A. Fox. J. Am. Chem. Soc. **125**, 6491 (2003).
9. (*a*) M.J. Hostetler, A.C. Templeton, and R.W. Murray. Langmuir, **15**, 3782 (1999); (*b*) R.H. Terrill, T.A. Postlethwaite, C.H. Chen, C.D. Poon, A. Terzis, A.D. Chen, J.E. Hutchison, M.R. Clark, G. Wignall, J.D. Londono, R. Superfine, M. Falvo, C.S. Johnson, E.T. Samulski, and R.W. Murray. J. Am. Chem. Soc. **117**, 12537 (1995); (*c*) A.J. Kell, R.L. Donkers, and M.S. Workentin. Langmuir, **21**, 735 (2005).
10. (*a*) A. Badia, L. Cuccia, L. Demers, F. Morin, and R.B. Lennox. J. Am. Chem. Soc. **119**, 2682 (1997); (*b*) A. Badia, W. Gao, S. Singh, L. Demers, L. Cuccia, and L. Reven. Langmuir, **12**, 1262 (1996).
11. M.C. Bourg, A. Badia, and R.B. Lennox. J. Phys. Chem. B, **104**, 6562 (2000).
12. D. Zanchet, B.D. Hall, and D.J. Ugarte. J. Phys. Chem. B, **104**, 11013 (2000).
13. M. Jose-Yacaman, M. Marin-Almazo, and J.A. Ascencio. J. Mol. Catal. A: Chem. **173**, 61 (2001).
14. W.W. Weare, S.M. Reed, M.G. Warner, and J.E. Hutchison. J. Am. Chem. Soc. **122**, 12890 (2000).
15. T.G. Schaaff, M.N. Shafigullin, J.T. Khoury, I. Vezmar, R.L. Whetten, W.G. Cullen, P.N. First, C. Gutierrez-Wing, J. Ascensio, and M.J.J. Jose-Yacaman. J. Phys. Chem. B, **101**, 7885 (1997).
16. W. Lu, B. Wang, K.D. Wang, X.P. Wang, and J.G. Hou. Langmuir, **19**, 5887 (2003).
17. M.J. Hostetler, J.J. Stokes, and R.W. Murray. Langmuir, **12**, 3604 (1996).
18. M.M. Alvarez, J.T. Khoury, T.G. Schaaff, M.N. Shafigullin, I. Vezmar, and R.L.J. Whetten. J. Phys. Chem. B, **101**, 3706 (1997).
19. J.C. Love, D.B. Wolfe, R. Haasch, M.L. Chabinyc, K.E. Paul, G.M. Whitesides, and R.G. Nuzzo. J. Am. Chem. Soc. **125**, 2597 (2003).

© 2006 NRC Canada

4-Aminophenyldiphenylphosphinite (APDPP), a new heterogeneous and acid scavenger phosphinite — Conversion of alcohols, trimethylsilyl, and tetrahydropyranyl ethers to alkyl halides with halogens or *N*-halosuccinimides

Nasser Iranpoor, Habib Firouzabadi, and Mohammad Gholinejad

Abstract: A new heterogeneous phosphinite, 4-aminophenyldiphenylphosphinite (APDPP), is prepared and used for the efficient conversion of alcohols, trimethylsilyl ethers, and tetrahydropyranyl ethers to their corresponding bromides, iodides, and chlorides in the presence of molecular halogens or *N*-halosuccinimides. The amino group in this phosphinite acts as an acid scavenger and removes the produced acid. A simple filtration easily removes the phosphinate by-product.

Key words: 4-aminophenyldiphenylphosphinite, alcohol, trimethylsilyl ether, tetrahydropyranyl ether, alkyl halide.

Résumé : On a préparé un nouveau phosphinite hétérogène, le phosphinite de 4-aminophényle et de diphényle, et on l'a utilisé pour la conversion efficace d'alcools et d'éthers triméthylsyles ou tétrahydropyranyles en bromures, chlorures et iodures correspondants en présence d'halogènes moléculaires ou de *N*-halogénosuccinimides. La groupe amino de ce phosphinite agit comme piège et permet d'enlever l'acide qui est produit. Une filtration simple permet d'enlever la phosphinate obtenu comme sous-produit.

Mots clés : phosphinite de 4-aminophényle et de diphényle, alcool, éther triméthylsilyle, éther tétrahydropyranyle, halogénure d'alkyle.

[Traduit par la Rédaction]

Introduction

The very useful application of tertiary phosphines as oxophiles has been widely studied in organic synthesis. Conversion of alcohols into alkyl halides using triphenylphosphine, one of the most popular phosphines under Mitsunobu conditions, or in the presence of molecular halogens has been widely studied (1–12). Isolation of the phosphine oxide by-product is considered a drawback of using homogeneous phosphine reagents. To simplify the workup procedure for the removal of phosphine oxides, the use of a limited number of heterogeneous phosphines is reported. The use of polymer-supported triphenylphosphine has the usual problem of lower efficiency of the polymeric reagents compared with monomeric ones (6*a*, 13–17). Tris{4-(1*H*,1*H*-perfluorooctyloxy)phenyl]phosphine has been reported as another heterogeneous phosphine (18). Using diphos-1,2-bis(diphenylphosphino)ethane as an interesting source of phosphines for this purpose still suffers from the problem that only 75% of diphos oxide can be removed under optimized conditions (19). Recently, we prepared a silica-based inorganic phosphine reagent (silphos) and applied it to the conversion of alcohols into their corresponding alkyl halides (17). Another drawback of using phosphines in conjunction with molecular halogens for the preparation of alkyl halides from alcohols is the production of HX in the reaction mixture, which may cause problems for acid-sensitive functional groups.

Received 8 March 2006. Accepted 12 June 2006. Published on the NRC Research Press Web site at http://canjchem.nrc.ca on 13 September 2006.

N. Iranpoor,[1] H. Firouzabadi,[2] and M. Gholinejad. Department of Chemistry, Faculty of Sciences, Shiraz University, Shiraz 71454, Iran.

[1]Corresponding author (e-mail: iranpoor@chem.susc.ac.ir).
[2]Corresponding author (e-mail: firouzabadi@chem.susc.ac.ir).

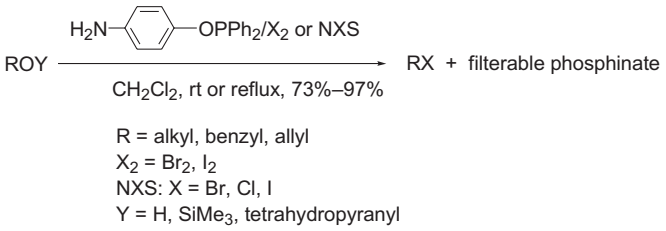
Results and discussion

In this work, we introduce 4-aminophenyldiphenylphosphinite (APDPP) as a new heterogeneous monomeric phosphinite reagent. In the presence of molecular halogens, this reagent efficiently converts alcohols into alkyl halides. The presence of an amino group makes this reagent an efficient acid scavenger and removes the HX produced from the reaction mixture. A simple filtration separates the ammonium salt of the produced phosphinate and leaves the pure product.

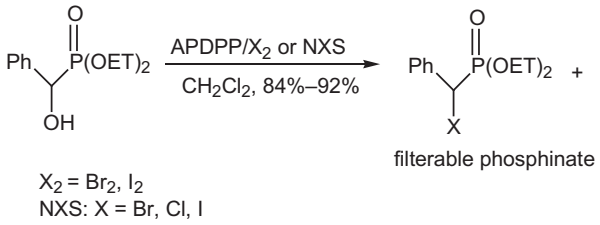
We successfully applied this easily prepared heterogeneous phosphinite to the conversion of different classes of alcohols to alkyl halides in the presence of molecular bromine, iodine, and *N*-halosuccinimides (NXS, X = Cl, Br, I) in dichloromethane at room temperature (Scheme 1).

 doi:10.1139/V06-120 © 2006 NRC Canada

Scheme 1.



Scheme 2.



The optimized molar ratios of benzyl alcohol – APDPP – halogen were found to be 1:1.2:1.2 for bromination and 1:1.5:1.5 for iodination reactions. Primary, secondary, and tertiary alcohols were converted into their corresponding alkyl bromides and iodides in excellent yields using these optimized conditions (Table 1). The HX produced in this reaction reacts with the amino group of the reagent and its phosphinate is easily removed by filtration. To extend the applicability of this reagent, we replaced the molecular halogens with *N*-halosuccinimides (NXS, X = Cl, Br, I) as safer sources of halogens for the conversion of alcohols to their corresponding halides. Here again, the produced phosphinate is insoluble and can be removed by filtration.

α-Functionalized phosphonates are important organophosphorous compounds in biology, pharmacology, and organic chemistry. A few methods for the conversion of diethyl α-hydroxyphosphinates into their corresponding diethyl α-halophosphinates have been reported in the literature (20, 21*a*–21*c*). Among these methods, the use of PPh_3–Br_2 in the presence of pyridine as an acid scavenger has been also reported (21*a*).

We successfully applied APDPP to the conversion of diethyl α-hydroxyphosphinates into their corresponding diethyl α-halophosphinates in the presence of molecular halogens or *N*-halosuccinimides (Scheme 2, Table 1, entries 13 and 14). The presence of an acid scavenger amino group in the structure of APDPP for the conversion of diethyl α-hydroxyphosphinates into their corresponding diethyl α-halophosphinates eliminates the use of toxic pyridine, as reported in the literature (21*a*). The results of this study are tabulated in Table 1.

In continuation of this work, we used this new phosphinite reagent for the efficient conversion of trimethylsilyl and tetrahydropyranyl ethers to their corresponding alkyl halides in conjunction with molecular halogens or *N*-halosucinimides under heterogeneous conditions (Scheme 1). The conversion of trimethylsilyl and tetrahydropyranyl ethers to their corresponding alkyl halides with this reagent occurs at room temperature with high to excellent yields. The results are shown in Tables 2 and 3.

To show the stability of acid-sensitive compounds during the course of the reaction, we converted benzyl alcohol to its bromide and iodide in the presence of equimolar amounts of 2-phenyl-1,3-dioxolane as a highly acid-sensitive compound. The conversion of benzyl alcohol to its halides occurred quantitatively, but the 2-phenyl-1,3-dioxolane remained intact. Similarly, addition of styrene oxide to a mixture of benzyl alcohol, APDPP, and Br_2 in CH_2Cl_2 did not show the formation of any product from the ring opening of styrene oxide. These results show that the acid produced in the course of the reaction of alcohols with APDPP and halogens can be removed by the amino group of the reagent before affecting the acid-sensitive groups.

In summary, the present investigation has demonstrated the applicability of APDPP as a new heterogeneous phosphinite for the efficient conversion of alcohols, trimethylsilyl ethers, and tetrahydropyranyl ethers to their corresponding alkyl halides. α-Hydroxyphosphonates can also be converted heterogeneously into their α-halophosphonates without the need to use an additional base such as pyridine. In addition, the stability, heterogeneous nature, easy preparation, and acid-scavengering properties are considered other advantages of using APDPP for these transformations.

Experimental

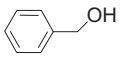
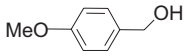
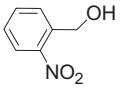
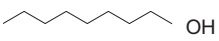
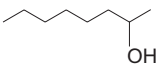
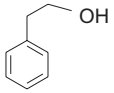
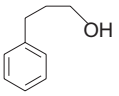
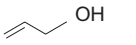
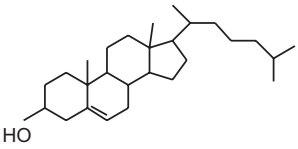
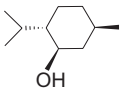
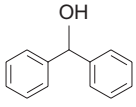
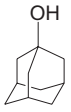
Chemicals were either prepared in our laboratory or obtained from Fluka (Buchs, Switzerland) and Merck (Darmstadt, Germany) chemical companies. IR spectra were recorded on a PerkinElmer 781 spectrometer. NMR spectra were recorded on an Avance DPX 250 MHz spectrometer. GC analyses were recorded on a Shimadzu GC-14A. Mass spectra were run on Shimadzu GC-Mass-QP 1000 EX at 70 eV.

Preparation of 4-aminophenyldiphenylphosphinite (APDPP)

To a flask containing *t*-BuOH (15 mL) was added potassium (0.43 g, 11 mmol), which was stirred slowly until the potassium was completely consumed. 4-Aminophenol (1.09 g, 10 mmol) was added and the solution was stirred with a mechanical stirrer for 30 min at room temperature. To the resulting dark syrup, chlorodiphenylphosphine (1.9 mL, 10 mmol) was added dropwise for a period of 10 min at room temperature. The reaction was completed after 5 min. The obtained product was washed with 30 mL of water to remove the produced KCl. The filtered cake was washed with diethyl ether (2 × 20 mL) and dried under vacuum at room temperature. 4-Aminophenyldiphenylphosphinite was obtained as a milky white solid (0.27 g, 93%). IR (KBr): 3340 (w), 3250 (w), 2915 (m), 2361 (m), 1498 (s), 1434 (m), 1281(w), 1213 (m), 865 (m), 690 (s), 511 (m). ^{1}H NMR (DMSO, 250 MHz, ppm) δ: 4.5 (b, 2H, NH_2), 6.4–6.5 (AA′BB′, pattern, 4H), 7.1–7.74 (complex, 10H). EI-MS (70 eV) *m/e*: 293 (2.07%), 292 (4.08%), 201 (53.4%), 183 (100%), 152 (13.9%), 107 (16%), 77 (26%), 51 (14%). Anal. calcd. for $C_{18}H_{16}NOP$: C 73.71, H 5.50, N 4.78; found: C 73.35, H 5.36, N 4.65.

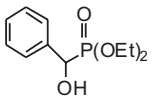
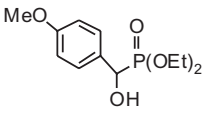
© 2006 NRC Canada

Table 1. Conversion of alcohols to their corresponding alkyl halides in the presence of APDPP and Br_2, I_2, NBS, NCS, and NIS.

Entry	Substrate	Reagent (Time)	Conversion (%)	Isolated yield (%)
1		Br_2 (immediately)	100	95
		I_2 (immediately)	100	95
		NBS (1.5 h)	100	95
		NCS (1.5 h)	95	95
		NIS (1.5 h)	100	95
2		Br_2 (immediately)	100	95
		I_2 (immediately)	100	94
		NBS (1.5 h)	100	95
		NCS (1.5 h)	96	95
		NIS (1.5 h)	100	96
3		Br_2 (25 min)	100	97
		I_2 (2 h)	100	98
		NBS (2 h)	100	96
		NCS (10 h)	86	90
		NIS (2 h)	97	93
4		Br_2 (3 h)	100	92
		I_2 (20 min)	100	93
5		Br_2 (7 h)	94	86[a]
		I_2 (30 min)	100	91.8
		NBS (5 h)	98	89
		NCS (9 h)	87	90
		NIS (2.5 h)	97	90
6		Br_2 (2.5 h)	100	93
		I_2 (25 min)	100	91.6
		NBS (2.5 h)	92	87
		NCS (3 h)	94	87
		NIS (3.5 h)	94	85
7		Br_2 (3 h)	100	92
		I_2 (25 min)	100	92
8		Br_2 (5 min)	100	-
		I_2 (5 min)	100	-
9		Br_2 (90 min)	100	92
		I_2 (45 min)	100	95
10		Br_2 (3 h)	85	80
		I_2 (2 h)	100	92.5
11		Br_2 (2 h)	89.7	86
		I_2 (2.30 h)	95	87
		NBS (10 h)	92	82
		NCS (15 h)	95	88
		NIS (10 h)	95	88
12		Br_2 (10 h)	100	96[b]
		I_2 (24 h)	92	85[c]
		NBS (18 h)	80	75[d]
		NCS (24 h)	79	73[e]
		NIS (10 h)	77	73[f]

© 2006 NRC Canada

Table 1 (*concluded*).

Entry	Substrate	Reagent (Time)	Conversion (%)	Isolated yield (%)
13		Br_2 (6 h)	100	90
		I_2 (4 h)	100	92
		NBS (10 h)	97	88
		NCS (14 h)	95	84
		NIS (10 h)	95	87
14		Br_2 (3.5 h)	100	91
		I_2 (1.5 h)	100	95
		NBS (8.5 h)	98	89
		NCS (10 h)	95	85
		NIS (9 h)	95	87

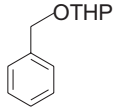
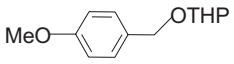
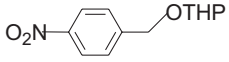
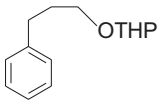
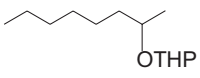
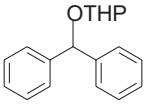
Note: The molar ratios of ROH–APDPP–Br_2, ROH–APDPP–I_2, and ROH–APDPP–NXS are 1:1.2:1.2, 1:1.5:1.5, and 1:2:2, respectively.

[a]The molar ratio of ROH–APDPP–Br_2 is 1:1.4:1.4.

[b,c]The molar ratio of ROH–APDPP–$Br_2(I_2)$ is 1:1.5:1.5.

[d,e,f]The molar ratio of ROH–APDPP–NXS is 1:2.5:2.5.

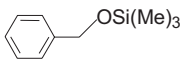
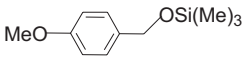
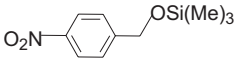
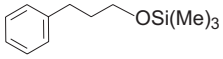
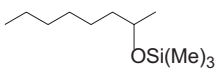
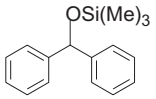
Table 2. Conversion of THP ethers to alkyl halides in the presence of APDPP and Br_2, I_2, NBS, NCS, and NIS

Entry	Substrate	Reagent (Time)	Conversion (%)	Isolated yield (%)
1		Br_2 (40 min)	100	94
		I_2 (30 min)	100	95
		NBS (2 h)	100	95
		NCS (1.5 h)	100	95
		NIS (1.5 h)	100	95
2		Br_2 (30 min)	100	95
		I_2 (5 min)	100	95
		NBS (1.5 h)	100	95
		NCS (1.5 h)	100	95
		NIS (1.5 h)	100	96
3		Br_2 (75 min)	100	95
		I_2 (1 h)	100	97
		NBS (3.5 h)	95	91
		NCS (5 h)	91	85
		NIS (4 h)	93	88
4		Br_2 (5 h)	100	93
		I_2 (3 h)	100	95
		NBS (3 h)	100	95
		NCS (4 h)	89	80
		NIS (3 h)	100	95
5		Br_2 (7 h)	95	85
		I_2 (4 h)	96	87
		NBS (9 h)	88	80
		NCS (14 h)	76	70
		NIS (8.5 h)	96	87
6		Br_2 (14 h)	95	86
		I_2 (10 h)	93	84
		NBS (10 h)	90	84
		NCS (15 h)	81	75
		NIS (11 h)	92	86

Note: The molar ratios of ROTHP–APDPP–Br_2, ROTHP–APDPP–I_2, and ROTHP–APDPP–NXS are 1:1.3:1.3, 1:1.5:1.5, and 1:2:2, respectively.

© 2006 NRC Canada

Table 3. Conversion of trimethylsilyl ethers to alkyl halides in the presence of APDPP and Br_2, I_2, NBS, NCS and NIS.

Entry	Substrate	Reaction (Time)	Conversion (%)	Isolated yield (%)
1		Br_2 (immediately)	100	95
		I_2 (immediately)	100	95
		NBS (1 h)	100	95
		NCS (1 h)	100	95
		NIS (1 h)	100	95
2		Br_2 (immediately)	100	95
		I_2 (immediately)	100	96
		NBS (1 h)	100	95
		NCS (1 h)	100	96
		NIS (1 h)	100	95
3		Br_2 (50 min)	100	95
		I_2 (20 min)	100	97
		NBS (2 h)	95	91
		NCS (3 h)	90	87
		NIS (3.5 h)	95	91
4		Br_2 (5 min)	100	94
		I_2 (immediately)	100	96
		NBS (1.5 h)	100	95
		NCS (2 h)	100	95
		NIS (2.5 h)	95	86
5		Br_2 (25 min)	100	93
		I_2 (10 min)	100	95
		NBS (2 h)	100	94
		NCS (3 h)	100	94
		NIS (3 h)	100	93
6		Br_2 (1 h)	95	87
		I_2 (70 min)	100	96
		NBS (5 h)	91	81
		NCS (8 h)	86	82
		NIS (6 h)	94	88

Note: The molar ratios of $ROSiMe_3$–APDPP–Br_2, $ROSiMe_3$–APDPP–I_2, and $ROSiMe_3$–APDPP–NXS are 1:1.2:1.2, 1:1.5:1.5, and 1:2:2, respectively.

Typical procedure for the conversion of benzyl alcohol to benzyl bromide using APDPP–Br_2.

To a flask containing APDPP (0.35 g, 1.2 mmol) was added Br_2 (0.06 mL, 1.2 mmol) at room temperature in CH_2Cl_2 (7 mL) and stirred. Then benzyl alcohol (0.1 mL, 1 mmol) was added. The progress of the reaction was monitored by TLC and GC analysis. Benzyl alcohol was completely converted to benzyl bromide immediately. The reaction mixture was filtered to remove the produced insoluble phosphinate and enough powdered sodium thiosulfate was added to the solution, with vigorous stirring, to react with excess bromine. After filtration, the solvent was evaporated under vacuum in a rotary evaporator. For further purification, the product was washed over a silica gel pad (2 cm thick) using *n*-hexane – ethyl acetate as eluent. Benzyl bromide was obtained as a colourless liquid (0.16 g, 95% yield), bp 195 to 196 °C (lit. value (22) bp 196–198 °C).

Typical procedure for the conversion of benzyl alcohol to benzyl bromide with APDPP–*N*-bromosuccinimide.

To a two-necked flask containing APDPP (0.58 g, 2 mmol) and benzyl alcohol (0.1 mL, 1 mmol) in reflux dichloromethane (10 mL) was added dropwise a solution of *N*-bromosuccinimide (0.35 g, 2 mmol) in CH_2Cl_2 (10 mL) for a 1.5 h period. After the addition, GC analysis of the reaction mixture indicated when the reaction was complete. The reaction mixture was then filtered to remove the insoluble phosphinate and enough powdered sodium thiosulfate was added, with vigorous stirring, to remove any bromine produced. After filtration, the solvent was evaporated under vacuum in a rotary evaporator. The purification of the product was achieved using chromatography over a silica gel pad using *n*-hexane – ethyl acetate as eluent. Benzyl bromide was obtained as colourless liquid (0.16 g, 90% yield).

Typical procedure for the conversion of 1-octanol to 1-iodooctane using APDPP–I_2

To a flask containing a stirring mixture of APDPP (0.44 g, 1.5 mmol) in dichloromethane (20 mL) was added I_2 (0.38 g, 1.5 mmol) at room temperature. After 5 min, 1-octanol (0.15 mL, 1 mmol) was added. GC analysis showed completion of the reaction after 20 min. After removal of the produced phosphinate by filtration, enough powdered sodium thiosulfate was added, with vigorous stirring, to react with the unreacted iodine. After filtration, the solvent was evaporated under vacuum in a rotary evaporator. For further purification, the product was washed over a silica gel pad (2 cm thick) using *n*-hexane as eluent to give 1-iodooctane

© 2006 NRC Canada

(0.18 g, 93% yield, bp 226 to 227 °C (lit. value (22) bp 225 to 226 °C).

Typical procedure for the conversion of benzyltrimethylsilyl ether to benzyl bromide using APDPP–Br_2

To a flask containing a stirring mixture of APDPP (0.35 g, 1.2 mmol) was added Br_2 (0.06 mL, 1.2 mmol) at room temperature in dichloromethane (15 mL), after which benzyltrimethylsilyl ether (0.18 g, 1 mmol) was also added. TLC monitoring of the reaction showed completion of the reaction after 1 min. After filtration of the reaction mixture, enough powdered sodium thiosulfate was added, with vigorous stirring, to react with the unreacted bromine. The reaction mixture was filtered and the solvent was evaporated under vacuum in a rotary evaporator. The product was chromatographed on a short silica gel pad (2 cm thick) using *n*-hexane as eluent. Benzyl bromide was produced (0.12 g, 95% yield).

Typical procedure for the conversion of benzyltetrahydropyranyl ether to benzyl iodide by APDPP–I_2

To a stirring mixture of APDPP (0.44 g, 1.5 mmol) and I_2 (0.38 g, 1.5 mmol) in CH_2Cl_2 (10 mL) was added benzyltetrahydropyranyl ether (0.18 g, 1 mmol) at room temperature. After 30 min, TLC and GC analysis indicated that the reaction was complete. The reaction mixture was filtered and the unreacted iodine was removed by the addition, with vigorous stirring, of enough powdered sodium thiosulfate. The mixture was then filtered and the resulting solution was evaporated. To purify the product, it was passed through a short column of silica gel using *n*-hexane – ethyl acetate as eluent. Benzyl iodide was obtained (0.2 g, 95% yield). It was identified by comparison with a known sample.

Typical procedure for the conversion of diethyl α-hydroxybenzylphosphinate to diethyl α-bromobenzylphosphinate using APDPP–Br_2

To a flask containing a stirring mixture of APDPP (2 mmol, 0.58 g) was added Br_2 (2 mmol, 0.1 mL) in CH_2Cl_2 (7 mL) at room temperature. Then, diethyl α-hydroxyphosphinate (0.24 g, 1 mmol,) was added. After 6 h, the reaction mixture was filtered to remove the insoluble phosphinate and enough powdered sodium thiosulfate was added to the solution, with vigorous stirring, to react with the unreacted bromine. After filtration, the product was washed over a silica gel pad (2 cm thick) using *n*-hexane – ethyl acetate (4:1) as eluent to give α-bromophosphinate (0.275 g. 90% yield). ^{1}H NMR ($CDCl_3$, 250 MHz, ppm) δ: 1.08 (t, 3H, $^3J_{HH}$ = 7.1 Hz, 2-OCH_2CH_3), 1.26 (t, H, $^3J_{HH}$ = 7.1 Hz, 2-OCH_2CH_3), 3.79–4.00 (m, 2H, 2-OCH_2CH_3), 4.03–4.17 (m, 2H, 2-OCH_2CH_3), 4.79 (d, 1H, $^2J_{PH}$ = 12.5 Hz, -CH), 7.25–7.28 (m, 3H, -C_6H_5), 7.47–7.49 (m, 2H, -C_6H_5). ^{13}C NMR ($CDCl_3$, TMS, 62.9 MHz) δ: 16.57 (d, $^3J_{CP}$ = 5.8 Hz, 2-OCH_2CH_3), 16.78 (d, $^3J_{CP}$ = 5.8 Hz, 2-OCH_2CH_3), 41.85 (d, $^1J_{CP}$ = 159.2 Hz, -CH), 64.46 (d, $^2J_{CP}$ = 4.2 Hz, 2-OCH_2CH_3), 64.57 (d, $^2J_{CP}$ = 4.2 Hz, 2-OCH_2CH_3), 129.05–129.95, 134.94, 134.99 (-C_6H_5). MS (70 eV) *m/e*: 307 [M^+], 227 [M – Br], 90 [227 – P(O)$(OEt)_2$]. Anal. calcd. for $C_{11}H_{16}BrO_3P$ (%): C 43.00, H 5.21; found: C 43.10, H, 5.30.

Typical procedure for the preparation of diethyl α-iodobenzylphosphinate from diethyl α-hydroxybenzylphosphinate using APDPP–NIS

A two-necked flask, equipped with a dropping funnel and a reflux condenser, was charged with APDPP (0.67 g, 2.3 mmol) and α-hydroxybenzylphosphinate (0.24 g, 1 mmol) in CH_2Cl_2 (10 mL) in reflux condition. Then a solution of *N*-iodosuccinimide (2.3 mmol) in CH_2Cl_2 (10 mL) was added dropwise for a 1.5 h period. TLC monitoring showed the completion of the reaction after 10 h. After filtration of the reaction mixture, the residue was chromatographed on a silica gel column, using *n*-hexane – ethyl acetate (4:1) as eluent, to give α-iodobenzylphosphinate (0.31 g, 87% yield). ^{1}H NMR ($CDCl_3$, TMS, 250 MHz, ppm) δ: 3.80–4.08 (m, 2H, 2-OCH_2CH_3), 4.18–4.27 (m, 2H, 2-OCH_2CH_3), 4.98 (d, 1H, $^2J_{PH}$ = 13.4 Hz, -CH), 7.28–7.31 (m, 3H, -C_6H_5), 7.56–7.59 (m, 2H, -C_6H_5). ^{13}C NMR ($CDCl_3$, TMS, 62.9 MHz, ppm) δ: 15.41 (d, $^1J_{CP}$ = 139.9 Hz, -CH), 16.57 (d, $^3J_{CP}$ = 5.9 Hz, 2-OCH_2CH_3), 16.7 (d, $^3J_{CP}$ = 5.9 Hz, 2-OCH_2CH_3), 64.42 (d, $^2J_{CP}$ = 8.6 Hz, 2-OCH_2CH_3), 64.55 (d, $^2J_{CP}$ = 8.6 Hz, 2-OCH_2CH_3), 128.95–130.04 (-C_6H_5). MS (70 eV) *m/e*: 354 [M], 226 [M – Br], 89 [226 – P(O)$(OEt)_2$]. Anal. calcd. for $C_{11}H_{16}IO_3P$ (%): C 37.29, H, 4.52; found: C 37.5, H, 4.48.

References

1. J.P. Schaefer, J.G. Higgins, and P.K. Shenoy. Org. Synth. **49**, 6 (1969).
2. J. Drabowicz, J. Luczak, and M. Mikolajczyk. J. Org. Chem. **63**, 9565 (1998).
3. G.A. Wiley, R.L. Hershkowitz, B.M. Rein, and B.C. Chung. J. Am. Chem. Soc. **86**, 964 (1964).
4. T. Oshikawa and M. Yamashita. Bull. Chem. Soc. Jpn. **57**, 2675 (1984).
5. A.K. Bose and B. Lal. Tetrahedron Lett. **40**, 3937 (1973).
6. (*a*) C.R. Harrison, P. Hodhe, B.J. Hunt, E. Khoshdel, and G. Richarson. J. Org. Chem. **48**, 3721 (1983); (*b*) D.L.J. Clive and C.V. Denyer. J. Chem. Soc. Chem. Commun. 773 (1972); (*c*) I.W.J. Still, G.W. Kutuney, and D. McLean. J. Org. Chem. **47**, 560 (1982).
7. N. Belkhouya, C. Frechou, M. Benazza, D. Beaupere, R. Uzan, and G. Demailly. Tetrahedron Lett. **32**, 3977 (1991).
8. J. Hooz and S.S.H. Gilani. Can. J. Chem. **46**, 86 (1968).
9. R.G. Wiess and E.I. Synder. J. Chem. Soc. Chem. Commun. 1358 (1968).
10. J.B. Lee and T.J. Nolan. Can. J. Chem. **44**, 1331 (1966).
11. (*a*) A.J. Burns and J.I.G. Cadogan. J. Chem. Soc. 5788 (1963); (*b*) O. Sugimoto, M. Mori, and K. Tanji. Tetrahedron Lett. **40**, 7477 (1999).
12. S. Trippet. J. Chem. Soc. 2337 (1962).
13. G. Anilkumar, H. Nambu, and Y. Kita. Org. Process Res. Dev. **6**, 190 (2002).
14. S.L. Regen and D.P. Lee. J. Org. Chem. **40**, 1669 (1975).
15. E. Arsted, A.G.M. Barrett, B.T. Hopkins, and J. Kobberling. Org. Lett. **4**, 1975 (2002).
16. M. Caldarelli, J. Habermann, and S.V. Ley. J. Chem. Soc. Perkin Trans. 1, 107 (1999).
17. N. Iranpoor, H. Firouzabadi, A. Jamalian, and F. Kazemi. Tetrahedron, **61**, 5699 (2005).
18. L. Desmaris, N. Percina, L. Cottier, and D. Sinou. Tetrahedron Lett. **44**, 7589 (2003).

© 2006 NRC Canada

19. M.P. Pollastri, J.F. Sagal, and G. Chang. Tetrahedron Lett. **42**, 2459 (2001).
20. H. Firouzabadi, N. Iranpoor, and S. Sobhani. Tetrahedron, **60**, 203 (2004).
21. (*a*) T. Gajda. Phosphorus Sulfur Silicon Relat. Elem. **53**, 327 (1990); (*b*) S. Kumaraswamy, R. Senthamizh Selvi, and K.C. Kumaraswamy. Synthesis, 207 (1997); (*c*) D. Green, S. Elgendy, G. Patel, J.A. Baban, E. Skordalakes, W. Husman, V.V. Kakkar, and J. Deadman. Tetrahedron, **52**, 10215 (1996).
22. Fluka Chemie. Chemica – Biochemica 1993–1994.

© 2006 NRC Canada

DISCUSSION / DISCUSSION

Discussion of "Efficient, microwave-assisted intramolecular 1,3-dipolar cycloadditions of oximes and *N*-methylnitrones derived from *o*-alkenylmethoxyacetophenones"[1]

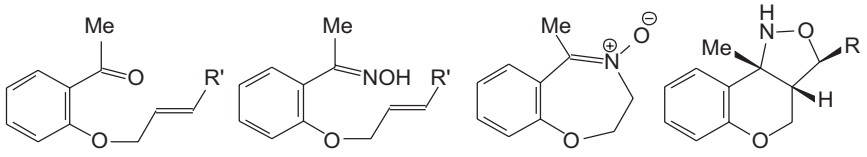
Frances Heaney and Linda Doyle

The following discussion note arises in defence of comments and assertions made upon our work (1) in the paper entitled "Efficient, microwave-assisted intramolecular 1,3-dipolar cycloadditions of oximes and *N*-methylnitrones derived from *o*-alkenylmethoxy-acetophenones", published in the *Canadian Journal of Chemistry* (2). Ishar and co-workers (2) include in their publication a number of inaccuracies and contradictions of our previously published work (1), the details of which are outlined in the following paragraphs.

Firstly, the inaccuracies. The abstract of the paper begins "Contrary to literature reports oximes (**2a**, **2b**) are transformed to nitrones, which undergo regio- and stereoselective intramolecular 1,3-dipolar cycloadditions, both on microwave heating under solvent free conditions and refluxing in toluene, to afford novel cycloadducts (**5a**, **5b**); the oxazepine *N*-oxide (**3a**) reported to be formed in 98% yield was obtained only as a minor product (~10%)." The final sentence of the introductory paragraph continues in the same vane, stating "Recently, it has been reported that the oximation of *o*-allyloxy-acetophenone and -benzophenone (**1**) affords *E*-oximes (**2**), which are quantitatively converted to dipoles (**3**, Scheme 1) on refluxing in xylene for 14 h (5)." The implication being that our cited work (1) included results on the behaviour of oximes **2**, i.e, **2a**–**2c**. This is in error, our publication concerned only the reaction of oxime **2a**, it did not include any data on **2b** or **2c**.

Secondly, the contradictions. The reaction of **2a** described in the publication by Ishar and co-workers (2) involves heating in toluene at 110 °C for 72 h, whilst our cited work (1) refers to thermal reaction of **2a** following 14 h heating in refluxing xylene (140 °C). Within the Results and discussion section of this paper (2), the authors contradict our work (1) no less than four times. The changes in experimental conditions, in terms of both reaction temperature (30 °C lower) and reaction duration (58 h longer) between that reported by Ishar and co-workers (2) and our cited work (1) are of sufficient magnitude to make it completely unreasonable for Ishar and co-workers to conclude that the result of their reaction contradicts our cited result. Indeed, following the publication of the paper by Ishar and co-workers, a researcher in our laboratory, not previously involved with the initial reactions of **2a**, repeated our reported work (1); thus, we can confirm that **2a** transforms (xylene, 140 °C, 14 h) smoothly to **3a** in excellent yield as we previously described (1).

The publication of the paper by Ishar and co-workers has publicly and inaccurately discredited our work on the important topic of the relationship between oxime geometry and reactivity. Moreover, this paper has already been cited by respected researchers in our field (3) and we welcome the opportunity to clarify our position with regard to the reaction of oxime **2a**.



1 **2** **3a, 3c** **5a, 5b**

a, R' = H; **b**, R' = Me; **c**, R' = Ph

Received 10 April 2006. Accepted 10 April 2006. Published on the NRC Research Press Web site at http://canjchem.nrc.ca on 21 July 2006.

F. Heaney[2] and L. Doyle. Department of Chemistry, National University of Ireland, Maynooth, Ireland.

[1]Appears in Can. J. Chem. **83**: 260–265.

[2]Corresponding author (e-mail: mary.f.heaney@nuim.ie).

 doi:10.1139/V06-104 © 2006 NRC Canada

References

1. F. Heaney and C. O'Mahony. J. Chem. Soc. Perkin Trans. 1, 341 (1998).
2. S. Singh, M.P.S. Ishar, G. Singh, and R. Singh. Can. J. Chem. **83**, 260 (2005).
3. O. Tamura, T. Mitsuya, X. Huang, Y. Tsutsumi, S. Hattori, and H. Ishibashi. J. Org. Chem. **70**, 10720 (2005).

© 2006 NRC Canada

DISCUSSION / DISCUSSION

Reply to the discussion by Heaney and Doyle on "Efficient, microwave-assisted intramolecular 1,3-dipolar cycloadditions of oximes and *N*-methylnitrones derived from *o*-alkenylmethoxyacetophenones"[1]

M.P.S. Ishar

This relates to the objections raised by Dr. Heaney and Linda Doyle regarding the use of the phrase "Contrary to literature reports" in our publication (1), which according to her has discredited their work (2).

I would like to make clear that our aim was never to discredit anyone's work. However, we had to contradict any over generalization, which was contrary to our observations.

We performed the reaction for the oximes under microwave heating because under these conditions the oximes are known to undergo a proton shift to generate nitrones in situ that can be trapped intramolecularly through 1,3-dipolar cycloadditions. As the observed outcome was in contradiction with the thermal transformations of related oximes reported by Heaney and O'Mahony (2), to compare our result with the thermal transformation, we carried out the corresponding thermal reactions by refluxing the oximes in toluene, wherein we obtained 1,3-dipolar cycloadducts as the major products in some cases. Therefore, we had no option but to contradict the literature reports.

If one goes through the abstract of the paper (2) by Heaney and O'Mahony, it reads "Thermally induced cyclization of *anti*-alkenyl oximes *E*-**7a**,**b** and *E*-**17a**,**b** affords cyclic α-alkoxycarbonylnitrones **8** and the 6,7-bicyclic nitrones **18**, respectively." This statement clearly generalizes the thermal behavior of similar oximes and no mention is made of reaction conditions. Heaney and O'Mahony have further asserted that the reaction outcome is related to the configuration (geometry) of oximes and that these oximes are configurationally stable under reaction conditions (refluxing xylene). However, in their Discussion, Heaney and Doyle have attributed the difference in reaction outcomes to possible differences in reaction conditions and reaction times, which is in contradiction with their own hypothesis that these oximes are configurationally stable under these reaction conditions (in refluxing xylene); we used a lower reaction temperature (refluxing toluene).

We have now repeated this reaction. The ^{1}H NMR spectra of the crude products obtained by refluxing oxime **2a** (**17a** in their case) in both toluene (72 h, spectrum A) and xylene (72 h, spectrum B) are presented here. It is obvious that intramolecular 1,3-dipolar cycloadducts are formed as the major products under both conditions and the nitrone **3a** derived from intramolecular alkylation is the minor product in both cases, although relative yields may be different; the spectra of the pure products, i.e., **5a** (spectrum D) and **3a** (spectrum E) are also presented for comparison. The ^{1}H NMR spectrum (C) obtained after refluxing oxime **2a** in xylene for 14 h is also presented. In this case, it is apparent that unreacted oxime **2a** is the major component, whereas Heaney and O'Mahony (2) reported the formation of nitrone **3a** (**18a** in their case) in excellent yield under the same conditions of temperature and time. Obviously, there is a great difference between our result and the results reported by Heaney and O'Mahony (2).

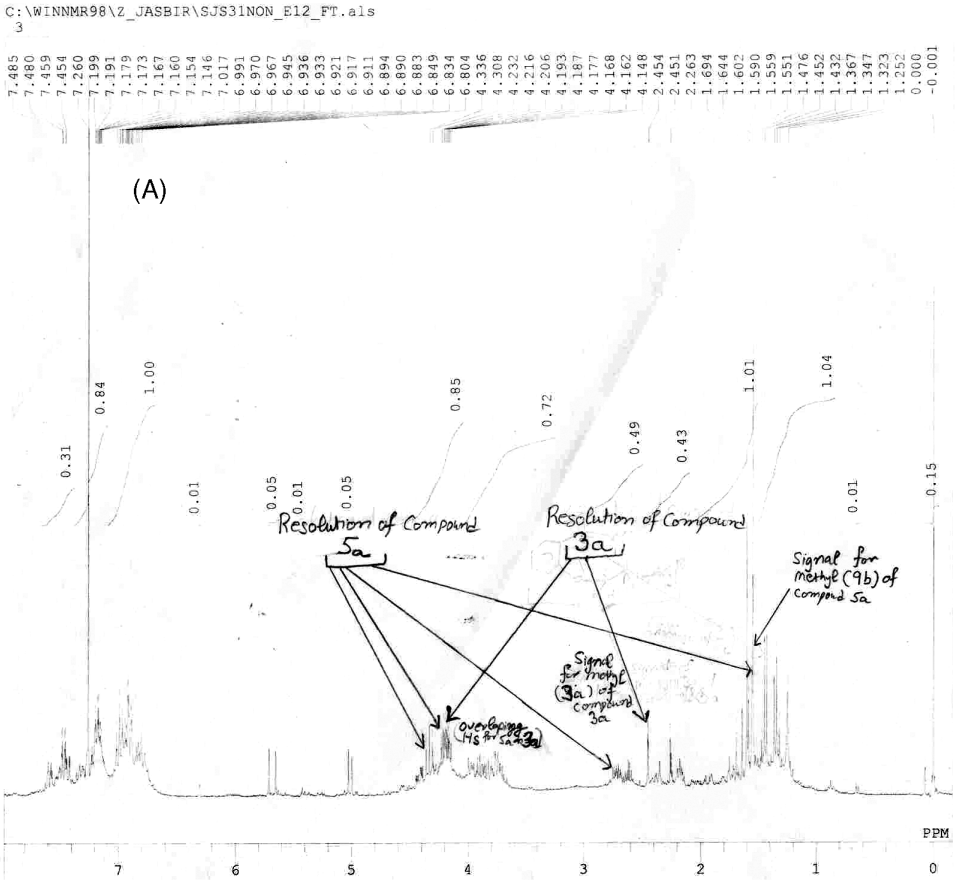
Even if it is accepted that the mode of transformation is specific to the configuration of the oxime, then the assertion that oximes are configurationally stable may not be correct or oxime **2a** does not preferably exist in the *E* form. Alternatively, the configuration is not important and the mode of transformation is temperature-dependent. Oxime **2a** gave the same spectral data as reported for **17a** by Heaney and O'Mahony (2), although they did not report the melting point and the crude solid obtained on trituration is used as such; however, they reported the assignment of the configuration of the oxime by ^{1}H nOe measurements. Interestingly, in one case, i.e., *o*-cinnamyloxyacetophenone oxime **3c** (in

Received 23 May 2006. Accepted 7 June 2006. Published on the NRC Research Press Web site at http://canjchem.nrc.ca on 21 July 2006.

M.P.S. Ishar. Department of Pharmaceutical Sciences, Guru Nanak Dev University, Amritsar-143005, Punjab, India (e-mail: mpsishar@yahoo.com).

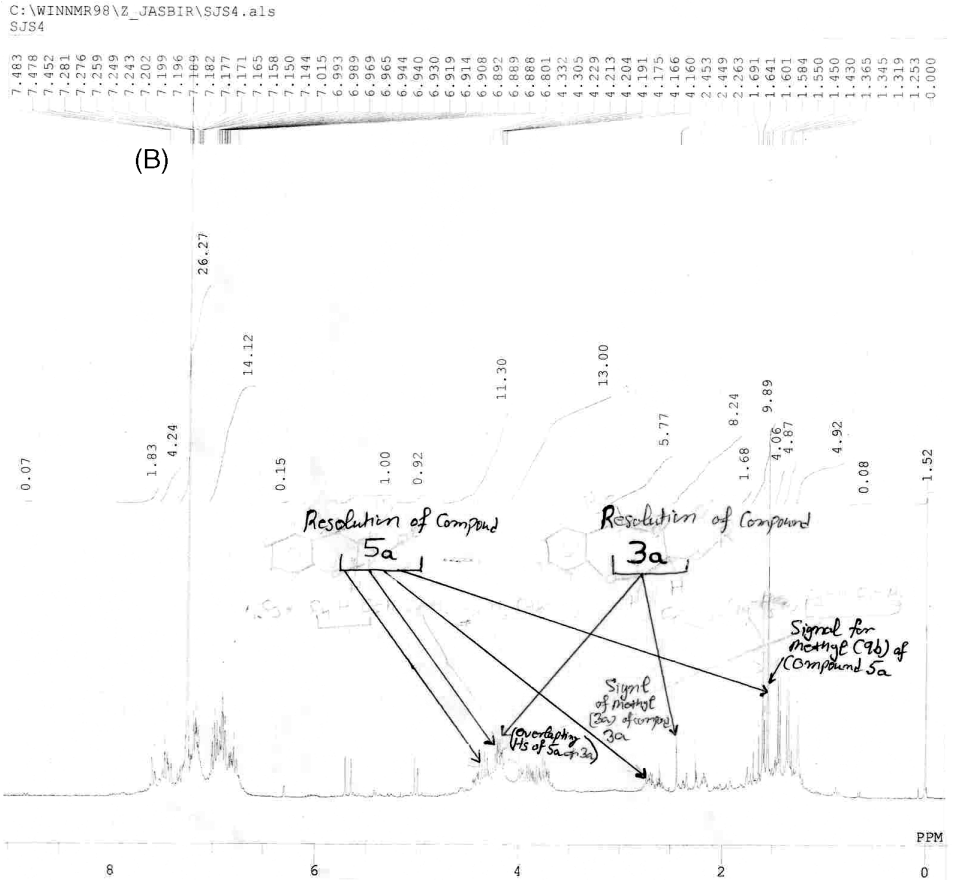
[1]Appears in Can. J. Chem., **84**. This issue.

 doi:10.1139/V06-105 © 2006 NRC Canada



JEOL FT-NMR AL-300 MHZ
CHEMISTRY DEPTT. G.N.D.U
OPERATOR :- JASBIR SINGH
DFILE C:\WINNMR98\Z_JASBIR\SJS31NON_E1:
COMNT 3
DATIM Tue Apr 25 11:35:35 2006
OBNUC 1H
EXMOD NON
OBFRQ 300.40 MHz
OBSET 130.00 KHz
OBFIN 1150.0 Hz
POINT 32768
FREQU 6016.8 Hz
SCANS 12
ACQTM 5.446 sec
PD 1.547 sec
PW1 6.3 us
IRNUC 1H
CTEMP 16.1 c
SLVNT CDCL3
EXREF 0.00 ppm
BF 0.12 Hz
RGAIN 17

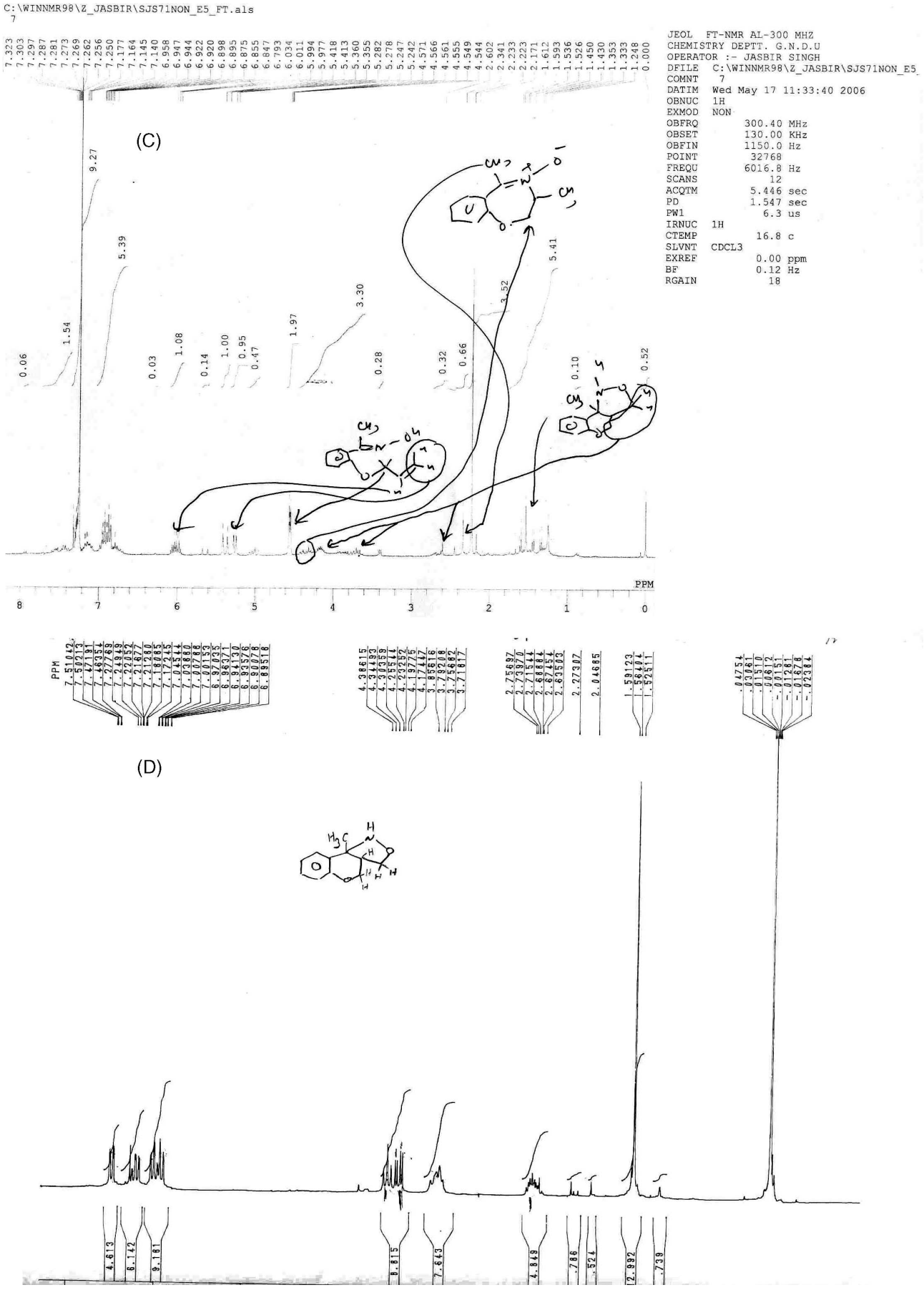
In Toluene Reflux



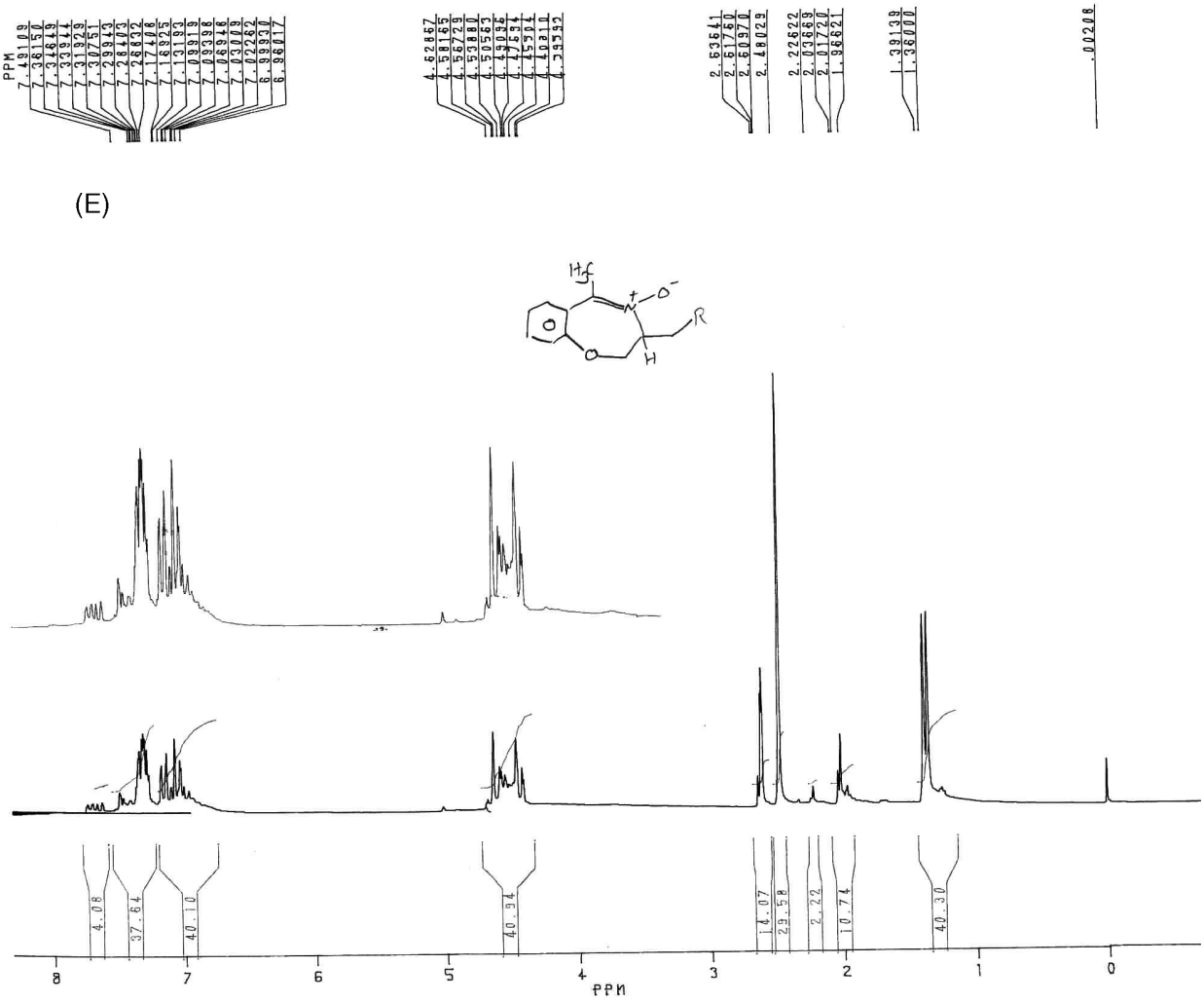
JEOL FT-NMR AL-300 MHZ
CHEMISTRY DEPTT. G.N.D.U
OPERATOR :- JASBIR SINGH
DFILE C:\WINNMR98\Z_JASBIR\SJS4.als
COMNT SJS4
DATIM Fri Apr 28 11:58:34 2006
OBNUC 1H
EXMOD NON
OBFRQ 300.40 MHz
OBSET 130.00 KHz
OBFIN 1150.0 Hz
POINT 32768
FREQU 6016.8 Hz
SCANS 14
ACQTM 5.446 sec
PD 1.547 sec
PW1 6.3 us
IRNUC 1H
CTEMP 18.0 c
SLVNT CDCL3
EXREF 0.00 ppm
BF 0.12 Hz
RGAIN 14

In xylene Reflux.

© 2006 NRC Canada



© 2006 NRC Canada



our paper, ref. 1), we obtained exclusive formation of a nitrone from intramolecular alkylation, thereby indicating that the nature of the alkene moiety dictates the mode of transformation.

It is true that only one example, i.e., oxime **17a** in their case (2) and **2a** in our paper (1) is identical. The generalization, if proved wrong in one case, can be rejected. Therefore, there is nothing wrong in using the phrase "Contrary to literature reports". Again, we would like to mention here again that our aim is not to discredit anyone's work, but to advance the understanding of the subject.

References

1. S. Singh, M.P.S. Ishar, G. Singh, and R. Singh. Can. J. Chem. **83**, 260 (2005).
2. F. Heaney and C. O'Mahony. J. Chem. Soc. Perkin Trans. 1, 341 (1998).

© 2006 NRC Canada

Stereoselective debromination and selective reduction of *vic*-dibromides with nickel boride

Jitender M. Khurana, Bhaskar M. Kandpal, Gagan Kukreja, and Purnima Sharma

Abstract: A simple procedure is reported for the stereoselective debromination of *vic*-dibromides with nickel boride at ambient temperature. Debromination with concomitant reduction of *vic*-dibromides to give dihydro products in a one-pot reaction is also reported. α,β-Dibromoketones can also be converted to their corresponding alcohols.

Key words: debromination, *vic*-dibromides, stereoselective, reduction, *E*-alkenes.

Résumé : On a mis au point une méthode simple de débromuration stéréosélective de dibromures *vicinaux* impliquant l'utilisation du borure de nickel à la température ambiante. On rapporte aussi la réaction monotope de débromuration avec réduction concomitante des dibromures *vicinaux* qui conduit à la formation des produits dihydrogénés. On peut aussi transformer les α,β-dibromocétones en alcools correspondants.

Mots clés : débromuration, dibromures *vicinaux*, stéréosélective, réduction, *E*-alcènes.

[Traduit par la Rédaction]

Introduction

The protection–deprotection of olefins via bromination and debromination (1) has been studied and different reagents and reaction conditions exist for debrominating *vic*-dibromides (2–9). Solvolytic stereoselective debromination has also been reported by DMF (10) and HMPA (11) without the aid of any reagents. The efficiency of a reagent greatly depends upon its selectivity and compatibility with other functionalities present in the substrate. Nickel boride is a versatile reducing agent reported to bring about a number of transformations, e.g., reduction, deoxygenation, desulfurization (12). It is known to behave differently under different reaction conditions and therefore we decided to explore its application for the debromination and (or) reduction of *vic*-dibromides.

Results and discussion

This is the first report on (*i*) stereoselective debromination of *vic*-dibromides to olefins and (*ii*) debromination with concomitant reduction of *vic*-dibromides in a one-pot reaction with nickel boride by changing the stoichiometric ratios and the solvent. Chalcone dibromides (benzylideneacetophenone dibromides/benzalacetophenone dibromides) also undergo chemoselective debromination to chalcones or undergo debromination with concomitant reduction to selectively give either dihydrochalcones or tetrahydrochalcones in methanol in one-pot reactions by changing the stoichiometric ratios.

A variety of stilbene dibromides and other *vic*-dibromides (Table 1, runs 1–16), soluble in tetrahydrofuran, undergo quantitative debromination with nickel boride generated in situ from nickel chloride and sodium borohydride using a molar ratio of 1:2:6 (substrate–$NiCl_2$–$NaBH_4$) in THF to give the corresponding alkenes (eq. [1]). The reactions were complete in 30–120 min at ambient temperature as monitored by TLC. Chalcone dibromides and other α,β-dibromoketones did not undergo complete debromination under these conditions. Smooth debromination of different chalcone dibromides and other α,β-dibromoketones, which were soluble in methanol, was successfully achieved to afford the corresponding chalcones or enones (Table 2, runs 17–28) in quantitative yields using a molar ratio of 1:5:2 (substrate–$NiCl_2$–$NaBH_4$) in methanol at ambient temperature for 15–60 min (eq. [1]). The carbonyl, carboxylic, carbmethoxy, highly sensitive furan and benzopyrone rings remained unaffected under these conditions. Even steroidal derivatives could be readily debrominated. The debrominations are stereoselective as (*E*)-stilbene was obtained from *meso*- and *dl*-stilbene dibromides, and fumaric acid was obtained from *meso*- and *dl*-α,β-dibromosuccinic acids. The possibility of any isomerization of (*Z*)-stilbene to (*E*)-stilbene or maleic acid to fumaric acid has been ruled out by independent reactions of (*Z*)-stilbene and maleic acid with nickel boride under identical conditions. The debrominations were undoubtedly due to the involvement of nickel boride generated in situ as starting *meso*-stilbene dibromide was recovered unchanged when treated with nickel chloride or sodium borohydride separately.

[1] $$\underset{\textbf{Ia–Iq, IIIa–IIIk}}{\text{RCHBr-CHBrR'}} \xrightarrow[\text{THF/MeOH, rt}]{NiCl_2,\ NaBH_4} \underset{\textbf{IIa–IIp, IVq, IVa–IVk}}{\text{RCH=CHR'}}$$

Received 20 April 2006. Accepted 1 August 2006. Published on the NRC Research Press Web site at http://canjchem.nrc.ca on 3 October 2006.

J.M. Khurana,[1] B.M. Kandpal, G. Kukreja, P. Sharma. Department of Chemistry, University of Delhi, Delhi 110007, India.

[1]Corresponding author (e-mail: jmkhurana@chemistry.du.ac.in; jmkhurana1@yahoo.co.in).

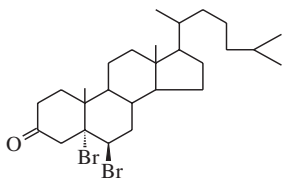
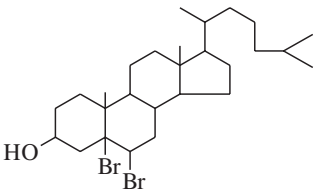
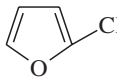
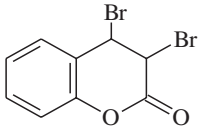
 doi:10.1139/V06-125 © 2006 NRC Canada

Table 1. Debromination of *vic*-dibromides with nickel boride in THF at ambient temperature.

Run	Substrate	Time (min)	Isolated yield (**II**) (%)
1	*meso*-$C_6H_5CHBrCHBrC_6H_5$ (**Ia**)	30	96
2	*dl*-$C_6H_5CHBrCHBrC_6H_5$ (**Ib**)	40	94
3	*meso*-4-$CH_3C_6H_4CHBrCHBrC_6H_5$ (**Ic**)	40	89
4	*meso*-4-$ClC_6H_4CHBrCHBrC_6H_5$ (**Id**)	40	88
5	*meso*-4-$ClC_6H_4CHBrCHBrC_6H_4Cl$-4 (**Ie**)	120	87
6	*meso*-4-$OCH_3C_6H_4CHBrCHBrC_6H_5$ (**If**)	40	76
7	$C_6H_5CHBrCHBrCOOH$ (**Ig**)	40	96
8	$C_6H_5CHBrCHBrCOOCH_3$ (**Ih**)	60	84
9	*meso*-COOHCHBrCHBrCOOH (**Ii**)	45	89
10	*dl*-COOHCHBrCHBrCOOH (**Ij**)	60	90
11	$CH_2BrCHBr(CH_2)_3CH_3$ (**Ik**)	60	80
12	*trans*-$CH_2BrCHBr(CH_2)_5CH_2$ (**Il**)	60	90
13	*trans*-$CH_2BrCHBr(CH_2)_3CH_2$ (**Im**)	30	75
14	*threo*-$CH_3(CH_2)_7CHBrCHBr(CH_2)_7COOH$ (**In**)	60	90
15	*threo*-$CH_3(CH_2)_7CHBrCHBr(CH_2)_7COOCH_3$ (**Io**)	45	88
16	$CH_3CHBrCHBrCOOCH_3$ (**Ip**)	35	90

Note: Seventy-five millilitres of solvent were used per gram of substrate. Molar ratio is 1:2:6 (substrate–$NiCl_2$–$NaBH_4$).

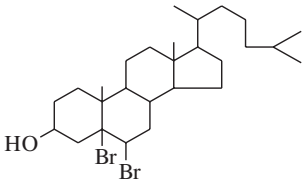
Table 2. Debromination of chalcone dibromides and α,β-dibromoketones with nickel boride in MeOH at ambient temperature.

Run	Substrate	Time (min)	Isolated yield (**IV**) (%)
17	$C_6H_5COCHBrCHBrC_6H_5$ (**IIIa**)	45	90
18	4-$CH_3C_6H_4COCHBrCHBrC_6H_5$ (**IIIb**)	35	88
19	4-$ClC_6H_4CHBrCHBrCOC_6H_5$ (**IIIc**)	20	90
20	4-$ClC_6H_4COCHBrCHBrC_6H_4Cl$-4 (**IIId**)	15	92
21	4-$OCH_3C_6H_4COCHBrCHBrC_6H_4CH_3O$-4 (**IIIe**)	25	88
22	4-$BrC_6H_4CHBrCHBr\ COC_6H_5$ (**IIIf**)	40	90
23	$C_6H_5CHBrCHBrCOCH_3$ (**IIIg**)	30	90
24	 (**IIIh**)	60	69
25	 (**Iq**)	20	92
26	 CH(Br)CH(Br)$COCH_3$ (**IIIi**)	45	88
27	 (**IIIj**)	15	90
28	$C_6H_5CHBrCHBrCOCHBrCHBrC_6H_5$ (**IIIk**)	35	85

Note: Thirty millilitres of methanol were used per gram of substrate. Molar ratio is 1:5:2 (substrate–$NiCl_2$–$NaBH_4$).

© 2006 NRC Canada

Table 3. Reduction of *vic*-dibromides with nickel boride in MeOH at ambient temperature.

Run	Substrate	Time (min)	Isolated yield (**V**) (%)
29	*meso*-$C_6H_5CHBrCHBrC_6H_5$ (**Ia**)	10	92
30	*dl*-$C_6H_5CHBrCHBrC_6H_5$ (**Ib**)	15	94
31	*meso*-4-$CH_3C_6H_4CHBrCHBrC_6H_5$ (**Ic**)	15	90
32	*meso*-4-$ClC_6H_4CHBrCHBrC_6H_5$ (**Id**)	10	94
33	*meso*-4-$ClC_6H_4CHBrCHBrC_6H_4Cl$-4 (**Ie**)	40	83
34	*meso*-4-$OCH_3C_6H_4CHBrCHBrC_6H_5$ (**If**)	25	85
35	$C_6H_5CHBrCHBrCOOH$ (**Ig**)	15	92
36	$C_6H_5CHBrCHBrCOOCH_3$ (**Ih**)	10	82
37	*meso*-COOHCHBrCHBrCOOH (**Ii**)	20	77
38	$CH_2BrCHBr(CH_2)_3CH_3$ (**Ik**)	15	85
39	*trans*-$CH_2BrCHBr(CH_2)_5CH_2$ (**Il**)	15	85
40	*trans*- $CH_2BrCHBr(CH_2)_5CH_2$ (**Im**)	20	86
41	*threo*-$CH_3(CH_2)_7CHBrCHBr(CH_2)_7COOH$ (**In**)	15	88
42	*threo*-$CH_3(CH_2)_7CHBrCHBr(CH_2)_7COOCH_3$ (**Io**)	15	91
43	$CH_3CHBrCHBrCOOCH_3$ (**Ip**)	15	81
44	 (**Iq**)	15	85

Note: Fifty millilitres of solvent were used per gram of substrate. Molar ratio is 1:3:9 (substrate–$NiCl_2$–$NaBH_4$).

We also report herein the debromination with concomitant reduction of *vic*-dibromides with nickel boride generated in situ. Since the activity, selectivity, and the physical and chemical properties of nickel boride depend on its method of preparation, and the amount of H_2 adsorbed in the crystal lattice of nickel boride depends upon the metal–boron ratio (12), the stoichiometric ratios of substrate–$NiCl_2$–$NaBH_4$ were varied to achieve the goal. *vic*-Dibromides (**Ia**–**Ii**, **Ik**–**Iq**) can be debrominated and reduced concomitantly in a one-pot reaction with nickel boride using a molar ratio of 1:3:9 in methanol to give the corresponding reduced product (Table 3, runs 29–44) in high yields (eq. [2]). Reactions of *meso*- and *dl*-stilbene dibromides using molar ratios of 1:2:6 or 1:1:3 of substrate – nickel chloride – sodium borohydride in methanol resulted in the formation of a mixture of (*E*)-stilbene and bibenzyl, implying that the reductions must be proceeding via the corresponding alkenes. The acid and ester groups were unaffected under these conditions.

[2] $$\underset{\textbf{Ia–Ii, Ik–Iq}}{RCHBr\text{-}CHBrR'} \xrightarrow[MeOH,\ rt]{NiCl_2,\ NaBH_4} \underset{\textbf{Va–Vi, Vk–Vq}}{RCH_2CH_2R'}$$

Chalcone dibromides and other α,β-dibromoketones gave corresponding alcohols (eq. [3]) rather than ketones under these conditions (Table 4, runs 45–53). Reactions of chalcone dibromide using molar ratios of 1:1:3 or 1:2:6 were incomplete and showed the presence of chalcone, dihydrochalcone, and tetrahydrochalcone. Selective debromination and reduction of the double bond could not be achieved under these conditions without affecting the carbonyl group. However, selective debromination was achieved using a molar ratio of 1:10:15 (substrate–$NiCl_2$–$NaBH_4$). High yields of dihydrochalcones were obtained under these conditions in methanol at ambient temperature (eq. [4]) (Table 5, runs 54–58). *p*-Bromochalcone dibromide (**IIIf**) also underwent competitive aryl debromination under these conditions.

[3] $$\underset{\textbf{IIIa–IIIe, IIIg–IIIj}}{RCHBr\text{-}CHBrC(=O)\text{-}R'} \xrightarrow[MeOH,\ rt]{NiCl_2,\ NaBH_4} \underset{\textbf{VIa–VIe, VIg–VIj}}{RCH_2CH_2\text{-}CH(OH)\text{-}R'}$$

[4] $$\underset{\textbf{IIIa–IIIe}}{RCHBr\text{-}CHBrC(=O)\text{-}R'} \xrightarrow[MeOH,\ rt]{NiCl_2,\ NaBH_4} \underset{\textbf{VIIa–VIIe}}{RCH_2CH_2\text{-}C(=O)\text{-}R'}$$

We conclude that nickel boride is an efficient and versatile reagent for debromination of *vic*-dibromides to the corresponding (*E*)-olefins and for debromination with concomitant reduction to give dihydro products at ambient temperature. Chalcone dibromides and other α,β-dibromoketones undergo debromination with complete reduction to give alcohols or undergo debromination with selective reduction to give dihydrochalcones.

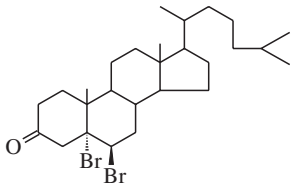
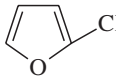
Experimental

General procedure for reactions of stilbene dibromides with $NiCl_2$ and $NaBH_4$ (molar ratio 1:2:6, Table 1) in THF

In a typical general procedure, *meso*-stilbene dibromide (1 g, 2.94 mmol) was dissolved in THF (75 mL) in a 250 mL round-bottomed flask mounted over a magnetic stir-

© 2006 NRC Canada

Table 4. Reduction of chalcone dibromides and α,β-dibromoketones with nickel boride in MeOH to their tetrahydro derivatives at ambient temperature.

Run	Substrate	Time (min)	Isolated yield (**VI**) (%)
45	$C_6H_5COCHBrCHBrC_6H_5$ (**IIIa**)	15	91
46	4-$CH_3C_6H_4COCHBrCHBrC_6H_5$ (**IIIb**)	5	80
47	4-$ClC_6H_4CHBrCHBrCOC_6H_5$ (**IIIc**)	10	96
48	4-$ClC_6H_4COCHBrCHBrC_6H_4$Cl-4 (**IIId**)	10	83
49	4-$OCH_3C_6H_4COCHBrCHBrC_6H_4CH_3$O-4 (**IIIe**)	10	78
50	$C_6H_5CHBrCHBrCOCH_3$ (**IIIg**)	15	82
51	 (**IIIh**)	10	83
52	 (**IIIi**)	45	75
53	$C_6H_5CHBrCHBrCOCHBrCHBrC_6H_5$ (**IIIj**)	45	75

Note: Forty millilitres of methanol were used per gram of substrate. Molar ratio is 1:3:9 (substrate–$NiCl_2$–$NaBH_4$).

Table 5. Reduction of chalcone dibromides with nickel boride in MeOH to their dihydrochalcones at ambient temperature.

Run	Substrate	Time (min)	Isolated yield (**VII**) (%)
54	$C_6H_5COCHBrCHBrC_6H_5$ (**IIIa**)	10	87
55	4-$CH_3C_6H_4COCHBrCHBrC_6H_5$ (**IIIb**)	10	86
56	4-$ClC_6H_4CHBrCHBrCOC_6H_5$ (**IIIc**)	15	83
57	4-$ClC_6H_4COCHBrCHBrC_6H_4$Cl-4 (**IIId**)	15	79
58	4-$OCH_3C_6H_4COCHBrCHBrC_6H_4CH_3$O-4 (**IIIe**)	10	82
59	4-$BrC_6H_4CHBrCHBrCOC_6H_5$ (**IIIf**)	—	—[a]

Note: Forty millilitres of methanol were used per gram of substrate. Molar ratio is 1:10:15 (substrate–$NiCl_2$–$NaBH_4$).
[a]A mixture of dihydrochalcone (56%) and *p*-bromodihydrochalcone (28%) was obtained.

rer. $NiCl_2$ (1.39 g, 5.88 mmol) was added followed by the addition of $NaBH_4$ (0.67 g, 17.64 mmol) while vigorously stirring the solution. The progress of the reaction was monitored by TLC using petroleum ether as eluent. The reaction was found to be complete in 30 min. The reaction mixture was filtered through a Celite pad (~1 in, 1 in = 25.4 mm) and washed with THF (2 × 10 mL). The combined filtrate was reduced to half and diluted with water (~150 mL). The product was extracted with ethyl acetate (3 × 15 mL). The combined extract was dried over anhydr. $MgSO_4$, filtered, and concentrated on a rotary evaporator to afford a white solid, which was identified as (*E*)-stilbene (0.5 g, 96%) with a mp of 112 °C (lit. value (13*a*) mp 114 °C) as demonstrated by the mixed mp, IR, and NMR spectra.

General procedure for reactions of chalcone dibromides with $NiCl_2$ and $NaBH_4$ (molar ratio 1:5:2, Table 2) in methanol

In a 100 mL round-bottomed flask mounted over a magnetic stirrer was placed a mixture of chalcone dibromide (1 g, 2.71 mmol), methanol (30 mL), and $NiCl_2$ (3.22 g, 13.55 mmol). $NaBH_4$ (0.206 g, 5.43 mmol) was added with continuous stirring. Disappearance of starting material was monitored by TLC using petroleum ether – benzene (50:50) as eluent. The reaction was complete after 45 min. The reaction mixture was filtered through a Celite pad (~1 in) and washed with methanol (2 × 15 mL). The combined filtrate was diluted with water (~150 mL) and extracted with ethyl acetate (3 × 15 mL). The combined extract was dried over anhydr. $MgSO_4$, filtered, and concentrated on a rotary evaporator to yield chalcone (0.508 g, 90%), confirmed with a mp of 55 °C (lit. value (13*b*) mp 56–58 °C) as demonstrated by the mixed mp, IR, and NMR spectra.

Reactions of stilbene dibromides with $NiCl_2$ and $NaBH_4$ (molar ratio 1:3:9, Table 3) in methanol

A mixture of *meso*-stilbene dibromide (1 g, 2.94 mmol), methanol (50 mL), and $NiCl_2$ (2.090 g, 8.82 mmol) was placed in a 100 mL round-bottomed flask and fitted with a reflux condenser and a guard tube. $NaBH_4$ (1.005 g, 26.46 mmol) was carefully added with continuous stirring. The progress of the reaction was monitored using petroleum ether as an eluent. The starting material disappeared in 10 min. The reaction was worked up as in previous proce-

© 2006 NRC Canada

dures. The product obtained was identified to be 1,2-diphenylethane (0.48 g, 92%) by IR and NMR spectra.

Reactions of chalcone dibromides with $NiCl_2$ and $NaBH_4$ (molar ratio 1:3:9, Table 4) in methanol

Chalcone dibromide (1 g, 2.71 mmol), $NiCl_2$ (1.926 g, 13 mmol), and methanol (40) mL were placed in a 100 mL conical flask fitted with a condenser. The flask was mounted over a magnetic stirrer. Sodium borohydride (0.929 g, 24.39 mmol) was added very cautiously while vigorously stirring the solution. The progress of the reaction was monitored by TLC using petroleum ether – benzene (50:50) as eluent. The starting material disappeared after 15 min and then the reaction was worked up as in previous procedures. The product obtained was identified to be tetrahydrochalcone (0.50 g, 91%) by IR and NMR spectra.

Reaction of chalcone dibromide with $NiCl_2$ and $NaBH_4$ (molar ratio 1:10:15, Table 5) in methanol

Chalcone dibromide (1 g, 2.71 mmol), $NiCl_2$ (6.422 g, 27.1 mmol), and methanol (40 mL) were added to a 100 mL round-bottomed flask fitted with a reflux condenser. The reaction mixture was stirred at room temperature and $NaBH_4$ (1.54 g, 40.65 mmol) was added very cautiously. The progress of the reaction was monitored by TLC using petroleum ether – benzene (50:50) as eluent. The starting material disappeared completely after 30 min and the reaction was worked up as in previous procedures. Dihydrochalcone (0.49 g, 87%) was isolated and identified with a mp of 70 to 71 °C (lit. value (13*c*) mp 72–75 °C) as demonstrated by IR, and NMR spectra.

In the case of aliphatic and cyclic *vic*-dibromides, because of high solubility in water, the reaction mixture was filtered through a Celite pad and washed with methanol or THF (2 × 15 mL). The combined extract was dried over anhydr. $MgSO_4$, filtered, and concentrated on a rotary evaporator. The product was extracted by triturating with dry ether.

Acknowledgements

We are pleased to acknowledge the financial support for this work by the Council of Scientific and Industrial Research (CSIR, New Delhi, India), project No. 01(1567)/99/EMR-II. BMK and GK also wish to thank CSIR, PS, and the University Grants Commission (UGC), New Delhi, for providing fellowships.

References

1. M.B. Smith and J. March. Advanced organic chemistry: Reactions, mechanisms, and structures. 5th ed. McGraw Hill International, New York. 1996. p. 1343, and refs. citied therein.
2. (*a*) R.C. Larock. Comprehensive organic transformations. 2nd ed. Wiley-VCH, New York. 1999. p. 259; (*b*) J. Vadecard, J.-C. Plaquevent, L. Duhamel, P. Duhamel, and L. Toupet. J. Org. Chem. **59**, 2285 (1994); (*c*) V. Montanari and D.D. DesMarteau. J. Org. Chem. **57**, 5018 (1992).
3. T. Norris, C. Dowdeswell, N. Johnson, and D. Daia. Org. Process Res. Dev. **9**, 792 (2005), and refs. cited therein.
4. D.A. Jackson, A. Edmunds, M.C. Bowden, and B. Brockbank. PCT Int. Appl. 143 459792 (2005).
5. B.C. Ranu and R. Jana. J. Org. Chem. **70**, 8621(2005).
6. A. Marfat. US Patent 4 761 485, 2 August 1988.
7. P.-H. Li, W.-P. Rao, M. Wang, and L. Wang. Chem. Res. Chin. Univ. **20**, 598 (2004).
8. B.C. Ranu, S. Guchhait, and A. Sarkar. Chem. Commun. (Cambridge), **19**, 2113 (1998).
9. T.S. Butcher and M.R. Detty. J. Org. Chem. **63**, 177 (1998).
10. (*a*) J.M. Khurana and G.C. Maikap. J. Org. Chem. **56**, 2582 (1991); (*b*) J.M. Khurana, G.C. Maikap, and P.K. Sahoo. Synthesis, 827 (1991).
11. J.M. Khurana, G. Bansal, and S. Chauhan. Bull. Chem. Soc. Jpn. **74**, 1089 (2001).
12. J.M. Khurana. J. Indian Chem. Soc. **81**, 733 (2004).
13. (*a*) Beilstein Institute. Handbuch Der Organischen Chemie. 5th Supp. p. 630; (*b*) 7th Supp. p. 478; (*c*) p. 2150.

© 2006 NRC Canada

Theoretical study on six-fold coordinated silicon in silicophosphate compounds

Hassan Rabaâ and Fatima Bkiri

Abstract: Extended Hückel tight-binding (EHTB) calculations were performed on silicophosphate compounds with six-coordinated silicon. Speculative structures related to silicon coordination in SiP_2O_7 are reported. To account for the particular structural distortion caused by the presence of SiO_6 in the silicon pyrophosphate, it is important to examine how the stability and the band gap of the extended structure of SiP_2O_7 are affected. Different theoretical tools are used (EHTB, ab initio Hartree–Fock, and density functional theory DFT-B3LYP). To obtain detailed descriptions of the incorporation of hexacoordinated silicon in this material, the band structures in SiP_2O_7 and $[P_2O_7]^{4-}$ were analyzed. It seems that the diffuse orbitals of silicon and the high energy of the Si 3p orbital lead to higher energy coordination and contribute to the breaking of the P-O-P bridge and the forming of a Si-O-P entity in this material. In addition, to provide more evidence of the existence of the octahedral silicon coordination in SiP_2O_7 (**1**), two model clusters $[P_4Si_2O_{23}H_{18}]$ (**2**) and $[P_4Si_2O_{19}H_{10}]$ (**3**) involving silicon atoms in octahedral and tetrahedral sites were investigated using Hartree–Fock and DFT theories. A remarkable agreement between calculated and experimental bond lengths for Si—O and P—O is obtained using the DFT calculation. The model cluster **2** corroborates the structural change in the Si-O-P and P-O-P fragments seen in **1**. The IR vibrational frequencies are calculated for both model clusters and are predicted to shift towards lower frequencies in the octahedral Si sites, which is consistent with experimental data.

Key words: silicophosphate, SiO_6, band structure, tight-binding calculations, Hartree–Fock, DFT, B3LYP, model cluster, IR frequencies.

Résumé : On a effectué des calculs étendus de Hückel à liaison serrée (EHTB) sur des silicophosphates comportant un silicium hexacoordiné. On rapporte les structures proposées pour la coordination du silicium dans le SiP_2O_7. Pour tenir compte de la distorsion particulière de la structure provoquée par la présence du SiO_6 dans le pyrophosphate de silicium, il est important d'examiner comment la stabilité et la bande interdite de la structure étendue du SiP_2O_7 sont affectées. On a étudié divers outils théoriques (calculs ab initio de Hartree–Fock, EHBT et théorie de la densité fonctionnelle, DFT-B3LYP). Dans le but d'obtenir des descriptions détaillées de l'incorporation du silicium hexacoordiné dans ce composé, on a analysé les structures de bande du SiP_2O_7 et du $[P_2O_7]^{4-}$. Il semble que les orbitales diffuses du silicium et l'énergie élevée de l'orbitale Si (3p) conduisent à une énergie de coordination plus élevée et qu'elles contribuent à une rupture du pont P-O-P et à la formation de l'entité Si-O-P dans ce produit. De plus, dans le but d'obtenir plus d'information sur l'existence d'une coordination octaédrique du silicium dans le SiP_2O_7 (**1**), et faisant appel aux théories de Hartree–Fock et de la densité fonctionnelle, on a étudié deux agrégats modèles $[P_4Si_2O_{23}H_{18}]$ (**2**) et $[P_4Si_2O_{19}H_{10}]$ (**3**) impliquant des atomes de silicium dans des sites octaédriques et tétraédriques. Avec la théorie de la densité fonctionnelle, on a obtenu un accord remarquable entre les valeurs calculées et expérimentales des liaisons Si—O et P—O. L'agrégat modèle **2** permet de corroborer le changement structural des fragments Si-O-P et P-O-P observés dans le produit **1**. On a calculé les fréquences vibrationnelles en infrarouge pour les deux composés modèles et ces calculs permettent de prédire un déplacement vers des fréquences plus basses pour les sites de silicium octaédrique, ce qui est en accord avec les données expérimentales.

Mots clés : silicophosphate, SiO_6, structure de bande, calculs.

[Traduit par la Rédaction]

Introduction

Silicophosphate compounds have been the subject of intensive study for their important applications (1–5). These materials have good reactivity and easy resorbance for natural bone in animals (1). For example, a calcium silicophosphate ceramic was tested for use in orthopaedic implants (3). High-silica glasses containing P_2O_5 have been recognized as promising materials for optical fibre communications (2). Vitreous ionic conducting materials have also been investigated as electrolytes in high-density solid-state alkaline batteries (6–8).

The addition of oxides such as Li_2O, Na_2O, or K_2O to the SiO_2–P_2O_5 binary system regulates the degree of SiO_6 formation and stimulates the copolymerisation of silicate compounds by forming a metaphosphate group and pyro-

Received 22 June 2005. Accepted 13 July 2006. Published on the NRC Research Press Web site at http://canjchem.nrc.ca on 3 October 2006.

H. Rabaâ[1] and F. Bkiri. Université Ibn Tofail, LCTA, Département de Chimie, P.O. Box 133, 14000 Kénitra, Morocco.

[1]Corresponding author (e-mail: hrabaa@yahoo.com).

 doi:10.1139/V06-126 © 2006 NRC Canada

phosphate linked by SiO_4 tetrahedra and SiO_6 octahedra (5–11). Molecular mechanics (12) and ab initio studies (13) on alkali phosphates have also been reported. The authors optimized different small clusters that contain the P-O-P unit with different alkali atoms (13*a*).

Silicon pyrophophosphate is of special interest because of the similarity of P and Si coordination environments. For example, phosphates and silicates exhibit similar crystalline structures based on $[PO_4]^{3-}$ and $[SiO_4]^{4-}$ tetrahedral units (11–20). Moreover, it is experimentally interesting to see how the low-temperature structure phases of SiP_2O_7 (**1**) differ from the high-temperature ones (14 and15). Eight crystal phases exist for **1** including the monoclinic and cubic structures that were prepared at high temperature. From an experimental viewpoint, several attempts to characterize **1** have been reported utilizing solid state NMR (9) and X-ray powder diffraction (20). The characterization of the structure and nature of the P-O-Si bond fragment in **1** remains a difficult task (12–20).

The first aim of this work is to study the electronic structural changes induced by a six-coordinate silicon atom in the silicon pyrophosphate phase obtained at low temperature. An understanding of the band structure of **1** using an extended Hückel tight-binding (EHTB) approach (21 and 22) is required. Our theoretical investigation focuses on the detailed description of the Si—O and P—O bonds of the SiO_6 building blocks with respect to binding energy, orbital overlap, and the band widths of the Si and P atoms in **1**. The second aim is to understand the changes that occur in this material using two cluster models $[P_4Si_2O_{23}H_{18}]$ (**2**) (Si in octahedral site) and $[P_4Si_2O_{19}H_{10}]$ (**3**) (Si in tetrahedral site) within an ab initio Hartree–Fock framework and also employing density functional theory, i.e., B3LYP. Finally, we analyze IR vibrational frequencies by comparing calculated frequencies with experimental data.

Computational details

The first part of this work focuses on the structure–property relationship of **1** by studying the one-electron band structure determined from a tight-binding approximation based on the extended Hückel method (EHTB) (21). The methodology is described in detail elsewhere and has been found to be quite satisfactory in describing a wide range of organic and inorganic structural problems (22). Both periodic (YAeHMOP, yet another extended Hückel molecular orbital package) (23) and molecular (CACAO, computer-aided composition of atomic orbitals) extended Hückel (24) software were used. The parameters employed in our YAeHMOP calculation are listed in Table 1. The off-diagonal elements of the Hamiltonian matrix were evaluated with the Wolfsberg–Helmholtz formula (26). Numerical integrations over the symmetry-unique section of the Brillouin zone of the three-dimensional structure were performed using a set of 36 k-points. DOS and COOP signify density of states and crystal orbital overlap population, respectively. The positive and negative regions shown in the COOP curves represent the bonding and antibonding zone between atoms. The *x* axes in Figs. 1 and 2 correspond to the DOS peaks. Their total integration fixes the main bonding encountered in the corresponding bands and is estimated generally between 0% and 100%.

Table 1. Parameters used in the EHTB calculations with a weighted H_{ij} approximation.

Atoms	Orbital	H_{ij} (eV)	ξ
P	3s	–18.6	1.75
	3p	–14.0	1.30
O	2s	–32.3	2.275
	2p	–14.8	2.275
Si	3s	–17.3	1.383
	3p	–9.20	1.383

Note: H_{ij} = orbital energy, ξ = Slater exponent. The k-points are generated according to the geometrical methods of Ramirez and Böhm (25).

Fig. 1. DOS of **1** from EHTB calculations. (*a*) Total DOS of **1**. Shaded areas represent the projection of individual atoms in, (*b*) silicon, (*c*) phosphorus, and (*d*) bridging oxygens in P-O-P. For clarity, the antibonding bands are not plotted. The same scaling factor is used for all plots. (X axes correspond to DOS peaks).

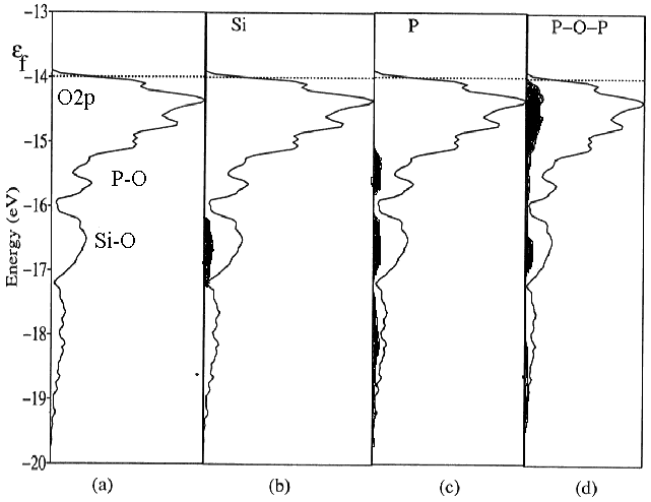
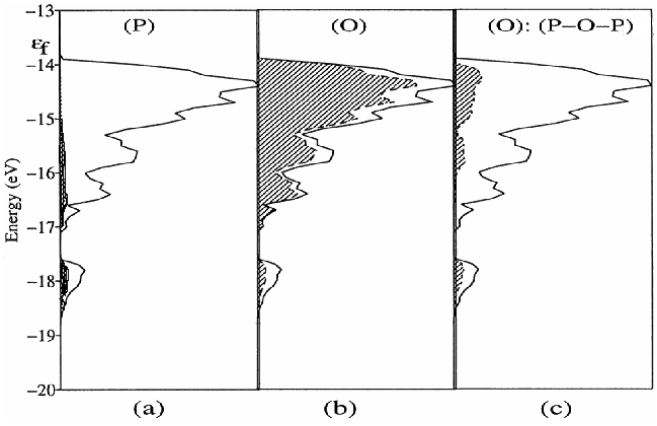


Fig. 2. DOS of 4 from EHTB calculations. The contributions of individual atoms are shown in shaded areas: (a) phosphorus (b) total of oxygens, and (c) bridging oxygens in P-O-P.



The second part concerns the model cluster using ab initio Hartree–Fock calculations in the Gaussian 98 package (27). The choice of this method was made for several reasons. For one, it was used in different theoretical investigations and in

© 2006 NRC Canada

cluster modeling by several authors (13). In addition, our model clusters **1** and **2** represent the real unit cell in pyrophosphate and metaphosphate compounds, respectively. Thus, two model clusters with four- and six-coordinate silicon are investigated, **2** and **3**, respectively. The cluster geometries were optimized at the Hartree–Fock (HF) level with the standard 6-31G* basis set for H, O, Si, and P atoms. Hydrogen atoms were used to terminate the dangling bonds that would otherwise result in open valences. To account for the electron correlation effects, supplementary calculations with DFT (27) using the same basis quoted above were undertaken for both clusters. Harmonic frequencies were calculated to determine the stationary points and the active band in the infrared spectra.

Results and discussion

Crystal structure of 1

Different speculations about powder structure resolution and coordination of SiO_6 in the crystal structure of SiP_2O_7 have been reported (5 and 6, 14 and 15). We begin by analyzing the crystal structure of **1**, synthesized at low temperature, according to the X-ray powder diffraction obtained by Clearfield and co-workers (20) (Fig. 3). It belongs to the hexagonal space group $P6_3$. The Si and P atoms are, respectively, octahedrally and tetrahedrally coordinated with oxygen atoms. The layers in **1** are held together by a linear P-O-P angle. From Fig. 3, it is clear that an oxygen atom that binds to any silicon is shared by six pyrophosphate groups. In other words, each pyrophosphate group binds to six different silicon atoms.

In Table 2, the important bond lengths and bond angles of **1** are summarized (20). The averages of the P—O_b (O_b, bridging oxygen, corresponds to O_2 in Table 2) and P=O_t (O_t, terminal oxygen, corresponds to O_1 and O_3) bond lengths are 1.56 Å and 1.49 Å, respectively. We observe that the PO_4 tetrahedral units possess three phosphorus–oxygen bonds (P—O_1, P—O_3, and P—O_2), two longer and one shorter. Moreover, a careful investigation of the data presented in Table 2 and a comparison of other compounds with tetrahedral silicon (4), shows an important structural change in **1** induced by the presence of the six-coordinated silicons; some Si—O bonds are elongated (1.77–1.70 Å vs. 1.62 Å) while P—O bonds are shortened (1.48 Å vs. 1.60 Å). The variation in the range of O-Si-O angles from 81° to 102° involves the distortion away from an ideal octahedron. Moreover, the P-O-P angle is equal to 180°. In accounting for such a structural change in this material (28–35), it was interesting to examine variation, stability, band gap, and binding energy by using tight-binding calculations in the extended structure of **1** or the cluster model.

Tight-binding calculations

We begin by exploring the EHTB-derived band structure of **1** Figures 1*a*–1*d* show, respectively, a plot of the total DOS for **1** with different DOS projections for Si and P atoms and the bridging oxygen atoms within the P-O-P fragment. In Fig. 1, we choose an energy window from –13 to –20 eV that represents the most important zone of P—O and Si—O bonding analysis including the band gap and the Fermi level (ε_f).

Fig. 3. Polyhedral representation of **1** as derived from ref. 20. The tetrahedra are PO_4 and the octahedra are SiO_6. The small red circles are O while the P-O-P bonds form linear bridges between the layers. The crystals belong to the hexagonal space group $P6_3$, with projection in the *ac* plane.

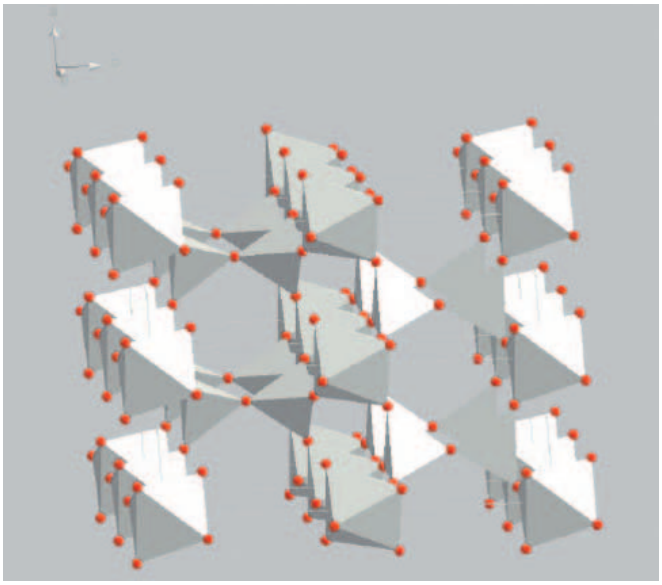


Table 2. Summary of the important bond lengths and angles for **1** from ref. 20.

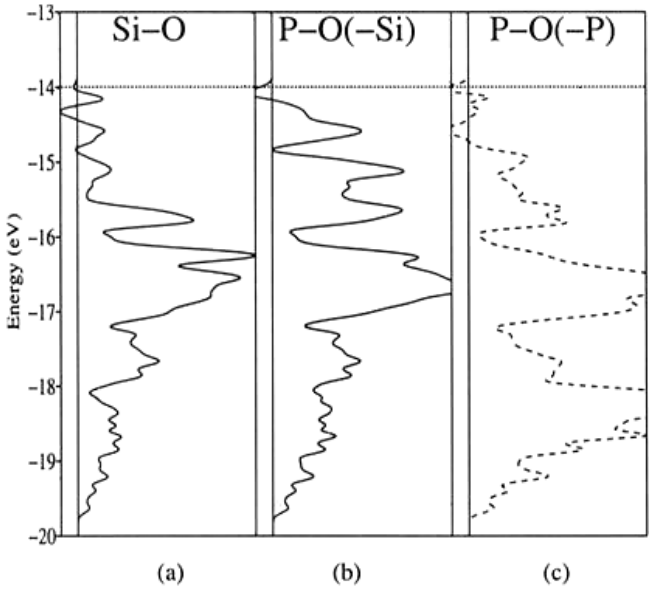
Bond lengths (Å)	
Si—O_1	1.77(1)
Si—O_3	1.70(2)
P_1—O_2	1.58(2)
P_1—O_3	1.48(1)
P_2—O_2	1.53(2)
P_2—O_1	1.48(1)
Bond angles (°)	
P_1-O_1-Si	152(2)
P_2-O_3-Si	141(1)
O_1-Si-O_1	81(1)
O_1-Si-O_3	86(1)
O_1-Si-O_3	102(1)
O_3-Si-O_3	93(1)
O_3-P_1-O_3	115(1)
O_3-P_1-O2	103(1)
P_2-O_2-P_1	180

Note: O_1 and O_3 are O_t and O_2 is O_b.

As a first observation of Fig. 1, it is clear that **1** displays a large band gap (3.5 eV), consistent with an insulator material. Just below the Fermi level (ε_f) at –13.7 eV, a large band formed by the lone pairs of terminal atoms with a small admixture of P (P—O bonds) appears. From –16.0 to –19.6 eV, the band contains a small contribution from silicon atoms, enough to show the presence of Si—O bonds. In this DOS portion, the dispersion of the silicon band reveals (Fig. 1*b*) a large Si—O interaction involving the diffuse orbital of silicon property and represents the interaction of Si-O_6 in the silicophophate.

© 2006 NRC Canada

Fig. 4. Average COOP plots for **1**. The contribution of each bond is shown: (*a*) P—O, (*b*) P—O (—Si) with an oxygen linked to the silicon atoms, and (*c*) P—O (—P) with an oxygen linked to the phosphorus atoms.



In Fig. 4, the COOP curves confirm this Si—O bond interaction. We show the binding of Si—O in SiO_6 and two types of P—O bonds, one related to a P-O-P linkage and another to a Si-O-P linkage. In addition, we notice a large Si—O and Si-O-P bonding contribution with an interesting overlap of silicon and oxygen concentrated in the region from –16.0 to –19.6 eV. The overlap averages of Si—O and P—O are 0.30 and 0.50, respectively. Meanwhile, the average silicon and phosphorus atomic charges are 2.77 and 2.44, respectively, showing a big difference between the silicon and phosphorus environments in terms of the silicon octahedral and phosphorus tetrahedral sites. In addition, the charges of O_b in P-O_b–P and Si-O_b–P, are equal to –1.22 and –0.99, respectively, indicating that the bridging oxygen charges in the Si-O-P bridges are more delocalized than in the P-O-P units. A similar extended Hückel calculation also shows the presence of a silicon molecular orbital (MO) at high energy around –15 eV (36).[2] Thus according to this analysis, the silicon orbitals should contribute significantly to the stability of **1** by an important interaction with the six surrounding atoms of oxygen and the latter probably explains the crystallization of **1** with six-fold coordinated silicon.

However, to understand the six-fold silicon coordination in **1** let us analyze the DOS and silicon binding energy of the hypothetical sublattice $[P_2O_7]^{-4}$ (**4**) obtained by removing the silicon atoms from the extended structure of **1**. We calculated the density of state of **4** (Fig. 2) and observed a higher-energy part of the valence band that is characterized by the O(2p) nonbonding levels of **4**. Below this band, another band has O(2s) oxygen and phosphorus P(3p) bonding character. The Fermi level moves down to around –13.8 eV in **4.** This shift is largely due to the removal of Si—O interactions in **4**. Also, the P—O band around –18 eV is less dispersed than in **1** (–17 to –20 eV). The difference in curve shape (Figs. 1 and 2) comes from the formation of the incoming Si—O bonds and P=O destruction. In addition, the computed binding energy of the hexacoordinated silicon (Si-O_6) in **1** was estimated at 1.1 eV. But this energy is insufficient to give a more stable compound at ambient temperature and explains the difficulty in synthesizing a hexacoordinated silicon. Moreover, the hypervalency (diffuse orbital) of Si atoms should also strongly modify the environment of phosphorus by breaking P=O bonds and forming Si—O bonds because of the closer energy level between oxygen and silicon atoms (37).

Table 3. Ab initio HF optimized bond lengths and angles of **2** (Si in octahedral sites, linear chains) and **3** (Si in tetrahedral sites, linear chains).

	2	**3**
Average bond lengths (Å)		
Si—O_b	1.893	1.612
Si—O_t	1.782	1.649
P=O_n	—	1.541
P—O_b	1.599	1.619
P—O_t	1.639	1.656
O—H	0.926	0.946
Average bond angles (°)		
O-Si-O	87.0	110
Si-O_b-P	121.4	146
O-P-O	103	110
P-O-P	158.1	140

Model clusters

Ab initio calculation

Besides the extended Hückel calculations, our aim is to complete our previous electronic analysis of the hexacoordinated silicon with an ab initio methodology (HF) using two model clusters **2** and **3**. The models were chosen for the following reasons: **2** represents a model of the pyrophosphate chain (a linear chain with Si atoms in octahedral sites) while **3** models the linear chain usually found in metaphosphates (a linear chain with silicon in tetrahedral sites). As a first result, the middle column in Table 3 lists the optimized bond lengths and angles of **2**. The optimized cluster is presented in Fig. 5. In comparing the structures of **1** and **2,** we observe an increase of the Si—O (1.89 Å) and P—O_b bond lengths (1.64 Å) in **2**, which indicates a substantial change in bond and dihedral angles. In addition, the mean angle of O-Si-O is closer to 87° in **2** and involves distortion away from an ideal octahedron of SiO_6, in agreement with the X-ray data of **1.**

The computed P-O-P angle of 158° is not surprising because different studies have found P-O-P angles ranging from 140° to 180° (29). This can also be interpreted in terms of the change in the π bonding character of the P—O bond, which depends on the average π bonding in the cluster. The lone pair orbital of oxygen (O_b) is substantially stabilized by

[2] Rabaâ. Unpublished work.

© 2006 NRC Canada

Fig. 5. Ab initio HF optimized structure of **2** with Si atoms in the octahedral site. The red circles represent oxygen atoms, blue circles represent silicon, big yellow circles represent phosphorus, and small gray circles represent hydrogen. P-O-P and Si-O-P angles are 158° and 121°, respectively.

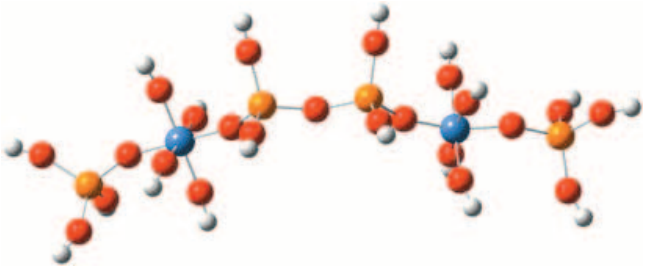
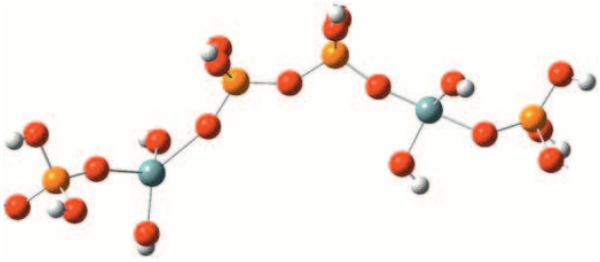


Fig. 6. Ab initio HF optimized structure of **3** with Si in tetrahedral coordination. The red circles represent oxygen atoms, blue circles represent silicon, yellow circles represent phosphorus, and small gray circles represent hydrogen. P-O-P and Si-O-P angles are 147° and 146°, respectively.



mixing with the $\sigma^*_{P\text{-}O}$ acceptor orbital and induces the linearity of P-O-P angles.

To complete our analyses, we compared the hexa- and tetra-coordinated silicon electronic structures. Thus, a new cluster **3** with silicon in the tetrahedral site was calculated. The optimized geometry of **3** is shown in Fig. 6.

The right column of Table 3 shows the calculated P—O_b, P—O_t, Si—O_b, and Si—O_n (O_n, nonbridging) bonds, which are equal to 1.612 Å, 1.649 Å, 1.619 Å, and 1.656 Å, respectively. The P=O bond is equal to 1.54 Å. Our calculations confirm a relative shortening of the Si—O and P—O bonds in **3** and a decrease of the P-O-P bond angles (146°). O'Keeffe et al. (34) reported similar values for the optimized distances of P—O and P=O in **4**, 1.65 Å and 1.57 Å, respectively.

DFT calculation

The previous model was also simulated using the B3LYP hybrid functional (27), which takes the electric correlation effects into account. The geometries of both model clusters **2** and **3** were optimized. A comparison of DFT and HF calculations reveals that the optimization of **2** and **3** in DFT converge to shorter bond lengths for Si—O and P—O and smaller bond angles for O-Si-O and Si-O-P (Table 4). Again, we observe a large difference between Si tetrahedral and octahedral sites in agreement with HF calculations. The conclusion of these calculations is that cluster **2** exhibits a structure similar to the unit cell of **1** and demonstrates the existence of SiO_6 bonding in accordance with the powder diffraction structure of **1** (20).

Infrared vibrational frequencies

We were quite interested in computing the infrared vibrational frequencies of the model clusters **2** and **3** and comparing them with the experimental IR data of **1**, which is available both for the cubic and monoclinic structures (38 and 39). For example, the IR spectra of several varieties of **1** are given by Ferraro et al. (38). Four crystalline polymorphs having the space groups $P2_1/n$, $P2_1/c$, $Pa3$ as well as one tetragonal and one vitreous phase are described. All IR spectra displayed strong lines at 500, 700, 1050, and 1200 cm^{-1} for the crystals. Selected computed IR frequencies of **2** and **3** are listed in Table 5 and compared with experimental data.

Table 4. DFT optimized bond lengths and angles of **2** (Si in octahedral sites, linear chains) and **3** (Si in tetrahedral sites, linear chains).

	2	**3**
Average bond lengths (Å)		
Si—O_b	1.807	1.656
Si—O_t	1.727	1.639
P=O_n	—	1.483
P—O_b	1.578	1.593
P—O_t	1.610	1.594
O—H	0.991	0.997
Average bond angles (°)		
O-Si-O	93.7	109.3
Si-O_b-P	129.1	146.4
P-O-P	121.2	134.3

The first calculation for **2** gives a band at 1245 cm^{-1}, assigned primarily to the P—O stretching because of the large overlap between O and P. The bands localized from 1133 to 1095 cm^{-1} are assigned to the P—O vibrational frequencies. The bands localized at 888 cm^{-1} are assigned to the coupled P—O and Si—O vibrational frequencies. Moreover, the band ranging from 893 to 875 cm^{-1} is assigned to P=O in **3.** The vibration frequencies in **2** within the range 800–809 cm^{-1} are assigned to Si—O_t and confirm the existence of hexacoordinated silicon. In contrast, in **3** the large band located between 923 to 909 cm^{-1} is assigned to tetrahedral silicon. In addition, the peaks at 708 cm^{-1} in **2** and 826 cm^{-1} in **3** are assigned to coupled Si—O and P—O stretching vibrations. Those at 708 and 826 cm^{-1} are attributed to P-O-P, respectively in **2** and **3.** The frequency at 515 cm^{-1} corresponds to pure bonding modes of the bridging oxygens in Si-O-Si in **2** while their signals frequency in **3** is equal to 557 cm^{-1}. As expected in **2**, the Si—O stretching vibrations involving the SiO_6 octahedral units and Si-O-P appear at much lower wave numbers (331 cm^{-1}).

Conclusion

We computed the band structure of **1** using an extended Hückel tight-binding calculation giving the DOS and the COOP and showing the principal interaction of P-O-P and

© 2006 NRC Canada

Table 5. Selected IR frequencies (cm^{-1}) of **2** and **3**.

	Monoclinic[a]	Cubic[a]	**2**	**3**
P—O[b]	1200	1230–1195	1245	1280
P—O	140–1100	—	1133–1095	1149–1092
P—O and Si—O	740	732	888	689
Si—O_t	790–700	798[c]	800–809	923–909[d]
P=O	550[e]	—	540	893–875[f]
P-O-P	515[g]	765[h]	708	826
Si-O-Si	—	510–473[i]	515	557
Si—O[j]	362	—	331	—

[a]Experimental IR spectra by Ferraro (38).
[b]Primarily stretching.
[c]In SiO_6.
[d]In SiO_4.
[e]Bending P-O-P and Si-O-P.
[f]P=O.
[g]Bending mode.
[h]Coupled Si—O and P—O stretching.
[i]Bending Si—O mode.
[j]Stretching.

Si-O-P linkage. Furthermore, we demonstrated that the crystal structure possesses a relative stability and large overlapping of Si-O_6 because of a large dispersion in the silicon pyrophosphate. The distortion seen in the parent compound **1** should be attributed to the presence of hexacoordinated silicon in this material and the diffuse character of Si atoms. From ab initio molecular and DFT calculations on model clusters, we confirmed that the hexacoordinated silicon in **2** imparts a structural change in bond lengths and bond angles in accordance with the crystal data of **1** Also, the vibrational frequency involving the octahedral Si—O stretching motions in **2** appears at lower wavenumbers, corroborating the experimental data.

Acknowledgements

We would like to thank the Moroccan–American Commission for Education and Cultural Exchange, which provided the facilities in the USA and Morocco. Special thanks go out to Prof. J-Y Saillard (Rennes University, Rennes, France) and Dr. Tom Cundari (University of North Texas, Denton, Texas) for their kind help.

References

1. A. Ignatius, K. Unterricker, K. Wenger, M. Richter, L. Claes, P. Lohse, and H. Hirst. J. Mater. Sci.: Mater. Med. **753**, 8 (1997).
2. T. Miya, Y. Terunuma, T. Hosaka, and T. Miyashita. Rev. Electr. Commun. Lab. **27**, 497 (1979).
3. T.L. Weeding, B.H.W.S. De Jong, W.S. Veeman, and B.G. Aitken. Nature (London), **318**, 352 (1985).
4. S. Muthupari and M.E. Fleet. J. Non-Cryst. Solids, **238**, 259 (1998).
5. W.H. Baur and A.A. Khan. Acta Crystallogr. Sect. B: Struct. Crystallogr. Cryst. Chem. **27**, 2133 (1977).
6. D. Li, G.M. Bancroft, and M.E. Fleet. Am. Mineral. **81**, 111 (1996).
7. R. Dupree, D. Holland, M.G. Mortuza, J.A. Collins, and M.W.G. Lockyer. J. Non-Cryst. Solids, **106**, 403 (1988).
8. D. Li, M.E. Fleet, G.M. Bancroft, M. Kasrai, and Y. Pan. J. Non-Cryst. Solids, **188**, 181 (1995).
9. J. Peters, H. Jain, O. Kanert, R. Kuchler, and V. Blache. J. Non-Cryst. Solids, **113**, 222 (1997).
10. Y. Vaugeois, R. De Jaeger, J. Levalois-Mitjaville, A. Mazzah, M. Wörle, and H. Grützmacher. New J. Chem. 783 (1998).
11. R. Dupree, D. Holland, and M.G. Motuza. Nature (London), **328**, 416 (1987).
12. J-J. Liang, R.T. Cygan, and T.M. Alam. J. Non-Cryst. Solids, **263–264**, 167 (2000).
13. (*a*) T. Uchino and T. Yoko. J. Non-Cryst. Solids, **263–264**, 180 (2000); (*b*) D. Li, G.M. Bancroft, M. Kasrai, M.E. Fleet, X.H. Feng, and K.H. Tan. Am. Mineral. **79**, 785 (1994); (*c*) M.M. Branda and N.J. Castellani. Surf. Sci. **393**, 171 (1997); (*d*) G. Pacchioni and G. Ierano. J. Non-Cryst. Solids, **216**, 1 (1997).
14. (*a*) E. Tillmanns, W. Gibert, and W.H. Baur. J. Solid State Chem. **7**, 69 (1973); (*b*) H. Makart. Helv. Chim. Acta, **399**, 50 (1967).
15. (*a*) V. Gertrud and F. Liebeau. Acta Crystallogr. Sect. B: Struct. Crystallogr. Cryst. Chem. **26**, 233 (1970); (*b*) F. Liebau, G. Bisset, and N. Koppen. Z. Anorg. Allg. Chem. **359**, 113 (1968).
16. S. Prabaker, K.J. Rao, and C.N.R. Rao. J. Mater. Res. **6**, 592 (1991).
17. F. Tian, L. Pan, F. Wu, and X. Wu. J. Non-Cryst. Solids, **104**, 129 (1988).
18. S. G. Kosiniski, D.M. Krol, T.M., Duncan, D.C. Douglass, J.B. MacChesney, and J.R. Simpson. J. Non-Cryst. Solids, **105**, 45 (1988).
19. I.N. Chakraborty and R.A. Condrate. Phys. Chem. Glasses, **26**, 68 (1985).
20. D.M. Poojary, R.B. Bordate, F.L. Cambell, and A. Clearfield. J. Solid State Chem. **112**, 106 (1994).
21. (*a*) R. Hoffmann and W.N. Libscomb. J. Chem. Phys. **36**, 2179 (1962); (*b*) R. Hoffmann and W.N.J. Libscomb. Chem. Phys. **36**, 3489 (1962); (*c*) R. Hoffmann and W.N.J. Libscomb. J. Chem. Phys. **37**, 590 (1963); (*d*) R. Hoffmann. J. Chem. Phys. **39**, 1397 (1963).
22. (*a*) M.H. Whangbo, R. Hoffmann, and R.B. Woodward. Proc. R. Soc. London, Ser. A, **366**, 23 (1979), (*b*) M.H. Whangbo and R. Hoffmann. J. Am. Chem. Soc. **100**, 6093 (1978).

© 2006 NRC Canada

23. G.A. Landrum and W.V. Glassey. YAeHMOP. Version 3.0 [computer program]. Avalaible from http://hamiltonian.chem.cornell.edu/.
24. (*a*) C. Mealli and D.M. Proserpio. J. Chem. Educ. **67**, 399 (1990); (*b*) C. Mealli, A. Ienco, and D.M. Proserpio. Book of abstracts of the XXXIII International Conference on Coordination Chemistry, Florence, Italy. (1998). p. 510.
25. R. Ramirez and M.C. Böhm. Int. J. Quantum. Chem. **30**, 391 (1986).
26. J.H. Ammeter, M. Elian, R.H. Summerville, and R. Hoffmann. J. Am. Chem. Soc. **100**, 3686 (1978).
27. M.J. Frisch, G.W. Trucks, H.B. Schlegel, G.E. Scuseria, M.A. Robb, J.R. Cheeseman, V.G. Zakrzewski, J.A. Montgomery Jr., R.E. Stratmann, J.C. Burant, S. Dapprich, J.M. Millam, A.D. Daniels, K.N. Kudin, M.C. Strain, O. Farkas, J. Tomasi, V. Barone, M. Cossi, R. Cammi, B. Mennucci, C. Pomelli, C. Adamo, S. Cliord, J. Ochterski, G.A. Petersson, P.Y. Ayala, Q. Cui, K. Morokuma, D.K. Malick, A.D. Rabuck, K. Raghavachari, J.B. Foresman, J. Cioslowski, J.V. Ortiz, B.B. Stefanov, G. Liu, A. Liashenko, P. Piskorz, I. Komaromi, R. Gomperts, R.L. Martin, D.J. Fox, T. Keith, M.A. Al-Laham, C.Y. Peng, A. Nanayakkara, C. Gonzalez, M. Challacombe, P.M.W. Gill, B. Johnson, W. Chen, M.W. Wong, J.L. Andres, C. Gonzalez, M. Head-Gordon, E.S. Replogle, and J.A. Pople. Gaussian 98. Revision A.6 [computer program]. Gaussian Inc., Pittsburgh, Penn. 1998.
28. R.J. Iuliucci and B.H. Meier. J. Am. Chem. Soc. **120**, 9059 (1998).
29. N. Khosrovani, V. Korhis, A.W. Sleight, and T. Vogt. Inorg. Chem. **7**, 412 (1996).
30. E. Tillmanns, W. Gibert, and W.H. Baur. J. Solid State Chem. **7**, 69 (1973).
31. A. Clearfield and G.D. Smith. Inorg. Chem. **8**, 421 (1969).
32. W.H. Zachariase. J. Am. Chem. Soc. **54**, 3841 (1932).
33. G. Alberti and V. Costantino. J. Mol. Catal. **27**, 235 (1984).
34. M. O'Keeffe, B. Domenges, and G.V. Gibbs. J. Phys. Chem. **89**, 2304 (1985).
35. B.M.C. Meredith and H.F Schaeffer, III. J. Phys. Chem. **98**, 8216 (1994).
36 F. Bkiri. Ph.D. thesis. Department of Chemistry, University Ibn Tofail, Kénitra, Morocco. 2005 and refs. cited therein.
37. T.A. Albright, J.K. Burdett, and M.-H. Whangbo. In Orbital interaction in chemistry. John Wiley & Sons, New York. 1985. pp. 258–269.
38. J.R. Ferraro, C.F. Chenuit, Sr., R.A. Condrate, and N. Chakraborty. J. Solid State Chem. **68**, 94 (1987).
39. P. Massiot, M.A. Centeno, I. Carrizosa, and J.A. Odriozola. J. Non-Cryst. Solids, **292**, 158 (2001).

© 2006 NRC Canada

Regio- and stereo-selectively kinetic resolution of four stereoisomers of 1-phenylbutan-1,3-diol by *Candida rugosa* lipase

Yi-Hui Chen, S. Joly, Pin-Mei Huang, and Kuangsen Sung

Abstract: Regio- and stereo-selective *Candida rugosa* lipase (CRL)-catalyzed acetylations of (±)-*syn*-1-phenylbutan-1,3-diols ((±)-*syn*-**1**) generated two monoacetates, (+)-*syn*-**2** and (–)-*syn*-**3**, whereas that of (±)-*anti*-**1** produced a monoacetate, (+)-*anti*-**3,** and an unreacted (–)-*anti*-**1**.

Key words: Candida rugosa lipase, kinetic resolution, 1,3-diols.

Résumé : Les acétylations régio- et stéréo-sélectives catalysées par la lipase *Candida rugosa* de (±)-*syn*-1-phénylbutane-1,3-diol, (±)-*syn*-**1**, conduisent à la formation de deux monoacétates, les (+)-*syn*-**2** et (–)-*syn*-**3**, alors que celles du (±)-*anti*-**1** conduisent à la formation d'un seul monoacétate, le (+)-*anti*-**3**, et qu'on retrouve du (–)-*anti*-**1** qui n'a pas réagi.

Mots clés : lipase *Candida rugosa*, résolution cinétique, 1,3-diols.

[Traduit par la Rédaction]

Introduction

Enzymes are unique and efficient catalysts for the preparation of many chiral molecules. Their reactions are environment-friendly and have a practical work-up with low costs (1*a*–1*d*). Lipases are one of the most commonly used enzymes in asymmetric synthesis. They have resolved racemic carboxylic acids and alcohols (1*e*), and demonstrated chemoselective O-acylation in aminoalcohols (1*f*) and regioselective O-acylation of nonequivalent hydroxy groups (1*g*).

The subunit 1,3-diol is present in several natural products and biologically active compounds, such as polyenemacrolide antibiotics (2). Some stereo-selective syntheses of chiral 1,3-diols have been developed in the last two decades (2*e*, 3–5). The 1,3-diols are known to protect ketones and aldehydes (6), so chiral 1,3-diols have the potential to become a chiral auxiliary in asymmetric synthesis. In spite of the fact that the lipases have often been employed for the resolution of several secondary alcohols (1), they have not been extensively used for the resolution of the 1,3-diols. It was reported that 1,3-diarylpropan-1,3-diols were resolved by *Candida rugosa* lipase (CRL) (4). Dynamic kinetic resolution of 1,3-diols was carried out by *Candida antarctica* lipase B (CAL-*B*) (5). We were interested in CRL-catalyzed resolution of an unsymmetrical 1,3-diol, 1-phenylbutan-1,3-diol (**1**) (see Scheme 1), with vinyl acetate as an acyl donor. The substrate **1**, with one large phenyl group and one small methyl group at either end, consists of four stereoisomers and has two nonequivalent chiral secondary alcohol groups. Clearly, it opens up several attractive prospects such as regio-selectivity with the two nonequivalent hydroxyl groups and stereo-selectivity with each of the two hydroxyl groups.

Received 15 April 2006. Accepted 23 August 2006. Published on the NRC Research Press Web site at http://canjchem.nrc.ca on 4 October 2006.

Y.-H. Chen, S. Joly, P.-M. Huang, and K. Sung.[1]
Department of Chemistry, National Cheng Kung University, Tainan, Taiwan.

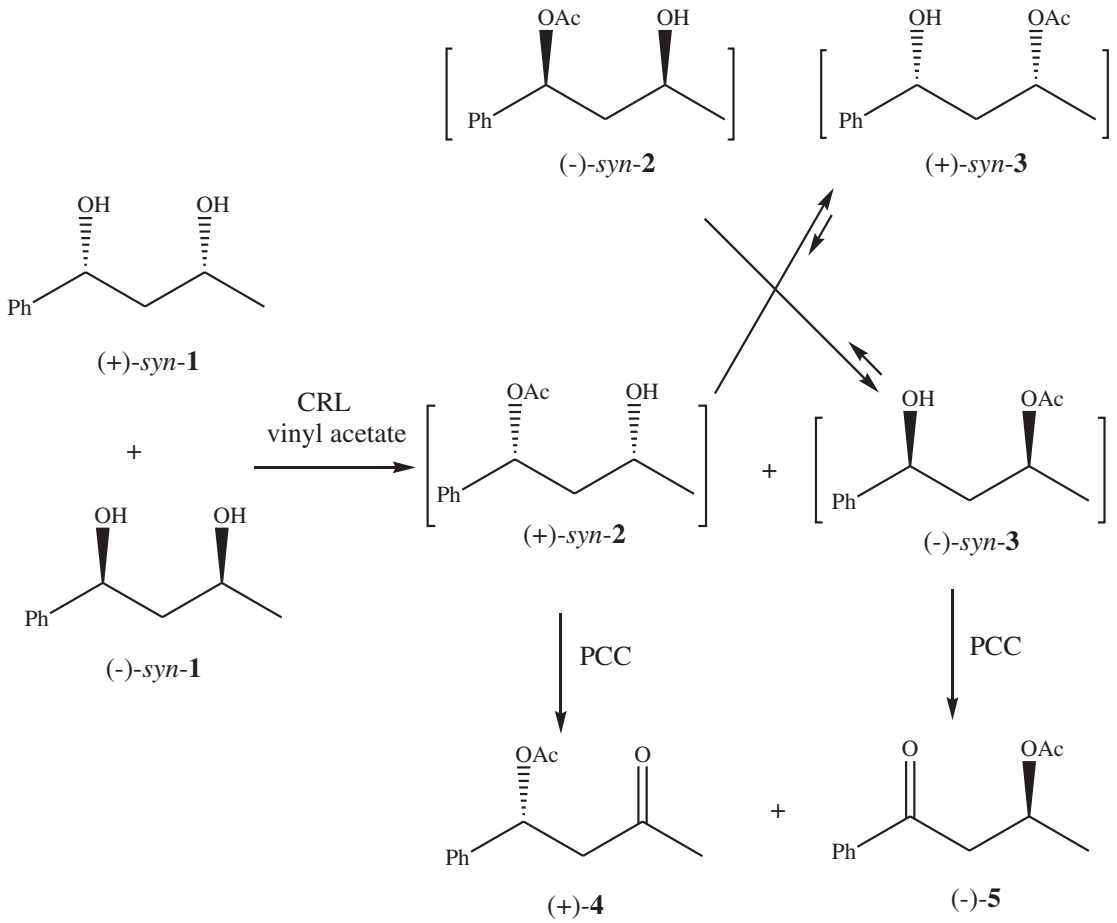
[1]Corresponding author (e-mail: kssung@mail.ncku.edu.tw).

Results and discussion

Kinetic resolution of (±)-*syn*-**1** was carried out by CRL with vinyl acetate as an acyl donor and generated two monoacetates, (+)-*syn*-**2** and (–)-*syn*-**3**, along with some unreacted (±)-*syn*-**1**. (Scheme 1). NMR spectroscopy showed that no diacetate product has been found in this reaction. For (+)-*syn*-**2** and (–)-*syn*-**3,** intramolecular transesterification has not been observed in vinyl acetate or in $CDCl_3$ after a period of 24 h. However, it was observed in the presence of CRL, silica gel, aluminum oxide, methanol, and aqueous acetonitrile. Consequently, to minimize this intramolecular transesterification, we tried to derivatize (+)-*syn*-**2** and (–)-*syn*-**3** with phenyl isocyanate. However, the corresponding carbamate isomers were difficult to separate by column chromatography and preparative HPLC. The next strategy we chose was the oxidation of (+)-*syn*-**2** and (–)-*syn*-**3** with pyridinium chlorochromate (PCC) right after this enzymatic reaction. The oxidation products, (+)-**4** and (–)-**5**, could be purified by column chromatography. Oxidation of the mixture of (+)-*syn*-**2** and (–)-*syn*-**3** at a ratio of 1:2.3 by PCC generated the mixture of (+)-**4** and (–)-**5** at a ratio of 1:2.6, indicating that very little intramolecular transesterification occurred during the oxidation. The isomer ratios were determined by ^{1}H NMR spectroscopy with $CDCl_3$ as a solvent. Thus, information regarding approximate enantiomeric excess (ee) values and configurations of (+)-*syn*-**2** and (–)-*syn*-**3** can be obtained from those of (+)-**4** and (–)-**5**.

 doi:10.1139/V06-131 © 2006 NRC Canada

Scheme 1.



The ee values of (+)-**4** have been determined by chiral HPLC,[2] and the ee values of (–)-**5** have been determined by NMR chiral shift reagent of (+)-Eu(hfc)$_3$. To confirm the configuration of (+)-**4**, it was synthesized by another reported procedure (7a). According to the chiral HPLC analysis, (+)-**4** indirectly produced from this enzymatic reaction is exactly the same as the one prepared by the reported procedure (7a), indicating that its configuration is (*R*) and the configuration of (+)-*syn*-**2** should be (*R*,*R*). According to the optical rotation and chiral HPLC analysis,[3] reduction of (+)-*syn*-**2** and (–)-*syn*-**3** with $LiAlH_4$ generated (+) and (–)-*syn*-**1**, respectively. The configurations of (+)-*syn*-**1** and (–)-*syn*-**1** are (*R*,*R*) and (*S*,*S*), respectively, (3*b–d*, 3*h*). Therefore, the configuration of (+)-*syn*-**2** is (*R*,*R*) and the configuration of (–)-*syn*-**3** is (*S*,*S*).

Two possible mechanisms operated in the kinetic resolution of (±)-*syn*-**1**. The first is enzymatic acetylation of one hydroxyl group of (±)-*syn*-**1**, followed by intramolecular transesterification to the other hydroxyl group. The second mechanism is that the enzymatic acetylation occurred in both one hydroxyl group of one enantiomer of (±)-*syn*-**1** and the other hydroxyl group of the other enantiomer. If this kinetic resolution had followed the former mechanism, the configurations of (+)-*syn*-**2** enantiomers would have been the same as those of (–)-*syn*-**3**. As previously stated, the reduction of (+)-*syn*-**2** and (–)-*syn*-**3** with $LiAlH_4$ generated opposite enantiomers of (±)-*syn*-**1**, respectively, implying that this kinetic resolution follows the latter mechanism and the enzymatic acetylation reactions are regio- and stereoselective.

As shown in Table 1, enzymatic acetylation of (±)-*syn*-**1** with CRL and vinyl acetate for 3 h produced (+)-*syn*-**2** with an ee >99% and a yield of 36%, and (–)-*syn*-**3** with an ee of 69% and a yield of 49%. When the reaction ran for a longer time, ee values of both (+)-*syn*-**2** and (–)-*syn*-**3** decreased, indicating that the highly regio- and stereo-selective acetylations of (±)-*syn*-**1** carried out by CRL and vinyl acetate were deteriorated by intramolecular transesterifications. For example, treatment of a mixture of (+)-*syn*-**2** and (–)-*syn*-**3** at a ratio of 8.1:1 with CRL and vinyl acetate for 24 h generated *syn*-**2** and *syn*-**3** at a ratio of 1:1.6; whereas, treatment of another mixture of (+)-*syn*-**2** and (–)-*syn*-**3** at a ratio of 1:39 with CRL and vinyl acetate for 24 h produced *syn*-**2** and *syn*-**3** at a ratio of 1:4.6. Each of the products, *syn*-**2** and *syn*-**3**, has much worse optical purity than the corresponding starting materials (+)-*syn*-**2** and (–)-*syn*-**3**. In addition, no

[2] Chiral HPLC analysis of (±)-**4**: Chiralcel OD-RH column; mobile phase: water/acetonitrile = 7:3; flow rate: 0.4 mL/min; detection UV wavelength: 263 nm; retention time for (+)-(*R*)-**4** and (–)-(*S*)-**4**: 27.9, 30.0 min.

[3] Chiral HPLC analysis of (±)-*syn*-**1**: Chiralcel OD-RH column; mobile phase: water/acetonitrile = 8:2; flow rate: 0.4 mL/min; detection UV wavelength: 257 nm; retention time for (+)-(1*R*,3*R*)-*syn*-**1** and (–)-(1*S*,3*S*)-*syn*-**1**: 14.0, 15.0 min.

© 2006 NRC Canada

Table 1. Kinetic resolution of (±)-*syn*-**1** by CRL and vinyl acetate at 25 °C.

		(+)-*syn*-**2**		(–)-*syn*-**3**	
Time (h)	Solvent and reagent (mL)	Yield (%)[a]	ee (%)[b]	Yield (%)[a]	ee (%)[c]
2	Vinyl acetate (2.5)	30	>99	45	69
3	Vinyl acetate (2.5)	36	>99	49	62
6	Vinyl acetate (2.5)	32	93	58	45
4	*i*-Pr_2O (2.0), vinyl acetate (0.5)	17	66	53	45

[a]The yields were based on ^{1}H NMR analysis of the reaction mixtures right after the enzymatic reactions.
[b]This was determined indirectly on (+)-**4** by chiral HPLC analysis.
[c]This was determined indirectly on (–)-**5** by NMR chiral shift reagent (+)-Eu(hfc)$_3$.

Scheme 2.

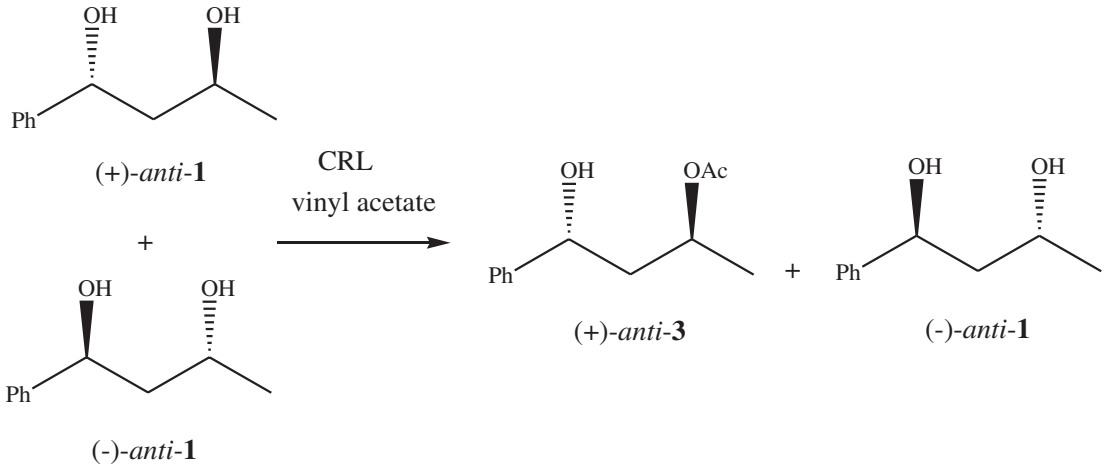


Table 2. Kinetic resolution of (±)-*anti*-**1** by CRL and vinyl acetate at 25 °C.

		(+)-*anti*-**3**		(–)-*anti*-**1**	
Time	Solvent (mL)	Yield (%)[a]	ee (%)[b]	Yield (%)[a]	ee (%)[b]
20 min	Vinyl acetate (2.5)	49	94	51	74
6 h	Vinyl acetate (2.5)	57	71	43	>99
18 h	Vinyl acetate (2.5)	59	48	41	>99
24 h	Vinyl acetate (2.5)	60	35	40	>99

[a]The yields were based on ^{1}H NMR analysis of the reaction mixtures right after the enzymatic reactions. The reaction conversion is the same as the yield of *anti*-**3**.
[b]This was determined on its diacetate derivative by chiral HPLC analysis. E = 72 at 20 min, according to the equation $E = \{\ln[1 - c(1 + ee_p)]/\ln[1 - c(1 - ee_p)]\}$ (7*a*).

hydrolyzed product, (±)-*syn*-**1**, was observed in these two reactions. When the mixtures of (+)-*syn*-**2** and (–)-*syn*-**3** were stirred in ethyl acetate – hexane containing silica gel or in aqueous acetonitrile for 24 h, similar results were found. Based on these experimental results, we suggest the presence of intramolecular transesterification equilibria between (+)-*syn*-**2** and (+)-*syn*-**3** and between (–)-*syn*-**2** and (–)-*syn*-**3** in vinyl acetate with CRL, ethyl acetate – hexane containing silica gel, or aqueous acetonitrile. The equilibria lie far to (±)-*syn*-**3**. This explains the low ee values for both products, (+)-*syn*-**2** and (–)-*syn*-**3**, in the CRL-catalyzed acetylations of (±)-*syn*-**1** at a longer reaction time, especially for the product of (–)-*syn*-**3**.

As shown in Scheme 2, kinetic resolution of (±)-*anti*-**1** with CRL and vinyl acetate generated monoacetate (+)-*anti*-**3** and unreacted (–)-*anti*-**1**. The results are shown in Table 2. As the reaction time increases, the ee value of (+)-*anti*-**3** decreases but the ee value of the unreacted (–)-*anti*-**1** increases, indicating that the CRL-catalyzed acetylation occurs at the 3-hydroxyl group of both (+)-*anti*-**1** and (–)-*anti*-**1** and one is much faster than the other. The kinetic resolution of (±)-*anti*-**1** is best stopped after 20 min. Intramolecular transesterification of (±)-*anti*-**3** was too slow to be observed in presence of vinyl acetate, $CDCl_3$, CRL, silica gel, aluminum oxide, methanol, or aqueous acetonitrile. The configuration of the unreacted (–)-*anti*-**1** with an ee of >99% was determined to be (1*S*,3*R*) by comparing its optical rotation with the reported data (3*d*, 3*g*, 3*h*). The ee values of the CRL-catalyzed acetylation products, (+)-*anti*-**3** and (–)-*anti*-**1**, were determined by chiral HPLC analysis[4] of their

[4]Chiral HPLC analysis for diacetate of (+)-*anti*-**3** and (–)-*anti*-**1**: Chiralcel OD-RH column; mobile phase: water/i-PrOH/acetonitrile = 6:3:1; flow rate: 0.24 mL/min; detection UV wavelength: 257 nm; retention time: 39.5, 46.0 min.

© 2006 NRC Canada

diacetate derivatives that were prepared by reaction with acetic anhydride and pyridine. According to the chiral HPLC analysis[4] of their diacetate derivatives, the configurations of (+)-*anti*-**3** and (–)-*anti*-**1** are opposite. The configuration of (–)-*anti*-**1** was determined to be (1*S*,3*R*), so the configuration of (+)-*anti*-**3** is (1*R*,3*S*) and the optical rotation is exactly opposite to that of the known (–)-anti-**3** (5*b*).

In conclusion, we have developed kinetic resolutions for four stereoisomers of 1-phenylbutan-1,3-diol by CRL. These chiral 1,3-diols have potential to be chiral auxiliaries in asymmetric synthesis.

Experimental

General

All the reagents were obtained from commercial suppliers and used as received. The 1,3-diols, (±)-*syn*-**1**, and (±)-*anti*-**1** were prepared according to the literature (8). *Candida rugosa* lipase (Type VII, 700–1500 unit/mg solid) was purchased from Sigma Chemical Co. (St. Louis, MO, USA).

CRL-catalyzed acetylation of (±)-*syn*-1, followed by oxidation with PCC

To a solution of (±)-*syn*-**1** (50 mg, 0.3 mmol) in 2.5 mL of vinyl acetate, CRL (51 mg) was added. The mixture was stirred at room temperature for some time. The reaction was stopped by filtration of the mixture, and the filtrate was concentrated by a rotary evaporator. The ratios of the products, (+)-*syn*-**2**,(–)-*syn*-**3**, and the unreacted diol (±)-*syn*-**1** were determined by ^{1}H NMR spectroscopy. The ee value of the unreacted diol (±)-*syn*-**1** was determined by chiral HPLC.[3] The residue was dissolved in 5 mL of dichloromethane, and this solution was added to a solution of PCC (120 mg, 0.556 mmol) in 5 mL of dichloromethane. The reaction was stirred for 2 h. Then the reaction mixture was diluted with 30 mL of diethyl ether and passed through a short pad of silica. After evaporation of the solvent, the crude reaction mixture was purified by column chromatography with a mobile phase of 10% ethyl acetate in hexane to yield (+)-**4** and (–)-**5** as colourless oily liquid. Their characterizations agreed with those reported (7*a*–7*d*). The enantiomeric excess of (+)-**4** was determined by chiral HPLC analysis.[2] The enantiomeric excess of (–)-**5** was determined by the ^{1}H NMR spectroscopy in the presence of 25 mg of chiral shift reagent (+)-Eu(hfc)$_3$.

syn-3-Hydroxy-1-phenylbutyl acetate (*syn*-2)

IR ($CDCl_3$, cm^{-1}): 1730 (C=O). ^{1}H NMR ($CDCl_3$) δ: 1.19 (d, J = 6.0 Hz, 3H, CH_3), 1.83–1.89 (m, 1H, CH), 2.05 (s, 3H, CH_3), 2.10–2.17 (m, 1H, CH), 3.70 (m, 1H, CH), 5.91 (t, J = 7.2 Hz, 1H, CH), 7.26–7.37 (m, 5H, PhH). ^{13}C NMR ($CDCl_3$) δ: 21.26, 23.81, 45.35, 65.18, 74.41, 126.59, 128.01, 128.48, 140.21, 170.24. HR-MS (EI) *m*/*z* calcd. for $C_{12}H_{16}O_3$: 208.1099; found: 208.1097.

syn-4-Hydroxy-4-phenylbutan-2-yl acetate (*syn*-3)

IR ($CDCl_3$, cm^{-1}): 1730 (C=O). ^{1}H NMR ($CDCl_3$) δ: 1.22 (d, J = 6.3 Hz, 3H, CH_3), 1.77–1.83 (m, 1H, CH), 1.94 (s, 3H, CH_3), 2.09–2.17 (m, 1H, CH), 2.91 (s, 1H, OH), 4.71 (t, J = 7.2 Hz, 1H, CH), 4.88–4.94 (m, 1H, CH), 7.21–7.32 (m, 5H, PhH). ^{13}C NMR ($CDCl_3$) δ: 20.04, 21.16, 44.86, 68.98, 71.62, 125.70, 127.51, 128.38, 144.02, 170.68. HR-MS (EI) *m*/*z* calcd. for $C_{12}H_{16}O_3$: 208.1099; found: 208.1094.

3-Oxo-1-phenylbutyl acetate (4)

^{1}H NMR ($CDCl_3$) δ: 2.02 (s, 3H, CH_3), 2.14 (s, 3H, CH_3), 2.92 (dd, J = 8.7, 5.0 Hz, 1H, CH), 3.00 (dd, J = 8.7, 5.0 Hz, 1H, CH), 6.18 (m, 1H, CH), 7.26–7.34 (m, 5H, PhH). Its characterization agreed with that reported in the literature (7*d*).

4-Oxo-4-phenylbutan-2-yl acetate (5)

^{1}H NMR ($CDCl_3$) δ: 1.37 (d, J = 6.4 Hz, 3H, CH_3), 1.99 (s, 3H, CH_3), 3.03 (dd, J = 6.4, 16.5 Hz, 1H, CH), 3.42 (dd, J = 6.4, 16.5 Hz, 1H, CH), 5.41–5.50 (m, 1H, CH), 7.41–7.59 (m, 3H, PhH), 7.93–7.97 (m, 2H, PhH). Its characterization agreed with that reported in the literature (7*c*).

CRL-catalyzed acetylation of (±)-*anti*-1

To a solution of (±)-*anti*-**1** (50 mg, 0.3 mmol) in 2.5 mL vinyl acetate, CRL (50 mg) was added. The reaction mixture was stirred at room temperature for some time. The reaction was stopped by filtration of the enzyme, and the filtrate was concentrated by rotary evaporator. The residue was purified by column chromatography with a mobile phase of 20% ethyl acetate in hexane to yield (+)-*anti*-**3** and (–)-*anti*-**1**. The optical rotation of (–)-*anti*-**1** was measured to be $[\alpha]^{26}_D$ –51.8° (*c* 0.96, $CHCl_3$, >99% ee), which is close to the literature data (3*d*, 3*g*, 3*h*). Characterization of (+)-*anti*-**3** is the same as that found in the literature (5*b*). The conversion was determined from the ^{1}H NMR spectrum of the reaction mixture. Derivatization of (+)-*anti*-**3** and (–)-*anti*-**1** was achieved by treating them with acetic anhydride (1 mmol) and pyridine (1.2 mmol) at room temperature for 24 h. The reaction mixture was neutralized with dilute hydrochloric acid, followed by extraction with diethyl ether. The ether solution was dried over anhydrous sodium sulfate. After evaporation of the ether, the residue was purified by column chromatography, followed by analysis with chiral HPLC.[4]

(+)-*anti*-4-Hydroxy-4-phenylbutan-2-yl acetate ((+)-*anti*-3)

$[\alpha]^{26}_D$ +11.3° (*c* 1.015, $CHCl_3$, 94% ee). IR ($CDCl_3$, cm^{-1}): 1715 (C=O). ^{1}H NMR ($CDCl_3$) δ: 1.26 (d, J = 6.4 Hz, 3H, CH_3), 1.87–1.91 (m, 2H, CH_2), 2.04 (s, 3H, CH_3), 2.96 (s, 1H, OH), 4.61–4.66 (m, 1H, CH), 5.17–5.23 (m, 1H, CH), 7.23–7.36 (m, 5H, PhH). ^{13}C NMR ($CDCl_3$) δ: 20.63, 21.21, 46.00, 68.33, 70.23, 125.59, 127.40, 128.40, 143.95, 171.59. HR-MS (EI) *m*/*z* calcd. for $C_{12}H_{16}O_3$: 208.1099; found: 208.1092.

Acknowledgments

This work is supported by NSC of Taiwan, ROC (NSC 94–2113-M-006–009).

References

1. (*a*) U.T. Bornscheuer and R.J. Kazlauskas. Hydrolases in organic synthesis. Wiley-VCH, Weinheim, 1999; (*b*) K. Drauz and H. Waldmann. Enzyme catalysis in organic synthesis. Wiley-VCH, Wienheim, 2002; (*c*) U. Hanefeld. Org. Biomol. Chem. **1**, 2405 (2003); (*d*) G. Carrea and S. Riva. Angew.

© 2006 NRC Canada

Chem., Int. Ed. Engl. **39**, 2226 (2000); (*e*) N.W. Fadnavis, R.L. Babu, K. Vadivel, A.A. Deshpande, and U.T. Bhalerao. Tetrahedron: Asymmetry, **9**, 4109 (1998); (*f*) K. Lundell, P. Lehtinen, and L.T. Kanerva. Adv. Synth. Catal. **345**, 790 (2003); (*g*) G. Pedrocchi-Fantoni and S. Servi. J. Chem. Soc., Perkin Trans. 1, 1029 (1992).

2. (*a*) S. Omura and H. Tanaka. *In* Macrolide antibiotics: Biology and practice. *Edited by* S. Omura. Academic Press, New York, 1984, pp. 351–404; (*b*) T. Nakata, N. Hata, and T. Oishi. Tetrahedron Lett. **31**, 381 (1990); (*c*) S.L. Schreiber and M.T. Goulet. J. Am. Chem. Soc. **109**, 8120 (1987); (*d*) J. Pawlak, K. Nakanishi, T. Iwashita, and E. Borowski. J. Org. Chem. **52**, 2896 (1987); (*e*) T. Oishi and T. Nakata. Synthesis, 635 (1990).
3. (*a*) S.E. Bode, M. Wolberg, and M. Muller. Synthesis, 557 (2006); (*b*) T.H. Chan and K.T. New. J. Org. Chem. **57**, 6107 (1992); (*c*) A. Bachki, F. Foubelo, and M. Yus. Tetrahedron: Asymmetry, **6**, 1907 (1995); (*d*) K. Ahmad, S.C. Taneja, A.P. Singh, M. Kapoor, R. Hassan, V. Verma, and G.N. Qazi. Tetrahedron: Asymmetry, **15**, 1685 (2004); (*e*) M. Kitamura, T. Ohkuma, S. Inoue, N. Sayo, H. Kumobayashi, S. Akutagawa, T. Ohta, and H. Takaya. J. Am. Chem. Soc. **110**, 629 (1998); (*f*) A. Barbero, D.C. Blakemore, I. Fleming, and R.N. Wesley. J. Chem. Soc., Perkin Trans. 1, 1329 (1997); (*g*) P.R. Chopade, T.A. Davis, E. Prasad, and R.A. Flowers II. Org. Lett. **6**, 2685 (2004), (*h*) M. Takeshita, M. Miura, and Y. Unuma. J. Chem. Soc., Perkin Trans. 1, 2901 (1993).
4. F. Levayer, C. Rabiller, and C. Tellier. Tetrahedron: Asymmetry, **6**, 1675 (1995).
5. (*a*) M. Edin and J.-E. Backvall. J. Org. Chem. **68**, 2216 (2003); (*b*) M. Edin, J. Steinreiber, and J.-E. Backvall. Proc. Natl. Acad. Sci. U.S.A. **101**, 5761 (2004).
6. (*a*) M. Guiso, C. Procaccio, M.R. Fizzano, and F. Piccioni. Tetrahedron Lett. **38**, 4291 (1997), (*b*) T.W. Greene and P.G.M. Wuts. Protective groups in organic synthesis. 2nd ed. John Wiley & Sons, New York, 1991.
7. (*a*) M.S. Nair and S. Joly. Tetrahedron: Asymmetry, **11**, 2049 (2000); (*b*) J. Iqbal and R.R. Srivastava. J. Org. Chem. **57**, 2001 (1992); (*c*) A. Abate, E. Brenna, G. Fronza, C. Fuganti, S. Ronzani, and S. Serra. Helv. Chim. Acta, **86**, 592 (2003); (*d*) J.P. Guthrie and S. O'Leary. Can. J. Chem. **53**, 2150 (1975).
8. (*a*) K. Shokat, T. Uno, and P.G. Schultz. J. Am. Chem. Soc. **116**, 2261 (1994); (*b*) K. Ahmad, S. Koul, S.C. Taneja, A.P. Singh, M. Kapoor, R. Hassan, V. Verma, and G.N. Qazi. Tetrahedron: Asymmetry, **15**, 1685 (2004).

© 2006 NRC Canada

Buffer capacity in multiple chemical reaction systems involving solid phases

Ilie Fishtik and Igor Povar

Abstract: The buffer capacity of a chemical species in a multiple chemical reaction system is discussed in terms of a special class of stoichiometrically unique reactions referred to as response reactions (RERs). More specifically, it is shown that the buffer capacity may be partitioned into a sum of contributions associated with RERs. This finding provides a deeper understanding of the factors that determine the buffer capacity. In particular, the main contributions to the buffer capacity come from the RERs involving the most abundant species. Concomitantly, the RERs approach provides a simple stoichiometric algorithm for the derivation and analysis of the buffer capacity that may be easily implemented into a computer software.

Key words: buffer capacity, response reaction, heterogeneous system, stoichiometric coefficient.

Résumé : La capacité d'une espèce chimique à agir comme tampon dans un système à multiples réactions chimiques est discuté en termes d'une classe spéciale de réactions à stoechiométrie unique appelées réactions de réponse (RER). D'une façon plus spécifique, on démontre que la capacité à agir comme tampon peut être divisée en une somme de contributions associées aux réactions de réponse. Cette conclusion permet de mieux comprendre les facteurs qui déterminent la capacité à agir comme tampon. En particulier, les contributions principales à cette capacité proviennent des réactions de réponse impliquant les espèces les plus abondantes. D'une façon concomitante, l'approche par les réactions de réponse fournit un algorithme stoechiométrique simple qui permet de dériver et analyser la capacité à agir comme tampon et qui peut être facilement appliqué par le biais d'un programme informatique.

Mots clés : capacité à agir comme tampon, réaction de réponse, système hétérogène, coefficient stoechiométrique.

Introduction

Buffer capacity is an important concept in many areas of science: analytical chemistry, geochemistry, biochemistry, medicine, water treatment, environment, and so forth. Initially, it was introduced to characterize the response of an acid–base system to changes in pH (1). Later on, the buffer capacity was extended to redox (2) and complex formation reactions (3–5) as well as reactions involving solid phases (6–8). Recently, several simple and elegant treatments of the buffer capacity have been presented (9, 10). The derivation of the buffer capacity formulae in multiple reaction systems may be performed in a straightforward manner using the simple rules of differentiation of implicit functions (11, 12). Alternatively, the buffer capacity may be easily evaluated employing numerical methods. In the meantime, by its very essence, it is clear that the buffer capacity is a particular case of a more general theoretical approach known as sensitivity analysis. As is well known, sensitivity analysis is a means to study the system's response to various perturbations. Within this approach, the buffer capacity may be treated as the sensitivity of the system with respect to a change in the concentration of a particular species.

A recent general study of the sensitivity of equilibrium multiple chemical reaction systems with respect to different perturbations revealed that the system's response may be partitioned into a sum of contributions. These contributions were associated with a special class of stoichiometrically unique reactions referred to as response reactions (RERs) (13, 14). This finding was shown to provide a deeper insight into the nature of chemical interactions in multiple chemical reaction systems. In particular, within the RERs formalism, the buffer capacity may be partitioned into certain stoichiometric and compositional factors associated with RERs. Consequently, these factors may be evaluated explicitly (15). As a result, one may select the RERs that dominate the buffer capacity of a complex system. Concomitantly, the RERs approach provides a simple stoichiometric algorithm for computer generation of the buffer capacity in complex systems starting from a list of species. In heterogeneous multiple chemical reaction systems, the RERs approach requires a substantial modification. The purpose of this work

Received 6 February 2006. Accepted 26 June 2006. Published on the NRC Research Press Web site at http://canjchem.nrc.ca on 4 October 2006.

I. Fishtik.[1] Department of Chemical Engineering, Fuel Cell Center, Worcester Polytechnic Institute, MA 01609, USA.
I. Povar. Department of Chemistry, The University of Western Ontario, London, ON N6A 5B7, Canada.

[1]Corresponding author (e-mail: ifishtik@wpi.edu).

 doi:10.1139/V06-127 © 2006 NRC Canada

is to point out the particularities of the RERs approach to the analysis of buffer capacity as applied to heterogeneous multiple chemical reaction systems.

Notation and definitions

We consider the general case of a heterogeneous multiple chemical reaction system comprising n chemical species B_1, B_2, ..., B_n. For simplicity, we assume that the system obeys an ideal behavior, that is, pure condensed phases (activity is one), dilute water solutions (activity of water is one), and ideal gas phases.

Let C_k^0 and $[B_k]$ ($k = 1, 2, ..., n$) be the initial and equilibrium concentrations of the species, respectively. The buffer capacity of the species B_k is defined as

$$[1] \qquad \beta_k = \left(\frac{\partial C_k^0}{\partial \ln[B_k]} \right)_{C_{k \neq i}}$$

This definition is slightly different from the conventional one in that we use the natural logarithm rather than the ten-based logarithm. Obviously, these two definitions differ by a factor of 2.303.

Let the species B_1, B_2, ..., B_n consist of s elements E_1, E_2, ..., E_s, where "elements" means any stoichiometrically appropriate atomic, molecular, or ionic set that may be used to construct the species, i.e.,

$$[2] \qquad B_1 = \varepsilon_{11}E_1 + \varepsilon_{21}E_2 + \ldots + \varepsilon_{s1}E_s$$

$$B_2 = \varepsilon_{12}E_1 + \varepsilon_{22}E_2 + \ldots + \varepsilon_{s2}E_s$$

$$B_n = \varepsilon_{1n}E_1 + \varepsilon_{2n}E_2 + \ldots + \varepsilon_{sn}E_s$$

Here ε_{li} ($l = 1, 2, ..., s$, $i = 1, 2, ..., n$), is the number of elements E_l in the species B_i. Let the rank of the formula matrix $\boldsymbol{\varepsilon}$ be

$$[3] \qquad \text{rank } \boldsymbol{\varepsilon} = \text{rank} \begin{bmatrix} \varepsilon_{11} & \varepsilon_{12} & \cdots & \varepsilon_{1s} \\ \varepsilon_{21} & \varepsilon_{22} & \cdots & \varepsilon_{2s} \\ \cdots & \cdots & \cdots & \cdots \\ \varepsilon_{n1} & \varepsilon_{n2} & \cdots & \varepsilon_{ns} \end{bmatrix} = s$$

From chemical stoichiometry, it is known that the number m of the stoichiometrically independent reactions is $m = n - \text{rank}\varepsilon = n - s$.

Response reactions (RERs)

A reaction involving no more than rank $\boldsymbol{\varepsilon} + 1 = s + 1$ species is called a response reaction (RER). Let the $s + 1$ species involved in a RER be $B_{i_1}, B_{i_2}, \ldots, B_{i_s}, B_{i_{s+1}}$ where i_1, i_2, …, i_s, i_{s+1} is an $(s + 1)$-tuple set of integers satisfying the condition $1 \leq i_1 < i_2 < \ldots < i_{s+1} \leq n$. A RER is denoted by $\rho(B_{i_1}, B_{i_2}, \ldots, B_{i_{s+1}})$ and its general equation is given by

$$[4] \qquad \rho(B_{i_1}, B_{i_2}, \ldots, B_{i_s}, B_{i_{s+1}}) = \begin{vmatrix} \varepsilon_{i_1,1} & \varepsilon_{i_2,2} & \cdots & \varepsilon_{i_1,s} & B_{i_1} \\ \varepsilon_{i_2,1} & \varepsilon_{i_2,2} & \cdots & \varepsilon_{i_2,s} & B_{i_2} \\ \cdots & \cdots & \cdots & \cdots & \cdots \\ \varepsilon_{i_s,1} & \varepsilon_{i_s,2} & \cdots & \varepsilon_{i_s,s} & B_{i_s} \\ \varepsilon_{i_{s+1},1} & \varepsilon_{i_{s+1},2} & \cdots & \varepsilon_{i_{s+1},s} & B_{i_{s+1}} \end{vmatrix} = 0$$

Thus, a complete set of RERs may be generated by selecting all of the possible combinations of $(s + 1)$ species from the total of n. Consequently, the number of RERs N is

$$[5] \qquad N = \binom{n}{s+1} = \frac{n!}{(s+1)!(n-s-1)!}$$

Clearly, the stoichiometric coefficients in the RERs are not necessarily equal to the smallest integers. If so, every RER $\rho(B_{i_1}, B_{i_2}, \ldots, B_{i_s}, B_{i_{s+1}})$ may be presented as

$$[6] \qquad \rho(B_{i_1}, B_{i_2}, \ldots, B_{i_s}, B_{i_{s+1}}) = \gamma(\rho_0)\,\rho_0(B_{i_1}, B_{i_2}, \ldots, B_{i_s}, B_{i_{s+1}})$$

Here, $\rho_0(B_{i_1}, B_{i_2}, \ldots, B_{i_s}, B_{i_{s+1}})$ is a RER in which the stoichiometric coefficients are the smallest integers while $\gamma(\rho_0)$ is a constant. The constant $\gamma(\rho_0)$ is a fundamental stoichiometric characteristic of a RER and is called the stoichiometric factor of a RER. It is not the absolute value of $\gamma(\rho_0)$ that counts but the ratios of $\gamma(\rho_0)$ for different RERs. Thus, for a complete set of RERs we choose the values of $\gamma(\rho_0)$ as the smallest integers. Furthermore, in all quantitative applications (formulae) of RERs, the stoichiometric factors appear as $\gamma^2(\rho_0)$. Because the sign of $\gamma(\rho_0)$ is not important, the directionality of the RERs is also arbitrary.

Although the RERs are linearly dependent, they have the remarkable property of being *stoichiometrically unique*, in that they only depend upon a given list of species. In other words, for a given set of species, one arrives at the same set of RERs no matter how they are derived.

For our purposes,we need to consider all of the RERs involving a certain species B_k ($k = 1, 2, \ldots, n$). The respective subset of RERs may be selected from a complete set of RERs by fixing one of the species, for example, $B_{i_{s+1}} = B_k$. Hence, the subset of RERs involving a given species B_k is simply $\rho(B_{i_1}, B_{i_2}, \ldots, B_{i_s}, B_k)$, where i_1, i_2, … , i_s is an s-tuple set of integers satisfying the conditions $1 \leq i_1 < i_2 < \ldots < i_s \leq n$ and i_1, i_2, …, $i_s \neq k$, we introduce further two quantities that characterize a RER $\rho_0(B_{i_1}, B_{i_2}, \ldots, B_{i_s}, B_k)$, namely,

$$[7] \qquad \pi_k(\rho_0) \equiv [B_{i_1}][B_{i_2}] \ldots [B_{i_s}]$$

$$[8] \qquad g_k(\rho_0) \equiv \frac{\nu_{i_1}{}^2(\rho_0)}{[B_{i_1}]} + \frac{\nu_{i_2}{}^2(\rho_0)}{[B_{i_2}]} + \ldots \frac{\nu_{i_s}{}^2(\rho_0)}{[B_{i_s}]}$$

These relations contain contributions coming from all species involved in a RER except species B_k.

Remark

Generally, the enumeration of RERs may be performed without reference to the activity of the species. For the special case of systems involving dilute aqueous solutions and pure condensed phases, the RERs need to be defined in a special way. Namely, the water and pure condensed phase

© 2006 NRC Canada

species are always among the $(s + 1)$ species that are involved in a RER $\rho_0(B_{i_1}, B_{i_2}, \ldots, B_{i_s}, B_{i_{s+1}})$. Because the activity of water and pure condensed phases is equal to one, these species should be disregarded in eqs. [7] and [8].

Buffer capacity in terms of RERs

We are now in a position to formulate the following result

$$[9] \qquad \beta_k = [B_k] + \frac{1}{\Delta_k} \sum_{\rho_0} \gamma^2(\rho_0)\, \nu_k{}^2(\rho_0)\, \pi_k(\rho_0)$$

$$[10] \qquad \Delta_k = \frac{1}{m} \sum_{\rho_0} \gamma^2(\rho_0) g_k(\rho_0)\, \pi_k(\rho_0)$$

Here, the summation runs over all RERs involving the species B_k. The proof of eqs. [9] and [10] follows the same lines as that used in our previous work and, therefore, is not given here. Obviously, the buffer capacity is a sum of two terms. The first term may be regarded as the own buffer capacity of the species B_k, e.g., the buffer capacity of a system containing no other species but B_k. The second term is a contribution coming from chemical reactions and may be regarded as reaction buffer capacity. In turn, the reaction buffer capacity of a multiple chemical reaction system may be partitioned into contributions coming from a subset of RERs involving the species B_k. The remarkable feature of this result is that the contributions of the RERs to the reaction buffer capacity may be evaluated explicitly. As indicated by eq. [9], the reaction buffer capacity depends on two factors. One of them is purely stoichiometric, i.e., it reflects the stoichiometric structure of the system. Namely, the contribution of the system's stoichiometry to the reaction buffer capacity is expressed through the stoichiometric factors $\gamma(\rho_0)$ and stoichiometric coefficients $\nu_k(\rho_0)$ of RERs. The other factor that determines the reaction buffer capacity is a compositional one, i.e., a function of the species concentrations, and is given explicitly by $\pi_k(\rho_0)$. Normally, the compositional factor is the dominant one. Because $\pi_k(\rho_0)$ is equal to the product of species concentrations involved in a RER, we immediately conclude that the most important contributions to the buffer capacity should be expected from the RERs involving the most abundant species.

The partition of the reaction buffer capacity into a sum of contributions associated with RERs concomitantly provides a simple algorithm for the computer generation of the analytical expressions of the buffer capacity. This algorithm includes the following steps. First, starting from a list of species, i.e., the formula matrix (eq. [3]), a complete set of RERs along with their stoichiometric factors $\gamma(\rho_0)$ is generated according to eqs. [4] and [6]. A subset of RERs involving a given species B_k ($k = 1, 2, \ldots, n$) is further selected from the complete set of RERs. The functions $\pi_k(\rho_0)$ and $g_k(\rho_0)$ are next generated according to eqs. [7] and [8]. The final equation for the buffer capacity is obtained by summing the contributions coming from RERs according to eqs. [9] and [10].

Examples

Buffer capacity with respect to H^+ in carbonate system

This system comprises $n = 8$ species: $CaCO_3$(s), H_2O(l), H^+(aq), Ca^{2+}(aq), CO_2(aq), HCO_3^-, CO_3^{2-}, and CO_2(g). An appropriate set of "elements" may be selected such as Ca^{2+}, C^{4+}, H^+, and O^{2-} resulting into the following formula matrix

$$\boldsymbol{\varepsilon} = \begin{array}{c} \begin{matrix} Ca^{+2} & C^{4+} & H^+ & O^{2-} \end{matrix} \\ \begin{bmatrix} 1 & 1 & 0 & 3 \\ 0 & 0 & 2 & 1 \\ 0 & 0 & 1 & 0 \\ 1 & 0 & 0 & 0 \\ 0 & 1 & 0 & 2 \\ 0 & 1 & 1 & 3 \\ 0 & 1 & 0 & 3 \\ 0 & 1 & 0 & 2 \end{bmatrix} \end{array} \begin{matrix} CaCO_3 \\ H_2O \\ H^+ \\ Ca^{2+} \\ CO_2(g) \\ HCO_3^- \\ CO_3^{2-} \\ CO_2(g) \end{matrix}$$

Obviously, this selection of the elements is not unique; however, it results in a formula matrix whose rank is equal to the number of elements, i.e., rank $\boldsymbol{\varepsilon} = s = 4$. Thus, the number of linearly independent reactions is equal to $m = n - \text{rank}\varepsilon = 8 - 4 = 4$ while a RER in this system involves no more than rank $\boldsymbol{\varepsilon} + 1 = 4 + 1 = 5$ species. The assumption that $CaCO_3$ is a pure solid phase and the activity of H_2O is equal to one requires these species to be involved in every RER. The other three species involved in a RER need to be selected from the remaining species H^+(aq), Ca^{2+}(aq), CO_2(aq), HCO_3^-, CO_3^{2-}, and CO_2(g). Here, we consider only the buffer capacity with respect to H^+; therefore, we need to generate a complete set of RERs involving H^+. Thus, each RER will involve two more species from the remaining five species: Ca^{2+}(aq), CO_2(aq), HCO_3^-, CO_3^{2-}, and CO_2(g). There are $5!/(3!/2!) = 10$ ways to select two species from a total of five, whereas the number of RERs involving concomitantly $CaCO_3$, H_2O and H^+ is equal to 10. For example, the five species, $CaCO_3$, H_2O, H^+, Ca^{2+} and CO_2(aq), define the following RER $\rho(CaCO_3, H_2O, H^+, Ca^{2+}, CO_2(aq))$. Applying eq. [4] to the formula matrix we obtain

$$\rho(CaCO_3,\ H_2O,\ H^+,\ Ca^{2+},\ CO_2(aq)) = \begin{vmatrix} 1 & 1 & 0 & 3 & CaCO_3 \\ 0 & 0 & 2 & 1 & H_2O \\ 0 & 0 & 1 & 0 & H^+ \\ 1 & 0 & 0 & 0 & Ca^{2+} \\ 0 & 1 & 2 & 3 & CO_2(aq) \end{vmatrix} = -\,CaCO_3 + H_2O - 2H^+ + Ca^{2+} + CO_2(aq) = 0$$

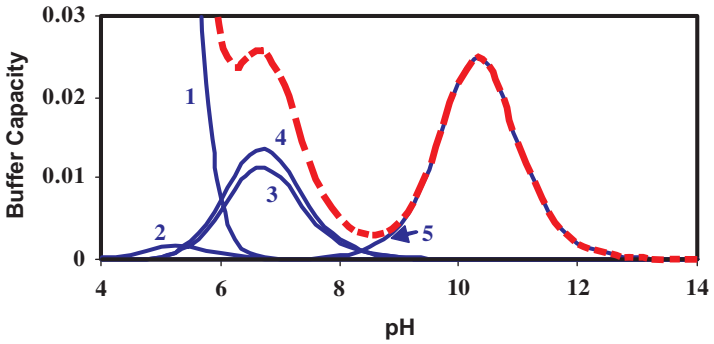
© 2006 NRC Canada

Table 1. Contributions to the buffer capacity with respect to H^+ in the carbonate system.

RERs	$\gamma(\rho_0)$	$\nu_{H^+}(\rho_0)$	$\pi_{H^+}(\rho_0)$	$g_{H^+}(\rho_0)$
1. ρ_0 ($CaCO_3$, H_2O, H^+, Ca^{2+}, $CO_2(aq)$) = – $CaCO_3$ + H_2O – $2H^+$ + Ca^{2+} + $CO_2(aq)$ = 0	1	–2	$[Ca^{2+}][CO_2(aq)]$	$\frac{1}{[Ca^{2+}]}+\frac{1}{[CO_2(aq)]}$
2. ρ_0 ($CaCO_3$, H_2O, H^+, Ca^{2+}, HCO_3^-) = – $CaCO_3$ – H^+ + Ca^{2+} + HCO_3^- = 0	1	–1	$[Ca^{2+}][HCO_3^-]$	$\frac{1}{[Ca^{2+}]}+\frac{1}{[HCO_3^-]}$
3. ρ_0 ($CaCO_3$, H_2O, H^+, Ca^{2+}, CO_3^{2-}) = – $CaCO_3$ + Ca^{2+} + CO_3^{2-} = 0	1	0	$[Ca^{2+}][CO_3^{2-}]$	$\frac{1}{[Ca^{2+}]}+\frac{1}{[CO_3^{2-}]}$
4. ρ_0 ($CaCO_3$, H_2O, H^+, Ca^{2+}, $CO_2(g)$) = – $CaCO_3$ – $2H^+$ + Ca^{2+} + $CO_2(g)$ + H_2O = 0	1	–2	$[Ca^{2+}][CO_2(g)]$	$\frac{1}{[Ca^{2+}]}+\frac{1}{[CO_2(g)]}$
5. ρ_0 ($CaCO_3$, H_2O, H^+, $CO_2(aq)$, HCO_3^-) = – H^+ – HCO_3^- + H_2O + $CO_2(aq)$ = 0	1	–1	$[CO_2(aq)][HCO_3^-]$	$\frac{1}{[CO_2(aq)]}+\frac{1}{[HCO_3^-]}$
6. ρ_0 ($CaCO_3$, H_2O, H^+, $CO_2(aq)$, CO_3^{2-}) = – $2H^+$ – CO_3^{2-} + H_2O + $CO_2(aq)$ = 0	1	–2	$[CO_2(aq)][CO_3^{2-}]$	$\frac{1}{[CO_2(aq)]}+\frac{1}{[CO_3^{2-}]}$
7. ρ_0 ($CaCO_3$, H_2O, H^+, $CO_2(aq)$, $CO_2(g)$) = – $CO_2(g)$ + $CO_2(aq)$ = 0	1	0	$[CO_2(aq)][CO_2(g)]$	$\frac{1}{[CO_2(aq)]}+\frac{1}{[CO_2(g)]}$
8. ρ_0 ($CaCO_3$, H_2O, H^+, CO_3^{2-}) = – H^+ – CO_3^{2-} + HCO_3^- = 0	1	–1	$[HCO_3^-][CO_3^{2-}]$	$\frac{1}{[HCO_3^-]}+\frac{1}{[CO_3^{2-}]}$
9. ρ_0 ($CaCO_3$, H_2O, H^+, HCO_3^-, $CO_2(g)$) = – $CO_2(g)$ – H_2O + HCO_3^- + H^+ = 0	1	1	$[HCO_3^-][CO_2(g)]$	$\frac{1}{[HCO_3^-]}+\frac{1}{[CO_2(g)]}$
10. ρ_0 ($CaCO_3$, H_2O, H^+, CO_3^{2-}, $CO_2(g)$) = – $CO_2(g)$ – H_2O + CO_3^{2-} + $2H^+$ = 0	1	2	$[CO_3^{2-}][CO_2(g)]$	$\frac{1}{[CO_3^{2-}]}+\frac{1}{[CO_2(g)]}$

© 2006 NRC Canada

Fig. 1. Overall reaction buffer capacity (dashed line) and individual contributions coming from various RERs (lines 1–5) for carbonate sustem discussed in Example 1. The total carbonate concentration is 0.1 mol/L. Equilibrium constants from ref. (6). 1. $CaCO_3(s) + 2H^+ = Ca^{2+} + CO_2(aq) + H_2O$, and $CaCO_3(s) + 2H^+ = Ca^{2+} + CO_2(g) + H_2O$; 2. $CaCO_3(s) + H^+ = Ca^{2+} + HCO_3^-$; 3. $HCO_3^- + H^+ = CO_2(aq) + H_2O$; 4. $HCO_3^- + H^+ = CO_2(g) + H_2O$; 5. $CO_3^{2-} + H^+ = HCO_3^- + H_2O$.



Clearly, the stoichiometric coefficients in this RERs are equal to the smallest integers and, consequently, the stoichiometric factor is equal to $\gamma(\rho_0) = 1$. To determine the contribution of this RER to the buffer capacity we need to further evaluate the functions $\pi_{H^+}(\rho_0)$ and $g_{H^+}(\rho_0)$. For the above RER these functions are

$$\pi_{H^+}(\rho_0) = [Ca^{2+}][CO_2(aq)]$$

$$g_{H^+}(\rho_0) = \frac{1}{[Ca^{2+}]} + \frac{1}{[CO_2(aq)]}$$

Continuing this procedure over the remaining RERs, we ultimately arrive at a complete set of RERs that, along with their stoichiometric and compositional factors, is presented in Table 1. Notice, the stoichiometric coefficients of H^+ in two RERs, namely, RERs 3 and 7 are equal to zero and consequently, the contributions to the buffer capacity with respect to H^+ coming from these RERs vanish. The buffer capacity with respect to H^+ is readily derived according to eqs. [9] and [10] and using the information presented in Table 1. The final result is

$$\beta_{H^+} = [H^+] + [OH^-] + \frac{1}{\Delta_{H^+}}(4[Ca^{2+}][CO_2(aq)] + [Ca^{2+}][HCO_3^-] + 4[Ca^{2+}][CO_2(g)] + [CO_2(aq)][HCO_3^-] + 4[CO_2(aq)][CO_3^{2-}] + [HCO_3^-][CO_3^{2-}] + [HCO_3^-][CO_2(g)] + 4[CO_3^{2-}][CO_2(g)])$$

where

$$\Delta_{H^+} = [Ca^{2+}] + [CO_2(aq)] + [HCO_3^-] + [CO_3^{2-}][CO_2(g)]$$

Here, the species concentrations are the equilibrium ones; hence, they may be evaluated by finding the equilibrium position in the system. Also, the units of $[CO_2]$ are mol/L. For ideal systems, the volumetric concentration of CO_2 may be converted to partial pressure via

$$[CO_2] = \frac{P_{CO_2}}{RT}$$

A numerical evaluation of the overall reaction buffer capacity along with contributions coming from individual RERs is presented in Figure 1. Clearly, the carbonate dominates the buffer capacity at low pH via the reactions:

$$CaCO_3(s) + 2H^+ = Ca^{2+} + CO_2(aq) + H_2O$$

$$CaCO_3(s) + 2H^+ = Ca^{2+} + CO_2(g) + H_2O$$

$$CaCO_3(s) + H^+ = Ca^{2+} + HCO_3^-$$

At a higher pH, the effect of carbonate rapidly decreases and the buffer capacity is controlled by reactions involving only aqueous and gas phase species:

$$HCO_3^- + H^+ = CO_2(aq) + H_2O$$

$$HCO_3^- + H^+ = CO_2(g) + H_2O$$

$$CO_3^{2-} + H^+ = HCO_3^- + H_2O$$

© 2006 NRC Canada

Table 2. A complete list of RERs and their stoichiometric factors in the system kaolinite–anorthite aqueous solution.

RERs	$\gamma(\rho_0)$
1. ρ_0 ($Al_2Si_2O_5(OH)_4$, $CaAl_2Si_2O_8$, H_2O, H^+, Ca^{2+}, Al^{3+}) = $- Al_2Si_2O_5(OH)_4 - Ca^{2+} + CaAl_2Si_2O_8 + H_2O + 2H^+ = 0$	2
2. ρ_0 ($Al_2Si_2O_5(OH)_4$, $CaAl_2Si_2O_8$, H_2O, H^+, Ca^{2+}, H_4SiO_4) = $- Al_2Si_2O_5(OH)_4 - Ca^{2+} + CaAl_2Si_2O_8 + H_2O + 2H^+ = 0$	2
3. ρ_0 ($Al_2Si_2O_5(OH)_4$, $CaAl_2Si_2O_8$, H_2O, H^+, Al^{3+}, H_4SiO_4) = $- Al_2Si_2O_5(OH)_4 - 6H^+ + 2Al^{3+} + 2H_4SiO_4 + H_2O = 0$	1
4. ρ_0 ($Al_2Si_2O_5(OH)_4$, $CaAl_2Si_2O_8$, H_2O, Ca^{2+}, Al^{3+}, H_4SiO_4) = $- 4Al_2Si_2O_5(OH)_4 - 3Ca^{2+} + 3CaAl_2Si_2O_8 + 2Al^{3+} + 2H_4SiO_4 + 4H_2O = 0$	2

Kaolinite–anorthite aqueous solution

This system comprises $n = 7$ species: $Al_2Si_2O_5(OH)_4$ (kaolinite), $CaAl_2Si_2O_8$ (anorthite), H_2O, H^+, Ca^{2+}, Al^{3+}, and H_4SiO_4. An appropriate set of elements for this system may be selected as Ca^{2+}, Al^{3+}, Si^{4+}, H^+, and O^{2-}. In this case, the rank formula matrix

$$\boldsymbol{\varepsilon} = \begin{array}{c} \begin{matrix} Ca^{2+} & Al^{3+} & Si^{4+} & H^+ & O^{2-} \end{matrix} \\ \begin{bmatrix} 0 & 2 & 2 & 4 & 9 \\ 1 & 2 & 2 & 0 & 8 \\ 0 & 0 & 0 & 2 & 1 \\ 0 & 0 & 0 & 1 & 0 \\ 1 & 0 & 0 & 0 & 0 \\ 0 & 1 & 0 & 0 & 0 \\ 0 & 0 & 1 & 4 & 4 \end{bmatrix} \end{array} \begin{matrix} Al_2Si_2O_5(OH_4) \\ CaAl_2Si_2O_8 \\ H_2O \\ H^+ \\ Ca^{2+} \\ Al^{3+} \\ H_4SiO_4 \end{matrix}$$

is equal to the number of elements, i.e., rank $\boldsymbol{\varepsilon} = s = 5$ and the number of linearly independent reactions is $m = n - s = 7 - 5 = 2$. A RER in this system is, therefore, defined by $s + 1 = 5 + 1 = 6$ species. The assumption that kaolinite and anorthite are pure solid phases while the aqueous solution is dilute implies that kaolinite, anorthite, and water should be involved in all of the RERs. The other three species need to be selected from the remaining four species, i.e., H^+, Ca^{2+}, Al^{3+}, and H_4SiO_4. Thus, we have a total of 4!/(3!/1!) = 4 RERs. The latter may be readily generated using eq. [4]. For example, the RER ρ ($Al_2Si_2O_5(OH)_4$, $CaAl_2Si_2O_8$, H_2O, H^+, Ca^{2+}, Al^{3+}) is given by

$$\rho(Al_2Si_2O_5(OH)_4, CaAl_2Si_2O_8, H_2O, H^+, Ca^{2+}, Al^{3+}) = \begin{vmatrix} 0 & 2 & 2 & 4 & 9 & Al_2Si_2O_5(OH)_4 \\ 1 & 2 & 2 & 0 & 8 & CaAl_2Si_2O_8 \\ 0 & 0 & 0 & 2 & 1 & H_2O \\ 0 & 0 & 0 & 1 & 0 & H^+ \\ 1 & 0 & 0 & 0 & 0 & Ca^{2+} \\ 0 & 1 & 0 & 0 & 0 & Al^{3+} \end{vmatrix} = 2Al_2Si_2O_5(OH)_4$$

$$- 2CaAl_2Si_2O_8 - 2H_2O - 4H^+ + 2Ca^{2+} + 0Al^{3+} = 0$$

Clearly, the stoichiometric numbers in this RER may be factorized by a factor of two. Hence, requiring the stoichiometric coefficients in the RER to be the smallest integers, we have to introduce a stoichiometric factor $\gamma(\rho_0)$ equal to two, i.e.,

$$\rho(Al_2Si_2O_5(OH)_4, CaAl_2Si_2O_8, H_2O, H^+, Ca^{2+}, Al^{3+}) = 2\rho_0(Al_2Si_2O_5(OH)_4, CaAl_2Si_2O_8, H_2O, H^+, Ca^{2+}, Al^{3+})$$

where

$$\rho_0(Al_2Si_2O_5(OH)_4, CaAl_2Si_2O_8, H_2O, H^+, Ca^{2+}, Al^{3+}) = -Al_2Si_2O_5(OH)_4 - Ca^{2+} + CaAl_2Si_2O_8 + H_2O + 2H^+ = 0$$

A complete set of RERs for this system along with their stoichiometric factors is presented in Table 2. Based on this complete set of RERs, one can easily derive the buffer capacity for all of the aqueous species. As an example, consider the buffer capacity for H^+. From the complete set of RERs, we select the subset of RERs involving H^+. Next, for every RER we evaluate the functions $\pi_{H^+}(\rho_0)$ and $g_{H^+}(\rho_0)$. These calculations are summarized in Table 3. Substituting the values of $\gamma(\rho_0)$, $\nu_{H^+}(\rho_0)$, $\pi_{H^+}(\rho_0)$ and $g_{H^+}(\rho_0)$ into eqs. [9] and [10] and summing over the three RERs gives

© 2006 NRC Canada

Table 3. Contributions to the buffer capacity with respect to H^+ in the kaolinite–anorthite aqueous solution.

RERs	$\gamma(\rho_0)$	$\nu_{H^+}(\rho_0)$	$\pi_{H^+}(\rho_0)$	$g_{H^+}(\rho_0)$
1. ρ_0 ($Al_2Si_2O_5(OH)_4$, $CaAl_2Si_2O_8$, H_2O, H^+, Ca^{2+}, Al^{3+}) = – $Al_2Si_2O_5(OH)_4$ – Ca^{2+} + $CaAl_2Si_2O_8$ + H_2O + $2H^+$ = 0	2	2	$[Ca^{2+}][Al^{3+}]$	$\frac{1}{[Ca^{2+}]}$
2. ρ_0 ($Al_2Si_2O_5(OH)_4$, $CaAl_2Si_2O_8$, H_2O, H^+, Ca^{2+}, H_4SiO_4) = – $Al_2Si_2O_5(OH)_4$ – Ca^{2+} + $CaAl_2Si_2O_8$ + H_2O + $2H^+$ = 0	2	2	$[Ca^{2+}][H_4SiO_4]$	$\frac{1}{[Ca^{2+}]}$
3. ρ_0 ($Al_2Si_2O_5(OH)_4$, $CaAl_2Si_2O_8$, H_2O, H^+, Al^{3+}, H_4SiO_4) = – $Al_2Si_2O_5(OH)_4$ – $6H^+$ + $2Al^{3+}$ + $2H_4SiO_4$ + H_2O = 0	1	–6	$[Al^{3+}][H_4SiO_4]$	$\frac{4}{[Al^{3+}]} + \frac{4}{[H_4SiO_4]}$

Table 4. Buffer capacity with respect to aqueous species in the kaolinite–anorthite aqueous solution.

Species	Buffer capacity
H+	$[H^+] + [OH^-] + 4[Ca^{2+}] + \frac{9[Al^{3+}][H_4SiO_4]}{[Al^{3+}] + [H_4SiO_4]}$
Ca^{2+}	$[Ca^{2+}] + 1/4[H+] + 9/4\ \frac{[Al^{3+}][H_4SiO_4]}{[Al^{3+}] + [H_4SiO_4]}$
Al^{3+}	$[Al^{3+}] + \frac{[H^+][H_4SiO_4] + 4[Ca^{2+}][H_4SiO_4]}{[H^+] + 4[Ca^{2+}] + 18[H_4SiO_4]}$
H_4SiO_4	$[H_4SiO_4] + \frac{[H^+][Al^{3+}] + 4[Ca^{2+}][Al^{3+}]}{[H^+] + 4[Ca^{2+}] + 18[Al^{3+}]}$

$$\beta_{H^+} = [H^+] + [OH^+] + 4[Ca^{2+}] + \frac{9[Al^{3+}][H_4SiO_4]}{[Al^{3+}] + [H_4SiO_4]}$$

The meaning of each term in this equation is evident. Namely, the first two terms are associated with the presence of H^+ and water dissociation while the last two terms are associated with the reactions

$$Al_2Si_2O_5(OH)_4 + Ca^{2+} = CaAl_2Si_2O_8 + H_2O + 2H^+$$

$$Al_2Si_2O_5(OH)_4 + 6H^+ = 2Al^{3+} + 2H_4SiO_4 + H_2O$$

Similarly, one can derive the buffer capacity for the remaining aqueous species. The buffer capacity with respect to all aqueous species is given in Table 4.

Pyrite–O_2 aqueous solution

This system comprises (n = 8) species: FeS_2(s), $Fe(OH)_3$(s), H_2O(l), H^+(aq) SO_4^{2-}(aq), Fe^{2+}(aq), Fe^{3+}(aq), and O_2(aq). An appropriate set of elements for this system is:

$$\boldsymbol{\varepsilon} = \begin{array}{c} \begin{matrix} Fe & S & H & O & e \end{matrix} \\ \begin{bmatrix} 1 & 2 & 0 & 0 & 0 \\ 1 & 0 & 3 & 3 & 0 \\ 0 & 0 & 1 & 2 & 0 \\ 0 & 0 & 1 & 0 & -1 \\ 0 & 1 & 0 & 4 & 2 \\ 1 & 0 & 0 & 0 & -2 \\ 1 & 0 & 0 & 0 & -3 \\ 0 & 0 & 0 & 2 & 0 \end{bmatrix} \end{array} \begin{matrix} FeS_2 \\ Fe(OH)_3 \\ H_2O \\ H^+ \\ SO_4^{2-} \\ Fe^{2+} \\ Fe^{3+} \\ O_2 \end{matrix}$$

It is easy to show that rank $\boldsymbol{\varepsilon}$ = 5 and m = 8 – 5 = 3. A RER in this system is thus defined by rank $\boldsymbol{\varepsilon}$ + 1 = 5 +1 = 6 species. Two of the species comprising the system, namely, FeS_2 and $Fe(OH)_3$, are assumed to be pure condensed phases, while the activity of H_2O is assumed to be unity. This means that these three species should be involved in every RER. The remaining three species need to be selected from H^+, SO_4^{2-}, Fe^{2+}, Fe^{3+}, and O_2. Thus, the number of RERs in this system is equal to 5!/(3!/2!) = 10. For instance, the RER ρ (FeS_2, $Fe(OH)_3$,H_2O, H^+, SO_4^{2-}, Fe^{2+}) is given by

© 2006 NRC Canada

Table 5. A complete set of RERs for the pyrite–O_2 aqueous solution.

RERs	$\gamma(\rho_0)$
1. $\rho_0(FeS_2, Fe(OH)_3, H_2O, H^+, SO_4^{2-}, Fe^{2+}) = -FeS_2 - 14Fe(OH)_3 - 26H^+ + 2SO_4^{2-} + 15Fe^{2+} + 34H_2O = 0$	1
2. $\rho_0(FeS_2, Fe(OH)_3, H_2O, H^+, SO_4^{2-}, Fe^{3+}) = -Fe(OH)_3 - 3H^+ + 3Fe^{3+} + 3H_2O = 0$	15
3. $\rho_0(FeS_2, Fe(OH)_3, H_2O, H^+, SO_4^{2-}, O_2) = -4FeS_2 - 15O_2 - 14H_2O + 4Fe(OH)_3 + 8SO_4^{2-} + 16H^+ = 0$	1
4. $\rho_0(FeS_2, Fe(OH)_3, H_2O, H^+, Fe^{2+}, Fe^{3+}) = -Fe(OH)_3 - 3H^+ + 3Fe^{3+} + 3H_2O = 0$	2
5. $\rho_0(FeS_2, Fe(OH)_3, H_2O, H^+, Fe^{2+}, O_2) = -4Fe^{2+} - O_2 - 10H_2 + 4Fe(OH)_3 + 8H^+ = 0$	2
6. $\rho_0(FeS_2, Fe(OH)_3, H_2O, H^+, Fe^{3+}, O_2) = -Fe(OH)_3 - 3H^+ + 3Fe^{3+} + 3H_2O = 0$	8
7. $\rho_0(FeS_2, Fe(OH)_3, H_2O, SO_4^{2-}, Fe^{2+}, Fe^{3+}) = -3FeS_2 - 16Fe(OH)_3 - 26Fe^{3+} + 45Fe^{2+} + 6SO_4^{2-} + 24H_2O = 0$	1
8. $\rho_0(FeS_2, Fe(OH)_3, H_2O, SO^{2-}_4, Fe^{2+}, O_2) = -4FeS_2 - 4Fe(OH)_3 - 13O_2 + 8Fe^{2+} + 8SO_4^{2-} + 6H_2O = 0$	2
9. $\rho_0(FeS_2, Fe(OH)_3, H_2O, SO_4^{2-}, Fe^{3+}, O_2) = -12FeS_2 - 4Fe(OH)_3 - 45O_2 + 16Fe^{3+} + 24SO_4^{2-} + 6H_2O = 0$	1
10. $\rho_0(FeS_2, Fe(OH)_3, H_2O, Fe^{2+}, Fe^{3+}, O_2) = -12Fe^{2+} - 3O_2 - 6H_2O + 4Fe(OH)_3 + 8Fe^{3+} = 0$	2

Table 6. Contributions to the buffer capacity with respect to H^+ in the pyrite–O_2 aqueous system.

RERs	$\gamma(\rho_0)$	$\nu_{H^+}(\rho_0)$	$\pi_{H^+}(\rho_0)$	$g_{H^+}(\rho_0)$
1. $\rho(FeS_2, Fe(OH)_3, H_2O, H^+, SO_4^{2-}, Fe^{2+}) = -FeS_2 - 14Fe(OH)_3 - 26H^+ + 2SO_4^{2-} + 15Fe^{2+} + 34H_2O = 0$	1	–26	$[SO_4^{2-}][Fe^{2+}]$	$\frac{4}{[SO_4^{2-}]} + \frac{225}{[Fe^{2+}]}$
2. $\rho(FeS_2, Fe(OH)_3, H_2O, H^+, SO_4^{2-}, Fe^{3+}) = -Fe(OH)_3 - 3H^+ + 3Fe^{3+} + 3H_2O = 0$	15	–3	$[SO_4^{2-}][Fe^{3+}]$	$\frac{9}{[Fe^{3+}]}$
3. $\rho(FeS_2, Fe(OH)_3, H_2O, H^+, SO_4^{2-}, O_2) = -4FeS_2 - 15O_2 - 14H_2O + 4Fe(OH)_3 + 8SO_4^{2-} + 16H^+ = 0$	1	16	$[SO_4^{2-}][O_2]$	$\frac{64}{[SO_4^{2-}]} + \frac{225}{[O^2]}$
4. $\rho(FeS_2, Fe(OH)_3, H_2O, H^+, Fe^{2+}, Fe^{3+}) = -Fe(OH)_3 - 3H^+ + 3Fe^{3+} + 3H_2O = 0$	1	–3	$[Fe^{2+}][Fe^{3+}]$	$\frac{9}{[Fe^{3+}]}$
5. $\rho(FeS_2, Fe(OH)_3, H_2O, H^+, Fe^{2+}, O_2) = -4Fe^{2+} - O_2 - 10H_2O + 4Fe(OH)_3 + 8H^+ = 0$	2	8	$[Fe^{2+}][O_2]$	$\frac{16}{[Fe^{2+}]} + \frac{1}{[O^2]}$
6. $\rho(FeS_2, Fe(OH)_3, H_2O, H^+, Fe^{3+}, O_2) = -Fe(OH)_3 - 3H^+ + 3Fe^{3+} + 3H_2O = 0$	8	–3	$[Fe^{3+}][O_2]$	$\frac{9}{[Fe^{3+}]}$

$$\rho(FeS_2,\ Fe(OH)_3,\ H_2O,\ H^+,\ SO_4^{2-},\ Fe^{2+}) = \begin{vmatrix} 1 & 2 & 0 & 0 & 0 & FeS_2 \\ 1 & 0 & 3 & 3 & 0 & Fe(OH)_3 \\ 0 & 0 & 1 & 2 & 0 & H_2O \\ 0 & 0 & 1 & 0 & -1 & H^+ \\ 0 & 1 & 0 & 4 & 2 & SO_4^{2-} \\ 1 & 0 & 0 & 0 & -2 & Fe^{2+} \end{vmatrix}$$

$$= -7FeS_2 + 4Fe(OH)_3 - 34H_2O + 22H^+ + 14SO_4^{2-} + 3Fe^{2+} = 0$$

The stoichiometric coefficients in this RER are equal to the smallest integers, therefore, $\gamma(\rho_0) = 1$. A complete list of RERs for this system along with their stoichiometric factors is given in Table 5. The complete set of RERs may now be used to build up the buffer capacity expressions for all aqueous species. To do this, we need to select the RERs involving a certain species and evaluate the functions $\pi_k(\rho_0)$ and $g_k(\rho_0)$. For instance, the buffer capacity for H^+ may be derived based on the data presented in Table 6. Summing the contributions coming from these RERs according to eqs. [9] and [10] gives

$$\beta_{H^+} = [H^+] + [OH^+] + \frac{1}{\Delta_{H^+}}(676[SO_4^{2-}][Fe^{2+}] + 2025[SO_4^{2-}][Fe^{3+}] + 256[Fe^{2+}][O_2]$$
$$+ 36[Fe^{2+}][Fe^{3+}] + 256[Fe^{2+}][O_2] + 576[Fe^{2+}][O_2])$$

© 2006 NRC Canada

Table 7. Buffer capacity with respect to aqueous species in the pyrite–O_2 aqueous solution.

Species	Buffer capacity
H^+	$[H^+] + [OH^-] + \frac{3(676[SO_4^{2-}][Fe^{2+}] + 2025[SO_4^{2-}][Fe^{2+}] + 256[SO_4^{2-}][O_2] + 36[Fe^{2+}][Fe^{3+}] + 256[Fe^{2+}][O_2] + 576[Fe^{2+}][O_2])}{(2475[SO_4^{2-}] + 44[Fe^{2+}] + 704[O_2])}$
SO_4^{2-}	$[SO_4^{2-}] + \frac{3(4[H^+][Fe^{2+}] + 64[H^+][O_2] + 36[Fe^{2+}][Fe^{3+}] + 256[Fe^{2+}][O_2] + 576[Fe^{3+}][O_2]}{(2475[H^+] + 3337[Fe^{2+}] + 4726[Fe^{3+}] + 768[O_2])}$
Fe^{2+}	$[Fe^{2+}] + \frac{3(225[H^+][SO_4^{2-}] + 64[H^+][O_2] + 2025[SO_4^{2-}][Fe^{3+}] + 256[SO_4^{2-}][O_2] + 576[Fe^{2+}][O_2]}{(6075[SO_4^{2-}] + 136[Fe^{3+}] + 1728[O_2])}$
Fe^{3+}	$[Fe^{3+}] + \frac{3(2025[H^+][SO_4^{2-}] + 36[H^+][Fe^{2+}] + 576[H^+][O_2] + 676[SO_4^{2-}][Fe^{2+}] + 256[SO_4^{2-}][O_2] + 256[Fe^{2+}][O_2]}{(6075[SO_4^{2-}] + 136[Fe^{2+}] + 1728[O_2]}$
O_2	$[O_2] = \frac{3(225[H+][SO_4^{2-}] + 4[H^+][Fe^{2+}] + 676[SO_4^{2-}][Fe^{2+}] + 2025[SO_4^{2-}][Fe^{3+}] + 36[Fe^{2+}][Fe^{3+}])}{(794[H^+] + 768[SO_4^{2-}] + 768[Fe^{2+}] + 1728[Fe^{3+}])}$

where

$$\Delta_{H^+} = \frac{1}{3}(2475[SO_4^{2-}] + 44[Fe^{2+}] + 704[O_2])$$

The buffer capacity for other aqueous species may be derived in a similar manner. The results are summarized in Table 7.

Discussion and concluding remarks

The buffer capacity in multiple chemical reaction systems is a complex function of the equilibrium composition. Explicit equations for the buffer capacity may be easily derived by differentiating the equilibrium conditions with respect to species concentrations. However, for complex, multiple chemical reaction systems, this procedure results in cumbersome expressions that lack a clear physicochemical meaning. In this work, we showed that the buffer capacity may be partitioned into a sum of contributions coming from RERs. This partition allows an easy way to generate analytical expressions for the buffer capacity based on a purely stoichiometric analysis. Concomitantly, this partition may be used to determine the reactions that contribute dominantly to the buffer capacity.

References

1. J. van Slyke. J. Biol. Chem. **52**, 525 (1922).
2. E.R. Nightingale. Anal. Chem. **30**, 267 (1958).
3. D.D. Perrin and D. Dempsey. Buffers for pH and metal ion control. Chapman and Hall, London. 1987.
4. I. Povar and C. Luca. Rev. Chim. **54**, 312 (2003).
5. I. Povar. Russ. J. Inorg. Chem. (Engl. Transl.), **45**, 1628 (2000).
6. J.N. Butler. Ionic equilibrium. Solubility and pH calculations. John Wiley and Sons, New York. 1998.
7. I. Povar. Russ. J. Inorg. Chem. (Engl. Transl.), **45**, 1632 (2000).
8. I. Povar. Russ. J. Inorg. Chem. (Engl. Transl.), **41**, 1167 (1996).
9. R. de Levie. J. Chem. Educ. **76**, 574 (1999).
10. E.T. Urbansky and M.R. Schock. J. Chem. Educ. **77**, 1640 (2000).
11. M.T. Beck and I. Nagypal. Chemistry of complex equilibria. Academiai Kiado, Budapest. 1990.
12. A.A. Bugaevsky. Raschet Khimicheskikh Ravnovesii v Rastvore. Kharkov, Vischa Shkola. 1980. [In Russian.]
13. I. Fishtik, I. Nagypal, and I. Gutman. J. Chem Soc. Faraday Trans. **90**, 3245 (1994).
14. I. Fishtik, I. Nagypal, and I. Gutman. J. Chem Soc. Faraday Trans. **92**, 3523 (1996).
15. I. Fishtik. Z. Phys. Chem. (Muenchen), **205**, 253 (1998).

© 2006 NRC Canada

A DFT study of spherands containing five anisyl groups — Highly preorganized to bind the alkali metal

Shabaan A.K. Elroby, Kyu Hwan Lee, Seung Joo Cho, and Alan Hinchliffe

Abstract: Although anisyl units are basically poor ligands for metal ions, the rigid placements of their oxygens during synthesis rather than during complexation are undoubtedly responsible for the enhanced binding and selectivity of the spherand. We used standard B3LYP/6-31G** (5d) density functional theory (DFT) to investigate the complexation between spherands containing five anisyl groups, with CH_2–O–CH_2 **(2)** and CH_2–S–CH_2 **(3)** units in an 18-membered macrocyclic ring, and the cationic guests (Li^+, Na^+, and K^+). Our geometric structure results for spherands **1**, **2**, and **3** are in good agreement with the previously reported X-ray diffraction data. The absolute values of the binding energy of all the spherands are inversely proportional to the ionic radius of the guests. The results, taken as a whole, show that replacement of one anisyl group by CH_2–O–CH_2 **(2)** and CH_2–S–CH_2 **(3)** makes the cavity bigger and less preorganized. In addition, both the binding and specificity decrease for small ions. The spherands **2** and **3** appear beautifully preorganized to bind all guests, so it is not surprising that their binding energies are close to the parent spherand **1**. Interestingly, there is a clear linear relation between the radius of the cavity and the binding energy (R^2 = 0.999).

Key words: spherands, preorganization, density functional theory, binding energy, cavity size.

Résumé : Même si les unités anisyles sont d'une façon inhérente de mauvais ligands pour les ions métalliques, les placements rigides de leur atome d'oxygène au cours des synthèses plutôt que durant la complexation sont sans aucun doute plus responsables pour l'augmentation de la fixation et de la sélectivité du sphérand. On a fait appel à la théorie de la densité fonctionnelle B3LYP/6-31G** (5d) standard pour étudier la complexation entre des espèces cationiques invitées (Li^+, Na^+ et K^+) et des sphérands macrocycliques à dix-huit membres comportant cinq groupes anisyles avec des unités CH_2–O–CH_2 **(2)** et CH_2–S–CH_2 **(3)**. Les résultats pour la structure géométrique des sphérands **1**, **2** et **3** sont en bon accord avec les données de diffraction des rayons X trouvées dans la littérature. Les valeurs absolues pour l'énergie de liaison de chacun des sphérands est inversement proportionnelle au rayon ionique des molécules invitées. Pris dans leur ensemble, les résultats montrent que le remplacement d'un groupe anisyle par des unités CH_2–O–CH_2 **(2)** et CH_2–S–CH_2 **(3)** fait que la cavité est agrandie et moins préorganisée. De plus, la fixation et la spécificité diminuent toutes les deux avec les petits ions. Les sphérands **2** et **3** semblent bien préorganisés pour se lier à toutes les molécules invitées; il n'est donc pas surprenant que les énergies de fixation des sphérands **2** et **3** soient proches de celle du sphérand fondamental **1**. Il est intéressant de noter qu'il existe clairement une relation linéaire entre le rayon de la cavité et l'énergie de liaison (R^2 = 0,999).

Mots clés : sphérands, préorganisation, théorie de la densité fonctionnelle, énergie de liaison, rayon de la cavité.

[Traduit par la Rédaction]

Introduction

Supramolecular chemistry and the quantification of noncovalent interaction offer the basis for novel approaches in medicine, host–guest chemistry (1), chromatography (2), and biocatalysis (3). The development of artificial receptors capable of forming complexes with specific guests (4–6) is important to the progress of supramolecular host–guest chemistry.

In host–guest complexation, the concave surface of a host complements the convex surface of a guest. Similarly, the receptor sites of enzymes frequently contain rigid cavities whose internal surfaces complement the convex surfaces of substrates or inhibitors.

The spherands, exemplified by **1** (Chart 1), are a specific type of cavitands. Unlike the chorands (crowns) or cryptands, they contain rigid cavities formed during their syntheses rather than during their complexation. The spherands' preorganization results in the highest binding and selectivity yet observed for the alkali metal ions (7). There is a vast chemical literature describing studies of the binding proper-

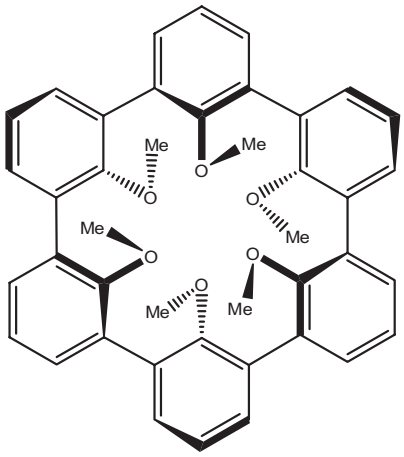
Received 22 May 2006. Accepted 30 August 2006. Published on the NRC Research Press Web site at http://canjchem.nrc.ca on 4 October 2006.

S.A.K. Elroby,[1] K.H. Lee, and S.J. Cho.[2] Korea Institute of Science and Technology, PO Box 131, Cheongryang, Seoul 130-650, Korea.
A. Hinchliffe. School of Chemistry, University of Manchester, Oxford Road, Manchester, M13 9PL, UK.

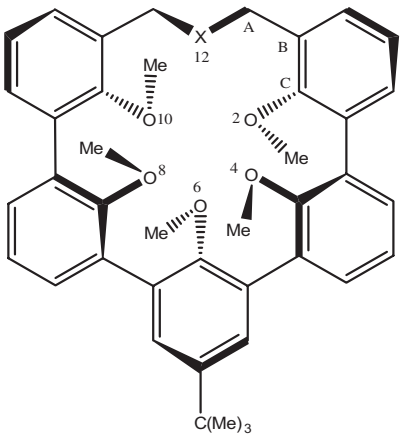
[1]Present address: Department of Chemistry, Faculty of Science, Beni Suef University, Beni Suef, Egypt.
[2]Corresponding author (e-mail: chosj@kist.re.kr).

 doi:10.1139/V06-130 © 2006 NRC Canada

Chart 1.



1



X = O 2
S 3

ties for the host–guest complexation ion involving such spherands.

The syntheses, characterization, and binding properties of four new spherands were reported by Cram and co-workers (8). These spherands contain five meta-linked anisyl binding sites incorporated in an 18-membered macrocyclic ring. The 18-membered macrocycles were completed with conformationally mobile CH_2–O–CH_2 and CH_2–S–CH_2 units. The crystal structure of the spherands indicated that the anisyl groups' CH_3O possess an up-down-up-down-up-down conformation when proceeding clockwise around the ring. All six oxygens' unshared electron pairs line forming an elongated spherical cavity preorganized to bind the smaller alkali metal cations (9).

To our knowedge, ab initio studies concerning the spherands compounds are very rare, presumably because of the large size of these hosts. Furthermore, ab initio studies in the gas phase would give a zero-order, yet valuable, opportunity to understand the intrinsic factors affecting the complexation without including the effects of solvation.

To understand the complexation of spherands, we have undertaken a density functional theory (DFT) study of spherands containing five anisyl groups and their complexes with Li^+, Na^+, and K^+ ions. The results can be compared with the results obtained experimentally. Hosts **2** and **3** are spherands in which one anisyl group is replaced by one group of CH_2–O–CH_2 or CH_2–S–CH_2, respectively. The main purpose of the present work is to provide accurate theoretical information on the structures of spherands **2** and **3** and their metal complexes and to analyze how the presence of CH_2–O–CH_2 or CH_2–S–CH_2 modifies the binding capacities relative to spherand **1**.

Computational method

All DFT calculations were carried out using the G03 suite of programs (10). We used the standard B3LYP/6-31G** (5d) model (11). All structures were fully optimized. Because the crystal structure of the analogous macrocycle (4-$MeC_6H_2OMe)_6$ shows D_{3d} symmetry, the OMe–spherands $(C_6H_3OMe)_6$ are thought to be of D_{3d} symmetry (9). Basis set superposition error corrections (BSSEC) (12) were used to obtain more reasonable binding energies. All the calculations were done using KIST teraflops Linux cluster.

Result and discussion

In spherand **1**, the acyclohexmetaphenylene system provides a framework that holds the oxygens of six methoxyl groups in a perfect octahedral arrgement by their attachment to six convergent positions of the aryl group. In the present work, we studied the effect of replacement of one anisyl group by CH_2–O–CH_2 (**2**) and CH_2–S–CH_2 (**3**) on the binding energies and the preorganization toward Li^+, Na^+, and K^+ guests. Because of the importance of Li^+, Na^+, and K^+ in physiological chemistry, the ability of hosts to differentiate between these ions in complexation is interesting.

Spherands **2** and **3** were examined for their differential binding properties toward the alkali metal and compared to spherand **1**. In both molecules, the five anisyl CH_3O groups and one CH_2–O–CH_2 and CH_2–S–CH_2 group possess an up-down-up-down-up-down conformation proceeding clockwise around the ring (18).

We defined the binding energy (E_{BE}) of the complexation (eq. [1]) as the measure of the enthalpic contribution to the thermodynamic stability of the host–guest complex:

$$[1] \qquad E_{BE} = E_{complex} - (E_{host} + E_{guest})$$

All binding energies, with and without the BSSEC, are listed in Table 1. Amongst the hosts of this study, those containing 18-membered rings (**1–3**) exhibit both the highest binding energy values and, generally, demonstrate the most discrimination between the guest ions studied.

Clearly, the absolute value of binding energy is inversely proportional to the ionic radius. As expected, Li^+ was found to be the strongest guest to **1**. Spherand **1** complexed Li^+ with a binding energy of 134.16 kcal/mol, which is 29 and 71.4 kcal/mol greater than those of **1**·Na^+ and **1**·K^+, respec-

© 2006 NRC Canada

Table 1. The energies of the spherands and their cation complexes.

Compound	E_{opt}[a] (hartree)	E_{bind}[b] (kcal/mol)	E_{CP}[c] (hartree)	$E_{CP,\ bind}$[d] (kcal/mol)
1	–2073.40849			
1·Li^+	–2080.91330	138.21	–2080.90685	–134.16
1·Na^+	–2235.66845	112.16	–2235.65951	–106.55
1·K^+	–2673.24596	71.20	–2673.23251	–62.75
2	–2038.93013			
2·Li^+	–2046.42868	–134.29	–2046.42126	–129.63
2·Na^+	–2201.18952	–111.80	–2201.17963	–105.60
2·K^+	–2638.76078	–66.92	–2638.75081	–60.67
3	–2361.91417			
3·Li^+	–2369.40926	–132.12	–2369.40355	–128.53
3·Na^+	–2524.14151	–91.70	–2524.13397	–86.96
3·K^+	–2961.73751	–62.34	–2961.72833	–56.58

[a]Optimized energy
[b]Binding energy
[c]Basis set superposition error corrected energy
[d]Binding energy with basis set superposition error correction.

Table 2. Distances and angles in the geometric structures of the spherands and their complexes.

Compound	12–A–B–C (°)	Average M^+–O (Å)	Diameter (Å)	O2–O8 (Å)	O4–O10 (Å)	O6–O12 (Å)
1			4.458		4.458	
1·Li^+	53.1	2.156	4.312			
1·Na^+	60.2	2.296	4.593			
1·K^+	74.8	2.600	5.201			
2	82.1		5.149	5.202 (4.084)[a]	4.799 (4.697)[a]	5.445 (5.447)[a]
2·Li^+	64.1	2.271	4.544	4.223	4.230	5.182
2·Na^+	67.4	2.393	4.750	4.647	4.648	4.956
2·K^+	86.1	2.884	5.473	5.224	6.141	5.045
3	92.5		5.281	5.117 (3.843)[a]	4.828 (4.939)[a]	5.899 (5.958)
3·Li^+	75.0	2.350	4.712	4.314	4.312	5.510
3·Na^+	90.3	2.592	5.296	4.680	5.918	5.292
3·K^+	105.1	2.820	5.709	5.214	6.154	5.758

Note: The average diameter of the resulting cavities was calculated by averaging the distances between the three sets of oxygen pairs most distant from one another (e.g., oxygens at 2 and 8, at 4 and 10, and at 6 and 12 o'clock).
[a] Experimental data from ref. 8.

tively. Spherand **2** complexed Li^+ with a binding energy of 129.63 kcal/mol which is 58.96 kcal/mol greater than the binding energy value for **2**·K^+(60 kcal/mol). As expected from the DFT calculations, host **1** is more preorganized and strongly binding than hosts **2** and **3**. The spherands **2** and **3** and their complexes are shown in Fig. 1, and the set of geometric parameters are gathered in Table 2 along with some experimental results. It is interesting to note how the diameter of sphere changes.

The DFT calculations predicted that the distance between the sulfur at 12 o'clock and the oxygen at 6 o'clock (see Chart 1) was 5.869 and 5.449 Å which is in good agreement with the experimental data (18). The calculations also predicted the distance between the oxygen at 12 o'clock and the oxygen at 6 o'clock to be 5.445 Å which is very close to the O12–O6 distance of 5.447 Å obtained from X-ray studies (18).

The predicted O2–O8 distances in hosts **2** and **3** of 5.202 and 5.117 Å differ from the experimentally derived values of 4.084 and 3.843 Å, respectively; this is within the experimental error margin. The experimental data show that O2 is below the mean plane thus accounting for the differences in the theoritical and experimental data.

The average diameter of the resulting cavities was calculated by averaging the distances between the three sets of oxygen pairs most distant from one another (e.g., oxygens at two and eight, at four and 10, and at six and 12 o'clock). The spherical diameter of **1** is 4.46 Å. It is interesting to note the changes in the diameter of the sphere that comprises six oxygen atoms. When complexed with Li^+, it shrinks slightly to 4.31 Å, while it enlarges to 4.59 and 5.20 Å with Na^+ and K^+, respectively. The contraction of **1** upon Li^+ complexation indicates the electrostatic attraction between Li^+ and its surrounding oxygen atoms. In conclusion, **1** stretched to accommodate K^+ and Na^+ and contracted to complex Li^+.

The cavity diameters in free **2** and **3** were 5.15 and 5.28 Å, respectively as compared with 5.470 and 5.709 Å in the case of K^+ complexes. Thus, spherand **2** and **3** appear beautifully preorganized to bind all guests and it is not surprising that their binding energies are close to that of the host **1**.

© 2006 NRC Canada

Fig. 1. The Na^+ complexes structures of the spherands studied. All H atoms are removed to improve visualization.

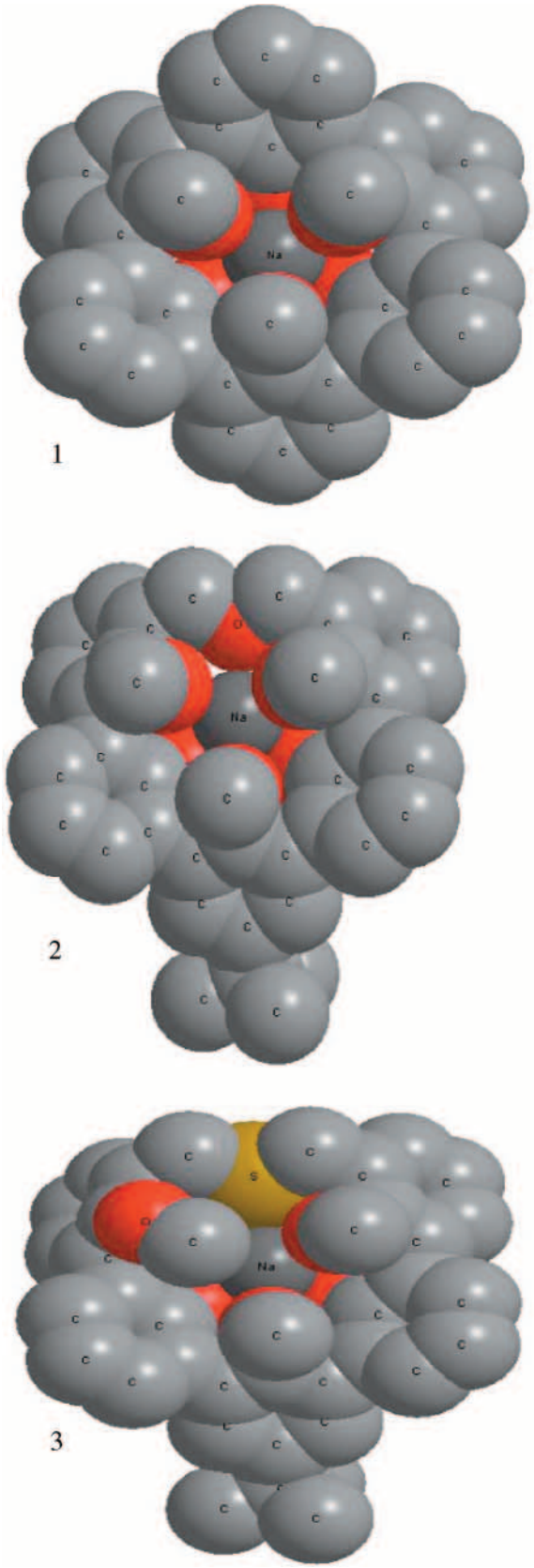
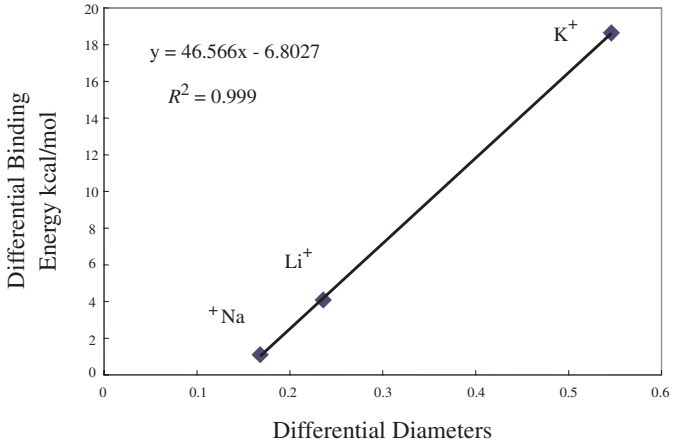


Fig. 2. The correlation between differential diameter and differential binding energy of hosts **2** and **3** complexes.



The diameter of the cavity of **2** in spheraplexes **2**·Na^+ and **2**·K^+ was 4.75 Å and 5.47 Å, respectively, compared with 5.149 Å in the case of free **2**. Thus, **2** stretched to accommodate K^+ and contracted to complex Li^+. Our calculations suggest that only the four OCH_3 oxygens and CH_2–O–CH_2 or CH_2–S–CH_2 can contact K^+ in **2**·K^+ and **3**·K^+, which correlates with the lower binding for these spheraplexes of 60.66 and 56.57 kcal/mol, respectively. The much lower binding energy with **2** and **3** compared with **1** is attributed to the fact that the presence of the respective CH_2–O–CH_2 and CH_2–S–CH_2 units in **2** and **3** not only expands the cavity but also introduces a flexibility into the 18-membered macroring, thus providing measurable binding for Na^+ and Li^+. The respective values for **2** and **3** complexing these ions are as follows: Li^+, 129.63 and 128.53 kcal/mol; Na^+, 105.59 and 86.96 kcal/mol. Thus, host **2** binds Na^+ better than host **3.** The cavity of **3** is larger than that of **2** because of the longer bonds in CH_2–S–CH_2 as compared to CH_2–O–CH_2. The softer character of S compared to O means bond angle deformations involving S are less costly than those involving O.

The effect of complexation of **2** and **3** on their geometric parameters is apparent from the comparisons in Table 2. Some structural parameters of the three complexes of the alkali metal ions are also listed in Table 2. The Na^+ ion in **3**·Na^+ exhibits a strong interaction compared to the host **3**. The average Na^+–O distances for **2**·Na and **3**·Na^+ are 2.39 and 2.59 Å, respectively. Comparisons of Na^+–O average distances in **2**·Na^+ and **3**·Na^+ with the standard value of 2.35 Å (19) show that Na^+ has stronger interactions with host **2** than host **3**. Because of constraints, the cavity of **3** is unable to contract enough to allow all six of its oxygen atoms to legate the Na^+ at the same time as K^+ ion. This is demonstrated by the fact that the diameter of **3**·Na^+ is 5.296 Å, much greater than normal, but in **2**·Na^+ the diameter is 4.75 Å, lower than normal. Thus, the O12–Ar dihedral angle (12–A–B–C) expands in **2**·Na^+ by 3.3° and shrinks in **3**·Na^+ by 2.2°. Also, we see a strong correlation between the differential diameter and differential binding energy of the complexes of hosts **2** and **3**. Figure 2 illustrates this relation and gives a good fitting equation with R^2 = 0.999. A comparison of the geometric parameters of the parent spherand

© 2006 NRC Canada

complexes with those of **2** and **3** is instructive. The Na^+–O distance in spherand **1** complexes is 2.296 Å, which is less than the standard value of 2.35 Å.

Comparisons of the Na^+–O distance of spherand **1** complexes with the standard value of 2.35 Å[3] and average distance of spherands **2** and **3** complexes show that spherand **1** has stronger interactions with all metal ions than hosts **2** and **3** (see Table 1).

Conclusion

This work reports results for the binding properties of spherands **2** and **3** based on the B3LYB/6-31G** (5d) level of theory. Results for the structures are compared with available X-ray diffraction data of spherands. A good agreement is observed between theoretical predictions and experimental data for hosts **2** and **3**. The results taken as a whole show that as the number of anisyl units increases, the cavity becomes smaller and more preorganized. Also, binding and specificity increase for the small ions, and the rates of equilibration among spherand, guest, and spheraplex decrease. Systems that contain five and six self-organizing anisyl groups are less specific for Li^+ over Na^+ and K^+ passing from **1** to **3**, respectively. Also, spherands **2** and **3** appear beautifully preorganized to bind all guests, so it is not surprising that their binding energies are close to that of the host **1**.

References

1. (*a*) H. Plenio and R. Diodone. J. Am. Chem. Soc. **118**, 356(1996); (*b*) X.X. Zhang, A.V. Bordunov, J.S. Bradshaw, N.K. Dalley, X. Kou, and R.M. Izatt. J. Am. Chem. Soc**. 117**, 11507(1995); (*c*) C.J. Pedersen. Science (Washington, D.C.). **241**, 536 (1988); (*d*) D.J. Cram. Science (Washington, D.C.). **219**, 1177 (1983); (*e*) J.-M. Lehn. Acc. Chem. Res. **11**, 49 (1978); (*f*) D.A. Dougherty and D.A. Stauffer. Science (Washington, D.C.). **250**, 1558 (1990).
2. C.J. Pedersen. *In* Synthetic multidentate macrocyclic compounds. *Edited by* R.M. Izatt and J.J. Christensen. Academic Press, New York. 1978. pp. 1–51.
3. J.-M. Lehn. Struct. Bonding (Berlin). **76**, 1 (1973).
4. (*a*) B.C. Pressman. Annu. Rev. Biochern. **45**, 501 (1976); (*b*) W. Simon, W.E. Morf, and P. Ch. Meier. Struct. bonding (Berlin). **76**, 113 (1973); (*c*) S. Lindenbaum, J.H. Rytting, and L.A. Sternson. *In* Progress in macrocyclic chemistry. *Edited by* R.M. Izatt and J.J. Christensen. Wiley & Sons, New York. 1979. pp. 219–254.
5. N.K. Dalley. *In* Synthetic multidentate macrocyclic compounds. *Edited by* R.M. Izatt and J.J. Christensen. Academic Press, New York. 1978. pp. 207–243.
6. I. Goldberg. Acta Crystallogr., Sect. B. **31**, 754 (1975).
7. (*a*) D.J. Cram, G.M. Lein, T. Kaneda, R.C. Helgeson, C.B. Knobler, E. Maverick, and K.N. Trueblood. J. Am. Chem. Soc. **103**,6228 (1981); (*b*) G. M Lein and D.J. Cram. J. Chem. Soc. Chem. Commun. 301 (1982).
8. K.N. Trueblood, C.B. Knobler, E. Maverick, R.C. Helgeson, S.B. Brown, and D.J. Cram. J. Am. Chem. Soc. **103**, 5594 (1981).
9. C.H. Roger, J.S. Beverly, G. Israel, B.K. Carolyn, and D.J. Cram. J. Am. Chem. Soc. **115**, 11506 (1993).
10. M.J. Frisch, G.W. Trucks, H.B. Schlegel, G.E. Scuseria, M.A. Robb, J.R. Cheeseman, J.A. Montgomery, Jr., T. Vreven, K.N.Kudin, J.C. Burant, J.M. Millam, S.S. Iyengar, J. Tomasi, V. Barone, B. Mennucci, M. Cossi, G. Scalmani, N. Rega, G.A. Petersson, H. Nakatsuji, M. Hada, M. Ehara, K. Toyota, R. Fukuda, J. Hasegawa, M. Ishida, T. Nakajima, Y. Honda, O. Kitao, H. Nakai, M. Klene, X. Li, J.E. Knox, H.P. Hratchian, J.B. Cross, C. Adamo, J. Jaramillo, R. Gomperts, R.E. Stratmann, O. Yazyev, A.J. Austin, R. Cammi, C. Pomelli, J.W. Ochterski, P.Y. Ayala, K. Morokuma, G.A. Voth, P. Salvador, J.J. Dannenberg, V.G. Zakrzewski, S. Dapprich, A.D. Daniels, M.C. Strain, O. Farkas, D.K. Malick, A.D. Rabuck, K. Raghavachari, J.B. Foresman, J.V. Ortiz, Q. Cui, A.G. Baboul, S. Clifford, J. Cioslowski, B.B. Stefanov, G. Liu, A. Liashenko, P. Piskorz, I. Komaromi, R.L. Martin, D.J. Fox, T. Keith, M.A. Al-Laham, C.Y. Peng, A. Nanayakkara, M. Challacombe, P.M.W. Gill, B. Johnson, W. Chen, M.W. Wong, C. Gonzalez, and J.A. Pople. GAUSSIAN 03. Revision B.04 [computer program]. Gaussian, Inc., Pittsburgh, Penn. 2003.
11 C. Lee, W. Yang, and R.G. Parr. Phys. Rev. B, **37**, 785 (1988).
12. S.F. Boys and F. Bernardi. Mol. Phys. **19**, 553 (1970).

[3] These values were obtained by adding the ionic radii of the metal ions to the van der Waals radii of the ligating atoms. Values were taken from L.C. Pauling. *Nature of the chemical bond*, 2nd ed. Cornell University Press, Ithaca, New York. 1940. pp. 189, 350.

© 2006 NRC Canada

Microwave-assisted synthesis of β-$Co(OH)_2$ and Co_3O_4 nanosheets via a layered precursor conversion method

Zhen-Hua Liang, Ying-Jie Zhu, Guo-Feng Cheng, and Yue-Hong Huang

Abstract: Single crystalline β-$Co(OH)_2$ nanosheets have been synthesized from a layered precursor cobalt(II) acetate hydroxide by microwave heating. The average thickness of β-$Co(OH)_2$ nanosheets is ~10 nm, with particle sizes up to 360 nm. The layered precursor was prepared using $Co(CH_3COO)_2{\cdot}4H_2O$, ethylene glycol, and H_2O in some cases by microwave heating. Co_3O_4 nanosheets have been synthesized by hydrothermal oxidation of the layered precursor cobalt(II) acetate hydroxide using H_2O_2.

Key words: nanosheets, microwave, cobalt hydroxide, cobalt oxide.

Résumé : On a réalisé la synthèse de nanofeuillets de β-$Co(OH)_2$ monocristallins en chauffant à l'aide de microondes une couche de son précurseur, l'hydroxyde de l'acétate de cobalt(II). L'épaisseur moyenne des nanofeuillets de β-$Co(OH)_2$ varie d'environ 10 nm jusqu'à 360 nm. La couche de précurseur a été préparée en chauffant, à l'aide de microondes, un mélange de $Co(OCOCH_3)_2{\cdot}4H_2O$, d'éthylèneglycol et (ou) d'eau. Les nanofeuillets de Co_3O_4 ont été synthétisés en procédant à une oxydation hydrothermique à l'aide de H_2O_2 de la couche d'hydroxyde de l'acétate de cobalt(II) précurseur.

Mots clés : nanofeuillets, microonde, hydroxyde de cobalt, oxyde de cobalt.

[Traduit par la Rédaction]

Introduction

The properties of nanostructured materials are dependent on the shape of building blocks. Although many examples have been demonstrated, controlling the shape of building blocks is still a great challenge. In the past decade, one-dimensional nanostructures such as nanorods, nanowires, and nanotubes have been intensively studied because of their novel properties and potential applications (1). Two-dimensional nanosheets possess interesting properties because of their high anisotropy and ultrathin thickness (2, 3). Nanosheets are considered as ideal systems for the investigation of dimensionally confined transport phenomena and as the ideal bases upon which to build functional devices.Therefore, it would be interesting to develop new methods for the synthesis of nanosheets of a variety of compounds.

Recently, cobalt hydroxide $Co(OH)_2$ has attracted increasing attention (4–6) because of its electric and magnetic applications. When added to nickel oxide electrodes, β-$Co(OH)_2$ can improve the electrochemical performance by enhancing the electrode conductivity and chargeability (7–10). There have been some reports on the synthesis of β-$Co(OH)_2$ nanostructures (11–13).

Co_3O_4 with a spinel structure is an important magnetic p-type semiconductor. Co_3O_4 has received considerable attention because of its diverse applications in fields such as solar selective absorber (14–15), catalysis (16, 17), batteries (18, 19), solid-state sensors (20, 21), magnetic materials (22, 23), and electrochromic devices (24). Different nanostructures of Co_3O_4 such as nanoparticles (25), nanocubes (26, 27), and nanotubes (28) have been reported. Recently, the preparation of Co_3O_4 nanoplatelets by thermal decomposition of $Co(OH)_2$ nanoplatelets was also reported (29).

The layered precursor conversion method is an effective method for the preparation of nanosheets of metal oxides such as CuO (30). In this paper, we demonstrate that powders of β-$Co(OH)_2$ single crystalline nanosheets can be synthesized by a simple microwave-assisted layered precursor conversion method. The application of microwave heating in synthetic chemistry is a fast-growing research area, and microwave heating has been accepted as a promising heating method. As a result, this has opened up the possibility of realizing reactions in a very short time. Co_3O_4 nanosheets have been synthesized by hydrothermal oxidation of the layered precursor cobalt(II) acetate hydroxide using H_2O_2.

Experimental

Chemicals and synthesis

Cobalt acetate $Co(CH_3COO)_2{\cdot}4H_2O$, H_2O_2 (Shanghai Chemical Reagents Company, Shanghai), and ethylene glycol (EG, Shanghai Lingfeng Chemical Reagents Co., Ltd.,

Received 1 March 2006. Accepted 28 August 2006. Published on the NRC Research Press Web site at http://canjchem.nrc.ca on 4 October 2006.

Z.-H. Liang,[1] Y.-J. Zhu,[2] G.-F. Cheng, and Y.-H. Huang. State Key Laboratory of High Performance Ceramics and Superfine Microstructure, Shanghai Institute of Ceramics, Chinese Academy of Sciences, Shanghai 200050, P. R. China.

[1]Present address: School of Chemistry and Chemical Engineering, Guangxi Normal University, Guilin, 541005, P. R. China.

[2]Corresponding author (e-mail: y.j.zhu@mail.sic.ac.cn).

 doi:10.1139/V06-134 © 2006 NRC Canada

Shanghai) were of analytical grade and used as purchased without further purification. Deionized water was used as the solvent in all experiments. In a typical experiment for the preparation of the precursor, 0.5 g of $Co(CH_3COO)_2{\cdot}4H_2O$ was dissolved in 20 mL of ethylene glycol (EG) and 0.4 mL of H_2O was added. The resulting solution was microwave heated to 170 °C and held at this temperature for 5 min. The microwave oven used was a focused single-mode microwave synthesis system (Discover, CEM, Matthews, USA). The microwave synthesis system was equipped with a water-cooled condenser outside the microwave cavity and a magnetic stirring system. After the solution was cooled to room temperature, the pink product (precursor) was centrifuged and washed with absolute ethanol. The precursor was redispersed in 20 mL of deionized water, microwave-heated to 100 °C, and held at 100 °C for 20 min. The product (sample 1) was separated by centrifugation, washed twice with deionized water, and dried in vacuum. Other samples were prepared by a procedure similar to that of sample 1, but under different conditions. Co_3O_4 was synthesized using the following procedure: the precursor and 20 mL deionized water were added in a 40 mL Teflon-lined stainless steel autoclave, then 1 mL 1 mol/L H_2O_2 was added while stirring. The autoclave was sealed, heated to 140 °C and maintained at this temperature for 12 h. Then, it was allowed to cool to room temperature. The black product was separated by centrifugation, washed with deionized water, and dried in vacuum.

Instruments and characterization

X-ray powder diffraction (XRD) patterns were recorded using a Rigaku D/max 2550V X-ray diffractometer with high-intensity Cu Kα radiation (λ = 1.54178 Å) and a graphite monochromator. TEM micrographs were taken with JEOL JEM-2010, JEOL JEM-200CX, selected area electron diffraction (SAED) patterns, and HITACHI H-800 transmission electron microscope.

Results and discussion

Cobalt acetate $Co(CH_3COO)_2{\cdot}4H_2O$ could dissolve in an EG solution and hydrolyze at elevated temperatures. The partially hydrolyzed product, cobalt acetate hydroxide, formed during the microwave heating process. The formation process of the cobalt acetate hydroxide may be described by the following reaction:

$$Co(CH_3COO)_2{\cdot}4H_2O + nH_2O \rightarrow Co(CH_3COO)_{2-x}(OH)_x{\cdot}yH_2O + xCH_3COOH$$

The presence of a small amount of water in EG is favorable for the formation of the layered precursor because it is a hydrolysis process. EG acts as a solvent with a high boiling point of ~198 °C, allowing the hydrolysis reaction to occur at a relatively high temperature.

Figure 1*a* shows the XRD pattern of the precursor cobalt(II) acetate hydroxide. It is typical of a layered structure, with an interlayer spacing of 8.4 Å. The sharp peak at a small angle and broad and asymmetric peaks at high angles indicate that the precursor was a lamellar compound with a brucite structure. Such features can be explained on the basis of stacking order of brucite-like sheets. This behavior was observed for α-$Co(OH)_2$ and layered hydroxide cobalt acetate (31, 32). Figure 1*b* shows that sample 1 consists of well-crystallized β-$Co(OH)_2$ with a hexagonal structure. No peaks due to α-$Co(OH)_2$ were observed in the XRD pattern.

Fig. 1. XRD patterns of the products: (*a*) the precursor, (*b*) β-$Co(OH)_2$ nanosheets, and (*c*) Co_3O_4 nanosheets.

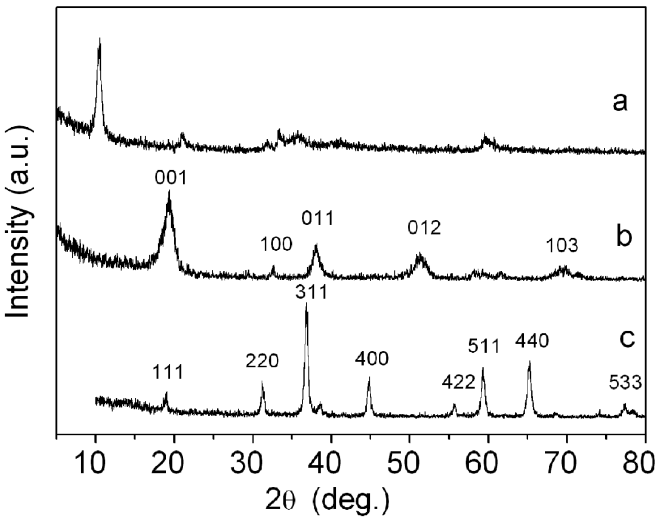


Figure 2 shows TEM micrographs of four samples of $Co(OH)_2$ nanosheets. Figures 2*a* and 2*b* show TEM micrographs of sample 1. One can see hexagonally shaped β-$Co(OH)_2$ nanosheets with angles of 120° between adjacent edges and with particle sizes up to 360 nm. We suggest that the surface of the nanosheets is parallel to the (0001) planes of the hexagonal β-$Co(OH)_2$. An SAED pattern of an individual nanosheet in Fig. 2*b* shows that the nanosheet was single-crystalline. In addition to the nanosheets, small particles were also observed. Figures 2*c* and 2*d* show TEM micrographs of sample 2 prepared under the same conditions as sample 1 except that the microwave heating time for the preparation of the precursor was 10 min instead of 5 min. In addition to hexagonal nanosheets, irregular and circular nanosheets with sizes in the range of 200–360 nm were observed. The sizes of nanosheets in sample 2 increased compared with those in sample 1.

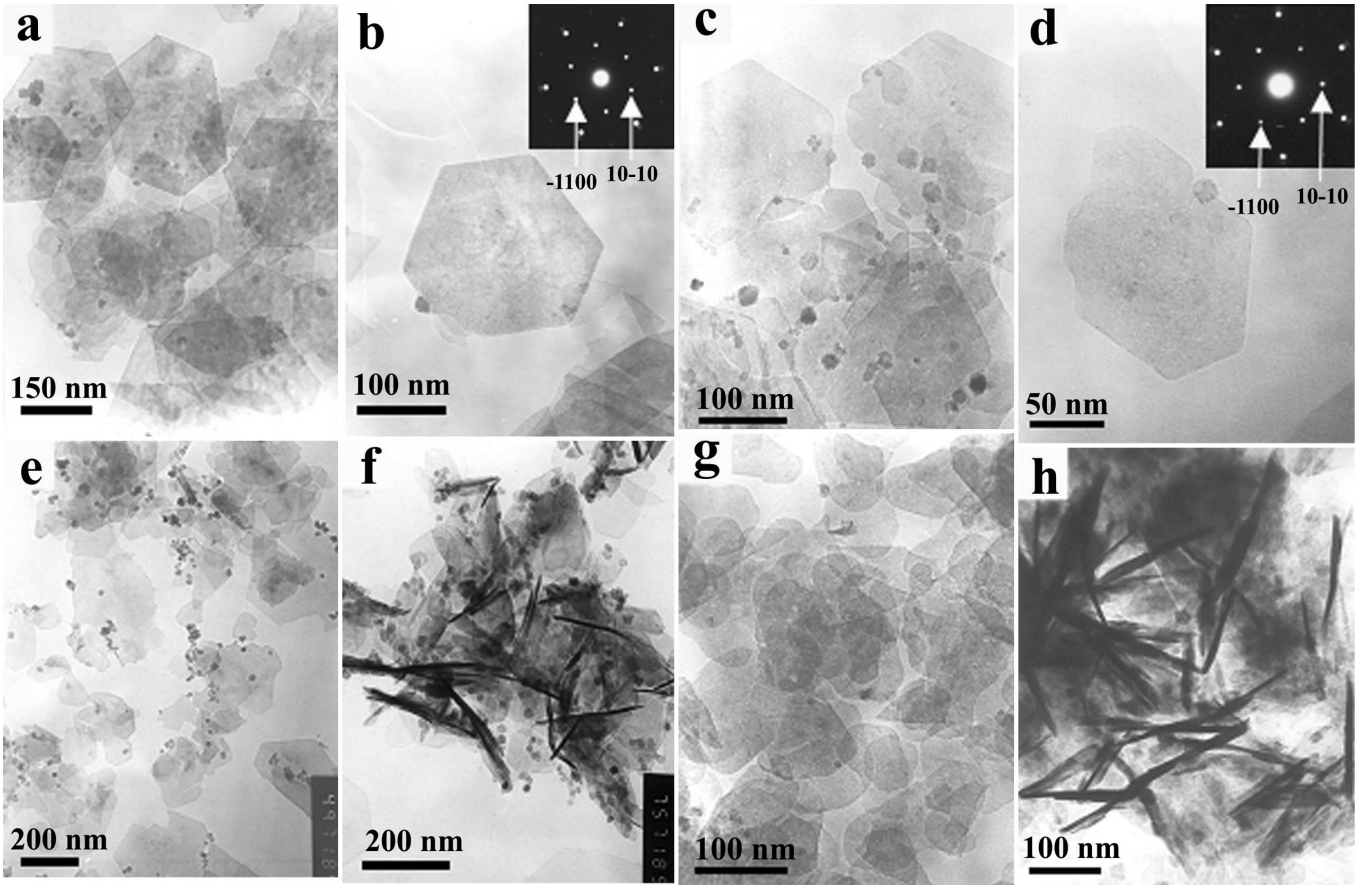
Figures 2*e* and 2*f* show the TEM micrographs of sample 3 prepared under the same conditions as sample 1 except that no water was added in EG. The product consisted of irregularly shaped nanosheets with sizes in the range of 120–300 nm and some having 120° angles between their adjacent edges. In a few cases, some curled nanostructures were also observed (Fig. 2*f*) because of the thin nanosheets. The average thickness of β-$Co(OH)_2$ nanosheets was about 10 nm, estimated from either the curled nanostructures or the standing nanosheets.

Figures 2*g* and 2*h* show the TEM micrographs of sample 4 prepared under the same conditions as sample 3 except that the microwave heating time for the preparation of the precursor was 10 min. It is interesting that the product consisted of circular nanosheets with diameters up to 150 nm. Figure 2*h* shows the curled nanostructures with lengths up to 300 nm. The average thickness of nanosheets was about 10 nm, estimated from the curled nanostructures.

Our experimental results show that the layered precursor

© 2006 NRC Canada

Fig. 2. TEM micrographs of four β-$Co(OH)_2$ samples: (*a*) and (*b*) sample 1; (*c*) and (*d*) sample 2; (*e*) and (*f*) sample 3; (*g*) and (*h*) sample 4. The insets of (*b*) and (*d*) are SAED patterns of an individual nanosheet by focusing electron beam along [0001] zone axis.



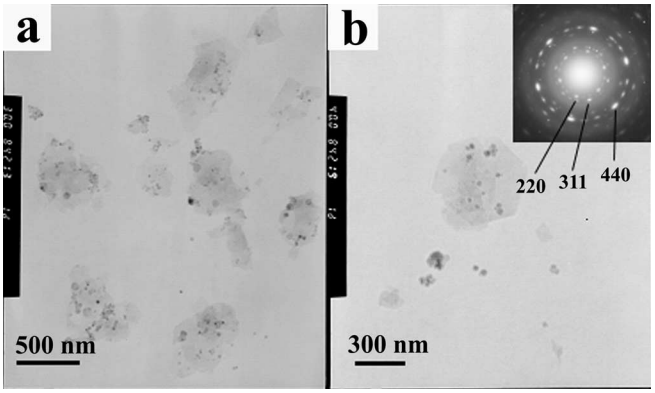
cobalt acetate hydroxide had an important effect on the morphology of β-$Co(OH)_2$. The presence of water in EG favored the formation of nanosheets with a hexagonal shape (sample 1). An increase in the microwave heating time for the preparation of the layered precursor resulted in the formation of irregularly shaped nanosheets (sample 2) instead of hexagonal nanosheets (sample 1). When EG was used as the only solvent without adding water, no hexagonal nanosheets were obtained, yet many curled nanostructures were observed.

The spinel Co_3O_4 with a cubic structure rarely forms sheet-like morphology by a direct synthesis method. We have successfully synthesized Co_3O_4 nanosheets by the hydrothermal oxidation of the layered precursor using H_2O_2. XRD pattern of the product (Fig. 1*c*) shows that it was a single phase of Co_3O_4 with a cubic structure (JCPDS 80-1545). No peaks from $Co(OH)_2$ were observed by XRD. The conversion from the layered precursor to Co_3O_4 nanosheets was achieved by a partial oxidation of Co^{2+} to Co^{3+} by H_2O_2. From TEM micrographs of the Co_3O_4 sample (Fig. 3), one can observe the formation of Co_3O_4 nanosheets.

Conclusion

In summary, we have successfully synthesized β-$Co(OH)_2$ nanosheets from a layered precursor cobalt(II) acetate hydroxide by the microwave heating method. The average thickness of β-$Co(OH)_2$ nanosheets is ~ 10 nm, with particle size up to 360 nm. The layered precursor was prepared using $Co(CH_3COO)_2{\cdot}4H_2O$, ethylene glycol, and H_2O in some cases by microwave heating. Co_3O_4 nanosheets were synthesized by the hydrothermal oxidation of the layered precursor cobalt(II) acetate hydroxide using H_2O_2. We expect that the layered precursor conversion method may be extended to synthesize nanosheets of other kinds of metal hydroxides and oxides.

Fig. 3. TEM micrographs of Co_3O_4 nanosheets. The inset of (*b*) is an SAED pattern of Co_3O_4 nanosheets.



Acknowledgments

Financial support from the National Natural Science

© 2006 NRC Canada

Foundation of China (50472014) and from the Chinese Academy of Sciences under the Program for Recruiting Outstanding Overseas Chinese (Hundred Talents Program) is gratefully acknowledged. We thank the Fund for Innovation Research from Shanghai Institute of Ceramics, Chinese Academy of Sciences.

References

1. Y.N. Xia, P.D. Yang, Y.G. Sun, Y.Y. Wu, B. Mayers, B. Gates, Y.D. Yin, F. Kim, and Y.Q. Yan. Adv. Mater. (Weinheim, Ger.), **15**, 353 (2003).
2. T. Sasaki, Y. Ebina, Y. Kitami, M. Watanabe, and T. Oikawa. J. Phys. Chem. B, **105**, 6116 (2001).
3. T. Sasaki and M. Watanabe. J. Phys. Chem. B, **101**, 10159 (1997).
4. L. Cao, Y.Y. Liang, L.B. Kong, and H.L. Li. J. Mater. Sci. **39**, 4697 (2004).
5. Z.P. Xu and H.C. Zeng. Chem. Mater. **11**, 67 (1999).
6. H. Itahara, S. Tajima, and T. Tani. J. Ceram. Soc. Jpn. **110**, 1048 (2002).
7. J. Ismail, M.F. Ahmed, P.V. Kamath, G.N. Subbanna, S. Uma, and J. Gopalakrishnan. J. Solid State Chem. **114**, 550 (1995).
8. M. Butel, L. Gautier, and C. Delmas. Solid State Ionics, **122**, 271 (1999).
9. J. Ismail, M.F. Ahmed, and P.V. Kamath. J. Power Sources, **41**, 223 (1993).
10. P.V. Kamath and M.F. Ahmed. J. Appl. Electrochem. **23**, 225 (1993).
11. X.L. Li, J.F. Liu, and Y.D. Li. Mater. Chem. Phys. **80**, 222 (2003).
12. Y.C. Zhu, H.L. Li, Y. Koltypin, and A. Gedanken. J. Mater. Chem. **12**, 729 (2002).
13. J.T. Sampanthar and H.C. Zeng. J. Am. Chem. Soc. **124**, 6668 (2002).
14. E. Barrera, L. Huerta, S. Muhl, and A. Avila. Sol. Energy Mater. Sol. Cells, **88**, 17 (2005).
15. A. Gulino, P. Dapporto, P. Rossi, and I. Fragala. Chem. Mater. **15**, 3748 (2003).
16. A.A.F. Grupioni and T.A.F. Lassali. J. Electrochem. Soc. **148**, A1015 (2001).
17. T. Suzuki, Y. Mayama, T. Hirai, and S. Hayashi. Int. J. Hydrogen Energy, **18**, 979 (1993).
18. Y.M. Kang, K.T. Kim, K.Y. Lee, S.J. Lee, J.H. Jung, and J.Y. Lee. J. Electrochem.Soc. **150**, A1538 (2003).
19. P.K. Shen, A.C.C. Tseung, and C. Kuo. J. Power Sources, **47**, 119 (1994).
20. R.J. Wu, C.H. Hu, C.T. Yeh, and P.G. Su. Sens. Actuators B, **96**, 596 (2003).
21. Y. Shimizu and Y. Furuta. Solid State Ionics, **115**, 241 (1998).
22. S. Takada, M. Fujii, S. Kohiki, T. Babasaki, H. Deguchi, M. Mitome, and M. Oku. Nano Lett. **1**, 379 (2001).
23. S.A. Makhlouf. J. Magn. Magn. Mater. **246**, 184 (2002).
24. F. Svegl, B. Orel, M.G. Hutchins, and K. Kalcher. J. Electrochem. Soc. **143**, 1532 (1996).
25. H.M. Yang, Y.H. Hu, X.C. Zhang, and G.Z. Qiu. Mater. Lett. **58**, 387 (2004).
26. J. Feng and H.C. Zeng. Chem. Mater. **15**, 2829 (2003).
27. R. Xu and H.C. Zeng. J. Phys. Chem. B, **107**, 926 (2003).
28. X.Y. Shi, S.B. Han, R.J. Sanedrin, C. Galvez, D.G. Ho, B. Hernandez, F.M. Zhou, and M. Selke. Nano Lett. **2**, 289 (2002).
29. Y.L. Hou, H. Kondoh, M. Shimojo, T. Kogure, T. Ohta. J. Phys. Chem. B, **109**, 19094 (2005).
30. Z.H. Liang and Y.J. Zhu. Chem. Lett. **34**, 214 (2005).
31. M. Dixit, G.N. Subbanna, and P.V. Kamath. J. Mater. Chem. **6**, 1429 (1996).
32. L. Poul, N. Jouini, and F. Fievet. Chem. Mater. **12**, 3123 (2000).

© 2006 NRC Canada

Solvent-free synthesis of 5-oxo-5,6,7,8-tetrahydro-4*H*-benzo-[*b*]-pyran derivatives under microwave irradiation

Xue Yuan Hu, Xue Sen Fan, Xin Ying Zhang, Gui Rong Qu, and Yan Zhen Li

Abstract: Several benzo-[*b*]-pyran derivatives were prepared via microwave irradiation under solvent-free conditions in the presence of $InCl_3 \cdot 4H_2O$. The advantages of this method include simple operational process, environmental benignancy, and high efficiency. Moreover, the catalyst can be recovered and reused effectively for at least six times.

Key words: benzo-[*b*]-pyran derivatives, indium trichloride, microwave irradiation.

Résumé : On a préparé plusieurs dérivés du benzo[*b*]pyrane par irradiation à l'aide de micro-ondes, dans des conditions sans solvant et en présence de $InCl_3 \cdot 4H_2O$. Cette méthode présente l'avantage d'être écologique, très efficace et de comporter un processus opérationnel simple. De plus, le catalyseur peut être récupéré et réutilisé d'une façon efficace au moins six fois.

Mots clés : dérivés du benzo-[*b*]-pyrane, trichlorure d'indium, irradiation à l'aide de microonde.

[Traduit par la Rédaction]

Introduction

Currently, research on the tetrahydropyran skeleton is of great interest in organic synthesis because the tetrahydropyran ring occurs in a number of natural products (1). Tetrahydropyran derivatives have also been extensively studied because they possess a wide range of biological activities and pharmacological properties, such as anticancer (2) and antihypertensive activities (3). Many procedures have been reported for the preparation of such compounds (4*a*); one of them is the condensation of α,β-unsaturated ketones with 5,5-dimethyl-1,3-cyclohexandione promoted by various catalysts. In this regard, anhydrous zinc chloride was recently utilized to catalyze this reaction to produce the substituted benzo-[*b*]-pyran derivatives. However, this method gives a low yield over a long reaction time (4*b*). A combination of glacial acetic acid and phosphoric anhydride could efficiently catalyze this reaction (4*c*), but the use of strongly acidic compounds is undesirable in view of green chemistry and may exclude some acid-sensitive substrates. Therefore, it is desirable to develop more efficient and greener synthetic methods for the preparation of benzo-[*b*]-pyran derivatives.

Recently, indium halides have emerged as mild Lewis acids imparting high regio- and chemo-selectivity in a variety of chemical transformations such as the Diels–Alder reaction (5), rearrangement reaction (6), Friedel–Crafts acylation reaction (7), Mukaiyama aldol reaction (8), Mannich-type reaction (9), and Biginelli reaction (10). Compared with conventional Lewis acids, indium halides possess advantages such as water stability, recyclability, and simplicity in operation. On the other hand, microwave-assisted organic syntheses have attracted considerable interests in recent years (11) because they offer several environmental and economic benefits, e.g., avoiding use of expensive and (or) toxic solvents, saving energy and time, and easier work-up after the reactions are completed. As part of our program aimed at developing environment-friendly methodologies for organic synthesis, we describe a simple, green, and efficient method for the synthesis of benzo-[*b*]-pyran derivatives. Treatments of chalcones (**1**) with 5,5-dimethyl-1,3-cyclohexandione (**2**) in the presence of $InCl_3 \cdot 4H_2O$ under microwave irradiation produced the corresponding 5-oxo-5,6,7,8-terahydro-4*H*-benzo-[*b*]-pyran derivatives (**3**) (Scheme 1) in excellent yields.

Received 3 November 2004. Accepted 2 August 2006. Published on the NRC Research Press Web site at http://canjchem.nrc.ca on 5 October 2006.

X.Y. Hu School of Chemical and Environmental Sciences, Henan Key Laboratory for Environmental Pollution Control, Henan Normal University, Xinxiang, Henan 453007, P.R. China. Chongqing University of Medical Sciences, Chongqing 400016, P. R. China.
X.S. Fan,[1] X.Y. Zhang, G.R. Qu, and Y.Z. Li. School of Chemical and Environmental Sciences, Henan Key Laboratory for Environmental Pollution Control, Henan Normal University, Xinxiang, Henan 453007, P.R. China.

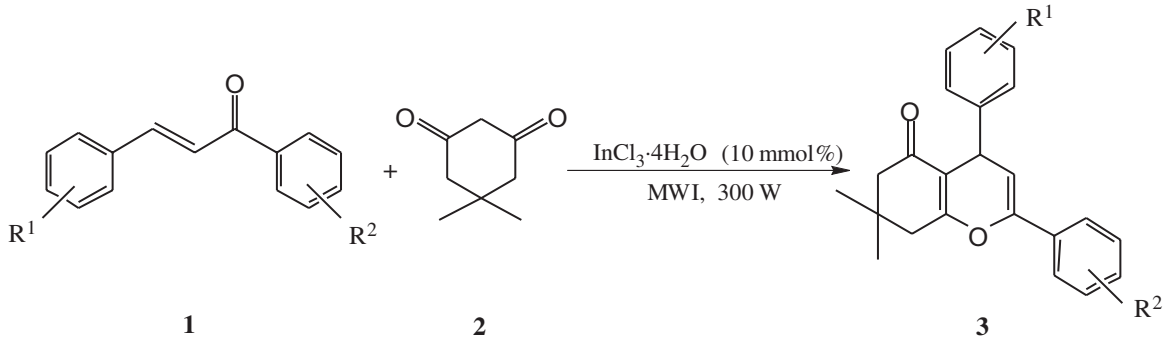
[1]Corresponding author (e-mail: fanxs88@263.net).

Results and discussion

At the outset of this study, we examined the condensation process by employing 1,3-diphenyl-propenone **(1a)** (Scheme 2) and **2** as model substrates. A summary of the optimization experiments is provided in Table 1. When **1a** (1 mmol) was treated with **2** (1 mmol) in the presence of a catalytic amount of $InCl_3 \cdot 4H_2O$ (10 mol%) under the microwave irradiation power of 495 W for 10 min, the desired

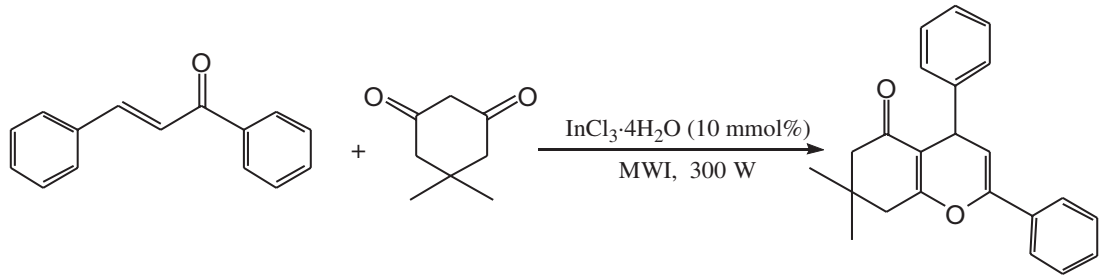
 doi:10.1139/V06-132 © 2006 NRC Canada

Scheme 1.



1 **2** **3**

Scheme 2.



1a **2** **3a**

Table 1. $InCl_3·4H_2O$-catalyzed synthesis of **3a** under different reaction conditions.

Entry	Microwave power (W)	Amount of $InCl_3·4H_2O$ (mol%)	Reaction time (min)	Isolated yields (%)
1	698	10	5	—
2	495	10	10	54
3	300	10	13	86
4	300	20	13	85
5	300	5	20	67
6	300	2.5	25	50
7	300	0	25	41

product **3a** was obtained with a moderate yield (54%), together with some unidentified by-products (Table 1, entry 2). However, no product could be obtained, and almost all the materials involved were carbonized when the reaction was carried out under a much higher irradiation power (698 W) (Table 1, entry 1). Under lower irradiation power (300 W), a much higher yield (86%) (Table 1, entry 3) was realized by treating the mixture of **1a** and **2** together with $InCl_3·4H_2O$ (10 mol%) for 13 min. On the other hand, the effect of the amount of $InCl_3·4H_2O$ on the output of this reaction was also investigated and the optimum concentration was determined to be 10 mol% (Table 1, entries 3–7). It should also be noted that the absence of $InCl_3·4H_2O$ would result in a much lower yield even over a longer reaction period (Table 1, entry 7).

With this exhilarating result, we extended this method to a variety of substituted chalcones to investigate its scope and generality.The results are listed in Table 2. A wide range of chalcones could react with **2** to give **3** with good yields (Table 2, entries 1–11). It is noted that the electronic property of the aromatic ring of chalcone affects the rate of this condensation process. In general, a shorter reaction time was needed with substrates bearing electron-withdrawing groups on the aromatic rings (Table 2, entries 2, 5–9). Substrates bearing electron-donating groups can also produce the corresponding products with satisfactory yields. However, a longer period was needed to complete the reaction (Table 2, entries 4, 10).

In view of green chemistry, recovery and reuse of the catalyst are highly preferable. To test this possibility, water was added to the reaction mixture upon completion of the reaction, and the product was extracted with ethyl acetate. The catalyst remaining in the aqueous phase was recovered by removing water under reduced pressure. Its reusability was investigated by using **1a** and **2** again as the model substrates. The corresponding product could be obtained with good yield even in the sixth round by using the catalyst recovered from the fifth round (Table 3, entry 6).

To compare conventional heating with solvent-free microwave irradiation for the synthesis of **3a**, a mixture of **1a** and **2** was dissolved in several organic solvents and the solution was refluxed using a classic heating method (oil bath in this case) in the presence of 10 mol% $InCl_3·4H_2O$. When the mixture of **1a** and **2** was refluxed in anhydrous ethanol for 5 h, no **3a** was formed (Table 4, entry 2). Although **3a** could be obtained with other solvents, a much longer reaction time was needed and the yield was much lower. Therefore, solvent-free microwave irradiation is more efficient compared with conventional heating in terms of reaction time and yield.

In conclusion, we have presented a new method for the preparation of benzo-[*b*]-pyran derivatives in the presence of $InCl_3·4H_2O$ under microwave irradiation. This simple and reproducible technique produces various benzo-[*b*]-pyran de-

© 2006 NRC Canada

Table 2. Preparation of **3** promoted by $InCl_3·4H_2O$ under microwave irradiation.

Entry	R_1	R_2	Time (min)	Products	Isolated yields (%)
1	H	H	13	**3a**	86
2	H	*p*-Cl	10	**3b**	85
3	H	*p*-Br	15	**3c**	86
4	H	*p*-CH_3O	15	**3d**	83
5	H	*p*-NO_2	10	**3e**	80
6	*p*-NO_2	H	10	**3f**	92
7	*m*-NO_2	*p*-Cl	10	**3g**	91
8	*p*-Cl	*p*-NO_2	10	**3h**	93
9	*m*-NO_2	H	10	**3i**	90
10	*p*-CH_3	H	15	**3j**	83
11	*p*-Cl	H	10	**3k**	81

Note: Reactions performed in the presence of 10 mol% $InCl_3·4H_2O$ and irradiated at 300 W.

Table 3. Reusability of the catalyst.

Round	Catalyst recovered (%)	Isolated yields of **3a** (%)
1	99	86
2	99	85
3	98	85
4	99	84
5	97	83
6	98	83

Note: Reaction conditions: microwave power of 300 W and reaction time of 13 min.

rivatives in a few minutes with excellent yields without the involvement of toxic materials or the formation of undesirable side products. Moreover, the catalyst can be recovered conveniently and reused efficiently. With all these advantages, this method provides an attractive alternative for the preparation of benzo-[*b*]-pyran derivatives.

Experimental

Melting points were measured by a Kofler micromelting point apparatus and were uncorrected. Infrared spectra were recorded on a Bruker Vector 22 spectrometer in KBr with absorption in cm^{-1}. ^1H NMR spectra were determined on a Bruker AC 400 spectrometer as $CDCl_3$ or DMSO solutions. Chemical shifts (δ) were expressed in ppm downfield from the internal standard tetramethylsilane, and coupling constants *J* were given in Hz. Mass spectra were obtained by a HP5989B mass spectrometer.

General procedure for the preparation of 5-oxo-5,6,7,8-tetrahydro-4*H*-benzo-[*b*]- pyran derivatives

Chalcones **1** (1 mmol), 5,5-dimethyl-1,3-cyclo-hexanedione **2** (1 mmol), and $InCl_3·4H_2O$ (0.1 mmol) were mixed without solvent in a 10 mL open flask and placed in a domestic microwave oven. The mixture was irradiated at 300 W for a certain period of time, as required to complete the reaction (monitored by TLC). Upon completion, the reaction mixture was cooled down to room temperature. Water was added, and the mixture was extracted with ethyl acetate. After the organic layer was dried (Na_2SO_4) and concentrated, the residue was recrystallized from a mixture of ethyl acetate and hexane to give 3 (Table 2). All the products were fully characterized by IR, ^1H NMR, and MS. The catalyst remaining in the aqueous phase was recovered for reuse by removing water under reduced pressure.

Table 4. Comparison between the conventional heating and solvent-free microwave irradiation (MWI) for the synthesis of compound **3a**.

Entry	Solvents	Heating methods	Reaction time (min)	Isolated yields (%)
1	None	MWI	13	86
2	Ethanol	Reflux	300	—
3	Acetic acid	Reflux	480	70[a]
4	THF	Reflux	660	51[b]
5	Toluene	Reflux	480	64[b]
6	Ethyl acetate	Reflux	360	55[b]

[a]At completion, water was added to the mixture and the product was obtained by filtration and recrystallization with hexane – ethyl acetate (10:1).

[b]The products were obtained by preparative chromatography on silica gel using cyclohexane–EtOAc (5:1) as an eluent.

3a: mp 140–142 °C (lit. value (4c) mp 140 °C). IR (KBr, cm^{-1}): 3070, 3024, 2956, 2872, 1679, 1658, 1627, 1468, 1380, 1289, 1215, 1166, 1056, 975, 824, 769. ^1H NMR (400 MHz, $CDCl_3$, ppm): 1.06 (s, 3H, CH_3), 1.17 (s, 3H, CH_3), 2.23–2.59 (m, 4H, $2CH_2$), 4.49 (d, 1H, *J* = 4.8 Hz, CH), 5.70 (d, 1H, *J* = 4.8 Hz, =CH), 7.14–7.18 (m, 1H, ArH), 7.25–7.38 (m, 7H, ArH), 7.57–7.59 (m, 2H, ArH). MS (70 eV) *m*/*z* (%): 330 (M^+, 93.75), 253 (100), 197 (10.94), 141 (10.94), 105 (9.38), 77 (9.38).

3b: mp 172–174 °C (lit. value (4*b*) mp 175–176 °C). IR (KBr, cm^{-1}): 3078, 3042, 2955, 2868, 1680, 1658, 1626, 1490, 1380, 1273, 1215, 1166, 1057, 1015, 825, 765. ^1H NMR (400 MHz, $CDCl_3$, ppm): 1.09 (s, 3H, CH_3), 1.16 (s, 3H, CH_3), 2.22 –2.63 (m, 4H, 2 H_2), 4.51 (d, 1H, *J* = 4.8 Hz, CH), 5.74 (d, 1H, *J* = 4.8 Hz, =CH), 7.20–7.34 (m, 5H, ArH), 7.36 (d, 2H, *J* = 8.4 Hz, ArH), 7.53 (d, 2H, *J* = 8.4 Hz, ArH). MS (70 eV) *m*/*z* (%): 364 (M^+, 97.37), 287 (100), 231 (9.21), 202 (7.89), 175 (7.24), 139 (18.42), 111 (6.58), 83 (3.94).

3c: mp 180–182 °C. IR (KBr, cm^{-1}): 3078, 3024, 2956, 2869, 1679, 1659, 1627, 1489, 1453, 1382, 1311, 1299, 1265, 1212, 1169, 1125, 1054, 977, 831, 769. ^1H NMR (400 MHz, $CDCl_3$, ppm): 1.10 (s, 3H, CH_3), 1.17 (s, 3H, CH_3), 2.22–2.62 (m, 4H, $2CH_2$), 4.51 (d, 1H, *J* = 4.8 Hz, CH), 5.73 (d, 1H, *J* = 4.8 Hz, =CH), 7.19–7.22 (m, 1H, ArH), 7.29–7.34 (m, 4H, ArH), 7.46–7.53 (m, 4H, ArH). MS (70 eV) *m*/*z* (%): 409 (M^+, 100), 331 (92.96), 275 (8.45), 253 (7.04), 215 (14.08), 168 (14.08), 139 (8.45), 115 (7.04), 83 (5.63).

3d: mp 134–136 °C. IR (KBr, cm^{-1}): 3068, 3020, 2980, 2868, 1680, 1660, 1620, 1450, 1370, 1263, 1211, 1160, 1030, 973, 840, 762. ^1H NMR (400 MHz, DMSO, ppm): 1.06 (s, 3H, CH_3), 1.13 (s, 3H, CH_3), 2.18–2.58 (m, 4H, $2CH_2$), 3.81 (s, 3H, OCH_3), 4.47 (d, 1H, *J* = 4.8 Hz, CH), 5.57 (d, 1H, *J* = 4.8 Hz, =CH), 6.89 (d, 2H, *J* = 9.6 Hz, ArH), 7.14–7.18 (m, 1H, ArH), 7.25–7.33 (m, 4H, ArH),

© 2006 NRC Canada

7.51 (d, 2H, *J* = 9.6 Hz, ArH). MS (70 eV) *m*/*z* (%): 360(M^+, 77.03), 283 (100), 171 (5.41), 135 (9.46) 115 (2.03), 77 (4.05).

3e: mp 148–150 °C. IR (KBr, cm^{-1}): 3078, 3024, 2955, 2863, 1674, 1658, 1625, 1594, 1514, 1381, 1346, 1285, 1212, 1168, 1123, 1053, 977, 849, 754. ^{1}H NMR (400 MHz, $CDCl_3$, ppm): 1.12 (s, 3H, CH_3), 1.18 (s, 3H, CH_3), 2.24–2.67 (m, 4H, $2CH_2$), 4.57 (d, 1H, *J* = 4.8 Hz, CH), 5.94 (d, 1H, *J* = 4.8 Hz, =CH), 7.22–7.33 (m, 5H, ArH), 7.77 (d, 2H, *J* = 8.4 Hz, ArH), 8.24 (d, 2H, *J* = 8.4 Hz, ArH). MS (70 eV) *m*/*z* (%): 374 (M^+, 75.18), 297 (100), 252 (96.38), 231 (8.74), 202 (5.98), 175 (5.86), 139 (13.43), 111 (4.95), 83 (4.93).

3f: mp 130–132 °C. IR (KBr, cm^{-1}): 3089, 3051, 2959, 2874, 1678, 1652, 1625, 1592, 1515, 1382, 1344, 1278, 1217, 1167, 1130, 1058, 975, 846, 767. ^{1}H NMR (400 MHz, $CDCl_3$, ppm): 1.09 (s, 3H, CH_3), 1.18 (s, 3H, CH_3), 2.22–2.61 (m, 4H, $2CH_2$), 4.65 (d, 1H, *J* = 4.8 Hz, CH), 5.67 (d, 1H, *J* = 4.8 Hz, =CH), 7.40–7.42 (m, 3H, ArH), 7.52 (d, 2H, *J* = 8.0 Hz, ArH), 7.61–7.62 (m, 2H, ArH), 8.17 (d, 2H, *J* = 8.0 Hz, ArH). MS (70 eV) *m*/*z* (%): 374 (M^+, 20.30), 358 (100), 328 (43.31), 253 (96.45), 197 (8.47), 141 (8.47), 105 (7.85), 77 (7.22).

3g: mp 194–196 °C. IR (KBr, cm^{-1}): 3073, 3062, 2960, 2868, 1680, 1662, 1631,1529, 1490, 1380, 1349, 1295, 1262, 1214, 1166, 1127, 1091, 1053, 976, 831, 743. ^{1}H NMR (400 MHz, $CDCl_3$, ppm): 1.11 (s, 3H, CH_3), 1.18 (s, 3H, CH_3), 2.23–2.66 (m, 4H, $2CH_2$), 4.65 (d, 1H, *J* = 4.8 Hz, CH), 5.67 (d, 1H, *J* = 4.8 Hz, =CH), 7.37 (d, 2H, *J* = 8.4 Hz, ArH), 7.48 (t, 1H, *J* = 8.0 Hz, ArH), 7.54 (d, 2H, *J* = 8.4 Hz, ArH), 7.70 (d, 1H, *J* = 7.6 Hz, ArH), 8.06 (d, 1H, *J* = 8.0 Hz, ArH), 8.17 (s, 1H, ArH). MS (70 eV) *m*/*z* (%): 409 (M^+, 22.86), 392 (100), 362 (40.00), 287 (85.71), 231 (9.52), 202 (5.71), 175 (9.05), 139 (20.00), 111 (6.67), 83 (4.76).

3h: mp 202–204 °C. IR (KBr, cm^{-1}): 3073, 3061, 2960, 2874, 1678, 1660, 1629, 1596, 1490, 1381, 1347, 1280, 1213, 1167, 1125, 1054, 977, 854, 755. ^{1}H NMR (400 MHz, $CDCl_3$, ppm): 1.10 (s, 3H, CH_3), 1.18 (s, 3H, CH_3), 2.23 – 2.60 (m, 4H, $2CH_2$), 4.54 (d, 1H, *J* = 4.8 Hz, CH), 5.89 (d, 1H, *J* = 4.8 Hz, =CH), 7.25–7.30 (m, 4H, ArH), 7.76 (d, 2H, *J* = 8.8 Hz, ArH), 8.25 (d, 2H, *J* = 8.8 Hz, ArH). MS (70 eV) *m*/*z* (%): 409 (M^+, 81.35), 374 (37.71), 358 (100), 329 (69.21), 253 (12.89), 197 (9.24), 141 (9.33) 105 (6.59), 77 (3.91).

3i: mp 138–140 °C. IR (KBr, cm^{-1}): 3094, 3070, 2953, 2874, 1683, 1658, 1629, 1527, 1494, 1382, 1348, 1318, 1275, 1217, 1169, 1125, 1056, 976, 874, 761. ^{1}H NMR (400 MHz, $CDCl_3$, ppm): 1.11 (s, 3H, CH_3), 1.18 (s, 3H, CH_3), 2.23–2.67 (m, 4H, $2CH_2$), 4.66 (d, 1H, *J* = 4.8 Hz, CH), 5.68 (d, 1H, *J* = 4.8 Hz, =CH), 7.37–7.49 (m, 4H, ArH), 7.62 (d, 2H, *J* = 7.6 Hz, ArH), 7.72 (d, 1H, *J* = 7.6 Hz, ArH), 8.07 (d, 1H, *J* = 8.4 Hz, ArH), 8.19 (s, 1H, ArH). MS (70 eV) *m*/*z* (%): 374 (M^+, 20.48), 358 (100), 328 (43.37), 253 (96.38), 197 (8.43), 141 (8.43), 105 (7.83), 77 (7.23).

3j: mp 84–86 °C. IR (KBr, cm^{-1}): 3051, 3024, 2956, 2871, 1678, 1656, 1627, 1512, 1449, 1380, 1272, 1214, 1165, 1125, 1056, 973, 854, 811, 769. ^{1}H NMR (400 MHz, $CDCl_3$, ppm): 1.06 (s, 3H, CH_3), 1.13 (s, 3H, CH_3), 2.18–2.58 (m, 7H, CH_3, $2CH_2$), 4.56 (d, 1H, *J* = 4.8 Hz, CH), 5.69 (d, 1H, *J* = 4.8 Hz, =CH), 7.08 (d, 2H, *J* = 7.6 Hz, ArH), 7.21 (d, 2H, *J* = 7.6 Hz, ArH), 7.30–7.37 (m, 3H, ArH), 7.58 (d, 2H, *J* = 8.0 Hz, ArH). MS (70 eV) *m*/*z* (%): 344 (M^+, 100), 329 (26.23), 253 (81.97), 197 (9.84), 141 (9.84), 105 (11.48), 77 (9.02).

3k: mp 108–110 °C. IR (KBr, cm^{-1}): 3078, 3040, 2890, 2868, 1679, 1658, 1627, 1490, 1380, 1273, 1215, 1167, 1057, 857, 721. ^{1}H NMR (400 MHz, $CDCl_3$, ppm): 1.08 (s, 3H, CH_3), 1.16 (s, 3H, CH_3), 2.22–2.58 (m, 4H, $2CH_2$), 4.51 (d, 1H, *J* = 4.8 Hz, CH), 5.70 (d, 1H, *J* = 4.8 Hz, =CH), 7.26–7.31 (m, 4H, ArH), 7.35–7.42 (m, 3H, ArH), 7.61(d, 2H, *J* = 7.6 Hz, ArH). MS (70 eV) *m*/*z* (%): 364 (M^+, 100), 287 (35.35), 253 (85.26), 202 (7.87), 197(9.80), 141 (9.80), 105 (11.37), 77 (11.02).

Acknowledgement

This work was financially supported by the National Natural Science Foundation of China (No. 20372018) and the Science Foundation of Henan Normal University for Young Scholars (No. 0307032).

References

1. S. Hatokeyama, N. Ochi, H. Numata, and S. Takano. Chem. Commun. **17**, 1202 (1998).
2. (*a*) T. Hyama and H. Saimoto. JP 62181276, (1987); Chem. Abstr. **108**, 37645p (1988); (*b*) L.J. Wang, D. Liu, Z.J. Zhang, S. Shan, X. Han, S.M. Srinivasulu, C.M. Croce, E.S. Alnemri, and Z. Huang. Proc. Natl. Acad. Sci. U.S.A. **97**, 7124 (2000).
3. E.C. Witte, P. Neubert, and A. Roesoh. DE 3427985, (1986); Chem. Abstr. **104**, 224915f (1986).
4. (*a*) T.P. Loh, L.C. Feng, and J.Y. Yang. Synthesis, **7**, 937 (2002); (*b*) M.G. Ahmed, S.A. Ahmed, U.K.R. Romman, T. Sultan, M.A. Hena, and S. Kiyooka. Indian J. Chem. B, **41**, 368 (2002), (*c*) V.K. Ahluwalia, S. Kiran, R. Aggarwal, and K.K. Arora. Indian J. Chem. B, **30**, 1095 (1991).
5. G. Babu, R. Nagarajan, R. Natarajan, and P.T. Perumal. Synthesis, **5**, 661 (2000).
6. T.P. Loh, Q.Y. Hu, and L.T. Ma. J. Am. Soc. **123**, 2450 (2001).
7. C.J. Chapman, C.G. Frost, J.P. Hartley, and A.J. Whittle. Tetrahedron Lett. **42**, 773 (2001).
8. T. Mukaiyama, J.S. Ohno, and J.S. Kobayashi. Chem. Lett. 949 (1991).
9. S.L. Chen, S.J. Ji, and T.P. Loh. Tetrahedron Lett. **44**, 2405 (2003).
10. B.C. Ranu, A. Hajra, and U. Jana. J. Org, Chem. **65**, 6270 (2000).
11. (*a*) S. Caddick. Tetrahedron, **51**, 10403 (1995); (*b*) R. Laurent, A. Laporterie, J. Dubac, J. Berlan, S. Lefeuvre, and M. Audhuy. J. Org. Chem. **57**, 7099 (1992); (*c*) A. Loupy, A. Petit, J. Hamelin, F. Texier-Boullet, P. Jacquault, and D. Mathe. Synthesis, 1213 (1998); (*d*) P. Lidstrom, J. Tierney, B. Wathey, and J. Westman. Tetrahedron, **57**, 9225 (2001); (*e*) N. Kuhnert. Angew. Chem., Int. Ed. Engl. **41**, 1863 (2002).

© 2006 NRC Canada

Chemoenzymatic synthesis of the chiral herbicide: (*S*)-metolachlor

Liangyu Zheng, Suoqin Zhang, Fang Wang, Gui Gao, and Shugui Cao

Abstract: A chemoenzymatic approach for the production of (*S*)-metolachlor, one of the most widely used herbicides, has been developed. The starting material (*S*)-*N*-(2-ethyl-6-methylphenyl)alanine was obtained by the use of lipase-catalyzed hydrolytic kinetic resolution. Under the optimal conditions, the good activity and excellent enantioselectivity of lipase B from *Candida antarctica* (CAL-B, $E > 100$) are achieved in diethyl ether – water (15% *v*/*v*), which is about 9.7-fold more enantioselective than that in a pure buffered aqueous solution ($E = 12.1$). After a simple extraction procedure is used to separate the acid product from the remaining ester, the remaining ester is racemized, providing the basis for the continuous resolution process. Then (*S*)-metolachlor is synthesized by a simple chemical method using the enantiomerically pure (*S*)-acid.

Key words: (*S*)-metolachlor, herbicide, CAL-B, (*S*)-*N*-(2-ethyl-6-methylphenyl)alanine, resolution.

Résumé : On a mis au point une approche chimioenzymatique à la production du (*S*)-métolachlore, un des herbicides les plus utilisés. Le produit de départ, la (*S*)-*N*-(2-éthyl-6-méthylphényl)alanine, a été préparé en faisant appel à une résolution par hydrolyse cinétique catalysée par une lipase. Dans des conditions optimisées, la meilleure activité et l'excellente énantiosélectivité de la lipase B provenant de la *Candida antartica* (CAL-B, $E > 100$) sont obtenues en opérant dans un mélange d'éther éthylique et d'eau (15% *v*/*v*), une énantiosélectivité qui est environ 9,7 fois plus élevée que dans une solution aqueuse pure ($E = 12,1$). Après avoir utilisé une simple procédure d'extraction pour éliminer le produit acide et récupérer de l'ester résiduel, ce dernier peut être racémisé et servir dans un processus continue de résolution. La synthèse du (*S*)-métolachlore est ensuite complétée par une méthode chimique simple en utilisant l'acide (*S*) énantiomériquement pur.

Mots clés : (*S*)-métolachlore, herbicide, CAL-B, (*S*)-*N*-(2-éthyl-6-méthylphényl)alanine, dédoublement.

[Traduit par la Rédaction]

Introduction

As optically pure single enantiomers are often more specific targets and have fewer side effects than their corresponding racemates, there is a real driving force for the production of new drugs and agrochemicals with high optical purity (1). The herbicide metolachlor (*N*-(1′-methyl-2′-methoxyethyl)-*N*-chloroacetyl-2-ethyl-6-methylaniline) has been widely used for over 20 years with a main strength in the control of weeds following pre-emergence application. In addition, weed resistance has not been developed, making metolachlor an important option in weed-management strategies (2). Metolachlor comprises four stereoisomers, the isomerism of which is based on a combination of a chiral center in the aliphatic side chain and a chiral axis between the phenyl group and the nitrogen atom. Although the four stereoisomers differ in their ability to inhibit the growth of weeds, it is reported that the herbicidal activity is mainly influenced by the chiral center, the (*S*)-enantiomers (Fig. 1) providing higher herbicidal activity than the (*R*)-enantiomers (3). Consequently, it is recognized that enriching the isomeric ratio in favor of the (*S*)-enantiomer will increase the biological activity of the herbicide. Thus, providing excellent weed control at rates substantially lower than those for racemic metolachlor and showing a reduced risk of environmental contamination. Therefore, it is necessary to develop a new catalyst system to allow the production of enantiomercially enriched (*S*)-metolachlor on a commercial scale.

(*S*)-*N*-(2-ethyl-6-methylphenyl)alanine ((*S*)-**2**) is an important precursor in the synthesis of (*S*)-metolachlor, which is currently produced by chemical synthesis in large quantities (4). The chemical method presently used requires drastic reaction conditions that may cause racemization, decomposition, or side reactions. The high energy consumption required for a long reaction time at a high temperature is unfavorable especially for industrial processes (5). As alternative to such processes, a highly active biocatalyst could be used in a very efficient manner. Among various commercial enzymes, lipases are attractive in terms of availability, the fact that there is no need of cofactors, high stability, and activity in organic media (6–8). The resolution of racemates by enzyme is still the most important approach in the industrial synthesis of optically pure compounds (9,10), as it is often

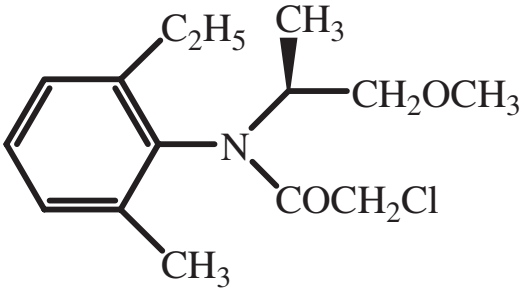
Received 11 June 2006. Accepted 2 August 2006. Published on the NRC Research Press Web site at http://canjchem.nrc.ca on 12 October 2006.

L. Zheng, G. Gao, and S. Cao. Key Laboratory for Molecular Enzymology and Engineering of Ministry of Education, Jilin University, Changchun, 130021, People's Republic of China.
S. Zhang[1] and F. Wang. College of Chemistry, Jilin University, Changchun, 130021, People's Republic of China.

[1]Corresponding author (e-mail: zhangsq@jlu.edu.cn).

 doi:10.1139/V06-129 © 2006 NRC Canada

Fig. 1. Structure of (*S*)-metolachlor.



the most economical and convenient way to prepare enantiomerically pure compounds. The main disadvantage of a resolution process compared with an enantioselective synthesis is that the maximum theoretical yield is 50%. Therefore, racemization of the unwanted enantiomer is of critical importance for economically and environmentally acceptable resolutions. A combination of classical resolution processes with racemization to give asymmetric transformations will be necessary to keep up with the advances in asymmetric synthesis (11).

Herein, we first report a practical lipase-catalyzed hydrolytic kinetic resolution of (*S*)-**2**, the key intermediate for (*S*)-metolachlor. To obtain the higher enantiomercially pure (*S*)-acid, the catalytic properties of different lipases are compared, the conditions of lipase-catalyzed hydrolysis are optimized, and the remaining ester is racemized. Then, (*S*)-metolachlor is synthesized by a chemical method based on (*S*)-**2**.

Experimental

Materials

Pseudomonas sp. lipase (PSL) and *Candida cylindracea* A.Y. lipase (AYL) were purchased from Amano Pharmaceutical Co., Ltd. (Nagoya, Japan). *Candida antarctica* lipase B (CAL-B) was kindly donated by Novo Nordisk Industries (Guangzhou, China). *Porcine pancreatic* lipase (PPL) was purchased from Shanghai Dongfeng biochemical reagent Co., Ltd. (Shanghai, China). *Candida lipolytic* lipase (CLL) was provided by Wuxi enzyme preparation plant (Wuxi, China). *Penicillium expansum* lipase (PEL) was provided by Nantong Pharmaceutical Co., Ltd. (Nantong, China). The authenticity of compounds prepared during the study was confirmed by spectroscopic analysis, including 300 MHz NMR (Mercury-300B, VARIAN, Palo Alto, USA), and GC–MS (Saturn 220, VARIAN, Palo Alto, USA). Reactions were routinely monitored on silica gel plates (Qingdao Haiyang Chemical Co., LTD., Qingdao, China) using UV light for detection of the spots. Optical rotation was measured with a WZZ-1S digital automatic polarimeter (Shanghai, China). All the organic solvents were reagent grade and used without further purification. Other reagents were all analytical grade or better.

Determination of conversion and enantiomeric excess (ee_p)

The analysis of the reaction mixtures and the determination of enantiomeric excesses of (*S*)-**2** were performed by capillary zone electrophoresis (P/ACE MDQ, Beckman, Fullerton, USA) with a 59 cm (49 cm to detector) × 50 μm i.d. eCAP^{TM} neutral capillary (Beckman, Fullerton, USA). The conversion of the reaction was determined by using 100 mmol/L triethylamine – acetic acid buffer (TEAA, pH = 5.5) as the background electrolyte. The enantiomeric excess of (*S*)-**2** was successfully analyzed in the buffer by using 40 mmol/L 2,6-di-*O*-methyl-β-cyclodextrin (DM-β-CD, Beckman, Fullerton, USA) as a buffer additive. The analysis was performed with an applied voltage of –20 kV, and the absorbance was recorded at 200 nm.

Enantiomeric ratio (*E*) of the hydrolysis of racemic *N*-(2-ethyl-6-methylphenyl) alanine methyl ester was calculated from the conversion (c) and enantiomeric excess (ee_p) of (*S*)-**2**, using the equation

$$E = \ln[1 - c(1 + ee_p)]/\ln[1 - c(1 - ee_p)]$$

where $ee_p = (c_S - c_R)/(c_S + c_R)$, where c_S and c_R are concentrations of the (*S*)- and (*R*)-enantiomers, respectively (12). The absolute configuration of the enantiomers was established by comparison of the measured optical rotation with the literature data (4).

Preparation of (*R*,*S*)-*N*-(2-ethyl-6-methylphenyl) alanine methyl ester: (*R*,*S*)-1

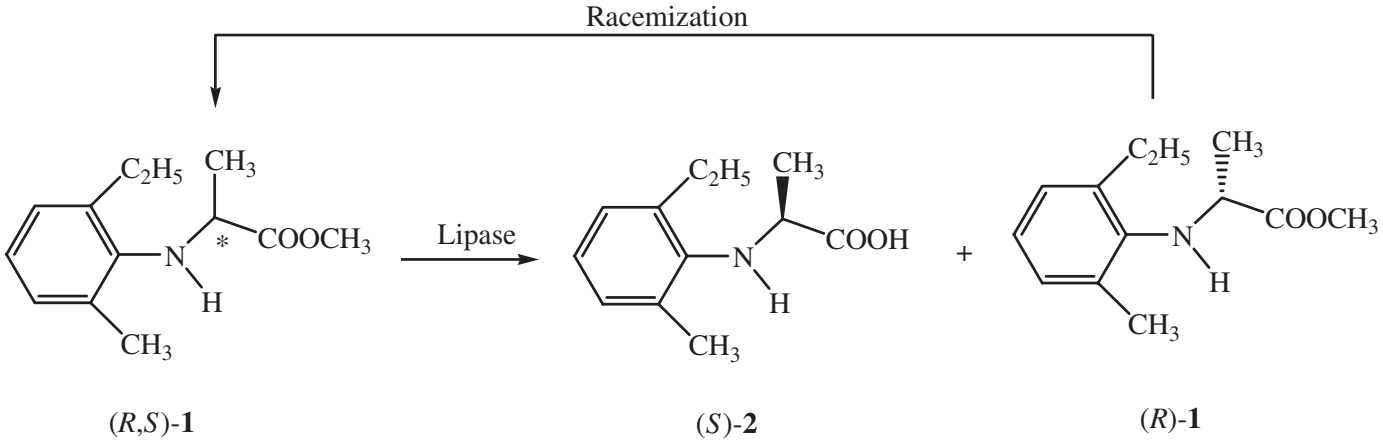
The reaction mixture of 2-ethyl-6-methylaniline (8.4 mL, 60 mmol), $NaHCO_3$ (5.5 g, 65 mmol), and methyl 2-bromopropionate (180 mmol) was stirred under nitrogen atmosphere and slowly heated to 120–125 °C in 1 h. Then, the dark reaction mixture was continually kept at the same temperature for 18 h with stirring. After cooling, the reaction mixture was transferred into 30 mL of ice water and extracted with ethyl acetate. The ethyl acetate fractions were dried over anhydrous Na_2SO_4 and concentrated in a rotary evaporator at 40 °C. After normal work-up, the resulting ester was purified by column chromatography on silica gel using ethyl acetate – petroleum ether (1:5) as the eluant to furnish the corresponding ester. *N*-(2-ethyl-6-methylphenyl) alanine methyl ester (8.9 g, 67.2% yield): ^{1}H NMR ($CDCl_3$) δ: 7.02–6.96 (m, 2H, aromatic H), 6.88–6.83 (t, 1H, J = 7.2 Hz, aromatic H), 3.96–3.94 (q, 1H, J = 6.9 Hz, $CHCH_3$), 3.81 (s, 1H, NH), 3.66 (s, 3H, OCH_3), 2.69–2.66 (m, 2H, CH_2CH_3), 2.30 (s, 3H, aromatic CH_3), 1.38–1.35 (d, 3H, J = 6.9 Hz, CH_2CH_3), 1.26–1.21 (t, 3H, J = 7.5 Hz, $CHCH_3$).GC–MS *m*/*z* (%): 221(M^+, 25), 162 (100), 133 (30), 77 (11); GC: 98% area.

Biocatalytic hydrolysis of (*R*,S)-1 in aqueous buffer with organic compound

CAL-B (200 mg) and (*R*,*S*)-**1** (2.2 g, 10 mmol) were added to the aqueous phosphate buffer (100 mmol/L, pH 8.0) containing diethyl ether (15% *v*/*v*) 100 mL. The mixture was stirred at 25 °C and the pH was maintained using 0.1 mol/L NaOH solution. When the hydrolysis reached 49% conversion, a saturated solution of $NaHCO_3$ (100 mL) was added to the reaction mixture. The mixture was then extracted with ether (3 × 100 mL) to remove the unchanged ester. The aqueous mixture was then acidified to pH 5.5 with 0.1 mol/L HCl and was extracted again with ether (3 × 100 mL) to remove the acid product. Acid extracts were

© 2006 NRC Canada

Scheme 1. Lipase-catalyzed hydrolysis of (*R*,*S*)-**1** and chemical racemization.



dried over anhydrous Na_2SO_4 and evaporated to give (*S*)-**2** (1.0 g, ee_p > 98%).

Racemization of (*R*)-*N*-(2-ethyl-6-methylphenyl) alanine methyl ester: (*R*)-1

The solution of (*R*)-**1** (1.0 g, 4.5 mmol) in toluene (5 mL) was added to a mixture of *n*-butyraldehyde (0.32 g, 4.5 mmol) and benzoic acid (0.22 g, 1.8 mmol) under nitrogen atmosphere. After refluxing for 3 h, the mixture was cooled to room temperature and washed with 5% Na_2CO_3 (3×5 mL) and H_2O (5 mL). The organic layer was separated, dried over anhydrous Na_2SO_4, and concentrated under reduced pressure. The resulting products were purified by silica gel chromatography using ethyl acetate – petroleum ether (1:5) as the eluant to produce the corresponding (*R*, *S*)-**1** (0.9 g, 90% yield, *R*:*S* = 50:50).

Preparation of (*S*)-*N*-(1′-methyl-2′-hydroxyethyl)-2-ethyl-6-methylaniline: (*S*)-3

To a stirred solution of $NaBH_4$ (0.9 g, 23 mmol) in anhydrous THF (20 mL) under nitrogen atmosphere, a solution of (*S*)-**2** (ee_p > 98%, 1.9 g, 9 mmol) in anhydrous THF (10 mL) was added dropwise. Then, the concentrated H_2SO_4 (0.7 mL) was added slowly below 20 °C. The reaction mixture was stirred at room temperature overnight, and the reaction was quenched by slow addition of methanol (20 mL). After concentrating the mixture in vacuo, 5 mol/L sodium hydroxide (10 mL) was added, and the reaction mixture was heated under reflux for 3 h. The crude mixture was filtered and extracted with $CHCl_3$ (3 × 20 mL). The organic layer was dried over anhydrous Na_2SO_4 and concentrated under reduced pressure to give (*S*)-**3** (1.6 g, 92% yield): $[\alpha]^{20}_D$ +6.8° (*c* 2.0%, methanol), 97.1% ee_p based on $[\alpha]^{20}_D$ +7° (*c* 1.941%, methanol) reported in literature (4). GC–MS *m*/*z* (%): 193.1 (M^+, 13.2), 162.2 (100); GC: 90% area.

Preparation of (*S*)-*N*-(1′-methyl-2′-hydroxyethyl)-*N*-chloroacetyl-2-ethyl-6-methylaniline: (*S*)-4

To a solution of (*S*)-**3** (1.6 g, 8.3 mmol) and Na_2CO_3 (0.88 g, 8.3 mmol) dissolved in benzene (10 mL) under nitrogen atmosphere, chloroacetyl chloride (0.94 g, 8.3 mmol) was slowly added at 15–20 °C with efficient stirring. The reaction mixture was then stirred for 3 h at room temperature and filtered. The filtrate was washed with 10% HCl, 10% Na_2CO_3, and saturated NaCl. The organic phase was dried over anhydrous Na_2SO_4, and subsequent concentration under reduced pressure afforded the yellow oil (*S*)-**4** (2.1 g, 95% yield): $[\alpha]^{20}_D$ +11.6°(*c* 1.1%, methanol), 96.6% ee_p based on $[\alpha]^{20}_D$ +12° (*c* 1.166%, methanol) reported in literature (4). GC–MS *m*/*z* (%): 269.2 (M^+, 12), 162.2 (100), 133.1 (21); GC: 92% area.

Preparation of (*S*)-*N*-(1′-methyl-2′-methoxyethyl)-*N*-chloroacetyl-2-ethyl-6-methylaniline: (*S*)-5

The reaction mixture of (*S*)-**4** (2.0 g, 7.4 mmol), 2,2-dimethoxypropane (1.69 g, 14.8 mmol), and *p*-toluenesulfonic acid (0.26 g, 1.1 mmol) dissolved in methanol (5 mL) was heated under reflux for 36 h. After cooling the reaction mixture to room temperature, methanol was evaporated under reduced pressure. The residue was taken up in ethyl acetate (10 mL), and the solution was washed with 10% Na_2CO_3 and water. The organic layer was dried over anhydrous $MgSO_4$ and concentrated in vacuo. The residual oil was purified by column chromatography on silica gel using ethyl acetate – petroleum ester (1:6) as the eluant to furnish the corresponding (*S*)-metolachlor, (*S*)-**5** (1.4 g, 66% yield): $[\alpha]^{20}_D$ –8.2 ± 1° (*c* 2.1%, *n*-hexane), 91.1% ee_p based on $[\alpha]^{20}_D$ –9.0 ± 1° (*c* 2.073%, *n*-hexane) reported in literature (4). ^1H NMR ($CDCl_3$), δ: 7.24–7.13 (m, 3H, aromatic H), 4.22 (m, 1H, $CHCH_3$), 3.94 (dd, *J* = 4.2 and 9.4 Hz) and 3.75 (dd, *J*= 4.2 and 9.4 Hz) for one diastereomeric proton of $CHCH_2OCH_3$), 3.62–3.61 (s, 2H, CH_2Cl), 3.51 (dd, *J* = 4.2 and 9.4 Hz) and 3.49 (dd, *J* = 4.2 and 6.5 Hz) for one diastereomeric proton of $CHCH_2OCH_3$, 3.27–3.26 (d, 3H, OCH_3), 2.62–2.54 (m, 2H, CH_2CH_3), 2.26 (s, 1H, aromatic CH_3), 2.24 (s, 2H, aromatic CH_3), 1.28–1.23 (t, 3H, *J* = 7.5 Hz, CH_2CH_3), 1.17–1.14 (q, 3H, *J* = 7.0 Hz, $CHCH_3$). GC–MS *m*/*z* (%): 284 (M^+, 60), 252 (38), 250 (100), 218 (47), 178 (25), 162 (37), 73 (60); GC: 98% area.

Results and discussion

In a general experimental procedure, readily accessible racemic methyl ester **1** was used as a substrate in the identification of a suitable lipase for the enantioselective hydrolysis (Scheme 1), and the screening results were listed in Table 1. The lipase CAL-B was very active, and 48.2% of

© 2006 NRC Canada

Table 1. Lipase-catalyzed hydrolysis of (*R*,*S*)-**1**.

Lipase	Time (h)	Conversion (%)	ee_p (%)	*E* value	Major enantiomer
CAL-B	2	48.2	69.4	10.6	*S*-(–)
PSL	60	48.2	99.0	>100	*R*-(+)
PPL	72	1.7	99.0	>100	*R*-(+)
CLL	72	0.24	98.0	99.2	*S*-(–)
AYL	72	2.0	78.8	8.6	*S*-(–)
PEL	72	0.12	58.5	3.8	*S*-(–)

Note: Reaction conditions: buffer: 100 mmol/L phosphate buffer (pH = 8.0, 5.0 mL); substrate: 0.5 mmol; enzyme: 105 U; temperature: 37 °C.

Table 2. CAL-B-catalyzed hydrolysis of (*R*,*S*)-**1** in different aqueous-organic media.

Organic solvent	Log *P*	Time (h)	Conversion (%)	ee_p (%)	*E* value
None	—	2	32.5	78.7	12.1
Acetonitrile	–0.33	2	29.7	83.7	15.9
Acetone	–0.23	2	31.7	82.9	15.5
THF	0.49	2	28.2	82.8	14.6
Diethyl ether	0.85	2	19.6	87.8	19.0
DIPE	1.90	2	28.3	84.8	16.8
Toluene	2.50	2	17.4	84.3	13.9
Cyclohexane	3.20	2	27.1	82.1	13.7
n-Hexane	3.50	2	25.1	87.6	20.1
n-Heptane	4.00	2	23.1	86.5	17.9

Note: Reaction conditions: substrate: 0.5 mmol; CAL-B: 10 mg; organic compound/phosphate buffer (100 mmol/L, pH= 8.0, 5.0 mL) 1:9; temperature: 25 °C.

(*R*,*S*)-**1** was hydrolyzed only after 2 h at 37 °C; however, it displayed poor enantioselectivity (*E* = 10.6) towards the (*S*)-enantiomer of the acid. The *E* value of >100 and enantiomeric excess (ee_p) of >98% were obtained by lipase PSL and PPL, but they preferably produced the (*R*)-acid and needed longer reaction time. Other enzymes investigated in this work gave both low conversion and enantioselectivity, making them practically useless. As a result of its higher activity and stereospecificity towards the (*S*)-enantiomer, the lipase CAL-B was chosen from the enzymes screened for further study.

Initially we investigated the influence of the microenvironment on the CAL-B-catalyzed resolution and found that the enantioselectivity of CAL-B was still too low for a large-scale preparation (data not shown). This may be ascribed to the ability of CAL-B to catalyze the hydrolysis of both (*R*)- and (*S*)-enantiomers of substrate, thus leading to the low enantioselectivity of enzyme. According to this assumption, if we take measures to enantioselectively inhibit the reaction rate of CAL-B-catalyzed hydrolysis, and as a result, the (*S*)-enantiomer becomes overwhelmingly the faster reacting enantiomer, the enantioselectivity of CAL-B may be enhanced.

The strategy of enantioselective inhibition by adding an organic compound to the reaction medium to enhance the selectivity of lipase had previously been reported by our group (13). So, in this study, organic compounds with different hydrophobicities (log *P*) (14, 15) were added to the reaction system to observe their effect on CAL-B-catalyzed hydrolysis (Table 2). In all experiments, the biocatalytic system shows the same stereopreference for (*R*,*S*)-**1** giving (*S*)-acid. Also, the addition of organic compounds generally enhanced the enantioselectivity of CAL-B compared with that in a pure buffered medium, despite a decrease in enzyme activity.

According to the previously mentioned results, it is worthy to note that the use of diethyl ether and *n*-hexane as additives is preferred (*E* = 19.0 and 20.1, respectively). Herein, the effects of diethyl ether and *n*-hexane amounts on the activity and enantioselectivity of CAL-B were studied. The additive amount of the organic compound is an important parameter worthy of careful optimization because it may have a strong influence on enzyme activity and enantioselectivity. When diethyl ether was added to the reaction medium, the maximum *E* value of CAL-B was obtained at 15% (*v*/*v*) (*E* > 100, Fig 2), which was approximately 9.7-fold more enantioselective than that in the pure buffered medium. For *n*-hexane, the results differed and the maximum enantioselectivity of CAL-B was stabilized at the additive amount ranging from 10 to 15% (*v*/*v*) (*E* = 20.1, Fig 3). The conversion ratios of reactions for various amounts of organic compounds were also measured and it was found that the ratio decreased with an increase of additive amount of organic compound. Based on these results, we presume that diethyl ether is a stronger and more (*R*)-selective inhibitor than *n*-hexane.

After CAL-B-catalyzed hydrolysis finished under the optimized conditions, the enantiomercially pure (*S*)-**2** (>98% ee_p) and the remaining ester (*R*)-**1** were extracted with ether. The two compounds can be separated easily by partitioning in ether or water. This simple extraction–partition procedure is especially convenient and suitable for a large-scale operation. The remaining ester can be recycled by chemical racemization, which is achieved through treatment with a mixture of *n*-butyraldehyde and benzoic acid dissolved in toluene (Scheme 1). The aldehyde-catalyzed racemization of

© 2006 NRC Canada

Fig. 2. Effect of different volume fractions of diethyl ether on the conversion and enantioselectivity of CAL-B-catalyzed hydrolysis of (*R*,*S*)-**1**.

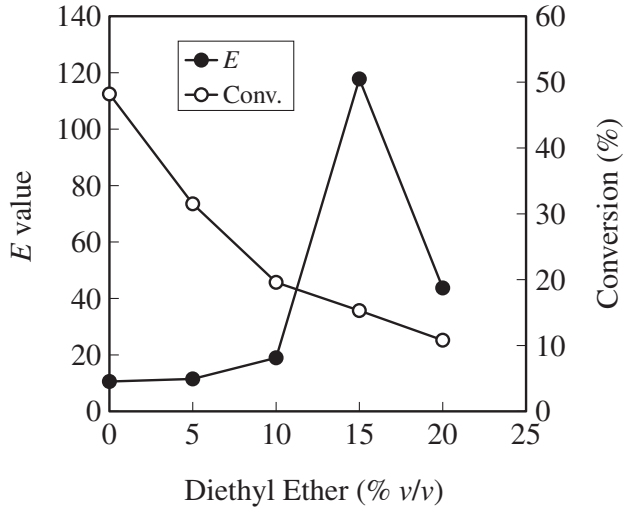
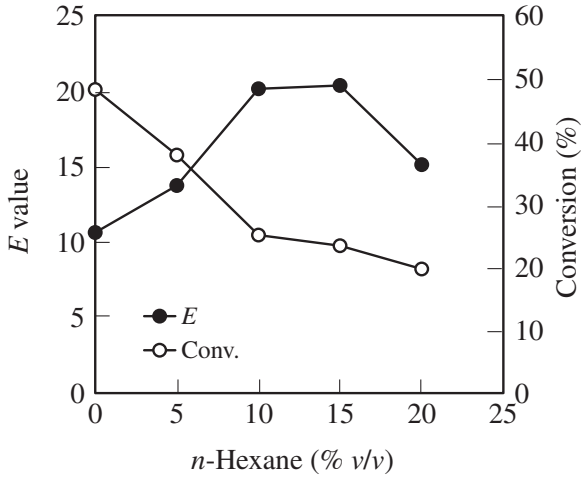
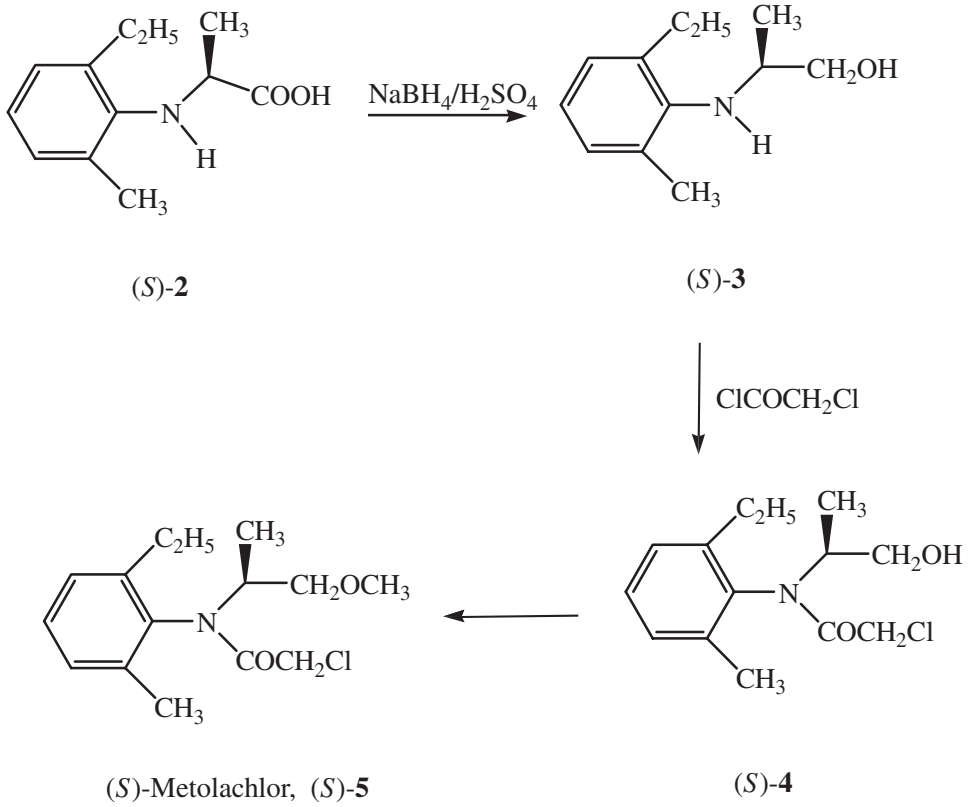


Fig. 3. Effect of different volume fractions of *n*-hexane on the conversion and enantioselectivity of CAL-B-catalyzed hydrolysis of (*R*,*S*)-**1**.



Scheme 2. Synthesis of (*S*)-metolachlor from enzymatically prepared (*S*)-**2**.



amino acids and derivatives is the most prominent example of how to derive a functional group connected to a chiral center and affect optical stability. Herein, we also investigated the effects of other aldehydes including formaldehyde, acetaldehyde, propionaldehyde, *n*-valeraldehyde, and benzaldehyde on the racemization, and found that the experimental results were similar. However, considering the economic factor and the boiling point of the aldehyde, we selected *n*-butyraldehyde as the racemic reagent. Very similar results were also reported by Park et al. (6).

The chemical synthesis of (*S*)-metolachlor was then carried out using enantiomercially pure (*S*)-**2** as a substrate via a number of pathways, which included reduction, chloroacetylation, and etherification (Scheme 2). The reduction of (*S*)-**2** to (*S*)-**3** is conveniently carried out in an inert solvent. Suitable reducing agents are lithium aluminium hydride and

© 2006 NRC Canada

sodium borohydride, but the selectivity of lithium aluminium hydride towards the functional group of the compound is poor and it is rather expensive. Thus, it is preferable to use sodium borohydride in the form of a complex, especially as a sodium borohydride – tetrahydrofuran complex. The conversion of (*S*)-**3** into (*S*)-**4** is carried out in an inert solvent by the reaction with a chloroacetylating agent, such as chloroacetyl chloride, in the presence of a base. Suitable bases may be alkali metal carbonates, triethylamine, and pyridine. Suitable inert solvents may be hydrocarbons, such as hexane, cyclohexane, benzene, toluene, and chlorobenzene. In this work, Na_2CO_3 and benzene were selected as the base and inert solvent, respectively. The reaction was carried out at a low or moderately elevated temperature. The etherification of the 2-hydroxy group of (*S*)-**4** was carried out by heating the reaction mixture, dissolved in methanol, in the presence of a strong acid at a reflux temperature. A strong acid suitable for the reaction is *p*-toluenesulfonic acid. Then (*S*)-metolachlorwas obtained with the optical purity of 91.1% ee_p. Compared with racemic metolachor, (*S*)-metolachlor has a markedly superior herbicidal action against weeds without increasing phytotoxicity towards cultivated plants.

Conclusion

We successfully developed a chemoenzymatic procedure for the synthesis of enantiomerically pure (*S*)-metolachlor. We took advantage of the higher activity and excellent enantioselectivity of lipase CAL-B, chemical racemization of the remaining ester, and chemical reactions including reduction, chloroacetylation, and etherification. The method is easy to perform with standard equipment and can be widely applied. At the same time, we found that organic compounds strongly influenced the selectivity of CAL-B. Diethyl ether, in particular, was found to achieve the highest enantioselectivity of CAL-B ($E > 100$) in the hydrolysis of (*R*,*S*)-**1**. Further work in this area, including the repeated use of enzymes to decrease the enzymatic cost and scale-up results of the process, is being done in our laboratory and will be reported soon.

Acknowledgements

The authors are grateful for the financial support from the National Natural Science Foundation of China (No.20432010) and the Foundation of Research Program of Jilin University, China.

References

1. J. Liu, Y. Zhang, L. Qiu, F. Yang, L. Ye, and Y. Xia. J. Ind. Microbiol. Biotechnol. **31**, 495 (2004).
2. P.J. O'Connell, C.T. Harms, and J.R.F. Allen. Crop Protection, **17**, 207 (1998).
3. B.T. Cho and Y. S.Chun. Tetrahedron: Asymmetry, **3**, 337 (1992).
4. H. Moser and C.Vogel. US Patent 5-002-606, 1991.
5. I. Osprian, M.H. Fechter, and H. Griengl. J. Mol. Catal. B, **24–25**, 89 (2003).
6. O.J. Park, S.H. Lee, T.Y. Park, S.W. Lee, and K.H. Cho. Tetrahedron: Asymmetry, **16**, 1221 (2005).
7. K.E. Jaeger and T. Eggert. Curr. Opin. Biotechnol. **13**, 390 (2002).
8. H. Stamatis, A. Xenakis, and F.N. Kolisis. Biotechnol. Adv. **17**, 293 (1999).
9. Y. Chikusa, Y. Hirayama, M. Ikunaka, T. Inoue, S. Kamiyama, M. Moriwaki, Y. Nishimoto, F. Nomoto, K. Ogawa, T. Ohno, K. Otsuka, A.K. Sakota, N. Shirasaka, A. Uzura, and K. Uzura. Org. Process Res. Dev. **7**, 289 (2003).
10. M. Kinoshita and A.Ohno. Tetrahedron, **52**, 5397 (1996).
11. E.J. Ebbers, G.J.A. Ariaans, J.P.M. Houbiers, A. Bruggink, and B. Zwanenburg. Tetrahedron, **53**, 9417 (1997).
12. C.S. Chen, Y. Fujimoto, G. Girdaukas, and C.J. Sih. J. Am. Chem. Soc. **104**, 7294 (1982).
13. L.Y. Zheng, S.Q. Zhang, Y. Feng, S.G. Cao, J.S. Ma, L.F. Zhao, and G. Gao. J. Mol. Catal. B, **31**, 117 (2004).
14. A. Cipiciani, M. Cittadini, and F. Fringuelli. Tetrahedron, **54**, 7883 (1998).
15. T.W. Chiou, C.C. Chang, C.T. Lai, and D.F. Tai. Bioorg. Med. Chem. Lett. **7**, 433 (1997).

© 2006 NRC Canada

A new and efficient one-pot solid-supported synthesis of 1,2,4,6-tetraaryl-1,4-dihydropyridines

Anil K. Verma, Summon Koul, Tej K. Razdan, and Kamal K. Kapoor

Abstract: 1,2,4,6-Tetraaryl-1,4-dihydropyridines were obtained by the one-pot reaction of chalcones and substituted anilines on the surface of Bi(III)nitrate-Al_2O_3. The reaction seems to proceed via β-oxygenation of Bi(III) enolised chalcones followed by Michael addition and heteroannulation with simultaneous retro aldol disproportionation. The presence of the ring-activating groups at ortho and para positions in the aniline seems to be essential for the reaction.

Key words: 1,2,4,6-tetraryl-1,4-dihydropyridines, chalcones, substituted anilines, Bi(III) nitrate-alumina catalyst.

Résumé : On a réalisé la synthèse de 1,2,4,6-tétraaryl-1,4-dihydropyridines par le biais d'une réaction monotope de chalcones avec des anilines substituées à la surface d'un catalyseur de nitrate de Bi(III)-Al_2O_3. La réaction semble impliquer une β-oxygénation des sels de Bi(III) des chalcones énolisées, suivie d'une addition de Michael et d'une héteroannelation accompagnée d'une dismutation simultanée rétroaldolique. Il semble que la présence de groupes activants dans les positions ortho et para de l'aniline soit essentielle à la réalisation de la réaction.

Mots clés : 1,2,4,6-tétraaryl-1,4-dihydropyridines, chalcones, anilines substituées, catalyseur de nitrate de Bi(III)-alumine.

[Traduit par la Rédaction]

Introduction

1,4-Dihydropyridine derivatives participate actively in biochemical oxidoreductase (1) and transaminase (2) reactions. They serve as key intermediates in the biogenesis of indole alkaloids (3) as well as the synthesis of several naturally occurring bioactive alkaloids (4) and substituted pyridines (5). These products are primarily potent calcium antagonists (6) and the activity is dictated by the stereochemistry at C-4 (7). The compounds also exhibit a wide range of other therapeutic properties such as antioxidant (8), antimutagenic (9), antidiabetic (10), hepatoprotective (11), antiaddictive (12), bronchodilating (13), herbicidal (14), and anticancer (15) activity. Therefore, the synthesis of 1,4-dihydropyridine derivatives continues to be a subject of fruitful research. These products, especially the calcium channel regulators, are synthesized chiefly by Hantzsch synthesis (14) or its modifications and by the reduction of pyridine derivatives or pyridinium salts. Several reviews (16) have exhaustively dealt with the synthesis, chemistry, pharmacology, and industrial utility of 1,4-dihydropyridine derivatives.

Our interest in the synthesis of 1,2,4,6-tetraaryl-1,4-dihydropyridines originated from the presumption that because of the planarity of the 1,4-dihydropyridine nucleus (17) these products may display the photodynamic activity akin to the symmetrical 2,4,6-triarylthiopyrylium, selenopyrylium, and telluropyrylium photosensitizers, which have been recommended for cell-specific cancer therapy (18). Moreover, since most of the known syntheses (16) of 1,4-dihydropyridine derivatives are multistage laborious processes and involve harsh or environmentally hazardous reaction conditions, together with the fact that the alkyl and the aryl primary amines have not gained popularity in their synthesis, we opined that a new and straightforward catalytic method, employing aryl primary amine as one of the substrates, was needed for the synthesis of 1,2,4,6-tetraaryl-1,4-dihydropyridines. Herein, we report a simple, convenient, and cost-effective one-pot solid-supported synthesis of these compounds from chalcones and substituted anilines using the hitherto unexplored Bi(III) nitrate-Al_2O_3 reagent.

Received 3 April 2006. Accepted 26 June 2006. Published on the NRC Research Press Web site at http://canjchem.nrc.ca on 12 October 2006.

A.K. Verma, S. Koul,[1] T.K. Razdan,[2] and K.K. Kapoor. Department of Chemistry, University of Jammu, Ambedkar Road, Jammu 180006, India.

[1]Present address: Department of Organic Chemistry, Simon Fraser University, Burnaby, BC V5A 1S6, Canada.
[2]Corresponding author (e-mail: tk_razdan@rediffmail.com).

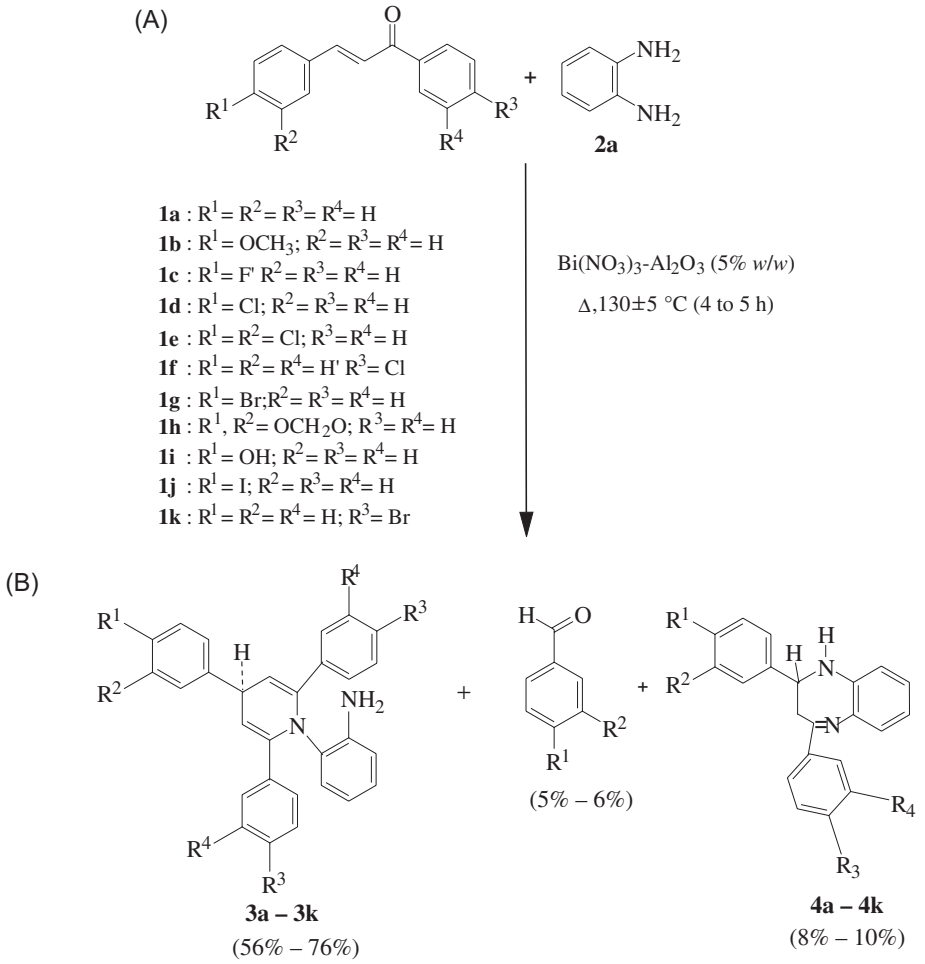
Results and discussion

Although Bi(III) nitrate is easily available in pure form and has negligible toxicity (19) and high stability in air and moisture, its catalytic efficacy has not been thoroughly explored. This led us to evaluate the possible catalytic utility of Bi(III) nitrate immobilized on neutral alumina in the synthesis of the title products. The catalyst was selected on the assumption that Bi(III) ions, being moderately acidic (20) in nature, could bind efficiently to the surface of neutral alumina, prevent its restructuring, synergise its catalytic activity (21), and initiate a reaction under mild conditions. The catalyst was prepared by adsorbing Bi(III) nitrate·$5H_2O$ (5% *w*/*w*) on neutral alumina and activation of the air-dried mixture in a hot air oven at 110 ± 5 °C, for six hours. The catalyst was reactivated each time before use.

The chalcone substrates **1a**–**1k** were prepared from the appropriate benzaldehyde and acetophenone by classical

 doi:10.1139/V06-128 © 2006 NRC Canada

Scheme 1. 1,2,4,6-Tetraaryl-1,4-dihydropyridines from chalcones.



(C)

	3a/4a	3b/4b	3c/4c	3d/4d	3e/4e	3f/4f	3g/4g	3h/4h	3i/4i	3j/4j	3k/4k
R^1	H	OCH_3	F	Cl	Cl	H	Br	–O–	OH	I	H
R^2	H	H	H	H	Cl	H	H	CH_2	H	H	H
								–O–			
R^3	H	H	H	H	H	Cl	H	H	H	H	Br
R^4	H	H	H	H	H	H	H	H	H	H	H

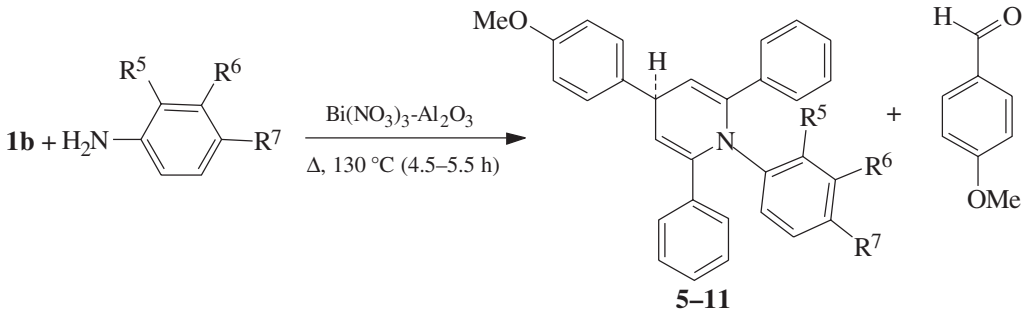
Claisen–Schmidt condensation (22). Subsequent reactions of **1a**–**1k** with *o*-phenylenediamine, **2a**, (2:1 mol/L), and Bi(III) nitrate-Al_2O_3 (Scheme 1), in the proportion by weight of chalcones, were carried out in a thermostatically controlled hot air oven at 130 ± 5 °C, for 4 to 5 h. The resulting product mixtures were isolated with chloroform and separated by column chromatography to yield the major products **3a**–**3k** (56%–76%) (Table 1) and the minor products **4a**–**4k** (8%–10%). These reactions also afforded the aldehyde (5%–6%) from which **1a**–**1k** were prepared. The compounds **3a**–**3k** and **4a**–**4k** were analysed by spectral methods, HREI-MS, IR, ^{1}H NMR, ^{13}C NMR and DEPT 135°. The spectra established the structures of **3a**–**3k** as 1,2,4,6-tetraaryl-1,4-dihydropyridine derivatives (Scheme 1). The expanded peak segregated ^{1}H NMR spectra of the products showed a characteristic one proton triplet (J = 3.8 Hz) near δ 5.37 because of the α proton (5*a*, 23) at C-4, δ_C 54.7, coupled to the protons at C-3 and C-5, δ 6.80–7.1 (d, J = 3.9 Hz, 2H), δ_C 145.2, of the dihydropyridine nucleus. The IR absorption band at υ_{max} 3455 cm^{-1} and a broad singlet near δ 7.23 (2H) in the ^{1}H NMR spectra revealed the presence of a free amino group in the compounds. The ^{13}C NMR signals were assigned on the basis of DEPT 135 experiments. The mass spectra of **3a**–**3k** exhibited fragmentations typical of 1,4-dihydropyridines (24) and displayed abundant ion peaks corresponding to the loss of an aryl radical from the C-4 of the

© 2006 NRC Canada

Table 1. Yield of the products **3a**–**3k** and **4a**.

Compound	Oven yield (%)	MW yield (%)	Compound	Oven yield (%)	MW yield (%)	MW time (min)
3a	70.0	72.4	**4a**	8	6	20
3b	76.0	78.3	**4b**	8	7	22
3c	56.2	59.1	**4c**	10	12	20
3d	60.8	61.2	**4d**	10	10	23
3e	64.5	68.0	**4e**	9	12	22
3f	61.0	65.0	**4f**	10	12	23
3g	67.5	67.4	**4g**	8	14	19
3h	72.0	73.5	**4h**	8	6	23
3i	70.0	71.2	**4i**	9	9	25
3j	62.5	65.0	**4j**	9	10	25
3k	65.7	66.5	**4k**	7	9	26

Scheme 2. Reaction of **1b** with different substituted anilines.



5–11

2b : R^5= OH; R^6= R^7= H

2c : R^6= OH; R^5= R^7= H

2d : R^7= OH; R^5= R^6= H

2e : R^5= Br; R^6= R^7= H

2f : R^6= Br; R^5= R^7= H

2g : R^7= Br; R^5= R^6= H

2h : R^6= NO_2; R^5= R^7= H

2i : R^5= NO_2; R^6 = R^7= H (No reaction)

2j : R^7= NO_2; R^5= R^7= H (No reaction)

2k : R^5= R^6= R^7 = H (No reaction)

5: R^5= OH; R^6= R^7= H

6: R^6= OH; R^5= R^7= H

7: R^7= OH; R^5= R^6= H

8: R^5= Br; R^6= R^7= H

9: R^6= Br; R^5= R^7= H

10: R^7= Br; R^5= R^6= H

11: R^6= NO_2; R^5= R^7= H

molecular ion. The base peak fragment ion at *m/z* 246 resulted from the loss of the second aryl radical from the C-2 or C-6 position of the (M^+ – $Ar^·$) fragment ion. Except for compounds **3f** and **3k**, which possessed two monosubstituted aryl rings at positions 2 and 6 of the 1-(2-aminophenyl)-1,4-dihydropyridine nucleus, and compound **3a**, which possessed unsubstituted phenyl rings at positions 2,4, and 6 of the nucleus, all products had a lone substituted phenyl ring at position 4 of the nucleus.

The ^{1}H NMR spectra of the minor products **4a**–**4k** displayed resonance signals near δ 3.0 (dd, *J* = 8.2, 11.5 Hz, H_a-6), 3.20 (dd, *J* = 4.1, 11.5 Hz, H_b-6), 5.10 (dd, *J* = 4.1, 8.2 Hz, H-7), and 3.80–3.90 (s, br, 1H, NH) typical of benzo-1,4-diazepines. These compounds were known and their spectral data and melting points were consistent with the literature (25).

To generalize this reaction and assess the influence of the ring-activating and ring-deactivating substituents in anilines on the percentage yield of the products, chalcone **1b** was reacted separately but under identical conditions with *ortho*-, *meta*-, and *para*-hydroxyaniline **2b**–**2d**, bromoaniline **2e**–**2g**, nitroaniline **2h**–**2j**, and aniline **2k** (Scheme 2). Aniline, *o*-

© 2006 NRC Canada

Scheme 3. Probable mechanism for formation of 1,2,4,6-tetraaryl-1,4-dihydropyridine.

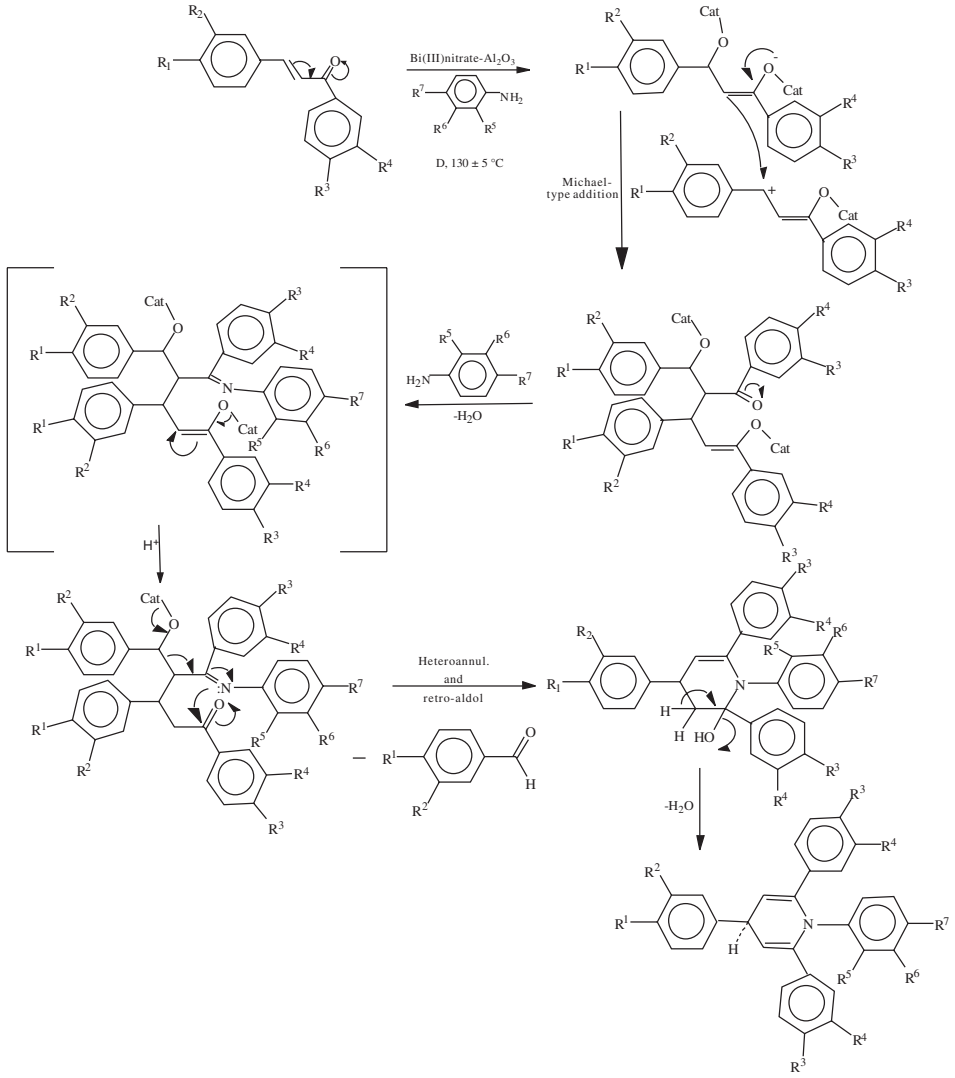


Table 2. Yield of the products of **1b** with different anilines **2b**–**2h**.

Product	Oven yield (%)	MW yield (%)	MW time (min)
5	65.6	68.2	20
6	22.5	26.0	26
7	72.0	74.3	25
8	73.4	75.4	18
9	19.5	19.8	25
10	76.5	78.5	20
11	32.5	33.0	20

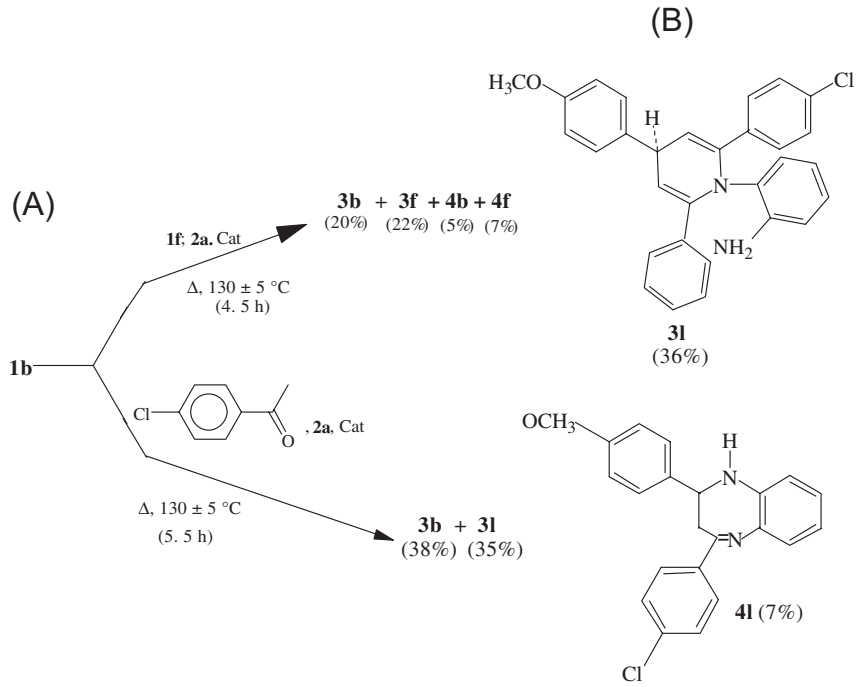
nitroaniline, and *p*-nitroaniline failed to afford the desired 1,2,4,6-tetraaryl-1,4-dihydropyridines while *meta*- nitroaniline afforded the product **11**, albeit in low yield (Table 2). The ring-activating groups in anilines seem to favour the reaction and formed compounds **5**–**10** with the percentage yield in the expected order of para > ortho > meta substituted anilines (Table 2).

Since crystalline bismuth nitrate exists as $Bi(NO_3)_3{\cdot}5H_2O$ and alumina also chemisorbs water readily (25) and retains some of it even after activation at 110 ± 5 °C, the mechanism of the reaction may be rationalised as involving β-oxygenation of the Bi(III) nitrate activated chalcone enolate, which may then undergo a Michael addition to a second α,β-unsaturated ketone (Scheme 3) to form a 1,5-diketone enolate adduct. Subsequent heteroannulation with substituted anilines via condensation and retro-aldol disproportionation (26) may form 2-hydroxy-1,2,4,6-tetraaryl-1,2,3,4-tetrahydropyridine derivatives, which may undergo dehydration to yield 1,2,4,6-tetraaryl-1,4-dihydropyridines. This mechanism is supported by the fact that the products obtained from 4-substituted chalcones, like **3b**, possessed only one substituted phenyl group at position 4-4 of the 1-(2-aminophenyl)-1,4-dihydropyridines nucleus.

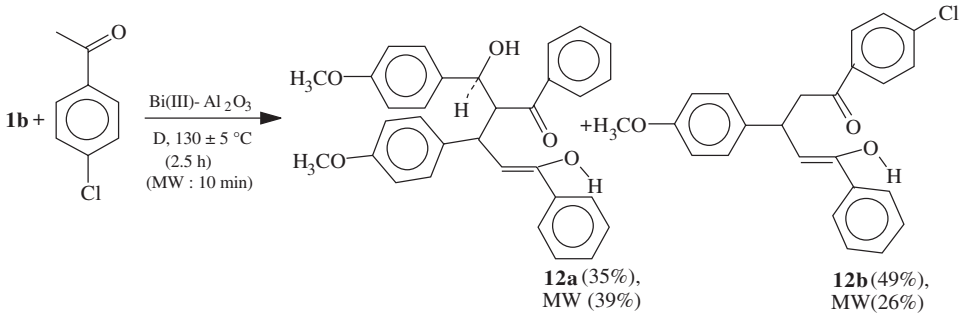
To substantiate the proposed mechanism, cross-reactions of chalcones **1b** and **1f** and also **1b** and *p*-chloroacetophenone (1:1 mol/L) with equimolar amounts of **2a** and 5% Bi(III) nitrate-Al_2O_3, in proportion by weight of the substrates, were carried out at 130 ± 5 °C (Scheme 4). The reaction of **1b**, **1f**, and **2a** yielded **3b** (20%), **3f** (22%), **3l** (36%),

© 2006 NRC Canada

Scheme 4. Cross reaction of **1b**.



Scheme 5. Reaction of **1b** and *p*-chloroacetophenone in the absence of aniline derivatives.



4b (5%), and **4f** (7%). The reaction involving **1b**, *p*-chloroacetophenone, and **2a** gave **3b** and **3l** in nearly equal proportions and **4l** (13%).

We attempted the reaction of equimolar quantities of **1b**, *p*-chloroacetophenone, and equal mass of Bi(III)nitrate-Al_2O_3 at 130 ± 5 °C (Scheme 5) in the absence of arylamines. The reaction afforded two products, **12a** and **12b**, which were separated by column chromatography and identified by spectral methods as 2-(4-methoxyphenyl)hydroxymethyl-3-(4-methoxy)phenyl-1,5-diphenylpentan-4-en-5-ol-1-one (**12a**) and 1-(4-chloro)phenyl-3-(4-methoxy)phenyl-5-phenylpentan-4-en-5-ol-1-one (**12b**) (Scheme 5). The ^{1}H NMR, ^{13}C NMR and DEPT 135 spectra for **12a** and **12b** showed the presence of a carbonyl group, δc 197.3, and an enol hydroxyl, δ 12.9 (s br, exch. D_2O, 1H). The spectra of **12a** revealed the absence of a methylene carbon whose presence in **12b** was evident from the resonance signals at δ 2.69 (d, J = 4.5 Hz, 2H) in its ^{1}H NMR spectrum and δ_C 25.3 in its ^{13}C NMR and DEPT 135 spectra. The spectra of **12a** showed the presence of a secondary hydroxyl displaying resonance signals at δ 2.80 (s br, exch. D_2O, 1H) and 5.01 (d, J = 3.6 Hz, 1H, -CH-OH), δ_C 83.2. These signals were absent in the spectra of **12b**. These observations were consistent with the proposed mechanism and indicated that the retro-aldol disproportionation is probably triggered by the heteroannulation of the Michael adduct with substituted anilines, especially the anilines having a ring-activating group at the ortho or para position.

The reaction is sensitive to temperature with the optimum temperature being 130 ± 5 °C. The reaction failed to proceed in solution or when neat Al_2O_3 or Bi(III) nitrate were used as the reagent. We repeated all the reactions in a domestic microwave (2450 MHz) using 60% power and followed the procedure of Mukhopadhyay et al. (27), which allows the temperature to remain at ca. 130 °C. The reactions were completed in 19–26 min without any appreciable improvement in the yield of the 1,2,4,6-tetraaryl-1,4-dihydropyridines (Tables 1 and 2).

Conclusion

In conclusion, we have devised a new one-pot environmentally benign and general solid-supported catalytic method for the synthesis of 1,2,4,6-tetraaryl–1,4-dihydropyridines

© 2006 NRC Canada

from the easily accessible chalcones and substituted anilines using Bi(III) nitrate immobilized on Al_2O_3 as a reagent. An advantage of this method is the low toxicity (19) and the antiulcerative (28) properties of bismuth compounds. Further studies on the scope and limitations of immoblized Bi(III) nitrate in organic transformations are under way.

Experimental

General

Melting points are uncorrected and were determined on Perfit melting point apparatus. IR, on KBr discs, were taken on a Brucker 4800 IR spectrometer. ^{1}H NMR (200 MHz) and ^{13}C NMR (50.3 MHz) were recorded in DMSO or $CDCl_3$ using a Brucker Ac DPX-200 spectrometer; some spectra were recorded on Varian Gemini 300 MHz instrument. HREI-MS were recorded on JEOL D-300 mass spectrometer at 70 eV. TLC was performed on 0.5 mm thick plates using BDH silica gel-G adsorbent. Column chromatography was performed on silica gel (BDH, mesh size 60–120) using graded solvent systems of petroleum ether (40–60 °C), petroleum ether – $CHCl_3$ and $CHCl_3$–EtOAc. Microwave irradiations were carried out in a domestic microwave oven (LG Model No. MS-255R, No. 4140W1A347A) with frequency 2450 MHz and R_f output of 900W.

Preparation of catalyst

Bi(III) nitrate·$5H_2O$ (2.5 g) was dissolved in 50% MeOH (150 mL) and the solution was added to neutral alumina (50 g) and stirred for 12 h at room temperature. The mixture was air dried and then heated at 110 ± 5 °C in a thermostatic hot air oven for 6 h. The activated Bi(III) nitrate-Al_2O_3 mixture was cooled in a dessicator and preserved. The catalyst was reactivated at 110 ± 5 °C for 0.5 h each time before use.

Preparation of chalcones 1a–1k

Chalcones **1a**–**1k** were prepared from the appropriate benzaldehyde and acetophenone by the well known procedure for Claisen–Schmidt condensation (22). Chalcones were purified by CC on silica gel using petroleum ether – CH_2Cl_2 (9:1, 7:3, and 1:1 *v*/*v*, 40–60 °C) followed by crystallization from $CHCl_3$ –MeOH.

General procedure for the preparation of 3a–3k, 5–11 and cross-reactions of 1b

The solution of chalcone **1a**–**1k** (2×10^{-3} mol/L) and *o*-phenylenediamine **2a** (1×10^{-3} mol/L) in chloroform (10 mL) were adsorbed on a Bi(III) nitrate-Al_2O_3 mixture in proportion by weight of the chalcones. The solvent was evaporated in air and the air-dried solid mixture was charged into a stoppered flask. The flask was heated in a thermostatically controlled hot air oven and maintained at 130 ± 5 °C. Simultaneously, separate experiments were conducted to monitor the reaction by comparative TLC of the ethylacetate extracts of the aliquots drawn out from the reaction flask at 0.5 h intervals, using petroleum ether – CH_2Cl_2 (9:1, 7:3, and 3:7 *v*/*v*, 40–60 °C) as solvent systems. The plates were developed by spraying with Ce(IV) ions and heating at 110 ± 5 °C for 10 min when dark purple spots of the Ce(IV) complexes of 1,2,4,6-tetraaryl-1,4-dihydropyridines and yellow spots of the 1,4-benzodiazepines were observed against a white background. On completion of the reaction (4–5 h) the product mixtures were extracted with hot $CHCl_3$ in a soxhlet extractor, freed from the solvent, and separated by CC, using petroleum ether – CH_2Cl_2 (40–60 °C) graded solvent systems. Twenty milliliter fractions were collected and TLC identical fractions were pooled. The solvent was distilled and the residue was purified by crystallization from $CHCl_3$ – petroleum ether (40–60 °C) and $CHCl_3$–MeOH. This gave **3a**–**3k** as major product and **4a**–**4k** (25) as the minor product (Table 1). In addition to these compounds, minor quantities of aldehydes from which **1a**–**1k** were prepared were also obtained. Compounds **5**–**11** (Scheme 3) were prepared by reacting **1b** (2×10^{-3} mol/L) and 2-aminophenol (**2b**), 3-aminophenol (**2c**), 4-aminophenol (**2d**), 2-bromoaniline (**2e**), 3-bromoaniline (**2f**), 4-bromoaniline (**2g**), and 3-nitroaniline (**2h**) (1×10^{-3} mol/L), respectively, with Bi(III) nitrate-Al_2O_3 in proportion by weight of the substrates using the previously described procedure. The same procedure was adopted in the reaction of **1b** (1×10^{-3} mol/L), **1f** (1×10^{-3} mol/L), and Bi(III) nitrate-Al_2O_3 and a mixture of **3b**, **3f**, **3l**, **4b**, and **4f** were obtained (Scheme 4). The mixture was separated by CC as described earlier. A similar procedure was used in the reaction of **1b** (1×10^{-3} mol/L), *p*-chloroacetophenone (1×10^{-3} mol/L), and Bi(III) nitrate-Al_2O_3 (Scheme 4) when a mixture of **3b**, **3l**, and **4l** was recovered by adopting the previously described procedure for the isolation, separation, and purification of the compounds.

Preparation of 12a and 12b

To a mixture of **1b** (0.238 g, 1×10^{-3} mol/L) and *p*-chloroacetophenone (0.15 g, 1×10^{-3} mol/L) dissolved in $CHCl_3$ (10 mL) was added the reagent Bi(III)nitrate-Al_2O_3 (0.388 g). The mixture was dried in air and heated in a thermostatically controlled hot air oven at 130 ± 5 °C. A separate experiment was simultaneously conducted to monitor the reaction by TLC of the chloroform extract of the aliquots drawn from the reaction mixture at 0.5 h intervals. On completion of the reaction (2.5 h) the products were isolated with chloroform and filtered, and the filtrate was washed with water and dried over anhydr. $MgSO_4$. TLC (silica gel G, solvent C_6H_6) of the product mixture showed the presence of two products **12a** and **12b**, which were separated by CC (silica gel), using petroleum ether – benzene (1:1) and benzene and were crystalized from chloroform–methanol.

General procedure for microwave irradiation

The solid mixtures of chalcones, anilines, and Bi(III)nitrate- Al_2O_3 in the same proportions as were used during the reactions carried out in a thermostatically controlled hot air oven were heated in a domestic microwave (2450 MHz) using 60% power (540 W) using the procedure of Mukhopadhyay et al. (27), which permits the control of temperature at 130 °C. The reactions were monitored by TLC as described earlier. The reactions were completed within 18–26 min (Tables 1 and 2). The products were extracted and purified as before and were identified by co-TLC, mp, and mmp as **3a**–**3k**, **3l**, **4a**–**4k**, **4l**, **5**–**11**, **12a**, and **12b**.

1-(2-Aminophenyl)-2,4,6-triphenyl-1,4-dihydropyridine (3a)

Colourless crystals, mp 162 to163 °C. IR (cm^{-1}) υ_{max}: 3430, 3036, 3004, 2945–2669 (m), 1611, 1500, 1476, 1454,

© 2006 NRC Canada

1434, 1399, 1371, 1294, 1253, 1178, 1033, 965, 744. ^{1}H NMR (200 MHz, $CDCl_3$) δ: 5.32 (t, *J* = 3.9 Hz, 1H), 7.02 (d, *J* = 3.9 Hz, 2H), 7.17 (d, *J* = 8.4 Hz, 4H), 7.25 (s br, 2H, NH_2), 7.49 (dd, *J* = 8.4, 3.2 Hz, 6H), 7.70 (m, 7H), 8.10 (d, *J* = 8.5 Hz, 2H). ^{13}C NMR ($CDCl_3$) δ: 54.8, 114.5, 121.6, 122.3, 127.9, 128.4, 129.7, 131.5, 139.4, 151.1. HR EI-MS *m/z*: 400.1979 (M^+, 5) (calcd. for $C_{29}H_{24}N_2$: 400.1939), 323 ([$M^+ - C_6H_5$], 36), 246 (100), 154 (33), 101 (47), 88 (65). Anal. calcd. for $C_{29}H_{24}N_2$: C 86.95, H 6.05, N 6.99; found: C 87.38, H 5.98, N 6.72.

1-(2-Aminophenyl)-4(4-methoxyphenyl)-2,6-diphenyl-1,4-dihydropyridine (3b)

Colourless crystals, mp 183 °C. IR (cm^{-1}) υ_{max}: 3435, 3036, 3004, 2940–2673 (m), 1610, 1500, 1470, 1455, 1435, 1399, 1371, 1294, 1253, 1030, 967. ^{1}H NMR (DMSO-d_6) δ: 3.84 (s, 3H), 5.35 (t, *J* = 3.8 Hz, 1H), 7.15 (d, *J* = 3.8 Hz, 2H), 7.17 (d, *J* = 8.4 Hz, 2H), 7.33 (ddd, *J* = 6.9, 8.4, 3.9 Hz, 6H), 7.35 (s, br, 2H), 7.69 (d, *J* = 8.4 Hz, 6H), 7.80 (d, *J* = 6.9 Hz, 4H). ^{13}C NMR (DMSO-d_6) δ_C: 54.8, 55.3, 114.6, 116.5, 127.6, 127.7, 128.4, 128.6, 131.2, 143.0, 149.1, 158.6. HR EI-MS *m/z*: 430.2015 (20) (calcd. for $C_{30}H_{26}N_2O$: 430.2045), 416 (35), 353 (40), 246 (100), 154 (45), 101 (53), 88 (71). Anal. calcd. for $C_{30}H_{26}N_2O$: C 83.68, H 6.09, N 6.50; found: C 83.72, H 6.12, N 6.20.

1-(2-Aminophenyl)-4(4-fluoro)phenyl-2,6-diphenyl-1, 4-dihydropyridine (3c)

Colourless crystals, mp 102 °C. IR (cm^{-1}) υ_{max}: 3436, 3035, 3004, 2943–2675 (m), 1618, 1500, 1470, 1455, 1430, 1398, 1371, 1294, 1253, 1030, 967. ^{1}H NMR (DMSO-d_6) δ: 5.75 (d, *J* = 3.9 Hz, 1H), 7.09 (t, *J* = 3.9 Hz, 1H), 7.16 (d, *J* = 8.7 Hz, 3H), 7.18 (m, 10H), 7.35 (sbr, 2H), 7.49 (dd, J = 8.7, 3.9 Hz, 4H), 8.10 (d, *J* = 3.9 Hz, 2H). ^{13}C NMR (DMSO-d_6) δ_C: 57.2, 114.3, 115.8, 121.7, 122.6, 124.6, 128.9, 129.8, 130.1, 134.9, 143.7, 151.2, 160.5. HR EI-MS *m/z*: 418.1846 (18) (calcd. for $C_{29}H_{23}FN_2$: 418.1851), 323 ([$M^+ - C_6H_4F$], 46), 246 ([$M^+ - C_6H_4F - C_6H_5$], 100), 92 (70), 77 (76). Anal. calcd for $C_{29}H_{23}FN_2$: C 83.22, H 5.55, N 6.69; found: C 83.35, H 5.42, N 6.20.

1-(2-Aminophenyl)-4(4-chloro)phenyl-2,6-diphenyl-1,4-dihydropyridine (3d)

Colourless crystals, mp 189 °C. IR (cm^{-1}) υ_{max}: 3437, 3010, 2945–2669 (m), 1620, 1480, 1456, 1434, 1399, 1370, 1295, 1253, 1178, 1033, 965, 745. ^{1}H NMR (DMSO-d_6) δ: 5.37 (d, *J* = 3.9 Hz, 1H), 7.09 (t, *J* = 3.9 Hz, 1H), 7.26 (d, *J* = 8.2 Hz, 4H), 7.46 (m, 13H), 7.37 (s br, 2H), 8.0 (d, *J* = 3.9 Hz, 2H). ^{13}C NMR (DMSO-d_6) δ_C: 55.8, 111.2, 118.7, 121.5, 122.4, 126.3, 128.8, 129.7, 130.0, 134.9, 143.7, 151.1. HR EI-MS *m/z*: 436.1535, 434.1540 (M^+, 6) (calcd. for $C_{29}H_{23}ClN_2$: 436.1520, 334.1520), 222 ([$M^+ - C_6H_5Cl$], 30), 246 ([$M^+ - C_6H_5Cl - C_6H_5$], 100), 92 (73), 77 (67). Anal. calcd. for $C_{29}H_{23}ClN_2$: C 79.79, H 5.34, N 6.45; found: C 80.20, H 4.95, N 5.98.

1-(2-Aminophenyl)-4-(3,4-dichlorophenyl)-2,6-diphenyl-1,4-dihydropyridine (3e)

Colourless crystals, mp 235 °C. IR (cm^{-1}) υ_{max}: 3435, 3050, 2945–2669 (m), 1605, 1550, 1497, 1387, 1350, 1148, 1090, 1018, 970, 730. ^{1}H NMR (DMSO-d_6) δ: 5.38 (t, *J* = 3.9 Hz, 1H), 7.17 (d, *J* = 3.9 Hz, 1H), 7.38 (m, 8H), 7.50 (ddd, *J* = 8.3, 7.9, 2.9 Hz, 2H), 7.55 (s br, 2H), 7.57 (ddd, *J* = 8.3, 7.9, 2.9 Hz, 3H), 7.64 (ddd, *J* = 8.3, 7.9, 2.2 Hz, 2H), 7.89 (d, *J* = 8.3Hz, 1H), 8.02 (dd, *J* = 8.2, 2.2 Hz, 2H). ^{13}C NMR(DMSO-d_6) δ_C: 54.3, 108.9, 111.7, 121.9, 123.0, 123.8, 126.4, 125.3, 128.0, 128.9, 129.8, 130.7, 133.5, 135.6, 143.9,151.1. HR EI-MS *m/z*: 470, 468.1109 (M^+, 13) (calc. for $C_{29}H_{22}Cl_2N_2$, 468.1120), 323 ([$M^+ - C_6H_3Cl_2$], 30), 246 ([$M^+ - C_6H_3Cl_2 - C_6H_5$], 100), 169 (56), 155 (41), 77 (70). Anal. calcd. for $C_{29}H_{22}Cl_2N_2$: C 74.34, H 4.74, N 5.98; found: C 75.01, H 4.68, N 6.30.

1-(2-Aminophenyl)-2,6-di(4-chloro)phenyl-4-phenyl-1,4-dihydropyridine (3f)

Colourless crystals, mp 202 °C. IR (cm^{-1}) υ_{max}: 3456, 3030, 2669–2945 (m), 1610, 1475, 1496, 1387, 1350, 1140, 1090, 1072, 926. ^{1}H NMR (DMSO-d_6) δ: 5.35 (t, *J* = 3.9 Hz, 1H), 7.06 (d, *J* = 3.9 Hz, 2H), 7.26 (d, *J* = 8.2 Hz, 4H), 7.45 (m, 5H), 7.55 (s br, 2H), 7.63 (dd, *J* = 8.2, 2.2 Hz, 2H), 7.64 (dd, *J* = 8.2, 2.2 Hz, 4H), 8.02 (dd, *J* = 8.2, 1.6 Hz, 2H). ^{13}C NMR (DMSO-d_6) δ: 54.1, 111.3, 118.7, 121.6, 122.5, 126.4, 128.9, 129.8, 130.1, 135.0, 143.7, 151.2. HR EI-MS *m/z* (rel. int): 468.1110 (10) (calcd. for $C_{29}H_{22}Cl_2N_2$: 468.1101), 391 [M^+- Ph], 280 (100), 188 (57), 169 (46), 77 (62). Anal. calcd. for CHN: not found.

1-(2-Aminophenyl)-4-(4-bromo)phenyl-2,6-diphenyl-1,4-dihydropyridine (3g)

Colourless crystals, mp 178 °C. IR (cm^{-1}) υ_{max}: 3435, 3050, 1605, 1545, 1490, 1387, 1350, 1150, 1095, 920, 760. ^{1}H NMR ($CDCl_3$) δ: 5.37 (t, *J* = 3.9 Hz, 6H), 7.16 (d, *J* = 3.9 Hz, 2H), 7.26 (m, 4H), 7.36 (s br, 2H), 7.39 (dd, *J* = 8.7, 3.9 Hz, 2H), 7.51 (s, br, 2H), 7.58 (ddd, *J* = 8.3, 2.4, 8.3 Hz, 4H), 7.72 (d, *J* = 8.7 Hz, 2H), 8.28 (ddd, *J* = 8.3, 2.4, 8.3 Hz, 2H). ^{13}C NMR (DMSO-d_6) δ_C: 55.9, 111.6, 118.9, 122.3, 125.6, 128.3, 129.7, 130.1, 131.9, 143.9, 151.1, 160.3. HR EI-MS *m/z*: 480.1018(13), 478.1030 (M^+, 10) (calcd. for $C_{29}H_{23}BrN_2$: 478.1025), 323 ([$M^+ - C_6H_5Br$], 40), 246 (100), 169 (58), 144 (67), 77 (70). Anal. calcd. for $C_{29}H_{23}BrN_2$: C 72.79, H 4.8, N 5.8; found: C 73.01, H 5.23, N 4.26.

1-(2-Aminophenyl)-4(3,4-dioxymethylene)phenyl-2,6-diphenyl-1,4-dihydropyridine (3h)

Colourless crystals, mp 173 °C. IR (cm^{-1}) υ_{max}: 3439, 3165, 3047, 2964–2531 (m), 1590, 1494, 1385, 1350, 1260, 1140, 1096, 920 760. ^{1}H NMR ($CDCl_3$) δ: 5.45 (t, *J* = 3.9 Hz, 1H), 6.02 (s, 2H), 7.10 (d, *J* = 3.9 Hz, 1H), 7.23 (s br, 2H, NH_2), 7.26 (dd, *J* = 8.5, 3.9 Hz, 4H), 7.35 (ddd, *J* = 8.1, 2.2, 8.3 Hz, 6H), 7.50 (ddd, *J* = 8.3, 2.4, 8.3 Hz, 5H), 7.53 (d, *J* = 8.3 Hz, 2H), 8.25 (d, *J* = 8.3 Hz, 1H). ^{13}C NMR (DMSO-d_6) δ_C: 55.3, 101.2, 114.5, 118.6, 122.8, 126.7, 128.3, 129.5, 135.5, 135.8, 147.3, 147.9, 149.3, 153.3. HR EI-MS *m/z* (rel.int): 444.1830 (M^+, 7) (calcd. for $C_{30}H_{24}N_2O_2$: 444.1839), 414 ([M^+ – HCHO], 20), 323 (15), 293 (21), 246 (100), 169 (52), 144 (56), 77 (70). Anal. calcd. C 81.04, H 5.44, N 6.30; found: C 82.10, H 5.70, N 5.85.

1-(2-Aminophenyl)-4(4-hydroxy)phenyl-2,6-diphenyl-1,4-dihydropyridine (3i)

Colourless crystals, mp 235 °C. IR (cm^{-1}) υ_{max}: 3560, 3430, 3265, 3050, 2964–2531 (m), 1605, 1550, 1485, 1380, 1345, 1280, 1140, 1096, 920, 750. ^{1}H NMR (DMSO-d_6) δ:

© 2006 NRC Canada

2.40 (s br, 1H), 5.10 (t, *J* = 3.8 Hz, 1H), 6.77 (dd, *J* = 8.3, 3.8 Hz, 4H), 7.26 (s br, 2H), 7.35 (ddd, *J* = 8.3, 5.6, 3.9 Hz, 6H), 7.50 (ddd, *J* = 8.6, 5.6 Hz, 6H), 7.56 (ddd, *J* = 8.3, 5.6, 8.5 Hz, 2H), 8.25 (d, *J* = 8.3 Hz, 2H). ^{13}C NMR (DMSO-d_6) δ_C: 54.8, 116.1, 122.6, 127.1, 127.2, 128.6, 128.8, 135.1, 135.7, 139.9, 151.8, 160.5. HR EI-MS *m/z* (rel. int.): 416.1896 (13) (calc. for $C_{29}H_{24}N_2O$: 416.1889), 323 (30), 246 (100), 169 (55), 144 (43), 77 (60). Anal. calcd. for CHN: not found.

1-(2-Aminophenyl)-4(4-iodo)phenyl-2,6-diphenyl-1, 4-dihydropyridine (3j)

Colourless crystals, mp 182 °C. IR (cm^{-1}) υ_{max}: 3453, 3052, 1605, 1549, 1490, 1382, 1357, 1148, 1090, 1018, 927, 730. ^{1}H NMR (DMSO-d_6) δ: 5.09 (t, *J* = 3.7 Hz, 1H), 6.80 (dd, *J* = 8.5, 3.7Hz, 4H), 7.20 (s br, 2H), 7.36 (ddd, *J* = 8.5, 2.4, 8.3 Hz, 4H), 7.52 (ddd, *J* = 8.6, 2.4, 8.3 Hz, 2H), 7.69 (dd, *J* = 8.6, 2.4 Hz, 6H), 7.86 (dd, *J* = 8.3, 8.5 Hz, 2H), 8.17 (d, *J* = 8.3 Hz, 2H). ^{13}C NMR (DMSO-d_6) δ: 53.9, 111.10, 116.3, 116.5, 122.8, 127.2, 128.3, 131.1, 135.5, 139.3, 143.2, 152.1. HR EI-MS *m/z* (rel. int.): 526.1870 (5) (calcd. for $C_{29}H_{23}IN_2$: 526.1861), 323 (34), 246 (100), 165 (45), 144 (36), 77 (68). Anal. calcd. for CHN: not found.

1-(2-Aminophenyl)-2,6-di(4-bromo)phenyl-4-phenyl-1,4-dihydropyridine (3k)

Colourless crystals, mp 208 °C. IR (cm^{-1}) υ_{max}: 3443, 3050, 2967–2953 (m), 1605, 1545, 1487, 1360, 1350,1140, 1090, 1075, 930, 725. ^{1}H NMR (DMSO-d_6) δ: 5.74 (t, *J* = 3.8 Hz, 1H), 7.00 (d, *J* = 3.8 Hz, 2H), 7.26 (s br, 2H), 7.40 (5H), 7.52 (ddd, *J* = 8.8, 2.5, 8.3 Hz, 4H), 7.64 (dd, *J* = 8.5, 2.4 Hz, 2H), 7.80 (s, 2H), 8.06 (dd, *J* = 8.7, 1.6 Hz, 2H), 8.25 (d, *J* = 3.9 Hz, 2H). ^{13}C NMR (DMSO-d_6) δ_C: 55.4, 114.1, 116.3, 116.5, 126.8, 127.2, 128.3, 131.0, 139.1, 143.2, 149.7, 151.3, 160.5. HR EI-MS *m/z* (rel. int.): 556.1020 (5), 558.0123 (M$^+$) (calcd. for $C_{30}H_{22}N_2Br_2$: 556.0109, 558.0109) 481 (5), 479 (10) 222 (9), 323 (100), 218 (40), 126 (60), 77 (71). Anal. calcd. for $C_{30}H_{22}N_2Br_2$: C 62.36, H 3.9, N 5.01; found: C 63.06, H 4.32, N 4.91.

1-(2-Aminophenyl)-2(4-chloro)phenyl-4(4-methoxy)phenyl-6-phenyl-1,4-dihydropyridine (3l)

Colourless compound, mp 184 °C. IR (cm^{-1}) υ_{max}: 3430, 2966–2576 (m), 1610, 1605, 1540, 1490, 1385, 1350, 1140, 1080, 940. ^{1}H NMR (DMSO-d_6) δ: 3.82 (s, 3H), 5.32 (t, *J* = 3.9 Hz, 1H), 7.06 (dd, *J* = 8.70, 3.9 Hz, 4H), 7.23 (s br, 2H), 7.28 (d, *J* = 8.7 Hz, 4H), 7.41 (d, *J* = 6.5 Hz, 2H), 7.55 (ddd, *J* = 8.7, 3.7, 2.1 Hz, 2H), 7.75 (dd, *J* = 8.7, 2.4 Hz, 2H), 7.82 (s, 1H), 8.08 (dd, *J* = 8.7, 1.6 Hz, 2H), 8.25 (d, *J* = 3.9 Hz, 2H). ^{13}C NMR (DMSO-d_6) δ_C: 55.4, 58.5, 114.4, 116.8, 122.3, 125.6, 128.5, 128.9, 130.1, 139.9, 147.6, 157.8, 160.4. HR EI-MS *m/z* (rel. int.): 466.1640, 464.1634 (M$^+$, 15) (calcd. for $C_{30}H_{25}ClN_2O$: 466.1626, 464.1626) 357 (25), 246 (100), 169 (42), 144 (56), 77 (68). Anal. calcd. for $C_{30}H_{25}ClN_2O$: C 77.58, H 5.38, N 6.03; found: C 78.2, H 4.91, N 5.80.

1-(2-Hydoxyphenyl)-4(methoxyphenyl)-2,6-diphenyl-1,4-dihydropyridine (5)

Colourless needles, mp 276 °C. IR (cm^{-1}) υ_{max}: 3572, 3056, 3002, 1605, 1540, 1490, 1385, 1350, 1140, 1080, 940, 790. ^{1}H NMR (DMSO-d_6) δ: 3.80 (s, 3H), 5.57 (t, *J* = 3.8 Hz, 1H), 6.67 (d, *J* = 7.9 Hz, 2H), 6.77 (d, *J* = 7.9 Hz, 2H), 6.80 (dd, *J*= 7.9 Hz, 2.9 Hz, 3H), 7.0 (d, *J* = 3.9 Hz, 2H), 7.20–7.29 (m, 6H), 7.30 (dd, *J* = 8.2, 2.9 Hz, 2H), 7.32 (dd, *J* = 8.2, 2.8 Hz, 2H), 8.20 (dd, *J* = 8.2, 2.8 Hz, 1H), 10.90 (s br, 1H). ^{13}C NMR (DMSO-d_6) δ_C: 55.6, 57.9, 113.7, 115.9, 122.5, 128.6, 130.1, 138.2, 138.7, 143.3, 143.7, 151.4. HR EI-MS *m/z* (rel. int.): 431.1892 (M$^+$, 7) (calcd. for $C_{30}H_{25}NO_2$: 431.1885), 416 (13), 323 (30), 246 (100), 180 (66), 164 (68), 90 (75). Anal. calcd. for CHN: not found.

1-(3-Hydroxyphenyl)-4(methoxyphenyl)-2,6-diphenyl-1,4-dihydropyridine (6)

Colourless needles, mp 230 °C. IR (cm^{-1}) υ_{max}: 3570, 3056, 3002, 1610, 1540, 1480, 1376, 1350, 1140, 1085, 945, 790. ^{1}H NMR (DMSO-d_6) δ: 3.81 (s, 3H), 5.37 (t, *J* = 3.8Hz, 1H), 6.78 (s br, 1H), 6.80 (dd, *J* = 8.0, 3.8 Hz, 3H), 6.92 (dd, *J* = 8.0, 2.8Hz, 2H), 7.12 (m, 8H), 7.30 (d, *J* = 3.8 Hz, 2H), 7.32 (dd, *J* = 8.2, 2.8 Hz, 3H), 8.00 (d, *J* = 8.2 Hz, 1H), 10.92 (s, 1H). ^{13}C NMR (DMSO-d_6) δ_C: 55.4, 58.1, 104.3, 110.2, 122.6, 131.2, 137.5, 138.2, 143.7, 151.4. HR EI-MS *m/z* (rel. int.): 431.1876 (M$^+$, 12) (calcd. for $C_{30}H_{25}NO_2$: 431.1885), 416 (24), 334 (36), 247 (100), 180 (57), 164 (68), 90 (75). Anal. calcd. for CHN: not found.

1-(4-Hydroxyphenyl)-4(methoxyphenyl)-2,6-diphenyl-1,4-dihydropyridine (7)

Colourless needles, mp 230 °C. IR (cm^{-1}) υ_{max}: 3554, 3050, 3005, 1610, 1540,1480, 1370, 1140, 1085, 940, 790. ^{1}H NMR (DMSO-d_6) δ: 3.85 (s, 3H), 5.56 (t, *J* = 3.9 Hz, 1H), 6.86 (d, *J* = 8.2 Hz, 4H), 7.00 (dd, *J* = 8.2, 3.9 Hz, 3H), 7.25 (m, 7H), 7.30 (dd, *J* = 3.9, 8.2 Hz, 2H), 7.32 (dd, *J* = 8.2, 2.9 Hz, 3H), 8.20 (dd, *J* = 8.5, 3.0 Hz, 1H), 10.76 (s, 1H). ^{13}C NMR (DMSO-d_6) δ_C: 55.6, 58.5, 104.6, 111.2, 116.5, 121.8, 122.6, 136.2, 137.1, 138.2, 143.1, 151.4, 156.5. HR EI-MS *m/z* (rel. int.): 441.1892 (M$^+$, 16) (calcd. for $C_{30}H_{25}NO_2$: 441.1885), 427 (13), 334 (26), 257 (100), 180 (45), 164 (52), 90 (61), 77 (63). Anal. calcd. for CHN: not done).

1-(2-Bromophenyl)-4(4-methoxy)phenyl-2,6-diphenyl-1,4-dihydropyridine (8)

Colourless crystals, mp 162 °C. IR (cm^{-1}) υ_{max}: 3005, 2964–2538 (m), 1605, 1543, 1480, 1370, 1150, 1110, 1085, 940, 790. ^{1}H NMR (DMSO-d_6) δ_C: 3.86 (s, 3H), 5.37 (t, *J* = 3.9Hz, 1H), 7.20 (d, *J* = 3.9 Hz, 2H), 7.27 (m, 8H), 7.37 (dd, *J* = 8.2, 2.9 Hz, 5H), 7.57 (dd, *J* = 8.2, 2.9 Hz, 4H), 7.97 (d, *J* = 8.2 Hz, 1H). ^{13}C NMR (DMSO-d_6) δ: 55.3, 58.2, 113.1, 116.2, 123.2, 123.5, 131.4, 136.9, 137.3, 138.1, 143.5, 151.8. HR EI-MS *m/z* (rel. int.): 495, (3), 493.1030 (M$^+$, 11) (calcd. for $C_{30}H_{24}BrNO$: 495.1021, 493.1021), 388 (9), 386 (27), 311 (41), 309 (100), 234 (27), 232 (20), 146 (15), 144 (56), 77 (56). Anal. calcd. for $C_{30}H_{24}BrNO$: C 73.02, H 4.86, N 2.8; found: C 74.1, H 3.9, N 3.01.

1-(3-Bromophenyl)-4(4-methoxy)phenyl-2,6-diphenyl-1, 4-dihydropyridine (9)

Colourless crystals, mp 127 °C. IR (cm^{-1}) υ_{max}: 3000, 2950–2623 (m), 1605, 1543, 1480, 1370, 1150, 1110, 1085, 940, 790. ^{1}H NMR (DMSO-d_6) δ: 3.81 (s, 3H), 5.35 (t, *J* = 3.9 Hz, 1H), 7.0 (d, *J* = 8.2 Hz, 2H), 7.16 (dd, *J* = 8.2, 3.9 Hz, 4H), 7.26 (d, *J* = 8.2 Hz, 2H), 7.29 (m, 6H), 7.37 (d, *J* = 8.2 Hz, 3H), 7.57 (d, *J* = 8.2 Hz, 2H), 8.00 (s, 1H). ^{13}C

© 2006 NRC Canada

NMR (DMSO-d_6) δ_C: 58.1, 114.1, 116.3, 121.6, 123.2, 123.5, 132.2, 136.9, 137.3, 138.1, 143.5, 151.9. HR EI-MS *m/z* (rel. int.): 495 (7), 493.1010 (M^+, 21). (calcd. for $C_{30}H_{24}BrNO$: 493.1021), 388 (16), 386 (27), 311(20), 309 (100), 234 (48), 232 (20), 146 (15), 144 (36), 77 (66). Anal. calcd. for CHN: not found.

1-(4-Bromophenyl-4(4-methoxy)phenyl-2,6-diphenyl-1, 4-dihydropyridine (10)

Colourless crystals, mp 148 °C. IR (cm^{-1}) υ_{max}: 3010, 2952–2623 (m), 1605, 1543, 1480, 1370, 1150, 1110, 1085, 940, 790. ^1H NMR (DMSO-d_6) δ: 3.86 (s, 3H), 5.36 (t, *J* = 3.9 Hz, 1H), 7.0 (dd, *J* = 8.2, 3.9 Hz, 2H), 7.20 (m, 5H), 7.31 (d, *J* = 8.2 Hz, 2H), 7.35 (d, *J* = 8.2 Hz, 4H), 7.45 (dd, *J* = 8.2, 2.4 Hz, 6H), 8.02 (d, *J* = 8.4 Hz, 1H). ^{13}C NMR (DMSO-d_6) δ: 58.7, 114.3, 116.5, 121.1, 123.7, 128.4, 130.9, 138.1, 143.2, 143.5, 151.3. HR EI-MS *m/z* (rel. int.): 495(10), 493.103 (M^+, 31) (calcd. for $C_{30}H_{24}BrNO$: 493.1021), 388 (27), 386 (36), 311 (10), 309 (100), 234 (29), 232 (15), 146 (15), 144 (67), 77 (63). Anal. calcd. for CHN: not found.

1-(3-Nitrophenyl-4(4-methoxy)phenyl-2,6-diphenyl-1,4-dihydropyridine (11)

Pale yellow crystals, mp 121 °C. IR (cm^{-1}) υ_{max}: 3020, 2695–2559 (m), 2215, 1605, 1600, 1485, 1415, 1375, 1360, 1150, 1090, 940, 790, 665. ^1H NMR ($CDCl_3$) δ: 3.57 (s, 3H), 5.10 (t, *J* = 3.9 Hz, 1H), 7.10 (dd, *J* = 8.1,3.9 Hz, 4H), 7.20 (d, *J* = 8.2 Hz, 2H), 7.26 (m, 9H), 7.45 (d, *J* = 8.0 Hz, 2H), 7.77 (dd, *J* = 8.1, 2.3 Hz, 2H), 8.09 (d, *J* = 8.2 Hz, 1H). ^{13}C NMR ($CDCl_3$) δ_C: 54.8, 55.6, 105.3, 118.6, 122.5, 124.2, 130.1, 131.2, 137.4, 139.1, 146.7, 153.2, 156.4. HR EI-MS *m/z* (rel. int.): 460.1792 (M^+, 10) (calcd. for $C_{30}H_{24}N_2O_3$: 460.1787), 393 (25), 316 (100), 239 (40), 194 (33), 77 (56). Anal calcd. for $C_{30}H_{24}N_2O_3$: C 78.26, H 5.21, N 6.08; found: C 78.31, H 4.85, N 5.91.

Hydroxymethyl-(4-methoxyphenyl-3-(4-methoxy)phenyl-1,5-diphenyl-pentan-4-en-5-ol-1-one, (12a)

Colourless crystals, mp 132 °C. IR (cm^{-1}) υ_{max}: 3590, 3423, 3010, 2810, 1700, 1640, 1580, 1410, 1245, 1090, 920, 750. ^1H NMR (200 MHz, $CDCl_3$) δ: 2.70 (d, *J* = 3.3 Hz, 1H), 2.80 (s br, 1H, OH), 3.05 (dd, *J* = 3.0, 3.6 Hz, 1H), 3.86 (s, 6H), 5.01 (dd, *J* = 3.0 Hz, 1H), 6.9 (s, 1H), 7.10–7.20 (m, 10H), 7.23 (dd, *J* = 3.2, 8.9 Hz, 4H), 7.65 (dd, *J* = 3.2, 8.6 Hz, 4H), 12.9 (s br, 1H). ^{13}C NMR ($CDCl_3$) δ_C: 55.6, 64.6, 77.2, 83.2, 114.4, 116.5, 124.9, 127.0, 128.9, 131.2, 138.5, 139.6, 149.5, 159.4, 197.3. HR EI-MS *m/z* (rel. int.): 494.2071 (M^+, 30) (calcd. for $C_{32}H_{30}O_5$: 494.2085), 493 (29), 476 (42), 466 (31), 371 (45), 239 (66), 224 (27), 134 (76), 133 (58), 105 (100), 92 (91), 77 (70), 64 (87).

1-(4-Chloro)phenyl-3-(4-methoxy)phenyl-5-phenyl-pentan-4-en-5-ol-1-one, (12b)

Colourless compound, mp 135 °C. IR (cm^{-1}) υ_{max}: 3020, 2816, 1715, 1580, 1640, 1420, 1250, 1090, 1075, 925, 780. ^1H NMR (200 MHz, $CDCl_3$) δ: 2.69 (d, *J* = 4.5 Hz, 2H), 3.08 (t, *J* = 4.5 Hz, 1H), 3.86 (s, 3H) 6.9 (s, 1H), 7.20 (m, 5H), 7.23 (dd, *J* = 3.2, 8.6 Hz, 2H), 7.41 (d, 2H, *J* = 6.5 Hz, 2H), 7.55 (d, *J* = 6.5 Hz, 2H), 7.66 (dd, *J* = 3.2, 8.6 Hz, 2H), 12.9 (s, 1H). ^{13}C NMR ($CDCl_3$) δ_C: 25.3, 42.6, 556, 114.4, 116.6, 116.8, 124.9, 127.0, 127.3, 128.6, 128.9, 130.1, 131.3, 138.5, 139.9, 149.5, 159.3, 160.4, 197.3. HR EI-MS *m/z* (rel. int.): 392.1172 (M^+, 28) (calc. for $C_{24}H_{21}O_3Cl$: 392.1165), 391 (25), 378 (48), 24 (26), 139 (68), 134 (56), 119 (62), 108 (38), 105 (100), 93 (76), 65 (80).

Acknowledgements

The authors are highly thankful to Professor S. Chanderasekran and Dr. R. G. Bhatt (IISC, Bangalore) and to Mrs. Poornima Wakhlu (RRL, Jammu) for providing spectral facilities.

References

1. (*a*) F.H. Westheimer. Advan. Enzymol. **24**, 469 (1962); (*b*) H. Sund, K. Diekmam, and K. Wallenfels. Advan. Enzymol. **26**, 115 (1964); (*c*) S.P. Colourick, J. Van Eys, and J.H. Park. Compr. Biochem. **14**, 1 (1966).
2. R.J. Kill and D.A. Widdowson. *In* Biorganic chemistry. Series 4. *Edited by* E.E. Van Tamelen. Academic Press, New York. 1978. pp. 239–75.
3. (*a*) A.A. Qureshi and A.I. Scott. Chem. Commun. (Cambridge), 945 (1968); (*b*) 947 (1968); (*c*) 948 (1968); (*d*) E. Wenkert. Acc. Chem. Res. **1**, 78 (1968).
4. (*a*) E. Wenkert, T.D.J. Halls, G. Kunesch, K. Orito, R.L. Stephens, W.A. Temple, J.S. Yadav. J. Am. Chem. Soc. **101**, 5370 (1979); (*b*) E. Wenkert, J. St. Pyerk, S. Uesato, Y.D. Vankar. J. Am. Chem. Soc. **104**, 2244 (1982); (*c*) D. Wenkert, C.J. Chang, H.P.S. Chawla, D.W. Cocharan, E.W. Hagaman, J.C. King, and O. Kazuhiko. J. Am. Chem. Soc. **98**, 3645 (1976); (*d*) M.J. Wanner, G.J. Kamen, and U.K. Pandit. Heterocycles, **15**, 377 (1981); (*e*) D.D. Weller, G.R. Luellen, and D.L. Weller. J. Org. Chem. **48**, 3061 (1983); (*f*) R. Kumar and R. Chandra. Adv. Heterocycl. Chem. **78**, 269 (2001).
5. (*a*) K. Akiba, Y. Iseki, and M. Wada. Tetrahedron Lett. **23**, 3935 (1982); (*b*) D.L. Comins and N.B. Mantlo. Tetrahedron Lett. **24**, 3683 (1983); (*c*) K. Reuter and W. Neumann. Tetrahedron Lett. **19**, 5235 (1978); (*d*) A. Gilbert and S. Krestonosich. J. Chem. Soc. Perkin Trans. 1, 2531 (1980); (*e*) N. Finch and C. Gemenden. J. Org. Chem. **40**, 569 (1975); (*f*) N. Ono, R. Tamura, and A. Kaji. J. Am. Chem. Soc. **102**, 2851 (1980).
6. (*a*) D.J. Triggle and D. Rampe. Trends Pharmacol. Sci. **10**, 507 (1989); (*b*) D.J. Triggle. Can. J. Physiol. Pharmacol. **68**, 1474 (1990); J. Cardiovasc. Pharmacol. **8**, 11 (1991); Am. J. Hypertens. **4**, 422 (1991); Chirality, **8**, 35 (1996); (*c*) N. Bandur, A. Rutledge, and D.J. Triggle. J. Med. Chem **36**, 3743 (1993); (*d*) S. Tang, A. Yatani, A. Bahinski, Y. Mori, and A. Schwartz. Neuron, **11**, 1013 (1993); (*e*) B.Z. Peterson, T.N. Tanada, and W.A. Catterall. J. Biol. Chem. **271**, 5293 (1996); (*f*) T. Tamazawa, H. Arima, T. Kojima, Y. Isomura, M. Okada, S. Fujita, T. Furuya, T. Takenaka, O. Inagaki, and M. Terai. J. Med. Chem. **29**, 2504 (1986); (*g*) R. Peri, S. Padmanabhan, A. Rutledge, S. Singh, and D.J. Triggle. J. Med. Chem. **43**, 2906 (2000).
7. R. Peri, S. Padmanabhan, A. Rutledge, S. Singh, and D.J. Triggle. J. Med. Chem. **43**, 2906 (2000).
8. E.J. Finkelstein, E.A. Alekseev, and E.J. Kozlov. Zh. Org. Chim. 792 (1980).
9. R.I. Goncharova, T.D. Kuzhir, G. Duburs, and J. Uldrikis. Dokl. Akad. Nauk SSSR, **255**, 1483 (1980).
10. W.J. Malaise and P.C.F. Mathias. Diabetologia, **28**, 153 (1985).

© 2006 NRC Canada

11. A. Majore, T.N. Kopylova, L. Saldava, G. Duburs, Z. Ogle, and J. Uldrikis. Eksper. Med. **14**, 97 (1982).
12. D. Gaskell. Chem. Br. **12**, 27 (1998).
13. R.W. Chapman, G. Danko, and M.I. Siegel. Pharmacology, **29**, 282 (1984).
14. A. Sausins and G. Duburs. Heterocycles, **27**, 269 (1988).
15. (*a*) K.V. Honn, J.M. Onodo, C.A. Diglo, M.M. Carufel, and J.D. Taylor. Clin. Exp. Metastasis, **2**, 61 (1984); (*b*) T. Tsuruo, H. Iida, M. Nojiri, S. Tsukagashi, and Y. Sakurai. Cancer Res. **43**, 2905 (1983).
16. (*a*) U. Eisner and J. Kuthan. Chem. Rev. **72**, 1 (1972); (*b*) J.P. Kutney. Heterocycles, **7**, 593 (1977); (*c*) D.M. Stout and A.I Meyers. Chem. Rev. **82**, 223 (1982); (*d*) A. Sausins and G. Duburs. Heterocycles, **27**, 269 (1988); Heterocycles, **27**, 291 (1988); (*e*) R. Kumar and R. Chandra. Adv. Heterocycl. Chem. **78**, 269 (2001).
17. (*a*) I.L. Karle. Acta Crystallogr. **14,** 497 (1961); (*b*) H. Koyama, J.M.M. Robinson, and F. Laves. Nature (London), **50**, 40 (1961).
18. K.A. Leonard, M.I. Nelen, T.P. Simard, S.R. Davies, S.O. Gollnick, A.R. Oseroff, S.L. Gibson, R. Hilf, L.B. Chen, M.R. Detty. J. Med. Chem. **42**, 3953 (1999).
19. (*a*) A. Cornelis, L. Delaude, A. Germans, and P. Laszlo. Tetrahedron Lett. **29**, 5909 (1988); (*b*) H. Suzuki, T. Ikegami, and Y. Matano. Synthesis, **24**9 1977 (1977).
20. J. March. Advanced organic chemistry. 4th Ed. John Wiley and Sons, New York. 1999. p. 262.
21. (*a*) C.N. Satterfield. Heterogeneous catalysis in practice. McGraw Hill, New York. 1980. Sect. 4.5; (*b*) H. Knozinger and P. Ratnasamy. Catal. Rev. Sci. Eng. **17**, 31 (1978).
22. B.S. Furniss, A.J. Hannaford, and P.W.J. Smith. Vogel's text book of practical organic chemistry. 5th ed. XXXX. 1989. p. 1034.
23. (*a*) T. Chennat and U. Eisner. J. Chem. Soc. Perkin Trans. 1, **75**, 926 (1975); (*b*) G.D. Hartman, W. Halezenko, and B.T. Phillips. J. Org. Chem. **50**, 2427 (1985); (*c*) M. Saunder and E.H. Gould. J. Org. Chem. **27**, 1439 (1962); (*d*) H. Diekmann, G. Englert, and K. Wallenfels. Tetrahedron, **20**, 281 (1964); (*e*) N.C. Cook and J.E. Lyons. J. Am. Chem. Soc. **87**, 3283 (1965); **88,** 3396 (1966); (*f*) E.M. Kosower and T.S. Sorensen. J. Org. Chem. **27**, 3764 (1962).
24. (*a*) B.J.S. Wang and E.R. Thornton. J. Am. Chem. Soc. **90**, 1216 (1968); (*b*) R.E. Lyle and E. White. Tetrahedron Lett. 1871 (1970); J. Org. Chem. **36**, 772 (1971).
25. (*a*) M.S. Balakrishna and B. Kaboudine. Tetrahedron Lett. **42**, 1127 (2001); (*b*) P. Stahlofen and W. Reid. Chem. Ber. **90**, 815 (1957); (*c*) J.A. Herbert and L. Suschitzky. J. Chem. Soc. Perkins Trans. 1, 2657 (1974); (*d*) H.R. Morals and A. Bulbarela. Heterocycles, **24**, 135 (1986); (*e*) D.I. Jung, T.W. Choi, Y.Y. Kim, I.S. Kim, Y.M. Park, Y.g. Lee, D.H. Jug. Synth. Commun. **29**, 1941 (1999); (*f*) M.S. Balakrishna and B. Kaboudin. Tetrahedron Lett. **42**, 1127 (2001); (*g*) B. Kaboudin and B. Navace. Heterocycles, **55**, 1443 (2001); (*h*) J.S. Yadav, B.V.S. Reddy, P.S. Kumar, K. Nagarah, N. Ungauah, and S.P. Sriprasad. Synthesis, **6**, 901 (2004).
26. (*a*) J.B. Peri. J. Phys. Chem. **69**, 220 (1965); **69**, 231 (1965); (*b*) H. Knozinger and P. Ratnasamy. Catal. Rev. Sci. Eng. **17**, 31 (1978); (*c*) A.A. Tsgyanenko and P.P. Mardilovich. J. Chem. Soc. Faraday Trans. **92**, 4843 (1996).
27. C. Mukhopadhyay, F.F. Becker, and B.K. Banik. J. Chem. Res. Synop. 28 (2001), and refs. 10 and 11 therein and footnote 16.
28. G.G. Briand and N. Burford. Chem. Rev. **99**, 2601 (1999).

© 2006 NRC Canada

Isomerization of 4-amino-6,7-diphenylbicyclo[2.2.2]octan-2-ones

Werner Seebacher, Robert Saf, Reto Brun, Marcel Kaiser, and Robert Weis

Abstract: Under strongly basic conditions (6*SR*,7*SR*)-4-amino-6,7-diphenylbicyclo[2.2.2]octan-2-ones isomerized regioselectively in position 6 giving their (6*RS*,7*SR*) analogues. The structure of the new products was established with the aid of NMR experiments.

Key words: aminobicyclo[2.2.2]octanones, isomerization, structure elucidation.

Résumé : Faisant appel à des bases fortes, les (6*SR*,7*SR*)-4-amino-6,7-diphénylbicyclo[2.2.2]octan-2-ones peuvent être isomérisées d'une façon régiosélective en position 6 pour conduire à la formation de leurs analogues (6*RS*,7*SR*). Les structures des nouveaux produits ont été déterminées à l'aide de la résonance magnétique nucléaire.

Mots clés : animobicyclo[2.2.2]octanones, isomérisation, élucidation de structures.

[Traduit par la Rédaction]

Introduction

Previously, we reported the formation of 4-aminobicyclo-[2.2.2]octan-2-ones **1a**–**1d** from the reaction of ammonium thiocyanates and benzylidene acetone (1, 2). Those compounds were used as starting materials for derivatives with antiplasmodial and antitrypanosomal activity (3–5). So far, structural modifications have been restricted to different substitutions of the aromatic rings, of the amino nitrogen, and in ring positions 1 and 2. To synthesize new derivatives with a substituent in ring position 3 of compounds **1a**–**1d**, we subjected the above-mentioned ketones to strong alkaline conditions for preliminary deprotonation experiments (Fig. 1). During these investigations, we observed transformations to new products. The yields of these reactions were improved by modification of the reaction conditions and structural evidence of the new compounds was achieved by use of NMR experiments.

Results and discussion

For deprotonation, we treated the 4-aminobicyclo-[2.2.2]octan-2-one **1a** with sodium *tert*-butylate in *tert*-butanol at 145 °C and observed the formation of a new compound. After 3 h, ca. 35% of **1a** was transformed into the new product. The rest of the mixture contained unchanged **1a**. No formation of side products was observed in the ^{1}H NMR spectra of the mixture. Longer reaction periods (overnight) or higher reaction temperature (200 °C for 4 h in an autoclave) did not increase the yield of the new product. Higher yields were obtained when the conversion was done without solvent at 200 °C. The reaction mixture contained up to 80% of the isomerized product, leaving 20% unchanged starting material. Still, no side products were detectable. Compounds **1b**–**1d** were converted in the same way. The new products were separated from **1** and purified by repeated recrystallization of their hydrochlorides. From NMR experiments it was evident that a symmetric molecule was formed. In ^{1}H NMR spectra the signals for the protons in positions 5 and 8 appeared as two, instead of four, separated signals as in compounds **1**. Therefore, we assumed that one of the symmetric ketones **2** or **3** had been formed, which is only possible by a change of the configuration in position 6 or 7. The protons 5-H′ and 8-H′ resonate at a higher field because of the shielding of the aromatic rings. Those protons show NOEs to aromatic protons as well as to the protons in position 3, ruling out structure **3** and furnishing the evidence of structure **2** (Fig. 1).

Muir and Stothers (6) proposed the following mechanism for homoenolization reactions of bicyclic compounds without enolizable protons in the α-position at 185 °C using *t*-BuO$^-$/*t*-BuOH. Proton abstraction from the bicyclo-[2.2.2]octan-2-one (**4**) was reported to give the tricyclic β-enolate (**5**) as an intermediate. When the bond between positions 2 and 6 is cleaved (**a**), compound **4** was re-formed, whereas splitting of the the bond between positions 1 and 2 (**b**) led to the bicyclo[3.2.1]octan-6-one (**6**) (Scheme 1).

Nickon et al. (7) proved that homoenolate ions can be generated in ketones with enolic protons and also that chiral centers β to a carbonyl can be epimerized via such ions. Therefore, deprotonation in position 6 of compounds **1** is expected to give β-enolates **7** as intermediates, which should undergo conversion to mixtures of **1** and **8**. However, the bicyclo[2.2.2]octane ring system was re-formed by selective addition of a proton in position 6, giving mixtures of bicyclo[2.2.2]octanes **1** and **2** that have reverse configurations in position 6 (Scheme 2). There are two possible rea-

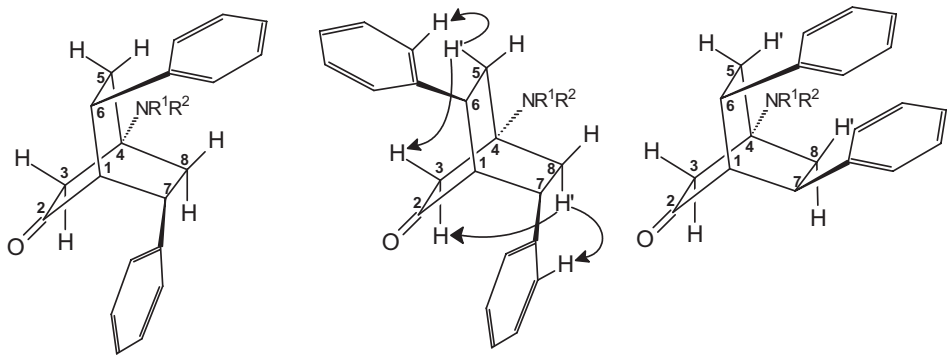
Received 28 March 2006. Accepted 6 September 2006. Published on the NRC Research Press Web site at http://canjchem.nrc.ca on 17 October 2006.

W. Seebacher,[1] R. Saf, R. Brun, M. Kaiser, and R. Weis. Institute of Pharmaceutical Sciences, Pharmaceutical Chemistry, Karl-Franzens-University, Universitätsplatz 1, A-8010 Graz, Austria.

[1]Corresponding author (e-mail: we.seebacher@uni-graz.at).

 doi:10.1139/V06-135 © 2006 NRC Canada

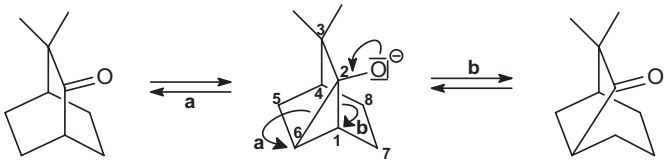
Fig. 1. Structures of compounds **1–3** with NOEs observed in compounds **2**.



1a–1d **2a–2d** **3**

a: $R^1 = R^2 = CH_3$
b: $R^1 + R^2 = -(CH_2)_2-O-(CH_2)_2-$
c: $R^1 + R^2 = -(CH_2)_4-$
d: $R^1 + R^2 = -(CH_2)_5-$

Scheme 1.



4 **5** **6**

sons why isomers **3** did not emerge from **7**. Either the proton in position 7 is not accessible by the used base or compounds **3** cannot be formed because of the sterical interaction of the two phenyl rings. Besides, the expected conversion of **7** to bicyclo[3.2.1]octanes (**8**) by cleavage of the bond between positions 1 and 2 was not observed in ^1H NMR spectra of the reaction mixtures. This could be due to better resonance stabilization of the benzylic anion, which is formed from **7** prior to the formation of compounds **2**.

Using this method, a complete conversion of compounds **1** to their isomers **2** is not possible. This was demonstrated by the reaction of **2d** with potassium *tert*-butylate. In this case, 15% of **1d** were formed showing that the isomerization is a balanced reaction.

Furthermore, we verified the essential role of the oxo group of compound **1a** in the isomerization process. We removed the oxo group of **1a** via a Wolff–Kishner reduction giving **9a** (8). When the latter was treated with *t*-BuOK at 200 °C, no isomerization was observed ruling out a simple proton abstraction in the benzyl position as an initial step of the isomerization. This observation established the formation of β-enolates in the proposed mechanism.

The antiplasmodial properties of the new ketones **2** were determined in an in vitro assay as described (3) and compared with those of ketones **1**. The results are presented in Table 1. A distinct increase of the activity against *Plasmodium falciparum* strain K1 of compounds **2** compared with compounds **1**, due to isomerization in position 6, is worthy of note. Compound **2c** exhibits the highest antiplasmodial activity and at the same time the lowest toxicity of this series.

Conclusion

(6*SR*,7*SR*)-6,7-diphenylbicylo[2.2.2]octan-2-ones **1** isomerized under strong alkaline conditions regioselectively to their (6*RS*,7*SR*) analogues. The mechanism of their formation contains a tricyclic enolate. The new compounds **2** show a distincly higher antiplasmodial activity compared with compounds **1**. Therefore the (6*RS*,7*SR*) analogues of the most active derivatives of compounds **1** will be synthesized.

Experimental

General

Melting points were obtained on a digital melting point apparatus Electrothermal IA 9200 and are uncorrected. IR spectra were obtained using a PerkinElmer 2000 FT IR spectrometer system. UV–vis were obtained using a PerkinElmer Lambda 17 UV spectrometer. NMR spectra were obtained using a Varian Inova 400 (300 K) with 5 mm tubes and TMS resonance as internal standard. ^1H and ^{13}C resonances were assigned using $^1H,^1H$ and $^1H,^{13}C$ correlation spectra. HMBC spectra were optimized for 8 Hz. For NOE measurements, oxygen was carefully removed by bubbling Ar through the solutions. ^1H and ^{13}C resonances are numbered as given in the formulas. Assignments marked with an asterisk are interchangeable. MS was measured using a Varian MAT 711 spectrometer with 70 eV electron impact and a Kratos profile spectrometer with 70 eV electron impact. GC-MS measurements were done with a Hewlett-Packard HP-6890 with 70 eV electron impact. Microanalyses were obtained by a EA 1108 CHNS–O apparatus (Carlo Erba) at the Microanalytical Laboratory at the Institute of Physical Chemistry, Vienna. Materials used for column chromatography (CC): silica gel 60 (Merck, 70–230 mesh), pore diameter 60 Å; thin-layer chromatography (TLC): TLC plates (Merck, silica

© 2006 NRC Canada

Scheme 2.

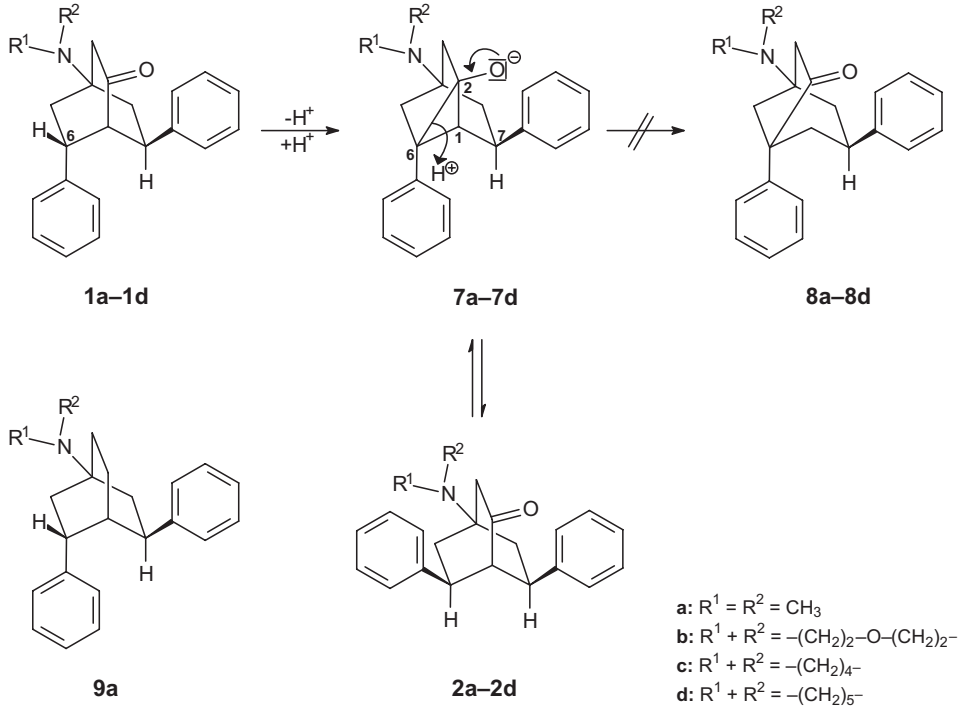


Table 1. Antiprotozoal activities of compounds **1a**–**1d** and **2a**–**2d** expressed as IC_{50} (μmol/L).

Compound	*P. falciparum* K1	*T.b.rhodesiense*	Cytotoxicity L-6
1a	>10.57	9.99	24.57
1b	>11.89	116.3	Nd[a]
1c	1.19	8.03	26.45
1d	3.95	8.12	46.82
2a	1.17	10.82	158.8
2b	11.79	45.45	193.1
2c	0.71	14.01	>235.6
2d	1.90	12.52	114.7
Standard[b]	0.0064	0.0039	11.37

Note: Values represent the average of four determinations (two determinations of two independent experiments).

[a]Nd (Not determined)

[b]Substances used as standard are mentioned in the experimental section.

gel 60 F_{254}, 0.2 mm, 200 mm × 200 mm); the substances were detected in UV light of 254 nm.

Synthesis of (6*SR*,7*SR*)-(±)-4-amino-6,7-diphenylbicyclo-[2.2.2]octan-2-ones 1a–1d

The synthesis of compounds **1a**–**1d** from acyclic starting material is described previously (1, 2).

Synthesis of (6*RS*,7*SR*)-(±)-4-amino-6,7-diphenylbicyclo-[2.2.2]octan-2-ones 2a–2d

Method A: Ketones **1** were dissolved in dry *tert*-butanol and potassium *tert*-butylate was added. The mixture was refluxed overnight at 145 °C and then cooled to room temperature. Brine was added and the resulting solution was extracted 4 times with ether. The combined organic layers were washed with water, dried over sodium sulfate, filtered, and the solvent evaporated. The residue contained 35% of the isomerization product and 65% of the starting product (^{1}H NMR) and was dissolved in the minimum amount of EtOH, treated with 10 mL of concd HCl, and evaporated. This process was repeated once more. Small amounts of the hydrochloride of the isomerization product were isolated by repeated crystallization from ethyl acetate – EtOH.

Method B: Ketones **1a**–**1d** were mixed with potassium *tert*-butylate and heated to 200 °C for 3 h. After cooling to room temperature, the dark red solid residue was dissolved in the minimum amount of EtOH and brine was added. The mixture was extracted 4 times with ether, the organic phases were combined, washed with water, and dried over sodium sulfate. After filtration from the solid, the solvent was evaporated in vacuo. The residue contained 80% of the isomerization product and 20% of the starting material. For further purification, the residue was dissolved in EtOH and 10 mL of concd HCl were added and the solvents evapo-

© 2006 NRC Canada

rated. The treatment of the residue with hydrochloric acid was repeated and the solvent evaporated. The residue was dissolved in a mixture of EtOH – ethyl acetate and the hydrochloride of the pure isomerization product crystallized. The bases were set free by treatment of the hydrochloride with 2N NaOH and repeated extraction with ether. The combined organic phases were washed with water, dried over sodium sulfate, filtered, and the solvent evaporated. The resinous residue was dried under reduced pressure.

(6*RS*,7*SR*)-(±)-4-Dimethylamino-6,7-diphenylbicyclo-[2.2.2]octan-2-one 2a

Method A: 3.5 g (11 mmol) of **1a** in 32 g of dry *tert*-butanol with 4.9 g (44 mmol) of potassium *tert*-butylate gave 300 mg (7.7%) of the hydrochloride of **2a**.

Method B: 4.8 g (15 mmol) of **1a** with 6.5 g (53 mmol) of potassium *tert*-butylate gave 2.97 g (56%) of the hydrochloride of **2a**.

Melting point (HCl) 261 °C. UV–vis (HCl, CH_3OH, nm) λ (logε): 210 (4.169). IR (HCl, KBr, cm^{-1}): 3422 (w), 2494 (w), 2363 (s), 1720 (s), 1493 (m), 1458 (m), 1354 (m), 1227 (w), 1138 (w), 1074 (w), 1008 (w), 771 (w), 758 (s), 702 (s). ^{1}H NMR (base, 400 MHz, $CDCl_3$, ppm) δ: 1.96 (br, dd, J = 13.7, 5.5 Hz, 2H, 5-H′, 8-H′), 2.37 (s, 6H, $N(CH_3)_2$), 2.42 (s, 2H, 3-H), 2.44 (br, t, J = 13.7 Hz, 2H, 5-H, 8-H), 2.79 (t, J = 2.1 Hz, 1H, 1-H), 3.51 (br, dd, J = 10.9, 3.8 Hz, 2H, 6-H, 7-H), 7.18–7.31 (m, 10 aromatic H). ^{13}C NMR (base, 100 MHz, $CDCl_3$, ppm) δ: 33.92 (C-5, C-8), 38.60 ($N(CH_3)_2$), 42.50 (C-6, C-7), 45.97 (C-3), 54.60 (C-1), 57.60 (C-4), 126.63, 126.93, 128.68, 143.81 (aromatic C), 212.39 (C-2). MS (EI$^+$) *m*/*z* (%): 319 (62.3) [M$^+$], 215 (100.0), 200 (17.5), 187 (91.1), 172 (37.4), 159 (14.0), 131 (19.5), 115 (21.0), 103 (28.0), 91 (20.2), 70 (20.6). Anal. calcd. for $C_{22}H_{26}ClNO$ (355.90): C 74.24, H 7.36, Cl 9.96, N 3.94; found: C 74.11, H 7.43, Cl 9.93, N 3.93. HRMS (EI$^+$) calcd. for $C_{22}H_{25}NO$: 319.193 61; found: 319.195 72.

(6*RS*,7*SR*)-(±)-4-Morpholino-6,7-diphenyl-bicyclo[2.2.2]octan-2-one 2b

Method A: 14.6 g (40 mmol) of **1b** in 128 g of dry *tert*-butanol with 7 g (62 mmol) of potassium *tert*-butylate gave 1.7 g (11.8%) of pure **2b** after purification by CC using benzene – ethyl acetate (1:1) as eluent.

Method B: 7.9 g (24 mmol) of **1b** with 2.67 g (22 mmol) of potassium *tert*-butylate gave 2.05 g (23%) of the pure hydrochloride of **2b**.

Melting point (HCl, decomp.) 274–278 °C. UV–vis (HCl, CH_3OH, nm) λ (logε): 209 (4.221). IR (HCl, KBr, cm^{-1}): 3501 (m), 3420 (s), 2521 (w), 2456 (w), 1722 (s), 1496 (w), 1453 (w), 1349 (w), 1266 (w), 1123 (m), 1075 (m), 900 (w), 759 (w), 745 (w) 700 (s). ^{1}H NMR (base, 400 MHz, $CDCl_3$, ppm) δ: 1.93 (br, dd, J = 12.1, 4.8 Hz, 2H, 5-H′, 8-H′), 2.40 (s, 2H, 3-H), 2.44 (dd, J = 13.5, 11.8 Hz, 2H, 5-H, 8-H), 2.66–2.68 (m, 4H, $N(CH_2)_2$), 2.81 (t, J = 2.4 Hz, 1H, 1-H), 3.50 (ddd, J = 11.0, 5.6, 2.1 Hz, 2H, 6-H, 7-H), 3.72–3.74 (m, 4H, $O(CH_2)_2$), 7.17–7.31 (m, 10 aromatic H). ^{13}C NMR (base, 100 MHz, $CDCl_3$, ppm) δ: 34.09 (C-5, C-8), 42.32 (C-6, C-7), 46.33 ($N(CH_2)_2$), 46.46 (C-3), 54.52 (C-1), 57.85 (C-4), 67.50 ($O(CH_2)_2$), 126.67, 126.90, 128.69, 143.69 (aromatic C), 212.08 (C-2). MS (EI$^+$) *m*/*z* (%): 361 (45.1) [M$^+$], 257 (100.0), 242 (12.5), 229 (72.4), 215 (23.3), 166 (11.7), 131 (42.0), 115 (40.1), 104 (79.4), 91 (66.9), 78 (36.6). Anal. calcd. for $C_{24}H_{28}ClNO_2 \times 0.5H_2O$ (406.95): C 70.83, H 7.18, Cl 8.71 N 3.44; found: C 71.10, H 7.16, Cl 8.63, N 3.36. HRMS (EI$^+$) calcd. for $C_{24}H_{27}NO_2$: 361.204 18; found: 361.202 66.

(6*RS*,7*SR*)-(±)-6,7-Diphenyl-4-pyrrolidinobicyclo-[2.2.2]octan-2-one 2c

Method B: 6.9 g (20 mmol) of **1c** with 2.4 g (20 mmol) of potassium *tert*-butylate gave 2.8 g (37%) of the hydrochloride of **2c**.

Melting point (HCl, decomp.) 275–278 °C. UV–vis (HCl, CH_3OH, nm) λ (logε): 209 (4.231). IR (HCl, KBr, cm^{-1}): 2952 (w), 2541 (m), 2425 (s), 1721 (s), 1495 (m), 1454 (m), 1359 (w), 1082 (w), 754 (m), 698 (s). ^{1}H NMR (base, 400 MHz, $CDCl_3$, ppm) δ: 1.78– 1.82 (m, 4H, $(CH_2)_2$), 2.00 (br, dd, J = 11.4, 5.7 Hz, 2H, 5-H′, 8-H′), 2.44–2.50 (m, 4H, 3-H, 5-H, 8-H), 2.72–2.76 (m, 4H, $N(CH_2)_2$), 2.77 (t, J = 2.4 Hz, 1H, 1-H), 3.52 (ddd, J = 11.4, 5.7, 2.4 Hz, 2H, 6-H, 7-H), 7.18–7.36 (m, 10 aromatic H). ^{13}C NMR (base, $CDCl_3$, 100 MHz, ppm) δ: 23.61 ($(CH_2)_2$), 34.96 (C-5, C-8), 42.69 (C-6, C-7), 45.71 ($N(CH_2)_2$), 46.61 (C-3), 54.90 (C-1), 56.32 (C-4), 126.59, 126.97, 128.29, 128.65, 143.94 (aromatic C), 212.60 (C-2). MS (EI$^+$) *m*/*z* (%): 345 (27.2) [M$^+$], 241 (87.2), 226 (21.8), 213 (100.0), 199 (27.2), 115 (39.7), 104 (77.0), 96 (26.5), 91 (48.2), 78 (40.5), 70 (27.2). Anal. calcd. for $C_{24}H_{28}ClNO$ (381.94): C 75.47, H 7.39, Cl 9.28, N 3.67; found: C 75.34, H 7.53, Cl 9.14, N 3.57. HRMS (EI$^+$) calcd. for $C_{24}H_{27}NO$: 345.209 26; found: 345.208 55.

(6*RS*,7*SR*)-(±)-6,7-Diphenyl-4-piperidinobicyclo-[2.2.2]octan-2-one 2d

Method B: 7.67 g (21 mmol) of **1d** with 2.6 g (21 mmol) of potassium *tert*-butylate gave 2.9 g (35%) **2d** as a hydrochloride.

Melting point (HCl, decomp.) 275–285 °C. UV–vis (HCl, CH_3OH, nm) λ (logε): 209 (4.191). IR (HCl, KBr, cm^{-1}): 2949 (w), 2457 (m), 2392 (w), 1721 (s), 1495 (w), 1453 (w), 1356 (w), 755 (w), 698 (s). ^{1}H NMR (base, 400 MHz, $CDCl_3$, ppm) δ: 1.43–1.48 (m, 2H, CH_2), 1.57–1.63 (m, 4H, $2CH_2$), 1.96 (br, dd, J = 12.2, 4.8 Hz, 2H, 5-H′, 8-H′), 2.41–2.47 (m, 4H, 3-H, 5-H, 8-H), 2.60–2.62 (m, 4H, $N(CH_2)_2$), 2.79 (t, J = 2.3 Hz, 1H, 1-H), 3.48 (ddd, J = 11.5, 5.5, 2.3 Hz, 2H, 6-H, 7-H), 7.17–7.35 (m, 10 aromatic H). ^{13}C NMR (base, 100 MHz, $CDCl_3$, ppm) δ: 24.75 (CH_2), 26.75 ($2CH_2$), 34.29 (C-5, C-8), 42.44 (C-6, C-7), 46.61 (C-3), 46.95 ($N(CH_2)_2$), 54.50 (C-1), 58.17 (C-4), 126.53, 126.92, 128.26, 128.60, 143.89 (aromatic C), 212.79 (C-2). MS (EI$^+$) *m*/*z* (%): 359 (49.4) [M$^+$], 255 (100.0), 240 (20.2), 227 (77.0), 213 (23.3), 136 (32.7), 128 (21.8), 104 (57.6), 91 (33.5), 78 (18.7). Anal. calcd. for $C_{25}H_{30}ClNO$ (395.97): C 75.83, H 7.64, Cl 8.95, N 3.54; found: C 75.71, H 7.80, Cl 8.86, N 3.49. HRMS (EI$^+$) calcd. for $C_{25}H_{29}NO$: 359.224 91; found: 359.224 91.

Biology

IC_{50} values are given in Table 1.

© 2006 NRC Canada

Antimalarial activity of compounds 1a–1d and 2a–2d

Antiplasmodial activity was determined using the K1 strain of *P. falciparum* (resistant to chloroquine and pyrimethamine). A modification of the [^{3}H]-hypoxanthine incorporation assay was used (9). Briefly, infected human red blood cells in an RPMI 1640 medium with 5% Albumax were exposed to serial drug dilutions in microtiter plates for 48 h. Viability was assessed by measuring the incorporation of [^{3}H]-hypoxanthine by liquid scintillation counting 24 h after the addition of the radiolabel. The counts were expressed as percentage of the control cultures, sigmoidal inhibition curves were drawn, and IC_{50} values calculated. The standard was artemisinine.

Activity of compounds 1a–1d and 2a–2d against *Trypanosoma b. rhodesiense* and cytotoxicity

Minimum essential medium (50 μL) supplemented according to Baltz et al. (10) with 2-mercaptoethanol and 15% heat-inactivated horse serum was added to each well of a 96-well microtiter plate. Serial drug dilutions were added to the wells. Then, 50 μL of trypanosome suspension (*T.b.rhodesiense* STIB 900) was added to each well and the plate incubated at 37 °C under a 5% CO_2 atmosphere for 72 h. Alamar Blue (10 μL) was then added to each well and incubation continued for a further 2–4 h. The plate was then read with a Millipore Cytofluor 2300 using an excitation wavelength of 530 nm and an emission wavelength of 590 nm (11). Fluorescence development was expressed as percentage of the control and IC_{50} values were determined. Melarsoprol served as the standard. Cytotoxicity was assessed using the same assay and L-6 cells using mefloquine as standard.

Acknowledgements

This work was supported by the Fonds zur Förderung der wissenschaftlichen Forschung (Austrian Science Fund, grant no. P-15928).

References

1. R. Weis, K. Schweiger, W. Seebacher, and F. Belaj. Tetrahedron, **54**, 14015 (1998).
2. R. Weis, R. Brun, R. Saf, and W. Seebacher. Monatsh. Chem. **134**, 1019 (2003).
3. W. Seebacher, R. Brun, and R. Weis. Eur. J. Pharm. Sci. **21**, 225 (2004).
4. W. Seebacher, C. Schlapper, R. Brun, M. Kaiser, R. Saf, and R. Weis. Eur. J. Pharm. Sci. **24**, 281 (2005).
5. W. Seebacher, R. Brun, M. Kaiser, R. Saf, and R. Weis. Eur. J. Med. Chem. **40**, 888 (2005).
6. D.J. Muir and J.B. Stothers. Can. J. Chem. **71**, 1099 (1993).
7. A. Nickon, J.L. Lambert, J.E. Oliver, D.F. Covey, and J. Morgan. J. Am. Chem. Soc. **98**, 2593 (1976).
8. W. Seebacher, R. Brun, R. Saf, and R. Weis. Monatsh. Chem. **134**, 1411 (2003).
9. H. Matile and J.R.L. Pink. *In* Immunological methods. *Edited by* I. Lefkovits and B. Pernis. Academic Press, San Diego. 1990. pp. 221–234.
10. T. Baltz, D. Baltz, C. Giroud, and J. Crockett. EMBO J. **4**, 1273 (1985).
11. B. Räz, M. Iten, Y. Grether-Bühler, R. Kaminsky, and R. Brun. Acta Trop. **68**, 139 (1997).

© 2006 NRC Canada

A simple and facile solventless procedure for the cyclization of 2′-amino- and 2′-hydroxy-chalcones using silica-supported sodium hydrogen sulphate as heterogenous catalyst

K. Hemanth Kumar and P. T. Perumal

Abstract: A simple environmentally friendly method for the cyclization of 2′-amino- and 2′-hydroxy-chalcones under solventless conditions using silica-supported sodium hydrogen sulphate has been reported.

Key words: 2′-aminochalcones, 2′-hydroxychalcones, silica gel, sodium hydrogen sulphate, quinolones and flavanones.

Résumé : On a mis au point une méthode simple et écologique de cyclisation des 2′-amino- et 2′-hydroxychalcones dans des conditions sans solvant en présence de sulfate acide de sodium déposé sur de la silice qui agit comme catalyseur.

Mots clés : 2′-aminochalcones, 2′-hydroxychalcones, gel de silice, sulfate acide de sodium, quinoléones, flavones.

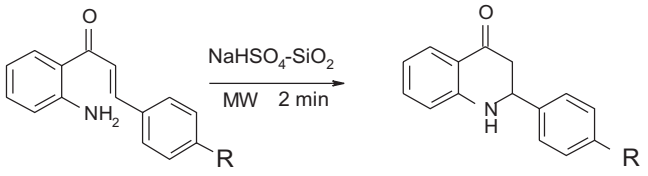
[Traduit par la Rédaction]

Introduction

Substituted tetrahydroquinolones and flavanones display various pharmacological activities (1, 2) and can be prepared (3, 4) by acid or base catalyzed reactions. Many of these procedures involve the use of corrosive reagents such as orthophosphoric acid, acetic acid, or strong alkali. Furthermore, many of them are of limited synthetic scope because of lower yields, extended reaction time, and the amount of catalyst or solvent used. In recent years, there has been increasing interest in solid-supported reagents coupled with microwave irradiation owing to the benefits of enhanced reaction rates, improved yields, cleaner reaction profiles, greater selectivity, and operational simplicity (5).

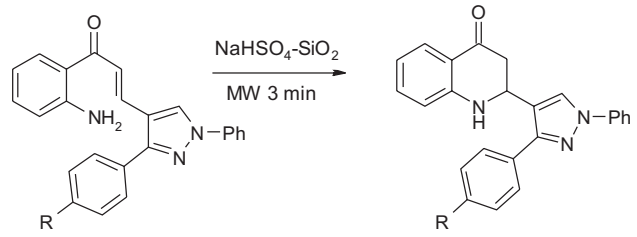
In continuation of our studies on the synthesis of heterocyclic compounds with medicinal potential from 2′-aminochalcones (6) and 2′-hydroxychalcones (7), we report an efficient and simple method for the synthesis of tetrahydroquinolones and flavanones through the cyclization of the corresponding chalcones using silica-supported sodium hydrogen sulphate under solventless conditions. The catalyst $NaHSO_4$-SiO_2 can be easily prepared (8), safely handled and removed from the reaction mixture, is inexpensive, and works under heterogeneous conditions.

Scheme 1.



R = H, Me, Cl, OMe

Scheme 2.



R = Cl, H, OMe, OEt

Results and discussion

2′-Aminochalcone was uniformly mixed with silica gel (finer than 200 mesh), preimpregnated with $NaHSO_4$, transferred into a glass vial, and irradiated by microwaves until (2 min) the reaction was complete (TLC). The reaction mixture was directly charged on a small silica gel column and eluted with a mixture of ethyl acetate – hexane (1:9) to afford the product 2-aryltetrahydro-4-quinolone in excellent yield (Scheme 1). To extend the scope of the reaction, a wide range of substituted and structurally diverse 2′-aminochalcones were subjected to similar conditions (Scheme 2). The reactions proceeded in a similar fashion

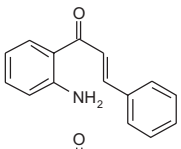
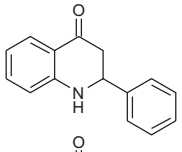
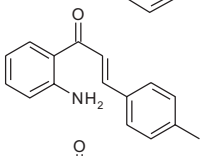
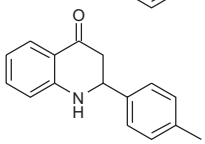
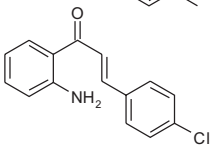
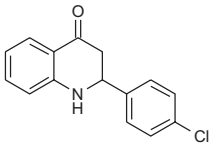
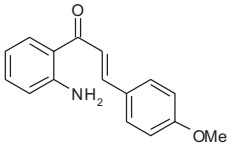
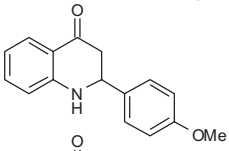
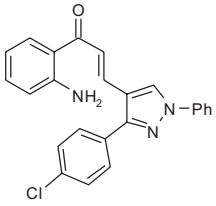
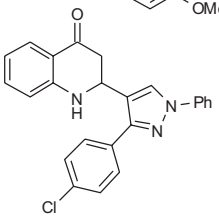
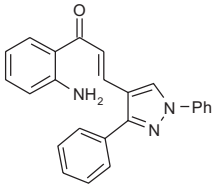
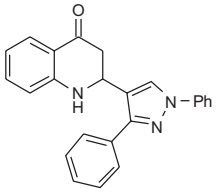
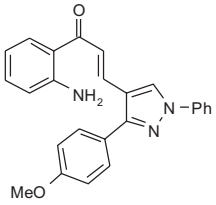
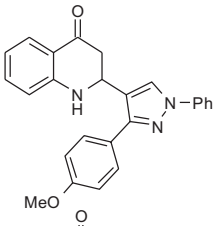
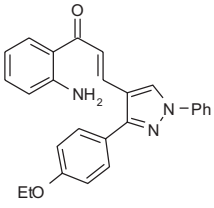
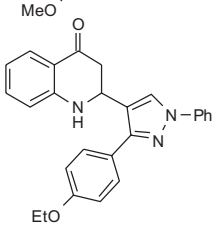
Received 12 May 2006. Accepted 23 August 2006. Published on the NRC Research Press Web site at http://canjchem.nrc.ca on 20 October 2006.

K.H. Kumar and P.T. Perumal.[1] Organic chemistry Division, Central Leather Research Institute, Adyar, Chennai 600 020, India.

[1]Corresponding author (e-mail: ptperumal@hotmail.com).

 doi:10.1139/V06-133 © 2006 NRC Canada

Table 1. $NaHSO_4$-SiO_2 catalyzed cyclization of 2′-aminochalcones under solventless conditions.

Entry	2′-Aminochalcone	Product	Microwave time (yield)[a]	Conventional heating time (yield)
1			2 min (95)	2 h (72)
2			2 min (90)	2 h (68)
3			2 min (88)	2 h (70)
4			2 min (96)	2 h (75)
5			3 min (86)	4 h (70)
6			3 min (80)	4 h (65)
7			3 min (92)	4 h (74)
8			3 min (87)	4 h (70)

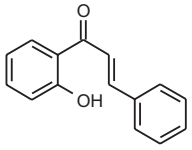
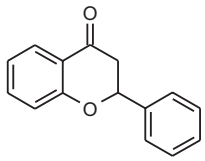
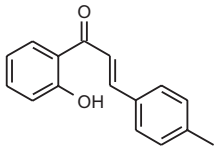
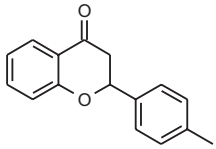
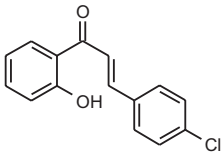
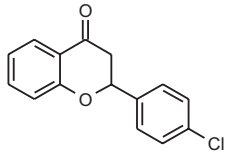
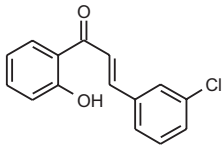
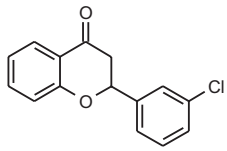
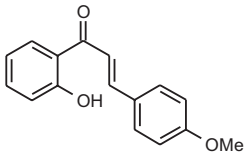
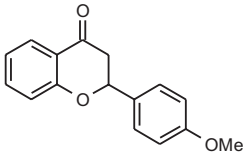
[a]Microwave irradiation was carried out at 650 W (BPL, India).

and substituted tetrahydro-4-quinolones were obtained in good yields (Table 1). The reaction rates and yields were dramatically enhanced by microwave irradiation.

Flavanones form a large and important group of naturally occurring secondary metabolites and are important intermediates for the synthesis of biologically active flavones and isoflavones (9). The conventional methods for the cyclization of 2′-hydroxychalcones involve prolonged time and the use of corrosive reagents such as sulphuric acid, hydrochloric acid, and strong alkalis (10), furnishing flavanones in not more than 50% yields. Hence, we attempted to synthesize flavanones by using $NaHSO_4$ on silica gel under solvent-free conditions as a mild catalyst for the cyclization of 2′-hydroxychalcones (Scheme 3), which fur-

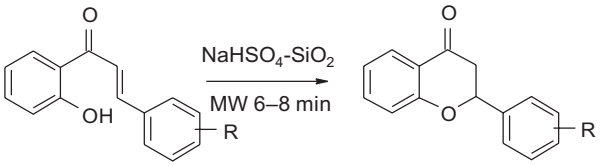
© 2006 NRC Canada

Table 2. $NaHSO_4$-SiO_2 catalyzed cyclization of 2′-hydroxychalcones under solventless conditions.

Entry	2'-Hydroxychalcone	Product	Microwave time (yield)[a]	Conventional heating time (yield)
1			6 min (75)	6 h (60)
2			6 min (70)	6 h (60)
3			8 min (72)	7 h (55)
4			8 min (68)	7 h (52)
5			6 min (75)	5 h (62)

[a]Microwave irradiation was carried out at 650 W (BPL, India).

Scheme 3.



nished the flavanones in good yields (Table 2). Here too, the use of microwave irradiation significantly enhanced the reaction rates as well as the yields.

Conclusion

In conclusion, the present procedure catalyzed by $NaHSO_4$ impregnated with silica gel provides an efficient and rapid synthesis of tetrahydroquinolones and flavanones by the cyclization of the corresponding 2′-aminochalcones and 2′-hydroxychalcones. The notable advantages of this procedure are (*i*) operational simplicity, (*ii*) fast and clean reaction, (*iii*) high yield, and (*iv*) safe and inexpensive catalyst. We believe that this procedure will provide a better scope and a more practical alternative to the existing procedures for the synthesis of tetrahydroquinolones and flavanones.

Experimental

2′-Amino- and 2′-hydroxy-chalcones were prepared using appropriate aldehyde and corresponding *o*-substituted acetophenones by earlier reported procedures (11, 12). 2-Amino- and 2-hydroxy-acetophenones (Sigma-Aldrich) were used as purchased. Sodium hydrogen sulphate and aromatic aldehydes were obtained from E-Merck (India) Ltd. Melting points were determined in capillary tubes and are uncorrected. Analytical TLC was performed on precoated plastic sheets of silica gel G/UV-254 of 0.2 mm thickness (Macherey-Nagel, Germany). FT-IR spectra were taken as KBr pellets on a PerkinElmer Spectrum RXI FT-IR spectrophotometer. ^{1}H NMR (500 MHz) and ^{13}C NMR (125 MHz) spectra were recorded in $CDCl_3$ solution with TMS as an internal standard. Column chromatography was performed on silica gel (60–120 mesh, SRL, India).

Cyclization of 2′-amino- or 2′-hydroxy-chalcones under microwave irradiation — Typical procedure A

The chalcone (1 mmol) was added to 2 g of silica gel (100–200 mesh activated by heating for 8 h at 150 °C before

© 2006 NRC Canada

use) impregnated with sodium hydrogen sulphate (2 g). The whole mixture was stirred for 5 min for uniform mixing and was then transferred to a glass tube and inserted in an alumina bath (100 g, 60 GF254, Fisher Scientific bath 6.8 cm diameter) inside the microwave oven. The compound was irradiated in a domestic microwave oven (BPL, India) at 650 W for the appropriate time. On completion, the reaction mixture was directly charged on a small silica gel column and eluted with a mixture of ethyl acetate – hexane (1:9 for quinolones, 2:8 for flavanones) to afford the corresponding products in high yields. The results are summarized in Tables 1 and 2.

Cyclization of 2′-amino- or 2′-hydroxy-chalcones by conventional means — Typical procedure B

The chalcone (1 mmol) was added to 2 g of silica gel (100–200 mesh activated by heating for 8 h at 150 °C before use) impregnated with sodium hydrogen sulphate (2 g). The whole mixture was stirred for 5 min for uniform mixing and was then transferred to a 100 mL RB flask and kept in a water bath for the appropriate time. On completion, the reaction mixture was directly charged on a small silica gel column and eluted with a mixture of ethyl acetate – hexane (1:9 for quinolones, 2:8 for flavanones) to afford the corresponding products in high yields. The results are summarized in Tables 1 and 2.

Spectral data

2-Phenyl-2,3-dihydroquinolin-4(1H)-one (Table 1, entry 1)

Pale yellow solid, mp 149 to 150 °C (lit. value (3*c*) 148–150 °C). IR (cm^{-1}) ν_{max}: 3303, 1650, 1605, 1480, 1308, 1152. ^{1}H NMR δ 2.85 (m, 2H), 4.60 (br s, NH, 1H), 4.74 (dd, *J* = 3.14, 13.2 Hz, 1H, H-2), 6.70–7.50 (m, 8H), 7.86 (dd, *J* = 1.72, 8.05 Hz, 1H, H-5). ^{13}C NMR δ 46.5, 58.2, 116.1, 118.4, 119.2, 126.8, 127.6, 128.6, 129.1, 135.5, 141.1, 151.7, 193.4. MS *m/z*: 223 (M^+). Anal. calcd. for $C_{15}H_{13}NO$: C 80.69, H 5.87, N 6.27; found: C 80.60, H 5.73, N 6.12.

2-(4-Methylphenyl)-2,3-dihydroquinolin-4(1H)-one (Table 1, entry 2)

Pale yellow solid, mp 148 to 149 °C (lit. value (3*b*) 149 °C). IR (cm^{-1}) ν_{max}: 3318, 1660, 1602, 1580, 1298, 1142. ^{1}H NMR δ 2.36 (s, 3H, CH_3), 2.84 (m, 2H), 4.67 (br s, NH, 1H), 4.70 (dd, *J* = 3.8, 11.9 Hz, 1H, H-2), 6.69–7.48 (m, 7H), 7.84 (dd, *J* = 1.14, 8.02 Hz, 1H, H-5). ^{13}C NMR δ 21.4, 46.5, 58.3, 116.1, 118.4, 119.0, 126.6, 127.7, 129.8, 129.1, 135.5, 138.2, 151.1, 193.6. MS *m/z*: 237 (M^+). Anal. calcd. for $C_{16}H_{15}NO$: C 80.98, H 6.37, N 5.90; found: C 80.92, H 6.31, N 5.86.

2-(4-Chlorophenyl)-2,3-dihydroquinolin-4(1H)-one (Table 1, entry 3)

Pale yellow solid, mp 168 °C (lit. value (3*c*) 167 to 168 °C). IR (cm^{-1}) ν_{max}: 3325, 1625, 1608, 1540, 1238, 1152. ^{1}H NMR δ 2.90 (m, 2H), 4.54 (br s, NH, 1H,), 4.81 (dd, *J* = 4.0, 13.7 Hz, 1H, H-2), 6.72–7.39 (m, 7H), 7.86 (d, *J* = 8.0 Hz, 1H, H-5). ^{13}C NMR δ 46.3, 57.3, 116.1, 118.1, 119.1, 127.4, 128.2, 129.2, 134.3, 135.6, 139.6, 151.9, 193.2. MS *m/z*: 257 (M^+). Anal. calcd. for $C_{15}H_{12}NOCl$: C 69.91, H 4.69, N 5.43; found: C 69.82, H 4.60, N 5.35.

2-(4-Methoxyphenyl)-2,3-dihydroquinolin-4(1H)-one (Table 1, entry 4)

Pale yellow solid, mp 147 °C (lit. value (3*c*) 146 to 147 °C). IR (cm^{-1}) ν_{max}: 3332, 1632, 1596, 1529, 1226, 1113. ^{1}H NMR δ 2.85 (m, 2H), 3.81 (s, 3H, OCH_3), 4.50 (br s, NH, 1H), 4.70 (dd, *J* = 3.4, 13.7 Hz, 1H, H-2), 6.68–7.37 (m, 7H), 7.86 (dd, *J* = 1.15, 7.98 Hz, 1H, H-5). ^{13}C NMR δ 44.6, 55.5, 58.0, 114.4, 116.0, 118.5, 119.1, 127.7, 127.9, 133.1, 135.5, 151.7, 159.7, 193.7. MS *m/z*: 253 (M^+). Anal. calcd. for $C_{16}H_{15}NO_2$: C 75.87, H 5.97, N 5.53; found: C 75.82, H 5.90, N 5.48.

2-[3-(4-Chlorophenyl)-1-phenyl-1H-pyrazol-4-yl]-2,3-dihydroquinolin-4(1H)-one (Table 1, entry 5)

Pale white solid, mp 190–192 °C. IR (cm^{-1}) ν_{max}: 3344, 1656, 1585, 1534, 1219, 1140. ^{1}H NMR δ 2.84–2.91 (m, 2H), 4.60 (s, br s, NH, 1H), 4.92–4.95 (m, 1H), 6.65 (d, *J* = 8.4 Hz, 1H, H-8), 6.77–6.8 (m, 1H, H-7), 7.28–7.87 (m, 10H), 7,85–7.87 (dd, *J* = 1.5, 7.65 Hz, 1H, H-5), 8.05 (s, 1 H, pyrazole-CH). ^{13}C NMR δ 45.6, 49.3, 116.1, 118.9, 119.2, 119.3, 121.8, 126.7, 127.1, 127.7, 129.2, 129.5, 129.6, 131.3, 134.6, 135.6, 139.7, 150.0, 151.5, 193.1. MS *m/z*: 400 (M^+). Anal. calcd. for $C_{24}H_{18}ClN_3O$: C 72.09, H 4.54, N 10.51; found: C 72.01, H 4.48, N 10.45.

2-(1,3-Diphenyl-1H-pyrazol-4-yl)-2,3-dihydro-quinolin-4(1H)-one (Table 1, entry 6)

Pale white solid, mp 128 to 129 °C. IR (cm^{-1}) ν_{max}: 3346, 1645, 1595, 1523, 1205, 1133. ^{1}H NMR δ 2.86–2.94 (m, 2H, H-3), 4.59 (s, br s, NH, 1H), 4.94–4.97 (m, 1H), 6.65 (d, *J* = 8.4 Hz, 1H, H-8), 6.81 (t, 1H, *J* = 7.65 Hz, H-7), 7.29–7.47 (m, 7H), 7.58 (d, *J* = 8.4 Hz, 2H), 7.69 (d, *J* = 7.65 Hz, 2H) 7.86 (d, *J* = 6.8 Hz, 1H, H-5), 8.0 (s, 1H, pyrazole-CH). ^{13}C NMR δ 45.6, 49.3, 116.1, 118.9, 119.1, 119.3, 121.8, 122.8, 126.7, 127.1, 127.7, 129.6, 129.8, 131.8, 132.1, 135.6, 139.7, 150.0, 151.2, 193.2. MS *m/z*: 365 (M^+). Anal. calcd. for $C_{24}H_{19}N_3O$: C 78.88, H 5.24, N 11.50; found: C 78.80, H 5.18, N 11.42.

2-[3-(4-Methoxyphenyl)-1-phenyl-1H-pyrazol-4-yl]-2,3-dihydroquinolin-4(1H)-one (Table 1, entry 7)

Pale white solid, mp 175–177 °C. IR (cm^{-1}) ν_{max}: 3330, 1642, 1577, 1509, 1234, 1116. ^{1}H NMR δ 2.89–2.91 (m, 2H), 3.83 (s, 3H, OCH_3), 4.61 (s, br s, NH, 1H), 4.94–4.96 (m, 1H), 6.62 (d, *J* = 8.05 Hz, 1H, H-8), 6.76 (m, 1H, H-7), 6.95–7.7 (m, 10H), 7.85 (d, *J* = 8.0 Hz, 1H, H-5), 8.04 (s, 1H, pyrazole-CH). ^{13}C NMR δ 45.0, 49.3, 56.5, 114.0, 114.8, 115.8, 118.3, 119.1, 120.3, 124.9, 126.0, 126.4, 127.3, 128.5, 129.4, 134.4, 138.9, 152.3, 154.3, 159.1, 193.2. MS *m/z*: 395 (M^+). Anal. calcd. for $C_{25}H_{21}N_3O_2$: C 75.93, H 5.35, N 10.63; found: C 75.82, H 5.30, N 10.58.

2-[3-(4-Ethoxyphenyl)-1-phenyl-1H-pyrazol-4-yl]-2,3-dihydroquinolin-4(1H)-one (Table 1, entry 8)

Pale white solid, mp 178 to 179 °C. IR (cm^{-1}) ν_{max}: 3349, 1658, 1569, 1519, 1227, 1136. ^{1}H NMR δ 1.41 (t, *J* = 6.9 Hz, 3H), 2.8–2.84 (m, 2H, H-3), 4.0 (q, *J* = 6.9, 13.75 Hz, 2H) 4.64 (s, br s, NH, 1H), 4.94–4.97 (m, 1H), 6.62 (d, *J* = 8.45 Hz, 1H, H-8), 6.76–7.86 (m, 11H), 7.84 (d,

© 2006 NRC Canada

J = 7.65 Hz, 1H, H-5), 8.03 (s, 1H, pyrazole-CH). ^{13}C NMR δ 14.9, 45.6, 49.3, 63.6, 114.5, 114.9, 116.1, 118.7, 119.0, 121.5, 125.1, 126.4, 126.7, 127.7, 129.5, 130.6, 135.5, 139.8, 151.0, 151.3, 159.3, 193.4. MS *m*/*z*: 409 (M^+). Anal. calcd. for $C_{26}H_{23}N_3O_2$: C 76.26, H 5.66, N 10.26; found: C 76.19, H 5.58, N 10.18.

2-Phenyl-2,3-dihydro-4*H*-chromen-4-one (Table 2, entry 1)

Pale white solid, mp 75 to 76 °C (lit. value (10*a*) 78 to 77 °C). IR (cm^{-1}) ν_{max}: 1691, 1606, 1517, 1464, 1223, 1174. ^{1}H NMR δ 2.84–3.12 (m, 2H), 5.46 (dd, *J* = 2.85, 13.15 Hz, 1H, H-2), 7.04–7.07 (m, 2H), 7.37–7.52 (m, 6H), 7.90 (dd, *J* = 1.75, 8.05 Hz, 1H, H-5). ^{13}C NMR δ 44.8, 77.4, 118.2, 121.0, 121.7, 126.3, 127.2, 128.9, 135.0, 136.3, 138.8, 161.7, 192.1. MS *m*/*z*: 224 (M^+). Anal. calcd. for $C_{15}H_{12}O_2$: C 80.34, H 5.39; found: C 80.27, H 5.32.

2-(4-Methylphenyl)-2,3-dihydro-4*H*-chromen-4-one (Table 2, entry 2)

Pale white solid, mp 82 to 83 °C (lit. value (10*a*) 83 to 84 °C). IR (cm^{-1}) ν_{max}: 1696, 1595, 1520, 1459, 1225, 1162. ^{1}H NMR δ 2.38 (s, 3H), 2.89–3.12 (m, 2H), 5.43 (dd, *J* = 1.95, 13.75 Hz, 1H, H-2), 7.03–7.06 (m, 2H), 7.23 (d, *J* = 8 Hz, 2H), 7.36 (d, *J* = 8 Hz, 2H), 7.48 (m, 1H, H-6), 7.92 (dd, *J* = 1.7, 8.55 Hz, 1H, H-5). ^{13}C NMR δ 21.3, 44.7, 77.4, 118.3, 121.0, 121.6, 126.3, 127.1, 129.6, 135.8, 136.3, 138.8, 161.7, 192.3. MS *m*/*z*: 238 (M^+). Anal. calcd. for $C_{16}H_{14}O_2$: C 80.65, H 5.92; found: C 80.58, H 5.84.

2-(4-Chlorophenyl)-2,3-dihydro-4*H*-chromen-4-one (Table 2, entry 3)

Pale white solid, mp 95 to 96 °C (lit. value (4) 94 to 95 °C). IR (cm^{-1}) ν_{max}: 1692, 1575, 1519, 1464, 1256, 1162. ^{1}H NMR δ 2.84–3.05 (m, 2H), 5.43–5.46 (m, 1H), 7.03–7.06 (m, 2H), 7.38–7.52 (m, 5H), 7.90 (dd, *J* = 1.55, 7.65 Hz, 1H, H-5). ^{13}C NMR δ 44.7, 77.4, 118.2, 121.0, 121.9, 127.2, 127.6, 128.3, 129.1, 136.4, 137.4, 161.4, 191.6. MS *m*/*z*: 258 (M^+). Anal. calcd. for $C_{15}H_{11}ClO_2$: C 69.64, H 4.29; found: C 69.59, H 4.21.

2-(3-Chlorophenyl)-2,3-dihydro-4*H*-chromen-4-one (Table 2, entry 4)

Pale white solid, mp 98 to 99 °C (lit. value (4) 99 to 100 °C). IR (cm^{-1}) ν_{max}: 1697, 1568, 1523, 1454, 1297, 1145. ^{1}H NMR δ 2.83–3.15 (m, 2H), 5.44–5.47 (m, 1H, H-2), 7.1–7.3 (m, 2H), 7.36–7.58 (m, 5H), 7.90 (dd, *J* = 1.65, 8.45 Hz, 1H, H-5). ^{13}C NMR δ 45.3, 76.4, 118.1, 119.4, 120.8, 121.9, 124.7, 127.0, 127.8, 128.0, 129.6, 136.4, 136.9, 160.4, 193.1. MS *m*/*z*: 258 (M^+). Anal. calcd. for $C_{15}H_{11}ClO_2$: C 69.64, H 4.29; found: C 69.57, H 4.22.

2-(4-Methoxyphenyl)-2,3-dihydro-4*H*-chromen-4-one (Table 2, entry 5)

Pale white solid, mp 87 to 88 °C (lit. value (4) 88 to 89 °C) IR (cm^{-1}) ν_{max}: 1689, 1588, 1513, 1443, 1243, 1123. ^{1}H NMR δ 2.86–3.0 (m, 2H), 3.8 (s, 3H), 5.39 (dd, *J* = 2.8, 13.70 Hz, 1H, H-2), 6.96 (d, *J* = 8.0 Hz, 1H), 7.01–7.05 (m, 2H), 7.39 (d, *J* = 8.6 Hz, 2H), 7.36 (d, *J* = 8 Hz, 2H), 7.91 (dd, *J* = 1.7, 8.0 Hz, 1H, H-5). ^{13}C NMR δ 44.5, 55.5, 77.4, 114.3, 118.2, 121.0, 121.6, 127.1, 130.9, 136.3, 160.1, 161.7, 192.3. MS *m*/*z*: 254 (M^+). Anal. calcd. for $C_{16}H_{14}O_3$: C 75.57, H 5.55; found: C 75.50, H 5.48.

Acknowledgement

One of the authors, KHK expresses gratitude to the Council of Scientific and Industrial Research (CSIR, New Delhi, India) for financial support.

References

1. (*a*) O.V. Singh and R.S. Kapil. Synth. Commun. **23**, 227 (1993); (*b*) L. Li, H.K. Wang, S.C. Kuo, T.S. Wu, D. Lednicer, C. Lin, E. Hamel, and K.H. Lee. J. Med. Chem. **37**, 3400 (1944).
2. (*a*) M. Ito, S. Ishimoto, Y. Nishida, T. Shiramizu, and H.Yunoki. Agric. Biol. Chem. **50**, 1073 (1986); (*b*) N. De Meyer, A. Haemers, L. Mishra, I.A.C. Pandey, L.A.C. Pieters, D.A.V. Berghe, A.J. Viletinck. J. Med. Chem. **34**, 736 (1991).
3. (*a*) J.A. Donnelly and D.F. Farell. Tetrahedron, **46**, 885 (1990); (*b*) A.L. Tokes and L. Szilagyi. Synth. Commun. **22**, 2433 (1992); (*c*) R.S. Varma and R.K. Sani. Synlett, 857 (1997).
4. S. Rajgopalan, C.R. Row, and T.R. Seshadri. Proc. Indian Acad. Sci. Sect. A, **23**, 97 (1946).
5. (*a*) J.C. Lee and Y.H Bae. Synlett, 507 (2003); (*b*) M. Chakrabarty, R. Basak, and N. Ghosh. Tetrahedron Lett. **42**, 3913 (2001); (*c*) J.S. Yadav, B.V. Subba Reddy, G. Mahesh, and C. Madan. Synlett, 1781 (2001); (*d*) B.C. Ranu, A. Hajra, S.S. Dey, and J. Umasish. Tetrahedron, **59**, 813 (2003).
6. (*a*) K. Hemanth Kumar, D. Muralidharan, and P.T. Perumal. Synthesis, **63**, (2004); (*b*) K. Hemanth Kumar, S. Selvi, and P.T. Perumal. J. Chem. Res. Synop. 218 (2004); (*c*) K. Hemanth Kumar, D. Muralidharan, and P.T. Perumal. Tetrahedron Lett. **45**, 7903 (2004).
7. K. Hemanth Kumar and P.T. Perumal. Chem. Lett. **34**, 1346 (2005).
8. T. Nishguchi and C. Kamio. J. Chem. Soc. Perkin Trans. 1, 707, (1989).
9. L. Jurd. In The chemistry of flavonoid compounds. *Edited by* T.A. Geissman. Pergamon Press, NewYork. 1962. p. 107.
10. (*a*) A. Lowenbein. Chem. Ber. **57**, 1515 (1924); (*b*) K. Maruyama, K. Tamanaka, and A. Nishinaga. Tetrahedron Lett. **30**, 4145 (1989); (*c*) A. Binaco, C. Cavarischia, A. Farina, M. Guiso, and C. Marra. Tetrahedron Lett. **44**, 9107 (2003).
11. W. S. Murphy and S. Watanasin. Synthesis, 647 (1980).
12. (*a*) N.S. Poonia, K. Chhabra, C. Kumar, and U.W. Bhagvat. J. Org. Chem. **42**, 3311(1977); (*b*) S.B. Lohiya and B.J. Ghiya. Indian. J. Chem. Sect. B: Org. Chem. Incl. Med. Chem. **25**, 279 (1986).

© 2006 NRC Canada

Experimental and theoretical study of the electrochemical behavior of N-protonated dopamine at Nafion multiwalled carbon nanotubes (MWNTs) modified glassy carbon (GCE) electrode

Yuanzhi Song and Yang Song

Abstract: The electrochemistry of N-protonated dopamine (DAH^+) was studied by cyclic voltammetry (CV) at a glassy carbon electrode modified by Nafion multiwalled carbon nanotubes (MWNTs) in phosphate buffers (pH 5.50) and the results show that the standard electrode potential of half reaction for $DAH^+_{(O)},H^+/\ DAH^+_{(R)}$ is 0.74 V. Calculations are performed using DFT B3LY/6-31G(d,p) for nine conformers of N-protonated dopamine ($DAH^+_{(R)}$) and three conformers of oxidized N-protonated dopamine ($DAH^+_{(O)}$). The energies of solvation and sum of electronic and thermal free energies of $DAH^+_{(R)}$, $DAH^+_{(O)}$, *p*-benzoquinone (*p*-BQ), and *p*-hydroquinone (*p*-HQ) are calculated at same level. The theoretical weighted average of the standard electrode potential (0.732 V) for $DAH^+_{(O)},H^+/\ DAH^+_{(R)}$, using the transformed Gibbs free energies of the stable $DAH^+_{(R)}$ and $DAH^+_{(O)}$ with a *p*-BQ, H^+/*p*-HQ reference electrode, is consistent with the experimental one of 0.74 V.

Key words: dopamine, DFT, cyclic voltammetry, standard electrode potential.

Résumé : Opérant dans des solutions tamponnées (pH de 5,50) de phosphate, on a étudié l'électrochimie de la dopamine N-protonée (DAH^+) en faisant appel à la voltampérométrie cyclique au niveau d'une électrode de carbone vitreuse modifiée par des nanotubes de carbone à plusieurs épaisseurs de Nafion; les résultats montrent que le potentiel d'électrode standard de la demie réaction pour $DAH^+_{(O)}/DAH^+_{(R)}$ est de 0,74 V. On a effectué des calculs de théorie de la fonctionnelle de densité au niveau B3LY/6-31G(d,p) pour neuf conformères de la dopamine N-protonée ($DAH^+_{(R)}$) et trois conformères de la dopamine N-protonée ($DAH^+_{(O)}$) et on a calculé au même niveau les énergies de solvatation et la somme des énergies libres électroniques et thermiques de dopamine N-protonée $DAH^+_{(R)}$, $DAH^+_{(o)}$, de la *p*-benzoquinone (*p*-BQ) et de la *p*-hydroquinone (*p*-HQ). Il existe une bonne corrélation entre la valeur expérimentale de 0,74 V et le potentiel d'électrode standard moyen théorique (0,7372 V) pour la réaction $DAH^+_{(O)},H^+/DAH^+_{(R)}$ lorsqu'on utilise les énergies libres de Gibbs transformées pour les formes stables du $DAH^+_{(R)}$ et du $DAH^+_{(O)}$ avec un électrode de référence *p*-BQ,H^+/*p*-HQ.

Mots clés : dopamine, théorie de la fonctionnelle de densité, voltampérométrie cyclique, potentiel d'électrode standard.

[Traduit par la Rédaction]

Introduction

Dopamine (DA) is very important catecholamine neurotransmitter in the mammalian central nervous system and is often electrochemically monitored in vivo with microfibre electrodes. The oxidation of these compounds is interesting and this process occurs in the human body. Catecholamine drugs are also used to treat hypertension, bronchial asthma, organic heart disease, and are used in cardiac surgery and myocardial infarction (1, 2). In addition, the N-protonated form is a preferred candidate for the formation of a drug-receptor complex through a reinforced electrostatic interaction (3).

Conformational studies of dopamine have been performed using experimental NMR techniques (4) and theoretical quantum chemical calculations (5, 6). No information could be obtained from these studies regarding the orientation of the catechol ring because of the rapid rotation of the aminoethyl chain.

An understanding of the electrochemical reactions of dopamine is necessary to develop a method for studying their physiological function and to aid in the diagnosis of some diseases. In clinical medicine, it is often desirable to develop an electroanalytical method to study electron transfer processes. Numerous observations of the electrochemical behaviour of dopamine and its analogs such as epinephrine have been made by many research groups (7–13). Figure 1 illustrates the reaction scheme for the case of DAH^+ at an electrode.

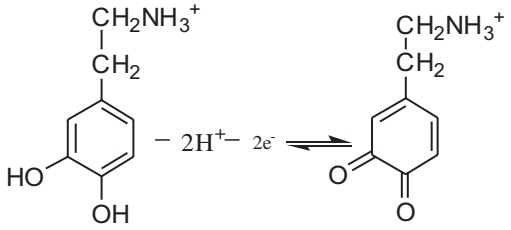
Received 2 May 2006. Accepted 11 September 2006. Published on the NRC Research Press Web site at http://canjchem.nrc.ca on 25 October 2006.

Y. Song.[1] Jiangsu Province Key Laboratory for Chemistry of Low-Dimensional Materials, Chemistry Department, Huaiyin Teachers College, Huai An 223300, People's Republic of China.
Y. Song. College of Materials Science and Engineering, Beijing Chemistry and Engineering University, Beijing 100021, People's Republic of China.

[1]Corresponding author (e-mail: songyuanzhi@sina.com, songyuanzhi@126.com).

 doi:10.1139/V06-136 © 2006 NRC Canada

Fig. 1. Reaction scheme for the electrochemical oxidation of $DAH^+_{(R)}$.



Based on the studies mentioned earlier, this article describes the CV of N-protonated dopamine (pH 5.50) at a glassy carbon electrode modified by Nafion multiwalled carbon nanotubes (Nafion-MWNTs) and discusses the electrochemical properties using quantum chemistry.

DFT using hybrid functionals has emerged as very powerful theoretical method to investigate electrochemical properties (14–19). Thus, we selected the B3LYP method, using 6-31G(d,p), to study the geometries of $DAH^+_{(R)}$ and its oxidized forms ($DAH^+_{(O)}$) and to compute the standard electrode potential for $DAH^+_{(O)}$,H^+/$DAH^+_{(R)}$.

Experimental

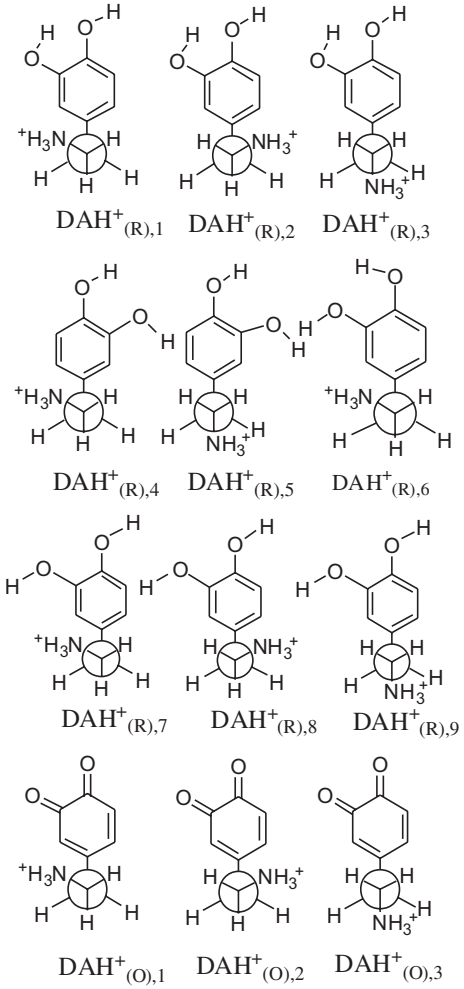
Chemicals and reagents

The phosphate buffer solution was made from 0.1 mol/L of NaH_2PO_4 and adjusted to the desired pH by adding 1 mol/L NaOH or HNO_3 solution. DA and Nafion solutions were from Sigma-Aldrich. All solutions were prepared with double-distilled water. The MWNTs were from Central Normal University (China). The MWNTs were depurated following the literature method (20). The MWNTs (50 mg) were dispersed in 50 cm^3 of concentrated nitric acid (68%, analytical grade), heated for 24 h, and left to stand for a further 24 h at room temperature. Then, the solution mixture was filtered with a PTFE membrane disc filter (1 μm pore size) under vacuum, followed by several washings with double-distilled water until neutralized. The MWNTs on the membrane disc were dried in an oven at 60 °C for 12 h. The prepared sample is named acid-treated MWNTs. The peaks of 1735 and 1690 cm^{-1} of the sample in the FTIR spectrum revealed that the carboxylic acid groups were present on the surface of acid-treated MWNTs.

Electrode preparation

A cylindrical glassy carbon electrode (GCE), 3 mm in diameter and 50 mm in length, was used for the preparation of the modified electrode as follows. The GCE was prepared by polishing to a mirrorlike appearance, first with fine wet emery papers (grain size 4000) and then with 1.0 mm and 0.3 mm alumina slurry on micro cloth pads (Buehler, Lake Bluff, IIlinois). After the initial polishing, the GCEs were resurfaced using 0.05 mm alumina slurry. The GCEs were sonicated in water twice, then in a 1:1 (*v*/*v*) isopropyl alcohol – acetonitrile (IPA + MeCN) mixture for 10 min each, respectively. The polished and cleaned GCE surface was modified with a 10 uL solution (1mg MWNTs, 5 mL of 1% Nafion in ethanol). To compare with the CV of an electrode modified with MWNTs, a polished and cleaned GCE surface was also modified with a 10 uL solution of the mixture (5 mL of 1% Nafion).

Fig. 2. The initial geometry of $DAH^+_{(R)}$ and $DAH^+_{(O)}$.



Instrumentation

A polarograph (Jiangsu Electrochemistry Analysis Instrument Corp., China) with MEC-12B analytical software was used to test electrochemical behaviour. A conventional three-electrode cell system was used. Silver chloride in 3 mol/L KCl solution, a platinum wire, and the GCE modified with MWNTs were used as the reference, auxiliary, and working electrodes, respectively. All CV experiments were carried out at a temperature of 25 °C.

Calculation methods

According to their molecular structure and symmetry, the initial geometries of nine conformers for $DAH^+_{(R)}$ and three conformers for $DAH^+_{(O)}$, shown in Fig. 2, are optimized. Both $DAH^+_{(R)}$ and $DAH^+_{(O)}$ exhibit conformational equilibrium by the rotation of an amine group about the C–C bond in the side chain. Furthermore, the asymmetrical substitution of the phenol ring provides possible further conformations for $DAH^+_{(R)}$. There is an antipode corresponding to each isomer and the energy of each isomer shown in Fig. 2 will be same for its antipode. Therefore, we need not study the antipode.

All the calculations were performed by using the DFT method B3LYP (21) with the split-polarized 6–31(d,p) using

© 2006 NRC Canada

Table 1. Comparison of experimental standard electrode potential from the literature.

Electrode	CAV-GCE (7)	PDDA/MWNT5-GCE (8)	*N*-Acetylcysteine SAM electrode (9)	Current work	
E_{pa} (V)	0.44	0.28	0.31	0.245	0.300
E_{pc} (V)	0.06	0.14	0.22	0.220	0.161
pH	6.00	7.00	5.70	5.50	5.50
Reference electrode	SCE	SCE	Ag/AgCl	Ag/AgCl	Ag/AgCl
$(E_{pa}+E_{pc})/2$	0.25	0.21	0.26	0.232	0.230
$E^0{}_1$ (V)	0.60	0.62	0.60	0.551	0.549
$E^0{}_2$ (V)	0.82	0.84	0.79	0.74	0.74

Note: SCE, saturated calomel electrode; CAV-GCE, GCE modifed by carbon atom wires; (CAWs) PDDA, diallyldimethylammonium chloride; *N*-acetylcysteine SAM electrode, gold electrode modified with *N*-acetylcysteine self-assembled monolayer.

the Gaussian 03 suite of programs (22). Optimized geometries of $DAH^+_{(O)}$ and $DAH^+_{(R)}$ were calculated with no geometrical restriction. All optimized geometries were further examined through vibrational frequency analysis. The energies of solvation of $DAH^+_{(O)}$ and $DAH^+_{(R)}$ at 298.15 K and 1 atm (1 atm = 101.325 kPa) were calculated by the polarized continuum (overlapping spheres) model (PCM) of Tomasi and co-workers (23–25) for analytic energies at the same levels. *p*-Benzoquinone (*p*-BQ) and *p*-hydroquinone (*p*-HQ), as reference electrodes, are also calculated at same level.

Results and discussion

Electrochemical investigation of dopamine at the modified GCE

The standard electrode potential E^0 of half reaction for reversible redox couple with CV is calculated as (26)

$$[1] \qquad E^0 = (E_{pa} + E_{pc})/2$$

where E_{pa} and E_{pc} represent oxidation potential and reduction potential, respectively.

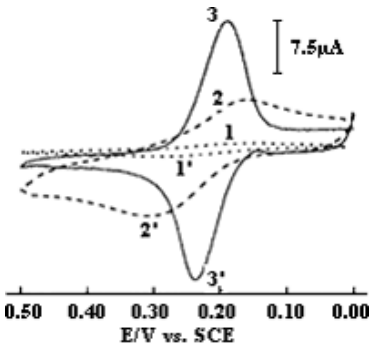
As shown in Fig. 3, for the phosphate buffer (0.1 mol/L, pH 5.50) no redox peak appears for the bare GCE. When $DA_{(R)}$ (1.0×10^{-4} mol/L) was added to the solution and the first CV scan toward the positive direction was performed, a pair of redox peaks appeared at about 0.200 V (E_{pc}) and 0.245 V (E_{pa}) for the Nafion- MWNTs-GCE, as well as 0.161 V (E_{pc}) and 0.300 V (E_{pa}) for the Nafion-GCE, respectively. In comparison, the peak currents at the modified electrode are much greater than those at the bare GCE. This means that the electrochemical behavior of DA can be improved by this modified electrode. Moreover, this electrochemical response has good stability as the peaks remain unchanged after 10 consecutive CV scans. The conditional potential of $DAH^+_{(O)}$,H^+/ $DAH^+_{(R)}$, estimated from the average values of the anodic and cathodic peak potentials *E* (26), $(E_{pa} + E_{pc})/2$, were 0.222 V and 0.230 V vs. Ag/AgCl, corresponding to the Nafion-MWNTs-GCE electrode and the Nafion-GCE, respectively. DAH^+ is undergoing two-electron oxidation during the two processes occurring at the modified electrode.

The standard electrode potential ($E^0{}_1$) vs. Ag/AgCl is written as

$$[2] \qquad E = E^0{}_1 + 0.059\text{l g}[H^+] \text{ (1 atm, 25 °C)}$$

then

Fig.3. The cyclic voltammogramms dopamine (1.0×10^{-4} mol/L) in phosphate buffer (pH 5.50). 1,1′ at bare GCE; 2,2′ at Nafion modified GCE (Nafion-GCE); 3,3′ at 3 Nafion multiwalled carbon nanotubes modified GCE (Nafion-MWNTs-GCE). Scanning rate = 50 mV/s.



$$[3] \qquad \text{at pH} = 5.50,\ E^0{}_1 = 0.551 \text{ V (1 atm, 25 °C)}$$
for Nafion-MWNTs-GCE

$$[4] \qquad \text{at pH} = 5.50,\ E^0{}_1 = 0.549 \text{ V (1 atm, 25 °C)}$$
for Nafion-GCE

The standard electrode potential $E^0{}_2$ vs. the normal hydrogen electrode (NHE) is given as

$$[5] \qquad E^0{}_2 = E^0{}_1 + E_{Ag/AgCl(3M\ KCl)}$$

$$[6] \qquad E_{Ag/AgCl(3M\ KCl)} = E^0{}_{AgCl/Ag} - 0.059\text{l g}[Cl^-] = 0.222 \text{ V} - 0.059\text{l g}[3] = 0.194 \text{ V (1 atm, 25 °C)}$$

where $E^0{}_{AgCl/Ag}$ represents the standard electrode potential for Ag/AgCl (27). Therefore, $E^0{}_2$ is calculated as

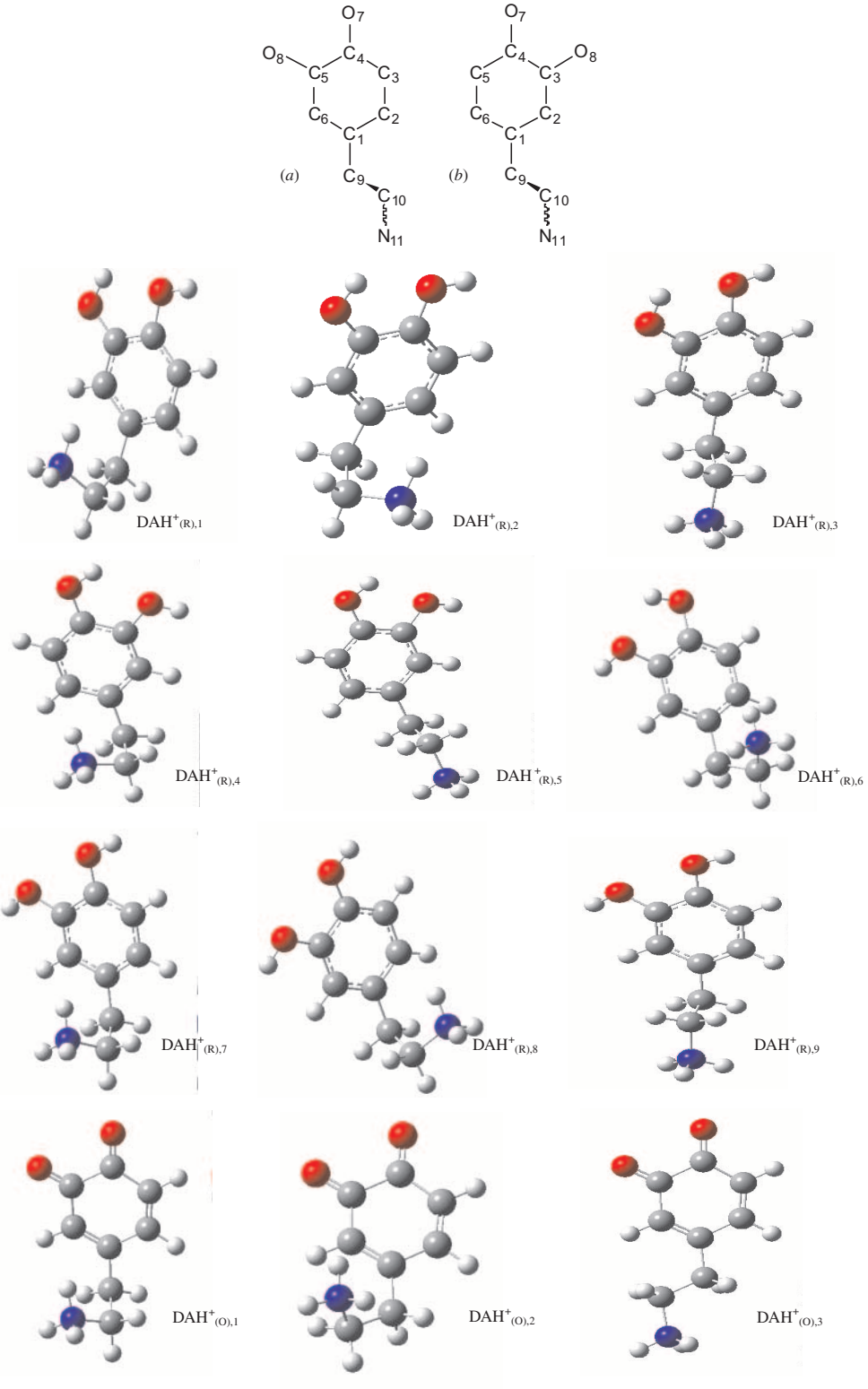
$$[7] \qquad E^0{}_2 = 0.517 \text{ V} + 0.194 \text{ V} = 0.74 \text{ V (1 atm, 25 °C)}$$
for Nafion-MWNTs-GCE

$$[8] \qquad E^0{}_2 = 0.525 \text{ V} + 0.194 \text{ V} = 0.74 \text{ V (1 atm, 25 °C)}$$
for Nafion-GCE

In a comparison with literature results (7–9), Table 1 shows the standard electrode potential as calculated earlier, indicating that the standard electrode potential for the reversible redox couple of DAH^+ at Nafion-GCE and Nafion-MWNTs-GCE with CV is in agreement with that at the different modi-

© 2006 NRC Canada

Fig. 4. Numbering in both $DA_{(R)}$ and $DA_{(O)}$ with geometries optimized at the B3LYP/6-31G(d,p) level.



fied electrodes and that the error in standard electrode potential is due to the irreversible reaction with CV.

Geometry of DAH^+

The geometries were optimized using BLYP/6–31G(d,p) and the numeration of atoms in both $DAH^+_{(R)}$ and $DAH^+_{(O)}$ shown in Fig. 4. The structure (Fig. 4*b*) of the two conformers, $DAH^+_{(R),4}$ and $DAH^+_{(R),5}$, is different from that of the others (Fig. 4*a*). All atoms of the benzene ring with OH atoms in both $DAH^+_{(O)}$ and $DAH^+_{(R)}$ are nearly planar.

The bond lengths and bond angles of both $DAH^+_{(R)}$ and $DAH^+_{(O)}$ optimized with B3LYP/6–31G(d,p) are listed in

© 2006 NRC Canada

Table 2. The geometrical parameters of $DA_{(R)}$ and $DA_{(O)}$ at the B3LYP/6-31G(d,p) level.

	$DAH^{+}_{(R),1}$	$DAH^{+}_{(R),2}$	$DAH^{+}_{(R),3}$	$DAH^{+}_{(R),4}$	$DAH^{+}_{(R),5}$	$DAH^{+}_{(R),6}$	$DAH^{+}_{(R),7}$	$DAH^{+}_{(R),8}$	$DAH^{+}_{(R),9}$	$DAH^{+}_{(O),1}$	$DAH^{+}_{(O),2}$	$DAH^{+}_{(O),3}$
Bond lengths (Å)												
R(1,2)	1.395	1.403	1.396	1.407	1.405	1.404	1.397	1.401	1.394	1.471	1.470	1.471
R(1,6)	1.411	1.405	1.404	1.404	1.398	1.407	1.412	1.407	1.406	1.358	1.357	1.352
R(1,9)	1.515	1.516	1.516	1.515	1.516	1.520	1.516	1.515	1.516	1.516	1.520	1.519
R(2,3)	1.399	1.404	1.399	1.389	1.389	1.397	1.397	1.403	1.397	1.349	1.348	1.347
R(3,4)	1.391	1.388	1.390	1.416	1.411	1.393	1.395	1.391	1.393	1.481	1.480	1.479
R(3,8)	—	—	—	1.363	1.368	—	—	—	—	—	—	—
R(4,5)	1.411	1.416	1.412	1.391	1.393	1.412	1.416	1.421	1.416	1.554	1.553	1.554
R(4,7)	1.363	1.362	1.365	1.347	1.350	1.348	1.350	1.350	1.353	1.214	1.214	1.214
R(5,6)	1.396	1.391	1.390	1.400	1.395	1.391	1.397	1.392	1.392	1.482	1.481	1.479
R(5,8)	1.350	1.348	1.353	—	—	1.364	1.353	1.350	1.355	1.214	1.215	1.215
R(9,10)	1.536	1.536	1.528	1.537	1.529	1.535	1.536	1.537	1.529	1.536	1.526	1.524
R(10,11)	1.524	1.524	1.538	1.523	1.539	1.523	1.525	1.524	1.539	1.525	1.526	1.528
Bond angles (°)												
A(2,1,6)	119.0	119.2	119.6	118.7	119.2	118.6	118.6	118.7	119.1	121.0	120.9	121.1
A(2,1,9)	121.1	120.7	120.7	120.6	120.4	121.4	121.0	120.7	120.6	118.1	116.0	115.3
A(6,1,9)	119.8	120.0	119.6	120.6	120.3	112.0	120.3	120.5	120.3	120.9	123.3	123.6
A(1,2,3)	120.4	120.5	120.2	120.4	120.2	120.9	120.4	120.4	120.2	122.5	122.7	122.7
A(2,3,4)	120.3	119.9	120.0	120.6	120.4	120.3	121.2	120.8	120.9	121.1	121.1	121.0
A(2,3,8)	—	—	—	125.2	125.2	—	—	—	—	—	—	—
A(4,3,8)	—	—	—	114.2	114.5	—	—	—	—	—	—	—
A(3,4,5)	120.0	120.1	120.2	119.2	119.3	119.2	119.1	119.2	119.3	116.9	116.7	116.7
A(3,4,7)	125.6	125.6	125.4	120.7	120.7	120.0	124.4	124.6	124.3	122.8	123.0	122.9
A(5,4,7)	114.4	114.2	114.4	120.1	120.0	120.8	116.5	116.2	116.5	120.3	120.3	120.3
A(4,5,6)	119.4	119.6	119.4	120.1	120.2	120.4	119.3	119.6	119.4	117.0	117.1	117.3
A(4,5,8)	121.0	120.6	120.8	—	—	114.4	116.5	116.2	116.5	121.1	121.2	120.9
A(6,5,8)	119.7	119.8	119.8	—	—	125.1	124.2	124.2	124.2	122.0	121.8	121.8
A(1,6,5)	120.8	120.6	120.5	121.0	120.7	120.5	121.4	121.3	121.1	121.5	121.7	121.3
A(1,9,10)	111.5	111.3	109.5	111.6	109.5	112.7	111.4	111.5	109.5	111.6	115.9	113.9
A(9,10,11)	109.3	108.7	111.2	109.0	111.3	109.2	108.9	108.8	111.3	109.7	110.3	110.5
Dihedral angles (°)												
D(6,1,2,3)	–0.7	–0.9	–0.3	–0.7	–0.3	–0.3	–0.5	–0.4	–0.0	–0.5	–0.1	–0.0
D(9,1,2,3)	–176.9	–177.8	–178.4	–177.3	–0.3	–179.9	–177.0	–177.1	–177.9	–178.4	179.1	180.0
D(2,1,6,5)	0.5	1.0	0.1	0.1	0.0	1.290	1.3	1.0	0.3	–0.6	–0.8	–0.0
D(9,1,6,5)	176.8	178.0	178.3	176.6	178.0	–179.1	177.9	177.6	178.2	177.3	–179.9	180.0
D(2,1,9,10)	85.2	97.4	97.6	84.0	94.4	52.8	76.4	94.2	87.1	81.2	160.5	–180.0
D(6,1,9,10)	–91.1	–79.5	–80.5	–92.5	–83.6	–126.8	–100.1	–82.4	–90.8	–96.7	–20.3	–0.0
D(1,2,3,4)	0.7	0.4	0.3	1.2	0.6	–0.4	0.1	0.1	–0.0	1.2	0.8	0.0
D(1,2,3,8)	—	—	—	–179.3	–179.6	—	—	—	—	—	—	—
D(2,3,4,5)	–0.5	–0.0	–0.2	–1.1	–0.5	0.1	–0.5	–0.3	–0.2	–0.7	–0.7	0.0
D(2,3,4,7)	179.9	–179.9	–179.9	179.5	179.3	–179.8	–179.8	–179.7	–179.7	178.7	178.9	–180.0
D(8,3,4,5)	—	—	—	179.4	179.7	—	—	—	—	—	—	—

© 2006 NRC Canada

Table 2 (*concluded*).

	$DAH^+_{(R),1}$	$DAH^+_{(R),2}$	$DAH^+_{(R),3}$	$DAH^+_{(R),4}$	$DAH^+_{(R),5}$	$DAH^+_{(R),6}$	$DAH^+_{(R),7}$	$DAH^+_{(R),8}$	$DAH^+_{(R),9}$	$DAH^+_{(O),1}$	$DAH^+_{(O),2}$	$DAH^+_{(O),3}$
D(8,3,4,7)	—	—	—	0.03	0.2	—	—	—	—	—	—	—
D(3,4,5,6)	0.3	0.1	0.1	0.4	0.2	0.9	1.3	0.8	0.5	–0.3	–0.1	–0.0
D(3,4,5,8)	–179.4	–179.9	–179.7	—	—	179.8	–179.1	–179.4	–179.4	178.6	179.3	180.0
D(7,4,5,6)	179.9	–180.0	179.8	179.8	179.7	–179.2	–179.3	–179.7	–179.9	–179.8	–179.7	180.0
D(7,4,5,8)	0.3	–0.1	0.0	—	—	–0.3	0.3	0.1	0.2	–0.8	–0.3	0.1
D(4,5,6,1)	–0.3	–0.6	–0.0	0.1	0.0	–1.6	–1.7	–1.1	–0.6	0.9	0.8	0.0
D(8,5,6,1)	179.4	179.4	179.8	—	—	179.6	178.7	179.1	179.3	–178.0	–178.6	–180.0
D(1,9,10,11)	55.1	–55.1	178.2	54.9	178.3	46.0	53.5	–54.8	–179.4	61.0	–58.0	180.0

Table 2. From Table 2, it can be seen that the bond lengths and bond angles of each isomer in both $DAH^+_{(R)}$ (except $C_4C_5C_8$, $C_3C_4C_7$, and $C_6C_5C_8$) and $DAH^+_{(O)}$ (except $C_2C_1C_9$ and $C_6C_1C_9$) are in a good agreement with that of other isomers. However, the dihedral angles of $C_2C_1C_9C_{10}$, $C_6C_1C_9C_{10}$, and $C_1C_9C_{10}N_{11}$ in both $DAH^+_{(R)}$ and $DAH^+_{(O)}$ conformers change markedly. From Table 2, the bond lengths of C_5C_8, C_4C_7, and C_2C_3 in $DAH^+_{(O)}$ are shorter than those in $DAH^+_{(R)}$ because of two carbonyls, however the bond lengths of C_1C_2, C_3O_4, and C_5O_6 in $DAH^+_{(O)}$ are longer than those in $DAH^+_{(R)}$. So, the bond angles of $C_2C_1C_9$, $C_6C_1O_9$, $C_1C_2C_3$, and $C_4C_5C_6$ as well as the dihedral angles of $C_2C_1C_9C_{10}$, $C_6C_1C_9C_{10}$, and $C_1C_9C_{10}C_{11}$ also change markedly with the changes in bond lengths.

Calculated standard electrode potential

The theoretical calculation of standard electrode potential for N-protonated dopamine versus *p*-BQ,H^+/*p*-HQ can be written as

[9] $DAH^+_{(O),g} + 2e^- + 2H^+_g = DAH^+_{(R),g}$

[10] $p\text{-}BQ_g + 2H^+_g + 2e^-_g = p\text{-}HQ_g$

where $DAH^+_{(O),g}$, $DAH^+_{(R),g}$, $p\text{-}BQ_g$, and $p\text{-}HQ_g$ represent $DAH^+_{(O)}$, $DAH^+_{(R)}$, *p*-BQ, and *p*-HQ in the gas state, respectively.

[11] $DAH^+_{(O),g} + p\text{-}HQ_g = DAH^+_{(R),g} + p\text{-}BQ_g$

The transformed Gibbs free energy of [11] is written as

[12] $$\Delta rG^0{}_1\ (298.15\ \text{K}) = G^0{}_{DAH^+(R),g} + G^0{}_{p\text{-}BQg} - G^0{}_{DAH^+(O),g} - G^0{}_{p\text{-}HQg}$$

where G^0 represents standard Gibbs free energies at 298.15 K and 1 atm, which is calculated using the Gaussian 03 package.

The redox reaction in solution is designed as (Fig. 5) where $\Delta rG^0{}_{aq,DAH^+(O)}$, $\Delta rG^0{}_{aq,DAH^+(R)}$, $\Delta rG^0{}_{aq,p\text{-}HQ}$, and $\Delta rG^0{}_{aq,p\text{-}BQ}$ are energies of solvation of $DAH^+_{(O)}$, $DAH^+_{(R)}$, *p*-HQ, and *p*-BQ in water at 298.15 K and 1 atm, respectively.

[13] $$\text{If } \Delta rG^0{}_2 = \Delta rG^0{}_{aq,DAH^+(R)} + \Delta rG^0{}_{aq,p\text{-}BQ} - \Delta rG^0{}_{aq,DAH^+(O)} - \Delta rG^0{}_{aq,p\text{-}HQ}$$

then the standard transformed Gibbs energy of reaction in solution is written as

[14] $\Delta rG^0\ (298.15\ \text{K, 1 atm}) = \Delta rG^0{}_1 + \Delta rG^0{}_2$

The standard electrode potential (E^0) of half reaction for $DA_{(O)}$,H^+/ $DA_{(R)}$ is calculated as

[15] $$\Delta rG^0\ (298.15\ \text{K, 1 atm}) = -nF\ (E^0 - E^0{}_{p\text{-}BQ,H^+/\,p\text{-}HQ})$$

where F is the Faraday constant (96.485 C/mol), n is number of electrons transferred, $E^0{}_{p\text{-}BQ,H^+/\,p\text{-}HQ}$ (0.699 V (27)) represents the standard electrode potential of half reaction for *p*-BQ,H^+/*p*-HQ.

The electron energies (ε_0), zero point energies (E_{ZPE}), total energies E_t ($\varepsilon_0 + E_{ZPE}$), relative energies (ΔE) in gas state compared with the lowest total energies, Gibbs free energies

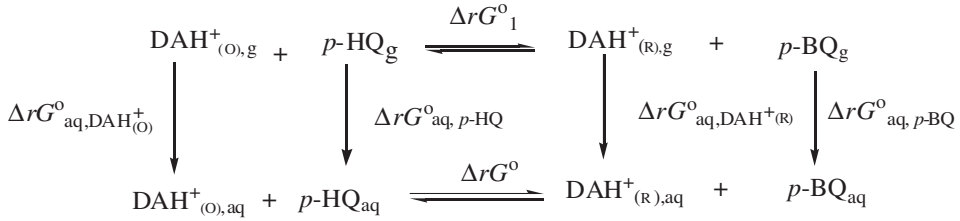
© 2006 NRC Canada

Table 3. Calculated thermochemistry values, ΔrG (298.15 K, 1 atm), standard electrode potential E^0, and the distribution coefficient a.

		$DAH^+_{(R),1}$	$DAH^+_{(R),2}$	$DAH^+_{(R),3}$	$DAH^+_{(R),4}$	$DAH^+_{(R),5}$	$DAH^+_{(R),6}$	$DAH^+_{(R),7}$
	ϵ_0[a]	–517.064 332	–517.063 956	–517.05 6477	–517.062 488	–517.054 000	–517.060 684	–517.054 486
	E_{ZPE}[a]	0.198 119	0.198 085	0.197 916	0.198 061	0.197 821	0.197 978	0.197 946
	E_t[a]	–516.866 214	–516.865 871	–516.858 560	–516.864 427	–516.856 179	–516.862 706	–516.856 541
	ΔE (kJ/mol)	0.0	0.90	20.10	4.69	26.35	9.21	25.40
	G^0 [a]	–516.902 263	–516.902 073	–516.895 556	–516.900 472	–516.893 151	–516.899 620	–516.892 899
	ΔrG^0_{aq} [a]	–0.100 777	–0.102 259	–0.112 813	–0.104 216	–0.116 922	–0.105 458	–0.112 321
	G^0_{aq} [a]	–517.003 04	–517.004 332	–517.008 369	–517.004 688	–517.010 073	–517.005 078	–517.005 220
	ΔG^0_{aq} (kJ/mol)	18.65	15.26	4.66	14.33	0.19	13.30	12.93
	N_i/N_o	5.403×10^{-4}	2.121×10^{-3}	0.153	3.087×10^{-3}	0.926	4.677×10^{-3}	5.429×10^{-3}
	a	2.574×10^{-4}	1.010×10^{-3}	0.0729	1.471×10^{-3}	0.4411	2.228×10^{-3}	2.586×10^{-3}
$DAH^+_{(O),1}$	ΔrG^0_1 (kJ/mol)	–90.04	–89.54	–72.43	–85.33	–66.11	–83.10	–65.45
	ΔrG^0_2 (kJ/mol)	87.62	83.73	56.02	78.59	45.23	75.33	57.31
	ΔrG^0 (kJ/mol)	–2.42	–5.81	–16.41	–6.74	–20.88	–7.77	–8.14
	E^0 (V)	0.712	0.729	0.784	0.734	0.807	0.739	0.741
$DAH^+_{(O),2}$	ΔrG^0_1 (kJ/mol)	–93.72	–93.22	–76.11	–89.02	–69.80	–86.78	–69.13
	ΔrG^0_2 (kJ/mol)	89.50	85.61	57.90	80.47	47.11	77.21	59.19
	ΔrG^0 (kJ/mol)	–4.22	–7.61	–18.21	–8.55	–22.69	–9.57	–9.94
	E^0 (V)	0.721	0.738	0.793	0.743	0.817	0.749	0.750
$DAH^+_{(O),3}$	ΔrG^o_1 (kJ/mol)	–103.78	–103.27	–86.17	–99.07	–79.86	–96.84	–79.19
	ΔrG^0_2 (kJ/mol)	115.54	111.64	83.93	106.50	73.14	103.24	85.22
	ΔrG^0 (kJ/mol)	11.76	8.37	–2.24	7.43	–6.71	6.40	4.03
	E^0 (V)	0.638	0.656	0.711	0.660	0.734	0.666	0.668

[a]Hartree

Fig. 5. Design of redox reaction of $DAH^+_{(R)}$ in solution, where g and aq denote gas and solution, respectively.



in water ($G^0_{aq} = G^0 + \Delta rG^0_{aq}$), relative Gibbs free energies in water ΔG^0_{aq}, G^0, ΔrG^0_{aq}, ΔrG^0_1, ΔrG^0_2, and $E^0_{DAH^+(O),H^+DAH^+(R)}$ are shown in Table 3. From Table 3, the most stable $DAH^+_{(R)}$ and $DAH^+_{(O)}$ in the gas state are $DAH^+_{(R),1}$ and $DAH^+_{(O),1}$, respectively. However, the lowest Gibbs free energies in water (G^0_{aq}) are ascribed to $DAH^+_{(R),9}$ and $DAH^+_{(O),3}$ because of the energies of solvation, respectively. The standard electrode potential calculated by $DAH^+_{(R),9}$ and $DAH^+_{(O),3}$ is 0.735 (V), which is in good agreement with the experimental value of 0.74 (V) at pH 5.50. From Table 3, it is found that the calculated standard electrode with a combination of stable $DAH^+_{(R),5}$, $DAH^+_{(R),9}$, and $DAH^+_{(O),3}$ is very close to our experimental value. However, there are more deviations from the theoretical values with a other combinations.

According to the Boltzmann distribution, the molecular number of excited states, N_i, the molecular number of ground states, N_o, the quantum number of the excited state at same energy level, $g_i = 2$, the quantum number of the ground state at same energy level, $g_o = 2$, Boltzmann constant, k, temperature, T (298.15 K), and the Gibbs free energy difference of the excited state, and the ground state for each molecule, ΔG_{aq}, are related by the equation (28)

$$[16] \quad N_i/N_o = g_i/g_o \exp(-\Delta G_{aq}/kT)$$

The N_i/N_o values of $DAH^+_{(R),1}$, $DAH^+_{(R),2}$, $DAH^+_{(R),3}$, $DAH^+_{(R),4}$, $DAH^+_{(R),5}$, $DAH^+_{(R),6}$, $DAH^+_{(R),7}$, and $DAH^+_{(R),8}$, shown in Table 3, are 5.403×10^{-4}, 2.121×10^{-3}, 0.153, 3.087×10^{-3}, 0.926, 4.677×10^{-3}, 5.429×10^{-3}, and 4.367×10^{-3}, respectively. The N_i/N_o values of $DAH^+_{(O),1}$ and $DAH^+_{(O),2}$ are 3.273×10^{-3} and 1.574×10^{-3}, respectively.

Suppose

$$[17] \quad N_o + \sum N_i = N_o + (5.403 \times 10^{-4}) \times N_o + (2.121 \times 10^{-3}) \times N_o + 0.153N_o + (3.087 \times 10^{-3}) \times N_o + 0.926N_o + (4.677 \times 10^{-3}) \times N_o + (5.429 \times 10^{-3}) \times N_o + (4.367 \times 10^{-3}) \times N_o = 1000$$

then $N_o = 476.4$. The distribution coefficients (a_R) of $DAH^+_{(R),1}$, $DAH^+_{(R),2}$, $DAH^+_{(R),3}$, $DAH^+_{(R),4}$, $DAH^+_{(R),5}$,

© 2006 NRC Canada

$DAH^+_{(R),8}$	$DAH^+_{(R),9}$	$DAH^+_{(O),1}$	$DAH^+_{(O),2}$	$DAH^+_{(O),3}$	*p*-BQ	*p*-HQ
–517.055 880	–517.047 575	–515.790 748	–515.789 560	–515.785 087	–381.457 744	–382.695 758
0.197 992	0.197 714	0.173 941	0.173 986	0.173 909	0.085 181	0.108 718
–516.857 889	–516.849 861	–516.616 807	–515.615 574	–515.611 178	–381.372 563	–382.587 040
21.86	42.93	0	3.22	14.76	—	—
–516.893 921	–516.886 919	–515.653 450	–515.652 04	–515.648 217	–381.403 087	–382.617 607
–0.111 095	–0.123 226	–0.121 889	–0.122605	–0.132 523	–0.006 319	–0.018 579
–517.005 016	–517.010 145	–515.775 339	–515.774 645	–515.780 740	–381.409 406	–382.636 186
13.47	0.00	14.18	16.00	0.00	—	—
4.367×10^{-3}	—	3.273×10^{-3}	1.574×10^{-3}	—	—	—
2.080×10^{-3}	0.4764	3.257×10^{-3}	1.566×10^{-3}	0.995	—	—
–68.13	–49.75	—	—	—	—	—
60.53	28.68	—	—	—	—	—
–7.60	–21.68	—	—	—	—	—
0.738	0.808	—	—	—	—	—
–71.82	–53.43	—	—	—	—	—
62.41	30.56	—	—	—	—	—
–9.41	–22.87	—	—	—	—	—
0.748	0.817	—	—	—	—	—
–81.87	–64.39	—	—	—	—	—
88.45	56.59	—	—	—	—	—
6.58	–6.90	—	—	—	—	—
0.665	0.735	—	—	—	—	—

$DAH^+_{(R),6}$, $DAH^+_{(R),7}$, $DAH^+_{(R),8}$, and $DAH^+_{(R),9}$, shown in Table 3, are 2.574 0^{-4}, 1.010×10^{-3}, 0.0729, 1.471×10^{-3}, 0.4411, 2.228×10^{-3}, 2.586×10^{-3}, 2.080×10^{-3}, and 0.4764, respectively. The distribution coefficient (*a*) of $DAH^+_{(O),1}$, $DAH^+_{(O),2}$, and $DAH^+_{(O),3}$, calculated similarly, shown in Table 3, are 3.257×10^{-3}, 1.566×10^{-3}, and 0.995, respectively. These results indicate that the redox reaction ascribes mainly to $DAH^+_{(R),5}$, $DAH^+_{(R),9}$, and $DAH^+_{(O),3}$.

We calculated the weighted average of the standard electrode potential E^0 as

[18] $$E^0 = \sum E^0_{i,j} \times a_{Ri} \times a_{Oj} = 0.732 \text{ (V)}$$

This result is in excellent agreement with the experimental value of 0.74 V and thus we believe that our theoretical calculation is reliable.

Conclusion

The geometries of $DAH^+_{(O)}$ and $DAH^+_{(R)}$ are optimized at the B3LYP/6–31G(d,p) level and nine conformers of $DAH^+_{(R)}$ and three conformers of $DAH^+_{(O)}$ are obtained. The predicted weighted average of standard electrode potentials (0.732 V) are in best agreement with experimental data (0.74 V at pH 5.50). This method is very useful in predicting unknown standard potentials of such compounds because the theoretical method is very simple and inexpensive.

Acknowledgements

This research was supported by National Sciences Foundation of China (grant No. 20405011), Opened Science Foundation of Jiangsu Province Key Laboratory for Chemistry of Low- Dimensional Materials (grant No. JSKC06031), and Science Foundation of the education department of Jiangsu province of China (grant No. 04KJD150038).

References

1. M.E. El-Kommos, F.A. Mohamed, and A.S.K. Khedr. J. Assoc. Off. Anal. Chem. **73**, 516 (1990).
2. M.H. Sorouraddin, J.L. Manzoori, E. Kargarzadeh, and A.M. Haji Shabani. J. Pharm. Biomed. Anal. **18**, 877 (1998).
3. D.D. Miller, M. Harold, R.A. Wallace, L.J. Wallace, and N.J. Uretsky. Trends Pharmacol. Sci. **9**, 282 (1998).
4. T.M. Bustard and R.S. Egan. Tetrahedron, **27**, 4457 (1971).
5. J.J. Urban, C.J. Cramer, and G.R. Famini. J. Am. Chem. Soc. **114**, 8226 (1992).
6. J.J. Urban and G.R. Famini. J. Comput. Chem. **14**, 353 (1993).
7. K.H. Xue, F.F. Tao, W. Xu, S.Y. Yin, and J.M. Liu. J. Electroanal. Chem. **578**, 323 (2005).
8. M. Zhang, K.P. Gong, H.W. Zhang, and L.Q. Mao. Biosens. Bioelectron. **20**, 1270 (2005).
9. T. Liu, M.X. Li, and Q.Y. Li. Talanta, **63**, 1053 (2004).
10. K.H. Xue, F.F. Tao, S.Y. Yin, W. Shen, and W. Xu. Chem. Phys. Lett. **391**, 243 (2004).
11. H. Razmi, M. Agazadeh, and B. Habibi-A. J. Electroanal. Chem. **547**, 25 (2003).
12. J.M. Zen and I.L. Chen. Electroanalysis, **9**, 537 (1997).
13. C.X. Cai and K.H. Xue. Microchem. J. **61**, 183 (1999).
14. N. S. Datta, J. Sudhamsu, and A. Pandey. J. Phys. Chem. B, **108**, 8007 (2004).
15. A. Pandey and S.N. Datta. J. Phys. Chem. B, **109**, 9066 (2005).
16. M.H.M. Olsson, G. Hong, and A. Warshel. J. Am. Chem. Soc. **125**, 5025 (2003).
17. Y.Z. Song, J.M. Xie, Y. Song, H.M. Shu, G.Q. Zhao, X.M. Lv, and W. Xie. Spectrochim. Acta Part A, **65**, 333 (2006).

© 2006 NRC Canada

18. M.J. Marsella, R.J. Reid, S. Estassi, and L.S. Wang. J. Am. Chem. Soc. **124**, 12507 (2002).
19. Y.Z. Song, J.F. Zhou, S.J. Zi, J.M. Xie, and Y. Ye. Bioorg. Med. Chem. **13**, 3169 (2005).
20. P. Zhang, F.H. Wu, G.C. Zhao, and X.W. Wei. Bioelectrochemistry, **67**, 109 (2005).
21. A.D. Becke. J. Chem. Phys. **98**, 5648 (1993).
22. M.J. Frisch, G.W. Trucks, H.B. Schlegel, G.E. Scuseria, M.A. Robb, J.R. Cheeseman, J.A. Montgomery, Jr., T. Vreven, K.N. Kudin, J.C. Burant, J.M. Millam, S.S. Iyengar, J. Tomasi, V. Barone, B. Mennucci, M. Cossi, G. Scalmani, N. Rega, G.A. Petersson, H. Nakatsuji, M. Hada, M. Ehara, K. Toyota, R. Fukuda, J. Hasegawa, M. Ishida, T. Nakajima, Y. Honda, O. Kitao, H. Nakai, M. Klene, X. Li, J.E. Knox, H.P. Hratchian, J.B. Cross, C. Adamo, J. Jaramillo, R. Gomperts, R.E. Stratmann, O. Yazyev, A.J. Austin, R. Cammi, C. Pomelli, J.W. Ochterski, P.Y. Ayala, K.Morokuma, G.A. Voth, P. Salvador, J.J. Dannenberg, V.G. Zakrzewski, S. Dapprich, A.D. Daniels, M.C. Strain, O. Farkas, D.K. Malick, A.D. Rabuck, K. Raghavachari, J.B. Foresman, J.V. Ortiz, Q. Cui, A.G. Baboul, S. Clifford, J. Cioslowski, B.B. Stefanov, G. Liu, A. Liashenko, P. Piskorz, I. Komaromi, R.L. Martin, D.J. Fox, T. Keith, M.A. Al-Laham, C.Y. Peng, A. Nanayakkara, M. Challacombe, P.M. W. Gill, B. Johnson, W. Chen, M.W. Wong, C. Gonzalez, and J.A. Pople. Gaussian [computer program]. Gaussian, Inc., Pittsburgh Penn., 2003.
23. R. Bonaccorsi, R. Cimiraglia, and J. Tomasi. Comput. Chem. **4**, 288 (1983).
24. J.L. Pascualahuir, E. Silla, J. Tomasi, and R.J. Bonaccorsi. Comput. Chem. **8**, 778 (1987).
25. S. Miertus, E Scrocco, and J. Tomasi. Chem. Phys. **55**, 117 (1981).
26. J. Wang. *In* Analytical electrochemistry. 2nd ed. John Wiley & Sons Inc., New York. 2000. p. 31.
27. D. Dobos. *In* Electrochemical data. Elsevier, New York. 1975. pp.1–26.
28. Y. Jiang. *In* Physical chemistry. Central China Normal University Publishing Company, Wuhan, China. 1987. pp. 290–300.

© 2006 NRC Canada

AWARD LECTURE / CONFÉRENCE D'HONNEUR

CIC Medal Award Lecture — Molecular keystones: Lessons from bioorganic reaction mechanisms[1]

Ronald Kluger

Abstract: The work of the author is reviewed in terms of "keystone molecules" that serve as figurative points of support to understand the interactions of smaller molecules within biological macromolecules. The review emphasizes lessons learned in carboxylation of biotin, reactions of cyclic phosphates, the uses of acyl phosphate monoesters, and the mechanism of decarboxylation of thiamin-derived intermediates.

Key words: CIC medal, biotin, ATP, mechanisms, cyclic phosphates, thiamin, acyl phosphates, catalysis.

Résumé : Ce rapport résume les travaux de l'auteur en fonction de molécules "clés de voûte" qui servent d'une façon figurative de support pour comprendre les interactions de molécules plus petites dans les macromolécules biologiques. Cette revue met en relief les leçons tirées de la carboxylation de la biotine, des réactions des phosphates cycliques, des utilisations des monoesters des phosphates d'acyle et du mécanisme de décarboxylation des intermédiaires dérivés de la thiamine.

Mots clés : médaille de l'ICC, biotine, ATP, mécanismes, phosphates cycliques, thiamine, phosphates d'acyle, catalyse.

[Traduit par la Rédaction]

Introduction

I was delighted to be designated the 2006 recipient of the CIC Medal; the Institute has been a central part of my scientific life. I gave the medal address as part of the Canadian Chemistry Conference in June 2006. This paper summarizes much of the talk and makes some clarifications while omitting some sections that do not follow an intelligible script. I organized the presentation around specific organic molecules that relate to mechanisms in biological chemistry. My objectives as a scientist result from approaching complex problems with the tools afforded by finding the right molecule to answer a question or target a larger system. I chose the phrase "molecular keystones" to describe species that are the basis of conceptual developments and built the talk around each of these as a section. The term "molecular keystone" has also been used to describe a structural role for a small molecule within a larger species (1).

In general, we chose molecular keystones as the simplest synthetic molecule containing the reacting functionality of a more complex biomolecule. This includes molecules designed to mimic biological interactions on a small scale and those that formed a basis for extended mechanism-based molecular design.

My interest in doing this work was the result of a perspective that goes back to my earliest days as a university student. I began doing organic chemistry research in my second undergraduate year at Columbia University in New York. Gilbert Stork hired me to work in his research group on projects that were odds and ends — preparing materials for others to use in their complex syntheses as well as changing the oil in the vacuum pumps. I was chosen for this from the many students taking introductory organic chemistry midway through the course. My teaching assistant was an undergraduate who had been with Stork and was leaving for graduate studies at mid-year. He designated me as his replacement. Of course, at the time I had no idea who Gilbert Stork was or how fortunate I was. The 3 years I spent in that lab were wonderful; Professor Stork's attitude was inspiring and amusing. I quickly became an expert at changing the pump oil and making the highly mutagenic precursor used at the time for making diazomethane. The department obtained its first routine NMR machine (a Varian-A60), and it was an immediate hit. But the only deuterated solvent that could be purchased was deuterium oxide. So I was given a project: make deuterochloroform so members of the Stork group could use it as a solvent for the new NMR. The synthesis was in a collection, "Organic Syntheses with Isotopes" (2) and seemed straightforward: combine chloral and sodium deuteroxide in deuterium oxide with anhydrous chloral. I could purchase chloral but not sodium deuteroxide. Stork

Received 28 July 2006. Accepted 5 September 2006. Published on the NRC Research Press Web site at http://canjchem.nrc.ca on 31 October 2006.

R. Kluger. Davenport Chemistry Laboratories, Department of Chemistry, University of Toronto, Toronto, ON M5S 3H6, Canada. (e-mail: rkluger@chem.utoronto.ca).

[1]Based on the CIC medal address.

 doi:10.1139/V06-149 © 2006 NRC Canada

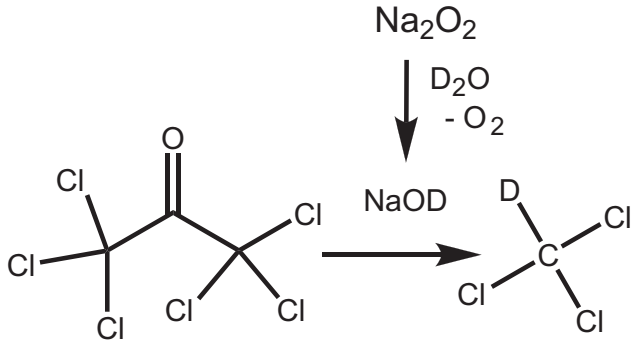
and I discussed the obvious and dangerous route involving adding pieces of sodium to deuterium oxide. The by-product is deuterium gas, which reacts just as hydrogen does, potentially combining explosively with oxygen. This process also loses an equivalent of deuterium from the solvent for each equivalent of deuteroxide produced. I recalled a high school chemistry experiment in which oxygen is generated from sodium peroxide and water, with sodium hydroxide as a by-product. I suggested that I try making sodium deuteroxide from sodium peroxide and deuterium oxide, and I was encouraged to try it. It worked well and cleaving chloral worked well. We had a lot of deuterochloroform. However, chloral is very wet and usually a hydrate. So I tried hexaxchloroacetone instead. This chemical is a powerful tear gas but is anhydrous. There was none in the department, so I called City Chemical in lower Manhattan. They had it in stock. I took the subway to their location, bought a gallon bottle of practical grade hexachloroacetone (it was inexpensive) and rode back to Columbia on the subway with my starting material. I was happy to finance my own research. I then made kilos of deuterochloroform. The word quickly spread throughout the department, and we were giving away many bottles of the solvent. The NMR was instantly busy. Professor Stork was very pleased and he encouraged me in my desire to describe the procedure in a journal article — an experience that I found exciting (Scheme 1).

It appeared in the *Journal of Organic Chemistry* during my third year as an undergraduate (3). My skill at making deuterochloroform did not remain in demand for long. Merck, Sharp and Dohme Isotopes (MSD) of Dorval, Quebec, started selling it for a low price soon after. Several years later a friend of mine interviewed there for a job. Recalling my deuterochloroform story, he asked how they made theirs. The answer was that they follow an unpatented procedure that had appeared in the *Journal of Organic Chemistry* a few years before, a fact I confirmed with Irwin Lesk of MSD when I met him after my arrival in Toronto. Just a year ago, I received a note from a professor in Wales who said he thought a student of his had a new and efficient synthesis of deuterochloroform. Then he had been referred to me and to my old article. He said that his method was not as good, and he had tried to learn how Aldrich currently made theirs. They wouldn't tell him. I called the technical department of Cambridge Isotope Labs and asked how they made their deuterochloroform. The answer was satisfying: by cleaving hexachloroacetone with sodium deuteroxide. When I asked how they came to do it that way, the answer was that they had always done it that way.

While I was at Columbia I also had the pleasure of taking a course in organic reaction mechanisms with Ronald Breslow and later asked for advice about what to do in organic chemistry. His response was that while it is satisfying to make molecules, it is even more satisfying to use them to test ideas. This was inspiring and has been my guiding principle. Professor Stork told me as I left that since I had learned how to make molecules in the time I was with him, I should do something that would use that as a background and that I should take advantage of opportunities to use mathematical applications to study reactions in more detail.

My graduate education involved studies of cyclic peptides with Elkan Blout and phosphate reaction mechanisms with

Scheme 1.



Frank Westheimer. I was a postdoc with Bob Abeles at Brandeis and learned to work on enzyme mechanisms. Regrettably, I was off to my first job at the University of Chicago only a short time after I started with Bob Abeles. This was because I had an interview at Chicago while I was still a student for a job I hadn't applied for. After a short time in Chicago, I moved to Toronto where I have had a most exciting and pleasant time with excellent students and colleagues. Some of the molecular keystones from my career in Toronto will be the focal points of the remainder of this review.

N-Carboxybiotin

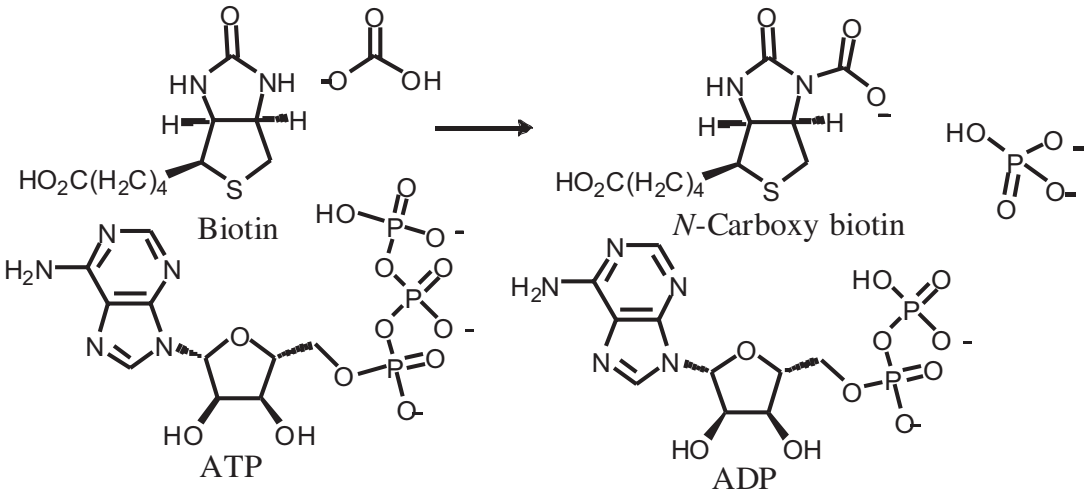
Biological processes involving synthesis are often associated with the hydrolysis of the terminal phosphate of ATP to give ADP and inorganic phosphate. The hydrolysis reaction is exergonic. Somehow, the energetically favored hydrolysis through the intervention of enzymes becomes the driving force for an apparently unrelated chemical synthetic process. Lipmann set these out in terms of the artifice of "high energy phosphate bonds" (4). One notable case is the formation of dicarboxylic acids from monocarboxylic acids and bicarbonate. Enzymes that catalyze the reaction do this in solution and accomplish this at the expense of ATP hydrolysis, using biotin as a cofactor. Lynen showed that the involvement of ATP hydrolysis is in an initial stage when bicarbonate and biotin react to form *N*-carboxybiotin. Oxygen from bicarbonate is transferred to the phosphate that is cleaved from ATP (5). Thus, the formation of *N*,1′-carboxybiotin creates a single chemical bond while dehydrating bicarbonate along with ATP hydrolysis (6).

The role of ATP in the process is direct; if bicarbonate is uniformly labeled with ^{18}O, a labeled oxygen atom appears in the phosphate that results from the reaction that produces *N*-carboxybiotin (5). Kinetic and isotope-exchange studies indicated that the reaction requires all components and that there are no partial exchange reactions. The overall process is summarized in Scheme 2.

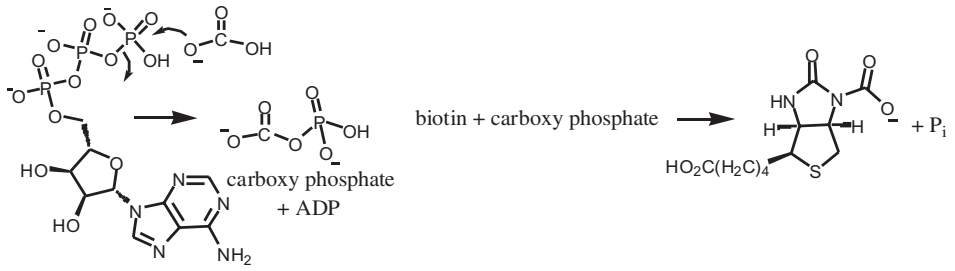
There are three reactants and three products, and no intermediate has been isolated. The lack of exchange is consistent with a fully concerted reaction of all three, but there is nothing chemically reasonable about any transition state that would be implied. The alternative is to break the process into more steps and to propose intermediates that have not been detected. The first two-step mechanism that was proposed involves the initial reaction of ATP and bicarbonate to give the mixed anhydride of carbonic and phosphoric acids,

© 2006 NRC Canada

Scheme 2.



Scheme 3.



carboxy phosphate and ADP (7). This reacts with the nitrogen of the conjugate base of biotin to give *N*-carboxybiotin (Scheme 3).

In this mechanism, carboxy phosphate is formed in the first step and transfers its carboxyl group to biotin in the second step. This mechanism is found in textbooks and accommodates much of the data. It is consistent with later studies on the stereochemical course at the terminal phosphate of ATP (8). Yet, the intermediate has never been observed and the there are aspects that are questionable in terms of chemical reactivity. In a study of half esters of carbonic acid, it was reported that carboxy phosphate is too unstable to produce synthetically, with an expected half-life in the millisecond time scale (9). Jencks proposed that upon formation, carboxy phosphate would convert to unsolvated carbon dioxide, which would react rapidly with the conjugate base of biotin. However, others suggested that the conjugate base of biotin would react with carboxy phosphate, since carbon dioxide does not react with biotin (10). Another problem in that case is that carboxy phosphate is a poorer electrophile than bicarbonate. Despite the shortcomings, it is normally the only mechanism presented when this system is reviewed. The fact that a mechanism is widely cited does not mean that it is correct. In Popper's view, hypotheses can only be tested by negation or risky prediction: consider all the possibilities and do experiments that challenge them. So, with biotin carboxylation, we should seek all possibilities and then challenge them with experiments.

An alternative two-step mechanism is the addition of biotin to ATP to form *O*-phosphobiotin (Scheme 4, structure **1**) (11). If the urea oxygen of biotin reacts with ATP, the intermediate is a functional analogue of the addition product from DCC and a phosphate. This could react with bicarbonate to generate carboxy phosphate adjacent to the reacting nitrogen. The steps are consistent with all the experimental information. To get an adjacent attack, the addition product would undergo pseudorotation at the phosphorus, leading to a mechanism with the same overall stereochemistry as reported.

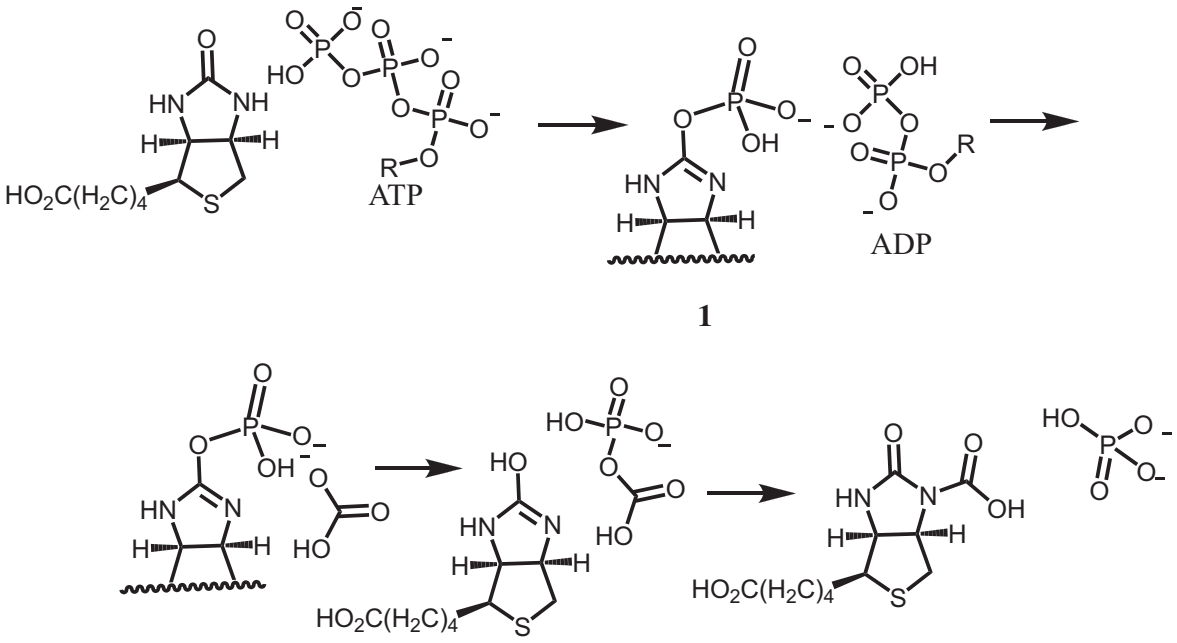
This raises the question of whether the urea is sufficiently nucleophilic to attack the phosphorus and displace the leaving group. By joining the two species to minimize the entropy barrier, Paul Davis and Prakash Adawadkar showed that such a reaction is very likely to occur rapidly. Hydrolysis of the phosphonate ester with an adjacent urea is very rapid, indicative of the formation of a cyclized covalent intermediate (Scheme 5) (12).

We have so far presented two mechanisms involving an initial reaction of two of the three reactant species. There is one remaining combination involving two initial reactants: bicarbonate reacts with biotin and the addition product reacts with ATP. A reaction through this combination is shown in Scheme 6.

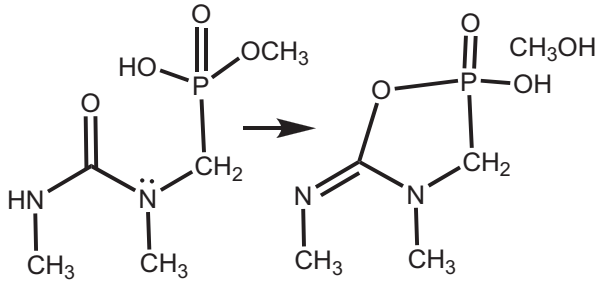
The addition of the conjugate base of biotin to bicarbonate should occur more readily than the addition to carboxy phosphate. Such a reaction had been established in an excellent model by Kirby and co-workers (13). In the next step, the remaining reactant, ATP, is the subject of nucleophilic substitution to produce a second addition intermediate and ADP. Loss of phosphate generates *N*-carboxybiotin. In this

© 2006 NRC Canada

Scheme 4.



Scheme 5.



mechanism, ATP is cleaved only when the addition to bicarbonate has occurred. The initial oxyanion addition product is a stronger base than bicarbonate. Will such a reaction occur at phosphorus (14)? Scott Taylor produced a phosphate ester derived from acetoin that reacts rapidly via just such a pathway (Scheme 7) (15).

This established that if biotin were to add to bicarbonate, the resulting product would be reactive toward ATP. The addition product is the same as would be formed in the reaction of biotin with carboxy phosphate, but it avoids the generation of such an unstable species that could simply consume ATP and give off CO_2. The matter of which mechanism is correct for an enzyme has yet to be established, although many authors believe it has. It is good to note that in Silverman's text (16), all the possibilities remain as possibilities.

Methyl ethylene phosphate

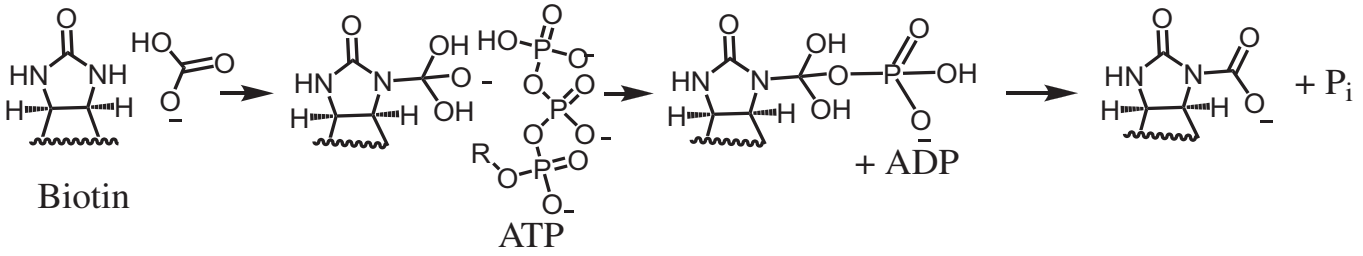
The hydrolysis of the ester linkages in RNA is catalyzed by ribonuclease enzymes from many sources. The immediate product of chain cleavage is the formation of a 2′,3′-cyclic derivative of the 5′-nucleotide from which the remaining chain continues. The cyclic ester is much more reactive than the open-chain material. The cyclic material undergoes relatively rapid spontaneous hydrolysis. Why is the cyclic species so much more reactive? Westheimer determined that the heat of hydrolysis of the cyclic ester, methyl ethylene phosphate (MEP), exceeds that of the comparable acyclic ester by about 5 kcal/mol (17, 18). The 5-coordinate phosphorus intermediate formed upon the addition of water to MEP is a high energy species and should closely resemble the transition states that lead to its formation and decomposition. Molecular mechanics computations suggested that the ring strain is negligible in the intermediate because of the change in hybridization of the bonding orbitals in the higher coordination state (19, 20). The kinetic acceleration of the reaction is about 10^6 in the observed first-order rate constant. The reduced strain in the transition state corresponds to about half the acceleration, although there are undocumented reports of strain up to 9 kcal/mol in MEP (21). This raises the question: if the strain accounts for only half the acceleration, what is the source of the rest (19)?

In Scheme 8, hydrolysis of MEP is shown to lead to two distinct sets of co-existing products. One product is ethylene phosphate in which the original ring is retained. Thus, it is clear that the acceleration can occur due to ring strain without the need for the ring to be cleaved. The formation of EP requires the pseudorotation of the intermediate because the attack and departure require the leaving–attacking groups to be in apical positions while the small ring must span an apical and an equatorial position (22). The yield of EP and methanol as a fraction of total products is expressed as the percent exocyclic cleavage. Analysis of the relationship of pH of hydrolysis to products showed that pseudorotation competes with other processes and can be rate-limiting for exocyclic cleavage (23). In alkaline solutions (Scheme 9), the electronegativity of the ionized hydroxyl in the intermediate supports direct expulsion of the ring as a leaving group and there is no exocyclic cleavage.

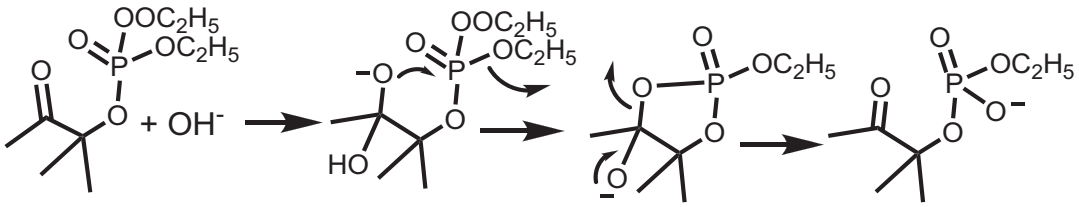
Exocylic cleavage occurs in neutral and in dilute acid solutions but not in dilute base solutions. In more concentrated

© 2006 NRC Canada

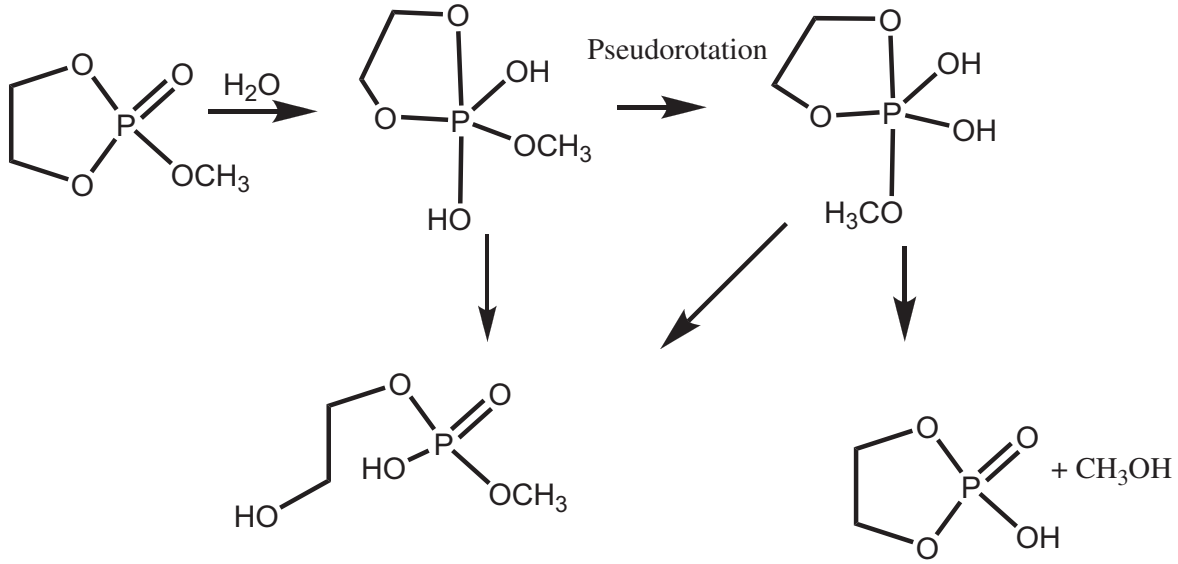
Scheme 6.



Scheme 7.



Scheme 8.



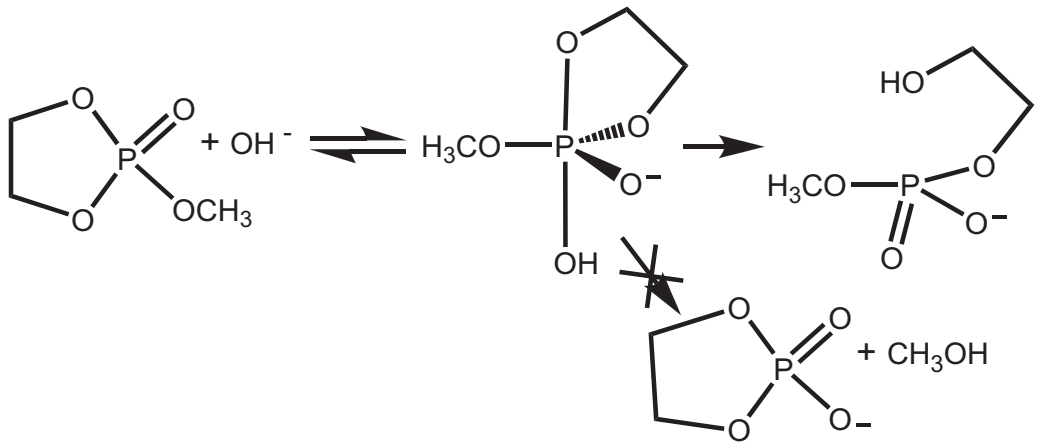
solutions of hydroxide, exocyclic cleavage increases in proportion to the concentration of added base. Because the overall reaction is first-order in hydroxide, the additional cleavage is second-order in base. This can be explained by the formation of the dianion, which forces a pseudorotation to accommodate its anionic oxygens in equatorial positions (Scheme 10).

Gorenstein developed a theory (24) that extended Lehn's application (25) of the Deslongchamps anti-periplanar lone pair hypothesis (ALPH) (26) to account for the increased reactivity of cyclic phosphates; leaving groups anti-periplanar to the greatest number of nonbonding lone pairs of electrons on oxygen will react fastest because of the nature of specific orbital interactions (27). However, the results that led to the mechanism in Scheme 10 appear to contradict that suggestion. The dianionic five-coordinate phosphorus intermediate that has undergone pseudorotation contains more lone electron pairs anti-periplanar to the ring O–P bond, yet the product distribution includes an increasing amount of exocyclic cleavage, which would violate the firm prediction from the Gorenstein version of ALPH.

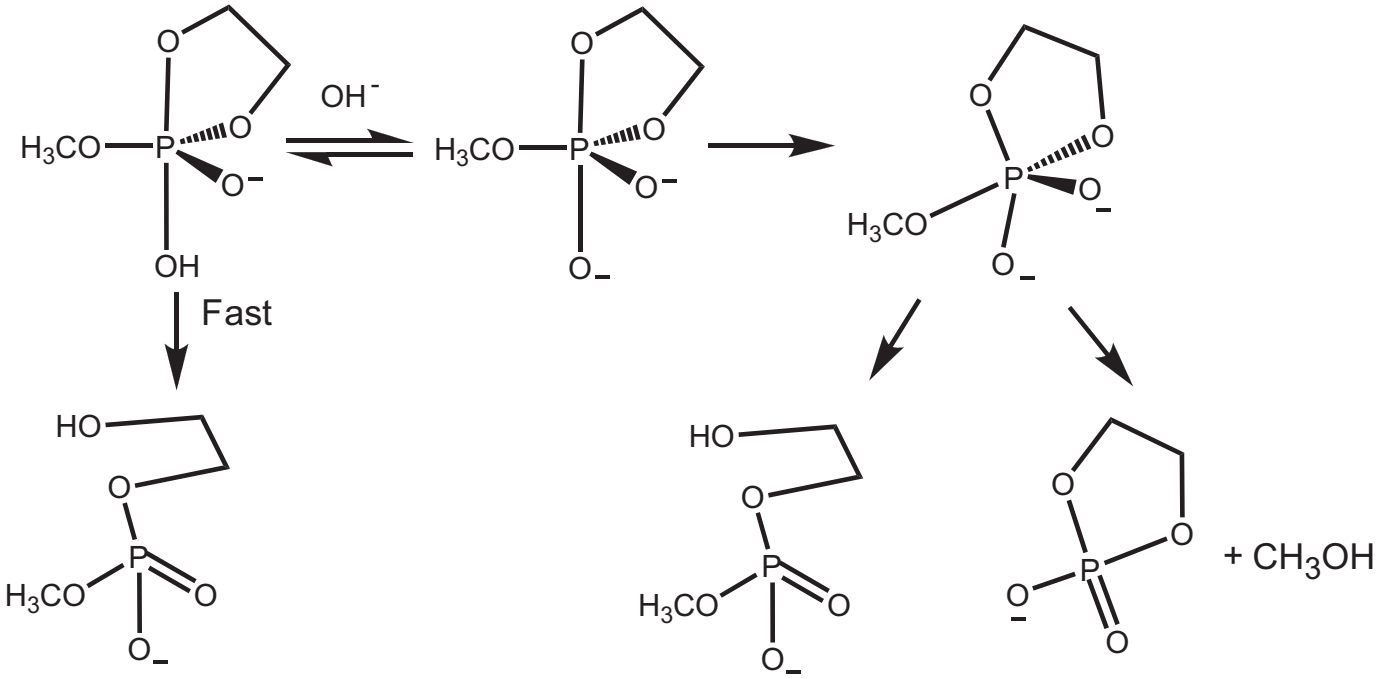
Our observations and explanation preceded the theoretical work by almost a decade. The results were based on careful analysis of methanol produced under both concentrated and dilute reaction conditions (to avoid possible polymerization of the product (28)) and with extrapolation to the time of mixing of the reactants. Thus, it seemed that the theory was not correct on this fundamental point. I noted this in correspondence with David Gorenstein whose paper reported that there is no exocylic cleavage in the hydrolysis of ethyl ethylene phosphate in strongly basic solutions confirming the predictions of ALPH but contradicting our own work (29). To my dismay, in 1983, Frank Westheimer contacted me and said that he had received a preprint of a paper from Gorenstein and Taira reporting results of using a rapid-quench method and ^{31}P NMR to re-examine the products of

© 2006 NRC Canada

Scheme 9.



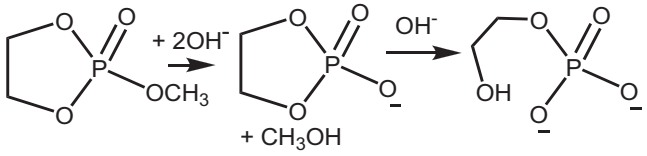
Scheme 10.



the reaction of MEP in a strongly basic solution (30). They concluded that our report in 1969 (31) was incorrect; that there is no exocyclic cleavage and, therefore, their ALPH theory is correct. He told me that it was my responsibility to reinvestigate that work and find out where I went wrong or he would do it. The Taira–Gorenstein publication appeared with these results: "We also now find no exocyclic cleavage (0 ± 3%) for methyl ethylene phosphate between pH 8 and 15. Even in 5 mol/L NaOH, a rapid freeze/acid quench (after less than 2 s of reaction) led to 100% endocyclic cleavage". The product analysis is based exclusively on ^{31}P NMR spectra, and the conclusion is based on the apparent absence of a signal for 2-hydroxyethyl phosphate, the product that would result from the further hydrolysis of the immediate product of exocyclic cleavage, ethylene phosphate (Scheme 11).

There is no mention of the signal of ethylene phosphate, which should be the product of interest from this method if a quench is used to stop any further reaction. Why would they not mention it? The rapid freeze – acid quench method is not

Scheme 11.



described in this paper but is presented in an earlier paper and applied to a similar compound, ethyl ethylene phosphate: "A 50 μL sample of 0.155 mol/L ethyl ethylene phosphate in dry dioxane was added to 0.49 mL of 5.0 mol/L NaOH at room temperature, and the solution was quickly frozen in an acetone/dry ice bath. To the almost frozen solution, was carefully added 66.6 μL of 36 N H_2SO_4. The pH of the solution was adjusted to about 9 with a Tris buffer solution. Up to this point everything was carried out within a minute. Some inorganic precipitate was filtered through a ni-

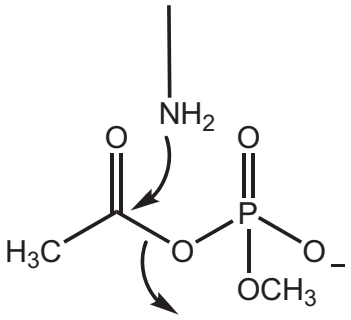
© 2006 NRC Canada

tric acid and EDTA solution treated disposable pipet plugged with EDTA-treated cotton and Chelex-100 (Bio-Rad) ion exchange resin". Gorenstein's graduate student, Kazunari Taira, also reported these results in his Ph.D. thesis. He wrote "I remember the day I asked Dr. Gorenstein frankly, 'Do you mind if I try to disprove your stereoelectronic theory by examining Westheimer's system in more detail?' He answered 'No, of course not. I just want to know the truth. Go ahead!!' I am glad that I have gotten the results which are consistent with the stereoelectronic theory, which constitutes my thesis" (32).

I asked Greg Thatcher, who was a graduate student in my lab in Toronto at the time, to duplicate the Gorenstein–Taira experiments and to analyze the products more completely. Greg synthesized MEP and attempted the quench reaction. It did not work at all as had been reported. Concentrated sulfuric acid flows very slowly from a pipet and reacts violently with concentrated sodium hydroxide, giving a massive solid of sodium sulfate with no liquid remaining (sodium sulfate forms hydrates). We changed the quench to use concentrated hydrochloric acid and worked as fast as possible. The results were the same as without a quench. Methanol is clearly present and can be seen and quantified in the ^{1}H NMR. Ethylene phosphate is easily seen in the ^{31}P NMR and in the amounts one would expect from the methanol produced (33). After running many controls (multiple synthetic routes, concentration dependence of every species), we concluded that whatever results were reported by Gorenstein and Taira were suspect and our original observation was correct; there is substantial exocyclic cleavage from MEP in a strong base, and this means that ALPH fails this test. Therefore, the question remains as to whether strain alone accounts for the increased rate of hydrolysis of cyclic phosphates.

While our results showed that it is not ALPH that accelerates the reaction, the actual difference in heats of reaction of comparable cyclic and acyclic phosphates remained uncertain. If the value is what was originally reported, 5 to 6 kcal mol, there is a significant additional factor beyond strain. If the value is a larger, then there isn't. Scott Taylor joined my group and took on this problem. He measured rates of reaction at various temperatures to obtain activation parameters for the hydrolysis of cyclic and acyclic esters. He used adiabatic precision calorimetry, taking advantage of newly developed computer interfacing to control the experiment and deal with the data. He first measured and compared the activation parameters for hydrolysis of MEP and related acyclic esters (34). The acceleration in MEP relative to the acyclic ester is entirely due to a lower enthalpy of activation; entropies of activation were identical. Therefore, there is no advantage in the cyclic compound from its restricted conformational space. Scott's precise calorimetry also confirmed that the originally reported value of strain energy of about 5 kcal/mol for MEP is correct (34). So, strain accounts only for about half of the enhanced reactivity of cyclic phosphates. Analyzing the reaction in terms of these results leads to the necessary conclusion that the transition state of the cyclic reaction is lower in energy than the transition state of the acyclic reaction. The explanation based on strain assumed that the cyclic ground state is higher in energy than in the acyclic case, but the transition states were of the same energy. This alteration makes sense on steric grounds; addition to a four-coordinate center is sterically demanding, and the five-coordinate intermediate (and thus transition state) is very crowded. By joining two of the coordinated groups into a ring, the crowding is dramatically relieved and the strain is increased. The combination quantitatively accounts for the nonenzymic reactivity of the cyclic phosphate intermediate in RNA hydrolysis.

Scheme 12.



Methyl acetyl phosphate and acyl phosphate monoesters

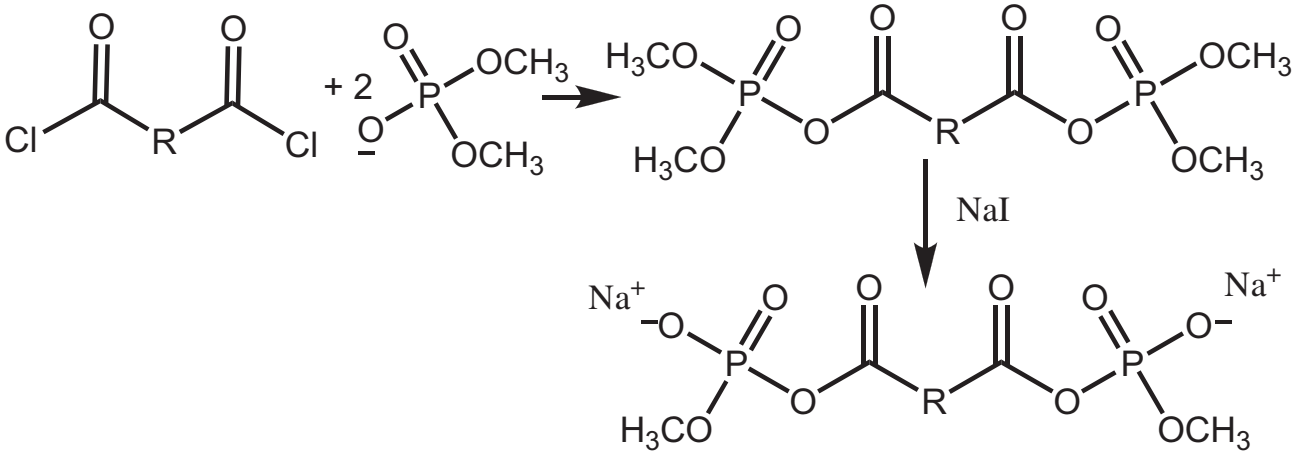
Carboxylic acids are not reactive in substitution reactions in neutral solution. Nature often activates carboxylic acids for substitution in enzymic reactions with ATP to give mixed anhydrides of AMP and the carboxylic acid. These intermediates are acyl adenylates. When we began our work in the area, there was no reliable route to acyl phosphate monoesters. Wing-Cheong Tsui developed the first reliable route to the simplest member of this class of materials, methyl acetyl phosphate (MAP) (Scheme 12) (35).

MAP was designed to react with amino groups in enzyme active sites that bind anionic groups and adjacent carbonyl groups (36). The reactivity of MAP is ideal for that purpose. Its half life for hydrolysis in neutral water is over 100 h at room temperature, but it reacts very rapidly with amines to form an amide. It is interesting that MAP is a reactive anionic electrophile; the functional group is divided into an electrophilic part and an anionic part. The electrophilic part makes it an acylating agent, while the anionic part produces the overall charge. We used that observation to give the original report a catchy title "Methyl Acetyl Phosphate. A Small Anionic Acetylating Agent" (35). Soon after the publication appeared, I was contacted by Professor James Manning, he had been working on the reactions of anionic acylating agents with hemoglobin. The protein contains a polycationic site that associates with 2,3-diphosphoglycerate (DPG), which is a penta-anion. Association of DPG with hemoglobin red blood cells causes a lowering in the oxygen affinity of hemoglobin, permitting the red blood cells to deliver oxygen efficiently. Manning and Ueno used our MAP and showed that it acetylated groups in the DPG-binding site of hemoglobin (37).

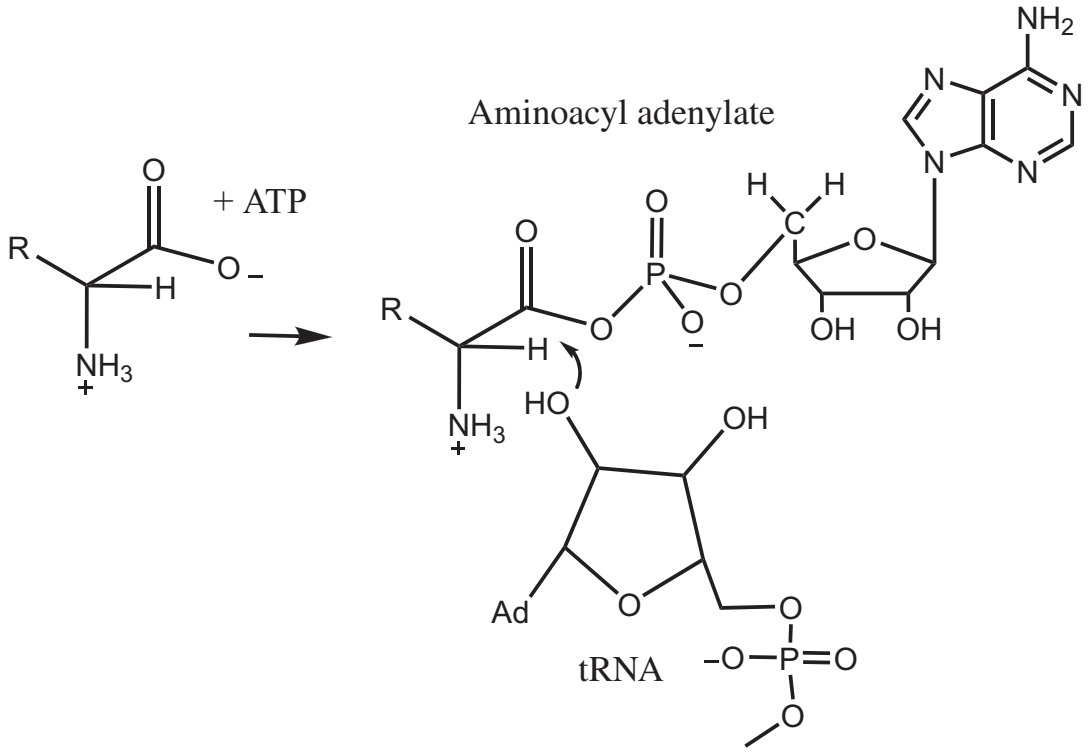
The idea that acyl phosphate monoesters will modify hemoglobin in the DPG-binding site became well established, and the potential for treatment of sickle cell disease was also noted. Soon after that, it occurred to me that a bifunctional version of MAP might serve to introduce a specific chemical cross-link into hemoglobin, which would then serve as a cir-

© 2006 NRC Canada

Scheme 13.



Scheme 14.



culating oxygen carrier, a potential replacement for red blood cells in transfusions. The general strategy for synthesis of these species was developed by Stephen Bearne, Andrew Grant, and Marcel Trachsel (Scheme 13) (38). This was carried further by Jolanta Wodzinska (39) and others and has reached its current state from the work of Nik Goruianov (40, 41) and Amer Alagic (42).

This method permits the efficient synthesis of simple and complex materials, including derivatives of triacids and tetra-acids. Many of these compounds react efficiently with hemoglobin, producing stable and specifically cross-linked species whose properties are easily investigated. A key discovery came from measuring the oxygen-binding and dissociation curves for a number of cross-linked hemoglobins with varying cross-links lengths. We have provided several summary reviews (42, 43). Our work has now been extended to create arrays of cross-linked hemoglobins, with linkages between cross-linked tetramers as well as conjugates of hemoglobin and other molecules.

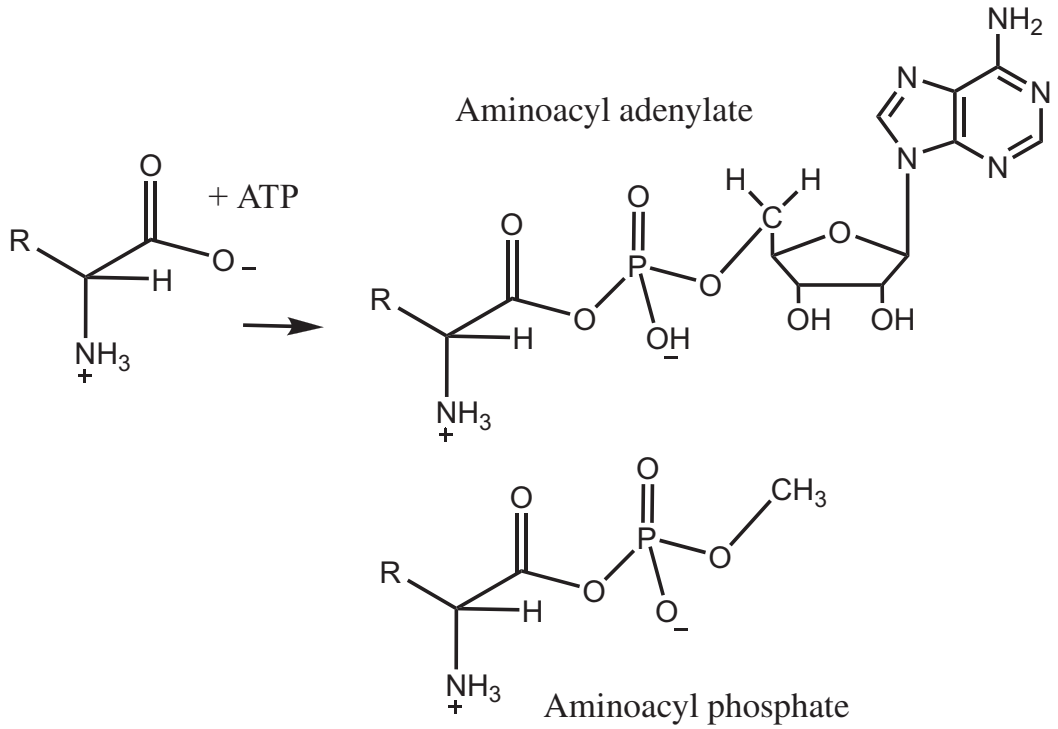
Aminoacyl phosphate monoesters

Amino acids are activated for ester formation in biochemical reactions within the cell by an initial reaction with the α-phosphoryl (Scheme 14) with catalysis and specificity provided by aminoacyl tRNA synthetases. In a second step on the same enzyme, the amino acid is transferred to the 3′-terminal hydroxyl group of the cognate tRNA

The intermediate is an aminoacyl adenylate (44), which is an aminoacyl phosphate monoester, a more complex version of the general class of acyl phosphate monoesters described earlier. The possibility of using a synthetically produced

© 2006 NRC Canada

Scheme 15.



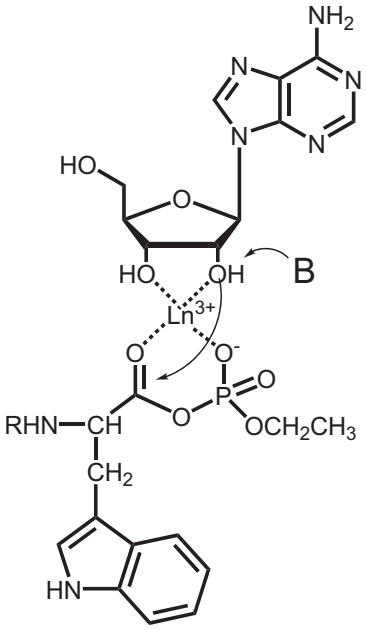
aminoacyl tRNA to alter the composition of a protein produced by a ribosome was proposed by Hecht (45) and actively pursued by him as well as by Schultz (45). Their methods involved rather complex syntheses, cleaving and reconnecting the tRNA. Because enzymes promote the synthesis by a route that simply brings the reactants together, we sought a way to take advantage of the aminoacyl phosphate ester to achieve similar results (Scheme 15).

The inherent reactivity of amines and acyl phosphate monoesters with one another led to the use of an amino-protecting group to prevent such reactions. The first examples were prepared by Neil Branda as an undergraduate project.

The normal nonenzymic reaction patterns of acyl phosphates are not suitable for the purpose of selective acylation of tRNA. These molecules react rapidly with amines and very slowly with oxygen-centered nucleophiles, as evidenced by their very slow spontaneous hydrolysis. We suspected that metal ions could serve as Lewis acid catalysts to enhance the reactivity of the carbon of the carboxyl center by coordination to the carbonyl oxygen and to the phosphate. However, this would also enhance the hydrolysis if successful. We found that a series of divalent metal ions did promote the hydrolysis, but there was no indication of enhanced reactivity with respect to alcohols (46). The structure of tRNA presents some built-in distinctions among the many hydroxyl groups within the chain compared with those of the ribosyl group at the 3′-terminus. Those within the chain are next to anionic phosphates, which would repel the anionic acyl phosphate. The terminal hydroxyls are the only diol in the macromolecule. Derived from ribose, the 2′ and 3′ groups are *cis*, and set up to form a chelate. By using a metal ion that can form a bis-bidentate chelate of the nucleotide diol and the aminoacyl phosphate, we might induce the desired reaction by proximity (Scheme 16).

Lisa Cameron discovered that lanthanide ions can very

Scheme 16.



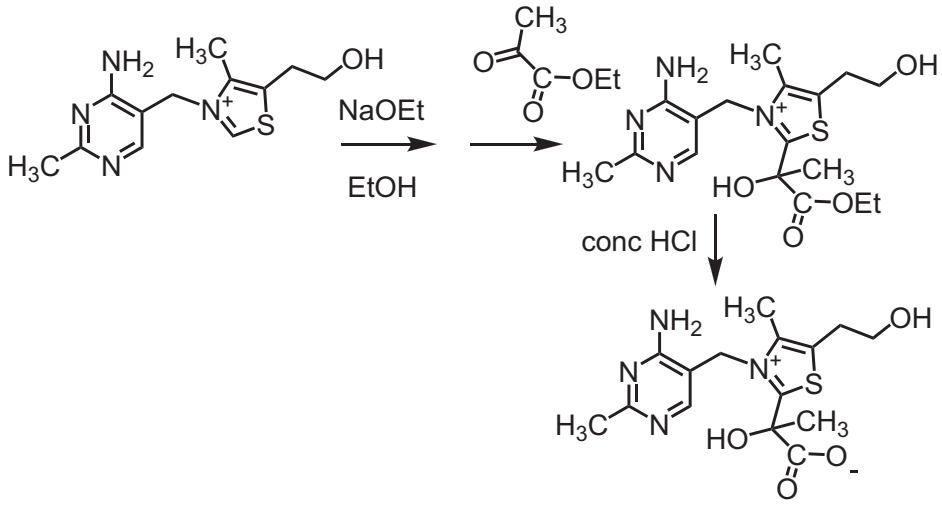
likely be used to achieve the desired specific result. They promote the base-catalyzed addition of methanol or water to acyl phosphates. Diols are acylated much more rapidly and at lower concentrations (47, 48). The work has recently been extended to the reactions of nucleotides and dinucleotides by Amber Asad and to tRNA with aminoacyl phosphates by Svetlana Tzvetkova.

α-Lactylthiamin

One of the major focuses of my research from the begin-

© 2006 NRC Canada

Scheme 17.



ning of my independent career has been the reactivity of the thiamin diphosphate (TDP) addition products in enzymes and how this reactivity compares to nonenzymic reactivity. Breslow had solved the basic puzzle of thiamin catalysis in 1957 by establishing that the C2 position of a thiazolium is a relatively acidic carbon acid (49). Nucleophilic addition of the carbanion from C2 of TDP to the keto group of 2-keto acids gives an intermediate that is set up for decarboxylation. The existence of such specific and reactive coenzyme-derived intermediates presented a unique opportunity to calibrate the effects of a protein on the reactivity of an intermediate. My presentation touched very briefly on this area because it had been the focus of another talk in the Enzyme Mechanisms symposium. The treatment here is especially brief to reflect that.

α-Lactylthiamin is a somewhat simplified analogue of the intermediate formed from TDP and pyruvate, α-lactylthiamin diphosphate, in enzymes that catalyze the decarboxylation of 2-ketoacids. Tim Smyth developed the first synthesis of α-lactylthiamin as well as α-lactylthiamin diphosphate (Scheme 17) (50). Jik Chin measured the nonenzymic reactivity while Smyth studied the interactions with the enzyme (51). We found that the enzyme activates the decarboxylation process by a factor of about 10^6 compared with the reaction of the intermediate itself. Furthermore, the enzyme binds the intermediate tightly, so addition of the synthetic intermediate is blocked. David Pike made the phosphonate analogues of pyruvate and found that they would be excellent inhibitors if they joined with TDP to form an impotent intermediate: one that is not able to do anything but reverse its addition (52).

2-1-(Hydroxybenzyl)thiamin

Washabaugh reported that the conversion of 2-1-(hydroxybenzyl)thiamin (HBnT) to benzaldehyde and thiamin is general-base catalyzed (53). I examined the molecule and its possible reaction pathways but could find none that would result in a mechanism that gives observed kinetics of general-acid catalysis. John Lam and C.-S. Kim studied the reaction and found that the products were not the expected benzaldehyde and thiamin but rather fragmentation products from a process Oka observed from the combination of benzaldehyde and thiamin in basic ethanol, giving a substituted phenyl thiazole ketone (PTK) and a dimethyl amino pyrimidine (DMAP) (Scheme 18) (54, 55). PTK absorbs strongly at 328 nm so it is readily observed by UV–vis spectroscopy.

Ian Moore studied the kinetic patterns of these reactions and found that the fragmentation step is very fast, with a first-order rate constant of about 10^4 s^{-1} (56). This is about 100 times larger than k_{cat} of the enzyme benzoylformate decarboxylase, which functions through the diphosphate of HBnT as an intermediate. How does the enzyme promote decarboxylation and suppress fragmentation?

α-Mandelylthiamin

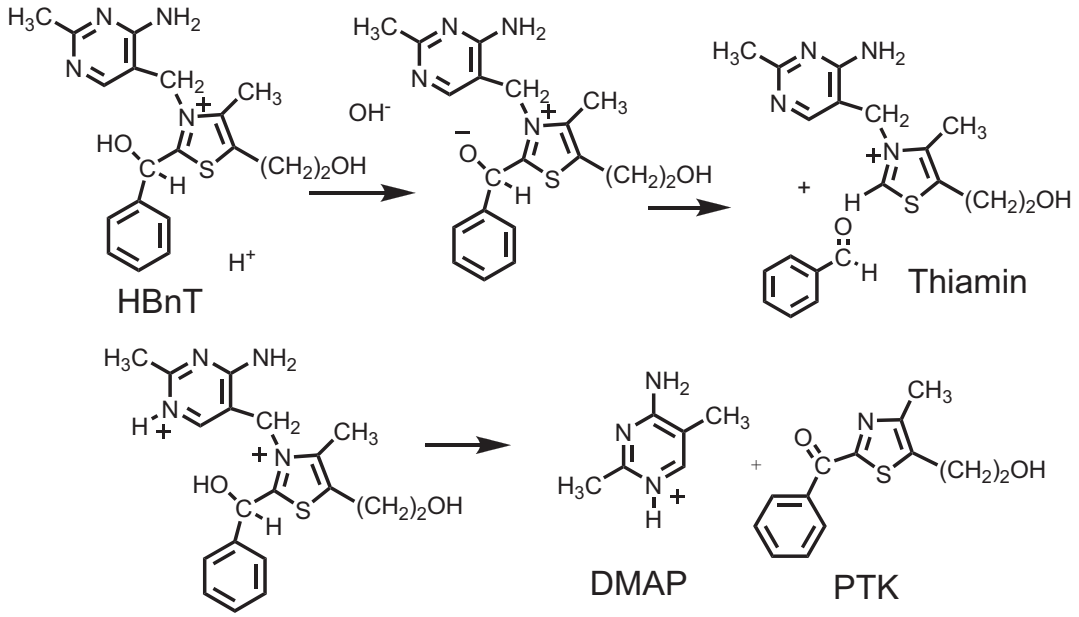
The enzymic precursor to HBnTDP is the compound α-mandelyl-TDP. Its inherent reaction patterns should answer important questions as to how the enzyme affects its reactivity. Qingyan (Jane) Hu developed a synthesis of the very elusive α-mandelylthiamin through a combination of determination and careful assessment of reactivity (Scheme 19) (57).

The rate of decarboxylation of MT is about 10^6 times less than the enzyme's k_{cat} and it undergoes rapid fragmentation after decarboxylation (Scheme 20) (58).

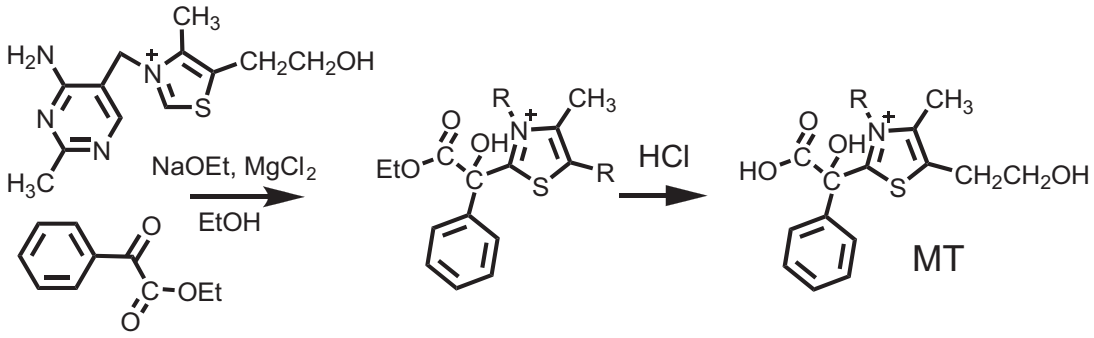
How does the enzyme enhance decarboxylation and prevent fragmentation of its similar intermediate? Jane studied the effects of buffers on product distribution, because Brønsted acids are expected to protonate the decarboxylation product and, thus, suppress fragmentation. Surprisingly, she discovered that the conjugate acid of pyridine accelerates the decarboxylation process, while other Brønsted acids that are not pyridine derivatives do not provide catalysis. There is no obvious place to add a proton to enhance the rate of bond-breaking in the decarboxylation step. When we looked up what is known about decarboxylation, we came across the work of Jiali Gao describing the theoretical analysis of decarboxylation related to another enzyme. The theory indicated that carbon dioxide in association with a carbanion will result in the reformation of the C–C bond, with a very low energy barrier. Separation of carbon dioxide is limited

© 2006 NRC Canada

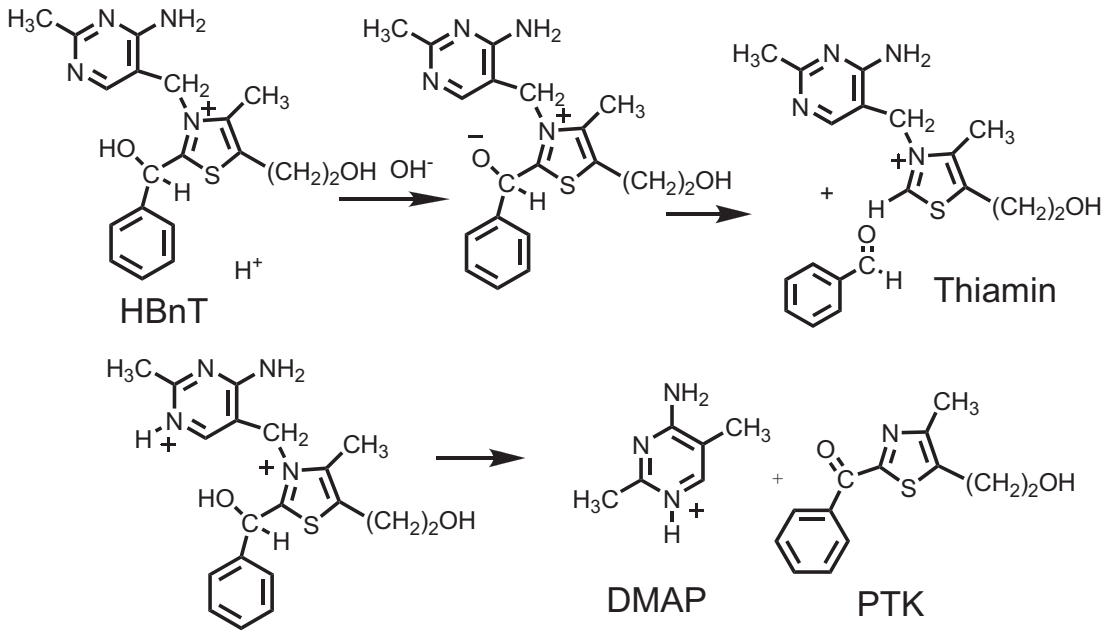
Scheme 18.



Scheme 19.



Scheme 20.



© 2006 NRC Canada

by its diffusion rate. Because a reaction with no barrier has a rate constant of about 10^{13} s^{-1}, while diffusion of carbon dioxide has a rate constant of about 10^{8} s^{-1}, there is a possibility for catalysis if a proton could be added prior to the departure of carbon dioxide after the C–C bond is broken. Because HBnT contains a benzene ring, pyridine could associate with HBnT by π-stacking and provide a proton without having to travel into the complex as it will be pre-associated. An enzyme could readily achieve similar catalysis by transferring protons from nearby groups to the nascent carbanion (59). The presence of two essential catalytic histidines at the active site of the enzyme is consistent with this (60).

Concluding remarks

The molecular keystones provide a point of strength and a point for departure. By using simple molecules as a starting point and analyzing complex environments, we continue to see that the methods and concepts of organic chemistry have unlimited prospects in the biochemical world. Once again I thank those who attended my talk and now add my thanks to those who have read this account.

Acknowledgements

My work has primarily and continuously been supported by the Natural Sciences and Engineering Research Council of Canada (NSERC) through operating and discovery grants, collaborative health research projects, and strategic projects. Mike Smith invited me to be a founding member of The Protein Engineering Networks of Centres of Excellence, and that period not only helped with funding but also gave me many new scientific interactions. I thank the students whose work has been mentioned and those who are specifically cited as well. All their contributions helped enormously. I thank those in the scientific community of Canada who have always been available to answer my naïve questions about reaction mechanisms, in particular, Peter Guthrie, Jerry Kresge, and the late John Bunting, to whom I dedicated my talk. I thank the CSC and CIC for keeping chemistry in Canada alive as a national interest and for giving me this recognition. Finally, I thank my family for accepting my abnormal interest in molecules with a smile.

References

1. S. Niranjanakumari, T. Stams, S.M. Crary, D.W. Christianson, and C.A. Fierke. Proc. Natl. Acad. Sci. U.S.A, **95**, 15212 (1998).
2. A. Murray III and D.L. Williams. Organic syntheses with isotopes. Part II: Organic compounds labeled with isotopes of the halogens, hydrogen, nitrogen, oxygen, phosphorus, and sulfur. Interscience Publishers, New York. 1958.
3. R. Kluger. J. Org. Chem. **29**, 2045 (1964).
4. F. Lipmann. *In* Symposium on The mechanism enzyme action. McCollum–Pratt Inst., Johns–Hopkins Univ., Baltimore. 1954. pp. 599–604.
5. Y. Kaziro, L.F. Hase, P.D. Boyer, and S. Ochoa. J. Biol. Chem. **237**, 1460 (1962).
6. J. Knappe, E. Ringelmann, and F. Lynen. Biochem. Z. **335**, 168 (1961).
7. S.G. Powers and A. Meister. Proc. Natl. Acad. Sci. U.S.A, **73**, 3020 (1976).
8. D.E. Hansen and J.R. Knowles. J. Biol. Chem. **257**, 14 and 795 (1982).
9. C.K. Sauers, W.P. Jencks, and S. Groh. J. Am. Chem. Soc. **97**, 5546 (1975).
10. J.R. Knowles. Annu. Rev. Biochem. **58**, 195 (1989).
11. M. Calvin and N.G. Pon. J. Cell. Comp. Physiol. **54**, 51 (1959).
12. R. Kluger, P.P. Davis, and P.D. Adawadkar. J. Am. Chem. Soc. **101**, 5995 (1979).
13. I.B. Blagoeva, I.G. Pojarlieff, and A.J. Kirby. J. Chem. Soc., Perkin Trans. 2, 745, (1984).
14. R. Kluger. Bioorg. Chem. **17**, 287 (1989).
15. S.D. Taylor and R. Kluger. J. Am. Chem. Soc. **115**, 867 (1993).
16. R.B. Silverman. The organic chemistry of enzyme-catalyzed reactions. Academic Press, San Diego. 2000.
17. J.R. Cox, Jr., R.E. Wall, and F.H. Westheimer. Chem. Ind. (London), 929 (1959).
18. E.T. Kaiser, M. Panar, and F.H. Westheimer. J. Am. Chem. Soc. **85**, 602 (1963).
19. D.A. Usher, E.A. Dennis, and F.H. Westheimer. J. Am. Chem. Soc. **87**, 2320 (1965).
20. F.H. Westheimer. Chem. Soc. (London), (Spec. Publ.), No. 8, 1 (1959).
21. J.A. Gerlt, F.H. Westheimer, and J.M. Sturtevant. J. Biol. Chem. **250**, 5059 (1975).
22. F.H. Westheimer. Acc. Chem. Res. **1**, 70 (1968).
23. R. Kluger, F. Covitz, E.A. Dennis, L.D. Williams, and F.H. Westheimer. J. Am. Chem. Soc. **91**, 6066 (1969).
24. D.G. Gorenstein, B.A. Luxon, J.B. Findlay, and R. Momii. J. Am. Chem. Soc. **99**, 4170 (1977).
25. J. Lehn and G. Wipff. J. Chem. Soc., Chem. Commun. 800 (1975).
26. M.L. Sinnott. Adv. Phys. Org. Chem. **24**, 113 (1988).
27. D.G. Gorenstein, B.A. Luxon, and J.B. Findlay. J. Am. Chem. Soc. **101**, 5869 (1979).
28. A. Munoz and J.P. Vives. Comp. Rend. **253**, 1693 (1961).
29. D.G. Gorenstein and K. Taira. J. Am. Chem. Soc. **104**, 6130 (1982).
30. K. Taira, T. Fanni, and D.G. Gorenstein. J. Org. Chem. **49**, 4531 (1984).
31. R. Kluger, F. Covitz, E. Dennis, L.D. Williams, and F.H. Westheimer. J. Am. Chem. Soc. **91**, 6066 (1969).
32. K. Taira. Ph.D. thesis, Department of Chemistry, University of Illinois at Chicago, Chicago. 1984.
33. R. Kluger and G.R.J. Thatcher. J. Am. Chem. Soc. **107**, 6006 (1985).
34. R. Kluger and S.D. Taylor. J. Am. Chem. Soc. **112**, 6669 (1990).
35. R. Kluger and W.-C. Tsui. J. Org. Chem. **45**, 2723 (1980).
36. R. Kluger and W.-C. Tsui. Biochem. Cell Biol. **64**, 434 (1986).
37. H. Ueno, M.A. Pospischil, R. Kluger, and J.M. Manning. J. Chromatogr. **359**, 193 (1986).
38. R. Kluger, A.S. Grant, S.L. Bearne, and M.R. Trachsel. J. Org. Chem. **55**, 2864 (1990).
39. R. Kluger, J. Wodzinska, R.T. Jones, C. Head, T.S. Fujita, and D.T. Shih. Biochemistry, **31**, 7551 (1992).
40. N. Gourianov and R. Kluger. J. Am. Chem. Soc. **125**, 10885 (2003).
41. N. Gourianov and R. Kluger. Biochemistry, **44**, 14989 (2005).
42. R. Kluger and A. Alagic. Bioorg. Chem. **32**, 451(2004).
43. R. Kluger. Can. J. Chem. **72**, 2193 (1994).
44. P. Berg. J. Biol. Chem. **233**, 608 (1958).

© 2006 NRC Canada

45. S.M. Hecht, B.L. Alford, Y. Kuroda, and S. Kitano. J. Biol. Chem. **253**, 4517 (1978).
46. R. Kluger, R.W. Loo, and V. Mazza. J. Am. Chem. Soc. **119**, 12089 (1997).
47. L.L. Cameron, S.C. Wang, and R. Kluger. J. Am. Chem. Soc. **126**, 10721 (2004).
48. R. Kluger and L.L. Cameron. J. Am. Chem. Soc. **124**, 3303 (2002).
49. R. Breslow. J. Am. Chem. Soc. **79**, 1762 (1957).
50. R. Kluger, J. Chin, and T. Smyth. J. Am. Chem. Soc. **103**, 884 (1981).
51. R. Kluger and T. Smyth. J.Am. Chem. Soc. **103**, 1214 (1981).
52. T.A. O'Brien, R. Kluger, D.C. Pike, and R.B. Gennis. Biochim. Biophys. Acta, **613**, 10 (1980).
53. E.J. Crane, III and M.W. Washabaugh. Bioorg. Chem. **19**, 351 (1991).
54.Y. Oka, S. Kishimoto, and H. Hirano. Chem. Pharm. Bull. **18**, 527 (1970).
55. R. Kluger, J.F. Lam, and C.S. Kim. Bioorg. Chem. **21**, 275 (1993).
56. R. Kluger and I.F. Moore. J. Am. Chem. Soc. **122**, 6145 (2000).
57. Q. Hu and R. Kluger. J. Am. Chem. Soc. **124**, 14858 (2002).
58. Q. Hu and R. Kluger. J. Am. Chem. Soc. **126**, 68 (2004).
59. Q. Hu and R. Kluger. J. Am. Chem. Soc. **127**, 12242 (2005).
60. E.S. Polovnikova, M.J. McLeish, E.A. Sergienko, J.T. Burgner, N.L. Anderson, A. K. Bera, F. Jordan, G.L. Kenyon, and M.S. Hasson. Biochemistry, **42**, 1820 (2003).

© 2006 NRC Canada

Synthesis and insulin-sensitizing activity of (*S*)-2-ethoxy-3-phenylpropanoic acid derivatives

Xiao-hua Cai and Bing Xie

Abstract: A series of (*S*)-2-ethoxy-3-phenylpropanoic acid derivatives were synthesized and their insulin-sensitizing activities were evaluated in 3T3-L1 cells. Compounds **1b** ($EC_{30} = 9.43 \times 10^{-3}$ μmol/L), **1d** ($EC_{30} = 7.45 \times 10^{-3}$ μmol/L), **1e** ($EC_{30} = 6.22 \times 10^{-3}$ μmol/L), and **1f** ($EC_{30} = 7.76 \times 10^{-3}$ μmol/L) exhibited more potent insulin-sensitizing activity than rosiglitazone ($EC_{30} = 2.06 \times 10^{-2}$ μmol/L).

Key words: (*S*)-2-ethoxy-3-phenylpropanoic acid derivatives, type 2 diabetes, insulin-sensitizing agents.

Résumé : On a réalisé la synthèse d'une série de dérivés de l'acide (*S*)-éthoxy-3-phénylpropanoïque et on a évalué leur activité de sensibilisation à l'insuline à l'aide de cellules 3T3-L1. Les composés **1b** ($EC_{30} = 9{,}43 \times 10^{-3}$ μmol/L), **1d** ($EC_{30} = 7{,}45 \times 10^{-3}$ μmol/L), **1e** ($EC_{30} = 6{,}22 \times 10^{-3}$ μmol/L), et **1f** ($EC_{30} = 2{,}06 \times 10^{-2}$ μmol/L) présentent une plus grande activité sensibilisatrice de l'insuline que la rosiglitazone ($EC_{30} = 2{,}06 \times 10^{-2}$ μmol/L).

Mots clés : dérivés de l'acide (*S*)-éthoxy-3-phénylpropanoïque, diabète de type 2, agents de sensibilisation de l'insuline.

[Traduit par la Rédaction]

Introduction

Type 2 diabetes is a complex metabolic disorder that affects between 6% and 20% of the populations in industrial societies. It is characterized by insulin resistance, hyperglycemia, and defects in insulin secretion and is usually associated with dyslipidemia, hypertension, and obesity (1–4). The peroxisome proliferator-activated receptors (PPARα, PPARγ, PPARδ) belong to the nuclear receptor superfamily and function as ligand-activated transcription factors (5).These receptors play a key role controlling the expresssion of genes involved in lipid and carbohydrate metabolism in various tissues. Interest in the PPARs has increased with the discovery of insulin sensitizers (e.g., TZD, pioglitazone, and rosiglitazone), which are potent and selective PPARγ agonists used in the treatment of type 2 diabetes. However, the success of these drugs has been hampered by cases of liver toxicity and side-effects such as fluid retention and weight gain (6). This has prompted the search for non-TZD ligands with different characteristics compared with the glitazones.

We were interested in developing a series of non-thiazolidinedione insulin-sensitizing activities, which might surmount the hepatic toxicity problems associated with the known non-thiazolidinedione. A few (*S*)-2-ethoxy-3-phenylpropanoic acid derivatives could increase insulin-sensitizing activities and have been reported to be useful in the treatment of hyperglycemia and hyperlipidemia. Of them, ragaglitazar (7) is in phase III and tesaglitazar (8) is in phase II clinical trials. Ragaglitazar (DRF-2725) has a binding affinity of 0.98 μmol/L at hPPARα and 0.092 μmol/L at hPPARγ and transactivates PPARα and PPARγ with EC_{50} values of 3.2 and 0.57 μmol/L, respectively. Ragaglitazar also displays good in vivo antidiabetic activity in db/ob mice and is reported to have 77% oral bioavailability in Wistar rats. Ragaglitazar was co-licensed by Novo Nordisk and completed phase II clinical trials. However, the clinical development of ragaglitazar has been terminated because of an incidence of bladder tumors in rodents. Our ongoing efforts to find a drug substance in the non-TZD class. As we know, molecular structures of many drugs contain bisphenyl moieties; therefore, using the dual PPARα/γ ragaglitazar as a structural template combined with the structural characteristics of rosiglitazone (Scheme 1), we demonstrate that insulin-sensitizing agents can be designed by using (*S*)-2-ethoxy-3-phenylpropanoic acid as the acidic moiety and bisphenyl as the lipophilic moiety of the molecule. A few bisphenyl-containing compounds **1a**–**1f** were designed and synthesized, and their insulin-sensitizing activities were evaluated with 3T3-L1 cells in vitro.

Chemistry

Compounds **1a**–**1f** were synthesized as outlined in Scheme 2. Intermediate **8** was prepared starting from diaryl methanol by chlorination, condensation with 2-methylaminoethanol, and mesylation (7). Then, **8** condensed with

Received 15 May 2006 Accepted 12 September 2006. Published on the NRC Research Press Web site at http://canjchem.nrc.ca on 25 October 2006.

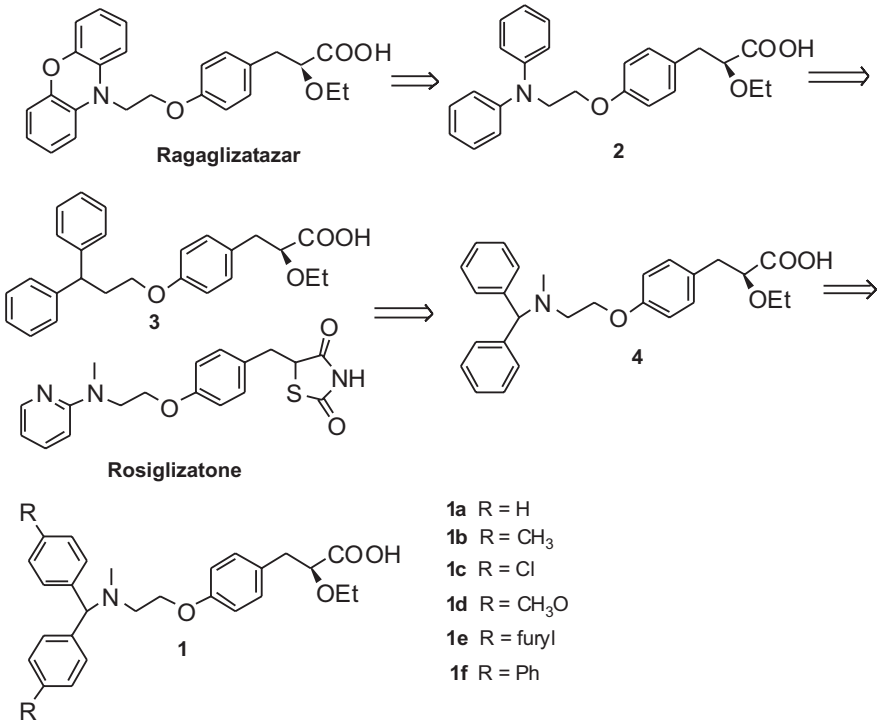
X.-h. Cai[1,2] and B. Xie. College of Chemistry and Environmental Science, Guizhou University for Nationalitives, Guiyang 550025, People's Republic of China.

[1]Also at: Department of Pharmaceuticals, Huaihua Medical College, Huaihua 418000, People's Republic of China.

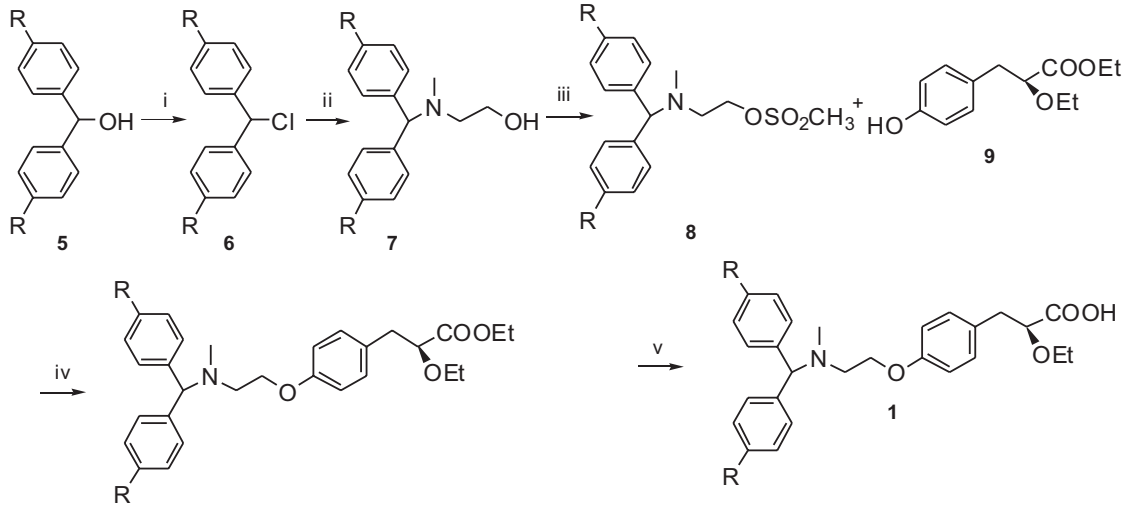
[2]Corresponding author (e-mail: caixh1111@163.com).

 doi:10.1139/V06-145 © 2006 NRC Canada

Scheme 1.



Scheme 2. (*i*) $SOCl_2$, benzene, reflux. (*ii*) $CH_3NHCH_2CH_2OH$, 100 °C. (*iii*) CH_3SO_2Cl, CH_2Cl_2, Et_3N, RT, 88–92%. (*iv*) Toluene, K_2CO_3, reflux. (*v*) MeOH, NaOH, RT.



ethyl (*S*)-3-(4-hydroxyphenyl)-2-ethoxy-propionate **(9)** (7) to give the ethyl esters of the desired products. Hydrolysis of the esters afforded the target compounds.

Experimental

Melting points were determined on XRC-1 micromelting point apparatus and are uncorrected. Columnn chromatography was carried out on silical (200–300 mesh, Qingdao Haiyang Chemical Co. Ltd., Qingdao, China). ^1H NMR and ^{13}C NMR spectra were recorded on a Bruker Avance 600 spectrometer with TMS as internal standard. IR spectra were given by a PerkinElmer spectrum one FTIR spectrometer (KBr discs), ESI-MS and HRESI-MS were obtained on a Finnigan LCQ^{DECA} and a Bruker Bio-TOF IIIQ, respectively.

7a

Thionyl chloride (2.38 g, 20 mmol) was added dropwise to a solution of diaryl methanol **5a** (1.84 g, 10 mmol) and benzene (15 mL) and the mixture was refluxed for 12 h. The solution was concentrated under reduced pressure to give **6a**. 2-Methylaminoethanol (4 mL) was added to **6a** and the mixture was heated to 100 °C and kept at that temperature for 8 h. After the completion (monitored by TLC), water (50 mL) was added to the reation mixture followed by ex-

© 2006 NRC Canada

Table 1. Screening data of insulin-sensitizing activity for (*S*)-2-ethoxy-3-phenylpropanoic acid derivatives.

		Insulin-sensitizing activity	
Compound	*R*	Triglyceride accumulation at 1 μmol/L[a]	EC_{30}[b] (μmol/L)
1a	H	96	3.82×10^{-2}
1b	CH_3	113	9.43×10^{-3}
1c	Cl	87	8.92×10^{-1}
1d	MeO	125	7.45×10^{-3}
1e	Furyl	138	6.22×10^{-3}
1f	Ph	131	7.76×10^{-3}
Rosiglitazone	—	100	2.06×10^{-2}

[a]% activity of rosiglitazone at 1 μmol/L. Values are the means of three experiments.
[b]Effective concentration (μmol/L) for 30% enhancement of insulin-induced triglyceride accumulation in 3T3-L1 cells.

traction with ethyl acetate (20 mL × 4). The extracted liquid was washed with water, dried over magnesium sulfate, and concentrated. The residue was purified by silica gel column chromatrography (petroleum ether – ethyl acetate, 10:1) to afford a colorless liquid **7a**: 1.06 g (44%). IR (KBr, cm^{-1}) ν_{max}: 3401, 3060, 3026, 2965, 2879, 2847, 1598, 1492, 1452, 1268, 1080, 1017, 759, 746, 706. ^1H NMR (600 MHz, $CDCl_3$) δ 2.18 (s, 3H), 2.56 (t, *J* = 7.2 Hz, 2H), 3.64 (t, *J* = 7.2 Hz, 2H), 4.50 (s, 1H), 7.21 (t, *J* = 7.2 Hz, 2H), 7.32 (t, *J* = 7.6 Hz, 4H), 7.39 (d, *J* = 7.2 Hz, 4H). ESI-MS *m/z* (%): 243 ($[M + H + 1]^+$, 8), 242 ($[M + H]^+$, 67).

1a

A mixture of ethyl (*S*)-2-ethoxy-3-(4-hydroxyphenyl)propionate **(9)** (0.357 g, 1.5 mmol), mesylate of **7a** (0.481 g, 1.5 mmol), potassium carbonate (0.828 g, 6 mmol), and toluene (15 mL) was refluxed for 12 h. After completion (monitored by TLC), the reaction mixture was poured into ice water and the toluene layer was separated while the aqueous layer was extracted with toluene. The combined organic layer was washed with water and concentrated under reduced pressure to afford an oil, which was dissolved in methanol (20 mL). Then, 2 mol/L sodium hydroxide (1.5 mL) aqueous solution was added slowly to the solution at room temperature. The reaction mixture was stirred for 8 h. The progress of the reaction was monitored by TLC. After completion of the hydrolysis, the reaction mixture was diluted with water (40 mL) and washed with ether to remove the impurities. The aqueous layer was adjusted to pH 2.5–3.0 with dilute hydrochloric acid and extracted with ethyl acetate (20 mL). The combined organic solution was washed with water and concentrated under reduced pressure to give a colorless solid **1a**: 0.558g (86%). IR (KBr, cm^{-1}) ν_{max}: 3430, 3028, 2973, 2923, 2870, 2783, 1730, 1612, 1583, 1512, 1454, 1241, 1178, 1115, 1021, 924, 827, 746, 706. ^1H NMR (600 MHz, $CDCl_3$) δ 1.20 (t, *J* = 6.8 Hz, 3H, OCH_2CH_3), 2.30 (s, 3H, NCH_3), 2.83 (s, 2H, NCH_2CH_2O-), 2.95 (dd, *J* = 14.4, 7.6 Hz, 1H, CH_2CH), 3.09 (dd, *J* = 14.4, 4.2 Hz, 1H, CH_2CH), 3.46–3.51 (m, 1H, OCH_2CH_3), 3.56–3.61 (m, 1H, OCH_2CH_3), 4.06–4.09 (m, 3H, NCH_2CH_2O, CH_2CH), 4.51 (s, 1H, $CHNCH_3$), 6.79 (d, *J* = 8.4 Hz, 2H), 7.13 (d, *J* = 8.4 Hz, 2H), 7.19 (t, *J* = 7.2 Hz, 2H), 7.29 (t, *J* = 7.6 Hz, 4H), 7.45 (d, *J* = 7.2 Hz, 4H). ^{13}C NMR (150 MHz, CDCl3,) δ 15.1, 37.5, 41.5, 53.8, 66.3, 67.0, 75.9, 79.8, 114.3, 127.0, 128.1, 128.4, 130.5, 142.8, 157.9, 172.8. ESI-MS *m/z* (%): 435 ($[M + H + 1]^+$, 27), 434 ($[M + H]^+$, 100), 433 ($[M^-]$, 28), 432 ($[M - H]^-$, 100); HRESI-MS *m/z* (%): 456.2147 ($[M + Na]^+$, calcd. for 456. 2145).

Insulin-sensitizing assay

All compounds were screened for insulin-sensitizing activity by measuring the triglyceride accumulation resulting from insulin-regulated differentiation of 3T3-L1 cells (9). Confluent 3T3-L1 cells were incubated in 5% fetal calf serum with isobutylmethylxanthine (0.5 mmol/L) and dexamethasone (1 μmol/L) for 48 h. Cultures were then incubated in Dulbecco's modified Eagle's medium – 2% fetal calf serum for 4 days with insulin (10 ng/mL) and the test compounds. Cellular triglycerides were extracted with 2-propanol and assayed by the enzymatic method using a commercially available kit (MPR2 Triglycerides GPO-PAP, Boehringer Mannheim, Mannheim, Germany). The marketed insulin-sensitizing drug rosiglitazone was selected as a positive control. All compounds activities in Table 1 are given as a percentage of rosiglitazone response for insulin-sensitizing activity at 1 μmol/L concentration, and the EC_{30} values (effective concentration for 30% enhancement of insulin-induced triglyceride accumulation in 3T3-L1 cells) of some compounds are also given.

Discussions

As indicated in Table 1, compounds **1b**, **1d**, **1e**, and **1f** exhibited more potent insulin-sensitizing activity than rosiglitazone according to their EC_{30} values. The primary structure–activity relationship study of these compounds indicated that the substituents at the *p*-position of the bisphenyl moiety play a key role in the potency of their activity, and the eletron-donating or aryl substituents (**1b**, **1d**, **1e**, and **1f**) lead to enhancement of the activity, whereas eletron-withdrawing substituents reduce the activity (**1c**).

Conclusion

In summary, we discovered a novel class of (*S*)-2-ethoxy-3-phenylpropanoic acid derivatives, which possesses potent insulin-sensitizing activity. This could be used as a lead structure in the search of non-thiazolidinedione insulin-sensitizing agents.

© 2006 NRC Canada

Acknowledgement

We thank the National Natural Science Foundation of China and the Science Foundation of the Guizhou Province Education Department for financial support.

References

1. P.Z. Zimmet, K.G.M.M. Alberti, and J. Shaw. Nature (London), **414**, 782 (2001).
2. J.S. Skyler. J. Med. Chem. **47**, 4112 (2004).
3. K.F. Petersen, R. Hendler, T. Price, G. Perseghin, D.L. Rothman, N. Held, J.M. Amatruda, and G.I. Shulman. Diabetes, **47**, 381 (1998).
4. G. Boden. Curr. Opin. Endocrinol. Diabetes, **8**, 235 (2001).
5. D.J. Mangelsdorf and R.M. Evans. Cell, **83**, 841 (1995).
6. A.B. King. Diabetes Care, **23**, 557b (2000).
7. S. Ebdrup, I. Pettersson, H.B. Rasmussen, H.J. Deussen, A.F. Jensen, S.B. Mortensen, J. Fleckner, L. Pridal, L. Nygaard, and P. Sauerberg. J. Med. Chem. **46**, 1306 (2003).
8. A. Kjellstedt, N. Oakes, and L. Svensson. Diabetes, **50** (suppl. 2), A121 (2001).
9. H. Shinkai, S. Onogi, M. Tanaka, T. Shibata, M. Iwao, K. Wakitani, and I. Uchida. J. Med. Chem. **41**, 1927 (1998).

© 2006 NRC Canada

Synthesis and evaluation of methyl 2-methoxycarbonyl-3-phenylpropionate derivatives as a new type of angiotensin converting enzyme inhibitors

Xiao-hua Cai, Bing Xie, and Hui Guo

Abstract: Methyl 2-methoxycarbonyl-3-phenylpropionate derivatives were prepared, and their inhibitory activities for angiotensin converting enzyme (ACE) were evaluated. Compounds **5b** (IC_{50} = 0.0039 μmol/L), **5d** (IC_{50} = 0.0027 μmol/L), **5e** (IC_{50} = 0.0021 μmol/L), and **5f** (IC_{50} = 0.0052 μmol/L) exhibited more potent ACE inhibitiory activity than the control drug Captopril® (IC_{50} = 0.0075 μmol/L).

Key words: hypertension, 2-methoxycarbonyl-3-phenyl propionate derivative, ACE inhibitor.

Résumé : On a préparé des dérivés du 2-méthoxycarbonyl-3-phénylpropionate de méthyle et on a évalué leurs activités inhibitrices pour l'enzyme de conversion de l'angiotensine (ECA). Les composés **5b** (IC_{50} = 0,0039 μmol/L), **5d** (IC_{50} = 0,0027 μmol/L), **5e** (IC_{50} = 0,0021 μmol/L), et **5f** (IC_{50} = 0,0052 μmol/L) présentent des activités inhibitrices vis-à-vis l'ECA qui sont supérieures à celle du médicament de contrôle, le Captopril® (IC_{50} = 0,0075 μmol/L).

Mots clés : hypertension, dérivés du 2-méthoxycarbonyl-3-phénylpropionate de méthyle, inhibiteur de l'ECA.

[Traduit par la Rédaction]

Introduction

Hypertension is a major risk factor for the development of cardiovascular diseases and mortality in Western countries (1). Although some of these risk factors can be unchanged, one factor that can be controlled and has the greatest impact on the etiology of stroke is high blood pressure (2). There are several classes of agents that have been used in the treatment of hypertension (3). Angiotensin I converting enzyme (ACE, EC 3.4.15.1), is responsible for hypertension by producing vasoconstrictor angiotensin II and degrading vasodilator, bradykinin. Therefore, inhibition of ACE is considered to be an important therapeutic approach for controlling hypertension. Initial interest in ACE inhibitors began with the discovery of snake venom peptides that could compete well with angiotensin I, the natural substrate of ACE (4, 5). With the model development of catalytic structure of ACE, specific inhibitors that bind more precisely to the enzyme active site were developed (6). Certain functional foods containing ACE inhibitory compounds have exhibited the ability to act as alternative treatment for hypertension (7). Even though the clinical ACE inhibitors are remarkably effective as antihypertensive drugs, they often cause adverse side effects or some of them are difficult to be synthesized (8). Therefore, the development of new ACE inhibitors is still important.

Methyl 2-methoxycarbonyl-3-phenylpropionate derivatives, such as JTP-20993 (9) and compound **1** (10) (Scheme 1), are PPARα/γ agonists used in the treatment of hyperglycemia and hyperlipidemia. Initially, we wish to design and synthesize some methyl 2-methoxycarbonyl-3-phenylpropionate derivatives (**5a**–**5f**) containing bisphenyl in the lipophilic moiety of the molecules and to investigate their PPARα/γ agonistic activity. Accidently, all the compounds showed ACE inhibitory activities.

Received 15 May 2006. Accepted 10 August 2006. Published on the NRC Research Press Web site at http://canjchem.nrc.ca on 25 October 2006.

X.-h. Cai[1,2] and H. Guo. Department of Pharmaceuticals, Huaihua Medical College, Huaihua, 418000, People's Republic of China.
B. Xie. College of Chemistry and Environmental Science, Guizhou University for Nationalitives, Guiyang 550025, People's Republic of China.

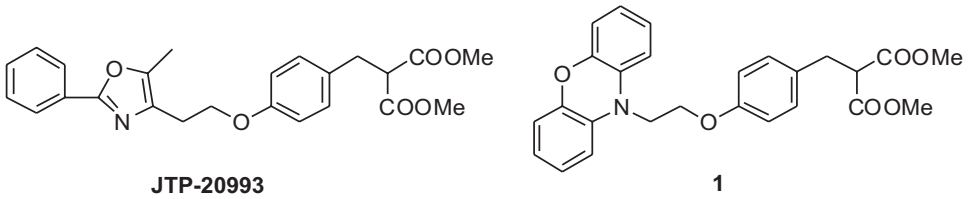
[1]Also at: College of Chemistry and Environmental Science, Guizhou University for Nationalitives, Guiyang 550025, People's Republic of China.
[2]Corresponding author (e-mail: caixh1111@163.com).

Chemistry

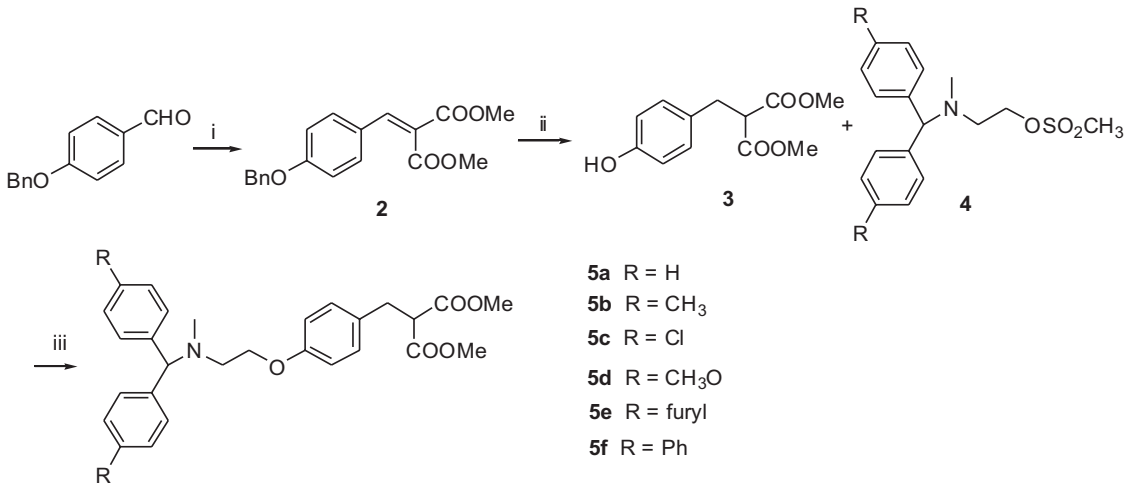
Compounds **5a**–**5f** were synthesized as outlined in Scheme 2. 4-Benzoxybenzaldehyde was condensed with dimethyl malonate using catalytic quantity of pipiridinium acetate to give 2-(4-benzyloxybenzylidene)malonic acid dimethyl ester (**2**), which was hydrogenated with 5% Pd–C and produced methyl 3-(4-hydroxyphenyl)-2-methoxycarbonylpropionate (**3**). Compound **3** was condensed with compound (**4**) to afford the desired products **5a**–**5f**. Compound 4 was prepared starting from diaryl ketones by reduction (11), chlorination, and condensation with 2-methylaminoethanol followed by mesylation (12) (Scheme 3).

 doi:10.1139/V06-146 © 2006 NRC Canada

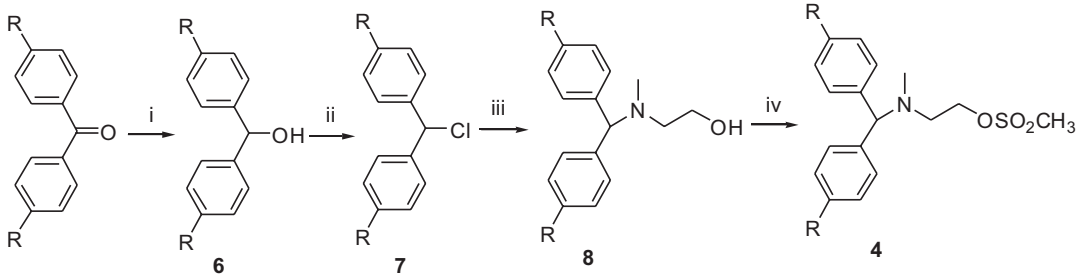
Scheme 1.



Scheme 2. (*i*) Toluene, $CH_2(COOMe)_2$, pipiridinium acetate, reflux, 88%. (*ii*) Dioxane, Pd/C, H_2, RT, 95%. (*iii*) Toluene, K_2CO_3, reflux, 78–86%.



Scheme 3.



Experimental

All starting compounds were used as received from commercial sources without further purification. Melting points were determined on XRC-1 micromelting point apparatus and are uncorrected. Columnn chromatography was carried out on silical (200–300 mesh, Qingdao Haiyang Chemical Co. Ltd., Qingdao, China). ^{1}H NMR and ^{13}C NMR spectra were recorded on a Bruker Avance 600 spectrometer with TMS as internal standard. IR spectra were given by a PerkinElmer spectrum one FTIR spectrometer (KBr discs), ESI-MS and HRESI-MS were obtained on a Finnigan LCQ^{DECA} and a Bruler Bio-TOF IIIQ, respectively.

2

A solution of benzyloxybenaldehyde (4.24 g, 20 mmol) and dimethyl malonate (2.64 g, 20 mmol) in toluene (40 mL) containing a catalytic quantity of pipridinium acetate was refluxed in a Dean–Stark trap for 12 h. After cooling to room temperature, the solution was concentrated. The residue was crystallized from ethyl acetate – hexane to give white solid **2**: 5.74 g (88%), mp 134–135 °C. IR (KBr, cm^{-1}) ν_{max}: 3440, 3031, 2949, 2871, 1734, 1634, 1604, 1571, 1512, 1435, 1379, 1319, 1256, 1205, 1175, 1154, 1104, 1026, 843, 750, 714, 695. ^{1}H NMR (600 MHz, $CDCl_3$) δ: 3.84 (s, 3H, OC*H*$_3$), 3.87 (s, 3H, OC*H*$_3$), 5.10 (s, 2H, OC*H*$_2$Bn), 6.97 (d, *J* = 8.4 Hz, 2H), 7.34–7.36 (t, *J* = 7.2 Hz, 1H), 7.38–7.43 (m, 6H), 7.72 (s, 1H, C*H*=). ESI-MS *m/z* (%): 365 ([M + K]$^+$, 32), 349 ([M + Na]$^+$, 100), 327 ([M + H]$^+$, 11), 325 ([M – H]$^-$, 89).

3

A solution of **2** (3.44 g, 10 mmol) in dioxane (30 mL) was hydrogenated with 5% Pd–C under atmospheric pressure and at room temperature for 12 h. The reaction mixture was filtered, and the filtrate was evaporated under vacuum to yield a brown oil **3**: 2.26 g (95%). IR (KBr, cm^{-1}) ν_{max}: 3440, 3019, 2955, 1735, 1614, 1596, 1516, 1437, 1349, 1235,

© 2006 NRC Canada

1173, 1155, 1104, 1026, 829, 772. ^{1}H NMR (600 MHz, $CDCl_3$) δ: 3.15 (d, *J* = 7.9 Hz, 2H, C*H*$_2$CH), 3.64 (t, *J* = 7.9 Hz, 1H, CH_2CH-), 3.70 (s, 6H, OC*H*$_3$), 5.89 (br s, 1H, O*H*), 6.72 (d, *J* = 8.2 Hz, 2H), 7.03 (d, *J* = 8.2 Hz, 2H). ESI-MS *m*/*z* (%): 277 ([M + K]$^+$, 17), 261([M + Na]$^+$, 97), 237 ([M – H]$^-$, 66).

8a

Thionyl chloride (2.38 g, 20 mmol) was added dropwise to a solution of **6a** (1.84g, 10 mmol) and benzene (15 mL) and the mixture was refluxed for 12 h. The solution was concentrated under reduced pressure to give brown oil **7a**. 2-Methylaminoethanol (4 mL) was added to **7a** and the mixture was heated to 100 °C for 8 h. After the reaction completion (monitored by TLC), water (50 mL) was added to the reaction mixture that was then extracted with ethyl acetate (20 mL × 4). The organic layer was washed with water, dried over magnesium sulfate, and concentrated. The residue was purified by silica gel column chromatrography (petroleum ether – ethyl acetate, 10:1) to afford **8a**: 1.06 g (44%) as a colorless liquid. IR (KBr, cm^{-1}) ν_{max}: 3401, 3060, 3026, 2965, 2879, 2847, 1598, 1492, 1452, 1268, 1080, 1017, 759, 746, 706. ^{1}H NMR (600 MHz, $CDCl_3$) δ: 2.18 (s, 3H), 2.56 (t, *J* = 7.2 Hz, 2H), 3.64 (t, *J* = 7.2 Hz, 2H), 4.50 (s, 1H), 7.21 (t, J = 7.2 Hz, 2H), 7.32 (t, *J* = 7.6 Hz, 4H), 7.39 (d, *J* = 7.2 Hz, 4H). ESI-MS *m*/*z* (%): 243 ([M + H + 1]$^+$, 8), 242 ([M + H]$^+$, 67).

5a

The mixture of **3** (2 mmol), mesylate of **8a** (**4a**, 2 mmol), potassium carbonate (8.28 g, 6 mmol), and toluene (20 mL) was refluxed for 10 h. The progress of the reaction was monitored by TLC. After completion, the reaction mixture was poured into ice water and the toluene layer was separated while the aqueous layer was extracted with toluene. The combined organic layer was washed with water and concentrated under vacuum. The residue was purified by silica gel column chromatography (petroleum ether – EtOAc, 6:1) to give **5a**: 0.787 g (85%) as a colorless liquid. IR (KBr, cm^{-1}) ν_{max}: 3060, 3027, 2953, 2848, 2782, 1753, 1737, 1612, 1512, 1492, 1452, 1436, 1343, 1244, 1178, 1152, 1023, 926, 828, 760, 747, 708. ^{1}H NMR (600 MHz, $CDCl_3$) δ: 2.28 (s, 3H, NC*H*$_3$), 2.80 (t, *J* = 6.0 Hz, 2H, NC*H*$_2$CH$_2$O), 3.16 (d, *J* = 7.8 Hz, 2H, C*H*$_2$CH), 3.63 (t, *J* = 7.8 Hz, 2H, CH$_2$C*H*), 3.71 (s, 6H, OC*H*$_3$), 4.06 (t, *J* = 6.1 Hz, 2H, NCH$_2$C*H*$_2$O), 4.48 (s, 1H, C*H*NCH$_3$), 6.77 (d, *J* = 8.6 Hz, 2H), 7.09 (d, *J* = 8.6 Hz, 2H), 7.19 (t, *J* = 7.6 Hz, 2H), 7.28 (t, *J* = 7.6 Hz, 4H), 7.44 (d, *J* = 7.6 Hz, 4H). ^{13}C NMR (150 MHz, $CDCl_3$) δ: 34.0, 41.5, 52.5, 53.8, 53.9, 66.3, 75.9, 114.5, 126.9, 128.0, 128.4, 129.7, 129.8, 142.9, 157.7, 169.3. ESI-MS *m*/*z* (%): 485 ([M + Na + 1]$^+$, 8.5), 484 ([M + Na]$^+$, 27), 462 ([M + H]$^+$, 25); HRESI-MS *m*/*z* (%): 484.2116 ([M + Na]$^+$, calcd. for $C_{28}H_{31}NNaO_5$: 484.2094).

ACE inhibitory assay

ACE inhibitory activity was determined spectrometrically following the reported procedure using hippuryl-*L*-histidyl leucine (HHL) as the substrate (13, 14). Appropriate solutions of HHL, inhibitor, and ACE were obtained by dissolving them in 50 mmol/L sodium borate buffer (pH 8.3) and a mixture containing 50 mL of inhibitor and 50 μL of ACE solution (25 mU/mL) was preincubated for 10 min at 37 °C. For ACE activity determination, 150 μL of 4.15 mmol/L HHL was added to the mixture followed by incubation for 30 min at 37 °C, and the reaction was terminated by addition of 250 μL of 1 mol/L HCl. The hippuric acid formed by the action of ACE was extracted into 500 μL of ethyl acetate. After centrifugation for 10 min, 200 μL of supernatant was separated from the upper layer and subjected to evaporation at room temperature under vacuum for 2 h. Distilled water (1.0 mL) was added to dissolve the hippuric acid, and the absorbance of the solution at 228 nm was monitored by a spectrophotometer. The sample added before mixing with ACE was used as a blank, while the sample replaced by the same volume of distilled water was treated as a control. The inhibitory ratio (%) of ACE was calculated as (C-A)/(C-B) × 100%, where A is A_{228} of the inhibitor, B is A_{228} of the blank, and C is A_{228} of the control. Captopril® was used as a positive control for ACE inhibitor.

Table 1. ACE inhibitory activity of **5a**–**5f**.

Compound	IC_{50} (μmol/L)
5a	0.0083
5b	0.0039
5c	0.0132
5d	0.0027
5e	0.0021
5f	0.0052
Captopril®	0.0075

Discussion

The ACE inhibitory activity of these compounds is summarized in Table 1, Captopril® was used as a positive control. Compounds (**5a**–**5f**) show ACE inhibitory activity, and the inhibitiory activities of compounds **5b** (IC_{50} = 0.0039 μmol/L), **5d** (IC_{50} = 0.0027 μmol/L), **5e** (IC_{50} = 0.0021 μmol/L), and **5f** (IC_{50} = 0.0052 μmol/L) were higher than that of the control drug Captopril® (IC_{50} = 0.0075 μmol/L). The primary structure–activity relationship study indicated that the substituents at the *p*-position of the bisphenyl moiety play a key role in determining the potency of ACE inhibitory activity, and the eletron-donating or aryl substituents at the *p*-position of the bis(diphenyl) moiety enhanced the activity (**5b**, **5d**, **5e**, and **5f**), whereas eletron-withdrawing substituents reduced the activity (**5c**).

Conclusion

We developed a new type of potent ACE inhibitory compounds. These results encouraged the continued synthesis and evaluation of compounds in the chemical series with the purpose of increasing in vitro potency.

Acknowledgement

We thank the National Natural Science Foundation of China and the Natural Foundation of Guizhou and Hunan Province Education Department for financial support.

© 2006 NRC Canada

References

1. D. Duprez, P. Van Helshoecht, D.W. Van Eynde, and M.J. Leeman. J. Hum. Hypertension, **16**, 47 (2002).
2. D. Dunbabin. Pharmacoeconomics, **2**, 468 (1992).
3. K.S. Mark and T.P. Davis. Peptides, **21**, 1965 (2000).
4. A. Rousseau-Plasse, M. Lenfant, and P. Potier. Bioorg. Med. Chem. **4**, 1113 (1996).
5. M.A. Ondetti, N.J. Williams, E.F. Sabo, J. Pluscec, E.R. Weaver, and O. Kocy. Biochemistry, **10**, 4033 (1971).
6. D.W. Cushman and M.A. Ondetti. Hypertension, **17**, 589 (1991).
7. (*a*) M. Bala, E. Qadar, M.A. Pasha, D.K. Bhardwaj, and S. Pasha. Bioorg. Med. Chem. **10**, 3685 (2002); (*b*) F.-L. Hsu, Y.-H. Lin, M.-H. Lee, C.-L. Lin, and W.C. Hou. J. Agric. Food Chem. **50**, 6109 (2002); (*c*) T.-L. Chen, Y.-C. Lo, W.-T. Hu, M.-C. Wu, S.-T. Chen, and H.-M. Chang. J. Agric. Food Chem. **51**, 1671 (2003).
8. R.H. Huang, E. Mendisa, and S.-K. Kim. Bioorg. Med. Chem. **13**, 3649 (2005).
9. H. Shinkai, S. Onogi, M. Tanaka, T. Shibata, M. Iwao, K. Wakitani, and I. Uchida. J. Med. Chem. **41**, 1927 (1998).
10. L. Jeppesen, P. Sauerberg, A. Murray, and P.S. Bury. US Patent 6-369-055, 9 April (2002).
11. M. Nishida. J. Org. Chem. **32**, 2692 (1967).
12. S. Ebdrup, I. Pettersson, H.B. Rasmussen, H.-J. Deussen, A.F. Jensen, S.B. Mortensen, J. Fleckner, L. Pridal, L. Nygaard, and P. Sauerberg. J. Med. Chem. **46**, 1306 (2003).
13. D.W. Cushman and H.S. Cheung. Biochem. Pharmacol. **20**, 1637 (1971).
14. A.C. Duncan, A.K. Jager, and J. Staden. J. Ethnopharmacol. **68**, 63 (1999).

© 2006 NRC Canada

Theoretical study of one- and two-photon absorption properties of olefin-linked paracyclophane oligomers

Xiang-Biao Zhang, Ji-Kang Feng, Ai-Min Ren, and Chia-Chung Sun

Abstract: The electronic structures and the one- and two-photon absorption (TPA) properties of two series of the olefin-linked paracyclophane (pCp) oligomers have been studied using AM1 and ZINDO-SOS methods. The relationship between the TPA cross sections and the molecular chain length is obtained. The maximum TPA cross section increases in proportion to N^{α} (N denotes the number of repeat units) and the values of α depend on different molecular structures. The olefin-linked pCp oligomers, which have good transparency and large TPA cross sections, are promising candidates for TPA materials.

Key words: two-photon properties, paracyclophane oligomer, AM1, ZINDO-SOS.

Résumé : Faisant appel aux méthodes AM1 et ZINDO-SOS, on a fait une étude théorique des structures électroniques et des propriétés d'absorption d'un photon et de deux photons (ADP) de deux séries d'oligomères de paracyclophane (pCp) reliés par des oléfines. On a pu établir la relation entre les sections droites de l'ADP et la longueur de la chaîne moléculaire. L'augmentation de la valeur maximale de la section droite de l'ADP est proportionnelle à N^{α} où N correspond au nombre d'unités alors que les valeurs de α dépendent des diverses structures moléculaires. Les oligomères de pCp liés par des oléfines, qui présentent une bonne transparence et des sections droites d'ADP, sont des candidats offrant beaucoup de possibilités comme matériaux d'ADP.

Mots clés : propriété à deux photons, oligomère de paracyclophane, méthode AM1, méthode ZINDO-SOS.

[Traduit par la Rédaction]

Introduction

New two-photon absorption (TPA) materials are under intense investigation because of their potential use in emerging applications such as upconverted lasing (1–3), optical power limiting (4–6), three-dimensional (3D) microfabrication (7–9), and photodynamic therapy (10). Extensive studies have revealed that some basic structural motifs are important with respect to TPA-active molecular construction (11, 12). Molecular structures containing a π center with electron donors or acceptors on the terminal sites of the conjugation systems are expected to exhibit good TPA response (12, 13). Particularly, the conjugation length, π electron center, and chemical functional groups at the end of electron conjugation are recognized as three important factors for structure–property optimization (11, 14). Quadrupolar molecules still receive considerable attention (10, 12, 13), though many recent studies have focused on octupolar and multibranched structures (15–18).

Typical organic nonlinear optical systems, based on intramolecular charge transfer (ICT) from a donor toward an acceptor moiety through a π system, require a compromise in properties (19). Most strategies to increase the degree of ICT require greater conjugation length. Although greater ICT typically leads to a greater nonlinearity in the optical response, the increased conjugation leads to a lower transparency in the spectral region of interest, limiting the potential usefulness of the material. Paracyclophane-based molecules may afford advantages in this tradeoff by generating a strong NLO response while providing favourable displacement of the region of transparency. Zyss et al. (20) investigated the NLO properties of substituted paracyclophane and pointed out that the paracyclophane core leads to significant ICT while preserving transparency. Our group have designed a series of paracyclophane derivatives and studied their TPA properties (21). The results showed that the paracyclophane core, as a multidimensional tunneling barrier, remarkably increases the TPA cross section of molecules. Bartholomew et al. (22, 23) have studied 3D nonlinear optical chromophores based on (2.2)paracyclophane (pCp) and have pointed out that the interplay between through-bond ICT and through-space ICT processes gives rise to large quadratic hyperpolarizability values. However, for practical application of such materials, they have to be incorporated into polymer to form thin films (24). An ideal approach for this would be to design the polymer structure in such a way as to allow maxi-

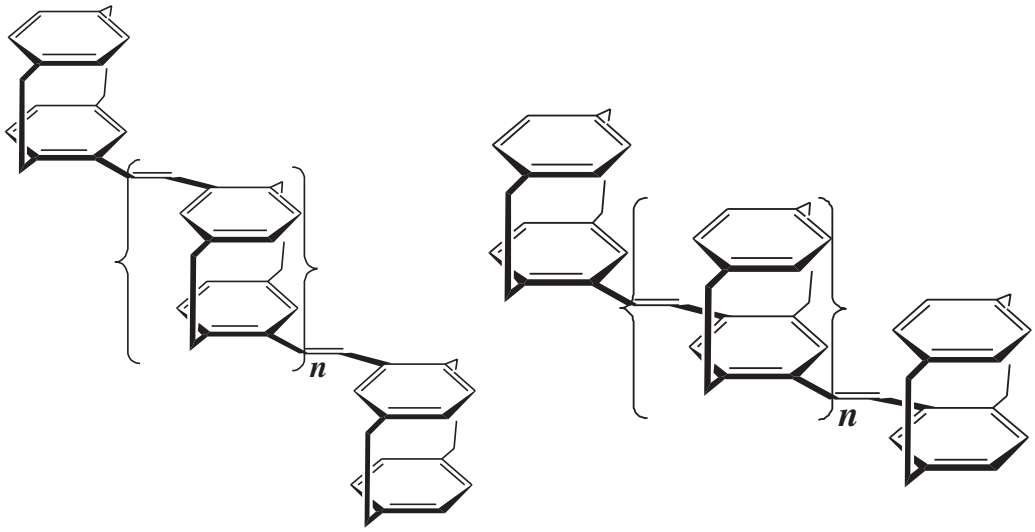
Received 3 June 2006. Accepted 30 August 2006. Published on the NRC Research Press Web site at http://canjchem.nrc.ca on 25 October 2006.

X.-B. Zhang, J.-K. Feng,[1, 2] A.-M. Ren, C.-C. Sun. State Key Laboratory of Theoretical and Computational Chemistry, Institute of Theoretical Chemistry, JiLin University, Changchun, 130023, China.

[1]College of Chemistry, JiLin University, Changchun, 130023, China
[2]Corresponding author (e-mail address: jikangf@yahoo.com).

 doi:10.1139/V06-139 © 2006 NRC Canada

Fig. 1. Chemical structures of the oligomers under study.



meso-*n* (*n* = 0–5) **rac-*n* (*n* = 0–7)**

mum utilization of monomeric or oligomeric TPA properties. The polymers containing pCp repeat units have been experimentally synthesized (25–27). In this paper, to provide useful information for the practical application of the pCp polymers, two series of the olefin-linked paracyclophane oligomers (see Fig. 1) have been designed and their electronic structures and TPA properties have been comparatively studied. The structure–property relationship of these molecules has been established.

Computational methods

The TPA process corresponds to simultaneous absorption of two photons. The TPA efficiency of an organic molecule, at optical frequency $\omega/2\pi$ can be characterized by the TPA cross section $\delta(\omega)$. It can be directly related to the imaginary part of the second hyperpolarizability $\gamma(-\omega; \omega, \omega, -\omega)$ (28),

$$[1] \qquad \delta(\omega) = \frac{8\pi^2\hbar\omega^2}{n^2c^2} L^4 \operatorname{Im}\gamma(-\omega; \omega, \omega, -\omega)$$

where $\hbar$ is Planck's constant divided by 2π, ω is the photon frequency, c is the speed of light, and n is the refractive index of the medium. L corresponds to the local-field factor. In the calculations presented here, n and L are set to 1 (isolated molecule in vacuum).

The sum-over-states (SOS) expression to evaluate the components of the second hyperpolarizability $\gamma_{\alpha\beta\gamma\delta}$ can be deduced using perturbation theory. By considering a Taylor expansion of energy with respect to the applied field, the $\gamma_{\alpha\beta\gamma\delta}$ Cartesian components are given by (29, 30)

$$[2] \quad \gamma_{\alpha\beta\gamma\delta}(-\omega_\sigma; \omega, \omega, -\omega) = \hbar^{-3} \sum \mathrm{P}_{1,2,3} \left\{ \sum_K{}' \sum_L{}' \sum_M{}' \left[\frac{\langle 0|\mu_\alpha|K\rangle\langle K|\overline{\mu_\beta}|L\rangle\langle L|\overline{\mu_\gamma}|M\rangle\langle M|\mu_\delta|0\rangle}{(\omega_K - i\Gamma_K/2 - \omega)(\omega_L - i\Gamma_L/2 - \omega_2 - \omega_3)(\omega_M - i\Gamma_L/2 - \omega_3)} \right.\right.$$
$$+ \frac{\langle 0|\mu_\beta|K\rangle\langle K|\overline{\mu_\alpha}|L\rangle\langle L|\overline{\mu_\gamma}|M\rangle\langle M|\mu_\delta|0\rangle}{(\omega_K + i\Gamma_K/2 + \omega_1)(\omega_L - i\Gamma_L/2 - \omega_2 - \omega_3)(\omega_M - i\Gamma_M/2 - \omega_3)} + \frac{\langle 0|\mu_\beta|K\rangle\langle K|\overline{\mu_\gamma}|L\rangle\langle L|\overline{\mu_\alpha}|M\rangle\langle M|\mu_\delta|0\rangle}{(\omega_K + i\Gamma_K/2 + \omega_1)(\omega_L + i\Gamma_L/2 + \omega_1 + \omega_2)(\omega_M - i\Gamma_M/2 - \omega_3)}$$
$$\left. + \frac{\langle 0|\mu_\beta|K\rangle\langle K|\overline{\mu_\gamma}|L\rangle\langle L|\overline{\mu_\alpha}|M\rangle\langle M|\mu_\delta|0\rangle}{(\omega_K + i\Gamma_K/2 + \omega_1)(\omega_L + i\Gamma_L/2 + \omega_1 + \omega_2)(\omega_M + i\Gamma_M/2 + \omega_\sigma)} \right] - \sum_K{}' \sum_L{}' \left[\frac{\langle 0|\mu_\alpha|K\rangle\langle K|\mu_\beta|0\rangle\langle 0|\mu_\gamma|L\rangle\langle L|\mu_\delta|0\rangle}{(\omega_K - i\Gamma_K/2 - \omega_\sigma)(\omega_K - i\Gamma_K/2 - \omega_1)(\omega_L - i\Gamma_L/2 - \omega_3)} \right.$$
$$+ \frac{\langle 0|\mu_\alpha|K\rangle\langle K|\mu_\alpha|0\rangle\langle 0|\mu_\gamma|L\rangle\langle L|\mu_\delta|0\rangle}{(\omega_K - i\Gamma_K/2 - \omega_1)(\omega_L + i\Gamma_L/2 + \omega_2)(\omega_L + i\Gamma_L/2 - \omega_3)} + \frac{\langle 0|\mu_\beta|K\rangle\langle K|\mu_\alpha|0\rangle\langle 0|\mu_\gamma|L\rangle\langle L|\mu_\delta|0\rangle}{(\omega_K + i\Gamma_K/2 + \omega_1)(\omega_K + i\Gamma_K/2 + \omega_\sigma)(\omega_L + i\Gamma_L/2 - \omega_2)}$$
$$\left.\left. + \frac{\langle 0|\mu_\beta|K\rangle\langle K|\mu_\alpha|0\rangle\langle 0|\mu_\gamma|L\rangle\langle L|\mu_\delta|0\rangle}{(\omega_K + i\Gamma_K/2 + \omega_1)(\omega_L + i\Gamma_L/2 + \omega_2)(\omega_L - i\Gamma_L/2 - \omega_3)} \right] \right\}$$

© 2006 NRC Canada

Table 1. HOMO and LUMO energies as well as the energy gaps between them (ΔE_{H-L}) for **meso-*n***.

Molecule	**meso-0**	**meso-1**	**meso-2**	**meso-3**	**meso-4**	**meso-5**
E_{HOMO}	–6.362 32	–6.323 13	–6.305 80	–6.297 37	–6.291 90	–6.288 01
E_{LUMO}	–0.063 43	–0.136 49	–0.164 59	–0.178 19	–0.186 43	–0.191 62
ΔE_{H-L}	6.298 89	6.186 64	6.141 21	6.119 18	6.105 47	6.096 39

Note: Energy values are given in eV.

Table 2. HOMO and LUMO energies as well as the energy gaps between them (ΔE_{H-L}) for **rac-*n***.

Molecule	**rac-0**	**rac-1**	**rac-2**	**rac-3**	**rac-4**	**rac-5**	**rac-6**	**rac-7**
E_{HOMO}	–6.379 54	–6.285 95	–6.175 46	–6.192 32	–6.140 29	–6.157 67	–6.124 71	–6.144 86
E_{LUMO}	–0.001 52	–0.231 74	–0.400 00	–0.387 16	–0.443 06	–0.443 60	–0.461 18	–0.455 06
ΔE_{H-L}	6.378 02	6.054 21	5.775 46	5.805 16	5.697 23	5.714 07	5.663 53	5.689 80

Note: Energy values are given in eV.

In this formula, α, β, γ, and δ refer to the molecular axes; ω_1, ω_2, and ω_3 are optical frequencies; and $\omega_\sigma = \omega_1 + \omega_2 + \omega_3$ is the polarization response frequency; $\Sigma P_{1,2,3}$ indicates a sum over the terms obtained by the six permutations of the pairs (ω_1/μ_β) and (ω_3/μ_δ); *K*, *L*, and *M* denote excited states and 0 denotes the ground state; $|K\rangle$ is an electronic wavefunction with energy $\hbar\omega_K$ relative to the ground electronic state; μ_α is the αth (= x, y, z) component of the dipole operator, $\langle K|\bar{\mu}_\alpha|L\rangle = \langle K|\mu_\alpha|L\rangle - \langle 0|\mu_\alpha|0\rangle\delta_{KL}$; the primes on the summation over the electronic states indicate exclusion of the ground state. Γ_K is the damping factor of excited state *K* and in the present work all damping factors Γ are set 0.14 eV. To compare the calculated δ value with the experimental value measured in solution, the orientationally averaged (isotropic) value of γ is evaluated. It is defined as,

$$[3] \qquad \langle\gamma\rangle = \frac{1}{15}\sum_{i,j}(\gamma_{iijj} + \gamma_{ijij} + \gamma_{ijji})$$

Substituting the imaginary part of $\langle\gamma\rangle$ into eq. [1], an expression for $\delta(\omega)$ is obtained that can be used to compare with the experimental value.

Generally, the position and relative strength of the two-photon response are predicted using the following simplified form of the SOS expression (31),

$$[4] \qquad \delta \propto \frac{M_{0k}^2 M_{kn}^2}{(E_{0k} - E_{0n}/2)^2\Gamma} + \frac{M_{0n}^2 \Delta\mu_n^2}{(E_{0n}/2)^2\Gamma}$$

where M_{ij} is the transition dipole moment from state *i* to *j*; E_{ij} is the corresponding excitation energy; the subscripts 0, *k*, and *n* refer to the ground state S_0, the intermediate state S_k, and the TPA final state S_n, respectively; and $\Delta\mu_n$ is the dipole moment difference between S_0 and S_n, which is zero in centrosymmetric molecules. So for centrosymmetric molecules, eq. [4] becomes

$$[5] \qquad \delta \propto \frac{M_{0k}^2 M_{kn}^2}{(E_{0k} - E_{0n}/2)^2\Gamma}$$

In this paper, taking into account the sizes of the molecules, all the geometries of the molecules are optimized with Austin Model 1 (AM1) method (32), which has been successfully applied to calculate many molecular structures (11). The properties of electronic excited states were then obtained by 196 single electron excitation and 54 double electron excitation configuration interactions (SDCI) using the ZINDO program. Furthermore, the transition energies and transition dipole moments that are needed to predict TPA were also provided. Then, using eqs. [1-3], the second hyperpolarizability γ and TPA cross section $\delta(\omega)$ were calculated, including the contributions of 200 lowest-lying excited states.

Results and discussions

Molecular geometries and electronic structures

The chemical structures of the studied molecules are shown in Fig. 1. As shown in Fig. 1, these molecules can be classified into two groups: **meso-*n*** (***n* = 1–5**) and **rac-*n*** (***n* = 0–7**). In the **meso-*n*** (***n* = 0–5**) repeat unit, the pCp cores are positioned in an "up/down" steplike configuration with one pCp above the plane of the ethylene linkage and the other pCp below the plane. In the **rac-*n*** (***n* = 1–7**) repeat unit, the pCp cores adopt an "up/up" configuration, in which both pCp cores are above the plane of the ethylene linkage. All the molecular geometries have been calculated with the AM1 method using the Gaussian 03 program suite. At the AM1 level in the studied molecules, the plane of the ethylene linkage is distorted about 30° from the adjacent phenyl rings in the pCp core and the ring strain distorts the phenyl rings in the pCp core. The distance between the bridgehead carbons on the opposing rings is about 2.7 Å while the distance between the nonbridging carbons is about 3.1 Å, which are in agreement with the experimental values of 2.78 and 3.09 Å (33). The middle two pCp cores in **rac-*n*** (***n* = 0, 2, 4, 6**) form a nearly perpendicular configuration with a dihedral angle of about 80°.

Tables 1 and 2 summarize the energies of the highest occupied molecular orbitals (HOMO), the lowest unoccupied molecular orbitals (LUMO), as well as the HOMO–LUMO energy gaps (ΔE_{H-L}) of **meso-*n*** (***n* = 0–5**) and **rac-*n*** (***n* = 0–7**), respectively. As can be seen in Table 1, in **meso-*n*** (***n* = 0–5**), the HOMO energy increases with ***n***, the molecular length, from –6.362 eV for **meso-0** to –6.288 eV for **meso-5**. Conversely, the LUMO energy decreases with the molecular length from –0.063 eV for **meso-0** to –0.192 eV for **meso-5**. In **rac-*n*** (***n* = 0–7**), the HOMO energy increases in the order of **rac-0** (–6.379 eV) < **rac-1** (–6.285 eV) < **rac-3**

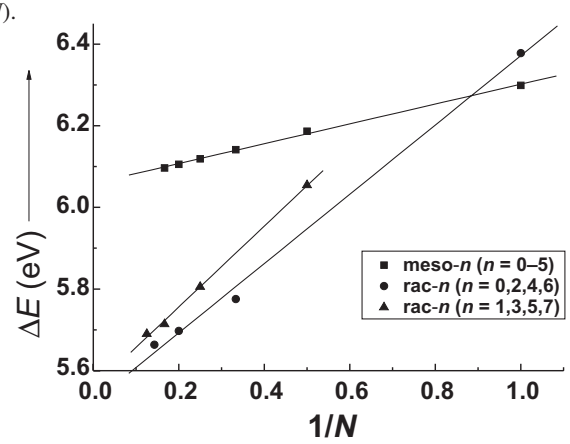
© 2006 NRC Canada

Table 3. The OPA properties for **meso-*n***.

Molecule	λ^{O}_{max} (nm)	Transition nature	Oscillator strength (*f*)	Configuration coefficient
meso-0	425.5	$S_0 \rightarrow S_1$	0.023	0.51 (H-1→L+3) + 0.56 (H→L) + 0.43 (H→L+2)
	375.6	$S_0 \rightarrow S_3$	0.030	0.61 (H-1→L+1) – 0.54 (H→L) + 0.55 (H→L+2)
	330.7	$S_0 \rightarrow S_5$	0.425	0.49 (H-1→L) – 0.53 (H-1→L+2) – 0.68 (H→L+1)
meso-1	436.8	$S_0 \rightarrow S_2$	0.032	0.34 (H-2→L+1) + 0.41 (H-1→L) + 0.40 (H-1→L+5)
	389.6	$S_0 \rightarrow S_5$	0.032	–0.40 (H-2→L+3) + 0.34 (H-1→L) – 0.60 (H-1→L+2) –0.33 (H→L+1) + 0.35 (H→L+3)
	352.2	$S_0 \rightarrow S_7$	0.561	–0.41 (H-2→L+1) – 0.54 (H→L+1) – 0.36 (H→L+6)
	331.0	$S_0 \rightarrow S_9$	0.519	–0.37 (H-2→L+6) – 0.35 (H-1→L) – 0.32 (H-1→L+7)
meso-2	438.7	$S_0 \rightarrow S_1$	0.002	0.32 (H-3→L+7) + 0.53 (H→L)
	434.3	$S_0 \rightarrow S_3$	0.026	–0.34 (H-3→L+1) – 0.34 (H-2→L)
	343.5	$S_0 \rightarrow S_9$	1.213	–0.57 (H→L+2)
meso-3	433.5	$S_0 \rightarrow S_2$	0.006	–0.41 (H-1→L) – 0.37 (H→L+1)
	430.1	$S_0 \rightarrow S_4$	0.024	–0.34 (H-4→L+1) + 0.32 (H-3→L)
	393.8	$S_0 \rightarrow S_9$	0.026	0.37 (H-3→L+4) – 0.37 (H-2→L+5) + 0.39 (H-1→L+4)
	340.5	$S_0 \rightarrow S_{11}$	2.019	–0.37 (H-1→L+2) – 0.51 (H→L+3)
meso-4	428.5	$S_0 \rightarrow S_1$	0.031	0.44 (H→L)
	334.2	$S_0 \rightarrow S_{15}$	0.648	0.37 (H-7→L+1)
	332.7	$S_0 \rightarrow S_{17}$	1.655	–0.44 (H→L+4)
meso-5	399.7	$S_0 \rightarrow S_6$	0.026	0.37 (H-4→L+7) + 0.32 (H-3→L+6)
	325.8	$S_0 \rightarrow S_{18}$	0.090	–0.32 (H-10→L) – 0.33 (H→L+3)
	319.1	$S_0 \rightarrow S_{20}$	1.915	–0.35 (H-2→L+3) – 0.37 (H-1→L+4) – 0.37 (H→L+5)
M	326.7 (322)(34)	$S_0 \rightarrow S_1$	1.349	0.96 (H→L)

Note: (H→L) denotes the single excitation from HOMO to LUMO.

Fig. 2. Energy gaps (ΔE) between HOMO and LUMO for the oligomers under study vs. the reciprocal numbers of repeat units ($1/N$).



(–6.192 eV) < **rac-2** (–6.175 eV) < **rac-5** (–6.158 eV) < **rac-7** (–6.145 eV) < **rac-4** (–6.140 eV) < **rac-6** (–6.125 eV). It can be seen that while ***n*** is even or odd, the HOMO energy increases as the molecular length increases. The LUMO energy in **rac-*n*** (***n* = 0–7**) decreases in the order of **rac-0** (–0.002 eV) > **rac-1** (–0.232 eV) > **rac-3** (–0.387 eV) > **rac-2** (–0.4 eV) > **rac-4** (–0.443 eV) > **rac-5** (–0.444 eV) > **rac-7** (–0.455 eV) > **rac-6** (–0.461 eV). As shown in Fig. 2, the HOMO–LUMO energy gaps of **meso-*n*** and **rac-*n*** (***n*** is even or odd) are inversely proportional to the number of the repeat units N (N = n + 1) and can be predicted with the following equations:

$$\text{L1: } \Delta E_{H-L} = 6.058\ 81 + 0.242\ 83/N \text{ (for } \textbf{meso-}\boldsymbol{n}\text{)}$$

$$\text{L2: } \Delta E_{H-L} = 5.557\ 87 + 0.990\ 48/N \text{ (for } \textbf{rac-}\boldsymbol{n}\text{, } \boldsymbol{n} \text{ even)}$$

$$\text{L3: } \Delta E_{H-L} = 5.522\ 94 + 0.8486\ 4/N \text{ (for } \textbf{rac-}\boldsymbol{n}\text{, } \boldsymbol{n} \text{ odd)}$$

Observing the slopes of L1, L2, and L3 (Fig. 2), one can see that the slope of L2 is greater than the slope of L3 and L1 has the smallest slope, which indicates that the **rac-*n*** (***n*** odd) reach a saturation limit for ΔE_{H-L} vs. the reciprocal of the number of repeat units more easily than the **rac-*n*** (***n*** even), and that the **meso-*n*** reach saturation most easily. The intercepts 6.058 81, 5.557 87, and 5.522 94 may be assigned to the HOMO–LUMO energy gaps of the infinite **meso-*n*** and **rac-*n*** (***n*** even and odd), respectively, corresponding to the HOMO–LUMO energy gaps of the corresponding polymers, respectively. The decrease of ΔE_{H-L} with the increase in the repeat units indicates that as the number of repeat units increases the electron conjugated scope enlarges, which is a favourable factor for the increase of TPA cross section of the molecule.

One-photon absorption

On the basis of the optimized molecular structures determined by the AM1 method, we calculated the OPA spectra of all the oligomers using the ZINDO program. Tables 3 and 4

© 2006 NRC Canada

Table 4. The OPA properties for **rac-*n***.

Molecule	λ^{O}_{max} (nm)	Transition nature	Oscillator strength (*f*)	Configuration coefficient
rac-0	442.7	$S_0 \rightarrow S_1$	0.016	–0.52 (H-1→L+3) + 0.58 (H→L) – 0.41 (H→L+2)
	373.3	$S_0 \rightarrow S_3$	0.018	0.64 (H-1→L+1) – 0.49 (H→L) – 0.57 (H→L+2)
	329.1	$S_0 \rightarrow S_5$	0.351	–0.33 (H-1→L+7) + 0.40 (H→L) + 0.50 (H→L+4)
rac-1	442.0	$S_0 \rightarrow S_1$	0.107	0.40 (H-2→L+5) – 0.59 (H→L) + 0.34 (H→L+3)
	392.4	$S_0 \rightarrow S_4$	0.138	0.40 (H-2→L+2) – 0.49 (H→L) – 0.55 (H→L+3)
	352.5	$S_0 \rightarrow S_7$	0.820	–0.60 (H-3→L) + 0.37 (H→L)
rac-2	454.9	$S_0 \rightarrow S_1$	0.327	0.71 (H→L)
	402.1	$S_0 \rightarrow S_5$	0.271	–0.41 (H→L) + 0.53 (H→L+4)
	365.9	$S_0 \rightarrow S_9$	0.807	0.58 (H-4→L)
rac-3	449.9	$S_0 \rightarrow S_1$	0.423	–0.67 (H→L)
	366.2	$S_0 \rightarrow S_{11}$	1.055	–0.56 (H-5→L)
rac-4	452.5	$S_0 \rightarrow S_1$	0.608	0.33 (H-1→L+1) + 0.70 (H→L)
	365.3	$S_0 \rightarrow S_{13}$	0.773	0.33 (H-7→L+1) + 0.57 (H-6→L)
rac-5	449.4	$S_0 \rightarrow S_1$	0.799	–0.36 (H-1→L+1) – 0.67 (H→L)
	364.5	$S_0 \rightarrow S_{15}$	0.714	0.34 (H-8→L+1) + 0.55 (H-7→L)
rac-6	435.5	$S_0 \rightarrow S_1$	1.201	–0.73 (H→L)
	413.0	$S_0 \rightarrow S_2$	0.303	0.37 (H-2→L+1) + 0.46 (H-1→L) + 0.34 (H-1→ L+2) – 0.42 (H→L+1)
	407.4	$S_0 \rightarrow S_3$	0.245	–0.42 (H-2→L) – 0.32 (H-2→L+2) – 0.48 (H-1→ L+1) + 0.32 (H→L+2)
	352.1	$S_0 \rightarrow S_{17}$	0.695	0.35 (H-9→L+1) – 0.62 (H-8→L)
rac-7	428.7	$S_0 \rightarrow S_1$	1.380	0.33 (H-1→L+1) – 0.68 (H→L)
	412.2	$S_0 \rightarrow S_2$	0.296	0.45 (H-1→L) – 0.43 (H→L+1)
	406.9	$S_0 \rightarrow S_3$	0.208	0.38 (H-2→L) + 0.43 (H-1→L+1) – 0.34 (H→L+2)
	346.7	$S_0 \rightarrow S_{15}$	0.283	–0.36 (H-1→L+13) + 0.35 (H→L+12)

Note: (H→L) denotes the single excitation from HOMO to LUMO.

show the maximum OPA wavelengths (λ^{O}_{max}), the corresponding oscillator strengths, and the transition natures for the **meso-*n*** (***n* = 0–5**) and the **rac-*n*** (***n* = 0–7**), respectively. To examine the calculation method, we chose 4,4′-bis (dimethylamino)stilbene (molecule **M** in Table 3) as a comparison sample. As shown in Table 3, the calculated results are in agreement with experimental values. There are two absorption bands in the OPAs of the studied molecules, one at 400–450 nm and another at 320–370 nm. For the molecules **meso-*n*** (***n* = 0–5**), the absorption of the low-energy bands is weaker so that we focus on the absorption of the high-energy bands. In Table 3, **meso-0** to **meso-5** exhibited the maximum absorptions at 330.7, 352.2, 343.5, 340.5, 332.7, and 319.1 nm, respectively. Apparently, the **meso-1** has the largest red-shifted wavelength of 352.2 nm. Subsequently, the absorption is blue-shifted as the molecular length increases, which is correlated to the energy level increase of the absorption state. The oscillator strength increases with the molecular length from 0.425 for **meso-0** to 1.915 for **meso-5**, but **meso-3** is an exception and its oscillator strength (2.019) is largest among the studied molecules. Compared with the molecule **meso-*n*** (***n* = 0–5**), the absorption of **rac-*n*** (***n* = 0–5**) is red-shifted. It can be seen in Table 4 that for the molecules **rac-*n*** (***n*** even), the low- and high-energy absorptions of **rac-2** are red-shifted by 12.2 and 36.8 nm relative to **rac-0**, respectively. Subsequently, the absorptions are blue-shifted from 454.9 and 365.9 nm for **rac-2** to 435.5 and 352.1 nm for **rac-6**. For the molecules **rac-*n*** (***n*** odd), the low- and high-energy absorptions of **rac-3** are red-shifted by 7.9 and 13.7 nm relative to **rac-1**, respectively. Subsequently, the absorptions are blue-shifted from 449.9 and 366.2 nm for **rac-3** to 428.7 and 346.7 nm for **rac-7**. The oscillator strength of the low-energy absorption of the **rac-*n*** increases with the molecular length. While ***n*** is even or odd, the oscillator strength reaches a saturation for **rac-2** and **rac-3**, respectively, and then decreases with the molecular length.

Two-photon absorption

Using eqs. [1–3], we calculated the third-order nonlinear susceptibilities γ and the TPA cross sections δ of the oligomers **meso-*n*** (***n* = 0–5**) and **rac-*n*** (***n* = 0–5**). Tables 5 and 6 summarize the maximum TPA wavelengths (λ^{T}_{max}), the maximum TPA cross sections (δ^{T}_{max}), the imaginary parts of third-order nonlinear susceptibilities (Imγ), and the transition natures. The curves of the TPA cross sections δ vs. the energies of the photons are plotted in Fig. 3. It should be noted that the TPA and OPA of the **meso-*n*** (***n* = 0–5**) have different final states because of the centrosymmetric structures of the molecules, while the TPAs of the **rac-*n*** (***n* = 0–5**) are more or less accompanied by OPA because they are noncentrosymmetric molecules. As shown in Tables 5 and 6, our calculated TPA cross sections and wavelengths are in agreement with experimental values. The maximum TPA

© 2006 NRC Canada

Table 5. The TPA properties for **meso-*n***.

Molecule	λ^{T}_{max} (nm)	Transition nature	δ^{T}_{max} (GM)	Imγ (10^{-34} esu)[a]	Configuration coefficient
meso-0	573	$S_0 \rightarrow S_{11}$	85.07	16.93	0.55 (H→L+3)
meso-1	576.8	$S_0 \rightarrow S_{17}$	233.26	46.94	–0.35 (H-5→L) – 0.32 (H→L+5)
meso-2	551.6	$S_0 \rightarrow S_{25}$	440.2	81.18	–0.44 (H→L+12)
meso-3	554	$S_0 \rightarrow S_{27}$	615.57	114.74	–0.38 (H-4→L) – 0.45 (H→L+9) – 0.35 (H→L+11)
meso-4	537	$S_0 \rightarrow S_{33}$	722.92	126.48	–0.36 (H-11→L+2)
meso-5	513.6	$S_0 \rightarrow S_{41}$	997.07	151.19	0.45 (H→L)
M	518.6	$S_0 \rightarrow S_4$	414.23	67.47	–0.91 (H-1→L)
	(529)(34)		(411)(34)		

Note: (H→L) denotes the single excitation from HOMO to LUMO.
[a]1 esu = 0.333 564 nC

Table 6. The TPA properties for **rac-*n***.

Molecule	λ^{T}_{max} (nm)	Transition nature	δ^{T}_{max} (GM)	Imγ (10^{-34} esu)	Configuration coefficient
rac-0	570.6	$S_0 \rightarrow S_{10}$	72.41	14.33	0.40 (H-3→L+1) + 0.43 (H-2→L) – 0.65 (H-2→L+2)
rac-1	612.4	$S_0 \rightarrow S_{13}$	310	70.39	0.34 (H-5→L) + 0.35 (H-4→L+1) + 0.49 (H-3→L+2)
rac-2	605.8	$S_0 \rightarrow S_{17}$	889.76	198.48	–0.36 (H-5→L+5) + 0.56 (H-4→L+4)
rac-3	622.2	$S_0 \rightarrow S_{16}$	1496.99	350.18	–0.48 (H-4→L) – 0.38 (H→L+9)
rac-4	608	$S_0 \rightarrow S_{21}$	2406.23	539.92	0.37 (H-6→L+9)
rac-5	606.4	$S_0 \rightarrow S_{24}$	3028	675.45	0.34 (H-8→L+8)

Note: (H-3→L+1) denotes the single excitation from HOMO-3 to LUMO+3.

peaks of the **meso-*n*** (***n* = 0–5**) and **rac-*n*** (***n* = 0–5**) are positioned at 510–580 nm and 570–630 nm, respectively. The molecules **meso-0** and **meso-1** have almost the same TPA positions (573 nm for **meso-0** and 576.8 nm for **meso-1**, respectively). Subsequently, the TPA position of the **meso-*n*** (***n* > 1**) are blue-shifted as the molecular length increases from 576.8 nm for **meso-1** to 513.6 nm for **meso-5**. For the **rac-*n*** (***n*** even or odd), the absorption reaches saturation for **rac-2** or **rac-3** and then slightly blue-shifts as the molecular length increases.

As shown in Tables 5 and 6, the TPA cross sections of the **meso-*n*** and **rac-*n*** increase as the molecular length increases. The enhancement of the TPA cross sections of the **meso-*n*** and **rac-*n*** with the molecular length can be expressed as $\delta_{TPA}(N) = N^{\alpha}\,\delta_{TPA}$ ($N = 1$). To obtain the values of α, we plotted $\lg\delta_{TPA}(N)$ vs. $\lg N$ according to $\lg\delta_{TPA}(N) = \alpha\lg N + \lg\delta_{TPA}(N = 1)$ (Fig. 4) and the linear equations are as follows:

$$\text{L3: } \lg\delta_{TPA}(N) = 1.356\,71 \times \lg N + 1.951\,97 \quad \text{(for } \textbf{meso-}\boldsymbol{n}\text{)}$$

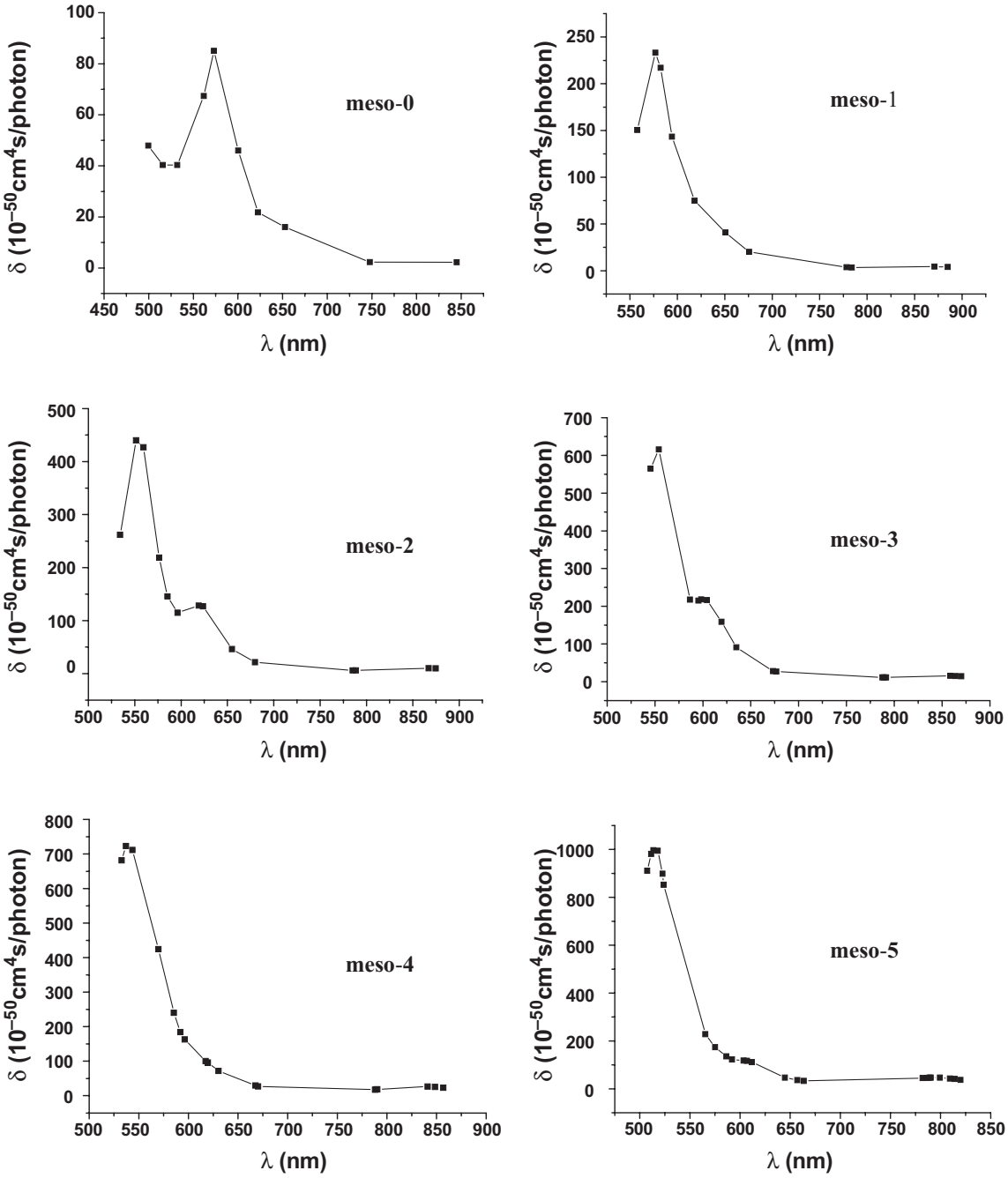
$$\text{L4: } \lg\delta_{TPA}(N) = 2.135\,55 \times \lg N + 1.872\,69 \quad \text{(for } \textbf{rac-}\boldsymbol{n}\text{)}$$

The equations show that α values for the **meso-*n*** and **rac-*n*** are 1.356 71 and 2.135 55, respectively. The calculated equations can be used to predict the values of the TPA cross sections of the **meso-*n*** and **rac-*n*** with different repeat units. We can find from the slope of two straight lines that the slope of L4 is greater than that of L3, indicating the enhancement of the TPA cross section of **rac-*n*** with the molecular length is greater than that of **meso-*n***. P. Najechalski et al. (35) give an approximate explanation of this relationship using the exciton model combined with the three-state expression of the TPA cross section.

In OPAs of **meso-*n***, the high-energy absorption has greater oscillator strength, indicating that the high-energy absorption state can be regarded as the intermediate state of the TPA of the **meso-*n***. For the **rac-*n***, the oscillator strength of the low-energy absorption increases with the molecular length; for ***n* > 2**, the low-energy absorption state becomes the intermediate state of TPA of the **rac-*n***. Though **rac-0** to **rac-5** are noncentrosymmetric molecules, we still use eq. [5] to explain the change of their TPA cross sections because of the smaller dipole moment difference between S_0 and $S_n(\Delta\mu_n)$. According to eq. [5], the excitation energies of the intermediate states (S_k) and the final states (S_n) of TPAs of the **meso-*n*** (***n* = 0–5**) and **rac-*n*** (***n* = 0–5**) and the transition dipole moments of $S_0 \rightarrow S_k$ and $S_k \rightarrow S_n$ (M_{ok} and M_{kn}) are collected in Figs. 5*a* and 5*b*. From eq. [5], it can be found that the TPA cross section is proportional to the squares of M_{ok} and M_{kn} and is inversely proportional to the square of the energy detuning term ($E_{ok} - E_{0n}/2$). As shown in Fig. 5*a*, the increase of TPA cross sections from **meso-0** to **meso-1** is mainly due to the decrease of the excitation energy of the intermediate states E_{0k} (3.75 eV for **meso-0** and 3.52 eV for **meso-1**). For **meso-2** to **meso-5**, the excitation energies of

© 2006 NRC Canada

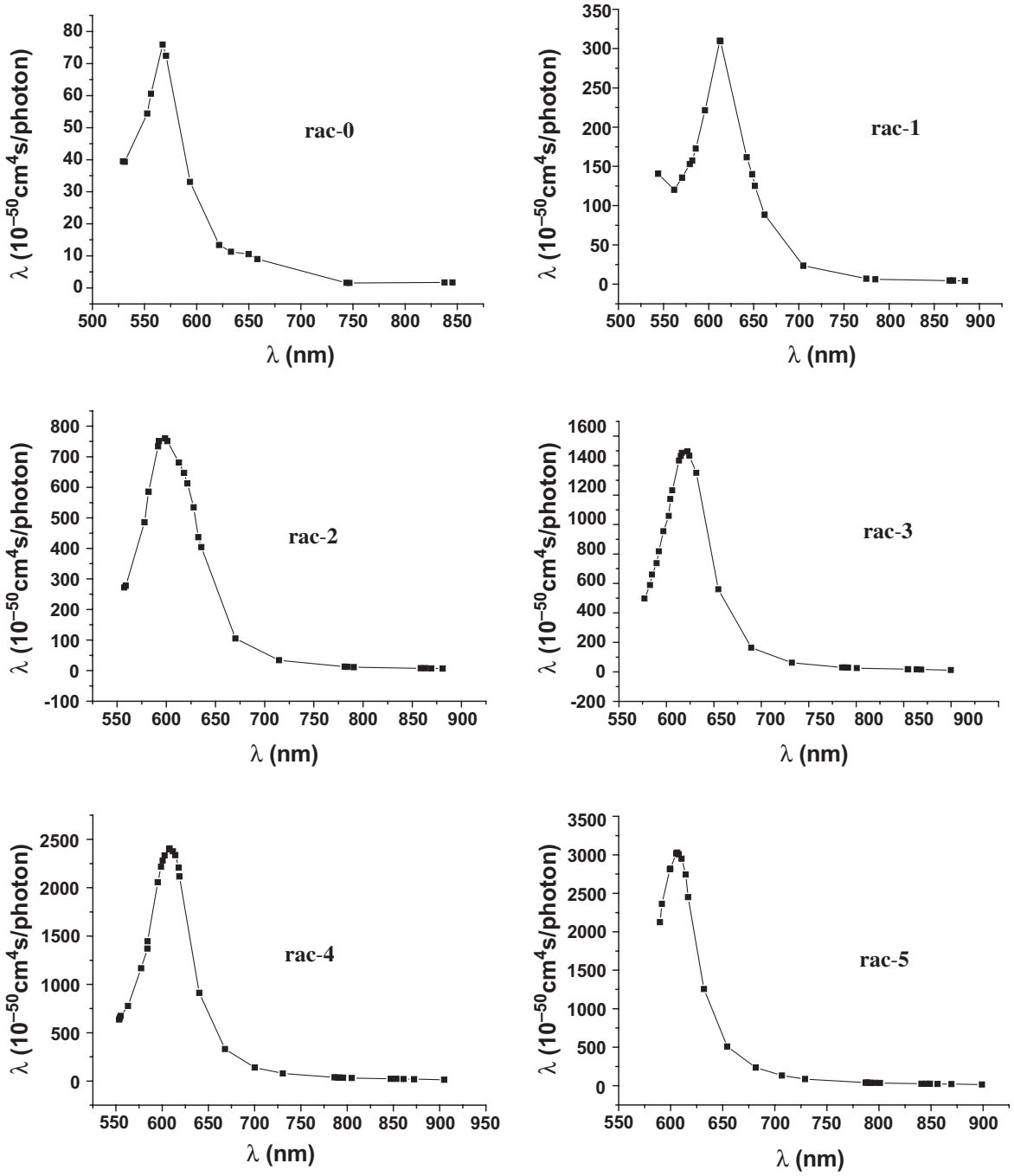
Fig. 3. The OPA and TPA spectra of the oligomers under study.



the intermediate states gradually increase (3.52, 3.60, 3.64, 3.73, and 3.88 eV for **meso-1**, **meso-2**, **meso-3**, **meso-4**, and **meso-5**, respectively). The enhancement of TPA cross section of the **meso-*n*** is mainly ascribed to the increased transition dipole moments M_{0k} (from 6.5 D for **meso-1** to 11.4 D for **meso-5**) and M_{kn} (from 4.8 D for **meso-1** to 12.0 D for **meso-5**). Though the **meso-3** has the largest M_{0k} (12.1 D) and M_{kn} (13.2 D), its TPA cross section is smaller than that of **meso-4** and **meso-5**. This is correlated to the smaller excitation energy of the TPA final state E_{0n} of **meso-3** compared with **meso-4** and **meso-5**. We can see from Fig. 5*b* that the excitation energies of the intermediate states of **rac-2** to **rac-5** are far smaller than that of **rac-0** and **rac-1**, so that **rac-*n*** (***n* > 1**) will have the smaller values of ($E_{0k} - E_{0n}/2$), which are the main reason for the remarkable enhancement of TPA cross sections for **rac-0** or **rac-1** to **rac-*n*** (***n* > 1**). From **rac-2** to **rac-5**, the transition dipole moments M_{0k} and M_{kn} increase with the molecular length and lead to the increased TPA cross sections. As shown in Tables 5 and 6, in comparison with the **meso-*n***, the **rac-*n*** have larger TPA cross sections because of the smaller excitation energy of the intermediate state.

© 2006 NRC Canada

Fig 3 (*concluded*).



It can be seen from Tables 3–6 that the studied ethylene-linked pCp oligomers have good transparency λ^{O}_{max} (< 460 nm) and large TPA cross sections that are proportional to N^{α} (α = 1.35671 for **meso-*n*** and α = 2.13555 for **rac-*n***, respectively). The TPA cross sections of **meso-5** and **rac-5** reach 997.07 GM (1 GM = 1×10^{-50} cm^4 sec) and 3028 GM, respectively. Their maximum OPA wavelengths are 399.7 and 449.4 nm, respectively. Therefore, the olefin-linked paracyclophane oligomers are promising TPA materials in terms of transparency and large third-order nonlinear responses.

Conclusions

In this paper, the electronic structures and the OPA and TPA properties of the olefin-linked paracyclophane oligomers have been studied by using AM1 and ZINDO methods. The results show that the HOMO–LUMO energy gaps of the olefin-linked paracyclophane oligomers are inversely proportional to the molecular length. And a power law $\delta_{TPA}(N) = N^{\alpha}$ δ_{TPA} (α = 1.35671 for the **meso-*n*** and 2.13555 for **rac-*n***) has been obtained. The enhancement of the TPA cross sections

© 2006 NRC Canada

Fig. 4. Plot of $lg\delta_{TPA}(N)$ vs. lg$N$ for the oligomers under study.

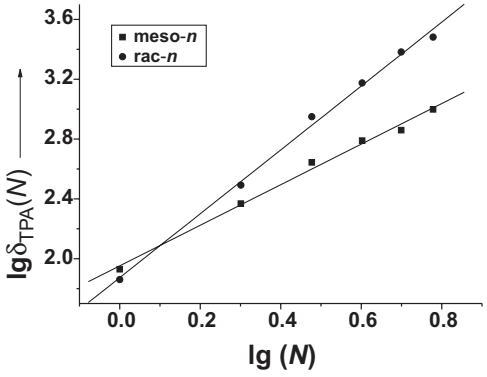
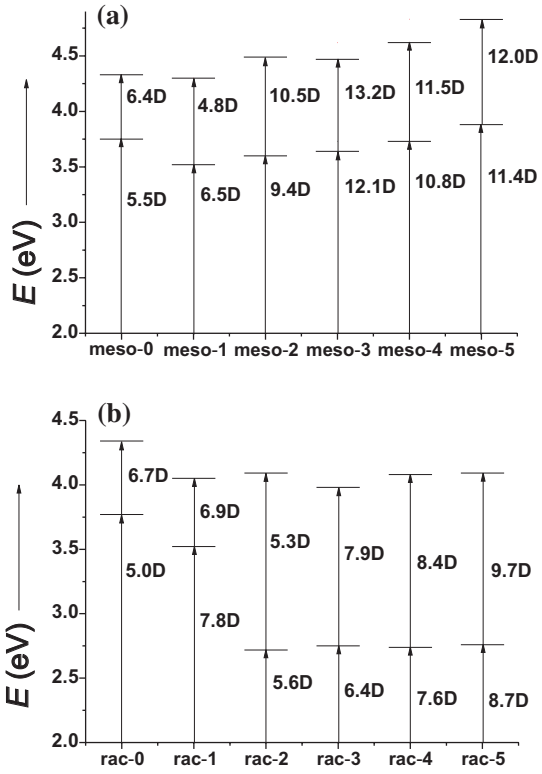


Fig. 5. Scheme of the calculated energy levels for (*a*) **meso-*n*** and (*b*) **rac-*n***.



is related to the increase of the transition dipole moments between the ground state and the intermediate state as well as between the intermediate state and the TPA final state and the decrease of the energy detuning term. The olefin-linked paracyclophane oligomers have good transparency and large TPA cross sections and, therefore, are promising TPA materials.

Acknowledgments

This work is supported by the National Nature Science Foundation of China and the Key Laboratory for Supramolecular Structure and Materials of Jilin University.

References

1. J.D. Bhawalkar, G.S. He, and P.N. Prasad. Rep. Prog. Phys. **59**, 1041 (1996).
2. G.S. He, C.-F. Zhao, J.D. Bhawalkar, and P.N. Prasad. Appl. Phys. Lett. **67**, 3703 (1995).
3. C.-F. Zhao, G.S. He, J.D. Bhawalkar, C.K. Park, and P.N. Prasad. Chem. Mater. **7**, 1979 (1995).
4. P.A. Fleitz, R.A. Sutherland, F.P. Stroghendl, F.P. Larson, and L.R. Dalton. SPIE Proc. **372**, 91 (1998).
5. G.S. He, J.D. Bhawalkar, C.-F. Zhao, and P.N. Prasad. Appl. Phys. Lett. **67**, 2433 (1995).
6. J.E. Ehrlich, X.-L. Wu, I.-Y.S. Lee, Z.-Y. Hu, H. Röeckel, S. R. Marder, and J.W. Perry. Opt. Lett. **22**, 1843 (1997).
7. M. Denk, J.H. Strickler, and W.W. Webb. Science (Washington, D.C.), **48**, 73 (1990).
8. C.M. Xu and W.W. Webb. Opt. Lett. **20**, 2532 (1995).
9. E.S. Wu, J.H. Stricker, W.R. Harrell, and W.W. Webb. SPIE Proc. **1674**, 776 (1992).
10. J.D. Bhawalkar, N.D. Kumar, C.-F. Zhao, and P.N. Prasad. J. Clin. Laser Med. Surg. **15**, 201 (1997).
11. M. Albota, D. Beljonne, J.-L. Brédas, J.E. Ehrlich, J.-Y. Fu, A.A. Heikal, S.E. Hess, T. Kogej, M.D. Levin, S.R. Marder, D. McCord-Maughon, J.W. Perry, H. Röckel, M. Rumi, G. Subramaniam, W.W. Webb, X.L. Wu, and C. Xu. Science (Washington, D.C.), **281**, 1653 (1998).
12. M. Rumi, J.E. Ehrlich, A.A. Heikal, J.W. Perry, S. Barlow, Z. Hu, D. McCord-Maughon, T.C. Parker, H. Röckel, S. Thayumanavan, S.R. Marder, D. Beljonne, and J.-L. Brédas. J. Am. Chem. Soc. **122**, 9500 (2000).
13. J.E. Enrlich, X.L. Wu, L.Y.S. Lee, Z.Y. Hu, H. Rockel, S.R. Marder, and J.W. Perry. Opt. Lett. **22**, 1843 (1997).
14. B.A. Reinhardt, L.L. Brott, and S.J. Clarson. Chem. Mater. **10**, 1863 (1998).
15. S.J. Chung, K.S. Kim, T.C. Lin, G.S. He, J. Swiatkiewicz, and P.N. Prasad. J. Phys. Chem. B, **103**, 10741 (1999).
16. S. Brasselet and J.J. Zyss. J. Opt. Soc. Am. B, **15**, 257 (1998).
17. J. Zyss and I. Ledoux. Chem. Rev. **94**, 77 (1994).
18. W.-H. Lee, H. Lee, J.-A. Kim, J.-H. Choi, M. Cho, S.-J. Jeon, and B.R. Cho. J. Am. Chem. Soc. **123**, 10658 (2001).
19. M. Blanchard-Desce, J.M. Lehn, M. Barzoukas, I. Ledoux, and J. Zyss. Chem. Phys. **181**, 281 (1994).
20. J. Zyss, I. Ledoux, S. Volkov, V. Chernyak, S. Mukamel, G.P. Bartholomew, and G.C. Bazan. J. Am. Chem. Soc. **122**,11956 (2000).
21. X. Zhou, A.-M. Ren, J.-K. Feng, and X.-J. Liu. J. Phys. Chem. A, **107**, 1850 (2003).
22. G.P. Bartholomew, I. Ledoux, S. Mukamel, G.C. Bazan, and J. Zyss. J. Am. Chem. Soc. **12**4 13480 (2002).
23. G.P. Bartholomew, M. Rumi, S.J.K. Pond, J.W. Perry, S. Tretiak, and G.C. Bazan. J. Am. Chem. Soc. **126**, 11529 (2004).
24. C. Samyn, T. Verbiest, and A. Persoons. Macromol. Rapid Comm. **21**, 1(2000).
25. Y. Morisaki and Y. Chujo. Macromolecules, **35**, 587 (2002).
26. Y. Morisaki, T. Ishida, and Y. Chujo. Macromolecules, **35**, 7872 (2002).
27. F. Salhi and D. Collard. Adv. Mater. (Weinheim, Ger.), **15**, 81 (2003).
28. C.L. Caylor, I. Dobrianow, C. Kimmr, R.E. Thome, W. Zipfel, and W.W. Webb. Phys. Rev. E, **59**, 3831 (1999).
29. B. Dick, R.M. Hochstrasser, and H.P. Trommsdorff. *In* Nonlinear optical properties of organic molecules and crystals. Vol. 2. Academic Press, Orlando, Fla. 1987. p. 167.

© 2006 NRC Canada

30. B.J. Orr and J.F. Ward. Mol. Phys. **20**, 513 (1971).
31. D. Beljonne, W. Wenseleers, E. Zojer, Z. Shuai, H. Vogel, S.J.K. Pond, J.W. Perry, S.R. Marder, and J.-L. Brédas. Adv. Funct. Mater. **12**, 631 (2002).
32. M.J.S. Dewar, E.G. Zoebisch, E.F. Healy, and J.J.P. Stewart. J. Am. Chem. Soc. **107**, 3902 (1995).
33. F. Voegtle. Cyclophane Chem. J. Wliley & Sons, New York, 1993.
34. Y. Morel, A. Irimia, P. Najechalski, Y. Kervella, O. Stephan, P.L. Baldeck, and C. Andraud. J. Chem. Phys. **114**, 5391 (2001).
35. P. Najechalski, Y. Morel, O. Stéphan, and P.L. Baldeck. Chem. Phys. Lett. **343**, 44 (2001).

© 2006 NRC Canada

Ionization potentials of nitriles — Photoelectron spectra of succinonitrile and glutaronitrile

Heidi M. Muchall and Nick H. Werstiuk

Abstract: The He(I) photoelectron spectra of succinonitrile (**1**) and glutaronitrile (**2**), both with extensive overlap of ionization bands in the low-energy region, are reported. To assign ionizations, we studied the conformational behaviour and resulting ionization energy dependence of **1** and **2** computationally with the B3LYP/6-31+G(d) model chemistry based on the fact that it reliably reproduces the ionization potentials of eleven mono- and di-nitriles, both saturated and unsaturated. The correlation of proton affinities with observed ionization potentials of **1**, **2**, and malononitrile establishes the orbital sequence of four C≡N π orbitals followed by two nitrogen lone pair orbitals as the highest occupied molecular orbitals for all three compounds.

Key words: photoelectron spectrum, ionization potential, conformational dependence, nitrile, DFT.

Résumé : On a déterminé les spectres photoélectroniques He(I) du succinonitrile (**1**) et du glutaronitrile (**2**) qui présentent tous les deux un recouvrement important des bandes d'ionisation dans la région de basse énergie. Pour attribuer les ionisations, en se basant sur le fait qu'ils permettent de reproduire fidèlement les potentiels d'ionisation de onze mono- et di-nitriles, tant saturés qu'insaturés, on a fait appel à des calculs théoriques au niveau B3LYP/6-31+G(d) pour effectuer une étude du comportement conformationnel des composés **1** et **2** et de la dépendance d'énergie d'ionisation qui en résulte. La corrélation des affinités protoniques avec les potentiels d'ionisation observés pour les composés **1**, **2** et pour le malonitrile permettent d'établir que, pour les trois composés, la séquence orbitalaire des orbitales moléculaires hautes occupées sont les quatre orbitales π du C≡N, suivies par les orbitales de deux orbitales de paires célibataires de l'azote.

Mots clés : spectre photoélectronique, potentiel d'ionisation, dépendance conformationnelle, nitrile, théorie de la théorie de la fonctionnelle de densité.

[Traduit par la Rédaction]

Introduction

This study was prompted by a request for the ionization potentials (IPs) of succinonitrile (**1**), which were needed for a comparison with those from 1,2-dicyanocyclopropanes (1). As explained in the following, the interpretation of the photoelectron (PE) spectrum of **1**, as well as that of glutaronitrile (**2**), turned into the comprehensive study reported here.

Two major problems have been reported with respect to the assignment of ionizations in nitriles. Firstly, Koopmans' theorem (2) seems to break down when model chemistries do not include electron correlation, which affected earlier analyses that made use of semiempirical or Hartree–Fock methods (3). Secondly, hole-mixing effects are reported to potentially further complicate the assignment of ionization events, even though the valence region seems to be little affected (4).

Received 11 July 2006. Accepted 14 September 2006. Published on the NRC Research Press Web site at http://canjchem.nrc.ca on 27 October 2006.

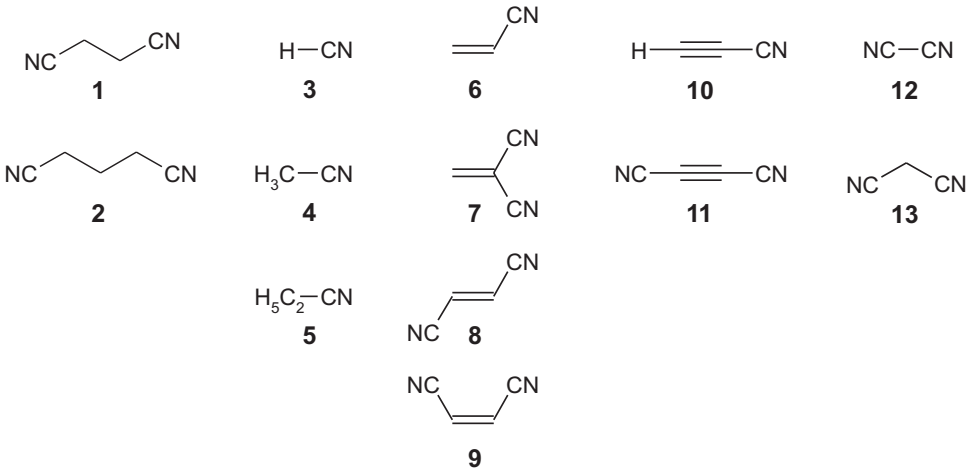
H.M. Muchall.[1] Centre for Research in Molecular Modeling and Department of Chemistry and Biochemistry, Concordia University, Montreal, QC H4B 1R6, Canada.
N.H. Werstiuk. Department of Chemistry, McMaster University, Hamilton, ON L8S 4M1, Canada.

[1]Corresponding author (e-mail: muchall@alcor.concordia.ca).

We expected to be able to make use of the methodology that we developed for the reliable calculation of ionization potentials of carbenes (5). The first ionization potential can be readily obtained as the difference in energy between a molecule and its radical cation at the geometry of the molecule (first vertical IP, $IP_{v,1}$) or the optimized radical geometry of the cation (first adiabatic IP, $IP_{a,1}$). Once the difference between the $IP_{v,1}$ and the energy of the highest occupied molecular orbital (HOMO) is added onto the energies of all occupied molecular orbitals, "calculated IPs" are obtained that can be compared to those obtained from a PE spectrum. Because the correlation between the two sets of IPs is usually of high accuracy, with both slopes and correlation coefficients of a linear regression close to 1.0, the calculated values are of tremendous aid in the interpretation of a PE spectrum in the case of multiple overlapping bands. A goal of this study was, therefore, to evaluate whether the low-energy ionizations of nitriles could be calculated reliably at the B3LYP/6-31+G(d) level of theory, as this model chemistry is highly efficient. Numerous PE spectra of nitriles are published and available for comparison with computational data and we chose nitriles **3**–**13** for our study because of their widely varying electronic structures.

In the following, we first evaluate the B3LYP/6-31+G(d) model chemistry for the determination of the low-energy ionization potentials of eleven nitriles, **3**–**13**, whose PE spectra are available in the literature. Next, the PE spectra of **1** and **2** are reported for the first time (to the best of our

 doi:10.1139/V06-141 © 2006 NRC Canada



knowledge) and the assignment of their ionization bands is discussed with particular emphasis on the molecular flexibility and its implications. Finally, the matter of the relative position of π and n type ionizations in the dinitrile series, malono- (**13**), succino- (**1**), and glutaronitrile (**2**), is addressed.

Experimental and computational details

The He(I) photoelectron spectra were recorded on a locally built instrument (6). Linearity of the scale was ensured through calibrations with iodomethane (9.54 and 10.16 eV) (7) and nitrogen (15.60 eV) (7) performed prior to the experiments. To remove water from succinonitrile and glutaronitrile (both purchased from Sigma-Aldrich), samples were pumped in the PE spectrometer at elevated probe temperatures (50–60 °C) and the process was followed by monitoring the PE spectra until the prominent ionization of water at 12.62 eV (7) had disappeared and no further change between subsequent spectra was discernible. The final spectra (averages of 20 scans) were also run with a probe temperature of 50–60 °C with nitrogen as an internal calibrant as well as make-up gas (8) to increase the pressure and improve the signal-to-noise ratio.

All calculations were performed using the Gaussian 98 (9) or Gaussian 03 (10) suite of programs. Geometries of the (protonated) nitriles were fully optimized with the Becke3 (11) – Lee, Young, and Parr (12) hybrid density functional (B3LYP) with the 6-31+G(d) basis set; only indicated torsional angles were frozen in the torsional analyses. All minima were confirmed by harmonic vibrational frequency analyses and wave functions were checked for stability. Synthetic spectra were generated with a Fortran program PESPEC (13). The temperature was set to 300 K and ionization potentials are convoluted with a Gaussian line-shape with a full width at half height of 0.2. Molecular orbitals were plotted using GaussView 3.0 (14). All energies, total and otherwise, used in the calculation of ionization potentials and proton affinities are given in Table S1 in the Supplementary Information.[2]

Results and discussion

Ionization potentials of nitriles 3–13

We decided to use the already published PE spectra of eleven mono- and di-nitriles, saturated and unsaturated, to evaluate our methodology for the calculation of ionization potentials (5). The prominent low-energy ionizations from n and π orbitals of **3**–**13** and ionizations from the onset of the σ-region reported in the literature are given in Table 1. We have calculated the first vertical ionization potentials ($IP_{v,1}$) of **3**–**13**. These are also given in Table 1 together with the calculated orbital energies ε and calculated IPs (obtained as explained in the introduction and in a footnote in Table 1).

As can be seen from Table 1, our calculated values for $IP_{v,1}$ are within 0.5 eV of the experimental values and in many cases the deviation is significantly less. Overall there is a very good agreement between experimental and calculated $IP_{v,1}$ with a correlation coefficient R^2 of 0.9664.

Individual plots of calculated vs. experimental IP_v for mononitriles **3**–**5** (10 data points) and alkenes **6**–**9** (25 data points) suggest that two of the values reported in the literature should be revised. In Fig. 1*a*, the fifth ionization for propionitrile (**5**), reported at 14.25 eV (7) and indicated with the symbol ×, is more likely to be at 13.8 eV and a close re-examination of the PE spectrum seems to confirm this. This suggested shift, pointed out by the arrow in Fig. 1*a*, improves the correlation coefficient from 0.9781 to 0.9884. In Fig. 1*b*, the third ionization for alkene **9**, reported at 13.35 eV (indicated with the symbol ×) (15), should probably be at a smaller value. While the onset of the second band in the PE spectra of alkenes **6**–**8** is sharp and starts from the baseline, there seems to be a shoulder on the low-energy side of the second band in the PE spectrum of **9**, indicating a somewhat broader ionization band under the one given at 12.77 eV (15). We suggest that the third ionization should then be located at 12.8 eV instead, which improves the correlation coefficient from 0.9684 to 0.9818.

In Fig. 2, we show the plot of calculated vs. experimental IP_v with the previously mentioned revised values for nitriles **3**–**13**. With a slope of close to one and an intercept near

[2] Supplementary data for this article are available on the journal Web site (http://canjchem.nrc.ca) or may be purchased from the Depository of Unpublished Data, Document Delivery, CISTI, National Research Council Canada, Ottawa, ON K1A 0R6, Canada. DUD 5086. For more information on obtaining material refer to http://cisti-icist.nrc-cnrc.gc.ca/irm/unpub_e.shtml.

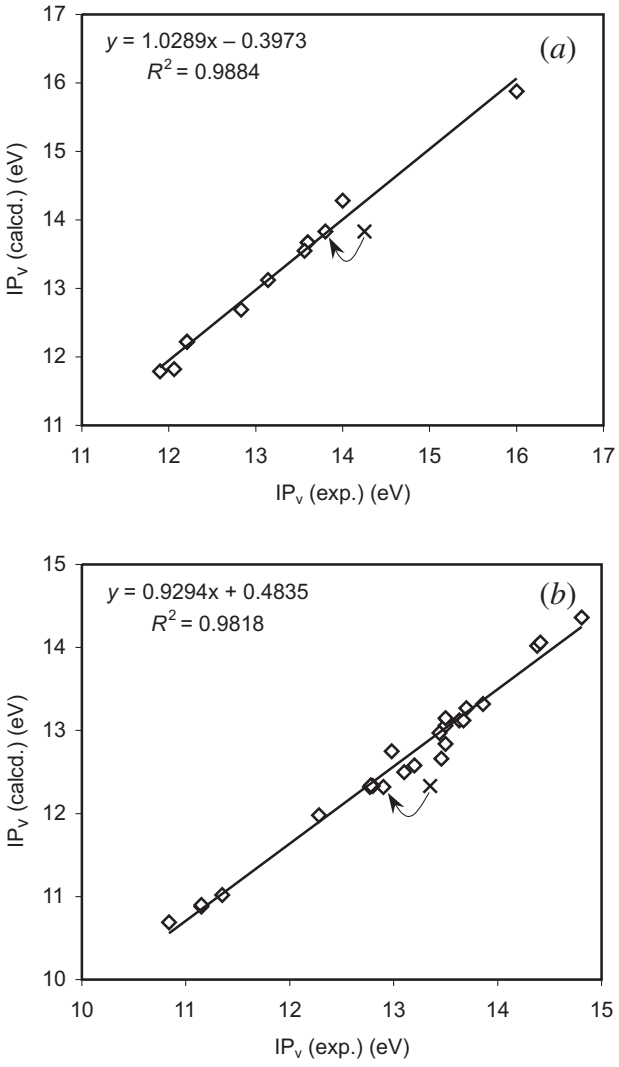
© 2006 NRC Canada

Table 1. Vertical ionization potentials and orbital energies (eV) of nitriles **3**–**13**.

	Exp. IP_v	$IP_{v,1}$[a]	–ε	Calcd. IP[b]	Refs.[c]
3	13.60	13.67	10.09	13.67	(7)
			10.09	13.67	
	14.0		10.70	14.28	
4	12.21	12.22	9.18	12.22	(7)
			9.18	12.22	
	13.14		10.08	13.12	
	16		12.84	15.88	
5	11.90	11.79	9.05	11.79	(7)
	12.06		9.08	11.82	
	12.83		9.95	12.69	
	13.56		10.81	13.55	
	14.25[d]		11.09	13.83	
6	10.84	10.69	8.16	10.84	(15)
	12.28		9.45	12.28	
	12.98		10.22	12.98	
	13.51		10.60	13.51	
7	11.35	11.02	8.75	11.02	(15)
	12.90		10.05	12.32	
	13.20		10.31	12.58	
	13.46		10.39	12.66	
	13.63		10.85	13.12	
	13.86		11.05	13.32	
	14.81		12.09	14.36	
8	11.15	10.90	8.65	10.90	(15)
	12.78		10.09	12.34	
	13.10		10.25	12.50	
	13.44		10.72	12.97	
			10.87	13.12	
	13.67		11.02	13.27	
	14.41		11.81	14.06	
9	11.15	10.88	8.61	10.88	(15)
	12.77		10.05	12.32	
	13.35[e]		10.06	12.33	
	13.5		10.57	12.84	
	13.5		10.79	13.06	
	13.5		10.88	13.15	
	14.38		11.75	14.02	
10	11.75	11.38	8.72	11.38	(16)
			8.72	11.38	
	13.54		10.83	13.49	
	14.18		11.18	13.84	
			11.18	13.84	
	18.3		15.52	18.18	
11	11.99	11.49	9.19	11.49	(16)
			9.19	11.49	
	13.91		11.30	13.60	
			11.30	13.60	
	14.00		11.51	13.81	
	14.16		11.55	13.85	
	15.00		12.41	14.71	
12	13.51	13.15	10.33	13.15	(16)
			10.33	13.15	
	14.49		11.70	14.52	
	14.86		12.05	14.87	
	15.6		12.51	15.33	
			12.51	15.33	
13	12.72	12.28	9.81	12.28	(17)
	13.14		10.01	12.48	
	13.42		10.26	12.73	
	13.59		10.35	12.82	
	13.91		10.88	13.35	
	14.06		11.01	13.48	

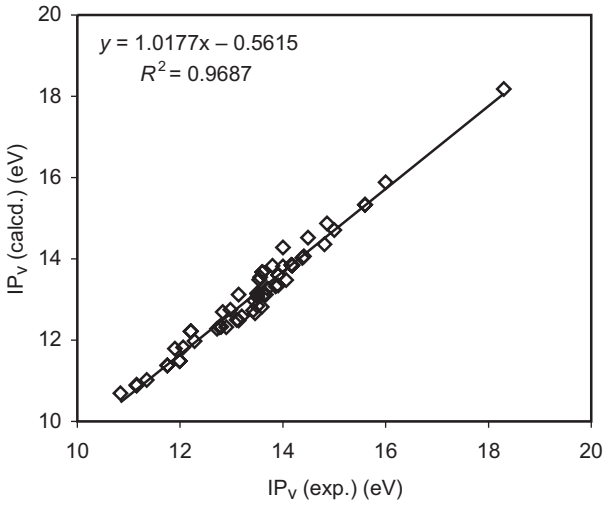
[a]Difference in electronic energy between a molecule and its radical cation at the geometry of the molecule.
[b]Obtained by a uniform shift of all orbital energies so that the HOMO energy matches the calculated $IP_{v,1}$.
[c]Experimental values.
[d]Should be at 13.8 eV, see text.
[e]Should be at 12.8 eV, see text.

Fig. 1. Correlation of calculated vs. experimental vertical ionization potentials for (*a*) mononitriles **3**–**5** and (*b*) alkenes **6**–**9**. Data points given with the symbol × were included in the correlations only after they were shifted as indicated by the arrows.



© 2006 NRC Canada

Fig. 2. Correlation of calculated and experimental vertical ionization potentials for nitriles **3**–**13**.



zero, this correlation demonstrates that our choice of model chemistry reliably reproduces the vertical ionization potentials of nitriles. Neither a larger basis set (6-311+G(2d,p)) nor a switch to the Perdew–Burke–Ernzerhof (PBE0) (18) functional with either basis set produced a significant improvement over the results presented here (we performed calculations on selected nitriles only; the results for $IP_{v,1}$ are given in Table S2 in the Supplementary Information).[2]

Photoelectron spectra of 1 and 2

The recorded photoelectron spectra of **1** and **2** are reported in Fig. 3. Owing to the relatively low vapour pressure of both **1** and **2** even at 50–60 °C, nitrogen was used as a make-up gas during the acquisition of the spectra. The intense first ionization of nitrogen at 15.6 eV is cut off arbitrarily in both spectra in Fig. 3. Both spectra exhibit extensive overlap of multiple ionization bands in the low-energy region (below 15 eV for **1** and below 13.5 eV for **2**) and an interpretation of the spectra is only possible with the help of computational results. Accordingly, the assignment of the observed bands for **1** and **2** is performed in the following sections, taking the calculated ionization potentials and conformational flexibility of the molecules into account. The resulting interpretation in terms of low-energy ionization bands of **1** and **2** is given in Tables 2 and 3 and as vertical bars in Fig. 3.

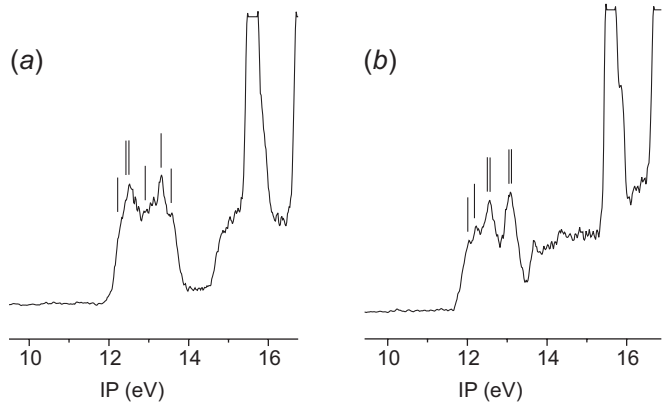
Interpretation of the PE spectra of 1 and 2

While nitriles **3**–**13** do not possess conformational flexibility (apart from methyl group rotations that are irrelevant for our purposes), **1** and **2** can exist in several conformations and this can affect the appearance of the PE spectra if the conformers are close in energy and their orbital energies differ sufficiently (19, 20).

Succinonitrile (1)

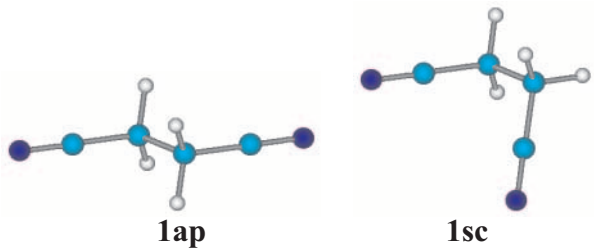
The conformations of **1** have been studied computationally with ab initio methods as early as 1978 (21), with even earlier work on its torsional potential (22). For **1**, a 1,2-disubstituted ethane, two low-energy conformations can be identified, antiperiplanar **1ap** and synclinal **1sc**. While **1sc**

Fig. 3. He(I) photoelectron spectra of (*a*) succinonitrile (**1**) and (*b*) glutaronitrile (**2**). The N_2 (make-up gas) signal at 15.6 eV is cut off. Assigned band positions are given by vertical bars.



(C–C–C–C torsional angle is 69° with B3LYP/6-31+G(d), 75° from experiment (23)) is the form present in the solid below –43.7 °C (24, 25), in the gas phase we calculate a destabilization with respect to **1ap** of 1.2 kcal/mol (B3LYP/6-31+G(d) based on either electronic energies or Gibbs free energies, 1 cal = 4.184 J) in line with an early prediction (25). We find a similar destabilization of 1.1 kcal/mol with B3LYP/6-311+G(2d,p) and PBE0/6-311+G(2d,p) model chemistries, thus confirming that the smaller basis set is adequate for the description of **1**. The energy difference leads to an equilibrium population of 78% **1ap** and 22% **1sc** (combined amount for the two indistinguishable conformers +sc and –sc) at 300 K, which is in excellent agreement with the 74% **ap** equilibrium at 170 °C found by electron diffraction in the gas phase (23).

Table 2 gives the calculated orbital energies and ionization potentials of **1ap** and **1sc** and it is obvious that even a small amount of **1sc** in the equilibrium should influence the appearance of the PE spectrum of **1**. To assess the IP dependence on the change in torsional angle that converts **1ap** into **1sc**, we have performed a relaxed potential energy scan twisting the C–C–C–C torsional angle through 180° and optimizing the rest of the molecule. The plot is shown in Fig. 4 for the first six calculated IPs (energies for HOMO to HOMO–5 shifted so that the HOMO energy for a torsional angle equals its first vertical ionization potential), which correspond to ionizations from the characteristic nitrile π and n orbitals. Orbital energies and calculated IPs for the different torsional angles are given in Table S3 in the Supplementary Information.[2] Figure 4 demonstrates the predicted significant changes in IPs upon twisting of **1**. Plots of the molecular orbitals of the C_{2h}-symmetrical **1ap** are given in Fig. 5; the order of the orbitals is the same in **1sc**. HOMO to HOMO–3



© 2006 NRC Canada

Table 2. Vertical ionization potentials and orbital energies (eV) of **1**.

	1ap			**1sc**		
Exp. IP_v	$IP_{v,1}$[a]	–ε	Calcd. IP_v[b]	$IP_{v,1}$[a]	–ε	Calcd. IP_v[b]
12.3	11.80	9.56	11.80	11.72	9.44	11.72
12.5		9.67	11.91		9.54	11.82
		9.72	11.96		9.62	11.90
13.0		10.03	12.27		9.90	12.18
13.41		10.53	12.77		10.44	12.72
13.50		10.68	12.92		10.47	12.75

Note: The IPs reported here from re-recorded spectra differ slightly from the preliminary values given in (1). Also, see the included structures for the naming of the conformers.

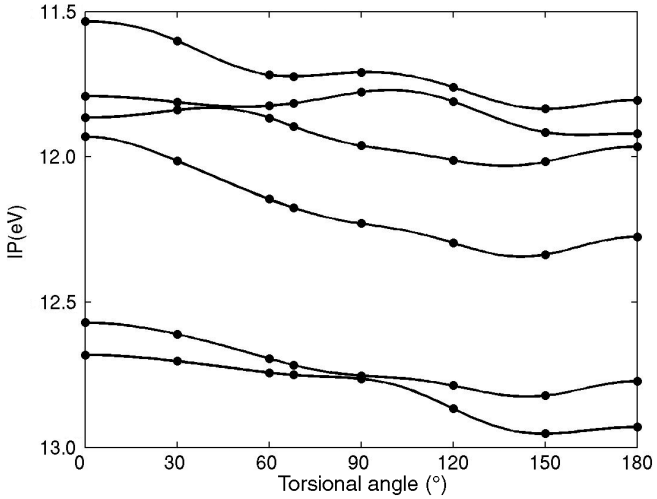
[a]Difference in electronic energy between a molecule and its radical cation at the geometry of the molecule.
[b]Obtained by a uniform shift of all orbital energies so that the HOMO energy matches the calculated $IP_{v,1}$.

Table 3. Vertical ionization potentials and orbital energies (eV) of **2**.

	2gg			**2ag**			**2aa**		
Exp. IP_v	$IP_{v,1}$[a]	–ε	Calcd. IP_v[b]	$IP_{v,1}$[a]	–ε	Calcd. IP_v[b]	$IP_{v,1}$[a]	–ε	Calcd. IP_v[b]
12.04	11.45	9.33	11.45	11.36	9.25	11.36	11.39	9.31	11.39
12.22		9.34	11.46		9.37	11.48		9.43	11.51
12.5		9.50	11.62		9.54	11.65		9.50	11.58
		9.59	11.71		9.71	11.82		9.68	11.76
13.1		10.28	12.40		10.26	12.37		10.31	12.39
		10.32	12.44		10.40	12.51		10.42	12.50

Note: See the included structures for the naming of the conformers.
[a]Difference in electronic energy between a molecule and its radical cation at the geometry of the molecule.
[b]Obtained by a uniform shift of all orbital energies so that the HOMO energy matches the calculated $IP_{v,1}$.

Fig. 4. Angular dependence of the first six ionization potentials of **1**. Orbital energies for the torsional angle were uniformly shifted so that the HOMO energy equals the first calculated IP_v.



are π type orbitals with additional coefficients on the linking CH_2 groups; HOMO–4 and HOMO–5 are the two lone pair combinations, n_N^+ and n_N^-. Ionizations arising from HOMO–1 and HOMO–2, the two out-of-plane orbitals π^-_{CNoop} and π^+_{CNoop}, as well as those from n_N^+ and n_N^- show only a small splitting that could be attributed to through-bond interactions in the molecular orbitals. On the other hand, ionizations from HOMO and HOMO–3, the two in-plane orbitals π^+_{CNip} and π^-_{CNip}, exhibit a somewhat constant splitting of about 0.4 eV throughout the torsion.

The fitted potential for the torsion in **1** is shown in Fig. 6*a* and we have simulated the PE spectrum of **1**, given in Fig. 6*b*, based on this potential and the six IPs given in Fig. 4. A comparison between the experimental and the simulated spectrum shows good agreement in the low-energy part and it can be seen that six ionizations lie under the first two broad bands in the experimental spectrum of **1** (Fig. 3*a*). As well, the simulated spectrum suggests that the first ionization in Fig. 3*a* should not be attributed to the maximum of the first band (12.5 eV) but rather to a shoulder on its low-energy side at 12.3 eV. The first adiabatic IP (IP_a) of **1** is at 11.9 eV (Fig. 3*a*) and so the experimentally determined energy gap between first IP_a and IP_v of 0.4 eV matches the calculated one (the IP_a calculated for **1ap** from 0–K enthalpies is 11.52 eV).

The final band assignment for the ionizations of **1** is given in Table 2 and their position as vertical bars in Fig. 3*a*. As a final note, and keeping in mind that the discrimination in count rate between high- and low-energy electrons is different for the two spectrometers used, our spectrum of **1** resembles that of *trans*-1,2-dicyanocyclopropane (**14**) (1) with one fundamental exception. The major difference is caused by the stabilization of HOMO and HOMO–1 of **1** as compared to these orbitals in **14** by 0.8 and 0.5 eV, respectively, because in **14** π_{CN} coefficients on the two nitrile groups are combined with two high-lying Walsh orbitals of the cyclopropyl group, ω_S and ω_A. The stabilization of the two orbitals in **1** leads to a shift of the first two ionizations towards higher potentials and the subsequent extensive overlap

© 2006 NRC Canada

Fig. 5. The six highest occupied molecular orbitals (HOMO to HOMO–5) of conformer **1ap**, their characters and symmetries.

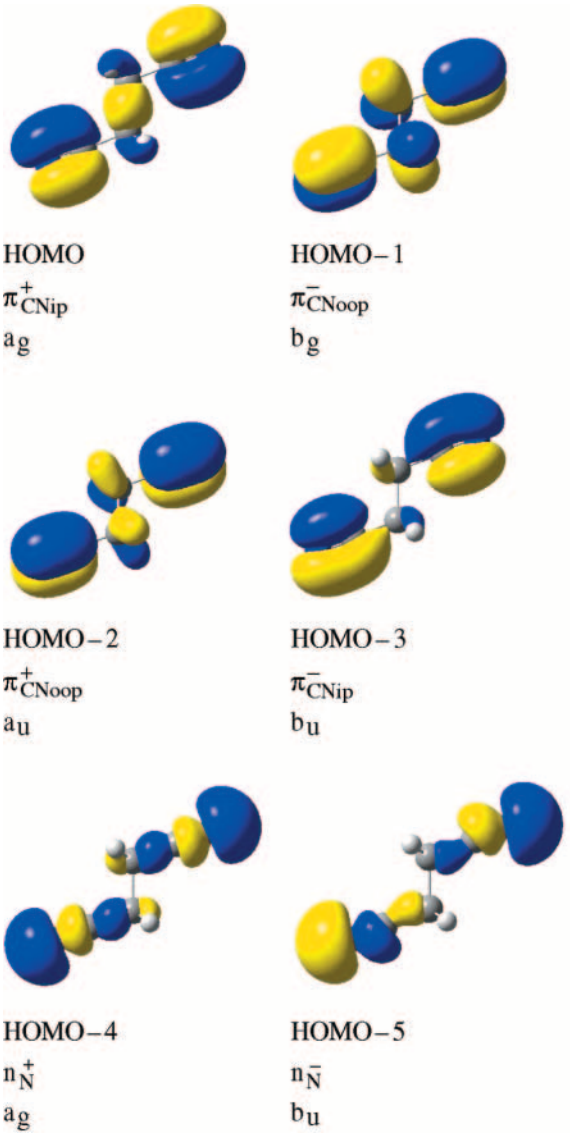
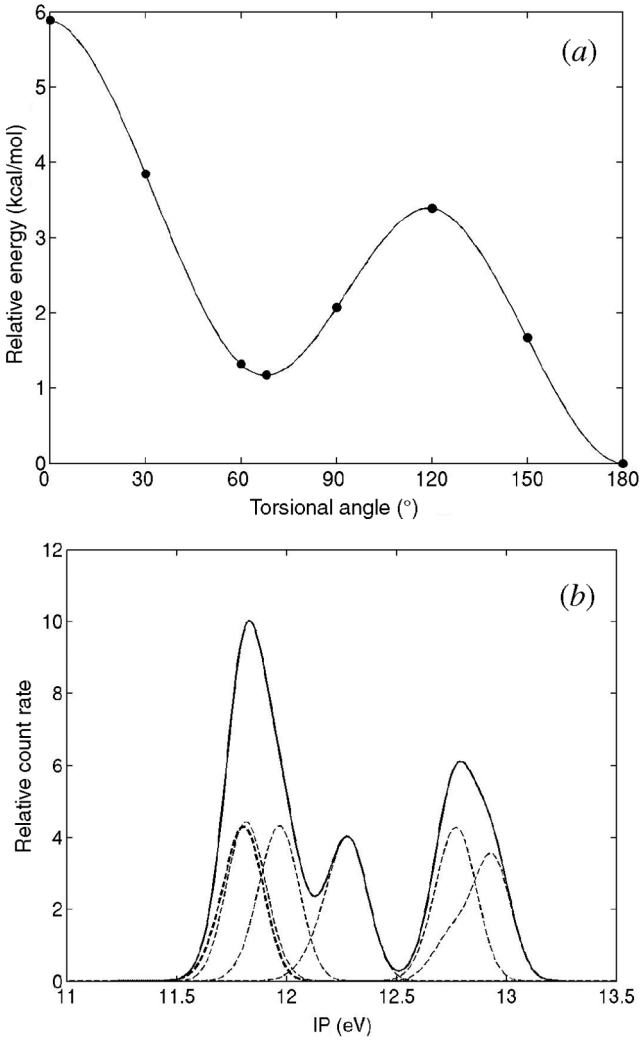


Fig. 6. (*a*) Torsional potential for twisting about the central C–C bond in **1** and (*b*) partial simulated PE spectrum of **1** based on the potential in (*a*). Dashed lines in (*b*) show the deconvoluted ionizations.



of bands in the spectrum of **1** that is not present in the spectrum of **14**.

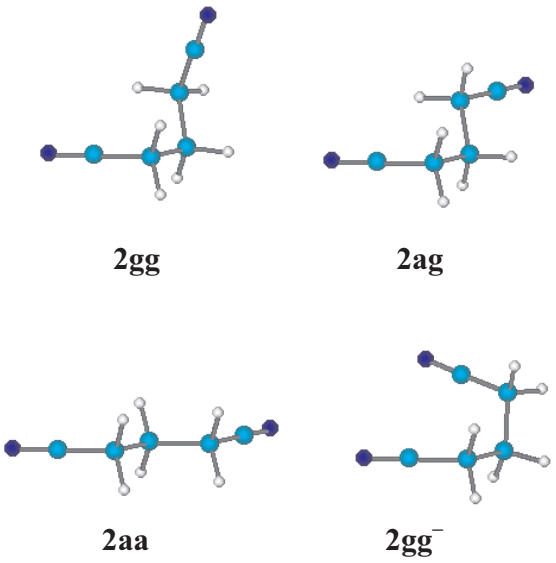
Glutaronitrile (2)

For **2**, a 1,3-disubstituted propane, there are two torsional angles and conformations can be described as antiperiplanar (a) or synclinal/gauche (g) for either substituent (26) or using the trans (T) and gauche (G) notation in the older literature (27). The four possible conformers for **2** from B3LYP/631+G(d) electronic energies are **2gg** (global minimum), **2ag** (+0.4 kcal/mol), **2aa** (+1.0 kcal/mol), and **2gg**$^{-}$ (+3.8 kcal/mol). From these relative stabilities, with a statistical weight of two for a **gg** and four for an **ag** conformer, at 300 K the equilibrium is composed of 48% **2gg**, 47% **2ag**, and 5% **2aa**. The conformer **2gg**$^{-}$ is too high in energy to contribute significantly.[3] An approximately equimolar mixture of **2gg** and **2ag** was also reported from an electron diffraction study at 448 K in the gas phase, but evidence for the presence of a small amount of **2aa** was not found (28).

The MO sequence in the C_2-symmetrical **2gg** is π^{+}_{CNip} (a symmetry), π^{-}_{CNoop} (b symmetry), π^{-}_{CNip} (b), π^{+}_{CNoop} (a), n_N^{-} (b), n_N^{+} (a). Pictures of the orbitals are similar to those given in Fig. 5. Some of these combinations are lost in **2ag** and π and n orbitals are localized on the individual CN groups, π^{+}_{CN}, π_{CN}, π_{CN}, π^{-}_{CN}, n_N, n_N. Table 3 shows that orbital energies for the two conformers are very similar. To simulate the PE spectrum of **2**, two torsional angles would have to be considered, a CN–C–C–C that converts **2gg** into **2ag** and another for conversion of **2gg** into **2aa**. We have checked the orbital energy dependence on the CN–C–C–C torsional angle that relates the two major contributors, **2gg** and **2ag**. Not surprisingly, we find the dependence to be sim-

[3] As **2gg** and **2ag** are approximately equal in energy, their equilibrium composition is about 1:1. This does not change when Gibbs free energies are considered even though **2ag** is now more stable by 0.1 kcal/mol.

© 2006 NRC Canada



ilar to that in **1** but less pronounced (plot not shown). For these reasons we have not simulated the PE spectrum of **2**.

With its onset (IP_a) at 11.7 eV and its maximum (IP_v) at 12.0 eV (Fig. 3*b*), the slope of the first ionization band is similar to that in the spectrum of **1**. Unlike for **1**, though, the adiabatic first IP for **2** is more difficult to assess computationally. A radical cation with a geometry close to that of **2gg** does not exist at the B3LYP/6-31+G(d) level and removal of an electron from **2gg** and geometry optimization leads to the transition state for a double hydride transfer instead. The calcd. IP_a for **2ag** (for which the optimized radical cation is a proper minimum) is 11.04 eV and with calculated IP_v values of 11.45 for **2gg** and 11.36 eV for **2ag**, the width-at-half-height of the first ionization band should be as is found experimentally. Overall, because of the similar IPs of **2gg** and **2ag** the presence of a second major conformer, be it **2gg** or **2ag**, is not detectable. Because **2aa** only contributes 5% to the equilibrium, its presence would only be noticeable if its first ionization potential were considerably lower than those of **2gg** and **2ag**. Table 3 shows that this is not the case. The final band assignment for the ionizations of **2** is given in Table 3 and their position as vertical bars in Fig. 3*b*.

Lone pair ionizations in dinitriles 1, 2, and 13

The question of which are the lone pair ionizations in **1** and **2** is easier to answer than in malononitrile (**13**), for which several orbital sequences have been given (4, 17, 29, 30). For **1**, the two n_N ionizations are degenerate at a C–C–C–C torsional angle of 90° (Fig. 4) and so the orbital energy dependence confirms the assignment given in Fig. 5. For **2**, the two functional groups are far enough apart that they show hardly any interaction and consequently the energy gap between π and n ionizations (0.7 eV calculated for **2gg**) is similarly pronounced as those in the mononitriles **4** and **5** (0.9 eV calculated). In contrast, the reported order of orbitals and peak assignments for the first six ionization bands in **13** varies from π, π, n_N^+, n_N^-, π, π (29) to π, π, π, n_N^+, n_N^-, π (17) to π, π, π, π, n^-, n^+ (4); i.e., the potentials for the lone pair ionizations are progressively increased.

Staley et al. (30) have shown a linear correlation between the proton affinity (PA) of a nitrile and its n_N ionization potential. While the data points for most mononitriles investigated (among these **3**–**6**) fall close to the correlation line, the two IPs for the dinitrile **13** (n_N^+ and n_N^-) are 6 and 10 kcal/mol too small when the original orbital sequence from Stafast and Bock (29) is used (30). This, among other reasons, led to a reassignment of the orbital order (17). We decided to use a similar correlation that would include **1** and **2** to confirm the orbital sequences we determined earlier. Calculating the proton affinity as the difference between the 0–K enthalpies of the neutral and protonated molecules (for our purposes we can ignore temperature effects (31)), we find a good linear correlation ($y = 1.419x - 82.83$, values in kcal/mol, $R^2 = 0.9945$, raw data are given in Table S4 in the Supplementary information)[2] between calculated and experimental PAs for the mononitriles **3**–**6**. From this, our calculated PAs for **1ap** (176.2 kcal/mol) and **2gg** (182.6 kcal/mol) give estimated experimental PAs of 182.5 and 187.0 kcal/mol, respectively. With these values, Fig. 7 allows the confirmation of the assigned lone pair ionizations in **1** and **2**. It shows good linear correlation between the experimental n_N ionization potential (Table 1) and the experimental PA of nitriles **3**–**6** (30). Superimposed are the first six ionization potentials of **1** and **2** at their estimated experimental PAs. Clearly, IPs around 13.5 eV for **1** and around 13.2 eV for **2** lie close to the regression line, confirming our assignment of these IPs to n_N orbitals. In addition, Fig. 7 seems to support the orbital assignment of Cambi and von Niessen for **13**, with four π orbitals followed by two n_N orbitals (4). At an experimental PA of 178.0 kcal/mol, the fifth ionization, attributed to the higher-lying lone pair combination, lies close to the correlation line. The orbital sequence of **13** is thus in perfect agreement with that given above for both **1** and **2**.

Conclusions

We have presented the He(I) photoelectron spectra of succinonitrile (**1**) and glutaronitrile (**2**). Even though the low-energy regions of both spectra exhibit extensive overlap of bands, it is possible to assign individual bands with the aid of calculated ionization potentials. Both **1** and **2** exhibit four π orbitals followed by two nonbonding orbitals as the six highest occupied molecular orbitals. This orbital sequence was also established for the related malononitrile.

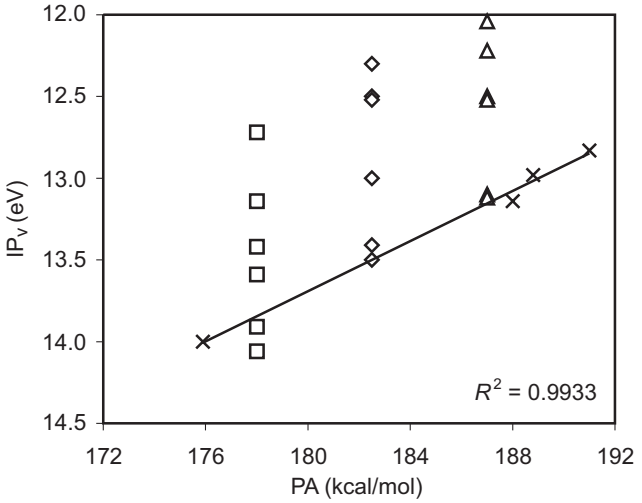
Finally, for nitriles of varying electronic structure (mono- and di-nitriles, either saturated or unsaturated), the B3LYP/6-31+G(d) model chemistry allows vertical ionization potentials to be reproduced reliably. A violation of Koopmans' theorem for dinitriles is not found with this density functional theory method.

Acknowledgements

Calculations were performed at the Centre for Research in Molecular Modeling (CERMM), which was established with the financial support of the Concordia University Faculty of Arts and Science, the Ministère de l'Éducation du Québec (MEQ), and the Canada Foundation for Innovation (CFI). We also thank SHARCNET (Shared Hierarchical Academic

© 2006 NRC Canada

Fig. 7. Linear regression of the measured n_N ionization potential versus the experimental proton affinity (30) of nitriles **3**–**6** (×). Superimposed are the experimental IPs for the first six ionization events of **1** (◇), **2** (Δ), and **13** (□) at their (estimated) PA values (see text).



Research Computing Network of Ontario) for providing computing resources at McMaster University. This work was supported by research grants from the Natural Sciences and Engineering Research Council of Canada (NSERC).

References

1. P. Rademacher. Eur. J. Org. Chem. **7**, 1572 (2004).
2. T. Koopmans. Physica, **1**, 104 (1934).
3. P. Rosmus, H. Stafast, and H. Bock. Chem. Phys. Lett. **34**, 275 (1975), and refs. cited therein.
4. R. Cambi and W. von Niessen. J. Electron. Spectrosc. Relat. Phenom. **42**, 245 (1987).
5. H.M. Muchall, N.H. Werstiuk, and B. Choudhury. Can. J. Chem. **76**, 221 (1998).
6. N.H. Werstiuk, D.N. Butler, and E. Shahid. Can. J. Chem. **65**, 760 (1986).
7. K. Kimura, S. Katsumata, Y. Achiba, T. Yamazaki, and S. Iwata. *In* Handbook of HeI photoelectron spectra of fundamental organic molecules. Halsted Press, New York. 1981.
8. N.H. Werstiuk, H.M. Muchall, J. Ma, and M.T.H. Liu. Can. J. Chem. **76**, 1162 (1998).
9. M.J. Frisch, G.W. Trucks, H.B. Schlegel, G.E. Scuseria, M.A. Robb, J.R. Cheeseman, V.G. Zakrzewski, J.J.A. Montgomery, R.E. Stratmann, J.C. Burant, S. Dapprich, J.M. Millam, A.D. Daniels, K.N. Kudin, M.C. Strain, O. Farkas, J. Tomasi, V. Barone, M. Cossi, R. Cammi, B. Mennucci, C. Pomelli, C. Adamo, S. Clifford, J. Ochterski, G.A. Peterson, P.Y. Ayala, Q. Cui, K. Morokuma, N. Rega, P. Salvador, J.J. Dannenberg, D.K. Malick, A.D. Rabuck, K. Raghavachari, J.B. Foresman, J. Cioslowski, J.V. Ortiz, A.G. Baboul, B.B. Stefanov, G. Liu, A. Liashenko, P. Piskorz, I. Komaromi, R. Gomperts, R.L. Martin, D.J. Fox, T. Keith, M.A. Al-Laham, C.Y. Peng, A. Nanayakkara, M. Challacombe, P.M.W. Gill, B. Johnson, W. Chen, M.W. Wong, J.L. Andres, C. Gonzalez, M. Head-Gordon, E.S. Replogle, and J.A. Pople. Gaussian 98 [computer program]. Revision A.11.4. Gaussian, Inc., Pittsburgh, Pa. 2002.
10. M.J. Frisch, G.W. Trucks, H.B. Schlegel, G.E. Scuseria, M.A. Robb, J.R. Cheeseman, J.A. Montgomery, Jr., T. Vreven, K.N. Kudin, J.C. Burant, J.M. Millam, S.S. Iyengar, J. Tomasi, V. Barone, B. Mennucci, M. Cossi, G. Scalmani, N. Rega, G.A. Petersson, H. Nakatsuji, M. Hada, M. Ehara, K. Toyota, R. Fukuda, J. Hasegawa, M. Ishida, T. Nakajima, Y. Honda, O. Kitao, H. Nakai, M. Klene, X. Li, J.E. Knox, H.P. Hratchian, J.B. Cross, C. Adamo, J. Jaramillo, R. Gomperts, R.E. Stratmann, O. Yazyev, A.J. Austin, R. Cammi, C. Pomelli, J.W. Ochterski, P.Y. Ayala, K. Morokuma, G.A. Voth, P. Salvador, J.J. Dannenberg, V.G. Zakrzewski, S. Dapprich, A.D. Daniels, M.C. Strain, O. Farkas, D.K. Malick, A.D. Rabuck, K. Raghavachari, J.B. Foresman, J.V. Ortiz, Q. Cui, A.G. Baboul, S. Clifford, J. Cioslowski, B.B. Stefanov, G. Liu, A. Liashenko, P. Piskorz, I. Komaromi, R.L. Martin, D.J. Fox, T. Keith, M.A. Al-Laham, C.Y. Peng, A. Nanayakkara, M. Challacombe, P.M.W. Gill, B. Johnson, W. Chen, M.W. Wong, C. Gonzalez, and J.A. Pople. Gaussian 03 [computer program]. Revision B.02. Gaussian, Inc., Pittsburgh, Pa. 2003.
11. A.D. Becke. J. Chem. Phys. **98**, 5648 (1993).
12. C. Lee, W. Young, and R.G. Parr. Phys. Rev. B, **37**, 785 (1988).
13. N.H. Werstiuk, G. Timmins, J. Ma, and T.A. Wildman. Can. J. Chem. **70**, 1971 (1992).
14. R. Dennington, II, T. Keith, J. Millam, K. Eppinnett, W.L. Hovell, and R. Gilliland. GaussView [computer program]. Version 3.09. Semichem, Inc., Shawnee Mission, Kans. 2003.
15. H. Stafast and H. Bock. Tetrahedron, **32**, 855 (1976).
16. L. Åsbrink, W. von Niessen, and G. Bieri. J. Electron Spectrosc. Relat. Phenom. **21**, 93 (1980).
17. C.B. Macdonald, D.S. Waddell, and N.P.C. Westwood. J. Mol. Struct. **162**, 341 (1987).
18. J.P. Perdew, K. Burke, and M. Ernzerhof. Phys. Rev. Lett. **77**, 3865 (1996); J.P. Perdew, K. Burke, and M. Ernzerhof. Phys. Rev. Lett. **78**, 1396 (1997); J.P. Perdew, M. Ernzerhof, and K. Burke. J. Chem. Phys. **105**, 9982 (1996).
19. E. Honegger and E. Heilbronner. Chem. Phys. Lett. **81**, 615 (1981).
20. H.M. Muchall, N.H. Werstiuk, J. Ma, T.T. Tidwell, and K. Sung. Can. J. Chem. **75**, 1851 (1997).
21. K. Kveseth. Acta Chem. Scand. Ser. A, **32**, 51 (1978).
22. L. Radom and P.J. Styles. J. Chem. Soc. Chem. Commun. 190 (1974).
23. L. Fernholt and K. Kveseth. Acta Chem. Scand. Ser. A, **33**, 335 (1979).
24. T. Fujiyama, K. Tokumaru, and T. Shimanouchi. Spectrochim. Acta, **20**, 415 (1964).
25. W.E. Fitzgerald and G.J. Janz. J. Mol. Spectrosc. **1**, 49 (1957).
26. E.L. Eliel and S.H. Wilen. *In* Stereochemistry of organic compounds. Wiley Interscience, New York. 1994. Chap. 10.
27. I. Matsubara. J. Chem. Phys. **35**, 373 (1961).
28. P.J. Stavnebrekk. J. Mol. Struct. **213**, 271 (1989).
29. H. Stafast and H. Bock. Z. Naturforsch. B, **28**, 746 (1973).
30. R.H. Staley, J.E. Kleckner, and J.L. Beauchamp. J. Am. Chem. Soc. **98**, 2081 (1976), and refs. cited therein.
31. E.I. von Nagy-Felsobuki and K. Kimura. J. Phys. Chem. **94**, 8041 (1990).

© 2006 NRC Canada

Electrochemically formed passive layers on titanium — Preparation and biocompatibility assessment in Hank's balanced salt solution

Baodong Zhao and Gregory Jerkiewicz

Abstract: Uniform and crack-free passive layers on Ti are prepared using AC voltage in 7.5 wt.% aq. $NH_4{\cdot}BF_4$ at 25 °C. The passive layers possess coloration (wide spectrum of colors) that depends on the experimental conditions. The biocompatibility of such prepared passive layers is evaluated using corrosion science and analytical techniques. Their corrosion behavior, Ti-ion release, surface roughness, and wettability in Hank's Balanced Salt Solution (HBSS) at 37 °C are the main focus of this work. Open-circuit potential and polarization measurements demonstrate that the corrosion potential (E_{corr}) of the passive layers becomes more positive than that of the untreated Ti. The value of E_{corr} increases as we increase the AC voltage (V_{AC}). Their corrosion rate (CR) is lower than that of the untreated Ti, and they reduced the Ti-ion release level from 230 to 15 ppb. An increase in the AC voltage frequency (f) leads to a slightly higher level of the Ti-ion release (~50 ppb). Surface profilometry, optical microscopy, and scanning electron microscopy (SEM) analyses show that prolonged exposure of the passive layers to HBSS results in changes to their surface topography. The passive layers prepared by the application of AC voltage are rougher and more hydrophilic than the untreated Ti. Our methodology of preparing biocompatible passive layers on Ti might be applied as a new surface treatment procedure for Ti implants.

Key words: titanium, metal surface treatment, surface roughness, corrosion, metal ion release, contact angle.

Résumé : Utilisant un voltage de courant alternatif dans une solution aqueuse à 7,5% (p/p) de $NH_4{\cdot}BF_4$, à 25 °C, on a préparé des couches passives uniformes et sans fissure sur du titane. Les couches passives possèdent des colorations qui s'étalent sur un large spectre de couleur et qui dépendent des conditions expérimentales. On a évalué la biocompatibilité des couches passives préparées de cette façon en faisant appel à la science de la corrosion et des techniques analytiques. Les orientations principales de cette étude sont le comportement de corrosion, la libération d'ion de titane, la rugosité de leur surface et la capacité de mouillage dans une solution de sel balancée de Hanck (SSBH) , à 37 °C. Le potentiel en circuit ouvert et les mesures de polarisation démontrent que le potentiel de corrosion (E_{corr}) des couches passives devient plus positif que celui du titane qui n'a pas été traité. La valeur de E_{corr} augmente avec une augmentation du voltage du courant alternatif (V_{CA}). Leur vitesse de corrosion (VC) est inférieure à celle du titane qui n'a pas été traité et le niveau de libération du titane est réduit de 230 à 15 ppb. Une augmentation de la fréquence (f) du voltage du courant alternatif conduit à un niveau légèrement supérieur de libération de l'ion titane (~50 ppb). Des analyses de profilométrie de surface, de microscopie optique et de microscopie électronique à balayage (MEB) montrent que des expositions prolongées des couches passives à une SSBH conduit à des changements de la topographie de la surface. Les couches passives préparées par l'application d'un voltage de courant alternatif sont plus rugueuses et plus hydrophiles que le titane qui n'a pas été traité. Il est possible que notre méthodologie de préparation de couches passives biocompatibles puisse trouver une application dans le développement d'une nouvelle façon de produire des implants au titane.

Mots clés : titane, traitement de la surface métallique, rugosité de la surface, corrosion, libération d'ion métallique, angle de contact.

[Traduit par la Rédaction]

Introduction

Titanium of commercial purity (CP) and its alloys are widely used as biomedical materials and find applications in bone and joint replacement, orthopedic treatment, dental implants, cardiovascular devices, external prostheses, and surgical instruments because of their suitable chemical, physical, and biological properties (1). The biological response of the human body to implant materials is directly related to their interfacial properties. Corrosion resistance, metal-ion release, surface roughness, and wettability are

Received 6 June 2006. Accepted 27 August 2006. Published on the NRC Research Press Web site at http://canjchem.nrc.ca on 27 October 2006.

B. Zhao and G. Jerkiewicz.[1] Department of Chemistry, Queen's University, 90 Bader Lane, Kingston, ON K7L 3N6, Canada.

[1]Corresponding author (e-mail: gregoryj@chem.queensu.ca).

 doi:10.1139/V06-142 © 2006 NRC Canada

among the most important properties that need to be considered in the fabrication and surface treatment of new biomaterials. The two main factors that determine the biocompatibility of a material are the host reaction induced by the material and the material's degradation in the body environment (2). Corrosion of the implanted metal by the body fluids changes its mechanical and interfacial properties and results in the release of undesired metal ions. The latter may interfere in physiological processes and subsequently induce rejection reactions, such as toxicity and allergy (3, 4). This is why metallic implants are selected based on their corrosion resistance or their ability to form a protective passive film. It was reported that in some cases large amounts of Ti compounds are found in tissues surrounding the implant device (5, 6), in spite of its good corrosion resistance. Suitable surface modification procedures are indispensable prior to the application of Ti or Ti-based alloys as implants, and surface treatment and biocompatibility evaluation of these materials have been a subject of extensive research (5–18).

The oxide layer that covers Ti is very stable and determines the corrosion behavior of Ti implants and their high tissue compatibility. Surface treatment procedures modify the composition, morphology, and thickness of the oxide layer; thus, they subsequently influence the corrosion behavior of such treated implants. It is the oxide's uniformity and chemical stability that are predominant factors in the protection of implants against biological corrosion. The corrosion resistance of implants does not only depend on the oxide's thickness (15).

Several different surface treatment methods have been used to improve the corrosion resistance and biocompatibility of Ti and Ti-based alloys. Thermal treatment involves heating at an elevated temperature, and oxides formed under such conditions lack uniformity or deform and subsequently cause swelling or cracking of the oxide layer due to the differing thermal expansion coefficients of Ti and its oxide. These phenomena are of major concern in the design and preparation of biocompatible passive layers. Electrochemical techniques have advantages over other surface treatment methods. They can be applied at the ambient temperature and form passive layers that are highly adhesive, uniform, and crack-free. In addition, typical electrochemical instrumentation and procedures are relatively simple and facilitate the formation of compact passive layers within seconds or minutes. Moreover, electrochemical methods allow one to easily control the oxide thickness.

Our previous work (19, 20) indicated that brightly and uniformly colored passive layers on Ti can be obtained by the application of AC (alternating current) voltage in aqueous $NH_4{\cdot}BF_4$. The coloration and thickness of these passive layers can be controlled by varying the concentration and pH of the electrolyte, adjusting the separation between electrodes, selecting the passivation time, and tuning the magnitude of the applied AC voltage. We examined the morphology, chemical composition, and electrochemical characteristics of the colored Ti passive layers using scanning electron microscopy (SEM), X-ray photoelectron spectroscopy (XPS), and electrochemical techniques. We concluded that the coloration of the passive layers originated from iridescence; thus, depended on their thickness. We also reported a linear relation between the oxide thickness (that is in the 50–310 nm range) and the applied AC voltage (V_{AC}, from 10 to 60 V_{AC}). XPS measurements showed that Ti^{z+} (z varies from 4 to 2 depending on the layer depth), O^{2-}, and F^- were the main constituents of the passive layers. We also determined that the colored passive layers on Ti were more corrosion resistant than Ti in 1.0 mol/L aq. H_2SO_4.

In this paper, we report new results that show how the frequency of the AC voltage affects the visual properties, thickness, and morphology of the passive layers. We analyze the influence of different pretreatments (such as etching, micro-sandblasting, and polishing) on their surface morphology, and study their biocompatibility by evaluating their biocorrosion behavior, Ti-ion release, surface roughness, and wettability in Hank's Balanced Salt Solution (HBSS) at 37 °C. Finally, we compare these results with those obtained for the untreated Ti.

Experimental

Preparation of Ti specimens

We used disc- and wire-shaped titanium specimens. The disc specimens were used to study the surface morphology and wettability, and to examine the Ti-ion release in immersion tests; whereas the wire specimens were used for electrochemical characterization that primarily involved monitoring the open-circuit potential and recording polarization curves. The disc specimens were prepared from a Ti foil (Johnson-Matthey, Ward Hill, MA, USA, 99.7% Ti, 0.0875% Fe, 0.1225% O, 0.0015% N, 0.0095% C, 0.0023% H) and were 13.0 mm in diameter and 0.89 mm in thickness; their geometric surface area was 3.0 cm^2. They were spot-welded to a Ti wire of 0.81 mm in diameter (Johnson-Matthey, Ward-Hill, MA, USA, 99.7% Ti, 0.031% Fe, 0.012% C, 0.009% N, 0.054% O, 0.0047% H) for electrical contact. The Ti wire was insulated with shrinkable Teflon and sealed at the connection point using epoxy resin. The wire-shaped specimens were prepared from a Ti wire (Johnson-Matthey, Ward Hill, MA, USA, composition as above) of 0.81 mm in diameter. They were connected to a copper wire using a special electrical connector and sealed at the connection point using epoxy resin. The Cu wire was insolated and never left in contact with the electrolyte. The Ti wire was cut to a length of 10.0 mm, and the cut surface was mechanically polished with 2400 grade silicon carbide grinding paper using a mechanical polisher (Struers, Copenhagen, Denmark) to obtain a flat end. These wire specimens were pretreated according to the following procedure: (*i*) degreasing in acetone under reflux for 2 h to remove any organic impurities and rinsing with Nanopure water (Millipore, Molshem, France); (*ii*) etching for 5 min in a HNO_3–HF solution, or (*ii′*) micro-sandblasting with 90 μm aluminum oxide using a Macro Cab (Danville Engineering, Inc., San Ramon, CA, USA) micro-sandblaster, or (*ii″*) mechanical polishing (in the case of Ti discs only) with 4000 grade silicon carbide grinding paper; and (*iii*) rinsing with Nanopure water, sonicating for 5 min in an ultrasonic bath (Branson, Danbury, CT, USA), and drying in the air.

© 2006 NRC Canada

Formation of passive layers

Titanium disc- and wire-shaped specimens, prepared according to the previous procedure, were placed in a single-compartment electrochemical cell containing 7.5 wt.% aq. $NH_4{\cdot}BF_4$ at 25 °C, and were passivated using either AC or DC voltages. The AC voltage was applied using a variable AC power supply (3KVA AC Power Source Model 3001iM, 0–300 V, 16–500 Hz, California Instruments, San Diego, CA, USA), while the DC voltage was applied using a DC power supply (Kepco, Flushing, NY, USA, 0–125 V). The counter electrode was a Pt foil (Johnson-Matthey, Ward Hill, MA, USA, 99.99%) in the case of wire-shaped specimens and a Ti foil (Johnson-Matthey, Ward Hill, MA, USA, 99.7% Ti) in the case of disc-shaped specimens. The separation between the Ti specimen and the counter electrode was ~10 cm, which was sufficient to allow for effective circulation of the electrolyte between the electrodes and for removal of the gases generated during the passivation. The passivation time was 10 s. To obtain uniform oxide thickness and coloration of the Ti specimens, the passivation was performed at well-controlled temperature conditions, i.e., the temperature was maintained at 25 °C using water circulation (Haake, Thermal Electron Corporation, Waltham, MA, USA) and the electrolyte was rigorously stirred using a magnetic stirrer. Following the passivation, the Ti specimens were rinsed with Nanopure water and sonicated for 5 min in an ultrasonic bath. This procedure ensured good reproducibility of the experimental results.

Surface morphology analysis

The uniformity of the surface coloration and the morphology of the colored Ti passive layers were examined by means of optical microscopy (SEIWA Optical, Correct Metallurgical Microscope, SDM-TR, Tokyo, Japan) and scanning electron microscopy (MICROLAB 310-F, Thermo Electron Co., East Grinstead, West Sussex, England). The average surface roughness (R_a) of the specimens prior to and after the passivation as well as after the immersion test was measured using a stylus surface profiler (Dektak8, Veeco, Veeco Tucson Inc., Tucson, AZ, USA). In the case of the surface profilometry data, we report a mean R_a value of at least 10 reproducible individual measurements.

Potentiodynamic polarization test

Potentiostatic polarization tests were carried out using a Princeton Applied Research (PAR) 263A Potentiostat and a standard three-compartment electrochemical cell. The PAR PowerCorr electrochemical software package was used to control the experimental parameters, and to collect and process the data. Platinum gauze served as a counter electrode, and its surface area was at least five times that of the working electrode to minimize any polarizability effects. A saturated calomel electrode (SCE) was used as a reference electrode. The electrolyte used in the tests was HBSS, that is, a simulated body fluid of the following composition: NaCl: 8.00 g L^{-1}; KCl: 0.40 g L^{-1}; $NaHCO_3$: 0.35 g L^{-1}; KH_2PO_4: 0.06 g L^{-1}; Na_2HPO_4: 0.0475 g L^{-1}; glucose: 1.00 g L^{-1}; and pH: 7.4 (13). The electrolyte was held at a constant temperature of 37 °C by immersing the cell in a Haake water bath. We followed the ASTM G5 standard test method in our measurements (21). The electrolyte was deaerated with ultra-high purity (UHP) N_2 for at least 1 h before immersing the test specimen in it, and the purging was maintained during the test. The open circuit potential, i.e., the corrosion potential (E_{corr}) of the test specimen, was continuously recorded for 1 h, starting immediately after the specimen's immersion. Potentiodynamic polarization transients were recorded by conducting a forward scan from a potential that was 0.25 V below E_{corr} up to an upper limit of 3.00 V vs. SCE at a scan rate of 0.166 mV s^{-1}. Tafel extrapolation was done in the ±0.25 V range of E_{corr} (E_{corr} – 0.25; E_{corr} + 0.25) in accordance with the procedure described by S. Hrapovic and co-workers (20); the anodic and cathodic Tafel parameters (β_A and β_C, respectively) were determined. The polarization resistance (R_P) was determined on the basis of potentiodynamic polarization resistance curves in the potential range (E_{corr} – 0.20; E_{corr} + 0.20) (21–24). Then, the corrosion current density (i_{corr}) in μA cm^{-2} and the corrosion rate (CR) in μm $year^{-1}$ at E_{corr} were calculated using the PowerCorr software. This program uses the Stern–Geary equation, the relation between CR and i_{corr}, the values of β_A, β_C, R_P, equivalent weight (EW) in g, the surface area, and the density of the test specimen (eqs. [1–3]).

$$[1] \qquad I_{corr} = \frac{\beta_A \beta_C}{2.3 R_P (\beta_A + \beta_C)}$$

$$[2] \qquad CR = \frac{3.27 i_{corr} EW}{d}$$

$$[3] \qquad EW = \frac{1}{N_{EQ}} = \frac{1}{\sum_i \left(\frac{f_i n_i}{a_i} \right)}$$

where d is the metal or alloy density in g cm^{-3}, N_{EQ} is the total number of equivalents, f_i is the mass fraction, a_i is the atomic weight, and n_i is the number of electrons exchanged. According to the AMS standards (24), the value of EW for Ti is 16 under reducing acid conditions and 12 under oxidizing conditions. These values are determined based on the assumption that the corrosion rate is uniform across the entire Ti surface. Finally, in these measurements, all i_{corr} values are reported with respect to the geometric surface area of the specimens. The E_{corr}, R_P, and CR values are the mean values of at least three reproducible individual measurements with a maximum uncertainty of 10%.

Immersion test and the Ti-ion release analysis

The disc-shaped specimens (3.0 cm^2) were placed in test tubes each containing 40.0 mL of HBSS and sealed with a silicone stopper. The specimens were suspended in the solution by using an insulated Ti wire attached to the silicone stopper to avoid any contact of the specimens with the test tube. The test tubes were immersed in a Haake water bath maintained at 37 °C. The specimens were taken out of the test tubes after 2 weeks, and a 2.0 mL aliquot of concentrated nitric acid was added to each tube to maintain low pH and to prevent any precipitation of insoluble Ti compounds. An inductively coupled plasma mass spectrometer (ICP-MS, Renaissance, LECO, St. Joseph, MI, USA) was used to measure the amount of Ti ions released during the immersion test. The detection limit of Ti was 0.5 ppb.

© 2006 NRC Canada

Fig. 1. Relation between the coloration of the Ti passive layers, the applied AC voltage, and surface pretreatment; the $NH_4 \cdot BF_4$ concentration is 7.5 wt.%, the polarization time is 10 s, and the AC frequency is 60 Hz.

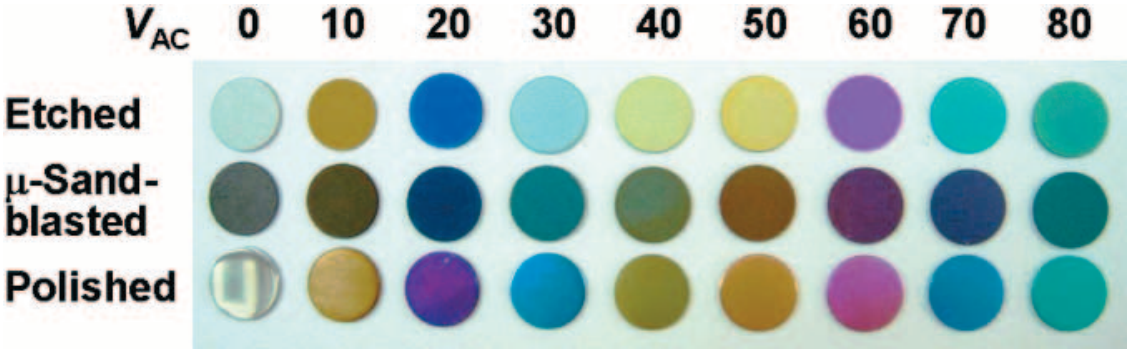
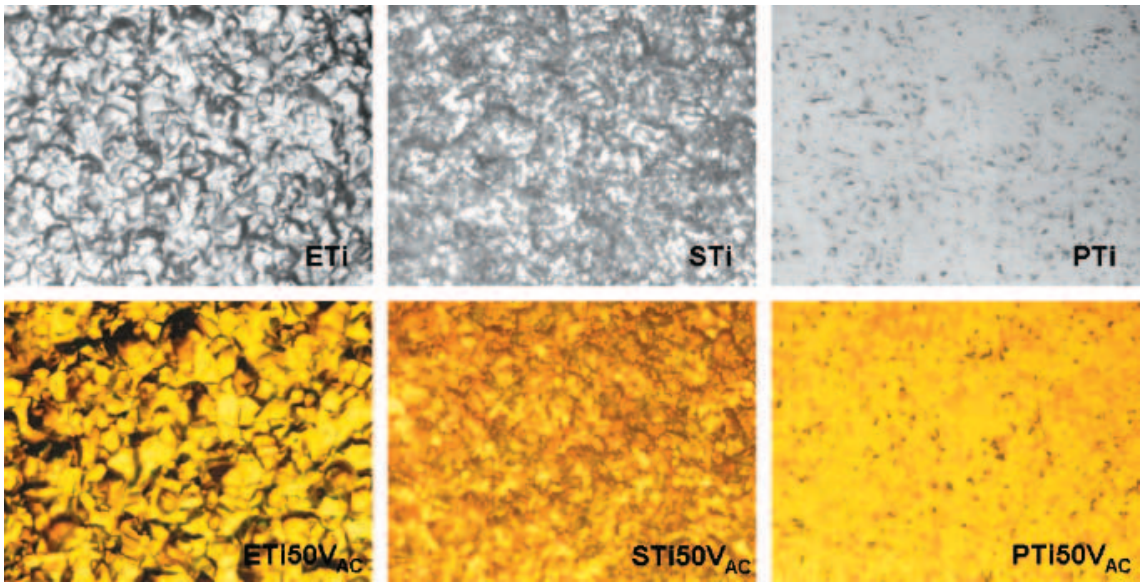


Fig. 2. Surface morphology of the etched, micro-sandblasted, and polished Ti (ETi, STi, and PTi, respectively) and their passive layers formed at 50 V_{AC} ($ETi50V_{AC}$, $STi50V_{AC}$, and $PTi50V_{AC}$, respectively) examined by optical microscopy at a magnification of 400×; the $NH_4 \cdot BF_4$ concentration is 7.5 wt.%, the polarization time is 10 s, and the AC frequency is 60 Hz.



Static contact angle (SCA) measurement

Static contact angle measurements were performed at the room temperature (22 °C ± 1) using a video contact angle system (VCA Optima, AST Products, Inc., Billerica, MA, USA). A 1.5 μL droplet of HBSS was placed on the specimen surface and the contact angle was analyzed. We report an average of at least 10 reproducible individual measurements.

Results and discussion

Influence of pretreatment, AC and DC voltage, and AC frequency on the visual properties and morphology of passive layers on Ti

Figure 1 shows the coloration of passive layers formed at different V_{AC} values up to 80 V_{AC} and at f = 60 Hz on Ti pretreated using three methods, i.e., chemical etching, micro-sandblasting, and mechanical polishing. In the first column, we show etched, micro-sandblasted, and polished Ti specimens without any electrochemical treatment (0 V_{AC}); they serve as respective references. We observe that the AC polarization of the Ti specimens at $10 \leq V_{AC} \leq 80$ V_{AC} results in a wide spectrum of bright, uniform, well-defined colors; the coloration varies in the following order (from the lowest to the highest value of V_{AC}): brown, blue, light blue, yellow, golden yellow, purple, olive green, and turquoise. Similar colors were obtained in the case of micro-sandblasted and mechanically polished specimens. However, the colors of the micro-sandblasted specimens were different in shade and less bright than those of either polished or etched specimens; the polished specimens revealed a shiny finish. The different colors and shades provide a wide range of choices for biomedical and decorative applications if a visual aspect is required, as in the case of orthodontic archwires or dental implants placed under the gum skin. Figure 2 shows the surface morphology of etched (E), micro-sandblasted (S), and mechanically polished (P) Ti specimens prior to and after the formation of a passive layer at 50 V_{AC}. The micrographs were obtained by means of optical microscopy at a 400× magnification. The results reveal that the passive layers are uniform and free of any cracks or flakes that could be observed using optical microscopy. The passive layers grow in registry with the underlying metal. Thus,

© 2006 NRC Canada

Table 1. Average surface roughness (R_a) in μm.

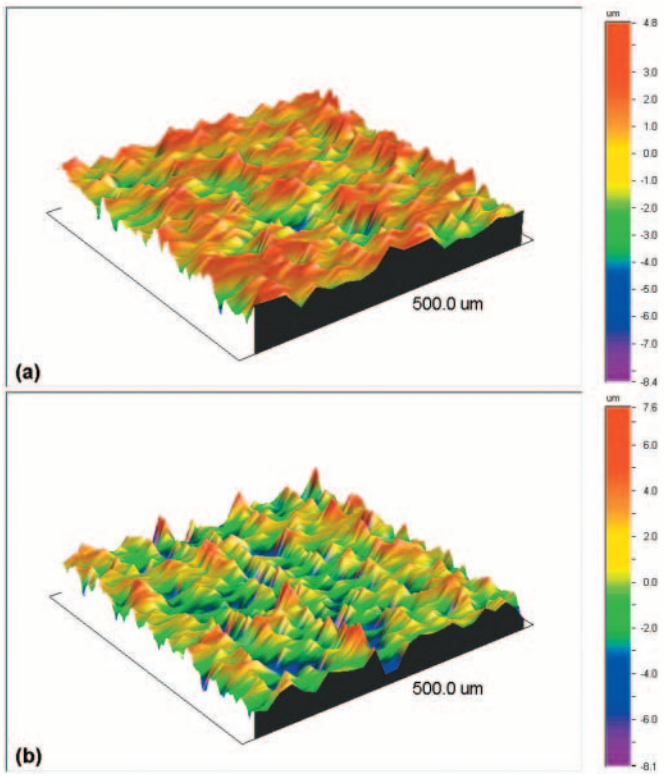
		Ti sample passivated at		
Specimen	Ti	10 V_{AC}	30 V_{AC}	50 V_{AC}
Polished	0.048 ± 0.008	—	—	0.13
Micro-sandblasted	0.89 ± 0.05	—	—	0.94
Etched	1.30 ± 0.03	1.43 ± 0.06	1.50 ± 0.06	1.58 ± 0.05
Etched and exposed to HBSS for 2 weeks	1.46 ± 0.06	1.52 ± 0.06	1.63 ± 0.05	1.71 ± 0.05

surface morphology of the passive layers resembles that of the corresponding untreated Ti specimen although the surface roughness slightly increases (see a later section dealing with surface profilometry studies). The etched specimens reveal a clearly discernible grain structure that comprises crystals and grain boundaries. In all cases, the coloration of each grain is uniform and identical to that of the adjacent grains. The micro-sandblasted Ti specimens show smaller features because of the micro-erosion caused by the 90 μm alumina particles; their morphology does not reveal any well-defined crystals or grain boundaries that are observed in the case of etched specimens. Clearly, the surface of the etched specimens is rougher than that of micro-sandblasted or polished specimens, and this observation is corroborated by the surface profilometry analysis (the values of the average surface roughness are reported in Table 1). We observed that the average surface roughness increases in the following order: mechanically polished Ti (0.048 μm), micro-sandblasted Ti (0.89 μm), and chemically etched Ti (1.30 μm). We also measured the surface roughness of three specimens that were pretreated as described previously and subsequently passivated at 50 V_{AC} (60 Hz). The results indicated that the passivation increased the surface roughness compared with non-passivated but identically pretreated specimens. The values of the average surface roughness increased in the following order: mechanically polished Ti (0.13 μm), micro-sandblasted Ti (0.94 μm), and chemically etched Ti (1.58 μm). We observed that this order is the same for the untreated and passivated Ti specimens.

We also analyzed the effect of the magnitude of V_{AC} on the surface roughness. This series of experiments was carried out using etched Ti specimens that were passivated at 10, 30, and 50 V_{AC}. The results revealed that the average surface roughness increased from 1.30 μm for Ti to 1.58 μm for the passive layer formed at 50 V_{AC} (Table 1). Figures 3*a* and 3*b* show three-dimensional surface profiles for an etched Ti specimen prior to and after passivation at 50 V_{AC}, respectively. The possibility of increasing and controlling the surface roughness of Ti specimens is of interest in the surface treatment of biocompatible materials. Specifically, roughened surfaces increase bone-implant contact, promote tissue and bone ingrowth, and create the interlock between the bone and implants, thus improving the bone-healing process (25). Because chemical etching and passivation provide the roughest Ti samples, we selected this pretreatment in our further tests.

It was important to evaluate whether passive layers on Ti of similar visual properties could be prepared by the application of DC voltage in the same electrolyte. Therefore, we applied both AC (f = 60 Hz) and DC voltage of the same magnitude to prepare passive layers on Ti (the other experimental parameters were the same). Figure 4 shows the passive layers prepared at several V_{AC} and V_{DC} values that ranged from 10 to 80 V_{AC} or V_{DC}. The results reveal that DC polarization also led to uniformly colored passive layers; however, their colors are different from those prepared using AC voltage. We observe that the color obtained at 30 V_{DC} is similar to that obtained at 20 V_{AC}; the other "V_{DC} – V_{AC} pairs of values" that gave the same surface coloration are as follows: 40 V_{DC} – 30 V_{AC}, 50 V_{DC} – 40 V_{AC}, 60 V_{DC} – 50 V_{AC}, 70 V_{DC} – 60 V_{AC}, and 80 V_{DC} – 70V_{AC}. We observe that, in general, a higher V_{DC} is required to obtain the same coloration as that achieved using an AC voltage (with other parameters being the same). This observation may at first seem counterintuitive, but it is the nature of the AC and DC voltage, properties and composition of the oxide layers, and associated electrochemical processes that determine the growth mechanism of passive layers and their thickness. As a passive layer on Ti develops at a given anodic V_{DC}, it imposes a barrier to the charge transfer (anodically formed ox-

Fig. 3. Three-dimensional surface profiles of (*a*) the etched Ti (R_a = 1.30 μm) and (*b*) its passive layer formed at 50 V_{AC} (60 Hz) (R_a = 1.58 μm).



© 2006 NRC Canada

Fig. 4. Relation between the coloration of the passive layers formed on etched Ti and the applied AC or DC voltage; the $NH_4{\cdot}BF_4$ concentration is 7.5 wt.%, the polarization time is 10 s, and AC frequency is 60 Hz.

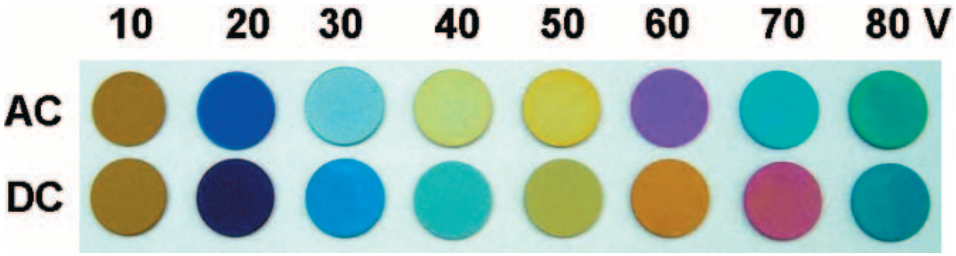
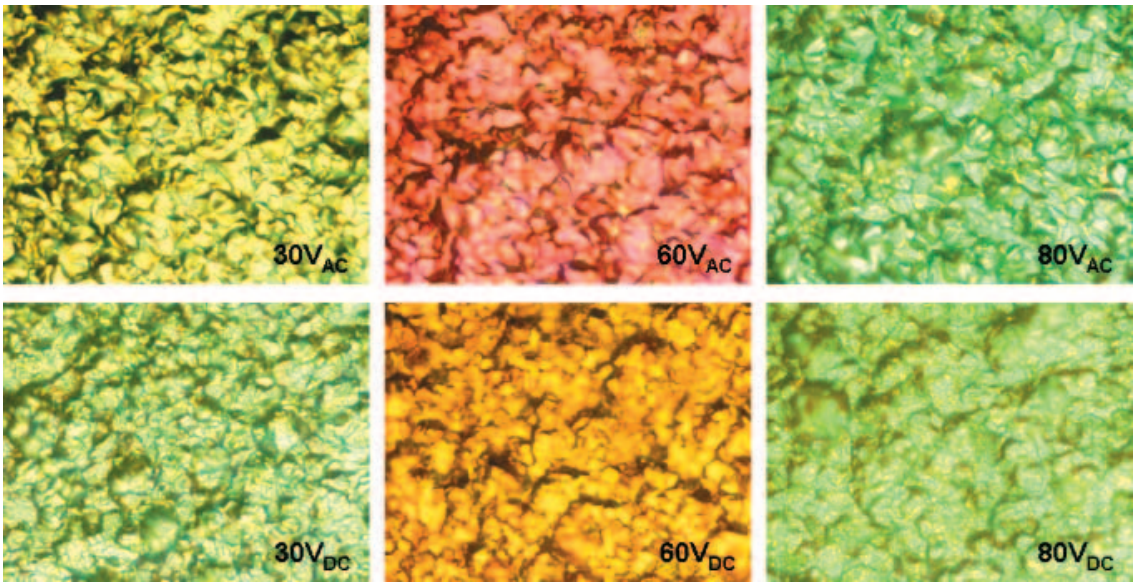


Fig. 5. Surface morphology of the passive layers formed on etched Ti using different V_{AC} (60 Hz) and V_{DC} values examined by optical microscopy at a 400× magnification; $NH_4{\cdot}BF_4$ concentration is 7.5 wt.% and the polarization time is 10 s.



ide layers have semiconducting properties), thus making the interface a less efficient electronic conductor. This translates into a gradual decrease of the oxidation current, which is eventually reduced to a very small value; thus, the passive layer grows to a limiting thickness for a given V_{DC} (26). In the case of AC polarization, we repetitively apply anodic and cathodic voltages whose magnitude is a sinusoidal function of time (the number of the anodic and cathodic voltages applied per unit time equals the AC frequency, f). Clearly, anodic and cathodic voltages result in oxidation (oxide formation and oxygen generation) and reduction (partial oxide reduction and hydrogen generation) reactions. If the anodically formed oxide is partially reduced, then its electronic properties are modified. In the case of Ti, the AC polarization results in the formation of a passive layer that contains Ti_2O_3 sandwiched between Ti and a thin surface layer of TiO_2 (19, 20). At present, we are unable to quantify the amount of Ti oxides that was reduced during cathodic transients of AC polarization because a specialized experimental setup is being constructed (this will be reported in a subsequent paper).

Figure 5 shows surface micrographs for the chemically etched and then passivated Ti specimens obtained using optical microscopy at a magnification of 400×; the applied AC and DC voltages were 30, 60, and 80 V_{AC} and V_{DC}, respectively. The results demonstrate that the DC polarization-formed passive layers are uniformly colored and are free of cracks or flakes. The morphology of the DC voltage-formed passive layers closely resembles that of the AC voltage-formed ones.

Another parameter that affects the growth of passive layers on Ti, and their coloration and thickness, is the frequency (f) of the applied AC voltage. Figure 6 presents 36 specimens that show the surface coloration for a set of V_{AC} and f values, namely, $10 \leq V_{AC} \leq 60$ V_{AC} and $16 \leq f \leq 500$ Hz. These results reveal that a wider spectrum of colors is created and the surface coloration becomes more uniform as f decreases; the most visually appealing specimens are those obtained at the lowest value of f (here, $f = 16$ Hz). Elsewhere, we showed that there is a well-defined relationship between the passive layers' coloration and thickness (20). According to those results and the data presented in Fig. 6, we may conclude that for a given V_{AC}, the thickness of the passive layers decreases as we increase f. Clearly, in the case of $f = 500$ Hz, we do not observe any passive layer formation up to $V_{AC} = 30$ V_{AC}. This observation is consistent with our proposal that a cathodic transient can reduce oxidized Ti species formed during a very short anodic transient

© 2006 NRC Canada

Fig. 6. Relation between the coloration of the Ti passive layers, the applied AC voltage, and its frequency; the $NH_4{\cdot}BF_4$ concentration is 7.5 wt.% and the polarization time is 10 s.

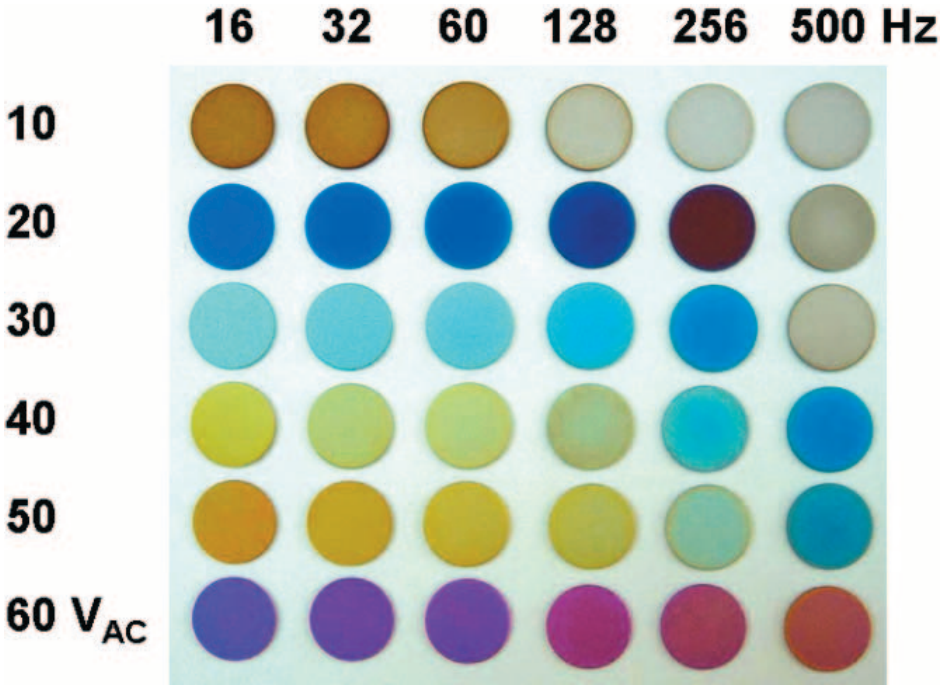
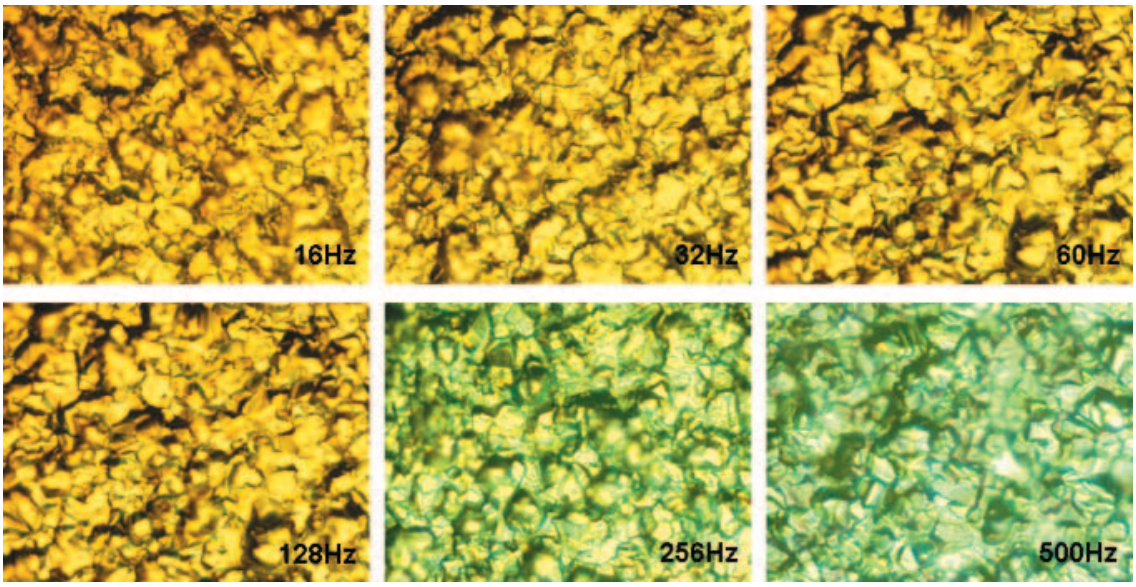


Fig. 7. Surface morphology of the passive layers formed on etched Ti at 40 V_{AC} and at different frequencies (16–500 Hz) examined by optical microscopy at a magnification of 400×; $NH_4{\cdot}BF_4$ concentration is 7.5 wt.% and the polarization time is 10 s.

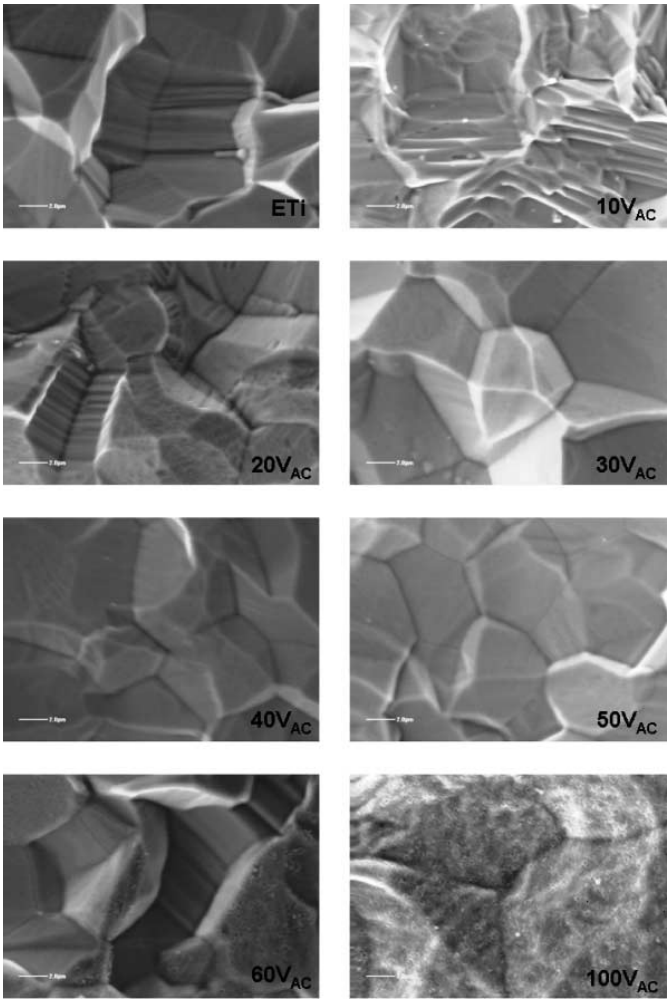


(here, 1 ms). For instance, in the case of V_{AC} = 10 V_{AC}, there is hardly any noticeable formation of a passive layer for 128 ≤ f ≤ 500 Hz. In the case of V_{AC} = 60 V_{AC}, the passive layer is the thickest for f = 16 Hz and the thinnest for f = 500 Hz. Consequently, the thickest passive layers are obtained at the highest V_{AC} and the lowest f value. Figure 7 shows surface micrographs obtained at a 400× magnification for passive layers formed at 40 V_{AC} and at six different values of f, namely, 16, 32, 60, 128, 256, and 500 Hz. In all cases, the passive layers have a uniform coloration and are free of cracks or flakes. Their surface morphology is similar, and there are no specific features that could be assigned to the frequency variation; their topography resembles that of the etched Ti (see Fig. 2).

Figure 8 shows SEM micrographs for disc-shaped Ti specimens at a magnification of 6000× that were prepared by the application of 10, 20, 30, 40, 50, 60, and 100 V_{AC} (60 Hz); the first micrograph refers to the etched Ti (ETi) and serves as a reference. The results indicate that the passive layers grow in registry with the underlying substrate and

© 2006 NRC Canada

Fig. 8. SEM micrographs for the disc-shaped etched Ti (ETi) and seven passive layers formed at 10, 20, 30, 40, 50, 60, and 100 V_{AC} (60 Hz) examined at a magnification of 6000×; the $NH_4{\cdot}BF_4$ concentration is 7.5 wt.% and the polarization time is 10 s.



there are only small changes in the surface morphology caused by the passive layer formation. We observe that in the case of the etched Ti and the specimens passivated at $10 < V_{AC} \leq 50$ V_{AC}, the morphology of each grain is uniform. However, the specimen prepared at 60 V_{AC} reveals sub-micrometre circular pores that become even more pronounced and denser in the case of passivation at 100 V_{AC}. We relate these features to the non-uniformity and (or) electrical breakdown that took place when an AC voltage of 60 V_{AC} or more was applied.

During the specimen preparation, we observed that the passive layers were not always uniform and that the applied AC voltage also resulted in a gas generation that occurred concurrently with the passive layer formation. To achieve uniform passivation, the electrolyte had to be efficiently cooled because the application of high voltages resulted in high currents and consequently in resistive heating of the electrolyte and a rise in its temperature. We also observed that the Ti disc became red-hot when polarized at very high V_{AC} values (≥60 V_{AC}) despite rigorous cooling. Such high localized temperatures (at the Ti surface) can affect the adhesion of the passive layers, as we explain in the following statements. The passive layer is formed at a localized high temperature, and as the process terminates, the specimens subsequently cool down to the ambient temperature. Because Ti and its oxides have different thermal expansion coefficients, the metal and the oxides contract in a different way (with a possible crack development), thus affecting their adhesion. Another factor that needs to be considered is the electrical breakdown that was manifested by audible cracking and (or) visible sparking at the electrode surface (26, 27). It is reported by James and Straumanis that the application of $V_{DC} \geq 60$ V_{DC} in 20% aqueous H_2SO_4 at 20 °C causes an electric breakdown of the anodic passive layer on Ti (26). Our results are consistent with those reported because we observed that the electrical breakdown of the passive layers occurred each time we heard cracking or observed sparking. We observed the same phenomena when using the wire-shaped Ti electrodes, but they manifested themselves already at voltages ≥ 50 V_{AC} and the sparking occurred only at the wire tip (regions of greater current density). In the following sections, we discuss the evaluation of the corrosion behavior, metallic ion release, and wettability of the Ti passive layers. The data reported next refer to the Ti specimens that were chemically etched and passivated using AC voltage for one frequency, namely, $f = 60$ Hz.

Corrosion behavior in HBSS

We studied the corrosion behavior of the passive layers by recording polarization curves in HBSS over a wide potential range, typically from E_{corr} –0.25 V to +3.00 V. A typical polarization curve consists of the following regions, starting from the most negative to the most positive potential: hydrogen generation, active, active–passive transition, passive, and transpassive with concurrent oxygen generation (20). An analysis of the polarization curves allows us to identify these regions (not all polarization curves reveal all of them) and to determine important corrosion parameters, such as the corrosion current density (i_{corr}) at corrosion potential (E_{corr}), critical potential (E_{cr}), critical current density (i_{cr}), passive current density (i_{pass}), and breakdown potential (E_b). The value of i_{corr} allows us to calculate the material's corrosion rate (CR) using eq. [2]. The value of E_{corr} is a measure of the material's stability, and the more positive E_{corr}, the more stable the material; the i_{corr} and CR are measures of the material's tendency to undergo corrosion. The value of i_{corr} is used to calculate CR and represents the amount of material that is lost because of corrosion per unit time, typically per year in corrosion studies. The higher the value of i_{corr}, the greater the material's loss (13).

Corrosion potential measurements and polarization curves for Ti specimens

Figure 9 shows the variation of the open circuit potential (OCP) with time in HBSS at 37 °C for etched Ti (ETi) and for passive layers on etched Ti formed at 10, 20, 30, 40, and 50 V_{AC} (60 Hz). The shape of the OCP versus time profile for the etched Ti indicates that it develops a passive layer upon contact with HBSS. In the case of the passive layers formed at 10, 20, 30, and 40 V_{AC}, we observe a continuous

© 2006 NRC Canada

Fig. 9. Variation of the open circuit potential (OCP) with time in HBSS at 37 °C for the etched Ti (ETi) and five passive layers formed at 10, 20, 30, 40, and 50 V_{AC} (60 Hz).

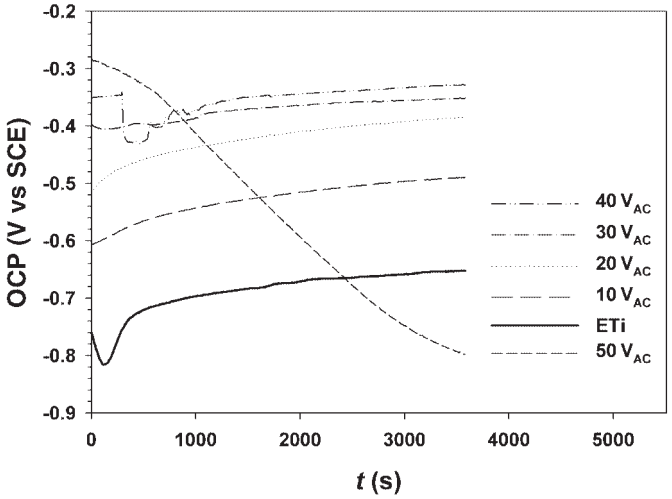
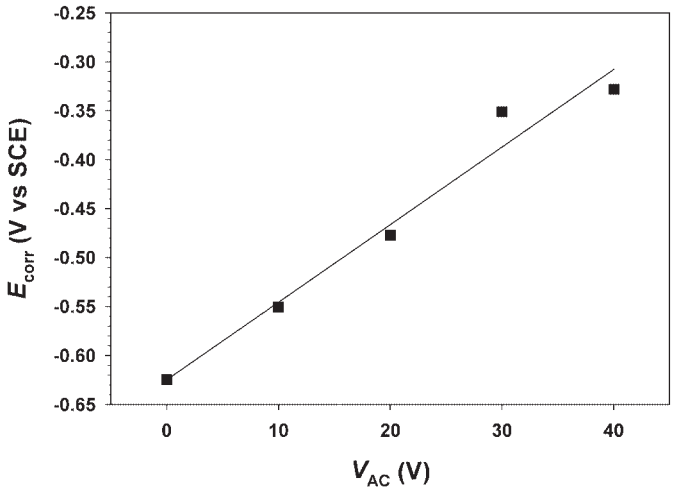


Fig. 10. Relation between the corrosion potential (E_{corr}) and the applied AC voltage (V_{AC}) for the etched Ti and four passive layers formed at 10, 20, 30, and 40 V_{AC} (60 Hz) in HBSS at 37 °C.



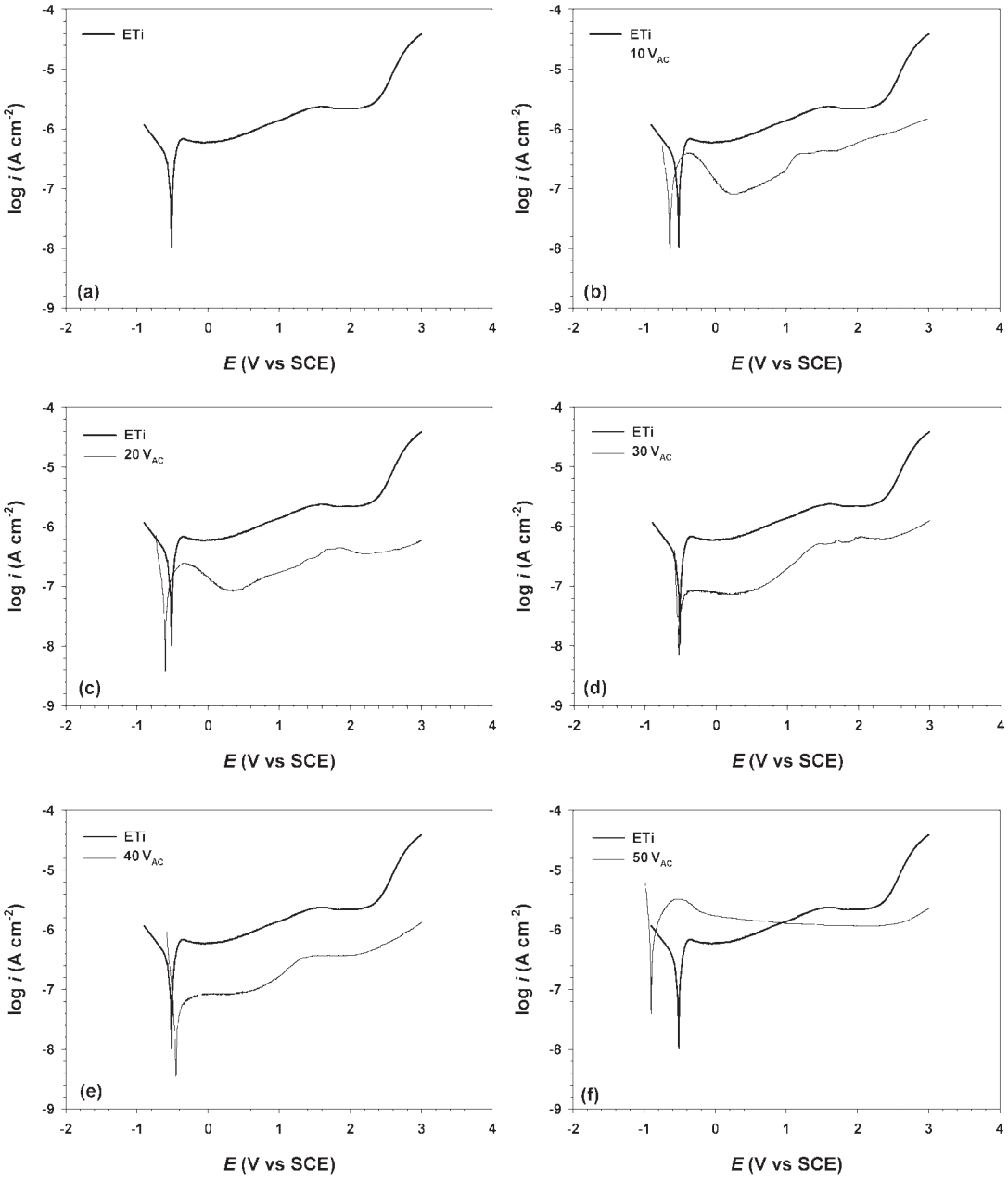
increase of OCP which indicates that the existing passive layers became more stable. These curves tend to a steady-state potential after 1 h of immersion in HBSS; the limiting OCP is referred to as the corrosion potential (E_{corr}). Figure 10 shows a relationship between E_{corr} and V_{AC} for V_{AC} up to 40 V_{AC}; we observe a linear rise of E_{corr} which indicates that the passive layers are more stable than the etched Ti. The curve for the passive layer prepared at 50 V_{AC} (Fig. 9) shows a different trend. At the onset, OCP is higher than all the other values; however, it decreases monotonously and reaches a value of –0.798 V versus SCE after 1 h. This value is more negative than any other value reported in Fig. 9 and still does not seem to tend to a steady-state value (consequently, we do not report E_{corr} for this passive layer). The decrease of OCP for the layer formed at 50 V_{AC} from –0.284 to –0.798 V points to its rapidly deteriorating corrosion resistance (see the discussion of the non-uniformity of the passive layers and their electrical breakdown).

Figure 11*a* shows a polarization curve for an etched, wire-shaped Ti specimen recorded in HBSS at 37 °C at a scan rate (*s*) of 0.166 mV s^{-1}; the potential range is (E_{corr} –0.25 to +3.00 V). The transient reveals the following features: (*i*) hydrogen generation and active region from –0.90 to –0.35 V; (*ii*) active–passive transition at the critical potential (E_{cr}) of –0.35 V; (*iii*) a passive region from –0.35 to +2.40 V; and (*iv*) a transpassive region beyond +2.40 V. The magnitude of the current density in the transpassive region is well below the value of 5 mA cm^{-2} that would be expected if pitting corrosion were to be present (28). Therefore, we may conclude that our experimental conditions do not trigger the development of pits, even in the transpassive region where the oxygen evolution takes place; we do not observe any breakdown potential either (6, 29). This polarization curve serves as a reference in the subsequent evaluation of the corrosion behavior of the passive layers in the same environment. Figures 11*b*–11*f* show polarization curves for the passive layers formed at 10, 20, 30, 40, and 50 V_{AC}, respectively, (f = 60 Hz). The transients for the passive layers formed at 10–40 V_{AC} reveal the following new features: (*i*) the shape of the polarization curves for the passive layers resembles that of Ti, but the current density values are lower; (*ii*) the critical potential (E_{cr}) that refers to the active–passive transition is in the –0.35 to –0.10 V range; (*iii*) the critical current density (i_{cr}) decreased from 0.686 μA m^{-2} for the etched Ti to 0.085 μA cm^{-2} for the passivated layer formed at 40 V_{AC}; the i_{cr} values decrease as V_{AC} rises; (*iv*) the passive current density (i_{pass}) decreased by approximately one order of magnitude upon the formation of the passive layers, thus from ~10^{-6} (for etched Ti) to 10^{-7} A cm^{-2} (for passive layer formed at 40 V_{AC}), which means that the corrosion rate of Ti decreases almost 10 times after the AC polarization; (*v*) the extent of the passive region for the passive layers is wider than that for the etched Ti. These results and, in particular, the passive region's extent and the passive current density value show that the growth of the passive layer on Ti accomplished by AC voltage improves its corrosion resistance. The passive layer formed at 50 V_{AC} reveals different characteristics; its E_{cr} (–0.52 V) is more negative and i_{cr} (3.277 μA cm^{-2}) is higher than the corresponding values for the etched Ti. In addition, i_{pass} is up to an order of magnitude higher than the analogous values for the other passive layers.

Figures 12 and 13 show the polarization resistance (R_P) and the corrosion rate (CR) values at E_{corr} for the etched Ti and the passive layers formed on Ti wires at 10, 20, 30, and 40 V_{AC}. We observe that the R_P values increase linearly with increasing V_{AC}, indicating that the passive layers are more corrosion-resistant than the etched Ti. We also observe that the higher the V_{AC} value, the more corrosion resistant the specimen. The trend of CR values confirms that the passive layers increase the corrosion resistance of Ti. The corrosion rate in HBSS drops from 1.12 μm $year^{-1}$ for the etched Ti to 0.30 μm $year^{-1}$ for the passive layer formed at 40 V_{AC}, i.e, by a factor of ~3. The passive layer formed at 50 V_{AC} has an R_P of 41.2 kΩ cm^2, a value that is lower than that for the etched Ti (190.9 kΩ cm^2). Its CR of 6.23 μm $year^{-1}$ is much higher than that of the etched Ti (1.11 μm $year^{-1}$). These re-

© 2006 NRC Canada

Fig. 11. Polarization curve for the etched Ti (ETi) and five sets of two polarization curves, one for ETi and one for a passive layer formed at a given V_{AC} value (10, 20, 30, 40, and 50 V_{AC}; f = 60 Hz). The polarization curves were recorded in HBSS at 37 °C at a scan rate s = 0.166 mV s^{-1}.



sults point to the non-uniformity and electrical breakdown of the passive layer formed at 50 V_{AC}.

Figure 14 shows four pictures, each containing two specimens, that demonstrate changes in the surface coloration of the etched Ti (ETi) and three passive layers (20, 40, and 50 V_{AC}, f = 60 Hz) prior to (left) and after (right) recording polarization curves in HBSS. The etched Ti and the passive layers formed at 20 and 40 V_{AC} are uniform and reveal only a minor change in the coloration brought about by the corrosion test. However, the passive layer formed at 50 V_{AC} shows significant changes in the coloration and its uniformity, which are assigned to the corrosion of the electrically broken-down passive layer. Figure 15 shows SEM micrographs for etched Ti (ETi) and three passive layers (30, 40, and 50 V_{AC}, f = 60 Hz) after recording polarization curves in HBSS. The etched Ti and the passive layers formed at 30 and 40 V_{AC} are free of damage after the corrosion test, but the passive layer formed at 50 V_{AC} shows damage at the specimen's tip. The passive layer formed at 50 V_{AC} is more prone toward corrosion-induced damage.

Titanium-ion release in HBSS

Figure 16 shows the Ti-ion release level as a function of the applied V_{AC} for the disc-shaped Ti specimens after immersion in HBSS at 37 °C for 2 weeks. The data show that the amount of the released Ti-ion decreases from 230

© 2006 NRC Canada

Fig. 12. Relation between the polarization resistance (R_P) and the applied AC voltage (V_{AC}) for the etched Ti and four passive layers formed at 10, 20, 30, and 40 V_{AC} in HBSS at 37 °C.

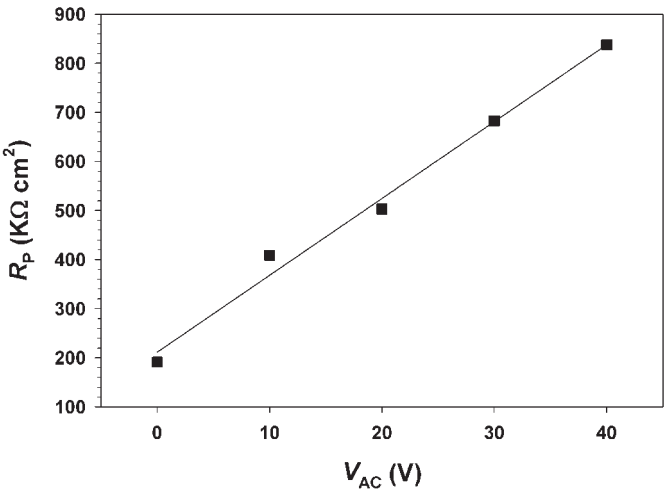


Fig. 13. Relation between the corrosion rate (CR) and the applied AC voltage (V_{AC}) for the etched Ti and four passive layers formed at 10, 20, 30, and 40 V_{AC} in HBSS at 37 °C.

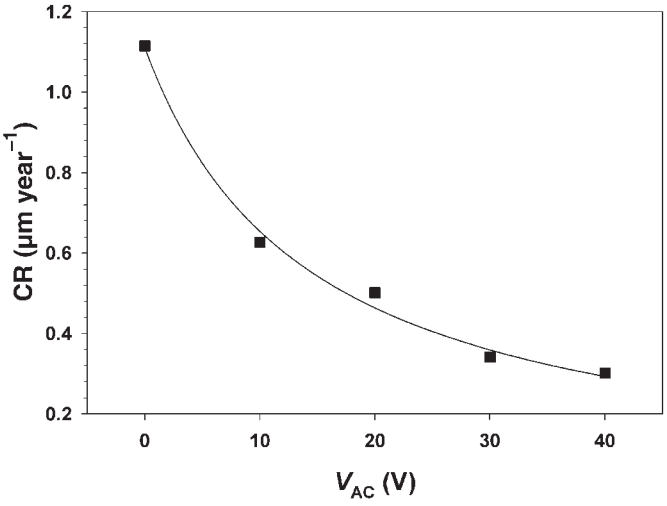
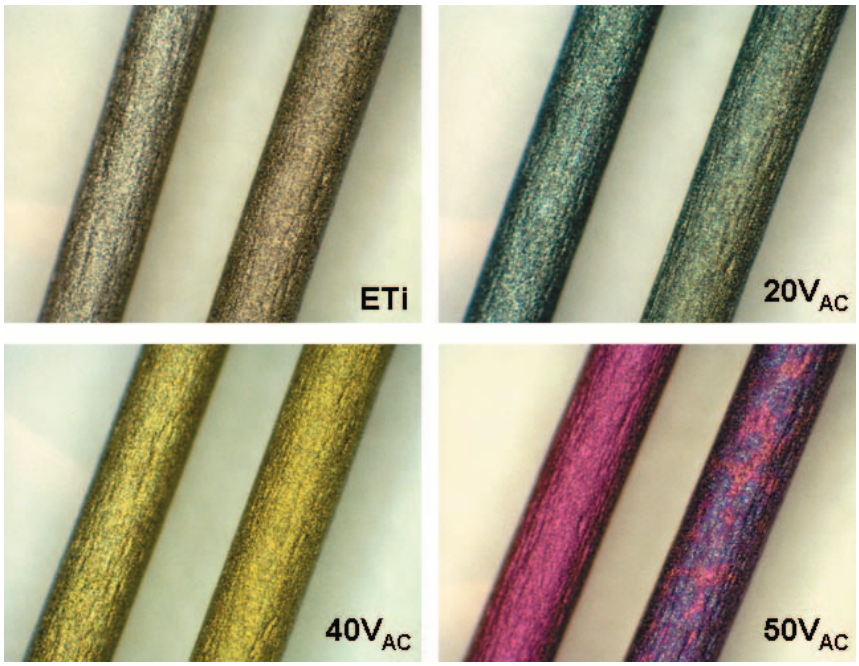


Fig. 14. Comparison of the surface morphology of the wire-shaped etched Ti (ETi) and three passive layers formed at 20, 40, and 50 V_{AC} (60 Hz) examined by optical microscopy at a magnification of 30× prior to (left) and after (right) recording polarization curves in HBSS at 37 °C.



(etched Ti, represented as 0 V_{AC}) to 15 ppb (passive layer formed at 50 V_{AC}); the results reveal that the higher the applied V_{AC} value, the lower the Ti-ion release level. The results presented in Figs. 13 and 16 and obtained using two different experimental approaches follow each other, therefore, demonstrating that the corrosion rate and the Ti-ion release data are in very good agreement. Figure 17 shows the Ti-ion release level as a function of the AC frequency ($16 \leq f \leq 500$ Hz) for the passive layer formed at 30 V_{AC} in comparison to the etched Ti (square symbol in Fig. 17). The data show that the Ti-ion release level for the etched Ti is much higher than for the AC voltage-treated specimens. They also reveal that a gradual increase of f from 16 to 500 Hz increases the Ti-ion release from 46 to 53 ppb, thus about 15%. Knowledge of the Ti-ion release allows us to calculate the corrosion rate. The outcome of such calculations shows that the amount of released Ti-ion ranges from 0.22 μg cm^{-2} d^{-1} for the etched Ti to 0.01 μg cm^{-2} d^{-1} for the passive layer formed at 50 V_{AC} (60 Hz); these results are in good agreement with the data reported in ref. 11. Figure 18 shows SEM micrographs for the etched Ti (ETi) and the passive layers formed at 20, 40, and 50 V_{AC} (60 Hz) after the Ti-ion release test obtained at a magnification of 6000×; the specimens were disc-shaped. These micrographs

© 2006 NRC Canada

Fig. 15. SEM micrographs for wire-shaped etched Ti (ETi) and three passive layers formed at 30, 40, and 50 V_{AC} (60 Hz) after recording polarization curves examined at a magnification of 500×.

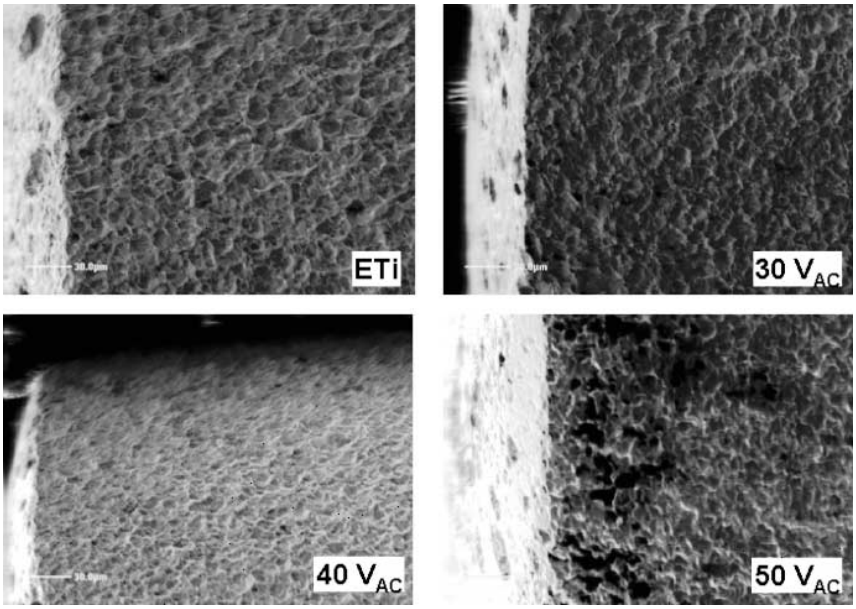


Fig. 16. Relationship between the Ti-ion release and the applied AC voltage (V_{AC}) for the etched Ti and five passive layers formed at 10, 20, 30, 40, and 50 V_{AC} (60 Hz); the specimens were immersed in 40 mL of HBSS at 37 °C for 2 weeks; the surface area of each specimen was 3.00 cm^2.

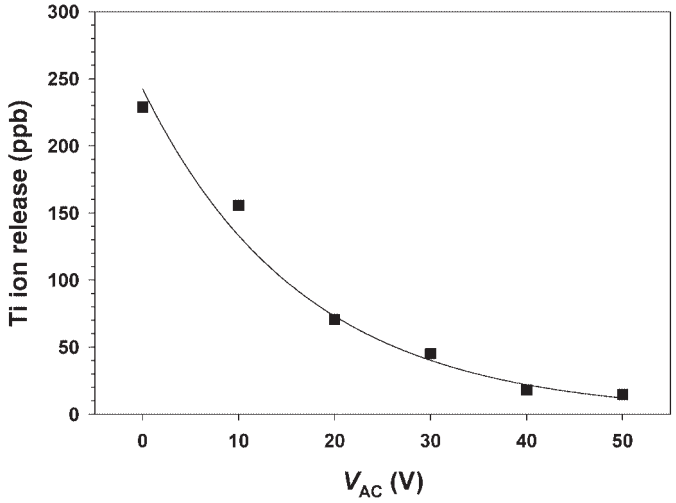
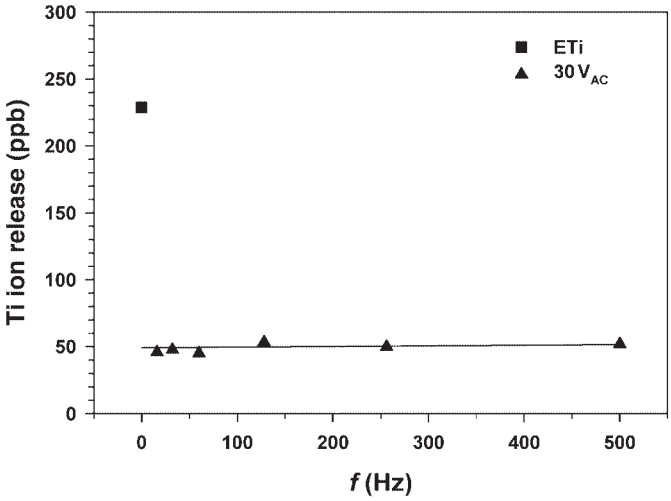


Fig. 17. Relationship between the Ti-ion release and the frequency (f) of the applied AC voltage (30 V_{AC}) for the etched Ti (ETi) and six passive layers formed at six different frequencies (16, 32, 64, 128, 256, and 500 Hz); the specimens were immersed in 40 mL of HBSS at 37 °C for 2 weeks; the surface area of each specimen was 3.00 cm^2.



reveal only small morphology changes that are assigned to the increase of surface roughness; all specimens are uniform and free of any other morphological features such as cracks or flakes. We also analyzed the surface roughness of these specimens after the Ti-ion release test (Table 1) using surface profilometry. The results reveal that the surface of all the specimens becomes rougher after the immersion test because of corrosion in HBSS.

Static contact angles

Table 2 shows the values of the static contact angle formed between HBSS and several Ti specimens, namely, the etched Ti and the passive layers formed at 10, 30, and 50 V_{AC}. The results reveal that the contact angle decreases upon the formation of passive films by up to 5° for the highest value of V_{AC}. Although the variation of the contact angle is small in magnitude, it still indicates that the passive layers on Ti slightly increase the surface wettability of Ti in HBSS; thus, the Ti surface becomes more hydrophilic.

Conclusions

(1) Uniform and crack-free passive layers were formed on Ti surface by applying AC or DC voltage in aqueous

© 2006 NRC Canada

Fig. 18. SEM micrographs for the etched Ti (ETi) and three passive layers formed at 20, 40, and 50 V_{AC} (60 Hz) after an immersion test in HBSS at 37 °C for 2 weeks.

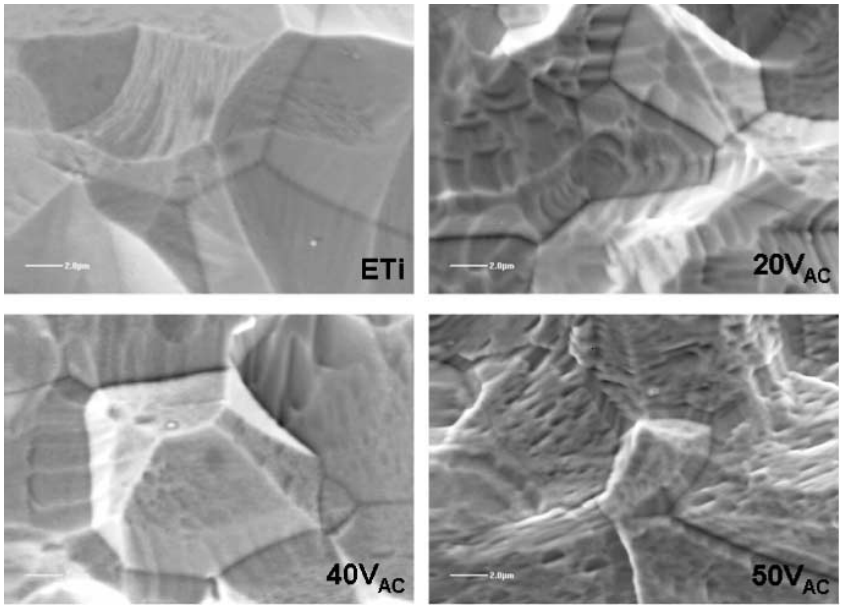


Table 2. Contact angle in HBSS.

Sample	Contact angle (°)
Etched Ti	67.7 ± 0.5
Passive layer formed at 10 V_{AC}	64.3 ± 0.4
Passive layer formed at 30 V_{AC}	63.5 ± 0.4
Passive layer formed at 50 V_{AC}	62.4 ± 0.5

$NH_4{\cdot}BF_4$. Their coloration and thickness could be modified by adjusting the experimental parameters.

(2) Higher DC voltages were required to prepare passive layers of similar coloration and thickness as those obtained using AC.

(3) The colored passive layers grew in registry with the underlying Ti substrate and no cracks or flakes were observed.

(4) The surface modification of Ti accomplished by the formation of passive layers made the surface rougher and slightly more hydrophilic.

(5) The passive layers revealed an enhanced corrosion resistance in HBSS at 37 °C when compared with the untreated Ti. These passive layers reduced the corrosion rate of Ti in HBSS by a factor of 3.

(6) The passive layers effectively reduced the Ti-ion release level in HBSS at 37 °C by a factor of 15; the higher the applied V_{AC}, the lower the Ti-ion release level.

Acknowledgements

We wish to acknowledge financial support from the Natural Sciences and Engineering Research Council of Canada (NSERC) and Queen's University. B.D. Zhao acknowledges an R.S. McLaughlin Fellowship. We thank Prof. D. Beauchemin and Dr. C. Y. Huang for their help in performing ICP-MS measurements. We acknowledge the assistance of Prof. A. Docoslis in conducting contact angle measurements.

References

1. B.D. Ratner. *In* Titanium in medicine. *Edited by* D.M. Brunette, P. Tengvall, M. Textor, and P. Thomsen. Springer, New York. 2001. pp. 2–24.
2. S.A. Shabalovskaya. Bio-Med. Mater. Eng. **12**, 69 (2002).
3. D.L. Mitchell, S.S. Synnott, and J.A. VanDercreek. Int. J. Oral Maxillofac. Implants. **5**, 79 (1990).
4. A. Yamamoto, R. Honma, and M. Sumita. J. Biomed. Mater. Res. **39**, 331 (1998).
5. J.F. Osborn, P. Willich, and N. Meenen. *In* Clinical implant materials. *Edited by* G. Heimke, U. Soltesz, and A.J.C. Lee. Elsevier, Amsterdam. 1990. pp. 75–80.
6. R.J. Solar, S.R. Pollack, and E. Korostoff. *In* ASTM STP 684, 1979. *Edited by* B.C. Syrett and A. Acharya. ASTM STP 684. 1979. pp. 161–172.
7. N. Schiff, B. Grosgogeat, M. Lissac, and F. Dalard. Biomaterials, **25**, 4535 (2004).
8. B. Yang, M. Uchida, H.M. Kim, X.D. Zhang, and T. Kokubo. Biomaterials, **25**, 1003 (2004).
9. H.H. Huang, Y.H. Chiu, T.H. Lee, S.C. Wu, H.W. Yang, K.H. Su, and C.C. Hsu. Biomaterials, **24**, 3585 (2003).
10. RG. Rondelli and B. Vicentini. Biomaterials, **20**, 785 (1999).
11. R. Strietzel, A. Hosch, H. Kalbfleisch, and D. Buch. Biomaterials, **19**, 1495 (1998).
12. A. Wisbey, P.J. Gregson, and L.M. Peter. Biomaterials, **12**, 470 (1991).
13. O. Cisse, O. Savadogo, M. Wu, and L.H. Yahia. J. Biomed. Mater. Res. **61**, 339 (2002).
14. Y.Z. Yang, J.M. Tian, J.T. Tian, Z.Q. Chen, X.J. Deng, and D.H. Zhang. J. Biomed. Mater. Res. **52**, 333 (2000).
15. C. Trepanier, M. Tabrizian, L.H. Yahia, L. Bilodeau, and D.L. Piron. J. Biomed. Mater. Res. **43**, 433 (1998).
16. S. Nishiguchi, H. Kato, M. Neo, M. Oka, H.M. Kim, T. Kokubo, and T. Nakamura. J. Biomed. Mater. Res. **54**, 198 (2001).

© 2006 NRC Canada

17. D.J. Blackwood and S.K.M. Chooi. Corros. Sci. **44**, 395 (2002).
18. T. Hepel, M. Hepel, R.A. Osteryoung. J. Electrochem. Soc. **129**, 2132 (1982).
19. G. Jerkiewicz, H. Strzelecki, and A. Wieckowski. Langmuir. **12**, 1005 (1996).
20. S. Hrapovic, B.L. Luan, M. D'Amours, G. Vatankhah, and G. Jerkiewicz. Langmuir. **17**, 3051 (2001).
21. ASTM G 5–94 (Reapproved 2004). Annual Book of ASTM Standards. American Society for Testing and Materials, Philadelphia. 1995. Vol. 03.02. pp. 48–58.
22. D.A. Jones. *In* Principles and prevention of corrosion. Macmillan Pub. Co. New York. 1992. pp. 142–152.
23. E.L. Liening. *In* Process industry corrosion. National Association of Corrosion Engineers. Houston, Texas, USA. 1986. pp. 85–122.
24. R.W. Schutz and D.E. Thomas. *In* ASM Handbook. *Edited by* J.R. Davis, J.D. Destefani, H.J. Frissell, and G.M. Crankovic. ASM Handbook, 9th Edition, ASM International. Metals Park, Ohio, USA. 1987. Vol. 13. pp. 669–706.
25. D.H. Li, S.J. Ferguson, T. Beutler, D.L. Cochran, C. Sittig, H.P. Hirt, and D. Buser. J. Biomed. Mater. Res. **60**, 325 (2002).
26. W.J. James and M.E. Straumanis. *In* Encyclopedia of electrochemistry of elements. *Edited by* A.J. Bard. Marcel Dekker, New York. 1976. Vol. 7. pp. 345–396.
27. K.C. Kalra, K.C. Singh, and M. Singh. J. Electroanal. Chem. **371**, 73 (1994).
28. Y.Y. Su. Wire Journal International, **2**, 106 (998).
29. P. Kovacs. Trans. Soc. Biomat. **19**, 272 (1993).

© 2006 NRC Canada

The photochemistry of ring-substituted cinnamyl acetates

S.A. Fleming, L. Renault, E.C. Grundy, and J.A. Pincock

Abstract: The photochemistry of the (*E*)-cinnamyl acetates ((*E*)-1-aryl-3-propenyl acetates, **8a**–**8e**) with substituents H, 4-CH_3O, 3-CH_3O, 4-CF_3, and 3-CF_3, respectively, was examined in both cyclohexane and methanol solvents. Alkene isomerization (*E* to *Z*) occurred more efficiently than other reactions and evidence is presented that this process occurs from the excited triplet state. In a slower process, 1,3-migration of the acetoxy group led to the rearranged 3-aryl-3-propenyl acetate isomers (**9a**–**9e**) as the major pathway, particularly in cylohexane. In methanol, the isomeric ethers 3-aryl-3-methoxypropene (**14**) and 1-aryl-3-methoxypropene (**15**) were formed by reaction of methanol with the photochemically generated cation. The combined yield of **14** and **15** (95% and 5%, respectively) was quantitative for the 4-methoxyphenyl compound (**8b**). Independent irradiations of the isomers **9a**–**9c** demonstrated that the ethers **14** and **15** were primary photoproducts from **8** and not secondary photoproducts from **9**. Fluorescence quantum yields and excited singlet state lifetimes indicated that the reactions, other than the *E* to *Z* isomerization, are from the excited singlet state.

Key words: cinnamyl acetates, photochemistry, *E*/*Z* isomerization, photocleavage, fluorescence.

Résumé : Opérant tant dans le cyclohexane que dans le méthanol comme solvants, on a étudié la photochimie des acétates de (*E*)-cinnamyle (acétates de (*E*)-1-aryl-3-propényle, **8a**–**8e**) portant des substituants H, 4-OCH_3, 3-OCH_3, 4-CF_3, et 3-CF_3. L'isomérisation de l'alcène (*E* à *Z*) est la réaction qui se produit de la façon la plus efficace par rapport aux autres et on présente des données qui montrent que cette réaction se produit à partir de l'état triplet excité. Dans un processus plus lent, particulièrement dans le cyclohexane, la voie réactionnelle principalement provoque un réarrangement avec migration-1,3 du groupe acétoxy qui conduit aux acétates de 3-aryl-3-propényle isomères (**9a**–**9e**). Dans le méthanol, les éthers isomères 3-aryl-3-méthoxypropène (**14**) et 1-aryl-3-méthoxypropène (**15**) se forment par réaction du méthanol avec le cation généré photochimiquement. Le rendement combiné des composés **14** et **15** (95 % et 5 %) est quantitatif pour le composé 4-méthoxyphényle (**8b**). Des irradiations indépendantes des isomères **9a**–**9c** ont démontré que les éthers **14** et **15** correspondent aux photoproduits primaires des composés **8** et non pas des photoproduits secondaires des composés **9**. Les rendements quantiques de fluorescence et les temps de vie de l'état excité singulet indiquent que les réactions, à l'exception de l'isomérisation *E* à *Z*, se font à partir de l'état singulet excité.

Mots clés : acétates de cinnamyle, photochimie, isomérisation *E*/*Z*, photoclivage, fluorescence.

[Traduit par la Rédaction]

Introduction

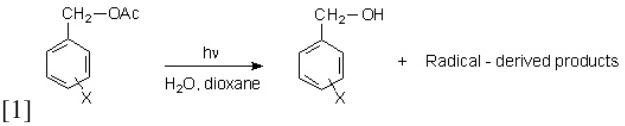
For some time, we have been interested in the effect that substitutents on aromatic rings have on photochemical processes. In particular, we have examined the photocleavage reactions of arylmethyl systems with leaving groups ($ArCH_2$-LG), the competition between radical and ion-derived products in polar nucleophilic solvents like alcohols, Scheme 1, and the pathway for their formation (1–3).

Received 14 July 2006. Accepted 7 September 2006. Published on the NRC Research Press Web site at http://canjchem.nrc.ca on 2 November 2006.

S.A. Fleming. Department of Chemistry and Biochemistry, C100 BNSN, Brigham Young University, Provo, UT 84602, USA.
L. Renault, E.C. Grundy, and J.A. Pincock.[1] Department of Chemistry, Dalhousie University, Halifax, NS B3H 4J3, Canada.

[1]Corresponding author (e-mail: james.pincock@dal.ca).

The initial report of the "meta effect" for these reactions by Zimmerman and coworkers (4, 5) presented the observation that 3-methoxybenzyl acetate (**1b**) gives a higher chemical (29%–35%) and quantum yield (0.13) of formation of the ion-derived alcohol product than 4-methoxybenzyl acetate (**1a**) ("minor" amount and 0.016, respectively) on photolysis in aqueous dioxane (eq. [1]). This observation is contrary to expectations on the basis of ground state stability of the corresponding cations, the 4-methoxybenzyl cation being considerably more stable than the 3-methoxy substituted one.



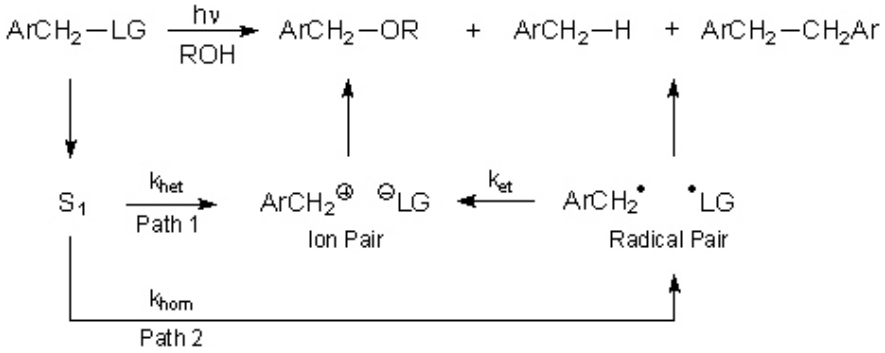
[1]

1a: X = 4-OCH_3
1b: X = 3-OCH_3

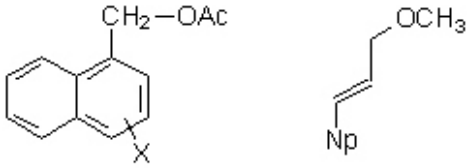
As outlined in Scheme 1, two quite different mechanistic proposals have been advanced to explain this observation.

 doi:10.1139/V06-140 © 2006 NRC Canada

Scheme 1.

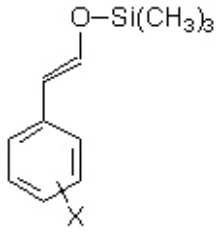


Path 1, as initially proposed and reinforced by more recent computational results by Zimmerman (6, 7) assumes that the ion pair is formed directly from the first excited singlet state, S_1, of the substrate and that the 3-methoxybenzyl cation is formed more efficiently than the 4-methoxy substituted one. Path 2, as developed by us, assumes that the ion pair is formed by redox electron transfer from an initially formed radical pair; direct formation of the ion pair from S_1 is, at most, a minor process. The yield of the ion pair is then determined by k_{et}, the rate constant for electron transfer that converts the radical pair to the ion pair and therefore by the driving force as determined by the reduction potential of the acyloxy radical and the oxidation potential of the arylmethyl radical. Results for substituted benzyl and 1- naphthylmethyl acetates **1**, **2** have been particularly important in developing this mechanism (1).

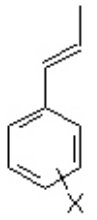


2a: X = 4-OCH_3
2b: X = 3-OCH_3

7



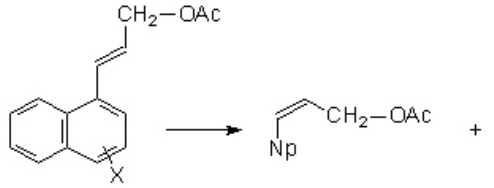
10b: X = 4-OCH_3
10c: X = 3-OCH_3
10d: X = 4-CF_3
10e: X = 3-CF_3



11a: X = H

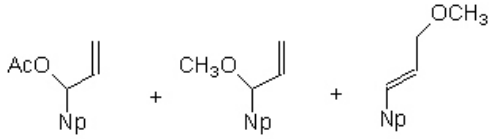
More recently, Rao et al. (8) reported on the photochemistry[2] of (*E*)-1-naphthylallyl acetates (**3**) for X = H, 4–CH_3 and 4–OCH_3 (eq. [2]) in hexane, methanol, and acetonitrile. In hexane, *E* to *Z* isomerization was the major process observed although low yields of the rearranged acetate **5** were reported for **3b** and **3c**. In acetonitrile, the efficiencies of conversion were similar but the major product was now the rearranged acetate **5** for all three cases. In methanol, the major photosolvolysis product for all three was the methyl ether **6** with yields of 30% from **3a**, 36% from **3b**, and 80% from **3c**. The ether **7**, resulting from direct substitution, was not observed. Remarkably, the 4-methoxy substrate **3c** reacted considerably more efficiently than either of the other two in methanol (conversion after 30 min of 40%, 43%, and 95% for **3a**, **3b**, and **3c**, respectively). No products obviously derived from radical intermediates were reported for any of the three substrates, even in cyclohexane as solvent, although the rearranged acetates **5** could be so formed.

[2]



3a: X = H
3b: X = 4-CH_3
3c: X = 4-OCH_3

4



5 **6** **7**

We have observed (9) a similar high yield (74% of the methyl ether) of ion-derived product for the photolysis in methanol of the 4-methoxy-1-naphthyl substrate **2a**, compared with the corresponding 3-methoxy derivative **2b** (31%).

We now report on the photochemistry in both cyclohexane and methanol of the cinnamyl acetates **8a**–**8e** (eq. [3]).

[2] For 30 min irradiations of 10^{-3} mol/L solutions of substrate in a Rayonet reactor with 300 nm lamps.

© 2006 NRC Canada

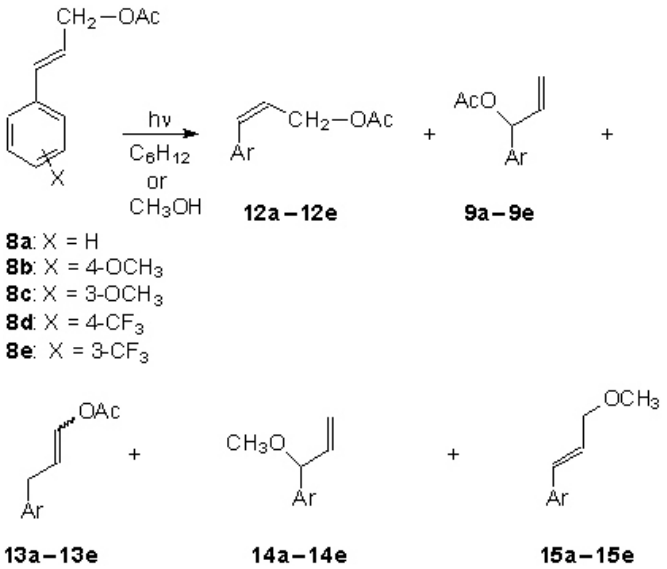
Table 1. Product yields for the photolysis of esters **8a**–**8e** for 1 h at 25 °C.

Compound	X	Solvent[a]	**8** (*E* + *Z*)	**9**	**13** (*E* + *Z*)	**14**	**15** (*E* + *Z*)
8a	H	C	24 + 46	30	—		
8b	4-CH_3O	C	—	96	4		
8c	3-CH_3O	C	30 + 43	16	11		
8d	4-CF_3	C	7 + 16	50	20 + 7		
8	3-CF_3	C	11 + 28	56	3		
8a	H	M	—	57	—	43	—
8b	4-CH_3O	M	—	—	—	95	5
8c	3-CH_3O	M	—	24	—	52	23
8d	4-CF_3	M	5 + 14	38	21 + 13	6	3
8	3-CF_3	M	7 + 15	58	5 + 5	9	2

Note: Product yields are in % and normalized to 100% (see text). A dash indicates that the yield was less than 1%.
[a]C = cyclohexane, M = methanol.

These compounds were chosen to examine both the "meta effect" for a system with extended conjugation relative to the prototypical benzyl acetates **1** and the connection between the arylmethyl compounds **1** and **2** and those with more extended allylic conjugation, **3** and **8**. The CF_3-substituted cases were included to examine the contrast in reactivity with substrates having electron-withdrawing substituents.

[3]



Results and discussion

Synthesis and photolysis experiments

The synthesis of the (*E*)-1-aryl-3-propenyl acetates **8a**–**8e** was performed as described in the literature (10). The corresponding commercially available cinnamic acids were converted to their ethyl esters, reduced with DIBAL, and the resulting alcohols were esterified by reacting with acetyl chloride. The acetates (100 mg in 100 mL of solvent) were irradiated at 25 °C in a Rayonet apparatus equipped with 254 nm lamps. The reaction progress was monitored by GCMS and product ratios (by GC and ^{1}H NMR) are reported in Table 1 after 1 hour of irradiation. Dark control experiments in methanol resulted in no alkene isomerization or solvolysis for any of the compounds **8**. For photolysis of all substrates, the mass balance for volatile products was low (e.g., typical of most cases only 55% after 85% conversion of **8a** in methanol). The nonvolatile products are assumed to be oligomers formed from the arylallyl radical and ionic intermediates. This suggestion is supported by the observation of broad structureless signals in the aromatic and aliphatic region of the ^{1}H NMR spectra of crude reaction mixtures. Therefore, the values of product yields in Table 1 have been normalized to 100%. On the basis of product yields, the most reactive compound in both cyclohexane and methanol is the 4-methoxy one, similar to the previous observations (8) for the 1-naphthyl derivatives **3** (eq. [2]).

A main photoproduct for each of the substrates was the isomeric 3-aryl-3-propenyl acetate (**9**). Although they could be isolated by chromatography from the photolysis mixtures, **9a**–**9c** were also prepared by the reaction of vinylmagnesium bromide with the appropriate substituted benzaldehyde followed by quenching with acetyl chloride.

Photophysical properties of 8a–8e and the siloxanes 10b–10e in cyclohexane and methanol

The photophysical properties of the esters **8** in both cyclohexane and methanol are reported in Table 2 along with those for the corresponding siloxanes **10**, which serve as useful models because they have the same chromophore but are photochemically unreactive to C–O bond cleavage. The siloxanes **10b**–**10e** were available in our laboratory because they had been prepared for a related project on the photochemistry of dicinnamyl siloxanes. Another good model for the chromophore of the esters are 1-arylpropenes, which have been studied previously; literature values for the spectra of 1-phenylpropene **11a** are also included in Table 1.

The UV absorption spectra of compounds **8**, **10**, and **11** are as expected on the basis of the reported values for 1-arylpropenes (11, 12) with a longer wavelength lower intensity band with vibrational structure for the S_0 to S_1 transition and a higher intensity broad structureless band for the S_0 to S_2 transition at shorter wavelength. As an example, for cinnamyl acetate **8a** in methanol the bands observed are at 291 nm (ε = 780 $(mol/L)^{-1}$ cm^{-1}) and 282 nm (ε = 1190 $(mol/L)^{-1}$ cm^{-1}) for the S_1 transition and 252 nm (ε = 16 100

© 2006 NRC Canada

Table 2. Photophysical properties of the compounds **8–11** at 25 °C.

Compound	X	Solvent[a]	λ_{max}, $\varepsilon/10^3$ (nm, (mol/L)$^{-1}$ cm^{-1})	Φ_f	τ (ns)	k_f (10^7 s^{-1})[b]
8a	H	C	253, 15.5	0.22	7.2	3.0
8a	H	M	252, 16.1	0.16	5.6	2.9
11a[c]	H	H	250[c]	0.35	11.8	3.0
9a	H	M	256, 0.23	0.026	7.2	0.36
8b	4-CH_3O	C	263, 22.2	0.23	1.8	12.7
10b	4-CH_3O	C	261, 22.5	0.59	6.1	9.7
8b	4-CH_3O	M	262, 22.1	0.029	—[d]	
10b	4-CH_3O	M	260, 24.4	0.34	3.2	10.6
9b	4-CH_3O	M	281, 1.58	0.098	5.25	1.9
8c	3-CH_3O	C	253, 14.0	0.50	6.5	7.7
10c	3-CH_3O	C	253, 15.2	0.44	5.8	7.6
8c	3-CH_3O	M	252, 14.4	0.091	0.89	10.2
10c	3-CH_3O	M	252, 14.0	0.64	6.8	9.3
9c	3-CH_3O	M	271, 1.66	0.008	1.1	0.72
8d	4-CF_3	C	255, 19.0	0.24	4.0	6.0
10d	4-CF_3	C	254, 18.8	0.25	3.8	6.6
8d	4-CF_3	M	253, 20.0	0.22	4.0	5.5
10d	4-CF_3	M	254, 20.9	0.16	3.5	4.6
8	3-CF_3	C	249, 16.6	0.24	4.8	5.0
10	3-CF_3	C	254, 18.4	0.21	4.2	5.0
8	3-CF_3	M	249, 17.9	0.24	5.4	4.4
10	3-CF_3	M	249, 18.3	0.27	5.0	5.4

[a]C = cyclohexane, M = methanol, H = hexane
[b]$k_f = \Phi_f / \tau$.
[c]From ref. 11.
[d]<0.5 ns.

(mol/L)$^{-1}$ cm^{-1}) for the S_2 transition. The irradiation experiments were done at 254 nm into the S_2 transition and only those bands are reported in Table 1. This band is shifted to longer wavelength (263 nm) and higher molar absorptivity (ε = 22 200 (mol/L)$^{-1}$ cm^{-1}) by the conjugating 4-methoxy substituent **8b** but affected only slightly by the other substituents. The change in solvent from cyclohexane to methanol also has little effect. A comparison of the absorption bands and the molar absorptivities for the esters **8** and the siloxanes **10** indicates that, as expected, the chromophores are essentially the same for the two.

In contrast, the quantum yields of fluorescence (Φ_f) for the methoxy substituted esters **8b** and **8c** are considerably lower than for the corresponding siloxanes **10b** and **10c**, particularly in methanol. This quantum yield is defined by eq. [4], where k_f and k_t are the rate constants for fluorescence and the total rate of decay for the excited singlet state, respectively. The rate constant k_t (the reciprocal of τ_S) is defined by eq. [5], where k_{ic}, k_{isc}, and k_r are the rate constants for internal conversion, intersystem crossing, and reaction, respectively. The decreases in Φ_f are a consequence of the fact that the excited singlet states of the esters have a pathway, C–O bond cleavage, for deactivation that competes with fluorescence but is unavailable for the silanes. In agreement with this concept, the excited singlet state lifetimes (τ_s) are also considerably shorter for the esters. The parallel decrease in the quantum yield of fluorescence and singlet state lifetime means that k_f remains nearly constant, again indicating the similarity of the excited states of the esters and the model siloxanes. This similarity is also apparent for the trifluoromethyl substituted compounds **8d** and **8e**, but now the Φ_f and τ_s values suggest that excited state C–O bond cleavage is a relatively inefficient process in both cyclohexane and methanol.

$$[4] \qquad \Phi_f = k_f / k_t = k_f \tau_s$$

$$[5] \qquad 1 / \tau_s = k_t = k_f + k_{isc} + k_{ic} + k_r$$

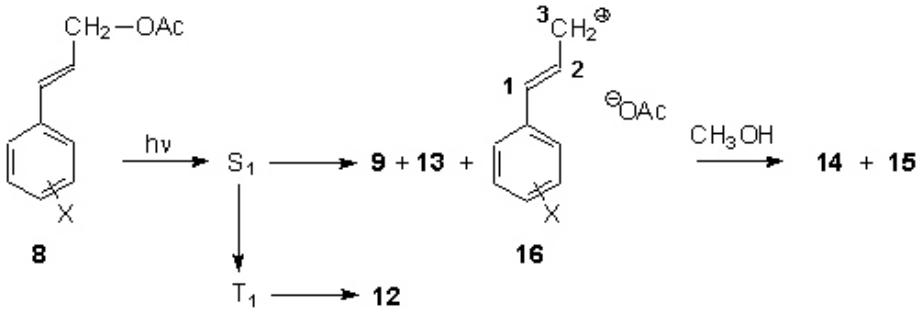
Photolysis of esters 8 in cyclohexane

Although the main goal of this study was to examine the ion-derived products formed by photosolvolysis of the cinnamyl esters, the results in cyclohexane provide important information on other mechanisms. Several observations and trends are worth noting. First, from percent conversion vs. time plots, *E* to *Z* isomerization occurs more rapidly than other photochemical processes to give mixtures enriched in the *Z* isomer. This result is apparent from the photolysis yield results shown in Table 1 for those substrates that are not completely consumed after one hour of irradiation. Further product formation then occurs from this equilibrated mixture, which is rich in the *Z* isomer. Because the secondary photochemistry must compete with the more rapid isomerization process, the photoreactions are relatively inefficient.

On the basis of results by Lewis and Zuo (11) for *(E)*- and (*Z*)-1-phenylpropene, which have an analogous chromophore

© 2006 NRC Canada

Scheme 2.



to the unsubstituted cinnamyl acetate **8a**, the *E* isomer should have a high barrier (~9 kcal/mol, 1 cal = 4.184 J) in the excited singlet state for rotation about the C=C double bond. At room temperature, the dominant mode of the excited singlet state decay should be intersystem crossing and isomerization would then occur by a barrierless process in the triplet manifold. In contrast, the *Z* isomer should have a lower barrier (~4 kcal/mol) for excited singlet state rotation and this process would be the dominant mode for its decay at room temperature.

Attempts to confirm that the triplet state of **8a** did undergo *E* to *Z* isomerization were unsuccessful because of rapid reaction of the sensitizers, either benzophenone or xanthone with the solvent cyclohexane. However, a previous report (13) on the triplet sensitization of the photochemistry of cinnamyl acetate **8a** in acetonitrile indicated that only isomerization occurred to give a ratio of 35% *E* and 65% *Z*. A very small amount (2.5%) of the rearranged isomer **9a** was also reported but it was ascribed to direct absorption of the incident light by **8a** rather than by the sensitizer.

Second, the predominate product for the irradiations in cyclohexane is the 3-aryl-3-propenyl acetate **9** that results from a 1,3-shift of the acetoxy group (eq. [3]). This observation is similar to that reported recently (8) for the formation of the products **5** on photolysis in hexane of the 1-(1-naphthyl)-3-propenyl acetate derivatives **3** (eq. [2]). However, in contrast to the high yields observed in the current study (94% for **8b**; X = 4-CH_3O, for example, the compound where this process is the most efficient) the yields reported for the naphthyl derivatives are very low (3% for **3c**; X = 4-CH_3O). Because these products are being formed in cyclohexane where ionic intermediates are unlikely to be formed, the mechanism for their formation must be by a radical or concerted pathway similar to a photo-Claisen rearrangement.

The other major product of the photolyses in cyclohexane is **13**, another deconjugated isomer of the starting material but formed by a 1,3-hydogen shift and as a mixture of *E* and *Z* isomers. The yield is highest (27%) for the 4-trifluoromethyl substrate **8d**. Again, this process does not likely involve ion pairs.

An important point to make here is that no products resulting from radical coupling were obtained. In the photochemistry of both benzyl and 1-naphthylmethyl acetates, products (ethylbenzene and ethylnaphthalene derivatives) resulting from the loss of carbon dioxide from the acetyloxy radical followed by coupling of the methyl radical with the arylmethyl radical are always observed (1). The lack of analogous products for the photolysis of **8** suggests that the formation of the rearranged isomers **9** and **13** in cyclohexane as solvent occurs by a concerted process without discrete intermediates.

Photolysis of esters 8 in methanol

Photolysis of each of the substrates **8** in methanol resulted in the formation of the ion-derived products **13** and **14** along with, in most cases, those obtained in cyclohexane irradiations. However, for the 4-methoxy compound **8b** the ethers **13** and **14** are the only products observed with a high selectivity for unconjugated isomer **14**. The evidence that these products are derived from the excited singlet state is provided by a sensitized irradiation in methanol for **8a**. Xanthone, as opposed to benzophenone, was chosen as the sensitizer on the basis of the fact that its triplet state is not efficiently quenched by methanol (14). Irradiation using a Pyrex filter, conditions that led to no reaction in the absence of xanthone, resulted in efficient *E* to *Z* isomerization. No other products were detected indicating that the excited triplet state of **8a** does not react by C–O bond cleavage in contrast to direct irradiations, which proceed through the excited singlet state. As discussed previously, this proposal is supported by the decreases in Φ_f and τ_f for **8a** (Table 1) relative to the *(E)*-1-phenylpropene **11a**.

None of the compounds irradiated in methanol, as in cyclohexane, gave observable quantities of radical coupling products. Therefore, the observed photochemistry is consistent with three possible mechanisms: (*i*) heterolytic cleavage of the C–O bond from S_1 to form the ion pair directly, (*ii*) homolytic cleavage from S_1 followed by electron transfer that is faster than decarboxylation of the acetyloxy radical, and (iii) bimolecular reaction of methanol with S_1 to form **14** (S_N2') or **15** (S_N2). The second would require that electron transfer be more than an order of magnitude faster than 10^9 s^{-1}, the rate of decarboxylation of the acetyloxy radical (15) and therefore faster than previously determined rates for benzyl systems (1). The third also seems unlikely because, to our knowledge, convincing evidence for this possibility in photosolvolysis reactions has not been reported. The first possibility, direct heterolytic cleavage from S_1, is therefore most probable. This suggestion is supported by the greater efficiency of reaction for the methoxy substituted compounds, which should favour cation formation relative to those with trifluoromethyl substituents.

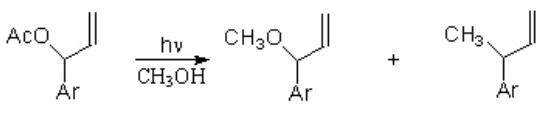
By reaction of the solvent at the aryl-substituted end C1 of the allylic cation, Scheme 2, the photosolvolysis products primarily give the unconjugated ether **14**. The same observation was made for the 1-naphthylmethyl derivatives **3**

© 2006 NRC Canada

(eq. [2]) with **6** formed in preference to **7**. Moreover, irradiation of the conjugated ether **15a** in methanol did not result in formation of the unconjugated isomer **14a**. If the two isomers were equilibrating photochemically then **14a**, with the weaker chromophore, would have been the major one in the mixture. Finally, because the conjugated isomers **15** will be more stable than the unconjugated ones **14**, any explanation for the preference for **14** must be a kinetic rather than a thermodynamic one.

This selective regiochemistry could simply be the result of the distribution of the positive charge in the cationic intermediate **16**. However, calculated positive charges (Mulliken, with attached hydrogens summed into the carbons) by Gaussian 03 (B3LYP, 6-31G(d), optimized geometry) (16) for **16** gave values (X, charge at C1, charge at C3) that were significantly higher at C3 than C1: **16a** (H, 0.091, 0.200), **16b** (4-methoxy, 0.055, 0.155), **16c** (3-methoxy, 0.081, 0.192), **16d** (4-trifluoromethyl, 0.098, 0.214), **16e** (3-trifluoromethyl, 0.099, 0.215). This result leads to a prediction opposite to that observed. However, examination of the LUMO, a pure π orbital dominated by contributions from the AO's at C1 and C3 so that it resembles an allyl system, was more satisfactory. The values for **16** were (X, contribution from $2p_x + 3p_x$ at C1, contribution from $2p_x + 3p_x$ at C3, difference): **16a** (H, 0.710, –0.614, 0.096), **16b** (4-methoxy, 0.694, –0.579, 0.115), **16c** (3-methoxy, 0.0.723, –0.617, 0.105), **16d** (4-trifluoromethyl, 0.718, –0.616, 0.102), **16e** (3-trifloromethyl, 0.725, –0.620, 0.105). Therefore, the LUMO is dominated by the contribution from C1 for all substituents, the largest difference being for the 4-methoxy compound where the selectivity is also high for reaction at C1 to give **14** (95%) over C3 to give **15** (5%) (Table 1). A similar observation that LUMO coefficients are better than positive charge distribution at predicting the regioselectivity of cation reactivity with methanol has been reported previously for photosolvolysis reactions (17). The asymmetry of the allyl fragment in the cations **16** is also apparent from the calculated bond lengths. The C1–C2 bond is significantly longer (1.420 ± 0.002) than that for C2–C3 (1.358 ± 0.0023), this difference being essentially independent of substituent.

The possibility that the methyl ethers **14** and **15** were formed as secondary photoproducts from the initially formed rearranged esters **9** was also independently tested by studying the photochemistry of **9**. As indicated in Table 2 and as expected, the esters **9a**–**9c** absorbed at similar wavelengths to **8a**–**8c**, but the molar absorptivity of compounds **9** was more than one order of magnitude lower. Therefore, competitive photochemistry of **9** is unlikely because it cannot be absorbing a significant percentage of the photons until very high conversion. Moreover, the rearranged acetate **9b** was not even observed in the photolysis of **8b** in methanol. The other interesting observation from the photochemistry of compounds **9** is that the products were exclusively the unconjugated ethers **14** and the radical coupling products **17** (eq. [6]). As discussed above, these latter products were not observed as photoproducts in methanol from compounds **8**. This implies that the excited states of **8** and **9** behave quite differently, the latter being comparable to normal benzylic ester photochemistry.

[6] 

9 **14** **17**

For irradiation of the 3- or 4-trifluoromethyl substituted compounds **8d** and **8e** in methanol, photosolvolysis is not the major pathway. In both cases the major photoproducts are the rearranged acetates **9** and **13**, the former being preferred. This result is consistent with a less efficient heterolytic cleavage because the electron-withdrawing groups do not assist with the bond breaking process. As discussed previously, this conclusion is supported by their small changes in fluorescence quantum yield and excited singlet state lifetime (Table 1) relative to the siloxanes **10d** and **10e**. The reversed polarity of the excited states as a consequence of the electron-withdrawing groups may also explain the preference for 1,3-hydrogen and 1,3-acetoxy migrations to give compounds **9** and **13**, respectively.

Conclusions

The photochemistry of the *(E)*-cinnamyl acetates is similar to that of benzylic esters in that processes involving C–O bond cleavage occur, including photosolvolysis in methanol. These processes from the excited singlet state are in competition with the more efficient intersystem crossing followed by *E* to *Z* isomerization from the triplet state. In contrast to benzylic systems, where 3-methoxy derivatives react considerably more efficiently than the 4-methoxy substituted ones in polar protic solvents, both methoxy compounds give high yields of photosolvolysis for the cinnamyl derivative. In fact, the 4-methoxy compound gives essentially 100% yield of ion-derived ethers in methanol.

In both cyclohexane and methanol, no evidence for radical-derived products was obtained. The rearranged acetates appear to be derived from concerted 1,3-hydrogen or acetoxy migrations.

Experimental

Materials and instruments

All NMR spectra were obtained in $CDCl_3$ using a Bruker 250 MHz instrument unless otherwise noted. High resolution mass spectrometry (HRMS) was performed on a CEC 21-110B sector instrument using electron impact ionization. Solvent extractions were dried with magnesium sulfate. Toluene was distilled from CaH. Ethyl acetate and hexane were flash distilled prior to chromatography. All other solvents were used without further purification. Solvents used for photochemical experiments were obtained commercially as HPLC grade. Column chromatography was performed using 60–250 mesh silica gel under flash conditions. Chiral chromatography was performed on a Varian Star #1 instrument using a Chiracel AD-RH column eluted with methanol–water.

Irradiations

A solution of ~100 mg of the appropriate compound in 100 mL of methanol or cyclohexane was purged with nitrogen and then irradiated in a Rayonet photochemical reactor using 16 lamps (75 W, 254 nm). The temperature was con-

© 2006 NRC Canada

trolled (±1 °C) by circulating water in an immersion tube. Reaction progress was monitored by GC followed by NMR analysis after solvent evaporation. For sensitized reactions in methanol, ~250 mg of **8a** and xanthone (3.6×10^{-4} mol/L, A = 2.3 at 340 nm) in 280 mL of solvent was irradiated in the well of a 450 W Hanovia lamp using a Pyrex filter. In the absence of the sensitizer, no reaction occurred under these conditions.

GC method

GCMS analyses were done a PerkinElmer Autosystem using a Supelco 30 mm × 0.25 mm MDN-5S 5% phenyl methylsiloxane column, film thickness 0.50 µm, temperature programmed as follows: 60 °C for 1min, 20 °C/min to 240 °C, 240 °C for 10 min.

Absorbance measurements

Absorbance spectra were recorded at 1 nm resolution using a Cary 100 UV–vis spectrometer thermostated at 25 °C.

Fluorescence measurements

All samples were degassed by three freeze-pump-thaw cycles and then thermostated at 25 °C. Fluorescence intensity measurements were done using a PTI-210M fluorescence spectrometer with dual Model 101 monochromators, a 75W Xenon lamp, and a Model 814 photomultiplier detector. Corrected spectra were obtained.

Singlet lifetimes were measured by monitoring fluorescence decay using a PRA time-correlated single photon counting apparatus with a hydrogen flash lamp with pulse width of about 1.8 ns. The cell compartment was thermostated at 25.0 °C with circulating water from a constant temperature bath.

General synthetic procedure for substituted (*E*)-cinnamyl acetates 8

(E)-Cinnamyl acetate **8a** is commercially available. For the other acetates, the commercially available substituted *(E)*-cinnamic acid was converted to its respective ester by refluxing in 100% ethanol in the presence of a catalytic amount of *p*-toluenesulfonic acid for 24–36 h. The isolated ester was then treated with 3 equiv. of diisobutyl aluminum hydride (DIBAL) in toluene in an ice bath. The reaction was allowed to stir for 2 h. The reaction was quenched with aq HCl (5%) and extracted with ether. The organic layer was washed with aq HCl (5%), water, brine, and then dried. The resulting alcohol was purified by recrystallization or chromatography to give the known X-substituted cinnamyl alcohols: X = 4-methoxy (18), X = 3-methoxy (19), X = 4-trifluoromethyl (20), X = 3-trifluoromethyl (21). Treatment of the alcohol with excess acetyl chloride in benzene then purification by chromatography yielded the substituted *(E)*-cinnamyl acetate.

4-Methoxycinnamyl acetate 8b

^{1}H NMR δ 7.32 (d, 2H, *J* = 8.5 Hz), 6.85 (d, 2H, *J* = 8.7 Hz), 6.60 (d, 1H, *J* = 16 Hz), 6.15 (dt, 1H, *J* = 16 and 6.2 Hz), 4.69 (d, 2H, *J* = 6.5 Hz), 3.80 (s, 3H), 2.01 (s, 3H). ^{13}C NMR (62.5 MHz) δ 171.1, 159.8, 134.2, 129.1, 128.0, 121.0, 114.2, 65.5, 55.4, 21.2. HRMS calcd. for $C_{12}H_{14}O_3$: 206.0943; found: 206.0939. The literature reference for the synthesis provides no spectral data (22).

3-Methoxycinnamyl acetate 8c

^{1}H NMR δ 7.25 (m, 1 H), 6.95 (d, 1H), 6.92 (bs, 1H), 6.83 (dd, 1H), 6.63 (d, 1H), 6.27 (dt, 1H), 4.73 (dd, 2H), 3.81 (s, 3H), 2.10 (s, 3H). ^{13}C NMR (62.5 MHz) δ 171.0, 160.1, 137.8, 134.3, 129.8, 123.8, 119.5, 114.0, 112.1, 65.2, 55.4, 21.2. The literature reference for the synthesis provides no spectral data (10).

4-Trifluoromethylcinnamyl acetate 8d

^{1}H NMR δ 7.57 (d, 2H, *J* = 7 Hz), 7.47 (d, 2H, *J* = 8 Hz), 6.67 (d, 1H, *J* = 16 Hz), 6.37 (dt, 1H, *J* = 16 and 6 Hz), 4.75 (d, 2H, *J* = 6 Hz), 2.11 (s, 3 H). ^{13}C NMR (62.5 MHz) δ 170.8, 139.9 (q, *J* = 1 Hz), 132.4, 129.9 (q, *J* = 32 Hz), 126.9, 126.2, 125.7 (q, *J* = 3.6 Hz), 124.3 (q, *J* = 270 Hz), 64.7, 21.0. HRMS calcd. for $C_{12}H_{11}F_3O_2$: 244.0711; found: 244.0714 (23).

3-Trifluoromethylcinnamyl acetate 8e

^{1}H NMR δ 7.7–7.4 (m, 4H), 6.67 (d, 1H, *J* = 16 Hz), 6.36 (dt, 1H, *J* = 16 and 6 Hz), 4.35 (d, 2H, *J* = 6 Hz), 2.11 (s, 3 H). ^{13}C NMR (62.5 MHz) δ 170.9, 137.1, 132.5, 131.2 (q, *J* = 32.3), 129.8 (q, *J* = 1.3), 129.2, 125.5, 124.7 (q, *J* = 3.7), 124.2 (q, *J* = 271), 123.4 (q, *J* = 4.0), 64.7, 21.0. HRMS calcd. for $C_{12}H_{11}F_3O_2$: 244.0711; found: 244.0713.

General synthetic procedure for substituted 3-aryl-3-propenyl acetates 9a–9c

The aldehyde (9.5 mmol) in 100 mL of anhydrous ether was cooled in an ice bath and 8.5 mL (8.5 mmol) of vinyl magnesium bromide was added. The reaction mixture was stirred for 3 h followed by the addition of acetyl chloride (2.4 mL, 38 mmol) followed by further stirring for 20 h. The reaction mixture was then poured into aq NaOH (5%) and extracted with ether. The extract was washed with water and saturated brine and then dried with magnesium sulfate. The crude ester was then purified by column chromatography with yield approximately 75%. Spectral data agreed with those reported previously: X = H (24), X = 4-methoxy (25), X = 3-methoxy (26).

Characterization of photoproducts from irradiation of the cinnamyl esters 8

The following compounds were isolated from photolysis mixtures by separation using column chromatography. Spectra were compared with those from the literature. Other photoproducts were not obtained in pure form but were identified by GCMS and analysis of ^{1}H NMR of mixtures.

3-(4-Trifluoromethylphenyl)-3-propenyl acetate 9d (26)

^{1}H NMR δ7.62 (d, 2H, *J* = 8.5 Hz), 7.46 (d, 2H, *J* = 8.5 Hz), 6.28 (bd, 1H, *J* = 6 Hz), 5.98 (ddd, 1H, *J* = 17, 10.3 and 6 Hz), 5.30 (m, 2H, =CH_2), 2.13 (s, 3H). GCMS *m/z* (rel. intensity): 244 (1), 202 (11), 165 (49), 164 (19), 145 (29, 133 (31), 116 (24), 115 (100), 75 (14), 69 (25), 63 (13).

3-(3-Trifluoromethylphenyl)-3-propenyl acetate 9e

^{1}H NMR δ 7.7–7.4 (m, 4 H), 6.35 (bd, 1 H, *J* = 7 Hz), 5.94 (ddd, 1 H, *J* = 17, 10 and 7 Hz), 5.30 (m, 2H, =CH_2), 2.12 (s, 3 H). GCMS *m/z* (rel. intensity): 244 (3), 202 (33),

© 2006 NRC Canada

185 (12), 184 (20), 165 (38), 164 (19), 145 (22), 133 (24), 116 (202), 115 (100), 69 (12).

3-Methoxy-3-phenylpropene 14a (27)

^{1}H NMR δ 7.5–7.2 (m, 5H), 5.93 (ddd, 1H, *J* = 17, 10.4 and 6.8 Hz), 5.23 (m, 2H, =CH_2), 4.61 (bd, H, *J* = 6.8 Hz), 3.43 (s, 3H). GCMS *m/z* (rel. intensity): 148 (1), 116 (30), 115 (86), 91 (53), 89 (15), 77 (68), 63 (38), 62 (20), 51 (100).

3-Methoxy-3-(4-methoxyphenyl)propene 14b (28)

^{1}H NMR δ 7.24 (d, 2H, *J* = 8.7 Hz), 6.88 (d, 2H, *J* = 8.7 Hz), 5.93 (ddd, 1H, *J* = 17.3, 10.2 and 6.5 Hz), 5.23 (m, 2H, =CH_2), 4.57 (bd, H, *J* = 6.5 Hz), 3.79 (s, 3H), 3.30 (s, 3H). GCMS *m/z* (rel. intensity): 178 (89), 177 (28), 163 (14), 151 (44), 148 (17), 147 (100), 146 (94), 135 (32), 132 (15), 131 (69), 117 (15), 116 (13), 115 (45), 104 (18), 103 (97), 102 (26), 91 (51), 89 (14), 78 (24), 77 (67), 76 (15), 65 (20), 63 (30), 55 (230, 51 (34).

3-Methoxy-3-(3-methoxyphenyl)propene 14c (26)

^{1}H NMR δ 7.3–6.7 (m, 4H), 5.92 (ddd, 1H, *J* = 16.7, 10.7 and 6.5 Hz), 5.27 (dt, 1H, *J* = 16.7 and 1.5 Hz), 5.19 (bd, 1H, *J* = 10.7 Hz), 4.59 (bd, H, *J* = 6.5 Hz), 3.80 (s, 3H), 3.33 (s, 3H). GCMS *m/z* (rel. intensity): 178 (75), 177 (18), 163 (19), 151 (32), 148 (15), 147 (63), 146 (100), 135 (22), 131 (50), 117 (12), 115 (32), 104 (13), 103 (63), 102 (15), 91 (28), 78 (13), 77 (30), 63 (15), 51 (12).

3-Methoxy-3-(3-trifluoromethylphenyl)propene 14e

^{1}H NMR δ 7.6–7.4 (m, 4H), 5.88 (m, H), 5.26 (m, 2H), 4.66 (bd, H, *J* = 7.1 Hz), 3.36 (s, 3H). GCMS *m/z* (rel. intensity): 218 (1), 189 (15), 73 (13), 165 (96), 164 (18), 147 (50), 145 (56), 141 (97), 133 (59), 117 (23), 116 (23), 115 (100), 109 (10), 91 (12), 89 (16), 75 (23), 69 (60), 63 (33), 55 (19), 51 (22), 50 (21).

(E)-3-Methoxy-1-(3-methoxyphenyl)propene 15c

^{1}H NMR δ 7.23 (t, 1H, *J* = 7.8 Hz), 6.98 (d, 1H, *J* = 7.8 Hz), 6.92 (d, 1H, *J* = 1.5 Hz), 6.81 (dd, 1H, *J* = 8 and 1 Hz), 6.58 (bd, 1H, *J* = 15.8 Hz), 6.27 (dt, 1H, *J* = 15.8 and 6 Hz), 4.09 (dd, 2H, *J* = 6 and 1 Hz), 3.81 (s, 3H), 3.39 (s, 3H).

(Z)-3-Methoxy-1-(3-methoxyphenyl)propene 15c

^{1}H NMR δ: 7.25 (t, 1 H, *J* = 8.5 Hz), 6.84–6.76 (m, 3 H), 6.57 (d, 1 H, *J* = 12 Hz), 5.84 (dt, 1 H, *J* = 12 and 6.5 Hz), 4.19 (d, 2 H, *J* = 6.3 Hz), 3.81 (s, 3 H), 3.36 (s, 3H).

(E)-3-(4-Trifluoromethylphenyl)-1-propenyl acetate 13d

^{1}H NMR δ: 7.55 (d, 2H, *J* = 8 Hz), 7.31 (d, 2H, *J* = 8 Hz), 7.20 (dt, 1H, *J* = 13 and 1.5 Hz), 5.50 (dt, 1H, *J* = 13 and 7.5 Hz), 3.39 (bd, 2H, *J* = 7.5 Hz), 2.07 (s, 3H).

(Z)-3-(4-Trifluoromethylphenyl)-1-propenyl acetate 13d

^{1}H NMR δ 7.55 (d, 2H, *J* = 8 Hz), 7.31 (d, 2H, *J* = 8 Hz), 7.19 (dt, 1H, *J* = 6.5 and 1.7 Hz), 5.07 (dt, 1H, *J* = 7.7 and 6.5 Hz), 3.55 (bd, 2H, *J* = 7.7 Hz), 2.13 (s, 3H). The two last isomers have not been previously reported but their spectra match (*E*)- and (*Z*)-3-phenyl-1-propenyl acetate (29).

Acknowledgements

We thank Natural Sciences and Engineering Research Council (NSERC) of Canada for financial support. SAF also thanks the Department of Chemistry and Biochemistry, Brigham Young University, for the leave necessary to pursue this research.

References

1. J.A. Pincock. Acc. Chem. Res. **30**, 43 (1997).
2. J.A. Pincock. *In* the CRC Handbook of organic photochemistry and photobiology. 2nd Ed. *Edited by* W. Horspool and F. Lenci. CRC Press. Boca Raton, Fla. 2004. pp. 66.1–66.17.
3. S.A. Fleming and J.A. Pincock. *In* Organic molecular photochemistry. Vol. 3. *Edited by* V. Ramamurthy and K.S. Schanze. Marcel Dekker, New York. 1999. p. 211.
4. H.E. Zimmerman and V.R. Sandel. J. Am. Chem. Soc. **85**, 915 (1963).
5. H.E. Zimmerman and S. Somasekhara. J. Am. Chem. Soc. **85**, 922 (1963).
6. H.E. Zimmerman. J. Am. Chem. Soc. **117**, 8988 (1995).
7. H.E. Zimmerman. J. Phys. Chem. A, **102**, 5616 (1998).
8. G.V. Rao, M.J.K. Reddy, K. Srinivas, M.J.K. Reddy, K.M. Bushan, and V.J. Rao. **76**, 29 (2002).
9. D.P. DeCosta and J.A. Pincock. J. Am. Chem. Soc. **115**, 2180 (1993).
10. H. Matsuzaka, Y. Hiroe, M. Iwasaki, Y. Ishii, Y. Koyasu, and M. Hidai. J. Org. Chem. **53**, 3832 (1988).
11. F.D. Lewis and X. Zuo. J. Am. Chem. Soc. **116**, 10477 (1994).
12. J.C. Roberts and J.A. Pincock. J. Org. Chem. **71**, 1480 (2005).
13. G.A. Lee and S.H. Israel. J. Org. Chem. **48**, 4557 (1983).
14. J.C. Scaiano. J. Am. Chem. Soc. **102**, 7747 (1980).
15. J.W. Hilborn and J.A. Pincock. J. Am. Chem. Soc. **113**, 2683 (1991).
16. M.J. Frisch, G.W. Trucks, H.B. Schlegel, G.E. Scuseria, M.A. Robb, J.R. Cheeseman, J.A. Montgomery, Jr., T. Vreven, K.N. Kudin, J.C. Burant, J.M. Millam, S.S. Iyengar, J. Tomasi, V. Barone, B. Mennucci, M. Cossi, G. Scalmani, N. Rega, G.A. Petersson, H. Nakatsuji, M. Hada, M. Ehara, K. Toyota, R. Fukuda, J. Hasegawa, M. Ishida, T. Nakajima, Y. Honda, O. Kitao, H. Nakai, M. Klene, X. Li, J.E. Knox, H.P. Hratchian, J.B. Cross, C. Adamo, J. Jaramillo, R. Gomperts, R.E. Stratmann, O. Yazyev, A.J. Austin, R. Cammi,C. Pomelli, J.W. Ochterski, P.Y. Ayala, K. Morokuma, G.A. Voth, P. Salvador, J.J. Dannenberg, V.G. Zakrzewski, S. Dapprich, A.D. Daniels, M.C. Strain, O. Farkas, D.K. Malick, A.D. Rabuck, K. Raghavachari, J.B. Foresman, Ortiz, J.V. Q. Cui, A.G. Baboul, S. Clifford, J. Cioslowski, B.B. Stefanov, G. Liu, A. Liashenko, P. Piskorz, I. Komaromi, R.L. Martin, D.J. Fox, T. Keith, M.A. Al-Laham, C.Y. Peng, A. Nanayakkara, M. Challacombe, P.M.W. Gill, B. Johnson, W. Chen, M.W. Wong, C. Gonzalez, and J.A. Pople. Gaussian 03 [computer program]. Revision B.05. Gaussian, Inc., Wallingford, Conn. 2004.
17. E.S. Krijnen, H. Zuilhof, and G. Lodder. J. Org. Chem. **59**, 8138 (1994).
18. T. Kim, G.A. Mirafzal, J. Liu, and N.A. Bauld. J. Am. Chem. Soc. **115**, 7653 (1993).
19. D.A. Evans, J.A. Gauchet-Prunet, E.M. Carreira, and A.B. Charette. J. Org. Chem. **56**, 741 (1991).
20. S. Oida, Y. Tajima, T. Konosu, Y. Nakamura, A. Somada, T. Tanaka, S. Habuki, T. Harasaki, Y. Kamai, T. Fukuoka, S. Ohya, and H. Yasuda. Chem. Pharm. Bull. **48**, 694 (2000).

© 2006 NRC Canada

21. B. Goument, L. Duhamel, and R. Mauge. Tetrahedron, **50**, 171 (1994).
22. A. Citterio, C. Arnoldi, C. Giordano, and G. Castaldi. J. Chem. Soc. Perkin Trans. 1, 891 (1983).
23. M.J. Kang, J.-S. Jang, and L.S.-G. Lee. Tetrahedron Lett. **36**, 8829 (1996).
24. Z. Rappoport, S. Winstein, and W.G. Young. J. Am. Chem. Soc. **94**, 2320 (1972).
25. Y.D. Ward, L.A. Villanueva, G.D. Allred, S.C. Payne, M.A. Semones, and L.S. Liebeskind. Organometallics, **14**, 4132 (1995).
26. L.F. Tietze, T. Hippo, and A. Steinmetz. Chem. Commun. (Cambridge), 793 (1998).
29. L.J. Gazzard, W.B. Motherwell, and D.A. Sandham. J. Chem. Soc. Perkin Trans. 1, 979 (1999).

© 2006 NRC Canada

The recognition and sensing of anions by a novel phenanthroline-bridged diamide

Yan-Hong Qiao, Hai Lin, and Hua-Kuan Lin

Abstract: A novel neutral anion recognition receptor **1** with the additional capability of selectively sensing anionic guest species has been synthesized and examined for its anion-binding abilities by UV–vis absorption spectroscopy. The results of nonlinear curve fitting and Job plot indicate that **1** forms 1:1 stoichiometric complexes with fluoride, chloride, bromide, iodide, and acetate, respectively. Their UV–vis absorption spectra in DMSO indicate the presence of anions such as F^-, Cl^-, Br^-, I^-, and AcO^- with high affinity ability and selectivity toward F^-, and also show dramatic colour changes from colourless to yellow in the presence of TBAX (1×10^{-5} mol/L, X= F^-, Cl^-, Br^-, I^-, and AcO^-). Receptor **1** has almost no affinity abilities for $H_2PO_4^-$ and OH^-.

Key words: phenanthroline-bridged diamide, synthesis, UV–vis spectrum, anion recognition.

Résumé : On a réalisé la synthèse d'un nouveau récepteur (**1**) qui peut reconnaître un anion neutre tout en possédant aussi la capacité de détecter la présence d'espèces invitées anioniques et, faisant appel à la spectroscopie UV-vis, on a étudié ses capacités à se lier aux anions. Les résultats d'un ajustement de courbe non linéaire et une courbe de Job indiquent que le composé **1** forme des complexes de stoechiométrie 1:1 respectivement avec les ions fluorure, chlorure, bromure, iodure et acétate. Leurs spectres d'absorption UV–vis dans le DMSO montrent qu'ils répondent avec une possibilité d'affinité élevée à la présence des anions tels que F^-, Cl^-, Br^-, I^- et AcO^-, avec sélectivité à la présence de F^- et avec un changement dramatique de couleur, d'incolore à jaune en présence de TBAX (1×10^{-5} mol/L, X = F^-, Cl^-, Br^-, I^- et AcO^-). Le récepteur **1** n'a pratiquement pas de possibilité d'affinité pour le $H_2PO_4^-$ ou le OH^-.

Mots clés : diamide à pont phénanthroline, synthèse, spectre UV–vis, reconnaissance d'anions.

[Traduit par la Rédaction]

Introduction

The development of neutral receptors for the recognition of anions has attracted much attention in organic as well as inorganic chemistry during recent years (1–11). There are a number of reasons for the sudden growth in this new area. Anions are ubiquitous throughout biological systems. Inorganic anions such as fluoride, chloride, bromide, iodide, dihydrogenphosphate, acetate, or hydroxide ion play an important role in energy transduction in organisms and control metabolic processes via participation in enzymatic reactions. They carry genetic information (DNA is a polyanion). The majority of enzyme substrates and cofactors are anionic. Anions also play roles in the areas of medicine and catalysis. Anions are larger than isoelectronic cations (12) and therefore have a lower ratio of charge to radius. This means that electrostatic binding interactions of anions are less effective than for the smaller cations. The design of anion receptors is particularly challenging. The design and synthesis of fluorescent or colorimetric sensors (13–18) are of vital importance because of their potential applications. In general, the performance of a chemosensor can be improved either by (*i*) increasing its selectivity through the preorganization of the receptor or (*ii*) through the improved signal transduction (read-out) that leads to a reliable substrate specific response. Aromatic scaffolds for amide groups are common motifs in anion receptors. The effectiveness of such building blocks was shown by Crabtree and coworkers with isophthalamide (11) and dipicolinic bisamide (19), followed by Gale et al. with pyrrole derivatives (20, 21). We decided to extend this family of aromatic building blocks to phenanthroline derivatives. In this note, we report the result of an anion recognition study of our novel *N*,*N*-(*p*-nitro-phenyl)-1,10-phenanthroline-2,9-dimethanamide receptor (Scheme 1).

Experimental

Reagents

All anions, in the form of tetrabutylammonium salts, were purchased from Sigma-Aldrich Chemical Co., stored in a desiccator under vacumm containing self-indicating silica,

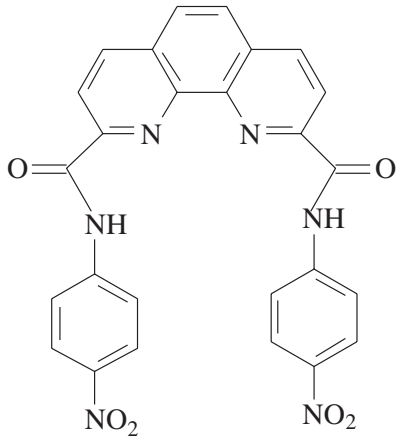
Received 10 July 2006. Accepted 7 September 2006. Published on the NRC Research Press Web site at http://canjchem.nrc.ca on 28 October 2006.

Y.-H. Qiao and H.-K. Lin.[1] Department of Chemistry, Nankai University, Tianjin 300071, P. R. China.
H. Lin. State Key Laboratory of Functional Polymer Materials for Absorption and Separation, Nankai University, Tianjin 300071, P. R. China.

[1]Corresponding author (e-mail: hklin@nankai.edu.cn).

 doi:10.1139/V06-138 © 2006 NRC Canada

Scheme 1.



used without any further purification, and dried with P_2O_5 in a vacumm desiccator at 353 K for 24 h prior to use. Dimethyl sulfoxide was dried with calcium hydride and distilled at reduced pressure prior to use. Unless stated otherwise, AR grade chemicals were purchased and used without further purification. The 1,10-phenanthroline-2,9-dicarboxylic acid was prepared according to the known method (22).

Instruments

Elemental analyses for C, H, and N were carried out on a PerkinElmer 240C element analyzer at the Institute of Elemento-Organic Chemistry, Nankai University. The ^{1}H NMR spectra were recorded using a Varian UNITY-plus 400 MHz spectrometer at the State Key Laboratory of Functional Polymer Materials for Absorption and Separation, Nankai University. UV–vis absorption spectra were performed on a General 1900 spectrophotometer. The spectrophotometer was standardized.

Synthesis

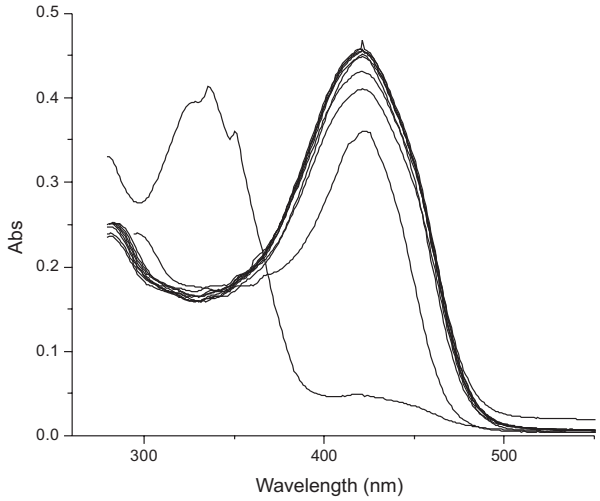
N,N′-(p-*nitro-phenyl)-1,10-phenanthroline-2,9-dimethanamide (1)*

The receptor *N*,*N*′-(*p*-nitro-phenyl)-1,10-phenanthroline-2,9-dimethanamide (**1**) was prepared by a method similar to that in the literature (23). To 1,10-phenanthroline-2,9-dicarboxylic acid (1.1 g, 4 mmol) was added thionyl chloride (25 mL) and the mixture refluxed for 6 h. The solution was concentrated under reduced pressure to dryness. The residue was added to 4-nitro-phenylamine (1.12 g, 8.1 mmol) in dry dichloromethane (50 mL) followed by the addition of triethylamine (2.5 mL). The solution was stirred for 72 h at room temperature, poured into sodium bicarbonate – deionized water, filtered, and washed with water to give a white solid, which was recrystallized from DMF to yield 0.68 g of **1** (yield 34.3%). ^{1}H NMR (DMSO-d_6) δ: 11.86 (s, 2H, NH), 8.87 (d, 2H, phen-H), 8.64 (d, 2H, phen-H), 8.45 (m, 8H, phenyl-H), 8.31 (d, 2H phen-H). Anal. calcd. for $C_{26}H_6N_6O_6.H_2O$: C 59.32, H 3.42, N15.97; found: C 59.79, H 3.88, N 15.86.

Anion titration of 1

Spectrophotometric titrations were performed on solutions of compound **1** (1.0×10^{-5} mol/dm^3) in DMSO (redistilled before use). Typically, increasing concentrations (0–10 equiv.) of a standard fresh tetrabutylammonium salt solution of the required anion F^-, Cl^-, Br^-, I^-, AcO^-, $H_2PO_4^-$, and OH^- were added, respectively, and the UV-vis absorption of the samples were recorded.

Fig. 1. UV–vis spectrum of **1** (1.0×10^{-5} mol/dm^3) in the presence of fluoride in DMSO. The equiv. of the fluoride anion are: 0, 0.05, 0.1, 0.2, 0.5, 0.8, 1, 2, 3, 4, and 5.



Results and discussion

Figure 1 shows the changes in the UV–vis spectra of **1** at a concentration of $1 \times 1.0\ 0^{-5}$ mol /dm^3 in DMSO upon addition of the fluoride anion. When the fluoride anion was introduced to the solution of **1**, a new absorption peak was observed at 422 nm and the absorbances at 336 and 351 nm were significantly decreased. Similar phenomena were observed when Cl^-, Br^-, I^-, or AcO^- were added to the solution of **1**. A satisfactory result was achieved when nonlinear curve fitting (absorbance at 422 nm against the fluoride anion equivalent) confirmed that **1** and fluoride anion formed a 1:1 complex, as shown in Fig. 2.

A continuous variation method was used to determine the stoichiometric ratios of the receptor **1** and the fluoride anion guest. Figure 3 shows a Job plot of the difference between the observed absorbance and the absorbance of the free receptor **1** (422 nm with the molar fraction of host {[H] / ([H] + [G])}) for a series of solutions in which the total concentration of host and fluoride anion guest was constant (2.0×10^{-5} mol /dm^3), while the molar fraction of the host was continuously varyied (24). The result illustrates that the receptor–anion complex concentration approaches a maximum when the molar fraction of the host {[H] / ([H] + [G])} is about 0.50, meaning that the receptor formed a 1:1 complex with the fluoride anion. In the same way, it was deduced that the receptor **1** and other halide anions (Cl^-, Br^-, and I^-) also formed 1:1 complexes. Though the shape of the acetate anion is different from the halide anions, the Job plot (Fig. 4) still proved that it would bind to the receptor in 1:1 stochiometry, as in the fluoride case.

For a complex of 1:1 stoichiometry, the relation in eq. [1] could be derived easily, as reported formerly (25), where *X*

© 2006 NRC Canada

Table 1. Association constants (K_{ass}) of receptor **1** with anions in DMSO.

Anion	Fluoride	Chloride	Bromide	Iodide	Acetate	Phosphate	Hydroxy
K_{ass} ((mol/L)$^{-1}$)	5.64×10^6	3.33×10^5	1.89×10^5	1.24×10^4	1.96×10^5	Nd	Nd

Note: Nd indicates that the spectra showed little or no change with the addition of the anion so that the affinity constant cannot be determined using the spectra.

Fig. 2. Nonlinear curve at 422 nm vs. equiv. of fluoride anion. The correlation coefficient (R^2) of the nonlinear curve fit is 0.99809.

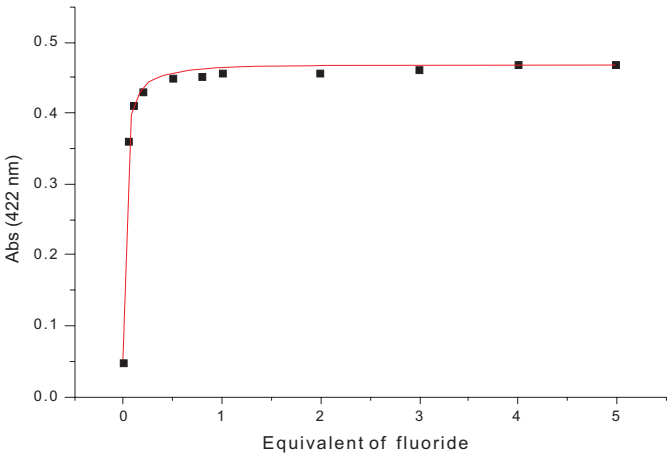
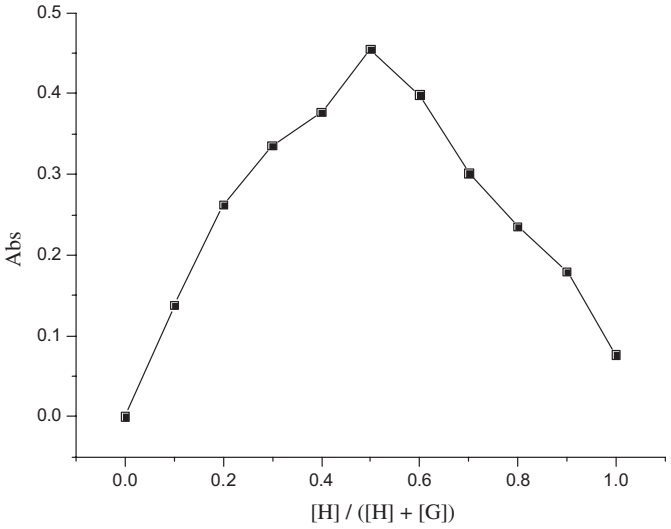


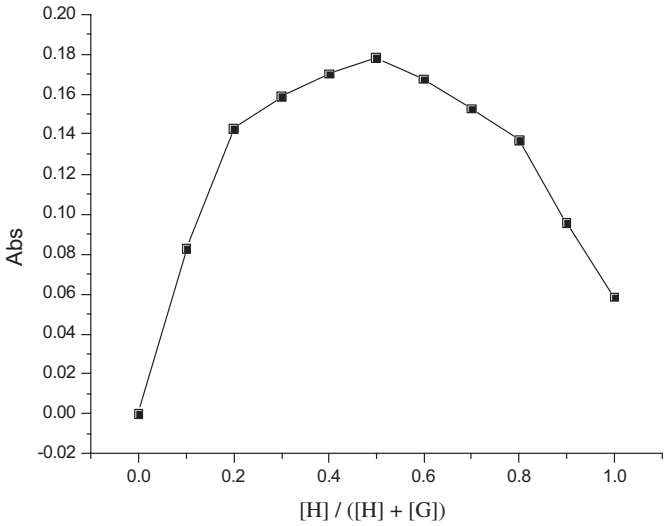
Fig. 3. Job plot of receptor **1** with fluoride anion at 422 nm. The total concentration of the host and guest was 2.0×10^{-5} mol/dm^3.



is the absorption intensity, and c_H or c_G is the concentration of the host or the anion guest, respectively.

$$[1] \quad X = X_0 + (X_{lim} - X_0)\{c_H + c_G + 1/K_{ass} - [(c_H + c_G + 1/K_{ass})^2 - 4c_Hc_G]^{1/2}\}/2c_H$$

Fig. 4. Job plot of receptor **1** with acetate anion at 423 nm. The total concentration of the host and guest was 2.0×10^{-5} mol/dm^3.



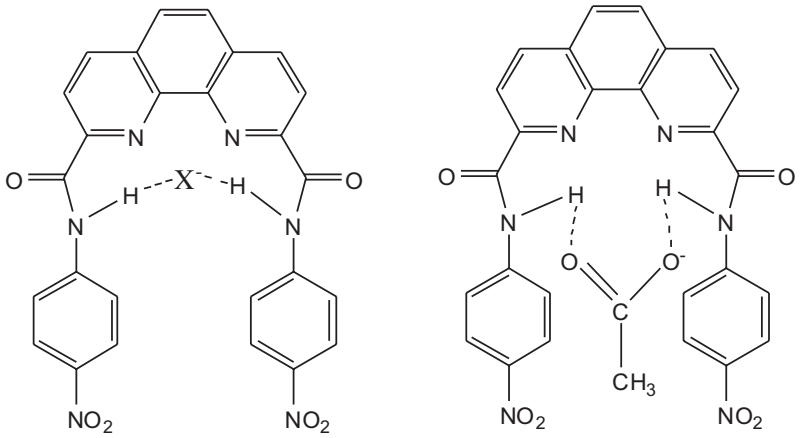
The affinity constants determined by UV–vis titration, summarized in Table 1, illustrate that the receptor can bind anions in the order $F^- > Cl^- > AcO^- > Br^- > I^- > H_2PO_4^- \sim OH^-$. In particular, receptor **1** can recognize fluoride anions with higher selectivity (over 10 times) than other halide anions, which is better than some fluorogenic receptors or colorimetric sensors reported previously (13–18). This indicates that the selective recognition for halide anions is related to the size of the anions.

Conclusion

In summary, a neutral anion receptor **1**, bearing diamide binding sites, was synthesized. The receptor **1** forms 1:1 complexes with anions. The receptor **1**, with a cleft forming a rigid cavity with two rigid arms, binds preferably with anions through effective hydrogen bonding. The sensitivity for the recognition of halide anions is related to the size of the anions. The cleft between the hydrogen of NH in receptor **1** is able to bind well to small anions, such as fluoride. Acetate (a triangular anion) is too big to enter the cleft, but binds via two O's with the two H's of NH on the cavity plane of receptor **1**. The proposed binding mode of receptor **1** is shown in Scheme 2. The receptor **1** selectively binds F^-, Cl^-, Br^-, I^-, and AcO^-, in particular the fluoride anion, with high affinity. Upon the addition of anions (F^-, Cl^-, Br^-, I^-, or AcO^-) to a solution of **1**, the response shows dramatic colour changes from colourless to yellow and selectivity toward F^-.

© 2006 NRC Canada

Scheme 2.



Acknowledgements

This project was supported by the National Natural Science Foundition of China (grant No. 20371028) and Natural Science Foundition of Tianjin (grant No. 023605811).

References

1. P.A. Gale. Coord. Chem. Rev. **240**, 191 (2003).
2. P.A. Gale. Coord. Chem. Rev. **213**, 79 (2001).
3. F.P. Schmidtchen and M.Berger. Chem. Rev. **97**, 1609 (1997).
4. J.L. Atwood, J.T. Holman, and J.W. Steed. Chem. Commun. (Cambridge), 1401 (1996).
5. M.F. Hawthorne, X. Yang, and C. Knubler. Angew. Chem. Int. Ed. Engl. **30**, 1507 (1991).
6. A. Bencini, P. Bianchi, E. Dapporto, E. Garcia-Espana, M. Micheloni, J.A. Ramirez, P. Paoletti, and P. Paoli. Inorg. Chem. **31**, 1902 (1992).
7. D.M. Rudkevich, W. Verboom, Z. Brzozka, M.J. Palys, W.P.R.V. Stauthamer, G.J. van Hummel, S.M. Franken, S. Harkema, J.F.J. Engbersen, and D.N. Reinhoudt. J. Am. Chem. Soc. **116**, 4341 (1994).
8. K.T. Holman, M.M. Halihan, J.W. Steed, S.S. Jurisson, and J.L. Atwood. J. Am. Chem. Soc. **117**, 7848 (1995).
9. X. Xu, J.J. Vittal, and R.J. Puddephatt. J. Am. Chem. Soc. **117**, 8362 (1995).
10. P.A. Gale, J.L. Sessler, V. Král, and V. Lynch. J. Am. Chem. Soc. **118**, 5140 (1996).
11. K. Kavallieratos, S.R. Gala, D.J. Austin, and R.H. Crabtree. J. Am. Chem. Soc. **119**, 2325 (1997).
12. R.D. Shannon. Acta Crystallogr. Sect. A, **32**, 751 (1976).
13. R. Martinez-Manez and F. Sancenon. Chem. Rev. **103**, 4419 (2003).
14. T. Gunnlaugsson, P.E. Kruger, T.C. Lee, R. Parker, F.M. Pfeffer, and G.M. Hussey. Tetrahedron Lett. **44**, 6575 (2003).
15. J.L. Wu, Y.B. He, Z.Y. Zeng, L.H. Wie, L.Z. Meng, and T.X.Yang. Tetrahedron, **60**, 4309 (2004).
16. M. Vazquez, L. Fabbrizzi, A. Taglietti, R.M. Pedrido, A.M. Gonzalez-Noya, and M.R. Bermejo. Angew. Chem. Int. Ed. **43**, 1962 (2004).
17. A.M. Costero, M.J. Banuls, M.J. Aurell, M.D. Ward, and S. Argent. Tetrahedron, **60**, 9471 (2004).
18. J. Kang and J. Kim. Tetrahedron Lett. **46**, 1759 (2005).
19. K. Kavallieratos, Ch.M. Bertoo, and R.H. Crabtree. Org. Chem. **64**, 1675 (1999).
20. P.A. Gale, S. Camiolo, C.P. Chapman, M.E. Light, and M.B. Hursthouse. Tetrahedron Lett. **42**, 5095 (2001).
21. P.A. Gale, S. Camiolo, G.J. Tizzard, C.P. Chapman, M.E. Light, S.J. Coles, and M.B. Hursthouse. J. Org. Chem. **66**, 7849 (2001).
22. J.Ch. Christopher, W.D. Leslie, and A.R. James. J. Heterocycl. Chem. **18**, 599 (1981).
23. M. S. Adel, Garas, S. V. arobert, J. Heterocycl. Chem. **37**, 151 (2000).
24. J.S. Kim, O.J. Shon, S.H. Yang, J.Y. Kim, and M.J. Kim. J. Org. Chem. **67**, 6514 (2002).
25. B. Valeur, J. Pouget, and J. Bourson. J. Phys. Chem. **96,** 6545 (1992).

© 2006 NRC Canada

Catalyzed β scission of a carbenium ion II — Variations leading to a general mechanism

Qingbin Li and Allan L.L. East

Abstract: The β-scission mechanisms of catalytically chemisorbed carbenium ions are further investigated using density functional theory computations and explicit-contact modelling, but with slightly larger catalyst fragment models than in our previous work. Some variations are seen, including the existence of formal one-step and three-step (rather than two-step) mechanisms. The activation barriers are most affected by the basicity of the catalyst model than by any other characteristics: the stronger the base, the greater the barrier. A general mechanism for β scission is presented, as are the specific mechanisms for all the step variations observed from computations to date.

Key words: C–C bond fission, β scission, carbenium ion, catalysis, chloroaluminate, mechanism.

Résumé : Faisant encore appel à des calculs de théorie de la densité fonctionnelle, on a étudié à nouveau les mécanismes de scission-β d'ions carbénium catalytiquement chimisorbés en faisant de la modélisation de contact explicite et en examinant des modèles de fragments de catalyseur légèrement supérieurs à ceux examinés antérieurement. On a observé des variations, y compris l'existence des mécanismes formels à une et à trois étapes, plutôt que deux étapes. La basicité du modèle du catalyseur est le facteur qui affecte le plus les paramètres d'activation; plus la base est forte, plus grande est la barrière. On présente un mécanisme général pour les scissions β ainsi que des mécanismes spécifiques pour toutes les variétés d'étapes qui ont été observées jusqu'à maintenant à partir des calculs.

Mots clés : scission d'une liaison C–C, scission β, ion carbénium, catalyse, chloroaluminate, mécanisme.

[Traduit par la Rédaction]

Introduction

Catalyzed β scission of the secondary carbenium ion *s*-$C_5H_{11}^+$ on small aluminum-containing anions ($AlH_2(OH)_2^-$ and $AlHCl_3^-$) has been computationally studied by us recently (1). That study filled the holes left by earlier studies of aluminum oxide catalysis of β scission (2–4) and demonstrates qualitative differences in the mechanism due to the different strengths of basicity of the two anions. We have also published β-scission steps found for the larger *s*-$C_6H_{13}^+$ ion on $AlHCl_3^-$ (5).

Real catalytic systems involve condensed phases and are much more difficult to model. Two examples of current interest are solid aluminosilicate zeolites and chloroaluminate ionic liquids. To date, calculations using periodic boundary conditions (6) have been forced to use approximate transition-state-finding algorithms (7) and await improvements. Continuum dielectric models have been problematic for proton-transfer phenomena and may be more so for ionic liquids, although new improvements look promising (8–10).

In this current study, we obtained more B3LYP computational results of minimum-energy pathways for β scission of secondary carbenium ions, initially chemisorbed to various anions. Five systems were studied, $C_5H_{11}^+$ on $Al(OH)(OSiH_3)_3^-$, $C_5H_{11}^+$ on $Al_2Cl_7^-$, $C_6H_{13}^+$ on $Al_2Cl_7^-$, $C_6H_{13}^+$ with a two-fragment catalyst model $AlCl_4^-$ + $AlHCl_3^-$, and $C_6H_{13}^+$ with a three-fragment catalyst model $AlCl_4^-$ + $AlHCl_3^-$ + Na^+. These systems are still poor mimics of real zeolite or ionic liquid systems. However, that is not the point. First, these systems allow us to explore how transition states and mechanisms may change as the models get larger without having to compromise on the accuracy in energy and transition-state calculations. Second, and most importantly, with these 22 new transition states added to the 12 found in our first paper and the 10 relevant ones from ref. 5, we feel we have enough examples to be able to present a truly proper discussion of the β scission of a secondary carbenium ion.

Received 11 July 2006. Accepted 1 September 2006. Published on the NRC Research Press Web site at http://canjchem.nrc.ca on 31 October 2006.

Q. Li and A.L.L. East.[1] Department of Chemistry and Biochemistry, University of Regina, Regina, SK S4S 0A2, Canada.

[1]Corresponding author (e-mail: Allan.East@uregina.ca).

Methods, models, and terminology

Calculations were performed to locate transition states (and the intermediates that they connect) for the β scission of chemisorbed 2-pentenium and 2-hexenium ions, catalyzed by various catalyst models in explicit contact. All computational methods and procedures are the same as before (1), based on the density functional theory model B3LYP (11, 12) with the 6-31G(d,p) basis set (13) and using the PQS 3.0 (14) and Gaussian 98-03 (13) codes. The energies reported have no ZPVE corrections attached, both for consistency with ref. 1 and to maintain focus on the underlying potential energy surface (PES).

For a more zeolite-like aluminosilicate fragment, the 18-atom cluster $Al(OH)(OSiH_3)_3^-$ containing four tetrahedral atoms (denoted T4 model, T=Si, Al), was employed.

 doi:10.1139/V06-143 © 2006 NRC Canada

Compared with the T1 model $AlH_2(OH)_2^-$ used in our previous study (1), the T4 model can better represent the surface of a zeolite, having three surface oxygen atoms and each of these bonded to a silicon atom to make the electron density near the Al and the basicity of the oxygen atoms more realistic. This T4 model has been used in other quantum chemical studies as a zeolite mimic. For example, Svelle et al. used T4 to investigate methylation of methylbenzenes and alkenes by halomethanes and methanol over acidic zeolites (15, 16) and the dimerization of linear alkenes over acidic zeolites (4). Arstad et al. (17, 18) studied the methylation, ethylation, and iso-propylation of methylbenzenes on T4 zeolites. Moreover, Rozanska et al. (19, 20) showed that the relative order of the activation energies of isomerization and transalkylation reactions of toluene and xylenes is conserved when comparing results obtained from T4 with results from larger models using periodic boundary conditions and plane wave basis sets.

For a chloroaluminate ionic liquid fragment, $Al_2Cl_7^-$ was chosen as a first extension over the previously used $AlHCl_3^-$. This choice was motivated by the work in the Johnson group (21). Using B3LYP/6-31G(d,p), Hunter thoroughly examined ionic liquid ion cluster systems involving $AlCl_3$, pyridine (Pyr), and HCl in various ratios and the resulting energies suggested that $PyrH^+$, $Al_2Cl_7^-$, and $AlCl_4^-$ were the predominant species in these mixtures, with extra HCl units complexed to the anions (22).

Further extension of an ionic liquid model was explored using two- and three-fragment catalysis models. The two-fragment model employed both $AlHCl_3^-$ and $AlCl_4^-$ placed on either side of the hydrocarbon and was first tried in an exploration of intermediates (ref. 5, Fig. 9). Since this model produces an overall –1 charge for the system, a three-fragment overall-neutral model was also tested, simply by adding a Na^+ spectator ion to the model. These models were designed to explore the possibility of a lowering of the β-scission barrier by providing a more flexible product chemisorption site option.

As before, we refer to the conversion from chemisorbed to physisorbed structures as ascension and the opposite as descension. We will use single and double slashes to denote chemisorbed and physisorbed complexes, respectively, (eg. $C_6H_{13}^+/AlHCl_3^-$ vs. $C_6H_{13}^+//AlHCl_3^-$). Our atom-numbering convention will be to count the carbon atoms as C_1, C_2, C_3, C_4, and C_5, or for hexane cracking to C_6, such that the C_2 atom is initially bound to the O_1 or Cl_1 atom of the catalyst in the chemisorbed state. A common abbreviation we use is PCP^+ for protonated dialkylcyclopropane, the prevalent form of a physisorbed or gas-phase secondary carbenium ion.

Results

The Cartesian coordinates of the 22 new transition states are provided as Supplementary Material, for purposes of reproducibility.[2] Specific bond distances are not reported in this paper because the important ones hardly differ from the values reported earlier, found with smaller Al-O and Al-Cl anion models (1). The structural results are presented in this section; the energies are left for the Discussion section.

One-fragment catalyst models $T4^-$ and $Al_2Cl_7^-$

Seven transition states (and the minima they connect) were found for the reaction $C_5H_{11}^+ \rightarrow C_2H_5^+ + C_3H_6$ on the T4 zeolite catalyst fragment $Al(OH)(OSiH_3)_3^-$. Five of the seven steps are qualitatively the same as those observed with the T1 model (ref. 1, Figs. 1, 3, and 5). Images of the two qualitatively new steps appear in Fig. 1. The first one (top row), a physi-to-physi β scission, is in comforting agreement with Svelle et al. (4), who observed it with this T4 model and a smaller (6-31G(d)) basis set. Hence, β scission of chemisorbed $C_5H_{11}^+/T4^-$ first rises to physisorbed $C_5H_{10}//T4$, but then could step to either chemisorbed $C_2H_5^+$ or physisorbed C_2H_4. The second row of Fig. 1 shows an extra descension step for the C_2H_4 product, so that we can consider this physi-to-physi β-scission route as a step in a complete chemi-to-chemi mechanism (see Discussion).

Two transition states were found for the two-step scission of $C_6H_{13}^+$ on $AlCl_4^-$. They are no different qualitatively than the two steps found earlier on $AlHCl_3^-$ (1).

Five transition states were found for the reactions $C_5H_{11}^+ \rightarrow C_2H_5^+ + C_3H_6$ (two) and $C_6H_{13}^+ \rightarrow C_3H_7^+ + C_3H_6$ (three) on the $Al_2Cl_7^-$ fragment. Four are qualitatively the same as the two-step "2Cl" (involving two Cl atoms) pathways observed previously for both these carbenium ions on $AlHCl_3^-$ (1, 5). Images for the qualitatively new step appear in the bottom row of Fig. 1. In this step, a physi-to-chemi β-scission step, the physisorbed ion-pair $C_6H_{13}^+//Al_2Cl_7^-$ intermediate undergoes scission, isomerization (p-$C_3H_7^+$ to s-$C_3H_7^+$), and descension (to a chemisorbed s-$C_3H_7^+$ fragment). These three processes are concerted (all in the one step) but not fully synchronous, as the descension occurs in the later part of the step. A similar-looking transition state exists in the $AlHCl_3^-$ fragment pathway (5), but there the forward direction resulted in a proton transfer to the catalyst (generating $HCl{\cdot}AlHCl_2$) rather than to a neighbouring C atom. This discrepancy in product may be due to catalyst basicity or the orientations chosen. In any event, the higher barrier associated with this step (see Discussion) suggests that this isomerization step during β scission will be rare.

Two-fragment catalyst model $AlHCl_3^-$ + $AlCl_4^-$

Figure 2 shows 3D images of the stationary-point geometries obtained for the β scission $C_6H_{13}^+ \rightarrow C_3H_7^+ + C_3H_6$ catalyzed by separated $AlHCl_3^-$ + $AlCl_4^-$ fragments. This model system has an overall charge of –1.

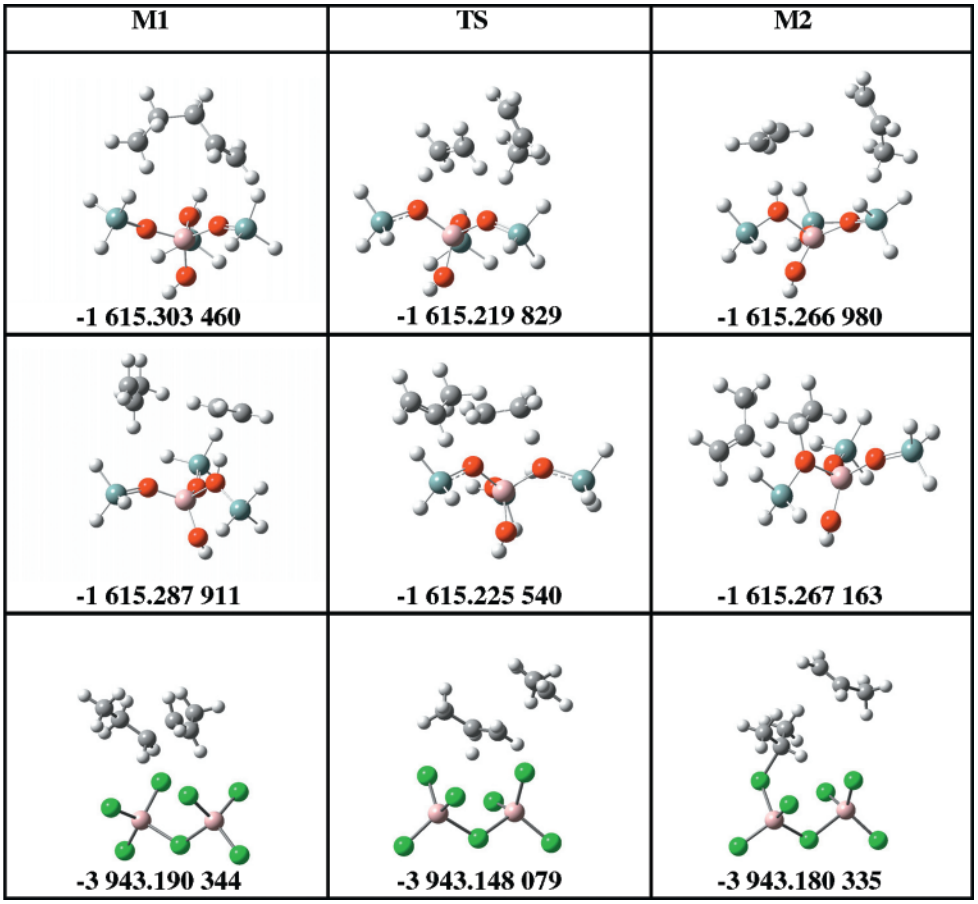
The top two rows of Fig. 2 show the two-step path, as seen with single-fragment catalysis. Here, $AlHCl_3^-$ was chosen as the chemisorbing fragment with $AlCl_4^-$ acting as a spectator fragment physisorbed near the reaction center.

In the third row, concerted one-step chemi-to-chemi β scission is observed, analogous to a one-step mechanism seen before (ref. 1, Fig. 9). Here in Fig. 2, $AlCl_4$ is the chemisorbing fragment with $AlHCl_3^-$ as the physisorbed spectator ion. The ascension of chemisorbed C2 from Cl1 occurs in concert with the S_N2-like migration of the C4 atom

[2] Supplementary data for this article are available on the journal Web site (http://canjchem.nrc.ca) or may be purchased from the Depository of Unpublished Data, Document Delivery, CISTI, National Research Council Canada, Ottawa, ON K1A 0R6, Canada. DUD 5088.

© 2006 NRC Canada

Fig. 1. B3LYP/6-31G(d,p) stationary points for the three qualitatively new steps observed for carbenium ion scission on single anion fragment models. Top row: physi-to-physi scission of 1-pentene on the T4 zeolite catalyst fragment. Middle row: descension of ethene to a chemisorbed ethenium ion. Bottom row: a one-step scission/isomerization/descension of $C_5H_{11}^+$ to C_3H_6 and a chemisorbed *s*-$C_3H_7^+$ fragment on $Al_2Cl_7^-$.



from C3 to Cl2. Subtleties in orientation of the initial structure likely control whether the β scission will be one-step or two-step, since the simpler $AlHCl_3^-$ single-fragment model also exhibited both possibilities (1).

In the last row of Fig. 2, we see another concerted one-step chemi-to-chemi β scission, but here the hydrocarbon migrates from one catalyst fragment ($AlCl_4^-$) to the other ($AlHCl_3^-$). This was the qualitatively new step we hoped to find with the two-fragment catalyst model.

Three-fragment catalyst model $Na^+ + AlHCl_3^- + AlCl_4^-$

Figure 3 shows 3D images of the stationary-point geometries obtained for β scission ($C_6H_{13}^+ \rightarrow C_3H_7^+ + C_3H_6$) in the presence of Na^+ as well as $AlHCl_3^-$ and $AlCl_4^-$ ions. The Na^+ was added to have a neutral charge model system for comparison to the negatively charged model of the previous section. Several choices for the location of the Na^+ ion were tested before settling on one particular choice.

The first two rows show the usual two-step mechanism seen in all chloroaluminate models, here having $AlCl_4^-$ as the chemisorbing fragment and $Na^+ \cdot AlHCl_3^-$ as a spectator complex. The only noteworthy item concerns the first minimum, which shows a peculiar rotation of the tight $Na^+ \cdot AlHCl_3^-$ complex that places the Na^+ near the hydrocarbon.

In the following two rows of Fig. 3, two different one-step chemi-to-chemi β scissions are presented. Unlike the ones in Fig. 2, however, *both* these examples involve a migration from one anion to another, the first from $AlCl_4^-$ to $AlHCl_3^-$ and vice versa for the second. To complicate matters, the addition of Na^+ to the model has created more variety of possible structures, including a saltlike catalyst surface (Fig 3., bottom row). This suggests that the use of three ions in explicit-contact modelling is still a poor model for mimicking liquid-phase transition states.

Discussion

β scission — The general mechanism and its finer details

Our convention considers the reactant and products to be chemisorbed because chemisorbed states are the lower-energy "storage states" of carbenium ions in the presence of oxide and chloride sites. This convention also allows a direct relationship between the reaction activation energy and the strength of the conjugate base of the original Bronsted catalyst (see later).

Given this convention, the general β-scission mechanism is shown in Fig. 4 and consists of three mechanistic components, ascension of the hydrocarbon (A), C–C bond scission

© 2006 NRC Canada

Fig. 2. B3LYP/6-31G(d,p) stationary points for scission of $C_6H_{13}^+$ catalyzed by $AlCl_4^-$ + $AlHCl_3^-$. Top row: ascension from $AlHCl_3^-$. Second row: scission and descension of physisorbed hexenium ion. Third row: one-step scission involving $AlCl_4^-$. Bottom row: one-step scission with migration from $AlCl_4^-$ to $AlHCl_3^-$.

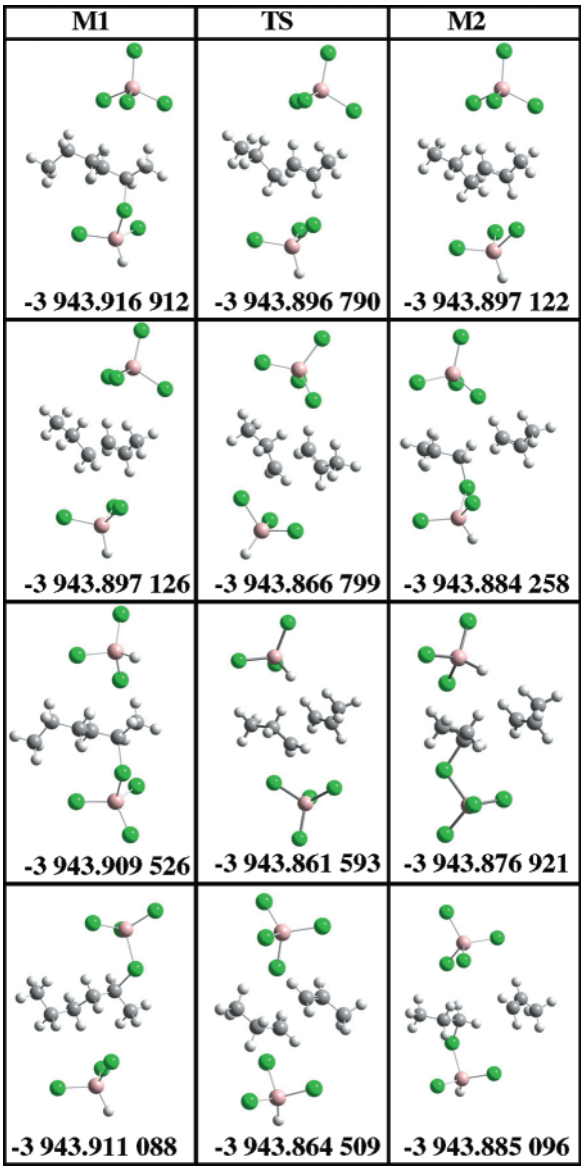
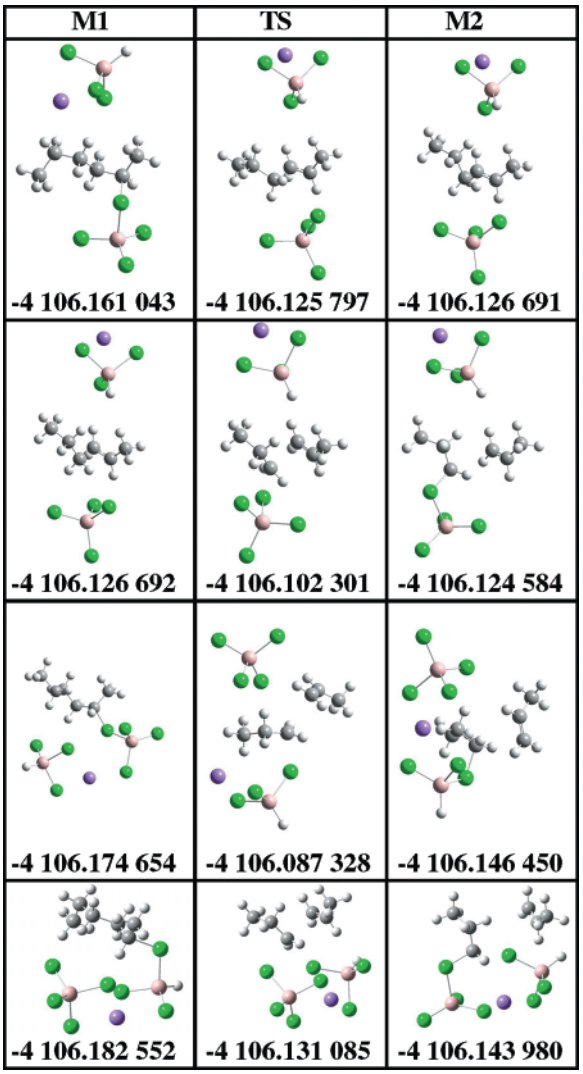


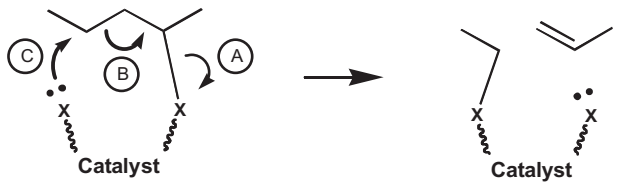
Fig. 3. B3LYP/6-31G(d,p) stationary points for scission of $C_6H_{13}^+$ catalyzed by Na^+ + $AlCl_4^-$ + $AlHCl_3^-$. Top row: ascension from $AlCl_4^-$. Second row: scission and descension of physisorbed hexenium ion. Third row: one-step scission with migration from $AlCl_4^-$ to $AlHCl_3^-$. Bottom row: one-step scission with migration from $AlHCl_3^-$ to $AlCl_4^-$ along a saltlike surface.



(B), and descension of the resulting primary carbenium ion product (C). In paper I (1), we found the mechanism to be two-step, with ascension to a higher-energy intermediate occurring as a separate step, followed by a concerted scission and descension step. From the work in this paper, we discover that the mechanism could also be one-step or even three-step, depending on catalyst and conformer orientation. Hence, we use the labels "ABC", "A,BC", and "A,B,C" to denote one-step, two-step, and three-step mechanisms.

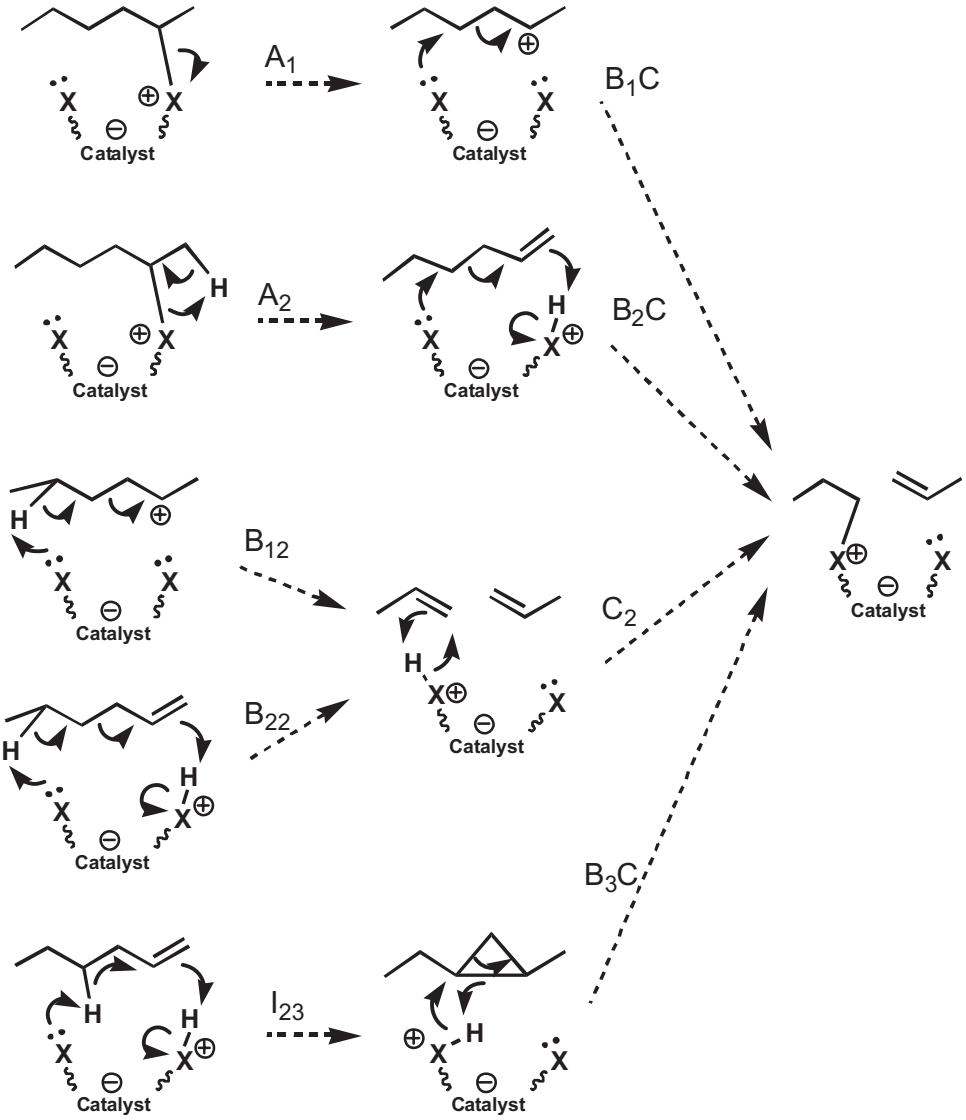
In addition, Paper I showed that there is some variation in the nature of the physisorbed intermediates. We will denote these here with subscripts, 1 for carbenium ions (PCP^+), 2 for alkenes, and 3 for cyclopropanes. Hence, A_1 will denote

Fig. 4. The general β-scission mechanism from chemisorbed reactant to chemisorbed product. The three components of the mechanism we call ascension (A), scission (B), and descension (C). The mechanism could be one-step, two-step, or three-step, depending on the degree of concertedness of these components.



© 2006 NRC Canada

Fig. 5. The various reaction steps seen to date in two-step and three-step β-scission mechanisms from B3LYP calculations using hexenium ion as the example. A, B, C are defined in Fig. 4, while I refers to an isomerization. The subscript labels refer to the type of physisorbed intermediate: 1, carbenium ion (PCP^+); 2, alkene; 3, dialkylcyclopropane.



ascension to a physisorbed PCP^+ ion and B_1C will denote concerted scission and descension of this PCP^+ ion. Fig. 5 shows the mechanism for each variation of the steps observed so far.

The B3LYP/6-31G(d,p) relative energies for present and previously published β-scission results are presented in Tables 1 (AlO-containing catalysts) and 2 (AlCl-containing catalysts). Several things are worth commenting on here. First, there is almost no difference in energetics between $C_5H_{11}^+$ and $C_6H_{13}^+$ β scission and there should be no qualitative differences in mechanism either; the A_2 ascensions found with $C_6H_{13}^+/AlHCl_3^-$ also likely exist with $C_5H_{11}^+/AlHCl_3^-$. Second, note the higher energy barriers for both A and BC steps on AlO-containing catalysts vs. AlCl-containing ones. Third, note the qualitative change in intermediates with AlCl-based catalysts; the intermediates can be carbenium ions (note the subscript 1's), unlike the ones with small AlO-based catalysts in which the intermediates are exclusively neutral (subscript 2's and 3's). This was emphasized in paper I and still holds true with the slightly larger catalyst fragments studied here. Fourth, note that the physisorbed carbenium ions of the AlCl-based systems are precariously stable, with barriers of less than 1 kcal mol^{-1} (1 cal = 4.184 J) to returning to the original chemisorbed state.

Single-fragment catalysis

There is a direct relationship between the overall activation barrier for the complete chemi-to-chemi β scission and the strength of the Lewis base sites on the catalyst. A simple indicator of the Lewis base strength of these sites is their proton affinity (PA): the higher the PA, the more basic the nucleophilic site must be. In our tables, we call this calculated PA the conjugate-base proton affinity (CBPA) to remind the reader that the original catalyst for C–C bond cracking is assumed to be a Bronsted acid that has been de-

© 2006 NRC Canada

Table 1. Relative and activation energies (E and E_a, in kcal mol^{-1}) for β-scission steps on AlO-containing catalysts.

Step label	Step	E (M1)	E (TS)	E (M2)	E_a
$C_5H_{11}^+$ on $AlH_2(OH)_2^-$ (CBPA = 338), ref. 1					
A_2	Ascension (1O path)	0.00	46.46	12.76	46.46
A_2	Ascension (2O path)	2.13	36.76	13.07	34.63
I_{23}	Pentene to dialkylcyclopropane	12.93	51.75	19.54	38.81
B_3C	Scission of dialkylcyclopropane	19.75	66.57	21.56	46.82
B_2C	Scission of pentene	12.61	66.75	21.34	54.15
$C_5H_{11}^+$ on $Al(OH)(OSiH_3)_3^-$ (CBPA = 311), this work					
A_2	Ascension (1O path)	0.00	41.70	10.53	41.70
A_2	Ascension (2O path)	0.93	34.22	10.66	33.29
I_{23}	Pentene to dialkylcyclopropane	10.67	44.15	17.56	33.47
B_3C	Scission of dialkylcyclopropane	17.57	60.00	21.01	42.43
B_2C	Scission of pentene	10.73	58.51	20.71	47.78
B_{22}	ph–ph Scission[a]	11.18	63.70	34.08	52.52
C_2	Descension of product[a]	33.97	60.11	20.94	26.14

Note: M1 = first minimum, TS = transition state, M2 = second minimum, and CBPA = conjugate-base proton affinity of the catalyst in kcal mol^{-1}, a measure of base strength (calcd. using B3LYP/6-31(d,p)).

[a]Structural images of these steps are presented in Fig. 1.

activated to its conjugate-base anion form before the β-scission reaction occurs. This consideration is not a moot one because these conjugate-base "catalyst fragments" actually inhibit, rather than accelerate, the β-scission reaction: the more basic the fragment, the more energy is required to rise from the chemisorbed state to the rate-determining transition state (which, in all cases, is an ion-pair complex). This apparent anomaly arises only when considering the β-scission reaction alone, for when the complete cracking of a neutral hydrocarbon is considered, these bigger barriers seen with stronger conjugate bases are actually bigger barriers in overall reactions with weaker acids.

Table 3 summarizes the overall ΔE and E_a values for complete chemi-to-chemi β scission on single-fragment catalysts, together with the CPBA values of the catalysts. The reaction energy is 20–22 kcal mol^{-1}, independent of catalyst. However, the activation barriers vary systematically with basicity of the catalyst, roughly following the linear relation E_a = CBPA/2 – 100. Curiously, an equally simple relation between the base strength and the E_a for simple ascension could not be found.

Aluminum chloride catalysis — Multiple-fragment models

For the two-fragment $AlHCl_3^-$ + $AlCl_4^-$ model (Table 2, 6th section), the first two rows describe the now familiar two-step β scission involving a single fragment ($AlHCl_3^-$ in this case with $AlCl_4^-$ as a spectator ion). The energies are closer to those of $Al_2Cl_7^-$ catalysis than $AlHCl_3^-$ catalysis. One-step chemi-to-chemi β scission was also found, analogous to the one-step scission on $AlHCl_3^-$ with no spectator anion, but with the two-fragment model the energies are closer to that of the two-step $Al_2Cl_7^-$ catalysis. Both of these two-fragment mechanisms give an overall ΔE of 20.5 kcal mol^{-1}, changing little from single-fragment models. The fourth row is the migratory two-fragment step we desired with ascension from $AlCl_4^-$ and descension of the product $C_3H_7^+$ onto $AlHCl_3^-$. The E_a dropped only from 30 to 29 kcal mol^{-1}, indicating little benefit to a two-fragment process. The noticeable decrease in ΔE, from 20.5 to 16.3 kcal mol^{-1}, is merely due to the change of the chemisorption host from a weaker base ($AlCl_4^-$) to a stronger one ($AlHCl_3^-$).

A further step in mimicking an ionic liquid might be to add a cation, making the entire model neutrally charged as it is in our single-fragment modelling. With Na^+ added to the $AlHCl_3^-$ side of the hydrocarbon, we again found the two-step mechanism (involving chemisorbed structures solely with $AlCl_4^-$). Interestingly, the energies for this (Table 2, 7th section) look more similar to those of $AlCl_4^-$ catalysis than those from two-fragment modelling with Na^+ absent. We tried to find two-fragment paths, but these revealed dramatic effects of the Na^+ ion. Saltlike structures of the inorganic ions were seen to offer 8–13 kcal mol^{-1} energy stabilization for the intermediates M1 and M2, for both one-step chemi-to-chemi paths. Such structures are more like solids than liquids and reveal the difficulties in trying to mimic ionic liquids in this way.

Conclusions

β scission, considered here to start and finish with carbenium ions chemisorbed to a catalyst, involves three fundamental components, which are ascension, bond scission, and descension. The lowest-energy pathways on AlO- and AlCl-containing catalyst fragments, as computed with B3LYP/6-31G(d,p), are generally two-step mechanisms, with ascension to a physisorbed intermediates preceding the concerted scission-plus-descension second step. A nearly linear relationship exists between the overall barrier height and the proton affinity of the anion catalyst fragment (the conjugate-base of the hypothetical original Bronsted-acid catalyst).

The extension of an AlO-containing catalyst model from $AlH_2(OH)_2^-$ to $Al(OH)(OSiH_3)_3^-$ reduces the catalyst basicity

© 2006 NRC Canada

Table 2. Relative and activation energies (E and E_a, in kcal mol^{-1}) for β-scission steps on AlCl-containing catalysts.

Step label	Step	E (M1)	E (TS)	E (M2)	E_a
$C_5H_{11}^+$ on $AlHCl_3^-$ (CBPA = 276), ref. 1					
A_1	Ascension	0.00	25.28	24.34	25.28
B_1C	Scission	24.34	38.43	21.27	14.09
ABC	ch-ch Scission	0.02	39.66	21.56	39.64
$C_6H_{13}^+$ on $AlHCl_3^-$ (CBPA = 276), ref. 5					
A_1	Ascension	0.00	23.93	23.19	23.93
B_1C	Scission	23.19	37.00	20.23	13.81
A_2	Ascension to 2-hexene (1Cl)	–0.45	25.66	15.76	26.11
A_2	Ascension to 2-hexene (2Cl)	–1.34	18.19	14.89	19.54
B_{12}	ph-ph Scission	22.57	44.76	37.35	22.19
$C_6H_{13}^+$ on $AlCl_4^-$ (CBPA = 268), this work					
A_1	Ascension	0.00	22.07	21.54	22.07
B_1C	Scission	21.54	35.99	20.45	14.45
$C_5H_{11}^+$ on $Al_2Cl_7^-$ (CBPA = 259), this work					
A_1	Ascension	0.00	12.11	11.33	12.11
B_1C	Scission	11.32	29.97	22.33	18.65
$C_6H_{13}^+$ on $Al_2Cl_7^-$ (CBPA = 259), this work					
A_1	Ascension	0.00	10.92	10.42	10.92
B_1C	Scission	10.42	28.46	21.31	18.04
$B_1I_{ps}C$	Scission + isomerization[a]	10.66	37.20	16.94	26.54
$C_6H_{13}^+$ on $AlHCl_3^-$ + $AlCl_4^-$, this work, Fig. 2					
A_1	Ascension	0.00	12.64	12.43	12.64
B_1C	Scission	12.43	31.47	20.51	19.05
ABC	ch-ch One fragment scission	4.64	34.74	25.11	30.10
ABC	ch-ch Two fragment scission	3.66	32.91	19.98	29.25
$C_6H_{13}^+$ on Na^+ + $AlHCl_3^-$ + $AlCl_4^-$, this work, Fig. 3					
A_1	Ascension	0.00	22.13	21.57	22.13
B_1C	Scission	21.57	36.89	22.90	15.32
ABC	ch-ch Two fragment scission	–8.55	46.29	9.16	54.84
ABC	ch-ch Salt scission	–13.51	18.81	10.72	32.32

Note: M1 = first minimum, TS = transition state, M2 = second minimum, and CBPA = conjugate-base proton affinity of the catalyst in kcal mol^{-1}, a measure of base strength (calcd. using B3LYP/6-31(d,p)).

[a]Structural images of this step is presented in Fig. 1.

Table 3. Overall reaction energies and activation energies for chemi-to-chemi β scission (ΔE and E_a, in kcal mol^{-1}) on single-fragment AlO- and AlCl-containing catalyst anion fragments.

Catalyst	Mechanism	CBPA	E_a	ΔE
$AlH_2(OH)_2^-$	A_2,B_2C	338	67	21
$Al(OH)(OSiH_3)_3^-$	A_2,B_2C	311	59	21
$AlHCl_3^-$	A_1,B_1C	276	37–38	20–21
$AlCl_4^-$	A_1,B_1C	268	36	20
$Al_2Cl_7^-$	A_1,B_1C	259	28–30	21–22

Note: For each catalyst, the lowest-energy pathway to lowest-energy products is considered. CBPA = conjugate-base proton affinity of the catalyst in kcal mol^{-1}, a measure of base strength (calcd. using B3LYP/6-31(d,p)).

but not enough to change qualitative aspects of the reaction. The physisorbed intermediates are neutral-pair complexes of either alkene or disubstituted cyclopropane with catalyst, with two-step or three-step mechanisms observed to date. The overall barrier for β scission from the chemisorbed state is lowered from 67 to 59 by using the larger and less basic anion model.

Chloroaluminate catalysis of the β-scission reaction is also hardly changed qualitatively with moderate extension of the models. The physisorbed intermediates that lead to C–C scission are ion-pair $PCP^+//Al_xCl_y^-$ complexes present with each catalyst model, which are always bound by less than 1 kcal mol^{-1} relative to descension to a chemisorbed state. Hence, the formally two-step A_1,B_1C mechanisms might kinetically appear little different from the one-step chemi-to-chemi β-scission paths, which have been found in both

© 2006 NRC Canada

single-fragment and multiple-fragment modelling. Finally, a truly liquid state proved difficult to mimic with multiple ions, which tended to form saltlike (crystalline) complexes on one side of the hydrocarbon.

Acknowledgments

This research was funded by Natural Sciences and Engineering Research Council of Canada (NSERC) and the Canada Foundation for Innovation (CFI). The Laboratory of Computational Discovery (University of Regina) is thanked for computational resources.

References

1. Q. Li and A.L.L. East. Can. J. Chem. **83**, 1146 (2005).
2. M.V. Frash, V.B. Kazansky, A.M. Rigby, and R.A. van Santen. J. Phys. Chem. B, **102**, 2232 (1998).
3. P.J. Hay, A. Redondo, and Y. Guo. Catal. Today, **50**, 517 (1999).
4. S. Svelle, S. Kolboe, and O. Swang. J. Phys. Chem. B, **108**, 2953 (2004).
5. Q. Li, K.C. Hunter, and A.L.L. East. J. Phys. Chem. A, **109**, 6223 (2005).
6. T. Demuth, X. Rozanska, L. Benco, J. Hafner, R. A. van Santen, and H. Toulhoat. J. Catal. **214**, 68 (2003).
7. G. Mills, H. Jonsson, and G.K. Schenter. Surf. Sci. **324**, 305 (1995).
8. C. Lim, D. Bashford, and M. Karplus. J. Phys. Chem. **95**, 5610 (1991).
9. C.P. Kelly, C.J. Cramer, and D.G. Truhlar. J. Phys. Chem. A, **110**, 2493 (2006).
10. M. Namazian, F. Kalantary-Fotooh, M.R. Noorbala, D.J. Searles, and M.L. Coote. THEOCHEM. **758**, 275 (2006).
11. A.D. Becke. J. Chem. Phys. **98**, 5648 (1993).
12. C. Lee, W. Yang, and R.G. Parr. Phys. Rev. B, **37**, 785 (1988).
13. M.J. Frisch, G.W. Trucks, H.B. Schlegel, G.E. Scuseria, M.A. Robb, J.R. Cheeseman, V.G. Zakrzewski, J.A. Montgomery, R.E. Stratmann, J.C. Burant, S. Dapprich, J.M. Millam, A.D. Daniels, K.N. Kudin, M.C. Strain, O. Farkas, J. Tomasi, V. Barone, M. Cossi, R. Cammi, B. Mennucci, C. Pomelli, C. Adamo, S. Clifford, J. Ochterski, G.A. Petersson, P.Y. Ayala, Q. Cui, K. Morokuma, D.K. Malick, A.D. Rabuck, K. Raghavachari, J.B. Foresman, J. Cioslowski, J.V. Ortiz, B.B. Stefanov, G. Liu, A. Liashenko, P. Piskorz, I. Komaromi, R. Gomperts, R.L. Martin, D.J. Fox, T. Keith, M.A. Al-Laham, C.Y. Peng, A. Nanayakkara, C. Gonzalez, M. Challacombe, P.M.W. Gill, B.G. Johnson, W. Chen, M.W. Wong, J.L. Andres, M. Head-Gordon, E.S. Replogle, and J.A. Pople. Gaussian 98. Rev. A.9 [computer program]. Gaussian Inc., Pittsburgh, Penn. 1998.
14. PQS 3.0 [computer program]. Parallel Quantum Solutions, Fayetteville, Ark. 2004.
15. S. Svelle, S. Kolboe, U. Olsbye, and O. Swang. J. Phys. Chem. B, **107**, 5251 (2003).
16. S. Svelle, B. Arstad, S. Kolboe, and O. Swang. J. Phys. Chem. B, **107**, 9281 (2003).
17. B. Arstad, S. Kolboe, and O. Swang. J. Phys. Chem. B, **106**, 12722 (2002).
18. B. Arstad, S. Kolboe, and O. Swang. J. Phys. Chem. B, **108**, 2300 (2004).
19. X. Rozanska, X. Saintigny, R.A. van Santen, and F. Hutschka. J. Catal. **202**, 141 (2001).
20. X. Rozanska, R.A. van Santen, F. Hutschka, and J. Hafner. J. Am. Chem. Soc. **123**, 7655 (2001).
21. J.L. Campbell and K.E. Johnson. J. Am. Chem. Soc. **117**, 7791 (1995).
22. K.C. Hunter. M. Sc. Thesis, University of Regina, Regina, Sask. 2002.

© 2006 NRC Canada

Some oxidation products of lycoctonine revisited

Doaa Abdelrahman, Michael Benn, Ryan Hellyer, Masood Parvez, and Oliver E. Edwards

Abstract: The structure of a chromic acid oxidation product of the norditerpenoid alkaloid lycoctonine (**1**) was established as hydroxylycoctonal (**3**) by spectrometric analyses and X-ray crystallography of its reduction product, hydroxylycoctonine (**5**); the structure of lycoxonine, a chromic acid oxidation product of the lactam, lycoctonam (**7**), was similarly confirmed as *N*-ethyl-4,7,8-trihydroxy-1α,6β,14α,16β-tetramethoxy-19-oxoaconitane (**8**). Reduction of lycoxonine with lithium aluminium hydride gave the 1,14-di-*O*-methyl ether (**12**) of the bisnorditerpenoid alkaloid delbine (**9**).

Key words: norditerpenoid, bisnorditerpenoid, alkaloids, lycoctonine, lycoctonam, hydroxylycoctonal, lycoxonine. 1,14-di-*O*-methyldelbine, semisynthesis.

Résumé : Faisant appel à des analyses spectroscopiques et à la diffraction des rayons X sur son produit de réduction, l'hydroxylycoctonine (**5**), on a établi que le produit d'oxydation à l'aide de l'acide chromique de l'alcaloïde norditerpénoïde lycoctonine (**1**) correspond à l'hydroxylycoctonal (**3**); de la même manière, on a établi que la lycoxonine, un produit d'oxydation chromique de la lactame, lycoctoname (**7**), correspond au *N*-éthyl-4,7,8-trihydroxy-1α,6β,14α,16β-tétraméthoxy-19-oxoaconitane (**8**). La réduction de la lycoxonine à l'aide d'hydrure double de lithium et d'aluminium conduit à l'éther 1,14-di-*O*-méthyle (**12**) de l'alcaloïde bisnorditerpénoïde, delbine (**9**).

Mots clés : norditerpénoïde, bisnorditerpénoïde, alcaloïdes, lycoctonine, lycoctoname, hydroxylycoctonal, lycoxonine, 1,14-di-*O*-méthyldelbine, semisynthèse.

[Traduit par la Rédaction]

Introduction

We report here the solutions to two long-standing puzzles in the chemistry of the alkaloid lycoctonine.

Initially described in 1886 as a constituent of *Aconitum lycoctonum* L (1), lycoctonine (**1**) is also the parent aminopolyol core of various ester-alkaloids present in this and other species of *Aconitum* and *Delphinium*. About 50 years ago, during the work directed at establishing the structures of these alkaloids, several of which are pharmacologically active, the oxidation products of lycoctonine received much attention (2–5) and it was X-ray crystallography of one such derivative at the National Research Council (NRC) in Ottawa (6) that first established the norditerpenoid skeleton that characterizes them. However, at that time the techniques for separations and spectrometric characterizations that are now routinely employed were unavailable and several products were left poorly characterized. We have had occasion to reexamine two such substances with the results that we now describe.

Received 16 June 2006. Accepted 8 September 2006. Published on the NRC Research Press Web site at http://canjchem.nrc.ca on 31 October 2006.

D. Abdelrahman, M. Benn,[1] R. Hellyer, and M. Parvez. Department of Chemistry, University of Calgary, 2500 University Drive, N.W., Calgary, AB T2N 1N4, Canada. **O.E. Edwards.** 678 Portage Ave., Ottawa, ON K1G 1T4, Canada.

[1]Corresponding author (e-mail: benn@ucalgary.ca).

Results and discussion

The first of these compounds had been encountered as a side product during the preparation of the aldehyde lycoctonal (**2**) by the oxidation of **1** with sodium dichromate in acetic acid. This procedure afforded **2** as crystalline hydrate in about 55% yield along with another base (**3**), which resisted crystallization but gave a crystalline perchlorate salt (**4**).

When it was isolated in 1959, the only data collected for this salt were an elemental analysis and an IR spectrum that contained an intense carbonyl-stretch absorption band. Recently, reinvestigation of this product revealed the presence of an aldehyde attached to a quaternary centre, as shown by NMR signals (δ_H 9.20 (1H, s) and δ_C 201.5 (*d*) ppm, cross-correlated in a HMQC spectrum). Additionally, the ^{1}H NMR spectrum contained signals for an ethyl and four methoxyl groups, while the ^{13}C NMR spectrum contained a total of 25 resonances (shown by DEPT-90 and 135 spectra to be due to 5 methyls, 6 methylenes, 10 methines, and 4 quaternary carbons). This implied that all the carbons of **1** were present in the product. Also notable were the presences in the ^{13}C NMR spectrum of a methine resonance at δ_C 183.9, which cross-correlated in HMQC spectra with a proton signal at δ_H 8.79 (1H, br s), and a quaternary carbon at δ_C 210.4 ppm. Strikingly, when **4** was converted to the free base (**3**) these signals disappeared, although that of the aldehyde (now δ_C 203.4, δ_H 9.44 ppm) remained. As before, the free base (**3**) was shown to be comprised of 5 methyls, 6 methylenes, 10 methines, and 4 quaternary carbons. When compared with the ^{13}C NMR data for **1** it was seen that a quaternary-

 doi:10.1139/V06-144 © 2006 NRC Canada

carbon resonance ascribed to C-7 had moved downfield from 88.3 to 96.0 ppm, although the resonance ascribed to C-8 showed little difference (77.3 ppm in **3**, 77.5 ppm in **1**).

These findings recalled hydroxylycoctonine (**5**), an unfortunately named compound prepared by the oxidation of lycoctonine with silver(I) oxide (2, 3), lead(IV) acetate (7), or potassium ferricyanide (2). Upon treatment with strong acid this forms ring-opened immonium ion salts (**6**), which, upon basification in aqueous media, hydrate and recyclise to **5** (8, 9). Thus, our observations were consistent with **3** being hydroxylycoctonal, the aldehyde of **5,** and **4** being the corresponding ring-opened immonium ion salt. That this was correct was demonstrated by the sodium borohydride reduction of **3** to provide in high yield a crystalline dihydro product, whose structure was proven to be hydroxylycoctonine (**5**) by X-ray crystallography and comparison with authentic material.

The formation of hydroxylycoctonal (**3**) in the Cr(VI) oxidation of lycoctonine (**1**) can be rationalized in terms of the formation of a chromate ester at C-7, the fragmentation of which affords an immonium ketone that upon work-up yields the hydroxybase. We did not observe hydroxylycoctonine (**5**) among the products of our oxidation of lycoctonine, which suggests that hydroxylycoctonal (**3**) is mainly, if not entirely, formed as an overoxidation product of lycoctonal (**2**) rather than by oxidation of the primary alcohol function of **5**.

In contrast to its behaviour with chromic acid, oxidation of lycoctonine with permanganate in neutral, weakly acidic, or alkaline solution affords the lactam, lycoctonam, 19-oxolycoctonine (**7**), a matter to which we will return. Suginome et al. (5) reported that the further oxidation of this product with chromic acid gave another neutral substance, lycoxonine, isolated as a crystalline hydrate together with formic acid. Microanalyses, including Zeisel and Hertzig–Meyer procedures, suggested that lycoxonine had the elemental composition $C_{24}H_{37}NO_8$ and contained an *N*-ethyl and four methoxyl groups. When heated with acetyl chloride or acetic anhydride, lycoxonine hydrate yielded a monoacetyl anhydro compound, which could be deacetylated to afford anhydrolycoxonine. These observations were taken to indicate that the di-tertiary 7,8-diol system of lyoctonam was still present in lycoxonine, i.e., the anhydro compound was formed via a pinacolic rearrangement. Largely on the basis of this information, Suginome proposed that lycoxonine had the structure (**8**) (5).

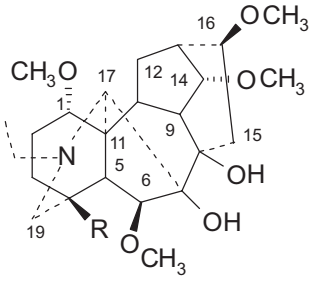
Relatively recently, this bisnorditerpenoid skeleton has been encountered in some *Delphinium* alkaloids, e.g., delbine (**9**), isolated from *Delphinium bonvalottii* Franchet (10). As Suginome's lycoxonine appeared to afford a semisynthetic entry to such alkaloids, we reinvestigated its preparation and structure.

The immediate precursor, lycoctonam (**7**), was originally prepared by adding solid potassium permanganate to a solution of lycoctonine in aqueous acetone containing acetic acid to prevent the reaction mixture becoming strongly alkaline as potassium hydroxide is generated (3). Suginome et al. (5) reported better yields when the acetic acid was omitted, but when we repeated their procedure, which involves leaving the reaction mixture overnight, we found that diacetone alcohol was formed in considerable amount, complicating the work-up. Subsequently, the NRC group showed that norditerpenoid alkaloids carrying a 6-methoxyl substituent were rapidly oxidized by a solution of potassium permanganate in aqueous acetone with the outcome determined by the orientation of the methoxyl; a β geometry steered the products towards lactams. Lycotonam (**7**) was obtained from lycoctonine (**1**) by this procedure in very high yield within 4 min (11). We found that a similarly fast and efficient nonaqueous oxidation was obtained by adding benzyltriethylammonium permanganate (12) in dichloromethane to lycoctonine in the same solvent. When benzyltriethylammomium chloride was used as a phase-transfer catalyst in a two-phase water–dichloromethane system with lycoctonine and potassium permanganate, the result was the same. The catalyst is known to be unstable in an alkaline solution and this induced us to try the two-phase oxidation without it. After a brief induction period the oxidation was complete within a few minutes. Following the destruction of excess reagent and manganese dioxide with dilute sulfuric acid and sodium metabisulfite, the only product isolated upon removal of the dichloromethane was **7**, formed in the same high yield as in the procedure of Achmatowicz et al. (11). The work–up of the two-phase reaction is simpler than that of the homogeneous aqueous acetone oxidation and it became our preferred route for conversion of **1** to **7**.

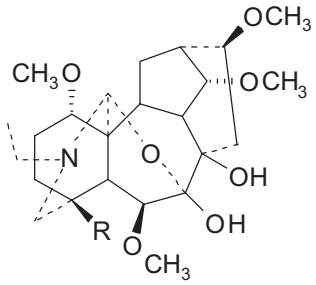
As Strassner and Houk have commented (13), although potassium permanganate is a venerable reagent remarkably little is known about the mechanistic details of the oxidations that it performs. In those oxidations that produce manganese(IV) oxide a three-electron reduction process is involved, indicating a multistep process, as with oxidations involving the reduction of Cr(VI) to Cr(III). For the oxidation of hydrocarbons there is evidence that the initial step involves hydrogen atom abstraction by the permanganate anion (14). In the oxidations of amines in nonaqueous media, the amide oxygen derives from the reagent and it seems reasonable to suppose that this is generally true. The selectivity seen in the oxidation of tertiary amines can then be rationalized either by an initial hydrogen atom transfer from a site adjacent to nitrogen (which would stabilize the resultant radical more than that obtained by abstraction from some other site) to give a radical pair that collapses ("oxygen rebound") to form a manganate(V) ester in a process similar to that proposed for the oxidations of hydrocarbons with permanganate (13, 14), or via an initial one-electron transfer from nitrogen to permanganate anion followed by a hydrogen atom transfer to generate an immonium ion and a manganate(V) anion that combine to yield the ester. Direct evidence that the H transfer step is rate-controlling is provided by the observation of a substantial kinetic isotope effect in the hexadecyltrimethylammonium permanganate oxidation of α-deuterated benzylamines in dichloromethane (15).

The manganate ester might fragment reversibly to the immonium ion pair or irreversibly to form an amide and an Mn(III) species, which then reacts with permanganate to form Mn(IV) dioxide and a manganate(VI) ion. Amide formation dominates in the case of lycoctonine (**1**), but the intermediacy of an immonium ion has been invoked (16) to account both for the N-dealkylations sometimes observed when the permanganate oxidation of other diterpenoid alkaloids is conducted in aqueous media (trapping of water gen-

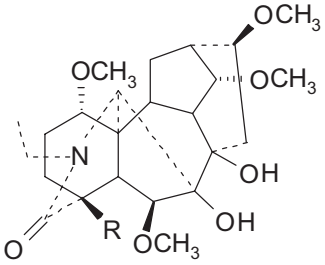
© 2006 NRC Canada



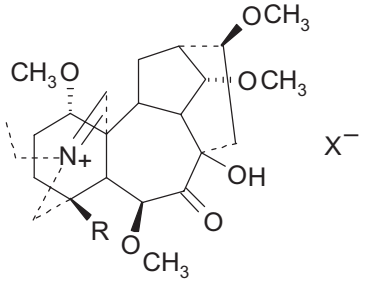
1 R = CH_2OH
2 R = CHO



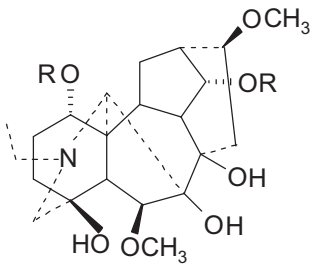
3 R = CHO
5 R = CH_2OH



7 R = CH_2OH
8 R = OH
10 R = CHO
11 R = CO_2H



4 R = CHO, X= ClO_4^-
6 R = CH_2OH



9 R = H
12 R = CH_3

erates a carbinolamine, which then decomposes to aldehyde and secondary amine) and for the fact that intramolecular cyclisation to a carbinolamine-ether may occur when when a hydroxyl group is in suitable proximity to the nitrogen (via its trapping by the immonium ion).

Suginome et al. (5) did not specify the ratio of chromic acid to lycoctonam used for their preparation of lycoxonine but when we used a 3:4 ratio of lycoctonam to chromium trioxide (in accordance with eq. [1]) we obtained a neutral crystalline product in about the same yield as they had reported.

[1] $3R_3CCH_2OH + 4CrO_3 + 12\ H^+ \rightarrow 3R_3COH + 3HCOOH + 4Cr^{3+} + 6H_2O$

The ^1H and ^{13}C NMR spectra of our product were in accord with the structure proposed for lycoxonine. In particular, there were only 24 ^{13}C resonances of which 3 could be attributed to tert alcohols and there was no longer one corresponding to the carbon of a hydroxymethylene group. The matter was clinched by X-ray crystallography, which revealed the structure of our product to indeed be **8**, as proposed by Suginome (5).

No explanation was suggested for the formation of **8**; however, carbon–carbon bond fission accompanying chromium(VI) oxidations of alcohols are precedented (17, 18). The mechanism of the reaction appears to involve a homolytic process induced by chromium(IV), evidence for which includes the inhibition of the cleavage reaction by oxalic acid (18). When we carried out the oxidation of

© 2006 NRC Canada

lycoctonam in aqueous acetone in the the presence of oxalic acid, as described by Müller and Blanc (19), there was nearly complete suppression of lycoxonine formation, the major products now being lycoctonamal (**10**) and lycoctonamic acid (**11**) together with recovered lycoctonam (**7**). As another experiment revealed that chromic acid oxidized lycoctonamal to lycoctonamic acid, rather than lycoxonine, we excluded the possibility that **8** was formed via a Baeyer–Villiger type cleavage involving a chromate ester of hydrated lycoctonamal and conclude that it is, as in other such cases, the result of chromium(IV) oxidation of the alcohol **7.**

Lithium aluminum hydride reduction of lycoxonine then afforded **12**, which corresponds to the 1,14-di-*O*-methyl ether of delbine. Variations in the extent of the degree of methoxylation are commonly observed in the norditerpenoid alkaloids so although **12** has not yet been isolated from a plant source we predict that it will be ultimately be discovered as a natural product.

Experimental

General procedures

NMR spectra were collected using a Bruker DRX 400 spectrometer (400 MHz ^{1}H, 100 MHz ^{13}C) in $CDCl_3$, using residual $CHCl_3$ (δ_H 7.25 ppm) and the centre line of the $CDCl_3$ multiplet (δ_C 77.0 ppm) as internal references. Sodium 3-(trimethylsilyl)propionate-2,2,3,3-d_4 was used as reference for solutions in D_2O. Melting points were measured with a Leitz hot-stage microscope and are uncorrected. Analytical and preparative TLC were carried out using Merck silica gel 60 F254 on glass plates (5 cm × 20 cm × 0.25 mm and 20 cm × 20 cm × 0.25 mm respectively), using I_2/silica gel powder (20) to detect spots and locate bands by the dusting of PTLC plate edges. Column chromatography was performed using Woelm neutral alumina, activity III. Lycoctonine (**1**) was isolated by saponifying methyllycaconitine obtained from *Delphinium glaucum* growing locally in the foothills of the Rocky Mountains (21). It was obtained as the crystalline hydrate, mp 112 to 113 °C, with ^{1}H and ^{13}C NMR spectra as recorded in the literature (22).

Hydroxylycoctonal (3)

(*a*) Lycoctonine (5 g) was dissolved in acetic acid (150 mL) and divided into 10 aliquots. To each of these was added a 5% (*w*/*v*) solution of $Na_2Cr_2O_7{\cdot}5H_2O$ in acetic acid (2.3 mL) over a period of 3 h. After another 4 h, by which time all of the oxidant appeared to have been reduced, the aliquots were combined and the bulk of the solvent removed under reduced pressure. The dark green residual solution was diluted with 1.5 mol/L aq. H_2SO_4 and extracted with $CHCl_3$ (5 × 30 mL). The combined $CHCl_3$ extracts were backwashed with 0.5 mol/L aq. H_2SO_4 (30 mL) and water (30 mL). Sufficient ice was added to the combined aqueous extract and washings to chill the mixture to below RT. Concentrated aqueous ammonia (ca. 17 mol/L) was added dropwise until the mixture was alkaline (pH 10–12, indicator paper) and the solution was then extracted with $CHCl_3$ (7 × 30 mL). The combined $CHCl_3$ extracts were dried (MgSO4) and the solvent removed to give a pale yellow glass (4.7 g). This was taken up in a little hot MeOH (ca. 3 mL) and hot water was added dropwise until permanent turbidity was just apparent. Crystals of lycoctonal (**2**) slowly separated and after the suspension had been kept overnight at RT, these were collected by filtration and air-dried (2.44 g). An additional amount of crystals (0.31 g) was obtained by evaporation of the mother liquors, redisolving the residue in MeOH, and adding H_2O as before. Total yield ca. 55% (2.75 g), mp 90–93 °C. ^{1}H NMR δ_H: 9.46 (1H, s), 3.58 (3H, m), 3.39 (3H, s), 3.32 (3H, s), 3.25 (3H, s), 3.17 (1H, m), 3.1–2.8 (6H, m), 2.78 (1H, d, J = 12.4 Hz), 2.58 (1H, dd, J = 9.0 and 15.3 Hz), 2.41 (1H, dd, J = 4.6 and 14.3 Hz), 2.32 (1H, dd, J = 4.6 and 16.1 Hz), 2.1 (2H, br m), 2.05–1.8 (3H, m), 1.63 (2H, m), 1.5 (1H, m), 1.05 (3H, t, J = 7.1 Hz). ^{13}C NMR δ_C: 203.7d, 91.9d, 88.5s, 83.8d, 83.6d, 82.6d, 77.6s, 64.7d, 59.3q, 57.8q, 56.3q, 56.0q, 50.9t, 49.9t, 49.7s, 48.8d, 48.4s, 46.0d, 43.3d, 38.1d, 33.5t, 29.9t, 29.0t, 25.2t, 14.0q.

Attempts to obtain more crystalline material by further concentration of the mother liquors was unsuccessful so these were taken to dryness under reduced pressure and the residue distributed between aqueous citric acid – sodium dihydrogen phosphate buffer (pH 6.6, 30 mL) and benzene (30 mL). The benzene extract was re-extracted with the buffer solution (pH 6, 30 mL) and both aqueous extracts were backwashed with benzene (30 mL). The combined benzene extracts and washings were then washed with 1 mol/L aq. NH_4OH, dried ($MgSO_4$), and evaporated to give a colourless glass (0.66 g). This was dissolved in MeOH (2 mL) and treated with a solution of 70% aq. $HClO_4$ (0.25 mL) in MeOH (2 mL) until pH 2 to 3 (indicator paper) to yield crystalline hydroxylycoctonal perchlorate (**4**) (0.22 g). Melting point 208–210 °C. IR (KBr, cm^{-1}) ν_{max}: 3998 br s, 2933s, 2830s, 1731s. ^{1}H NMR (D_2O) δ_H: 9.20 (1H, s), 8.79 (1H, br s), 4.4–4.0 (6H, m), 3.64 (4H, m), 3.47 (3H, s), 3.41 (3H, s), 3.33 (3H, s), 3.21 (3H, s), 2.97 (1H, m), 2.77 (1H, d, J = 9.8 Hz), 2.66m (1H, m), 2.54 (3H, m), 1.96 (1H, d, J = 16.8 Hz), 1.95–1.7 (2H, m), 1.59 (3H, t, J = 7.2 Hz), 1.45 (1H, m), 1.12 (1H, m). ^{13}C NMR δ_C: 210.4s, 201.5d, 183.9d, 89.8d, 87.0d, 82.2s, 81.7d, 81.6d, 61.5t, 61.1q, 60.7q, 60.6q, 59.4q, 56.3t, 53.4s, 50.3s, 44.0d, 42.7d, 42.2d, 37.9d, 35.0t, 32.8t, 31.5t, 26.3t, 16.0q.

Hydroxylycoctonal (**3**) was obtained from the salt by suspending it in 1 mol/L aq. Na_2CO_3 followed by extraction with $CHCl_3$. Removal of the solvent from the dried ($MgSO_4$) $CHCl_3$ extracts gave the free base as a colourless glass, which resisted crystallization. IR ($CHCl_3$, cm^{-1}) ν_{max}: 1725. ^{1}H NMR δ_H: 9.44 (1H, s), 4.83 (1H, s), 3.66 (1H, t, J = 4.5 Hz), 3.40 (3H, s), 3.39 (3H, s), 3.30 (3H, s), 3.25 (3H, s), 3.20 (1H, m), 3.04 (1H, dd, J = 6.2 and 10.9 Hz), 3.0 (1H, br d, J = 12.6 Hz), 2.85 (1H, dq, J = 7.1 and 12.9 Hz), 2.7–2.5 (4H, m), 2.38 (1H, m), 2.17 (1H, m), 2.05 (1H, dq, J = 7.1 and 12.9 Hz), 2.0–1.8 (3H, m), 1.7–1.5 (4H, m), 1.08 (3H, t, J = 7.1 Hz). ^{13}C NMR δ_C: 203.4d, 96.0s, 88.7d, 87.1d, 85.9d, 84.4d, 82.5d, 78.0s, 60.6q, 57.8q, 56.8q, 56.4q, 49.5s, 48.4t, 49.0d, 47.1t, 44.9d, 44.0d, 42.4s, 38.1d, 33.0t, 29.8t, 29.5t, 23.9t, 12.9q. HR EI-MS *m*/*z* for $C_{25}H_{39}NO_8$: 481.2698; req. 481.2676.

(*b*) To a magnetically stirred solution of lycoctonine hydrate (500 mg) dissolved in AcOH (7.5 mL) was added a 5% (*w*/*v*) solution of $Na_2Cr_2O_7{\cdot}5H_2O$ in AcOH (1.5 mL). After 1 h, more oxidant (1 mL) was added and after a further 3 h a

© 2006 NRC Canada

little more (0.2 mL). The mixture was allowed to stir for a total of 5 h and then poured into H_2O (50 mL) containing $Na_2S_2O_5$ (25 mg). The solution was acidified (pH 1, indicator paper) with 3 mol/L aq. H_2SO_4 and extracted with $CHCl_3$ (3 × 20 mL) to removed neutral byproducts, then made alkaline with Na_2CO_3 (s) (pH 9 to 10, indicator paper) and extracted with $CHCl_3$ (3 × 25 mL). After removal of solvent, the combined dried (Na_2SO_4) $CHCl_3$ extracts gave the basic products as a colourless glass (411 mg). TLC ($CHCl_3$–MeOH, 7:1 *v/v*) revealed 3 major components, R_F 0.15, 0.51, and 0.70. A portion of the mixture (ca. 20 mg) was subjected to PTLC on a 20 cm × 20 cm × 0.25 mm plate of Merck silica gel 60 F254, using the same solvent system. The individual components were then examined by NMR. This resulted in the following identifications: R_F 0.10, lycoctonine (**1**) (5 mg); R_F 0.45, lycoctonal (**2**) (13 mg); and R_F 0.70, hydroxylycoctonal (**3**) (4 mg).

Sodium borohydride reduction of hydroxylycoctonal — Formation of hydroxylycoctonine (5)

The free base (404 mg) obtained by chloroform extraction of a solution of the perchlorate salt in water, which was basified with aq. 1 mol/L Na_2CO_3, was dissolved in MeOH (15 mL) and $NaBH_4$ (100 mg) was added in 3 equal portions at 10 min intervals. After a further 30 min, the reaction mixture was diluted with H_2O (45 mL) and the resultant milky alkaline solution was extracted with $CHCl_3$ (5 × 10 mL). The combined dried ($MgSO_4$) $CHCl_3$ extracts were evaporated to a colourless glass (424 mg), which crystallized from moist ether and recrystallized from acetone–hexanes in plates. Melting point 123–125 °C. That this product was hydroxylycoctonine (**5**), despite the difference in mp observed here and the value of 150–153 °C reported for the anhydrous compound (2, 7), was established by X-ray crystallography as well as the following data. ^{1}H NMR δ_H: 4.83 (1H, s), 4.11 (1H, br s, exchanged by D_2O), 3.81 (1H, br s, exchanged by D_2O), 3.67 (1H, t, J = 4.5 Hz), 3.67 (3H, s), 3,57 (1H, br s), 3.54 (1H, d, J = 7 Hz), 3.41 (3H, s), 3.31 (3H, s), 3.24 (3H, s), 3.00 (1H, dd, J = 6.1 and 11.1 Hz), 2.83 (1H, dq, J= 7.1 and 12.9 Hz), 2.78 (1H, dd, J = 8.5 and 15.0 Hz), 2.71 (1H, t, J = 4.8 Hz), 2.58 (1H, dq, J = 7.1 and 12.9 Hz), 2.5–2.3 (4H, m), 2.2–2.1 (1H, m), 2.1–1.9 (3H, m), 1.7–1.5 (6H, m), 1.06 (3H, t, J = 7.1Hz). ^{13}C NMR δ_C: 96.4s, 89.5d, 86.5d, 85.8d, 84.4d, 82.5d, 77.6s, 68.5t, 59.7q, 57.8q, 56.6q, 65.4q, 50.2t, 49.3d and 49.3t, 44.5d, 43.9d, 42.8s, 38.2s, 37.6d, 33.2t, 32.3t, 29.5t, 24.8t, 12.9q. HR EI-MS *m/z* found for highest mass ion $C_{25}H_{41}NO_8$: 483.2834; req. 483.2832. Crystal data: $C_{25}H_{41}NO_8{\cdot}H_20$; MW = 501.60; monoclinic; space group $P2_1$; cell dimensions a = 7.842(2), b = 10.170(3), c = 15.656(4) Å, and β = 99.79(2)°; V = 1230.4(6) Å^3; Z = 2; dx = 1.354 Mg/m^3; μ = 0.102 mm^{-1}; F(000) = 544; λ (mo Kα) = 0.71073 Å; T = 173(2) K; R = 0.065 (for 3717 $I > 2.0\sigma(I)$); and wR = 0.99 (all data); goodness of fit S = 1.04. The absolute structure could not be established by the Flack method.[2]

Lycoctonam (7)

To lycoctonine (**1**) (1.14 g, 2.35 mmol) in CH_2Cl_2 (30 mL) was added a solution of powdered $KMnO_4$ (502 mg, 3.18 mmol) in H_2O (5 mL) and the mixture was stirred vigorously (magnet) for 30 min. Excess oxidant was destroyed by adding $Na_2S_2O_5$ to the stirred mixture until all of the MnO_2 had dissolved and a clear two-phase system remained. The organic layer was separated and the aqueous phase was extracted with CH_2Cl_2 (2 × 15 mL). The organic layers were combined, dried (Na_2SO_4), and the solvent evaporated in vacuo yielding lycoctonam (**7**) in quantitative yield as a near colourless oil, which set to a solid white cake of crystals on addition of drop of water. Melting point 98–100 °C (lit. value (3) 95 °C for the dihydrate). ^{1}H NMR (400 MHz, $CDCl_3$, ppm) δ: 3.38 (d, J = 2.1 Hz, 6H, MeO), 3.32 (s, 3H, MeO), 3.17 (s, 3H, MeO), 1.07 (t, J = 7.1 Hz, 3H, NEt). ^{13}C NMR (100 MHz, $CDCl_3$, ppm) δ: 173.6s, 91.1d, 85.8s, 83.4d, 81.9d, 81.2d, 76.4s, 66.8t, 63.1d, 58.5q, 57.7q, 56.2q, 55.0q, 50.7d, 48.0s, 47.0s, 44.7d, 43.2t, 42.6d, 37.3d, 33.1t, 28.6t, 28.4t, 24.4t, 11.9q.

Lycoxonine (8)[3]

To lycoctonam (**7**) (2.055 g, 4.283 mmol) in 0.5 mol/L aqueous sulfuric acid (57 mL) was added chromium trioxide (1.14 g, 11.4 mmol) in 0.5 mol/L aq. H_2SO_4 (11.5 mL) with stirring. The resulting solution was left to stir for 48 h and then extracted with $CHCl_3$ (3 × 100 mL). The organic extracts were washed with H_2O–ammonia (4:1, 1 × 40 mL) and brine (1 × 80 mL) and the solvent was evaporated in vacuo. Chromatographic separation (on alumina) of the obtained crude oil, with 0.5% MeOH–$CHCl_3$ as eluent, afforded lycoxonine (**8**) (247.1 mg, 25.7%) as a white crystalline solid, shown by X-ray crystallography to be chloroform solvate. Melting point 98–91 °C (lit. value (8) 80–83 °C for a hydrate). ^{1}H NMR (400 MHz, $CDCl_3$, ppm) δ: 3.44 (s, 3H, MeO), 3.36 (s, 3H, MeO), 3.23 (s, 3H, MeO), 1.14 (t, J = 7.3 Hz, 3H, NEt). ^{13}C NMR (100 MHz, $CDCl_3$, ppm) δ: 172.6s, 90.4d, 86.0s, 83.5d, 82.2d, 81.4d, 76.6s, 74.9s, 63.8d, 58.7q, 58.0q, 56.4q, 55.5q, 53.0t, 49.0s, 45.8d, 43.3t, 43.0d, 38.0d, 34.4t, 32.9t, 27.8t, 27.1t, 12.3q. Crystal data: $C_{24}H_{37}NO_8{\cdot}CHCl_3$; MW = 586.91; orthorhombic; space group $P2_12_12_1$; cell dimensions a = 9.273(2), b = 16.111(4), and c= 18.218(5) Å; V = 2721.7(12) Å^3; Z = 4; dx = 1.432 Mg/m^3; μ = 0.39 mm^{-1}; F(000) = 1240; λ (mo Kα) = 0.71073 Å; T = 170(2) K; R = 0.046 (for 5260 $I > 2.0\sigma(I)$); wR = 0.136 (all data); goodness of fit S = 1.04.

[2] Supplementary data for this article are available on the journal Web site (http://canjchem.nrc.ca) or may be purchased from the Depository of Unpublished Data, Document Delivery, CISTI, National Research Council Canada, Ottawa, ON K1A 0R6, Canada. DUD 5089. For more information on obtaining material refer to http://cisti-icist.nrc-cnrc.gc.ca/irm/unpub_e.shtml. CCDC 611409 and 611410 contain the crystallographic data for this manuscript. These data can be obtained, free of charge, via http://www.ccdc.cam.ac.uk/conts/retrieving.html (Or from the Cambridge Crystallographic Data Centre, 12 Union Road, Cambridge CB2 1EZ, UK; fax +44 1223 336033; or deposit@ccdc.cam.ac.uk).

[3] Chemical Abstracts Services has assigned the name aconitane to the hexacyclic ring system, which characterizes many of the norditerpenoid alkaloids of *Aconitum* and *Delphinium*, as exemplified by lycoctonine (**1**) (23). Lycoxonine is then semisytematically named as *N*-ethyl-4,7,8-trihydroxy-1α,6β,14α,16β-tetramethoxy-19-oxoaconitane.

© 2006 NRC Canada

The absolute structure was established by the Flack method.[2]

Co-oxidation of lycoctonam and oxalic acid — Preparation of lycoctonamal (10)

Lycoctonam hydrate (350 mg, 0.70 mmol) and oxalic acid dehydrate (690 mg, 5.48 mmol) were dissolved with stirring (magnet) in 60% (*v*/*v*) aqueous acetone containing concd. H_2SO_4 (40 μL). To the stirred homogeneous solution, cooled in ice water, was added dropwise from a syringe over 20 min a solution of CrO_3 (195 mg, 1.95 mmol) in H_2O (220 μL). There was rapid production of a purple solution and concomitant gas evolution. The syringe was rinsed into the reaction mixture with 60% aqueous acetone (ca. 200 μL) and stirring continued for a further 3 h. The mixture was diluted with water (ca. 30 mL) and extracted with CH_2Cl_2 (3 × 20 mL). The combined CH_2Cl_2 extracts were washed with H_2O (5 mL) and then with aq. NH_4OH (NH_4OH–H_2O, 1:5 *v*/*v*, 2 × 5 mL) and water (3 mL). The combined aq. NH_4OH and final H_2O washes were acidified to pH 1 (indicator paper) with 3M aq. H_2SO_4 and extracted with CH_2Cl_2 (3 × 5 mL). Evaporation of the dried (Na_2SO_4) CH_2Cl_2 extract remaining after the aq. NH_4OH washes yielded the neutral fraction (**N**) as a colourless foam (299 mg), while the CH_2Cl_2 extracts obtained after acidification of the aq. NH_4OH washes similarly yielded the acidic products (**A**) as a white crystalline solid (43 mg).

TLC (Al_2O_3, MeOH–$CHCl_3$ 1:50) of the neutral fraction (**N**) revealed two components, R_f 0.56 and 0.38, the slower running corresponding to recovered lycoctonam (**7**). Flash chromatography of the material (on Woelm neutral Al_2O_3 grade III, 23 cm × 1.2 cm), eluting with $CHCl_3$–MeOH (50:1 *v*/*v*, collecting 25 mL fractions), resulted in the rapid elution of lycoctonamal (**10**) obtained, after removal of solvents under reduced pressure, as a colourless glass (220 mg). ^{1}H NMR δ_H: 10.22 (1H, s), 4.12 (1H, dq, *J*= 7.2 and 14.4 Hz), 4.03 (1H, br s), 3.65 (1H, t, *J* = 4.5 Hz), 3.41 (3H, s), 3.38 (1H, d, *J* = 1.6 Hz), 3.36 (3H, s), 3.27 (1H, d, *J* = 3 Hz), 3.34 (3H, s), 3.21 (3H, s), 3.06 (1H, dq, *J* = 7.2 and 14.4 Hz), 2.92 (1H, dd, *J* = 4.6 and 6.8 Hz), 2.56 (1H, dd, *J* = 8.9 and 15.5 Hz), 2.42 (1H, br t, *J* = 4.6 Hz), 2.19 (1H, d, *J* = 1.1 and 3.1 Hz), 2.1 (3H, m), 1.95 (3H, m), 1.74 (1H, dd, *J* = 8.9 and 15. 5 Hz), 1.5 (4H, m), 1.4 (1H, m), 1.13 (3H, t, *J* = 7.2 Hz). ^{13}C NMR δ_C: 204.7d, 168.7s, 94.3d, 85.8s, 83.6d, 82.2d, 81.0d, 76.9s 62.9d, 60.7s, 59.9q, 57.9q, 56.4q, 55.5q, 49.2d 47.7s, 44.9d, 43.6t, 42.8d, 37.7d, 33.2t, 29.7t, 28.6t, 24.5t, 11.9q. No lycoxonine could be detected in this material by TLC, ^{1}H NMR, or ^{13}C NMR. ES MS *m*/*z*: 502 (M + Na) with MS-MS on this ion revealing its fragmentation to an ion *m*/*z*: 474 (likely loss of CO or C_2H_4). HR EI-MS highest mass ion *m*/*z* calcd. for $C_{23}H_{33}NO_8$: 451.2186, 451.2206 (M – C_2H_4).

Lycoctonam (**7**) (71 mg) was eluted in later fractions and identified by ^{1}H and ^{13}C NMR.

The acidic material (**A**) was similarly identified as lycoctonamic acid (**11**). ^{1}H NMR δ_H: 4.13 (1H, br s), 4.10 (1H, dq, *J* = 7.2 and 14.4 Hz), 3.64 (1H, t, *J* = 4.5 Hz), 3.54 (1H, d, *J* = 4.9 Hz), 3.44 (3H, s), 3.38 (3H, s), 3.33 (3H, s), 3.25 (1H, d, *J* = 2.9 Hz), 3.18 (3H, s), 3.12 (1H, m), 3.10 (1H, dq, *J* = 7.2 and 14.4 Hz), 2.94 (1H, br t, *J* = 4.6 and 6.9 Hz), 2.54 (1H, dd, *J* = 8.9 and 15.4 Hz), 2.43 (1H, d, *J* = 2.0 Hz), 3.40 (1H, dd, *J* = 4.6 and 6.9 Hz), 2.17 (1H, m), 2.12 (1H, m), 1.73 (1H, *J* = 7.1 and 15.4 Hz), 1.54 (1H, m), 1.12 (3H, t, *J* = 7.2 Hz). ^{13}C NMR δ_C: 173.1s, 172.0s, 94.5d, 86.0s, 82.0d, 83.3d, 82.0d, 80.2d, 76.7s, 63.9d, 60.0d, 57.7q, 56.2q, 55.5q, 55.4q, 49.1s, 47.3s, 44.5t, 44.3d, 42.5d, 37.4d, 33.0t, 32.5t, 28.6t, 23.9t, 11.5q.

Chromic acid oxidation of lycoctonamal — Formation of lycoctonamic acid (11)

To a stirred solution of lycoctonamal (**10**) (27 mg) in 0.5 mol/L aq. H_2SO_4 (3 mL) was added CrO_3 (9 mg) and the mixture was stirred at RT overnight. A few crystals of $Na_2S_2O_5$ were added to destroy excess oxidant and the mixture was extracted with $CHCl_3$ (3 × 3 mL). The combined $CHCl_3$ extracts were washed with aq. Na_2CO_3 (2 × 2 mL), then dried (Na_2SO_4) and evaporated to yield a trace of neutral materials (2 mg), which was not lycoxonine (by ^{1}H and ^{13}C NMR). Acidification of the Na_2CO_3 extracts with concd. aq. HCl (to pH 1, indicator paper) followed by extraction with $CHCl_3$ (3 × 2 mL) and removal of solvent from the combined dried (Na_2SO_4) extracts gave the acidic products (18 mg) as a white solid. The ^{1}H and ^{13}C NMR spectra revealed it to be lycoctonamic acid (**11**).

1,14-Di-*O*-Methyldelbine (12)

To freshly powdered $LiAlH_4$ (212.6 mg, 5.607 mmol) in anhydr. THF (7.4 mL) was added lycoxonine (**8**) (132.6 mg, 283.9 μmol) in THF (3.2 mL). The reaction mixture was stirred and boiled under reflux. After 6 h, the reaction mixture was cooled to RT and H_2O (300 μL) was added followed by 15% *w*/*w* sodium hydroxide – H_2O (600 μL). The mixture was filtered and the granular residue of white inorganic material was washed with $CHCl_3$ (5 mL). The combined filtrate and washings were evaporated in vacuo and then partitioned between $CHCl_3$ (3 mL) and 0.5 mol/L aq. H_2SO_4 (3 mL). The $CHCl_3$ phase was re-extracted with 0.5 mol/L aq. H_2SO_4 (2 × 3 mL). The combined aq. H_2SO_4 extracts were bacified to pH 10 (indicator paper) with aq. NH_4OH and extracted with $CHCl_3$ (4 × 5 mL). The combined $CHCl_3$ extracts were combined and the solvent removed in vacuo affording 1,14-di-*O*-methyldelbine (**12**) (101.6 mg, 79%) as a golden oil. ^{1}H NMR (400 MHz, $CDCl_3$, ppm) δ: 4.20 (s, 1H, OH), 4.06 (s, 1H, H-6), 3.39 (s, 6H, MeO), 3.31 (s, 3H, MeO), 3.22 (s, 3H, MeO), 1.02 (t, *J* = 7.1 Hz, 3H, NEt). ^{13}C NMR (ppm) δ_C: 89.9d, 88.8s, 83.9d, 83.8d, 82.7, 77.6s, 70.0s, 64.0d, 58.3q, 57.8t, 57.7q, 56.2q, 56.1q, 56.0d, 50.6s, 50.4t, 45.9d, 43.4d, 38.3d, 37.5t, 33.3t, 28.7t, 27.0t, 14.1q.

Acknowledgements

We thank R.Yamdagni, D. Fox and Q. Wu for the provision of mass spectrometric data and assistance with the measurement of NMR spectra; we also thank Professor A. Rauk for his views on the theoretical aspects of the oxidation of amines by permanganate ion. Financial support was provided by MB.

© 2006 NRC Canada

References

1. F. Hűbschmann. Wittsteins Vierteljahrsschr. **15**, 22 (1886); a good abstract of this difficult to obtain paper is provided in Chem. Zentralbl. **37**, 79 (1886); the first detailed investigation of lycoctonine was provided by H. Schultze and E. Bierling. Arch. Pharm. **251**, 8 (1913); for the suggestion that the plant source may actually have been *A.vulparia* Reich, see T.A. Henry. The plant alkaloids. 4th ed. J.& A. Churchill, London. 1949. p. 692. footnote 57.
2. H. Suginome and K. Ohno. J. Fac. Sci. Hokkaido Univ. Ser. 3, **4**, 36 (1950); Chem. Abstr. **46**, 5594 (1952).
3. O.E. Edwards and L. Marion. Can. J. Chem. **30**, 627 (1952).
4. O.E. Edwards, L. Marion, and D.K.R. Stewart. Can. J. Chem. **34**, 1315 (1956).
5. H. Suginome, S. Imato, S. Yamada, and N. Katsui. Bull. Chem. Soc. Jpn. **32**, 819 (1959).
6. (*a*) M. Przybylska and L. Marion. Can. J. Chem. **34**, 185 (1956); **37**, 1843 (1959), however, this structure incorrectly assigned a β configuration to the methoxyl at C-1, an error that was subsequently corrected; (*b*) S.W. Pelletier, N.V. Mody, K.I. Varughese, J.A. Maddry, and H.K. Desai. J. Am. Chem. Soc. **103**, 6536 (1981); (*c*) O.E. Edwards. Can. J. Chem. **59**, 3039 (1981); (*d*) O.E. Edwards and M. Pryzybylska. Can. J. Chem. **60**, 2661 (1982).
7. R.C. Cookson and M.E. Trevett. Chem. Ind. (London), 276 (1956).
8. O.E. Edwards, M. Los, and L. Marion. Can. J. Chem. **37**, 1998 (1959).
9. (*a*) Z. Valenta. Chem. Ind. (London), 633, (1959); (*b*) Z. Valenta and I.G. Wright. Tetrahedron, **9**, 284 (1960).
10. Q.-P. Jiang and W.L. Sung. Heterocycles, **23**, 11 (1985).
11. O. Achmatowicz, Jr., Y. Tsuda, and L. Marion. Can. J. Chem. **43**, 2336 (1965).
12. H.-J. Schmidt and H.J. Schäfer. Angew. Chem. Int. Ed. Engl. **20**, 104 (1981).
13. T. Strassner and K.N. Houk. J. Am. Chem. Soc. **122**, 7821 (2000).
14. (*a*) J.I. Brauman and A.J. Pandell. J. Am. Chem. Soc. **92**, 329 (1969); (*b*) J.M. Mayer. Acc. Chem. Res. **31**, 441 (1998).
15. R. Shukla, P.K. Sharma, L. Kotai, and K. Banerji. Proc. Indian. Acad. Sci. Chem. Sci. **115**, 129 (2003).
16. For a review, see: F.-P. Wang and X.-T. Liang. *In* The alkaloids. Vol. 42. *Edited by* G.A. Cordell. Academic Press, Inc., New York. 1992. pp. 151–247.
17. W.A. Mosher and F. Whitmore. J. Am. Chem. Soc. **70**, 2544 (1948).
18. F. Hasan and J. Roček. J. Am. Chem. Soc. **96**, 534 (1974).
19. P. Műller and J. Blanc. Helv. Chim. Acta, **62**, 1980 (1979).
20. J. Robertson. J. Chem. Educ. **62**, 156 (1985).
21. L. Marion and R.H.F. Manske. Can. J. Res. Sect. B, **24**, 1 (1946).
22. S.W. Pelletier, N.V. Mody, B.S. Joshi, and L.C. Schramm. *In* Alkaloids: chemical and biological perspectives. Vol 2. *Edited by* S.W. Pelletier. J. Wiley and Sons, New York. 1984. p. 205.
23. Aconitane. *In* Chemical abstracts. 9th Collected Chemical Substance Index, American Chemical Society, Columbus, Ohio. **75–85**, (1972–76).

© 2006 NRC Canada

Ruthenium(III) acetylacetonate [$Ru(acac)_3$] — An efficient chemoselective catalyst for the tetrahydropyranylation (THP) of alcohols and phenols under solvent-free conditions

Ravi Varala and Srinivas R. Adapa

Abstract: A catalytic amount of ruthenium(III) acetylacetonate (2 mol%) [$Ru(acac)_3$] enables solvent-free tetrahydropyranylation of different types of alcohols and phenols at ambient temperature in moderate to excellent yields. Notably, selective monoprotection of diols can be achieved chemoselectively. Furthermore, the catalyst could be recovered and reused if necessary.

Key words: tetrahydropyranyl ethers, protecting groups, ruthenium(III) acetylacetonate, alcohols, thiols.

Résumé : L'addition de quantités catalytiques (2 mol %) d'acétylacétonate de ruthénium(III) [$Ru(acac)_3$] permet d'effectuer un tétrahydropyranylation sans solvant de divers types d'alcools et de phénols, à la température ambiante, avec des rendements allant de modérés à excellents. Il est à noter que la monoprotection sélective de diols peut être réalisée chimiosélectivement. De plus, si cela est nécessaire, le catalyseur peut être récupéré et réutilisé.

Mots clés : oxydes de tétrahydropyranyle, groupes protecteurs, acétylacétonate de ruthénium(III), alcools, thiols.

[Traduit par la Rédaction]

Introduction

The choice of the protection and deprotection strategy in a synthetic sequence is inevitable owing to the chemoselective transformations in the presence of various functional groups (1). Tetrahydropyran (THP) ethers are one of the most widely used protecting groups employed during a multistep organic synthesis because of their low cost, easy removal under mild acidic conditions, and stability in various reaction conditions such as strong bases, Grignard reagents, hydrides, redox reagents, alkylating, acylating agents, and catalytic hydrogenation (2). Furthermore, tetrahydropyranyl ethers are synthetically useful as building blocks for the synthesis of biologically important compounds such as nucleosides, carbohydrates, steroids,and alkaloids. They can also be used in perfume formulations (3). A variety of protonic as well as Lewis acid catalysts, including amberlyst, zeolites, montmorillonite K-10, sulfuric acid on silica gel, $ZnCl_2$, tetrabutylammonium bromide, PTSA, $BF_3{\cdot}Et_2O$, $ZrCl_4$, I_2, $In(OTf)_3$, $NbCl_5$, $InCl_3$, $PdCl_2(CH_3CN)_2$, lithium perchlorate – diethyl ether, TBATB, $Bi(OTf)_3$, $La(NO_3)_3{\cdot}6H_2O$, $Fe_2(SO_4)_3{\cdot}xH_2O$, $VO(OAc)_2$, $AlCl_3{\cdot}6H_2O$, and $CeCl_3{\cdot}7H_2O$ – NaI, have been developed for tetrahydropyranylation of hydroxy functions (4). However, several reported methods are associated with drawbacks including long reaction times under reflux, high catalyst to substrate ratios, the use of large amounts of solid support (which eventually results in the generation of large amount of toxic waste, harsh and acidic conditions), the use of expensive and toxic reagents or solvents, and incompatability with other acid-sensitive functional groups. Despite a number of precedents, a solvent-free and catalytically efficient practical alternative for this very important transformation is highly desirable and subject to further improvement.[2]

Recently, we reported CuBr-catalyzed chemoselective thioacetalization of carbonyl compounds (5). As part of our ongoing research program to develop novel synthetic methodologies, particularly carbon–carbon and carbon–heteroatom bond formations (6), we herein present our preliminary results using an efficient ruthenium(III) acetylacetonate [$Ru(acac)_3$]-catalyzed solvent-free tetrahydropyranylation of hydroxy and thiol functions. The procedure, based on the Lewis acid catalytic activity of [$Ru(acac)_3$], represents an environmentally benign alternative to current chemical processes that use water-intolerant Lewis acids.

The screening of a few acetylacetonates allowed us to select [$Ru(acac)_3$] as the versatile catalyst to affect this transformation (Table 1).

Among the reagents tested, the addition product of

Received 23 May 2006. Accepted 6 September 2006. Published on the NRC Research Press Web site at http://canjchem.nrc.ca on 2 November 2006.

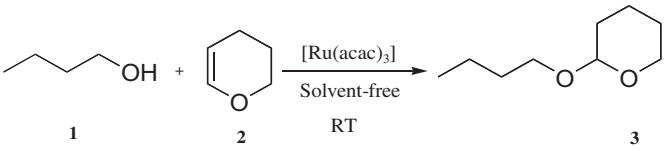
R. Varala and S.R. Adapa.[1] Indian Institute of Chemical Technology, Hyderabad-500 007, India.

[1]Corresponding author (e-mail: rvarala_iict@yahoo.co.in).

[2]Exothermicity of a large-scale reaction should be controlled by maintaining the temperature and using an appropriate solvent if necessary.

 doi:10.1139/V06-137 © 2006 NRC Canada

Table 1. Comparison of various acetylacetonates for the tetrahydropyranylation of *n*-butanol with DHP under solvent-free conditions.



1 **2** **3**

Catalyst	Time (min)	Yield (%)[a]
$VO(acac)_2$	30	90
$Pd(acac)_2$	45	68
$Co(acac)_3$	40	80
$[Ru(acac)_3]$	30	>99

[a]Isolated yields.

Table 2. Comparison of reaction rates of DHP with **1** in different solvents.

Entry	Solvent	Time (min)	Yield (%)[a]
1	MeOH	40	70
2	CH_3CN	30	87
3	Toluene	45	–
4	THF	30	88
5	Dioxane	60	62
6	CCl_4	30	90
7	DCM	45	–
8	DMSO	45	72
9	No solvent	30	>99

Note: All reactions were carried out by stirring mixtures of **1** (1 mmol), DHP (1.1 mmol), and a catalyst for the appropriate times.
[a]Isolated yields.

$[Ru(acac)_3]$ was obtained in >99% yield in 30 min at ambient temperature by using solvent-free conditions (Table 1, entry 4). Next, our efforts focused on achieving the optimum conditions for tetrahydropyranylation of *n*-butanol (**1**) as a model hydroxy compound in the presence of $[Ru(acac)_3]$ as Lewis acid. The results are summarized in Table 2. From the results obtained, we noted that the optimum concentration of 2 mol% of $[Ru(acac)_3]$ is sufficient to carry forward the reaction. The reaction is found to be sluggish when carried out using even stoichiometric – 0.5 equiv. of catalyst amounts. Among the various solvents tested for the THP protection of **1**, toluene and DCM did not furnish the expected product (Table 2, entries 3, 7), whereas other solvents gave moderate to good yields of the addition product. We have also adopted a solvent-free procedure, and to our surprise, the reaction can be carried out in a shorter time with almost quantitative yield (Table 2, entry 9). This allowed us to adopt a simple work-up procedure by employing ether to dissolve the organic material and not the catalyst, which could be easily removed by filtration.

With optimized experimental conditions for the reaction between *n*-butanol (**1**) and DHP, this process was investigated for a wide range of aromatic and aliphatic alcohols and phenols. The results are listed in Table 3.

One of the important features of this protocol for the formation of THP ethers is that absolute anhydrous conditions are not required. The reaction conditions are mild enough not to induce any isomerization of the double bonds of allylic systems (Table 3, entries 2, 4–6, 8). The reactions are reasonably fast, which holds well even with hindered alcohols like geranial and menthol (Table 3, entries 8–9). We investigated the substrate scope and tolerance of electronically divergent alcohols including those that contain sensitive functionalities, for example, epoxy (Table 3, entry 17), C=C, C≡C (Table 3, entries 3, 7), NO_2 (Table 3, entry 32), and Cl (Table 3, entry 33). Another remarkable feature of this method is the chemoselective monotetrahydropyranylation of symmetrical 1,*n*-diols (Table 3, entries 14–16, with 7–8% of di-THP ethers), which is a difficult transformation to accomplish via conventional methods. A primary alcohol has been selectively protected in the presence of a secondary alcohol (Table 3, entry 14). Benzylic alcohols are also smoothly tetrahydropyranylated when reacting with DHP (Table 3, entries 10, 28) to give the corresponding THP ethers in good yields. Furthermore, alcohols bearing the hydroxy group bonded to a carbon stereogenic centre (Table 3, entries 9, 16, 18) can be protected, giving adducts with a complete retention of configuration. However, low diastereoselectivity is observed.

We also investigated the electronic effects on the phenol moiety in the THP protection reaction (Table 3, entries 19–27, 29–33). No apparent difference in the rate of reactivity was observed in the presence of electron donating and withdrawing groups on the aromatic ring. However, no or less reaction occurred between entries 20–23 and 3,4-dihydro-2*H*-pyran. Interestingly, *p*-hydroxy benzaldehyde and *o*-aminophenol (Table 3, entries 27, 30) did not react as expected, even after stirring for 2 days.

The efficiency and generality of the present $[Ru(acac)_3]$-catalyzed protocol can be realized at a glance by comparing our results for the chosen model substrates with those of some recently developed procedures (Table 4). The reactions have been compared with respect to the reaction times, mol% of the catalyst used, and the yields.

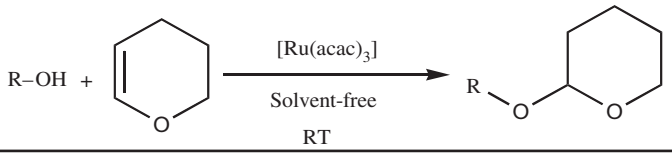
In conclusion, we have developed a mild, efficient, and highly selective methodology for the tetrahydropyranylation of alcohols using $[Ru(acac)_3]$ as a catalyst (2 mol%). Notable features of the protocol include clean and simple reaction conditions, nonaqueous work-up, and environmentally benign reagents. This work widens the scope of using transition metal salts and complexes in organic synthesis because of the nontoxic nature of the catalyst. We believe that this work will be a valuable addition to modern synthetic methodologies.

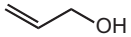
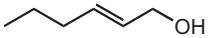
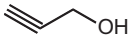
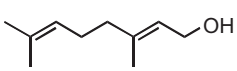
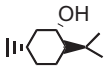
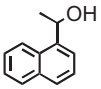
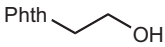
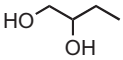
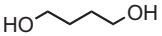
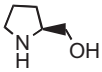
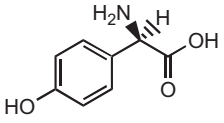
Typical experimental procedures

The hydroxy compound (1–33, 1.0 mmol), 3,4-dihydro-2*H*-pyran (1.1 mmol), and $[Ru(acac)_3]$ (2 mol%) were placed successively in a flask. After stirring, the reaction mixture was treated with Et_2O (2 × 10 mL), and the catalyst was removed by filtration. The filtrate extracts were concentrated under reduced pressure, and the crude product was then purified by silica gel chromatography (hexane – ethyl acetate). All the obtained tetrahydropyranyl ethers were characterized by IR, ^1H NMR spectroscopy, and mass spectrometry, and

© 2006 NRC Canada

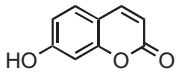
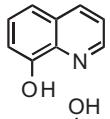
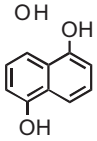
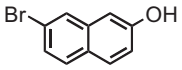
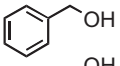
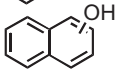
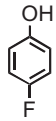
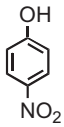
Table 3. Tetrahydropyranylation of hydroxy compounds in the presence of 2 mol% of $[Ru(acac)_3]$ under solvent-free conditions.



Entry	Substrate	Time (min/h)	Yield (%)[a]
1		30 min	>99
2		6 h	82
3		12 h	74
4		14 h	72
5		24 h	95
6		22 h	92
7		18 h	68
8		8 h	62
9		1.5 h	90
10		2 h	78
11		24 h	92
12		1.75 h	86
13		45 min	>95
14		8 h	>99
15		30 min	78/08[b]
16		1.5 h	82/07[b]
17		24 h	28
18		16 h	94
19		15 h	>99

© 2006 NRC Canada

Table 3 (*continued*).

Entry	Substrate		Time (h)	Yield (%)[a]
20			48 h	12
21			48 h	–
22			48 h	–
23			24 h	42
24			13 h	88
25		*o*- *m*- *p*-	14 h 16 h 12 h	85 78 72
26		*o*- *p*-	24 h 24 h	48 52
27		*o*- *m*- *p*-	24 h 24 h 24 h	50 32 –
28			16 h	80
29		1- 2-	22 h 8 h	30 56
30		*o*- *p*-	48 h 48 h	– 17
31			24 h	78
32			24 h	32
33			12 h	74

[a]Isolated yields.
[b]Ratio of mono-:di-THP ether.

their structures are consistent with the published physical data.

Spectral data for selected compounds

Entry 3

^{1}H NMR (300 MHz, $CDCl_3$, ppm) δ: 1.32–1.38 (m, 6H), 2.25 (t, 1H), 3.29–4.01 (m, 2H), 4.14 (d, 2H), 4.78 (br s, 1H).

Entry 4

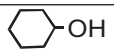
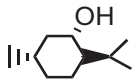
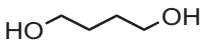
^{1}H NMR (300 MHz, $CDCl_3$, ppm) δ: 1.49–1.91 (m, 6H), 3.52 (m, 1H), 3.86 (m, 1H), 4.01 (m, 1H), 4.25 (m, 1H), 4.66 (br s, 1H), 5.24 (dd, 2H), 5.96 (m, 1H).

Entry 9

^{1}H NMR (300 MHz, $CDCl_3$, ppm) δ: 0.75–1.08 (m, 12H), 1.18–1.83 (m, 10H), 2.06–2.35 (m, 2H), 3.30–3.48 (m, 2H),

© 2006 NRC Canada

Table 4. Comparison of the results of tetrahydropyranylation of alcohols with other catalysts (see ref. 4).

Entry	Alcohol (Phenol)	Catalyst	mol%	Time	Yield (%)
1		$CeCl_3·7H_2O$ – NaI	2–5	26 h	73 (neat)
		$NbCl_5$ – DCM	10	3 h	85
		$PdCl_2(CH_3CN)_2$ – THF	10	1 h	49
		$LiClO_4$ – ether	5 mmol/1 mL	12 h	80
		$VO(OAc)_2$	27	1.5 h	88
		TBATB	2.5	1 h	75
		$Bi(OTf)_3$	0.1	3.25 h	83
		$AlCl_3·6H_2O$	1	30 min	88
		$In(OTf)_3$	0.5	30 min	85
		[Ru(acac)$_3$]	**2**	**40 min**	**>95 (neat)**
2		$CeCl_3·7H_2O$ – NaI	2–5	24 h	90 (neat)
		$Bi(OTf)_3$	0.1	2 h	74
		TBATB	2.5	1 h	74
		$VO(OAc)_2$	27	1.5 h	94
		[Ru(acac)$_3$]	**2**	**1 h**	**90 (neat)**
3		$VO(OAc)_2$	27	30 min	75
		$AlCl_3·6H_2O$	1	30 min	75
		[Ru(acac)$_3$]	**2**	**30 min**	**78 (neat)**

3.85–3.99 (m, 1H), 4.60–4.81 (m, 1H). EI-MS *m*/*z* (%): 139 (M^+ – 101).

Entry 13

^{1}H NMR (300 MHz, $CDCl_3$, ppm) δ: 4.66 (br s, 1H), 3.79–3.94 (m, 1H), 3.41–3.62 (m, 2H), 1.11–1.90 (m, 16H). EI-MS *m*/*z* (%): 184 (M^+).

Entry 24

^{1}H NMR (300 MHz, $CDCl_3$, ppm) δ: 1.62–2.07 (m, 6H), 3.64 (m, 1H), 3.96 (m, 1H), 5.46 (br s, 1H), 6.99–7.34 (m, 5H).

Entry 25 (catechol)

^{1}H NMR (300 MHz, $CDCl_3$, ppm) δ: 1.21–2.01 (m, 12H), 3.02–3.94 (m, 4H), 5.09 (m, 2H), 6.46–7.03 (m, 4H).

Entry 26 (p-hydroxy)

^{1}H NMR (300 MHz, $CDCl_3$, ppm) δ: 1.45–2.05 (m, 6H), 2.55 (s, 3H), 3.48–3.66 (m, 1H), 3.76–3.90 (m, 1H), 5.51 (br s, 1H), 7.07 (d, *J* = 8.8 Hz, 2H), 7.90 (d, *J* = 8.8 Hz, 2H).

Entry 28

^{1}H NMR (400 MHz, $CDCl_3$, ppm) δ: 1.49–1.89 (m, 6H), 3.51 (m, 1H), 3.90 (m, 1H), 4.42 (d, *J* = 11.6 Hz, 1H), 4.71 (m, 1H), 4.80 (d, *J* = 12.0 Hz, 1H) 7.22–7.26 (m, 5H). EI-MS *m*/*z* (%): 192 (M^+).

Entry 29 (2-naphthol)

^{1}H NMR (300 MHz, $CDCl_3$, ppm) δ: 1.60–1.73 (m, 3 H), 1.89–1.92 (m, 2H), 1.99–2.08 (m, 1 H), 3.62–3.66 (m, 1 H), 3.90–3.97 (m, 1 H), 5.56 (t, *J* = 3.3 Hz, 1H), 7.22–7.27 (m, 1H), 7.32 (d, *J* = 8.0 Hz, 1H), 7.40–7.44 (m, 2H), 7.72–7.77 (m, 3H). EI-MS *m*/*z* (%): 228 (M^+).

Entry 32

^{1}H NMR (300 MHz, $CDCl_3$, ppm) δ: 1.42–2.08 (m, 6H), 3.43–3.95 (m, 2H), 5.52 (br s, 1H), 7.11 (d, *J* = 9.3 Hz, 2H), 8.16 (d, *J* = 9.3 Hz, 2H).

Acknowledgments

We thank Dr. J.S. Yadav, Director, Indian Institute of Chemical Technology, and the Council of Scientific Industrial Research (CSIR, India) for financial support.

References

1. P.J. Kocienski. Protecting groups. 3rd ed. Goerg Thieme Verlag, Stuttgart, 2005.
2. C.B. Reese. *In* Protecting groups in organic chemistry. *Edited by* J.F.W. McOmie. Plenum Press, London, 1973. Chap. 3.
3. (*a*) E.J. Corey and R.H. Wollenberg. J. Org. Chem. **40**, 2665 (1975); (*b*) S. Hoyer and P. Laszlo. Synthesis, 655 (1986).
4. (*a*) Amberlyst: A. Bongini, G. Cardillo, M. Orena, and S. Sandri. Synthesis, 618 (1979); (*b*) Zeolites: I. Rodriguez, M.J. Clement, S. Iborra, V. Fornes, A. Corma. J. Catal. **192**, 441 (2000); (*c*) Montmorillonite K-10: S. Hoyer, P. Laszlo, M. Orlovic, and E. Polla. Synthesis, 655 (1986); (*d*) Sulfuric acid on silica gel: M.M. Heravi, D. Ajami, and M. Ghassemzadeh. Synth. Commun. **29**, 1013 (1999); (*e*) $ZnCl_2$: B.C. Ranu and M. Saha. J. Org. Chem. **59**, 8269 (1994); (*f*) Tetrabutylammonium bromide: S. Naik, R. Gopinath, and B.K. Patel. Tetrahedron Lett. **42**, 7679 (2001); (*g*) PTSA: E.J. Corey, H. Niwa, and J. Knolle. J. Am. Chem. Soc. **100**, 1942 (1978); K.F. Bernardy, M.B. Floyd, J.F. Poletto, and M.J. Weiss. J. Org. Chem. **44**, 1438 (1979); (*h*) $BF_3·Et_2O$: H. Alper and L. Dinker. Synthesis, 81 (1972); (*i*) $ZrCl_4$: N. Rezai, F.A. Meybodi, and P. Salehi. Synth. Commun. **30**, 1799 (2000); (*j*) I_2: N. Deka and J.C. Sarma. Synth. Commun. **30**, 4435 (2000); (*k*) $In(OTf)_3$: T. Mineno. Tetrahedron Lett. **43**, 7975

© 2006 NRC Canada

(2002); (*l*) lithium perchlorate – diethyl ether: S.M. Reddy, Y.V. Reddy, and Y. Venkateswarlu. Tetrahedron Lett. **46**, 7439 (2005); (*m*) $Bi(OTf)_3$: J.R. Stephens, P.L. Butler, C.H. Clow, M.C. Oswald, R.C. Smith, R.S. Mohan. Eur. J. Org. Chem. 3827 (2003); (*n*) $La(NO_3)_3{\cdot}6H_2O$: T.S. Reddy, K. Ravinder, N. Suryakiran, M. Narasimhulu, K. Chinni Mahesh, and Y. Venkateswarlu. Tetrahedron Lett. **47**, 2341 (2006); (*o*) $CeCl_3{\cdot}7H_2O$–NaI: G. Bartoli, R. Giovannini, A. Giuliani, E. Marcantoni, M. Massaccesi, P. Melchiorre, M. Paoletti, and L. Sambri. Eur. J. Org. Chem., 1476 (2006); (*p*) $Fe_2(SO_4)_3{\cdot}xH_2O$: L. Li, L. Zhu, X. Zhang, G. Zhang, and G. Qu. Can. J. Chem. **83**, 1120 (2005); (*q*) $PdCl_2(CH_3CN)_2$: Y.-G. Wang, X.-X. Wu, and Z.-Y. Jiang. Tetrahedron Lett. **45**, 2973 (2004); (*r*) $NbCl_5$: K. Nagaiah, B.V.S. Reddy, D. Sreenu, and A. Venkat Narsaiah. Arkivoc, 192 (2005); (*s*) $InCl_3$ immobilized in ionic liquids: J.S. Yadav, B.V.S. Reddy, and D. Gnaneshwar. New J. Chem. **27**, 202 (2003); (*t*) $AlCl_3{\cdot}6H_2O$: V.V. Namboodiri and R.S. Varma. Tetrahedron Lett. **43**, 1143 (2002); (*u*) $VO(OAc)_2$: B.M. Choudary, V. Neeraja, and M.L. Kantam. J. Mol. Catal. A, **175**, 169 (2001); (*v*) TBATB: S. Naik, R. Gopinath, B.K. Patel. Tetrahedron Lett. **42**, 7679 (2001).

5. R. Varala, N. Sreelatha, and S.R. Adapa. Bull. Korean Chem. Soc. **27**, 1079 (2006).
6. (*a*) R. Varala, E. Ramu, and S.R. Adapa. Bull. Chem. Soc. Jpn. **79**, 140 (2006), and refs cited therein; (*b*) R. Varala, E. Ramu, N. Sreelatha, and S.R. Adapa. Tetrahedron Lett. **47**, 877 (2006); (*c*) R. Varala, E. Ramu, and S.R. Adapa. Chin. J. Chem. **24**, 807 (2006); (*d*) R. Varala, E. Ramu, N. Sreelatha, and S.R. Adapa. Synlett, **7**, 1009 (2006); (*e*) R. Varala, N. Sreelatha, and S.R. Adapa. Synlett, **10**, 1549 (2006); (*f*) M.M. Alam, R. Varala, E. Ramu, and S.R. Adapa. Lett. Org. Chem. **3**, 187 (2006); (*g*) R. Varala, E. Ramu, and S.R. Adapa. Synthesis. In press; (*h*) R. Varala, N. Sreelatha, and S.R. Adapa. J. Org. Chem. **71**, 8283 (2006).

© 2006 NRC Canada

Monometallic, homo-, and hetero-bimetallic complexes of a siloxy-bis(phosphinimide) ligand

Gema Martinez and Douglas W. Stephan

Abstract: Deprotonation of $Me_3SiNP(t\text{-}Bu)_2Me$ with BuLi generates $[Me_3SiNP(t\text{-}Bu)_2CH_2Li]$ (**1**), which reacts with $(Me_2SiCl)_2O$ to give the new siloxyl-bis(phosphinimine) ligand $[Me_3SiNP(t\text{-}Bu)_2CH_2SiMe_2]_2O$ (**2**). This ligand reacts with 1 or 2 equiv. of $CpTiCl_3$ to give $[CpTiCl_2NP(t\text{-}Bu)_2CH_2SiMe_2OCH_2SiMe_2P(t\text{-}Bu)_2NSiMe_3]$ (**3**) and $[CpTiCl_2NP(t\text{-}Bu)_2CH_2SiMe_2]_2O$ (**4**), similar to the species $[CpNbCl_3NP(t\text{-}Bu)_2CH_2SiMe_2]_2O$ (**5**) and $[CpTiCl_2NP(t\text{-}Bu)_2(\mu\text{-}O\text{-}(CH_2SiMe_2)_2)\text{-}P(t\text{-}Bu)_2NCpNbCl_3]$ (**6**). Subsequent alkylations of these metal-halide derivatives afforded the analogous permethylated analogs **7**–**10**, respectively. Reaction of **8** with $B(C_6F_5)_3$ generates $[(CpTiMe_2NP(t\text{-}Bu)_2CH_2SiMe_2)(CpTiMeNP(t\text{-}Bu)_2CH_2SiMe_2)O][MeB(C_6F_5)]$ (**11**). Benzylation of **4** give the species $[CpTiBz_2NP(t\text{-}Bu)_2CH_2SiMe_2]_2O$ (**12**), which reacts subsequently with $NC(2,6\text{-}Me_2C_6H_3)$ to give a 1:1 mixture of the diastereoisomers of $[CpTiBz(N{=}C(CH_2Ph)(2,6\text{-}Me_2C_6H_3))NP(t\text{-}Bu)_2CH_2SiMe_2]_2O$ **13a** and **13b**. These synthetic routes are described and the implications considered. X-ray structural data for compounds **2**, **4**, **8**, and **10** are reported.

Key words: phosphinimide ligands, bimetallic species, heterobimetallic compounds.

Résumé : La déprotonation du $Me_3SiNP(t\text{-}Bu)_2Me$ à l'aide de BuLi génère du $[Me_3SiNP(t\text{-}Bu)_2CH_2Li]$ (**1**) qui réagit avec du $(Me_2SiCl)_2O$ pour conduire à la formation du nouveau ligand siloxyl-bis(phosphinimine) $[Me_3SiNP(t\text{-}Bu)_2CH_2SiMe_2]_2O$ (**2**). Ce ligand réagit avec un ou deux équivalents de $CpTiCl_3$ pour conduire à la formation des complexes $[CpTiCl_2NP(t\text{-}Bu)_2CH_2OCH_2SiMe_2P(t\text{-}Bu)_2NSiMe_3]$ (**3**) et $[CpTiCl_2NP(t\text{-}Bu)_2CH_2SiMe_2]_2O$ (**4**) et de la même manière aux espèces $[CpNbCl_3NP(t\text{-}Bu)_2CH_2SiMe_2]_2O$ (**5**) et $[CpTiCl_2NP(t\text{-}Bu)_2(\mu\text{-}OCH_2Me_2)_2P(t\text{-}Bu)_2CpNbCl_3]$ (**6**). Des alkylations subséquentes ces halogénures métalliques conduisent aux analogues perméthylés **7**–**10** respectivement. La réaction du composé **8** avec du $B(C_6F_5)_3$ fournit le complexe $[CpTiMe_2NP(t\text{-}Bu)_2CH_2SiMe_2)(CpTiMeNP(t\text{-}Bu)_2CH_2SiMe_2)O][MeB(C_6F_5)]$ (**11**). La benzylation du composé **4** fournit l'espèce $[CpTiBz_2NP(t\text{-}Bu)_2CH_2SiMe_2]_2O$ (**12**) qui peut réagir subséquemment avec le $NC(2,6\text{-}Me_2C_6H_3)$ pour conduire à un mélange 1:1 des diastéréoisomères **13a** et **13b** du $[CpTiBz(N{=}C(CH_2Ph)(2,6\text{-}Me_2C_6H_3))NP(t\text{-}Bu)_2CH_2SiMe_2]_2O$. On rapporte les voies de synthèses de ces composés et les implications considérées des données relatives aux structures de composés **2**, **4**, **8** et **10** déterminées par diffraction des rayons X.

Mots clés : ligands phosphinimide, espèces bimétalliques, composés hétérobimétalliques.

[Traduit par la Rédaction]

Introduction

The utility of monometallic early metal phosphinimide complexes of the general form $CpTi(NPR_3)X_2$ and $(R_3PN)_2TiX_2$ in olefin polymerization has been established (1–4). Such complexes have been shown to result in high activity single-site polymerization catalysts under commercially relevant conditions. In efforts to both develop new catalysts as well as glean a deeper understanding of the structure–reactivity relationships, considerable effort has been put into the synthesis and study of a variety of new phosphinimide derivatives. Much of the work on such phosphinimide-based complexes to date has been recently reviewed (5).

One avenue for examination that has drawn some recent attention has been the effort to prepare and utilize bis(phosphinimide) ligands (Scheme 1). One motivation involves the analogy between bis(phosphinimide) complexes and ansa-metallocene systems. However, the synthesis of such compounds has proved challenging. Bochmann and coworkers (6) have shown that bis(diphenylphosphinimino)ethane affords bimetallic bis(phosphinimide) complexes as well as chelate complexes (**A**) in which the ligand backbone is metallated (**B**). In the related bis(phosphinimino)methane chemistry, Cavell and coworkers (8–10) have described related bimetallic species (**C**) (7) as well as a number of species in which double activation of the central carbon of the ligand gives rise to reactive carbene derivatives (**D**). Bimetallic Ti-phosphinimide complexes have also been recently obtained by Fryzuk and coworkers (11) from the oxidation of a phosphine during dinitrogen cleavage chemistry (**E**). Contrived synthesis of bis(phosphinimide) ligands derived from $p\text{-}C_6H_4(CH_2PR_2)_2$ have been used to prepare bimetallic titanium derivatives (**F**), while more recently we (12) and

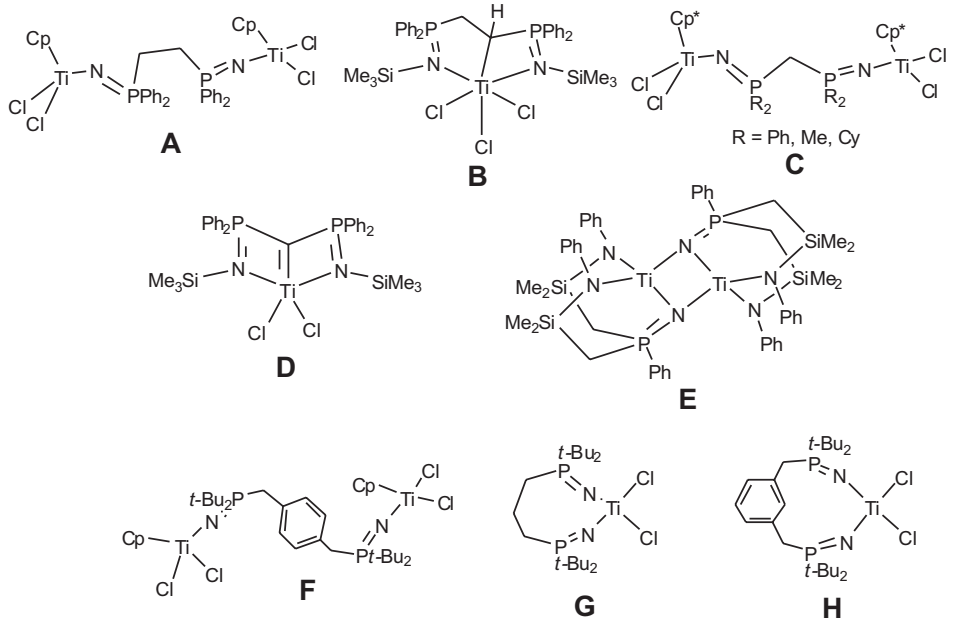
Received 25 July 2006. Accepted 17 September 2006. Published on the NRC Research Press Web site at http://canjchem.nrc.ca on 2 November 2006.

G. Martinez and D.W. Stephan.[1] Department of Chemistry & Biochemistry, University of Windsor, Windsor, ON N9B 3P4, Canada.

[1]Corresponding author (e-mail: stephan@uwindsor.ca).

 © 2006 NRC Canada

Scheme 1. Examples of known Ti bis(phosphinimine) and bis(phosphinimide) complexes.



others (13, 14) showed that the phosphinimines derived from *m*-$C_6H_4(CH_2PR_2)_2$ and $CH_2(CH_2P$*t*-$Bu_2)_2$ provide access to chelate complexes (**G**, **H**) (Scheme 1). In this paper, we explore the potential of a new siloxy-bis(phosphinimide) ligand in the synthesis of monometallic as well as bimetallic complexes. In addition, this ligand is employed to prepare a rare example of heterobimetallic phosphinimide complexes.

Experimental

General data

All preparations were done under an atmosphere of dry O_2-free N_2 employing both Schlenk line techniques and an MBraun or Vacuum Atmospheres inert atmosphere glove box. Solvents were purified employing a Grubbs type solvent purification system manufactured by Innovative Technologies. All organic reagents were purified by conventional methods. ^{1}H, ^{31}P{^{1}H}, ^{11}B{^{1}H}, and ^{13}C{^{1}H} NMR spectra were recorded on Bruker Avance-300 and 500 spectrometers. All spectra were recorded in C_6D_6 at 25 °C unless otherwise noted. Trace amounts of protonated solvents were used as reference and chemical shifts are reported relative to $SiMe_4$. ^{31}P{^{1}H} and ^{11}B{^{1}H} NMR spectra were referenced to external 85% H_3PO_4 and $BF_3{\cdot}Et_2O$, respectively, and are reported in ppm. Additionally, to make the correct assignation for each signal in ^{1}H and ^{13}C NMR, all complexes were characterized by HMQC and DEPT. Combustion analyses were performed in-house employing a PerkinElmer CHN Analyzer. The species $Me_3SiNP(t\text{-}Bu)_2Me$ was prepared by literature methods (5). $(Me_2SiCl)_2O$ was purchased from the Sigma-Aldrich Chemical Co.

Generation of [$Me_3SiNP(t\text{-}Bu)_2CH_2Li$] 1

This intermediate reagent was generated and used in situ by reaction of a THF solution of $Me_3SiNP(t\text{-}Bu)_2Me$ with a stoichiometric amount of *n*-BuLi and used in situ. ^{31}P{^{1}H} NMR δ: 58.9.

Synthesis of [$Me_3SiNP(t\text{-}Bu)_2CH_2SiMe_2]_2O$ 2

A solution of $(Me_2SiCl)_2O$ (0.38 g, 1.97 mmol) in THF (10 mL) was added to a solution of the lithium salt **1** (1.00 g, 3.95 mmol) in THF (20 mL) at RT. The mixture was stirred for 18 h. The solvent was removed under vacuum and the residue extracted with hexanes (30 mL). The solvent was removed under vacuum to produce **2** as a microcrystalline white solid. Yield 1.97 g, 3.16 mmol, 80%. ^{1}H NMR δ: 0.35 (s, 18H, $SiMe_3$), 0.47 (s, 12H, $SiMe_2$), 1.07 (d, $^3J_{PH}$ = 14 Hz, 36H, *t*-Bu), 1.13 (d, $^3J_{PH}$ = 14 Hz, 4H, CH_2). ^{13}C{^{1}H} NMR δ: 3.4 (s, $SiMe_2$), 4.9 (s, $SiMe_3$), 13.6 (d, $^1J_{PC}$ = 60 Hz, CH_2), 27.7 (s, *t*-Bu), 37.3 (d, $^1J_{PC}$ = 60 Hz, *t*-Bu). ^{31}P{^{1}H} NMR δ: 27.7. EA calcd. for $C_{28}H_{70}Si_4ON_2P_2$: C 53.79, H 11.29, N 4.48; found: C 53.71, H 11.04, N 4.63. X-ray quality crystals were obtained from hexanes at –30 °C.

Synthesis of [$CpTiCl_2NP(t\text{-}Bu)_2CH_2SiMe_2OSiMe_2CH_2P(t\text{-}Bu)_2NSiMe_3$] 3

To a solution of **2** (3.00 g, 4.78 mmol) in toluene (15 mL) was added $CpTiCl_3$ (0.70 g, 3.19 mmol) at 25 °C. The mixture was stirred for 7 h. The volume of the solution was reduced under vacuum and the residue was washed with pentane (30 mL) and dried under vacuum to give a yellow crystalline solid. Yield 1.75 g, 2.39 mmol, 75%. ^{1}H NMR ($CDCl_3$, 25 °C) δ: –0.03 (s, 9H, $SiMe_3$), 0.31 (s, 6H, $SiMe_2$), 0.42 (s, 6H, $SiMe_2$), 1.10 (d, $^3J_{PH}$ = 14 Hz, 2H, CH_2), 1.15 (d, $^3J_{PH}$ = 15 Hz, 18H, *t*-Bu), 1.17 (d, $^3J_{PH}$ = 13 Hz, 2H, CH_2), 1.39 (d, $^3J_{PH}$ = 15 Hz, 18H, *t*-Bu), 6.46 (s, 10H, Cp). ^{13}C{^{1}H} NMR ($CDCl_3$, 25 °C) δ: 4.0 (s, $SiMe_2$), 4.6 (s, $SiMe_2$), 5.6 (s, $SiMe_3$), 12.3 (d, $^1J_{PC}$ = 50 Hz, CH_2), 12.3 (d, $^1J_{PC}$ = 58 Hz, CH_2), 28.3 (s, *t*-Bu), 28.4 (s, *t*-Bu), 38.2 (d, $^1J_{PC}$ = 58 Hz, *t*-Bu), 40.2 (d, $^1J_{PC}$ = 54 Hz, *t*-Bu), 116.3 (s, Cp). ^{31}P{^{1}H} NMR δ: 21.1, 41.0. EA calcd. for $C_{30}H_{60}Cl_2N_2P_2OSi_3Ti$: C 49.37, H 8.29, N 3.84; found: C 49.24, H 8.57, N 3.64.

Synthesis of [$CpTiCl_2NP(t\text{-}Bu)_2CH_2SiMe_2]_2O$ 4

To a solution of **2** (2.00 g, 3.19 mmol) in toluene (50 mL) was added $CpTiCl_3$ (1.40 g, 6.39 mmol) at 25 °C. The re-

© 2006 NRC Canada

sulting suspension was stirred for 18 h. The volume of the solution was reduced under vacuum to cause the formation of a solid that was washed with hexanes (40 mL) and dried under vacuum to give a yellow crystalline solid. Yield 2.33 g, 2.62 mmol, 89%. ^{1}H NMR ($CDCl_3$, 25 °C) δ: 0.49 (s, 12H, $SiMe_2$), 1.17 (d, $^3J_{PH}$ = 13 Hz, 4H, CH_2), 1.38 (d, $^3J_{PH}$ = 15 Hz, 36H, *t*-Bu), 6.45 (s, 10H, Cp). ^{13}C{^{1}H} NMR ($CDCl_3$, 25 °C) δ: 3.5 (s, $SiMe_2$), 11.0 (d, $^1J_{PC}$ = 49 Hz, CH_2), 27.2 (s, *t*-Bu), 39.1 (d, $^1J_{PC}$ = 54 Hz, *t*-Bu), 115.4 (s, Cp). ^{31}P{^{1}H} NMR δ: 43.5. EA calcd. for $C_{32}H_{62}Cl_4Si_2ON_2P_2Ti_2$: C 45.40, H 7.35, N 3.31; found: C 45.20, H 7.15, N 2.99. X-ray quality crystals were obtained by slow evaporation of a toluene solution.

Synthesis of [CpNbCl$_3$NP(*t*-Bu)$_2$CH$_2$SiMe$_2$]$_2$O 5

To a solution of **2** (0.50 g, 0.79 mmol) in THF (30 mL) was added $CpNbCl_4$ (0.48 g, 1.59 mmol). The resulting suspension was stirred at 25 °C for 18 h. The volume of the solution was reduced under vacuum to cause the formation of a yellow solid that was washed with hexanes (20 mL) and dried under vacuum to give **5** as a microcrystalline solid. Yield 0.66 g, 0.65 mmol, 82%. ^{1}H NMR ($CDCl_3$, 25 °C) δ: 0.53 (s, 12H, $SiMe_2$), 1.45 (d, $^3J_{PH}$ = 16 Hz, 36H, *t*-Bu), 1.51 (d, $^3J_{PH}$ = 15 Hz, 4H, CH_2), 6.59 (s, 10H, Cp). ^{13}C{^{1}H} NMR ($CDCl_3$, 25 °C) δ: 4.8 (s, $SiMe_2$), 10.0 (d, $^1J_{PC}$ = 47 Hz, CH_2), 28.6 (s, *t*-Bu), 40.59 (d, $^1J_{PC}$ = 50 Hz, *t*-Bu), 118.5 (s, Cp). ^{31}P{^{1}H} NMR δ: 65.5. EA calcd. for $C_{32}H_{62}Cl_6Si_2ON_2P_2Nb_2$: C 38.14, H 6.20, N 2.78; found: C 37.96, H 6.56, N 2.75.

Synthesis of [CpTiCl$_2$NP(*t*-Bu)$_2$CH$_2$SiMe$_2$OSiMe$_2$CH$_2$P(*t*-Bu)$_2$NCpNbCl$_3$] 6

To a solution of **3** (0.50 g, 0.68 mmol) in THF (30 mL) was added $CpNbCl_4$ (0.20 g, 0.68 mmol) at 25 °C. The reaction suspension was stirred at 25 °C for 18 h and slowly became a yellow solution. The volume of the solvent was reduced under vacuum to give a yellow solid that was washed with a mixture of toluene and hexanes in proportion 3 to 1 (3 × 40 mL) and dried under vacuum. Yield 0.53 g, 0.57 mmol, 85%. ^{1}H NMR ($CDCl_3$, 25 °C) δ: 0.49 (s, 6H, $SiMe_2$), 0.53 (s, 6H, $SiMe_2$), 1.22 (m, 4H, CH_2), 1.39 (d, $^3J_{PH}$ = 15 Hz, 18H, *t*-Bu), 1.46 (d, $^3J_{PH}$ = 16 Hz, 18H, *t*-Bu), 6.44 (s, 5H, Cp), 6.61 (s, 5H, Cp). ^{13}C{^{1}H} NMR ($CDCl_3$, 25 °C) δ: 3.6 (s, $SiMe_2$), 3.9 (s, $SiMe_2$), 9.2 (d, $^1J_{PC}$ = 47 Hz, CH_2), 11.2 (d, $^1J_{PC}$ = 49 Hz, CH_2), 27.4 (s, *t*-Bu), 27.6 (s, *t*-Bu), 40.5 (d, $^1J_{PC}$ = 54 Hz, *t*-Bu), 40.1 (d, $^1J_{PC}$ = 50 Hz, *t*-Bu), 115.5 (s, Cp), 117.6 (s, Cp). ^{31}P{^{1}H} NMR δ: 41.2, 66.3. EA calcd for $C_{32}H_{62}Cl_5Si_2ON_2P_2NbTi$: C 41.46, H 6.74, N 3.02; found: C 41.26, H 6.66, N 2.95.

Synthesis of [CpTiMe$_2$NP(*t*-Bu)$_2$CH$_2$SiMe$_2$OSiMe$_2$CH$_2$P(*t*-Bu)$_2$NSiMe$_3$] 7

To a suspension of **3** (0.50 g, 0.68 mmol) in hexanes (30 mL) was added 3.0 mol/L MeMgCl in THF (0.50 mL, 1.50 mmol) at 25 °C. The reaction mixture was stirred for 18 h. The light yellow solution was filtered and the solvent removed under vacuum to give a yellow microcrystalline solid that was washed with cold pentane (2 mL). Yield 0.38 g, 0.55 mmol, 82%. ^{1}H NMR δ: 0.44 (s, 9H, $SiMe_3$), 0.57 (s, 12H, $SiMe_2$), 0.71 (s, 6H, TiMe), 1.17 (d, $^3J_{PH}$ = 14 Hz, 18H, *t*-Bu), 1.17 (d, $^3J_{PH}$ = 14 Hz, 2H, CH_2), 1.27 (d, $^3J_{PH}$ = 14 Hz, 18H, *t*-Bu), 1.27 (d, $^3J_{PH}$ = 14 Hz, 2H, CH_2), 6.30 (s, 10H, Cp). ^{13}C{^{1}H} NMR δ: 3.2 (s, $SiMe_2$), 3.4 (s, $SiMe_2$), 5.0 (s, $SiMe_3$), 12.1 (d, $^1J_{PC}$ = 49 Hz, CH_2), 13.5 (d, $^1J_{PC}$ = 63 Hz, CH_2), 27.1 (s, *t*-Bu), 27.3 (s, *t*-Bu), 37.4 (d, $^1J_{PC}$ = 59 Hz, *t*-Bu), 38.9 (d, $^1J_{PC}$ = 56 Hz, *t*-Bu), 42.5 (s, TiMe), 110.2 (s, Cp). ^{31}P{^{1}H} NMR δ: 25.9, 27.3. EA calcd. for $C_{32}H_{66}N_2P_2OSi_3Ti$: C 55.79, H 9.66, N 4.07; found: C 55.22, H 9.70, N 4.01.

Synthesis of [CpTiMe$_2$NP(*t*-Bu)$_2$CH$_2$SiMe$_2$]$_2$O 8

To a suspension of complex **4** (0.10 g, 0.12 mmol) in hexanes (20 mL) was added 3.0 mol/L MeMgCl in THF (0.16 mL, 0.50 mmol). The reaction mixture was stirred for 18 h. The light yellow solution was filtered and the solvent removed under vacuum to produce a yellow solid that was washed with cold pentane (2 × 2mL) and dried under vacuum. Yield 0.06 g, 0.08 mmol, 66%. ^{1}H NMR δ: 0.50 (s, 12H, $SiMe_2$), 0.65 (s, 12H, TiMe), 1.11 (d, $^3J_{PH}$ = 12 Hz, 4H, CH_2), 1.15 (d, $^3J_{PH}$ = 15 Hz, 36H, *t*-Bu), 6.21 (s, 10H, Cp). ^{13}C{^{1}H} NMR δ: 3.9 (s, $SiMe_2$), 12.5 (d, $^1J_{PC}$ = 49 Hz, CH_2), 27.6 (s, *t*-Bu), 38.9 (d, $^1J_{PC}$ = 55 Hz, *t*-Bu), 42.6 (s, TiMe), 111.5 (s, Cp). ^{31}P{^{1}H} NMR δ: 36.3. EA calcd. for $C_{36}H_{84}Si_2ON_2P_2Ti_2$: C 56.53, H 9.75, N 3.66; found: C 56.13, H 9.23, N 3.55. X-ray quality crystals were obtained from pentane at –30 °C.

Synthesis of [CpNbMe$_3$NP(*t*-Bu)$_2$CH$_2$SiMe$_2$]$_2$O 9

To a suspension of complex **5** (0.22 g, 0.21 mmol) in hexanes (20 mL) was added 3.0 mol/L MeMgCl in THF (0.50 mL, 1.30 mmol). The reaction mixture was stirred for 18 h. The light yellow solution was filtered and the solvent removed under vacuum to produce a yellow solid that was washed with cold pentane (2 × 2 mL) and dried under vacuum. Yield 0.15 g, 0.17 mmol, 81%. ^{1}H NMR δ: 0.42 (s, 12H, $SiMe_2$), 1.01 (s, 18H, NbMe), 1.04 (d, $^3J_{PH}$ = 14 Hz, 36H, *t*-Bu), 1.05 (d, $^3J_{PH}$ = 14 Hz, 4H, CH_2), 5.62 (s, 10H, Cp). ^{13}C{^{1}H} NMR δ: 3.7 (s, $SiMe_2$), 11.8 (d, $^1J_{PC}$= 49 Hz, CH_2), 27.5 (s, *t*-Bu), 34.0 (s, NbMe), 38.7 (d, $^1J_{PC}$ = 55 Hz, *t*-Bu), 107.1 (s, Cp). ^{31}P{^{1}H} NMR δ: 39.6. EA calcd. for $C_{38}H_{80}Si_2ON_2P_2Nb_2$: C 51.57, H 9.11, N 3.17; found: C 51.96, H 8.86, N 2.75.

Synthesis of [CpTiMe$_2$NP(*t*-Bu)$_2$CH$_2$SiMe$_2$OSiMe$_2$CH$_2$P(*t*-Bu)$_2$NCpNbMe$_3$] 10

A 3.0 mol/L THF solution of MgMeCl (0.95 mL, 2.80 mmol) was added at 25 °C to a suspension of **6** (0.50 g, 0.53 mmol) in hexanes (30 mL). The reaction mixture was stirred for 18 h. After filtration the solvent was removed under vacuum and the residue was extracted with pentane (20 mL). The solvent was removed from the filtrate under vacuum to produce **12** as a microcrystalline yellow solid. Yield 0.30 g, 0.36 mmol, 68%. ^{1}H NMR δ: 0.41 (s, 6H, $SiMe_2$), 0.50 (s, 6H, $SiMe_2$), 0.62 (s, 6H, TiMe), 0.93 (d, $^3J_{PH}$ = 14, 2H, CH_2), 1.01 (d, $^3J_{PH}$ = 14 Hz, 18H, *t*-Bu), 1.03 (s, 9H, NbMe), 1.16 (d, $^3J_{PH}$ = 14, 2H, CH_2), 1.19 (d, $^3J_{PH}$ = 14 Hz, 18H, *t*-Bu), 5.63 (s, 5H, Cp), 6.20 (s, 5H, Cp). ^{13}C{^{1}H} NMR δ: 3.7 (s, $SiMe_2$), 3.8 (s, $SiMe_2$), 11.7 (d, $^1J_{PC}$ = 48 Hz, CH_2), 12.3 (d, $^1J_{PC}$ = 49 Hz, CH_2), 27.4 (s, *t*-Bu), 27.6 (s, *t*-Bu), 35.1 (s, NbMe), 38.6 (d, $^1J_{PC}$ = 56 Hz, *t*-Bu), 38.9 (d, $^1J_{PC}$ = 56 Hz, *t*-Bu), 42.6 (s, TiMe), 107.0 (s, Cp), 111.4 (s, Cp). ^{31}P{^{1}H} NMR δ: 39.4, 25.7. EA calcd.

© 2006 NRC Canada

Table 1. Crystallography parameters.

Compound	**2**	**4**	**8**	**10**
Formula	$C_{28}H_{70}N_2OP_2Si_4$	$C_{32}H_{62}Cl_4N_2OP_2Si_2Ti_2$	$C_{36}H_{74}N_2OP_2Si_2Ti_2$	$C_{37}H_{77}N_2NbOP_2Si_2Ti$
Formula weight	625.16	846.56	764.89	824.94
Crystal system	Monoclinic	Triclinic	Monoclinic	Triclinic
Space group	$P2_1/c$	P-1	$P2_1/n$	P-1
a (Å)	9.6813(16)	8.960(5)	17.375(5)	17.0801(18)
b (Å)	28.143(5)	15.693(9)	15.544(4)	17.4142(19)
c (Å)	15.203(3)	16.182(9)	18.889(5)	17.3733(19)
α (°)		107.051(8)		90.019(2)
β (°)	95.915(2)	93.929(9)	115.739(3)	115.5840(10)
γ (°)		90.108(8)		89.988(2)
V (Å^3)	4120.1(12)	2170(2)	4595(2)	4660.8(9)
Z	4	2	4	4
d_{calcd} (g/cm)	1.011	1.296	1.106	1.176
μ, (mm^{-1})	0.242	0.77	0.495	0.564
Data collected	39 088	20 267	43 218	30 974
Data $F_O^2 > 3\sigma(F_O^2)$	7249	7633	8088	9768
Variables	334	406	406	797
R	0.0688	0.0907	0.0523	0.0794
Rw	0.1944	0.1968	0.1372	0.2048
GOF	1.051	1.184	1.059	1.021

for $C_{37}H_{77}Si_2ON_2P_2NbTi$: C 53.87, H 9.41, N 3.40; found: C 53.66, H 9.33, N 3.25. X-ray quality crystals were obtained by slow evaporation of pentane.

Generation of [(CpTiMe$_2$NP(*t*-Bu)$_2$CH$_2$SiMe$_2$OSiMe$_2$CH$_2$P(*t*-Bu)$_2$)TiCpMe][MeB(C$_6$F$_5$)] 11

An equimolar mixture of **8** (34.00 mg, 0.04 mmol) and $B(C_6F_5)_3$ (0.022 g, 0.04 mmol) was charged into a Teflon-valved NMR tube and BrC_6D_5 was added at 25 °C. Complex **11** was highly sensitive to air and moisture and only characterized by NMR techniques. ^{1}H NMR (BrC_6D_5, 25 °C) δ: –0.04 (s, 3H, TiMe), 0.14 (s, 6H, $SiMe_2$), 0.31 (s, 6H, $SiMe_2$), 0.55 (s, 6H, TiMe), 0.99 (m, 4H, CH_2). 1.02 (d, $^3J_{PH}$ = 14 Hz, 18H, *t*-Bu), 1.03 (d, $^3J_{PH}$ = 14 Hz, 18H, *t*-Bu), 5.99 (s, 10H, Cp). ^{13}C{^{1}H} NMR (BrC_6D_5, 25 °C) δ: 3.3 (s, $SiMe_2$), 3.4 (s, $SiMe_2$), 11.3 (d, $^1J_{PC}$ = 50 Hz, CH_2), 26.6 (s, *t*-Bu), 26.8 (s, *t*-Bu), 37.6 (d, $^1J_{PC}$ = 51 Hz, *t*-Bu), 38.3 (d, $^1J_{PC}$ = 54 Hz, *t*-Bu), 42.1 (s, TiMe), 49.3 (s, TiMe), 113.2 (s, Cp). ^{19}F NMR (BrC_6D_5, 25 °C) δ: –132.1 (d, F_o), –164.4, (t, F_p), –166.8 (t, F_m). ^{11}B{^{1}H} NMR (BrC_6D_5, 25 °C) δ: –14.9. ^{31}P{^{1}H} NMR (BrC_6D_5, 25 °C) δ: 39.5, 39.6.

Synthesis of [CpTiBz$_2$NP(*t*-Bu)$_2$CH$_2$SiMe$_2$]$_2$O 12

A 2 mol/L THF solution of BzMgCl (0.25 mL, 0.49 mmol) was added at 25 °C to a solution of complex **4** (0.10 g, 0.12 mmol) in Et_2O (20 mL). The resulting suspension was stirred for 18 h. The orange solution formed was filtered. After removal the solvent under vacuum the residue was washed with hexanes (2 × 20 mL) and dried under vacuum to give an orange solid. Yield 0.08 g, 0.07 mmol, 65%. ^{1}H NMR δ: 0.48 (s, 12H, $SiMe_2$), 1.10 (d, $^3J_{PH}$ = 13 Hz, 4H, CH_2), 1.11 (d, $^3J_{PH}$ = 15 Hz, 36H, *t*-Bu), 2.69 (d, J_{HH} = 10 Hz, 4H, $TiCH_2$), 2.82 (d, J_{HH} = 10 Hz, 4H, $TiCH_2$), 5.95 (s, 10H, Cp), 6.92 (m, 4H, H_p Ph), 7.03 (m, 8H, H_o Ph), 7.24 (m, 8H, H_m Ph). ^{13}C{^{1}H} NMR (C_6D_6, 25 °C) δ: 4.2 (s, $SiMe_2$), 13.2 (d, $^1J_{PC}$ = 48 Hz, CH_2), 27.8 (s, *t*-Bu), 38.7 (d, $^1J_{PC}$ = 55 Hz, *t*-Bu), 71.7 (s, $TiCH_2$), 114.2 (s, Cp), 121.2 (s, C_p Ph), 126.4 (s, C_o Ph), 128.6 (s, C_m Ph), 153.7 (s, C_{ipso} Ph). ^{31}P{^{1}H} NMR δ: 36.3. EA calcd. for $C_{60}H_{80}Si_2ON_2P_2Ti_2$: C 67.40, H 8.48, N 2.61; found: C 67.11, H 8.37, N 2.81.

Synthesis of [CpTiBz(N=C(CH$_2$Ph)(2,6-Me$_2$C$_6$H$_3$))NP(*t*-Bu)$_2$CH$_2$SiMe$_2$]$_2$O 13

To an orange solution of **12** (0.40 g, 0.52 mmol) in toluene (20 mL) was added NC(2,6-$Me_2C_6H_3$) (0.13 g, 1.04 mmol). The mixture was stirred for 1 h at 25 °C. After removal of the solvent under vacuum the residue was washed with hexanes (10 mL) and dried under vacuum to give complex **5** as a mixture of two diastereomers **13a** and **13b** (assignments to the two isomers are denoted with [a] and [b]). Yield 0.34 g, 0.25 mmol, 68%. ^{1}H NMR δ: 0.50[a]/0.51[b] (s, 6H, $SiMe_2$), 0.55[a]/0.56[b] (s, 6H, $SiMe_2$), 1.07[a]/1.08[b] (d, $^3J_{PH}$ = 14 Hz, 18H, *t*-Bu), 1.10[a]/1.11[b] (d, $^3J_{PH}$ = 14 Hz, 18H, *t*-Bu), 1.13[a,b] (m, 4H, CH_2), 1.53[a,b] (s, 3H, $Me_2C_6H_3$), 2.20[a,b] (s, 3H, $Me_2C_6H_3$), 3.04[a,b] (d, J_{HH} = 8 Hz, 2H, $TiCH_2$), 3.13[a,b] (d, J_{HH} = 7 Hz, 2H, $TiCH_2$), 3.72[a,b] (d, J_{HH} = 14 Hz, 2H, CH_2Ph), 3.79[a,b] (d, J_{HH} = 14 Hz, 2H, CH_2Ph), 5.82/[a]5.83[b] (s, 10H, Cp), 6.80–7.20[a,b] (m, 26H, $Me_2C_6H_3$ and C_6H_5). ^{13}C{^{1}H} NMR δ: 4.5[a,b] (s, $SiMe_2$), 14.8[a,b] (d, $^1J_{PC}$ = 44 Hz, CH_2), 19.2[a,b] (s, $Me_2C_6H_3$), 20.1[a,b] (s, $Me_2C_6H_3$), 28.0[a]/28.2[b] (s, *t*-Bu), 37.6[a]/38.2[b] (d, $^1J_{PC}$ = 56 Hz, *t*-Bu), 44.8[a,b] (s, CH_2Ph), 52.9[a]/53.1[b] (s, $TiCH_2$), 109.3[a]/109.6[b] (s, Cp), 125.7[a,b], 126.1[a,b], 127.1[a,b], 127.8[a,b], 128.8[a,b], 128.9[a,b], 129.5[a,b], 130.5[a,b], (s, C_p, C_o, C_m, Ph), 137.1[a,b] (s, C_{ipso} CH_2Ph), 147.1[a,b] (s, C_{ipso} $TiCH_2Ph$), 157.0[a,b] (s, N=C). ^{31}P{^{1}H} NMR δ: 26.5. EA calcd. for $C_{78}H_{108}Si_2ON_4P_2Ti_2$: C 70.36, H 8.18, N 4.21; found: C 70.25, H 8.11, N 4.11.

X-ray data collection and reduction

Crystals were manipulated and mounted in capillaries in a glove box, thus maintaining a dry O_2-free environment for each crystal. Diffraction experiments were performed on a Siemens SMART System CCD diffractometer. The data

© 2006 NRC Canada

were collected in a hemisphere of data in 1448 frames with 10 s exposure times. The observed extinctions were consistent with the space groups in each case. The data sets were collected for the range $4.5° < 2\theta < 45–50.0°$. The intensities of reflections within these frames showed no statistically significant change over the duration of the data collections. The data were processed using the SAINT and XPREP processing packages. An empirical absorption correction based on redundant data was applied to each data set. Subsequent solution and refinement was performed using the SHELXTL solution package.

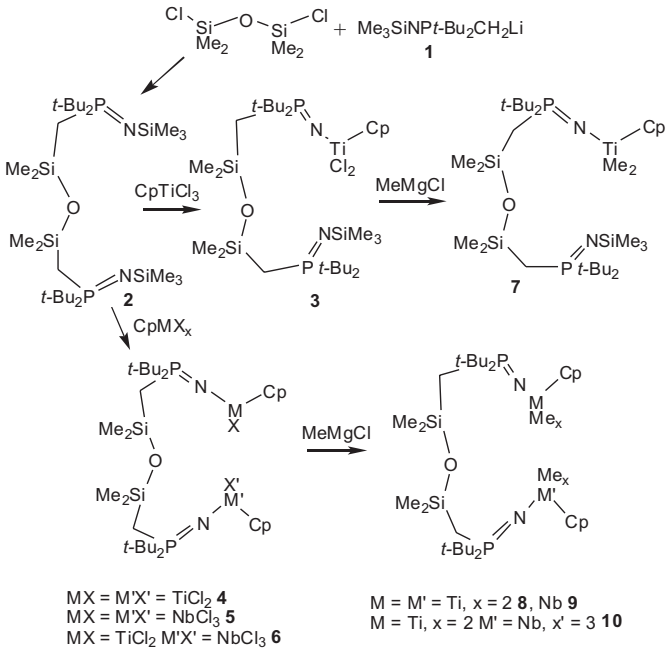
Structure solution and refinement

Non-hydrogen atomic scattering factors were taken from the literature (15). The heavy atom positions were determined using the SHELXTL direct methods routine. The remaining non-hydrogen atoms were located from successive Fourier map difference calculations. The refinements were carried out by using full-matrix least-squares techniques on *F*, minimizing the function $\omega (F_o\text{-}F_c)^2$ where the weight ω is defined as $4F_o^2/2\sigma (F_o^2)$ and F_o and F_c are the observed and calculated structure factor amplitudes. In the final cycles of each refinement, all non-hydrogen atoms were assigned anisotropic temperature factors. In the case of **10**, the cell parameters suggested the possibility of an alternative refinement using a monoclinic cell. All attempts to refine models in higher symmetry space groups provided unsatisfactory refinements. Thus, it was concluded that the correct space group was indeed the reported triclinic cell. In all cases, hydrogen atom positions were calculated and allowed to ride on the carbon to which they are bonded, assuming a C–H bond length of 0.95 Å. H atom temperature factors were fixed at 1.10 times the isotropic temperature factor of the C atom to which they are bonded. The H atom contributions were calculated but not refined. The locations of the largest peaks in the final Fourier map difference calculation as well as the magnitude of the residual electron densities in each case were of no chemical significance. Addition details are provided in the Supplementary data.[2]

Results and discussion

Deprotonation of a P-bound methyl group has been shown in the past to be a straightforward manner for the generation of a carbon-based P-containing nucleophile (16). In this fashion, the reaction of $Me_3SiNP(t\text{-}Bu)_2Me$ with BuLi was employed to generate solutions of the lithium salt $[Me_3SiNP(t\text{-}Bu)_2CH_2Li]$. Subsequent reaction of this reagent with $(Me_2SiCl)_2O$ afforded, after suitable work-up, the new siloxyl-bis(phosphinimine) ligand $[Me_3SiNP(t\text{-}Bu)_2CH_2SiMe_2]_2O$ **2** in 80% isolated yield (Scheme 2). This species gives rise to a single $^{31}P\{^1H\}$ NMR signal at 27.7 ppm and the expected ^1H and $^{13}C\{^1H\}$ NMR resonances. X-ray quality crystals were obtained from hexanes at

Scheme 2. Synthesis of compounds **1**–**10**.



–30 °C. The crystallographic structure (Fig. 1) confirmed the above formulation and revealed the new average C–Si bond length of 1.865(4) Å, while the N–Si distances averaged 1.653(4) Å. The central Si–O bond length was found to be 1.631(3) Å, while the Si–O–Si angle was 144.7(2)°.

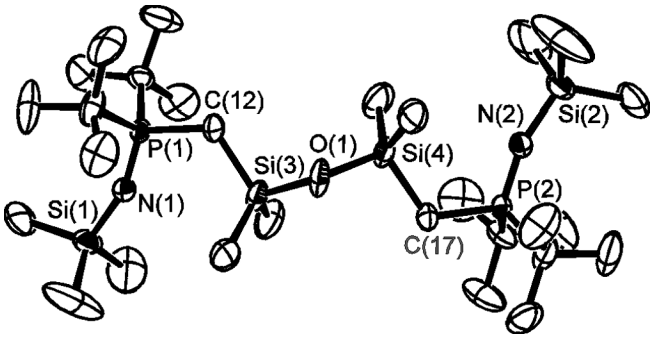
Initial attempts to utilize this ligand **2** involved reactions with MCl_4 (M = Ti, Zr). In these cases, refluxing conditions gave complex mixtures of products. ^{31}P NMR resonances attributed to $HNP(t\text{-}Bu)_2Me$, $Me_3SiNP(t\text{-}Bu)_2Me$, and $OP(t\text{-}Bu)_2Me$ were consistent with ligand fragmentation. In constrast, the ligand precursor **2** reacts cleanly and stoichiometrically with $CpTiCl_3$. Reaction of **2** with 1 equiv. of $CpTiCl_3$ proceeded smoothly at 25 °C in toluene to give a yellow crystalline solid **3** in 75% yield. The $^{31}P\{^1H\}$ NMR spectrum of **3** gave rise to two resonances at 21.1 and 41.0 ppm. These data together with the ^1H and ^{13}C NMR data were consistent with the formulation of **3** as $[CpTiCl_2NP(t\text{-}Bu)_2CH_2SiMe_2OCH_2SiMe_2P(t\text{-}Bu)_2NSiMe_3]$ (Scheme 2).

In an analogous manner, the reaction of **2** with 2 equiv. of $CpTiCl_3$ proceeded to give a yellow crystalline solid **4** in 89% yield. The $^{31}P\{^1H\}$ NMR resonance for **4** is shifted downfield to 43.5 ppm. The simplicity of the ^1H NMR spectrum is notable; resonances at 6.45, 1.38, 1.17, and 0.49 ppm are attributable to cyclopentadienyl, methylene, *t*-Bu, and Me protons respectively. The corresponding resonances are observed in the $^{13}C\{^1H\}$ NMR spectrum. These assignments support the notion of reactions of both ends of the ligand with Ti. This results in the formulation of **4** as bimetallic

[2] Supplementary data for this article are available on the journal Web site (http://canjchem.nrc.ca) or may be purchased from the Depository of Unpublished Data, Document Delivery, CISTI, National Research Council Canada, Ottawa, ON K1A 0R6, Canada. DUD 5090. For more information on obtaining material refer to http://cisti-icist.nrc-cnrc.gc.ca/irm/unpub_e.shtml. CCDC 607211 and 607214 contain the crystallographic data for this manuscript. These data can be obtained, free of charge, via http://www.ccdc.cam.ac.uk/conts/retrieving.html (Or from the Cambridge Crystallographic Data Centre, 12 Union Road, Cambridge CB2 1EZ, UK; fax +44 1223 336033; or deposit@ccdc.cam.ac.uk).

© 2006 NRC Canada

Fig. 1. ORTEP drawing of **2**; 30% thermal ellipsoids are shown. Hydrogen atoms are omitted for clarity. Selected distances (Å) and angles (°) are Si(1)–N(1) 1.659(3), Si(2)–N(2) 1.668(3), Si(3)–O(1) 1.640(3), Si(3)–C(12) 1.863(4), Si(4)–O(1) 1.630(3), Si(4)–C(17) 1.865(4), P(1)–N(1) 1.535(3), P(2)–N(2) 1.526(3), Si(4)–O(1)–Si(3) 144.8(2).



species $[CpTiCl_2NP(t\text{-}Bu)_2CH_2SiMe_2]_2O$. Recrystallization of **4** from toluene gave well-formed crystals for X-ray diffraction studies. The crystallography confirmed the bimetallic nature of **4** (Fig. 2). The Ti–Cl distances averaged 2.315(4) Å with Cl–Ti–Cl averaging 100.9(1)°. The *Ti*-phosphinimide linkages are typical, with average Ti–N and N–P bond lengths of 1.767(6) Å and 1.620(6) Å, respectively. The corresponding Ti–N–P angles were found to be 171.2(4)° and 167.7(3)°. The central Si–O linkage gave rise to an average Si–O distance of 1.649(4) Å and an Si–O–Si angle of 149.3(3)°.

In an analogous synthetic method, the ligand **2** was reacted with 2 equiv. of $CpNbCl_4$ at 25 °C to give a yellow solid **5** in 82% yield. The resulting $^{31}P\{^1H\}$ NMR resonance for **5** was observed at 65.5 ppm while the ^1H resonance at 6.59 ppm was attributed to the cyclopentadienyl ligands. These data were consistent with the formulation of **5** as diniobium complex$[CpNbCl_3NP(t\text{-}Bu)_2CH_2SiMe_2]_2O$ (Scheme 2).

In a similar fashion, the species **3** reacts with $CpNbCl_4$ to give a yellow solid **6** in 85% yield formulated as the heterobimetallic complex $[CpTiCl_2NP(t\text{-}Bu)_2\{\mu\text{-}O\text{-}(CH_2SiMe_2)_2\}P(t\text{-}Bu)_2NCpNbCl_3]$. The $^{31}P\{^1H\}$ NMR of **6** showed two resonances at 41.2 and 66.3 ppm while the ^1H NMR spectrum showed resonances attributable to cyclopentadienyl ligands at 115.5 and 117.6 ppm (Scheme 2). It is also noteworthy that attempts to react **4**–**6** with an additional equivalent of the siloxyl-bis(phosphinimine) ligand **2** failed to give either isolable macrocyclic or oligomeric products.

Subsequent alkylations of these metal halide derivatives **3**–**5** were probed. In the case of **3**, alkylation was effected by reaction with MeMgCl in THF to give an 82% yield of a yellow microcrystalline solid **7**. The $^{31}P\{^1H\}$ NMR spectrum of **7** gave rise to two resonances at 25.9 and 27.3 ppm. The ^1H NMR of **7** shows the ligand resonances as well as signals at 0.71 and 6.30 ppm, attributable to Ti-bound methyl and cyclopentadienyl groups. The presence of two sets of resonances at 0.44 and 0.57 ppm, attributable to $SiMe_2$ fragments, and at 1.17 and 1.27 ppm, arising from the $P(t\text{-}Bu)_2$ groups, were consistent with the monosubstitution of the ligand (Fig. 3). These data confirm the formulation of **7** as $[CpTiMe_2NP(t\text{-}Bu)_2CH_2SiMe_2OSiMe_2CH_2\ P(t\text{-}Bu)_2NSiMe_3]$.

Fig. 2. ORTEP drawing of **4**; 30% thermal ellipsoids are shown. Hydrogen atoms are omitted for clarity. Selected distances (Å) and angles (°) are Ti(1)–N(1) 1.767(6), Ti(1)–Cl(2) 2.315(2), Ti(1)–Cl(1) 2.323(2), Ti(2)–N(2) 1.767(5), Ti(2)–Cl(3) 2.306(2), Ti(2)–Cl(4) 2.316(2), P(1)–N(1) 1.611(6), P(2)–N(2) 1.628(5), Si(2)–O(1) 1.649(4), Si(2)–O(1) 1.649(4), N(1)–Ti(1)–Cl(2) 103.86(19), N(1)–Ti(1)–Cl(1) 102.82(19), Cl(2)–Ti(1)–Cl(1) 101.18(10), N(2)–Ti(2)–Cl(3) 102.15(18), N(2)–Ti(2)–Cl(4) 105.21(17), Cl(3)–Ti(2)–Cl(4) 100.78(9), P(1)–N(1)–Ti(1) 171.2(4), P(2) N(2)–Ti(2) 167.7(3), Si(1)–O(1)–Si2 149.3(3).

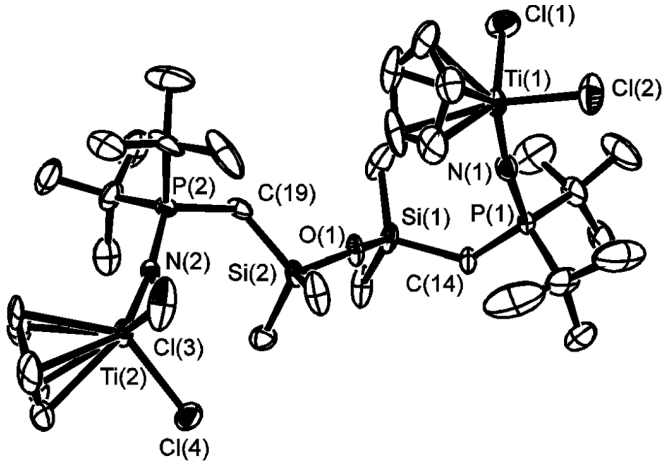
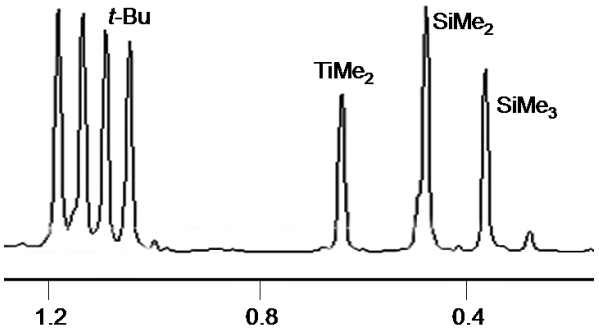


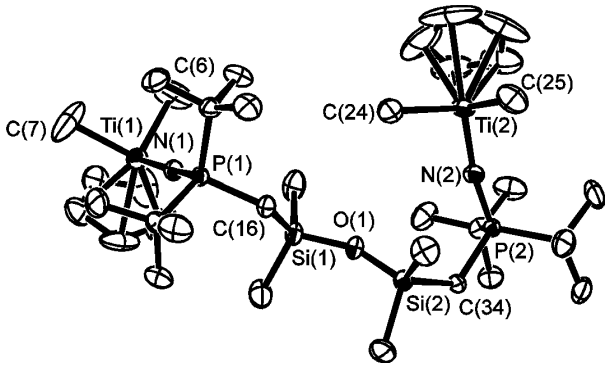
Fig. 3. Methyl region of the ^1H NMR spectrum of **7**.



In a similar fashion, akylation of **4** afforded the new species **8** in 73% yield. The compound **8** is soluble in aromatic and hydrocarbon solvents and gives rise to a $^{31}P\{^1H\}$ NMR resonance at 36.3 ppm as well as a ^1H NMR signal at 0.65 ppm, attributable to the Ti-bound methyl groups. The resulting formulation of **8** as $[CpTiMe_2NP(t\text{-}Bu)_2CH_2SiMe_2]_2O$ was subsequently confirmed by X-ray crystallography (Fig. 4). The metric parameters for **8** showed Ti–N distances of 1.802(3) and 1.805(3) Å, slightly longer than that seen in **4**. The corresponding P–N distances were shorter in **8** than those in **4**, averaging 1.585(3) Å, while the Ti–N–P angles in **8** were in a similar range to those in **4** being 170.98(19)° and 169.93(19)°. These metric differences were consistent with the replacement of the chlorine atoms by the electron-donating methyl groups. The Ti–C distances in **8** range from 2.114(5) to 2.136(5) Å, while the C–Ti–C angles were found to be 97.8(3)° and 95.3(2)°. The Si–O bonds in **7** were found to be only slightly shorter than those

© 2006 NRC Canada

Fig. 4. ORTEP drawing of **8**; 30% thermal ellipsoids are shown. Hydrogen atoms are omitted for clarity. Selected distances (Å) and angles (°) are Ti(1)–N(1) 1.802(3), Ti(1)–C(6) 2.126(6), Ti(1)–C(7) 2.128(6), Ti(2)–N(2) 1.805(3), Ti(2)–C(24) 2.114(5), Ti(2)–C(25) 2.136(5), Si(1)–O(1) 1.628(2), Si(2)–O(1) 1.625(3), P(1)–N(1) 1.586(3), P(2)–N(2) 1.583(3), N(1)–Ti(1)–C(6) 103.29(17), N(1)–Ti(1)–C(7) 103.2(2), C(6)–Ti(1)–C(7) 97.8(3), N(2)–Ti(2)–C(25) 103.51(18), C(24)–Ti(2)–C(25) 95.3(2), P(1)–N(1)–Ti(1) 170.98(19), P(2)–N(2)–Ti(2) 169.93(19), Si(2)–O(1)–Si(1) 155.10(18).

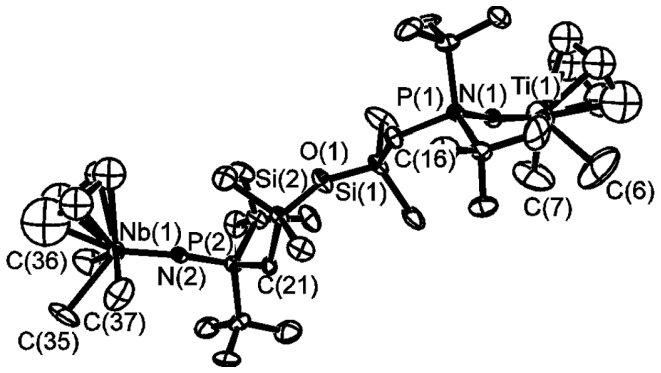


in **4**, being 1.628(2) and 1.625(3) Å, while the Si–O–Si angle is slightly larger at 155.10(18)°.

Alkylation of **5** with excess MeMgCl was also readily accomplished in a hexane suspension. The yellow product **9** was obtained in 81% yield and gave rise to a new $^{31}P\{^{1}H\}$ NMR signal at 39.6 ppm. The ^{1}H NMR spectrum revealed resonances at 1.01 and 5.62 ppm, attributable to Nb-bound methyl and cyclopentadienyl ligands, respectively. These data affirmed the formulation of **9** as $[CpNbMe_3NP(t\text{-}Bu)_2CH_2SiMe_2]_2O$ (Scheme 2). In a similar fashion, the full methylation of **6** resulted in the formation of a yellow crystalline solid **10**. Isolation afforded an overall yield of 68%. Two resonances were observed in the $^{31}P\{^{1}H\}$ NMR spectrum at 39.4 and 25.7ppm. Similarly, the ^{1}H and $^{13}C\{^{1}H\}$ NMR spectra reflected the dissymmetry of the molecule and confirmed the formulation of **10** as $[CpTiMe_2NP(t\text{-}Bu)_2CH_2SiMe_2OSiMe_2CH_2P(t\text{-}Bu)_2NCpNbMe_3]$. X-ray quality crystals were obtained by slow evaporation of a pentane solution. The dissymmetry of the molecule is reflected in the crystallographic data (Fig. 5). The Nb–N distance was found to be 1.850(8) Å, slightly longer than the corresponding Ti–N distance of 1.804(9) Å. Interestingly, the corresponding P–N distances are not distinct, both being 1.58(1) Å. This Nb–N is similar to that found in $NbCl_3(NPR_3)_2$ (R = Ph 1.827(4) (17), i-Pr 1.835(7) (18)). The corresponding metal–C distances were found to be 2.192(12), 2.236(14), and 2.249(14) Å for Nb and 2.097(17) and 2.25(2) Å for Ti. The remaining metric parameters of the ligand are similar to those seen above with a Si–O–Si angle of 150.7(5)°.

Reactivity of the bimetallic species was briefly probed. The complex **8** was shown to react with 1 equiv. of $B(C_6F_5)_3$ in BrC_6D_5. The resulting product **11** exhibits two $^{31}P\{^{1}H\}$ NMR signals at 39.5 and 39.6 ppm. ^{1}H NMR data for **11** shows signals at –0.04 and 0.55 ppm in a 1:2 ratio, which were attributed to Ti-bound methyl groups. These data support the formation of inequivalent Ti centers, although only one resonance at 5.99 ppm was attributable to the cyclopentadienyl ligands. ^{19}F resonances at –132.1, –164.4, and –166.8 ppm, together with the $^{11}B\{^{1}H\}$ resonance at –14.9 ppm, were consistent with the formation of the free anion $[MeB(C_6F_5)]$ and the formulation of **11** as $[(CpTiMe_2NP(t\text{-}Bu)_2CH_2SiMe_2)(CpTiMeNP(t\text{-}Bu)_2CH_2SiMe_2)O][MeB(C_6F_5)]$. It is noteworthy that monometallic cations exhibit a downfield shift of the $^{31}P\{^{1}H\}$ resonance relative to that of monometallic precursors $CpTi(NPR_3)Me_2$ (19). In the case of **11**, the similarity of the two $^{31}P\{^{1}H\}$ NMR signals and the symmetry of the ^{1}H NMR spectrum suggests the possibility of cyclic structure (Scheme 3 (a)) where the ^{1}H NMR resonance at –0.04 ppm is attributable to the bridging methyl group. Further spectral data collected at –30 °C yielded no further structural information for this very sensitive product. Repeated attempts to isolate X-ray quality crystals of this product were unsuccessful and thus precluded the unambiguous confirmation of this structural proposition. Attempts to probe the related chemistry of **10** afforded complex mixtures of products, suggesting that methyl abstraction from either Ti or Nb results in the formation of mixture of methyl-bridged oligomers. However, this proposition could not be confirmed.

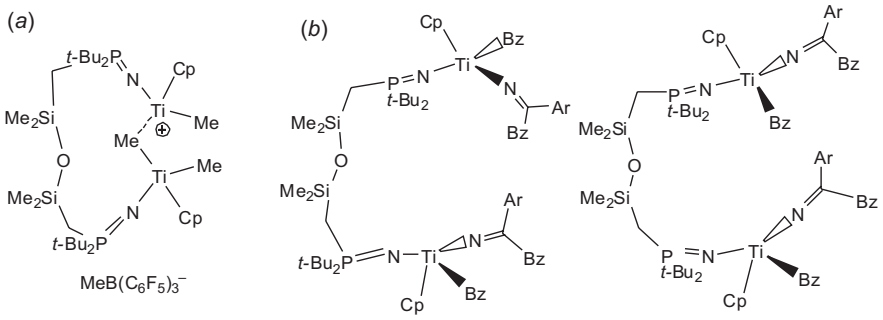
Fig. 5. ORTEP drawing one of the two molecules in the asymmetric unit of **10**; 30% thermal ellipsoids are shown. Hydrogen atoms are omitted for clarity. Selected distances (Å) and angles (°) are Nb(1)–N(2) 1.850(8), Nb(1)–C(37) 2.192(12), Nb(1)–C(36) 2.236(14), Nb(1)–C(35) 2.249(14), Ti(1)–N(1) 1.804(9), Ti(1)–C(7) 2.097(17), Ti(1)–C(6) 2.25(2), P(1)–N(1) 1.575(9), P(1)–C16 1.803(10), P(2)–N(2) 1.574(8), Si(1)–O(1) 1.616(7), Si(1)–C17 1.846(13), Si(1)–C16 1.863(11), Si(1)–C18 1.876(14), Si(2)–O(1) 1.624(7), N(2)–Nb(1)–C(37) 92.6(5), N(2)–Nb(1)–C(36) 95.8(5), C(37)–Nb(1)–C(36) 135.5(8), N(2)–Nb(1)–C(35) 122.9(7), C(37)–Nb(1)–C(35) 70.0(8), C(36)–Nb(1)–C(35) 68.8(8), N(1)–Ti(1)–C(7) 107.0(7), N(1)–Ti(1)–C(6) 102.2(9), C(7)–Ti(1)–C(6) 77.9(12), P(1)–N(1)–Ti(1) 169.0(6), P(2)–N(2)–Nb(1) 173.5(5), Si(1)–O(1) Si(2) 150.7(5).



Compound **4** was also alkylated with BzMgCl to give the species $[CpTiBz_2NP(t\text{-}Bu)_2CH_2SiMe_2]_2O$ **12** in 65% yield as an orange solid. The $^{31}P\{^{1}H\}$ NMR spectrum of **12** was observed as a singlet at 36.3 ppm. The ^{1}H NMR data showed the expected resonances including two doublets at 2.69 and 2.82 ppm attributable to the metal-bound methylene groups. The corresponding $^{13}C\{^{1}H\}$ resonance was seen at 71.7 ppm. Compound **12** was shown to react with 2 equiv. of $NC(2,6\text{-}Me_2C_6H_3)$ upon stirring for 1 h at 25 °C in toluene. Work-up afforded a new species **13** in 68% yield, which gave rise to a single new $^{31}P\{^{1}H\}$ resonance at 26.5 ppm.

© 2006 NRC Canada

Scheme 3. (*a*) Proposed structures of **11** and (*b*) diastereomers of 13.



The ^{1}H and $^{13}C\{^{1}H\}$ NMR data are consistent with the formation of a 1:1 mixture of diastereoisomers formulated as $[CpTiBz(N{=}C(CH_2Ph)(2,6\text{-}Me_2C_6H_3))NP(t\text{-}Bu)_2CH_2SiMe_2]_2O$ **13a** and **13b** (Scheme 3(b)). The chirality results from the insertion of the nitrile into one of the Ti-Bz groups on each of the Ti centers of **13**. As an example, this is evidenced by the observation of benzylic ^{1}H resonances observed at 3.04, 3.13, 3.72, and 3.79 ppm as well as peaks at 5.82 and 5.83 attributable to the cyclopentadienyl rings.

In summary, the new bis(phosphinimide) siloxy-based ligand described herein affords synthetic pathways to linked phosphinimide mono- and bi-metallic complexes as well as heterobimetallic species. The chemistry of related phosphinimide compounds continues to be the subject of study in our laboratories.

Acknowledgments

Financial support from the Natural Sciences and Engineering Research Council of Canada (NSERC) and NOVA Chemicals Corporation (Calgary, Alberta) is gratefully acknowledged.

References

1. D.W. Stephan, F. Guerin, R.E.v.H. Spence, L. Koch, X. Gao, S.J. Brown, J.W. Swabey, Q.Wang, W. Xu, P. Zoricak, and D.G. Harrison. Organometallics, **18**, 2046 (1999).
2. D.W. Stephan, J.C. Stewart, S.J. Brown, J.W. Swabey, and Q. Wang. *In* High temperature solution polymerization of olefins in the presence of metallocene catalyst system. EP, 983043134. 1998.
3. D.W. Stephan, J.C. Stewart, F. Guerin, R.E.v.H. Spence, W. Xu, and D.G. Harrison. Organometallics, **18**, 1116 (1999).
4. D.W. Stephan, J.C. Stewart, and D.G. Harrison. *In* Supported phosphinimine-cyclopentadienyl catalysts for polymerization of olefins. EP, 983053521. 1998.
5. D.W. Stephan. Organometallics, **24**, 2548 (2005).
6. M.J. Sarsfield, M. Said, M. Thornton-Pett, L.A. Gerrard, and M. Bochmann. J. Chem. Soc. Dalton Trans. 822 (2001).
7. R.P.K. Babu, R. McDonald, and R.G. Cavell. J. Chem. Soc. Dalton Trans. 2210 (2001).
8. R.P.K. Babu, R. McDonald, and R.G. Cavell. Chem. Commun. (Cambridge), 481 (2000).
9. R.P.K. Babu, R. McDonald, S.A. Decker, M. Klobukowski, and R.G. Cavell. Organometallics, **18**, 4226 (1999).
10. R.G. Cavell, R.P.K. Babu, A. Kasani, and R. McDonald. J. Am. Chem. Soc. **121**, 5805 (1999).
11. L. Morello, P. Yu, C.D. Carmichael, B.O. Patrick, and M.D. Fryzuk. J. Am. Chem. Soc. **127**, 12796 (2005).
12. E. Hollink, J.C. Stewart, P. Wei, and D.W. Stephan. J. Chem. Soc. Dalton Trans. 3968 (2003).
13. U. Siemeling, L. Koelling, O. Kuhnert, B. Neumann, A. Stammler, H.-G. Stammler, H.G. Fink, E. Kaminski, A. Kiefer, and R.R. Schrock. Z. Anorg. Allg. Chem. **629**, 781 (2003).
14. U. Siemeling, L. Koelling, A. Stammler, and H.-G. Stammler. J. Chem. Soc. Dalton Trans. 3277 (2002).
15. D.T. Cromer and J.B. Mann. Acta Crystallogr. Sect. A, **24**, 321 (1968).
16. H. Schmidbaur and W. Tronich. Chem. Ber. **101**, 3556 (1968).
17. F. Weller, D. Nusshar, and K. Dehnicke. Z. Anorg. Allg. Chem. **615**, 1563 (1992).
18. G. Philipp, K. Harms, K. Dehnicke, C. Maichle-Mossmer, and U. Abram. Z. Anorg. Allg. Chem. **622**, 1927 (1996).
19. D.W. Stephan, J.C. Stewart, F. Guerin, S. Courtenay, J. Kickham, E. Hollink, C. Beddie, A. Hoskin, T. Graham, P. Wei, R.E.v.H. Spence, W. Xu, L. Koch, X. Gao, and D.G. Harrison. Organometallics, **22**, 1937 (2003).

© 2006 NRC Canada

Regioselectivity of glycoluril-directed Claisen condensations — A kinetic and mechanistic study of substituent effects in the nucleophilic acyl group

Mei Chen, Katie Won, Robert S. McDonald, and Paul H.M. Harrison

Abstract: The Claisen-like condensation of a series of 1-arylacetyl-6-acetyl-3,4,7,8-tetramethylglycolurils (Ar = Ph, *p*-$OMeC_6H_4$, and *p*-ClC_6H_4) was studied in preparative experiments and by analysis of kinetic data. The reactions proceeded in virtually quantitative yield and were highly regioselective: the corresponding *N*-(2′-aryl-3′-ketobutanoyl)-3,4,7,8-tetramethylglycolurils were obtained in all cases, with none of the 4′-aryl regioisomers being detected. Clean bimolecular kinetics were observed for each conversion using UV spectroscopy. Reaction rates followed the order Ar = *p*-$OMeC_6H_4$ < Ph < *p*-ClC_6H_4. The results are explained by a mechanism in which the deprotonation of the substrates is rate-limiting; thus, deprotonation of the arylacetyl groups is favoured. The ensuing enolate reacts rapidly in the C–C bond-forming step.

Key words: glycoluril, biomimetic, Claisen condensation, regioselectivity, kinetics, mechanism, substituent effects.

Résumé : On a étudié la condensation de type Claisen d'une série de 1-arylacétyl-6-acétyl-3,4,7,8-tétraméthylglycoluriles (Ar = Ph, *p*-$MeOC_6H_4$ et *p*-ClC_6H_4) dans des expériences préparatives ainsi que par l'analyse de données cinétiques. Les réactions se produisent avec des rendements pratiquement quantitatifs et un grande régiosélectivité; dans tous les cas, on a obtenu les *N*-(2′-aryl-3′-cétobutanoyl)-3,4,7,8-tétraméthylglycoluriles et on n'a pas pu détecter la présence du régioisomère 4′-aryle. Pour chacune des conversions, en faisant appel à la spectroscopie UV, on a observé une cinétique bimoléculaire propre. Les vitesses des réactions sont dans l'ordre Ar = *p*-$MeOC_6H_4$ < Ph < *p*-ClC_6H_4. Les résultats sont expliqués par un mécanisme dans lequel la déprotonation des substrats correspond à l'état cinétiquement limitante; la déprotonation des groupes arylacétyles est donc favorisée. L'énolate qui en résulte réagit rapidement dans l'étape de formation de la liaison C–C.

Mots clés : glycourile, biomimétique, condensation de Claisen, régiosélectivité, cinétique, mécanisme, effets de substituants.

[Traduit par la Rédaction]

Introduction

The Claisen condensation is one of the fundamental C–C bond forming reactions in organic chemistry (1). However, remarkably, the mechanism of this process has not been extensively explored by kinetics experiments despite a number of studies of the related aldol and Claisen–Schmidt reactions (2). This may be in part a result of problems associated with the characteristics of enolates, such as self association and variation of metal coordination, which can give rise to complex kinetic schemes (3).

Although there are reports of catalysts that circumvent the problem of regioselectivity, the modest yields and mixtures of the products obtained in many crossed-Claisen condensations have discouraged the use of this method in synthesis (4). Nonetheless, many natural processes, e.g., the formation of acetoacetyl-coenzyme A from two moles of acetyl-CoA by acetoacetyl-CoA thiolase, proceed through highly efficient Claisen-like mechanisms (5). A related reaction in vivo, which occurs during the biosynthesis of polyketides and fatty acids, is the Claisen-like decarboxylative condensation of malonate and acyl units attached to the fatty acid synthase (FAS) or polyketide synthase (PKS) (6).

Some time ago, we developed an efficient intramolecular Claisen-like condensation between two acyl groups, that were pre-assembled onto 3,4,7,8-tetramethylglycoluril (**1a**) (7) or its dithio congener (**1b**) (8) (Scheme 1); this process allows efficient and selective monoacylation to afford, e.g., **2a**, then a second acylation to give, e.g., **3a** ensues under

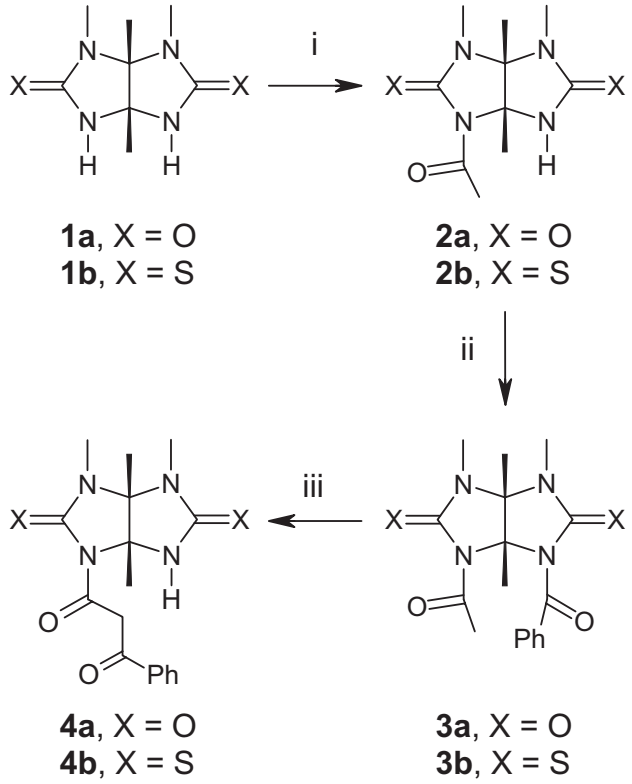
Received 12 July 2006. Accepted 9 September 2006. Published on the NRC Research Press Web site at http://canjchem.nrc.ca on 3 November 2006.

M. Chen, Department of Chemistry, McMaster University, 1280 Main Street West, Hamilton, ON L8S 4M1, Canada; School of Chemistry and Chemical Engineering, Sun Yat-Sen University, Guangzhou 510275, People's Republic of China.
K. Won, and P.H.M. Harrison.[1] Department of Chemistry, McMaster University, 1280 Main Street West, Hamilton, ON L8S 4M1, Canada.
R.S. McDonald.[2] Department of Chemistry and Physics, Mount St. Vincent University, Halifax, NS B3M 2J6 Canada.

[1]Corresponding author (email: pharriso@mcmaster.ca).
[2]Joint principal corresponding author.

 doi:10.1139/V06-147 © 2006 NRC Canada

Scheme 1. Reagents: (*i*) $(CH_3CO)_2O$, reflux or *n*-BuLi, THF, reflux, then CH_3COCl, RT; (*ii*) *n*-BuLi, THF, 0 °C, then PhCOCl, 0 °C to RT; (*iii*) KO*t*-Bu, THF, 0 °C to RT; for kinetics experiments: 50:50 *tert*-BuOH – THF, 25 °C, then KO*t*-Bu.



more forcing conditions. The condensation between the acetyl and aroyl moieties to give the β-ketoacyl derivatives, which mimics some features of FAS and PKS, was shown to proceed efficiently in >95% yield; thus, **3a** gives, e.g., **4a** (9). The methodology is amenable to an iterative approach to the chemical synthesis of fatty acids and polyketides in a sequence of reactions that mimics several features of the biosynthesis of this important class of natural products. The regioselectivity of the condensation reaction was examined in preparative experiments (7, 8); although the regioselectivity could be altered and even reversed by altering the glycoluril, the results generally showed a preference for deprotonation at the smaller of two acyl groups. However, the mechanistic origin of the observed regioselectivity was unclear. Because an understanding of regiocontrol is important in designing improved methodology based on the glycoluril, we initiated a program to explore the mechanism of the reaction.

In previous work, we demonstrated that the progress of this Claisen-like condensation could be monitored readily by UV spectroscopy. The kinetics of this reaction were explored for acetyl aroyl glycolurils (e.g., **3a**) (10) and their dithio congeners (e.g., **3b**) (11); the results showed that substituents on the aroyl moiety influenced the overall rate of condensation, with electron-withdrawing groups accelerating the process. These and other results, from deuterium isotope effects in the acetyl methyl group, support a mechanism in which initial deprotonation of substrate (step 1, k_1) is partially reversible, and is followed by nucleophilic attack of the ensuing enolate (**5**) onto the acceptor aroyl moiety, which behaves as the electrophile in this case (step 2, k_2) (Scheme 2). Depending on the aroyl substituent and the glycoluril structure, step 1 or step 2 were shown to be the rate-limiting steps. The collapse of tetrahedral intermediate **6** via **7** to **8** was assumed to be fast, based on precedents found in the literature (12). The conjugated enolate **8** is the species observed as the final product in the kinetics experiments in the UV cell; neutral products **4** are formed during acidic work-up in preparative experiments.

We were intrigued to determine whether substituents on the nucleophilic donor acyl moiety might influence the rate of condensation, as opposed to the previously studied effects on the electrophilic acyl acceptor unit. We expected that knowledge of this influence would shed mechanistic light on the origin of regioselectivity in the condensation process. Therefore, we prepared a series of acetyl arylacetyl glycoluril derivatives (**9**–**11**) for further kinetic analysis. However, prior to performing the kinetics experiments, it was unclear whether these compounds would condense with the desired regioselectivity, i.e., would these reactions proceed under thermodynamic or kinetic control, and, if the latter, would deprotonation occur at the phenylacetyl group to give **12**–**14**, or at the acetyl moiety to give **15**–**17** (Scheme 3)? Therefore, we first investigated the regiochemical outcome of these condensations in preparative experiments and then used kinetics to explain the observed regiochemistry. The results of these experiments are described herein.

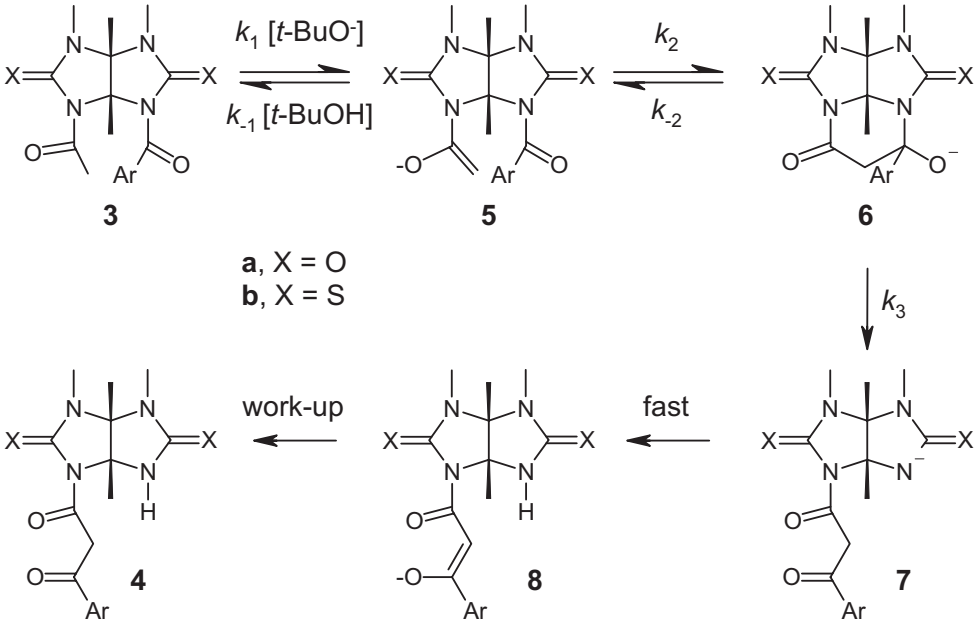
Results

Compounds **9**–**11** were readily prepared by treatment of monoacetylglycoluril **2a** with the appropriate acid chloride. Each compound was then treated with potassium *tert*-butoxide in a preparative experiment. The condensation products were isolated and purified.

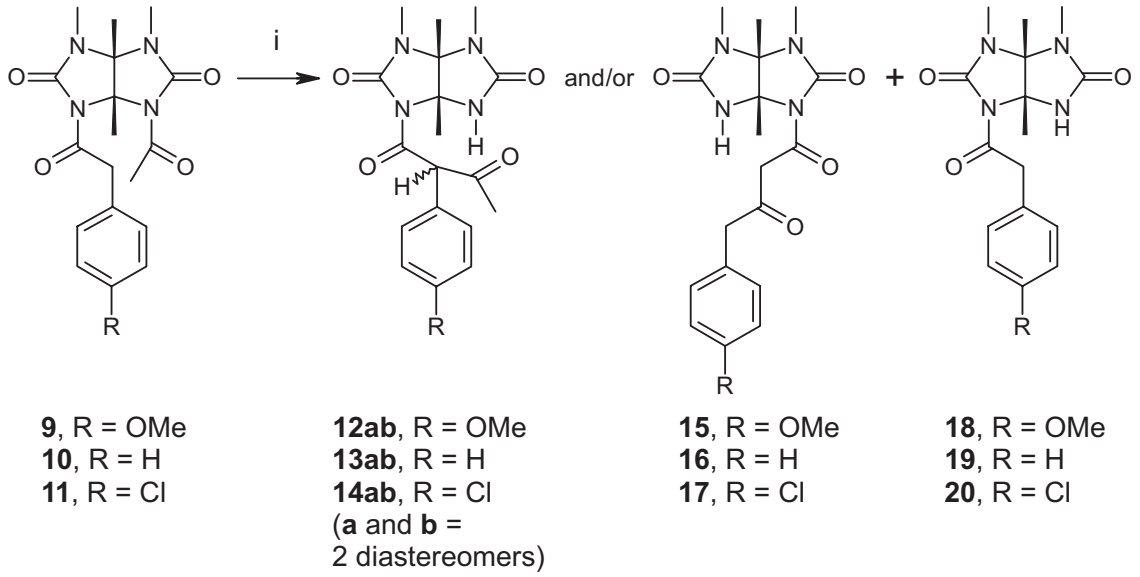
NMR analysis of these samples showed, in all three cases, a pair of closely related products in a ratio of approx.1:2 (**12**–**14a**, **12**–**14b**, respectively). A trace impurity was detected in all cases; however, this did not correspond to the regioisomeric condensation products **15**–**17**, which were clearly absent from the spectra, but rather to the arylacetylglycolurils (**18**–**20**) in which the acetyl group had been cleaved from the starting material, presumably by solvolysis. Notably, each proton NMR spectrum showed two singlets at about 5.8 ppm, which were tentatively assigned to H-2′ in the two diastereomeric forms of **12**–**14** (Table 1), along with a pair of singlets at 2.1 ppm, which by chemical shift comparison with previous condensation products could be assigned to methyl groups C-4′ in the two diastereomers. Further purification and NMR examination, including COSY, HSQC, and HMBC experiments, confirmed each structure unambiguously. The results of these experiments for the side-chain part-structure of **13** are shown in Fig. 1; a full spectral assignment for **13** is given in Table 1. NMR data for **12** and **14** were essentially identical to that for **13**, except in the aryl group. Mass spectral data further confirmed the structures; each sample exhibited a prominent fragment ion at *m*/*z* [M – 42] corresponding to the loss of CH_2CO, a fragmentation that is possible for **12**–**14**, but not for regioisomers **15**–**17**. Intriguingly, there was no evidence for

© 2006 NRC Canada

Scheme 2. Proposed mechanism for the intramolecular Claisen-like condensation of **3** to give **4**.



Scheme 3. Intramolecular Claisen-like condensations of acetyl arylacetyl glycolurils **9–11** to give the observed products **12–14** as a mixture of diastereomers **a** and **b**. Regioisomers **15–17** were not observed. Reagent: KO*t*-Bu, THF, 0 °C to RT; for kinetics experiments: 50:50 *tert*-BuOH – THF, 25 °C, then KO*t*-Bu.



enolization of any of the three condensation products, despite the observation of enol contents up to ~50% in other β-ketoacylglycolurils that we prepared in previous work (7–11).

Nonetheless, when a dilute solution of condensation products **12–14** in THF–*tert*-butanol was treated with excess potassium *tert*-butoxide in a quartz UV cell, substantial spectral changes occurred. For example, a new strong absorbance peak centred at 309 nm was observed in the base-treated solution of **13** (Fig. 2, panels B vs. D), indicating the formation of the enolate by deprotonation of the condensation product. The spectrum of the starting diacylglycoluril **10** was recorded in the same solvent (Fig. 2, panel A), and then the sample was treated with KO*t*-Bu. After completion of reaction, the spectrum in panel C was recorded. In this case, the spectrum resembles that of panel D, indicating that KO*t*-Bu induced the conversion of **10** to **13**. Similar results were obtained for conversion of **9** to **12** and **11** to **14**.

Next, the yield for the conversion in the cell was estimated. The extinction coefficient for the enolate of product **13** was calculated from the UV spectrum, assuming complete deprotonation. This coefficient was then used to determine the concentration of condensation product that had been formed by the base treatment of **10**. Comparing this concentration with the known starting concentration of **10** in the spectrometer cell gave an estimate of the yield of the conversion of **10** to **13** in the cell, namely 81%. A similar

© 2006 NRC Canada

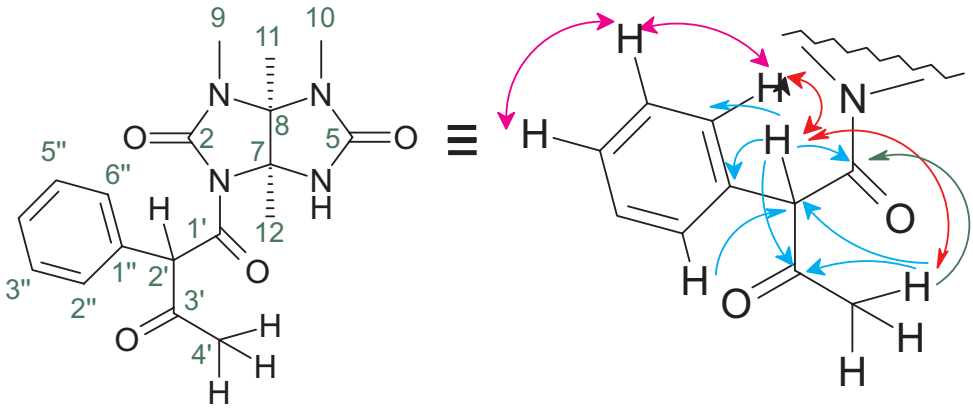
Table 1. ^{13}C and ^{1}H NMR assignments of the diastereomeric condensation products **13a** and **13b**.

Carbon[a]	δ ^{13}C (**13a**)	δ ^{13}C (**13b**)	δ ^{1}H (**13a**) (minor)	δ ^{1}H (**13b**) (major)
3′	201.64	202.73		
1′	168.71	168.57		
5	156.99	157.14		
2	153.15	153.15		
1″	132.01	131.53		
2″/6″	130.33	130.40	7.20–7.29 (m, 2H)	7.20–7.29 (m, 2H)
4″	128.80	128.80	7.30–7.40 (m, 3H)	7.30–7.40 (m, 3H)
3″/5″	128.33	128.39	7.30–7.40 (m, 3H)	7.30–7.40 (m, 3H)
7	78.74	78.87		
8	76.70	76.70		
6-NH			6.07 (s, 1H)	5.88 (s, 1H)
2′	65.64	65.93	5.89 (s, 1H)	5.72 (s, 1H)
4′	28.95	28.95	2.11 (s, 3H)	2.14 (s, 3H)
9	27.14	27.14	2.96 (s, 3H)	2.97 (s, 3H)
10	26.64	26.44	2.85 (s, 3H)	2.82 (s, 3H)
12	19.92	19.05	1.60 (s, 3H)	1.75 (s, 3H)
11	15.93	15.74	1.52 (s, 3H)	1.53 (s, 3H)

Note: The diastereomers are formed as a racemic mixture. It was not possible to determine relative stereochemistry in the present work; the compounds are designated a and b for the minor and major products, respectively.

[a]For the compound numbering system, see Fig. 1.

Fig. 1. Structure of diastereomers (**13a** and **13b**) showing the numbering sequence. Critical connectivities identified within the β-ketoacyl group are shown: magenta = COSY; red = weaker, long-range correlation observed in the COSY spectrum; cyan = HMBC; green = weaker, 4-bond correlation observed by HMBC. 1-bond heteronuclear shift correlations were also observed for each protonated carbon, but are not shown for clarity. Each correlation was observed in both of the diastereomers (**a** and **b**).



calculation for the conversion of **9** to **12** gave a value of 86% (Table 2). Although the errors in these calculations are estimated to be ~10% (largely due to errors in weighing the two substrates), it is apparent that in each case the condensation reaction within the UV cell proceeds in high yield and with at least predominantly the same regioselectivity as was observed in the preparative experiments. Therefore, the dramatic change in conditions (temperature, solvent, and concentrations) between the preparative and the kinetics experiments does not alter the reaction outcome.

The kinetics of each reaction was observed through monitoring the conversion of each substrate into product, i.e., at the λ_{max} of the product enolate determined as described above. In the presence of excess base, the reaction progress curves were readily observed and could be fit to pseudo first-order kinetics, giving a pseudo first-order rate constant k_{obs}, as we described previously (7). Next followed a series of experiments using **9** and **10** as substrates in which the [KO*t*-Bu] was varied. Both plots of k_{obs} vs. base concentration were linear, indicating that the processes were first-order in base. Therefore, the apparent second-order rate constant, k_{app}, could be determined for each substrate, either from the slope of the plots, or by dividing measured k_{obs} values by base concentration. The results are summarized in Table 2, along with an estimate of error in k_{app} from three replicate experiments. Also shown is k_{rel}, the rate constant relative to that for **9**, from a separate series of experiments with each substrate in which the same stock solution of base was used. This latter treatment removes errors in the estimation of the base concentration between different base stock solutions and gives values which allow for a better comparison between the three analogues. Although the results vary

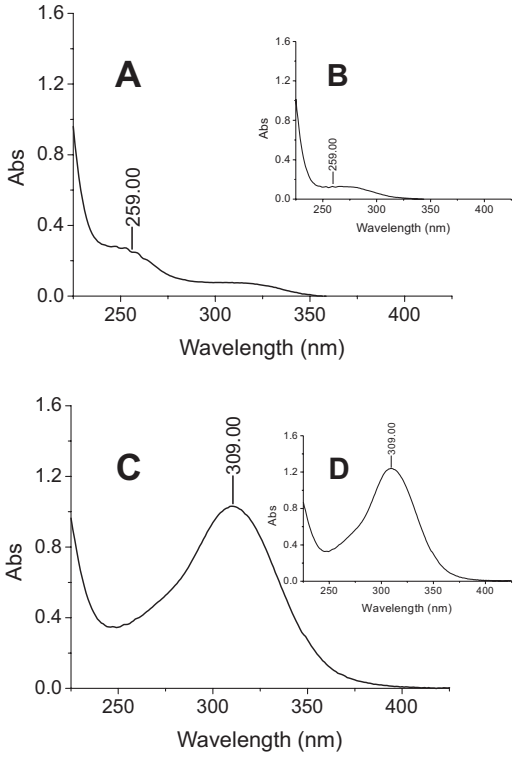
© 2006 NRC Canada

Table 2. Rate constants for conversion of diacylglycolurils **9–11** to β-ketoacylglycolurils **12–14**, respectively.

Compound	Substituent in the aryl group	λ_{max}[a] (nm)	k_{app}[b] (L mol^{-1}s^{-1})	k_{rel}[c] (L mol^{-1}s^{-1})	yield %[d]
9	*p*-OMe	310	71±10	1	86±10
10	H	309	148±5	1.6	81±10
11	*p*-Cl	311	165±15	2.1	ND[e]

[a]Wavelength of maximum absorption of the product, used for monitoring all kinetics experiments; determined by treatment of synthetic product with potassium *tert*-butoxide (5–10 equiv.).
[b]Apparent rate constant determined from an average of three experiments (/compound).
[c]Relative rate constant determined by the comparison of **9** (k_{rel} = 1), **10**, and **11** using the same base solution.
[d]Value obtained by the comparison of spectra from kinetic runs with those of authentic, synthetic product.
[e]Not determined.

Fig. 2. UV spectra for (A) substrate **10** (acetyl phenylacetyl glycoluril) in THF–*t*-BuOH (50:50); (B) synthetic condensation product **13** in the same solvent; (C) sample in A treated with excess KO*t*-Bu and allowed to react; (D) sample in B treated with excess KO*t*-Bu.



quantitatively depending on the method of determination, in all cases the qualitative order of reactivity was **9 < 10 < 11**.

Discussion

At the outset of this investigation, we had shown in preparative experiments that the glycolurils **1a** and **1b** acted as efficient auxiliaries to allow high-yield Claisen-like condensations between two acyl groups. The present results extend these observations. Although the yields for attachment of the arylacetyl moieties to the glycoluril were not optimized, the key C–C bond forming reaction, i.e., the condensation step, proceeds with the same high efficiency observed in previous cases, giving isolated yields of 80–96%. It is also noteworthy that these yields are not reduced by dilution, even under the highly diluted conditions of the kinetics experiments. The chemical yields were shown by UV spectroscopy to be in excess of 80%.

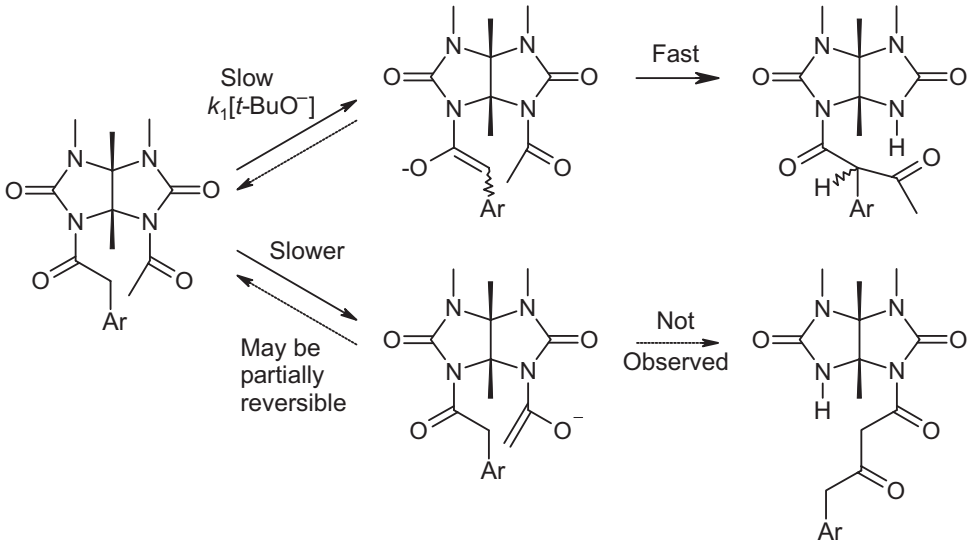
Furthermore, previous synthetic experiments in which the two acyl groups were not equivalent showed that the condensation process was moderately regioselective, e.g., in a competition between an acetyl and a butanoyl group attached to **1**, the dominant product was that in which the acetyl group was deprotonated, and the butanoyl group acted as the electrophilic partner in the condensation. Because it was unclear which of the regioisomers would predominate for **9–11**, we initially explored the condensation reaction in preparative experiments. The results illustrate an unprecedented level of regiocontrol, with clean conversion to condensation products **12–14** and no detectable amounts of regioisomers **15–17** being formed (Scheme 4). Thus, the reactions are highly selective in favour of deprotonation at the arylacetyl group, with nucleophilic attack of the ensuing enolates onto the carbonyl group of the acetyl moieties. This is clearly the case even with electron-donating groups in the aromatic ring. All three compounds studied gave products of the same regiochemical orientation. Together with the high chemical yield, these results illustrate the ruggedness of the glycoluril methodology and bode well for further applications in synthesis.

Despite the prior and current observations of regioselectivity in this system, the mechanistic origin of this effect remained speculative. We formerly discussed the possibility that the deprotonation of acetyl butanoyl glycoluril was under kinetic control, and thus the easiest formed enolate, i.e., that of the acetyl moiety, would dominate. However, we also noted that the process could be controlled by the condensation step (step 2). In this case, the deprotonation could be reversible, but the enolate that reacts fastest in step 2 (i.e., presumably also the acetyl enolate on steric grounds) would lead to the dominant product. Finally, the process could be under overall thermodynamic control, with the relative stability of the two regioisomeric enolate products determining their ratio. These possibilities could not be readily distinguished from the preparative experiments but are important to resolve to make logical predictions in applying this methodology in synthesis.

We investigated the mechanism of the condensation reaction using kinetics experiments. The glycoluril system provided clean, bimolecular kinetics, and this was also observed for each compound in the present study. Thus, there is no need to take into account the association of the enolate in the present case, allowing for simpler interpretation of the data. This lack of apparent association may be the result of the low enolate concentration in the present experiments: the

© 2006 NRC Canada

Scheme 4. Proposed kinetic scheme for the intramolecular Claisen-like condensations of **9–11** to give **12–14**.



enolate reacts as soon as it is formed. A variety of previous results indicated that either step 1, i.e., deprotonation of substrate, or step 2, i.e., the key C–C bond forming step, could control the rate of the overall reaction (Scheme 2). Notably, if step 1 is endothermic and rate-limiting, then $k_{app} = k_1$, while a pre-equilibrium with step 2 as the rate-limiting step has kinetics of the same order but a different value for k_{app}, i.e., $k_{app} = (k_1k_2 / k_{-1})/[t\text{-BuOH}]$. These different situations are reflected in different substituent effects, deuterium kinetic isotope effects, and deuterium exchange.

However, all substrates reported in kinetics experiments to date were either symmetric (two acetyl groups) or had an acetyl and an aroyl group. In these cases, there is only one possible product, and so the issue of regioselectivity and its control had not been explored. Therefore, we wished to extend the kinetics approach to explore a system that could potentially lead to two regioisomeric condensation products; to measure the rates of reaction for quantitative comparison with the known systems; to determine what step(s) control(s) the rate and, therefore, the regiochemical outcome; and to provide a facile method to explore whether reaction conditions can be varied to control the regiochemical outcome.

We selected the acetyl arylacetyl glycolurils **9–11** for kinetic exploration, reasoning that the anticipated conjugation of the aryl moieties with the enolates of one regioisomeric condensation product (**12–14**) would give rise to UV absorption at a substantially different wavelength than that for the enolates of regioisomers **15–17**, where the aryl unit is isolated from the enolate component. Furthermore, the aryl moiety allows the introduction of substituents at the remote *p*-position to explore electronic effects on the reaction rate.

While deprotonation at the arylacetyl moiety should be favoured because of the greater thermodynamic stability of the resonance-stabilized enolate over the unstabilized enolate formed by deprotonation of the acetyl moiety (Scheme 4, step 1), this stabilized enolate might also be expected to react more slowly in the condensation step (Scheme 4, step 2). Furthermore, if the deprotonation were to occur under kinetic control, it is less obvious which enolate would be favoured. Sterically, the acetyl moiety is more accessible, but the aryl group might also stabilize the transition state leading to deprotonation at the phenylacetyl group.

In the control experiments, we compared the UV spectra of the observed enolates produced from the kinetics experiments with those obtained from deprotonation of the authentic, synthetic products. They were qualitatively identical, and a quantitative comparison of the spectra showed that the kinetics experiments were forming the same regioisomer as the synthetic work, in a yield of at least 80–90%. Therefore, the measured rate constants represent those for the dominant reaction, i.e., for the formation of **12–14**.

As seen in Table 2, all three rate constants k_{app} for the acetyl arylacetyl glycolurils are 10-fold to 20-fold larger than that for the diacetyl analogue (8.6 L mol^{-1} s^{-1} (11)); therefore, the presence of the aryl group accelerates the overall reaction. It follows that the observed regioselectivity results from an overall rate *acceleration* relative to the diacetyl analogue because of the presence of the aryl moiety and *not* from a reduction in the rate of condensation of the acetyl enolate (i.e., it is not due to a smaller rate constant for step 2 (Scheme 2, k_2) for the acetyl enolate than for the phenylacetyl enolate, Scheme 4). The latter effect might reasonably have accounted for selectivity because the nucleophilic attack of the acetyl enolate onto the phenylacetyl group might be expected to suffer from steric effects compared with the corresponding reaction of the diacetyl compound. The observed rate acceleration also argues against the reaction proceeding through initial fast formation of **15–17**, followed by thermodynamic rearrangement to **12–14**. Because deprotonation at the acetyl group would be the obligatory first step, this process would be expected to proceed at an overall rate comparable to or slower than that for the diacetylglycoluril. Therefore, the regioselectivity is determined kinetically.

A comparison of the three rate constants for **9**, **10**, and **11** is also revealing: the values for k_{app} are larger with an electron-withdrawing group (*p*-Cl) and smaller with an electron-donating group in the aryl ring. These observations are consistent with the stabilization of the negative charge in the key rate-determining transition state, and imply that step 1,

© 2006 NRC Canada

i.e., the deprotonation of the substrate, is important in determining the overall rate of reaction (Scheme 4). The results are not consistent with a rate-determining step 2 for the reaction of the aryl enolate, where an inverse effect of substituent would be expected, but rather are best described in terms of a rate-limiting deprotonation followed by a rapid intramolecular C–C bond forming step. Assuming that the deprotonation of the acetyl group of **9**–**11** proceeds at approximately the same rate as for the diacetyl analogue, then the regioselectivity of the condensation can be estimated from the relative rates after allowing for the two acetyl groups in the diacetyl compound. This gives a predicted selectivity, ranging from 21:1 for **9** to 42:1 for **11**, consistent with the high level of selectivity observed in the preparative experiments.

We note that the reactions described herein can proceed through either an *E* or a *Z* enolate and that there is a number of diastereomeric transition states for step 2. The present results do not shed light on these issues, and it must be noted that the rate constants are overall constants for each step irrespective of whether the reaction proceeds through a single stereoisomeric path or multiple ones. We hope to investigate the cryptic stereochemistry of this process through further experiments.

In summary, the results show that the condensation reaction under the conditions used in the kinetics experiments proceeds by slow enolate formation at the phenylacetyl group to give a stabilized enolate, a process that is nonetheless fast compared with deprotonation at the acetyl moiety. The enolate is still capable of rapid intramolecular attack onto the acetyl carbonyl group in step 2. The high rate of this step, compared with the acetyl aroyl glycolurils where step 2 is at least partially rate-determining, may be due to the higher electrophilicity of the acetyl moiety compared with the aroyl carbonyl group. Thus, step 1 is the rate-determining step, but we cannot yet establish unambiguously whether this is a kinetic or an equilibrium effect, i.e., whether $k_2 > k_{-1}[t\text{-BuOH}] > k_1$ or $k_{-1}[t\text{-BuOH}] > k_2 > k_1$. Further work to explore the latter issue, as well as whether other factors can alter the rate-determining step, including a study of the temperature dependence of the reaction rates, are in progress. The results will be reported soon.

Conclusion

The crossed-Claisen-like condensation of an arylacetyl and an acetyl group is promoted by the attachment of these moieties to the N1 and N6 positions of 3,4,7,8-tetramethylglycoluril. The process proceeds rapidly under mild conditions to give exclusively the regioisomer resulting from the deprotonation at the arylacetyl group. Kinetics experiments show that the first deprotonation step is rate-determining and that the origin of the regioselectivity lies in the ease of deprotonation of the phenylacetyl versus the acetyl moiety. Because the C–C bond forming step is fast, the relative rates of this step leading to each regioisomer do not influence the overall regiochemical outcome of the reaction.

Experimental

General

General conditions for the preparation and characterization of the glycoluril derivatives were as previously described. THF was distilled from sodium–benzophenone. *tert*-Butanol was purchased from Fisher (Nepean, ON, Canada). Potassium *tert*-butoxide was obtained from Alfa Aesar (Ward Hill, MA, USA). All glassware was oven-dried prior to use for all the reactions. All air- and moisture-sensitive reagents were transferred by syringe. NMR spectra were recorded on Bruker AM-600 and Bruker AM-200 spectrometers. IR spectra were recorded on a Biorad FTS-40 spectrophotometer. Mass spectra were determined on a Finnigan 4500 mass spectrometer. UV spectroscopy was performed on a Cary 300 spectrophotometer with the temperature controlled to 25 °C. Quartz UV cells bearing a screw cap and a septum were obtained from Aldrich (Oakville, ON, Canada); they were dried by evacuation over phosphorus pentoxide in a desiccator.

General procedure for kinetic determinations

Stock solutions of each predried acetyl (substituted) phenylacetyl glycoluril and the condensation product were prepared by the dissolution of a carefully determined mass (~2.5 mg) in 1:1 *v*/*v* anhydrous THF–*tert*-butanol in a volumetric flask (5 mL). The resulting solutions (0.3 mL) were further diluted with 2.4 mL of the stock solvent in a quartz UV cell equipped with a magnetic stir bar and a septum. The reference cell contained 1:1 *v*/*v* anhydrous THF–*tert*-butanol. After equilibration of the temperature to 25 °C within the spectrophotometer, the UV spectrum was recorded in scanning mode. The resulting solutions had concentrations of 9.11×10^{-5} to 13.96×10^{-5} mol/L.

The base solution was prepared with potassium *tert*-butoxide (~25 mg) in the same stock solvent in a volumetric flask (25 mL). The kinetic measurements were recorded by monitoring the absorbance at λ_{max} at 25 °C after adding 0.3 mL of the base solution by syringe to the substrate solution in the UV cell with rapid stirring. The observed rate constant, k_{obs}, was determined for each compound by the spectrometer computer after the kinetic data were fit to a pseudo first-order kinetic plot. Then the apparent second-order rate constant, k_{app}, was obtained by dividing the corresponding value by the calculated base concentration. Values of k_{app} and k_{rel} were also determined from plots of k_{obs} vs. [Base] and from experiments using the same base solution, respectively, as described in the text.

General procedure for preparation of acetyl (substituted) phenylacetyl glycolurils 9–11

To a solution of acetyl-3,4,7,8-tetramethylglycoluril (**2a**) in anhydrous THF (8 mL per mmol **2a**), which had been cooled to 0 °C, 1.2 equiv. of lithium bis(trimethylsilyl)-amide (1.0 mol/L solution in tetrahydrofuran) was added by syringe. The mixture was stirred for 30 min. Then (substituted) phenylacetyl chloride (1.1–1.5 equiv.) was added, and stirring was continued for 1 h at 0 °C. After quenching the reaction mixture with 1 mol/L $NaHSO_4$ aqueous solution (1.5 mL per mmol **2a**), most of the THF was removed on the rotary evaporator and the aqueous residue was extracted

© 2006 NRC Canada

three times with $CHCl_3$. The combined organic layers were washed with an equal volume of sodium bicarbonate and then water and saturated sodium chloride in sequence, dried over Na_2SO_4, filtered, and concentrated. The product was purified by flash chromatography on silica gel using ethyl acetate as the eluent.

Acetyl 4-methoxyphenylacetyl glycoluril (9)

Compound **2a** (1.5 g, 6.3 mmol) and 4-methoxyphenylacetyl chloride (1.44 mL) gave 300 mg (12%) of **9**; mp 150–152 °C. UV (50:50 THF–*t*-BuOH) λ_{max} (nm) (ε): 213, 275 (17 738, 3069); when treated with excess KO*t*-Bu: λ_{max} = 213, 310 (12 146, 6170). IR ($CHCl_3$ cast, cm^{-1}): 2938, 2839 (C–H str.), 1728 (C=O), 1613, 1514, 1406, 1368, 1247, 1115, 1093, 1033, 952, 822. ^{1}H NMR (200 MHz, $CDCl_3$) δ: 7.20 (d, *J* = 7 Hz, 2H, ArH), 6.84 (d, *J* = 7 Hz, 2H, ArH), 4.33 (d, *J* = 16 Hz, 1H, $OCCH_2$), 3.81 (d, *J* = 16 Hz, 1H, $OCCH_2$), 3.77 (s, 3H, OCH_3), 2.94 (s, 6H, $2NCH_3$), 2.46 (s, 3H, $OCCH_3$), 1.91 (s, 3H, CH_3), 1.45 (s, 3H, CH_3). ^{13}C NMR (50 MHz, $CDCl_3$) δ: 172.18 (C=O), 170.46 (C=O), 158.53 (urea, C=O), 153.13 (urea, C=O), 130.90, 126.49, 113.87 (aryl, 2 signals overlapped), 80.76, 77.95 (C bridgehead), 55.31 (OCH_3), 43.19 (CH_2), 26.87 (2C), 26.17, 19.15, 14.66. EI-MS *m*/*z*: 388, 295, 282, 225, 168, 149, 148, 121, 120, 78, 43. HR-MS calcd. for $C_{19}H_{24}N_4O_5$: 388.1747; found: 388.1736.

Acetyl phenylacetyl glycoluril (10)

Compound **2a** (2.8 g, 11.7 mmol) and phenylacetyl chloride (2.1 mL) gave 340 mg (8%) of **10**; a yield of 38% was obtained using *n*-BuLi as the base; mp 51–54 °C. UV (50:50 THF–*t*-BuOH) λ_{max} (nm) (ε): 212, 259 (13 446, 1807); when treated with excess KO*t*-Bu: λ_{max} = 212, 309 (12 328, 6888). IR ($CHCl_3$ cast, cm^{-1}): 3031 (Ar–H str.), 2932 (C–H str.), 1732 (C=O), 1406, 1373, 1254, 1116, 1094. ^{1}H NMR (200 MHz, $CDCl_3$) δ: 7.26 (m, 5H, C_6H_5), 4.38 (d, *J* = 16 Hz, 1H, $OCCH_2$), 4.05 (d, *J* = 16 Hz, 1H, $OCCH_2$), 2.90 (s, 6H, $2NCH_3$), 2.44 (s, 3H, $COCH_3$), 1.88 (s, 3H, CH_3), 1.41 (s, 3H, CH_3). ^{13}C NMR (50 MHz, $CDCl_3$) δ: 171.61 (C=O), 170.30 (C=O), 152.94 (2 urea C=O), 134.37, 129.75, 128.28, 126.71 (aryl), 80.60, 77.81 (C bridgehead), 43.90 (CH_2), 26.72 (2C), 26.02, 18.98, 14.47. EI-MS *m*/*z*: 358, 323, 316, 284, 245, 244, 225, 199, 168, 140, 126, 125, 118, 91, 90, 56. HR-MS calcd. for $C_{18}H_{22}N_4O_4$: 358.1641; found: 358.1638.

Acetyl 4-chlorophenylacetyl glycoluril (11)

Compound **2a** (3 g, 12.5 mmol) and 4-chlorophenylacetyl chloride (2 mL) gave 300 mg (6%) of **11**; mp 126–128 °C. UV (50:50 THF – *t*-BuOH) λ_{max} (nm) (ε): 215 (22 757); when treated with excess KO*t*-Bu: λ_{max} = 212, 311 (15 614, 7918). IR ($CHCl_3$ cast, cm^{-1}): 2920, 2851 (C–H str.), 1729 (C=O), 1653, 1559, 1492, 1406, 1345, 1116, 1093, 1017, 809. ^{1}H NMR (200 MHz, $CDCl_3$) δ: 7.26–7.14 (m, 4H, ArH), 4.35 (d, *J* = 17 Hz, 1H, $OCCH_2$), 3.99 (d, *J* = 16 Hz, 1H, $OCCH_2$), 2.92 (s, 6H, $2NCH_3$), 2.44 (s, 3H, $OCCH_3$), 1.88 (s, 3H, CH_3), 1.45 (s, 3H, CH_3). ^{13}C NMR (50 MHz, $CDCl_3$) δ: 171.47 (C=O), 170.40 (C=O), 153.00 (urea, 2C=O), 132.96, 132.70, 131.36, 128.48 (aryl), 80.68 (2C, C bridgehead), 43.46 (CH_2), 26.86 (2C), 26.06, 19.11, 14.63. EI-MS *m*/*z*: 392, 350, 307, 279, 240, 199, 163, 154, 152, 118, 86, 84. HR-MS calcd. for $C_{18}H_{21}N_4O_4Cl$: 392.1251; found: 392.1247.

General procedure for preparative condensations of acetyl (substituted) phenylacetyl glycolurils 9–11 giving 12a–12b, 13a–13b, 14a–14b

The acetyl (substituted) phenylacetyl glycoluril was dissolved in anhydrous THF and the mixture was cooled to 0 °C. Then, potassium *tert*-butoxide (2 equiv.) in THF was added to the solution by syringe, and the mixture was stirred for 20 min at 0 °C. The reaction mixture was quenched with 1 mol/L $NaHSO_4$, then the organic solvents were removed using a rotary evaporator, and the residue was extracted with $CHCl_3$. The extracts were dried over Na_2SO_4, filtered, and concentrated. The product was purified by flash chromatography on silica gel using ethyl acetate as the eluent.

N^1-[2′-(4″-Methoxy)-phenyl-3′-oxo-butanoyl]-3,4,7,8-tetramethylglycoluril (diastereomers 12a, 12b)

Compound **9** (100 mg, 0.26 mmol) in THF (20 mL) with potassium *tert*-butoxide (58 mg) gave 80 mg (80%) of a mixture of **12a** and **12b**. UV (50:50 THF–*t*-BuOH) λ_{max} (nm) (ε): 214, 275 (10 515, 1957); when treated with excess KO*t*-Bu: λ_{max} = 213, 310 (11 233, 7198). IR ($CHCl_3$ cast, cm^{-1}): 3337 (N–H), 2922 (C–H str.), 1718 (C=O), 1512, 1458, 1413, 1387, 1251, 1111, 1035, 929. ^{1}H NMR (600 MHz, $CDCl_3$) δ: 7.19 (d, *J* = 9 Hz, 0.67H, ArH of **12a**), 7.16 (d, *J* = 9 Hz, 1.33H, ArH of **12b**), 6.92 (d, *J* = 8.4 Hz, 1.33H, ArH of **12b**), 6.91 (d, *J* = 9 Hz, 0.67H, ArH of **12a**), 6.02 (s, 0.33H, NH of **12a**), 5.84 (s, 0.33H, COCHCO of **12a**), 5.83 (s, 0.67H, NH of **12b**), 5.67 (s, 0.67H, COCHCO of **12b**), 3.81 (s, 3H, OCH_3), 3.00 (s, 3H, NCH_3), 2.91 (s, 1H, NCH_3 of **12a**), 2.86 (s, 2H, NCH_3 of **12b**), 2.17 (s, 2H, CH_3CO of **12b**), 2.14 (s, 1H, CH_3CO of **12a**), 1.78 (s, 2H, CH_3 of **12b**), 1.63 (s, 1H, CH_3 of **12a**), 1.56 (s, 3H, CH_3 of **12b**), 1.55 (s, sh, CH_3 of **12a**). ^{13}C NMR (150 MHz, $CDCl_3$) δ: 202.96 (C=O of **12b**), 201.81 (C=O of **12a**), 168.95 (C=O), 159.68 (urea, C=O of **12a**), 159.62 (urea, C=O of **12b**), 157.10 (urea, C=O of **12a**), 156.94 (urea, C=O of **12b**), 153.13 ($COCH_3$), 131.44, 131.40 (Ar), 123.35 (Ar of **12a**, CCHCO), 123.33 (Ar of **12b**, CCHCO), 114.28 (Ar), 78.80, 78.67 (C bridgehead), 65.11 (COCH of **12b**), 64.81 (COCH of **12a**), 55.27 (OCH_3), 28.78 ($COCH_3$), 27.10 (NCH_3), 26.62 (NCH_3 of **12a**), 26.42 (NCH_3 of **12b**), 19.92 (CH_3 of **12a**), 19.03 (CH_3 of **12b**), 15.92 (CH_3 of **12a**), 15.73 (CH_3 of **12b**). EI-MS *m*/*z*: 388, 347, 346, 326, 279, 214, 213, 202, 190, 155, 148, 128, 85, 69, 57, 43. HR-MS calcd. for $C_{19}H_{24}N_4O_5$: 388.1747; found: 388.1710.

N^1-(2′-Phenyl-3′-oxo-butanoyl)-3,4,7,8-tetramethylglycoluril (diastereomers 13a, 13b)

Compound **10** (130 mg, 0.36 mmol) in THF (20 mL) with potassium *tert*-butoxide (81 mg) gave 120 mg (92%) of a mixture of **13a** and **13b**. UV (50:50 THF – *t*-BuOH) λ_{max} (nm) (ε): 214, 259 (14 167, 925); when treated with excess KO*t*-Bu: λ_{max} = 213, 309 (10913, 8554). IR ($CHCl_3$ cast, cm^{-1}): 3431, 3354 (N–H), 3007 (Ar–H str.), 2924, 2852 (C–H str.), 1734 (C=O), 1599, 1455, 1353, 1263, 1112, 1035, 991, 962, 867. ^{1}H NMR (600 MHz, $CDCl_3$) δ: 7.30–7.40 (m, 3H, ArH), 7.20–7.29 (m, 2H, ArH), 6.07 (s, 0.33H, NH of **13a**), 5.89 (s, 0.33H, COCHCO of **13a**), 5.88 (s,

© 2006 NRC Canada

0.67H, NH of **13b**), 5.72 (s, 0.67H, COCHCO of **13b**), 2.97 (s, 2H, NCH_3 of **13b**), 2.96 (s, 1H, NCH_3 of **13a**), 2.85 (s, 1H, NCH_3 of **13a**), 2.82 (s. 2H, NCH_3 of **13a**), 2.14 (s, 2H, CH_3CO of **13b**), 2.11 (s, 1H, CH_3CO of **13a**), 1.75 (s, 2H, CH_3 of **13b**), 1.60 (s, 1H, CH_3 of **13a**), 1.53 (s, 2H, CH_3 of **13b**), 1.52 (s, 1H, CH_3 of **13a**). ^{13}C NMR (150 MHz, $CDCl_3$) δ: 202.73 (C=O of **13b**), 201.64 (C=O of **13a**), 168.71 (C=O of **13a**), 168.57 (C=O of **13b**), 157.14 (C=O of **13b**), 156.99 (C=O of **13a**), 153.15 (C=O), 132.01 (Ar of **13a**, CCH), 131.53 (Ar of **13b**, CCH), 130.40 (Ar of **13b**), 130.33 (Ar of **13a**), 128.80 (Ar of **13a**, **13b**), 128.39 (Ar of **13b**), 128.33 (Ar of **13a**), 78.87 (C bridgehead of **13b**), 78.74 (C bridgehead of **13a**), 76.70 (C bridgehead), 65.93 (COCHPh of **13b**), 65.64 (COCHPh of **13a**), 28.95 ($COCH_3$), 27.14 (NCH_3), 26.64 (NCH_3 of **13a**), 26.44 (NCH_3 of **13b**), 19.92 (CH_3 of **13a**), 19.05 (CH_3 of **13b**), 15.93 (CH_3 of **13a**), 15.74 (CH_3 of **13b**). EI-MS *m*/*z*: 358, 340, 335, 318, 317, 316, 315, 297, 285, 284, 283, 268, 259. HR-MS calcd. for $C_{18}H_{22}N_4O_4$: 358.1641; found: 358.1630.

N[1]-[2′-(4″-Chloro)-phenyl-3′-oxo-butanoyl]-3,4,7,8-tetramethylglycoluril (diastereomers 14a, 14b)

Compound **11** (51 mg, 0.13 mmol) in THF (10 mL) with potassium *tert*-butoxide (30 mg) gave 49 mg (96%) of a mixture of **14a** and **14b**. UV (50:50 THF–*t*-BuOH) λ_{max} (nm) (ε): 214, 222 (17 564, 17 519); when treated with excess KO*t*-Bu: λ_{max} = 214, 310 (18 769, 8881). IR ($CHCl_3$ cast, cm^{-1}): 3362 (N–H), 3009, 2928 (C–H str.), 1718 (C=O), 1490, 1411, 1387, 1350, 1263, 1150, 1111, 1092, 1017, 961. ^1H NMR (200 MHz, $CDCl_3$) δ: 7.38–7.34 (m, 2H, ArH), 7.23–7.16 (m, 2H, ArH), 6.02 (s, 0.4H, NH of **14a**), 5.89 (s, 0.4H, COCHCO of **14a**), 5.83 (s, 0.6H, NH of **14b**), 5.70 (s, 0.6H, COCHCO of **14b**), 2.99 (s, 3H, NCH_3), 2.88 (s, 1.2H, NCH_3 of **14a**), 2.85 (s, 1.8H, NCH_3 of **14b**), 2.16 (s, 1.8H, CH_3CO of **14b**), 2.14 (s, 1.2H, CH_3CO of **14a**), 1.77 (s, 1.8H, CH_3 of **14b**), 1.62 (s, 1.2H, CH_3 of **14a**), 1.56 (s, 3H, CH_3). ^{13}C NMR (50 MHz, $CDCl_3$) δ: 202.42 (C=O of **14b**), 201.22 (C=O of **14a**), 168.45 (C=O of **14a**), 168.24 (C=O of **14b**), 157.19 (urea, C=O of **14b**), 157.00 (urea, C=O of **14a**), 153.16 (urea, C=O), 134.73 (Ar of **14b**), 134.63 (Ar of **14a**), 131.81 (Ar), 130.47 (Ar of **14a**, CCHCO), 130.00 (Ar of **14b**, CCHCO), 129.13 (Ar), 78.98 (C bridgehead of **14b**), 78.85 (C bridgehead of **14a**), 65.29 (COCH of **14b**), 64.94 (COCH of **14a**), 29.81 ($COCH_3$ of **14a**), 29.06 ($COCH_3$ of **14b**), 27.28 (NCH_3), 26.77 (NCH_3 of **14a**), 26.55 (NCH_3 of **14b**), 19.98 (CH_3 of **14a**), 19.12 (CH_3 of **14b**), 16.05 (CH_3 of **14a**), 15.85 (CH_3 of **14b**). EI-MS *m*/*z*: 392, 352, 350, 276, 225, 199, 194, 152, 125, 111, 86, 56. HR-MS calcd. for $C_{18}H_{21}N_4O_4Cl$: 392.1251; found: 392.1234.[3]

Acknowledgments

We thank the Natural Sciences and Engineering Research Council of Canada (NSERC) for financial support. MC was partially supported by a Kaisi Overseas Scholarship.

References

1. M.B. Smith and J. March. *In* Advanced organic chemistry, 5th ed. Wiley, New York 2001, and refs. cited therein.
2. For a discussion of the mechanism and an early example, see: S.M. McElvain. J. Am. Chem. Soc. **51**, 3124 (1929). For an example of heterogeneous catalysis, see: A. Guida, M.H. Lhouty, D. Tichit, F. Figueras, and P. Geneste. Appl. Cat. A, **164**, 251 (1997).
3. For a review, see: (*a*) D.B. Collum. Acc. Chem. Res. **25**, 448 (1992); (*b*) S.S.-W. Leung and A. Streitwieser. J. Am. Chem. Soc. **120**, 10557 (1998); (*c*) Y.-J. Kim and A. Streitwieser. Org. Lett. **4**, 573 (2002), and refs. cited therein; for an example of non first-order kinetics in the reaction of a ketone enolate with an ester, see: (*d*) D.G. Hill, J. Burkus, and C.R. Hauser. J. Am. Chem. Soc. **81**, 602 (1959); for an example in the aldol condensation, see: (*e*) J.D. Gettler and L.P. Hammett. J. Am. Chem. Soc. **65**, 1824 (1943).
4. For an example, see: Y. Tanabe. Bull. Chem. Soc. Jpn. **62**, 1917 (1989).
5. For recent reviews, see: (*a*) A.M. Haapalainen, G. Merilainen, and R.K. Wierenga. Trends Biochem. Sci. **31**, 64 (2006); (*b*) R.J. Heath and C.O. Rock. Nat. Prod. Rep. **19**, 581 (2002).
6. For selected recent reviews, see: (*a*) Y. Tang and C. Khosla. *In* Exploiting chemical diversity for drug discovery. *Edited by* P.A. Bartlett and M. Entzeroth. Royal Society of Chemistry, Cambridge, UK. 2006. pp. 57–90; (*b*) K. Weissman and P.F. Leadlay. Nat. Rev. Microbiol. **3**, 925 (2005); (*c*) R. McDaniel, M. Welch, and C.R. Hutchinson. Chem. Rev. **105**, 543 (2005); (*d*) J. Staunton and K. Weissman. Nat. Prod. Rep. **18**, 380 (2001); (*e*) B. Rawlings. Nat. Prod. Rep. **18**, 190 (2001), and refs. cited therein.
7. (*a*) S. Sun and P.H.M. Harrison. Tetrahedron Lett. **33**, 7715 (1992); (*b*) S. Sun and P.H.M. Harrison. J. Chem. Soc., Chem. Commun. 2235 (1994); (*c*) S. Sun, L. Edwards, and P.H.M. Harrison. J. Chem. Soc., Perkin Trans. 1. 437 (1998); (*d*) C. Cow, D. Valentini, and P. Harrison. Can. J. Chem. **75**, 884 (1997).
8. C.N. Cow and P. Harrison. J. Org. Chem. **62**, 8834 (1997).
9. C.F. Matta, C.N. Cow, and P. Harrison. J. Mol. Struct. **660**, 81 (2003).
10. M. Rahimizadeh, K. Kam, S.I. Jenkins, R.S. McDonald, and P.H.M. Harrison. Can. J. Chem. **80**, 517 (2002).
11. K. Kam, M. Rahimizadeh, R.S. McDonald, P.H.M. Harrison, H. Chen, S.I. Jenkins, and A. Pedrech. Can. J. Chem. **83**, 1253 (2005).
12. T. Nishimura, M. Sunagawa, T. Okajima, and Y. Fukazawa. Tetrahedron Lett. **38**, 7063 (1997).

[3] Supplementary data for this article are available on the journal Web site or may be purchased from the Depository of Unpublished Data, Document Delivery, CISTI, National Research Council Canada, Ottawa, ON K1A 0S2, Canada. DUD 5091. For more information on obtaining material refer to http://cisti-icist.nrc-cnrc.gc.ca/irm/unpub_e.shtml.

© 2006 NRC Canada

IN MEMORIAM \ NÈCROLOGIE



Professor David A. Armstrong

David Anthony Armstrong, FCIC, passed away suddenly at his home in Calgary on July 24, 2006 in his 76th year. He is survived by his wife, Ruth, three children, and one grandchild. With his passing, the University of Calgary and the scientific community have lost a highly respected member, a kind mentor, a true gentleman, and a good friend.

He was born in Barbados on August 27, 1930 and studied at McGill University, completing a B.Sc. (Honours Chemistry) degree in 1952. He completed his Ph.D. degree in physical chemistry at McGill in 1955 with research on the kinetics of active nitrogen reactions, under the supervision of Professor C. A. Winkler. During his undergraduate years he was introduced to western Canada through a student exchange program, spending the year 1950-51 at the University of Alberta. From 1955 to 1957 he was Brotherton Research Lecturer at the University of Leeds in England and did research on the radiation chemistry of water with Professor F. S. Dainton. Following a two-year NRC postdoctoral fellowship with Professor J. W. T. Spinks at the University of Saskatchewan, he joined the staff of the University of Alberta, Calgary as an Assistant Professor in 1958. He was promoted to Associate Professor in 1963 and to Professor in 1968.

He was a key figure in the small group of academics who developed the foundations for the Department of Chemistry

Le 24 juillet 2006, **David Anthony Armstrong**, MICC, est décédé soudainement chez lui, à Calgary, un mois avant son 76e anniversaire. Il laisse dans le deuil sa conjointe Ruth, ses trois enfants et un petit enfant. À l'Université de Calgary et dans le milieu scientifique, son départ marque la perte d'un homme très respecté, d'un mentor apprécié, d'un vrai gentleman et d'un bon ami.

M. Armstrong est né à la Barbade le 27 août 1930. Il a étudié à l'Université McGill, où il a obtenu un baccalauréat spécialisé en chimie en 1952. Il a terminé son doctorat en chimie physique à McGill en 1955. Ses recherches, sous la supervision du professeur C. A. Winkler, portaient sur la cinétique des réactions de l'azote actif. Durant ses études de premier cycle, il a fait la découverte de l'ouest du Canada en participant à un échange d'étudiants, qui lui a permis d'étudier à l'Université de l'Alberta en 1950-1951. Bénéficiaire d'une bourse de recherche Brotherton de l'Université de Leeds, en Angleterre, de 1955 à 1957, il a étudié la radiolyse de l'eau avec le professeur F. S. Dainton. Après avoir obtenu une bourse de recherche postdoctorale du CNRC pour travailler deux ans avec le professeur J. W. T. Spinks à l'Université de la Saskatchewan, il s'est joint au personnel de l'Université de l'Alberta, à Calgary, à titre de professeur adjoint, en 1958. Il est devenu professeur agrégé en 1963, et professeur en 1968.

M. Armstrong était au cœur du petit groupe d'universitaires qui ont jeté les fondations du Département de chimie de

© 2006 NRC Canada

at the University of Calgary, which was established in 1966. He served as Head of the Department of Chemistry during its formative years and also as Dean of the Faculty of Science at the University of Calgary from 1984 to 1989. He retired in 1991 and was awarded emeritus status; he was appointed as a Faculty Professor in 1994. In 2000, he was named to the Order of the University of Calgary for his contributions to the development of the University. His continuing recent research in radiation chemistry and chemical kinetics focused on the radical reactions that occur during oxidative damage in living cells and on reactions between electrons and clusters of molecules.

The international recognition of his research led to a number of Visiting Scientist appointments at research institutions in Canada, Europe, Australia, and China. He also held a Visiting Professor appointment at the University of Notre Dame.

In 1998, the *Polish Radiation Research Society* awarded the Marie Skłodowska-Curie Medal to him for his contributions to radiation chemistry. He was appointed to the Research and Development Advisory Panel of Atomic Energy of Canada Ltd. and the IUPAC Chemistry Task Group on Radical Reduction Potentials, continuing his active participation until his death.

A total of 13 graduate theses were completed under his supervision (including the first Ph.D. thesis completed at the University of Alberta, Calgary in 1963) and 18 postdoctoral fellows and research associates worked in his laboratory over the years. His research was presented in 96 invited lectures and conference papers and in more than 160 refereed journal articles.

Peter J. Krueger, FCIC

l'Université de Calgary, établi en 1966. D'ailleurs, il a été directeur de ce département durant les premières années de sa mise sur pied, puis doyen de la Faculté des sciences de l'Université de Calgary, de 1984 à 1989. En 1991, il a pris sa retraite et a reçu le titre de professeur émérite. Par la suite, il a été nommé professeur à la Faculté (titre honorifique) en 1994. En 2000, il a été nommé à l'ordre de l'Université de Calgary pour sa contribution au développement de l'Université. Ses recherches récentes en chimie sous rayonnement et en cinétique chimique portaient principalement sur les réactions des radicaux dans les cellules vivantes soumises à un stress oxydatif et sur les réactions entre des électrons et des agrégats de molécules.

La reconnaissance internationale de ses recherches lui a valu plusieurs nominations à titre de chercheur invité dans des établissements de recherche du Canada, d'Europe, d'Australie et de Chine. Il était aussi professeur invité à l'Université de Notre Dame.

En 1998, la *Polish Radiation Research Society* lui a remis la médaille Marie Skłodowska-Curie pour sa contribution à la chimie sous rayonnement. Il a été nommé au Comité consultatif de recherche et développement d'Énergie atomique du Canada limitée et au groupe de travail sur les potentiels de réduction des radicaux de l'Union internationale de chimie pure et appliquée, et y est demeuré actif jusqu'à son décès.

Treize étudiants des cycles supérieurs ont rédigé leur mémoire ou leur thèse sous sa supervision. De ce nombre, on trouve le premier titulaire d'un doctorat décerné par l'Université de l'Alberta, à Calgary, en 1963. En outre, 18 boursiers de recherche postdoctorale et associés de recherche ont travaillé dans son laboratoire au fil des ans. Par ailleurs, M. Armstrong a présenté ses recherches dans le cadre de 96 conférences et communications sur invitation, et plus de 160 articles de revue à comité de lecture.

Peter J. Krueger, MICC

© 2006 NRC Canada

AWARD LECTURE / CONFÉRENCE D'HONNEUR

2005 Alfred Bader Award Lecture Diaminopimelate and lysine biosynthesis — An antimicrobial target in bacteria[1,2]

John C. Vederas

Abstract: The development of bacterial resistance to current antibiotic therapy has stimulated the search for novel antimicrobial agents. The essential peptidoglycan cell wall layer in bacteria is the site of action of many current drugs, such as β-lactams and vancomycin. It is also a target for a number of very potent bacterially produced antibiotic peptides, such as nisin A and lacticin 3147, both of which are highly posttranslationally modified lantibiotics that act by binding to lipid II, the peptidoglycan precursor. Another set of potential targets for antibiotic development are the bacterial enzymes that make precursors for lipid II and peptidoglycan, for example, those in the pathway to diaminopimelic acid (DAP) and its metabolic product, L-lysine. Among these, DAP epimerase is a unique nonpyridoxal phosphate (PLP) dependent enzyme that appears to use two active site thiols (Cys73 and Cys217) as a base and an acid to deprotonate the α-hydrogen of LL-DAP or meso-DAP from one side and reprotonate from the other. This process cannot be easily duplicated in the absence of the enzyme. A primary goal of our work was to generate inhibitors of DAP epimerase that would accurately mimic the natural substrates (meso-DAP and LL-DAP) in the enzyme active site and, through crystallographic analysis, provide insight into mechanism and substrate specificity. A series of aziridine-containing DAP analogs were chemically synthesized and tested as inhibitors of DAP epimerase from *Haemophilus influenzae*. Two diastereomers of 2-(4-amino-4-carboxybutyl)aziridine-2-carboxylic acid (AziDAP) act as rapid irreversible inactivators of DAP epimerase; the AziDAP analog of LL-DAP reacts selectively with the sulfhydryl of Cys73, whereas the corresponding analog of meso-DAP reacts with Cys217. AziDAP isomers are too unstable to be useful antibiotics. However, mass spectral and X-ray crystallographic analyses of the inactivated enzymes confirm that the thiol attacks the methylene group of the aziridine with concomitant ring opening to give a DAP analog bound in the active site. Further crystallographic analyses should yield useful mechanistic insights.

Key words: enzyme mechanism, enzyme inhibition, antibiotics, aziridines, amino acids.

Résumé : Le fait que les bactéries aient développé de la résistance aux antibiotiques actuels a stimulé la recherche de nouveaux agents antimicrobiens. La paroi cellulaire essentielle des bactéries qui est formée de peptidoglycane est le site d'action de plusieurs médicaments actuels, y compris les β-lactames et la vancomycine. C'est aussi la cible d'un certain nombre de peptides antibiotiques très puissant produits par des bactéries, telles la nisine A et la lacticine 3147 qui sont toutes les deux des antibiotiques fortement modifiés d'une façon post-translationnelle qui agissent en se liant au lipide II, le précurseur du peptidoglycane. Un autre ensemble de cibles potentielles pour le développement d'antibiotiques sont les enzymes bactériens qui fabriquent des précurseurs du lipide II ou du peptidoglycane, dont ceux qui se retrouvent dans la voie conduisant à l'acide diaminopimélique (ADP) et à son produit de métabolisme, la L-lysine. Dans cette catégorie, l'épimérase de l'ADP est un enzyme unique qui ne dépend pas du phosphate de pyridoxyal (PLP) et qui semble utiliser les deux sites thiols actifs (Cys73 et Cys217) comme acide et base pour déprotoner l'hydrogène α des LL-ADP et méso-ADP à partir d'un côté pour le reprotoner de l'autre. Il n'est pas possible de réaliser ce processus en l'absence d'un enzyme. Un des objectifs primaires de notre travail a été de générer des inhibiteurs de l'épimérase d'ADP qui pourraient imiter correctement les substrats naturels (méso-ADP et LL-ADP) dans le site enzymatique actif et, par le biais d'études cristallographiques, pourraient nous donner une idée sur le mécanisme et sur la spécificité du substrat. On a réalisé la synthèse d'une série d'analogues de l'ADP contenant une aziridine et on les a

Received 9 January 2006. Accepted 8 February 2006. Published on the NRC Research Press Web site at http://canjchem.nrc.ca on 30 June 2006.

J.C. Vederas. Department of Chemistry, University of Alberta, Edmonton AB T6G 2G2, Canada. (e-mail: john.vederas@ualberta.ca).

[1]This article is part of a Special Issue dedicated to Dr. Alfred Bader.
[2]Presented at the Canadian Society for Chemistry Conference, Saskatoon, Sask. May 2005.

 doi:10.1139/V06-072 © 2006 NRC Canada

testés comme inhibiteurs de l'épimérase d'ADP provenant du *Haemophilus influenzae*. Deux diastéréoisomères de l'acide 2-(4-amino-4-carboxybutyl)aziridine-2-carboxylique (AziADP) agissent comme inactivateurs irréversibles rapides de l'épimérase d'ADP; l'analogue AziADP du LL-ADP réagit d'une façon sélective avec le groupe sulfhydryle du site Cys73 alors que l'analogue correspondant du méso-ADP réagit avec celui du site Cys217. Les isomères du AziADP sont trop instables pour être utiles comme antibiotiques. Toutefois, les spectres de masse et les analyses par diffraction des rayons X des enzymes inactivés confirment que le thiol attaque le groupe méthylène de l'aziridine avec une ouverture de cycle concomitante qui conduit à la formation d'un analogue ADP lié au site actif. Des études cristallographiques ultérieures devraient permettre d'obtenir un nouvel éclairage sur le mécanisme.

Mots clés : mécanisme enzymatique, inhibition enzymatique, antibiotiques, aziridines, acides aminés.

[Traduit par la Rédaction]

Introduction

Resistance to common antibiotics was observed shortly after their introduction into clinical practice in the late 1940s and early 1950s, and has become a serious and costly problem in health care. Although it is well-understood that overuse of antibiotics produces resistance, it is estimated that currently about half of the 100 million prescriptions per year written by office-based physicians in the United States are unnecessary because they are prescribed for the common cold and other viral infections, against which antibiotics are not active (1). The approximate direct cost of antibiotic resistance may be more than $3 billion annually with an associated indirect cost of perhaps 10 times that amount (2). Another concern that exacerbates this problem is that the market for antibiotics is a fragile one. Unlike medicines for chronic conditions, such as high cholesterol or high blood pressure, that are taken daily for long periods of time, antibiotics are only taken for a short time and only when a patient suffers particular diseases. Thus, the profitability of this class of medications is limited and it has become even more limited because the costs and standards for regulatory approval match those for the more profitable drugs that see daily use.

Formation of peptidoglycan, the netlike cell wall layer in bacteria, is a primary target for many antibiotics, including the β-lactams (e.g., penicillins, cephalosporins) as well as vancomycin and related glycopeptides (3). Interestingly, lipid II, the monomer unit that is polymerized to form peptidoglycan, is also a target for antimicrobial agents (Fig. 1). The topical peptide antibiotic bacitracin inhibits utilization and processing of its lipid portion (4), whereas a number of lantibiotics (lanthionine-containing peptides), such as nisin A, bind to it (5). Nisin A (Fig. 2), which is approved for use as a food preservative, uses lipid II as a docking molecule not only to inhibit peptidoglycan formation, but also to create pores in bacterial cell membranes. Although nisin A is many orders of magnitude more potent than conventional antibiotics, its instability at neutral pH and its tendency to be inactivated by Michael addition of ubiquitous thiols, such as glutathione, to its dehydroamino acid residues precludes its therapeutic use in mammals (6). Fortunately, lacticin 3147, a very potent two-peptide lantibiotic consisting of A1 and A2 peptides and certain other lantibiotics, appears to be much more stable and may be useful in such applications (7, 8).

Lipid II in Gram-negative bacteria contains a *meso*-diaminopimelic acid (meso-DAP) residue that acts as a cross-linking amino acid in peptidoglycan via attack at the penultimate D-alanine amide bond of a nearby pentapeptide moiety (Fig. 3) (9). In most Gram-positive bacteria, the DAP moiety is replaced by its metabolic product, L-lysine, which serves the analogous function. For some time, we and others have been interested in targeting the DAP pathway to L-lysine (Fig. 4), which occurs in bacteria and higher plants, for possible development of new antibiotics (10). The DAP pathway is absent in mammals, which require L-lysine in their diet as an essential amino acid. Hence, it is likely that specific inhibitors of the bacterial enzymes in this metabolic route could be potent antimicrobial agents against bacteria resistant to conventional antibiotics and would be nontoxic to humans and animals. Limited antibiotic activity has already been demonstrated for an heterocyclic analog of DAP that inhibits DAP dehydrogenase (11).

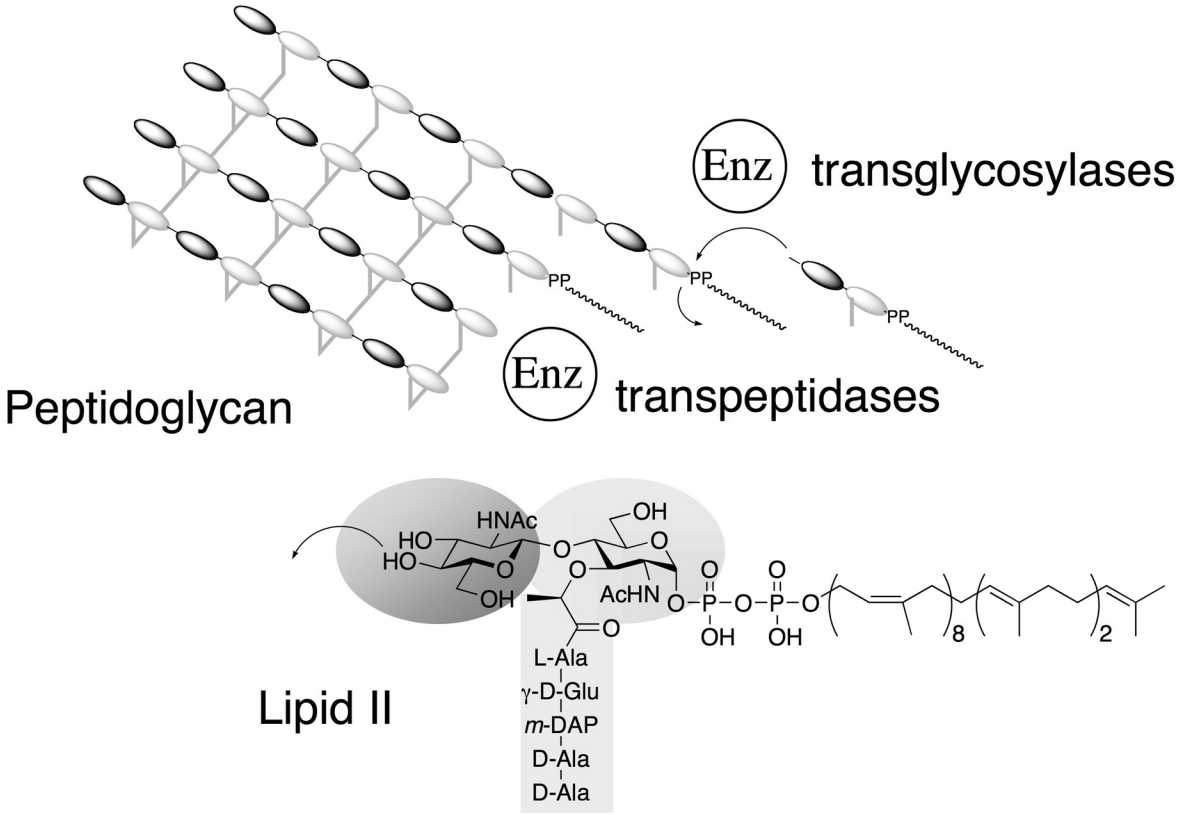
DAP epimerase and its properties

DAP epimerase is an enzyme of particular interest because of its unusual mechanism, although it may not be the best target for antibiotic development as it appears late in the pathway and its function may be circumvented (12). The enzyme reversibly interconverts LL-DAP and meso-DAP without the use of cofactors, metals, or keto or imine intermediates (13). Although a number of enzymes racemize amino acids using pyridoxal phosphate (PLP) (14, 15), DAP epimerase belongs to the class of PLP-independent racemases, which includes aspartate racemase (16), glutamate racemase (17, 18), and proline racemase (19). Based on early work by Albery and Knowles (19), Wiseman and Nichols (13) proposed that DAP epimerase uses two cysteines in the active site (Fig. 5) as an acid and a base to remove the α-proton and reprotonate from the opposite side. During this process, a primary kinetic isotope effect is observed and the α-hydrogen exchanges with solvent via the thiol (13, 20). DAP epimerase is highly specific and does not transform the DD-isomer of DAP or any isomer of lanthionine (the 3-thia analog of DAP). All substrate carboxyl and amino groups of DAP must be present for successful binding and neither the D- or L-isomers of lysine or α-aminopimelic acid are substrates or effective inhibitors (21).

This type of epimerization is not a trivial process and the half-life for such a transformation in the absence of enzyme is estimated to be in excess of 1500 years (22). Several major obstacles block this reaction in the absence of enzyme. The most important is the inherent lack of acidity of the α-hydrogen in a free α-amino acid compared with the much

© 2006 NRC Canada

Fig. 1. Simplified schematic of the formation of peptidoglycan from lipid II. In Gram-positive bacteria, *m*-DAP is usually replaced by L-lysine.



more acidic hydrogens on the carboxyl oxygen in a fully protonated amino acid or on the ammonium group in the zwitterionic form. The pK_a of the α-hydrogen has been estimated to be 34 for the deprotonated anionic amino acid, about 29 for the zwitterionic form, and 21 for the corresponding fully protonated version (23). Thus, a free base in solution will rapidly take a proton first from the carboxyl oxygen and then from the ammonium group, at which point removal of the α-hydrogen requires an extremely strong base. A second major problem is that the free thiol of a cysteine residue typically has a pK_a of ca. 10 and, as a result, the corresponding thiolate is a poor base for deprotonation at the α-carbon.

Nevertheless, the formation of an α-anion in the epimerization process could be confirmed by elimination of hydrogen fluoride from pure β-fluoro-DAP stereoisomers (24). Interestingly, the loss of HF proceeds very rapidly from isomers **1** and **3**, but diasteromers **2** and **4** epimerize reversibly and only slowly undergo elimination of hydrogen fluoride (Fig. 6).

These results indicate not only that anionic character forms at the α-carbon, but also that the substrate, which is normally conformationally mobile, is rigidly held in the enzyme active site so as to orient the cleaving bonds at the α- and β-carbons synperiplanar or antiperiplanar in the rapidly eliminating isomers. Subsequent experiments with β-fluoro-DAP stereoisomers **1** and **2**, using site-specific mutants Cys73Ala and Cys217Ala, demonstrate that Cys73 is the base that removes the α-proton from LL-DAP, whereas Cys217 performs the analogous function on meso-DAP (25).

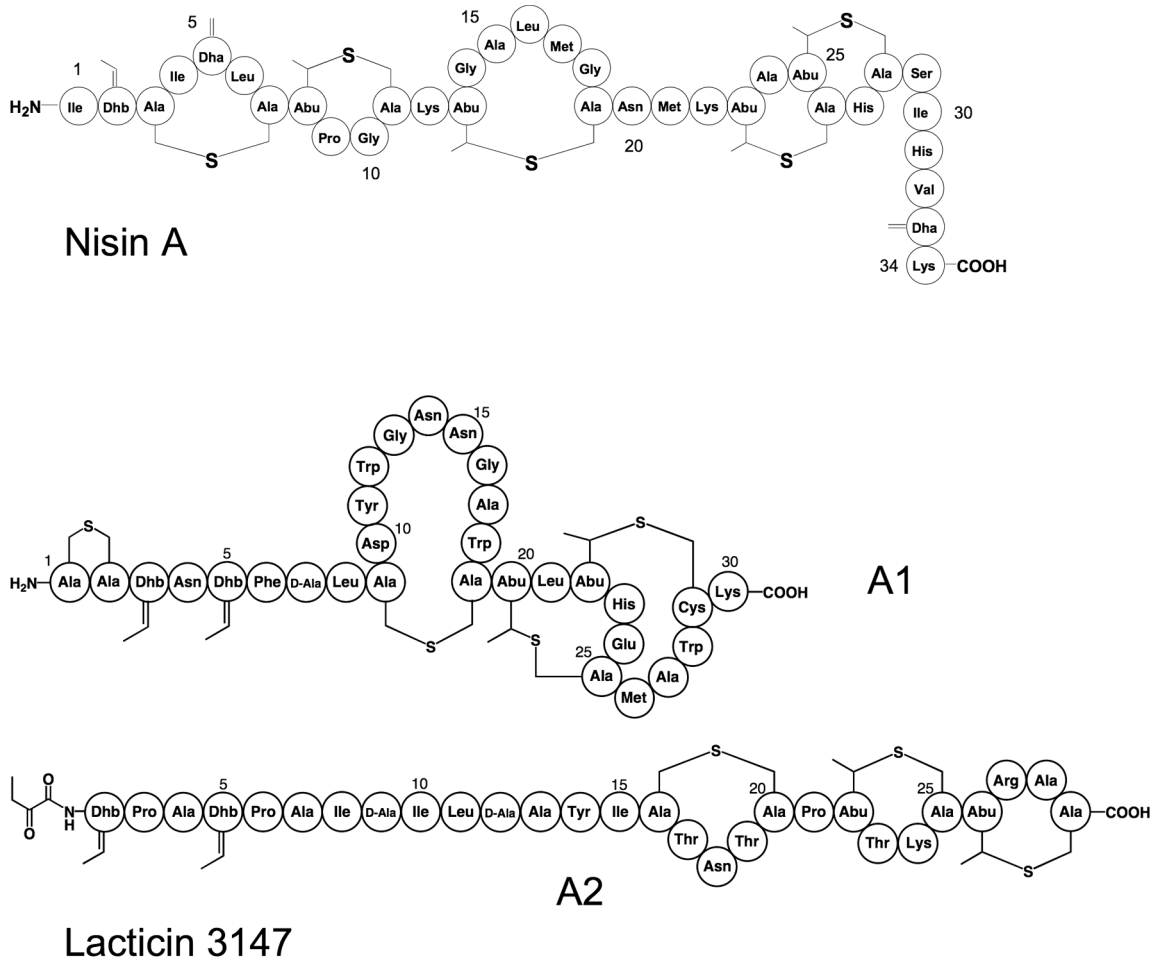
A major breakthrough in the understanding of this unusual enzyme was the elucidation by Blanchard and co-workers (26) of the crystal structure (2.7 Å) of an inactive form of DAP epimerase from *Haemophilus influenzae* in which Cys73 and Cys217 formed a disulfide. This was subsequently refined by Roper and co-workers (27) to 1.75 Å. The monomeric enzyme (274 amino acid residues) displays an unusual pseudo twofold symmetry axis around the central cleft that forms the putative active site. Unfortunately, unambiguous modeling of DAP isomers as substrates in the active site is not readily accomplished using this inactive disulfide structure. Subsequent crystallographic structures of related PLP-independent racemases such as aspartate racemase (16) and glutamate racemase (17, 28), also do not permit definitive placement of substrate (29) in the active sites in such a way as to elucidate the catalytic mechanism. Thus, a primary goal of our work was to generate inhibitors of DAP epimerase that would accurately mimic the natural substrates (meso-DAP and LL-DAP) in the enzyme active site and provide mechanistic insight through crystallographic analysis.

Synthesis of AziDAP isomers

In 1990, Higgins and co-workers (30) reported that a crude mixture of all possible diastereomers of 2-(4-amino-4-carboxybutyl)aziridine-2-carboxylic acid (AziDAP), generated by heating a mixture of α-halomethyl DAP isomers, caused irreversible inactivation of DAP epimerase (Fig. 7). Enzymatic digestion of the inactivated enzyme indicated that Cys73 had been alkylated by the inhibitor through an attack

© 2006 NRC Canada

Fig. 2. Structures of nisin A and lacticin 3147 (a two-component antibiotic consisting of A1 and A2 peptides).



by the thiol on the methylene of the aziridine ring in AziDAP. Subsequently, an elegant study by Tanner and Miao (31) employed an aziridino analog of glutamic acid to inactivate the PLP-independent glutamate racemase. A diastereomeric mixture of oxa analogues of AziDAP was also found to irreversibly inactivate DAP epimerase, probably by thiol opening of the epoxide moiety (32). We reasoned that the synthesis of pure AziDAP isomers **5** and **6**, corresponding to the natural substrates LL-DAP and meso-DAP, respectively, would provide probes that could give crystallographic pictures of the DAP epimerase active site with a bound substrate analog. These would have a stereochemically locked DAP skeleton. Although the AziDAP isomers **5** and **6** are quite small molecules, their synthesis provides a considerable challenge because of high reactivity of the aziridine ring under acidic conditions. This sensitivity is exacerbated by the presence of five internal nucelophiles (four carboxyl oxygens and the distal amino group). In addition, complete stereochemical purity at well-separated centers is required. We also embarked on the synthesis of the DAP derivatives **7** and **8**, having an internal aziridine moiety, to test their ability to analogously inactivate DAP epimerase.

Analog **8** could be prepared by aziridination of an α,β-unsaturated amide bearing a chiral auxiliary. We had earlier reported (33) the diastereoselective aziridination of *N*-enoylbornane[10,2]sultams by *N*-aminophthalimide mediated by lead tetraacetate. This reaction subsequently proved feasible with oxoalkenyloxazolidinone (34) and camphor auxilliaries (35). Hence, we targeted an analogous route with the use of 3-amino-2-ethyl-3,4-dihydroquinazolin-4-one (**15**) to provide the stereoselective synthesis of the internal aziridine moiety to be followed by deprotection using N—N bond reduction with metal in ammonia. As shown (Fig. 8), reaction of the chiral phosphonate ester with *N*,*N*-di-Boc glutamate semialdehyde (**9**) gives exclusively the *trans*-alkene. One Boc protecting group could then be cleaved with TFA to generate the desired precursor **10** for aziridination. Lead tetraacetate aziridination with quinazolin-4-one at –40 °C gives a diastereomeric ratio of 9:1. The major isomer **11** is readily isolated by recrystallization. Although the absolute stereochemistry of this aziridine could not be directly confirmed by X-ray crystallography, it is known that addition to *N*-enoylbornane[10,2]sultams occurs by syn attack from the re face of the α-carbon (33). Removal of the Boc group, base hydrolysis, and reductive cleavage of the N—N bond with Li and ammonia affords the target **8**. With stereochemically pure **8** available, we also synthesized a 1:1 mixture of **8** and its diastereomer **7** to test for irreversible in-

© 2006 NRC Canada

Fig. 3. Expanded view of a pentapeptide chain of peptidoglycan showing DAP and sites that form cross-links to adjacent pentapeptide moieties.

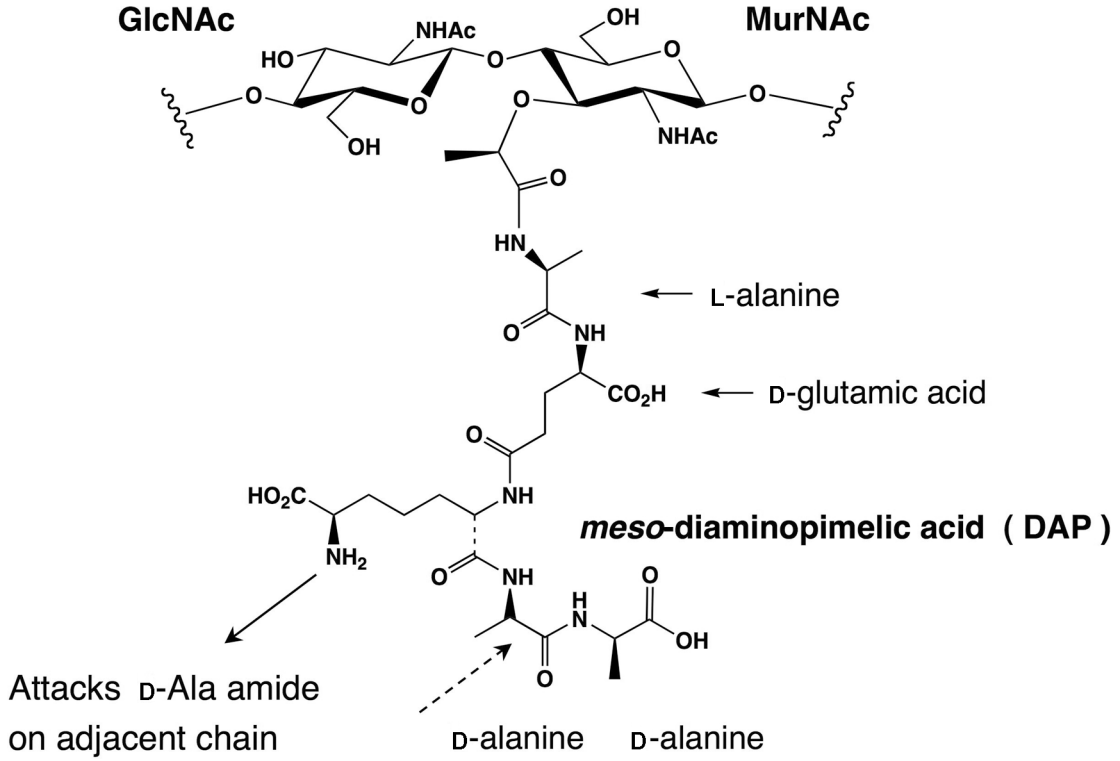
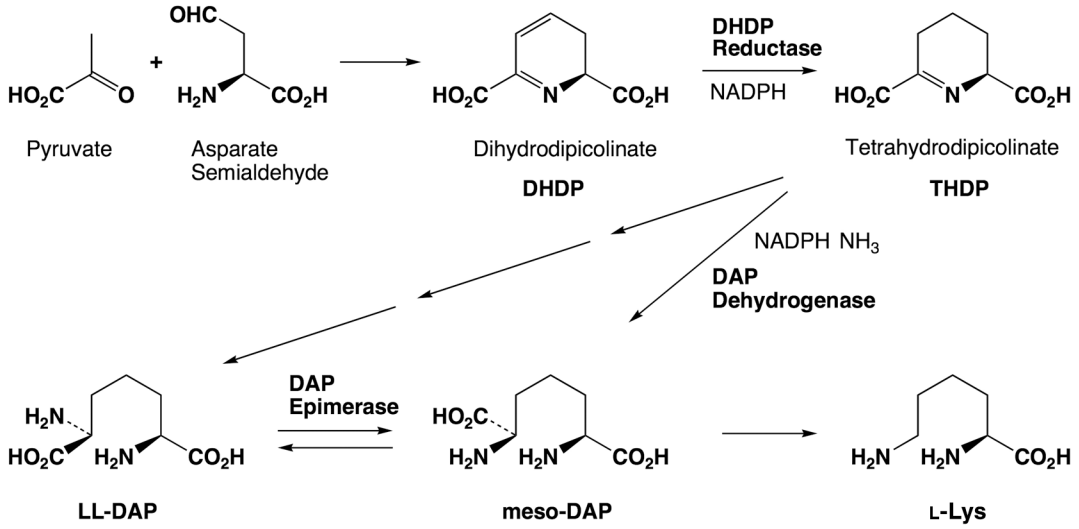


Fig. 4. Diaminopimelate pathway to L-lysine in bacteria. Most bacteria use the route via LL-DAP, but some Gram-positive bacteria employ a shortcut to meso-DAP via DAP dehydrogenase.



activation of DAP epimerase. This mixture was made by by nonstereospecific aziridination of the dimethyl ester **12** followed by analogous deprotection (Fig. 8).

Numerous approaches for synthesis of stereochemically pure **5** and **6** were tried, and the most successful method involved the tethering of a chiral aziridinating moiety via an ester linkage (36, 37) to the unsaturated amino acid framework to allow intramolecular reaction. The required unsaturated α-aminopimelic ester **16** was constructed by photolysis of the Barton ester of *N*-Cbz-L-glutamic acid α-methyl ester with methyl α-thiophenol methylacrylate to give a 68% yield over three steps (Fig. 9) (38). The chiral aziridinating portion, (*R*)-aminoquinazolin-4(3*H*)-one (**18**), was then coupled to the monoacid **17**, which was made by saponification of **16** and selective monoesterification using methanol and polymer-bound PTSA (39). Although the tethering of the aziridinating agent to form **20** works reasonably well using DCC–DMAP, several cycles of flash chromatography are re-

© 2006 NRC Canada

Fig. 5. Proposed mechanism for DAP epimerase.

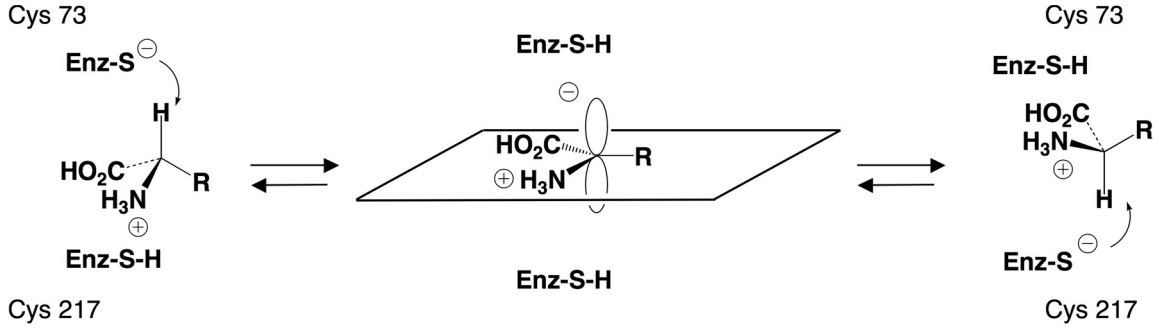
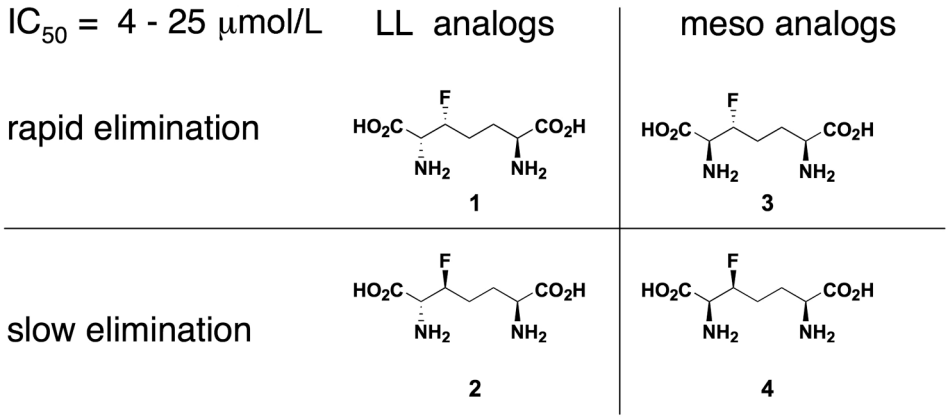
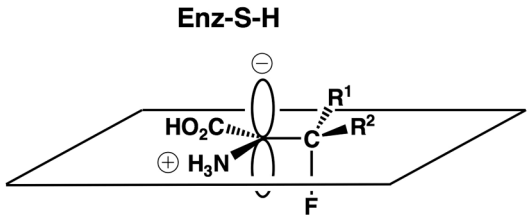
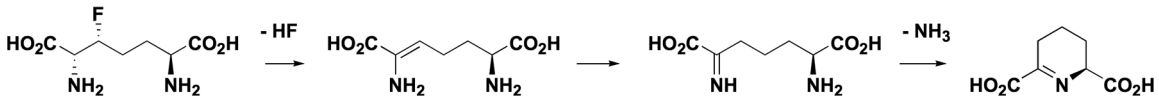


Fig. 6. Interaction of β-fluoro analogs of DAP with DAP epimerase.



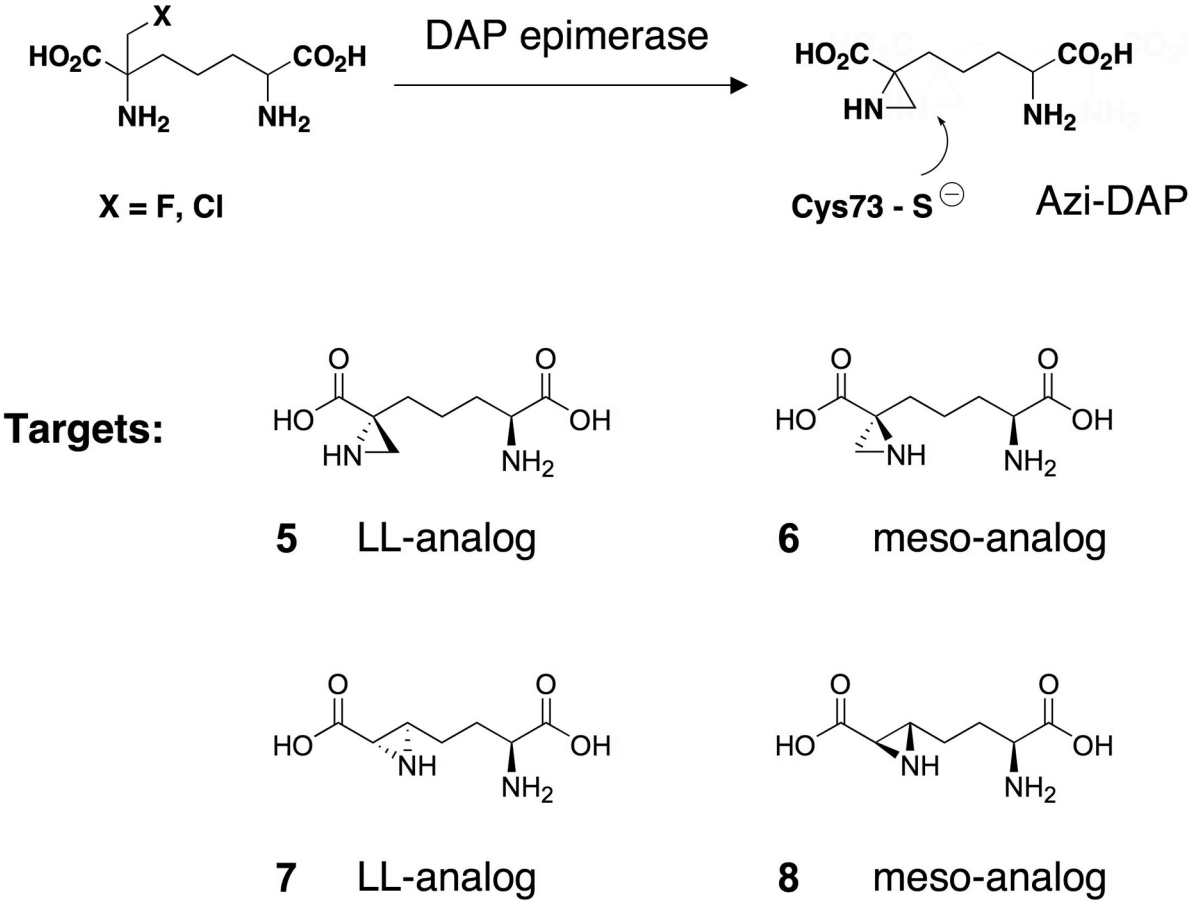




quired to remove the unwanted urea by-product. In contrast, resin-bound *N*-benzyl-*N*-cyclohexylcarbodiimide reagent (PS-DCC) (40) permits facile purification after coupling of acid **17** to the (*S*)-aminoquinazolin-4(3*H*)-one (**19**) to give **22** in 51% yield. Intramolecular aziridination of **22** progresses rapidly upon treatment with lead tetraacetate at 0 °C to give the target **23** with complete diastereoselectivity (>99:1 dr). NOE studies confirm the stereochemical outcome of this reaction. In particular, there is a strong (3%) NOE interaction of the hydrogen on the stereogenic centre bearing the methyl group across the face of the 10-membered ring with the methylene hydrogens of the side chain (Fig. 10). Preparation of the diastereomeric aziridine **21** under analogous conditions is slightly less selective (98:2 dr), but the minor diastereomer can be removed by careful column chromatography to give a >99:1 dr. Interestingly, the diastereomeric compounds **21** and **23** can be distinguished by ^{13}C NMR spectroscopy despite the relatively wide separation of the stereogenic centres. Hydrolysis of the fully protected AziDAP **23**, using lithium hydroxide or sodium hydroxide, results in decomposition. Fortunately, sodium carbonate (41) in methanol–water allows quantitative generation of the salt of the diacid. Subsequent deprotection with sodium or lithium in ammonia at –78 °C gives AziDAP isomer **6** as the major product along with ε-methyl-α-aminopimelic acid in a 5.6:1 ratio. This undesired product is formed as a 1:1 mixture of diastereomers at the carbon bearing the methyl. It may result from reductive aziridine ring cleavage to generate an anion α to the carboxylate followed by elimination of nitrogen and further reduction of the resulting conjugated olefin. Separation of the crude reaction mixture using preparative TLC under basic conditions gives

© 2006 NRC Canada

Fig. 7. Inactivation of DAP epimerase by a mixture of AziDAP isomers and synthetic targets.



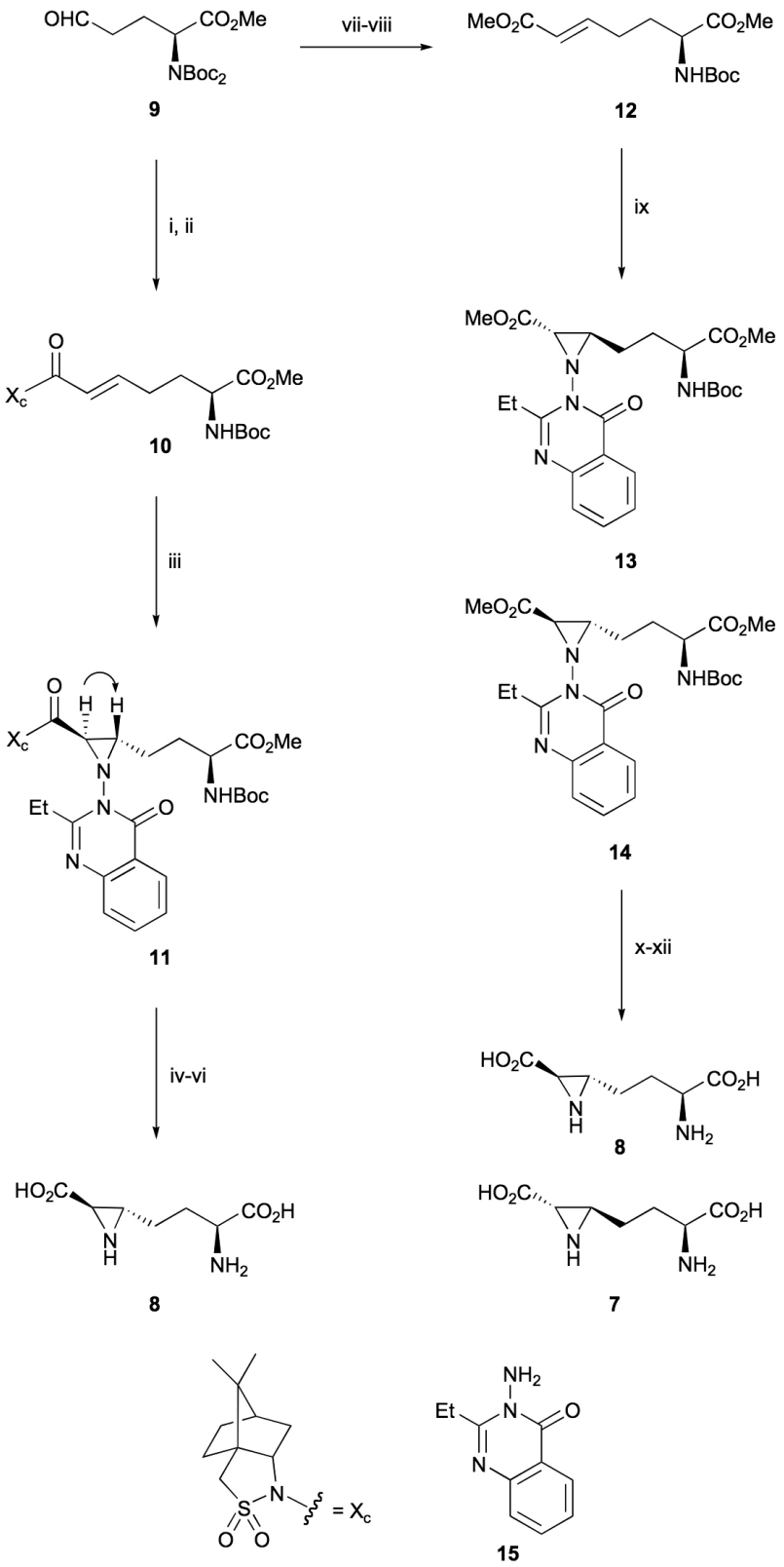
a low isolated yield (23% for AziDAP **6**). Pure AziDAP **5** could be prepared in improved yield (30%) by direct reduction, without preliminary HPLC purification of the diacid salt. AziDAP isomers **5** and **6** are extremely sensitive compounds that are stable in a strong base, but decompose quickly under acidic or neutral conditions. The multiple internal nucleophiles (four carboxylate oxygens and the distal amino group) promote rapid intramolecular aziridine ring opening. As solid carboxylate salts, **5** and **6** decompose somewhat more slowly at room temperature, with half-lives of about 2 weeks. They are stable for longer periods only under cryogenic (–80 °C) conditions, but this propensity to decompose in aqueous media precludes evaluation of their antimicrobial activity in bacterial cultures.

Interaction of DAP epimerase from *H. influenzae* with AziDAP isomers

As mentioned previously, Higgins and co-workers (30) reported that a crude mixture of all possible diastereomers of AziDAP caused irreversible inactivation of DAP epimerase with covalent modification of Cys73 in the enzyme active site. Exposure of cloned and overexpressed (*Eschrichia coli*) DAP epimerase from *H. influenzae* (25) to **5**, **6**, **7**, and **8** demonstrates that the compounds with the internal aziridine ring (**7** and **8**) are weak reversible inhibitors (IC_{50} for **8** is 2.88 mmol/L) that do not bind permanently in the active site. In contrast, the AziDAP isomers **5** and **6** rapidly and irreversibly inactivate the enzyme at low concentration and show both time and concentration dependence. The covalent attachment of both isomers to the enzyme can be demonstrated by electrospray mass spectroscopy. Because of the instability of these compounds in aqueous media, it is not possible to obtain accurate kinetic constants, an observation already reported by the Higgins group with the isomeric mixture (30). Earlier studies (25) suggested that pure LL-AziDAP **5** should result in selective attachment to Cys73 of DAP epimerase, whereas DL-AziDAP **6** would react with Cys217. Inactivation of DAP epimerase with individual AziDAP isomers, followed by treatment with thermolysin and trypsin, generates fragments that afford excellent sequence coverage (89%) by MS–MS and allow separate examination of both active site cysteines. The reaction of **5** with Cys73 of the enzyme is readily demonstrated by this approach. In contrast, analysis of DAP epimerase inhibited with a large excess (10- to 100-fold) of AziDAP **6** reveals that in addition to the expected alkylation of Cys217, attack also occurs at Cys73 to a certain extent. In principle, it is possible that a single diasteroisomer of AziDAP (i.e., 29) reacts with both cysteines. However, the excess of inhibitor **6** could possibly be contaminated by very small amounts (<1.0%) of the other AziDAP diastereomer **5**, which is not easily detectable and could act on the DAP epimerase. The use of such a large excess of inhibitor was initially prompted

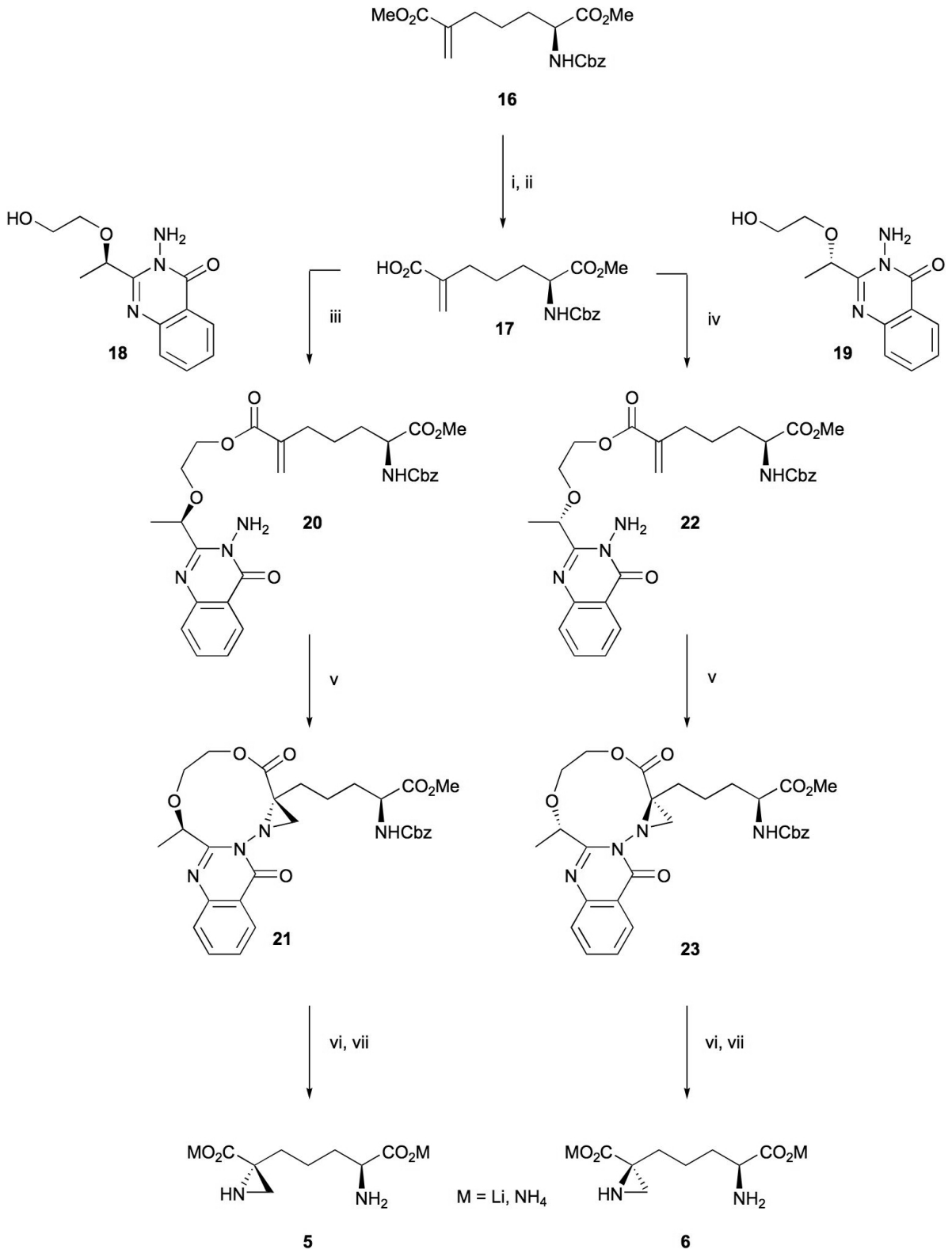
© 2006 NRC Canada

Fig. 8. Synthesis of **7** and **8**. See ref. 37. Reagents: (*i*) **Xc**-$COCH_2PO(OEt)_2$, DBU, LiCl (85%); (*ii*) TFA (94%); (*iii*) **15**, $Pb(OAc)_4$, HMDS (72%); (*iv*) TFA (99%); (*v*) LiOH, $MeOH–H_2O$ (85%); (*vi*) Li, NH_3 (48%); (*vii*) $MeO_2CCH{=}PPh_3$ (88%); (*viii*) TFA (88%); (*ix*) **15**, $Pb(OAc)_4$, HMDS (83%); (*x*) TFA (quant.); (*xi*) LiOH, $MeOH–H_2O$, (84%); (*xii*) Li, NH_3 (48%).



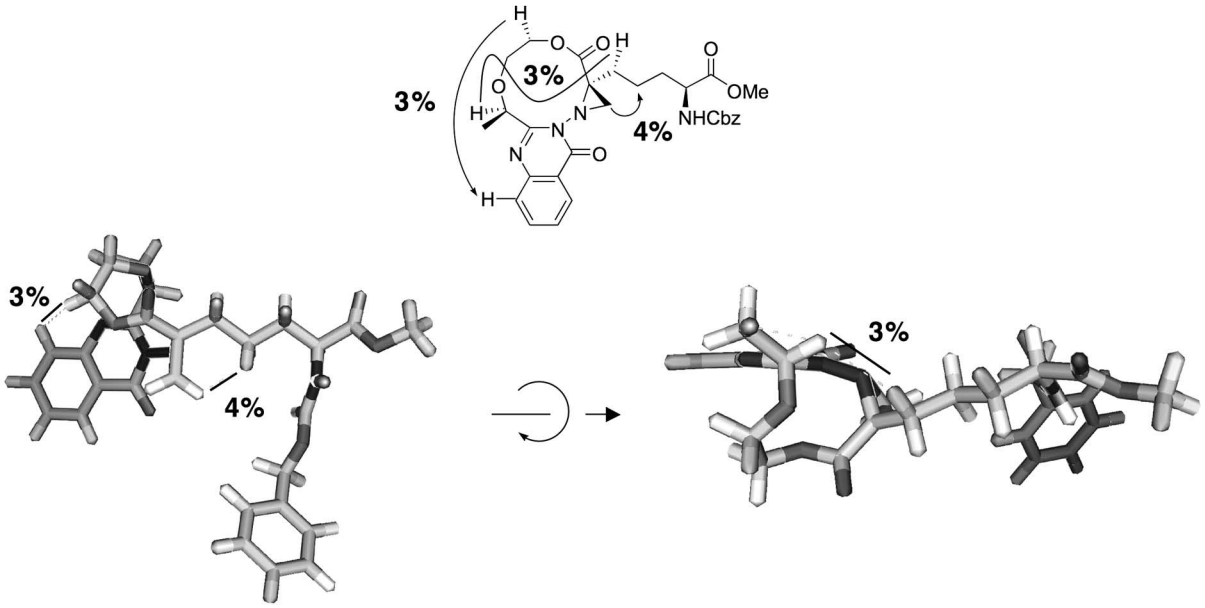
© 2006 NRC Canada

Fig. 9. Synthesis of **5** and **6**. See ref. 37. Reagents: (*i*) LiOH, MeOH–H_2O (82%); (*ii*) PS-PTSA, MeOH (95%); (*iii*) **18**, DCC, DMAP (62%); (*iv*) **19**, PS-DCC, DMAP (51%); (*v*) $Pb(OAc)_4$, HMDS (**21**, 55%; **23**, 87%); (*vi*) Na_2CO_3, MeOH–H_2O (from **23**, 69%); (*vii*) Li, NH_3 (**5**, 30% over two steps; **6**, 23%).



© 2006 NRC Canada

Fig. 10. Determination of aziridination stereochemistry by NOE effects. Selected NOE enhancements for **21** are shown with its calculated preferred conformation (two views).



by the desire to completely and rapidly inactivate the enzyme for crystallographic studies prior to its facile aerobic oxidation to form the internal disulfide between Cys73 and Cys217.

Fortunately, X-ray crystallography studies by our collaborators, Professor Michael James and Dr. Bindu Pillai (Department of Biochemistry, University of Alberta), on DAP epimerase separately inhibited with the individual AziDAP isomers showed that LL-AziDAP **5** bound exclusively to Cys73 and that DL-AziDAP **6** attached only to Cys217. In both cases, inactivation proceeds as predicted by attack of the thiolate on the aziridine methylene. Although these three-dimensional structures will be the subject of a separate report (submitted for publication), the key features essential for the unusual catalysis are readily evident. As one of the active site thiols in DAP epimerase has a considerably reduced pK_a (6 to 7) (20), the two cysteines are likely to exist as a thiolate–thiol pair prior to substrate binding. Binding of AziDAP and ring opening by the thiolate gives an analog of the substrate–enzyme complex in which the α-hydrogen of the corresponding DAP substrate is replaced by a methylene group. The enzyme–inactivator complex shows a significant domain shift, compared with the inactive disulfide version of the enzyme (26, 27), to enclose the DAP analog, similar to what has been very recently reported for glutamate racemase with D-glutamate in the active site (42). This creates a very tight-fitting pocket for binding the substrate, which is lined with hydrophobic side chains and also has a series of hydrogen bond donors and acceptors to recognize and interact with the substrate–inhibitor carboxyl and amino functionalities. As expected, the carboxylate attached to the α-carbon that undergoes epimerization is fully hydrogen bonded to allow electron delocalization. The amino group at the α-carbon is also protonated and α-helices near the carboxylate assist dispersion of negative charge. Finally, relatively rigid binding of substrate–inhibitor with exclusion of solvent, and location of the thiolate base close to the α-hydrogen with separation from the carboxyl and amino groups, enables catalysis with minimal movement. The crystallographic details will be reported in a forthcoming publication (43).

Acknowledgements

I am deeply grateful to the Canadian Society for Chemistry for selecting me to receive the Alfred Bader Award. I would particularly like to acknowledge the continuing contributions that Alfred Bader has made in supporting scientific endeavours internationally, not only through generous donations to national societies and universities, but also by his career-long efforts to make useful laboratory chemicals routinely available. Co-workers and collaborators cited in the references are gratefully acknowledged for their dedicated work in this project. I especially thank John Blanchard (Albert Einstein College of Medicine, Yeshiva University), Michael James, Bindu Pillai, Paul Semchuk, and Maia Cherney (Department of Biochemistry, University of Alberta), and Andrew Sutherland and Christopher Diaper of our group. This research has been supported by the Natural Sciences and Engineering Research Council of Canada (NSERC), Merck Frosst Canada, the Canada Research Chair in Bioorganic and Medicinal Chemistry, and the Alberta Heritage Foundation for Medical Research.

References

1. L.R. Peterson and A. Dalhoff. J. Antimicrob. Chemother. **53**, 902 (2004).
2. J.E. McGowan, Jr. Emerging Infect. Dis. **7**, 286 (2001).
3. C. Walsh. *In* Antibiotics, actions, origins, resistance. American Society for Microbiology Press, Washington, D.C. 2003.
4. M. El Ghachi, A. Bouhss, D. Blanot, and D. Mengin-Lecreulx. J. Biol. Chem. **279**, 30106 (2004).
5. S.T.D. Hsu, E. Breukink, E. Tischenko, M.A.G. Lutters, B. de Kruijff, R. Kaptein, A.M.J.J. Bonvin, and N.A.J. van Nuland. Nat. Struc. Mol. Biol. **11**, 963 (2004).

© 2006 NRC Canada

6. N.L. Rose, P. Sporns, H.M. Dodd, M.J. Gasson, F.A. Mellon, and L.M. McMullen. J. Agric. Food Chem. **51**, 3174 (2003).
7. N.I. Martin, T. Sprules, M.R. Carpenter, P.D. Cotter, C. Hill, R.P. Ross, and J.C. Vederas. Biochemistry, **43**, 3049 (2004), and refs. cited therein.
8. P.D. Cotter, C. Hill, and R.P. Ross. Curr. Protein Pept. Sci. **6**, 61 (2005).
9. J. Van Heijenoort. Nat. Prod. Rep. **18**, 503 (2001).
10. R.J. Cox, A. Sutherland, and J.C. Vederas. Bioorg. Med. Chem. **8**, 843 (2000).
11. S.D. Abbott, P. Lane-Bell, K.P.S. Sidhu, and J.C. Vederas. J. Am. Chem. Soc. **116**, 6513 (1994).
12. D. Mengin-Lecreulx, D. Blanot, and J. van Heijenoort. J. Bacteriol. **176**, 4321 (1994).
13. J.S. Wiseman and J.S. Nichols. J. Biol. Chem. **259**, 8907 (1984).
14. M.E. Tanner. Acc. Chem. Res. **35**, 237 (2002).
15. T. Yoshimura and N. Esaki. J. Biosci. Bioeng. **96**, 103 (2003).
16. L. Liu, K. Iwata, A. Kita, Y. Kawarabayasi, M. Yohda, and K. Miki. J. Mol. Biol. **319**, 479 (2002).
17. S. Glavas and M.E. Tanner. Biochemistry, **40**, 6199 (2001).
18. H. Mobitz and T.C. Bruice. Biochemistry, **43**, 9685 (2004).
19. W.J. Albery and J.R. Knowles. Biochemistry, **25**, 2572 (1986).
20. C.W. Koo and J.S. Blanchard. Biochemistry, **38**, 4416 (1999).
21. Y. Gao, P. Lane-Bell, and J.C. Vederas. J. Org. Chem. **63**, 2133 (1998).
22. J.P. Richard and T.L. Amyes. Bioorg. Chem. **32**, 354 (2004), and refs. cited therein.
23. J.P. Richard and T.L. Amyes. Curr. Opin. Chem. Biol. **5**, 626 (2001).
24. M.H. Gelb, Y. Lin, M.A. Pickard, Y. Song, and J.C. Vederas. J. Am. Chem. Soc. **112**, 4932 (1990).
25. C.W. Koo, A. Sutherland, J.C. Vederas, and J.S. Blanchard. J. Am. Chem. Soc. **122**, 6122 (2000).
26. M. Cirilli, R. Zheng, G. Scapin, and J.S. Blanchard. Biochemistry, **37**, 16452 (1998).
27. A.J. Lloyd, T. Huyton, J. Turkenburg, and D.I. Roper. Acta Crystallogr. Sect. D, Biol. Crystallogr. **60**, 397 (2004).
28. M. Anderson. PCT Int. Application (AstraZeneca AB, Sweden, AstraZeneca Pharmaceuticals LP). WO 2004/061097, 1125 pp.
29. E. Puig, M. Garcia-Viloca, A. Gonzalez-Lafont, I. Lopez, X. Daura, and J.M. Lluch. J. Chem. Theory Comput. **1**, 737 (2005).
30. F. Gerhart, W. Higgins, C. Tardif, and J.B. Ducep. J. Med. Chem. **33**, 2157 (1990).
31. M.E. Tanner and S. Miao. Tetrahedron Lett. **35**, 4073 (1994).
32. R.J. Cox, J. Durston, and D.I. Roper. J. Chem. Soc. Perkin Trans. 1, 1029 (2002).
33. J.T. Kapron, B.D. Santarsiero, and J.C. Vederas. J. Chem. Soc. Chem. Commun. 1074 (1993).
34. T.K. Chakraborty and A. Ghosh. Indian J. Chem. Sect. B: Org. Chem. **40**, 895 (2001).
35. K.-S. Yang and K. Chen. J. Org. Chem. **66**, 1676 (2001).
36. R.S. Atkinson, R.D. Draycott, D.J. Hirst, M.J. Parratt, and T.M. Raynham. Tetrahedron Lett. **43**, 2083 (2002).
37. C.M. Diaper, A. Sutherland, B. Pillai, M.N.G. James, P. Semchuk, J.S. Blanchard, and J.C. Vederas. Org. Biomol. Chem. **3**, 4402 (2005).
38. D.H.R. Barton, S.D. Gero, B. Quiclet-Sire, and M. Samadi. J. Chem. Soc. Perkin Trans. 1, 981 (1991).
39. P. Gogoi. Synlett, 2263 (2005).
40. S.V. Ley, I.R. Baxendale, R.N. Bream, P.S. Jackson, A.G. Leach, D.A. Longbottom, M. Nesi, J.S. Scott, R.I. Storer, and S.J. Taylor. J. Chem. Soc. Perkin Trans. 1, 3815 (2000).
41. K.L. Kaestle, M.K. Anwer, T.K. Audhya, and G. Goldstein. Tetrahedron Lett. **32**, 327 (1991).
42. S.N. Ruzheinikov, M.A. Taal, S.E. Sedelnikova, P.J. Baker, and D.W. Rice. Structure, **13**, 1707 (2005).
43. B. Pillai, M.M. Cherney, C.M. Diaper, A. Sutherland, J.S. Blanchard, J.C. Vederas, M.N.G. James, Proc. Natl. Acad. Sci. U.S.A. 103, 8668 (2006).

© 2006 NRC Canada

Mechanism of cyclopropanol to cyclopropanol isomerization mediated by Ti(IV) and a Lewis acid[1]

Charles P. Casey and Neil A. Strotman

Abstract: Isomerization of *trans*-3-deutero-*r*-1-methyl-*cis*-2-phenylcyclopropan-1-ol (**1-trans-d**) to three isomeric cyclopropanols was facilitated by reaction with a mixture of Ti(O-*i*-Pr)$_4$ and $BF_3{\cdot}OEt_2$. The more Lewis acidic Cl_2Ti(O-*i*-Pr)$_2$ catalyzed this reaction in the absence of $BF_3{\cdot}OEt_2$. This cyclopropanol to cyclopropanol rearrangement involves reversible ring opening to a β-titanaketone. When the major species in solution prior to quenching was a titanium cyclopropoxide, a 40:40:10:10 mixture of cyclopropanols **1-trans-d**:**1-cis-d**:**2-trans-d**:**2-cis-d** was obtained; this is close to the equilibrium ratio of the titanium cyclopropoxides. When a catalytic quantity of Ti(O-*i*-Pr)$_4$ and a large excess of cyclopropanol was used, quenching gave a 29:29:21:21 mixture; this is closer to the equilibrium ratio of the cyclopropanols than the cyclopropoxides. Extrapolation to 0% and to 100% cyclopropoxide gave equilibrium constants for both cyclopropanols (K_{eq} = [**2**]/[**1**] = 1.3) and cyclopropoxides (K_{eq} = [**2-Ti**]/[**1-Ti**] = 0.18). A mechanism for these isomerization processes that involves ring opening and (or) ring closing with both retention and inversion of configuration at the carbon bearing phenyl is proposed.

Key words: cyclopropanol, titanium isopropoxide, Kulinkovich hydroxycyclopropanation.

Résumé : L'isomérisation du *trans*-3-deutéro-*r*-1-méthyl-2-phénylcyclopropan-1-ol (**1-trans-d**) en trois cyclopropanols isomères est facilitée par une réaction avec un mélange de Ti(O-*i*-Pr)$_4$ et de $BF_3{\cdot}OEt_2$. Le Cl_2Ti(O-*i*-Pr)$_2$, un acide de Lewis plus acide, catalyse cette réaction sans $BF_3{\cdot}OEt_2$. Ce réarrangement d'un cyclopropanol en un autre implique une ouverture de cycle réversible en β-titanacétone. Quand l'espèce principale en solution avant le captage le cyclopropylate de titane, on obtient un mélange 40 : 40 : 10 : 10 des cyclopropanols **1-trans-d** : **1-cis-d** : **2-trans-d** : **2-cis-d**, une proportion qui se rapproche du rapport à l'équilibre des cyclopropylates de titane. Quand on utilise une quantité catalytique de Ti(O-*i*-Pr)$_4$ avec un large excès de cyclopropanol, le piégeage conduit à un mélange 29 : 29 : 21 : 21 qui est plus près du rapport d'équilibre des cyclopropanols que de celui des cyclopropylates. Une extrapolation à des quantités égales à 0 % et à 100 % de cyclopropylate permet d'obtenir les constantes d'équilibre tant pour les cyclopropanols ($K_{éq}$ = [**2**]/[**1**] = 1,3) que pour les cyclopropanolates ($K_{éq}$ = [**2-Ti**]/[**1-Ti**] = 0,18). On propose un mécanisme pour ces processus d'isomérisation qui impliquent des ouvertures et des fermetures de cycle impliquant des rétentions et des inversions de configuration au niveau du carbone portant le noyau phényle.

Mots clés : cyclopropanol, isopropylate de titane, hydroxycyclopropanation de Kulinkovich.

[Traduit par la Rédaction]

Introduction

The Kulinkovich hydroxycyclopropanation, discovered in 1989, allows for the one-step preparation of polysubstituted cyclopropanols from esters, Grignard reagents, and Ti(O-*i*-Pr)$_4$ (Scheme 1) (1). Advances in this methodology have resulted in the employment of catalytic quantities of titanium (2), highly diastereoselective (3), and enantioselective (4) variants of this reaction and a widely broadened substrate scope.

This reaction is believed to involve a Ti(II)-alkene complex (**B**), formed via alkane loss from an unstable dialkyl-Ti(IV) intermediate (**A**) (Scheme 2). In the presence of an added alkene, exchange occurs, leading to increased product diversity. Reductive coupling of the alkene and the ester carbonyl by Ti(II) leads to metallacycle **C**. This metallacycle fragments with alkoxide loss to give β-titanaketone (**D**). Attack of the nucleophilic carbon bound to titanium on this γ-carbonyl moiety results in ring closure to form cyclopropoxide.

We recently demonstrated that the final step of the Kulinkovich hydroxycyclopropanation reaction involves frontside attack of the carbon–titanium bond on the γ-carbonyl to form a cyclopropoxide (Scheme 3) (5). Deuterium labelling revealed that the carbon bound to titanium retained its configuration throughout this process to give *trans*-3-

Received 8 August 2005. Accepted 19 September 2005. Published on the NRC Research Press Web site at http://canjchem.nrc.ca on 27 May 2006.

Dedicated to Dr. Alfred Bader on the occasion of his 80th birthday. As a Past President of the American Chemical Society, I want to express the thanks of all our members to Dr. Bader for his generous support of the ACS Project Seed, the Bader Scholars program, and the ACS World Reach Fund and for sponsoring the Alfred Bader Award in Bioinorganic or Bioorganic Chemistry.

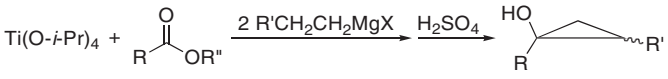
C.P. Casey[2] and N.A. Strotman. Department of Chemistry, University of Wisconsin-Madison, Madison, WI 53706, USA.

[1]This article is part of a Special Issue dedicated to Dr. Alfred Bader.

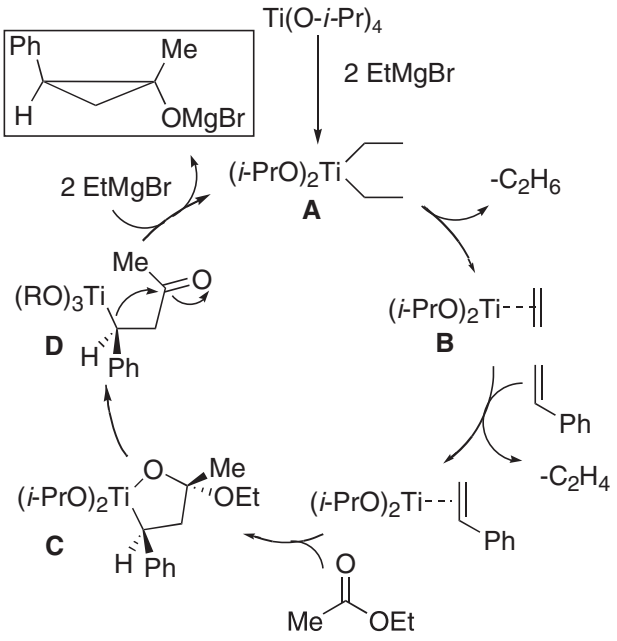
[2]Corresponding author (e-mail: casey@chem.wisc.edu).

 doi:10.1139/V06-069 © 2006 NRC Canada

Scheme 1.



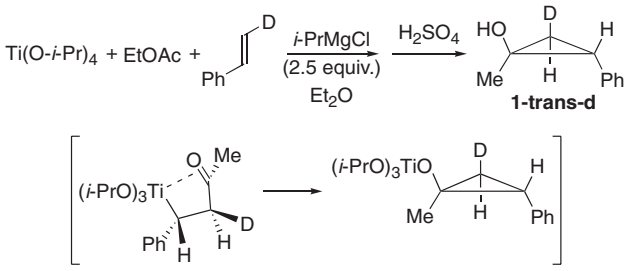
Scheme 2.



deutero-*r*-1-methyl-*cis*-2-phenylcyclopropan-1-ol (**1-trans-d**)[3] as the only observed product (5, 6).

We wondered whether introduction of a Lewis acid into this reaction, prior to cyclopropoxide formation, might result in a different ring closure mechanism. It seemed likely that the carbonyl oxygen would bind more tightly to an electron deficient Lewis acid, such as BF_3, than intramolecularly to the electron rich alkyltitanium triisopropoxide unit (Scheme 4). This would inhibit coordination of the carbonyl oxygen to titanium and would cause the alkyltitanium species to adopt a less sterically demanding transition structure. This opens the possibility that ring closure might occur with inversion of configuration at the carbon bound to titanium. An analogous transition structure, in addition to being involved in iron- (7), tin- (8), and zirconium-mediated (5) cyclopropane formation, was consistent with the inversion of configuration that we observed at the carbon–titanium bond in de Meijere's cyclopropylamine synthesis (5, 9) (Scheme 4). The addition of BF_3 during the Kulinkovich reaction produced additional cyclopropanol isomers. Here, we report an

Scheme 3.



unusual cyclopropanol to cyclopropanol rearrangement, catalyzed by Ti(O-*i*-Pr)$_4$ and $BF_3{\cdot}OEt_2$, that is responsible for the observation of additional isomers (10).[4] This isomerization is shown to require reversible ring opening of a cyclopropoxide. Moreover, two different mechanisms for the reversible ring opening are required; one involves retention and the other involves inversion of configuration at the carbon bound to titanium in the ring-opened intermediate.

Results

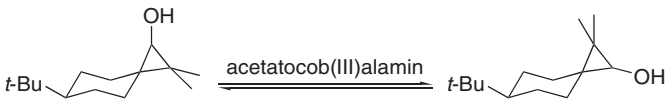
To test our hypothesis that a Lewis acid could affect a different ring closure mechanism in the Kulinkovich hydroxycyclopropanation, we modified the cyclopropanation procedure (3*d*). In the original Kulinkovich procedure, 2.5 equiv. of *i*-PrMgCl were added to a solution of Ti(O-*i*-Pr)$_4$, EtOAc, and *trans*-β-deuterostyrene in refluxing ether over a 1 h period. However, in our variation, the Grignard reagent was added over 5 min at 0 °C, followed by the addition of 2.5 equiv. of $BF_3{\cdot}OEt_2$ and stirred for 1 h (Scheme 5).

Formation of two deuterium-scrambled cyclopropanols in the presence of BF_3

In contrast to the reaction in the absence of $BF_3{\cdot}OEt_2$, which produced only a single cyclopropanol (**1-trans-d**), the addition of $BF_3{\cdot}OEt_2$ led to the formation of three additional isomeric cyclopropanols: *cis*-3-deutero-*r*-1-methyl-*cis*-2-phenylcyclopropan-1-ol (**1-cis-d**), *trans*-3-deutero-*r*-1-methyl-*trans*-2-phenylcyclopropan-1-ol (**2-trans-d**), and *cis*-3-deutero-*r*-1-methyl-*trans*-2-phenylcyclopropan-1-ol (**2-cis-d**). ^{1}H NMR spectroscopy of the crude product mixture showed the formation of **1-trans-d** and **1-cis-d** (δ 2.31) and **2-trans-d** and **2-cis-d** (δ 1.98) in 37% and 19% yields, respectively. ^{2}H NMR spectroscopy showed a 1:1:0.46:0.46 mixture of **1-trans-d**:**1-cis-d**:**2-trans-d**:**2-cis-d**. A mixture of **1-trans-d** and **1-cis-d** was isolated as a white solid (35%) by

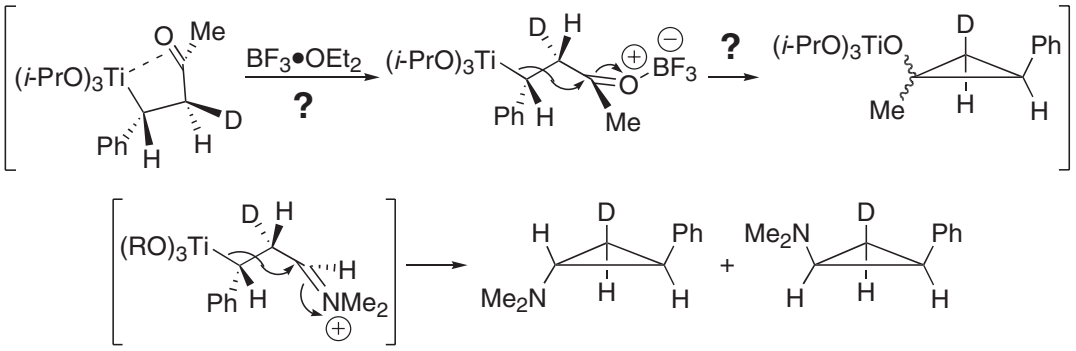
[3] The stereochemistry of cyclopropanes is specified using the IUPAC reference system where *r*- is used to specify the reference substituent.

[4] This isomerization from one cyclopropanol to another is very unusual. We found only two other reports containing evidence of a cyclopropanol to cyclopropanol rearrangement. Kasatkin and Sato (3*b*) observed a temperature dependence on the cis/trans product ratio of cyclopropanols generated from homoallyl esters, Ti(O-*i*-Pr)$_4$, and 2 *i*-PrMgBr. When the reaction mixture was allowed to equilibrate at room temperature for 1.5 h before quenching, the trans product was favored greatly with a 95:5 trans:cis ratio, compared with a 41:59 ratio obtained without this equilibration period. In a second example, acetatocob(III)alamin catalyzed the equilibrium isomerization of a spiro-fused cyclopropanol in a maximum of 29% yield (eight other products from oxidation of the cyclopropanol were also seen).

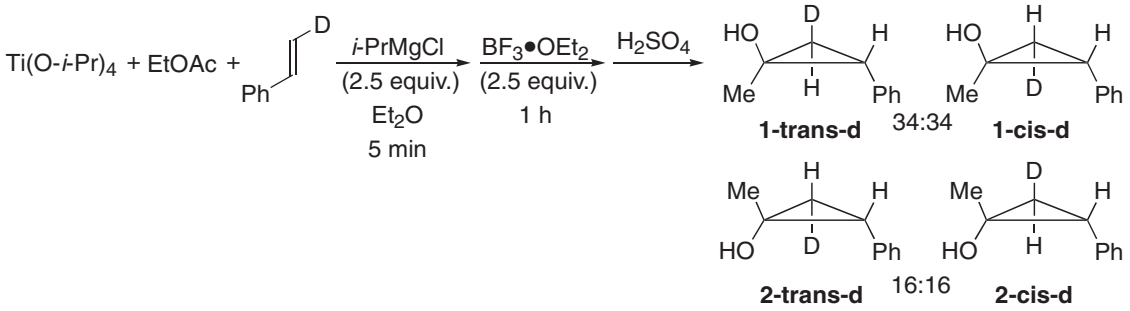


© 2006 NRC Canada

Scheme 4.



Scheme 5.



recrystallization. Since *r*-1-methyl-*trans*-2-phenylcyclopropan-1-ol (**2**) could not be obtained by crystallization, it was eventually isolated by preparative TLC (see the following).

The ^{1}H NMR spectrum of recrystallized **1-trans-d** and **1-cis-d** was similar to that of the undeuterated analog *r*-1-methyl-*cis*-2-phenylcyclopropan-1-ol (**1**) except that the two cyclopropyl protons at C-3 (δ 1.21 and 0.97) each gave integrations of 0.5H and each showed coupling only to the benzylic proton. Proton-decoupled ^{2}H NMR spectroscopy showed peaks at δ 1.21 and δ 0.98 of equal integration corresponding to a 1:1 mixture of **1-trans-d** and **1-cis-d**. ^{13}C NMR spectroscopy showed the cyclopropyl carbon bearing the deuterium at δ 18.9 (J_{CD} = 24 Hz) as a 1:1:1 triplet. The absence of a larger central peak or any overlapping quintet indicated that no d_0 or d_2 analog was present.

In a similar experiment, preparative TLC led to the isolation of **2**, which was free of **1**. However, the 1:1 mixture of **2-trans-d**:**2-cis-d** also contained ~30% decomposition products.[5] The ^{1}H NMR chemical shifts were consistent with those previously reported for compound **2** (11). The proton decoupled ^{2}H NMR spectrum of the impure mixture of **2-trans-d** and **2-cis-d** showed equal integrations for the peaks at δ 1.05 and δ 1.18, corresponding to deuterium on C-3 of the cyclopropane.

While this BF_3 modification of the Kulinkovich procedure is clearly of no synthetic utility, it suggests the interesting possibility that an unusual cyclopropanol to cyclopropanol isomerization might be occurring. The formation of cyclopropanols **1** and **2** and the 1:1 ratio of deuterium on C-3 of each cyclopropanol strongly suggested that some type of equilibration process had occurred. It seemed highly unlikely that a 1:1 ratio of retention:inversion at the carbon–titanium bond had occurred in the formation of each cyclopropanol. We suspected that isomerization might have occurred *after* cyclopropanol formation, possibly by reversible ring opening.

To determine whether the majority of cyclopropane was formed stereospecifically prior to the addition of BF_3, we conducted an analogous experiment in which 2.5 equiv. of *i*-PrMgCl were added to Ti(O-*i*-Pr)$_4$, EtOAc, and *trans*-β-deuterostyrene at 0 °C over 5 min and then quenched with acid and water. In this experiment, with no BF_3·OEt_2 added, a 57% NMR yield of **1-trans-d** was obtained. There was no evidence of other cyclopropanol isomers detected by either ^{1}H or ^{2}H NMR spectroscopy in the crude product mixture. This demonstrated that rapid ring closure (<5 min at 0 °C) to form cyclopropoxide had occurred before Lewis acid addition and that BF_3·OEt_2 was involved in the isomerization of the cyclopropoxide rather than in the initial ring closure step.

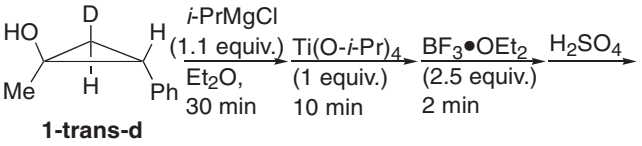
Cyclopropanol to cyclopropanol isomerization with *i*-PrMgCl, Ti(O-*i*-Pr)$_4$, and BF_3·OEt_2

We next tested whether pure cyclopropanol **1-trans-d** (5) could undergo cyclopropanol to cyclopropanol rearrangement. Deprotonation of the cyclopropanol **1-trans-d** with 1.1 equiv. of *i*-PrMgCl was followed by the sequential addition of 1.0 equiv. of Ti(O-*i*-Pr)$_4$ and 2.5 equiv. of BF_3·OEt_2 and quenching with H_2SO_4 (Scheme 6). When the reaction was quenched after 2 min, ^{1}H NMR spectroscopy showed both **1** and **2** and integration vs. an internal standard showed quantitative recovery of cyclopropanols. Integration of the ^{2}H NMR peaks for the CHD resonances of **1** and **2** at δ 1.22,

[5] The low recovered yields were due to decomposition on the silica gel as well as incomplete separation of TLC bands.

© 2006 NRC Canada

Scheme 6.



1-trans-d:1-cis-d:2-trans-d:2-cis-d
38:38:12:12

0.98, 1.04, and 1.18 indicated a 38:38:12:12 mixture of **1-trans-d**:**1-cis-d**:**2-trans-d**:**2-cis-d**.[6]

At longer times before H_2SO_4 quenching (>60 min), the ratio of deuterated cyclopropanols remained the same, but the yield of recovered cyclopropanols decreased.

Several recrystallizations from pentane at –78 °C of a mixture obtained from isomerization of **1** led to the isolation of a mixture of pure cyclopropanols greatly enriched in **2**. When this 25:75 mixture of **1**:**2** was subjected to our standard isomerization conditions, a 71:29 mixture of **1**:**2** was obtained (Scheme 7). The observation of the same ratio of isomers of **1**:**2** starting from either **1** or **2** demonstrates that equilibrium between the salts of **1** and **2** was reached.

Attempts to isomerize *cis*-2-butyl-*r*-1-methylcyclopropanol (2), bearing a butyl group in place of the phenyl in **1**, failed under our standard conditions and gave only starting material. This indicates that only a bond to a benzylic carbon can cleave during rearrangement.

Cyclopropanol to cyclopropanol isomerization with *i*-PrMgCl and $Cl_2Ti(O\text{-}i\text{-}Pr)_2$

The isomerization of **1-trans-d** did not occur in the presence of $Ti(O\text{-}i\text{-}Pr)_4$ or BF_3 alone; only the starting cyclopropanol was recovered. Our hypothesis was that both a titanium salt and a Lewis acid were required for isomerization. This hypothesis suggested that the more electron deficient $Cl_2Ti(O\text{-}i\text{-}Pr)_2$ might be used alone to serve this dual purpose.

Deprotonation of **1-trans-d** with *i*-PrMgCl, addition of 2 equiv. $Cl_2Ti(O\text{-}i\text{-}Pr)_2$, and quenching after 30 min led to incomplete equilibration and observation of an 85:8:3:3 ratio of **1-trans-d**:**1-cis-d**:**2-trans-d**:**2-cis-d** (Scheme 8). When the reaction mixture was quenched after 3.5 h, more extensive isomerization to a 46:34:10:10 ratio was seen. This ratio is similar to the equilibrium ratio seen in the $Ti(O\text{-}i\text{-}Pr)_4$–$BF_3$ mediated isomerization. Although $Cl_2Ti(O\text{-}i\text{-}Pr)_2$ proved a competent catalyst for this isomerization, it facilitated rearrangement much more slowly.

Equilibrium formation of titanium cyclopropoxides

We wondered whether irreversible deprotonation of the cyclopropanol by *i*-PrMgCl was necessary for the $Ti(O\text{-}i\text{-}Pr)_4$–$BF_3$ catalyzed isomerization. We first examined the equilibrium for cyclopropanol exchange with $Ti(O\text{-}i\text{-}Pr)_4$. The ^{1}H NMR spectrum of a solution of equimolar amounts of $Ti(O\text{-}i\text{-}Pr)_4$ and cyclopropanol **1** in $Et_2O\text{-}d_{10}$ showed an equilibrium mixture of titanium alkoxides (Scheme 9). No change in the NMR spectrum of this solution was seen over 80 min, indicating that equilibrium had been rapidly achieved. In addition, no isomerization to the cyclopropoxide of **2** (**2-Ti**) and no ring opening of the cylopropanol was observed. The cyclopropanol **1** and titanium cyclopropoxide **1-Ti** were differentiated by their benzylic proton resonances at δ 2.22 and 2.45, respectively; $Ti(O\text{-}i\text{-}Pr)_4$ and *i*-PrOH were distinguished by their CHO proton resonances at δ 4.52 and 3.87, respectively.[7] At equilibrium, the benzylic protons at δ 2.45 and 2.22 integrated to 89:11 when equimolar amounts of **1** and $Ti(O\text{-}i\text{-}Pr)_4$ were used (K_{eq} = ~65). Apparently, deprotonation of the cyclopropanol by a Grignard reagent is not required to generate titanium cyclopropoxides without deleterious side reactions.

While NMR spectroscopy allowed ready distinction between cyclopropanol and cyclopropoxides, it did not provide a way to distinguish between the various $Ti(O\text{-}i\text{-}Pr)_n(OR)_{4-n}$ species. To determine whether multiple cyclopropoxy units bind to a single titanium center, we studied the equilibrium between cyclopropanol and cyclopropoxides at high ratios of cyclopropanol:titanium by ^{1}H NMR spectroscopy (Table 1).

In all cases, more cyclopropoxide was seen than predicted by statistics, indicating that **1** is more acidic than isopropanol. Multiple cyclopropoxy groups can clearly bind to titanium. There does not appear to be any significant difference in the selectivity of cyclopropoxide binding to the various $Ti(O\text{-}i\text{-}Pr)_n(OR)_{4-n}$ species.

Cyclopropanol to cyclopropanol isomerization with $Ti(O\text{-}i\text{-}Pr)_4$ and $BF_3{\cdot}OEt_2$

1-trans-d was combined with 1.0 equiv. of $Ti(O\text{-}i\text{-}Pr)_4$ followed by 2.5 equiv. of $BF_3{\cdot}OEt_2$ and the reaction was quenched after 2 min. NMR spectroscopy showed the ratio of **1-trans-d**:**1-cis-d**:**2-trans-d**:**2-cis-d** was 40:40:10:10 (Scheme 10). This shows that $Ti(O\text{-}i\text{-}Pr)_4$ and $BF_3{\cdot}OEt_2$ are sufficient for cyclopropanol to cyclopropanol isomerization and that prior irreversible deprotonation by a Grignard reagent is not necessary.

Both $Ti(O\text{-}i\text{-}Pr)_4$ and $BF_3{\cdot}OEt_2$ are required for isomerization. No isomerization of **1-trans-d** was seen with $Ti(O\text{-}i\text{-}Pr)_4$ alone. Similarly, $BF_3{\cdot}OEt_2$ alone did not catalyze cyclopropanol epimerization although a small amount of decomposition (<10%) of **1-trans-d** was seen.

This equilibrium ratio of products is approximately representative of the relative energies of the cyclopropoxides of **1** and **2** (**1-Ti** and **2-Ti**), since little of the free cyclopropanols exists at equilibrium. This indicates that a $(i\text{-PrO})_3$TiO- unit is more sterically bulky than a methyl group, making the titanium alkoxide **1-Ti** with phenyl cis to methyl slightly more stable than the titanium alkoxide **2-Ti** with phenyl cis to $(i\text{-PrO})_3$TiO-.

Using only a catalytic amount of $Ti(O\text{-}i\text{-}Pr)_4$ should allow direct measurement of the equilibrium ratio of **1**:**2** rather than the equilibrium ratio of the titanium alkoxides **1-Ti**:**2-**

[6] The ratio of cyclopropanols **1** and **2** varied between 83:17 and 72:28 and showed no relationship to reaction time. This variation between runs may be due to the exact ratio of titanium:magnesium employed and the extent of precipitation of magnesium salts. The identity of the metal would affect the relative energies of the cyclopropoxides **1** and **2**.

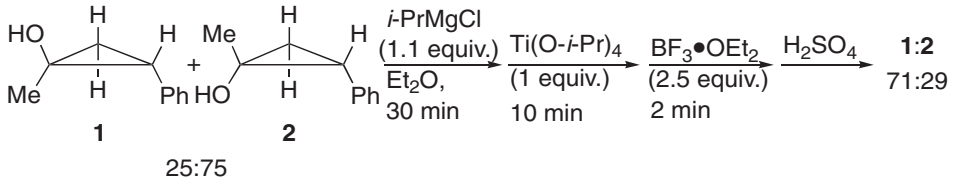
[7] The resonance at δ 4.52 corresponds to $Ti(O\text{-}i\text{-}Pr)_4$ as well as $(RO)Ti(O\text{-}i\text{-}Pr)_3$ (**1-Ti**).

© 2006 NRC Canada

Table 1. Percent of material present as titanium cyclopropoxide as a function of ratio of **1** : Ti(O-*i*-Pr)4.

1 : $Ti(O\text{-}i\text{-}Pr)_4$	% as **1-Ti**	Expected statistical (% as **1-Ti**)	Theoretical maximum (% as **1-Ti**)
1.0:1	89	80	100
4.0:1	62	50	100
10:1	36	29	40

Scheme 7.

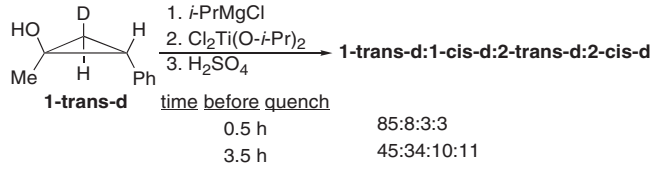


Ti, since most of the material would be in the protonated form. When **1-trans-d** was combined with 0.10 equiv. of $Ti(O\text{-}i\text{-}Pr)_4$ followed by 0.25 equiv. of $BF_3{\cdot}OEt_2$ and quenched after 1 h, the ratio of **1-trans-d**:**1-cis-d**:**2-trans-d**:**2-cis-d** was 30:30:20:20 (Scheme 10). Allowing the same reaction to proceed for 3 h before quenching gave an almost identical ratio 29:29:21:21, demonstrating that equilibrium had been reached after 1 h. To obtain a closer approximation of the equilibrium amounts of cyclopropanols, we attempted to further decrease the amount of $Ti(O\text{-}i\text{-}Pr)_4$. However, catalyst deactivation, indicated by incomplete isomerization of **1-trans-d** to **1-cis-d** even at long reaction times, was seen below 0.1 equiv. of $Ti(O\text{-}i\text{-}Pr)_4$ and 0.25 equiv. of $BF_3{\cdot}OEt_2$.

Equilibrium ratios of cyclopropanols and of cyclopropoxides are both involved in determining the ratios of cyclopropanols upon quenching (Scheme 11). When a 1:1 ratio of cyclopropanol–$Ti(O\text{-}i\text{-}Pr)_4$ was employed (Scheme 10), 89% of the material is present as a titanium cyclopropoxide (Table 1) and the observed 80:20 ratio of **1**:**2** obtained on quenching mainly reflects the equilibrium ratio of cyclopropoxides. When a 10:1 ratio of cyclopropanol:$Ti(O\text{-}i\text{-}Pr)_4$ was employed (Scheme 10), 64% of the material is present as a free cyclopropanol (Table 1) and the observed 58:42 ratio of **1**:**2** obtained on quenching has an increased contribution from the equilibrium ratio of cyclopropanols. The greater equilibrium amount of **2** seen at lower titanium levels indicates that the equilibrium ratio of cyclopropanols **1**:**2** must be substantially less than that of the corresponding cyclopropoxides. The ratio of **1**:**2** obtained upon quenching is the weighted average of the ratios of **1**:**2** and **1-Ti**:**2-Ti** existing in solution. At high titanium concentrations, the equilibrium in Scheme 11 is shifted toward cyclopropoxides **1-Ti** and **2-Ti**, whereas at low titanium concentrations this equilibrium is shifted toward cyclopropanols **1** and **2**.

A linear plot of **1** (in %) in the quench vs. cyclopropoxides **1-Ti** and **2-Ti** (in %) in the solution being quenched was obtained (Fig. 1). [8,9]Extrapolation of the plot to 100% cyclopropoxides gives the percentage of **1-Ti** at equilibrium (**1-Ti**:**2-Ti** = 85:15; K_{eq} = [**2-Ti**]/[**1-Ti**] = 0.18; ΔG = 1.0 kcal mol^{-1} (1 cal = 4.184 J)). Similarly, extrapolation of the plot to 0% cyclopropoxides gives the percentage of free alcohol **1** at equilibrium (**1**:**2** = 43:57; K_{eq} = [**2**]/[**1**] = 1.3, ΔG = –0.17 kcal mol^{-1}).

Scheme 8.



These equilibration studies show that cyclopropoxide **1-Ti** is more stable than **2-Ti**, indicating that an $O\text{-}Ti(OR)_3$ group is more sterically bulky than a methyl group. In contrast, equilibration showed that the free cyclopropanol **2** is more stable than **1**, reaffirming that an OH group has less steric bulk than a methyl group. The order of decreasing steric bulk is : $O\text{-}Ti(OR)_3$ > Me > OH.

Since both cyclopropoxide **2-Ti** and cyclopropanol **2** are present in substantial amounts at equilibrium, the formation of cyclopropanol **1** as the only product of the Kulinkovich hydroxycyclopropanation[9] must be a kinetic phenomenon.

Discussion

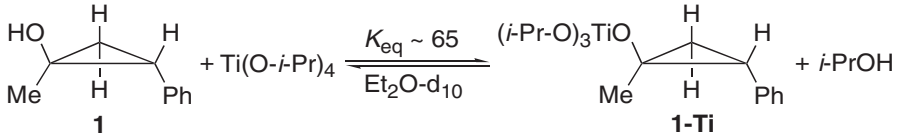
Cyclopropanol to cyclopropanol rearrangements, such as the one reported here, are very unusual (10). Normally, cyclopropanols undergo rearrangement to ketones and epimerization is not observed. For example, DePuy (12) observed that **1** undergoes ring-opening isomerization in protic solvents to 4-phenylbutan-2-one by different stereospecific pathways in acidic and basic solution. Ring opening of **1** un-

[8] This analysis does not take into account any effect of BF_3 on the cyclopropoxide:cyclopropanol ratio, the cyclopropanol:cyclopropanol ratio, or the cyclopropoxide:cyclopropoxide ratio. ^1H NMR spectroscopy of a mixture of cyclopropanol with $Ti(O\text{-}i\text{-}Pr)_4$ and $BF_3{\cdot}OEt_2$ was unable to resolve any relevant resonances.

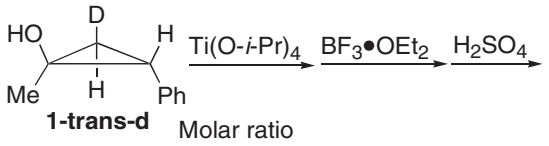
[9] Supplementary material provides a derivation of the equation for the plot of the percentage of **1** in quench vs. the percentage of cyclopropoxides **1-Ti** and **2-Ti**. Supplementary data for this article are available on the journal Web site (http://canjchem.nrc.ca) or may be purchased from the Depository of Unpublished Data, Document Delivery, CISTI, National Research Council Canada, Ottawa, ON K1A 0R6, Canada. DUD 5034. For more information on obtaining material refer to http://cisti-icist.nrc-cnrc.gc.ca/irm/unpub_e.shtml.

© 2006 NRC Canada

Scheme 9.

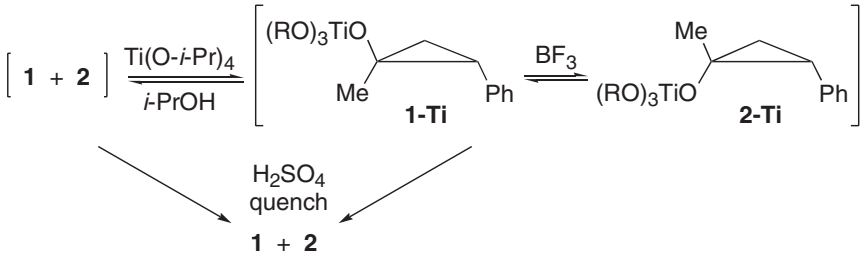


Scheme 10.



Molar ratio			
1.0	1.0	2.5	40:40:10:10
4.0	1.0	2.5	34:34:16:16
10.0	1.0	2.5	29:29:21:21

Scheme 11.



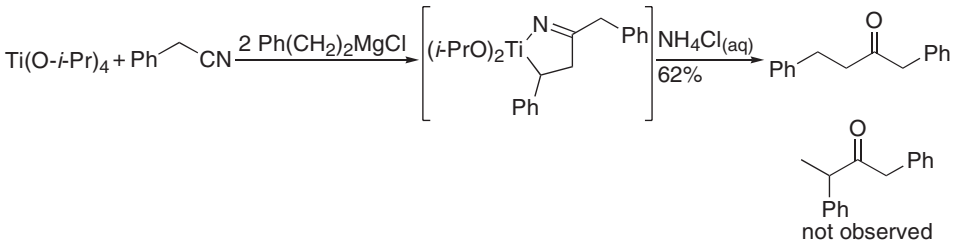
der basic conditions in 1:1 dioxane–D_2O occurred "almost instantaneously" to give 4-phenylbutan-2-one with inversion of configuration, corresponding to corner protonation of the cyclopropane (Scheme 12). Under acidic conditions in 1:1 dioxane:D_2O, slower ring opening of **1** gave a 40:60 mixture of 4-phenylbutan-2-one–3-phenylbutan-2-one; 4-phenylbutan-2-one was formed with exclusive retention of stereochemistry, corresponding to edge protonation of the cyclopropane.

It is interesting that while ring opening of **1** occurs rapidly in the presence of base in 1:1 dioxane–D_2O, we did not observe any ring opening of titanium cyclopropoxide **1-Ti** in the presence of alcohols in Et_2O or CH_2Cl_2. Apparently, titanium alkoxides are more covalent and stable than "free" alkoxide ions. The kinetic stability of titanium cyclopropoxides was confirmed by the calculation of a large barrier (28.8 kcal mol^{-1}) for the ring opening of *cis*-1,2-dimethylcyclopropoxytitanium trimethoxide (6).

Mechanism of cyclopropanol to cyclopropanol isomerization with $Ti(O\text{-}i\text{-}Pr)_4$ and BF_3OEt_2

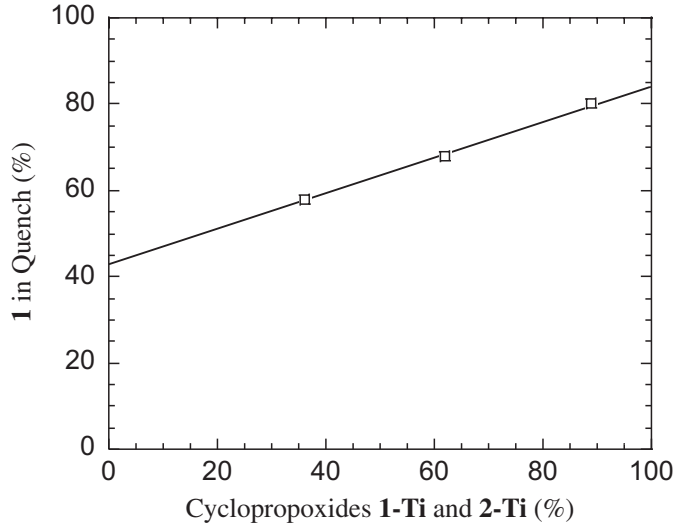
Any valid mechanism must account for three key observations (13).[10] (*i*) BF_3 is required as a Lewis acid for isomerization; titanium cyclopropoxides are stable in its absence. (*ii*) A 2-phenyl substituent on the cyclopropanol ring is required; *cis*-2-butyl-*r*-1-methylcyclopropanol, bearing a butyl group in place of the phenyl, did not isomerize. This suggests that breaking a bond to the carbon bearing the phenyl group is involved in the isomerization. (*iii*) Since all possible diastereomers of the deuterated cyclopropanol are obtained, at least two of the three ring carbons must undergo epimerization.

[10]At one point we considered the possibility that this apparent scrambling of the deuterium stereochemistry was occurring by deprotonation by an alkoxide α to the carbonyl in the ring-opened intermediate. However, this would lead to d_0 and d_2 products, which is inconsistent with our ^{13}C NMR results showing only d_1 compounds. The possibility of the phenyl substituent being β to titanium and α to the carbonyl has been excluded based on (*i*) computational results (6), (*ii*) analogy with quenching studies of the reaction of ketones (*a*) or imides (*b*) with alkenes, and (*iii*) our quenching experiment with a nitrile and alkene.



© 2006 NRC Canada

Fig. 1. 1 (in %) in quench vs. cyclopropoxides **1-Ti** and **2-Ti** (in %).

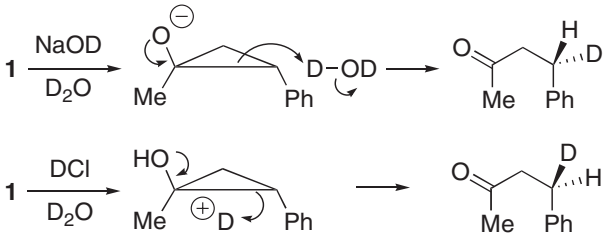


Kasatkin and Sato (3*b*), who observed a temperature dependence on the cis/trans product ratio of cyclopropanols generated from homoallyl esters, Ti(O-*i*-Pr)$_4$, and 2*i*-PrMgBr, attributed this apparent cyclopropoxide isomerization to reversible dissociation of the TiO—C(cyclopropyl) bond. However, the involvement of cyclopropyl cations in our rapid cyclopropanol to cyclopropanol isomerizations can be excluded. While reversible Lewis acid mediated cleavage of the cyclopropyl C—O bond might lead to interconversion of **1** and **2**, this process alone cannot alter the relative stereochemistry of phenyl and deuterium. Although reversible ring opening of the cyclopropyl cation to an allyl cation could, in principle, have isomerized phenyl relative to deuterium, cyclopropyl ring opening is highly exothermic (ΔH°_{expt} = –30 kcal mol^{-1}) (14) and is irreversible. Moss and Chu (15) recently generated the 2-phenyl-1-methylcyclopropyl cation in question and found that ring opening to allyl chlorides was competitive with ion pair collapse to a chlorocyclopropane. In addition, we demonstrated that **1-trans-d** is not isomerized by $BF_3{\cdot}OEt_2$ or Ti(O-*i*-Pr)$_4$ alone.

It is possible to directly convert any one of the four cyclopropoxide diastereomers to each of the other three by distinct processes (Scheme 13).

All of the interconversions begin with an electrophilic attack on the cyclopropoxide. The electrophile could be

Scheme 12.

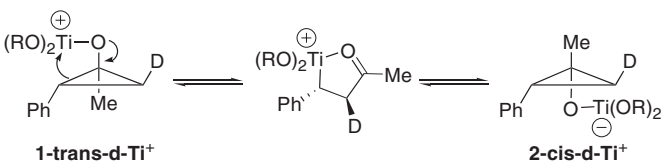


$Ti(OR)_3^+$, generated by the reaction of BF_3 with $Ti(OR)_4$, or another reactive titanium species.[11] Our proposed mechanism for these cyclopropanol isomerization reactions involves two different stereochemistries for the attack of the electrophile on the cyclopropoxide and two different stereochemistries for the microscopic reverse, cyclopropanol ring closing. Electrophilic attack on the cyclopropane bond linking the -OTi and phenyl-bearing carbons leads to retention of configuration at the carbon bearing the phenyl group (Scheme 14); this process is analogous to edge protonation of a cyclopropane. Electrophilic attack on the backside of the same cyclopropane bond leads to inversion of configuration and is analogous to corner protonation of a cyclopropane. The microscopic reverse of this process is responsible for the inversion of configuration at the titanium center in the formation of cyclopropylamines in the de Meijere reaction (5). In both cases, the bond linking the -OTi and phenyl-bearing carbons is attacked and a stabilized benzylic titanium species is generated.

The processes shown in Scheme 14 epimerize the CHPh ring carbon via cyclopropanol ring opening by the backside attack of the electrophile on the phenyl-bearing carbon (inversion of configuration at this carbon), rotation about the C—CHPhTi bond, and frontside ring closure with retention of configuration. Reversing the order of these processes to frontside ring opening with retention, rotation about the C—CHPhTi bond, and backside ring closure with inversion, produces the same result. This corresponds to the processes shown in blue in Scheme 13 that interconverts **1-trans-d** with **2-trans-d** and **1-cis-d** with **2-cis-d**.

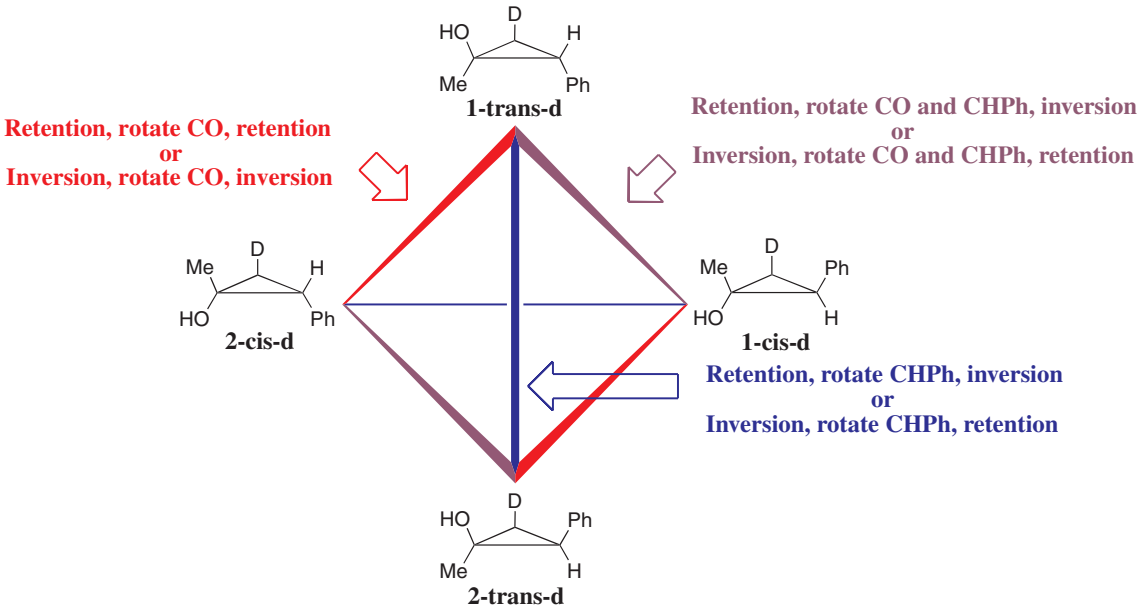
The processes shown in Scheme 15 epimerize the CMeOTi ring carbon by electrophilic cyclopropanol ring opening, rotation about the TiOMeC—C bond, and ring closure with the same stereochemistry as the ring opening. There are two different pathways, one involving ring open-

[11]It is also possible that cationic titanium cyclopropoxide **1-trans-d-Ti$^+$**, generated by BF_3 abstraction of an isopropoxy group from **1-trans-d-Ti**, can ring open in an intramolecular fashion involving only a single titanium. Migration of the benzylic carbon to the highly electrophilic cationic titanium center during cleavage of the carbon–carbon bond should be more favorable than carbon migration to a neutral titanium center. This could explain why isomerization to other cyclopropanols via ring opening is not observed in the Kulinkovich hydroxycyclopropanation, but is made accessible with the addition of BF_3. This suggests that production of only **1-Ti** through the Kulinkovich hydroxycyclopropanation is a kinetic phenomenon, and that when BF_3 is present, ring closure to **1-Ti** is made reversible. Even if only a very small fraction of ring closures lead to **2-Ti**, successive ring closure and ring-opening cycles would eventually lead to a an equilibrium mixture of **1-Ti** and **2-Ti**. Epimerization of the benzylic carbon requires the involvement of two titanium centers.

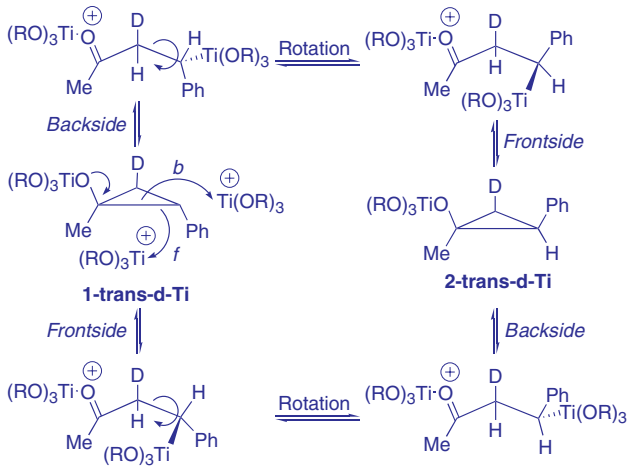


© 2006 NRC Canada

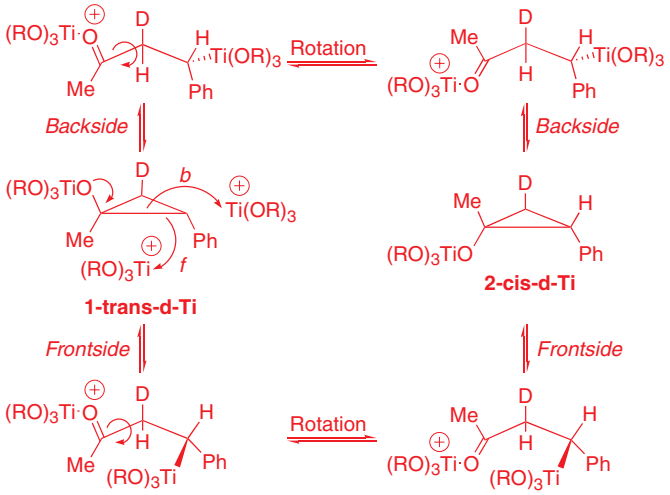
Scheme 13.



Scheme 14.



Scheme 15.



ing and ring closing with inversion of configuration and the other involving ring opening and ring closing with retention. These are the red processes in Scheme 13 that interconvert **1-trans-d** with **2-cis-d** and **1-cis-d** with **2-trans-d**.

The processes shown in Scheme 16 simultaneously epimerize both the CHPh and the CMeOTi ring carbons by electrophilic cyclopropanol ring opening, rotation about both the C—CHPhTi and TiOMeC—C bonds, and ring closure with the opposite stereochemistry. Microscopic reversibility requires equal rates for the processes of retention-double, rotation–inversion, and inversion-double rotation–retention. These are the purple processes in Scheme 13 that interconvert **1-trans-d** with **1-cis-d** and **2-trans-d** with **2-cis-d**.

The isomerizations of **1-trans-d** catalyzed by $Ti(O\text{-}i\text{-}Pr)_4$ and $BF_3{\cdot}OEt_2$ occur so rapidly that only fully equilibrated mixtures are seen. Therefore, it is not possible to tell whether any one of the three processes in Scheme 13 occurs more rapidly than another. In the slower isomerization catalyzed by *i*-PrMgCl and $Cl_2Ti(O\text{-}i\text{-}Pr)_2$ (Scheme 8), all three isomerized cyclopropanes formed at rates proportional to their equilibrium distributions. Therefore, it seems likely that the three processes of Scheme 13 all occur at similar rates.

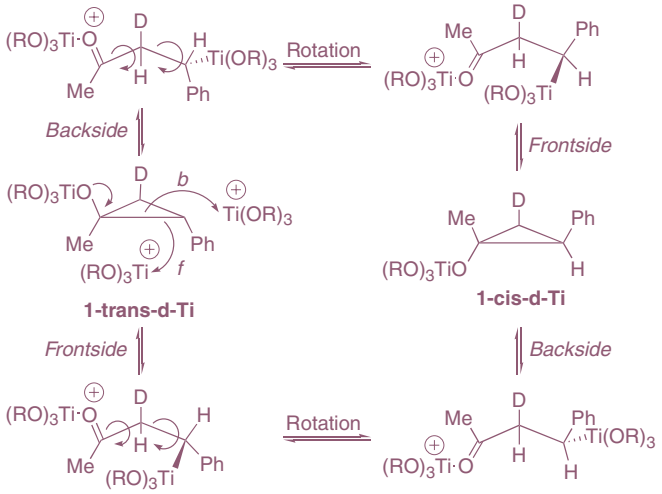
It should be noted that the processes shown in Schemes 14–16 all involve ring opening, rotation, and ring closing. Two of these processes require that ring opening and ring closing occur with opposite stereochemistries. An alternative would be to have the ring opening and closing occur with only a single stereochemistry and to invert the -CHPhTi center by transmetallation. Normally, transmetallation occurs with retention of stereochemistry, but there are examples where inversion has been demonstrated (16).

Conclusions

We have demonstrated a rapid $Ti(O\text{-}i\text{-}Pr)_4$–$BF_3{\cdot}OEt_2$ catalyzed isomerization of cyclopropanols involving epimeriza-

© 2006 NRC Canada

Scheme 16.



tion at two cyclopropyl carbons. This double epimerization requires reversible opening of the cyclopropyl ring to a β-titanaketone and is consistent with two competing stereochemistries for ring closing and opening. Equilibrium constants between epimeric cyclopropoxides and between epimeric cyclopropanols were determined by measuring the effects of catalyst concentration on product ratios.

Experimental section

Kulinkovich hydroxycyclopropanation employing $BF_3{\cdot}OEt_2$

i-PrMgCl (4.2 mL, 2.0 mol/L solution in Et_2O, 8.4 mmol) in Et_2O (5 mL) was added dropwise over 5 min to a 0 °C solution of Ti(O-*i*-Pr)$_4$ (0.99 mL, 3.5 mmol), EtOAc (0.33 mL, 3.4 mmol), and *trans*-β-deuterostyrene (0.71 g, 6.7 mmol) in Et_20 (15 mL). After stirring for 1 min, $BF_3{\cdot}OEt_2$ (1.06 mL, 8.4 mmol) was added and the reaction mixture was allowed to warm to room temperature over 1 h. The reaction mixture was poured into a 10% aq. H_2SO_4 solution (20 mL) and was extracted with Et_2O (3 × 15 mL). The Et_2O extract was washed with a satd. aq. $NaHCO_3$ solution (20 mL) and H_2O (20 mL) and was dried ($MgSO_4$). Solvent was removed by rotary evaporation to give a colorless oil. ^{1}H NMR spectroscopy showed the formation of **1-trans-d** and **1-cis-d** (37%) and of **2-trans-d** and **2-cis-d** (19%), based on integration vs. THF added after workup as an internal standard. Recrystallization from pentane gave a 1:1 mixture of **1-trans-d** and **1-cis-d** (177 mg, 35%).

In a similar experiment, a 1:1 mixture of **1-trans-d** and **1-cis-d** (62 mg, 12%) was obtained by preparative TLC (silica gel, 10:1 pentane–ether, R_f = 0.2) along with a 1:1 mixture of **2-trans-d** and **2-cis-d** (R_f = 0.3) as an impure mixture with decomposition products. The ^{1}H NMR spectrum of this mixture of **2-trans-d** and **2-cis-d** was consistent with the chemical shifts previously reported for unlabelled cyclopropanol **2** (11).

For a 1:1 mixture of **1-trans-d** and **1-cis-d**: ^{1}H NMR (300 MHz, CD_2Cl_2) δ: 7.28 (t, *J* = 7.5 Hz, 2H), 7.21–7.13 (m, 3H), 2.31 (br d, *J* = 9.3 Hz, 1H, CHPh), 2.13 (br s, 1H, OH), 1.21 (d, *J* = 10.2 Hz, 0.5 H, CHD), 1.16 (s, 3H, Me), 0.97 (d, *J* = 6.6 Hz, 0.5 H, CDH). ^{2}H{^{1}H}NMR (76.7 MHz, CH_2Cl_2) δ: 1.21 (s, 1.00D), 0.98 (s, 1.01D). ^{13}C{^{1}H}NMR (75 MHz, CD_2Cl_2) δ: 139.4, 128.9 (2C), 128.7 (2C), 126.4, 57.8, 31.2, 20.9, 18.9 (t, J_{HD} = 24 Hz). HRMS (EI) calcd. for $C_{10}H_{11}D^{\cdot+}$ ($M^{\cdot+}$): 149.0950; found: 149.0950.

For a 1:1 mixture of **2-trans-d** and **2-cis-d**: ^{2}H {^{1}H} NMR (76.8 MHz, CH_2Cl_2) δ: 1.18 (s, 1.00D), 1.05 (s, 1.02D).

Isomerization of cyclopropanols 1 and 2 *with* deprotonation by a Grignard reagent

A solution of cyclopropanol **1** (25.0 mg, 0.168 mmol) in Et_2O (0.8 mL) was added by syringe over 1 min to a stirred solution of *i*-PrMgCl (92 μL, 2.0 mol/L solution in Et_2O, 0.18 mmol) in Et_2O (1.5 mL). After stirring for 30 min, Ti(O-*i*-Pr)$_4$ (47.8 mg, 0.168 mmol) in Et_2O (0.5 mL) was added. After 10 min, $BF_3{\cdot}OEt_2$ (53 μL, 0.42 mmol) was added and the reaction mixture was stirred for ~2 min before quenching. The mixture was cooled to ~5 °C and cold 10% aq. H_2SO_4 (4 mL) was added. This mixture was extracted with Et_2O (3 × 2 mL) and the combined Et_2O extracts were washed with satd. aq. $NaHCO_3$ (2 mL) and H_2O (3 mL) and dried over 4Å molecular sieves. Evaporation of the solvent gave a 4:1 mixture of cyclopropanols **1** and **2**, which were shown to be >95% pure by ^{1}H and ^{2}H NMR spectroscopy.

When the isomerization of **1** was performed on a 100 mg scale, recrystallization from pentane at –30 °C allowed separation of pure crystalline **1**. Successive crystallizations of the mother liquor at –78 °C gave a mixture of **2** and **1** in a 75:25 ratio that was free of any additional impurities.

For cyclopropanol **2** (11): ^{1}H NMR (500 MHz, CD_2Cl_2) δ: 7.31 (t, *J* = 7.4 Hz, 2H), 7.19–7.26 (m, 3H), 1.98 (dd, *J* = 9.5, 7.0 Hz, 1H, CHPh), 1.72 (br s, 1H, OH), 1.54 (d, *J* = 0.6 Hz, 3H, Me), 1.19 (tq, *J* = 6.6, 0.6 Hz, 1H, CH*H*), 1.05 (dd, *J* = 9.5, 5.9 Hz, 1H, C*H*H). ^{13}C {^{1}H} NMR (126 MHz, CD_2Cl_2) δ: 138.6, 129.0 (2C), 128.6 (2C), 126.4, 57.1, 30.8, 26.2, 20.4. NOESY 1D ^{1}H NMR (500 MHz, CD_2Cl_2): The methyl protons at δ 1.54 were pulsed and integrated for –3.000H, the resonance at δ 1.98 for the benzylic hydrogen cis to the methyl group integrated as +0.035H (3.5%), the resonance at δ 1.05 for the proton on C-3 cis to the methyl group integrated as +0.020H (2.0%), and the resonance at δ 1.18 for the proton on C-3 trans to the methyl group integrated as +0.004H (0.4%).

Isomerization of cyclopropanols 1 and 2 *without* deprotonation by a Grignard reagent

$BF_3{\cdot}OEt_2$ (53 μL, 0.42 mmol) was added to a solution of **1** (25.0 mg, 0.168 mmol) and Ti(O-*i*-Pr)$_4$ (47.8 mg, 0.168 mmol) in Et_2O (2.3 mL). After 2 min, the solution was cooled to 5 °C and quenched by the addition of cold 10% aq. H_2SO_4 (4 mL). This mixture was extracted with Et_2O (3 × 2 mL) and the combined Et_2O extracts were washed with satd. aq. $NaHCO_3$ (2 mL) and H_2O (3 mL) and dried over 4 Å molecular sieves. Evaporation of the solvent gave a quantitative yield of a 4:1 mixture of cyclopropanols **1** and **2**, which were shown to be >97% pure by ^{1}H and ^{2}H NMR spectroscopy.

Reaction of 1-trans-d with $BF_3{\cdot}OEt_2$ in the absence of Ti(O-*i*-Pr)$_4$

$BF_3{\cdot}OEt_2$ (53 μL, 0.42 mmol) was added to a solution of **1** (25.0 mg, 0.168 mmol) in Et_2O (0.8 mL). After 2 min, the

© 2006 NRC Canada

solution was cooled to 5 °C and quenched by the addition of cold 10% aq. H_2SO_4 (4 mL). This mixture was extracted with Et_2O (3 × 2 mL) and the combined Et_2O extracts were washed with satd. aq. $NaHCO_3$ (2 mL) and H_2O (3 mL) and dried over 4 Å molecular sieves. Evaporation of the solvent gave an oily solid that was >90% **1-trans-d** by ^1H and ^2H NMR spectroscopy and contained no other cyclopropanols.

Measurement of cyclopropanol–Titanium cyclopropoxide equilibria

In an NMR tube, cyclopropanol **1** (25 or 50 mg) was combined with Ti(O-*i*-Pr)$_4$ (1.0, 0.25, or 0.10 equiv.) in Et_2O-d_{10} (0.65 mL). Equilibrium was established immediately and spectra of the samples taken directly after the addition or after 20 min showed no differences. Peaks for the methine proton of the isopropanol and titanium isopropoxide were visible at δ 3.9 and 4.5, respectively.[12] The peaks for the benzylic protons of cyclopropanol **1** and the titanium cyclopropoxides of **1** gave resonances at δ 2.22 and 2.5, respectively. The percentage of **1** in the cyclopropanol form relative to the percentage in the titanium cyclopropoxide form was determined from the relative integrations of these two peaks (Table 1).

Acknowledgement

Financial support from the National Science Foundation is gratefully acknowledged.

References

1. O.G. Kulinkovich, S.V. Sviridov, D.A. Vasilevskii, and T.S. Prityts kaya. Zh. Org. Khim. **25**, 2244 (1989).
2. O.G. Kulinkovich, S.V. Sviridov, and D.A. Vasilevski. Synthesis, **234** (1991).
3. (*a*) O.G. Kulinkovich, A.I. Savchenko, S.V. Sviridov, and D.A. Vasilevski. Mendeleev Commun. **230** (1993); (*b*) A. Kasatkin and F. Sato. Tetrahedron Lett. **36**, 6079 (1995); (*c*) J. Lee, C.H. Kang, H. Kim, and J.K. Cha. J. Am. Chem. Soc. **118**, 291 (1996); (*d*) O.L. Epstein, A.I. Savchenko, and O.G. Kulinkovich. Tetrahedron Lett. **40**, 5935 (1999).
4. E.J. Corey, S.A. Rao, and M.C. Noe. J. Am. Chem. Soc. **116**, 9345 (1994).
5. C.P. Casey and N.A. Strotman. J. Am. Chem. Soc. **126**, 1699 (2004).
6. It has been demonstrated elsewhere (3*a*, 3*d*, 4) and observed in our lab that the Kulinkovich hydroxycyclopropanation yields exclusively cyclopropanol isomer **1**, bearing phenyl cis to methyl and does not give any of isomer **2**, where phenyl is trans to methyl. The origin of this stereochemical preference has been addressed computationally. Y.-D. Wu and Z.-X. Yu. J. Am. Chem. Soc. **123**, 5777 (2001).
7. (*a*) C.P. Casey and L. Smith. Organometallics, **8**, 2288 (1989); (*b*) M. Brookhart and Y. Liu. Organometallics, **8**, 1569 (1989); (*c*) M. Brookhart and Y. Liu. J. Am. Chem. Soc. **113**, 939 (1991); (*d*) C.P. Casey and L.J.S. Vosejpka. Organometallics, **11**, 738 (1992).
8. (*a*) D.D. Davis, R.L. Chambers, and H.T. Johnson. J. Organomet. Chem. **25**, C13 (1970); (*b*) D.D. Davis and R.H. Black. J. Organomet. Chem. **82**, C30 (1974); (*c*) D.D. Davis and H.T. Johnson. J. Am. Chem. Soc. **96**, 7576 (1974); (*d*) I. Fleming and C.J. Urch. Tetrahedron Lett. **24**, 4591 (1983); (*e*) I. Fleming and C.J. Urch. J. Organomet. Chem. **285**, 173 (1985).
9. (*a*) V. Chaplinski and A. de Meijere. Angew. Chem. Int. Ed. Engl. **35**, 413 (1996); (*b*) V. Chaplinski, H. Winsel, M. Kordes, and A. de Meijere. Synlett, 111 (1997); (*c*) C.M. Williams and A. de Meijere. J. Chem. Soc. Perkin Trans. 1, 3699 (1998); (*d*) A. de Meijere, V. Chaplinski, F. Gerson, P. Merstetter, and E. Haselbach. J. Org. Chem. **64**, 6951 (1999); (*e*) A. de Meijere, C.M. Williams, A. Kourdioukov, S.V. Sviridov, V. Chaplinski, M. Kordes, A.I. Savchenko, C. Stratmann, and M. Noltemeyer. Chem. Eur. J. **8**, 3789 (2002).
10. T.S. Wan and A. Fischli. Helv. Chim. Acta, **67**, 1461 (1984).
11. C.H. DePuy and R.J. Van Lanen. J. Org. Chem. **39**, 3360 (1974).
12. (*a*) C.H. DePuy and F.W. Breitbeil. J. Am. Chem. Soc. **85**, 2176 (1963); (*b*) C.H. DePuy, F.W. Breitbeil, and K.R. DeBruin. J. Am. Chem. Soc. **88**, 3347 (1966).
13. (*a*) N. Morlender-Vais, N. Solodovnikova, and I. Marek. Chem. Commun. Cambridge, 1849 (2000); (*b*) J. Lee, J.D. Ha, and J.K. Cha. J. Am. Chem. Soc. **119**, 8127 (1997).
14. (*a*) P.A. Arnold and B.K. Carpenter. Chem. Phys. Lett. **328**, 90 (2000); (*b*) W.G. Mallard (*Editor*). NIST Chemistry Webbook [online]. National Institute of Standards and Technology, Gaithersburg, Maryland. Available from http://webbook.nist. gov. 2005.
15. R.A. Moss and G. Chu. Tetrahedron Lett. **45**, 3321 (2004).
16. Transmetallation with inversion of configuration at carbon has been observed. (*a*) Sn to Pd: J.W. Labadie and J.K. Stille. J. Am. Chem. Soc. **105**, 669 (1983); (*b*) Sn to Pd: J.W. Labadie and J.K. Stille. J. Am. Chem. Soc. **105**, 6129 (1983); (*c*) Li to Zn: S. Klein, I. Marek, and J.-F. Normant. J. Org. Chem. **59**, 2925 (1994); (*d*) Li to Sn: A. Carstens and D. Hoppe. Tetrahedron, **50**, 6097 (1994); (*e*) Li to Hg: C. Strohmann, B.C. Abele, K. Lehmen, F. Villafañe, L. Sierra, S. Martín-Barrios, and D. Schildbach. J. Organomet. Chem. **661**, 149 (2002).

[12]The peak positions varied slightly for isopropanol and for **1** ($\Delta\delta < 0.02$ ppm) and were dependent on changes in the bulk solvent as catalyst loading increased. The isopropoxides and cyclopropoxides showed more variation ($\Delta\delta < 0.09$ ppm) at different ratios of **1**:Ti(O-*i*-Pr)$_4$. These systematic variations in frequency can be attributed to the changing mix of alkoxides bound to titanium.

© 2006 NRC Canada

Tetraazaoctaphyrin — A biimidazole-containing expanded porphyrin[1]

Jonathan L. Sessler, Bobbi L. Rubin, Marcin Stępień, Thomas Köhler, G. Dan Pantos, and Vladimir Roznyatovskiy

Abstract: A series of expanded porphyrins, incorporating biimidazoles and bipyrroles within their macrocyclic framework, has been synthesized. Insights into the complex conformational characteristics of these systems were obtained from two-dimensional NMR spectroscopic studies. The relative energy values for the various asymmetric structures inferred from these analyses were compared using DFT molecular modeling calculations.

Key words: macrocycles, expanded porphyrins, imidazoles, pyrroles, biimidazoles, supramolecular chemistry, heterocycles.

Résumé : On a réalisé la synthèse d'une série de porphyrines agrandies qui incorporent des biimidazoles et des bipyrroles dans le squelette de leur macrocycle. Sur les bases des études de spectroscopie RMN bidimensionnelle, on a extrait des donnés qui permettent de mieux comprendre les caractéristiques conformationnelles complexes de ces systèmes. On a comparé les valeurs relatives d'énergie de diverses structures asymétriques déduites de ces analyses à celles obtenues par des calculs de modélisation moléculaire sur la base de la théorie de la fonctionnelle de densité.

Mots clés : macrocycles, porphyrines agrandies, imidazoles, pyrroles, biimidazoles chimie macromoléculaire, hétérocycles.

[Traduit par la Rédaction]

Introduction

A new subdiscipline of porphyrin chemistry, involving the synthesis and study of large oligopyrrole macrocycles, so-called expanded porphyrins, was instigated by the serendipitous discovery of sapphyrin by Woodward and co-workers in the mid 1960s (1). In the decades since that time, the field of expanded porphyrin chemistry has grown into a large and vibrant subfield of macrocyclic chemistry (2). Expanded porphyrins have been studied in the context of molecular recognition with anionic, cationic, and neutral substrates (3). Part of what is driving this research is the promise that these systems show in various practical applications, ranging from drug development to anion recognition (4–7). Work in this area has also been inspired by less prosaic motivations, including the synthetic challenge of constructing new oligopyrrolic macrocycles and their inherent aesthetic appeal.

Received 11 October 2005. Accepted 30 November 2005. Published on the NRC Research Press Web site at http://canjchem.nrc.ca on 8 June 2006.

J.L. Sessler,[2] B.L. Rubin, M. Stępień, T. Köhler, G.D. Pantos, and V. Roznyatovskiy.[3] Department of Chemistry and Biochemistry, The University of Texas at Austin, 1 University Station A5300, Austin, TX 78712-0165, USA.

[1]This article is part of a Special Issue dedicated to Dr. Alfred Bader.

[2]Corresponding author (e-mail: sessler@mail.utexas.edu).
[3]Present address: Department of Chemistry, M.V. Lomonosov Moscow State University, Leninskie Gory, 119899 Moscow, Russian Federation.

[4]J.L. Sessler and J.T. Lee. Unpublished results.

Most known expanded porphyrins, with the exception of Schiff-base macrocycles, have been constructed from pyrrole and its closely related heterocyclic analogues, furan, thiophene, and selenophene. Recently, efforts have shifted towards incorporating imidazoles and biimidazoles into porphyrin-like structures. Youngs et al. (8) reported the synthesis of a series of cyclophane complexes, or porphyrinoids, which contained imidazoliums incorporated into the skeletal framework of the macrocycle. In 2003, the research groups of Allen (9) and Nonell (10) separately reported the first biimidazole-based porphycene analog, imidacene. There have also been a number of reports that describe the incorporation of imidazole or imidazolium cations into other macrocyclic structures (11–14). These systems show great promise in both anionic and cationic recognition and are made especially interesting because they are potentially capable of recognition both inside and outside the skeletal framework. In spite of this promise, biimidazoles, as opposed to imidazoles, have yet to be incorporated into expanded porphyrin-type frameworks. We report here the first example of such a system, namely 3,6,21,24-tetraaza[32]octaphyrin(1.0.1.0.1.0.1.0).

Results and discussion

The synthesis of tetraazaoctaphyrin target **3** was carried out in a single step via the condensation of biimidazole **1** with bis-α-free bipyrrole **2** under dilute conditions (Scheme 1). Biimidazole **1a** was prepared according to the literature and **1b** was synthesized using an extension of this same basic methodology (10). Bipyrroles **2a**–**2c** were synthesized according to the literature (15, 16).[4] The condensation of biimidazole **1** with bipyrrole **2** was performed in a

 doi:10.1139/V06-068 © 2006 NRC Canada

methanol–tetrahydrofuran (THF) mixture using trifluoroacetic acid (TFA) as the acid catalyst. After column chromatographic work-up over silica gel, tetraazaoctaphyrins **3a**–**3e** were obtained in yields ranging from 26% to 69%, depending on the substrates used. The compounds obtained in this way are unstable when exposed to oxygen and decompose over time. Thus, they were stored in a freezer under a blanket of argon. Under these conditions, little decomposition was seen for a period of 1 week. Elemental analysis was used as a means of characterization and repeatedly resulted in total carbon, hydrogen, and nitrogen counts of 95%–96% of the theoretical values. XPS analysis revealed the presence of silicon and oxygen, which is supported by a singlet near 0 ppm observed in the ^{1}H NMR spectra of **3a**–**3e**, attributable to a dimethyl siloxane compound. Efforts to remove the impurity included recrystallization, trituration, and extraction, but unfortunately all proved unsuccesful. If, however, the carbon, hydrogen, and nitrogen percentage is normalized to 100% and compared with a theoretical percentage of the same elements, thus accounting for the amount of impurity in these percentages, the experimental results fall within acceptable error values (i.e., $\Delta < 0.20\%$). In an additional experiment, the solvent was passed through a blank column under identical conditions and the siloxane was identified in the eluate by XPS and ^{1}H NMR spectroscopy, thus establishing the silica gel as the likely source of the impurity.

The UV–vis absorption spectrum of **3b**, the prototypical tetraazaoctaphyrin chosen for detailed study, is characterized by a Soret-type band at 299 nm and a Q-type band at 633 nm (Fig. 1). These features, particularly the latter long-wavelength absorption band, are considered diagnostic of an extended conjugated system (17). Dilute solutions of tetraazaoctaphyrin **3** in methylene chloride are blue and fluoresce red (Fig. 2). For the fluorescence emission experiments, excitation was performed at 578 nm, while the emission maximum was observed at 670 nm.

The one-dimensional ^{1}H NMR spectrum of **3b** recorded in dichloromethane-d_2 is shown in Fig. 3. It is apparent from an inspection of this spectrum that the solution structure of **3b** does not exhibit the fourfold symmetry implied by the representation of the macrocycle given in Scheme 1. The actual conformation has only twofold symmetry, which can be inferred from the doubled number of peaks in the aromatic and alkyl regions. The signal at 9.87 ppm integrates to two protons and most likely corresponds to a pyrrole NH proton. When studied as a solution in DMSO-d_6, an additional peak with the same integral intensity can be observed at 10.8 ppm. In dichloromethane-d_2, this signal is broadened by exchange and cannot be observed. Such a solvent dependence is typically found for imidazole NH protons. Based on these findings, the signal is assigned as an imidazole NH; however, its exact placement on the biimidazole unit could not be determined. Chemical shifts of the NH and meso protons indicate an absence of overall macrocyclic aromaticity.

The doubled spectral pattern, indicative of symmetry lowering, is also seen for the other tetraazaoctaphyrin derivatives. It should, however, be noted that the doubled signals assigned to the dominant species present in solution are often accompanied by ones ascribable to an impurity, which gives rise to a single set of peaks. The admixture inferred on this basis cannot be separated by chromatography (all samples yield a single peak on the HPLC chromatogram). While the identity of the additional species could not be ascertained, it is thought that it may correspond to a different symmetrical conformation for each of the different derivatives of **3**.

Fig. 1. Absorbance (—) and fluorescence spectra (----) of **3b** in CH_2Cl_2.

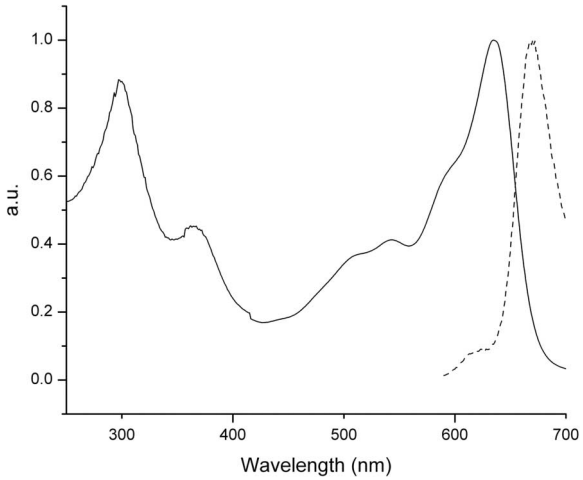


Fig. 2. Dilute solution tetraazaoctaphyrin **3b** in methylene chloride in the absence (left) and presence (right) of an illuminating black light (365 nm).



The assignment of the signals presented in Fig. 3 follows the labeling pattern given in Scheme 2. These assignments were deduced using two-dimensional NMR spectroscopy (COSY and ROESY maps). Figure 4 shows representative expansions of the COSY spectrum, used to establish connectivity within the aryl rings and alkyl chains. There is a significant crowding of signals in the alkyl region, which was resolved on the COSY map. Further insight into the structure and conformation of **3b** was gained from an analysis of the ROESY spectrum (Fig. 5).

Based on selected ROE cross-peaks, it was possible to assign unequivocally each of the signals to one of the two

© 2006 NRC Canada

Scheme 1. Synthesis of tetraazaoctaphyrin **3**.

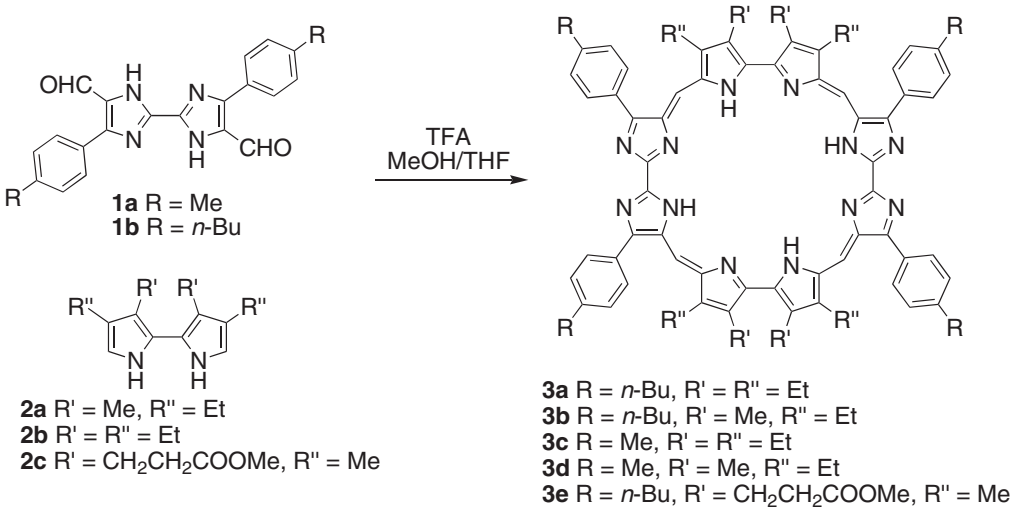
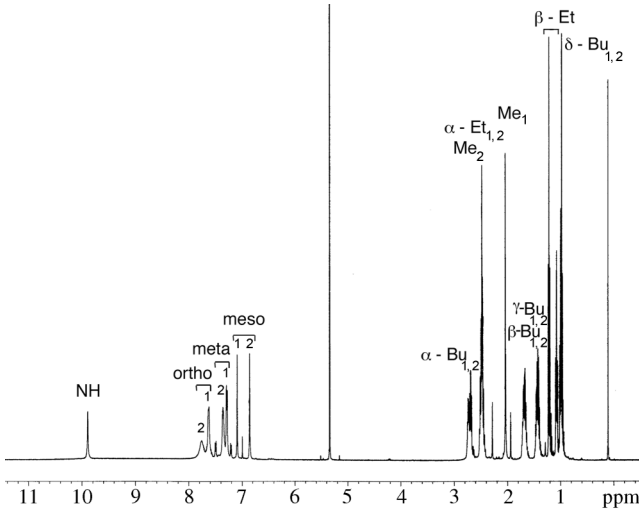
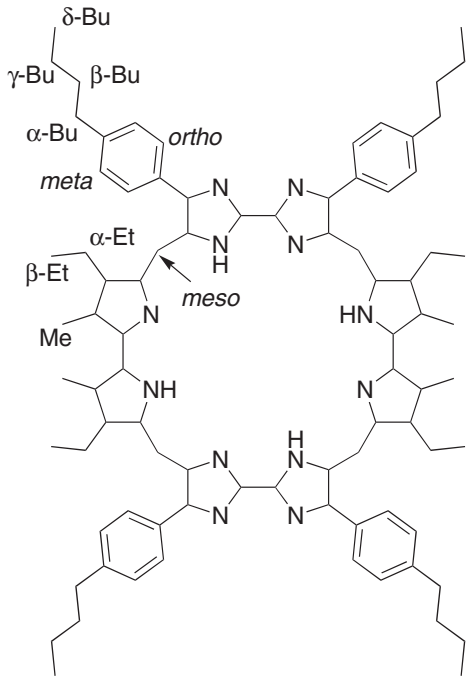


Fig. 3. ^{1}H NMR spectrum of compound **3b** (500 MHz, CD_2Cl_2, 298 K). Labeling of peaks follows that given in Scheme 2.



Scheme 2. Labeling scheme used in the analysis of ^{1}H NMR spectra of **3b**. For simplification, π bonding in the macrocycle is not shown. Placement of pyrrole and imidazole NH protons is arbitrary.



nonequivalent subunits 1 and 2 (Scheme 3). Each of the subunits contains one pyrrole ring and one imidazole ring linked by a meso-bridging carbon atom. In addition, four special ROE correlations provided the information necessary to determine the arrangement of constituent rings in each subunit. The meso signal of subunit 1 ($meso_1$, 7.04 ppm) correlates with the ortho signal of the adjacent aryl ring ($ortho_1$, 7.59 ppm, peak A in Fig. 5), as well as with one of the ethyl CH_3 signals (β-Et1, 1.04 ppm, peak C). In the other subunit, the meso signal ($meso_2$, 6.95 ppm) only correlates with the respective ethyl group (β-Et2, 1.21 ppm, peak D) and shows no cross-peak to the ortho signal ($ortho_2$, 7.72 ppm). However, the latter yields an unexpected correlation with the pyrrolic NH (peak B). This latter correlation can be rationalized by assuming a "kinked" conformation for subunit 2, in which the meso CH fragment is turned away from the aryl ring (Scheme 3).

Macrocycle **3** should contain two subunits of type 1 and two of type 2 combined in such a way that the entire structure exhibits twofold symmetry. The four arrangements that meet the above criterion are shown in Fig. 6. In arrangements A and B, the sequence of subunits in the ring is 1–2–1–2, whereas, in arrangements C and D, the sequence is 1–1–2–2. Furthermore, the aryl rings pointing towards the inside of the macrocycle are positioned on the same side of the macrocyclic plane (in arrangements A and C) or on the opposite sides (B and D). As a result, we obtain four distinct conformers, two of which are chiral (A and D).

Inspection of the molecular models leads to the inference that arrangement B is the least congested of the four conformers and hence the one with the lowest energy. This conclusion is supported by DFT calculations performed at the TZ2p atomic level. Optimized geometries and relative

© 2006 NRC Canada

Fig. 4. ^{1}H COSY spectrum of **3b** (500 MHz, CD_2Cl_2, 298 K). Parts (*A*) and (*B*) show expansions of the aromatic and aliphatic regions, respectively. Peaks corresponding to the symmetrical form are not labeled.

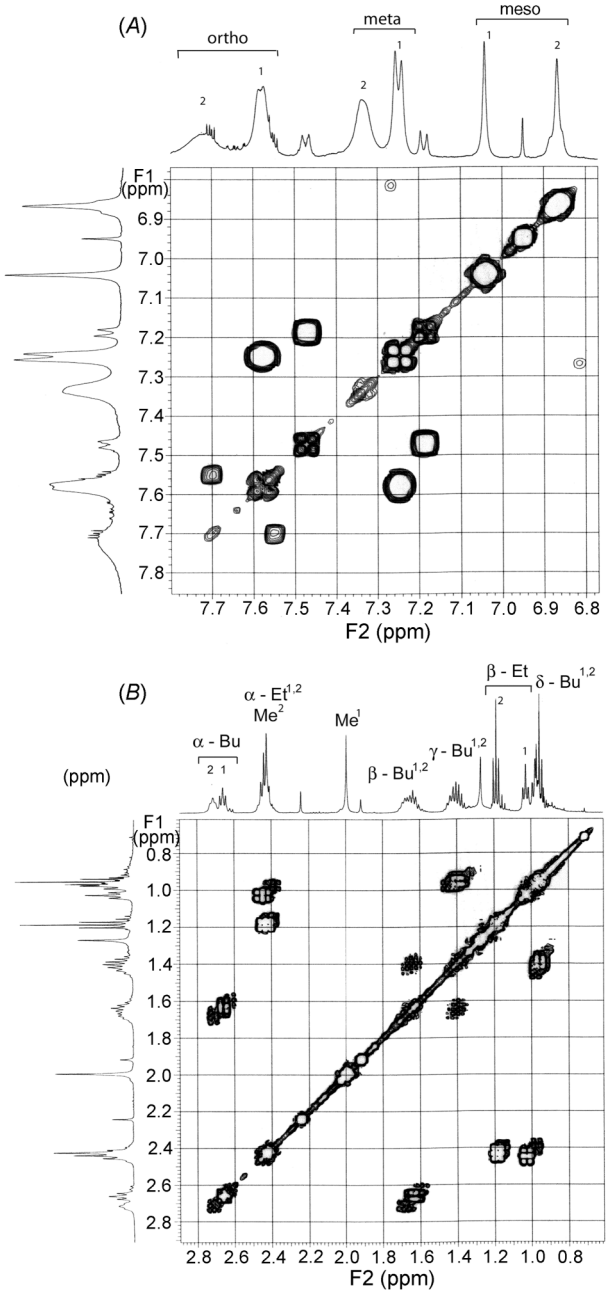
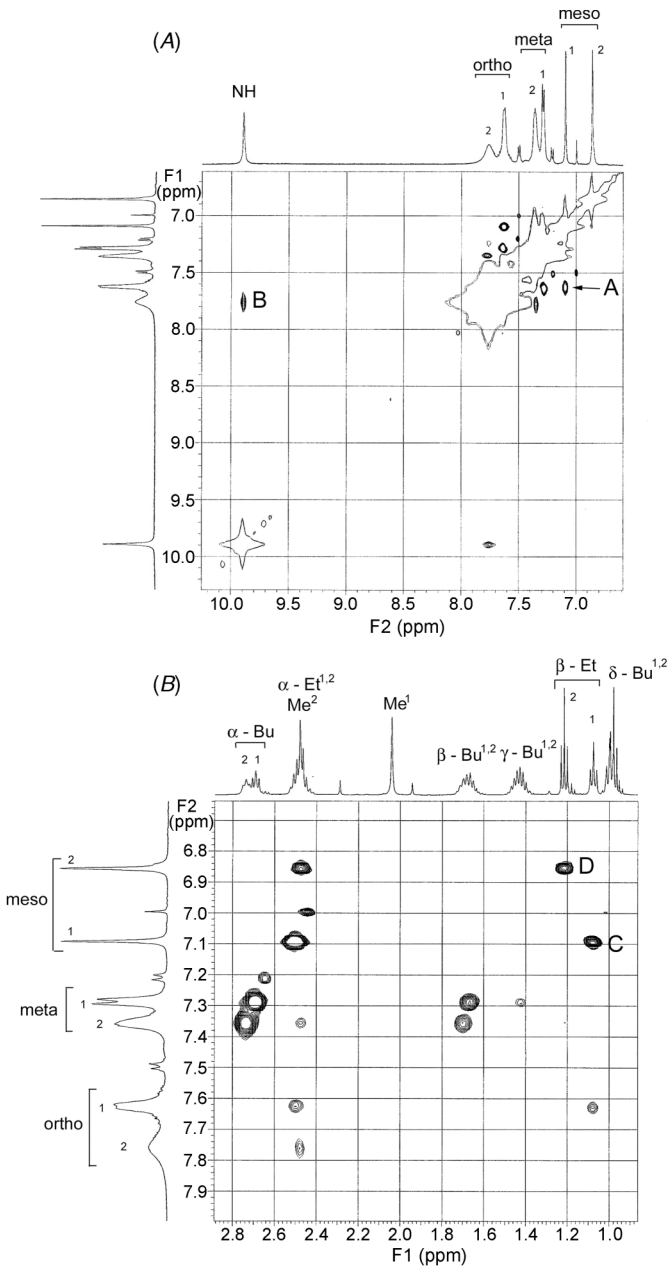


Fig. 5. ^{1}H ROESY spectrum of **3b** (500 MHz, CD_2Cl_2, 298 K). Parts (*A*) and (*B*) show the expansions of aromatic–aromatic and aliphatic–aromatic regions, respectively. The spectrum is phased to give positive ROE crosspeaks.



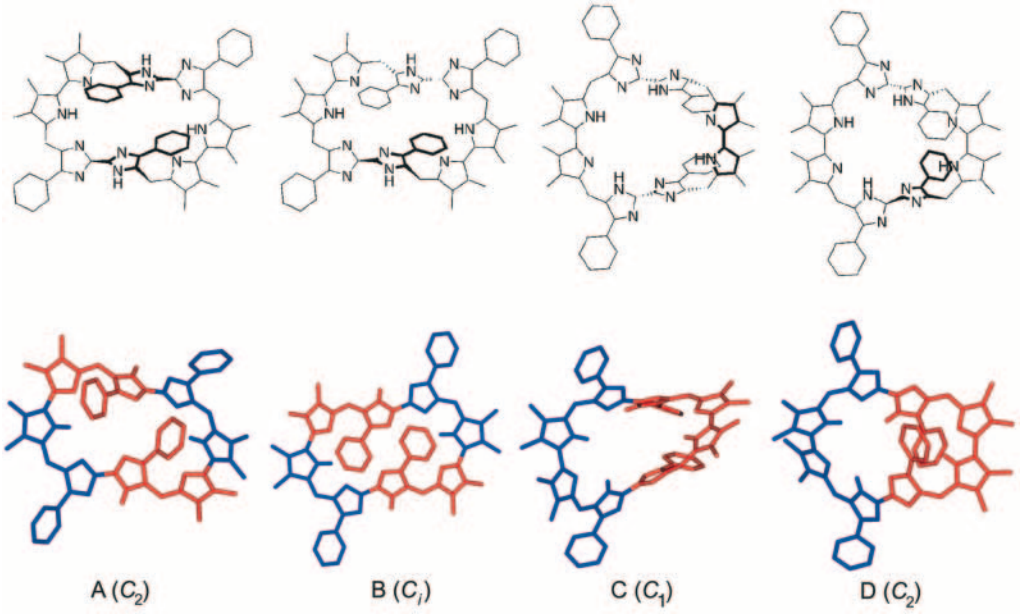
energy values are given in Table 1. Conformer B is the most stable, closely followed in energy by conformer D (Fig. 6); not surprisingly, conformations A and C are higher in energy, likely reflecting the cis arrangement of the phenyl rings within the cavity. Additionally, conformer C, expected to have a symmetry plane (C_s symmetry), collapsed upon optimization into a completely nonsymmetrical geometry.

The conformation of **3** observed in solution appears to be rigid. No exchange cross-peaks in the room temperature ROESY and NOESY spectra have been observed between topologically equivalent signals (e.g., meso$_1$ and meso$_2$); nor has any exchange been noted between the major asymmetrical form and the symmetrical admixture mentioned earlier. In point of fact, the lines remain sharp even at 130 °C in DSMO-d_6. However, significant broadening is observed at room temperature for the ortho and meta signals of the aryl rings (Fig. 3). This broadening is most readily interpreted in terms of the aryl moieties being in an unsymmetrical environment and undergoing slow rotation, conclusions that are consistent with the nonplanar conformation noted above.

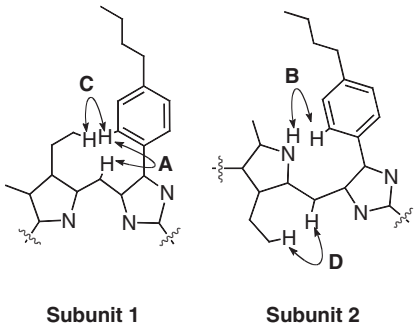
Interestingly, the conformation proposed for **3** has no apparent precedent among the structures of octaphyrins

© 2006 NRC Canada

Fig. 6. Possible conformers of tetraazaoctaphyrin **3** (top). The bottom part shows the DFT optimized structures and their point symmetries. Within the optimized structures, subunit 1 is highlighted in blue, while subunit 2 is highlighted in red for clarity. With the exception of the NH hydrogen atoms, all the hydrogen atoms have been removed for clarity.



Scheme 3. Illustration of the two subunit structure of **3b**, as determined from the interpretation of the ROESY spectrum. The π electron extended conjugation is removed for clarity.



reported to date. For [32]octaphyrin(1.0.1.0.1.0.1.0), reported by Vogel and co-workers (18), a D_2-symmetrical figure eight conformation with transoid bipyrrole subunits located at the figure eight intersection was observed in the crystal structure. A similar conformation was conjectured for a closely related macrocycle obtained by Setsune et al. (19). Another type of figure eight conformation was observed for [36]octaphyrin(1.1.1.1.1.1.1.1), reported by Furuta, Osuka and co-workers. (20), and for its thiophene analogue obtained by Spruta and Latos-Grażyński (21). However, the presence of four imidazole rings in system **3** and a different substitution pattern (aryl groups at the β-pyrrole positions) may explain why this new macrocycle adopts a conformation different from that of its all-pyrrole analogue (18).

Conclusion

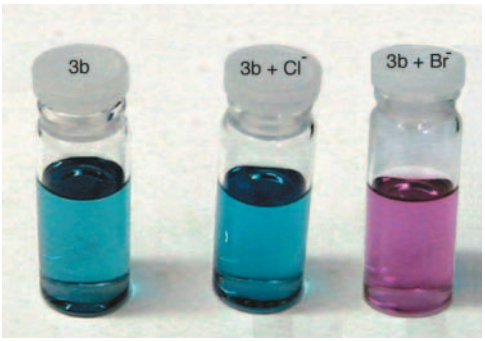
The design and synthesis of a novel expanded porphyrin has been described. The series of tetraazaoctaphyrins **3a**–**3e** were formed from the condensation of biimidazole dialdehydes **2a** and **2b** with bis-α-free bipyrroles **2a**–**2c**. The high density of NH functionality makes these systems of potential interest as anion receptors. Initial qualitative tests of this postulate have been performed on tetraazaoctaphyrin **3**. We have found that the neutral host (**3b**) undergoes a naked-eye detectable color change in the presence of fluoride, bromide

Table 1. Minimization energy values for molecular arrangements A–D.

Arrangement	Energy (kcal/mol)	Relative energy
A	–321 084.01	16.76
B	–321 067.25	0
C	–321 053.80	13.45
D	–321 064.63	2.62

Note: 1 cal = 4.184 J.

Fig. 7. Tetraazaoctaphyrin **3b** in acetonitrile in the absence (left) and presence of tetrabutylammonium chloride (middle) and tetrabutylammonium bromide (right).



© 2006 NRC Canada

(Fig. 7), cyanide, hydroxyde, acetate, nitrate, dihydrogenphosphate anions (studied in the form of their respective tetrabutylammonium salts). On the other hand, no change in the spectral properties of **3b** was noted upon addition of chloride, iodide, hypochlorate, nitrite, benzoate, and hydrogensulfate anions. Such observations lead us to propose that this or other neutral biimidazole-incorporated expanded porphyrins may emerge as useful anion sensors.

Experimental

General information

All reagents and solvents were purchased from Sigma-Aldrich Corporation, Fischer Scientific, or Fluka and used without further purification with the following exceptions. Dichloromethane was dried by distillation under argon over calcium hydride. Dimethylformamide was dried by passage through two columns of molecular sieves. Tetrahydrofuran (THF) was dried by passage through two columns of activated alumina. Toluene was dried by passage through two columns of activated alumina. *N*-Bromosuccinimide was recrystallized from boiling water. For column chromatography, silica gel (Scientific Adsorbents Inc., particle size 32–63 μm) was used as the immoble phase.

*1-((2-(Trimethylsilyl)ethoxy)methyl)-2-(1-((2-(trimethylsilyl)ethoxy)methyl)-5-formyl-4-*p*-tolyl-1*H*-imidazol-2-yl)-4-*p*-tolyl-1*H*-imidazole-5-carbaldehyde*

4,4′-Dibromo-1,1′-bis[(trimethylsilyl)ethoxymethyl]-2,2′-biimidazole-5,5′-dicarbaldehyde (10) (1.68 mmol) and *p*-methylphenyl boronic acid (3.36 mmol) were degassed for 20 min in 9.2 mL of 2 mol/L sodium carbonate and 4 mL of ethanol by purging the solution with argon. Palladium tetrakistriphenylphosphine (10% mol) was added and the reaction was heated to reflux for 7 h using an oil bath. The reaction flask was removed from the oil bath, cooled, and the mixture was diluted with ethyl acetate, dried with sodium sulfate, filtered, and concentrated in vacuo to give an oil. Column chromatography was performed using silica gel as the solid support, eluting initially with hexanes and slowly increasing the polarity to 20% ethyl acetate in hexanes. Desired fractions were combined, concentrated in vacuo, and dried to give an off-white solid in 89% yield. ^{1}H NMR ($CDCl_3$, 400 MHz) δ: –0.13 (m, 9H), –0.08 (m, 9H), 2.02 (s, 3H), 2.42 (s, 3H), 3.58 (m, 4H), 4.10 (m, 4H), 6.31 (s, 2H), 6.37 (s, 2H), 7.30 (d, J = 8.0 Hz, 4H), 7.61 (d, J = 7.6 Hz, 4H), 9.88 (s, 1H), 9.96 (s, 1H). ^{13}C NMR δ: 14.17, 17.86, 21.35, 60.39, 66.41, 127.14, 127.55, 128.75, 128.95, 129.29, 120.49, 129.525, 139.71, 141.16, 154.49, 171.17, 181.00. HR-MS (CI^+) m/z ($M + H^+$) calcd. for $C_{22}H_{18}N_4O_2$: 371.1508; found: 371.1521.

*2-(5-Formyl-4-*p*-tolyl-1*H*-imidazol-2-yl)-4-*p*-tolyl-1*H*-imidazole-5-carbaldehyde (1a)*

The previous compound (0.457 mmol) was dissolved in 10 mL ethanol. Ten milliliters of 10% HCl was added and the reaction was heated to reflux for 1 h using an oil bath. The flask was removed from the oil bath, cooled, and the solution was carefully neutralized with 10% aqueous sodium carbonate. At this juncture, a solid precipitated out of solution. It was filtered and washed with ice-cold water, and dried under vacuum to give the desired compound in the form of a white solid in 78% yield; mp 160–180 °C. ^{1}H NMR (400 MHz, DMSO-d_6) δ: 2.37 (s, 6H), 7.33 (d, J = 7.6 Hz, 4H), 7.79 (d, J = 8.4 Hz, 4H), 9.88 (s, 2H). ^{13}C NMR (500 MHz, DMSO-d_6) δ: 21.00, 125.30, 126.81, 128.73, 128.97, 129.30, 129.58, 129.72, 133.12, 139.25, 140.01, 182.60. HR-MS (CI^+) m/z ($M + H^+$) calcd. for $C_{22}H_{18}N_4O_2$: 371.1508; found: 371.1521.

General procedure for the preparation of tetraazaoctaphyrin derivatives (3)

Biimidazole dialdehyde **1** (0.184 mmol) was dissolved in 200 mL of dry 2:1 methanol–THF containing 1 mL of TFA. Bipyrrole **2** (0.184 mmol) was separately dissolved in 40 mL of the same solvent ratio and placed in an addition funnel. The bipyrrole solution was added dropwise to the biimidazole solution over 30 min and after several hours of stirring at room temperature, an additional 1 mL of TFA was added to the reaction. Stirring was continued overnight with the reaction left open to the atmosphere. After 12 h, the deep blue-black solution was concentrated in vacuo to give a deep purple oil, which was taken to dryness on the vacuum line to remove any residual trifluoroacetic acid. Column chromatography was performed twice over silica gel, eluting initially with methylene chloride before the polarity of the eluent was slowly increased to 3% methanol in methylene chloride. The desired fractions were combined and concentrated in vacuo to give a lustrous blue-black solid. The material was then redissolved in methylene chloride, washed with 5% aqueous sodium bicarbonate, dried over sodium sulfate, filtered, concentrated in vacuo to a blue-black solid, and dried under vacuum. The solid was triturated with distilled pentane to remove any remaining grease. The desired tetraazaoctaphyrin was obtained as a blue-black lustrous solid.

Elemental analysis was pursued as a means of characterization and repeatedly resulted in carbon, hydrogen, and nitrogren counts of 95%–96% of the theoretical values. XPS analysis revealed the presence of 3.14% silicon in the sample of **2.5b**. Taking into account this silicon percentage, the calculated impurity reveals 1.40 equiv. of the siloxane for each equivalent of the host **2.5b**. Anal. calcd. for $C_{84}H_{92}N_{12}\cdot 1.4SiO_2(CH_3)_2$: C 74.72, H 7.20, N 12.05; found: C 74.71, H 7.09, N 12.22. Efforts to remove the impurity included recrystallization, trituration, and extraction, but unfortunately all proved unsuccesful.

*2,7,20,25-Tetra-*p*-butylphenyl-11,12,15,16,29,30,33,34-octaethyl–3,6,21,24-tetraaza[32]octaphyrin(1.0.1.0.1.0.1.0) (3a)*

The compound was obtained from the condensation of biimidazole **1b** (10) with bipyrrole **2b** (16)[4] in 69% yield, following the general procedure given above. UV–vis (CH_3CN, nm (ε)) λ_{max}: 296 (85 800), 534 (41 100), 631 (94 300). ^{1}H NMR (500 MHz, CD_2Cl_2) δ: 0.95–1.09 (comp, 24H, CH_2CH_3, $CH_2CH_2CH_2CH_3$), 1.13–1.21 (comp, 8H, CH_2CH_3), 1.39–1.49 (comp, 8H, $CH_2CH_2CH_2CH_3$), 1.61–1.75 (comp, 8H, $CH_2CH_2CH_2CH_3$), 2.34 (m, 8H, CH_2CH_3), 2.65–2.77 (comp, 12H, CH_2CH_3 & $CH_2CH_2CH_2CH_3$), 2.97 (m, 4H, $CH_2CH_2CH_2CH_3$), 6.94 (s, 2H, *meso-H*), 7.080 (s, 2H, *meso-H*), 7.27 (d, J = 8.0 Hz, 4H), 7.38 (d, J = 8.5 Hz, 4H), 7.53 (d, J = 8.0 Hz, 4H), 7.82 (d, J = 8.0 Hz, 4H), 9.98

© 2006 NRC Canada

(s, 2H, *NH*), 11.70 (br, *NH*). ^{13}C NMR (500 MHz, CD_2Cl_2) δ: 12.95, 13.095, 13.18, 15.12, 16.33, 17.11, 17.21, 18.19, 21.44, 21.59, 32.26, 32.43, 34.59, 34.64, 117.92, 123.68, 126.87, 127.59, 128.09, 128.45, 134.20, 134.86, 136.08, 137.16, 139.27, 141.34, 144.15, 144.29, 148.18, 150.13, 158.59.

2,7,20,25-Tetra*-p-*butylphenyl-11,16,29,34-tetraethyl-12,15,30,33-tetramethyl-3,6,21,24-tetraaza[32]octaphyrin-(1.0.1.0.1.0.1.0) (3b)

The compound was obtained from the condensation of biimidazole **1b** (10) with bipyrrole **2a** (16)[4] in 54% yield, following the general procedure given above. UV–vis (CH_3CN, nm (ε)) λ_{max}: 299 (139 000), 536 (68 500), 633 (142 000). ^{1}H NMR (500 MHz, CD_2Cl_2) δ: 0.93–1.04 (comp, 18H, CH_2CH_3, $CH_2CH_2CH_2CH_3$), 1.16–1.21 (m, 6H, CH_2CH_3), 1.36–1.47 (m, 8H, $CH_2CH_2CH_2CH_3$), 1.59–1.69 (comp, 8H, $CH_2CH_2CH_2CH_3$), 2.00 (s, 6H, CH_3), 2.39–2.47 (comp, 14H, CH_3 and $CH_2CH_2CH_2CH_3$), 2.61–2.72 (comp, 8H, $CH_2CH_2CH_2CH_3$), 6.87 (br, 2H, *meso-H*), 6.95 (s, 1H, *meso-H*), 7.04 (br, 1H, *meso-H*), 7.19 (m, 2H), 7.25 (m, 2H), 7.46 (br, 4H), 7.49 (m, 2H), 7.59 (br, 2H), 7.72 (br, 4H), 9.87 (br, 2H). ^{13}C NMR (500 MHz, CD_2Cl_2) δ: 10.95, 11.67, 14.11, 14.38, 15.64, 18.16, 18.69, 22.81, 33.98, 35.84, 119.71, 121.37, 126.50, 128.68, 129.10, 129.14, 129.42, 137.88, 143.97, 144.85, 147.48, 159.16.

2,7,20,25-Tetra*-p-*methylphenyl-11,12,15,16,29,30,33,34-octaethyl-3,6,21,24-tetraaza[32]octaphyrin(1.0.1.0.1.0.1.0) (3c)

The compound was obtained from the condensation of biimidazole **1a** with bipyrrole **2b** (16)[4] in 62% yield, following the general procedure given above. UV–vis (CH_3CN, nm (ε)) λ_{max}: 299 (78 400), 540 (40 900), 634 (92 400). ^{1}H NMR (400 MHz, CD_2Cl_2) δ: 0.90–1.25 (comp, 24H, CH_2CH_3), 2.36–2.99 (comp, 28H, CH_3, CH_2CH_3), 6.89 (s, 1H, *meso-H*), 6.99 (s, 2H, *meso-H*), 7.06 (s, 1H, *meso-H*), 7.22–7.31 (comp, 4H), 7.39 (d, J = 7.6 Hz, 2H), 7.54 (m, 4H), 7.72 (d, J = 8.4 Hz, 2H), 7.84 (d, J = 7.6 Hz, 4H), 10.02 (s, 2H). ^{13}C NMR (500 MHz, CD_2Cl_2) δ: 14.81, 15.22, 15.30, 16.86, 18.17, 18.61, 19.18, 19.54, 21.50, 127.81, 128.92, 129.73, 135.12, 138.73, 147.10, 148.25. HR-MS (FAB$^+$) m/z (M + H$^+$) calcd. for $C_{76}H_{77}N_{12}$: 1157.6394; found: 1157.6383.

2,7,20,25-Tetra*-p-*methylphenyl-11,16,29,34-tetraethyl-12,15,30,33-tetramethyl-3,6,21,24-tetraaza[32]octaphyrin-(1.0.1.0.1.0.1.0) (3d)

The compound was obtained from the condensation of biimidazole **1a** with bipyrrole **2a** (16)[4] in 59% yield, following the general procedure given above. UV–vis (CH_3CN, nm (ε)) λ_{max}: 296 (253 000), 531 (140 000), 633 (326 000). ^{1}H NMR (500 MHz, CD_2Cl_2) δ: 1.02 (t, J = 7.5 Hz, 6H), 1.18 (m, 6H), 1.97 (s, 6H), 2.38–2.45 (comp, 6H, CH_3, CH_2CH_3), 6.80 (s, 2H), 7.02 (s, 2H), 7.23 (m, 4H), 7.33 (br, 4H), 7.56 (m, 4H), 7.27 (br, 4H), 9.85 (br, 2H). ^{13}C NMR (500 MHz, CD_2Cl_2) δ: 10.87, 11.55, 14.18, 15.63, 18.17, 18.66, 21.44, 119.89, 121.28, 123.17, 124.99, 126.40, 128.69, 129.44, 129.74, 131.69, 137.54, 138.09, 138.83, 139.80, 147.35, 148.89, 150.94.

2,7,20,25-Tetra*-p-*butylphenyl-11,16,29,34-tetramethyl-12,15,30,33-tetracarboxylate-3,6,21,24-tetraaza[32]octaphyrin(1.0.1.0.1.0.1.0) (3e)

The compound was obtained from the condensation of biimidazole **1b** (10) with bipyrrole **2c** (17) in 26% yield, following the general procedure given above. UV–vis (CH_3CN, nm (ε)) λ_{max}: 275 (34 300), 609 (4790). ^{1}H NMR (400 MHz, CD_2Cl_2) δ: 0.98 (m, 12H, $CH_2CH_2CH_2CH_3$), 1.44 (m, 8H, $CH_2CH_2CH_2CH_3$), 1.67 (m, 8H, $CH_2CH_2CH_2CH_3$), 2.05 (s, 12H, CH_3), 2.45 (t, J = 7.4 Hz, 4H, CH_2CH_2), 2.62–2.77 (comp, 12H, CH_2CH_2), 3.02 (t, J = 7.6 Hz, $CH_2CH_2CH_2CH_3$), 3.21 (t, J = 7.2 Hz, 4H, $CH_2CH_2CH_2CH_3$), 3.30 (s, 6H, CO_2CH_3), 3.56 (s, 6H, CO_2CH_3), 7.00 (s, 2H, *meso-H*), 7.13 (s, 2H, *meso-H*), 7.30 (d, J = 7.6 Hz, 4H), 7.41 (d, J = 8.0 Hz, 4H), 7.62 (d, J = 8 Hz, 4H), 7.82 (d, J = 8 Hz, 4H), 10.02 (s, 2H, *NH*).

Molecular modelling studies

Molecular modelling studies were performed using semi-empirical calculations at the PM3 level, using HyperChem® V7.1, for preoptimization. Density functional theory (DFT) calculations were then performed using PRIRODA-04 (22). A PBE functional that includes the electron density gradient was used. The TZ2p atomic basis sets of grouped Gaussian functions were used to solve the Kohn–Sham equations. The criterion for convergence was to reach a difference in energy gradient between two sequential structures below 0.01 kcal/mol/Å (1 cal = 4.184 J). A PDB file for each optimized structure is included in the Supplementary information.[5]

Acknowledgements

This project was supported by the National Science Foundation Integrative Graduate Education and Research Traineeship Program (grant No. DGE 9870653) and the National Science Foundation (grant No. CHE 0515670 to JLS). We would also like to acknowledge Mr. Jeong Tae Lee for providing bipyrrole **2c** and Dr. Dmitri Laikov for providing the DFT software PRIRODA-04.

References

1. R.B. Woodward. *In* Aromaticity conference. Sheffield, UK. 1966.
2. J.L. Sessler and D. Seidel. Angew. Chem. Int. Ed. **42**, 5134 (2003).
3. J.L. Sessler and S. Weghorn. Expanded, contracted, and isomeric porphyrins. Pergamon, New York. 1997.
4. J.L. Sessler and W.E. Allen. Chemtech, **9**, 16 (1999).
5. J.L. Sessler, M. Cyr, H. Furuta, V. Kral, T. Mody, T. Morishima, M. Shionoyam, and S. Weghorn. Pure Appl. Chem. **3**, 393 (1993).
6. H. Ali and J.E. Van Lier. Chem. Rev. **9**, 2379 (1999).
7. J. Jasat and D. Dolphin. Chem. Rev. **6**, 2267 (1997).

[5] Supplementary data for this article are available on the journal Web site (http://canjchem.nrc.ca) or may be purchased from the Depository of Unpublished Data, Document Delivery, CISTI, National Research Council Canada, Ottawa, ON K1A 0R6, Canada. DUD 5038. For more information on obtaining material refer to http://cisti-icist.nrc-cnrc.gc.ca/irm/unpub_e.shtml.

© 2006 NRC Canada

8. W.J. Youngs, R.S. Simmons, J.C. Garrisoon, W.G. Kofron, and C.A. Tessier. Tetrahedron Lett. **43**, 3423 (2002).
9. A.L. Sargant, I.C. Hawkins, W.E. Allen, H. Liu, J.L. Sessler, and C.J. Fowler. Chem. Eur. J. **9**, 3065 (2003).
10. S. Nonell, J.I. Borrell, S. Borros, C. Colominas, O. Rey, N. Rubio, D. Sanchez-Garcia, and J. Teixido. Chem. Eur. J. **9**, 1635 (2003).
11. J.P. Street. Tetrahedron Lett. **28**, 3333 (1991).
12. Y.D. Choi and J.P. Street. J. Org. Chem. **57**, 1258 (1992).
13. K. Chellappan, N.J. Singh, I. Hwang, J.W. Lee, and K.S. Kim. Angew. Chem. Int. Ed. **44**, 2899 (2005).
14. J. Yoon, S.K. Kim, N.J. Singh, J.W. Lee, Y.J. Yang, K. Chellappan, and K.S. Kim. J. Org. Chem. **69**, 581 (2004).
15. J.L. Sessler and M.C. Hoehner. Synlett, **3**, 211 (1994).
16. M. Ringuet and J. Gagnon. Can. J. Chem. **63**, 2420 (1985).
17. K.M. Kadish, K.M. Smith, and R. Guilard. *In* The porphyrin handbook. Vol. 16. Academic Press, San Diego. 2003.
18. M. Bröring, J. Jendrny, L. Zander, H. Schmickler, J. Lex, Y-D. Wu, M. Nendel, J.G. Cheng, D.A. Plattner, K.N. Houk, and E. Vogel. Angew. Chem. Int. Ed. Engl. **34**, 2511 (1995).
19. J. Setsune, Y. Katakami, and N. Iizuna. J. Am. Chem. Soc. **121**, 8957 (1999).
20. Y-J. Shin, H. Furuta, K. Yoza, S. Igarashi, and A. Osuka. J. Am. Chem. Soc. **123**, 7190 (2001).
21. N. Sprutta and L. Latos-Grażyński. Chem. Eur. J. **7**, 5099 (2001).
22. D.N. Laikov. Chem. Phys. Lett. **281**, 151 (1997).

© 2006 NRC Canada

Toward the total synthesis of lophotoxin — New methodologies and synthetic strategies[1]

Peter Wipf and Michel Grenon

Abstract: Our recent progress toward the synthesis of the furanocembranolide lophotoxin (**1**) is disclosed. Strategies for the stereoselective incorporation of the C_{13} stereocenter by a catalytic desymmetrization of a cyclic *meso*-anhydride, as well as a novel 1,6-addition reaction of organocuprates to unsaturated [1,3]dioxin-4-ones are discussed. Preliminary results on the development of a rhodium-catalyzed asymmetric 1,6-addition reaction are also mentioned. Finally, modifications of a previously reported transition-metal-catalyzed cyclization reaction involving α-propargyl β-keto esters allow furan ring formation either under thermal conditions or by microwave irradiation.

Key words: 1,6-addition, organocuprates, catalytic desymmetrization, furan cyclization, microwave.

Résumé : Nos plus récents progrès concernant la synthèse totale du furanocembranolide lophotoxine (**1**) sont décrits. Des stratégies pour l'incorporation stéréosélective du substituant en C_{13} par la désymétrisation catalytique d'un anhydride cyclique *meso*, ainsi qu'une nouvelle réaction d'addition 1,6-conjuguée d'organocuprates sur des [1,3]dioxin-4-ones insaturées sont discutées. Des résultats préliminaires sur le dévelopement d'une réaction d'addition 1,6-conjugée asymétrique catalysée par le rhodium sont aussi mentionnés. Finalement, la modification d'une réaction de cyclisation catalysée par un métal de transition et mettant en jeu l'α-propargyl β-céto ester permet la formation d'un furane soit sous certaines conditions thermiques ou par irradiation aux micro-ondes.

Mots clés : addition 1,6-, organocuprates, désymétrisation catalytique, cyclisation de furane, microonde.

Introduction

Lophotoxin (**1**) is a member of the furanocembranolides (1), a growing class of natural products that comprise a number of highly functionalized cyclic diterpenes (Fig. 1). This compound is found in a number of marine invertebrates (gorgonian octocorals) located in tropical and subtropical waters (2). Lophotoxin acts as a potent neurotoxin by binding selectively and irreversibly to the Tyr^{190} residue present in the α-subunit of nicotinic acetylcholine receptors, leading to respiratory depression, paralysis, asphyxia, and ultimately death (3). SAR studies have demonstrated that the key structural elements responsible for this unique biological activity can be attributed to the C_7–C_8 epoxide and the lactone oxygens, allowing for a direct structural correlation of the pharmacophore in **1** with acetylcholine (4).

Received 2 November 2005. Accepted 21 December 2005. Published on the NRC Research Press Web site at http://canjchem.nrc.ca on 6 July 2006.

Dedicated to Dr. Alfred Bader, in recognition of his spirit for entrepreneurship, and his appreciation for the legacy of human accomplishment!

P. Wipf[2] and M. Grenon. Department of Chemistry, University of Pittsburgh, 219 Parkman Avenue, Pittsburgh, PA 15260, USA.

[1]This article is part of a Special Issue dedicated to Dr. Alfred Bader.

[2]Corresponding author (e-mail: pwipf@pitt.edu).

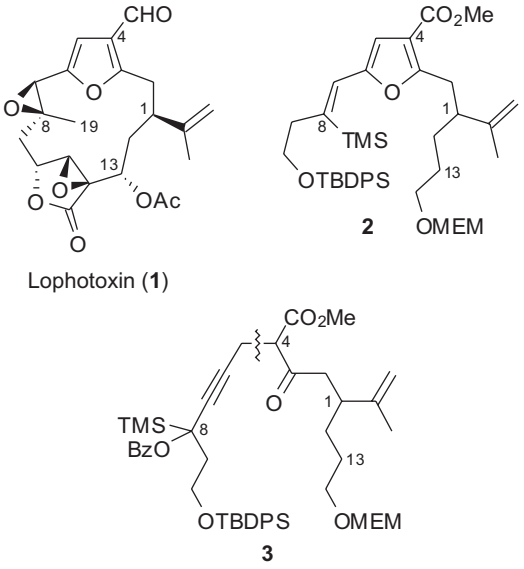
The presence of a 2,3,5-trisubstituted furan ring adjacent to a trans-trisubstituted epoxide, along with an epoxidized butenolide imbedded in a strained 14-membered macrocycle are the most prominent structural features of this molecule. In addition to the interesting biological activity displayed by this compound, the synthetic challenge offered to organic chemists has prompted a number of research groups to develop strategies aimed at the total synthesis of lophotoxin (5, 6) and other furanocembranolides (7–10).

Our research group has been interested in this class of molecules for a few years and we have recently disclosed a method to construct the 2-alkenyl-3,5-trisubstituted furan (**2**) from the simple acyclic α-propargyl β-keto ester (**3**) (Fig. 1) (11). This method is based on a general strategy for the construction of five-membered heterocycles (12) and features the use of a palladium catalyst and an inorganic base to induce the 5-exo-dig cyclization and concomitant aromatization to the furan ring. High levels of selectivity for the (*Z*)-isomer **2** were obtained as a result of the facial-selective protonation of an allene intermediate. With the furan in hand, the vinylsilane moiety was further elaborated to the C_{19} methyl group attached to the trans-trisubstituted epoxide in lophotoxin.

Some issues that were not addressed in our previous communication concern the installation of the C_{13} acetate group as well as a method to introduce the C_1 isopropenyl group in a stereoselective way. Previous synthetic work by others has either exploited the chiral pool (8, 9), a diastereoselective alkylation (5), or an intramolecular Nozaki–Hiyama–Kishi reaction (7) to introduce the isopropenyl group, whereas the

 doi:10.1139/V06-073 © 2006 NRC Canada

Fig. 1. Lophotoxin and the structures of synthetic intermediates.



configuration of the C_{13} substituent was not addressed (5, 6) or of no concern (7–9). In this paper, we wish to report on our findings for the stereoselective introduction of these two stereogenic carbons. A modification of our initial set of conditions, which uses microwave irradiation for the furan cyclization reaction, is also disclosed.

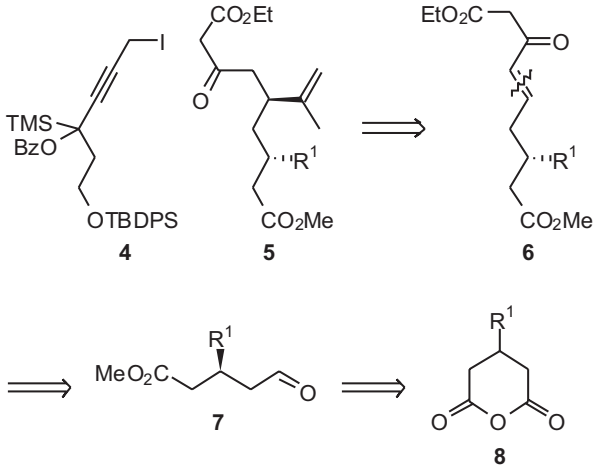
Results and discussions

β-Keto esters, such as **3**, are rapidly constructed by an alkylation reaction with propargylic iodide (**4**) (11) (Scheme 1). Segment **5** would need to be constructed in a stereocontrolled fashion. Further simplification of **5** provides **6**, which can be assembled from aldehyde **7** and an appropriate phosphonate by a Horner–Wadsworth–Emmons olefination. Finally, the highly symmetrical nature of aldehyde **7** led us to consider the use of a catalytic desymmetrization reaction of cyclic *meso*-anhydride (**8**) with an alcohol (13) to create the stereocenter at C_{13}.

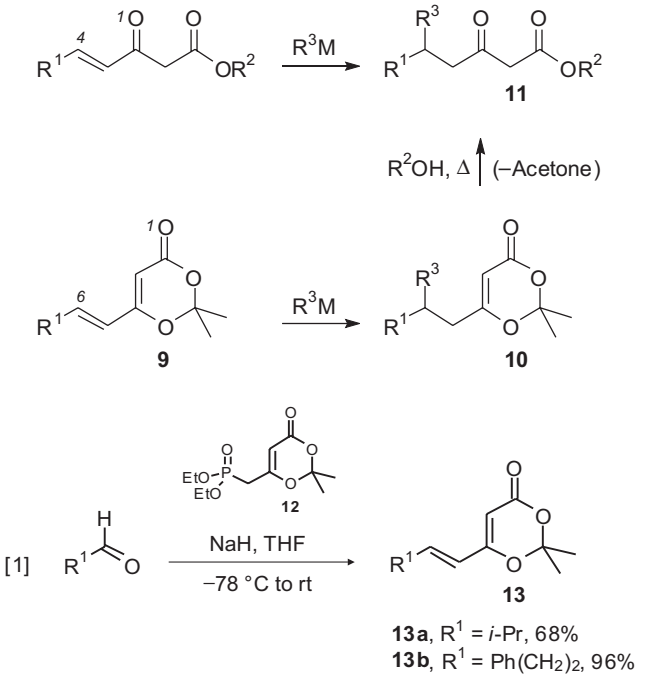
We initially envisioned that a conjugate 1,4-addition of an isopropenyl group to the unsaturated β-keto ester would be a straightforward means to introduce the C_1 side chain in **6**. However, owing to the ease of enolization of this particular type of substrate, we opted for an indirect route in which the 1,3-dicarbonyl unit would be revealed at a later stage (Scheme 2). We further anticipated that confinement of the β-keto ester to a [1,3]dioxin-4-one ring system, such as in **9**, would solve the problem, however, instead of a conjugate 1,4-addition, this required an extended 1,6-additon reaction. Thermolysis of adduct **10** in the presence of an alcohol (R^2OH) would then provide a number of different β-keto esters **11**, and an even greater number of derivatives could be obtained if other heteronucleophiles such as thiols or amines were to be used instead.

To test the feasibility of this route, [1,3]dioxin-4-ones (**13**) were prepared from phosphonate (**12**) (14) and either isobutyraldehyde or hydrocinnamaldehyde according to a literature procedure (15) and used as model substrates (eq. [1]).

Scheme 1. Strategy for the incorporation of the C_{13} stereogenic carbon center.



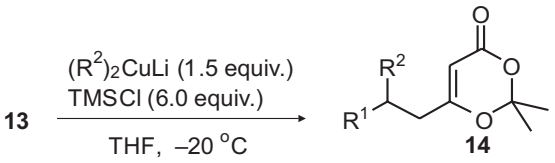
Scheme 2. Strategy for the incorporation of the C_1 stereogenic carbon center.



After some optimization of the reaction conditions, it was found that the addition of these extended Michael acceptors to solutions of Gillman-type organocuprates (R_2CuLi) containing chlorotrimethylsilane (16) at low temperature cleanly afforded the desired 1,6-addition products in high yields (Table 1). A small survey of different organocuprates revealed that simple alkyl groups were readily added (Table 1, entries 1–4), as were aromatic (Table 1, entries 5 and 6) and even silicon-based groups (17) (Table 1, entries 7 and 8). The addition of sterically encumbered organocuprates such as $(t\text{-Bu})_2CuLi$ also proceeded to afford the 1,6-addition adduct, albeit in low yields (Table 1, entries 9 and 10). However, the low yields observed were not because of a lack of reactivity during the 1,6-addition, but rather the result of a

© 2006 NRC Canada

Table 1. 1,6-Addition of organocuprates to [1,3]dioxin-4-ones **13**.



Entry	Substrate	$(R^2)_2CuLi$	Yield (%)
1	**13a**	Me_2CuLi	91
2	**13b**	Me_2CuLi	77
3	**13a**	Et_2CuLi	88
4	**13b**	Et_2CuLi	92
5	**13a**	Ph_2CuLi	79
6	**13b**	Ph_2CuLi	66
7	**13a**	$(PhMe_2Si)_2CuLi$	60
8	**13b**	$(PhMe_2Si)_2CuLi$	61
9	**13a**	*t*-Bu_2CuLi	17
10	**13b**	*t*-Bu_2CuLi	43

nonselective protonation step of the intermediate extended silyl enol ether formed after the 1,6-addition. No reaction occured when less reactive sp-hybridized organocopper reagents (RC≡CCu) or organocuprates [$(RC{\equiv}C)_2CuLi$] were used. It should be pointed out that in all cases studied using these sets of conditions, no adducts derived from 1,4- or 1,2-addition were isolated (18).

Having established that the extended conjugate addition reaction was possible, we next turned our attention toward the preparation of fragment **5** for our synthesis of lophotoxin. As we discussed previously, we planned on introducing the stereocenter at C_{13} by a catalytic desymmetrization reaction on cyclic *meso*-anhydrides **8** (Scheme 3). These were conveniently prepared according to a literature procedure (19) from commercially available diethyl 3-hydroxyglutarate by protection of the free hydroxyl group as a silyl ether to give **15**, followed by exhaustive saponification and dehydration of the resulting disodium acid salt with acetic anhydride. The TBDMS-protected cyclic anhydride **8a** was obtained as an off-white solid upon recrystallization of the crude material after the dehydration step, whereas the TBDPS-protected anhydride **8b** had to be filtered rapidly over a pad of silica gel pretreated with acetic anhydride to remove silanes before recrystallization was successful.[3]

Although there are a number of reported procedures to effect the desymmetrization of the cyclic anhydride **8a** (20–22), we opted for a method recently developed by Deng and co-workers (23) that employs modified cinchona alkaloids, initially adapted for the catalytic asymmetric dihydroxylation of alkenes (24) (Table 2). Using substoichiometric amounts (30 mol%) of $(DHQD)_2AQN$ in the presence of an excess of methanol at low temperature, Deng and co-workers (23) converted cyclic *meso*-anhydrides **8** (R^1 = Me, *i*-Pr) to acids **16** in good yields and high values of ee (Table 2, entries 1 and 2). When these optimized conditions were applied to the TBDMS-protected cyclic anhydride **8a**, a similar conversion to the desired acid was obtained (Table 2, entry 3). Longer reaction times resulted in higher conversions (Table 2, entry 4), however extensive desilylation of the product in both cases precluded the use of this substrate. Fortunately, when the TBDPS-protected cyclic anhydride **8b** was submitted to the desymmetrization reaction, conversions of 75%–85% were obtained, and more importantly, ^{1}H NMR analysis of the crude mixture indicated that no desilylation of **16** had occurred (Table 2, entry 5). An aliquot of the crude acid, accumulated from seven desymmetrizations under identical conditions, was reduced to the corresponding alcohol and treated with dil. HCl to provide the cyclic lactone **18** (Scheme 4) (25). Comparison of the chiral HPLC trace of this material with the racemic material prepared using quinuclidine as the organocatalyst (Table 2, entry 7) showed that the desymmetrization reaction occurred with a high level of enantioselectivity (95% ee). Finally, conducting the desymmetrization of **8b** at a higher temperature (–20 °C, Table 2, entry 6) resulted in a com-

Scheme 3. Preparation of cyclic anhydrides **8**. Reagents and conditions: (*a*) chlorosilane, imidazole, CH_2Cl_2, rt (**15a**, R^1 = OTBDMS, 92%; **15b**, R^1 = OTBDPS, 96%); (*b*) NaOH, MeOH, rt, 24–40 h; (*c*) Ac_2O, C_6H_6, Δ, 1.5 h (**8a**, R^1 = OTBDMS, 80%; **8b**, R^1 = OTBDPS, 46%).

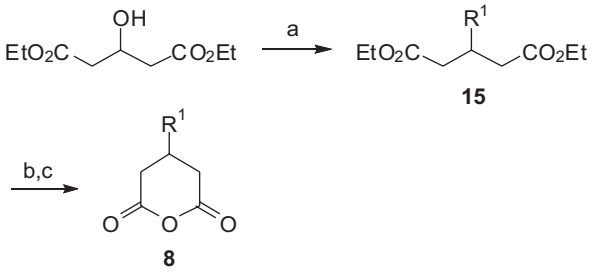
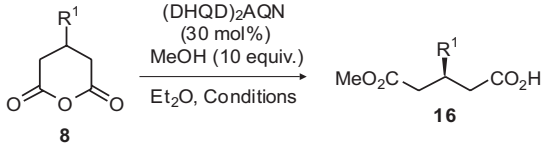


Table 2. Catalytic desymmetrization of cyclic *meso*-anhydrides **8** with $(DHQD)_2AQN$.



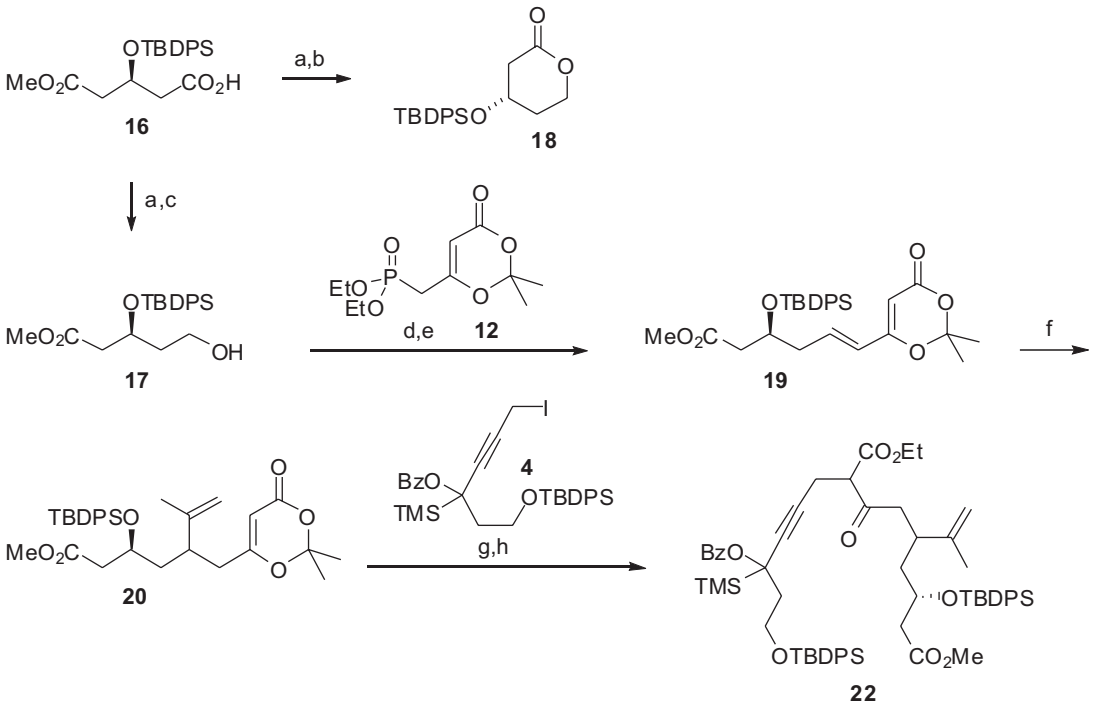
Entry	R^1	Conditions (°C, h)	Conversion (%)	ee (%)
1[a]	Me	–40, 43[a]	70[a,b]	91
2[a]	*i*-Pr	–40, 43[a]	72[a,b]	90
3	OTBDMS (**8a**)	–40, 41	65[c]	Nd[d]
4	OTBDMS (**8a**)	–40, 70	90–95[c]	Nd
5	OTBDPS (**8b**)	–40, 70	75–85[e]	95
6	OTBDPS (**8b**)	–20, 70	100	88
7	OTBDPS (**8b**)	–40, 70	96[f]	—

[a]Data from ref. 23.
[b]Isolated yield.
[c]Extensive desilylation of the product was observed.
[d]Nd (not determined).
[e]Conversions from seven desymmetrizations under identical conditions.
[f]Quinuclidine was used as a catalyst.

[3] Extensive desilylation occurs during the two-step sequence leading to lower yields of **8b**.

© 2006 NRC Canada

Scheme 4. Preparation of furan cyclization precursor **22**. Reagents and conditions: (*a*) BH_3·DMS, THF, rt, 15–17 h; (*b*) 10% HCl, rt, 1 h (38% from **8b**); (*c*) satd. aq. $NaHCO_3$, rt, 20 min (71% from **8b**); (*d*) TPAP (5 mol%), NMO, 4 Å MS, MeCN–CH_2Cl_2 (1:9), 30 min; (*e*) **12**, NaH, THF, –78 °C to rt, 1 h (49%, two steps); (*f*) CuI, 2-lithiopropene, TMSCl, THF, –20 °C, 16 h (94%, 1:1 dr); (*g*) EtOH, toluene, Δ; (*h*) NaH, **4**, THF, 0 °C to rt (77%, two steps).



plete conversion to the acid, albeit with lower selectivity (88% ee).

With an efficient and stereoselective solution for introducing the protected alcohol at C_{13}, we proceeded with our synthesis of fragment **5**. Reduction of the acid function in **16** with the borane – dimethyl sulfide complex followed by basic aqueous work up gave the alcohol **17** in good overall yield from cyclic *meso*-anhydride **8b**. Ley–Griffith oxidation of this alcohol to the aldehyde (26) followed by a Horner–Wadsworth–Emmons olefination with the stabilized phosphonate **12** (15) provided the 1,6-addition precursor **19** as a single isomer. Using 3 equiv. of the organocuprate derived from 2-lithiopropene, addition to the extended Michael acceptor occurred smoothly to provide **20** in high yield as a 1:1 mixture of diastereomers. Thermolysis of the [1,3]dioxin-4-one ring with ethanol in refluxing toluene revealed the β-keto ester (**21**) (see Table 3) that was then alkylated with the previously reported iodide **4** (11) to give the furan cyclization precursor **22** in good yield as a mixture of stereoisomers.

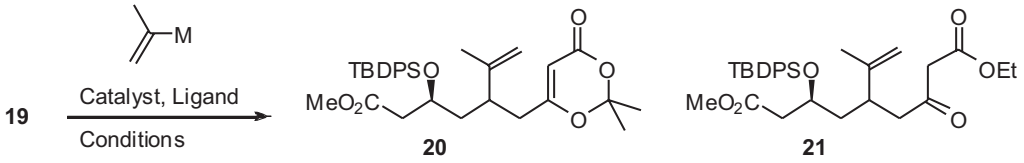
We were not surprised by the lack of stereocontrol obtained for the 1,6-addition of the organocuprate to [1,3]dioxin-4-one (**19**) (Scheme 4). By analogy to the diastereoselective 1,4-addition of copper-based organometallic reagents to Michael acceptors possessing a stereogenic center at the δ position under substrate control (27), we anticipated low levels of selectivity for the 1,6-addition. This gave us the opportunity to develop a catalytic asymmetric variant of the 1,6-addition reaction, and since stoichiometric copper-based reagents were effective, we initially screened for copper catalysts (Table 3). These studies proved quite disappointing; indeed, using conditions optimized for the catalytic asymmetric 1,4-addition of diorganozincs to enones (28), no reaction occurred and the starting material was recovered unchanged (Table 3, entry 1). The addition of chlorotrimethylsilane had no effect on the outcome of the reaction and even the use of Et_2Zn, which is often employed as a nucleophile in catalytic asymmetric conjugate additions, failed as well.

Over the past decade, rhodium catalysts have received increasing attention as alternatives to copper catalysts for the catalytic asymmetric 1,4-addition reaction, especially since the pioneering work by the research groups of Miyaura and Hayashi (29). However, a serious concern arises when considering the experimental conditions employed; most of the procedures involve heating at elevated temperatures in a binary solvent mixture composed of water and a cosolvent. We feared that thermal fragmentation of the [1,3]dioxin-4-one ring would lead to the α,β-unsaturated methyl ketone derived from **19** by a sequence that involves addition of 1 equiv. of water to an acyl ketene intermediate, followed by intramolecular decarboxylation of the resulting β-keto acid. As shown in Table 3 (entry 2), these concerns were confirmed when an addition of lithium 2-propenylborate in the presence of 1 equiv. of water (30) resulted in hydrolysis of **19** and isolation of the α,β-unsatured ester (65%).

Recent findings by Feringa and co-workers (31) and Genêt and co-workers (32) have shown that potassium organotrifluoroborates (RBF_3K), a class of air- and moisture-stable organometallic reagents, can be used as substitutes for boronic acids in the rhodium-catalyzed asymmetric 1,4-addition to enones using phosporamidites or

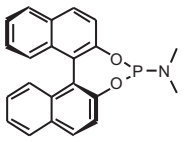
© 2006 NRC Canada

Table 3. Catalytic asymmetric 1,6-addition to [1,3]dioxin-4-one **19**.

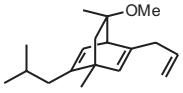


Entry	Substrate	M	Catalyst (mol%), Ligand (mol%)	Conditions	Yield **20**,**21** (%)	dr[a]
1	**19**	$(\text{Zn})_2$	$Cu(OTf)_2$ (5), **L_1** (10)	Toluene, –20 °C	0	—
2	**19**	$B(OMe)_3Li$	$Rh(acac)(eth)_2$ (4), Binap (6.5)	Dioxane H_2O (1 equiv.), Δ	0	—
3	**19**	BF_3K	$Rh(acac)(eth)_2$ (4), **L_1** (13)	EtOH, 83 °C	23,41	1.7:1
4	**19**		$Rh(acac)(eth)_2$ (4), **L_2** (6)	EtOH, 82 °C	21,38	4.0:1
5	**24**[b]		$Rh(acac)(eth)_2$ (4), **L_2** (6)	EtOH, 78 °C	27,32	3.7:1

[a] Diastereomeric ratio determined by ^{1}H NMR.
[b] Reaction performed on the acetate-protected derivative.



L_1 (MonoPhos™)



L_2 (Carreira's diene)

bidentate phosphines as chiral ligands. Of particular interest to us was the fact that these reactions can be performed in the absence of water (pure EtOH) and at lower temperatures (70 °C) (31), so that addition could occur before any significant cleavage of the [1,3]dioxin-4-one ring could take place. Gratifyingly, on our first try with Monophos™ (**L_1**, see bottom of Table 3) in a heated ethanolic solution, we obtained a mixture of 1,6-addition products **20** and **21** in a moderate combined yield, albeit in low diastereoselectivity (Table 3, entry 3). We then turned our attention to chiral bidentate phosphine ligands such as (*R*)-Binap, (*R*,*R*)-Me-Duphos, and (*S*,*S*)-Chiraphos, however, the use of these ligands seemed to considerably diminish the activity of the catalytic system and only starting material was recovered.

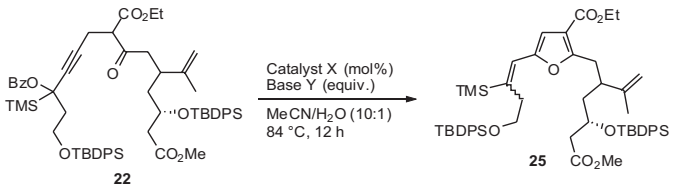
Another class of promising chiral ligands for the catalytic asymmetric 1,4-addition are chiral dienes (33), which have been disclosed recently by Hayashi et al. (34) and Carreira and co-workers (35). We chose to prepare Carreira's diene (see **L_2**, bottom of Table 3) from commercially available carvone. After heating **19** with the organotrifluoroborate in the presence of a rhodium catalyst, we were able to isolate the addition products **20** and **21** in a moderate combined yield as a 4:1 mixture of isomers (Table 3, entry 4) (36). Performing the reaction with a different neutral rhodium catalyst, $\{[RhCl(eth)_2]_2\}$ gave similar results (64% combined yield, 3.1:1 dr), whereas lower temperatures (57–60 °C) resulted in lower conversions.[4] We also attempted the reaction with the acetate-protected derivative **24** (Table 3, entry 5) as well as the free-hydroxyl derivative **23**, however, no increase in selectivity was observed with the former and the latter appeared to be unreactive.

Since we were unable to prepare the 1,6-addition products **20** and (or) **21** with high levels of stereoselectivity, we decided to resume our synthesis of lophotoxin with the 1:1 mixture of diastereomers obtained in high yield from the organocuprate addition (Scheme 4). The stage was now set for the key cyclization step that would produce the 2,3,5-trisubstituted furan ring and stereoselectively generate the olefin with the appropriate geometry, all in a single transition-metal-catalyzed event. Unfortunately, treatment of the α-propargyl β-keto ester **22** under our previously optimized conditions (11) gave only trace amounts of furan **25** (Table 4, entry 1). Although the starting material had been completely consumed, as judged by ^{1}H NMR analysis, no identifiable products could be isolated from the crude reaction mixture. After a number of unsuccessful attempts, we decided to conduct control experiments and we were quite surprised to see that treatment of **22** with only K_2CO_3, present under otherwise identical reaction conditions, resulted in rapid desilylation (TMS group) of the starting material (ca. 1 h, Table 4, entry 2). In light of this result, we decided to screen for other catalyst–base combinations and we were pleased to see that the use of $Pd(PPh_3)_4$ and $NaOAc{\cdot}3H_2O$ provided a reasonable yield of furan **25** as a 6.8:1 mixture of isomers (Table 4, entry 3). The addition of more base (Table 4, entry 4) or the use of related bases (Table 4, entries 5

[4] Comparable diastereomeric ratios (3.9:1) were obtained.

© 2006 NRC Canada

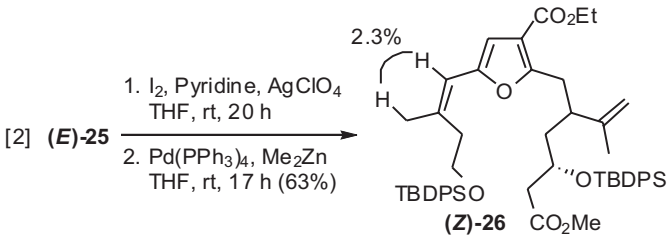
Table 4. Transition-metal-catalyzed cyclization of α-propargyl β-keto ester **22**.



Entry	Catalyst X (mol%)	Base Y (equiv.)	*E*/*Z* (ratio)[a]	Yield (%)
1	$Pd(OAc)_2$ (5), dppf (6)	K_2CO_3 (1.1)	—	Nd[b]
2	none	K_2CO_3 (1.1)	—	0
3	$Pd(PPh_3)_4$ (15)	$NaOAc{\cdot}3H_2O$ (1.1)	6.8:1	49
4	$Pd(PPh_3)_4$ (15)	$NaOAc{\cdot}3H_2O$ (5.0)	6.8:1	51
5	$Pd(PPh_3)_4$ (15)	NaOBz (1.1)	5.4:1	44
6	$Pd(PPh_3)_4$ (15)	$NaOPiv{\cdot}H_2O$ (1.1)	5.5:1	53
7	$Pd(PPh_3)_4$ (15)	$NaOAc{\cdot}3H_2O$ (1.1), 2,6-lutidine (1.1)	6.6:1	56

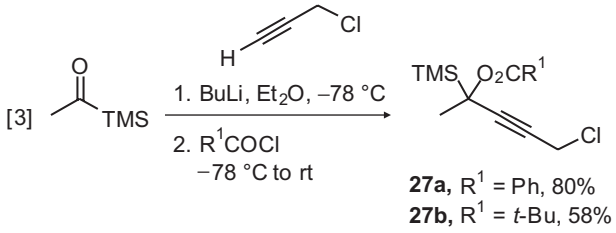
and 6) led to almost identical results, as did the combination of $NaOAc{\cdot}3H_2O$ and an organic base (Entry 7).

Comparison of the ^1H NMR spectra of **25** with our previously described furan **2** (Fig. 1) indicated that the major isomer formed during the reaction was the undesired (*E*)-isomer.[5] To verify the olefin configuration, we converted the vinylsilane moiety to the corresponding iodide and performed a Negishi cross-coupling reaction with dimethylzinc that yielded furan **26** (eq. [2]). A 1D-nOe analysis allowed us to assign the stereochemistry of the major isomer as **(*Z*)-26** since an nOe enhancement was observed between the hydrogen atoms of the newly introduced methyl group and the hydrogen atom of the alkene, establishing that the TMS group in **25** was located *trans* to the furan ring.



Our inability to gain access to **(*Z*)-25** forced a reconsideration of our strategy to close the macrocyclic ring in lophotoxin. Instead of relying on the furan cyclization reaction to set the stereochemistry as shown in **(*Z*)-25** and then attach the C_{19} methyl group, we decided to prepare furan **(*E*)-29** (Table 5) that already had an attached C_{19} methyl group and to use the vinylsilane moiety for further transformations. In addition to being more convergent, this approach gave us the opportunity to focus on a different bond disconnection in which C_8 and C_9 would be joined together by a transition-metal-catalyzed intramolecular cross-coupling reaction. In any event, we prepared the α-propargyl β-keto esters **28** from β-keto ester **21** and the appropriate halides **27** (eq. [3]).

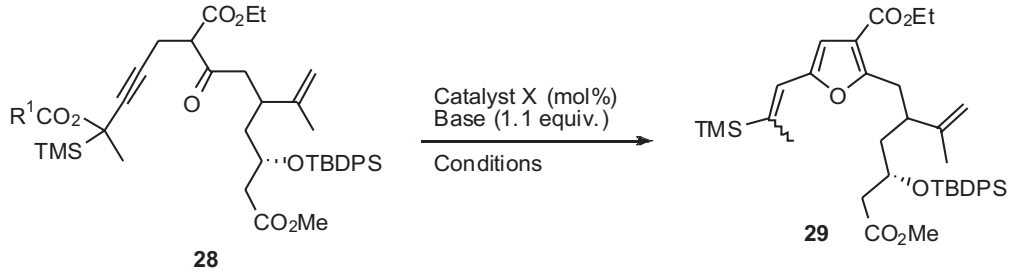
When substrate **28a** (R^1 = Ph) was subjected to the original cyclization conditions, virtually no furan was formed and the starting material decomposed (Table 5, entry 1). Using the modified set of conditions [$Pd(PPh_3)_4$–$NaOAc{\cdot}3H_2O$] we were pleased to see that cyclization had occured, although we were alarmed by the much lower isolated yield (Table 5, entry 2). Another product, possibly arising from migration of the benzoate group across the alkyne, was recovered from this reaction in ca. 32% yield. Since the benzoate might be too readily eliminated, we prepared the pivaloate derivative **28b** (R^1 = *t*-Bu) and were relieved to see that under the new set of conditions, the desired furan **29** was formed once again in moderate yield (Table 5, entry 3). To decrease the reaction times and possibly minimize side reactions, we next turned our attention to the use of microwave irradiation to promote the cyclization reaction. Gratifyingly, heating **28b** for only 40 min in the microwave under otherwise identical reaction conditions led to furan **29** in a comparable yield and high selectivity (Table 5, entry 4). While screening for other transition-metal catalysts, we were pleased to find that the allylpalladium chloride dimer was also an effective catalyst for the cyclization. In this case, both pivalate and benzoate derivatives could be used and the furan was obtained in acceptable yields (Table 5, entries 5 and 6). Although the (*E*/*Z*) selectivity was severely diminished, isomerization of the furan mixture with a catalytic amount (5–10 mol%) of $(PhSe)_2$ in THF at reflux produced pure **(*E*)-29** in high yield (Table 5, entry 5). With a more practical route to this furan in hand, we are currently exploring a strategy that involves further modification of the protected β-hydroxy ester fragment followed by an intramolecular transition-metal-



[5] The ^1H NMR chemical shift of the TMS group is particularly diagnostic. Indeed, in **2** the TMS group has a δ of 0.11 ppm, whereas the major isomer in **25** has a δ of 0.00 ppm and the minor isomer has a δ of 0.09 ppm.

© 2006 NRC Canada

Table 5. Transition-metal-catalyzed cyclization of α-propargyl β-keto esters **28**.



28 **29**

Entry	R^1	Catalyst X (mol%)	Base (1.1 equiv.)	Conditions[a]	E/Z (ratio)[b]	Yield (%)
1	Ph (**28a**)	$Pd(OAc)_2$ (5), dppf (6)	K_2CO_3	A	—	Nd[c]
2	Ph (**28a**)	$Pd(PPh_3)_4$ (15)	$NaOAc{\cdot}3H_2O$	A	5.1:1	30
3	*t*-Bu (**28b**)	$Pd(PPh_3)_4$ (15)	$NaOAc{\cdot}3H_2O$	A	6.6:1	53
4	*t*-Bu (**28b**)	$Pd(PPh_3)_4$ (15)	$NaOAc{\cdot}3H_2O$	B	8.6:1	51
5	*t*-Bu (**28b**)	$[(\eta^3\text{-}C_3H_5)PdCl]_2$ (7.5), dppf (15)	None	C	1.4:1	59 (50[d])
6	Ph (**28a**)	$[(\eta^3\text{-}C_3H_5)PdCl]_2$ (7.5), dppf (15)	None	C	1.5:1	54

[a]Reagents and conditions: (A) MeCN–H_2O (10:1); (B) MeCN–H_2O (10:1), 100 °C, μW, 40 min; (C) THF, 100 °C, μW, 20 min.
[b]Isomeric ratio determined by ^1H NMR.
[c]Nd (not determined).
[d]Yield of pure (***E*)-29** from **28** after isomerization with $(PhSe)_2$.

catalyzed cross-coupling reaction with the vinylsilane moiety. These results will be disclosed in due course.

Conclusion

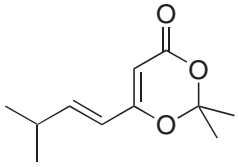
We have shown that a catalytic desymmetrization reaction using a modified cinchona alkaloid allows for the stereoselective incorporation of the C_{13} substituent present in lophotoxin from a simple prochiral cyclic anhydride. A newly developed, highly regioselective 1,6-addition reaction of organocuprates to unsaturated [1,3]dioxin-4-ones provided a means to introduce the C_1 isopropenyl group, and encouraging preliminary results have established that a rhodium-catalyzed asymmetric 1,6-addition reaction provides moderate levels of diastereocontrol. Problems encountered with the transition-metal catalyzed furan cyclization reaction have led to modifications of our original thermal procedure and to the development of a microwave-assisted variant. We are currently applying these modifications toward the total synthesis of lophotoxin and other members of the furanocembranolide family of natural products.

Experimental

General methods

All moisture-sensitive reactions were performed under an atmosphere of N_2 and glassware was flame-dried under vacuum prior to use. Et_2O and THF were dried by distillation over Na–benzophenone. Distilled hexane and ethyl acetate were used for chromatographic purifications. Toluene and CH_2Cl_2 were purified by filtration through activated alumina. TMSCl was distilled over CaH_2 and kept in a dessicator. $(DHQD)_2AQN$ was prepared according to a literature procedure (24). Unless otherwise stated, all other reagents and solvents were used as received. Analytical thin layer chromatography (TLC) was performed on precoated silica gel 60 F-254 plates (particle size 0.040–0.055 mm, 230–400 mesh) and visualization was accomplished with a 254 nm UV light and (or) by staining with a basic $KMnO_4$ solution (1.5 g of $KMnO_4$ and 1.5 g of K_2CO_3 in 100 mL of a 0.1% aq. NaOH solution). NMR spectra were recorded at 300 MHz and 76 MHz for ^1H NMR and ^{13}C NMR, respectively, using a Bruker AVANCE 300 MHz spectrometer at 21 °C in $CDCl_3$ unless stated otherwise. Chemical shifts (δ) are reported as follows: chemical shift, multiplicity (singlet (s), doublet (d), triplet (t), quartet (q), quintet (qn), hextet (hex), multiplet (m), broad (b)), coupling constants, and integration. IR spectra were obtained on a Nicolet AVATAR 360 FT-IR ESP spectrometer. Mass spectra were obtained on a Micromass Autospec double focusing instrument. Optical rotations were measured on a PerkinElmer 241 polarimeter. Microwave reactions were run on a CEM Discover instrument.

2,2-Dimethyl-6-(3-methylbut-1-enyl)[1,3]dioxin-4-one (13a)

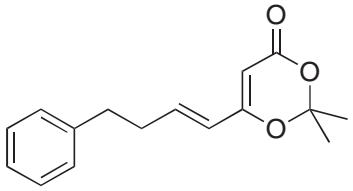


To a solution of phosphonate **12** (1.11 g, 3.99 mmol) in THF (20 mL) cooled to 0 °C was added NaH (192 mg of a 60% mineral dispersion, 4.80 mmol). The ice bath was removed and the reaction mixture was stirred at rt for 30 min, cooled to –78 °C, and treated with isobutyraldehyde (400 μL, 4.4 mmol). The solution was allowed to gradually warm to rt and stirred for 1 h. One drop of satd. aq. $NaHCO_3$ was added and the mixture was stirred for 5 min (to complete the deprotonation step). After adding satd. aq. $NaHCO_3$ (50 mL), the reaction was transferred to a separatory funnel and extracted with Et_2O (3 × 50 mL). The organic layers were combined, dried (Na_2SO_4), filtered,

© 2006 NRC Canada

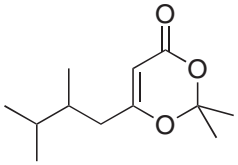
concentrated under reduced pressure, and purified by chromatography on SiO_2 to afford 532 mg of **13a** (68%) as a colourless oil. R_f 0.26 (20% EtOAc–hexane). FT-IR (neat, cm^{-1}): 2963, 2872, 1731, 1653, 1592, 1391, 1374, 1273, 1206, 1018. ^1H NMR ($CDCl_3$) δ: 6.54 (dd, J = 15.6, 6.8 Hz, 1H), 5.85 (dd, J = 15.6, 1.4 Hz, 1H), 5.26 (s, 1H), 2.46 (hexd, J = 6.8, 1.4 Hz, 1H), 1.72 (s, 6H), 1.08 (d, J = 6.8 Hz, 6H). ^{13}C NMR ($CDCl_3$) δ: 163.5, 161.8, 148.5, 119.6, 106.0, 93.1, 31.1, 24.8 (2), 21.3 (2). HR-MS (EI) *m/e* calcd. for $C_{11}H_{16}O_3$: 196.1099; found: 196.1102.

2,2-Dimethyl-6-(4-phenylbut-1-enyl)[1,3]dioxin-4-one (13b)



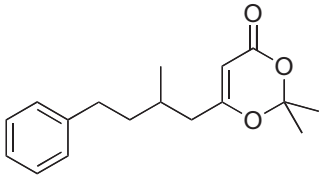
To a solution of phosphonate **12** (1.95 g, 7.01 mmol) in THF (50 mL) cooled to 0 °C was added NaH (240 mg of a 60% mineral dispersion, 6.00 mmol). The ice bath was removed and the reaction mixture was stirred at rt for 30 min, cooled to –78 °C, and treated with hydrocinnamaldehyde (730 μL, 5.0 mmol). The solution was allowed to gradually warm to rt and stirred for 1 h. One drop of satd. aq. $NaHCO_3$ was added and the mixture was stirred for 5 min (to complete the deprotonation step). After adding satd. aq. $NaHCO_3$ (50 mL), the reaction was transferred to a separatory funnel and extracted with Et_2O (4 × 50 mL). The organic layers were combined, dried (Na_2SO_4), filtered, concentrated under reduced pressure, and purified by chromatography on SiO_2 to afford 1.23 g of **13b** (96%) as a colourless oil. R_f 0.20 (20% EtOAc–hexane). FT-IR (neat, cm^{-1}): 2999, 2941, 1725, 1653, 1592, 1390, 1274, 1205, 1020. ^1H NMR ($CDCl_3$) δ: 7.34–7.18 (m, 5H), 6.61 (dt, J = 15.5, 7.1 Hz, 1H), 5.93 (dt, J = 15.6, 1.4 Hz, 1H), 5.25 (s, 1H), 2.82–2.76 (m, 2H), 2.58–2.50 (m, 2H), 1.72 (s, 6H). ^{13}C NMR ($CDCl_3$) δ: 163.1, 161.9, 141.2, 140.6, 128.4 (2), 128.2 (2), 126.1, 122.9, 106.2, 93.4, 34.6, 34.4, 24.9 (2). HR-MS (EI) *m/e* calcd. for $C_{16}H_{18}O_3$: 258.1256; found; 258.1254.

6-(2,3-Dimethylbutyl)-2,2-dimethyl[1,3]dioxin-4-one (14a)



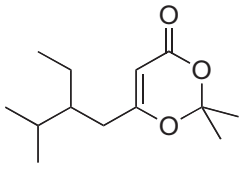
To a suspension of CuI (143 mg, 0.751 mmol) in THF (2.5 mL) cooled to –78 °C was added dropwise a solution of MeLi in Et_2O (1.6 mol/L, 940 μL, 1.5 mmol). The cold bath was removed and the mixture was stirred at rt for 30 min. The resulting colourless solution was then cooled to –78 °C and TMSCl (380 μL, 3.0 mmol) was added. After stirring for ca. 5 min, a solution of **13a** (98.8 mg, 0.503 mmol) in THF (1.5 mL, 1.0 mL rinse) was added. The mixture was stirred at –78 °C for 30 min, then at –20 °C for ca. 18 h. The reaction was stopped by adding satd. aq. $NaHCO_3$ (30 mL) at –20 °C, then warmed to rt, transferred to a separatory funnel, and extracted with Et_2O (4 × 30 mL). The organic layers were combined, dried (Na_2SO_4), filtered, concentrated under reduced pressure, and purified by chromatography on SiO_2 to afford 97 mg of **14a** (91%) as a colourless oil. R_f 0.36 (20% EtOAc–hexane). FT-IR (neat, cm^{-1}): 2961, 2876, 1735, 1633, 1390, 1272, 1205, 1013. ^1H NMR ($CDCl_3$) δ: 5.23 (s, 1H), 2.29 (dd, J = 14.1, 5.0 Hz, 1H), 1.96 (dd, J = 14.1, 9.4 Hz, 1H), 1.75–1.70 (m, 1H), 1.70 (s, 3H), 1.69 (s, 3H), 1.65–1.59 (m, 1H), 0.91 (d, J = 6.8 Hz, 3H), 0.87 (d, J = 6.8 Hz, 3H), 0.86 (d, J = 6.8 Hz, 3H). ^{13}C NMR ($CDCl_3$) δ: 171.7, 161.2, 106.1, 94.0, 38.5, 36.0, 31.8, 25.2, 24.7, 19.8, 17.7, 15.0. HR-MS (ESI–POS) *m/e* calcd. for $C_{12}H_{20}O_3Na$: 235.1310 [M + Na]; found: 235.1299.

2,2-Dimethyl-6-(2-methyl-4-phenylbutyl)[1,3]dioxin-4-one (14b)



Following the previous procedure for the 1,6-addition of Me_2CuLi, [1,3]dioxin-4-one **13b** (124 mg, 0.480 mmol) gave 101 mg (77%) of **14b** as a colourless oil. R_f 0.29 (20% EtOAc–hexane). FT-IR (neat, cm^{-1}): 2998, 2929, 1732, 1633, 1390, 1272, 1204, 1014. ^1H NMR ($CDCl_3$) δ: 7.32–7.27 (m, 2H), 7.22–7.15 (m, 3H), 5.22 (s, 1H), 2.73–2.67 (m, 1H), 2.63–2.57 (m, 1H), 2.28 (dd, J = 14.2, 6.1 Hz, 1H), 2.07 (dd, J = 14.2, 7.9 Hz, 1H), 1.86 (hex, J = 6.4 Hz, 1H), 1.73–1.67 (m, 1H), 1.67 (s, 3H), 1.66 (s, 3H), 1.56–1.47 (m, 1H), 1.02 (d, J = 6.7 Hz, 3H). ^{13}C NMR ($CDCl_3$) δ: 170.8, 161.1, 141.9, 128.3 (2), 128.2 (2), 125.8, 106.1, 94.2, 41.0, 38.3, 33.1, 30.1, 25.0, 24.9, 19.3. HR-MS (ESI–POS) *m/e* calcd. for $C_{17}H_{22}O_3Na$ [M + Na]: 297.1467; found: 297.1447.

6-(2-Ethyl-3-methylbutyl)-2,2-dimethyl[1,3]dioxin-4-one (14c)

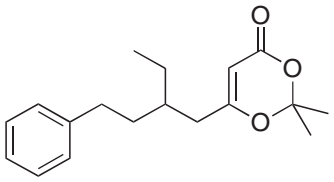


To a suspension of CuI (143 mg, 0.751 mmol) in THF (2.0 mL) cooled to 0 °C was added dropwise a 0.39 mol/L solution of EtLi in benzene–cyclohexane (90:10, 3.8 μL, 1.5 mmol) and the mixture was stirred at 0 °C for 30 min. The resulting dark black solution was then cooled to –78 °C and TMSCl (380 μL, 3.0 mmol) was added. After stirring for ca. 5 min, a solution of **13a** (97.6 mg, 0.497 mmol) in THF (1.5 mL, 1.0 mL rinse) was added. The mixture was stirred at –78 °C for 30 min, then at –20 °C for ca. 17 h. The reaction was stopped by adding satd. aq. $NaHCO_3$ (30 mL) at –20 °C, then warmed to rt, transferred to a separatory funnel, and extracted with Et_2O (3 × 30 mL). The organic layers were combined, dried (Na_2SO_4), filtered, concentrated under

© 2006 NRC Canada

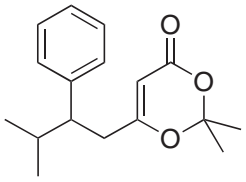
reduced pressure, and purified by chromatography on SiO_2 to afford 99 mg of **14c** (88%) as a colourless oil. R_f 0.35 (20% EtOAc–hexane). FT-IR (neat, cm^{-1}): 2961, 2876, 1735, 1632, 1464, 1389, 1272, 1205, 1015. ^1H NMR ($CDCl_3$) δ: 5.24 (s, 1H), 2.21 (dd, *J* = 14.4, 6.0 Hz, 1H), 2.06 (dd, *J* = 14.4, 7.7 Hz, 1H), 1.82–1.72 (m, 1H), 1.69 (s, 6H), 1.53–1.42 (m, 1H), 1.42–1.17 (m, 2H), 0.89 (t, *J* = 7.5 Hz, 3H), 0.88 (d, *J* = 7.3 Hz, 3H), 0.86 (d, *J* = 7.0 Hz, 3H). ^{13}C NMR ($CDCl_3$) δ: 172.3, 161.3, 106.1, 94.0, 42.8, 34.9, 28.6, 25.1, 24.9, 22.8, 19.0, 18.6, 11.6. HR-MS (EI) *m/e* calcd. for $C_{10}H_{16}O_2$: 168.1150 [M – CH_3COCH_3]; found: 168.1148.

6-(2-Ethyl-4-phenylbutyl)-2,2-dimethyl[1,3]dioxin-4-one (14d)



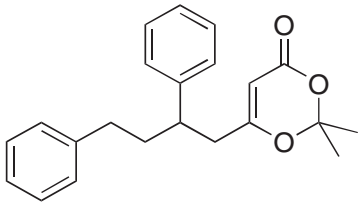
Following the previous procedure for the 1,6-addition of Et_2CuLi, [1,3]dioxin-4-one **13b** (131 mg, 0.507 mmol) gave 134 mg (92%) of **14d** as a colourless oil. R_f 0.28 (20% EtOAc–hexane). FT-IR (neat, cm^{-1}): 2998, 2935, 1731, 1631, 1455, 1390, 1272, 1204, 1014. ^1H NMR ($CDCl_3$) δ: 7.32–7.26 (m, 2H), 7.22–7.14 (m, 3H), 5.23 (s, 1H), 2.67–2.57 (m, 2H), 2.26–2.19 (m, 2H), 1.73–1.60 (m, 3H), 1.67 (s, 3H), 1.65 (s, 3H), 1.49–1.36 (m, 2H), 0.92 (t, *J* = 7.4 Hz, 3H). ^{13}C NMR ($CDCl_3$) δ: 171.2, 161.2, 142.0, 128.3 (2), 128.2 (2), 125.8, 106.2, 94.2, 37.7, 36.1, 34.7, 32.7, 25.5, 25.0, 24.9, 10.4. HR-MS (EI) *m/e* calcd. for $C_{18}H_{24}O_3$: 288.1725; found: 288.1727.

2,2-Dimethyl-6-(3-methyl-2-phenylbutyl)-[1,3]dioxin-4-one (14e)



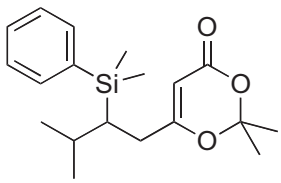
To a suspension of CuI (143 mg, 0.751 mmol) in THF (2.5 mL) cooled to 0 °C was added dropwise a solution of PhLi (1.0 mol/L) in cyclohexane–Et_2O (70:30, 1.5 mL, 1.5 mmol). After stirring at 0 °C for 30 min, the mixture was cooled to –78 °C, at which point a dense precipitate formed. TMSCl (380 μL, 3.0 mmol) was added and after ca. 5 min a solution of **13a** (99.2 mg, 0.506 mmol) in THF (1.5 mL, 1.0 mL rinse) was added. The mixture was stirred at –78 °C for 30 min, then at –20 °C for ca. 18 h. The reaction was stopped by adding satd. aq. $NaHCO_3$ (30 mL) at –20 °C, then warmed to rt, transferred to a separatory funnel, and extracted with Et_2O (4 × 30 mL). The organic layers were combined, dried (Na_2SO_4), filtered, concentrated under reduced pressure, and purified by chromatography on SiO_2 to afford 110 mg of **14e** (79%) as a colourless oil. R_f 0.31 (20% EtOAc–hexane). FT-IR (neat, cm^{-1}): 2960, 2873, 1731, 1633, 1454, 1390, 1272, 1204, 1014. ^1H NMR ($CDCl_3$) δ: 7.29–7.24 (m, 2H), 7.22–7.17 (m, 1H), 7.10–7.06 (m, 2H), 5.05 (s, 1H), 2.76 (dd, *J* = 14.2, 4.3 Hz, 1H), 2.73–2.66 (m, 1H), 2.52 (dd, *J* = 14.2, 11.1 Hz, 1H), 1.84 (apparent hex, *J* = 6.8 Hz, 1H), 1.51 (s, 3H), 1.32 (s, 3H), 0.98 (d, *J* = 6.7 Hz, 3H), 0.77 (d, *J* = 6.7 Hz, 3H). ^{13}C NMR ($CDCl_3$) δ: 170.7, 161.2, 141.4, 128.4 (2), 128.1 (2), 126.6, 106.2, 94.5, 49.5, 36.9, 33.6, 25.4, 24.0, 20.6, 20.1. HR-MS (EI) *m/e* calcd. for $C_{14}H_{16}O_2$: 216.1150 [M – CH_3COCH_3]; found: 216.1150.

6-(2,4-Diphenylbutyl)-2,2-dimethyl[1,3]dioxin-4-one (14f)



Following the previous procedure for the 1,6-addition of Ph_2CuLi, [1,3]dioxin-4-one **13b** (128 mg, 0.496 mmol) gave 110 mg (66%) of **14f** as a colourless oil. R_f 0.24 (20% EtOAc–hexane). FT-IR (neat, cm^{-1}): 3027, 2999, 2939, 2858, 1728, 1632, 1495, 1454, 1390, 1272, 1204, 1014. ^1H NMR ($CDCl_3$) δ: 7.36–7.31 (m, 2H), 7.29–7.23 (m, 3H), 7.21–7.15 (m, 3H), 7.12–7.07 (m, 2H), 5.07 (s, 1H), 2.97–2.89 (m, 1H), 2.60 (dd, *J* = 14.5, 6.4 Hz, 1H), 2.56–2.40 (m, 3H), 2.05–1.88 (m, 2H), 1.53 (s, 3H), 1.46 (s, 3H). ^{13}C NMR ($CDCl_3$) δ: 169.8, 161.0, 142.6, 141.6, 128.6 (2), 128.29 (2), 128.26 (2), 127.5 (2), 126.8, 125.8, 106.3, 94.5, 42.3, 40.7, 38.1, 33.3, 25.0, 24.6. HR-MS (EI) *m/e* calcd. for $C_{19}H_{18}O_2$: 278.1307 [M – CH_3COCH_3]; found: 278.1303.

6-[2-(Dimethylphenylsilanyl)-3-methylbutyl]-2,2-dimethyl[1,3]dioxin-4-one (14g)

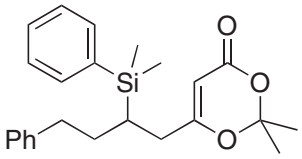


To a suspension of CuI (143 mg, 0.751 mmol) in THF (1.0 mL) cooled to –20 °C was added dropwise a solution of $PhMe_2SiLi$ in THF (0.40 mol/L, 3.8 μL, 1.5 mmol), and the mixture was stirred at –20 °C for 4 h. TMSCl (380 μL, 3.0 mmol) was added and the mixture was stirred for ca. 5 min after which a solution of **13a** (95.4 mg, 0.486 mmol) in THF (1.5 mL, 1.0 mL rinse) was added. The reaction mixture was stirred at –20 °C for ca. 15 h, stopped by adding satd. aq. $NaHCO_3$ (30 mL) at –20 °C, then warmed to rt, transferred to a separatory funnel, and extracted with Et_2O (4 × 30 mL). The organic layers were combined, dried (Na_2SO_4), filtered, concentrated under reduced pressure, and purified by chromatography on SiO_2 to afford 97 mg of **14g** (60%) as a colourless oil. R_f 0.42 (20% EtOAc–hexane). FT-IR (neat, cm^{-1}): 2998, 2957, 2872, 1732, 1630, 1427, 1389, 1271, 1205, 1111, 1016. ^1H NMR ($CDCl_3$) δ: 7.54–7.47 (m,

© 2006 NRC Canada

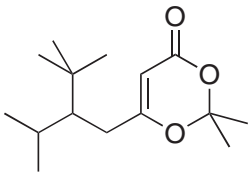
2H), 7.39–7.33 (m, 3H), 5.17 (s, 1H), 2.30–2.22 (m, 2H), 1.98–1.92 (m, 1H), 1.63 (s, 3H), 1.60 (s, 3H), 1.31–1.26 (m, 1H), 0.95 (d, J = 6.9 Hz, 3H), 0.88 (d, J = 7.0 Hz, 3H), 0.36 (s, 6H). ^{13}C NMR ($CDCl_3$) δ: 172.6, 161.2, 138.3, 133.7 (2), 129.0, 127.8 (2), 106.1, 93.5, 31.4, 29.8, 28.7, 25.2, 24.6, 22.0, 21.3, –2.2, –3.1. HR-MS (EI) *m/e* calcd. for $C_{18}H_{25}O_3Si$: 317.1573 [M – CH_3]; found: 317.1557.

6-(2-(Dimethyl(phenyl)silyl)-4-phenylbutyl)-2,2-dimethyl-4H-1,3-dioxin-4-one (14h)



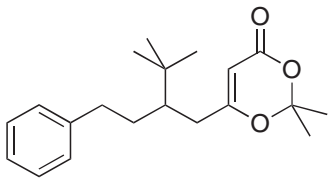
Following the previous procedure for the 1,6-addition of $(PhMe_2Si)_2CuLi$, [1,3]dioxin-4-one **13b** (129 mg, 0.499 mmol) gave 121 mg (61%) of **14h** as a colourless oil. R_f 0.26 (20% EtOAc–hexane). FT-IR (neat, cm^{-1}): 2999, 2950, 2859, 1729, 1629, 1389, 1272, 1204, 1112, 1014. ^{1}H NMR ($CDCl_3$) δ: 7.53–7.48 (m, 2H), 7.42–7.36 (m, 3H), 7.28–7.23 (m, 2H), 7.20–7.16 (m, 1H), 7.05–7.01 (m, 2H), 5.19 (s, 1H), 2.61–2.53 (m, 1H), 2.53–2.46 (m, 1H), 2.38 (dd, J = 14.9, 4.5 Hz, 1H), 2.16 (dd, J = 14.9, 9.6 Hz, 1H), 1.83–1.75 (m, 1H), 1.67–1.59 (m, 1H, hidden under two s), 1.65 (s, 3H), 1.64 (s, 3H), 1.32–1.25 (m, 1H), 0.363 (s, 3H), 0.360 (s, 3H). ^{13}C NMR ($CDCl_3$) δ: 171.9, 161.0, 141.8, 137.2, 133.8 (2), 129.3, 128.3 (2), 128.1 (2), 127.9 (2), 125.8, 106.2, 93.8, 35.2, 34.3, 31.9, 25.1, 24.7, 22.1, –4.1, –4.2. HR-MS (EI) *m/e* calcd. for $C_{24}H_{30}O_3Si$: 394.1964; found: 394.1953.

6-(2-Isopropyl-3,3-dimethylbutyl)-2,2-dimethyl[1,3]dioxin-4-one (14i)



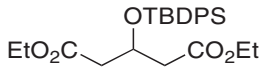
To a suspension of CuI (143 mg, 0.751 mmol) in THF (2.5 mL) cooled to –78 °C was added dropwise a solution of *t*-BuLi in pentane (1.4 mol/L, 1.1 µL, 1.5 mmol). The mixture was stirred at –78 °C for 30 min and then TMSCl (380 µL, 3.0 mmol) was added. After stirring for ca. 5 min, a solution of **13a** (101 mg, 0.515 mmol) in THF (1.5 mL, 1.0 mL rinse) was added. The mixture was stirred at –78 °C for 30 min, then at –20 °C for ca. 15 h. The reaction was stopped by adding satd. aq. $NaHCO_3$ (30 mL) at –20 °C, then warmed to rt, transferred to a separatory funnel, and extracted with Et_2O (3 × 30 mL). The organic layers were combined, dried (Na_2SO_4), filtered, concentrated under reduced pressure, and purified by chromatography on SiO_2 to afford 22 mg of **14i** (17%) as a colourless oil. R_f 0.53 (20% EtOAc–hexane). FT-IR (neat, cm^{-1}): 2960, 1733, 1630, 1389, 1271, 1205, 1016. ^{1}H NMR ($CDCl_3$) δ: 5.29 (s, 1H), 2.22 (d, J = 5.6 Hz, 2H), 2.11–2.06 (m, 1H), 1.69 (s, 6H), 1.50 (td, J = 5.7, 1.9 Hz, 1H), 0.93–0.92 (m, 12H), 0.87 (d, J = 6.8 Hz, 3H). ^{13}C NMR ($CDCl_3$) δ: 174.1, 161.5, 106.1, 93.2, 49.9, 34.9, 30.4, 28.6 (3), 27.7, 25.2, 25.0, 24.4, 18.3. HR-MS (EI) *m/e* calcd. for $C_{15}H_{27}O_3$: 255.1960 [M + H]; found: 255.1964.

6-(3,3-Dimethyl-2-phenethylbutyl)-2,2-dimethyl[1,3]dioxin-4-one (14j)



Following the previous procedure for the 1,6-addition of $(t\text{-Bu})_2CuLi$, [1,3]dioxin-4-one **13b** (130 mg, 0.503 mmol) gave 68 mg (43%) of **14j** as a colourless oil. R_f 0.33 (20% EtOAc–hexane). FT-IR (neat, cm^{-1}): 3026, 2960, 1732, 1630, 1454, 1389, 1272, 1204, 1014. ^{1}H NMR ($CDCl_3$) δ: 7.32–7.25 (m, 2H), 7.22–7.13 (m, 3H), 5.32 (s, 1H), 2.74–2.67 (m, 1H), 2.58–2.51 (m, 1H), 2.47 (dd, J = 15.0, 4.2 Hz, 1H), 2.07 (dd, J = 15.0, 7.5 Hz, 1H), 1.90–1.82 (m, 1H), 1.71 (s, 6H), 1.53–1.48 (m, 1H), 1.46–1.37 (m, 1H), 0.91 (s, 9H). ^{13}C NMR ($CDCl_3$) δ: 172.7, 161.2, 142.1, 128.4 (2), 128.2 (2), 125.9, 106.2, 93.8, 45.1, 35.9, 35.6, 33.9, 33.4, 27.5 (3), 25.3, 24.9. HR-MS (EI) *m/e* calcd. for $C_{17}H_{22}O_2$: 258.1620 [M – $(CH_3)_2CO$]; found: 258.1616.

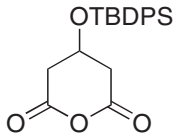
3-(tert-Butyldiphenylsilanyloxy)pentanedioic acid diethyl ester (15, R^1 = OTBDPS)



To a solution of imidazole (1.36 g, 20.0 mmol) in CH_2Cl_2 (20 mL) at rt was added TBDPSCl (2.47 mL, 9.50 mmol). After stirring for 10 min at rt, a solution of diethyl 3-hydroxyglutarate (2.04 g, 10.0 mmol) in CH_2Cl_2 (5, 2, and 1 mL rinses) was added to the white suspension. The reaction was stirred at rt for 16 h after which it was stopped by the addition of water (25 mL) and diluted with Et_2O (125 mL). The mixture was then transferred to a separatory funnel, extracted, the layers separated, and the organic layer was washed with brine (25 mL). The aqueous layers were combined and extracted with Et_2O (50 mL). The organic layers were combined, dried (Na_2SO_4), filtered, concentrated under reduced pressure, and purified by chromatography on SiO_2 to afford 4.05 g of **15** (96%) as a white solid; mp 44–46 °C. R_f 0.48 (20% EtOAc–hexane). FT-IR (KBr, cm^{-1}): 2966, 1740, 1378, 1268, 1227, 1145, 1107, 1026. ^{1}H NMR ($CDCl_3$) δ: 7.70–7.66 (m, 4H), 7.47–7.35 (m, 6H), 4.55 (qn, J = 6.0 Hz, 1H), 4.08–3.97 (m, 4H), 2.60 and 2.54 (AB of ABX, J = 15.2, 6.3 and 15.2, 5.9 Hz, 4H), 1.19 (t, J = 7.1 Hz, 6H), 1.03 (s, 9H). ^{13}C NMR ($CDCl_3$) δ: 170.8 (2), 135.8 (4), 133.5 (2), 129.7 (2), 127.6 (4), 67.2, 60.3 (2), 41.8 (2), 26.8 (3), 19.2, 14.1 (2). HR-MS (EI) *m/e* calcd. for $C_{24}H_{31}O_5Si$: 427.1941 [M – CH_3]; found: 427.1931.

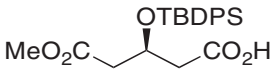
© 2006 NRC Canada

3-[(*tert*-Butyldiphenylsilyl)oxy]pentanedioic anhydride (8b, R^1 = OTBDPS)



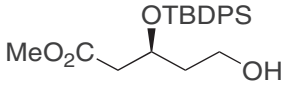
To a solution of diester **15** (8.85 g, 20.0 mmol) in MeOH (30 mL) was added NaOH pellets (2.00 g, 50.0 mmol) and the mixture was stirred vigorously at rt for 38 h. The resulting yellowish suspension was concentrated under reduced pressure and kept under high vacuum. The flaky solid was then crushed into smaller pieces, suspended in a mixture of benzene (40 mL) and Ac_2O (30 mL) and heated to reflux for 1.5 h. During this time, the colour changed to a deep purple. After cooling to rt, the reaction was stopped by the addition of brine (200 mL) and the mixture was transferred to a separatory funnel with $CHCl_3$ (400 mL). After extraction, the layers were separated and the organic layer was washed with satd. aq. $NaHCO_3$ (3 × 200 mL). The organic layer was then dried ($MgSO_4$), filtered, concentrated under reduced pressure, and purified by chromatography on SiO_2 [pretreated with hexane containing 1% Ac_2O, solvent gradient from pure hexane (+1% Ac_2O) to 20% EtOAc–hexane (+1% Ac_2O)] to afford 3.40 g of **8b** (46%) as a white solid. Recrystallization from a hot mixture of hexane–EtOAc (20:1) provided white needles; mp 107 to 108 °C (hexane–EtOAc 20:1). R_f 0.27 (20% EtOAc–hexane containing 1% Ac_2O). FT-IR (KBr, cm^{-1}): 2932, 1817, 1765, 1429, 1348, 1262, 1191, 1111, 1070, 1044. ^{1}H NMR ($CDCl_3$) δ: 7.71–7.56 (m, 4H), 7.55–7.35 (m, 6H), 4.31 (qn, *J* = 3.2 Hz, 1H), 2.86 (dd, *J* = 16.0, 3.6 Hz, 2H), 2.58 (dd, *J* = 16.0, 2.4 Hz, 2H), 1.05 (s, 9H). ^{13}C NMR ($CDCl_3$) δ: 165.3 (2), 135.8 (4), 132.4 (2), 130.6 (2), 128.3 (4), 62.9, 38.9 (2), 26.9 (3), 19.2. HR-MS (EI) *m/e* calcd. for $C_{17}H_{15}O_4Si$: 311.0740 [M – C_4H_9]; found: 311.0744.

(S)-((3-*tert*-Butyldiphenylsilyl)oxy)pentanedioic acid monomethyl ester (16)



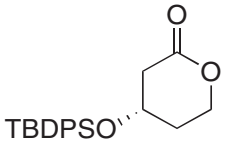
To a previously dried flask containing cyclic anhydride **8b** (1.09 g, 2.96 mmol) was added Et_2O (100 mL). The solution was cooled to –40 °C, $(DHQD)_2AQN$ (760 mg, 0.887 mmol) was added and the mixture was stirred for about 20 min. MeOH (1.20 mL, 29.6 mmol) was then added and the reaction was stirred at –40 °C for 70–72 h, stopped by the addition of 10% aq. HCl (90 mL) at –40 °C, and allowed to warm to rt. After transferring to a separatory funnel, the mixture was extracted, the layers were separated, and the aqueous layer was reextracted with EtOAc (2 × 100 mL). The organic layers were combined, dried (Na_2SO_4), filtered, and concentrated under reduced pressure to provide 1.25 g of the crude acid **16** as a pale yellow oil. ^{1}H NMR ($CDCl_3$) δ: 7.70–7.65 (m, 4H), 7.48–7.35 (m, 6H), 4.51 (qn, *J* = 6.1 Hz, 1H), 3.56 (s, 3H), 2.69–2.53 (m, 4H), 1.03 (s, 9H). The ^{1}H NMR spectra was identical with the one reported in ref. 25. This material was combined with other crude desymmetrized material to provide 7.29 g of product. The catalyst was recovered by basifying the acidic aqueous layer with KOH pellets (a yellow precipitate formed). The aqueous layer was then extracted with Et_2O until the organic layer remained colourless. The organic layers were combined, dried (Na_2SO_4), filtered, and concentrated under reduced pressure. The recovered catalyst was purified by chromatography on SiO_2 with 5% MeOH–$CHCl_3$ containing 0.5% aq. NH_4OH before being reused.

(S)-3-((*tert*-Butyldiphenylsilyl)oxy)-5-hydroxypentanoic acid, methyl ester (17)



To a solution of crude acid **16** (7.29 g, 19.8 mmol) in THF (100 mL) at rt was added a solution of BH_3·DMS in THF (2.0 mol/L, 30 mL, 60 mmol) and the mixture was stirred for 15 h. The reaction was stopped by slowly adding satd. aq. $NaHCO_3$ (350 mL) and stirred vigorously for 20 min. The mixture was then transferred to a separatory funnel and extracted with Et_2O (3 × 300 mL). The organic layers were combined, dried (Na_2SO_4), filtered, concentrated under reduced pressure, and purified by chromatography on SiO_2 to afford 5.41 g of **17** (71%) as a colourless oil. ^{1}H NMR ($CDCl_3$) δ: 7.74–7.65 (m, 4H), 7.48–7.37 (m, 6H), 4.38 (qn, *J* = 5.9 Hz, 1H), 3.70–3.61 (m, 2H), 3.54 (s, 3H), 2.55 (d, *J* = 6.4 Hz, 2H), 1.86–1.80 (m, 1H), 1.78–1.72 (m, 1H), 1.62 (bt, *J* = 5.5 and 5.2 Hz, 1H), 1.06 (s, 9H). The ^{1}H NMR spectra was identical with the one reported in ref. 25.

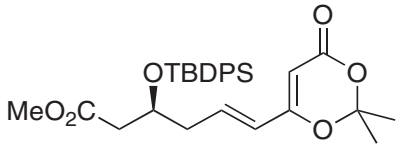
(S)-3-((*tert*-Butyldiphenylsilyl)oxy)-5-hydroxypentanoic acid lactone (18)



To a solution of crude acid **16** (115 mg, 0.287 mmol) in THF (2.0 mL) at rt was added a solution of BH_3·DMS in THF (2.0 mol/L, 430 μL, 0.86 mmol) and the mixture was stirred for 17 h. The reaction was stopped by slowly adding 10% HCl (3.5 mL) and stirred vigorously for 1 h. The mixture was then transferred to a separatory funnel and extracted with Et_2O (3 × 5 mL). The organic layers were combined, dried (Na_2SO_4), filtered, concentrated under reduced pressure, and purified by chromatography on SiO_2 to afford 38 mg of **18** (38%) as a colourless oil. $[\alpha]_D$ –12.3 (*c* 7.55, $CHCl_3$). ^{1}H NMR ($CDCl_3$) δ: 7.67–7.62 (m, 4H), 7.50–7.37 (m, 6H), 4.63 (ddd, *J* = 11.3, 8.6, 4.5 Hz, 1H), 4.28–4.18 (m, 2H), 2.59 (d, *J* = 4.9 Hz, 2H), 1.94–1.75 (m, 2H), 1.08 (s, 9H). The ^{1}H NMR spectra was identical with the one reported in ref. 25. The enantiomeric excess was determined by chiral HPLC (Chiralcel OD) using *i*-PrOH–hexane (1.0%) at a flow rate of 1.0 mL/min (R_t minor = 22.8 min, R_t major = 24.5 min).

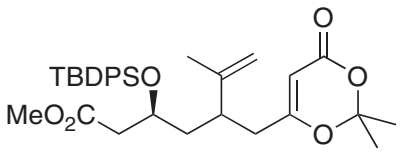
© 2006 NRC Canada

3-(tert-Butyldiphenylsilanyloxy)-6-(2,2-dimethyl-6-oxo-6H-[1,3]dioxin-4-yl)hex-5-enoic acid methyl ester (19)



To a stirred solution of alcohol **17** (5.41 g, 14.0 mmol) in a mixture of CH_2Cl_2 (63 mL) and CH_3CN (7 mL) at rt was added NMO (2.46 g, 21.0 mmol) and 4 Å molecular sieves (7.0 g). TPAP (246 mg, 0.700 mmol) was added in three portions over a period of 20 min and the resulting mixture was stirred for 30 min at rt. The dark black mixture was then filtered over Celite with CH_2Cl_2 and the filtrate was concentrated under reduced pressure. The resulting oil was rapidly purified by chromatography on SiO_2 with EtOAc–hexanes (20%) to afford 4.23 g of the corresponding aldehyde (79%) as a colourless oil. A solution of phosphonate **12** (4.28 g, 15.4 mmol) in THF (100 mL) cooled to 0 °C was treated with 95% NaH (317 mg, 13.2 mmol). The cold bath was removed and the mixture was stirred at rt for 20 min. After cooling to –78 °C, a solution of the aldehyde (4.23 g, 11.0 mmol) in THF (5 mL, 5 mL rinse) was added, the bath was removed, and the reaction was allowed to gradually warm to rt and was stirred at that temperature for 1 h. One drop of satd. aq. $NaHCO_3$ was added and the mixture was stirred for 5 min (to complete the deprotonation step). After adding additional satd. aq. $NaHCO_3$ (300 mL), the mixture was transferred to a separatory funnel and extracted with Et_2O (3 × 300 mL). The organic layers were combined, dried (Na_2SO_4), filtered, concentrated under reduced pressure, and purified by chromatography on SiO_2 to afford 3.50 g of **19** (49% from alcohol) as a colourless oil. $[\alpha]_D$ 58.0 (*c* 0.21, $CHCl_3$). R_f 0.33 (30% EtOAc–hexane). FT-IR (neat, cm^{-1}): 2932, 2858, 1728, 1655, 1592, 1428, 1390, 1274, 1206, 1111, 1020. ^1H NMR ($CDCl_3$) δ: 7.76–7.60 (m, 4H), 7.52–7.33 (m, 6H), 6.44 (dt, *J* = 15.5, 7.5 Hz, 1H), 5.78 (d, *J* = 15.6 Hz, 1H), 5.18 (s, 1H), 4.29 (qn, *J* = 6.0 Hz, 1H), 3.57 (s, 3H), 2.54 (A of ABX, J_{AB} = 15.2, J_{AX} = 6.4 Hz, 1H), 2.48–2.36 (m, 3H), 1.67 (s, 6H), 1.04 (s, 9H). ^{13}C NMR ($CDCl_3$) δ: 171.3, 162.7, 161.9, 137.4, 135.81 (2), 135.78 (2), 133.4, 133.3, 129.8 (2), 127.6 (4), 125.2, 106.2, 93.8, 69.5, 51.5, 41.7, 40.2, 26.8 (3), 24.9 (2), 19.2. HR-MS (EI) *m/e* calcd. for $C_{25}H_{27}O_6Si$: 451.1577 [M – C_4H_9]; found: 451.1575.

(3S)-Methyl 3-(tert-butyldiphenylsilyloxy)-5-((2,2-dimethyl-4-oxo-4H-1,3-dioxin-6-yl)methyl)-6-methylhept-6-enoate (20)

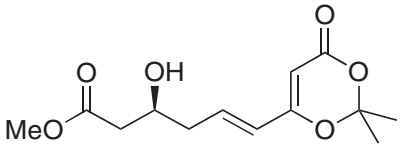


A solution of *t*-BuLi in pentane (1.2 mol/L, 33 mL, 40 mmol) cooled to –78 °C was diluted with THF (33 mL) and 2-bromopropene (1.78 mL, 20.0 mmol) was added dropwise. The mixture was stirred at –78 °C for 30 min, then at 0 °C for 30–45 min. To a suspension of CuI (1.10 g, 5.78 mmol) in THF (20 mL) cooled to –78 °C was added the solution of 2-lithiopropene (39 mL, 12 mmol). The dark black mixture was stirred at –78 °C for 30 min and then TMSCl (3.0 mL, 24 mmol) was added. After stirring for ca. 5 min, a solution of **19** (981 mg, 1.93 mmol) in THF (6.0 mL, 2 × 2.0 mL rinse) was added. The mixture was stirred at –78 °C for 30 min, then at –20 °C for ca. 16 h. The reaction was stopped by adding satd. aq. $NaHCO_3$ (100 mL) at –20 °C, then warmed to rt, transferred to a separatory funnel, and extracted with Et_2O (4 × 100 mL). The organic layers were combined, dried (Na_2SO_4), filtered, concentrated under reduced pressure, and purified by chromatography on SiO_2 to afford 999 mg of **20** (94%) as a colourless oil. R_f 0.38 (30% EtOAc–hexane). FT-IR (neat, cm^{-1}): 2933, 2858, 1732, 1633, 1428, 1390, 1272, 1205, 1111, 1015. ^1H NMR ($CDCl_3$) δ: 7.75–7.62 (m, 4H), 7.51–7.34 (m, 6H), 5.08 and 5.05 (s, 1H), 4.66–4.62 (m, 1H), 4.54 and 4.41 (br s, 1H), 4.14–4.03 (m, 1H), 3.59 and 3.54 (s, 3H), 2.65–2.26 (m, 3H), 2.11–1.97 (m, 2H), 1.67–1.47 (m, 2H), 1.65 and 1.64 (s, 3H), 1.60 and 1.58 (s, 3H), 1.49 and 1.21 (s, 3H), 1.04 and 1.02 (s, 9H). ^{13}C NMR ($CDCl_3$) δ: 171.6 [171.3], 170.0 [169.8], 161.16 [161.09], 144.4 [144.3], 135.9 (8), 133.9 [133.7], 133.6 [133.5], 129.8 (4), 127.6 (8), 113.9 [113.3], 106.3 (2), 94.2 [94.1], 68.6 [68.4], 51.41 [51.36], 42.6 [41.2], 40.8 [40.7], 40.8 [40.4], 37.8 [37.4], 26.9 (3) [26.8 (3)], 25.40 [25.36], 25.0 [24.9], 19.3 [19.2], 17.6 [17.3]. HR-MS (ESI–POS) *m/e* calcd. for $C_{32}H_{42}O_6NaSi$: 573.2648 [M + Na]; found: 573.2642.

Rhodium-catalyzed asymmetric 1,6-addition of potassium isopropenyl organotrifluoroborate to 19 in the presence of Carreira's diene

To a dry sealed tube was added the diene ligand (3.6 mg, 0.014 mmol), $Rh(acac)(eth)_2$ (3 mg, 0.01 mmol), and EtOH (0.5 mL) and the mixture was stirred at rt for 15 min. A solution of **19** (117 mg, 0.230 mmol) in EtOH (0.75 mL, 0.75 mL rinse) was then added, followed by potassium isopropenyl organotrifluoroborate (37) (102 mg, 0.689 mmol). The reaction mixture was stirred at 82 °C for 24 h, cooled to rt, and treated with satd. aq. $NaHCO_3$ (15 mL). The mixture was transferred to a separatory funnel and extracted with Et_2O (3 × 15 mL). The organic layers were combined, dried (Na_2SO_4), filtered, concentrated under reduced pressure, and purified by chromatography on SiO_2 to afford 27.2 mg (21%) of **20** and 47.5 mg of **21** (38%).

6-(2,2-Dimethyl-6-oxo-6H-[1,3]dioxin-4-yl)-3-hydroxyhex-5-enoic acid methyl ester (23)

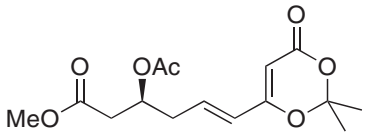


To a solution of **19** (234 mg, 0.460 mmol) in THF (5.5 mL) in a plastic tube was added HF·pyridine (600 µL, 23 mmol) and the mixture was stirred vigorously at rt for 3 days. The reaction was stopped by dropwise addition to

© 2006 NRC Canada

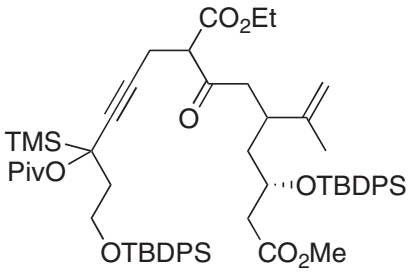
satd. aq. $NaHCO_3$ (75 mL). After adding solid $NaHCO_3$ to the aqueous solution, the mixture was transferred to a separatory funnel and extracted with Et_2O (4 × 30 mL). The organic layers were combined, dried (Na_2SO_4), filtered, concentrated under reduced pressure, and purified by chromatography on SiO_2 to afford 34 mg (15%) of starting material **19** and 101 mg of **23** (81%) as a colourless oil. $[\alpha]_D$ 5.9 (*c* 2.38, CH_2Cl_2). R_f 0.17 (50% EtOAc–hexane). FT-IR (neat, cm^{-1}): 3454, 2999, 2952, 1728, 1651, 1592, 1392, 1276, 1204, 1067, 1020. ^1H NMR ($CDCl_3$) δ: 6.59 (dt, *J* = 15.6, 7.6 Hz, 1H), 6.01 (d, *J* = 15.6 Hz, 1H), 5.28 (s, 1H), 4.23–4.13 (m, 1H), 3.74 (s, 3H), 3.10 (d, *J* = 3.6 Hz, 1H), 2.54 (A of ABX, J_{AB} = 16.7, J_{AX} = 3.4 Hz, 1H), 2.51–2.40 (m, 3H), 1.72 (s, 6H). ^{13}C NMR ($CDCl_3$) δ: 172.8, 162.7, 161.9, 137.2, 125.1, 106.4, 93.9, 66.9, 51.8, 40.6, 39.4, 24.9 (2). HR-MS (EI) *m/e* calcd. for $C_{13}H_{16}O_5$: 252.0998 [M – H_2O]; found: 252.0999.

(S,E)-Methyl 3-acetoxy-6-(2,2-dimethyl-4-oxo-4H-1,3-dioxin-6-yl)hex-5-enoate (24)



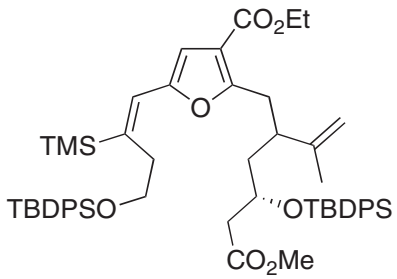
To a solution of **23** (51.2 mg, 0.189 mmol) in pyridine (1.56 mL, 19.3 mmol) was added Ac_2O (910 μL, 9.6 mmol) and the mixture was stirred at rt for 6.5 h. After concentrating under reduced pressure, the resulting mixture was purified by chromatography on SiO_2 to afford 56.4 mg (95%) of **24** as a colourless oil. $[\alpha]_D$ 11.9 (*c* 1.96, CH_2Cl_2). R_f 0.37 (50% EtOAc–hexane). FT-IR (neat, cm^{-1}): 2999, 2954, 1732, 1656, 1594, 1438, 1376, 1244, 1020. ^1H NMR ($CDCl_3$) δ: 6.45 (dt, *J* = 15.5, 7.5 Hz, 1H), 5.98 (dt, *J* = 15.6, 1.3 Hz, 1H), 5.36–5.27 (m, 1H), 5.28 (s, 1H), 3.69 (s, 3H), 2.64 (A of ABX, J_{AB} = 15.8, J_{AX} = 7.3 Hz, 1H), 2.59–2.52 (m, 2H), 2.04 (s, 3H), 1.71 (s, 6H). ^{13}C NMR ($CDCl_3$) δ: 170.3, 170.1, 162.5, 161.9, 135.6, 125.8, 106.5, 94.3, 68.8, 51.9, 38.2, 37.0, 25.0, 24.9, 20.9. HR-MS (EI) *m/e* calcd. for $C_{13}H_{16}O_5$: 252.0998 [M – CH_3CO_2H]; found: 252.0998.

(7S)-Dimethyl 2-(4-(benzoyloxy)-6-(tert-butyldiphenylsilyloxy)-4-(trimethylsilyl)hex-2-ynyl)-7-(tert-butyldiphenylsilyloxy)-3-oxo-5-(prop-1-en-2-yl)nonanedioate (22)



To a solution of [1,3]dioxin-4-one **20** (999 mg, 1.81 mmol) in toluene (20 mL) was added EtOH (530 μL, 9.1 mmol). The solution was heated at reflux for ca. 1.5 h until TLC analysis showed complete consumption of the starting material. The solution was then concentrated under reduced pressure and kept under high vacuum. The crude β-keto ester was redissolved in THF (20 mL) and cooled to 0 °C. The septum was temporarily removed to allow the quick introduction of 98% NaH (52 mg, 2.2 mmol) and the mixture was stirred at 0 °C for ca. 20 min. Afterwards, a solution of iodide **4** [prepared from the corresponding chloride (1.86 g, 3.30 mmol) and NaI (679 mg, 4.53 mmol) in refluxing acetone (15 mL)] in THF (6.0 mL, 6.0 mL rinse) was added and the reaction was gradually warmed to rt, while maintaining the flask in the cold bath. After stirring overnight, the reaction mixture was concentrated under reduced pressure and filtered over a pad of SiO_2 with EtOAc–hexane (20%). This material was then purified by chromatography on SiO_2 to afford 1.50 g of **22** (77%, two steps) as a colourless oil. Since this α-propargyl β-keto ester exists as a mixture of up to four different diastereomers, it was not characterized.

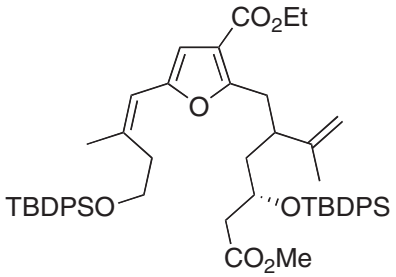
Ethyl 5-((E)-4-(tert-butyldiphenylsilyloxy)-2-(trimethylsilyl)but-1-enyl)-2-((4S)-4-(tert-butyldiphenylsilyloxy)-6-methoxy-6-oxo-2-(prop-1-en-2-yl)hexyl)furan-3-carboxylate (25)



A solution of α-propargyl β-keto ester **22** (76.0 mg, 0.0713 mmol) in a mixture of MeCN (1.0 mL) and H_2O (100 μL) was subjected to three freeze–pump–thaw cycles. Afterwards, $NaOAc{\cdot}3H_2O$ (10.7 mg, 0.0784 mmol) and $Pd(PPh_3)_4$ (12 mg, 0.010 mmol) were added and the mixture was stirred at 87 °C for 2 h. After cooling to rt, the crude mixture was filtered over a pad of SiO_2 with 20% EtOAc–hexane and concentrated under reduced pressure. This material was then purified by chromatography on SiO_2 to afford 33.2 mg of **25** (49%, 6.8:1 mixture of (*E*)–(*Z*)-isomers) as a colourless oil. R_f 0.28 (10% EtOAc–hexane). FT-IR (neat, cm^{-1}): 3071, 2931, 2857, 1741, 1716, 1590, 1428, 1388, 1230, 1111. ^1H NMR ($CDCl_3$) δ: 7.75–7.59 (m, 8H), 7.46–7.31 (m, 12H), 6.75 and 6.71 (s, 1H), 6.45 and 6.42 (s, 1H), 4.58 and 4.46 (brs, 1H), 4.46 and 4.41 (brs, 1H), 4.32–4.20 (m, 2H), 4.18–4.03 (m, 1H), 3.71–3.61 (m, 2H), 3.55 and 3.49 (s, 3H), 2.94–2.72 (m, 4H), 2.61–2.33 (m, 2H), 1.75–1.48 (m, 3H), 1.57 and 1.21 (s, 3H), 1.33 and 1.30 (t, *J* = 7.2 Hz, 3H), 1.063 and 1.056 (s, 9H), 1.00 (s, 9H), –0.003 and –0.004 (s, 9H). ^{13}C NMR ($CDCl_3$) δ: 172.0 [171.5], 163.8 [163.7], 160.0 [159.7], 151.1 [151.0], 145.7 [144.9], 140.04 [139.99], 135.94, 135.88, 135.8, 135.6, 135.2, 134.8, 134.2, 133.8, 133.62, 133.58, 129.5, 127.7, 127.6, 127.5, 127.4, 126.6 [126.4], 115.6, 112.85 [112.80], 110.0, 69.0 [68.9], 62.5, 60.1, 51.33 [51.27], 43.2, 43.0, 42.5 41.0, 40.1, 39.6, 34.7, 32.4 [32.3], 26.9, 26.8, 26.5, 19.2, 19.1, 19.0, 18.0, 16.9, 14.33 [14.28], 0.14, –1.8.

© 2006 NRC Canada

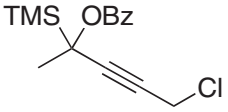
Ethyl 5-((Z)-4-(*tert*-butyldiphenylsilyloxy)-2-methylbut-1-enyl)-2-((4S)-4-(*tert*-butyldiphenylsilyloxy)-6-methoxy-6-oxo-2-(prop-1-en-2-yl)hexyl)furan-3-carboxylate (26)



To a solution of I_2 (105 mg, 0.414 mmol) in THF (0.5 mL) was added pyridine (50 μL, 0.62 mmol) followed by $AgClO_4$ (85 mg, 0.41 mmol). The mixture was stirred at rt for 15 min, then a solution of furan **25** (97.4 mg, 0.103 mmol) in THF (1.0 mL, 2 × 0.5 mL rinse) was added. After stirring at rt for 19 h, the crude reaction mixture was filtered over a pad of Celite with Et_2O (25 mL). The solution was transferred to a separatory funnel and extracted with a mixture of 10% aq. $Na_2S_2O_3$ (10 mL) and satd. aq. $NaHCO_3$ (10 mL). The layers were separated and the aqueous layer was extracted again with Et_2O (2 × 10 mL). The combined organic layers were dried (Na_2SO_4), filtered, and concentrated under reduced pressure to afford 113 mg of crude vinyl iodide. The iodide was redissolved in THF (1.0 mL) and subjected to two freeze–pump–thaw cycles. The degassed solution was then cooled to 0 °C and $Pd(PPh_3)_4$ (6.0 mg, 0.0052 mmol) was added, followed by a 2.0 mol/L solution of Me_2Zn in toluene (160 μL, 0.32 mmol). The cold bath was removed and the reaction was stirred at rt for ca. 17 h, stopped by adding H_2O (5 mL), and transferred to a separatory funnel. The aqueous layer was extracted with Et_2O (3 × 5 mL), the organic layers were combined, washed with brine (10 mL), dried (Na_2SO_4), filtered, concentrated under reduced pressure, and purified by chromatography on SiO_2 to afford 57.5 mg of **26** (63%, 4.7:1 mixture of (*Z*)–(*E*)-isomers) as a colourless oil. R_f 0.28 (10% EtOAc–hexane). FT-IR (neat, cm^{-1}): 3071, 2931, 2857, 1740, 1715, 1600, 1428, 1385, 1227, 1111. ^1H NMR ($CDCl_3$) δ: 7.74–7.61 (m, 8H), 7.45–7.33 (m, 12H), 6.47 and 6.45 (s, 1H), 6.02 and 6.00 (s, 1H), 4.54 and 4.43 (brs, 1H), 4.43 and 4.37 (brs, 1H), 4.31–4.20 (m, 2H), 4.16–4.04 (m, 1H), 3.87–3.79 (m, 2H), 3.55 and 3.50 (s, 3H), 2.98–2.77 (m, 2H), 2.77–2.59 (m, 2H), 2.55–2.35 (m, 2H), 1.86 and 1.85 (s, 3H), 1.71–1.50 (m, 3H), 1.56 and 1.09 (s, 3H), 1.32 and 1.30 (t, J = 7.2 Hz, 3H), 1.041 and 1.038 (s, 9H), 1.01 and 1.00 (s, 9H). ^{13}C NMR ($CDCl_3$) δ: 172.0 [171.5], 163.93 [163.90], 159.2 [158.9], 151.05 [150.97], 145.8 [145.0], 137.43 [137.38], 135.91, 135.88, 135.81, 135.6, 135.2, 134.8, 134.2, 133.9, 133.7, 133.6, 133.5, 129.5, 127.7, 127.6, 127.5, 127.4, 115.37 [115.24], 115.15 [115.08], 112.7, 107.7 [107.6], 69.0 [68.9], 62.3, 60.0, 51.31 [51.25], 43.3, 43.0, 42.4, 41.0, 40.3, 39.7, 36.6, 32.3 [32.2], 26.9, 26.8, 26.5, 25.2, 19.2, 19.1, 18.4, 18.0, 17.0, 14.4 [14.3].

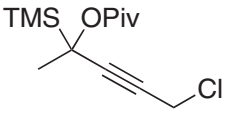
5-Chloro-2-(trimethylsilyl)pent-3-yn-2-yl benzoate (27a)

A solution of *n*-BuLi (1.6 mol/L, 4.4 mL, 7.0 mmol) in Et_2O (40 mL) was cooled to –78 °C and treated with propargyl chloride (540 μL, 7.5 mmol). After stirring at



–78 °C for 20 min, acetyltrimethylsilane (720 μL, 5.0 mmol) was added dropwise. The mixture was stirred at –78 °C for 30 min and benzoyl chloride (870 μL, 7.8 mmol) was added. The reaction was allowed to gradually warm up to rt, while maintained in the cold bath and stirred overnight. The reaction was stopped by adding H_2O (50 mL) and the mixture was transferred to a separatory funnel. After extraction, the organic layer was separated and the aqueous layer was extracted once more with Et_2O (50 mL). The organic layers were combined, dried (Na_2SO_4), filtered, concentrated under reduced pressure, and purified by chromatography on SiO_2 to afford 1.2 g of **27a** (80%) as a yellow-orange oil. For the full spectral characterization of this compound, see ref. 11.

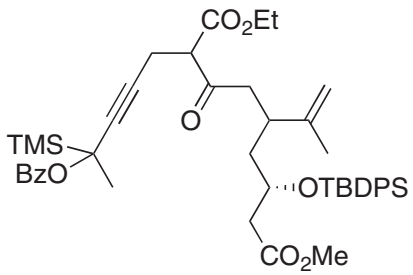
5-Chloro-2-(trimethylsilyl)pent-3-yn-2-yl pivalate (27b)



A solution of *n*-BuLi (1.6 mol/L, 8.8 mL, 14 mmol) in Et_2O (80 mL) cooled to –78 °C was treated with propargyl chloride (1.09 mL, 15.0 mmol). After stirring at –78 °C for 20 min, acetyltrimethylsilane (1.43 mL, 9.98 mmol) was added dropwise. The mixture was stirred at –78 °C for 30 min and trimethylacetyl chloride (1.85 mL, 15.0 mmol) was added. The reaction mixture was allowed to gradually warm up to rt, while maintained in the cold bath and stirred overnight. The reaction was stopped by adding H_2O (100 mL) and transferred to a separatory funnel. After extraction, the organic layer was separated and the aqueous layer was extracted once more with Et_2O (100 mL). The organic layers were combined, dried (Na_2SO_4), filtered, concentrated under reduced pressure, and purified by chromatography on SiO_2 to afford 1.59 g of **27b** (58%) as a yellow-orange oil. R_f 0.22 (5% EtOAc–hexane). FT-IR (neat, cm^{-1}): 2970, 1737, 1479, 1367, 1262, 1144, 1060. ^1H NMR ($CDCl_3$) δ: 4.24 (s, 2H), 1.62 (s, 3H), 1.19 (s, 9H), 0.19 (s, 9H). ^{13}C NMR ($CDCl_3$) δ: 177.1, 87.6, 82.4, 67.2, 39.2, 31.3, 27.1 (3), 21.1, –4.2. HR-MS (EI) *m/e* calcd. for $C_{13}H_{23}O_2SiCl$: 274.1156; found: 274.1154.

(7S)-1-Ethyl 9-methyl 2-(4-(benzoyloxy)-4-(trimethylsilyl)pent-2-ynyl)-7-(*tert*-butyldiphenylsilyloxy)-3-oxo-5-(prop-1-en-2-yl)nonanedioate (28a)

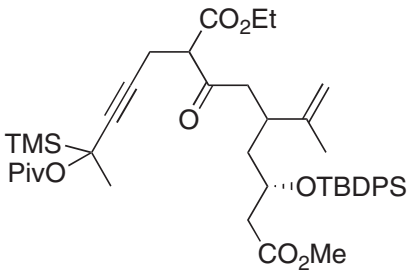
Following the same procedure as for the preparation of α-propargyl β-keto ester **22**, the alkylation of β-keto ester **21**



© 2006 NRC Canada

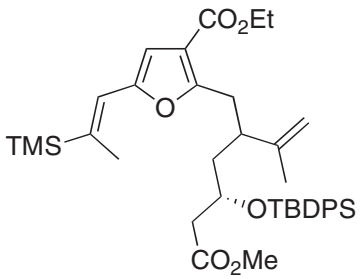
[prepared from [1,3]dioxin-4-one **20** (422 mg, 0.765 mmol)] with the iodide derived from **27a** (406 mg, 1.38 mmol) gave 580 mg (95%, two steps) of **28a** as a colourless oil. Since this α-propargyl β-keto ester exists as a mixture of up to four different diastereomers, it was not characterized.

(7S)-1-Ethyl 9-methyl 7-(tert-butyldiphenylsilyloxy)-3-oxo-2-(4-(pivaloyloxy)-4-(trimethylsilyl)pent-2-ynyl)-5-(prop-1-en-2-yl)nonanedioate (28b)



Following the same procedure as for the preparation of α-propargyl β-keto ester **22**, the alkylation of β-keto ester **21** [prepared from [1,3]dioxin-4-one **20** (387 mg, 0.703 mmol)] with the iodide derived from **27b** (349 mg, 1.27 mmol) gave 350 mg (64%, two steps) of **28b** as a colourless oil. Since this α-propargyl β-keto ester exists as a mixture of up to four different diastereomers, it was not characterized.

Ethyl 2-((4S)-4-(tert-butyldiphenylsilyloxy)-6-methoxy-6-oxo-2-(prop-1-en-2-yl)hexyl)-5-((E)-2-(trimethylsilyl)prop-1-enyl)furan-3-carboxylate (29)



In a microwave tube, a solution of **28b** (84.3 mg, 0.108 mmol) in THF (500 μL) was subjected to three freeze–pump–thaw cycles. To the degassed solution was then added allylpalladium chloride dimer (3.0 mg, 0.0082 mmol) and dppf (9.0 mg, 0.016 mmol) and the mixture was stirred vigorously at rt for ca. 5 min (during this time a voluminous precipitate formed). The microwave tube was then heated with stirring in the microwave reactor for 20 min (100 °C, 300 W) and then cooled to rt. The crude, wine-red reaction mixture was filtered over a pad of SiO_2 with 20% EtOAc–hexane. This material was then purified by chromatography on SiO_2 to afford 43.5 mg of **29** (59%) as a colourless oil. The diastereomeric mixture of furans was dissolved in THF (500 μL) and $(PhSe)_2$ (1.0 mg, 0.0032 mmol) was added. The solution was heated at 70 °C for 16 h in a sealed tube, then cooled to rt, and concentrated under reduced pressure. This material was purified by chromatography on SiO_2 to afford 36.8 mg of pure ***E*-29** (50% from **28b**) as a colourless oil. R_f 0.55 (20% EtOAc–hexane). FT-IR (neat, cm^{-1}): 3072, 2954, 2857, 1742, 1715, 1597, 1428, 1229, 1111. ^1H NMR ($CDCl_3$) δ: 7.73–7.60 (m, 4H), 7.45–7.31 (m, 6H), 6.55 and 6.54 (s, 1H), 6.44 and 6.37 (apparent q, J = 1.5 and 1.6 Hz, 1H), 4.59 and 4.48 (bs, 1H), 4.46 and 4.43 (bs, 1H), 4.31–4.19 (m, 2H), 4.18–4.04 (m, 1H), 3.56 and 3.50 (s, 3H), 3.00–2.75 (m, 2H), 2.63–2.36 (m, 2H), 2.01 and 2.00 (d, J = 1.6 and 1.6 Hz, 3H), 1.75–1.49 (m, 3H), 1.56 and 1.16 (s, 3H), 1.34 and 1.31 (t, J = 7.1 and 7.1 Hz, 3H), 1.00 (s, 9H), 0.14 (s, 9H). ^{13}C NMR ($CDCl_3$) δ: 171.9 [171.5], 163.9 [163.8], 159.4 [159.1], 151.83 [151.79], 145.7 [145.1], 140.2 [140.0], 135.92 (2) [135.88 (2)], 135.85 (2) [135.77 (2)], 134.2 [133.8], 133.6 (2), 129.6 (3), 129.5, 127.5 (6), 127.4 (2), 124.3 [124.2], 115.5 (2), 112.8 [112.6], 109.74 [109.71], 69.0 [68.8], 60.0 (2), 51.3 [51.2], 43.0 [42.9], 42.5 [41.0], 40.1 [39.6], 32.3 (2), 26.9 (3) [26.8 (3)], 19.2 (2), 18.0 [17.1], 17.1 (2), 14.34 [14.28], –2.3 (6). HR-MS (ESI–POS) *m/e* calcd. for $C_{39}H_{54}O_6NaSi_2$: 697.3357 [M + Na]; found: 697.3303.

Acknowledgements

This work was supported by a postdoctoral fellowship from the Natural Sciences and Engineering Research Council of Canada (NSERC) and a research grant from the National Institutes of Health (US Department of Health and Human Services; No. GM55433).

References

1. For other examples of furanocembranolides, see: (*a*) M.G. Missakian, B.J. Burreson, and P.J. Scheuer. Tetrahedron, **31**, 2513 (1975); (*b*) M. D'Ambrosio, D. Fabbri, A. Guerriero, and F. Pietra. Helv. Chim. Acta, **70**, 63 (1987); (*c*) D. Williams and R.J. Andersen. J. Org. Chem. **52**, 332 (1987); (*d*) A.E. Wright, N.S. Burres, and G.K. Schulte. Tetrahedron Lett. **30**, 3491 (1989); (*e*) W.R. Chan, W.F. Tinto, R.S. Laydoo, P.S. Manchand, W.F. Reynolds, and S. McLean. J. Org. Chem. **56**, 1773 (1991); (*f*) A. Rudi, T.L.-A. Dayan, M. Aknin, E.M. Gaydou, and Y. Kashman. J. Nat. Prod. **61**, 872 (1998); (*g*) J. Marrero, A.D. Rodríguez, P. Baran, and R.G. Raptis. Org. Lett. **5**, 2551 (2003); (*h*) M. Gutiérrez, T.L. Capson, H.M. Guzmán, J. González, E. Ortega-Barría, E. Quiñoá, and R. Riguera. J. Nat. Prod. **68**, 614 (2005).
2. W. Fenical, R. K. Okuda, M.M. Bandurraga, P. Culver, and R.S. Jacobs. Science (Washington, D.C.), **212**, 1512 (1981).
3. (*a*) P. Culver, W. Fenical, and P. Taylor. J. Biol. Chem. **259**, 3763 (1984); (*b*) R.S. Jacobs, P. Culver, R. Langdon, T. O'Brien, and S. White. Tetrahedron, **41**, 981 (1985); (*c*) S.N. Abramson, P. Culver, T. Kline, Y. Li, P. Guest, L. Gutman, and P. Taylor. J. Biol. Chem. **263**, 18568 (1988).
4. S.N. Abramson, J.A. Trischman, D.M. Tapiolas, E.E. Harold, W. Fenical, and P. Taylor. J. Med. Chem. **34**, 1798 (1991).
5. (*a*) M. Cases, F. González-López de Turiso, and G. Pattenden. Synlett, 1869 (2001); (*b*) M. Cases, F. González-López de Turiso, M.S. Hadjisoteriou, and G. Pattenden. Org. Biomol. Chem. **3**, 2786 (2005).
6. (*a*) I. Paterson, M. Gardner, and B.J. Banks. Tetrahedron, **45**, 5283 (1989); (*b*) I. Paterson, R.E. Brown, and C.J. Urch. Tetrahedron Lett. **40**, 5807 (1999).
7. L.A. Paquette and P.C. Astles. J. Org. Chem. **58**, 165 (1993).
8. J.A. Marshall and C.A. Sehon. J. Org. Chem. **62**, 4313 (1997).
9. J.A. Marshall and E.A Van Devender. J. Org. Chem. **66**, 8037 (2001).

© 2006 NRC Canada

10. For other relevant synthetic work on furanocembranolides, see: (*a*) M.A. Tius and S. Trehan. J. Org. Chem. **51**, 767 (1986); (*b*) J. Leonard and G. Ryan. Tetrahedron Lett. **28**, 2525 (1987); (*c*) A. Kondo, T. Ochi, H. Iio, T. Tokoroyama, and M. Siro. Chem. Lett. 1491 (1987); (*d*) M.P. Astley and G. Pattenden. Synlett, 335 (1991); (*e*) M.P. Astley and G. Pattenden. Synthesis, 101 (1992); (*f*) M. Tsubuki, K. Takahashi, and T. Honda. J. Org. Chem. **68**, 10183 (2003); (*g*) M. Tsubuki, K. Takahashi, K. Sakata, and T. Honda. Heterocycles, **65**, 531 (2005); (*h*) C. Stock, F. Höfer, and T. Bach. Synlett, 511 (2005).
11. P. Wipf and M.J. Soth. Org. Lett. **4**, 1787 (2002).
12. P. Wipf, L.T. Rahman, and S.R. Rector. J. Org. Chem. **63**, 7132 (1998).
13. For a short review on the subject, see: A.C. Spivey and B.I. Andrews. Angew. Chem. Int. Ed. **40**, 3131 (2001).
14. R.K. Boeckman, R.B. Perni, J.E. Macdonald, and A.J. Thomas. Org. Synth. **66**, 194 (1988).
15. R.K. Boeckman and A.J. Thomas. J. Org. Chem. **47**, 2823 (1982).
16. E.J. Corey and N.W. Boaz. Tetrahedron Lett. **26**, 6019 (1985).
17. D.J. Ager, I. Fleming, and S.K. Patel. J. Chem. Soc. Perkin Trans. 1, 2520 (1981).
18. For examples of 1,4-addition to [1,3]dioxin-4-ones, see: D. Seebach, J. Zimmermann, U. Gysel, R. Ziegler, and T.-K. Ha. J. Am. Chem. Soc. **110**, 4763 (1988).
19. T. Rosen, M. Watanabe, and C.H. Heathcock. J. Org. Chem. **49**, 3657 (1984).
20. For the desymmetrization with a stoichiometric amount of a chiral alcohol or amine, see: (*a*) T. Rosen and C.H. Heathcock. J. Am. Chem. Soc. **107**, 3731 (1985); (*b*) C.H. Heathcock, C.R. Hadley, T. Rosen, P.D. Theisen, and S.J. Hecker. J. Med. Chem. **30**, 1858 (1987); (*c*) P.D. Theisen and C.H. Heathcock. J. Org. Chem. **53**, 2374 (1988); (*d*) D.S. Karanewsky, M.F. Malley, and J.Z. Gougouttas. J. Org. Chem. **56**, 3744 (1991); (*e*) T. Konoike and Y. Araki. J. Org. Chem. **59**, 7849 (1994).
21. For the desymmetrization with a stoichiometric amount of a chiral oxazolidinone, see: R. Verma, S. Mithran, and S.K. Ghosh. J. Chem. Soc. Perkin Trans. 1, 257 (1999).
22. For the desymmetrization with a stoichiometric amount of a chiral complex derived from (–)-sparteine and EtMgBr, see: R. Shintani and G.C. Fu. Angew. Chem. Int. Ed. **41**, 1057 (2002).
23. Y. Chen, S.-K. Tian, and L. Deng. J. Am. Chem. Soc. **122**, 9542 (2000).
24. H. Becker and B.K. Sharpless. Angew. Chem. Int. Ed. Engl. **35**, 448 (1996).
25. D.W. Brooks, R.P. Kellogg, and C.S. Cooper. J. Org. Chem. **52**, 192 (1987).
26. S.V. Ley, J. Norman, W.P. Griffith, and S.P. Marsden. Synthesis, 639 (1994).
27. B. Breit and P. Demel. *In* Modern organocopper chemistry. *Edited by* N. Krause. Wiley-VCH, Weinheim, Germany. 2002. p. 200.
28. (*a*) A.H.M. de Vries, A. Meetsma, and B.L. Feringa. Angew. Chem. Int. Ed. Engl. **35**, 2374 (1996); (*b*) B.L. Feringa, M. Pineschi, L.A. Arnold, R. Imbos, and A.H.M. de Vries. Angew. Chem. Int. Ed. Engl. **36**, 2620 (1997); (*c*) L.A. Arnold, R. Imbos, A. Mandoli, A.H.M. de Vries, R. Naasz, and B.L. Feringa. Tetrahedron, **56**, 2865 (2000).
29. For an overview of earlier work by Miyaura and Hayashi, see: T. Hayashi. Synlett, 879 (2001).
30. Y. Takaya, T. Senda, H. Kurushima, M. Ogasawara, and T. Hayashi. Tetrahedron: Asymmetry, **10**, 4047 (1999).
31. A. Duursma, J.-G. Boiteau, L. Lefort, J.A.F. Boogers, A.H.M. de Vries, J.G. de Vries, A.J. Minnaard, and B.L. Feringa. J. Org. Chem. **69**, 8045 (2004).
32. M. Pucheault, S. Darses, and J.-P. Genêt. Eur. J. Org. Chem. 3552 (2002).
33. For a mini-review, see: F. Glorius. Angew. Chem. Int. Ed. **43**, 3364 (2004).
34. T. Hayashi, K. Ueyama, N. Tokunaga, and K. Yoshida. J. Am. Chem. Soc. **125**, 11508 (2003).
35. (*a*) C. Defieber, J.-F. Paquin, S. Serna, and E.M. Carreira. Org. Lett. **6**, 3873 (2004); (*b*) J.-F. Paquin, C. Defieber, C.R.J. Stephenson, and E.M. Carreira. J. Am. Chem. Soc. **127**, 10850 (2005); (*c*) J.-F. Paquin, C.R.J. Stephenson, C. Defieber, and E.M. Carreira. Org. Lett. **7**, 3821 (2005).
36. This is the first example of a catalytic asymmetric 1,6-addition reaction to a 2,4-dien-1-oate. For a recent report on the rhodium-catalyzed asymmetric 1,6-addition of arylzinc reagents to 2,4-dien-1-ones, see: T. Hayashi, S. Yamamoto, and N. Tokunaga. Angew. Chem. Int. Ed. **44**, 4224 (2005). For a report on the rhodium-catalyzed asymmetric 1,6-addition of aryltitanates to 3-alkynyl-2-en-1-ones, see: T. Hayashi, N. Tokunaga, and K. Inoue. Org. Lett. **6**, 305 (2004). Attempts to extend these procedures to our system were unsuccessful.
37. G.A. Molander and M.R. Rivero. Org. Lett. **4**, 107 (2002).

© 2006 NRC Canada

Synthesis of a hindered C_2-symmetric hydrazine and diamine by a crisscross cycloaddition of citronellal azine[1]

Barry B. Snider, James F. Grabowski, Roger W. Alder, Bruce M. Foxman, and Lin Yang

Abstract: Crisscross cycloaddition of citronellal azine (**6**) with 2 equiv. of TFA and powdered 3 Å molecular sieves in CH_2Cl_2 at reflux for 22 h afforded 37% of the desired C_2-symmetric hydrazine **7** and 5%–10% of diastereomer **8** in which one of the 6–5 ring fusions is cis. Methylation of the hydrazine of **7** and reduction of the resulting salt (**9**) with Li in NH_3 cleaved the N—N bond to give secondary tertiary amine **10** in 97% yield. Eschweiler–Clarke methylation afforded the C_2-symmetric bis tertiary amine **11** in 69% yield. Racemic products were obtained in initial attempts at asymmetric catalysis using **7** or **11** as asymmetric bases, using bistertiary amine **11** as a ligand analogous to sparteine for alkyllithiums, or using the lithium amide from secondary tertiary amine **10** as an asymmetric base. Apparently, the proton is buried in the core of **11**, leaving a hydrophobic surface; the free counterion is not an asymmetric catalyst. Diamine **11** may be too hindered to complex to *s*-BuLi. Tertiary amine **11** (pK_{a1} = 24.7) is more basic than DBU (pK_a = 24.3) in CH_3CN, in good agreement with theory.

Key words: crisscross cycloaddition, azine, dipolar cycloaddition, calculation of pK_a.

Résumé : La cycloaddition croisée de l'azine du citronellal (**6**) à l'aide de 2 équivalents d'acide trifluoroacétique et de tamis moléculaires 3 Å en poudre, dans du CH_2Cl_2 au reflux, pendant 22 heures, conduit à la formation de l'hydrazine (**7**) de symétrie C_2 recherchée avec un rendement de 37 % ainsi qu'à environ 5 % à 10 % du diastéréomère **8** dans lequel la fusion des cycles à cinq et à six chaînons est cis. La méthylation de l'hydrazine **7** et la réduction du sel **9** qui en résulte avec du Li dans de l'ammoniac permet de clivé la liaison N—N pour conduire à la formation de l'amine secondaire tertiaire **10** avec un rendement de 97 %. Une méthylation de Eschweiler–Clarke fournit la bisamine tertiaire de symétrie C_2 (**11**) avec un rendement de 60 %. On n'a obtenu que des produits racémiques dans les essais initiaux de catalyse asymétrique en utilisant les bases asymétriques **7** ou **11**, en utilisant la bisamine tertiaire **11** comme ligand analogue à la spartéine pour les alkyllithiens ou en utilisant l'amide de lithium dérivé de l'amine secondaire tertiaire **10** comme base asymétrique. Il semble que le proton est enfoui à l'intérieur du composé **11** qui ne laisse qu'une surface hydrophobe; le contre-ion libre n'est pas un catalyseur asymétrique. Il est possible que la diamine **11** soit trop encombrée pour se complexer au *s*-BuLi. L'amine tertiaire **11** (pK_{a1} = 24,7) est plus basique que la DBU (pK_a = 24,3) dans le CH_3CN, ce qui est en bon accord avec la théorie.

Mots clés : cycloaddition croisée, azine, cycloaddition dipolaire, calcul de pK_a.

[Traduit par la Rédaction]

Introduction

Both inter- and intra-molecular crisscross cycloadditions of azines with two alkenes are well-known as routes to 1,5-diazabicyclo[3.3.0]octanes, which are tetralkylhydrazines embedded in the ring fusion of a bicyclo[3.3.0] ring system (see Scheme 1) (1, 2). In an intermolecular example, the azine of hexafluoroacetone (**1**) reacted with 2 equiv. of methyl acrylate in benzene at 80 °C for 8 days to give 64% of adduct **2** and minor amounts of regio- and stereo-isomers (2*b*). Reaction of 2-allyloxy-1-naphthalenecarboxaldehyde (**3**) with 0.5 equiv. of hydrazine dihydrochloride in EtOH at

Received 10 November 2005. Accepted 21 December 2005. Published on the NRC Research Press Web site at http://canjchem.nrc.ca on 7 July 2006.

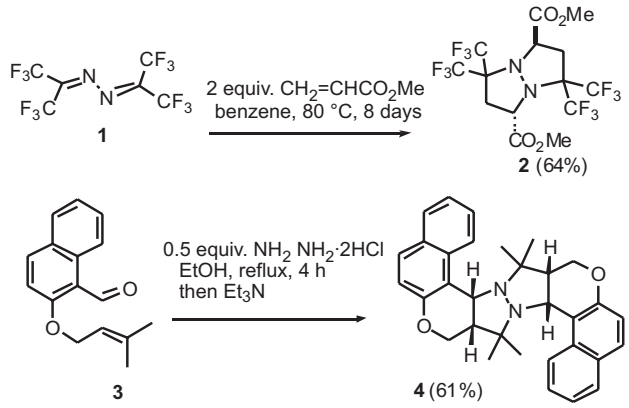
Dedicated to Alfred Bader in honor of the contributions that he and the Aldrich Chemical Company, which he founded and developed, have made to the development of organic chemistry over the past half century. RWA thanks Alfred Bader for his enthusiastic promotion of Proton Sponge®.

B.B. Snider,[2] J.F. Grabowski, B.M. Foxman, and L. Yang. Department of Chemistry MS 015, Brandeis University, Waltham, Massachusetts, 02454-9110, USA.
R.W. Alder. School of Chemistry, University of Bristol, Cantock's Close, Bristol BS8 1TS, UK.

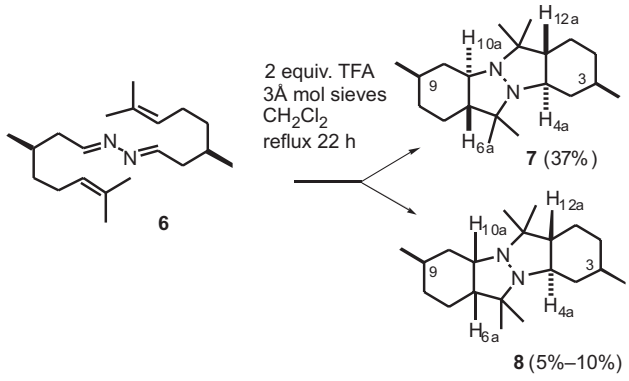
[1]This article is part of a Special Issue dedicated to Dr. Alfred Bader.
[2]Corresponding author (e-mail: snider@brandeis.edu).

 doi:10.1139/V06-084 © 2006 NRC Canada

Scheme 1. Examples of crisscross cycloadditions.



Scheme 2. Crisscross cycloaddition of azine **6**.



reflux for 4 h provided the azine, which underwent a crisscross cycloaddition to give **4** in 61% yield (2*a*, 2*c*). We were intrigued by the possibility of using this reaction with the azine of a readily available chiral aldehyde, such as citronellal, to obtain a chiral C_2-symmetric product that might be of value as an asymmetric catalyst. C_2-Symmetric diamines have been widely used in asymmetric synthesis (3), as has sparteine, which is not C_2-symmetric (4). The intramolecular cycloaddition of citronellal phenylhydrazone has been reported, although the stereochemistry of the product has not been well-characterized (5). Kobayashi et al. (6) have also explored asymmetric cycloadditions of related unsaturated acylhydrazones.

Results and discussion

Crisscross cycloaddition of 6

Initial attempts at forming the azine **6** of (*R*)-citronellal (**5**) with hydrazine dihydrochloride under various conditions afforded complex mixtures of azine **6**, hydrazones, hemiacetals, hemiaminals, and (or) the ene adduct, isopulegol. Eventually we found that treatment of neat (*R*)-citronellal (**5**) with 0.5 equiv. of anhydrous hydrazine for 10 min at 0–25 °C afforded azine **6** quantitatively as a 100:20:1 mixture of *E*,*E*-, *E*,*Z*-, and *Z*,*Z*-isomers, respectively, as determined by analysis of the chemical shift of the CH=N protons (7).

Heating a solution of azine **6** with 2 equiv. of TFA and powdered 3 Å molecular sieves in CH_2Cl_2 at reflux for 22 h afforded 37% of the desired C_2-symmetric hydrazine **7** and 5%–10% of diastereomer **8** in which one of the 6–5 ring fusions is cis (see Scheme 2). Lower yields were obtained without molecular sieves, with either more or less TFA, with other acids or $BF_3{\cdot}Et_2O$, or by combining azine formation and crisscross cycloaddition in a single step.

The structures of both **7** and **8** were established by spectroscopic analysis and X-ray structure determination. The ^{13}C NMR spectrum of **7** has only 10 different carbons, establishing that the molecule is symmetrical. The ^1H NMR spectrum of **7** is also simple. H_{4a} and H_{10a} both absorb at δ 2.65 as a ddd (J = 11.0, 11.0, 3.7 Hz). The 11.0 Hz coupling constant between both H_{4a} and H_{12a} and H_{10a} and H_{6a} establishes that the ring fusions are trans with antiperiplanar hydrogens. The cycloaddition should proceed preferentially to give products with the methyl groups attached to C_3 and C_9 equatorial, permitting the assignment of **7** as the major product.

The ^{13}C NMR spectrum of the minor product **8** has 20 different carbons. H_{4a} absorbs at δ 2.17 as a ddd (J = 11.0, 11.0, 3.1 Hz). The 11.0 Hz coupling constant between H_{4a} and H_{12a} establishes that the ring fusion is trans. H_{10a} absorbs at δ 3.01 as a ddd (J = 8.5, 8.5, 5.5 Hz), establishing that the other ring fusion is cis. Assuming that the cycloaddition gave only products with equatorial methyl groups, the minor product must be **8**.

Crystallographic analysis[3]

Figures 1 and 2 show the structures of **7** and **8** determined by X-ray crystallographic analysis. The orientation of the lone pairs in the core 1,5-diazabicyclo[3.3.0]octanes is quite different in the two adducts. In the major adduct **7**, the lone pairs are syn with a calculated torsion angle of 12° (see Scheme 3). The numbering corresponds to that used for the crystallographic data. The nitrogens are pyramidal and are 0.45 and 0.44 Å above the plane formed by the three substituents. In the minor adduct **8**, the lone pairs are anti with a calculated torsion angle of 177°. The molecule is flattened with the nitrogens only 0.11 and 0.23 Å above the plane formed by the three substituents. In syn isomers such as **7**, the torsion angles C_1-N_1-N_2-C_{11} (117.8°) and C_{17}-N_1-N_2-C_7 (141.4°) are much less than 180° and differ significantly. In anti isomers, such as **8**, the torsion angles C_1-N_1-N_2-C_{11} (169.3°) and C_{17}-N_1-N_2-C_7 (174.7°) are both close to 180°. In syn isomers such as **7**, the torsion angle between the lone pairs (12°) is calculated to be the average of C_1-N_1-N_2-C_7 (12.2°) and C_{17}-N_1-N_2-C_{11} (11.4°). In anti isomers such as **8**, the torsion angle between the lone pairs (177°) is calculated

[3] Supplementary data for this article are available on the journal Web site (http://canjchem.nrc.ca) or may be purchased from the Depository of Unpublished Data, Document Delivery, CISTI, National Research Council Canada, Ottawa, ON K1A 0R6, Canada. DUD 5052. For more information on obtaining material refer to http://cisti-icist.nrc-cnrc.gc.ca/irm/unpub_e.shtml. CCDC 289019 and 28920 contain the crystallographic data for this manuscript. These data can be obtained, free of charge, via http://www.ccdc.cam.ac.uk/conts/retrieving.html (Or from the Cambridge Crystallographic Data Centre, 12 Union Road, Cambridge CB2 1EZ, UK; fax +44 1223 336033; or deposit@ccdc.cam.ac.uk).

© 2006 NRC Canada

Fig. 1. Molecular structure of **7**.

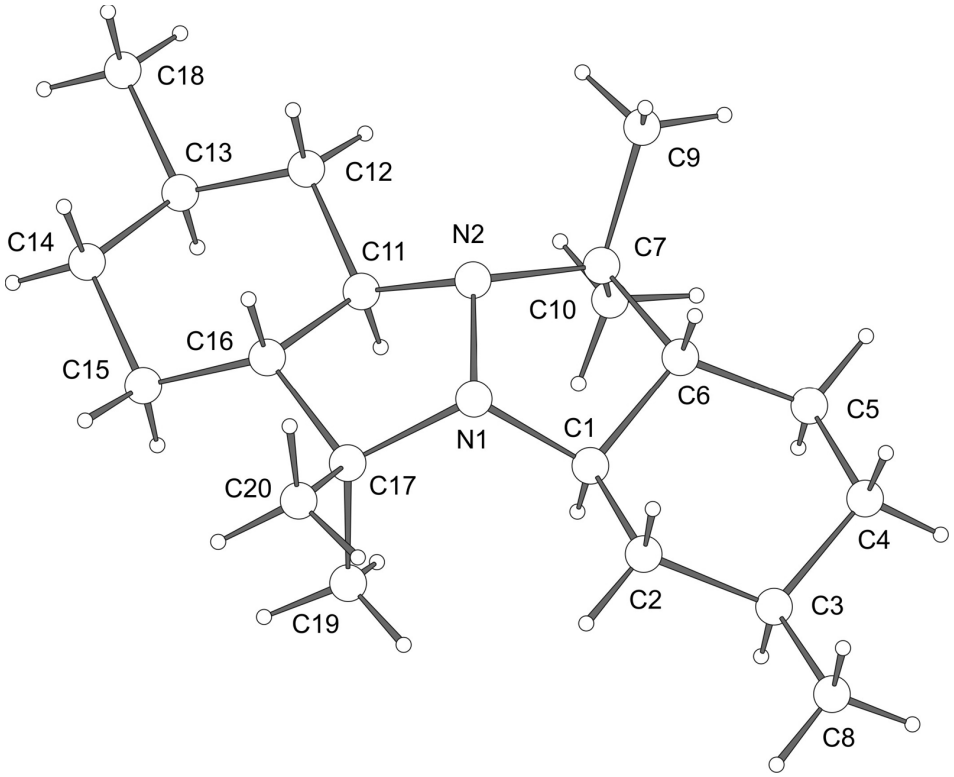
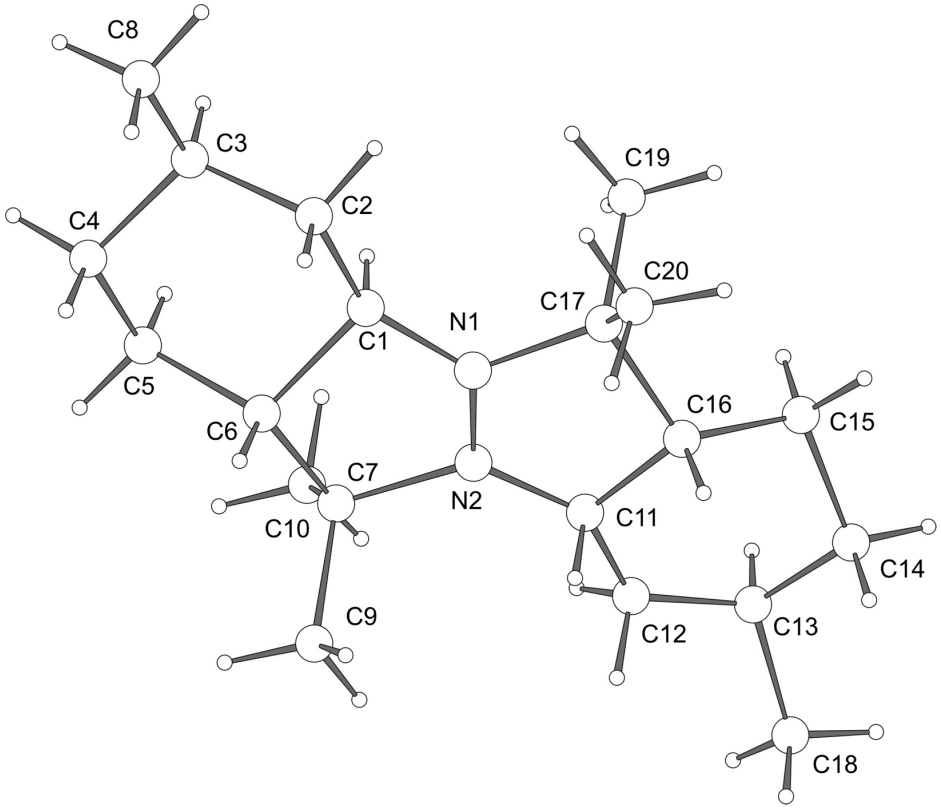
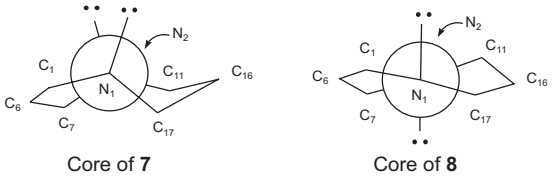


Fig. 2. Molecular structure of **8**.



© 2006 NRC Canada

Scheme 3. 1,5-Diazabicylo[3.3.0]octane cores of **7** and **8** showing lone pair torsion angles.



to be 180° minus half the difference between C_1-N_1-N_2-C_7 (23.9°) and C_{17}-N_1-N_2-C_{11} (18.5°).

A search of the Cambridge Structural Database (CSD) found structures of seven 1,5-diazabicyclo[3.3.0]octanes whose CSD refcodes, lone pair torsion angles, and out of plane distances, respectively, are listed in the following. Five of these have syn lone pairs comparable to **7**: BETGOW, 48.3°, 0.45 Å, 0.45 Å (2*b*); BETGUC, 23.8°, 0.35 Å, 0.35 Å (2*b*); BETHAJ, 23.2°, 0.35 Å, 0.35 Å (2*b*); FEDYAP, 44.8°, 0.54 Å, 0.56 Å (2*i*); and WIWFAJ, 36.6°, 0.52 Å, 0.52 Å (2*g*). The other two have anti lone pairs comparable to **8**: LEKHIS, 179.8°, 0.44 Å, 0.43 Å (2*e*); and LEKHIS, 175.3°, 0.46 Å, 0.42 Å (2*e*).

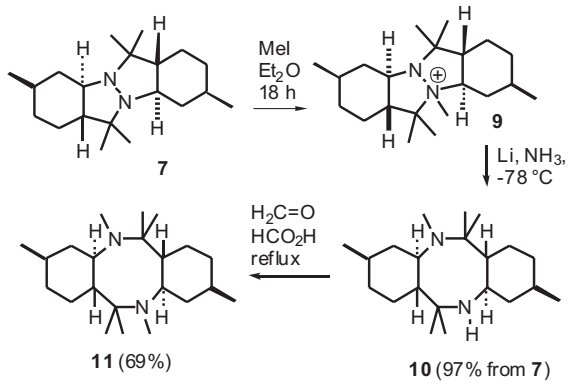
Preparation of 10 and 11

Hydrazines are less basic than amines (8) and are sensitive to oxidation. We therefore explored the reductive cleavage of **7** to give a bis secondary amine. Although hydrazines have been reduced hydrogenolytically (9) or by dissolving metal reductions (10), initial attempts to reduce **7** by either method were unsuccessful. Apparently, steric hindrance and the electron-donating alkyl substituents retard the reduction. We activated the system toward reduction by methylation (11). A solution of **7** was treated with excess (10 equiv.) MeI in ether for 18 h at 25 °C to give **9** (see Scheme 4). Slow addition of a THF solution of **9** to excess Li in NH_3 at –78 °C afforded secondary tertiary amine **10** in 97% yield from **7**. It is important to make sure that excess Li is present because $LiNH_2$ acts as a nucleophile to convert **9** back to **7** with the formation of $MeNH_2$. Eschweiler–Clarke methylation (12) of **10** with formic acid and aqueous formaldehyde at reflux for 19 h afforded the C_2-symmetric tertiary amine **11** in 69% yield.

Evaluation of 7, 10, and 11 as catalysts

We now turned our attention to exploring the use of hydrazine **7** and amines **10** and **11** for asymmetric catalysis. Methanolysis of *cis*-1,2-cyclohexanedicarboxylic anhydride in ether (13) was very slow with **7** as the catalyst and very rapid with **11** as the catalyst. In both cases racemic product was obtained. Attempted deprotonation of *N*-Boc pyrrolidine with *s*-BuLi and **11**, analogously to that reported with *s*-BuLi and sparteine (14) was unsuccessful. Attempted asymmetric deprotonation of cyclohexene oxide with LDA and **10** as described by Asami for other chiral secondary tertiary amines (15) gave racemic 2-cyclohexen-1-ol. The nitrogens of **11** are very basic and quite hindered. The NMR spectrum of diamine **11** in CD_3OD is identical to that of the monotrifluoroacetate salt indicating that the free amine is fully converted to the ammonium methoxide. Apparently, the proton is buried in the core leaving a hydrophobic surface and the reactive methoxide is not an asymmetric catalyst.

Scheme 4. Conversion of hydrazine **7** to amines **10** and **11**.



Diamine **11** may be too hindered to complex to *s*-BuLi. It is also possible that the distance between and (or) alignment of the lone pairs make **11** a poor ligand for Li. The presence of the two geminal dimethyl groups makes the nitrogens very hindered so that **11** is not effective as an asymmetric catalyst or ligand.

Determination of the pK_a of 11 in MeCN

Cyclic diamines are much more basic than simple amines because there is lone pair repulsion in the free diamine and the ammonium salt is stabilized by a strong intramolecular hydrogen bond. 1,4-Dimethyl-1,4-diazacyclooctane has a pK_{a1} in H_2O of 11.9 (15). We determined the pK_{a1} of **11** relative to DBU (**12**) in CD_3CN by adding 0.4 equiv. of TFA to a CD_3CN solution of 1 equiv. of DBU and 1 equiv. of **11**. The NMR spectrum showed three species. Amine **11** (0.72 equiv.) and **11-H$^+$** (0.28 equiv.) are observed as separate species that equilibrate slowly on the NMR timescale as has been previously observed for other polyamines (16). DBU is observed as a single rapidly equilibrating species that is 14% protonated by comparison with values for DBU and DBU-H$^+$. We established that this mixture was at equilibrium by adding the components in various orders. These data establish that **11** is more basic than DBU by 0.4 pK_a units. Using a value of 24.3 for the pK_a of DBU in CH_3CN (17), the pK_{a1} of **11** is 24.7. A similar experiment in DMSO showed that only DBU was protonated, indicating that DBU (pK_a = 13.9, ref. 17) is much more basic than **11** in DMSO.

Calculation of the pK_a of 11

Calculation of proton affinities (PA), gas-phase basicities (GB), and solution pK_a values have been extensively developed in recent years and might help us understand the basicity of **11**. Liptak and Shields (18) have shown that it is possible to calculate absolute aqueous pK_a values with chemical accuracy and their methods have been applied with considerable success to calculate pK_a values in several solvents for one special class of strong neutral bases, the diaminocarbenes, by Magill et al. (19). Unfortunately, the most reliable methods (e.g., CBS-QB3) are far too computationally intensive to be applied to molecules the size of **11**. Magill and Yates' (20) recent results suggest that two good options for larger species are (*a*) CBS-4M and (*b*) B3LYP/6-311+G** and method (*b*) has been used here. This procedure uses geometries, zero point energies, and thermal and entropy corrections from the well-established B3LYP/6-

© 2006 NRC Canada

Table 1. Calculated (B3LYP/6-311+G**//B3LYP/6-31G*) PA and pK_a values for amines **11**–**15**.

Diamine	Gas-phase PA (kJ mol^{-1})	pK_a (MeCN)[a]	pK_a (DMSO)[b]	$\Delta E(1)$ (kJ mol^{-1})	$\Delta E(2)$ (kJ mol^{-1})
11	1074	24.4	14.7	98	59
12	1052	23.9	12.1		
13a	1028	18.1	8.5		
13b	1089	23.2	11.1		
14	1046	23.5	14.0	1	–9
15	1078	28.3	18.7	42	–6
16	1105	30.4	20.9	43	–23

[a]Relative to Me_3N, pK_a = 17.61.
[b]Relative to Me_3N, pK_a = 8.4.

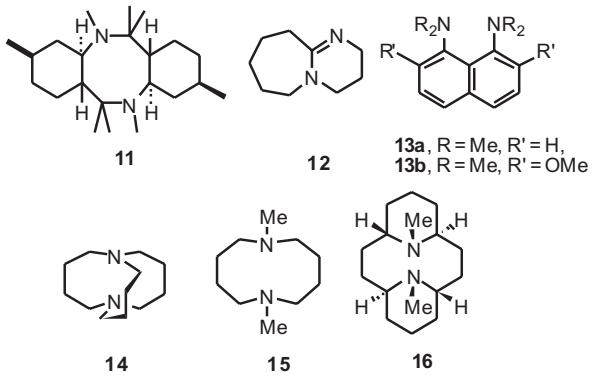
31G* level of theory. pK_a values have been calculated relative to the pK_a values for Me_3NH^+ of 17.61 in MeCN and 8.4 in DMSO, as described previously (21).

DFT calculations were performed with the Jaguar program package (22), using Becke's three-parameter exchange functional (23) with the correlation functional of Lee et al. (B3LYP) (24). All species were characterized by full geometry optimization with the standard 6-31G* basis set, and minima were characterized by analytical frequency calculations. Single point calculations were then carried out with the 6-311+G** basis set. Calculations simulating the solvents MeCN and DMSO employed the Poisson–Boltzmann continuum solvent model as implemented in the Jaguar program, with the assumption that geometries, zero point energy, and thermodynamic parameters could be transferred from the gas-phase calculations. These procedures lead to pK_a values of 11.9 (H_2O), 18.1 (MeCN), and 8.5 (DMSO) for the original proton sponge **13a** compared with experimental values of 12.1 (25), 18.62 (17*a*), and 7.5 (26, 27), respectively. The pK_a value of **13b** in DMSO is calculated to be 11.1 (experimental value, 11.5, ref. 28). While the general level of agreement in MeCN seems relatively good, it is worth noting that the calculated pK_a difference between **13b** and **15** in DMSO is 3.9, compared with a measured value of only 0.4 (15, 21).

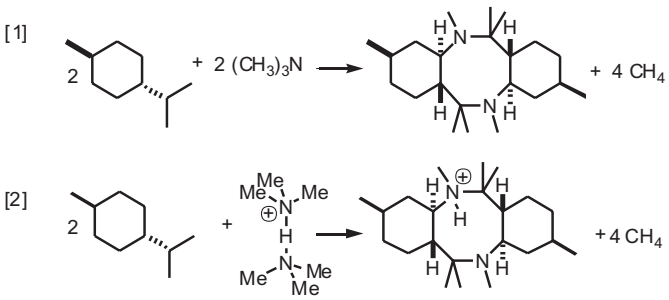
Monte Carlo multiple minimum conformational searches (29, 30) were carried out to find low energy conformations for diamine **11** and the monoprotonated ion, using the MMFFs force field in MacroModel (31, 32). One conformation was clearly preferred for the ion, with a strong N···H-N$^+$ bond (2.66 Å distance between nitrogens; N···H-N angle, 140.9°). The cyclohexane rings are in the expected chair form, and the eight-membered ring is in a twist boat form. The conformational situation for diamine **11** was less clear and therefore, five low energy structures from a MacroModel search for the diamine were submitted to B3LYP/6-31G* calculation. The preferred structure was found to have the same conformation as the protonated ion, with the nitrogen atoms separated by 2.90 Å; this structure was used for the PA and pK_a calculations.

PA and pK_a values for amines **11**–**16** (see Chart 1) are listed in Table 1. The gas-phase PA results should be regarded as rather reliable. They show that diamine **11** is a substantially stronger base than the flexible 10-membered ring diamine **14**, in spite of having a hydrogen bond that is further from the linear ideal. This presumably reflects greater strain relief on protonation.

Chart 1. Structures of amines whose calculated PA and pK_a values are shown in Table 1.



Scheme 5. Theoretical eqs. [1] and [2] used for assessing strain relief in calculations of PA and pK_a values.



As described previously (21), a convenient way to assess this strain relief is by comparison of the calculated energy changes associated with eqs. [1] and [2] in which the strained diamine and protonated ion are formally constructed from unstrained components (see Scheme 5). The B3LYP/6-31G* computed vales for $\Delta E(1)$ and $\Delta E(2)$ are shown in Table 1. The value of $[\Delta E(1) - \Delta E(2)]$ for **11** (39 kJ mol^{-1}) is considerably greater than for **14** and approaches that for **15**, but is still much smaller than that for **16** (66 kJ mol^{-1}). We conclude that this strain relief is the major factor that determines the PA of these diamines. The increased strain in diamine **11**, when compared with its protonated ion, will be partly due to lone pair – lone pair repulsion, but forcing the nitrogen atoms to move to 2.90 Å, compared with 2.66 Å in the protonated ion, necessarily increases the strain elsewhere in the molecule.

There is much more uncertainty about the calculated pK_a values, since these rely on the performance of the solvation

© 2006 NRC Canada

model. In fact, the calculated pK_a values in MeCN for **11** and **12** are in reasonable agreement with the experimental relative pK_a data. Note that the calculations suggest that, in this solvent, **11** has a rather low pK_a value considering its PA, and is nearer to **14** than **15** in calculated pK_a. This of course reflects a relatively high (calculated) solvation energy for the diamine. There is no simple way of assessing whether this is correct, but we note that diamine **11** has a larger purely hydrophobic surface than the other diamines being used for comparison. While the calculated pK_a values in MeCN are in (possibly fortuitously) quite good agreement with experiment, the calculated values in DMSO are in poor agreement. We can offer no simple explanation, beyond noting that results for DMSO, using the Poisson–Boltzmann continuum solvent model, as implemented in the Jaguar program, have been less satisfactory than for MeCN, as noted earlier.

Conclusion

We have developed an efficient route to C_2-symmetric hydrazine **7** and diamine **11**. Initial trials suggest that the bis tertiary amine **11** is too hindered to function as an asymmetric catalyst or ligand. We are currently exploring routes to less hindered C_2-symmetric tricyclic amines that lack the two geminal dimethyl substituents.

Experimental section

General procedures

NMR spectra were recorded at 400 MHz in $CDCl_3$ unless otherwise indicated, chemical shifts are reported in δ, and coupling constants in Hz. The silica gel used for chromatography was deactivated with methanol unless otherwise indicated. IR spectra are reported in cm^{-1}.

(*R*)-Citronellal azine (6)

Anhydrous hydrazine (0.28 mL, 9.0 mmol) was added dropwise to (*R*)-(+)-citronellal (**5**, 3.26 mL, 2.77 g, 18.0 mmol) at 0 °C and the resulting mixture was stirred at 25 °C for 10 min. The mixture was diluted with CH_2Cl_2 (20 mL), dried over $MgSO_4$, and concentrated under reduced pressure to give 2.637 g (98%) of **6** as a 100:20:1 mixture of *E*,*E*-, *E*,*Z*-, and *Z*,*Z*-isomers (7), respectively, as a clear oil. IR (neat): 1651. ^{1}H NMR: 7.88 (t, 2, *J* = 6.1, *E*,*E*-isomer), 7.56 (t, 1, *J* = 5.8, *E*,*Z*-isomer), 7.15 (t, 1, *J* = 5.5, *E*,*Z*-isomer) 7.07–7.02 (t, 2, *J* = 5, *Z*,*Z*-isomer), 5.09 (tq, 2, *J* = 8.5, 1.2), 2.35 (ddd, 2, *J* = 14.0, 8.5, 6.1, *E*,*E*-isomer), 2.19 (ddd, 2, *J* = 14.0, 8.0, 6.1, *E*,*E*-isomer), 2.07–1.95 (m, 4), 1.84–1.76 (m, 2), 1.68 (s, 6), 1.60 (s, 6), 1.45–1.36 (m, 2), 1.30–1.21 (m, 2), 0.97 (d, 6, *J* = 6.7). ^{13}C NMR: 165.0 (2C), 131.5 (2C), 124.3 (2C), 39.6 (2C), 36.8 (2C), 30.9 (2C), 25.7 (2C), 25.4 (2C), 19.6 (2C), 17.6 (2C).

(3*R*,4a*R*,6a*R*,9*R*,10a*R*,12a*R*)-Dodecahydro-3,6,6,9,12,12-hexamethyl-1*H*,6*H*-indazolo[2,1-*a*]indazole (7) and (3*R*,4a*R*,6a*R*,9*R*,10a*S*,12a*R*)-dodecahydro-3,6,6,9,12,12-hexamethyl-1*H*,6*H*-indazolo[2,1-*a*]indazole (8)

TFA (1.4 mL, 18 mmol) was added to a suspension of azine **6** (2.616 g, 8.591 mmol) and 3 Å powdered molecular sieves (1.024 g) in dry CH_2Cl_2 (300 mL) and the resulting suspension was stirred and heated at reflux for 22 h. The suspension was cooled and water (60 mL) was added. The phases were separated and the aqueous layer was extracted with CH_2Cl_2 (3 × 60 mL). The combined organic phases were dried over Na_2SO_4 and concentrated under reduced pressure to give 3.632 g of a yellow oil. Flash chromatography on silica gel (hexanes–acetone, 3:2) and subsequent deprotonation with satd. $NaHCO_3$ solution gave 495 mg (19%) of 60% pure **8** as a clear wax. Elution with MeOH and subsequent deprotonation with satd. $NaHCO_3$ solution gave 975 mg (37%) of **7** as an orange wax. Data for **7**: IR (CH_2Cl_2): 1688. ^{1}H NMR: 2.65 (ddd, 2, *J* = 11.0, 11.0, 3.7, H_{4a}, H_{10a}), 1.84–1.60 (m, 8), 1.44–1.41 (m, 2), 1.19–1.09 (m, 2), 1.14 (s, 6), 0.98–0.87 (m, 4), 0.96 (s, 6), 0.92 (d, 6, *J* = 6.7). ^{13}C NMR: 58.2 (2C), 58.1 (2C), 57.6 (2C), 41.1 (2C), 34.5 (2C), 30.9 (2C), 28.4 (2C), 24.3 (2C), 22.2 (2C), 19.3 (2C). HRMS (EI) calcd. for $C_{20}H_{36}N_2$: 304.2878 (M^+); found: 304.2882

TFA (2 drops, excess) was added to a solution of **7** in $CDCl_3$ to give **7**·TFA: ^{1}H NMR: 2.92 (ddd, 2, *J* = 11.7, 11.4, 4.0, $H_{4a(10a)}$), 2.20 (ddd, 2, *J* = 12.3, 11.4, 3.2, $H_{12a(6a)}$), 1.91 (br d, 2, *J* = 11.7, $H_{4eq(10eq)}$), 1.78 (br d, 2, *J* = 13.2, $H_{2eq(8eq)}$), 1.73 (br dd, 2, *J* = 11.5, 3.2, $H_{1eq(7eq)}$), 1.44–1.38 (m, 2, $H_{3ax(9ax)}$), 1.41 (s, 6), 1.36 (ddd, 2, *J* = 11.7, 11.7, 11.4, $H_{4ax(10ax)}$), 1.15 (s, 6), 1.15 (br ddd, 2, *J* = 12.3, 11.5, 2.9, $H_{1ax(7ax)}$), 1.05 (m, 2, $H_{2ax(8ax)}$), 0.99 (d, 6, *J* = 6.2). A 1D NOESY experiment showed NOEs from $H_{4a(10a)}$ at δ 2.9 to $H_{12a(6a)}$ at δ 2.2 (small), to $H_{4eq(10eq)}$ at δ 1.91 (large), to $H_{3ax(9ax)}$ at δ 1.44–1.38 (small), to $H_{4ax(10ax)}$ at δ 1.36 (small), to $H_{1ax(7ax)}$ at δ 1.15 (small), and to the methyl group at δ 1.15.

Flash chromatography of 495 mg of 60% pure **8** on silica gel (Et_2O) gave 118 mg (5%) of **8** as a clear wax. ^{1}H NMR: 3.01 (ddd, 1, *J* = 8.5, 8.5, 5.5, H_{10a}), 2.17 (ddd, 1, *J* = 11.0, 11.0, 3.1, H_{4a}), 1.94–1.90 (m, 2, H_{6a}, H_{12a}), 1.86–1.78 (m, 2), 1.76–1.69 (m, 1), 1.58–1.48 (m, 3, including H_{10eq}), 1.47–1.39 (m, 1, H_{4eq}), 1.36–1.31 (m, 2), 1.27–1.18 (m, 2, including H_{10ax}), 1.12–1.05 (m, 1), 1.11 (s, 3), 1.10 (s, 3, 12-CH_3), 1.00 (s, 3, 6-CH_3), 0.98–0.86 (m, 1, H_{4ax}), 0.93 (d, 3, *J* = 6.7), 0.90 (d, 3, *J* = 6.1, 9-CH_3), 0.90 (s, 3, 6-CH_3), 0.77–0.72 (m, 1). ^{13}C NMR: 60.7, 58.5, 56.7, 54.2, 50.2, 38.2, 35.3, 34.2, 31.2, 31.1, 28.7, 26.5, 25.2, 25.0, 23.2, 22.42, 22.41, 21.8, 16.7 (one carbon was not observed). A 1D NOESY experiment showed NOEs from H_{10a} at δ 3.01 to H_{6a} at δ 1.94–1.90 (large), to H_{10eq} at δ 1.58–1.48 (small), to H_{10ax} at δ 1.27–1.18 (large), to 12-CH_3 at δ 1.10, and to 9-CH_3 at δ 0.90 (small). A 1D NOESY experiment showed NOEs from H_{4a} at δ 2.17 to H_{12a} at δ 1.94–1.90 (small), to H_{4eq} at δ 1.47–1.39 (large), to 6-CH_3 at δ 1.00 (large), to H_{4ax} at δ 0.98–0.86 (small), and to 6-CH_3 at δ 0.90 (small).

(3*R*,4a*R*,6a*R*,9*R*,10a*R*,12a*R*)-Hexadecahydro-3,5,6,6,9,12,12-heptamethyldibenzo[*b*,*f*][1,5]diazocine (10)

Iodomethane (0.56 mL, 9.06 mmol) was added to a solution of **7** (276 mg, 0.906 mmol) in dry Et_2O (18 mL) and the resulting solution was stirred at 25 °C for 18 h. The solution was concentrated under reduced pressure to give monomethylated iodide **9** as a white residue.

Crude **9** was dissolved in dry THF (12 mL) and the solution was added dropwise to a dark blue mixture of dry NH_3 (30 mL) and lithium metal at –78 °C. More lithium was

© 2006 NRC Canada

added immediately after the solution became lighter blue so that an excess of solvated electrons was always present. After the addition was complete, the mixture was stirred at reflux (–33 °C) for 1 h. NH_4Cl (3 g) was added and the NH_3 was evaporated. The residue was dissolved in water (20 mL) and the aqueous layer was extracted with CH_2Cl_2 (3 × 50 mL). The combined organic phases were washed with 1 mol/L NaOH solution (100 mL) and dried over Na_2SO_4. The resulting solution was concentrated under reduced pressure to give 283 mg (97%) of >95% pure **10** as a red liquid. IR (neat): 3349. ^{1}H NMR: 3.83 (br s, 1, NH), 2.83 (br dd, 1, J = 11.0, 11.0), 2.49 (br dd, 1, J = 10.4, 10.4), 2.37 (s, 3), 2.12–1.93 (m, 4), 1.76–1.64 (m, 4), 1.44–1.18 (m, 5), 1.17 (s, 3), 1.12–1.01 (m, 1), 1.04 (s, 3), 1.00–0.78 (m, 2), 0.96 (s, 3), 0.95 (s, 3), 0.934 (d, 3, J = 6.7), 0.927 (d, 3, J = 6.1). ^{13}C NMR: 68.7, 60.1, 59.8, 56.4, 50.8, 49.0, 43.6, 38.5, 37.0, 36.0, 35.8, 34.6, 34.1, 31.3, 30.6, 29.7, 28.6, 25.4, 23.8, 22.6, 21.9.

(3*R*,4a*R*,6a*R*,9*R*,10a*R*,12a*R*)-Hexadecahydro-3,5,6,6,9,11,12,12-octamethyldibenzo[*b*,*f*][1,5]diazocine (11)

Formic acid (0.17 mL, 4.42 mmol) and 37% formaldehyde in water (0.17 mL, 2.30 mmol) were added in succession to **10** (283 mg, 0.883 mmol) at 0 °C. The resulting solution was heated at reflux for 19 h. The solution was cooled and 2 mol/L HCl (3 mL) was added. The aqueous solution was extracted with Et_2O (2 × 5 mL) to remove less polar impurities and made basic with 2 mol/L NaOH solution. The aqueous solution was saturated with NaCl and extracted with EtOAc (3 × 10 mL). The combined organic phases were dried over Na_2SO_4 and concentrated under reduced pressure to give 205 mg (69%) of **11** as a white wax. IR (CH_2Cl_2): 2956, 2921, 2772. ^{1}H NMR: 2.38–2.27 (m, 2), 2.32 (s, 6), 2.18–1.98 (m, 4), 1.81–1.73 (m, 2), 1.72–1.62 (m, 2), 1.35–1.15 (m, 4), 1.12–0.82 (m, 4), 0.97 (s, 6), 0.92 (d, 6, J = 6.7), 0.89 (s, 6). ^{1}H NMR (CD_3CN): 2.40–2.29 (m, 2), 2.37 (s, 6), 2.25–2.10 (m, 2), 2.09–2.00 (m, 2), 1.82–1.72 (m, 2), 1.71–1.62 (m, 2), 1.38–1.24 (m. 2), 1.22–1.12 (m, 2), 1.11–0.92 (m, 4) 1.00 (s, 6), 0.94 (s, 6), 0.92 (d, 6, J = 6.7). ^{1}H NMR (CD_3OD): 3.07 (ddd, 2, J = 11.6, 11.3, 2.4), 2.67 (s, 6), 2.44 (ddd, 2, J = 11.3, 11.0, 3.1), 2.18 (br dd, 2, J = 11.6, 2.4), 1.90 (br ddd, 2, J = 12.2, 6.7, 3.0), 1.77 (br d, 2, J = 12.2), 1.54–1.40 (m, 2), 1.41 (ddd, 2, J = 11.6, 11.6, 11.6), 1.27 (s, 6), 1.26 (s, 6), 1.31–1.08 (m, 4), 1.03 (d, 6, J = 6.1). ^{13}C NMR: 67.0 (2C), 58.5 (2C), 49.9 (2C), 38.4 (2C), 36.8 (2C), 36.5 (2C), 34.3 (2C), 30.1 (2C), 22.6 (2C), 22.4 (2C), 22.3 (2C). HRMS (EI) calcd. for $C_{22}H_{42}N_2$: 334.3348 (M^+); found: 334.3356.

TFA (120 µL, 10^{-1} mol/L in $CDCl_3$, 12 µmol, 1 equiv.) was added to a solution of 4 mg (12 µmol) **11** in $CDCl_3$ to give **11**·TFA. ^{1}H NMR: 3.00 (br dd, 2, J = 11.9, 11.5), 2.71 (s, 6), 2.27 (ddd, 2, J = 11.5, 10.4, 2.4), 2.16 (br d, 2, J = 11.0), 1.89–1.79 (m, 4), 1.56–1.42 (m, 2), 1.28 (s, 6), 1.23 (s, 6), 1.23 (br ddd, 2, J = 11.9, 10.4, 9.8), 1.16 (br ddd, 2, J = 14.0, 14.0, 11.9), 1.08–0.94 (m, 2), 1.01 (d, 6, J = 6.7). The NMR spectrum did not change on addition of an additional 120 µL of TFA solution.

TFA (2 drops, excess) was added to a solution of **11** in CD_3CN to give **11**·TFA. ^{1}H NMR (CD_3CN): 2.97 (ddd, 2, J = 11.6, 11.3, 2.4), 2.57 (d, 6, J = 3.1), 2.36 (ddd, 2, J = 11.3, 10.6, 3.1), 2.10 (ddd, 2, J = 10.6, 1.8, 1.8), 1.85–1.74 (m, 2), 1.71 (br d, 2, J = 9.2), 1.49–1.30 (m, 4), 1.28–1.02 (m, 2), 1.18 (s, 12), 1.01–0.88 (m, 2), 0.97 (d, 6, J = 6.1).

Determination of the pK_a of 11 in CH_3CN

TFA (3.5 µmol, 0.4 equiv., 2.7 µL of a 1.3 mol/L solution in CD_3CN prepared by diluting TFA (100 µL, 148 mg, 1.3 mmol) to a final volume of 1 mL) was added to a solution of DBU (8.7 µmol, 13 µL of a 6.7×10^{-1} mol/L solution in CD_3CN prepared by diluting DBU (100 µL, 102 mg, 0.67 mmol) to a final volume of 1 mL) and **11** (2.9 mg, 8.7 µmol) in CD_3CN (1.0 mL). The resulting solution was monitored for 4 days at 25 °C by ^{1}H NMR. DBU was calculated to be 14% protonated from the ^{1}H NMR shift (δ 3.155, t, J = 5.5) relative to $DBUH^+$ (δ 3.279, br s) and to the DBU/**5** solution (δ 3.135, t, J = 5.5) prior to adding TFA. Diamine **11** was calculated to be 28% protonated from an integration of **11** at δ 2.09–1.72 (m, 4) and **11**-H^+ at δ 2.97 (ddd, 2, J = 11.6, 11.3, 2.4). Based on the pK_a of DBU (24.34 (17*a*)), the pKa of **11** was calculated to be 24.7. An identical mixture was obtained adding DBU to a solution of TFA and diamine **11** in CD_3CN.

Determination of the pK_a of 11 in DMSO

TFA (3.5 µmol, 0.40 equiv., 2.7 µL of a 1.3 mol/L solution in DMSO-d_6, prepared by diluting TFA (100 µL, 148 mg, 1.3 mmol) to a final volume of 1 mL) was added to a solution of DBU (8.7 µmol, 13 µL of a 6.7×10^{-1} mol/L solution in DMSO-d_6, prepared by diluting DBU (100 µL, 102 mg, 0.67 mmol) to a final volume of 1 mL) and **11** (2.9 mg, 8.7 µmol) in DMSO-d_6 (1.0 mL) and the resulting solution was monitored for 3 h at 25 °C by ^{1}H NMR. DBU was calculated to be 37% protonated from the ^{1}H NMR shift (δ 3.150, br s) relative to $DBUH^+$ (δ 3.248, br s) and to the DBU/**11** solution (δ 3.093, t, J = 5.2) prior to adding TFA. Diamine **5** was calculated to be completely unprotonated. The peaks for **11** at δ 2.12–1.93 (m, 4) were present and those for **11**-H^+ at δ 2.99 (br dd, 2, J = 10.4, 10.4) were absent.

A solution of TFA (3.5 µmol, 2.7 µL of a 1.3 mol/L stock solution in DMSO-d_6) and **11** (2.9 mg, 8.7 µmol) in DMSO-d_6 (1.0 mL) showed the presence of a mixture of **11** and **11**-H^+ (48:52) based on integration of the peaks for **11** at δ 2.12–1.93 (m, 4) and for **11**-H^+ at δ 2.99 (br dd, 2, J = 10.4, 10.4). Addition of DBU (8.7 µmol, 13 µL of a 6.7×10^{-1} mol/L solution in DMSO-d_6) gave a spectrum identical to that described above with DBU absorbing at δ 3.151 and only unprotonated **11**.

Acknowledgements

We thank the National Institutes of Health (GM 50151) for financial support.

References

1. For reviews of crisscross cycloadditions, see: (*a*) R. Grashley. *In* 1,3-Dipolar cycloaddition chemistry. Vol. 1. *Edited by* A. Padwa. John Wiley and Sons, New York. 1984. pp. 757–763; (*b*) S. Rádl. Aldrichimica Acta, **30**, 97 (1997).

© 2006 NRC Canada

2. (*a*) S.S. Mathur and H. Suschitzky. J. Chem. Soc. Perkin Trans. 1, 2479 (1975); (*b*) K. Burger, H. Schickaneder, F. Hein, A. Gieren, V. Lamm, and H. Engelhardt. Liebigs Ann. Chem. 845 (1982); (*c*) T. Shimizu, Y. Hayashi, M. Miki, and K. Teramura. J. Org. Chem. **52**, 2277 (1987); (*d*) M. Potáček, R. Marek, Z. Žák, J. Trottier, Z. Janoušek, and H. Viehe. Tetrahedron Lett. **34**, 8341 (1993); (*e*) M.G. Barlow, R.G. Pritchard, N.S. Suliman, and A.E. Tripping. Acta Crystalogr. Sect. C, **50**, 553 (1994); (*f*) M.M. Abdul-Ghani and A.E. Tipping. J. Fluorine Chem. **73**, 203 (1995); (*g*) G. Maas and V. Gettwert. Tetrahedron, **56**, 4139 (2000); (*h*) É. Frank, J. Wölfing, B. Aukszi, V. König, T. Schneider, and G. Schneider. Tetrahedron, **58**, 6843 (2002); (*i*) A.P. Molchanov, D.I. Sipkin, Yu. B. Koptelov, J. Kopf, and R.R. Kostikov. Russ. J. Org. Chem. **40**, 67 (2004).
3. (*a*) A. Berkessel, M. Schröder, C.A. Sklorz, S. Tabanella, N. Vogl, J. Lex, and J.M. Neudörfl. J. Org. Chem. **69**, 3050 (2004); (*b*) J.-C. Kizirian, N. Cabello, L. Pinchard, J.-C. Caille, and A. Alexakis. Tetrahedron, **61**, 8939 (2005).
4. (*a*) D. Hoppe and T. Hense. Angew. Chem. Int. Ed. Engl. **36**, 2282 (1997); (*b*) P.-W. Phuan, J.C. Ianni, and M.C. Kozlowski. J. Am. Chem. Soc. **126**, 15473 (2004).
5. B. Fouchet, M. Joucla, and J. Hamelin. Tetrahedron Lett. **22**, 1333 (1981).
6. S. Kobayashi, H. Shimizu, Y. Yamashita, H. Ishitani, and J. Kobayashi. J. Am. Chem. Soc. **124**, 13678 (2002).
7. J. Elguero, R. Jacquier, and C. Marzin. Bull. Soc. Chim. Fr. 1374 (1969).
8. S.F. Nelsen, D.T. Rumack, L.W. Sieck, and M. Meot-Ner (Mautner). J. Am. Chem. Soc. **110**, 6303 (1988).
9. (*a*) H. Stetter and H. Spangenberger. Chem. Ber. **91**, 1982 (1958); (*b*) F.J. Weigert. J. Org. Chem. **43**, 622 (1978); (*c*) S.F. Nelsen and M.R. Willi. J. Org. Chem. **49**, 1 (1984); (*d*) F. Alonso, G. Radivoy, and M. Yus. Tetrahedron, **56**, 8673 (2000).
10. (*a*) J.M. Mellor and N.M. Smith. J. Chem. Soc. Perkin Trans. 1, 2927 (1984); (*b*) S.E. Denmark, O. Nicaise, and J.P. Edwards. J. Org. Chem. **55**, 6219 (1990).
11. S.F. Nelsen, J.T. Ippoliti, and P.A. Petillo. J. Org. Chem. **55**, 3825 (1990).
12. S.H. Pine and B.L. Sanchez. J. Org. Chem. **36**, 829 (1971).
13. Y. Chen, S.-K. Tian, and L. Deng. J. Am. Chem. Soc. **122**, 9542 (2000).
14. (*a*) M. Asami, T. Suga, K. Honda, and S. Inoue. Tetrahedron Lett. **38**, 6425 (1997); (*b*) P. O'Brien. J. Chem. Soc. Perkin Trans. 1, 1439 (1998).
15. R.W. Alder, P. Eastment, N.M. Hext, R.E. Moss, A.G. Orpen, and J.M. White. J. Chem. Soc. Chem. Commun. 1528 (1988).
16. G.R. Weisman, M.E. Rogers, E.H. Wong, J.P. Jasinski, and E.S. Paight. J. Am. Chem. Soc. **112**, 8604 (1990).
17. (*a*) I. Kaljurand, A. Kütt, L. Sooväli, T. Rodima, V. Mäemets, I. Lieto, and I.A Koppel. J. Org. Chem. **70**, 1019 (2005); (*b*) R. Schwesinger, H. Schlemper, C. Hasenfratz, J. Willaredt, T. Dambacher, T. Breuer, C. Ottaway, M. Fletschinger, J. Boele, H. Fritz, D. Putzas, H.W. Rotter, F.G. Bordwell, A.V. Satish, G.-Z. Ji, E.-M. Peters, K. Peters, H.G. von Schnering, and L. Walz. Liebigs Ann. 1055 (1996).
18. M.D. Liptak and G.C. Shields. J. Am. Chem. Soc. **123**, 7314 (2001).
19. A.M. Magill, K.J. Cavell, and B.F. Yates. J. Am. Chem. Soc. **126**, 8717 (2004).
20. A.M. Magill and B.F. Yates. Aust. J. Chem. **57**, 1205 (2004).
21. R.W. Alder. J. Am. Chem. Soc. **127**, 7924 (2005).
22. Schrödinger, LLC. Jaguar. Version 6.0 [computer program]. Schrödinger, LLC, New York. 2005.
23. A.D. Becke. J. Chem. Phys. **98**, 5648 (1993).
24. C. Lee W. Yang, and R.G. Parr. Phys. Rev. B, **37**, 785 (1988).
25. R.W. Alder, P.S. Bowman, W.R.S. Steele, and D.R. Winterman. J. Chem. Soc. Chem. Commun. 723 (1968).
26. A. Mucci, R. Domain, and R.L. Benoit. Can. J. Chem. **58**, 953 (1980).
27. R.L. Benoit, D. Lefebvre, and M. Fréchette. Can. J. Chem. **65**, 996 (1987).
28. A.F. Pozharskii, O.V. Ryabtsova, V.A. Ozeryanskii, A.V. Degtyarev, O.N. Kazheva, G.G. Alexandrov, and O.A. Dyachenko. J. Org. Chem. **68**, 10109 (2003).
29. G. Chang, W.C. Guida, and W.C. Still. J. Am. Chem. Soc. **111**, 4379 (1989).
30. M. Sauders, K.N. Houk, Y.D. Wu, W.C. Still, M. Lipton, G. Chang, and W.C. Guida. J. Am. Chem. Soc. **112**, 1419 (1990).
31. F. Mohamadi, N.G.J. Richards, W.C. Guida, R. Liskamp, M. Lipton, G. Caulfield, G. Chang, T. Hendrickson, and W.C. Still. J. Comput. Chem. **11**, 440 (1990).
32. Schrödinger, LLC. MacroModel. Version 9.0 [computer program]. Schrödinger, LLC, New York. 2005.

© 2006 NRC Canada

Bis(ether) derivatives of tetrakis(2-hydroxyphenyl)ethene — Direct synthesis of (*E*)- and (*Z*)-bis(2-hydroxyphenyl)-bis(2-methoxyphenyl)ethene via the McMurry olefination reaction[1]

Mee-Kyung Chung, Paul Fancy, and Jeffrey M. Stryker

Abstract: The direct synthesis of sterically hindered, partially etherified derivatives of tetrakis(2-hydroxyphenyl)ethene is reported by using the McMurry reductive olefination reaction on a range of differentially substituted 2,2′-dialkoxybenzophenone substrates. Three orthogonal protection strategies are demonstrated, incorporating β-silylethyl, 3-butenyl, and *tert*-butyl protecting groups, respectively, into the starting benzophenones. The latter proved most efficient, with both the McMurry coupling and deprotection steps occurring concomitantly under the McMurry conditions to directly yield the desired bis(2-hydroxyphenyl)-bis(2-methoxyphenyl)ethene as a 1:1 mixture of *E*- and *Z*-diastereoisomers.

Key words: preorganized polyaryloxide ligands, McMurry olefination, titanium trichloride, supramolecular chemistry, tetrakis(2-hydroxyphenyl)ethene, 2,2′-disubstituted benzophenone.

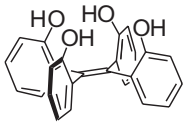
Résumé : On a réalisé la synthèse directe de dérivés stériquement encombrées et partiellement éthérifiés du tétrakis(2-hydroxyphényl)éthène en appliquant la réaction d'oléfination réductrice de McMurry à une large série de 2,2′-alkoxybenzophénones substituées. On a démontré les stratégies de protection orthogonale en incorporant respectivement des groupes protecteurs β-silyléthyle, butén-3-yle et *tert*-butyle dans les benzophénones de départ. Le dernier s'avère le plus efficace alors que les étapes de couplage de McMurry et de déprotection se produisent d'une façon concomitante dans les conditions de McMurry pour conduire directement au bis(2-hydroxyphényl)éthène-bis(2-methoxyphényl)éthène recherche sous la forme de mélange 1 : 1 des diastéréoisomères *E*- et *Z*-.

Mots clés : ligands polyaryloxydes préorganisés, oléfination de McMurry, trichlorure de titane, chimie supramoléculaire, tétrakis(2-hydroxyphényl)éthène, benzophénone 2,2′-disubstituée.

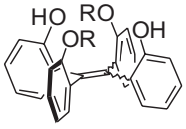
[Traduit par la Rédaction]

Introduction

Structurally preorganized polydentate ligands based on tetrakis(2-hydroxyphenyl)ethene (**I**) constitute a topologically distinct alternative to the ubiquitous calix[4]arene class (1, 2). The roughly square binding array and conformational rigidity imposed by the planarity of the ethylene core allows the construction of highly bridged polymetallic coordination complexes of unusual robustness, providing unique structural and functional models for oxo-surface coordination (1*a*, 3). To expand the potential of this system for applications to coordination chemistry, the preparation of partially etherified tetrakis(2-hydroxyphenyl)ethene ligands (e.g., **II**) has also been reported, both by direct synthesis and by selective dealkylation reactions starting with tetrakis(2-methoxyphenyl)ethene (4).



I



II

The original synthesis of tetrakis(2-hydroxyphenyl)ethene derivatives required a two-step conversion of a 2,2′-dialkoxybenzophenone to the corresponding diaryldiazomethane, followed by acid-catalyzed generation of the tetrakis(2-alkoxyphenyl)ethene. We recently introduced (5) an improved synthesis of tetrakis(2-substituted) tetraphenylethenes by direct conversion of the 2,2′-dialkoxybenzophenone into the corresponding tetraphenylethene using the McMurry reductive olefination reaction (6). Historically, bis(ortho-substituted) benzophenones have been identified as unsuitable for the McMurry reaction, leading instead to competitive reduction of the diarylketone and (or) formation of the

Received 24 January 2006. Accepted 11 April 2006. Published on the NRC Research Press Web site at http://canjchem.nrc.ca on 8 July 2006.

Dedicated to Dr. Alfred Bader, who did well, certainly, and then did good; with deepest admiration and respect. Eppes fun gornisht — "From nothing, something".

M.-K. Chung, P. Fancy, and J.M. Stryker.[2] Department of Chemistry, University of Alberta, Edmonton, AB T6G 2G2, Canada.

[1]This article is part of a Special Issue dedicated to Dr. Alfred Bader.

[2]Corresponding author (e-mail: jeff.stryker@ualberta.ca).

 doi:10.1139/V06-087 © 2006 NRC Canada

coupled but over-reduced tetrasubstituted ethane (7). 2,2′-Dimethoxybenzophenone itself is reported to produce tetrakis(2-methoxyphenyl)*ethane* nearly exclusively (7*a*), presumably a consequence of the high degree of steric congestion in the vicinity of the carbonyl functionality. Despite this negative precedent, however, meticulous optimization of McMurry reaction conditions has led to a remarkably general McMurry procedure for the preparation of sterically hindered tetrakis(2-substituted) tetraphenylethenes in moderate to excellent yields, a significant expansion in the scope of this important olefination reaction (5). To explain this success, the intervention of a previously unrecognized *substrate-based electronic effect* was postulated, contravening the steric limitations inherent to this substrate class.

To improve upon our syntheses of bis(ether) derivatives of tetrakis(2-hydroxyphenyl)ethene, our McMurry protocol has been challenged by a series of orthogonally protected 2,2′-dialkoxybenzophenones, some of considerable steric encumbrance. In this communication, we report the successful extension of the McMurry olefination protocol to this expanded range of unsymmetrically disubstituted substrates, culminating in a single-step olefination–deprotection procedure for the synthesis of (*E*)- and (*Z*)-bis(2-hydroxyphenyl)-bis(2-methoxyphenyl)ethene.

Results and discussion

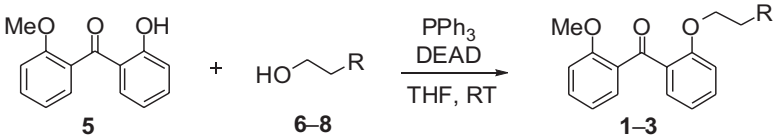
Thus, four unsymmetrically functionalized 2,2′-dialkoxybenzophenones (**1**–**4**) were selected for investigation, each designed to produce a tetrakis(2-alkoxyphenyl)ethene derivative capable of undergoing selective deprotection to give the targeted bis(2-hydroxyphenyl)-bis(2-methoxyphenyl)ethene. Benzophenones **1**–**3** were directly prepared by the dehydrative etherification of 2-hydroxy-2′-methoxybenzophenone [(2-hydroxyphenyl)(2-methoxyphenyl)methanone] (**5**) (4) and the corresponding functionalized alcohols **6**–**8** (8) under Mitsunobu-type conditions (eq. [1]) (9).[3] The final substrate, 2-*tert*-butoxy-2′-methoxybenzophenone (**4**), was prepared in good yield by the directed ortho-lithiation of *tert*-butoxybenzene (**9**) (*n*-BuLi, TMEDA) (10) followed by condensation with the known Weinreb amide, 2-methoxy-*N*-methoxy-*N*-methyl benzamide (**10**) (eq. [2]) (11, 12).

For each substrate, treatment under the previously optimized McMurry reaction conditions ($TiCl_3$ or $TiCl_3$·1.5DME, Zn(Cu), DME, RT)[3] proceeded in moderate to good yields to give the desired olefination product, albeit as an approximately 1:1 mixture of (*E*)- and (*Z*)-isomers (Table 1). The β-silylethyl and butenyl ethers **1**–**3** were converted to the expected bis(2-methoxyphenyl)-bis(2-alkoxyphenyl)ethene derivatives **11**–**13**, respectively (Table 1, entries 2–4). For comparison, the results obtained from McMurry coupling of the symmetrical 2,2′-dimethoxybenzophenone under the same conditions are also provided in Table 1 (entry 1) (5). Although it was anticipated that the steric bulk of the β-silylethyl protecting groups might produce a diastereoselective McMurry reaction, the reactions were entirely nonselective, suggesting that the silyl substituents are too remote from the reactive carbonyl functionality to influence the stereochemistry of the reaction.

For bis[2-(3-butenyloxyphenyl]-bis(2-methoxyphenyl)ethene (**13**), selective deprotection of the butenyloxy moiety was accomplished using catalytic $RhCl_3$·$3H_2O$ (13) in ethanol (reflux, 24 h).[3] In this way, the readily separable mixture of (*E*)- and (*Z*)-bis(2-hydroxyphenyl)-bis(2-methoxyphenyl)ethene (**14**) (ca. 1:1) was obtained, spectroscopically identical with authentic material (4). With due consideration of the attractive results obtained from the reactions of **4** (vide infra), the deprotection of the β-silylethyl ether derivatives **11** and **12** was not pursued in this investigation.

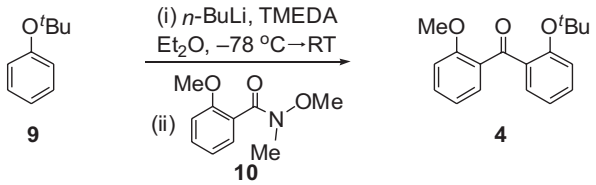
Among the four substrates, the *tert*-butyl ether derivative **4** provided the most compelling and, not coincidentally, the most synthetically valuable result. Despite our original expectation that the steric bulk of the *tert*-butyl substituent might completely inhibit the McMurry reaction, the desired olefination reaction nonetheless proceeds in good yield, *accompanied by the serendipitous in situ deprotection of the* tert*-butyl ether groups*. Thus, a mixture of (*E*)- and (*Z*)-bis(2-hydroxyphenyl)-bis(2-methoxyphenyl)ethenes (**14**) (ca. 1:1) was obtained *directly* from the McMurry reaction (Table 1, entry 5).[3]

A series of control experiments provides some insight into this unexpected transformation. Although the preparation of the low-valent titanium reagent by reduction of $TiCl_3$ with Zn(Cu) also produces $ZnCl_2$ as a by-product, the Lewis acid-

[1] 

5 **6–8** **1–3**

1/6: R = Si^tBuPh_2 **2/7**: R = $SiPh_3$ **3/8**: R = $CH{=}CH_2$

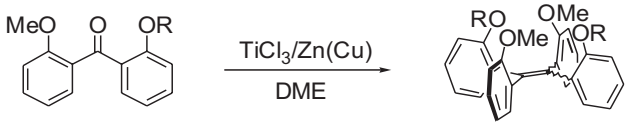
[2] 

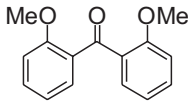
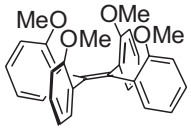
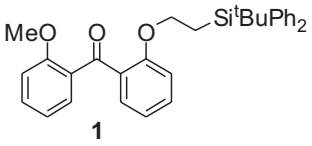
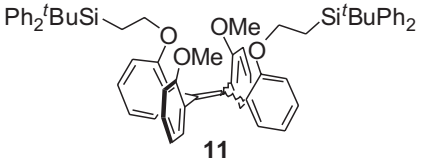
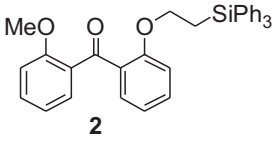
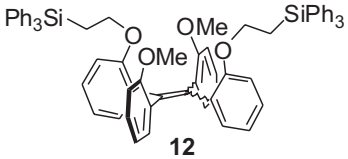
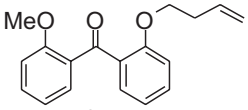
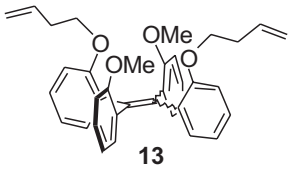
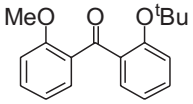
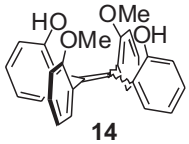
9 **10** **4**

[3] Supplementary data (experimental procedures for the preparation of unsymmetrical ketones (**1**-**4**) and McMurry reactions (**11**–**14**) and the deprotection of **13**; spectroscopic and analytical data) for this article are available on the journal Web site (http://canjchem.nrc.ca) or may be purchased from the Depository of Unpublished Data, Document Delivery, CISTI, National Research Council Canada, Ottawa, ON K1A 0R6, Canada. DUD 5056. For more information on obtaining material refer to http://cisti-icist.nrc-cnrc.gc.ca/irm/unpub_e.shtml.

© 2006 NRC Canada

Table 1. McMurry olefination reactions of 2,2′-bis(*ortho*-alkoxy)benzophenones **1**–**4**.



Entry	Ketone	Olefin derivatives[a]	Isolated yield (%)
1[b]			76[c], 73[d]
2	 **1**	 **11**	69[e] (*E*/*Z* = 1)
3	 **2**	 **12**	57[e] (*E*/*Z* = 1)
4	 **3**	 **13**	48[e] (*E*/*Z* = 1)
5	 **4**	 **14**	45[f,g] (*E*/*Z* = 1), 64[h] (*E*/*Z* = 1)

Note: Reagents and conditions: (*i*) $TiCl_3$ (6 equiv.), Zn(Cu) (3 equiv.), DME, 80 °C, 14 h; (*ii*) RT, substrate. Details provided as Supplementary information (see footnote 3).

[a]Product(s) and *E*/*Z* ratio by spectroscopic analysis. Complete characterization data are provided as Supplementary information (see footnote 3).

[b]See ref. 5.

[c]1,1,2,2-(2′-Methoxyphenyl)ethane was also isolated in 15% yield.

[d]Large-scale experiment (4.12 g, 17.0 mmol of ketone).

[e]The corresponding tetraarylethane was isolated in ~5% yield.

[f]1,2-Bis(2′-hydroxyphenyl)-bis(2′-methoxyphenyl)ethane was isolated in 17% yield.

[g]Product identification by comparison to literature data (see ref. 4).

[h]$TiCl_3$·1.5DME was used as the titanium source and the McMurry reagent preparation step was omitted in this procedure.

ity of this compound is significantly moderated by coordination to DME. In independent trials, anhydr. $ZnCl_2$ in DME only slowly mediates cleavage of the *tert*-butyl ether in **4**.[4] Moreover, the reaction of 2-hydroxy-2′-methoxybenzophenone (**5**) with $TiCl_3$–Zn(Cu) under otherwise identical reaction conditions produces no detectable olefination product; the McMurry reaction of **4** clearly involves the reductive coupling of the intact substrate.[5] Steric effects, evidently, do

[4]The conversion of **4** to **5** using equimolar anhydr. $ZnCl_2$ in DME proceeds 12% to completion after being left overnight at ambient temperature.

[5]After standard aqueous work up, **5** was recovered in 87% yield.

© 2006 NRC Canada

not significantly limit the scope of the McMurry reaction for the production of hindered tetraphenylethenes (5). Whether the in situ deprotection of the *tert*-butyl ether occurs on the surface of the low-valent titanium or by subsequent reaction with DME-solvated $ZnCl_2$ remains undetermined. The replacement of unsolvated $TiCl_3$ powder with the $TiCl_3$·1.5 DME complex and elimination of the reagent preparation period (14) provides significantly higher yields of bis(2-hydroxyphenyl)-bis(2-methoxyphenyl)ethene (**14**) (Table 1, entry 5), although the origin of this improvement is not obvious.[6] Finally, despite the close proximity of the sterically bulky *tert*-butyl substituents to the reactive carbonyl functionality, the McMurry olefination of **4** remains inexplicably stereorandom, consistently returning a 1:1 mixture of (*E*)- and (*Z*)-isomers.

Despite this lack of diastereoselectivity, the steric tolerance of this McMurry olefination protocol is quite remarkable, providing unexpectedly general access to sterically encumbered ortho-substituted tetraphenylethenes. Further extension in the scope of this reaction remains under investigation.

Optimized experimental procedure

McMurry reaction of 4 using $TiCl_3$·1.5 DME[3]

All operations were performed under an atmosphere of argon. In a glovebox, an oven-dried, 50 mL Schlenk flask was charged with $TiCl_3$·1.5 DME (0.62 g, 4.0 mmol) and Zn(Cu) (0.13 g, 2.0 mmol). After removal from the glovebox, anhydr. DME (12.0 mL) was added at ambient temperature under an argon flow. An oven-dried 25 mL Schlenk flask was charged with **4** (0.20 g, 0.69 mmol) and anhydr. DME (6.0 mL) under an atmosphere of argon. The resulting solution was transferred to the slurry of low-valent titanium by cannula under a flow of argon and the reaction mixture stirred at ambient temperature for 18 h, with the progress of the reaction monitored by analytical TLC. After completion of the reaction, the reaction mixture was quenched cautiously with 5 mL of water. The resulting suspension was extracted with diethyl ether (3 × 15 mL). The combined organic layers were dried over $MgSO_4$ and the volatiles removed on the rotary evaporator. Flash chromatography of the crude product on silica gel using a gradient solvent system of CH_2Cl_2–hexanes provided 0.220 g of 1,2-bis(2-hydroxyphenyl)-bis(2-methoxyphenyl)ethene (**14**) as a 1:1 mixture of (*E*)- and (*Z*)-isomers (64% yield). Stereochemical assignments and separation of the isomers by selective crystallization or column chromatography has been previously reported (4).

Acknowledgements

We are grateful to the Natural Sciences and Engineering Research Council of Canada Collaborative Research Opportunities (NSERC-CRO) Program and the University of Alberta for generous financial support. MKC acknowledges the Killam Trusts and the Province of Alberta (Alberta Ingenuity Foundation) for a postdoctoral fellowship and research allowance.

References

1. (*a*) U.H. Verkerk, M. Fujita, T.D. Dzwiniel, R. McDonald, and J.M. Stryker. J. Am. Chem. Soc. **124**, 9988 (2002); (*b*) U.H. Verkerk, R. McDonald, and J.M. Stryker. Can. J. Chem. **83**, 922 (2005).
2. (*a*) C.D. Gutsche. Calixarenes revisited. Royal Society of Chemistry, Cambridge, UK. 1998; (*b*) C. Wieser, C.B. Dielman, and D. Matt. Coord. Chem. Rev. **165**, 93 (1997); (*c*) M.P. Oude Wolbers, F.C. van Veggel, F.G.A. Peters, E.S.E. van Beelen, J.W. Hofstraat, F.A.J. Geurts, and D.N. Reinhoudt. Chem. Eur. J. **4**, 772 (1998).
3. M. Fujita, R. McDonald, and J.M. Stryker. Manuscript submitted for publication.
4. M. Fujita, G. Qi, U.H. Verkerk, T.L. Dzwiniel, R. McDonald, and J.M. Stryker. Org. Lett. **6**, 2653 (2004).
5. M.-K. Chung, G. Qi, and J.M. Stryker. Org. Lett. **6**, 1491 (2006).
6. Original references: (*a*) T. Mukaiyama, T. Sato, and J.J. Hanna. Chem. Lett. 1041 (1973); (*b*) S. Tyrlik and I. Wolochowicz. Bull. Soc. Chim. Fr. 2147 (1973); (*c*) J.E. McMurry and M.P. Fleming. J. Am. Chem. Soc. **96**, 4708 (1974); (*d*) Reviews: J.E. McMurry. Chem. Rev. **89**, 1513 (1989); J.E. McMurry, M.P. Fleming, K.L. Kees, and L.R. Krepski. J. Org. Chem. **43**, 3255 (1978); T. Lectka. *In* Active metals: Preparation, characterization, applications. *Edited by* A. Fürstner. VCH, New York. 1996. Chap. 3; A. Fürstner and B. Bogdanovic. Angew. Chem. Int. Ed. Engl. **35**, 2442 (1996).
7. (*a*) F.-A. von Itter and F. Vögtle. Chem. Ber. **118**, 2300 (1985); (*b*) R. Willem, H. Pepermans, K. Hallenga, M. Gielen, R. Dams, and H. J. Geise. J. Org. Chem. **48**, 1890 (1983); (*c*) F.A. Bottino, P. Finocchiaro, E. Libertini, A. Reale, and A. Recca. J. Chem. Soc. Perkin Trans. 2, 77 (1982).
8. β-Silylethanols **6**–**8** were synthesized by literature procedures: (*a*) S. Sato, J. Matsuda, and Y. Izumi. J. Organomet. Chem. **344**, 71 (1988); (*b*) A. Barbero, P. Cuadrado, A.M. González, F.J. Pulido, and I. Fleming. J. Chem. Soc. Perkin Trans. 1, 2811 (1991).
9. B. Ciommer and H. Schwartz. J. Organomet. Chem. **244**, 319 (1983).
10. S. Harder, J. Boersma, L. Brandsma, J.A. Kanters, A.J.M. Duisenberg, J.H. van Lenthe. Organometallics, **9**, 511 (1990).
11. J. Einhorn, C. Einhorn, and J.-L. Luche. Synth. Commun. **20**, 1105 (1990).
12. The preparation of 2-*tert*-butoxy-2′-methoxybenzophenone (**4**) is a modification of a literature procedure: S. Nohm, S. M. Weinreb. Tetrahedron Lett. **22**, 3815 (1981).
13. (*a*) P.A. Grieco and N. Marinovic. Tetrahedron Lett. 2545 (1978); (*b*) P.A. Grieco, M. Nishizawa, N. Marinovic, and W.J. Ehmann. J. Am. Chem. Soc. **98**, 7102 (1976).
14. This McMurry variant is informally referred to as the "instant method". (*a*) A. Fürstner and D.N. Jumbam. Tetrahedron, **48**, 5991 (1992); (*b*) A. Fürstner, A. Hupperts, A. Ptock, and E. Janssen. J. Org. Chem. **59**, 5215 (1994); (*c*) B. Bogdanovic and A. Bolte. J. Organomet. Chem. **502**, 109 (1995); (*d*) M. Stahl, U. Pidun, and G. Frenking. Angew. Chem. Int. Ed. Engl. **36**, 2234 (1997).

[6] The use of unsolvated $TiCl_3$ (rather than the $TiCl_3$·1.5 DME complex) in this so-called instant method leads to low yields of the desired product and the formation of unidentified, inseparable by-products.

© 2006 NRC Canada

Fabrication of patterned organic thin film by low-energy electron beam lithography and surface-initiated ring-opening metathesis polymerization[1]

Zhebo Ding and Bruce Ganem

Abstract: High densities of immobilized polymer brushes have been created on solid supports in a spatially addressable fashion. Octadecyltrichlorosilane was self-assembled on a silicon substrate to form an inert monolayer. The substrate was then patterned by low-energy electron beam lithography. Finally, the exposed region was back-filled with a second functionalized silane and the pattern was further amplified by surface-initiated ring-opening metathesis polymerization. The patterned substrate was imaged by scanning electron microscopy and atomic force microscopy.

Key words: patterned thin film, e-beam lithography, ring-opening metathesis polymerization, polymer brushes.

Résumé : On a préparé des brosses de polymères de hautes densités immobilisés sur des supports solides dans des arrangements qui peuvent être adressés d'une façon spatiale. On a réalisé un autoassemblage de l'octadécyltrichlorosilane sur un substrat de silicium qui à conduit à la formation d'une monocouche inerte. On a ensuite lithographié le substrat à l'aide de la méthode par faisceau d'électrons de basse énergie. Enfin, on a rempli la région exposée avec un deuxième silane fonctionnalisé et on a amplifié le patron par une polymérisation de métathèse avec ouverture de cycle initiée par la surface. On a obtenu une image du patron du substrat à l'aide de microscopie électronique à balayage et par microscopie des forces atomiques.

Mots clés : film mince avec un patron, lithographie à l'aide d'un faisceau électronique, polymérisation de métathèse avec ouverture de cycle, brosses de polymère.

[Traduit par la Rédaction]

Introduction

The ability to immobilize organic compounds on solid supports in a spatially addressable fashion is of interest in combinatorial chemistry, high-throughput screening, genetic analysis, controlled drug delivery, and trace analyte detection (1). High densities of surface-bound organic substances may be achieved using polymer brushes, which are long polymer chains anchored to the surface that extend away from the attachment sites. Such systems may be assembled either by grafting functionalized polymers onto the surface (2) or by inducing radical (3), cationic (4), or anionic (5) polymerization reactions at surface-bound initiators.

The use of ring-opening metathesis polymerization (ROMP) reactions catalyzed by well-defined and highly active metal alkylidenes (6) represents an attractive alternative approach. The living nature of ROMP reactions provides control of organic thin film thickness and chemical composition. Recently, Weck et al. (7*a*) and Kim et al. (8) reported successful surface-initiated ROMP reactions using an initiator anchored on gold and Si–SiO_2 surfaces, respectively. Pattern generation in polymeric films was achieved by combining microcontact printing (μ-CP) and surface-initiated polymerization (9). Recently, imprint lithography has been demonstrated to fabricate sub-100 nm features (10) for biotechnological applications such as antibody or cell–cell interaction assays (11). Here, we report a simple method for creating high densities of immobilized polymer brushes on solid supports in a spatially addressable fashion as an alternative to imprint lithographic technique.

Electron beam lithography is commonly used in semiconductor manufacturing and can produce precisely aligned, high-resolution patterns. Because direct substrate contact is not required, the method offers advantages over μ-CP or scanned probe lithography (SPL) for patterning surfaces that display complex features (12). Moreover, no mask is needed for electron beam lithography. The creation of features as small as 6 nm in width has been achieved by electron beam

Received 26 October 2005. Accepted 11 January 2006. Published on the NRC Research Press Web site at http://canjchem.nrc.ca on 14 July 2006.

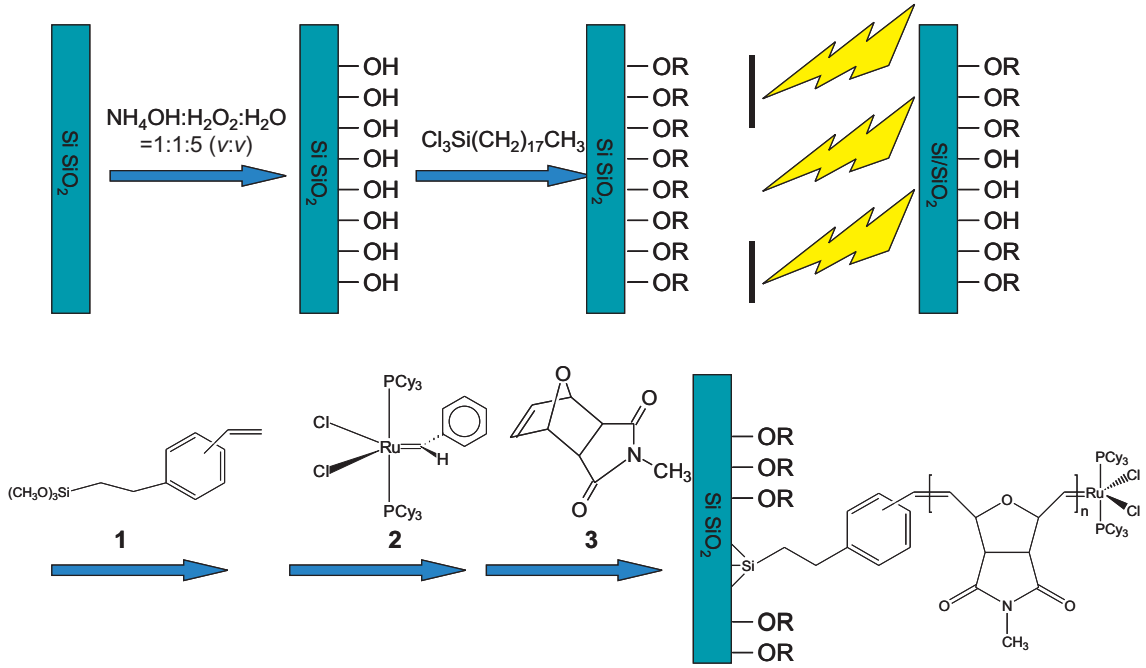
This paper is dedicated to Dr. Alfred Bader on the occasion of his 80th birthday.

Z. Ding and B. Ganem.[2] Department of Chemistry and Chemical Biology, Baker Laboratory, Cornell University, Ithaca, NY 14853-1301, USA.

[1]This article is part of a Special Issue dedicated to Dr. Alfred Bader.
[2]Corresponding author (e-mail: bg18@cornell.edu).

 doi:10.1139/V06-089 © 2006 NRC Canada

Fig. 1. Formation of patterned organic thin films by low-energy electron beam lithography and surface-initiated ring-opening metathesis polymerization.



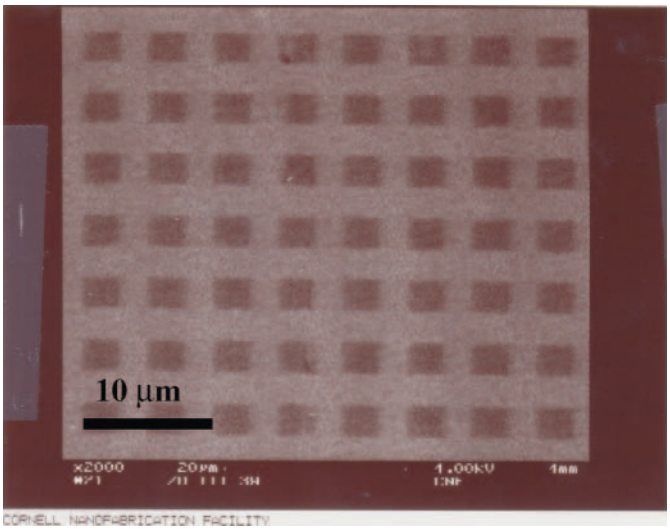
lithography on self-assembled monolayers (SAMs) (13). Low-energy electron beam lithography has recently attracted attention because of its easy operation, low cost, and biological compatibility. Here, we describe a simple and convenient method for fabricating patterned organic thin films using a combination of low-energy electron beam lithography and surface-initiated ROMP.

Methods

A monolayer of octadecyltrichlorosilane (OTS) was self-assembled on a Si–SiO_2 substrate (Fig. 1), then patterned sacrificially by low-energy electron beam lithography. Next, the exposed region was back-filled with a second functionalized silane and the pattern was further amplified by surface-initiated ROMP. Overall, the process is simple and compatible with simple dip and rinse laboratory protocols.

To prepare a hydroxyl group terminated Si–SiO_2 substrate for monolayer deposition, a silicon wafer was first rinsed several times with acetone and 2-propanol. The wafer was then immersed in a boiling solution containing 1:1:5 (by volume) of 30% aqueous hydrogen peroxide, 28%–30% ammonium hydroxide, and deionized water for 10 min, then rinsed with deionized water and dried with flowing argon gas. Self-assembled monolayers of OTS (Sigma-Aldrich) were formed on the clean silicon surface by immersing the cleaned substrate in a 2 mmol/L OTS solution in toluene overnight under argon. The sample was then sonicated in toluene for 5 min, rinsed with toluene, dried with argon, and annealed at 130 °C for 20 min. The contact angle of prepared OTS-modified silicon surfaces was measured to be 113 ± 3°, indicating the complete coverage of the self-assembled monolayers (14). Monolayers were judged to be stable for at least two months when stored in a desiccator at room temperature, since no significant decrease in contact angle was observed.

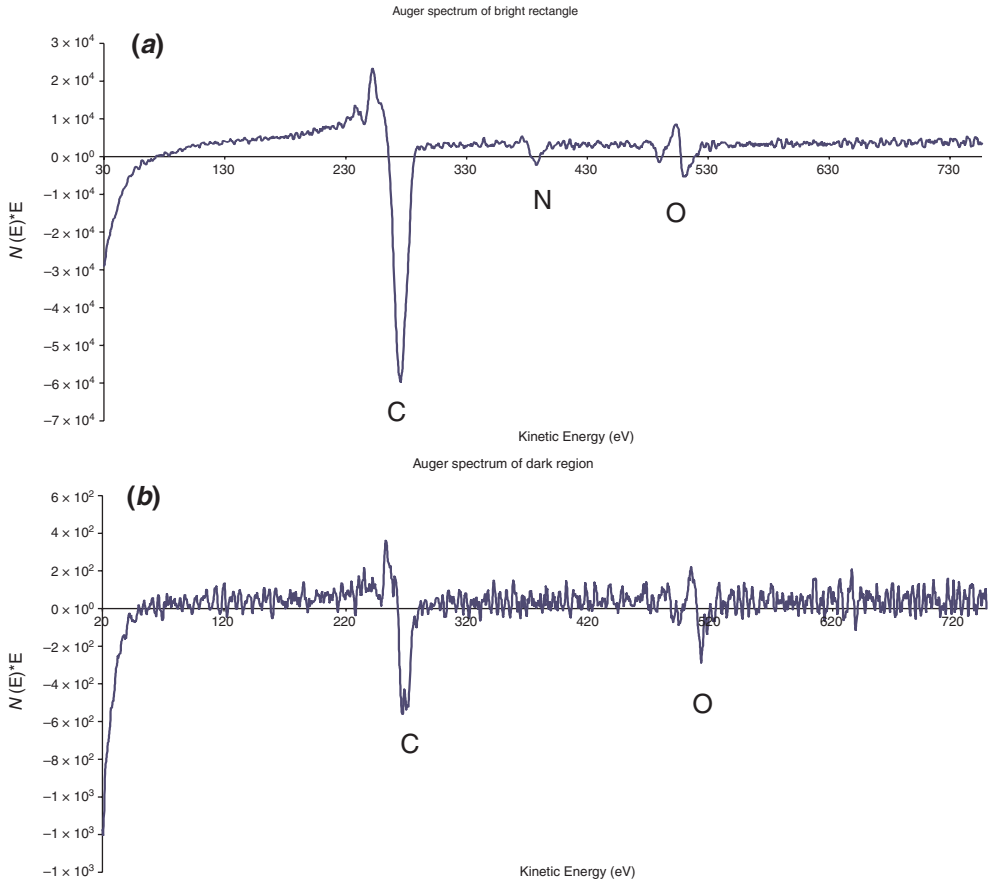
Fig. 2. SEM image of patterned polymer film of **3** on a Si–SiO_2 substrate.



A scanning electron microscope (LEO Electron Microscopy, Inc.Nano Technology Systems Division, Carl Zeiss SMT), equipped with a pattern generator and alignment system (JC Nabity Lithography Systems, Bozeman, Montana), was used for electron beam lithography. Typical electron beam exposures were conducted at an accelerating voltage of 2 kV and doses of 500 µC/cm^2. After electron beam exposure, the sample was further developed in the UV–ozone

© 2006 NRC Canada

Fig. 3. Auger electron spectra of (*a*) the region modified by polymer film of **3** and (*b*) the OTS-modified region. Spectra were taken at an extraction voltage of 3 kV and an electron current of 20 nA. Samples were tilted at a 60° angle.



cleaner (UVOCS Inc., Montgomeryville, Pennsylvania) for 45 s to remove the decomposed monolayer and to regenerate the chemically active hydroxyl groups. It has been shown (15) that UV–ozone exposure is sufficient to remove damaged monolayers without significantly reducing the hydrophobicity of unexposed areas. After surface cleaning, the substrate was immediately immersed in a toluene solution containing 4% (by volume) styrylethyltrimethoxysilane (**1**, SETS, Gelest Inc., Morrisville, Pennsylvania) and 2% (by volume) triethylamine (Fluka) overnight to back-fill the exposed area. The substrate was then sonicated in toluene for 5 min, rinsed with toluene, and dried with argon. Grubbs catalyst [$(Cy_3P)_2Cl_2Ru{=}CHPh$] (16) (**2**) was then immobilized at the styryl-terminated regions by dipping the patterned substrate into a 33 mmol/L CH_2Cl_2 solution of **2** for 3 h. After extensive rinsing with distilled CH_2Cl_2, the sample was subsequently exposed to a 0.4 mol/L CH_2Cl_2 solution of *exo*-*N*-methyl-7-oxabicyclo[2.2.1]hept-5-ene-2,3-dicarboximide (**3**) for 16 h to allow the growth of polymer brushes on the surface.

Spatially localized polymer brushes synthesized by surface-initiated ROMP on the patterned functionalized surfaces were imaged by scanning electron microscopy (SEM) and atomic force microscopy (AFM). Figure 2 shows a low-resolution SEM image of the patterned polymer film. The dark rectangles in the image (3 μm × 2 μm) represent regions where polymer brushes were formed, while light regions represent unaffected areas of OTS monolayers.

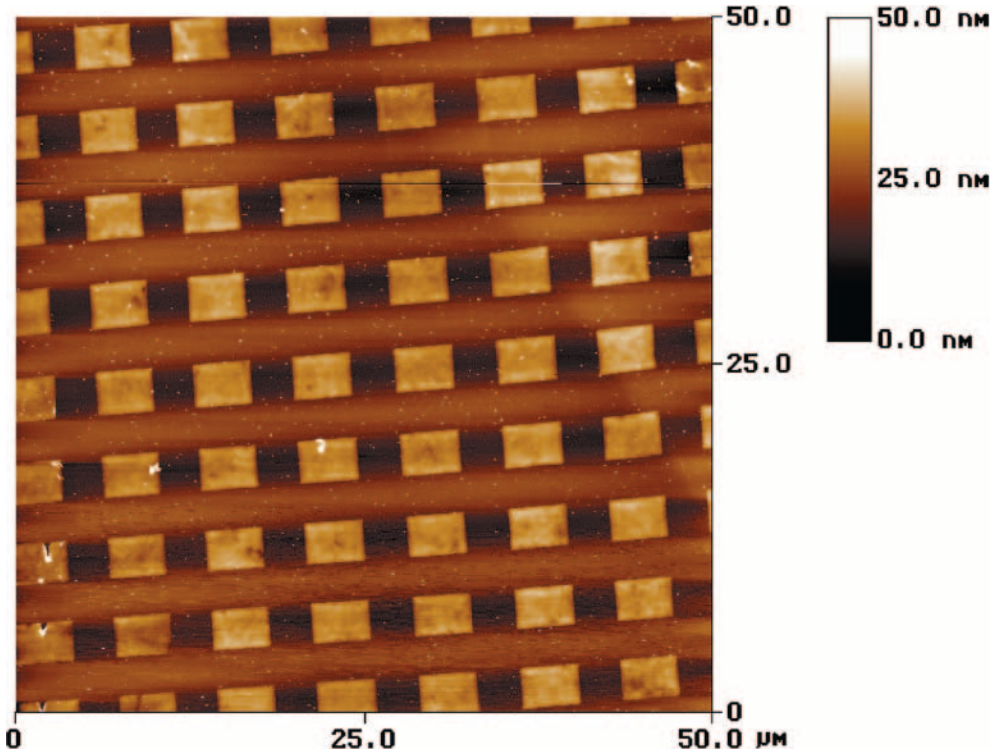
Insights into the chemical composition of the dark and light regions in Fig. 2 came from Auger electron spectroscopy. A scanning Auger microprobe (SAM) was used to establish unique elemental signatures in each region (Fig. 3). Using this technique, dark regions in the SEM image corresponded to polymer brushes, as confirmed by the carbon, nitrogen, and oxygen elemental signatures in the Auger spectrum (Fig. 3*a*). The Auger spectrum of light regions (Fig. 3*b*) matched spectra of authentic samples of uniform OTS monolayers.

Further analysis of the polymer brushes was carried out using AFM. A 50 μm × 50 μm tapping mode AFM scan of the patterned polymer film (Fig. 4) showed very well-defined boundaries between regions where polymer brushes were formed (bright rectangles) and regions covered with OTS (dark areas). The regions of the surface exposed to the electron beam were covered by uniform polymer films. Estimates from the AFM image indicated that the polymer brush thickness was ~30 nm, which is in good agreement with ellipsometry data.[3]

[3] Ellipsometry results were obtained using uniform polymer films produced under identical experimental conditions.

© 2006 NRC Canada

Fig. 4. Tapping mode AFM image of patterned polymer film of **3** on Si–SiO_2 substrate.



Conclusion

In conclusion, a simple surface chemical process has been developed for fabricating patterned organic thin films using low-energy electron beam lithography and surface-initiated ROMP. All processes were conducted in solution at ambient temperature by simple dip and rinse procedures. The use of low-energy electron beam lithography makes it possible to generate higher resolution patterns on surfaces, while locally varying the density of attached materials. The use of this technique for the site-specific anchoring of concentrated quantities of small-molecule drugs, peptides, or diagnostic proteins as polymer brush deposits on surfaces is currently being explored.

Acknowledgments

We are grateful for financial support through the Johnson & Johnson Focused Giving Program. This work was carried out in part at the Cornell NanoScale Science and Technology Facility (a member of the National Nanofabrication Users Network), which is supported by the National Science Foundation under Grant ECS-9731293. We thank Professor Harold Craighead (Department of Applied and Engineering Physics at Cornell University) and Dr. Cindy Harnett (Sandia National Laboratory, Livermore California), as well as Drs. George Papandreou and Pallassana Narayanan (Cordis Corporation, Miami Lakes, Florida) for experimental assistance and helpful discussions.

References

1. G.H. McCall, A.D. Barone, M. Diggelman, S.P.A. Fodor, E. Gentalen, and N. Ngo. J. Am. Chem. Soc. **119**, 5081 (1997); M. Biesalski and J. Ruhe. Macromolecules, **32**, 2309 (1999); R. Jordan, A. Ulman, A.J.F. Kang, M.H. Rafailovich, and J. Sokolov. J. Am. Chem. Soc. **121**, 1016 (1999); J.T. Yates, Jr. Science (Washington, D.C.), **279**, 335 (1998).
2. D. Albagli, G.C. Bazan, R.R. Schrock, and M.S. Wrighton. J. Am. Chem. Soc. **115**, 7328 (1993); J.M. Stouffer and T.J. McCarthy. Macromolecules, **21**, 1204 (1988); S. Al-Maawali, J. Bemis, B. Akhremitchev, R. Leecharoen, B. Janesko, and G. Walker. J. Phys. Chem. B, **105**, 3965 (2001); R. Jordan, K. Graf, H. Riegler, and K.K. Unger. Chem. Commun. (Cambridge), **9**, 1025 (1996); W. Zhao, G. Krausch, M.H. Rafailovich, and J. Sokolov. Macromolecules, **27**, 2933 (1994).
3. O. Prucker and J. Ruhe. Macromolecules, **31**, 592 (1998); T.E. Patten, J.H. Xia, T. Abernathy, and K. Matyjaszewski. Science (Washington, D.C.), **272**, 866 (1996); M. Husseman, E.E. Malmstrom, M. McNamara, M. Mate, D. Mecerreyes, D.G. Benoit, J.L. Hedrick, P. Mansky, E. Huang, T.P. Russell, and C.J. Hawker. Macromolecules, **32**, 1424 (1999); X. Huang and M.J. Wirth. Macromolecules, **32**, 1694 (1999); R.R. Shah, D. Merreceyes, M. Husemann, I. Rees, N.L. Abbott, C.J. Hawker, and J.L. Hedrick. Macromolecules, **33**, 597 (2000).
4. R. Jordan and A. Ulman. J. Am. Chem. Soc. **120**, 243 (1998), and refs. cited therein.
5. R. Jordan, A. Ulman, J.F. Kang, M.H. Rafailovich, and J. Sokolov. J. Am. Chem. Soc. **121**, 1016 (1999).
6. T.M. Trnka and R.H. Grubbs. Acc. Chem. Res. **34**, 18 (2001); R.H. Grubbs and T.M. Trnka. *In* Ruthenium in organic synthesis. *Edited by* S.-I. Murahashi. John Wiley and Sons, Weinheim, Germany. 2004. pp 153–177; R.H. Grubbs. Tetrahedron, **60**, 7117 (2004); R.R. Schrock. J. Mol. Catal. A: Chem. **213**, 21 (2004).
7. (*a*) M. Weck, J.J. Jackiw, R.R. Rossi, P.S. Weiss, and R.H. Grubbs. J. Am. Chem. Soc. **121**, 4088 (1999); see also: (*b*) A. Juang, O. Scherman, R.H. Grubbs, and N.S. Lewis. Langmuir, **17**, 1321 (2001).

© 2006 NRC Canada

8. N.Y. Kim, N.L. Jeon, I.S. Choi, S. Takami, Y. Harada, K.R. Finnie, G.S. Girolami, R.G. Nuzzo, G.M. Whitesides, and P.E. Laibinis. Macromolecules, **33**, 2793 (2000).
9. M. Husemann, D. Mecerreyes, C.J. Hawker, J.L. Hedrick, R. Shah, and N.L. Abbott. Angew. Chem. Int. Ed. **38**, 647 (1999); N.L. Jeon, I.S. Choi, G.M. Whitesides, N.Y. Kim, P.E. Laibinis, Y. Harada, K.R. Finnie, G.S. Girolami, and R.G. Nuzzo. Appl. Phys. Lett. **75**, 4201 (1999).
10. J.P. Rolland, E.C. Hagberg, G.M. Denison, K.R. Carter, and J.M. De Simone. Angew. Chem. Int. Ed. **43**, 5796 (2004).
11. D.J. Pritchard, H. Morgan, and J.M. Cooper. Anal. Chem. **67**, 3605 (1995); S.N. Bhatia, M.L. Yarmush, and M. Toner. J. Biomed. Mater. Res. **34**, 189 (1997).
12. C.K. Harnett, K.M. Satyalakshmi, and H.G. Craighead. Appl. Phys. Lett. **76**, 2466 (2000).
13. M.J. Lercel, C.S. Whelan, and H.G.J. Craighead. Vac. Sci. Technol. **14**, 4085 (1996).
14. Y. Wang and M. Lieberman. Langmuir, **19**, 1159 (2003).
15. C.K. Harnett, K.M. Satyalakshmi, and H.G. Craighead. Langmuir, **17**, 178 (2001).
16. P. Schwab, M.B. France, J.W. Ziller, and R.H. Grubbs. Angew. Chem. Int. Ed. Engl. **34**, 2039 (1995).

© 2006 NRC Canada

A silyl-mediated [3+2] photochemical cycloaddition[1]

Michael G. Organ and Debasis Mallik

Abstract: The generation of larger rings from intermediate cyclobutanes via a two-step [2+2] photocycloaddition – ring expansion, known as the de Mayo reaction, has been widely applied in synthesis. Herein a one-step synthesis of cyclopentanoids has been developed based on the photochemical irradiation of an enone in the presence of an allylsilane. The ability of the silyl moiety to stabilize the intermediate biradical is believed to be responsible for this unique transformation where one normally expects to see the [2+2] cyclobutane adduct.

Key words: [2+2] photocycloaddition – ring expansion, allylsilanes, cyclopentanoids, photochemical.

Résumé : La génération de cycles plus grands à partir d'intermédiaires cyclobutanes, par le biais d'une séquence en deux étapes comportant une photocycloaddition [2+2] suivie expansion de cycle, connue sous le nom de réaction de de Mayo, est très souvent utilisée en synthèse. Dans ce travail, on décrit une synthèse en une étape de cyclopentanoïdes qui repose sur l'irradiation photochimique d'une énone en présence d'un allylsilane. On croit que la possibilité pour la portion silane de stabiliser l'intermédiaire biradicalaire est responsable de cette transformation unique au cours de laquelle on s'attend normalement à obtenir une addition cyclobutane [2+2].

Mots clés : photocycloaddition [2+2] – expansion de cycle, allylsilanes, cyclopentanoïdes, photochimie.

[Traduit par la Rédaction]

Since the seminal work on the allylation reaction between allyltrimethylsilane and α,β-unsaturated ketones was disclosed by Hosomi and Sakurai (1), there has been a great deal published regarding the expansion of the scope and utility of allylsilanes in such reactions (2). This methodology has been expanded to include ring formation when the allylsilanes involved possess "bulky groups" on silicon to provide cyclobutane and cyclopentane products via Lewis acid catalyzed [2+2] and [3+2] annulation, respectively (3–5). The general addition process for allylsilanes onto unsaturated substrates is illustrated in Scheme 1. Siliranium ion intermediate **3** is central to all possible products of initial conjugate addition. In the case of enone substrates (X = alkyl), if Y is large (e.g., isopropyl) the principal product isolated is the five-membered ring adduct **6**, which appears to be both the thermodynamic and kinetic product (6, 7). When Y is methyl, the allylation product **4**, i.e., the Sakurai product, is the major adduct isolated. In the case of unsaturated ester substrates (e.g., X = OR), the formation of both four- and five-membered rings is also with precedent (8, 9). In these situations, the cyclobutane is typically the kinetic product and the cyclopentane **6** forms from **5** over time in the presence of the Lewis acid, presumably via intermediate **3**.

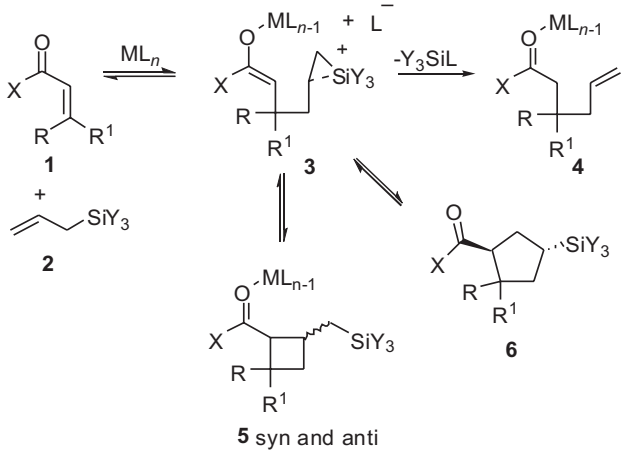
Received 14 October 2005. Accepted 12 April 2006. Published on the NRC Research Press Web site at http://canjchem.nrc.ca on 20 July 2006.

M.G. Organ[2] and D. Mallik. Department of Chemistry, York University, 4700 Keele Street, Toronto,ON M3J 1P3, Canada.

[1]This article is part of a Special Issue dedicated to Dr. Alfred Bader.

[2]Corresponding author (e-mail: organ@yorku.ca).

Scheme 1.

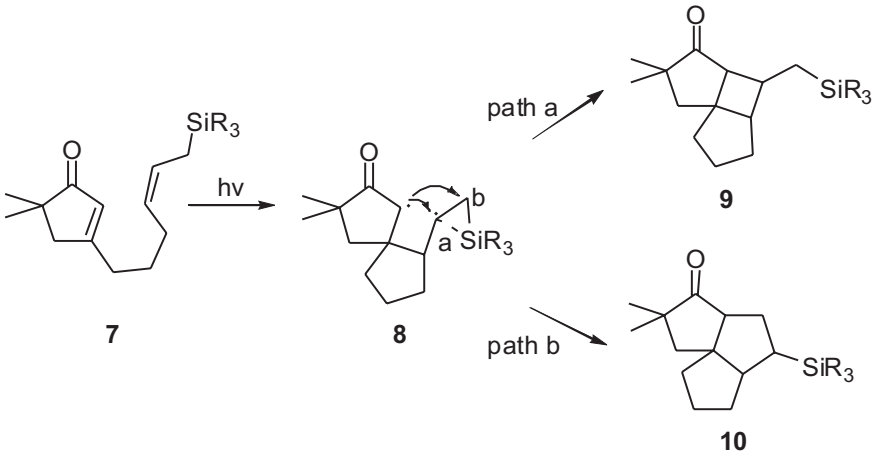


The primary driving force behind nucleophilic reactions involving allylsilanes is the presence of the silicon moiety, which activates the olefin and stabilizes the intermediate carbocation that is generated β to itself during the addition process by strong hyperconjugative effects (see intermediate **3**) (10). Thus, the silyl group is electron-rich and strongly σ-donating. The larger and more electron-rich the ligands on silicon, the more nucleophilic, hence reactive, the allylsilane becomes (11). Further, the larger the ligands on silicon, the more the silyl moiety resists protodesilylation.

It is known that radicals show similar stabilization as do cations when positioned β to silicon, but little has been done with this synthetically. We were interested in trying to exploit this feature of silicon in the development of new cyclization reactions. The photochemical excitation of enones in

 doi:10.1139/V06-077 © 2006 NRC Canada

Scheme 2.

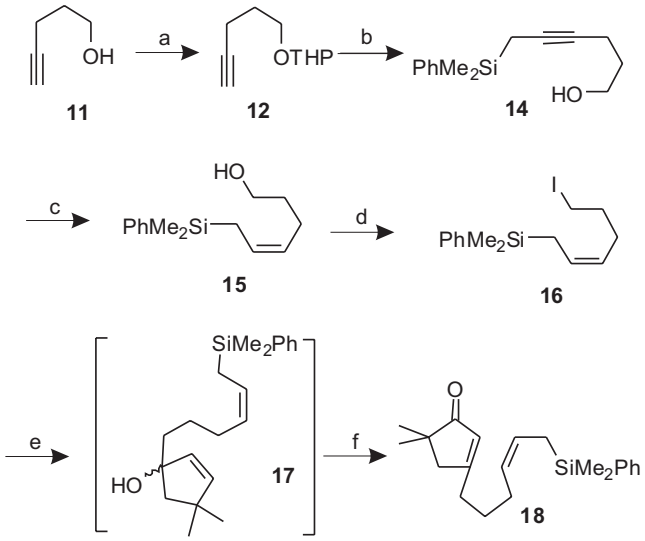


the presence of ground-state alkenes is a reliable and well-established method for the production of radicals. If the alkene was in fact an allylsilane, then the silyl component could become directly involved during the photoaddition itself, thus giving rise to new ringed structures directly upon irradiation. We envisioned that this methodology could be used for the production of five-membered rings and this is demonstrated in our approach to the angular triquinane framework shown in Scheme 2. In this case, it is an intramolecular photoaddition that would lead, presumably, to the intermediate biradical **8**, which would be stabilized by hyperconjugation. This would place radical character at both position *a* and *b*. Closure at *a* would lead to cyclobutane **9**, whereas *b* would provide cyclopentane **10**, which posseses the triquinane ring structure in one overall transformation from **7**.

Our synthetic approach to photoprecursor **18** began with 4-pentyn-1-ol (**11**, Scheme 3). Protection of the alcohol followed by alkyne deprotonation and electrophilic capture with dimethylphenylsilylmethyl iodide provided the corresponding allylsilane. Deprotection (**14**) and controlled hydrogenation with P2 catalyst provided the requisite *cis*-olefin geometry in **15**, which we determined was necessary to deliver the required stereochemistry in the triquinane structure through the ring-forming steps later on (see Scheme 4). Conversion of the alcohol to the corresponding iodide (**16**) provided the substrate for metal–halogen exchange and 1,2-addition to 4,4-dimethylcyclopent-2-en-1-one, yielding **17**. Finally, chromium-mediated [1,3] rearrangement and concomitant oxidation provided photoprecursor **18** cleanly and in good recovery.

The optimized photochemical step is outlined in Scheme 4. Initially, we attempted the reaction under a variety of conditions. In cyclohexane solvent, all other parameters being the same as those in Scheme 4, the Norrish type I cleavage product (i.e., the aldehyde) was the principal one isolated. All reactions attempted using a Hanovia 450 W Hg medium pressure lamp failed to provide any identifiable cycloadducts. However, we did observe isomerization of the allylsilane double bond geometry, which could happen by one of at least two possible mechanisms. The reaction could proceed to the biradical intermediate (**19**), but under these reaction conditions, reversion to starting material is faster than closure to product, thus scrambling olefin geometry.

Scheme 3. Reagents and conditions: (*a*) DHP, PPTS (cat.), CH_2Cl_2, rt, 82%; (*b*) (1*i*) *n*-BuLi, THF, –78 °C, (1*ii*) $PhMe_2SiCH_2I$ (**13**), reflux; (2) H_2SO_4 (cat.), MeOH, rt, 99%; (*c*) H_2 (1 atm, 1 atm = 101.325 kPa), $Ni(AcAc)_2$, $4H_2O$ (cat.), $NaBH_4$ (cat.), Et_3N, EtOH, rt, 75%; (*d*) I_2, PPh_3, Et_3N, MeCN, rt, 76%; (*e*) (*i*) *t*-BuLi (2.2 equiv.), Et_2O, –78 °C, (*ii*) 4,4-dimethylcyclopent-2-en-1-one; (*f*) PDC, CH_2Cl_2, rt, 99%.

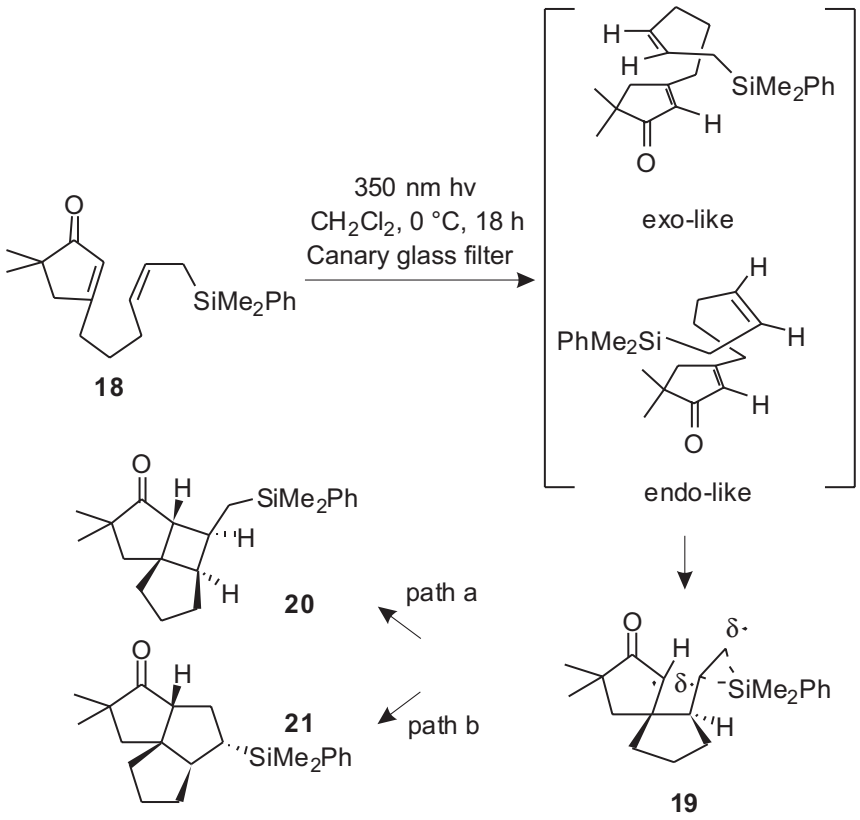


Conversely, and more likely, the double bond could be getting excited, either directly or by triplet transfer, and relaxation occurs with olefin scrambling. We reasoned that if we could eliminate light of wavelengths less than 300 nm, at least direct excitation of the allylsilane would be eliminated with certainty. This meant that Pyrex with a 280 nm cutoff was not a suitable filter, so we opted to use uranium (canary) glass that possesses a 314 nm cutoff (12). As mentioned, attempts with the Hg lamp failed, but prolonged irradiation with a low power Rayonet reactor equipped with 350 nm lamps led to two products (**20** and **21**) in equal amounts (yield = 60%) that were purified by preparative HPLC.

Assuming that the intramolecular addition followed the "rule of 5" (13), leading to the linearly fused and not crossfused photoadduct, the trajectory of the olefin to the enone could follow an "endo-like" or "exo-like" arrangement

© 2006 NRC Canada

Scheme 4.



(see Scheme 4). The endo approach would lead to a highly congested transition state, which is exacerbated by the presence of the *gem*-dimethyl moiety that we installed in the photoprecursor, which is present in the general structure of all angular triquinanes and is therefore necessary. Further to this mechanistic assessment, the structures of **20** and **21** were assigned on the basis of 1D and 2D proton NMR spectra, including COSY and nOe that are in the Supporting information.[3]

There are a few examples in the literature pertaining to the use of olefins that are substituted with structural moieties, which can lead to cycloadducts other than the expected [2+2] photoproducts from the biradical intermediates that are presumably formed on the reaction pathway (14). Indeed, vinylcyclopropane and 1,6-hexadiene derivatives have been used to directly produce six- and seven-membered rings during irradiation with suitable enones. These systems were used as mechanistic probes to determine the initial site of bond formation during the addition process itself. Interestingly, when compound **18** was treated with a variety of Lewis acids (i.e., Me_2AlCl, $EtAlCl_2$, and $TiCl_4$), decomposition of the substrate (**18**) was observed, indicating that the ring expansion is a unique photochemical outcome. To our knowledge, no photoaddition has been conducted that directly leads to the formation of a cyclopentane ring. Further, the silyl moiety is a latent alcohol that can be used to modify the photoadduct to deliver the methyl group and unsaturation at the C-9 site, which is common in the structure of triquinanes.

Acknowledgments

We thank the Ontario Research and Development Challenge Fund (ORDCF) and the Natural Sciences and Engineering Research Council of Canada (NSERC) for financially supporting our program.

References

1. A. Hosomi and H. Sakurai. J. Am. Chem. Soc. **99**, 1673 (1977).
2. For general reviews on the uses of silicon in organic synthesis, see: (*a*) I. Fleming. Chem. Soc. Rev. **10**, 83 (1981); (*b*) Z.N. Parnes and G.I. Bolestova. Synthesis, 991 (1984); (*c*) T.A. Blumenkopf and L.E. Overman. Chem. Rev. **86**, 857 (1986); (*d*) D. Schinzer. Synthesis, 263 (1988); (*e*) I. Fleming, J. Dunogues, and R. Smithers. Org. React. (N.Y.), **31**, 57 (1989); (*f*) T.H. Chan, D. Wang, P. Pellon, S. Lamothe, Z.Y. Wie, L.H. Li, and L.M. Chen. *In* Frontiers of organosilicon chemistry. The Royal Society of Chemistry, Cambridge. 1991. p. 344; (*g*) E.W. Colvin, M.A. Loreto, M. Montieth, and I. Tommasini. *In* Frontiers of organosilicon chemistry. The Royal Society of Chemistry, Cambridge. 1991. p. 356.
3. For approaches to four-membered rings using allylsilanes, see: (*a*) G.D. Hartman and T.G. Traylor. Tetrahedron Lett. **16**, 939 (1975); (*b*) M. Ochiai, M. Arimoto, and E. Fujita. J. Chem.

[3] Supplementary data for this article are available on the journal Web site (http://canjchem.nrc.ca) or may be purchased from the Depository of Unpublished Data, Document Delivery, CISTI, National Research Council Canada, Ottawa, ON K1A 0R6, Canada. DUD 5050. For more information on obtaining material refer to http://cisti-icist.nrc-cnrc.gc.ca/irm/unpub_e.shtml.

© 2006 NRC Canada

Soc. Chem. Commun. 460 (1981); (*c*) L.A. Paquette, R.S. Valpey, and G.D. Annis. J. Org. Chem. **49**, 1317 (1984); (*d*) T. Fujiwara, A. Suda, and T. Takeda. Chem. Lett. 1631 (1992); (*e*) M. Hojo, K. Tomita, Y. Hirohara, and A. Hosomi. Tetrahedron Lett. **34**, 8123 (1993); (*f*) T. Akiyama and M. Kirino. Chem. Lett. 723 (1995).

4. For approaches to five-membered ring carbocycles using allylsilanes, see: (*a*) R.L. Danheiser, B.R. Dixon, and R.W. Gleason. J. Org. Chem. **57**, 6094 (1992); (*b*) M. Hojo, K. Tomita, Y. Hirohara, and A. Hosomi. Tetrahedron Lett. **34**, 8123 (1993); (*c*) R.L. Danheiser, T. Takahashi, B. Bertók, and B.R. Dixon. Tetrahedron Lett. **34**, 3845 (1993); (*d*) H.J. Knölker and R. Graf. Tetrahedron Lett. **34**, 4765 (1993); (*e*) S. Kiyooka, Y. Shiomi, H. Kira, Y. Kaneko, and Tanimori. J. Org. Chem. **59**, 1958 (1994); (*f*) G.P. Brengel, C. Rithner, and A.I. Meyers. J. Org. Chem. **59**, 5144 (1994); (*g*) Y. Takahashi, K. Tanino, and I. Kuwajima. Tetrahedron Lett. **37**, 5943 (1996); (*h*) T. Akiyama, E. Hoshi, and S. Fujiyoshi. J. Chem. Soc. Perkin Trans. 1, 2121 (1998); (*i*) T. Akiyama and M. Yamanaka. Tetrahedron Lett. **39**, 7885 (1998).
5. For approaches to substituted furans using allylsilanes, see: (*a*) J.S. Panek and M. Yang. J. Am. Chem. Soc. **113**, 9868 (1991); (*b*) J.S. Panek and R. Beresis. J. Org. Chem. **58**, 809 (1993); (*c*) J.S. Panek and N.F. Jain. J. Org. Chem. **58**, 2345 (1993); (*d*) T. Akiyama, T. Yasusa, K. Ishikawa, and S. Ozaki. Tetrahedron Lett. **35**, 8401 (1994).
6. (*a*) H.J. Knölker, P.G. Jones, and J.B. Pannek. Synlett, 429 (1990); (*b*) H.J. Knölker, P.G. Jones, J.B. Pannek, and A. Weinkauf. Synlett, 147 (1991); (*c*) H.J. Knölker, N. Foitzik, R. Graf, and J.B. Pannek. Tetrahedron, **49**, 9955 (1993); (*d*) H.J. Knölker, N. Foitzik, H. Goesmann, and R. Graf. Angew. Chem. Int. Ed. Engl. **32**, 1081 (1993).
7. For an example detailing the formation of a (trimethylsilyl)methyl-substituted cyclobutane adduct, in addition to some of the trimethylsilyl-substituted cyclopentanoids, from the reaction of naphthaquinone and allyltrimethylsilane in the presence of the mild Lewis acid, Me_2AlCl, see: W.S. Murphy and D. Neville. Tetrahedron Lett. **38**, 7933 (1997).
8. H.-J. Knölker, G. Baum, and R. Graf. Angew. Chem. Int. Ed. Engl. **33**, 1612 (1994).
9. M.G. Organ, V. Dragan, M. Miller, R.D.J. Froese, and J.D. Goddard. J. Org. Chem. **65**, 3666 (2000).
10. For discussions regarding silyl-stabilized β-carbocations, see: (*a*) W. Hanstein, H.J. Berwin, and T.G. Traylor. J. Am. Chem. Soc. **92**, 829 (1970); (*b*) C. Eaborn. J. Chem. Soc. Chem. Commun. 1255 (1972); (*c*) I. Fleming. *In* Frontier orbitals and organic chemical reactions. Wiley, London. 1976. p. 81; (*d*) S.G. Wierschke, J. Chandrasekhar, and W.L. Jorgensen. J. Am. Chem. Soc. **107**, 1496 (1985); (*e*) J.B. Lambert, G.T. Wang, R.B. Finzel, and D.H. Teramura. J. Am. Chem. Soc. **109**, 7838 (1987); (*f*) J.B. Lambert. Tetrahedron, **46**, 2677 (1990); (*g*) J.B. Lambert and E.C. Chelius. J. Am. Chem. Soc. **112**, 8120 (1990); (*h*) A.J. Green, Y.L. Kuan, and J.M. White. J. Org. Chem. **60**, 2734 (1995); (*i*) V. Gabelica and A.J. Kresge. J. Am. Chem. Soc. **118**, 3838 (1996); (*j*) V.Y. Chan, C.I. Clark, J. Giordano, A.J. Green, A. Karalis, and J.M. White. J. Org. Chem. **61**, 5227 (1996).
11. For examinations of the β effect in relation to different groups on silicon, see: (*a*) M.A. Brook, M.A. Hadi, and A. Neuy. J. Chem. Soc. Chem. Commun. 957 (1989); (*b*) M.A. Brook and C. Henry. Tetrahedron, **52**, 861 (1996); (*c*) H. Mayr and G. Hagen. J. Chem. Soc. Chem. Commun. 91 (1989); (*d*) H. Mayr, J. Bartl, and G. Hagen. Angew. Chem. Int. Ed. Engl. **31**, 1613 (1992); (*e*) H. Mayr and M. Patz. Angew. Chem. Int. Ed. Engl. **33**, 938 (1994); (*f*) H. Mayr and G. Gorath. J. Am. Chem. Soc. **117**, 7862 (1995).
12. For photocyclization of conjugated enones using a uranium filter, see: (*a*) M.T. Crimmins and S.W. Mascarella. J. Am. Chem. Soc. **108**, 3435 (1987); (*b*) M.T. Crimmins and J.A. DeLoach. J. Am. Chem. Soc. **108**, 800 (1986).
13. A.C. Weedon. *In* Synthetic organic chemistry. *Edited by* W.M. Horspool. Plenum Press, New York. 1984.
14. (*a*) A. Rudolf and A.C. Weedon. Can. J. Chem. **68**, 1590 (1990); (*b*) D. Becker, N. Haddad, and Y. Sahali. Tetrahedron Lett. **30**, 2661 (1989); (*c*) D. Becker, N. Haddad, and Y. Sahali. Tetrahedron Lett. **30**, 4429 (1989).

© 2006 NRC Canada

Synthesis and characterization of 2,7-bis(2-pyridyl)-1,8-diazaanthraquinone — A redox-active ligand designed for the construction of supramolecular grids[1]

Rajsapan Jain, Sharon L. Caldwell, Anika S. Louie, and Robin G. Hicks

Abstract: Double condensation of 2-acetylpyridine with 1,3-diaminobenzene-4,6-dicarboxaldehyde affords 2,7-bis(2-pyridyl)-1,8-diazaanthracene, which was subsequently oxidized to the corresponding quinone. Electrochemical studies indicate two reversible reduction processes corresponding to semiquinone and hydroquinonate formation. Electron-withdrawing pyridine groups and the nitrogen atoms make this somewhat more easily reduced than anthraquinone. This compound is redox-active and can be reduced to its radical anion, a potential spin-bearing ligand for the construction of [2 × 2] metallo-grid structures.

Key words: quinone, grid, supramolecular, bistridentate, electrochemistry, metallosupramolecular chemistry.

Résumé : La double condensation de la 2-acétylpyridine avec du 1,3-diaminobenzène-4,6-dicarboxaldéhyde conduit à la formation de 2,7-bis(2-pyridyl)-1,8-diazaanthrène qui s'oxyde subséquemment en quinone correspondante. Des études électrochimiques indiquent qu'il existe deux processus de réductions réversibles qui correspondent à la formation de la semiquinone et de l'hydroquinonate. Par comparaison avec l'anthraquinone, les groupes pyridines et les atomes d'azote électroattracteurs rendent cette réduction plus facile. Ce composé est actif dans un système redox et il peut être réduit en anion radical, un ligand qui pourrait s'avérer utile comme porteur de spin dans la construction de structures en grilles métalliques [2 × 2].

Mots clés : quinone, grille, supramoléculaire, bistridentate, électrochimie, chimie métallosupramoléculaire.

[Traduit par la Rédaction]

Introduction

The designed assembly of metal–ligand architectures — metallosupramolecular chemistry — is an immensely popular contemporary facet of coordination chemistry. Judicious ligand design, coupled with the thermodynamic control that spurs the self-assembly of metal ions and multidentate receptor ligands, has led to a plethora of well-defined geometric shapes (1) as well as coordination polymers (2) and networks. The ultimate product is contingent on ligand topology in addition to its compatibility with different metal ions. This field of research is spurred by the promise of applications based on the potential function (magnetic, optical, catalytic, etc.) of these materials.

One of the more intensively studied classes of discrete metallosupramolecular structures are the so-called "grids" (3). This architectural class is characterized by ligands with multiple polydentate binding sites situated so as to enforce a regular $m \times n$ array of octahedrally or tetrahedrally coordinated metal ions. Figure 1 schematically depicts the assembly of a 2 × 2 grid based on bisbidentate or bistridentate ligands in conjunction with tetrahedrally or octahedrally coordinated metal ions, respectively. A huge number of grids have been prepared, many of which form in high yield simply from reactions of the free ligand and a metal ion source. The structural diversity is impressive and includes larger grids ($n \times n$, $n \geq 3$) (4), rectangular ($n \times m$, $n \neq m$) grids, grids with incompletely filled metal sites (5), and even grids with extraneous (noncoordinated) ligands intercalated into the grid (6).

Beyond their attractive structural features, the properties of grid molecules have been heavily studied. The incorporation of redox-active metals into grid structures can lead to a rich redox chemistry (7), and the magnetic (8) properties of these materials have also been investigated. In all these cases the redox- or spin-active component of the grids are the metal ions; the ligands play an important structural role but can be described as only passive contributors to the electronic functionality of the grids. No examples of metallosupramolecular grids based on redox-active or spin-containing ligands have yet been reported, although we have described the synthesis of a stable radical containing an analogue of **2** designed for such purposes (9).

Herein we present the design and synthesis of a new bistridentate ligand (**5**), which has been designed specifically

Received 22 November 2005. Accepted 12 January 2006. Published on the NRC Research Press Web site at http://canjchem.nrc.ca on 20 July 2006.

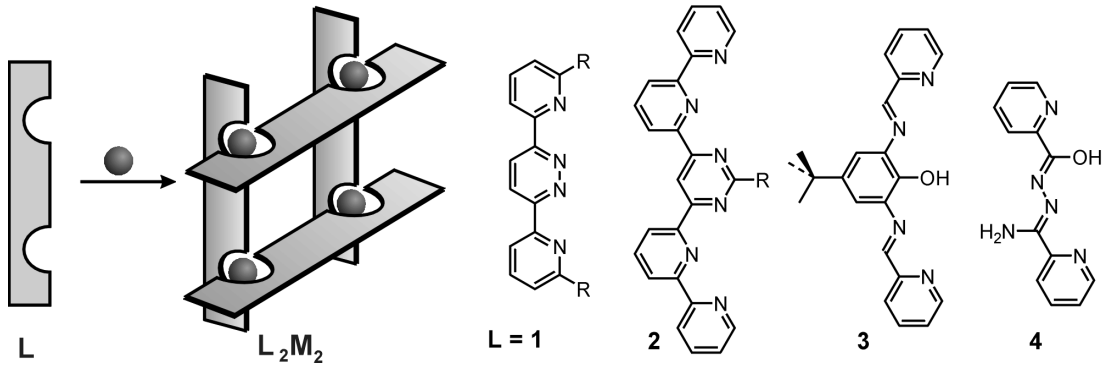
R. Jain, S.L. Caldwell, A.S. Louie, and R.G. Hicks.[2]
Department of Chemistry, University of Victoria,
P.O. Box 3065 STN CSC, Victoria, BC V8W 3V6, Canada.

[1]This article is part of a Special Issue dedicated to Dr. Alfred Bader.

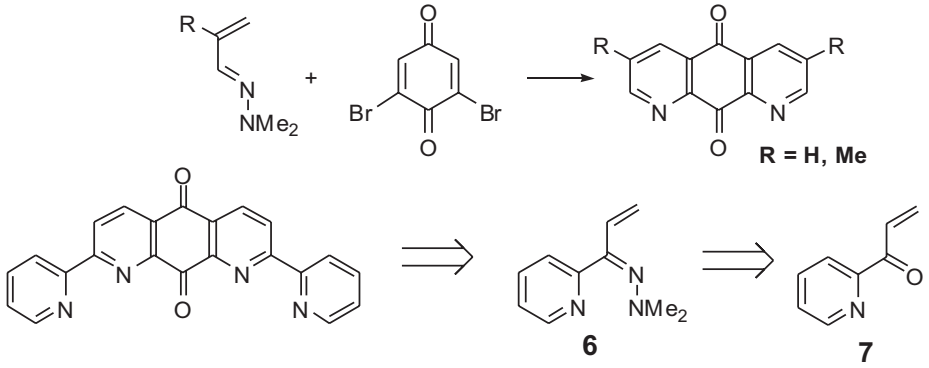
[2]Corresponding author (e-mail: rhicks@uvic.ca).

 doi:10.1139/V06-094 © 2006 NRC Canada

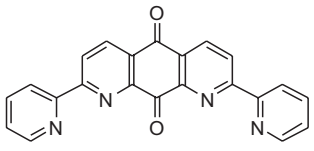
Fig. 1. Schematic of the assembly of a 2 × 2 grid with selected examples of L.



Scheme 1.



for 2 × 2 grid assembly and has the potential to play an active role in electronic (redox, magnetic, optical, etc.) properties of the assembled grid. The metal-binding sites present in **5** are analogous to those found in **3**, i.e., suited for 2 × 2 grid assembly based on octahedrally coordinated metals. However, **5** is distinguished by the presence of the *p*-(anthra)quinone functional unit embedded in the structure. Quinones are well-known to be redox active and form stable radical anions and dianions. Moreover, metal complexes of *o*-quinones possess a number of very interesting physicochemical properties such as strong magnetic exchange between metal- and semiquinone-based spins and molecular bistability (valence tautomerism) (10). The incorporation of quinone-type functional units into supramolecular assemblies is quite rare (11). The molecular structure of **5** has an appropriate topology of metal binding sites for the formation of 2 × 2 grid structures, and the presence of the *p*-quinone component offers the possibility of magnetically coupled metal–ligand arrays or even grid structures capable of exhibiting valence tautomerism.

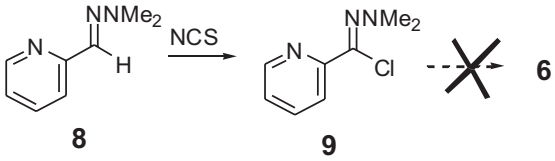


5

Synthesis

Diaza-9,10-anthraquinones are commonly prepared through hetero-Diels–Alder reactions of 1,4-benzoquinones or quinoline–diones and azadienes (Scheme 1) (12). Our initial attempts to construct **5** were based on this strategy, for which the azadiene **6** was identified as a key intermediate. However, attempts to prepare this substrate from the reaction of (2-pyridyl) vinyl ketone (**7**), prepared by oxidation of the corresponding secondary alcohol (13) with *N*,*N*-dimethylhydrazine, failed. We then turned to a different strategy to prepare **6**, outlined in Scheme 2. 2-Pyridinecarboxaldehyde-*N*,*N*-dimethylhydrazone (14) was chlorinated with NCS to give **9**. Attempts to convert **9** to azadiene **6** through reactions with vinyl nucleophiles (Grignard, lithium reagents) led to no reaction or extensive substrate decomposition. Addition of late metal catalysts did not improve these reactions. Therefore, a different route was sought.

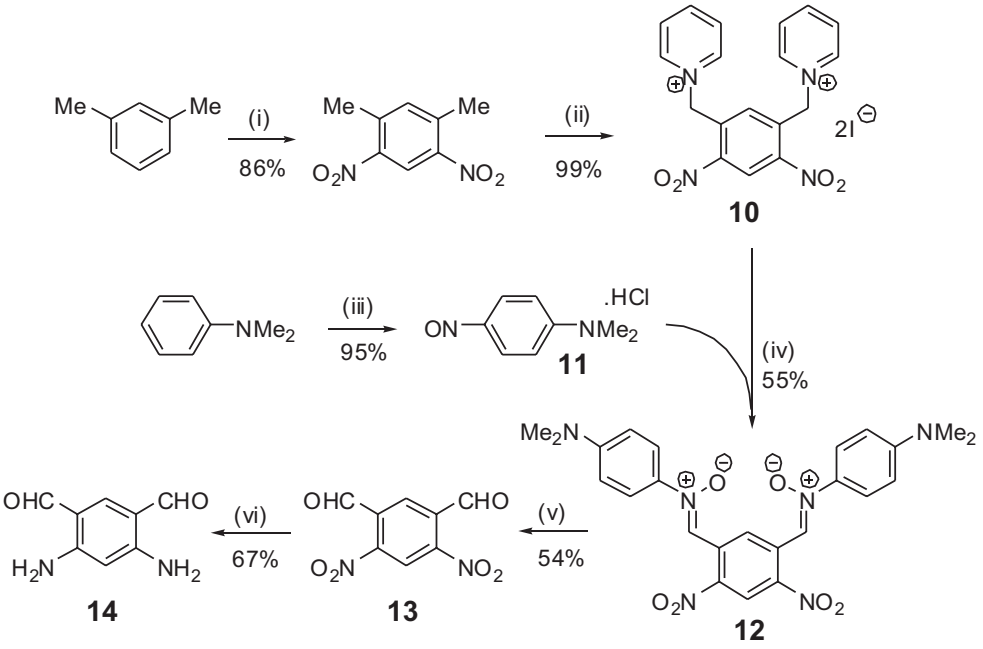
Scheme 2.



The successful synthesis of **5** is outlined in Schemes 3 and 4. The key intermediate is 4,6-diamino-1,3-benzenedicarboxaldehyde (**14**), which was made by slight modification of literature procedures (Scheme 3) (15). *m*-Xylene was bisnitrated and subsequently refluxed with I_2 for 16 h in pyridine to give the air-sensitive bis(pyridinium)diiodide salt (**10**). This salt was reacted with *p*-nitrosodimethylaniline hydrochloride (**11**) (16) to give the bis(imine) oxide (**12**), which was deprotected to give 4,6-dinitro-1,3-benzaldehyde (**13**). Attempts to reduce **13** to the diamine using the literature method (15) failed in our hands. This problem was solved by adopting the protocol described for the reduction of 6-nitro-

© 2006 NRC Canada

Scheme 3. Reagents and conditions: (*i*) HNO_3 (concd.) O °C to rt; (*ii*) pyridine–I_2, 95 °C; (*iii*) 2HCl, $NaNO_2$; (*iv*) **11**, EtOH – 10% NaOH (–5 to 5 °C); (*v*) H_2SO_4 (6 N), toluene, 65 °C; (*vi*) $FeSO_4{\cdot}7H_2O$, EtOH–H_2O–NH_4OH, 80 °C.



Scheme 4. Reagents and conditions: (*i*) 2-acetylpyridine (20 equiv.), 10% KOH, EtOH, 100 °C; (*ii*) CH_3COOH, CrO_3–H_2O, Δ.

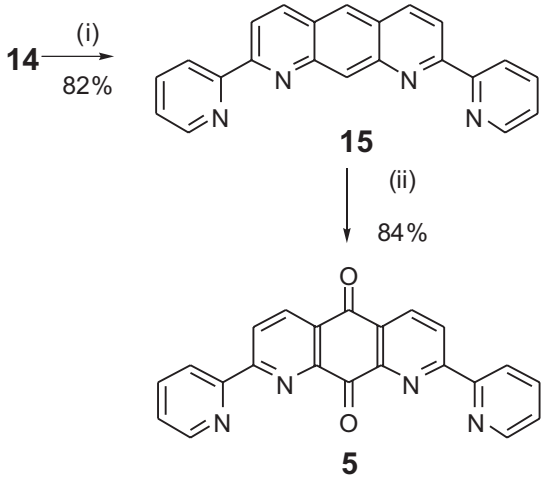
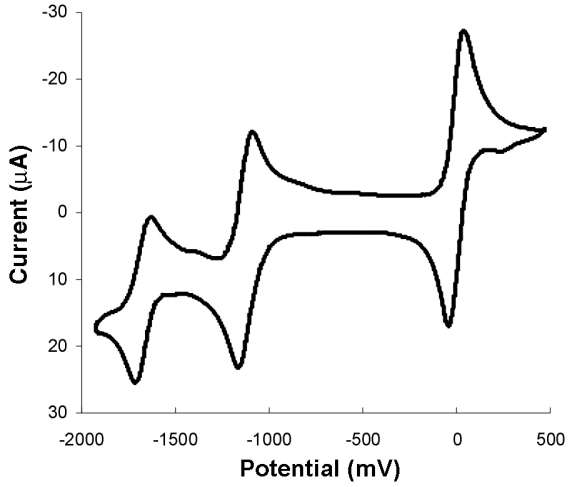


Fig. 2. Cyclic voltammogram of 2,7-dipyridyl-1,8-diaza-9,10-anthraquinone. The redox process at 0 mV is the ferrocene/ferrocenium redox couple, added as an internal reference.



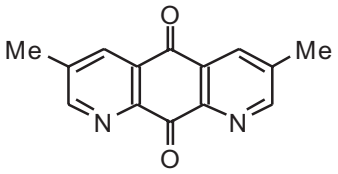
piperinal (17), i.e., aq. $FeSO_4{\cdot}7H_2O$ in EtOH–H_2O followed by addition of 30% NH_4OH at 80 °C. This facilitated formation of **14** in 67% yield.

Dialdehyde **14** then underwent a double condensation reaction with an excess of 2-acetylpyridine to give 2,7-bis(2-pyridyl)-1,8-diazaanthracene (**15**) in excellent yield. We note the potential use of this compound as a bisbidendate ligand in its own right. The oxidation of **15** to target quinone **5** was initially attempted using V_2O_5 and $NaClO_3$, similar to the oxidation of anthracene to anthraquinone (16), but this method was plagued with dismal conversions and recovery of mostly starting material. Aqueous chromium trioxide in glacial acetic acid proved to be a more effective alternative. Upon cooling the reaction after refluxing for 30 min, quinone **5** precipitated and was isolated in 84% yield. The IR spectrum of **5** shows two carbonyl stretches at 1703 and 1662 cm^{-1}. The UV–vis spectrum showed four intense absorptions at 230, 260, 285, and 315 nm. Other spectroscopic and analytical tools confirmed the structure and purity of **5**.

The redox properties of **5** were probed electrochemically. The cyclic voltammogram of **9** (Fig. 2) has two reversible reduction waves at potentials of E_1° = –1.13 V and E_2° = –1.67 V vs. the ferrocene/ferrocenium redox couple. Table 1 presents the reduction potentials of this compound along with corresponding data for several other compounds. 9,10-Anthraquinone is considerably more difficult to reduce (E_1° = –1.39 V, E_2° = –1.86 V) than 1,4-benzoquinone (E_1° = –0.96 V, E_2° = –1.56 V) because of the effects of annelation. The introduction of two nitrogen atoms at the 1,8 positions (i.e., 1,8-diazaanthraquinone (**16**); made according to literature methods (12*b*)) renders this compound slightly more easily

© 2006 NRC Canada

Table 1. Reduction potentials of *p*-quinones in CH_2Cl_2.



16

Compound	E_1° (V)	E_2° (V)
1,4-Benzoquinone	–0.96	–1.56
9,10-Anthraquinone	–1.39	–1.86
16	–1.24	–1.77
5	–1.13	–1.67

reduced (E_1° = –1.24 V, E_2° = –1.77 V) and the title compound has yet still higher reduction potentials (E_1° = –1.13 V, E_2° = –1.67 V) because of the electron-withdrawing 2-pyridyl substituents. Based on this, reduction of **5** should be chemically possible by reaction with cobaltocene (oxidation potential, E_1° = –1.33 V). This was found to be the case as evidenced by a striking color change from pale yellow to deep red on adding cobaltocene to a solution of **5**. However, the presumed cobaltocenium salt of the radical anion of **5** was exceptionally reactive and could not be isolated, as is often the case in *p*-quinones with low reduction potentials. Despite this shortcoming, we anticipate the radical anion of **5** to gain stability upon coordination as observed in other *p*-dioxolene systems (18).

Experimental

General considerations

All reagents were purchased from Sigma-Aldrich and used as received. All solvents were dried and distilled under argon prior to use (ether, Na–benzophenone, CH_2Cl_2, CaH_2). Infrared spectra were recorded on a PerkinElmer FT-IR spectrometer using KBr pellets. NMR spectra were acquired on a Bruker AMX500 spectrometer in $CDCl_3$. Mass spectra were recorded on a Kratos Concept IH mass spectrometer system. UV–vis data were collected on a Cary 100 SCAN spectrophotometer. The electrochemical experiments were performed using a CV-50W voltammetric analyzer (BAS) at room temperature (22 ± 2 °C). Cyclic voltammetry experiments were performed in CH_2Cl_2 containing 0.1 mol/L of *n*-Bu_4NBF_4 under argon. A carbon electrode (BAS, diameter 3.0 mm) was used as the working electrode. Platinum and silver wires were used as the auxiliary and reference electrodes, respectively. The working electrode was polished on alumina before use. *iR* compensations were applied for all experiments. All peak potentials are reported vs. an internal reference (ferrocene/ferrocenium). Elemental analyses were performed by Canadian Microanalytical Services Ltd., Vancouver, British Columbia.

Synthesis of 2-pyridyl-*N*,*N*-dimethylaminochloroimine (9)

A CH_2Cl_2 solution (35 mL) of 2-pyridinecarboxaldehyde dimethylhydrazone (2.03 g, 13.6 mmol) was slowly treated with *N*-chlorosuccinimide in small portions. After stirring overnight, the solvent was removed under reduced pressure and hexanes were added. The succinimide by-product precipitated and was filtered. The yellow-orange filtrate was cooled to afford crystals of **9**. Yield: 1.67 g (67%). ^{1}H NMR ($CDCl_3$, ppm) δ: 8.6 (d, 1H), 7.9 (d, 1H), 7.6 (dd, 1H), 7.2 (dd, 1H), 2.9 (s, 6H). ^{13}C NMR ($CDCl_3$, ppm) δ: 152.1, 149.0, 136.3, 131.9, 124.1, 122.3, 46.7.

Synthesis of 1,3-diamino-4,6-benzenedicarboxaldehyde (14)

A solution of 4,6-dinitro-1,3-benzaldehyde (**13**) (1.6 g, 7.1 mmol) in EtOH–H_2O (50:50, 80 mL) was brought to reflux and then a solution of ferrous sulfate heptahydrate (36.8 g, 0.132 mol) in H_2O (80 mL) was added to the vigorously stirred reaction mixture, followed by ammonium hydroxide (36 mL) while refluxing. The thick black slurry was refluxed for an additional hour. Thereafter, the hot solution was suction filtered using a large Büchner funnel. Finally, hot ethanol (approx. 50 mL) was used to wash the residue to make sure all the product was filtered through. The filtrate was then brought to a boil and refiltered to remove any metallic black residue that may not have been eliminated the first time. The resultant yellow filtrate was boiled to reduce the volume (to approximately one-third) and on cooling, crude **14** (light brown) precipitated, which was isolated by another filtration. The product was recrystallized using a H_2O–EtOH (5:1) mixture. Yield: 0.780 g (67%). Characterization data (^{1}H and ^{13}C NMR) of **14** was the same as reported previously (15).

Synthesis of 2,7-dipyridyl-1,8-diazaanthracene (15)

KOH (10%, 0.4 mL) was added to a solution of 1,3-diamino-4,6-benzenedicarboxaldehyde (**14**, 0.300 g 1.83 mmol) and of 2-acetylpyridine (4.432 g, 36.5 mmol) at 100–110 °C. The solution was stirred for an additional 15 min. Thereafter, 15 mL of ethanol was added to the mixture and boiled for a short time (~2 min). The reaction mixture was cooled, filtered, and the yellow residue washed with EtOH and dried in vacuo to give **15,** which was recrystallized from hot EtOH. Yield: 0.500 g (82%); mp 239 to 240 °C. ^{1}H NMR ($CDCl_3$, 500 MHz) δ: 7.40 (m, 2H, H18, H23), 7.92 (m, 2H, H17, H22), 8.37 (s, 1H, H10), 8.44 (d, 2H, H4, H5, ^3J = 8.8 Hz), 8.61 (d, 2H, H3, H6, ^3J = 8.8 Hz), 8.76–8.80 (m, 4H, H16, H19, H21, H24), 9.07 (s, 1H, H9). ^{13}C NMR ($CDCl_3$, 500 MHz) δ: 119.2 (C3, C6), 122.3 (C18, C23), 124.4 (C16, C21), 126.4 (C10), 127.0 (C11, C14), 129.3 (C9), 136.9, 137.0 (C4, C5, C17, C22), 146.7 (C12, C13), 149.1 (C19, C24), 155.9 (C15, C20), 157.5 (C2, C7). LSIMS: 335 $[M + H]^+$. Anal. calcd. for $C_{22}H_{14}N_4$ (%): C 79.02, H 4.22, N 16.76; found: C 78.73, H 4.23, N 16.74.

Synthesis of 2,7-dipyridyl-1,8-diaza-9,10-anthraquinone (2,7-DIP-DAAQ) (5)

To **15** (0.600 g, 1.80 mmol) in a two-necked flask, mounted by a reflux condenser, was added glacial acetic acid (6 mL), then the flask stoppered. The reaction mixture was brought to reflux, and while that was underway, CrO_3 (4 equiv. mol) were dissolved in H_2O (0.6 mL), followed by glacial acetic acid (3 mL). The heat source was removed from the reaction mixture and the mixture was dropped into the stirring reaction mixture over a course of ~10 min. The

© 2006 NRC Canada

reaction was then refluxed for a further 10–15 min. Pure 2,7-DIP-DAAQ usually precipitates on cooling, but if it did not, the reaction solution at room temperature was precipitated into ice-cold water (30 mL) with continued stirring for another 10–15 min (cold conditions must be maintained). Filtration afforded a crude yellow residue that was washed thoroughly with hot water, cold water, and diethyl ether. Recrystallization from glacial acetic acid afforded **5**. Yield: 0.550 g (84%); mp 316 °C. UV–vis (CH_2Cl_2, nm) λ_{max} (ε): 230 (20 100 (mol/L)$^{-1}$ cm^{-1}), 260 (22 100 (mol/L)$^{-1}$ cm^{-1}), 285 (23 100 (mol/L)$^{-1}$ cm^{-1}), 315 (27 500 (mol/L)$^{-1}$ cm^{-1}). Pertinent IR stetches (cm^{-1}): 1703 (m), 1662 (s), 1589 (s), 1330 (s). ^{1}H NMR ($CDCl_3$, 500 MHz) δ: 7.46 (m, 2H, H18, H23), 7.96 (m, 2H, H17, H22), 8.76–8.79 (m, 4H, H3–H6), 8.85 (d, 2H, H16, H21, ^3J = 8.1 Hz), 8.97 (d, 2H, H19, H24, ^3J = 8.1 Hz). ^{13}C NMR ($CDCl_3$, 500 MHz) δ: 123.2 (C18, C23), 125.4 (C3, C6, C16, C21), 129.8 (C11, C14), 136.4 (C17, C22), 137.4 (C4, C5), 148.8 (C12, C13), 149.4 (C19, C24), 154.1 (C15, C20), 161.2 (C2, C7), 180.1, 182.0 (C9, C10). HRMS calcd. for $C_{22}H_{12}N_4O_2$: 364.10; found: 364.0955 ± 0.0016. Anal. calcd. for $C_{22}H_{12}N_4O_2$ (%): C 72.52, H 3.32, N 15.38: found: C 72.77, H 3.38, N 15.37.

Acknowledgements

We thank the University of Victoria and the Natural Sciences and Engineering Research Council of Canada (NSERC) for support of this research.

References

1. E.C. Constable. Prog. Inorg. Chem. **42**, 67 (1994); C. Piguet, G. Bernardinelli, and G. Hopfgartner. Chem. Rev. **97**, 2005 (1997); M. Fujita. Chem. Soc. Rev. **27**, 417 (1998); S. Leininger, B. Olenyuk, and P.J. Stang. Chem. Rev. **100**, 853 (2000); G.F. Swiegers and T.J. Malefetse. Chem. Rev. **100**, 3483 (2000); B.J. Holliday and C.A. Mirkin. Angew. Chem. Int. Ed. **40**, 2022 (2001); M. Albrecht. Chem. Rev. **101**, 3457 (2001); L. Carlucci, G. Ciani, and D.M. Proserpio. Coord. Chem. Rev. **246**, 247 (2003).
2. A.J. Blake, N.R. Champness, R. Hubberstey, P.W.S. Li, M.A. Withersby, and M. Schroëder. Coord. Chem. Rev. **183**, 117 (1999); R. Robson. J. Chem. Soc. Dalton Trans. 3735 (2000); C. Janiak. Dalton Trans. 2781 (2003); S.L. James. Chem. Soc. Rev. 276 (2003).
3. M. Ruben, J. Rojo, F.J. Romero-Salguero, L.H. Uppadine, and J.-M. Lehn. Angew. Chem. Int. Ed. **43**, 3644 (2004); L.K. Thompson. Coord. Chem. Rev. **233–234**, 193 (2002).
4. A.M. Garcia, F.J. Romero-Salguero, D.M. Bassani, J.-M. Lehn, G. Baum, and D. Fenske. Chem. Eur. J. **5**, 1803 (1999); L. Zhao, Z. Xu, L.K. Thompson, S.L. Heath, D.O. Miller, and M. Ohba. Angew. Chem. Int. Ed. **39**, 3114 (2000); L.K. Thompson, L. Zhao, Z. Xu, D.O. Miller, and W.M. Reiff. Inorg. Chem. **42**, 128 (2003).
5. E. Breuning, G.S. Hanan, F.J. Romero-Salguero, A.M. Garcia, P.N.W. Baxter, J.-M. Lehn, E. Wegelius, K. Rissanen, H. Nierengarten, and A. van Dorsselaer. Chem. Eur. J. **8**, 3458 (2002); C.J. Matthews, S.T. Onions, G. Morata, M. Bosch Salvia, M.R.J. Elsegood, and D.J. Price. Chem. Commun. (Cambridge), 320 (2003); S.T. Onions, A.M. Frankin, P.N. Horton, M.B. Hursthouse, and C.J. Matthews. Chem. Commun. (Cambridge), 2864 (2003).
6. S. Toyota, C.R. Woods, M. Benaglia, R. Haldimann, K. Wärnmark, K. Hardcastle, and J.S. Siegel. Angew. Chem. Int. Ed. **40**, 751 (2001).
7. M.T. Youinou, N. Rahmouni, J. Fischer, and J.A. Osborn. Angew. Chem. **31**, 733 (1992); M. Ruben, E. Breuning, J.-P. Gisselbrecht, and J.-M. Lehn. Angew. Chem. Int. Ed. **39**, 4139 (2000); M. Ruben, E. Breuning, M. Barboiu, J.-P. Gisselbrecht, and J.-M. Lehn. Chem. Eur. J. **9**, 291 (2003); D.M. Bassani, J.-M. Lehn, S. Serroni, F. Puntoriero, and S. Campagna. Chem. Eur. J. **9**, 5936 (2003); L. Zhao, C.J. Matthews, L.K. Thompson, and S.L. Heath. Chem. Commun. (Cambridge), 265 (2000).
8. O. Waldmann, J. Hassmann, P. Müller, G.S. Hanan, D. Volkmer, U.S. Schubert, and J.-M. Lehn. Phys. Rev. Lett. **78**, 3390 (1997); O. Waldmann, J. Hassmann, P. Müller, D. Volkmer, U.S. Schubert, and J.-M. Lehn. Phys. Rev. B, **58**, 3277 (1998); J. Rojo, J.-M. Lehn, G. Baum, D. Fenske, O. Waldmann, and P. Müller. Eur. J. Inorg. Chem. 517 (1999); Z. Xu, L.K. Thompson, and D.O. Miller. Chem. Commun. (Cambridge), 1170 (2001); O. Waldmann, R. Koch, S. Schromm, P. Müller, L. Zhao, and L.K. Thompson. Chem. Phys. Lett. **332**, 73 (2000); O. Waldmann, L. Zhao, and L.K. Thompson. Phys. Rev. Lett. **88**, 066401 (2002); M. Ruben, E. Breuning, J.-M. Lehn, V. Ksenofontov, F. Renz, and P. Gütlich. Chem. Eur. J. **9**, 4422 (2003); L.K. Thompson, T.L. Kelly, L.N. Dawe, H. Grove, M.T. Lemaire, J.A.K. Howard, E.C. Spencer, C.J. Matthews, S.T. Onions, S.J. Coles, P.N. Horton, M.B. Hursthouse, and M.E. Light. Inorg. Chem. **43**, 7605 (2004); L.H. Uppadine, J.P. Gisselbrecht, N. Kyritsakas, K. Nattinen, K. Rissanen, and J.M. Lehn. Chem. Eur. J. **8**, 2549 (2005).
9. R.G. Hicks, B.D. Koivisto, and M.T. Lemaire. Org. Lett. **6**, 1887 (2004).
10. C.G. Pierpont and R.M. Buchanan. Coord. Chem. Rev. **38**, 45 (1981); (*b*) A. Dei and D. Gatteschi. Inorg. Chim. Acta, **198–200**, 813 (1992); C.G. Pierpont and C.Q. Lange. Prog. Inorg. Chem. **41**, 331 (1994); (*d*) P. Gütlich and A. Dei. Angew. Chem. Int. Ed. Engl. **36**, 2724 (1997); C.G. Pierpont. Coord. Chem. Rev. **219–221**, 415 (2001); E. Evangelio and D. Ruiz-Molina. Eur. J. Inorg. Chem. 2957 (2005).
11. P.J. Stang and B. Olenyuk. Angew. Chem. Int. Ed. Engl. **35**, 732 (1996).
12. (*a*) J.M. Pérez, P. López-Alvarado, C. Avendano, and J.C. Menéndez. Tetrahedron, **56**, 1561 (2000); (*b*) J.M. Pérez, C. Avendano, and J.C. Menéndez. Tetrahedron Lett. **38**, 4717 (1997); (*c*) K. Potts, E.B. Walsh, and D. Bhattacharjee. J. Org. Chem. **52**, 2285 (1987); (*d*) C. Gesto, E. de la Cuesta, and C. Avendano. Tetrahedron, **45**, 4477 (1989); (*e*) B. Serckx-Poncin, A.-M. Hesbain-Frisque, and L. Ghosez. Tetrahedron Lett. **23**, 3261 (1982).
13. J. Uenishi, T. Hiraoka, S. Hata, K. Nishiwaki, O. Yonemitsu, K. Nakamura, and H. Tsukube. J. Org. Chem. **63**, 2481 (1998); L. De Luca, G. Giacomelli, and A. Porcheddu. J. Org. Chem. **66**, 7907 (2001).
14. R.H. Wiley, S.G. Slaymaker, and H. Kraus. J. Org. Chem. **22**, 204 (1957).
15. H. Quast and N. Schön. Liebigs Ann. Chem. 133 (1984).
16. G.M Bennett and E.V. Bell. Org. Synth. Coll. Vol. II, 223 (1943).
17. I. Pendrak, R. Wittrock, and W.D. Kingsbury. J. Org. Chem. **60**, 2912 (1995).
18. A. Dei, D. Gatteschi, L. Pardi, and U. Russo. Inorg. Chem. **30**, 2589 (1991).

© 2006 NRC Canada

Synthesis and aldol cyclotrimerization of 4,7-di-*tert*-butylacenaphthenone[1]

Aaron W. Amick, Keith S. Griswold, and Lawrence T. Scott

Abstract: An efficient gram scale synthesis of the previously unknown 4,7-di-*tert*-butylacenaphthenone (**3b**) is reported. The facile isomerization of epoxide **9b** to ketone **3b** occurs simply on stirring a solution of **9b** with silica gel at room temperature. Aldol cyclotrimerization of **3b** with titanium tetrachloride gives 2,5,8,11,14,17-hexa-*tert*-butyldecacyclene (**1b**) in 58% isolated yield. X-ray crystal structures have been obtained for the synthetic intermediates 4,7-di-*tert*-butylacenaphthene (**2b**) and 4,7-di-*tert*-butylacenaphthylene (**8b**).

Key words: aromatic, decacyclene, hydrocarbon, nonalternant, polycyclic.

Résumé : On a mis au point une synthèse efficace au niveau du gramme de la 4,7-di-*tert*-butylacénaphténone, un composé antérieurement inconnu. L'isomérisation facile de l'époxyde **9b** en cétone **3b** se produit simplement en agitant une solution du composé **9b** avec du gel de silice, à la température ambiante. La cyclotrimérisation aldolique du composé **3b** en présence de tétrachlorure de titane conduit au 2,5,8,11,14,17-hexa-*tert*-butyldécacyclène (**1b**) qui a été isolé avec un rendement de 58 %. Faisant appel à la diffraction des rayons X, on a déterminé les structures cristallines des intermédiaires de synthèse 4,7-di-*tert*-butylacénaphtène (**2b**) et 4,7-di-*tert*-butylacénaphtylène (**8b**).

Mots clés : aromatique, décacyclène, hydrocarbure, nonalternant, polycyclique.

[Traduit par la Rédaction]

Introduction

Decacyclene (**1a**), annulated with additional aromatic rings and (or) substituted with strategically placed chlorine atoms, has served admirably in our laboratory for some years now as the core structure of synthetic precursors to geodesic polyarenes ranging from bowl-shaped polycyclic aromatic hydrocarbons to the I_h fullerene, C_{60} (1). The parent decacyclene (**1a**) was first prepared in 1883 (2) by an oxidative trimerization of acenaphthene (**2a**) (3), which, in turn, was isolated from coal tar. Unfortunately, this simple method is not well-suited for the regioselective cyclotrimerization of unsymmetrical acenaphthene derivatives (4). For this purpose, we have relied on the acid-catalyzed head-to-tail cyclic aldol trimerization of compounds related to acenaphthenone (**3a**, Fig. 1) (1).

Other triply annulated benzene rings with threefold symmetry have been prepared by aldol cyclotrimerizations of cyclic ketones since the 19th century (5); however, the success of the reaction depends on the particular system in ways that are still poorly understood. Some cases work spectacularly well, e.g., 1-indanone (**4**), 85% yield (6), whereas closely related systems sometimes fail miserably, e.g., 1-tetralone (**5**), 0% yield (7).

We recently surveyed the literature on such reactions in an attempt to uncover correlations between the outcome of attempted aldol cyclotrimerizations and structural features in the cyclic ketones, and at least one prerequisite for success did emerge (8). Some critical factors that can scuttle these reactions have been identified (8, 9); however, others remain obscure. Thus, it is still not possible to predict with confidence which cyclic ketones will give triply annulated benzene rings in high yield by aldol cyclotrimerizations.

Fortunately for us, the tricyclic and tetracyclic ketones **6** and **7** and certain chlorinated derivatives thereof, provide triply annulated benzene rings in high yield by aldol cyclotrimerizations (9, 10). We have been especially puzzled, however, by the relatively low yield of decacyclene (**1a**) produced under a variety of conditions from acenaphthenone (**3a**), a five-membered ring aromatic ketone that closely resembles both indanone (**4**) and the larger ketones **6** and **7** (11).

By following the buildup and disappearance of the various intermediates involved in this reaction, we hoped to learn more about what makes the aldol cyclotrimerization of acenaphthenone such a comparatively poor reaction. The low solubility of decacyclene and of the two aldol dimers (E and Z) of **3a**, unfortunately, hampered our ability to obtain reliable data, so we decided to incorporate solubilizing groups at the 4 and 7 positions, where they would not impose any steric hindrance to the reactions. The hexa-*tert*-butyldecacyclene (**1b**) expected from cyclotrimerization of 4,7-di-*tert*-butylacenaphthenone (**3b**), in fact, is already a known compound (3, 12) and its solubility in normal organic solvents bodes well for the mechanistic studies we have

Received 13 October 2005. Accepted 22 November 2005. Published on the NRC Research Press Web site at http://canjchem.nrc.ca on 20 July 2006.

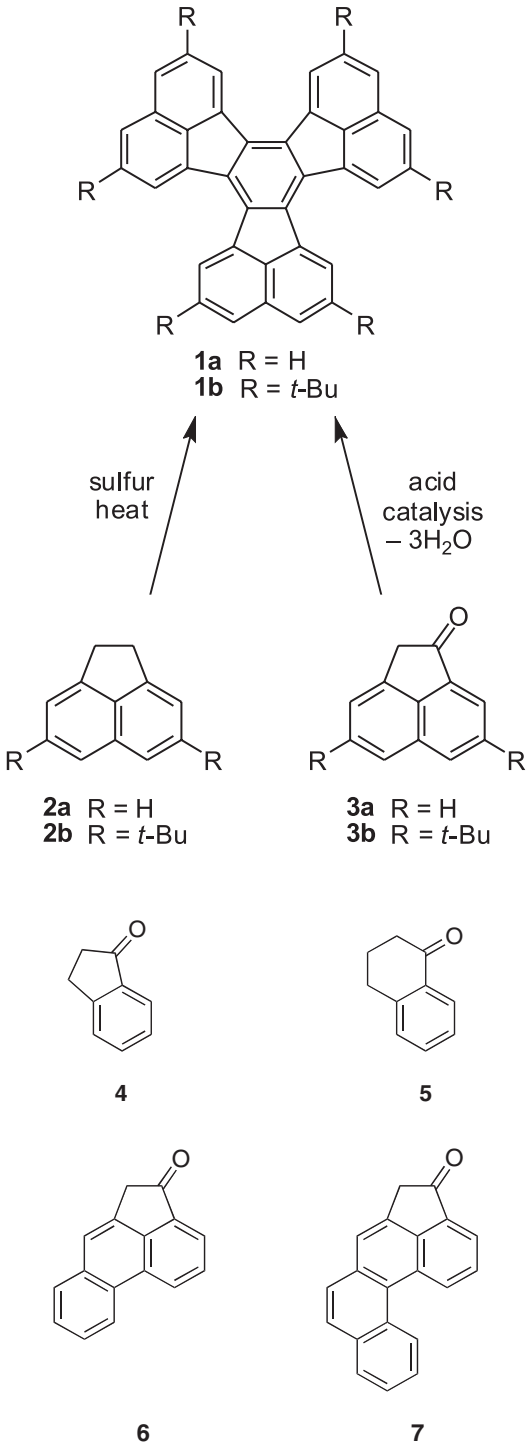
A.W. Amick, K.S. Griswold, and L.T. Scott.[2] Merkert Chemistry Center, Boston College, Chestnut Hill, MA 02467-3860, USA.

[1]This article is part of a Special Issue dedicated to Dr. Alfred Bader.

[2]Corresponding author (e-mail: lawrence.scott@BC.edu).

 doi:10.1139/V06-062 © 2006 NRC Canada

Fig. 1. Decacyclenes (**1**) by oxidative cyclotrimerization of acenaphthenes (**2**) and by aldol cyclotrimerization of acenaphthenones (**3**).



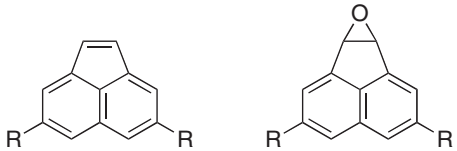
planned. Our purpose is not to compete with the published syntheses of **1b**, which have been achieved both by direct Friedel–Crafts alkylation of **1a** (12) and by oxidative cyclotrimerization of **2b** (3). Rather, we hope to use the alternative synthesis of **1b** from **3b** as a case study with which to probe the factors that influence the interconnected maze of competing pathways involved in aldol cyclotrimerization reactions.

Synthesis and cyclotrimerization of 4,7-di-*tert*-butylacenaphthenone (3b)[3]

The di-*tert*-butylation of acenaphthene (**2a**) under Friedel–Crafts conditions to give 4,7-di-*tert*-butylacenaphthene (**2b**) was first reported by Peters in 1942 (13). The structure of the product was initially misassigned, but Peters corrected the assignment himself in 1950 to the one shown (**2b**) (14).

A further complication in the literature on compounds of this class derives from the intermingling of at least three different numbering schemes for the acenaphthene ring system. Peters consistently refers to compound **2b** as "2 : 5-di-*tert*-butylacenaphthene", in accord with "Richter's numbering of the acenaphthene system",[4] which numbers the carbon atoms of the five-membered ring last. In this paper, we use the *Chemical Abstracts* numbering scheme, which numbers the two carbon atoms of the five-membered ring first.

The unsaturated hydrocarbon, 4,7-di-*tert*-butylacenaphthylene (**8b**), has been prepared from **2b** by dehydrogenation with DDQ in refluxing benzene (15). A third numbering scheme led the authors who first reported this reaction to name the compound "3,6-di-*tert*-butylacenaphthylene", but the structure is the one shown here (**8b**). We have made no significant modifications to the procedures for synthesizing **2b** and **8b**, but report here the UV–vis spectra of both hydrocarbons and the ^{13}C NMR spectrum of **8b** for the first time. Because there are some discrepancies concerning the melting points and NMR chemical shifts of **2b** (13, 14, 16–19) and **8b** (15), we report our melting points and NMR data as well, including copies of the full spectra for the first time in the Supplementary material.[5]



8a R = H
8b R = *t*-Bu

9a R = H
9b R = *t*-Bu

The usual route to substituted acenaphthenones involves benzylic acetoxylation with Pb_3O_4 in acetic acid, followed

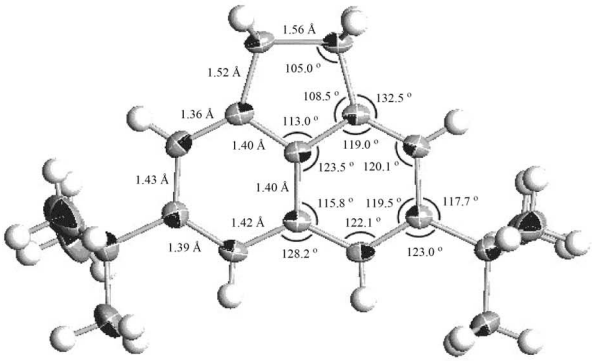
[3] *Chemical Abstracts* name: 4,7-bis(1,1-dimethylethyl)-1(2*H*)-acenaphthylenone or 4,7-di-*tert*-butyl-1(2*H*)-acenaphthylenone.

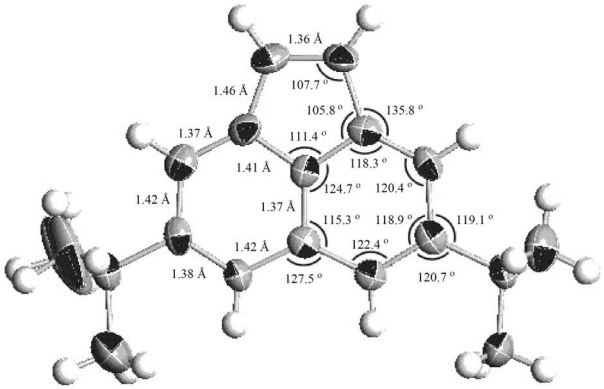
[4] See footnote on page 729 in ref. 14.

[5] Supplementary data for this article are available on the journal Web site (http://canjchem.nrc.ca) or may be purchased from the Depository of Unpublished Data, Document Delivery, CISTI, National Research Council Canada, Ottawa, ON K1A 0R6, Canada. DUD 5051. For more information on obtaining material refer to http://cisti-icist.nrc-cnrc.gc.ca/irm/unpub_e.shtml. CCDC 279886 (**2b**) and 279887 (**8b**) contain the crystallographic data for this manuscript. These data can be obtained, free of charge, via http://www.ccdc.cam.ac.uk/conts/retrieving.html (Or from the Cambridge Crystallographic Data Centre, 12 Union Road, Cambridge CB2 1EZ, UK; fax +44 1223 336033; or deposit@ccdc.cam.ac.uk).

© 2006 NRC Canada

Fig. 2. X-ray crystal structures of 4,7-di-*tert*-butylacenaphthene (**2b**, left) and 4,7-di-*tert*-butylacenaphthylene (**8b**, right).

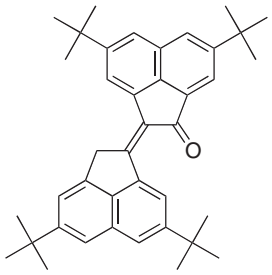




by saponification of the acetate to the alcohol and oxidation to the ketone (17). In the present case, we have found that the readily available epoxide (**9b**) rearranges in high yield to 4,7-di-*tert*-butylacenaphthenone (**3b**) under exceptionally mild conditions (i.e., stirring in solution with silica gel at room temperature).

Preliminary attempts to promote an aldol cyclotrimerization of the substituted acenaphthenone **3b** by treatment with various Lewis acids and Brønsted acids gave only low yields of hexa-*tert*-butyldecacyclene (**1b**). The best conditions found so far (58% isolated yield) entail heating a solution of **3b** and titanium tetrachloride (6 equiv.) in 1,2-dichloroethane to reflux for 4.5 h, with a constant flow of N_2 bubbling through the solvent to sweep out the HCl that is formed.

From a reaction run under other conditions, we isolated and characterized the aldol dimer, 4,7,4′,7′-tetra-*tert*-butyl-1,1′-biacenaphthylenyliden-2-one (**10**), a presumed intermediate in the trimerization. The solubility imparted by the *tert*-butyl groups to all the species present in this reaction has allowed us to begin monitoring these aldol cyclotrimerizations by NMR spectroscopy, and detailed studies that are currently underway with a variety of catalysts, stoichiometries, solvents, temperatures, times, etc., will be reported in due course.



10

X-ray crystal structures of 2b and 8b

Through our ongoing collaboration with the solid-state NMR group of Grant and Pugmire and co-workers in Utah (20), we learned that the motion of individual molecules in crystals of acenaphthylene (**8a**) has prevented the experimental determination of chemical shift tensors for the carbon atoms in this archetypal nonalternant hydrocarbon. We speculated that the *tert*-butyl groups on **8b** should anchor the molecules in the crystal and thereby eliminate the motion. As an added bonus, the incorporation of so many aliphatic hydrogen atoms near the acenaphthylene core would be expected to shorten the relaxation times for the carbon nuclei and allow faster data acquisition. Grant and Pugmire expressed an interest in both the saturated and the unsaturated hydrocarbons, so we supplied them with samples of both **2b** and **8b**.

When we were informed that analysis of the solid-state NMR data would be facilitated by a knowledge of the exact geometries of the molecules, we obtained X-ray crystal structures for both **2b** and **8b** (Fig. 2).[5]

Conclusions

The previously unknown 4,7-di-*tert*-butylacenaphthenone (**3b**) can now be prepared on a gram scale by an efficient three-step synthesis from commercially available acenaphthene (**2a**). The facile isomerization of epoxide **9b** to ketone **3b** occurs simply on stirring a solution of **9b** with silica gel at room temperature. Preliminary efforts to effect the aldol trimerization of **3b** have given the substituted decacyclene **1b** in 58% isolated yield, and the stage is now set for more detailed mechanistic studies. X-ray crystal structures have been obtained for the synthetic intermediates **2b** and **8b**.

Experimental

General

Melting points are corrected.

4,7-Di-*tert*-butylacenaphthene (2b)

The synthesis was carried out in a manner similar to that reported by Gill et al. (18) and the product was obtained as colorless needles by recrystallization from glacial acetic acid (twice) and ethanol (95%, once); mp 162.5–163.5 °C (lit. value (13) mp 162 to 163 °C; lit. value (14) mp 162.5–163.5 °C; lit. value (16) mp 162 to 163 °C; lit. value (17) mp 167.0–168.0 °C; lit. value (19) mp 164 °C). UV–vis (CH_2Cl_2) λ_{max} (log ε): 235 (5.61), 284 (4.50). ^{1}H NMR (400 MHz, $CDCl_3$, ppm) δ: 7.58 (s, 2H), 7.39 (s, 2H), 3.39 (s, 4H), 1.42 (s, 18H). ^{13}C NMR (100 MHz, $CDCl_3$, ppm) δ: 151.08, 144.88, 136.11, 130.56, 117.34, 117.27, 35.43,

© 2006 NRC Canada

31.80, 30.66. HRMS ESI (*m/z*) calcd. for $C_{20}H_{26}$: 266.2034 $[M]^+$; found: 266.2035.

4,7-Di-*tert*-butylacenaphthylene (8b)

A 250 mL round bottom flask was charged with 4,7-di-*tert*-butylacenaphthene (**2b**, 5.16 g, 19.3 mmol), DDQ (6.61 g, 29.1 mmol), and benzene (100 mL). The mixture was heated to reflux, and the progress of the reaction was monitored by GC–MS until it reached completion (ca. 4 h). The benzene was evaporated from the reaction mixture under reduced pressure to give a dark blue solid. This solid was then redissolved in dichloromethane and run through an alumina plug to remove any latent DDQ and hydroquinone. This organic solution was evaporated under reduced pressure to give 4.41 g of a yellow crystalline solid (88% yield); mp 114.5–117 °C (lit. value (15) mp 108 to 109 °C). UV–vis (CH_2Cl_2) λ_{max} (log ε): 235 (5.51), 331 (4.39). ^{1}H NMR (400 MHz, $CDCl_3$, ppm) δ: 7.79 (d, *J* = 1.1 Hz, 2H), 7.76 (d, *J* = 1.1 Hz, 2H), 7.08 (s, 2H), 1.46 (s, 18H). ^{13}C NMR (100 MHz, $CDCl_3$, ppm) δ: 150.90, 138.84, 129.40, 127.09, 125.26, 122.42, 121.93, 35.61, 31.79. HRMS ESI (*m/z*) calcd. for $C_{20}H_{24}$: 264.1878 $[M]^+$; found: 264.1882.

4,7-Di-*tert*-butylacenaphthenone (3b)

A sample of 4,7-di-*tert*-butylacenaphthylene (2.00 g, 7.60 mmol) was added to a solution of freshly washed *m*-chloroperoxybenzoic acid (2.00 g, 11.4 mmol), dichloromethane (50 mL), and saturated aqueous sodium bicarbonate (50 mL). The reaction mixture was stirred and the reaction progress was monitored by GC–MS. Upon completion of the reaction (2 h), the organic layer was separated, dried over anhydrous magnesium sulfate, filtered, and evaporated under reduced pressure. The product was redissolved in dichloromethane and silica gel (ca. 50 g) was added. This slurry was stirred at 25 °C for approximately 6 h. The silica gel was filtered off and washed with dichloromethane. Evaporation of the organic solvent under reduced pressure gave a reddish-orange, oily solid. This product was dissolved in hexanes and evaporated under reduced pressure yielding 1.70–1.91 g (80%–90% over several runs) of a reddish-orange, crystalline solid; mp 81–83 °C. UV–vis (CH_2Cl_2) λ_{max} (log ε): 234 (5.45), 287 (4.47). IR (KBr, cm^{-1}): 1718 (C=O). ^{1}H NMR (400 MHz, $CDCl_3$, ppm) δ: 8.06 (d, *J* = 1.4 Hz, 1H), 8.02 (d, *J* = 1.4 Hz, 1H), 7.74 (s, 1H), 7.52 (d, *J* = 1.0 Hz, 1H), 3.82 (s, 2H), 1.46 (s, 9H), 1.45 (s, 9H). ^{13}C NMR (125 MHz, $CDCl_3$, ppm) δ: 203.72, 151.90, 151.86, 140.25, 134.14, 134.07, 130.45, 127.16, 119.44, 119.24, 118.72, 42.50, 35.66, 35.64, 31.67, 31.47. HRMS ESI (*m/z*) calcd. for $C_{20}H_{24}O$: 280.1827 $[M]^+$; found: 280.1823.

2,5,8,11,14,17-Hexa-*tert*-butyldecacyclene (1b)

A 100 mL two-necked flask was charged with 4,7-di-*tert*-butylacenaphthenone (0.200 g, 0.714 mmol), dichloroethane (16 mL), and titanium tetrachloride (4.3 mmol, 0.47 mL). The reaction mixture was heated to reflux for 4.5 h with a constant flow of N_2 bubbling through the solvent. When the reaction was complete, as determined by TLC, the mixture was poured into a solution of 10% HCl and ice and extracted with dichloromethane. The organic extracts were dried over anhydrous magnesium sulfate, filtered, and concentrated to dryness under reduced pressure.The dark product thus obtained was purified by column chromatography on neutral alumina with hexane–dichloromethane (75:25) to give 0.097 g of a dark yellow crystalline solid (58%). UV–vis (CH_2Cl_2) λ_{max} (log ε): 234 (5.53), 280 (4.86), 350 (4.70). ^{1}H NMR (400 MHz, $CDCl_3$, ppm) δ: 8.97 (s, 6H), 7.93 (s, 6H), 1.66 (s, 54H). ^{13}C NMR (125 MHz, $CDCl_3$, ppm) δ: 151.00, 137.01, 136.37, 131.37, 129.57, 122.14, 121.80, 35.84, 31.99. HRMS ESI (*m/z*) calcd. for $C_{60}H_{66}$: 786.5165 $[M]^+$; found: 786.5168.

4,7,4′,7′-Tetra-*tert*-butyl-1,1′-biacenaphthylenyliden-2-one (10)

A sample of 4,7-di-*tert*-butylacenaphthenone (0.200 g, 0.714 mmol) and anhydrous ethanol (16 mL) were added to a pressure vessel under N_2 and the mixture was cooled to –78 °C. Titanium tetrachloride (0.034 g, 0.178 mmol) was added via syringe and the vessel was sealed. The reaction mixture was stirred in an oil bath at 90 °C for 1 h and subsequently quenched with 10% HCl. The product was extracted into dichloromethane, which was then dried over anhydrous magnesium sulfate, filtered, and evaporated under reduced pressure. The crude product was purified by preparative TLC on alumina with hexane–dichloromethane (75:25) as the eluent, yielding 0.005 g (2.4%) of a bright yellow solid; mp 246–256 °C (dec). UV–vis (CH_2Cl_2) λ_{max} (log ε): 234 (5.28), 289 (4.56), 440 (4.25). IR (KBr, cm^{-1}): 1692 (C=O). ^{1}H NMR (400 MHz, $CDCl_3$, ppm) δ: 10.03 (d, *J* = 1.6 Hz, 1H), 8.19 (d, *J* = 1.6 Hz, 1H), 8.05 (d, *J* = 1.6 Hz, 1H), 8.03 (s, 1H), 7.92 (d, *J* = 1.2 Hz, 1H), 7.82 (d, *J* = 0.8 Hz, 1H), 7.71 (s, 1H), 7.64 (d, *J* = 0.8 Hz, 1H), 4.68 (s, 2H), 1.60 (s, 9H), 1.58 (s, 9H), 1.49 (s, 9H), 1.48 (s, 9H). ^{13}C NMR (125 MHz, $CDCl_3$, ppm) δ: 193.39, 152.27, 151.76, 151.69, 151.18, 150.92, 138.78, 138.27, 138.21, 136.53, 135.94, 133.52, 130.68, 130.33, 129.89, 126.33, 126.30, 123.84, 119.91, 119.88, 119.26, 118.65, 118.06, 41.00, 35.94, 35.88, 35.71, 35.44, 31.88, 31.73, 31.66. HRMS ESI (*m/z*) calcd. for $C_{40}H_{46}O$: 542.3549 $[M]^+$; found: 542.3558.

The stereochemistry around the double bond in this dimer is assigned as (Z) on the basis of ^{1}H NMR chemical shift arguments. Both dimers can be seen in solution, although only this one was isolated and characterized. The lowest field chemical shift for the E-dimer is seen at δ 8.98 ppm, which is very close to lowest field chemical shift for the cyclic trimer (**1b**, 8.90 ppm). The structural similarity between the sterically crowded fjord regions of **1b** and the E-dimer accounts for the near coincidence of their lowest field proton chemical shifts. By contrast, the lowest field chemical shift for the Z-dimer is seen at δ 10.03 ppm, more than 1.00 ppm lower field than that for the E-dimer and for **1b**. The proximity of the fjord region hydrogen in the Z-dimer to the carbonyl group (**10**) accounts for its exceptionally low field chemical shift. Presumably, the E-and Z-dimers interconvert through a common dienol during the aldol trimerization reaction.

Acknowledgments

We thank the National Science Foundation and the Department of Energy for financial support of this research. We are also indebted to the Schering-Plough Corporation for support of the Boston College X-ray facility, to Restek Corp.

© 2006 NRC Canada

for a capillary GC column, and to Kathleen Kilway and Robert Clevenger for helpful advice on the Friedel–Crafts alkylation of acenaphthene.

References

1. (*a*) L.T. Scott. Angew. Chem. Int. Ed. **43**, 4994 (2004); (*b*) R.B.M. Ansems and L.T. Scott. J. Am. Chem. Soc. **122**, 2719 (2000).
2. P. Rehländer. Ph.D. dissertation, University of Berlin, Berlin, Germany, 1883; cited by: P. Rehländer. Chem. Ber. **36**, 1583 (1903).
3. For a synthesis of **1b** from **2b** by the same method, see: J.A. Watson, R.A. Pascal, D.M. Ho, and K.V. Kilway. Tetrahedron Lett. **41**, 5005 (2000).
4. M. Sarobe, R.H. Fokkens, T.J. Cleij, L.W. Jenneskens, N.M.M. Nibbering, W. Stas, and C. Versluis. Chem. Phys. Lett. **313**, 31 (1999).
5. (*a*) S. Gabriel and A. Michael. Ber. Dtsch. Chem. Ges. **10**, 1551 (1877); (*b*) W. Wislicenus. Ber. Dtsch. Chem. Ges. **20**, 589 (1887); (*c*) F.S. Kipping. J. Chem. Soc. **65**, 480 (1894), and refs. cited therein.
6. (*a*) An 85% isolated yield of analytically pure product has been reported by: O. De Frutos, B. Gomez-Lor, T. Granier, M.A. Monge, E. Gutierrez-Puebla, and A.M. Echavarren. Angew. Chem. Int. Ed. **38**, 204 (1999); (*b*) An even higher yield (98%) of unpurified product prepared by the same method was reported earlier by: E.V. Dehmlow and T. Kelle. Synth. Commun. **27**, 2021 (1997).
7. S. Hagen and L.T. Scott. J. Org. Chem. **61**, 7198 (1996), and refs. cited therein.
8. M.M. Boorum and L.T. Scott. *In* Modern arene chemistry. *Edited by* D. Astruc. Wiley, New York. 2002. Chap. 1.
9. L.T. Scott, M.M. Boorum, B.J. McMahon, S. Hagen, J. Mack, J. Blank, H. Wegner, and A. de Meijere. Science, **295**, 1500 (2002).
10. M.M. Boorum, Y.V. Vasil'ev, T. Drewello, and L.T. Scott. Science, **294**, 828 (2001).
11. (*a*) M.S. Bratcher. Ph.D. dissertation, Boston College, Chestnut Hill, Massachusetts. 1996; (*b*) R.B.M. Ansems. Ph.D. dissertation, Boston College, Chestnut Hill, Massachusetts. 2004.
12. K. Zimmermann, R. Goddard, C. Krueger, and M.W. Haenel. Tetrahedron Lett. **37**, 8371 (1996).
13. A.T. Peters. J. Chem. Soc. 562 (1942).
14. H.E. Nursten and A.T. Peters. J. Chem. Soc. 729 (1950).
15. S.F. Nelsen and J.P. Gillespie. J. Am. Chem. Soc. **95**, 1874 (1973).
16. M. Barfield, C.J. Fallick, K. Hata, S. Sternhell, and P.W. Westerman. J. Am. Chem. Soc. **105**, 2178 (1983).
17. K. Ohashi, T. Kubo, T. Masui, K. Yamamoto, K. Nakasuji, T. Takui, Y. Kai, and I. Murata. J. Am. Chem. Soc. **120**, 2018 (1998).
18. H.S. Gill, M. Harmjanz, J. Santamaria, I. Finger, and M.J. Scott. Angew. Chem. Int. Ed. **43**, 485 (2004).
19. A. Altieri, F.G. Gatti, E.R. Kay, D.A. Leigh, D. Martel, F. Paolucci, A.M.Z. Slawin, and J.K.Y. Wong. J. Am. Chem. Soc. **125**, 8644 (2003).
20. A.M. Orendt, J.C. Facelli, S. Bai, A. Rai, M. Gossett, L.T. Scott, J. Boerio-Goates, R.J. Pugmire, and D.M. Grant. J. Phys. Chem. A, **104**, 149 (2000).

© 2006 NRC Canada

Effect of crown ether ring size on binding and fluorescence response to saxitoxin in anthracylmethyl monoazacrown ether chemosensors[1]

Hua Mao, John B. Thorne, Jennifer S. Pharr, and Robert E. Gawley

Abstract: Convenient macrocyclization synthetic routes for the preparation of different-sized monoaza anthracylmethyl crown ether chemosensors (15-crown-5, 18-crown-6, 21-crown-7, 24-crown-8, and 27-crown-9) are described. Evaluation of these crowns as chemosensors for saxitoxin revealed that the larger crowns have moderately higher binding constants, with the 27-crown-9 chemosensor having the largest binding constant (2.29×10^5 $(mol/L)^{-1}$). Fluorescence enhancements of 100% were observed at saxitoxin concentrations of 5 μmol/L, which is close to the detection limit in mouse bioassay.

Key words: anthracene, crown ethers, saxitoxin, paralytic shellfish poison (PSP), binding constants; chemosensors.

Résumé : On décrit des voies de synthèse pratiques à base de macrocyclisations pour la préparation de senseurs chimiques à base des monoaza anthracylméthyl éthers couronnes de tailles différentes, 15-courone-5, 18-couronne-6, 21-couronne-7, 24-couronne-8 et 27-couronne-9. L'évaluation de ces couronnes comme senseurs chimiques pour la saxitoxine révèle que les couronnes les plus grosses présentent les constantes de fixation les plus élevées, alors que le senseur chimique à base de 27-couronne-9 est associée à la constante de fixation la plus élevée, soit $2{,}29 \times 10^{-5}$ $(mol/L)^{-1}$. On a observé des augmentations de la fluorescence de 100 % à des concentrations de 5 μmol/L, valeur qui est proche de la limite de détection dans les bioessais à l'aide de souris.

Mots clés : anthracène, éthers couronnes, saxitonine, intoxication paralysante par les mollusques, constantes de fixation, senseurs chimiques.

[Traduit par la Rédaction]

Harmful algal blooms (HABs) are linked to many cases of human poisoning each year. Economic losses and costs to the fishing industry, public health, and tourism are estimated to be $40 000 000US annually as of the late 1990s (1). The toxins produced by HABs, as well as many other analytes of interest to members of the biomedical community, are "small molecules". Saxitoxin (STX) (Fig. 1) is such a small molecule because of its neurotoxicity and is the most toxic component of the paralytic shellfish poisons (PSPs) (2). Its activity is manifested through the binding of the toxin to voltage-gated sodium channels and blocking sodium ion transport across neuronal membranes. In 1996, saxitoxin was included on the United States government's list of "Select Agents" (potential terrorist weapons). It is one of only three small molecules on the list; the rest are viruses (e.g., Ebola), bacteria (e.g., *Yersenia pestis*), and proteins (e.g., ricin, abrin).

Mouse bioassay is the current method used by government agencies to detect saxitoxin and its derivatives (3), but for both ethical and economic reasons, an alternative would be highly beneficial. We have been working for several years to develop fluorescent chemosensors for the detection of saxitoxin and have recently made significant advances. Specifically, we have shown that arylmethylcrowns are selective for the detection of saxitoxin over sodium, potassium, and calcium ions (4), as well as several organic analytes (5), including tetrodotoxin (Fig. 1) (6). The latter point is clinically relevant since saxitoxin and tetrodotoxin bind, competitively, to the same site on voltage-gated sodium channels and produce the same clinical symptoms (7, 8).

Received 11 November 2005. Accepted 24 January 2006. Published on the NRC Research Press Web site at http://canjchem.nrc.ca on 20 July 2006.

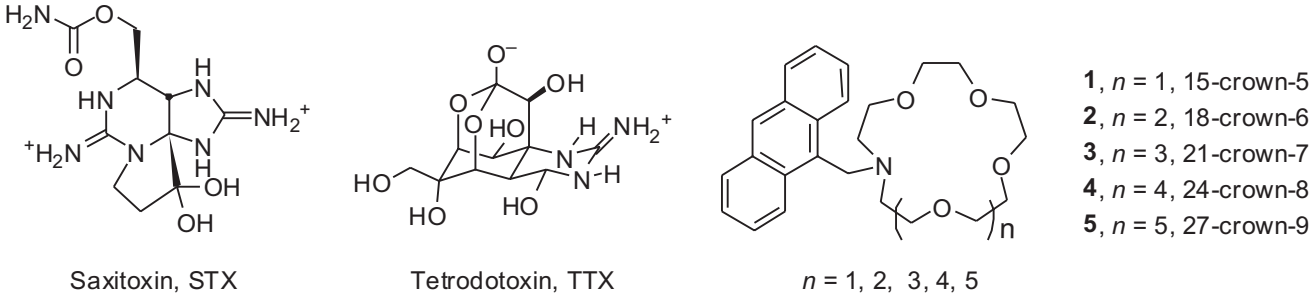
This paper is dedicated to Alfred Bader in recognition of his many contributions, both personal and professional, to the chemical enterprise.

H. Mao, J.B. Thorne, J.S. Pharr, and R.E. Gawley.[2] Department of Chemistry and Biochemistry, University of Arkansas, Fayetteville, AR 72701, USA.

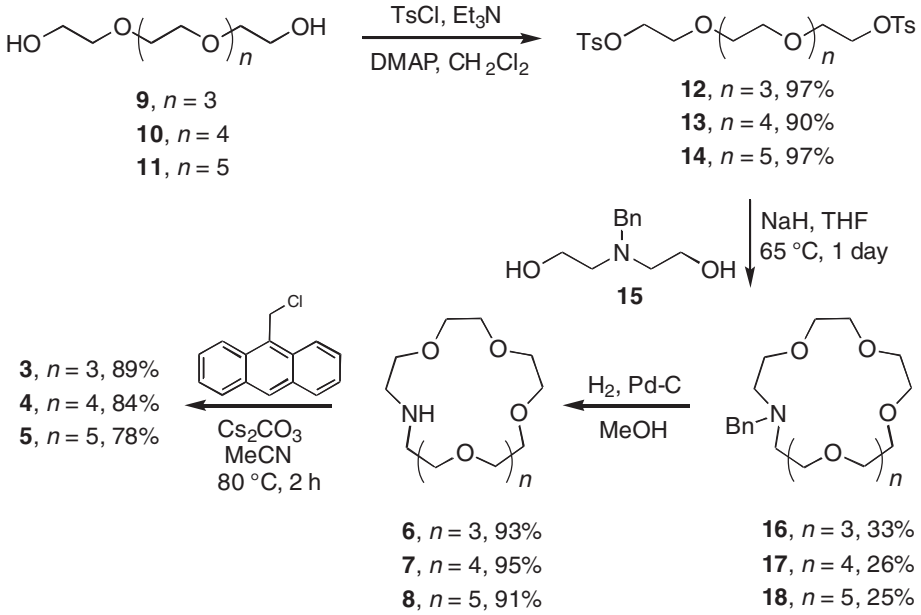
[1]This article is part of a Special Issue dedicated to Dr. Alfred Bader.
[2]Corresponding author (e-mail: bgawley@uark.edu).

 doi:10.1139/V06-093 © 2006 NRC Canada

Fig. 1.



Scheme 1.



Until now we have focused on the 18-crown-6 monoaza- or diaza-crown ethers, with anthracene, coumarin, or acridine fluorophores. In early work, Cram and co-workers showed that 27-crown-9 crown ether is the optimum size to host a guanidinium guest (9, 10). Since saxitoxin (Fig. 1) is a bisguanidinium dication, we explored larger crown sizes to determine the effect on binding, using the anthracene fluorophore as sensor. Thus, crown ethers **1**–**5** were prepared and evaluated for fluorescence response to saxitoxin: 15-crown-5 (**1**, n = 1), 18-crown-6 (**2**, n = 2), 21-crown-7 (**3**, n = 3), 24-crown-8 (**4**, n = 4), and 27-crown-9 (**5**, n = 5) (Fig. 1).

Synthesis

Anthracylmethyl crown ethers **1** and **2** were originally prepared by de Silva and co-workers (11). They were made by alkylation of monoazacrowns with 9-(chloromethyl)anthracene. Anthracylmethyl crowns **3**–**5** were similarly prepared by alkylation of monoazacrowns **6**–**8**, as shown in Scheme 1. The diols **9** and **10** are commercially available. Diol **11** was prepared in three steps from diethylene glycol and triethylene glycol according to a literature procedure (12) with some modifications (using benzyl instead of allyl as the protecting group). Ditosylation of polyethylene glycols **9**–**11** afforded ditosylates **12** (13), **13** (14), and **14**, respectively, which were cyclized with *N*-benzyldiol **15** using sodium hydride to afford the *N*-benzyl crowns **16**–**18** in modest yields. Hydrogenolysis of **16**–**18** to crowns **6**–**8** proceeded smoothly and alkylation with chloromethyl anthracene afforded the sensors **3**–**5**. The synthetic steps all proceeded in excellent yields with the exception of the macrocyclization, which is typically low-yielding (10).[3]

Titrations

A solution of each crown ether in methanol was titrated against saxitoxin using the fluorescence response of anthracene at an excitation wavelength of 372 nm and an emission wavelength of 420 nm. The concentration of the crown ethers was held constant at 10^{-6} mol/L, while the

[3] Supplementary data (^{1}H and ^{13}C NMR spectra for compounds **3**–**8** and **12**–**18** and typical binding isotherms for the titration of crowns **1**–**4**) for this article are available on the journal Web site (http://canjchem.nrc.ca) or may be purchased from the Depository of Unpublished Data, Document Delivery, CISTI, National Research Council Canada, Ottawa, ON K1A 0R6, Canada. DUD 5060. For more information on obtaining material refer to http://cisti-icist.nrc-cnrc.gc.ca/irm/unpub_e.shtml.

© 2006 NRC Canada

concentration of the toxin was varied by successive dilutions with a 10^{-6} mol/L solution of the crown ether. Beginning with 150 µL of a solution of 1 µmol/L crown sensor (**1**–**5**) and a starting STX concentration of 100 µmol/L, binding isotherms were obtained by successive removal of 50 µL aliquots and replacement with 50 µL of a 1 µmol/L crown solution. Fluorescence measurements for each dilution were made after a 4 min equilibration. Binding constants for each anthracylmethyl crown ether were obtained by curve fitting of the intensity at 420 nm to a standard rectangular hyperbolic equation for 1:1 binding (15). The binding constant was determined according to the equation

$$\frac{F}{F_0} = \frac{1 + \left(\frac{k_{11}}{k_{crown}}\right) K_{11}[STX]}{1 + K_{11}[STX]}$$

where F and F_0 are the observed fluorescence intensities in the presence and absence of STX, respectively, k_{crown} and k_{11} are constants related to fluorescence intensities of the crown and the 1:1 crown·STX complex, respectively, K_{11} is the binding constant for the 1:1 complex, and [STX] is the equilibrium concentration of unbound saxitoxin (15). The equation describes a hyperbolic binding isotherm and the binding constant (K_{11}) was obtained by a nonlinear least-squares curve-fitting program. One of the isotherms for saxitoxin binding to **5** is shown in Fig. 2. The binding constants (K_{11}) for the five crown sensors are listed in Table 1. Each value is the average of at least two runs and each run had a correlation coefficient for the least-squares fit of ≥0.98.

Discussion

The sensing mechanism is illustrated by the following equilibrium

$$\text{Toxin} + \text{Crown} \underset{}{\overset{K_{11}}{\rightleftharpoons}} \text{Toxin·Crown}$$

where K_{11} is the binding (equilibrium) constant for formation of the 1:1 Toxin·Crown complex. In sensors such as **1**–**5**, the fluorescent chromophore having a benzylic nitrogen is only weakly fluorescent owing to photoinduced electron transfer (PET) (16). Upon complexation of the toxin, PET is turned off and the chromophore fluoresces normally. The usual mechanism invoked for this type of PET quenching is complexation of a ligand to the benzylic nitrogen lone pair. The binding model that we believe is operative in saxitoxin sensing involves hydrogen bonding of the crown ether to one of the guanidiniums (C-8, Fig. 1), as shown in Fig. 3 (5). Monte Carlo searching of possible docked structures failed to identify a low energy structure having a hydrogen bond to the benzylic nitrogen (5). Note that the second guanidinium appears to π stack with the anthracene fluorophore. We suggest that this π stacking perturbs the relative energies of the chromophore HOMO and the nitrogen lone pair, thus "turning off" the PET (5). This hypothesis is supported by the fact that sodium, potassium, calcium (4), guanidinium (5, 17), and ammonium ions (5, 17), all of which are known to bind to crown ethers, produce no fluorescence enhancement with these sensors in alcohol solvents containing small amounts of water. Further support is found in the failure of

Fig. 2. Typical binding isotherm for titration of saxitoxin from 10^{-4} mol/L to 5×10−7 mol/L vs. anthracylmethyl 27-crown-9 chemosensor **5** (10^{-6} mol/L). A 50% fluorescence enhancement is observed at 1 µmol/L [STX] and 100% enhancement is observed at 5 µmol/L [STX].

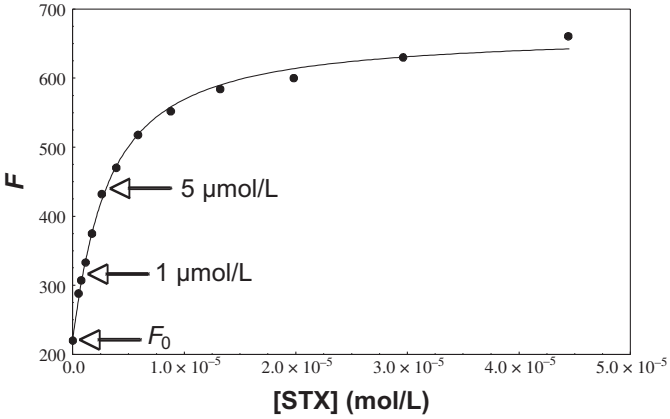
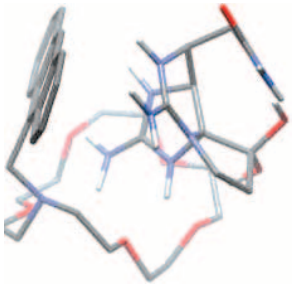


Table 1. Binding constants of saxitoxin to crown sensors **1**–**5** in methanol.

Crown sensor	Binding constant (K_b, $(mol/L)^{-1}$)
1	4.93×10^4
2	5.3×10^4
3	4.68×10^4
4	1.07×10^5
5	2.29×10^5

Note: Each K_{11} is the average of at least two runs. Correlation coefficients of ≥0.98 were calculated for each fit.

Fig. 3. Molecular mechanics model of STX docked to anthracylmethyl 18-crown-6 (global minimum) (5). Note the absence of a hydrogen bond to the benzylic nitrogen.



tetrodotoxin (Fig. 1), a toxin having many hydrogen bond donors but only one guanidinium and which binds competitively to saxitoxin in sodium channels to produce any fluorescence enhancement (6).

Three factors can contribute to an increase in fluorescence intensity upon binding of the toxin: (1) a large binding constant, which increases the relative concentration of the fluorescing Toxin·Crown complex over the unbound Crown; (2) a chromophore having a high molar absorptivity (extinction coefficient); and (3) a high fluorescence quantum yield, such that a high fraction of incident light is absorbed and a high fraction of absorbed light is emitted when PET is turned off. Anthracene has one of the highest fluorescence quantum

© 2006 NRC Canada

yields known (~0.4–0.8, depending on conditions). The fluorescence enhancement by saxitoxin in these sensors has not shown significant dependence on the chromophore (anthracene (5, 17), coumarin (4), or acridine (6)), so our efforts have focussed primarily on increasing the binding constant by making modifications to the crown ether.

In a full paper (5), we reported the synthesis and binding constants of 11 anthracylmethyl 18-crown-6 ethers, 10 of which were diazacrowns with additional substituents added to the crown ring — opposite the anthracylmethyl group — in the hope of increasing the binding constant. Although replacement of one oxygen with a nitrogen doubled the binding constant, further substitution failed to produce any improvement.

In early work on the binding of guanidinium ions to crown ethers, molecular models were used to postulate six hydrogen bonds between guanidinium ion and 27-crown-9 ethers (9, 10). The hypothesis was supported by the solubilization of (otherwise insoluble) guanidinium ion in chloroform by benzo-27-crown-9. The binding model invoked hydrogen bonding between the six guanidinium N-Hs and six of the nine oxygens of the crown ether. Although this binding model cannot be employed for saxitoxin, the large number of hydrogen bond donors in the toxin prompted the question whether a larger crown might show enhanced binding. Interestingly, neither ammonium ion nor guanidinium ion produced any fluorescence enhancement in **2** in ethanol (5, 17). The results of the current study reveal increased binding as the size of the crown ring increases. A control experiment shows that guanidinium ion fails to enhance the fluorescence of **5**; if anything, a slight suppression is observed in methanol.

Summary

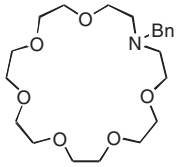
Anthracylmethyl crown ether chemosensors show enhanced binding over smaller crowns. This may be due to the fact that there are more heteroatoms in the crown and (or) that the larger crown is simply more flexible. Either effect could offer more sites for hydrogen bonding to the toxin. Our results show that simple chemosensors such as these could be developed for the detection of saxitoxin and possibly other PSP toxins, at concentrations comparable to those at which mice are sensitive.

Experimental section

General methods

IR spectra were recorded as thin films between NaCl plates or as KBr pellets. ^{1}H and ^{13}C NMR were recorded at 300 MHz for ^{1}H and 75 MHz for ^{13}C. ^{1}H and ^{13}C NMR chemical shifts are reported in ppm relative to residual chloroform; coupling constants are reported in Hz. ESI mass spectra were obtained by flow injection on a quadrupole ion trap mass spectrometer with methanol as the carrier solvent. High-resolution ESI mass spectra (HRMS/ESI) were obtained by using direct flow injection on a 9.4 T Fourier transform mass spectrometer. Dry solvents were freshly distilled before use: dichloromethane was distilled from calcium hydride and THF from sodium–benzophenone. Methanol, acetonitrile, and ethyl acetate were used as received. The hexane used in column chromatography was distilled before use. Water refers to high purity water that was obtained from the Milli-Q purification system. All reactions were performed under a nitrogen atmosphere.

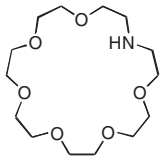
N-Benzyl monoaza-21-crown-7 (16)



To a solution of pentaethylene glycol (5.00 g, 21.0 mmol) in CH_2Cl_2 (120 mL) was added Et_3N (8.8 mL, 63.0 mmol), DMAP (1.28 g, 10.5 mmol), and TsCl (8.41 g, 44.1 mmol) at 0 °C. After stirring at RT for 1 h, NH_4Cl (satd. aq. sol., 50 mL) was added. The reaction mixture was extracted three times with CH_2Cl_2 (3 × 20 mL), the organic phase was dried with $MgSO_4$ and evaporated under reduced pressure. The residue was purified on silica gel using EtOAc–hexane (50%:50%), which gave **12** as an oil (11.2 g, 97%).

To a solution of bistosylate **12** (11.2 g, 20.5 mmol) in anhydr. THF (150 mL) was added *N*-benzyl diol **15** (4.00 g, 20.5 mmol) and NaH (2.46 g, 61.4 mmol; 60% dispersion in mineral oil, the oil was removed from the product chromatographically). The mixture was heated at 65 °C for 18 h. After cooling to RT, NH_4Cl (satd. aq. sol., 100 mL) was added. The reaction mixture was extracted three times with CH_2Cl_2 (3 × 30 mL). The organic phase was dried with $MgSO_4$, evaporated under reduced pressure, and the residue was purified on alumina using EtOAc–hexane (50%:50%), which gave an oil (2.69 g, 33%). IR ($CHCl_3$, cm^{-1}) ν_{max}: 3523, 2870, 1643, 1453, 1124. ^{1}H NMR (300 MHz, $CDCl_3$) δ: 2.78 (t, 4H, J = 5.8 Hz, CH_2), 3.57–3.68 (m, 26H, CH_2), 7.19–7.33 (m, 5H, CH-Ar). ^{13}C NMR (75 MHz, $CDCl_3$) δ: 53.78 (*C*H_2), 59.66 (*C*H_2-Bn), 70.00, 70.63, 70.78, 70.83, 70.90 (*C*H_2), 126.78, 128.11, 128.83 (*C*H-Ar), 139.71 (*C*-Ar). MS *m*/*e*: 398 [M^+ + 1]. HRMS calcd. for $C_{21}H_{36}NO6$ 398.2542 [MH^+]; found: 398.2531. Anal. calcd. for $C_{21}H_{35}NO_6$: C 63.45, H 8.87; found: C 63.29, H 8.88.

1-Aza-21-crown-7 (6)

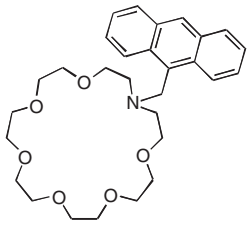


A solution of **16** (2.69 g, 6.76 mmol) in MeOH (50 mL) containing Pd-C (10%, 200 mg) was stirred under 1 atm H_2 (balloon, 1 atm = 101.325 kPa) overnight. The catalyst was filtered through Celite and washed with MeOH (5 × 10 mL). After evaporation, the residue was purified on alumina using MeOH–EtOAc (15%:85%), which gave a colorless oil (1.94 g, 93%). IR ($CHCl_3$, cm^{-1}) ν_{max}: 3504, 2874, 1648, 1460, 1353, 1110. ^{1}H NMR (300 MHz, $CDCl_3$) δ: 2.71

© 2006 NRC Canada

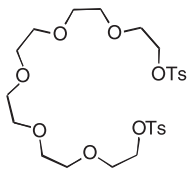
(t, 4H, J = 4.9 Hz, CH_2), 2.90 (1H, br, NH), 3.51–3.59 (m, 24H, CH_2). ^{13}C NMR (75 MHz, $CDCl_3$) δ: 49.25 (CH_2), 70.53, 70.57, 70.69, 70.75 (CH_2). MS *m/e*: 308 [M^+ + 1]. HRMS calcd. for $C_{14}H_{30}NO_6$: 308.2073 [MH^+]; found: 308.2061.

1-(Anthracen-9-ylmethyl)-aza-21-crown-7 (3)



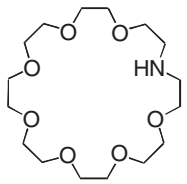
To a solution of **16** (0.301 g, 0.976 mmol) in anhydr. CH_3CN (30 mL) was added 9-(chloromethyl)anthracene (0.221 g, 0.976 mmol) and Cs_2CO_3 (0.954 g, 2.93 mmol). The mixture was heated at 80 °C for 2 h. After cooling to RT, NH_4Cl (satd. aq. sol., 30 mL) was added. The reaction mixture was extracted three times with CH_2Cl_2 (3 × 20 mL), the organic phase was dried with $MgSO_4$ and evaporated under reduced pressure. The residue was purified on SiO_2 using EtOAc–MeOH (90%:10%), to give an oil (0.432 g, 89%). IR ($CHCl_3$, cm^{-1}) ν_{max}: 3487, 2868, 1630, 1451, 1117. ^1H NMR (300 MHz, $CDCl_3$) δ: 2.90 (t, 4H, J = 5.7 Hz, CH_2), 3.56–3.73 (m, 24H, CH_2), 4.64 (s, 2H, CH_2), 7.44–7.55 (m, 4H, CH-Ar), 8.00 (d, 2H, J = 8.9 Hz, CH-Ar), 8.41 (s, 1H, CH-Ar), 8.60 (d, 2H, J = 8.9 Hz, CH-Ar). ^{13}C NMR (75 MHz, $CDCl_3$) δ: 51.75 (CH_2), 53.86 (CH_2), 70.10, 70.44, 70.85 (CH_2), 124.80, 125.35, 125.52, 127.41, 128.89 (*C*H-Ar), 130.57, 131.41, 131.43 (*C*-Ar). MS *m/e*: 498 [M^+ + 1]. HRMS calcd. for $C_{29}H_{40}NO_6$: 498.2855 [MH^+]; found: 498.2838.

Hexaethylene glycol ditosylate (13)



To a solution of hexaethylene glycol (3.36 g, 11.9 mmol) in CH_2Cl_2 (50 mL) at 0 °C was added Et_3N (5.0 mL, 35.7 mmol), DMAP (1.45 g, 5.96 mmol), and TsCl (5.68 g, 29.78 mmol). After stirring at RT for 30 min, NH_4Cl (satd. aq. sol., 20 mL) was added. The reaction mixture was extracted three times with CH_2Cl_2 (3 × 20 mL) and the combined organic phase was dried with $MgSO_4$, condensed, and the residue was purified on silica gel using EtOAc–hexane (80%:20%) to EtOAc (100%), which gave a colorless oil (6.34 g, 90%). IR ($CHCl_3$, cm^{-1}) ν_{max}: 2957, 2871, 1596, 1450, 1361, 1181. ^1H NMR (300 MHz, $CDCl_3$) δ: 2.41 (s, 6H, CH_3-Ts), 3.54 (s, 8H, CH_2), 3.56–3.62 (m, 8H, CH_2), 3.63–3.66 (m, 4H, CH_2), 4.10–4.13 (m, 4H, CH_2), 7.30–7.33 (m, 4H, CH-Ts), 7.74–7.77 (m, 4H, CH-Ts). ^{13}C NMR (75 MHz, $CDCl_3$) δ: 21.61 (CH_3-Ts), 68.60, 69.31, 70.45, 70.50, 70.55, 70.66 (6 × CH_2), 127.92 and 129.84 (8 × *C*H-Ar), 132.90 and 144.84 (4 × *C*-Ar). MS *m/e*: 591 [M^+ + 1]. Anal. calcd. for $C_{26}H_{38}O_{11}S_2$: C 52.87, H 6.48; found: C 52.75, H 6.59.

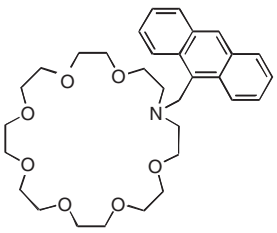
1-Aza-24-crown-8 (7)



To a solution of bistosylate **13** (19.56g, 33.1 mmol) in anhydr. THF (150 mL) was added *N*-benzyl diol **15** (6.45 g, 33.1 mmol) and NaH (3.97 g, 99.3 mmol; 60% dispersion in mineral oil, the oil was removed from the product chromatographically). The mixture was heated at 65 °C for 18 h. After cooling to RT, NH_4Cl (satd. aq. sol., 100 mL) was added. The reaction mixture was extracted three times with CH_2Cl_2 (3 × 30 mL) and the combined organic phase was dried with $MgSO_4$, condensed, and the residue was purified on alumina using EtOAc–hexane (80%:20%), which gave compound **17** as an oil (3.85 g, 26%).

A solution of **17** (3.85 g, 8.71 mmol) in MeOH (50 mL) containing Pd-C (10%, 200 mg) was stirred under 1 atm H_2 (balloon) overnight. The catalyst was filtered through Celite and washed with MeOH (5 × 10 mL). After evaporation, the residue was purified on alumina using MeOH–EtOAc (15%:85%), which gave a colorless oil (2.91 g, 95%). IR ($CHCl_3$, cm^{-1}) ν_{max}: 3490, 2872, 1649, 1461, 1352, 1109. ^1H NMR (300 MHz, $CDCl_3$) δ: 2.39 (s, br, NH), 2.72 (t, 4H, J = 5.1 Hz, CH_2), 3.51–3.60 (m, 28H, CH_2). ^{13}C NMR (75 MHz, $CDCl_3$) δ: 49.09 (CH_2), 70.44, 70.56, 70.66, 70.67, 70.70, 70.80 (CH_2). MS *m/e*: 352 [M^+ + 1]. HRMS calcd. for $C_{16}H_{34}NO_7$: 352.2335 [MH^+]; found: 352.2326.

1-(Anthracen-9-ylmethyl)-aza-24-crown-8 (4)

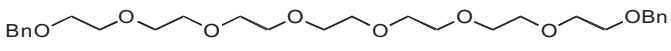


To a solution of **7** (0.837 g, 2.38 mmol) in anhydr. CH_3CN (50 mL) was added 9-(chloromethyl)anthracene (0.450 g, 1.98 mmol) and Cs_2CO_3 (1.29 g, 3.96 mmol). The mixture was heated at 80 °C for 2 h. After cooling to RT, NH_4Cl (satd. aq. sol., 30 mL) was added. The reaction mixture was extracted three times with CH_2Cl_2 (3 × 20 mL) and the combined organic phase was dried with $MgSO_4$, evaporated, and purified on alumina using EtOAc–hexane (60%:40%), which gave an oil (0.903 g, 84%). IR ($CHCl_3$, cm^{-1}) ν_{max}: 3486, 2868, 1636, 1452, 1119. ^1H NMR (300 MHz, $CDCl_3$) δ: 2.90 (t, 4H, J = 5.7 Hz, CH_2), 3.55–

© 2006 NRC Canada

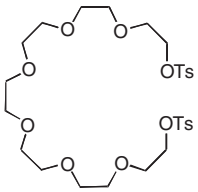
3.69 (m, 28H, CH_2), 4.64 (s, 2H, CH_2), 7.43–7.54 (m, 4H, CH-Ar), 8.00 (d, 2H, J = 8.9 Hz, CH-Ar), 8.40 (s, 1H, CH-Ar), 8.58 (d, 2H, J = 8.9 Hz, CH-Ar). ^{13}C NMR (75 MHz, $CDCl_3$) δ: 51.84 (*C*H_2), 53.79 (*C*H_2), 70.08, 70.46, 70.80, 70.82, 70.84, 70.87 (*C*H_2), 124.81, 125.36, 125.52, 127.41, 128.89 (*C*H-Ar), 130.58, 131.41, 131.43 (*C*-Ar). MS *m/e*: 542 [M^+ + 1]. HRMS calcd. for $C_{31}H_{44}NO_7$: 542.3118 [MH^+]; found: 542.3099.

1-((2-(2-(2-(2-(2-(2-(benzyloxy)ethoxy)ethoxy)-ethoxy)ethoxy)ethoxy)ethoxy)ethoxy)methyl)benzene



To a solution of triethylene glycol bistosylate (5.02 g, 10.93 mmol, synthesized according to literature procedure (13) with some modifications) in anhydr. THF (100 mL) was added 2-(2-(benzyloxy)ethoxy)ethanol (4.50 g, 22.96 mmol) and NaH (2.20 g, 54.68 mmol; 60% dispersion in mineral oil, the oil was removed from the product chromatographically). The mixture was heated at 65 °C for 1.5 h. After cooling to RT, NH_4Cl (satd. aq. sol., 100 mL) was added. The reaction mixture was extracted three times with CH_2Cl_2 (3 × 30 mL) and the combined organic phase was dried with $MgSO_4$, evaporated, and the residue was purified on SiO_2 using EtOAc, which gave the product as an oil (4.825 g, 87%). IR ($CHCl_3$, cm^{-1}) ν_{max}: 3572, 2870, 1454, 1106. ^{1}H NMR (300 MHz, $CDCl_3$) δ: 3.62–3.71 (m, 28H, CH_2), 4.58 (s, 4H, CH_2), 7.26–7.34 (m, 10H, CH-Ar). ^{13}C NMR (75 MHz, $CDCl_3$) δ: 69.44, 70.59, 70.61, 70.66, 73.23 (*C*H_2), 127.59, 127.74, 128.36 (*C*H-Ar), 138.29 (*C*-Ar). MS *m/e*: 507 [M^+ + 1]. Anal. calcd. for $C_{28}H_{42}O_8$: C 66.38, H 8.36; found: C 66.09, H 8.30.

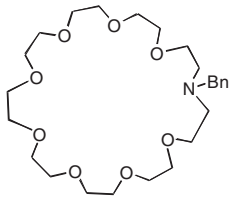
Heptaethylene glycol ditosylate (14)



The bisbenzyl ether prepared above (4.825 g, 9.52 mmol) was dissolved in MeOH (50 mL) containing Pd-C (10%, 300 mg) and stirred under 1 atm H_2 pressure (balloon) overnight. The catalyst was filtered through Celite and washed with MeOH (5 × 20 mL). After evaporation, the product (heptaethylene glycol) was obtained as a colorless oil (2.52 g, 81%) and used without further purification or characterization.

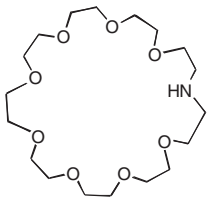
To this heptaethylene glycol (2.52 g, 7.73 mmol) in CH_2Cl_2 (50 mL) was added Et_3N (3.2 mL, 23.2 mmol), DMAP (0.472 g, 3.87 mmol), and TsCl (3.09 g, 16.23 mmol) at 0 °C. After stirring at RT for 1 h, NH_4Cl (satd. aq. sol., 20 mL) was added. The reaction mixture was extracted three times with CH_2Cl_2 (3 × 30 mL) and the combined organic phase was dried with $MgSO_4$, evaporated, and the residue was purified on silica gel using EtOAc to afford a colorless oil (4.71 g, 96%). IR ($CHCl_3$, cm^{-1}) ν_{max}: 3525, 2872, 1598, 1457, 1182. ^{1}H NMR (300 MHz, $CDCl_3$) δ: 2.43 (s, 6H, CH_3-Ts), 3.56–3.68 (m, 24H, CH_2), 4.12–4.15 (m, 4H, CH_2), 7.32–7.34 (m, 4H, CH-Ts), 7.76–7.79 (m, 4H, CH-Ts). ^{13}C NMR (75 MHz, $CDCl_3$) δ: 21.63 (*C*H_3-Ts), 68.63, 69.28, 70.48, 70.52, 70.54, 70.58, 70.70 (*C*H_2), 127.95 and 129.84 (*C*H-Ar), 132.95 and 144.82 (*C*-Ar). MS *m/e*: 635 [M^+ + 1]. Anal. calcd. for $C_{28}H_{42}O_{12}S_2$: C 52.98, H 6.67; found: C 53.16, H 6.59.

***N*-Benzyl monoaza-27-crown-9 (18)**



To a solution of bistosylate **14** (2.164 g, 3.41 mmol) in anhydr. THF (50 mL) was added *N*-benzyl diol **15** (0.798 g, 4.09 mmol) and NaH (0.545 g, 13.6 mmol; 60% dispersion in mineral oil, the oil was removed from the product chromatographically). The mixture was heated at 65 °C for 18 h. After cooling to RT, NH_4Cl (satd. aq. sol., 50 mL) was added. The reaction mixture was extracted three times with CH_2Cl_2 (3 × 30 mL) and the combined organic phase was dried with $MgSO_4$, evaporated, and the residue was purified on alumina using EtOAc–hexane (80%:20%), which gave an oil (0.414 g, 25%). IR ($CHCl_3$, cm^{-1}) ν_{max}: 3525, 2871, 1644, 1456, 1113. ^{1}H NMR (300 MHz, $CDCl_3$) δ: 2.79 (t, 4H, J = 5.9 Hz, CH_2), 3.52–3.71 (m, 34H, CH_2), 7.23–7.40 (m, 5H, CH-Ar). ^{13}C NMR (75 MHz, $CDCl_3$) δ: 53.79 (*C*H_2), 59.85 (*C*H_2-Bn), 69.93, 70.53, 70.75 (*C*H_2), 126.84, 128.15, 128.88 (*C*H-Ar), 139.45 (*C*-Ar). MS *m/e*: 486 [M^+ + 1]. HRMS calcd. for $C_{25}H_{44}NO_8$: 486.3067 [MH^+]; found: 486.3049. Anal. calcd. for $C_{25}H_{43}NO_8$: C 61.83, H 8.93; found: C 61.81, H 9.06.

1-Aza-27-crown-9 (8)

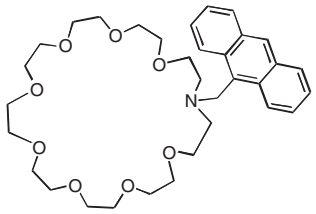


A solution of **18** (0.369 g, 0.759 mmol) in MeOH (15 mL) containing Pd-C (10%, 50 mg) was stirred under 1 atm of H_2 (balloon) overnight. The catalyst was filtered through Celite and washed with MeOH (5 × 10 mL). After evaporation, the residue was purified on alumina using MeOH–EtOAc (15%:85%), which gave a colorless oil (0.274 g, 91%). IR ($CHCl_3$, cm^{-1}) ν_{max}: 3452, 2915, 1649, 1461, 1103. ^{1}H NMR (300 MHz, $CDCl_3$) δ: 2.35 (s, br, NH), 2.80 (t, 4H, J = 5.0 Hz, CH_2), 3.58–3.69 (m, 32H, CH_2). ^{13}C NMR (75 MHz, $CDCl_3$) δ: 49.16 (*C*H_2), 70.52, 70.60, 70.71, 70.75

© 2006 NRC Canada

(CH_2). MS *m/e*: 396 [M^+ + 1]. HRMS calcd. for $C_{18}H_{38}NO_8$: 396.2597 [MH^+]; found: 396.2580. Anal. calcd. for $C_{18}H_{37}NO_8$: C 54.66, H 9.43; found: C 54.38, H 9.48.

1-(Anthracen-9-ylmethyl)-aza-27-crown-9 (5)



To a solution of **8** (0.210 g, 0.530 mmol) in anhydr. CH_3CN (20 mL) was added 9-(chloromethyl)anthracene (0.109 g, 0.482 mmol) and Cs_2CO_3 (0.314 g, 0.964 mmol). The mixture was heated at 80 °C for 2 h. After cooling to RT, NH_4Cl (satd. aq. sol., 30 mL) was added. The reaction mixture was extracted three times with CH_2Cl_2 (3 × 20 mL) and the combined organic phase was dried with $MgSO_4$, evaporated, and the residue was purified on alumina using EtOAc–hexane (60%:40%), which gave an oil (0.221 g, 78%). IR ($CHCl_3$, cm^{-1}) ν_{max}: 3449, 2870, 1646, 1108. ^1H NMR (300 MHz, $CDCl_3$) δ: 2.89 (t, 4H, *J* = 5.8 Hz, CH_2), 3.50–3.67 (m, 32H, CH_2), 4.64 (s, 2H, CH_2), 7.44–7.54 (m, 4H, CH-Ar), 7.99 (d, 2H, *J* = 8.8 Hz, CH-Ar), 8.41 (s, 1H, CH-Ar), 8.58 (d, 2H, *J* = 8.8 Hz, CH-Ar). ^{13}C NMR (75 MHz, $CDCl_3$) δ: 51.94 (CH_2), 53.79 (CH_2), 70.02, 70.32, 70.51, 70.69 (CH_2), 124.82, 125.33, 125.53, 127.42, 128.89 (*C*H-Ar), 130.52, 131.39, 131.42 (*C*-Ar). MS *m/e*: 586 [M^+ + 1]. HRMS calcd. for $C_{33}H_{48}NO_8$: 586.3380 [MH^+]; found: 586.3354.

Acknowledgements

This work was supported by the US EPA Science to Achieve Results (STAR) program (R82959902 and GR83238201). We are also grateful to Dr. Sherwood Hall, US Food and Drug Administration, for a gift of saxitoxin. Core facilities were funded by the US National Institutes of Health (P20 R15569) and the Arkansas Biosciences Institute.

References

1. J. Tibbets. Environ. Health Persp. **106**, A326 (1998).
2. L.M. Botana (*Editor*). Seafood and freshwater toxins: Pharmacology, physiology, and detection. Marcel Dekker, New York. 2000.
3. M.A. Quilliam. J. AOAC Int. **80**, 131 (1997).
4. P. Kele, J. Orbulescu, T.L. Calhoun, R.E. Gawley, and R.M. Leblanc. Tetrahedron Lett. **43**, 4413 (2002).
5. R.E. Gawley, S. Pinet, C.M. Cardona, P.K. Datta, T. Ren, W.C. Guida, J. Nydick, and R.M. Leblanc. J. Am. Chem. Soc. **124**, 13448 (2002).
6. R.E. Gawley, M. Shanmugasundaram, J.B. Thorne, and R.M. Tarkka. Toxicon, **45**, 783 (2005); Erratum, **46**, 477 (2005).
7. C.Y. Kao. Pharmacol. Rev. **18**, 211 (1966).
8. C.Y. Kao. *In* Molecular basis of drug action. *Edited by* T.P. Singer and R.N. Ondarza. Elsevier, Amsterdam. 1981. pp. 283–297.
9. K. Madan and D.J. Cram. J. Chem. Soc. Chem. Commun. 427 (1975).
10. K.P. Kyba, R.C. Helgeson, K. Madan, G.W. Gokel, T.L. Tarnowski, S.S. Moore, and D.J. Cram. J. Am. Chem. Soc. **99**, 2564 (1977).
11. R.A. Bissell, E. Calle, A.P. de Silva, S.A. de Silva, H.Q.N. Gunaratne, J.-L. Habib-Jiwan, S.L.A. Peiris, R.A.D.D. Rupasinghe, T.K.S.D. Samarasinghe, K.R.A.S. Sandanayake, and J.-P. Soumillion. J. Chem. Soc. Perkin Trans. 2, 1559 (1992).
12. B.A. Burkett and T.H. Chan. Synthesis, 1007 (2004).
13. H.M. Colquhoun, E.P. Goodings, J.M. Maud, J.F. Stoddart, J.B. Wolstenholme, and D.J. Williams. J. Chem. Soc. Perkin Trans. 2, 607 (1985).
14. P. Bandyopadhyay, P. Bandyopadhyay, and S.L. Regen. J. Am. Chem. Soc. **124**, 11254 (2002).
15. K.A. Connors. *In* Binding constants: The measurement of molecular complex stability. Wiley-Interscience, New York. 1987. pp. 339–343.
16. R.A. Bissell, A.P. de Silva, H.Q.N. Gunaratne, P.L.M. Lynch, G.E.M. Maguire, C.P. McCoy, and K.R.A.S. Sandanayake. Top. Curr. Chem. **168**, 223 (1993).
17. R.E. Gawley, Q. Zhang, P.I. Higgs, S. Wang, and R.M. Leblanc. Tetrahedron Lett. **40**, 5461 (1999); Erratum, **40**, 6135 (1999).

© 2006 NRC Canada

1,4,8,11-Tetra[2-aryl-1-diazenyl]-1,4,8,11-tetraazacyclotetradecanes — Synthesis, characterization, and X-ray crystallography of the first tetrakistriazenes to be reported[1]

Jeffery D. Clarke, Keith Vaughan, and Valerio Bertolasi

Abstract: The reactions of a series of arene diazonium salts with 1,4,8,11-tetraazacyclotetradecane (cyclam) afford the novel compounds, the 1,4,8,11-tetra[2-aryl-1-diazenyl]-1,4,8,11-tetraazacyclotetradecanes (**1a**–**1f**), which are the first examples of tetrakistriazenes to be reported. The tetrakistriazenes were characterized by IR spectroscopy, proton and carbon NMR, elemental analysis, high resolution electrospray mass spectrometry, and X-ray crystallography. The analogous reaction of a diazonium salt with 1,4,7-triazacyclononane or 1,5,9-triazacyclododecane yields the tristriazenes **2**, **3a**, and **3b**. The structures of compounds **1c** and **1e** were solved by X-ray crystallography at low temperature (150 K). Both molecules display a conformation where the four phenyltriazenyl groups point alternately upwards and downwards with respect to the mean macrocyclic plane.

Key words: triazene, tetrakistriazene, cyclam, tetraazacyclotetradecane, X-ray, NMR, cyclic polyamines.

Résumé : Les réactions d'une série de sels d'arènediazonium avec le 1,4,8,11-tétraazacyclotétradécane (= cyclame) conduit à la formation de nouveaux composés, les 1,4,8,11-tétra[2-aryl-1-diazényl]-1,4,8,11-tétraazatétradécanes (**1a**–**1f**) qui sont les premiers exemples de tétrakistriazènes à être rapportés. On a caractérisé les tétrakistriazènes par spectroscopie IR, par RMN du ^{1}H et du ^{13}C, par analyse élémentaire, par spectrométrie de masse à haute résolution à l'aide d'une ionisation par électronébulisation, et par diffraction des rayons X. La réaction analogue d'un sel de diazonium avec le 1,4,7-triazacyclononane ou le 1,5,9-triazacyclododécane conduit à la formation des tristriazènes **2**, **3a** et **3b**. Les structures des composés **1c** et **1e** ont été résolues par diffraction des rayons X à basse température (150 K). Les deux molécules présentent chacune une conformation dans laquelle les quatre groupes phényltriazényles sont orientés alternativement vers le haut et vers le bas par rapport au plan macromoléculaire moyen.

Mots clés : triazène, tétrakistriazène, cyclame, tétraazacyclotétradécane, rayons X, RMN, polyamines cycliques.

[Traduit par la Rédaction]

Introduction

1,4,8,11-Tetraazacyclotetradecane (cyclam) forms the most stable complexes with transition metal ions from both a thermodynamic and a kinetic viewpoint, among cyclic polyamines of varying ring size (1). The proclivity of cyclam to coordinate to Ni^{II} has been used to advantage in the template synthesis reaction (2), whereas covalent attachment of cyclam to a DNA-intercalator molecule, such as anthraquinone (3), influences interaction with DNA, causing substantially enhanced unwinding of the DNA. Metal complexation to the cyclam portion of the adduct increases the effect still further and metal-binding to DNA can cause sequence selective binding (4). Bicyclam derivatives composed of two cyclam units linked by an aliphatic linker have been identified as potent inhibitors of HIV type 1 and type 2 (5). This is just a fragment of the intense and vast literature dealing with the chemistry and pharmacology of cyclam. Surprisingly, the potential of cyclam to undergo diazo coupling reactions has apparently not been explored previously.

The reaction of a diazonium salt with a simple secondary amine is the conventional way to synthesize a stable triazene, e.g., $ArN{=}N{-}NR_2$ (6). Many triazenes have been shown to possess antitumor properties in experimental models (7) and a few triazenes are used clinically in the treatment of human malignant melanoma (8) and brain tumors (9). Bistriazenes are compounds that contain two triazene units in the same molecule; the chemistry of bistriazenes has recently been reviewed (10). Compounds that contain three or four triazene units per molecule, i.e., tristriazenes and

Received 5 October 2005. Accepted 31 March 2006. Published on the NRC Research Press Web site at http://canjchem.nrc.ca on 28 July 2006.

This paper is dedicated to the invaluable contribution of Dr. Alfred Bader, whose entrepreneurial skills have provided starting materials for the pursuit of organic synthesis in laboratories everywhere.

J.D. Clarke and K. Vaughan.[2] Department of Chemistry, Saint Mary's University, Halifax, NS B3H 3C3, Canada.
V. Bertolasi. Dipartimento di Chimica and Centro di Strutturistica Diffrattometrica, Universita' di Ferrara, Via L. Borsari, 46, 44100 Ferrara, Italy.

[1]This article is part of a Special Issue dedicated to Dr. Alfred Bader.

[2]Corresponding author (email: keith.vaughan@smu.ca).

 doi:10.1139/V06-090 © 2006 NRC Canada

tetrakistriazenes, are hitherto unknown, so it is with great satisfaction that we report here the synthesis of the first known examples of the classes of tristriazenes and tetrakistriazenes from the diazonium coupling reaction with the cyclic polyamines, 1,4,7-triazacyclononane, 1,5,9-triazacyclododecane, and 1,4,8,11-tetraazacyclotetradecane (cyclam). The potential medicinal chemistry resulting from the combination of the polyamine and triazene units in the same drug molecule is an exciting prospect.

Experimental

Melting points were determined on a hot-stage melting point apparatus and are uncorrected. IR spectra were obtained using Nujol mulls. ^{1}H and ^{13}C NMR chemical shifts were recorded in $CDCl_3$ or d_6-DMSO solutions at 27 °C (unless stated otherwise) and are relative to TMS as internal standard. Accurate mass measurements were performed by ESI-MS. The sample was dissolved in methanol or methanol–chloroform. The solution concentration was approximately 50–100 μmol/L. It was infused at a flow rate of 30 μL/min. For accurate mass measurement of $(M + H)^+$, tetralysine KKKK or Angiotensin III was used as the reference compound. The mass of $(M + H)^+$ from tetralysine was used as the lock mass.

Synthesis of the 1,4,8,11-tetra[2-aryl-1-diazenyl]-1,4,8,11-tetraazacyclotetradecanes (1a–1f)

General procedure

A solution of the aromatic amine (0.005 mol) in 3 mol/L hydrochloric acid (5.0 mL) was cooled to 0 °C and diazotized with a solution of sodium nitrite (0.38 g) in water (1.5 mL). A solution of 1,4,8,11-tetraazacyclotetradecane (0.20 g) in water (2.0 mL), with 3 mol/L HCl (0.5 mL) added, was added slowly with stirring to the cold diazonium salt solution and the mixture was left stirring for 0.5 h. The solution was then neutralized with saturated sodium bicarbonate solution, stirred in the cold for a further 1.0 h, and then filtered by vacuum filtration to afford the following tetrakistriazenes.

*1,4,8,11-Tetra[2-(*p*-cyanophenyl)-1-diazenyl]-1,4,8,11-tetraazacyclotetradecane (1a)*

Off-white powder, yield 80%, mp 251–254 °C (ethyl acetate). IR (cm^{-1}) ν_{max}: 2223 (CN), 844 (OOP). ^{1}H NMR (500 MHz, d_6-DMSO) δ: 2.17 (4H, v br), 3.84 (8H, br), 4.15 (8H, br s, H_a), 7.45 (8H, d, J = 6.7 Hz), 7.75 (8H, d, J = 6.7 Hz). MS (ESI+) m/z calcd. for $C_{38}H_{36}N_{16}$: 716 $(M + Na)^+$; found: 739.2.

*1,4,8,11-Tetra[2-(*p*-nitrophenyl)-1-diazenyl]-1,4,8,11-tetraazacyclotetradecane (1b)*

Yellow powder, yield 90%, mp 263 to 264 °C (from dimethylsulfoxide). IR (cm^{-1}) ν_{max}: 1514, 1333 (nitro group), 854 (OOP). ^{1}H NMR (500 MHz, d_6-DMSO) δ: 2.18 (4H, br), 3.93 (8H, br), 4.20 (8H, br s), 7.57 (8H, d, J = 9.0 Hz), 8.24 (8H, d, J = 9.5 Hz). Second species (rotamer with 40% relative intensity) δ: 2.94 (br), 3.99 (br), 4.20 (br), 7.42 (br), 8.31 (d, J = 9.0 Hz). Anal. calcd. for $C_{34}H_{36}N_{16}O_8$: C 51.25, H 4.55; found: C 51.14, H 4.57.

*1,4,8,11-Tetra[2-(*p*-methoxycarbonylphenyl)-1-diazenyl]-1,4,8,11-tetraazacyclotetradecane (1c)*

Pale yellow prisms, yield 75%, mp 215–217 °C (toluene). IR (cm^{-1}) ν_{max}: 1716 (C=O), 1278 (C-O), 859 (OOP). ^{1}H NMR (500 MHz, 47 °C, $CDCl_3$) δ: 2.19 (4H, quintet, J = 6.7 Hz), 3.79 (8H, t, J = 6.7 Hz), 3.91 (12H, s), 4.11 (8H, s), 7.33 (8H, d, J = 8.5 Hz), 7.92 (8H, d, J = 8.6 Hz). ^{13}C NMR (15 MHz, $CDCl_3$) δ: 30.40, 51.76, 120.21, 130.50, 145.03, 153.61, 166.75. HRMS (ESI) m/z calcd. for $C_{42}H_{49}N_{12}O_8$: 849.3796 $(M + H)^+$; found: 849.3799. Anal. calcd. for $C_{91}H_{104}N_{24}O_{16}$: C 61.07, H 5.82, N 18.79; found: C 61.24, H 5.95, N 18.45.

*1,4,8,11-Tetra[2-(*p*-acetylphenyl)-1-diazenyl]-1,4,8,11-tetraazacyclotetradecane (1d)*

Reddish-brown powder, yield 65%, mp 182–184 °C (ethanol). IR (cm^{-1}) ν_{max}: 1672 (C=O), 841 (OOP). ^{1}H NMR (500 MHz, $CDCl_3$) δ: 2.19 (4H, br), 2.58 (12H, s), 3.80 (8H, br), 4.15 (8H, s), 7.35 (8H, d, J = 8.2 Hz), 7.84 (8H, d, J = 8.2 Hz). Anal. calcd. for $C_{42}H_{48}N_{12}O_4$: C 64.26, H 6.16; found: C 63.84, H 6.31.

*1,4,8,11-Tetra[2-(*p*-methylphenyl)-1-diazenyl]-1,4,8,11-tetraazacyclotetradecane (1e)*

White needles, yield 40%, mp 139 to 140 °C (ethanol). IR (cm^{-1}) ν_{max}: 825 (OOP). ^{1}H NMR (500 MHz, $CDCl_3$) δ: 2.14 (4H, quintet, J = 6.7 Hz), 2.33 (12H, s), 3.73 (8H, t, J = 6.8 Hz), 4.02 (8H, s), 7.07 (8H, d, J = 8.2 Hz), 7.26 (8H, d, J = 8.2 Hz). ^{13}C NMR (125.77 MHz, $CDCl_3$) δ: 21.04, 27.09, 49.54, 120.53, 129.44, 135.37, 148.32. HSQC NMR (125.77 MHz, $CDCl_3$) δ: 51.38 correlates with proton signal at 3.73 ppm. HRMS (ESI) m/z calcd. for $C_{38}H_{49}N_{12}$: 673.4203 $(M + H)^+$; found: 673.4202.

*1,4,8,11-Tetra[2-(*p*-bromophenyl)-1-diazenyl]-1,4,8,11-tetraazacyclotetradecane (1f)*

Off-white powder, yield 86%, mp 198 to 199 °C (propanol). IR (cm^{-1}) ν_{max}: 828 (OOP). ^{1}H NMR (500 MHz, $CDCl_3$) δ: 2.12 (4H, quintet, J = 6.6 Hz), 3.72 (8H, t, J = 6.6 Hz), 4.04 (8H, s), 7.18 (8H, d, J = 8.5 Hz), 7.365 (8H, d, J = 8.5 Hz). ^{13}C NMR (125.77 MHz, $CDCl_3$) δ: 26.99, 49.44, 119.18, 122.15, 131.92, 149.25. Anal. calcd. for $C_{34}H_{36}N_{12}Br_4$: C 43.90, H 3.89, N 18.03; found: C 44.07, H 3.87, N 17.74.

Application of this procedure with 1,5,9-triazacyclododecane in place of cyclam afforded the tristriazene **2**.

*1,5,9-Tri[2-(*p*-cyanophenyl)-1-diazenyl]-1,5,9-triazacyclododecane (2)*

Red-brown powder, yield 57%, mp 172–175 °C (ethanol). IR (cm^{-1}) ν_{max}: 2221 (CN), 844 (OOP). ^{1}H NMR (500 MHz, $CDCl_3$) δ: 2.32 (6H, br quintet), 3.88 (12H, t, J = 6.0 Hz), 7.47 (6H, d, J = 8.5 Hz), 7.61 (6H, d, J = 8.5 Hz). Anal. calcd. for $C_{30}H_{30}N_{12}$: C 64.50, H 5.41; found: C 64.26, H 5.39.

Application of the general procedure with 1,4,7-triazacyclononane in place of cyclam afforded the tristriazenes **3a** and **3b**.

© 2006 NRC Canada

Table 1. Crystal data of compounds **1c** and **1e**.

Compound	**1c**	**1e**
Formula	$C_{42}H_{48}N_{12}O_8 \cdot {}^{1/2}(C_7H_8)$	$C_{38}H_{48}N_{12}$
M_r	894.99	672.88
Crystal system	Triclinic	Triclinic
Space group	*P*-1	*P*-1
a (Å)	11.6051(4)	11.7168(3)
b (Å)	11.9153(5)	17.2582(5)
c (Å)	17.1696(8)	20.0360(7)
α (°)	95.044(2)	106.296(1)
β (°)	94.902(2)	103.975(1)
γ (°)	106.145(3)	100.614(2)
V (Å^3)	2 256.7(2)	3 632.9(2)
Z	2	4
$D_{calcd.}$ (g cm^{-3})	1.317	1.230
F(000)	946	1440
μ (cm^{-1})	0.93	0.77
Temperature (K)	150	150
Crystal form, color	Irregular, colorless	Prismatic, colorless
Crystal size (mm)	0.16 × 0.10 × 0.07	0.25 × 0.10 × 0.05
θ_{min}–θ_{max} (°)	2.48–20.81	2.55–22.21
Measured reflections	33 849	53 975
Index ranges	$-11 \le h \le 11$, $-11 \le k \le 11$, $-17 \le l \le 17$	$-12 \le h \le 12$, $-18 \le k \le 18$, $-21 \le l \le 20$
Unique reflections	4 695	9 150
R_{int}	0.090	0.123
Obs. reflections [$F^2 \ge 2\sigma(F^2)$]	2 738	5 277
$R(F^2)$ (Obs. reflections)	0.0504	0.0566
$wR(F^2)$ (All reflections)	0.1294	0.1393
No. of parameters	617	901
GOF	0.969	1.006
$\Delta\rho_{min}$, $\Delta\rho_{max}$	–0.20, 0.19	–0.24, 0.27

*1,4,7-Tri[2-(*p*-cyanophenyl)-1-diazenyl]-1,4,7-triazacyclononane (3a)*

Light-brown powder, yield 88%, mp 253–256 °C (ethanol). IR (cm^{-1}) ν_{max}: 2222 (CN), 845 (OOP). ^{1}H NMR (500 MHz, $CDCl_3$) δ: 3.95–4.37 (12H, m), 7.45 (6H, d, *J* = 8.4 Hz), 7.60 (6H, d, *J* = 8.4 Hz). Anal. calcd. for $C_{27}H_{24}N_{12}$: C 62.78, H 4.68, N 32.54; found: C, 62.87, H 4.64, N 31.84.

*1,4,7-Tri[2-(*p*-methylphenyl)-1-diazenyl]-1,4,7-triazacyclononane (3b)*

Cream-coloured needles, yield 61.5%, mp 152–155 °C (ethanol). IR (cm^{-1}) ν_{max}: 822 (OOP). ^{1}H NMR (500 MHz, $CDCl_3$) δ: 2.34 (9H, s), 3.91 (6H, v br), 4.19 (6H, v br), 7.12 (6H, d, *J* = 8.1 Hz), 7.31 (6H, d, *J* = 8.2 Hz). ^{13}C NMR (125.77 MHz, 223 K, $CDCl_3$) δ: 21.51, 53.18, 120.54, 129.83, 135.75, 148.10. Second species (rotamer) δ: 21.51, 49.28, 120.6, 129.7, 135.9, 147.9. Anal. calcd. for $C_{27}H_{33}N_9$: C 67.06, H 6.88, N 26.07; found: C 66.76, H 6.60, N 25.82.

Crystallography

X-ray diffraction data for compounds **1c** and **1e** were collected at low temperature (150 K) on a Nonius Kappa CCD diffractometer with graphite monochromated Mo Kα radiation (λ = 0.7107 Å).[3] The structures were solved by direct methods (SIR97) (11) and refined (SHELXL-97) (12) by full-matrix least-squares with anisoptropic non-H and hydrogen atoms included on calculated positions riding on their carrier atoms. The methoxy carbonyl moiety C41, O7, O8, C42 in **1c** is disordered and the methyl group $C42H_3$ has been refined over two positions with the respective occupancies of 0.579(9) and 0.421(9). The crystal contains half a molecule of toluene per molecule of **1c**, disordered around a crystallographic centre of symmetry. It has been refined over

[3] Supplementary data for this article are available on the journal Web site (http://canjchem.nrc.ca) or may be purchased from the Depository of Unpublished Data, Document Delivery, CISTI, National Research Council Canada, Ottawa, ON K1A 0R6, Canada. DUD 5059. For more information on obtaining material refer to http://cisti-icist.nrc-cnrc.gc.ca/irm/unpub_e.shtml. CCDC 276886 and 292214 contain the crystallographic data for this manuscript. These data can be obtained, free of charge, via http://www.ccdc.cam.ac.uk/conts/retrieving.html (Or from the Cambridge Crystallographic Data Centre, 12 Union Road, Cambridge CB2 1EZ, UK; fax +44 1223 336033; or deposit@ccdc.cam.ac.uk).

© 2006 NRC Canada

Table 2. Selected bond distances and angles in 1,4,8,11-tetra[2-(*p*-methoxycarbonylphenyl)-1-diazenyl]-1,4,8,11-tetraazacyclotetradecane (**1c**).

Bond distances (Å)	
N1—N2	1.340(4)
N1—C1	1.469(5)
N1—C10	1.463(5)
N2—N3	1.277(5)
N3—C11	1.427(5)
N4—N5	1.309(4)
N4—C2	1.457(5)
N4—C3	1.467(4)
N5—N6	1.287(4)
N6—C19	1.428(5)
N7—N8	1.341(4)
N7—C5	1.465(5)
N7—C6	1.465(5)
N8—N9	1.277(5)
N9—C27	1.426(4)
N10—N11	1.314(4)
N10—C7	1.466(4)
N10—C8	1.456(5)
N11—N12	1.283(5)
N12—C35	1.419(4)
Bond angles (°)	
N2-N1-C1	114.3(3)
N2-N1-C10	123.5(3)
C1-N1-C10	120.8(3)
N1-N2-N3	113.2(3)
N2-N3-C11	112.9(3)
N5-N4-C2	123.8(3)
N5-N4-C3	117.3(3)
C2-N4-C3	118.7(3)
N4-N5-N6	114.9(3)
N5-N6-C19	110.7(3)
N8-N7-C5	114.7(3)
N8-N7-C6	121.6(3)
C5-N7-C6	119.7(3)
N7-N8-N9	112.7(3)
N8-N9-C27	112.9(3)
N11-N10-C7	122.3(3)
N11-N10-C8	118.0(3)
C7-N10-C8	119.2(3)
N10-N11-N12	115.2(3)
N11-N12-C35	110.8(3)

Table 3. Selected bond distances and angles in 1,4,8,11-tetra[2-(*p*-methylphenyl)-1-diazenyl]-1,4,8,11-tetraazacyclotetradecane (**1e**).

	Molecule A	Molecule B
Bond distances (Å)		
N1—N2	1.344(3)	1.332(4)
N1—C1	1.453(5)	1.464(4)
N1—C10	1.474(4)	1.472(5)
N2—N3	1.273(4)	1.274(4)
N3—C11	1.426(4)	1.430(4)
N4—N5	1.322(4)	1.336(4)
N4—C2	1.449(5)	1.446(5)
N4—C3	1.461(4)	1.465(5)
N5—N6	1.284(5)	1.268(5)
N6—C18	1.426(4)	1.434(4)
N7—N8	1.345(4)	1.337(4)
N7—C5	1.469(5)	1.473(4)
N7—C6	1.458(5)	1.462(5)
N8—N9	1.272(5)	1.278(3)
N9—C25	1.430(4)	1.413(4)
N10—N11	1.347(4)	1.330(4)
N10—C7	1.449(4)	1.456(4)
N10—C8	1.456(5)	1.456(5)
N11—N12	1.279(5)	1.279(5)
N12—C32	1.427(4)	1.435(4)
Bond angles (°)		
N2-N1-C1	121.8(3)	122.0(3)
N2-N1-C10	114.6(3)	115.3(3)
C1-N1-C10	121.6(3)	118.7(3)
N1-N2-N3	113.4(3)	115.4(3)
N2-N3-C11	112.1(3)	111.3(3)
N5-N4-C2	122.3(3)	122.3(3)
N5-N4-C3	118.6(3)	116.3(3)
C2-N4-C3	119.1(3)	119.4(3)
N4-N5-N6	114.6(3)	113.6(3)
N5-N6-C18	111.0(3)	112.2(3)
N8-N7-C5	114.1(3)	114.3(3)
N8-N7-C6	120.8(3)	121.5(3)
C5-N7-C6	119.9(3)	118.8(3)
N7-N8-N9	113.8(3)	114.5(3)
N8-N9-C25	112.3(3)	112.0(3)
N11-N10-C7	120.9(3)	122.4(3)
N11-N10-C8	117.4(3)	115.6(3)
C7-N10-C8	119.1(3)	119.8(3)
N10-N11-N12	112.6(3)	114.8(3)
N11-N12-C32	113.2(3)	110.4(3)

two positions with occupancies of 0.5. All other calculations were performed using the PARST system of programs (13).

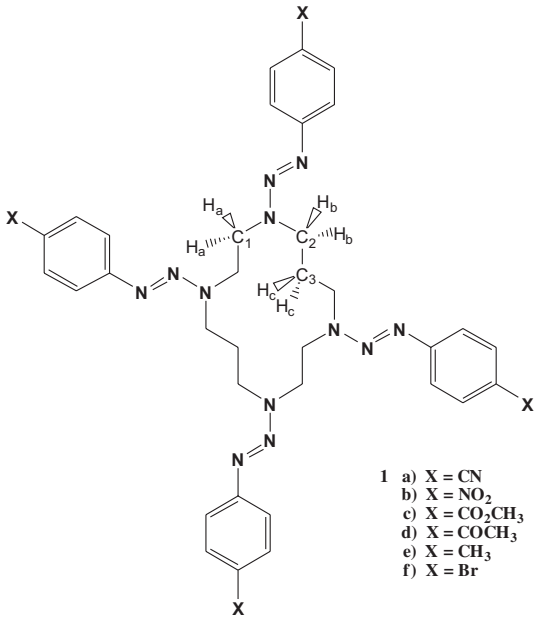
The crystal data and refinement parameters are summarized in Table 1. Selected bond distances and angles are given in Tables 2 and 3.

Results and discussion

1,4,8,11-Tetraazacyclotetradecane (cyclam) reacted favorably in aqueous solution with a variety of diazonium salts to afford the novel 1,4,8,11-tetra[2-aryl-1-diazenyl]-1,4,8,11-tetraazacyclotetradecanes (**1a**–**1f**) in excellent yields, as high as 90%. The diazonium salt was used in 25% excess above the required stoichiometric ratio of 4:1. Raising the amount of diazonium salt to 50% excess had little effect on the yield, with the exception of the *p*-bromo derivative (**1f**) that went from 35% to 86% yield. The 1,4,8,11-tetra[2-aryl-1-diazenyl]-1,4,8,11-tetraazacyclotetradecanes are stable solids that crystallize, mostly from polar solvents, and it was possible to grow small crystals from two of the compounds in the series for X-ray crystallography. The tetrakistriazenes have been identified by spectroscopic methods. The IR spectra display the characteristic bands of the particular aryl substituents, e.g., nitrile, carbonyl, and nitro groups. The ^{1}H NMR spectra are consistent with the assigned structures, although significant broadening of NMR signals was evident

© 2006 NRC Canada

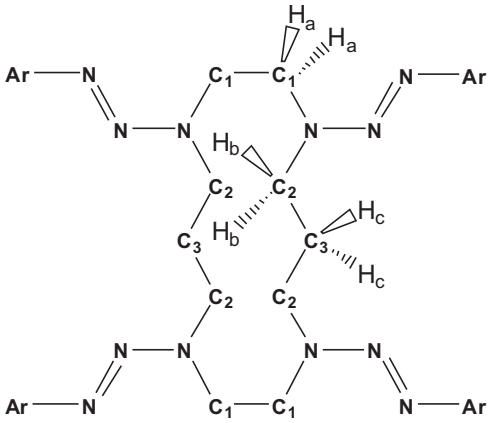
owing to the familiar phenomenon of restricted rotation around the N—N bonds of the triazene moieties (14). The protons attached to the carbon atoms of the 14-membered macrocyclic ring are clearly distinguished (see proton and carbon labelling in Fig. 1 to clarify the following discussion).



The eight equivalent protons of the ethylene spacers, labeled H_a attached to C_1, give rise to a singlet at ca. 4.2 ppm, integrating for 8H as expected, with varying line width from quite sharp in **1e** and **1f** to very broad in **1b**. The multiplicity of the protons of the propylene spacers, H_b and H_c, is resolved in compounds **1c**, **1e**, and **1f**. In these spectra, the H_b protons appear as an eight-proton triplet at ca. 3.8 ppm and the H_c protons are resolved as a four-proton quintet at ca. 2.2 ppm. The analogous signals in the spectra of **1a**, **1b**, and **1d** are too broad for the multiplicity to show. In all compounds (**1a**–**1f**) the aromatic protons give rise to the expected AA′BB′ pattern and the protons of the methyl groups in the X-substituents of **1c**–**1e** are observed at the predicted chemical shifts.

A VT NMR experiment was conducted with compound **1c** in $CDCl_3$ to attempt to slow down the rotational equilibrium in the triazene units so that resolution would be improved. However, lowering the temperature of the solution of **1c** resulted in further broadening of the proton signals, while raising the temperature to 47 °C gave a nicely resolved spectrum with the triplet of H_b and the quintet of H_c clearly evident. Evidently, raising the temperature of the solution causes the faster exchange of rotamers and individual multiplets are observed. A different manifestation of the dynamic rotation is observed in the case of the *p*-nitro derivative (**1b**); this tetrakistriazene affords a proton spectrum with two clear sets

Fig. 1. Proton and carbon labelling in structures **1a**–**1f**.



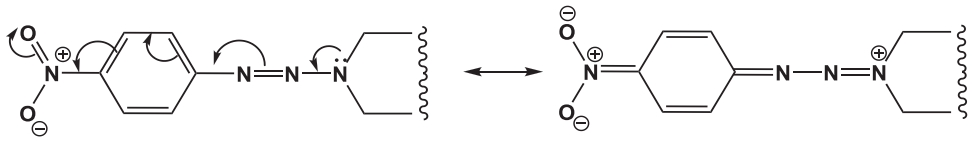
of broad signals that we ascribe to the rotamers resulting from the restricted rotation around the N—N bond (14). This total doubling of the spectra is only seen in the case of the *p*-nitro compound; the strongly electron-withdrawing nitro group promotes the resonance (eq. [1]) that gives the N—N bond greater double-bond character.

^{13}C NMR analysis was not feasible with compounds **1a**, **1b**, and **1d** owing to the combination of low solubility and the broadening of NMR signals because of rotational dynamics. However, compounds **1c** and **1f** gave partial ^{13}C NMR spectra with not all macrocyclic ring carbons showing. Only compound **1e** gave a complete set of ^{13}C signals, with the aid of HSQC spectroscopy (Fig. 2) to detect the signal from C2. These limited data give the general assignments of C1 at 49.5 ppm, C2 at 51.0 ppm, and C3 at ca. 27.0 ppm, together with the predicted aromatic carbon signals.

Further analytical evidence for the structures of the tetrakistriazenes was obtained from elemental analysis of compounds **1b**–**1f** and from electrospray mass spectrometry with compounds **1a**, **1c**, and **1e**. The molecular ions of these compounds did not survive the conditions of electron ionization mass spectrometry. Unequivocal proof of the novel tetrakistriazene structure is evident in the X-ray crystallography of compounds **1c** and **1e**.

An ORTEP (15) view of the molecule of the tetrakistriazene **1c** is shown in Fig. 3, in which the molecule is viewed more or less through the plane of the cyclam core. The best view of the 14-membered macrocycle (without substituents for the sake of clarity) is shown in the ORTEP diagram of Fig. 4. The molecule of **1c** displays a conformation where the four phenyltriazenyl groups point alternately upwards and downwards with respect to the mean macrocyclic plane. All the phenyltriazenyl groups are almost planar and those on the same side are roughly parallel, but the phenyl ring couples (C11-C16)–(C27-C32) and (C19-C24)–(C35-C40) form angles of 11.0(2)° and 10.2(1)°, respectively. An important point to make regarding this structure is the conjugation degree within the triazene moieties that is greater for

[1]



© 2006 NRC Canada

Fig. 2. High-field region of the HSQC ($CDCl_3$) spectrum of 1,4,8,11-tetra[2-(*p*-tolyl)-1-diazenyl]-1,4,8,11-tetraazacyclotetradecane (**1e**), showing the correlation of protons H_a, H_b, and H_c with carbons C1, C2, and C3, respectively.

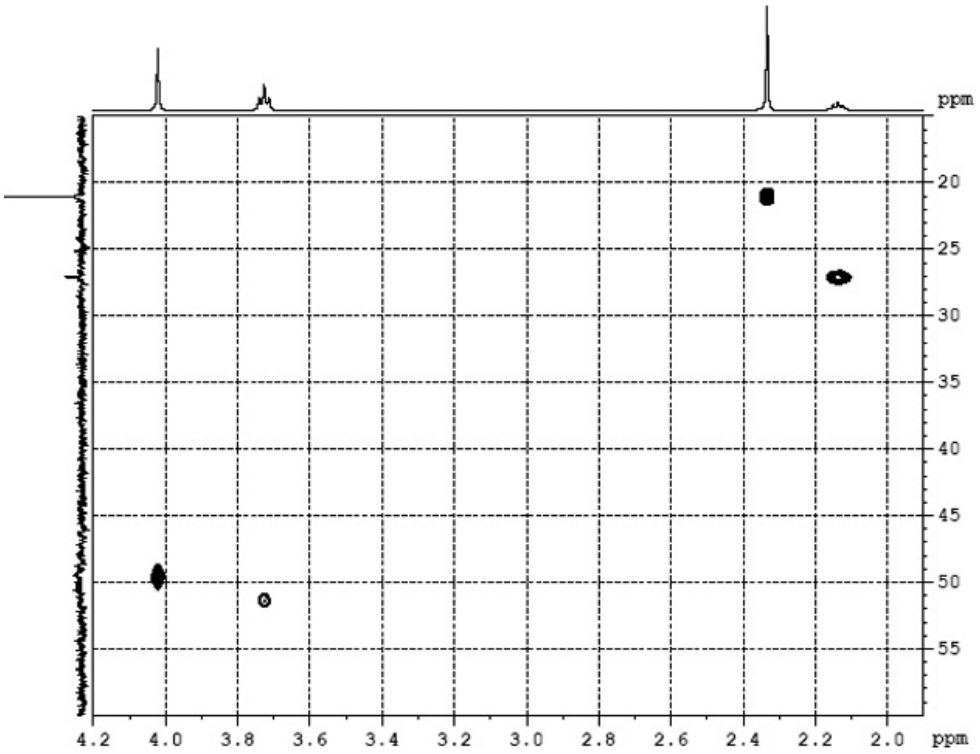
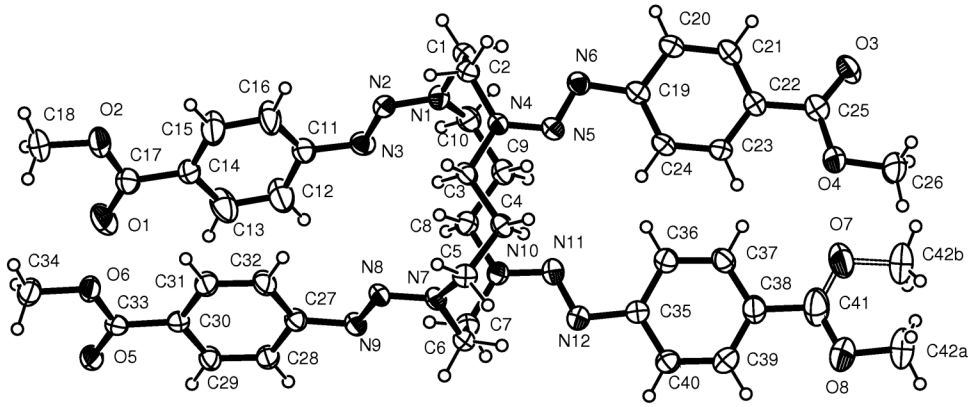


Fig. 3. ORTEP view of 1,4,8,11-tetra[2-(*p*-methoxycarbonyl-phenyl)-1-diazenyl]-1,4,8,11-tetraazacyclotetradecane (**1c**), displaying the thermal ellipsoids at 40% probability.



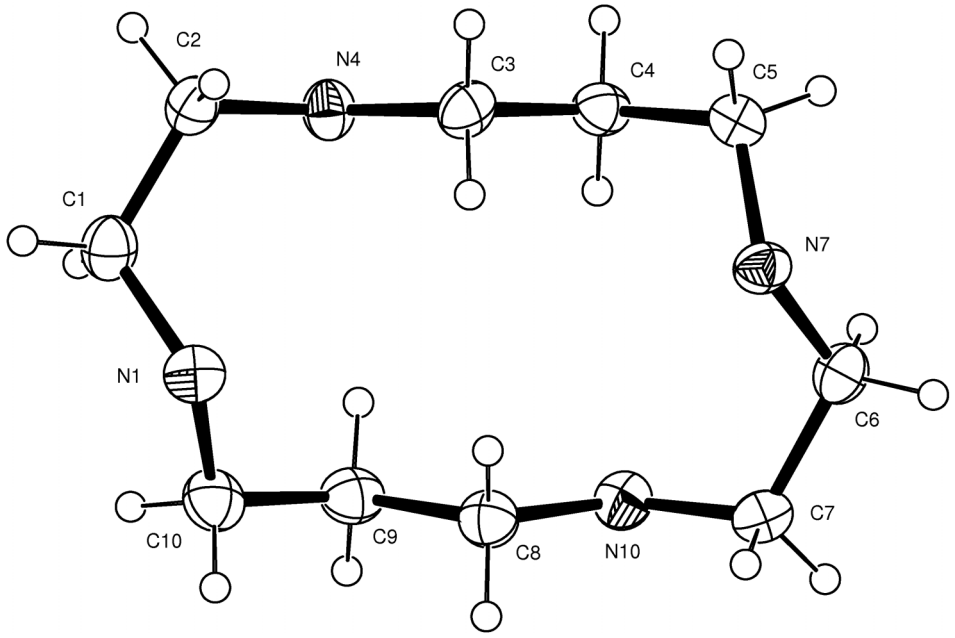
N4-N5=N6 and N10-N11=N12 situated on one side with respect to N1-N2=N3 and N7-N8=N9 on the other side.

Although the N1—N2 and N7—N8 single bonds of 1.340(4) and 1.341(4) Å and the N2=N3 and N8=N9 double bonds of 1.277(5) and 1.277(5) Å indicate significant conjugation within the triazene moieties, the corresponding distances for the other triazenes, N4—N5 = 1.309(4) Å, N5=N6 = 1.287(4) Å, N10—N11 = 1.314(4) Å, and N11=N12 = 1.283(5) Å, show, however, a much more pronounced degree of conjugation. The macrocycle shown in Fig. 3 displays a rectangular cavity with the following internal distances: N1···N7 = 5.311(4) Å, N4···N10 = 4.527(4) Å, N4···C9 = 3.609(5) Å, and N10···C4 = 3.623(5) Å.

The structure of the *p*-tolyl analogue in the series (**1e**) is quite complicated because the asymmetric unit contains two independent molecules; the ORTEP diagrams of these two species are shown in Figs. 5*a* and 5*b*, which clearly support our conclusions that the connectivity in this compound is the tetrakistriazene structure. The best projections of the 14-membered macrocycles (without substituents) are shown in Figs. 6*a* and 6*b*. Both molecules display similar conformations with respect to those observed in compound **1c**, where the four phenyltriazenyl groups point alternately upwards and downwards from the mean macrocyclic plane. All the phenyltriazenyl groups are almost planar and the phenyl groups, on the same sides, form the following dihedral angles: C11-C16-C25-C30 of 15.9(1)° and 3.7(1)° and C18-C23-C32-C37 of 10.4(1)° and 11.8(1)° for molecules A and B, respectively. All the triazene groups display similar conjugations with N—N single bonds in the range 1.32–1.35 Å

© 2006 NRC Canada

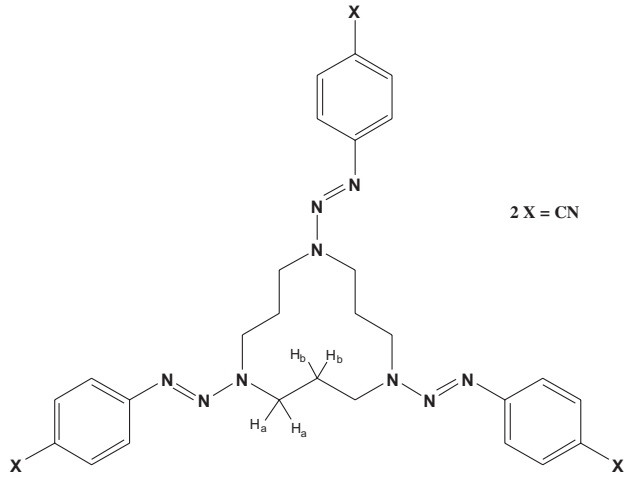
Fig. 4. ORTEP view of the heterocyclic cyclam core of the molecule of **1c**.



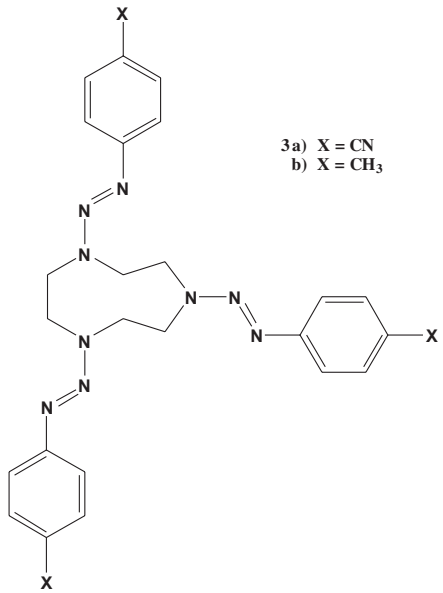
and N=N double bonds in the range 1.27–1.28 Å. The macrocycles, shown in Figs. 6*a* and 6*b*, exhibit slightly different conformations displaying cavities with the following internal distances: N1···N7 = 5.378(4) Å, N4···N10 = 4.470(4) Å, N4···C9 = 3.564(5) Å, and N10···C4 = 3.586(5) Å for molecule A; N1···N7 = 5.346(4) Å, N4···N10 = 4.556(4) Å, N4···C9 = 3.665(5) Å, and N10···C4 = 3.663(5) for molecule B.

This paper represents a major advance in the chemistry of triazenes, moving in one leap from the bistriazene front to the previously unknown tetrakistriazene. Of course, there is a missing link in this picture, which is the tristriazene represented by structures **2** and **3**. Accordingly, we investigated the reaction of 1,5,9-triazacyclododecane with *p*-cyanobenzenediazonium chloride, which afforded the tristriazene, 1,5,9-tri[2-(*p*-cycanophenyl)-1-diazenyl]-1,5,9-triazacyclododecane (**2**). The ^{1}H NMR spectrum of **2** is decidedly simple and consistent with the tristriazene structure. The protons of the three equivalent three-carbon spacers appear as the expected six-proton quintet at 2.32 ppm, assigned to the protons H_b of the central methylene groups, and a 12-proton triplet at 3.88 ppm, assigned to the protons H_a of the N-CH_2 groups.

Reaction of 1,4,7-triazacyclononane with diazonium salts afforded the tristriazenes **3a** and **3b**. However, the NMR spectra of these molecules are not as simple as expected; in principle, the protons of the triazacyclononane methylene groups should be equivalent. In the ^{1}H NMR spectrum of **3b**, the peaks are broad but, significantly, they integrate for the correct number of protons. The tolyl methyl protons resonate at 2.34 ppm with an integration for nine protons and the broadened aromatic AA′BB′ system integrates for 12 protons. The methylene protons of the heterocyclic ring appear as two very broad signals at 3.91 and 4.19 ppm, each integrating for 6H. We suggest that these two methylene signals can be assigned to the axial and equatorial hydrogen atoms



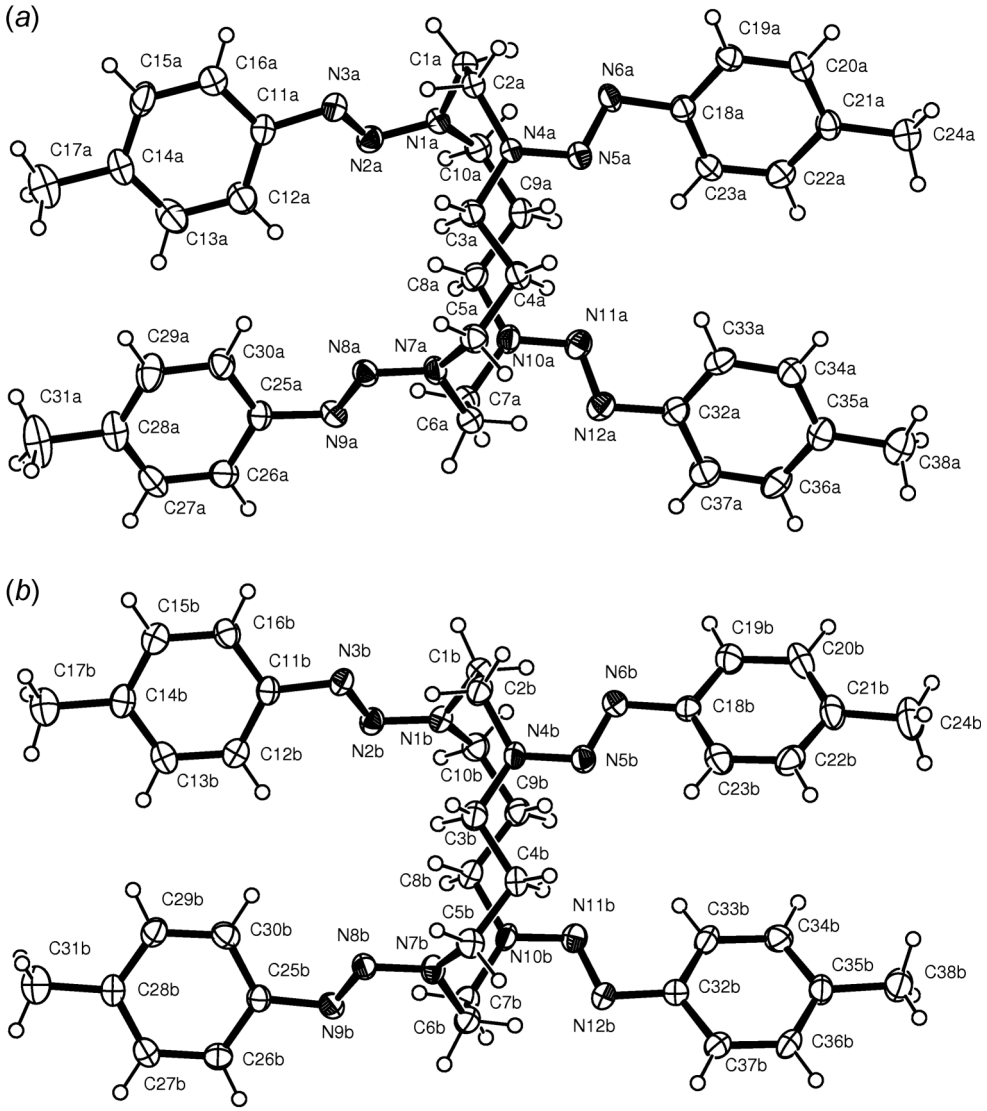
2 X = CN



3a) X = CN
b) X = CH_3

© 2006 NRC Canada

Fig. 5. ORTEP views of the two independent molecules of 1,4,8,11-tetra[2-(*p*-methylphenyl)-1-diazenyl]-1,4,8,11-tetraazacyclotetradecane (**1e**), displaying the thermal ellipsoids at 40% probability.



in the nine-membered ring (see Fig. 7). The broadening of the signals is ascribed to the rotational dynamics of the triazene moieties (14). Indeed, the two rotameric forms of **3b** are clearly seen in the ^{13}C NMR spectrum, and each carbon atom is detected. The relative intensity of the signals from the two rotamers indicates that the major rotamer is present in 60%–70% abundance. Significantly, the equivalent carbon atoms of the heterocyclic ring are detected at 49.28 and 53.18 ppm.

Tristriazene **3a** did not have sufficient solubility to enable ^{13}C NMR analysis, but the ^{1}H NMR spectrum of **3a** showed a complex set of signals for the methylene protons of the heterocyclic ring. The multiplet observed in the range 3.95–4.37 ppm could be interpreted as a group of signals centred around 4.03 ppm and a second group around 4.25 ppm. The two groups are assigned to the axial and equatorial hydrogens (Fig. 6) and the multiple peaks in each group could be assigned to the various rotamers arising from the restricted rotation around the N—N bond in the triazenes (14).

Conclusion

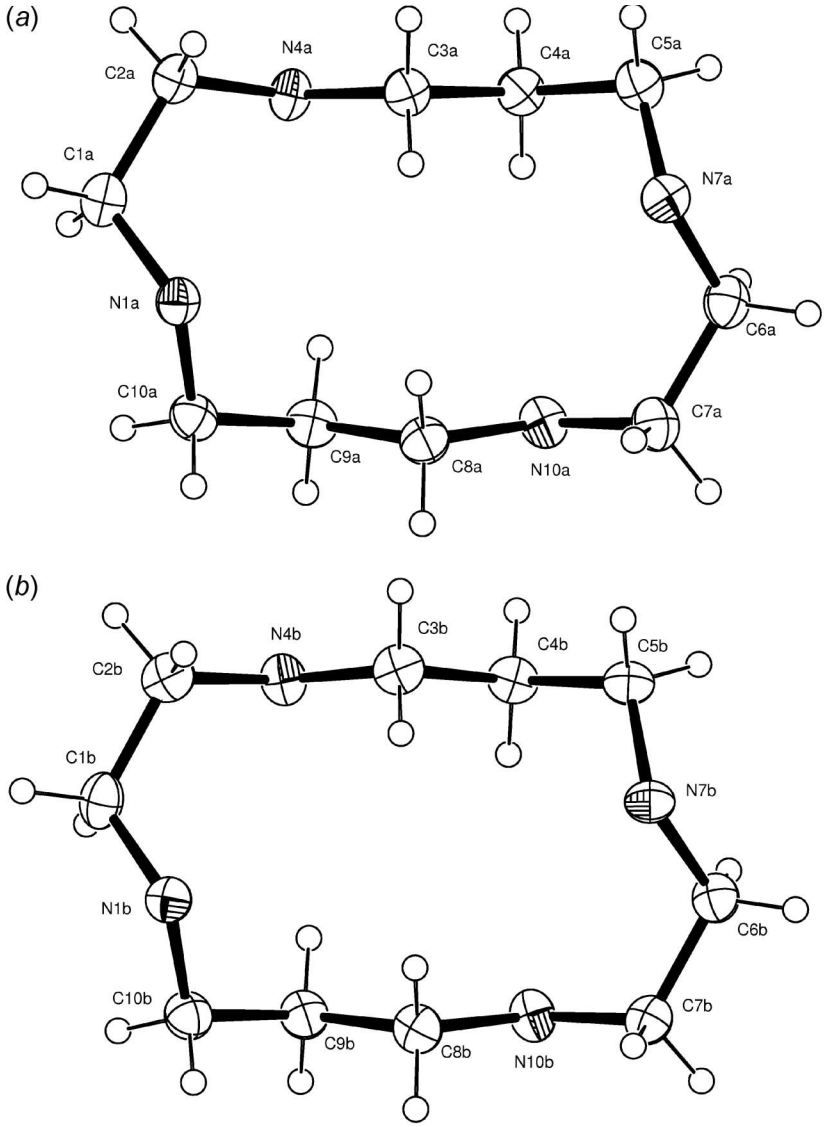
The results reported in this paper clearly show that tristriazenes and tetrakistriazenes can be synthesized and characterized. These results further our extensive research into the synthesis of bistriazenes of various types. Notably, our recent studies have been involved with the general synthesis of triazene derivatives of 1,*x*-diazacycloalkanes. For example, diazonium coupling with piperazine affords the stable bis-1,4-di-(2-aryl-1-diazenyl)-piperazines (**4**) (16). Analogous coupling of diazonium salts with homopiperazines affords the bistriazene series **5** (17).

Acknowledgements

The authors are grateful to the Natural Sciences and Engineering Research Council of Canada (NSERC) for a Discovery Grant to the principal author (KV) and an Undergraduate Summer Research Award (2004) to Jeff Clarke. Financial

© 2006 NRC Canada

Fig. 6. ORTEP views of the best projections of the 14-membered macrocycles (without substituents) of compound **1e**.



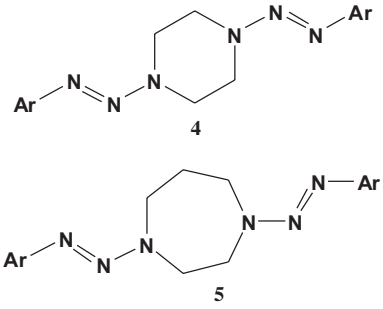
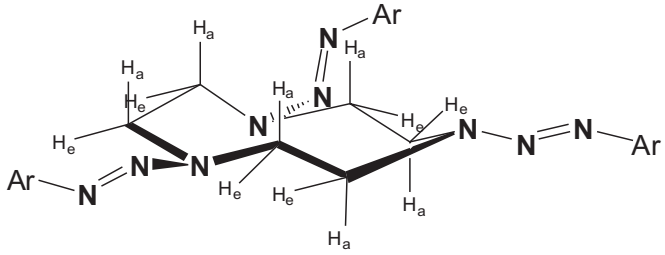


Fig. 7. A representation of the tristriazene structure **3** showing the orientation of the axial (H_a) and equatorial (H_e) hydrogen atoms of the triazacyclononane ring.



support was also provided by the Student Employment Experience Program (SEEP) at Saint Mary's University. We are also grateful to the Atlantic Region Magnetic Resonance Centre (ARMRC) at Dalhousie University for providing NMR spectra; in particular, we would like to thank Dr. Bob Berno for assistance with interpretation of the NMR spectral data. We are indebted to Dr. J. Wilson Quail of the Department of Chemistry, University of Saskatchewan, for his skilful contribution to the refinement of X-ray structures displaying poor diffraction data.

References

1. D.H. Busch. Acc. Chem. Res. **11**, 392 (1978).

© 2006 NRC Canada

2. E.K. Barefield, F. Wagner, A.W. Herlinger, and A.R. Dahl. Inorg. Synth. **16**, 220 (1976).
3. L.T. Ellis, D.F. Perkins, P. Turner, and T.W. Hambley. J. Chem. Soc. Dalton Trans. 2728 (2003).
4. E. Kimura, T. Ikeda, and M. Shionoya. Pure Appl. Chem. **69**, 2187 (1997).
5. E. de Clercq, N. Yamamoto, R. Pauwels, M. Baba, D. Schols, H. Nakashima, J. Balzarini, Z. Debyser, B.A. Murrer, and D. Schwarz. Proc. Natl. Acad. Sci. U.S.A. **89**, 5286 (1992).
6. P. Griess. Ann. **121**, 258 (1862); O. Dimroth. Ber. **38**, 670 (1905).
7. R.C.S. Audette, T.A. Connors, H.G. Mandel, K. Merai, and W.C.J. Ross. Biochem. Pharmacol. **22**, 1855 (1973).
8. S.K. Carter and M.A. Friedman. Eur. J. Cancer, **8**, 85 (1972); R. Ridolfi, V. Chiarion-Sileni, M. Guida, A. Romanini, R. Labianca, A. Freschi, G.L. Re, R. Nortilli, S. Brugnara, P. Vitali, and O. Nanni. J. Clin. Oncol. **20**, 1600 (2002).
9. E.S. Newlands, M.F.G. Stevens, S.R. Wedge, R.T. Wheelhouse, and C. Brock. Cancer Treat. Rep. **23**, 35 (1997); W.K. Yung, R.E. Albright, J. Olson, R. Fredericks, K. Fink, M.D. Prados, M. Brada, A. Spence, R.J. Hohl, and W. Shapiro. Br. J. Cancer, **83**, 588 (2000).
10. K. Vaughan. Org. Prep. Proced. Int. **33**, 59 (2001).
11. A. Altomare, M.C. Burla, M. Camalli, G. Cascarano, C. Giacovazzo, C. Guagliardi, A.G. Moliterni, C. Polidori, and R. Spagna. J. Appl. Crystallogr. **32**, 115 (1999).
12. G.M. Sheldrick. SHELXL97 [computer program]. University of Göttingen, Göttingen, Germany. 1997.
13. M. Nardelli. J. Appl. Crystallogr. **28**, 659 (1995).
14. M. Barra, S. Srivastava, and E. Brockman. J. Phys. Org. Chem. **17**, 1057 (2004); B.T. Golding, T.J. Kemp, R. Narayanaswamy, and B.W. Waters. J. Chem. Res. Synop. 130 (1984).
15. M.N. Burnett and C.K. Johnson. ORTEP-III [computer program]. Oak Ridge National Laboratory, Oak Ridge, Tenn. 1996.
16. V.R. Little, R. Tingley, and K. Vaughan. Can. J. Chem. **83**, 471 (2005).
17. S.L. Moser and K. Vaughan. Can. J. Chem. **82**, 1725 (2004).

© 2006 NRC Canada

A chiral auxiliary cleavable by ring-closing alkene metathesis — Efficient synthesis of chiral nonracemic cycloalkenes[1]

Luc Boisvert, Francis Beaumier, and Claude Spino

Abstract: *p*-Menthane-3-carboxaldehyde is a readily available chiral auxiliary used to prepare cycloalkenes and heterocycles bearing a chiral tertiary or quaternary carbon of high enantiomeric purity. The auxiliary is available in both enantiomeric forms and is inexpensive and recyclable. It is cleaved by a ring-closing alkene metathesis reaction directly yielding the cycloalkene.

Key words: chiral auxiliary, cleavage reaction, cyclization, ring-closing alkene metathesis, enantioenriched cycloalkenes.

Résumé : Le *p*-menthane-3-carboxaldéhyde est utilisé comme auxiliaire chiral pour fabriquer des cycloalcènes et des hétérocycles contenant un centre carboné tertiaire ou quaternaire de pureté énantiomérique élevée. L'auxiliaire est disponible dans les deux séries énantiomériques et est peu dispendieux et recyclable. Il est clivé par une réaction de fermeture de cycle par métathèse d'alcènes menant directement au cycloalcène.

Mots clés : auxiliaire chiral, réaction de clivage, cyclisation, fermeture de cycle par métathèse d'alcènes, cycloalcènes énantioenrichis.

Introduction

Chiral auxiliaries are exceptionally useful tools in synthetic organic chemistry because many of them achieve high levels of asymmetric induction on a wide range of substrates (1). One inherent drawback to their use is the need to install and cleave the auxiliary, which adds two chemical steps to the synthesis of the target molecule. This disadvantage can, however, be minimized if one of these two steps consists of a chemical transformation that would have been carried out eventually as part of the synthetic plan. This is not the case for the majority of chiral auxiliaries found in the literature that are cleaved either by addition–elimination reactions on polarized π systems (e.g., hydride reduction of C=O functional groups) or by hydrolysis of acetal-like functionalities (1). In addition, while other auxiliary-specific cleaving reactions have been developed (e.g., ozonolysis of C=C bonds (2) or hydrogenolysis of benzylic groups (3)), there is still a need to widen the arsenal of available methods to cleave chiral auxiliaries.

In this report, we disclose the cleavage of a chiral auxiliary by ring-closing alkene metathesis (RCM) (4) to yield highly enantioenriched cycloalkenes. To the best of our knowledge, this constitutes the first example of a chiral auxiliary cleavable by a RCM reaction (5, 6). Using our strategy, the cleavage of the auxiliary becomes intrinsic to the synthetic strategy and does not add extra steps en route to the final target.

Synthesis of RCM precursors[3]

The sequence of reactions starts with the synthesis of allylic alcohols **7a**–**7e** from *p*-menthane-3-carboxaldehyde **3** (7). These allylic alcohols were prepared by one of three methods (Scheme 1 and Table 1).

Method A involves the $AlMe_3$-promoted addition of vinyllithium reagents **6a** to aldehyde **3** (8). In this manner, a mixture of diastereomeric allylic alcohols, which are easily separated by flash chromatography, is obtained with selectivities ranging from ca. 10:1 to more than 100:1, favouring the Felkin–Ahn adducts (i.e., **7** as illustrated). Method B involves the addition of vinylalanes **6b**, generated by the zirconium-catalyzed methylalumination of alkynes (9) to aldehyde **3**. In Method C, lithium acetylides **2** are added to aldehyde **3** in the presence of dry cerium trichloride to afford a mixture of diastereomeric propargylic alcohols **4** (10).

Received 19 October 2005. Accepted 13 December 2005. Published on the NRC Research Press Web site at http://canjchem.nrc.ca on 28 July 2006.

This article is dedicated to Dr. Alfred Bader for his precious contributions to the science of chemistry.

L. Boisvert, F. Beaumier, and C. Spino.[2] Université de Sherbrooke, Département de Chimie, 2500 Boul. Université, Sherbrooke, QC J1K 2R1, Canada.

[1]This article is part of a Special Issue dedicated to Dr. Alfred Bader.
[2]Corresponding author (e-mail: claude.spino@USherbrooke.ca).
[3]Supplementary data for this article are available on the journal Web site (http://canjchem.nrc.ca) or may be purchased from the Depository of Unpublished Data, Document Delivery, CISTI, National Research Council Canada, Ottawa, ON K1A 0R6, Canada. DUD 5067. For more information on obtaining material refer to http://cisti-icist.nrc-cnrc.gc.ca/irm/unpub_e.shtml.

 doi:10.1139/V06-095 © 2006 NRC Canada

Scheme 1.

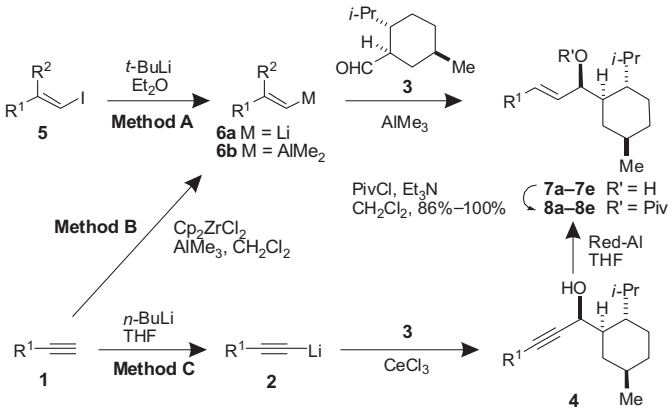


Table 1. Preparation of allylic alcohols **7a**–**7e** (cf. Scheme 1).

Entry	R1	R2	Compound	Yield of **7**[a] (%), (dr)
1	Bn	H	**7a**	64,[b] 170:1
2	$TBSOCH_2$	H	**7b**	43,[c] 3.5:1[d]
3	Bn	Me	**7c**	76,[e] 11:1
4	$TBSO(CH_2)_4$	Me	**7d**	68,[e] 11:1
5	$MOMOCH_2$	H	**7e**	37,[c] 3.1:1[d]

[a]Isolated yield of diastereomerically pure allylic alcohol **7**.
[b]Method A.
[c]Method C (yield of **7** over two steps).
[d]DR of **4** from the addition of **2** to **3**.
[e]Method B.

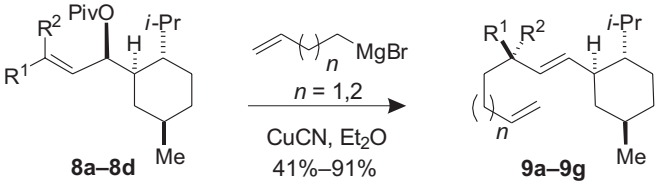
These propargylic alcohols are easily separated and converted to geometrically pure *E* allylic alcohols **7** by reduction with Red-Al. The alcohols **7a**–**7e** were then converted to the corresponding allylic pivalate esters **8a**–**8e** in excellent yields.

Cyanocuprates, derived from Grignard reagents, displaced the pivalate esters stereospecifically (anti to the leaving group with complete transfer of chirality) with 100% stereoselectivity (reaction on the conformer with minimized $A^{1,3}$ strain, yielding *E* alkenes) and with exclusive S_N2' regioselectivity (no S_N2 adduct detected by GC) (7, 11). Thus, cuprate adducts **9a**–**9g** (precursors to five- and six-membered rings for the subsequent RCM reactions) were prepared from pivalate esters **8a**–**8d** (Scheme 2). It should be noted that both absolute stereochemistries at the newly created chiral center in adducts **9** are accessible since both enantiomers of *p*-menthane-3-carboxaldehyde **3** are available, the double-bond geometry in **8** can be controlled, and the order of introduction of the different substituents on the new chiral center can be varied (7).

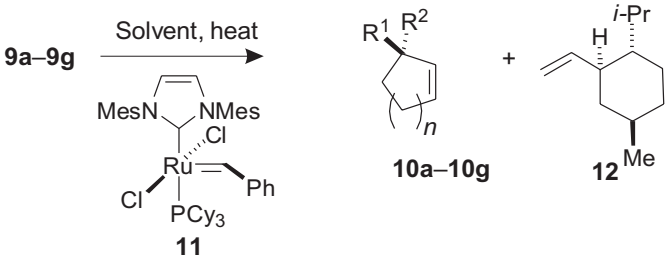
RCM reactions

After screening different ruthenium-based metathesis catalysts (see Supplementary data),[3] it was found that the formation of cycloalkenes **10** by a RCM reaction was best performed using the Grubbs–Nolan catalyst **11** (12) (Scheme 3). For precursors of five-membered rings bearing a tertiary carbon center (**9a** and **9c**) very mild conditions (**11** (1 mol%), CH_2Cl_2, 40 °C, 3 h) resulted in smooth transformation to cycloalkenes **10a** and **10c** (Table 2, entries 1 and

Scheme 2.



Scheme 3.



3). The only detectable (^{1}H NMR) products in the crude reaction mixtures were the cycloalkenes **10** and compound **12**.

Cyclization of precursors of six-membered rings bearing a tertiary carbon center (**9b** and **9d**) necessitated harsher conditions (**11** (10 mol%), $ClCH_2CH_2Cl$, 83 °C, 3 h) to avoid the formation of the corresponding dimers **13b** and **13d** by a competitive cross-metathesis reaction (Fig. 1). Under these conditions, the RCM reactions occurred smoothly to provide cycloalkenes **10b** and **10d** in good yields (Table 2, entries 2 and 4), with only trace amounts of **13** being detected.

Adducts **9e**–**9g**, bearing a quaternary carbon, presented a greater challenge. Minimizing the production of dimer **13** was crucial because when **13e** (derived from **9e**) was treated under RCM conditions (with or without an atmosphere of ethylene), no useful amount of **10e** could be obtained. Ultimately, it was found that higher dilution and temperatures were efficient in decreasing the amount of **13**. However, these conditions sometimes caused side-reactions, like the well-documented alkene isomerization (13), such that cycloalkenes **10e** and **10g** were contaminated with small amounts of inseparable alkene regioisomers **14e** and **14g**, respectively (Fig. 1).

Many strategies were tried to inhibit the formation of **14** (see Supplementary data),[3] but none gave reproducible results. Although the isomerization could not be completely suppressed, cycloalkene **10e** could be obtained in 79% yield as an acceptable 31:1 mixture of **10e** and **14e** by maintaining strictly anhydrous conditions and limiting the reaction time. In the same manner, **10g** was obtained in 70% yield as a 42:1 mixture of **10g** and **14g**. The fact that the RCM proceeds at all on substrates **9e** and **9g** is very satisfying, given the presence of an allylic quaternary center and a bulky menthyl fragment on each side of the *E* double bond (14).

It is perhaps not surprising, given the above results, that we have not yet succeeded in forming six-membered rings bearing a quaternary carbon. Compound **9f** afforded mostly dimer **13f** and degradation products under various conditions; RCM adduct **10f** was never observed, nor was by-product **12** (Table 2, entry 6).

The enantiomeric purity (determined by GC or HPLC analysis against racemic samples) of each RCM adduct was

© 2006 NRC Canada

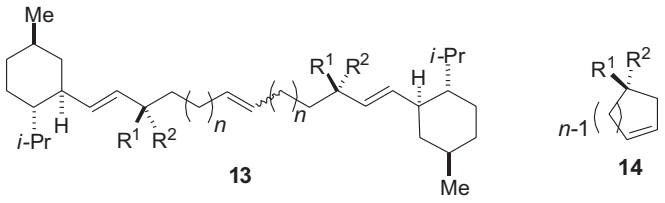
Table 2. Yields and enantiomeric ratios of cycloalkenes **10a**–**10g**.

Entry	9	R1	R2	*n*	10	Yield of **10** (%)[a]	er (%)
1	**9a**	Bn	H	1	**10a**	81	—[b]
2	**9b**	Bn	H	2	**10b**	84	>99:1[c]
3	**9c**	$TBSOCH_2$	H	1	**10c**	87	>98:2[d]
4	**9d**	$TBSOCH_2$	H	2	**10d**	73	>98:2[d]
5	**9**	Bn	Me	1	**10**	79[b]	97:3[e]
6	**9f**	Bn	Me	2	**10f**	0	—
7	**9g**	$TBSO(CH_2)_4$	Me	1	**10g**	70[b]	—[b]

Note: General conditions: **11** (1–10 mol%), CH_2Cl_2 or $ClCH_2CH_2Cl$ (0.01–0.002 mol/L), reflux, 3 h (see Supplementary data).[3]

[a]Isolated yield of **10** after flash chromatography.
[b]See text.
[c]Determined by HPLC analysis.
[d]Determined by GC analysis on the free alcohol.
[e]Determined by HPLC analysis on the allylic oxidation derivative.

Fig. 1. By-products from RCM reactions.



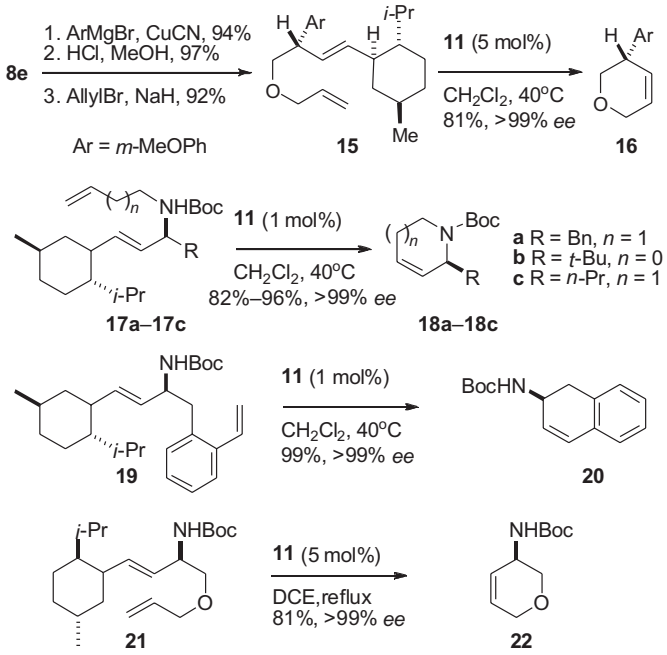
found to be excellent. For entries 1 and 7 of Table 2, we were unable to achieve complete resolution of the cycloalkene enantiomers, but their enantiomeric ratios are likely to be equally high. By-product **12** can be easily recovered by flash chromatography in yields of 70%–80% and, if desired, can be recycled back to aldehyde **3** by ozonolysis.

It is possible to envisage the application of our strategy to the preparation of a wide variety of highly enantioenriched cycloalkenes. Among the most interesting candidates, heterocycles are highly desirable (15). As an example, diene **15** (obtained in three steps from pivalate ester **8e**) was submitted to a RCM reaction to furnish dihydropyran **16** in 81% yield and >99% ee (as determined by HPLC analysis) (Scheme 4). *N*-Heterocycles, prepared by a different route (16), were also obtained by a similar RCM cleavage strategy as shown in Scheme 4. Dehydropiperidine **18a** and **18c**, pyrrolidine **18b**, and dihydroquinoline **20** were formed in excellent yield under much milder conditions (1 mol% catalyst in refluxing dichloromethane). Dihydropyran **22** required higher catalyst loading and higher temperature. We are currently embarked on the total synthesis of several alkaloids using this methodology.

Conclusion

We have achieved the first cleavage of a chiral auxiliary by a RCM reaction. This unprecedented method of cleavage has the merit of increasing the complexity of the substrate during the cleavage of the auxiliary, while not adding any extra steps to a synthetic plan aimed at synthesizing cycloalkenes. The sequence described herein allows the synthesis of enantioenriched cycloalkenes bearing a tertiary or quaternary chiral carbon in just four steps starting from readily available starting materials (vinyliodides or alkynes).

Scheme 4.



We are currently expanding the methodology to include more diverse and complex structures.

Acknowledgement

We thank the Natural Sciences and Engineering Research Council of Canada (NSERC), the ACS Petroleum Research Fund (Grant No. 36256-AC1), and the Université de Sherbrooke for financial support.

References

1. (*a*) J. Seyden-Penne. Chiral auxiliaries and ligands in asymmetric synthesis. John Wiley and Sons, New York. 1995; (*b*) R.E. Gawley and J. Aubé. Principles of asymmetric synthesis. Elsevier Science, New York. 1996.
2. (*a*) C. Spino, C. Beaulieu, and J. Lafrenière. J. Org. Chem. **65**, 7091 (2000); (*b*) M. Braun. Angew. Chem. Int. Ed. **37**, 430 (1998).

© 2006 NRC Canada

3. Y. Aoyagi, R.P. Jain, and R.M. Williams. J. Am. Chem. Soc. **123**, 3472 (2001).
4. Recent reviews: (*a*) R.H. Grubbs (*Editor*). Handbook of metathesis. *Edited by* Wiley-VCH, Weinheim, Germany. 2003; (*b*) K.C. Nicolaou, P.G. Bulger, and D. Sarlah. Angew. Chem. Int. Ed. **44**, 4490 (2005); (*c*) R.H. Grubbs. Tetrahedron, **60**, 7117 (2004); (*d*) A.H. Hoveyda, D.G. Gillingham, J.J. Van Veldhuizen, O. Kataoka, S.B. Garber, J.S. Kingsbury, and J.P.A. Harrity. Org. Biomol. Chem. **2**, 8 (2004).
5. Although we know of no other RCM-cleavable chiral auxiliary, the underlying concept is similar to RCM-cleavable linkers developed for solid-phase synthesis. For example, see: (*a*) M.S.M. Timmer, J.D.C. Codée, H.S. Overkleeft, J.H. van Boom, and G.A. van der Marel. Synlett, 2155 (2004); (*b*) J.-D. Moriggi, L.J. Brown, J.L. Castro, and R.C.D. Brown. Org. Biomol. Chem. **2**, 835 (2004).
6. While RCM reactions on dienes attached to a chiral auxiliary are numerous, in these systems the auxiliary is cleaved by transformations different from the RCM reaction. For example, see: M.T. Crimmins and B.W. King. J. Org. Chem. **61**, 4192 (1996).
7. (*a*) C. Spino and C. Beaulieu. Angew. Chem. Int. Ed. **39**, 1930 (2000); (*b*) C. Spino, C. Godbout, C. Beaulieu, M. Harter, T.M. Mwene-Mbeja, and L. Boisvert. J. Am. Chem. Soc. **126**, 13312 (2004).
8. C. Spino, M.-C. Granger, and M.-C. Tremblay. Org. Lett. **4**, 4735 (2002).
9. E.-I. Negishi and D.Y. Kondalov. Chem. Soc. Rev. **25**, 417 (1996).
10. The use of carefully dried $CeCl_3$ was beneficial in increasing both the yields of the propargylic alcohols **4** and the Felkin–Ahn selectivity. For discussions on the drying of $CeCl_3$ and its effects, see: (*a*) N. Takeda and T. Imamoto. Org. Synth. **76**, 228 (1999); (*b*) V. Dimitrov, K. Kostova, and M. Genov. Tetrahedron Lett. **37**, 6787 (1996); (*c*) D.A. Conlon, D. Kumke, C. Moeder, M. Hardiman, G. Hutson, and L. Sailer. Adv. Synth. Catal. **346**, 1307 (2004); (*d*) P.E. Harrington and M.A. Tius. J. Am. Chem. Soc. **123**, 8509 (2001).
11. For the use of CuCN in the S_N2' displacement of allylic esters with Grignard reagents, see: C.C. Tseng, S.D. Paisley, and H.L. Goering. J. Org. Chem. **51**, 2884 (1986).
12. (*a*) J. Huang, E.D. Stevens, S.P. Nolan, and J.L. Peterson. J. Am. Chem. Soc. **121**, 2674 (1999); (*b*) M. Scholl, T.M. Trnka, J.P. Morgan, and R.H. Grubbs. Tetrahedron Lett. **40**, 2247 (1999).
13. For recent discussions, see: (*a*) C.D. Edlin, J. Faulkner, D. Fengas, C.K. Knight, J. Parker, I. Preece, P. Quayle, and S.N. Richards. Synlett, 572 (2005); (*b*) S.H. Hong, M.W. Day, and R.H. Grubbs. J. Am. Chem. Soc. **126**, 7414 (2004); (*c*) B. Schmidt. Eur. J. Org. Chem. 1865 (2004).
14. Successful RCM reactions on such sterically demanding substrates are rare in the literature. For RCM on substrates with the same general features, see: (*a*) S. Suga, M. Watanabe, and J.-I. Yoshida. J. Am. Chem. Soc. **124**, 14824 (2002); (*b*) E. Roulland, C. Monneret, J.-C. Florent, C. Bennejean, P. Renard, and S. Léonce. J. Org. Chem. **67**, 4399 (2002); (*c*) Y. Chong, G. Gumina, and C.K. Chu. Tetrahedron: Asymmetry, **11**, 4853 (2000). In all cases, the terminal alkyl group (opposite a quaternary center) on the *E* alkene is much less hindered than in our case (i.e., menthyl fragment) and the RCM proceeds much more easily than here, allowing the use of the less active catalyst, $Cl_2(Cy_3P)_2Ru{=}CHPh$.
15. For the synthesis of heterocycles by RCM and other methods, see the thematic issue on heterocycles: Chem. Rev. **104**(5), (2004).
16. D. Gagnon, S. Lauzon, C. Godbout, and C. Spino. Org. Lett. **7**, 4769 (2005).

© 2006 NRC Canada

Triazene derivatives of (1,*x*-)diazacycloalkanes. Part VI. 3-({5,5-Dimethyl-3-[2-aryl-1-diazenyl]-1-imidazolidinyl}methyl)-4,4-dimethyl-1-[2-aryl-1-diazenyl]imidazolidines — Synthesis, characterization, and X-ray crystal structure[1,2]

Keith Vaughan, Shasta Lee Moser, Reid Tingley, M. Brad Peori, and Valerio Bertolasi

Abstract: Reaction of a series of diazonium salts with a mixture of formaldehyde and 1,2-diamino-2-methylpropane affords the 3-({5,5-dimethyl-3-[2-aryl-1-diazenyl]-1-imidazolidinyl}methyl)-4,4-dimethyl-1-[2-aryl-1-diazenyl]imidazolidines (**1a**–**1f**) in excellent yield. The products have been characterized by IR and NMR spectroscopic analysis, elemental analysis, and X-ray crystallography. The X-ray crystal structure of the *p*-methoxycarbonyl derivative (**1c**) establishes without question the connectivity of these novel molecules, which can be described as linear bicyclic oligomers with two imidazolidinyl groups linked together by a one-carbon spacer. This is indeed a rare molecular building block. The molecular structure is corroborated by ^{1}H and ^{13}C NMR data, which correlates with the previously published data of compounds of types **5** and **6** derived from 1,3-propanediamine. The triazene moieties in the crystal of **1c** display significant π conjugation, which gives the N—N bond a significant degree of double-bond character. This in turn causes restricted rotation around the N—N bond, which leads to considerable broadening of signals in both the ^{1}H and ^{13}C NMR spectra. The molecular ion of the *p*-cyanophenyl derivative (**1b**) was observed using electrospray mass spectrometry (ES + Na). The mechanism of formation of molecules of type **1** is proposed to involve diazonium ion trapping of the previously unreported bisimidazolidinyl methane (**13**).

Key words: triazene, bistriazene, imidazolidine, synthesis, X-ray crystallography, NMR spectroscopy.

Résumé : Les réactions d'une série de sels de diazonium avec un mélange de formaldéhyde et de 1,2-diamino-2-méthylpropane conduit à la formation des 3-({5,5-diméthyl-3-[2-aryl-1-diazényl]-1-imidazolidinyl}méthyl)-4,4-diméthyl-1-[2-aryl-1-diazényl]imidazolidines (**1a**–**1f**) avec d'excellents rendements. On a caractérisé les produits par leurs spectres IR et RMN, par analyse élémentaire et par diffraction des rayons X. La structure cristalline ainsi déterminée pour le dérivé *p*-méthoxycarbonyle (**1c**) permet d'établir sans ambiguïté la connectivité dans ces nouvelles molécules qui peuvent être décrites comme des oligomères bicycliques linéaires comportant deux groupes imidazolidinyles reliés par un groupe d'espacement formé d'un atome de carbone, ce qui est un élément moléculaire d'assemblage assez rare. La structure moléculaire est corroborée par les données de la RMN du ^{1}H et du ^{13}C qui permettent d'établir une corrélation avec les données publiées antérieurement au sujet de composés des types **5** et **6** dérivés de la 1,3-propanediamine. Dans les portions triazènes présentes dans la structure cristalline du composé **1c** on retrouve une conjugaison π importante qui donne à la liaison N—N un caractère important de double liaison. Ce caractère provoque une restriction autour de la liaison N—N et, par voie de conséquence, un élargissement considérable dans les spectres RMN du ^{1}H et du ^{13}C. Dans le spectrogramme de masse obtenu en faisant appel à une ionisation par électronébulisation, on peut observer l'ion moléculaire du dérivé *p*-cyanophényle (**1b**). On suggère que le mécanisme de formation des molécules de type **1** implique un piégeage par l'ion diazonium du bisimidazolidinyméthane (**13**) qui n'avait pas encore été rapporté antérieurement.

Mots clés : triazène, bistriazène, imidazolidine, synthèse, cristallographie à l'aide de rayons X, spectroscopie RMN.

[Traduit par la Rédaction]

Received 26 August 2005. Accepted 16 February 2006. Published on the NRC Research Press Web site at http://canjchem.nrc.ca on 1 August 2006.

This paper is dedicated to the work of Dr. Alfred Bader for his contribution to the advancement of the science of organic synthesis.

K. Vaughan,[3] S.L. Moser, R. Tingley, and M.B. Peori. Department of Chemistry, Saint Mary's University, Halifax, NS B3H 3C3, Canada.
V. Bertolasi. Dipartimento di Chimica and Centro di Strutturistica Diffrattometrica, Universita' di Ferrara, Via L. Borsari, 46, 44100 Ferrara, Italy.

[1]This article is part of a Special Issue dedicated to Dr. Alfred Bader.
[2]For Part V, see: Can. J. Chem. **83**, 1799 (2005).
[3]Corresponding author (e-mail: keith.vaughan@smu.ca).

 doi:10.1139/V06-091 © 2006 NRC Canada

Introduction

Imidazolidines are ubiquitous in pharmacology, medicinal chemistry, biochemistry, and various chemical studies. A number of imidazolidine carbonyl derivatives have recently been shown to exhibit antinociceptive activity (1) and several substituted thioxo-imidazolidine compounds have been evaluated for schistosomicidal activity (2). A structure–activity relationship of some new antiarrhythmic 5-arylideneimidazolidine-2,4-diones has been established (3) and the compounds were devoid of significant side effects. In the area of asymmetric synthesis, chiral imidazolidine ligands have been synthesized from *N*,*N*′-dialkylated cyclohexanediamine derivatives with excellent levels of enantiomeric excess (4). A novel imidazolidine derivative is formed spontaneously from the reaction of triethylenetetramine, salicylaldehyde, and benzaldehyde in methanol (5); this reaction has some significance to the chemistry reported in this paper. On a different playing field, a pentamethylimidazolidine embedded in polyethylene has been used as a radical probe to investigate the orientation distribution function of certain anisotropic paramagnetic species (6), and in a theoretical study, structural, electronic, and energetic information has been elucidated for three imidazolidinone derivatives (7).

This paper reports the synthesis and characterization of a series of new bis(imidazolyl)methanes, the novel 3-({5,5-dimethyl-3-[2-aryl-1-diazenyl]-1-imidazolidinyl}methyl)-4,4-dimethyl-1-[2-aryl-1-diazenyl]imidazolidines (**1a**–**1f**), from the diazonium coupling reaction with a mixture of formaldehyde and 1,2-diamino-2-methylpropane. These new bistriazenes exhibit the linear bicyclic structure similar to other bistriazenes derived from 1,3-propanediamines previously reported (8). However, these structures are diametrically different from the molecules of type **2**, obtained by analogous reaction with ethylenediamine (9), which have a distinctly different bridged bicyclic (or "cagelike") structure. Evidently, we have discovered a crossover in the molecular architecture of the products (**2**) derived from ethylenediamine itself (**3**) compared with the products (**1**) derived from the branched chain molecule, 1,2-diamino-2-methylpropane (**4**) (Scheme 1).

Experimental section

All reagents were reagent grade materials purchased from the Sigma-Aldrich Chemical Co. Ltd. and were used without further purification. Melting points were determined on a Fisher-Johns melting point apparatus (Fisher Scientific Inc.) and are uncorrected. Infrared spectra were obtained using Nujol mulls, unless otherwise stated, on a PerkinElmer 299 spectrophotometer or with a Brucker Vector 22 spectrometer. ^{1}H and ^{13}C NMR spectra were obtained using either the Anasazi Instruments 60 MHz EFT spectrometer at Saint Mary's University or the Bruker 250 MHz spectrophotometer at the Atlantic Regional Magnetic Resonance Centre at Dalhousie University, both located in Halifax, Nova Scotia. Chemical shifts were recorded in $CDCl_3$ solutions at 20 °C and are relative to TMS as the internal standard. Elemental analysis was carried out at the Canadian Microanalytical Laboratory, Delta, British Columbia.

Synthesis of the 3-({5,5-dimethyl-3-[2-aryl-1-diazenyl]-1-imidazolidinyl}methyl)-4,4-dimethyl-1-[2-aryl-1-diazenyl]imidazolidines (1a–1f)

General procedure

The appropriate aromatic amine (0.015 mol) was dissolved in 3 mol/L of hydrochloric acid (20.0 mL) and the resulting solution was cooled to 0 °C. The hydrochloride solution was diazotized with a solution of sodium nitrite (1.15 g) in water (minimum volume) and the diazonium salt solution was left in the cold with stirring for 0.5 h. The solution was neutralized with saturated sodium bicarbonate solution and then 37% aqueous formaldehyde (5.0 mL) was added, while the temperature was kept below 0 °C. An aliquot of 1,2-diamino-2-methylpropane (0.015 mol) was dissolved in water and was then slowly added to the neutralized formaldehyde – diazonium salt mixture. After stirring for a further 0.5 h, the mixture was again basified with saturated sodium bicarbonate and the product that precipitated at this point was isolated by vacuum filtration, dried, and recrystallized from either ethanol, an ethanol – ethyl acetate mixture, or a hexanes – ethyl acetate mixture, to afford the following products.

*3-({5,5-Dimethyl-3-[2-(*p*-nitrophenyl)-1-diazenyl]-1-imidazolidinyl}methyl)-4,4-dimethyl-1-[2-(*p*-nitrophenyl)-1-diazenyl]imidazolidine (1a)*

Yellow crystals; yield 87%; mp 135–138 °C (ethanol – ethyl acetate). IR (Nujol, cm^{-1}) ν_{max}: 848, 1338, 1507. ^{1}H NMR ($CDCl_3$, 250 MHz) δ: 1.27 (12H, s), 3.51 (2H, s), 3.88 (4H, br s), 4.59 (4H, br s), 7.48 (4H, d, J = 9.0 Hz), 8.17 (4H, d, J = 9.0 Hz). ^{13}C NMR ($CDCl_3$, 62.9 MHz, ppm) δ: 22.0, 58.2, 120.7, 125.0, 145.0. Anal. calcd. for $C_{23}H_{30}N_{10}O_4$ (%): C 54.1, H 5.9, N 27.5; found: C 53.9, H 5.8, N 27.1.

*3-({5,5-Dimethyl-3-[2-(*p*-cyanophenyl)-1-diazenyl]-1-imidazolidinyl}methyl)-4,4-dimethyl-1-[2-(*p*-cyanophenyl)-1-diazenyl]imidazolidine (1b)*

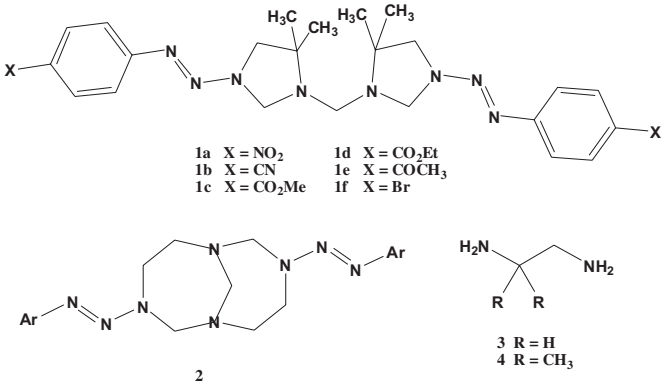
Cream prisms; yield 97%; mp 198–200 °C (hexanes – ethyl acetate). IR (Nujol, cm^{-1}) ν_{max}: 848, 2219. ^{1}H NMR ($CDCl_3$, 250 MHz) δ: 1.26 (12H, s), 3.50 (2H, s), 3.65 (4H, br s), 4.59 (4H, br s), 7.46 (4H, d, J = 8.5 Hz), 7.59 (4H, d, J = 8.4 Hz). ^{13}C NMR ($CDCl_3$, 62.9 MHz, ppm) δ: 22.0 (br), 58.3, 60.0 (br), 68.0 (br), 69.4 (br), 108.5, 119.6, 121.3, 133.3, 154.3. MS (ES$^+$ + Na) m/z: 493 (M$^+$ + 23). Anal. calcd. for $C_{25}H_{30}N_{10}$ (%): C 63.8, H 6.4, N 29.8; found: C 63.7, H 6.3, N 29.8.

*3-({5,5-Dimethyl-3-[2-(*p*-methoxycarbonylphenyl)-1-diazenyl]-1-imidazolidinyl}methyl)-4,4-dimethyl-1-[2-(*p*-methoxycarbonylphenyl)-1-diazenyl]imidazolidine (1c)*

Amber needles; yield 87%; mp 178–181 °C (ethanol – ethyl acetate). IR (Nujol, cm^{-1}) ν_{max}: 860, 1710. ^{1}H NMR ($CDCl_3$, 250 MHz) δ: 1.25 (12H, s), 3.49 (2H, s), 3.75 (4H, br s), 3.89 (6H, s, O-Me), 4.67 (4H, br s), 7.46 (4H, d, J = 8.5 Hz), 8.00 (4H, d, J = 8.6 Hz). ^{13}C NMR ($CDCl_3$, 62.9 MHz, ppm) δ: 22.0, 26.7, 58.2, 60.5, 120.5, 125.5, 129.7, 154.7, 197.6. Anal. calcd. for $C_{27}H_{36}N_8O_4$ (%): C 60.4, H 6.7, N 20.9; found: C 59.6, H 6.7, N 20.2.

© 2006 NRC Canada

Scheme 1.



*3-({5,5-Dimethyl-3-[2-(*p*-ethoxycarbonylphenyl)-1-diazenyl]-1-imidazolidinyl}methyl)-4,4-dimethyl-1-[2-(*p*-ethoxycarbonylphenyl)-1-diazenyl]imidazolidine (1d)*

Yellow needles; yield 92%; mp 139–144 °C (ethanol). IR (Nujol, cm^{-1}) ν_{max}: 860, 1708. ^1H NMR ($CDCl_3$, 250 MHz) δ: 1.22 (12H, s), 1.36 (6H, t, J = 7.0 Hz), 3.46 (2H, s), 3.72 (4H, br s), 4.33 (4H, q, J = 7.1 Hz), 4.66 (4H, br s), 7.44 (4H, d, J = 8.6 Hz), 8.00 (4H, d, J = 8.6 Hz). ^{13}C NMR ($CDCl_3$, 62.9 MHz, ppm) δ: 14.4, 21.7, 58.1, 60.3, 60.8, 68.0 (br), 70.0 (w br), 120.3, 127.2, 130.6, 154.4, 166.6. Anal. calcd. for $C_{29}H_{40}N_8O_4$ (%): C 61.7, H 7.1, N 19.8; found: C 61.6, H 7.2, N 19.3.

*3-({5,5-Dimethyl-3-[2-(*p*-acetylphenyl)-1-diazenyl]-1-imidazolidinyl}methyl)-4,4-dimethyl-1-[2-(*p*-acetylphenyl)-1-diazenyl]imidazolidine (1e)*

Cream-coloured needles; yield 60%; mp 159–163 °C (ethanol). IR (Nujol, cm^{-1}) ν_{max}: 833, 1672. ^1H NMR ($CDCl_3$, 250 MHz) δ: 1.25 (12H, s), 2.58 (6H, s), 3.49 (2H, s), 3.75 (4H, br s), 4.68 (4H, br s), 7.46 (4H, d, J = 8.5 Hz), 7.94 (4H, d, J = 8.6 Hz). ^{13}C NMR ($CDCl_3$, 62.9 MHz, ppm) δ: 22.0, 26.7, 58.2, 60.6, 120.5, 125.5, 129.7, 154.7, 197.6. Anal. calcd. for $C_{27}H_{36}N_8O_2$ (%): C 64.3, H 7.2, N 22.2; found: C 64.5, H 7.1, N 22.4.

*3-({5,5-Dimethyl-3-[2-(*p*-bromophenyl)-1-diazenyl]-1-imidazolidinyl}methyl)-4,4-dimethyl-1-[2-(*p*-bromophenyl)-1-diazenyl]imidazolidine (1f)*

Pale yellow needles; yield 91%; mp 157–160 °C (ethanol). IR (Nujol, cm^{-1}) ν_{max}: 831. ^1H NMR ($CDCl_3$, 250 MHz) δ: 1.23 (12H, s), 3.46 (2H, s), 3.70 (4H, br s), 4.63 (4H, br s), 7.28 (4H, d, J = 8.8 Hz), 7.45 (4H, d, J = 8.5 Hz). ^{13}C NMR ($CDCl_3$, 62.9 MHz, ppm) δ: 21.9, 58.2, 60.4, 68.0, 119.0, 122.2, 132.0, 150.0. Anal. calcd. for $C_{23}H_{30}N_8Br_2$ (%): C 47.7, H 5.2, N 19.4; found: C 47.3, H 5.1, N 19.1.

Crystallography

X-ray diffraction data were collected on a Nonius Kappa CCD diffractometer with graphite-monochromated Mo Kα radiation (λ = 0.7107 Å). Data sets were integrated using the Denzo-SMN package (10) and corrected for Lorentz and polarization effects. The structure was solved by direct methods (SIR97) (11) and refined (SHELXL-97) (12) by full-matrix least-squares with anisotropic non-H and the hydrogen atoms included on calculated positions, riding on their carried atoms. All other calculations were accomplished using the PARST system of programs (13). Crystal data are given in Table 1.[4] Selected bond distances and angles are given in Table 2.

Table 1. Crystal data of compound **1c**.

Compound	**1c**
Formula	$C_{27}H_{36}N_8O_4$
M_r	536.64
Crystal system	Monoclinic
Space group	$P2_1/a$
a (Å)	13.9425(3)
b (Å)	7.1444(2)
c (Å)	28.6998(9)
β (°)	97.272(1)
V (Å^3)	2835.82(13)
Z	4
$D_{calcd.}$ (g cm^{-3})	1.257
F(000)	1 144
μ (cm^{-1})	0.874
Temperature (K)	295
Crystal form, colour	Prismatic, colourless
Crystal size (mm)	0.43 × 0.19 × 0.12
θ_{min}–θ_{max} (°)	3.4–27.5
Measured reflections	8624
Index ranges	$-18 \le h \le 18$; $-9 \le k \le 9$; $-37 \le l \le 36$
Unique reflections	6502
R_{int}	0.027
Obs. reflections [$F^2 \ge 2\sigma(F^2)$]	3792
$R(F^2)$ (Obs. reflections)	0.0466
$wR(F^2)$ (All reflections)	0.1311
No. of parameters	358
GoF	1.017
$\Delta\rho_{min}$, $\Delta\rho_{max}$	–0.129, 0.135

Results and discussion

Reaction of a mixture of 1,2-diamino-2-methylpropane and formaldehyde with an arene diazonium salt afforded the new bistriazene series, the 3-({5,5-dimethyl-3-[2-aryl-1-diazenyl]-1-imidazolidinyl}methyl)-4,4-dimethyl-1-[2-aryl-1-diazenyl]imidazolidines (**1a**–**1f**); in all but one case, the yields are very high, in the range 87%–97%. These new bistriazenes have two 4,4-dimethylimidazolidinyl moieties connected together via a single methylene group bridging

[4] Supplementary data for this article are available on the journal Web site (http://canjchem.nrc.ca) or may be purchased from the Depository of Unpublished Data, Document Delivery, CISTI, National Research Council Canada, Ottawa, ON K1A 0R6, Canada. DUD 5065. For more information on obtaining material refer to http://cisti-icist.nrc-cnrc.gc.ca/irm/unpub_e.shtml. CCDC 246660 contains the crystallographic data for this manuscript. These data can be obtained, free of charge, via http://www.ccdc.cam.ac.uk/conts/retrieving.html (Or from the Cambridge Crystallographic Data Centre, 12 Union Road, Cambridge CB2 1EZ, UK; fax +44 1223 336033; or deposit@ccdc.cam.ac.uk).

© 2006 NRC Canada

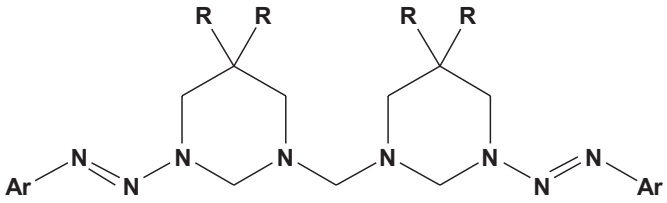
Table 2. Selected bond lengths and angles in compound **1c**.

Bond lengths (Å)	
N1—C1	1.423(2)
N1—N2	1.276(2)
N2—N3	1.319(2)
N3—C9	1.448(2)
N3—C11	1.440(2)
N4—C10	1.486(2)
N4—C11	1.456(2)
N4—C14	1.444(2)
C9—C10	1.520(3)
N8—C20	1.426(2)
N7—N8	1.274(2)
N6—N7	1.329(2)
N6—C16	1.447(2)
N6—C17	1.446(2)
N5—C15	1.488(2)
N5—C17	1.454(2)
N5—C14	1.450(2)
C15—C16	1.532(2)
Bond angles (°)	
N2-N1-C1	112.2(2)
N1-N2-N3	113.3(2)
N1-N3-C9	124.7(1)
N2-N3-C11	119.8(2)
C9-N3-C11	112.6(1)
C10-N4-C11	107.2(1)
C10-N4-C14	116.5(1)
C11-N4-C14	113.0(1)
N4-C14-N5	109.0(1)
N7-N8-C20	111.9(1)
N6-N7-N8	112.8(1)
N7-N6-C16	124.4(1)
N7-N6-C17	118.0(1)
C16-N6-C17	111.8(1)
C15-N5-C17	106.5(1)
C14-N5-C15	116.3(1)
C14-N5-C17	112.0(1)

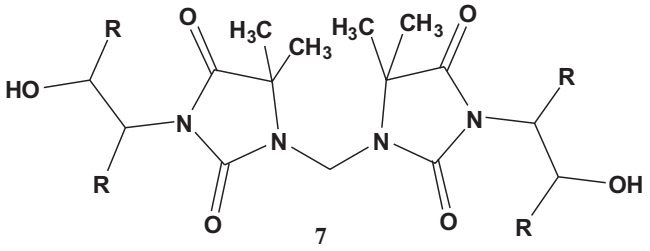
the N3 nitrogens; the available N1 nitrogens are coupled to the aryldiazenyl groups. This is a very similar type of molecular architecture to that previously reported (8) for the hexahydropyrimidine series, **5** and **6**. Molecules of types **1**, **5**, and **6** can be described as linear bicyclic bistriazenes, whereas the contrasting structure (**2**) can be described as a bridged bicyclic bistriazene with a cagelike structure. All compounds in the series **1a**–**1f** are stable crystalline solids, whereas the compounds of series **5** and **6** showed variable stability with a certain tendency to decompose (Scheme 2).

Molecules of type **1**, with two imidazole groups bridged by a single carbon atom are quite rare. Habermeier and Porret (14) reported a series of 1,1′-methylene-bis(hydantoins) (**7**). It is intriguing to note that the dimethyl branching positions in **1** are identical to those in the hydantoin (**7**), which raises the question regarding the possible existence of isomers of the new compounds of series **1**. Such isomers would have the structures shown in **8** and **9**; however, it is clear from the crystal structure elucidation of

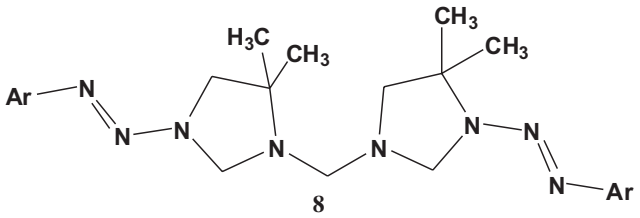
Scheme 2.



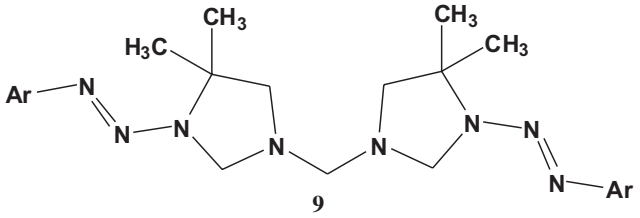
5 R = H
6 R = CH_3



7



8



9

compound **1c** that we do indeed have the novel structure **1** in which the methyl branches essentially face each other in an intuitively unlikely stereochemical combination.

An ORTEP (15) view of compound **1c** is shown in Fig. 1. The compound is built up by two equivalent fragments in the S-cis orientation, with respect to the N4-C14-N5 bridge. The planar phenyltriazenyl groups are mutually slightly rotated by an angle of 39.57(6)° and both the triazene moieties in the anti configuration display significant π conjugation. Both the imidazolidine five-membered rings adopt a twist conformation as shown in Table 3 (16).

The intuitive reasoning that suggests that structure **1c** should be sterically crowded is not supported by the ORTEP diagram in Fig. 1. The molecule of **1c** adopts a folded conformation that brings the triazene moieties fairly close together, but not close enough to invoke π–π stacking interactions. This folding of the molecule, which is similar to the folding observed in the X-ray structures of molecules of types **5** and **6** (17, 18), relieves any steric strain that would build up between the methyl branching groups. The folded conformation is also seen clearly in the crystal packing diagram, as displayed in Fig. 2, which is determined only by

© 2006 NRC Canada

Fig. 1. Thermal ellipsoid plot (ORTEP) of **1c**. Thermal ellipsoids are drawn at the 30% probability level.

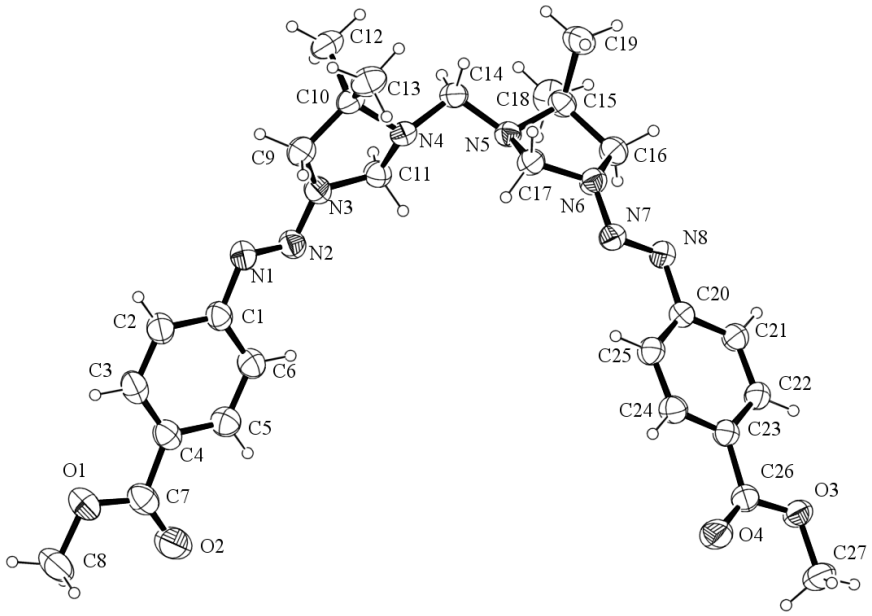


Fig 2. The crystal packing of **1c** viewed down the crystallographic *b* axis.

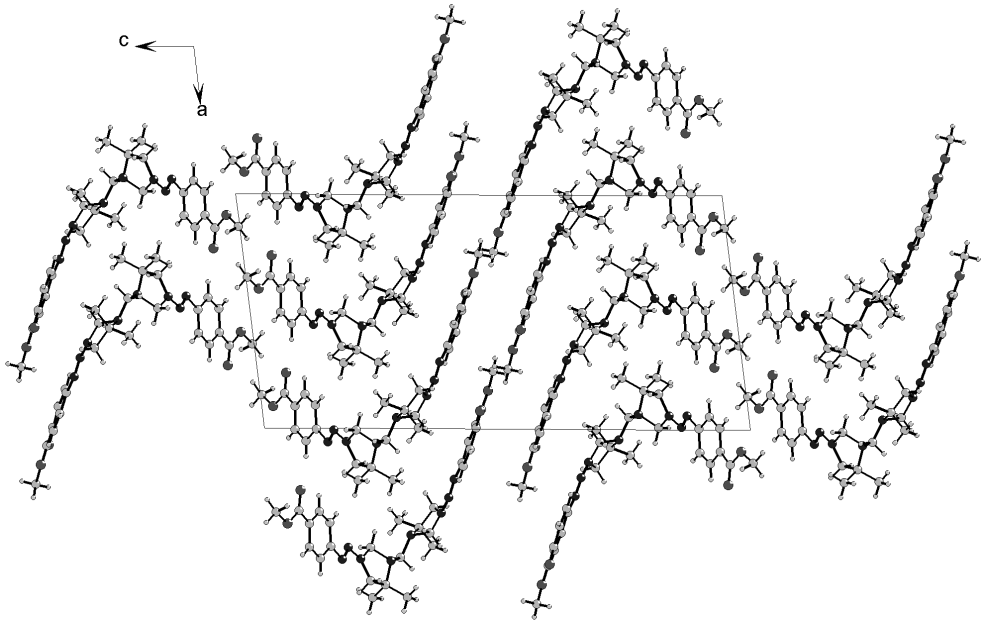


Table 3. Puckering parameters and ring conformations (16).

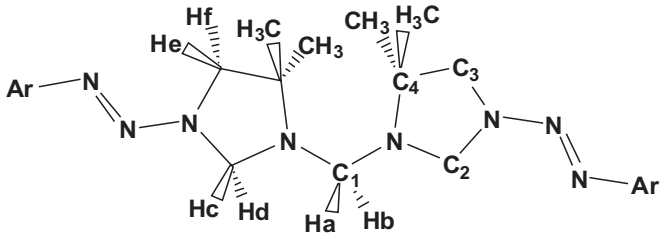
Ring	ϕ_2 (°)	q_2 (Å)	Conformation
N3-C9-C10-N4-C11	–88.6(3)	0.349(2)	$^4T_3$
N6-C16-C15-N5-C17	–83.3(2)	0.368(2)	$^4T_3$

van der Waals interactions. There is an inherent flow to the 3D structure shown in Fig. 2; the crystal is built up of layers of strings of molecules, but each string is like a sine wave. This repeating sine curve is made possible by the inherent curvature of each molecule derived from the folded conformation. It would appear that the ends of the molecules in each string are held together by the van der Waals attraction between the dipole moments of the terminal ester (COOMe) groups.

Further identification of the compounds in the series **1a**–**1f** is based on spectroscopic evidence. In the IR spectra of the new bistriazenes, the functional groups in the parasubstituents give rise to the predicted bands of either nitro, cyano, or carbonyl groups. Discussion of the supporting NMR data will be facilitated with reference to the proton and carbon labels in Fig. 3. In the ^{1}H NMR spectra, the protons of the methyl substituents give rise to a 12-proton singlet at ca. 1.25 ppm and the protons (H_a, H_b) of the bridging methylene group also give a sharp singlet at ca. 3.5 ppm. The equivalent methylene groups (H_c, H_d) give rise to a somewhat broadened singlet at ca. 4.6–4.7 ppm. The singlet

© 2006 NRC Canada

Fig. 3. Labelling of some hydrogen and carbon atoms in structure **1** to assist with the discussion of NMR data.



arising from the other methylene protons (H_e, H_f) at ca. 3.7–3.9 ppm is similarly broadened. This broadening of the signals of protons in close proximity to the triazene moiety is quite familiar and is attributed to the restricted rotation around the N—N bond in the triazene because of the partial double bond character of this group (19). The aromatic protons appear as the predictable AA′BB′ patterns.

The ^{13}C NMR spectra also show signs of the rotational dynamics in the triazene units referred to in the preceding paragraph. The carbon signals of carbon atoms C1, C2, and C3 are often so broad as to be impossible to detect. The carbon atom at C4, well away from the triazene units, is clearly seen in all spectra at ca. 58 ppm. The carbon atoms of the methyl substituents are also clearly evident at ca. 22 ppm. The C3 carbon is visible in four out of six spectra and is readily assigned to the chemical shift at ca. 60 ppm. The carbon atoms at C1 and C2 are more difficult to detect and when they are seen, the signals are weak and broad, but we can say with reasonable certainty that C1 occurs at ca. 68 ppm and C2 occurs at ca. 70 ppm. These chemical shift assignments show a strong correlation with the chemical shift assignments previously reported (8) for the compounds of series **5**.

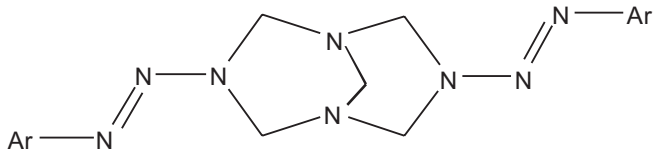
The stability of the compounds of series **1** did not extend to the analysis by mass spectrometry. Attempts to record mass spectra of these compounds by EI instrumentation did not succeed; no molecular ions were observed. However, in one case, that of **1b**, we were successful in seeing the molecular ion under ES^+ conditions with sodium as the charged cation.

Conclusion

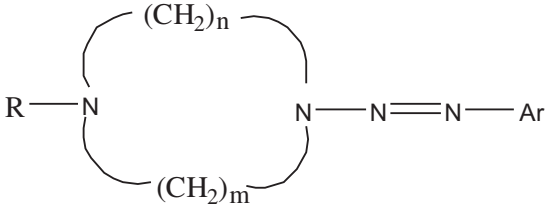
It appears, from our ongoing studies, that the interaction of a diazonium salt with a mixture of formaldehyde and an alkanediamine [$NH_2(CH_2)_nNH_2$] gives rise to two distinct types of oligomer. Bistriazenes of types **2** (9) and **10** (20) are examples of the bridged bicyclic bistriazene, whereas the compounds of series **1** and **5** exemplify the linear bicyclic bistriazene. The new compounds of series **1**, reported here, clearly belong to the linear bicyclic class, providing further evidence that there is a crossover in the molecular architecture going from ethylenediamine (**3**) (two-carbon spacer) to the branched two-carbon spacer (**4**). This type of crossover was also observed in the transition from ethylenediamine to propanediamine in structures **5** and **6** (17, 18) (Scheme 3).

This paper is part VI in a series that describes the synthesis of a variety of triazenes and bistriazenes that fit the general classification of 1-aryldiazenyl-(1,*x*)-diazacycloalkanes

Scheme 3.



10



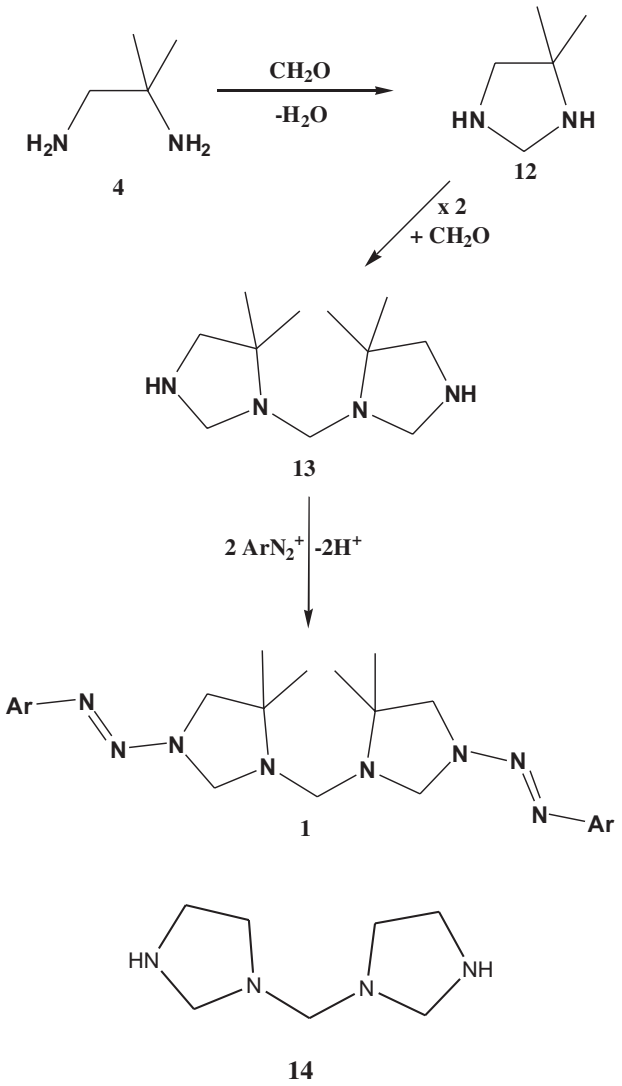
11

described by the general structure **11**, where m = 1 or 2 and n = 2, 3, 4, or 5. The new compounds of series **1** fit to the general structure **11** where m = 1 and n = 2. Previously, we reported new triazenes derived from piperazine (21, 22) ($m = n = 2$) and homopiperazine (23) (m = 2, n = 3). In future papers in this series, we will report more examples of the linear bicyclic bistriazene derived from other diamines, such as 1,4-diaminobutane and 1,5-diaminopentane. Evidently, the linear bicyclic bistriazene, reported here in the new compounds of series **1**, appears to be the normal type of molecular architecture in this field of chemistry.

However, there may be a more prevailing reason why these new compounds of type **1** are significant and that is the presence of the imidazolidine ring. Although well-known stable molecules like imidazolidine-2,4-dione ("hydantoin") (used to prepare amino acids (24)) and the essential growth factor, biotin, contain a 2-oxoimidazolidine ring in their structure, the parent imidazolidine is not so well-known. Direct hydrogenation of imidazole is difficult and it has been said by no less a figure of heterocyclic chemistry than Adrien Albert (25) that "imidazolidine appears to be unknown". However, the *N*,*N*′-diethyl derivative is readily prepared by reaction of *N*,*N*′-diethylethylenediamine and formaldehyde. This observation, and the work of Bera et al. (5), gives us a clue as to how the molecules of type **1** are formed (Scheme 4). Condensation of **4** with formaldehyde could afford the 4,4-dimethylimidazolidine (**12**), which in turn undergoes a dimerization–condensation to give the dimer **13**. Reaction of **13** with the diazonium ion then affords the observed product **1**. It would seem that the importance of the results reported here lies in the fact that the diazonium coupling reaction "traps out" the elusive intermediate bisimidazolidinyl methane **13**, which has previously not been reported. In fact, it would appear that the central moiety of our new compounds of series **1**, i.e., the saturated bis(imidazolidinyl)-methane unit (**14**), is virtually unknown. Although the CA files contain numerous molecules that contain the skeleton of **14**, all known compounds with this skeleton are either oxo-substituted derivatives, i.e., hydantoin-like molecules, such as **7**, or they are aromatic benzimidazolidine derivatives.

© 2006 NRC Canada

Scheme 4.



References

1. K. Sztanke, S. Fidecka, E. Kedzierska, Z. Karczmarzyk, K. Pihlaja, and D. Matosiuk. Eur. J. Med. Chem. **40**, 127 (2005).
2. M.C. Albuquerque, T.G. Silva, M.G. Pitta, A.C. Silva, P.G. Silva, and E. Malagueno. Pharmazie, **60**, 7 (2005).
3. E. Pekala, K. Stadnicka, A. Broda, M. Zygmunt, B. Filipek, and K. Kiec-Kononowicz. Eur. J. Med. Chem. **40**, 259 (2005).
4. E.-K. Lee, S.-H. Kim, B.-H. Jung, W.-S. Ahn, and G.-J. Kim. Tetrahedron Lett. **44**, 1971 (2003).
5. M. Bera, U. Mukhopadhyay, and D. Ray. Inorg. Chim. Acta, **358**, 437 (2005).
6. A.Kh. Vorobiev and N.A. Chumakova. J. Magn. Reson. **175**, 146 (2005).
7. M.V.P. Santos, M.R. Silva, Jr., S.M. Oliviera, J.B.P. da Silva, M.T.C. Lima, M.C.A. Lima, S.L. Galdino, and I.R. Pitta. J. Mol. Struct: THEOCHEM, **715**, 191 (2005).
8. S.L. Moser, R. Church, M.B. Peori, and K. Vaughan. Can. J. Chem. **83**, 1071 (2005) (Part IV in this series).
9. M.B. Peori, K. Vaughan, and D.L. Hooper. J. Org. Chem. **63**, 7437 (1998).
10. Z. Otwinowski and W. Minor. *In* Methods in enzymology. Vol. 276. Part A. *Edited by* C.W. Carter and R.M. Sweet. Academic Press, London. 1997. pp 307–326.
11. A. Altomare, M.C. Burla, M. Camalli, G.L. Cascarano, C. Giacovazzo, C. Guagliardi, A.G. Moliterni, G. Polidori, and R. Spagna. J. Appl. Crystallogr. **32**, 115 (1999).
12. G.M. Sheldrick. SHELXL97 [computer program]. University of Göttingen, Göttingen, Germany. 1997.
13. M. Nardelli. J. Appl. Crystallogr. **28**, 659 (1995).
14. J. Habermeier and D. Porret. Helv. Chim. Acta, **55**, 686 (1972).
15. M.N. Burnett and C.K. Johnson. ORTEP-III [computer program]. Oak Ridge National Laboratory, Oak Ridge, Tenn. 1996.
16. D. Cremer and J.A. Pople. J. Am. Chem. Soc. **97**, 1354 (1975).
17. M.B. Peori, K. Vaughan, and V. Bertolasi. J. Chem. Crystallogr. **35**, 297 (2005).
18. S.L. Moser, V. Bertolasi, and K. Vaughan. J. Chem. Crystallogr. **35**, 307 (2005).
19. (*a*) M. Barra, S. Srivastawa, and E. Brockman. J. Phys. Org. Chem. **17**, 1057 (2004); (*b*) B.T. Golding, T.J. Kemp, R. Narayanaswamy, and B.W. Waters. J. Chem. Res. Synop. 130 (1984).
20. R.D. Singer, K. Vaughan, and D.L. Hooper. Can. J. Chem. **64**, 1567 (1986).
21. V.R. Little and K. Vaughan. Can. J. Chem. **82**, 1294 (2004).
22. V.R. Little, R. Tingley, and K. Vaughan. Can. J. Chem. **83**, 471 (2005).
23. S.L. Moser and K. Vaughan. Can. J. Chem. **82**, 1725 (2004).
24. M.H. Palmer. *In* The structure and reactions of heterocyclic compounds. Edward Arnold Publishers, London. 1967. p. 377.
25. A. Albert. Heterocyclic chemistry. 2nd ed. Athlone Press, London. 1968. p. 42.

© 2006 NRC Canada

The regioselective α-alkylation of the benzophenone imine of glycinamide, alaninamide, and related derivatives[1]

Martin J. O'Donnell, Jeremy D. Keeton, Vien Van Khau, and John C. Bollinger

Abstract: The benzophenone imine of glycinamide was alkylated using ion pair extraction (RX, 10% aq. NaOH, Bu_4NHSO_4 (1 equiv.), CH_2Cl_2, rt) to give the α-monosubstituted products, which were then alkylated a second time using stronger basic conditions (KO-*t*-Bu, THF, 0 °C, RX). Crystal structures of the Schiff bases of glycinamide, an α-monosubstituted and an α,α-disubstituted product were reported.

Key words: benzophenone imines, Schiff bases, alkylation, ion pair extraction (IPE), phase-transfer catalysis (PTC), anhydrous base, X-ray crystal structures.

Résumé : L'alkylation de la benzophénone imine du glycinamide par extraction par paire d'ions (RX, NaOH aqueux à 10%, Bu_4HSO_4 (1 équiv.), CH_2Cl_2, température ambiante) conduit à des produits α-monosubstitués qui sont alkylés une deuxième fois dans des conditions plus basiques (KO-*t*-Bu, THF, 0 °C, RX). Les structures cristallines des bases de Schiff du glycinamide, d'un produit α-monosubstitué et d'un produit α,α-disubstitué ont été déterminées.

Mots clés : imines de la benzophénone, bases de Schiff, alkylation, extraction par paire d'ions (EPI), catalyse par transfert de phase (CTP), base anhydre, structures cristallines par diffraction des rayons X.

[Traduit par la Rédaction]

Introduction

The development of new methods for the synthesis of unnatural α-amino acids has been the focus of our research for many years. The first general synthesis of α-amino acids by phase-transfer catalysis (PTC) was reported in 1978 (1). On treatment with base, the benzophenone imines of glycine alkyl esters (**1**) function as glycine anion equivalents for reaction with electrophiles to yield higher amino acid derivatives **2** (Scheme 1, pK_a experimental (calculated), refs. 2 and 3)) (4). A key tenet in this chemistry is the ability to achieve selective monoalkylation of **1** to give **2** under mild ("normal") PTC conditions, although a second alkylation to form **3** can be accomplished using stronger basic conditions (5). The possibility of stopping the reaction at the monoalkylation stage is attributed to $A_{1,3}$ strain in products **2** (6). The lower acidity of the monoalkylation product **2** compared with starting material **1** (2) has also been applied for the selective monophenylation of **1** (7), in the catalytic enantioselective alkylation for the synthesis of monoalkyl products without concomitant racemization under basic PTC conditions (8–10), and in the regioselective solution (**1**, OR = amino acid ester (11)) and on-resin (**1**, R = Merrifield, Wang, Rink, or Weinreb resin (l2)) monoalkylation of a benzophenone-protected glycine residue in a peptide without either N-alkylation or alkylation of a C-terminal glycine or higher amino acid residue. Additionally, the on-resin enantioselective syntheses of α-alkyl amino acids have been achieved by both alkylation and Michael addition reactions (13).

While monoalkylations of the aldimines of glycine esters ($ArCH{=}NCH_2CO_2R$, **4a**, Ar = 4-ClC_6H_4, R = Et; pK_a (DMSO) 18.8 (19) (refs. 2 and 3)) are possible (14), the similar acidities of the unsubstituted (e.g., **4a**) and monosubstituted (e.g., **5a**) derivatives (2) can lead to overalkylation and (or) racemization of products **5** by deprotonation–reprotonation. In contrast, PTC alkylation of the aldimine of a monoalkyl amino ester is generally the method of choice to prepare α,α-dialkylated amino acid derivatives (Scheme 2) (15). Similarly, the aldimine activating group has been used for preparation of α-phenyl-α-alkyl amino acid derivatives by phenylation of the α-alkyl derivatives (16) and the regioselective solution (11) and on-resin (17) N-terminal α-carbon alkylation of peptides containing an N-terminal non-

Received 6 February 2006. Accepted 31 March 2006. Published on the NRC Research Press Web site at http://canjchem.nrc.ca on 1 August 2006.

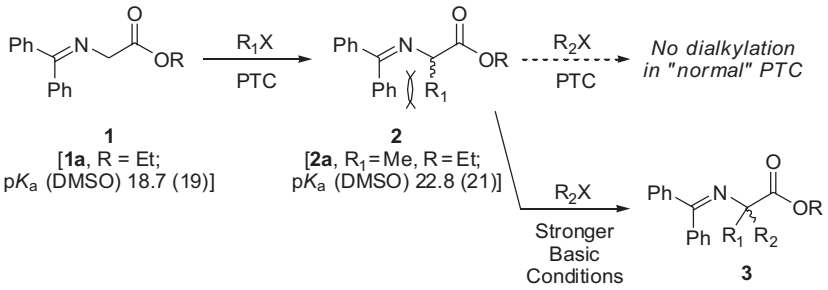
Dedicated to Dr. Alfred Bader for his contributions to humanity.

M.J. O'Donnell,[2] J.D. Keeton, and V. Van Khau. Department of Chemistry and Chemical Biology, Indiana University – Purdue University Indianapolis, 402 N. Blackford St., Indianapolis, IN 46202-3274, USA.
J.C. Bollinger. Department of Chemistry, Indiana University, Bloomington, IN 47405-4001, USA.

[1]This article is part of a Special Issue dedicated to Dr. Alfred Bader.
[2]Corresponding author (e-mail: odonnell@chem.iupui.edu).

 doi:10.1139/V06-088 © 2006 NRC Canada

Scheme 1. Selective monoalkylation of benzophenone imine glycinates.



glycine residue. A limitation of this methodology for the preparation of α,α-dialkyl amino acids from their glycine counterparts is the need to change activating groups from ketimine (Ph_2C=N-) (Scheme 1, **1** to **2**) to aldimine (ArCH=N-) (Scheme 2). As noted earlier (5), stronger base may be used to prepare the α,α-dialkylated products (Scheme 1, **2** to **3**). Additionally, on-resin tandem alkylations of benzophenone imine protected glycinates have been achieved by initial alkylation under PTC-like conditions followed by introduction of a second group at the α-carbon using stronger base (18).

The successful alkylation chemistry of the Schiff bases of glycine alkyl esters (**1**) and higher amino acid esters (**5**) prompted us to extend this methodology to the selective α-carbon alkylations of amino amides as a route to α-substituted and α,α-disubstituted amides (19). Reports of the enantioselective synthesis of monosubstituted amino amides by PTC have recently appeared (20).

Enzymatic resolution of racemic α-substituted and α,α-disubstituted amino acid amides has been developed by the DSM group (21) for preparing these important compounds and their associated α-amino acids in optically pure form from the racemic or optically enriched products. One synthetic route involves alkylation of **1b**, hydrolysis of the monoalkylated benzophenone imine of glycine methyl ester (**2**, R = Me, R_1 = alkyl), and conversion to the amide by treatment with ammonia (21*g*). A route to the α,α-disubstituted derivatives involved preparation of the aldimine of a monosubstituted amino acid amide (**7**) followed by alkylation under PTC conditions to give **8** (Scheme 3) (21*c*).

A more efficient route to the α,α-disubstituted derivatives of amino acid amides would be to start with the benzophenone imine of glycinamide (**10**) (prepared from benzophenone imine (**9**) and glycinamide), carry out a selective monoalkylation to (**11**), and then, *without changing the imine-protecting group*, do a second alkylation to give **12**. In this paper we report the successful accomplishment of this goal (Scheme 4).

Results and discussion

Prediction of the acidities of the benzophenone imines of glycinamide and their monoalkylated derivatives

Although the experimental acidities of the imines of glycinamide and their monoalkyl derivatives are not available, it was possible to use CAMEO to obtain qualitative theoretical acidities (DMSO) of these compounds (Fig. 1).[3]

Scheme 2. Alkylation of a higher amino acid derivative by PTC.

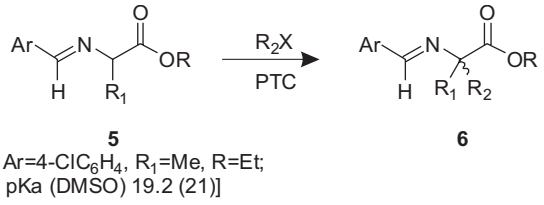
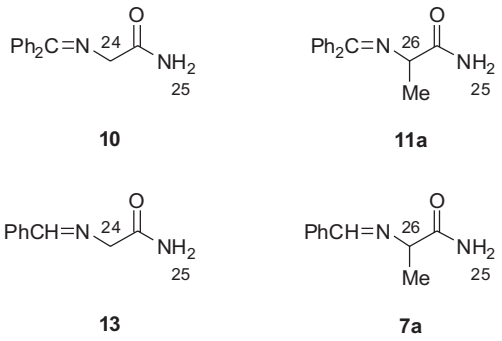


Fig. 1. Calculated acidities (pK_a in DMSO) using CAMEO for the benzophenone imines of glycinamide and alaninamide.

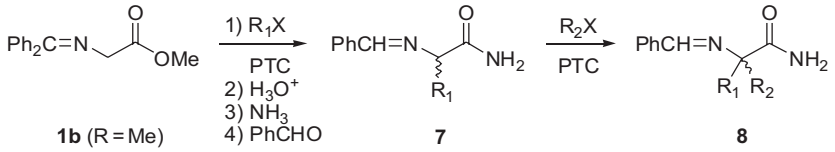


The predicted acidities of the α-protons in glycinamide imines (**10** or **13**, α-CH pK_a = 24) are only an order of magnitude greater than the acidities of the NH protons on the unsubstituted amides (**10** or **13**, NH pK_a = 25). This small effect is certainly not, by itself, sufficient to predict selective α-monoalkylation over N-alkylation. Additionally, as in the amino acid ester cases (2*a*), both the benzophenone imines and aldimines were predicted to have the same acidities and the monoalkyl derivatives were both predicted to be 10^2 less acidic than their glycinamide counterparts. As in the ester cases, the potential major acid-weakening effect in the benzophenone imine of alaninamide (**11a**) was not predicted. If this effect were taken into account, one would predict that the α-proton in **11a** would be even less acidic (higher pK_a) than those in **10**. Thus, it would be expected that the second alkylation of **10** would occur at nitrogen rather than at the α-carbon. Even though these qualitative theoretical predictions do not bode well for achieving the desired selective mono- and di-alkylations in the amino acid amide imines, we proceeded with experimental studies of these alkylation reactions.

[3] Previous alkylation and Michael addition studies of three active methylene derivatives (cyanoacetamide, acetoacetamide, and malonamide) containing an unsubstituted amide and the predicted pK_as (DMSO) of these compounds are summarized in the Supplementary material.

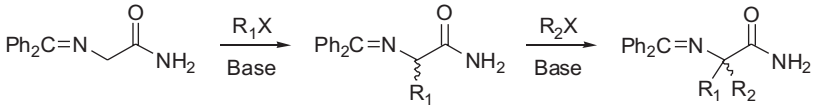
© 2006 NRC Canada

Scheme 3. DSM route to α-alkyl amino amides and α,α-dialkyl amino amides.



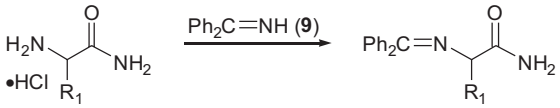
1b (R = Me) **7** **8**

Scheme 4. Selective mono- and di-alkylation of the benzophenone imine of glycinamide.



10 **11** **12**

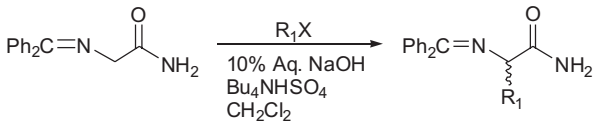
Scheme 5. Synthesis of the Schiff base of glycinamide (**10**) and alaninamide (**11a**) by transimination.



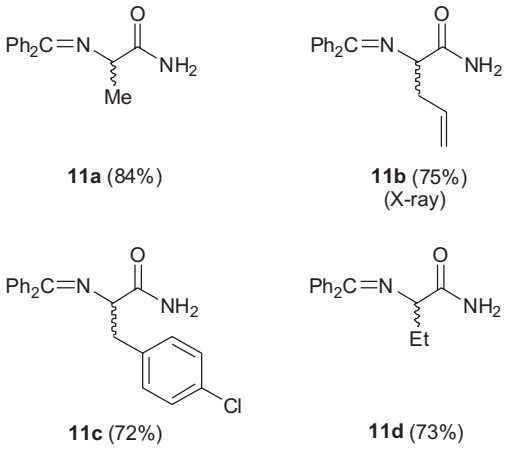
14 (R_1 = H)
15 (R_1 = Me)

10 (R_1 = H) (70%, X-ray)
11a (R_1 = Me) (96%)

Scheme 6. Alkylation of the benzophenone imine of glycinamide (**10**) by ion pair extraction to form the α-monosubstituted derivatives **11**.



10 **11**



11a (84%) **11b** (75%) (X-ray)

11c (72%) **11d** (73%)

Preparation and monoalkylation of the benzophenone imine of glycinamide

The benzophenone imine of glycinamide (**10**) (22, 23) was prepared from glycinamide hydrochloride **14** and benzophenone imine by transimination following a protocol similar to that developed for preparation of the related imines of glycine and monoalkyl amino acid esters (Scheme 5) (24). Since glycinamide hydrochloride is relatively insoluble in dichloromethane, the reaction was refluxed overnight in 1,2-dichloroethane with triethylamine (1 equiv.). Removal of solvent followed by recrystallization gave **10** (70%) as white crystals. An X-ray crystal structure, which will be discussed later, was obtained for **10**.

Alkylations of the Schiff base of glycinamide **10** were accomplished by ion pair extraction (IPE) using representative active (methyl, allyl, or benzyl) or less active (ethyl) halides, 10% aq. NaOH, and tetrabutylammonium hydrogen sulfate (TBAH, 1.2 equiv.) in dichloromethane at room temperature overnight (Scheme 6) (1*a*, 25). After work-up, the crude products were purified by column chromatography (silica gel was prewashed with 1% triethylamine because of the acid lability of the imine). Notably, under these mild alkylation conditions, the Cα-monoalkylated products (**11a**–**11d**) were obtained in good yield (72%–84%). An X-ray crystal structure, to be discussed later, was obtained of the α-monoalkylated product **11b**.

Alternatively, **11a** was prepared in 96% yield by transimination of alaninamide hydrochloride with benzophenone imine (DMF, rt, overnight).

Model study — Allylation of the benzophenone imine of alaninamide

A model alkylation study for the proposed regioselective Cα-alkylation of the Schiff base of alaninamide (**11a**) to prepare the α,α-dialkylated product was conducted using allyl bromide as the alkylating agent with a variety of bases and reaction conditions (Scheme 7). In addition to the desired C-monoalkylated product **12a**, four other alkylation products are possible in this reaction (**16**–**19**) (Fig. 2). The calculated pK_a values (CAMEO) of the α-CH and NH protons in these products are given for reference (see Fig. 1 for predicted pK_a values of **10** and **11a**).

The reactions were conveniently monitored by TLC (Fig. 3). The optimized TLC system provides for separation of the starting material (**11a**), the desired C-allylated target (**12a**), the N-allylated product (**16**), the two possible diallylated derivatives (**17** and **18**), and the triallylated compound (**19**), as well as the hydrolysis product, benzophenone. Identities of the various spots were determined using mass spectral analysis and ^{1}H NMR.

Allylation of Schiff base **11a** was studied using a variety of bases and reaction conditions (Table 1). The alkylation was first conducted using IPE conditions, however no reaction was observed (Table 1, entry 1) (1*a*, 25). IPE conditions using 50% aq. NaOH gave only trace amounts of desired

© 2006 NRC Canada

Scheme 7. Model study for regioselective α-C alkylation of the Schiff base of alaninamide (**11**a).

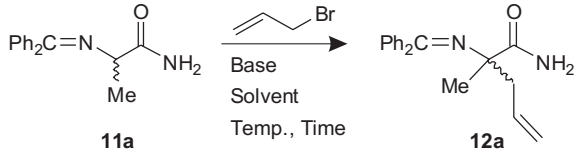
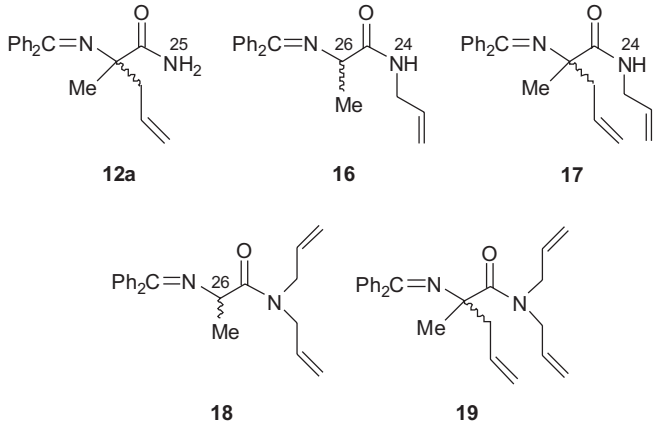
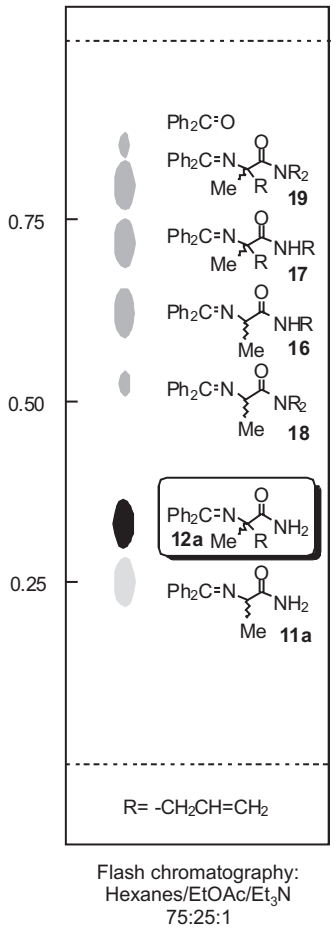


Fig. 2. Possible products from the alkylation of the Schiff base of alaninamide (**11a**) with allyl bromide.



product (**12a**) (Table 1, entry 2). Next, alkylation was performed under nonaqueous conditions using the Schwesinger base BTPP (*tert*-butylimino-tri(pyrrolidino)phosphorane, 0.9 equiv.) to again give only trace amounts of product. BTPP is a relatively strong, organic soluble, nonionic base used successfully for the α-alkylation of resin-bound Schiff base derivatives of amino acids and peptides (26). From these first experiments, it was apparent that stronger conditions were needed to effect α-alkylation. Thus, alkylation was next attempted using sodium ethoxide (in EtOH) in the presence of catalytic TBAB in anhydrous acetonitrile (Table 1, entry 4) (5). In this case, no reaction was observed because of the insolubility of **11a** in acetonitrile. In a second set of reactions using the same reagents, the EtOH was first removed from NaOEt and then acetonitrile was added, but again the reaction was unsuccessful because of the insolubility of the starting Schiff base (Table 1, entry 4). LDA in anhydr. THF gave only trace amounts of product (Table 1, entry 5). The same conditions were applied using LiHMDS, but again only trace amounts of desired product were observed (Table 1, entry 6) (27). With KHMDS, the target α-monoalkylated product (**12a**) was obtained in 24% yield (Table 1, entry 7). The final and most effective base used was KO-*t*-Bu (Table 1, entries 8–10) (27). When the reaction was carried out at ambient temperature or –78 °C, 42%–46% and 34%–48% yields, respectively, of **12a** were obtained (Table 1, entries 8 and 9). Optimal conditions were obtained using Schiff base **11a** (1 equiv.), KO-*t*-Bu (1.2 equiv.), and allyl bromide (1.2 equiv.) in THF at 0 °C for 3 h to give product **12a** in 55%–61% yield (Table 1, entry 10). The addition of LiCl (5 equiv.), which has often proven to be an effective additive in alkylation and other anionic reactions (28), using the KO-*t*-Bu conditions at rt, 0 °C, or –78 °C gave only trace amounts of product as did other solvents (DMF or *tert*-butyl alcohol) with KO-*t*-Bu (TLC, LC–MS, and ^{1}H NMR).

Fig. 3. TLC data for products from the allylation of the Schiff base of alaninamide (**11a**).



The reaction conditions were studied further by using 0.9 equiv. of both allyl bromide and KO-*t*-Bu to understand which of the various possible alkylations was occurring and in what order. Hopefully, selective monoalkylation at the α position to form **12a** would occur first and further alkylation would not be problematic when less than 1 equiv. of base and alkylating reagent was used. If more than 1 equiv. of base and alkylating agent was used, selective Cα-monoalkylation (**12a**) could occur followed by N-alkylation (to **17**), and possibly N,N-dialkylation (to **19**).

The results from the model experiment showed that, even when less than 1 equiv. of base and alkylating reagent were used, the reaction gave mixtures of mono-, di-, and trialkylation products (Fig. 2). From the earlier experimental results (Table 1), in which the desired C-allylated product was obtained in up to 61% yield, it is apparent that the predicted pK_a values (Figs. 1 and 2) provide only a very qualitative estimate of the various pK_as.

Finally, the alkylation reaction of **11a** with allyl bromide was examined after 5 min by TLC to see if the product distribution was affected by time. At this time, all of the products shown in Fig. 3 were present.

© 2006 NRC Canada

Table 1. α-Allylation of the benzophenone imine of alaninamide (**11a**) to form **12a** (base study).

Entry	Base	Solvent	Other	Temp. (°C)	Time (h)	**12a** (%)
1	10% Aq. NaOH	CH_2Cl_2	TBAH[a]	rt	18	No rxn.
2	50% Aq. NaOH	CH_2Cl_2	TBAH[a]	rt	18	Trace
3	BTPP[b]	CH_2Cl_2	—	rt	18	Trace
4	NaOEt	CH_3CN	TBAB[c]	—	—	No rxn.[d]
5	LDA	THF	—	–78	3	Trace
6	LiHMDS	THF	—	–78	3	Trace
7	KHMDS	THF	—	–78	3	24
8	KO-*t*-Bu	THF	—	rt	3	42–46
9	KO-*t*-Bu	THF	—	–78	3	34–48
10	KO-*t*-Bu	THF	—	0	3	55–61

[a] Bu_4NHSO_4 (1 equiv.).
[b] *tert*-Butylimino-tri(pyrrolidino)phosphorane.
[c] Bu_4NBr (cat.).
[d] Starting material insoluble.

Alkylation of the Schiff base of monosubstituted amino amides to give α,α-disubstituted derivatives

Using the optimized results from the model alkylation study described previously, several target molecules were made by following the general procedure for alkylation of the benzophenone imine of a monosubstituted amino amide. Further alkylations included benzylation and alkylation with less reactive alkyl halides as well as a Michael addition. The model conditions used, unless otherwise noted, were as follows: KO-*t*-Bu (2.38 mmol) was added to the benzophenone imine of a monosubstituted α-amino amide (1.98 mmol) dissolved in anhydr. THF at 0 °C and the reaction mixture was stirred at 0 °C for 20 min. The alkylating agent (2.38 mmol) was added and the reaction mixture was stirred at 0 °C for an additional 3 h. After work-up, the crude product was purified by flash chromatography using silica that was prewashed with hexanes–EtOAc–triethylamine (75:25:1). The product was then recrystallized from dichloromethane–hexanes (1:15). Four monoalkylated starting materials (**11a**–**11d**, Scheme 6) were used to prepare 10 new α,α-disubstituted products (**12a**–**12e** and **12g–12k**, Fig. 4).

The alkylation of **11a** with allyl derivatives gave the highest yields for all alkylations studied (Fig. 4, products **12a**–**12d**). Alkylation of Schiff base **11a** with allyl bromide, 4-bromo-2-methyl-2-butene, 3-bromo-2-methylpropene, and cinnamyl bromide, gave the respective Schiff bases (**12a**–**12d**) in 36%–61% isolated yield. An X-ray crystal structure, which will be discussed later, was obtained for dialkylated product **12b**.

The alkylation of Schiff base **11a** using non-allylic halides was examined next (Fig. 4, products **12e**–**12h**). Alkylation with 4-chlorobenzyl bromide gave the Schiff base **12e** (53%) while methylation gave a complex mixture of products, likely owing to the reactivity and small size of the methyl group. Alkylation of **11a** with iodoethane gave **12g** (24%) while 1-iodo-2-methylpropane gave **12h** (25%). Alkylation with two α-haloesters, methyl bromoacetate, and *tert*-butyl bromoacetate, did not give the desired α-alkylated products (LC–MS and ^{1}H NMR).

Alkylation of the Schiff base of higher amino amides using the general procedure for the alkylation of **11a** was also studied (Fig. 4, products **12i**–**12k**). The Schiff base starting materials (**11b**–**11d**) were prepared earlier by IPE from the Schiff base of glycinamide (**10**, Scheme 6). These three monoalkylated Schiff base glycinamides (**11b**–**11d**) were then subjected to allylation and benzylation. In all cases, the allylation of the benzophenone imines of these higher amino amides did yield the desired products, although in low yields. Allylation of Schiff base **11b** gave **12i** (21%), **11c** yielded **12j** (25%), and **11d** gave **12k** (13%). For the synthesis of Schiff base **12j**, the addition of 4-chlorobenzyl bromide to Schiff base **11b** gave only a 10% yield of product. This compared with the higher yield (25%) of the same product (**12j**) obtained by allylation of the benzylated starting material **11c**.

Methylation of Schiff bases **11b** and **10** gave a mixture of products (TLC and LC–MS) and it was not possible to isolate the desired α-alkylated product, which was present only in trace amounts, from the crude reaction mixture. Methylation of **11d** gave the N-monoalkylated product (45%) and methylation of **11c** yielded less than 10% of product **12e**, compared with the 53% yield for the reverse order of alkylation of the Schiff base alaninamide **11a** using *p*-chlorobenzyl bromide.

Michael addition of the Schiff base of alaninamide

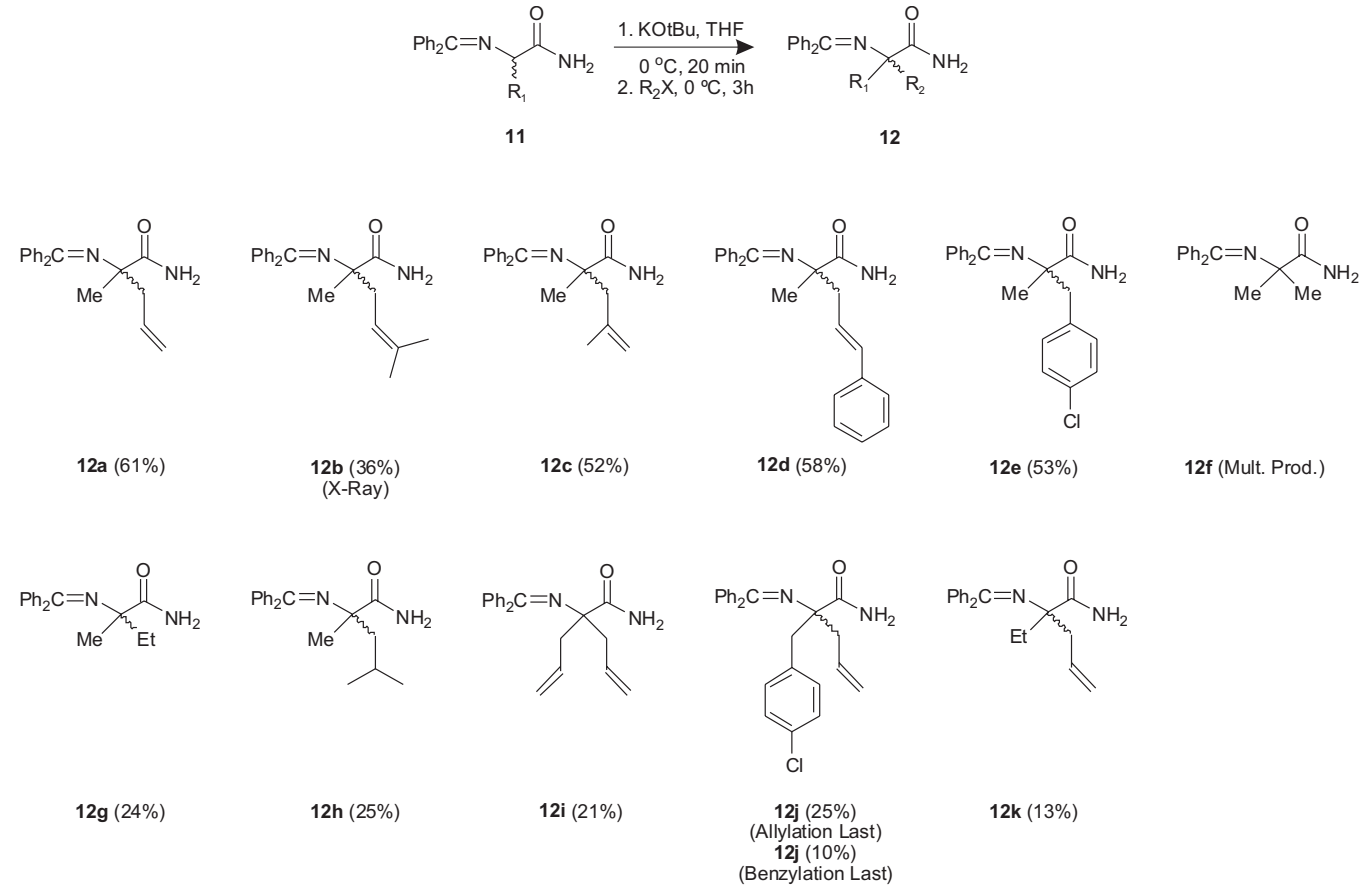
The Schiff base of alaninamide (**11a**) was reacted with the Michael acceptor (*tert*-butyl acrylate) to give the Schiff base **20** (32%) (Scheme 8). Schiff base **11a** (1.98 mmol) was dissolved in anhydr. THF, then *tert*-butyl acrylate (2.38 mmol) was added, followed by KO-*t*-Bu (0.238 mmol), and the reaction mixture was stirred at 0 °C for 3 h. This reaction was optimal with 0.12 molar equiv. of KO-*t*-Bu rather than the normal 1.2 equiv. in the case of alkylation. Attempted Michael addition with methyl acrylate did not give the desired product as monitored by LC–MS, while use of acrylonitrile gave the N,N-dialkylated product (^{1}H NMR and LC–MS) and only trace amounts of monoalkylated product (LC–MS).

X-ray crystal structures of the benzophenone imine of amino amides

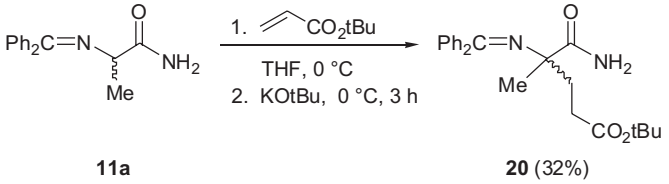
The X-ray crystal structures of the benzophenone imines of the unsubstituted (**10**), a monosubstituted (**11b**), and a disubstituted (**12b**) amino amide were obtained (Fig. 5). A

© 2006 NRC Canada

Fig. 4. Alkylation of the benzophenone imines of monosubstituted amino amides (**11**) with KO-*t*-Bu to form the α,α-disubstituted products **12**.



Scheme 8. Michael addition of the benzophenone imine of alaninamide with *tert*-butyl acrylate.



summary of the crystallographic data is given in Table 2.[4] In addition to confirming the structures of these products, several other points are of interest in this series of compounds.

The *cis*-phenyl group (Ph_c) on the imine is considerably farther out of planarity with the imine double bond than is the *trans*-phenyl group (Ph_t). This is due to $A_{1,3}$ strain (6) in the mono- and di-substituted derivatives, where the effect is more pronounced than in the unsubstituted case. Interestingly, the sum of these two values (Σ) increases in going from **10** (Σ = 88°) to **11b** (Σ = 92°) to **12b** (Σ = 99°). As a comparison, in the unsubstituted Schiff base esters ($Ph_2C{=}NCH_2CO_2Et$, **1a**, Σ = 71°; $Ph_2C{=}NCH_2CO_2$-*t*-Bu, **1c**, Σ = 86° (4)) and in the α-benzyl or α-phenyl substituted Schiff base esters ($Ph_2C{=}NCH(CH_2C_6H_4$-4-Cl$)CO_2$-*t*-Bu, **2c**, Σ = 97° (4); $Ph_2C{=}NCH(Ph)CO_2Et$, **2d**, Σ = 82° (7)). The X-ray structure of an α,α-disubstituted Schiff base ester in this series was not determined.

The bond lengths to the quaternary α-carbon in the disubstituted Schiff base amide (**12b**) relative to the other two compounds in the series are also of interest. Three of the four bonds to the α-carbon are the longest in the series: the Cα—N_{imine} bond(1.477 Å), the Cα—Me bond (1.536 Å), and the Cα-C_{CO} bond (1.555 Å), which is a result of the steric congestion about the quaternary α-carbon in **12b**.

Experimental

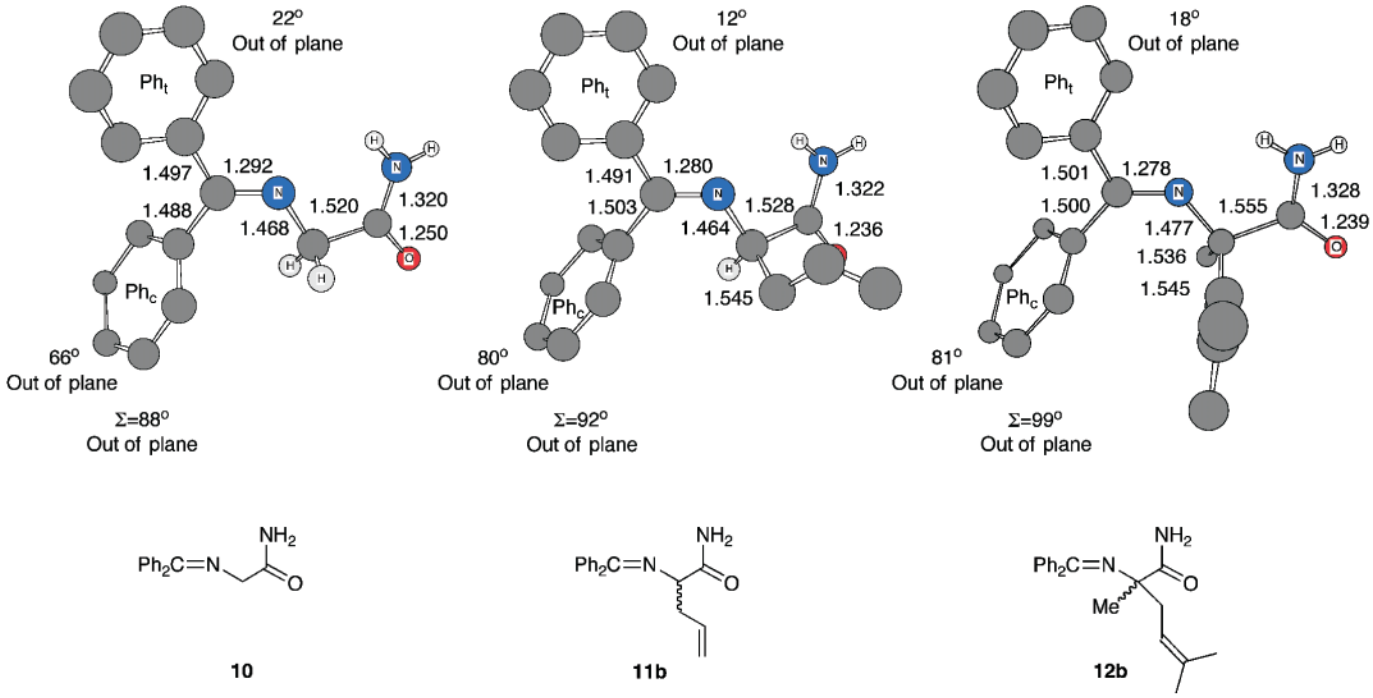
General

Unless otherwise noted, all manipulations were carried out under an inert atmosphere (argon) in glassware dried

[4] Supplementary data for this article are available on the journal Web site (http://canjchem.nrc.ca) or may be purchased from the Depository of Unpublished Data, Document Delivery, CISTI, National Research Council Canada, Ottawa, ON K1A 0R6, Canada. DUD 5057. For more information on obtaining material refer to http://cisti-icist.nrc-cnrc.gc.ca/irm/unpub_e.shtml. CCDC 296438, 296439, and 296437 (compounds **10**, **11b**, and **12b**, respectively) contain the crystallographic data for this manuscript. These data can be obtained, free of charge, via http://www.ccdc.cam.ac.uk/conts/retrieving.html (Or from the Cambridge Crystallographic Data Centre, 12 Union Road, Cambridge CB2 1EZ, UK; fax +44 1223 336033; or deposit@ccdc.cam.ac.uk).

© 2006 NRC Canada

Fig. 5. Crystal structures of representative unsubstituted, α-monosubstituted, and α,α-disubstituted amino amide derivatives.



with a heat gun. THF was freshly distilled before use from sodium benzophenone ketyl. Sure Seal™ bottles of potassium *tert*-butoxide (1.0 mol/L in THF and 1.0 mol/L in *tert*-butyl alcohol), sodium ethoxide (21 wt% in denatured ethyl alcohol), lithium diisopropylamine (2.0 mol/L in heptane–THF–ethylbenzene), potassium bis(trimethylsilyl)amide (0.5 mol/L in toluene), lithium bis(trimethylsilyl)amide (1.0 mol/L in THF), and all solvents other than THF were purchased from the Sigma-Aldrich Chemical Co.

Nuclear magnetic resonance (NMR) spectra were recorded on a 300 MHz Varian Gemini spectrometer. Infrared (IR) spectra were obtained neat in thin films on NaCl plates (oils) using a Matteson Genesis FT-IR. Elemental analyses were performed by Midwest Microlabs, Indianapolis, Indiana. High-resolution mass spectrometry was run in the FAB mode at Indiana University. Melting points were determined in open-end capillaries using a Thomas-Hoover Unimelt melting apparatus and are uncorrected. Thin layer chromatography (TLC) was performed on silica gel 60 F254 aluminum sheets with UV visualization. Column chromatography was performed using silica gel (60 Å, 40–63 μm standard grade gel) with the solvent systems described in the individual procedures. Liquid chromatography – mass spectrometry (LC–MS) was performed on a Waters 2795 liquid chromatograph, a Waters 996 photodiode array, a Sedex 75 light scatterer, and a Waters Micromass ZQ mass spectrometer. The mobile-phase solvent was 90% H_2O – 5% ACN – 5% – 0.2% formic acid buffer at approximately pH 3.0.

X-ray crystallography was performed at the Molecular Structure Center at Indiana University. X-ray diffraction data were collected using a Bruker diffractometer with SMART 6000 CCD detector. Structures were solved via the SHELXTL program suite (29). Further structure determination details are available in CIF form in the Supplementary material.[4]

Preparation of the benzophenone imines of glycinamide and alaninamide by transimination

2-[(Diphenylmethylene)amino]acetamide (10)

Glycinamide hydrochloride (**14**, 5.00 g, 45.2 mmol) and 1,2-dichloroethane (60 mL) were added to a dried 250 mL three-necked round-bottomed flask equipped with a reflux condenser, a magnetic stirrer, and an argon source. Diphenylketimine (7.6 mL, 45.2 mmol), triethylamine (6.93 mL, 49.7 mmol), and 1,2-dichloroethane (20 mL) were added by syringe to a separate dry 50 mL round-bottomed flask equipped with an argon source. The mixture was stirred for 5 min and was added slowly by cannula under argon to the reaction flask. The mixture was refluxed under argon overnight, cooled, filtered, and the solvent was removed under reduced pressure to give a light yellow solid. Recrystallization from hexanes–EtOAc (2:3 by volume) gave **10** as white crystals (7.55 g, 70%); mp 160–163 °C (lit value (22) mp 162 to 163 °C). IR (cm^{-1}): 1681, 3442. ^1H NMR δ: 3.96 (s, 2H, CH_2), 5.55–5.75 (br s, 2H, NH_2), 7.10–7.70 (m, 10H, aromatic). ^{13}C NMR ($CDCl_3$) δ: 58.2, 128.9, 129.8, 130.0, 130.1, 130.5, 130.6, 132.3, 137.6, 140.4, 156.7, 172.0, 175.1.

(±)-2-[(Diphenylmethylene)amino]propanamide (11a)

(±)-Alaninamide hydrochloride (**15**, 1.00 g, 8.03 mmol) followed by anhydr. DMF (50 mL) were added to a dried 250 mL round-bottomed flask equipped with a magnetic stirrer. The solution was stirred at room temperature under argon for 30 min or until the solid was completely dissolved. Benzophenone imine (1.45 g, 8.03 mmol) was added dropwise via syringe to the alaninamide solution under argon at room temperature. The reaction mixture was stirred at room temperature under argon overnight. The solution was

© 2006 NRC Canada

Table 2. Crystallographic data.

Crystal	**10**	**11b**	**12b**
Emperical formula	$C_{15}H_{14}N_2O$	$C_{18}H_{18}N_2O$	$C_{21}H_{24}N_2O$
Formula mass	238.28	278.34	320.42
Colour, habit	Multifaceted, colourless	Plate, colourless	Colourless, block
Crystal dimensions (mm)	0.5×0.5×0.25	0.5×0.3×0.08	0.26×0.18×0.14
Crystal system	Monoclinic	Triclinic	Triclinic
Space group	*C*2/*c*	*P*-1	*P*-1
Z	8	6	4
a (Å)	26.640(6)	11.1428(3)	8.9409(7)
b (Å)	5.9821(14)	12.9776(3)	11.6696(8)
c (Å)	18.643(4)	16.5402(4)	17.8861(13)
α (°)	90.00	92.3530(10)	102.943(2)
β (°)	118.543(5)	99.9610(10)	95.127(2)
γ (°)	90.00	101.0850(10)	97.676(2)
Collection ranges	$-31 \le h \le 27$, $-7 \le k \le 7$, $-20 \le l \le 22$	$-15 \le h \le 15$, $-18 \le k \le 18$, $-23 \le l \le 23$	$-12 \le h \le 12$, $-16 \le k \le 16$, $25 \le l \le 25$
Temperature (K)	120(2)	120(2)	117(2)
Volume (Å^3)	2609.8(10)	2304.97(10)	1788.7(2)
D_{calcd} (Mg m^{-3})	1.213	1.203	1.190
Radiation (Å)	MoKα (λ = 0.710 73)	MoKα (λ = 0.710 73)	MoKα (λ = 0.710 73)
Absorption coeff (μ, mm^{-1})	0.078	0.075	0.073
Absorption correction	Semiempirical	Semiempirical	Numerical
F(000)	1008	888	688
θ range for data (°)	2.44–29.97	2.07–30.01	3.50–29.86
Observed reflections	7106	42 952	38 005
Independent reflections	2302	13 452	7930
Data/restraints/parameters	2302/0/219	13452/0/815	7930/0/625
Maximum shift/error	0.003	0.002	0.001
GOF on F^2	0.995	1.462	1.553
Final *R* indices [$I > 2\sigma(I)$]	R_1 = 0.0698, wR_2 = 0.1749	R_1 = 0.0461, wR_2 = 0.0960	R_1 = 0.0457, wR_2 = 0.1007
R indices (all data)	R_1 = 0.1109, wR_2 = 0.2293	R_1 = 0.0739, wR_2 = 0.1038	R_1 = 0.0648, wR_2 = 0.0963
Absolute structure parameter	NA	NA	NA
Extinction coefficient	NA	NA	NA
Largest diff peak and hole (e Å^{-3})	0.368 and –0.395	0.352 and –0.227	0.432 and –0.215

quenched with H_2O (100 mL), Et_2O (100 mL) was added, the layers were separated, and the aqueous layer was extracted with Et_2O (3 × 75 mL). The combined organic layers were washed with H_2O (3 × 100 mL) and brine (50 mL), dried over $MgSO_4$, filtered, and the solvent was removed under reduced pressure. The solid was washed with hexanes (5 × 20 mL) to give **11a** as a white solid (1.94 g, 96%). Recrystallization from CH_2Cl_2–hexanes (1:15) gave the product as a fine white powder (see the following analytical data).

General procedure for the alkylation of the benzophenone imine of glycinamide (10) by IPE to form the α-monosubstituted products 11

Aqueous NaOH (10%, 2.52 mmol) followed by tetrabutylammonium hydrogen sulfate (1.03 mmol) were added to a dried 25 mL round-bottomed flask equipped with a magnetic stirrer and the reaction mixture was stirred for 5 min. The benzophenone imine of glycinamide (**10**, 0.84 mmol) was dissolved in dichloromethane (1.5 mL) and then added dropwise via syringe to the reaction mixture. The solution was stirred for 3 min and then the system was placed under argon. The alkylating agent (4.2 mmol) was added dropwise via syringe and the reaction mixture was stirred at room temperature under argon overnight. The reaction mixture was transferred to a separatory funnel and distilled water (10 mL) and dichloromethane (10 mL) were added. The layers were separated and the aqueous layer was extracted with dichloromethane (3 × 5 mL). The organic layer was washed with distilled water (3 × 10 mL), dried over $MgSO_4$, filtered, and the solvent was removed under reduced pressure to give the crude product. The product was purified by flash column chromatography (SiO_2, first washed with hexanes–EtOAc–Et_3N (90:10:1)) using EtOAc–hexanes (50:50) to EtOAc–hexanes (85:15) gave the purified products **11**.

(±)-2-[(Diphenylmethylene)amino]propanamide (11a)

The general procedure described in the previous section using 10% aq. NaOH (0.9 g, 2.52 mmol), tetrabutylammonium hydrogen sulfate (0.351 g, 1.03 mmol), **10** (0.200 g, 0.84 mmol) in dichloromethane (1.5 mL), and

© 2006 NRC Canada

iodomethane (0.593 g, 4.2 mmol) gave solid product **11a** (177 mg, 84%); mp 120–123 °C. IR (cm^{-1}): 1651, 3451. ^1H NMR δ: 1.35 (d, 3H, J = 7.4 Hz, CH_3), 4.00 (q, 1H, J = 6.9 Hz, CH), 5.30–5.45 (br s, 2H, NH_2), 7.00–7.70 (m, 10H, aromatic). ^{13}C NMR ($CDCl_3$) δ: 22.3, 63.0, 128.9, 129.8, 130.1, 130.3, 130.4, 130.5, 132.2, 137.2, 140.7, 170.5, 178.5. Anal. calcd. for $C_{16}H_{16}N_2O$: C 76.17, H 6.39, N 11.10; found: C 76.36, H 6.50, N 11.14.

(±)-2-[(Diphenylmethylene)amino]-4-pentenamide (11b)

The general procedure described previously using 10% aq. NaOH (11.65 g, 31.5 mmol), tetrabutylammonium hydrogen sulfate (4.38 g, 12.9 mmol), **10** (2.50 g, 10.5 mmol) in dichloromethane (20 mL), and allyl bromide (5.07 g, 42.0 mmol) gave a glassy oil, which was purified by flash column chromatography (SiO_2, first washed with hexanes–EtOAc–Et_3N (90:10:1)) using EtOAc–hexanes (50:50) to EtOAc–hexanes (85:15) to give **11b** as a white solid (2.20 g, 75%); mp 78–80 °C. IR (cm^{-1}): 1686, 3448. ^1H NMR δ: 2.54 (t, 2H, J = 6.6 Hz, CH_2), 4.07 (t, 1H, J = 5.9 Hz, CH), 5.04 (m, 2H, CH_2), 5.44 (br s, 1H, NH), 5.68 (m, 1H, CH), 6.82 (br s, 1H, NH), 7.10–7.66 (m, 10H, aromatic). ^{13}C NMR ($CDCl_3$) δ: 39.8, 65.9, 117.7, 127.8, 128.2, 128.6, 128.7, 128.9, 130.6, 134.0, 135.7, 139.3, 169.8, 175.3. Anal. calcd. for $C_{18}H_{18}N_2O$: C 77.67, H 6.52, N 10.06; found: C 77.36, H 6.52, N 10.00.

(±)-2-[(Diphenylmethylene)amino]-3-(4-chlorophenyl)propanamide (11c)

The general procedure described previously using 10% aq. NaOH (11.6 g, 31.5 mmol), tetrabutylammonium hydrogen sulfate (4.38 g, 12.9 mmol), **10** (2.50 g, 10.5 mmol) in dichloromethane (22 mL), and 4-chlorobenzyl bromide (2.65 g, 12.9 mmol) gave a white solid, which was purified by flash column chromatography (SiO_2, first washed with hexanes–EtOAc–Et_3N (90:10:1)) using EtOAc–hexanes (50:50) to EtOAc–hexanes (85:15) to give the alkylated product **11c** as a white solid (2.74 g, 72%); mp 181 to 182 °C. IR (cm^{-1}): 1681, 3441. ^1H NMR δ: 3.01 (dd, 1H, J = 9.6, 13.2 Hz, CH), 3.15 (dd, 1H, J = 3.3, 12.9 Hz, CH), 4.17 (q, 1H, J = 4.2 Hz, CH), 5.38 (br s, 1H, NH), 6.55 (d, 2H, J = 6.6 Hz, CH), 6.73 (br s, 1H, NH), 6.94–7.59 (m, 14H, aromatic). ^{13}C NMR ($CDCl_3$) δ: 42.4, 69.1, 128.9, 129.8, 130.1, 130.2, 132.3, 132.9, 133.9, 136.8, 137.8, 140.7, 171.9, 176.5. HRMS m/z calcd. for $C_{22}H_{20}N_2OCl$: 363.1186 ($M + Na^+$); found: 363.1252.

(±)-2-[(Diphenylmethylene)amino]butanamide (11d)

The general procedure described previously using 10% aq. NaOH (11.6 g, 31.5 mmol), tetrabutylammonium hydrogen sulfate (4.38 g, 12.9 mmol), **10** (2.50 g, 10.5 mmol) in dichloromethane (25 mL), and iodoethane (2.01 g, 12.9 mmol) gave a light yellow solid, which was purified by flash column chromatography (SiO_2, first washed with hexanes–EtOAc–Et_3N (90:10:1)) using EtOAc–hexanes (50:50) to EtOAc–hexanes (85:15) to give **11d** as a white solid (2.05 g, 73%); mp 116 to 117 °C. IR (cm^{-1}): 1686, 3451. ^1H NMR δ: 0.88 (t, 3H, J = 7.4 Hz, CH_3), 1.78–1.85 (m, 2H, CH_2), 3.93 (q, 1H, J = 3.9 Hz, CH), 5.41 (br s, 1H, NH), 6.80 (br s, 1H, NH), 7.10–7.68 (m, 10H, aromatic). ^{13}C NMR ($CDCl_3$) δ: 11.7, 30.3, 68.8, 129.3, 129.8, 130.2, 130.3, 130.4, 132.2, 137.4, 140.9, 171.0, 177.6. Anal. calcd. for $C_{17}H_{18}N_2O$: C 76.66, H 6.81, N 10.52; found: C 76.94, H 6.84, N 10.55.

General procedure for the alkylation of the benzophenone imines of α-monosubstituted amino amides (11) using KO-*t*-Bu to form the α,α-disubstituted products 12

The benzophenone imine of a monosubstituted α-amino amide (**11**, 1.98 mmol) and anhydr. THF (5 mL) were added at room temperature to a dried 15 mL round-bottomed flask containing a magnetic stirrer and an argon source. The solution was cooled to 0 °C and KO-*t*-Bu (1.0 mol/L in THF, 2.38 mmol) was added dropwise via syringe. The reaction mixture was stirred at 0 °C for 20 min. The alkylating agent (2.38 mmol) was added dropwise via syringe to the reaction mixture at 0 °C and the solution was stirred for 3 h. The reaction mixture was quenched with satd. NH_4Cl (5 mL), H_2O (10 mL), and CH_2Cl_2 (15 mL) were added. The layers were separated, the organic layer was washed with H_2O (2 × 10 mL), and the aqueous layer was extracted with CH_2Cl_2 (3 × 15 mL). The combined organic layers were washed with brine (10 mL), dried over $MgSO_4$, filtered, and the solvent was removed under reduced pressure. The product was purified by flash column chromatography (silica was washed with hexanes–EtOAc–Et_3N, 75:25:1) to give, in most cases, a solid product. Recrystallization from CH_2Cl_2–hexanes (1:15) gave the purified products **12**.

(±)-2-[(Diphenylmethylene)amino]-2-methyl-4-pentenamide (12a) and by-products (16–19)

The general procedure described in the previous section using **11a** (0.500 g, 1.98 mmol) and allyl bromide (0.287 g, 2.38 mmol) gave product **12a** as a white solid (0.35 g, 61%); mp 127–129 °C. R_f 0.39 (hexanes–EtOAc, 7:3). IR (cm^{-1}): 1682, 3438. ^1H NMR δ: 1.23 (s, 3H, CH_3), 2.25 (dd, 1H, J = 6.3, 14.3 Hz, CH), 2.69 (dd, 1H, J = 7.4, 14.7 Hz, CH), 5.05 (m, 2H, CH_2), 5.56 (bs, 1H, NH), 5.71–5.82 (m, 1H, CH), 7.12–7.52 (m, 10H, aromatic). ^{13}C NMR ($CDCl_3$) δ: 24.7, 43.9, 67.8, 117.6, 127.9, 128.0, 128.1, 128.6, 130.3, 133.6, 138.3, 166.9, 179.1. Anal. calcd. for $C_{19}H_{20}N_2O$: C 78.05, H 6.89, N 9.58; found: C 77.94, H 6.93, N 9.62.

Selected analytical data for the by-products

N-Allylated product **16**: R_f 0.62 (hexanes–EtOAc, 7:3). Selected ^1H NMR signals: 1.30 (d, 3H, CH_3), 4.00 (q, 1H, CH), 5.0–6.0 (m, 3H, vinyl of one allyl). LC–MS: 293. Cα,N-Diallylated product **17**: R_f 0.71 (hexanes–EtOAc, 7:3). Selected ^1H NMR signals: 1.23 (s, 3H, CH_3), 5.0–6.0 (m, 6 H, vinyls of two allyls). LC–MS: 333. N,N-Diallylated product **18**: R_f 0.52 (hexanes–EtOAc, 7:3). Selected ^1H NMR signals: 1.30 (d, 3H, CH_3), 4.00 (q, 1H, CH), 5.0–6.0 (m, 6H, vinyls of two allyls). LC–MS: 333. Cα,N,N-Triallylated product **19**: R_f 0.77 (hexanes–EtOAc, 7:3). Selected ^1H NMR signals: 1.23 (s, 3H, CH_3), 5.0–6.0 (m, 9H, vinyls of three allyls). LC–MS: 373.

(±)-2-[(Diphenylmethylene)amino]-2,5-dimethyl-4-hexenamide (12b)

The general procedure described previously using **11a** (0.500 g, 1.98 mmol) and 4-bromo-2-methyl-2-butene (0.355 g, 2.38 mmol) gave product **12b** as a white solid

© 2006 NRC Canada

(0.226 g, 36%); mp 127–129 °C. IR (cm^{-1}): 1638, 3442. ^1H NMR δ: 1.21 (s, 3H, CH_3), 1.50 (s, 3H, CH_3), 1.67 (s, 3H, CH_3), 2.12 (dd, 1H, J = 5.9, 14.7 Hz, CH), 2.70 (dd, 1H, J = 7.3, 15.5 Hz, CH), 5.09 (m, 1H, CH), 5.59 (br s, 1H, NH), 7.18–7.53 (m, 10H, aromatic), 7.96 (br s, 1H, NH). ^{13}C NMR ($CDCl_3$) δ: 18.0, 24.5, 25.9, 38.6, 67.8, 119.2, 127.9, 128.1, 128.4, 130.2, 134.1, 138.4, 141.2, 179.6. Anal. calcd. for $C_{21}H_{24}N_2O$: C 78.71, H 7.55, N 8.74; found: C 78.51, H 7.59, N 8.74.

(±)-2-[(Diphenylmethylene)amino]-2,4-dimethyl-4-pentenamide (12c)

The general procedure described previously using **11a** (0.500 g, 1.98 mmol) and 3-bromo-2-methylpropene (0.320 g, 2.38 mmol) gave product **12c** as a white solid (0.314 g, 52%); mp 122 to 123 °C. IR (cm^{-1}): 1686, 3443. ^1H NMR δ: 1.28 (s, 3H, CH_3), 1.61 (s, 3H, CH_3), 1.96 (d, 1H, J = 16.2 Hz, CH), 2.80 (d, 1H, J = 16.2 Hz, CH), 4.76 (d, 2H, J = 26.5 Hz, CH_2), 5.56 (br s, 1H, NH), 7.21–7.52 (m, 10H, aromatic), 8.13 (br s, 1H, NH). ^{13}C NMR ($CDCl_3$) δ: 25.7, 28.5, 47.5, 68.8, 114.7, 129.3, 129.5, 129.6, 129.8, 130.1, 131.8, 139.9, 142.8, 143.2, 167.7, 181.3. HRMS *m/z* calcd. for $C_{20}H_{23}N_2O$: 307.1732 for (M + Na^+); found: 307.1797.

(±)-2-[(Diphenylmethylene)amino]-2-methyl-(5E)-phenyl-4-pentenamide (12d)

The general procedure described previously using **11a** (0.500 g, 1.98 mmol) and cinnamyl bromide (0.466 g, 2.38 mmol) gave product **12d** as a white solid (0.423 g, 58%); mp 149 to 150 °C. IR (cm^{-1}): 1686, 3442. ^1H NMR δ: 1.26 (s, 3H, CH_3), 2.40 (dd, 1H, J = 7.0, 13.6 Hz, CH), 2.84 (dd, 1H, J = 7.4, 14.0 Hz, CH), 5.55 (br s, 1H, NH), 6.15 (m, 1H, CH), 6.39 (d, 1H, J = 14.6 Hz, CH), 7.16–7.53 (m, 15H, aromatic), 7.94 (br s, 1H, NH). ^{13}C NMR ($CDCl_3$) δ: 26.4, 44.8, 69.8, 126.9, 127.8, 128.7, 129.5, 129.7, 129.8, 130.0, 130.3, 131.9, 134.4, 139.2, 140.0, 142.7, 168.7, 180.6. Anal. calcd. for $C_{25}H_{24}N_2O$: C 81.49, H 6.57, N 7.60; found: C 81.29, H 6.61, N 7.63.

(±)-2-[(Diphenylmethylene)amino]-2-(4-chlorophenyl)propanamide (12e)

The general procedure described previously using **11a** (0.500 g, 1.98 mmol) and 4-chlorobenzyl bromide (0.490 g, 2.38 mmol) in anhydr. THF (1 mL) gave product **12e** as a white solid (0.392 g, 53%); mp 147–149 °C. IR (cm^{-1}): 1686, 3444. ^1H NMR δ: 1.14 (s, 3H, CH_3), 2.87 (d, 1H, J = 14.0 Hz, CH), 3.25 (d, 1H, J = 13.2 Hz, CH), 5.39 (bs, 1H, NH), 7.05–7.50 (m, 14H, Ar). ^{13}C NMR ($CDCl_3$) δ: 26.4, 44.8, 69.8, 126.9, 127.8, 128.7, 129.5, 129.7, 129.8, 130.0, 131.9, 134.4, 139.2, 140.0, 142.7, 168.7, 180.6. Anal. calcd. for $C_{23}H_{21}ClN_2O$: C 73.30, H 5.62, Cl 9.41, N 7.43; found: C 73.06, H 5.62, Cl 9.52, N 7.43.

(±)-2-[(Diphenylmethylene)amino]-2-methylbutanamide (12g)

The general procedure described previously using **11a** (0.500 g, 1.98 mmol) and iodoethane (0.371 g, 2.38 mmol) gave of product **12g** as a white solid (0.129 g, 24%); mp 137 to 138 °C. IR (cm^{-1}): 1680, 3436. ^1H NMR δ: 0.87 (t, 3H, J = 7.6 Hz, CH_3), 1.22 (s, 3H, CH_3), 1.45 (m, 1H, CH), 1.96 (m, 1H, CH), 6.20 (br s, 1H, NH), 7.20–7.53 (m, 10H, aromatic), 8.14 (br s, 1H, NH). ^{13}C NMR ($CDCl_3$) δ: 10.7, 26.7, 33.9, 69.9, 129.3, 129.6, 129.7, 130.1, 131.8, 140.1, 142.8, 167.9, 181.7. Anal. calcd. for $C_{18}H_{20}N_2O$: C 77.11, H 7.19, N 9.99; found: C 76.83, H 7.28, N 9.82.

(±)-2-[(Diphenylmethylene)amino]-2,4-dimethylpentanamide (12h)

The general procedure described previously using **11a** (0.500 g, 1.98 mmol) and 1-iodo-2-methylpropane (0.437 g, 2.38 mmol) gave product **12h** as a white solid (0.150 g, 25%); mp 136–138 °C. IR (cm^{-1}): 1700, 3061. ^1H NMR δ: 0.86 (d, 3H, J = 6.6 Hz, CH_3), 0.93 (d, 3H, J = 6.6 Hz, CH_3), 1.16 (s, 3H, CH_3), 1.42 (dd, 1H, J = 5.1, 14.0 Hz, CH), 1.80 (m, 1H, CH), 1.97 (dd, 1H, J = 8.1, 14.0 Hz, CH), 5.57 (br s, 1H, NH), 7.19–7.53 (m, 10H, aromatic), 8.19 (br s, 1H, NH). ^{13}C NMR ($CDCl_3$) δ: 24.2, 25.8, 26.9, 28.4, 49.6, 68.9, 129.0, 129.6, 129.7, 129.8, 130.1, 130.2, 131.8, 140.1, 142.8, 167.8, 182.2. HRMS *m/z* calcd. for $C_{20}H_{25}N_2O$: 309.1889 (M + Na^+); found: 309.1961.

2-[(Diphenylmethylene)amino]-2-(2-propenyl)-4-pentenamide (12i)

The general procedure described previously using **11b** (0.500 g, 1.79 mmol) and allyl bromide (0.266 g, 2.16 mmol) gave the product **12i** as a solid (0.119 g, 21%); mp 138–140 °C. IR (cm^{-1}): 1691, 3435. ^1H NMR δ: 2.23 (dd, 2H, J = 6.3, 14.3 Hz, CH_2), 2.67 (dd, 2H, J = 7.4, 13.2 Hz, CH_2), 5.05 (m, 4H, CH_2), 5.73 (m, 2H, CH), 7.26–7.48 (m, 10H, aromatic), 8.72 (br s, 1H, NH). ^{13}C NMR ($CDCl_3$) δ: 43.6, 72.7, 119.3, 128.9, 129.7, 129.8, 130.5, 131.9, 134.7, 139.9, 142.8, 168.7, 179.4. Anal. calcd. for $C_{21}H_{22}N_2O$: C 79.21, H 6.96, N 8.80; found: C 79.34, H 7.01, N 8.80.

(±)-2-(4-Chlorobenzyl)-2-[(diphenylmethylene)amino]-4-pentenamide (12j) by allylation

The general procedure described previously using **11c** (0.500 g, 1.38 mmol) and allyl bromide (0.196 g, 1.65 mmol) gave product **12j** as a solid (0.139 g, 25%); mp 143 to 144 °C. IR (cm^{-1}): 1686, 2360, 3442. ^1H NMR δ: 2.27 (dd, 1H, J = 5.9, 14.7 Hz, CH), 2.71 (dd, 1H, J = 7.4, 14.7 Hz, CH), 2.89 (d, 1H, J = 14.0 Hz, CH), 3.23 (d, 1H, J = 14.7 Hz, CH), 5.05 (d, 2H, J = 12.5 Hz, CH_2), 5.53 (br s, 1H, NH), 5.72 (m, 1H, CH), 7.09–7.49 (m, 14H, aromatic), 7.93 (br s, 1H, NH). ^{13}C NMR ($CDCl_3$) δ: 43.3, 45.3, 72.8, 119.7, 128.9, 129.7, 129.8, 129.9, 130.6, 132.1, 132.6, 133.8, 134.4, 137.2, 139.8, 142.6, 168.7, 178.7. HRMS *m/z* calcd. for $C_{25}H_{24}N_2OCl$: 403.1499 (M + Na^+); found: 403.1595.

(±)-2-(4-Chlorobenzyl)-2-[(diphenylmethylene)amino]-4-pentenamide (12j) by benzylation

The general procedure described previously using **11b** (0.250 g, 0.90 mmol) and 4-chlorobenzyl bromide (0.222 g, 1.08 mmol) in THF (1 mL) gave product **12j** as a solid (0.036 g, 10%). See previous analytical data.

(±)-2-[(Diphenylmethylene)amino]-2-ethyl-4-pentenamide (12k)

The general procedure described previously using **11d** (0.500 g, 1.87 mmol) and allyl bromide (0.273 g,

© 2006 NRC Canada

2.25 mmol) gave the product **12k** as a solid (0.075 g, 13%); mp 136 to 137 °C. IR (cm^{-1}): 1679, 3447. ^1H NMR δ: 0.85 (t, 3H, J = 7.4 Hz, CH_3), 1.43 (m, 1H, CH), 1.94 (m, 1H, CH), 2.20 (dd, 1H, J = 6.6, 14.7 Hz, CH), 2.64 (dd, 1H, J = 7.4, 14.7 Hz, CH), 5.03 (m, 2H, CH_2), 5.74 (m, 2H, CH_2), 7.24–7.49 (m, 10H, aromatic), 8.33 (br s, 1H, NH). ^{13}C NMR ($CDCl_3$) δ: 1.6, 10.3, 32.3, 44.1, 44.2, 119.0, 128.6, 129.6, 129.7, 129.8, 129.9, 130.3, 131.6, 131.8, 133.9, 135.0, 168.2, 187.5. Anal. calcd. for $C_{20}H_{22}N_2O$: C 78.40, H 7.24, N 9.14; found: C 78.28, H 7.26, N 9.13.

Michael addition of the benzophenone imine of alaninamide

1,1-Dimethylethyl (±)-5-amino-4-[(diphenylmethylene)amino]-4-methyl-5-oxopentanoate (20)

2-[(Diphenylmethylene)amino]propanamide (**11a**, 0.500 g, 1.98 mmol) and anhydr. THF (5 mL) were added at room temperature to a dried 15 mL round-bottomed flask containing a magnetic stirrer and an argon source. The solution was cooled to 0 °C and *tert*-butyl acrylate (0.305 g, 2.38 mmol) followed by KO-*t*-Bu (1.0 mol/L in THF, 0.238 mL, 0.238 mmol) were added dropwise via syringe. The reaction mixture was stirred at 0 °C for 3 h. The reaction mixture was quenched with satd. NH_4Cl (5 mL), H_2O (10 mL), and CH_2Cl_2 (15 mL) were added. The layers were separated, the organic layer was washed with H_2O (2 × 10 mL), and the aqueous layer was extracted with CH_2Cl_2 (3 × 15 mL). The combined organic layers were washed with brine (10 mL), dried over $MgSO_4$, filtered, and the solvent was removed under reduced pressure. The product was purified by flash column chromatography (silica was washed with hexanes–EtOAc–Et_3N, 75:25:1) to give product **20** as a white solid (0.242 g, 32%). Recrystallization from CH_2Cl_2–hexanes (1:15) gave the purified product; mp 161 to 162 °C. IR (cm^{-1}): 1686, 3438. ^1H NMR δ: 1.20 (s, 3H, CH_3), 1.38 (s, 9H, *tert*-butyl), 1.77–1.81 (m, 2H, CH_2), 6.10 (br s, 1H, NH), 7.22–7.52 (m, 10H, aromatic), 8.03 (br s, 1H, NH). ^{13}C NMR ($CDCl_3$) δ: 24.3, 24.9, 28.0, 30.5, 31.1, 33.1, 34.7, 62.1, 66.8, 125.8, 125.9, 127.7, 128.1, 128.2, 128.4, 128.5, 128.6, 130.4, 138.1, 140.9, 145.3, 146.0, 167.3, 172.2, 172.7, 179.4, 179.8. HRMS m/z calcd. for $C_{23}H_{29}N_2O_3$: 381.2100 ($M + Na^+$); found: 381.2187.

Acknowledgements

We thank the National Institutes of Health (R01 GM028193) and Eli Lilly and Company for financial support of this work. We acknowledge helpful discussions with H.E. Schoemaker, Q.B. Broxterman, and B. Kaptein of DSM Research (Geleen, The Netherlands). A generous gift of (±)-alaninamide hydrochloride from DSM Research is gratefully acknowledged.

References

1. (*a*) M.J. O'Donnell, J.M. Boniece, and S.E. Earp. Tetrahedron Lett. 2641 (1978); (*b*) M.J. O'Donnell and T.M. Eckrich. Tetrahedron Lett. 4625 (1978).
2. (*a*) M.J. O'Donnell, W.D. Bennett, W.A. Bruder, W.N. Jacobsen, K. Knuth, B. LeClef, R.L. Polt, F.G. Bordwell, S.R. Mrozack, and T.A. Cripe. J. Am. Chem. Soc. **110**, 8520 (1988); (*b*) F.G. Bordwell. Acc. Chem. Res. **21**, 456 (1988).
3. (*a*) Computer-assisted mechanistic evaluation of organic reactions (CAMEO): A.J. Gushurst and W.L. Jorgensen. J. Org. Chem. **51**, 3513 (1986); (*b*) For a recent paper on first-principle predictions of absolute pK_as of organic acids in DMSO, see: Y. Fu, L. Liu, R.-Q. Li, R. Liu, and Q.-X. Guo. J. Am. Chem. Soc. **126**, 814 (2004).
4. M.J. O'Donnell, I.A. Esikova, A. Mi, D.F. Shullenberger, and S. Wu. *In* Phase-transfer catalysis: Mechanisms and syntheses. *Edited by* M.E. Halpern. American Chemical Society, Washington, D.C. 1997. Chap. 10. pp 124–135.
5. A. López, M. Moreno-Mañas, R. Pleixats, A. Roglans J. Ezquerra, and C.Pedregal. Tetrahedron, **52**, 8365 (1996).
6. R.W. Hoffmann. Chem. Rev. **89**, 1841 (1989).
7. M.J. O'Donnell, W.D. Bennett, W.N. Jacobsen, and Y.-a. Ma. Tetrahedron Lett. **30**, 3909 (1989).
8. Early development of enantioselective PTC alkylations of the benzophenone imine of glycine *tert*-butyl ester with Cinchona-derived quaternary ammonium salts: (*a*) M.J. O'Donnell, W.D. Bennett, and S. Wu. J. Am. Chem. Soc. **111**, 2353 (1989); (*b*) M.J. O'Donnell, S. Wu, and J.C. Huffman. Tetrahedron, **50**, 4507 (1994); (*c*) E.J. Corey, F. Xu, and M.C. Noe. J. Am. Chem. Soc. **119**, 12414 (1997); (*d*) B. Lygo and P.G. Wainwright. Tetrahedron Lett. **38**, 8595 (1997).
9. Reviews from the author's laboratory. Asymmetric PTC reactions: (*a*) M.J. O'Donnell. *In* Catalytic asymmetric synthesis. *Edited by* I. Ojima. VCH, New York. 1993. Chap. 8. pp. 389–411; (*b*) M.J. O'Donnell. *In* Catalytic asymmetric synthesis. 2nd Ed. *Edited by* I. Ojima. Wiley-VCH, New York. 2000. Chap. 10. pp. 727–755; (*c*) Preparation of optically active α-amino acids from the benzophenone imine of glycine derivatives: M.J. O'Donnell. Aldrichimica Acta, **34**, 3 (2001); (*d*) Enantioselective synthesis of α-amino acids by PTC with achiral Schiff base esters: M.J. O'Donnell. Acc. Chem. Res. **37**, 506 (2004).
10. Selected reviews or lead references for enantioselective PTC reactions of the benzophenone imine of glycine alkyl esters for the preparation of optically active α-amino acids: (*a*) C. Nájera. Synlett, 1388 (2002); (*b*) B. Lygo and B.I. Andrews. Acc. Chem. Res. **37**, 518 (2004); (*c*) Y. Fukuta, T. Ohshima, V. Gnanadesikan, T. Shibuguchi, T. Nemoto, T. Kisugi, T. Okino, and M. Shibasaki. Proc. Nat. Acad. Sci. U.S.A. **101**, 5433 (2004); (*d*) M.-S. Yoo, B.-S. Jeong, J.-H. Lee, H.-g. Park, and S.-s. Jew. Org. Lett. **7**, 1129 (2005); (*e*) K. Maruoka. Pure Appl. Chem. **77**, 1285 (2005).
11. M.J. O'Donnell, T.P. Burkholder, V.V. Khau, R.W. Roeske, and Z. Tian. Pol. J. Chem. **68**, 2477 (1994).
12. (*a*) M.J. O'Donnell, C. Zhou, and W.L. Scott. J. Am. Chem. Soc. **118**, 6070 (1996); (*b*) M.J. O'Donnell, C.W. Lugar, R.S. Pottorf, C. Zhou, W.L. Scott, and C.L. Cwi. Tetrahedron Lett. **38**, 7163 (1997); (*c*) W.L. Scott, F. Delgado, K. Lobb, R.S. Pottorf, and M.J. O'Donnell. Tetrahedron Lett. **42**, 2073 (2001); (*d*) M.J. O'Donnell, M.D. Drew, R.S. Pottorf, and W.L. Scott. J. Comb. Chem. **2**, 172 (2000).
13. M.J. O'Donnell, F. Delgado, and R.S. Pottorf. Tetrahedron, **55**, 6347 (1999).
14. L. Ghosez, J.-P. Antoine, E. Deffense, M. Navarro, V. Libert, M.J. O'Donnell, W.A. Bruder, K. Willey, and K. Wojciechowski. Tetrahedron Lett. **23**, 4255 (1982).
15. M.J. O'Donnell, B. LeClef, D.B. Rusterholz, L. Ghosez, J.-P. Antoine, and M. Navarro. Tetrahedron Lett. **23**, 4259 (1982).
16. M.J. O'Donnell, W.D. Bennett, W.N. Jacobsen, and Y.-a. Ma. Tetrahedron Lett. **30**, 3913 (1989).

© 2006 NRC Canada

17. W.L. Scott, C. Zhou, Z. Fang, and M.J. O'Donnell. Tetrahedron Lett. **38**, 3695 (1997).
18. D.L. Griffith, M.J. O'Donnell, R.S. Pottorf, W.L. Scott, and J.A. Porco, Jr. Tetrahedron Lett. **38**, 8821 (1997).
19. Taken in part from: (*a*) J.D. Keeton. M.S. thesis, Purdue University, Indianapolis, Indiana. 2002; (*b*) V. Van Khau. M.S. thesis, Purdue University, Indianapolis, Indiana. 1988.
20. (*a*) S. Kumar and U. Ramachandran. Tetrahedron: Asymmetry, **14**, 2539 (2003); (*b*) T. Ooi, D. Sakai, M. Takeuchi, E. Tayama, and K. Maruoka. Angew. Chem. Int. Ed. **42**, 5868 (2003); (*c*) S. Kumar and U. Ramachandran. Tetrahedron Lett. **46**, 19 (2005); (*d*) T. Ooi, M. Takeuchi, D. Kato, Y, Uematsu, E. Tayama, D. Sakai, and K. Maruoka. J. Am. Chem. Soc. **127**, 5073 (2005).
21. (*a*) Review: H.E. Schoemaker, W.H.J. Boesten, B. Kaptein, E.C. Roos, Q.B. Broxterman, W.J.J. van den Tweel, and J. Kamphuis. Acta. Chem. Scand. **50**, 225 (1996); (*b*) Review: H.E. Schoemaker, W.H.J. Boesten, Q.B. Broxterman, E.C. Roos, B. Kaptein, W.J.J. van den Tweel, J. Kamphuis, E.M. Meijer, and F.P.J.T. Rutjes. Chimia, **51**, 308 (1997); (*c*) B. Kaptein, W.H.J. Boesten, Q.B. Broxterman, H.E. Schoemaker, and J. Kamphuis. Tetrahedron Lett. **33**, 6007 (1992); (*d*) B. Kaptein, H.M. Moody, Q.B. Broxterman, and J. Kamphuis. J. Chem. Soc. Perkin Trans. 1, 1495 (1994); (*e*) F.P.J.T. Rutjes and H.E. Schoemaker. Tetrahedron Lett. **38**, 677 (1997); (*f*) J. Van Betsbrugge, D. Tourwé, B. Kaptein, H. Kierkels, and R. Broxterman. Tetrahedron, **53**, 9233 (1997); (*g*) F.P.J.T. Rutjes, K.C.M.F. Tjen, L.B. Wolf, W.F.J. Karstens, H.E. Schoemaker, and H. Hiemstra. Org. Lett. **1**, 717 (1999); (*h*) F.P.J.T. Rutjes, J.J.N. Veerman, W.J.N. Meester, H. Hiemstra, and H.E. Schoemaker. Eur. J. Org. Chem. 1127 (1999); (*i*) B. Kaptein, Q.B. Broxterman, H.E. Schoemaker, F.P.J.T. Rutjes, J.J.N. Veerman, J. Kamphuis, C. Peggion, F. Formaggio, and C. Toniolo. Tetrahedron, **57**, 6567 (2001).
22. E.C. Taylor, N.F. Haley, and R.J. Clemens. J. Am. Chem. Soc. **103**, 7743 (1981).
23. Amination (7 mol/L NH_3, MeOH) of the benzophenone imine of glycine methyl ester (**1b**) gave **10**, see: D.J. Hyett, D. Mink, Q.B. Broxterman, B. Kaptein, and H.J.M. Zeegers. PCT Int. Appl. 078702, 2004; Chem. Abstr. CAN 141:243830, AN 2004:756676.
24. For the use of transimination for the preparation of the benzophenone Schiff bases of amino esters, see: M.J. O'Donnell and R.L. Polt. J. Org. Chem. **47**, 2663 (1982).
25. A. Brändström. Preparative ion pair extraction. Apotekarsocieteten/Hässle, Läkemedel, Sweden. 1974.
26. M.J. O'Donnell, F. Delgado, C. Hostettler, and R. Schwesinger. Tetrahedron Lett. **39**, 8775 (1998).
27. G. Guillena, B. Mancheño, C. Nájera, J. Ezquerra, and C. Pedregal. Tetrahedron, **54**, 9447 (1998).
28. G. Guillena and C. Nájera. Tetrahedron: Asymmetry, **9**, 3935 (1998).
29. Bruker Analytical X-ray Systems. SHELXTL. Version 6.12 [computer program]. Bruker Analytical X-ray Systems, Madison, Wisconsin. 2001.

© 2006 NRC Canada

Cyclotrimerization approach to unnatural structural modifications of pancratistatin and other amaryllidaceae constituents — Synthesis and biological evaluation[1]

Tomas Hudlicky, Michael Moser, Scott C. Banfield, Uwe Rinner, Jean-Charles Chapuis, and George R. Pettit

Abstract: The phenanthridone core of pancratistatin lacking all aromatic oxygenation was prepared by cyclotrimerization of acetylene-containing scaffolds **30** and **41**, reflecting the natural and the C-1 epi configuration, respectively, of the amino inositol moiety. The cobalt-catalyzed formation of the aromatic core led to bisTMS derivatives **39** and **48**, as well as bisacetyl derivative **51**. The effectiveness of cyclotrimerization of the natural or trans series was compared with that of the cis series. In addition, the yields of cyclotrimerization were compared for propargylic amines and propargylic amides. Eleven derivatives, including the fully hydroxylated phenantridone **39**, were tested against seven cancer cell lines. Three of the compounds displayed activities only an order of magnitude less than those of 7-deoxypancratistatin. Full experimental and spectral details are provided for all key compounds and future projections for the preparation of unnatural analogs of Amaryllidaceae constituents are advanced, along with some new insight into the minimum pharmacophore of pancratistatin.

Key words: cyclotrimerization, alkaloids, cobalt catalyst.

Résumé : Faisant appel à une cyclotrimérisation des dérivés acétyléniques **30** et **41** qui reflètent respectivement les configurations naturelle et C-1-épi, on a préparé la phénanthridone, le squelette fondamental de la pancratistatine ne comportant pas d'oxygène aromatique. La formation catalysée par le cobalt du noyau fondamental à conduit aux dérivés bisTMS **39** et **48** ainsi qu'au dérivé bisacétylé **51**. On a comparé l'efficacité de la cyclotrimérisation de la série nature ou trans avec celle de la série cis. De plus, on a comparé les rendements des cyclotrimérisations avec des amines et des amides propargyliques. Onze dérivés, y compris la phénantridone totalement hydroxylé (**39**) ont été évalués contre sept souches de cancer. Trois de ces composés présentent des activités qui ne sont qu'un ordre de grandeur inférieures à celle de la 7-désoxypancratistatine. On rapporte l'ensemble des détails expérimentaux et spectraux relatifs à tous les intermédiaires clés. Les projections relatives à la préparation d'analogues non naturels des constituants de l'Amaryllidaceae sont avancées et l'on possède déjà de nombreuses pistes nouvelles concernant la nature du pharmacophore minimal de la pancratistatine.

Mots clés : cyclotrimérisation, alcaloïdes, catalyseur de cobalt.

[Traduit par la Rédaction]

Introduction

Pancratistatin (**1**) and its congeners (Fig. 1) have been at the forefront of activities in both synthetic and medicinal communities (1). All four naturally occurring constituents have been synthesized by many creative approaches (2–5), and significant effort has been devoted to the investigation of the mode of action (6), active pharmacophore (7), and more bioavailable agents (8). To date many truncated versions of the key constituents have been prepared (9) and evaluated for activities against several cancer cell lines. From the results of these evaluations, several generalizations

Received 7 November 2005. Accepted 4 March 2006. Published on the NRC Research Press Web site at http://canjchem.nrc.ca on 1 August 2006.

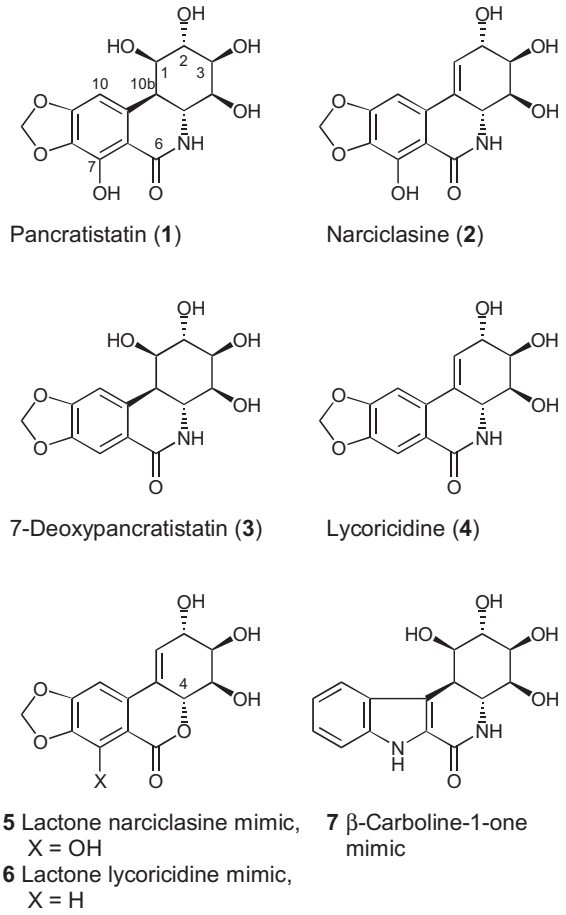
Dedicated to Dr. Alfred Bader in recognition of his service to the organic chemistry community.

T. Hudlicky,[2] M. Moser, and S. Banfield. Department of Chemistry and Centre for Biotechnology, Brock University, 500 Glenridge Avenue, St. Catharines, ON L2S 3A1, Canada.
U. Rinner. Institut für Organische Chemie, Universität Wien, Währinger Strasse 38, 1090 Wien, Austria.
G.R. Pettit. Department of Chemistry and Biochemistry and the Cancer Research Institute, Arizona State University, Tempe, Arizona 85287, USA.

[1]This article is part of a Special Issue dedicated to Dr. Alfred Bader.
[2]Corresponding author (e-mail: thudlicky@brocku.ca).

 doi:10.1139/V06-078 © 2006 NRC Canada

Fig. 1. Amaryllidaceae constituents (**1**–**4**) and some recently synthesized unnatural mimics (**5**–**7**).



have emerged with regard to the structural elements essential to activity. First, the hydroxyphenanthridone moiety is thought to be essential to high activity of pancratistatin and narciclasine; its deletion, as in 7-deoxypancratistatin and lycoricidine, leads to a significant drop in activity (10). Second, the amino inositol motif is also essential, save for small changes at C-1 and C-2; deletion of the hydroxyls at these positions or altering substitution patterns at C-1 does not altogether eliminate activity (7, 11). Various unnatural derivatives with specific deletions in the hydroxylated ring have been tested. A recent article established that the minimum requirement for activity is the 2,3,4-triol pattern found in all active constituents (11). Third, deletion of some of the aromatic oxygenation lowers activity significantly (12). Fourth, recently synthesized lactone mimics **5** and **6**, in both configurations at C-4, were found inactive, suggesting that the phenanthridone unit is essential for retention of activity (13). Finally, an indole mimic of pancratistatin (**7**) recently prepared in our laboratory possessed borderline activity against one cell line (Table 1) (14).

These observations, as well as the bioavailability studies, indicate that the greatest opportunity for structural alterations exists in modifications of the aromatic core of the natural product. To prepare a large number of derivatives, a diversity-oriented synthesis strategy (DOS) is the most efficient way to generate libraries of compounds for testing. Rather than synthesize uniquely functionalized aryl residues for eventual attachment to the amino inositol unit, we have chosen the cyclotrimerization approach portrayed in Fig. 2, which is based on acetylene- and nitrile-containing scaffolds and their cobalt-catalyzed trimerization to aromatic (15) and heteroaromatic (16) variants of the pancratistatin type. This unique transformation was discovered in 1864 by Berthelot (17), who prepared benzene by passing acetylene over hot copper. We note that Berthelot's paper, published in 1866, is usually cited as the event of original discovery (17*b*, 17*c*). This is not the correct citation and for historical interest we include the original description of his 1864 experiment here:

Il est un cas de condensation de l'acetylene naissant très-remarquable et qui mérite un examen particulier, bien que la démonstration en soit plutôt vraisemblable que rigoureusement établie: c'est la condensation de l'acétylène en benzine. Entre la formule de l'acétylène, C^4H^2, et celle de la benzine $C^{12}H^6$, c'est-à-dire entre les poids de ces deux corps ramenés à l'état gazeux et au même volume, il existe une relation très-simple; la deuxième formule est triple de la première :

$$3\ C^4H^2 = C^{12}H^6.$$

Or cette relation n'existe pas seulement entre les formulas des deux corps; mais on peut admettre que, dans certaines circonstances que nous allons signaler, l'acétylène naissant se transforme réellement en benzine. Voici ces circonstances.

Nous avons vu précédemment (p. 286) qu'en faisant passer un courant de vapeur de formène trichloré (chloroforme), C^2HCl^3, sur du cuivre chauffé au rouge, le chlore est absorbé et l'acétylène prend naissance. Répétons cette expérience avec le formène tribromé (bromoforme), C^2HBr^3, nous obtiendrons de la benzine. Nous sommes donc autorisés à penser que 3 molécules d'acétylène naissant peuvent se condenser en une seule molécule de benzine : la benzine serait alors du triacétylène.

This is an example of condensation of the nascent acetylene that is very remarkable and deserves a close examination, even though the demonstration is rather plausible then rigorously established: it is the condensation of the acetylene into benzene. There is a very simple relationship between the formula of acetylene, C_4H_2, and the formula of benzene, $C_{12}H_6$, specifically between the weight of equal volumes of those two bodies in the gas state: the second formula is triple of the first:

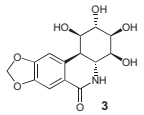
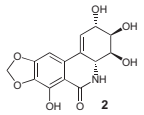
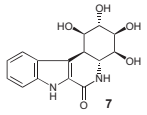
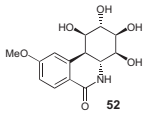
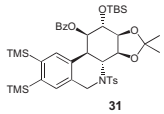
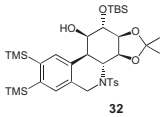
$$3\ C_4H_2 = C_{12}H_6.$$

Now such relation does not just exist between the formulas of the two bodies; but we can admit that under certain particular circumstances that we may point to, nascent acetylene is actually transformed to benzene. We have already seen (p.286) that by passing a stream of gaseous trichlorinated formene (chloroform), C_2HCl_3, over red-hot copper, chlorine is absorbed and acetylene is generated. By repeating this experience with tribrominated formene (bromofrom), C_2HBr_3, we would obtain some benzene. This leads us to think that three molecules of nascent acetylene could combine to form a single molecule of benzene. Thus benzene would be a triacetylene.

The reaction enjoyed moderate attention and, indeed, exhibited moderate yields in most of the documented examples in the literature, including recent applications (18). An ex-

© 2006 NRC Canada

Table 1. Evaluation of the activities of aromatic deoxygenated TMS derivatives of 7-deoxypancratistatin.

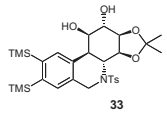
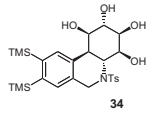
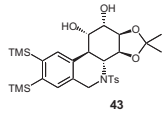
		Murine P388 lumphocytic leukemia and human cancer cell results (GI_{50} values in μg/mL)						
Entry	Compound	Murine P388 lymphocytic leukemia	Pancreas BXPC-3	Breast MCF-7	CNS SF-268	Lung NCI-H460	Colon KM20L2	Prostate DU-145
2		0.44				0.29	0.22	
3		0.0012	0.026	0.019	0.021	0.032	0.021	0.011
4		18.3	>10	>10			>10	
5		4.3	4.9	4.4	3.3	2.8	3.6	2.6
6		> 10	> 10	> 10	> 10	> 10	> 10	> 10
7			3.6	2.2	3.8	4.7	3.1	13.1

ception to such critique is found in the classic application of cyclotrimerization to the total synthesis of estrone by Funk and Vollhardt in 1977 (19), shown in Fig. 3. Despite the attention this synthesis received, only once more was this technique featured in a total synthesis effort — an approach to morphine also disclosed by Vollhardt and co-workers (20) (Fig. 3). In the estrone synthesis, the initial cyclization furnished a low yield of **13** in addition to the intermediate benzocyclobutane, which, under the conditions of the reaction, underwent [4+2] cyclization to **13** in a total yield of 71%. In the approach to morphine, benzofuran **15** yielded the tetracyclic morphine skeleton as a single diastereomer with C-5, C-9, and C-13 correctly set, indicating the potential for adjustment to the total synthesis of morphine itself, once appropriate substitution parameters for the incipient quaternary center at C-13 were designed. The emphasis on multicomponent reactions and cascade processes, so prevalent in the last decade or so (21, 22), seemed in sharp contrast to the apparent underutilization of cyclotrimerization techniques that satisfy both of these criteria. We reasoned that the modest yields reported in most of the applications could be addressed though appropriate reaction engineering and optimization of conditions. The benefits that would be harvested in the area of structure and activity relationships (SAR) for the analogs of the pancratistatin group of compounds seemed to outweigh the uncertainty and expectations of moderate yields in the construction of aromatic nuclei of the analogs.

In this manuscript we report the successful synthesis of several pancratistatin analogs by a high-yielding cyclotri-

© 2006 NRC Canada

Table 1 (*concluded*).

		Murine P388 lumphocytic leukemia and human cancer cell results (GI_{50} values in μg/mL)						
Entry	Compound	Murine P388 lymphocytic leukemia	Pancreas BXPC-3	Breast MCF-7	CNS SF-268	Lung NCI-H460	Colon KM20L2	Prostate DU-145
8	 **33**	3.0	1.7	1.5	1.6	1.7	1.6	1.6
9	 **34**	3.3	1.7	1.7	1.6	1.7	1.4	1.8
10	 **43**	3.9						

Note: Compounds 36, 37, 38, 39, 44, and 48 are marginally inactive to completely inactive in the p388 leukemia cell lines.

merization protocol from fully functionalized scaffolds of type **9** (23). The biological evaluation of the analogs, also reported herein, provided some surprising results and cast some uncertainty on the previously held views regarding some of the structural features deemed essential for biological function.

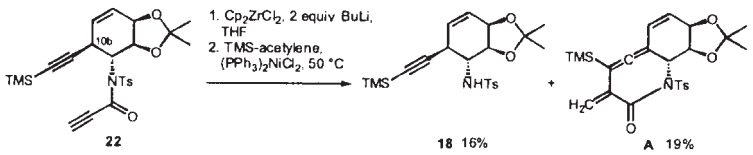
Results and discussion

The original intent of our study was the investigation of a de *novo* approach to pancratistatin (**1**) from scaffold **9** in which the acetylene partners would provide a triply silylated arene that could be converted to the fully oxygenated core of pancratistatin. Portrayed in Scheme 1 are the results of this particular approach, which met with abject failure because of the steric issues associated with multiply silylated sites or perhaps random desilylation processes similar to those observed when Rainier used an iron-based catalyst (24). Only the cobalt-coordinated tetracycle **20** was isolated in low yield from the reactions of bisacetylene **19** (Scheme 1). The final cycloaddition of bis(trimethylsilyl)acetylene (BTMSA) did not lead to the fully silylated arene **21**, presumably because of steric crowding.

When $Ni(COD)_2$ was employed as a catalyst, the cyclotrimerization of **22** gave an interesting dimeric product (**23**) in 47% yield. The use of a zirconium catalyst (25) did not lead to dimeric **23** and gave other products.[3]

Adjustments in the strategic plan led to the construction of simpler scaffolds unencumbered by TMS groups and cyclotrimerization attempts to attain a 7-deoxypancratistatin

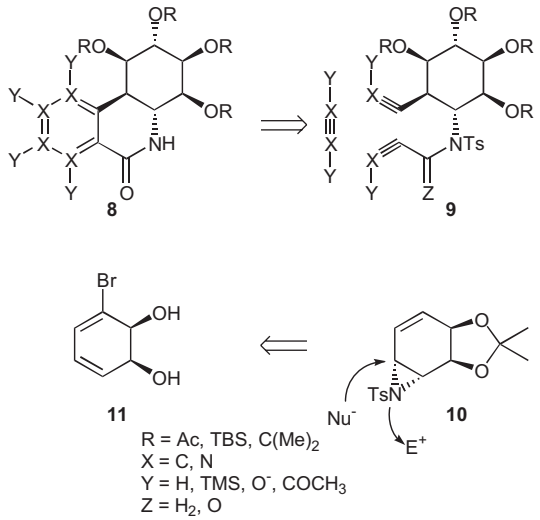
[3] The exposure of propargylic amide **22** to a zirconium-based catalyst led to some unusal results. The propargylic amide was lost and tosylamide **18** was recovered, in addition to an unusual structure, tentatively identified as cyclic allene **A**, which may result in an ene reaction between the propargyl group and the hydrogen at 10b.



A [(1*R*,2*S*,6*R*)-4,4-Dimethyl-12-methylene-14-(4-methylphenylsulfonyl)-11-trimethylsilyl-3,5-dioxa-14-azatricyclo-[7.5.0.$0^{2,6}$]tetradeca-7,9,10-trien-13-one]: $[\alpha]^{28}_D$ +79.0 (c 0.95, $CHCl_3$). R_f 0.81 (hexanes – ethyl acetate, 4:1). IR ($CHCl_3$, cm^{-1}) ν: 3683, 3020, 2962, 2932, 2401, 2167, 1736, 1660, 1598, 1509, 1374, 1308, 1278, 1251, 1216, 1189, 1176, 1091, 1063, 950, 908, 847, 757, 669, 582. ^{1}H NMR (300 MHz, $CDCl_3$, 50 °C, ppm) δ: 8.00 (d, *J* = 8.2 Hz, 2H), 7.33 (d, *J* = 8.1 Hz, 2H), 6.11 (s, 1H), 5.80 (dd, *J* = 9.9, 3.1 Hz, 1H), 5.64 (d, *J* = 10.2 Hz, 1H), 4.71 (t, *J* = 5.0 Hz, 1H), 4.63 (d, *J* = 4.8 Hz, 1H), 4.40 (m, 1 H), 2.43 (s, 3H), 1.53 (s, 3H), 1.43 (s, 3H), 0.14 (s, 9H). ^{13}C NMR (75 MHz, $CDCl_3$, ppm) δ: 145.6, 142.7, 135.5, 129.8, 128.9, 128.0, 125.1, 121.5, 110.7, 104.0, 77.5, 74.4, 69.8, 62.9, 41.0, 28.1, 27.0, 22.0, 0.0. MS (EI) *m/z* (relative intensity): 456 ($M^+ - CH_3$, 30), 415 (10), 414 (30), 413 (23), 259 (11), 258 (30), 242 (7), 230 (10), 220 (5), 215 (5), 161 (6), 156 (8), 155 (29), 149 (11), 140 (5), 139 (13), 129 (6), 108 (5), 107 (7), 106 (12), 105 (9), 99 (6), 98 (11). HRMS (EI) calcd. for $C_{23}H_{26}O_5NSSi$-CH_3: 456.1301; found: 456.1289.

© 2006 NRC Canada

Fig. 2. Cyclotrimerization approach to aromatic core variants of pancratistatin.



substitution pattern instead. These efforts were divided into three distinct areas: (*i*) synthesis of building blocks exhibiting the stereochemistry of the "natural" or trans series, with respect to stereochemical configuration at C-1 and C-2; (*ii*) synthesis of the corresponding "unnatural" or cis series; and (*iii*) comparison of the overall efficiency of these two approaches with one that would employ propargyl amides vs. propargyl amines. Upon attaining the nucleus of Amaryllidaceae constituents, all of these approaches would be evaluated and the best one chosen for the eventual production of analogs.

Cyclotrimerization of scaffolds in the trans or natural series

The intermediate reflecting the natural amino inositol configuration was synthesized as shown in Scheme 2 (23). Vinylaziridine **10** (26) was reacted with the aluminum complex prepared from lithium (trimethylsilyl)acetylene to provide **18** in 69% yield. After column chromatography, the product of this reaction was treated with 2,2-dimethoxypropane (DMP) and acetone to reprotect the diol liberated in the portion of the mixture by the action of $AlCl_3$. The reprotected compound was used without further purification. The tosylaziridine **18** was first converted to the cis-diol **24** by the action of OsO_4 and *N*-methylmorpholine-*N*-oxide (NMO) (44% yield, 76% conversion), and the cyclic sulfate **25** was then generated in 82% yield by treatment with SO_2Cl_2 and NEt_3. Cyclic sulfates, whose reactivity resembles that of epoxides (27), are easily opened with weak nucleophiles such as ammonium benzoate. Such opening generates the required trans relationship at C-1/C-2 of pancratistatin, as has been previously demonstrated (27*b*). Treatment of **25** with ammonium benzoate generated, surprisingly, a mixture of the desired **26**, as a minor product accompanied by the elimination product **27**, displaying the substitution parameters of narciclasine or lycoricidine. Investigation of this reaction revealed that **27** does not originate in **26** nor is it derived from **25** by syn elimination. Careful experimentation revealed that the likely source of **27** is the intramolecular elimination of proton at C-10b by the intermediate sulfate anion **25a** as shown in Fig. 4. Further study is required to optimize the production of either **26** or **27**, the latter containing the structural features of narciclasine.

The TMS group was removed with tetrabutylammonium triphenyldifluorosilicate (TBAT) in 84% yield from acetylene **26** to avoid previously encountered problems with steric bulk at the incipient C-10 of the aromatic nucleus. Following the protection of the C-2 alcohol as a TBS ether (89%), tosylamide **29** was alkylated with propargyl bromide to yield the required compound **30** in 79% yield. As mentioned above, the prospects for high yields in the cyclotrimerization were not promising based on the rather modest yields reported throughout the literature. Yet, after optimization, acetylene derivative **30** was converted to tetracyclic tosylamide **31** in 83% yield (slow addition over 36 h of a mixture of **30**, catalyst, and BTMSA to a heated solution of BTMSA, which was recovered by distillation upon completion of the reaction). Tosylamide **31** was converted to fully deprotected tetraol **34** (as shown in Scheme 3) to provide compounds lacking the phenanthridone carbonyl group for biological evaluation. Oxidation of **31** to the state of phenanthridone proved somewhat arduous, proceeding in 15% yield to **35** with $NaIO_4$–$RuCl_3$. Oxidation studies on bisbenzoate **37** led to the same results under these conditions. With the reaction buffered by solid Na_2CO_3, the oxidation occurred more slowly to give **38** in 33% yield. This material was subjected to reductive detosylation with sodium naphthalide, during which a partial loss of the benzoate groups occurred as a result of the basic conditions. The crude material was treated first under stronger basic conditions CH_3ONa in MeOH) then under acidic conditions (Dowex 50WX8-100 in MeOH) to provide the 7-deoxypancratistatin nucleus having TMS groups in place of the aromatic oxygenation. The preparation of this key compound in 14 steps and 0.3% overall yield starting from aziridine **10** signified the successful validation of the cyclotrimerization strategy as an approach to compounds with variations in the aromatic core.

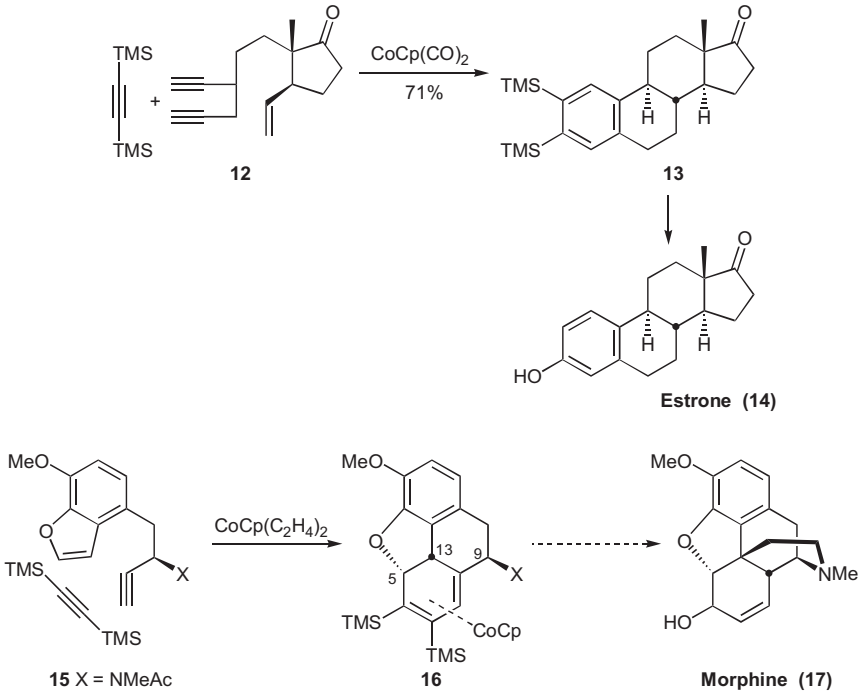
Cyclotrimerization of scaffolds in the cis or unnatural series

The unnatural or cis series intermediate was synthesized as shown in Scheme 4. The purpose of this approach was twofold. First, it would avoid the lack of selectivity in the cyclic sulfate opening encountered with **25**, leaving this reaction for the latter part of the synthesis. Second, it would provide the analogs with unnatural C-1 configuration for biological testing. The bisbenzoate **41** was subjected to cyclotrimerization under the optimized conditions applied to compound **30** in the trans series and provided tetracycle **42** in 87% yield (as shown in Scheme 5).

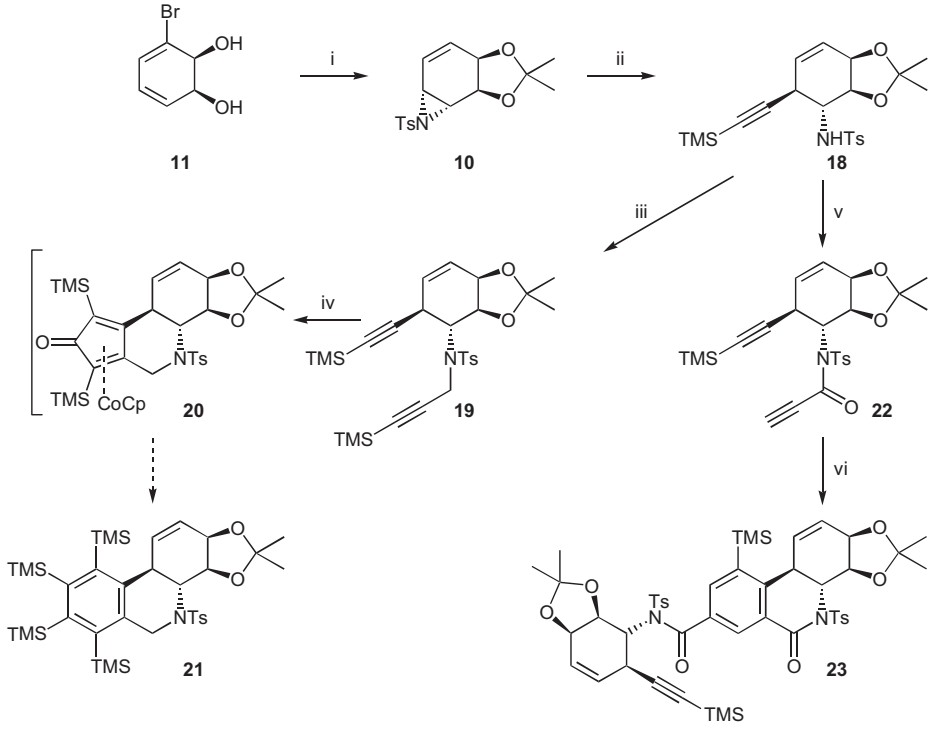
Deprotection of the benzoate and generation of the cyclic sulfate was accomplished in high yield and *trans*-benzoate alcohol **36** was generated in essentially quantitative yield. Upon exposure of **44** to ammonium benzoate in dimethylformamide (DMF) in this series, the elimination to the narciclasine/lycoricidine manifold was not observed. A possible explanation may lie in the relative acidities of propargylic vs. benzylic protons at C-10b in **25** vs. **44**, respectively. Fully deprotected analogs **34** (lacking the phenanthridone carbonyl) and **39** (containing the amide) were ob-

© 2006 NRC Canada

Fig. 3. Applications of cyclotrimerization strategy in total synthesis (Vollhardt's estrone and morphine).



Scheme 1. Cyclotrimerization approach to fully silylated aromatic core. Reagents and conditions: (*i*) DMP, *p*-TSA, acetone, rt, then PhINTs, $Cu(acac)_2$, H_3CCN, 0 °C to rt, then *n*-Bu_3SnH, AIBN, THF, reflux, 25% over three steps; (*ii*) BuLi, TMS–acetylene, $AlCl_3$, toluene, 0 °C to rt, then DMP, *p*-TSA, acetone, rt, 69% over two steps; (*iii*) BuLi, TMS – propargyl bromide, $(n\text{-}Bu)_4NI$, THF, rt, 46% (66% by conversion); (*iv*) $CpCo(CO)_2$, BTMSA, 140 °C; (*v*) BuLi, propiolic acid anhydride, THF, 0 °C to rt, 46%; (*vi*) $Ni(COD)_2$, PPh_3, toluene, BTMSA, rt, 47%.



© 2006 NRC Canada

Scheme 2. Scaffold for cyclotrimerization in the trans or natural series. Reagents and conditions: (*i*) BuLi, TMS–acetylene, $AlCl_3$, toluene, 0 °C to rt; (*ii*) DMP, acetone, rt, 69% over two steps; (*iii*) OsO_4, NMO, CH_2Cl_2, rt, 44% (76% by conversion); (*iv*) SO_2Cl_2, NEt_3, CH_2Cl_2, 0 °C to rt, 82%; (*v*) $H_5C_6COONH_4$, DMF, 70 °C, then H_2O, H_2SO_4, THF, rt; (*vi*) TBAT, H_3CCN, rt, 84%; (*vii*) TBSCl, imidazole, DMF, rt, 89%; (*viii*) NaHMDS, propargyl bromide, $(n\text{Bu})_4NI$, THF, –0 °C to rt, 79%.

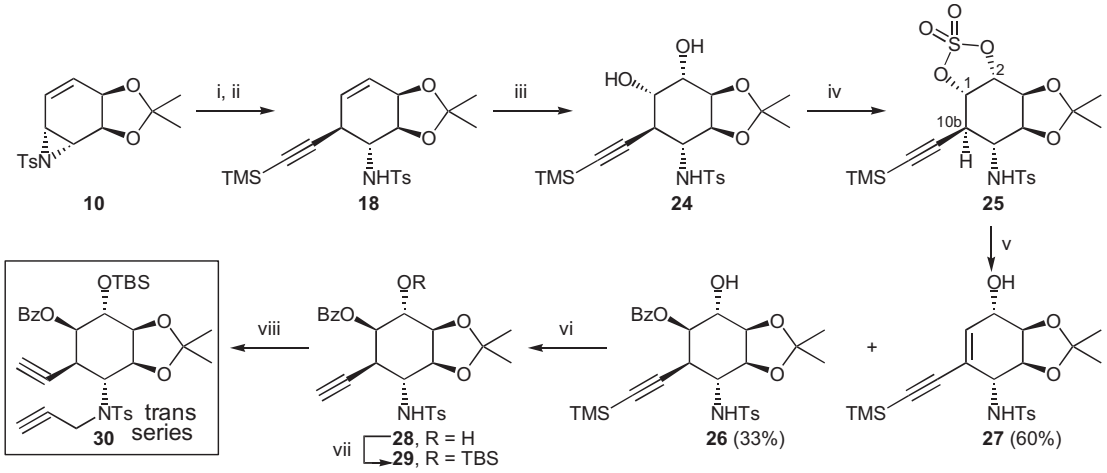
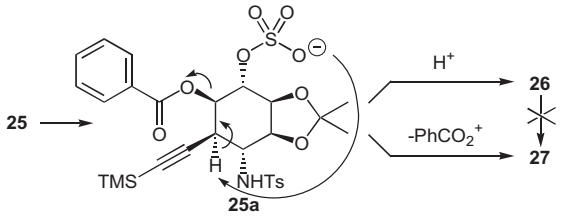


Fig. 4. Generation of enyne **25**.



tained in a manner similar to that employed in the trans series. Overall, the cis series synthesis of phenanthridone **48** proved to be three times higher yielding because of higher selectivity in the cyclic sulfate opening. The eventual synthesis of C-1 epimeric analogs would originate in the cis-diol **24**.

Cyclotrimerization of propargyl amides

To avoid the modest yields of benzylic oxidation in the tetracycles **31** and **37**, we chose to investigate the cyclotrimerization protocol on propargylic amides, which could be easily generated by acylation of tosylamide **18**. Initially, the enyne **45**, obtained by acylation of **18** with propiolic acid anhydride, was chosen for this purpose (as shown in Scheme 6). Cyclotrimerization of this material furnished metal complex **46** in 11% yield and with apparent isomerization of the olefin to the configuration representing 2-deoxylycoricidine. When **47** was synthesized from **40** in 35% yield over two steps (cis series) and subjected to the same optimized conditions for cyclotrimerization, the tetracyclic phenanthridone **48** was obtained in 5% yield. It remains unclear whether these low yields are a function of unfavorable rotamer population of the imides such as **45** or **47** or whether the additional basic oxygen interferes with the catalytic cycle by complexation with the catalyst. Apparently these issues did not prevent the aforementioned cyclotrimerization of amide **22** to the dimeric phenanthridone **23** obtained in 47% yield (Scheme 1).

Synthesis of the bisacetyl derivative of 7-deoxypancratistatin

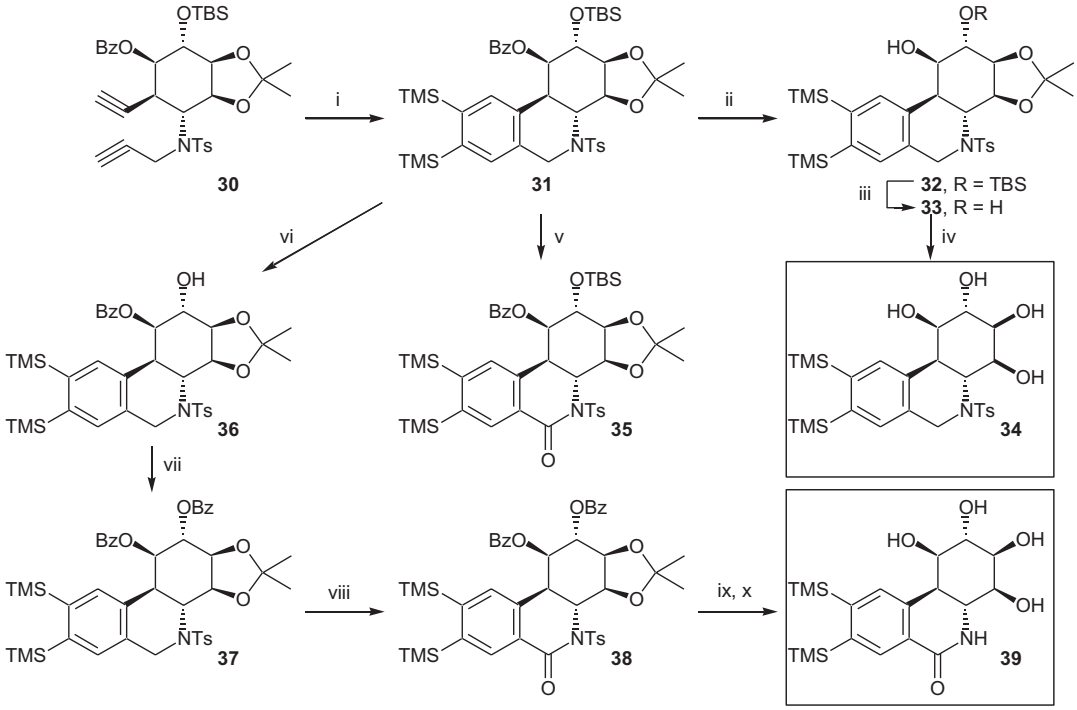
As a prelude to a de novo synthesis of one of the Amaryllidaceae constituents, we decided to prepare the bisacetyl derivative **51** shown in Scheme 7. Both arylsilanes and acetophenones should respond to Tamao oxidation (28) or Baeyer–Villiger oxidation (29), respectively, as means of generating the required oxygenation of the aromatic nucleus. Having noticed the experimental difficulties experienced by Vollhardt and Funk (19) in establishing the phenolic unit in estrone from a TMS group, we thought the bis(acetyl)arene would provide an alternative way to accomplish this task. To this end, the cyclotrimerization of bisacetylene **41** (cis series) was performed with hex-3-yne-2,5-diol protected as a bisTBS ether **49**. Tetracycle **50** was obtained as a mixture of diastereomers in 31% yield. The mixture was treated with tetrabutylammonium fluoride (TBAF) and oxidized to the bisacylated tetracycle **51** in 51% yield over two steps. In future endeavors, the oxidation of this compound to acetyl catechols will be pursued as the means of establishing the C-8/C-9 oxygenation of pancratistatin-type constituents.

Biological evaluation

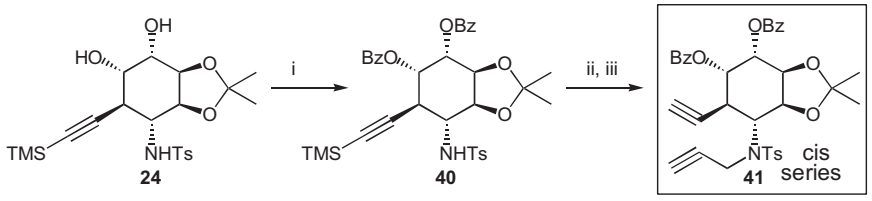
Several of the compounds in both the trans or natural and the C-1 epimeric series were evaluated in the cancer cell line series listed in Table 1. The activity profiles of pancratistatin, 7-deoxypancratistatin, and narciclasine (Table 1, entries 1, 2, and 3, respectively) are shown for comparison, along with two unnatural analogs previously synthesized in our laboratory (Table 1, entries 4 and 5). Some rather surprising and unexpected results were obtained. While the fully protected core of 7-deoxypancratistatin (Table 1, entry 6) is essentially inactive, the partially deprotected intermediates (Table 1, entries 7 and 8), as well as the fully deprotected tetraol (Table 1, entry 9) are quite active, having activities only 10-fold less than those of 7-deoxypancratistatin. This is surprising for several reasons: First, it has been widely held that the phenathridone amide carbonyl is essential for activity, since Chapleur and co-workers (13) demonstrated that

© 2006 NRC Canada

Scheme 3. Cyclotrimerization of the trans scaffold. Reagents and conditions: (*i*) $CpCo(CO)_2$, BTMSA, xylene, 140 °C, 83%; (*ii*) NaOMe, MeOH, rt, 99%; (*iii*) TBAF, THF, rt, 85%; (*iv*) Dowex 50WX8-100, MeOH, 70 °C, 79%; (*v*) $NaIO_4$, $RuCl_3$, CH_3CN–CCl_4–H_2O, rt, 15%; (*vi*) TBAF, THF, rt, 84%; (*vii*) BzCl, pyridine, rt, 86%; (*viii*) $NaIO_4$, $RuCl_3$, Na_2CO_3, CH_3CN–CCl_4–H_2O, rt, 33%; (*ix*) Na-naphthalide, THF, –65 °C, then NaOMe, MeOH, rt, 32%; (*x*) Dowex 50WX8-100, MeOH, 70 °C, 94%.



Scheme 4. Scaffold for cyclotrimerization in the cis or unnatural series. Reagents and conditions: (*i*) BzCl, pyridine, 0 °C to rt, 80%; (*ii*) TBAT, H_3CCN, rt, 76%; (*iii*) NaHMDS, propargyl bromide, $(n\text{Bu})_4NI$, THF, –70 °C to rt, 94%.



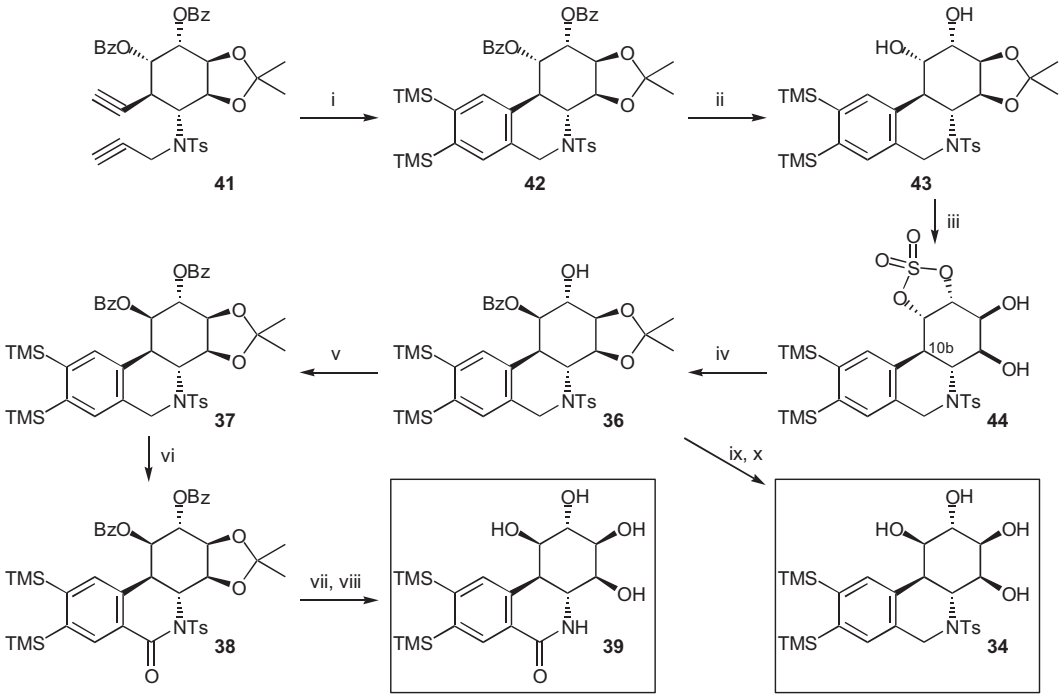
the lactone analogs **5** and **6** are inactive. Second, these compounds represent the first examples of pancratistatin analogs that retain activity despite the absence of all aromatic oxygenation, in addition to lacking the amide moiety. Third, and very surprising, these derivatives have shown greater activity than the fully deprotected bisTMS derivative **39** (Table 1, entry 16) in which the phenanthridone amide is present. This difference in activity may also be ascribed to the fact that a tosyl group is a common pharmacophore and several truncated derivatives of pancratistatin containing tosyl groups were shown to be more active than those lacking it (9*c*). As it has been assumed that the phenolic hydroxyl and the amide may be required as a donor–acceptor pair for hydrogen bonding, our results indicate that these requirements may be offset by other structural features. The only other active compound was the C-1 epimeric diol (Table 1, entry 10), where activity supports the observation that changes at C-1 of the pharmacophore do not drastically alter biological profiles. The fact that four of the intermediates displayed profiles only an order of magnitude lower that those of 7-deoxypancratistatin is promising and will guide us in further design of unnatural analogs with variable functionality in the aromatic core.

Summary and conclusion

The successful synthesis of several analogs of pancratistatin was achieved by the cobalt-catalyzed cyclotrimerization of acetylenic scaffolds with BTMSA and protected 2,5-hex-3-yne. Both configurations at the C-1 hydroxylated aminoinositol unit were examined, with the unnatural, or cis series, being clearly a higher-yielding and more efficient process. The cyclotrimerizations of bisacetylenes with *N*-propargylic substituents were also much higher yielding than the corresponding processes that employed the propargylic amides. The attainment of bisacetyl derivative **51** bodes well for eventual installation of the methylenedioxy unit via the Baeyer–Villiger reaction in a de novo synthesis of 7-

© 2006 NRC Canada

Scheme 5. Cyclotrimerization of the cis scaffold. Reagents and conditions: (*i*) $CpCo(CO)_2$, BTMSA, xylene, 140 °C, 87%; (*ii*) 1% NaOH, MeOH, rt, 99%; (*iii*) SO_2Cl_2, NEt_3, CH_2Cl_2, 0 °C to rt, 70%; (*iv*) $H_5C_6COONH_4$, DMF, 70 °C, 99%; (*v*) BzCl, pyridine, rt, 86%; (*vi*) $NaIO_4$, $RuCl_3$, Na_2CO_3, CH_3CN–CCl_4–H_2O, rt, 33%; (*vii*) Na-naphthalide, THF, –65 °C, then NaOMe, MeOH, rt, 32%; (*viii*) Dowex 50WX8-100, MeOH, 70 °C, 94%; (*ix*) NaOMe, MeOH, rt, 99%; (*x*) Dowex 50WX8-100, MeOH, 70 °C, 79%.

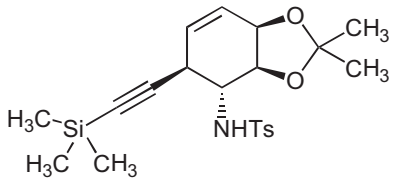


deoxypancratistatin. Based on the surprising and promising results of biological activity, it now seems prudent to proceed further with the preparation of diversely functionalized analogs of Amaryllidaceae constituents.

Experimental section

All nonaqueous reactions were conducted in an argon atmosphere using standard Schlenk techniques for the exclusion of moisture and air. Methylene chloride was distilled from calcium hydride; THF and toluene were dried over potassium/benzophenone. Analytical thin-layer chromatography was performed on Silicycle 60 Å 250 μm TLC plates with F-254 indicator. Flash column chromatography was performed using silica gel 60 (230–400 mesh). Melting points were recorded on a Hoover Unimelt apparatus and are uncorrected. IR spectra were obtained on a PerkinElmer One FT-IR spectrometer. Optical rotation was measured on a PerkinElmer 341 polarimeter at a wavelength of 589 nm. ^1H and ^{13}C NMR spectra were recorded on a 300 MHz Brucker spectrometer. All chemical shifts are referenced to TMS or residual undeuterated solvent ($CHCl_3$). The data for the proton spectra are reported as follows: chemical shift (multiplicity, singlet (s), doublet (d), triplet (t), quartet (q), and multiplet (m), coupling constants (Hz), integration). Carbon spectra were recorded with complete proton decoupling and the chemical shifts are reported in ppm (δ) relative to solvent resonance as internal standard. Combustion analysis were performed by Chemisar Laboratories Inc., Guelph, Ontario. Mass spectra and high-resolution mass spectra were performed by the analytical division at Brock University, St. Catharines, Ontario.

_N_-[(1_R_,2_R_,5_R_,6_S_)-2-(2-Trimethylsilylethynyl)-5,6-(isopropylidenedioxy)cyclohex-3-en-1-yl]-4-methylbenzenesulfonamide (18)

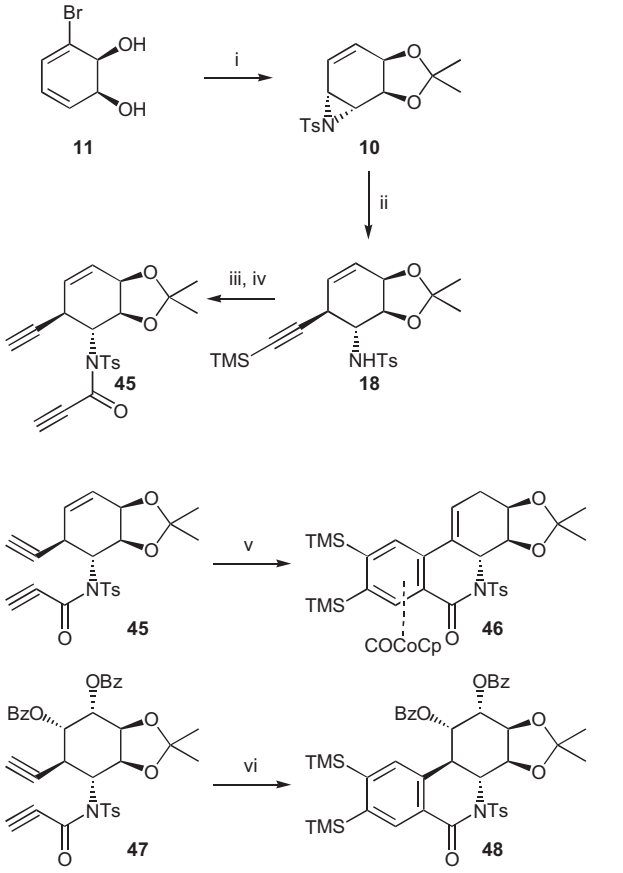


$C_{21}H_{29}NO_4SSi$
419.61 g/mol

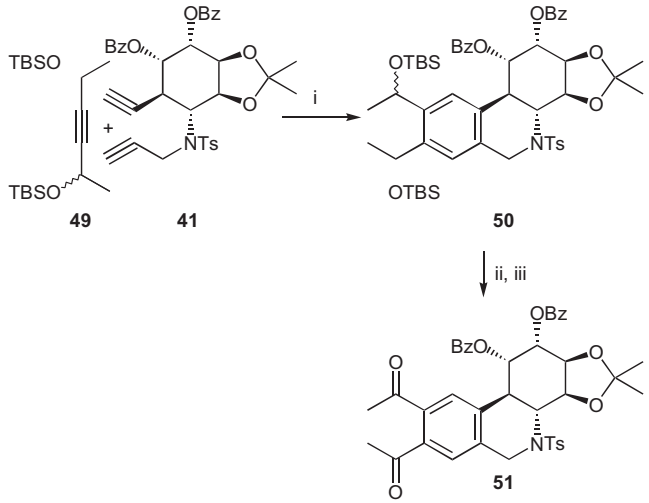
To a solution of of (trimethylsilyl)acetylene (2.75 g, 28.00 mmol) in 40 mL toluene was added BuLi (1.6 mol/L, 17.50 mL, 28.00 mmol) at 0 °C. During the addition, a heavy white precipitate formed. The reaction mixture was stirred at 0 °C for 10 min before $AlCl_3$ (1.24 g, 9.33 mmol) was added. After stirring for a further 10 min, aziridine **10** (1.00 g, 3.11 mmol), dissolved in 5 mL toluene, was added dropwise. Additional $AlCl_3$ (622 mg, 4.67 mmol) was added and the suspension was allowed to warm to room temperature over 18 h. The reaction was quenched by addition of 1 mol/L HCl (100 mL) and diluted with ethyl acetate (50 mL). The layers were separated and the aqueous layer was extracted with ethyl acetate (3 × 50 mL). The combined organic layers were washed with brine (40 mL), dried over

© 2006 NRC Canada

Scheme 6. Propargyl amide series. Reagents and conditions: (*i*) DMP, *p*-TSA, acetone, rt, then PhINTs, $Cu(acac)_2$, H_3CCN, 0 °C to rt, then *n*-Bu_3SnH, AIBN, THF, reflux, 25% over three steps; (*ii*) BuLi, TMS–acetylene, $AlCl_3$, toluene, 0 °C to rt, then DMP, *p*-TSA, acetone, rt, 69% over two steps; (*iii*) BuLi, propiolic acid anhydride, THF, 0 °C to rt, 46%; (*iv*) TBAT, H_3CCN, rt, 61%; (*v*) $CpCo(CO)_2$, BTMSA, xylene, 140 °C, 11%; (*vi*) $CpCo(CO)_2$, BTMSA, xylene, 140 °C, 5%.

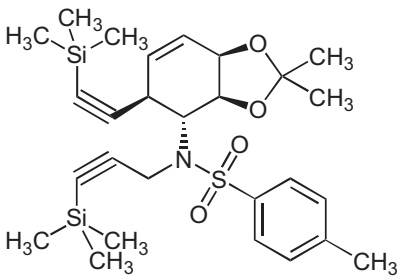


Scheme 7. Bisketone approach. Reagents and conditions: (*i*) $CpCo(CO)_2$, xylene, 140 °C, 31%; (*ii*) TBAF, THF, rt, 72%; (*iii*) IBX, DMSO, rt, 71%.



$MgSO_4$, and the solvent was removed under reduced pressure. Flash column chromatography of the residue (hexanes – ethyl acetate, 2:1 to 1:2) afforded the title compound and the corresponding free diol. The diol was dissolved in 40 mL of acetone and protected by addition of 2,2-dimethoxypropane (486 mg, 4.67 mmol) and *p*-TSA (0.2 g). After 15 min the solution was diluted with ethyl acetate (200 mL), washed with satd. aq. $NaHCO_3$ (3 × 40 mL) and brine (40 mL). The organic phase was dried over $MgSO_4$ and the solvent was removed under reduced pressure affording 900 mg of pure acetonide **18** (2.14 mmol, 69%); mp 168 °C. $[\alpha]^{21}_D$ +30.2 (*c* 0.20, CH_2Cl_2). R_f 0.48 (hexanes – ethyl acetate, 2:1). IR ($CHCl_3$, cm^{-1}) ν: 3269, 3020, 2401, 2176, 1600, 1427, 1375, 1330, 1251, 1216, 1159, 1094, 1075, 972, 928, 846, 759, 669. ^{1}H NMR (300 MHz, $CDCl_3$, ppm) δ: 7.83 (d, *J* = 8.0 Hz, 2H), 7.26 (d, *J* = 7.5 Hz, 2H), 5.83 (m, 2H), 4.63 (d, *J* = 8.0 Hz, 1H), 4.50 (m, 1H), 4.05 (dd, *J* = 8.5, 6.1 Hz, 1H), 3.60 (q, *J* = 8.3 Hz, 1H), 3.14 (d, *J* = 8.4 Hz, 1H), 2.41 (s, 3H), 1.34 (s, 3H), 1.26 (s, 3H), 0.14 (s, 9H). ^{13}C NMR (75 MHz, $CDCl_3$, ppm) δ: 143.2, 138.9, 130.4, 129.4, 127.5, 124.6, 110.1, 103.5, 87.9, 76.5, 71.8, 56.8, 34.6, 27.9, 25.9, 21.6, 0.0. MS (EI) *m*/*z* (relative intensity): 420 (MH^+, 0.6), 419 (M^+, 1.6), 255 (12), 254 (76), 253 (17), 207 (20), 191 (11), 190 (20), 175 (26), 171 (10), 155 (28), 149 (16), 147 (11), 139 (43), 124 (17), 123 (10), 121 (16), 117 (7), 107 (10), 105 (10), 100 (10), 99 (82), 98 (57), 97 (11), 92 (15), 91 (100), 89 (10), 85 (10), 84 (13), 83 (15), 77 (12), 75 (24), 73 (64), 65 (16), 59 (11), 58 (14), 57 (10), 45 (14), 44 (18), 43 (56), 41 (11). HRMS (EI) calcd. for $C_{21}H_{29}O_4NSSi$: 419.1587; found: 419.1582. Anal. calcd. for $C_{21}H_{29}O_4NSSi$: C 60.11, H 6.97; found: C 60.33, H 7.07.

(3a*S*,4*R*,5*R*,7a*R*)-2,2-Dimethyl-4-[4-methylphenyl(3-trimethylsilyl-2-propynyl)sulfonamido]-5-(2-trimetylsilyl-1-ethynyl)-3a,4,5,7a-tetrahydro-1,3-benzodioxole (19)



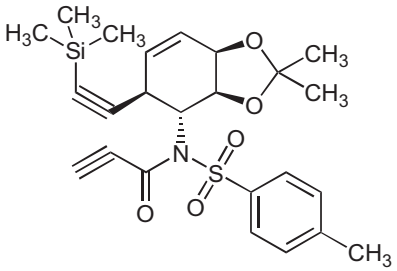
$C_{27}H_{39}NO_4SSi2$
529.84 g/mol

To a solution of of tosylamide **18** (200 mg, 0.48 mmol) in 3 mL THF was added BuLi (1.6 mol/L, 0.30 mL, 0.48 mmol) at 0 °C under argon. The solution was stirred for 5 min and trimethylsilyl propargyl bromide (0.37 mL, 2.38 mmol) and a catalytic amount of N(*n*-Bu)$_4$I were added. The reaction mixture was allowed to stir for 1 h at 0 °C and then it was warmed to room temperature and stirred for 16 h. The reaction was quenched by the addition of satd. aq. NH_4Cl (20 mL) and extracted with ethyl acetate (4 × 20 mL). The combined organic phases were washed with brine (10 mL), dried over $MgSO_4$, and the solvent was

© 2006 NRC Canada

removed under reduced pressure. Flash column chromatography of the residue (hexanes – ethyl acetate, 7:1 to 2:1) afforded sulfonamide **19** (115 mg, 0.22 mmol, 46%) and starting material **18** (40 mg, 20%). R_f 0.63 (hexanes – ethyl acetate, 5:1). IR ($CHCl_3$, cm^{-1}) ν: 2959, 2926, 2180, 1599, 1497, 1381, 1347, 1249, 1216, 1159, 1095 1068, 1016, 1000, 972, 920, 843, 814, 760, 734, 699, 666, 642, 596, 568, 544, 482. ^{1}H NMR (300 MHz, $CDCl_3$, ppm) δ: 8.01 (d, J = 8.3 Hz, 2H), 7.25 (d, J = 8.0 Hz, 2H), 5.91 (m, 2H), 4.62 (m, 2H), 4.17 (m, 1H), 4.10 (d, J = 7.3 Hz, 2H), 3.77 (d, J = 10.5 Hz, 1H), 2.42 (s, 3H), 1.53 (s, 3H), 1.34 (s, 3H), 0.18 (s, 9H), 0.08 (s, 9H). ^{13}C NMR (75 MHz, $CDCl_3$, ppm) δ: 143.0, 138.0, 132.8, 129.1, 128.5, 123.3, 109.8, 104.2, 100.6, 90.5, 88.0, 77.3, 74.0, 72.7, 61.3, 33.2, 28.0, 25.8, 21.6, 0.0, –0.4. MS (EI) *m/z* (relative intensity): 529 (M^+, 0.2), 514 ($M^+ - CH_3$, 4.1), 366 (12), 365 (27), 364 (100), 347 (12), 215 (16), 209 (28), 207 (15), 168 (11), 155 (10), 149 (17), 139 (66), 111 (15), 97 (11), 91 (47), 84 (10), 83 (33), 75 (16), 73 (86), 71 (12), 59 (16), 53 (13), 43 (32). HRMS (EI) calcd. for $C_{27}H_{39}O_4NSSi$: 529.2138; found: 529.2144.

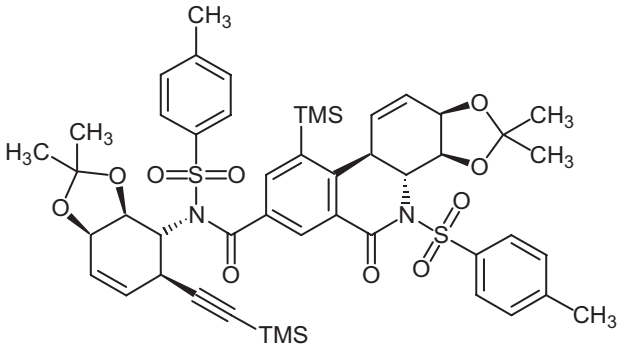
N-[(1*R*,2*R*,5*R*,6*S*)-2-(2-Trimethylsilylethynyl)-5,6-(isopropylidenedioxy)cyclohex-3-en-1-yl]-*N*-propioloyl-4-methylbenzenesulfonamide (22



$C_{24}H_{29}NO_5SSi$
471.64 g/mol

To a solution of of acetonide **18** (250 mg, 0.60 mmol) in 5 mL THF was added BuLi (1.6 mol/L, 0.41 mL, 0.66 mmol) at 0 °C under argon. Propiolic acid anhydride (87 mg, 0.72 mmol) was added and the solution was allowed to warm to room temperature overnight. The reaction was quenched by the addition of satd. aq. NH_4Cl (20 mL) and extracted with ethyl acetate (4 × 20 mL). The combined organic phases were washed with brine (10 mL), dried over $MgSO_4$, and the solvent was removed under reduced pressure. Flash column chromatography of the residue (hexanes – ethyl acetate, 3:1) afforded the tosylamide **22** (128 mg, 0.27 mmol, 46%) as a slightly yellow foam. $[\alpha]^{21}_D$ +29.2 (*c* 0.25, CH_2Cl_2). R_f 0.71 (hexanes – ethyl acetate, 3:1). IR ($CHCl_3$, cm^{-1}) ν: 3297, 3021, 2988, 2961, 2177, 2110, 1932, 1795, 1739, 1675, 1597, 1494, 1457, 1366, 1307, 1250, 1216, 845, 756. ^{1}H NMR (300 MHz, $CDCl_3$, ppm) δ: 8.03 (d, J = 8.1 Hz, 2H), 7.31 (d, J = 8.0 Hz, 2H), 5.98 (m, 2H), 5.11 (m, 1H), 4.74 (m, 2H), 4.25 (d, J = 10.8 Hz, 1H), 3.23 (s, 1H), 2.43 (s, 3H), 1.53 (s, 3H), 1.43 (s, 3H), 0.02 (s, 9H). ^{13}C NMR (75 MHz, $CDCl_3$, ppm) δ: 153.7, 145.2, 136.0, 132.6, 130.1, 129.2, 123.3, 110.6, 103.4, 89.6, 82.7, 75.5, 73.7, 72.8, 65.8, 34.0, 27.9, 25.8, 21.9, –0.2. MS (EI) *m/z* (relative intensity): 471 (MH^+, 0.1), 456 (9), 306 (19), 258 (7), 248 (16), 242 (7), 224 (7), 207 (7), 191 (24), 190 (72), 176 (8), 175 (35), 161 (7), 159 (7), 157 (7), 156 (10), 155 (90), 151 (6), 149 (9), 147 (9), 139 (15), 131 (7), 124 (11), 123 (8), 121 (7), 119 (5), 117 (6), 115 (6), 112 (8), 109 (5), 108 (6), 107 (5), 105 (7), 100 (7), 99 (7), 98 (9), 97 (10), 92 (13), 91 (100), 90 (5), 89 (9), 85 (7), 84 (7), 83 (12), 79 (5), 77 (8), 75 (19), 74 (10), 73 (77), 71 (6), 70 (7), 69 (9), 65 (13), 64 (10), 63 (5), 60 (6), 59 (12), 58 (8), 57 (9), 56 (5), 55 (8), 53 (30), 51 (5), 45 (14), 44 (17), 43 (49), 42 (6), 41 (10). HRMS (EI) calcd. for $C_{21}H_{29}O_4NSSi$: 471.1536; found: 471.1527.

N-[(1*R*,2*R*,5*R*,6*S*)-2-Trimethylsilylethynyl-5,6-(isopropylidenedioxy)cyclohex-3-en-1-yl]-*N*-(4-methylphenylsulfonyl)-(3a*S*,3b*R*,9b*R*,10*R*,11a*S*)-2,2-dimethyl-5-oxo-9-trimethylsilyl-3a,3b,4,5,9b,11a-hexahydro[1,3]dioxolo[4,5-*c*]phenanthridine-10-en-7-carboxamide (23)



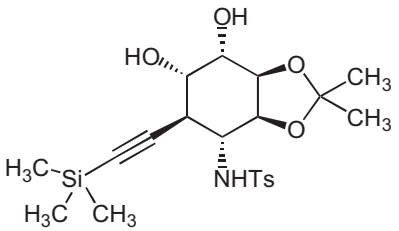
$C_{48}H_{58}N_2O_{10}S_2Si_2$
943.28 g/mol

To a solution of of bis(cyclooctadiene)nickel(0) (15 mg, 0.06 mmol) and triphenylphosphine (57 mg, 0.22 mmol) in 5 mL toluene was added bisacetylene **22** (86 mg, 0.18 mmol), immediately followed by of (trimethylsilyl)acetylene (27 mg, 0.27 mmol, 39 μL) at room temperature under argon. The solution was stirred overnight, quenched by the addition of satd. aq. NH_4Cl (20 mL) and extracted with ethyl acetate (4 × 20 mL). The combined organic phases were washed with brine (10 mL), dried over $MgSO_4$, and the solvent was removed under reduced pressure. Flash column chromatography of the residue (hexanes – ethyl acetate, 5:1) afforded the cyclotrimerized dimer **23** (40 mg, 0.04 mmol, 47%) as a slightly yellow oil. $[\alpha]^{28}_D$ +53.6 (*c* 0.74, $CHCl_3$). R_f 0.64 (hexanes – ethyl acetate, 4:1). IR ($CHCl_3$, cm^{-1}) ν: 3430, 3020, 2172, 1686, 1677, 1598, 1374, 1253, 1216, 1171, 1076, 845, 756. ^{1}H NMR (300 MHz, $CDCl_3$, 50 °C, ppm) δ: 8.30 (d, J = 8.2 Hz, 2H), 7.71 (d, J = 7.9 Hz, 1H), 7.49 (m, 2H), 7.31 (d, J = 8.1 Hz, 2H), 7.16 (m, 2H), 7.08 (d, J = 7.9 Hz, 1H), 5.16 (m, 4H), 5.55 (m, 1H), 4.76 (m, 3H), 4.58 (m, 1H), 4.42 (m, 1H), 4.20 (d, J = 10.8 Hz, 1H), 3.63 (t, J = 10.5 Hz, 1H), 2.45 (s, 3H), 2.43 (s, 3H), 1.38 (m, 12H), 0.49 (s, 9H), 0.16 (s, 9H). MS (EI) *m/z* (relative intensity): 943 (M^+, 0.1), 927 (0.1), 456 (9), 256 (7), 255 (8), 254 (47), 253 (12), 231 (5), 229 (15), 207 (19), 206 (6), 191 (12), 190 (27), 189 (6), 176 (7),

© 2006 NRC Canada

175 (18), 161 (6), 156 (6), 155 (32), 151 (5), 149 (20), 147 (8), 145 (5), 140 (6), 139 (39), 135 (6), 133 (5), 131 (10), 129 (6), 123 (6), 121 (10), 119 (9), 117 (8), 116 (6), 115 (5), 109 (5), 108 (6), 107 (7), 105 (7), 100 (8), 99 (45), 98 (36), 97 (12), 95 (7), 93 (7), 92 (13), 91 (86), 90 (6), 89 (9), 86 (5), 85 (10), 84 (16), 83 (12), 82 (5), 81 (8), 79 (6), 77 (10), 75 (24), 74 (12), 73 (100), 71 (15), 70 (13), 69 (19), 67 (7), 65 (17), 64 (6). HRMS (EI) calcd. for $C_{48}H_{58}O_{10}N_2S_2Si_2$-$CH_3$: 927.2837; found: 927.2824.

(3a*S*,4*R*,5*R*,6*S*,7*S*,7a*S*)-6,7-Dihydroxy-2,2-dimethyl-4-(4-methylphenylsulfonamido)-5-(2-trimethylsilyl-1-ethynyl)perhydro-1,3-benzodioxole (24)

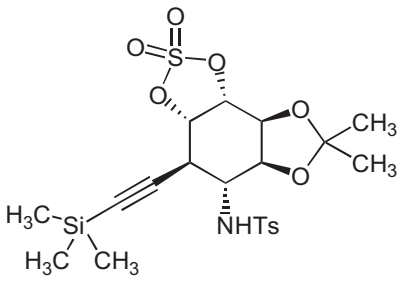


$C_{21}H_{31}NO_6SSi$
453.63 g/mol

To a solution of of (trimethylsilyl)acetylene **18** (1.55 g, 3.68 mmol) in 40 mL CH_2Cl_2 was added *N*-methylmorpholine-*N*-oxide (5.18 mg, 4.42 mmol) and six small crystals of OsO_4. The reaction mixture was stirred for 3 h at room temperature. The reaction was quenched by the addition of satd. aq. $NaHSO_3$ (50 mL), the organic and the aqueous phases were separated, and the aqueous phase was extracted with ethyl acetate (3 × 50 mL). The combined organic phases were washed with brine (20 mL), dried over Na_2SO_4, and the solvent was removed under reduced pressure. Flash column chromatography of the residue (hexanes – ethyl acetate, 1:1) afforded diol **24** (768 mg, 1.69 mmol, 46%) as white crystals (mp 87 °C) and the starting material (488 mg, 1.16 mmol, 32%). $[\alpha]^{21}_D$ +32.5 (*c* 0.45, $CHCl_3$). R_f 0.37 (hexanes – ethyl acetate, 1:1). IR ($CHCl_3$, cm^{-1}) ν: 3684, 3577, 3359, 3020, 2991, 2962, 2903, 2401, 2178, 1731, 1599, 1519, 1423, 1383, 1375, 1334, 1306, 1250, 1216, 1160, 1093, 1066, 929, 848, 814, 771, 669, 627, 598, 557, 512, 460. ^{1}H NMR (300 MHz, $CDCl_3$, ppm) δ: 7.79 (d, *J* = 8.1 Hz, 2H), 7.29 (d, *J* = 8.1 Hz, 2H), 5.80 (d, *J* = 9.4 Hz, 1H), 4.11 (m, 3H), 4.01 (d, *J* = 5.8, 1H), 3.89 (m, 1H), 3.26 (s, 2H), 2.80 (t, *J* = 5.5 Hz, 1H), 2.42 (s, 3H), 1.41 (s, 3H), 1.25 (s, 3H), 0.13 (s, 9H). ^{13}C NMR (75 MHz, $CDCl_3$, ppm) δ: 143.5, 138.4, 129.8, 127.2, 109.5, 102.5, 89.6, 78.1, 77.4, 72.5, 69.9, 54.9, 36.9, 27.9, 25.9, 21.7, 0.0. MS (EI) *m*/*z* (relative intensity): 438 (M^+ – CH_3, 28), 380 (7), 366 (11), 351 (7), 322 (15), 282 (6), 254 (12), 242 (6), 226 (13), 225 (24), 224 (8), 222 (9), 212 (6), 211 (9), 194 (7), 193 (6), 180 (7), 178 (8), 172 (5), 171 (8), 157 (6), 156 (6), 155 (60), 154 (5), 153 (7), 152 (6), 151 (6), 150 (6), 149 (16), 141 (7), 140 (11), 139 (27), 129 (8), 128 (5), 125 (12), 124 (8), 123 (6), 109 (5), 108 (7), 107 (7), 101 (14), 100 (16), 99 (15), 98 (14), 97 (7), 92 (14), 91 (100), 90 (5), 89 (6), 86 (5), 85 (11), 84 (14), 83 (8), 77 (8), 75 (29), 74 (10), 73 (84), 72 (5), 71 (8), 70 (33), 69 (9), 65 (15), 64 (6), 63 (5), 61 (7), 60 (6), 59 (29), 58 (9), 55 (10), 53 (8), 45 (14), 44 (9), 43 (57), 42 (6), 41 (8). HRMS (EI) calcd. for $C_{21}H_{31}O_6NSSi$-CH_3: 438.1407; found: 438.1400. Anal. calcd. for $C_{21}H_{31}O_6NSSi$: C 55.60, H 6.89; found: C 55.20, H 7.02.

(3a*S*,4*R*,5*R*,5a*S*,8a*S*,8b*S*)-*N*-(7,7-Dimethyl-2,2-dioxo-4-trimethylsilanylethynyl hexahydro-1,3,6,8-tetraoxa-2λ^6-thia-*as*-indacen-5-yl)-4-methylbenzenesulfonamide (25)

To a solution of diol **24** (150 mg, 0.33 mmol) in 5 mL dry



$C_{21}H_{29}NO_8S_2Si$
515.67 g/mol

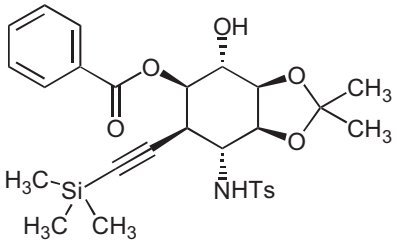
CH_2Cl_2 was added triethylamine (0.37 mL, 2.65 mmol) at 0 °C. The solution was stirred for 10 min and SO_2Cl_2 (0.99 mL, 1.0 mol/L solution, 0.99 mmol) was added dropwise. After the addition, the solution was allowed to warm to room temperature and was stirred for 3 h. Further addition of triethylamine (0.37 mL, 2.65 mmol) and SO_2Cl_2 (0.99 mL, 1.0 mol/L solution, 0.99 mmol) led to total consumption of the starting material (2 h). The reaction mixture was diluted with CH_2Cl_2 (30 mL) and extracted with water (2 × 10 mL). The organic phase was dried over Na_2SO_4, filtered, and the solvent was removed under reduced pressure. Purification by flash column chromatography (hexanes – ethyl acetate, 2:1) afforded cyclic sulfate **25** (140 mg, 0.27 mmol, 82%); mp 169 °C. $[\alpha]^{26}_D$ –51.5 (*c* 1.40, $CHCl_3$). R_f 0.89 (hexanes – ethyl acetate, 3:7). IR ($CHCl_3$, cm^{-1}) ν: 3684, 3617, 3374, 3020, 2964, 2928, 2401, 2182, 1721, 1599, 1520, 1496, 1404, 1334, 1307, 1291, 1252, 1216, 1160, 1093, 1013, 985, 924, 848, 813, 759, 669, 548, 505, 475, 462, 454. ^{1}H NMR (300 MHz, $CDCl_3$, ppm) δ: 7.81 (d, *J* = 8.2 Hz, 2H), 7.28 (d, *J* = 8.3 Hz, 2H), 5.03 (m, 3 H), 4.48 (m, 1H), 4.14 (m, 1H), 3.52 (m, 1H), 3.04 (m, 1H), 2.43 (s, 3H), 1.38 (s, 3H), 1.19 (s, 3H), 0.21 (s, 9H). ^{13}C NMR (75 MHz, $CDCl_3$, ppm) δ: 143.6, 138.3, 129.5, 127.5, 110.6, 98.1, 93.3, 82.4, 80.7, 77.3, 73.4, 54.4, 36.0, 27.4, 25.2, 21.7, –0.2. MS (EI) *m*/*z* (relative intensity): 500 (M^+ – CH_3, 15), 391 (16), 309 (7), 244 (5), 243 (35), 242 (100), 238 (6), 234 (5), 233 (5), 231 (6), 229 (9), 228 (8), 225 (8), 222 (6), 207 (5), 206 (6), 205 (8), 204 (18), 191 (6), 190 (7), 180 (6), 178 (6), 177 (8), 176 (8), 175 (6), 171 (6), 169 (5), 167 (9), 165 (12), 164 (8), 163 (13), 162 (7), 161 (9), 160 (5), 159 (5), 156 (7), 155 (34), 153 (7), 152 (6), 151 (10), 150 (9), 149 (41), 147 (6), 140 (6), 139 (16), 138 (5), 137 (11), 135 (10), 133 (7), 129 (7), 127 (6), 126 (8), 125 (8), 124 (9), 123 (11), 122 (5), 121 (7), 119 (9), 115 (5), 113 (8), 112 (9), 111 (15), 110 (7), 109 (12), 108 (7), 107 (7), 105 (7), 102 (6), 100 (7), 99 (10), 98 (10), 97 (21), 96 (9), 95 (15), 93 (5), 92 (9), 91 (42), 89 (6), 85 (21), 84 (13), 83 (23), 82 (10), 81 (16), 80 (7), 79 (7), 77 (6), 76 (8), 75 (11), 73 (26), 72 (6), 71 (48), 70 (23), 69 (45), 68 (9), 67 (12), 65

© 2006 NRC Canada

(9), 64 (6), 59 (8), 58 (13), 57 (48), 56 (18), 55 (40), 54 (6), 53 (9), 51 (5), 45 (5), 43 (65), 42 (8), 41 (29). HRMS (EI) calcd. for $C_{21}H_{29}O_8NS_2Si$-CH_3: 500.0869; found: 500.0846. Anal. calcd. for $C_{21}H_{29}O_8NS_2Si$: C 48.91, H 5.67; found: C 49.32, H 5.86.

(3a*S*,4*S*,5*R*,6*R*,7*R*,7a*S*)-4-Hydroxy-2,2-dimethyl-7-(4-methylphenylsulfonamido)-5-phenylcarbonyloxy-6-(2-trimethylsilyl-1-ethynyl)perhydro-1,3-benzodioxole (26)

To a solution of cyclic sulfate **25** (462 mg, 0.90 mmol) in 5 mL dry DMF was added ammonium benzoate (312 mg,

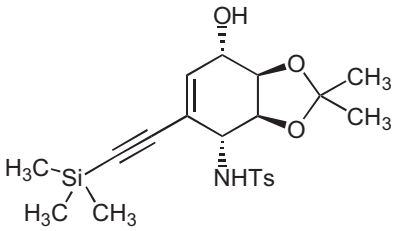


$C_{28}H_{35}NO_7SSi$
557.73 g/mol

2.24 mmol). The reaction mixture was heated to 70 °C for 2 h, then cooled to 40 °C and the DMF was removed under reduced pressure. The residue was suspended in 25 mL THF before 3 drops of H_2O and H_2SO_4 were added. The resulting mixture was stirred for 1.5 h and then quenched with satd. aq. $NaHCO_3$ (25 mL) and diluted with CH_2Cl_2. The aqueous phase was extracted with CH_2Cl_2 (3 × 10 mL). The combined organic phases were dried over Na_2SO_4 and evaporated at reduced pressure. Column chromatography (hexanes – ethyl acetate, 2:1) afforded benzoate **26** (167 mg, 0.30 mmol, 33%); mp 105 °C. $[\alpha]^{22}_D$ –38.4 (*c* 0.98, $CHCl_3$). R_f 0.19 (hexanes – ethyl acetate, 2:1). IR ($CHCl_3$, cm^{-1}) ν: 3275, 2924, 2853, 2323, 2177, 1702, 1601, 1452, 1383, 1332, 1275, 1249, 1219, 1159, 1119, 1093, 1069, 1027, 845, 814, 761, 712, 664, 568, 550. ^{1}H NMR (300 MHz, $CDCl_3$, ppm) δ: 8.07 (d, *J* = 7.2 Hz, 2H), 7.85 (d, *J* = 8.2 Hz, 2H), 7.58 (m, 1H), 7.45 (m, 2H), 7.28 (d, *J* = 7.2 Hz, 2H), 5.75 (d, *J* = 7.1 Hz, 1H), 5.31 (dd, *J* = 4.2, 7.7 Hz, 1H), 4.30 (m, 1H), 4.23 (m, 1H), 4.08 (m, 2H), 3.26 (m, 1H), 3.16 (s, 1H), 2.41 (s, 3H), 1.50 (s, 3H), 1.24 (s, 3H), 0.10 (s, 9H). ^{13}C NMR (75 MHz, $CDCl_3$, ppm) δ: 166.7, 143.7, 138.1, 133.7, 130.3, 129.9, 128.7, 127.6, 110.0, 101.1, 90.5, 78.5, 77.5, 72.2, 70.5, 66.6, 54.3, 36.2, 28.2, 26.0, 21.8, 0.0. MS (EI) *m*/*z* (relative intensity): 542 (M^+ – CH_3, 2.1), 366 (10), 351 (8), 276 (16), 264 (6), 263 (27), 225 (8), 224 (8), 212 (5), 180 (5), 179 (6), 169 (6), 155 (22), 151 (6), 150 (8), 149 (8), 141 (8), 140 (8), 139 (14), 137 (7), 135 (6), 133 (7), 132 (7), 127 (12), 126 (8), 125 (13), 124 (8), 123 (13), 122 (37), 121 (9), 120 (7), 113 (11), 112 (12), 111 (23), 110 (7), 109 (14), 108 (30), 107 (7), 106 (9), 105 (58), 104 (12), 101 (6), 100 (8), 99 (19), 98 (18), 97 (38), 96 (10), 95 (17), 94 (7), 93 (10), 92 (13), 91 (60), 89 (5), 87 (5), 86 (7), 85 (61), 84 (21), 83 (53), 82 (13), 81 (19), 80 (11), 79 (9), 78 (9), 77 (32), 75 (8), 74 (6), 73 (15), 72 (7), 71 (65), 70 (34), 69 (53), 68 (11), 67 (15), 65 (16), 64 (7), 63 (6), 60 (7), 59 (12), 58 (11), 57 (100), 56 (22), 55 (57), 54 (7), 53 (11), 52 (9), 51 (19), 50 (12), 47(6), 45 (11), 44 (27), 43 (94), 42 (15), 41 (38). HRMS (EI) calcd. for $C_{28}H_{35}O_7NSSi$-CH_3: 542.1669; found: 542.1660.

(3a*S*,4*R*,7*S*,7a*R*)-7-Hydroxy-2,2-dimethyl-4-(4-methylphenylsulfonamido)-5-(2-trimethylsilyl-1-ethynyl)-3a,4,7,7a-tetrahydro-1,3-benzodioxole (27)

To a solution of cyclic sulfate **25** (462 mg, 0.90 mmol) in 5 mL dry DMF was added ammonium benzoate (312 mg,



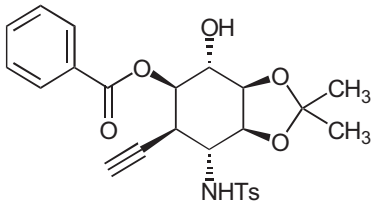
$C_{21}H_{29}NO_5SSi$
435.61 g/mol

2.24 mmol). The reaction mixture was heated to 70 °C for 2 h, then cooled to 40 °C and the excess DMF was removed under reduced pressure. The residue was suspended in 25 mL THF and 3 drops of H_2O and H_2SO_4 were added. The resulting mixture was stirred for 1.5 h, quenched with satd. aq. $NaHCO_3$ (25 mL), and diluted with CH_2Cl_2. The aqueous phase was extracted with CH_2Cl_2 (3 × 10 mL). The combined organic phases were dried over Na_2SO_4 and evaporated at reduced pressure. Column chromatography (hexanes – ethyl acetate, 2:1) afforded allyl alcohol **27** (234 mg, 0.54 mmol, 60%); mp 131 °C. $[\alpha]^{22}_D$ –42.7 (*c* 0.30, $CHCl_3$). R_f 0.33 (hexanes –ethyl acetate, 2:1). IR ($CHCl_3$, cm^{-1}) ν: 3318, 3020, 2928, 2401, 2149, 1726, 1600, 1424, 1384, 1332, 1251, 1216, 1158, 1094, 1060, 926, 865, 846, 814, 771, 669, 603, 550, 515. ^{1}H NMR (300 MHz, $CDCl_3$, ppm) δ: 7.80 (d, *J* = 8.2 Hz, 2H), 7.28 (d, *J* = 8.0 Hz, 2H), 6.37 (d, *J* = 5.2 Hz, 1H), 5.76 (d, *J* = 9.5 Hz, 1H), 4.51 (m, 1H), 4.38 (m, 1H), 4.32 (m, 1H), 3.96 (dd, *J* = 3.2, 9.4 Hz, 1H), 3.16 (s, 1H), 2.42 (s, 3H), 1.33 (s, 3H), 1.28 (s, 3H), 0.22 (s, 9H). ^{13}C NMR (75 MHz, $CDCl_3$, ppm) δ: 143.3, 137.8, 137.3, 129.6, 127.4, 125.0, 109.0, 102.3, 98.0, 77.6, 77.6, 66.2, 53.9, 26.4, 24.5, 21.7, –0.2. MS (EI) *m*/*z* (relative intensity): 420 (M^+ – CH_3, 6), 349 (9), 337 (7), 336 (15), 335 (61), 212 (16), 206 (6), 205 (7), 204 (8), 192 (6), 190 (6), 181 (8), 180 (43), 178 (12), 177 (9), 176 (11), 175 (6), 165 (5), 155 (14), 150 (6), 149 (18), 139 (15), 120 (13), 107 (8), 105 (6), 104 (6), 101 (6), 100 (7), 97 (13), 96 (6), 95 (5), 92 (12), 91 (75), 90 (5), 85 (16), 84 (7), 83 (9), 81 (5), 77 (8), 75 (25), 74 (12), 73 (100), 71 (13), 70 (6), 69 (12), 65 (13), 60 (6), 59 (13), 58 (7), 57 (12), 55 (11), 45 (11), 44 (6), 43 (44), 42 (8), 41 (13). HRMS (EI) calcd. for $C_{21}H_{29}O_5NSSi$: 435.1536; found: 435.1534. Anal. calcd. for $C_{21}H_{29}O_5NSSi$: C 57.90, H 6.71; found: C 57.45, H 7.00.

(3a*S*,4*S*,5*R*,6*R*,7*R*,7a*S*)-4-Hydroxy-2,2-dimethyl-7-(4-methylphenylsulfonamido)-5-phenylcarbonyloxy-6-(1-ethynyl)perhydro-1,3-benzodioxole (28)

To a solution of TMS-protected acetylene **26** (436 mg, 0.78 mmol) in 15 mL dry acetonitrile was added TBAT (633 mg, 1.17 mmol). The reaction mixture was stirred at

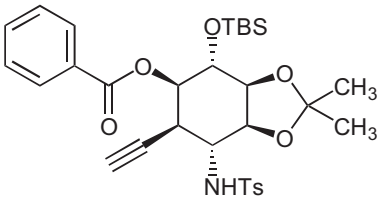
© 2006 NRC Canada



$C_{25}H_{27}NO_7S$
485.55 g/mol

room temperature for 4 h, quenched with satd. aq. NH_4Cl (25 mL), and extracted with ethyl acetate (3 × 20 mL). The combined organic phases were dried over Na_2SO_4, filtered, and evaporated at reduced pressure. Column chromatography (hexanes – ethyl acetate, 1:1) afforded alcohol **28** (318 mg, 0.65 mmol, 84%) as white crystals; mp 103 °C. $[\alpha]^{19}_D$ –23.4 (*c* 0.85, $CHCl_3$). R_f 0.41 (hexanes – ethyl acetate, 1:1). IR ($CHCl_3$, m^{-1}) ν: 440, 3288, 3155, 2988, 2254, 1726, 1697, 1600, 1453, 1375, 1331, 1279, 1247, 1222, 1163, 1119, 1095, 1069, 908, 815, 734, 651, 545.^{1}H NMR (300 MHz, $CDCl_3$, ppm) δ: 8.06 (d, *J* = 7.5 Hz, 2H), 7.84 (d, *J* = 8.2 Hz, 2 H), 7.58 (m, 1H), 7.44 (m, 2H), 7.28 (d, *J* = 8.1 Hz, 2H), 5.59 (d, *J* = 8.0 Hz, 1H), 5.31 (dd, *J* = 3.6, 6.8 Hz, 1H), 4.33 (m, 1H), 4.23 (m, 1H), 4.08 (m, 2H), 3.19 (m, 1H), 3.03 (s, 1H), 2.38 (s, 3H), 2.02 (d, *J* = 2.7 Hz, 1H), 1.51 (s, 3H), 1.24 (s, 3H). ^{13}C NMR (75 MHz, $CDCl_3$, ppm) δ: 166.7, 143.6, 138.2, 133.7, 130.2, 129.7, 129.5, 128.7, 127.6, 109.9, 79.6, 78.5, 77.4, 73.2, 72.4, 69.4, 54.3, 34.6, 28.0, 26.1, 21.7. MS (EI) *m*/*z* (relative intensity): 470 (M^+ – CH_3, 3.2), 377 (6), 362 (5), 263 (7), 225 (8), 179 (16), 155 (17), 150 (7), 139 (9), 134 (8), 132 (5), 123 (5), 122 (24), 108 (8), 106 (13), 105 (100), 92 (8), 91 (48), 85 (6), 80 (6), 78 (7), 77 (34), 75 (8), 73 (11), 71 (5), 70 (11), 69 (7), 65 (11), 59 (7), 58 (5), 57 (8), 55 (8), 53 (5), 51 (13), 50 (7), 45 (7), 44 (13), 43 (25), 41 (11). HRMS (EI) calcd. for $C_{25}H_{27}O_7NS$-CH_3: 470.1273; found: 470.1283. Anal. calcd. for $C_{25}H_{27}O_7NS$: C 61.84, H 5.60; found: C 61.45, H 5.36.

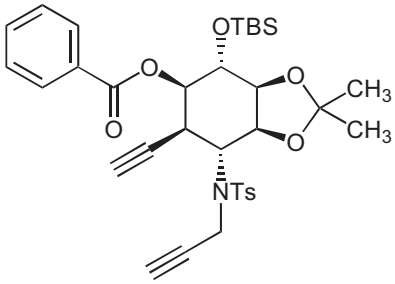
(3a*S*,4*S*,5*R*,6*R*,7*R*,7a*S*)-2,2-Dimethyl-7-(4-methylphenyl-sulfonamido)-4-(*tert*-butyldimethylsilyloxy)-5-phenyl-carbonyloxy-6-(1-ethynyl)perhydro-1,3-benzodioxole (29)



$C_{31}H_{41}NO_7SSi$
599.81 g/mol

To a solution of alcohol **28** (290 mg, 0.60 mmol) in 4 mL dry DMF were added imidazole (204 mg, 2.99 mmol) and TBSCl (451 mg,2.99 mmol). The reaction mixture was stirred at room temperature for 18 h, quenched with water (20 mL) and, after stirring for an additional 10 min, extracted with CH_2Cl_2 (3 × 20 mL). The combined organic phases were dried over Na_2SO_4 and evaporated at reduced pressure. Column chromatography (hexanes – ethyl acetate, 9:1) afforded TBS-protected alcohol **29** (319 mg, 0.53 mmol, 89%) as white crystals; mp 83 °C. $[\alpha]^{19}_D$ –36.9 (*c* 1.20, $CHCl_3$). R_f 0.33 (hexanes – ethyl acetate, 5:1). IR ($CHCl_3$, cm^{-1}) ν: 3309, 3066, 2988, 2955, 2931, 2896, 2859, 2254, 1720, 1601, 1586, 1495, 1472, 1463, 1452, 1383, 1373, 1328, 1272, 1221, 1160, 1112, 1094, 1081, 1054, 1027, 1005, 987, 909, 840, 814, 781, 734, 664, 650, 579, 564, 549, 514, 466. ^{1}H NMR (300 MHz, $CDCl_3$, ppm) δ: 8.08 (d, *J* = 8.2 Hz, 2H), 7.86 (d, *J* = 8.2 Hz, 2H), 7.58 (m, 1H), 7.46 (m, 2H), 7.22 (d, *J* = 8.1 Hz, 2H), 5.29 (d, *J* = 7.5 Hz, 1H), 5.23 (m, 1H), 4.32 (m, 1H), 4.10 (m, 1H), 4.08 (m, 2H), 3.09 (m, 1H), 2.38 (s, 3H), 1.83 (d, *J* = 2.3 Hz, 1H), 1.52 (s, 3H), 1.26 (s, 3H), 0.86 (s, 9H), 0.15 (s, 3H), 0.13 (s, 3H). ^{13}C NMR (75 MHz, $CDCl_3$, ppm) δ: 165.8, 143.1, 139.2, 133.5, 130.1, 129.9, 129.3, 128.6, 127.7, 109.6, 80.1, 78.5, 77.7, 73.8, 72.7, 67.4, 55.0, 33.3, 28.1, 26.2, 25.8, 21.7, 18.1, –4.8, –4.9. MS (EI) *m*/*z* (relative intensity): 584 (M^+ – CH_3, 3.7), 420 (9), 378 (5), 377 (18), 363 (6), 362 (20), 288 (5), 207 (7), 206 (7), 192 (6), 191 (32), 181 (5), 180 (15), 179 (89), 155 (12), 139 (5), 129 (5), 106 (9), 105 (100), 91 (34), 85 (5), 77 (20), 75 (14), 73 (32), 59 (6), 57 (9), 43 (13), 41 (7). HRMS (EI) calcd. for $C_{31}H_{41}O_7NSSi$-CH_3: 584.2138; found: 584.2150. Anal. calcd. for $C_{31}H_{41}O_7NSSi$: C 62.08, H 6.89; found: C 61.86, H 6.64.

(3a*S*,4*S*,5*R*,6*R*,7*R*,7a*S*)-2,2-Dimethyl-7-(4-methylphenyl(2-propynyl)sulfonamido)-4-(*tert*-butyldimethylsilyloxy)-5-phenylcarbonyloxy-6-(1-ethynyl)perhydro-1,3-benzodioxole (30)



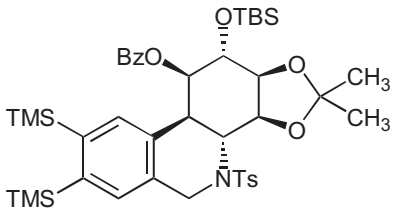
$C_{34}H_{43}NO_7SSi$
637.86 g/mol

To a solution of tosylamide **29** (411 mg, 0.69 mmol) in 11 mL of dry THF was added NaHMDS (0.82 mL, 0.82 mmol) at –70 °C. The reaction mixture was stirred for 0.5 h, while warming up to 0 °C. TMS – propargyl bromide (408 mg, 3.43 mmol) and $(n\text{-Bu})_4NI$ (252 mg, 0.69 mmol) were added. The reaction mixture was stirred at room temperature for 6 h, quenched with satd. aq. NH_4Cl (30 mL), extracted with ethyl acetate (3 × 30 mL), dried over Na_2SO_4, and the solvent was evaporated at reduced pressure. Column chromatography (hexanes – ethyl acetate, 9:1) afforded imide **30** (345 mg, 0.54 mmol, 79%) as colourless foam. $[\alpha]^{19}_D$ –37.5 (*c* 0.24, $CHCl_3$). R_f 0.54 (hexanes – ethyl acetate, 3:1). IR ($CHCl_3$, cm^{-1}) ν: 3309, 3068, 2987, 2956, 2931, 2896, 2859, 2255, 2125, 1722, 1601, 1586, 1495, 1472, 1463, 1453, 1384, 1373, 1351, 1331, 1308, 1269, 1221, 1159, 1095, 1027, 1006, 990, 961, 910, 865, 840, 815, 781, 734, 712, 666, 650, 599, 583, 546, 467. ^{1}H NMR (300 MHz,

© 2006 NRC Canada

$CDCl_3$, ppm) δ: 8.18 (d, *J* = 8.1 Hz, 2H), 8.00 (d, *J* = 8.2 Hz, 2H), 7.59 (m, 1H), 7.47 (m, 2H), 7.28 (d, *J* = 8.1 Hz, 2H), 5.35 (m, 1H), 4.84 (m, 2H), 4.42 (m, 1H), 4.15 (m, 3H), 3.64 (m, 1H), 2.42 (s, 3H), 2.22 (m, 1H), 2.00 (d, *J* = 2.2 Hz, 1H), 1.64 (s, 3H), 1.36 (s, 3H), 0.94 (s, 9H), 0.25 (s, 3H), 0.18 (s, 3H). ^{13}C NMR (75 MHz, $CDCl_3$, ppm) δ: 165.9, 143.5, 137.8, 133.4, 130.2, 129.9, 129.4, 128.6, 128.5, 109.7, 80.5, 78.7, 78.5, 74.9, 74.7, 73.9, 73.0, 66.6, 58.7, 30.9, 28.2, 26.3, 25.8, 25.8, 21.7, 18.1, –4.8, –5.0. MS (EI) *m*/*z* (relative intensity): 622 ($M^+ - CH_3$, 2.6), 522 (7), 401 (6), 400 (19), 245 (7), 222 (9), 192 (7), 191 (35), 181 (6), 180 (15), 179 (94), 167 (7), 155 (18), 150 (7), 149 (23), 139 (15), 137 (8), 135 (6), 129 (8), 122 (5), 113 (6), 111 (6), 109 (5), 106 (9), 105 (100), 97 (10), 95 (8), 92 (9), 91 (48), 85 (14), 84 (6), 83 (14), 81 (10), 77 (19), 75 (13), 73 (41), 71 (18), 70 (12), 69 (23), 67 (6), 66 (6), 65 (7), 59 (6), 57 (34), 56 (12), 55 (22), 53 (5), 43 (27), 41 (21). HRMS (EI) calcd. for $C_{34}H_{43}O_7NSSi$-CH_3: 622.2295; found: 622.2284. Anal. calcd. for $C_{34}H_{43}O_7NSSi$: C 64.02, H 6.79; found: C 63.82, H 6.94.

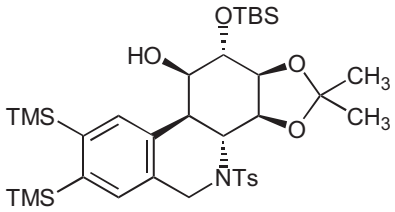
(3a*S*,3b*R*,9b*R*,10*R*,11*S*,11a*S*)-2,2-Dimethyl-4-(4-methylphenylsulfonyl)-10-phenylcarbonyloxy-11-(*tert*-butyldimethylsilyloxy)-7,8-di(trimethylsilyl)-3a,3b,4,5,9b,10,11,11a-octahydro[1,3]dioxolo[4,5-*c*]phenanthridine (31)



$C_{42}H_{61}NO_7SSi_3$
808.26 g/mol

To a solution of $CpCo(CO)_2$ (5 μL) in BTMSA (12 mL) were added dropwise with a syringe pump bisacetylene **30** (324 mg, 0.51 mmol) and $CpCo(CO)_2$ (5 μL) dissolved in xylene (2 mL) and BTMSA (8 mL) at 140 °C over 30 h. During this slow addition, extra catalyst was added directly into the reaction mixture in aliquots: 5 μL after 5 h and 3 μL after 20 and 29 h. The reaction mixture was heated under argon for further 12 h. BTMSA and xylene were removed under high vacuum and the residue was purified by column chromatography (hexanes – ethyl acetate, 9:1). The cyclotrimerized product **31** was isolated as crystalline foam in 83% yield (341 mg, 0.42 mmol); mp 97 °C. $[\alpha]^{22}_D$ +17.6 (*c* 0.65, $CHCl_3$). R_f 0.60 (hexanes – ethyl acetate, 3:1). IR ($CHCl_3$, cm^{-1}) ν: 2956, 2930, 2857, 1724, 1601, 1511, 1452, 1348, 1267, 1251, 1219, 1160, 1109, 957, 839, 757, 712, 670, 627, 560, 536, 515. ^{1}H NMR (300 MHz, $CDCl_3$, ppm) δ: 8.15 (d, *J* = 7.6 Hz, 2H), 7.73 (m, 1H), 7.58 (m, 2H), 7.38 (m, 4H), 6.63 (d, *J* = 7.9 Hz, 2H), 5.96 (s, 1H), 4.85 (m, 2H), 4.49 (m, 4H), 3.12 (d, *J* = 11.9 Hz, 1H), 2.21 (s, 3H), 1.91 (s, 3H), 1.59 (s, 3H), 1.05 (s, 9H), 0.45 (s, 9H), 0.35 (m, 12H), 0.33 (s, 3H). ^{13}C NMR (75 MHz, $CDCl_3$, ppm) δ: 165.6, 145.9, 143.6, 141.9, 137.1, 134.5, 133.2, 132.7, 130.7, 130.1, 129.6, 128.5, 128.4, 127.5, 109.1, 79.4, 77.3, 76.1, 71.6, 68.5, 57.0, 48.5, 35.8, 28.2, 26.1, 25.7, 21.3, 18.0, 1.8, 1.8, –4.9, –5.2. MS (EI) *m*/*z* (relative intensity): 750 ($M^+ - C(CH_3)_3$, 15), 692 (6), 653 (6), 652 (11), 596 (8), 595 (16), 594 (12), 572 (5), 571 (10), 570 (19), 562 (8), 496 (7), 495 (5), 472 (6), 471 (6), 430 (6), 415 (6), 414 (12), 179 (22), 167 (7), 155 (8), 151 (5), 150 (5), 149 (29), 139 (7), 137 (6), 135 (6), 129 (5), 127 (5), 125 (10), 123 (9), 121 (6), 113 (8), 112 (8), 111 (18), 110 (7), 109 (13), 106 (6), 105 (55), 99 (9), 98 (12), 97 (34), 96 (11), 95 (20), 91 (14), 88 (6), 87 (5), 86 (37), 85 (32), 84 (65), 83 (35), 82 (13), 81 (20), 77 (10), 75 (10), 74 (5), 73 (41), 72 (6), 71 (51), 70 (29), 69 (54), 68 (10), 67 (16), 60 (7), 59 (7), 58 (8), 57 (96), 56 (37), 55 (80), 54 (7), 53 (7), 51 (6), 49 (12), 47 (14), 45 (9), 44 (7), 43 (100), 42 (17), 41 (73). HRMS (EI) calcd. for $C_{42}H_{61}O_7NSSi_3$-$C(CH_3)_3$: 750.2772; found: 750.2772.

(3a*S*,3b*R*,9b*R*,10*R*,11*S*,11a*S*)-2,2-Dimethyl-4-(4-methylphenylsulfonyl)-11-(*tert*-butyldimethylsilyloxy)-7,8-di(trimethylsilyl)-3a,3b,4,5,9b,10,11,11a-octahydro[1,3]dioxolo[4,5-*c*]phenanthridin-10-ol (32)



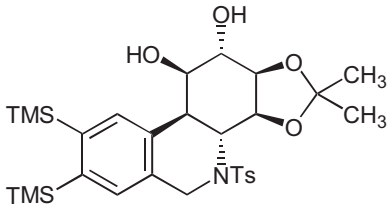
$C_{35}H_{57}NO_6SSi_3$
704.15 g/mol

To a solution of benzoate **31** (110 mg, 0.13 mmol) in 1 mL THF was added 0.5 mL of a 2.25 mol/L solution of freshly prepared sodium methoxide in methanol. The reaction was stirred for 10 min, quenched with NH_4Cl (3 mL), and diluted with ethyl ether (10 mL). The organic phase was separated and washed with $NaHCO_3$ (3 mL) and satd. NaCl solution (3 mL). After drying over $MgSO_4$ and filtration, the solvent was removed under vacuum and the residue was purified by column chromatography (hexanes – ethyl acetate, 3:1). The product **32** was isolated as crystalline foam in 99% yield (88 mg, 0.12 mmol); mp 97 °C. $[\alpha]^{22}_D$ +14.2 (*c* 0.60, CH_2Cl_2). R_f 0.40 (hexanes – ethyl acetate, 3:1). IR (CH_2Cl_2, cm^{-1}) ν: 3516, 2986, 2954, 2931, 2898, 2859, 2253, 1912, 1738, 1599, 1553, 1495, 1471, 1463, 1455, 1407, 1383, 1371, 1361, 1346, 1308, 1250, 1220, 1161, 1122, 1091, 1007, 977, 948, 910, 858, 839, 811, 780, 756, 734, 700, 675, 656, 628, 605, 577, 559, 540, 513, 472. ^{1}H NMR (300 MHz, $CDCl_3$, ppm) δ: 7.36 (d, *J* = 8.1 Hz, 2H), 7.24 (s, 1H), 7.15 (s, 1H), 6.86 (d, *J* = 7.8 Hz, 2H), 5.07 (m, 1H), 4.65 (dd, J_1 = 75.0 Hz, J_2 = 17.1 Hz, 2H), 4.26 (m, 3H), 4.04 (m, 1H), 2.82 (d, *J* = 12.9 Hz, 1H), 2.34 (m, 1H), 2.24 (s, 3H), 1.57 (s, 3H), 1.41 (s, 3H), 0.92 (s, 9H), 0.33 (s, 9H), 0.28 (s, 9H), 0.16 (s, 3H), 0.13 (s, 3H). ^{13}C NMR (75 MHz, $CDCl_3$, ppm) δ: 144.7, 143.7, 142.3, 137.8, 134.0, 133.2, 133.0, 132.2, 128.6, 127.4, 109.4, 79.1, 75.3, 73.5, 69.2, 58.5, 51.4, 36.3, 28.5, 26.1, 25.6, 21.4, 17.9, 1.8, 1.8, –5.0, –5.1. MS (EI) *m*/*z* (relative intensity): 689 ($M^+ - CH_3$, 5), 688 (7), 648 (10), 647 (18), 646 (32), 588 (7), 550 (11), 549 (22), 548 (50), 491 (9), 490 (14), 476 (5), 460 (9), 459

© 2006 NRC Canada

(14), 458 (33), 457 (34), 433 (8), 432 (9), 430 (10), 428 (6), 414 (7), 385 (5), 316 (6), 315 (7), 304 (6), 303 (7), 302 (5), 276 (8), 275 (15), 274 (24), 258 (5), 243 (5), 202 (8), 159 (14), 149 (10), 139 (9), 131 (10), 129 (11), 124 (9), 123 (6), 121 (6), 119 (7), 117 (8), 115 (6), 105 (10), 101 (7), 100 (7), 98 (5), 97 (6), 92 (8), 91 (21), 88 (9), 86 (45), 85 (10), 84 (69), 82 (6), 81 (11), 77 (9), 75 (35), 74 (13), 73 (100), 71 (6), 70 (5), 69 (10), 59 (11), 58 (6), 57 (11), 56 (8), 55 (10), 51 (6), 49 (9), 47 (18), 45 (9), 43 (24), 41 (15). HRMS (EI) calcd. for $C_{35}H_{57}O_6NSSi_3$-CH_3: 688.2980; found: 688.3006. Anal. calcd. for $C_{35}H_{57}O_6NSSi_3$: C 59.70, H 8.16; found: C 59.36, H 7.83.

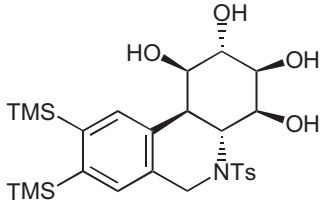
(3a*S*,3b*R*,9b*R*,10*R*,11*S*,11a*S*)-2,2-Dimethyl-4-(4-methylphenylsulfonyl)-7,8-di(trimethylsilyl)-3a,3b,4,5,9b,10,11,11a-octahydro[1,3]dioxolo[4,5-*c*]phenanthridin-10,11-diol (33)



$C_{29}H_{43}NO_6SSi_2$
589.89 g/mol

To a solution of TBS-protected alcohol **32** (49 mg, 0.07 mmol) in 0.1 mL THF was added 84 µL of a 1.0 mol/L solution of TBAF in THF. The reaction was stirred for 10 min at room temperature, quenched with NH_4Cl (3 mL) and diluted with ethyl ether (5 mL). The organic phase was separated and extracted three times with ethyl ether (3 mL). After drying over $MgSO_4$ and filtration, the solvent was removed under vacuum and the residue was purified by column chromatography (pentane –ethyl ether, 3:1). The deprotected diol **33** was isolated as crystalline foam in 85% yield (35 mg, 0.06 mmol); mp 91 °C. $[\alpha]^{22}_D$ +33.7 (*c* 0.39, CH_2Cl_2). R_f 0.57 (hexanes – ethyl acetate, 1:2). IR (CH_2Cl_2, cm^{-1}) ν: 3469, 2987, 2956, 2931, 2253, 1771, 1725, 1634, 1599, 1495, 1453, 1384, 1376, 1342, 1307, 1250, 1221, 1159, 1121, 1091, 1058, 974, 911, 872, 856, 840, 811, 790, 734, 675, 650, 626, 578, 561, 542. ^{1}H NMR (300 MHz, $CDCl_3$, ppm) δ: 7.45 (d, J = 8.4 Hz, 2H), 7.36 (s, 1H), 7.19 (s, 1H), 6.95 (d, J = 8.4 Hz, 2H), 4.88 (dd, J_1 = 8.7 Hz, J_2 = 6.0 Hz, 1H), 4.45 (m, 3H), 4.28 (t, J = 5.4 Hz, 1H), 4.18 (m, 1H), 4.07 (dd, J_1 = 12.0 Hz, J_2 = 8.7 Hz, 1H), 2.88 (dd, J_1 = 12.0 Hz, J_2 = 2.4 Hz, 1H), 2.58 (d, J = 2.7 Hz, 1H), 2.27 (s, 3H), 2.21 (d, J = 4.8 Hz, 1H), 1.58 (s, 3H), 1.37 (s, 3H), 0.32 (s, 9H), 0.30 (s, 9H). ^{13}C NMR (75 MHz, $CDCl_3$, ppm) δ: 145.4, 143.8, 142.5, 137.3, 134.5, 132.9, 132.6, 131.8, 128.9, 127.6, 109.9, 78.3, 76.2, 72.5, 71.4, 57.3, 49.2, 38.4, 28.1, 25.7, 21.5, 1.9, 1.9. MS (EI) *m*/*z* (relative intensity): 574 (M^+ – CH_3, 0.1), 458 (5), 155 (5), 149 (15), 111 (11), 109 (6), 105 (7), 99 (6), 98 (19), 97 (37), 96 (9), 95 (10), 91 (9), 87 (18), 86 (6), 85 (29), 84 (23), 83 (38), 82 (10), 81 (15), 77 (5), 75 (14), 73 (19), 72 (5), 71 (50), 70 (45), 69 (87), 68 (13), 67 (11), 60 (8), 59 (9), 58 (11), 57 (82), 56 (45), 55 (72), 54 (6), 53 (5), 44 (5), 43 (100), 42 (15), 41 (60). HRMS (EI) calcd. for $C_{29}H_{43}O_6NSSi_2$: 589.2350; found: 589.2322. Anal. calcd. for $C_{29}H_{43}O_6NSSi_2$: C 59.05, H 7.35; found: C 58.72, H 6.92.

(1*S*,2*S*,3*S*,4*S*,4a*R*,10b*R*)-5-(4-Methylphenylsulfonyl)-8,9-di(trimethylsilyl)-1,2,3,4,4a,5,6,10b-octahydro-1,2,3,4-phenanthridinetetraol (34)



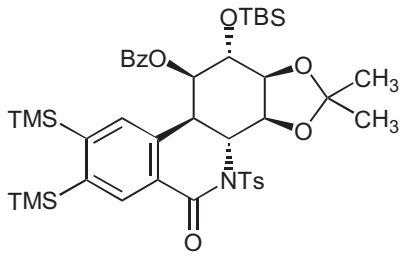
$C_{26}H_{39}NO_6SSi_2$
549.83 g/mol

To a solution of acetonide **33** (27 mg, 0.05 mmol) in MeOH (0.5 mL) was added 1 drop of water and a spatula tip of strong acidic Dowex 50WX8-100 ion exchange resin. The reaction was heated for 4 h at 70 °C, dried by addition of $MgSO_4$, and filtered. The solvent was removed under vacuum and the residue was diluted in $CHCl_3$ and filtered again. After removal of the solvent, the deprotected tetraol **34** was isolated as an oily solid in 79% yield (20 mg, 0.04 mmol). $[\alpha]^{22}_D$ +23.9 (*c* 0.61, CH_2Cl_2). R_f 0.44 (hexanes – ethyl acetate, 1:2). IR (CH_2Cl_2, cm^{-1}) ν: 3410, 2954, 2926, 2902, 2253, 1793, 1646, 1599, 1494, 1450, 1409, 1331, 1307, 1289, 1265, 1249, 1186, 1153, 1122, 1089, 1063, 1020, 970, 909, 856, 840, 811, 735, 673, 650, 629, 582, 565, 539, 481. ^{1}H NMR (300 MHz, $CDCl_3$, ppm) δ: 7.42 (s, 1H), 7.25 (d, J = 6.0 Hz, 2H), 7.14 (s, 1H), 6.85 (d, J = 8.1 Hz, 2H), 4.69 (d, J = 16.2 Hz, 1H), 4.49 (s, 1H), 4.36 (m, 3H), 4.27 (d, J = 10.5 Hz, 1H), 4.03 (m, 1H), 3.57 (brs, 4H) 2.91 (d, J = 11.7 Hz, 1H), 2.21 (s, 3H), 0.32 (s, 9H), 0.28 (s, 9H). ^{13}C NMR (75 MHz, $CDCl_3$, ppm) δ: 145.5, 143.0, 143.0, 134.7, 134.3, 133.9, 132.2, 131.3, 128.9, 127.6, 74.9, 70.8, 70.4, 69.6, 55.3, 47.9, 38.9, 21.4, 1.9, 1.9. MS (EI) *m*/*z* (relative intensity): 534 (M^+ – CH_3, 5), 467 (5), 466 (11), 460 (8), 459 (15), 458 (36), 457 (5), 450 (6), 430 (6), 396 (6), 395 (12), 394 (35), 387 (8), 386 (26), 342 (6), 324 (6), 323 (5), 322 (13), 316 (5), 304 (7), 303 (7), 302 (8), 288 (6), 287 (5), 286 (6), 276 (6), 275 (10), 274 (21), 273 (5), 272 (7), 258 (6), 257 (5), 256 (8), 252 (6), 244 (6), 242 (6), 234 (9), 232 (6), 231 (8), 230 (8), 229 (8), 228 (11), 216 (6), 215 (17), 214 (52), 213 (21), 212 (5), 206 (9), 205 (7), 204 (12), 203 (8), 202 (15), 200 (6), 193 (10), 191 (5), 190 (7), 189 (6), 188 (9), 187 (14), 186 (15), 185 (7), 184 (5), 181 (6), 171 (5), 167 (6), 162 (6), 159 (6), 158 (7), 157 (8), 156 (11), 155 (8), 149 (19), 143 (6), 141 (6), 140 (10), 139 (15), 138 (6), 137 (37), 136 (16), 135 (8), 134 (6), 133 (8), 132 (5), 131 (12), 130 (10), 129 (13), 128 (8), 127 (7), 126 (7), 124 (15), 122 (5), 116 (6), 115 (7), 113 (7), 112 (5), 111 (10), 110 (9), 109 (10), 108 (8), 107 (10), 105 (7), 99 (11), 98 (31), 97 (18), 96 (8), 95 (13), 93 (10), 92 (22), 91 (52), 90 (5), 83 (8), 81 (22), 80 (8), 79 (8), 78 (5), 77 (13), 76 (5), 75 (27), 74 (13), 73 (100), 71 (31), 69 (22), 68 (8), 67 (12), 65 (14), 64 (9), 63 (6), 60 (11), 59 (5), 57 (56), 56 (15), 55 (38), 54

© 2006 NRC Canada

(6), 53 (7), 45 (23), 43 (43), 41 (28). HRMS (EI) calcd. for $C_{26}H_{39}O_6NSSi_2$: 549.2037; found: 549.2031.

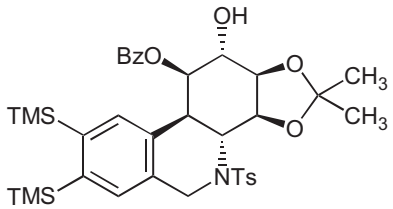
(3a*S*,3b*R*,9b*R*,10*R*,11*S*,11a*S*)-2,2-Dimethyl-4-(4-methylphenylsulfonyl)-5-oxo-10-phenylcarbonyloxy-11-(*tert*-butyldimethylsilyloxy)-7,8-di(trimethylsilyl)-3a,3b,4,5,9b,10,11,11a-octahydro[1,3]dioxolo[4,5-*c*]phenanthridine (35)



$C_{42}H_{59}NO_8SSi_3$
822.24 g/mol

To a suspension of tosylamide **31** (20 mg, 0.02 mmol) in CH_3CN–CCl_4–H_2O (2:2:3, 0.5 mL) were added $NaIO_4$ (22 mg, 0.10 mmol) and a catalytic amount of $RuCl_3 \cdot H_2O$. After 3 h, $NaIO_4$ (15 mg) and another catalytic amount of $RuCl_3 \cdot H_2O$ were added. The reaction mixture was stirred at room temperature overnight. After another addition of $NaIO_4$ (15 mg) and another catalytic amount of $RuCl_3 \cdot H_2O$ the next day, the starting material was fully converted. The heterogeneous reaction was diluted with CH_2Cl_2 (25 mL) and extracted with water. The organic phase was dried with Na_2SO_4, filtered, and purified by flash chromatography (hexanes – ethyl acetate, 2:1). The oxidized product **35** was isolated as colorless oil in 15% yield (3 mg, 0.003 mmol). $[\alpha]^{22}_D$ –97.8 (*c* 0.09, CH_2Cl_2). R_f 0.63 (hexanes – ethyl acetate, 3:1). IR ($CHCl_3$, cm^{-1}) ν: 3055, 2986, 2957, 2930, 2857, 2305, 1721, 1697, 1600, 1581, 1509, 1452, 1422, 1363, 1265, 1221, 1175, 1148, 1108, 1068, 939, 895, 880, 840, 739, 705, 656, 636, 603, 544, 516, 476. ^{1}H NMR (300 MHz, $CDCl_3$, ppm) δ: 8.38 (m, 3H), 7.64 (m, 3H), 7.44 (m, 1H), 7.34 (d, *J* = 8.1 Hz, 2H), 7.24 (m, 2H), 5.93 (s, 1H), 5.74 (m, 1H), 4.57 (m, 1H), 4.44 (s, 1H), 4.34 (m, 1H), 3.94 (m, 1H), 2.45 (s, 3H), 1.41 (s, 3H), 1.39 (s, 3H), 0.99 (s, 9H), 0.32 (s, 3H), 0.25 (m, 21H). MS (EI) *m*/*z* (relative intensity): 764 (M^+ – $C(CH_3)_3$, 4), 610 (7), 445 (5), 432 (6), 431 (11), 430 (25), 422 (5), 421 (12), 358 (6), 356 (9), 332 (10), 331 (28), 307 (9), 302 (7), 217 (5), 215 (7), 189 (8), 181 (6), 180 (11), 179 (43), 169 (6), 167 (10), 165 (5), 155 (8), 151 (7), 150 (8), 141 (9), 140 (7), 139 (11), 137 (8), 135 (10), 129 (8), 127 (8), 126 (6), 125 (11), 124 (11), 123 (16), 122 (9), 121 (20), 119 (24), 117 (9), 113 (9), 112 (10), 111 (21), 110 (8), 109 (16), 107 (7), 106 (10), 105 (100), 100 (7), 99 (13), 98 (16), 97 (38), 96 (13), 95 (25), 93 (8), 92 (11), 91 (35), 89 (6), 88 (98), 87 (12), 86 (37), 85 (55), 84 (44), 83 (46), 82 (36), 81 (32), 80 (6), 79 (9), 78 (5), 77 (27), 76 (6), 75 (14), 74 (10), 73 (73), 72 (11), 71 (65), 70 (44), 69 (71), 68 (14), 67 (20), 65 (10). HRMS (EI) calcd. for $C_{42}H_{59}O_8NSSi_3$-$C(CH_3)_3$: 764.2565; found: 764.2597. HRMS (EI) calcd. for $C_{42}H_{59}O_8NSSi_3$-CH_3: 806.3034; found: 806.3073.

(3a*S*,3b*R*,9b*R*,10*R*,11*S*,11a*S*)-11-Hydroxy-2,2-dimethyl-4-(4-methylphenylsulfonyl)-10-phenylcarbonyloxy-7,8-di(trimethylsilyl)-3a,3b,4,5,9b,10,11,11a-octahydro[1,3]dioxolo[4,5-*c*]phenanthridine (36)



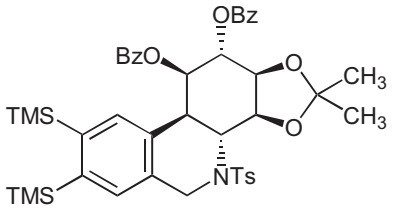
$C_{36}H_{47}NO_7SSi_2$
694.00 g/mol

To a solution of cyclic sulfate **44** (344 mg, 0.53 mmol) in dry DMF (8 mL) was added ammonium benzoate (184 mg, 1.32 mmol). The reaction mixture was heated to 70 °C for 2 h, then cooled to 40 °C, and the DMF was removed under reduced pressure. The residue was suspended in THF (8 mL) before 1 drop each of H_2O and H_2SO_4 were added. The resulting mixture was stirred for 1.5 h and then quenched with satd. aq. $NaHCO_3$ (30 mL) and diluted with CH_2Cl_2. The aqueous phase was extracted with CH_2Cl_2 (3 × 30 mL). The combined organic phases were dried over Na_2SO_4, filtered, and evaporated at reduced pressure. Benzoate **36** (410 mg, 0.59 mmol, 99%) was obtained as foamy white crystals and used without further purification; mp 91 °C. $[\alpha]^{27}_D$ +63.7 (*c* 1.00, CH_2Cl_2). R_f 0.38 (hexanes – ethyl acetate, 2:1). IR (CH_2Cl_2, cm^{-1}) ν: 3019, 2954, 2401, 1719, 1602, 1494, 1452, 1384, 1346, 1318, 1269, 1250, 1216, 1159, 1115, 1091, 1070, 955, 876, 841, 810, 757, 714, 669, 627, 564, 456. ^{1}H NMR (300 MHz, $CDCl_3$, ppm) δ: 7.92 (d, *J* = 8.1 Hz, 2H), 7.59 (t, *J* = 7.5 Hz, 1H), 7.43 (t, *J* = 7.5 Hz, 2H), 7.32 (d, *J* = 7.2 Hz, 2 H), 7.18 (d, *J* = 7.8 Hz, 2 H), 6.59 (d, *J* = 8.1 Hz, 2 H), 5.87 (m, 1 H), 4.66 (m, 2H), 4.35 (m, 4H), 3.04 (m, 2H), 2.10 (s, 3H), 1.71 (s, 3H), 1.40 (s, 3H), 0.28 (s, 9H), 0.12 (s, 9H). ^{13}C NMR (75 MHz, $CDCl_3$, ppm) δ: 166.8, 146.0, 143.9, 142.2, 137.2, 134.8, 133.7, 132.8, 132.4, 130.8, 129.9, 128.8, 128.7, 127.7, 109.8, 78.3, 76.9, 73.0, 71.0, 56.7, 47.6, 37.0, 29.9, 28.1, 25.9, 21.6, 1.9, 1.8. MS (EI) *m*/*z* (relative intensity): 693 (2), 484 (8), 472 (9), 471 (23), 317 (12), 316 (37), 285 (5), 169 (20), 155 (6), 149 (8), 147 (6), 139 (5), 123 (8), 122 (44), 121 (5), 119 (14), 111 (6), 106 (7), 105 (74), 97 (10), 95 (7), 91 (22), 88 (11), 86 (63), 85 (12), 84 (100), 83 (11), 82 (9), 81 (10), 78 (6), 77 (44), 75 (9), 74 (10), 73 (56), 71 (12), 70 (7), 69 (26), 67 (7), 65 (6), 60 (6), 59 (8), 57 (21), 56 (7), 55 (19), 52 (5), 51 (25), 50 (13), 49 (21), 47 (25), 45 (12), 44 (8), 43 (34), 42 (6), 41 (18). HRMS (EI) calcd. for $C_{36}H_{47}O_7NSSi_2$: 693.9979; found: 693.2603. Anal. calcd. for $C_{36}H_{47}O_7NSSi_2$: C 62.30, H 6.83; found: C 62.18, H 6.70.

(3a*S*,3b*R*,9b*R*,10*R*,11*S*,11a*S*)-2,2-Dimethyl-4-(4-methylphenylsulfonyl)-10,11-di(phenylcarbonyloxy)-7,8-di(trimethylsilyl)-3a,3b,4,5,9b,10,11,11a-octahydro[1,3]dioxolo[4,5-*c*]phenanthridine (37)

To a solution of of alcohol **36** (142 mg, 0.21 mmol) in pyridine (1 mL) was added benzoyl chloride (35 μL,

© 2006 NRC Canada

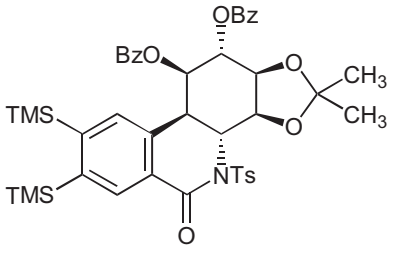


$C_{43}H_{51}NO_8SSi_2$
798.10 g/mol

0.31 mmol) at 0 °C. The ice bath was removed and the reaction mixture was stirred for 4 h at room temperature. The reaction was quenched with 5 drops of MeOH, diluted with ethyl acetate (50 mL), and washed with 1.0 mol/L HCl (2 × 20 mL) and brine (20 mL). The organic phase was dried over Na_2SO_4, filtered, and the solvent was removed under reduced pressure. Flash column chromatography of the residue (hexanes – ethyl acetate, 5:1) afforded dibenzoate **37** (140 mg, 0.18 mmol, 86%) as foamy white crystals; mp 107 °C. $[\alpha]^{25}_D$ –12.7 (*c* 1.39, CH_2Cl_2). R_f 0.62 (hexanes – ethyl acetate, 2:1). IR ($CHCl_3$, cm^{-1}) ν: 3020, 2954, 1726, 1602, 1585, 1493, 1452, 1407, 1384, 1373, 1349, 1316, 1249, 1218, 1170, 1159, 1093, 1070, 1027, 983, 954, 858, 841, 811, 711, 670, 627, 578, 562, 550, 532, 514, 462. ^{1}H NMR (300 MHz, $CDCl_3$, ppm) δ: 8.10 (m, 4H), 7.59 (m, 2H), 7.48 (m, 4H), 7.25 (m, 4H), 6.45 (d, *J* = 8.1 Hz, 2H), 6.21 (s, 1H), 5.74 (t, *J* = 2.4 Hz, 1H), 4.77 (d, *J* = 16.5 Hz, 1H), 4.71 (dd, J_1 = 5.4 Hz, J_2 = 10.2 Hz, 1H), 4.50 (m, 2H), 4.34 (d, *J* = 16.2 Hz, 1H), 3.04 (d, *J* = 11.7 Hz, 1H), 2.05 (s, 3H), 1.84 (s, 3H), 1.47 (s, 3H), 0.31 (s, 9H), 0.20 (s, 9H). ^{13}C NMR (75 MHz, $CDCl_3$, ppm) δ: 165.1, 164.3, 146.3, 144.0, 141.9, 136.6, 134.6, 133.6, 133.4, 132.6, 131.9, 130.3, 130.1, 129.8, 129.7, 128.8, 128.5, 128.4, 128.4, 128.3, 127.4, 109.8, 76.3, 70.0, 68.3, 56.1, 47.4, 38.0, 27.9, 25.9, 21.3, 1.7, 1.6. MS (EI) *m*/*z* (relative intensity): 798 (M^+, 4), 797 (6), 642 (6), 476 (7), 340 (7), 179 (5), 149 (5), 123 (6), 122 (31), 106 (8), 105 (100), 97 (8), 95 (5), 91 (10), 84 (6), 83 (9), 77 (37), 74 (6), 73 (23), 71 (10), 70 (5), 69 (10), 67 (6). HRMS (EI) calcd. for $C_{43}H_{51}O_8NSSi_2$: 797.2874; found: 797.2863. Anal. calcd. for $C_{43}H_{51}O_8NSSi_2$: C 64.71, H 6.44; found: C 64.71, H 6.50.

(3a*S*,3b*R*,9b*R*,10*R*,11*S*,11a*S*)-2,2-Dimethyl-4-(4-methylphenylsulfonyl)-5-oxo-10,11-di(phenylcarbonyloxy)-7,8-di(trimethylsilyl)-3a,3b,4,5,9b,10,11,11a-octahydro[1,3]dioxolo[4,5-*c*]phenanthridine (38)

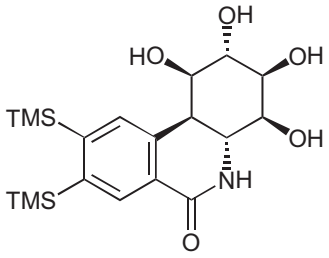
To a suspension of tosylamide **37** (141 mg, 0.18 mmol) in CH_3CN–CCl_4–H_2O (4:4:3, 11 mL) was added a solution of



$C_{43}H_{49}NO_9SSi_2$
812.09 g/mol

Na_2CO_3 (60 mg) and $NaIO_4$ (340 mg, 1.59 mmol) in H_2O (3 mL). A catalytic amount of $RuCl_3 \cdot H_2O$ (1 mg) was added and the reaction was stirred at room temperature. After 3 h, the same amount of $NaIO_4$ buffered with Na_2CO_3 and another catalytic amount of $RuCl_3 \cdot H_2O$ were added. The reaction mixture was stirred at room temperature overnight. After another addition of the same amount of oxidant the next day and one additional hour, the starting material was fully converted. The heterogeneous reaction was diluted with CH_2Cl_2 (25 mL) and washed with water and brine. The organic phase was dried with Na_2SO_4, filtered, and purified by flash chromatography (hexanes – ethyl acetate, 3:1). The oxidized product **38** was isolated as colorless oil in 33% yield (48 mg, 0.059 mmol); mp 105 °C. $[\alpha]^{23}_D$ –72.5 (*c* 0.65, CH_2Cl_2). R_f 0.74 (hexanes – ethyl acetate, 2:1). IR (CH_2Cl_2, cm^{-1}) ν: 3057, 2956, 2927, 2856, 2306, 1968, 1729, 1698, 1600, 1582, 1494, 1452, 1365, 1315, 1266, 1221, 1176, 1093, 1070, 1027, 955, 857, 843, 740, 710, 666, 637, 608, 587, 545. ^{1}H NMR (300 MHz, $CDCl_3$, ppm) δ: 8.35 (s, 1H), 8.34 (d, *J* = 6.9 Hz, 2H), 8.11 (d, *J* = 6.9 Hz, 2H), 7.62 (m, 3H), 7.48 (m, 4H), 7.34 (d, *J* = 8.4 Hz, 2H), 7.25 (m, 2H), 6.17 (t, *J* = 3.3 Hz, 1H), 5.82 (t, *J* = 3.6 Hz, 1H), 5.70 (dd, J_1 = 5.7 Hz, J_2 = 8.4 Hz, 1H), 4.69 (dd, J_1 = 8.7 Hz, J_2 = 12.6 Hz, 1H), 4.52 (m, 1H), 3.94 (dd, J_1 = 3.3 Hz, J_2 = 12.6 Hz, 1H), 2.45 (s, 3H), 1.47 (s, 3H), 1.40 (s, 3H), 0.25 (s, 9H), 0.19 (s, 9H). ^{13}C NMR (75 MHz, $CDCl_3$, ppm) δ: 166.9, 165.1, 164.6, 154.8, 146.0, 144.1, 138.5, 135.6, 133.8, 133.3, 131.6, 130.0, 129.6, 129.1, 129.0, 128.9, 128.7, 128.2, 127.3, 109.9, 74.6, 73.5, 68.8, 68.5, 63.0, 40.1, 28.3, 26.1, 21.7, 1.6, 1.3 (two signals missing). MS (EI) *m*/*z* (relative intensity): 796 (M^+ – CH_3, 0.4), 477 (6), 356 (5), 355 (6), 331 (6), 179 (6), 122 (5), 106 (8), 105 (100), 97 (7), 91 (13), 85 (6), 83 (8), 81 (7), 77 (19), 73 (19), 71 (8), 69 (14), 67 (5). HRMS (EI) calcd. for $C_{43}H_{49}O_9NSSi_2$-CH_3: 796.2432; found: 796.2444.

(1*R*,2*S*,3*S*,4*S*,4a*R*,10b*R*)-1,2,3,4-Tetrahydroxy-8,9-di(trimethylsilyl)-1,2,3,4,4a,5,6,10b-octahydro-6-phenanthridinone (39)



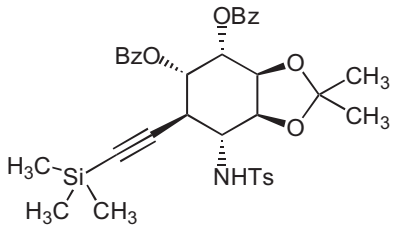
$C_{19}H_{31}NO_5Si_2$
409.62 g/mol

To a solution of of tosylate **38** (39 mg, 0.05 mmol) in THF (0.5 mL) under argon was added a 0.4 mol/L solution of sodium naphthalide (at –65 °C) until the green colour persisted. The reaction was quenched with satd. aq. NH_4Cl and extracted with CH_2Cl_2 (6 × 10 mL). The combined organic phases were dried over $MgSO_4$, filtered, and the organic solvent was removed under reduced pressure. The residue was dissolved in MeOH. After addition of a 2.25 mol/L solution

© 2006 NRC Canada

of sodium methoxide (64 μL), the reaction mixture was stirred for 20 min. The solution was quenched with satd. aq. NH_4Cl and extracted with CH_2Cl_2 (6 × 10 mL). The combined organic phases were dried over $MgSO_4$, filtered, and the organic solvent was removed under vacuum. Flash column chromatography of the residue (pentane – diethyl ether, 1:2) afforded a diol (7 mg, 0.02 mmol, 32%). The diol (6 mg, 0.01 mmol) was dissolved in MeOH and heated to reflux for 4 h after addition of a spatula tip of Dowex 50WX8-100. The ion exchange resin was removed by filtration and the solvent was removed under reduced pressure. Flash column chromatography of the residue ($CHCl_3$–MeOH, 6:1) afforded tetraol **39** (5 mg, 0.01 mmol, 25% over three steps); mp 213 °C. $[\alpha]^{23}_D$ +60.5 (*c* 0.15, MeOH). R_f 0.38 ($CHCl_3$–MeOH, 6:1). IR ($CHCl_3$, cm^{-1}) ν: 3385, 2953, 2926, 1705, 1652, 1600, 1586, 1447, 1410, 1375, 1318, 1250, 1217, 1155, 1128, 1093, 1055, 955, 857, 838, 757, 667, 630, 572, 549. ^{1}H NMR (300 MHz, CD_3OD, ppm) δ: 8.31 (s, 1H), 7.79 (s, 1H), 4.87 (s, 5H), 4.61 (m, 1H), 4.22 (t, *J* = 3.3 Hz, 1H), 4.05 (m, 1H), 3.95 (m, 2H), 3.33 (m, 1H), 0.41 (s, 9H), 0.40 (s, 9H). ^{13}C NMR (75 MHz, $CDCl_3$, ppm) δ: 168.3, 153.0, 145.3, 139.0, 134.9, 132.7, 129.1, 75.1, 72.1, 72.0, 70.2, 51.6, 41.1, 2.0, 1.9. MS (ESI) *m/z* (relative intensity): 454 ([M + formate]$^-$, 72), 444 ([M + Cl]$^-$, 100), 408 ([M – H]$^-$, 2), 394 (7), 311 (5), 265 (8), 171 (17), 111 (7), 89 (12). HRMS (ESI) calcd. for $C_{42}H_{61}O_7NSSi_3$ + Cl^-: 444.1429; found: 444.1429.

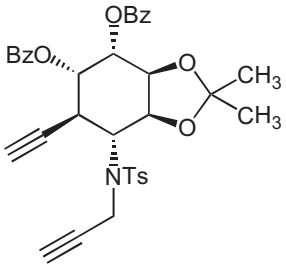
(3a*S*,4*S*,5*S*,6*R*,7*R*,7a*S*)-2,2-Dimethyl-7-(4-methylphenylsulfonamido)-4,5-di(phenylcarbonyloxy)-6-(2-trimethylsilyl-1-ethynyl)perhydro-1,3-benzodioxole (40)



$C_{35}H_{39}NO_8SSi$
661.84 g/mol

To a solution of of diol **24** (721 mg, 1.59 mmol) in pyridine (5 mL) was added benzoyl chloride (0.44 mL, 3.82 mmol) at 0 °C. The ice bath was removed and the reaction mixture was stirred for 1.5 h at room temperature. The reaction was quenched with 10 drops of MeOH, diluted with ethyl acetate (150 mL), and washed with 1.0 mol/L HCl (3 × 20 mL), water (20 mL), and brine (20 mL). The organic phase was dried over Na_2SO_4 and the solvent was removed under reduced pressure. Flash column chromatography of the residue (hexanes – ethyl acetate, 6:1 to 3:1) afforded dibenzoate **40** (840 mg, 1.27 mmol, 80%) as white crystals; mp 149 °C. $[\alpha]^{23}_D$ –99.9 (*c* 4.50, CH_2Cl_2). R_f 0.71 (hexanes – ethyl acetate, 2:1). IR ($CDCl_3$, cm^{-1}) ν: 3673, 3264, 3066, 3034, 2988, 2961, 2938, 2901, 2255, 2183, 1966, 1911, 1728, 1601, 1585, 1493, 1452, 1384, 1374, 1329, 1316, 1274, 1248, 1222, 1162, 1094, 1070, 1026, 1003, 910, 848, 814, 792, 734, 711, 686, 662, 650, 575, 548, 512, 466. ^{1}H NMR (300 MHz, $CDCl_3$, ppm) δ: 7.95 (m, 4H), 7.79 (d, *J* = 8.1 Hz, 2H), 7.56 (m, 2H), 7.42 (m, 4H), 7.28 (d, *J* = 8.4 Hz, 2H), 5.86 (dd, J_1 = 2.7 Hz, J_2 = 4.2 Hz, 1H), 5.68 (dd, J_1 = 2.7 Hz, J_2 = 8.1 Hz, 1H), 5.04 (d, *J* = 7.5, 1H), 4.38 (m, 2H), 3.87 (m, 1H), 3.23 (t, *J* = 7.8 Hz, 1H), 2.42 (s, 3H), 1.51 (s, 3H), 1.31 (s, 3H), 0.06 (s, 9H). ^{13}C NMR (75 MHz, $CDCl_3$, ppm) δ: 165.3, 165.3, 143.6, 138.8, 133.9, 133.7, 130.1, 130.1, 129.8, 129.7, 129.6, 128.9, 128.8, 127.6, 110.6, 101.6, 90.5, 78.1, 75.1, 71.8, 69.7, 57.4, 36.4, 28.1, 26.3, 21.9, 0.0. MS (EI) *m/z* (relative intensity): 646 (M^+ – CH_3, 3), 282 (6), 214 (11), 155 (7), 122 (9), 106 (10), 105 (100), 91 (15), 77 (21), 73 (8), 69 (9), 57 (6), 55 (6), 43 (11), 41 (6). HRMS (EI) calcd. for $C_{35}H_{39}O_8NSSi$: 661.2166; found: 661.2158. Anal. calcd. for $C_{35}H_{39}O_8NSSi$: C 63.52, H 5.94; found: C 63.97, H 5.95.

(3a*S*,4*S*,5*S*,6*R*,7*R*,7a*S*)-6-(1-Ethynyl)-2,2-dimethyl-7-[4-methylphenyl(propynyl)sulfonamido]-4,5-di(phenylcarbonyloxy)perhydro-1,3-benzodioxole (41)



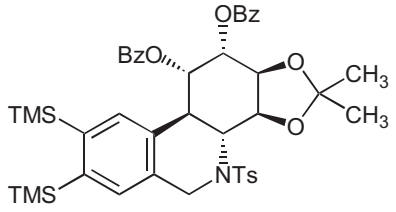
$C_{35}H_{33}NO_8S$
627.70 g/mol

To a solution of TMS-protected acetylene **40** (976 mg, 1.48 mmol) in dry acetonitrile (35 mL) was added TBAT (1.19 g, 2.21 mmol). The reaction mixture was stirred at room temperature for 1.5 h, quenched with satd. aq. NH_4Cl (50 mL), and extracted with ethyl acetate (3 × 50 mL). The combined organic phases were dried over Na_2SO_4 and evaporated at reduced pressure. Column chromatography (hexanes – ethyl acetate, 4:1 to 2:1) afforded unprotected acetylene (664 mg, 1.13 mmol, 76%) as white crystals. To these crystals (418 mg,0.71 mmol) dissolved in THF (2 mL) was added NaHMDS (1.0 mol/L, 0.85 mL, 0.85 mmol) at –70 °C under argon. The reaction mixture was allowed to warm up to 0 °C over a period of 20 min and was further stirred for 10 min at this temperature. Propargyl bromide (422 mg, 3.54 mmol) and $(n\text{Bu})_4NI$ (262 mg, 0.71 mmol) were added and the solution was allowed to warm to room temperature overnight. The reaction was quenched by addition of satd. aq. NH_4Cl (40 mL) and extracted with ethyl acetate (4 × 40 mL). The combined organic phases were washed with brine (20 mL), dried over $MgSO_4$, and the solvent was removed under reduced pressure. Flash column chromatography of the residue (hexanes – ethyl acetate, 3:2) afforded tosylamide **41** (419 mg, 0.67 mmol, 94%; 71% over two steps) as crystalline foam ; mp 86 °C. $[\alpha]^{23}_D$ –99.0 (*c* 1.40, CH_2Cl_2). R_f 0.29 (hexanes – ethyl acetate, 3:1). IR (CH_2Cl_2, cm^{-1}) ν: 3300, 3064, 2988, 2939, 2593, 2126, 1918, 1732, 1602, 1586, 1494, 1452, 1386, 1374, 1352,

© 2006 NRC Canada

1328, 1274, 1247, 1222, 1157, 1097, 1071, 1037, 1003, 921, 894, 854, 817, 736, 710, 667, 578, 564, 545, 526, 460. ^{1}H NMR (300 MHz, $CDCl_3$, ppm) δ: 8.04 (d, J = 7.5 Hz, 2H), 7.92 (m, 4H), 7.52 (m, 1H), 7.43 (m, 3H), 7.30 (m, 4H), 5.95 (m, 1H), 5.70 (dd, J_1 = 2.1 Hz, J_2 = 9.6 Hz, 1H), 4.99 (dd, J_1 = 5.7 Hz, J_2 = 8.7 Hz, 1H), 4.40 (m, 1H), 4.22 (m, 3H), 4.00 (m, 1H), 2.38 (s, 3H), 2.22 (s, 1H), 2.05 (d, J = 1.5 Hz, 1H), 1.65 (s, 3H), 1.36 (s, 3H). ^{13}C NMR (75 MHz, $CDCl_3$, ppm) δ: 165.0, 164.8, 143.6, 137.2, 133.5, 133.1, 129.8, 129.7, 129.3, 129.0, 128.5, 128.3, 128.0, 110.6, 79.9, 78.1, 75.0, 75.0, 74.2, 73.3, 71.3, 68.5, 62.6, 36.5, 36.4, 33.2, 28.0, 26.0, 21.5. MS (EI) *m*/*z* (relative intensity): 612 ($M^+ - CH_3$, 1), 472 (11), 414 (5), 355 (7), 246 (5), 232 (5), 214 (8), 190 (16), 189 (97), 173 (7), 171 (6), 170 (7), 155 (7), 149 (14), 139 (8), 137 (11), 136 (5), 129 (5), 123 (7), 122 (9), 121 (9), 119 (5), 106 (11), 105 (100), 97 (7), 95 (8), 92 (9), 91 (24), 85 (7), 83 (9), 82 (6), 81 (26), 78 (6), 77 (21), 73 (11), 71 (12), 70 (6), 69 (61), 68 (8), 67 (7), 65 (7), 60 (10), 59 (5), 57 (23), 56 (9), 55 (19), 45 (8), 43 (32), 41 (24), 40 (9), 39 (10). HRMS (EI) calcd. for $C_{35}H_{33}O_8NS$-CH_3: 612.1692; found: 612.1682.

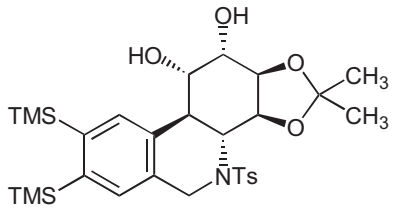
(3a*S*,3b*R*,9b*R*,10*S*,11*S*,11a*S*)-2,2-Dimethyl-4-(4-methylphenylsulfonyl)-10,11-di(phenylcarbonyloxy)-7,8-di(trimethylsilyl)-3a,3b,4,5,9b,10,11,11a-octahydro[1,3]dioxolo[4,5-*c*]phenanthridine (42)



$C_{43}H_{51}NO_8SSi_2$
798.10 g/mol

To a solution of $CpCo(CO)_2$ (5 μL) in BTMSA (12 mL) bisacetylene **41** (370 mg, 0.59 mmol), $CpCo(CO)_2$ (5 μL) dissolved in xylene (2 mL), and BTMSA (8 mL) were added dropwise with a syringe pump at 140 °C over 30 h. During this slow addition, extra catalyst was added directly into the reaction mixture in aliquots: 3 μL after 5 h, 5 μL after 20 h, and 3 μL after 29 h. The reaction mixture was heated under argon for further 12 h. BTMSA and xylene were removed under high vacuum and the residue was purified by column chromatography (hexanes – ethyl acetate, 9:1). The cyclotrimerized product **42** was isolated as crystalline foam in 87% yield (407 mg, 0.51 mmol); mp 131 °C. $[\alpha]^{23}_D$ +43.1 (*c* 0.75, CH_2Cl_2). R_f 0.37 (hexanes – ethyl acetate, 3:1). IR ($CDCl_3$, cm^{-1}) ν: 3065, 3034, 2986, 2954, 2901, 2255, 1911, 1729, 1602, 1586, 1493, 1452, 1384, 1374, 1348, 1316, 1272, 1251, 1218, 1178, 1162, 1120, 1093, 1069, 1027, 1002, 971, 910, 874, 856, 839, 812, 784, 734, 670, 649, 628, 564, 519. ^{1}H NMR (300 MHz, $CDCl_3$, ppm) δ: 7.89 (d, J = 7.5 Hz, 2H), 7.85 (d, J = 8.7 Hz, 2H), 7.52 (m, 4H), 7.34 (m, 4H), 7.26 (m, 2H), 7.04 (d, J = 8.1 Hz, 2H), 6.19 (dd, J_1 = 5.4 Hz, J_2 = 8.4 Hz, 1H), 5.70 (dd, J_1 = 5.1 Hz, J_2 = 9.3 Hz, 1H), 4.98 (t, J = 7.5 Hz, 1H), 4.76 (dd, J_1 = 7.2 Hz, J_2 = 9.0 Hz, 1H), 4.59 (dd, J_1 = 16.5 Hz, J_2 = 60.0 Hz, 2H), 4.03 (dd, J_1 = 8.4 Hz, J_2 = 12.6 Hz, 1H), 3.28 (dd, J_1 = 8.7 Hz, J_2 = 12.6 Hz, 1H), 2.31 (s, 3H), 1.56 (s, 3H), 1.37 (s, 3H), 0.39 (s, 9H), 0.12 (s, 9H). ^{13}C NMR (75 MHz, $CDCl_3$, ppm) δ: 165.4, 165.3, 146.2, 144.3, 142.7, 137.4, 133.6, 133.3, 133.1, 132.6, 132.5, 131.4, 129.7, 129.7, 129.3, 129.1, 129.0, 128.3, 128.1, 127.5, 110.7, 76.9, 73.7, 69.7, 69.5, 58.1, 48.0, 39.4, 27.5, 25.1, 21.4, 1.8, 1.6. MS (EI) *m*/*z* (relative intensity): 430 (2), 256 (5), 230 (11), 167 (5), 149 (19), 137 (11), 136 (6), 129 (15), 123 (9), 122 (5), 121 (7), 113 (6), 112 (10), 111 (7), 109 (8), 197 (6), 105 (19), 98 (7), 97 (12), 96 (6), 95 (15), 93 (9), 91 (8), 87 (5), 85 (12), 84 (13), 83 (19), 82 (10), 81 (41), 79 (7), 77 (10), 73 (23), 71 (26), 70 (21), 69 (100), 68 (16), 67 (15), 61 (6), 60 (19), 58 (6), 57 (49), 56 (31), 55 (46), 54 (6), 53 (8), 45 (12), 44 (12), 43 (59), 42 (15), 41 (67). HRMS (EI) calcd. for $C_{43}H_{51}O_8NSSi_2$: 797.2874; found: 797.2885.

(3a*S*,3b*R*,9b*R*,10*S*,11*S*,11a*S*)-2,2-Dimethyl-4-(4-methylphenylsulfonyl)-7,8-di(trimethylsilyl)-3a,3b,4,5,9b,10,11,11a-octahydro[1,3]dioxolo[4,5-*c*]phenanthridine-10,11-diol (43)



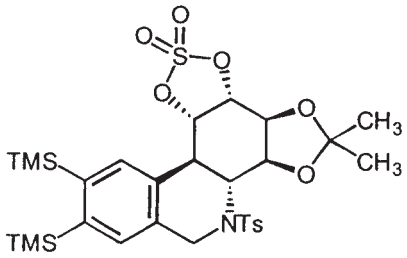
$C_{29}H_{43}NO_6SSi_2$
589.89 g/mol

Protected diol **42** (100 mg, 0.13 mmol) was dissolved in a 1% sodium hydroxide solution in methanol (2 mL) and stirred for 1 h at room temperature. The reaction was quenched with NH_4Cl and extracted with CH_2Cl_2. The organic solvents were dried over Na_2SO_4 and removed under high vacuum. The residue was purified by column chromatography (hexanes – ethyl acetate, 3:1 to 1:1). The diol **43** was isolated as foamy crystals in 99% yield (73 mg, 0.12 mmol); mp 121 °C. $[\alpha]^{25}_D$ +35.5 (*c* 1.50, CH_2Cl_2). R_f 0.18 (hexanes – ethyl acetate, 2:1). IR (CH_2Cl_2, cm^{-1}) ν: 3406, 3055, 2954, 2927, 2871, 1727, 1599, 1495, 1455, 1376, 1347, 1266, 1250, 1213, 1160, 1124, 1091, 1072, 1042, 1002, 972, 931, 877, 858, 840, 740, 704, 672, 656, 602, 563, 546, 519, 486, 479, 467, 463, 455. ^{1}H NMR (300 MHz, $CDCl_3$, ppm) δ: 7.65 (s, 1H), 7.43 (d, J = 8.1 Hz, 2H), 7.21 (s, 1H), 6.98 (d, J = 8.1 Hz, 2H), 4.74 (t, J = 7.8 Hz, 1H), 4.56 (d, J = 16.2 Hz, 1H), 4.35 (m, 3H), 3.91 (m, 1H), 3.75 (m, 1H), 3.11 (s, 1H), 2.87 (s, 1H), 2.67 (dd, J_1 = 8.1 Hz, J_2 = 12.3 Hz, 1H), 2.29 (s, 3H), 1.54 (s, 3H), 1.33 (s, 3H), 0.33 (s, 9H), 0.32 (s, 9H). ^{13}C NMR (75 MHz, $CDCl_3$, ppm) δ: 145.6, 143.9, 142.5, 137.4, 133.9, 133.8, 132.3, 132.1, 128.9, 127.4, 110.3, 77.1, 75.8, 70.3, 68.8, 57.0, 47.6, 41.0, 27.7, 25.0, 21.5, 1.9, 1.9. MS (EI) *m*/*z* (relative intensity): 574 ($M^+ - CH_3$, 13), 471 (12), 459 (10), 458 (22), 435 (23), 434 (65), 432 (11), 429 (13), 428 (29), 342 (11), 335 (17), 322 (20), 285 (21), 274 (12), 185 (10), 169

© 2006 NRC Canada

(79), 155 (30), 150 (15), 149 (19), 147 (27), 139 (15), 133 (10), 131 (13), 129 (17), 125 (14), 124 (14), 123 (14), 119 (45), 111 (21), 109 (21), 105 (15), 97 (38), 96 (17), 95 (28), 92 (12), 91 (65), 85 (23), 84 (14), 83 (32), 82 (17), 81 (31), 79 (14), 77 (14), 73 (51), 71 (33), 70 (21), 69 (75), 68 (14), 67 (22), 65 (15), 59 (12), 57 (55), 56 (19), 55 (61), 53 (11), 45 (15), 44 (15), 43 (100), 42 (15), 41 (54). HRMS (EI) calcd. for $C_{29}H_{43}O_6NSSi_2$-CH_3: 574.2115; found: 574.2099. Anal. calcd. for $C_{29}H_{43}O_6NSSi_2$: C 59.05, H 7.35; found: C 58.77, H 7.37.

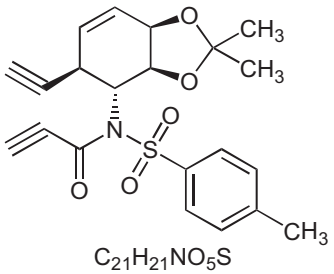
(3a*S*,3b*R*,6a*S*,6b*R*,12b*R*,12c*S*)-5,5-Dimethyl-7-(4-methylphenylsulfonyl)-10,11-di(trimethylsilyl)-3a,3b,6a,6b,7,8,12b,12c-octahydro-1,3,4,6-tetraoxa-2-thia-7-azadicyclopenta[*a*,*c*]phenanthrene-2,2-dioxide (44)



$C_{29}H_{41}NO_8S_2Si_2$
651.94 g/mol

To a solution of diol **43** (494 mg, 0.84 mmol) in dry CH_2Cl_2 (20 mL) was added triethylamine (5 mL) at 0 °C. The solution was stirred for 10 min and SO_2Cl_2 (1.0 mol/L solution, 15 mL) were added dropwise via syringe pump over a period of 2 h. Additional NEt_3 (5 mL) and SO_2Cl_2 (15 mL) were added over a period of 2 h for full conversion (TLC). The reaction mixture was diluted with CH_2Cl_2 (30 mL), quenched with satd. aq. NH_4Cl (50 mL), and extracted with CH_2Cl_2 (3 × 50 mL). The organic phase was dried over Na_2SO_4, filtered, and the solvent was removed under reduced pressure. Purification by flash column chromatography (hexanes – ethyl acetate, 5:1) afforded cyclic sulfate **44** (383 mg, 0.59 mmol, 70%); mp 110 °C. $[\alpha]^{26}_D$ +24.6 (*c* 0.40, CH_2Cl_2). R_f 0.66 (hexanes – ethyl acetate, 2:1). IR ($CHCl_3$, cm^{-1}) ν: 3462, 3021, 2963, 2870, 1732, 1597, 1456, 1385, 1355, 1308, 1249, 1213, 1182, 1162, 1127, 1090, 1056, 995, 919, 883, 840, 795, 756, 669, 627, 562. ^{1}H NMR (300 MHz, $CDCl_3$, ppm) δ: 7.42 (m, 3H), 7.28 (s, 1H), 7.00 (d, J = 8.1 Hz, 2H), 5.35 (dd, J_1 = 7.2 Hz, J_2 = 9.6 Hz, 1H), 5.04 (t, J = 7.2 Hz, 1H), 4.75 (m, 2H), 4.63 (d, J = 16.2 Hz, 1H), 4.27 (d, J = 16.2 Hz, 1H), 3.69 (dd, J_1 = 8.1 Hz, J_2 = 12.3 Hz, 1H), 2.99 (t, J = 10.8 Hz, 1H), 2.30 (s, 3H), 1.57 (s, 3H), 1.34 (s, 3H), 0.34 (s, 9H), 0.33 (s, 9H). ^{13}C NMR (75 MHz, $CDCl_3$, ppm) δ: 145.0, 144.0, 141.3, 135.1, 131.7, 130.8, 129.6, 128.8, 127.3, 125.6, 109.8, 80.9, 78.0, 75.1, 73.0, 54.3, 45.2, 36.5, 25.5, 22.9, 19.7, 0.0, 0.0. MS (EI) *m*/*z* (relative intensity): 636 (M^+ – CH_3, 1), 88 (11), 86 (65), 84 (100), 73 (6), 69 (6), 49 (21), 47 (27), 43 (6). HRMS (EI) calcd. for $C_{29}H_{41}O_8NS_2Si_2$-CH_3: 636.1577; found: 636.1556. Anal. calcd. for $C_{29}H_{41}O_8NS_2Si_2$: C 53.43, H 6.34; found: C 53.52, H 6.47.

(3a*S*,4*R*,5*R*,7a*R*)-5-(1-Ethynyl)-2,2-dimethyl-4-[4-methylphenyl(propioloyl)sulfonamido]-3a,4,5,7a-tetrahydro-1,3-benzodioxolone (45)



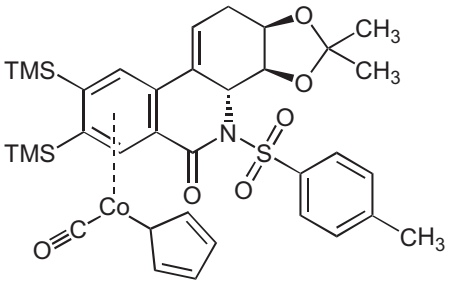
$C_{21}H_{21}NO_5S$
399 46 g/mol

To a solution of acetonide **18** (250 mg, 0.60 mmol) in THF (5 mL) was added BuLi (1.6 mol/L, 0.41 mL, 0.66 mmol) at 0 °C under argon. Propiolic acid anhydride (87 mg, 0.72 mmol) was added and the solution was allowed to warm to room temperature overnight. The reaction was quenched by addition of satd. aq. NH_4Cl (20 mL) and the aqueous phase extracted with ethyl acetate (4 × 20 mL). The combined organic phases were washed with brine (10 mL), dried over $MgSO_4$, and the solvent was removed under reduced pressure. Flash column chromatography of the residue (hexanes – ethyl acetate, 3:1) afforded a bisacetylene (128 mg, 0.27 mmol, 46%) as a slightly yellow foam. To a solution of this bisacetylene (150 mg, 0.32 mmol) in acetonitrile (5 mL) was added TBAT (340 mg, 0.63 mmol). The reaction mixture was stirred at room temperature for 30 h, then diluted with 30 mL ethyl acetate, and washed with satd. aq. NH_4Cl (3 × 10 mL) and with brine (10 mL). The organic phase was dried over $MgSO_4$ and the solvent was removed under reduced pressure. Flash column chromatography of the residue (hexanes – ethyl acetate, 3:1) afforded the bisacetylene **45** (77 mg, 0.19 mmol, 61%) as a colorless oil. $[\alpha]^{21}_D$ +30.3 (*c* 0.25, CH_2Cl_2). R_f 0.40 (hexanes – ethyl acetate, 3:1). IR ($CHCl_3$, cm^{-1}) ν: 3298, 3021, 2989, 2937, 2876, 2591, 2403, 2109, 1917, 1732, 1674, 1597, 1511, 1495, 1485, 1456, 1429, 1399, 1366, 1309, 1270, 1246, 1216, 1189, 1172, 1141, 1120, 1085, 1067, 1027, 1019, 998, 971, 946, 923, 897, 865, 830, 813, 757. ^{1}H NMR (300 MHz, $CDCl_3$, ppm) δ: 7.97 (d, J = 8.0 Hz, 2H), 7.40 (d, J = 9.5 Hz, 2H), 5.98 (m, 2H), 5.07 (m, 1H), 4.70 (m, 2H), 4.21 (d, J = 10.4 Hz, 1H), 3.24 (s, 1H), 2.39 (s, 3H), 2.16 (s, 1H), 1.48 (s, 3H), 1.38 (s, 3H). ^{13}C NMR (75 MHz, $CDCl_3$, ppm) δ: 153.6, 145.4, 136.0, 132.6, 129.7, 129.2, 123.6, 110.6, 83.0, 81.5, 75.2, 73.4, 72.9, 72.7, 65.4, 32.9, 27.8, 25.8, 21.9. MS (EI) *m*/*z* (relative intensity): 384 (MH^+ – CH_3, 8), 306 (18), 248 (11), 228 (7), 224 (10), 204 (12), 170 (9), 156 (8), 155 (77), 152 (9), 139 (11), 135 (20), 119 (22), 118 (46), 107 (5). HRMS (EI) calcd. for $C_{21}H_{21}O_5NS$-CH_3: 384.0906; found: 384.0898.

Carbonyl-η^1-cyclopentadienyl-η^6-(3a*S*,3b*R*,11a*R*)-2,2-dimethyl-4-(4-methylphenylsulfonyl)-7,8-di(trimethylsilyl)-3a,3b,4,5,11,11a-hexahydro[1,3]dioxolo[4,5-*c*]-phenanthridin-5-onylcobalt (46)

A solution of bisacetylene **45** (165 mg, 0.43 mmol) and $CpCo(CO)_2$ (10 μL) in BTMSA (10 mL) and xylene (10 mL) was added with a syringe pump to a refluxing solu-

© 2006 NRC Canada

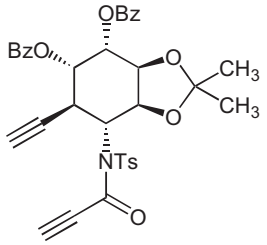


$C_{35}H_{44}CoNO_6SSi_2$
721.91 g/mol

tion of $CpCo(CO)_2$ (10 μL) in BTMSA (25 mL) over a period of 35 h. After the addition was completed, the reaction mixture was refluxed for an additional 6 h. The solvent was removed under reduced pressure (0.1 mbar, 1 bar = 100 kPa). The reddish brown residue was purified by flash column chromatography (pentane to ether – pentane, 1:1) and afforded the cobalt complex **46** (33 mg, 0.05 mmol, 11%) as a yellow oil. $[\alpha]^{26}_D$ +27.6 (*c* 0.23, $CHCl_3$). R_f 0.53 (hexanes –ethyl acetate, 3:1). IR ($CHCl_3$, cm^{-1}) ν: 3261, 3019, 2958, 2934, 2873, 2401, 1693, 1599, 1521, 1496, 1456, 1383, 1375, 1328, 1287, 1272, 1251, 1216, 1158, 1096, 1071, 969, 928, 857, 841, 812, 757, 669. ^{1}H NMR (300 MHz, $CDCl_3$, ppm) δ: 8.00 (s, 1H), 7.51 (s, 1H), 7.36 (d, *J* = 8.2 Hz, 2H), 6.96 (d, *J* = 8.1 Hz, 2H), 6.01 (d, *J* = 7.7 Hz, 1H), 5.91 (m, 1H), 5.71 (d, *J* = 9.8 Hz, 1H), 4.57 (m, 1H), 4.18 (m, 3H), 4.00 (m, 1H), 3.61 (m, 1H), 2.18 (s, 3H), 1.58 (m, 2H), 1.33 (s, 3H), 1.18 (s, 3H), 0.23 (s, 9H), 0.21 (s, 9H). ^{13}C NMR (75 MHz, $CDCl_3$, ppm) δ: 169.5, 152.6, 144.8, 141.7, 141.0, 140.0, 136.3, 136.1, 135.7, 129.5, 129.1, 128.8, 126.9, 124.3, 109.9, 79.5, 79.3, 72.7, 65.9, 60.4, 41.8, 30.5, 28.7, 28.2, 26.2, 25.9, 21.6, 1.9, 1.8. MS (FAB) *m*/*z* (relative intensity): 744 (M^+ + Na, 0.1). MS (EI) *m*/*z* (relative intensity): 656 (M^+ – Cp, 4.8), 614 (5), 613 (11), 505 (7), 501 (8), 500 (20), 460 (9), 459 (21), 458 (8), 420 (6), 419 (14), 418 (38), 358 (6), 357 (13), 356 (7), 343 (6), 341 (7), 340 (7), 329 (5), 325 (8), 294 (7), 288 (6), 279 (5), 255 (8), 254 (37), 253 (23), 228 (6), 205 (6), 171 (6), 155 (18), 149 (17), 141 (5), 140 (7), 139 (33), 124 (8), 100 (11), 99 (65), 98 (52), 97 (6), 95 (8), 92 (11), 91 (58), 85 (7), 83 (9), 81 (5), 77 (6), 75 (18), 74 (11), 73 (100), 71 (13), 69 (13), 67 (5), 65 (10). HRMS (EI) calcd. for $C_{35}H_{44}O_6NSSi_2Co$-CO: 693.1811; found: 693.1807.

(3a*S*,4*S*,5*S*,6*R*,7*R*,7a*S*)-6-(1-Ethynyl)-2,2-dimethyl-7-[4-methylphenyl(propioloyl)sulfonamido]-4,5-di(phenylcarbonyloxy)perhydro-1,3-benzodioxole (47)

To a solution of TMS-protected acetylene **40** (976 mg, 1.48 mmol) in dry acetonitrile (35 mL) was added TBAT (1.19 g, 2.21 mmol). The reaction mixture was stirred at room temperature for 1.5 h, quenched with satd. aq. NH_4Cl (50 mL), and extracted with ethyl acetate (3 × 50 mL). The combined organic phases were dried over Na_2SO_4 and evaporated under reduced pressure. Column chromatography (hexanes – ethyl acetate, 4:1 to 2:1) afforded unprotected acetylene (664 mg, 1.13 mmol, 76%) as white crystals. To a solution of this material (210 mg, 0.36 mmol) in THF (6 mL) was added NaHMDS (1.0 mol/L, 0.43 mL, 0.43 mmol) at –70 °C under argon. The reaction mixture was allowed to warm to 0 °C over a period of 20 min and was further stirred for 10 min at this temperature. Propiolic acid anhydride (130 mg, 1.07 mmol) was added and the solution was allowed to warm to room temperature overnight. The reaction was quenched by addition of satd. aq. NH_4Cl (20 mL) and the aqueous phase extracted with ethyl acetate (4 × 20 mL). The combined organic phases were washed with brine (10 mL), dried over $MgSO_4$, and the solvent was removed under reduced pressure. Flash column chromatography of the residue (hexanes – ethyl acetate, 3:2) afforded an unseparable 3:2 rotamer mixture of tosylamide **47** (128 mg, 0.27 mmol, 46%) as oily white crystals; mp 121 °C. $[\alpha]^{23}_D$ –124.6 (*c* 1.05, CH_2Cl_2). R_f 0.62 (hexanes – ethyl acetate, 2:1). IR (CH_2Cl_2, cm^{-1}) ν: 3292, 3055, 2987, 2831, 2686, 2522, 2411, 2306, 2113, 1731, 1677, 1602, 1551, 1422, 1363, 1266, 1189, 1173, 1116, 1095, 1071, 1055, 1027, 896, 853, 740, 705, 618, 574, 546. ^{1}H NMR (300 MHz, $CDCl_3$, ppm) δ: 8.15 (m, 3H), 8.02 (m, 1H), 7.97 (m, 2H), 7.58 (m, 1H), 7.49 (m, 3H), 7.40 (m, 4H), 6.06 (m, 1H), 5.72 (dd, J_1 = 2.1 Hz, J_2 = 10.2 Hz, 1H), 5.35/4.96 (m, 1H), 4.96 (m, 1H), 4.46 (m, 2H), 3.30/3.18 (m, 1H), 2.45/2.43 (s, 3H), 2.19/2.14 (m, 1H), 1.74/1.64 (s, 3H), 1.42 (s, 3H). ^{13}C NMR (75 MHz, $CDCl_3$, ppm) δ: 165.3, 165.1/164.9, 153.2, 145.4/145.2, 136.7, 133.7, 133.3/133.2, 130.9/130.0, 129.9, 129.9, 129.6, 129.4/129.3, 129.2/129.0, 128.7, 128.4/128.3, 111.2/111.0, 83.6/83.2, 79.4/79.0, 75.9/75.4, 75.2/75.1, 74.4/74.1, 74.0/73.2, 71.2/71.1, 68.3/68.1, 62.8, 33.8/31.5, 27.9/27.8, 26.2/26.0, 21.7. MS (EI) *m*/*z* (relative intensity): 626 (M^+ – CH_3, 1), 122 (9), 119 (5), 105 (47), 91 (8), 88 (19), 86 (100), 84 (100), 77 (14), 64 (16), 53 (15), 51 (11), 49 (31), 48 (6), 47 (37), 44 (7), 43 (17). HRMS (EI) calcd. for $C_{35}H_{31}O_9NS$-CH_3: 626.1485; found: 626.1495.

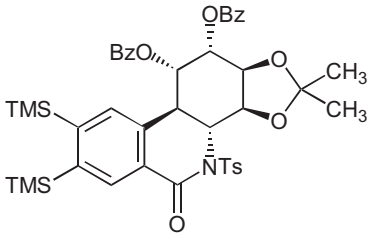


$C_{35}H_{31}NO_9S$
641.69 g/mol

(3a*S*,3b*R*,9b*R*,10*S*,11*S*,11a*S*)-2,2-Dimethyl-4-(4-methylphenylsulfonyl)-5-oxo-10,11-di(phenylcarbonyloxy)-7,8-di(trimethylsilyl)-3a,3b,4,5,9b,10,11,11a-octahydro[1,3]dioxolo[4,5-*c*]phenanthridine (48)

To a solution of $CpCo(CO)_2$ (2 μL) in BTMSA (6 mL), bisacetylene **47** (105 mg, 0.16 mmol) and $CpCo(CO)_2$ (2 μL) dissolved in xylene (1 mL) and BTMSA (4 mL) were added dropwise with a syringe pump at 140 °C over 30 h. During this slow addition, extra catalyst was added directly into the reaction mixture in aliquots: 2 μL after 5 h and after 20 h, and 1 μL after 29 h. After 5 h and after 20 h, additional $CpCo(CO)_2$ (2 μL) was added, and after 29 h, additional $CpCo(CO)_2$ (1 μL) was added. The reaction mixture was heated under argon for a further 12 h. BTMSA and

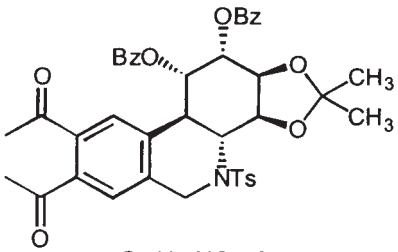
© 2006 NRC Canada



$C_{43}H_{49}NO_9SSi_2$
812.09 g/mol

xylene were removed at high vacuum and the residue was purified by column chromatography (hexanes – ethyl acetate, 9:1). The cyclotrimerized product **48** was isolated as a colourless oil in 5% yield (7 mg, 0.01 mmol). $[\alpha]^{22}_D$ –20.9 (*c* 0.25, CH_2Cl_2). R_f 0.32 (hexanes – ethyl acetate, 4:1). IR (CH_2Cl_2, cm^{-1}) ν: 3061, 2987, 2957, 2928, 2856, 1728, 1704, 1601, 1584, 1494, 1452, 1405, 1366, 1316, 1266, 1219, 1189, 1175, 1094, 1027, 1003, 963, 841, 816, 739, 712, 672, 660, 638, 602, 572, 545, 512. ^{1}H NMR (300 MHz, $CDCl_3$, ppm) δ: 8.44 (s, 1H), 8.30 (d, *J* = 8.4 Hz, 2H), 8.13 (s, 1H), 8.07 (m, 2H), 7.99 (m, 2H), 7.64 (m, 1H), 7.52 (m, 3H), 7.39 (m, 2H), 7.34 (d, *J* = 8.4 Hz, 2H), 6.44 (s, 1H), 5.85 (dd, J_1 = 7.2 Hz, J_2 = 10.8 Hz, 1H), 5.25 (dd, J_1 = 2.4 Hz, J_2 = 7.2 Hz, 1H), 4.98 (t, *J* = 7.2 Hz, 1H), 3.90 (t, *J* = 11.1 Hz, 1H), 3.76 (d, *J* = 12.0 Hz, 1H), 2.45 (s, 3H), 1.49 (s, 3H), 1.32 (s, 3H), 0.44 (s, 9H), 0.39 (s, 9H). ^{13}C NMR (75 MHz, $CDCl_3$, ppm) δ: 166.4, 165.5, 165.5, 155.6, 146.7, 144.2, 138.4, 137.9, 136.7, 133.8, 133.4, 131.1, 129.9, 129.8, 129.3, 129.2, 129.0, 128.8, 128.8, 128.4, 126.8, 110.4, 75.4, 73.5, 72.0, 70.5, 66.1, 46.1, 27.6, 25.5, 21.7, 1.7, 1.6. MS (EI) *m*/*z* (relative intensity): 796 ($M^+ - CH_3$, 1), 525 (6), 477 (5), 179 (5), 149 (7), 129 (8), 106 (9), 105 (100), 98 (7), 97 (13), 96 (6), 95 (8), 91 (13), 85 (10), 84 (9), 83 (17), 82 (8), 81 (13), 77 (16), 73 (25), 71 (17), 70 (10), 69 (30), 68 (6), 67 (8). HRMS (EI) calcd. for $C_{43}H_{49}O_9NSSi_2$-CH_3: 796.2432; found: 796.2399. Anal. calcd. for $C_{43}H_{49}O_9NSSi_2$: C 63.60, H 6.08; found: C 63.46, H 6.00.

(3a*S*,3b*R*,9b*R*,10*S*,11*S*,11a*S*)-7,8-Diacetyl-2,2-dimethyl-4-(4-methylphenylsulfonyl)-10,11-di(phenylcarbonyloxy)-3a,3b,4,5,9b,10,11,11a-octahydro[1,3]dioxolo[4,5-*c*]phenanthridine (51)



$C_{41}H_{39}NO_{10}S$
737.82 g/mol

To a solution of 2,5-di(*tert*-butyldimethylsilyloxy)-3-hexyne (1.00 g) in $CpCo(CO)_2$ (5 μL), bisacetylene **41** (108 mg, 0.17 mmol) and $CpCo(CO)_2$ (5 μL) dissolved in xylene (5 mL) were added dropwise with a syringe pump at 140 °C over 30 h. During and after this slow addition, extra catalyst was added directly into the reaction mixture in aliquots: 5 μL after 5, 17, 29, and 41 h. The reaction mixture was heated under argon for a further 12 h. Xylene was removed at high vacuum and the residue was purified by column chromatography (hexanes – ethyl acetate, 9:1 to 6:1). All four diastereoisomers of the cyclotrimerized product **50** were isolated as crystalline foam in 31% overall yield (52 mg, 0.05 mmol). MS (EI) *m*/*z* (relative intensity): 954 ($M^+ - CH_3$, 0.1), 912 (10), 526 (12), 253 (12), 179 (12), 147 (11), 106 (12), 105 (100), 91 (16), 77 (17), 75 (27), 73 (33).

The mixture of diastereoisomers was dissolved in THF (0.5 mL), treated with TBAF (1.0 mol/L solution in THF, 0.55 mL) and stirred for 2 h. The reaction mixture was quenched with satd. NH_4Cl solution and extracted three times with diethyl ether. The combined organic phases were dried over $MgSO_4$, filtered, and evaporated to dryness. Column chromatography (hexanes – ethyl acetate, 1:2) gave a mixture of four diastereomeric diols (29 mg, 0.04 mmol, 72%), used immediately in the next step. IR ($CDCl_3$, cm^{-1}) ν: 3417, 3019, 2978, 2929, 2857, 1727, 1601, 1452, 1384, 1375, 1347, 1316, 1276, 1216, 1160, 1092, 1070, 1027, 758, 713, 668.

To the diastereomeric diols (17 mg, 0.02 mmol) dissolved in DMSO (1 mL) was added *o*-iodoxybenzoic acid (IBX, (75 mg, 0.28 mmol). The reaction mixture was stirred for 1 day, diluted with diethyl ether, and washed four times with water. The ether phase was dried over $MgSO_4$, filtered, and evaporated to dryness. The pure product **51** was obtained by column chromatography (ethyl ether – pentane, 2:1) as a white crystalline single diastereomer in 71% yield (12 mg, 0.02 mmol); mp 119 °C. $[\alpha]^{23}_D$ +38.6 (*c* 0.06, CH_2Cl_2). R_f 0.48 (hexanes – ethyl acetate, 1:1). IR ($CDCl_3$, cm^{-1}) ν: 3020, 2926, 2855, 1759, 1727, 1602, 1510, 1452, 1316, 1273, 1216, 1162, 1092, 1068, 1027, 933, 814, 758, 710, 667, 548. ^{1}H NMR (600 MHz, $CDCl_3$, ppm) δ: 7.89 (2m, 4H), 7.62 (d, *J* = 8.3 Hz, 2H), 7.58 (m, 1H), 7.52 (m, 1H), 7.52 (s, 1H), 7.40 (t, *J* = 7.8 Hz, 2H), 7.33 (t, *J* = 7.9 Hz, 2H), 7.15 (d, *J* = 8.1 Hz, 2H), 7.08 (s, 1H), 6.12 (dd, J_1 = 4.8 Hz, J_2 = 8.6 Hz, 1H), 5.74 (dd, J_1 = 4.7 Hz, J_2 = 7.9 Hz, 1H), 5.03 (dd, J_1 = 6.8 Hz, J_2 = 8.8 Hz, 1H), 4.73 (t, *J* = 7.4 Hz, 1H), 4.62 (d, *J* = 16.8 Hz, 1H), 4.53 (d, *J* = 16.7 Hz, 1H), 4.00 (dd, J_1 = 8.9 Hz, J_2 = 12.6 Hz, 1H), 3.43 (dd, J_1 = 8.9 Hz, J_2 = 12.6 Hz, 1H), 2.41 (s, 3 H), 2.35 (s, 3H), 2.20 (s, 3H), 1.54 (s, 3H), 1.36 (s, 3H). ^{13}C NMR (150 MHz, $CDCl_3$, ppm) δ: 201.7, 200.0, 165.4, 165.3, 143.8, 139.3, 138.6, 137.7, 137.4, 136.4, 133.8, 133.5, 129.8, 129.8, 129.4, 128.6, 128.4, 127.5, 126.2, 125.1, 110.8, 96.1, 76.2, 74.1, 70.1, 69.8, 59.4, 48.5, 39.6, 30.3, 29.2, 27.8, 27.7, 25.4, 21.5. MS (EI) *m*/*z* (relative intensity): 737 (M^+, 0.1), 133 (14), 105 (6), 89 (41), 87 (18), 73 (11), 59 (12), 45 (100). HRMS (EI) calcd. for $C_{41}H_{39}O_{10}NS$: 737.2295; found: 737.2306.

Acknowledgements

The authors wish to thank Professor Peter Vollhardt (University of California, Berkeley) for helpful discussions and advice related to cyclotrimerization. The following agencies are gratefully appreciated for financial support of this work: Natural Sciences and Engineering Research Council of Can-

© 2006 NRC Canada

ada (NSERC), Canada Foundation for Innovation (CFI), Ontario Innovation Trust (OIT), Brock University, TDC Research Foundation, Inc. (fellowship to Michael Moser), and TDC Research, Inc. Professor George R. Pettit is pleased to acknowledge the financial assistance from Grant No. R01 CA90441-01-05 awarded by the Division of Cancer Treatment and Diagnosis, National Cancer Institute, DHHS, and the Arizona Biomedical Research Commission.

References

1. For reviews of synthetic strategies, see: (*a*) S.F. Martin. *In* The alkaloids. Vol. 40. *Edited by* A.R. Bross. Academic Press, New York. 1987. p. 251; (*b*) R. Polt. Organic synthesis: Theory and applications. Vol. 3. *Edited by* T. Hudlicky. JAI Press, Greenwich, Conn. 1997. p. 109; (*c*) S. Prabhakar and M.R. Tavares. Alkaloids Chem. Biol. Perspect. **15**, 433 (2001); (*d*) Z. Jin. Nat. Prod. Rep. **20**, 606 (2003); (*e*) Z. Jin. Nat. Prod. Rep. **22**, 111 (2005); (*f*) U. Rinner and T. Hudlicky. Synlett, 365 (2005); (*g*) Y. Chapleur. Curr. Org. Chem. In press.
2. For total syntheses of pancratistatin, see: (*a*) S. Danishefsky and J.Y. Lee. J. Am. Chem. Soc. **111**, 4829 (1989); (*b*) X.R. Tian, T. Hudlicky, and K. Königsberger. J. Am. Chem. Soc. **117**, 3643 (1995); (*c*) B.M. Trost and S.R. Pulley. J. Am. Chem. Soc. **117**, 10143 (1995); (*d*) G.E. Keck, S.F. McHardy, and J.A. Murry. J. Am. Chem. Soc. **117**, 7289 (1995); (*e*) T. Hudlicky, X.R. Tian, K. Königsberger, R. Maurya, J. Rouden, and B. Fan. J. Am. Chem. Soc. **118**, 10752 (1996); (*f*) N. Chida, M. Jitsuoka, Y. Yamamoto, M. Ohtsuka, and S. Ogawa. Heterocycles, **43**, 1385 (1996); (*g*) T.J. Doyle, M. Hendrix, D. VanDerveer, S. Javanmard, and J. Haseltine. Tetrahedron, **53**, 11153 (1997); (*h*) P. Magnus and I.K. Sebhat. Tetrahedron, **54**, 15509 (1998); (*i*) P. Magnus and I.K. Sebhat. J. Am. Chem. Soc. **120**, 5341 (1998); (*j*) J.H. Rigby, U.S.M. Maharoof, and M.E. Mateo. J. Am. Chem. Soc. **122**, 6624 (2000); (*k*) G.R. Pettit, N. Melody, and D.L. Herald. J. Org. Chem. **66**, 2583 (2001); (*l*) S. Kim, H. Ko, E. Kim, and D. Kim. Org. Lett. **4**, 1343 (2002); (*m*) H. Ko, E. Kim, J.E. Park, D. Kim, and S. Kim. J. Org. Chem. **69**, 112 (2004).
3. For total syntheses of 7-deoxypancratistatin, see: (*a*) S. Ohta and S. Kimoto. Chem. Pharm. Bull. **24**, 2977 (1976); (*b*) S. Ohta and S. Kimoto. Chem. Pharm. Bull. **24**, 2969 (1976); (*c*) H. Paulsen and M. Stubbe. Liebigs Ann. Chem. 535 (1983); (*d*) X.R. Tian, R. Maurya, K. Königsberger, and T. Hudlicky. Synlett, 1125 (1995); (*e*) G.E. Keck, S.F. McHardy, and J.A. Murry. J. Am. Chem. Soc. **117**, 7289 (1995); (*f*) N. Chida, M. Jitsuoka, Y. Yamamoto, M. Ohtsuka, and S. Ogawa. Heterocycles, **43**, 1385 (1996); (*g*) G.E. Keck, T.T. Wager, and S.F. McHardy. J. Org. Chem. **63**, 9164 (1998); (*h*) G.E. Keck, T.T. Wager, S.F. McHardy, and J.A. Murry. J. Org. Chem. **64**, 4465 (1999); (*i*) J.L. Acena, O. Arjona, M.L. Leon, and J. Plumet. Org. Lett. **2**, 3683 (2000); (*j*) for *ent*-7-deoxypancratistatin, see: H. Akgun and T. Hudlicky. Tetrahedron Lett. **40**, 3081 (1999).
4. For total syntheses of narciclasine, see: (*a*) J.H. Rigby and M.E. Mateo. J. Am. Chem. Soc. **119**, 12655 (1997); (*b*) G.E. Keck, T.T. Wager, and J.F.D. Rodriquez. J. Am. Chem. Soc. **121**, 5176 (1999); (*c*) D. Gonzales, T. Martinot, and T. Hudlicky. Tetrahedron Lett. **40**, 3077 (1999); (*d*) J.H. Rigby, U.S.M. Maharoof, and M.E. Mateo. J. Am. Chem. Soc. **122**, 6624 (2000); (*e*) S. Elango and T.H. Yan. J. Org. Chem. **67**, 6954 (2002).
5. For total syntheses of lycoricidine, see: (*a*) S. Ohta and S. Kimoto. Chem. Pharm. Bull. **24**, 2977 (1976); (*b*) H. Paulsen and M. Stubbe. Tetrahedron Lett. **23**, 3171 (1982); (*c*) H. Paulsen and M. Stubbe. Liebigs Ann. Chem. 535 (1983); (*d*) N. Chida, M. Ohtsuka, and S. Ogawa. Tetrahedron Lett. **32**, 4525 (1991); (*e*) T. Hudlicky and H.F. Olivo. J. Am. Chem. Soc. **114**, 9694 (1992); (*f*) N. Chida, M. Ohtsuka, and S. Ogawa. J. Org. Chem. **58**, 4441 (1993); (*g*) S.F. Martin and H.H. Tso. Heterocycles, **35**, 85 (1993); (*h*) T. Hudlicky, H.F. Olivo, and B. McKibben. J. Am. Chem. Soc. **116**, 5108 (1994); (*i*) for *ent*-lycoricidine, see: G.E. Keck and T.T. Wager. J. Org. Chem. **61**, 8366 (1996); (*j*) G.E. Keck, T.T. Wager, and J.F.D. Rodriquez. J. Am. Chem. Soc. **121**, 5176 (1999); (*k*) S. Elango and T.H. Yan. Tetrahedron, **58**, 7335 (2002); (*l*) A. McLachlan, N. Kekre, J. McNulty, and S. Pandey. Apoptosis, **10**, 619 (2005); (*m*) N. Kekre, C. Griffin, J. McNulty, and S. Pandey. Cancer Chemother. Pharmacol. **56**, 29 (2005).
6. F. Dall'Acqua, G. Rodighiero, and G. Ceriotti. Farmaco Ed. Sci. **32**, 67 (1977).
7. J. McNulty, R. Mao, R. Mo, S. Wolf, G.R. Pettit, D.L. Herald, and M.R. Boyd. Bioorg. Med. Chem. Lett. **11**, 169 (2001).
8. (*a*) G.R. Pettit, N. Melody, and D.L. Herald. J. Nat. Prod. **67**, 322 (2004); (*b*) G.R. Pettit, B. Orr, and S. Ducki. Anti-Cancer Drug Des. **15**, 389 (2001).
9. (*a*) F. Chretien, S.I. Ahmed, A. Masion, and Y. Chapleur. Tetrahedron, **49**, 7463 (1993); (*b*) G. Pandey, A. Murugan, and M. Balakrishnan. Chem. Commun. (Cambridge), 624 (2002); (*c*) T. Hudlicky, U. Rinner, D. Gonzales, H. Akgun, S. Schilling, P. Siengalewicz, T.A. Martinot, G.R. Pettit. J. Org. Chem. **67**, 8762 (2002); (*d*) A.N. Phung, M.T. Zannetti, G. Whited, and W.D. Fessner. Angew. Chem. Int. Ed. **42**, 4821 (2003); (*e*) T. Hudlicky, U. Rinner, K.J. Finn, and I. Ghiviriga. J. Org. Chem. **70**, 3490 (2005).
10. B. Gabrielsen, T.P. Monath, J.W. Huggins, D.F. Kefauver, G.R. Pettit, G. Groszek, M. Hollingshead, J.J. Kirsi, W.M. Shannon, E.M. Schubert, J. Dare, B. Ugarkar, M.A. Ussery, and M.J. Phelan. J. Nat. Prod. **55**, 1569 (1992).
11. J. McNulty, V. Larichev, and S. Pandey. Bioorg. Med. Chem. Lett. **15**, 5315 (2005).
12. U. Rinner, H.L. Hillebrenner, D.R. Adams, T. Hudlicky, and G.R. Pettit. Bioorg. Med. Chem. Lett. **14**, 2911 (2004).
13. S. Ibn-Ahmed, M. Khaldi, F. Chretien, and Y. Chapleur. J. Org. Chem. **69**, 6722 (2004).
14. U. Rinner, T. Hudlicky, H. Gordon, and G.R. Pettit. Angew. Chem. Int. Ed. **43**, 5342 (2004).
15. (*a*) N.E. Schore. Chem. Rev. **88**, 1081 (1988); (*b*) M. Lautens, W. Klute, and W. Tam. Chem. Rev. **96**, 46 (1996); (*c*) S. Saito and Y. Yamamoto. Chem. Rev. **100**, 2901 (2000).
16. J.A. Varela and C. Saá. Chem. Rev. **103**, 3787 (2003).
17. (*a*) M. Berthelot. Leçons sur les methods générales de syntheses en chimie organique. Gauthier-Villars, Paris. 1864. p. 308 to 309; (*b*) M.C.R. Berthelot. Acad. Sci. **62**, 905 (1866); (*c*) M. Berthelot. Liebigs Ann. **139**, 272 (1866).
18. (*a*) N. Saino, D. Kogure, and S. Okamoto. Org. Lett. **7**, 3065 (2005); (*b*) K. Tanaka, G. Nishida, M. Ogino, M. Hirano, and K. Noguchi. Org. Lett. **7**, 3119 (2005); (*c*) U. Groth, T. Huhn, C. Kesenheimer, and A. Kalogerakis. Synlett, 1758 (2005); (*c*) D.H. Kim and Y.K. Chung. Synlett, 1889 (2005).
19. (*a*) R.L. Funk and K.P.C. Vollhardt. J. Am. Chem. Soc. **99**, 5483 (1977); (*b*) R.L. Funk and K.P.C. Vollhardt. J. Am. Chem. Soc. **102**, 5253 (1980).
20. D. Perez, B.A. Siesel, M.J. Malaska, E. David, and K.P.C. Vollhardt. Synlett, 306 (2000).

© 2006 NRC Canada

21. I. Ugi and S. Heck. Comb. Chem. High Throughput Screening, **4**, 1 (2001).
22. L.F. Tietze. Chem. Ind. (London), **12**, 453 (1995).
23. For a preliminary account of this work, see: M. Moser, X. Sun, and T. Hudlicky. Org. Lett. **7**, 5669 (2005).
24. J.D. Rainier and J.E. Imbriglio. J. Org. Chem. **65**, 7272 (2000).
25. (*a*) E. Negishi, F.E. Cederbaum, and T. Takahashi. Tetrahedron Lett. **27**, 2829 (1986); (*b*) X. Zhou, Z. Li, H. Wang, M. Kitamura, K. Kanno, K. Nakajima, and T. Takahashi. J. Org. Chem. **69**, 4559 (2004).
26. T. Hudlicky, X. Tian, K. Königsberger, and J. Rouden. J. Org. Chem. **59**, 4037 (1994).
27. (*a*) B.B. Lohray. Synthesis, 1035 (1992); (*b*) U. Rinner, P. Siengalewicz, and T. Hudlicky. Org. Lett. **4**, 115 (2002).
28. K. Tamao, N. Ishida, Y. Ito, and M. Kumada. Org. Synth. Coll. **8**, 315 (1993).
29. G.R. Krow. Org. React. (N.Y.), **43**, 251 (1993).

© 2006 NRC Canada

Novel electrophilic ipso acylation – detosylation reaction of pyrroles[1]

Erin T. Pelkey and Gordon W. Gribble

Abstract: A pyrrole and two pyrroloindoles that are substituted with a *p*-toluenesulfonyl group undergo an ipso acylation – detosylation reaction with acid chlorides and aluminum chloride to afford the corresponding acyl-substituted pyrroles and pyrroloindoles.

Key words: pyrrole, pyrroloindole, ipso acylation, detosylation, Friedel–Crafts reaction.

Résumé : Sous l'action de chlorures d'acides et de chlorure d'aluminium, un pyrrole et deux pyrroindoles substitués par un groupe *p*-toluènesulfonyle subissent des réactions d'acétylation-détosylation ipso qui conduisent à la formation des pyrroles et pyrroindoles correspondants substitués par un groupe acyle.

Mots clés : pyrrole, pyrroindole, acétylation ipso, détosylation, réaction de Friedel–Crafts.

[Traduit par la Rédaction]

Introduction

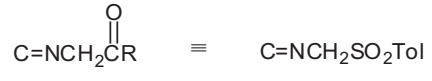
Whereas electrophilic ipso substitution (1) of aromatic and heteroaromatic compounds, including organosilanes (2), organostannanes (3), and several other substrates (4), is well-documented, there appear to be no examples of organosulfones undergoing electrophilic ipso substitution. For example, treatment of 3-phenyl-4-(*p*-toluenesulfonyl)furan with acetyl chloride and $AlCl_3$ gives only the expected electrophilic product, 2-acetyl-3-phenyl-4-(*p*-toluenesulfonyl)furan (5). On the other hand, free radical ipso stannylation – detosylation reactions of 1-(phenylsulfonyl)-2-(*p*-toluenesulfonyl) indole and related heterocycles have been described (6).

Results and discussion

In connection with our interest in the closely related Barton–Zard (7), van Leusen (8), and Montforts (9) syntheses of pyrroles (10), we had occasion to examine the Friedel–Crafts acylation of 4-ethyl-2-(*p*-toluenesulfonyl)pyrrole (**4**). This compound was readily prepared by treating either 2-nitrobutyl acetate (**1**) (11) or 2-nitro-1-butene (**2**) (12) with TosMIC (**3**) (13) and DBU in the presence of isopropanol Scheme 1). Treatment of **4** with acetyl chloride in the presence of aluminum chloride affords 2-acetyl-4-ethylpyrrole (**5**) and not the expected 2-acetyl-3-ethyl-5-(*p*-toluenesulfonyl)pyrrole (**6**). The characteristic odor of *p*-toluenesulfonyl chloride (**7**) in the reaction mixture was indicative of this novel transformation. To confirm the regiochemistry of **5**, we synthesized 2-acetyl-3-ethylpyrrole (**8**) by hydrolysis (K_2CO_3, MeOH, reflux, 78%) of the known 2-acetyl-3-ethyl-1-(phenylsulfonyl)pyrrole (14). Direct comparison of these two pyrroles reveals that the product of the acetylation of **4** was clearly **5** and not **8**. We view this ipso acylation – detosylation reaction as involving ipso electrophilic attack at C-5 in **4** followed by chloride attack on the sulfonyl group to give *p*-toluenesulfonyl chloride and pyrrole **5**.

This ipso acylation – detosylation was extended to the synthesis of acylated pyrroloindoles (Scheme 2). Thus, treatment of pyrrolo[2,3-*b*]indole **10** and pyrrolo[3,4-*b*]indole **13** with acetyl chloride and valeryl chloride in the presence of aluminum chloride affords the acylated analogues **11** and **14**, respectively. Pyrroloindoles **10** and **13** were synthesized with TosMIC from indoles **9** and **12**, respectively, according to our earlier method (10).

In summary, we have discovered a novel electrophilic ipso acylation – detosylation reaction of α-tosylpyrroles. In the context of van Leusen and Barton–Zard pyrrole syntheses, the reagent TosMIC (**3**) can be viewed as a synthetic equivalent for α-isocyanoketones (**15**). Compounds related to **15** have previously been generated from α-metalated oxazoles (15), but they have not been employed in these pyrrole ring syntheses.



15 **3**

Received 14 November 2005. Accepted 31 March 2006. Published on the NRC Research Press Web site at http://canjchem.nrc.ca on 12 August 2006. Reposted on the Web site with correction on 25 August 2006.

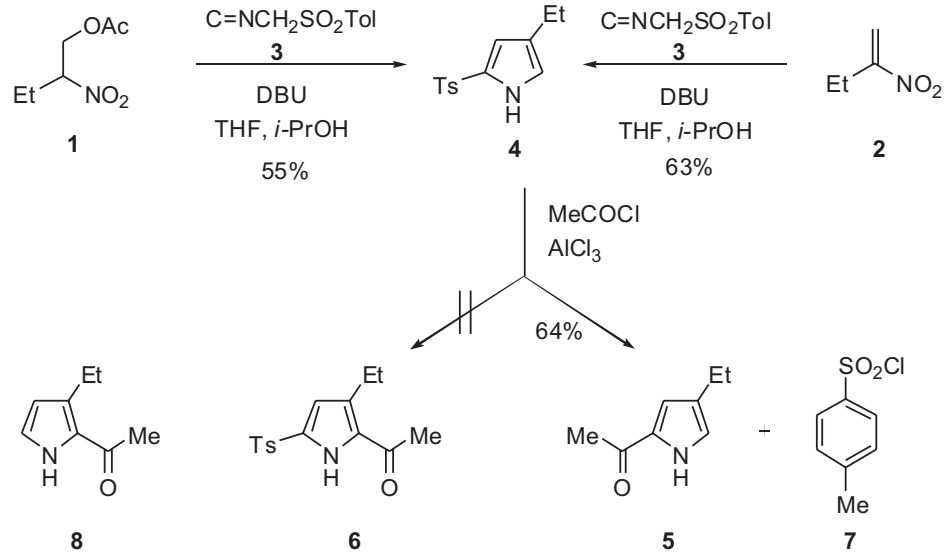
Dedicated to Dr. Alfred Bader, organic chemistry pioneer and art connoisseur extraordinaire. Thank you for giving us decades of wonderful service and for rejuvenating our appreciation of art.

E.T. Pelkey and G.W. Gribble.[2] Department of Chemistry, Dartmouth College 6128 Burke Laboratory, Hanover, NH 03755, USA.

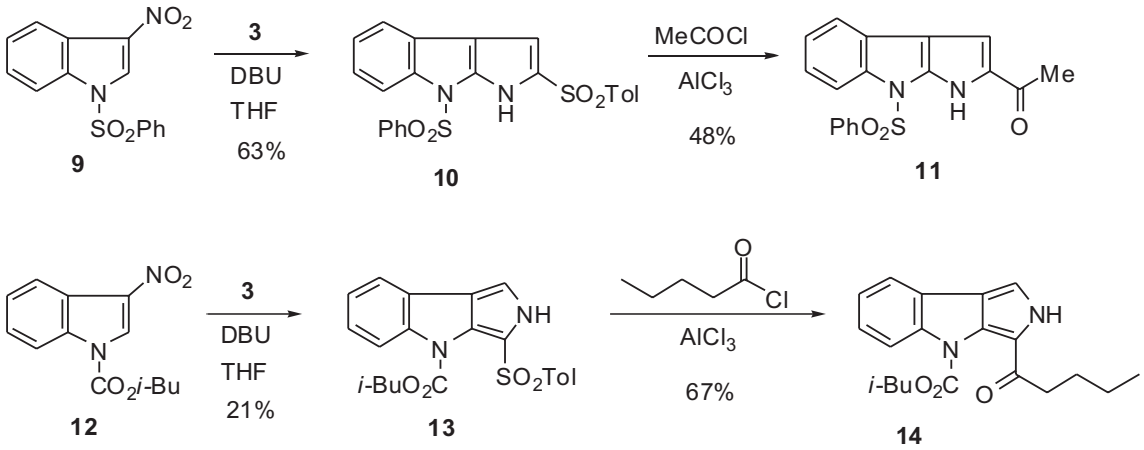
[1]This article is part of a Special Issue dedicated to Dr. Alfred Bader.

 doi:10.1139/V06-075 © 2006 NRC Canada

Scheme 1.



Scheme 2.



Experimental

Melting points were determined using open capillary tubes and are uncorrected. Thin-layer chromatography (TLC) was performed on regular TLC plates. Visualization of developed plates was achieved with a 254 nm UV lamp and (or) with iodine. Flash chromatography utilized 230–400 mesh silica gel 60. ^{1}H NMR and ^{13}C NMR were run at 300 and 75 MHz, respectively. Chemical shifts (δ) are reported in ppm using the solvent residual proton or carbon signal ($CDCl_3$: H, 7.27, C, 77.23) as an internal reference. The apparent multiplicity (singlet (s), doublet (d), triplet (t), quartet (q), septet (sept), multiplet (m), broad (br)), number of protons, and coupling constants (in Hz) are reported in that order in parenthesis after the chemical shift. Infrared spectra (IR) are reported in reciprocal centimeters and were obtained using neat compounds (neat), solid KBr pellets (KBr), polyethylene IR cards (PE), or polytetrafluoroethylene IR cards (PTFE). High-resolution mass spectrometry (HRMS) was performed at the University of Illinois (Urbana-Champaign, Illinois) mass spectrometry laboratory or by the SOCAL Mass Spectrometry Facility at the University of California (Riverside, California). Elemental analyses were performed by Atlantic Microlabs, Inc. (Norcross, Georgia). Tetrahydrofuran (THF) and diethyl ether (ether) were distilled from sodium-benzophenone ketyl. Diisopropylamine, dichloromethane, xylenes, and triethylamine were distilled from calcium hydride. Acetyl chloride, hexanoyl chloride, trimethylsilyl chloride, and valeryl chloride were distilled from 0.1% quinoline. Unless otherwise indicated, all other reagents and solvents were purchased from commercial sources and were used without further purification. All reactions were performed under a positive nitrogen atmosphere with magnetic stirring unless otherwise noted. All glassware was oven-dried at >130 °C and allowed to cool in a desiccator (Drierite®) before assembly under positive nitrogen.

2-Nitro-1-butanol

A modification of a literature procedure was utilized (11). To a 0 °C stirred solution of sodium hydroxide (4.20 g, 105 mmol) dissolved in distilled water (40 mL) was added 1-nitropropane (8.91 g, 100 mmol) dropwise. The reaction mixture was stirred at 0 °C for 30 min and then at room temperature (rt) for 1 h. Upon recooling to 0 °C, the reaction mixture was treated with an aqueous solution of formalin

© 2006 NRC Canada

(37%, 8.52 g, 105 mmol) dropwise via addition funnel over 10 min and then the reaction mixture was stirred at rt for 7 h. Upon recooling to 0 °C, the reaction mixture was treated with acetic acid (6.60 g, 110 mmol) dropwise and stirred for 3 h. The aqueous solution was extracted with ether (5 × 50 mL) and the combined organic extracts were washed with brine (200 mL) and dried over sodium sulfate. Removal of the solvent in vacuo gave a yellow oil (20 g) that was purified by vacuum distillation through a Vigreux column. The desired product was obtained as a colorless oil. Yield: 6.57 g, 55.1 mmol, 55%; bp 124 to 125 °C at 10 Torr (1 Torr = 133.322 4 Pa) (lit. value (11) bp 90–92 °C at 3 Torr). ^{1}H NMR ($CDCl_3$) δ: 4.51–4.59 (m, 1H) 3.89–4.10 (m, 2H), 1.81–2.06 (m, 3H), 1.02 (t, J = 7.2 Hz, 3H). ^{13}C NMR ($CDCl_3$) δ: 90.8, 63.1, 23.5, 10.4.

2-Nitrobutyl acetate (1)

A modification of the literature procedure for synthesizing β-nitroacetates was utilized (16). To a 0 °C stirred solution of 2-nitro-1-butanol (5.59 g, 47.0 mmol) dissolved in CH_2Cl_2 (50 mL) was added acetic anhydride (5.72 g, 56.0 mmol) followed by *p*-toluenesulfonic acid monohydrate (380 mg, 2.0 mmol). The reaction mixture was stirred at 0 °C and then at rt for 8 h. Removal of the solvent in vacuo gave a residue (10 g) that was purified by vacuum distillation through a Vigreux column. The desired product **1** was obtained as a light yellow oil. Yield: 6.57 g, 40.1 mmol, 86%; bp 88 to 89 °C at 4 Torr (lit. value (11) bp 70–72 °C at 2 Torr). ^{1}H NMR ($CDCl_3$) δ: 4.62–4.69 (m, 1H), 4.41–4.43 (m, 2H), 2.07 (s, 3H), 1.80–2.06 (m, 2H), 1.03 (t, J = 7.2 Hz, 3H). ^{13}C NMR ($CDCl_3$) δ: 170.5, 87.8, 63.8, 23.9, 20.8, 10.2.

2-Nitro-1-butene (2) (Caution: Lachrymator and foul smelling)

A modification of the literature procedure for the synthesis of 2-nitropropene was utilized (17). A round-bottomed flask (100 mL) fitted with a Vigreux column and short-path distillation apparatus was charged with 2-nitro-1-butanol (11.9 g, 0.100 mol) and phthalic anhydride (29.6 g, 0.200 mol) and was partially evacuated (under water aspirator pressure). The reaction mixture was heated in an oil bath to 150 °C for 30 min and then to 200 °C. The desired product **2** distilled over with water into an ice-cooled receiving flask. The aqueous layer was separated and the organic layer was dried over sodium sulfate. The desired product **2** was obtained as a blue-green oil. Yield: 4.48 g, 0.0443 mol, 44%; bp 76–84 °C at 40 Torr (lit. value (12) bp 108 °C at 61 Torr). IR (neat, cm^{-1}) υ_{max}: 3132, 2980, 2942, 2882, 1524, 1465, 1436, 1347, 1258. ^{1}H NMR ($CDCl_3$) δ: 6.44 (s, 1H), 5.55 (s, 1H), 2.64 (q, J = 7.2 Hz, 2H,), 1.18 (t, J = 7.2 Hz, 3H,). ^{13}C NMR ($CDCl_3$) δ: 159.8, 116.3, 23.6, 11.8.

4-Ethyl-2-(*p*-toluenesulfonyl)pyrrole (4)

To a rt stirred solution of 2-nitro-1-butene (**2**) (202 mg, 2.00 mmol) and tosylmethyl isocyanide (**3**) (586 mg, 3.00 mmol) dissolved in THF (3 mL) and 2-propanol (3 mL) was added a solution of DBU (457 mg, 3.00 mmol) dissolved in THF (3 mL) and 2-propanol (3 mL). The reaction mixture was stirred at rt for 20 h. Removal of the solvent in vacuo gave a brown oil (1.8 g) that was purified by flash chromatography (hexanes; CH_2Cl_2–hexanes, 1:1; CH_2Cl_2–hexanes, 3:1). After eluting a brightly colored yellow impurity (R_f 0.38; CH_2Cl_2–hexanes, 3:1), the desired product **4** was obtained as a yellow amorphous solid. Yield: 372 mg, 80% pure by ^{1}H NMR, 1.25 mmol, 63% yield based on NMR integration. Recrystallization (CH_2Cl_2–hexanes, 1:4) gave **4** as off-white needles; mp 94 to 95 °C. R_f 0.15 (CH_2Cl_2–hexanes, 3:1). IR (PTFE, cm^{-1}) υ_{max}: 3306 (NH), 2964, 2924, 2872, 1595, 1494, 1440, 1379, 1301, 1202, 1146. ^{1}H NMR ($CDCl_3$) δ: 8.90 (br s, 1H), 7.80–7.83 (m, 2H), 7.26 (m, 2H), 6.70–6.75 (m, 2 H), 2.45 (q, 2H, J = 7.5 Hz), 2.39 (s, 3H), 1.15 (t, 3H, J = 7.5 Hz). ^{13}C NMR ($CDCl_3$) δ: 143.9, 139.9, 130.0, 129.0, 127.7, 127.0, 121.1, 114.8, 21.7, 20.0, 15.0. MS *m*/*z* (%): 250 (M^+ + 1), 249 (M^+), 234 (100%), 184, 170, 142, 127, 110, 91, 78, 65. Anal. calcd. for $C_{13}H_{15}NO_2S$: C 62.63, H 6.06, N 5.62, S 12.83; found: C 62.57, H 6.05, N 5.56, S 12.95.

2-Acetyl-4-ethylpyrrole (5)

To a 0 °C stirred suspension of aluminum chloride (333 mg, 2.50 mmol) in CH_2Cl_2 (5 mL) was added freshly distilled (from quinoline) acetyl chloride (79 mg, 1.00 mmol) and the mixture was stirred for 15 min and then treated with a solution of 4-ethyl-2-(*p*-toluenesulfonyl)pyrrole (**4**) (125 mg, 0.500 mmol) dissolved in CH_2Cl_2 (5 mL) dropwise. The reaction mixture was stirred at 0 °C for 1 h and then was poured onto ice (20 g). The organic layer was separated and the aqueous layer was extracted with CH_2Cl_2 (3 × 20 mL). The combined organic extracts were washed with brine (60 mL) and dried over sodium sulfate. Removal of the solvent in vacuo gave an orange oil (0.3 g) that was purified by flash chromatography (hexanes; CH_2Cl_2). The title compound **5** was obtained as a yellow oil. Yield: 44 mg, 0.32 mmol, 64%. R_f 0.16 (CH_2Cl_2–EtOAc, 10:1). UV (EtOH) λ_{max} (nm): 208, 250, 302. IR (PTFE, cm^{-1}) υ_{max}: 3257 (NH), 2960, 2920, 2851, 1633 (C=O), 1568, 1479, 1432, 1397, 1322. ^{1}H NMR ($CDCl_3$) δ: 9.82 (br s, 1H), 6.77–6.87 (m, 2H), 2.52 (q, 2H, J = 7.5 Hz), 2.42 (s, 3H), 1.17–1.26 (m, 3H). ^{13}C NMR ($CDCl_3$) δ: 188.1, 132.0, 128.6, 122.8, 116.5, 25.5, 20.0, 15.4. MS *m*/*z* (%): 138 (M^+ + 1), 137 (M^+), 122 (100%), 104, 94, 77, 67. HRMS *m*/*z* calcd. for $C_8H_{11}NO$: 137.0841 (M^+); found: 137.0841.

2-Acetyl-3-ethylpyrrole (8)

To a rt stirred solution of 3-ethyl-2-acetyl-1-(phenylsulfonyl)pyrrole (14) (83 mg, 0.30 mmol) dissolved in methanol (5 mL) was added potassium carbonate (170 mg, 1.2 mmol) and the reaction mixture was heated to reflux for 7 h and then allowed to cool to rt. Removal of the solvent in vacuo gave an orange oil (0.5 g) that was partitioned between distilled water (20 mL) and ether (20 mL). The organic layer was separated and the aqueous layer was extracted with ether (2 × 20 mL). The combined organic extracts were washed with brine (60 mL) and dried over sodium sulfate. Removal of the solvent in vacuo gave a yellow oil (40 mg) that was purified by flash chromatography (hexanes; CH_2Cl_2). The desired product **8** was obtained as a light yellow amorphous solid. Yield: 32 mg, 0.23 mmol, 78%; mp 64 to 65 °C. R_f 0.18 (CH_2Cl_2). UV (EtOH) λ_{max} (nm): 206, 292. IR (PTFE, cm^{-1}) υ_{max}: 3271 (NH), 2967, 1622 (C=O), 1532, 1478, 1407, 1325, 1201, 1136. ^{1}H NMR ($CDCl_3$) δ:

© 2006 NRC Canada

9.43 (br s, 1H), 6.92–6.94 (m, 1H), 6.17–6.19 (m, 1H), 2.82 (q, 2H, J = 7.5 Hz), 2.47 (s, 3H), 1.30 (t, 3H, J = 7.5 Hz). ^{13}C NMR ($CDCl_3$) δ: 187.9, 134.2, 123.3, 111.5, 111.4, 28.0, 21.3, 15.1. MS m/z (%): 138 (M^+ + 1), 137 (M^+), 122 (100%), 94, 80, 67. HRMS m/z calcd. for $C_8H_{11}NO$: 137.0841 (M^+); found: 137.0842.

1,8-Dihydro-4-(phenylsulfonyl)-2-(*p*-toluenesulfonyl)pyrrolo[2,3-*b*]indole (10)

To a stirred solution of 3-nitro-1-(phenylsulfonyl)indole (**9**) (18) (151 mg, 0.500 mmol) dissolved in THF (10 mL) was added a solution of tosylmethyl isocyanide (**3**) (117 mg, 0.600 mmol) dissolved in THF (5 mL) followed by neat DBU (183 mg, 1.20 mmol). The clear yellow reaction mixture was stirred at rt for 22 h. Removal of solvent in vacuo gave a crude orange oil (500 mg) that was purified by flash chromatography (hexanes; CH_2Cl_2–hexanes, 3:1; CH_2Cl_2). The desired product **10** was obtained as a white amorphous solid (150 mg). Trituration (hexanes, 2 × 5 mL) gave **10** as a gray flaky solid. Yield: 142 mg, 0.315 mmol, 63%; mp 212–214 °C (dec). Two recrystallizations (CH_2Cl_2–cyclohexane, 2:1) gave **10** as white crystals; mp 236–238 °C. R_f 0.50 (CH_2Cl_2). UV (EtOH) λ_{max} (nm): 210, 274 (sh), 300, 346 (sh). IR (KBr, cm^{-1}) υ_{max}: 3256 (NH), 2928, 1540, 1528, 1447, 1419, 1374, 1318, 1181. ^{1}H NMR ($CDCl_3$) δ: 9.78 (bs, 1H), 7.88–7.92 (m, 3H), 7.74–7.76 (m, 2H), 7.48–7.54 (m, 2H), 7.22–7.37 (m, 6H), 7.11 (d, 1H, J = 1.8 Hz), 2.41 (s, 3H). ^{13}C NMR ($CDCl_3$) δ: 144.3, 139.6, 138.5, 137.6, 136.4, 134.8, 130.2, 129.6, 128.8, 127.2, 126.9, 125.0, 124.6, 124.3, 120.1, 114.8, 113.4, 107.6, 21.8. MS m/z (%): 473.1 $(M + Na)^+$. Anal. calcd. for $C_{23}H_{18}N_2O_4S_2$: C 61.32, H 4.03, N 6.22, S 14.23; found: C 61.35, H 4.04, N 6.23, S 14.36.

2-Acetyl-1,8-dihydro-8-(phenylsulfonyl)pyrrolo[2,3-*b*]indole (11)

To a 0 °C stirred suspension of aluminum chloride in CH_2Cl_2 (5 mL) was added acetyl chloride (79 mg, 1.0 mmol) and the mixture was stirred for 15 min. The reaction mixture was treated with a solution of 1,8-dihydro-2-(*p*-toluenesulfonyl)-4-(phenylsulfonyl)pyrrolo[2,3-*b*]indole (**10**) (225 mg, 0.500 mmol) dissolved in CH_2Cl_2 (5 mL). The reaction mixture was stirred at 0 °C for 2 h and then at rt for 30 min. The reaction was poured onto ice (20 g) and extracted with CH_2Cl_2 (3 × 30 mL). The combined organic extracts were washed with a saturated aqueous solution of sodium bicarbonate (100 mL) and brine (100 mL) and dried over sodium sulfate. Removal of the solvent in vacuo gave a yellow oil (0.6 g) that was purified by flash chromatography (hexanes; CH_2Cl_2–hexanes, 1:1; CH_2Cl_2–hexanes, 3:1). The desired product **11** was obtained as a white amorphous solid. Yield: 82 mg, 0.24 mmol, 48%; mp 222–225 °C. Recrystallization (CH_2Cl_2–hexanes) gave **11** as light brown crystals; mp 230 to 231 °C. R_f 0.18 (CH_2Cl_2). UV (EtOH) λ_{max} (nm): 206, 224, 254 (sh), 332. IR (PTFE, cm^{-1}) υ_{max}: 3304 (NH), 2917, 2851, 1633, 1555, 1488, 1440, 1380, 1285, 1201, 1171. ^{1}H NMR ($CDCl_3$) δ: 9.87 (br s, 1H), 7.93–7.96 (m, 1H), 7.81–7.85 (m, 2H), 7.27–7.59 (m, 6H), 7.11 (d, 1H, J = 1.5 Hz), 2.51 (s, 3H). ^{13}C NMR ($CDCl_3$) δ: 187.9, 139.1, 139.0, 136.9, 134.7, 132.9, 129.6, 127.0, 124.9, 124.7, 124.4, 120.0, 114.9, 113.5, 108.2, 25.3. MS m/z (%): 338 (M^+), 197 (100%), 169, 155, 127, 101, 77. Anal. calcd. for $C_{18}H_{14}N_2O_3S$: C 63.89, H 4.17, N 8.28, S 9.47; found: C 64.04, H 4.07, N 8.20, S 9.34.

2-Methyl-1-propyl 2,4-dihydro-3-(*p*-toluenesulfonyl)pyrrolo[3,4-*b*]indole-4-carboxylate (13)

To a rt stirred solution of 2-methyl-1-propyl 3-nitroindole-1-carboxylate (**12**) (18) (1.84 g, 7.00 mmol) and tosylmethyl isocyanide (**3**) (1.56 g, 8.00 mmol) dissolved in THF (50 mL) was added DBU (1.22 g, 8.00 mmol) and the reaction mixture was stirred at rt for 20 h. Removal of the solvent in vacuo gave a brown oil (4 g) that was purified by flash chromatography (hexanes; CH_2Cl_2–hexanes, 3:1; CH_2Cl_2). The desired product **13** was obtained as a brown amorphous solid (615 mg, 1.50 mmol, 21%) that was purified by a second round of column chromatography (hexanes; CH_2Cl_2–hexanes, 1:1). The yellow powder thus obtained was recrystallized (CH_2Cl_2–hexanes) to give **13** as fine yellow needles; mp 177 to 178 °C. R_f 0.23 (CH_2Cl_2). UV (EtOH) λ_{max} (nm): 206, 222 (sh), 254 (sh), 278, 315 (sh), 324. IR (PTFE, cm^{-1}) υ_{max}: 3283 (NH), 2958, 1731 (C=O), 1595, 1515, 1448, 1417, 1379, 1317, 1199, 1139. ^{1}H NMR ($CDCl_3$) δ: 9.60 (br s, 1H), 8.32 (br s, 1H), 8.24–8.26 (m, 1H), 7.89 (d, 2H, J = 8.1 Hz), 7.34–7.49 (m, 2H), 7.24 (d, 2H, J = 8.1 Hz), 7.03 (br s, 1H), 4.23 (d, 2H, J = 4.8 Hz), 2.35 (s, 3H), 2.14 (br s, 1H), 1.06 (d, 6H, J = 6.6 Hz). ^{13}C NMR ($CDCl_3$) δ: 151.4, 144.2, 143.2, 139.7, 131.4, 130.1, 127.4, 126.6, 123.8, 122.8, 121.5, 120.0, 116.1, 115.5, 107.2, 73.1, 28.1, 21.7, 19.3. HRMS m/z calcd. for $C_{22}H_{22}N_2O_4S$: 410.1300 (M^+); found: 410.1294. Anal. calcd. for $C_{22}H_{22}N_2O_4S$: C 64.37, H 5.40, N 6.82, S 7.81; found: C 64.46, H 5.51, N 6.85, S 7.76.

2-Methyl-1-propyl 2,4-dihydro-3-valerylpyrrolo[3,4-*b*]-indole-4-carboxylate (14)

To a 0 °C stirred suspension of aluminum chloride (200 mg, 1.50 mmol) in CH_2Cl_2 (5 mL) was added freshly distilled (from 0.1% quinoline) valeryl chloride (72 mg, 0.60 mmol) and this was stirred for 15 min. The reaction mixture was treated with a solution of 2-methyl-1-propyl 2,4-dihydro-3-(*p*-toluenesulfonyl)pyrrolo[3,4-*b*]indole-1-carboxylate (**13**) (123 mg, 0.300 mmol) dissolved in CH_2Cl_2 (10 mL) dropwise. The reaction mixture was stirred at 0 °C for 15 min and then was poured onto ice (20 g). The aqueous solution was extracted with CH_2Cl_2 (3 × 30 mL) and the combined organic extracts were washed with a saturated aqueous solution of sodium bicarbonate (100 mL) and brine (100 mL) and dried over sodium sulfate. Removal of the solvent in vacuo gave a tan amorphous solid (0.2 g) that was purified by flash chromatography (hexanes; CH_2Cl_2–hexanes, 1:1; CH_2Cl_2–hexanes, 3:1). The desired product **14** was obtained as an off-white amorphous solid (68 mg, 0.20 mmol, 67%, mp 166–168 °C). Recrystallization (EtOAc–hexanes) gave **14** as white needles; mp 173 to 174 °C. R_f 0.48 (H_2Cl_2–MeOH, 98:2). UV (EtOH) λ_{max} (nm): 206, 233 (sh), 246 (sh), 277 (sh), 286, 311 (sh), 344 nm. IR (KBr) υ_{max} (cm^{-1}): 3236 (NH), 2956, 2870, 1728 (C=O), 1627 (C=O), 1506, 1460, 1402, 1390, 1319, 1268, 1219. ^{1}H NMR ($CDCl_3$) δ: 10.04 (br s, 1H), 8.43 (br s, 1H), 8.00–8.02 (m, 1H), 7.43–7.48 (m, 1H), 7.33–7.38 (m, 1H), 7.13 (br s, 1H), 4.27 (d, 2H, J = 6.3 Hz), 3.12 (t, 2H, J = 7.2 Hz), 2.12–2.22 (m, 1H), 1.82–1.92 (m, 2H), 1.48–1.60 (m, 2H), 1.10 (d, 6H, J =

© 2006 NRC Canada

6.9 Hz), 1.02 (t, 3H, J = 7.2 Hz). ^{13}C NMR ($CDCl_3$) δ: 190.1, 151.6, 143.4, 131.8, 126.8, 123.5, 122.6, 122.5, 121.0, 118.5, 116.3, 107.5, 73.2, 40.5, 28.2, 26.7, 22.8, 19.4, 14.3. MS *m/z* (%): 340 (M^+, 100%), 298, 283, 242, 198, 183, 156, 127, 101, 77. Anal. calcd. for $C_{20}H_{24}N_2O_3$: C 70.57, H 7.11, N 8.23; found: C 70.32, H 7.11, N 8.13.

Acknowledgements

The authors would like to acknowledge the Donors of the Petroleum Research Fund (PRF), administered by the American Chemical Society, Pfizer, and Wyeth-Ayerst, for support of this project, Smith-Kline Beecham for sponsoring a Division of Organic Chemistry American Chemical Society Graduate Fellowship to ETP, and Professor Daniel M. Ketcha (Wright State University, Dayton, Ohio) for a gift of **8**.

References

1. (*a*) C.L. Perrin and G.A. Skinner. J. Am. Chem. Soc. **93**, 3389 (1971); (*b*) J.G. Traynhan. J. Chem. Educ. **60**, 937 (1983).
2. (*a*) J.R. Pratt, F.H. Pinkerton, and S.F. Thames. J. Organomet. Chem. **38**, 29 (1972); (*b*) A.G.M. Barrett, D. Dauzonne, I.A. O'Neil, and A. Renaud. J. Org. Chem. **49**, 4409 (1984); (*c*) M. Speranza, C.-Y. Shiue, A.P. Wolf, D.S. Wilbur, and G. Angelini. J. Fluorine Chem. **30**, 97 (1985); (*d*) M.W. Majchrzak and G. Simchen. Synthesis, 956 (1986); (*e*) D.M. Ketcha, B.A. Lieurance, D.F.J. Homan, and G.W. Gribble. J. Org. Chem. **54**, 4350 (1989); (*f*) B. Bennetau and J. Dunogues. Synlett, 171 (1993).
3. (*a*) J.R. Pratt, F.H. Pinkerton, and S.F. Thames. J. Organomet. Chem. **38**, 29 (1972); (*b*) J. Einhorn, P. Demerseman, and R. Royer. Synthesis, 978 (1984); (*c*) F. Favresse, V. Fargeas, P. Charrue, B. Lebret, M. Piteau, and J.-P. Quintard. J. Organomet. Chem. **598**, 187 (2000); (*d*) V. Fargeas, F. Favresse, D. Mathieu, I. Beaudet, P. Charrue, B. Lebret, M. Piteau, and J.-P. Quintard. Eur. J. Org. Chem. 1711 (2003).
4. (*a*) ArX: D.M. Ketcha, B.A. Lieurance, D.F.J. Homan, and G.W. Gribble. J. Org. Chem. **54**, 4350 (1989); (*b*) $ArCO_2H$: A.H. Jackson, G.W. Kenner, and K.M. Smith. J. Chem. Soc. C, 502 (1971); A.K. Bose, S.N. Ganguly, M.S. Manhas, V. Srirajan, A. Bhattacharjee, S. Rumthao, and A.H. Sharma. Tetrahedron Lett. **45**, 1179 (2004); (*c*) $ArCH_2OH$: A. Bravo, F. Fontana, B. Dordi, and F. Minisci. J. Org. Chem. **65**, 3880 (2000); (*d*) Ar-*t*-Bu: T. Yamato, T. Furukawa, S. Saito, K. Tanaka, and H. Tsuzuki. New J. Chem. **26**, 1035 (2002); (*e*) $ArB(OH)_2$: H.G. Kuivila and E.K. Easterbrook. J. Am. Chem. Soc. **73**, 4629 (1951); G.M. Davies, P.S. Davies, W.E. Paget, and J.M. Wardleworth. Tetrahedron Lett. 795 (1976); C. Thiebes, G.K.S. Prakash, N.A. Petasis, and G.A. Olah. Synlett, 141 (1998); J. Simon, S. Salzbrunn, G.K.S. Prakash, N.A. Petasis, and G.A. Olah. J. Org. Chem. **66**, 633 (2001); E. Shoji and M.S. Freund. Langmuir, **17**, 7183 (2001); G.K.S. Prakash, C. Panja, T. Mathew, V. Surampudi, N.A. Petasis, and G.A. Olah. Org. Lett. **6**, 2205 (2004).
5. S.W. McCombie, B.B. Shankar, and A.K. Ganguly. Tetrahedron Lett. **28**, 4123 (1987).
6. (*a*) S. Caddick, K. Aboutayab, and R. West. Synlett, 231 (1993); (*b*) Y. Antonio, M.E. De La Cruz, E. Galeazzi, A. Guzman, B.L. Bray, R. Greenhouse, L.J. Kurz, D.A. Lustig, M.L. Maddox, and J.M. Muchowski. Can. J. Chem. **72**, 15 (1994); (*c*) K. Aboutayab, S. Caddick, K. Jenkins, S. Joshi, and S. Khan. Tetrahedron, **52**, 11329 (1996); (*d*) Y. Watanabe, Y. Ueno, T. Araki, T. Endo, and M. Okawara. Tetrahedron Lett. **27**, 215 (1986).
7. (*a*) D.H.R. Barton and S.Z. Zard. J. Chem. Soc. Chem. Commun. 1098 (1985); (*b*) D.H.R. Barton, J. Kervagoret, and S.Z. Zard. Tetrahedron, **46**, 7587 (1990); (*c*) For a review, see: G.W. Gribble. Name reactions in heterocyclic chemistry. *Edited by* J.J. Li. Wiley-Interscience Inc., Hoboken, New Jersey. 2005. p. 70.
8. A.M. van Leusen, H. Siderius, B.E. Hoogenboom, and D. van Leusen. Tetrahedron Lett. 5337 (1972).
9. (*a*) G. Haake, D. Struve, and F.-P. Montforts. Tetrahedron Lett. **35**, 9703 (1994); (*b*) Y. Abel, E. Haake, G. Haake, W. Schmidt, D. Struve, A. Walter, and F.-P. Montforts. Helv. Chim. Acta, **81**, 1978 (1998).
10. (*a*) E.T. Pelkey, L. Chang, and G.W. Gribble. Chem. Commun. (Cambridge), 1909 (1996); (*b*) E.T. Pelkey and G.W. Gribble. Chem. Commun. (Cambridge), 1873 (1997).
11. H. Feuer and R. Miller. J. Org. Chem. **26**, 1348 (1961).
12. D.H. Lloyd and D.E. Nichols. J. Org. Chem. **51**, 4294 (1986).
13. A.M. van Leusen, G.J.M. Boerma, R.B. Helmholdt, H. Siderius, and J. Strating. Tetrahedron Lett. 2367 (1972).
14. D. Xiao, J.A. Schreier, J.H. Cook, P.G. Seybold, and D.M. Ketcha. Tetrahedron Lett. **37**, 1523 (1996).
15. (*a*) D. Hoppe. Angew. Chem. Int. Ed. Engl. **13**, 789 (1974); (*b*) U. Schöllkopf. Angew. Chem. Int. Ed. Engl. **16**, 339 (1977); (*c*) H. Kojima, K. Yamamoto, Y. Kinoshita, and H. Inoue. J. Heterocycl. Chem. **30**, 1691 (1993).
16. N. Ono, H. Katayama, S. Nisyiyama, and T. Ogawa. J. Heterocycl. Chem. **31**, 707 (1994).
17. M. Miyashita, T. Yanami, and A. Yoshikoshi. Org. Syn. Coll. Vol. VII, 396 (1990).
18. E.T. Pelkey and G.W. Gribble. Synthesis, 1117 (1999).

© 2006 NRC Canada

Catalysis with palladium colloids supported in poly(acrylic acid)-grafted polyethylene and polystyrene[1]

David E. Bergbreiter, Andrew Kippenberger, and Zhenqi Zhong

Abstract: Grafts of poly(acrylic acid) on polyethylene powder (PE-*g*-PAA) or polystyrene (PS-*g*-PAA) can be used to support Pd(0) crystallites that function like a homogeneous Pd(0) catalyst in some reactions. These Pd–PE-*g*-PAA catalysts were active in allylic substitution reactions in the presence of added phosphine ligand. A catalyst analogous to the Pd–PE-*g*-PAA powder catalyst on polystyrene (Pd–PS-*g*-PAA) was similarly active for allylic substitution and could also be used in Heck reactions at 80–100 °C in *N*,*N*-dimethylacetamide (DMA). Analysis of the product solutions for Pd leachate and a correlation of the Pd leaching with product formation in the allylic substitution chemistry for both types of catalysts suggests that the active catalysts in these reactions are leached from the support. In the case of the allylic substitution reaction, external triphenylphosphine and substrate together are required for the chemistry and Pd leaching.

Key words: catalysis, palladium, allylic substitution, grafted polystyrene, supported catalysts.

Résumé : Les produits de greffage d'acide polyacrylique sur de la poudre de polyéthylène (PE-*g*-APA) ou de polystyrène (PS-*g*-APA) peuvent être utilizés comme support de cristallites de Pd(0) qui, dans certaines réactions, peuvent fonctionner comme catalyseur de Pd(0). Ces catalyseurs de Pd–PE-*g*-APA mis en présence d'un ligand phosphine sont actifs dans les réactions de substitution allylique. Un catalyseur analogue au catalyseur en poudre Pd–PE-*g*-APA sur du polystyrène (Pd–PS-*g*-APA) est aussi actif pour la réaction de substitution allylique et il peut aussi être utilizé dans les réactions de Heck, à des températures allant de 80 à 100 °C, dans le *N*,*N*-diméthylacétamide (DMA). Une analyse des solutions de produits pour rechercher la présence de Pd qui aurait été lessivé ainsi qu'une corrélation du Pd de lessivage avec la formation de produit dans la chimie de la substitution allylique pour les deux types de catalyseur suggère que les catalyseurs actifs dans ces réactions sont lessivés de leur support. Dans le cas de la réaction de substitution allylique, la présence simultanée de la triphénylphosphine externe et du substrat sont requis pour la chimie et le lessivage du Pd.

Mots clés : catalyse, palladium, substitution allylique, polystyrène greffé, catalyseurs sur un support.

[Traduit par la Rédaction]

Introduction

The use of supported heterogeneous catalysts is well-established. Palladium catalysts are among the most common examples of such species. For example, catalysts like Pd–C are widely used for hydrogenation of alkenes (1). They have the virtue of wide availability, relatively low costs for handling and preparation, and activity that is often as good or better than that of the more "novel" hydrogenation catalysts reported from time to time.

While hydrogenation is an important reaction, other palladium-catalyzed processes, such as allylic substitutions and cross-coupling chemistry, are of more current interest. A variety of palladium catalysts have been developed for these purposes (2). Some years ago we had noted that classical Pd–C catalysts, under relatively mild conditions (i.e., at reaction temperatures <100 °C) (3, 4), exhibit reactivity resembling that of the well-established homogeneous Pd catalyst, tetrakis(triphenylphosphine)palladium(0). Specifically, we found that both a supported Pd(0) species prepared from an organometallic derivative of cross-linked polystyrene (5) and simple Pd–C could effectively catalyze allylic substitution of allyl acetates by nucleophiles like secondary amines. In these cases, catalysis was most effective in the presence of a soluble phosphine with reactions sometimes occurring at room temperature.

The importance of new sorts of catalysts, including adventitiously formed or designed colloidal metal catalysts for various catalytic reactions including cross-coupling reactions, has recently received increased attention (6–11). For example, we and others have noted the exceptional reactivity of Pd(0) colloidal catalysts, presumably generated in situ from Pd(II) palladacycle compounds during cross-coupling chemistry (12–17). These studies suggest that further explo-

Received 31 October 2005. Accepted 28 February 2006. Published on the NRC Research Press Web site at http://canjchem.nrc.ca on 12 August 2006.

D.E. Bergbreiter,[2] A. Kippenberger, and Z. Zhong. Department of Chemistry, P.O. Box 30012, College Station, TX 77842-3012, USA.

[1]This article is part of a Special Issue dedicated to Dr. Alfred Bader.

[2]Corresponding author (e-mail: bergbreiter@tamu.edu).

 doi:10.1139/V06-076 © 2006 NRC Canada

ration of ways to support and use Pd colloids merit attention. Our studies of these putative Pd colloids formed from SCS–Pd(II) precursors noted that those species were more soluble in polar phases than in nonpolar phases (14). Since we recently developed some new sorts of immobilized polar poly(acrylic acid) graft phases on polyethylene powders and on DVB cross-linked polystyrene resins, we have sought to explore these supported phases as supports for catalytically active Pd colloids. We have shown that Pd colloids formed and supported in these poly(acrylic acid) phases are active catalysts. While they are competent catalysts for hydrogenations, their activity is not significantly different then the more readily available and simpler Pd–C catalysts in hydrogenation catalysis.

While catalytic activity, especially reactivity in a reaction as simple as alkene hydrogenation, is often easy to demonstrate and assay, the identity of the actual species that leads to catalysis is not always clear. Indeed, it can even be difficult to determine whether the actual catalyst is soluble or insoluble (18). Such issues are even more complex when the chemistry is carried out with supported palladium colloids. For example, while we assumed a soluble Pd species was generated in our earlier studies (3, 4), a three-phase test using a polymer-supported Pd species (a soluble phosphine) and a second polymer-supported substrate failed to detect a soluble catalyst. We rationalized this result at the time on the basis that the actual phosphine-ligated Pd colloidal catalyst could still be present but could be unreactive to a second insoluble supported substrate (3). More recent work from several laboratories using various procedures, including Rebek's three-phase test (19), has been more successful in showing that homogeneous catalysts are responsible for the catalysis seen in other systems with "heterogeneous" catalysts (12, 19–24).

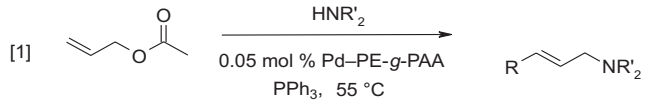
Here we describe work where we have shown that the Pd colloids in poly(acrylic acid) grafted polystyrene, which we used previously in hydrogenation reactions, are active in Heck catalysis and also in allylic substitution chemistry. While the analogous polyethylene-supported catalysts cannot be used in Heck chemistry (the required temperatures are incompatible with the underlying polymer), the polyethylene-bound catalysts exhibit Pd(0)-like reactivity in allylic substitutions of allylic acetates and amines. While we did not achieve the sort of notable reactivity we and others have seen in other putative Pd colloidal catalysts (12–17), we have been able to show that, in the case of these Pd colloids in a grafted polystyrene matrix or supported on polyethylene powder, Pd leaching is associated with the observed Pd(0)-like chemistry. The simplest explanation for these results is that soluble phosphine-free (Heck catalysis) or phosphine-ligated Pd species (allylic substitutions), derived from the interfacially supported Pd colloids in both the poly(acrylic acid)-grafted polyethylene powder and the poly(acrylic acid)-grafted DVB cross-linked polystyrene resin, are the active catalysts.

Results and discussion

We recently described several sorts of supported palladium catalysts using a poly(acrylic acid) graft on polyethylene powder (PE-*g*-PAA) or a poly(acrylic acid) graft within DVB cross-linked polystyrene beads (PS-*g*-PAA) as supports (19, 20, 25). Such colloidal catalysts have precedent both in our earlier work with polystyrene-supported palladium colloids (3, 4) and in other reports where supported thin films or inorganic matrices support analogs of homogeneous catalysts (3, 4, 8, 26–31).

The synthesis and characterization of both the PE-*g*-PAA and PS-*g*-PAA supports and catalysts were previously described, and the syntheses of these catalysts are summarized in Schemes 1 and 2. As shown in both schemes, the formation of a PE-*g*-PAA or a PS-*g*-PAA supported Pd colloid involved ion exchange of palladium acetate onto a PE- or PS-bound carboxylate group with subsequent reduction of the Pd(II) carboxylate ionically attached to the polymer graft. The Pd–PE-*g*-PAA and Pd–PS-*g*-PAA catalysts contained about 0.01 or 1.1 mmol of Pd per gram of support, respectively, based on digestion of the polymers and analysis of the residue for Pd by ICP metal analysis. In the case of the Pd–PE-*g*-PAA catalyst, imaging of the catalyst by XPS spectroscopy showed that the Pd colloids were distributed throughout a 50–100 μm region on the surface of the powder (Fig. 1). In the case of the Pd–PS-*g*-PAA, the Pd colloidal particles were mostly within the polystyrene bead.

The use of the Pd–PE-*g*-PAA and Pd–PS-*g*-PAA catalysts for catalytic hydrogenation reactions were described previously (19, 20). Both catalysts were found to be fully recyclable and no Pd leachate was detected in those studies. Of more interest in this study was that these catalysts also catalyze some Pd(0)-like reactions. Specifically, the PE-bound Pd colloids were effective in promoting allylic substitution reactions between secondary amines and allyl acetate (eq. [1]). Such reactions were not successful if no added phosphine was present in solution, but were successful in the presence of 5 mol% added triphenylphosphine (Table 1).

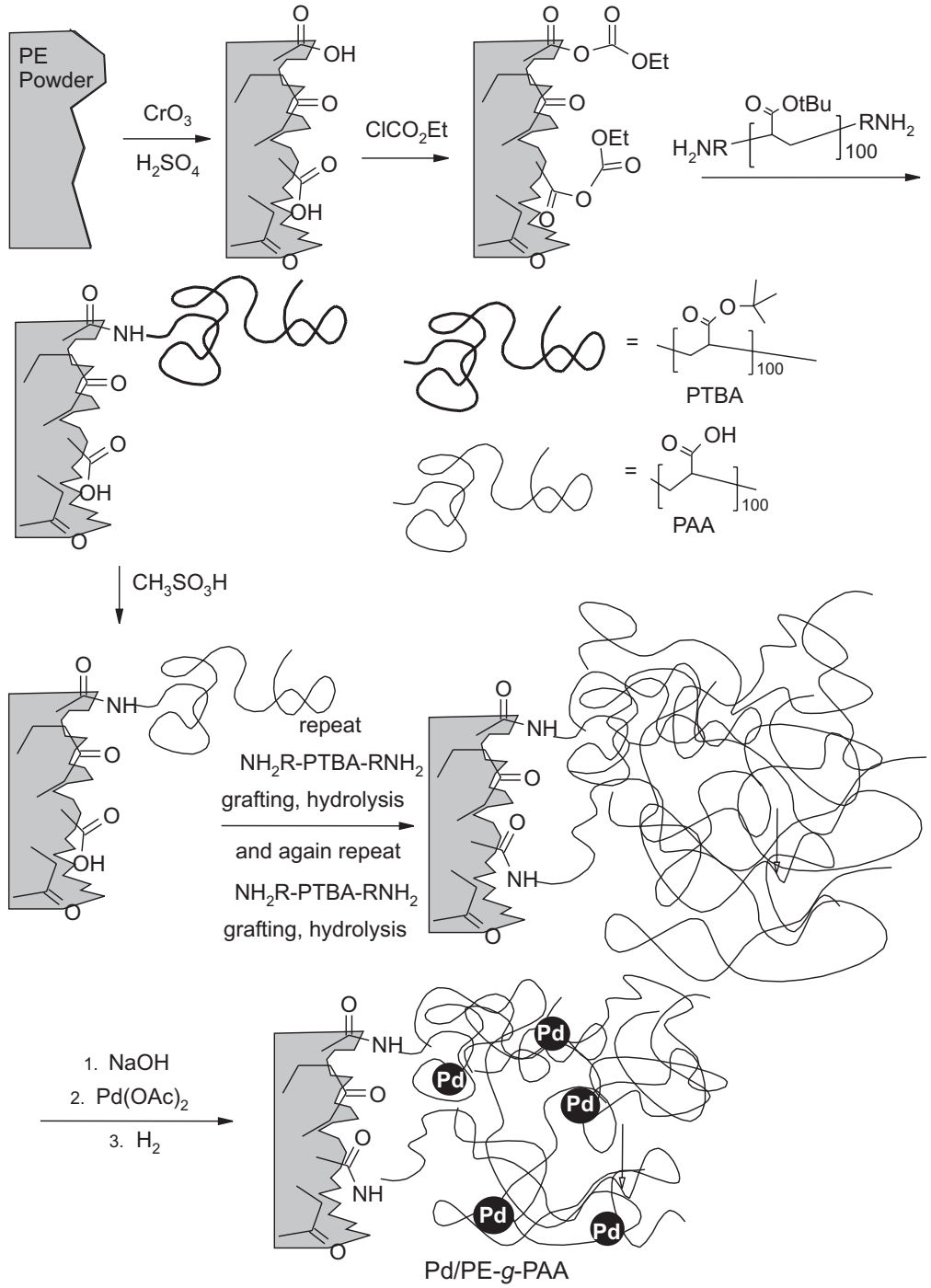


The reactivity in the presence of added phosphine ligands of the Pd–PE-*g*-PAA catalyst could be due to activation of the Pd colloids within the polymer matrix by the added triphenylphosphine. Alternatively, formation of tetrakis(triphenylphosphine)palladium or formation of some less-defined soluble phosphine-ligated Pd(0) species could explain the observed chemistry. As noted above, we had previously been unsuccessful at using a three-phase test to detect such soluble intermediates in a related system (3). Here we used several other approaches that together provide convincing evidence that a soluble Pd species is formed in these catalytic reactions.

To ascertain the origin of the catalysis, several experiments were performed. First, XPS analysis of Pd crystallites in a hyperbranched graft of Pd–PE-*g*-PAA showed a Pd $3d^{3/2}$ peak at 333.3 eV. This peak was discernibly different than the peak for a previously described immobilized molecular catalyst — a Pd(0) complex prepared using the same polymer that had been further modified to contain aminodiphenylphosphinopropyl ligands (i.e., Pd(0)-DPPA–PE-*g*-PAA; DPPA is diphenylphosphinopropylamide containing a phosphine ligand that was covalently coupled to poly(acrylic

© 2006 NRC Canada

Scheme 1. Synthesis of Pd–PE-*g*-PAA catalysts.



acid)-grafted PE via an amide bond) (25). No evidence was obtained for the presence of phosphine in the recovered PE support after a reaction, suggesting that added phosphine was not sorbed into the resin. Catalysts analogous to the Pd–PE-*g*-PAA could also be prepared by deliberate oxidation of the phosphine ligands in a Pd(0)-DPPA–PE-*g*-PAA catalyst — a process that converted the light yellow Pd(0)-DPPA–PE-*g*-PAA powder into a grey powder and produced a new peak for oxidized phosphine in XPS spectroscopy and a Pd(0) species with a Pd $3d^{3/2}$ peak such as that seen for the Pd crystallites in Pd–PE-*g*-PAA.

While the original Pd(0)-DPPA–PE-*g*-PAA catalyst was active in allylic substitution, after oxidation, both this recovered catalyst, now containing Pd(0) colloids, and the Pd–PE-*g*-PAA catalyst behaved similarly in that they had no activity in allylic substitution unless external phosphine was present (Fig. 2). These reactions catalyzed by Pd(0) colloids were also accompanied by Pd leaching. Using ICP–MS (inductively coupled plasma – mass spectroscopy) analysis, ca. 2% to 3% Pd leaching was seen in the reaction between allyl acetate and diethylamine with external phosphine. Pd leaching was not seen with Pd(0)-DPPA–PE-*g*-PAA catalysts that

© 2006 NRC Canada

Scheme 2. Synthesis of Pd–PAA-*g*-PS catalysts.

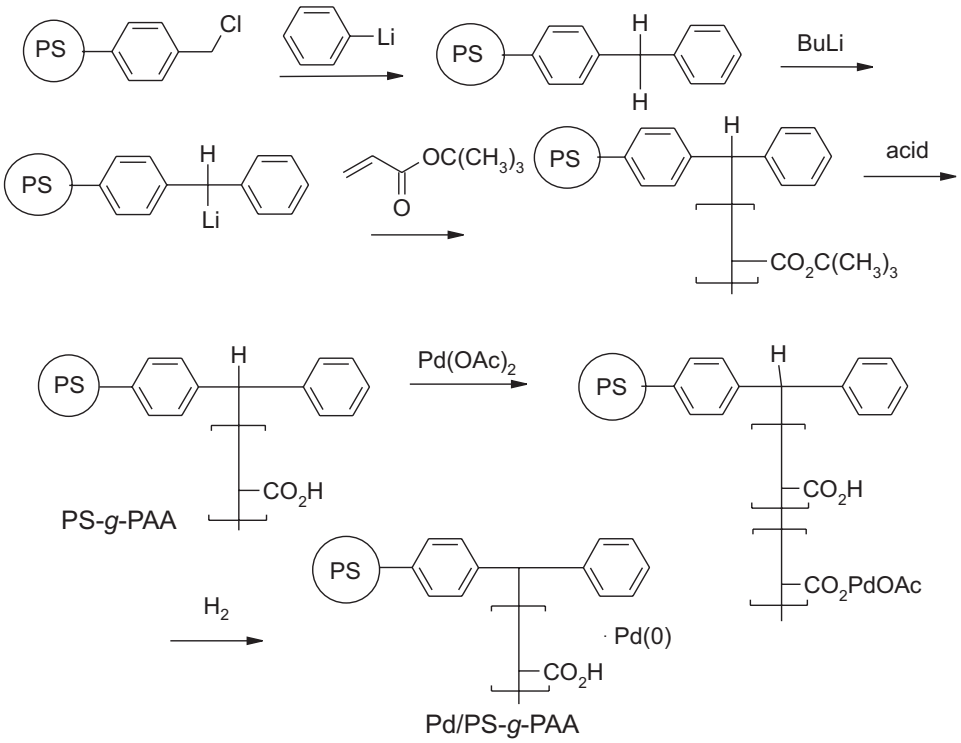
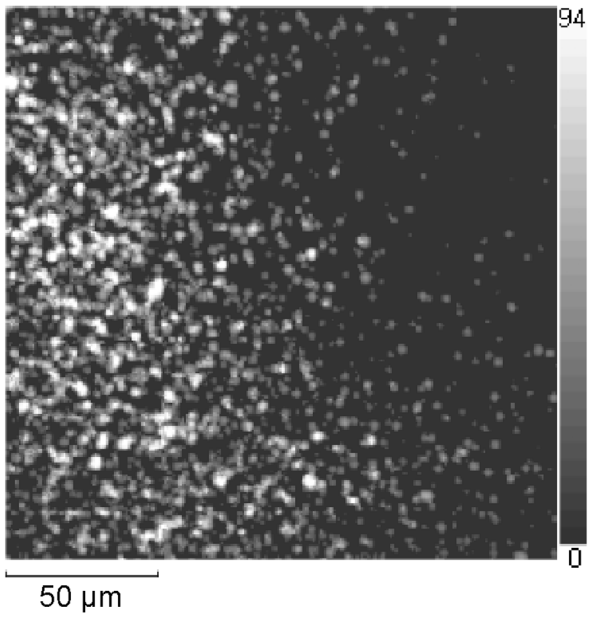


Fig. 1. XPS image of a Pd–PE-*g*-PAA powder. The white regions represent the presence of Pd 3d electrons. The left side of the image is focused on a Pd–PE-*g*-PAA particle, and the edge of the three-dimensional particle roughly transects the photograph.



contained covalently bound phosphine ligands within the functional polymer support that formed analogs of a molecular Pd(0) catalyst (25). Taken together, these results are consistent with an explanation such as that proposed previously (3) for the activity of these Pd–PE-*g*-PAA colloidal catalysts, which is based on leaching of a phosphine-ligated Pd catalyst or a Pd cluster.

Table 1. Allylic substitution reactions of allyl acetate with Pd–PE-*g*-PAA.

-R″	PPh_3 (mol%)	Time (h)	Conversion (%)[a]
Diethylamine	0.00	24	—[b]
Diethylamine	0.05	6/6	99, 99[c]
Pyrrolidine	0.05	20	99

Note: Reactions were carried out at 55 °C on a 20 mmol scale, typically without any added solvent.

[a]GC analysis showed that the conversion of starting material to product was 99%. Isolated yields of allylic amines in similar reactions were typically ca. 90%.

[b]No product was detected.

[c]Conversions for a second cycle using the Pd–PE-*g*-PAA catalyst with a fresh addition of 5 mol% triphenylphosphine.

These PE-bound Pd(0) species could not be used in Heck catalysis. No Heck catalysis was seen at 55 °C, and heating to higher temperatures led to thermal reorganization of the grafted PE powder (melting that produced a material that became inactive in hydrogenation or allylic substitution with or without added phosphine). However, immobilized poly(acrylic acid) grafts on a more thermally robust polymer, which are analogous to the Pd–PE-*g*-PAA powder catalysts described previously, can be prepared on DVB crosslinked polystyrene supports as shown in Scheme 2. Ion exchange of $Pd(OAc)_2$ with the immobilized poly(acrylic acid) followed by reduction, produced immobilized Pd(0) colloids that had hydrogenation activity analogous to that seen with Pd–C or to Pd crystallites immobilized within hyperbranched poly(acrylic acid) grafts on PE powder (20).

While the PE-supported Pd colloids could not be used in Heck catalysis because of temperature limitations, Pd colloids supported on more thermally robust DVB crosslinked polystyrene were active in Heck catalysis (eq. [2]).

© 2006 NRC Canada

Table 2. Heck catalysis with Pd–PS-*g*-PAA.

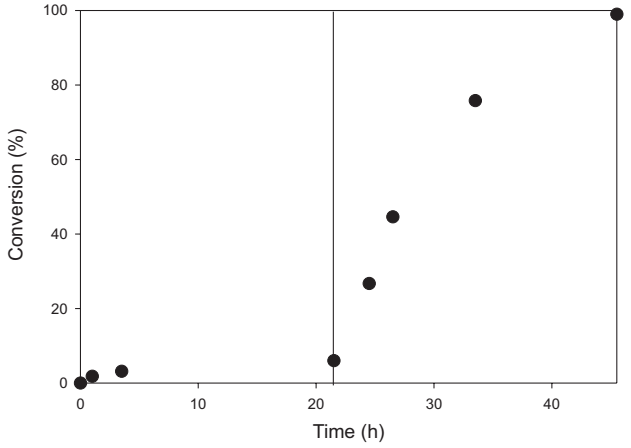
Substrate aryl iodide	Heck acceptor	Catalyst	Yield (%)[a]
4-Iodotoluene	*tert*-Butyl acrylate	Pd–PS-*g*-PAA	99
4-Iodotoluene	*tert*-Butyl acrylate	Pd–C[b]	75
Iodobenzene	*tert*-Butylstyrene	Pd–PS-*g*-PAA	100
4-Iodoanisole	*tert*-Butylbenzene	Pd–PS-*g*-PAA	94
4-Iodoanisole	*N*,*N*-Dimethylacrylamide	Pd–PS-*g*-PAA	95
4-Iodoanisole	*N*,*N*-Dimethylacrylamide	Pd–C	36
Iodobenzene	*tert*-Butyl acrylate	Pd–PS-*g*-PAA	100
4-Bromoacetophenone	*tert*-Butyl acrylate	Pd–PS-*g*-PAA	81
4-Bromoacetophenone	*N*,*N*-Dimethylacrylamide	Pd–PS-*g*-PAA	66

Note: Reactions were carried out on a 2 mmol scale in 10 mL of *N*,*N*-dimethylacrylamide using 2.5 mmol of Et_3N as a base at 80 °C for 36 h (or at 100 °C for 24 h). The Heck acceptor was present in 20 mol% excess. The PS-*g*-Pd catalyst contained 0.11 mol% of Pd. The Pd–C species used was 10% Pd–C (Sigma-Aldrich). Yields were measured by GC using dodecane as an internal standard. The catalyst was present at 0.1 mol%.

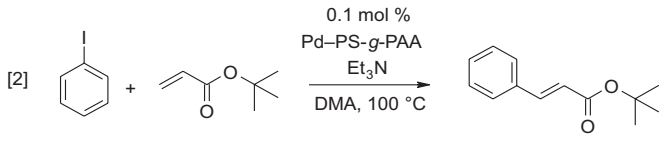
[a]Isolated yields were typically 10% lower for reactions carried out on a 5 or 10 mmol scale.

[b]The catalyst was present at 0.5 mol%.

Fig. 2. Allylic substitution of allyl acetate using diethylamine with a Pd(0) catalyst containing Pd(0) crystallites and no phosphine ligands within the interface. After 24 h, external PPh_3 was introduced to the reaction mixture, a step that did lead to allylic substitution product formation.



As shown in Table 2, good yields in small scale reactions were obtained with a variety of aryl iodides. However, unactivated aryl bromides and aryl chlorides were not substrates, even if added to a reaction along with a more reactive aryl iodide. The activity of the Pd–PS-*g*-PAA catalysts was also compared to Pd–C — a simple catalyst that also has modest activity in Heck catalysis. The PS-*g*-PAA immobilized Pd colloids were found to be more active. These cross-coupling reactions occurred without any added phosphine ligand present.



Recycling the Pd species in a polystyrene resin in Heck catalysis was tested using the Heck reaction between iodobenzene and *tert*-butyl acrylate (eq. [2]) as a model reaction. The first cycle was complete in 6 h by GC analysis. The catalyst was recovered by pouring off the reaction solution after centrifugation. Fresh reagents and solvent were then added to the catalyst for the second cycle (Table 3). After 6 h, the reaction had proceeded to 95% conversion by GC analysis. During the third recycling experiment the reaction went to only 46% conversion after 6 h. After washing the catalyst by Soxhlet extraction with MeOH for 24 h, a fourth cycle went to 99% conversion after 9 h. Presumably, the reaction salts had built up in the resin, inhibiting the reaction. Such fouling of a recovered catalyst by salt byproducts is a potential general problem for any recoverable catalyst that employs a relatively polar phase.

Table 3. Recycling experiments using Pd–PS-*g*-PAA in the Heck reaction of *tert*-butyl acrylate and iodobenzene (eq. [2]).

Cycle	Conversion (%)	Time (h)
1	99	6
2	95	6
3	46	6
4	99	9

Note: After the third cycle, the catalyst was recovered and washed in a Soxhlet apparatus with MeOH for 24 h.

Trace metal analysis (ICP–MS) of an acid-digested aliquot from the first reaction cycle showed 2.1% leaching of Pd. This result is in accord with other suggestions that activity of a heterogeneous Pd catalyst involves oxidative addition and formation of a soluble Pd species (2).

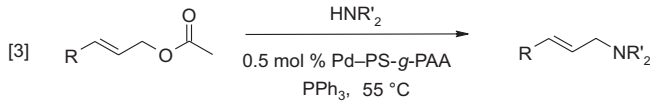
The Pd–PS-*g*-PAA catalyst is also active for allylic substitution chemistry (Table 4). As was true for Pd–PE-*g*-PAA catalysts, the presence of external triphenylphosphine is required for these reactions to proceed. A series of allylic substitution reactions using allyl acetate or cinnamyl acetate reacting with diethylamine or piperidine were performed (eq. [3]). The reaction between allyl acetate and diethylamine went to only 38% conversion in 18 h without the presence of external triphenylphosphine. With external phosphine, the reaction goes to complete conversion in 1 h. The reaction between cinnamyl acetate and diethylamine was even more dependant on external phosphine. After 24 h without any external phosphine, no reaction was seen by GC analysis. A reaction in the presence of added triphenylphosphine was completed within 8 h.

© 2006 NRC Canada

Table 4. Results for allylic substitution reactions with Pd–PS-*g*-PAA.

-R	-R′	PPh_3 (mmol)	Time (h)	Conversion (%)
-H	$-CH_2CH_3$	—	18	38
-H	$-CH_2CH_3$	0.1	1	99
-Ph	$-CH_2CH_3$	—	24	0
-Ph	$-CH_2CH_3$	0.1	8	99
-H	$-CH_2CH_2CH_2CH_2CH_2-$	0.05	1	99

Note: These reactions were carried out in THF at 60 °C on a 10 or 20 mmol scale.

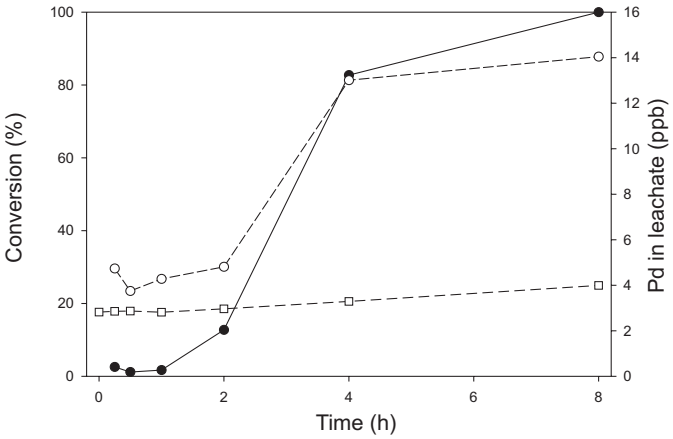


A more detailed study showed that these reactions appear to involve Pd leachates as the active catalyst. An induction period of ca. 2 h was observed for the formation of the cinnamyl acetate and diethylamine product. Interestingly, the progress of these allylic substitution reactions using Pd–PS-*g*-PAA catalysts with added triphenylphosphine were correlated with leaching of palladium into solution. In these studies, the first experiment was designed to monitor the Pd leaching into solution from the Pd–PS-*g*-PAA catalyzed allylic substitution reaction between cinnamyl acetate and diethylamine with triphenylphosphine present. During the course of the 8 h reaction between cinnamyl acetate and diethylamine, aliquots were removed from solution. The aliquots were digested in acid and analyzed by ICP–MS. Figure 3 shows the results from this experiment. The results show very little Pd leaching into solution during the induction period. As product forms, the Pd concentration in the reaction mixture increases. A second control reaction that had only triphenylphosphine and Pd–PS-*g*-PAA catalyst showed almost no palladium leaching for 8 h, the time required for complete conversion of starting materials to product. This suggests that the substrates cause the leaching of Pd and that the active catalytic species is generated with the presence of triphenylphosphine. In this case the Pd–PS-*g*-PAA catalyst serves as a reservoir of Pd for the reaction. These results are in accord with previous results from our group where the three-phase test for a soluble Pd catalyst failed using a polymer-supported allylic ester substrate and Pd–C- and polystyrene-supported Pd(0) catalysts (3). These results showed no reaction between a polystyrene-bound allyl ester and diethylamine using a heterogeneous Pd catalyst with triphenylphosphine in solution. However, as shown here, that result is understandable since in that experiment the substrate and Pd source were both heterogeneous. Assuming that this is also the case presently, the soluble phosphine alone would not cause the Pd leaching and no reaction would occur.

Conclusion

Hyperbranched grafts of poly(acrylic acid) on polyethylene powder or polystyrene can be used to support Pd(0) crystallites that function as a homogeneous Pd(0) catalyst in some reactions. These Pd–PE-*g*-PAA catalysts were active in allylic substitution reactions in the presence of added phosphine ligand. A catalyst analogous to the Pd–PE-*g*-PAA powder catalyst on polystyrene (Pd–PS-*g*-PAA) was similarly active for allylic substitution and could also be used in Heck reactions at 80 °C in *N*,*N*-dimethylacetamide (DMA). Analysis of the solution for Pd and a correlation of the Pd leaching with product formation in the allylic substitution chemistry for both types of catalysts suggests that the active catalysts in these reactions are leached from the support. In the case of the allylic substitution reaction, external triphenylphosphine and substrate together are required for the chemistry and Pd leaching.

Fig. 3. A Pd–PS-*g*-PAA catalyzed allylic substitution reaction between cinnamyl acetate and diethyl amine carried out in the presence of 0.5 mol% of added triphenylphosphine in THF at 60 °C. The various plots show the extent of reaction in the presence of added triphenylphosphine as a function of reaction time (●), the concentration of Pd in the leachate as a function of time (○), and the concentration of leachate in a reaction with the same catalyst and the same amount of triphenylphosphine and amine but no cinnamyl acetate substrate (□). No reaction was observed in the absence of triphenylphosphine over a 24 h period under the same reaction conditions.



Experimental section

General methods

Merrifield Resin (RGEN100) was obtained from the American Peptide Company, Inc. (Sunnyvale, California) as a 100–200 mesh resin and had a loading of 1.05 mmol of $ClCH_2$ groups per gram. Other reagents and solvents were obtained from the Sigma-Aldrich Chemical Company and were used as received unless noted otherwise. X-ray photoelectron spectra were obtained on a Kratos Axis Ultra XPS

© 2006 NRC Canada

(Manchester, UK) using a monochromatic Al K_α source (400 W) in a UHV environment (ca. 5×10^{-9} torr (1 torr = 133.3224 Pa). During acquisition, surfaces were kept from charging by the application of low energy electrons. Surface elemental composition was determined by normalized integration of the resulting peaks using Kratos software (Kratos Analytical, Chestnut Ridge, New York). ^{1}H and ^{13}C NMR spectroscopy experiments were carried out using Mercury 300, Unity 300, or Unity 500 spectrometers. GC analyses were carried out using a Shimazdu Model 2010 GC. All glassware used in the experiments in which trace metal analysis was performed was soaked in a 1 mol/L HNO_3 acid bath for at least 12 h prior to the experiment.

Preparation of Pd–PS-*g*-PAA

A reported procedure was used (20). The product Pd catalyst was prepared on a 12 g scale. The Pd loading of the Pd(II)–PS-*g*-PAA prepared in this manner was 1.27 mmol/g, based on gravimetric analysis of the exchange of $Pd(OAc)_2$ and the sodium salt of the poly(acrylic acid)-grafted polystyrene. Subsequent reduction of this Pd(II) salt in the poly(acrylic acid) graft produces a product (Pd–PS-*g*-PAA) that was used in the catalytic studies. Analysis by ICP–MS of a solution of the residue after combustion and acid digestion of this Pd–PS-*g*-PAA product in triplicate showed that the Pd loading of this polystyrene-supported Pd product was 1.1 mmol of Pd per gram of Pd–PS-*g*-PAA.

Preparation of Pd–PE-*g*-PAA powder

Following a literature procedure (19), a poly(acrylic acid) hyperbranched graft on a PE powder sample (1.3 g) was first stirred with a pH 9 buffer for 2 h to deprotonate the -CO_2H groups of the graft. The resulting carboxylate-containing polymer was then suspended in 25 mL of an acetone–water (4:1) mixture with 20 mg of $Pd(OAc)_2$. This solution was stirred at room temperature for 24 h then filtered and washed with dilute acidic ethanol and ethanol. The yellowish powder was suspended in EtOH and reduced with H_2 in a Parr apparatus to yield the Pd–PE-*g*-PAA catalyst that was used in these studies. To determine the Pd loading, this powder sample was combusted in a crucible at 650 °C for 2 h. The residue was digested in acid and ICP–MS analysis of the residue for Pd showed that Pd loading was ca. 0.01 mmol of Pd per gram of Pd–PE-*g*-PAA powder.

Typical procedure for Heck catalysis with 10% Pd–C or Pd–PS-*g*-PAA

An aryl iodide such as iodotoluene (2.0 mmol), 2.4 mmol (0.3139 g, 98%) of *tert*-butyl acrylate, 2.5 mmol of triethylamine, along with 0.01 mmol of the Pd catalyst (e.g., 9 mg of Pd–PS-*g*-PAA) were added to a 50 mL flask. Then 10 mL of DMA was added to the mixture and the reaction was heated to 80 °C.

Typical procedure for allylic substitutions with Pd–PS-*g*-PAA

A mixture of 2.0 mmol (0.36 g) of cinnamyl acetate, 2.4 mmol (0.21 g) of morpholine, 0.1 mmol (0.264 g) of triphenylphosphine, and 0.01 mmol (9.0 mg) of Pd–PS-*g*-PAA were added to a 50 mL reaction flask along with 10 mL of THF. The reaction mixture was heated to 60 °C and agitated with a wrist-action shaker. The progress of the reaction was checked using GC.

General procedure for Heck catalysis, recycling, and leachate analysis using Pd–PS-*g*-PAA

Iodobenzene (5 mmol), *tert*-butyl acrylate (6 mmol), triethylamine (7.5 mmol), and 0.5 mol% Pd(0)-PAA–PS (0.025 mmol of Pd, 22.5 mg of resin) were added to a 40 mL centrifuge tube along with 25 mL of DMA. This mixture was heated to 100 °C and agitated using a wrist-action shaker until GC analysis showed the reaction was complete. After the reaction was complete, the catalyst was separated by centrifugation and decantation. The catalyst isolated in this manner could then be reused in a subsequent reaction. To analyze for Pd leaching, ca. 25% of the decanted solution from this reaction was evaporated to dryness and then heated on a hot plate with 20 mL of concentrated sulfuric acid for 24 h. The solution was diluted to 50 mL using 1% HCl and analyzed by ICP–MS. In a typical analysis, a reaction that started with 2.65 mg of Pd had 56 μg of Pd in total in this solution corresponding to 2.1% leaching.

General procedure for allylic substitution reactions and leachate analysis using Pd–PS-*g*-PAAC

Cinnamyl acetate (10 mmol, 1.76 g) and diethylamine (24 mmol, 1.75 g) were combined with triphenylphosphine (0.2 mmol, 52.4 mg) and Pd(0)-PAA–PS (0.5 mol%, 45 mg of resin) in 20 mL of distilled THF in a 40 mL centrifuge tube. This mixture was degassed by freeze–pump–thaw cycles three times and then backfilled with N_2. The reaction tube was heated to 55 °C and agitated using a wrist-action shaker. A control reaction was also carried out at the same time using the same amount of catalyst, phosphine, and solvent but without any cinnamyl acetate. GC analysis of aliquots was carried out as the reaction progressed. The remainder of each aliquot was digested by heating in concd. H_2SO_4 for 24 h. The concentrated digest was diluted to 25 mL with 1% HCl and then analyzed by ICP–MS.

Pd–PE-*g*-PAA catalyzed allylic substitution reactions

Allyl acetate (18.8 mmol, 1.8852 g), piperidine (37.8 mmol, 3.2125 g), triphenylphosphine (0.01 mmol, 26.4 mg), and 400 mg of Pd–PE-*g*-PAA powder were combined in a 20 mL flask. This mixture was degassed three times by freeze–pump–thaw, backfilled with N_2, and then heated to 55 °C. After 20 h, the allyl acetate had been completely consumed based on GC analysis.

Acknowledgments

We thank the Robert A. Welch Foundation (A-0639) and the National Science Foundation (CHE-0446107) for support of this research.

References

1. R.L. Augustine. Heterogeneous catalysis for the synthetic chemist. Dekker, New York. 1995.
2. V. Farina. Adv. Synth. Catal. **346**, 1553 (2004).
3. D.E. Bergbreiter, B. Chen, and D. Weatherford. J. Mol. Catal. **74**, 409 (1992).

© 2006 NRC Canada

4. D.E. Bergbreiter and B. Chen. J. Chem. Soc. Chem. Commun. 1238 (1983).
5. D.E. Bergbreiter, B. Chen, and T.J. Lynch. J. Org. Chem. **48**, 4179 (1983).
6. M.T. Reetz and J.G. de Vries. Chem. Commun. (Cambridge), 1559 (2004).
7. B.H. Lipshutz. Adv. Synth. Catal. **343**, 313 (2001).
8. C.K.Y. Lee, A.B. Holmes, S.V. Ley, I.F. McConvey, B. Al-Duri, G.A. Leeke, R.C.D. Santos, and J.P.K. Seville. Chem. Commun. (Cambridge, U.K.), 2175 (2005).
9. S.J. Broadwater, S.L. Roth, K.E. Price, M. Kobaslija, and D.T. McQuade. Org. Biomol. Chem. **3**, 2899 (2005).
10. P.D. Stevens, J. Fan, H.M.R. Gardimalla, M. Yen, and Y. Gao. Org. Lett. **7**, 2085 (2005).
11. F. Wen, H. Bonneman, J.Y. Jiang, D.M. Lu, Y.H. Wang, and Z.L. Jin. Appl. Organomet. Chem. **19**, 81 (2005).
12. I.P. Beletskaya and A.V. Cheprakov. J. Organomet. Chem. **689**, 4055 (2004).
13. K. Yu, W. Sommer, J.M. Richardson, M. Weck, and C.W. Jones. Adv. Synth. Catal. **347**, 161 (2005).
14. D.E. Bergbreiter, P. Osburn, and J.D. Frels. Adv. Synth. Catal. **347**, 172 (2005).
15. W. Sommer, K. Yu, J.S. Sears, Y. Ji, X. Zhang, R.J. Davis, D.C. Sherrill, C.W. Jones, and M. Weck. Organometallics, **24**, 4351 (2005).
16. D. Olsson, P. Nilsson, M. El Masnaouy, and F.O. Wendt. Dalton Trans. 1924 (2005).
17. C.S. Consorti, F.R. Flores, and J. Dupont. J. Am. Chem. Soc. **127**, 12054 (2005).
18. D.E. Bergbreiter, J.G. Franchina, and K. Kabza. Macromolecules, **32**, 4993 (1999).
19. D.E. Bergbreiter, G. Tao, and A.M. Kippenberger. Org. Lett. **2**, 2853 (2000).
20. D.E. Bergbreiter and Z. Zhong. Ind. Eng. Chem. Res. **44**, 8616 (2005).
21. C.M. Hagen, J.A. Widegren, P.M. Maitlis, and R.G. Finke. J. Am. Chem. Soc. **127**, 4423 (2005).
22. J. Rebek, Jr. Tetrahedron, **35**, 723 (1979).
23. I.W. Davies, L. Matty, D.L. Hughes, and P.J. Reider. J. Am. Chem. Soc. **123**, 10139 (2001).
24. A. Corma, D. Das, H. Garcia, and A. Leyva. J. Catal. **229**, 322 (2005).
25. D.E. Bergbreiter, A.M. Kippenberger, and G. Tao. Chem. Commun. (Cambridge), 2158 (2002).
26. C.M. Crudden, M. Sateesh, and R. Lewis. J. Am. Chem. Soc. **127**, 10045 (2005).
27. J.P. Arhancet, M.E. Davis, J.S. Merola, and B.E. Hanson. J. Catal. **121**, 327 (1990).
28. F. Quignard, A. Choplin, and A. Domard. Langmuir, **16**, 9106 (2000).
29. S.-I. Fujita, Y. Sano, M.B. Bhanage, and M. Arai. J. Catal. **225**, 95 (2004).
30. Z.M. Michalska, L. Rogalski, K. Rozga-Wijas, J. Chojnowski, W. Fortuniak, and M. Scibiorek. J. Mol. Catal. A: Chem. **208**, 187 (2004).
31. C.P. Mehnert. Chem. Eur. J. **11**, 50 (2005).

© 2006 NRC Canada

Design and synthesis of selenonium and sulfonium ions related to the naturally occurring glucosidase inhibitor salacinol[1]

Hui Liu and B. Mario Pinto

Abstract: Four series of analogues of the naturally occurring glucosidase inhibitor salacinol were synthesized for structure–activity studies with different glycosidase enzymes. The target zwitterionic compounds were synthesized by means of nucleophilic attack at the least-hindered carbon atom of the 1,3-cyclic sulfates derived from D-glucose and D-mannose by the isopropylidene-protected 1,4-anhydro-4-thio- and seleno-D-allitols and the 4-thio- and seleno-L-allitols. Deprotection of the coupled products afforded the novel sulfonium and selenonium ions containing polyhydroxylated acyclic chains of four and six carbons, with different stereochemistry at the stereogenic centers and with 1,4-anhydro-4-seleno or 4-thio-D- or L- alditol heterocyclic rings. The compounds showed no significant activity against recombinant human maltase glucoamylase (MGA), a critical intestinal glucosidase involved in the processing of oligosaccharides of glucose into glucose itself.

Key words: glycosidase inhibitors, zwitterionic, selenonium salts, sulfonium salts, cyclic sulfates, L-ascorbic acid, D-gulonic-γ-lactone.

Résumé : Afin de pouvoir faire des études de structure–activité avec divers enzymes glycosides, on a réalisé la synthèse de quatre séries d'analogues du salacinol, un inhibiteur naturel de glucosidase. Les composés zwitterioniques cibles ont été synthétisés par le biais d'une attaque nucléophile au niveau de l'atome de carbone le moins encombré de sulfates 1,3-cycliques obtenus à partir du D-glucose et du D-mannose par des 1,4-anhydro-4-thio- et 1,4-anhydro-4-séléno-D-allitols et des 4-thio- et 4-séléno-L-allitols. La déprotection des produits de couplage fournit des nouveaux ions sulfonium et sélénonium qui contiennent des chaînes acycliques polyhydroxylées de quatre et de six carbones, avec des stéréochimies différentes au niveau des centres stéréogènes et hétérocycles 1,4-anhydro-4-séléno- et 1,4-anhydro-4-thio-D- ou L-alditols. Ces composés ne présentent aucune activité significative contre la maltase glucoamylase humaine recombinante (MGA), une glucosidase intestinale critique dans la transformation des oligosaccharides du glucose en glucose.

Mots clés : inhibiteurs de glycosidase, zwitterion, sels de sélénonium, sels de sulfonium, sulfates cycliques, acide L-ascorbique, γ-lactone de l'acide D-gulonique.

[Traduit par la Rédaction]

Introduction

Glycosidases are responsible for the hydrolysis of poly- and oligo-saccharides into monomers or the cleavage of bonds between sugars and non-carbohydrate aglycons. In recent years, much attention has focused on the synthesis and development of glycosidase inhibitors because of an increasing awareness of the vital role played by sugars in biological processes and because of their therapeutic potential (1, 2). In the case of patients suffering from Type II diabetes, the management of blood glucose levels is crucial since their insulin secretion may be normal, but the entry into cells of glucose (normally mediated by insulin) is compromised (3). Glycosidase inhibitors can be used to inhibit the activity of intestinal glucosidases that break down oligosaccharides to glucose. This enzyme inhibition delays glucose absorption into the blood and results in a lowering or smoothing of the blood glucose levels (4, 5).

There are two generally accepted mechanisms for the enzymatic hydrolysis of a glycosidic bond, proceeding either with the inversion or retention of configuration at the anomeric center (6, 7). In either case, protonation of the exocyclic oxygen leads to cleavage of the glycosidic bond with subsequent formation of an oxacarbenium ion. To generate potent glycosidase inhibitors, an attractive approach is to create compounds that mimic the oxacarbenium ion transition state in the enzyme-catalyzed reaction. Some naturally occurring compounds, such as acarbose (**1**) and voglibose (**2**) (Chart 1), are potent glycosidase inhibitors and presumably mimic the oxacarbenium ion, at least in binding to active site carboxylate residues via the protonated nitrogen atom (8, 9).

Received 11 November 2005. Accepted 21 December 2005. Published on the NRC Research Press Web site at http://canjchem.nrc.ca on 19 September 2006.

Dedicated, with respect, to Dr. Alfred Bader for his impact on the field of chemistry.

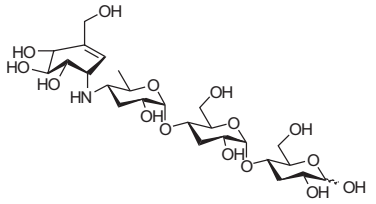
H. Liu and B.M. Pinto.[2] Department of Chemistry, Simon Fraser University, Burnaby, BC V5A 1S6, Canada.

[1]This article is part of a Special Issue dedicated to Dr. Alfred Bader.

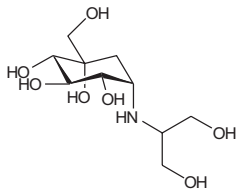
[2]Corresponding author (e-mail: bpinto@sfu.ca).

 doi:10.1139/V06-100 © 2006 NRC Canada

Chart 1.

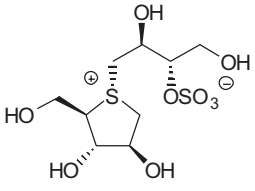


acarbose (**1**)

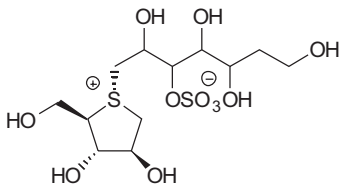


voglibose (**2**)

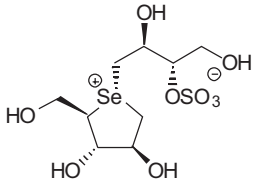
Chart 2.



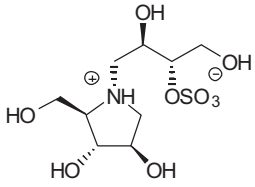
salacinol (**3**)



kotalanol (**4**)



blintol (**5**)

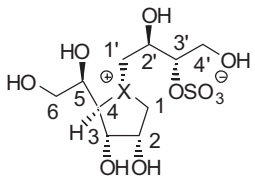


ghavaminol (**6**)

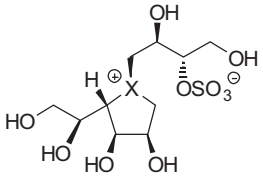
Recently, a new class of glycosidase inhibitors, including salacinol (**3**) and kotalanol (**4**) (Chart 2), with an intriguing inner-salt sulfonium sulfate structure was isolated from the roots and stems of the plant *Salacia reticulata* (10–12). The compounds were shown to be inhibitors of intestinal glucosidase enzymes that attenuate the undesirable spike in blood glucose that is experienced by diabetics after consuming a meal rich in carbohydrates. It is postulated that the inhibition of glucosidases by salacinol and kotalanol is due to their ability to mimic both the shape and charge of the oxocarbenium ion-like transition state involved in the enzymatic reactions.

In our current research program, we have undertaken a limited structure–activity study of salacinol and related compounds. The synthesis of salacinol and its ammonium and selenonium analogues have been reported by us and others (13–17). Analogues containing six-membered heterocyclic rings and some chain-extended analogues of salacinol have also been synthesized (18–21). Some of these analogues exhibited inhibitory activities in the micromolar range for recombinant human maltase glucoamylase, an intestinal glucosidase (20, 21). The studies also showed an interesting variation in the inhibitory power of these compounds against glycosidase enzymes of different origin (14–17, 22). In particular, the stereochemistry at the different stereogenic centers as well as the nature of the heteroatom play significant roles in discrimination between glycosidase enzymes. The molecular basis for this selectivity is being investigated through structural studies of the enzyme-bound inhibitors using molecular modeling in conjunction with conformational analysis by NMR techniques (23) and X-ray crystallography (24).

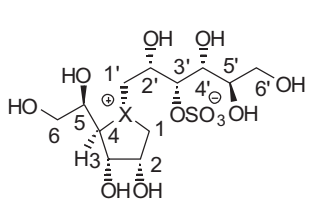
Chart 3.



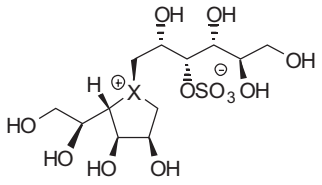
7 X = Se
8 X = S



9 X = Se
10 X = S



11 X = Se
12 X = S



13 X = Se
14 X = S

To further understand the enzyme discrimination of related compounds, we now describe the synthesis of new analogues of salacinol analogues **7**–**14** based on novel seleno- and thio-alditols derived from D-gulonic-γ-lactone and L-ascorbic acid (Chart 3).

Results and discussion

The analogues **7**–**14** can be synthesized by alkylation of a protected anhydroalditol at the ring heteroatom with terminal 1,3-cyclic sulfates. The protected anhydroalditols and the cyclic sulfates can be synthesized from the appropriate carbohydrate starting materials (Scheme 1).

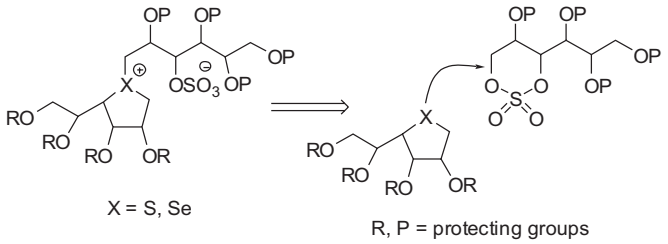
The choice of protecting groups for the thio- and selenoanhydroalditols and the cyclic sulfates, however, merited careful consideration, especially in the case of the selenonium analogues. Hydrogenolysis and strongly basic conditions proved to be problematic deprotection steps for similar selenonium analogues; thus, these conditions needed to be avoided (15–17). Therefore, we chose to use isopropylidene and benzylidene acetals as the protecting groups for the thio- and seleno-anhydroalditols **15**–**18** and the cyclic sulfates **19** and **20** since these acetals are both labile to acidic hydrolysis (Chart 4).

Our previous work also suggested that the release of ring strain in the opening of bicyclic sulfates was beneficial (14–17). Therefore, the benzylidene acetal at the 2,4-positions of the cyclic sulfates **19** and **20** played dual roles as protecting groups and reaction facilitators for the coupling reactions with compounds **15**–**18**. After the coupling reactions, the products could then be readily deprotected by simple treatment with trifluoroacetic acid.

The synthesis of the isopropylidene-protected 1,4-anhydro-4-seleno-D-allitol (**15**) and 1,4-anhydro-4-thio-D-allitol (**16**) started from the commercially available D-gulonic-γ-lactone (**21**, Scheme 2). 2,3,5,6-Di-*O*-isopropylidene-D-gulonic-γ-lactone (**22**) (25) was reduced with sodium borohydride to afford the corresponding diol **23**. Compound

© 2006 NRC Canada

Scheme 1.



Scheme 2.

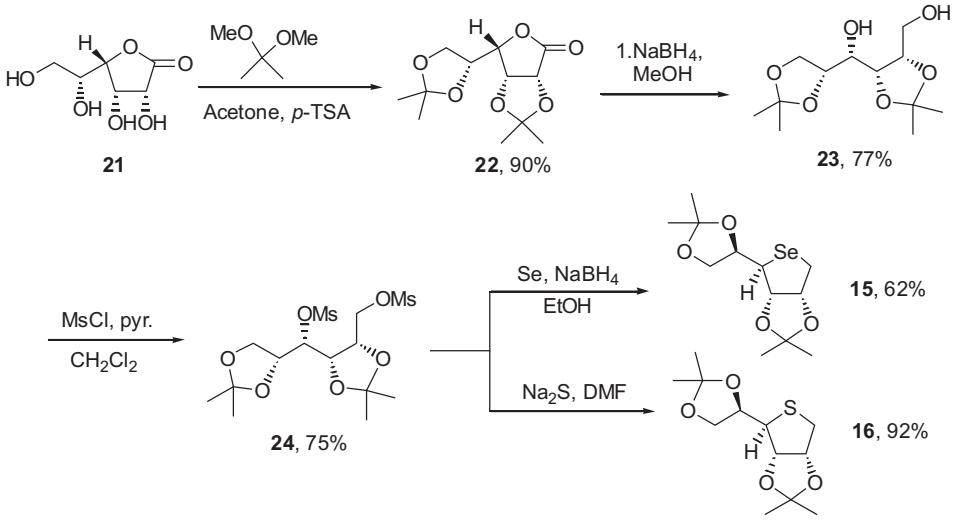
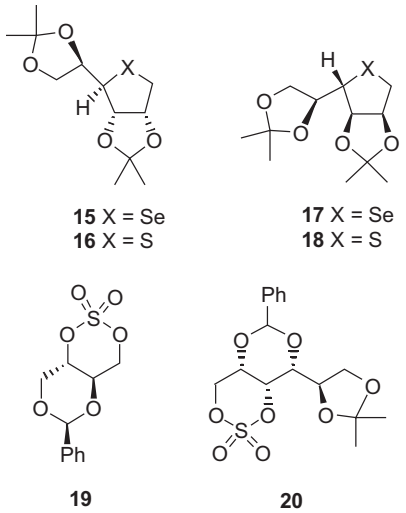


Chart 4.



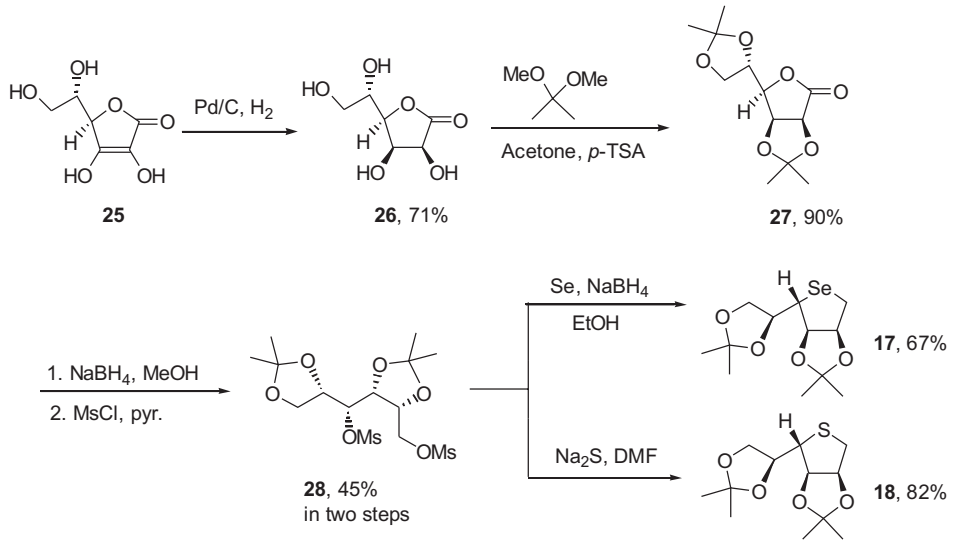
23 was then converted to the dimesylate **24** by treatment with methanesulfonyl chloride and pyridine in 80% yield (26). When the dimesylate **24** was reacted with selenium metal and sodium borohydride in EtOH at 60–65 °C, the isopropylidene-protected 1,4-anhydro-4-seleno-D-allitol **15** was obtained in 62% yield. The isopropylidene-protected 1,4-anhydro-4-thio-D-allitol **16** was prepared in 92% yield by treatment of the dimesylate **24** with sodium sulfide in DMF (Scheme 2).

Although the enantiomeric isopropylidene-protected 1,4-anhydro-4-seleno-L-allitol (**17**) and 1,4-anhydro-4-thio-L-allitol (**18**) could, in principle, be prepared from L-gulonic-γ-lactone, the high cost of this starting material made these syntheses unrealistic. Thus, inexpensive and commercially available L-ascorbic acid (**25**) was used as the starting material to give the L-gulonic-γ-lactone (**26**) in 71% yield (27) (Scheme 3). Compound **26** was then treated with 2,2-dimethoxypropane in dry acetone containing *p*-toluenesulfonic acid as a catalyst to give 2,3,5,6-di-*O*-isopropylidene-L-gulonic-γ-lactone (**27**) (25). The lactone **27** was subsequently reduced with sodium borohydride to afford the corresponding diol that was, in turn, converted to the dimesylate **28** by treatment with methanesulfonyl chloride and pyridine. When the dimesylate **28** was reacted with selenium metal and sodium borohydride in EtOH at 60–65 °C, the isopropylidene-protected 1,4-anhydro-4-seleno-L-allitol **17** was obtained in 67% yield. The isopropylidene-protected 1,4-anhydro-4-thio-L-allitol **18** was prepared in 82% yield by treatment of the dimesylate **28** with sodium sulfide in DMF.

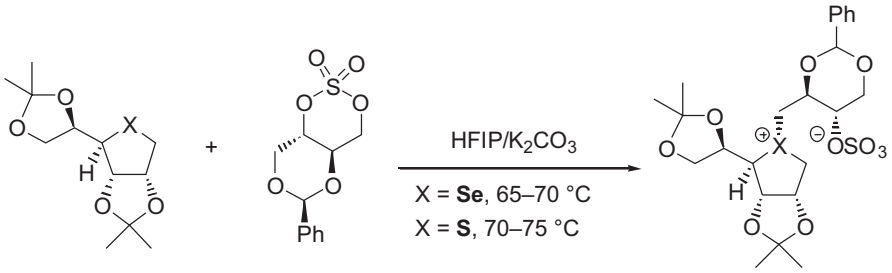
Since salacinol **3** and its selenonium analogue, blintol (**5**) (Chart 2), are the most active, so far, of this class of glycosidase inhibitors against human maltase glucoamylase, we first concentrated on the coupling reactions of **15** and **16** with the cyclic sulfate **19**, which would yield the identical side chain present in salacinol and blintol (Scheme 4). The solvent chosen for the coupling reactions was the unusual solvent 1,1,1,3,3,3-hexafluoroisopropanol (HFIP), which offers significant advantage in these types of coupling reactions compared with other solvents (15–17). The cyclic sulfates **19**, prepared as described previously (16), were reacted with **15** and **16**, to give the corresponding protected

© 2006 NRC Canada

Scheme 3.



Scheme 4.



selenonium and sulfonium sulfates **29** and **30**, respectively (Scheme 4).

The coupling reactions of enantiomeric **17** and **18** with the cyclic sulfate **19** were carried out analogously, to give the corresponding protected selenonium and sulfonium sulfates **31** and **32**, respectively (Scheme 5).

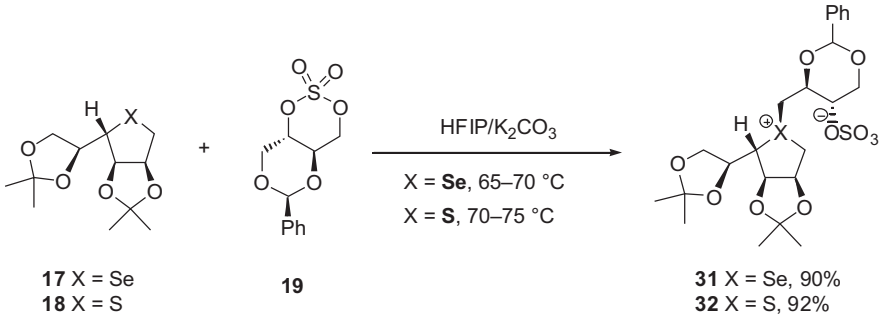
We next turned our attention to the possibility of attaching longer side chains to the anhydroalditols **15**–**18**. Our interest in longer side chains stemmed from the fact that kotalanol **4**, which has a seven-carbon side chain instead of four-carbon side chain of the salacinol, exhibits stronger inhibitory activities toward certain glycosidase enzymes. Since the exact stereochemistry of kotalanol **4** is not yet known, it is necessary and important to study the structure–activity relationships of these types of compounds systematically by attaching side chains with different chain lengths and different stereochemistry at the stereogenic centers to the heterocyclic rings of the anhydroheteroalditols. The cyclic sulfate **20**, which consisted of a protected polyhydroxylated six-carbon chain (19), was chosen for this purpose. The cyclic sulfate **20** reacted with **15** and **16** and their enantiomers **17** and **18** in HFIP to give the corresponding protected selenonium and sulfonium compounds **33**–**36**, respectively (Scheme 6).

The reactivity of **15**–**18** with cyclic sulfates **19** and **20** varied slightly. With the same anhydroalditols, the cyclic sulfate **19** was more reactive than the cyclic sulfate **20**, also resulting in higher yields of the coupling reactions. Thus, the coupling reactions with the cyclic sulfate **19** usually proceeded in yields of 90%–95%, while the cyclic sulfate **20** typically gave yields of 70%–80%, with the remainder consisting of starting materials and a small amount of decomposition products. With the same cyclic sulfate, the selenoalditols were slightly more reactive than their sulfur counterparts, as demonstrated by the different reaction temperatures required in the coupling reactions. The reactivities of the enantiomeric pairs, compounds **15**–**17** and **16**–**18** with the cyclic sulfates **19** and **20** were virtually the same. Selectivity for attack at the primary center of the cyclic sulfates **19** and **20** over possible alternative attack at the secondary center by compounds **15**–**18** was invariably excellent, and in no case were isolable quantities of the regioisomers detected. In the case of the coupling reaction of **15** and L-allitol **17** with the cyclic sulfates **19** and **20**, there was a small amount (5%–10%) of the stereoisomer formed through electrophilic attack on the β face of the seleno-D-allitol **15** and the α face of the seleno-L-allitol **17** to give products that were diastereomeric at the selenonium center, but could not be isolated in pure form. However, this type of minor product was not detected in the reactions of the corresponding thioallitols.

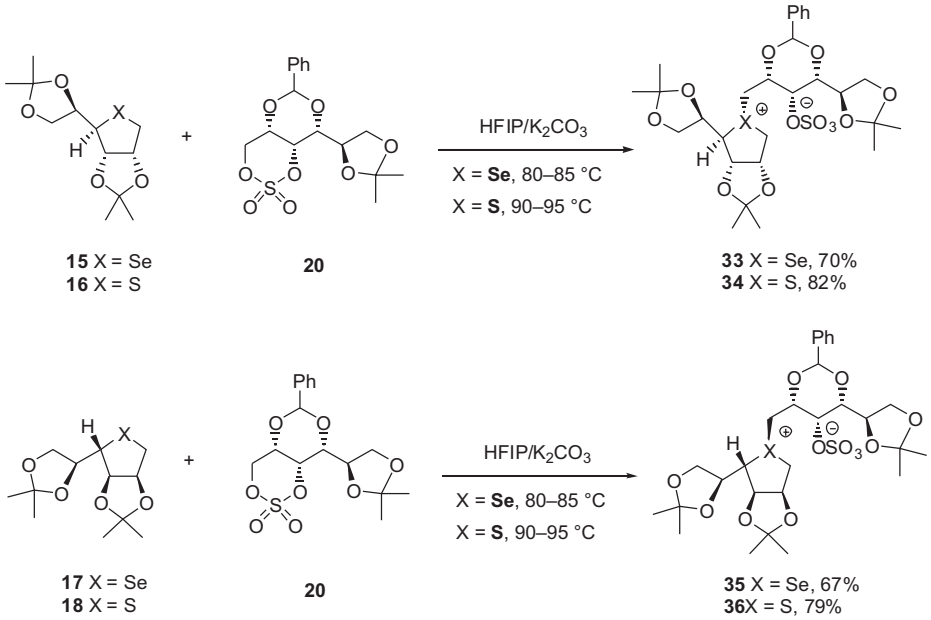
The deprotection of the coupled products **29**–**36** was carried out by treatment with trifluoroacetic acid (Scheme 7). After rinsing away the cleaved protecting groups with dichloromethane, the resulting residues were purified by flash

© 2006 NRC Canada

Scheme 5.



Scheme 6.



chromatography to yield compounds **7**–**10** as amorphous, hygroscopic solids. In the cases of compounds **33**–**36**, however, some of the benzylidene acetal protecting group (up to 30% by NMR measurements) remained even after prolonged (up to 48 h) treatment with TFA. The remaining benzylidene acetal was eventually cleaved by hydrogenolysis in 80% acetic acid to give the corresponding deprotected products **11**–**14** as amorphous, hygroscopic solids. The yields of compounds **11**–**14** were low, partly because of the adsorption of the products on the Pd–C catalyst. Compounds **7**–**14** were characterized by spectroscopic methods. The MALDI-TOF mass spectra of compounds **7**–**14** showed major fragmentation peaks ($M + Na^+ - SO_3$) together with the molecular ion peaks ($M + Na^+$) of much lower intensities.

The absolute stereochemistry at the heteroatom center of compounds **7**–**14** was established by 1D-NOE NMR spectroscopy. For example, in the 1D-NOE spectrum of compound **8** (Fig. 1), the H-4 to H-1′b correlation was clearly exhibited, implying that these two hydrogens are syn-facial. Therefore, C-1′ of the side chain must be anti to C-5 of the sulfonium salt ring.

As a final point of interest, compounds **7**–**14** were screened against recombinant human maltase glucoamylase (MGA), a critical intestinal glucosidase involved in the processing of oligosaccharides of glucose into glucose itself. The compounds showed no significant activity.[3]

Conclusions

Four series of analogues of the naturally occurring glucosidase inhibitor salacinol were synthesized. These analogues contained the acyclic chains of salacinol and extended acyclic chains of six carbons, as well as ring heteroatom substitution (Se, S). In addition, the heterocyclic ring bore the D- or L-allitol configuration. These syntheses utilized the 1,3-cyclic sulfates derived from commercially available D-glucose and D-mannose. The isopropylidene and benzylidene acetal protecting groups on the coupled products ensured facile deprotection with TFA to yield the final compounds **7**–**14**. The compounds showed no inhibitory activity against human maltase glucoamylase.

Experimental section

General

Optical rotations were measured at 23 °C. ^1H and ^{13}C

[3] L. Sim and D.R. Rose. Unpublished data.

© 2006 NRC Canada

Scheme 7.

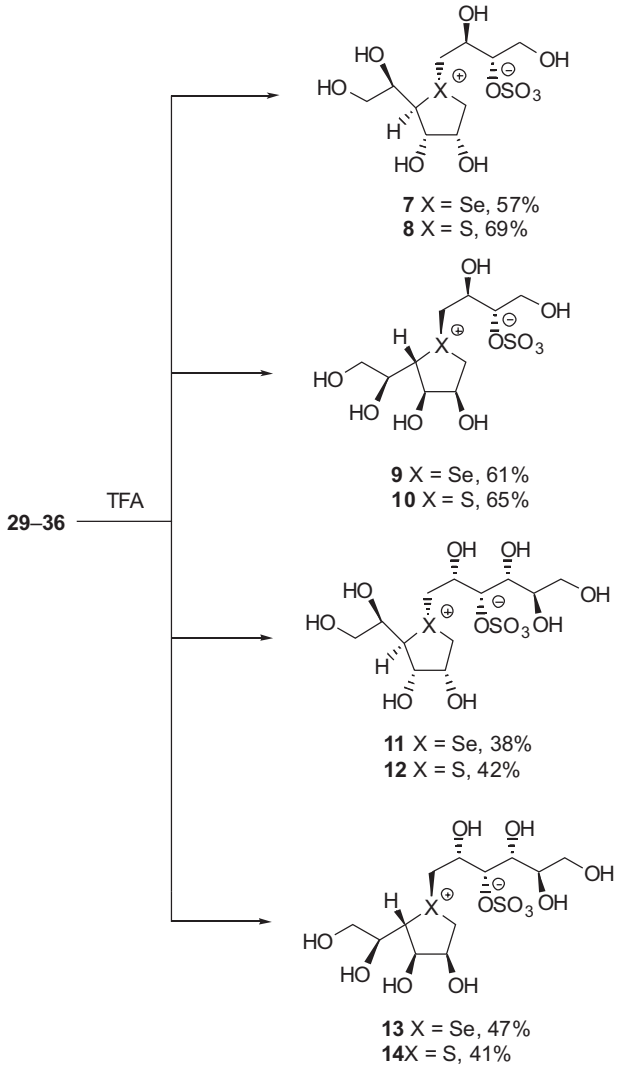
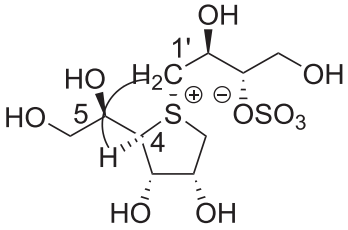


Fig. 1. NOE correlation observed in the 1D-NOE spectrum of compound **8**.



NMR spectra were recorded at 500 and 125 MHz, respectively. All assignments were confirmed with the aid of two-dimensional ^{1}H and ^{1}H (COSYDFTP) or ^{1}H and ^{13}C (INVBTP) experiments using standard Bruker pulse programs. Column chromatography was performed with Merck silica gel 60 (230–400 mesh). MALDI mass spectra were obtained on a PerSeptive Biosystems Voyager DE time-of-flight spectrometer for samples dispersed in a 2,5-dihydroxybenzoic acid matrix. High-resolution mass spectra were obtained by the electrospray ionization (ESI) technique, using a ZabSpec oaTOF mass spectrometer at 10 000 RP.

2,3,5,6-Di-*O*-isopropylidene-1,4-di-*O*-methanesulfonyl-D-gulitol (24)

2,3,5,6-Di-*O*-isopropylidene-1,4-di-*O*-methanesulfonyl-D-gulitol (**24**) was prepared by the literature method (26) with slight variations. To a solution of commercially available D-gulonic-γ-lactone **21** (10.0 g, 56.1 mmol) in dry acetone (200 mL), 2,2-dimethoxypropane (40 mL, 0.32 mmol) was added at RT. To this solution, *p*-toluenesulfonic acid (200 mg) was added as a catalyst. The progress of the reaction was followed by TLC analysis of the aliquots (hexane–EtOAc, 1:1). When the starting material **21** had been essentially consumed, the reaction was stopped by addition of triethylamine (1 mL) to the reaction mixture. The solvent was then evaporated under reduced pressure and the residue was purified by column chromatography (hexane–EtOAc, 1:1) to give compound **22** as a white solid (13.1 g, 90%). The NMR spectrum of compound **22** matched that of the published data (25). The lactone **22** (5.0 g, 19.3 mmol) was dissolved in THF (20 mL) and MeOH (50 mL) was then added. To this solution, $NaBH_4$ was added portionwise at 0 °C. The progress of the reaction was followed by TLC analysis of the aliquots (hexane–EtOAc, 1:1). When the starting material **22** had been consumed, the solvent was evaporated under reduced pressure. The residue was redissolved in EtOAc (50 mL), washed with aqueous tartaric acid solution (2 × 10 mL) and brine (50 mL), and dried over Na_2SO_4. Purification by column chromatography (hexane–EtOAc, 2:1) yielded compound **23** as a colourless syrup (3.9 g, 77%). The NMR spectrum of compound **23** matched that of the published data (26). The diol **23** (5.0 g, 19.1 mmol) was dissolved in CH_2Cl_2 (50 mL) and the solution was added dropwise to a mixture of pyridine (100 mL) and methanesulfonyl chloride (6 mL, 77.5 mmol) and cooled to 0 °C. The reaction mixture was stirred at 0 °C for 30 min and then allowed to warm to RT for 6 h. When TLC analysis of the aliquots (hexane–EtOAc, 1:1) showed total consumption of the starting material, the reaction mixture was poured into ice water, extracted with CH_2Cl_2 (3 × 100 mL), washed with brine (50 mL), and dried over Na_2SO_4. Purification by column chromatography (hexane–EtOAc, 2:1) yielded compound **24** as a colourless syrup (5.9 g, 75%). $[\alpha]^{22}_{D}$ –46° (*c* 1, CH_2Cl_2). ^{1}H NMR ($(CD_3)_2O$) δ: 4.87 (dd, 1H, $J_{3,4}$ = 5.8 Hz, $J_{4,5}$ = 4.7 Hz, H-4), 4.56 (ddd, 1H, $J_{1b,2}$ = 6.0 Hz, $J_{1a,1b}$ = 12.0 Hz, H-1b), 4.56–4.48 (m, 2H, H-2, H-3, H-1a), 4.48 (dd, 1H, H-1a), 4.46 (ddd, 1H, H-5), 4.14 (dd, 1H, $J_{5,6b}$ = 6.8 Hz, $J_{6a,6b}$ = 8.7 Hz, H-6b), 4.02 (dd, 1H, $J_{5,6a}$ = 6.7 Hz, H-6a), 3.23, 3.14 (2 s, 6H, 2 × OSO_2CH_3), 1.51, 1.41, 1.38, 1.34 (4 s, 12H, 4 × CH_3). ^{13}C NMR ($(CD_3)_2O$) δ: 110.1, 109.6 ($(CH_3)_2C(OR)_2$), 79.1 (C-4), 75.6 (C-3), 75.0 (C-2), 74.9 (C-1), 68.7 (C-5), 65.4 (C-6), 38.8, 36.7 (2 × OSO_2CH_3), 26.9, 25.6, 25.1, 25.0 (4 × CH_3). Anal. calcd. for $C_{14}H_{26}O_{10}S_2$: C 40.18, H 6.26; found: C 40.35, H 6.14.

2,3,5,6-Di-*O*-isopropylidene-1,4-di-*O*-methanesulfonyl-L-gulitol (28)

To a solution of commercially available L-ascorbic acid **25** (30.0 g, 0.17 mmol) in distilled water (200 mL), palladium

© 2006 NRC Canada

on activated carbon (10%, 1.0 g) was added as a catalyst at RT. The reaction mixture was placed in a steel reaction vessel and underwent hydrogenation (100 psi, 1 psi = 6.894 757 kPa) at 60 °C for 48 h. The progress of the reaction was followed by TLC analysis of the aliquots (EtOAc–MeOH–H_2O, 10:3:1). When the starting material **25** had been essentially consumed, the reaction was stopped and the reaction mixture was filtered under vacuum and washed with water (2 × 50 mL). The filtrate and the wash were combined and the water was then evaporated under reduced pressure. The residue was recrystallized from methanol – ethyl acetate to give compound **26** as a white solid (21.5 g, 71%). The NMR spectrum of compound **26** matched that of the published literature (26). To a suspension of the lactone **26** (10.0 g, 56.1 mmol) in dry acetone (200 mL), 2,2-dimethoxypropane (40 mL, 0.32 mmol) was added at RT. To this mixture, *p*-toluenesulfonic acid (200 mg) was added as a catalyst. The progress of the reaction was followed by TLC analysis of the aliquots (hexane–EtOAc, 1:1). When the starting material **26** had been essentially consumed, the reaction was stopped by addition of triethylamine (1 mL). The solvent was then evaporated under reduced pressure and the residue was purified by column chromatography (hexane–EtOAc, 1:1) to give compound **27** as a white solid. The NMR spectrum of compound **26** matched that of the published data (25). Lactone **27** (5.0 g, 19.3 mmol) was dissolved in THF (20 mL) and MeOH (50 mL) was then added. To this solution, $NaBH_4$ was added portionwise at 0 °C. The progress of the reaction was followed by TLC analysis of the aliquots (hexane–EtOAc, 1:1). When the starting material **27** had been consumed, the solvent was evaporated under reduced pressure. The residue was redissolved in EtOAc (50 mL), washed with aqueous tartaric acid solution (2 × 10 mL) and brine (50 mL), and dried over Na_2SO_4. After evaporating the solvent, the crude diol was used directly in the next step. The crude diol was dissolved in CH_2Cl_2 (50 mL). The solution was added dropwise to a mixture of pyridine (100 mL) and methanesulfonyl chloride (6 mL, 77.5 mmol) and cooled to 0 °C. The reaction mixture was stirred at 0 °C for 30 min, then allowed to warm to RT for 6 h. When TLC analysis of the aliquots (hexane–EtOAc, 1:1) showed total consumption of the starting material, the reaction mixture was poured into ice water, extracted with CH_2Cl_2 (3 × 100 mL), washed with brine (50 mL), and dried over Na_2SO_4. Purification by column chromatography (hexane–EtOAc, 2:1) yielded compound **28** as a colourless syrup (3.6 g, 45% for two steps). $[\alpha]^{22}_D$ +54° (*c* 4, CH_2Cl_2). ^{1}H NMR (($CD_3)_2O$) δ: 4.87 (dd, 1H, $J_{3,4}$ = 6.1 Hz, $J_{4,5}$ = 4.8 Hz, H-4), 4.57 (ddd, 1H, $J_{1b,2}$ = 6.0 Hz, $J_{1a,1b}$ = 12.0 Hz, H-1b), 4.56–4.48 (m, 3H, H-2, H-3, H-1a), 4.45 (ddd, 1H, H-5), 4.13 (dd, 1H, $J_{5,6b}$ = 6.7 Hz, $J_{6a,6b}$ = 8.6 Hz, H-6b), 4.03 (dd, 1H, $J_{5,6a}$ = 6.6 Hz, H-6a), 3.24, 3.15 (2 s, 6H, 2 × OSO_2CH_3), 1.52, 1.41, 1.38, 1.34 (4 s, 12H, 4 × CH_3). ^{13}C NMR (($CD_3)_2O$) δ: 114.3, 113.8 (($CH_3)_2C(OR)_2$), 83.3 (C-4), 79.7 (C-3), 79.0 (C-2), 78.9 (C-1), 72.9 (C-5), 69.6 (C-6), 43.0, 40.9 (2 × OSO_2CH_3), 31.3, 29.9, 29.3, 29.2 (4 × CH_3). Anal. calcd. for $C_{14}H_{26}O_{10}S_2$: C 40.18, H 6.26; found: C 39.89, H 6.02.

1,4-Anhydro-2,3,5,6-di-*O*-isopropylidene-4-seleno-D-allitol (15)

To a suspension of grey selenium metal (1.6 g, 20.2 mmol) and 95% EtOH (100 mL), $NaBH_4$ was added portionwise until the black Se color disappeared. To this mixture, a solution of the dimesylate **24** (7.0 g, 16.8 mmol) in THF (10 mL) was added and the reaction mixture was heated at 70 °C for 12 h. The solvent was evaporated under reduced pressure, the residue was redissolved in EtOAc, washed with water (20 mL) and brine (20 mL), and dried over Na_2SO_4. After evaporating the solvent, the crude product was purified by column chromatography (hexane–EtOAc, 3:1) to give **15** as a colourless oil (3.2 g, 62%). $[\alpha]^{22}_D$ +152° (*c* 1, CH_2Cl_2). ^{1}H NMR (($CD_3)_2O$) δ: 4.98 (ddd, 1H, $J_{1b,2}$ = 4.5 Hz, H-2), 4.91 (dd, 1H, $J_{2,3}$ = 5.6 Hz, H-3), 4.12 (dd, 1H, $J_{6a,6b}$ = 8.4 Hz, $J_{5,6b}$ = 6.4 Hz, H-6b), 4.04 (ddd, 1H, $J_{5,6a}$ = 5.9 Hz, $J_{4,5}$ = 5.8 Hz, H-5), 3.71 (dd, 1H, H-6a), 3.18 (m, 1H, H-4), 3.16 (dd, 1H, $J_{1a,1b}$ = 12.8 Hz, H-1b), 2.78 (dd, 1H, H-1a), 1.42, 1.38, 1.29, 1.28 (4 s, 12H, 4 × CH_3). ^{13}C NMR (($CD_3)_2O$) δ: 110.3, 109.8 (($CH_3)_2C(OR)_2$), 85.6 (C-3), 83.9 (C-2), 76.4 (C-5), 69.0 (C-6), 57.7 (C-4), 37.4 (C-1), 26.5, 26.0, 25.1, 24.1 (4 × CH_3). Anal. calcd. for $C_{12}H_{20}O_4Se$: C 46.91, H 6.56; found: C 46.67, H 6.37.

1,4-Anhydro-2,3,5,6-di-*O*-isopropylidene-4-thio-D-allitol (16)

To a solution of the dimesylate **24** (5.0 g, 11.9 mmol) in DMF (80 mL), $Na_2S{\cdot}9H_2O$ (4.0 g, 16.7 mmol) was added and the reaction mixture was heated at 90 °C for 12 h. The reaction mixture was poured into water (100 mL), extracted with Et_2O (4 × 50 mL), washed with water (10 × 20 mL), and dried over Na_2SO_4. After evaporating the solvent, the crude product was purified by column chromatography (hexane–EtOAc, 3:1) to give **16** as a colourless oil (2.9 g, 92%). $[\alpha]^{22}_D$ +127° (*c* 1, CH_2Cl_2). ^{1}H NMR (($CD_3)_2O$) δ: 5.04 (ddd, 1H, $J_{1b,2}$ = 4.7 Hz, H-2), 4.91 (dd, 1H, $J_{2,3}$ = 5.6 Hz, H-3), 4.15–4.12 (m, 1H, H-4), 4.13 (dd, 1H, H-6b), 3.68 (ddd, 1H, $J_{5,6a}$ = 6.7 Hz, $J_{4,5}$ = 9.2 Hz, $J_{5,6b}$ = 8.2 Hz, H-5), 3.45 (dd, 1H, $J_{6a,6b}$ = 8.5 Hz, H-6a), 3.29 (dd, 1H, $J_{1a,1b}$ = 11.2 Hz, H-1b), 2.92 (dd, 1H, H-1a), 1.42, 1.38, 1.29, 1.27 (4 s, 12H, 4 × CH_3). ^{13}C NMR (($CD_3)_2O$) δ: 109.9, 109.8 (($CH_3)_2C(OR)_2$), 87.1 (C-3), 85.3 (C-2), 77.1 (C-5), 69.6 (C-6), 52.6 (C-4), 29.7 (C-1), 26.6, 26.2, 25.2, 24.1 (4 × CH_3). Anal. calcd. for $C_{12}H_{20}O_4S$: C 55.36, H 7.74; found: C 55.64, H 7.72.

1,4-Anhydro-2,3,5,6-di-*O*-isopropylidene-4-seleno-L-allitol (17)

To a suspension of grey selenium metal (1.4 g, 18.7 mmol) and EtOH (100 mL, 95%), $NaBH_4$ was added portionwise until the black Se color disappeared. To this mixture, a solution of the dimesylate **28** (6.0 g, 14.3 mmol) in THF (10 mL) was added and the reaction mixture was heated at 65–70 °C for 12 h. The solvent was evaporated under reduced pressure and the residue was redissolved in EtOAc, washed with water (20 mL) and brine (20 mL), and dried over Na_2SO_4. After evaporating the solvent, the crude product was purified by column chromatography (hexane–EtOAc, 3:1) to give **17** as a colourless oil (2.9 g, 67%). $[\alpha]^{22}_D$ −143° (*c* 1, CH_2Cl_2). ^{1}H NMR (($CD_3)_2O$) δ: 5.03 (ddd, 1H, H-2), 4.91 (dd, 1H, $J_{2,3}$ = 5.6 Hz, H-3), 4.15–4.10 (m, 2H, H-5, H-6b), 3.68 (dd, 1H, $J_{5,6a}$ = 8.9 Hz, $J_{6a,6b}$ = 11.4 Hz, H-6a), 3.45 (dd, 1H, H-4), 3.27 (dd, 1H, $J_{1b,2}$ = 4.7 Hz, $J_{1a,1b}$ = 12.0 Hz, H-1b), 2.92 (dd, 1H, $J_{1b,2}$ = 0.7 Hz,

© 2006 NRC Canada

H-1a), 1.42, 1.37, 1.29, 1.27 (4 s, 12H, 4 × CH_3). ^{13}C NMR ($(CD_3)_2O$) δ: 110.0, 109.8 ($(CH_3)_2C(OR)_2$), 87.1 (C-3), 85.3 (C-2), 77.1 (C-5), 69.6 (C-6), 52.6 (C-4), 29.8 (C-1), 26.6, 26.2, 25.3, 24.1 (4 × CH_3). Anal. calcd. for $C_{12}H_{20}O_4Se$: C 46.91, H 6.56; found: C 46.76, H 6.66.

1,4-Anhydro-2,3,5,6-di-*O*-isopropylidene-4-thio-L-allitol (18)

To a solution of the dimesylate **28** (5.0 g, 11.9 mmol) in DMF (80 mL), $Na_2S·9H_2O$ (4.0 g, 16.7 mmol) was added and the reaction mixture was heated at 90 °C for 12 h. The reaction mixture was poured into water (100 mL), extracted with Et_2O (4 × 50 mL), washed with water (10 × 20 mL), and dried over Na_2SO_4. After evaporating the solvent, the crude product was purified by column chromatography (hexane–EtOAc, 3:1) to give **18** as a colourless oil (2.5 g, 82%). $[\alpha]^{22}_D$ –139° (*c* 1, CH_2Cl_2). ^{1}H NMR ($(CD_3)_2O$) δ: 4.99 (ddd, 1H, H-2), 4.92 (dd, 1H, $J_{2,3}$ = 5.6 Hz, H-3), 4.12 (dd, 1H, $J_{6a,6b}$ = 8.2 Hz, $J_{5,6b}$ = 6.4 Hz, H-6b), 4.04 (ddd, 1H, H-5), 3.71 (dd, 1H, $J_{5,6a}$ = 5.9 Hz, H-6a), 3.19–3.15 (m, 1H, H-4), 3.17 (dd, 1H, H-1b), 2.80 (dd, 1H, $J_{1a,1b}$ = 12.9 Hz, H-1a), 1.42, 1.38, 1.29, 1.28 (4 s, 12H, 4 × CH_3). ^{13}C NMR ($(CD_3)_2O$) δ: 110.3, 109.8 ($(CH_3)_2C(OR)_2$), 85.6 (C-3), 83.9 (C-2), 76.3 (C-5), 69.0 (C-6), 57.7 (C-4), 37.4 (C-1), 26.5, 26.0, 25.1, 24.1 (4 × CH_3). Anal. calcd. for $C_{12}H_{20}O_4S$: C 55.36, H 7.74; found: C 55.16, H 7.58.

General procedure for the preparation of sulfonium and selenonium sulfates 29–36

A mixture of **15**, **16**, **17**, or 1**8**, and the cyclic sulfate **19** or **20** in HFIP (1,1,1,3,3,3-hexafluoroisopropanol) was placed in a reaction vessel and K_2CO_3 (20 mg) was added. The stirred reaction mixture was heated in a sealed tube at the indicated temperature for the indicated time, as given later. The progress of the reaction was followed by TLC analysis of the aliquots (EtOAc–MeOH, 10:1). When the limiting reagent had been essentially consumed, the mixture was cooled, diluted with CH_2Cl_2, and evaporated to give a syrupy residue. Purification by column chromatography (EtOAc to EtOAc–MeOH, 10:1) gave the purified sulfonium salts and selenonium salts **29**–**36**.

1,4-Anhydro-2,3,5,6-di-*O*-isopropylidene-1-[(S)-[(2′S,3′S)-2′,4 -benzylidenedioxy-3′-(sulfooxy)butyl]selenonio]-D-allitol inner salt (29)

The reaction of compound **15** (500 mg, 1.63 mmol) with the cyclic sulfate **19** (530 mg, 1.94 mmol) in HFIP (2.0 mL) for 12 h at 80–85 °C gave compound **29** as a colourless, amorphous solid (850 mg, 90% based on **15**). $[\alpha]^{22}_D$ +12° (*c* 0.5, CH_2Cl_2). ^{1}H NMR ($(CD_3)_2O$) δ: 7.56–7.38 (m, 5H, H-Arom.), 5.74 (s, 1H, C*H*Ph), 5.52 (ddd, 1H, $J_{1b,2}$ = 5.2 Hz, $J_{2,3}$ = 5.7, H-2), 5.27 (dd, 1H, H-3), 4.78 (ddd, 1H, ddd, 1H, $J_{5,6b}$ = 7.3 Hz, $J_{5,6a}$ = 5.2 Hz, $J_{4,5}$ = 3.8 Hz, H-5), 4.62 (dd, 1H, H-4), 4.46–4.37 (m, 4H, H-1′b, H-2′, H-3′, H-4′b), 4.28 (dd, 1H, $J_{1'a,1'b}$ = 13.4 Hz, $J_{1'a,2'}$ = 3.8 Hz, H-1′a), 4.25 (dd, 1H, $J_{6a,6b}$ = 9.5 Hz, $J_{5,6b}$ = 7.3 Hz, H-6b), 4.10 (dd, 1H, $J_{1b,2}$ = 5.2 Hz, $J_{1a,1b}$ = 15.4 Hz, H-1b), 3.97 (dd, 1H, H-1a), 3.96 (dd, 1H, $J_{5,6a}$ = 5.2 Hz, H-6a), 3.78 (m, 1H, H-4′a), 1.64, 1.42, 1.38, 1.32 (4 s, 18H, 4 × CH_3). ^{13}C NMR ($(CD_3)_2O$) δ: 142.3, 133.9, 133.0, 131.1 (C-Ar), 116.9, 115.7 (2 $(CH_3)_2C(OR)_2$), 106.1 (*C*HPh), 89.9 (C-3), 89.8 (C-2), 81.3 (C-2′), 79.0 (C-5), 73.9 (C-4), 73.5 (C-4′), 71.8 (C-6), 71.5 (C-3), 52.8 (C-1), 50.4 (C-1′), 30.3, 30.1, 28.2, 27.1 (4 × *C*H_3). HRMS calcd. for $C_{23}H_{33}O_{10}SSe$: 581.0594 (M + H^+); found: 581.0597.

1,4-Anhydro-2,3,5,6-di-*O*-isopropylidene-1-[(S)-[(2′S,3′S)-2′,4′-benzylidenedioxy-3′-(sulfooxy)butyl]sulfonio]-D-allitol inner salt (30)

The reaction of compound **16** (500 mg, 1.92 mmol) with the cyclic sulfate **19** (630 mg, 2.31 mmol) in HFIP (2.0 mL) for 12 h at 70–75 °C gave compound **30** as a colourless, amorphous solid (960 mg, 94% based on **16**). $[\alpha]^{22}_D$ +1.2° (*c* 0.1, CH_2Cl_2). ^{1}H NMR ($(CD_3)_2O$) δ: 7.56–7.38 (m, 5H, H-Arom.), 5.74 (s, 1H, C*H*Ph), 5.52 (ddd, 1H, $J_{1b,2}$ = 5.2 Hz, $J_{2,3}$ = 5.7 Hz, H-2), 5.26 (dd, 1H, H-3), 4.79 (ddd, 1H, ddd, 1H, $J_{5,6b}$ = 7.4 Hz, $J_{5,6a}$ = 5.1 Hz, $J_{4,5}$ = 3.9 Hz, H-5), 4.63 (dd, 1H, H-4), 4.49–4.36 (m, 4H, H-1′b, H-2′, H-3′, H-4′b), 4.28 (dd, 1H, $J_{1'a,1'b}$ = 13.4 Hz, $J_{1'a,2'}$ = 3.7 Hz, H-1′a), 4.25 (dd, 1H, $J_{6a,6b}$ = 9.4 Hz, H-6b), 4.10 (dd, 1H, $J_{1b,2}$ = 5.2 Hz, $J_{1a,1b}$ = 14.4 Hz, H-1b), 3.97 (dd, 1H, H-1a), 3.97 (dd, 1H, $J_{5,6a}$ = 5.1 Hz, H-6a), 3.78 (m, 1H, H-4′a), 1.64, 1.42, 1.38, 1.32 (4s, 18H, 4 × CH_3). ^{13}C NMR ($(CD_3)_2O$) δ: 138.5, 129.3, 128.4, 126.5 (C-Ar), 112.3, 111.1 (2 $(CH_3)_2C(OR)_2$), 101.4 (*C*HPh), 85.3 (C-3), 85.2 (C-2), 76.7 (C-2′), 74.4 (C-5), 69.2 (C-4′), 68.8 (C-4), 67.1 (C-6), 67.0 (C-3′), 48.2 (C-1), 45.8 (C-1′), 25.7, 25.5, 23.6, 22.5 (4 × *C*H_3). Anal. calcd. for $C_{23}H_{32}O_{10}S_2$: C 51.86, H 6.06; found: C 52.06, H 5.87. HRMS calcd. for $C_{23}H_{33}O_{10}S_2$: 533.1510 (M + H^+); found: 533.1512.

1,4-Anhydro-2,3,5,6-di-*O*-isopropylidene-1-[(S)-[(2′S,3′S)-2′,4 -benzylidenedioxy-3′-(sulfooxy)butyl]selenonio]-L-allitol inner salt (31)

The reaction of compound **17** (500 mg, 1.63 mmol) with the cyclic sulfate **19** (530 mg, 1.94 mmol) in HFIP (2.0 mL) for 12 h at 65–70 °C gave compound **31** as a colourless, amorphous solid (850 mg, 90% based on **17**). $[\alpha]^{22}_D$ +18° (*c* 1.0, CH_2Cl_2). ^{1}H NMR (CD_2Cl_2) δ: 7.48–7.38 (m, 5H, H-Arom.), 5.61 (s, 1H, C*H*Ph), 5.41 (ddd, 1H, H-2), 5.15 (dd, 1H, $J_{2,3}$ = 5.3 Hz, H-3), 4.81 (ddd, 1H, $J_{4,5}$ = 2.0 Hz, $J_{5,6a}$ = 4.6 Hz, $J_{5,6b}$ = 7.8 Hz, H-5), 4.60 (m, 1H, H-4), 4.55 (ddd, 1H, H-3′), 4.52 (dd, 1H, H-4′b), 4.42 (d, 2H, H-1′b, H-1′a), 4.38–4.32 (m, 1H, H-2′), 4.20 (dd, 1H, $J_{5,6b}$ = 7.8 Hz, $J_{6a,6b}$ = 9.6 Hz, H-6b), 3.95 (dd, 1H, $J_{5,6a}$ = 4.6 Hz, H-6a), 3.85 (dd, 1H, $J_{4'a,4'b}$ = 10.0 Hz, H-4′a), 3.63 (dd, 1H, H-1b), 3.60 (dd, 1H, $J_{1a,2}$ = 5.1 Hz, $J_{1a,1b}$ = 13.9 Hz, H-1a), 1.60, 1.44, 1.36, 1.32 (4 s, 12H, 4 × CH_3). ^{13}C NMR (CD_2Cl_2) δ: 137.0, 129.5, 128.6, 126.3 (C-Ar), 112.1, 111.2 (2 $(CH_3)_2C(OR)_2$), 101.8 (*C*HPh), 87.8 (C-2), 85.7 (C-3), 76.9 (C-3′), 74.7 (C-5), 70.5 (C-4), 69.3 (C-4′), 67.7 (C-2′), 67.2 (C-6), 44.5 (C-1′), 43.2 (C-1), 26.2, 26.0, 23.3, 22.9 (4 × *C*H_3). Anal. calcd. for $C_{23}H_{32}O_{10}SSe$: C 47.67, H 5.57; found: C 47.89, H 5.67.

1,4-Anhydro-2,3,5,6-di-*O*-isopropylidene-1-[(S)-[(2′S,3′S)-2′,4′-benzylidenedioxy-3′-(sulfooxy)butyl]sulfonio]-L-allitol inner salt (32)

The reaction of compound **18** (500 mg, 1.92 mmol) with the cyclic sulfate **19** (630 mg, 2.31 mmol) in HFIP (2.0 mL) for 12 h at 80–85 °C gave compound **32** as a colourless, amorphous solid (940 mg, 92% based on **18**). $[\alpha]^{22}_D$ +10° (*c* 0.5, CH_2Cl_2). ^{1}H NMR ($(CD_3)_2O$) δ: 7.48–7.39 (m, 5H, H-

© 2006 NRC Canada

Arom.), 5.59 (s, 1H, C*H*Ph), 5.26 (ddd, 1H, H-2), 5.10 (dd, 1H, $J_{2,3}$ = 5.8 Hz, H-3), 4.88 (ddd, 1H, $J_{4,5}$ = 7.6 Hz, H-5), 4.68 (ddd, 1H, H-3′), 4.54 (m, 1H, H-4), 4.50 (dd, 1H, $J_{3',4'}$ = 1.8 Hz, H-4′), 4.40 (d, 2H, H-1′b, H-1′a), 4.34 (m, 1H, H-2′), 4.32 (dd, 1H, $J_{5,6b}$ = 7.9 Hz, $J_{6a,6b}$ = 9.8 Hz, H-6b), 4.01 (dd, 1H, $J_{5,6a}$ = 4.6 Hz, H-6a), 3.82 (dd, 1H, H-4′a), 3.68 (dd, 1H, $J_{1b,2}$ = 5.3 Hz, $J_{1a,1b}$ = 15.0 Hz, H-1b), 3.62 (dd, 1H, H-1a), 1.60, 1.44, 1.36, 1.34 (4 s, 12H, 4 × CH_3). ^{13}C NMR ($(CD_3)_2O$) δ: 136.9, 129.6, 128.6, 126.3 (C-Ar), 112.8, 111.5 (2 $(CH_3)_2C(OR)_2$), 101.9 (*C*HPh), 86.2 (C-2), 84.1 (C-3), 76.9 (C-3′), 74.8 (C-5), 71.4 (C-4), 69.2 (C-2), 67.3 (C-6), 65.7 (C-4′), 47.7 (C-1), 45.9 (C-1′), 26.0, 25.9, 23.3, 22.6 (4 × *C*H_3). HRMS calcd. for $C_{23}H_{33}O_{10}S_2$: 533.1510 ($M + H^+$); found: 533.1515.

1,4-Anhydro-2,3,5,6-di-*O*-isopropylidene-1-[(S)-[(2′R,3′S,4′R,5′R)-2′,4′-benzylidenedioxy-5′,6′-isopropylidenedioxy-3′-(sulfooxy)hexyl]selenonio]-D-allitol inner salt (33)

The reaction of compound **15** (500 mg, 1.63 mmol) with the cyclic sulfate **20** (730 mg, 1.96 mmol) in HFIP (2.0 mL) for 12 h at 80–85 °C gave compound **33** as a colourless, amorphous solid (770 mg, 70% based on **15**). $[\alpha]^{22}_D$ +8° (*c* 0.5, CH_2Cl_2). ^{1}H NMR ($(CD_3)_2O$) δ: 7.58–7.32 (m, 5H, H-Arom.), 5.90 (s, 1H, C*H*Ph), 5.63 (ddd, 1H, $J_{2,3}$ = 5.4 Hz, H-2), 5.26 (dd, 1H, H-3), 4.92 (m, 1H, H-2′), 4.82 (ddd, 1H, $J_{5,6b}$ = 7.7 Hz, $J_{5,6a}$ = 4.9 Hz, $J_{4,5}$ = 3.2 Hz, H-5), 4.62 (dd, 1H, $J_{1'a,1'b}$ = 12.2 Hz, $J_{1'b,2'}$ = 5.9 Hz, H-1′ b), 4.59–4.57 (m, 2H, H-3′, H-4), 4.46 (ddd, 1H, $J_{4',5'}$ = 2.3 Hz, $J_{5',6'a}$ = 8.1 Hz, $J_{5',6'b}$ = 6.8 Hz, H-5′), 4.40 (m, 1H, H-4′), 4.29 (dd, 1H, $J_{6'a,6'b}$ = 8.5 Hz, H-6′b), 4.28 (dd, 1H, H-6b), 4.18 (dd, 1H, H-1′a), 4.16 (dd, 1H, H-6′a), 4.08 (dd, 1H, $J_{6a,6b}$ = 9.5 Hz, H-6a), 3.76 (dd, 1H, $J_{1a,1b}$ = 14.1 Hz, $J_{1b,2}$ = 5.4 Hz, H-1b), 3.60 (dd, 1H, H-1a), 1.59, 1.43, 1.36, 1.33, 1.31, 1.29, 1.28 (6 s, 18H, 6 × CH_3). ^{13}C NMR ($(CD_3)_2O$) δ: 138.2, 129.1, 128.4 and 126.3 (C-Ar), 111.3, 110.6, 107.5 (3 × $(CH_3)_2C(OR)_2$), 100.6 (*C*HPh), 88.1 (C-2), 85.9 (C-3), 78.9 (C-4′), 76.5 (C-5′), 74.8 (C-5), 74.0 (C-2′), 71.1 (C-3′), 69.1 (C-4), 67.1 (C-6), 64.6 (C-6′), 43.9 (C-1′), 43.6 (C-1), 26.0, 25.7, 25.6, 25.5, 23.4, 22.5 (6 × *C*H_3). Anal. calcd. for $C_{28}H_{40}O_{12}SSe$: C 49.48, H 5.93; found: C 49.16, H 6.09.

1,4-Anhydro-2,3,5,6-di-*O*-isopropylidene-1-[(S)-[(2′R,3′S,4′R,5′R)-2′,4′-benzylidenedioxy-5′,6′-isopropylidenedioxy-3′-(sulfooxy)hexyl]sulfonio]-D-allitol inner salt (34)

The reaction of compound **16** (500 mg, 1.92 mmol) with the cyclic sulfate **20** (860 mg, 2.30 mmol) in HFIP (2.0 mL) for 12 h at 90–95 °C gave compound **34** as a colourless, amorphous solid (1.0 g, 82% based on **16**). $[\alpha]^{22}_D$ +5.4° (*c* 0.1, CH_2Cl_2). ^{1}H NMR ($(CD_3)_2O$) δ: 7.60–7.38 (m, 5H, H-Arom.), 5.89 (s, 1H, C*H*Ph), 5.50 (ddd, 1H, H-2), 5.26 (dd, 1H, $J_{2,3}$ = 5.8 Hz, H-3), 4.88 (ddd, 1H, $J_{2',3'}$ = 5.0 Hz, $J_{1'b,2'}$ = 5.0 Hz, $J_{1'a,2'}$ = 2.1 Hz, H-2′), 4.83 (ddd, 1H, $J_{5,6b}$ = 2.8 Hz, $J_{5,6a}$ = 5.1 Hz, $J_{4,5}$ = 7.6 Hz, H-5), 4.59 (dd, 1H, $J_{3,4}$ = 2.4 Hz, H-4), 4.57–4.52 (m, 2H, H-1′b, H-3′), 4.50 (ddd, 1H, $J_{4',5'}$ = 2.1 Hz, $J_{5',6'a}$ = 9.1 Hz, $J_{5',6'b}$ = 7.1 Hz, H-5′), 4.42 (dd, 1H, $J_{3',4'}$ = 1.8 Hz, H-4′), 4.33 (dd, 1H, H-6′b), 4.30 (dd, 1H, $J_{5,6b}$ = 2.8 Hz, H-6b), 4.28 (m, 1H, H-1′a), 4.18 (dd, 1H, $J_{6'a,6'b}$ = 8.4 Hz, H-6′a), 4.11 (dd, 1H, $J_{6a,6b}$ = 9.6 Hz, H-6a), 3.90 (dd, 1H, $J_{1b,2}$ = 5.4 Hz, H-1b), 3.75 (dd, 1H, $J_{1a,1b}$ = 14.3 Hz, H-1a), 1.61, 1.43, 1.37, 1.30, 1.29, 1.28 (6 s, 18H, 6 × CH_3). ^{13}C NMR ($(CD_3)_2O$) δ: 138.2, 129.1, 128.4, 126.3 (C-Ar), 112.1, 110.9, 107.5 (3 × $(CH_3)_2C(OR)_2$), 100.7 (*C*HPh), 86.2 (C-2), 84.5 (C-3), 79.0 (C-4), 76.7 (C-5′), 74.7 (C-5), 74.1 (C-2′), 70.3 (C-3′), 70.0 (C-4′), 67.1 (C-6), 64.6 (C-6′), 47.9 (C-1), 46.1 (C-1′), 23.9, 25.6, 25.5, 25.4, 23.4, 22.4 (6 × *C*H_3). Anal. calcd. for $C_{28}H_{40}O_{12}S_2$: C 53.15, H 6.37; found: C 52.92, H 6.17.

1,4-Anhydro-2,3,5,6-di-*O*-isopropylidene-1-[(S)-[(2′R,3′S,4′R,5′R)-2′,4′-benzylidenedioxy-5′,6′-isopropylidenedioxy-3′-(sulfooxy)hexyl]selenonio]-L-allitol inner salt (35)

The reaction of compound **17** (500 mg, 1.63 mmol) with the cyclic sulfate **20** (730 mg, 1.96 mmol) in HFIP (2.0 mL) for 12 h at 80–85 °C gave compound **35** as a colourless, amorphous solid (740 mg, 67% based on **17**). $[\alpha]^{22}_D$ –12° (*c* 1, CH_2Cl_2). ^{1}H NMR ($(CD_3)_2O$) δ: 7.60–7.38 (m, 5H, H-Arom.), 5.92 (s, 1H, C*H*Ph), 5.55 (ddd, 1H, H-2), 5.21 (dd, 1H, $J_{2,3}$ = 5.4 Hz, $J_{3,4}$ = 1.8 Hz, H-3), 4.96–4.92 (m, 1H, H-2′), 4.60 (dd, 1H, H-3′), 4.53 (dd, 1H, $J_{1'b,2'}$ = 6.4 Hz, $J_{1'b,1'a}$ = 12.2 Hz, H-1′ b), 4.45 (ddd, 1H, $J_{4,5}$ = 2.3 Hz, $J_{5,6'a}$ = 9.2 Hz, $J_{5,6'b}$ = 6.9 Hz, H-5′), 4.41 (dd, 1H, H-4′), 4.40–4.36 (m, 1H, H-5), 4.34 (dd, 1H, $J_{6'a,6'b}$ = 8.6 Hz, H-6′b), 4.24–4.18 (m, 3H, H-4, H-1′a, H-6′a), 3.99 (dd, 1H, 1H, $J_{5,6b}$ = 7.3 Hz, $J_{6a,6b}$ = 9.3 Hz, H-6b), 3.96 (dd, 1H, $J_{1b,2}$ = 5.2 Hz, H-1b), 3.90 (dd, 1H, $J_{1a,1b}$ = 14.2 Hz, H-1a), 3.76 (dd, 1H, $J_{5,6a}$ = 5.2 Hz, H-6a), 1.59, 1.39, 1.35, 1.30, 1.29, 1.25 (6 s, 18H, 6 × C*H*$_3$). ^{13}C NMR ($(CD_3)_2O$) δ: 142.9, 133.9, 133.1, 131.0 (C-Ar), 116.1, 115.3, 112.1 (3 × $(CH_3)_2C(OR)_2$), 105.0 (*C*HPh), 91.5 (C-3), 91.0 (C-2), 83.4 (C-4′), 81.2 (C-5′), 78.7 (C-5), 78.5 (C-2′), 75.5 (C-3′), 72.3 (C-4), 71.6 (C-6), 69.3 (C-6′), 49.3 (C-1), 48.0 (C-1′), 30.7, 30.6, 30.3, 30.2, 28.1, 27.5 (6 × *C*H_3). Anal. calcd. for $C_{28}H_{40}O_{12}SSe$: C 49.48, H 5.93; found: C 49.31, H 5.90.

1,4-Anhydro-2,3,5,6-di-*O*-isopropylidene-1-[(S)-[(2′R,3′S,4′R,5′R)-2′,4′-benzylidenedioxy-5′,6′-isopropylidenedioxy-3′-(sulfooxy)hexyl]sulfonio]-L-allitol inner salt (36)

The reaction of compound **18** (500 mg, 1.92 mmol) with the cyclic sulfate **20** (860 mg, 2.30 mmol) in HFIP (2.0 mL) for 12 h at 90–95 °C gave compound **36** as a colourless, amorphous solid (960 mg, 77% based on **18**). $[\alpha]^{22}_D$ –15° (*c* 0.5, CH_2Cl_2). ^{1}H NMR (CD_2Cl_2) δ: 7.56–7.40 (m, 5H, H-Arom.), 5.76 (s, 1H, C*H*Ph), 5.19 (ddd, 1H, H-2), 4.98 (dd, 1H, $J_{2,3}$ = 5.7 Hz, H-3), 4.68–4.62 (m, 2H, H-2′, H-3′), 4.51 (ddd, 1H, H-5′), 4.42 (dd, 1H, $J_{1'b,2'}$ = 5.7 Hz, $J_{1'b,1'a}$ = 13.5 Hz, H-1′b), 4.28 (dd, 1H, $J_{1'a,2'}$ = 2.3 Hz, H-1′a), 4.28–4.25 (m, 1H, H-5), 4.25–4.18 (m, 3H, H-6′a, H-6′b, H-4′), 4.14 (m, 1H, H-4), 3.90 (dd, 1H, $J_{1a,1b}$ = 15.4 Hz, H-1b), 3.86 (dd, 1H, $J_{1a,2}$ = 4.6 Hz, H-1a), 3.86 (dd, 1H, 1H, $J_{5,6b}$ = 7.8 Hz, H-6b), 3.71 (dd, 1H, $J_{5,6a}$ = 5.1 Hz, $J_{6a,6b}$ = 9.5 Hz, H-6a), 1.62, 1.39, 1.38, 1.37, 1.34, 1.24 (6 s, 18H, 6 × C*H*$_3$). ^{13}C NMR (CD_2Cl_2) δ: 137.4, 129.7, 128.6, 126.3 (C-Ar), 112.7, 111.5, 108.5 (3 × $(CH_3)_2C(OR)_2$), 100.9 (*C*HPh), 85.2 (C-2), 84.8 (C-3), 79.1 (C-4′), 75.5 (C-5′), 74.3 (C-5), 74.0 (C-3′), 70.5 (C-2′), 69.8 (C-4), 67.0 (C-6), 65.0 (C-6′), 47.8 (C-1), 45.9 (C-1′), 26.4, 26.1, 25.9, 25.5, 23.3, 22.8 (6 × *C*H_3). Anal. calcd. for $C_{28}H_{40}O_{12}S_2$: C 53.15, H 6.37; found: C 53.36, H 6.41.

© 2006 NRC Canada

General procedure for the deprotection of the coupled products to yield the final compounds 7–14

The protected coupled products **29**–**36** were dissolved in CH_2Cl_2 (2 mL), TFA (10 mL) was then added, and the mixture was stirred for 6–8 h at RT. The progress of the reaction was followed by TLC analysis of the aliquots (EtOAc–MeOH–H_2O, 7:3:1). When the starting material had been consumed, the TFA and CH_2Cl_2 were removed under reduced pressure. The residue was rinsed with CH_2Cl_2 (4 × 2 mL) and the CH_2Cl_2 was decanted to remove the cleaved protecting groups. The remaining gum was dissolved in water and purified by column chromatography (EtOAc and EtOAc–MeOH, 2:1) to give the purified compounds **7**–**10** as colourless, amorphous, and hygroscopic solids. In the cases of **33**–**36**, the benzylidene groups were not completely cleaved. The residue was then dissolved in 80% AcOH (10 mL) and Pd–C (10%, 200 mg, in two portions) was added and the reaction mixture was subjected to hydrogenolysis for 48 h at RT. After filtering the Pd–C, the filtrate was mixed with water (100 mL) and the solvents were removed under reduced pressure. The remaining gum was dissolved in water and purified by column chromatography (EtOAc and EtOAc–MeOH, 2:1) to give the purified compounds **11**–**14** as colourless, amorphous, and hygroscopic solids.

1,4-Anhydro-1-[(S)-[(2′S,3′S)-2′,4′-dihydroxy-3′-(sufooxy)butyl]selenonio]-D-allitol inner salt (7)

To a solution of **29** (500 mg, 0.86 mmol) in CH_2Cl_2 (2 mL) was added TFA (10 mL) to yield the compound **7** as a colourless, amorphous, and hygroscopic solid (202 mg, 57%). $[\alpha]^{22}_D$ +54° (*c* 2, H_2O). ^{1}H NMR (D_2O) δ: 4.74 (m, 1H, H-2), 4.34 (dd, 1H, $J_{2,3}$ = 9.1 Hz, $J_{3,4}$ = 3.1 Hz, H-3), 4.28 (ddd, 1H, H-3′), 4.25–4.18 (m, 2H, H-2′, H-5), 4.05 (dd, 1H, $J_{4,5}$ = 4.3 Hz, H-4), 3.97 (dd, 1H, $J_{1'b,2'}$ = 3.6 Hz, $J_{1'a,1'b}$ = 12.6 Hz, H-1′b), 3.82 (dd, 1H, $J_{3',4'b}$ = 6.4 Hz, H-4′b), 3.80 (dd, 1H, $J_{1'a,2'}$ = 3.2 Hz, H-1′a), 3.73 (dd, 1H, $J_{3',4'a}$ = 3.3 Hz, 1H, $J_{4'a,4'b}$ = 12.8 Hz, H-4′a), 3.68 (m, 2H, H-6a, H-6b), 3.55 (dd, 1H, $J_{1b,2}$ = 3.7 Hz, H-1b), 3.33 (dd, 1H, $J_{1a,2}$ = 2.1 Hz, $J_{1a,1b}$ = 13.1 Hz, H-1a). ^{13}C NMR (D_2O) δ: 80.8 (C-3′), 76.0 (C-2), 75.9 (C-3), 68.4 (C-5), 66.0 (C-2′), 65.1 (C-4), 63.4 (C-6), 60.1 (C-4′), 48.5 (C-1′), 40.5 (C-1). HRMS calcd. for $C_{10}H_{19}O_{10}SSe$: 410.9859 (M – H); found: 410.9861.

1,4-Anhydro-1-[(S)-[(2′S,3′S)-2′,4′-dihydroxy-3′-(sufooxy)butyl]sulfonio]-D-allitol inner salt (8)

To a solution of **30** (500 mg, 0.94 mmol) in CH_2Cl_2 (2 mL) was added TFA (10 mL) to yield the compound **8** as a colourless, amorphous, and hygroscopic solid (240 mg, 69%). $[\alpha]^{22}_D$ +39° (*c* 2, H_2O). ^{1}H NMR (D_2O) δ: 4.63 (m, 1H, H-2), 4.48 (dd, 1H, $J_{2,3}$ = 8.7 Hz, $J_{3,4}$ = 3.3 Hz, H-3), 4.36–4.30 (m, 2H, H-2′, H-5), 4.27 (ddd, 1H, H-3′), 4.12 (dd, 1H, $J_{1'b,2'}$ = 3.4 Hz, $J_{1'a,1'b}$ = 13.6 Hz, H-1′ b), 4.05 (dd, 1H, $J_{3,4}$ = 3.3 Hz, $J_{4,5}$ = 8.6 Hz, H-4), 3.86 (dd, 1H, $J_{3',4'b}$ = 2.8 Hz, H-4′b), 3.85 (dd, 1H, $J_{1'a,2'}$ = 8.3 Hz, H-1′a), 3.78 (dd, 1H, $J_{3',4'a}$ = 3.2 Hz, 1H, $J_{4'a,4'b}$ = 12.8 Hz, H-4′a), 3.70 (m, 2H, H-6a, H-6b), 3.69 (dd, 1H, $J_{1b,2}$ = 3.3 Hz, H-1b), 3.46 (dd, 1H, $J_{1a,2}$ = 1.6 Hz, $J_{1a,1b}$ = 14.4 Hz, H-1a). ^{13}C NMR (D_2O) δ: 79.8 (C-3′), 74.7 (C-2), 74.4 (C-3), 68.3 (C-2′), 65.6 (C-4), 65.5 (C-5), 63.0 (C-6), 59.9 (C-4′), 51.1 (C-1′), 44.2 (C-1). HRMS calcd. for $C_{10}H_{20}O_{10}S_2Na$: 387.0390 (M + Na); found: 387.0391.

1,4-Anhydro-1-[(S)-[(2′S,3′S)-2′,4′-dihydroxy-3′-(sufooxy)butyl]selenonio]-L-allitol inner salt (9)

To a solution of **31** (500 mg, 0.86 mmol) in CH_2Cl_2 (2 mL) was added TFA (10 mL) to yield the compound **9** as a colourless, amorphous, and hygroscopic solid (216 mg, 61%). $[\alpha]^{22}_D$ –17° (*c* 0.5, H_2O). ^{1}H NMR (D_2O) δ: 4.77 (ddd, 1H, H-2), 4.42 (dd, 1H, $J_{2,3}$ = 8.8 Hz, $J_{3,4}$ = 3.0 Hz, H-3), 4.33–4.25 (m, 2H, H-5, H-2′), 4.25–4.30 (ddd, 1H, H-3′), 4.13 (dd, 1H, $J_{4,5}$ = 8.7 Hz, H-4), 3.97 (dd, 1H, $J_{1'b,2'}$ = 4.0 Hz, $J_{1'a,1'b}$ = 12.4 Hz, H-1′b), 3.94 (dd, 1H, $J_{1'a,2'}$= 8.7 Hz, H-1′a), 3.83 (dd, 1H, $J_{3',4'b}$ = 3.2 Hz, H-4′b), 3.75 (dd, 1H, $J_{3',4'a}$ = 3.2 Hz, 1H, $J_{4'a,4'b}$ = 12.8 Hz, H-4′a), 3.68 (d, 2H, H-6a, H-6b), 3.58 (dd, 1H, $J_{1b,2}$ = 8.5 Hz, H-1b), 3.36 (dd, 1H, $J_{1a,2}$ = 2.2 Hz, $J_{1a,1b}$ = 13.3 Hz, H-1a). ^{13}C NMR (D_2O) δ: 81.0 (C-3), 75.8 (C-2), 75.5 (C-3), 68.7 (C-2), 66.5 (C-5), 65.5 (C-4), 63.4 (C-6), 60.0 (C-4), 48.4 (C-1), 40.4 (C-1). HRMS calcd. for $C_{10}H_{19}O_{10}SSe$: 410.9859 (M – H); found: 410.9857.

1,4-Anhydro-1-[(S)-[(2′S,3′S)-2′,4′-dihydroxy-3′-(sufooxy)butyl]sulfonio]-L-allitol inner salt (10)

To a solution of **32** (500 mg, 0.94 mmol) in CH_2Cl_2 (2 mL) was added TFA (10 mL) to yield the compound **10** as a colourless, amorphous, and hygroscopic solid (223 mg, 65%). $[\alpha]^{22}_D$ +6° (*c* 0.5, H_2O). ^{1}H NMR (D_2O) δ: 4.60 (m, 1H, H-2), 4.47 (dd, 1H, $J_{2,3}$ = 8.3 Hz, $J_{3,4}$ = 3.3 Hz, H-3), 4.32 (ddd, 1H, H-5), 4.28–4.24 (m, 1H, H-2′), 4.22 (ddd, 1H, H-3′), 4.07 (dd, 1H, $J_{4,5}$ = 8.5 Hz, H-4), 3.98 (dd, 1H, $J_{1'b,2'}$ = 3.5 Hz, H-1′b), 3.92 (dd, 1H, $J_{1'a,2'}$ = 8.8 Hz, $J_{1'a,1'b}$ = 13.6 Hz, H-1′a), 3.86 (dd, 1H, $J_{3',4'b}$ = 9.5 Hz, H-4′b), 3.74 (dd, 1H, $J_{3',4'a}$ = 3.2 Hz, 1H, $J_{4'a,4'b}$ = 12.8 Hz, H-4′a), 3.66 (d, 2H, H-6a, H-6b), 3.64–3.61 (m, 1H, H-1b), 3.44 (dd, 1H, $J_{1a,2}$ = 9.7 Hz, $J_{1a,1b}$ = 14.3 Hz, H-1a). ^{13}C NMR (D_2O) δ: 80.5 (C-3′), 74.6 (C-2), 74.5 (C-3), 68.8 (C-5), 66.6 (C-2′), 66.2 (C-4), 63.1 (C-6), 59.9 (C-4′), 50.9 (C-1′), 44.1 (C-1). HRMS calcd. for $C_{10}H_{20}O_{10}S_2Na$: 387.0390 (M + Na); found: 387.0389.

1,4-Anhydro-1-[(S)-[(2′R,3′S,4′R,5′R)-2′,4′,5′,6′-tetrahydroxy-3′-(sufooxy)hexyl]selenonio]-D-allitol inner salt (11)

To a solution of **33** (600 mg, 0.88 mmol) in CH_2Cl_2 (2 mL) was added TFA (10 mL). After removing the cleaved protecting groups, the remaining gum was then dissolved in AcOH (10 mL), Pd–C (10%, 100 mg) was added, and the reaction mixture was subjected to hydrogenolysis to give compound **11** as a colourless, amorphous, and hygroscopic solid (157 mg, 38%). $[\alpha]^{22}_D$ –8° (*c* 0.5, H_2O). ^{1}H NMR (D_2O) δ: 4.80 (m, 1H, H-2), 4.59 (dd, 1H, H-3′), 4.48 (ddd, 1H, H-2′), 4.43 (dd, 1H, $J_{2,3}$ = 8.9 Hz, $J_{3,4}$ = 2.8 Hz, H-3), 4.31 (ddd, 1H, H-5), 4.14 (dd, 1H, $J_{4,5}$ = 8.9 Hz, H-4), 4.08 (dd, 1H, $J_{1'b,2'}$ = 9.9 Hz, $J_{1'a,1'b}$ = 12.2 Hz, H-1′b), 3.95 (dd, 1H, $J_{1'a,2'}$ = 3.5 Hz, H-1′a), 3.84–3.74 (m, 3H, H-4′, H-5′, H-6′b), 3.72 (d, 2H, H-6a, H-6b), 3.62–3.57 (m, 2H, H-6′a, H-1b), 3.38 (dd, 1H, $J_{1a,2}$ = 1.9 Hz, $J_{1a,1b}$ = 13.0 Hz, H-1a). ^{13}C NMR (D_2O) δ: 78.5 (C-3′), 75.8 (C-2), 75.7 (C-3), 70.7 (C-5′), 69.6 (C-4′), 68.8 (C-5), 68.1 (C-2′), 65.5 (C-4), 63.4 (C-

© 2006 NRC Canada

6′), 62.8 (C-6), 47.7 (C-1′), 40.2 (C-1). HRMS calcd. for $C_{12}H_{25}O_9Se$: 393.0658 (M + H – SO_3); found: 393.0656.

1,4-Anhydro-1-[(S)-[(2′R,3′S,4′R,5′R)-2′,4′,5′,6′-tetrahydroxy-3′-(sufooxy)hexyl]sulfonio]-D-allitol inner salt (12)

To a solution of **34** (500 mg, 0.79 mmol) in CH_2Cl_2 (2 mL) was added TFA (10 mL). After removing the cleaved protecting groups, the remaining gum was then dissolved in AcOH (10 mL), Pd–C (10%, 100 mg) was added, and the reaction mixture was subjected to hydrogenolysis to give compound **12** as a colourless, amorphous, and hygroscopic solid (140 mg, 42%). $[\alpha]^{22}_D$ –32° (*c* 2, H_2O). ^{1}H NMR (D_2O) δ: 4.53 (m, 1H, H-2), 4.51 (dd, 1H, $J_{2',3'}$ = 5.1 Hz, $J_{3',4'}$ = 1.1 Hz, H-3′), 4.44 (ddd, 1H, H-2′), 4.26 (dd, 1H, $J_{2,3}$ = 9.6 Hz, $J_{3,4}$ = 3.1 Hz, H-3), 4.12 (ddd, 1H, H-5), 3.95 (dd, 1H, $J_{1b,2}$ = 10.8 Hz, $J_{1'a,1'b}$ = 13.4 Hz, H-1′b), 3.88 (dd, 1H, $J_{1'a,2'}$ = 2.8 Hz, H-1′a), 3.86 (dd, 1H, $J_{4,5}$ = 8.2 Hz, H-4), 3.74 (dd, 1H, $J_{4',5'}$ = 9.2 Hz, H-4′), 3.72 (dd, 1H, $J_{5,6b}$ = 3.1 Hz, $J_{6a,6b}$ = 11.9 Hz, H-6b), 3.67 (dd, 1H, $J_{5',6'b}$ = 2.5 Hz, $J_{6'a,6'b}$ = 11.8 Hz, H-6′b), 3.66–3.63 (m, 1H, H-5′), 3.59 (dd, 1H, $J_{5,6a}$ = 3.9 Hz, H-6a), 3.52–3.46 (m, 3H, H-1a, H-1b, H-6′a). ^{13}C NMR (D_2O) δ: 77.7 (C-3′), 76.1 (C-3), 72.8 (C-2), 70.4 (C-5′), 68.9 (C-4′), 67.8 (C-2′), 67.4 (C-5), 64.6 (C-6), 64.3 (C-4), 62.7 (C-6′), 49.3 (C-1′), 44.4 (C-1). HRMS calcd. for $C_{12}H_{25}O_9S$: 345.1214 (M + H – SO_3); found: 345.1214.

1,4-Anhydro-1-[(S)-[(2′R,3′S,4′R,5′R)-2′,4′,5′,6′-tetrahydroxy-3′-(sufooxy)hexyl]selenonio]-L-allitol inner salt (13)

To a solution of **35** (600 mg, 0.88 mmol) in CH_2Cl_2 (2 mL) was added TFA (10 mL). After removing the cleaved protecting groups, the remaining gum was then dissolved in AcOH (10 mL), Pd–C (10%, 100 mg) was added, and the reaction mixture was subjected to hydrogenolysis to give compound **13** as a colourless, amorphous, and hygroscopic solid (197 mg, 47%). $[\alpha]^{22}_D$ –22° (*c* 1, H_2O). ^{1}H NMR (D_2O) δ: 4.76 (ddd, 1H, H-2), 4.57 (dd, 1H, $J_{2',3'}$ = 5.2 Hz, H-3′), 4.50 (ddd, 1H, H-2′), 4.37 (dd, 1H, $J_{2,3}$ = 9.1 Hz, $J_{3,4}$ = 3.0 Hz, H-3), 4.25 (ddd, 1H, H-5), 4.06 (dd, 1H, $J_{4,5}$ = 7.9 Hz, H-4), 4.00 (dd, 1H, $J_{1'b,2'}$ = 4.0 Hz, $J_{1'a,1'b}$ = 12.4 Hz, H-1′b), 3.89 (dd, 1H, $J_{1'a,2'}$ = 9.0 Hz, H-1′a), 3.84–3.79 (m, 1H, H-5′), 3.72 (d, 2H, H-6a, H-6b), 3.63 (dd, 1H, H-4′), 3.60–3.50 (m, 3H, H-6′b, H-6′a, H-1b), 3.34 (dd, 1H, $J_{1a,2}$ = 2.7 Hz, $J_{1a,1b}$ = 13.0 Hz, H-1a). ^{13}C NMR (D_2O) δ: 78.3 (C-3′), 76.0 (C-3), 75.4 (C-2), 73.1 (C-5′), 69.8 (C-4′), 68.2 (C-5), 67.1 (C-2′), 64.7 (C-4), 62.8 (C-6), 62.6 (C-6′), 47.4 (C-1′), 40.2 (C-1). HRMS calcd. for $C_{12}H_{25}O_9Se$: 393.0658 (M + H – SO_3); found: 393.0656.

1,4-Anhydro-1-[(S)-[(2′R,3′S,4′R,5′R)-2′,4′,5′,6′-tetrahydroxy-3′-(sufooxy)hexyl]sulfonio]-L-allitol inner salt (14)

To a solution of **36** (600 mg, 0.95 mmol) in CH_2Cl_2 (2 mL) was added TFA (10 mL). After removing the cleaved protecting groups, the remaining gum was then dissolved in AcOH (10 mL), Pd–C (10%, 100 mg) was added, and the reaction mixture was subjected to hydrogenolysis to give compound **14** as a colourless, amorphous, and hygroscopic solid (165 mg, 41%). $[\alpha]^{22}_D$ –32° (*c* 1, H_2O). ^{1}H NMR (D_2O) δ: 4.58 (ddd, 1H, H-2), 4.55 (dd, 1H, $J_{2',3'}$ = 4.6 Hz, $J_{3',4'}$ = 0.7 Hz, H-3′), 4.49 (ddd, 1H, H-2′), 4.42 (dd, 1H, $J_{2,3}$ = 8.7 Hz, $J_{3,4}$ = 3.2 Hz, H-3), 4.25 (ddd, 1H, H-5), 4.03 (dd, 1H, $J_{1'b,2'}$ = 3.8 Hz, H-1′b), 4.04–3.99 (m, 1H, H-4), 3.92 (dd, 1H, $J_{1'a,2'}$ = 9.1 Hz, $J_{1'a,1'b}$ = 13.5 Hz, H-1′a), 3.79 (dd, 1H, $J_{4',5'}$ = 8.0 Hz, H-4′), 3.68 (dd, 1H, $J_{5',6'b}$ = 2.4 Hz, H-6′b), 3.68–3.64 (m, 1H, H-5′), 3.67 (d, 2H, H-6a, H-6b), 3.61 (dd, 1H, $J_{1b,2}$ = 3.2 Hz, $J_{1a,1b}$ = 14.2 Hz, H-1b), 3.52 (dd, 1H, $J_{5',6'a}$ = 5.6 Hz, $J_{6'a,6'b}$ = 11.5 Hz, H-6′a), 3.44 (dd, 1H, $J_{1a,2}$ = 8.0 Hz, H-1a). ^{13}C NMR (D_2O) δ: 77.7 (C-3′), 74.8 (C-3), 74.4 (C-2), 70.5 (C-5′), 69.1 (C-4′), 68.3 (C-5), 67.0 (C-2′), 65.0 (C-4), 62.8 (C-6′), 62.7 (C-6), 49.9 (C-1′), 43.9 (C-1). HRMS calcd. for $C_{12}H_{25}O_9S$: 345.1214 (M + H – SO_3); found: 345.1211.

Acknowledgements

We are grateful to the Natural Sciences and Engineering Research Council of Canada (NSERC) for financial support and to B.D. Johnston for helpful discussions. We are also grateful to D.R. Bundle for providing access to the high-resolution mass spectral facilities.

References

1. (*a*) B. Winchester and G.W.J. Fleet. Glycobiology, **2**, 199 (1992); (*b*) J.F. Kennedy and C.A. White. Bioactive carbohydrates in chemistry, biochemistry, and biology. Halsted Press, New York. 1983; (*c*) F. Garcia-Olmeda, G. Salcedo, R. Sanchez-Monge, L. Gomez, L. Royo, and P. Carbonero. Oxford Surv. Plant Molecular Cell Biol. **4**, 275 (1987); (*d*) C. Bompard-Gilles, P. Rousseau, P. Rouge, and F. Payan. Structure, **4**, 1441 (1996); (*e*) F. Vallee, A. Kadziola, Y. Bourne, M. Juy, K.W. Rodenburg, B. Svensson, and R. Haser. Structure, **6**, 649 (1998); (*f*) S. Strobl, K. Maskos, G. Wiegand, R. Huber, F-X. GomisRuth, and R. Glockshuber. Structure, **6**, 911 (1998).
2. (*a*) A. Varki, R. Cummings, J. Esko, H. Freeze, G. Hart, and J. Marth (*Editors*). Essentials of glycobiology. Cold Spring Harbor Laboratory Press, Cold Spring Harbor, NY. 1999; (*b*) A.D. Elbein, R.J. Molyneux and B.M. Pinto (*Editors*). Comprehensive natural products chemistry. Vol. 3. Elsevier, Oxford, UK. 1999. Chap. 7; (*c*) N. Asano, R.J. Nash, R.J. Molyneux, and G.W.J. Fleet. Tetrahedron: Asymmetry, **11**, 1645 (2000); (*d*) J.D. McCarter and S.G. Withers. Curr. Opin. Struct. Biol. **4**, 885 (1994); (*e*) H.D. Ly and S.G. Withers. Annu. Rev. Biochem. **68**, 487 (1999).
3. R.R. Holman, C.A. Cull, and R.C. Turner. Diabetes Care, **22**, 960 (1999).
4. G.S. Jacob. Curr. Opin. Struct. Biol., **5**, 605 (1995).
5. L. Sherwood. Fundamentals of physiology. 2nd ed. West Publishing Co., New York, NY. 1995. p. 517.
6. (*a*) M.L. Sinnott. Chem. Rev. **90**, 1171 (1990); (*b*) T.D. Henghman, A.T. Vasella. Angew. Chem. Int. Ed. **38**, 750 (1999).
7. (*a*) D. Zechel and S.G. Withers. Acc. Chem. Res. **33**, 11 (2000); (*b*) C.S. Rye and S.G. Withers. Curr. Opin. Chem. Biol. **4**, 573 (2000).
8. (*a*) K. Schoffling and I. Hillebrand. Dtsch. Med. Wochenschr. **106**, 1083 (1981); (*b*) J.L. Chiasson, R.G. Josse, A.H. Hunt, C. Palmason, N.W. Roger, S.A. Ross, E.A. Ryan, M.H. Tan, and T.M.S. Wolever. Ann. Intern. Med. **121**, 928 (1994).
9. (*a*) T. Kobatake, Y. Matsuzawa, K. Tokunaga, S. Fujioka, T. Kawamoto, Y. Keno, H. Odaka, T. Matsuo, and S. Tarui. Int. J. Obesity, **13**, 147 (1989); (*b*) T. Matsuo, H. Odaka, and H. Ikeda. Am. J. Clin. Nutr. **55**, 3145 (1992); (*c*) R.R. Holman, C.C. Cull, and R.C. Tyrner. Diabetes Care, **21**, 256 (1998).

© 2006 NRC Canada

10. M. Yoshikawa, T. Murakami, H. Shimada, H. Matsuda, J. Yamahara, G. Tanabe, and O. Muraoka. Tetrahedron Lett. **38**, 8367 (1997).
11. M. Yoshikawa, T. Murakami, K. Yashiro, and H. Matsuda. Chem. Pharm. Bull. **46**, 1339 (1998).
12. M. Yoshikawa, T. Murikawa, H. Matsuda, G. Tanabe, and O. Muraoka. Bioorg. Med. Chem. **10**, 1547 (2002).
13. H. Yuasa, J. Takada, and H. Hashimoto. Tetrahedron Lett. **41**, 6615 (2000).
14. A. Ghavami, B.D. Johnston, and B.M. Pinto. J. Org. Chem. **66**, 2312 (2001).
15. A. Ghavami, K.S. Sadalapure, B.D. Johnston, M. Lobera, B.B. Snider, and B.M. Pinto. Synlett, 1259 (2003).
16. A. Ghavami, B.D. Johnston, M.D. Maddess, S.M. Chinapoo, M.T. Jensen, B. Svensson, and B.M. Pinto. Can. J. Chem. **80**, 937 (2002).
17. B.D. Johnston, A. Ghavami, M.T. Jensen, B. Svensson, and B.M. Pinto. J. Am. Chem. Soc. **124**, 8245 (2002).
18. (*a*) H. Liu and B.M. Pinto. J. Org. Chem. **70**, 753 (2005); (*b*) B.M. Pinto, B.D. Johnston, A. Ghavami, M.G. Szczepina, H. Liu, and K. Sadalapure. US Patent 06 455 573, 24 September 2002.
19. (*a*) A. Ghavami, B.D. Johnston, M.T. Jensen, B. Svensson, and B.M. Pinto. J. Am. Chem. Soc. **123**, 6268 (2001); (*b*) O. Muraoka, S. Ying, K. Yoshikai, Y. Matsuura, E. Yamada, T. Minematsu, G. Tanabe, H. Matsuda, and M. Yoshikawa. Chem. Pharm. Bull. **49**, 1503 (2001).
20. (*a*) M.G. Szczepina, B.D. Johnston, Y. Yuan, B. Svensson, and B.M. Pinto. J. Am. Chem. Soc. **126**, 12458 (2004); (*b*) E. Gallienne, M. Benazza, G. Demailly, J. Bolte, and M. Lemaire. Tetrahedron, **61**, 4557 (2005).
21. (*a*) B.D. Johnston, H.H. Hensen, and B.M. Pinto. J. Org. Chem. **71**, 1111 (2005); (*b*) H. Liu and B.M. Pinto. Can. J. Chem. **84**, 497 (2006); (*c*) H. Liu, L. Sim, D.R. Rose, and B.M. Pinto. J. Org. Chem. **71**, 3007 (2006).
22. Y. Li, C.R. Scott, N.A. Chamoles, A. Chavami, B.M. Pinto, T. Frantisek, and M.H. Gelb. Clin. Chem. **50**, 1785 (2004).
23. X. Wen, Y. Yuan, D.A. Kuntz, D.R. Rose, and B.M. Pinto. Biochemistry, **44**, 6729 (2005).
24. D. Kuntz, A. Ghavami, B.D. Johnston, B.M. Pinto, and D.R. Rose. Tetrahedron: Asymmetry, **16**, 25 (2005).
25. G.W.J. Fleet, N.G. Ramsden, and D.R. Witty. Tetrahedron, **45**, 319 (1989).
26. L.S. Jeong, D.Z. Jin, H.O. Kim, D.H. Shin, H.R. Moon, P. Gunaga, M.W. Chun, Y.C. Kim, N. Melman, Z.G. Gao, and K.A. Jacobson. J. Med. Chem., **46**, 3775 (2003).
27. G.C. Andrews, T.C. Crawford, and B.E. Bacon. J. Org. Chem. **46**, 2976 (1981).

© 2006 NRC Canada

Synthesis of an 11-*cis*-locked biotinylated retinoid for sequestering 11-*cis*-retinoid binding proteins[1]

Hiroko Matsuda, Shenglong Zhang, Andrea E. Holmes, Sonja Krane, Yasuhiro Itagaki, Koji Nakanishi, and Nasri Nesnas

Abstract: The synthesis of a seven-membered ring locked analogue of 11-*cis*-retinol, tethered to a cross-linking moiety on C-15 and a lysine-extended biotin on the C-3, was accomplished for its utilization as a probe to fish out retinol binding proteins that may be involved in the reisomerization of retinal from all-*trans* to 11-*cis* in the visual cycle.

Key words: retinoids, biotin, 11-*cis*-locked, cross-linking, retinol binding proteins.

Résumé : La synthèse d'un analogue de 11-*cis*-rétinol sous la forme d'un anneau verrouillé, comportant sept membres, attachés en partie, au C-15, avec un groupe ayant la possibilité de se liér aux protéines a été réalisée. En plus, l'analogue est attaché de l'autre côté sur le C-3, avec une lysine biotine étendue. Cette synthèse a été réalisée afin d'utilizer le composé comme agent détecteur des protéines qui portent des rétinols et qui pourraient être impliquées dans la réisomerization du all-*trans* retinal au 11-*cis* dans le cycle de vision.

Mots clés : rétinoides, biotine, 11-*cis*-verrouillé, liés, protéines qui portent des rétinols.

Introduction

The basic process of vision, first elucidated by Wald (1), involves the light-triggered isomerization of retinal (or vitamin A aldehyde) from its 11-*cis* conformation to the all-trans conformation. Retinal, in its 11-*cis* geometry, is bound by the apoprotein opsin, a G-protein coupled receptor, forming a protonated Schiff base with Lys296, present in Helix G of the seven-membered transmembrane protein,which generates rhodopsin, the active photoreceptor unit in the cones and rods of eyes (2, 3). Upon absorption of a photon by 11-*cis*-retinal, the retinoid undergoes an isomerization to the all-trans geometry, resulting in a conformational change in the protein that leads to the activation of the G protein, which ultimately results in vision (4). The all-*trans*-retinal is subsequently hydrolyzed off the lysine residue, freeing the protein for a fresh 11-*cis*-retinal molecule. The completion of the visual cycle is ultimately dependent on the less well-understood proteins that are capable of binding all *trans*-retinoids and converting them to the 11-*cis*-retinal geometry (5). The latter proteins are collectively termed retinol binding proteins (RBPs). Their crucial involvement in the visual cycle warrants the need for the development of tools that enable their isolation and purification for further studies of their detailed function.

We have previously synthesized (6) a biotin-linked 11-*cis*-retinol analogue (structure **1** without the trimethylene bridge linking C-10 and C-13), as well as the all-*trans*-retinol analogue, **1a**. The latter derivative, bearing a biotin moiety and a chloroacetate cross-linking unit, enabled us to successfully isolate and characterize certain retinol binding proteins (7). We attempted to use the biotin-linked 11-*cis* analogue in the isolation of RBPs involved in the isomerization of all-*trans*-retinal to 11-*cis*-retinal. Despite the synthetic accomplishment (6), the retinoid was prone to undergoing an inevitable isomerization from 11-*cis* to all-trans upon incubation in the retinal pigment epithelial (RPE) cells, thus losing its affinity toward the RBPs of interest. To circumvent this problem, we resorted to ret7 (Fig. 1), the first of the 11-*cis*-locked analogues, which is comprised of a seven-membered ring locking the double bond at the C-11 position into a *cis*-conformation (8). This retinoid was particularly useful because it retains the full chromophore properties of native 11-*cis*-retinal and readily forms, with bovine opsin, the nonbleachable pigment, rhodopsin 7 or rh7. Both the UV–vis λ_{max} of 490 nm and the CD maxima at 330 and 488 nm

Received 31 October 2005. Accepted 24 January 2006. Published on the NRC Research Press Web site at http://canjchem.nrc.ca on 27 September 2006.

This article is part of a Special Issue dedicated to Dr. Alfred Bader in celebration of his 80th birthday.

H. Matsuda, S. Zhang, A.E. Holmes, S. Krane, Y. Itagaki, K. Nakanishi,[2] and N. Nesnas.[3,4] Department of Chemistry, Columbia University, New York, NY 10027, USA.

[1]This article is part of a Special Issue dedicated to Dr. Alfred Bader.
[2]Corresponding author (e-mail: kn5@columbia.edu).
[3]Corresponding author (e-mail: nesnas@fit.edu).
[4]Present address: Department of Chemistry, Florida Institute of Technology, Melbourne, FL 32901, USA.

 doi:10.1139/V06-092 © 2006 NRC Canada

Scheme 1. Retrosynthetic analysis for the biotinylated retinoid **1**.

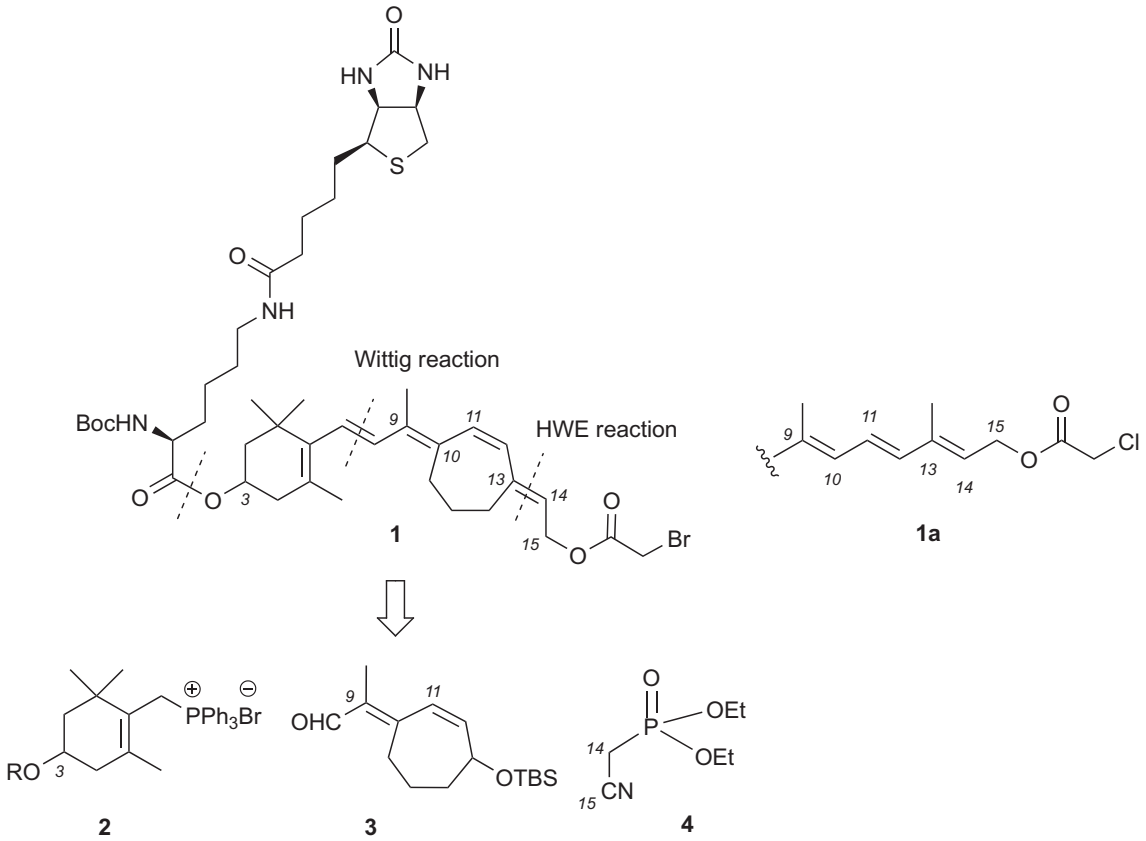
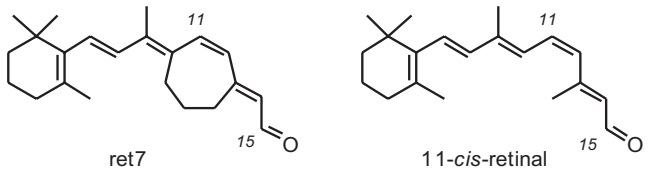


Fig. 1. The structures of ret7 and the native 11-*cis*-retinal.



(digitonin–phosphate buffer, pH 7) are similar to those of the native chromophore (UV–vis λ_{max} at 500 nm and CD maxima at 340 and 490 nm), indicating that the binding sites are the same. These aspects have made this pigment a popular substrate for various spectroscopic measurements (9–11).

We hereby report the synthesis of 11-*cis*-locked retinoid **1** bearing an appropriate functionality for isolation through cross-linking and which possesses the additional advantage of resisting isomerization under light conditions as well as in the media of RPE cells.

The target structure **1** has significant features that merit highlighting. It has the basic 11-*cis*-retinoid structure that can bind selectively to certain RBPs involved in the reisomerization of all-*trans*- to 11-*cis*-retinal. It also harbors an active cross-linking unit, the bromoacetate functionality, which can form a stable covalent bond with the RBPs and it also has the (Boc)Lys-biotinyl linker anchored at C-3, which will facilitate isolation of the covalently linked protein via an avidin affinity chromatography. Moreover, the ret7 moiety in the structure ensures its stability against light and (or) the RPE cell medium. Based on our earlier studies, the presence of the seven-membered ring would not prevent the retinoid from binding into the protein (8, 12, 13).

Results and discussion

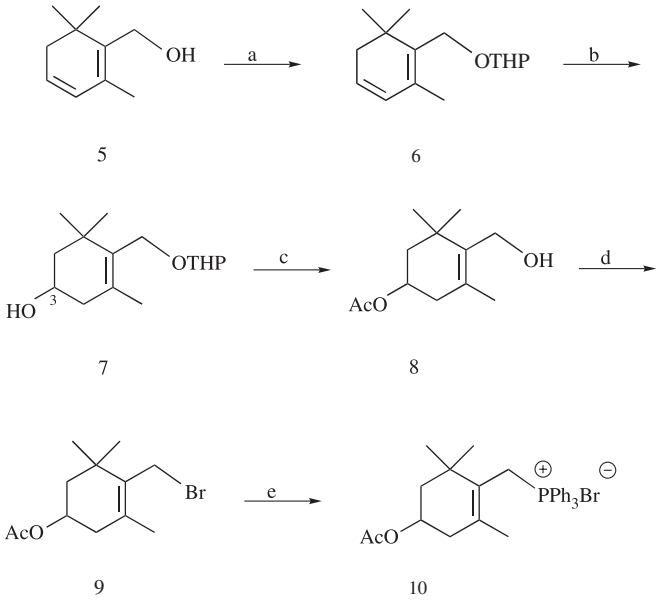
The retrosynthetic logic for **1** is shown in Scheme 1. It stems from our earlier work conducted on the seven-membered ring unit **3**, synthesized from 2-cyclohepten-1-one in five steps (14). The hydroxylated β-ionone ring structure can be introduced by employing a Wittig reaction between aldehyde **3** and synthon **2**, the latter being prepared from dehydro-β-cyclocitral (also known as safranal) in seven steps as outlined in Scheme 2. The Horner–Wadsworth–Emmons (HWE) reaction can be used to install a nitrile group at the C-14 position with reagent **4**, followed by its reduction to the corresponding aldehyde, which would be subjected to further reduction to the corresponding primary alcohol onto which a bromoester can be esterified in the final stages.

Synthon **3** has been prepared from the commercially available 2-cyclohepten-1-one, according to our earlier report (14). The synthesis featured an allylic oxidation of 2-cyclohepten-1-one, a three-carbon homologation by HWE reaction with the reagent bearing the nitrile functionality, and lastly, a partial reduction of the nitrile to the corresponding aldehyde.

The synthesis of **10** (the synthon **2** unit) is outlined in Scheme 2. Dehydro-β-cyclocitrol (**5**), prepared from dehydro-β-cyclocitral (15), was protected as the tetrahydropyranyl (THP) ether (→**6**, 81%) and subsequently treated

© 2006 NRC Canada

Scheme 2. Reagents and conditions: (*a*) DHP, *p*-TsOH, CH_2Cl_2, 0 °C (81%); (*b*) 9-BBN, THF, Δ, then MeOH, NaOH, H_2O_2, 0 °C → 50 °C (55%); (*c*) (*i*) Ac_2O, pyridine, CH_2Cl_2, rt, (*ii*) *p*-TsOH, MeOH, rt (60%, two steps); (*d*) PPh_3, CBr_4, THF (94%); (*e*) PPh_3, benzene, Δ (quant.).]



with 9-borabicyclo[3.3.1]nonane (9-BBN) to undergo a hydroboration reaction affording the 3-hydroxy **7** in 55% yield. As in the case of the biotinylated all-trans analogue **1a** (6, 7), no attempts were made to resolve the C-3 enantiomers. The 3-hydroxy group was protected as the acetate by treatment with acetic anhydride (Ac_2O) – pyridine. The allylic hydroxy group was then liberated by acidic cleavage of the THP group to give alcohol **8**, which was transformed to the corresponding bromide **9** using triphenylphosphine (PPh_3) and carbon tetrabromide (94% yield). The phosphonium salt **10** was synthesized from **9** by treatment with PPh_3 under reflux conditions.

Scheme 3 shows the critical steps that assemble the retinoid from synthons **3** and **10**. A Wittig reaction between aldehyde **3** and phosphonium salt **10** afforded the desired tetraene **11a** (33%), along with a considerable amount of **11b** (40%). The trans geometry of the olefin thus formed was confirmed from the coupling constant (J = 16 Hz) observed for the H-7 and H-8 protons. The TBS group of **11a** was removed using tetrabutylammonium fluoride (TBAF) to give the free allylic alcohol, which, upon treatment with MnO_2, underwent smooth oxidation to afford the conjugated ketone **12** in 84% yield. A two-carbon extension through HWE reaction was carried out on ketone **12** with cyanomethylphoshonate (**4**) to afford the (*E*)-isomer **13** in 27% yield (the (*Z*)-isomer, 53%). The *E*/*Z* geometry was determined by NOE experiments for the H-12 and H-14 protons. Nitrile **13** was subjected to partial reduction with diisobutylaluminum hydride (DIBAH) to the corresponding aldehyde accompanied by an inevitable reductive cleavage of the acetate group at the C-3 position. After reprotection of the free alcohol with an acetyl group, resulting in **14**, the aldehyde was further reduced to the corresponding primary alcohol by treatment with sodium borohydride and was then protected as a TBS ether to afford **15**. Basic cleavage of the 3-acetyl group gave the corresponding 3-OH followed by esterification with biotinyl-(Boc)Lys-OH to give **16** (78% yield, two steps). The TBS group was deprotected, releasing the primary alcohol, which was eventually subjected to esterification with bromoacetic acid to afford the target structure **1** in 66% yield.

Preliminary studies directed towards isolation and characterization of RBPs employing **1** performed by Rando's group (Harvard Medical School, Boston, Massachusetts) have shown that some RBPs have been sequestered and identified. The results of the isolation and characterization of the RBPs using **1** will be reported in a subsequent manuscript.

Conclusion

The synthesis of biotinylated retinoid **1** was accomplished via a series of Wittig reactions, esterification of a (Boc)Lys-biotin on the 3-hydroxy position of the β-ionone ring, and the final attachment of the active bromoester cross-linking unit. The significance of the seven-membered ring lock is evident as the preliminary biological studies using this molecule have already proven the robust nature of the 11-*cis*-olefin unit. The target structure will be able to cross-link to RBPs that are involved in the crucial isomerization process that regenerates 11-*cis*-retinal. Avidin affinity chromatography will enable facile purification of the sequestered protein, and basic hydrolysis will release the isolated protein from the affinity column by cleaving the ester at the C-15 position. The purified protein can be further studied and characterized for the elucidation of its detailed function.

Experimental section

General considerations

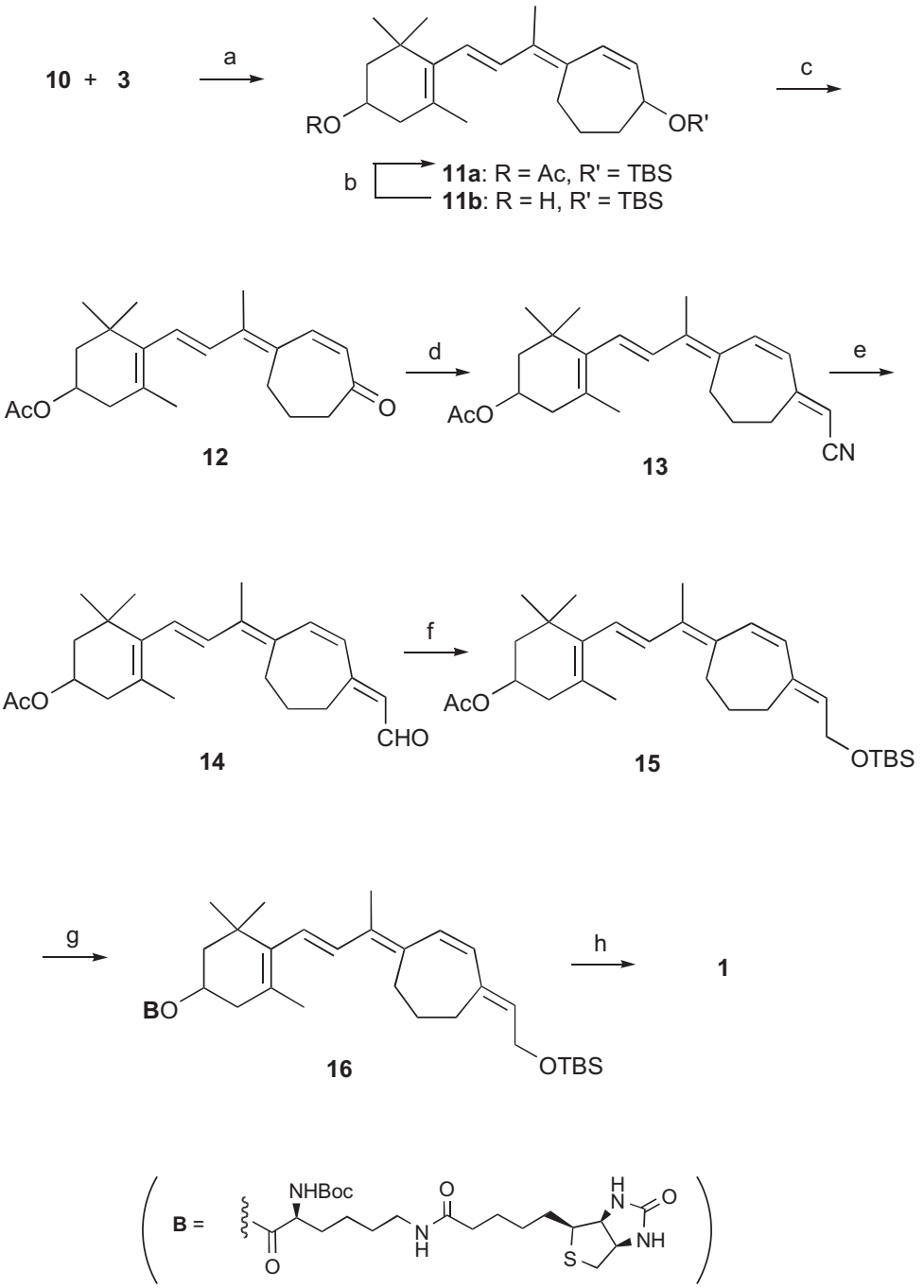
^{1}H NMR spectra were measured on a Bruker DMX 400 or Bruker DPX 300 spectrometer (400 or 300 MHz). The chemical shifts are expressed in ppm downfield from the signal of tetramethylsilane, used as an internal standard in the solvent $CDCl_3$. Splitting patterns are designated as s (singlet), d (doublet), t (triplet), q (quartet), qn (quintet), m (multiplet), and br (broad). High resolution mass spectrometry (HRMS) were measured on a JEOL (Tokyo) JMS-HX110/110 tandem mass spectrometer equipped with a Xe beam FAB gun (6 kV), using 3-nitrobenzyl alcohol as a matrix. Analytical and preparative thin layer chromatography (TLC) was carried out using precoated silica gel plates (Merck silica gel $60F_{254}$). The silica gel used for column chromatography was 230–400 mesh (Merck). All reactions were carried out under an Ar atmosphere using predried solvents. Anhydrous CH_2Cl_2, Et_2O, and THF were obtained from the solvent purification system via passage through an activated alumina cartridge.

Tetrahydropyranyl safranol (6)

To a solution of safranol **5** (7.67 g, 50.4 mmol) in CH_2Cl_2 (100 mL) was added 3,4-dihydro-2*H*-pyran (DHP, 8.48 g, 101 mmol). The mixture was stirred and cooled to –10 °C and *p*-toluenesulfonic acid monohydrate (*p*-TsOH, 190 mg, 1.00 mmol) was then added. After 10 min of stirring, triethylamine (1.0 mL) was added to quench the reaction.

© 2006 NRC Canada

Scheme 3. Reagents and conditions: (*a*) *n*-BuLi, THF, –78 °C → rt, (for **11a**, 33%; for **11b**, 40%); (*b*) Ac_2O, pyridine, DMAP, rt for **11b** (63%); (*c*) (*i*) TBAF, THF, 0 °C → rt (99%), (*ii*) MnO_2, CH_2Cl_2, 0 °C → rt (84%); (*d*) **4**, NaH, THF, 0 °C → rt (*E*:*Z*, 27%:53%); (*e*) (*i*) DIBAH, Et_2O, –78 °C → 0 °C (82%), (*ii*) Ac_2O, pyridine, CH_2Cl_2, 0 °C → rt (50%); (*f*) (*i*) $NaBH_4$, MeOH–$CHCl_3$ (1:10), 0 °C, (*ii*) TBSCl, imidazole, CH_2Cl_2, 0 °C (70%, two steps); (*g*) (*i*) K_2CO_3, MeOH, 0 °C → rt, (*ii*) biotinyl (Boc)lys-OH (**B**-OH), EDC, DMAP, CH_2Cl_2, 0 °C → rt (78%, two steps); (*h*) (*i*) TBAF, THF, 0 °C → rt (60%), (*ii*) $BrCH_2COOH$, EDC, DMAP, 0 °C → rt (66%).



The mixture was poured into water (150 mL) and extracted with Et_2O (3 × 150 mL). The organic layers were washed with brine, combined, dried over $MgSO_4$, and concentrated under reduced pressure. Purification of the residue by silica gel column chromatography (EtOAc–hexanes, 10:90) afforded the THP ether **6** (9.60 g, 40.8 mmol, 81%) as a colorless oil. ^{1}H NMR ($CDCl_3$, ppm) δ: 5.75 (2H), 4.61 (1H, brs), 4.31 (1H, d, *J* = 11.2 Hz), 4.07 (1H, d, *J* = 11.2 Hz), 3.91 (1H, m), 3.52 (1H, m), 2.05 (2H, s), 1.81 (3H, s), 1.81–1.69 (6H), 1.04, 1.01 (each 3H, s). ^{13}C NMR ($CDCl_3$, ppm) δ: 134, 129.9, 129.1, 126, 97.7, 63.4, 62.4, 40.3, 33.5, 31.0, 26.7 (2C), 25.9, 19.9, 18.4. FAB-HRMS calcd. for $C_{15}H_{24}O_2$ *m*/*z*: 236.1776 [M^+]; found: 236.1769.

Tetrahydropyranyl 3-hydroxysafranol (7)

To a solution of THP ether **6** (6.66 g, 28.2 mmol) in THF (40.0 mL), 9-BBN (0.5 mol/L solution in THF, 113 mL, 56.4 mmol) was added slowly over 20 min. The reaction

© 2006 NRC Canada

mixture was heated up to 60 °C and was stirred for 4 h. After the reaction mixture was cooled to room temperature, methanol (68.0 mL) and an aq. NaOH solution (3 mol/L, 9.4 mL) were added to it. Subsequently, H_2O_2 (30% solution, 8.0 mL) was added slowly to the stirring reaction mixture using an ice bath. The reaction mixture was heated for 2 h at 55 °C. The mixture was poured into water (100 mL) and extracted with EtOAc (3 × 100 mL). The organic layers were washed with brine, combined, dried over $MgSO_4$, and concentrated in vacuo. Purification of the residue by silica gel column chromatography (EtOAc–hexanes, 30:70) afforded a diastereomeric mixture of **7** (3.94 g, 15.5 mmol, 55%). The ^{1}H NMR spectra indicated that the sample consisted of a mixture of diastereomers (50:50). ^{1}H NMR ($CDCl_3$, ppm) δ: 4.55 (2 × 0.5H, dt, *J* = 3.2, 8.5 Hz), 4.26, 4.17, 3.80, 3.74 (each 0.5H, d, *J* = 10.7 Hz), 3.93–3.81 (0.5H × 2 × 2), 3.50 (0.5H × 2, m), 2.37 (0.5H × 2, brs), 2.27 (0.5H × 2, brdt), 2.01 (0.5H × 2, brdd), 1.78 (0.5H × 2, m), 1.69, 1.68 (each 1.5H, s), 1.70–1.62 (0.5H × 2 × 2), 1.56–1.40 (0.5H × 2 × 5), 1.06, 1.02, 1.00, 0.993 (each 1.5H, s). ^{13}C NMR ($CDCl_3$, ppm) δ: 134, 133, 131.5, 131.4, 98.9, 98.6, 64.9 (0.5C × 2), 63.5, 63.4, 62.4, 62.3, 48.2 (0.5C × 2), 42.3 (0.5C × 2), 36.8 (0.5C × 2), 30.7 (0.5C × 2), 29.4, 29.2, 28.7, 28.6, 25.5 (0.5C × 2), 19.7 (0.5C × 2), 19.69, 19.63. FAB-HRMS calcd. for $C_{15}H_{26}O_3$ *m*/*z*: 254.1882 [M^+]; found: 254.1891.

3-*O*-Acetoxysafranol (8)

To a solution of hydroxy **7** (1.00 g, 3.93 mmol) in pyridine (7.0 mL), acetic anhydride (3.5 mL) was added at 0 °C. The resultant mixture was stirred at room temperature. After 12 h of stirring, the mixture was azeotropically concentrated with toluene (×3) in vacuo. The crude sample was subjected to the next step without purification. The acetate was treated with a catalytic amount of *p*-TsOH (10.0 mg) in methanol (60.0 mL). The resultant mixture was allowed to stir for 12 h at room temperature. The mixture was neutralized with Et_3N (1.0 mL) and concentrated under reduced pressure. Silica gel purification of the residue (EtOAc–hexanes, 25:75) gave the 3-*O*-acetyl safranol **8** (576 mg, 2.72 mmol, 70%, in two steps). ^{1}H NMR ($CDCl_3$, ppm) δ: 4.97 (1H, m), 4.13, 4.07 (each 1H, d, *J* = 11.5 Hz), 2.35 (1H, dd, *J* = 5.7, 16.9 Hz), 2.04 (1H, dd, *J* = 9.4, 16.9 Hz), 2.00 (3H, s), 1.71 (1H, m) overlapping with 1.72 (3H, s), 1.52 (1H, t, *J* = 11.9 Hz), 1.45 (1H, br, CH_2OH), 1.09, 1.05 (each 3H, s). ^{13}C NMR ($CDCl_3$, ppm) δ: 170, 137, 127, 68.2, 58.2, 43.8, 38.2, 36.4, 29.2, 28.5, 21.5, 19.5.

3-*O*-Acetoxysafranyl bromide (9)

To a solution of alcohol **8** (576 mg, 2.72 mmol) in THF (20.0 mL) at 0 °C, PPh_3 (1.07 g, 4.08 mmol) and CBr_4 (1.35 g, 4.08 mmol) were added. The resultant mixture was stirred at room temperature for 1 h. The mixture was poured into water (50 mL) and extracted with Et_2O (3 × 50 mL). The organic layers were washed with brine, combined, dried over $MgSO_4$, and concentrated in vacuo. The residue was purified with silica gel chromatography (EtOAc–hexanes, 2:98) to afford the allyl bromide **9** (710 mg, 2.55 mmol, 94%). ^{1}H NMR ($CDCl_3$, ppm) δ: 4.99 (1H, m), 4.07, 3.96 (each 1H, d, *J* = 8.2 Hz), 2.43 (1H, dd, *J* = 4.5, 13.8 Hz), 2.11 (1H, dd, *J* = 7.4, 13.8 Hz), 2.02 (3H, s), 1.72 (1H, m) overlapping with 1.75 (3H, s), 1.58 (1H, t, *J* = 9.5 Hz), 1.20, 1.12 (each 3H, s). ^{13}C NMR ($CDCl_3$, ppm) δ: 169, 133.4, 144.2, 67.2, 43.5, 38.4, 36.7, 29.0, 28.6, 28.3, 21.1, 19.6. FAB-HRMS calcd. for $C_{12}H_1{}^{8}{}^{79}BrO_2$ *m*/*z*: 273.0490 [M – H]$^+$; found: 273.0497.

3-*O*-Acetoxysafranyl triphenylphosphonium bromide (10)

To a solution of allyl bromide **9** (710 mg, 2.55 mmol) in benzene (20.0 mL) at room temperature, PPh_3 (670 mg, 2.55 mmol) was added. The resultant mixture was heated up to the reflux temperature (~85 °C bath) for 12 h. After the mixture was cooled to room temperature, the volatiles were evaporated in vacuo. The residue was washed with benzene (×3) and dried under the reduced pressure for 1 day to give **10** (1.37 g, 2.55 mmol, quantitative yield). ^{1}H NMR ($CDCl_3$, ppm) δ: 7.9–7.6 (15H), 4.97 (1H, m), 4.58, 4.42 (each 1H, t, *J* = 14.0 Hz), 2.26 (1H, m), 2.04 (3H, s), 1.95 (1H, m), 1.71 (1H, dd, *J* = 2.0, 12.0 Hz), 1.51 (1H, t, *J* = 12.0 Hz), 1.07 (3H, d, *J* = 4.0 Hz), 0.88, 0.84 (each 3H, s). FAB-HRMS calcd. for $C_{30}H_{34}O_2P$ *m*/*z*: 457.2291 [M – Br]$^+$; found: 457.2285.

3-*O*-Acetyl-13-*O*-TBS (11a)

To a solution of the triphenylphosphonium bromide **10** (657 mg, 1.22 mmol) in THF (7.0 mL) at –78 °C, *n*-BuLi (2.5 mol/L solution in hexanes, 1.4 mL, 3.50 mmol) was added, and the resultant mixture was allowed to warm to room temperature and was stirred at this temperature for 1 h to generate the corresponding ylide. To a solution of aldehyde **3** (460 mg, 1.64 mmol) in THF (10.0 mL), the ylide solution was added. After 14 h of stirring at the same temperature, the mixture was poured into water and extracted with Et_2O (3 × 30 mL). The organic layers were washed with brine, combined, dried over $MgSO_4$, and concentrated in vacuo. Purification of the residue by silica gel column chromatography (EtOAc–hexanes, 5:95 and 20:80) afforded the acetyl **11a** (245 mg, 534 μmol, 33%) and alcohol **11b** (276 mg, 663 μmol, 40%) as a colorless oil. The ratio of diastereomers was not determined and this sample was used as a mixture.

To a solution of 3-hydroxy **11b** (294 mg, 706 μmol) in pyridine (3.0 mL) at room temperature, Ac_2O (1.5 mL) and *N*,*N*-dimethylaminopyridine (DMAP, 5.0 mg) were added, and the resultant mixture was stirred at the same temperature for 12 h. The mixture was poured into a satd. aq. solution of $NaHCO_3$ (30 mL) and extracted with Et_2O (3 × 30 mL). The organic layers were washed with brine, combined, dried over $MgSO_4$, and concentrated in vacuo. Purification of the residue by silica gel column chromatography (EtOAc–hexanes, 2:98) provided the acetyl **11a** (205 mg, 446 μmol, 63%) as a colorless oil. The ratio of diastereomers was not determined, and this sample was used as a diastereomeric mixture. ^{1}H NMR for **11a** ($CDCl_3$, ppm, major signals are only described.) δ: 6.49, 6.09 (each 1H, dd, *J* = 1.8, 16.0 Hz), 6.45, 5.69 (each 1H, dd, *J* = 2.2, 11.8 Hz), 5.06 (1H, m), 4.46 (1H, m), 2.67 (1H, dt, *J* = 5.0, 13.7 Hz), 2.44 (1H, dd, *J* = 5.8, 17.0 Hz), 2.23 (1H, m), 2.10 (1H, dd, *J* = 9.4, 16.6 Hz), 2.04 (3H, s), 1.87 (3H, s), 1.83–1.75 (2H), 1.72 (3H, s), 1.8–1.7 (2H), 1.58 (2H, t, *J* = 12.0 Hz), 1.10, 1.07 (each 3H, s), 0.906 (3H × 3, s), 0.090, 0.081 (each 3H, s). ^{13}C NMR

© 2006 NRC Canada

($CDCl_3$, ppm) δ: 170, 138, 137, 134, 132, 130, 129, 125.8, 125.0, 71.0, 68.4, 43.9, 38.3, 36.6, 35.6, 30.0, 29.8. 28.4, 25.8 (3C), 23.8, 21.4 (2C), 18.2, 14.3, –4.6 (2C). FAB-HRMS calcd for $C_{28}H_{46}O_3Si$ *m/z*: 458.3216 [M^+]; found: 458.3196. ^1H NMR for **11b** ($CDCl_3$, ppm, major signals are only described.) δ: 6.11, 6.49 (each 1H, d, *J* = 16.0 Hz), 5.69, 6.46 (each 1H, d, *J* = 11.9 Hz), 4.46 (1H, m), 4.01 (1H, m), 2.68 (1H, dt, *J* = 5.4, 8.8 Hz), 2.38 (1H, dd, *J* = 5.4, 16.6 Hz), 2.24 (1H, m), 2.04 (1H, m), 1.86 (3H, s), 1.71–1.85 (4H) overlapping with 1.73 (3H, s), 1.65 (1H, brs), 1.48 (1H, t, *J* = 11.9 Hz), 1.07 (3H × 2, s), 0.907 (3H × 3, s), 0.0815, 0.0914 (each 3H, s). ^{13}C NMR ($CDCl_3$, ppm) δ: 138, 136, 134, 132, 130, 130, 125.67, 125.64, 71.0, 64.9, 48.2, 42.4, 37.0, 35.6, 30.2, 29.8, 28.6, 25.8 (3C), 23.8, 21.5, 18.2, 14.4, –4.6 (2C). FAB-MS *m/z* (%, rel. int.): 416 (52, M^+), 398 (25, [M – H_2O]$^+$). FAB-HRMS calcd. for $C_{26}H_{44}O_2Si$ *m/z*: 416.3111 [M^+]; found: 416.3106.

13-Ketone (12)

To a solution of **11a** (205 mg, 446 mmol) in THF (10.0 mL) at 0 °C, tetrabutylammonium fluoride (TBAF, 1.0 mol/L solution in THF, 892 μL, 892 μmol) was added, and the resultant mixture was allowed to warm to room temperature and was continuously stirred at this temperature. After 3 h of stirring, the mixture was poured into water (30 mL) and extracted with Et_2O (3 × 30 mL). The organic layers were washed with brine, combined, dried over $MgSO_4$, and concentrated under reduced pressure. Purification of the residue by silica gel column chromatography (EtOAc–hexanes, 15:85) afforded the 13-hydroxy compound (145 mg, 425 μmol, 99%) as a colorless oil. ^1H NMR ($CDCl_3$, ppm) δ: 6.51, 5.73 (each 1H, d, *J* = 11.8 Hz), 6.47, 6.10 (each 1H, d, *J* = 15.8 Hz), 5.05 (1H, m), 4.47 (1H, m), 2.70 (1H, m), 2.44 (1H, dd, *J* = 5.4, 6.8 Hz), 2.23 (1H, m), 2.12 (1H, m), 2.05 (3H, s), 2.00–1.89 (2H), 1.88 (3H, s), 1.81–1.68 (2H, m), 1.71 (3H, s), 1.58 (2H, t, *J* = 11.9 Hz), 1.10, 1.07 (each 3H, s).

To a solution of the 13-hydroxy (209 mg, 607 μmol) in CH_2Cl_2 (15.0 mL) at 0 °C, MnO_2 (1.60 g, 18.2 mmol) was added, and the resultant mixture was stirred at this temperature. After 40 min of stirring at the same temperature, the mixture was filtered and the volatiles were removed under reduced pressure. Purification of the residue by silica gel column chromatography (EtOAc–hexanes, 20:80) afforded ketone **12** (174 mg, 507 μmol, 84%) as a colorless oil. ^1H NMR ($CDCl_3$, ppm) δ: 7.32, 5.92 (each 1H, d, *J* = 12.0 Hz), 6.55, 6.32 (each 1H, d, *J* = 18.0 Hz), 5.03 (1H, m), 2.63 (2H, t, *J* = 6.6 Hz), 2.57 (2H, t, *J* = 6.6 Hz), 2.45 (1H, dd, *J* = 5.4, 16.9 Hz), 2.11 (1H, dd, *J* = 9.6, 16.9 Hz), 2.04, 2.02 (each 3H, s), 1.87 (2H, qn, *J* = 6.6 Hz), 1.79 (1H, brt), 1.72 (3H, s), 1.58 (1H, t, *J* = 12.0 Hz), 1.10, 1.07 (each 3H, s). ^{13}C NMR ($CDCl_3$, ppm) δ: 203, 170, 143, 137.9, 137.0, 134, 132, 130, 129, 126, 68.1, 43.8, 42.9, 38.3, 36.5, 31.2, 29.9, 28.4, 23.1, 21.4, 21.3, 15.0. FAB–HRMS calcd. for $C_{22}H_{31}O_3^+$ *m/z*: 343.2273 [M + H]$^+$; found: 343.2266.

13-Nitrilemethylene (13)

To a solution of NaH (freshly prepared by washing with hexanes and drying under reduced pressure, 140 mg, 5.84 mmol) in THF (15.0 mL) at 0 °C, $(EtO)_2P(O)CH_2CN$ (**4**, 944 μL, 5.84 mmol) was added, and the resultant mixture was allowed to warm to room temperature and was stirred at this temperature for 1 h to generate the corresponding ylide. To a solution of ketone **12** (174 mg, 507 μmol) in THF (25.0 mL), the generated ylide was added. After 12 h of stirring at the same temperature, the mixture was poured into water (30 mL) and extracted with Et_2O (3 × 30 mL). The organic layers were washed with brine, combined, dried over $MgSO_4$, and concentrated in vacuo. Purification of the residue by silica gel column chromatography (EtOAc–hexanes, 7:93) afforded the (*E*)-nitrile **13** (47.1 mg, 135 μmol, 27%) and the (*Z*)-nitrile (99.3 mg, 265 μmol, 53%) as yellowish oils, respectively. ^1H NMR for (*E*)-isomer **13** ($CDCl_3$, ppm) δ: 6.82, 6.13 (each 1H, d, *J* = 11.3 Hz), 6.52, 6.25 (each 1H, d, *J* = 15.9 Hz), 5.15 (1H, s), 5.04 (1H, m), 2.67 (2H, t, *J* = 6.7 Hz), 2.52 (2H, t, *J* = 6.7 Hz), 2.46 (1H, dd, *J* = 5.9, 17.2 Hz), 2.12 (1H, dd, *J* = 9.5, 17.2 Hz), 2.05, 1.96 (each 3H, s), 1.87 (2H, qn, *J* = 6.7 Hz), 1.79 (1H, m), 1.73 (3H, s), 1.59 (1H, t, *J* = 12.2 Hz), 1.11, 1.08 (each 3H, s). ^{13}C NMR ($CDCl_3$, ppm) δ: 170, 162, 139, 138, 134 (2C), 132, 129, 128, 126, 117, 96.3, 68.2, 43.9, 38.4, 36.6, 33.0, 31.3, 30.0, 28.5, 26.9, 21.5, 21.4, 14.9. FAB–HRMS calcd. for $C_{24}H_{31}NO_2$ *m/z*: 365.2355 [M^+]; found: 365.2354. ^1H NMR for the (*Z*)-isomer ($CDCl_3$, ppm) δ: 6.94, 6.57 (each 1H, d, *J* = 11.4 Hz), 6.50, 6.25 (each 1H, d, *J* = 16.0 Hz), 5.07 (1H, s), 5.04 (1H, m), 2.51 (2H, t, *J* = 6.7 Hz), 2.46 (1H, m) 2.42 (2H, t, *J* = 6.7 Hz), 2.11 (1H, dd, *J* = 9.5, 17.0 Hz), 2.04, 1.97 (each 3H, s), 1.83 (2H, qn, *J* = 6.7 Hz), 1.72 (3H, s), 1.59 (2H, t, *J* = 11.9 Hz), 1.11, 1.08 (each 3H, s).

14-Aldehyde (14)

To a solution of the (*E*)-nitrile **13** (35.7 mg, 97.7 μmol) in Et_2O (3.0 mL) at –78 °C, DIBAH (1.0 mol/L solution in toluene, 900 μL, 900 μmol) was added, and the resultant mixture was stirred at 0 °C. After 40 min of stirring, methanol (0.63 mL) was carefully added, followed by a 30% aqueous solution of Rochelle salt (potassium sodium tartrate) (1.08 mL), the resultant mixture was then stirred for 40 min. The organic layer was washed with a 30% Rochelle salt aqueous solution (2 × 0.45 mL and 1 × 0.23 mL). The combined aqueous layer was back-extracted with Et_2O (3 × 30 mL). The organic layers were washed with brine, combined, dried over $MgSO_4$, and concentrated under reduced pressure. Purification of the residue by silica gel column chromatography (Et_2O–hexanes, 50:50) afforded the aldehyde without an acetyl group at C-3 (26.1 mg, 80.1 μmol, 82%) as an oil. ^1H NMR ($CDCl_3$, ppm) δ: 10.0 (1H, d, *J* = 8.2 Hz), 6.90, 6.24 (each 1H, d, *J* = 11.3 Hz), 6.53, 6.27 (each 1H, d, *J* = 15.9 Hz), 5.93 (1H, d, *J* = 8.2 Hz), 3.97 (1H, m), 2.85 (2H, t, *J* = 6.7 Hz), 2.56 (2H, t, *J* = 6.7 Hz), 2.40 (1H, dd, *J* = 6.2, 17.0 Hz), 2.05 (1H, dd, *J* = 10.0, 17.0 Hz), 1.98 (3H, s), 1.89 (2H, qn, *J* = 6.7 Hz), 1.83–1.74 (1H, m), 1.74 (3H, s), 1.49 (1H, t, *J* = 11.8 Hz), 1.08 (3H × 2, s).

To a solution of the aldehyde (26.1 mg, 80.0 μmol) in a mixture of CH_2Cl_2 (1.0 mL) and pyridine (0.2 mL) at 0 °C, Ac_2O (0.1 mL) and DMAP (2.0 mg) were added, and the resultant mixture was allowed to warm to room temperature and was stirred at this temperature. After 1 h of stirring, the volatiles were removed in vacuo. Purification of the residue by silica gel column chromatography (Et_2O–hexanes, 15:85) afforded the alcohol (14.5 mg, 39.3 μmol, 50%) as an oil.

© 2006 NRC Canada

^{1}H NMR ($CDCl_3$, ppm) δ: 10.0 (1H, d, *J* = 8.2 Hz), 6.90, 6.24 (each 1H, d, *J* = 11.3 Hz), 6.53, 6.25 (each 1H, d, *J* = 15.9 Hz), 5.93 (1H, d, *J* = 8.2 Hz), 5.05 (1H, m), 2.85 (2H, t, *J* = 6.7 Hz), 2.56 (2H, t, *J* = 6.7 Hz), 2.45 (1H, dd, *J* = 5.5, 16.4 Hz), 2.12 (1H, dd, *J* = 9.4, 16.4 Hz), 2.05 (3H, s), 1.98 (3H, s), 1.90 (2H, qn, *J* = 6.7 Hz), 1.79 (1H, m), 1.74 (3H, s), 1.59 (1H, t, *J* = 12.0 Hz), 1.11, 1.08 (each 3H, s). ^{13}C NMR ($CDCl_3$, ppm) δ: 190, 170, 160, 139, 138, 135, 134, 132.4, 132.2, 128.8, 128.5, 126, 68.2, 43.8, 38.4, 36.6, 31.2, 29.9, 29.0, 28.4 (2C), 21.4 (2C), 14.9. FAB–HRMS calcd. for $C_{24}H_{31}O_3$: 367.2273 $[M - H]^+$; found: 367.2271.

15-*O*-TBS (15)

To a solution of the aldehyde **14** (14.5 mg, 39.3 μmol) in a mixture of $CHCl_3$ (0.2 mL) and methanol (1.0 mL) at –10 °C, $NaBH_4$ (8.9 mg, 236 μmol) was added. After 2 min of stirring, a satd. aq. solution of NH_4Cl (20 mL) was added and the resultant mixture was extracted with EtOAc (3 × 20 mL). The organic layers were washed with brine, combined, and dried over $MgSO_4$. ^{1}H NMR ($CDCl_3$, ppm) δ: 6.50, 6.10 (each 1H, d, *J* = 15.9 Hz), 6.47, 6.12 (each 1H, d, *J* = 11.3 Hz), 5.66 (1H, t, *J* = 7.0 Hz), 5.04 (1H, m), 4.25 (2H, d, *J* = 7.0 Hz), 2.52 (2H, t, *J* = 6.7 Hz), 2.44 (1H, dd, *J* = 6.0, 17.6 Hz), 2.36 (2H, t, *J* = 6.7 Hz), 2.11 (1H, dd, *J* = 8.9, 17.6 Hz), 2.05 (3H, s), 1.92 (3H, s), 1.83–1.70 (3H), 1.72 (3H, s), 1.58 (1H, t, *J* = 11.9 Hz), 1.10, 1.07 (each 3H, s).

To a solution of the crude alcohol in CH_2Cl_2 (1.0 mL) at room temperature, imidazole (16.0 mg, 197 μmol) was added. The mixture was cooled to 0 °C, and TBSCl (11.8 mg, 78.6 μmol) was added at this temperature. After 2 h of stirring, the mixture was poured into water (20 mL) and the resultant mixture was extracted with Et_2O (3 × 20 mL). The organic layers were washed with brine, combined, dried over $MgSO_4$, and concentrated in vacuo. Purification of the residue by silica gel column chromatography (EtOAc–hexanes, 7:93) afforded **15** (13.4 mg, 27.6 μmol, 70%, in two steps) as a colorless oil. ^{1}H NMR ($CDCl_3$, ppm) δ: 6.51, 6.08 (each 1H, d, *J* = 16.0 Hz), 6.42, 6.11 (each 1H, d, *J* = 11.4 Hz), 5.57 (1H, t, *J* = 6.4 Hz), 5.05 (1H, m), 4.28 (2H, d, *J* = 6.4 Hz), 2.52 (2H, t, *J* = 6.7 Hz), 2.44 (1H, dd, *J* = 5.5, 17.0 Hz), 2.31 (2H, t, *J* = 6.7 Hz), 2.10 (1H, dd, *J* = 9.3, 17.0 Hz), 2.05, 1.91 (each 3H, s), 1.82–1.73 (3H), 1.72 (3H, s), 1.58 (1H, t, *J* = 12.0 Hz), 1.10, 1.07 (each 3H, s), 0.906 (3H × 3, s), 0.0813 (3H × 2, s). ^{13}C NMR ($CDCl_3$, ppm) δ: 170, 139, 138, 135, 134, 132, 131, 130.4, 130.3, 125.7, 125.0, 68.4, 59.9, 44.0, 38.5, 36.7, 31.3, 30.4, 30.1, 28.9, 28.6, 27.9, 26.1 (3C), 21.6, 18.5, 14.7, –4.80 (2C). FAB-HRMS calcd. for $C_{30}H_{48}O_3Si$ *m*/*z*: 484.3373 $[M^+]$; found: 484.3366.

3-*O*-Biotinyl (Boc)Lys-15-*O*-TBS (16)

To a solution of **15** (5.4 mg, 11.1 μmol) in methanol (1.0 mL) at 0 °C, K_2CO_3 (2.0 mg, 14.5 μmol) was added. The mixture was stirred and allowed to warm to room temperature. After 12 h of stirring, the mixture was poured into a satd. aq. solution of NH_4Cl (20 mL) and the resultant mixture was extracted with EtOAc (3 × 20 mL). The organic layers were washed with brine, combined, dried over $MgSO_4$, and concentrated under reduced pressure. ^{1}H NMR ($CDCl_3$, ppm) δ: 6.51, 6.11 (each 1H, d, *J* = 15.9 Hz), 6.43, 6.11 (each 1H, d, *J* = 11.4 Hz), 5.57 (1H, t, *J* = 6.3 Hz), 4.28 (2H, d, *J* = 6.3 Hz), 4.00 (1H, m), 2.52 (2H, t, *J* = 6.6 Hz), 2.38 (1H, dd, *J* = 5.0, 16.7 Hz), 2.31 (2H, t, *J* = 6.6 Hz), 2.04 (1H, dd, *J* = 9.7, 16.7 Hz), 1.91 (3H, s), 1.77 (1H, m), 1.73 (2H, qn, *J* = 6.7 Hz), 1.73 (3H, s), 1.47 (2H, t, *J* = 11.9 Hz), 1.07 (3H × 2, s), 0.906 (3H × 3, s), 0.0807 (3H × 2, s).

To a mixture of the crude 3-OH compound, biotinyl (Boc)Lys-OH (7.9 mg, 16.7 μmol),1-ethyl-3-(3-dimethylaminopropyl)carbodiimide (EDC, 6.4 mg, 33.3 μmol) at 0 °C, and CH_2Cl_2 (0.7 mL) were added. DMAP (2.0 mg) was also added at this temperature. The mixture was warmed to room temperature and stirred. After 3 h of stirring, the mixture was poured into a satd. aq. solution of $NaHCO_3$ (20 mL) and the resultant mixture was extracted with $CHCl_3$ (20 mL). The organic layer was washed with a satd. aq. NH_4Cl solution, water, and brine, followed by drying over $MgSO_4$. Purification of the residue by silica gel column chromatography (methanol–$CHCl_3$, 7:93) afforded **16** (7.8 mg, 8.69 μmol, 78%, in two steps) as a colorless oil. ^{1}H NMR ($CDCl_3$, ppm) δ: 6.52, 6.11 (each 1H, d, *J* = 16.1 Hz), 6.44, 6.13 (each 1H, d, *J* = 11.3 Hz), 6.24 (1H, brs), 6.18 (1H, brs), 5.59 (1H, t, *J* = 6.5 Hz), 5.45–5.38 (1H, m), 5.37 (1H,brs), 5.20 (1H, d, *J* = 6.5 Hz), 5.10 (1H, m), 4.53 (1H, dd, *J* = 4.8, 7.5 Hz), 4.37–4.28 (1H, m), 4.29 (2H, d, *J* = 6.5), 4.23 (1H, m), 3.23 (2H, qn, *J* = 5.9 Hz), 3.16 (1H, m), 2.92 (1H, dd, *J* = 4.8, 12.6 Hz), 2.75 (1H, d, *J* = 12.6 Hz), 2.52 (2H, t, *J* = 6.4 Hz), 2.44 (1H, m), 2.32 (2H, t, *J* = 7.4 Hz), 2.20 (2H, t, *J* = 7.4 Hz), 2.13 (1H, m), 1.91 (3H, s), 1.85–1.50 (15H), 1.73 (3H, s), 1.45 (3H × 3, s), 1.10, 1.08 (each 3H, s), 0.908 (3H × 3, s), 0.0813 (3H × 2, s). FAB-HRMS calcd. for $C_{49}H_{81}N_4O_7SSi^+$ *m*/*z*: 897.5590 $[M + H]^+$; found: 897.5574. FAB-HRMS calcd. for $C_{49}H_{81}N_4NaO_7SSi$: 920.5493 $[M + H + Na]^+$; found: 920.5489.

3-*O*-Biotinyl (Boc)Lys 15-*O*-bromoacetate (1)

To a solution of **16** (4.1 mg, 4.57 μmol) in THF (1.0 mL) at 0 °C, TBAF (1.0 mol/L solution in THF, 9.2 μL, 9.2 μmol) was added. The mixture was warmed to room temperature and stirred. After 2 h of stirring, the mixture was poured into water (20 mL) and the resultant mixture was extracted with $CHCl_3$ (3 × 20 mL). The organic layer was washed with brine, combined, dried over $MgSO_4$, and concentrated under reduced pressure. Purification of the residue by silica gel column chromatography (methanol–$CHCl_3$, 10:90) afforded the biotinylated alcohol (2.1 mg, 2.68 μmol, 60%) as a colorless oil. ^{1}H NMR ($CDCl_3$, ppm) δ: 6.52, 6.13 (each 1H, d, *J* = 15.3 Hz), 6.49, 6.15 (each 1H, d, *J* = 11.1 Hz), 5.90 (1H, brs), 5.68 (1H, t, *J* = 6.8 Hz), 5.56 (1H, brs), 5.17 (1H, d, *J* = 7.9 Hz), 5.10 (1H, m), 4.90 (1H, brs), 4.52 (1H, m), 4.33 (1H, m), 4.26 (2H, d, *J* = 6.8 Hz), 4.25 (1H, brs), 3.23 (2H, brs), 3.17 (1H, q, *J* = 4.4 Hz), 2.93 (1H, dd, *J* = 4.8, 12.9 Hz), 2.74 (1H, d, *J* = 12.9 Hz), 2.53 (2H), 2.44 (1H, m), 2.37 (2H, t, *J* = 6.6 Hz), 2.28–2.18 (2H), 2.18–2.10 (1H, m), 1.92 (3H, s), 1.85–1.48 (16H), 1.73 (3H, s), 1.45 (3H × 3, s), 1.10, 1.08 (each 3H, s).

To a solution of the biotinylated alcohol (2.1 mg, 2.68 μmol) in CH_2Cl_2 (0.7 mL) at room temperature, $BrCH_2COOH$ (2.0 mg, 14.4 μmol) was added. The mixture was cooled to –10 °C and EDC (3.1 mg, 16.1 μmol) and DMAP (1.0 mg) were added. After 15 min of stirring at the

© 2006 NRC Canada

same temperature, the mixture was poured into a satd aq. solution of $NaHCO_3$ (20 mL) and the resultant mixture was extracted with $CHCl_3$ (20 mL). The organic layer was washed with a satd aq. NH_4Cl solution, water and brine, followed by drying over $MgSO_4$. After concentration in vacuo, purification of the residue by silica gel column chromatography (methanol–$CHCl_3$, 7:93) afforded the biotinylated bromoacetate **1** (1.6 mg, 1.77 μmol, 66%) as a colorless oil. ^{1}H NMR ($CDCl_3$, ppm) δ: 6.53, 6.13 (each 1H, d, J = 11.4 Hz), 6.50, 6.12 (each 1H, d, J = 15.7 Hz), 5.86 (1H, t, J = 5.0 Hz), 5.58 (1H, t, J = 7.3 Hz), 5.51 (1H, brs), 5.16 (1H, d, J = 8.6 Hz), 5.10 (1H, m), 4.87 (1H, brs), 4.77 (2H, d, J = 7.3 Hz), 4.51 (1H, dd, J = 4.7, 7.8 Hz), 4.32 (1H, dd, J = 4.7, 7.6 Hz), 4.23 (1H, m), 3.83 (2H, s), 3.23 (2H, qn, J = 6.1 Hz), 3.16 (1H, m), 2.92 (1H, dd, J = 4.7, 12.6 Hz), 2.73 (1H, d, J = 12.6 Hz), 2.51 (2H, t, J = 7.0 Hz), 2.39 (2H, t, J = 6.5 Hz), 2.10 (1H, m), 2.14 (2H, t, J = 6.5 Hz), 2.10 (1H, m), 1.92 (3H, s), 1.88–1.30 (16H), 1.72 (3H, s), 1.45 (3H × 3, s), 1.10, 1.08 (each 3H, s).

Acknowledgement

We acknowledge the National Institutes of Health (GM 36564) for their generous support of this research.

References

1. G. Wald. Nature (London), **219**, 800 (1968).
2. N. Fishkin, N. Berova, and K. Nakanishi. Chem. Rec. **4**, 120 (2004).
3. K. Nakanishi. Chem. Pharm. Bull. **48**, 1399 (2000).
4. B. Borhan, M.L. Souto, H. Imai, Y. Shichida, and K. Nakanishi. Science, **288**, 2209 (2000).
5. R.R. Rando. Chem. Rev. **101**, 1881 (2001).
6. N. Nesnas, R.R. Rando, and K. Nakanishi. Tetrahedron, **58**, 6577 (2002).
7. W.J. Jahng, C. David, N. Nesnas, K. Nakanishi, and R.R. Rando. Biochemistry, **42**, 6159 (2003).
8. H. Akita, S.P. Tanis, M. Adams, V. Balogh-Nair, and K. Nakanishi. J. Am. Chem. Soc. **102**, 6370 (1980).
9. R.R. Birge, L.P. Murray, B.M. Pierce, H. Akita, V. Balogh-Nair, L.A. Findsen, and K. Nakanishi. Proc. Natl. Acad. Sci. U.S.A. **82**, 4117 (1985).
10. H. Kandori, S. Matuoka, Y. Shichida, T. Yoshizawa, M. Ito, K. Tsukida, V. Balogh-Nair, and K. Nakanishi. Biochemistry, **28**, 6460 (1989).
11. Y. Fujimoto, J. Ishihara, S. Maki, N. Fujioka, T. Wang, T. Furuta, N. Fishkin, B. Borhan, N. Berova, and K. Nakanishi. Chem. Eur. J. **7**, 4198 (2001).
12. Y. Fujimoto, N. Fishkin, G. Pescitelli, J. Decatur, N. Berova, and K. Nakanishi. J. Am. Chem. Soc. **124**, 7294 (2002).
13. R. Crouch, B.R. Nodes, J.I. Perlman, D.R. Pepperberg, H. Akita, and K. Nakanishi. Inv. Ophth. Vis. Sci. **25**, 419 (1984).
14. Y. Fujimoto, R. Xie, S.E. Tully, N. Berova, and K. Nakanishi. Chirality, **14**, 340 (2002).
15. E.K. Karvinen and A.M.P. Koskinen. Tetrahedron, **51**, 7555 (1995).

© 2006 NRC Canada

A theoretical and experimental investigation of some unusual intermolecular hydrogen-bond IR bands — Appearances can be deceptive[1]

Grzegorz Litwinienko, Gino A. DiLabio, and K.U. Ingold

Abstract: The IR spectra of the O-H stretch for hydrogen bonds (HBs) arising from complex formation between the HB donor (HBD), 4-fluorophenol, and the HB acceptors, peroxides and ethers, frequently show asymmetry that appears to arise from two incompletely resolved bands from two different complexes, but the O-H HB bands with the HBD methanol are symmetric (M. Berthelot, F. Bessau, and C. Laurence. Eur. J. Org. Chem. 925 (1998)). The present studies show that this difference in O-H HB band shapes also is true for other phenols and alcohols. However with ethylene oxide, 4-fluorophenol gives an almost symmetric O-H HB band with a very broad maximum, while alcohols give symmetric O-H HB bands with well-defined maxima. It is shown by experiment that the unusual O-H HB band shapes for the phenols are not due to Fermi resonance and are unrelated to the enthalpies of HB complex formation. Theoretical exploration of the potential energy (PE) surfaces for complexes of 4-fluorophenol and methanol with *tert*-butyl methyl ether and ethylene oxide reveals that O-H HB band asymmetry or broadness cannot be ascribed to the presence of two different HB complexes. For this ether, the PE surfaces for rotation about the HB and for up-and-down motion of the HBD with respect to the COC plane of the ether are relatively symmetric for methanol, but are strongly asymmetric for 4-fluorophenol, hence the differences in the O-H HB band shapes. The PE surfaces for the epoxide are effectively symmetric, but the PE for rotation about the HB has a single broad minimum for methanol, whereas with 4-fluorophenol there are two minima owing to attractive interactions between the phenyl group and the CH_2 groups of the epoxide. The previously unknown β_2^H values for ethylene oxide and tetramethylethylene oxide are 0.36 and 0.58, respectively.

Key words: asymmetric IR O-H bands, asymmetric potential energy surfaces, hydrogen-bonded complexes, hydrogen bond enthalpy, O-H frequency shift.

Résumé : Les spectres IR de l'élongation O-H des liaisons hydrogènes (LH) découlant de la formation de complexes entre le donneur de liaison hydrogène (DLH), 4-fluorophénol, et des accepteurs de LH, tels les peroxydes et les éthers, présentent fréquemment une asymétrie qui semble découler de la présence de deux bandes pas complètement résolues provenant de deux complexes différents, mais les bandes de LH O-H avec le DLH méthanol sont symétriques (M. Berthlot, F. Bessau, et C. Laurence. Eur J. Chem. 925 (1998)). La présente étude montre que cette différence dans les formes de la bande de LH O-H est aussi vraie pour d'autres phénols et d'autres alcools. Toutefois, avec l'oxyde d'éthylène, le 4-fluorophénol donne lieu à une bande de LH O-H qui est pratiquement symétrique avec un maximum très large alors que les alcools donnent lieu à des bandes de LH OH symétriques avec des maxima bien définis. On a montré sur la base d'expériences que les formes inhabituelles de la bande de LH OH des phénols ne sont pas causées par une résonance de Fermi et qu'elles ne sont pas associées aux enthalpies de formation du complexe de LH. Une étude théorique des surfaces d'énergie potentielle (EP) des complexes du 4-fluorophénol et du méthanol avec l'oxyde de *tert*-butyle et de méthyle et l'oxyde d'éthylène montre que l'asymétrie ou la largeur de la bande de LH O-H ne peut pas être attribuée à la présence de deux complexes différents de LH. Pour cet éther, les surfaces d'EP pour la rotation autour de la LH et pour les mouvements ascendant et descendant du DLH par rapport au plan COC de l'éther sont relativement symétriques pour le méthanol, mais fortement asymétriques pour le 4-fluorophénol; d'où les différences dans les formes des bandes des LH O-H. Les surfaces d'EP pour l'époxyde sont effectivement symétriques, mais l'EP pour la rotation autour de la LH ne présente qu'un seul minimum élargi pour le méthanol alors que pour le 4-fluorophénol on observe deux minima qui résultent d'interactions d'attraction entre le groupe phényle et les groupes CH_2 de l'époxyde. Les valeurs β_2^H qui n'était pas connues antérieurement pour l'oxyde d'éthylène et l'oxyde de

Received 31 October 2005. Accepted 12 January 2006. Published on the NRC Research Press Web site at http://canjchem.nrc.ca on 8 November 2006.

G. Litwinienko.[2] Department of Chemistry, Warsaw University, Pasteura 1, 02-093 Warsaw, Poland.
G.A. DiLabio.[3] National Institute for Nanotechnology, 11421 Saskatchewan Drive, Edmonton, AB T6G 2M9, Canada.
K.U. Ingold. National Research Council Canada, 100 Sussex Drive, Ottawa, ON K1A 0R6, Canada.

[1]This article is part of a Special Issue dedicated to Dr. Alfred Bader.
[2]Corresponding author (e-mail: litwin@chem.uw.edu.pl).
[3]Corresponding author (e-mail: gino.dilabio@nrc-cnrc.gc.ca).

 doi:10.1139/V06-097 © 2006 NRC Canada

tétraméthyléthylène sont respectivement égales à 0,36 et 0,58.

Mots clés : bandes O-H IR asymétriques, surfaces d'énergie potentielle asymétriques, complexes à liaisons hydrogènes, enthalpie d'une liaison hydrogène, déplacement d'une fréquence O-H.

[Traduit par la Rédaction]

Introduction

During a critical reevaluation of the O—H bond dissociation enthalpy of phenol (1), the relative hydrogen bond acceptor (HBA) activity of di-*tert*-butyl peroxide was required. This is best quantified using the β_2^H scale of HBA relative activities developed by Abraham et al. (2). This is a general, thermodynamically related scale of solute hydrogen bond basicities in CCl_4. Values of β_2^H are calculated from the equilibrium constants for 1:1 complex formation between the HBA and a "calibrated" hydrogen bond donor (HBD), XOH, measured by IR spectroscopy in CCl_4 at room temperature (2)

$$[1] \qquad XOH + HBA \rightleftharpoons XOH\cdots HBA$$

$$[2] \qquad K_{eq} = \frac{[XOH\cdots HBA]}{([XOH]_0 - [XOH\cdots HBA])([HBA]_0 - ([XOH\cdots HBA])}$$

where the subscript 0 refers to the concentrations of XOH and the HBA in the absence of complex formation. Phenol and 4-fluorophenol (4-F-phenol) are often used as the calibrated HBA, the latter being particularly popular because, for 4-F-phenol only, there is a very simple relation between β_2^H and K_{eq} (β_2^H = (log K_{eq} + 1.1)/4.636) (2).[4] Values of β_2^H range from 0.00 for saturated hydrocarbons to 1.00 for hexamethylphosphortriamide, the strongest organic base.

Berthelot et al. (3) had reported a β_2^H value of 0.33 for di-*tert*-butyl peroxide, which we confirmed (1). We also confirmed their report that hydrogen-bond (HB) formation between 4-F-phenol and di-*tert*-butyl peroxide gives an asymmetric O-H HB stretching band in the IR that appears to arise from two incompletely resolved bands. Very reasonably, Berthelot et al. assigned this asymmetry and the asymmetry they found in the O-H HB bands for HB complexes of 4-F-phenol with some, but not all, ethers to the existence of two stereoisomeric hydrogen bonded species. These were suggested to have structures **A** and **B** (Fig. 1).

The asymmetric ether (peroxide)$\cdots HOC_6H_4F$ O-H HB bands discovered by Berthelot et al. (3) are intriguing. Herein, an experimental study of some asymmetric (and symmetric) O-H HB bands, which confirms and extends the earlier report (3), is combined with theoretical calculations on the structures of the species responsible for them.

Experimental

Materials

With one exception, all compounds were purchased from Sigma-Aldrich. Anhydrous solvents and the phenols were of highest purity available (usually 99%+) and were used as received except as noted. Prior to their use, the phenols were kept in a desiccator over P_2O_5 and di-*tert*-butyl peroxide was passed over basic alumina. Gaseous ethylene oxide was dissolved in CCl_4 to obtain a stock solution. The ethylene oxide concentration in the stock solution was determined by ^1H NMR using a sample to which CH_3CN had been added as an internal standard. 1,1,2,2-Tetramethylethylene oxide (purity 98%) was purchased from ChemSampCo Inc., Trenton, New Jersey.

IR spectra

Spectra were measured in CCl_4 at ambient temperatures. Each spectrum was collected on a Shimadzu FTIR 8201PC apparatus using a 1.03 mm CaF_2 cell (20 scans with a resolution of 1 cm^{-1}), and the baseline was corrected using solutions having the same concentration of the HBA as in the HBD–HBA solution. For all HBD–HBA measurements, the HBD concentrations were kept below a level that would lead to HBD self-association.

Theoretical calculations

All calculations were performed using the Gaussian 03 program package (4). Structures, vibration frequencies, and hydrogen bond strengths were computed using B971/6-31+G**(5). This level of theory was shown to predict reasonable hydrogen-bond strengths (6). Hydrogen-bond strengths were corrected for basis set superposition error via the counterpoise technique (7). Additional calculations to generate approximate potential energy surfaces (PESs) were performed with MP2/6-31+G**. This level of theory was used to avoid any uncertainties associated with the use of a density functional theory method to describe effects owing to steric repulsion at the extrema of the PESs.

Results

IR spectra

Figure 2A shows the O-H stretching region with 4-F-phenol (11.5 mmol/L) and concentrations of di-*tert*-butyl peroxide ranging from 109 to 561 mmol/L. The asymmetry of the O-H HB band is very apparent at all HBA concentrations. Deconvolution of this O-H HB band by Berthelot et al. (3) yielded wavenumber differences from the band maximum for the non-hydrogen bonded (i.e., "free") 4-F-phenol (3614 cm^{-1}), $\Delta\nu$(OH) = 145 and 220 cm^{-1}. Additional support for the assignment of this asymmetric band entirely to hydrogen bonding was obtained by measurements using *O*-deuterio-4-F-phenol. The addition of a very small quantity of D_2O to CCl_4 containing 4-F-phenol (16.5 mmol/L) followed by the addition of di-*tert*-butyl peroxide produced the spectra shown in Fig. 2B. The O-H HB band in Fig. 2B has shifted roughly 900 cm^{-1} from that shown in Fig. 2A, but the two bands have the same asymmetric shape. This "makes

[4] From ref. 2, a solute hydrogen bond basicity scale against reference acids is established through the relationship log $K_{eq} = L_A$ log $K_B^H + D_A$. For the reference acid (4-F-phenol), L_A = 1.000 and D_A = 0.000 giving log K_B^H = log K_{eq}.

© 2006 NRC Canada

Table 1. Infrared spectral data for five phenols and three alcohols in CCl_4 and for their 1:1 hydrogen-bonded complexes with *tert*-butyl methyl ether, and the enthalpies of formation of these complexes.

			ν(OH) (cm^{-1})[b]			A ($(mol/L)^{-1}/cm^{-2}$)	$-\Delta H$
HBD	$\Sigma\sigma$[a]	α_2^H	Free	HB	Δν	Free	(kcal/mol)[c]
Phenols							
3,5-Cl_2	0.74	0.728[d]	3604	3224, **3253**	380, **351** (419)	6750	6.80 (7.69)
4-CF_3	0.54	0.680[d]	3607	3250, **3260**	357, **347** (392)	6430	6.32 (7.36)
4-F	0.06	0.629[e]	3615	3303, **3317**	312, **298** (341)	5090	5.80 (6.66)
C_6H_5OH	0.00	0.590[d]	3613	3315, **3319**	298, **294** (328)	4900	5.40 (6.16)
4-MeO	–0.27	0.550[d]	3618	3333, **3355**	285, **263** (307)	4200	5.00 (5.96)
Alcohols							
CF_3CH_2OH		0.567[e]	3622	3367	255 (306)	3340	5.17 (6.27)
MeOH		0.367[e]	3645	3482	163 (219)	2360	3.14 (4.44)
Me_3COH		0.320[e]	3618	3484	134 (177)	1870	2.66 (4.10)

Note: See text for the meaning of the column headers.
[a]From C. Hansch, A. Leo, and R.W. Taft. Chem. Rev. **91**, 165 (1991).
[b]Numbers in regular type refer to band maxima and numbers in boldface refer to the center of asymmetric O-H HB bands (defined as the frequencies at which 50% of the overall band is at higher, and 50% at lower, frequencies). Numbers in parentheses are values calculated using the B971 functional.
[c]Calculated using eq. [3] with $\beta_2^H = 0.494$ for *tert*-butyl methyl ether (3) and the values in parentheses were calculated using the B971 functional.
[d]From D.W. Snelgrove, J. Lusztyk, J.T. Banks, P. Mulder, and K.U. Ingold. J. Am. Chem. Soc. **123**, 469 (2001).
[e]From ref. 8.

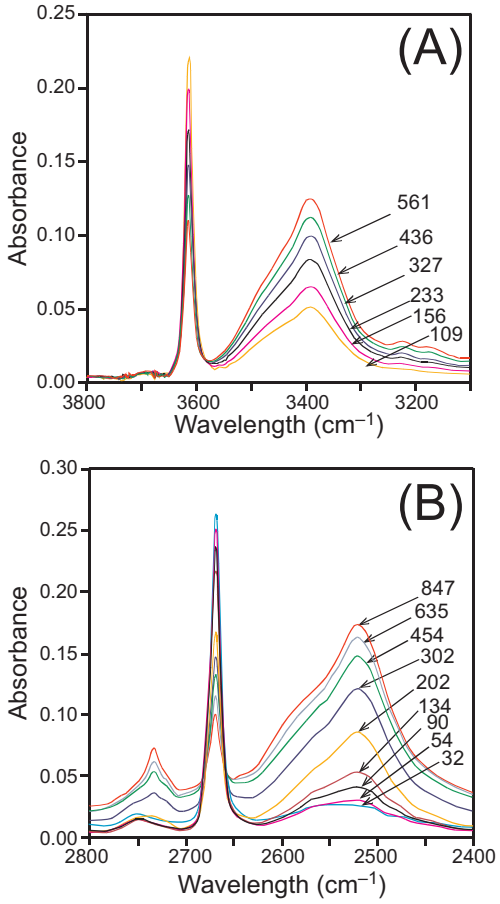
Fig. 1. The two possible structures of the l:1 comlex of an ether (or peroxide) with a hydrogen bond donor as proposed in ref. 3.



improbable the attribution of the doublet to a Fermi resonance" (3).

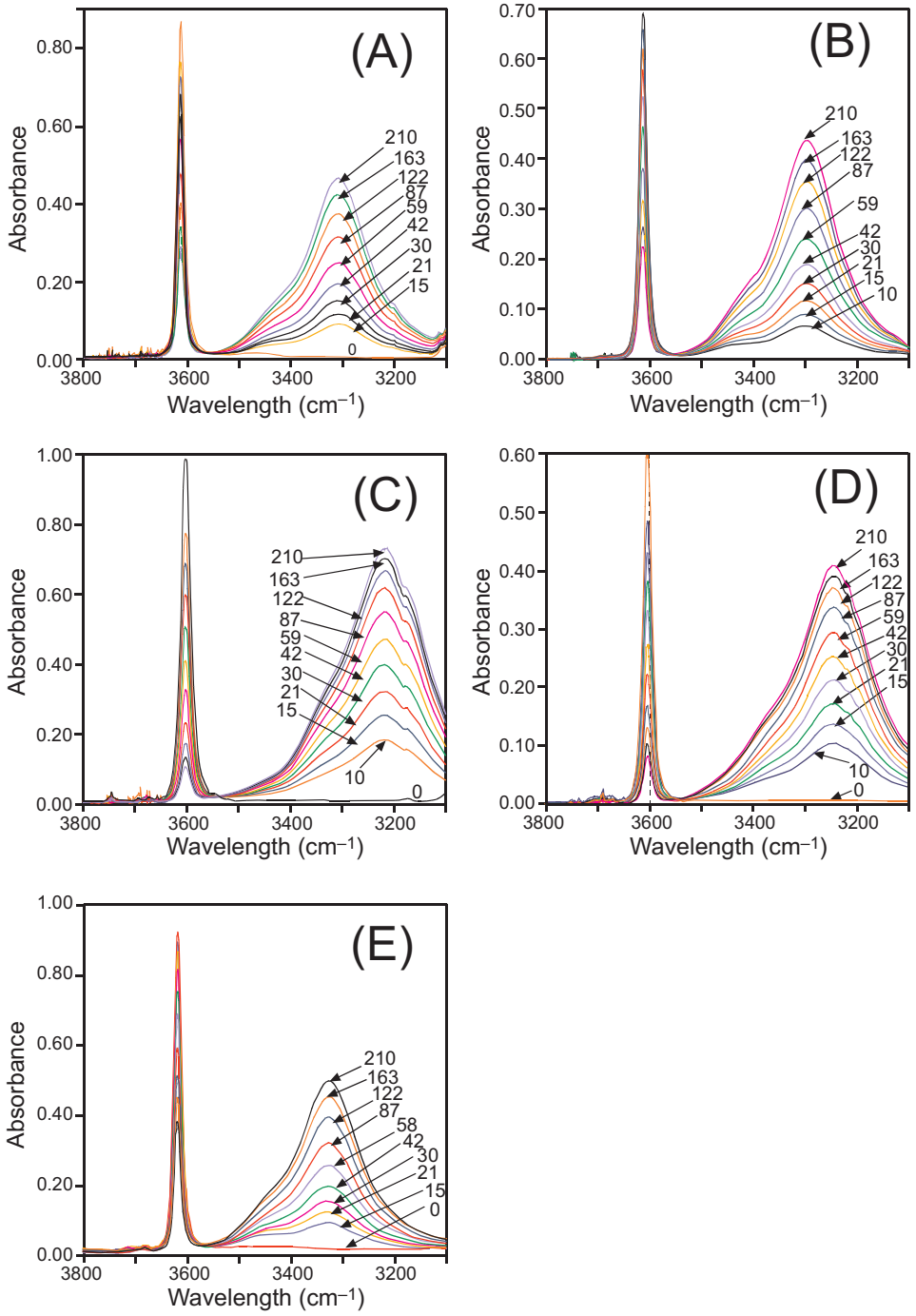
Next we demonstrated that asymmetric O-H HB bands are not specific to 4-F-phenol, and furthermore that their shape is more or less independent of the HBD activity of the phenol. Relative HBD activities are best quantified using the α_2^H scale developed by Abraham et al. (8). Like his β_2^H scale, the α_2^H scale is a general, thermodynamically related scale of solute hydrogen bond acidities in CCl_4. Values of α_2^H are also calculated from the equilibrium constants for 1:1 complex formation between the HBD and a calibrated HBA and are measured by IR spectroscopy in CCl_4 at room temperature. Values of α_2^H range from 0.00 for saturated hydrocarbons to nearly 1 for strong organic acids, e.g., 0.951 for CF_3COOH (8). As the HBDs, we chose five phenols covering a range of α_2^H values (Table 1.) As the HBA, we chose *tert*-butyl methyl ether ($\beta_2^H = 0.494$), which had been shown to give an asymmetric O-H HB band with 4-F-phenol that was deconvoluted into two bands with Δν(OH) = 186 and 315 cm^{-1}(3). Our results are presented in Fig. 3 and Table 1. Both the free O-H and O-H HB band maxima shift to higher wavenumbers as the electron-withdrawing ability of the substituents on the phenols decrease, i.e., on going down the list of phenols in Table 1. It has been shown (9) that for phenol

Fig. 2. OH stretching region of the IR spectrum of (A) 4-F-phenol (11.5 mmol/L) and (B) OD stretching region of *O*-deuterio-4-F-phenol (16.5 mmol/L) in $CC1_4$ containing mmol/L concentrations of di-*tert*-butyl perioxide as indicated.



© 2006 NRC Canada

Fig. 3. OH stretching region of the IR spectrum of (A) PhOH (13.6 mmol/L), (B) 4-F-phenol (12.5 mmol/L), (C) 3,5-Cl_2-phenol (15.8 mmol/L), (D) 4-CF_3-phenol (9.2 mmol/L), and (E) 4-MeO-phenol (20.1 mmol/L) in $CC1_4$ containing mmol/L concentrations of *tert*-butyl methyl ether as indicated.



and 17 meta- and para-substituted phenols in CCl_4, the free OH band maximum frequencies (ν(OH)) and the integrated intensities of their bands (*A*) correlate with Σσ where σ is the Hammett substituent constant. In Hammett plots, the frequencies decrease ($\rho = -13.9$ cm^{-1}) and the intensities increase ($\rho = 1930$ $(mol/L)^{-1}$ cm^{-2}) as σ increases (9). The present results on the free O-H stretching band (Table 1) are consistent with this earlier report. The magnitudes of the shifts in the O-H stretching frequencies upon H-bonding to *tert*-butyl methyl ether, $\Delta\nu$ = ν(OH free) – ν(OH HB), are also given in Table 1 using both the O-H HB band maximum and the "center" of those O-H HB bands that are asymmetric. The center is the frequency at which 50% of the area of the O-H HB band is at higher, and 50% at lower, frequencies. B971 calculated values of Δν have also been included.

In earlier work (1), an empirical equation was derived that relates ΔH_1 for 1:1 hydrogen bond complex formation (rxn.

© 2006 NRC Canada

[1]) between an HBD and an HBA to their α_2^H and β_2^H values, respectively. This equation (which is accurate to ±0.4 kcal/mol, 1 cal = 4.184 J) is

$$[3] \qquad \Delta H_1 = -20.56\alpha_2^H\beta_2^H + 0.59 \text{ kcal/mol}$$

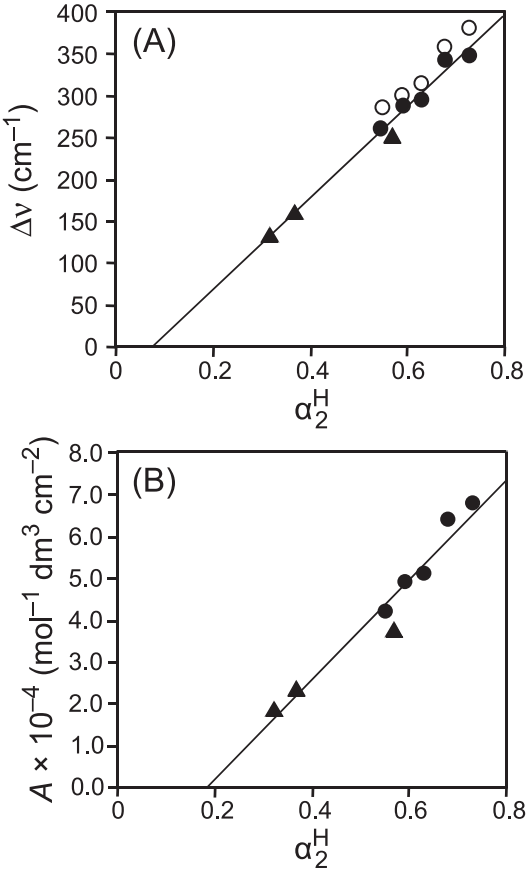
Values of ΔH_1 evaluated using eq. [3] and calculated using the B971 functional are included in Table 1.

The three quantities (Δν(OH), α_2^H, and ΔH_1) for each HBD – *tert*-butyl methyl ether combination (Table 1) are obviously interrelated. For example, a plot of experimental Δν(OH) vs. α_2^H yields an excellent straight line for the five phenol and three alcohol HBDs studied in the present work provided that the centers of the ν(OH HB) bands of the phenols are used rather than the band maxima (Fig. 4A). Such linear correlations are not surprising because the O-H and H···O moieties in hydrogen-bonded complexes are coupled oscillators (10). The integrated OH band areas for the free phenols (*A*) also correlate with α_2^H (Fig. 4B).

Asymmetric O-H HB bands have been observed for 4-F-phenol complexes with a number of ethers and peroxides (3) (Figs. 2 and 3). In contrast, methanol has been reported to give a single O-H HB band maximum with all but one of the same substrates (3).[5] Reported differences between the frequencies of the free OH band maxima for methanol and 4-F-phenol and their O-H HB band maxima for their 1:1 complexes with 40 ethers and 3 peroxides (3) reveal that Δν(OH) MeOH]/[Δν(OH) 4-F-phenol ~ 0.5 with all 43 bases. Obviously, methanol forms a weaker hydrogen bond to a particular base than does 4-F-phenol, as is fully consistent with their α_2^H values (0.367 and 0.629, respectively, Table 1). This suggested that HB bond asymmetry might only become obvious for strong HBDs.[6] To check this possibility we again chose *tert*-butyl methyl ether as the HBA and used three alcohols as HBDs: (*i*) methanol, (*ii*) the weaker HBD, *tert*-butanol, and (*iii*) the much stronger HBD, 2,2,2-trifluoroethanol (see α_2^H values in Table 1). The resulting IR spectra are shown in Fig. 5 and the spectral data together with the calculated values of ΔH_1 are collected in Table 1. None of these alcohols give rise to an asymmetric O-H HB band. This allows us to rule out a simple thermodynamic cause (i.e., the magnitude of ΔH_1) for O-H HB band asymmetry.

It was by now clear that an explanation for O-H HB band asymmetry would not come from experiment alone, it would require examination of some of the HBA···HBD complexes that gave asymmetric O-H HB bands by theory, and a simple, preferably fairly rigid, HBA would make high level calculations more practical. We therefore reexamined the data from Berthelot et al. These contain one epoxide[7] in which the epoxide ring plane was also a plane of symmetry for the whole molecule. This was 2,3-diadamant-2-yl oxirane.[8] With 4-F-phenol this epoxide gave an asymmetric O-H HB band

Fig. 4. Values of (A) Δν = ν(OH free) – ν(OH HB) and (B) *A* as functions of the α_2^H parameter of HBD. Alcohols (▲), phenols using ν(OH HB) band maxima (○), phenols using the center of the ν(OH HB) band (●). Note: There is, of course, only a single *A* value for each alcohol and phenol.



that was deconvoluted into two bands (Δν = 234 and 338 cm^{-1}). Unfortunately, this is too large a molecule for high-level calculations to be carried out in any reasonable time. However, this result of Berthelot et al. did encourage us to examine ethylene oxide and tetramethylethylene oxide, neither of which has previously been used in IR studies of hydrogen bonding. In the presence of 4-F-phenol, the spectra (Figs. 6A and 7A) showed O-H HB bands that were almost symmetric, but were very broad with maxima that are wide plateaus rather than the fairly sharp maxima seen for all the other O-H HB bands (Figs. 2, 3, and 5). In contrast, the O-H HB bands formed between alcohols and these two epoxides are not only symmetric, but also show distinct maxima (Figs. 6B, 6C, and 7B).

Deconvolution of the O-H HB bands shown in Figs. 6A and 7A using two Lorentzian functions yields two band

[5] The exception was 2,3-diadamant-2-yl oxirane. Deconvolution of the HB band yielded two band maxima (Δν(OH) = 129 and 180 cm^{-1}, ref. 3).

[6] However, this would not explain why 4-F-phenol does not give asymmetric HB bands with all ethers. That is, if chloroethers and dibenzyl ether are excluded because they contain two HBA moieties (chlorine and an aromatic ring) that could give rise to separate HB bands and hence to asymmetry, only 12 out of 36 ether–4-F-phenol HB bands were deconvoluted into two bands (3).

[7] Four epoxides were employed, but three of them (propylene oxide, cyclohexene oxide, and epichlorhydrin) lack the single plane of symmetry for the epoxide ring and the whole molecule desired to simplify the theoretical calculations.

[8] This is also the only HBA that gave an asymmetric HB band with methanol that was deconvoluted into two bands (Δν = 129 and 180 cm^{-1}, ref. 3).

© 2006 NRC Canada

Fig. 5. OH stretching region of the IR spectrum of (A) MeOH (10.9 mmol/L), (B) *t*-BuOH (13.9 mmol/L), and (C) CF_3CH_2OH (15.1 mmol/L) in $CC1_4$ containing mmol/L concentrations of *tert*-butyl methyl ether as indicated.

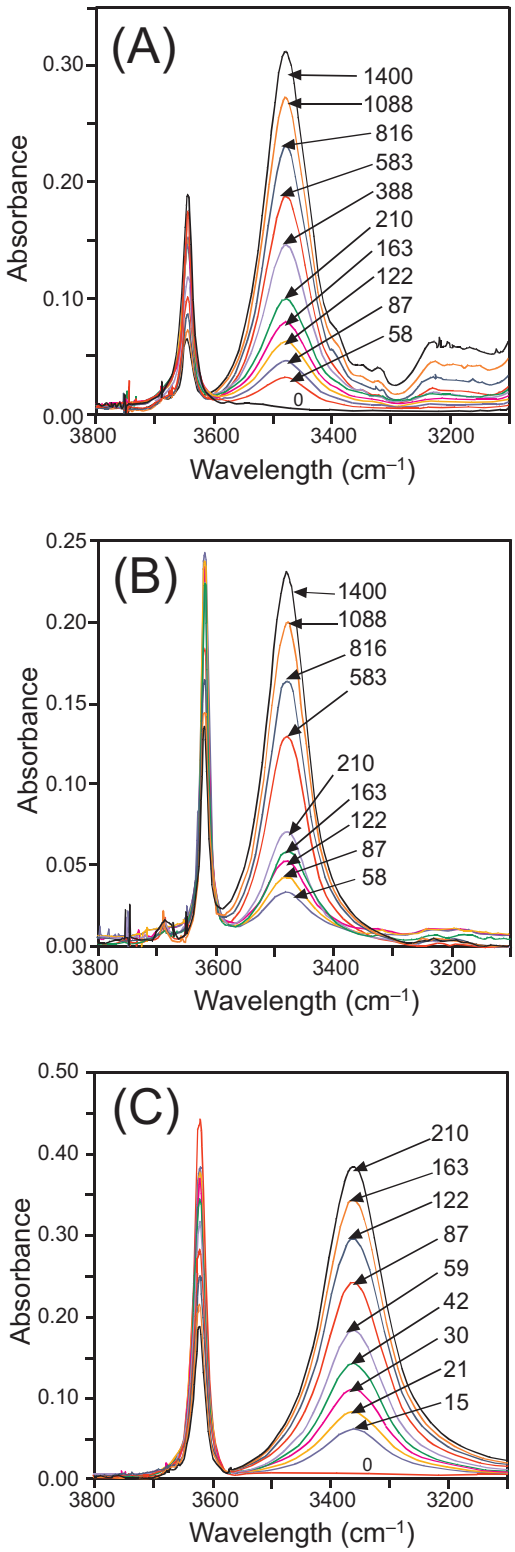
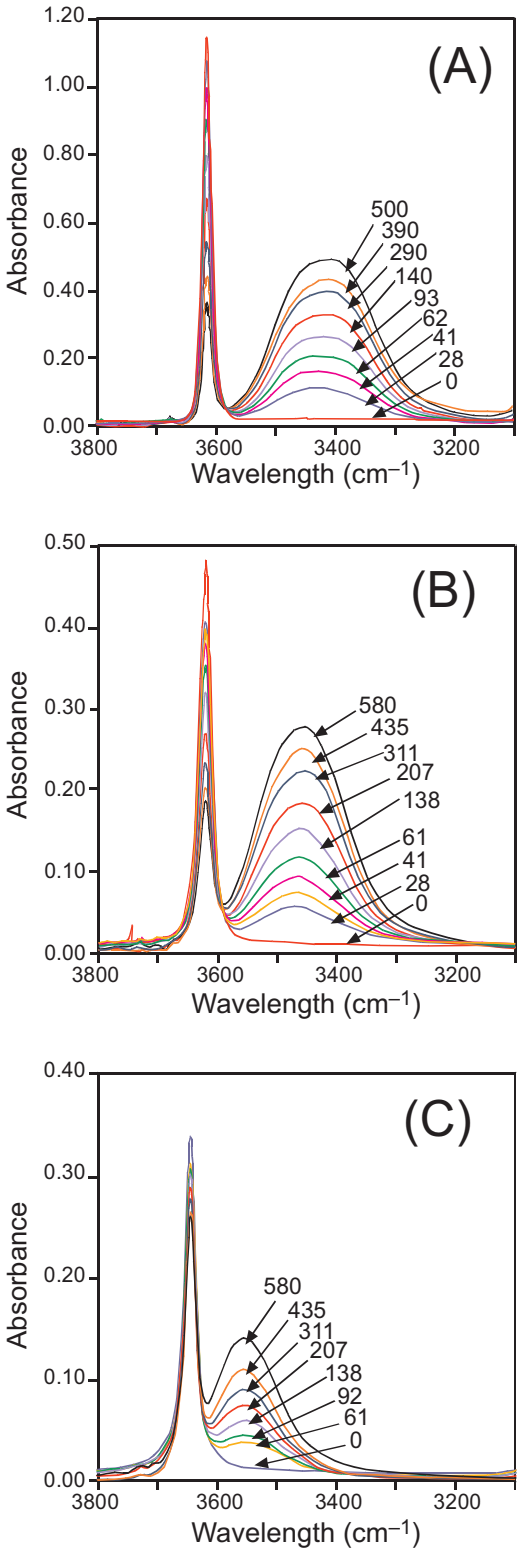


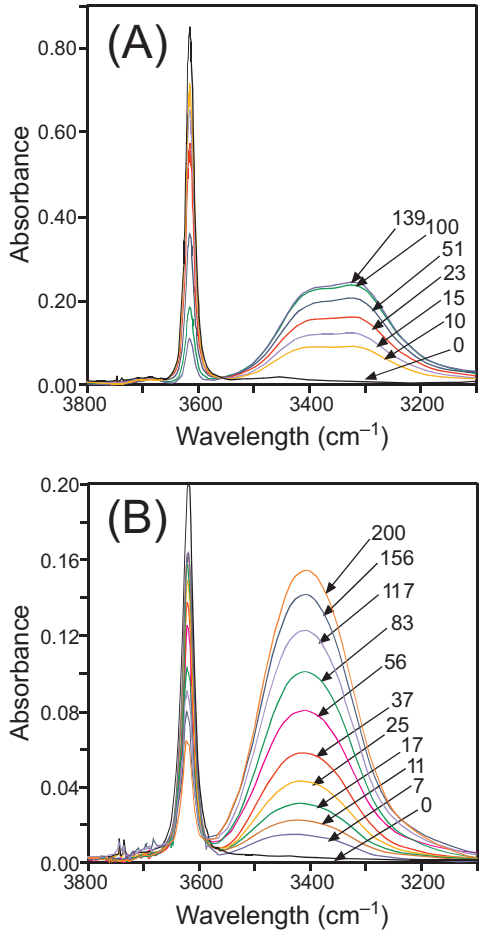
Fig. 6. OH stretching region of the IR spectrum of (A) 4-F-phenol (20.0 mmol/L), (B) CF_3CH_2OH (15.2 mmol/L), and (C) MeOH (15.4 mmol/L) in $CC1_4$ containing mmol/L concentrations of ethylene oxide as indicated.



maxima. However, not only would the implied existence of two HB complexes with different structures be inconsistent with theory (vide infra), but also the two deconvoluted band maximum frequencies vary with the concentration of the epoxide. For example, band maxima are found at 3382 and 3456 cm^{-1} with 41 mmol/L ethylene oxide and at 3392 and

© 2006 NRC Canada

Fig. 7. OH stretching region of the IR spectrum of (A) 4-F-phenol (14.6 mmol/L) and (B) CF_3CH_2OH (16.2 mmol/L) in CCl_4 containing mmol/L concentrations of 1,1,2,2-tetramethylethylene oxide as indicated.



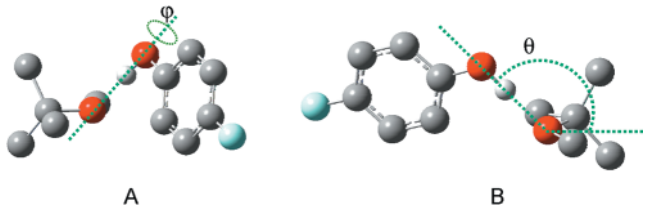
3471 cm^{-1} with 435 mmol/L ethylene oxide (see Supplementary data),[9] a result that can be attributed to differences in the permittivity (dielectric constant) of the two solvent mixtures.

The traces shown in Figs. 6 and 7 can be used to calculate the previously unknown β_2^H values for ethylene oxide (0.36) and tetramethylethylene oxide (0.58) (see Supplementary data).[9] The much larger β_2^H value for tetramethylethylene oxide compared with ethylene oxide is congruent with the β_2^H values for *tert*-butyl alcohol (0.49) vs. methanol (0.41) (2) and is undoubtedly due to the greater inductive electron-donating ability of $(CH_3)_nC$- groups compared with a CH_3 group.

Theoretical calculations

The changes in the potential energy as a function of the dihedral angle defined by R-O-H···O-C(methyl), i.e., as a function of rigid rotations of the molecules about their common hydrogen bond (structure **A**, Fig. 8), are shown in Figs. 9A and 10A, respectively. The results of relaxed

Fig. 8. The rotational potential energy surfaces (shown in Figs. 9A and 10A) were generated by rotation of the dihedral angle (φ) defined by R-O-H···O-C(methyl), as illustrated in structure **A** for the 4-F-phenol – *tert*-butyl methyl ether HB complex. The bending potentials shown in Figs. 9B and 10B were generated by changing the angle (θ) defined by the O—H bond of the HBD and the COC plane of the HBA, as illustrated in structure **B** for the same HB complex. Hydrogen atoms have been removed for clarity.



MP2/6-31+G** potential energy (PE) surface scans as a function of the bending angle (θ) defined by the O-H bond of the HBD and the COC plane of the HBA (structure **B**, Fig. 8) for the same two complexes are shown in Figs. 9B and 10B. This bending motion connects structures **A** and **B** in Fig. 1. These calculations reveal that structure **B** in Fig. 1 (with θ = 180°) is not even a metastable energy minimum. For methanol, but not for 4-F-phenol, the θ = 180° structure is close to the transition state for the shift of the HBD from the "upper" lone pair of electrons on the oxygen atom (structure **A** in Fig. 1) to the equivalent lower lone pair. These PE surfaces demonstrate that these H-bonded complexes must sample a large range of configurations at room temperature.

Discussion

The structures of the HB complexes of 4-F-phenol and methanol with *tert*-butyl methyl ether are similar. In both complexes, the HBDs are aligned so that the plane defined by their COH atoms is roughly perpendicular to and roughly bifurcates the plane defined by the COC atoms of the ether (see structure **A** in Fig. 1). The PE surfaces generated by changes in ϕ (structure **A**, Fig. 8), i.e., by rigid rotation about the HB in both HB complexes, are fairly similar (see Fig. 9A). They reflect repulsive steric interactions between the hydrocarbon moieties of the HBDs and the HBA at rotation angles that substantially deviate from those of the minimum energy structures. The differences in steric bulk of the HBD and HBA hydrocarbon groups (HBD: *tert*-butyl > methyl; HBA: phenyl > methyl) are evident in Fig. 9A.

In contrast, the PE surfaces associated with changes in θ, i.e., with the bending motion of the HBD up and down with respect to the COC plane of the ether (structure **B**, Fig. 8), are very different for the methanol – *tert*-butyl methyl ether and 4-F-phenol – *tert*-butyl methyl ether complexes (see Fig. 9B). For methanol, this PE surface has two degenerate minima that correspond to HB formation to each of the lone pairs of the oxygen atom of the HBA. Note that in the second minimum, the HBA is reoriented to the "trans" position by a 180° rotation about the HB. This reorientation is possi-

[9] Supplementary data for this article are available on the journal Web site (http://canjchem.nrc.ca) or may be purchased from the Depository of Unpublished Data, Document Delivery, CISTI, National Research Council Canada, Ottawa, ON K1A 0R6, Canada. DUD 5071. For more information on obtaining material refer to http://cisti-icist.nrc-cnrc.gc.ca/irm/unpub_e.shtml.

© 2006 NRC Canada

Fig. 9. Potential energy surface (PES) scans at the MP2/6-31+G** level of theory for 4-F-phenol – methyl *tert*-butyl ether (solid line, ■) and for methanol – methyl *tert*-butyl ether (dotted line, ▲). (A) Rigid PE surface associated with changes in φ, i.e., associated with rotation about the hydrogen bond, as illustrated in structure **A** of Fig. 8. The asymmetries of these PE surfaces are due to the different sizes of the methyl and *tert*-butyl groups. (B) Relaxed PE surface associated with changes in θ, the bend angle defined as illustrated in structure **B** of Fig. 8. This second PE surface connects structures **A** and **B** of Fig. 1. The dashed horizontal lines in the plots indicate the value of *RT* at 298.15 K. The arrows indicate that the potential anergies rise steeply toward the HB strength of the complex.

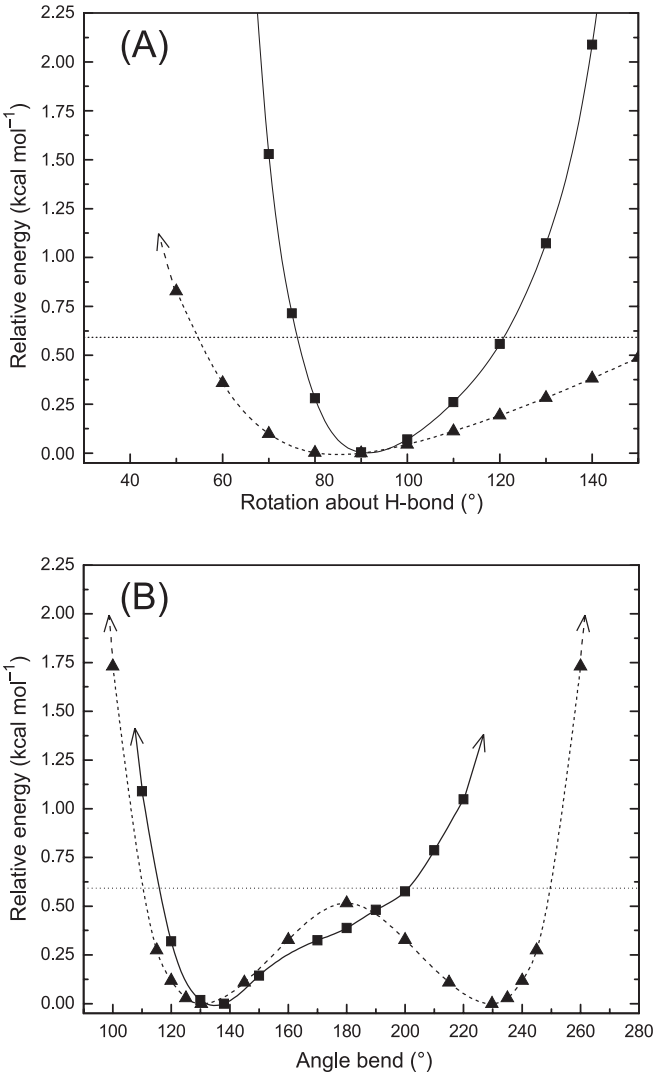
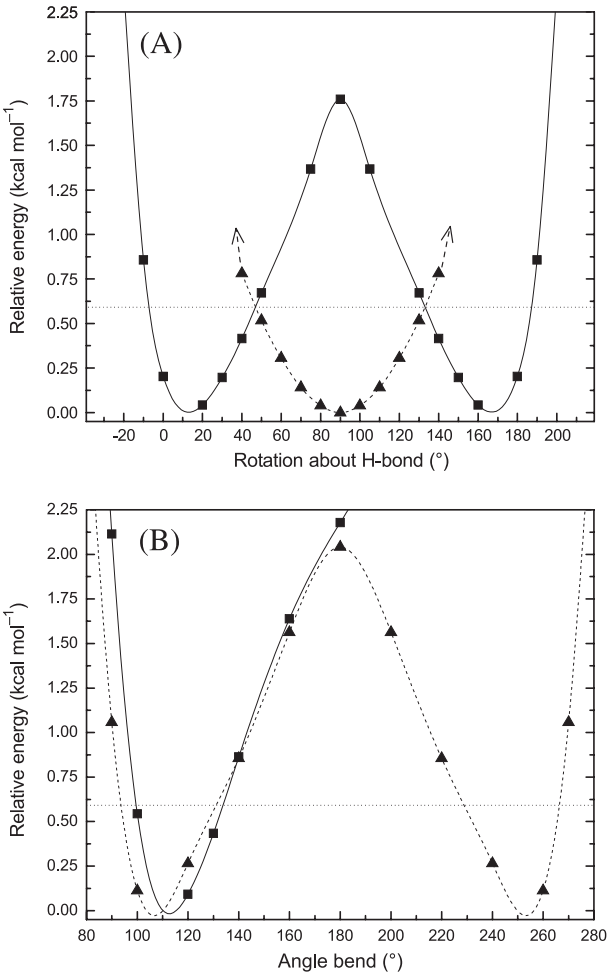


Fig. 10. Potential energy surface (PES) scans at the MP2/6-31+G** level of theory for 4-F-phenol – ethylene oxide (solid line, ■) and for methanol – ethylene oxide (dotted line, ▲). (A) Rigid PE surface associated with changes in φ, i.e., associated with rotation about the hydrogen bond, as illustrated in structure **A** of Fig. 8 for 4-F-phenol – methyl *tert*-butyl ether. (B) Relaxed PE surface associated with changes in θ, the bend angle defined as illustrated in structure **B** of Fig. 8 for 4-F-phenol – methyl *tert*-butyl ether. For methanol, this second PE surface connects structures **A** and **B** in Fig. 1, but for 4-F-phenol the PE continues to increase as θ increases above 180°. The dashed horizontal lines in the plots indicate the value of *RT* at 298.15 K. The arrows indicate that the potential energies rise steeply toward the HB strength of the complex.



ble because of the small size of the methyl group. However, the larger steric bulk of the phenyl ring in the 4-F-phenol complex prevents the facile reorientation of this HBD. Thus, the PE associated with changes in θ in the 4-F-phenol – *tert*-butyl methyl ether HB complex increases continuously from the minimum rather than reaching a local maximum at 180° as is the case for the methanol complex (Fig. 9B). This increase in PE is slow at first, but as the HB approaches the second lone-pair of the oxygen atom of the ether, steric repulsion becomes large and the PE increases more rapidly. A large portion of this asymmetric PE surface can be sampled at room temperature (*RT* = 0.59 kcal/mol at 298 K), and because the coupling between the O-H oscillator of the HBD and the O···H oscillator of the HB changes over this configuration sampling, an asymmetric O-H HB band is produced.

The situation is different for the ethylene oxide HB complexes. Figure 10A shows the PE surface associated with changes in ϕ, i.e., associated with rotation about the HB, in the methanol – ethylene oxide and the 4-F-phenol – ethylene oxide complexes. For the former complex, the COH plane of

© 2006 NRC Canada

the methanol bifurcates and is perpendicular to the plane of the ethylene oxide ring. Rotation about this HB produces a broader, single minimum PE surface analogous to that found for the similar motion in the methanol – *tert*-butyl methyl ether complex (Fig. 9A). In contrast, with 4-F-phenol the PE surface has two minima that are due to attractive interactions between the π electron cloud of the phenyl group and the CH_2 groups of the ethylene oxide.

The θ angle bend PE surface for the methanol – ethylene oxide HB complex has a similar shape to that found for the methanol – *tert*-butyl methyl ether complex (Fig. 10B). That is, two identical HB complexes of equal energy are formed in which the OH group of the HBD interacts with each lone pair on the oxygen atom of the epoxide. The minimum energy structures are transoid with the methyl group pointing away from the epoxide ring and are rather easily interconverted at room temperature. The methanol – ethylene oxide complex therefore yields a symmetric O-H HB band. For the 4-F-phenol – ethylene oxide HB complex, the strong secondary interactions that produce the double minimum shown in Fig. 10A prevent facile changes in the θ angle, i.e., the PE surface for this motion is quite steep. Both of the PE surfaces for the 4-F-phenol – ethylene oxide HB complex are effectively symmetric, which accounts for this complex having a symmetric O-H HB band. In this complex, the broadness of the O-H HB band results from the changes in coupling upon the interconversion of the two structures whose energy minima are shown in Fig. 10A.

Further evidence that two different HB complexes are not formed between *tert*-butyl methyl ether and 4-F-phenol comes from the plots in Fig. 4. The plots of $\Delta\nu$ against α_2^H (Fig. 4A) for the phenols, with their asymmetric O-H HB bands, and for the alcohols, with their symmetric O-H HB bands, yield a single straight line.[10] A least-squares fitting of the data presented in Table 1 gives $\Delta\nu(OH) = 54(-\Delta H) - 9$ cm^{-1} ($R^2 = 0.98$, SD = 11 cm^{-1}). If we now use the two $\Delta\nu$ values given by Berthelot et al. (3) for the deconvoluted 4-F-phenol – methyl *tert*-butyl ether O-H HB band (vide supra), we obtain $-\Delta H$ values of 3.6 ($\Delta\nu$ = 186 cm^{-1}) and 6.0 ($\Delta\nu$ = 315 cm^{-1}) kcal/mol. These HB enthalpies imply that if there really were two different complexes, the ratio of the weaker to the stronger would be ca. 2:98. Such a small population of the weaker HB complex would be unlikely to make an observable contribution to the O-H HB band and hence be the reason for the observed asymmetry.

In conclusion, although the asymmetries of the O-H HB bands for many phenol–ether complexes appear at first sight to be due to two (deconvolutable) overlapping bands that reflect the presence of two distinct HB complex configurations, this is not the true situation. In these cases, as in so many other aspects of science and life, appearances can be deceptive.

References

1. P. Mulder, H.-G. Korth, D.A. Pratt, G.A. DiLabio, L. Valgimigli, G.F. Pedulli, and K.U. Ingold. J. Phys. Chem. A, **109**, 2647 (2005).
2. M.H. Abraham, P.L. Grellier, D.V. Prior, J.J. Morris, and P.J. Taylor. J. Chem. Soc. Perkin Trans. 2, 521 (1990).
3. M. Berthelot, F. Bessau, and C. Laurence. Eur. J. Org. Chem. 925 (1998).
4. M.J. Frisch, G.W. Trucks, H.B. Schlegel, G.E. Scuseria, M.A. Robb, J.R. Cheeseman, J.A. Montgomery, Jr., T. Vreven, K.N. Kudin, J.C. Burant, J.M. Millam, S.S. Iyengar, J. Tomasi, V. Barone, B. Mennucci, M. Cossi, G. Scalmani, N. Rega, G.A. Petersson, H. Nakatsuji, M. Hada, M. Ehara, K. Toyota, R. Fukuda, J. Hasegawa, M. Ishida, T. Nakajima, Y. Honda, O. Kitao, H. Nakai, M. Klene, X. Li, J.E. Knox, H.P. Hratchian, J.B. Cross, V. Bakken, C. Adamo, J. Jaramillo, R. Gomperts, R.E. Stratmann, O. Yazyev, A.J. Austin, R. Cammi, C. Pomelli, J.W. Ochterski, P.Y. Ayala, K. Morokuma, G.A. Voth, P. Salvador, J.J. Dannenberg, V.G. Zakrzewski, S. Dapprich, A.D. Daniels, M.C. Strain, O. Farkas, D.K. Malick, A.D. Rabuck, K. Raghavachari, J.B. Foresman, J.V. Ortiz, Q. Cui, A.G. Baboul, S. Clifford, J. Cioslowski, B.B. Stefanov, G. Liu, A. Liashenko, P. Piskorz, I. Komaromi, R.L. Martin, D.J. Fox, T. Keith, M.A. Al-Laham, C.Y. Peng, A. Nanayakkara, M. Challacombe, P.M.W. Gill, B. Johnson, W. Chen, M.W. Wong, C. Gonzalez, and J.A. Pople. Gaussian 03. Revision C.02 [computer program]. Gaussian, Inc., Wallingford, Conn. 2004.
5. F.A. Hamprecht, A.J. Cohen, D.J. Tozer, and N.C. Handy. J. Chem. Phys. **109**, 6264 (1998).
6. E.R. Johnson and G.A. DiLabio. Chem. Phys. Lett. **419**, 333 (2006).
7. S.F. Boys and F. Bernardi. Mol. Phys. **19**, 553 (1970).
8. M.H. Abraham, P.L. Grellier, D.V. Prior, P.P. Duce, J.J. Morris, and P.J. Taylor. J. Chem. Soc. Perkin Trans. 2, 699 (1989).
9. K.U. Ingold. Can. J. Chem. **38**, 1092 (1960).
10. K.F. Purcell and R.S. Drago. J. Am. Chem. Soc. **89**, 2874 (1967).

[10]The point for CF_3CH_2OH deviates from the linear fit because this HBD undergoes a reorientation in the HB complex. This reorientation allows for a more favourable alignment of the H···O and C–F local dipoles than would be achieved if the HBD had an anti conformation.

© 2006 NRC Canada

Syntheses and characterization of phthalonitriles and phthalocyanines substituted with adamantane moieties[1]

Patrick W. Causey, Igor Dubovyk, and Clifford C. Leznoff

Abstract: The reaction of 3,4,5,6-tetrafluorophthalonitrile with 1-adamantanol, 1-adamantylamine, 1-adamantanemethanol, and 1-adamantaneethanol gave 4,5-di-(1-adamantyloxy)-3,6-difluorophthalonitrile, 4,5-di-(1-adamantylamino)-3,6-difluorophthalonitrile, 4-(1-adamantylamino)-3,5,6-trifluorophthalonitrile, 3,4,5,6-tetra-(1-adamantylmethoxy)phthalonitrile, and 3,4,5,6-tetra-(1-adamantylethoxy)phthalonitrile, respectively. The conversion of these tetrasubstituted phthalonitriles to magnesium, nickel, and metal-free phthalocyanines was demonstrated. These highly hindered phthalocyanines exhibited interesting red shifts in their UV–vis spectra.

Key words: highly hindered adamantane phthalocyanines, adamantylphthalonitriles.

Résumé : La réaction du 3,4,5,6-tétrafluorophtalonitrile avec l'adamantan-1-ol, l'adamantyl-1-amine, l'adamantane-1-méthanol et l'adamantane-1-éthanol conduit à la formation des 4,5-di-(adamantanyl-1-oxy)-3,6-difluorophtalonitrile, 4,5-di-(adamantanyl-1-amino)-3,6-difluorophtalonitrile, 4-(adamantanyl-1-amino)-3,5,6-trifluorophtalonitrile, 3,4,5,6-tétra-(adamantanyl-1-méthoxy)phtalonitrile, 3,4,5,6-tétra-(adamantanyl-1-éthoxy)phtalonitrile respectivement. On a démontré qu'il est possible de transformer ces phtalonitriles tétrasusbstitués en phtalocyanines libre ou complexées avec du nickel ou du magnésium. Les spectres UV–visible de ces phtalocyanines fortement empêchées présentent des déplacements intéressants vers le rouge.

Mots clés : phtalocyanines de l'adamantane fortement empêchées, adamantylphtalonitriles.

[Traduit par la Rédaction]

Introduction

Phthalocyanines (Pcs) are brilliantly coloured purple, blue, or green macrocyclic compounds that have been extensively studied, initially because of their extensive use as dyes (1), but more recently because of their interesting photochemistry (2), potential applications as chemical sensors (3), nonlinear optics (4), and as medicinal agents in photodynamic therapy (PDT) (5). Recently, red-coloured manganese Pcs for analogs, substituted with highly hindered, bulky hexadecaalkoxyl functional groups, have been reported (6, 7), while other red phthalocyanines bearing alkylthio (8) and phenyl groups (9) have been described. These analogs represent Pcs exhibiting pronounced red shifts. Previously, some highly red-shifted analogs of some Pcs had been prepared with some difficulty owing to insolubility (10) and decomposition problems (11).

A significant bathochromic red shift of the Pc chromophore has long been associated with analogs bearing electron-donating substituents at the 1, 4, 8, 11, 15, 18, 22, and 25 positions (nonperipheral), while less pronounced red shifts of the Q band are associated with substitution on the 2, 3, 9, 10, 16, 17, 23, and 24 positions (peripheral) (12, 13). For analogs fully substituted at both the peripheral and nonperipheral positions with alkoxy moieties, enhanced red shifts of the Q band have also been reported (14). It has been postulated that sterically bulky substituents at the peripheral positions around the Pc exert influence upon the nonperipheral positions, thereby effectively increasing the steric bulk of the nonperipheral substituents and further promoting a shifting of the Q band. Various metallated and nonmetallated Pcs bearing sterically bulky alkoxy moieties have been reported, including both neopentoxy and cyclohexylmethoxy groups (6, 7). In addition to the effect that these substitutions appear to have on the absorption spectra of the resulting Pcs, a disruption of the π stacking among the aromatic macrocycles increases the solubility of the molecule, even in nonpolar solvents.

One particular bulky alkyl moiety that has interested our research group is adamantane. In particular, amine-substituted adamantanes have been approved for treatment as an antiviral agent against influenza A (15) and adamantyl moieties have been investigated for their potential use as carrier groups for anticonvulsant (16) and anticancer drugs

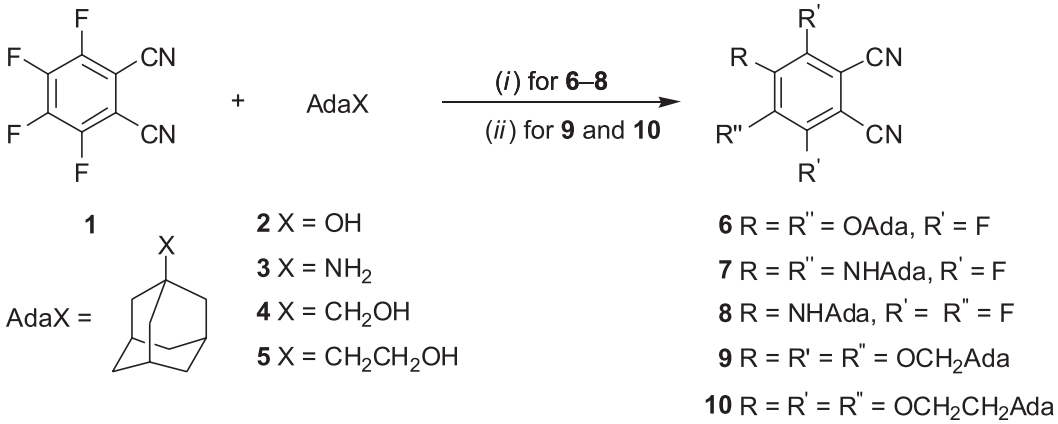
Received 4 October 2005. Accepted 8 December 2005. Published on the NRC Research Press Web site at http://canjchem.nrc.ca on 29 September 2006.

P.W. Causey, I. Dubovyk, and C.C. Leznoff.[2] Department of Chemistry, York University, Toronto, ON M3J 1P3, Canada.

[1]This article is part of a Special Issue dedicated to Dr. Alfred Bader.
[2]Corresponding author (e-mail: leznoff@yorku.ca).

 doi:10.1139/V06-096 © 2006 NRC Canada

Scheme 1. Reagents and conditions: (*i*) *n*-BuLi, THF, 25 °C, 1 h; (*ii*) K_2CO_3, DMF, 140 °C, 4 days.



(17). However, it is their more general physicochemical characteristics associated with large steric bulk and their close steric relationship to our favorite bulky group, the neopentoxy group, that have piqued our interest as related to the potential for substitution onto the Pc framework.

The synthesis of substituted Pcs can be accomplished through two distinct approaches, each involving nucleophilic aromatic substitution. A recent approach employed in our research group has focused upon directly reacting metallated hexadecafluorophthalocyanines with various heteroatom nucleophiles (18). A limit to this synthetic approach is the distribution of substituents replacing the fluorine atoms resulting in a range of products that are difficult to separate by flash chromatography. Furthermore, complete replacement of all 16 fluorine atoms is limited to sterically small, strong nucleophiles Alternatively, tetrasubstituted phthalonitriles bearing functionalities, such as the neopentoxy group, can be readily produced by nucleophilic aromatic substitution reactions on 3,4,5,6-tetrafluorophthalonitrile (**1**) despite the steric bulk of the substituents (19).

The general synthetic strategy employed for the synthesis of adamantyl-substituted Pcs follows the production and isolation of substituted phthalonitriles. Subsequent condensation of the adamantyl-substituted phthalonitriles gives the required phthalocyanines. In this research we were interested in systematically varying the bulk of the substitiuents so as to produce a series of hexadecasubstituted phthalocyanines and examining their spectroscopic properties.

Results and discussion

A novel series of phthalocyanine compounds were designed and synthesized bearing bulky adamantane-based substituents. Commercially available 3,4,5,6-tetrafluorophthalonitrile (**1**) was reacted with 1-adamantanol (**2**), 1-adamantylamine (**3**), 1-adamantanemethanol (**4**), or 2-(1-adamantanyl)ethanol (**5**) in the presence of a base to generate 4,5-di-(1-adamantyloxy)-3,6-difluorophthalonitrile (**6**), 4,5-di-(1-adamantylamino)-3,6-difluorophthalonitrile (**7**), 4-(1-adamantylamino)-3,5,6-trifluorophthalonitrile (**8**), 3,4,5,6-tetra-(1-adamantylmethoxy)phthalonitrile (**9**), or 3,4,5,6-tetra-[2-(1-adamantyl)ethoxy]phthalonitrile (**10**). For the synthesis of fully substituted adamantylmethoxyl and adamantylethoxyl (Scheme 1) derivatives, a previously reported synthetic approach was followed in which an excess of alkyl alcohol was combined with 3,4,5,6-tetrafluorophthalonitrile (**1**) in *N*,*N*-dimethylformamide (DMF) at 140 °C in the presence of potassium carbonate (19). Both tetrasubstituted crude products, purified by flash silica gel column chromatography, were eluted with dichloromethane–methanol and reduced to an amber-coloured oil under reduced pressure. These oils solidified under a stream of air yielding the desired final products, which were confirmed by EI mass spectra NMR and IR spectroscopic analysis and microanalyses.

Despite repeated attempts to synthesize the tetrasubstituted analog from 1-adamantanol and **1** using this synthetic approach, the reaction was not successful. Therefore, an alternative synthetic approach for the aromatic nucleophilic substitution of the phthalonitrile fluorine was implemented, in which *n*-butyllithium in tetrahydrofuran (THF) was used to deprotonate **2** (or **3**) to create the desired nucleophile. Although this modified approach did result in fluorine substitution, complete tetrasubstitution was not achieved, presumably because of the high degree of steric bulk associated with the adamantanyl cage. This steric hindrance is not so severe in the adamantanemethanol and adamantaneethanol homologs, thereby enabling complete substitution. An obvious colour change was noted immediately upon addition of 3,4,5,6-tetrafluorophthalonitrile to the activated adamantyloxide nucleophile, and despite allowing the reaction to continue for up to 72 h, substitution of more than two fluorine moieties was not observed (Scheme 1). TLC of the reaction mixture did reveal an additional spot that was presumed to be the monosubstituted analog, although isolation of this species was not achieved. As usual, a sharp intense absorbance at 2239 cm^{-1} was observed in the IR spectra and was attributed to CN stretching. Furthermore, EI mass spectroscopy and microanalysis confirmed that the product from this reaction is a disubstituted phthalonitrile. The ^1H NMR spectra for this compound revealed the expected resonances for the adamantyl protons between δ 1.68 and 2.24 ppm, while the ^{19}F NMR exhibited a singlet at δ –114.9 ppm. The singlet suggests that the two adamantyloxy substituents are positioned at the peripheral position.

The synthesis of derivatives substituted with nitrogen-containing adamantane analogs was accomplished through an approach similar to adamantanol involving the in situ

© 2006 NRC Canada

generation of an adamantamide anion from **3**, followed by subsequent addition of **1**. The desired disubstituted product was separated by flash silica gel column chromatography, yielding an amber-coloured oil that solidified under air. EI mass spectroscopy and elemental analysis confirmed the product, while fluorine NMR spectra for the species showed a singlet at $\delta \sim -119$ ppm.

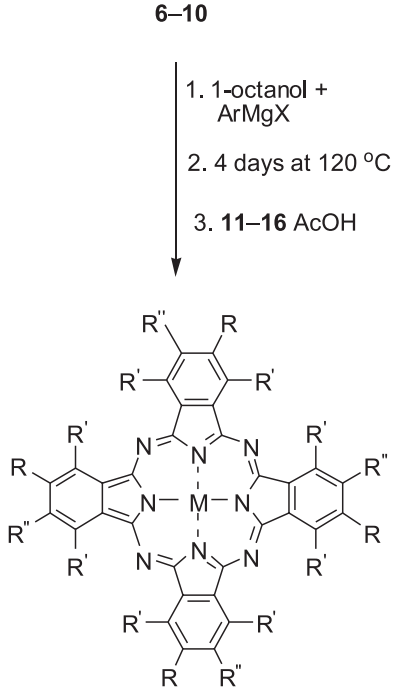
Subsequently, the reaction was repeated with 1 equiv. of adamantylamine (**3**) and **1** to generate the monosubstituted analog, **8**. Three distinct resonances (δ –118.7, –129.7, and –136.8) were identified in the ^{19}F NMR, corresponding to the three inequivalent fluorines from the monosubstituted phthalonitrile. Further characterization by EI mass spectroscopy, FT-IR spectroscopy, and elemental analysis confirm the synthesis of the monosubstituted adamantylamine-substituted analog.

Each of the above phthalonitriles (**6**–**10**) was condensed with 1-octanol and phenyl or 4-methoxyphenylmagnesium bromide to yield the corresponding magnesium phthalocyanine, as outlined in Scheme 2. The formed Pcs were all purified by flash silica gel column chromatography, eluting with a solvent mixture of hexane – ethyl acetate, and subsequently characterized by MALDI mass spectroscopy (MALDI-MS), elemental analyses, UV–vis spectrophotometry, and NMR analyses. The mass spectra of all magnesium phthalocyanines gave the expected parent ion clusters. In addition, daughter ion clusters corresponding to the loss of the adamantanyl fragments cleaved at the alkyl–heteroatom bond were also detected.

The ^{1}H NMR spectra for all magnesium phthalocyanines exhibited resonances for the adamantanyl protons between 1.6 and 2.3 ppm. In the OCH_2 region for the hexadeca-adamantylmethoxysubstituted analog **14**, a broad singlet was observed. A similar nickel phthalocyanine bearing hexadeca-cyclohexylmethoxyl moieties revealed temperature-dependant separation of the peripherally and nonperipherally substituted methylene protons and that at room temperature the two chemically different proton pairs appeared as a broad singlet (19) The peripheral and nonperipheral OCH_2 protons for the hexadecaadamantylethoxyphthalocyanine **15** are chemically inequivalent and appeared as distinct triplets at 4.27 and 4.16 ppm, respectively. As expected, the ^{19}F NMR for the hexadecasubstituted analogs showed no fluorine resonances, while the octaadamantyloctafluoro Pcs **11** and **12** exhibited singlets at approximately –120 ppm. However, the ^{19}F NMR for the tetrasubstituted analog **13**, which consists of a mixture of isomers, revealed multiple fluorine resonances corresponding to the multitude of inequivalent fluorines formed during the phthalocyanine condensation reaction.

A comparison of the UV–vis spectra for the Mg Pcs exhibits the expected red shifts owing to the substitution onto the macrocyclic aromatic ring, as shown in Table 1. Each of the hexadecasubstituted compounds exhibited a pronounced red shift of the Q band, with λ_{max} values similar to those reported in the literature for magnesium hexadecaneopentoxyphthalocyanine (754 nm) (6, 7). The tetrasubstituted derivative **13** was not red-shifted as greatly as the octaadamantylamine derivative, further supporting the association between large, sterically bulky substituents and the red shift of the corresponding UV–vis spectra. As compared

Scheme 2.



11 R = R'' = OAda, R' = F, M = Mg

12 R = R'' = NHAda, R' = F, M = Mg

13 R = NHAda, R' = R'' = F, M = Mg

14 R = R' = R'' = OCH_2Ada, M = Mg

15 R = R' = R'' = OCH_2CH_2Ada, M = Mg

16 R = R'' = OAda, R' = F, M = H_2

Table 1. Summary of the UV–vis spectra for the adamantane-substituted magnesium phthalocyanines.

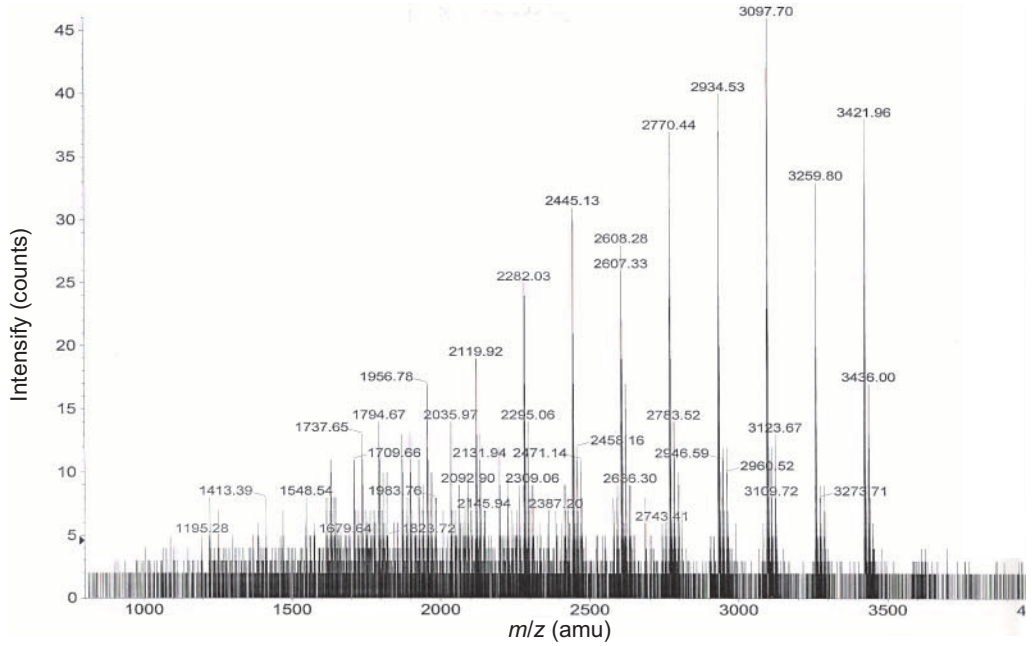
Mg Pc	λ_{max} (log ε)
11	708 (4.83)
12	794 (4.57)
13	714 (4.63)
14	752 (4.91)
15	744 (4.93)

with the tetrasubstituted analog, the octaadamantylamine-substituted derivative exhibited a red shift of 80 nm. It is possible that these bulky adamantylamino groups, even at the peripheral positions, distort the planar Pc ring, causing this red shift. Not surprisingly, a small decrease in the λ_{max} was detected upon insertion of a methylene unit for the hexadecasubstituted analogs **15**, as compared with **14**, as the extra methylene group in **15** will position the bulky adamantyl group further from the core of the Pc.

Metal-free Pcs are useful intermediates for transmetallating synthetically challenging complexes. A metal-free phthalocyanine analog **16** was synthesized after refluxing the magnesium derivative **11** in acetic acid. Purification was achieved by flash silica gel column chromatogra-

© 2006 NRC Canada

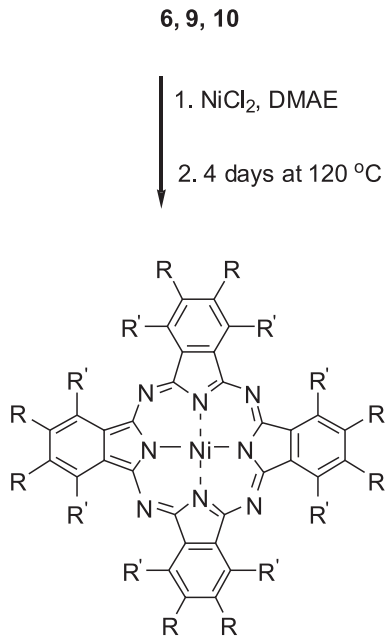
Fig. 1. MALDI-MS spectra for **19** showing parent ion cluster $[M + H]^+$ at 3418, along with daughter ion clusters separated by 163 amu ($C_{12}H_{19}$).



phy with hexane – ethyl acetate used as the mobile phase. This compound was characterized by MALDI-MS and again revealed the expected parent ion cluster at 1883 amu. A series of daughter ion clusters were observed separated by 135 amu, corresponding to the loss of an adamantanyl unit ($C_{10}H_{15}$). The complex was further characterized by NMR spectroscopy, elemental analysis, and UV–vis spectrophotometry, with the λ_{max} of the Q band red-shifted by 26–764 nm with respect to the magnesium derivative. Following the isolation and characterization of the metal-free derivative, repeated attempts to introduce manganese into the core of the phthalocyanine were unsuccessful.

Due to the difficulty associated with forming the metal-free phthalocyanines incorporating adamantane-based substituents, a multistep synthesis for transmetalating Pcs was not viable. Therefore, direct condensation of precursor phthalonitriles with nickel as the core metal ion was pursued. As previously described (19), the general synthetic approach is outlined in Scheme 3 in which **6**, **9**, or **10** was heated with $NiCl_2$ in *N*,*N*-dimethylaminoethanol (DMAE) for 4 days at 120 °C to give the nickel phthalocyanines **17**–**19**, respectively. Again, MALDI-MS revealed the expected parent ion clusters, in addition to daughter ion clusters corresponding to fragmentation between the alkyl substituents and oxygen. For the octaadamantyloctafluoro-nickel Pc **17**, the daughter ions were separated by 135 amu, while the daughter ion clusters for the hexadecaadamantylmethoxy-nickel Pc **18** were separated by 149 amu and the daughter ion peaks corresponding to hexadecaadamantylethoxy-substituted analog were separated by 163 amu, as shown in Fig. 1. Similar to the magnesium Pc analogs, the OCH_2 resonances for the adamantylmethoxyphthalocyanine **18** appeared as a broad signal at 4.21 ppm representing both the peripheral and nonperipheral substituents, while two clearly distinct triplet resonances at 4.78 and 4.53 ppm were observed for the peripheral and nonperipheral OCH_2 protons, respectively, of the adamantylethoxyl Pc **19**. UV–vis spectra were recorded for the three nickel phthalocyanines (summarized in Table 2), although the Q bands are not as red-shifted as the corresponding magnesium phthalocyanines. The most sterically congested nickel Pc (**18**) exhibited the greatest red

Scheme 3.



17 R = OAda, R' = F

18 R = R' = OCH_2Ada

19 R = R' = OCH_2CH_2Ada

© 2006 NRC Canada

Table 2. Summary of the UV–vis spectra for the adamantane-substituted nickel phthalocyanines.

Ni Pc	λ_{max} (log ε)
17	708 (4.91), 636 (4.23)
18	750 (4.93), 672 (4.43)
19	736 (4.88), 660 (4.25)

shift, while the octaadamantyloxy-octafluorophthalocyanine **17** was the least red-shifted nickel complex. Perhaps some aggregation in **17**–**19** resulted in somewhat lower log ε values than usual. This reinforces the association between large sterically hindered substitutions onto the aromatic macrocycle and the red shifting of the Q band for phthalocyanines, although the λ_{max} for **18** was slightly less red-shifted as compared with hexadecaneopentoxyphthalocynaninato nickel (750 vs. 758 nm) (19).

Experimental

General methods

Inert atmosphere conditions were maintained using Air Liquide prepurified argon. Magnetic stirring methods were utilized during all reactions. Flash chromatography was performed using silica gel of particle size 40–63 μm, with eluting solvents mixtures as described. Nuclear magnetic resonance (NMR) spectroscopy for proton and fluorine was performed using a Bruker 300 spectrometer at room temperature and was processed using XWIN-NMR 3.5 software. Chemical shifts are reported in parts per million (δ). Infrared (IR) spectra were recorded on a Mattson 3000 FT-IR spectrometer using KBr discs. UV–vis were recorded on a Hewlett-Packard HP8452A diode array spectrophotometer. For all phthalonitriles, low-resolution mass spectra (MS) were recorded in electron ionization (70 eV) mode on a Micromass/Waters GCT time-of-flight instrument. For all phthalocyanines, low-resolution MS were recorded using laser desorption ionization (LDI) on a PE Sciex Q-STAR XL or PerSeptive Biosystems Voyager – DE STR spectrometer. Microanalyses were performed by Guelph Chemical Laboratory Ltd., Guelph, Ontario.

Synthesis of 4,5-di-(1-adamantyloxy)-3,6-difluorophthalonitrile (6)

1-Adamantanol (**2**, 1.50 g, 9.85 mmol, 2 equiv.) was dissolved in 10 mL of THF and the solution was stirred under an argon atmosphere at room temperature. To this solution was added *n*-butyllithium in hexanes (4.94 mL, 2 mol/L, 2 equiv.). The reaction mixture initially turned cloudy and a fine white precipitate was observed. The mixture was stirred for 1 h before a solution of 3,4,5,6-tetrafluorophthalonitrile (**1**, 0.986 g, 4.93 mmol, 1 equiv.) in THF was added dropwise under argon. The reaction mixture turned reddish-purple and was stirred at room temperature for 4 h. After this period, 100 mL of water was added to the reaction mixture and the mixture was extracted with diethyl ether (3 × 50 mL). After drying over sodium sulfate, the solvent was removed under reduced pressure, resulting in an amber-coloured oil. The oil was then dissolved in a minimum of toluene and was passed through a flash silica gel column using toluene as eluant. The first fraction was collected and the solvent was removed under reduced pressure, yielding an oil that solidified upon sitting under a stream of air overnight. Yield: 76% (1.74 g); mp 196–198 °C. TLC (toluene): R_f 0.63. IR (KBr, cm^{-1}) ν: 2911, 2846, 2239 (CN), 1454, 1354, 1295, 1113, 1042. ^{1}H NMR ($CDCl_3$) δ :2.24 (br m, 6H, bridgehead C-H), 1.93 (m, 12H, CH_2), 1.68 (br m, 12H, CH_2). ^{19}F NMR ($CDCl_3$) δ: –114.9 (s). EI-MS *m*/*z* (rel. intensity): M^+ 464 (64). Anal. calcd. for $C_{28}H_{30}O_2N_2F_2$: C 72.39, H 6.51, N 6.03; found: C 72.42, H 6.34, N, 6.11.

Synthesis of 4,5-di-(1-adamantylamino)-3,6-difluorophthalonitrile (7)

1-Adamantylamine (**3**, 1.52 g, 10.1 mmol, 2 equiv.) was dissolved in 15 mL of THF and the solution was stirred under an argon atmosphere at room temperature. To this was added *n*-butyllithium in hexanes (4.0 mL, 2.5 mol/L, 2 equiv.). The reaction mixture initially turned cloudy and a fine white precipitate was observed. The mixture was stirred for 1 h before a solution of 3,4,5,6-tetrafluorophthalonitrile (**1**, 0.986 g, 4.93 mmol, 1 equiv.) in THF was added dropwise under argon. The reaction mixture turned dark red and was stirred at room temperature for 4 h. After this period, 100 mL of water was added to the reaction mixture and was extracted with diethyl ether (3 × 50 mL). After drying over sodium sulfate, the solvent was removed under reduced pressure, resulting in an amber-coloured oil. The oil was then dissolved in a minimum of toluene and was passed through a flash silica gel column using toluene for elution. The first fraction was collected and the solvent was removed under reduced pressure, yielding an oil that solidified upon sitting under a stream of air overnight. Yield: 52% (1.12 g); mp 184–186 °C. TLC (toluene): R_f 0.61. IR (KBr, cm^{-1}) ν: 3377, 2910, 2850, 2225 (CN), 1594, 1515, 1453, 1384, 1359, 1306. ^{1}H NMR ($CDCl_3$) δ: 4.05 (br s, 2H, N-H), 2.20 (br s, 6H, bridgehead C-H), 1.94 (m, 6H, CH_2), 1.85 (m, 6H, CH_2), 1.70(m, 12H, CH_2). ^{19}F NMR ($CDCl_3$) δ: –119.6. EI-MS *m*/*z* (rel. intensity): M^+ 462 (100). Anal. calcd. for $C_{28}H_{32}N_4F_2$: C 72.70, H 6.97, N 12.11; found: C 72.89, H 7.20, N 12.16.

Synthesis of 4-(1-adamantylamino)-3,5,6-trifluorophthalonitrile (8)

1-Adamantylamine (**3**, 0.76 g, 5.0 mmol, 1 equiv.) was dissolved in 15 mL of THF and the solution was stirred under an argon atmosphere at room temperature. To this solution was added *n*-butyllithium in hexanes (2.0 mL, 2.5 mol/L, 1 equiv.). The reaction mixture initially turned cloudy and a fine white precipitate was observed. The reaction was stirred for 1 h before a solution of 3,4,5,6-tetrafluorophthalonitrile (**1**, 0.986 g, 4.93 mmol, 1 equiv.) in THF was added dropwise under argon. It was then stirred at room temperature for 4 h and worked up as for **7**. IR (KBr, cm^{-1}) ν: 3418, 3382, 2912, 2854, 2231 (CN), 1566, 1452, 1382, 1108. Yield: 58% (0.95 g); mp 135–137 °C. TLC (toluene): R_f 0.65. ^{1}H NMR ($CDCl_3$) δ: 3.42 (br s, 1H, N-H), 2.19 (br s, 3H, bridgehead C-H), 1.93 (br s, 6H, CH_2), 1.71 (br s, 6H, CH_2). ^{19}F NMR ($CDCl_3$) δ: –118.7 (m), –129.7 (m), –136.8 (m). EI-MS *m*/*z* (rel. intensity): M^+ 331 (47). Anal. calcd. for $C_{18}H_{16}N_3F_3$: C 65.25, H 4.87, N 12.68; found: C 65.03, H 4.85, N 12.78.

© 2006 NRC Canada

Synthesis of 3,4,5,6-tetra-(1-adamantylmethoxy)phthalonitrile (9)

1-Adamantanemethanol (**4**, 5.0 g, 30.1 mmol, 24 equiv.), potassium carbonate (5 g, 36 mmol, 30 equiv.), and 3,4,5,6-tetrafluorophthalonitrile (**1**, 1.0 g, 5 mmol, 1 eq.) were dissolved in 12 mL DMF and the reaction mixture was heated to 120 °C for 4 days. After this period, 100 mL of water was added to the reaction mixture, which was subsequently extracted with diethyl ether (3 × 75 mL). After drying over sodium sulfate, the solvent was removed under reduced pressure, yielding an amber-coloured oil. The oil was dissolved in a minimum of dichloromethane and was passed through a flash silica gel column using dichloromethane–methanol (20:1) as eluant. The first fraction was collected and the solvent was removed under reduced pressure, yielding an amber oil that solidified to an off-white solid under a stream of air overnight. Yield: 78% (3.07 g); mp 173–176 °C. TLC (toluene): R_f 0.66. IR (KBr, cm^{-1}) ν: 2943, 2917, 2230 (CN), 1558, 1489, 1358, 1101. ^{1}H NMR ($CDCl_3$) δ: 3.69 (s, 4H, CH_2), 3.68 (s, 4H, CH_2), 2.04 (m, 12H, bridgehead C-H), 1.71 (m, 24H, CH_2), 1.67 (m, 24H, CH_2). EI-MS *m/z* (rel. intensity): M^+ 784 (41). Anal. calcd. for $C_{52}H_{68}O_4N_2$: C 79.55, H 8.73, N 3.57; found: C 79.14, H 9.07, N 3.59.

Synthesis of 3,4,5,6-tetra-(1-adamantylethoxy)phthalonitrile (10)

1-Adamantaneethanol (**5**, 5.0 g, 27.8 mmol, 8 equiv.), potassium carbonate (4.3 g, 32 mmol, 8 equiv.), and 3,4,5,6-tetrafluorophthalonitrile (**1**, 0.7 g, 3.5 mmol, 1 equiv.) were added to 12 mL of DMF and the reaction mixture was heated to 120 °C for 4 days. The work-up proceeded as for **9**, but dichloromethane–methanol (10:1) was used as eluant. Yield: 81% (2.39 g); mp 166–168 °C. TLC (toluene): R_f 0.68. IR (KBr, cm^{-1}) ν: 2935, 2846, 2231 (CN), 1559, 1448, 1382, 1371, 1244, 1106. ^{1}H NMR ($CDCl_3$) δ: 4.19 (m, 8H, OCH_2), 1.98 (br s, 12H, bridgehead C-*H*), 1.67 (m, 24H, CH_2), 1.56 (m, 32H, OCH_2CH_2 and adamantyl CH_2). EI-MS *m/z* (rel. intensity): M^+ 840 (51). Anal. calcd. for $C_{56}H_{76}O_4N_2$: C 79.96, H 9.11, N 3.33; found: C 79.60, H 9.35, N 3.32.

Synthesis of magnesium 2,3,9,10,16,17,23,24-octa-(1-adamantyloxy)-1,4,8,11,15,18,22,25-octafluorophthalocyanine (11)

4-Methoxyphenylmagnesium bromide (2 mL, 0.5 mol/L in THF) was added to 3 mL of 1-octanol and the mixture was stirred for 0.5 h under argon at room temperature. To this was added 4,5-di-(1-adamantyloxy)-3,6-difluorophthalonitrile (**6**) (0.250 g, 0.53 mmol) and the mixture was heated under argon to 120 °C. Upon heating, the clear, colourless mixture turned green. After heating for 24 h, 50 mL of methanol was added and a green solid precipitated out of solution. The solid was collected by centrifugation and was washed with water and methanol. The crude product was then passed through a flash silica gel column eluting with hexane – ethyl acetate (9:1). The first fraction was collected and the solvent was removed under reduced pressure, yielding a dark green solid. Yield: 34% (0.085 g); mp >300 °C. TLC (hexane – ethyl acetate, 5:1): R_f 0.72. UV–vis (dichloromethane) λ_{max} (log ε) (nm): 708 (4.83), 636 (4.06), 364 (4.43), 318 (4.37). ^{1}H NMR ($CDCl_3$) δ: 2.50 (br s, 24H, bridgehead C-H), 2.31 (m, 48H, CH_2), 2.22 (m, 48H, CH_2). ^{19}F NMR ($CDCl_3$) δ: –119.2. MALDI-MS *m/z* (rel. intensity): 1883 $[M]^+$ (10), 1748 $[M - C_{10}H_{15}]^+$ (21), 1613 $[M - 2(C_{10}H_{15})]^+$ (25), 1478 $[M - 3(C_{10}H_{15})]^+$. Anal. calcd. for $C_{112}H_{120}O_8N_8F_8Mg$: C 71.46, H 6.43, N 5.95; found: C 71.48, H 6.44, N, 6.11

Synthesis of magnesium 2,3,9,10,16,17,23,24-octa-(1-adamantylamino)-1,4,8,11,15,18,22,25-octafluorophthalocyanine (12)

4-Methoxyphenylmagnesium bromide (2 mL, 0.5 mol/L in THF) was added to 3 mL of 1-octanol and the mixture was stirred for 0.5 h under argon at room temperature. To this was added 4,5-di-(1-adamantylamino)-3,6-difluorophthalonitrile (**7**, 0.250 g, 0.53 mmol) and the mixture was heated under argon to 120 °C. Upon heating, the clear, colourless mixture turned red and was worked up as for **11**, yielding a dark green solid. Yield: 17% (0.042 g); mp >300 °C. TLC (hexane – ethyl acetate, 5:1): R_f 0.72. UV–vis (dichloromethane) λ_{max} (log ε) (nm): 794 (4.57), 708 (4.09), 478 (4.04), 358 (4.34), 322 (4.34). ^{1}H NMR ($CDCl_3$) δ: 2.11 (m, 24H, bridgehead C-H), 1.87 (m, 48H, CH_2), 1.68 (m, 48H, CH_2). MALDI-MS *m/z* (rel. intensity): 1872 $[M]^+$ 100. Anal. calcd. for $C_{112}H_{128}N_{16}F_8Mg$: C 71.76, H 6.88, N 11.95; found: C 71.87, H 7.27, N 11.24.

Synthesis of magnesium 2,9,16,23-tetra-(1-adamantylamino)-1,3,4,8,10,11,15,17,18,22,24,25-dodecafluorophthalocyanine (13)

4-Methoxyphenylmagnesium bromide (2 mL, 0.5 mol/L in THF) was added to 3 mL of 1-octanol and the mixture was stirred for 0.5 h under argon at room temperature. To this was added 4-(1-adamantylamino)-3,5,6-trifluorophthalonitrile (**8**, 0.250 g, 0.75 mmol) and the mixture was heated under argon to 120 °C. Upon heating, the clear, colourless mixture turned green. After heating for 24 h, 50 mL of methanol was added and a green solid precipitated out of solution and was worked up as for **11**, yielding a dark green solid. Yield: 21% (0.053 g); mp >300 °C. TLC (hexane – ethyl acetate, 9:1): R_f 0.62. UV–vis (dichloromethane) λ_{max} (log ε) (nm): 714 (4.63), 646 (4.07), 362 (4.37). ^{1}H NMR ($CDCl_3$) δ: 3.82 (br s, 4H, NH), 2.18 (m, 12H, bridgehead C-H), 1.71–1.96 (m, 24H, CH_2), 1.58 (br s, 24H, CH_2). ^{19}F NMR ($CDCl_3$) δ: –128 (m), –138 (m). MALDI-MS *m/z* (rel. intensity): 1348 $[M]^+$ (100), 1213 $[M - C_{10}H_{15}]^+$ (63), 1078 $[M - 2(C_{10}H_{15})]^+$ (53), 943 $[M - 4(C_{10}H_{15})]^+$ (24). Anal. calcd. for $C_{72}H_{64}N_{12}F_{12}Mg$: C 64.07, H 4.78, N 12.45; found: C 64.44, H 4.94, N 12.78

Synthesis of magnesium 1,2,3,4,8,9,10,11,15,16,17,18,22,23,24,25-hexadeca-(1-adamantylmethoxy)phthalocyanine (14)

4-Methoxyphenylmagnesium bromide was added (2 mL, 0.5 mol/L in THF) to 3 mL of 1-octanol and the mixture was stirred for 0.5 h under argon at room temperature. To this was added 3,4,5,6-tetraadamantylmethoxyphthalonitrile (**9**, 0.250 g, 0.32 mmol) and the mixture was heated under argon to 120 °C. Upon heating, the clear, colourless mixture turned green. After heating for 24 h, 50 mL of methanol was added and a green solid precipitated out of solution and was worked up as for **11**, yielding a dark green solid. Yield: 15%

© 2006 NRC Canada

(0.039 g); mp >300 °C. TLC (hexane – ethyl acetate, 15:1): R_f 0.52. UV–vis (dichloromethane) λ_{max} (log ε) (nm): 752 (4.91), 672 (4.12), 364 (4.19). ^{1}H NMR ($CDCl_3$) δ: 3.49 (br s, 32H, OCH_2), 2.00 (m, 48H, bridgehead C-H), 1.70–1.90 (m, 192H, CH_2). MALDI-MS *m/z* (rel. intensity): 3160 $[M]^+$ (49), 3011 $[M - C_{11}H_{17}]^+$ (57), 2862 [M – 2(C11H17)]$^+$ (100), 2713 $[M - 3(C_{11}H_{17})]^+$ (96). Anal. calcd. for $C_{208}H_{272}O_{16}N_8Mg$: C 78.94, H 8.66, N 3.54; found: C 78.50, H 8.47, N, 3.28.

Synthesis of magnesium 1,2,3,4,8,9,10,11,15,16,17,18, 22,23,24,25-hexadeca-(1-adamantaneethoxy)phthalocyanine (15)

4-Methoxyphenylmagnesium bromide (2 mL, 0.5 mol/L in THF) was added to 3 mL of 1-octanol and the mixture was stirred for 0.5 h under argon at room temperature. To this was added 3,4,5,6-tetra-(1-adamantylethoxy)phthalonitrile (**10**, 0.250 g, 0.30 mmol) and the mixture was heated under argon to 120 °C. Upon heating, the clear, colourless mixture turned green. After heating for 24 h, 50 mL of methanol was added and a green solid precipitated out of solution. The solid was collected by centrifugation and was washed with water and methanol. The crude product was then passed through a flash silica gel column eluting with hexane – ethyl acetate (9:1). The first fraction was collected and the solvent was removed under reduced pressure, yielding a dark green solid. Yield: 20% (0.051 g); mp >300 °C. TLC (hexane – ethyl acetate, 15:1): R_f 0.49. UV–vis (dichloromethane) λ_{max} (log ε) (nm): 744 (4.93), 668 (4.09), 328 (4.10). ^{1}H NMR ($CDCl_3$) δ: 4.27 (t, 16H, J = 9.0 Hz, OCH_2), 4.16 (t, 16H, J = 9.0 Hz, OCH_2), 1.99 (br s, 48H, bridgehead C-*H*), 1.76 (m, 96H, CH_2), 1.61 (m, 128H, OCH_2OCH_2- and CH_2). MALDI-MS *m/z* (rel. intensity): 3384 $[M]^+$ (68), 3221 $[M - C_{12}H_{19}]^+$ (71), 3058 $[M - 2(C_{12}H_{19})]^+$ (95), 2895 $[M - 3(C_{12}H_{19})]^+$ (89), 2732 $[M - 4(C_{12}H_{19})]^+$ (83), 2569 $[M - 5(C_{12}H_{19})]^+$ (83), 2406 $[M - 6(C_{12}H_{19})]^+$ (100). Anal. calcd. for $C_{224}H_{304}O_{16}N_8Mg$: C 79.38, H 9.04, N 3.31; found: C 78.77, H 9.41, N 3.78

Synthesis of metal-free 2,3,9,10,16,17,23,24-octa-(1-adamantyloxy)-1,4,8,11,15,18,22,25-octafluorophthalocyanine (16)

Magnesium 2,3,9,10,16,17,23,24-octa-(1-adamantyloxy)-1,4,8,11,15,18,22,25-octafluorophthalocyanine (**11**, 0.502 g, 0.27 mmol) was dissolved in glacial acetic acid (5 mL) and the mixture was refluxed under air. After 4 days, the crude product was precipitated out of solution following the addition of absolute ethanol (50 mL). The dark green precipitate was washed with ethanol (2 × 30 mL) and methanol (1 × 30 mL). The crude product was purified by flash silica gel column chromatography using hexane – ethyl acetate (4:1) as eluant. The first fraction was collected and the solvent was removed under reduced pressure. Yield: 11% (55 mg); mp >300 °C. TLC (hexane – ethyl acetate, 4:1): R_f 0.80. UV–vis (dichloromethane) λ_{max} (log ε) (nm): 734 (4.02), 704 (4.01), 670 (3.51), 636 (3.40), 358 (3.63). ^{1}H NMR ($CDCl_3$) δ: 2.25 (m, 24H, bridgehead C-H), 1.52–1.98 (m, 96H, CH_2). ^{19}F ($CDCl_3$) δ: –119.2. IR (KBr, cm^{-1}) ν: 3275, 2915, 2853, 1732, 1653, 1456, 1300, 1281, 1048, 967. MALDI-MS *m/z* (rel. intensity): 1858 $[M]^+$ (28), 1723 $[M - C_{10}H_{15}]^+$ (51), 1588 $[M - 2(C_{10}H_{15})]^+$ (87), 1453 $[M - 3(C_{10}H_{15})]^+$ (100). Anal. calcd. for $C_{112}H_{122}O_8N_8F_8$: C 72.31, H 6.61, N 6.02; found: C 71.90, H 6.75, N 5.96.

Synthesis of nickel 2,3,9,10,16,17,23,24-octa-(1-adamantyloxy)-1,4,8,11,15,18,22,25-octafluorophthalocyanine (17)

4,5-Di-(1-adamantyloxy)-3,6-difluorophthalonitrile (**6**, 0.306 g, 0.65 mmol) and nickel(II) chloride (90 mg, 0.7 mmol) were added to 4 mL of *N*,*N*-dimethylaminoethanol (DMEA). The mixture was heated to 145 °C and stirred under argon. After stirring for 24 h, a green solid was precipitated following the addition of 40 mL of water. The precipitate was collected by centrifugation. The crude product was purified by flash silica gel column chromatography with hexane – ethyl acetate (4:1) as eluant. The first fraction was collected and the solvent was removed under reduced pressure. Yield: 24% (0.076 g); mp >300 °C. TLC (hexane – ethyl acetate, 2:1): R_f 0.81. UV–vis (dichloromethane) λ_{max} (log ε) (nm): 708 (4.91), 636 (4.23), 342 (4.34), 304 (4.47). ^{1}H NMR ($CDCl_3$) δ: 2.41 (br s, 24H, bridgehead C-H), 2.36 (br m, 48H, CH_2), 1.74 (m, 48H, CH_2). ^{19}F NMR ($CDCl_3$) δ: –126.1. MALDI-MS *m/z* (rel. intensity): 1914 $[M]^+$ (10), 1779 $[M - C_{10}H_{15}]^+$ (23), 1644 $[M - 2(C_{10}H_{15})]^+$ (42), 1509 $[M - 2(C_{10}H_{15})]^+$ (67), 1374 $[M - 4(C_{10}H_{15})]^+$ (91). Anal. calcd. for $C_{112}H_{120}O_8N_8F_8Ni$: C 70.18, H 6.31, N 5.85; found: C 69.91, H 6.78, N 5.74.

Synthesis of nickel 1,2,3,4,8,9,10,11,15,16,17,18, 22,23,24,25-hexadeca-(1-adamantylmethoxy)phthalocyanine (18)

3,4,5,6-Tetra-(1-adamantylmethoxy)phthalonitrile (**9**, 0.202 g, 0.26 mmol) and nickel(II) chloride (36 mg, 0.28 mmol) were added to 4 mL of DMEA. The mixture was heated to 145 °C and allowed to stir under argon. After stirring for 24 h, a green solid was precipitated following the addition of 40 mL of water and was worked up as for **17**. Yield: 14% (29 mg); mp >300 °C. TLC (hexane – ethyl acetate, 9:1): R_f 0.71. UV–vis (dichloromethane) λ_{max} (log ε) (nm): 750 (4.93), 672 (4.43), 386 (4.55), 314 (4.77). ^{1}H NMR ($CDCl_3$) δ: 4.21 (br m, 32H, OCH_2), 2.10 (br m, 24H, bridgehead CH), 1.98 (br m, 24H, bridgehead CH), 1.61–1.88 (m, 192H, CH_2). MALDI-MS *m/z* (rel. intensity): 3214 $[M + H_2O]^+$ (38), 3065 $[M + H_2O - C_{11}H_{17}]^+$ (52), 2916 $[M + H_2O - 2(C_{11}H_{17})]^+$ (53), 2769 $[M + H_2O - 3(C_{11}H_{17})]^+$ (94). Anal. calcd. for $C_{208}H_{272}O_{16}N_8Ni$: C 77.65, H 8.58, N 3.48; found: C 77.48, H 9.03 N, 3.61.

Synthesis of nickel 1,2,3,4,8,9,10,11,15,16,17,18, 22,23,24,25-hexadeca-(1-adamantaneethoxy)phthalocyanine (19)

3,4,5,6-Tetra-(1-adamantaneethoxy)phthalonitrile (**10**, 0.260 g, 0.31 mmol) and nickel(II) chloride (40 mg, 0.31 mmol) were added to 4 mL of DMEA. The mixture was heated to 145 °C and allowed to stir under argon. After stirring for 24 h, a green solid was precipitated following the addition of 40 mL of water and was worked up as for **17**. Yield: 32% (85 mg); mp >300 °C. TLC (hexane – ethyl acetate, 9:1): R_f 0.73. UV–vis (dichloromethane) λ_{max} (log ε) (nm): 736 (4.85), 660 (4.25), 372 (4.40), 340 (4.48), 312 (4.61). ^{1}H NMR ($CDCl_3$) δ: 4.78 (t, 16H, J = 7.1 Hz, OCH_2CH_2), 4.53 (t, 16H, J = 7.1 Hz, OCH_2CH_2), 2.12 (t, 16H, J = 7.1 Hz,

© 2006 NRC Canada

OCH_2CH_2), 2.05 (two br m, 48H, bridgehead CH), 1.94 (t, 16H, J = 7.1 Hz, OCH_2CH_2), 1.62–1.85 (m, 192H, adamantyl-CH_2). MALDI-MS m/z (rel. intensity): 3418 $[M + H]^+$ (83), 3256 $[M + H - C_{12}H_{19}]^+$ (72), 3094 $[M + H - 2(C_{12}H_{19})]^+$ (100), 2930 $[M + H - 3(C_{12}H_{19})]^+$ (85). Anal. calcd. for $C_{224}H_{304}O_{16}N_8Ni$: C 78.59, H 8.95, N 3.27; found: C 78.07, H 9.29, N 3.64.

Conclusions

Phthalocyanines bearing large bulky substituents have previously shown interesting physicochemical properties, including a red shifting of the Q band. A series of metallated and nonmetallated Pcs have been synthesized incorporating large bulky substituents based upon analogs of adamantane. These complexes exhibit interesting characteristics, notably pronounced red shifting of the Q band.

Acknowledgement

We thank the Natural Sciences and Engineering Research Council of Canada (NSERC) for grants in support of this research.

References

1. F.H. Moser and A.L. Thomas. *In* Phthalocyanine compounds. Reinhold, New York. 1963.
2. C.C. Leznoff and A.B.P. Lever. *In* Phthalocyanines: properties and applications. Vols. 1–4. Wiley-VCH, New York. 1989–1996.
3. C. Peichocki, J. Simon, A. Skoulious, D. Guillon, and P. Weber. J. Am. Chem. Soc. **104**, 5254 (1982).
4. J.S. Shirk, R.G.F. Pong, H. Heckmann, and M. Hanack. J. Phys. Chem. A, **104**, 1438 (2000).
5. I. Rosenthal and E. Ben-Hur. *In* Phthalocyanines: Properties and applications. Vol. 1. *Edited by* C.C. Leznoff and A.B.P. Lever. Wiley-VCH, New York. 1989.
6. A.B.P. Lever and C.C. Leznoff. US prov. Patent Appl. 60/474 301, 30 May 2003; A.B.P. Lever and C.C. Leznoff. PCT/CA2004/000808 (WO2004/106436 A1).
7. C.C. Leznoff, S. Black, A. Hiebert, P.W. Causey, D. Christendat, and A.B.P Lever. Inorg. Chim. Acta, **359**, 2690 (2006).
8. P.M. Burnham, M.J. Cook, L.A. Gerrard, M.J. Heeney, and D.L. Hughes. Chem Commun. (Cambridge), 2064 (2003).
9. T. Fukuda, K. Ono, S. Homma, and N. Kobayashi. Chem. Lett. **32**, 736 (2003); T. Fukuda, T. Ishigura, and N. Kobayashi. Tetrahedron Lett. **46**, 2970 (2005).
10. N. Kobayashi. *In* Phthalocyanines: Properties and applications. Vol 2. *Edited by* C.C. Leznoff and A.B.P. Lever. Wiley-VCH, New York. 1992.
11. A.K. Sobbi, D. Wohrle, and D. Schlettwein. J. Chem. Soc. Perkin Trans. 2, 481 (1993).
12. P.J. Duggan and P.F. Gordon. Eur. Patent Appl. EP 155780, 1985.
13. M.J. Cook, A.J. Dunn, S.D. Howe, and A.J. Thomson. J. Chem. Soc. Perkin Trans. 1, 2453 (1998).
14. W. Eberhardt and M. Hanack. Synthesis, 95 (1997).
15. L.V. Gubareva, L. Kaiser, F.G. Hayden. Lancet, **335**, 827 (2000).
16. S.M. Antonov, J.W. Johnson, N.Y. Lukomskaya, N.N. Potapyeva, V.E. Gmiro, and L.G. Magazanik. Mol. Pharmacol. **47**, 559 (1995).
17. J.J. Wang, Y.C. Chen, C.W. Chi, K.T. Huang, and Y.T. Chern. Anti-Cancer Drugs, **15**, 697 (2004).
18. C.C. Leznoff and J.L. Sosa-Sanchez. Chem. Commun. (Cambridge), 338 (2004).
19. N. Bhardwaj, J. Andraos, and C.C. Leznoff. Can. J. Chem. **80**, 141 (2002).

© 2006 NRC Canada

Synthesis and Lewis acid induced isomerization of mono-, di-, and tri-spiro α-keto tetrahydro-furans and -pyrans[1]

David G. Hilmey, Peter R. Selvaraj, and Leo A. Paquette

Abstract: The stereoselectivity of the acid-catalyzed ring expansion of dihydrofuranyl and dihydropyranyl 1,2-adducts to spirocyclic ketones 8 and **9** has been examined. These substrates have become readily available by the utilization of 1,3-dichloroacetone as a synthetic equivalent of cyclopropanone. The kinetically controlled isomerizations result in ring expansion to dispirocyclopentanones. Third-stage conversion to trispirocyclohexanones was shown to be possible in select examples. On a different front, the syn and anti pairs proved capable of interconversion by heating in the presence of boron trifluoride etherate. A push–pull fragmentation of the ketone ring is proposed to account for these epimerizations. Calculations have been performed to simulate transition state energies in the oxonium ion intermediates and to gain some idea of the preferred ground-state geometries of the final products.

Key words: oxonium ion rearrangements, ring expansions, acid-catalyzed epimerizations, cyclopropanone equivalent, spirocyclic ethers.

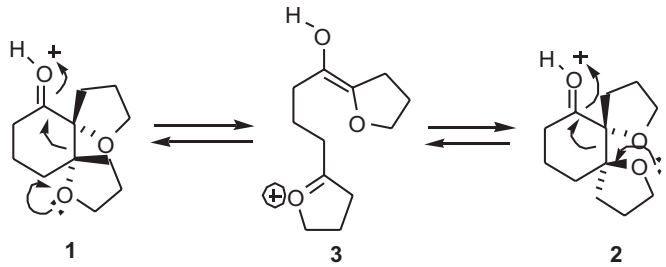
Résumé : On a étudié la stéréosélectivité de l'expansion de cycle acidocatalysée de 1,2-adduits dihydrofuranyles et dihydropyranyles en cétones spirocycliques **8** et **9**. Ces substrats sont facilement disponibles à partir de la 1,3-dichloroacétone utilisée comme équivalent de synthèse de la cyclopropanone. Les isomérisations sous contrôle cinétique conduisent à une expansion de cycle qui fournit des dispirocyclopentanones. On a démontré la possibilité de réaliser le troisième stade de conversion en trispirocyclopentanones en utilisant des exemples choisis. On a par ailleurs démontré que les paires syn et anti peuvent subir des interconversions par chauffage en présence d'éthérate de trifluorure de bore. On propose une fragmentation de type « push–pull » du cycle cétonique pour expliquer ces épimérisations. Des calculs ont été effectués pour simuler les énergies de l'état de transition dans les ions oxonium intermédiaires et pour mieux comprendre les géométries de l'état fondamental privilégié des produits finaux.

Mots clés : réarrangement d'ion oxonium, expansion de cycle, épimérisation acidocatalysée, équivalent de cyclopropanone, éthers spirocycliques.

[Traduit par la Rédaction]

Introduction

The feasibility of inducing epimerization in molecules constructed of two neighbouring quaternary carbon centers is seldom encountered. One way to drive this process is to suitably position a heteroatom such as an ether oxygen or a divalent sulfur β to a carbonyl group (1, 2). This structural arrangement allows for the operation under acidic conditions of a push–pull fragmentation of the cycloalkanone, with subsequent reconstitution of the original but now stereochemically scrambled substrate (3). The interconversion of **1** with **2** via **3** is illustrative of the process. Since **1** and **2** are chiral and amenable to resolution while **3** is not, the cyclization of this tethered oxonium ion – enol intermediate results in racemization as has been observed experimentally (3). Rotation of either terminus of the chain relative to the other prior to ring closure provides the enabling means for losing stereochemical "memory".



1 3 2

Studies involving such molecular frameworks have previously been limited to di- and tri-spirocyclic cyclohexanone systems because of synthetic constraints. To explore a more representative array of congeners, it became imperative that cyclopropanone replace cyclobutanone as the key building

Received 1 September 2005. Accepted 4 December 2005. Published on the NRC Research Press Web site at http://canjchem.nrc.ca on 29 September 2006.

This paper is dedicated with respect and admiration to Alfred Bader who has been so instrumental in fostering with his entrepreneurship the enormous growth of our discipline.

D.G. Hilmey, P.R. Selvaraj, and L.A. Paquette.[2] Evans Chemical Laboratories, The Ohio State University, Columbus, OH 43210, USA.

[1]This article is part of a Special Issue dedicated to Dr. Alfred Bader.

[2]Corresponding author (e-mail: paquette.1@osu.edu).

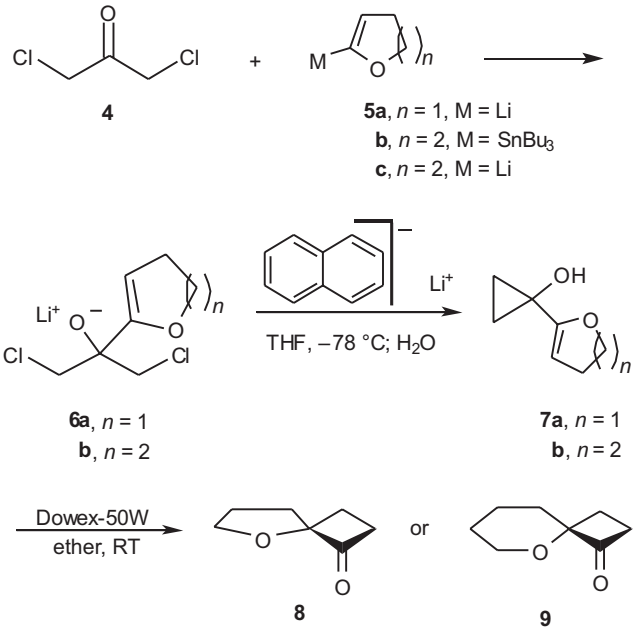
 doi:10.1139/V06-103 © 2006 NRC Canada

block. However, the highly reactive nature of this compound does not lend itself to being accessible in preparative quantities in a standard laboratory setting (4, 5). Most often, recourse has been made to release of the three-membered cyclic ketone from its ethyl hemiketal (6), 1-acetoxycyclopropanol (7), or a select carbinolamine (8). None of these alternatives was considered to be particularly desirable in the present context.

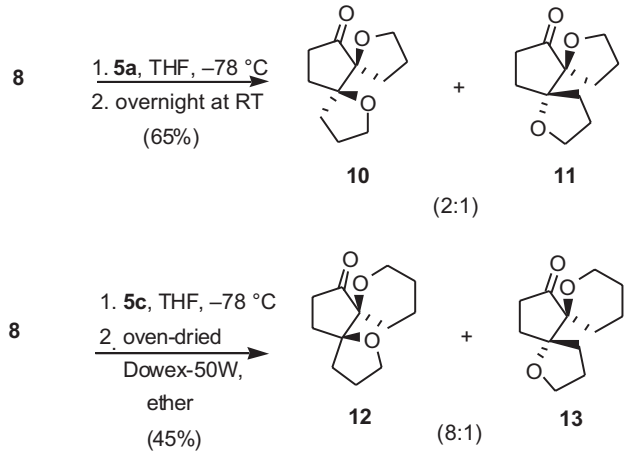
A more promising alternative originated from reports that appeared several decades ago indicating that 1,3-dichloroacetone **4** (Scheme 1) undergoes a straightforward 1,2-addition in the presence of Grignard reagents. Subsequent exposure of these adducts to ethylmagnesium bromide and iron(III) chloride then furnished 1-substituted cyclopropanols (9, 10). At a later date, Barluenga et al. (11) discovered that the initial Grignard adducts are amenable to reductive cyclization when admixed with $MgBr_2$ and lithium powder, or more conveniently with lithium naphthalenide in THF. We have come to favour the latter approach to reactive three-membered carbinols and detail here the advantages that materialize when this chemistry precedes application of the oxonium ion initiated pinacolic ring expansion (12). The use of 1,3-dichloroacetone in this manner offers an experimentally simple and versatile means for varying not only the dimensions of the central ring, but the number of spirocycles attached thereto as well as their individual size (13).

Also addressed herein is the extent to which the end products are subject to solution-phase epimerization in the presence of boron trifluoride etherate. MM3 calculations have also been performed to gauge the relative stabilities of the isomer pairs in the gas phase, and in combination with AM1 semiempirical calculations, the thermodynamically preferred geometry of the putative oxonium ion intermediates.

Scheme 1.



Scheme 2.



Synthetic efforts

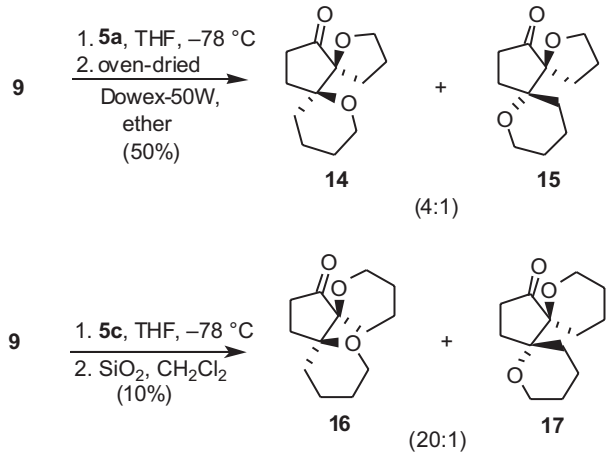
The deprotonation of 2,3-dihydrofuran with *tert*-butyllithium (14) proceeds efficiently to produce **5a** whose condensation with **4** gives rise to alkoxide **6a** (Scheme 1). Direct reductive dechlorination of **6a** with a solution of lithium naphthalenide in THF at –78 to 20 °C promoted conversion to cyclopropanol **7a** after workup. Overnight stirring of **7a** with a small quantity of Dowex-50W resin at room temperature resulted in smooth isomerization to the volatile spiro ketone **8**, which was isolated in 65% overall yield from **4**. When comparable direct use was made of 3,4-dihydropyran as the anticipated precursor to organometallic **5c**, a diverse array of products was formed in low yield following exposure to **4**. This situation was remedied by effecting transmetalation instead via stannane **5b** (15). This alternative means for the generation of **5c** and its further processing as in Scheme 1 furnished **9** with an overall efficiency of 75%.

In the case of **8**, second-stage coupling to **5a** led to a diastereomeric mixture of two tertiary carbinols intended to serve as precursors to **10** and **11** (Scheme 2). Fortunately, the pinacol rearrangement of these adducts occurred spontaneously on standing in neat condition at room temperature. Attempts to bring about this isomerization with acid promoters under more customary conditions (3, 16) resulted instead in hydrolysis of the enol ether functionality. Consequently, cyclopentanones **10** and **11** were formed as a chromatographically separable 2:1 mixture in a single laboratory manipulation (65%). The second example, involving the combination of **5c** with **8**, produced carbinols that proved amenable to ring expansion in the presence of oven-dried Dowex-50W resin. The dominance of the more polar syn isomer **12** by the margin of 8:1 is noteworthy.

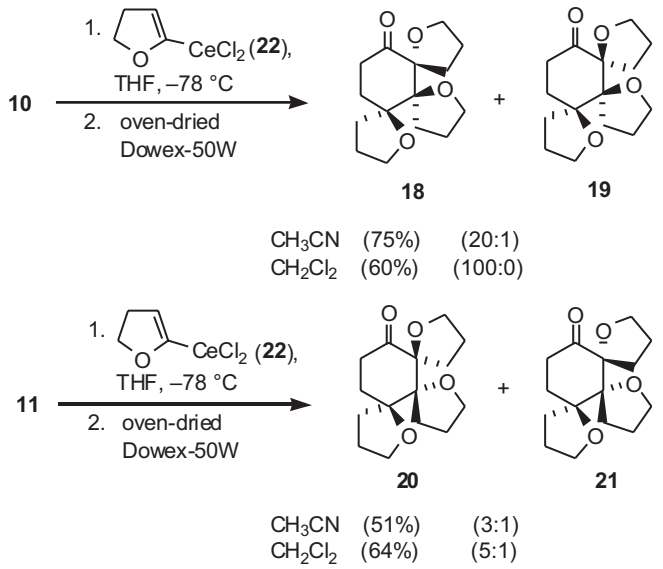
Our attention was next directed to the acquisition of analogs characterized by the presence of a spirotetrahydropyranyl unit β to the ketone carbonyl. The response of **9** to the action of **5a** and subsequent ring expansion proceeded in a manner closely comparable to the precedent set by **8**. Once again, the syn isomer **14** was more prevalent in the product mixture than **15** (4:1, Scheme 3). A striking difference in behaviour was encountered following preparation of the tertiary carbinol from 1,2-addition of **5c** to **9**. In contrast to its congeners, this intermediate proved to be unusually sensitive to the presence of Dowex-50W. When the targeted ring enlargement could not be brought about in this manner, other promoters were sought and silica gel slurried in CH_2Cl_2

© 2006 NRC Canada

Scheme 3.



Scheme 4.



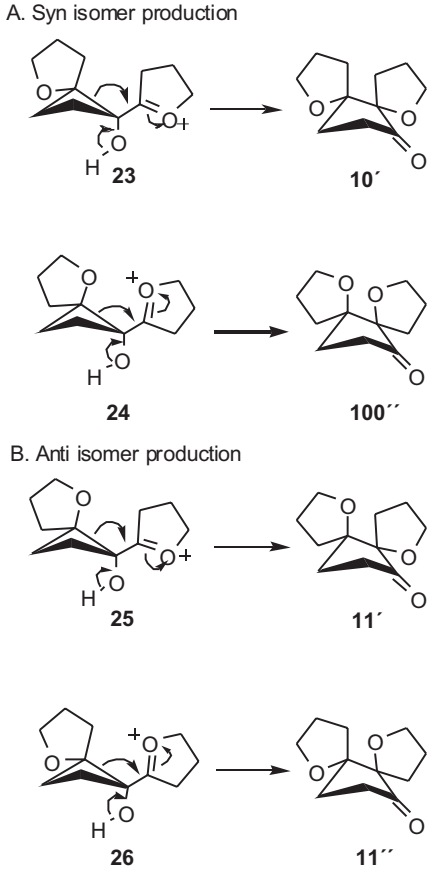
proved to be workable. With this catalyst, isomerization proceeded slowly. After 3 days, a mixture of **16** and **17** richer in the syn isomer was generated and chromatographically separated. The diminished efficiencies of the ring expansions involving **9** are a likely reflection of enhanced steric congestion in the vicinity of the reaction centers. The stereochemical assignments to all of the di- and tri-spiro ketones have been documented elsewhere (13), based on distinctive ^{1}H NMR spectral features and polarity considerations.

Compounds **10** and **11** proved amenable to a third-stage enhancement of the core ring size to the cyclohexanone level provided that the cerate reagent **22** was used to curtail the significant tendency of these cyclopentanones to experience competitive enolization (17, 18). Two important issues emerge from the data compiled in Scheme 4. The more obvious finding is the preference exhibited for introducing the third spirotetrahydrofuran anti to that positioned at the adjacent β-carbon. For **20** and **21**, the stereoselectivity gap is modest (3–5:1) and of comparable magnitude in the two solvents. Where **18** and **19** are concerned, the bias for producing **18** is quite substantial and is particularly dominant when the reaction is performed in CH_2Cl_2. Under the latter conditions, no **19** was observed. In these examples, the trispiro product ratios are reversed relative to those witnessed for the dispiro analogs such as **10/11**, **12/13**, **14/15**, and the like. We also call attention to the brevity with which **18**–**21** can be prepared from 1,3-dichoroacetone, thus doing away with issues surrounding their availability.

Stereoselectivity considerations

In line with ample precedent, the migratory aptitudes associated with 1,2-shifting to the oxonium ion center strongly favour translocation of the more electron-rich neighbouring carbon atom (1, 12, 19, 20). The end result is therefore a preferred migration of that adjacent carbon atom, which is the more highly alkylated. The only restriction is the requirement that the migrating bond be capable of being properly aligned with the pπ orbital, resident at the electrophilic center. In the present examples, the degrees of freedom are such that two modes of structural staging are possible for each product isomer. The conformational facets of the conversion of **8** to **10** and **11** are exemplified in Scheme 5. At issue is the diastereoselectivity of oxonium ion capture, a

Scheme 5.

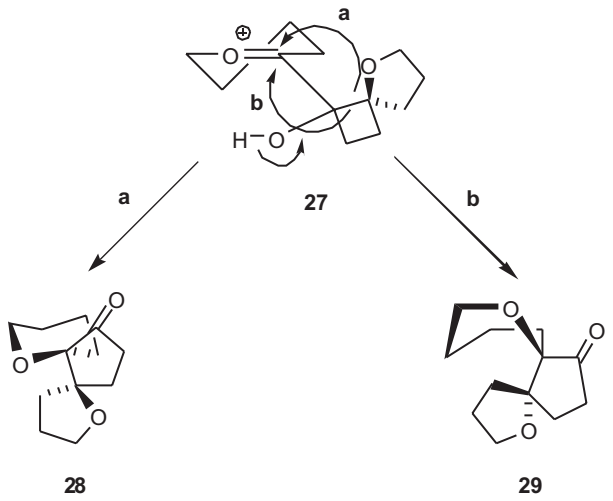


phenomenon that holds considerable fascination (21). One sees that **23** and **24** are capable of arriving at **10′** and **10″**, while **25** and **26** lead instead to **11′** and **11″**, respectively. The possibility exists, of course, that the relative magnitude and direction of stereoselectivity is founded only on steric grounds, an analysis made acceptable by the kinetically irreversible nature of the conversion to products. In this con-

© 2006 NRC Canada

nection, it is perhaps insignificant that the ratio of diastereomeric tertiary carbinols (e.g., the precursors to **23/26** and **24/25**) is not known with precision. The key outcome is the favoured proximal placement of the methylene groups, as in **10′**, or of the ether oxygen atoms, as in **10″**, relative to the pair of alternatives **11′** and **11″** where nonbonded CH_2–O interaction develops.

The change from a flexible envelope arrangement having pseudorotational capability as in tetrahydrofurans to a well-defined axial–equatorial status in tetrahydropyrans, because of the adoption of chairlike arrangements, is a dramatic one. As a result, the diastereoselectivity associated with migrations involving six-membered oxonium ions can be projected to be more pronounced. Thus, the conversion of **27** to **28** should occur more readily and its formation not deterred as in **29** because of the development of boatlike features.

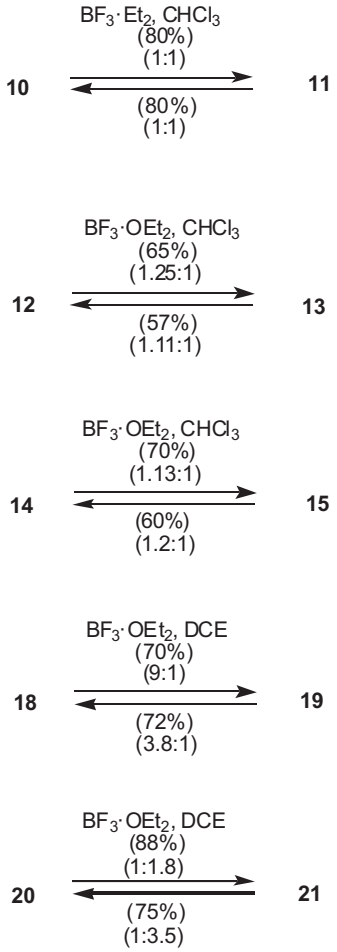


Calculations show that the oxonium functionality preferentially orients its oxygen antiperiplanar to the hydroxyl substituent (22) , as seen in **24**. This conformer will then rearrange to syn isomer **10″**, which would explain, in part, the overall preference for more prevalent formation of dispirocyclopentanones **10**, **12**, **14**, and **16**. On the other hand, the enhanced ability of the oxonium intermediate derived from the chelation-controlled adduct of **10** to adopt a synperiplanar relationship with the hydroxyl group explains the preferences for the formation of **18**. Relevantly, when the addition to **10** is nonchelation-controlled, the preferred conformation of the oxonium unit reverts back to antiperiplanar with respect to the hydroxyl, again giving **18** after ring expansion. These conformational preferences, regardless of the facial selectivity of the addition process, concisely account for the very high selectivity noted in the formation of **18** over **19**.

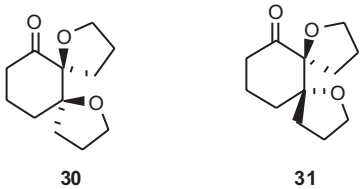
Lewis acid induced isomerizations

On an allied front, the ability of the various syn–anti isomer pairs to interconvert when heated in the presence of boron trifluoride etherate has been examined. An important distinction to be made regarding isomerizations of the type **1** ⇄ **2** is that kinetic control is not operative. All of the ketones prepared in the course of this investigation were treated in a comparable manner involving either chloroform or 1,2-dichloroethane as solvent. The results are compiled in Table 1. Chlorinated solvents proved most well-suited to these processes, with interconversion being optimal in the indicated medium. Except perhaps for the **10** ⇄ **11** example, complete equilibration was not reached for the majority of the isomerizations. Higher temperatures and longer reaction times only enhanced the extent of the accompanying decomposition. Under no circumstances did **16** and **17** interconvert.

Table 1. BF_3·OEt_2-induced equilibrations.

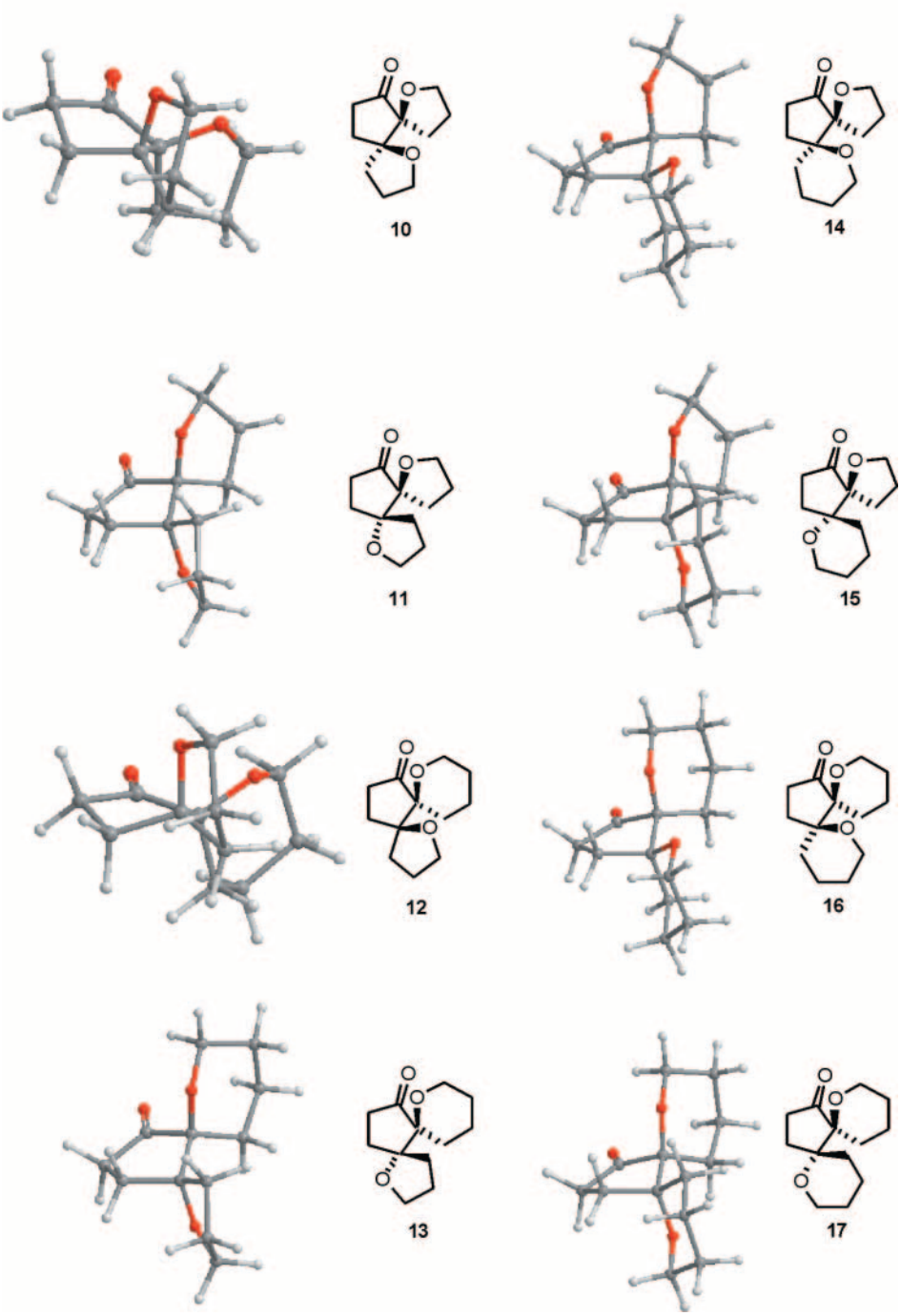


Molecular mechanics (MM3) calculations were performed on seven sets of isomers, including the **30/31** pair for the sake of completeness. The conformational searching was performed with recourse to the Monto Carlo simulation capability in MacroModel version 5.0 (23). A minimum of 1000 simulations were determined per structure and involved operations featuring one bond closure (1.0–3.0 Å) in all rings. The minimum energy diagrams were visualized with Chem 3D Ultra (24).



© 2006 NRC Canada

Fig. 1. Perspective drawings of the minimal energy conformations of **10**–**31**. Note that the representations for **18**–**21** are enantiomeric to those depicted in the text.



A conformational model of the lowest energy conformation of each of the 14 structures is illustrated in Fig. 1, and the associated steric energy values are compiled in Table 2. These data reveal the cyclopentanone systems **10**–**17** to have rather similar strain energy differences ranging from 2.6–2.8 kcal/mol (1 cal = 4.184 J). These values indicate the anti isomers to be thermodynamically advantaged to the extent of 95:5 at RT. For the cyclohexanone systems, the energy differences between pairs is considerably smaller (ca. 1 kcal/mol), thus reducing the energy gaps to a factor of only three- to six-fold. In addition, the **20/21** pair alone exhibits greater stability for its syn diastereomer.

Whereas **11** has both of its heteroatoms oriented pseudoaxially, isomer **10** projects its α C—O bond in a pseudoequatorial fashion. The latter preference persists when the α-spirocycle is expanded to the tetrahydropyranyl level as seen in **12**. We conclude that the [4.4] and [4.5] dispiro systems, including **14/15** and **16/17**, have lower energy when the capability exists to orient the α- and β-heteroatoms pseudoaxially. In the mixed systems, the

© 2006 NRC Canada

Fig. 1 (*concluded*).

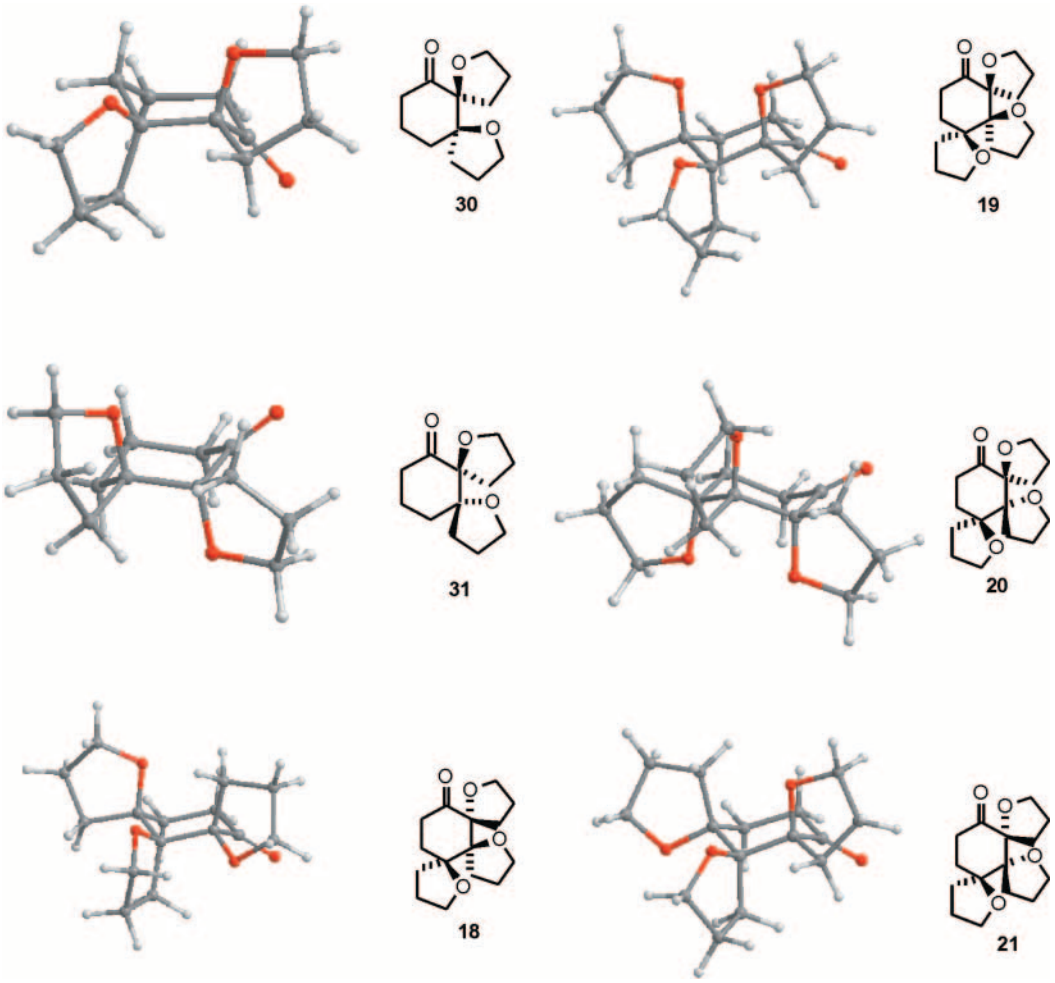


Table 2. MM3-derived steric energies.

Compound	E_{steric} (kcal/mol)	ΔE (kcal/mol)
10	57.5	
11	54.8	–2.7
12	52.1	
13	49.3	–2.8
14	46.7	
15	44.1	–2.6
16	51.9	
17	49.3	–2.6
30	52.6	
31	51.9	–0.7
19	74.1	
18	72.9	–1.2
21	72.8	
20	73.8	+1.0

Note: The syn isomer is cited first.

tetrahydropyranyl ring, whether situated α or β to the ketone as in **12** and **14**, likewise prefers to adopt a pseudoaxial orientation placing the tetrahydrofuranyl ring in a seemingly less favourable equatorial position. This conformational dominance by the six-membered heteroring is noteworthy.

The anti isomer of the **30/31** pair is modestly lower in energy (0.7 kcal/mol). This small but significant difference can be traced back to the axial character of the C—O bonds that is adopted twice in **31** and only once in **30**. Finally, in the remaining cyclohexanones **18**–**21**, the spiroannulated tetrahydrofuran rings orient themselves in a fashion opposite to that reflected in the cyclopentanone systems. In these trispirocyclic examples, increased equatorial placement of the C—O bonds serves to lower the level of steric strain in the system, as noted in other contexts (25–27).

At the experimental level, the acid-catalyzed equilibrations of pure samples of **10**–**14** gave rise to product mixtures approximating 1:1. In light of the energy differences determined in the gas phase for these syn–anti isomer pairs, these distributions appear not to be controlled by ground state energetics. We can hypothesize, though, that the final distribution is influenced by solvent effects and more strongly by coordination with the one equivalent of $BF_3{\cdot}OEt_2$. This latter association is likely leveling the energetic differences seen between syn and anti isomers, either through altered conformation or steric and electronic factors. On the other hand, the epimerizations have proven quite utilitarian as a means for funneling one stereoisomer into another. The initial experiments, which were performed with catalytic levels of $BF_3{\cdot}OEt_2$, fared poorly. Subsequently, the use of catalytic

© 2006 NRC Canada

quantities was abandoned in favor of a full equivalent of Lewis acid, despite the possibility that such high levels of promoter could play a role in leveling the relative amounts of isomers in each subset.

For **18**–**21**, it proved possible to make use of 0.3 equiv. of catalyst. This reduced loading resulted in the generation of isomer ratios more reflective of the theoretical equilibrium values. The discrepancies that remain might stem from the tight binding of boron trifluoride to one-third of the respective starting cyclohexanone.

In conclusion, the isomerization of **10**–**15** with stoichiometric amounts of Lewis acid does not adhere to thermodynamic control largely through acid coordination and solvent effects. Ketones **18**–**21** perform better at approaching equilibrium, although very slowly, while **16** and **17** are unresponsive to these conditions. The energetic preference is biased in favour of the anti relationship of the C—O bonds with one exception. The THF and THP spirocycles favour axial oxygen orientations in the dispiro examples regardless of ring size, while an equatorial preference is seen in the trispirocycles.

Experimental

1-Oxaspiro[3.4]octan-6-one (8)

Dry tetrahydrofuran (100 mL) and freshly distilled 2,3-dihydrofuran (7.15 mL, 94.5 mmol) were placed in a 500 mL flame-dried flask, purged with N_2, and cooled to –78 °C. After 15 min, *tert*-butyllithium (55.6 mL of 1.7 mol/L in pentane, 94.5 mmol) was introduced via cannula. After 30 min, the solution was brought to 0 °C (ice bath) and after an additional 30 min introduced into a solution of 1,3-dichloroacetone (10.0 g, 78.8 mmol) in anhydrous ether (200 mL) at –78 °C. The yellow reaction mixture was stirred in the cold for 2 h before a solution of lithium naphthalenide (197 mL of 1 mol/L in THF) was added via cannula. After 4 h, the green solution was allowed to warm to rt and then cooled to 0 °C before being quenched with sat. $NaHCO_3$ solution. The separated aqueous phase was extracted with ether (3 × 150 mL) and the combined organic phases were dried and filtered. The filtrate was admixed with Dowex-50W resin (8 g), stirred overnight, and filtered again. The solvent was removed by bulb-to-bulb distillation to a volume of about 150 mL, followed by rotatory evaporation (no heat) until a solid–oil mixture was seen. Addition of toluene (25 mL), column chromatography on silica gel (elution with 5%–20% ether in petroleum ether), and subsequent fractional distillation to remove solvent afforded **8** as a pale yellow oil (6.4 g, 65%). IR (neat, cm^{-1}): 1790, 1058. ^1H NMR (300 MHz, $CDCl_3$) δ: 3.93 (t, J = 6.6 Hz, 2H), 2.79–2.70 (m, 2H), 2.22–2.05 (m, 3H), 2.02–1.90 (m, 3H). ^{13}C NMR (75 MHz, $CDCl_3$) δ: 211.7, 96.8, 70.1, 39.7, 33.8, 26.6, 25.6. EI-MS m/z calcd.: 144.07 [$M^+ - H_2O$]; found: 144.05. Anal. calcd. for $C_7H_{10}O_2$: C 66.64, H 7.99; found: C 66.52, H 8.23.

1-Oxaspiro[3.5]nonan-7-one (9)

A solution of **5b** (14.93 g, 40.0 mmol) in dry THF (150 mL) was blanketed with N_2, cooled to –78 °C, and treated dropwise with *n*-butyllithium (29.2 mL of 1.3 mol/L in pentane, 0.038 mol). Upon completion of the addition, the reaction mixture was stirred in the cold for 30 min prior to being added to a solution of 1,3-dichloroacetone (5.08 g, 0.040 mol) in dry THF (100 mL) at –78 °C. After 1 h at this temperature, a solution of lithium naphthalenide (from lithium (0.69 g, 0.10 mol) and naphthalene (19.22 g, 0.15 mol)) in THF (200 mL) was added. The reaction mixture was maintained at –78 °C for 2 h, quenched with water, diluted with petroleum ether (200 mL), and extracted with ether (3 × 300 mL). The organic extracts were washed with brine, treated with Dowex-50W (3 g), and stirred for 3 h. The resin was separated by filtration, the solvent removed by bulb-to-bulb distillation, and the residue purified by chromatography on silica gel (elution with 4:1 petroleum ether – ether) to furnish 4.0 g (75%) of **9** as a colourless, volatile oil. IR (neat, cm^{-1}): 1732, 1464, 1282. ^1H NMR (300 MHz, $CDCl_3$) δ: 4.18–4.10 (m, 1H), 3.65–3.59 (m, 1H), 2.56–2.32 (m, 2H), 1.90–1.80 (m, 1H), 1.44–1.28 (m, 7H). ^{13}C NMR (75 MHz, $CDCl_3$) δ: 208.3, 87.5, 64.9, 39.1, 34.2, 30.1, 29.8, 25.8, 25.4, 20.2. ES-HRMS m/z calcd.: 163.0735 [M + Na]$^+$; found: 163.0735.

Dispirocyclopentanones 10 and 11

A solution of 2,3-dihydrofuran (5.2 mL, 69.0 mmol) in dry THF (75 mL) was cooled to –78 °C under N_2, treated with *tert*-butyllithium (46 mL of 1.5 mol/L in pentane), and stirred for 0.5 h at –78 °C followed by 0.5 h at 0 °C. A solution of **8** (5.8 g, 46.0 mmol) in THF (25 mL) was introduced dropwise at this temperature and the reaction mixture was allowed to warm to rt after 2 h. While being cooled in an ice bath, the mixture was quenched with sat. $NaHCO_3$ solution and diluted with ether. The separated aqueous phase was extracted with ethyl acetate, and the combined organic phases were dried and evaporated. After 2 days, chromatography on silica gel (elution with 25%–50% ethyl acetate in hexanes) afforded 4.17 g of the polar **10** and 2.0 g of **11**, both as colourless oils.

10

IR (neat, cm^{-1}): 1751, 1078. ^1H NMR (300 MHz, $CDCl_3$) δ: 4.10 (m, 1H), 3.95–3.80 (m, 3H), 2.38 (q, J = 9.7 Hz, 1H), 2.23 (ddd, J = 2.8, 9.3, 19.2 Hz, 1H), 2.10–1.65 (series of m, 10H). ^{13}C NMR (75 MHz, $CDCl_3$) δ: 216.5, 90.7, 88.6, 70.1, 68.4, 32.2, 31.0, 30.4, 29.9, 25.8, 25.3. ES-HRMS m/z calcd.: 219.0992 [M + Na]$^+$; found: 219.0998.

11

IR (neat, cm^{-1}): 1750, 1067. ^1H NMR (300 MHz, $CDCl_3$) δ: 3.95–3.79 (m, 4H), 2.48–2.23 (m, 2H), 2.20–1.80 (series of m, 9H), 1.70–1.61 (m, 1H). ^{13}C NMR (75 MHz, $CDCl_3$) δ: 216.4, 89.7, 88.4, 69.5, 68.5, 33.4, 31.7, 30.8, 27.1, 26.3, 26.1. ES-HRMS m/z [M + Na]$^+$ calcd.: 219.0992; found: 219.0990.

Dispirocyclopentanones 12 and 13

n-Butyllithium (29 mL of 1.54 mol/L, 45 mmol) was added to a solution of **5b** (18.65 g, 50 mmol) in anhydr. THF (100 mL) at –78 °C. After 30 min, the mixture was added to a solution of **8** (5.0 g, 39.7 mmol) in THF (50 mL) and stirring was maintained in the cold for 2 h. Water was slowly added, the products were extracted into ether, and the combined organic layers were washed with brine and dried.

© 2006 NRC Canada

Oven-dried Dowex-50W resin (2 g) was added and ultimately filtered off when isomerization was complete (TLC analysis). The filtrate was evaporated and the residue chromatographed on silica gel (gradient elution with hexanes – ethyl acetate). Ketone **12** eluted with a 2:1 solvent mixture while **13** eluted with a 10:1 solvent system. **12** (3.33 g, 40%) and **13** (0.42 g, 5%) were isolated as colourless oils.

12

IR (neat, cm^{-1}): 1743, 1450. ^1H NMR (300 MHz, $CDCl_3$) δ: 4.33–4.24 (m, 1H), 3.90–3.79 (m, 3H), 2.45–2.32 (m, 1H), 2.22–2.05 (m, 2H), 1.96–1.46 (series of m, 11H). ^{13}C NMR (75 MHz, $CDCl_3$) δ: 216.4, 89.9, 81.4, 68.6, 64.2, 33.5, 30.3, 30.1, 26.2, 25.7, 25.3, 18.6. ES-HRMS *m/z* calcd.: 233.1148 $[M + Na]^+$; found: 233.1148.

13

IR (neat, cm^{-1}): 1741, 1443. ^1H NMR (300 MHz, $CDCl_3$) δ: 3.80–3.56 (m, 4H), 2.30–1.99 (m, 5H), 1.94–1.83 (m, 3H), 1.77–1.61 (m, 3H), 1.54–1.34 (m, 3H). ^{13}C NMR (75 MHz, $CDCl_3$) δ: 215.9, 90.4, 79.8, 68.3, 64.1, 34.1, 31.4, 28.9, 26.1, 25.8, 23.0, 18.3. ES-HRMS *m/z* calcd.: 233.1148 $[M + Na]^+$; found: 233.1158.

Dispirocyclopentanones 14 and 15

A solution of 2,3-dihydrofuran (2.64 mL, 35 mmol) in anhydr. THF (100 mL) was cooled to –78 °C, treated with *tert*-butyllithium (17.6 mL of 1.7 mol/L, 30 mmol), stirred in the cold for 1 h, and allowed to warm to rt for 30 min. The reaction mixture was returned to –78 °C at which point it was added to a solution of **9** (4.0 g, 28.5 mmol) in dry THF (50 mL). Once TLC analysis indicated the ketone to be consumed, water was slowly introduced and the product was extracted into ether (3 × 100 mL). The combined organic layer was washed with brine and dried. Oven-dried Dowex-50W resin (2.5 g) was added to the filtrate. When the reaction was complete (TLC analysis), the resin was filtered off, the filtrate was concentrated, and the residue was chromatographed on silica gel (gradient elution from hexane to ethyl acetate – hexane) to afford **14** (2.40 g, 40%) and **15** (0.59 g, 10%), both as colourless oils.

14

IR (neat, cm^{-1}): 1752, 1448. ^1H NMR (300 MHz, $CDCl_3$) δ: 4.13–3.92 (m, 2H), 3.82–3.77 (dd, *J* = 10.5, 3.5 Hz, 1H), 3.60–3.52 (dt, *J* = 11, 3.0 Hz, 1H), 2.53–2.44 (ddd, *J* = 3.3, 9.0, 10.3 Hz, 1H), 2.33–2.11 (m, 2H), 2.02–1.54 (series of m, 11H). ^{13}C NMR (75 MHz, $CDCl_3$) δ: 216.7, 92.0, 80.3, 70.1, 62.1, 30.8, 29.0, 27.2, 25.5, 25.1, 24.0, 19.2. ES-HRS *m/z* calcd.: 233.1154 $[M + Na]^+$; found: 233.1143.

15

IR (neat, cm^{-1}): 1750, 1446. ^1H NMR (300 MHz, $CDCl_3$) δ: 3.88–3.54 (m, 4H), 2.45–2.11 (m, 3H), 2.04–1.72 (m, 6H), 1.62–1.46 (m, 5H). ^{13}C NMR (75 MHz, $CDCl_3$) δ: 216.1, 89.8, 80.5, 77.5, 77.0, 69.0, 61.6, 32.0, 27.2, 26.5, 26.1, 24.8, 18.9. ES-HRMS *m/z* calcd.: 233.1154 $[M + Na]^+$; found: 233.1156.

Reaction of 5c with 9

n-Butyllithium (20.1 mL of 1.54 mol/L in hexane, 31 mmol) was added to a solution of **5b** (11.94 g, 32 mmol) in anhydr. THF (100 mL) at –78 °C. After being stirred for 30 min, this solution was added to a solution of **9** (2.8 g, 20 mmol) in the same medium (50 mL) and at the same temperature. After the disappearance of **9** (TLC), water was slowly introduced, the products were extracted into ethyl acetate (3 × 200 mL), and the combined organic layers were washed with brine and dried. The residue remaining after solvent evaporation was dissolved in dry CH_2Cl_2 (250 mL). Silica gel (4 g) was added and stirring was maintained at rt for 3 days. After filtration, solvent removal, and chromatographic separation on silica gel (hexane – ethyl acetate, 25–5:1), less polar **17** (20 mg, 0.5%) and more polar **16** (400 mg, 9%) were isolated.

16

Colourless solid, mp 70–72 °C. IR (neat, cm^{-1}): 1745, 1443, 1219. ^1H NMR (300 MHz, C_6D_6) δ: 4.57–4.48 (dt, *J* = 2.8, 11.4 Hz, 1H), 3.83–3.71 (m, 2H), 3.40–3.31 (dt, *J* = 2.7, 8.5 Hz, 1H), 2.29–2.17 (m, 1H), 2.12–2.03 (m, 1H), 1.87–1.76 (m, 2H), 1.63–1.53 (dt, *J* = 4.2, 12.5 H, 1H), 1.49–1.12 (m, 10H), 1.03–0.97 (m, 1H). ^{13}C NMR (75 MHz, C_6D_6) δ: 214.9, 82.6, 80.8, 63.4, 61.8, 32.4, 27.2, 25.8, 25.7,24.8, 23.8, 19.1, 18.8. ES-HRMS *m/z* calcd.: 247.1310 $[M + Na]^+$; found: 247.1308.

17

Colourless oil. IR (neat, cm^{-1}): 1743, 1441, 1094. ^1H NMR (300 MHz, C_6D_6) δ: 3.69–3.64 (m, 2H), 3.50–3.44 (m, 1H), 3.30–3.21 (dt, *J* = 11.6, 2.8 Hz, 1H), 2.56–2.40 (m, 1H), 2.27–2.00 (m, 4H), 1.77–1.21 (m, 11H). ^{13}C NMR (75 MHz, C_6D_6) δ: 214.4, 82.3, 80.3, 63.9, 61.0, 32.6, 27.2, 26.4, 26.2, 23.7, 22.5, 19.1, 18.8. ES-HRMS *m/z* calcd.: 247.1310 $[M+Na]^+$; found: 247.1310.

Ring expansion of 10 with 2,3-dihydrofuran

Cerium trichloride heptahydrate (31.3 g, 41.8 mmol) was dried overnight under high vacuum at 140 °C, admixed with dry THF (125 mL), and stirred at rt for 2 h. The resulting slurry was cooled to –78 °C and *tert*-butyllithium (1.6 mol/L in pentane) was added until a pink color persisted at which point a solution of **5a** (from 2,3-dihydrofuran (4.8 mL, 63.4 mmol)) in THF (75 mL) was introduced. Stirring was maintained at –78 °C for 2 h prior to the addition of **10** (8.2 g, 41.8 mmol) dissolved in THF (50 mL) via syringe pump over 45 min. After 2 h of stirring in the cold, the reaction mixture was warmed to 0 °C, quenched with sat. $NaHCO_3$ solution, and filtered through Celite after 30 min. The separated aqueous phase was extracted with CH_2Cl_2 (3×) and the combined organic phases were dried and evaporated. The resulting oil was dissolved in acetonitrile (200 mL), admixed with oven-dried Dowex-50W resin (8 g), and stirred overnight. The mixture was filtered through Celite and freed of solvent to leave a residue that was chromatographed on silica gel (elution with 30% ethyl acetate in hexane) to give 8.0 g of **18** and 0.35 g of **19** (total 75%), both of which were spectroscopically identical with earlier recorded data. When the last step was performed in CH_2Cl_2, a 60% yield of **18**, exclusively, was isolated.

© 2006 NRC Canada

Ring expansion of 11 with 2,3-dihydrofuran

Reaction of cerium trichloride heptahydrate (14.0 g, 37.4 mmol), 2,3-dihydrofuran (1.8 mL, 23.8 mmol), *tert*-butyllithium in pentane (14 mL, 1.6 mol/L), and **11** (2.2 g, 11.2 mmol) in the predescribed manner, and performance of the final step in acetonitrile gave rise to the isolation of 1.5 g of **20** and 0.5 g of **21** for a combined yield of 51% in a ratio of 3:1. Use of CH_2Cl_2 as solvent led to the isolation of **20** and **21** in 64% combined yield in a ratio of 5:1. The spectral features of these products proved identical to those previously reported.

Isomerization of 10 and 11 — Prototypical procedure

Ketone **10** (4.5 g, 22.9 mmol) dissolved in $CHCl_3$ (100 mL) was treated with boron trifluoride etherate (2.9 mL, 23 mmol), refluxed for 6 h, cooled to 0 °C, and quenched with water. The separated organic phase was dried and freed of solvent to leave a residue that was chromatographed on silica gel. Elution with 25%–50% ethyl acetate in hexane furnished 1.7 g of **10** and 1.9 g (80% total) of **11**.

An identical procedure was adopted starting from **11** (500 mg, 2.65 mmol) in $CHCl_3$ (10 mL) and the subsequent introduction of boron trifluoride etherate (0.37 mL, 2.91 mmol). A parallel workup protocol furnished 206 mg of **10** and 1.93 mg of **11** (total of 80%).

Acknowledgment

We thank the Astellas USA Foundation (Deerfield, Illinois) for financial support.

References

1. L.A. Paquette, J.F.P. Andrews, C. Vanucci, D.E. Lawhorn, J.T. Negri, and R.D. Rogers. J. Org. Chem. **57**, 3956 (1992).
2. B.M. Branan and L.A. Paquette. J. Am. Chem. Soc. **116**, 7658 (1994).
3. L.A. Paquette, B.M. Branan, D. Friedrich, S.D. Edmondson, and R.D. Rogers. J. Am. Chem. Soc. **116**, 506 (1994).
4. N.J. Turro. Acc. Chem. Res. **2**, 25 (1969).
5. H.H. Wasserman, G.M. Clark, and P.C. Turley. Top. Curr. Chem. **47**, 73 (1974).
6. (*a*) J. Salaün. Chem. Rev. **83**, 619 (1983); (*b*) J. Salaün and J. Marguerite. Org. Synth. **63**, 147 (1985).
7. N.J. Turro and W.B. Hammond. Tetrahedron, **24**, 6029 (1968).
8. (*a*) H.H. Wasserman, H.W. Adickes, and O. Espejo de Ochoa. J. Am. Chem. Soc. **93**, 5586 (1971); (*b*) H.H. Wasserman and E.A. Glazer. J. Org. Chem. **40**, 1505 (1975).
9. C.H. De Puy, G.M. Dappen, K.L. Eilers, and R.A. Klein. J. Org. Chem. **29**, 2813 (1964).
10. J. Salaün and J.M. Conia. Tetrahedron Lett. 2849 (1972).
11. J. Barluenga, J. Florez, and M. Yus. J. Chem. Soc. Chem. Commun. 1153 (1982).
12. (*a*) L.A. Paquette. Recent Res. Dev. Chem. Sci. **1**, 1 (1997); (*b*) L.A. Paquette, J.C. Lanter, and J.N. Johnston. J. Org. Chem. **62**, 1702 (1997).
13. L.A. Paquette, D.G. Hilmey, and P.R. Selvaraj. Heterocycles, in press.
14. R.K. Boeckman, Jr. and K.J. Bruza. Tetrahedron, **37**, 3997 (1981).
15. R.W. Friesen, C.F. Sturino, A.K. Daljeet, and A. Kolaczewska. J. Org. Chem. **56**, 1944 (1991).
16. (*a*) J.T. Negri, R.D. Rogers, and L.A. Paquette. J. Am. Chem. Soc. **113**, 5073 (1991); (*b*) L.A. Paquette, J.T. Negri, and R.D. Rogers. J. Org. Chem. **57**, 3947 (1992).
17. T. Imamoto, N. Takiyama, K. Nakamura, T. Hatajima, and Y. Kamiya. J. Am. Chem. Soc. **111**, 4392 (1989).
18. L.A. Paquette, W. He, and R.D. Rogers. J. Org. Chem. **54**, 2291 (1989).
19. (*a*) M.D. Lord, J.T. Negri, and L.A. Paquette. J. Org. Chem. **60**, 191 (1995); (*b*) L.A. Paquette, M.D. Lord, and J.T. Negri. Tetrahedron Lett. **34**, 5693 (1993).
20. (*a*) L.A. Paquette and H.-L. Wang. Tetrahedron Lett. **36**, 6005 (1995); (*b*) L.A. Paquette, J.C. Lanter, and H.-L. Wang. J. Org. Chem. **61**, 1119 (1996).
21. L.A. Paquette, J.C. Lanter, and J.N. Johnston. J. Org. Chem. **62**, 1702 (1997).
22. The molecular mechanics program is incapable of directly handling molecules containing oxonium cations and realistic energy values must be arrived at in a two-step manner. We have followed the protocol outlined earlier: L.A. Paquette, C.K. Seekamp, A.L. Kahane, D.G. Hilmey, and J.C. Gallucci. J. Org. Chem. **69**, 7442 (2004).
23. Shrödinger™. MacroModel. Version 5.0 [computer program]. Shrödinger™, New York, N.Y.
24. CyberChem, Inc. Chem 3D Ultra [computer program]. CyberChem, Inc., Gainesville, Fla.
25. L.A. Paquette. *In* Chemistry for the 21st century. *Edited by* E. Keinan and I. Shechter. Wiley-VCH, Weinheim, Germany. 2001. pp 37–53.
26. L.A. Paquette, M. Stepanian, B.M. Branan, S.D. Edmondson, C.B. Bauer, and R.D. Rogers. J. Am. Chem. Soc. **118**, 4504 (1996).
27. (*a*) L.A. Paquette, J. Tae, E.R. Hickey, W.E. Trego, and R.D. Rogers. J. Org. Chem. **65**, 9160 (2000); (*b*) L.A. Paquette, J. Tae, B.M. Branan, D.G. Bolin, and S.W.E. Eisenberg. J. Org. Chem. **65**, 9172 (2000); (*c*) P.R. Rablen, L.A. Paquette, and W.T. Borden. J. Org. Chem. **65**, 9180 (2000).

© 2006 NRC Canada

Deprotonation of β,β-disubstituted α,β-unsaturated amides — Mechanism and stereochemical consequences[1]

James R. Green, Marek Majewski, and Victor Snieckus

Abstract: A detailed study of the lithium dialkylamide induced deprotonation of β,β-disubstituted α,β-unsaturated amides is presented. The preferential γ-*Z*-deprotonation and stereochemical outcome of substituents on the γ-*Z* carbon atom are rationalized in terms of a cyclic eight-membered transition state, which is supported by DFT calculations. Analogous deprotonations on cyclohexylidenecarboxamides reveal a delicate balance of the preference for the eight-membered cyclic transition state with the effects of existing substituents on the ring and the intervention of a twist-boat transition state.

Key words: dienolate, amide, deprotonation mechanism, transition state, enolization, regioselectivity, stereoselectivity.

Résumé : On a effectué une étude détaillée de la déprotonation induite par les dialkylamides de lithium d'amides α,β-insaturés et β,β-disubstitués. La déprotonation préférentielle en γ-*Z*- et le résultat stéréochimique des substitutions sur l'atome de carbone γ-*Z* sont rationalisés en termes d'un état de transition cyclique à huit chaînons qui est supporté par des calculs de la théorie de la densité fonctionnelle. Des déprotonations analogues sur les cyclohexylidènecarboxamides mettent en évidence la délicate balance de la préférence en faveur de l'état de transition cyclique à huit chaînons avec les effets des substituants déjà présents sur le cycle et l'intervention d'un état de transition en forme de bateau croisé.

Mots clés : diénolate, amide, déprotonation, mécanisme, état de transition, énolisation, régiosélectivité, stéréosélectivité.

[Traduit par la Rédaction]

Introduction

The prediction of the stereochemistry of enolate formation is of fundamental significance to the large number of valuable C—C bond-forming synthetic strategies of which the aldol condensation is arguably the most prominent (1). A body of data (2) on the stereoselection of enolization has been rationalized by the pericyclic chairlike transition state model (structure 1 in Fig. 1) originally proposed by Ireland et al. (3) in which deprotonation occurs perpendicular to the plane of the carbonyl coordinated to the lithium dialkylamide (4). This model is based on allylic strain (5) and stereoelectronic (4, 6) considerations. Compelling kinetic (7, 8) and spectroscopic (9) evidence for lithium base carbonyl complexation associated with proton abstractions has been advanced (10), although the strict cyclohexane-like chair nature of the transition state has required revision in light of computational analysis (11).

In spite of the extensive synthetic use of β,β-disubstituted, α,β-unsaturated carbonyl compounds (**2**) and related derivatives (12, 13), the stereoselectivity aspects of dienolate formation (γ-*Z* or γ-*E* proton abstraction) have not been systematically addressed (14–17). Although the preferential deprotonation of γ-*Z* over equivalently substituted γ-*E* protons has been established (12*a*, 14*a*–14*c*, 18, 19), the scope and limitations of this feature as it pertains to differential substitution at the γ-*Z* and γ-*E* sites, a systematic study of the stereochemical fate of γ-*Z* substituents, and the stereochemical disposition of the proton undergoing abstraction have not been dealt with in depth. Originating with our interest in the synthetic utility of α,β-unsaturated amides (16*k*), we addressed this question (18, 19) and herein present extended detailed studies, which significantly amplify our preliminary results, may have broader application to other α,β-unsaturated functionalized systems (20), and thereby may shed further light on this interesting question, which has considerable synthetic and mechanistic interest.

Concerning the site of deprotonation of senecioamides

Previous work using unsaturated esters does not allow unambiguous generalization concerning the *syn* vs. *anti* γ-H site of deprotonation to analogous systems (14*r*, 14*m*, 14*q*,

Received 24 February 2006. Accepted 19 May 2006. Published on the NRC Research Press Web site at http://canjchem.nrc.ca on 29 September 2006.

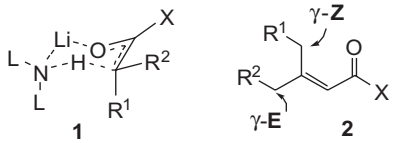
Dedicated to Alfred Bader, for the chemistry he created amongst all chemists and in appreciation of his tenacious support of Canadian chemistry.

J.R. Green. Department of Chemistry, University of Windsor, Windsor, ON N9B 3P4, Canada.
M. Majewski. Department of Chemistry, University of Saskatchewan, Saskatoon, SK S7N 5C9, Canada.
V. Snieckus.[2,3] Department of Chemistry, University of Waterloo, Waterloo, ON N21 3G1, Canada.

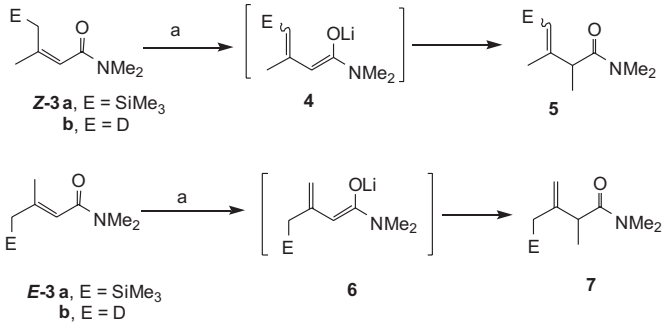
[1]This article is part of a Special Issue dedicated to Dr. Alfred Bader.
[2]Current address: Department of Chemistry, Queen's University, Kingston, ON K7L 3N6, Canada.
[3]Corresponding author (e-mail: cjc@chem.queensu.ca).

 doi:10.1139/V06-112 © 2006 NRC Canada

Fig. 1. Deprotonation in carbonyls and unsaturated carbonyls.



Scheme 1. Reagents and conditions: (*a*) (*i*) LDA, THF; (*ii*) MeI, 0 °C to room temperature.



14*n*, 14*k*, 14*a*–14*d*, 19). We decided to approach this question for unsaturated amides in conjunction with ongoing studies. γ-Silylated carboxamides ***Z*-3a** and ***E*-3b** (Scheme 1), available as a result of our work on amide dienolate reactivity (13*c*, 21), were subjected to LDA deprotonation at room temperature (RT) and the resulting dienolates **4a** and **6a** were quenched with methyl iodide to give products **5a** (*Z*, *E*) and **7a** in 90% and 84% yields, respectively. The products were readily distinguished by ^{1}H NMR spectroscopy (see the Experimental section), which showed that compounds ***Z*-3a** and ***E*-3a** gave exclusively compounds **5a** and **7a**, respectively. The issues of acidifying and steric effects led us to consider replacement of silicon by deuterium as a positional γ marker that would minimally perturb the system under study.

Using conditions previously developed in our laboratories for regio- and stereo-selective introduction of electrophiles into γ-*cis* methyl positions of senecioamdies (16*k*), the dimethyl amide **8** (Scheme 2) was subjected to LDA deprotonation at –78 °C followed by treatment with CuI, according to the protocol of Katzenellenbogen for favoring γ-functionalization, and D_2O in sequence to give a mixture of γ- and α-deuterated products ***Z*-3b** and **9** in a 57:43 ratio. Exclusion of CuI in this sequence led to lower γ:α product ratios. The corresponding ***E*-3b** isomer was prepared according to the excellent and dependable Sum and Weiler procedure (22) involving γ-deuteration of **10** to give **11** followed by stereoselective β-methylation via the enol phosphonate **12**. The location and content of deuterium in the products depicted in Scheme 2 were determined by MS and ^{2}H NMR (see the Experimental section). For compound ***E*-3b**, ^{2}H NMR analysis showed approximately 5% contamination with the ***Z*-3b** isomer.

Deprotonation of ***Z*-3b** and ***E*-3b** under identical conditions (LDA, THF, 0 °C, 0.5 h) and subsequent methylation of the resulting dienolates gave **5b** (78%) and **7b** (68%), respectively. The ^{1}H NMR spectrum of ***Z*-5b** showed significant deuteration in the vinyl site but not in the allylic methyl group, while the corresponding spectrum of ***E*-5b** indicated

Scheme 2. Reagents and conditions: (*a*) (*i*) LDA, THF, –78 °C; (*ii*) CuI; (*iii*) MeOD, –78 °C. (*b*) (*i*) NaH; (*ii*) *n*-BuLi: (*iii*) F_3CCO_2D + D_2O; (*iv*) NH_4Cl. (*c*) (*i*) NaH; (*ii*) $ClP(O)(OEt)_2$. (*d*) (*i*) Me_2CuLi, –78 to –40 °C; (*ii*) NH_4Cl.

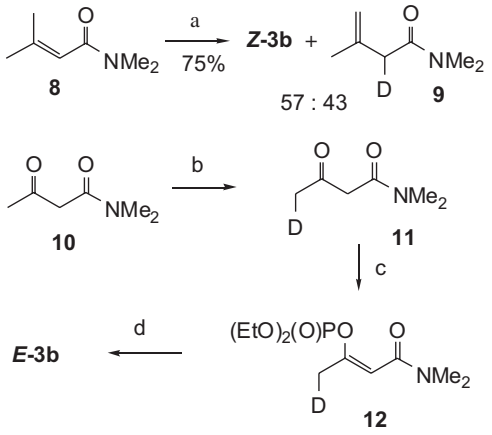
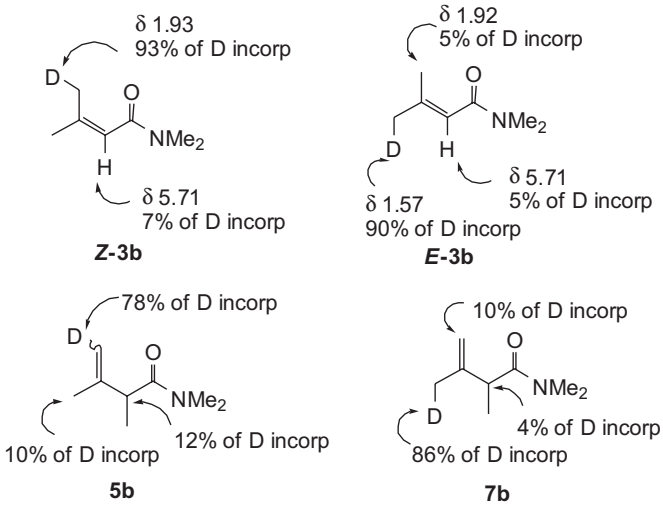


Fig. 2. ^{2}H NMR based relative deuterium incorporation levels.



essentially no deuteration in the vinyl group but significant deuterium incorporation in the allylic methyl group (see the Experimental section and Fig. 2). More conclusive data was obtained from the ^{2}H NMR spectra (Fig. 2), which showed relative deuterium incorporation at the vinyl, α-carbon, and allylic methyl in a ratio of 78:12:10 for **5b** and 10:4:86 for **7b**. These results indicate that γ-*Z* over γ-*E* deprotonation has occurred to the extent of 89% and 96% in the two substrates ***Z*-3b** and ***E*-3b**, respectively, and therefore implicate the intermediacy of the dienolates **4b** and **6b**, respectively. Thermodynamic deprotonation of these systems is ruled out by the observation that ***E*-3a** did not proceed via dienolate **4a**. The results of our studies with ***Z*-3b** and ***E*-3b** mirror the observations of Harris and Weiler (19) on the corresponding carboxylic acids and esters.

Substituent effects on γ-deprotonation

In seeking a more detailed understanding of the factors affecting the geometry of dienolate formation, we investigated

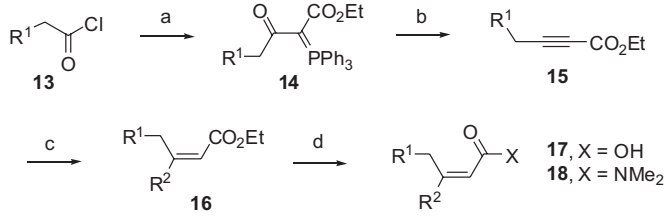
© 2006 NRC Canada

Table 1. Stereoselectivity in deprotonations of ***Z*-3a** and **18**.

Entry	Amide	R^1	R^2	Product[a]	trans:cis Ratio
1	**18g**	Me	Et	**19g** (80)	79:21
2[b]	**18g**	Me	Et	**19g** (71)	92:8
3	**18a**	Me	*n*-Bu	**19a** (54)	79:21
4	**18b**	Me	*s*-Bu	**19b** (89)	41:59
5	**18c**	Me	*t*-Bu	**19c** (75)	<3:>97
6	**18d**	*i*-Pr	*s*-Bu	**19d** (54)	8:92
7	**18f**	OMe	*n*-Bu	**19e** (84)	<3:>97
8	***Z*-3a**	$SiMe_3$	Me	**5a** (90)	79:21

[a]Yields in parentheses.
[b]Reaction conducted at 78 °C.

Scheme 3. Reagents and conditions: (*a*) $2Ph_3P{=}CHCO_2Et$. (*b*) 270 °C, ~0.4 Torr. (*c*) (*i*) R^2R^3CuLi, THF, –78 °C; (*ii*) H_3O^+; (*iii*) $SoCl_2$, C_6H_6; (*iv*) $HNMe_2$, Et_2O.

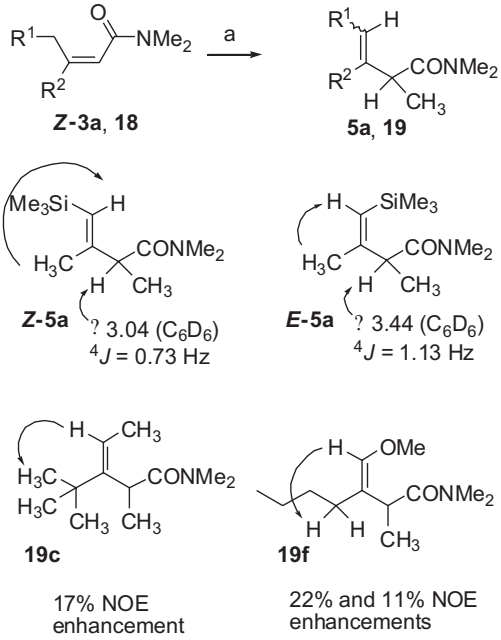


For **13**–**15** **a**, $R^1 = CH_3$; **b**, $R^1 = {}^iPr$; **c**, $R^1 = {}^tBu$; **d**, $R^1 = OMe$
For **16**–**18** **a**, $R^1 = CH_3$, $R^2 = R^3 = {}^nBu$; **b**, $R^1 = CH_3$, $R^2 = R^3 = {}^sBu$; **c**, $R^1 = CH_3$, $R^2 = {}^tBu$, $R^3 = Me$; **d**, $R^1 = {}^iPr$, $R^2 = R^3 = {}^sBu$; **e**, $R^1 = {}^tBu$, $R^2 = R^3 = {}^sBu$; **f**, $R^1 = OMe$, $R^2 = R^3 = {}^nBu$

the deprotonation chemistry of a variety of β,γ-disubstituted acrylamides. In particular, we were interested in the effect of substituents anchored at the site of deprotonation. For this purpose, a series of stereochemically homogeneous β,β-disubstituted acrylamides **18** were prepared by adapting cuprate-addition chemistry to ethyl-2-alkynoates (Scheme 3) (23). Condensation of acyl halides **13a**–**13d** with carboethoxymethylene triphenylphosphorane using the procedure described by Hanack et al. (24) as modified by Markl (25) afforded the acyl phosphoranes **14a**–**14d**, which normally were not isolated but directly pyrolyzed to give the 2-alkynoate esters **15a**–**15d**. Treatment of esters **15a**–**15d** with lithium dialkyl cuprates furnished the stereochemically pure α,β-unsaturated esters **16a**–**16f** in variable yields (37%–81%). The conversion of esters **16a**–**16f** into the requisite dimethyl amides **18a**–**18f** was carried out under standard conditions via the intermediate carboxylic acids **17a**–**17f**. Amide **18g** (R^1 = Me, R^2 = Et) was prepared using a Horner–Wadsworth–Emmons procedure (see the Experimental section). The structures and stereochemistry of all amides **18** were assigned by ^1H NMR spectroscopy: with one exception (**18f**), the CH_2 group cis to the amide carbonyl appears as expected downfield (δ 2.3) from the one located trans to the carbonyl (δ 2.15). Furthermore, the *cis*-CH_2 resonances experienced an aromatic solvent-induced shift to lower field (δ 2.47) upon replacement of $CDCl_3$ with C_6D_6 as solvent (26).

Compounds **18a**–**18g** were deprotonated with LDA in THF at room temperature, except for entry 2, and quenched with methyl iodide to give mixtures of products *trans*-**19a**–**19d**, **19f**, and **19g** and *cis*-**19a**–**19d**, **19f**, and **19g**[4] (Scheme 4, Table 1). Attempted deprotonation of **18e** resulted in extensive decomposition and thus was not pursued further. For the sake of completeness, the deprotonation of ***Z*-3a** is included (Table 1, entry 8). The trans to cis ratio was established by integration of the ^1H NMR methine resonance of the two isomers with chemical shifts δ separated by a consistent value of approximately 0.3 ppm (3.3 ppm for trans and 3.6 ppm for cis isomers). Stereochemical assignments at the newly formed double bond were determined by the four-bond vinyl-to-methyl coupling constant in accordance with the literature (Scheme 4) (27). In addition, the stereochemistry of compounds *trans*-**19c** and *trans*-**19f** was confirmed by NOE difference experiments.

Scheme 4. Reagents and conditions: (*a*) (*i*) LDA, THF; (*ii*) MeI, 0 °C to room temperature.



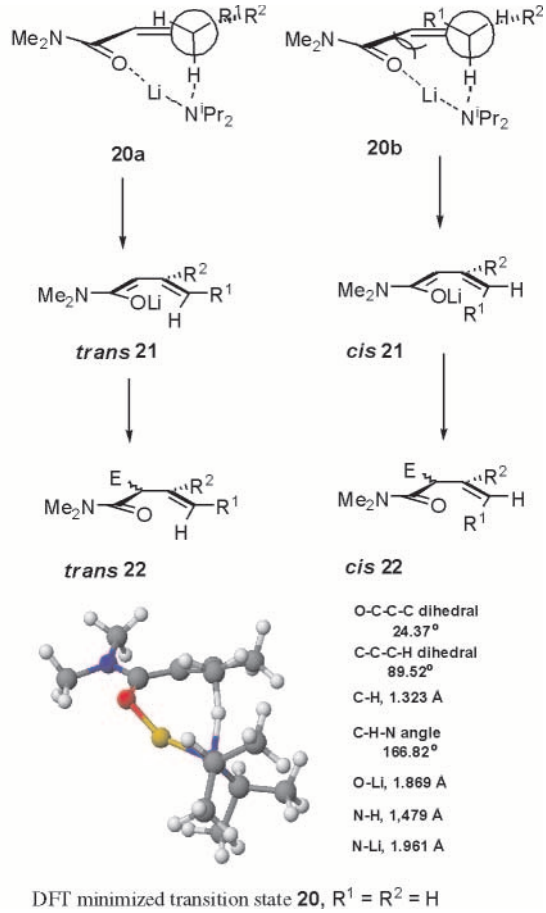
The mechanism of γ-deprotonation

On the basis of the above results, we propose that deprotonation of β,β-disubstitued α,β-unsaturated amides oc-

[4]*Z*/*E* nomenclature is not used because of priority changes in R^2 in the progression of the series.

© 2006 NRC Canada

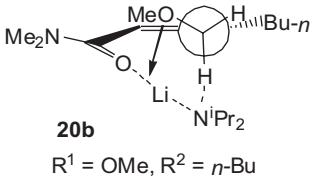
Scheme 5.



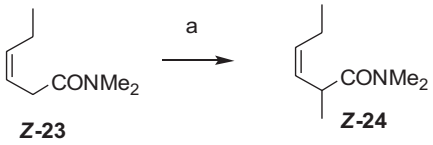
DFT minimized transition state **20**, $R^1 = R^2 = H$

curs through a cyclic eight-membered ring transition state (**20a** and **20b**), which highlights lithium carboxamide oxygen coordination according to the established complex-induced proximity effect (CIPE) (7) (Scheme 5). Since the γ-*Z* carbon is in closer proximity to the amide carbonyl than the γ-*E* carbon atom, deprotonation occurs preferentially from the former leading to dienolates *cis*-**21** and *trans*-**21**, which undergo reaction with the electrophile at the α site to give products *cis*-**22** and *trans*-**22**. To rationalize substitutent effects, we begin with the assumption that deprotonation occurs perpendicular to the plane of the unsaturated amide (3). While semiempirical calculations (MNDO) have indicated a H-C-C-O torsion angle for ketone deprotonation of only about 60° (11), DFT[5] calculations on **20** reveal that the eight-membered ring transition state incorporates an optimal H-C-C-C torsion angle (89.5°) for senecioamide deprotonation, with a minimal twist (24.4°) from coplanarity of the unsaturated carbonyl. With small R^2 substituents, the γ-R^1 group prefers to be oriented away from the carboxamide in transition state **20a**, leading preferentially to dienolate *trans*-**21** and ultimately to alkylated product *trans*-**22**. As the size of the R^2 group is increased (Et < *s*-Bu < *t*-Bu), the steric repulsion between R^1 and R^2 increases, giving rise to greater amounts of deprotonation from transition state **20b**, which cascades to dienolate *cis*-**21** and product *cis*-**22**. Comparison

Fig. 3. Deprotonation transition state for **18f**.



Scheme 6. Reagents and conditions: (*a*) (*i*) LDA, THF, RT; (*ii*) MeI, 0 °C to room temperature.



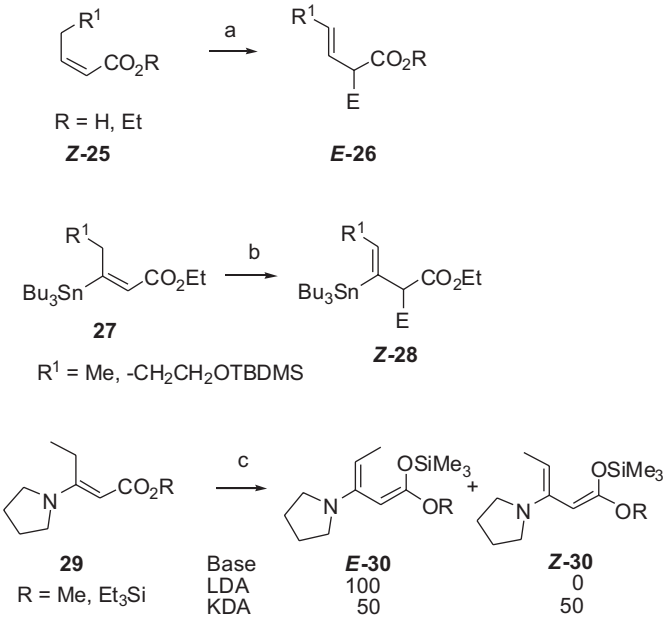
of entries 4 and 6 (Table 1) suggests that an increase in the size of R^1 enhances the energy difference between transition states **20a** and **20b**. In this context, the result obtained with the TMS (entry 8) shows no size effect in spite of the fact that this group has an A value similar to *i*-Pr (28). The case of the OMe substituent (Table 1, entry 7) is striking in that, on the basis of steric arguments, preferential formation of *trans*-**19f** was expected. The exclusive formation of *cis*-**19f** strongly suggests that lithium–OMe coordination (Fig. 3) in the transition state is significant although the tentative nature of this proposal is recognized in view of reports on the dimeric (29) and tetrameric (30) nature of dienolates in the solid state. Finally, a comparison of the results of deprotonation of **19g** at –78 °C and room temperature (Table 1, entries 1 and 2) shows the expected enhancement in selectivity with decreased temperature consistent with a 0.8–0.95 kcal/mol (1 kcal = 4184 J) difference in activation energy for the respective dienolate isomer formation. To confirm that the products result from kinetic deprotonation and that double bond isomerization about Cβ—Cγ does not occur in the dienolate, the β,γ-unsaturated amide ***Z*-23** was prepared according to Baldwin and co-workers (16*j*) and subjected to the standard LDA deprotonation conditions. The product ***Z*-24** showed retention of double bond geometry, which must stem from the thermodynamically less stable dienolate, thereby providing confirmation of kinetic deprotonation (Scheme 6). Because of the lack of proximity of the carbonyl oxygen and the deprotonation site, our model clearly does not contribute to an understanding of the mechanism of deprotonation of *E*-α,β-unsaturated esters and acids (16*a*, 16*f*, 16*j*).

The earlier observations of Pfeffer and Silbert (16*u*), Krebs (16*r*), and Kende and Toder (16*p*) on the deprotonation of *Z*-unsaturated esters and acids (***Z*-25** to ***E*-26** in Scheme 7) are in agreement with our proposed model of deprotonation (Scheme 5). In all these earlier investigations, compounds with no β-*E* substitutents were employed (Scheme 5, R^2 = H). As a consequence, the R^1 – carbonyl oxygen interaction constitutes the only significant repulsive interaction. A transition state analogous to **20a** is therefore expected, which ultimately leads to the corresponding

[5] DFT calculations were carried out using the B88-PW91 method, and a DZVP basis set, using CAChe® version 6.1.12.33 (see Supporting information). All stationary points were confirmed via frequency calculations.

© 2006 NRC Canada

Scheme 7. Reagents and conditions: (*a*) (*i*) LDA, HMPA, THF, –78 °C; (*ii*) E^+. (*b*) (*i*) LDA, THF; (*ii*) H^+, –98 °C. (*c*) (*i*) base, THF, –78 °C; (*ii*) Me_3SiCl.

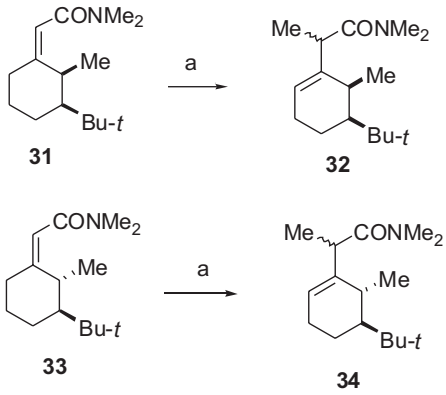


dienolate *trans*-**21** and product *trans*-**22**. In addition, Piers and Gavai (16*l*) and Schlessinger and co-workers (15*d*) have reported on the low-temperature deprotonation of β-stannyl (**27**) and β-pyrrolidino (**29**) substituted unsaturated esters. Piers and Gavai found that LDA deprotonation of **27** followed by proton quench produced only the ***Z*-28** isomer, which is consistent with the relatively small conformational *A* value of tin (either 0.94 (31)) or 1.06 (32)). Piers and Gavai also observed that the presence of an oxygen function in **27**, R = $CH_2CH_2OTBDMS$, does not alter the stereochemical outcome of deprotonation. This may be due to the oxygen function being too distant to participate in coordination to lithium or the inhibition of coordination by the bulky TBDMS group. In the Schlessinger study, deprotonation of the β-pyrrolidino system **29** with LDA gave exclusively the *cis*-enolate as reflected in the formation of the *O*-silyl dienolate product ***E*-30**, a result in qualitative agreement with our results (Table 1) if one considers the large *A* value (2.1) of a dialkylamino group (33). The lack of selectivity shown by KDA in the deprotonation of **29** to give ***E*-30** and ***Z*-30** may reflect an earlier transition state and weaker metal-to-carbonyl coordination. Our study of the effect of base on the deprotonation of **18g** led to inconclusive results (13*c*).

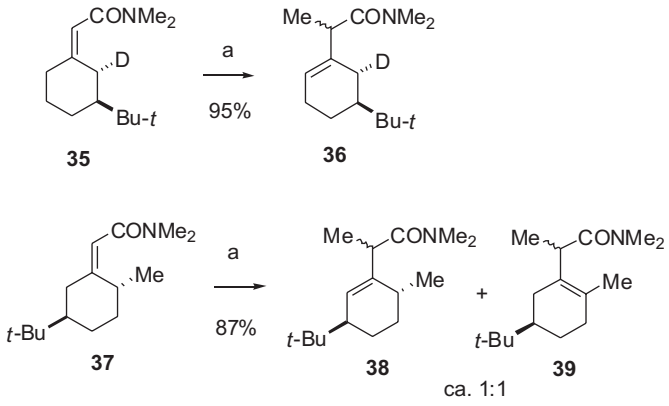
These arguments concerned with substituent effects on γ-deprotonation appear to be applicable and lead to similar conclusions for α,β-unsaturated systems with other carbonyl acidifying functionality (20), such as phosphonates and phosphine oxides (34) and sulfones (35).

At this point in the study, we were interested in determining whether the requirement for perpendicular C-H orientation would manifest itself in axial proton abstraction in cyclohexylidene carboxamides. For this purpose, we prepared diastereomers **31** and **33** using cuprate conjugate addition and Peterson olefination chemistry (see Supplementary material)[6] and subjected them to the standard LDA deprotonation – methyl iodide quench conditions to give the deconjugated amides **32** and **34**, respectively (Scheme 8). Disappointingly, deprotonation had occurred at the γ-*E* methylene to the exclusion of γ-*Z* methine proton. We considered that the factor responsible for the unwanted γ-*E* deprotonation is the presence of the equatorial γ-methyl or the δ-*t*-Bu groups. Therefore, we prepared (see Supplementary material)[6] γ-deuterated (**35**) and the *t*-Bu γ-methyl (**37**) derivatives and treated these under the normal deprotonation–methylation conditions. Unfortunately, compound **35** also underwent deprotonation at the γ-*E*-methylene site to give deconjugated product **36** (Scheme 9). Furthermore, compound **37** gave a mixture of compounds **38** and **39** (approx. 1:1) indicating γ-*E*-methylene and γ-*Z*-methine deprotonation, respectively. We surmise that the presence of the γ-methyl function in the cyclohexylidene amides either causes the six-membered ring to adopt a twist-boat conformation or prevents the proper orientation of the

Scheme 8. Reagents and conditions: (*a*) (*i*) LDA, THF, RT; (*ii*) MeI, 0 °C to room temperature.



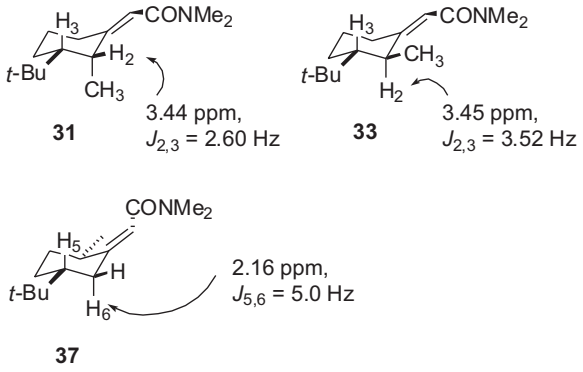
Scheme 9. Reagents and conditions: (*a*) (*i*) LDA, THF, RT; (*ii*) MeI, 0 °C to room temperature.



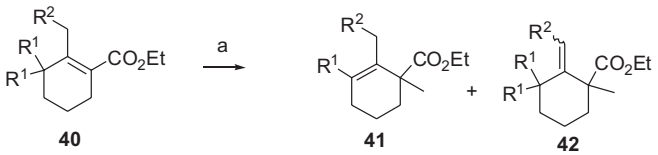
[6] Supplementary data for this article are available on the journal Web site (http://canjchem.nrc.ca) or may be purchased from the Depository of Unpublished Data, Document Delivery, CISTI, National Research Council Canada, Ottawa, ON K1A 0R6, Canada. DUD 5078. For more information on obtaining material, refer to http://cisti-icist.nrc-cnrc.gc.ca/irm/unpub_e.shtml.

© 2006 NRC Canada

Fig. 4. Selected ^{1}H NMR spectral data of cyclohexylidene amides.



Scheme 10. Reagents and conditions: (*a*) (*i*) base, THF, –78 °C; (*ii*) MeI.

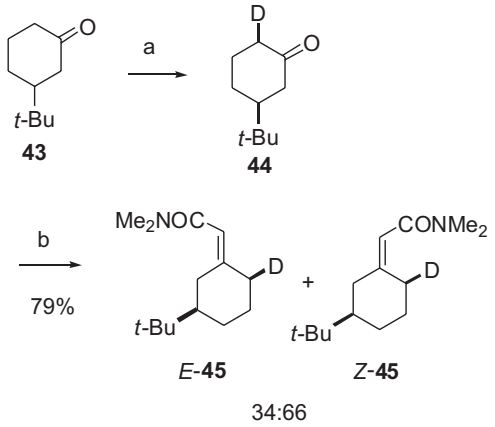


Entry	Base	**41**:**42** Ratio	
1. R^1 = H, R^2 = H	LiICA	0	100
2. R^1 = H, R^2 = Me	LDA/HMPA	100	0
3. R^1 = D, R^2 = Me	LDA/HMPA	40	60
4. R^1 = H, R^2 = Me	LDA	0	100

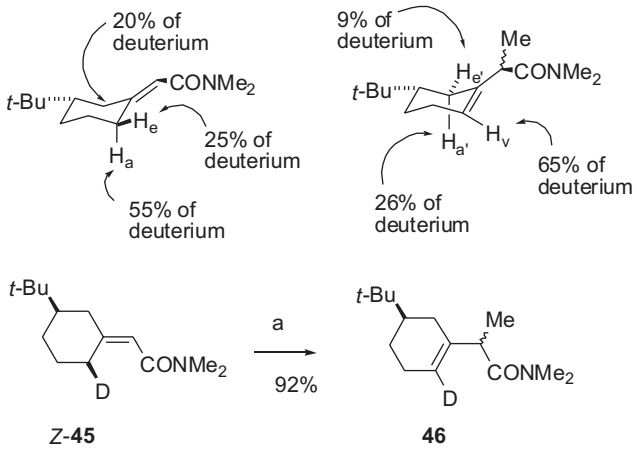
amide carbonyl for formation of the required transition state **20** (Scheme 5). In the ^{1}H NMR of cyclohexanones, axial hydrogens resonate at lower fields than the corresponding equatorial hydrogen (36). This is clearly not the case for the corresponding hydrogens H_2 in the cyclohexylidene amides **31** and **33** (Fig. 4). Similarly, the axial hydrogen H_6 in **37** resonates at δ 2.16, but more importantly shows coupling with the adjacent methine hydrogen with J = normal practice 5 Hz. Spectroscopic characterization of **35** does not allow the identification of the conformation of the cyclohexane ring. It appears, however, that the *tert*-butyl function at the position γ to the carbonyl is sufficient to block deprotonation at the γ-*Z* site.

Our difficulties in deprotonating cyclohexylidene amide systems are reminiscent of the results observed by White (14*t*), Gesson (14*o*), and Weiler (14*h*) and their co-workers on cyclohexene carboxylate esters **40** (Scheme 10). Examination of the entries shows that the seemingly trivial modification of substituents of the base (compare entries 2 and 3 or 2 and 4 in Table 1) leads to dramatic changes in ratios of deconjugated products **41** and **42**. Considering that the γ-*Z* deprotonation in the unperturbed cases has been demonstrated by our previous results (Table 1 and Scheme 1), we chose to prepare compound **43** (Scheme 11), which incorporates a *t*-Bu group in a location remote from the site of deprotonation. Treatment of 3-*tert*-butylcyclohexanone **43** with LDA followed by deuteration afforded **44**, albeit with modest incorporation of deuterium (d_1 = 40%, d_2 = 10%) (37). Peterson olefination of **44** with the lithio enolate of α-silyl acetamide gave a mixture of ***Z*-45** and ***E*-45** in a ratio of

Scheme 11. Reagents and conditions: (*a*) (*i*) LDA, THF, –78 °C; (*ii*) CF_3CO_2D + D_2O. (*b*) (*i*) $Me_3SiCH_2CONMe_2$, LDA, THF, –78 °C; (*ii*) **44**, –78 °C to room temperature.



Scheme 12. Reagents and conditions: (*a*) (*i*) LDA, THF; (*ii*) MeI, 0 °C to room temperature.

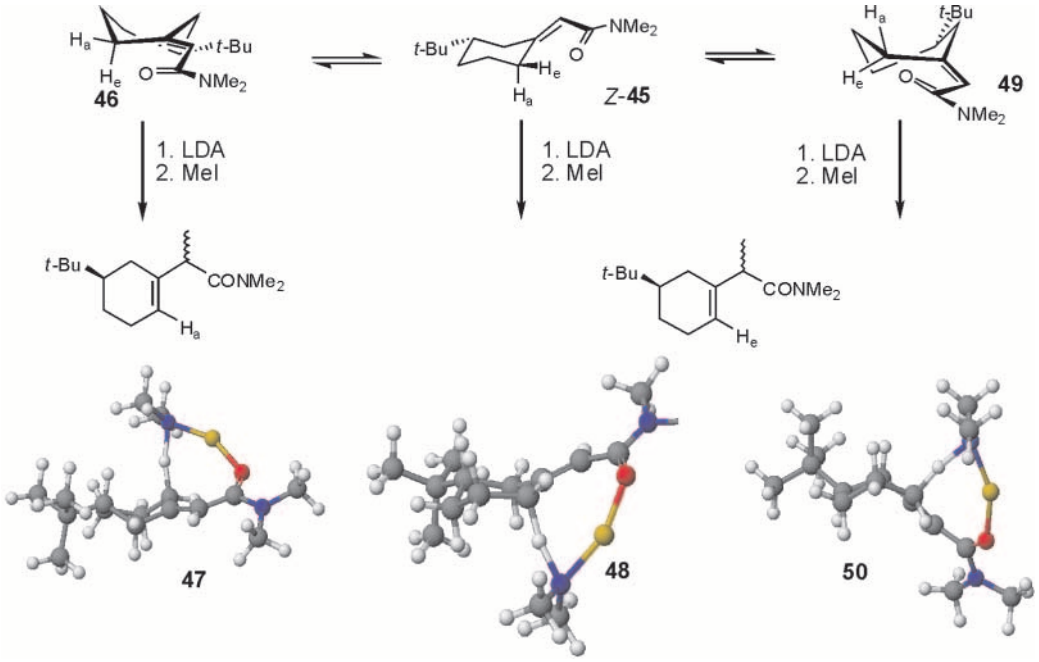


66:34, which were separated by column chromatography to give pure ***Z*-45**. The mass spectrum of ***Z*-45** indicated 37% d_1 and 9% d_2 incorporation, while the ^{2}H NMR showed approximately 55%, 25%, and 20% relative deuteration at H_a, H_e, and γ-*E* sites, respectively. When ***Z*-45** was subjected to deprotonation and methylation under normal conditions, compound **46** was obtained in high yield and its ^{2}H NMR spectrum showed relative deuterium incorporation of 65%, 26%, and 9% at H_v, H_a, and H_e, respectively (Scheme 12). This corresponds to an approximately 20:80 ratio favoring equatorial deprotonation. The mass spectrum of **46** showed 27% d_1 and 8% d_2 content, which is consistent with predominant equatorial deprotonation.

We believe that the explanation of these results lies in the classic work of Fraser and Champagne (4) who demonstrated that protonation or deprotonation in conformationally locked systems can occur via perpendicular attack by base through a twist-boat transition state, and in the proposal that these transition states are responsible for equatorial protonation or deprotonation in cyclohexanones (38). The predominant equatorial deprotonation of **Z-45** is due to an analogous twist-boat cyclohexylidene conformation **46** (Scheme 13) in which the axial hydrogen H_e is suitably ori-

© 2006 NRC Canada

Scheme 13. Twist-boat deprotonation model of ***Z*-45**.



ented. DFT calculations[5] on the transition state for the deprotonation of protio-***Z*-45**, employing lithium dimethylamide for simplification of the calculations, support the assertion that H_e deprotonation occurs through a twist-boat transition state (**47**). As the transition state for H_a deprotonation through the chair (**48**) is 2.2 kcal/mol lower in energy relative to **47** according to DFT calculations (again employing lithium dimethylamide), it is entirely possible that the observed results are due to a primary deuterium isotope effect in ***Z*-45** impeding axial H_a deprotonation via **48**; the degree of the contribution of this isotope effect, however, is unknown at this time. Deprotonation of H_a through a complementary twist-boat conformation (**49**) may also be deduced computationally (**50**), with approximately the same energy as **47** (within 0.1 kcal/mol).

Conclusions

We believe that the results reported herein advance our understanding of vinylogous deprotonation reactions in α,β-unsaturated carbonyl systems. The conditions for regio- and stereoselective γ-deprotonation of systems **2** (X = NR_2) followed by simple electrophile quench may be usefully extended to functionalized, and therefore more useful, electrophiles and thereby lead to γ-chain extended intermediates of synthetic value. As one illustration, the construction of terpenoid frameworks could be achieved in a direct manner rather than in several steps. Finally, in view of the progress in the area of enantioselective deprotonation chemistry (39), potentially important results for construction of chiral building blocks may be anticipated.

Experimental section

General methods

Elemental analyses were performed by M-H-W Laboratories, Phoenix, Arizona. Melting points were determined on a Büchi SMP-20 instrument and are uncorrected. Infrared spectra were determined on a PerkinElmer 983 spectrophotometer. ^{1}H NMR spectra were determined with Bruker WP-80 and Bruker AM-250 spectrometers. The spectra were recorded at 80 or 250 MHz in $CDCl_3$ with tetramethylsilane as an internal standard unless otherwise stated. ^{2}H NMR spectra were determined using a Bruker AM-250 spectrometer in C_6H_6 or $CHCl_3$, with C_6D_6 or $CDCl_3$, respectively, as internal standards. Spectral features are tabulated in the following order: chemical shift (δ, ppm); multiplicity (singlet (s), doublet (d), triplet (t), quartet (q), septet (sept), multiplet (m), broad (br)), coupling constant (*J*, Hz); number of protons; assignment. Low-resolution mass spectra were determined on a VG 7070F instrument at 20 eV (1 eV = 1.602 19 × 10^{-19} J) unless otherwise stated. High-resolution mass spectra were determined on a VG ZAB-E spectrometer. Analytical gas chromatography (GC) was performed on either a Hewlett Packard 5840 A instrument or a Varian 6500 instrument using commercially available 10% SE-30 packed and capillary columns, respectively. Preparative HPLC was done on a Waters PREP-500 with an SiO_2 column. Analytical thin layer chromatography (TLC) was performed using Merck precoated silica gel 60F-254 or aluminum oxide 150F-254 neutral (type T) sheets. Preparative TLC was performed using Merck silica gel 60GF-254 with a plate thickness of 1 mm. Column chromatography was carried out using silica gel 60 (0.063–0.20 mm and 0.04–0.063 mm). Flash chromatography refers to the method reported by Still et al. (40).

All dry solvents were employed after distillation from the appropriate drying agent (41). Diethyl ether (Et_2O), benzene, and tetrahydrofuran (THF) were distilled from benzophenone-ketyl immediately prior to use. Solutions of *n*-BuLi, *s*-BuLi, and *t*-BuLi were titrated with 2,5-dimethoxybenzyl alcohol (42) as a standard. Diisopropylamine was dried and distilled over CaH_2 and stored in brown bottles over 4 Å mo-

© 2006 NRC Canada

lecular sieves in a dessicator containing $CaCl_2$. All other reagents were purified according to literature procedures (41). All lithiation reactions were carried out under high purity nitrogen or argon.

The term "–78 °C" refers to the temperature of a CO_2–acetone bath (normally –75° to –78 °C). The phrase "workup in the usual manner" or "standard workup" refers to the addition of satd. aq. NH_4Cl to the reaction mixture, followed by evaporation of the organic solvent under reduced pressure, extraction of the residue with CH_2Cl_2 or diethyl ether (Et_2O), drying of the organic extract over $MgSO_4$, filtration, and then evaporation to dryness under reduced pressure to afford the crude product. Subsequent chromatography and (or) recrystallization and (or) distillation of the crude material afforded pure products.

Cuprate reactions were worked up in the following manner. The organic solvent was evaporated under reduced pressure, diethyl ether was added, and the mixture was filtered. The ethereal layer was separated and the remaining aqueous layer was further extracted with diethyl ether. The combined ether layers were then back-extracted with aq. NH_4OH and satd. NaCl, then dried over $MgSO_4$, filtered, and concentrated under reduced pressure.

General procedure for the formation of lithium dienolates

Preparation of LDA

Diisopropylamine (5 mmol, 0.70 mL) was dissolved in THF (25 mL), and cooled to 0 °C. *n*-BuLi (5 mmol) was added by syringe injection over a period of about 30 s. The solution was then stirred for a further 0.5 h at 0 °C.

Lithiation with LDA — Procedure A

The amide in question was added by syringe to 1.05 equiv. of LDA in THF at –78 °C so that the concentration in solution was roughly 0.2 mol/L. This solution was stirred at –78 °C for 1 h prior to electrophile addition.

Lithiation with LDA — Procedure B

The amide in question was added by syringe to 1.05 equiv. of LDA in THF at 0 °C so that the concentration in solution was roughly 0.2 mol/L. This solution was stirred at 0 °C for 0.5 h prior to electrophile addition.

Lithiation with LDA — Procedure C

The amide in question was added by syringe to 1.05 equiv. of LDA in THF at room temperature (RT) so that the concentration of the amide or amide dienolate in solution was roughly 0.2 mol/L. This solution was stirred at RT for 1 h prior to electrophile addition.

Alkylation of lithium dienolates

The temperature of the solution of the lithium dienolate was adjusted to 0 °C at which time an excess of the electrophile was added by syringe. The resulting mixture was allowed to stir for 0.5 h at 0 °C before the ice bath was removed. The mixture was allowed to come to room temperature, after which a standard workup was performed.

***Z*- and *E*-*N*,*N*,2,3-Tetramethyl-4-trimethylsilyl-3-butenamide (*Z*- and *E*-5a)**

Compound ***Z*-3a** (0.9212 g, 4.62 mmol) was lithiated according to procedure C and alkylated with iodomethane (0.4 mL) in the normal manner. After a standard workup, the crude product was subjected to column chromatography (ethyl acetate – hexane, 1:1–2:1) to give a mixture of ***Z*-** and ***E*-5a** (0.8860 g, 90%); bp 40–43 °C at 0.005 Torr (1 Torr = 133.322 4 Pa). IR (neat, cm^{-1}) ν_{max}: 1649, 1611. ^1H NMR (C_6D_6) δ: 0.10 and 0.07 (2s, 9H, $3SiCH_3$), 1.35, 1.38 (2d, J = 7 Hz, 3H, CH_3), 1.75, 1.79 (2d, J = 0.73, 1.17 Hz, 3H, CH_3), 2.40, 2.67 (2s, 6H, $2NCH_3$), 3.04, 3.41 (2q, J = 7 Hz, 1H, CH), 5.26, 5.36 (2m, 1H, vinyl CH). MS *m*/*e* (rel. intensity): 213 (M^+, 9), 199(33), 198(100), 140(24), 101(36), 73(43). Anal. calcd. for $C_{11}H_{23}NOSi$: C 61.91, H 10.86, N 6.56; found: C 62.10, H 11.05, N 6.73.

Preparative HPLC (hexane – ethyl acetate, 3:1) successfully separated small amounts of ***Z*-5a** and ***E*-5a**. The following peaks in the ^1H NMR spectrum were assigned to represent the *E* isomer: 0.10, 1.35, 1.75 (J = 0.73 Hz), 3.04, 5.36. The following peaks in the ^1H NMR spectrum were assigned to represent the *Z* isomer: 0.079, 1.38, 1.79 (J = 1.17 Hz), 3.41, 5.26. By peak heights of the various distinguishable signals and the integrated areas under the δ 3.04 and δ 3.41 peaks, the ratio of ***E*-5a** to ***Z*-5a** in the unseparated mixture was established to be 79:21.

***N*,*N*,2-Trimethyl-3-trimethylsilylmethyl-3-butenamide (7a)**

Compound ***E*-3a** (0.7191 g, 3.61 mmol) was lithiated according to procedure B and alkylated with iodomethane (0.4 mL) in the normal manner. After a standard workup, the crude product was subjected to flash chromatography (CH_2Cl_2–acetone,15:1) to give 0.6993 g (84%) of **7a**; bp 60–62 °C at 0.01 Torr (lit. value (15*k*) bp 65–70 °C at 0.015 Torr).

4-Deuterio-*N*,*N*,3-trimethyl-2-butenanide (*Z*-3b)

N,*N*-Dimethylsenecioamide (1.34 mL, 9.8 mmol) was lithiated according to procedure A. To the resulting dienolate at –78 °C was added CuI (1.822 g, 9.6 mmol). The mixture was stirred for a further 1 h at –78 °C and 1.7 mL (excess) MeOD was added. The reaction was allowed to warm to RT over 6 h, before 2.0 mL of D_2O was added. After a standard workup, the crude product was subjected to column chromatography (ethyl acetate – hexane, 3:2) to give 0.9562 g (75%) of a 57:43 mixture of ***Z*-3b** and its double bond isomer **9**, as determined by the relative areas of vinyl resonances in the ^1H NMR spectrum. Preparative HPLC (CH_2Cl_2–acetone, 10:1) enabled the separation of a small amount of pure ***Z*-3b**; bp 35–40 °C at 0.004 Torr (lit. value (43) bp 62–64 °C at 3.0 Torr). ^1H NMR (C_6D_6) δ: 1.55 (s, 3H, CH_3), 1.96 (s, 2.45H, CH_2D). ^2H NMR (C_6H_6, decoupled) δ: 1.93 (86% of D, CH_2D), 2.84 (7% of D, CHD from **9**), 5.71 (7% of D, CD). MS *m*/*e* (rel. intensity): 129, 128, 127 (M^+, d_2:d_1:d_0, corrected, 1:75:24).

***N*,*N*-Dimethyl-3-oxobutanamide (10)**

Compound **10** was prepared by literature methods (44) in 67% yield; bp 80–83 °C at 0.9 Torr (lit. value (44) bp 109° at 10 Torr).

© 2006 NRC Canada

4-Deuterio-*N*,*N*-dimethyl-3-oxobutanamide (11)

To a suspension of NaH (1.6917 g, 66 mmol) in THF (125 mL) was slowly added **10** (4.2925 g, 33.2 mmol). After stirring for 20 min, the resulting white gel was cooled to 0 °C and *n*-BuLi (36.5 mmol) added. The resulting mixture was stirred for 20 min at 0 °C. In a separate flask, D_2O (3 mL) was added to trifluoroacetic anhydride (7 mL) at 0 °C and the resulting solution was rapidly added to the first flask. After stirring for 15 min at 0 °C, the reaction was worked up in the following manner. Saturated aqueous ammonium chloride was added and the mixture was concentrated under reduced pressure. The resulting mixture was extracted several times with CH_2Cl_2. The combined CH_2Cl_2 layers were washed with saturated aq. $NaHCO_3$, dried over $MgSO_4$, filtered, and concentrated under reduced pressure. The resulting crude product was distilled to give **11** (2.8935, g, 67%); bp 95 to 96 °C at 1.9 Torr. ^{1}H NMR δ: 1.91, 2.24 (2m, 2H, CH_2D), 2.98, 3.00 (2s, 6H, $2NCH_3$), 3.54 (s, 1.15H, CH_2), 4.14 (s, 0.43H, vinyl CH). MS *m*/*e* (rel. intensity): 131, 130, 129 (M^+, d_2:d_1:d_0, corrected, 9:72:19).

Z-4-Deuterio-3-[(diethylphosphoryl)oxy]-*N*,*N*-dimethyl-2-butenamide (12) and *E*-4-deuterio-*N*,*N*,3-trimethyl-2-butenamide (*E*-3b)

To a suspension of NaH (0.5780 g, 26.1 mmol) in THF (125 mL) was slowly added **11** (2.8363 g, 21.8 mmol). After stirring for 20 min, diethyl chlorophosphate (3.40 mL, 22.9 mmol) was added. The resulting yellow suspension was stirred for 0.5 h. A standard workup gave **12**. IR (neat, cm^{-1}) ν_{max}: 1679, 1631, 1275. ^{1}H NMR δ: 1.35 (td, *J* = 7, 1.0 Hz, 6H, $2CH_3$), 2.11 (br s, 2H, CH_2D), 2.96, 3.05 (2s, 6H, $2NCH_3$), 4.18 (dq, *J* = 7, 7 Hz, 4H, $2OCH_2$), 5.42 (s, 1H, CH). MS *m*/*e* (rel. intensity): 267, 266, 265 (M^+, d_2:d_1:d_o, corrected, 14:68:17), 266 (M^+, 20), 222(29), 194(22), 166(44), 156(36), 155(100), 127(72). The crude **12** was not purified, but was carried on directly to the next step.

To a solution of lithium dimethylcuprate (46.4 mmol) in Et_2O (125 mL) at –78 °C was added **12** (6.5361 g). The suspension was stirred for 2 h at –78 °C, then for 1 h at –45 °C and finally warmed to 0 °C for 15 min. After a standard workup, column chromatography of the crude reaction product gave ***E*-3b** (1.8574 g, 67%); bp 45–50 °C at 0.05 Torr. ^{1}H NMR (C_6D_6) δ: 1.54 (br s, 2H, CH_2D), 1.97 (d, *J* = 1.2 Hz, 3H, CH_3), 2.39, 2.70 (2br s, 6H, $2NCH_3$), 5.65 (br s, 1H, CH). ^{2}H NMR (C_6H_6, decoupled) δ: 1.57 (90% of D, CH_2D), 1.92 (5% of D, CH_2D), 5.72 (5% of D, CD). MS *m*/*e* (rel. intensity): 129, 128, 127 (M^+, d_2:d_1:d_0, corrected, 10:71:19), 85, 84, 83 (M^+ – 44, d_2:d_1:d_0, corrected, 8:70:22).

4-Deuterio-*N*,*N*,2,3-tetramethyl-3-butenanide (*E*-5b)

Compound ***Z*-3b** (0.10 mL, 0.72 mmol) was lithiated according to procedure B and the resulting dienolate was alkylated in the normal manner with iodomethane (0.08 mL). After a standard workup, distillation of the crude product gave ***E*-5b** (0.0803 g, 78%); bp 40–50 °C at 0.004 Torr. ^{1}H NMR δ: 1.26 (d, *J* = 7 Hz, 3H, CH_3), 1.73 (s, 3H, CH_3), 2.93, 2.98 (2s, 6H, $2NCH_3$), 3.34 (q, *J* = 7 Hz, 1H, CH), 4.79, 4.86 (2m, 1.3H, CHD). ^{2}H NMR (C_6H_6) δ: 1.60 (t, *J* = 2.2 Hz, 10% of D), 2.93 (s, 12% of D, CD), 4.72 (s, 78% of D, CHD). MS *m*/*e* (rel. intensity): 128, 127, 126 (M^+ – 15, d_2:d_l:d_0, corrected, 4:65:31).

3-Deuteriomethyl-*N*,*N*,2-trimethyl-3-butenanide (7b)

Compound ***E*-3b** (0.4149 g, 3.24 mmol) was lithiated according to procedure B and the resulting dienolate was alkylated with iodomethane (0.30 mL) in the normal manner. Following a standard workup, the crude product was subjected to column chromatography (ethyl acetate – hexane, 4:1) to give **7b** (0.3124 g, 68%); bp 30–35 °C at 0.08 Torr (Kugelrohr). ^{1}H NMR (C_6D_6) δ: 1.26 (d, *J* = 7 Hz, 3H, CH_3), 1.62 (m, 2H, CH_2D), 2.42, 2.67 (2br s, 6H, $2NCH_3$), 3.03 (q, *J* = 7 Hz, 1H, CH), 4.72 (s, 2H, CH_2). ^{2}H NMR (C_6H_6, decoupled) δ: 1.60 (87% of D, CH_2D), 2.97 (4% of D, CD), 4.72 (10% of D, CHD). MS *m*/*e* (rel. intensity): 85, 84, 83 (M^+ – 59, d_2:d_1:d_0, corrected, 11:65:24).

Ethyl 3-oxo-2-triphenylphosphoranylidenepentanoate (14a) and ethyl 2-pentynoate (15a)

Ethyl 3-oxo-2-triphenylphosphoranylidenepentanoate(**14a**) was prepared from the reaction of ethyl phosphoranylidene acetate and propanoyl chloride as described by Hanack et al. (24). Compound **14a** was identified by ^{1}H NMR only. ^{1}H NMR δ: 0.85 (t, *J* = 7 Hz, 3H, CH_3), 1.40 (t, *J* = 8 Hz, 3H, CH_3), 3.17 (q, *J* = 8 Hz, 2H, CH_2), 3.81 (q, *J* = 7 Hz, 2H, OCH_2), 7.71 (m, *J* = 15 Hz, 3H, C_6H_5). The crude **14a** was heated in a flask fitted with a Vigreux column at 260–280 °C and 0.4 Torr for 4 h and the distillate was collected in a flask at –78 °C. The distillate was redistilled under reduced pressure to give **15a** (2.7577 g, 71% based on propanoyl chloride); bp 64–66 °C at 9 Torr (lit. value (45) bp 178.5 °C).

Ethyl *E*-3-ethyl-2-heptenoate (16a)

To a solution of lithium di-*n*-butylcuprate (5.5 mmol) in THF (25 mL) at –78 °C was added **15a** (0.6341 g, 5.03 mmol) in a minimum amount of THF (~2 mL). The mixture was stirred at –78 °C for 1.5 h, after which ethanol and then satd. aq. NH_4Cl were added dropwise. The mixture was then allowed to warm to room temperature overnight. After the normal workup for cuprate reactions, the crude product was purified by distillation under reduced pressure to give **16a** (0.6843 g, 75%); bp 96–98 °C at 8 Torr. IR (neat, cm^{-1}) ν_{max}:1715, 1642. ^{1}H NMR δ: 0.8–1.6 (m, 13H, $3CH_3$ + $2CH_2$), 2.16 (br m, 2H, CH_2), 2.61 (q, *J* = 8 Hz, 2H, CH_2), 4.15 (q, *J* = 7 Hz, 2H, OCH_2), 5.61 (br s, 1H, CH). MS *m*/*e* (rel. intensity): 184 (M^+, 35), 155(59), 142(75), 139(100), 127(23), 114(51). Anal. calcd. for $C_{11}H_{20}O_2$: C 71.70, H 10.94; found: C 71.68, H 11.01.

***E*-3-Ethyl-2-heptenoic acid (17a) and *E*-3-ethyl-*N*,*N*-dimethyl-2-heptenamide (18a)**

To a solution of KOH (0.8695 g) in methanol–water (15 mL, H_2O–MeOH, 10:1) was added ester **16a** (0.6563 g, 3.56 mmol). The reaction mixture was heated under reflux for 5 h, extracted with diethyl ether (50 mL), acidified with HCl, and extracted with CH_2Cl_2 (4 × 25 mL). The combined CH_2Cl_2 extracts were dried over $MgSO_4$, filtered, and concentrated under reduced pressure to give **17a** (0.5091 g, 92%). Compound **17a** was identified spectroscopically by IR ((neat, cm^{-1}) ν_{max}: 1690, 1636 (lit. value (46) ν_{max} 1690, 1640)), then dissolved in benzene (25 mL) and treated with

© 2006 NRC Canada

thionyl chloride (0.9 mL) for 40 h. The excess thionyl chloride and benzene were removed under reduced pressure, the residue dissolved in diethyl ether (25 mL), and dimethylamine bubbled through the solution for 0.5 h at 0 °C. The mixture was made basic with 10% aq. NaOH, the organic layer separated, and the aqueous layer extracted with CH_2Cl_2 (3 × 25 mL). The combined organic extracts were dried over $MgSO_4$, filtered, and concentrated under reduced pressure. Distillation of the crude product gave **18a** (0.5028 g, 84%); bp 78–80 °C at 0.3 Torr. IR (neat, cm^{-1}) ν_{max}: 1628. ^1H NMR δ: 0.8–1.2 (m, 6H, $2CH_3$), 1.3–1.6 (m, 4H, $2CH_2$), 2.12 (m, 2H, CH_2), 2.31 (q, J = 7 Hz, 2H, CH_2), 2.97, 3.01 (2s, 6H, $2NCH_3$), 5.74 (br s, 1H, CH). MS *m/e* (rel. intensity): 183 (M^+, 51), 153(32), 139(100), 72(83). Anal. calcd. for $C_{11}H_{21}NO$: C 72.08, H 11.55, N 7.64; found: C 71.94, H 11.33, N, 7.66.

3-Ethyl-*N*,*N*-dimethyl-2-pentenamide (18g)

To a suspension of NaH (0.6032 g, 25.1 mmol) in benzene (125 mL) was added diethyl 2- (dimethylamino)-2-oxoethylphosphonate (4.92 mL, 25.0 mmol). The mixture was stirred for 45 min and then 3-pentanone (28 mL, 26 mmol) was added. The reaction mixture was heated under reflux for 21 h and the reaction worked up in the normal manner. The crude product was subjected to flash chromatography (ethyl acetate – hexane, 4:1) to give one fraction, which was shown to be **18g** (1.7642 g, 46%); bp 64 to 65 °C at 0.6 Torr. IR (neat, cm^{-1}) ν_{max}: 1630. ^1H NMR δ: 1.05 (m, 6H, $2CH_3$), 2.15 (q, J = 8 Hz, 2H, CH_2), 2.32 (q, J = 8 Hz, 2H, CH_2), 2.98, 3.00 (2s, 6H, $2NCH_3$), 5.73 (br s, 1H, CH). MS *m/e* (rel. intensity): 155 (M^+, 57), 111(100), 72(27). Anal. calcd.for $C_9H_{17}NO$: C 69.63,H 11.04, N 9.02; found: C 69.59, H 11.13, N 9.01.

***Z*- and *E*-3-(1-Butyl)-*N*,*N*,2-trimethyl-3-pentenamide (19a)**

Compound **18a** (0.5028 g, 2.743 mmol) was lithiated according to procedure C and the resulting dienolate was alkylated with iodomethane (0.35 mL) in the normal manner. Following a standard workup, the crude reaction product was subjected to preparative TLC (ethyl acetate – hexane, 95:2) to afford two fractions. The first fraction was shown to be **19a** (0.2925 g, 54%); bp 60–65 °C at 0.2 Torr. IR (neat, cm^{-1}) ν_{max}: 1645. ^1H NMR (250 MHz) δ: 0.85–1.05 (m, 3H, CH_3), 1.21 (d, J = 7 Hz, 3H, CH_3), 1.32 (m, 2H, CH_2), 1.61, 1.66 (2d, J = 7 Hz, 2H, CH_2 from ***E*-** and ***Z*-19a**, respectively), 2.06 (m, 2H, CH_2), 2.90, 2.91, 2.94, 2.97 (2 × 2s, 6H, $2NCH_3$ from ***Z*-** and ***E*-19a**, respectively), 3.28, 3.62 (2q, J = 7 Hz, 1H, CH from ***E*-** and ***Z*-19a**, respectively, relative area 79:21), 5.29 (q, J = 7 Hz, 2H, vinyl CH). MS *m/e* (rel. intensity): 197 (M^+, 5), 182(94), 72(100), 59(100). Anal. calcd. for $C_{12}H_{23}NO$: C 73.04, H 11.75, N 7.10; found: C 72.83, H 11.77, N 7.36. The second fraction proved to be starting **18a** (0.1276 g, 25%).

***Z*- and *E*-3-(2-Butyl)-*N*,*N*,-2-trimethyl-3-pentenamide (19b)**

Compound **18b** (0.1260 g, 0.6784 mmol) was lithiated according to procedure C and the resulting dienolate was alkylated with iodomethane (0.15 mL) in the normal manner. Following a standard workup, the crude reaction product was subjected to column chromatography (hexane – ethyl acetate, 3:1). After a small forerun containing dialkylated material, the one significant fraction proved to be **19b** (0.1212 g, 89%); bp 65–70 °C at 0.2 Torr. IR (neat, cm^{-1}) ν_{max}: 1646. ^1H NMR (250 MHz) δ: 0.7–1.5 (m, 11H, $3CH_3$ + CH_2), 1.66, 1.69 (2d, J = 7 Hz, 3H, CH_3 for ***E*-** and ***Z*-19b**, respectively), 2.06, 2.46 (2m, 1H,CH for ***Z*-** and ***E*-19b**, respectively), 2.92, 2.93 and 2.94, 3.02 (2× 2s, 6H, $2NCH_3$, for ***Z*-** and ***E*-19b**, respectively). MS *m/e* (rel. intensity): 197(M^+, 4), 182(100), 72(45). Anal. calcd. for $C_{12}H_{23}NO$: C 73.04, H 11.75, N 7.10; found: C 73.23, H 11.73, N 6.93.

***E*-3-(1,1-Dimethylethyl)-*N*,*N*-2-trimethyl-3-pentenamide (19c)**

Compound **18c** (0.1160 g, 0.6328 mmol) was lithiated according to procedure C and the resulting dienolate alkylated with iodomethane (0.20 mL) in the normal manner. Following a standard workup, the crude reaction mixture was subjected to column chromatography (hexane – ethyl acetate, 3:1) to give only one fraction, which was shown to be **19c** (0.0940 g, 75%); bp 60–65 °C at 0.05 Torr. IR (neat, cm^{-1}) ν_{max}: 1648. NMR (250 MHz) δ: 1.09 (s, 9H, $3CH_3$), 1.32 (d, J = 7 Hz, 3H, CH_3), 1.66 (d, J = 7 Hz, 3H, CH_3), 2.93 (s, 6H, $2NCH_3$), 3.56 (q, J = 7 Hz, 1H, CH), 5.54 (q, J = 7 Hz, 1H, CH). MS *m/e* (rel. intensity): 197 (M^+, 2), 182(100), 72(83). Anal. calcd. for $C_{12}H_{23}NO$: C 73.04, H 11.75, N 7.10; found: C 72.89, H 11.51, N, 7.28.

***Z*- and *E*-3-(2-Butyl)-*N*,*N*,2,5-tetramethyl-3-hexenamide (19d)**

Compound **18d** (0.4405 g, 2.084 mmol) was lithiated according to procedure C and the resulting dienolate alkylated with iodomethane (0.30 mL) in the normal manner. Following a standard workup, the crude reaction product was subjected to preparative TLC (ethyl acetate – hexane, 1:1) to give two fractions. The first fraction was shown to be **19d** (0.2254 g, 54%); bp 60–64 °C at 0.02 Torr. IR (neat, cm^{-1}) ν_{max}: 1643. ^1H NMR (250 MHz) δ: 7.15 (m, 17H, $5CH_3$ + CH_2), 2.03 (m, 1H, CH), 2.65 (m, 1H, CH), 2.94 (m, 6H, $2NCH_3$), 3.25, 3.71 (m, 1H, CH). MS *m/e* (rel. intensity): 225 (M^+, 3), 210(100), 100(23), 72(66). Anal. calcd. for $C_{14}H_{27}NO$: C 74.61, H 12.08, N 6.21; found: C 74.61, H 11.88, N 6.01. The second fraction was found to contain starting material **18d** (0.1657 g, 38%).

***Z*-3-(1-Butyl)-4-methoxy-*N*,*N*,2-trimethyl-3-butenanide (19f)**

Compound **18f** (0.1365 g, 0.6849 mmol) was lithiated according to procedure C and the resulting dienolate alkylated with iodomethane (0.15 mL) in the normal manner. Following a standard workup, the crude reaction product was subjected to flash chromatography (fine silica, ethyl acetate – hexane, 1:1) to afford **19f** (0.1234 g, 84%); bp 59–62 °C at 0.007 Torr. IR (neat, cm^{-1}) ν_{max}: 1647. ^1H NMR (250 MHz) δ: 0.87 (m, 3H, CH_3), 1.17 (d, J = 7 Hz, 3H, CH_3), 1.29 (m, 4H, $2CH_2$), 1.82 (m, 2H, CH_2), 2.91, 2.94 (2s, 6H, $2NCH_3$), 3.58 (s, 3H, OCH3), 3.90 (q, J = 7 Hz, 1H, CH), 5.76 (m, 1H, CH). Irradiation of the δ 5.76 resonance resulted in a 22% integrated enhancement of the δ 1.82 resonance; irradiation of the δ 1.82 resonance resulted in an 11% integrated enhancement in the δ 5.76 signal. MS *m/e* (rel. intensity):

© 2006 NRC Canada

213 (M^+, 26), 198(27), 141(100), 99(62). Anal. calcd. for $C_{13}H_{23}NO$: C 67.57, H 10.87, N 6.57; found: C 67.68, H 10.76, N 6.63.

_Z_- and _E_-3-Ethyl-_N_,_N_,3-trimethyl-3-pentenamide (19g)

Compound **18g** (0.1220 g, 0.7858 mmol) was lithiated according to procedure C and the resulting dienolate alkylated with iodomethane (0.20 mL) in the normal manner. Following standard workup, column chromatography (hexane – ethyl acetate, 5:2) afforded one fraction, which was shown to be **19g** (0.1057 g, 80%); bp 58–62 °C at 0.2 Torr. IR (neat, cm^{-1}) ν_{max}: 1645. ^1H NMR (250 MHz) δ: 0.96 (t, J = 8 Hz, 3H, CH_3), 1.18, 1.21 (2d, J = 7 Hz, 3H, CH_3 for ***Z***- and ***E*-19g**, respectively), 1.62, 1.67 (2d, J = 7, 3H, CH_3 for ***E***- and ***Z*-19g**, respectively), 2.10 (q, J = 8 Hz, 2H, CH_2), 2.96 (m, 6H, $2NCH_3$), 3.29, 3.64 (2q, J = 7 Hz, 1H, CH for ***E***- and ***Z*-19g**, respectively, relative area 79:21), 5.27 (q, J = 7 Hz, 1H, CH). MS *m*/*e* (rel. intensity): 169 (M^+, 4), 154(100), 74(69), 72(89). Anal. calcd. for $C_{10}H_{19}NO$: C 70.96, H 11.31, H 8.28; found: C 70.86, H 10.89, N 8.63.

Compound **18g** (0.4156 g, 268 mmol) was lithiated according to procedure C and alkylated at –78 °C with iodomethane (0.4 mL). After allowing the reaction to warm overnight to RT, a standard workup was performed and the crude reaction product was subjected to preparative TLC (ethyl acetate – hexane, 5:2) to yield **19g** (0.3213 g, 71%) as the only isolated fraction. Integration of the δ 3.29 and δ 3.64 resonances in the ^1H NMR spectrum established the ratio of ***E*-19g**:***Z*-19g** as 92:8.

***Z*-_N_,_N_-Dimethyl-3-hexenamide (23)**

Compound **23** was prepared by the method reported by Baldwin and co-workers (16*j*) in 35% yield based on methyl sorbate; bp 46–48 °C at 2 Torr.

***Z*-_N_,_N_,-2-Trimethyl-3-hexenamide (24)**

Compound **23** (0.1394 g, 0.987 mmol) was lithiated according to procedure A and the resulting dienolate alkylated with iodomethane (0.20 mL) in the normal manner. Following a standard workup, column chromatography (hexane – ethyl acetate, 5:2) of the crude product gave, after a forerun that contained a trace amount of dialkylated material, compound **24** (0.1281 g, 84%); bp 75–80 °C at 2.0 Torr. IR (neat, cm^{-1}) ν_{max}: 1643. ^1H NMR (250 MHz) δ: 1.00 (t, J = 8 Hz, 3H, CH_3), 1.81 (d, J = 7 Hz, 3H, CH_3), 2.10 (m, 2H, CH_2), 2.94, 3.01 (2s, 6H, $2NCH_3$), 3.61 (qd, J = 7, 7 Hz, 1H, CH), 5.04 (m, 2H, $2CH_2$); a signal at δ 3.33 (qd, m, CH for ***E*-24**) was barely perceptible and ***E*-24** was therefore estimated to be present to the extent of 5%. MS *m*/*e* (rel. intensity): 155 (M^+, 16), 140(22), 83(100). Anal. calcd. for $C_9H_{17}NO$: C 69.63, H 11.04, N 9.02; found: C 69.63, H 11.16, N 9.08.

_N_,_N_-Dimethyl-2-[*cis*-5-(1,1-dimethylethyl)-6-methyl-1-cyclohexenyl]propanamide (32)

Compound **31** (0.2468 g, 1.04 mmol) was lithiated according to procedure C and the resulting dienolate alkylated with iodomethane (0.18 mL) in the normal manner. Following a standard workup, the crude product was subjected to column chromatography (hexane – ethyl acetate, 4:1) to give one fraction, which was shown to contain **32** as a pair of diastereomers (0.2480 g, 95%); bp 89–94° at 0.02 Torr. IR (neat, cm^{-1}) ν_{max}: 1646. ^1H NMR (250 MHz) δ: 0.87, 0.89 (2s, 9H, $3CH_3$), 1.03, 1.15 (2d, J = 7 Hz, 3H, CH_3), 1.26 (d, J = 7 Hz, 3H, CH_3), 1.4–2.1 (m, 5H, $2CH_2$ + CH), 2.23 (q, J = 7 Hz, 1H, CH), 2.93, 3.06 and 2.95, 2.97 (4s, 6H, $2NCH_3$), 3.32, 3.37 (2q, J = 7 Hz, 1H, CH), 5.45, 5.73 (2dd, J = 7, 7 Hz, 1H, CH). MS *m*/*e* (rel. intensity): 251 (M^+, 9), 236(33), 194(100), 101(25), 72(136). Anal. calcd. for $C_{16}H_{29}NO$: C 76.44, H 11.63, N 5.57; found: C 76.36, H 11.72, N 5.48.

_N_,_N_-Dimethyl-2-[*trans*-5-(1,1-dimethylethyl)-6-methyl-1-cyclohexenyl]propanamide (34)

Compound **33** (0.198 g, 0.808 mmol) was lithiated according to procedure C and the resulting dienolate alkylated with iodomethane (0.10 mL) in the normal manner. Following a standard workup, the crude reaction product was subjected to flash chromatography (fine silica, hexane – ethyl acetate, 9:2) to give one major fraction, which contained **34** as a pair of diastereomers (0.1670 g, 82%); bp 90–95 °C at 0.02 Torr. IR (neat, cm^{-1}) ν_{max}: 1646. ^1H NMR δ: 0.84 (s, 9H, $3CH_3$), 0.9–2.3 (m, 12H, $2CH_3$ + $2CH_2$ + 2CH), 2.93, 2.97 (2s, 6H, $2NCH_3$), 3.1–3.6 (m, 1H, CH), 5.34, 5.58 (2br s, 1H, CH). MS *m*/*e* (rel. intensity): 251 (M^+, 12), 236(39), 194(100), 101(38), 72(147). Anal. calcd. for $C_{16}H_{29}NO$: C 76.44, H 11.63, N, 5.57; found: C 76.21, H 11.50, N 5.64.

***trans*-6-Deuterio-5-(1,1-dimethylethyl)-1-cyclohexenyl-_N_,_N_-dimethylpropanamide (36)**

Compound ***Z*-35** (0.1666 g, 0.743 mmol) was lithiated according to procedure C and the resulting dienolate alkylated with iodomethane (0.15 mL) in the normal manner. Following standard workup, the crude product was subjected to flash chromatography (fine silica, hexane – ethyl acetate, 4:1) to afford one fraction, which contained **36** as a pair of diastereomers (0.1667 g, 95%); bp 90–95 °C at 2 Torr. IR (neat, cm^{-1}) ν_{max}: 1646. ^1H NMR (250 MHz) δ: 0.87 (s, 9H, $3CH_3$), 1.22 (d, J = 7 Hz, 3H, CH_3), 1.0–1.35 (partially obscured m, 1H, CH), 1.65–2.2 (m, 5H, CH_2 + 3CH), 2.95, 2.96, 2.97, 2.98 (4s, 6H, $2NCH_3$), 3.18 (m, 1H, CH), 5.47 (m, 1H, CH). ^2H NMR δ: 1.92 (s, approx. 89% of D), 3.07 (s, approx. 8% of D), 5.49 (s, approx. 3% of D). MS *m*/*e* (rel. intensity): 239, 238, 237 (M^+, d_2:d_1:d_0, corrected, 5:93:22), 238 (M^+, 36), 223(38), 181(100), 167(35), 100(40), 72(173).

_N_,_N_-Dimethyl-2-[*trans*-3-(1,1-dimethylethyl)-6-methyl-1-cyclohexenyl]propanamide (38) and _N_,_N_-dimethyl-2-[5-(1,1-dimethylethyl)-2-inethyl-1-cyclohexenyl]propanamide (39)

Compound **Z-37** (0.1442 g, 0.607 mmol) was lithiated according to procedure C and the resulting dienolate alkylated with iodomethane (0.15 mL) in the normal manner. Following a standard workup, the reaction product was subjected to column chromatography (hexane – ethyl acetate, 5:1) to give one fraction. The contents of this fraction were shown by GC and ^1H NMR spectroscopy to be a roughly 1:1 mixture of **38** and **39** (0.1328 g, 87%); bp 89–94 °C at 0.05 Torr. IR (neat, cm^{-1}) ν_{max}: 1648. ^1H NMR (250 MHz) δ: 0.83, 0.83 (2s, 9H, $3CH_3$), 1.0–2.3 (m, 12 protons of **38** and 13 protons of **39**, $2CH_3$ + $2CH_2$ + 2CH of **38** and $2CH_3$ + $3CH_2$ + CH

© 2006 NRC Canada

of 39), includes 1.65 (s, CH_3 of **39**), 2.9–3.0 (m, 6H, $2NCH_3$), 3.17, 3.3, 3.57 (q, J = 7 Hz, q, J = 7 Hz and m, 1H, CH), 5.33, 5.57 (2s, 1 proton of **38**, CH). MS *m/e* (rel. intensity): 251 (M^+, 12), 236(52), 194(100), 180(52), 101(36), 84(20), 72(171). Anal. calcd. for $C_{16}H_{29}NO$: C 76.44, H 11.63, N 5.57; found: C 76.56, H 11.75, N 5.56.

***cis*-2-Deuterio-5-(1,1-dimethylethyl)cyclohexanone (44)**

To a solution of LDA (13 mmol) in THF (65 mL) at –78 °C was added 3-(1,1-dimethylethyl)cyclohexanone (0.9988 g, 6.48 mmol) in a minimum amount of THF (~5 mL). The solution was stirred for 1 h at –78 °C. In a separate flask, D_2O (0.25 mL) was added to a stirred solution of trifluoroacetic anhydride (0.92 mL, 13 mmol) at –78 °C and the solution allowed to warm to RT. The contents of the latter flask were then added to the former flask, the mixture was stirred at –78 °C for 10 min, and $MgSO_4$ added. After warming to RT, the mixture was filtered through Celite and concentrated under reduced pressure. Distillation of the crude reaction product gave **44** (0.4614 g, 46%); bp 96–98 °C at 10 Torr. MS *m/e* (rel. intensity): 155, 154, 153 (M^+, d_2:d_1:d_0 = 10:40:50).

***Z*- and *E*-(*cis*-2-Deuterio-5-(1,1-dimethylethyl)cyclohexylidene]-*N*,*N*-dimethylacetamide (*Z*- and *E*-45)**

N,*N*-Dimethyltrimethylsilylacetamide (0.9543 g, 5.99 mmol) was lithiated according to procedure A. To a –78 °C solution of the resulting enolate was added **44** (0.9301 g, 5.99 mmol) in a minimum amount of THF (~3 mL). The reaction mixture was stirred for 3 h at –78 °C, warmed to RT, and two drops of water and $MgSO_4$ were added. After filtration through Celite and concentration of the filtrate under reduced pressure, the crude reaction product was subjected to flash chromatography (fine silica, hexane–Et_2O, 2:1). Four fractions were isolated. The first fraction contained starting material **44** (0.0530 g, 6%). The second fraction proved to be ***E*-45** (6.2084 g, 27% including fraction No. 3, see compound ***Z*-35**) contaminated with a small amount (4%) of ***Z*-45**. The third fraction was a 34:66 mixture of ***E*-45** and ***Z*-45** (0.2084 g). The final fraction was shown to contain ***Z*-45** (0.3805 g, 52% including fraction Nos. 2 and 3); bp 85–90 °C at 0.1 Torr. IR (neat, cm^{-1}) ν_{max}: 1628. ^1H NMR (250 MHz) δ: 0.87 (s, 9H, $3CH_3$), 1.0–1.3 (m, 2H, CH_2), 1.65–2.1 (m, 4.5H, CH_2 + 2CH + CD), 2.30 (d, J = 13 Hz, 1H, CH), 2.93 (obscured d, 1H, CH), 5.71 (s, 1H, CH). ^1H NMR (250 MHz, C_6D_6) δ: 0.79 (s, 9H, $3CH_3$), 0.8–1.8 (m, 6H, $2CH_2$ + 2CH + CD), 2.21 (br d, J = 13 Hz, 1H, CH), 2.24, 2.72 (2s, 6H, $2NCH_3$), 3.57 (br d, J = 11 Hz, 1H, CH), 5.68 (s, 1H, CH). ^2H NMR (C_6D_6, decoupled) δ: 1.60 (55% of D), 2.16 (20% of D), 3.48 (25% of D). MS *m/e* (rel. intensity): 225, 224, 223 (M^+, d_2:d_1:d_0, corrected, 9:37:54), 223 (M^+, 100), 180(69), 166(86), 121(46), 95(87), 81(49), 72(115). Anal. calcd. for $C_{14}H_{25}NO$: C 75.28, H 11.28, N 6.27; found: C 74.98, H 11.24, N 6.25.

2-Deuterio-5-(1,1-dimethyl ethyl)-1-cyclohexenyl-*N*,*N*-2-trimethylacetamide (46)

Compound ***Z*-45** (0.1601 g, 0.714 mmol) was lithiated according to procedure C and the resulting dienolate alkylated with iodomethane (0.15 mL) in the usual manner. Following a standard workup, the crude reaction product was subjected to column chromatography (hexane – ethyl acetate, 1:1) to afford one fraction, which contained **46** as a pair of diastereomers (0.1562 g, 92%); bp 85–90 °C at 0.2 Torr. IR (neat, cm^{-1}) ν_{max}: 1644. ^1H NMR δ: 0.87 (s, 9H, $3CH_3$), 1.0–1.35 (partially obscured m, 1H, CH), 1.6–2.2 (m, 6H, $2CH_2$ + 2CH), 2.95, 2.96, 2.97, 2.98 (4s, 6H, $2NCH_3$), 3.18 (m, 1H, CH), 5.47 (m, 0.65H, CD). ^2H NMR (decoupled) δ: 1.72 (9% of D), 2.28 (26% of D), 3.60 (65% of D). MS *m/e* (rel. intensity): 239, 238, 237 (M^+, d_2:d_1:d_0, corrected, 8:27:65), 237 (M^+, 27), 222(26), 181(100), 166(31), 101(50), 72(38). Anal. calcd. for $C_{15}H_{27}NO$: C 75.90, H 11.46, N 5.90; found: C 76.02, H 11.72, N 6.38.

Material on deposit

The experimental procedures and spectral data for the preparation of **14b–14d**, **15b–15d**, **16b–16f**, **17b–17f**, **18b–18f**, (diethylamino)-2-oxoethylphosphonate, the precursors to **31**, **33**, **35**, and **37**, and the minimized structures, final Cartesian coordinates, and energies for the calculated transition states for senecioamide deprotonation (**47**, **49**, and **50**) have been deposited as Supplementary material.[6]

Acknowledgements

We are grateful to the Natural Sciences and Engineering Research Council of Canada (NSERC) for support of our synthetic programs. JRG was a NSERC 1967 Fellowship awardee. We also wish to thank James Gauld for assistance with the DFT calculations on the deprotonation transition states.

References

1. (*a*) R. Mahrwald (*Editor*). Modern aldol reactions. Wiley-VCH, Weinheim, Germany. 2004; (*b*) C.H. Heathcock. *In* Asymmetric synthesis. Vol. 3. *Edited by* J.D. Morrison. Academic Press, New York. 1983. pp. 111–212.
2. (*a*) D.A. Evans. *In* Asymmetric synthesis. Vol. 3. *Edited by* J.D. Morrison. Academic Press, New York. 1983. pp. 1–110; (*b*) see also: R.M. Pollack. Tetrahedron, **45**, 4913 (1989); (*c*) J.R. Green. *In* Science of synthesis. Vol. 8a. *Edited by* M. Majewski and V. Snieckus. Georg Thieme Verlag, Stuttgart, Germany. 2005. pp. 427–486.
3. R.E. Ireland, R.H. Mueller, and A.K. Willard. J. Am. Chem. Soc. **98**, 2868 (1976).
4. R.R. Fraser and P.J. Champagne. J. Am. Chem. Soc. **100**, 657 (1978).
5. (*a*) F. Johnson. Chem. Rev. **68**, 375 (1968); (*b*) G.J. Karabatsos and D.J. Fenoglio. Top. Stereochem. **5**, 167 (1970).
6. (*a*) A.J. Kirby (*Editor*). Stereoelectronic effects. Oxford University, Oxford. 1996; (*b*) P. Deslongchamps. Stereoelectronic effects in organic chemistry. Pergamon Press, Oxford, UK. 1983. p. 274; (*c*) A.J. Kirby. Adv. Phys. Org. Chem. **29**, 87 (1994).
7. For reviews, see: (*a*) M.C. Whisler, S. MacNeil, V. Snieckus, and P. Beak. Angew. Chem. Int. Ed. **43**, 2206 (2004); (*b*) P. Beak and A. I. Meyers. Acc. Chem. Res. **19**, 356 (1986).
8. (*a*) A. Sun and D.B. Collum. J. Am. Chem. Soc. **122**, 2452 (2000); (*b*) D.J. Miller and W.H. Saunders, Jr. J. Org. Chem. **47**, 5039 (1982).
9. (*a*) A. Sun and D.B. Collum. J. Am. Chem. Soc. **122**, 2459 (2000); (*b*) M. Al-Aseer, P. Beak, D. Hay, D.J. Kempf, S.

© 2006 NRC Canada

Mills, and S.G. Smith. J. Am. Chem. Soc. **105**, 2080 (1983); (*c*) A.I. Meyers, W.F. Rieker, and L.M. Fuentes. J. Am. Chem. Soc. **105**, 2082 (1983).

10. (*a*) For the modified Ireland–Narula model, see: H.P. Beutelman, L. Xie, and W.H. Saunders, Jr. J. Org. Chem. **54**, 1703 (1989).
11. (*a*) F.E. Romesberg and D.B. Collum. J. Am. Chem. Soc. **117**, 2166 (1995); (*b*) J.M. Hayes, J.C. Greer, and F.S. Mair. New J. Chem. **25**, 262 (2001).
12. (*a*) In the construction of the carbacyclic prostacyclic analogue isocicaprost, see: M. Lerm, H.-J. Gais, K. Cheng, and C. Vermeeren. J. Am. Chem. Soc. **125**, 9653 (2003); (*b*) in the stereoselective construction of oxetanes and ring fused tetrahydrofurans, see: P. Galatsis, S.D. Millan, and G. Ferguson. J. Org. Chem. **62**, 5048 (1997).
13. (*a*) For reviews, see: S. Gil and M. Parra. Curr. Org. Chem. **6**, 283 (2002); (*b*) G. Casiraghi, F. Zanardi, G. Appendino, and G. Rassu. Chem. Rev. **100**, 1929 (2000); (*c*) J.R. Green. Ph.D. thesis, University of Waterloo, Waterloo, Ontario. 1987.
14. For studies concerning the site of deprotonation, see: (*a*) M. Iguchi and K. Tomioka. Org. Lett. **4**, 4329 (2002); (*b*) M.J. Aurell, L.R. Domingo, R. Mestres, E. Muñoz, and R.J. Zaragoza. Tetrahedron, **55**, 815 (1999); (*c*) D.W. Cameron, M.G. Looney, and J.A. Patterman. Tetrahedron Lett. **36**, 7555 (1995); (*d*) S.Y. Lee, Y.S. Kulkarni, B.W. Burbaum, M.L. Johnston, and B.B. Snider. J. Org. Chem. **53**, 1848 (1988); (*e*) C. Fehr and J. Galindo. J. Org. Chem. **53**, 1828 (1988); (*f*) V. Guay and P. Brassard. Synthesis, 294 (1987); (*g*) S. Tsuboi, K. Muranaka, T. Sakai, and A. Takeda. J. Org. Chem. **51**, 4944 (1986); (*h*) F.L. Harris and L. Weiler. J. Chem. Soc. Chem. Commun. 1124 (1985); (*i*) Y. Thebtaranonth and C. Yenjai. Tetrahedron Lett. **26**, 4097 (1985); (*j*) A.E. Greene, F. Coelho, J.-P. Deprés, and T.J. Brocksom. J. Org. Chem. **50**, 1973 (1985); (*k*) J.-P. Gesson, J.-C. Jacquesy, and B. Renoux. Tetrahedron, **40**, 4743 (1984); (*l*) E. Block, V. Eswarakrisknan, and K. Gebreyes. Tetrahedron Lett. **25**, 5469 (1984); (*m*) P. Brownbridge, P.G. Hunt, and S. Warren. Tetrahedron Lett. **24**, 3391 (1983); (*n*) F.L. Harris and E.-P. Krebs. Helv. Chim. Acta, **64**, 1023 (1984); (*o*) J.-P. Gesson, J.-C. Jacquesy, and M. Mondon. Tetrahedron Lett. **21**, 2509 (1980); (*p*) T.A. Hase and R. Kukkola. Synth. Commun. **10**, 451 (1980); (*q*) J.J. Eisch and J.E. Galle. J. Org. Chem. **44**, 3279 (1979); (*r*) W.G. Dauben, G.T. Rivers, and W.J. Zimmerman. J. Am. Chem. Soc. **99**, 3414 (1977); (*s*) J.A. Katzenellenbogen and A.L. Crumrine. J. Am. Chem. Soc. **98**, 4925 (1976); (*t*) J.D. White and W.L. Sung. J. Org. Chem. **39**, 2323 (1974); (*u*) M.S. Newman, V. De Vries, and R. Darlak. J. Org. Chem. **31**, 2171 (1976).
15. For direct evidence of dienolate structure, see: (*a*) L.R. Domingo, S. Gil, and M. Parra. Tetrahedron: Asymmetry, **12**, 915 (2001); (*b*) L.R. Domingo, S. Gil, R. Mestres, and M.T. Picher. Tetrahedron, **52**, 11105 (1996); (*c*) P.G. Williard, J.R. Tata, R.H. Schlessinger, A.D. Adams, and E.J. Iwanowicz. J. Am. Chem. Soc. **110**, 7901 (1988); (*d*) A.D. Adams, R.H. Schlessinger, J.R. Tata, and J.J. Venit. J. Org. Chem. **51**, 3068 (1986); (*e*) A. Bongini, M. Orena, and S. Sandri. J. Chem. Soc. Chem. Commun. 50 (1986); (*f*) R. Amstutz, J.D. Dunitz, J.P. Laube W.B. Schweizer, and D. Seebach. Chem. Ber. **119**, 434 (1986); (*g*) M.-E. Tran Huu Dau, M. Fétizon, and N.T. Anh. Tetrahedron Lett. 855 (1973); (*h*) G.J. Heiszwolf and H. Kloosterziel. Recl. Trav. Chim. Pays–Bas, **86**, 807 (1967); (*i*) D. Ivanoff, B. Jordanov, and B. Blagoev. Naturwissenschaften, **51**, 286 (1964); (*j*) E.J. Corey and R.A. Sneen. J. Am. Chem. Soc. **78**, 6269 (1956); (*k*) M. Majewski. Ph.D. thesis, University of Waterloo, Waterloo, Ontario. 1982.
16. For evidence based on product analysis, see: (*a*) S.K. Guha, A. Shibayama, D. Abe, M. Sakaguchi, Y. Ukaji, and K. Inomata. Bull. Chem. Soc. Jpn. **77**, 2147 (2004); (*b*) F. Bargiggia and O. Piva. Tetrahedron: Asymmetry, **14**, 1819 (2003); (*c*) M. Hiersemann, C. Lauterbach, and A. Pollex. Eur. J. Org. Chem. 2713 (1999); (*d*) K. Tomooka, A. Nagasawa, and T. Nakai. Chem. Lett. 1049 (1998); (*e*) K. Tomooka, A. Nagasawa, S.-Y. Wei, and T. Nakai. Tetrahedon Lett. **37**, 8895 (1996); (*f*) P. Galatsis, J.J. Manwell, and S.C. Millan. Tetrahedron Lett. **37**, 5261 (1996); (*g*) Y. Yamamoto, S. Hatsuya, and J.-i. Yamada. J. Org. Chem. **55**, 3118 (1990); (*h*) S. Fier, R.W. Sullivan, and B. Rickborn. J. Org. Chem. **53**, 2353 (1988); (*i*) A. Bongini, M. Orena, and S. Sandri. J. Chem. Soc. Chem. Commun. 50 (1986); (*j*) S.G. Alcock, J.E. Baldwin, R. Bohlmann, L.M. Harwood, and J.I. Seeman. J. Org. Chem. **50**, 3526 (1985); (*k*) S.H. Bell, D.W. Cameron, and G.I. Feutrill. Tetrahedron Lett. **26**, 6519 (1985); (*l*) E. Piers and A.V. Gavai. J. Org. Chem. **56**, 2374 (1990); (*m*) Y. Ikeda and H. Yamamoto. Tetrahedron Lett. **25**, 5181 (1984); (*n*) W. Oppolzer, R. Pitteloud, G. Bernardinelli, and K. Baetlig. Tetrahedron Lett. **24**, 4975 (1983); (*o*) A.I. Meyers, W.F. Rieker, and L.M. Fuentes. J. Am. Chem. Soc. **105**, 2082 (1983); (*p*) A.S. Kende and B.H. Toder. J. Org. Chem. **47**, 163 (1982); (*q*) M. Majewski, G.B. Mpango, M.T. Thomas, A. Wuand, and V. Snieckus. J. Org. Chem. **46**, 2029 (1981), and refs. cited therein; (*r*) E.-P. Krebs. Helv. Chim. Acta, **64**, 1023 (1981); (*s*) M. Hayashi, Y. Arai, H. Wakatsuka, M. Kawamura, Y. Konishi, T. Tsuda, and K. Matsumoto. J. Med. Chem. **23**, 525 (1980); (*t*) H. Koyama, K. Kogure, K. Mori, and M.P. Zimmerman. Synth. Commun. **7**, 189 (1977); (*u*) P.E. Pfeffer and L.S. Silbert. J. Org. Chem. **36**, 3290 (1971); (*v*) P.v.R. Schleyer, J.D. Pill, and J.A. Pople. Tetrahedron, **33**, 2497 (1977); (*w*) S.R. Wilson and R.S. Myers. J. Org. Chem. **40**, 3309 (1975); (*x*) A.S. Kende, D. Constantinides, S.J. Lee, and L. Liebeskind. Tetrahedron Lett. 405 (1975); (*y*) M. Matsui. Agr. Biol. Chem. **36**, 792 (1972).
17. P. Beak, D.J. Kempf, and K.D. Wilson. J. Am. Chem. Soc. **107**, 4745 (1985).
18. To avoid overlap, we exclude presentation of our results on **3b**, which are in complete agreement with those reported by Harris and Weiler (ref. 19). For a preliminary communication, see: M. Majewski, J. R. Green, and V. Snieckus. Tetrahedron Lett. **27**, 531 (1986).
19. Weiler and Harris have reported an analogous investigation of α,β-unsaturated acids and esters: (*a*) F.L. Harris and L. Weiler. Tetrahedron Lett. **25**, 1333 (1984); (*b*) F.L. Harris and L. Weiler. Tetrahedron Lett. **26**, 1939 (1985).
20. For a review, see: A.R. Katritzky, M. Piffl, H. Lang, and E. Anders. Chem. Rev. **99**, 665 (1999).
21. J.R. Green, M. Majewski, B.I. Alo, and V. Snieckus. Tetrahedron Lett. **27**, 535 (1986).
22. F.-W. Sum and L. Weiler. Can. J. Chem. **57**, 1431 (1979).
23. (*a*) E. Corey and J.A. Katzenellenbogen. J. Am. Chem. Soc. **91**, 1851 (1969); (*b*) J.B. Siddall, M. Biskup, and J.H. Fried. J. Am. Chem. Soc. **91**, 1854 (1969).
24. M. Hanack, C.J. Collins, H. Stutz, and B.M. Benjamin. J. Am. Chem. Soc. **103**, 2356 (1981).
25. G. Markl. Chem. Ber. **94**, 3005 (1961).
26. C.J. Timmons. J. Chem. Soc. Chem. Commun. 576 (1965).
27. (*a*) B.B. Snider, M. Karras, and R.S.E. Conn. J. Am. Chem. Soc. **100**, 4264 (1978); (*b*) B.B. Snider, R.S.E. Conn, and M. Karras. Tetrahedron Lett. 1679 (1979).
28. W. Kitching, H.A. Olszowy, G.M. Drew, and W. Adcock. J. Org. Chem. **47**, 5153 (1982).

© 2006 NRC Canada

29. R. Amstutz, J.D. Dunitz, J.P. Laube, W.G. Schweizer, and D. Seebach. Chem. Ber. **119**, 434 (1986).
30. (*a*) D. Seebach, R. Amstutz, and J.D. Dunitz. Helv. Chim. Acta, **64**, 2622 (1981); (*b*) H.D. Zook and J.A. Miller. J. Org. Chem. **36**, 1112 (1976).
31. T.I. Moder, C.C.K. Hsu, and F.R. Jensen. J. Org. Chem. **45**, 1008 (1980).
32. W. Kitching, H.A. Olszowy, and K. Harvey. J. Org. Chem. **47**, 893 (1982).
33. J. Sicher, J. Jonáš, and M. Tichý. Tetrahedron Lett. 825 (1963). A value of $A = 1.53$ in a different solvent system has been cited; see: H. Booth and M.L. Jozefowicz. J. Chem. Soc. Perkin Trans. 2, 895 (1976).
34. (*a*) S. Hanessian, A. Gomtsyan, and N. Malek. J. Org. Chem. **65**, 5623 (2000); (*b*) S.E. Denmark and J.E. Marlin. J. Org. Chem. **56**, 1003 (1991).
35. (*a*) T.G. Back and K. Nakajima. J. Org. Chem. **65**, 4543 (2000); (*b*) T.G. Back, M.V. Krishna, and K.R. Muralidharan. J. Org. Chem. **54**, 4146 (1989).
36. (*a*) K. Dawes, N.J. Turro, and J.M. Conia. Tetrahedron Lett. 1377 (1971); (*b*) B.J.L. Huff, T.N. Tuller, and D. Caine. J. Org. Chem. **34**, 3070 (1969).
37. The low deuterium content may be due to internal proton return from $(i\text{-Pr})_2$NH-enolate complexes; see: T. Laube, J.D. Dunitz, and D. Seebach. Helv. Chim. Acta, **68**, 1373 (1985).
38. (*a*) J. Toullec. *In* Advances in physical organic chemistry. Vol. 18. *Edited by* V. Gold and L. Bethell. Academic Press, London. 1982. pp. 1–77; (*b*) G. Lamaty. *In* Isotopes in organic chemistry. Vol. 2. *Edited by* E. Buncel and C.C. Lee. Elsevier. Amsterdam. 1976. pp. 33–88.
39. (*a*) D.M. Hodgson and M.A.H. Stent. Top. Organometal. Chem. **5**, 1 (2003); (*b*) J. Eames. Eur. J. Org. Chem. 393 (2002); (*c*) M. Majewski. *In* Advances in asymmetric synthesis. Vol. 3. *Edited by* A. Hassner. JAI, Stamford. 1998. pp. 39–76; (*d*) N.S. Simpkins. *In* Advanced asymmetric synthesis. *Edited by* G.R. Stephenson. Chapman and Hall, London, UK. 1996. pp. 111–125.
40. W.C Still, M. Kahn, and A. Mitra. J. Org. Chem. **43**, 2923 (1978).
41. D.D. Perrin, W.L. Amarego, and A. Mitra. Purification of laboratory chemicals. 2nd ed. Pergamon, Oxford, UK. 1980.
42. M.R. Winkle, J.M. Lansinger, and R.C. Ronald. J. Chem. Soc. Chem. Commun. 87 (1980).
43. G.B.W. Mpango. Ph.D. dissertation, University of Waterloo, Waterloo, Ontario. 1980.
44. H. Brederick, R. Gompper, and K. Klemm. Chem. Ber. **92**, 1456 (1959).
45. E. Schzanberg. Z. Phys. Chem. **A181**, 430 (1938).
46. G. Cahiez, D. Bernard, and J.F. Normant. Synthesis, 247 (1976).

© 2006 NRC Canada

Synthesis and characterization of a series of novel phenol- and polyphenol-based glycerolipids[1]

Rolf Schmidt, Joseph G. Carrigan, and Christine E. DeWolf

Abstract: A building block approach was used to design a modular synthetic route for the preparation of novel glycerolipids with phenolic and polyphenolic headgroups. Based on this scheme, it is possible to vary the substitution pattern of the headgroup, the stereochemistry of the backbone, and the length of the sidechains. Five glycerolipids with different headgroups and identical backbone stereochemistry and chain length have been prepared.

Key words: glycerolipid, polyphenol, hydrogen bonding, lipid-protein interaction, self-adhering.

Résumé : On a développé une méthode modulaire de synthèse de nouveaux glycérolipides comportant des têtes phénoliques et polyphénoliques. En se basant sur ce schéma, il est possible de faire varier la nature du groupe de tête, la stéréochimie du squelette et la longueur des chaînes latérales. On a préparé cinq glycérolipides dont la stéréochimie du squelette et la longueur de la chaîne sont les mêmes, mais qui diffèrent par la nature de leur groupe de tête.

Mots clés : glycérolipide, polyphénol, liaison hydrogène, interaction lipide-protéine, autoadhérente.

[Traduit par la Rédaction]

Introduction

It is well-known that polyphenols bind and precipitate proteins and (or) peptides and can act as antioxidants (Handique and Baruah (1) provide a comprehensive review of natural and synthetic polyphenols). Furthermore, poly(phenol) films have been used as protective coatings for proteins immobilized onto electrodes (2). A novel synthetic lipid, 1,2-dipalmitoylgalloylglycerol (DPGG), has been prepared (3) that incorporates a polyphenol as the headgroup. The authors suggest that this lipid has the potential to exhibit comparable protein-binding properties (4) so that Langmuir–Blodgett films of such lipids could prove useful as biocompatible coatings. Pollastri et al. (3) demonstrated the self-adhesive nature of DPGG bilayers and proposed both strong inter- and intra-bilayer hydrogen bonding between gallic acid headgroups. We have recently shown that DPGG monolayers exhibit strong lateral cohesion and high rigidity, which can also be attributed to lateral hydrogen bonding (5). The influence of hydrogen bonding on monolayer and bilayer phase behaviour has been previously documented for lipids such as phosphatidylethanolamines and cerebrosides (3, 6, 7). To probe and understand the lateral cohesion in monolayers due to a hydrogen bonding network requires systematic chemical modification with respect to hydrogen bonding sites. In contrast to phosphatidylethanolamines and cerebrosides, DPGG provides an ideal template for a library of analogous lipids. We have employed a building block approach to design a modular synthetic route for the preparation of this library of novel glycerolipids with phenolic and polyphenolic headgroups. We report here the preparation of DPGG analogues with headgroups varying in number and position of hydroxyl groups (Fig. 1).

Received 14 November 2005. Accepted 21 December 2005. Published on the NRC Research Press Web site at http://canjchem.nrc.ca on 11 October 2006.

R. Schmidt, J.G. Carrigan, and C.E. DeWolf.[2] Department of Chemistry and Biochemistry, Concordia University, 7141 Sherbrooke St. West, Montréal, QC H4B 1R6, Canada.

[1]This article is part of a Special Issue dedicated to Dr. Alfred Bader.

[2]Corresponding author (e-mail: cdewolf@alcor.concordia.ca).

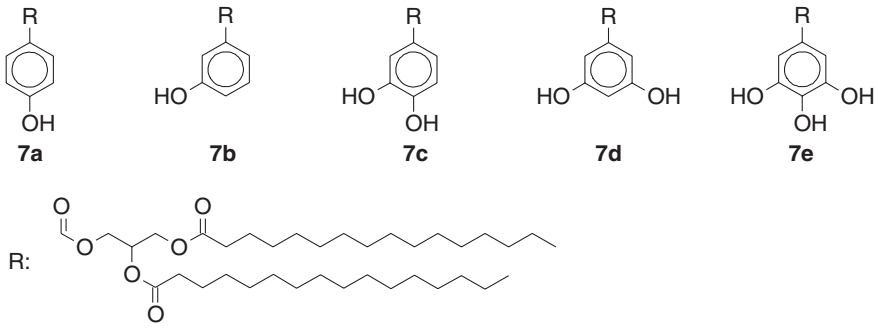
Results and discussion

The preparation of DPGG in two steps from tri-O-benzylgalloyl chloride and dipalmitoylglycerol has been described in the literature (3). The key features of this synthesis are the use of the benzyl protecting group and the introduction of a side chain bearing glycerol moiety. We report a more modular synthetic route to DPGG and some of its analogues, which allows for easy variation not only of the headgroup (number and position of hydroxyl groups) but also the stereochemistry of the backbone (R or S) and the chemical character of the side chains (chain length, units of unsaturation, functionalization, etc.) (Scheme 1). All of these parameters are known to influence monolayer phase behaviour and more generally, lipid self-assembly properties.

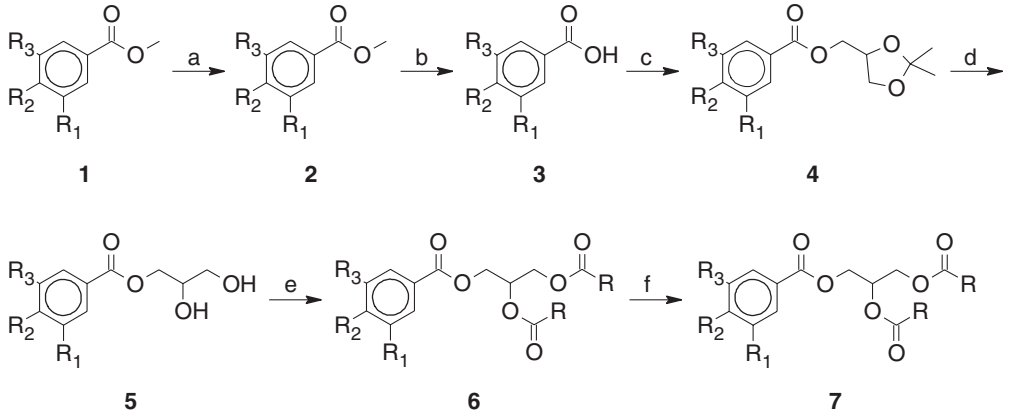
Compounds **3a**, **3c**, and **3e** are commercially available in gram quantities. Compounds **3b** and **3d** were prepared by well-known methods from 3-hydroxybenzoic acid methyl ester and 3,4-dihydroxybenzoic acid, respectively. Therefore, it is easy to alter the headgroup structure of the title compounds by varying the substitution pattern of the starting material. In the first step of the synthesis of the title compounds, phenol-bearing benzoic acids **3** are reacted with a racemic mixture of 2,2-dimethyl-1,3-dioxolane-4-methanol (solketal, a protected glycerol) to give compounds **4**. Importantly, the same procedure could be used to prepare the enantiomerically pure analogues starting from commercially

 doi:10.1139/V06-102 © 2006 NRC Canada

Fig. 1. Chemical structure of DPGG (**7e**) and prepared analogues.



Scheme 1. Reagents: (*a*) BnBr, K_2CO_3, CH_2Cl_2–MeOH, (*b*) KOH, THF–H_2O, (*c*) solketal, 1-methylimidazole, *p*-TsCl, MeCN, (*d*) Amberlyst® 15, MeOH–H_2O, (*e*) hexadecanoic acid, DMAP, EDCI, CH_2Cl_2, (*f*) H_2, 10% Pd–C.



1, 7	R_1	R_2	R_3
a	H	OH	H
b	OH	H	H
c	OH	H	OH
d	OH	OH	H
e	OH	OH	OH

2–6	R_1	R_2	R_3
a	H	OBn	H
b	OBn	H	H
c	OBn	H	OBn
d	OBn	OBn	H
e	OBn	OBn	OBn

available (*R*)-(-)- or (*S*)-(+)-2,2-dimethyl-1,3-dioxolane-4-methanol instead of the racemic mixture, provided that the pH is held between 7 to 8 to retain optical purity (8). The isopropylidene and benzyl protecting groups were chosen from orthogonal sets to provide selective deprotection of the isopropylidene in step d (Fig. 1). The protected benzoates **4** were not isolated, but the glycerol moiety was deprotected by treatment with wet Amberlyst® 15, a strongly acidic resin that allows for easy removal from the reaction mixture by gravity filtration. The advantage of Amberlyst® 15, aside from easy removal, is the fact that the sulfonic residues bound to the resin beads provide significant steric hindrance to prevent ester cleavage (9). Cleavage of the isopropylidene protecting group with I_2 in methanol (10) or under acidic conditions using aqueous acetic acid (11) was not successful. It has to be noted that a similar approach has previously been employed by Schmidt and Blank (12) for the preparation of compounds **4e** and **5e**. However, reaction times are generally much shorter and workup much simpler for our synthetic scheme with similar yields. In the next step, the palmitoyl side chains were introduced by coupling **5** with palmitic acid in the presence of *N*-(3-dimethylaminopropyl)-*N*-ethylcarbodiimide hydrochloride (EDCI) and 4-dimethylaminopyridine (DMAP) (13, 14). This acylation method was shown to be superior to the coupling of acid chlorides or anhydrides with the corresponding aliphatic acids (15). Furthermore, excess EDCI and the 1-(3-dimethylamino-propyl)-3-ethyl-urea formed during the reaction can easily be removed from the reaction mixture by liquid–liquid extraction because of their good solubility in water. The reaction has also been successfully carried out with the corresponding myristoyl and stearoyl side chains (data not shown). In addition, it is possible to selectively introduce two dissimilar side chains (e.g., palmitoyl and stearoyl) by successive coupling with the respective acids (15, 16).

Diacetylation in the first step as well as 1,2-acyl migration in the second step can be avoided by maintaining the reaction temperature between 0 and 20 °C (15). The benzyl protecting group is removed by catalytic hydrogenation under moderate pressure in the final step. The reaction time in-

© 2006 NRC Canada

creases with the number of benzyl groups to be removed. DPGG and its benzyl-protected precursor were also prepared by this method with comparable yields to the literature (3).

Conclusion

We have prepared a library of phenolic and polyphenolic glycerolipids according to a relatively simple modular reaction scheme. Moreover, the same scheme can be used to prepare glycerolipids that are enantiomerically pure and (or) have dissimilar side chains.

Experimental

All chemicals were purchased from commercial suppliers and used without further purification. 4-Benzyloxybenzoic acid, 3,5-di-benzyloxybenzoic acid, and 3,4,5-tris-benzyloxybenzoic acid were obtained from Tokyo Chemical Industry Co., Ltd. (TCI, Tokyo, Japan). ^{1}H spectra were obtained at 300 MHz and ^{13}C NMR spectra were obtained at 75 MHz in $CDCl_3$ unless otherwise noted using the NMR solvent as an internal reference. Abbreviations used in the descriptions of NMR spectra are singlet (s), doublet (d), triplet (t), multiplet (m), broad signal (br). The coupling constants (*J*) are given in Hertz. Mass spectrometry measurements were carried out on a MALDI mass spectrometer using dithranol as a matrix. IR measurements were carried out using a liquid cell equipped with KBr windows and in $CDCl_3$ unless otherwise noted. All melting points are uncorrected. Silica gel for flash chromatography was acquired from Life Force Inc. (Flushing, New York).

3,4-Dihydroxybenzoic acid methyl ester (1d)

3,4-Dihydroxybenzoic acid (1 g, 6.49 mmol) was dissolved in 40 mL of MeOH. After the addition of 2 drops of concd. H_2SO_4, the solution was refluxed for 7 days. The reaction was stopped by the addition of 300 mL of distilled H_2O. The mixture was extracted with ethyl acetate – hexanes (60:40). The organic layers were combined, dried over Na_2SO_4, and the solvent removed under reduced pressure to give 0.8 g of a light-brown solid in 73% yield.

3-Benzyloxybenzoic acid methyl ester (2b)

Compound **2b** was prepared according to the literature (17) with a reaction time of 6 h. The product was purified by flash chromatography on SiO_2 (hexanes – ethyl acetate, 80:20) to give 0.98 g of a white solid in 61% yield.

3,4-Bis-benzyloxybenzoic acid methyl ester (2d)

Compound **2d** was prepared in a manner analogous to **2b**. However, 2.3 equiv. of benzyl bromide were used and gave 1.19 g of a white solid in 77% yield.

3-Benzyloxybenzoic acid (3b)

Compound **2b** (0.75 g, 3.1 mmol) was dissolved in 35 mL of THF. A solution of KOH (1.04 g, 18.6 mmol, 6 equiv.) in 50 mL of distilled H_2O was added and the reaction was stirred for 24 h. The reaction mixture was added to 250 mL of distilled H_2O and acidified to pH 5 with 2N HCl. The mixture was extracted with diethylether. The organic layers were combined, dried over Na_2SO_4, and the solvent removed under reduced pressure to yield 0.67 g of a white solid in 95% yield.

3,4-Bis-benzyloxy-benzoic acid (3d)

Compound **3d** was prepared in a manner analogous to **3b** with a reaction time of 48 h. The reaction gave 0.67 g of a white solid in 70% yield.

Synthesis of the benzyloxybenzoic acid 2,3-dihydroxypropyl esters (5a–5d)

Typical procedure

Compound **3a** (1.0 g, 4.38 mmol), 1-methyl-imidazole (1.08 g, 13.14 mmol, 3 equiv.), and *p*-toluenesulfonyl chloride (1.17 g, 6.13 mmol, 1.4 equiv.) were dissolved in 45 mL of CH_3CN and stirred for 30 min. After the addition of racemic 2,2-dimethyl-1,3-dioxolane-4-methanol (0.58 g, 4.38 mmol, 1 equiv.), the solution was stirred under inert atmosphere for 3 h. The volume of the solution was reduced to approximately 4 mL under reduced pressure and the solution filtered through Al_2O_3 with 40 mL of CH_2Cl_2. The solvent was removed under reduced pressure to give 1.0 g of a white solid which was used without further purification. Compound **4a** (0.15 g, 0.438 mmol) was suspended in 40 mL of EtOH–H_2O (95:5). Wet Amberlyst® 15 (0.180 g, 1 equiv.) was added to the suspension and the suspension was refluxed for 24 h. The solution was allowed to cool to room temperature and 40 mL of CH_2Cl_2 and 300 mL of brine were added. The mixture was extracted with CH_2Cl_2 (2 × 20 mL). The organic layers were combined, dried over Na_2SO_4, and the solvent removed under reduced pressure. The crude was purified by flash chromatography on SiO_2 (ethyl acetate – hexanes, 70:30) to give 0.105 g of a white solid in 80% yield.

Data for 5a

Melting point 77–79 °C. IR (cm^{-1}) ν: 3614, 3036, 2952, 2886, 1713, 1606. ^{1}H NMR δ: 8.01 (m, 2H), 7.40 (m, 5H), 7.01 (m, 2H), 5.13 (s, 2H, Ar*CH*$_2$), 4.42 (m, 2H), 4.00 (m, 1H), 3.71 (m, 2H). ^{13}C NMR δ: 166.7, 162.8, 136.1, 131.8, 128.7, 128.2, 127.5, 122.1, 114.6, 70.45, 70.13, 65.5, 63.4. MS *m*/*z*: 325.3 $[M + Na]^+$

Data for 5b

Yield 80%, mp 76–78 °C. IR (cm^{-1}) ν: 3618, 3036, 2952, 2884, 1719, 1586. ^{1}H NMR δ: 7.68 (m, 2H), 7.40 (m, 6H), 7.19 (m, 1H), 5.11 (s, 2H, Ar*CH*$_2$), 4.42 (m, 2H), 4.06 (m, 1H), 3.72 (m, 2H). ^{13}C NMR δ: 166.8, 158.7, 136.4, 130.9, 129.6, 128.6, 128.1, 127.5, 122.4, 120.5, 115.4, 70.3, 70.2, 65.8, 63.4. MS *m*/*z*: 325.3 $[M + Na]^+$.

Data for 5c

Yield 85%, mp 94 to 95 °C. IR (cm^{-1}) ν: 3618, 3035, 2952, 2884, 1717, 1596. ^{1}H NMR δ: 7.38 (m,10H), 7.28 (d, 2H, *J* = 2.33 Hz), 6.82 (t, 1H, *J* = 2.34 Hz), 5.07 (s, 4H, Ar*CH*$_2$), 4.52 (m, 2H), 4.05 (m, 1H), 3.71 (m, 2H). ^{13}C NMR δ: 166.6, 159.8, 136.4, 131.4, 128.6, 128.2, 127.6, 108.6, 107.4, 70.4, 70.3, 65.9, 63.4. MS *m*/*z*: 431.4 $[M + Na]^+$.

© 2006 NRC Canada

Data for 5d

Yield 83%, mp 80 to 81 °C. IR (cm^{-1}) ν: 3613, 3034, 2951, 2885, 1712, 1601. ^{1}H NMR δ: 7.63 (m, 2H), 7.39 (m, 10H), 6.93 (m, 1H), 5.23 (s, 2H, ArCH_2), 5.20 (s, 2H, ArCH_2), 4.37 (m, 2H), 4.02 (m, 1H), 3.68 (m, 2H). ^{13}C NMR δ: 166.7, 153.3, 148.3, 136.7, 136.4, 128.6, 128.5, 128.0, 127.9, 127.4, 127.1, 124.3, 122.3, 115.7, 113.2, 71.3, 70.8, 70.4, 65.6, 63.3. MS *m/z*: 431.4 $[M + Na]^+$.

Data for 5e

Yield 57%.

Synthesis of benzyloxybenzoic acid 2,3-bis-hexadecanoyloxypropyl esters (6a–6e)

Typical procedure

Compound **5a** (0.38 g, 1.25 mmol) and hexadecanoic acid (0.73 g, 2.825 mmol, 2.26 equiv.) were dissolved in 20 mL of CH_2Cl_2. A suspension of DMAP (0.35 g, 2.825 mmol, 2.26 equiv.) and EDCI (0.58 g, 3 mmol, 2.4 equiv.) in 10 mL of CH_2Cl_2 was added to the reaction mixture and the mixture was stirred for 4 h. Brine (300 mL) was added and the reaction mixture was extracted with CH_2Cl_2 (2 × 20 mL). The organic layers were combined, dried over Na_2SO_4, and the solvent removed under reduced pressure. The product was purified by flash chromatography on SiO_2 (hexanes – ethyl acetate, 80:20) to give 0.80 g of a white solid in 82% yield.

Data for 6a

Melting point 64–66 °C. IR (cm^{-1}) ν: 2927, 2855, 1736, 1606. ^{1}H NMR δ: 7.98 (m, 2H), 7.39 (m, 5H), 7.01 (m, 2H), 5.41 (m, 1H), 5.12 (s, 2H, ArCH_2), 4.41 (m, 3H), 4.24 (m, 1H), 2.33 (t, 2H, *J* = 7.5 Hz, CH_2COO), 2.32 (t, 2H, *J* = 7.6 Hz, CH_2COO), 1.61 (m, 4H, CH_2CH_2COO), 1.27 (m, 48H), 0.88 (t, 6H, *J* = 6.70 Hz, CH_3). ^{13}C NMR δ: 173.3, 172.9, 165.7, 162.8, 136.2, 131.8, 128.7, 128.2, 127.4, 122.1, 114.6, 70.1, 68.9, 62.6, 62.3, 34.3, 34.1, 31.9, 29.7, 29.6, 29.5, 29.4, 29.3, 29.2, 29.1, 24.9, 24.8, 22.7, 14.1. MS *m/z*: 802.1 $[M + Na]^+$.

Data for 6b

Reaction time 6 h, yield 44%, mp 51 to 52 °C. IR (cm^{-1}) ν: 2927, 2855, 1735, 1586. ^{1}H NMR δ: 7.64 (m, 2H), 7.39 (m, 6H), 7.18 (m, 1H), 5.42 (m, 1H), 5.11 (s, 2H, ArCH_2), 4.43 (m, 3H), 4.24 (m, 1H), 2.33 (t, 2H, *J* = 7.5 Hz, CH_2COO), 2.32 (t, 2H, *J* = 7.6 Hz, CH_2COO), 1.61 (m, 4H, CH_2CH_2COO), 1.27 (m, 48H), 0.88 (t, 6H, *J* = 6.7 Hz, CH_3). ^{13}C NMR δ: 173.3, 172.9, 165.8, 158.8, 136.5, 130.8, 129.5, 128.6, 128.1, 127.5, 122.3, 120.5, 115.3, 70.2, 68.9, 63.0, 62.2, 34.3, 34.1, 31.9, 29.8, 29.7, 29.5, 29.4, 29.3, 29.2, 29.1, 24.9, 24.8, 22.7, 14.1. MS *m/z*: 802.1 $[M + Na]^+$.

Data for 6c

Reaction time 12 h, yield 94%, mp 66–68 °C. IR (cm^{-1}) ν: 2927, 2855, 1736, 1596. ^{1}H NMR δ 7.38 (m, 10H), 7.26 (d, 2H, *J* = 2.3 Hz), 6.81 (t, 1H, *J* = 2.3 Hz), 5.41 (m, 1H), 5.07 (s, 4H, ArCH_2), 4.45 (m, 3H), 4.22 (m, 1H), 2.33 (t, 4H, *J* = 7.5 Hz, CH_2COO), 1.61 (m, 4H, CH_2CH_2COO), 1.27 (m, 48H), 0.88 (t, 6H, *J* = 6.7 Hz, CH_3). ^{13}C NMR δ 173.3, 172.9, 165.7, 159.8, 136.4, 131.4, 128.6, 128.1, 127.6, 108.5, 107.5, 70.3, 68.8, 63.0, 62.1, 34.3, 34.1, 31.9, 29.7, 29.6, 29.5, 29.4, 29.3, 29.2, 29.1, 24.9, 24.8, 22.7, 14.1. MS *m/z*: 908.3 $[M + Na]^+$.

Data for 6d

Reaction time 12 h, yield 63%, mp 45–47 °C. IR (cm^{-1}) ν: 2927, 2855, 1736, 1601. ^{1}H NMR δ: 7.62 (m, 1H), 7.58 (d, 1H, *J* = 2.1 Hz), 7.42 (m, 10H), 6.93 (d, 1H, *J* = 8.5 Hz), 5.41 (m, 1H), 5.23 (s, 2H, ArCH_2), 5.20 (s, 2H, ArCH_2), 4.40 (m, 3H), 4.17 (m, 1H), 2.33 (t, 4H, *J* = 7.5 Hz, CH_2COO), 1.61 (m, 4H, CH_2CH_2COO), 1.27 (m, 48H), 0.88 (t, 6H, *J* = 6.7 Hz, CH_3). ^{13}C NMR δ: 173.3, 172.9, 165.6, 153.2, 148.4, 136.8, 136.5, 128.6, 128.5, 128.0, 127.9, 127.4, 127.1, 124.1, 122.3, 115.5, 113.2, 71.6, 70.8, 68.9, 62.7, 62.2, 34.3, 34.1, 31.9, 29.7, 29.6, 29.5, 29.4, 29.3, 29.2, 29.1, 24.9, 24.8, 22.7, 14.1. MS *m/z*: 908.3 $[M + Na]^+$.

Data for 6e

Reaction time 15 h, yield 70%.

Synthesis of hydroxybenzoic acid 2,3-bis-hexadecanoyloxypropyl esters (7a–7e)

Typical procedure

Compound **6a** (0.2 g, 0.257 mmol) was dissolved in 20 mL of dry THF. 10% Pd–C (0.07 g, 30 wt%) was added and the reaction mixture was placed in a pressure reactor and stirred under 3.5 atm (1 atm = 101.325 kPa) of hydrogen gas for 4 h. The mixture was filtered through Celite 545 and the solvent removed under reduced pressure to give 0.14 g of a white solid in 80% yield.

Data for 7a

Melting point 69–71 °C. IR (cm^{-1}) ν: 3587, 2927, 2855, 1736, 1610. ^{1}H NMR δ: 7.94 (m, 2H), 6.86 (m, 2H), 5.42 (m, 1H), 5.33 (br, 1H, *OH*), 4.44 (m, 3H), 4.24 (m, 1H), 2.33 (t, 2H, *J* = 7.5 Hz, CH_2COO), 2.32 (t, 2H, *J* = 7.5 Hz, CH_2COO), 1.61 (m, 4H, CH_2CH_2COO), 1.27 (m, 48H), 0.88 (t, 6H, *J* = 6.7 Hz, CH_3). ^{13}C NMR δ: 173.5, 173.1, 165.7, 160.0, 132.1, 122.1, 115.3, 69.0, 62.7, 62.3, 34.3, 34.1, 31.9, 29.7, 29.6, 29.5, 29.4, 29.3, 29.2, 29.1, 24.9, 24.8, 22.7, 14.1. MS *m/z*: 712.0 $[M + Na]^+$.

Data for 7b

Reaction time 6 h, 61% yield, mp 64 to 65 °C. IR (cm^{-1}) ν: 3594, 2927, 2855, 1734, 1593. ^{1}H NMR δ: 7.61 (m, 1H), 7.48 (m, 1H), 7.32 (m, 1H), 7.06 (m, 1H), 5.43 (m, 1H), 5.20 (br, 1H, *OH*), 4.43 (m, 3H), 4.24 (m, 1H), 2.33 (t, 2H, *J* = 7.4 Hz, CH_2COO), 2.32 (t, 2H, *J* = 7.5 Hz, CH_2COO), 1.61 (m, 4H, CH_2CH_2COO), 1.27 (m, 48H), 0.88 (t, 6H, *J* = 6.7 Hz, CH_3). ^{13}C NMR δ: 173.4, 173.1, 165.7, 155.8, 130.1, 129.8, 122.1, 120.5, 116.3, 68.9, 63.0, 62.2, 34.3, 34.1, 31.9, 29.7, 29.6, 29.5, 29.4, 29.3, 29.2, 29.1, 24.9, 24.8, 22.7, 14.1. MS *m/z*: 712.0 $[M + Na]^+$.

Data for 7c

Reaction time 7 h, 53% yield, mp 78 to 79 °C. IR (cm^{-1}) ν: 3594, 2927, 2855, 1733, 1605. ^{1}H NMR δ: 7.07 (d, 2H, *J* = 2.2 Hz), 6.59 (t, 1H, *J* = 2.3 Hz), 5.45 (m, 3H), 4.41 (m, 3H), 4.24 (m, 1H), 2.33 (t, 6H, *J* = 7.6 Hz, CH_2COO), 1.61 (m, 4H, CH_2CH_2COO), 1.27 (m, 48H), 0.88 (t, 6H, *J* = 6.7 Hz, CH_3). ^{13}C NMR δ: 173.6, 173.3, 165.4, 157.1, 131.6, 109.2, 107.8, 68.5, 63.1, 62.2, 34.3, 34.1, 31.9, 29.7, 29.6,

© 2006 NRC Canada

29.5, 29.4, 29.3, 29.2, 29.1, 24.9, 24.8, 22.7, 14.1. MS *m*/*z*: 728.0 $[M + Na]^+$.

Data for 7d

Reaction time 7 h, 50% yield, mp 92 to 93 °C. IR (cm^{-1}) ν: 3566, 2927, 2855, 1734, 1616. ^1H NMR δ: 7.07 (d, 2H, *J* = 2.2 Hz), 6.59 (t, 1H, *J* = 2.3 Hz), 5.45 (m, 3H), 4.41 (m, 3H), 4.24 (m, 1H), 2.33 (t, 6H, *J* = 7.6 Hz, CH_2COO), 1.61 (m, 4H, CH_2CH_2COO), 1.27 (m, 48H), 0.88 (t, 6H, *J* = 6.7 Hz, CH_3). ^{13}C NMR δ: 173.7, 173.4, 166.3, 149.8, 146.8, 123.1, 120.9, 115.9, 114.6, 68.9, 62.5, 62.2, 34.3, 34.1, 31.9, 29.7, 29.6, 29.5, 29.4, 29.3, 29.2, 29.1, 24.9, 24.8, 22.7, 14.1. MS *m*/*z*: 728.0 $[M + Na]^+$.

Data for 7e

Reaction time 8 h. The product was then adsorbed to silica in the presence of 1 mL of acetic acid and purified by flash chromatography on SiO_2 using a solvent gradient of hexanes – ethyl acetate from 90:10 to 30:70. The product was then extracted from 200mL of brine with $CHCl_3$ (5 × 20 mL). The organic layers were combined, dried over Na_2SO_4, and the solvent removed under reduced pressure to give 0.050 g of a white solid in 70% yield.

Acknowledgements

The authors acknowledge the Natural Science and Engineering Research Council (NSERC) of Canada and the Canada Foundation for Innovation for financial support. Dr. Heidi Muchall and Dr. Louis Cuccia are acknowledged for their contribution to discussions and provision of additional facilities.

References

1. J.G. Handique and J.B. Baruah. React. Funct. Polym. **52**, 163 (2002).
2. D.W.M. Arrigan and P.N. Bartlett. Biosens. Bioelectron. **13**, 293 (1998).
3. M.P. Pollastri, N.A. Porter, T.J. McIntosh, and S.A. Simon. Chem. Phys. Lipids, **104**, 67 (2000).
4. F. Davis and S.P.J. Higson. Biosens. Bioelectron. **21**, 1 (2005).
5. R. Schmidt and C.E. DeWolf. Langmuir, **20**, 3284 (2004).
6. T.J. McIntosh and S.A. Simon. Langmuir, **12**, 1622 (1996).
7. K. Kulkarni, D.S. Snyder, and T.J. McIntosh. Biochemistry, **38**, 15264 (1999).
8. K. Yamauchi, F. Une, S. Tabata, and M. Kinoshita. J. Chem. Soc. Perkin Trans. 1, 765 (1986).
9. C.C. Yu, Y.-S. Lee, B.S. Cheon, and S.H. Lee. Bull. Korean Chem. Soc. **24**, 1229 (2003).
10. W.A. Szarek, A. Zamojski, K.N. Tiwari, and E.R. Ison. Tetrahedron Lett. **27**, 3827 (1986).
11. S. Hanessian, D. Delorme, P.C. Tyler, G. Demailly, and Y. Chapleur. Can. J. Chem. **61**, 634 (1983).
12. O.T. Schmidt and W. Blank. Chem. Ber. **89**, 283 (1956).
13. J.C. Sheehan, P.A. Cruickshank, and G.L. Boshart. J. Org. Chem. **26**, 2525 (1961).
14. N. Hebert, A. Beck, R.B. Lennox, and G. Just. J. Org. Chem. **57**, 1777 (1992).
15. S.F. Martin, J.A. Josey, Y.-L. Wong, and D.W. Dean. J. Org. Chem. **59**, 4805 (1994).
16. J. Ohlsson and G. Magnusson. Tetrahedron, **56**, 9975 (2000).
17. K.M. Khan, M. Rasheed, Z. Ullah, S. Hayat, F. Kaukab, M.I. Choudhary, Atta-ur-Rahman, and S. Perveen. Bioorg. Med. Chem. **11**, 1381 (2003).

© 2006 NRC Canada

Hydrosilylation of ketones catalyzed by C_2-symmetric proline-derived complexes[1]

Li Gan and Michael A. Brook

Abstract: Extracoordinate chiral hydrosilanes were generated in situ from triethoxysilane and a C_2-symmetric ligand derived from bisproline 7. In the presence of a catalytic amount of ligand **7**, prochiral ketones were reduced in moderate yield with moderate enantioselectivity (up to 64% ee). Alternatively, TiF_4 complexes of **7** were used to provide higher enantioselectivity and with improved yields. The copper complex of ligand **7** and ^{29}Si NMR data provide some guidance as to the key factors responsible for the observed reactivity at the silicon and at the ligand centre.

Key words: extracoordinate chiral silane, C_2-symmetry, enantioselectivity, Lewis acid titanium catalysis.

Résumé : On a effectué une génération *in situ* d'hydrosilanes chiraux extracoordinés à partir du triéthoxysilane et d'un ligand de symétrie C_2 dérivé de la bisproline **7**. En présence d'une quantité catalytique du ligand **7**, les cétones prochirales sont réduites avec des rendements moyens et un énantiosélectivité modérée, allant jusqu'à 64 % d'excès énantiomère. D'une façon alternative, on a utilisé des complexes du tétrafluorure de titane du ligand **7** qui ont fourni une énantiosélectivité supérieure et de meilleurs rendements. Le complexe de cuivre du ligand **7** et les données de la RMN du ^{29}Si donnent des indications sur les facteurs clés responsables au niveau de l'atome de silicium et du centre du ligand pour la réactivité observée.

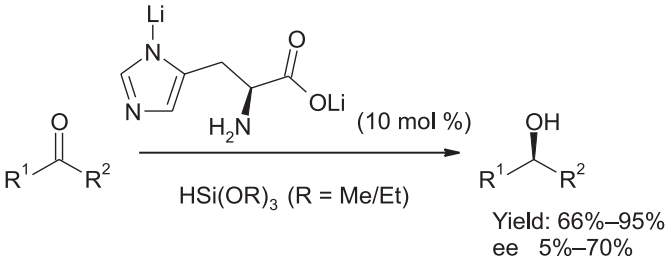
Mots clés : silane chiral extracoordiné, symétrie C_2, énantiosélectivité, catalyseur de titane agissant comme acide de Lewis.

[Traduit par la Rédaction]

Introduction

The enantioselective reduction of carbonyl groups remains one of the fundamental operations in organic synthesis (1). Typical catalytic systems utilize a chiral ligand complexed with a transition metal (2). With the exception of boron, such as the well-developed chiral boron catalyst (CBS) (3), the use of chiral catalytic motifs based on main group elements is uncommon (4). However, in a process related to that reported by Shiffers and Kagan (5) and Hosomi and co-workers (6), we previously demonstrated that the complex derived from hydrosilanes and a catalytic amount of amino acids can reduce ketones enantioselectively (Scheme 1) (7).

Scheme 1. Histidine-catalyzed ketone reduction.



These reactions with hydrosilanes occur via extracoordinate silicon in the presence of anionic catalysts. Sakurai and co-workers (8a, 8b) has demonstrated that diastereoselective allylation of carbonyl groups in the presence of pentacoordinate silicon hydrides, for example, can best be explained by invoking six-membered ring transition states (Scheme 2). Coordination of the nucleophile, the carbonyl group, to the extracoordinate silicon is followed by allyl group transfer. As a departure point, we proposed that a related assembly of ketone and carboxylate on an extracoordinate silicon 1 could be used to explain the observed stereoselectivity in the hydrosilane reduction of acetophenone, although related bidentate structures could also be envisaged. While the mechanisms of these reactions have not yet been clearly established, the presence of extracoordinate

Received 6 March 2006. Accepted 17 May 2006. Published on the NRC Research Press Web site at http://canjchem.nrc.ca on 11 October 2006.

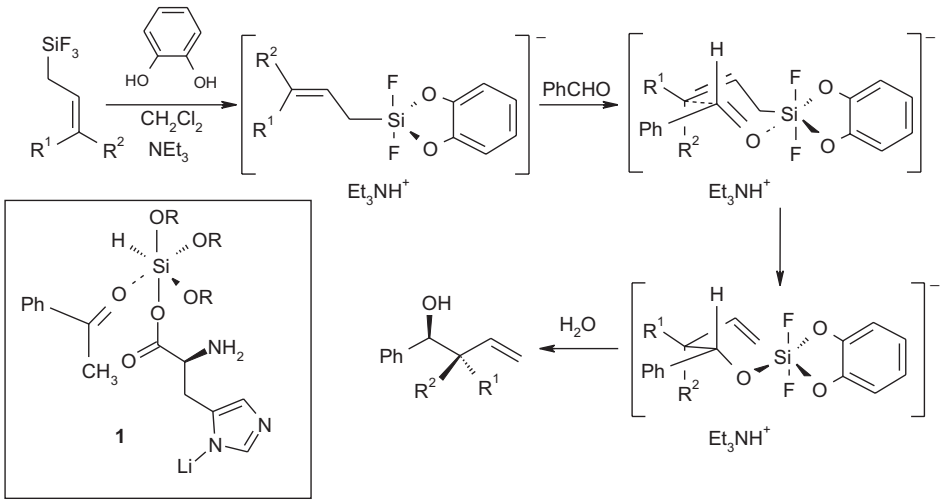
It is a great pleasure to dedicate this paper to the superb career of Alfred Bader. I learned about his passion for chemistry and chemists when we met several times when I was a graduate student and postdoctoral fellow. It meant a great deal to me then, and now, that "Please Bother Us" meant anyone interested in chemistry, not just the professors. I thank him for sharing his vision and enthusiasm for chemistry with me then and many times since. The example he set has profoundly affected the way my career has evolved.

L. Gan and M.A. Brook.[2] Department of Chemistry, McMaster University, Hamilton, ON L8S 4M1, Canada.

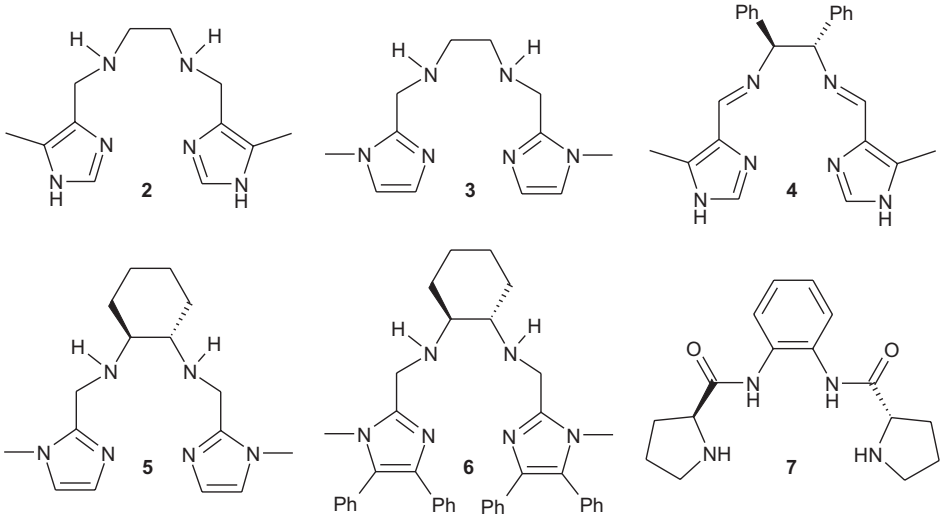
[1]This article is part of a Special Issue dedicated to Dr. Alfred Bader.
[2]Corresponding author (e-mail: mabrook@mcmaster.ca).

 doi:10.1139/V06-116 © 2006 NRC Canada

Scheme 2.



Scheme 3.



silicon, particularly the pentacoordinate species, is evident from Si NMR.

In an attempt to better understand the processes involved in the reduction, recent research has turned to the utilization of multidentate ligands that, on binding, would have fewer degrees of freedom and, additionally, would be more amenable to structural characterization. The use of C_2-symmetry, in particular, provides a more highly structured environment for enantioselective reactions (9), a strategy we recently utilized with silane-medicated reductions (**2**–**6**, Scheme 3) (10). Unfortunately, only moderate ee were observed in these reactions.

In this study, we developed a C_2-symmetric multidentate ligand that utilizes proline, perhaps the most widely utilized amino acid chiral template (11). We report the synthesis of the C_2-symmetric compound **7** (Scheme 3), the formation of pentacoordinate silicon complexes on reaction of **7** with $HSi(OEt)_3$, as shown by ^{29}Si NMR, the ability of this complex to reduce ketones, and the characterization of its copper complex **13** by an X-ray structure. In addition, the behaviour of the Lewis acidic derivative formed from the reaction of **7** with TiF_4 is described in the same carbonyl reduction process.[3]

Results and discussion

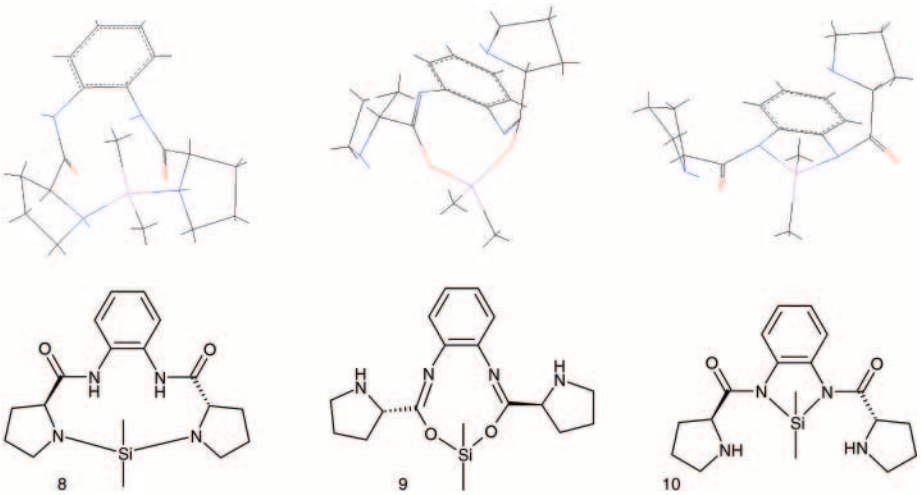
Preparation and characterization of the ligands

A series of molecular modeling experiments were undertaken with C_2-symmetric diamino acid derivatives. Preliminary studies compared the geometries of bidentate

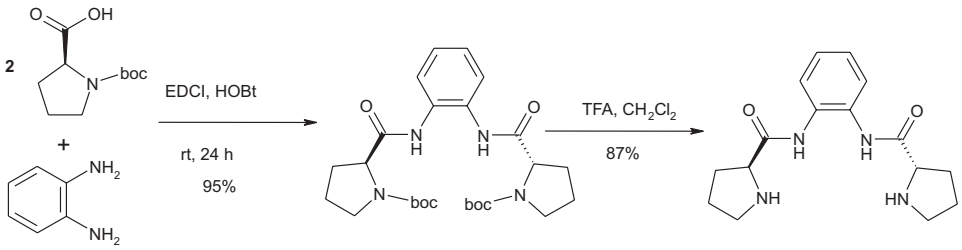
[3] Supplementary data for this article are available on the journal Web site (http://canjchem.nrc.ca) or may be purchased from the Depository of Unpublished Data, Document Delivery, CISTI, National Research Council Canada, Ottawa, ON K1A 0R6, Canada. DUD 5079. For more information on obtaining material refer to http://cisti-icist.nrc-cnrc.gc.ca/irm/unpub_e.shtml. CCDC 601366 and 601367 contain the crystallographic data for this manuscript. These data can be obtained, free of charge, via http://www.ccdc.cam.ac.uk/conts/retrieving.html (Or from the Cambridge Crystallographic Data Centre, 12 Union Road, Cambridge CB2 1EZ, UK; fax +44 1223 336033; or deposit@ccdc.cam.ac.uk).

© 2006 NRC Canada

Fig. 1. Molecular models of dimethylsilyl derivatives of **7.**



Scheme 4. Preparation of bisproline **7**.



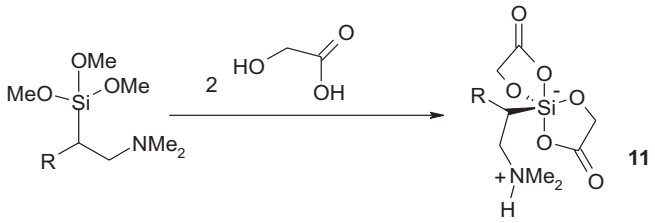
dimethylsilicon complexes based on various amino acid complexes of 1,2-diaminobenzene. Among the amino acids examined (phenylalanine, histidine, alanine, and proline), the latter had a more tightly constrained structure, irrespective of whether the linkages occurred through the proline nitrogen **8**, amide oxygen **9**, or amide nitrogen **10** (Fig. 1). All of the derivatives had more rigid and compact chiral environments than structures based on the structural motifs found in **4** or **5** (Scheme 3). Therefore, the bisproline ligand **7** was prepared by coupling 1,2-diaminobenzene with commercially available N-protected L-proline (Scheme 4). The optically pure ligand was obtained, after deprotection by trifluoroacetic acid, by recrystallization from methanol in an overall yield of 83% and structurally characterized by NMR (^{1}H, ^{13}C), HRMS, and IR.

Mechanistic study

Silicon compounds undergo extracoordination in the presence of silaphilic nucleophiles, particularly oxygen, fluoride, and aromatic amines (12). Coordination expansion is facilitated by electron-withdrawing groups on silicon, especially fluoride and oxygen ligands. Thus, the facility of trialkoxysilanes to undergo extracoordination lies between that of trialkyl- and trihalo-silanes (12). Tacke and co-workers (13), in a beautiful series of papers, demonstrated that bidentate nucleophiles are particularly efficacious in inducing coordination expansion. A broad variety of pentacoordinate amino and hydroxy acid derivatives, exemplified by **11**, have been isolated in crystalline form (Scheme 5) (13, 14).

Complexes of **7** and $HSi(OEt)_3$ were characterized by ^{29}Si NMR. The ^{29}Si NMR of the neutral mixture gave a singlet at

Scheme 5. Formation of extracoordinate silicon with α-hydroxy acids.



–58.68 ppm, consistent with reported data for triethoxysilane (15). Thus, the amine groups are insufficiently basic to engender extracoordination at silicon. By contrast, when the bisproline tetraanion of **7** was mixed with triethoxysilane in a ratio of 1:2 (sensitivity of the NMR precluded lower concentrations of the silicon compound and higher concentration of the bisproline tetraanion led to precipitates) ^{29}Si NMR showed two singlets at –84.27 and –98.83 ppm, respectively.

It is challenging to assign putative structures to compounds with these chemical shifts. Each exchange at silicon of H by O or N leads to an upfield shift, as does each exchange of N by O. For example, the addition of the anionic ligand of **7** to $HSi(OEt)_3$ to give a pentacoordinate species $(HSi(OEt)_3\text{-}N\mathbf{7})^-$ would lead to an upfield shift of about 20 ppm. However, displacement of the EtO^- by the same nitrogen to give a tetracoordinate species $(HSi(OEt)_2\text{-}N\mathbf{7})$ would lead to a downfield shift of about 15 ppm (16). The observed peaks are consistent with a pentacoordinate species ($HSiX_4^-$, –84.27 ppm) and an oxidized pentacoordinate species (SiX_5^-) or a hydrido hexacoordinate species ($HSiX_5^{2-}$,

© 2006 NRC Canada

Fig. 2. ORTEP drawing of the structure of **12**, a copper complex **13**, and a possible structure of the hydridosiliconate **14**.

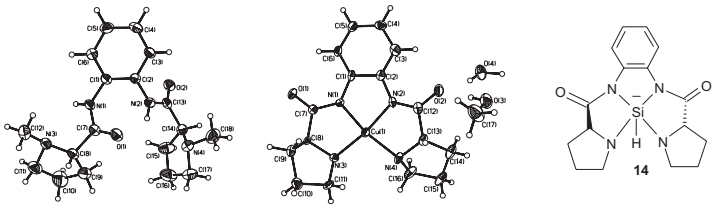


Table 1. Selected crystallographic data for ligand **7**.

Identification code	CCDC 601366
Empirical formula	$C_{18}H_{26}N_4O_2$
Formula weight (g mol^{-1})	330.43
Crystal system	Monoclinic
Space group	*C*2
a (Å)	20.259(8)
b (Å)	8.751(3)
c (Å)	10.929(4)
α (°)	90
β (°)	113.066(6)
γ (°)	90
Volume (Å^3)	1782.6(12)
Z	4
Density$_{calcd.}$ (Mg/m^3)	1.231
Absorption coefficient (mm^{-1})	0.082
F(000)	712
Crystal size (mm^3)	0.38 × 0.18 × 0.08
θ range for data collection (°)	2.03–26.48
Reflections collected	7556
Independent reflections	3346
R_{int}	0.0346
Data, restraints, parameters	3346, 1, 218
Goodness-of-fit on F^2	1.009
Final *R* indices [$I > \sigma(I)$]	R_1 = 0.0419, wR_2 = 0.0898
R indices (all data)	R_1 = 0.0702, wR_2 = 0.0993
Largest diff. peak and hole (e Å^{-3})	0.116 and –0.118

Table 2. Selected crystallographic data for **13**.

Identification code	CCDC 601367
Empirical formula	$C_{17}H_{24}CuN_4O_4$
Formula weight	411.94
Space group	*P*2(1)2(1)2(1)
Crystal system	Orthorhombic
Crystal size (mm^3)	0.20 × 0.18 × 0.06
a (Å)	8.3234(4)
b (Å)	11.7554(5)
c (Å)	18.5682(8)
α (°)	90
β (°)	90
γ (°)	90
Volume (Å^3)	1816.80(14)
Z	4
Density$_{calcd.}$ (Mg/m^3)	1.506
Absorption coefficient (mm^{-1})	1.233
F(000)	860
θ range for data collection (°)	2.05–28.31
Reflections collected	16 688
Independent reflections	4359
R_{int}	0.0891
Completeness to θ = 28.31° (%)	98.00
Data, restraints, parameters	4359, 0, 248
Goodness-of-fit on F^2	1.042
Final *R* indices [$I > 2\sigma(I)$]	R_1 = 0.0593, wR_2 = 0.1036
R indices (all data)	R_1 = 0.1041, wR_2 = 0.1152
Largest diff. peak and hole (e Å^{-3})	0.526 and –0.555

–98.83 ppm), respectively. Since extracoordinate hydridosiliconates are required to reduce ketones (see later), it is anticipated that these peaks represent penta- and hexacoordinate silicon hydrides; after the ketone reduction, ^{29}Si NMR showed only one peak at –82.39 ppm.

It did not prove possible to prepare crystals of sufficient quality for an X-ray analysis. By contrast, the *N*,*N*-dimethyl derivative **12** gave suitable crystals (Fig. 2, for crystallographic parameters and typical bond lengths and angles see Table 1). To explore complexed ligand structures that would be related to the reduction process, the copper complex **13** of ligand **7** was prepared by the reaction of the ligand with copper(II) chloride in methanol in the presence of excess potassium carbonate (Fig. 2). An X-ray crystal structure of the compound showed a nearly square planar arrangement of the C_2-symmetric nitrogen ligands around copper (Tables 2 and 3). The ligand in **13** forms a compact complex with short Cu—N bond lengths that brings the stereodirecting chiral centres in closer proximity to the metal centre. This structure was very encouraging as it suggests that analogous C_2-symmetric structures, such as **14**, may be formed. Extensive attempts to isolate various silicon complexes of **7** in crystalline form were unsuccessful.

Reductions of acetophenone

Previous work demonstrated that ketone reduction with hydrosilanes could be initiated with carboxylate or other anions to activate the silicon (7). A series of reductions of acetophenone was undertaken to establish the key factors required for efficacy in the presence of **7** (Table 4). Negative controls included a set of reactions in which each of the key ingredients was selectively absent. Notable among the results is the reduction of acetophenone with the proline anion, which resulted in 50% yield and 15% ee (Table 4, entry 3). This is a result that is related to, but less efficient than, reductions in the presence of anions of histidine and particularly phenylalanine that occurred in yields typically of 80% and ee up to 70% (7). A series of experiments demonstrated that the best compromise for yield and ee occurred at 55 °C, higher than would be expected for a reaction run under ki-

© 2006 NRC Canada

Table 3. Selected bond lengths (Å) and angles (°) for **13** (esds in parentheses).

Bond lengths (Å)	
Cu(1)—N(1)	1.924(4)
Cu(1)—N(4)	2.006(4)
C(12)—C(13)	1.526(7)
C(7)—C(8)	1.517(7)
N(3)—C(8)	1.525(6)
Cu(1)—N(2)	1.925(4)
N(1)—C(7)	1.342(6)
N(2)—C(2)	1.413(6)
N(2)—C(12)	1.305(6)
Cu(1)—N(3)	1.997(4)
N(1)—C(1)	1.410(6)
C(1)—C(2)	1.426(6)
N(4)—C(13)	1.511(6)
Bond angles (°)	
N(1)-Cu(1)-N(2)	83.38(16)
N(1)-Cu(1)-N(4)	168.95(17)
C(7)-N(1)-C(1)	127.5(4)
C(6)-C(1)-N(1)	127.5(4)
C(12)-N(2)-Cu(1)	116.8(3)
N(2)-C(2)-C(1)	114.4(4)
C(8)-N(3)-Cu(1)	106.5(3)
C(13)-N(4)-Cu(1)	107.2(3)
N(1)-C(7)-C(8)	113.5(4)
C(9)-C(8)-N(3)	103.8(4)
N(2)-C(12)-C(13)	115.2(4)
C(15)-C(14)-C(13)	103.8(5)
N(1)-Cu(1)-N(3)	85.66(17)
N(2)-Cu(1)-N(4)	85.60(16)
C(7)-N(1)-Cu(1)	116.7(3)
N(1)-C(1)-C(2)	113.0(4)
C(2)-N(2)-Cu(1)	114.2(3)
C(11)-N(3)-C(8)	106.4(4)
C(16)-N(4)-C(13)	105.5(4)
O(1)-C(7)-N(1)	128.0(4)
C(7)-C(8)-C(9)	114.1(4)
O(2)-C(12)-N(2)	127.3(5)
N(4)-C(13)-C(12)	112.3(4)
N(2)-Cu(1)-N(3)	166.91(16)
N(3)-Cu(1)-N(4)	105.17(17)
C(1)-N(1)-Cu(1)	115.1(3)
C(12)-N(2)-C(2)	127.9(4)
C(3)-C(2)-N(2)	125.8(4)
C(11)-N(3)-Cu(1)	118.2(3)
C(16)-N(4)-Cu(1)	117.7(3)
O(1)-C(7)-C(8)	118.5(4)
C(7)-C(8)-N(3)	113.0(4)
O(2)-C(12)-C(13)	117.5(4)
C(12)-C(13)-C(14)	114.3(4)

netic control. The reactions further confirmed that extracoordinate hydrosilanes are more reactive towards a variety of electrophiles than their four-coordinate counterparts (12). For example, neutral $HSi(OEt)_3$ is not able to reduce acetophenone in the absence of nucleophilic activation (Table 4, entry 1). Neutral bisproline **7** is similarly unable to activate triethoxysilane to undergo the reduction (Table 4, entry 2) as was also shown by ^{29}Si NMR experiments (see earlier). By contrast, the most effective reduction took place with the tetraanion of **7** (Table 3, entry 4). While the tetraanion of **7** can make a tight complex with silicon, it can do so with loss of chirality because of amino acid epimerization.

While the yields of these reactions were acceptable, the ee were marginal. Although the crystal structure of the copper complex **13** shows that the stereochemistry of the amino acids are maintained in the complex, it is also conceivable that α-amido epimerization occurs under the more basic conditions used for these reductions. To reduce this possibility, the efficacy of the reaction was tested as a function of the equivalents of base added (from 1 to 4 equiv.). The most interesting results came with 2 equiv. of base, which should deprotonate the amide NHs, possibly leading to bidentate complexes **15** (Table 4) and **16** (analogous to **9** and **10**, Fig. 3) without affecting the chiral centres. The reaction was more sluggish and it can be seen that, in one case, the ee improved, but at the expense of reaction yield (Table 4, entries 5–7).

Hydrosilanes are very stable at neutral conditions, but significantly less so away from neutrality, particularly under basic conditions. Exchangeable hydrogens under these conditions serve as excellent electrophiles, with the result that H_2 is normally released (e.g., $R_3SiH + HY \rightarrow R_3SiY + H_2$) (17). This process is particularly favoured when multidentate ligands are utilized (14) and can be exploited as a method for generating H_2 in situ on demand (18).

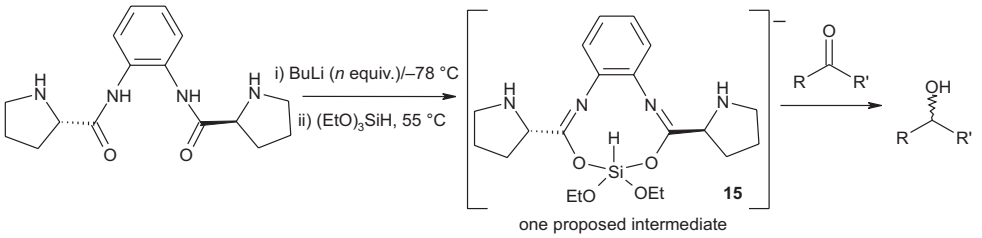
In the current case, the design of the ligand is challenged by this reactivity. Tetradentate complexation giving compounds such as **14** could also result in loss of chirality through epimerization **17**. By contrast, a bidentate chiral C_2-symmetric complex such as **16** is subject to loss of hydride through the processes just described (**16** → **18**, Fig. 3).

Si-H groups are significantly less reactive to acidic than basic conditions (19). It was reasoned that these problems could be mitigated or avoided by changing from basic to acidic conditions. That is, the same ligand could be complexed by a Lewis acid that would fit into the chiral pocket of the ligand and direct reduction. An important precedent for this approach is the observation by Cozzi and coworkers (20) that Lewis acidic titanium fluoride complexes **19**, based on readily accessible chiral bisoxazoline complexes of Evans, will catalyze carbonyl reductions (Scheme 6). The titanium complex of ligand **7** is expected to be tetradentate (Table 5) based on the structure of the copper complex **13**. Carbonyl complexation will preferentially occur at the more Lewis acidic site (titanium) and the locus of the reduction reaction will be taken away from silicon. These proposals were tested by complexing ligand **7** with titanium-based Lewis acids and examining the reduction reaction in the absence and presence of base (Table 5) in the presence of 5 mol% of the chiral catalyst.

The relative Lewis acidity of simple titanium catalysts follows the order $Ti(OiPr)_4 < TiCl_4 < TiF_4$. Replacement of halides or alkoxy groups with amines will further moderate Lewis acidity. No reduction was observed under any conditions when the first two less acidic compounds were employed as catalysts (Table 5). When 2 equiv. of BuLi were

© 2006 NRC Canada

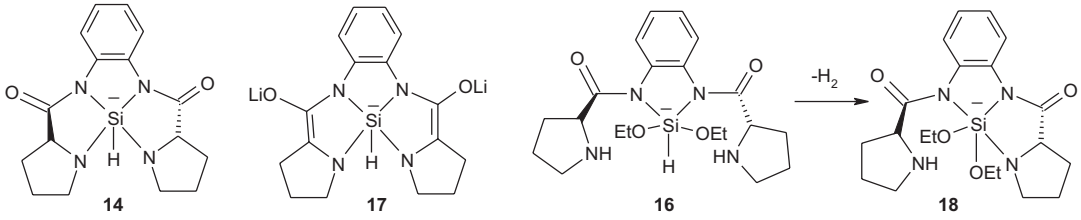
Table 4. Basic reduction of acetophenone by $(EtO)_3SiH$ in the presence of **7**.



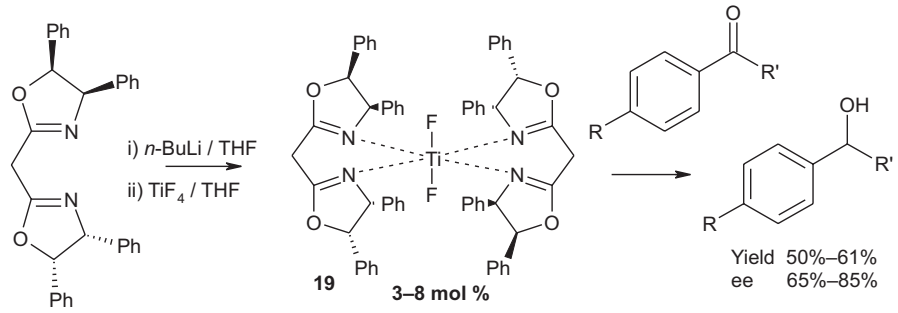
Entry	A	Conditions	*n* (equiv. base)	Yield (%)	ee (%)
1	Acetophenone	55 °C, 72 h	0	NR[a]	—
2	Acetophenone	**7**, 55 °C, 12 h	0	NR	—
3	Acetophenone	proline, BuLi, 55 °C, 24 h	2	50	15
4	Acetophenone	**7**, BuLi, rt, 12 h	4	85	5
5	Acetophenone	**7**, BuLi, rt, 72 h	2	35	64
6	2-Bromoacetophenone	**7**, BuLi, rt, 72 h	2	20	20
7	4-Methoxyacetophenone	**7**, BuLi, rt, 72 h	2	48	5

[a]NR = No reaction.

Fig. 3. Possible pentacoordinate intermediates prior to and following reduction.



Scheme 6.



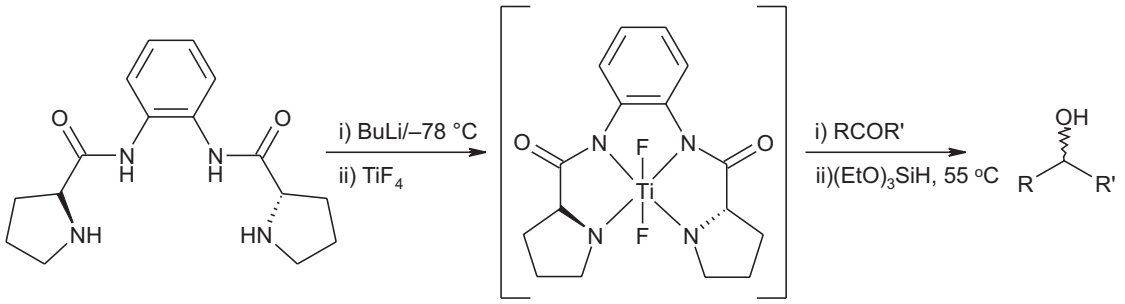
used to facilitate formation of the titanium–**7** complex, only marginal reduction yields were observed, in general worse than in the absence of the titanium compound (Table 4). Of the three reducing agents H_2, Ph_2SiH_2, and $HSi(OEt)_3$, only the last was somewhat efficient. H_2 was used as a negative control. Of the two silanes, $HSi(OEt)_3$ is generally more reactive than Ph_2SiH_2. It has a greater facility for coordination expansion, and as discussed earlier, silylhydrides are more reactive as five- rather than four-coordinate silicon. Improved results were obtained when 4 equiv. of base was used to create the titanium–**7** complex. Yields increased as did enantioselectivity as determined using Mosher ester synthesis (21), although not to levels sufficient for practical application.

A bidentate adduct could form from addition of the dianion **20** to TiF_4 (Scheme 7), which will be a less rigid structure than a tridentate complex such as **21** or the C_2-symmetric catalyst tetradentate titanium complex **22** that should form when 4 equiv. of base are added (Scheme 7). The more rigid structures with proximal chiral groups should have improved enantioselectivity, as was observed with the system derived from the tetraanion.

Several observations provide guidance about the role of the titanium complex **20**. Oxophilic titanium will preferentially jettison nitrogen groups to form a complex with the carbonyl oxygen to give a motif such as **21**, which is widely exploited in titanium-catalyzed aldol and related reactions (22), but in doing so will lose C_2-symmetry. The attempt to crystallize **20** or carbonyl complexes of it were unfortunately unfruitful. Hydrosilanes are normally insufficiently reactive

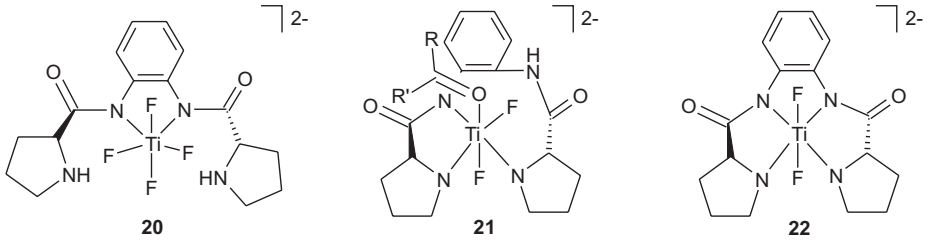
© 2006 NRC Canada

Table 5. Enantioselective reduction of ketones using a bisproline-Ti catalytic system.



Entry	Ketone	7 (mol%)	Metal catalyst (equiv.)	Reaction time (h)	Temp. (°C)	Reducing agent	*n* (equiv. BuLi)	Yield	ee
1	Acetophenone	5	None	12	25	$HSi(OEt)_3$	4	85	5
2	Acetophenone	0	TiF_4 (5)	24	55	$HSi(OEt)_3$	0	NR	—
3	Acetophenone	5	$TiCl_4$ (10)	24	55	$HSi(OEt)_3$	2	NR	—
4	Acetophenone	10	TiF_4 (10)	24	25	H_2	2	NR	—
5	Acetophenone	5	None	24	55	Ph_2SiH_2	2	NR	—
6	Acetophenone	5	TiF_4 (5)	24	55	Ph_2SiH_2	2	17	—
7	Acetophenone	5	TiF_4 (5)	24	55	$(EtO)_3SiH$	2	10	—
8	Acetophenone	5	$TiCl_4$ (5)	24	55	$(EtO)_3SiH$	4	NR	—
9	Acetophenone	5	$RhCl_3$ (5)	24	55	$HSi(OEt)_3$	4	20	—
10	Acetophenone	5	TiF_4 (5)	12	25	$HSi(OEt)_3$	4	80	2
11	Acetophenone	5	TiF_4 (5)	24	55	$HSi(OEt)_3$	4	80	20
12	Acetophenone	5	TiF_4 (5)	12	55	$(EtO)_3SiH$	4	80	20
13	2-Bromoacetophenone	5	TiF_4 (5)	12	55	$(EtO)_3SiH$	4	60	20
14	2-Methoxyacetophenone	5	TiF_4 (5)	12	55	$(EtO)_3SiH$	4	40	2
15	*trans*-4-Phenyl-3-buten-2-one	5	TiF_4 (5)	12	55	$(EtO)_3SiH$	4	90	2

Scheme 7.



to reduce such titanium carbonyl complexes. By contrast, carbocations can be trapped to give C—H bonds (23).

While the specific role of the hydrosilane has not yet been established in the Ti-catalyzed reductions, it seems likely, as with the basic conditions, that extracoordinate silicon is responsible for reduction. The inability of the $TiCl_4$ complex of **7** to catalyze reduction is instructive in this context. The formation of a Lewis acidic chiral complex will liberate the halide Cl^-, which is normally not able to facilitate extracoordination at silicon (12). Thus, while a chiral carbonyl–Ti complex may form, the only reducing agent present is $HSi(OEt)_3$, which is a not viable reducing agent for ketones.

As reported by many researchers, fluoride activates silicon hydrides to reduce carbonyls (24). Formation of compounds such as **22** with TiF_4 serves two purposes. It first provides a chiral Lewis acidic pocket that serves as the locus of reduction and further liberates 2 equiv. of F^-. Fluoride is key, as it can convert the hydrosilane into an active reducing agent, $HSi(OEt)_3F^-$. The obvious disadvantage of this process is that the activated fluoride complex $HSi(OEt)_3F^-$ can directly reduce the ketone outside the sphere of the chiral ligand, leading to a reduction in the overall enantioselectivity of the process.

Of the two very mild approaches examined, the Lewis acidic approach was more efficacious than the extracoordinate hydrosiliconate, with respect to both yields and enantioselectivity. Our current focus is to develop ligands that provide chirality and intramolecular activation to the silicon. Such a system will constrain all reactions to the proximity of the chiral environment.

Conclusion

A C_2-symmetric bisproline ligand can be used as a cata-

© 2006 NRC Canada

lyst to induce enantioselective induction as an anionic extracoordinate silicon complex or after complexation with TiF_4. The Lewis acid catalyzed route led to high yields because side reactions are reduced and showed higher ee.

Experimental section

Reagents and physical methods

The following materials were obtained from Sigma-Aldrich and were used without further purification: acetophenone, *n*-butyllithium (1.6 mol/L solution in cyclohexane), (*S*)-(+)-α-methoxy-α-(trifluoromethyl)phenylacetyl chloride (MTPA-Cl (+)), 2-methoxyacetophenone, *trans*-4-phenyl-3-buten-2-one, sodium sulfate, triethoxysilane, 1,2-diaminobenzene, *N*-BOC-(*S*)-proline, hydroxybenztriazole (HOBt), 1-(3-dimethylaminopropyl)-3-ethylcarbodiimide hydrochloride (EDC), rhodium(III) chloride, titanium(IV) fluoride, and titanium(IV) chloride.

All solvents were thoroughly dried before use; THF was dried from Na/benzophenone. All reactions were carried out in flame-dried apparatus under an argon atmosphere with the use of septa and syringes for the transfer of reagents.

^{1}H and ^{13}C NMR spectra were recorded on a Bruker AC-200 (at 200 MHz for protons, 50.32 MHz for ^{13}C) Fourier transform spectrometer. ^{29}Si NMR was performed on a Bruker DRX-300 (at 75.44 and 59.60 MHz for carbon and silicon, respectively). ^{1}H-NMR was also performed on a Bruker DRX-500 (at 500 MHz for hydrogen). ^{1}H chemical shifts are reported either with respect to tetramethylsilane as an external standard set to 0 ppm or $CDCl_3$ as an internal standard set to 7.26 ppm. ^{13}C NMR chemical shifts are reported either with respect to $CDCl_3$ as an internal standard set to 77.26 or THF-d_8 as an internal standard set to 67.57 ppm. Coupling constants (*J*) are recorded in Hertz (Hz). The abbreviations singlet (s), doublet (d), triplet (t), quartet (q), doublet of doublets (dd), doublet of triplets (dt), multiplet (m) are used to report spectra.

Electron impact (EI) and chemical ionization (CI, NH_3) mass spectra were recorded at 70 eV with a source temperature of 200 °C on a Micromass GCT (Waters Corporation, Milford, Massachusetts) mass spectrometer using a heated probe. High-resolution mass spectral (HRMS) data were obtained using the EI method calibrant with perfluorotributyl amine. Molecular modeling calculations were undertaken using the MM2 molecular mechanics parameter set, using Hyperchem 5.01 from Hypercube Inc. (Gainesville, Florida).

X-ray crystallographic data for **7** and **13** were collected from suitable samples mounted with epoxy on the end of thin glass fibers. Data collections were performed at 273 K.

Data for **7** were collected on a Bruker P4 diffractometer equipped with a Bruker SMART 1K CCD area detector (using the program SMART (25)) and a rotating anode utilizing graphite-monochromated Mo Kα radiation (λ = 0.710 73 Å). Data processing was carried out by use of the program SAINT (26), while the program SADABS (27) was utilized for the scaling of diffraction data, the application of a decay correction, and an empirical absorption correction based on redundant reflections. The structures were solved by using the direct methods procedure in the Bruker SHELXTL (28) program library and refined by full-matrix least-squares methods on F^2. All non-hydrogen atoms were refined using anisotropic thermal parameters and hydrogen atoms were added as fixed contributors at calculated positions, with isotropic thermal parameters based on the atom to which they are bonded.

Data for **13** were collected on a three-circle D8 Bruker diffractometer equipped with a Bruker SMART 6000 CCD area detector (using the program SMART (25)) and a rotating anode utilizing cross-coupled parallel focusing mirrors to provide monochromated Cu Kα radiation (λ = 1.541 78 Å). Data processing and structure solving were carried out as noted previously.

Preparation of the bis(L)prolinyl amide of 1,2-diaminobenzene

A solution of 1,2-diaminobenzene (0.36 g, 3.3 mmol) and *N*-(*tert*-butoxycarbonyl)-L-proline (1.5 g, 6.9 mmol) in CH_2Cl_2–DMF (10:1, 30 mL) was treated at 0 °C with HOBt (0.93 g, 6.9 mmol) and EDC (1.35 g, 6.9 mmol). The reaction mixture was stirred at 0 °C for 2 h and allowed to warm up to room temperature (rt) overnight. Solvents were removed under reduced pressure. CH_2Cl_2 (20 mL) was added to the yellow residue and stirred for 2 h. TFA (10 mL) was added dropwise at rt to the solution, which was stirred for another 2 h. Saturated K_2CO_3 solution (20 mL) neutralized the solution (pH 9). The aqueous layer was extracted with CH_2Cl_2 (3 × 20 mL). The combined organic layer was dried over anhydr. Na_2SO_4. After removing the solvents under reduced pressure, the product was recrystallized from methanol and dichloromethane (20:1). The product, a colourless crystal, was formed in 83% yield. ^{1}H NMR ($CDCl_3$, 500 MHz) δ: 1.73–1.80 (m, 4H, R_1-C*H*-R_2), 2.02–2.13 (m, 2H, NH), 2.18–2.24 (m, 4H, R_2-C*H*-R_3), 2.95–3.10 (m, 4H, CH_2-NH), 3.86–3.93 (q, 2H, *CH*-NH), 7.13–7.19 (m, 2H, Ph-*H*), 7.65–7.70 (m, 2H, Ph-*H*). ^{13}C NMR (d_6-DMSO, 200 MHz) δ: 33.27, 37.76, 54.07, 67.92, 131.03, 132.11, 137.72, 181.25. LRMS (EI) *m*/*z* (%): 302 (M^+, 13), 232 (62), 205 (53), 188 (100), 91 (92), 70 (83), 45 (87). HRMS (ES) *m*/*z* calcd. for $(C_{16}H_{23}N_4O_2)^+$: 303.1808; found: 303.1821.

Preparation of the *N*,*N*′-dimethyl bis(L)prolinyl amide of 1,2-diaminobenzene (12)

To a stirred solution of **7** (1 g, 3.3 mmol) and 37% aqueous formaldehyde (2 mL, 25 mmol) in 20 mL acetonitrile was added sodium cyanoborohydride (0.8 g, 10 mmol). Glacial acetic acid was added until the solution reached neutrality. The reaction was stirred at ambient temperature for 3 h. The reaction mixture was poured into 50 mL of ether and washed with 3 × 30 mL portions of 1 N KOH and one 30 mL portion of brine. The ether solution was dried (Na_2SO_4) and evaporated under reduced pressure. The desired product was recrystallized from MeOH and ether (1:10). The product, a colourless crystal, was formed in 80% yield, mp 206 °C. ^{1}H NMR ($CDCl_3$, 300 MHz) δ: 1.77–1.80 (m, 4H, R_1-CH_2-R_2), 1.82–1.99 (m, 2H, CH-CH_2-CH_2), 2.25–2.42 (m, 4H, CH-CH_2-CH_2), 2.46 (s, 6H, CH_3-N), 3.02 (q, 2H, *J* = 5.1, 10.2 Hz, CH_2-$NHCH_3$), 3.14–3.19 (m, 2H, CH_2-$NHCH_3$), 3.29–3.32 (m, 2H, C*H*-NCH_3), 7.20–7.25 (m, 2H, Ph-*H*), 7.62–7.67 (m, 2H, Ph-*H*), 9.38 (s, 2H, CON*H*). ^{13}C NMR ($CDCl_3$, 200 MHz) δ: 24.38, 31.15, 41.79, 56.67, 69.23, 124.25, 125.80, 129.77, 173.43. LRMS (ES) *m*/*z* (%): 331.6 (M^+, 100), 147.0 (5), 65 (10). HRMS (ES) *m*/*z* calcd.

© 2006 NRC Canada

for $(C_{18}H_{27}N_4O_2)^+$: 331.2134; found: 331.2139. For X-ray data, see Table 1.

Preparation of the copper complex of the bis(L)prolinyl amide of 1,2-diaminobenzene (13)

Ligand **7** (0.03 g, 0.1 mmol) was dissolved in methanol (5 mL) before the addition of anhydr. K_2CO_3 (0.055 g, 0.4 mmol) and $CuCl_2 \cdot 2H_2O$ (0.017 g, 0.1 mmol). The resulting system was stirred overnight, then the solid was filtered off and the clear blue solution was layered with ether. After 2 weeks, purple crystals were isolated, mp 295 °C (dec.). HRMS (ES) *m/z* calcd. for $(C_{16}H_{21}N_4O_2Cu)^+$: 364.0961; found: 364.0957. For X-ray data, see Tables 2 and 3.

General procedure for the ^{29}Si NMR experiment (example ligand 7–triethoxysilane, 1:2)

To a dry NMR tube was added **7** (0.039 g, 0.13 mmol) and d_8-THF (0.3 mL). This solution was cooled to –78 °C and *n*-butyllithium (0.16 mL, 1.6 mol/L solution in hexanes, 0.26 mmol) was added dropwise. The resulting yellowish solution was warmed to 0 °C for 15 min. To this yellow solution was added triethoxysilane (0.05 mL, 0.26 mmol). The solution was allowed to stand at 0 °C then warmed up to rt for 30 min. ^{29}Si NMR was examined in proton decoupled mode using the Bruker DRX-500.

General procedure for basic reduction of ketone in the presence of 7 (example acetophenone) (Table 4)

To a dry 10 mL round-bottomed flame-dried flask protected by argon was added **7** (0.016 g, 0.05 mmol) and THF (5 mL). This solution was cooled to –78 °C and *n*-butyllithium (0.13 mL, 1.6 mol/L solution in hexanes, 0.2 mmol) was added dropwise. The resulting yellowish solution was stirred for 5 min at –78 °C and then warmed to 0 °C for 15 min at which point $(EtO)_3SiH$ (0.38 mL, 2.06 mmol) was added. The resulting clear solution was stirred for 1 h at rt, then acetophenone (0.12 mL, 1.02 mmol) was added. The solution was stirred at rt and product development was monitored by TLC. The reaction mixture was acidified by adding 1 N HCl at 0 °C and carefully made to pH 6 (29). The organic phase collected. The aqueous phase was extracted with ethyl acetate (3 × 10 mL). The organic layers weree combined, dried over sodium sulfate, and then concentrated to give the crude product, which was purified by column chromatography eluting with hexanes – ethyl acetate (5:1). ^{1}H NMR ($CDCl_3$, 200 MHz) δ: 1.56 (d, 3H, *J* = 6.5 Hz, PhCH(OH)*CH*$_3$), 2.76 (bs, 1H, PhCH(*OH*)CH_3), 4.94 (q, 1H, *J* = 6.5 Hz, Ph*CH*(OH)CH_3), 7.32–7.45 (m, $5H_{arom}$). ^{13}C NMR ($CDCl_3$, 200 MHz) δ: 24.97, 69.99, 125.24, 127.14, 128.24, 145.75. MS (EI) *m/z* (%): 122 (M^+, 10), 121 (40), 104 (68), 79 (28), 57 (7), 43 (100). MS (CI) *m/z* (%): 140 ($(M + 18)^+$, 17), 122 (100), 105 (41), 78 (2), 52 (1), 44(1).

General procedure for Lewis acid catalyzed reduction of ketone (example acetophenone) (Table 5)

To a dry 10 mL round-bottomed flame-dried flask protected by argon was added **7** (0.016 g, 0.05 mmol) and THF (5 mL). This solution was cooled to –78 °C and *n*-butyllithium (0.13 mL, 1.6 mol/L solution in hexanes, 0.2 mmol) was added dropwise. The resulting yellowish solution was stirred for 5 min at –78 °C and warmed to 0 °C for 15 min. To this yellow solution was added TiF_4 (6 mg, 0.05 mmol) and the mixture was vigorously stirred until the salt was completely dissolved. The resulting yellow mixture was stirred for 1 h at rt and triethoxysilane (0.38 mL, 2.06 mmol) and acetophenone (0.12 mL, 1.02 mmol) were added. The solution was stirred at 55 °C and product development was monitored by TLC. The reaction mixture was diluted with ethyl acetate (5 mL) and carefully made basic (pH 9) with 1 mol/L of sodium hydroxide (30). The solid was separated by filtration and the organic phase was collected. The aqueous phase was extracted with ethyl acetate (3 × 10 mL). The organic layers were combined, dried over sodium sulfate, and then concentrated to give the crude product which was purified by column chromatography eluting with hexanes – ethyl acetate (5:1).

2-Bromophenethyl alcohol

^{1}H NMR ($CDCl_3$, 200 MHz) δ: 2.69 (bs, 1H, O*H*), 3.69–3.45 (m, 2H, CH_2Br), 4.90 (dd, *J* = 3.5, 8.6 Hz, 1H, Ph*CH*(OH)), 7.36 (s, $5H_{arom}$). ^{13}C NMR ($CDCl_3$, 200 MHz) δ: 40.12, 73.78, 125.95, 128.43, 128.65, 140.31. MS (EI) *m/z* (%): 202 ($(M + 2)^+$, 2), 200 (M^+, 2), 185 (5), 183 (5), 121 (5), 107 (100), 91 (10), 79 (78), 51 (29).

***trans*-4-Phenyl-3-buten-2-ol**

^{1}H NMR ($CDCl_3$, 200 MHz) δ: 1.38 (d, 3H, *J* = 6.4 Hz, PhCH=CHCH(OH)*CH*$_3$), 2.26 (bs, 1H, PhCH=CHCH(*OH*)CH_3), 4.48 (dp, 1H, *J* = 0.9, 6.3 Hz, PhCH=CHC*H*(OH)CH_3), 6.26 (dd, 1H, *J* = 6.3, 16.0 Hz, PhCH=C*H*CH(OH)CH_3), 6.56 (d, 1H, *J* = 16.0 Hz, PhC*H*=CHCH(OH)CH_3), 7.20–7.41 (m, $5H_{arom}$). ^{13}C NMR ($CDCl_3$, 200 MHz) δ: 23.27, 68.68, 126.34, 127.47, 128.44, 129.16, 133.51, 136.61. MS (EI) *m/z* (%): 148 (M^+, 63), 131 (66), 115 (26), 105 (100), 91 (49), 77 (37), 55 (15), 43 (71).

4-Methoxyphenethyl alcohol

^{1}H NMR ($CDCl_3$, 200 MHz) δ: 1.41 (d, 3H, *J* = 6.4 Hz, CH_3O-C_6H_4CH(OH)*CH*$_3$), 2.64 (bs, 1H, $CH_3OC_6H_4$CH(O*H*)CH_3), 3.74 (s, 3H, C$H_3OC_6H_4$-CH(OH)CH_3), 4.76 (q, 1H, *J* = 6.4 Hz, $CH_3OC_6H_4$*CH*(OH)CH_3), 6.85 (d, 2H, *J* = 8.0 Hz, 2 × CH_3OC-CH-*CH*), 7.25 (d, 2H, *J* = 8.0 Hz, 2 × CH_3OC-*CH*-CH). ^{13}C NMR ($CDCl_3$, 200 MHz) δ: 24.88, 55.09, 69.61, 113.62, 126.53, 138.00, 158.70. MS (EI) *m/z* (%): 152 (M^+, 6), 135 (37), 109 (78), 105 (50), 84 (17), 77 (74), 51 (42), 43 (100).

2-Methoxyphenethyl alcohol

^{1}H NMR ($CDCl_3$, 200 MHz) δ: 2.81 (s, 1H, OH), 3.43 (s, 3H, CH_3O), 3.53 (dd, 2H, *J* = 1.2, 4.1 Hz, CH_3O-CH_2-CH(OH)), 4.88 (dd, 1H, *J* = 1.2, 1.7 Hz, C*H*(OH)), 7.30–7.40 (m, $5H_{arom}$). ^{13}C NMR ($CDCl_3$, 200 MHz) δ: 24.12, 26.89, 57.69, 115.62, 129.53, 139.00. MS (EI) *m/z* (%): 144 (M^+, 9), 113 (31), 96 (68), 77 (78), 67 (70), 31 (100).

General procedure for reduction of ketone using rhodium chloride and titanium chloride

The general procedure for Table 5 was followed except that $RhCl_3$ (10 mg, 0.05 mmol) or $TiCl_4$ (9.5 mg, 0.05 mmol) were used, respectively.

© 2006 NRC Canada

General experimental procedure for preparation of Mosher esters (example (*S*)-1-phenylethanol)

(*S*)-1-Phenylethanol (2 mg, 0.02 mmol) and MTPA-Cl (+) (4 μL, 0.02 mmol) were mixed with carbon tetrachloride (3 drops) and dry pyridine (3 drops). The reaction mixture was allowed to stand in a stoppered flask for 12 h at ambient temperature. Water (1 mL) was added and the reaction mixture transferred to a separatory funnel and extracted with ether (20 mL). The ether solution, after washing successively with HCl (1 mol/L, 20 mL), saturated sodium carbonate solution (20 mL), and water (20 mL), was dried with sodium sulfate, filtered, and the solvent was removed in vacuo. The residue was dissolved in deuterated chloroform for NMR analysis. The integration of the hydrogen on the carbon bearing the hydroxyl group was used as a measure to assess the enantioselection.

References

1. (*a*) I. Ojima (*Editor*). Catalytic asymmetric synthesis. Wiley-VCH, New York. 1993; (*b*) R. Noyori. Asymmetric catalysis in organic synthesis. Wiley, New York. 1994.
2. W.-L. Duan, M. Shi, and G.-B. Rong. Chem. Commun. (Cambridge), 2916 (2003).
3. E.J. Corey and C.J. Helal. Angew. Chem. Int. Ed. **37**, 1986 (1998).
4. A. Berkessel and H. Gröger. Asymmetric organocatalysis — From biomimetic concepts to applications in asymmetric synthesis. Wiley-VCH, Germany. 2005. Chap. 1.
5. R. Shiffers and H.B. Kagan. Synlett, 1175 (1997).
6. S. Kohra, H. Hayashida, Y. Tominaga, and A. Hosomi. Tetrahedron Lett. **29**, 89 (1988).
7. F.J. LaRonde and M.A. Brook. Tetrahedron Lett. **40**, 3507 (1999).
8. (*a*) M. Kira, K. Sato, K. Sekimoto, R. Gewald, and H. Sakurai. Chem. Lett. 281 (1995); (*b*) K. Sato, M. Kira, and H. Sakurai. J. Am. Chem. Soc. **111**, 6429 (1989); (*c*) A. Hosomi, S. Kohra, K. Ogata, T. Yanagi, and Y. Tominaga. J. Org. Chem. **55**, 2415 (1990).
9. J.K. Whitesell. Chem. Rev. **89**, 1581 (1989).
10. F.J. LaRonde and M.A. Brook. Can. J. Chem. **81**, 1206 (2003).
11. (*a*) B. List, R.A. Lerner, and C.F. Barbas, III. J. Am. Chem. Soc. **122**, 2395 (2000); (*b*) W. Notz and B. List. J. Am. Chem. Soc. **122**, 7386 (2000); (*c*) B. List, P. Pojarliev, and C. Castello. Org. Lett. **3**, 573 (2001); (*d*) K. Sakthivel, W. Notz, T. Bai, and C.F. Barbas, III. J. Am. Chem. Soc. **123**, 5260 (2001).
12. M.A. Brook. Silicon in organic, organometallic, and polymer chemistry. Wiley, New York. 2000. Chap. 4.
13. (*a*) M. Mühleisen and R. Tacke. Organometallics, **13**, 3740 (1994); (*b*) R. Tacke and M. Mühleisen. Angew. Chem. Int. Ed. Engl. **106**, 1431 (1994); (*c*) R. Tacke and M. Mühleisen. Inorg. Chem. **33**, 4191 (1994); (*d*) R. Tacke, M. Mühleisen, and P.G. Jones. Angew. Chem. Int. Ed. Engl. **33**, 1186 (1994); (*e*) M. Mühleisen and R. Tacke. Chem. Ber. **127**, 1615 (1994); (*f*) R. Tacke, J. Becht, A. Lopez-Mras, and J. Sperlich. J. Organomet. Chem. **446**, 1 (1993).
14. (*a*) M.J. Roth, M.A. Brook, and H.B. Penny. J. Organomet. Chem. **521**, 65 (1996); (*b*) M.A. Brook, D. Chau, M.J. Roth, W. Yu, and H. Penny. Organometallics, **13**, 750 (1994).
15. F.J. LaRonde and M.A. Brook. Inorg. Chim. Acta, **296**, 208 (1999).
16. E.A. Williams. *In* The chemistry of organic silicon compounds. Vol. 1. *Edited by* S. Patai and Z. Rappoport. Wiley, Chichester, UK. 1989. Chap. 8. p. 524.
17. L.N. Lewis. J. Am. Chem. Soc. **112**, 5998 (1990), and refs. cited therein.
18. (*a*) J.M. Tour and S.L. Pendalwar. Tetrahedron Lett. **31**, 4719 (1990); (*b*) J.M. Tour, J.P. Cooper, and S.L. Pendalwar. J. Org. Chem. **55**, 3452 (1990).
19. W. Noll. Chemistry and technology of silicones. Academic Press, New York. 1968.
20. M. Bandini, P.G. Cozzi, L. Negro, and A. Umani-Ronchi. Chem. Commun. (Cambridge), 39 (1999).
21. J.A. Dale, D.L. Dull, and H.S. Mosher. J. Org. Chem. **34**, 2543 (1969).
22. (*a*) I. Marek (*Editor*). Titanium and zirconium in organic synthesis. Wiley-VCH, Weinheim, Germany. 2002; (*b*) H. Urabe and F. Sato. *In* Acids in organic synthesis. *Edited by* H. Yamamoto. Wiley-VCH, Weinheim, Germany. 2000. pp. 653–798.
23. S. Anwar and A.P. Davis. J. Chem. Soc. Chem. Commum. 831 (1986).
24. M. Fujita and F. Hiyama. J. Org. Chem. **53**, 5405 (1988).
25. G.M. Sheldrick. SMART. Release 6.45 [computer program]. Siemens Energy and Automation Inc., Madison, Wis. 2003.
26. G.M. Sheldrick. SAINT. Release 6.45 [computer program]. Siemens Energy and Automation Inc., Madison, Wis. 2003.
27. G.M. Sheldrick. SADABS [computer program]. Siemens Energy and Automation Inc., Madison, Wis. 2003.
28. G.M. Sheldrick. SHELXTL. Release 6.14 [computer program]. Siemens Crystallographic Research Systems, Madison, Wis. 2000.
29. H. Nishiyama, S. Yamaguchi, M. Kondo, and K. Itoh. J. Org. Chem. **57**, 4306 (1992).
30. B.H. Lipshutz, K. Noson, W. Chrisman, and A. Lower. J. Am. Chem. Soc. **125**, 8779 (2003).

© 2006 NRC Canada

Hydrogen-bonded networks in crystals built from bis(biguanides) and their salts[1]

Olivier Lebel, Thierry Maris, and James D. Wuest

Abstract: Biguanide groups and biguanidinium cations incorporate multiple sites that can donate or accept hydrogen bonds. To assess their ability to associate and to direct the formation of extended hydrogen-bonded networks, we examined the structure of crystals of four compounds in which two neutral biguanide groups or the corresponding cations are attached to the 1,4- and 1,3-positions of phenylene spacers. As expected, all four structures incorporate extensive networks of hydrogen bonds and reveal other reliable features. In particular, (1) neutral biguanide groups favor a roughly planar conformation with an intramolecular hydrogen bond, and they associate as hydrogen-bonded pairs, (2) despite coulombic repulsion, biguanidinium cations can also associate as hydrogen-bonded pairs, and (3) the 1,3-phenylenebis(biguanidinium) dication favors a pincerlike conformation that allows chelation of suitable counterions. However, the precise patterns of hydrogen bonding in the structures vary substantially, limiting the usefulness of biguanide and biguanidinium as groups for directing supramolecular assembly.

Key words: bis(biguanide), bis(biguanidinium), structure, hydrogen-bonded network, noncovalent interaction, supramolecular chemistry, crystal engineering.

Résumé : Des groupes biguanide et des cations biguanidinium incorporent de multiples sites qui peuvent donner ou accepter des liaisons hydrogène. Dans le but d'évaluer la capacité d'associer et de diriger la formation de réseaux étendus de liaisons hydrogène, on a étudié la structure cristalline de quatre composés dans lesquels deux groupes biguanide neutres, ou les cations correspondants, sont attachés aux positions 1,4- et 1,3- de groupes phénylènes. Comme prévu, les quatre structures permettent d'incorporer des réseaux de liaisons hydrogène et mettent en évidence d'autres caractéristiques fiables. En particulier, 1) les groupes biguanide neutres favorisent une conformation pratiquement plane avec une liaison hydrogène intramoléculaire et s'associent sous la forme de paires réunies par des liaisons hydrogène, 2) malgré une répulsion coulombique, les cations biguanidinium peuvent aussi former des paires associées par des liaisons hydrogène et 3) le dication phénylène-1,3-bis(biguanidinium) favorise une conformation en forme de pince qui permet d'effectuer une chélation avec des contre-ions appropriés. Toutefois, les régimes précis des liaisons hydrogène varient d'une façon substantielle, ce qui limite l'utilité des groupes biguanide et biguanidinium comme unités pouvant orienter un assemblage supramoléculaire.

Mots clés : bis(biguanide), bis(biguanidinium), structure, réseau à liaisons hydrogène, interaction non covalente, chimie supramoléculaire, génie cristallin.

[Traduit par la Rédaction]

Introduction

The general family of compounds that includes biguanide (**1**) has been known for over 100 years (1–3).[3] Members of the family have important applications as medicines, as ligands in coordination chemistry, as bases, and as precursors for the synthesis of various heterocyclic compounds (4). In addition, biguanide groups and biguanidinium cations incorporate characteristic patterns of sites that can donate or accept hydrogen bonds, thereby allowing them to associate and engage in supramolecular assembly (4).

A productive strategy for engineering predictably ordered supramolecular materials is to build them from compounds incorporating multiple sticky sites that participate in directional intermolecular interactions (5). These interactions tend to place adjacent molecules in specific positions, leading to the formation of extensive networks with predetermined architectures. In this paper, we assess the potential of multiple biguanide and biguanidinium groups to serve in this way as sticky sites, and we describe the hydrogen-bonded networks present in crystals of bis(biguanide) **2**, its dihydrochloride, and the dihydrochloride and carbonate of isomeric bis(biguanide) **3**. Previous use of such compounds in supramolecular chemistry has been limited to the chelation of metals by ethylenebis(biguanide) (6, 7).

Received 3 December 2005. Accepted 26 April 2006. Published on the NRC Research Press Web site at http://canjchem.nrc.ca on 17 October 2006.

Dedicated with respect and affection to Dr. Alfred Bader for his friendship, encouragement, generosity, entreprenurial spirit, love of art, and enduring service to chemistry.

O. Lebel, T. Maris, and J.D. Wuest.[2] Département de Chimie, Université de Montréal, Montréal, QC H3C 3J7, Canada.

[1]This article is part of a Special Issue dedicated to Dr. Alfred Bader.

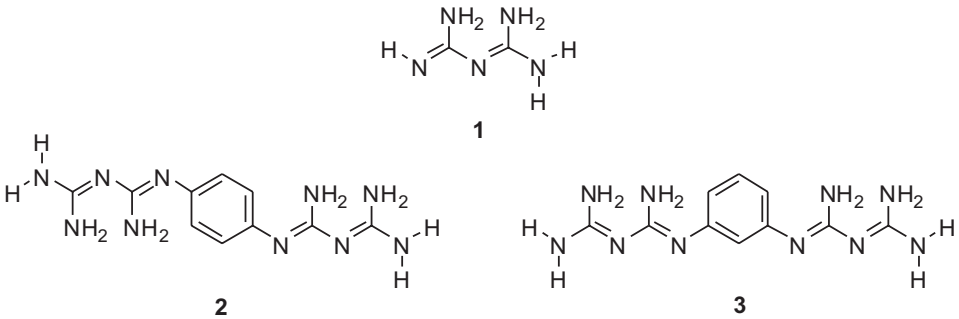
[2]Corresponding author (e-mail: james.d.wuest@umontreal.ca).

[3]For the sake of simplicity, biguanides and their salts are normally represented in this paper as single tautomers.

 doi:10.1139/V06-115 © 2006 NRC Canada

Table 1. Crystallographic data for bis(biguanide) **2**, its dihydrochloride, and the dihydrochloride and carbonate of isomeric bis(biguanide) **3**.

Compound	**2**·H_2O	**2**·2HCl·H_2O	**3**·2HCl·$3H_2O$	**3**·H_2CO_3·H_2O·0.5 dioxane
Temperature (K)	100	293	100	100
λ (Å)	1.54178	1.54178	1.54178	1.54178
Formula	$C_{10}H_{18}N_{10}O$	$C_{10}H_{20}Cl_2N_{10}O$	$C_{10}H_{24}Cl_2N_{10}O_3$	$C_{13}H_{24}N_{10}O_5$
Fw	294.34	367.26	403.29	400.42
F(000)	936	384	424	424
Crystal system	Triclinic	Triclinic	Triclinic	Triclinic
Z	6	2	2	2
d (g cm^{-3})	1.432	1.420	1.435	1.420
μ (mm^{-1})	0.863	3.591	3.437	0.947
Space group	*P*-1	*P*-1	*P*-1	*P*-1
a (Å)	10.0311(16)	5.8749(8)	9.3537(3)	9.9072(3)
b (Å)	10.8820(18)	12.036(5)	9.6015(3)	10.1769(3)
c (Å)	21.127(3)	13.084(5)	11.4402(4)	11.0195(5)
α (°)	88.090(7)	105.66(3)	82.983(2)	77.297(2)
β (°)	87.280(7)	95.65(3)	71.193(2)	67.906(2)
γ (°)	62.735(6)	102.12(2)	73.759(2)	65.826(2)
Volume ($Å^3$)	2047.5(6)	859.1(5)	933.19(5)	936.32(6)
θ max (°)	58.01	70.01	70.01	72.03
h, *k*, *l* max	10, 11, 23	7, 14, 15	11, 11, 14	12, 12, 13
Unique reflections	6951	3241	3545	3557
Observed reflections ($I > 2\sigma(I)$)	3715	2766	2583	2403
*R*1	0.0600	0.0456	0.0745	0.0487
*wR*2	0.0903	0.1109	0.2142	0.1277
*R*1 (all data)	0.1294	0.0463	0.0818	0.0699
*wR*2 (all data)	0.1012	0.1110	0.2351	0.1357
Diff. peak and hole (e, $Å^3$)	0.318, –0.360	0.323, –0.396	0.913, –0.626	0.397, –0.479
GoF	1.012	1.105	1.058	0.942



1

2 **3**

Results and discussion

Crystal structure of bis(biguanide) 2

Bis(biguanide) **2** was prepared by a published method (4) and was crystallized from hot water. X-ray diffraction established that the crystals belong to the triclinic space group *P*-1 and exist as a pair of nonmerohedral twins (8). The crystals have the composition **2**·H_2O and each unit cell contains six molecules of bis(biguanide) **2** and six molecules of H_2O. Crystallographic parameters are given in Table 1, views of the structure appear in Figs. 1 and 2, and additional information is provided as Supplementary data.[4] Multiple symmetry-independent biguanide groups are present in the unit cell, but all correspond to tautomeric form **I** (Scheme 1) and have a roughly planar geometry with internal torsion angles in the range 2.5(3)°–29.8(3)°. This geometry is enforced by an intramolecular NH···N hydrogen bond, with N···H distances of normal values (1.993(5)–2.263(5) Å). Similar features appear in all previous structural studies of neutral biguanides (4, 9–11), so a nearly planar geometry and an intramolecular hydrogen bond appear to be structural features of biguanides that can be used reliably by crystal engineers. The average

[4] Supplementary data for this article are available on the journal Web site (http://canjchem.nrc.ca) or may be purchased from the Directory of Unpublished Data, Document Delivery, CISTI, National Research Council Canada, Ottawa, ON K1A 0S2, Canada. DUD 3662. For more information on obtaining material refer to http://cisti-icist.nrc-cnrc.gc.ca/irm/unpub_e.shtml. CCDC 291494–291497 contain the crystallographic data for this manuscript. These data can be obtained free of charge via www.ccdc.cam.ac.uk/conts/retrieving.html (or from the Cambridge Crystallographic Data Centre, 12 Union Road, Cambridge CB2 1EZ, UK; fax +44 1223 336033; or deposit@ccdc.cam.ac.uk).

© 2006 NRC Canada

Fig. 1. View of the crstal structure of neutral bis(biguanide) **2** grown from water. The view reveals that each biguanide group incorporates an internal NH···N hydrogen bond and favors tautomeric form **I** (Scheme 1). In addition, the view shows bifurcated intermolecular hydrogen bonds that link compound **2** into continuous ribbons, as well as additional hydrogen bonds involving water. Hydrogen bonds are represented by broken lines. Hydrogen atoms appear in white, carbon in gray, nitrogen in blue, and oxygen in red.

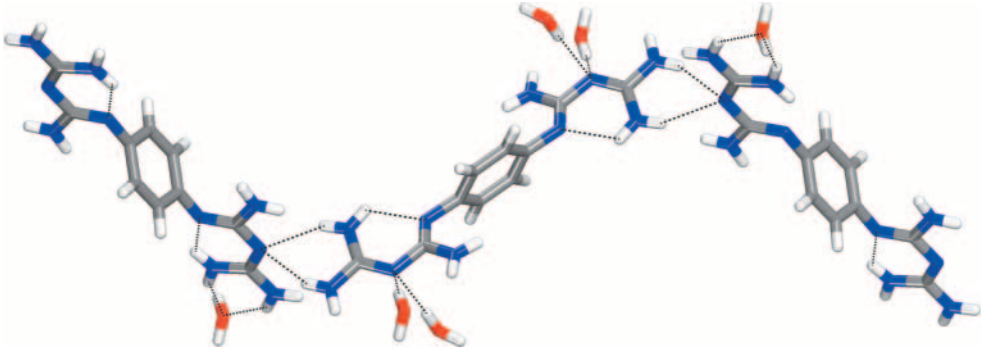
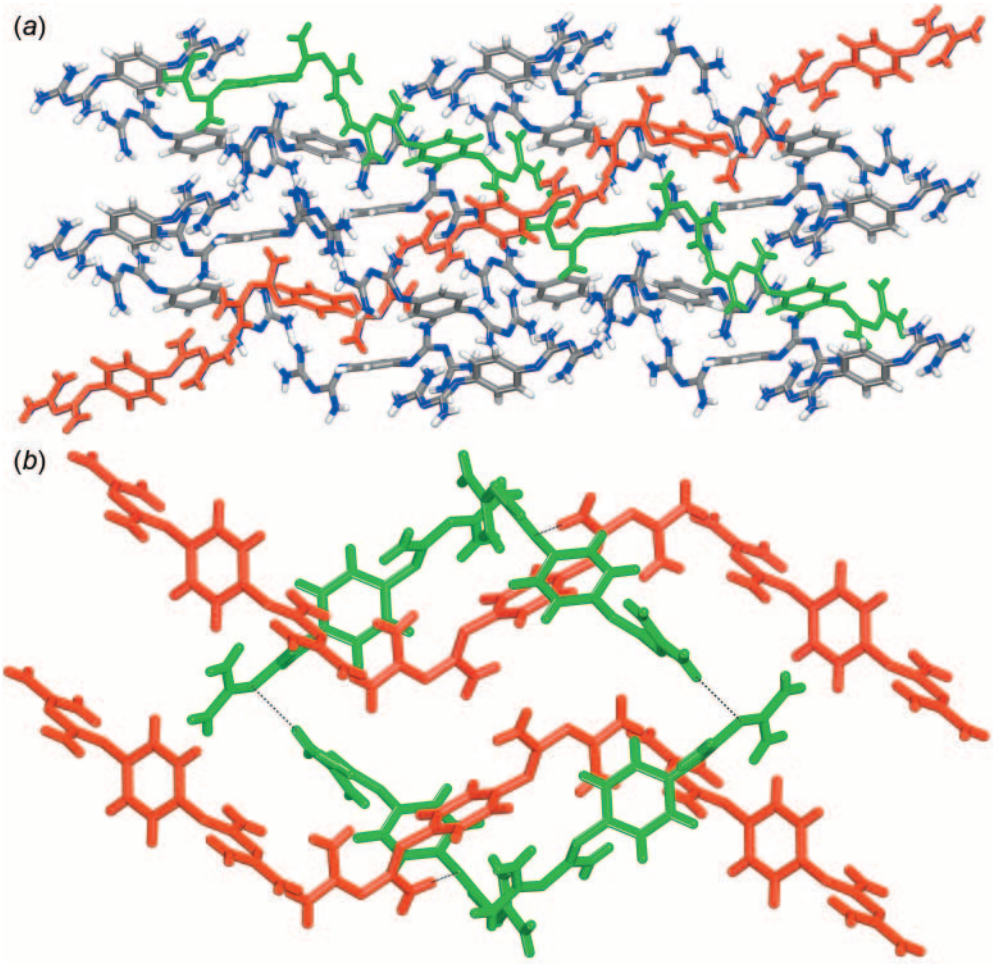


Fig. 2. (*a*) View along the *b* axis of the structure of crystals of neutral bis(biguanide) **2**, with hydrogen atoms shown in white, carbon in gray, and nitrogen in blue. Two hydrogen-bonded ribbons are highlighted in red and green. The two highlighted ribbons run in opposite directions along the *ac* diagonal. (*b*) View along the *a* axis showing secondary hydrogen bonds (represented by broken lines) between the characteristic ribbons. In both views, water molecules are omitted for clarity.



planes defined by the biguanide groups form dihedral angles in the range 67.6(1)°–88.7(1)° with respect to the plane of the central aromatic ring.

Intermolecular hydrogen bonds involving bis(biguanide) **2** and water create a complex network (Figs. 1 and 2), with over 40 hydrogen bonds per unit cell. A primary motif in this network is the ribbon shown in Fig. 1, which links molecules of bis(biguanide) **2** end-to-end by novel bifurcated

© 2006 NRC Canada

Scheme 1.

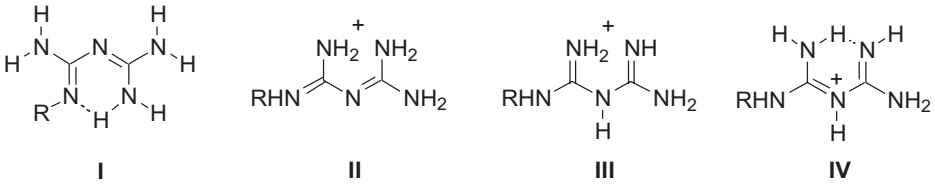
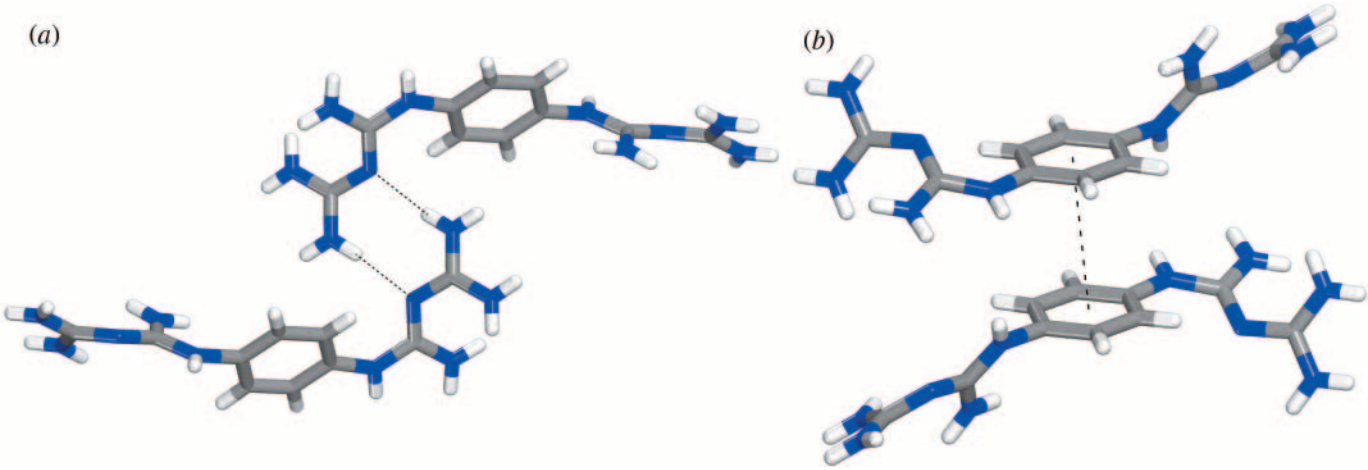


Fig. 3. Views of the crystal structure of the dihydrochloride salt of bis(biguanide) **2** grown from acetone–water. (*a*) The biguanidinium cations favour structure **II** (Scheme 1) and form hydrogen-bonded pairs. (*b*) Additional cohesion is contributed by slightly offset face-to-face aromatic interactions. Hydrogen bonds and the aromatic interaction are represented by broken lines and included water molecules are omitted for simplicity. Hydrogen atoms appear in white, carbon in gray, and nitrogen in blue.



hydrogen bonds. Each molecule in the ribbon serves either as a double acceptor or a double donor of these bifurcated bonds. The resulting ribbons are aligned with the *ac* diagonal and linked by additional hydrogen bonds between biguanide groups, as well as by bridging molecules of water (Fig. 2).

Crystal structure of the dihydrochloride salt of bis(biguanide) 2

Crystals were grown by allowing acetone to diffuse slowly into an aqueous solution of bis(biguanidinium) dichloride (**2**·2HCl), which was prepared by a known method (4). X-ray diffraction demonstrated that the crystals belong to the triclinic space group *P*-1 and have the composition **2**·2HCl·H_2O. Each unit cell contains two symmetry-equivalent molecules of bis(biguanidium) dichloride and two molecules of H_2O. There are four potential sites for H_2O, associated in pairs within van der Waals distances, but only half are occupied. Crystallographic parameters appear in Table 1, views of the structure are shown in Figs. 3 and 4, and additional information is given as Supplementary data.[4] The biguanidinium groups are extensively delocalized, as demonstrated by the similarity of the C-N distances (1.310(3)–1.366(2) Å). Each biguanidinium group can be represented by structure **II** (Scheme 1) and its resonance hybrids, and alternatives in which the central atom of nitrogen is protonated (structure **III**) or in which an intramolecular hydrogen bond is present (structure **IV**) are not favoured in the solid state. Similar conclusions have been reached in all previous structural analyses of biguanidinium cations (4, 10–21), so protonation of biguanides to give structure **II** (Scheme 1) appears to be a fundamental preference, both in solution (2) and in the solid state. Although the biguanidium groups in the dihydrochloride salt of compound **2** can be represented by structure **II**, they are not planar. The two guanidinium subunits that can be considered to be present in each biguanidinium group are individually planar, but their planes define dihedral angles of 39.2(1)° and 45.5(1)° in the two arms of each dication.

The structure of the dihydrochloride salt of bis(biguanide) **2** can be described as a complex network held together in part by hydrogen-bonded pairing of biguanidinium cations (Fig. 3*a*). The N··N distance in these cationic pairs is 3.033(3) Å. Intercationic hydrogen bonding is inhibited by coulombic repulsion and is absent in most biguanidinium salts (4, 11, 14, 15, 17, 19–21), although it has previously been observed in a few cases (12, 13, 18). Slightly offset face-to-face aromatic interactions are also observed in the structure of salt **2**·2HCl (Fig. 3*b*), with a center-to-center separation of 3.879(2) Å. In addition, the structure of the salt reveals multiple ionic hydrogen bonds between biguanidium cations and chloride (Fig. 4). There are two distinct types of chloride ion in the structure, each of which accepts hydrogen bonds from N-H groups provided by neighbouring bis(biguanidium) dications. One type (Cl1) accepts five hydrogen bonds from four dications (Fig. 4*a*) and the other type (Cl2) accepts six hydrogen bonds from four dications, two of which are involved in chelation of chloride (Fig. 4*b*). Each bis(biguanidinium) dication is linked by hydrogen bonding to eight chloride ions, two molecules of water, and one other bis(biguanidinium) dication. The resulting network defines small channels along the *a* axis that are occupied by included molecules of water.

© 2006 NRC Canada

Fig. 4. Views of the crystal structure of the dihydrochloride salt of bis(biguanide) **2** showing ionic hydrogen bonds involving chloride. (*a*) One type of chloride ions (Cl1) accepts hydrogen bonds donated by five N-H groups in four different bis(biguanidinium) dications. (*b*) The other type of chloride (Cl2) accepts six hydrogen bonds (four involving chelation), again contributed by N-H groups in four different bis(biguanidinium) dications. In both views, hydrogen bonds are represented by broken lines. Hydrogen atoms appear in white, carbon in gray, nitrogen in blue, and chlorine in green.

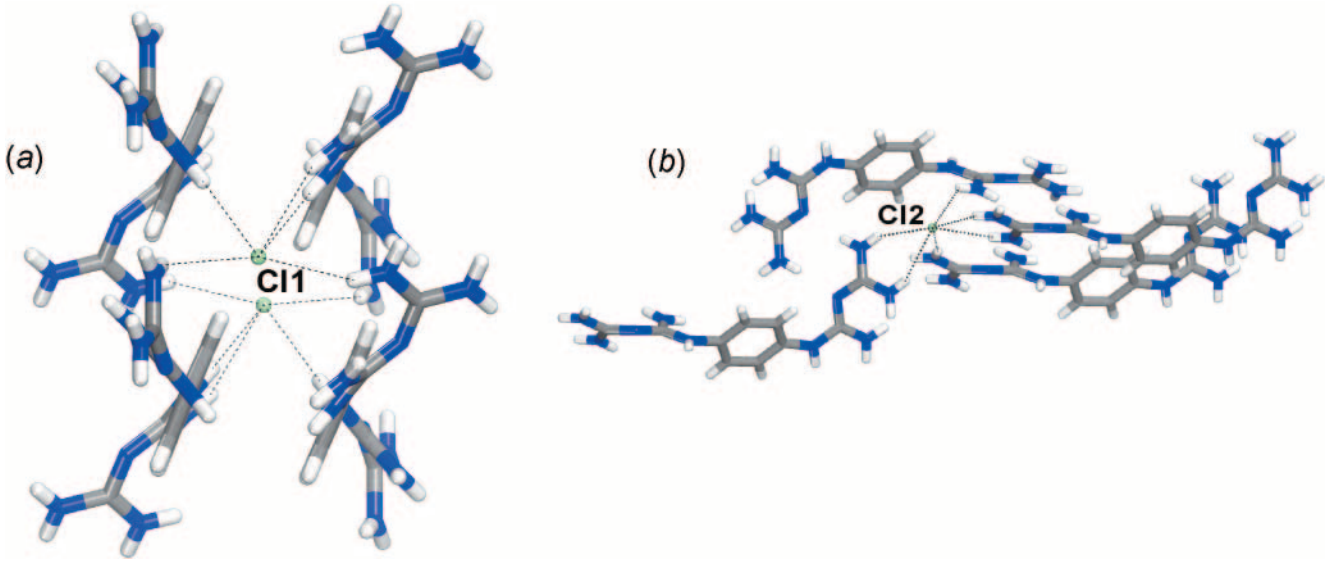
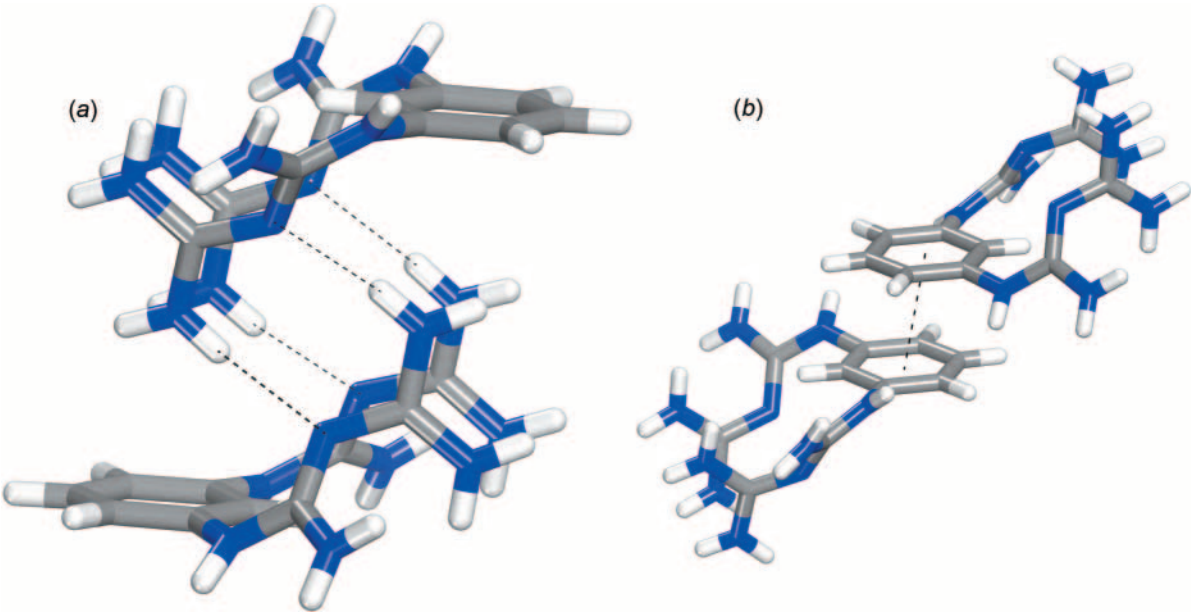


Fig. 5. Views of the crystal structure of the dihydrochloride salt of bis(biguanide) **3** grown from acetone–water. (*a*) The biguanidinium cations favor structure **II** (Scheme 1) and form hydrogen-bonded pairs. (*b*) Additional cohesion is contributed by face-to-face aromatic interactions. Hydrogen bonds and the aromatic interaction are represented by broken lines, and included water molecules are omitted for simplicity. Hydrogen atoms appear in white, carbon in gray, and nitrogen in blue.

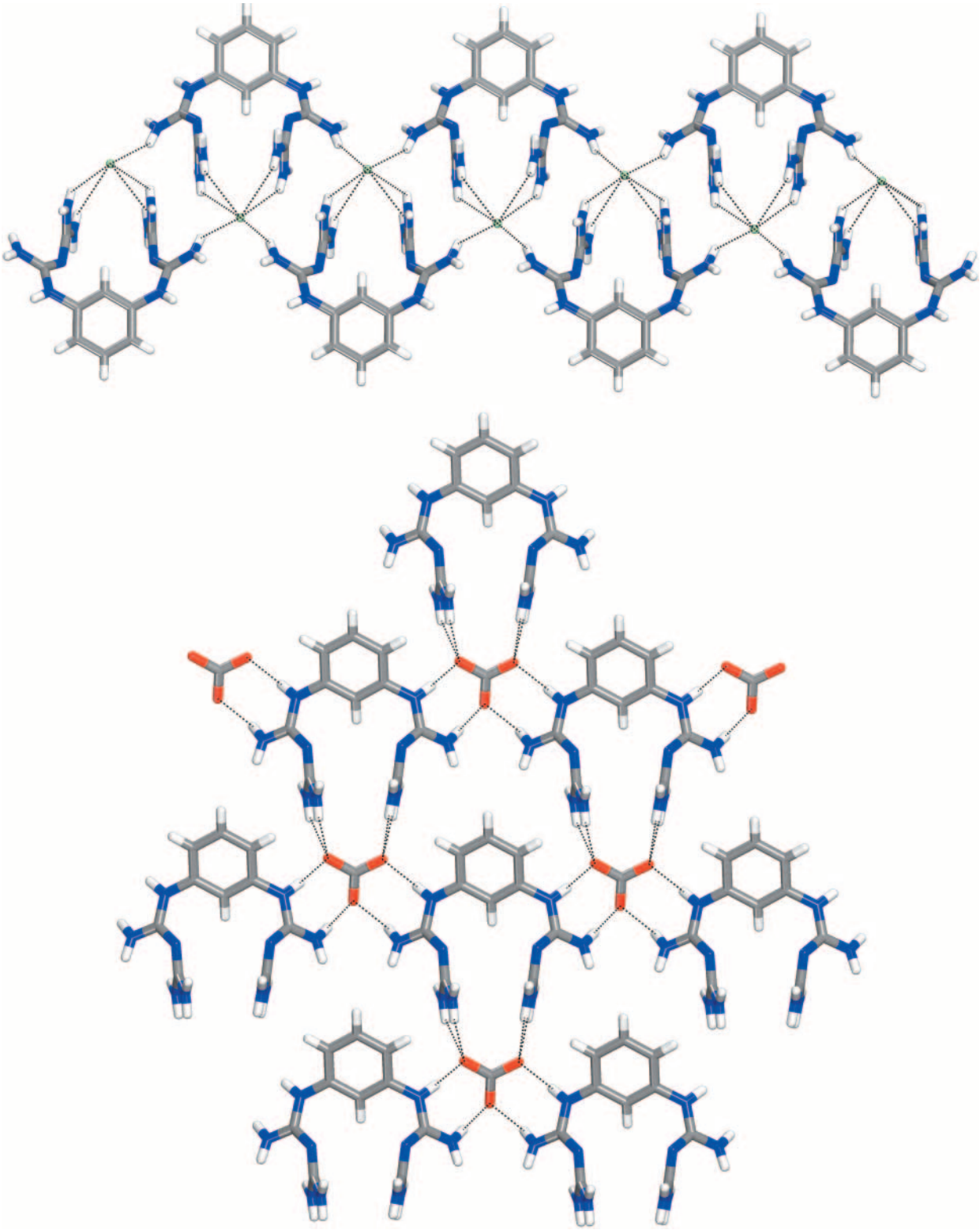


Crystal structure of the dihydrochloride salt of bis(biguanide) 3

Bis(biguanidinium) dichloride **3**·2HCl was prepared by a known method (4) and was crystallized from acetone–water. X-ray diffraction revealed that (*i*) the crystals belong to the triclinic space group *P*-1, (*ii*) their composition corresponds to **3**·2HCl·3H_2O, and (*iii*) each unit cell contains two equivalent molecules of bis(biguanidium) dichloride and six molecules of H_2O. Crystallographic parameters are given in Table 1, views of the structure appear in Figs. 5 and 6*a*, and additional information is provided in the Supplementary data.[4] As noted in other biguanidinium salts, the cations are extensively delocalized, and the C-N distances have similar values (1.320(5)–1.353(5) Å). Again, each biguanidinium

© 2006 NRC Canada

Fig. 6. (*a*) View along the *c* axis of the crystal structure of the dihydrochloride salt of bis(biguanide) **3** grown from acetone–water. The view shows a tape constructed by ionic hydrogen bonding involving one of the two types of chloride ions in the structure. Each bis(biguanidinium) dication adopts a pincerlike conformation that permits chelation of chloride by the simultaneous donation of four hydrogen bonds. (*b*) View along the *c* axis of the closely related structure of crystals of the carbonate salt of bis(biguanide) **3** grown from dioxane–water. In both views, hydrogen bonds are represented by broken lines. Hydrogen atoms appear in white, carbon in gray, nitrogen in blue, oxygen in red, and chlorine in green.



© 2006 NRC Canada

group can be represented by structure **II** (Scheme 1). This further reinforces the conclusion, drawn previously from analysis of salt **2**·2HCl and related compounds (4), that structure **II** is a fundamental preference of biguanidinium cations and can be used dependably by crystal engineers. As in the case of analogue **2**·2HCl, the two biguanidinium groups in each bis(biguanidinium) dication are distinctly nonplanar, and the planes of the guanidinium subunits that can be considered to be present define dihedral angles of 52.6(2)° and 54.8(2)°.

Various important interactions can be identified in the structure of the dihydrochloride salt of bis(biguanide) **3**. As in the structure of the analogous salt **2**·2HCl, a network is formed by hydrogen-bonded pairing of biguanidinium cations (Fig. 5*a*), with N···N distances similar to those observed previously (2.979(4) and 3.028(4) Å). It is noteworthy that this uncommon hydrogen-bonded dimeric motif is observed in the structures of both bis(biguanidinium) salts, despite its coulombic disadvantage. Nevertheless, its absence in the structures of most other biguanidinium salts (4, 11, 14, 15, 17, 19–21) suggests that it does not define a motif that can be used reliably in supramolecular construction.

Additional cohesive forces in the structure of salt **3**·2HCl, also observed in that of analogue **2**·2HCl, are contributed by face-to-face aromatic interactions with a center-to-center separation of 3.687(2) Å (Fig. 5*b*). The structure of salt **3**·2HCl, like that of analogue **2**·2HCl, reveals multiple ionic hydrogen bonds between biguanidium cations and chloride (Fig. 6*a*). Again, there are two distinct types of chloride ion in the structure. One accepts a total of six hydrogen bonds from N-H groups provided by three neighbouring bis(biguanidium) dications (Fig. 6*a*). This type of chloride accepts an additional hydrogen bond from one of the included molecules of water. The dications adopt a pincerlike conformation that favors the binding of chloride by allowing each biguanidinium group to donate two hydrogen bonds to a single chloride, resulting in a characteristic chelation (Fig. 6*a*). Binding of chloride in this way generates tapes that run along the *ab* diagonal. The second type of chloride forms additional ionic hydrogen bonds that help bridge the tapes, and further links between the tapes are created by the hydrogen-bonded pairing of biguanidinium cations (Fig. 5*a*).

Crystal structure of the carbonate salt of bis(biguanide) 3

In contact with air, solutions of bis(biguanide) **3** in dioxane–water yielded crystals of the corresponding carbonate. X-ray diffraction established that (*i*) the crystals belong to the triclinic space group *P*-1, (*ii*) their composition corresponds to **3**·H_2CO_3·H_2O·0.5 dioxane, and (*iii*) each unit cell contains two equivalent molecules of bis(biguanidium) carbonate. Crystallographic parameters are provided in Table 1, a view of the structure appears in Fig. 6*b*, and additional information is given in the Supplementary data.[4] The bis(biguanidinium) dications adopt essentially the same pincerlike conformation observed in dichloride **3**·2HCl, and the two structures are strikingly similar. Chelation of carbonate leads to the assembly of sheets rather than tapes (Fig. 6*b*). Hydrogen-bonded pairing of biguanidinium cations, also observed in the other salts of bis(biguanides) **2** and **3**, then joins the sheets in a three-dimensional network. Each carbonate also accepts an additional hydrogen bond from an adjacent sheet, and molecules of dioxane are held between the sheets by multiple hydrogen bonds.

Conclusions

Biguanides are an intrinsically interesting class of compounds with many known or potential applications. Because biguanides and biguanidinium salts incorporate multiple sites that can donate or accept hydrogen bonds, they are inherently disposed to associate, making them attractive candidates for applications in crystal engineering and other areas of supramolecular chemistry. To evaluate their potential, we have linked two biguanide or biguanidinium groups to rigid aromatic spacers, and we have determined how the resulting bis(biguanides) and bis(biguanidinium) dications interact in the crystalline state. These studies, along with previous structural analyses, have confirmed that the biguanide and biguanidinium groups can be counted on to engage in multiple hydrogen bonds, leading to the formation of extended networks. However, the precise patterns of hydrogen bonding vary significantly, suggesting that other groups are inherently more suitable for fully controlling molecular aggregation.

Experimental

Crystallization of bis(biguanide) 2

Bis(biguanide) **2** was prepared according to a published procedure (4) and crystallized from hot water.

Crystallization of the dihydrochloride salt of bis(biguanide) 2

The dihydrochloride salt of bis(biguanide) **2** was prepared according to a published procedure (4). Single crystals suitable for X-ray diffraction were grown by allowing acetone to diffuse slowly into an aqueous solution of the salt.

Crystallization of the dihydrochloride salt of bis(biguanide) 3

The dihydrochloride salt of bis(biguanide) **3** was prepared according to a published procedure (4). Single crystals suitable for X-ray diffraction were grown by allowing acetone to diffuse slowly into an aqueous solution of the salt.

Crystallization of the carbonate salt of bis(biguanide) 3

Bis(biguanide) **3** was prepared according to a published procedure (4). Single crystals of the carbonate salt suitable for X-ray diffraction were grown by allowing dioxane to diffuse slowly into an aqueous solution of compound **3** in contact with air.

X-ray crystallographic studies

The structures were solved by direct methods using SHELXS-97 (22) and refined with SHELXL-97 (23). All non-hydrogen atoms were refined anisotropically. Hydrogen atoms bonded to nitrogen atoms were located from difference Fourier maps, whereas hydrogen atoms bonded to the carbon atoms of aryl groups were placed in idealized positions. All hydrogen atoms were refined as riding atoms. The structure of bis(biguanide) **2** was refined as a two-

© 2006 NRC Canada

component twin with twin element scale factors of 0.512(1) and 0.488(1) (24).

Acknowledgements

We are grateful to the Natural Sciences and Engineering Research Council (NSERC) of Canada, the Ministère de l'Éducation du Québec, the Canada Foundation for Innovation, and the Canada Research Chairs Program for financial support. In addition, we thank Professor Jurgen Sygusch for providing access to a Bruker SMART 6000 CCD diffractometer equipped with a rotating anode.

References

1. P. Hubberstey and U. Suksangpanya. Struct. Bonding (Berlin, Ger.), **111**, 33 (2004).
2. F. Kurzer and E.D. Pitchfork. Fortschr. Chem. Forsch. **10**, 375 (1968).
3. P. Ray. Chem. Rev. **61**, 313 (1961).
4. O. Lebel, T. Maris, H. Duval, and J.D. Wuest. Can. J. Chem. **83**, 615 (2005).
5. J.D. Wuest. Chem. Commun. (Cambridge, U.K.), 5830 (2005).
6. A. Das and S. Mukhopadhyay. Polyhedron, **23**, 895 (2004).
7. A. De. Acta Crystallogr. Sect. C: Cryst. Struct. Commun. **46**, 1004 (1990).
8. C. Giacovazzo. Fundamentals of crystallography. Oxford University Press, New York. 1992. pp. 83–87.
9. A. Dalpiaz, V. Ferretti, P. Gilli, and V. Bertolasi. Acta Crystallogr. Sect. B: Struct. Sci. **52**, 509 (1996).
10. A.A. Pinkerton and D. Schwarzenbach. J. Chem. Soc. Dalton Trans. 989 (1978).
11. S.R. Ernst. Acta Crystallogr. Sect. B: Struct. Crystallogr. Cryst. Chem. **33**, 237 (1977).
12. G. López-Olvera and M. Soriano-García. Anal. Sci.: X-ray Struct. Anal. [online]. **20**, x151 (2004).
13. A. Martin, A.A. Pinkerton, and A. Schiemann. Acta Crystallogr. Sect. C: Struct. Commun. **52**, 966 (1996).
14. M. Hariharan, S.S. Rajan, and R. Srinivasan. Acta Crystallogr. Sect. C: Struct. Commun. **45**, 911 (1989).
15. J.M. Amigó, J.M. Martínez-Calatayud, A. Cantarero, and T. Debaerdemaeker. Acta Crystallogr. Sect. C: Struct. Commun. **44**, 1452 (1988).
16. J.M. Amigó, J. Martínez-Calatayud, and T. Debaerdemaeker. Bull. Soc. Chim. Belg. **94**, 119 (1985).
17. C.J. Brown and L. Sengier. Acta Crystallogr. Sect. C: Struct. Commun. **40**, 1294 (1984).
18. C. Herrnstadt, D. Mootz, and H. Wunderlich. J. Chem. Soc. Perkin Trans 2, 735 (1979).
19. R. Handa and N.N. Saha. Acta Crystallogr. Sect. B: Struct. Crystallogr. Cryst. Chem. **29**, 554 (1973).
20. R. Handa and N.N. Saha. J. Cryst. Mol. Struct. **1**, 235 (1971).
21. C.J. Brown. J. Chem. Soc. A, 60 (1967).
22. G.M. Sheldrick. SHELXS-97 [computer program]. Universität Göttingen, Göttingen, Germany. 1997.
23. G.M. Sheldrick. SHELXL-97 [computer program]. Universität Göttingen, Göttingen, Germany. 1997.
24. R. Herbst-Irmer and G.M. Sheldrick. Acta Crystallogr. Sect. B: Struct. Sci. **54**, 443 (1998).

© 2006 NRC Canada

Triazene derivatives of (1,*x*)-diazacycloalkanes. Part VII. Synthesis of a series of 1-aryl-2-[3-(3-[2-aryl-1-diazenyl]-1,3-diazepan-1-ylmethyl)-1,3-diazepan-1-yl]-1-diazenes from the reaction of diazonium salts with mixtures of formaldehyde and 1,4-diaminobutane[1,2]

Reid Tingley and Keith Vaughan

Abstract: A new series of bistriazenes, the 1-aryl-2-[3-(3-[2-aryl-1-diazenyl]-1,3-diazepan-1-ylmethyl)-1,3-diazepan-1-yl]-1-diazenes (**8**), has been synthesized from the reaction of diazonium salts with a mixture of 1,4-diaminobutane and formaldehyde. All new compounds of series **8** have been characterized by IR and NMR spectroscopy, and the elemental composition of selected examples has been verified by elemental analysis. The connectivity of the series has been unequivocally determined by X-ray crystallography. The new bistriazenes are important because the structure contains the novel saturated heterocycle, 1,3-diazepane. The general conclusion of this study is that alkanediamines with three or four carbon atoms in the spacer link between the nitrogen atoms give rise to the linear bicyclic molecules of type **2**, in contrast to the case of ethylenediamine (two carbon atoms in spacer link), which affords molecules of type **3**, which exemplify the cage structure of type **1**.

Key words: diazonium salt, triazene, bistriazene, diazepane, formaldehyde, nuclear magnetic resonance.

Résumé : On a réalisé la synthèse d'une nouvelle série de bistriazènes, les 1-aryl-2-[3-(3-[2-aryldiazén-1-yl]-1,3-diazépan-1-ylméthyl)-1,3-diazépan-1-yl]diaz-1-ènes (**8**) en faisant réagir les sels de diazonium avec un mélange de 1,4-diaminobutane et de formaldéhyde. On a caractérisé tous les nouveaux composés de la série **8** par spectroscopies IR et RMN et on a vérifié la composition élémentaire d'exemples choisis par le biais d'analyses élémentaires. La connectivité dans les produits de la série a été déterminée sans équivoque par diffraction des rayons X. Les nouveaux bistriazènes sont importants puisque leur structure comporte le nouvel hétérocycle saturé, 1,3-diazépane. La conclusion générale de cette étude est que les alcanediamines comportant 3 ou 4 atomes de carbones entre les atomes d'azote conduisent à des molécules bicycliques linéaires de type **2** alors que l'éthylènediamine, qui ne comporte que deux atomes de carbone entre les atomes d'azote, conduit à la formation de molécules de type **3** tel qu'on l'observe dans la structure en cage de type **1**.

Mots clés : sel de diazonium, triazène, bistriazène, diazépane, formaldéhyde, résonance magnétique nucléaire.

[Traduit par la Rédaction]

Introduction

The term "bistriazene" has been coined to describe any molecule that contains two triazene units in the same molecule with a link or spacer in between the triazene moieties. Recent progress in the synthesis of bistriazenes has been reviewed (1). One of the conclusions of recent work is that there are two distinct types of oligomer produced by the interaction of a diazonium salt with a mixture of formaldehyde and a bis-primary amine. The cage-type of bistriazene is exemplified by the general structure **1** (Chart 1) . Examples of this structural type are the bistriazenes (**3**), which arise from ethylene diamine (2) and the 3,7-di-[2-aryl-1-diazenyl]-1,3,5,7-tetraazabicyclo[3.3.1]nonanes (**4**), which are formed by the reaction of a diazonium ion with ammonia/formaldehyde mixtures (3). The alternate type of molecular geometry is the linear bicyclic structure (**2**).

The molecule of type **2** is exemplified by the structure **5a**, which describes the series of products that were obtained from the diazonium coupling reaction with a mixture of formaldehyde and 1,3-propanediamine. The description of the synthesis and characterization of the series **5a** was published in Part IV of this series (4) and the connectivity of one member of series **5a** (with X = *p*-CN) was established

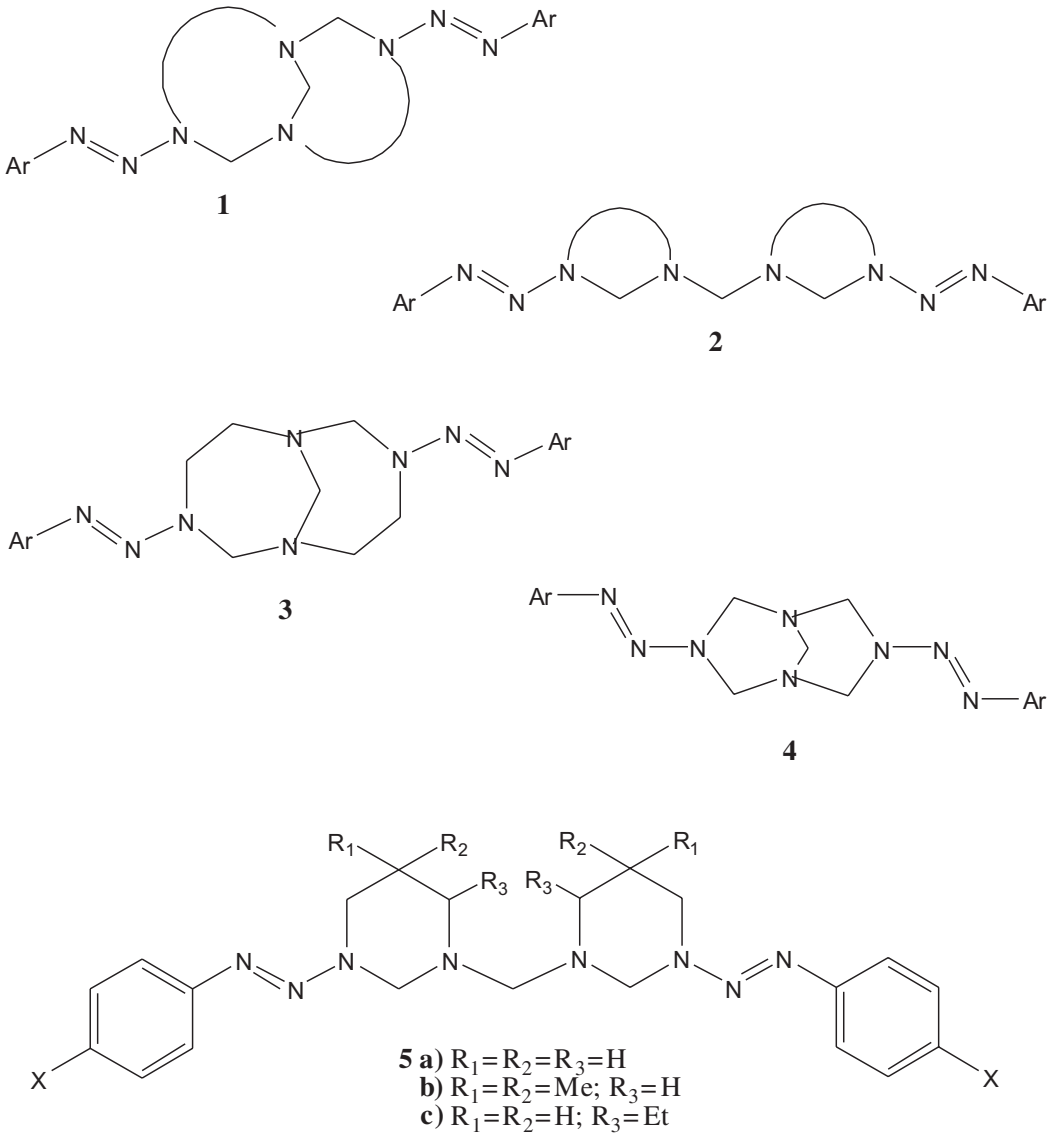
Received 17 April 2006. Accepted 30 June 2006. Published on the NRC Research Press Web site at http://canjchem.nrc.ca on 17 October 2006.

R. Tingley and K. Vaughan.[3] Department of Chemistry, Saint Mary's University, Halifax, NS. B3H 3C3, Canada.

[1]This article is part of a Special Issue dedicated to Dr. Alfred Bader.
[2]For Part VI, see: Can. J. Chem. 84 (2006). This issue.
[3]Corresponding author (e-mail: keith.vaughan@smu.ca).

 doi:10.1139/V06-123 © 2006 NRC Canada

Chart 1.



unequivocally by an X-ray structure determination (5). This work was extended to the dimethyl-substituted series **5b** by the analogous reaction with 2,2-dimethyl-1,3-propanediamine. This work was included in Part IV and an X-ray structure of the methyl benzoate analogue (**5b**, X = CO_2Me) was completed and published (6). The compounds of series **5a** and **5b** are important as new derivatives of the saturated heterocyclic hexahydropyrimidine system, in addition to being illustrations of the linear bicyclic genereal structure **2**.

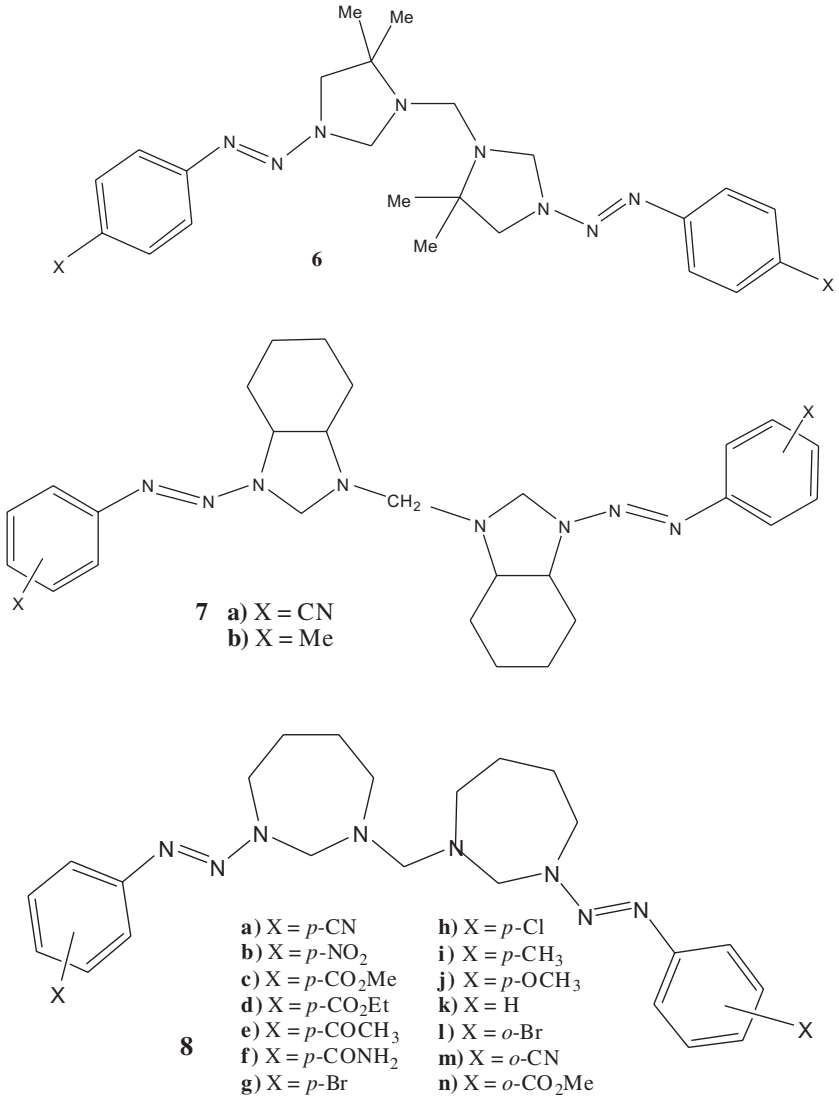
The linear bicyclic bistriazenes (**5c**) were obtained from the analogous reaction of diazonium salts with formaldehyde and 1,3-pentanediamine, which affords the 6-ethylhexahydropyrimidin-1-yl system. These results have been reported in Part V of this series (7) and an X-ray crystal structure of the *p*-bromo derivative of series **5c** has been published (8). Examples of the linear bicycles of type **2** are not restricted to the six membered ring pyrimidines (**5**). The bistriazene series (**6**) (Chart 2) , which are important and novel derivatives of the rare imidazolidine system, have been obtained from the reaction of diazonium salts with a mixture of formaldehyde and 2-methyl-1,2-propanediamine. The synthesis, characterization and X-ray crystal structure (of **6**, X = CO_2Me) have been published as Part VI of this series (9).

Further examples of imidazolidine-containing molecules of type **2** were found as products of the reaction of diazonium salts with a mixture of formaldehyde and 1,2-cyclohexanediamine. These products have been assigned the structure **7** (Chart 2). The synthesis and characterization of the series **7** has been published (10), and the X-ray structure of the *p*-cyano derivative (**7a**) has been reported (11). The X-ray structure of the second example of this series (**7b**, X = Me) has been published recently (12).

Thus, there seems to be a crossover in behaviour of the alkanediamine going from ethylenediamine to propanediamine and also in the introduction of a branching chain in the ethylenediamine. In the present study, we have extended these reactions with the next further homologue in the diamine series, specifically 1,4-butanediamine, and it is clear that the linear bicyclic molecule of type **2** is formed in preference to the cage structures of type **1**. The products of these

© 2006 NRC Canada

Chart 2.



reactions are seen in Chart 2 (**8a–8n).** In this paper, we report the details of the synthesis of series **8** and their characterization by IR, ^{1}H NMR, and ^{13}C NMR spectroscopy.

Experimental

All reagents were reagent grade materials purchased from the Sigma-Aldrich Chemical Co. Ltd. (Oakville, Ontario) and were used without further purification. Melting points were determined on a Fisher-Johns melting point apparatus and were uncorrected. IR spectra were obtained using Nujol mulls, unless otherwise stated, on a PerkinElmer 299 spectrophotometer or with a Brucker Vector 22 spectrometer. ^{1}H and ^{13}C NMR spectra were obtained using either the Anasazi Instruments 60 MHz EFT spectrometer at Saint Mary's University, or the Bruker 250 MHz spectrophotometer at the Atlantic Regional Magnetic Resonance Centre at Dalhousie University in Halifax, Nova Scotia. Chemical shifts were recorded in $CDCl_3$ or d_6-DMSO solutions at 20 °C, and are relative to TMS as internal standard. Multiplicities are reported as singlet (s), doublet (d), triplet (t), quartet (q), quintet (qu-intet), multiplet (m), and broad (br).

1-Aryl-2-[3-(3-[2-aryl-1-diazenyl]-1,3-diazepan-1-ylmethyl)-1,3-diazepan-1-yl]-1-diazenes (8a–8n)

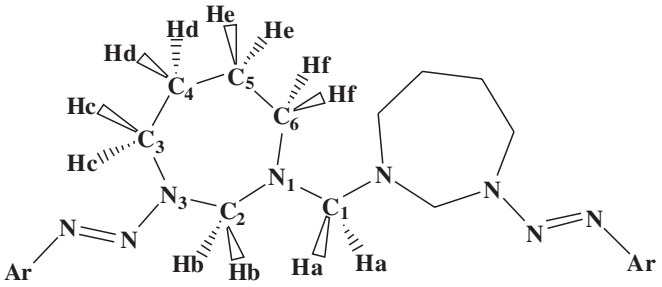
General procedure

Method A

The appropriate arylamine (0.010 mol) was dissolved in hydrochloric acid (3 mol/L, 40 ml) with heating if necessary to obtain a clear solution. This solution was then cooled in an ice/salt bath. The arylamine hydrochloride solution was diazotized at 0–5 °C with a solution of sodium nitrite (0.011 mol) in water and the resulting mixture was stirred in the cold for 0.5 h. Any insoluble impurities were removed by vacuum filtration. The mixture was brought to pH 7 using a saturated solution of sodium bicarbonate, at which point 37% aqueous formaldehyde solution (5 mL) was added. 1,4-Diaminobutane (0.010 mol) was slowly added to the solution, which was allowed to stir in the cold for a further 0.5 h. Occasionally, a slight precipitate was evident during the period of the addition, but was not removed. The mixture was then adjusted to alkaline pH with additional saturated sodium bicarbonate solution, whereupon the product precipi-

© 2006 NRC Canada

Fig. 1. Proton and carbon labels in **8** for the discussion of NMR assignments.



tated out of solution. Solid precipitates were isolated by vacuum filtration and purified by recrystallization from an appropriate solvent. The oil **8n** was recovered by extraction into dichloromethane (three 20 mL aliquots), dried over anhyd $MgSO_4$, and rotoevaporated under vacuum.

Method B

The procedure of Method A was followed exactly with the exception of the amount of formaldehyde used. A 40:1 molar ratio of formaldehyde–arylamine was used, i.e., approx. 32 mL of 37% aqueous formaldehyde was added at the appropriate time. Application of these procedures afforded compounds **8a–8n**.

1-(*p*-Cyanophenyl)-2-[3-{3-[2-(*p*-cyanophenyl)-1-diazenyl]-1,3-diazepan-1-ylmethyl}-1,3-diazepan-1-yl]-1-diazene (8a)

Method B: yield 100%; lustrous pale yellow prisms; from ethanol – ethyl acetate; mp 191–193 °C. IR (cm^{-1}) ν_{max}: 2220 (CN), 843 (OOP). ^1H NMR (250 MHz, $CDCl_3$, ppm): 1.64 (4H, br m, H_e), 1.96 (4H, br m, H_d), 2.93 (4H, t, J = 5.2 Hz, H_f), 3.25 (2H, s, H_a), 3.75 (4H, t, J = 6.0 Hz, H_c), 4.98 (4H, s, H_b), 7.42 (4H, d, J = 8.9 Hz, arom.), 7.56 (4H, d, J = 8.9 Hz, arom.) (See Fig. 1 for the key to the proton and carbon labels in the NMR spectra). ^{13}C NMR (62.9 MHz, $CDCl_3$, ppm): 24.7 (C-5), 28.0 (C-4), 49.9 (C-6), 53.2 (C-3), 64.7 (C-1), 69.9 (C-2), 107.9 (CN),119.6, 121.0, 133.1, 154.5 (arom.). Anal. calcd. for $C_{25}H_{30}N_{10}$: C 63.8, H 6.4, N 29.8; found: C 64.1, H 6.3, N 29.0%.

1-(*p*-Nitrophenyl)-2-[3-{3-[2-(*p*-nitrophenyl)-1-diazenyl]-1,3-diazepan-1-ylmethyl}-1,3-diazepan-1-yl]-1-diazene (8b)

Method A: 100%. Method B: 86%. Reddish brown prisms; from ethanol – ethyl acetate; mp 165–167 °C. IR (cm^{-1}) ν_{max}: 1507 and 1328 (NO_2), 855 (OOP). ^1H NMR (250 MHz, $CDCl_3$, ppm): 1.64–1.80 (4H, br m, H_e), 2.02 (4H, br m, H_d), 2.95 (4H, t, J = 5.3 Hz, H_f), 3.27 (2H, s, H_a), 3.80 (4H, t, J = 7.2 Hz, H_c), 5.00 (4H, s, H_b), 7.45 (4H, d, J = 9.2 Hz, arom.), 8.15 (4H, d, J = 9.2 Hz, arom.). ^{13}C NMR (62.9 MHz, $CDCl_3$, ppm): 24.7 (C-5), 28.1 (C-4), 49.8 (C-6), 53.4 (C-3), 64 (w) (C-1), 69.8 (C-2), 120.6, 129.7, 155.0 (arom.). Anal. calcd. for $C_{23}H_{30}N_{10}O_4$: C 54.1, H 5.9; found: C 55.5, H 6.0%.

Methyl-4-(2-{3-[(3-{2-[4-(methoxycarbonyl)phenyl]-1-diazenyl}-1,3-diazepan-1-yl)methyl]-1,3-diazepan-1-yl}-1-diazenyl)benzoate (8c)

Method B: 86%; off-white powder; from ethanol – ethyl acetate; mp 184–187 °C. IR (cm^{-1}) ν_{max}: 1715 (C=O), 859 (OOP). ^1H NMR (250 MHz, $CDCl_3$, ppm): 1.61 (4H, br m, H_e), 1.97 (4H, br m, H_d), 2.91 (4H, t, J = 4.9 Hz, H_f), 3.26 (2H, s, H_a), 3.73 (4H, t, J = 5.8 Hz, H_c), 3.89 (6H, s, O–Me), 4.98 (4H, s, H_b), 7.41 (4H, d, J = 8.5 Hz, arom.), 7.96 (4H, d, J = 8.5 Hz, arom.). ^{13}C NMR (62.9 MHz, $CDCl_3$, ppm): 24.8 (C-5), 28.1 (C-4), 49.7 (C-6), 52.0 (O–Me) 53.4 (C-3), 64.8 (C-1), 69.6 (C-2), 120.3, 126.5, 130.7, 154.9 (arom.), 167.2 (C=O). Anal. calcd. for $C_{27}H_{36}N_8O_4$: C 60.43 H 6.76, N 20.88 ; found: C 60.4, H 6.75, N 20.4%.

Ethyl 4-(2-{3-[(3-{2-[4-(ethoxycarbonyl)phenyl]-1-diazenyl}-1,3-diazepan-1-yl)methyl]-1,3-diazepan-1-yl}-1-diazenyl)benzoate (8d)

Method B: 99%; white needles; from ethanol – ethyl acetate; mp 152–154 °C. IR (cm^{-1}) ν_{max}: 1712 (C=O), 1266 and 1143 (CO), 863 (OOP). ^1H NMR (250 MHz, $CDCl_3$, ppm): 1.39 (6H, t, J = 7.2 Hz, C–CH_3), 1.61 (4H, br m, H_e), 2.01 (4H, br m, H_d), 2.93 (4H, t, J = 5.0 Hz, H_f), 3.26 (2H, s, H_a), 3.75 (4H, t, J = 6.0 Hz, H_c), 4.36 (4H, q, J = 7.1 Hz, O–CH_2), 4.98 (4H, s, H_b), 7.42 (4H, d, J = 8.5 Hz, arom.), 7.98 (4H, d, J = 8.5 Hz, arom.). ^{13}C NMR (62.9 MHz, $CDCl_3$, ppm): 14.5 (CH_3), 24.8 (C-5), 28.2 (C-4), 49.7 (C-6), 53.5 (C-3), 60.8 (O–CH_2), 64.8 (C-1), 69.6 (C-2), 120.3, 126.9, 130.7, 154.8 (arom.), 166.8 (C=O). Anal. calcd. for $C_{29}H_{40}N_8O_4$: C 61.7, H 7.1, N 19.9 ; found: C 61.6, H 7.2, N 19.8%.

1-(4-{2-[3-({3-[2-(4-Acetylphenyl)-1-diazenyl]-1,3-diazepan-1-yl}methyl)-1,3-diazepan-1-yl]-1-diazenyl}phenyl)-1-ethanone (8e)

Method A: 94%; off-white prisms; from ethanol; mp 175–177 °C. IR (cm^{-1}) ν_{max}: 1676 (C=O), 850 (OOP). ^1H NMR (60 MHz, $CDCl_3$, ppm): 1.82 (8H, br m, H_d and H_e), 2.56 (6H, s, acetyl Me), 2.95 (4H, br t, J = 4.7 Hz, H_f), 3.30 (2H, s, H_a), 3.77 (4H, br t, J = 5.3 Hz, H_c), 5.00 (4H, s, H_b), 7.42 (4H, d, J = 8.5 Hz, arom.), 7.90 (4H, d, J = 8.7 Hz, arom.). ^{13}C NMR (15.1 MHz, $CDCl_3$, ppm): 24.1 (C-5), 25.9 (acetyl Me), 27.4 (C-4), 49.0 (C-6), 52.6 (C-3), 64.3 (C-1), 69.2 (C-2), 119.9, 129.0, 133.3, 154.4 (arom.), 196.8 (C=O). Anal. calcd. for $C_{27}H_{36}N_8O_2$: C 64.28, H 7.14; found: C 63.7, H 6.8%.

4-(2-{3-[(3-{2-[4-(Aminocarbonyl)phenyl]-1-diazenyl}-1,3-diazepan-1-yl)methyl]-1,3-diazepan-1-yl}-1-diazenyl)benzamide (8f)

Method A: 100%; method B: 96%; pale yellow powder; from ethanol – ethyl acetate/toluene; mp 212–215 °C. IR (cm^{-1}) ν_{max}: 3388 (NH), 1655 (C=O), 856 (OOP). ^1H NMR (60 MHz, $CDCl_3$, ppm): 1.68 (8H, br m, H_d and H_e), 2.87 (4H, br, H_f), 3.35 (2H, s, H_a), 3.65 (4H, br m, H_c), 4.97 (4H, br s, H_b), 7.31 (4H, d, J = 8.2 Hz, arom.), 7.85 (4H, d, J = 8.9 Hz, arom.).

1-(*p*-Bromophenyl)-2-[3-{3-[2-(*p*-bromophenyl)-1-diazenyl]-1,3-diazepan-1-ylmethyl}-1,3-diazepan-1-yl]-1-diazene (8g)

Method B: 95%; off-white needles; from ethanol – ethyl acetate; mp 183–184 °C. IR (cm^{-1}) ν_{max}: 829 (OOP). ^1H NMR (400 MHz, $CDCl_3$, ppm): 1.63 (4H, br m, H_e), 1.90 (4H, br m, H_d), 2.91 (4H, br t, J = 6.0 Hz, H_f), 3.25 (2H, s, H_a), 3.70 (4H, quintet, J = 6.1 Hz, H_c), 4.93 (4H, s, H_b),

© 2006 NRC Canada

7.25 (4H, d, J = 9.8 Hz, arom.), 7.39 (4H, d, J = 8.6 Hz, arom.). ^{13}C NMR (100.6 MHz, $CDCl_3$, ppm): 25.0 (C-5), 29.9 (C-4), 49.5 (C-6), 53.6 (C-3), 64.8 (C-1), 69.6 (C-2), 122.3, 132.0, 150.3 (arom.). Anal. calcd. for $C_{23}H_{30}N_8Br_2$: C 47.77, H 5.19, N 19.38 ; found: C 46.9, H 5.2, N 19.3%.

1-(*p*-Chlorophenyl)-2-[3-{3-[2-(*p*-chlorophenyl)-1-diazenyl]-1,3-diazepan-1-ylmethyl}-1,3-diazepan-1-yl]-1-diazene (8h)

Method A: 90%; off-white needles; from ethanol – ethyl acetate; mp 163–167 °C. IR (cm^{-1}) ν_{max}: 839 (OOP). ^{1}H NMR (60 MHz, $CDCl_3$, ppm): 1.78 (8H, br m, H_d and H_e), 2.94 (4H, br t, J = 4.8 Hz, H_f), 3.34 (2H, br s, H_a), 3.75 (4H, br t, J = 5.4 Hz, H_c), 4.94 (4H, s, H_b), 7.26 (8H, m, arom.). Anal. calcd. for $C_{23}H_{30}N_8Cl_2$: C 56.5, H 6.1, N 22.9; found: C 56.4, H 6.3, N 22.5%.

1-(*p*-Tolyl)-2-[3-{3-[2-(*p*-tolyl)-1-diazenyl]-1,3-diazepan-1-ylmethyl}-1,3-diazepan-1-yl]-1-diazene (8i)

Method B: 68%; pale yellow prisms; from ethanol – ethyl acetate; mp 177–179 °C. IR (cm^{-1}) ν_{max}: 824 (OOP). ^{1}H NMR (250 MHz, $CDCl_3$, ppm): 1.60 (4H, br m, H_e), 1.93 (4H, br m, H_d), 2.32 (6H, s, tolyl Me), 2.92 (4H, t, J = 5.0 Hz, H_f), 3.29 (2H, br s, H_a), 3.71 (4H, br, H_c), 4.94(4H, s, H_b), 7.10 (4H, d, J = 8.2 Hz, arom.), 7.30 (4H, d, J = 8.2 Hz, arom.). ^{13}C NMR (62.9 MHz, $CDCl_3$, ppm): 21.1 (tolyl Me), 25.0 (C-5), 28.1 (C-4), 49.2 (C-6), 53.5 (C-3), 65 (w) (C-1), 69.3 (C-2),120.4, 129.5, 134.9, 149.0 (arom.). Anal. calcd. for $C_{25}H_{36}N_8$: C 67.0, H 8.0, N 25.0; found: C 67.1, H 8.1, N 24.7%.

1-(*p*-Methoxyphenyl)-2-[3-{3-[2-(*p*-methoxyphenyl)-1-diazenyl]-1,3-diazepan-1-ylmethyl}-1,3-diazepan-1-yl]-1-diazene (8j)

Method B: 48%; golden yellow plates; from ethanol – ethyl acetate; mp 183–184 °C. IR (cm^{-1}) ν_{max}: 1239 (C O), 833 (OOP). ^{1}H NMR (250 MHz, $CDCl_3$, ppm): 1.63 (4H, br m, H_e), 1.93 (4H, br m, H_d), 2.92 (4H, t, J = 5.2 Hz, H_f), 3.31 (2H, br s, H_a), 3.70 (4H, t, J = 7.0 Hz, H_c), 3.79 (6H, s, O–Me), 4.92 (4H, s, H_b), 6.87 (4H, d, J = 8.9 Hz, arom.), 7.36 (4H, d, J = 9.2 Hz, arom.). ^{13}C NMR (62.9 MHz, $CDCl_3$, ppm): 25.0 (C-5), 29.0 (C-4), 53.4 (C-3), 55.6 (O–Me), 114.1, 121.5, 145.2, 157.6 (arom.). Anal. calcd. for $C_{25}H_{36}N_8O_2$: C 62.5, H 7.5; found: C 61.9, H 7.5%.

1-Phenyl-2-[3-{3-[2-phenyl-1-diazenyl]-1,3-diazepan-1-ylmethyl}-1,3-diazepan-1-yl]-1-diazene (8k)

Method A: 58%; brown powder; mp 99–102 °C. IR (cm^{-1}) ν_{max}: 761 (OOP). ^{1}H NMR (60 MHz, $CDCl_3$, ppm): 1.74 (8H, br m, H_d and H_e), 2.92 (4H, t, J = 4.9 Hz, H_f), 3.35 (2H, s, H_a), 3.75 (4H, t, J = 5.6 Hz, H_c), 4.93 (4H, s, H_b), 7.06–7.60 (8H, m, arom.). ^{13}C NMR (15.1 MHz, $CDCl_3$, ppm): 24.6 (C-5), 27.7 (C-4), 48.8 (C-6), 53.0 (C-3), 64.9 (C-1), 69.1 (C-2), 1120.4, 125.1, 128.6, 151.0 (arom.).

1-(*o*-Bromophenyl)-2-[3-{3-[2-(*o*-bromophenyl)-1-diazenyl]-1,3-diazepan-1-ylmethyl}-1,3-diazepan-1-yl]-1-diazene (8l)

Method B: 96%; white needles; from ethanol – ethyl acetate; mp 117–120 °C. IR (cm^{-1}) ν_{max}: 754 (OOP). ^{1}H NMR (60 MHz, $CDCl_3$, ppm): 1.77 (8H, br m, H_d and H_e), 2.94 (4H, t, J = 4.8 Hz, H_f), 3.30 (2H, s, H_a), 3.78 (4H, t, J = 6.0 Hz, H_c), 4.96 (4H, s, H_b), 6.78–7.63 (8H, m, arom.).

1-(*o*-Cyanophenyl)-2-[3-{3-[2-(*o*-cyanophenyl)-1-diazenyl]-1,3-diazepan-1-ylmethyl}-1,3-diazepan-1-yl]-1-diazene (8m)

Method B: 67%; beige powder; from ethanol – ethyl acetate; mp 132–135 °C. IR (cm^{-1}) ν_{max}: 2226 (CN), 764 (OOP). ^{1}H NMR (250 MHz, $CDCl_3$, ppm): 1.25–1.78 (4H, br m, H_e), 2.01 (4H, br m, H_d), 2.95 (4H, t, J = 5.0 Hz, H_f), 3.27 (2H, s, H_a), 3.80 (4H, br, H_c), 4.97 (4H, s, H_b), 7.6–8.1 (8H, m, arom.).

Methyl 2-(2-{3-[(3-{2-[2-(methoxycarbonyl)phenyl]-1-diazenyl}-1,3-diazepan-1-yl) methyl]-1,3-diazepan-1-yl}-1-diazenyl)benzoate (8n)

Method A: 18%; oil. IR (cm^{-1}) ν_{max}: 1731 (C=O), 721 (OOP). ^{1}H NMR (60 MHz, $CDCl_3$, ppm): 1.76 (8H, br m, H_d and H_e), 2.90 (4H, br t, J = 4.7 Hz, H_f), 3.32 (2H, br s, H_a), 3.75 (4H, br t, J = 7.5 Hz, H_c), 4.91 (4H, s, H_b), 7.03–7.68 (8H, m, arom.).

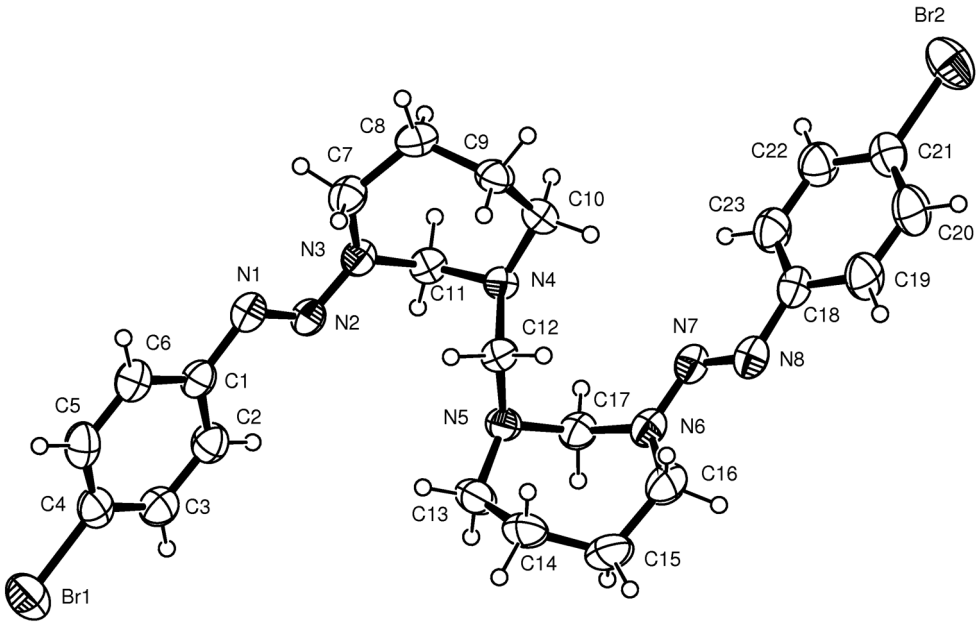
Results and discussion

The required diazonium salt, ArN_2^+, was prepared by diazotization of the appropriate arylamine. The diazonium salt solution was then treated with a mixture of formaldehyde and 1,4-diaminobutane ($NH_2(CH_2)_4NH_2$). On the basis of IR and NMR spectroscopic analysis, together with elemental analysis whenever possible, the products of this reaction have been identified unequivocally as the 1-aryl-2-[3-(3-[2-aryl-1-diazenyl]-1,3-diazepan-1-ylmethyl)-1,3-diazepan-1-yl]-1-diazenes (**8a**–**8n**). The connectivity in structure **8** has been established by X-ray crystyallography. The yields of the products are excellent, often in excess of 90%, and the solid products recrystallize in most cases from a mixture of ethanol and ethyl acetate. The pure compounds are generally colourless or pale in colour, crystallizing as needles, prisms, or plates. The IR spectra were recorded mainly to confirm the presence of the particular aryl substituent (X), such as the presence of a carbonyl band in **8c**–**8f** and **8n**, and also to confirm the substitution pattern as ortho or para from the measurements of the OOP bending vibrations.

The ^{1}H NMR spectra of the new bistriazenes are very informative about the structures of these molecules, in particular the presence of two identical 1,3-diazepanyl groups attached to a central methylene group. The detailed structure in Fig. 1 shows the proton labels from H_a to H_e, which is useful to interpret the following discussion. The central methylene group between the heterocyclic rings (H_a) appears universally as a two-proton singlet at ~3.30 ppm, sometimes broadened. The protons (H_b) of the two equivalent methylene groups situated between the N1 and N3 nitrogen atoms of the diazepane rings appear as a four-proton singlet at ~5.0 ppm. The protons (H_c) of the two equivalent *N*-methylene groups of the heterocyclic rings appear at ~3.70–3.80 ppm as a four-proton triplet with coupling constant J_{cd} in the range 5–7 Hz because of the anticipated coupling to the protons of the adjacent methylene group (H_d). Likewise, the protons (H_f) of the other equivalent *N*-methylene groups appear as a four-proton triplet with J_{ef} = ~5.0 Hz because of

© 2006 NRC Canada

Fig. 2. ORTEP view of 1-(*p*-bromophenyl)-2-[3-{3-[2-(*p*-bromophenyl)-1-diazenyl]-1,3-diazepan-1-ylmethyl}-1,3-diazepan-1-yl]-1-diazene (**8g**) showing the thermal ellipsoids at 40% probability level.



the coupling to H_e. However, the chemical shift of H_f is at a higher field (~2.90 ppm). The proximity of the triazene group to the H_c protons is presumably responsible for this difference. The protons of the other methylene groups of the diazepane rings appear as four-proton multiplets at ~1.6 ppm and 2.0 ppm. Other features of the NMR spectra, such as the AA′BB′ aromatic protons and the proton signals of the aryl substituent (X), are clearly evident.

^{13}C NMR analysis of the series **8a**–**8n** was not possible for all compounds because of the combination of limited solubility and the extreme broadening of carbon signals ubiquitous in triazenes of this type (4). Nevertheless, complete ^{13}C NMR spectral data was acquired for a significant number of these compounds. The assignment of carbon signals is based on the numbering scheme shown in Fig. 1. The carbon of the central methylene group (C1) in **8** is observed at ~64–65 ppm and C2 of the diazepane ring is observed in the narrow range 69.1–69.9 ppm. The assignments of C3, C4, C5, and C6 to the signals at ~53, 28, 25, and 49,respectively, is based on the proximity to the nitrogen atoms N1 and N3, and to the triazene moiety. The ^{13}C NMR data is a strong supporting evidence for the structure **8** assigned to these products.

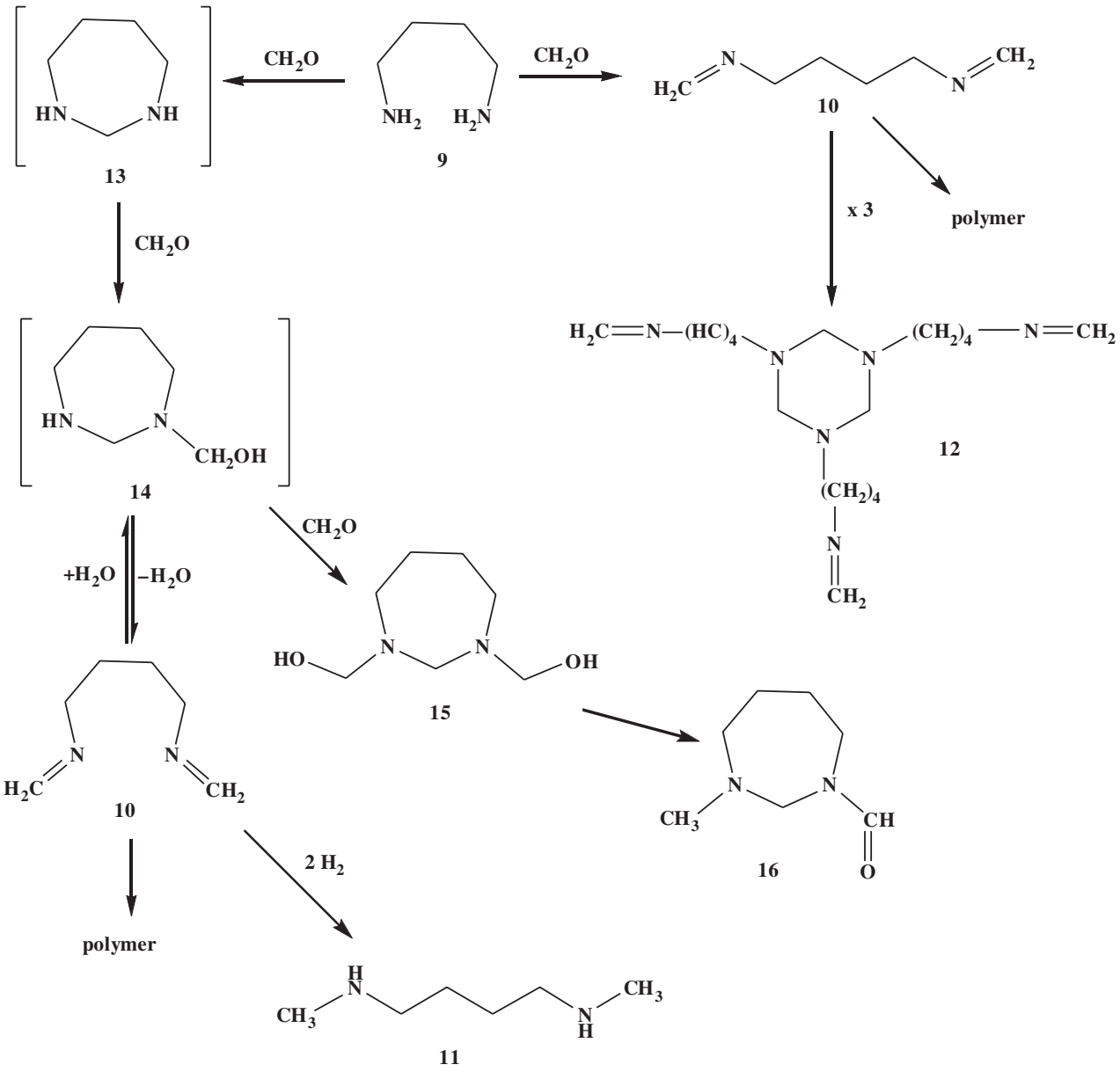
It should be noted that there is a wide range of stability for the compounds in the series **8a**–**8n**. These stability problems are not new to our experience with similar bistriazenes, such as those of type **5a**–**5c** (4, 7). Several products displayed a limited shelf-life when stored for a couple of years. Samples that were fine powders when fresh are now glass, such as **8d**, **8l**, and **8m**. Others like **8a**–**8c** and **8g** show little if any sign of decay. Compound **8j**, which afforded an X-ray crystallographic structure, is somewhat fickle in this regard. A crude sample that was stored for over two years showed definite signs of decomposition, whereas a purified sample of the same compound showed no sign of decomposition. It is possible that the stability of these bis(aryldiazenyl-1,3-diazepanyl)methanes is prolonged in the crystalline state compared with the amorphous state; however, we have not undertaken a systematic study of this question. This stability problem had a detrimental effect on the results of elemental analysis of several new compounds, which were not universally successful. There is an approximate correlation of the stability of the compounds in this series and either the success or lack of success of elemental analysis. However, elemental analysis of selected compounds in the series **8** did provide further evidence of the assigned structures. Unequivocal evidence of the connectivity of the compounds in series **8** has been obtained from the X-ray crystal structures of three compounds **8a**, **8g,** and **8j**. Full details of the X-ray analysis will be published elsewhere (13)and an ORTEP diagram of the *p*-bromo derivative (**8g**) is shown in Fig. 2.

In consideration of the possible reaction pathways that could be involved in the formation of molecules of type **8**, it is essential to examine the reported work on the reaction of 1,4-diaminobutane with formaldehyde. The earliest work of any consequence is that of Krassig (14), who concluded that the reaction of diaminobutane (**9**) with formaldehyde afforded viscose polymers, described as "poly-bismethylenetetramethylenediamines". He suggested that the initial condensation product (Scheme 1) has structure **10**, which can trimerise to the novel 1,3,5-triazine derivative (**12**). An evidence for the existence of **10** is the isolation and characterization of *N*,*N*′-dimethyl-1,4-diaminobutane (**11**) from the reductive amination of formaldehyde by **9**. Subsequent to Krassig's work, Evans and co-workers (15) investigated the reaction of 1,4-diaminobutane with acetamidine, which resulted in a synthetic method for a variety of substituted diazepines.

However, the most significant and enlightening work with relevance to the present study is the paper by Dale and Sigvartsen (16). The surprising result in their paper is that the final product after prolonged standing of the reactants is

© 2006 NRC Canada

Scheme 1.



the formamide (**16**), together with the initial polymer. They suggest that the formamide (**16**) is produced by the sequence of reactions starting with condensation to give the diazepane (**13**), which can hydroxymethylate to give **14**. This carbinolamine can either: (*i*) dehydrate reversibly to give Krassig's di-imine (**10**), which could be the source of the polymer, or (*ii*) condense further with formaldehyde to give the diol **15**. Cannizzaro-like redox disproportionation of **15** produces the final product **16**.

The work of Dale and Sigvartsen leads to a logical hypothesis (Scheme 2) for the formation of the novel bistriazenes (**8**). Reaction of a molecule of Krassig's diimine (**10**) with a molecule of the diazepane (**13**) affords the bis(1,3-diazepanyl)methane (**17**) by ring-closure dimerization. Reaction of **17** with two equivalents of the diazonium ion followed by deprotonation affords the observed product (**8**).

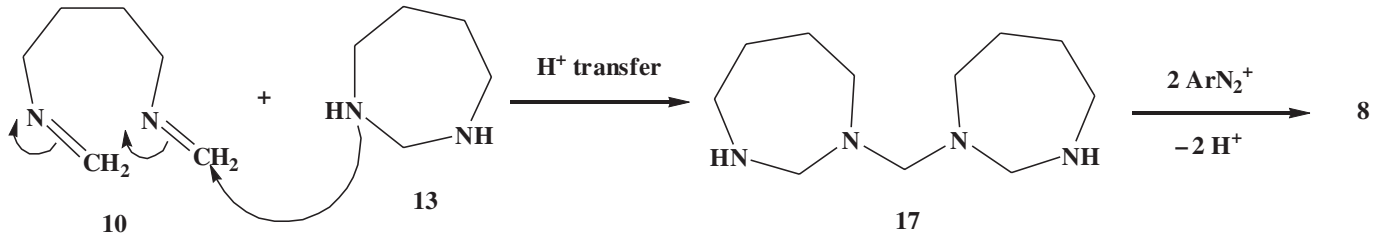
Conclusion

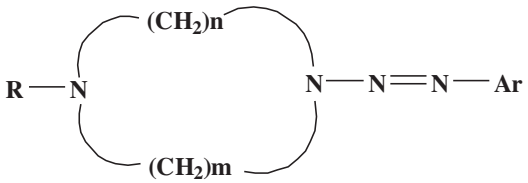
It appears, from our on-going studies, that the interaction of a diazonium salt with a mixture of formaldehyde and an alkanediamine [$NH_2(CH_2)_nNH_2$] gives rise to two distinct types of oligomer. Bistriazenes of types **3** (2) and **4** (3) are examples of the bridged bicyclic bistriazene, whereas the compounds of series **5** (5, 7) exemplify the linear bicyclic bistriazene. The new compounds of series **8**, reported here, clearly belong to the linear bicyclic class, providing further evidence that there is a crossover in the molecular architecture going from the two-carbon spacer of ethylenediamine to the three- or four-carbon spacer.

This paper is part VII in a series that describes the synthesis of a variety of triazenes and bistriazenes that fit the general classification of 1-aryldiazenyl-(1,x)-diazacycloalkanes described by the general structure **18**, where m = 1 or 2 and

© 2006 NRC Canada

Scheme 2.





18

n = 2, 3, 4 or 5. Previously, we reported new triazenes derived from imidazolidine (m = 1, n = 2) (9, 10), hexahydropyrimidine (m = 1, n = 3) (4), piperazine (m = n = 2) (17, 18), and homopiperazine (m = 2, n = 3) (19). The new diazepanes of series **8** fit to the general structure **18**, where m = 1 and n = 4. Future work in this field of chemistry will endeavour to further extend the family of (1,x)-diazacycloalkanes.

Acknowledgements

The authors are grateful to the Natural Sciences and Engineering Research Council of Canada (NSERC) for a Discovery Grant to the principal author (KV) and to Human Resources at Saint Mary's University for a Student Employment Experience Program (SEEP) award to Reid Tingley. We are also grateful to the Atlantic Regional Magnetic Resonance Centre (ARMRC) at Dalhousie University for providing NMR spectra.

References

1. K. Vaughan. Org. Prep. Proced. Int. **33**, 59 (2001).
2. M.B. Peori, K. Vaughan, and D.L. Hooper. J. Org. Chem. **63**, 7437 (1998).
3. R.D. Singer, K. Vaughan, and D.L. Hooper. Can. J. Chem. **64**, 1567 (1986).
4. S.L. Moser, R. Church, M.B. Peori, and K. Vaughan. Can. J. Chem. **83**, 1071 (2005).
5. M.B. Peori, K. Vaughan, and V. Bertolasi. J. Chem. Crystallogr. **35**, 297 (2005).
6. S.L. Moser, V. Bertolasi, and K. Vaughan. J. Chem. Crystallogr. **35**, 307 (2005).
7. R.Tingley, M.B. Peori, R. Church, and K. Vaughan. Can. J. Chem. **83**, 1799 (2005).
8. R. Tingley, V. Bertolasi, and K. Vaughan. J. Chem. Crystallogr. **35**, 821 (2005).
9. K. Vaughan, S.L. Moser, R. Tingley, M.B. Peori, and V. Bertolasi. Can. J. Chem. **84** (2006). This issue.
10. J.F. Glister and K. Vaughan. J. Heterocycl. Chem. **43**, 217 (2006).
11. J.F. Glister, K. Vaughan, and V. Bertolasi. J. Chem. Crystallogr. **34**, 175 (2004).
12. J.F. Glister, H. Jenkins, and K. Vaughan. J. Chem. Cryst. **36**, 445 (2006).
13. R. Tingley, V. Bertolasi, and K. Vaughan. J. Chem. Cryst. Accepted for publication.
14. H. Krassig. Makromol. Chem. **17**, 77 (1955).
15. J.M. DesMarchelier, N.A. Evans, R.F. Evans, and R.B. Jones. Aust. J. Chem. **24**, 257 (1968).
16. J. Dale and T. Sigvartsen. Acta. Chem. Scand. **45**, 1064 (1991).
17. V.R. Little and K. Vaughan. Can. J. Chem. **82**, 1294 (2004).
18. V.R. Little, R. Tingley, and K. Vaughan. Can. J. Chem. **83**, 471 (2005).
19. S.L. Moser and K. Vaughan. Can. J. Chem. **82**, 1725 (2004).

© 2006 NRC Canada

In situ nitrosonium ion generation — α-Oximinylation of enol ethers from steroidal spiroketals: Introduction of C23 (*R*)-OH in cephalostatin intermediates[1]

Seongmin Lee and Philip L. Fuchs

Abstract: Nitrosonium ion generated in situ from the reaction of *t*-$BuNO_2$ and $BF_3{\cdot}Et_2$ is an effective oximinylating agent for enol ethers derived from steroidal spiroketals. The scope and limitations of this method has been studied. The difficult reduction of C23 ketone to C23 (*R*)-alcohol has now been selectively achieved via L-Selectride® reduction. Application to cephalostatin intermediates is discussed.

Key words: oximinylation, nitrosonium ion, steroid spiroketal, cephalostatins.

Résumé : L'ion nitrosonium généré in situ par réaction du *t*-$BuNO_2$ avec le $BF_3{\cdot}OEt_2$ est un agent d'oximinylation efficace pour les éthers énoliques dérivés de spirocétals stéroïdaux. On a étudié la portée et les limitations de cette méthode. Faisant appel à une réduction à l'aide de L-Selectride®, on a maintenant réalisé la difficile réduction stéréosélective de la cétone C23 en alcool-(*R*) C23. On discute de l'application à des intermédiaires de la céphalostatine.

Mots clés : oximinylation, ion nitrosonium, spirocétal stéroïdal, céphalostatines.

[Traduit par la Rédaction]

Introduction

The 45 members of the cephalostatin and ritterazine family, along with analogs, afford the basis for elucidating some of the structure–activity relationships (SAR) of these potent cytotoxins (1). All members of the cephalostatin family possess two steroidal spiroketals connected by a pyrazine. The most active compounds bear a highly oxygenated north unit and a substantially less polar south unit. In terms of bioactivity, cephalostatin **1** (Fig. 1) shows average 1 nmol/L GI_{50}s in 2 day tests in the NCI 60-line screen and 10^{-14} mol/L GI_{50}s in 6day tests in the Purdue 6 line minipanel (2). Cephalostatin **1**, cephalostatin **7**, ritterazine **M**, and ritterazine **K** have been synthesized by our group (3), while we and others (4) have also been active in the synthesis and testing of analogs.

The mechanism of action of the cephalostatins and ritterazines is currently unknown, although recent data indicates that ritterazine **B** is an apoptotic agent like OSW-1 (5) and cephalostatin **7** (6). The role of spiroketals and sugars as hydrogen bond donors and (or) acceptors has been suggested (7). Although it is evident from the NIH 60-cell line COMPARE studies that cephalostatin 1 and OSW-1 are related, significant biological differences[3] and recent bioactivity data of C22 deoxy OSW-**1** analogs (8) suggest that they may have a modified mechanism of action. Correlation of cytotoxicity with energy for E-ring oxacarbenium ion access in cephalostatins and ritterazines has been proposed (9). SAR studies indicate that the hydroxyl groups of both north and south units of the cephalostatin family play an essential role in tumor eradication. Hydroxyl groups provide "polarity match" (10), a requirement for the exhibition of bioactivity, and affect the heat of formation of the E-ring oxacarbenium ion,[4] thus adjusting bioactivity. When the C17 alcohol, for instance, in the north unit of cephalostatin **1** was replaced by a hydrogen, the antitumor activity dropped dramatically.[5] The presence of the C23 hydroxyl group also contributes to the anticancer activity. The recently synthesized C23′-deoxy cephalostatin **1**(11) is about 10 times less potent than cephalostatin **1**.

Our second generation synthesis of cephalostatin **1** (**4**) uses a "redox" strategy(12), requiring a scalable protocol ca-

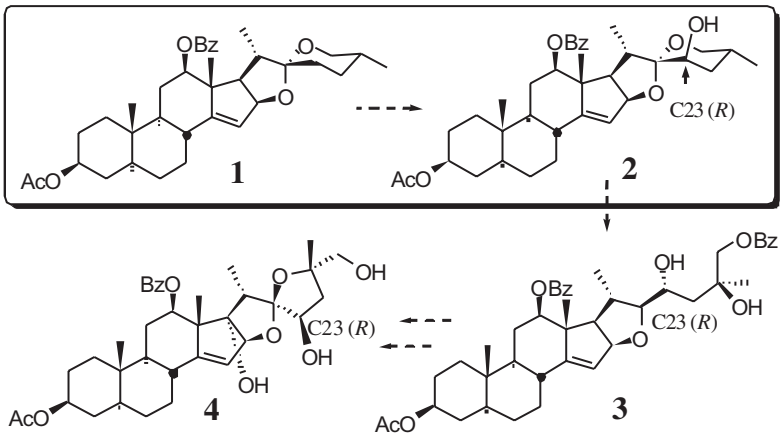
Received 21 December 2005. Accepted 29 April 2006. Published on the NRC Research Press Web site at http://canjchem.nrc.ca on 17 October 2006.

S.M. Lee and P.L. Fuchs.[2] Department of Chemistry, Purdue University, West Lafayette, IN 47097, USA.

[1]This article is part of a Special Issue dedicated to Dr. Alfred Bader.
[2]Corresponding author (e-mail: pfuchs@purdue.edu).
[3]P. Huang. Unpublished results.
[4]T.G. LaCour and P.L. Fuchs. Unpublished results.
[5]Compare, for example, ritterazine **A** (17 -OH, 24 nmol/L) and ritterazine **T** (17 -H, 590 nmol/L).

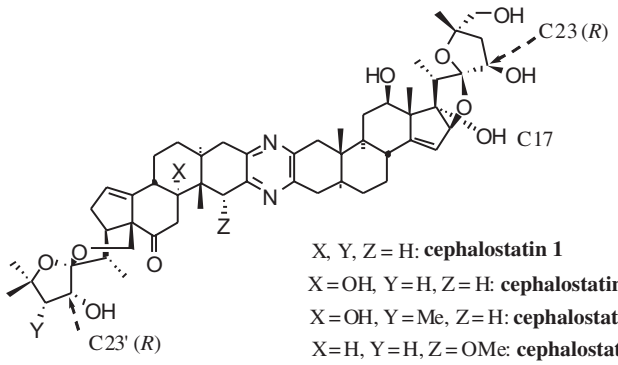
 doi:10.1139/V06-113 © 2006 NRC Canada

Scheme 1.



North unit of cephalosatin 1

Fig. 1.



pable of efficient introduction of the C23 (*R*)-alcohol (Scheme 1). Eighteen of nineteen known cephalostatins possess the north C23 (*R*)-alcohol and seventeen of those bear the south C23 (*R*)-alcohol (Fig. 1).

Many efforts have been made to introduce the C23 (*R*)-alcohol (13), such as the reduction of the C23 carbonyl group (14), sulfinylation of a C22,C23 enol ether with TFAA-activated DMSO followed by allylic rearrangement (15), and addition of allyl stannane to an aldehyde (16). However, none of these methods provided the requisite C23 (*R*)-alcohol in workable excess (de < 30%). At present, the only acceptable method is the dimethyldioxirane (DMDO) oxidation of an enone – vinyl ether to quantitatively achieve stereospecific cyclization to the prized (*R*)-alcohol. However, this method employs 750 mL of DMDO for the production of 15.7 g of C23 alcohol (17) and also requires the use of stoichiometric amounts of toxic selenium and stannyl reagents to prepare **2**. Herein, we describe a scalable pathway leading to C23 (*R*)-OH.

Results and discussion

The known methods for α-oxidation of ketones, enols, and spiroketals (Scheme 2) were initially surveyed to access the desired C23 ketone **7**. We first attempted the synthesis of a masked C23 ketone, such as nitroimine 5 or oxime 6. Although Suàrez and co-workers (18) recently demonstrated that the C14,C15-saturated spiroketal forms the nitroimine in acceptable yield, our attempts to use this procedure on substrate **1** only afforded the C23 nitroimine **5** in very low yield. We also investigated S_N2 chemistry with equatorial C23 bromide **8** and iodide **9**, prepared from **1** with phenyltrimethylammonium bromide (PTAB) or iodine monochloride, respectively. Unfortunately, numerous reagents that convert alkyl halides to alkoxy groups, including superoxide (19), KNO_2 (20), O_2–Bu_3SnH (21), $AgBF_4$–glyme–H_2O (22), AgOAc (23), and CsF–BzOH (24), were either unreactive or severely destructive.

The known methods for α-oximinylation of ketones were not applicable to our substrate (25). Thus, we were delighted that the formation of the desired oxime spiroketal **12** took place smoothly from the reaction of rockogenin diacetate **11** with *t*-$BuNO_2$ and $BF_3{\cdot}Et_2$. Optimization of this new procedure is summarized in Table 1. The choice of Lewis acid is critical for this event, as $BF_3{\cdot}Et_2$ gave the best yields while $FeCl_3$, $TiCl_4$, $SnCl_4$, $ZnBr_2$, $Sc(OTf)_3$, and TMSOTf failed to give reasonable conversions, probably because of their decreased oxophilic character relative to $BF_3{\cdot}OEt_2$.

Minimization of undesired lactone **13**, which comes from oxime spiroketal **12**, requires using excess *t*-BuONO (5 equiv.) and catalytic $BF_3{\cdot}OEt_2$ (0.5 equiv.) in acetic acid at ambient temperature for the minimum time. The use of less *t*-BuONO (Table 1, entries 1–5 and 7) and $BF_3{\cdot}Et_2$ (Table 1, entry 11), solvents other than AcOH (Table 1, entries 1, 3, and 4), lower temperature (Table 1, entry 2), or prolonged reaction time (Table 1, entry 10) results in the formation of significant amounts of lactone **13**.

The proposed mechanism of oximinylation involves nitrosonium ion (26) mediated nitrosylation of the enol ether **11a** formed via Lewis acid opening of the steroid spiroketal (Scheme 3). First, nitrosonium ion ($NO^+BF_4^-$) is generated in situ from a reaction of *t*-$BuNO_2$ and $BF_3{\cdot}OEt_2$. Then, the attack of enol ether **11a** on the nitrogen atom of nitrosonium ion takes place to produce nitroso spiroketal **12a**. Finally, the nitroso spiroketal **12a** is rapidly isomerized to give oxime spiroketal **12**. The presence of a $NOBF_4$ (–141.6 ppm, CD_3CN) peak in the ^{19}F NMR supports this mechanism. The reaction of spiroketal **11** with 3 equiv. of commercial $NOBF_4$ (Table 1, entry 19) in acetic acid affords the same

© 2006 NRC Canada

Scheme 2.

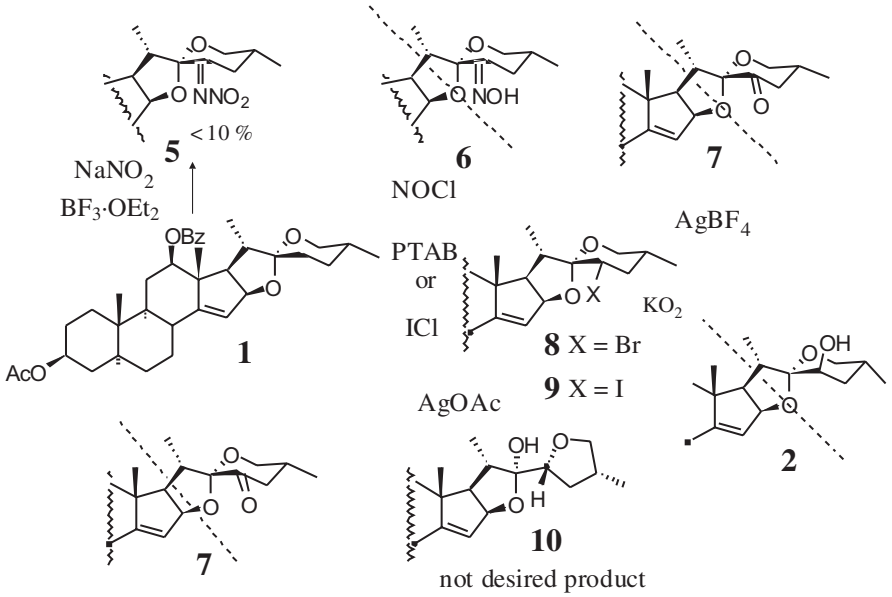
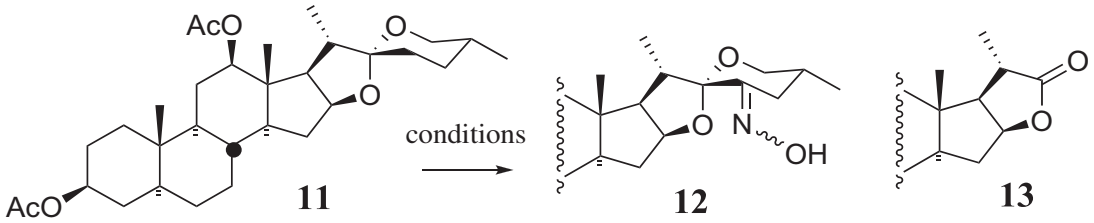


Table 1. Optimization of α-oximinylation.



Entry	Lewis acid (equiv.)	*t*-$BuNO_2$ (equiv.)	Solvent	*T* (°C)	Time (h)	Yields of **12** and **13** (%)
1	$BF_3{\cdot}OEt_2$ (1)	3	CH_2Cl_2	25	3	45, 31
2	$BF_3{\cdot}OEt_2$ (1)	3	CH_2Cl_2	0	3	NR
3	$BF_3{\cdot}OEt_2$ (1)	3	Toluene	25	3	40, 23
4	$BF_3{\cdot}OEt_2$ (1)	3	MeCN	25	3	35, 48
5	$BF_3{\cdot}OEt_2$ (1)	3	AcOH	25	0.5	62, 17
6	—	3	AcOH	25	1	NR
7	$BF_3{\cdot}OEt_2$ (2)	2	AcOH	25	1	37, 45
8	$BF_3{\cdot}OEt_2$ (0.5)	3	AcOH	25	1	32, 52
9	$BF_3{\cdot}OEt_2$ (0.5)	5	AcOH	25	0.2	92, 0
10	$BF_3{\cdot}OEt_2$ (0.5)	5	AcOH	25	2	50, 36
11	$BF_3{\cdot}OEt_2$ (0.2)	5	AcOH	25	2	41, 44
12	$NOBF_4$ (3)		AcOH	25	0.2	82, 0

Note: NR = No reation.

oxime spiroketal **12** in 82% yield after 10 min, thus exhibiting similar reactivity and product distribution pattern to that observed in the reaction of spiroketal **11** with $BF_3{\cdot}Et_2$ and *t*-BuONO (Table 1, entry 16). The Lewis acid promoted second-order Beckmann fragmentation (27) of α-oxygenated oxime spiroketal **12** appears to account for the formation of lactone **13**. The scope and limitation of the oximinylation of steroid spiroketals was then explored.[6] The results in Table 2 reveal some interesting features. First, C23 oximinylation works for only 5/6 spiroketals, not for 5/5 and 6/5 spiro systems, such as **21** and **22**. Hecogenin acetate (starting material for **15**) containing a C12 ketone, which is diffi-

[6] Supplementary data for this article are available on the journal Web site (http://canjchem.nrc.ca) or may be purchased from the Depository of Unpublished Data, Document Delivery, CISTI, National Research Council Canada, Ottawa, ON K1A 0R6, Canada. DUD 5081. For more information on obtaining material refer to http://cisti-icist.nrc-cnrc.gc.ca/irm/unpub_e.shtml.

© 2006 NRC Canada

Scheme 3.

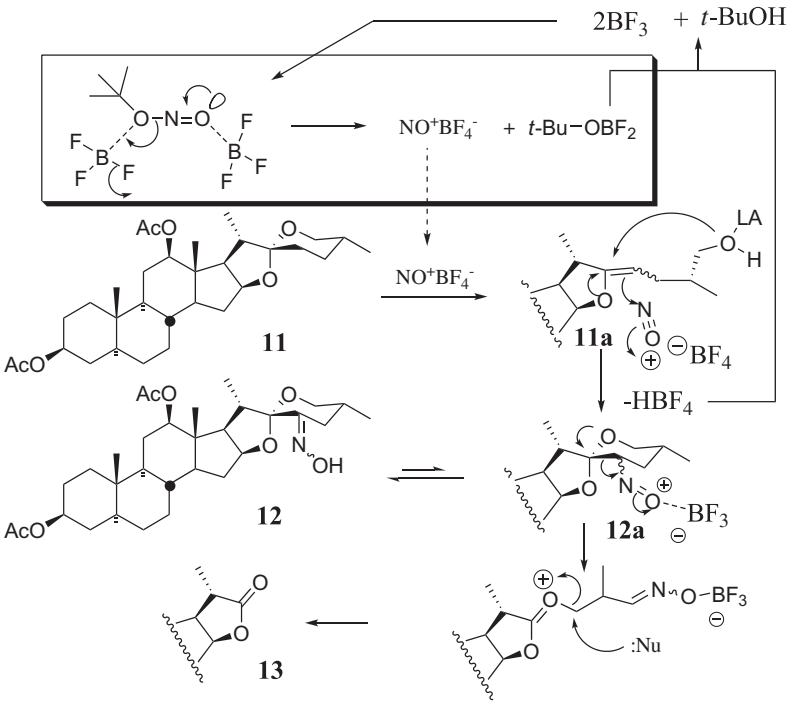
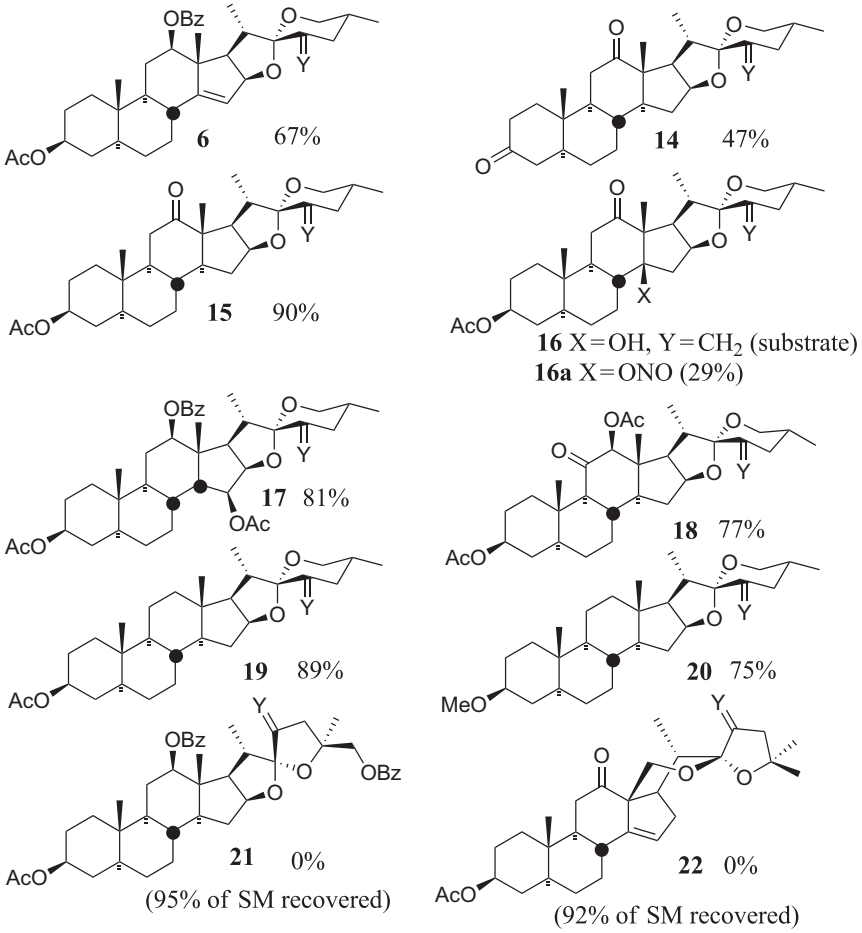


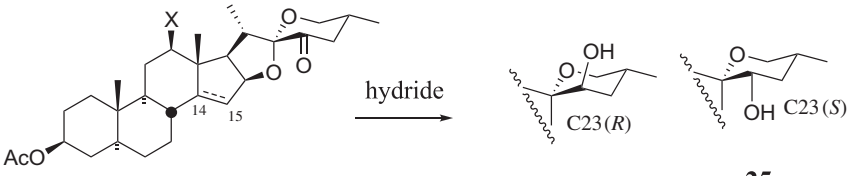
Table 2. α-Oximinylation of steroid spiroketals.



Note: isolated yields. Y = H_2 (substrates) or Y = NOH (products).

© 2006 NRC Canada

Table 3. Reduction of the C23 ketone.



23 X = OAc, C14–15 = 14α–H **24** **25**

7 X = OBz, C14–15 = Δ^{14} **2** **26**

Entry	Substrate	Hydride	Conditions	Products	Yield (%)	C23 (*R*):C23 (*S*)
1	23	$LiAl(OtBu)_3H$	0 °C, THF	**24**, **25**	93	1:20
2	23	$NaBH_4$	25 °C, MeOH	**24**, **25**	97	1:19
3	23	(*R*)-CBS/BH_3	25 °C, THF	**24**, **25**	85	1:11
4	23	$CeCl_3$/$NABH_4$	–78 °C, 2 h	**24**, **25**	94	1:4.2
5	23	LS-Selectride®	–78 °C, THF	**24**, **25**	81	1:1.4
6	23	L-Selectride®	–78 °C, THF	**24**, **25**	89	2.5:1
7	23	K-Selectride®	–78 °C, THF	**24**, **25**	83	4.6:1
8	23	(*S*)-CBS/BH_3	25 °C, 0.5 h, THF	**24**, **25**	91	6.2:1
9	7	L-Selectride®	–78 °C, 3 h, THF	**2**, **26**	87	10.3:1
10	7	(*S*)-CBS/BH_3	25 °C, 0.5 h, THF	**2**, **26**	92	7.3:1
11	7	L-Selectride®	–78 °C, 3 h, PhMe	**2**, **26**	85	5.5:1

cult to enolize, smoothly gave oxime spiroketal **15**. The presence of more readily enolized C3 ketone resulted in low yield of **14** because of the formation of by-products. It is notable that olefin moieties (**6** and **22**) are intact under the reaction conditions. Alcohol functionality was converted to nitrite **16a**. Most importantly, employing the new protocol, we were able to obtain a key intermediate (5/6 spiroketal **6**) in reasonable yield.

C23 ketones **23** and **7** were readily prepared by *p*-toluenesulfonic acid catalyzed deoximinylation. We next turned our attention to establishing the requisite C23 (*R*) stereochemistry (Table 3). In the case of C14,C15-saturated C23 ketone **23**, (*S*)-CBS best effected the desired reduction to afford C23 (*R*) and C23 (*S*) in a reproducible ratio of 6.2:1[7] (Table 3, entry 8, C23 (*R*) (78%) and C23 (*S*) (13%), isolated yield, 50 mmol scale; previous results (28) show formation of C23 (*R*) and C23 (*S*) in a ratio of 1.7:1 (72%)). We were pleased that the L-Selectride® reduction of C14,C15-unsaturated ketone **7** (Table 3, entry 9) delivered C23 axial alcohol **2** in a highly sterereoselective fashion.

In conclusion, an efficient and economical in situ method to generate nitrosonium fluoroborate is presented. This chemistry provides a large-scale pathway for the establishment of the C23 (*R*) stereochemistry of steroidal sapogenins. Further research is ongoing regarding the application of this method for the synthesis of the north unit of cephalostatin **1**.

Acknowledgments

This investigation was generously supported by funds provided by the National Institutes of Health (CA 60548). We acknowledge Arlene Rothwell and Karl Wood for providing MS data.

References

1. G.R. Pettit, R. Tan, J.P. Xu, Y. Ichihara, M.D. Williams, and M.R. Boyd. J. Nat. Prod. **61**, 953 (1998), and refs. therein.
2. T.G. LaCour, C. Guo, S. Ma, J. Jeong, M.R. Boyd, and P.L. Fuchs. Bioorg. Med. Chem. Lett. **9**, 2587 (1999), and refs. therein.
3. (*a*) T.G. LaCour, C. Guo, M.R. Boyd, and P.L. Fuchs. Org. Lett. **2**, 33 (2000); (*b*) W. Li, T.G. LaCour, M.R. Boyd, and P.L. Fuchs. J. Am. Chem. Soc. **124**, 4548 (2002), and refs. therein; (*c*) S.M. Lee, T.G. LaCour, D.A. Lantrip, and P.L. Fuchs. Org. Lett. **4**, 313 (2002).
4. (*a*) C.H. Heathcock and S.C. Smith. J. Org. Chem. **59**, 6828 (1994), and refs. therein; (*b*) R. Jautelat, A. Muller-Fahrnow, and E. Winterfeldt. Chem. Eur. J. **5**, 1226 (1999); (*c*) S. Basler, A. Brunck, R. Jautelat, and E. Winterfeldt. Helv. Chim. Acta. **83**, 1854 (2000), and refs. therein.
5. (*a*) Y. Mimaki, M. Kuroda, A. Kameyama, Y. Sashida, and T. Hirano. Bioorg. Med. Chem. Lett. **7**, 633 (1997); (*b*) S. Kubo, Y. Mimaki, M. Terao, Y. Sashida, T. Nikaido, and T. Ohmoto. Phytochemistry, **31**, 3969 (1992).
6. (*a*) T. Komiya, N. Fusetani, S. Matsugana, M. Kelley, and K. Nakagawa. Cancer Chemother. Pharmacol. **51**, 202 (2003); (*b*) V.M. Dirsch, I.M. Mueller, S.T. Eichhorst, G.R. Pettit, Y. Kamano, M. Inoue, and A.M. Vollmar. Cancer Res. **63**, 8869 (2003).
7. Y. Pan, R.L. Merriaman, L.R. Tanzer, and P.L. Fuchs. Bioorg. Med. Chem. Lett. **2**, 967 (1992).
8. (*a*) L. Deng, H. Wu, B. Yu, M. Jiang, and J. Wu. Bioorg. Med. Chem. Lett. **14**, 2781 (2004); (*b*) J. Morzycki, A. Wihtiekewicz, and S. Wolcznski. Bioorg. Med. Chem. Lett. **14**, 3323 (2004).
9. (*a*) T.G. LaCour, C. Guo, M.R. Boyd, and P.L. Fuchs. Org. Lett. **2**, 33 (2000); (*b*) C. Guo, T.G. LaCour, and P.L. Fuchs. Bioorg. Med. Chem. Lett. **9**, 419 (1999).

[7] Preincubation (~30 min) of (*S*)-CBS and BH_3 Me_2 in THF before the addition of **23** is critical to obtain good stereoselectivity.

© 2006 NRC Canada

10. S. Fukuzawa, S. Matsunaga, and N. Fusetani. J. Org. Chem. **62**, 4484 (1997), and refs. therein.
11. W. Li, T.G. LaCour, M.R. Boyd, and P.L. Fuchs. J. Am. Chem. Soc. **124**, 4548 (2002).
12. (*a*) S.M. Lee and P.L. Fuchs. J. Am. Chem. Soc. **124**, 13978 (2002); (*b*) S.M. Lee and P.L. Fuchs. Org. Lett. **4**, 313 and 317 (2002).
13. Hydroxylation of steroids — C5: (*a*) J.T. Dixon, C.W. Holzapfel, and F.R. Heerden. Synth. Commun. **23**, 135 (1993); (*b*) P. Bovicelli, A. Gambacorta, and E. Mincione. Tetrahedron Lett. **33**, 7411 (1992); hydroxylation of steroids — C14: (*c*) M.D. Kaufman, P.A. Grieco, and D.W. Bougie. J. Am. Chem. Soc. **115**, 11648 (1993); hydroxylation of steroids — C17: (*d*) F.A. Davies, L.C. Vischwarkarma, J.M. Billmers, and J. Finn. J. Org. Chem. **49**, 3243 (1984).
14. (*a*) C. Betancor, R. Freire, I. Perez-Martin, T. Prange, and E. Suàrez. Org. Lett. **4**, 1295 (2002); (*b*) D.H. Barton, P.G. Sammes, M.V. Taylor, and E. Werstiuk. J. Chem. Soc. Chem. Commun. 1977 (1970).
15. J. Jeong and P.L. Fuchs. J. Am. Chem. Soc. **116**, 773 (1994).
16. S. Kim, S.C. Sutton, C. Guo, T.G. LaCour, and P.L. Fuchs. J. Am. Chem. Soc. **121**, 2056 (1999).
17. J.S. Lee and P.L. Fuchs. Org. Lett. **5**, 2247 (2003).
18. A.G. Gonzalez, R. Frerire, M.G. Garcia-Estrada, and E. Suàrez. Tetrahedron, **28**, 1289 (1972).
19. E.J. Corey, K.C. Nicolaou, M. Shibasaki, Y. Machida, and C. Shiner. Tetrahedron Lett. **37**, 3183 (1975).
20. R.M. Moriarty and V.K. Singh. Tetrahedron Lett. **34**, 8029 (1993).
21. E. Nakamura, T. Inubushi, S. Aoki, and D. Machii. J. Am. Chem. Soc. **113**, 8980 (1991).
22. J. Morzycki and A. Jastrzebska. Tetrahedron Lett. **42**, 5989 (2001).
23. M. Zarraga and J.D. Martin. Tetrahedron Lett. **31**, 1633 (1990).
24. T. Sato and J. Otera. Synlett, 336 (1995).
25. (*a*) A.A. Mohammed and G. Nagendrappa. Tetrahedron Lett. **44**, 2753 (2003); (*b*) J. Rasmussen and A. Hassner. J. Org. Chem. **39**, 2558 (1974); (*c*) Y.H. Kim, Y.J. Park, and K. Kim. Tetrahedron Lett. **30**, 2833 (1989); (*d*) M.N. Mallya, G. Nagendrappa, J.S. Prasad, M.A. Sridhar, and M.K. Lokanath. Tetrahedron Lett. **42**, 2565 (2001).
26. (*a*) G.A. Olah. Aldrichimica Acta, **12**, 43 (1979); (*b*) M.P. Doyle and W. Wierenga. J. Am. Chem. Soc. **94**, 3896 (1972); (*c*) R.H. McGirk and E.H. White. J. Am. Chem. Soc. **95**, 3854 (1973); (*d*) G.A. Olah, J. Shih, B.P. Singh, and P.G. Gupta. J. Org. Chem. **48**, 3356 (1983).
27. (*a*) H. Tso, B.A. Gilbert, and J. Huw. J. Chem. Soc. Chem. Commun. 669 (1993); (*b*) P.A. Petukhov and A.V. Tkachev. Synlett, 580 (1993); (*c*) D. Miljkovic and J. Pedtrovic. J. Org. Chem. **38**, 3585 (1973); (*d*) A.F. Ferris, G.S. Johnson, and F.E. Gould. J. Org. Chem. **25**, 496 (1960).
28. C. Betancor, R. Freire, I. Perez-Martin, T. Prange, and E. Suàrez Org. Lett. **4**, 1295 (2002).

© 2006 NRC Canada

Preparation of enantiopure long chain *threo*-2-amino-3-hydroxyesters via chiral morpholinone-derived azomethine ylids[1]

Victoria A. Brome, Laurence M. Harwood, and Helen M.I. Osborn

Abstract: The synthetic approach to *threo*-2-amino-3-hydroxyesters possessing long alkyl chains outlined herein centres on the generation of chiral azomethine ylids by reaction of (5*R*)-5-phenyl-morpholin-2-one, (*R*)-(**1**), with long chain aldehydes. In the presence of a second equivalent of aldehyde, the azomethine ylid can be trapped to afford a cycloadduct with three new stereodefined centres. Degradation of the cycloadduct allows entry to β-substituted-α-amino acid derivatives, which have potential as building blocks for sphingosine synthesis.

Key words: sphingosine, morpholinone, chiral azomethine ylid, dipolar cycloaddition.

Résumé : On a mis au point une approche à la synthèse de *thréo*-2-amino-3-hydroxyesters d'acides à longues chaînes alkyles qui est centrée sur la génération d'ylures d'azométhines chiraux par la réaction de la (5*R*)-5-phénylmorpholin-2-one, (*R*)-(**1**) avec des aldéhydes à longues chaînes. En présence d'un deuxième équivalent d'aldéhyde, l'ylure d'azométhine peut être piégé pour conduire à la formation d'un cycloadduit comportant trois nouveaux centres stéréodéfinis. La dégradation du cycloadduit permet d'obtenir des dérivés d'acides α-aminés et β-substitués qui peuvent servir de blocs dans la synthèse de sphingosines.

Mots clés : sphingosine, morpholinone, ylure d'azométhine chiral, cycloaddition dipolaire.

[Traduit par la Rédaction]

Introduction

Glycosphingolipids have been isolated from a variety of natural sources, including marine sponge species of *Agelas* and *Axinella* (1, 2). Such compounds demonstrate interesting immunostimulatory activity, for example, the modulation of protein kinase C activities and the regulation of hormone receptors and nerve cells (3). The glycosphingolipid structure may be considered in two parts, namely, a sphingosine-related component and a carbohydrate component (Fig. 1). Generally, throughout the literature, the syntheses of the two constituent units are considered independently.

Developments in the synthesis of the sphingolipid moiety and its analogues have been recently reviewed (4), and since the first nonstere ocontrolled synthesis of sphinganine by Grob and Gadient (5), synthetic strategies have frequently utilized various carbohydrate precursors (6) or serine-derived building blocks for accessing this family of compounds (7).

The sphingosines can be looked upon as 3-hydroxy-2-amino acid derivatives, and detailed examples of enantio- and stereo-selective syntheses of β-hydroxy-α-amino acids have been reviewed by Duthaler (8). Drawing on the findings of Dellaria and Santarsiero's investigation into the alkylation of chiral glycine synthon equivalents in α-amino acid synthesis (9), much work carried out within our group has focused on the use of (*R*)- and (*S*)-5-phenyl-3,4,5,6-tetrahydro-2*H*-1,4-oxazin-2-one (**1**) (referred to herein as 5-phenylmorpholin-2-one) as a chiral relay system and its use as a chiral template in the area of α-amino acid synthesis (10). During the cycloaddition studies in which the ylid was generated using paraformaldehyde, a minor product was sometimes obtained, which neither corresponded to any of the possible cycloadducts nor the diketopiperizine resulting from dimerization of the template. Spectroscopic evidence pointed to the minor product being **2a**, a result of trapping the azomethine ylid by a second equivalent of formaldehyde. Confirmation that this was indeed the case was obtained when reaction between the (*S*)-morpholin-2-one template and excess paraformaldehyde yielded **2a** in essentially quantitative yield. As the trapping of the azomethine ylid with a second equivalent of aldehyde does not compete efficiently with electron deficient alkenes and alkynes, it was concluded that the rate of this reaction is appreciably slower than with carbon–carbon dipolarophiles. When aldehydes other than paraformaldehyde were used, a single adduct was observed in every case, and these adducts (**2b**–**2g**) could be deconstructed to liberate enantiomerically pure *threo*-β-hydroxy-α-

Received 2 February 2005. Accepted 7 March 2006. Published on the NRC Research Press Web site at http://canjchem.nrc.ca on 8 November 2006.

Dedicated with our best respects to Alfred Bader.

V.A. Brome, L.M. Harwood,[2] and H.M.I. Osborn.[3] School of Chemistry, University of Reading, Whiteknights, Reading, Berkshire, RG6 6AD, UK.

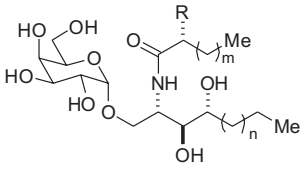
[1]This article is part of a Special Issue dedicated to Dr. Alfred Bader.

[2]Corresponding author (e-mail: l.m.harwood@reading.ac.uk).

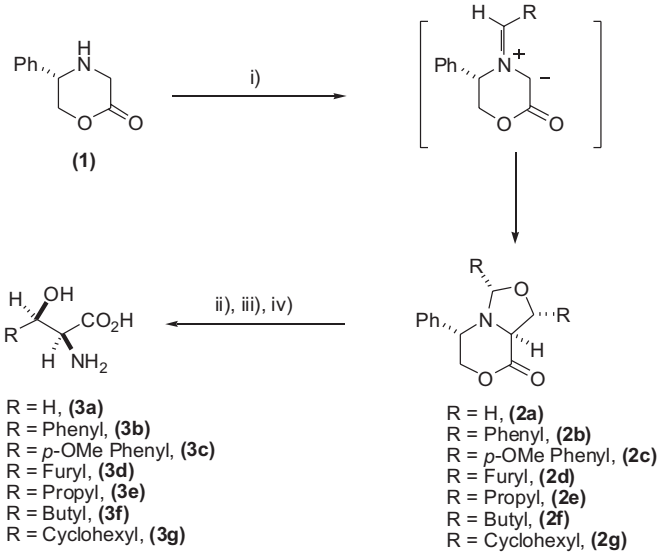
[3]Current address: School of Pharmacy, University of Reading, Whiteknights, Reading, Berkshire, RG6 6AD, UK.

 doi:10.1139/V06-121 © 2006 NRC Canada

Fig. 1. Representative structure for a galactosylsphingolipid.



Scheme 1. Reagents and conditions: (*i*) RCHO (excess), reflux; (*ii*) 1 mol/L HCl, MeOH, reflux; (*iii*) H_2 (5 atm), $Pd(OH)_2/C$, TFA (1 equiv.), aq. MeOH; (*iv*) basic ion-exchange resin.



R = H, **(3a)**
R = Phenyl, **(3b)**
R = *p*-OMe Phenyl, **(3c)**
R = Furyl, **(3d)**
R = Propyl, **(3e)**
R = Butyl, **(3f)**
R = Cyclohexyl, **(3g)**

R = H, **(2a)**
R = Phenyl, **(2b)**
R = *p*-OMe Phenyl, **(2c)**
R = Furyl, **(2d)**
R = Propyl, **(2e)**
R = Butyl, **(2f)**
R = Cyclohexyl, **(2g)**

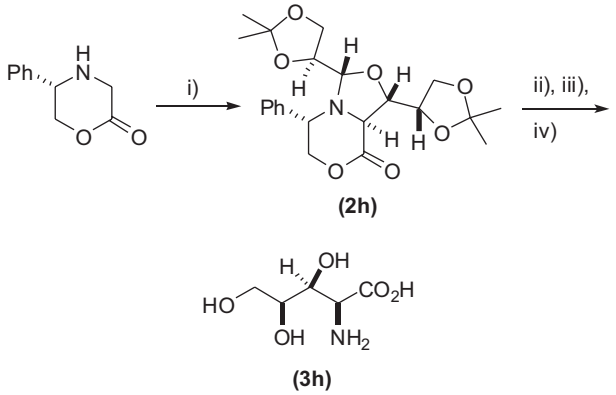
amino acids (**3b**–**3g**) (Scheme 1) in good yields (11). The value of this route was subsequently illustrated by a concise synthesis of (+)-polyoxamic acid (**3h**) (Scheme 2) (12).

Results and discussion

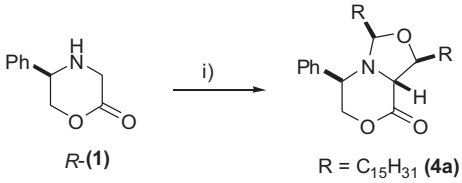
To extend this methodology to allow preparation of long chain hydroxyamino acids, which could act as precursors to sphingosine analogues, preliminary investigations focused on hexadecanal as a representative substrate, in terms of alkyl chain length. Following our previous protocol, 3 equiv. of the aldehyde were added to (5*R*)-5-phenylmorpholin-2-one ((*R*)-(**1**)) (i.e., 6 mmol aldehyde : 1 mmol (*R*)-(**1**)) in toluene and the mixture was heated to reflux for 48 h, after which time, TLC analysis indicated that all of the morpholinone had been consumed. As the hexadecanal proved to be far less polar than previous aldehydes employed in this reaction, the eluent chosen for chromatographic purification had to reflect this; a system of 19:1 petroleum – diethyl ether proving the most efficient. Unfortunately, only low yields (18%) of pure cycloadduct (**4a**) were isolated under these conditions, with much of the remaining product being contaminated with residual hexadecanal. NOE investigations of cycloadduct **4a** failed to determine conclusively the stereochemistry of the adduct, the very large signal representing the aliphatic protons masking important regions in the ^1H NMR spectrum. Additionally, the pure product was isolated as a waxy solid, which was unsuitable for X-ray analysis. However, as ^1H NMR data were in agreement with those of cycloadducts **2e**–**2f**, derived from lower homologue aliphatic aldehydes (12), the hexadecanal-derived cycloadduct was tentatively assigned as **4a** (Scheme 3). It was clear that use of excess aldehyde in the cycloaddition reaction was not only wasteful but was also hampering isolation and purification of the desired product. The reaction conditions were therefore examined with the objective of achieving higher yields of the pure hexadecanal-derived cycloadduct. To this end, the number of equivalents of hexadecanal to (5*R*)-5-phenylmorpholin-2-one was reduced from 3.0 to 1.5, the rationale being that reduced aldehyde contamination of the crude product could simplify isolation of the cycloadduct. TLC analysis of the reaction mixture after 72 h indicated that the starting material had been almost completely consumed and the crude reaction mixture was therefore purified, resulting in the isolation of 34% of pure cycloadduct. Further reduction to 1.1 equiv. of aldehyde required a reaction time of 5 days before all starting morpholinone had been consumed, but this resulted in a greatly improved yield of 65% of pure cycloadduct (**4a**) after a single purification (Table 1).

Thus, although reducing the number of equivalents of aldehyde in the reaction mixture necessitated an increase in

Scheme 2. Reagents and conditions: (*i*) Excess (*S*)-glyceraldehyde acetonide, 53%; (*ii*) 1 mol/L HCl, MeOH, reflux; (*iii*) H_2 (5 atm), $Pd(OH)_2/C$, TFA (1 equiv.), aq. MeOH; (*iv*) basic ion-exchange resin, 95% over 3 steps.



Scheme 3. Reagents and conditions: See Table 1.



R-(**1**) R = $C_{15}H_{31}$ **(4a)**

Table 1. Effect of the number of equivalents of the added aldehyde on reaction yield and time.

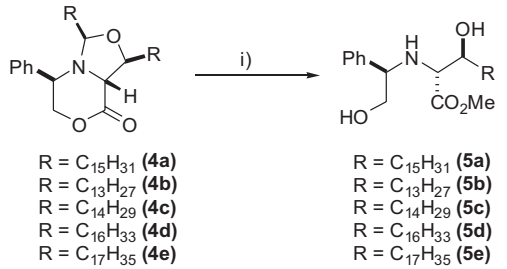
Hexadecanal (equiv.)	Reaction time	Isolated yield of **4a** (%)
3.0	48 h	18
1.5	72 h	34
1.1	5 d	65

© 2006 NRC Canada

Table 2. Optimized yields of the cycloadducts of (**4b**–**4e**).

Aldehyde	Yield of (**cycloadduct**) (%)
Tetradecanal	58 (**4b**)
Pentadecanal	68 (**4c**)
Heptadecanal	56 (**4d**)
Octadecanal	62 (**4e**)

Scheme 4. Reagents and conditions: (*i*) MeOH, 5 mol/L HCl, reflux 1 h.



R = $C_{15}H_{31}$ **(4a)**
R = $C_{13}H_{27}$ **(4b)**
R = $C_{14}H_{29}$ **(4c)**
R = $C_{16}H_{33}$ **(4d)**
R = $C_{17}H_{35}$ **(4e)**

R = $C_{15}H_{31}$ **(5a)**
R = $C_{13}H_{27}$ **(5b)**
R = $C_{14}H_{29}$ **(5c)**
R = $C_{16}H_{33}$ **(5d)**
R = $C_{17}H_{35}$ **(5e)**

reaction time, it resulted in a greater than three-fold increase in yield and involved less wastage of aldehyde.

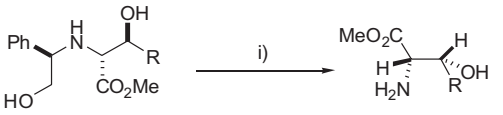
With the procedure for preparing the hexadecanal-derived cycloadduct optimized, a range of analogues derived from aldehydes with chain lengths between 14 and 18 carbon atoms was synthesized, utilizing 1.1 equiv. of aldehyde. In each case a single cycloadduct (**4b**–**4e**) was isolated in an acceptable yield after purification by column chromatography (Table 2).

The subsequent step of the synthesis was the opening of the cycloadduct to afford the corresponding amino esters (**5a**–**5e**). The two-step hydrolysis and hydrogenolysis sequence, previously shown to be the optimal procedure for aliphatic aldehyde-derived cycloadducts, was adopted. Previously, the hydrolysis had been carried out in methanol at reflux using 1 mol/L hydrochloric acid to release the amino ester, but when applied to the hexadecanal-derived cycloadduct (**4a**), the conditions failed to effect hydrolysis, leaving the starting material intact. It was observed that the starting material was only sparingly soluble in aqueous methanol at room temperature but was more soluble in hot methanol. Thus, the effect of the addition of 5 mol/L hydrochloric acid to a hot methanolic solution of the cycloadduct was investigated, and this furnished the corresponding methyl ester in 1 h. In the first instance, the lactone-opened products **5a**–**5e** were isolated for characterization purposes and were obtained in moderate to good yield (Scheme 4, Table 3). These derivatives were solids, as opposed to the oils obtained when using the lower homologue aldehydes. The proposed structure for the hexadecanal-derived methyl ester **5a**, (a representative example) was supported by characteristic ^{1}H NMR data, which displayed a multiplet at 7.30 ppm representing the five aromatic protons; a one proton doublet at 3.17 ppm corresponding to the proton α to the amino group and a one proton multiplet at 3.75–3.68 ppm for the methane proton α to the hydroxyl functionality. A set of overlapping multiplets, integrating to 30 protons, due to the aliphatic hydrogens of the long alkyl chain, dominated the spectrum.

Table 3. Methanolysis of the cyloadducts (**4a**–**4e**)

Cycloadduct	Yield of (**methyl ester**) %
4a	81 (**5a**)
4b	79 (**5b**)
4c	82 (**5c**)
4d	68 (**5d**)
4e	56 (**5e**)

Scheme 5. Reagents and conditions: (*i*) H_2 (5 atm), Pearlman's catalyst, TFA, MeOH (aq), 48 h.



R = $C_{15}H_{31}$ **(5a)**
R = $C_{13}H_{27}$ **(5b)**
R = $C_{14}H_{29}$ **(5c)**
R = $C_{16}H_{33}$ **(5d)**
R = $C_{17}H_{35}$ **(5e)**

R = $C_{15}H_{31}$ **(6a)**
R = $C_{13}H_{27}$ **(6b)**
R = $C_{14}H_{29}$ **(6c)**
R = $C_{16}H_{33}$ **(6d)**
R = $C_{17}H_{35}$ **(6e)**

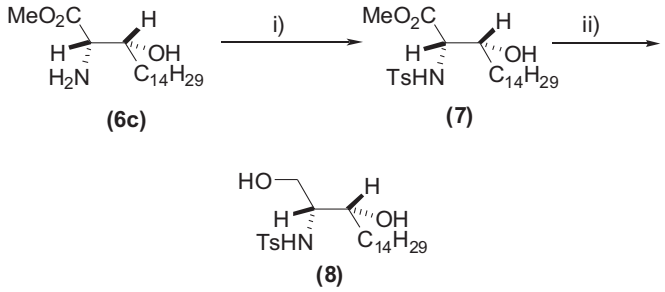
Table 4. Hydrogenolysis of the methyl esters (**5a**–**5e**).

Methyl ester precursor (**5**)	Yield of (**hydroxyamino ester**) (**6**) %
5a	53 (**6a**)
5b	60 (**6b**)
5c	54 (**6c**)
5d	66 (**6d**)
5e	69 (**6e**)

Following the previously developed reaction protocol (11*b*), it was envisaged that the crude hydrolysis reaction mixture would be concentrated and subjected directly to hydrogenolysis at 5 bar (1 bar = 100 kPa) using Pearlman's catalyst and TFA in methanol. The first complication encountered was the insolubility of the crude reaction mixture in methanol. Therefore, to aid solubility, a 10:1 ratio of methanol to ethyl acetate was used. Continuing with the standardized conditions, the amino ester was subjected to hydrogenolysis, but after 48 h there was no evidence of reaction. Gratifyingly, when the hydrolysis products (**5a**–**5e**) were purified by column chromatography prior to hydrogenation, the reactions proceeded efficiently. Presumably, components of the crude reaction mixtures were poisoning the catalyst. A further deviation from the original method when applied to the longer aliphatic chain analogues was the final purification procedure. The original method (11*b*) used ion exchange chromatography to afford the free amino acids as colourless solids in near quantitative yields, but the hexadecanal analogue could not be treated in the same way, as the hydrogenolysis product was insoluble in water, and so more conventional silica gel chromatography was implemented. As a result, the final product was isolated as the methyl ester **6a** (Scheme 5), as opposed to the free β-hydroxy-α-amino acid. In this way, all the long chain hydroxyamino esters (**6a**–**6e**) could be isolated in pure form and in acceptable yields (Table 4). In all cases, detailed

© 2006 NRC Canada

Scheme 6. Reagents and conditions: (*i*) *p*-TsCl, imidazole, DMAP, DCM, 43%; (*ii*) $LiBH_4$, THF, rt, 74%.



spectroscopic analysis showed these final products to be homogeneous with a resonance for the proton α- to the amino group, appearing as a doublet between 3.52 and 3.45 ppm, corresponding to the equivalent proton in the pentanal-derived material (3.45 ppm).

In a further illustrative extension of how these long chain hydroxyamino esters could be converted into *N*-protected sphingosine analogues, **6c** was *N*-tosylated to yield **7** in 43% isolated yield, and this was subsequently reduced to diol **8** in 74% yield using lithium borohydride in THF (Scheme 6).

Conclusions

In conclusion, we have developed protocols in which long chain aliphatic aldehydes will undergo 1,3-dipolar cycloadditions with (5*R*)-5-phenyl-morpholin-2-one to furnish cycloadducts containing three newly defined stereocentres in good yield. Degradation of these cycloadducts affords diastereomerically and enantiomerically pure β-substituted-α-amino acid derivatives, and further modification can furnish sphingosine analogues suitable for coupling to appropriate carbohydrate donors.

Experimental section

General techniques

^{1}H NMR spectra were recorded on either a Bruker AMX 400 NMR (400 MHz) or a Bruker DPX 250 (250 MHz) spectrometer in chloroform-*d* or dimethyl sulfoxide-*d* and referenced to the residual solvent residual proton. Signal positions were recorded in δ ppm with the abbreviations s, d, t, q, quint., br, and m denoting singlet, doublet, triplet, quartet, quintet, broad, and multiplet, respectively. ^{13}C NMR spectra were recorded on the same spectrometers listed above at either 100 or 62.5 MHz, respectively, and were referenced to chloroform-*d* or dimethyl sulfoxide-*d*. All NMR chemical shifts are quoted in ppm.

Infrared spectra were recorded on a PerkinElmer 1720-X. Spectra were analysed as either thin films between sodium chloride plates or as potassium bromide disks.

Mass spectra (*m*/*z*) and accurate mass (HR-MS) were recorded under conditions of electron impact (EI) or chemical ionization using ammonia as the ionizing source (CI). The instrument used was a Fisons VG Autospec mass spectrometer.

Specific rotations ($[\alpha]^{20}_D$) were recorded using the sodium D line (589.3 nm) in the appropriate solvent and are quoted in 10^{-1} deg cm^2 g^{-1}. Solution conentrations are given in the units g 100 mL^{-1}. Readings were measured using a PerkinElmer 341 polarimeter.

Melting points were obtained using a Reichert Kofler heated-stage microscope and are uncorrected. Flash column chromatography was performed according to the method of Still (13) with silica gel 60 (Merck 9385) using head pressure by the means of hand bellows. TLC analyses were carried out using 0.25 mm silica gel precoated aluminium or glass-backed plates with fluorescent indicator UV_{254}. Spots were visualized either by the quenching of UV fluorescence or by staining with an acidic ammonium heptamolydate solution.

Reagents obtained from Acros Organics (Loughborough, UK), Aldrich (Gillingham, UK), Avocado (Heysham, UK), Fluka (Gillingham, UK), and Lancaster fine chemicals (Morecombe, UK) suppliers were used directly as supplied or following purification according to standard procedures. Acetonitrile and dichloromethane were dried by distillation from calcium hydride under nitrogen. Tetrahydrofuran was dried by distillation from sodium-benzophenone ketyl under nitrogen. Petrol refers to light petroleum ether in the boiling point range 30–40 °C, which was fractionally distilled through a Vigreux column prior to use. (5*R*)-5-Phenylmorpholin-2-one was synthesized according to the literature procedure (9). The long chain aldehydes were obtained in quantitative yield from the corresponding commercially available alcohols by oxidation using 4-methylmorpholine-*N*-oxide (1.5 equiv.) and tetra-*n*-propylammonium perruthenate (5 mol%) in dichlorormethane at room temperature in the presence of 4A molecular sieves (14).

General method for preparation of cycloadducts (4a–4e)

The requisite aldehyde (2.2 mmol, 1.1 equiv.) was added to a solution of (5*R*)-5-phenylmorpholin-2-one ((*R*)-(**1**), 1.0 mmol, 1 equiv.) in anhydrous toluene (40 cm^3). The flask was fitted with a magnetic stir.bar, a Soxhlet extractor containing 4A molecular sieves, and a condenser. The reaction mixture was heated to reflux under nitrogen for 5 d. The solvent was removed in *vacuo*, and the resulting pale yellow oil was subjected to column chromatography (diethyl ether – petroleum ether, 1:19) to yield the corresponding cycloadduct.

(2R,6R,7S,9R)-2-Phenyl-7,9-dipentadecyl-1-aza-4,8-dioxabicyclo[4.3.0^{1,6}]nonan-5-one (4a)

Yield 65%; colourless needles; mp 53 to 54 °C. $[\alpha]^{20}_D$ –4.8 (*c* 1.0, $CHCl_3$). IR (KBr disc, cm^{-1}) ν_{max}: 2920, 1730 (lactone C=O). ^{1}H NMR (250 MHz, $CDCl_3$) δ: 0.94 (6H, t, *J* = 6.5, alkyl CH_3), 1.00–1.20 (60H, m, alkyl CH_2), 3.73 (1H, d, *J* = 8.2, H-6), 3.84 (1H, dd, *J* = 3.6, *J*′ = 10.5, H-3$_{eq}$), 4.10 (1H, dt, *J* = 3.3, *J*′ = 9.6, H-7), 4.18 (1H, dd, *J* = 3.5, *J*′ = 10.3, H-2), 4.23 (1H, t, *J* = 10.3, *J*′ = 10.5, H-3$_{ax}$), 4.32–4.26 (1H, m, H-9), 7.37–7.33 (5H, m, Ph-H). ^{13}C NMR (60 MHz, $CDCl_3$) δ: 14.5 (alkyl *C*H$_3$), 23.1, 24.8, 26.6, 29.6, 29.7, 29.8, 29.9, 30.1, 32.3, 35.3, 35.9 (alkyl *C*H$_2$), 60.1 (C-3), 63.7 (C-6), 72.9 (C-2), 79.2 (C-7), 97.3 (C-9), 128.5, 129.1, 129.2, 137.4 (Ar–*C*), 169.8 (C=O). CI-MS *m*/*z* (%): 640 ([M + NH_4]$^+$, 8), 400 (74), 252 (39), 216 (70), 104 (100). HR-MS calcd. for $C_{42}H_{77}O_3N_2$ ([M + NH_4]$^+$): 640.5669; found: 640.5665.

© 2006 NRC Canada

(2R,6R,7S,9R)-2-Phenyl-7,9-ditridecyl-1-aza-4,8-dioxabicyclo[4.3.0$^{1.6}$]nonan-5-one (4b)

Yield 58%; colourless solid; mp 46 to 47 °C. $[\alpha]^{20}_{D}$ –5.0 (*c* 1.0, $CHCl_3$); IR ($CHCl_3$, cm^{-1})ν_{max}: 2955 (Ph–H), 2850 (C–H), 1730 (C=O). ^{1}H NMR (250 MHz, $CDCl_3$) δ: 0.88 (6H, t, *J* = 6.7, alkyl C*H*$_3$), 1.01–1.62 (48H, m, alkyl C*H*$_2$), 3.81 (1H, d, *J* = 8.2, H-6), 3.92 (1H, dd, *J* = 3.5, *J′* = 10.7, H-3$_{eq}$), 4.17 (1H, dt, *J* = 3.2, *J′* = 8.3, H-7), 4.18 (1H, dd, *J* = 3.5, *J′* = 11.4, H-2), 4.26 (1H, dd, *J* = 10.7, *J′* = 11.4, H-3$_{ax}$), 4.31–4.34 (1H, m, H-9), 7.32–7.39 (5H, Ph–H). ^{13}C NMR (60 MHz, $CDCl_3$) δ: 14.1 (alkyl *C*H$_3$), 22.1, 22.7, 24.4, 26.2, 29.2, 29.4, 29.5, 29.6, 29.7, 31.9, 34.9, 35.5, 43.9 (alkyl *C*H$_2$), 59.7 (C-3), 63.3 (C-6), 72.5 (C-2), 78.8 (C-7), 96.9 (C-9), 128.1, 128.3, 128.7, 128.8, 137.1 (Ar–C), 169.4 (C=O). CI-MS *m*/*z* (%): 584 ([MH]$^+$, 24), 372 (100), 216 (44), 104 (47), 68 (27). HR-MS calcd. for $C_{37}H_{66}O_3N$ ([MH]$^+$): 584.5042; found: 584.5052.

(2R,6R,7S,9R)-2-Phenyl-7,9-ditetradecyl-1-aza-4,8-dioxabicyclo[4.3.0$^{1.6}$]nonan-5-one (4c)

Yield 68%; colourless solid; mp 57 to 58 °C. $[\alpha]^{20}_{D}$ –5.7 (*c* 1.0, $CHCl_3$). IR ($CHCl_3$, cm^{-1}) ν_{max}: 2920 (Ph–H), 2850 (C–H), 1730 (C=O). ^{1}H NMR (250 MHz, $CDCl_3$) δ: 0.87 (6H, t, *J* = 6.3, alkyl C*H*$_3$), 1.25–1.65 (52H, m, alkyl C*H*$_2$), 3.81 (1H, d, *J* = 8.2, C-6), 3.92 (1H, dd, *J* = 3.6, *J′* = 10.5, H-3$_{eq}$), 4.16 (1H, dt, *J* = 3.3, *J′* = 8.2, H-7), 4.24 (1H, dd, *J* = 3.6, *J′* = 11.5, H-2), 4.26 (1H, dd, *J* = 10.5, *J′* = 11.5, H-3$_{ax}$), 4.35–4.38 (1H, m, H-9), 7.32–7.39 (5H, m, Ph–H). ^{13}C NMR (60 MHz, $CDCl_3$) δ: 14.5 (alkyl *C*H$_3$), 23.1, 24.8, 26.6, 29.6, 29.8, 29.9, 30.0, 30.1, 32.3, 35.3, 35.9 (alkyl *C*H$_2$), 60.1 (C-3), 63.7 (C-6), 72.9 (C-2), 79.2 (C-7), 97.3 (C-9), 128.5, 129.1, 129.2, 137.5 (Ar–C), 169.8 (C=O). CI-MS *m*/*z* (%): 612 ([MH]$^+$, 10), 386 (100), 216 (47), 81 (27). HR-MS calcd. for $C_{40}H_{70}O_3N$ ([MH]$^+$): 612.5355; found: 612.5368.

(2R,6R,7S,9R)-2-Phenyl-7,9-dihexadecyl-1-aza-4,8-dioxabicyclo[4.3.0$^{1.6}$]nonan-5-one (4d)

Yield 56%; colourless solid; mp 67 to 68 °C. $[\alpha]^{20}_{D}$ –14.1 (*c* 1.0, $CHCl_3$). IR ($CHCl_3$, cm^{-1}) ν_{max}: 2920 (Ph–H), 2850 (C–H), 1730 (C=O). ^{1}H NMR (250 MHz, $CDCl_3$) δ: 0.88 (6H, t, *J* = 6.6, alkyl C*H*$_2$), 1.13–1.70 (64H, m, alkyl C*H*$_2$), 3.81 (1H, d, *J* = 8.2, H-6), 3.92 (1H, dd, *J* = 3.6, *J′* = 10.4, H-3$_{eq}$), 4.18 (1H, dt, *J* = 3.3, *J′* = 8.2, H-2), 4.24 (1H, dd, *J* = 3.6, *J′* = 11.4, H-2), 4.31 (1H, dd, *J* = 10.4, *J′* = 11.4, H-3$_{ax}$), 4.34–4.40 (1H, m, H-9), 7.31–7.40 (5H, m, Ph–H). ^{13}C NMR (60 MHz, $CDCl_3$) δ: 14.5 (alkyl *C*H$_3$), 23.1, 24.8, 26.6, 29.6, 29.7, 29.8, 29.9, 30.0, 30.1, 32.3, 35.3, 35.9 (alkyl *C*H$_2$), 60.1 (C-3), 63.7 (C-6), 72.8 (C-2), 79.2 (C-7), 97.3 (C-9), 128.5, 129.1, 129.2, 137.5 (Ph–H), 169.7 (C=O). CI-MS *m*/*z* (%): 668 ([MH]$^+$, 21), 414 (100), 266 (38), 216 (55), 104 (55). HR-MS calcd. for $C_{44}H_{77}O_3N$ ([MH]$^+$): 668.5981; found: 668.5972.

(2R,6R,7S,9R)-2-Phenyl-7,9-diheptadecyl-1-aza-4,8-dioxabicyclo[4.3.0$^{1.6}$]nonan-5-one (4e)

Yield 62%; colourless solid; mp 65 to 66 °C. $[\alpha]^{20}_{D}$ –9.1 (*c* 1.0, $CHCl_3$). IR ($CHCl_3$, cm^{-1}) ν_{max}: 2920 (Ph–H), 2850 (C–H), 1730 (C=O). ^{1}H NMR (250 MHz, $CDCl_3$) δ: 0.88 (6H, t, *J* = 6.4, alkyl C*H*$_3$), 1.13–1.55 (68H, m, alkyl C*H*$_2$), 3.81 (1H, d, *J* = 8.3, H-6), 3.92 (1H, dd, *J* = 3.6, *J′* = 10.5, H-3$_{eq}$), 4.16 (1H, dt, *J* = 3.5, *J′* = 8.3, H-7), 4.24 (1H, dd, *J* = 3.5, *J′* = 11.4, H-2), 4.31 (1H, dd, *J* = 10.5, *J′* = 11.4, H-3$_{ax}$), 4.34–4.38 (1H, m, H-9), 7.33–7.39 (5H, m, Ph–H). ^{13}C NMR (60 MHz, $CDCl_3$) δ: 14.5 (alkyl *C*H$_3$), 22.7, 23.1, 24.8, 26.6, 29.6, 29.8, 29.9, 30.1, 32.3, 35.3, 35.9 (alkyl *C*H$_2$), 60.1 (C-3), 63.7 (C-6), 72.9 (C-2), 79.2 (C-7), 97.3 (C-9), 128.5, 129.1, 129.2, 137.5 (Ar–C), 169.7 (C=O). CI-MS *m*/*z* (%): 696 ([MH]$^+$, 7), 428 (100), 216 (51), 131 (12), 81 (22). HR-MS calcd. for $C_{46}H_{82}O_3N$ ([MH]$^+$): 696.6294; found: 696.6299.

General procedure for the preparation of amino esters (5a–5e)

Cycloadduct **4** (100 mg) was dissolved in methanol (4 cm^3), and 5 mol/L of hydrochloric acid (1 cm^3) was added. The reaction mixture was heated to reflux and left to stir under nitrogen for 2 h. Saturated sodium carbonate solution (5 cm^3) was added, and the aqueous layer separated and extracted with ethyl acetate (5 × 5 cm^3). The organic phases were combined, washed with brine, dried ($MgSO_4$), filtered, and the excess solvent removed in *vacuo* to give a yellow oil, which was subjected to column chromatography (eluent petrol – diethyl ether, 4:1, then 10% methanol) to afford the corresponding amino ester.

Methyl (2R,3S,1′R)-(2N-2′-hydroxy-1′-phenylethylamino)-3-hydroxyoctadecanoate (5a)

Yield 81%; colourless solid; mp 61 to 62 °C. $[\alpha]^{20}_{D}$ –26.5 (*c* 1.0, MeOH). IR (KBr disc, cm^1) ν_{max}: 3335 (O–H), 2920 (Ar–H), 2850 (C–H), 1740 (C=O). ^{1}H NMR (250 MHz, $CDCl_3$) δ: 0.91 (3H, t, alkyl C*H*$_3$), 1.40–1.18 (26H, m, alkyl C*H*$_2$), 2.00 (2H, bs, NH and OH), 3.17 (1H, d, *J* = 5.3, C*H*CO$_2$CH$_3$), 3.48 (3H, s, CO$_2$C*H*$_3$), 3.66–3.64 (3H, m, C*H*$_2$OH and PhC*H*), 3.75–3.68 (1H, m, C*H*OH), 7.37–7.23 (5H, m, Ph–H). ^{13}C NMR (60 MHz, $CDCl_3$) δ: 14.9 (alkyl *C*H$_3$), 24.2, 27.1, 30.9, 31.0, 31.1, 31.2, 33.5, 35.2 (alkyl *C*H$_2$), 52.5 (CO$_2$*C*H$_3$), 67.2, 67.3 (*C*HCO$_2$CH$_3$ and *C*HOH), 68.0 (*C*H$_2$OH), 74.0 (Ph*C*H), 129.0, 129.4, 129.8, 142.3 (Ar–C), 176.0 (C=O). CI-MS *m*/*z* (%): 450 ([MH]$^+$, 2), 210 (60), 178 (100). HR-MS calcd. for $C_{27}H_{48}O_4N$ ([MH]$^+$): 450.3583; found: 450.3596.

Methyl (2R,3S,1′R)-(2N-2′-hydroxy-1′-phenylethylamino)-3-hydroxyhexadecanoate (5b)

Yield 79%; colourless solid; mp 52 to 53 °C. $[\alpha]^{20}_{D}$ –24.5 (*c* 1.0, MeOH). IR (thin film, cm^{-1}) ν_{max}: 1740 (C=O), 2850 (C–H), 2920 (Ph–H), 3320 br (O–H). ^{1}H NMR (250 MHz, MeOD) δ: 0.80 (3H, t, *J* = 6.3, alkyl C*H*$_3$), 1.19–1.36 (24H, m, alkyl C*H*$_2$), 3.07 (1H, d, *J* = 5.9, C*H*CO$_2$CH$_3$), 3.26 (3H, s, CO$_2$C*H*$_3$), 3.51 (2H, dd, *J* = 4.1, *J′* = 6.9, C*H*$_2$OH), 3.55–3.64 (2H, C*H*Ph and C*H*OH), 7.13–7.20 (5H, m, Ph–*H*). ^{13}C NMR (60 MHz, MeOD) δ: 14.6 (alkyl *C*H$_3$), 24.2, 27.1, 30.9, 31.0, 31.1, 31.2, 33.5, 35.2 (alkyl *C*H$_2$), 52.5 (CO$_2$*C*H$_3$), 67.2 (*C*HCO$_2$CH$_3$), 67.3 (*C*HPh), 68.1 (*C*H$_2$OH), 73.9 (*C*HOH), 129.1, 129.4, 129.8, 142.4 (Ar–*C*), 176.1 (*C*=O). CI-MS *m*/*z* (%): 422 ([MH]$^+$, 4), 210 (91), 178 (100), 118 (19). HR-MS calcd. for $C_{25}H_{44}O_4N$ ([MH]$^+$): 422.3270; found: 422.3274.

Methyl (2R,3S,1′R)-(2N-2′-hydroxy-1′-phenylethylamino)-3-hydroxyheptadecanoate (5c)

Yield 82%; colourless solid; mp 56 to 57.5 °C. $[\alpha]^{20}_{D}$ –23.6 (*c* 1.0, MeOH). IR (thin film, cm^{-1}) ν_{max}: 3370 (O–H),

© 2006 NRC Canada

3025 (Ar–H), 2870 (C–H), 1735 (C=O). ^{1}H NMR (250 MHz, $CDCl_3$) δ: 0.86 (3H, t, *J* = 7.0, CH_2CH_3), 1.25–1.41 (6H, m, alkyl CH_2), 3.12 (1H, d, *J* = 6.0, $CHCO_2CH_3$), 3.29 (3H, s, CO_2CH_3), 3.51–3.69 (4H, m, CH_2OH, PhC*H*, C*H*OH), 7.13–7.39 (5H, m, Ph–H). ^{13}C NMR (60 MHz, $CDCl_3$) δ: 14.8 (alkyl CH_3), 24.0, 29.4, 34.9 (alkyl CH_3), 52.5 (CO_2CH_3), 67.3, 67.4 ($CHCO_2CH_3$ and C*H*OH), 68.1 (CH_2OH), 73.9 (Ph*C*H), 129.1, 129.4, 129.8, 142.2 (Ar–C), 176.1 (C=O). CI-MS *m/z* (%): 296 ([MH]$^+$, 75), 264 (47), 210 (38), 178 (100), 118 (35). HR-MS calcd. for $C_{16}H_{26}O_4N$ ([MH]$^+$): 296.1862; found: 296.1864.

*Methyl (2**R**,3**S**,1′**R**)-(2**N**-2′-hydroxy-1′-phenylethylamino)-3-hydroxynonadecanoate (5d)*

Yield 68%; colourless solid; mp 64–65.5 °C. $[\alpha]^{20}_D$ –21.7 (*c* 1.0, $CHCl_3$). IR (KBr disc, cm^1) ν_{max}: 3351 (O–H), 2920 (Ar–H), 2855 (C–H), 1740 (C=O). ^{1}H NMR (250 MHz, MeOD) δ: 0.80 (3H, t, *J* = 6.2 alkyl CH_3), 1.36–1.19 (28H, m, alkyl CH_2), 3.07 (1H, d, *J* = 5.9, $CHCO_2CH_3$), 3.25 (3H, s, CO_2CH_3), 3.48–3.51 (3H, m, CH_2OH and PhC*H*), 3.56–3.64 (1H, m, C*H*OH), 7.12–7.20 (5H, m, Ph-H). ^{13}C NMR (60 MHz, MeOD) δ: 14.9 (alkyl CH_3), 24.2, 27.1, 30.9, 31.0, 31.1, 31.2, 33.5, 35.2 (alkyl CH_2), 52.5 (CO_2CH_3), 67.2, 67.3 ($CHCO_2CH_3$ and *C*HOH), 68.1 (CH_2OH), 74.0 (Ph*C*H), 129.1, 129.4, 129.8, 142.4 (Ar–C), 176.1 (C=O). CI-MS *m/z* (%): 446 ([MH]$^+$-H_2O, 9), 414 (19), 210 (10), 178 (100), 118 (15). HR-MS calcd. for $C_{28}H_{49}O_3N$ ([MH]$^+$-H_2O): 446.3634; found: 446.3448.

*Methyl (2**R**,3**S**,1′**R**)-(2**N**-2′-hydroxy-1′-phenylethylamino)-3-hydroxyicosanoate (5e)*

Yield 56%; colourless solid; mp 59–61 °C. $[\alpha]^{20}_D$ –23.8 (*c* 1.0, $CHCl_3$). IR ($CHCl_3$, cm^1) ν_{max}: 3315 (O-H), 2920 (Ar–H), 2850 (C–H), 1740 (C=O). ^{1}H NMR (250 MHz, MeOD) δ: 0.80 (3H, t, *J* = 6.2, alkyl CH_3), 1.19–1.36 (30H, m, alkyl CH_2), 3.07 (1H, d, *J* = 5.9, $CHCO_2CH_3$), 3.26 (3H, s, CO_2CH_3), 3.48–3.51 (3H, m, CH_2OH and PhC*H*), 3.56–3.62 (1H, m, C*H*OH), 7.13–7.20 (5H, m, Ph-H). ^{13}C NMR (60 MHz, MeOD) δ: 14.9 (alkyl CH_3), 24.2, 27.1, 30.9, 31.0, 31.1, 31.2, 33.5, 35.2 (alkyl CH_2), 52.5 (CO_2CH_3), 67.2, 67.3 ($CHCO_2CH_3$ and *C*HOH), 68.1 (CH_2OH), 74.0 (Ph*C*H), 129.1, 129.4, 129.8, 142.4 (Ar–C), 176.1 (C=O). CI-MS *m/z* (%): 460 ([MH]$^+$-H_2O, 12), 428 (76), 268 (16), 216 (25), 178 (100), 104 (37). HR-MS calcd. for $C_{29}H_{50}O_3N$ ([MH]$^+$-H_2O): 460.3790; found: 460.3799.

General method for the preparation of long chain amino acid methyl esters (6a–6e)

Amino ester (1 equiv.) was dissolved in methanol, and water (10:1) and Pearlman's catalyst were added (weight for weight of amino ester) followed by the addition of trifluoroacetic acid (1 equiv.). The system was degassed and hydrogen introduced. The system was once again degassed and hydrogen re-introduced. The reaction mixture was warmed to 50 °C and left to stir for 16 h. The hydrogen was released, and the reaction mixture filtered through Celite® and the filtrate concentrated in *vacuo*. The residue was subjected to column chromatography (eluent petrol – diethyl ether, 1:1, then 10% methanol) to afford the amino acid methyl ester.

*Methyl (2**R**,3**S**)-2-amino-3-hydroxyoctadecanoate (6a)*

Yield 53%; colourless solid; mp 74–76.5 °C. $[\alpha]^{20}_D$ –10.5 (*c* 1.0, $CHCl_3$). IR ($CHCl_3$, cm^{-1}) ν_{max}: 3355 (N–H), 3130 (O–H), 2915, 2840 (C–H), 1720 (C=O). ^{1}H NMR (250 MHz, D_6 acetone) δ: 0.82 (3H, t, *J* = 6.4 alkyl CH_3), 1.19–1.38 (28H, m, alkyl CH_2), 3.45 (1H, d, *J* = $CHNH_2$), 3.53 (3H, s, $COOCH_3$), 3.62–3.74 (1H, m, C*H*OH). ^{13}C NMR (60 MHz, D_6 acetone) δ: 14.8 (alkyl CH_3), 23.7, 27.3, 29.3, 33.0, 36.2 (alkyl CH_2), 52.9 ($COOCH_3$), 66.2 ($CHNH_2$), 81.5 (*C*HOH), 173.7 (C=O).

*Methyl (2**R**,3**S**)-2-amino-3-hydroxyhexadecanoate (6b)*

Yield 60%; colourless solid; mp 61–63 °C. $[\alpha]^{20}_D$ –14.3 (*c* 1.0, $CHCl_3$). IR ($CHCl_3$, cm^{-1}) ν_{max}: 3345 (O–H), 2920, 2850 (C–H), 1680 (C=O). ^{13}C NMR (250 MHz, D_6 acetone) δ: 0.75 (3H, t, *J* = 6.5, alkyl CH_3, 1.16–1.40 (24H, m, alkyl CH_2), 3.52 (1H, d, *J* = 7.7, $CHNH_2$), 3.60 (3H, s, CO_2CH_3), 3.64–3.72 (1H, m, C*H*OH). ^{13}C NMR (60 MHz, D_6 acetone) δ: 14.8 (alkyl CH_3), 23.7, 27.3, 29.3, 31.1, 33.0, 36.2 (alkyl CH_2),52.9 ($COOCH_3$), 66.1 ($CHNH_2$), 81.5 (*C*HOH), 173.5 (C=O). CI-MS *m/z* (%): 302 ([MH]$^+$, 89), 242 (10), 89 (100). HR-MS calcd. for $C_{17}H_{36}O_3N$ ([MH]$^+$): 302.2695; found: 302.2708.

*Methyl (2**R**,3**S**)-2-amino-3-hydroxyheptadecanoate (6c)*

Yield 54%; colourless solid; mp 75–77.5 °C. $[\alpha]^{20}_D$ –16.8 (*c* 1.0, $CHCl_3$). IR ($CHCl_3$, cm^{-1}) ν_{max}: 3135 (O–H), 2915, 2845 (C–H), 1735 (C=O). ^{1}H NMR (250 MHz, D_6 acetone) δ: 0.75 (3H, t, *J* = 6.4, alkyl CH_3), 1.25–1.45 (26H, m, alkyl CH_2), 3.48 (1H, d, *J* = 7.7, $CHNH_2$), 3.57 (3H, s, $COOCH_3$), 3.59–3.70 (1H, m, C*H*OH). ^{13}C NMR (60 MHz, D_6 acetone) δ: 14.8 (alkyl CH_3), 23.7, 27.3, 28.2, 33.0, 36.3 (alkyl *C*H), 52.8 ($COOCH_3$), 66.4 ($CHNH_2$), 81.7 (*C*HOH), 173.6 (C=O). CI-MS *m/z* (%): 316 ([MH]$^+$, 100), 256 (10), 89 (50). HR-MS calcd. for $C_{18}H_{38}O_3N$ ([MH]$^+$): 316.2852; found: 316.2847.

*Methyl (2**R**,3**S**)-2-amino-3-hydroxynonadecanoate (6d)*

Yield 66%; colourless solid; mp 84–86.5 °C. $[\alpha]^{20}_D$ –6.1 (*c* 1.0, $CHCl_3$). IR ($CHCl_3$, cm^{-1}) ν_{max}: 3130 (O–H), 1720 (C=O). ^{1}H NMR (250 MHz, acetone) δ: 0.75 (3H, t, *J* = 6.2, alkyl CH_3), 1.24–1.53 (30H, m, alkyl CH_2), 2.76 (3H, br s, NH_2 and O*H*), 3.47 (1H, d, *J* = 7.7, $CHNH_2$), 3.62 (3H, s, $COOCH_3$), 3.63–3.67 (1H, m, C*H*OH). ^{13}C NMR (60 MHz, D_6 acetone) δ: 14.7 (alkyl CH_3), 23.7, 27.3, 33.0, 36.3 (alkyl CH_2), 52.8 ($COOCH_3$), 66.3 ($CHNH_2$), 81.6 (*C*HOH), 173.6 (C=O). CI-MS *m/z* (%): 326 ([MH]$^+$-H_2O, 69), 266 (18), 115 (100), 82 (13), 56 (25). HR-MS calcd. for $C_{20}H_{39}O_2N$ ([MH]$^+$-H_2O): 326.3059; found: 326.3043.

*Methyl (2**R**,3**S**)-2-amino-3-hydroxyicosanoate (6e)*

Yield 69%; colourless solid; mp 86 to 87 °C. $[\alpha]^{20}_D$ –7.1 (*c* 1.0, $CHCl_3$). IR ($CHCl_3$, cm^{-1}) ν_{max}: 3140 (O–H), 2915, 2845 (C–H), 1720 (C=O). ^{1}H NMR (250 MHz, D_6 acetone) δ: 0.75 (3H, t, *J* = 6.2, alkyl CH_3), 1.28–1.54 (32H, m, alkyl CH_2), 2.76 (3H, br s, NH_2 and O*H*), 3.47 (1H, d, *J* = 7.7, $CHNH_2$), 3.59 (3H, s, $COOCH_3$), 3.62–3.65 (1H, m, C*H*OH). ^{13}C NMR (60 MHz, D_6 acetone) δ: 14.8 (alkyl CH_3), 23.7, 27.3, 33.0, 36.3 (alkyl CH_2), 52.8 ($COOCH_3$), 66.3 ($CHNH_2$), 81.6 (*C*HOH), 173.6 (C=O). CI-MS *m/z* (%): 358 ([MH]$^+$, 26), 90 (100). HR-MS calcd. for $C_{21}H_{44}NO_3$ ([MH]$^+$): 358.3321; found: 358.3313.

© 2006 NRC Canada

Methyl (2*R*,3*S*)-3-hydroxy-2-(toluenesulfonylamino)heptadecanoate (7)

Amino ester **6c** (74 mg, 0.0.23 mmol) was dissolved in anhydrous dichloromethane (5 cm^3), and freshly recrystallized *p*-toluenesulfonyl chloride (45 mg, 0.23 mmol, 1 equiv.) was added followed by dimethylaminopyridine (2 drops). The reaction mixture was left to stir under an atmosphere of nitrogen for 16 h. Water was added (5 cm^3), the organic layer was separated, and the aqueous phase extracted with dichloromethane (5 × 10 cm^3). The organic fractions were combined, dried ($MgSO_4$), filtered, and the solvent removed in *vacuo*. The residue was purified by column chromatography, eluting with dichloromethane–acetone (10:1), to afford the title compound as a colourless solid (47 mg, 43%), mp 85 to 86 °C. $[\alpha]^{20}_D$ –15.3 (*c* 1.0, $CHCl_3$). IR ($CHCl_3$, cm^{-1}) ν_{max}: 3400 (O–H), 2910, 2840 (C–H), 1710 (C=O), 1165 (SO_2). ^{1}H NMR (250 MHz, $CDCl_3$) δ: 0.81 (3H, t, *J* = 6.4, alkyl CH_3), 1.19–1.47 (26H, m, alkyl CH_2), 2.22 (1H, br s, O–H), 2.34 (3H, s, Ph–CH_3), 3.45 (3H, s, COOCH_3), 3.80–3.85 (2H, m, C*H*OH, C*H*NHTs), 5.58 (1H, d, *J* = 9.6, N*H*PhCH$_3$), 7.21 (2H, d, *J* = 8.4, *m*-Ph–H), 7.65 (2H, d, *J* = 8.4, *o*-Ph–H). ^{13}C NMR (60 MHz, $CDCl_3$) δ: 14.5 (alkyl *C*H$_3$), 21.9 (Ph–*C*H$_3$), 23.1, 25.8, 29.8, 29.9, 30.0, 30.1, 30.1, 32.3, 34.0 (alkyl *C*H$_2$), 53.0 (COO*C*H$_3$), 59.9 (*C*HNHTs), 72.8 (*C*HOH), 127.6 (*m*-Ar–C), 129.9 (*o*-Ar–C), 137.3 (*p*-Ar–C), 144.0 (*i*-Ar–C), 171.5 (C=O).

(2*S*,3*R*)-2-(Toluenesulfonylamino)heptadecan-1,3-diol (8)

The *N*-protected amino ester **7** (49 mg, 0.098 mmol) was dissolved in anhydrous THF (5 cm^3), and lithium borohydride (2 mg, 0.36 mmol) was added. The reaction mixture was left to stir under nitrogen for 16 h. Water (5 cm^3) was added, the organic phase separated, and the aqueous phase extracted with ethyl acetate (5 × 5 cm^3). The organic fractions were combined, dried ($MgSO_4$), filtered, and the solvent removed in *vacuo*, to afford the title compound as a colourless solid (32 mg, 74%), mp 80 to 81 °C. $[\alpha]^{20}_D$ +10.6 (*c* 1.0, $CHCl_3$). IR ($CHCl_3$, cm^{-1}) ν_{max}: 3415 (O–H), 2910, 2840 (C–H), 1160 (SO_2). ^{1}H NMR (250 MHz, $CDCl_3$) δ: 0.81 (3H, t, *J* = 6.3, alkyl CH_3), 1.04–1.27 (26H, m, alkyl CH_2), 2.35 (3H, s, Ph–CH_3), 2.87 (1H, br s, O–H), 3.09–3.16 (1H, m, C*H*NHTs), 3.64 (2H, d, *J* = 3.7, CH_2OH), 3.71–3.79 (1H, m, C*H*OH), 5.57 (1H, d, *J* = 7.9, N*H*Ts), 7.22 (2H, d, *J* = 8.2, *m*-Ph–H), 7.71 (2H, d, *J* = 8.2, *o*-Ph–H). ^{13}C NMR (60 MHz, $CDCl_3$) δ: 13.1 (alkyl *C*H$_3$), 20.5 (Ph–*C*H$_3$), 21.7, 24.4, 28.4, 28.5, 28.7, 28.7, 30.9, 32.8 (alkyl *C*H$_2$), 55.7 (*C*HNHTs), 64.4 (*C*H$_2$OH), 72.2 (*C*HOH), 126.1 (*o*-Ph–H), 128.7 (*m*-Ph–H), 136.6 (*p*-Ph–H), 142.5 (*i*-Ph–H). CI-MS *m*/*z* (%): 442 ([MH]$^+$, 100), 410 (15), 213 (15), 91 (7), 60 (10). HR-MS calcd. for $C_{24}H_{44}O_4SN$ ([MH]$^+$): 442.2991; found: 442.2979.

Acknowledgements

We are grateful to the University of Reading's Research Endowment Trust Fund for their financial support (studentship to VAB).

References

1. (*a*) V. Constantino, E. Fattorusso, and A. Mangoni. Tetrahedron, **52**, 1573 (1996); (*b*) T. Natori, M. Morita, K. Akimoto, and Y. Koezuka. Tetrahedron, **50**, 2771 (1994); (*c*) V. Constantino, E. Fattorusso, and A. Mangoni. Liebigs Ann. 2133 (1995); (*d*) U.V. Babu, S.P.S. Bhandari, and H.S. Garg. J. Nat. Prod. **60**, 732 (1997); (*e*) V. Constantino, E. Fattorusso, M. Menna, and O. Taglialatela-Scafati. Curr. Med. Chem. **11**, 1671 (2004); (*f*) V. Costantino, E. Fattorusso, C. Imperatore, and A. Mangoni. J. Org. Chem. **69**, 1174 (2004).
2. (*a*) H. Fukushima, Y. Koezuka, K. Motoki, M. Nakijima, T. Natori, T. Shimzu, A. Uchimura, and E. Ueno. Bioorg. Med. Chem. **5**, 1447 (1997); (*b*) V. Constatino, E. Fattorusso, A. Mangoni, M. Di Rosa, and A. Ianaro. Tetrahedron, **56**, 1393 (2000).
3. (*a*) R. Ishida, H. Shirahama, and T. Matsumoto. Chem. Lett. 9 (1993); (*b*) V. Constantino, E. Fattorusso, A. Mangoni, M. Di Rosa, and A. Ianaro. J. Am. Chem. Soc. **119**, 12465 (1997); (*c*) R. Durán, E. Zubía, M.J. Ortega, S. Naranjo, and J. Salvá. Tetrahedron, **54**, 14597 (1998); (*d*) V. Constantino, E. Fattorusso, A. Mangoni, M. Di Rosa, and A. Ianaro. Bioorg. Med. Chem. Lett. **9**, 271 (1999); (*e*) B. Zhang and F.L. Kiechle. Ann. Clin. Lab. Sci. **34**, 3 (2004); (*f*) M. Bektas and S. Spiegel. Glycoconjugate J. **20**, 39 (2003); (*g*) V. Costantino, M. D'Esposito, E. Fattorusso, A. Mangoni, N. Basilico, S. Parapini, and D. Taramelli. J. Med. Chem. **48**, 7411 (2005).
4. For representative reviews see: (*a*) P.M. Koskinen and A.M.P. Koskinen. Synthesis, 1075 (1998); (*b*) H. Gaubius and S. Gaubius. Glycosciences. Chapman and Hall, Weinheim. 1997; (*c*) T. Kolter and K. Sandhoff. Chem. Soc. Rev. **25**, 371 (1996); (*d*) Y.D. Vankar and R.R. Schmidt. Chem. Soc. Rev. **29**, 201 (2000).
5. C.A. Grob and F. Gadient. Helv. Chim. Acta, **40**, 1145 (1957).
6. (*a*) K. Koike, Y. Nakahara, and T. Ogawa. Agric. Biol. Chem. **54**, 663 (1990); (*b*) J. Gigg and R. Gigg. J. Chem. Soc. C, 1872 (1966); (*c*) R.R. Schmidt and P. Zimmermann. Tetrahedron Lett. **27**, 481 (1986); (*d*) R.R. Schmidt and T. Maier. Carbohydr. Res. **174**, 169 (1988); (*e*) P. Kumar and R.R. Schmidt. Synthesis, 33 (1997); (*f*) R. Wild and R.R. Schmidt. Tetrahedron: Asymmetry, **5**, 2195 (1994); (*g*) M. Kiso, A. Nakamura, Y. Tomita, and A. Hasegawa. Carbohydr. Res. **158**, 101 (1986); (*h*) K. Koike, M. Numata, M. Sugimoto, Y. Nakahara, and T. Ogawa. Agric. Biol. Chem. **54**, 663 (1990); (*i*) H. Hirata, Y. Yamagiwa, and T. Kamikawa. J. Chem. Soc. Perkin Trans. 1, 2279 (1991); (*j*) T. Mirkami, H. Minamikawa, and M. Hato. Tetrahedron Lett. **35**, 745 (1994); (*k*) J.W. Cornforth, R.H. Cornforth, and K.K. Mathew. J. Chem. Soc. 112 (1959); (*l*) M. Obayashi and M. Schlosser. Chem. Lett. 1715 (1985); (*m*) J.S. Yadav, D. Vidyanand, and D. Rajogopal. Tetrahedron Lett. **34**, 1191 (1993); (*n*) Y.L. Li, X.L. Sun, and Y.L. Wu. Tetrahedron, **50**, 10727 (1994); (*o*) D.H. Ball. J. Org. Chem. **31**, 220 (1966); (*p*) R.R. Scmidt, T. Bär, and R. Wild. Synthesis, 868 (1995).
7. (*a*) H. Newman. J. Am. Chem. Soc. **95**, 4098 (1993); (*b*) T.L. Cupps, R.H. Boutin, and H. Rapoport. J. Org. Chem. **50**, 3972 (1985); (*b*) R.H. Boutin and H. Rapoport. J. Org. Chem. **51**, 5320 (1996); (*c*) P. Garner, J.M. Park, and E. Malecki. J. Org. Chem. **53**, 4395 (1988); (*d*) S. Nimkar, D. Menaldino, A.H. Merrill, and D. Liotta. Tetrahedron Lett. **29**, 3037 (1988); (*e*) P. Herold. Helv. Chim. Acta, **71**, 354 (1988); (*g*) A.M.P. Koskinen and P.M. Koskinen. Tetrahedron Lett. **34**, 6765 (1993).

© 2006 NRC Canada

8. R.O. Duthaler. Tetrahedron, **50**, 1539 (1994).
9. (*a*) J.F. Dellaria, Jr. and B.D. Santarsiero. Tetrahedron Lett. **29**, 6079 (1988); (*b*) J.F. Dellaria, Jr. and B.D. Santarsiero. J. Org. Chem. **54**, 3916 (1989).
10. (*a*) A.S. Anslow, L.M. Harwood, H. Phillips, and D. Watkin. Tetrahedron: Asymmetry, **2**, 169 (1991); (*b*) A.S. Anslow, L.M. Harwood, H. Phillips, and D. Watkin. Tetrahedron: Asymmetry, **2**, 997 (1991); (*c*) A.S. Anslow, L.M. Harwood, H. Phillips, D. Watkin, and L.F. Wong. Tetrahedron: Asymmetry, **2**, 1343 (1991); (*d*) L.M. Harwood, A.C. Manage, S. Robin, S.F.G. Hopes, D.J. Watkin, and C.E. Williams. Synlett, 777 (1993).
11. (*a*) L.M. Harwood, J. Macro, D. Watkin, C.E. Williams, and L.F. Wong. Tetrahedron: Asymmetry, **3**, 1127 (1992); (*b*) D. Alker, G. Hamblett, L.M. Harwood, S.M. Robertson, D.J. Watkin, and C.E. Williams. Tetrahedron, **54**, 6089 (1998).
12. L.M. Harwood and S.M. Robertson. J. Chem. Soc. Chem. Commun. 2641 (1998).
13. W.C. Still, M. Khan, and A. Mitra. J. Org. Chem. **43**, 2923. (1978).
14. (*a*) W.P. Griffith, S.V. Ley, G.P. Whitcombe, and A.D. White. J. Chem. Soc. Chem. Commun. 1625 (1987); (*b*) W.P. Griffith and S.V. Ley. Aldrichimica Acta, **23**, 13 (1990); (*c*) S.V. Ley, J. Norman, W.P. Griffith, and S.P. Marsden. Synthesis, 639 (1994).

© 2006 NRC Canada

Intramolecular [4 + 3] cycloadditions — Stereochemical issues in the cycloaddition reactions of cyclopentenyl cations — A synthesis of (+)-dactylol[1]

Michael Harmata, Paitoon Rashatasakhon, and Charles L. Barnes

Abstract: Five cyclopentanones were prepared for the purpose of examining the effects of stereogenic centers on the course of the intramolecular [4 + 3] cycloaddition reactions of cyclopentenyl cations. One substrate reacted with very high levels of diastereoselectivity and was converted to (+)-dactylol. The cyclopentenone without stereogenic centers on the tether or the five-membered ring gave two cycloadducts, the endo isomer being only slightly favored over the exo. Other substrates reacted with generally good to poor stereoselectivity. An epimer of the substrate leading to (+)-dactylol afforded all possible isomers of the cycloadduct with relatively poor stereoselectivity.

Key words: cycloaddition, total synthesis, dactylol.

Résumé : On a préparé cinq cyclopentanones dans le but d'examiner les effets des centres stéréogènes sur le cours des réactions de cycloaddition [4 + 3] intramoléculaires des cations cyclopentényles. Un substrat réagit avec des degrés élevés de diastéréosélectivité et conduit à la formation du (+)-dactylol. La cyclopenténone sans centres stéréogènes sur la chaîne latérale ou sur le cycle à cinq chaînons conduit à la formation de deux cycloadduits dans lesquels l'isomère endo est légèrement favorisé par rapport à l'isomère exo. D'autres substrats réagissent avec des stéréosélectivités qui vont généralement de bonnes à mauvaises. Un épimère du substrat qui conduit au (+)-dactylol a permis d'isoler tous les isomères possibles du cycloadduit avec une stéréosélectivité relativement faible.

Mots clés : cycloaddition, synthèse totale, dactylol.

[Traduit par la Rédaction]

Introduction

The intramolecular [4 + 3] cycloaddition reaction of allylic cations and dienes has been shown to be a powerful route to polycyclic compounds (1). One variation on this theme involves the use of cyclic cations in the cycloaddition reaction. Appropriate modifications of the cycloadducts from such reactions can then provide useful routes to natural products (2). We and others realized the potential for this process in the context of the synthesis of cyclooctanoids (3). We recently reported a total synthesis of (+)-dactylol based on this chemistry (2*c*). This report is a more detailed description of that work, including studies to evaluate the effects of various stereocenters on the course of the cycloaddition reaction.

Received 1 September 2005. Accepted 4 December 2005. Published on the NRC Research Press Web site at http://canjchem.nrc.ca on 8 November 2006.

M. Harmata,[2] P. Rashatasakhon, and C.L. Barnes. Department of Chemistry, University of Missouri-Columbia, Columbia, MO 65211, USA.

[1]This article is part of a Special Issue dedicated to Dr. Alfred Bader.

[2]Corresponding author (e-mail: harmatam@missouri.edu).

Results and discussion

Diene synthesis

The basic approach for the preparation of substrates for this study consisted of the alkylation of cyclopentanone enolates with diene-containing electrophiles. The synthesis of the dienes used is shown in Scheme 1. Treatment of **1a**–**1c** with $TMSCH_2MgCl$–$CeCl_3$ followed by iodide formation afforded **3a**–**3c** in excellent yields (4, 5).

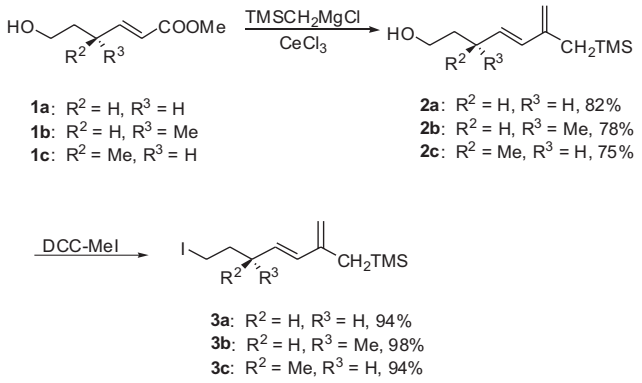
Ester **1a** was prepared by a literature procedure (6). Esters **1b** and **1c** were prepared as shown in Scheme 2. Protection of 1,4-butanediol with allyl bromide followed by oxidation gave the acid **5** in 69% yield from **4**. Oxazolidinones were formed from **5** in standard fashion and alkylated with high stereoselectivity and in good yields to afford **6b** and **6c**. Reduction with LAH gave the alcohols **7b** and **7c** in excellent yields. Swern oxidation, Wittig homologation, and deprotection (7) afforded esters **1b** and **1c** in 81% and 77% yields, respectively.

Preparation of cycloaddition substrates

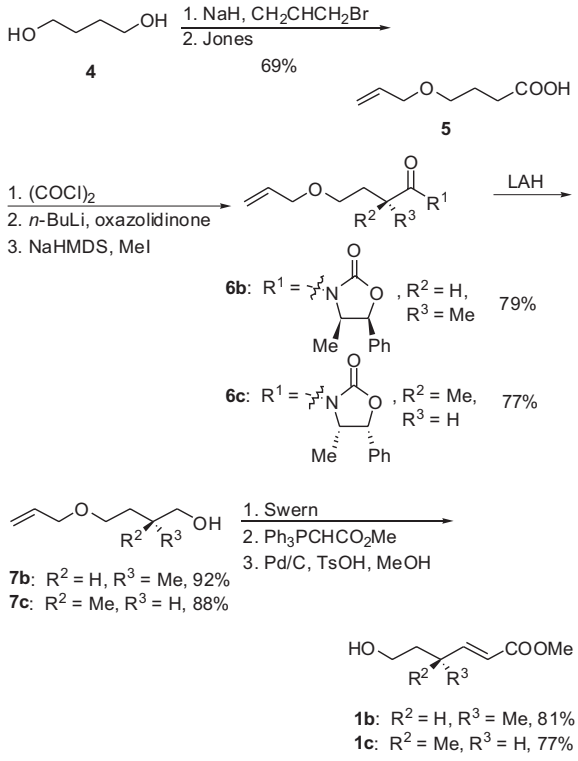
Cycloaddition substrates were easily prepared by alkylation. For example, the reaction of **8** with potassium carbonate in the presence of **3a** afforded the alkylation product **9** in good yield. This was converted to the ketone **11** in 66% yield via reaction with potassium cyanide in hot DMSO

 doi:10.1139/V06-122 © 2006 NRC Canada

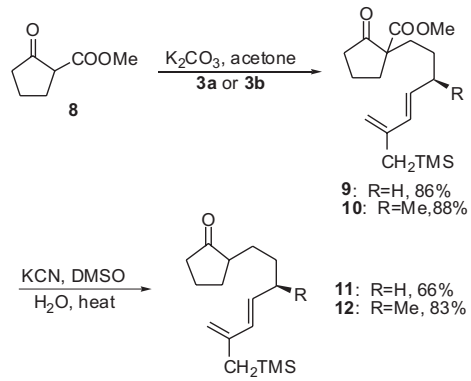
Scheme 1.



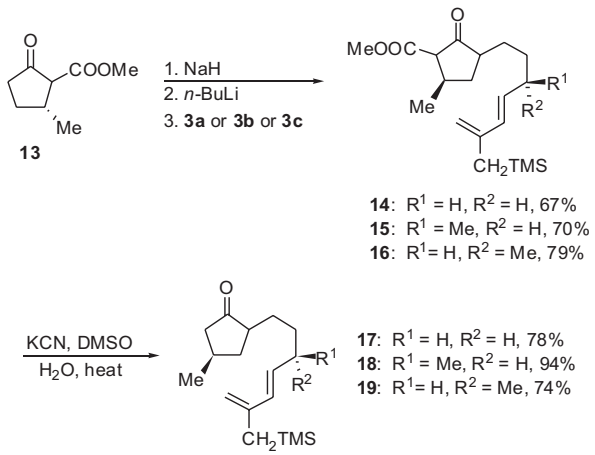
Scheme 2.



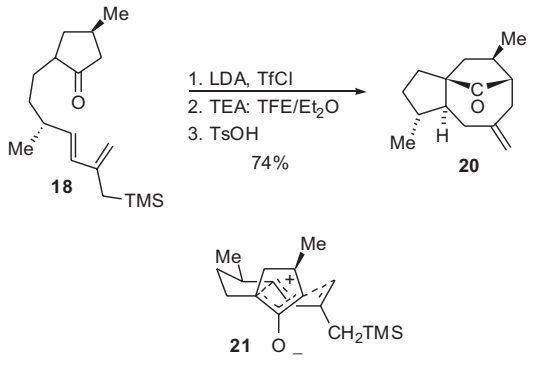
Scheme 3.



Scheme 4.



Scheme 5.



(8). Ketone **12** was prepared in a similar fashion in 73% overall yield (Scheme 3).

The ketoester **13** was readily prepared from (*R*)-pulegone by a known procedure (9). Dianion formation followed by alkylation and decarboalkoxylation afforded cycloaddition substrates **17**–**19**, as shown in Scheme 4.

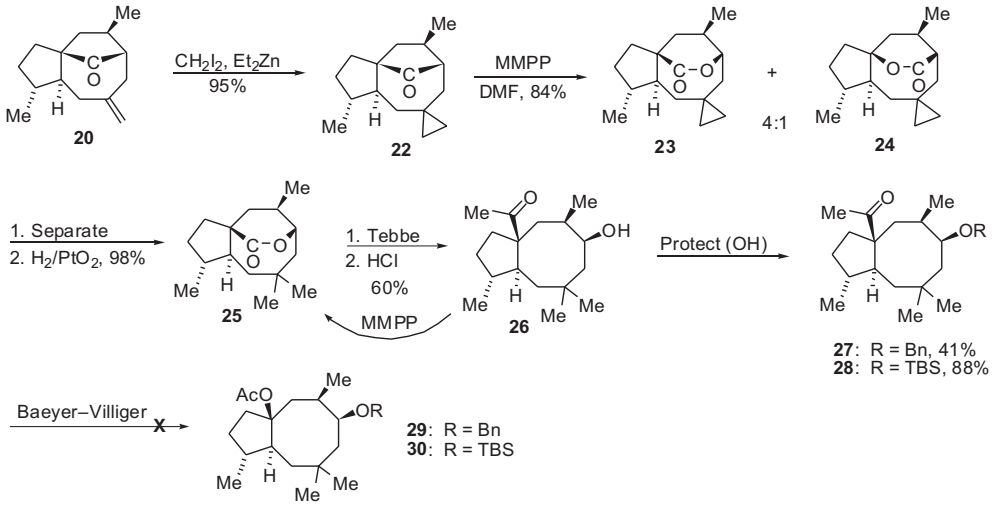
The synthesis of (+)-dactylol

We begin with the synthesis of dactylol, since that was indeed the first cycloaddition in this series that we examined. Treatment of **18** with Lithium diisopropylamide (LDA) and reacting the resultant enolate with triflyl chloride gave an α-chloroketone. This was not characterized but immediately subjected to typical cycloaddition conditions: stirring at –78 °C to room temperature in a 1:1 mixture of ether and trifluoroethanol in the presence of 3 equiv. of triethylamine (Scheme 5). Even though the purification of the cycloadduct could be carried out at this stage, we found that some desilylation and double bond migration occurred during the chromatography on silica gel.

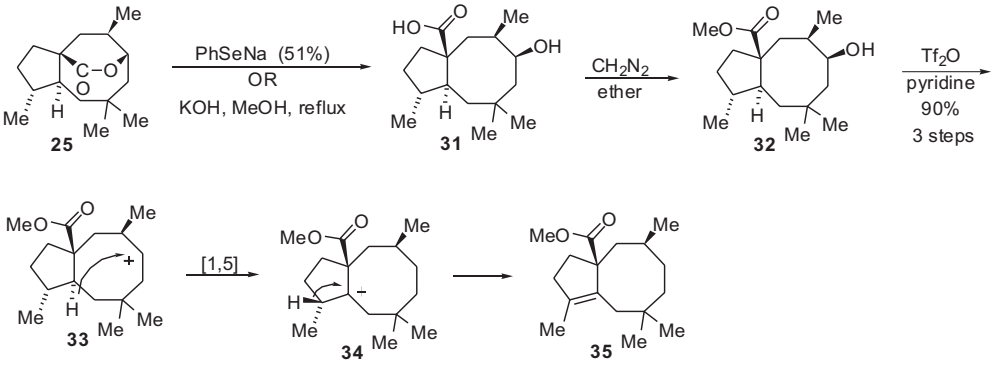
Therefore, the crude product was subsequently treated with tosic acid to give rise to alkene **20** as a 25:1 mixture of isomers in 74% yield for the three steps. The diastereomeric ratio was determined by GC and integration of the olefinic region of the ^{1}H NMR of a crude product mixture. The minor isomer has not been characterized. The rationalization for the favorable stereochemical outcome is depicted in structure **21**. We anticipated that the diene would approach the dienophile in an endo fashion on the less-hindered face of the dienophile. In addition, the methyl group on the tether

© 2006 NRC Canada

Scheme 6.



Scheme 7.



would occupy a pseudoequatorial orientation on the puckered, incipient five-membered ring with the diene oriented so as to minimize gauche interactions.

The next stage of the synthesis is shown in Scheme 6. Simmons–Smith cyclopropanation of **20** produced **22** in 95% yield. The Baeyer–Villiger reaction of **22** with MMPP in DMF afforded a 4:1 mixture of two regioisomers after purification. Surprisingly, the major product was that resulting from the migration of the less substituted carbon atom. Attempts to alter the regioselectivity using a variety of reaction conditions were unsuccessful, as some reagents gave higher regioselectivity but lower yields of the products.[3] Studies we have conducted suggest that the methyl substituent on the five-membered ring has a major, but not exclusive, influence on the regiochemistry of the reaction (10). The major isomer **23** was separated, and the cyclopropane ring was cleaved by hydrogenolysis to afford **25** in 98% yield. The structure and relative stereochemistry were established by X-ray crystallography.

Our first attempt to convert **25** into dactylol began with a methylenation reaction using Tebbe's reagent (11). Hydrolysis of the resultant enol ether afforded the ketone **26**, whose hydroxy group could be protected with either a benzyl or TBS group. We anticipated that a Baeyer–Villiger oxidation of either of these species would afford the corresponding acetate **29** or **30**.[4] Unfortunately, no reaction occurred between either **27** or **28** and MMPP, *m*-CPBA, or TFAA-H_2O_2 after a 24 h period at room temperature. Treatment of **26** with MMPP afforded lactone **25** (10). We also attempted a reaction between lactone **25** and sodium phenylselenide and expected to obtain a system suitable for further elaboration to (+)-dactylol. However, the hydroxy acid **31** was obtained as the sole product in 51% yield, via an apparent hydrolysis reaction. Even though this result was not satisfactory, it proved the existence and stability of the hydroxycarboxylic acid **31**, which became significant.

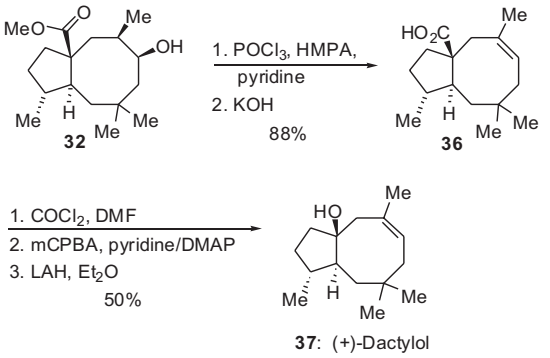
Thus, the next sequence to (+)-dactylol began with a hydrolysis of lactone **25** using KOH in refluxing aqueous methanol and esterification of the corresponding hydroxy acid with diazomethane (Scheme 7). The next challenging step was the introduction of the double bond in dactylol by dehydration of **32**. Regioselectivity was a problem, as were side reactions. For example, treatment of **32** with $POCl_3$ in pyridine, Tf_2O in pyridine, or Martin's sulfurane resulted in

[3] Reagent, ratio **23**:**24**, solvent, temperature, time, yield: (*a*) *m*-CPBA–$NaHCO_3$, 6:1, CH_2Cl_2, RT, 5 d, 67%; (*b*) TFAA–H_2O_2, 5:1, CH_2Cl_2, 0 °C – RT, 3 d, 36%; (*c*) *m*-CPBA–TFA, 4:1, CH_2Cl_2, 0 °C–rt, 48 h, 53%; (*d*) peracetic acid – NaOAc, 9:1, AcOH, RT, 48 h, 31%; (*e*) MMPP, 4:1, DMF, RT, 48 h, 84%.

[4] Without protection of the alcohol group, the Baeyer–Villiger reaction proceeded by an unexpected course. See ref. 10.

© 2006 NRC Canada

Scheme 8.



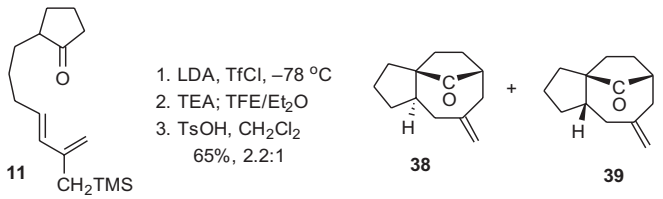
the formation of a compound identified as **35**. Presumably, these reagents induced cation formation, which was followed by a 1,5-transannular hydride shift to form **34**, and subsequent elimination to give tetra-substituted alkene **35**, whose structure was determined based on spectroscopic and analytical data. The ^{1}H NMR spectrum showed no signal for olefinic protons. The most downfield peak appeared at 3.59 ppm as a singlet, which corresponded to the methyl ester. There was also a singlet peak that integrated for three protons at 1.65 ppm, suggesting the presence of a methyl substituent on an olefin. The ^{13}C NMR spectrum confirmed the existence of ester and alkene (δ: 177.3, 136.9, 134.7).

By taking advantage of the dehydration procedure developed by Trost and Jungheim (12), we were able to overcome this problem (Scheme 8). Phosphorus oxychloride ($POCl_3$) was added to a solution of **32** in HMPA with slow heating from room temperature to 50 °C. After the white precipitate that formed dissolved, pyridine was added and heating was continued to 100 °C at which point the dehydration was complete. Subsequent hydrolysis of the sterically hindered methyl ester group using KOH in DMSO provided **36** as a single product (based on crude ^{1}H NMR) in 84% yield. At this point, we found that typical acid chloride formation procedures failed to give the acid chloride of the hindered acid **36**.[5] However, upon treatment with DMF and phosgene in refluxing toluene, **36** was cleanly converted to the corresponding acid chloride (13). In a benzene solution containing pyridine and DMAP, this acid chloride reacted with mCPBA to form a mixed anhydride, which rearranged upon stirring for 24 h at room temperature to a mixed carbonate with retention of configuration (14). Reduction of the mixed carbonate with LAH then afforded (+)-dactylol in 50% overall yield from **36**. The spectral, analytical, and optical rotation data were consistent with those reported in the literature (15).

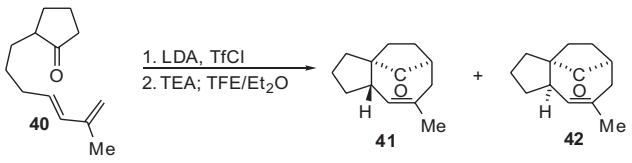
Simple diastereoselectivity

After the successful synthesis of (+)-dactylol, we decided to examine the influence of all stereocenters on the course of the reaction. First, however, we looked at simple diastereoselectivity. Past experience suggested that the intramolecular [4 + 3] cycloaddition reaction of cyclopentenyl cations with tethered butadienes would proceed with only a slight simple diastereoselectivity in favor of the endo product (3*b*). This was indeed the case.

Scheme 9.



Scheme 10.



The ketone **11** was treated with LDA and TfCl to furnish the corresponding α-chloroketone, which was subjected to the [4 + 3] cycloaddition and desilylation reactions (Scheme 9). Two diastereomeric cycloadducts (**38** and **39**) were obtained in 65% yield in a ratio of 2.2:1. The product ratio was determined by gas chromatographic analysis and integration of the crude product ^{1}H NMR spectrum. After purification by flash chromatography on silica gel, the major product was treated with excess $NH_2OH{\cdot}HCl$ and KOH in refluxing ethanol to form an oxime derivative. Recrystallization of this oxime from hexane and EtOAc afforded crystals of suitable quality for single crystal X-ray crystallographic analysis. Thus, the major product was assigned as the endo isomer **38**. It should be noted that cycloadditions of this type appear to take place under kinetic control.

We have examined simple diastereoselectivity computationally for the conversion of **40** to **41** and **42**. We found that while the lowest energy transition state corresponds to the endo product **41**, other transition state structures that lead to the exo product are close in energy, and thus, for unsubstituted systems at least, simple diastereoselectivity should not ever be expected to be substantial (Scheme 10) (16).

It is interesting to note that West and co-workers (3*a*) have reported very high simple diastereoselectivity in the formation of **44** via a domino Nazarov – [4 + 3] cycloaddition process as shown in Scheme 11. It is clear that many new features of this aspect of the intramolecular [4 + 3] cycloaddition reaction of cyclopentenyl cations remain to be uncovered.

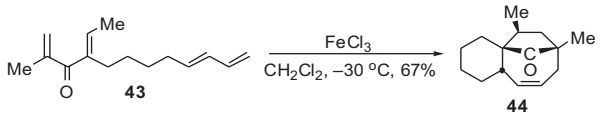
Relative stereoselection I — Cycloaddition of 12

The introduction of a stereogenic center in the tether joining the diene and dienophile in these reactions introduces a new complication. Our goal in pursuing the cycloaddition of **12** was essentially to discover the impact of the stereocenter on the course of the reaction in an effort to elucidate which of the stereocenters in **18** had a more profound impact on the stereochemical outcome on that compound's cycloaddition.

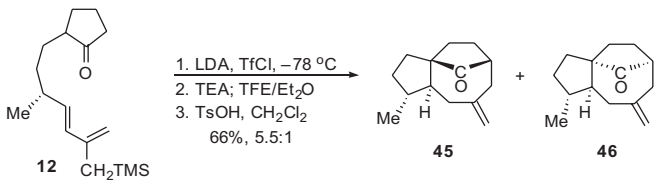
[5] For example, stirring the solution of **36** in hexane with 3 equiv. of oxalyl chloride or heating a hexane solution of **36** with excess thionyl chloride resulted in no change.

© 2006 NRC Canada

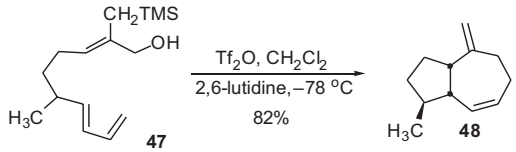
Scheme 11.



Scheme 12.



Scheme 13.



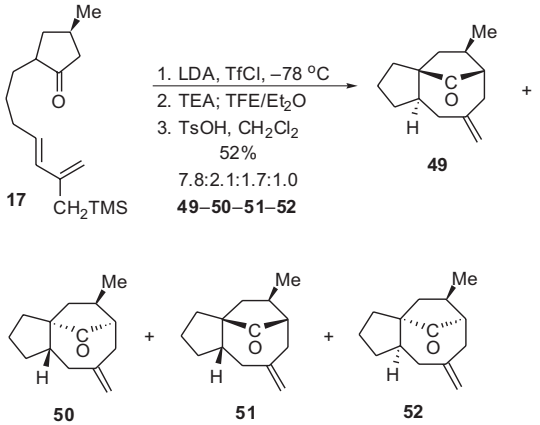
Cycloaddition of **12** afforded four products, only two of which, **45** and **46**, could be cleanly isolated (Scheme 12). Gas chromatographic analysis of the crude reaction mixture indicated a product ratio of 47.2(**45**):8.1(**46**):1:2.3. The major product of the reaction was **45**, as expected on the basis of the small but real endo preference observed in these systems and a report by Giguere and co-workers (17) on relative diastereoselection in intramolecular [4 + 3] cycloadditions. In that paper, Giguere and co-workers (17) reported that treatment of **47** with triflic anhydride afforded cycloadduct **48** as the major product of the reaction (Scheme 13). Regardless of the mechanistic basis for the outcome, one could assume that stereogenic centers adjacent to dienes would produce similar stereochemical outcomes in other intramolecular [4 + 3] cycloaddition reactions. This is what is observed in the formation of **45** and **46**. The structure of both compounds was established by X-ray analysis of the corresponding oximes.[6]

Relative stereoselection II — Cycloaddition of 17

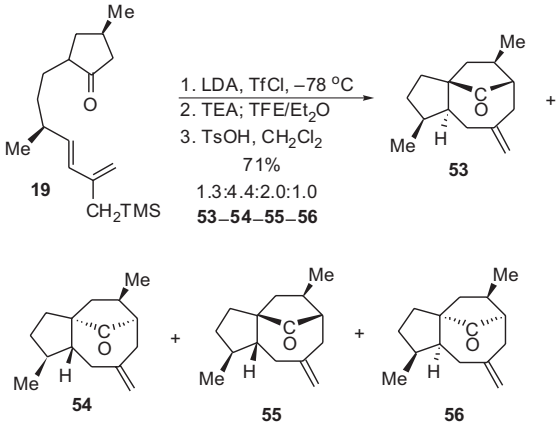
The cycloaddition reaction of **17** was anticipated to be reasonably selective. Endo–exo selectivity was not expected to be high but facial selectivity was expected to be reasonable, the diene approaching the less hindered face of the dienophile (i.e., on the face opposite the methyl substituent). There is a reasonable amount of precedent for this in the literature (18).

Surprisingly, the reaction produced all four possible isomeric products (**49**–**52**) in 52% yield overall from ketone **17** (Scheme 14). Gas chromatographic analysis of the crude product mixture suggested that the products were formed in a ratio of 7.8:2.1:1.7:1.0. They were separated by flash chromatography on silica gel and individually transformed into their oxime derivatives. Consistent with other data, the major

Scheme 14.



Scheme 15.



products were those derived from the transition states having the diene approaching from the opposite side of the methyl group on the stereogenic center. However, the level of facial selectivity in this reaction was approximately 3:1, while the endo–exo ratio was 3.4:1. The low level of facial selectivity is surprising, but larger substituents at the stereogenic centers should produce a better result.

Cycloaddition of 19 — The mismatched case

The last [4 + 3] cycloaddition in this study was the reaction of ketone **19**. Since the stereogenic center on the cyclopentanone remained the same (*R*) while the one on diene was switched from (*R*) to (*S*) compared with ketone **18**, we expected to see the diastereomer of **20** formed as the major isomer. In fact, the reaction produced all four isomers of cycloadduct (**53**–**56**) in 71% yield in a ratio of 1.3:4.4:2.0:1.0 (Scheme 15). Each product was purified, characterized, and converted into an oxime derivative, and the stereochemical assignment was made using X-ray crystallography. The major isomer (**54**) derived from a transition state having an endo approach of the diene with a tether conformation that minimized gauche interactions. However, at-

[6] The oxime derived from **46** gave poor quality X-ray data. Finding a suitable crystal was problematic and the one found turned out to be racemic, in spite of the fact that the bulk sample was clearly enantiomerically enriched based on optical rotation data. However, the data were sufficient to establish the relative stereochemistry.

© 2006 NRC Canada

tack occurred on what appears to be the more sterically hindered face of the oxyallylic cation intermediate.

Surprisingly, the overall facial selectivity in this case, (**53** + **55**):(**54** + **56**), was 1:1.6 in favor of the products derived from the approach of the diene to the more hindered face of the cyclopentanone. The endo–exo ratio, (**53** + **54**):(**55** + **56**) was 1.9:1 in favor of endo products. The relative stereoselectivity (**53** + **56**):(**54** + **55**) was 1:2.8 in favor of the products having a cis relationship between the angular hydrogen and the methyl group on the newly formed five-membered ring.

Conclusion

The intramolecular [4 + 3] cycloaddition of cyclopentenyl cations to dienes is a useful route to cyclooctanoids. High levels of stereocontrol in this reaction are possible, but it is clear that effects that might appear to be cooperative need not be and that further studies of these cycloadditions will be necessary to achieve results that are more generally suitable for applications in synthesis. This conclusion is true for acyclic dienes tethered to cyclopentenyl cations. High levels of simple diastereoselection are possible with tethered furans (3). Whether this inherent selectivity can be used to produce high levels of relative stereocontrol remains to be seen. We plan to perform further work to solve the problems that exist and continue to apply the methodology to the synthesis of cyclooctanoids. Further results will be reported in due course.[7]

Experimental

General procedure for Peterson olefination: synthesis of 2a–2c

A 500 mL round-bottomed flask was charged with powdered cerium(III) chloride heptahydrate ($CeCl_3$-$7H_2O$, 13.02 g, 34.96 mmol). The flask was immersed in an oil bath and evacuated to a full vacuum (about 0.1 mmHg (1 mmHg = 133.322 4)). The solid was magnetically stirred as the flask was heated at 150 °C for 2 h. After the flask was cooled to room temperature, it was vented to the atmosphere and quickly purged with a steam of argon for 30 s. The flask was capped with a rubber septum and 60 mL of THF was added. The white suspension was stirred at room temperature for 1 h, cooled to –78 °C in a dry ice – 2-propanol bath, and a 1 mol/L solution of trimethylsilylmethylmagnesium chloride (35 mL, 35 mmol) was added over a period of 15 min. After the cold mixture was stirred for an additional 15 min, 9.99 mmol of **1a**, **1b**, or **1c** was added dropwise and the mixture was allowed to warm slowly to room temperature over a period of 3 h. The reaction was quenched with ice-cold 1 mol/L HCl (60 mL) and stirred for 5 min. The layers were separated, and the aqueous phase was extracted with ether. The combined organic layers were washed with saturated sodium bicarbonate solution (100 mL), dried over magnesium sulfate, filtered, and the solvents were removed by rotavap. The crude product was purified by flash chromatography (hexane–EtOAc, 4:1).

6-Trimethylsilylmethyl-hepta-4,6-dien-1-ol (2a)

Yield: 82%, colorless oil. IR (neat, cm^{-1}): 3353 (ms), 2947 (s), 1252 (s), 859 (s). ^1H NMR (250 MHz, $CDCl_3$) δ: 6.09 (d, *J* = 15.6 Hz, 1H), 5.58 (dt, *J* = 7.0, 15.6 Hz, 1H), 4.78 (d, *J* = 1.5 Hz, 1H), 4.66 (s, 1H), 3.68–3.61 (m, 2H), 2.18 (q, *J* = 7.3 Hz, 1H), 1.77 (br t, *J* = 4.5 Hz, 1H), 1.72–1.61 (m, 2H), 1.69 (s, 2H), 0.00 (s, 9H). ^{13}C NMR (62.9 MHz, $CDCl_3$) δ: 143.7, 133.6, 129.7, 112.0, 62.3, 32.3, 29.0, 22.1, –1.2. HR-MS (EI) calcd. for $C_{11}H_{20}OSi$ (M^+): 198.1440; found: 198.1438.

(3R)-Methyl-6-trimethylsilylmethyl-hepta-4,6-dien-1-ol (2b)

Yield: 78%, colorless oil. $[\alpha]^{20}_D$ –24.42 (*c* 1.0, $CHCl_3$). IR (neat, cm^{-1}): 3334 (m), 2957 (s), 2929 (m), 2898 (m), 1596 (w), 1422 (w), 1250 (m), 1157 (m), 1054 (m), 967 (m), 853 (s). ^1H NMR (300 MHz, $CDCl_3$) δ: 6.07 (d, *J* = 15.7 Hz, 1H), 5.45 (dd, *J* = 8.3, 11.3 Hz, 1H), 4.80 (d, *J* = 1.9, 1H), 4.68 (s, 1H), 3.66 (br s, 1H), 2.37 (sept, *J* = 7.1 Hz, 1H), 1.70 (s, 2H), 1.66–1.35 (m, 2H), 1.35 (br s, 1H), 1.05 (d, *J* = 6.7 Hz, 3H), 0.00 (s, 9H). ^{13}C NMR (75 MHz, $CDCl_3$) δ: 143.7, 135.7, 132.0, 112.3, 61.2, 39.8, 34.0, 22.1, 21.0, –1.2. Anal. calcd. for $C_{12}H_{24}O_3Si$: C 67.86, H 11.39; found: C 67.92, H 11.47.

(3S)-Methyl-6-trimethylsilylmethyl-hepta-4,6-dien-1-ol (2c)

Yield: 75%, colorless oil. $[\alpha]^{20}_D$ +26.67 (*c* 1.0, $CHCl_3$). IR (neat, cm^{-1}): 3378 (s), 2957 (s), 2877 (s), 1459 (m), 1420 (m), 1380 (m), 1254 (s), 1055 (s), 853 (s). ^1H NMR (300 MHz, $CDCl_3$) δ: 6.07 (d, *J* = 15.7 Hz, 1H), 5.45 (dd, *J* = 8.3, 11.3 Hz, 1H), 4.80 (d, *J* = 1.9, 1H), 4.68 (s, 1H), 3.66 (br s, 1H), 2.37 (sept, *J* = 7.1 Hz, 1H), 1.70 (s, 2H), 1.66–1.35 (m, 2H), 1.35 (br s, 1H), 1.05 (d, *J* = 6.7 Hz, 3H), 0.00 (s, 9H). ^{13}C NMR (75 MHz, $CDCl_3$) δ: 143.7, 135.7, 132.0, 112.3, 61.2, 39.8, 34.0, 22.1, 21.0, –1.2. HR-MS (EI) calcd. for $C_{12}H_{24}OSi$ (M^+): 212.1596; found: 212.1610.

General procedure for conversion of alcohols to iodides: synthesis of 3a–3c

To a solution of **2a**, **2b**, or **2c** (4.70 mmol) in THF (47 mL) was added 9.42 mmol of DCC-MeI salt. The mixture was stirred in an oil bath at 35 °C for 6 h. The solvent was removed under reduced pressure, and the crude product was purified by flash chromatography (100% hexane). Due to the instability of the products, the characterizations were performed by NMR and IR only.

(7-Iodo-2-methylene-hept-3-enyl)-trimethylsilane (3a)

Yield: 94%, colorless oil. IR (neat, cm^{-1}): 3078 (w), 2945 (s), 2896 (s), 1597 (m), 1423 (m), 1241 (m), 1155 (s), 967 (m), 846 (s). ^1H NMR (250 MHz, $CDCl_3$) δ: 6.12 (d, *J* = 15.7 Hz, 1H), 5.51 (dt, *J* = 7.0, 15.6 Hz, 1H), 4.81 (d, *J* =

[7] Supplementary data for this article are available on the journal Web site (http://canjchem.nrc.ca) or may be purchased from the Depository of Unpublished Data, Document Delivery, CISTI, National Research Council Canada, Ottawa, ON K1A 0R6, Canada. DUD 5104. For more information on obtaining material refer to http://cisti-icist.nrc-cnrc.gc.ca/irm/unpub_e.shtml. CCDC 282839–282845 and 282856 contain the crystallographic data for this manuscript. These data can be obtained, free of charge, via http://www.ccdc.cam.ac.uk/conts/retrieving.html (or from the Cambridge Crystallographic Data Centre, 12 Union Road, Cambridge CB2 1EZ, UK; fax +44 1223 336033; or deposit@ccdc.cam.ac.uk).

© 2006 NRC Canada

2.0 Hz, 1H), 4.69 (s, 1H), 3.19 (t, J = 6.9 Hz, 2H), 2.21 (q, J = 7.0 Hz, 2H), 1.92 (quint, J = 7.0 Hz, 2H), 1.69 (d, J = 0.7 Hz, 2H), –0.48 (s, 9H). ^{13}C NMR (62.9 MHz, $CDCl_3$) δ: 143.6, 134.6, 128.0, 112.5, 33.3, 33.1, 22.1, 6.3, –1.2.

(7-Iodo-(5R)-methyl-2-methylene-hept-3-enyl)-trimethylsilane (3b)

Yield: 98%, colorless oil. $[\alpha]^{20}_D$ –43.94 (c 1.0, $CHCl_3$). IR (neat, cm^{-1}): 3078 (w), 2955 (s), 2927 (m), 2897 (m), 1597 (m), 1422 (m), 1249 (s), 1158 (m), 969 (m), 851 (s). ^{1}H NMR (300 MHz, $CDCl_3$) δ: 6.12 (d, J = 15.7 Hz, 1H), 5.35 (dd, J = 8.4, 15.6 Hz, 1H), 4.84 (d, J = 1.9 Hz, 1H), 4.71 (s, 1H), 3.23–3.09 (m, 2H), 2.35 (sept, J = 6.8 Hz, 1H), 1.90–1.80 (m, 2H), 1.70 (s, 2H), 1.05 (d, J = 6.7 Hz, 3H), 0.01 (s, 9H). ^{13}C NMR (75 MHz, $CDCl_3$) δ: 143.5, 134.0, 132.9, 112.7, 40.6, 38.0, 22.1, 20.3, 4.9, –1.2.

(7-Iodo-(5R)-methyl-2-methylene-hept-3-enyl)-trimethyl silane (3c)

Yield: 94%, colorless oil. $[\alpha]^{20}_D$ +39.71 (c 1.0, $CHCl_3$). IR (neat, cm^{-1}): 3079 (w), 2952 (s), 2927 (m), 2887 (m), 1594 (m), 1421 (m), 1252 (s), 1160 (m), 970 (m), 853 (s). ^{1}H NMR (300 MHz, $CDCl_3$) δ: 6.12 (d, J = 15.7 Hz, 1H), 5.35 (dd, J = 8.4, 15.6 Hz, 1H), 4.84 (d, J = 1.9 Hz, 1H), 4.71 (s, 1H), 3.23–3.09 (m, 2H), 2.35 (sept, J = 6.8 Hz, 1H), 1.90–1.80 (m, 2H), 1.70 (s, 2H), 1.05 (d, J = 6.7 Hz, 3H), 0.01 (s, 9H). ^{13}C NMR (75 MHz, $CDCl_3$) δ: 143.6, 134.0, 132.9, 112.7, 40.6, 38.0, 22.1, 20.3, 4.9, –1.2.

4-(2-Propenyloxy)-butanoic acid (5)

To a solution of 1,4-butanediol (54.0 g, 600 mmol) in dry DMF (400 mL) was added 60% NaH (5.76 g, 240 mmol) portionwise while the solution was stirred in an ice-water bath. After the addition of NaH, the reaction flask was removed from the bath. The mixture was stirred at room temperature for 30 min and cooled in the ice-water bath again. Allyl bromide (17.3 mL, 200 mmol) was added dropwise, and the mixture stirred for 1 h. The reaction was quenched with water (500 mL) and extracted with EtOAc. The organic phase was concentrated on a rotatory evaporator, and the residue dissolved in acetone (400 mL). The solution was cooled in the ice bath and Jones reagent (prepared from 133.6 g of CrO_3, 115 mL of H_2SO_4, and 350 mL of H_2O) was added dropwise with stirring until a red color persisted (approximately 70 mL of Jones reagent was used). Volatile solvents were removed under reduced pressure. The residue was diluted with water and extracted with EtOAc. The combined organic phases were washed with saturated $NaHCO_3$ solution (300 mL × 2), and the organic layer was discarded. The aqueous phase was acidified by addition of 6 mol/L HCl until pH ≤ 4, and extracted with ether (100 mL × 3). The combined organic phase was dried over $MgSO_4$ and filtered. The solvent was removed under reduced pressure, and the product was obtained as a colorless liquid (19.9 g, 69%). NMR and IR data were consistent with those published in literature (19).

(4*R*)-Methyl-(5*S*)-phenyl-3-(4-propenyloxy)butanoyl-oxazolidin-2-one and (4*S*)-methyl-(5*R*)-phenyl-3-(4-propenyloxy)butanoyl-oxazolidin-2-one

Oxalyl chloride (30 mL, 343.34 mmol) was added to a solution of acid **5** (16.5 g, 114.45 mmol) in hexane (220 mL) and the mixture was stirred at room temperature for 3 h. Volatile compounds were removed under reduced pressure, and the crude product was used in the next step without further purification. A solution of (4*R*)-methyl-(5*S*)-phenyl-oxazolidin-2-one or (4*S*)-methyl-(5*R*)-phenyl-oxazolidin-2-one (16.89 g, 95.31 mmol) in dried THF (320 mL) was cooled to –78 °C and 2.2 mol/L n-BuLi (43.3 mL, 95.31 mmol) was added dropwise. After the addition of n-BuLi, 4-(2-propenyloxy)butanoyl chloride (18.6 g, 114.38 mmol) was added in one portion. The reaction flask was moved into an ice-water bath and stirred for 30 min. The reaction was quenched with 1 mol/L K_2CO_3 (200 mL) and extracted with EtOAc. The combined organic phases were dried over $MgSO_4$, filtered, and concentrated. The crude product was purified by flash chromatography (hexane–EtOAc, 4:1) on silica gel.

(4R)-Methyl-(5S)-phenyl-3-(4-propenyloxy)butanoyl-oxazolidin-2-one

Yield: 94%, colorless oil. $[\alpha]^{20}_D$ +41.72 (c 1.0, $CHCl_3$). IR (neat, cm^{-1}): 3072 (w), 2932 (m), 2860 (m), 1783 (s), 1702 (s), 1455 (m), 1349 (s), 1198 (s), 1120 (m). ^{1}H NMR (300 MHz, $CDCl_3$) δ: 7.45–7.29 (m, 5H), 5.98–5.85 (m, 1H), 5.66 (d, J = 7.30 Hz, 1H), 5.28 (dq, J = 17.2, 1.5 Hz, 1H), 5.17 (dq, J = 10.4, 1.5 Hz, 1H), 4.76 (quint, J = 6.8 Hz, 1H), 3.97 (dm, J = 5.5 Hz, 2H), 3.52 (t, J = 6.3 Hz, 2H), 3.14–2.97 (m, 2H), 1.99 (sept, J = 7.1 Hz, 2H), 0.89 (d, J = 6.6 Hz, 3H). ^{13}C NMR (75 MHz, $CDCl_3$) δ: 172.7, 153.0, 134.8, 133.3, 128.7, 128.6, 125.6, 116.8, 78.9, 71.7, 69.1, 54.7, 32.5, 24.4, 14.5. Anal. calcd. for $C_{17}H_{21}NO_4$: C 67.31, H 6.98; found: C 67.55, H 6.81.

(4S)-Methyl-(5R)-phenyl-3-(4-propenyloxy)butanoyl-oxazolidin-2-one

Yield: 95%, colorless oil. $[\alpha]^{20}_D$ –40.00 (c 1.0, $CHCl_3$). IR (neat, cm^{-1}): 3074 (w), 2935 (m), 2861 (m), 1784 (s), 1708 (s), 1350 (s), 1198 (s), 1120 (m). ^{1}H NMR (300 MHz, $CDCl_3$) δ: 7.45–7.29 (m, 5H), 5.98–5.85 (m, 1H), 5.66 (d, J = 7.30 Hz, 1H), 5.28 (dq, J = 17.2, 1.5 Hz, 1H), 5.17 (dq, J = 10.4, 1.5 Hz, 1H), 4.76 (quint, J = 6.8 Hz, 1H), 3.97 (dm, J = 5.5 Hz, 2H), 3.52 (t, J = 6.3 Hz, 2H), 3.14–2.97 (m, 2H), 1.99 (sept, J = 7.1 Hz, 2H), 0.89 (d, J = 6.6 Hz, 3H). ^{13}C NMR (75 MHz, $CDCl_3$) δ: 172.7, 153.0, 134.9, 133.3, 128.7, 128.6, 125.6, 116.7, 78.9, 71.7, 69.1, 54.7, 32.5, 24.4, 14.5. Anal. calcd. for $C_{17}H_{21}NO_4$: C 67.31, H 6.98; found: C 67.42, H 6.79.

(4*R*)-Methyl-(5*S*)-phenyl-3-(4-propenyloxy-2(*R*)-methyl-butanoyl)-oxazolidine-2-one (6b) and (4*S*)-methyl-(5*R*)-phenyl-3-(4-propenyloxy-(2*S*)-methyl-butanoyl)-oxazolidine-2-one (6c)

To a flame-dried, 1 L, round-bottomed flask was placed 27.1 g (89.33 mmol) of (4*R*)-methyl-(5*S*)-phenyl-3-(4-propenyloxy)butanoyl-oxazolidin-2-one or (4*S*)-methyl-(5*R*)-phenyl-3-(4-propenyloxy)butanoyl-oxazolidin-2-one and freshly distilled THF (350 mL). The solution was cooled to –78 °C, and 2.0 mol/L NaHMDS in THF (53.6 mL, 107.2 mmol) was added dropwise over 20 min. The mixture was stirred at –78 °C for 30 min and MeI (38.0 mL, 268.0 mmol) was added. After stirring at –78 °C for an additional 4 h, the reaction was quenched with half-saturated NH_4Cl solution (300 mL). The organic phase was separated, and the aqueous

© 2006 NRC Canada

phase was extracted with EtOAc (200 mL × 3). The combined organic phases were dried over $MgSO_4$, filtered, and concentrated. The crude product was purified by flash chromatography (hexane–EtOAc, 10:1) on silica gel.

6b

Yield: 84%, colorless oil. $[\alpha]^{20}_D$ +9.59 (*c* 1.0, $CHCl_3$). IR (neat, cm^{-1}): 2980 (m), 2937 (m), 2872 (m), 1782 (s), 1700 (s), 1457 (m), 1347 (s), 1242 (s), 1197 (s). ^1H NMR (300 MHz, $CDCl_3$) δ: 7.42–7.29 (m, 5H), 5.99–5.84 (m, 1H), 5.63 (d, *J* = 7.1 Hz, 1H), 5.28 (dq, *J* = 1.7, 17.2 Hz, 1H), 5.17 (dq, *J* = 1.7, 8.9 Hz, 1H), 4.74 (quint, *J* = 6.9 Hz, 1H), 3.95–3.89 (m, 3H), 3.53–3.48 (m, 2H), 2.18–2.03 (m, 1H), 1.79–1.67 (m, 1H), 1.23 (d, *J* = 6.9 Hz, 3H), 0.88 (d, *J* = 6.6, 3H). ^{13}C NMR (75 MHz, $CDCl_3$) δ: 176.5, 152.6, 134.8, 133.4, 128.5, 125.5, 116.3, 78.6, 71.5, 68.1, 54.7, 35.1, 33.4, 17.5, 14.4. Anal. calcd. for $C_{18}H_{23}NO_4$: C 68.12, H 7.30; found: C 68.28, H 7.16.

6c

Yield: 81%, colorless oil. $[\alpha]^{20}_D$ –9.44 (*c* 1.0, $CHCl_3$). IR (neat, cm^{-1}): 2980 (m), 2932 (m), 2871 (m), 1784 (s), 1698 (s), 1459 (m), 1342 (s), 1244 (m), 1196 (s). ^1H NMR (250 MHz, $CDCl_3$) δ: 7.45–7.27 (m, 5H), 5.99–5.84 (m, 1H), 5.63 (d, *J* = 7.1 Hz, 1H), 5.28 (dq, *J* = 1.7, 17.2 Hz, 1H), 5.17 (dq, *J* = 1.7, 10.4 Hz, 1H), 4.74 (quint, *J* = 6.7 Hz, 1H), 3.95–3.87 (m, 3H), 3.53–3.46 (m, 2H), 2.18–2.04 (m, 1H), 1.79–1.67 (m, 1H), 1.23 (d, *J* = 6.9 Hz, 3H), 0.88 (d, *J* = 6.6, 3H). ^{13}C NMR (62.9 MHz, $CDCl_3$) δ: 176.7, 152.7, 134.9, 133.5, 128.6, 125.6, 116.5, 78.7, 71.6, 68.2, 54.8, 35.2, 33.5, 17.6, 14.5. Anal. calcd. for $C_{18}H_{23}NO_4$: C 68.12, H 7.30; found: C 67.81, H 7.51.

4-Allyloxy-(2*R*)-methyl-butan-1-ol (7b) and 4-allyloxy-(2*S*)-methyl-butan-1-ol (7c)

To a cooled solution (0 °C) **6b** or **6c** (25.27 g, 79.61 mmol) in diethyl ether (320 mL) was added 6.05 g (159.23 mmol) of $LiAlH_4$ portionwise over 40 min and stirred for 2 h. The reaction was quenched by a slow addition of water and 1 N NaOH (20 mL). The mixture was filtered, and the white precipitate was washed with ether (300 mL × 2). The combined ether solution was concentrated, and crude product was purified by vacuum distillation (bp = 60–65 °C, 0.1 mmHg).

7b

Yield: 92%, colorless oil. $[\alpha]^{20}_D$ +14.16 (*c* 1.0, $CHCl_3$). IR (neat, cm^{-1}): 3397 (s), 3081 (w), 2930 (s), 2870 (s), 1458 (m), 1097 (s), 1044 (m). ^1H NMR (300 MHz, $CDCl_3$) δ: 5.99–5.83 (m, 1H), 5.27 (dq, *J* = 1.6, 17.3 Hz, 1H), 5.18 (dq, *J* = 1.2, 10.4 Hz, 1H), 3.98 (d, *J* = 5.6 Hz, 2H), 3.60–3.40 (m, 4H), 2.87 (br t, *J* = 5.7 Hz, 1H), 1.83–1.50 (m, 3H), 0.93 (d, *J* = 6.7 Hz, 3H). ^{13}C NMR (75 MHz, $CDCl_3$) δ: 134.4, 117.1, 71.8, 68.6, 68.0, 34.1, 34.0, 17.1. Anal. calcd. for $C_8H_{16}O_2$: C 66.63, H 11.18; found: C 66.73, H 11.31.

7c

Yield: 88%, colorless oil. $[\alpha]^{20}_D$ –12.53 (*c* 1.0, $CHCl_3$). IR (neat, cm^{-1}): 3413 (s), 2957 (s), 2926 (s), 2870 (s), 1459 (m), 1099 (s), 1047 (s). ^1H NMR (250 MHz, $CDCl_3$) δ: 5.99–5.83 (m, 1H), 5.27 (dq, *J* = 1.6, 17.3 Hz, 1H), 5.18 (dq, *J* = 1.2, 10.4 Hz, 1H), 3.98 (d, *J* = 5.6 Hz, 2H), 3.60–3.40 (m, 4H), 2.87 (br t, *J* = 5.7 Hz, 1H), 1.83–1.50 (m, 3H), 0.93 (d, *J* = 6.7 Hz, 3H). ^{13}C NMR (75 MHz, $CDCl_3$) δ: 134.4, 117.1, 71.8, 68.6, 68.0, 34.1, 34.0, 17.1. Anal. calcd. for $C_8H_{16}O_2$: C 66.63, H 11.18; found: C 66.73, H 11.28.

Synthesis of 6-allyloxy-(4*R*)-methyl-hex-2-enoic acid methyl ester and 6-allyloxy-(4*S*)-methyl-hex-2-enoic acid methyl ester

DMSO (9.4 mL, 132.41 mmol) was added to a cooled solution (–78 °C) of oxalyl chloride (5.8 mL, 66.20 mmol) in methylene chloride (460 mL). After 5 min, a solution of **7b** or **7c** (6.80 g, 47.29 mmol) in 10 mL of methylene chloride was added. The mixture was stirred for 30 min at –78 °C, and triethylamine (29.0 mL, 208.08 mmol) was added. After stirring for an additional 1 h at –30 °C, the reaction was quenched and washed with water (200 mL × 2). The organic phase was dried over magnesium sulfate, filtered, and concentrated. The crude product was dissolved in 1,2-dichloroethane (50 mL), $Ph_2PCHCOOMe$ (16.56 g, 47.26 mmol) was added, and it was refluxed for 6 h. Volatile solvents were removed under reduced pressure, and the crude product was purified by flash chromatography (hexane–EtOAc, 4:1) on silica gel.

6-Allyloxy-(4R)-methyl-hex-2-enoic acid methyl ester

Yield: 88%, colorless oil. $[\alpha]^{20}_D$ –43.85 (*c* 1.0, $CHCl_3$). IR (neat, cm^{-1}): 2956 (s), 2867 (s), 1726 (s), 1658 (m), 1436 (m), 1273 (s), 1180 (m), 1103 (m). ^1H NMR (300 MHz, $CDCl_3$) δ: 6.87 (dd, *J* = 8.0, 15.7 Hz, 1H), 5.95–5.82 (m, 1H), 5.80 (dd, *J* = 1.0, 15.8 Hz, 1H), 5.26 (dq, *J* = 1.6, 17.2 Hz, 1H), 5.16 (dq, *J* = 1.6, 9.9 Hz, 1H), 3.93 (m, 2H), 3.73 (s, 3H), 3.45–3.39 (m, 2H), 2.52 (sept, *J* = 7.0 Hz, 1H), 1.65 (q, *J* = 6.7 Hz, 2H), 1.07 (d, *J* = 6.7 Hz, 3H). ^{13}C NMR (75 MHz, $CDCl_3$) δ: 167.1, 154.0, 134.7, 119.5, 116.7, 71.7, 67.7, 51.3, 35.7, 33.3, 19.3. Anal. calcd. for $C_{11}H_{18}O_3$: C 66.64, H 9.15; found: C 66.47, H 8.98.

6-Allyloxy-(4S)-methyl-hex-2-enoic acid methyl ester

Yield: 85%, colorless oil. $[\alpha]^{20}_D$ +45.35 (*c* 1.0, $CHCl_3$). IR (neat, cm^{-1}): 2957 (m), 2873 (m), 1730 (s), 1660 (m), 1435 (m), 1274 (m), 1183 (m), 1104 (m). ^1H NMR (300 MHz, $CDCl_3$) δ: 6.87 (dd, *J* = 8.0, 15.7 Hz, 1H), 5.95–5.82 (m, 1H), 5.80 (dd, *J* = 1.0, 15.8 Hz, 1H), 5.26 (dq, *J* = 1.6, 17.2 Hz, 1H), 5.16 (dq, *J* = 1.6, 9.9 Hz, 1H), 3.93 (m, 2H), 3.73 (s, 3H), 3.45–3.39 (m, 2H), 2.52 (sept, *J* = 7.0 Hz, 1H), 1.65 (q, *J* = 6.7 Hz, 2H), 1.07 (d, *J* = 6.7 Hz, 3H). ^{13}C NMR (75 MHz, $CDCl_3$) δ: 167.1, 154.0, 134.7, 119.5, 116.7, 71.7, 67.7, 51.3, 35.7, 33.3, 19.3. Anal. calcd. for $C_{11}H_{18}O_3$: C 66.64, H 9.15; found: C 66.81, H 9.36.

6-Hydroxy-(4*R*)-methyl-hex-2-enoic acid methyl ester (1b) and 6-hydroxy-(4*R*)-methyl-hex-2-enoic acid methyl ester (1c)

To a solution of 6-allyloxy-(4*R*)-methyl-hex-2-enoic acid methyl ester or 6-allyloxy-(4*S*)-methyl-hex-2-enoic acid methyl ester (8.25 g, 41.60 mmol) in anhydrous methanol (150 mL) was added 10% Pd–C (4.16 g) and *p*-toluenesulfonic acid (2.08 g). The mixture was stirred and heated under a reflux condition for 24 h, then filtered, and concentrated. The crude product was purified by flash chromatography (hexane–EtOAc, 2:1).

© 2006 NRC Canada

1b

$[\alpha]^{20}_D$ –40.73 (*c* 1.0, $CHCl_3$). IR (neat, cm^{-1}): 3437 (m), 2958 (s), 2879 (m), 1725 (s), 1657 (s), 1437 (m), 1275 (s), 1210 (s), 1175 (s). ^1H NMR (300 MHz, $CDCl_3$) δ: 6.88 (dd, *J* = 8.0, 15.7 Hz, 1H), 5.83 (dd, *J* = 1.0, 15.7 Hz, 1H), 3.73 (s, 3H), 3.68–3.61 (m, 2H), 2.53 (m, 1H), 2.24 (s, 1H), 1.064 (q, *J* = 6.78 Hz, 2H), 1.08 (d, *J* = 6.8 Hz, 3H). ^{13}C NMR (75 MHz, $CDCl_3$) δ: 167.2, 154.1, 119.5, 60.2, 51.4, 38.5, 33.0, 19.3. Anal. calcd. for $C_8H_{14}O_3$: C 60.74, H 8.92; found: C 60.91, H 8.77.

1c

$[\alpha]^{20}_D$ +44.08 (*c* 1.0, $CHCl_3$). IR (neat, cm^{-1}): 3429 (s), 2956 (s), 2879 (s), 1726 (s), 1658 (s), 1439 (s), 1276 (s), 1210 (s), 1175 (s). ^1H NMR (250 MHz, $CDCl_3$) δ: 6.88 (dd, *J* = 8.0, 15.7 Hz, 1H), 5.83 (dd, *J* = 1.0, 15.7 Hz, 1H), 3.73 (s, 3H), 3.68–3.61 (m, 2H), 2.53 (m, 1H), 2.24 (s, 1H), 1.064 (q, *J* = 6.78 Hz, 2H), 1.08 (d, *J* = 6.8 Hz, 3H). ^{13}C NMR (62.9 MHz, $CDCl_3$) δ: 167.2, 154.1, 119.6, 60.4, 51.4, 38.6, 33.1, 19.3. Anal. calcd. for $C_8H_{14}O_3$: C 60.74, H 8.92; found: C 60.60, H 8.96.

General procedure for the alkylation of ketoester 8: synthesis of 9 and 10

To a solution of **8** (5 mmol) in acetone (25 mL) was added alkyl iodide **3a** or **3b** (2.5 mmol) and K_2CO_3 (7.5 mmol). The mixture was heated under a reflux condition under N_2 for 12 h. After the mixture was cooled to room temperature, water (30 mL) was added and the mixture was extracted with Et_2O (30 mL × 3). Combined organic phases were washed with brine, dried over $MgSO_4$, filtered, and concentrated under reduced pressure. The crude product was purified by column chromatography (silica gel, pentane–ether, 20:1).

9

Yield: 86%, colorless oil. IR (neat, cm^{-1}): 3079 (w), 2956 (s), 2896 (s), 1751 (s), 1730 (s), 1436 (m), 1251 (m), 1159 (m), 855 (s). ^1H NMR (300 MHz, $CDCl_3$) δ: 6.06 (d, *J* = 15.6 Hz, 1H), 5.54 (dt, *J* = 7.0, 15.6 Hz, 1H), 4.78 (d, *J* = 2.0 Hz, 1H), 4.66 (s, 1H), 3.71 (s, 3H), 2.57–1.86 (m, 8H), 1.68 (s, 2H), 1.64–1.32 (m, 4H), 0.00 (s, 9H). ^{13}C NMR (75 MHz, $CDCl_3$) δ: 214.7, 171.5, 143.7, 133.7, 128.6, 112.0, 60.4, 52.5, 37.9, 33.6, 32.9, 32.8, 24.7, 22.1, 19.6, –1.2. Anal. calcd. for $C_{18}H_{30}O_3Si$: C 67.03, H 9.38; found: C 66.88, H 9.12.

10

Yield: 88%, colorless oil. IR (neat, cm^{-1}): 3080 (w), 2957 (s), 2928 (s), 1754 (s), 1729 (s), 1600 (m), 1460 (m), 1250 (s), 1157 (m), 856 (s). ^1H NMR (300 MHz, $CDCl_3$) δ: 6.05 and 6.01 (d, *J* = 15.7 and 15.7 Hz, 1H), 5.44–5.32 (m, 1H), 4.79 (d, *J* = 2.0 Hz, 1H), 4.66 (d, *J* = 2.0 Hz, 1H), 3.70 and 3.69 (s, 3H), 2.63–1.77 (m, 8H), 1.68 (s, 2H), 1.67–1.12 (m, 3H), 1.00 and 0.99 (d, *J* = 6.7 and 6.7 Hz, 3H). ^{13}C NMR (75 MHz, $CDCl_3$) δ: 214.71, 214.65, 171.6, 171.4, 143.74, 143.69, 135.5, 132.1, 132.0, 112.13, 112.08, 60.4, 60.3, 52.4, 38.0, 37.8, 37.5, 37.4, 32.9, 32.7, 32.0, 31.9, 31.8, 22.1, 22.0, 20.8, 20.7, 19.5, –1.2. HR-MS (EI) calcd. for $C_{19}H_{31}O_3Si$ (M^+): 336.2121; found: 336.2121.

General procedure for the alkylation of ketoester 13: synthesis of 14–16

To a flame-dried, 50 mL, round-bottomed flask equipped with a magnetic bar was placed 0.65 g (17 mmol) of 60% NaH in mineral oil and 27 mL of freshly distilled THF. The mixture was stirred in an ice bath, and a solution of **13** (15 mmol) in 3 mL of THF was added slowly. The mixture was stirred for 5 min, and 2.5 mol/L solution of *n*-BuLi (15 mmol) was added. After stirring for an additional 5 min, a solution of alkyl iodide **3a**, **3b**, or **3c** (10 mmol) in 3 mL of THF was added into the orange-yellow solution. The mixture was stirred and allowed to warm to room temperature overnight. The reaction was quenched with water (25 mL) and extracted with ether (30 mL × 3). The combined organic phases were dried over magnesium sulfate, filtered, and concentrated with a rotatory evaporator. The crude product was purified by column chromatography (silica gel, pentane–ether, 20:1) to give a mixture of diastereomers.

14

Yield: 67%, yellow oil. $[\alpha]^{20}_D$ +49.70 (*c* 1.0, $CHCl_3$). IR (neat, cm^{-1}): 3083 (w), 2957 (s), 2967 (s), 1753 (s), 1730 (s), 1436 (m), 1250 (m), 857 (s). ^1H NMR (250 MHz, $CDCl_3$) δ: 6.05 (d, *J* = 15.6 Hz, 1H), 5.55 (dt, *J* = 7.0, 15.6 Hz, 1H), 4.78 (d, *J* = 2.2 Hz, 1H), 4.66 (s, 1H), 3.75 and 3.74 (s, 3H), 2.86 and 2.74 (d, *J* = 10.0 and 11.44 Hz, 1H), 2.70–2.40 (m, 1H), 2.39–2.21 (m, 1H), 2.14–2.07 (m, 2H), 2.03–1.74 (m, 1H), 1.72–1.59 (m, 1H), 1.68 (s, 2H), 1.50–1.34 (m, 4H), 1.18 and 1.16 (d, *J* = 6.34 and 6.45 Hz, 3H), 0.00 (s, 9H). ^{13}C NMR (75 MHz, $CDCl_3$) δ: 213.6, 212.5, 169.63, 169.59, 143.8, 133.6, 129.8, 111.9, 111.2, 62.9, 62.8, 52.3, 50.5, 47.9, 36.2, 35.0, 34.1, 33.6, 32.6, 32.5, 30.4, 29.3, 27.8, 27.4, 27.3, 22.1, 19.7, 19.1, 15.8, –1.2. Anal. calcd. for $C_{19}H_{32}O_3Si$: C 67.81, H 9.58; found: C 67.66, H 9.52.

15

Yield: 70%, yellow oil. $[\alpha]^{20}_D$ +37.22 (*c* 1.0, $CHCl_3$). IR (neat, cm^{-1}): 2955 (s), 2874 (m), 1756 (s), 1731 (s), 1250 (m), 853 (s). ^1H NMR (300 MHz, $CDCl_3$) δ: 6.02 (d, *J* = 15.7 Hz, 1H), 5.47–5.35 (m, 1H), 4.78 (d, *J* = 1.7 Hz, 1H), 4.66 (s, 1H), 3.75 and 3.74 (s, 3H), 2.95 and 2.85 (d, *J* = 10.3 and 9.5 Hz, 1H), 2.75–2.42 (m, 1H), 2.35–2.13 (m, 2H), 1.99–1.59 (m, 2H), 1.68 (s, 2H), 1.39–1.23 (m, 3H), 1.18–1.06 (m, 4H), 1.00 (d, *J* = 6.7 Hz, 3H), 0.00 (s, 9H). ^{13}C NMR (75 MHz, $CDCl_3$) δ: 213.6, 212.6, 169.6, 169.6, 143.8, 143.8, 135.9, 135.8, 131.9, 131.8, 112.1, 112.0, 63.0, 62.8, 52.3, 50.5, 48.2, 37.2, 37.1, 36.2, 35.1, 35.1, 34.6, 34.1, 33.6, 28.8, 27.5, 22.1, 22.1, 20.9, 20.5, 19.2, –1.2. Anal. calcd. for $C_{20}H_{34}O_3Si$: C 68.52, H 9.78; found: C 68.70, H 9.85.

16

Yield: 79%, yellow oil. $[\alpha]^{20}_D$ +45.50 (*c* 1.0, $CHCl_3$). IR (neat, cm^{-1}): 3084 (w), 2956 (s), 2867 (s), 1759 (s), 1729 (s), 1444 (m), 1250 (s), 1158 (m), 849 (s). ^1H NMR (300 MHz, $CDCl_3$) δ: 5.97 (d, *J* = 15.7 Hz, 1H), 5.42–5.30 (m, 1H), 4.74 (d, *J* = 2.0 Hz, 1H), 4.61 (br s, 2H), 3.70 and 3.69 (s, 3H), 2.81 and 2.69 (d, *J* = 9.6 and 11.6 Hz, 1H), 2.65–2.10 (m, 4H), 1.97–1.53 (m, 2H), 1.64 (s, 2H), 1.40–1.19 (m, 3H), 1.12 and 1.11 (d, *J* = 6.3 and 6.4 Hz, 3H),

© 2006 NRC Canada

1.05–1.00 (m, 1H), 0.96 (d, *J* = 6.6 Hz, 3H), –0.04 (s, 9H). ^{13}C NMR (75 MHz, $CDCl_3$) δ: 213.3, 212.3, 169.5, 169.4, 143.6, 143.5, 135.7, 135.6, 131.8, 131.7, 111.93, 111.87, 62.8, 62.7, 52.1, 50.5, 47.8, 37.1, 36.8, 36.1, 35.0, 34.7, 34.6, 34.0, 33.4, 28.4, 27.6, 21.98, 21.96, 20.7, 20.5, 19.6, 19.0, –1.3. HR-MS (EI) calcd. for $C_{20}H_{34}O_3Si$ (M^+): 350.2277; found: 350.2241.

General procedure for decarbomethoxylation: synthesis of 11–12 and 17–19

To a solution of β-keto ester (3.0 mmol) in DMSO (6.0 mL) was added potassium cyanide (6.0 mmol) and water (6.0 mmol). The mixture was heated under reflux for 30 min, allowed to cool to room temperature, diluted with water (20 mL), and extracted with ether (20 mL × 3). The combined organic phases were dried over magnesium sulfate, filtered, and concentrated. The crude product was purified by flash chromatography (silica gel, pentane–ether, 20:1).

11

Yield: 66%, colorless oil. IR (neat, cm^{-1}): 3079 (w), 2956 (s), 1740 (s), 1250 (s), 1157 (m), 856 (s). ^{1}H NMR (300 MHz, $CDCl_3$) δ: 6.06 (d, *J* = 15.6 Hz, 1H), 5.57 (dt, *J* = 7.06, 15.6 Hz, 1H), 4.78 (d, *J* = 2.01, 1H), 4.66 (s, 1H), 2.36–1.93 (m, 7H), 1.88–1.72 (m, 2H), 1.69 (s, 2H), 1.62–1.21 (m, 4H), 0.39 (s, 9H). ^{13}C NMR (62.9 MHz, $CDCl_3$) δ: 221.3, 143.8, 133.5, 130.1, 111.8, 49.1, 38.1, 32.8, 29.6, 29.4, 27.5, 22.2, 20.7, –1.2. Anal. calcd. for $C_{16}H_{28}OSi$: C 72.66, H 10.67; found: C 72.50, H 10.49.

12

Yield: 83%, colorless oil. $[\alpha]^{20}_D$ –10.13 (*c* 1.0, $CHCl_3$). IR (neat, cm^{-1}): 3080 (w), 2956 (s), 2870 (s), 1738 (s), 1249 (s), 1160 (m), 857 (s). ^{1}H NMR (250 MHz, $CDCl_3$) δ: 6.02 (d, *J* = 15.7 Hz, 1H), 5.48–5.36 (m, 1H), 4.79 (d, *J* = 2.2 Hz, 1H), 4.66 (br s, 1H), 2.35–1.93 (m, 6H), 1.87–1.65 (m, 2H), 1.69 (s, 2H), 1.60–1.15 (m, 4H), 1.02 and 1.01 (d, *J* = 6.7 and 6.7 Hz, 3H), 0.00 (s, 9H). ^{13}C NMR (62.9 MHz, $CDCl_3$) δ: 221.3, 143.9, 143.8, 136.1, 136.0, 131.8, 131.6, 111.94, 111.89, 49.3, 49.1, 38.14, 38.11, 37.4, 37.1, 35.2, 34.8, 29.63, 29.59, 27.8, 27.5, 22.14, 22.12, 20.9, 20.7. 20.5, –1.2. HR-MS (EI) calcd. for $C_{17}H_{30}OSi$ (M^+): 278.2066; found: 278.2079.

17

Yield: 78%, colorless oil. $[\alpha]^{20}_D$ +71.31 (*c* 1.0, $CHCl_3$). IR (neat, cm^{-1}): 3081 (w), 2954 (s), 2862 (s), 1743 (s), 1459 (w), 1250 (s), 1158 (m), 857 (s). ^{1}H NMR (250 MHz, $CDCl_3$) δ: 6.06 (d, *J* = 15.3 Hz, 1H), 5.63–5.54 (m, 1H), 4.78 (d, *J* = 2.2 Hz, 1H), 4.66 (s, 1H), 2.52–2.03 (m, 6H), 1.97–1.62 (m, 2H), 1.69 (s, 2H), 1.51–1.20 (m, 3H), 1.18–1.05 (m, 1H), 1.14 and 1.09 (d, *J* = 6.4 and 6.7 Hz, 3H), 0.00 (s, 9H). ^{13}C NMR (62.9 MHz, $CDCl_3$) δ: 221.6, 220.7, 143.8, 133.5, 133.4, 130.1, 130.1, 111.8, 50.8, 47.0, 46.8, 46.4, 35.6, 36.9, 32.8, 32.7, 30.2, 29.7, 29.4, 28.3, 27.5, 22.2, 20.8, 20.3, –1.2. Anal. calcd. for $C_{17}H_{30}OSi$: C 73.31, H 10.86; found: C 73.41, H 10.68.

18

Yield: 94%, colorless oil. $[\alpha]^{20}_D$ +41.65 (*c* 1.0, $CHCl_3$). IR (neat, cm^{-1}): 3079 (w), 2955 (s), 2870 (s), 1740 (s), 1593 (m), 1458 (m), 1249 (s), 1158 (m), 968 (m), 854 (s). ^{1}H NMR (300 MHz, $CDCl_3$) δ: 6.02 (d, *J* = 15.6 Hz, 1H), 5.50–5.35 (m, 1H), 4.79 (d, *J* = 2.0 Hz, 1H), 4.66 (s, 1H), 2.50–2.05 (m, 4H), 1.95–1.60 (m, 2H), 1.69 (s, 2H), 1.40–1.18 (m, 5H), 1.13 and 1.09 (d, *J* = 6.4 and 6.5 Hz, 3H), 1.01 and 1.00 (d, *J* = 6.7 and 6.7 Hz, 3H), 0.00 (s, 9H). ^{13}C NMR (75 MHz, $CDCl_3$) δ: 221.7, 220.7, 143.9, 143.8, 136.2, 136.0, 131.8, 131.6, 112.0, 111.9, 50.9, 47.3, 46.9, 46.4, 38.5, 37.4, 37.1, 36.9, 35.2, 34.8, 29.7, 28.6, 28.3, 27.4, 22.2, 22.1, 20.9, 20.8, 20.5, 20.3, –1.2. Anal. calcd. for $C_{18}H_{32}OSi$: C 73.90, H 11.03; found: C 73.85, H 10.95.

19

Yield: 74%, colorless oil. $[\alpha]^{20}_D$ +66.45 (*c* 1.0, $CHCl_3$). IR (neat, cm^{-1}): 3081 (w), 2956 (s), 2923 (s), 2865 (m), 1744 (s), 1250 (s), 1158 (m), 850 (s). ^{1}H NMR (250 MHz, $CDCl_3$) δ: 6.02 (d, *J* = 15.7 Hz, 1H), 5.47–5.36 (m, 1H), 4.78 (d, *J* = 2.1 Hz, 1H), 4.65 (d, *J* = 1.4 Hz, 1H), 2.50–2.06 (m, 5H), 1.91–1.62 (m, 3H), 1.69 (s, 2H), 1.43–1.21 (m, 2H), 1.13 and 1.08 (d, *J* = 6.4 and 6.6 Hz, 3H), 1.17–1.06 (m, 1H), 1.02 and 1.00 (d, *J* = 6.7 and 6.7 Hz, 3H), 0.00 (s, 9H). ^{13}C NMR (62.9 MHz, $CDCl_3$): 221.6, 220.6, 143.8, 136.1, 136.0, 131.8, 131.7, 111.9, 51.0, 47.0, 46.8, 46.4, 38.6, 37.4, 37.1, 37.0, 35.1, 34.8, 29.7, 28.4, 28.3, 27.8, 22.1, 20.84, 20.76, 20.6, 20.3, –1.2. HR-MS (EI) calcd. for $C_{18}H_{32}OSi$ (M^+): 292.2222; found: 292.2241.

α-Chlorination of cyclopentanone, intramolecular [4 + 3] cycloaddition, and desilylation of allylsilane: synthesis of 20

To a cooled solution (–78 °C) of ketone **18** (2.0 mmol) in THF (15 mL) was slowly added a solution of LDA (prepared by adding a 2.5 mol/L solution of *n*-BuLi (2.5 mmol) into a solution of diisopropylamine (3.0 mmol) in THF (5 mL) at 0 °C). The mixture was stirred at –78 °C for 30 min and trifluoromethanesulfonyl chloride (2.5 mmol) was added dropwise. After stirring for 5 min, the reaction was quenched with water (20 mL) and extracted with ether (15 mL × 3). The combined organic phases were washed with water (20 mL), dried over magnesium sulfate, filtered, and concentrated. Volatile solvents were removed under high vacuum. The resulting colorless oil was dissolved in freshly distilled ether (10 mL), cooled to –78 °C, and diluted with trifluoroethanol (10 mL). The mixture was stirred for a few minutes and triethylamine (6.0 mmol) was added dropwise. The reaction was allowed to warm to room temperature overnight, quenched with water (20 mL), and extracted with ether (15 mL × 3). The combined organic phases were dried over magnesium sulfate, filtered, and concentrated. The crude product was dried under high vacuum. The resulting yellow oil was dissolved in methylene chloride (20 mL), and $TsOH{\cdot}H_2O$ (0.2 mmol) was added. The mixture was stirred at room temperature for 6 h and washed with water (20 mL). The organic phase was separated and dried over magnesium sulfate, filtered, and concentrated. The crude product was purified by flash chromatography on silica gel using hexane–EtOAc (30:1) as the eluent. Ketone **20** was obtained as a colorless oil in 74% yield. $[\alpha]^{20}_D$ +44.60 (*c* 1.0, $CHCl_3$). IR (neat, cm^{-1}): 3073 (w), 2952 (s), 2867 (s), 1735 (s), 1643 (w), 1455 (m), 1154 (w). ^{1}H NMR (300 MHz, $CDCl_3$) δ: 4.83 (d, *J* = 13.5 Hz, 2H), 2.46–1.68 (m, 8H), 1.58–0.92 (m,

© 2006 NRC Canada

6H), 1.04 (d, J = 6.4 Hz, 3H), 1.00 (d, J = 6.1 Hz, 3H). ^{13}C NMR (75 MHz, $CDCl_3$) δ: 220.8, 146.5, 115.0, 61.1, 58.6, 52.7, 46.9, 43.2, 39.9, 39.4, 35.1, 31.7, 28.0, 21.0, 18.3. Anal. calcd. for $C_{15}H_{22}O$: C 82.52, H 10.16; found: C 82.25, H 10.20.

Simmons–Smith cyclopropanation: synthesis of 22

To a cooled solution (0 °C) of **20** (2.29 mmol) in methylene chloride (5 mL) was added methylene iodide (5.4 mL, 5.8 mmol) and 1.0 mol/L solution of diethylzinc in hexane (23 mL, 23 mmol). The mixture was stirred vigorously for 12 h while it was allowed to warm to room temperature. The reaction was quenched with water (20 mL), 1 N HCl (5 mL) was added, and it was extracted with ether (20 mL × 3). The combined organic phases were dried over magnesium sulfate, filtered, and concentrated using a rotatory evaporator. The crude product was purified by flash chromatography (3:1, hexane–CH_2Cl_2). Ketone **22** was obtained in 95% yield as a colorless oil. $[\alpha]^{20}_D$ +12.63 (*c* 1.0, $CHCl_3$). IR (neat, cm^{-1}): 2956 (s), 2869 (s), 1728 (s), 1457 (m), 1390 (m), 1164 (m), 1114 (m). ^{1}H NMR (250 MHz, $CDCl_3$) δ: 2.63–2.51 (m, 1H), 2.28–2.11 (m, 3H), 1.99–1.94 (m, 4H), 1.84–1.77 (m, 1H), 1.56–1.43 (m, 1H), 1.36–1.13 (m, 5H), 1.03 (d, J = 6.88 Hz, 3H), 0.99–0.95 (m, 1H), 0.91 (d, J = 5.33 Hz, 3H), 0.83–0.75 (m, 1H), 0.51–0.39 (m, 2H), 0.31–0.15 (m, 2H). ^{13}C NMR (62.9 MHz, $CDCl_3$) δ: 220.1, 61.6, 55.0, 41.2, 42.8, 39.1, 35.1, 31.6, 27.3, 21.1, 18.4, 17.0, 14.7, 12.3. Anal. calcd. for $C_{16}H_{24}O$: C 80.70, H 10.41; found: C 82.60, H 10.30.

Baeyer–Villiger oxidation: synthesis of 23 and 24

To a solution of ketone **22** (2.15 mmol) in DMF (4 mL) was added MMPP (10.63 g, 21.50 mmol), and the resulted suspension was stirred at room temperature for 24 h. The mixture was diluted with water (20 mL) and extracted with ether (20 mL × 3). The combined ether solutions were dried over magnesium sulfate, filtered, and concentrated. The crude product was purified by flash chromatography (hexane–EtOAc, 10:1).

23

Yield: 68%, white solid (recrystallized from hexane–EtOAc), mp 52–54 °C. $[\alpha]^{20}_D$ +26.46 (*c* 1.0, $CHCl_3$). IR (KBr, cm^{-1}): 2956 (d), 2869 (d), 1728 (d), 1457 (m), 1390 (m), 1164 (m), 1114 (s). ^{1}H NMR (300 MHz, $CDCl_3$) δ: 4.36–4.31 (m, 1H), 2.70–2.46 (m, 3H), 2.03 (dd, J = 7.4, 13.5 Hz, 1H), 1.94–1.83 (m, 1H), 1.78–1.65 (m, 2H), 1.61–1.33 (m, 3H), 1.25–1.03 (m, 2H), 1.10 (d, J = 6.9 Hz, 3 H), 0.92 (br s, 1H), 0.88 (d, J = 6.0 Hz, 3H), 0.53–0.42 (m, 2H), 0.38–0.27 (m, 2H). ^{13}C NMR (75 MHz, $CDCl_3$) δ: 177.3, 85.4, 57.7, 51.1, 44.5, 42.0, 41.4, 38.0, 36.0, 33.0, 26.6, 22.2, 18.0, 16.7, 14.9, 14.7. Anal. calcd. for $C_{16}H_{24}O_2$: C 77.38, H 9.74; found: C 77.23, H 9.89.

24

Yield: 16%, white solid (recrystallized from hexane–EtOAc), mp 65–67 °C. $[\alpha]^{20}_D$ –103.65 (*c* 1.0, $CHCl_3$). IR (KBr, cm^{-1}): 2956 (s), 2917 (s), 2871 (s), 1722 (s), 1452 (w), 1374 (w), 1266 (w), 1098 (s). ^{1}H NMR (250 MHz, $CDCl_3$) δ: 2.66–2.38 (m, 3H), 2.21–1.79 (m, 5H), 1.67–1.53 (m, 2H), 1.39–1.21 (m, 2H), 1.13–0.96 (m, 1H), 1.02 (d, J = 6.8 Hz, 3H), 0.89 (d, J = 6.4 Hz, 3H), 0.79–0.73 (m, 1H), 0.55–0.28 (m, 4H). ^{13}C NMR (62.9 MHz, $CDCl_3$) δ: 178.0, 90.6, 56.8, 46.8, 43.5, 42.6, 41.7, 41.1, 35.6, 32.1, 25.4, 23.0, 18.6, 17.5, 15.1, 14.3. Anal. calcd. for $C_{16}H_{24}O_2$: C 77.38, H 9.74; found: C 77.50, H 9.71.

Hydrogenolysis of a cyclopropane: synthesis of 25

To a 20 mL hydrogenation vessel was placed 0.90 mmol of cyclopropane **23**, 9.0 mL of glacial acetic acid, PtO_2 (4 equiv.), and NaOAc (4 equiv.). The vessel was connected to a hydrogenation apparatus, and the system was flushed with H_2 gas for a few minutes. The hydrogen pressure was adjusted to 100 psi (1 psi = 6.894 757 kPa), and the mixture was stirred under hydrogen for 12 h. The vessel was vented, and the catalyst was filtered off. The filtrate was partitioned between ether (20 mL) and water (20 mL). The organic phase was separated, and the aqueous phase was extracted with ether (20 mL × 2). The combined organic phases were dried over magnesium sulfate, filtered, and concentrated. The crude product was purified by flash chromatography (hexane–EtOAc, 10:1). Lactone **25** was synthesized in 98% yield as a white crystalline solid. mp 91 to 92 °C. $[\alpha]^{20}_D$ +15.23 (*c* 1.0, $CHCl_3$). IR (KBr, cm^{-1}): 2955 (s), 2872 (s), 1720 (s), 1455 (m), 1113 (m). ^{1}H NMR (300 MHz, $CDCl_3$) δ: 4.36 (q, J = 3.5 Hz, 1H), 2.73–2.60 (m, 1H), 2.43–2.34 (m, 1H), 2.07 (dd, J = 8.3, 13.8 Hz, 1H), 1.93–1.82 (m, 2H), 1.75–1.16 (m, 8H), 1.12 (s, 3H), 1.09 (d, J = 6.9 Hz, 3H), 0.98–0.96 (m, 6H). ^{13}C NMR (75 MHz, $CDCl_3$) δ: 177.3, 85.3, 54.0, 51.3, 46.3, 43.0, 42.6, 42.0, 36.5, 36.4, 32.9, 32.5, 29.5, 27.3, 23.2, 18.3. Anal. calcd. for $C_{16}H_{26}O_2$: C 76.75, H 10.47; found: C 76.80, H 10.56.

Hydrolysis of lactone 25 and esterification of carboxylic acid 31: synthesis of 32

To a 10 mL round-bottomed flask equipped with a reflux condenser was placed **25** (0.05 g, 0.20 mmol), MeOH (2.0 mL), water (1.0 mL), and KOH (0.5 g). The mixture was heated and stirred under a reflux condition for 12 h. The mixture was allowed to cool to room temperature, was diluted with 2 N HCl (5 mL), and extracted with ether (10 mL × 3). The organic phase was dried over magnesium sulfate, filtered, and concentrated. The crude product was dissolved in 5 mL of ether; a solution of diazomethane in ether was added until a yellow color persisted. The mixture was stirred for 5 min, and the solvent was removed under reduced pressure. The crude product was purified by flash chromatography (hexane–EtOAc, 4:1). Ester **32** was obtained as a colorless oil (0.053 g, 95%). $[\alpha]^{20}_D$ –27.08 (*c* 1.0, $CHCl_3$). IR (neat, cm^{-1}): 3424 (m), 2960 (s), 2872 (s), 1720 (s), 1466 (m), 1175 (m). ^{1}H NMR (300 MHz, $CDCl_3$) δ: 3.80–3.74 (m, 1H), 3.67 (s, 3H), 2.26 (dd, J = 9.3, 15.0 Hz, 1H), 2.04–1.83 (m, 4H), 1.73–1.35 (m, 6H), 1.26–1.15 (m, 3H), 1.03 (d, J = 7.0 Hz, 3H), 0.96–0.93 (m, 9H). ^{13}C NMR (75 MHz, $CDCl_3$) δ: 178.6, 72.4, 55.4, 51.4, 49.7, 46.9, 41.4, 39.4, 37.7, 36.8, 35.9, 32.0, 31.9, 31.2, 24.1, 20.2, 19.3. Anal. calcd. for $C_{17}H_{30}O_3$: C 72.30, H 10.71; found: C 72.42, H 10.61.

Dehydration of alcohol 32 using Tf_2O–pyridine: synthesis of 35

To a solution of **32** (0.01 g, 0.04 mmol) in pyridine (1.0 mL) was added Tf_2O (0.013 mL, 0.08 mmol), and it

© 2006 NRC Canada

was stirred for 12 h at room temperature. The mixture was diluted with water (5 mL) and extracted with ether (5 mL × 3). Combined organic phases were washed with 0.5 N HCl (5 mL) and brine, dried over magnesium sulfate, filtered, and concentrated. After a chromatographic purification (silica gel, hexane–EtOAc, 10:1), **35** was obtained in 90% yield as a colorless oil. $[\alpha]^{20}_D$ +94.86 (*c* 1.0, $CHCl_3$). IR (neat, cm^{-1}): 2949 (s), 2918 (s), 1730 (s), 1467 (m), 1220 (m), 1158 (s). ^1H NMR (250 MHz, $CDCl_3$) δ: 3.59 (s, 3H), 2.50–2.30 (m, 1H), 2.25–1.59 (m, 8H), 1.65 (s, 3H), 1.44–1.35 (m, 2H), 1.20–1.10 (m, 2H), 0.97 (s, 3H), 0.87 (d, *J* = 6.5 Hz, 3H), 0.86 (s, 3H). ^{13}C NMR (62.9 MHz, $CDCl_3$) δ: 177.3, 136.9, 134.7, 61.7, 51.5, 38.1, 36.4, 35.7, 35.1, 34.43, 34.35, 29.6, 27.6, 26.2, 25.7, 22.1, 16.3. Anal. calcd. for $C_{17}H_{28}O_2$: C 77.22, H 10.67; found: C 77.34, H 10.44.

Dehydration of alcohol 32 using $POCl_3$–HMPA–pyridine and hydrolysis of ester: synthesis of 36

A 10 mL round-bottomed flask was charged with 0.053 g (0.19 mmol) of **32**, 2.0 mL of HMPA, and 0.2 mL of $POCl_3$. The resulting white suspension was stirred for 1 h at room temperature and for another 1 h in an oil bath at 50 °C. Pyridine (0.2 mL) was added, and the mixture was stirred at 50 °C for 1 h, at 75 °C for 45 min, and at 100 °C for 30 min. The mixture was allowed to cool to room temperature and was quenched by the dropwise addition of water (2 mL). The mixture was extracted with ether (5 mL × 3). The combined organic phases were washed with water (5 mL), dried over magnesium sulfate, filtered, and concentrated. The volatile compounds were removed under high vacuum, and the residue was dissolved in DMSO (2 mL). A few drops of water and 0.1 g of KOH were added, and the mixture was heated under reflux for 1 h. The reaction was allowed to cool to room temperature, 2 N HCl (5 mL) was added, and the mixture was extracted with ether (10 mL × 3). The organic phase was dried over magnesium sulfate, filtered, and concentrated. The crude product was purified by flash chromatography (hexane–EtOAc, 10:1). Acid **36** was obtained as a white solid (0.04 g, 88%). mp 133–135 °C. $[\alpha]^{20}_D$ +17.78 (*c* 1.0, $CHCl_3$). IR (KBr, cm^{-1}): 3435–2372 (s), 2952 (s), 1697 (s), 1466 (m), 1249 (m), 1205 (s). ^1H NMR (300 MHz, $CDCl_3$) δ: 12.00 (br, 1H), 5.50 (t, *J* = 8.4 Hz, 1H), 2.55 (d, *J* = 13.4 Hz, 1H), 2.31 (d, *J* = 13.5 Hz, 1H), 2.15–1.81 (m, 5H), 1.77 (s, 3H), 1.72–1.60 (m, 2H), 1.25–1.10 (m, 2H), 1.02 (d, *J* = 15.0 Hz, 1H), 0.95 (d, *J* = 6.5 Hz, 3H), 0.89 (s, 3H), 0.88 (s, 3H). ^{13}C NMR (75 MHz, $CDCl_3$) δ: 183.5, 135.4, 125.9, 58.2, 52.0, 40.7, 39.1, 38.9, 38.2, 34.7, 29.7, 28.1, 26.4, 20.1. Anal. calcd. for $C_{16}H_{26}O_2$: C 76.75, H 10.47; found: C 76.94, H 10.40.

Carboxy inversion: synthesis of (+)-dactylol (37)

A dried, 10 mL, round-bottomed flask was charged with 0.03 g (0.11 mmol) of acid **36**, 2.0 mL of 20% solution of $COCl_2$ in toluene, and four drops of DMF. The mixture was stirred at room temperature for 1 h, and then heated under reflux for 30 min. The mixture was allowed to cool to room temperature and was diluted with pentane (5 mL), filtered, and concentrated. The resulting colorless oil was dissolved in benzene (2.0 mL). *m*-CPBA (0.019 g, 0.11 mmol), pyridine (0.1 mL, 0.12 mmol), and DMAP (0.005 g) were added. The mixture was stirred at room temperature for 24 h, filtered, and concentrated. The volatile compounds were removed under high vacuum, and the residue was dissolved in ether (2 mL). The solution was cooled in an ice-water bath and 0.013 g (0.33 mmol) of $LiAlH_4$ was added. The suspension was stirred at 0 °C for 2 h and slowly quenched with water, filtered, and the white precipitate washed thoroughly with ether (5 mL × 3). The combined organic phases were concentrated, and the crude product was purified by flash chromatography (hexane–EtOAc, 10:1). (+)-Dactylol (**37**) was obtained as a white solid (0.012 g, 50%). mp 49 to 50 °C (lit. value (15e), mp 50.3–51.5 °C). $[\alpha]^{20}_D$ +21.38 (*c* 1.0, $CHCl_3$) (lit. value (15e)) $[\alpha]^{20}_D$ +22.5). IR (neat, cm^{-1}): 3500 (w), 2955 (s), 2872 (s), 1465 (m). ^1H NMR (300 MHz, $CDCl_3$) δ: 5.49 (t, *J* = 8.4 Hz, 1H), 2.21 (d, *J* = 13.4 Hz, 1H), 2.07 (d, *J* = 13.4 Hz, 1H), 1.95–1.85 (m, 2H), 1.82 (s, 3H), 1.80–1.71 (m, 1H), 1.70–1.60 (m, 1H), 1.57–1.49 (m, 2H), 1.46 (dd, *J* = 15.0, 7.9 Hz, 1H), 1.33 (br s, 1H), 1.09–0.95 (m, 2H), 0.91 (d, *J* = 6.6 Hz, 3H), 0.90 (s, 3H), 0.85 (s, 3H), 0.71 (d, *J* = 114.6 Hz, 1H). ^{13}C NMR (75 MHz, $CDCl_3$) δ: 135.9, 124.6, 82.8, 52.9, 43.1, 40.4, 39.4, 39.3, 36.5, 35.2, 29.5, 29.3, 28.9, 27.9, 19.2. Anal. calcd. for $C_{15}H_{26}O$: C 81.02, H 11.78; found: C 81.27, H 12.00.

[4 + 3] Cycloaddition of 11: synthesis of 38 and 39

Ketone **11** was subjected to an α-chlorination, [4 + 3] cycloaddition, and desilylation conditions using the procedure described in the synthesis of ketone **20**. Cycloadduct **38** and **39** were obtained and separated by hexane–EtOAC (20:1).

38

Yield: 47%, colorless oil. IR (neat, cm^{-1}): 3069 (m), 2950 (s), 2872 (s), 1730 (s), 1454 (m). ^1H NMR (250 MHz, $CDCl_3$) δ: 4.84 (s, 1H), 4.80–4.73 (m, 1H), 2.45–2.30 (m, 3H), 2.26–2.09 (m, 2H), 2.00–1.80 (m 3H), 1.79–1.40 (m, 6H), 1.39–1.29 (m, 1H), 1.21–1.09 (m, 1H). ^{13}C NMR (62.9 MHz, $CDCl_3$) δ: 221.3, 146.0, 115.4, 58.2, 51.7, 43.7, 41.5, 40.0, 36.7, 36.3, 33.8, 26.3, 19.8. Anal. calcd. for $C_{13}H_{18}O$: C 82.06, H 9.53; found: C 81.92, H 9.65.

39

Yield: 18%, colorless oil. IR (neat, cm^{-1}): 3071 (w), 2957 (s), 2870 (m), 1737 (s), 1451 (m). ^1H NMR (250 MHz, $CDCl_3$) δ: 4.80–4.65 (m, 2H), 2.70 (dd, *J* = 7.1, 15.0 Hz, 1H), 2.26–2.54 (m, 1H), 2.38 (dd, *J* = 3.2, 13.6 Hz, 1H), 2.30–2.07 (m, 5H), 1.91–1.27 (m, 8H). ^{13}C NMR (62.9 MHz, $CDCl_3$) δ: 221.4, 145.8, 114.6, 58.5, 51.6, 44.8, 38.9, 36.1, 33.2, 30.0, 27.8, 26.2, 21.6. Anal. calcd. for $C_{13}H_{18}O$: C 82.06, H 9.53; found: C 81.95, H 9.33.

[4 + 3] Cycloaddition of 12: synthesis of 45 and 46

Ketone **12** was subjected to an α-chlorination, [4 + 3] cycloaddition, and desilylation conditions using the procedure described in the synthesis of ketone **20**. Cycloadducts **45** and **46** were obtained and separated by pentane–Et_2O (20:1).

45

Yield: 57%, colorless oil. $[\alpha]^{20}_D$ +41.46 (*c* 1.0, $CHCl_3$). IR (neat, cm^{-1}): 3070 (w), 2950 (s), 2863 (m), 1733 (s), 1456 (m). ^1H NMR (250 MHz, $CDCl_3$) δ: 4.87 (br s, 1H), 4.80 (t,

© 2006 NRC Canada

J = 1.9 Hz, 1H), 2.49–2.36 (m, 3H), 2.30–2.13 (m, 2H), 1.99–1.62 (m, 5H), 1.55–1.22 (m, 4H), 1.16–1.05 (m, 1H), 1.00 (d, *J* = 6.2 Hz, 3H). ^{13}C NMR (62.9 MHz, $CDCl_3$) δ: 221.3, 145.8, 115.3, 59.1, 59.0, 43.7, 43.1, 40.3, 39.5, 37.4, 35.1, 31.9, 19.7, 18.2. HR-MS (EI) calcd. for $C_{14}H_{20}O$ (M^+): 204.1514; found: 204.1499.

46

Yield: 9%, colorless oil. $[\alpha]^{20}_D$ –108.75 (*c* 1.0, $CHCl_3$). IR (neat, cm^{-1}): 3070 (w), 2951 (s), 2866 (m), 1733 (s), 1449 (m). ^{1}H NMR (250 MHz, $CDCl_3$) δ: 4.80–4.73 (m, 2H), 2.72 (dd, *J* = 5.9, 12.5 Hz, 1H), 2.62–2.50 (m, 1H), 2.38 (dd, *J* = 2.9, 11.5 Hz, 1H), 2.27–1.61 (m, 8H), 1.40–1.22 (m, 2H), 1.09–0.95 (m, 2H), 1.00 (d, *J* = 5.4 Hz, 3H). ^{13}C NMR (62.9 MHz, $CDCl_3$) δ: 221.4, 145.7, 114.7, 59.3, 58.3, 44.8, 39.1, 37.1, 34.4, 31.3, 31.2, 29.2, 26.2, 18.6. HR-MS (EI) calcd. for $C_{14}H_{20}O$ (M^+): 204.1514; found: 204.1517.

[4 + 3] Cycloaddition of 17: synthesis of 49–52

Ketone **17** was subjected to an α-chlorination, [4 + 3] cycloaddition, and desilylation conditions using the procedure described in the synthesis of ketone **20**. Cycloadducts **49**–**52** were obtained and separated by pentane–Et_2O (20:1 to 10:1). Ketone **49** and **50** were not completely isolable. The mixture was obtained as slightly yellow oil (41%). Further chromatographic purification on silica gel (pentane–Et_2O, 30:1) afforded a sufficient amount of each isomer along with a mixture of the two isomers.

49

$[\alpha]^{20}_D$ +62.08 (*c* 1.0, $CHCl_3$). IR (neat, cm^{-1}): 3072 (w), 2949 (s), 2866 (s), 1731 (s), 1642 (m), 1452 (m). ^{1}H NMR (250 MHz, $CDCl_3$) δ: 4.83 (s, 1H), 4.77 (t, *J* = 2.0 Hz, 1H), 2.46–2.33 (m, 2H), 2.31–2.15 (m, 2H), 2.13–2.00 (m, 2H), 1.99–1.84 (m, 2H), 1.81–1.61 (m, 3H), 1.59–1.24 (m, 3H), 1.22–1.08 (m, 1H), 1.04 (d, *J* = 66 Hz, 3H). ^{13}C NMR (62.9 MHz, $CDCl_3$) δ: 220.8, 146.6, 115.1, 60.2, 52.7, 51.3, 46.1, 41.8, 39.2, 36.4, 33.6, 28.0, 26.3, 21.0. HR-MS (EI) calcd. for $C_{14}H_{20}O$ (M^+): 204.1514; found: 204.1510.

50

$[\alpha]^{20}_D$ +13.64 (*c* 1.0, $CHCl_3$). IR (neat, cm^{-1}): 3069 (w), 2934 (s), 2869 (m), 1733 (s), 1643 (m), 1456 (m). ^{1}H NMR (250 MHz, $CDCl_3$) δ: 4.91–4.88 (m, 1H), 4.85 (br s, 1H), 2.64 (dd, *J* = 4.7, 12.6 Hz, 1H), 2.54 (d, *J* = 13.6 Hz, 1H), 2.38–2.12 (m, 5H), 1.99–1.41 (m, 7H), 1.28–1.17 (m, 1H), 1.12 (d, *J* = 6.0 Hz, 3H). ^{13}C NMR (62.9 MHz, $CDCl_3$) δ: 223.5, 146.3, 114.2, 57.9, 55.0, 51.6, 47.3, 40.1, 36.9, 34.3, 34.2, 30.7, 25.8, 15.1. HR-MS (EI) calcd. for $C_{14}H_{20}O$ (M^+): 204.1514; found: 204.1520.

51

Yield: 7%, colorless oil. $[\alpha]^{20}_D$ +32.17 (*c* 1.0, $CHCl_3$). IR (neat, cm^{-1}): 3072 (w), 2953 (s), 2871 (s), 1737 (s), 1637 (w), 1457 (m). ^{1}H NMR (250 MHz, $CDCl_3$) δ: 4.78–4.71 (m, 2H), 2.75–2.63 (m, 1H), 2.48–2.34 (m, 2H), 2.29–2.04 (m, 5H), 1.89–1.26 (m, 6H), 1.13 (dd, *J* = 6.7, 20.7 Hz, 1H), 1.04 (d, *J* = 7.0 Hz, 3H). ^{13}C NMR (62.9 MHz, $CDCl_3$) δ: 221.0, 145.8, 114.8, 59.8, 54.2, 51.5, 38.3, 37.5, 36.5, 34.7, 33.9, 30.1, 23.9, 21.6. HR-MS (EI) calcd. for $C_{14}H_{20}O$ (M^+): 204.1514; found: 204.1503.

52

Yield: 4%, colorless oil. IR (neat, cm^{-1}): 3072 (w), 2948 (s), 2872 (s), 1738 (s), 1635 (w), 1455 (m). ^{1}H NMR (300 MHz, $CDCl_3$) δ: 4.79–4.74 (m, 2H), 2.52–1.52 (m, 13H), 1.44–1.19 (m, 2H), 1.13 (d, *J* = 6.8 Hz, 3H). ^{13}C NMR (75 MHz, $CDCl_3$) δ: 220.4, 145.6, 115.3, 59.6, 52.3, 50.8, 37.5, 35.7, 34.3, 30.7, 29.9, 29.6, 21.8, 15.6. HR-MS (EI) calcd. for $C_{14}H_{20}O$ (M^+): 204.1514; found: 204.1524.

[4 + 3] Cycloaddition of 19: synthesis of 53–56

Ketone **19** was subjected to an α-chlorination, [4 + 3] cycloaddition, and desilylation conditions using the procedure described in the synthesis of ketone **20**. Cycloadducts **53**–**56** were obtained and separated by pentane–Et_2O (30:1 to 10:1).

53

Yield: 11%, colorless oil. $[\alpha]^{20}_D$ +67.40 (*c* 1.0, $CHCl_3$). IR (neat, cm^{-1}): 2950 (s), 2927 (s), 2867 (m), 1732 (s), 1455 (m), 1379 (m). ^{1}H NMR (250 MHz, $CDCl_3$) δ: 4.85 (br s, 1H), 4.80–4.78 (m, 1H), 2.45–2.36 (m, 1H), 2.30–1.90 (m, 7H), 1.80–1.57 (m, 3H), 1.50–1.40 (m, 1H), 1.38–1.23 (m, 2H), 1.04 (d, *J* = 6.3 Hz, 3H), 0.83 (d, *J* = 7.2Hz, 3H). ^{13}C NMR (62.9 MHz, $CDCl_3$) δ: 221.1, 147.6, 115.2, 60.8, 53.4, 52.9, 46.6, 39.5, 39.3, 37.5, 34.1, 31.7, 28.1, 21.0, 15.1. Anal. calcd. for $C_{15}H_{22}O$: C 82.52, H 10.16; found: C 82.67, H 10.33.

54

Yield: 41%, colorless oil. $[\alpha]^{20}_D$ +34.55 (*c* 1.0, $CHCl_3$). IR (neat, cm^{-1}): 2950 (s), 2933 (s), 2868 (m), 1731 (s), 1452 (m), 1165 (w). ^{1}H NMR (250 MHz, $CDCl_3$) δ: 4.92–4.88 (m, 1H), 4.85 (br s, 1H), 2.64–2.53 (m, 2H), 2.35–2.12 (m, 5H), 1.94–1.81 (m, 2H), 1.60–1.18 (m, 5H), 1.12 (d, *J* = 6.2 Hz, 3H), 0.93 (d, *J* = 6.3 Hz, 3H). ^{13}C NMR (62.9 MHz, $CDCl_3$) δ: 223.6, 146.1, 114.2, 61.2, 58.7, 51.5, 48.0, 40.8, 28.3, 34.9, 34.8, 34.5, 30.7, 17.3, 15.1. Anal. calcd. for $C_{15}H_{22}O$: C 82.52, H 10.16; found: C 82.36, H 9.97.

55

Yield 12%, colorless oil. $[\alpha]^{20}_D$ +75.05 (*c* 1.0, $CHCl_3$). IR (neat, cm^{-1}): 2950 (s), 2932 (s), 2863 (m), 1732 (s), 1456 (m), 1375 (m). ^{1}H NMR (250 MHz, $CDCl_3$) δ: 4.77 (br s, 1H), 4.75–4.72 (m, 1H), 2.71 (dd, *J* = 7.6, 14.9 Hz, 1H), 2.50–1.60 (m, 10H), 1.43–1.07 (m, 3H), 1.02 (d, *J* = 6.9 Hz, 3H), 1.00 (d, *J* = 6.5 Hz, 3H). ^{13}C NMR (62.9 MHz, $CDCl_3$) δ: 220.8, 145.7, 114.8, 60.5, 58.1, 54.1, 38.7, 38.4, 37.2, 34.8, 34.6, 32.0, 31.3, 23.8, 18.6. Anal. calcd. for $C_{15}H_{22}O$: C 82.52, H 10.16; found: C 82.39, H 10.19.

56

Yield 7%, colorless oil. $[\alpha]^{20}_D$ +25.40 (*c* 1.0, $CHCl_3$). IR (neat, cm^{-1}): 2956 (s), 2868 (s), 1737 (s), 1460 (m), 1169 (m), 1121 (w). ^{1}H NMR (250 MHz, $CDCl_3$) δ: 4.82–4.76 (m, 2H), 2.53–1.61 (m, 12H), 1.50–1.18 (m, 2H), 1.11 (d, *J* = 6.7 Hz, 3H), 0.89 (d, *J* = 7.2 Hz, 3H). ^{13}C NMR (62.9 MHz, $CDCl_3$) δ: 220.5, 146.0, 115.7, 59.4, 54.3, 51.3, 36.9, 35.2, 35.0, 34.4, 33.4, 31.9, 29.4, 18.4, 15.4. Anal. calcd. for $C_{15}H_{22}O$: C 82.52, H 10.16; found: C 82.51, H 9.99.

© 2006 NRC Canada

Acknowledgment

This paper is dedicated to Dr. Alfred R. Bader on the occasion of his 80th birthday and as a tribute to his many contributions to organic chemistry, art, scholarship, and humanity. This work was supported by the National Science Foundation, to whom we are grateful.

References

1. (*a*) M. Harmata. Acc. Chem. Res. **34**, 595 (2001;. (*b*) M. Harmata. Tetrahedron, **53**, 6235 (1997); (*c*) M. Harmata. *In* Advances in cycloaddition. Vol. 4. *Edited by* M. Lautens. JAI, Greenwich. 1997. pp. 41–86.
2. (*a*) M. Harmata and S. Wacharasindhu. Org. Lett. **7**, 2563, (2005); (*b*) M. Harmata and G.J. Bohnert. Org. Lett. **5**, 59 (2003); (*c*) M. Harmata and P. Rashatasakhon. Org. Lett. **3**, 2533 (2001); (*d*) M. Harmata and P. Rashatasakhon. Org. Lett. **2**, 2913 (2000); (*e*) M. Harmata and K.W. Carter. Tetrahedron Lett. **38**, 7985 (1997); (*f*) J. Cha and J. Oh. Curr. Org. Chem. **2**, 217 (1998).
3. (*a*) Y. Wang, A.Yong, M. Atta, and F.G. West. J. Am. Chem. Soc. **121**, 876 (1999); (*b*) M. Harmata, S. Elomari, and C.L. Barnes. J. Am. Chem. Soc. **118**, 2860 (1996); (*c*) M. Harmata, S. Elahmad, and C.L. Barnes. J. Org. Chem. **59**, 1241 (1994); (*d*) F.G. West, C. Hartke-Karger, D.J. Koch, C.E. Kuehn, and A.M. Arif. J. Org. Chem. **58**, 6795 (1993).
4. W.H. Bunnelle and B.A. Narayanan. Org. Synth. **69**, 89 (1990).
5. R. Scheffold and E. Saladin. Angew. Chem. Int. Ed. Engl. **11**, 229 (1972).
6. S.E. Denmark and C.B.W. Senanayake. J. Org. Chem. **58**, 1853 (1993).
7. R. Boss and R. Scheffold. Angew. Chem. Int. Ed. Engl. **15**, 558 (1976).
8. (*a*) A.P. Krapcho. Synthesis, 805 (1982); (*b*) A.P. Krapcho. Synthesis, 893 (1982).
9. J.N. Marx and L.R. Norman. J. Org. Chem. **40**, 1602 (1975).
10. M. Harmata and P. Rashatasakhon. Tetrahedron Lett. **43**, 3641 (2002).
11. F.N. Tebbe, G.W. Parshall, and G.S. Reddy. J. Am. Chem. Soc. **100**, 3611 (1978).
12. B.M. Trost and L.N. Jungheim. J. Am. Chem. Soc. **102**, 7910 (1980).
13. C.M. Marson and P.R. Giles. Synthesis using Vilsmeier reagents. CRC, Boca Raton, Fl. 1994.
14. D.B. Denney and N. Sherman. J. Org. Chem. **30**, 3760 (1965).
15. (*a*) L.A. Paquette, W.H. Ham, and D.S. Dime. Tetrahedron Lett. **26**, 4983 (1985); (*b*) R.C. Gadwood, R.M. Lett, and J.E. Wissinger. J. Am. Chem. Soc. **108**, 6343 (1986); (*c*) K.S. Feldman, M.J. Wu, and D.P. Rotella. J. Am. Chem. Soc. **111**, 6457 (1989); (*d*) K.S. Feldman, M.J. Wu, and D.P. Rotella. J. Am. Chem. Soc. **112**, 8490 (1990); (*e*) G.A. Molander and P.R. Eastwood. J. Org. Chem. **60**, 4559 (1995); (*f*) A. Fürstner and K. Langemann. J. Org. Chem. **61**, 8746 (1996).
16. C.J. Cramer, M. Harmata, and P. Rashatasakhon. J. Org. Chem. **66**, 5641 (2001).
17. R.J. Giguere, S.M. Tassely, and M.I. Rose. Tetrahedron Lett. **31**, 4577 (1990).
18. J.H. Rigby and F.C. Pigge. Org. React. **51**, 351 (1997).
19. B. Simonot and G. Rousseau. J. Org. Chem. **59**, 5912 (1994).

© 2006 NRC Canada

Polycyclic oxonium ylides — Use of cyclic acetals as convenient scaffolds in the construction of fused bicyclic compounds containing a medium ring[1]

Graham K. Murphy, Fredrik P. Marmsäter, and F.G. West

Abstract: Cyclic mixed acetals with pendant diazoketone side chains undergo efficient rearrangement to ether-bridged cyclooctanoid and cycloheptanoid systems upon treatment with $Cu(hfacac)_2$. Stevens [1,2]-shift of an oxonium ylide furnishes the major product, in some cases accompanied by minor amounts of a product resulting from [1,2]-shift of a sulfonium ylide. These results demonstrate that hetero-substituted carbons are suitable migrating groups for the Stevens [1,2]-shift of oxonium ylides. In cases employing a mixed thioacetal, the resulting sulfide served as a trigger for cleavage of the bridging ether through one of two complementary strategies. In the hydrazulene series, the desired bicyclo[5.3.0]heptene was accompanied by the product of novel transannular S_N2' attack on the resulting allylic ketal.

Key words: [1,2]-shift, diazo, medium-sized ring, oxonium ylide, ring expansion.

Résumé : Les acétals cycliques mixtes portant des chaînes latérales diazocétones soumis à un traitement avec du $Cu(hfacac)_2$ subissent un réarrangement efficace en systèmes cyclooctanoïdes et cycloheptanoïdes à pont éther. Un déplacement [1,2] de Stevens d'un ylure d'oxonium conduit à la formation du produit principal qui est dans quelques cas accompagné de quantités mineures d'un produit qui résulte d'un déplacement [1,2] d'un ylure de sulfonium. Ces résultats démontrent que les carbones substitués par des hétéroatomes sont des groupes migratoires appropriés pour le déplacement [1,2] de Stevens d'ylures d'oxonium. Dans les cas où on fait appel à un acétal mixte, le sulfure qui en résulte sert à déclencher le clivage de l'éther de pont par le biais d'une des deux stratégies complémentaires. Dans la série de l'hydroazulène, le bicyclo[5.3.0]heptène est accompagné par le produit d'une nouvelle attaque transannulaire S_N2' sur le cétal allylique qui en résulte.

Mots clés : déplacement [1,2], diazo, cycle de taille moyenne, ylure d'oxonium, expansion de cycle.

[Traduit par la Rédaction]

Introduction

Stereocontrolled synthesis of medium-sized carbocycles is an important challenge in synthetic organic chemistry. We have had a long-standing interest in the chemical synthesis of natural products such as dactylol, traversianal, and phorbol (Fig. 1). Common structural features among these compounds include the presence of a functionalized medium-sized ring fused to one or more smaller rings, along with bridgehead oxygenation. Efforts towards the chemical synthesis of these compounds have resulted in many new methods (1). For example, use of a preexisting carbocyclic or heterocyclic ring as a scaffold could allow the formation of an intermediate bridged bicyclic compound by closure of a smaller second ring. Fragmentation of the bridge would then reveal a medium-ring skeleton and install a bridgehead hydroxyl group (2), although attempted cleavage of bridging ethers (3) or their carbon analogues (4) is not always a straightforward process.

The Stevens [1,2]-shift of fused bicyclic oxonium ylides can furnish medium-ring ethers or carbocycles with bridging ethers (5). Early examples typically involved the migration of aryl-substituted carbons, and the products were not well suited to synthetic manipulation. In an effort to broaden the synthetic potential of this approach, we have examined various hetero-substituted examples of the oxonium ylide ring expansion (6, 7). By this approach, bicyclic acetals with bridgehead diazoketone side chains could be used as convenient scaffolds for the construction of seven- and eight-membered carbocycles (Scheme 1). The key [1,2]-shift step is believed to involve a stepwise homolytic mechanism, with subsequent recombination of the intermediate biradical (8).

Here we present a full account of this work, an oxonium ylide-based method that permits the concise synthesis of

Received 8 February 2006. Accepted 7 June 2006. Published on the NRC Research Press Web site at http://canjchem.nrc.ca on 30 November 2005.

Dedicated to Dr. Alfred Bader in recognition of his immense impact on the field of organic chemistry and his lasting legacy to Canadian science.

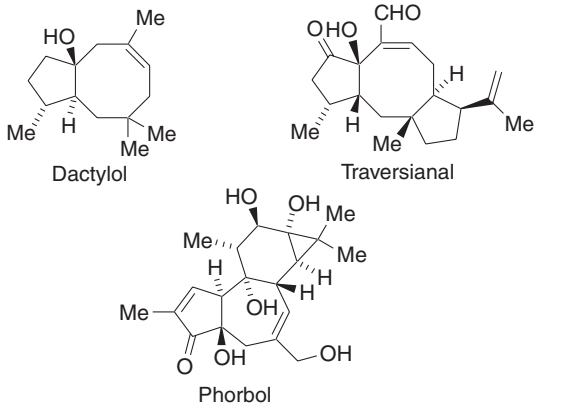
G.K. Murphy, F.P. Marmsäter, and F.G. West.[2]
Department of Chemistry, University of Alberta, W5-67 Gunning-Lemieux Chemistry Centre, Edmonton, AB T6G 2G2, Canada.

[1]This article is part of a Special Issue dedicated to Dr. Alfred Bader.

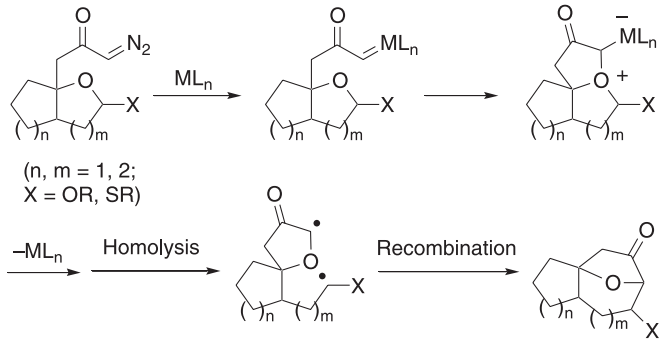
[2]Corresponding author (e-mail: frederick.west@ualberta.ca).

 doi:10.1139/V06-111 © 2006 NRC Canada

Fig. 1. Medium ring containing natural products possessing angular hydroxyls.



Scheme 1.



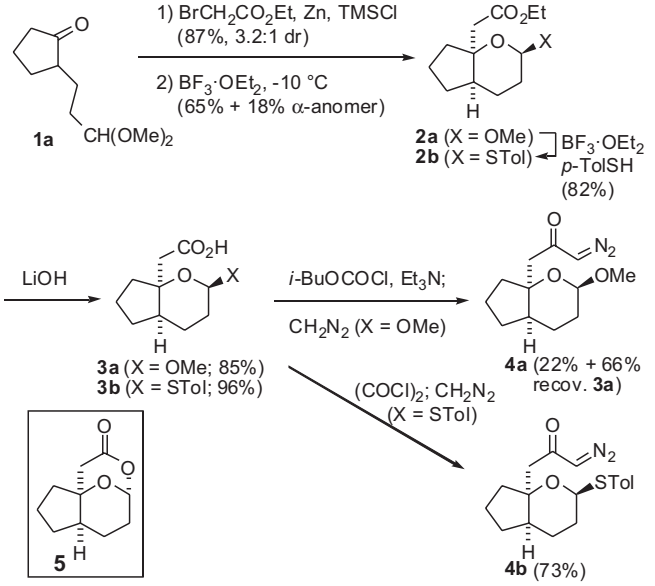
functionalized fused 5–8 and 5–7 bicyclic ring systems using a novel sulfur- or oxygen-directed Stevens rearrangement of oxonium ylides. In addition, convenient methodology is described for subsequent sulfur-mediated cleavage of the ether bridge to introduce a bridgehead alcohol.

Results and discussion

Substrate synthesis

Substrates were prepared in a straightforward fashion via cyclopentanone precursors **1** (Scheme 2). Reformatsky addition of ethyl bromoacetate to the known 2-(3,3)-dimethoxypropyl)-cyclopentanone **1a** (9) was followed by conversion to cyclic acetal **2a** with $BF_3{\cdot}OEt_2$. The methoxy group of the acetal could be exchanged for STol with careful control of temperature and stoichiometry to give mixed thioacetal **2b**. Both **2a** and **2b** were formed as the expected β anomers. Saponification to the acids **3a** and **3b** was uneventful and these intermediates were then converted to the desired diazoketones **4a** and **4b**. Diazoketone **4a** was formed via activation of **3a** as the mixed anhydride, followed by treatment with diazomethane. This method was not suitable in the case of **3b**, as the mixed anhydride was found to be insufficiently reactive. The corresponding acid chloride did furnish some of **4b**, but the process was complicated by the formation of lactone-bridged side product **5**. This material presumably results from acid-catalyzed decomposition of the

Scheme 2.



thioacetal with subsequent trapping by the carboxyl group. We eventually found that careful control of reaction temperature minimized the formation of **5**, allowing access to **4b** in 73% yield.

The lower homologue **1b** (10) was treated with the lithium enolate of ethyl acetate and the diastereomeric adducts were treated with $BF_3{\cdot}OEt_2$ (Scheme 3).[3] This effected cyclization of the cis isomer to the fused bicyclic mixed acetals **2c** and **2d** (4.4:1 mixture of anomers), while leaving the trans diastereomer unchanged. Thio exchange (HSTol, $BF_3{\cdot}OEt_2$) furnished the corresponding mixed thioacetals **2e** and **2f** in good yield. The esters **2c**–**2f** were subjected to saponification to give acids **3c**–**3f**, then converted to diazoketones **4c**–**4f**. As before, the methoxy acetals could be activated via the mixed anhydrides, but the thioacetals required the more reactive acid chlorides. In these cases, the presence of 2,6-lutidine was found to suppress acid-catalyzed decomposition, allowing the formation of **4e** and **4f** in 60% yield.

Finally, two substrates possessing additional carbonyl stabilization at the incipient ylide centre were prepared (Scheme 4). Mixed thioacetals **2b**, **2e**, and **2f** were condensed with ethyl acetate to furnish the corresponding keto esters **6a**–**6c**. Attempts to form **6a** more directly by the addition of the dianion of ethyl acetoacetate to **1a** and **1b**, cyclization to the mixed acetal, and thio exchange encountered a variety of undesired side reactions, so the crossed Claisen approach was followed in all three cases. Standard diazotransfer conditions with *p*-toluenesulfonyl azide (11) were then carried out on **6a** and the major five-membered anomer **6b** to yield the diazoketones **4g** and **4h**.

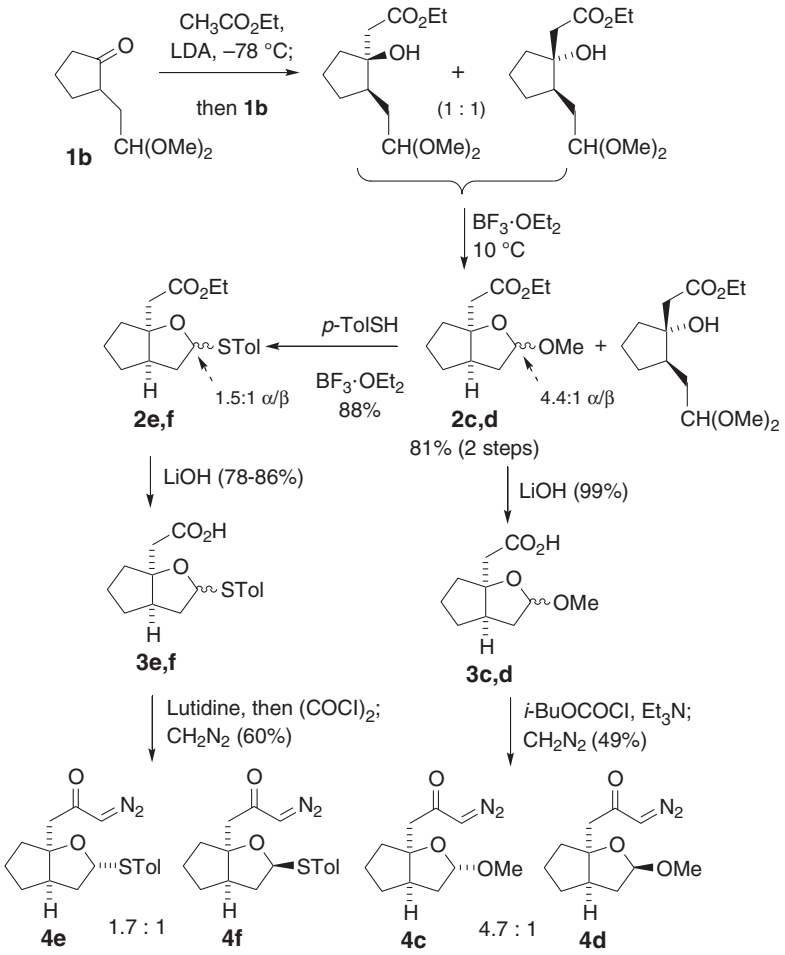
Oxonium ylide generation and rearrangement — Formation of bicyclo[6.3.0]undecanones and bicyclo[5.3.0]decanones

Substrates **4a**–**4h** were subjected to catalytic carbene transfer conditions to effect generation of the desired

[3] Use of Reformatsky conditions resulted in similar diastereromer ratios and lower yields.

© 2006 NRC Canada

Scheme 3.



oxonium ylide intermediates. Initial trials with thioacetal **4b** (Scheme 5) were conducted using several transition metal catalysts known to effect oxonium ylide formation (8, 12). Rhodium(II) catalysts were found to be ineffective: both rhodium(II) acetate dimer and the bulkier rhodium(II) triphenylacetate (13) gave a side product tentatively assigned as **8** and only minor amounts of the desired [1,2]-shift product **7b**.[4] There is considerable precedent for poor selectivity for oxonium ylide formation vs. C–H insertion with rhodium carbenoids (5*b*, 8, 12). The optimal conditions ($Cu(tfacac)_2$, CH_2Cl_2, reflux) for the generation and [2,3]-shift of allyl-substituted oxonium ylides (12, 14) gave only low yields of several unidentified products, consistent with the observation that this catalyst is not effective for 1,2]-shift processes (14). In contrast to the above, $Cu(hfacac)_2$ provided **7b** in high yield and with excellent diastereoselectvity. The major diastereomer of **7b** was the result of a [1,2]-shift with retention of configuration at the migrating anomeric centre.[5] Mixed acetal **4a** was also subjected to the optimized conditions found for **4b** and furnished the analogous [1,2]-shift product **7a** in good yield as a single diastereomer, again the result of migration with retention.

The five-membered acetal substrates **4c**–**4f** were next examined (Scheme 6). In each case, the desired ether-bridged bicyclo[5.3.0]octanone system was formed, although the degree of stereochemical retention observed was substantially lower than with **4a** and **4b**. Thus, either the α anomer (**4c**) or the β anomer (**4d**) of the methoxy mixed acetal provided a mixture of **7c** and **7d** in moderate yield, in each case with a small preference for the product of retention. In the case of **4c**, an additional very minor product was isolated and tentatively assigned as structure **9**.[6] Mixed thioacetal **4f** underwent conversion to **7e** and **7f** in excellent yield and with relatively good diastereoselectivity. The corresponding α anomer (**4e**) provided the same products in somewhat lower yield, but in this case a side product, **10e**, was isolated in significant quantities. This compound apparently results from formation of the alternative sulfonium ylide **A**, fol-

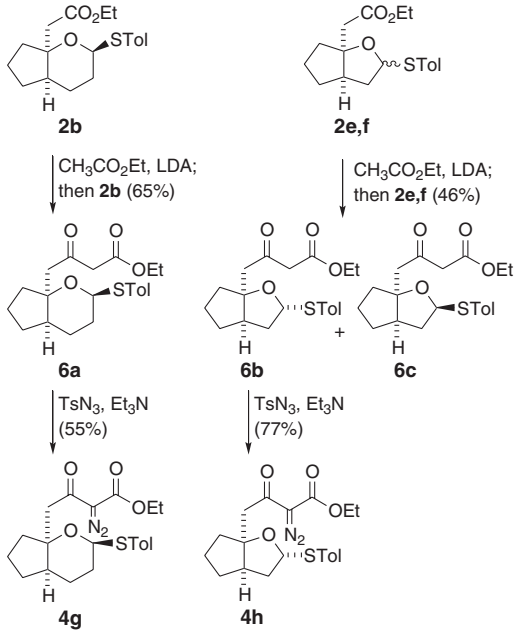
[4] Spectral data indicated a newly formed ketone and an intact thioacetal. Evidence for the proposed structure includes the apparent presence of an anomeric acetal-type proton in the ^1H NMR spectrum and a ^{13}C NMR carbonyl chemical shift consistent with a cyclopentanone.

[5] X-ray data confirming the structures of compounds **7b** and **12** can be found in CIF format in the Supporting Information of ref. 7*a*.

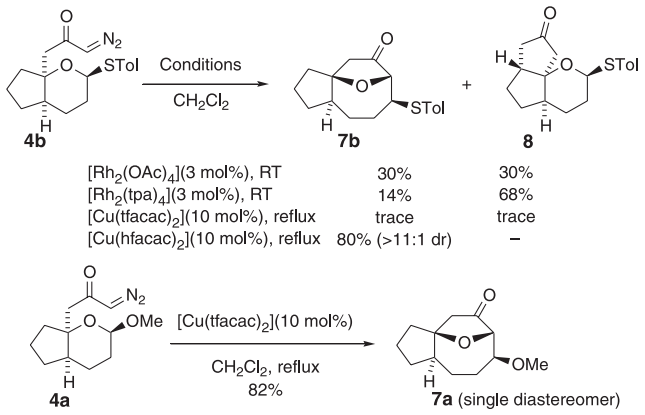
[6] Compound **9** may arise from competing formation of the oxonium ylide derived from the OMe group, followed by a 1,4-shift of the methyl substituent. Evidence for the proposed structure of this acid-labile substance includes the presence of both an enol ether and an anomeric carbon, and its silica gel-mediated conversion to an apparent α-methoxy aldehyde.

© 2006 NRC Canada

Scheme 4.



Scheme 5.



lowed by [1,2]-shift of the anomeric carbon with concomitant ring contraction.

Finally, the doubly stabilized diazoketoester substrates **4g** and **4h** were subjected to $Cu(hfacac)_2$ in refluxing toluene (Scheme 7). Six-membered thioacetal **4g** underwent conversion to **7g** (4.5:1 mixture of diastereomers) in moderate yield. The five-membered thioacetal **4h** gave dramatically different results: only minor amounts of the oxonium ylide-derived products **7h** and **7i** (8:1 dr) were obtained. Instead, the major product was **10h** (ca. 7:1 dr), resulting from selective formation and rearrangement of the sulfonium ylide.

In the key rearrangement steps, it appears that in most cases the oxonium ylide was formed efficiently with $Cu(hfacac)_2$ catalysis and underwent smooth a [1,2]-shift to give the ether-bridged medium-ring products. The exceptions are the doubly stabilized substrates **4g** and **4h**, which did not react in refluxing CH_2Cl_2 and required extended stirring in refluxing toluene to consume starting material. Carbene transfer from diazo compounds substituted with two electron-withdrawing groups is known to be relatively slow.[7] Although the diastereoselectivity varied substantially, in all cases the major product resulted from migration with retention of configuration. Most mechanistic evidence related to ylide [1,2]-shifts points to stepwise rearrangement via radical pair intermediates (8). However, rearrangement with moderate to high degrees of retention in the Stevens rearrangement of both oxonium (5) and ammonium (15) ylides has been observed. One possible explanation for migration with retention is rapid radical recombination as compared with bond rotation (16). However, direct involvement by the transition metal catalyst in the rearrangement step cannot be ruled out (8*b*, 17).

The origin of the lower levels of retention seen for the five-membered acetals **4c**–**4f** as compared with the six-membered substrates **4a**, **4b**, and **4g**, is unclear. Assuming a stepwise mechanism via a radical pair intermediate, this result suggests that the relative rate for recombination vs. bond rotation is greater for six-membered rings despite the presence of an additional freely rotating C–C bond in the side chain. A possible explanation may derive from the relative strain of the angularly fused tricyclic ylide precursors. Homolysis of the more strained 5-5-5 tricyclic ylide **B** could involve greater ring strain release, which might permit a higher amount of randomization by the biradical **C** prior to recombination than in the case of the higher homologues **D** and **E** (Scheme 8; shown for β anomers but also applicable to α anomers **4c**, **4e**, and **4h**). Recombination of **C** may also be slowed relative to that of **E** as a result of increased strain in the cyclization transition state due to the shorter tether. However, since involvement of the catalyst in the [1,2]-shift is also possible (8*b*, 14), this explanation must be viewed as tentative.

Competing formation of the ylide derived from the exocyclic XR group was observed in several cases. This was not seen for six-membered acetal substrates **4a**, **4b**, and **4g** due to the predominant or exclusive formation of the β anomers, with the XR group disposed trans to the diazoketone side chain. On the other hand, the five-membered acetals were formed as anomeric mixtures, and products apparently resulting from the alternative ylides were seen in each case with the α anomers (**4c**, **4e**,and **4h**). Notably, **4h** reacted mainly via the 7-membered sulfonium ylide, possibly as a result of the greater electrophilicity and (or) selectivity of the metallocarbene precursor. Equilibration between the two possible ylides may be possible, based on related competition experiments (4).

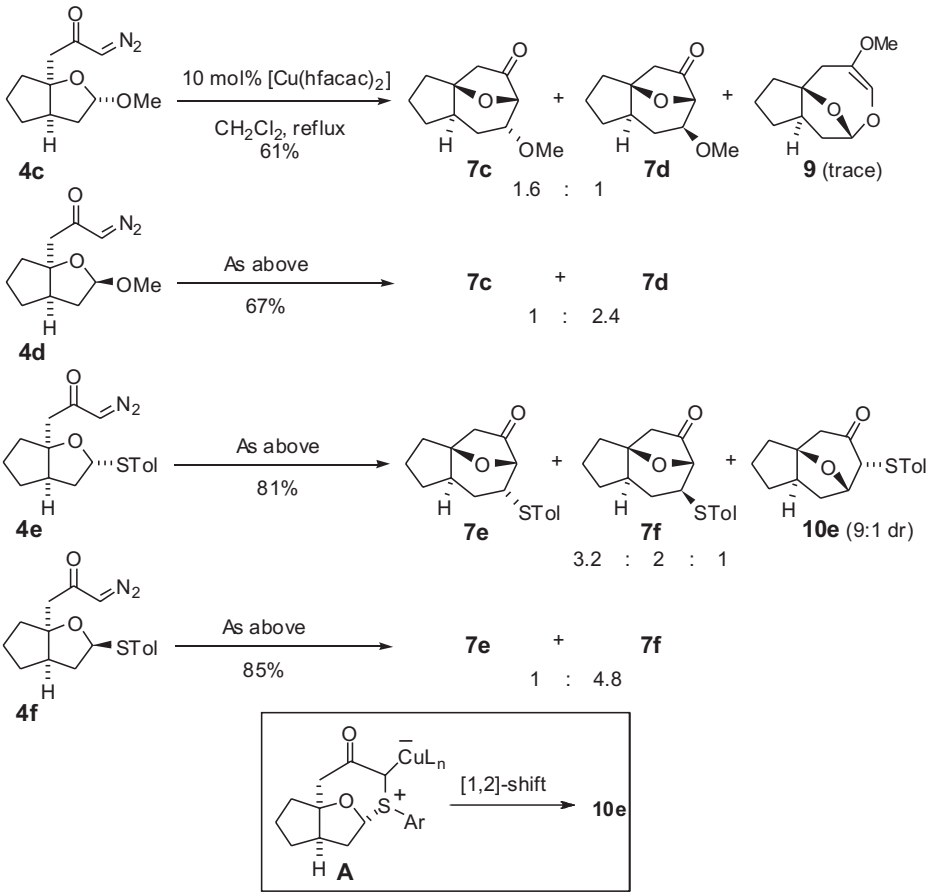
Cleavage of the ether bridge

The methodology described above allows for quick entry into a series of ether-bridged fused bicyclic skeletons containing a medium-sized ring. For application to natural product targets, an effective method for cleavage of the bridging ether is needed. We felt that the thioacetal-derived products **7b** and **7e** were well suited to this goal: the thioaryl group, which had effectively mediated the [1,2]-shift of the former anomeric carbon, could now be used as an anionic trigger for eliminative opening of the ether. First, the keto group of

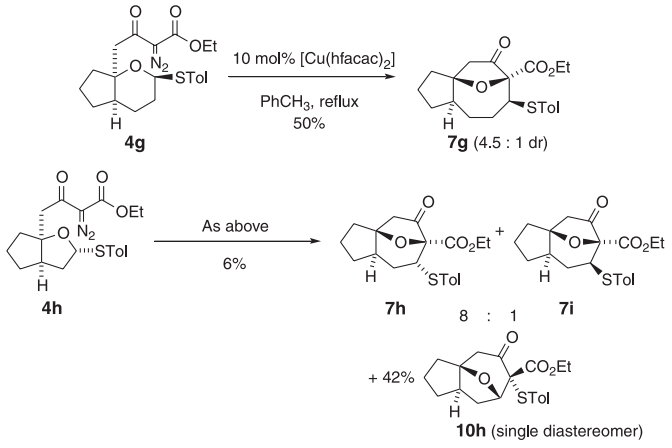
[7] See ref. 11, pp. 64–65.

© 2006 NRC Canada

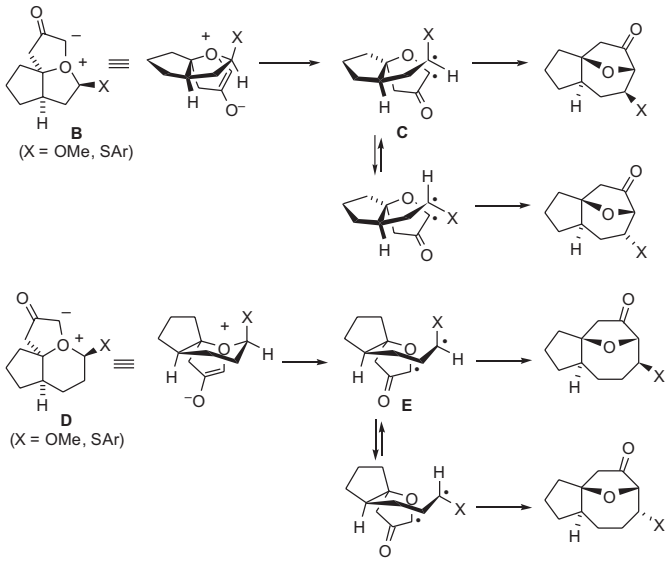
Scheme 6.



Scheme 7.



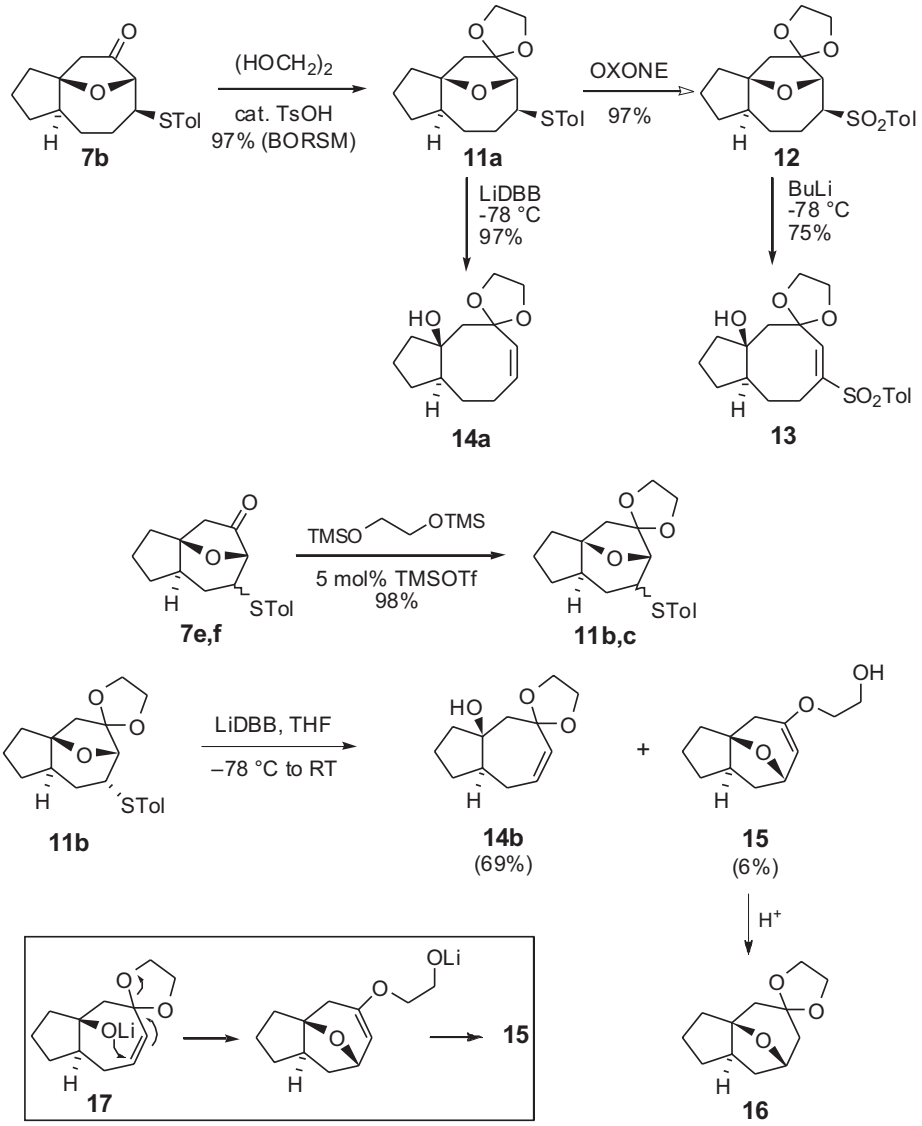
Scheme 8.



7b was protected as the ethylene ketal to give **11a**, and the thioaryl group oxidized to the corresponding sulfone **12** (18) (Scheme 9). Treatment of this compound with *n*-BuLi at low temperature effected the elimination of the ether to give unsaturated sulfone **13**. Alternatively, **11a** could be subjected to reductive desulfurization with LiDBB (19) to provide cyclooctene **14a** in excellent yield. A mixture of hydrazulenes **7e** and **7f** was converted to ketals **11b** and **11c**, and **11b** was also subjected to the reductive conditions. In this case, cycloheptene **14b** was obtained in good yield, accompanied by minor amounts of enol ether **15**, which underwent slow, acid-catalyzed conversion to ketal **16**. This compound is believed to arise from in situ transannular S_N2' attack by the initially formed lithium alkoxide **17** on the unsaturated ketal. Paquette et al. (20) reported a related case involving

© 2006 NRC Canada

Scheme 9.



transannular cyclization of a medium-ring enolate with concomitant with S_N2' displacement of a methoxy leaving group.

The methodology described here allows for the expeditious construction of fused bicyclic skeletons containing a medium-sized ring, starting with readily available mixed acetals. In cases involving mixed thioacetals, two convenient methods are available for cleavage of the bridging ethers found in the rearrangement products. Interesting reactivity differences are seen, depending upon ring size and anomeric configuration. Application of this chemistry to natural product targets is currently underway and will be reported in due course.

Experimental[8]

General information

Reactions were conducted in oven-dried (120 °C) or flame-dried glassware under a positive nitrogen atmosphere unless otherwise stated. Transfer of anhydrous solvents or mixtures was accomplished with oven-dried syringes or cannulae. Solvents were distilled before use: dichloromethane from calcium hydride; diethyl ether and tetrahydrofuran from sodium benzophenone ketyl. Thin layer chromatography (TLC) was performed on plates of silica precoated with 0.25 mm Kieselgel 60 F_{254}. Flash chro-

[8] Supplementary data for this article are available on the journal Web site (http://canjchem.nrc.ca) or may be purchased from the Depository of Unpublished Data, Document Delivery, CISTI, National Research Council Canada, Ottawa, ON K1A 0R6, Canada. DUD 5103. For more information on obtaining material refer to http://cisti-icist.nrc-cnrc.gc.ca/irm/unpub_e.shtml. CCDC 227793 and 227794 contain the crystallographic data for this manuscript. These data can be obtained, free of charge, via http://www.ccdc.cam.ac.uk/conts/retrieving.html (Or from the Cambridge Crystallographic Data Centre, 12 Union Road, Cambridge CB2 1EZ, UK; fax +44 1223 336033; or deposit@ccdc.cam.ac.uk).

© 2006 NRC Canada

matography columns were packed with 230–400 mesh silica gel. Where given, column dimensions include outer diameters. Radial chromatography was performed on plates of silica precoated with 1, 2, or 4 mm silica gel 60 PF_{254} containing gypsum.

Proton nuclear magnetic resonance spectra (^{1}H NMR) were recorded at 300, 400, or 500 MHz on Varian Inova 300, 400, and 500, Mercury 400, or Unity 500 spectrometers, and the chemical shifts are reported on the δ scale (ppm) downfield from tetramethylsilane. Coupling constants (*J*) are reported in Hz. Splitting patterns are designated as s, singlet; d, doublet; t, triplet; q, quartet; m, multiplet; br, broad; dd, doublet of doublets, etc. Carbon nuclear magnetic resonance spectra (^{13}C NMR) were obtained at 125 MHz and are reported (ppm) relative to the center line of a triplet at 77.23 ppm for deuterochloroform. Infrared spectra (IR) were measured with a Nicolet Magna 750 FT-IR infrared spectrophotometer. Mass spectra were determined on a Kratos Analytical MS-50 (EI) or Applied Biosystems Mariner Biospectrometry Workstation (ESI). Elemental analyses were obtained at the University of Alberta on a Carlo Erba CHNS-O EA 1108 Elemental Analyzer.

Substrate syntheses

Ethyl 2-(2-(3,3-dimethoxypropyl)-1-hydroxycyclopent-1-yl)acetate

To a two-necked flask equipped with a large stir bar and condenser, charged with a mixture of Zn (400 mg, 6.1 mmol) in Et_2O (6 mL), TMSCl (47 μL, 0.36 mmol) was added via syringe (21). The mixture was heated to reflux for 15 min and then stirred at RT for an additional 15 min. Freshly distilled ethyl bromoacetate (0.68 mL, 6.1 mmol) was added dropwise via syringe. The mixture was heated to reflux for 45 min and then stirred at RT for an additional 1 h. During this time, the mixture turned to a yellow tint and most of the solid Zn was consumed. The solution of Reformatsky reagent thus prepared was then transferred via cannula to a second flask, leaving behind any remaining solid Zn. The flask was then cooled to –10 °C (acetone – ice bath) and 2-((3,3)-methoxypropyl)cyclopentanone **1a** (8) (677 mg, 3.61 mmol) was slowly added as a solution in Et_2O (3 mL) via cannula. The reaction was stirred at –10 °C for 1 h and then for an additional 2 h at RT at which time the reaction had consumed the starting material as ascertained by TLC. The reaction was diluted with Et_2O (30 mL) and quenched by addition of satd. NH_4Cl solution (30 mL). The aqueous phase was extracted with Et_2O (3 × 30 mL) and the combined organic phase was dried with $MgSO_4$, filtered, and concentrated. The resulting oil was purified by flash chromatography (silica gel, 3 cm × 24 cm column, solvent ramp: 200 mL each of 20%, 30%, and 40% EtOAc–hexanes) to yield the desired alcohol (856 mg, 87%) as a 3.2:1 cis/trans mixture of diastereomers. R_f = 0.17 (30% EtOAc–hexanes). IR (CH_2Cl_2 cast, cm^{-1}): 3516, 2951, 2872, 1731, 1189, 1053. ^{1}H NMR (500 MHz, $CDCl_3$, major diastereomer) δ: 4.35 (t, *J* = 5.7 Hz, 1H), 4.17 (q, *J* = 7.2 Hz, 2H), 3.32 (s, 3H), 3.30 (s, 3H), 2.71 (d, J_{AB} = 15.7 Hz, 1H), 2.33 (d, J_{AB} = 15.4 Hz, 1H), 1.90–1.44 (m, 11H), 1.38–1.31 (m, 1H), 1.28 (t, *J* = 7.2 Hz, 3H). ^{13}C NMR (125 MHz, $CDCl_3$, major diastereomer) δ: 173.6, 105.1, 79.7, 60.9, 53.3, 52.7, 49.5, 40.0, 31.9, 29.9, 23.9, 21.3, 14.4. HR-MS (ESI) calcd. for $C_{13}H_{22}O_4$ (M – MeOH$^+$): 242.1518; found: 242.1521.

Mixed acetal 2a

To a solution of ethyl 2-(2-(3,3-dimethoxypropyl)-1-hydroxycyclopent-1-yl)acetate (812 mg, 2.96 mmol, 3.2:1 mixture of diastereomers) in CH_2Cl_2 (150 mL) cooled to –10 °C (acetone – ice bath), $BF_3{\cdot}OEt_2$ (376 μL, 2.96 mmol) was added via syringe. The reaction was stirred for 15 min at which time the reaction had consumed the starting material as ascertained by TLC. The reaction was quenched by addition of Et_3N (~1 mL) followed by H_2O (50 mL). The aqueous phase was extracted with CH_2Cl_2 (50 mL) and the combined organic phase was washed with brine (200 mL), dried with Na_2SO_4, filtered, and concentrated. The resulting oil was purified by flash chromatography (silica gel, 3 cm × 24 cm column, solvent ramp: 200 mL each of 2.5%, 5%, 10%, and 20% EtOAc–hexanes) to yield the minor (α) anomer of **2a** (99 mg, 18% based on 3.2:1 diastereomer ratio of starting material), major (β) anomer of **2a** (354 mg, 65% based on 3.2:1 diastereomer ratio of starting material), and a mixture of anomers derived from the minor trans diastereomer (131 mg, 77% based on 1:3.2 diastereomer ratio of starting material). Major anomer of **2a**: R_f = 0.49 (30% EtOAc – hexanes). IR (neat, cm^{-1}): 2953, 2870, 1734, 1368, 1225, 1150, 1016. ^{1}H NMR (500 MHz, $CDCl_3$, major anomer) δ: 4.62 (dd, *J* = 8.8, 3.2 Hz, 1H), 4.21 (dq, *J* = 10.8, 7.2 Hz, 1H), 4.09 (dq, *J* = 10.8, 7.2 Hz, 1H), 3.42 (s, 3H), 2.97 (d, J_{AB} = 13.4 Hz, 1H), 2.31 (d, J_{AB} = 13.3 Hz, 1H), 2.10–2.05 (m, 1H), 1.92–1.84 (m, 2H), 1.82–1.65 (m, 5H), 1.63–1.54 (m, 3H), 1.27 (t, *J* = 7.2 Hz, 3H). ^{13}C NMR (125 MHz, $CDCl_3$, major anomer) δ: 171.1, 98.6, 83.8, 60.5, 56.1, 41.1, 40.9, 39.9, 27.9, 25.9, 21.9, 21.8, 14.5. HR-MS (ESI) calcd. for $C_{13}H_{22}O_4$ (M$^+$): 242.1518; found: 242.1516.

Thioglycoside 2b

A solution of **2a** (275 mg, 1.14 mmol) and thiocresol (141 mg, 1.14 mmol) in CH_2Cl_2 (114 mL) was stirred for 10 min to ensure that the thiocresol was completely dissolved. The solution was cooled to –10 °C (acetone – ice bath) and $BF_3{\cdot}OEt_2$ (144 μL, 1.14 mmol) was added dropwise via syringe. The reaction was stirred for 10 min at which time the reaction had consumed the starting material as ascertained by TLC. The reaction was quenched by addition of Et_3N (~1 mL) followed by H_2O (50 mL). The aqueous phase was extracted with CH_2Cl_2 (50 mL) and the combined organic phase was washed with brine (200 mL), dried with Na_2SO_4, filtered, and concentrated. The resulting oil was purified by radial chromatography (4 mm plate, solvent ramp: 100 mL each of 2.5%, 5%, and 10% EtOAc–hexanes) to yield **2b** as a single anomer (313 mg, 82%). R_f = 0.53 (30% EtOAc–hexanes). IR (CH_2Cl_2 cast, cm^{-1}): 2951, 2869, 1733, 1221, 1044. ^{1}H NMR (500 MHz, $CDCl_3$) δ: 7.41 (d, *J* = 8.3 Hz, 2H), 7.08 (d, *J* = 7.8 Hz, 2H), 4.90 (dd, *J* = 10.6, 3.6 Hz, 1H), 4.05 (dq, *J* = 11.1, 7.3 Hz, 1H), 3.95 (dq, *J* = 10.9, 7.3 Hz, 1H), 2.88 (d, J_{AB} = 13.6 Hz, 1H), 2.45 (d, J_{AB} = 13.5 Hz, 1H), 2.31 (s, 3H), 2.10–2.05 (m, 1H), 1.92–1.55 (m, 10H), 1.19 (t, *J* = 7.1 Hz, 3H). ^{13}C NMR (125 MHz, $CDCl_3$) δ: 170.9, 137.6, 133.4, 130.1, 129.5, 84.6, 79.8, 60.5, 40.1, 39.9, 39.4, 27.7, 25.9, 22.7, 22.0,

© 2006 NRC Canada

21.3, 14.4. HR-MS (ESI) calcd. for $C_{12}H_{19}O_3$ (M – $CH_3C_6H_4S^+$): 211.1334; found: 211.1336.

Acid 3a

To a solution of hemiacetal **2a** (410 mg, 1.69 mmol) in THF (3.0 mL) and methanol (3.0 mL), a 2 mol/L solution of LiOH (1.7 mL) was added. The reaction was stirred for 16 h at RT, during which time the reaction mixture turned slightly yellow. The reaction was diluted with water (15 mL) and Et_2O (15 mL) and transferred to a separatory funnel. The layers were separated and the aqueous layer was washed with ether (15 mL). The aqueous layer was then acidified with 0.5 mol/L HCl to pH ~3, resulting in a cloudy suspension. Ethyl acetate (20 mL) was added to this and the resulting layers separated. The aqueous layer was washed with 3 portions of ethyl acetate (20 mL) and the combined organic extracts were washed with water and then brine, dried over magnesium sulfate, filtered, and concentrated to yield the acid, as a yellow oil (307 mg, 85%). IR (CH_2Cl_2 cast, cm^{-1}): 3500–2400, 2946, 2891, 2680, 1704, 1451, 1408, 1391, 1363, 1335, 1322, 1307. ^1H NMR (500 MHz, $CDCl_3$) δ: 10.90 (br s, 1H), 4.66–4.64 (m, 1H), 3.41 (s, 3H), 2.94 (d, J_{AB} = 14.1 Hz, 1H), 2.35 (d, J_{AB} = 14.1 Hz, 1H), 2.16 (m, 1H), 1.91–1.80 (m, 3H), 1.78–1.72 (m, 4H), 1.66–1.58 (m, 3H). ^{13}C NMR (125 MHz, $CDCl_3$) δ: 174.9, 98.9, 83.8, 56.0, 41.2, 41.0, 38.9, 28.1, 26.2, 21.7, 21.5. HR-MS (EI) calcd. for $C_{11}H_{18}O_4$ (M^+): 214.1205; found 214.1192. Anal. calcd. for $C_{11}H_{18}O_4$: C 61.66, H 8.73; found: C 61.31, H 8.47.

(1S,3S*,6R*)-3-Methoxy-2-oxabicycl[4.3.0]nonane-1-acetic acid isobutyrylcarbonic mixed anhydride*

To a solution of the acid (100 mg, 0.47 mmol) in Et_2O (2 mL) at 0 °C was added Et_3N (68 μL, 0.49 mmol) followed by isobutyl chloroformate (65 μL, 0.49 mmol). The reaction was stirred for 4 h, resulting in an off-white precipitate. The reaction mixture was filtered through a fritted filter (D), the residue was rinsed with Et_2O (20 mL), and the combined filtrates were concentrated to give the anydride as a yellow oil (149 mg, 100%) used directly in the next step. R_f = 0.66 (30% EtOAc–hexanes). IR (CH_2Cl_2 cast, cm^{-1}): 2956, 2874, 1819, 1735, 1457, 1392, 1369, 1336, 1307, 1230, 1207. ^1H NMR (500 MHz, $CDCl_3$) δ: 4.60 (dd, J = 8.8, 3.0 Hz, 1H), 4.04 (d, J = 6.7 Hz, 2H), 3.42 (s, 3H), 3.08 (d, J_{AB} = 13.6 Hz, 1H), 2.42 (d, J_{AB} = 13.6 Hz, 1H), 2.16 (m, 1H), 2.01 (sept, J = 6.7 Hz, 1H), 1.94–1.83 (m, 2H), 1.82–1.68 (m, 5H), 1.64–1.53 (m, 3H), 0.97 (d, J = 6.7 Hz, 6H). ^{13}C NMR (125 MHz, $CDCl_3$) δ: 165.4, 149.3, 98.7, 83.5, 75.7, 56.2, 41.2, 40.9, 39.7, 28.0, 27.8, 25.9, 21.9, 21.8, 19.0. HR-MS (EI) calcd. for $C_{16}H_{26}O_6$ (M^+): 314.1729; found: 314.1721.

Diazoketone 4a

Into a solution of freshly prepared diazomethane (12 mmol) in Et_2O (40 mL) at –15 °C was added a solution of the mixed anhydride (250 mg, 0.80 mmol) in Et_2O (10 mL), and the resulting mixture was allowed to stir overnight as the cold bath expired. A stream of N_2 was applied to the system to allow for slow evaporation of both excess diazomethane and solvent, and the resulting yellow oil was diluted in ether and passed through a short pad of silica gel in a fritted filter, eluting with ether. This was then concentrated and the resulting oil purified by radial chromatography (2 mm plate, solvent ramp: 100 mL each of 5%, 10% then 15% EtOAc–hexanes until the product was recovered) to yield starting material (152 mg) as well as **4a** (51 mg, 22%; 70% BRSM) as a yellow oil. R_f = 0.33 (3:7, EtOAc–hexanes). IR (CH_2Cl_2 cast, cm^{-1}): 3082, 2953, 2869, 2101, 1733, 1637, 1457, 1364, 1226, 1187. ^1H NMR (500 MHz, –20 °C, $CDCl_3$) δ: 5.50 (s, 1H), 4.64 (dd, J = 8.4, 3.1 Hz, 1H), 3.46 (s, 3H), 2.96 (d, J_{AB} = 13.7 Hz, 1H), 2.33 (d, J_{AB} = 13.7 Hz, 1H), 2.09 (ddd, J = 12.8, 8.2, 4.0 Hz, 1H), 1.86 (m, 2H), 1.82–1.66 (m, 5H), 1.66–1.54 (m, 3H). ^{13}C NMR (125 MHz, –60 °C, $CDCl_3$,) δ: 193.0, 98.2, 83.8, 56.7, 56.6, 46.0, 41.1, 39.2, 26.8, 25.2, 21.4, 21.0. HR-MS (EI) calcd. for $C_{12}H_{17}N_2O_3$ (M – H^+): 237.1239; found: 237.1225.

Acid 3b

To a solution of **2b** (850 mg, 2.54 mmol) in THF (2 mL) and MeOH (4 mL) was added a 2 N solution of LiOH (2.54 mL). The reaction was stirred for about 12 h during which time the reaction turned slightly yellow and the starting material was consumed as ascertained by TLC. The reaction was diluted by addition of Et_2O (50 mL) and H_2O (50 mL). The aqueous phase was washed with Et_2O (50 mL). After the layers were separated, EtOAc (50 mL) was added to the aqueous phase followed by the dropwise addition of 3 N HCl until the pH reached ~2. The cloudy aqueous phase was then extracted with EtOAc (3 × 30 mL), the combined organic phase was dried with Na_2SO_4, filtered, and concentrated to yield the desired acid as a white solid (743 mg, 96%), mp 122–124 °C. IR (CH_2Cl_2 cast, cm^{-1}): 3220, 3030, 2948, 1707, 1042, 979. ^1H NMR (500 MHz, $CDCl_3$) δ: 10.88 (br s, 1H), 7.42 (d, J = 8.1 Hz, 2H), 7.09 (d, J = 8.3 Hz, 2H), 4.89–4.86 (m, 1H), 2.98 (d, J_{AB} = 14.6 Hz, 1H), 2.39 (dd, J = 14.5, 1.9 Hz, 1H), 2.32 (s, 3H), 2.13–2.08 (m, 1H), 1.91–1.59 (m, 10H). ^{13}C NMR (125 MHz, $CDCl_3$) δ: 175.7, 138.1, 133.6, 129.6, 129.4, 84.6, 80.3, 40.4, 39.8, 38.9, 27.7, 25.8, 22.7, 21.9, 21.4. HR-MS (ESI) calcd. for $C_{17}H_{22}O_3S$ (M^+): 306.1289; found: 306.1284.

Diazoketone 4b

To a solution of oxalyl chloride (38 μL, 0.44 mmol) and the acid in CH_2Cl_2 (2.4 mL) cooled to –45 °C (acetonitrile – dry ice bath) was added 1 drop of DMF. The reaction was stirred at this temperature for 1 h then allowed to warm to –10 °C (acetone – ice bath; gas evolution was observed during the warming of the reaction) and stirred an additional 1 h at that temperature. The reaction was then directly transferred via cannula to a freshly prepared solution of diazomethane (~4 mmol) in Et_2O (~12 mL) and cooled to –45 °C (acetonitrile – dry ice bath). The bath was allowed to expire, and a stream of N_2 was introduced once the reaction reached RT The crude yellow oil thus obtained was passed through a short pad of silica gel (1 cm in a disposable pipette), eluting with 10 mL of 50% EtOAc–hexanes. The solvents were removed under reduced pressure and the resulting yellow oil was purified by radial chromatography (2 mm plate, solvent ramp: 100 mL each of 10%, 20%, and 30% EtOAc–hexanes) to yield **4b** as a yellow solid (88 mg, 73%), mp 93 to 94 °C. R_f = 0.30 (30% EtOAc–hexanes). IR (CH_2Cl_2 cast, cm^{-1}): 2949, 2868, 2100, 1635, 1363, 1044. ^1H NMR (400 MHz, $CDCl_3$) δ: 7.48 (d, J = 8.1 Hz, 2H), 7.12 (d, J = 8.2 Hz, 2H),

© 2006 NRC Canada

4.84–4.81 (m, 1H), 4.78 (br s, 1H), 2.97 (d, J_{AB} = 14.6 Hz, 1H), 2.31 (s, 3H), 2.09 (br app d, J_{AB} = 14.6 Hz, 1H), 1.95–1.54 (m, 11H). ^{13}C NMR (100 MHz, $CDCl_3$) δ: 193.0, 138.7, 135.1, 129.7, 129.5, 84.6, 80.6, 55.2, 45.7, 42.0, 39.0, 27.8, 25.8, 22.8, 21.9, 21.3. HR-MS (ESI) calcd. for $C_{18}H_{22}N_2O_2NaS$ ($M + Na^+$): 353.1300; found: 353.1295.

Ethyl acetate adducts of 1b

Into a stirring solution of diisopropyl amine (3.66 mL, 26.1 mmol) in THF (30 mL) at –78 °C, *n*-BuLi (10.9 mL of 2.4 mol/L solution, 26.1 mmol) was added and the resulting mixture was stirred at –78 °C for 30 min. This was then warmed to 0 °C over several minutes and stirred for another 30 min before being cooled once again to –78 °C. Ethyl acetate (2.44 mL, 25 mmol) was added dropwise, and the mixture was stirred for 1 h. A solution of 2-[(2,2-dimethoxy)ethyl]cyclopentanone **1b** (9) (4.0 g, 22.7 mmol) in THF (10 mL) was added dropwise to the above mixture and the reaction mixture was stirred at –78 °C until the reaction was complete by TLC analysis (4 h). The reaction mixture was quenched with saturated ammonium chloride (25 mL). After separation of the phases, the aqueous layer was extracted with Et_2O (3 × 15 mL) and the combined organic extracts were washed with water (50mL) and brine (50mL), dried ($MgSO_4$), filtered, and concentrated. The crude product (5.64 g, 95.3%), a 1.7:1 mixture of inseparable cis and trans isomers (ratio determined by ^{1}H NMR integration of methoxy singlets), was carried on without further purification.

Cis isomer

R_f = 0.23 (3:7 EtOAc–hexanes). IR (CH_2Cl_2 cast, cm^{-1}): 3513, 2953, 2830, 1731, 1447, 1371, 1334, 1190, 1125, 1057, 964. ^{1}H NMR (500 MHz, $CDCl_3$) δ: 4.37 (dd, J = 7.8, 3.5 Hz, 1H), 4.14 (q, J = 7.0 Hz, 2H), 3.28 (s, 6H), 3.23 (br s, 1H), 2.66 (d, J_{AB} = 15.5 Hz, 1H), 2.33 (d, J_{AB} = 15.5 Hz, 1H), 1.88–1.65 (m, 5H), 1.60–1.50 (m, 4H), 1.25 (t, J = 7.0 Hz, 3H). ^{13}C NMR (125 MHz, $CDCl_3$) δ: 220.7, 103.3, 53.4, 52.8, 45.7, 37.9, 32.7, 30.4, 21.0. LR-MS (ESI) calcd. for $C_{13}H_{24}O_5Na$ ($M + Na^+$): 283.1; found: 283.1. Anal. calcd. for $C_{13}H_{24}O_5$: C 59.98, H 9.29; found: C 59.58, H 10.01. (Data obtained from the inseparable mixture of diastereomers).

Trans isomer

R_f = 0.23 (3:7 EtOAc–hexanes). IR (CH_2Cl_2 cast, cm^{-1}): 3511, 2953, 2830, 1724, 1447, 1371, 1332, 1199, 1124, 1058, 966. ^{1}H NMR (500 MHz, $CDCl_3$) δ: 4.42 (dd, J = 7.1, 4.4 Hz, 1H), 4.15 (q, J = 7.2 Hz, 2H), 3.81 (br s, 1H), 3.30 and 3.26 (2s, 6H), 2.47 (d, J_{AB} = 15.6 Hz, 1H), 2.38 (d, J_{AB} = 15.6 Hz, 1H), 2.03–1.94 (m, 2H), 1.82–1.76 (ddd, J = 13.9, 7.1, 4.2 Hz, 1H), 1.75–1.65 (m, 3H), 1.61–1.51 (m, 2H), 1.29–1.20 (m, 2H), 1.26 (t, J = 7.2 Hz, 3H). ^{13}C NMR (125 MHz, $CDCl_3$) δ: 173.7, 103.8, 80.7, 61.0, 53.5, 52.2, 45.6, 39.7, 38.4, 33.2, 29.3, 20.8, 14.4. LR-MS (ESI) calcd. for $C_{13}H_{24}O_5Na$ ($M + Na^+$): 283.1; found: 283.1. Anal. calcd. for $C_{13}H_{24}O_5$: C 59.98, H 9.29; found: C 59.85, H 9.29. (Data obtained from a pure sample of the trans isomer recovered after the formation of **2c** and **2d** from the inseparable mixture of cis and trans isomers).

Mixed acetals 2c and 2d

To a solution of the cis and trans ethyl acetate adducts (11.2 g, 43.3 mmol) in CH_2Cl_2 (1.0 L) at –15 °C (acetone – ice bath), $BF_3{\cdot}OEt_2$ (5.50 mL, 43.3 mmol) was added and the reaction was stirred for 20 min, at which time TLC showed consumption of the cis isomer and a mixture of **2c** and **2d**, together with unreacted trans isomer. The reaction was quenched with Et_3N (6 mL) and water (500 mL) and the resulting phases were separated. The aqueous layer was extracted with CH_2Cl_2 and the combined organic extracts were washed with water and brine, then dried ($MgSO_4$), filtered, and concentrated. The crude product was purified by column chromatography (silica gel; 3:7, EtOAc–hexanes) to afford recovered trans adduct and **2c** and **2d** (3.85 g, 62%; 4.4:1 mixture of α and β anomers; ratio based on integration of OMe singlets) as a yellow oil. R_f = 0.53 (3:7, EtOAc–hexanes). IR (CH_2Cl_2 cast, cm^{-1}): 2950, 2868, 2829, 1735, 1467, 1447, 1369, 1342, 1300, 1208, 1103, 1049. ^{1}H NMR (500 MHz, $CDCl_3$) δ: 4.97 (d, J = 5.2 Hz, 0.8H) overlapping with 4.96 (m, 0.2H), 4.11 (q, J = 7.1 Hz, 2H), 3.30 (s, 2.4H), 3.28 (s, 0.6H), 2.85 (d, J_{AB} = 14.4 Hz, 0.8H), 2.67–2.61 (m, 0.8H), 2.64 (d, J_{AB} = 14.4 Hz, 0.2H), 2.63 (d, J_{AB} = 14.4 Hz, 0.8H), 2.56 (m, 0.2H), 2.52 (d, J_{AB} = 14.4 Hz, 0.2H), 2.27 (ddd, J = 13.3, 9.5, 5.7 Hz, 0.2H), 2.20 (dd, J = 13.3, 9.3 Hz, 0.8H), 1.96–1.87 (m, 1H), 1.73–1.56 (m, 4.8H), 1.46–1.41 (m, 1.2H), 1.24 (t, J = 7.2 Hz, 2.4H), 1.23 (t, J = 7.2 Hz, 0.6H). ^{13}C NMR (125 MHz, $CDCl_3$) δ: major anomer: 171.4, 106.7, 93.8, 60.4, 54.7, 46.2, 46.0, 41.4, 38.9, 33.6, 24.0, 14.5; minor anomer: 171.2, 107.0, 94.9, 60.5, 54.9, 45.4, 44.9, 40.5, 40.4, 34.2, 24.5, 14.5. HR-MS (EI) calcd. for $C_{12}H_{20}O_4$ (M^+): 228.1362; found: 228.1359. Anal. calcd. for $C_{12}H_{20}O_4$: C 63.14, H 8.83; found: C 62.90, H 9.43.

Mixed thioacetals 2e and 2f

To a solution of **2c** and **2d** (50 mg, 0.22 mmol) and *p*-thiocresol (27 mg, 0.22 mmol) in CH_2Cl_2 (22 mL) at –45 °C, $BF_3{\cdot}OEt_2$ (28 μL, 0.22 mmol) was added and the reaction was stirred until deemed complete by TLC. After 2 h only a trace of starting acetals was observed; the reaction was quenched with Et_3N (0.5 mL) and water (15 mL) and the resulting bi-layer was separated. The aqueous phase was extracted with CH_2Cl_2 (15 mL) and the combined organic extracts were washed with water (30 mL), brine (30 mL), dried with magnesium sulfate, filtered, and concentrated. The crude product was first passed through a pad of silica gel in a fritted filter, eluting with Et_2O, and then purified by radial chromatography (silica gel, 2 mm plate, solvent ramp: 100 mL each of 3%, 6%, and then 9% EtOAc–hexanes until the product was recovered) to afford the product, a yellow oil, as a 1:5:1 mixture of partially separable anomers (**2e** and **2f**) in 88% yield (57 mg) based on recovered **2c** and **2d** (4 mg).

Major anomer 2e (α)

R_f = 0.63 (3:7, EtOAc–hexanes). IR (CH_2Cl_2 cast, cm^{-1}): 2954, 2867, 1731, 1493, 1446, 1369, 1340, 1300, 1195, 1094, 1054, 1034. ^{1}H NMR (500 MHz, $CDCl_3$) δ: 7.35 (d, J = 8.2 Hz, 2H), 7.04 (d, J = 8.2 Hz, 2H), 5.51 (dd, J = 6.9, 5.4 Hz, 1H), 4.09 (q, J = 7.2 Hz, 2H), 2.94 (d, J_{AB} = 14.6 Hz, 1H), 2.85 (d, J_{AB} = 14.6 Hz, 1H), 2.74 (ddd, J =

© 2006 NRC Canada

8.4, 5.2, 3.2 Hz, 1H), 2.29–2.24 (m, 1H), 2.28 (s, 3H), 2.08 (ddd, J = 13.6, 6.8, 5.2 Hz, 1H), 1.97–1.92 (m, 1H), 1.84–1.76 (m, 1H), 1.73–1.58 (m, 3H), 1.49–1.44 (m, 1H), 1.22 (t, J = 7.2 Hz, 3H). ^{13}C NMR (125 MHz, $CDCl_3$) δ: 171.2, 137.2, 132.2, 131.8, 129.8, 95.0, 88.3, 60.5, 46.9, 44.8, 41.0, 39.2, 33.3, 24.5, 21.3, 14.4. HR-MS (EI) calcd. for $C_{18}H_{24}O_3S$ (M^+): 320.1446; found: 320.1419. Anal. calcd. for $C_{18}H_{24}O_3S$: C 67.47, H 7.55; found: C 67.24, H 7.57.

Minor anomer 2f (β)

R_f = 0.63 (3:7, EtOAc–hexanes). IR (CH_2Cl_2 cast, cm^{-1}): 3511, 2953, 2830, 1724, 1447, 1371, 1332, 1199, 1124, 1058, 966. ^{1}H NMR (500 MHz, $CDCl_3$) δ: 7.33 (d, J = 8.0 Hz, 2H), 7.04 (d, J = 8.0 Hz, 2H), 5.25 (dd, J = 8.2, 6.4 Hz, 1H), 4.09 (q, J = 7.2 Hz, 2H), 2.61 (s, 2H), 2.66–2.53 (m, 3H), 2.29 (s, 3H), 2.04 (m, 1H), 1.78–1.50 (m, 6H), 1.22 (t, J = 8.0 Hz, 3H). ^{13}C NMR (125 MHz, $CDCl_3$) δ: 171.1, 137.0, 131.7, 131.6, 129.7, 94.7, 86.2, 60.6, 46.8, 43.9, 41.0, 39.4, 33.8, 24.2, 21.3, 14.5. HR-MS (EI) calcd. for $C_{18}H_{24}O_3S$ (M^+): 320.1446; found: 320.1428.

Diazoketones 4c and 4d

To a solution of mixed acetals **2c** and **2d** (1.00 g, 4.38 mmol) in THF (8 mL) and methanol (8 mL) was added a 2.0 mol/L solution of LiOH (4.38 mL). The reaction was stirred for 16 h at RT, during which time the reaction mixture turned slightly yellow. The reaction was diluted with water (20 mL) and Et_2O (20 mL) and transferred to a separatory funnel. The layers were separated and the aqueous layer was washed with ether (20 mL). The aqueous layer was then acidified with 0.5 mol/L HCl to pH ~3, resulting in a cloudy suspension. This was then diluted with ethyl acetate (30 mL) and the resulting layers separated. The aqueous layer was washed with three portions of ethyl acetate (20 mL) and the combined organic extracts were washed with water then brine, dried over magnesium sulfate, filtered, and concentrated to give the acids **3c** and **3d** (mixture of anomers) as a yellow oil (870 mg, 99%). IR (CH_2Cl_2 cast, cm^{-1}): 3600–2500, 2949, 1708, 1468, 1440, 1409, 1339, 1300, 1218. ^{1}H NMR (500 MHz, $CDCl_3$) δ: 10.8 (br s, 1H), 4.99 (d, J = 5.2 Hz, 1.0H), 3.30 (s, 2.4H), 3.28 (s, 0.6H), 2.90 (d, J_{AB} = 14.9 Hz, 0.8H), 2.64 (d, J_{AB} = 14.6 Hz, 0.2H), 2.63 (d, J_{AB} = 14.9 Hz, 0.8H), 2.56 (d, J_{AB} = 14.6 Hz, 0.2H), 2.49 (ddd, J = 4.6, 1.2 Hz, 0.2H), 2.27 (ddd, J = 13.6, 9.8, 5.7 Hz, 0.2H), 2.20 (dd, J = 13.3, 9.2 Hz, 0.8H), 1.98–1.80 (m, 1.6H), 1.75–1.55 (m, 5.2H), 1.43 (m, 1.0H). ^{13}C NMR (125 MHz, $CDCl_3$) δ: major anomer: 176.0, 107.1, 93.5, 55.0, 46.5, 46.0, 41.1, 38.9, 33.7, 24.0; minor anomer: 176.0, 107.2, 94.7, 55.1, 44.8, 40.2, 40.1, 34.0, 24.6. HR-MS (EI) calcd. for $C_{10}H_{16}O_4$ (M^+): 200.1049; found: 200.1051.

To a solution of the anomeric acids **3c** and **3d** (800 mg, 4.0 mmol) in Et_2O (50 mL) at 0 °C was added Et_3N (585 μL, 4.4 mmol) followed by isobutyl chloroformate (574 μL, 4.4 mmol) and the reaction was stirred for 2.5 h, resulting in the formation of an off-white precipitate. The reaction mixture was filtered through a fritted filter (D), rinsed with Et_2O (50 mL), and concentrated to give the mixed anhydrides (1.09 g, 91%) as a yellow oil. R_f = 0.62 (3:7, EtOAc–hexanes). IR (CH_2Cl_2 cast, cm^{-1}): 2958, 2784, 2831, 1804, 1760, 1470, 1452, 1396, 1370. ^{1}H NMR (500 MHz, $CDCl_3$, major anomer) δ: 5.00 (d, J = 5.3 Hz, 1H), 4.03 (d, J = 7.1 Hz, 2H), 3.31 (s, 3H), 3.03 (d, J_{AB} = 15.3 Hz, 1H), 2.80 (d, J_{AB} = 15.3 Hz, 1H), 2.66 (m, 1H), 2.23 (dd, J = 13.3, 9.2 Hz, 1H), 2.01 (sept, J = 6.8 Hz, 1H), 2.00 (m, 1H), 1.76 (m, 1H), 1.68 (ddd, J = 12.0, 7.5, 5.3 Hz, 1H), 1.63 (m, 2H), 1.46 (m, 1H), 0.95 (d, J = 6.8 Hz, 6H). ^{13}C NMR (125 MHz, $CDCl_3$) δ: major anomer: 165.8, 149.4, 106.9, 93.1, 75.7, 54.8, 46.4, 45.7, 41.3, 38.8, 33.5, 27.8, 24.0, 19.0; minor anomer: 165.6, 149.4, 106.7, 94.4, 75.5, 54.8, 45.6, 44.6, 41.4, 38.9, 34.3, 33.6, 24.5, 19.0. HR-MS (EI) calcd. for $C_{15}H_{23}O_6$ ($M - H^+$): 299.1495; found: 299.1499.

A solution of anomeric mixed anhydrides (624 mg, 2.2 mmol) in Et_2O (10 mL) was added via cannula to a solution of freshly prepared diazomethane (20 mmol) in Et_2O (60 mL) at –15 °C, and the resulting mixture was stirred for 16 h as the cooling bath expired. A gentle stream of N_2 was applied to the system to allow for slow evaporation of both excess diazomethane and solvent, and the resulting yellow oil was diluted in ether (20 mL), passed through a short pad of silica gel in a fritted filter, eluting with copious ether. This was then concentrated and the resulting oil purified by radial chromatography (silica gel, 4 mm plate, solvent ramp: 100 mL each of 3%, 6%, 9%, and then 12% EtOAc–hexanes until the products were recovered) to yield **4c** and **4d**, an inseparable 4.7:1 mixture of anomers (228 mg, 49%) as a bright yellow oil, as well as a trace of starting material (not quantified). R_f = 0.23 (3:7, EtOAc–hexanes). IR (CH_2Cl_2 cast, cm^{-1}): 3087, 2949, 2868, 2829, 2102, 1817, 1735, 1637, 1440, 1361. ^{1}H NMR (500 MHz, –40 °C, $CDCl_3$) δ: 5.67 (s, 0.8H), 5.52 (s, 0.2H), 5.01 (m, J = 5.1 Hz, 1H), 3.36 (s, 2.4H), 3.30 (s, 0.6H), 2.94 (d, J_{AB} = 14.3 Hz, 0.8H), 2.69 (d, J_{AB} = 13.5 Hz, 0.2H), 2.60 (m, 1H), 2.55 (d, J_{AB} = 14.3 Hz, 0.8H), 2.47 (d, J_{AB} = 13.5 Hz, 0.2H), 2.20 (dd, J = 13.5, 9.5 Hz, 1H), 1.90 (m, 1H), 1.70–1.45 (m, 6H). ^{13}C NMR (125 MHz, $CDCl_3$, –60 °C) δ: major anomer: 194.1, 106.4, 93.4, 56.0, 54.9, 52.8, 46.4, 40.3, 38.1, 32.5, 23.4; minor anomer: 194.1, 106.5, 95.4, 56.8, 54.7, 50.8, 44.2, 40.3, 39.9, 33.6, 24.2; HR-MS (ESI) calcd. for $C_{11}H_{16}N_2O_3Na$ ($M + Na^+$): 247.1059; found: 247.1060.

Diazoketones 4e and 4f

Preparation and characterization of individual acid anomers is given below. For convenience, they were usually prepared as a mixture of anomers and converted into the separable diazoketones.

To a solution of mixed acetal **2e** (423 mg, 1.3 mmol) in THF (5 mL) and methanol (5 mL) was added a 2.0 mol/L solution of LiOH (1.3 mL). The reaction was stirred for 16 h at RT, during which time the reaction mixture turned slightly yellow. The reaction was diluted with water (20 mL) and Et_2O (20 mL) and transferred to a separatory funnel. The layers were separated and the aqueous layer was washed with ether (15 mL). The aqueous layer was then acidified with 0.5 mol/L HCl to pH ~3, resulting in a cloudy suspension. This was then diluted with ethyl acetate (40 mL) and the resulting layers separated. The aqueous layer was washed with three portions of ethyl acetate (20 mL) and the combined organic extracts were washed with water (50 mL) and then brine (50 mL), dried over magnesium sulfate, filtered, and concentrated to yield **3e** as a yellow oil (333 mg, 86%). IR (CH_2Cl_2 cast, cm^{-1}): 3500–2400, 2953, 2867,

© 2006 NRC Canada

1708, 1597, 1493, 1443, 1408, 1300, 1231, 1133, 1093. ^{1}H NMR (500 MHz, $CDCl_3$) δ: 7.34 (d, J = 8.2 Hz, 2H), 7.07 (d, J = 8.2 Hz, 2H), 5.56 (dd, J = 6.0, 6.0 Hz, 1H), 3.03 (d, J_{AB} = 14.8 Hz, 1H), 2.74 (d, J_{AB} = 14.8 Hz, 1H), 2.63 (m, 1H), 2.32–2.25 (m, 1H), 2.29 (s, 3H), 2.14 (ddd, J = 13.4, 6.8, 5.0 Hz, 1H), 1.98–1.92 (m, 1H), 1.88–1.79 (m, 1H), 1.70–1.58 (m, 3H), 1.52–1.46 (m, 1H), (COO*H* peak not measured). ^{13}C NMR (125 MHz, $CDCl_3$) δ: 186.8, 137.9, 132.5, 130.8, 130.0, 94.7, 88.7, 47.5, 44.9, 40.5, 39.0, 33.0, 24.5, 21.3. HR-MS (EI) calcd. for $C_{16}H_{20}SO_3$ (M^+): 292.1133; found: 292.1135.

Following the same procedure as the previous section, **2f** (142 mg, 0.44 mmol) was converted into the corresponding acid **3f** (100 mg, 78%) as a white solid, mp 115 to 116 °C. IR (CH_2Cl_2 cast, cm^{-1}): 3500–2500, 2949, 2865, 1707, 1493, 1439, 1411, 1299, 1232, 1146, 1093. ^{1}H NMR (500 MHz, $CDCl_3$) δ: 9.4 (br s, 1H), 7.34 (d, J = 8.4 Hz, 2H), 7.06 (d, J = 8.4 Hz, 2H), 5.28 (dd, J = 8.2, 5.6 Hz, 1H), 2.69 (d, J_{AB} = 14.8 Hz, 1H), 2.57 (d, J_{AB} = 14.8 Hz, 1H), 2.60–2.51 (m, 2H), 2.29 (s, 3H), 2.10 (m, 1H), 1.78–1.54 (m, 6H). ^{13}C NMR (125 MHz, $CDCl_3$) δ: 186.8, 137.7, 132.4, 130.7, 129.9, 94.4, 86.5, 47.6, 43.6, 40.6, 39.0, 33.6, 24.3, 21.3; HR-MS (EI) calcd. for $C_{16}H_{20}SO_3$ (M^+): 292.1133; found: 292.1141. Anal. calcd. for $C_{16}H_{20}O_3S$: C 65.72, H 6.89; found: C 65.21, H 7.07.

To a solution of both anomeric acids (**3e** and **3f**) (1.0 g, 3.42 mmol) in CH_2Cl_2 (140 mL) at –15 °C was added 2,6-lutidine (478 μL, 4.1 mmol) followed by oxalyl chloride (36 μL, 4.1 mmol) and DMF (2 drops, ~10 μL), resulting in the evolution of copious amounts of gas. The reaction was stirred for 4 h, and solvent was removed by rotary evaporation to give a yellow oil entrained in a white precipitate. This material was redissolved in ether (50 mL) and the suspension filtered through a fritted filter (D) and was then washed several times with ether (50 mL). The ethereal solution of the acid chloride was condensed to a lesser volume (~50 mL) and added via cannula to a solution of freshly prepared diazomethane (60 mmol) in Et_2O (200 mL) at –15 °C, and the resulting mixture stirred for 16 h as the cooling bath expired. A gentle stream of N_2 was applied to the system to allow for slow evaporation of both excess diazomethane and solvent, and the resulting yellow oil was diluted in ether (40 mL), passed through a short pad of silica gel in a fritted filter, eluting with copious ether. The filtrate was concentrated and the resulting oil purified by radial chromatography (silica gel, 4 mm plate, solvent ramp: 100 mL each of 3%, 6%, 9%, and then 12% EtOAc–hexanes until the products were recovered) to yield **4e** (410 mg) and **4f** (240 mg), as yellow oils in a combined overall yield of 60%.

Major anomer 4e (α)

R_f = 0.32 (3:7, EtOAc–hexanes). IR (CH_2Cl_2 cast, cm^{-1}): 3105, 2953, 2866, 2100, 1636, 1492, 1450, 1358, 1241, 1162, 1093, 1061, 1017. ^{1}H NMR (500 MHz, –60 °C, $CDCl_3$) δ: 7.36 (d, J = 8.0 Hz, 2H), 7.14 (d, J = 8.0 Hz, 2H), 5.81 (dd, J = 6.2, 2.7 Hz, 1H), 5.12 (s, 1H), 3.23 (d, J_{AB} = 13.2 Hz, 1H), 2.66 (approx. q, J = 7.3 Hz, 1H), 2.49 (d, J_{AB} = 13.2 Hz, 1H), 2.37–2.30 (m, 1H), 2.32 (s, 3H), 2.17–2.11 (m, 1H), 1.84–1.52 (m, 6H). ^{13}C NMR (125 MHz, –60 °C, $CDCl_3$) δ: 194.3, 136.5, 131.3, 129.8, 129.8, 95.0, 87.0, 56.2, 52.1, 47.4, 29.8, 98.0, 32.2, 23.5, 21.1. HR-MS (ESI) calcd. for $C_{17}H_{20}N_2O_2SNa$ (M + Na^+): 339.1143; found: 339.1147. Anal. calcd. for $C_{17}H_{20}N_2O_2S$: C 64.53, H 6.37, N 8.85; found: C 64.92, H 6.13, N 8.66.

Minor anomer 4f (β)

R_f = 0.26 (3:7, EtOAc–hexanes). IR (CH_2Cl_2 cast, cm^{-1}): 3081, 2952, 2865, 2100, 1636, 1492, 1449, 1358, 1161, 1093, 1051, 1016. ^{1}H NMR (500 MHz, –60 °C, $CDCl_3$) δ: 7.39 (d, J = 8.0 Hz, 2H), 7.13 (d, J = 8.0 Hz, 2H), 5.53 (s, 1H), 5.14 (dd, J = 9.7, 5.4 Hz, 1H), 2.66 (d, J_{AB} = 13.6 Hz, 1H), 2.60 (approx. q, J = 7.6 Hz, 1H), 2.53 (d, J_{AB} = 13.6 Hz, 1H), 2.48 (ddd, J = 13.0, 9.0, 5.5 Hz, 1H), 2.34 (s, 3H), 2.04–1.98 (br m, 1H), 1.66–1.46 (m, 6H). ^{13}C NMR (125 MHz, –60 °C $CDCl_3$) δ: 193.8, 137.5, 131.8, 129.7, 129.5, 94.0, 84.9, 56.7, 50.0, 46.8, 39.6, 38.5, 32.7, 23.4, 21.2. HR-MS (ESI) calcd. for $C_{17}H_{20}N_2O_2SNa$ (M + Na^+): 339.1143; found: 339.1143. Anal. calcd. for $C_{17}H_{20}N_2O_2S$: C 64.53, H 6.37, N 8.85; found: C 64.40, H 6.58, N 8.52.

Ethyl acetate adduct 6a

Into a stirring solution of diisopropyl amine (1.44 μL, 10.31 mmol) in THF (7 mL) at –78 °C, *n*-BuLi (4.37 mL of 2.36 mol/L solution, 10.31 mmol) was added, and the resulting mixture was stirred at –78 °C for 30 min. This was then warmed to 0 °C over several minutes and stirred for another 30 min before being cooled once again to –78 °C. Ethyl acetate (968 μL, 9.9 mmol) was added dropwise, and the mixture was stirred for 1 h. A solution of anomer **2b** (662 mg, 1.98 mmol, 1 equiv.) in THF (1 mL) was added dropwise to the mixture and the reaction mixture was stirred overnight, allowing the cooling bath to expire. The reaction was then diluted with ethyl ether (10 mL) and quenched by the addition of saturated ammonium chloride solution (10 mL). After separation of the phases, the aqueous layer was extracted with Et_2O (3 × 10 mL) and the combined organic extracts were washed with water (15 mL) and brine (15 mL), dried ($MgSO_4$), filtered, and concentrated. The crude β-ketoester product was then purified by radial chromatography (4 mm plate, solvent ramp: 100 mL each of 2%, 4%, 8%, and then 15% EtOAc–hexanes until the product was recovered) to afford 424 mg of the product **6a** as a yellow oil in 65% yield, based on recovered **2b** (77 mg). R_f = 0.65 (3:7, EtOAc–hexanes). IR (CH_2Cl_2 cast, cm^{-1}): 2952, 2870, 1743, 1712, 1492, 1449, 1366, 1318, 1236, 1152, 1096, 1041. ^{1}H NMR (500 MHz, $CDCl_3$) δ: 7.40 (d, J = 8.1 Hz, 2H), 7.06 (d, J = 8.2 Hz, 2H), 4.86 (dd, J = 8.0, 5.6 Hz, 1H), 4.12 (q, J = 7.2 Hz, 2H), 3.26 (d, J_{AB} = 14.0 Hz, 1H), 3.19 (d, J_{AB} = 15.8 Hz, 1H), 3.05 (d, J_{AB} = 15.8 Hz, 1H), 2.32 (s, 3H), 2.29 (d, J_{AB} = 14.0 Hz, 1H), 1.92–1.52 (m, 11H), 1.25 (t, J = 7.1 Hz, 3H). ^{13}C NMR (125 MHz, $CDCl_3$) δ: 201.8, 167.3, 138.3, 134.5, 129.5, 129.1, 84.5, 80.2, 61.1, 49.8, 46.4, 41.4, 39.0, 27.4, 25.7, 22.6, 21.8, 21.1, 14.1. HR-MS (EI) calcd. for $C_{21}H_{28}O_4S$ (M – $EtOH^+$): 330.1290; found: 330.12943.

Diazoketoester 4g

To a stirred solution of **6a** (91 mg, 0.24 mmol, 1 equiv.) and TEA (34 μL, 0.24 mmol, 1 equiv.) in CH_3CN (2 mL), *p*-TsN_3 (48 mg, 0.24 mmol, 1 equiv.) was added, and the mixture was vigorously stirred at RT for 2.5 h. The CH_3CN was then removed by rotary evaporation and the resulting oil dissolved in 10 mL ether. This solution was washed with 5 mL of 25% aq. KOH, 5 mL of 6% aq. KOH, and then 10 mL

© 2006 NRC Canada

water. The organic layer was then dried over sodium sulfate and concentrated by rotary evaporation. The product was purified by radial chromatography (2 mm plate, solvent ramp: 50 mL each of 1%, 2%, 5%, and then 10% EtOAc–hexanes until the product was recovered) to afford 54 mg (55%) of **4g** as a pale yellow oil. R_f = 0.62 (3:7, EtOAc–hexanes). IR (CH_2Cl_2 cast, cm^{-1}): 2948, 2869, 2133, 1712, 1652, 1492, 1371, 1300, 1220, 1145, 1040. ^1H NMR (500 MHz, $CDCl_3$) δ: 7.42 (d, J = 8.1 Hz, 2H), 7.07 (d, J = 8.0 Hz, 2H), 4.93 (dd, J = 8.0, 5.2 Hz, 1H), 4.21 (q, J = 7.2 Hz, 1H), 4.18 (q, J = 7.2 Hz, 1H), 4.01 (d, J_{AB} = 14.4 Hz, 1H), 2.52 (d, J_{AB} = 14.4 Hz, 1H), 2.31 (s, 3H), 2.13 (m, J = 8.5, 4.7 Hz, 1H), 1.98–1.84 (m, 3H), 1.80–1.54 (m, 7H), 1.30 (t, J = 7.1 Hz, 3H). ^{13}C NMR (125 MHz, $CDCl_3$) δ: 189.7, 161.2, 137.5, 133.8, 130.0, 129.1, 85.5, 80.2, 61.3, 41.3, 40.8, 40.0, 27.4, 25.7, 22.8, 22.0, 21.0, 14.1, (diazo carbon was not detected for this compound). HR-MS (EI) calcd. for $C_{21}H_{26}O_4S$ ($M - N_2^+$): 374.1552; found: 374.1548.

Ethyl acetate adducts 6b (α) and 6c (β)

Into a stirring solution of diisopropyl amine (409 μL, 2.92 mmol) in THF (1 mL) at –78 °C, *n*-BuLi (1.24 mL of 2.36M solution, 2.92 mmol) was added, and the resulting mixture was stirred at –78 °C for 30 min. This was then warmed to 0 °C over several minutes and stirred for another 30 min before being cooled once again to –78 °C. Ethyl acetate (280 μL, 2.86 mmol) was added dropwise, and the mixture was stirred for 1 h. A solution of anomers **2e** and **2f** (183 mg, 0.57 mmol, 1 equiv.) in THF (1 mL) was added dropwise to the mixture and the reaction mixture was stirred overnight, allowing the cooling bath to expire. The reaction was then diluted with ethyl ether (10 mL) and quenched by the addition of saturated ammonium chloride solution (5 mL). After separation of the phases, the aqueous layer was extracted with Et_2O (3 × 5 mL) and the combined organic extracts were washed with water (15 mL) and brine (15 mL), dried ($MgSO_4$), filtered, and concentrated. The crude β-ketoester product was then purified by radial chromatography (2 mm plate, solvent ramp: 50 mL each of 2%, 4%, 8%, and then 15% EtOAc–hexanes until the product was recovered) to afford the products as yellow oils and as a mixture of separable anomers **6b** (α) and **6c** (β) in 46% yield (51 and 38 mg, respectively), based on recovered **2** (13 mg).

Major anomer 6b (α)

R_f = 0.69 (3:7, EtOAc–hexanes). IR (CH_2Cl_2 cast, cm^{-1}): 2955, 2867, 1744, 1713, 1493, 1446, 1366, 1313, 1235 1153, 1094, 1031. ^1H NMR (500 MHz, $CDCl_3$) δ: 7.36 (d, J = 8.2 Hz, 2H), 7.11 (d, J = 8.2 Hz, 2H), 5.62 (dd, J = 6.2, 6.2 Hz, 1H), 4.16 (q, J = 7.1 Hz, 1H), 4.15 (q, J = 7.1 Hz, 1H), 3.51 (s, 2H), 3.26 (d, J_{AB} = 14.7 Hz, 1H), 2.87 (d, J_{AB} = 14.8 Hz, 1H), 2.62 (m, 1H), 2.32 (s, 3H), 2.27 (ddd, J = 12.7, 8.6, 5.6 Hz, 1H), 1.92–1.84 (m, 2H), 1.70–1.60 (m, 3H), 1.48 (m, 1H), 1.25 (t, J = 7.1 Hz, 3H). ^{13}C NMR (125 MHz, $CDCl_3$) δ: 202.1, 167.4, 136.8, 131.9, 130.8, 129.7, 95.0, 87.8, 61.1, 52.7, 50.5, 47.4, 40.5, 38.7, 32.7, 24.3, 21.0, 14.1. HR-MS (EI) calcd. for $C_{20}H_{26}O_4S$ (M^+): 362.1552; found: 362.1554.

Minor anomer 6c (β)

R_f = 0.62 (3:7, EtOAc–hexanes). IR (CH_2Cl_2 cast, cm^{-1}): 2955, 2867, 1742, 1717, 1493, 1446, 1367, 1305, 1236 1152, 1094, 1026. ^1H NMR (500 MHz, $CDCl_3$) δ: 7.39 (d, J = 8.1 Hz, 2H), 7.10 (d, J = 7.8 Hz, 2H), 5.30 (dd, J = 6.2, 6.3 Hz, 1H), 4.16 (q, J = 7.1 Hz, 2H), 3.52 (d, J_{AB} = 15.7 Hz, 1H), 3.46 (d, J_{AB} = 15.7 Hz, 1H), 2.89 (d, J_{AB} = 14.5 Hz, 1H), 2.74 (d, J_{AB} = 14.5 Hz, 1H), 2.62–2.50 (m, 2H), 2.32 (s, 3H), 2.00 (m, 1H), 1.80–1.52 (m, 6H), 1.26 (t, J = 7.1 Hz, 3H). ^{13}C NMR (125 MHz, $CDCl_3$) δ: 201.8, 167.2, 137.3, 132.3, 130.8, 129.5, 94.6, 86.4, 61.2, 51.4, 50.5, 47.5, 40.5, 39.0, 33.3, 24.0, 21.1, 14.1. HR-MS (EI) calcd. for $C_{20}H_{26}O_4S$ (M^+): 362.1552; found: 362.1554.

Diazoketone 4h

Ketoester **6b** (50 mg, 0.14 mmol) was subjected to the procedure as described previously for **4g**, to afford 41 mg (77%) of **4h** as a pale yellow oil. R_f 0.73 (3:7, EtOAc–hexanes). IR (CH_2Cl_2 cast, cm^{-1}): 2954, 2867, 2131, 1717, 1652, 1493, 1446, 1370, 1297, 1210, 1057. ^1H NMR (500 MHz, $CDCl_3$) δ: 7.37 (d, J = 8.1 Hz, 2H), 7.09 (d, J = 7.9 Hz, 2H), 5.51 (dd, J = 6.5, 6.3 Hz, 1H), 4.24 (q, J = 7.1 Hz, 2H), 3.48 (d, J_{AB} = 16.3 Hz, 1H), 3.44 (d, J_{AB} = 15.9 Hz, 1H), 2.76 (dddd, J = 12.6, 8.3, 4.0, 4.0 Hz, 1H), 2.30 (s, 3H), 2.25 (ddd, J = 14.6, 8.6, 6.1 Hz, 1H), 2.10 (ddd, J = 13.4, 6.6, 4.6 Hz, 1H), 2.04 (m, 1H), 1.89 (m, 1H), 1.72–1.56 (m, 3H), 1.47 (m, 1H), 1.28 (t, J = 7.1 Hz, 3H). ^{13}C NMR (125 MHz, $CDCl_3$) δ: 190.6, 161.3, 136.7, 132.0, 131.5, 129.5, 95.6, 87.8, 61.3, 48.3, 46.7, 40.8, 39.7, 32.9, 24.4, 21.1, 14.3, (diazo carbon was not detected for this compound). HR-MS (EI) calcd. for $C_{20}H_{24}O_4S$ ($M - N_2^+$): 360.13953; found: 360.13900.

Carbene transfer reactions of diazo compounds 4a–4h

Catalytic decomposition of diazoketone 4b with Cu(hfacac)$_2$; 8-(p-tolylthio)-12-oxatricyclo[7.2.1.0^{1,5}]undecan-10-one (7b)

To a solution of $Cu(hfacac)_2$ (11 mg, 0.017 mmol, 10 mol%) in CH_2Cl_2 (22 mL, 0.01 mol/L) heated to reflux, was added dropwise via cannula, a solution of diazoketone **4b** (56 mg, 0.17 mmol) in 2 mL of CH_2Cl_2. Following completion of addition, the reaction was stirred at reflux until complete consumption (ca. 30 min) of **4b** (TLC monitoring), after which the reaction was cooled to RT and a solution of 0.5 mol/L K_2CO_3 was added. The aqueous phase was then extracted with CH_2Cl_2 (2 × 15 mL) and the combined organic phase was dried with $MgSO_4$, filtered, condensed, and purified by radial chromatography to yield 41 mg (80%) of **7b** as a white crystalline solid, mp 75 to 76 °C. R_f = 0.53 (30% EtOAc–hexanes). IR (CH_2Cl_2 cast, cm^{-1}): 2934, 2866, 1753, 1492, 1081, 809. ^1H NMR (500 MHz, $CDCl_3$) δ: 7.35 (d, J = 8.2 Hz, 2H), 7.11 (d, J = 8.2 Hz, 2H), 4.27 (approx. br s, 1H), 3.59 (ddd, J = 6.6, 4.7, 1.4 Hz, 1H), 2.74 (dd, J = 17.5, 1.1 Hz, 1H), 2.38 (dd, J = 17.3, 1.1 Hz, 1H), 2.31 (s, 3H), 2.15–2.10 (m, 1H), 2.02–1.96 (m, 2H), 1.92–1.83 (m, 2H), 1.80–1.64 (m, 4H), 1.60–1.53 (m, 1H), 1.49–1.43 (m, 1H). ^{13}C NMR (125 MHz, $CDCl_3$) δ: 216.7, 137.6, 132.5, 130.1, 130.0, 91.1, 83.5, 51.7, 51.2, 49.1, 40.3, 32.1, 27.5, 26.3, 23.4, 21.3. HR-MS (EI) calcd. for $C_{18}H_{22}O_2S$ (M^+): 302.1341; found: 302.1342.

8-Methoxy-12-oxatricyclo[7.2.1.0^{1,5}]undecan-10-one (7a)

To a refluxing solution of $Cu(hfacac)_2$ (9.4 mg, 0.02 mmol, 10 mol%) in CH_2Cl_2 (15 mL) was added a solution of **4a** (46.9 mg, 0.20 mmol) in CH_2Cl_2 (5 mL), and the

© 2006 NRC Canada

resulting mixture was stirred at reflux until consumption of **4a** (~30 min), after which the reaction mixture was cooled to RT and quenched with 0.5 mol/L K_2CO_3 (10 mL). The layers were separated and the aqueous phase extracted with CH_2Cl_2 (2 × 10 mL). The organic extracts were combined and washed with water and brine, dried with magnesium sulfate, filtered, and concentrated. The crude product was purified by column chromatography (30% EtOAc–hexanes) to give **7a**, a yellow solid (34 mg), in 82% yield, m.p. 41 to 43 °C. R_f = 0.44 (3:7, EtOAc–hexanes). IR (CH_2Cl_2 cast, cm^{-1}): 2937, 2867, 2823, 1755, 1450, 1403, 1366, 1342, 1299, 1235. ^1H NMR (500 MHz, $CDCl_3$) δ: 4.05 (s, 1H), 3.50 (ddd, *J* = 6.2, 4.2, 1.2 Hz, 1H), 3.35 (s, 3H), 2.73 (d, J_{AB} = 17.7 Hz, 1H), 2.37 (d, J_{AB} = 17.7 Hz, 1H), 2.09 (m, 1H), 2.02–1.92 (m, 2H), 1.89–1.81 (m, 2H), 1.79–1.71 (m, 2H), 1.66 (m, 1H), 1.56 (m, 1H), 1.48 (ddd, *J*= 14.5, 10.2, 4.2 Hz, 1H), 1.37 (ddd, *J* = 13.7, 10.0, 3.2 Hz, 1H). ^{13}C NMR (125 MHz, $CDCl_3$) δ: 216.5, 90.9, 83.1, 81.6, 56.6, 51.3, 49.0, 40.4, 32.1, 27.0, 23.9, 23.5. HR-MS (EI) calcd. for $C_{12}H_{18}O_3$ (M^+): 210.1256; found: 210.1249. Anal. calcd. for $C_{12}H_{18}O_3$: C 68.60, H 8.60; found: C 68.20, H 9.06.

Carbene transfer reactions of 4c and 4d

Preparation of 7c and 7d

To a refluxing solution of Cu(hfacac)$_2$ (37 mg, 0.08 mmol, 10 mol%) in CH_2Cl_2 (55 mL) was added a solution of **4c** and **4d** (168 mg, 0.75 mmol, 4.4:1 mixture of anomers) in CH_2Cl_2 (25 mL), and the resulting mixture was monitored by TLC. Upon consumption of diazoketone **4a** (45 min), the reaction mixture was cooled to RT and quenched with 0.5 mol/L K_2CO_3 (25 mL). The layers were separated and the aqueous phase extracted with CH_2Cl_2 (2 × 15 mL). The organic extracts were combined and washed with water (20 mL), pre-dried with brine (20 mL), dried with magnesium sulfate, filtered, and concentrated. The resulting pale oil was purified by gradient column chromatograhy (silica gel; 5%, 10%, 15%, and then 20% EtOAc–hexanes until the products were recovered) to yield **7c** (68 mg) and **7d** (25 mg) as pale yellow oils, in an overall yield of 67%. (This reaction was also carried out on a small scale with pure samples of **4c** and **4d**. **4c** also furnished trace amounts of product **9**.).

Major diastereomer 7c (α)

R_f = 0.40 (3:7, EtOAc–hexanes). IR (CH_2Cl_2 cast, cm^{-1}): 2938, 2871, 2825, 1760, 1456, 1403, 1370, 1347, 1312. ^1H NMR (500 MHz, $CDCl_3$) δ: 4.04 (d, *J* = 4.9 Hz, 1H), 3.61 (ddd, *J* = 10.6, 5.3, 5.3 Hz, 1H), 3.34 (s, 3H), 2.54 (d, J_{AB} = 17.6 Hz, 1H), 2.19 (d, J_{AB} = 17.6 Hz, 1H), 2.06 (dd, *J* = 13.9, 5.7 Hz, 1H), 1.92–1.76 (m, 5H), 1.76–1.69 (m, 1H), 1.68–1.62 (m, 1H), 1.56 (ddd, *J* = 13.9, 9.1, 6.0 Hz, 1H). ^{13}C NMR (125 MHz, $CDCl_3$) δ: 214.4, 88.7, 78.3, 74.7, 56.8, 44.6, 44.4, 34.1, 28.9, 27.5, 21.3. HR-MS (ESI) calcd. for $C_{11}H_{16}O_3$ (M^+): 196.1099; found: 196.1097.

Minor anomer 7d (β)

R_f = 0.46 (3:7, EtOAc–hexanes). IR (CH_2Cl_2 cast, cm^{-1}): 2938, 2872, 2824, 1761, 1436, 1405, 1368, 1347, 1312. ^1H NMR (500 MHz, $CDCl_3$) δ: 4.19 (s, 1H), 3.28 (s, 3H), 3.23 (m, 1H), 2.60 (d, J_{AB} = 17.3 Hz, 1H), 2.22 (d, J_{AB} = 17.3 Hz, 1H), 2.03–1.74 (m, 7H), 1.66–1.54 (m, 2H). ^{13}C NMR (125 MHz, $CDCl_3$) δ: 215.8, 88.7, 80.3, 75.3, 56.4, 45.3, 41.9, 34.9, 30.9, 26.4, 21.8. HR-MS (ESI) calcd. for $C_{11}H_{16}O_3$ (M^+): 196.1099; found: 196.1092.

Side product 9 (partial data)

^1H NMR (500 MHz, $CDCl_3$) δ: 6.03 (d, *J* = 2.3 Hz, 1H), 5.56 (d, *J* = 4.5 Hz, 1H), 3.49 (s, 3H), 2.54 (dd, *J* = 14.1, 2.3 Hz, 1H), 2.42 (d, *J* = 14.1 Hz, 1H), 2.33 (dd, *J* = 13.2, 8.9 Hz, 1H), 2.24 (dddd, *J* = 9.8, 8.7, 6.4, 4.0 Hz, 1H), 2.01–1.83 (m, 3H), 1.74 (approx. dt, *J* = 13.2, 4.3 Hz, 1H), 1.70–1.56 (m, 2H), 1.35–1.27 (m, 1H). ^{13}C NMR (125 MHz, $CDCl_3$) δ: 136.2, 134.0, 102.9, 93.2, 60.1, 44.1, 40.9, 36.0, 34.2, 33.1, 25.7.

Carbene transfer reaction of 4e

Preparation of 7e, 7f, and 10e

To a refluxing solution of Cu(hfacac)$_2$ (16 mg, 0.03 mmol, 10 mol%) in CH_2Cl_2 (33 mL) was added a solution of **4e** (105 mg, 0.33 mmol) in CH_2Cl_2 (8 mL), and the resulting mixture was monitored by TLC. Upon consumption of diazoketone **4e** (30 min), the reaction mixture was cooled to RT and quenched with 0.5 mol/L K_2CO_3 (25 mL). The layers were separated and the aqueous phase extracted with CH_2Cl_2 (2 × 15 mL). The organic extracts were combined and washed with water (25 mL), pre-dried with brine (25 mL), dried with magnesium sulfate, filtered, and concentrated. The resulting pale yellow oil was diluted in ether (20 mL), and passed through a short pad of silica gel in a fritted filter while rinsing with excess ether. This was then concentrated and the resulting oil purified by radial chromatography (silica gel, 2 mm plate, solvent ramp: 100 mL each of 2%, 5%, 7%, and then 10% EtOAc–hexanes until the products were recovered) to yield a mixture of **7e** and **7f** (59 mg, 68%, ca. 2:1 ratio) as pale yellow oils, as well as **10e** (11 mg, 13%) as a white solid, in an overall yield of 80%. Minor diastereomer **7f** could be obtained as a white solid, mp 64–65 °C.

Diastereomers 7e and 7f

R_f = 0.41 (3:7, EtOAc–hexanes). IR (CH_2Cl_2 cast, cm^{-1}): 3019, 2955, 2869, 1785, 1711, 1492, 1447, 1401, 1343. ^1H NMR (500 MHz, $CDCl_3$) δ: 7.35 (d, *J* = 8.1 Hz, 2H), 7.28 (d, *J* = 8.1 Hz, 1H), 7.07 (d, *J* = 8.1 Hz, 1H), 7.06 (d, *J* = 8.1 Hz, 2H), 4.01 (s, 0.5H), 3.86 (d, *J* = 3.9 Hz, 1H), 3.50 (ddd, *J* = 13.2, 5.4, 4.2 Hz, 1H), 3.27 (ddd, *J* = 6.9, 13.5, 1.7 Hz, 0.5H), 2.60 (d, J_{AB} = 17.3 Hz, 0.5H), 2.57 (d, J_{AB} = 17.6 Hz, 1H), 2.29 (s, 4.5H), 2.24 (d, J_{AB} = 17.3 Hz, 0.5H), 2.23 (d, J_{AB} = 17.6 Hz, 1H), 2.16–2.06 (m, 2H), 1.96–1.77 (m, 7.5H), 1.75–1.62 (m, 4H). ^{13}C NMR (125 MHz, $CDCl_3$) δ: major diastereomer: 213.5, 138.0, 133.3, 130.1, 129.9, 88.5, 79.8, 44.8, 44.5, 44.2, 34.5, 28.1, 27.5, 21.3; minor diastereomer: 216.2, 137.8, 132.5, 131.4, 130.2, 89.1, 81.3, 45.8, 45.5, 43.0, 35.5, 31.4, 26.8, 22.3. HR-MS (EI) calcd. for $C_{17}H_{20}O_2S$ (M^+): 288.1184; found 283.1180. Anal. calcd. for $C_{17}H_{20}O_2S$: C 70.80, H 6.99; found: C 70.36, H 7.05.

Isomer 10e

Melting point 95 °C. R_f = 0.44 (3:7, EtOAc–hexanes). IR (CH_2Cl_2 cast, cm^{-1}): 2953, 2866, 1711, 1493, 1448, 1404,

© 2006 NRC Canada

1345, 1301. ^{1}H NMR (500 MHz, $CDCl_3$) δ: 7.32 (d, J = 8.0 Hz, 2H), 7.10 (d, J = 8.0 Hz, 2H), 4.75 (d, J = 7.3 Hz, 1H), 3.43 (d, J_{AB} = 14.8 Hz, 1H), 3.32 (s, 1H), 2.32 (s, 3H), 2.26–2.21 (m, 1H), 2.24 (d, J_{AB} = 14.8 Hz, 1H), 2.16 (m, 1H), 2.13 (dd, J = 12.4, 9.1 Hz, 1H), 1.93–1.84 (m, 3H), 1.67 (m, 1H), 1.51 (ddd, J = 13.4, 9.8, 7.5 Hz, 1H), 1.40 (m, 1H). ^{13}C NMR (125 MHz, $CDCl_3$) δ: 203.4, 138.4, 132.9, 130.1, 93.9, 60.9, 48.9, 45.3, 39.9, 37.1, 34.8, 25.4, 21.4. HR-MS (EI) calcd. for $C_{17}H_{20}O_2S$ (M^+): 288.1184; found: 283.1183. Anal. calcd. for $C_{17}H_{20}O_2S$: C 70.80, H 6.99; found: C 70.90, H 6.68.

Carbene transfer reaction of 4f — Preparation of 7e and 7f

Diazoketone **4f** was subjected to the procedure given previously for **4e**, to yield 85% of **7e** and **7f** in a 1:4.8 ratio. None of the isomeric product **10e** was isolated.

Carbene transfer reaction of 4g — Preparation of 7g

To a solution of **4g** (43 mg, 0.11 mmol) in toluene (9 mL) was added Cu(hfacac)$_2$ (9 mg, 0.01 mmol, 10 mol%), and the resulting mixture was heated to reflux. Upon consumption of diazoketone **4g** (14 h at reflux) the reaction mixture was cooled to RT and quenched with 0.5 mol/L K_2CO_3 (15 mL). The layers were separated and the aqueous phase extracted with CH_2Cl_2 (2 × 15 mL). The organic extracts were combined and washed with water (25 mL) and brine (25 mL), dried over $MgSO_4$, filtered, and concentrated. The resulting pale oil was diluted in ether (20 mL), and passed through a short pad of silica gel in a fritted filter while rinsing with excess ether. This was then concentrated and the resulting oil purified by radial chromatography (2 mm plate, solvent ramp: 50 mL each of 2%, 5%, 7%, and then 10% EtOAc–hexanes until the products were recovered) to yield 20 mg (50%) of **7g** as a pale oil, and as a 4.5:1 mixture of isomers by GC. This pale oil crystallized upon standing into a white solid. R_f = 0.42 (3:7, EtOAc–hexanes). IR (CH_2Cl_2 cast, cm^{-1}): 2952, 2934, 2867, 1769, 1746, 1492, 1443, 1400, 1269, 1254, 1143. ^{1}H NMR (500 MHz, $CDCl_3$; major diastereomer) δ: 7.34 (d, J = 8.1 Hz, 2H), 7.09 (d, J = 7.9 Hz, 2H), 4.19 (dq, J = 16.4, 7.1 Hz, 1H), 4.15 (dq, J = 16.4, 7.1 Hz, 1H), 4.04 (dd, J = 3.5, 3.5 Hz, 1H), 2.81 (d, J_{AB} = 17.0 Hz, 1H), 2.54 (d, J_{AB} = 17.0 Hz, 1H), 2.35 (m, 3H), 2.32 (s, 3H), 2.18 (dd, J = 11.5, 11.5 Hz, 1H), 2.03 (m, 1H), 1.97–1.84 (m, 3H), 1.80 (m, 1H), 1.63–1.46 (m, 3H), (t, J = 7.2 Hz, 3H). ^{13}C NMR (125 MHz, $CDCl_3$; major diastereomer) δ: 209.1, 166.1, 137.4, 132.4, 131.5, 129.7, 62.3, 55.8, 52.7, 50.8, 41.6, 35.2, 30.1, 26.7, 24.8, 21.1, 13.9. HR-MS (EI) calcd. for $C_{21}H_{26}O_4S$ (M^+): 374.1552; found: 374.1554.

Carbene transfer reaction of 4h — Preparation of 7h, 7i, and 10h

To a solution of **4h** (122 mg, 0.314 mmol) in toluene (31 mL) was added Cu(hfacac)$_2$ (16 mg, 0.03 mmol, 10 mol%), and the resulting mixture was heated to reflux. Upon consumption of diazoketone **4h** (14 h at reflux) the reaction mixture was cooled to RT and quenched with 0.5 mol/L K_2CO_3 (25 mL). The layers were separated and the aqueous phase extracted with CH_2Cl_2 (2 × 15 mL). The organic extracts were combined and washed with water (25 mL) and brine (25 mL), dried over $MgSO_4$, filtered, and concentrated. The resulting pale oil was diluted in ether (20 mL), and passed through a short pad of silica gel in a fritted filter while rinsing with excess ether. This was then concentrated and the resulting oil purified by radial chromatography (2 mm plate, solvent ramp: 50 mL each of 2%, 5%, 7%, and then 10% EtOAc–hexanes until the products were recovered) to yield 7 mg of a mixture of **7h** and **7i** (8:1 diastereomers by GC) and 48 mg of **10h** (single diastereomer by GC and NMR) as pale oils (49% combined yield).

7h

R_f = 0.57 (3:7, EtOAc–hexanes). IR (CH_2Cl_2 cast, cm^{-1}): 2941, 2871, 1774, 1743, 1493, 1448, 1401, 1342, 1277. ^{1}H NMR (500 MHz, $CDCl_3$) δ: 7.33 (d, J = 8.2 Hz, 2H), 7.07 (d, J = 7.9 Hz, 2H), 4.11 (m, 2H), 3.72 (dd, J = 11.4, 6.0 Hz, 1H), 2.78 (d, J_{AB} = 17.4 Hz, 1H), 2.36 (d, J_{AB} = 17.4 Hz, 1H), 2.31 (s, 3H), 2.17 (dd, J = 13.0, 5.9 Hz, 1H), 2.02–1.83 (m, 6H), 1.76–1.64 (m, 2H), 1.20 (t, J = 7.1 Hz, 3H). ^{13}C NMR (125 MHz, $CDCl_3$) δ: 208.4, 165.6, 137.7, 133.0, 130.4, 129.7, 87.8, 85.6, 62.1, 46.4, 45.5, 44.1, 34.3, 30.1, 28.5, 21.4, 21.1, 13.8. HR-MS (EI) calcd. for $C_{20}H_{24}O_4S$ (M^+): 360.1395; found: 360.1403.

10h

R_f = 0.52 (3:7, EtOAc–hexanes). IR (CH_2Cl_2 cast, cm^{-1}): 2955, 2869, 1750, 1717, 1492, 1448, 1402, 1346, 1241. ^{1}H NMR (500 MHz, $CDCl_3$) δ: 7.32 (d, J = 8.2 Hz, 2H), 7.10 (d, J = 8.2 Hz, 2H), 4.75 (d, J = 7.0 Hz, 1H), 4.11 (m, 1H), 3.47 (d, J_{AB} = 15.7 Hz, 1H), 2.33 (s, 3H), 2.32–2.27 (m, 3H), 2.16 (m, J = 6.0, 2.6 Hz, 1H), 1.93–1.82 (m, 3H), 1.68 (m, 1H), 1.52 (ddd, J = 16.9, 9.9, 7.7 Hz, 1H), 1.43 (m, 1H), 1.21 (t, J = 7.2 Hz, 3H). ^{13}C NMR (125 MHz, $CDCl_3$) δ: 196.3, 166.8, 140.3, 136.3, 129.7, 126.4, 93.9, 81.2, 67.3, 61.6, 48.3, 45.3, 38.6, 36.7, 34.4, 24.9, 21.3, 14.0. HR-MS (EI) calcd. for $C_{20}H_{24}O_4S$ (M^+): 360.1395; found: 360.1397.

Modification of rearrangement products

Ketal 11a

A flask containing a solution of **7b** (67 mg, 0.22 mmol), ethylene glycol (144 μL, 3.32 mmol), and TsOH (2 mg, 0.01 mmol) in toluene (5 mL) was equipped with a condenser and Dean-Stark trap (pre-filled with toluene), and then heated to reflux for 12 h. The reaction was cooled to RT and the solution was transferred to a separatory funnel and washed with satd. $NaHCO_3$ (10 mL). The organic phase was dried with $MgSO_4$, filtered, and the solvent was removed under reduced pressure. The crude white solid thus obtained was passed through a short pad of silica gel (1 cm in a disposable pipette) while eluting with 10 mL of 30% EtOAc–hexanes. The solvents were removed under reduced pressure and the resulting white solid was purified by radial chromatography (2 mm plate, solvent ramp: 100 mL of hexanes, 2.5%, 5%, and 10% EtOAc–hexanes) to yield recovered **7b** (16 mg, 25%) and **11a** (55 mg, 73%) as a white solid. R_f = 0.18 (5% EtOAc–hexanes). IR (CH_2Cl_2 cast, cm^{-1}): 2946, 2868, 1319, 1092. ^{1}H NMR (500 MHz, $CDCl_3$) δ: 7.35 (d, J = 8.1 Hz, 2H), 7.09 (d, J = 7.9 Hz, 2H), 4.11 (approx. br s, 1H), 3.93 (ddd, J = 8.0, 6.6, 4.9 Hz, 1H), 3.85 (approx. q, J = 7.3 Hz, 1H), 3.77 (ddd, J = 6.9, 6.9, 4.9 Hz, 1H), 3.62 (ddd, J = 7.9, 7.1, 7.1 Hz, 1H), 3.62–3.48 (m, 1H),

© 2006 NRC Canada

2.35 (d, J_{AB} = 14.2 Hz, 1H), 2.32 (s, 3H), 2.27 (d, J_{AB} = 14.2 Hz, 1H), 2.05–1.99 (m, 1H), 1.96–1.89 (m, 3H), 1.83–1.70 (m, 4H), 1.65–1.47 (m, 3H). ^{13}C NMR (125 MHz, $CDCl_3$) δ: 137.3, 132.9, 132.1, 129.9, 117.1, 92.0, 86.5, 65.4, 64.2, 50.9, 50.8, 48.0, 41.9, 32.4, 27.8, 26.6, 23.5, 21.3. HR-MS (EI) calcd. for $C_{20}H_{26}O_3S$ (M^+): 346.1603; found: 346.1600.

Tricyclic sulfone 12

To a mixture of **11a** (83 mg, 0.24 mmol) in MeOH (1 mL) cooled to 0 °C was added a mixture of OXONE® (295 mg) in a pH 4 buffer (1 mL) (18). After the addition, the cooling bath was removed and the slurry was stirred at RT for 10 h. The mixture was diluted with water (5 mL) and $CHCl_3$ (5 mL). The biphasic mixture was transferred to a separatory funnel, separated, and the aqueous phase was extracted with $CHCl_3$ (3 × 5 mL). The combined organic phase was washed with brine, dried with $MgSO_4$, and the solvents were removed under reduced pressure. Sulfone **12** was obtained as a white crystalline solid (88 mg, 97%) (homogenous by TLC and ^{1}H NMR analysis), and was used without further purification; mp 191–194 °C. R_f = 0.25 (30% EtOAc–hexanes). IR (CH_2Cl_2 cast, cm^{-1}): 2956, 1299, 1145, 1085. ^{1}H NMR (500 MHz, $CDCl_3$) δ: 7.76 (d, J = 8.4 Hz, 2H), 7.34 (d, J = 7.9 Hz, 2H), 4.46 (approx. d, J = 2.9 Hz, 1H), 4.01 (ddd, J = 8.0, 6.5, 4.4 Hz, 1H), 3.95–3.90 (m, 1H), 3.85 (approx. q, J = 7.0 Hz, 1H), 3.78 (approx. q, J = 7.4 Hz, 1H), 3.51 (dddd, J = 11.6, 3.3, 3.3, 3.3 Hz, 1H), 2.44 (s, 3H), 2.27 (dd, J = 14.3, 0.9 Hz, 1H), 2.10 (d, J_{AB} = 14.3 Hz, 1H), 1.98–1.90 (m, 2H), 1.80–1.50 (m, 9H). ^{13}C NMR (125 MHz, $CDCl_3$) δ: 144.7, 135.2, 129.9, 129.4, 117.3, 92.7, 79.5, 67.1, 65.4, 64.8, 47.2, 42.6, 39.7, 28.5, 25.2, 21.8, 20.9, 20.5.

Vinyl sulfone 13

To a solution of **12** (22 mg, 0.058 mmol) in THF (1.16 mL) cooled to –78 °C (isopropanol/dry ice bath) was added dropwise via syringe *n*-BuLi (35 μL, 2.52 mol/L in hexanes). The solution initially turned pale yellow, then dark yellow-orange. The starting material was consumed after 20 min as ascertained by TLC, and the reaction was stirred an additional 30 min. The cooling bath was removed and the reaction was immediately quenched by the addition of satd. NH_4Cl solution (4 mL) and Et_2O (5 mL). The biphasic mixture was transferred to a separatory funnel, separated, and the aqueous phase was extracted with Et_2O (3 × 5 mL). The combined organic phase was then washed with brine (10 mL), dried with $MgSO_4$, filtered, and the solvents were removed under reduced pressure. The resulting crude material was purified by radial chromatography (2 mm plate, solvent ramp: 100 mL each of 20%, 30%, and 40% EtOAc–hexanes) to yield **13** (16 mg, 75%) as a white solid; mp 120–122 °C. R_f = 0.11 (30% EtOAc–hexanes). IR (CH_2Cl_2 cast, cm^{-1}): 3534, 2948, 1301, 1143, 1086. ^{1}H NMR (500 MHz, $CDCl_3$) δ: 7.75 (d, J = 8.4 Hz, 2H), 7.33 (d, J = 8.3 Hz, 2H), 6.92 (approx. br s, 1H), 4.02–3.92 (m, 3H), 3.87–3.83 (m, 1H), 3.30 (br s, 1H), 3.16 (ddd, J = 14.2, 12.3, 6.7 Hz, 1H), 2.44 (s, 3H), 2.31 (ddd, J = 14.8, 7.3, 1.5 Hz, 1H), 2.26 (d, J_{AB} = 14.6 Hz, 1H), 2.06 (d, J_{AB} = 14.6 Hz, 1H), 1.76–1.73 (m, 2H), 1.67–1.57 (m, 3H), 1.51–1.46 (m, 1H), 1.35–1.19 (m, 3H). ^{13}C NMR (100 MHz, $CDCl_3$) δ: 144.9, 144.8, 140.1, 136.1, 130.1, 128.7, 108.8, 79.8, 65.5, 63.7, 50.2, 47.1, 44.0, 34.5, 28.8, 23.4, 23.2, 21.9. HR-MS (EI) *m/z* calcd. for $C_{20}H_{26}O_5S$: 378.1501; found: 378.1495.

Cyclooctenone ketal 14a

This procedure was carried out under an argon atmosphere. A large excess of LiDBB solution was prepared according to Cohen's procedure (Li (10 mg), di-*tert*-butylbiphenyl (DBB) (358 mg), THF (4.5 mL)) (19*b*). To a solution of **11a** (14 mg, 0.04 mmol) and a crystal of phenanthroline in THF (0.17 mL) cooled to –78 °C (isopropanol/dry ice bath) *n*-BuLi (~10 μL, 2.52 mol/L in hexanes) was added dropwise until the solution turned a red color (19*c*). LiDBB was then added dropwise via cannula to this solution until a persistent dark green color was observed, indicating an excess of LiDBB (exact volume of LiDBB added not measured). Starting material was consumed within 30 min (TLC). The reaction was allowed to stir for an additional 1 h at –78 °C, the cooling bath was then removed followed by the immediate addition of satd. NH_4Cl solution (5 mL) and Et_2O (5 mL). The mixture was then transferred to a separatory funnel, the aqueous phase was back extracted with Et_2O (5 mL), the combined organic phase was washed with brine (10 mL) and dried with $MgSO_4$, filtered, and the solvents were removed under reduced pressure. The resulting crude material was purified by radial chromatography (2 mm plate, solvent ramp: 100 mL each of hexanes, 5%, 15%, and 30% EtOAc–hexanes) to yield **14a** (9 mg, 97%) as a colorless oil. R_f = 0.32 (30% EtOAc–hexanes). IR (CH_2Cl_2 cast, cm^{-1}): 3542, 3018, 2948, 1061, 757. ^{1}H NMR (500 MHz, $CDCl_3$) δ: 5.78 (ddd, J = 11.5, 9.7, 7.6 Hz, 1H), 5.58 (dd, J = 11.5, 1.2 Hz, 1H), 4.00–3.98 (m, 1H), 3.94–3.90 (m, 3H), 3.39 (br s, 1H), 2.94–2.85 (m, 1H), 2.26 (d, J_{AB} = 14.4 Hz, 1H), 2.08–2.01 (m, 2H), 1.99 (d, J_{AB} = 14.4 Hz, 1H), 1.80–1.56 (m, 6H), 1.49–1.41 (m, 1H), 1.41–1.34 (m, 1H). ^{13}C NMR (125 MHz, $CDCl_3$) δ: 133.2, 132.8, 109.6, 80.3, 64.8, 63.4, 50.3, 46.9, 43.9, 34.8, 29.4, 24.3, 23.3. HR-MS (EI) calcd. for $C_{13}H_{20}O_3$ (M^+): 224.1413; found: 224.1412.

Ketalization of 7e and 7f

Formation of 11b and 11c

To a mixture of diastereomers **7e** and **7f** (340 mg, 1.2 mmol, ca. 2.5:1) in CH_2Cl_2 (6 mL) at 0 °C was added 1,2-bis(trimethylsiloxy)ethane (580 μL, 2.4 mmol) followed by TMSOTf (12 μL, 5 mol%), and the resulting mixture was warmed to RT over several hours. This was then heated to reflux for ca. 12 h, after which TLC showed consumption of starting materials. The reaction was quenched with pyridine (1 mL) and saturated aqueous $NaHCO_3$ (5 mL), diluted with Et_2O (10 mL), and the resulting layers were separated. The aqueous layer was washed with three portions of Et_2O (10 mL) and the combined organic extracts were washed with water (30 mL) and then brine (30 mL), dried over magnesium sulfate, filtered, and concentrated, giving the crude product as a yellow oil. This oil was diluted in ether (20 mL) and passed through a short pad of silica gel in a fritted filter while eluting with ether. This was then concentrated and the resulting oil purified by radial chromatography (silica gel, 2 mm plate, solvent ramp: 100 mL each of 3%, 6%, and then 10% EtOAc–hexanes until the products are recovered) to

© 2006 NRC Canada

yield **11b** (283 mg, 72%) as a pale oil and **11c** (102 mg, 26%) as a crystalline solid.

Ketal 11b

R_f = 0.63 (3:7, EtOAc–hexanes). IR (CH_2Cl_2 cast, cm^{-1}): 2945, 2869, 1492, 1434, 1398, 1344, 1323, 1291. ^1H NMR (500 MHz, $CDCl_3$) δ: 7.23 (d, J = 8.0 Hz, 2H), 7.06 (d, J = 8.0 Hz, 2H), 4.11 (m, 1H), 4.06 (m, 1H), 3.87, (d, J = 2.6 Hz, 1H), 3.84 (m, 1H), 3.76 (m, 1H), 3.31 (ddd, J = 12.7, 5.8, 3.5 Hz, 1H), 2.37 (d, J_{AB} = 13.7 Hz, 1H), 2.42–2.34 (m, 1H), 2.32 (s, 3H), 2.10 (d, J_{AB} = 13.7 Hz, 1H), 2.04 (dd, J = 14.0, 5.7 Hz, 1H), 1.80–1.74 (m, 5H), 1.65–1.57 (m, 2H). ^{13}C NMR (125 MHz, $CDCl_3$) δ: 136.8, 134.1, 131.1, 130.3, 116.9, 88.5, 83.1, 65.5, 64.6, 45.7, 45.3, 44.9, 34.6, 28.5, 28.4, 21.4, 21.2. HR-MS (EI) calcd. for $C_{19}H_{24}O_3S$ (M^+): 332.1146; found: 332.1438. Anal. calcd. for $C_{19}H_{24}O_3S$: C 68.64, H 7.28, S 9.60; found: C 68.78, H 7.05, S 9.79.

Ketal 11c

Melting point 78 to 79 °C. R_f = 0.54 (3:7, EtOAc–hexanes). IR (CH_2Cl_2 cast, cm^{-1}): 2951, 2871, 1492, 1445, 1433, 1398. ^1H NMR (500 MHz, $CDCl_3$) δ: 7.29 (d, J = 8.0 Hz, 2H), 7.05 (d, J = 8.0 Hz, 2H), 3.92–3.87 (m, 2H), 3.78 (approx. q, J = 7.2 Hz, 1H), 3.63 (ddd, J = 11.5, 7.0, 4.5 Hz, 1H), 3.53 (approx. q, J = 7.4 Hz, 1H), 3.38 (ddd, J = 7.8, 6.1, 1.7 Hz, 1H), 2.29 (s, 3H), 2.24 (d, J_{AB} = 13.4 Hz, 1H), 2.22 (m, 1H), 1.96 (d, J_{AB} = 13.4 Hz, 1H), 1.92–1.74 (m, 8H). ^{13}C NMR (125 MHz, $CDCl_3$) δ: 137.2, 132.5, 132.4, 129.9, 116.7, 89.0, 83.4, 65.4, 64.3, 46.1, 44.1,43.4, 36.5, 32.1, 27.4, 22.9, 21.3. HR-MS (EI) calcd. for $C_{19}H_{24}O_3S$ (M^+): 332.1446; found: 332.1445. Anal. calcd. for $C_{19}H_{24}O_3S$: C 68.64, H 7.28, S 9.60; found: C 68.61, H 7.01, S 9.76.

LDBB reduction of 11b

Formation of 14b and 15

A large excess of LDBB was prepared according to Cohen's procedure, using Li (8 mg, 6 equiv.) and di-*tert*-butylbiphenyl (300 mg) in THF (3.2 mL). To a solution of **11b** (57 mg, 0.19 mmol) and a crystal of phenanthroline in THF (0.7 mL) cooled to –78 °C was added *n*-BuLi until the color turned deep red. LDBB was then added dropwise (without quantification) to the reaction mixture until an intense green color persisted, indicating the presence of excess LDBB. The reaction was stirred until consumption of starting material was observed by TLC (ca. 2 h). The reaction was then quenched by addition of saturated aqueous ammonium chloride (5 mL), further diluted in Et_2O (15 mL), and the resulting bilayer was separated. The aqueous layer was back extracted once with Et_2O (10 mL) and the combined organic extracts were pre-dried with brine (30 mL), dried over anhydrous magnesium sulfate, filtered, and concentrated. The crude product was purified by gradient column chromatography (silica gel, 0%, 20%, and 60% EtOAc–hexanes) to give **14a** (25 mg, 69%) as a pale yellow oil, as well as a trace of isomer **15** (2 mg, 5.5%), in an overall yield of 75%. The ratio of product isomers depended on the time allowed for the reaction: if the reaction was quenched after 30 min, the ratio of the products is **14a** (19%) and isomer **15** (45%).

Alcohol 14b

R_f = 0.36 (3:7, EtOAc–hexanes). IR (CH_2Cl_2 cast, cm^{-1}): 3513, 3025, 2959, 1653, 1445, 1425, 1397, 1344, 1316, 1281. ^1H NMR (500 MHz, $CDCl_3$) δ: 5.89 (ddd, J = 12.2, 8.9, 3.5 Hz, 1H), 5.65 (ddd, J = 12.0, 3.1, 1.3 Hz, 1H), 4.19 (s, 1H) 3.93 (s, 4H), 2.29 (dddd, J = 16.1, 11.8, 3.1, 3.1 Hz, 1H), 2.21 (d, J_{AB} = 14.1 Hz, 1H), 2.04 (ddd, J = 16.0, 8.8, 2.3 Hz, 1H), 1.86 (d, J_{AB} = 14.1 Hz, 1H), 1.80–1.66 (m, 3H), 1.65–1.50 (m, 4H). ^{13}C NMR (125 MHz, $CDCl_3$) δ: 133.9, 133.6, 108.6, 78.6, 64.6, 63.9, 47.2, 44.9, 41.9, 30.9, 26.6, 19.8. HR-MS (ESI) calcd. for $C_{12}H_{18}O_3Na$ ($M + Na^+$): 233.1148; found: 233.1149.

Isomer 15

R_f = 0.09 (3:7, EtOAc–hexanes). IR (CH_2Cl_2 cast, cm^{-1}): 3428 (br), 2946, 2865, 1651, 1446, 1433, 1360, 1327. ^1H NMR (500 MHz, $CDCl_3$) δ: 5.89 (ddd, J = 12.2, 8.8, 3.5 Hz, 1H), 5.64 (d, J = 12.2 Hz, 1H), 4.18 (s, 1H), 3.94 (s, 4H), 2.29 (approx. ddt, J = 14.5, 11.3, 3.3, 3.3 Hz, 1H), 2.21 (d, J_{AB} = 14.1 Hz, 1H), 2.04 (ddd, J = 16.0, 8.8, 2.2 Hz, 1H), 1.86 (d, J_{AB} = 14.1 Hz, 1H), 1.80–1.48 (m, 7H). ^{13}C NMR (125 MHz, $CDCl_3$) δ: 153.2, 99.4, 90.8, 74.1, 67.8, 61.3, 46.0, 46.9, 39.9, 37.1, 33.0, 24.8. HR-MS (EI) calcd. for $C_{12}H_{18}O_3$ (M^+): 210.1256; found: 210.1253.

Isomer **15** was found to reketalize upon standing in $CDCl_3$ to give compound **16**. R_f = 0.40 (3:7, EtOAc–hexanes). IR (CH_2Cl_2 cast, cm^{-1}): 2951, 2869, 1350. ^1H NMR (500 MHz, $CDCl_3$) δ: 4.43 (dd, J = 7.6, 4.3 Hz, 1H), 3.92 (approx. t, J = 6.3 Hz, 2H), 3.81 (approx. t, J = 6.3 Hz, 2H), 2.67 (approx. tt, J = 9.2, 4.7 Hz, 1H), 2.31 (dd, J = 12.2, 9.0 Hz, 1H), 2.08 (d, J_{AB} = 13.5 Hz, 1H), 1.96–1.86 (m, 2H), 1.86–1.78 (m, 2H), 1.72 (dd, J = 13.5, 2.0 Hz, 1H), 1.65–1.61 (m, 1H), 1.64 (ddd, J = 13.8, 1.8, 1.8 Hz, 1H), 1.56–1.51 (m, 1H), 1.45–1.40 (m, 1H), 1.35–1.30 (m, 1H). ^{13}C NMR (125 MHz, $CDCl_3$) δ: 107.6, 91.5, 76.0, 64.3, 63.2, 44.5, 44.2, 40.7, 39.0, 37.4, 34.9, 25.1. HR-MS (EI) calcd. for $C_{12}H_{18}O_3$ (M^+): 210.1256; found: 210.1253.

Acknowledgments

We thank the Natural Sciences and Engineering Research Council of Canada (NSERC) for support of this work, and NSERC and Alberta Heritage Foundation for Medical Research for studentships (GKM).

References

1. Review: G. Mehta and V. Singh. Chem. Rev. **99**, 881 (1999).
2. (*a*) F. López, L. Castedo, and J.L. Mascarenas. J. Am. Chem. Soc. **124**, 4218 (2002); (*b*) K. Lee and J.K. Cha. J. Am. Chem. Soc. **123**, 5590 (2001); (*c*) P. de Armas, F. Carcia-Tellado, and J.J. Marrero-Tellado. Eur. J. Org. Chem. 4423 (2001); (*d*) P.A. Wender, C.D. Jesudason, H. Nakahira, N. Tamura, A.L. Tebbe, and Y. Ueno. J. Am. Chem. Soc. **119**, 12976 (1997); (*e*) P.A. Wender, K.D. Rice, and M.E. Schnute. J. Am. Chem. Soc., **119**, 7897 (1997); (*f*) H.M.L. Davies, G. Ahmed, and M.R. Churchill. J. Am. Chem. Soc. **118**, 10774 (1996); (*g*) D.R. Williams, J.W. Benbow, J.G. McNutt, and E.E. Allen. J. Org. Chem. **60**, 833 (1995); (*h*) Review: P. Chiu and M. Lautens. Top. Curr. Chem. **190**, 1 (1997).

© 2006 NRC Canada

3. (*a*) J.H. Rigby and J.A.Z. Wilson. J. Org. Chem. **52**, 34 (1987); (*b*) G.A. Molander and P.R. Eastwood. J. Org. Chem. **60**, 4559 (1995).
4. M. Harmata and P. Rashataskhon. Org. Lett. **2**, 2913 (2000).
5. (*a*) F.G. West, T.H. Eberlein, and R.W. Tester. J. Chem. Soc. Perkin Trans. 1, 2857 (1993); (*b*) R.W. Tester and F.G. West. Tetrahedron Lett. **39**, 4631 (1998).
6. (*a*) F.P. Marmsäter, G.K. Murphy, and F.G. West. J. Am. Chem. Soc. **125**, 14724 (2003); (*b*) G.K. Murphy and F.G. West. Org. Lett. **7**, 1801 (2005).
7. For other examples of efficient migration of heteroatom-substituted carbons in oxonium ylide [1,2]-shifts, see: (*a*) J.B. Brogan, C. Bauer, R.D. Rogers, and C.K. Zercher. J. Org. Chem. **62**, 3902 (1997); (*b*) J.B. Brogan and C.K. Zercher. Tetrahedron Lett. **39**, 1691 (1998); (*c*) Ref. 5*b*.
8. (*a*) T.H. Eberlein, F.G. West, and R.W. Tester. J. Org. Chem. **57**, 3479 (1992); (*b*) F.G. West, B.N. Naidu, and R.W. Tester. J. Org. Chem. **59**, 6892 (1994).
9. S. Ando, K.P. Minor, and L.E. Overman. J. Org.Chem. **63**, 6379 (1997).
10. (*a*) G.C. Hirst, P.N. Howard, and L.E. Overman. J. Am. Chem. Soc. **111**, 1514 (1989); (*b*) T.O. Johnson, Jr. Ph.D. thesis, University of California, Irvine, Calif. 1992.
11. For a representative diazotransfer procedure, see: M.P. Doyle, M.A. McKervey, and T. Ye. Modern catalytic methods for organic synthesis with diazo compounds. Wiley-Interscience, New York, N.Y. 1997. p. 10.
12. (*a*) F.P. Marmsäter and F.G. West. J. Am. Chem. Soc. **123**, 5144 (2001); (*b*) F.P. Marmsäter, J.A. Vanecko, and F.G. West. Tetrahedron, **58**, 2027 (2002).
13. (*a*) S. Hashimoto, N. Watanabe, and S. Ikegami. Tetrahedron Lett. **33**, 2709 (1992); (*b*) S. Hashimoto, N. Watanabe, and S. Ikegami. J. Chem. Soc. Chem. Commun. 1508 (1992); (*c*) S. Hashimoto, N. Watanabe, M. Anada, and S. Ikegami. J. Synth. Org. Chem. Jpn. **54**, 988 (1996).
14. F.P. Marmsäter, J.A. Vanecko, and F.G. West. Org. Lett. **6**, 1657 (2004).
15. (*a*) F.G. West and B.N. Naidu. J. Am. Chem. Soc. **116**, 8420 (1994); (*b*) B.N. Naidu and F.G. West. Tetrahedron, **53**, 16565 (1997); (*c*) J.A. Vanecko and F.G. West. Org. Lett. **4**, 2813 (2002); (*d*) Review: J.A. Vanecko, H. Wan, and F.G. West. Tetrahedron, **62**, 1043 (2006).
16. For early mechanistic studies showing retention of configuration in ammonium ylide [1,2]-shifts, see: W.D. Ollis, M. Rey, and I.O. Sutherland. J. Chem. Soc. Perkin Trans. 1, 1009 (1983).
17. (*a*) C.R. Johnson and E.J. Roskamp. J. Am. Chem. Soc. **108**, 6062 (1986); (*b*) N. Karche, S.M. Jachak, and D.D. Dhavale. J. Org. Chem. **66**, 6323 (2001).
18. B.M. Trost and D.P. Curran. Tetrahedron Lett. **22**, 1287 (1981).
19. (*a*) T. Cohen and M. Bhupathy. Acc. Chem. Res. **22**, 152 (1989); (*b*) B. Mudryk and T. Cohen. Org. Synth. **72**, 173 (1995); (*c*) S.D. Rychnovsky, A.J. Buckmelter, V.H. Dahankar, and D.J. Skalitzky. J. Org. Chem. **64**, 6849 (1999).
20. L.A. Paquette, J. Reagan, S.L. Schreiber, and C.A. Teleha. J. Am. Chem. Soc. **111**, 2331 (1989).
21. G. Picotin and P. Miginiac. J. Org. Chem. **52**, 4796 (1987).

© 2006 NRC Canada

An examination of VANOL, VAPOL, and VAPOL derivatives as ligands for asymmetric catalytic Diels–Alder reactions[1]

Douglas P. Heller, Daniel R. Goldberg, Hongqiao Wu, and William D. Wulff

Abstract: Several derivatives of the vaulted biaryl ligand VAPOL were prepared and evaluated as chiral ligands for aluminum Lewis acids in the catalytic asymmetric Diels–Alder reactions of methyl acrylate and methacrolein with cyclopentadiene. The substituents on VAPOL were introduced into the 6- and 6′-positions in an effort to further extend the chiral pocket of the major groove, which contains the phenol functions at the 4- and 4′-positions. The set of four new ligands that have been prepared have the following groups introduced into the 6- and 6′-positions of VAPOL: bromide, methyl, phenyl and 3,5-di-*t*-butylphenyl. All of these ligands give lower asymmetric inductions than the unsubstituted VAPOL for the Diels–Alder reactions of both methyl acrylate and methacrolein. The positive cooperativity of added carbonyl compounds on the autoinduction in the Diels–Alder reaction of methyl acrylate and cyclopentadiene were also investigated with the VANOL and VAPOL ligands as well as the 6,6′-dibromo and 6,6′-diphenyl derivatives of VAPOL. Only the reaction with VAPOL showed any significant positive cooperativity. The reaction with VANOL was sluggish at –78 °C, but at higher temperatures, the reaction did exhibit positive cooperativity that was similar to that of VAPOL. Finally, no positive cooperativity was observed with the VAPOL ligand for the reaction of methacrolein and cyclopentadiene.

Key words: Diels–Alder, asymmetric catalysis, vaulted biaryl ligands, VANOL, VAPOL.

Résumé : On a préparé plusieurs dérivés du ligand voûté VAPOL et on les a évalués comme ligands chiraux pour des acides de Lewis dérivés de l'aluminium à utiliser dans des réactions de Diels–Alder asymétrique catalytique de l'acrylate de méthyle et de la méthacroléine avec le cyclopentadiène. On a introduit des substituants sur les positions 6 et 6′ du VAPOL dans le but d'agrandir la poche chirale de la cannelure principale qui comporte les fonctions phénols dans les positions 4 et 4′. Dans l'ensemble des quatre nouveaux ligands qui ont été préparés, on a introduit les groupes suivants dans les positions 6 et 6′ du VAPOL: bromure; méthyle; phényle et 3,5-di-tert-butylphényle. Chacun de ces ligands conduit à des inductions asymétriques inférieures à celle observé avec le VAPOL non substitué, tant pour les réactions de Diels-Alder de l'acrylate de méthyle que celles de la méthacroléine. On a aussi étudié la coopération positive des composés carbonyles ajoutés sur l'autoinduction de la réaction de l'acrylate de méthyle et du cyclopentadiène à l'aide de ligands VANOL et VAPOL ainsi qu'avec les dérivés 6,6′-dibromo et 6,6′-diphényl du VAPOL. Seule la réaction avec le VAPOL a montré une coopération positive significative. La réaction avec le VANOL était lente à –78°C, mais à des températures plus élevées, la réaction présente une coopération positive semblable à celle du VAPOL. Enfin, on n'a observé aucune coopération positive avec le ligand VAPOL pour la réaction de la méthacroléine avec le cyclopentadiène.

Mots clés : Diels–Alder, catalyse asymétrique, ligands biaryles voûtés, VANOL, VAPOL.

[Traduit par la Rédaction]

Received 1 February 2006. Accepted 31 March 2006. Published on the NRC Research Press Web site at http://canjchem.nrc.ca on 1 December 2006.

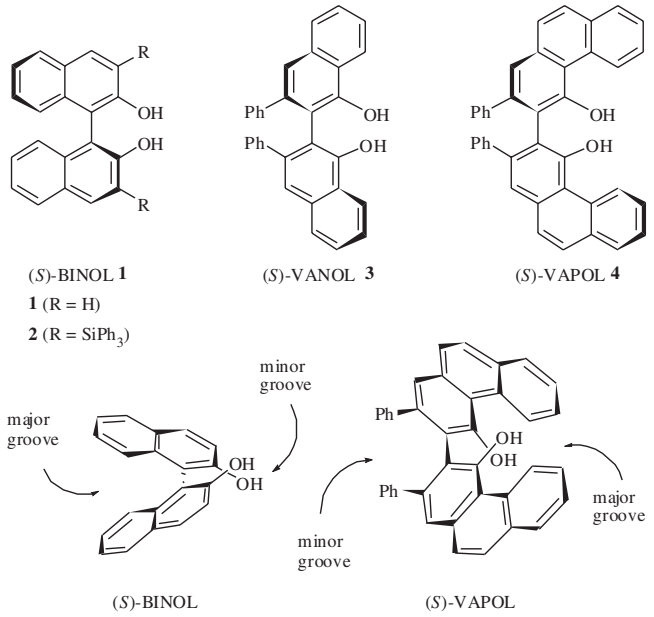
This manuscript is dedicated to Dr. Alfred Bader. Dr. Bader is many things to many people and included among them he is an entrepreneur, a lover of the arts, a champion of young scientists, and above all, a generous and gracious human being. When I was a beginning assistant professor in the early 1980s, he awarded me one of his young chemist awards. This was a greatly appreciated and needed boast to my program. A gift of $5000 was a significant sum in those days considering my start-up package was $25 000. His call came out of the blue one day when I was home in bed with a nasty fever. Having failed to reach me at work, he tracked me down at home and what I remember from my delirious state is my wife saying someone named Alfred Bader was on the phone. I think that I thanked him at the time, and if I didn't, I would certainly like to thank him now.

D.P. Heller, D.R. Goldberg, H. Wu, and W.D. Wulff.[2] Department of Chemistry, Michigan State University, East Lansing, MI 48864, USA.

[1]This article is part of a Special Issue dedicated to Dr. Alfred Bader.
[2]Corresponding author (e-mail: wulff@chemistry.msu.edu).

 doi:10.1139/V06-124 © 2006 NRC Canada

Scheme 1.

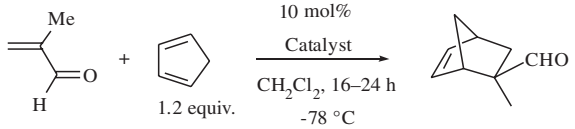


Introduction

One of the most widely used and successful ligands in asymmetric catalysis is 1,1′-binaphth-2,2′-ol, or BINOL 1 (1). In most applications, catalysts are generated from BINOL by the formation of covalent bonds to the two phenol functions with either a transition metal or a main group atom. In many applications it has been found that improved induction results from these catalysts if substituents are introduced in the 3- and 3′-positions of BINOL (such as **2**) (2). This is particularly true for catalysts that have only one BINOL ligand bound to the metal center (2). In the absence of substituents at the 3- and 3′-positions, the BINOL ligand provides a much smaller chiral pocket for the metal center since the phenol functions project into the minor groove of BINOL rather than the major groove (Scheme 1). Our approach to this problem is to design biaryls in which the phenol functions are projected into the major groove of the ligand (Scheme 1). To this end, we simply envisioned an extension of the aromatic system of BINOL out into the region of the phenol functions and as a result ultimately synthesized the vaulted biaryl ligands VANOL **3** and VAPOL **4** (3). These ligands have been demonstrated to be particularly successful in catalytic asymmetric Diels–Alder (4), aziridination (5), Mannich (6) reactions, as well as in Baeyer–Villiger oxidations (7) and imine amination reactions (8).

We have reported that a catalyst prepared from VAPOL and diethylaluminum chloride is effective in providing high asymmetric inductions in the reactions of methacrolein and methyl acrylate with cyclopentadiene (Table 1) (4). A comparison of a series of catalysts prepared from diethyl aluminum chloride and ligands **1**–**4** reveals that only the VAPOL-derived catalyst offers significant asymmetric induction in the reaction with methacrolein (Table 1) (4*a*). The data from a corresponding set of boron catalysts prepared from bromoborane dimethyl sulfide complex revealed that these catalysts are slower and that VANOL gave the catalyst with the superior enantioselectivities (4*b*). Based on the data in

Table 1. Diels–Alder reaction of methacrolein and cyclopentadiene.



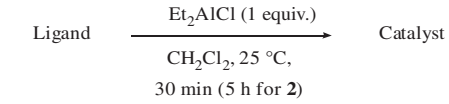
5 **6** (*2R*)-**7**

Ligand	Yield **7** (%)	exo–endo	ee% **7** (exo)[a]
(*S*)-BINOL	99	97:3	23
(*S*)-**2**	69	92:8	20
(*S*)-VANOL	84	93:7	5
(*S*)-VAPOL	100	98:2	91.4 (93.6)[b]

Note: All reactions use 1.0 mol/L in methacrolein.

[a]ee% was measured by conversion to chiral acetals as described in the experimental section.

[b]ee% in parentheses was measured by GC as described in the experimental section.



Scheme 2.

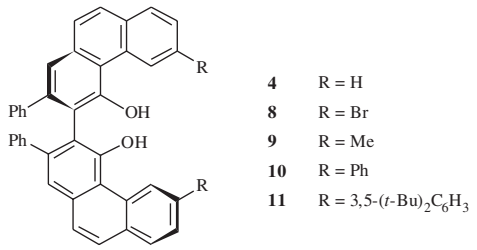
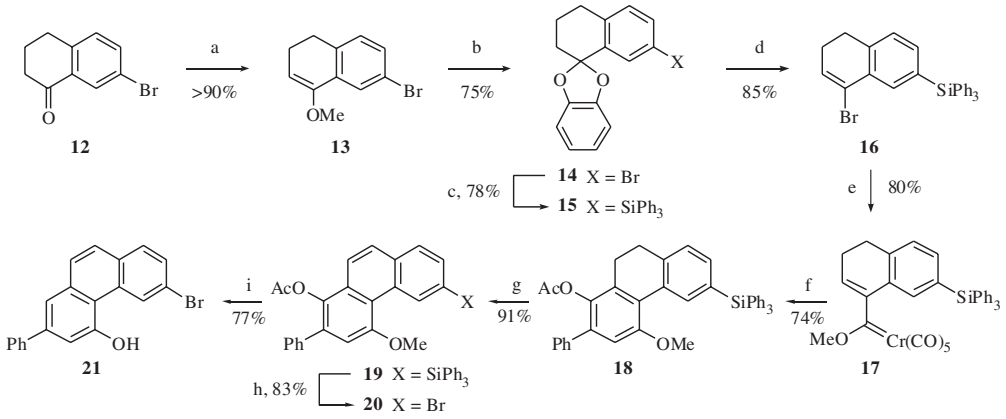


Table 1, we set out to prepare and evaluate the set of 6,6′-disubstituted VAPOL ligands **8**–**11** (Scheme 2) as precursors to aluminum catalysts in the asymmetric catalytic Diels–Alder reaction and to compare their selectivity profile with that of the unsubstituted VAPOL ligand **4**. Substituents in the 6- and 6′-positions would be expected to increase the size of the major groove of the VAPOL ligand (Scheme 1) and as a result, the asymmetric induction observed in reactions mediated by catalysts generated from these ligands. In addition, catalysts generated from the VANOL ligand **3** will be evaluated for the Diels–Alder reactions, given the recent findings that the VANOL ligand is equally as effective as the VAPOL ligand in asymmetric catalytic aziridination reactions and superior to the VAPOL ligand in Baeyer–Villiger reactions (7).

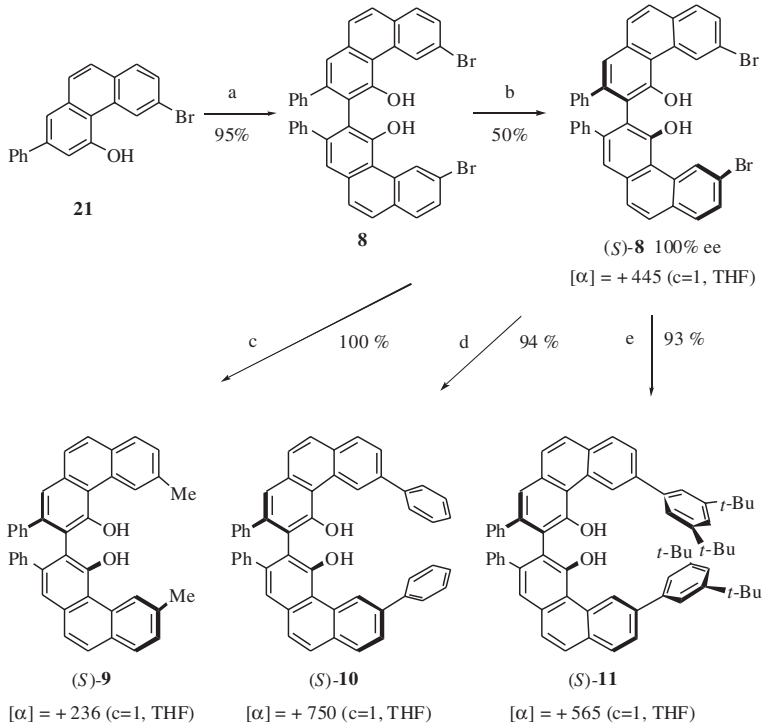
The retrosynthesis of the VAPOL derivatives **8**–**11** was envisioned to involve, first, the initial preparation of the 6,6′-dibromoVAPOL **8** and then after subsequent resolution, the utilization of this dibromo derivative as the intermediate through which the other derivatives will be prepared. The synthesis of the 6,6′-dibromo-VAPOL **8** was modeled after the original method that we developed for the synthesis of the VAPOL ligand (3) and involves the oxidative phenol coupling of the phenanthrol **21** (Scheme 3), whose synthesis in turn would involve the benzannulation reaction of the carbene complex **17** with phenylacetylene as the key step (Scheme 4). The synthesis of the alkenyl bromide **16** neces-

© 2006 NRC Canada

Scheme 3. (*a*) $HC(OMe)_3$, MeOH, cat CSA, benzene, reflux; (*b*) catechol, cat TsOH, benzene, reflux; (*c*) *i*. *n*-BuLi, THF, –78 °C, *ii*. Ph_3SiCl; (*d*) BBr_3, CH_2CL_2; (*e*) *i*. 2 equiv. *t*-BuLi, THF, –78 °C, *ii*. $Cr(CO)_6$, *iii*. MeOTf, CH_2CL_2; (*f*) *i*. PhC / CH, THF, 60 °C, 21 h, *ii*. Ac_2O, NEt_3, THF, 60 °C; (g) NBS, cat benzoyl peroxide, benzene, reflux; (*h*) Br_2, CH_2CL_2, reflux; (*i*) EtSH, $AlCl_3$, CH_2CL_2.



Scheme 4. (*a*) 195 °C, air; (*b*) *i*. (–)-sparteine, $CuCl_2$-$2H_2O$, MeOH–CH_2CL_2, *ii*. extract into hexane; (*c*) MeMgBr, cat Ni(II)(dpe)Cl_2, ether, reflux; (*d*) $PhB(OH)_2$, cat $Pd(PPh_3)_4$, benzene, aq. Na_2CO_3, reflux; (*e*) 3,5-(*t*-Bu)$_2C_6H_3B(OH)_2$, cat $Pd(PPh_3)_4$, benzene, aq. Na_2CO_3, reflux.



sary for the synthesis of the carbene complex **17** begins with 7-bromo-α-tetralone **12**, as indicated in Scheme 4. After evaluation of several methods for the conversion of ketones to alkenyl bromides, we found that the best procedure for the tetralone **12** was the method reported by Napolitano (9) involving the intermediacy of a catechol ketal, which was reported for α-tetralone in 40% overall yield. As reported by Napolitano for α-tetralone, we found that the direct conversion of 7-bromo-α-tetralone **12** to the catechol ketal **14** was inefficient. On a small scale, the direct reaction of **12** with catechol gave minimal yields of **14** and on a large scale this conversion failed completely. However, excellent yields of **14** could be obtained if **12** was first converted to the methyl enol ether **13**. The bromide function in the alkenyl bromide **16** is necessary for the preparation of the carbene complex **17**, but prior to the formation of the alkenyl bromide **16** by treatment of the ketal with boron tribromide the aryl bromide function in **14** was protected as its triphenylaryl silane **15**. The carbene complex **17** could then be generated by the standard Fischer procedure from **16** and chromium hexacarbonyl in 80% yield. The benzannulation of the carbene complex **17** with phenyl acetylene was carried out in two steps, (*i*) the reaction with phenylacetylene and (*ii*) the protection of the phenol function as its acetate. One attempt to carry out this transformation concurrently by the addition of acetic anhydride and triethylamine at the beginning of the reaction met with failure. Thus, this overall transformation must be carried in sequential steps. In the next step, oxida-

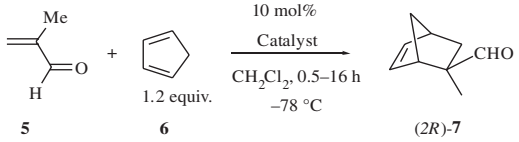
© 2006 NRC Canada

tion of the B ring with NBS under free-radical conditions afforded phenanthrene **19** in 91% yield. Initial attempts at this oxidation with palladium on carbon or DDQ were unsuccessful. One might wonder why we waited until after the benzannulation reaction to aromatize. We could have, for example, oxidized the compound **16** and carried the naphthyl system into the benzannulation. We chose this order because the benzannulation of alkenyl carbene complexes with alkynes is much less susceptible to side-product formation than aryl complexes (10). The triphenylsilyl group was then "deprotected" to the bromide by treatment with bromine, which after considerable optimization was found to be best achieved with two equivalents of bromine to give **20** in 83% yield. The monomer **21** was finally generated by the reaction of **20** with ethanethiol and aluminum chloride (3). It is critical to control the time of this reaction since prolonged times can lead to the reduction of the bromide in the product **21**. Since trace amounts of this reduced monomer would lead to cross-coupled products in the oxidative phenol coupling step, it was necessary to rigorously purify the monomer **21** by column chromatography.

The oxidative phenol coupling follows the procedure developed for the synthesis of VAPOL and VANOL (3). Melting **21** in the presence of air and heating at 195 °C until the monomer **21** was consumed gave racemic 6,6′-dibromo-VAPOL **8** in 95% yield. This compound was deracemized with (–)-sparteine and copper (II) according to a procedure originally reported by Kocovsky (11), which has recently been improved by our laboratory (12). This procedure gave 6,6′-dibromo-VAPOL **8** that was substantially enantioenriched (>90% ee). The optical purity could be easily improved by extracting with hexane. The racemates of VAPOL **4** and Br_2-VAPOL **8** are both substantially less soluble than the optically pure material. Thus, the pure enantiomer of **8** (>99% ee) could be easily obtained by stirring the enantioenriched **8** with enough hexane to leave only a small amount of residue undissolved. The hexane solution is decanted to leave the solid and then the hexane is removed to leave the optically pure ligand **8**. This ligand could also be crystallized from hexane and ethyl acetate to give X-ray quality crystals, which have two molecules of ethyl acetate per molecule of **8**. The conversion of the 6,6′-dibromo-VAPOL ligand **8** to the corresponding dimethyl derivative **9** was accomplished in 100% yield by the nickel-catalyzed coupling of **8** with methyl magnesium bromide (6 equiv.) (13). The two aryl-substituted VAPOL ligands **10** and **11** were prepared from the dibromide **8** by Suzuki coupling reactions in 94% and 93% yields, respectively (14).

The results from the asymmetric catalytic Diels–Alder reactions of methacrolein and cyclopentadiene with catalysts generated from VAPOL **4** and the VAPOL derivatives **8**–**11** are shown in Table 2. All of the VAPOL derivatives with substituents in the 6- and 6′-positions give lower asymmetric inductions than VAPOL. The best of these is the bis-(3,5-di-*t*-butylphenyl) derivative, which gives a 62% ee for the reaction. Interestingly, the diphenyl derivative **10** gives the product **7** with the opposite sense of induction to all of the other ligands. The catalyst was prepared in each case by treating the ligand with 1 equiv. of ethylaluminum dichloride at RT. The completion of catalyst formation was determined by ^{1}H NMR and it was found that for the ligands **4**, **8**, and **9** the

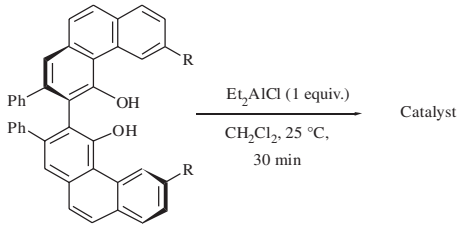
Table 2. Effect of vaulted biaryl catalysts on the reaction of **5** and **6**.



5 **6** (*2R*)-**7**

Ligand	R	Yield **7** (%)[a]	exo–endo[b]	ee% **7** (exo)[b]
(*S*)-**4**	H	>95	27	93
(*S*)-**8**	Br	>95	8.3	18
(*S*)-**9**	Me	>95	14.4	30
(*S*)-**10**	Ph[c]	76	11.7	–41
(*S*)-**11**	3,5-(*t*-Bu)$_2$C$_6$H$_3$[c]	>95	8.4	62

Note: All reactions use 0.5–1.0 mol/L in methacrolein.
[a]Determined by ^{1}H NMR with ligand as internal standard.
[b]Determined by GC of acetals prepared from (2*R*,4*R*)(–)pentanediol.
[c]Catalyst was prepared at 55 °C for 24 h.



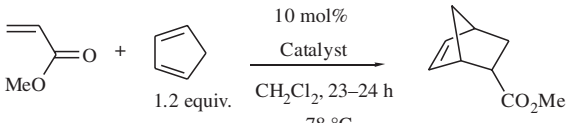
VAPOL was completely consumed within 30 min. However, for the more hindered ligands **10** and **11**, the complete consumption of the ligand required heating at 55 °C for 24 h.

Catalysts prepared from VAPOL-derived ligands **8**–**11** were also examined with the reaction of methyl acrylate and cyclopentadiene (Table 3). These reactions were slower than those with methacrolein but all are complete in 24 h except for the catalyst generated from the VANOL ligand, which only gave a 28% yield of the product **23** after 24 h. As with the reactions with methacrolein, all of the derivatives of VAPOL gave lower asymmetric inductions than VAPOL itself. Thus, for both sets of reactions it appears that the VANOL ligand does not provide a large enough chiral pocket. Furthermore, all of the 6,6′-substituted VAPOL derivatives form aluminum catalysts where either the bound substrate does not exist in a single conformation or the substrate does not have one of its faces sufficiently differentially shielded. The VAPOL ligand seems to be optimal for this particular aluminum catalyst.

The effect of solvents on the reaction of methyl acrylate with cyclopentadiene that is catalyzed by the VAPOL-derived catalyst is shown in Table 4. There was no reaction at all in THF and in ether the reaction was very sluggish giving only a 23% yield after 24 h with 10 mol% catalyst. Clearly, the best solvent for this reaction is toluene, which gives the product in 100% yield and 97% ee, whereas methylene chloride gives 87% yield and 82% ee. It was very curious indeed to find that if the reaction in methylene chloride was stopped after 15 min, the product was isolated with 48% ee. Furthermore, if the reaction was carried out by addition of only 10% of the dienophiles at the beginning of the reaction followed by slow addition of the remaining dienophiles, the asymmetric induction for **23** was higher at the end of the

© 2006 NRC Canada

Table 3. Effect of vaulted biaryl catalysts on the reaction of **22** and **6**.



22 **6** (*S*)-**23**

Ligand	R	Yield **23** (%)[a]	endo–exo[b]	ee% **23** (exo)[b]
(S)-**4**	H	87	112	82
(S)-**8**	Br	>95	51	16
(S)-**9**	Me	>95	92	28
(S)-**10**	Ph[c]	>95	129	35
(S)-**11**	3,5-(*t*-Bu)$_2$C$_6$H$_3$[c]	>95	44	29
(S)-**3**	VANOL	28	34	21

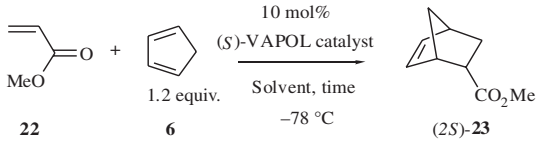
Note: All reactions use 0.5–1.0 mol/L in **22**. Unless otherwise specified the catalyst was prepared as indicated in Table 2.

[a]Determined by ^{1}H NMR with ligand as internal standard.

[b]Determined with a chiral GC column (J & W Cyclodex-B).

[c]Catalyst was prepared at 55 °C for 24 h.

Table 4. Solvent effect on the reaction of **22** and **6**.



22 **6** (2*S*)-**23**

Entry	Solvent	Time (h)	Yield **23** (%)[a]	endo–exo[b]	ee% **23** (exo)[b]
1	CH_2CL_2	24	87	112	82
2	CH_2CL_2	0.25[c]	21	—	48
3	CH_2CL_2	24[d]	80	—	89.4
4	Toluene	24	100	99	96.6
5	THF	24	0	—	—
6	Et_2O	24	23	—	—

Note: All reactions use 0.5–1.0 mol/L in **22**. Unless otherwise specified the catalyst was prepared as indicated in Table 2.

[a]Determined by ^{1}H NMR with ligand as internal standard.

[b]Determined with a chiral GC column (J & W Cyclodex-B).

[c]Reaction stopped at 20% conversion.

[d]10% of **22** was added at the beginning of the reaction and the rest was added slowly by syringe pump over 2.5 h.

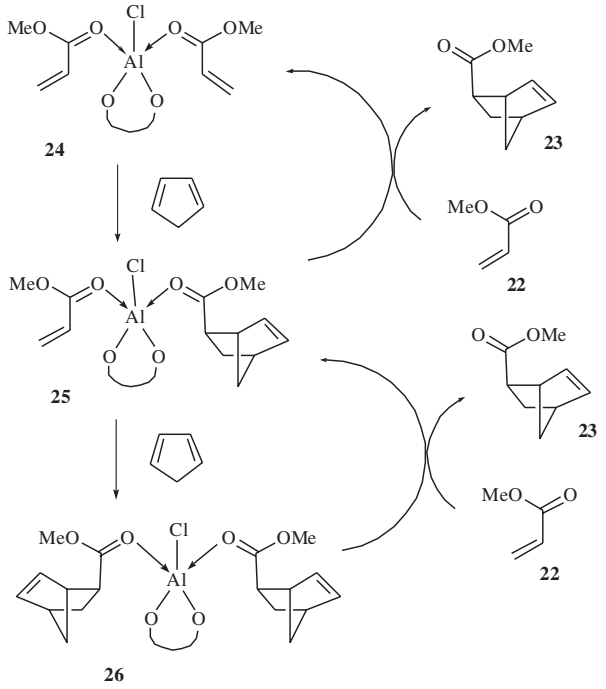
reaction. We had observed this same type of behaviour for the reaction of methacrolein and cyclopentadiene (4*a*). We interpreted this as an asymmetric autoinduction (15) and have investigated this in some detail for the reaction of methyl acrylate and cyclopentadiene (4*c*). We chose the reaction of methyl acrylate and cyclopentadiene over that of methacrolein and cyclopentadiene since the former reacts much slower and it would be easier to follow the time course of the reaction. Also, the asymmetric induction was lower for the reaction with methyl acrylate and thus changes in induction would be more easily detected and monitored over a greater range. It is also for this reason that we chose to investigate the reaction of methyl acrylate in methylene chloride rather than in toluene.

Our explanation for the autoinductive effect observed for these reactions is illustrated in Scheme 5 for the reaction of methyl acrylate with cyclopentadiene (4*c*). It was proposed that the aluminum in the chiral catalyst could coordinate to the carbonyl group of two molecules of the starting material as in **24**, two molecules of the product as in **26**, or one molecule of each as in **25**. The fact that the particular asymmetric autoinduction we observed involves an increase in the asymmetric induction as the reaction progresses can then be accounted for if the Diels–Alder reaction of the complex **25** with one molecule of methyl acrylate and one molecule of product coordinated to the aluminum occurs with a higher selectivity than complex **24** with two molecules of starting material coordinated to the aluminum. At the beginning of the reaction there was little or no product and thus the great majority of the reaction flux will be through complex **24**. As more and more of the product is formed, more of the flux will occur through complex **25** and thus the asymmetric induction will continue to climb as the reaction progresses. In fact we have previously reported that the asymmetric induction for the reaction of methyl acrylate with cyclopentadiene is 48% ee after 20% completion and slowly rises during the course of the reaction until its culmination at 82% ee when the reaction is complete (Table 4 and ref. 4*c*).

It was reasoned that if complex **25** gives higher induction than **24** because of the greater steric size of the product com-

© 2006 NRC Canada

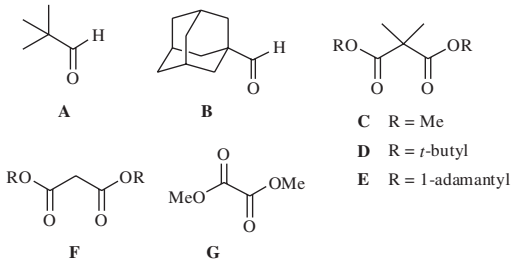
Scheme 5.



pared with that of the starting material, then one might be able to avoid the low asymmetric induction at the beginning of the reaction by the addition of a "dummy" carbonyl compound that is physically larger than methyl acrylate. This expectation was borne out in a series of experiments involving the carbonyl compounds indicated in Scheme 6. This study has been already communicated and some of this data is included in Table 5 (4*c*). As can be seen from the data in the first three entries, the addition of 0.5 equiv. of pivaldehyde at the beginning of the reaction increased the asymmetric induction at the end of the reaction from 82% to 96% ee. The larger adamantyl aldehyde B increased the induction still further to 98.5% ee. It was unexpected to find that 1,3-dicarbonyl compounds were even more effective. The di-*t*-butylmalonate D increased the induction to greater than 99% ee (Table 5, entry 5). These effects were more visible at higher temperatures. For example, the malonate E can increase the induction from 37% ee to 85% ee at 0 °C with 0.5 equiv. of E and to 92% ee with 1.0 equiv. This is quite remarkable when considering that the presence of this additive allows the temperature of the reaction to be increased by 80 °C and at the same time increases the induction from 82% ee to 92% ee. Since our initial report (4*c*) and as mentioned above, we have found that substantially increased asymmetric induction can be achieved in toluene as solvent. The asymmetric induction can be increased from 82% ee in CH_2Cl_2 to 97% ee in toluene at –78 °C (Table 5, entries 1 and 20). However, the additive effect is hardly observable in toluene. The reaction at 0 °C in toluene shows only a slight increase in induction from 46% ee to 58% ee in the presence of 0.5 equiv. of the malonate E.

The phenomenon of increased asymmetric induction with the addition of product mimics was termed "positive cooperativity" (4*c*). The strong effect that carbonyl additives had on the autoinduction for the reaction of methyl acrylate and cyclopentadiene with a catalyst generated from the VAPOL

Scheme 6.



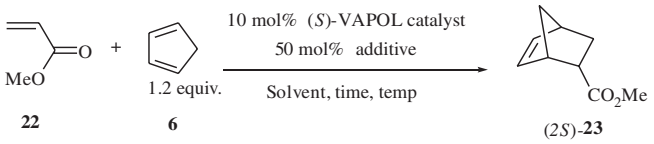
ligand prompted the study outlined in Table 6 to probe the extent to which added carbonyl compounds would exhibit positive cooperativity with the substituted VAPOL ligands **8** and **10** and with the VANOL ligand. These reactions were screened with 0.5 equiv. of the di-*t*-butyl malonate D added at the beginning of the reaction. Remarkably, the addition of malonate D had essentially no effect on the asymmetric induction with catalyst generated from 6,6′-dibromo-VAPOL **8** or from 6,6′-diphenyl-VAPOL **10**. Perhaps the major groove of these ligands (Scheme 1) is too hindered to allow for the coordination of two carbonyl groups at the same time. It was also found that the asymmetric induction from the VANOL-derived catalyst was not sensitive to the addition of the malonate D (Table 6, entries 8 and 9). In this case however, the yields were quite low with and without the additive. At this point we do not know if the structure of the active catalyst is the same from VAPOL and VANOL and, in fact, the ^1H NMR spectrum of the catalyst generated from Et_2AlCl and VAPOL reveals that there appears to be a mixture of several different species. In light of this fact, it is remarkable that very high asymmetric inductions can be achieved with this catalyst mixture for the reaction with methyl acrylate in toluene (Table 5, entry 20) or in CH_2Cl_2 in the presence of additives A-D (Table 5, entries 2–5).

The sluggishness of the reaction with the VANOL catalyst prompted a study of the effect of temperature on this catalyst to find conditions under which the reaction could be driven to completion and at the same time to determine the extent of any positive cooperativity with added carbonyl compounds leading to increased asymmetric induction. As the data in Table 7 shows, it was found that reasonable yields of the product could be observed in 24 h with 10 mol% catalyst if the temperature was raised to –40 °C and that at –20 °C the reaction was complete in the same time period. It is interesting to note that the VANOL and VAPOL ligands gave nearly identical results at –40 °C (Table 7, entry 7 vs. Table 5, entry 7) and at 0 °C (Table 7, entry 11 vs. Table 5, entry 13). In contrast to the VAPOL-derived ligands **8** and **10** (Table 6), the VANOL catalyst was significantly affected by the addition of additives. The degree of the effect of the malonate D was about the same as that on the VAPOL catalyst at 0 °C but the effect was less for the VANOL catalyst at –40 °C.

An investigation of the Diels–Alder reactions of cyclopentadiene with the *t*-butyl, *n*-propyl, and ethyl esters of acrylic acid was undertaken to compare the results with those of methyl acrylate. It was thought that if the steric bulk of the two carbonyls coordinated to the aluminum were important to the asymmetric induction of the Diels–Alder reaction (Scheme 5) then perhaps adjusting the size of the alkoxy group of the acrylate ester could have a similar ef-

© 2006 NRC Canada

Table 5. Effect of additives on the reaction of **22** and **6**.



22 **6** (2*S*)-**23**

Entry	Solvent	Additive	Temp (°C)	Yield **23** (%)[a]	endo–exo[b]	ee% **23** (exo)[b]
1	CH_2CL_2	None	–78	87	99	82
2	CH_2CL_2	A	–78	80	99	96
3	CH_2CL_2	B	–78	60	99	98.5
4	CH_2CL_2	C	–78	49	99	98
5	CH_2CL_2	D	–78	76	99	>99
6	CH_2CL_2	F	–78	<30	—	—
7	CH_2CL_2	None	–40	76	99	47
8	CH_2CL_2	B	–40	80	99	88
9	CH_2CL_2	C	–40	80	98	90
10	CH_2CL_2	D	–40	100	99	92
11	CH_2CL_2	E	–40	100	98	93
12	CH_2CL_2	G	–40	85	92	45
13	CH_2CL_2	None	0	84	99	37
14	CH_2CL_2	D	0	67	94	69
15	CH_2CL_2	E	0	90	95	85
16	CH_2CL_2	E[c]	0	80	99	92
17	CH_2CL_2	None	25	100	92	33
18	CH_2CL_2	D	25	80	99	56
19	CH_2CL_2	E	25	80	93	49
20	Toluene	None	–78	100	99	97
21	Toluene	E	–78	100	99	96
22	Toluene	None	0	77	99	46
23	Toluene	E	0	100	—	58

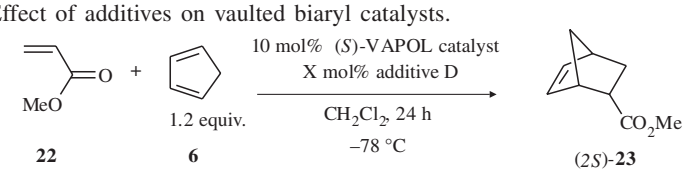
Note: All reactions use 0.5–1.0 mol/L in **22**. Unless otherwise specified the catalyst was prepared as indicated in Table 2. Reaction time for all reactions was 24 h except for those at 0 °C, which was 2 h and those at RT, which was 1 h.

[a]Determined by ^{1}H NMR with ligand as internal standard.

[b]Determined with a chiral GC column (J & W Cyclodex-B).

[c]100 mol% additive.

Table 6. Effect of additives on vaulted biaryl catalysts.



22 **6** (2*S*)-**23**

Entry	Ligand	X	Yield **23** (%)[a]	endo–exo[b]	ee% **23** (exo)[b]
1	**4**(*R*)-VAPOL	0	99	>100	82[c]
2	**4**(*R*)-VAPOL	50	94	>100	98[c]
3	**4**(*S*)-VAPOL	50	86	>100	99
4	**8**(*S*)-Br_2VAPOL	0	99	65	15
5	**8**(*S*)-Br_2VAPOL	50	95	56	16
6	**10**(*S*)-Ph_2VAPOL	0	99	122	35
7	**10**(*S*)-Ph_2VAPOL	50	58	145	31
8	**3**(*S*)-VANOL	0	28	34	21
9	**3**(*S*)-VANOL	50	11	42	17

Note: All reactions use 0.5–1.0 mol/L in **22**. Unless otherwise specified the catalyst was prepared as indicated in Table 2.

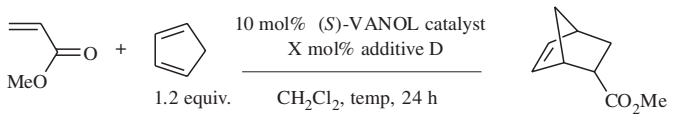
[a]Determined by ^{1}H NMR with ligand as internal standard.

[b]Determined with a chiral GC column (J & W Cyclodex-B).

[c](2*R*)-**23** was obtained.

© 2006 NRC Canada

Table 7. Reaction of **22** and **6** with a VANOL catalyst.



22 **6** (2*S*)-**23**

Entry	X	Temp (°C)	Yield **23** (%)[a]	endo–exo[b]	ee% **23** (exo)[b]
1	0	–78	28	34	21
2	50	–78	11	42	17
3	0	–60	25	47	19
4	50	–60	10	50	24
5	0	–50	38	132	39
6	50	–50	41	100	57
7	0	–40	74	38	42
8	50	–40	75	74	54
9	0	–20	100	30	35
10	50	–20	100	31	57
11	0	0	97	22	29
12	50	0	95	Nd[c]	60

Note: All reactions use 0.5–1.0 mol/L in **22**. Unless otherwise specified the catalyst was prepared as indicated in Table 2.

[a]Determined by ^{1}H NMR with ligand as internal standard.

[b]Determined with a chiral GC column (J & W Cyclodex-B).

[c]Not determined.

fect. As expected, the asymmetric induction observed for the ethyl and *n*-propyl esters (Table 8, entries 6 and 9) were greater than that for the methyl ester (Table 5, entry 1). However, the trend does not continue to the *t*-butyl ester as the induction with this substrate falls to 9% ee (Table 8, entry 1). While the reaction of the *t*-butyl ester was unresponsive to any positive cooperativity effect with any additive (B–E), it was found that both the ethyl and *n*-propyl esters responded to carbonyl additives to a degree very similar to that of methyl acrylate (Table 8 vs. Table 5).

Finally, the reaction of methacrolein and cyclopentadiene was investigated in the presence of carbonyl additives to look for positive cooperativity effects. The data in Table 9 suggests that this reaction is unaffected by the presence of adamantyl aldehyde B or the di-*t*-butyl malonate D. The asymmetric induction for this reaction in CH_2Cl_2 is higher at –78 °C (93.6% ee) than it is for the same reaction with methyl acrylate (82% ee). Nonetheless, the addition of either B or D to the reaction would have been expected to produce measurable increases in induction if the positive cooperativity effect was in play here. Furthermore, no significant positive cooperativity effect was observed if the reaction temperature was raised to –40 °C or even to 0 °C where the asymmetric induction of the reaction itself was 16.9% and 5.1% ee, respectively. This lack of a positive cooperativity effect for the reaction of methacrolein and cyclopentadiene was surprising since this reaction, like the reaction of methyl acrylate, exhibits autoinduction. The degree of autoinduction for methacrolein is not as strong as that for methyl acrylate. For example, the reaction of methacrolein and cyclopentadiene has been reported to give an 81% ee after 30% conversion under conditions where an 88% ee was observed at the end of the reaction (4*a*).

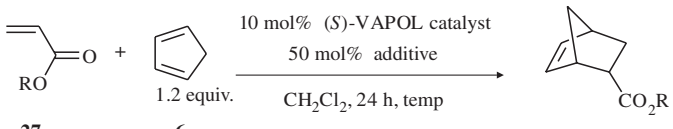
The results of the present studies suggest that the VAPOL ligand appears to be optimal in forming a catalyst with diethylaluminum chloride to effect asymmetric Diels–Alder reactions with methacrolein and methyl acrylate with cyclopentadiene. Catalyst derived from the 6,6′-disubstituted VAPOL derivatives **8**, **9**, **10**, and **11** all gave reduced enantioselectivities for both of these reactions. The VANOL ligand gave lower enantioselectivities and slower rates as well. Since this is a smaller ligand, the lower rates may be due to a different catalyst structure. It was also found that carbonyl additives displayed positive cooperativity with the VAPOL catalyst on the autoinduction for the reaction with methyl acrylate but not with the substituted VAPOL catalysts derived from **8** and **10** or with the catalyst derived from the VANOL ligand. In contrast, no positive cooperativity with carbonyl additives was observed with the VAPOL catalyst on the autoinduction in the reaction of methacrolein and cyclopentadiene.

Experimental

Syntheses were performed under dry argon unless otherwise stated. THF and ether were distilled from sodium benzophenone ketyl. Methylene chloride, 1,2-dichloroethane, and acetonitrile were distilled from CaH_2. Toluene was distilled from sodium. Methacrolein was distilled from CaO. Methyl acrylate and pivaldehyde were distilled from $MgSO_4$. Cyclopentadiene was freshly cracked from dicyclopentadiene over 4 Å MS. Whatman glass-backed TLC plates (part #4861–820, 250 mm thickness, K6F Silica gel) were used for reported R_f values, except in those noted cases in which Macherey–Nagel plastic-backed TLC plates (Polygram® Sil N-HR/UV_{254}, 250 mm thickness) were used. IR spectra were taken on a Nicolet 20SXB FTIR spectrometer. Melting points were taken on a Hoover Unimelt apparatus and are uncorrected. Mass spectra were run on a VG Analytical 70–70EQ Double Focusing Hybrid MS (EI @ 70 eV).

© 2006 NRC Canada

Table 8. Effect of ester substituent on the reaction of **27** and **6**.



27 **6** (2*S*)-**28**

Entry	R	Additive	Temp (°C)	Yield **28** (%)[a]	endo–exo[b]	ee% **28** (exo)[b]
1	*t*-butyl	None	–78	63	96	9
2		B	–78	Trace	—	—
3		C	–78	0	—	—
4		D	–78	32	96	19
5		E	–78	0	—	—
6	*n*-propyl	None	–78	33	99	92
7		B	–78	25	99	>99
8		C	–78	52	99	98
9	ethyl	None	–78	58	99	94
10		None	–40[c]	90	97	60
11		C	–40	72	98	92
12		D	–40[c]	100	Nd[d]	87
13		None	0[e]	100	93	33
14		C	0[e]	100	95	69

Note: All reactions use 0.5–1.0 mol/L in **22**. Unless otherwise specified the catalyst was prepared as indicated in Table 2.

[a]Determined by ^{1}H NMR with ligand as internal standard.

[b]Determined with a chiral GC column (J & W Cyclodex-B).

[c]The reaction time was 30 h.

[d]Not determined because of obscured integral.

[e]The reaction time was 2 h.

Elemental analyses were performed by Galbraith Laboratories, Knoxville, Tennessee.

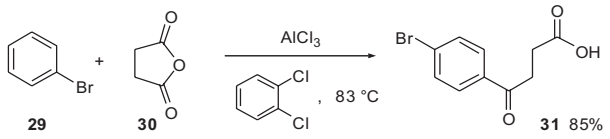
Chiral HPLC was done with a Pirkle covalent D-phenylglycine Rexchrom™ Regis column. Pump: Waters M-45 (ser. # 5615); operating pressure: 3100 psi (1 psi = 6.894 757 kPa); flow rate: 2.0 mL/min; solvent: 7:3 (*v*/*v*) hexane–isopropanol; detector (254 nm): Waters 440 Absorbance detector (ser. #07249); integrator: Spectra-Physics SP4270 (ser. #092–132).

Capillary GC was done on a Varian Star 3600 outfitted with an Alltech Econocap SE-54 column for nonchiral applications and a J & W Scientific Cyclodex-B column for chiral applications using helium carrier gas and FID detection.

Optical rotations were taken on a PerkinElmer Model 141 instrument using the sodium D line (589 nm). For ligand sample preparation, a 20 mg sample was dissolved in 2 mL THF. Concentration: 1 g/100 mL; temperature: 23 °C; path length: 1 dm; $[\alpha]_D = (100)\ a_{obs}$.

Preparation of 7-bromo-α-tetralone 12 (16)

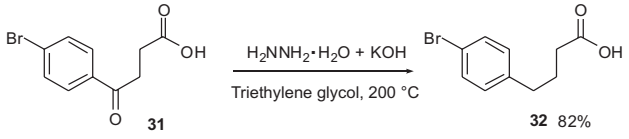
Friedel–crafts acylation of bromobenzene



29 **30** **31** 85%

A 1 L three-necked round-bottomed (RB) flask was fitted with a mechanical stirrer and was connected to an oil bubbler. It was charged with bromobenzene **29** (60.5 mL, 573 mmol), succinic anhydride **30** (37.6, 376 mmol), and *o*-dichlorobenzene (113 mL), and mechanically stirred. Aluminum trichloride (107 g, 804 mmol) was added in portions over 30 min. The solution turned rust red in colour and emitted a whitish smoke. It was warmed to 83 °C for 6 h, cooled to RT, and then poured into a mixture of HCl–ice in a 2 L Erlenmeyer flask whereupon a white curdish precipitate came out of solution. The precipitate was dissolved in ether, the entire contents were transferred in portions to a large separatory funnel, and the aqueous layer was removed. Concentration of the ether layer by distillation afforded crystals of product, which were suction filtered and then finely divided and spread out to dry in a pan in a 110 °C oven for two days. Yield: 82 g white-pinkish solid (85% yield). On a larger scale, it was not practical to dissolve the crude product in ether. In this case, crude product was allowed to oven dry directly, which took longer.

Wolff–Kischner reduction of 31

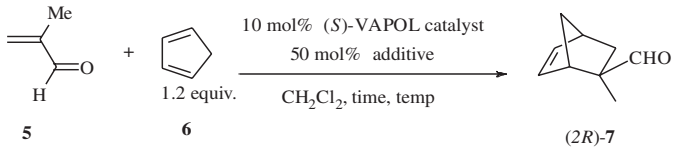


31 **32** 82%

A 1 L three-necked flask was equipped with a thermometer and a condenser–receiving flask. KOH (45 g, 804 mmol) and triethylene glycol (350 mL) were added and mechanically stirred. The mixture was warmed to 100 °C with a heating mantle to dissolve the KOH. It was then cooled to

© 2006 NRC Canada

Table 9. Effect of additives on the reaction of **5** and **6**.



5 **6** (2*R*)-**7**

Entry	Additive	Time	Temp (°C)	Yield **7** (%)[a]	exo–endo[b]	ee% **7** (exo)[b]
1	None	0.5 h	–78	51	93	93.6
2	B	0.5 h	–78	65	94	94.6
3	D	0.5 h	–78	53	92	93.7
4	None	1 h	–40	73	80	16.9
5	D	1 h	–40	80	81	17.3
6	None	15 min	0	84	71	5.1
7	D	15 min	0	80	77	10.8

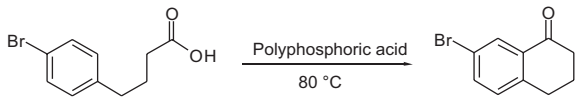
Note: All reactions use 0.5–1.0 mol/L in **5**. Unless otherwise specified the catalyst was prepared as indicated in Table 2.

[a]Determined by ^{1}H NMR with ligand as internal standard.

[b]Determined with a chiral GC column (Astec B-MB column) after reduction to the alcohol with $NaBH_4$.

80 °C, whereupon 68 g (265 mmol) of the keto acid **31** from the previous step and 34 mL of hydrazine monohydrate (702 mmol) were added. After stirring at 90–100 °C for 1 h, the mixture was warmed by a heating mantle to 200 °C and stirred at that temperature for 1 h. Liquid was distilled off into the receiving flask. The solution was cooled to near RT and poured into 400 mL of H_2O. Aq HCl (6 N, 220 mL) was added, which precipitated out a white suspension, and an oil settled on the bottom. On sitting overnight the oil solidified. The solid was filtered, then dissolved in ether (it was exceedingly soluble in ether), dried over $MgSO_4$, filtered, and left to crystallize in a crystallizing dish on air evaporation of ether to afford 52.98 g of **32** as a light tan solid (82% yield). ^{1}H NMR (500 MHz, $CDCl_3$) δ: 1.96 (quintet, 2H), 2.38 (t, 2H, *J* = 7.4 Hz), 2.64 (t, 2H), 7.04 (d, 2H, *J* = 8.2 Hz), 7.38 (d, 2H, *J* = 8.2 Hz), acid proton not reported.

Cyclization of carboxylic acid (32)

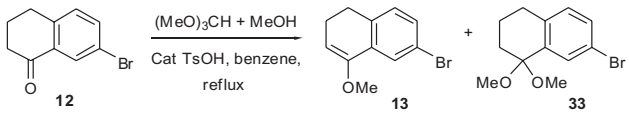


32 **12** 75%

This reaction was run in open air. Polyphosphoric acid (PPA, 250 g) was warmed in a 1 L Erlenmeyer flask to 70 °C. The bromoaryl carboxylic acid **32** (52.98 g, 218 mmol) was melted at 50 °C and then added to the PPA and the mixture was swirled with a glass rod for a few minutes while keeping the temp between 70 and 90 °C. Additional PPA (200 g) was added and the mixture was kept at 80 °C for 1 h and swirled occasionally and it became a dark orange color. Heat was removed and ice was added, which turned the mixture yellowish. The mixture was extracted three times with ether (1 × 200 mL, 2 × 100 mL). The combined ether layers were washed sequentially with 200 mL H_2O, 100 mL 5% aq KOH, 100 mL H_2O, 100 mL 3% aq HOAc, 100 mL 5% aq $NaHCO_3$, and 100 mL H_2O, then dried over $MgSO_4$ and filtered into a crystallizing dish. Air evaporation of ether afforded 36.8 g of clear blocky crystals covered with an orange thin film (75% yield). The product could be crystallized from MeOH to yield colourless crystals: mp 75 to 76 °C (lit. value (16) mp 71–73 °C). R_f = 0.23 (hexane–EtOAc, 9:1). IR (neat film, NaCl, cm^{-1}): 2946 (w), 1676 (s), 1585 (m), 1221 (m), 1190 (m). ^{1}H NMR (500 MHz, $CDCl_3$) δ: 2.10 (quintet, 2H, *J* = 6.3 Hz), 2.62 (t, 2H, *J* = 6.5 Hz), 2.88 (t, 2H, *J* = 6.0 Hz), 7.12 (d, 1H, *J* = 8.13 Hz), 7.53 (dd, 1H, *J* = 8.2, 1.9 Hz), 8.11 (d, 1H, *J* = 1.8 Hz). ^{13}C NMR (75 MHz, $CDCl_3$) δ: 22.9, 29.0, 38.6, 120.5, 129.8, 130.5, 133.9, 135.9, 143.0, 196.8.

Preparation of the catechol ketal 14 from 7-bromo-α-tetralone (12)

Preparation of methyl vinyl ether (13)



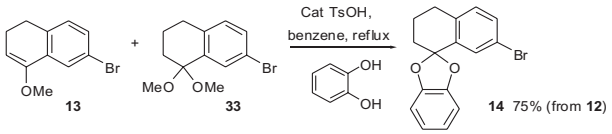
12 **13** **33**

A 250 mL three-necked RB flask equipped with a side arm adapter, to which was connected a condenser and receiving flask, was charged with 7-bromotetralone **12** (20 g, 88.8 mmol), trimethyl orthoformate (25 mL, 228.5 mmol), *p*-toluenesulfonic acid monohydrate (980 mg, 5.15 mmol), methanol (23 mL), and benzene (60 mL). The magnetically stirred solution was warmed under N_2 to gentle reflux for 40 h so that solvent distilled very slowly over into the receiving flask. After cooling to RT, it was partitioned between 500 mL ether and 250 mL satd. aq $NaHCO_3$. The organic layer was removed by separatory funnel and washed with 1 × 150 mL satd. aq $NaHCO_3$ and 1 × 150 mL brine, then dried over $MgSO_4$ and filtered. Solvent was removed in vacuo to afford 22 g of an orange oil, which was used in the next step without purification.

Conversion of 13 to ketal 14

A 250 mL three-necked RB flask equipped as described in the last step was charged with 22 g of the crude starting material **13**, catechol (11.75 g, 106.7 mmol), *p*-toluenesulfonic acid monohydrate (150 mg, 0.79 mmol), and benzene (150 mL) and was brought to reflux under N_2 for 4 h so that

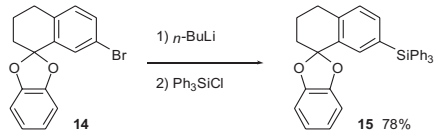
© 2006 NRC Canada



13 33 14 75% (from 12)

solvent distilled slowly into the receiving flask. After cooling to RT, 1.5 mL triethylamine was added. The mixture was partitioned between 200 mL ether and 100 mL water. The organic layer was removed by separatory funnel, washed with 1 × 100 mL H_2O, 2 × 75 mL 10% aq NaOH, 1 × 100 mL brine, then dried over $MgSO_4$, and filtered. The solvent was removed in vacuo to afford 27 g of a light tan crude product. The product was purified in portions by SiO_2 chromatography (hexane eluent) to yield 21 g of the white crystalline product **14** (75% yield): mp 101–104 °C. R_f = 0.45 (hexane–EtOAc, 9:1). ^{1}H NMR (300 MHz, $CDCl_3$) δ: 2.03–2.10 (m, 2H), 2.22–2.26 (m, 2H), 2.82 (t, 2H, J = 6.3 Hz), 6.81–6.88 (m, 4H), 7.04 (d, 1H, J = 8.3 Hz), 7.41 (dd, 1H, J = 8.3, 2.1 Hz), 7.68 (d, 1H, J = 2.1 Hz). ^{13}C NMR (75 MHz, $CDCl_3$) δ: 19.8, 28.4, 34.0, 108.6, 114.4, 120.0, 121.5, 129.3, 130.4, 132.7, 136.4, 137.1, 147.0. EI-MS m/z (%): 318 [M^+] (69, ^{81}Br), 316 [M^+] (69, ^{79}Br), 301 (16), 299 (17), 290 (16), 288 (17), 209 (22), 207 (22), 128 (100), 107 (36). Anal. calcd. for $C_{16}H_{13}O_2Br$: C 60.59, H 4.10; found: C 60.24, H 4.13.

Synthesis of the catechol ketal of 7-triphenylsilyl-α-tetralone (15)



14 15 78%

A 250 mL RB flask was charged with aryl bromide **14** (2.04 g, 6.4 mmol) and covered with Ar. It was dissolved in 50 mL THF and then cooled to –78 °C. *t*-BuLi in pentane (7.8 mL, 1.7 mol/L, 13.2 mmol) was added over 10 min whereupon the solution turned brown. After stirring at –78 °C for 40 min, a solution of triphenylsilylchloride (2.08 g, 7.1 mmol) in 20 mL THF was added dropwise over 5 min. After stirring an additional 1.25 h, the cold bath was removed. Over the next few hours the colour evolved from a dark blue, to a greenish olive, to a light brown, and finally to a clear light orange. The solution was stirred for 20 h at RT. Satd. aq $NaHCO_3$ (3 mL) was added and the THF was removed by rotory evaporator to leave a gummy residue. The residue was partitioned between 100 mL ether and 100 mL satd. aq $NaHCO_3$. The organic layer was washed with brine and then dried over $MgSO_4$. Purification by SiO_2 chromatography (hexanes–EtOAc, 9:1) afforded 2.5 g of a clear, colourless waxy oil, which foamed up under high vacuum (78% yield). On runs of larger scale, a white solid crystallized out on removal of solvent: mp 125.8–128 °C. R_f = 0.375 (hexane–EtOAc, 9:1). ^{1}H NMR (300 MHz, $CDCl_3$) δ: 2.05–2.09 (m, 2H), 2.25–2.29 (m, 2H), 2.87 (t, 2H, J = 6.2 Hz), 6.64–6.75 (m, 4H, catechol protons), 7.16 (d 1H, J = 7.6 Hz), 7.75 (s, 1H), 7.24–7.63 (m, 16 H). ^{13}C NMR (75 MHz, $CDCl_3$) δ: 20.1, 28.8, 34.6, 108.1, 115.0, 121.1, 127.8, 128.2, 129.5, 133.8, 134.1, 136.2, 136.36, 136.44, 137.2, 139.2, 147.2, (one sp^2 C not located). EI-MS m/z (%): 497 [M^++1] (43), 496 [M^+] (100), 416 (27), 339 (22), 259 (38), 181 (17).

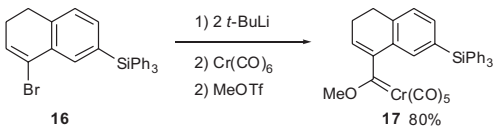
The preparation of vinyl bromide 16 (9)



15 16 85%

A 500 mL RB flask was charged with starting material **15** (5.0 g, 10.08 mmol) and was covered with Ar. Methylene chloride (200 mL) was added to dissolve the solid and the solution was cooled to between –30 and –35 °C. A 1 mol/L solution of BBr_3 (10.25 mL, 10.15 mmol) in CH_2Cl_2 was added over 5 min. The reaction was slowly warmed to –15 °C over 3 h and then to 0 °C over 2 h, after which time it was stored overnight at –15 °C. Satd. aq $NaHCO_3$ (10 mL) was added and the mixture was concentrated until ~50 mL CH_2Cl_2 remained. Hexane (300 mL) was added and the solution was washed sequentially with 1 × 150 mL H_2O, 1 × 100 mL 10% aq NaOH, 1 × 150 mL 5% aq KOH, 1 × 150 mL H_2O, then dried over $MgSO_4$, and filtered. The crude product was purified by SiO_2 chromatography (hexane–EtOAc, 9:1) to give 4.0 g of **16** as a white crystalline solid (85% yield): mp 146–148 °C. R_f = 0.38 (hexane–EtOAc, 9:1). ^{1}H NMR (500 MHz, $CDCl_3$) δ: 2.36 (dt, 2H, J = 4.8, 8.0 Hz), 2.84 (t, 2H, J = 8.0 Hz), 6.38 (t, 1H, J = 4.8 Hz), 7.05 (d, 1H, J = 7.3 Hz), 7.33 (t, 6H, J = 7.1 Hz), 7.38 (t, 3H, J = 7.0 Hz), 7.50 (d, 1H, J = 7.3 Hz), 7.53 (d, 6H, J = 7.1 Hz), 7.74 (s, 1H). ^{13}C NMR (75MHz, $CDCl_3$) δ: 25.3, 27.6, 121.6, 126.9, 127.9, 129.6, 130.7, 132.38, 132.45, 134.2, 136.3, 136.5, 137.9. EI-MS m/z (%): 469 [M^++1] (33, ^{81}Br), 468 [M^+] (97, ^{81}Br), 467 [M^++1] (36, ^{79}Br), 466 [M^+] (100, ^{79}Br), 391 (83), 389 (86), 312 (30), 259 (55), 181 (40), 105 (30). Anal. calcd. for $C_{28}H_{23}SiBr$: C 71.97, H 4.92; found: C 71.81, H 5.09.

Synthesis of chromium carbene complex (17)



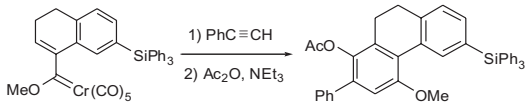
16 17 80%

A 100 mL RB flask with a stir bar was charged with vinyl bromide **16** (3.0 g, 6.42 mmol) and then covered with Ar. THF was added (32 mL) and after the solid dissolved the solution was cooled to –78 °C. A 1.7 mol/L solution of *t*-BuLi in pentane (12.84 mmol, 7.6 mL) was added over 5–10 min. The solution was stirred at –78 °C for 15 min, was warmed to 0 °C for 10 min, and was then transferred by cannula into a separate flask containing a stirred slurry of $Cr(CO)_6$ (1.41 g, 6.42 mmol) in 39 mL of THF under Ar. After stirring at RT for 1.7 h the solvent was removed by rotary evaporator and then high vacuum (19 h) to afford a light brown foam. The foam was dissolved in 45 mL argon-sparged (AS) CH_2Cl_2 under Ar and then cooled to 0 °C. Methyl triflate (1.09 mL, 9.63 mmol) was added over 5 min. The mixture was warmed to RT and stirred for 55 min. The deep red so-

© 2006 NRC Canada

lution was then concentrated down to a few mL of volume by rotary evaporator, applied to the top of a SiO_2 column, and eluted with hexane–EtOAc (9:1), which after removal of solvent afforded 3.2 g of carbene complex **17** as a red solid (80% yield). R_f = 0.275 (hexane–EtOAc, 9:1). IR (neat film, NaCl, cm^{-1}): 2062 (m), 1988 (w), 1940 (s). ^1H NMR (300 MHz, CD_2Cl_2) δ: 2.47 (m, 2H), 2.86 (m, 2H), 4.14 (br s, 3H, methoxy), 5.76 (t, 1H, J = 4.5 Hz), 7.38 (t, 6H, J = 7.0 Hz), 6.78 (s, 1H), 7.52 (d, 6H, J = 7.6 Hz), 7.24–7.57 (m, 5H). ^{13}C NMR (75 MHz, CD_2Cl_2) δ: 22.7, 27.8, 66.1, 123.4, 128.3, 128.6, 129.7, 130.0, 130.1, 132.2, 134.3, 135.9, 136.4, 136.6, 137.8, 216.5 (CO), 225.1 (CO), 358.6 (carbene C). MS (FAB, nitrobenzyl alcohol) *m/z* (%): 622 [M^+] (3), 594 [M^+ – CO] (5), 483 (44), 482 (87), 467 (37), 452 (18), 259 (100).

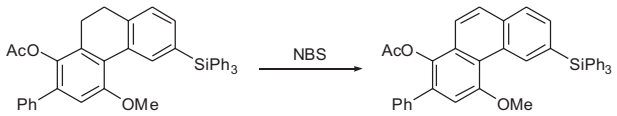
The benzannulation reaction of complex 17 with phenylacetylene (3)



17 **18** 74%

Carbene complex **17** (3.2 g, 5.15 mmol) was dissolved in 150 mL of THF in a 250 mL single-necked RB flask, which had the joint replaced with a threaded high-vacuum Teflon stopcock. Phenylacetylene (0.85 mL, 7.72 mmol) was added and the solution was deoxygenated by the freeze-pump-thaw method (3 cycles, –196 °C and 20 °C). The flask was charged with Ar at RT and then sealed and warmed at 60 °C for 21 h. After cooling to RT, triethylamine (1.79 mL, 12.87 mmol) and 1.19 mL acetic anhydride (12.6 mmol) were added. The flask was resealed and warmed to 60 °C for 8 h and then stirred at RT overnight. The crude mixture was concentrated down to a few mL of volume by rotorary evaporator, applied to the top of a SiO_2 column, and eluted with hexane–EtOAc 9:1). The product fraction was collected (R_f = 0.22, hexane–EtOAc (9:1)) as well as a more polar yellow band, which was the arene chromium tricarbonyl complex of the product. This yellow compound was dissolved in $CHCl_3$ and stirred overnight in open air to remove the chromium. This was then passed through a short SiO_2 pad to filter off the green flocculent chromium byproduct. The resulting product was combined with the earlier collected product to afford 2.3 g of a white crystalline solid (74% yield); mp 228–229.5 °C. IR (neat film, NaCl, cm^{-1}): 3067 (w), 3048 (w), 2933 (w), 1761 (ms), 1460 (m), 1428 (m), 1367 (m), 1211 (s), 1186 (s), 1108 (ms), 1059 (m), 701 (vs). ^1H NMR (500 MHz, $CDCl_3$) δ: 2.07 (s, 3H), 2.78 (t, 2H, J = 6.4 Hz), 2.50–2.85 (m, 2H), 3.56 (s, 3H), 6.76 (s, 1H), 7.21–7.29 (m, 2H), 7.31–7.39 (m, 14H), 7.58 (d, 6H, J = 7.0 Hz), 8.51 (s, 1H). ^{13}C NMR (75MHz, $CDCl_3$) δ: 20.5, 23.1, 28.9, 55.4, 111.6, 123.8, 127.0, 127.5, 127.8, 128.8, 129.4, 131.1, 131.5, 133.1, 134.1, 134.6, 135.1, 136.5, 136.9, 138.0, 138.5, 139.6, 154.7, 169.4. EI-MS *m/z* (%): 604 [M^+ + 2] (10), 603 [M^+ + 1] (27), 602 [M^+] (51), 562 (15), 561 (48), 560 [M^+ – ketene] (100), 483 (14), 259 Ph_3Si^+ (73), 230 (19), 181 (14). Anal. calcd. for $C_{41}H_{34}O_3Si$: C 81.70, H 5.64; found: C 81.53, H 5.62.

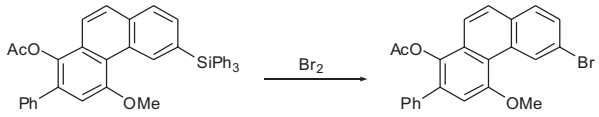
Aromatization of the B-ring of intermediate (18)



18 **19** 91%

A 500 mL RB flask was charged with starting material **18** (2.17g, 3.6 mmol), N-bromosuccinimide (673 mg, 3.78 mmol), benzoyl peroxide (89 mg, 0.36 mmol), and benzene (200 mL). The magnetically stirred solution was refluxed for 9 h. Upon cooling, the solution was filtered through a short plug of Al_2O_3 and then purified by SiO_2 chromatography (hexane–EtOAc, 5:1) to afford 1.97 g of **19** as a white crystalline solid (91% yield); mp 237 to 238 °C. R_f = 0.31 (hexane–EtOAc, 4:1). IR (neat film, NaCl, cm^{-1}): 3066 (w), 3048 (w), 2922 (w), 1763 (m), 1428 (m), 1197 (s), 1108 (ms), 1049 (mw). ^1H NMR (500 MHz, $CDCl_3$) δ: 2.14 (s, 3H), 3.61 (s, 3H), 6.98 (s, 1H), 7.28–7.39 (m, 11H), 7.47 (d, 2H, J = 7.3 Hz), 7.63 (d, 6H, J = 7.2 Hz), 7.73 (m, 4H), 7.83 (d, 1H, J = 7.8 Hz), 9.89 (s, 1H). ^{13}C NMR (75MHz, $CDCl_3$) δ: 20.7, 55.4, 109.6, 120.5, 120.8, 127.6, 127.9, 128.4, 128.8, 129.1, 129.5, 132.0, 132.8, 132.9, 133.0, 133.2, 134.6, 136.6, 136.9, 137.3, 137.8, 138.0, 156.6, 169.7, (1C not located). EI-MS *m/z* (%): 602 [M^+ + 2] (8), 601 [M^+ + 1] (15), 600 [M^+] (30), 560 (21), 559 (45), 558 [M^+ – ketene] (100), 481 (8), 465 (10), 387 (10), 260 (17), 259 Ph_3Si^+ (66,), 230 (19), 181 (14), 220 (15), 181 (8).

Bromo-desilylation of phenanthrene (19)



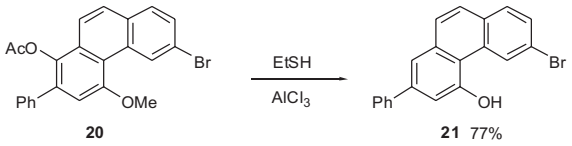
19 **20** 83%

A 100 mL RB flask with a stir bar was charged with phenanthrene **19** (342 mg, 0.57 mmol), CH_2Cl_2 (20 mL), and 5.1 mL of a 0.3 mol/L solution of Br_2 in CH_2Cl_2 (1.54 mmol). The mixture was brought to reflux for 3.5 h and then stirred at RT for 20 h. A small amount of SiO_2 was poured into the reaction mixture. Solvent was removed in vacuo to adsorb the crude reaction material on the silica. This SiO_2 adsorbate was applied to the top of a silica gel column and eluted with hexane–EtOAc (4:1) to afford 199 mg of **20** as a white solid (83% yield). The desired product elutes from the column after an orange impurity elutes. On scaling up the reaction, it was more efficacious to use slightly less Br_2 (~2 equiv.) to avoid this separation. Melting point 203.5–205 °C. R_f = 0.36 (hexane–EtOAc, 4:1). IR (neat film, NaCl, cm^{-1}): 2922 (w), 1761 (ms), 1589 (mw), 1440 (m), 1368 (m), 1212 (m), 1196 (vs), 1048 (m). ^1H NMR (300 MHz, $CDCl_3$) δ: 2.17 (s, 3H), 4.11 (s, 3H), 7.13 (s, 1H), 7.32–7.44 (m, 4 H), 7.56 (d, 1H, J = 7.9 Hz), 7.61 (dd, 1H, J = 7.6, 1.4 Hz), 7.64–7.68 (m, 1H), 7.70 (d, 2H, J = 9.5 Hz), 9.84 (s, 1H). ^{13}C NMR (75 MHz, $CDCl_3$) δ: 20.7, 55.9, 109.6, 120.5, 121.1, 127.7, 127.8, 127.9, 128.4, 128.6, 129.0, 129.4, 129.6, 130.0, 131.1, 132.7, 134.9, 136.5, 137.7, 156.4, 169.6. EI-MS *m/z* (%): 423 [M^+ + 1] (5,

© 2006 NRC Canada

^{81}Br), 422 [M$^+$] (18, ^{81}Br), 421 [M$^+$ + 1] (5, ^{79}Br), 420 [M$^+$] (19, ^{79}Br), 381 (23), 380 (99), 379 (25), 378 (100), 365 (14), 363 (14), 300 (19), 298 (14), 284 (32).

Reduction of 20 to the phenanthrol 21 (3)

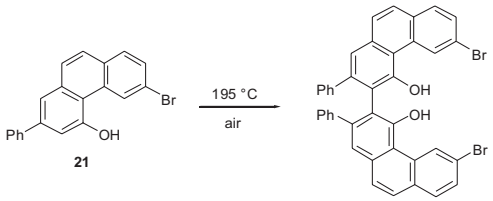


20 **21** 77%

A 200 mL RB flask with stir bar was charged with freshly sublimed $AlCl_3$ (405 mg, 3.03 mmol), CH_2Cl_2 (100 mL), and ethanethiol (0.475 mL, 6.4 mmol). Caution: flask needs to be openly vented to allow gases to escape on addition of ethanethiol. A gentle stream of N_2 was directed down into the open neck of the flask. After stirring for 5 min at RT, starting material (421 mg, 1.0 mmol) was added, which turned the mixture orange. The flask was then sealed with a septum and punctured with a needle connected to an N_2 bubbler. The mixture was stirred 9 h. The solution turned murky within 2 to 3 h after the addition of the starting material. The solution was carefully quenched with satd. aq $NaHCO_3$ (caution: vent flask to open air) and then partitioned between 50 mL H_2O and 100 mL ether. The aqueous layer was removed by separatory funnel and re-extracted with 50 mL ether. The combined organic layers were washed with 50 mL brine, dried over $MgSO_4$, filtered, and then stripped of volatiles. Trituration from CH_2Cl_2–hexane afforded a white powder that was contaminated with a small amount (ca. 5%) of a compound that resulted from reduction of the bromide in **21**. Repeated trial runs of this reaction indicated that the amount of this impurity increased with reaction times greater than 8 to 9 h. Reaction glassware was deodorized from the stench of EtSH by immersion in dilute aqueous bleach solution. Pure product was isolated by SiO_2 chromatography (hexane–EtOAc, 5:1). It elutes just before the bromine-reduced impurity. Yield: 270 mg (77%) of light peach-coloured powder, which could be crystallized to colourless needles by slow evaporation from ether; mp 178 to 179 °C (ether). R_f = 0.29 (hexane–EtOAc, 4:1). Note: the phenananthrol monomer **21** as well as the phenanthrol dimers described below are prone to decomposition as evidenced by their turning yellow and orange on handling. Chromatography should be done expeditiously. They should not be stored as solutions (especially CH_2Cl_2) open to air. They are more stable as solids. A useful method for crashing out solid is to dissolve the compound in CH_2Cl_2, add hexane, and then slowly remove solvent on a rotory evaporator. IR (neat film, NaCl, cm^{-1}): 3335 (br), 3052 (w), 2921 (w), 1587 (w), 1393 (w). ^{1}H NMR (500 MHz, $CDCl_3$) δ: 5.76–6.10 (variable) (s, 1H, O**H**), 7.20 (d, 2H, J = 5.9 Hz), 7.35 (t, 1H, J = 7.2 Hz), 7.44 (t, 2H, J = 7.5 Hz), 7.61–7.69 (m, 6H), 9.77 (s, 1H). ^{13}C NMR (75MHz, CD_2Cl_2) δ: 112.6, 117.8, 119.7, 121.0, 127.5, 127.9, 128.17, 128.23, 129.3, 129.9, 131.3, 131.5, 131.9, 135.7, 140.2, 155.5 (2C not located). EI-MS *m/z* (%): 351 [M$^+$ + 1] (24, ^{81}Br), 350 [M$^+$] (99, ^{81}Br), 349 [M$^+$ + 1] (24, ^{79}Br), 348 [M$^+$] (100, ^{79}Br), 270 (32), 269 (54), 268 (26), 241 (47), 239 (46), 120 (26).

Synthesis of (*S*)-6,6′-dibromo-2,2′-diphenyl-3,3′-bis(phenanthren-4-ol) 8 (3)

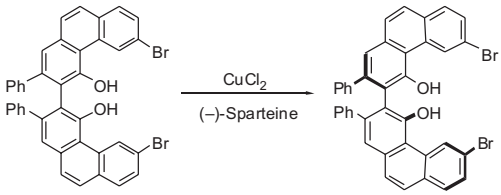
Oxidative coupling of 21



21 **8** 95%

Phenanthrene **21** (310.8 mg, 0.89 mmol) was added to a 25 × 150 mm test tube containing a micro stir bar. It was heated for a total of 14 h at 195 °C during which time it solidified to a dark brown cake. Heating was interrupted briefly after ca. 6 h to wash down sublimed starting material from the sides of the test tube with a small amount of EtOAc. (Care should be exercised in evaporating of the last of this EtOAc as it tends to spray the reaction mixture along the sides of the test tube.) The crude brown product was obtained (303 mg, 97% crude yield), which NMR indicated was the dimerized product **8** contaminated with ~5%–10% unreacted starting material. This material was used in the next step without purification. HPLC retention times for the two enantiomers: 11.33 and 17.45 min.

Deracemization of 8



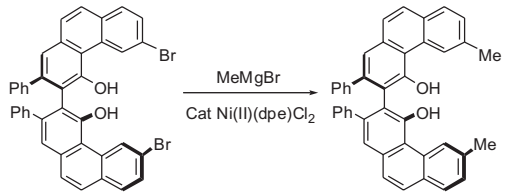
8 (*S*)-**8**

A sample of $CuCl_2 \cdot 2H_2O$ (73 mg, 0.428 mmol) was dissolved under Ar in 6.7 mL AS MeOH in a 100 RB flask. A solution of 200 mg (–)-sparteine (0.853 mmol) in 13 mL AS MeOH was added by cannula, which turned the solution a murky lime green. The solution was stirred for 0.5 h at RT. In a separate flask, 213 mg of the crude biphenanthrol **8** (–0.31 mmol) was partially dissolved in 10 mL AS CH_2Cl_2. This solution was transferred by cannula into the reaction mixture with concurrent addition of 10 mL AS MeOH. The remaining undissolved starting material was dissolved in 6.5 mL AS CH_2Cl_2 and transferred into the reaction flask with concurrent addition of 6.5 mL AS MeOH. The mixture turned black. It was stirred for 24 h, quenched with 1 mL concd HCl, and then partitioned between 50 mL H_2O and 50 mL CH_2Cl_2. The organic layer was dried over $MgSO_4$ and filtered, then adsorbed onto a small amount of SiO_2 and chromatographed (hexane–EtOAc, 5:1) to afford 108 mg of (*S*)-**8** as a white or pale yellow solid (50% yield). R_f = 0.38 (hexane–EtOAc, 4:1). The optical purity of **8** was determined to be >98% ee by chiral HPLC analysis on Pirkle D-phenyl glycine column with 70:30 mixture of hexane–*i*PrOH at 2 mL/min. The chiral HPLC retention time of (*S*)-**8** was 16.9 min. X-ray quality crystals were grown by dissolving a

© 2006 NRC Canada

sample in a minimum amount of hot EtOAc, allowing this to cool to RT, and then layering with hexane, which produced clear faintly pale green crystals. Crystallography as well as ^{1}H NMR indicated the crystal contained two equiv. of EtOAc. Absolute configuration is assigned to the (*S*)-isomer by analogy with the parent molecule VAPOL, which upon deracemization with (–)-sparteine–$CuCl_2$ affords (*S*)-(+)-VAPOL (12). On scaling up the reaction, the material obtained from the chromatography column was not always enantiopure. In this case the enantiopurity was upgraded by stirring the scalemic powder for 1 h in enough hexane to allow a small amount to remain undissolved. The decanted hexane was found to contain enantiopure material. $[\alpha]_D$ + 445° (*c* 1.0, THF). IR (neat film, NaCl, cm^{-1}): 3482 (s), 3139 (w), 3052 (w), 3027 (w). ^{1}H NMR (500 MHz, $CDCl_3$) δ: 6.60 (s, 2H), 6.64 (d, 4H, *J* = 7.5 Hz), 6.94 (t, 4H, *J* = 7.6 Hz), 7.05 (t, 2H, *J* = 7.3 Hz), 7.40 (s, 2H), 7.65 (d, 2H, *J* = 8.7 Hz), 7.69 (d, 2H, *J* = 8.3 Hz), 7.75 (t, 4H, *J* = 9.5 Hz), 9.91 (s, 2H). ^{13}C NMR (75 MHz, $CDCl_3$) δ: 116.0, 117.1, 121.3, 123.2, 126.9, 127.4, 127.6, 128.6, 128.8, 129.4, 129.6, 131.27, 131.35, 131.42, 135.3, 139.5, 142.2, 153.3. EI-MS *m*/*z* (%): 699 [M$^+$ + 1] (23, ^{81}Br), 698 [M$^+$] (65, ^{81}Br), 697 [M$^+$ + 1] (48, ^{81}Br^{79}Br), 696 [M$^+$] (100, ^{81}Br^{79}Br), 695 [M$^+$ + 1] (26, ^{79}Br, ^{79}Br), 694 [M$^+$] (41, ^{79}Br. ^{79}Br), 618 (22), 616 (18), 536 (5), 268 (72), 239 (27), 149 (42). Anal. calcd. for $C_{40}H_{24}O_2Br_2 \cdot 2(C_4H_8O_2)$: C 6.07, H 4.62; found: C 66.16, H 4.57.

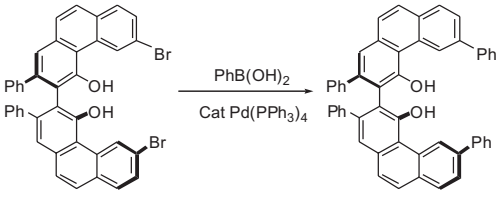
Coupling of (S)-8 with methyl Grignard reagent — Synthesis of (S)-9 (13)



(*S*)-**8** (*S*)-**9**

The optically pure dibromide (*S*)-**8** (10 mg, 14.4 μmol) and Ni(II)dpeCl_2 (1 mg,1.9 μmol) were added to a 5 mL RB flask and then covered with Ar. Ether (3 mL) was added via syringe and the solution was cooled to 0 °C. A 3 mol/L solution (29 μL) of CH_3MgBr in ether (86.4 μmol) was added dropwise. The solution was stirred for 0.5 h and was then warmed to reflux for 20.5 h. Additional ether (3 mL) was added during the reflux period to replace evaporated solvent. On cooling to RT, 3 mL of 10% aq HCl was added and the reaction mixture was partitioned between 20 mL ether and 5 mL H_2O. The organic layer was washed with brine and then dried over $MgSO_4$. Solvent was removed in vacuo to afford 7.6 mg (93% yield) of (*S*)-**9** as a pale tan solid that was pure by proton NMR. Chiral HPLC retention time: 23.3 min. $[\alpha]_D$ + 236° (*c* 1.0, THF). R_f = 0.34 (hexane–EtOAc, 9:1, plastic plate). IR (neat film, NaCl, cm^{-1}): 3480 (s), 3054 (w), 2922 (m). ^{1}H NMR (500 MHz, $CDCl_3$) δ: 2.60 (s, 6H), 6.60 (s, 2H), 6.64 (d, 4H, *J* = 7.8 Hz), 6.92 (t, 4H, *J* = 7.5 Hz), 7.03 (t, 2H, *J* = 7.5 Hz), 7.38 (s, 2H), 7.74 (d, 2H, *J* = 8.2 Hz), 7.80 (d, 2H, *J* = 7.9 Hz), 9.54 (s, 2H). ^{13}C NMR (75 MHz, $CDCl_3$) δ: 22.5, 115.6, 117.9, 123.2, 126.1, 126.7, 127.5, 127.9, 128.3, 128.6, 128.8, 129.1, 130.4, 130.7, 135.5, 136.8, 139.8, 141.4, 153.5. EI-MS *m*/*z* (%): 568 [M$^+$ + 2] (10), 567 [M$^+$ + 1] (44), 566 [M$^+$] (100), 552 (7), 475 (7), 383 (11), 283 (30), 255 (8).

Coupling of (*S*)-8 with phenyl boronic acid — Synthesis of (*S*)-10 (14)

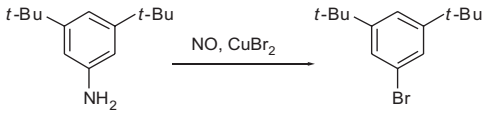


(*S*)-**8** (*S*)-**10**

Ethanol, aq Na_2CO_3 (2 mol/L), and benzene were sparged (>10 min) with inert gas (Ar or N_2) prior to use. A 25 mL RB flask was charged with $Pd(PPh_3)_4$ (2.3 mg, 2.2 μmol) and optically pure (*S*)-**8** (25 mg, 35.9 μmol). The flask was filled with Ar and 1.5 mL benzene and aq Na_2CO_3 (0.75 mL, 2 mol/L) was added by syringe. A solution of phenyl boronic acid (10.9 mg, 89.7 μmol) in 0.5 mL EtOH was added. The mixture was refluxed for 7 h and then stirred overnight at RT. The reaction mixture was diluted with 30 mL ether and washed with 25 mL brine containing a pipette tipful of HCl. The organic layer was dried over $MgSO_4$, filtered, adsorbed onto a small amount of SiO_2, and chromatographed (hexane–EtOAc, 9:1) to afford 23.4 mg of (*S*)-**10** as a white solid film (94% yield). $[\alpha]_D$ 749.5° (*c* 1.0, THF). R_f = 0.25 (hexane–EtOAc, 9:1, plastic plate). Chiral HPLC retention time: 22.4 min. IR (neat film, NaCl, cm^{-1}): 3481 (s), 3058 (w), 2923 (m), 2852 (w). ^{1}H NMR (500 MHz, $CDCl_3$) δ: 6.66 (d, 6H), 6.94 (t, 4H, *J* = 7.6 Hz), 7.04 (t, 2H, *J* = 7.1 Hz), 7.27, (t, 2H, *J* = 7.1 Hz), 7.39 (t, 6H), 7.64 (d, 2H, *J* = 8.7 Hz), 7.76 (d, 4H, *J* = 7.4 Hz), 7.81 (d, 2H, *J* = 8.5 Hz), 7.87 (d, 2H, *J* = 7.5 Hz), 7.96 (d, 2H, *J* = 8.3 Hz), 10.04 (s, 2H). ^{13}C NMR (75 MHz, $CDCl_3$) δ: 115.9, 118.2, 123.3, 125.5, 126.8, 127.1, 127.2, 127.5, 128.8, 130.6, 132.0, 135.6, 139.6, 139.7, 141.7, 153.5, (6 C not located). EI-MS *m*/*z* (%): 692 [M$^+$ + 2] (17), 691 [M$^+$ + 1] (57), 690 [M$^+$] (100), 672 (8), 614 (20), 615 (11), 446 (13), 346 (15), 345 (25).

Coupling of (*S*)-8 with 3,5-di-*t*-butylphenyl Grignard reagent — Synthesis of (*S*)-11

Synthesis of 3,5-di-t-butylbromobenzene (17).



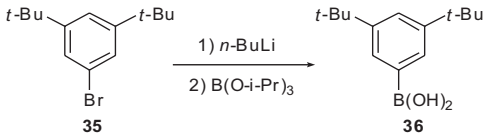
34 **35** 54%

A 25 mL RB flask with stir bar was charged with pulverized $CuBr_2$ (544 mg, 2.43 mmol) and 5 mL freshly distilled CH_3CN. NO gas was bubbled through the mixture for 10 min. The reaction mixture was then cooled to –30 °C, while maintaining NO gas bubbling. A solution of 500 mg of the *tert*-butylated aniline **34** (2.43 mmol) in 1.5 mL CH_3CN was added over 5 min. After stirring 5 additional minutes, the cold bath was removed, NO gas flow was

© 2006 NRC Canada

reduced to a trickle, and the solution stirred at RT for 1 h 10 min. The reaction was partitioned between 50 mL H_2O and 100 mL ether. The murky green organic layer was then washed with brine, dried over $MgSO_4$, filtered, and adsorbed onto a small amount of SiO_2. Purification by SiO_2 chromatography (hexane) afforded 355 mg of a clear, colourless oil, which crystallized on sitting at RT (54% yield). R_f = 0.40 (hexane). ^{1}H NMR (500 MHz, CD_3CN) δ: 1.09 (s, 18H), 7.13 (s, 2H), 7.19 (s, 1H). The aryl protons showed the same chemical shift in $CDCl_3$. EI-MS *m/z* (%): 271 (3), 270 [M^+] (24, ^{81}Br), 269 (3), 268 [M^+] (24, ^{79}Br), 256 (15), 255 (99), 254 (10), 253 (100).

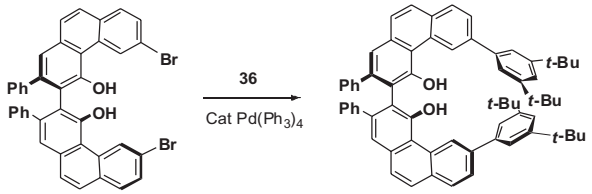
Synthesis of boronic acid 36 (18)



35 **36**

A 25 mL RB flask with stir bar was charged with 320 mg of aryl bromide **35** (1.19 mmol) and then covered with Ar. THF (5 mL) was added and after dissolution the flask was cooled to –78 °C, whereupon 0.48 mL of a 2.5 mol/L solution of *n*-BuLi in hexanes (1.2 mmol) was added dropwise. After stirring at –78 °C for 1 h, a solution of 0.68 mL triisopropyl borate in THF (1 mL, 2.9 mmol) was added all at once by syringe to give a clear solution. The cold bath was removed and while warming to RT the solution became cloudy. After stirring 1 h the mixture was poured into a vigorously stirred mixture of 10% aq HCl (30 mL) and ether (40 mL) and stirred a few minutes. Both the aqueous and organic layers were clear and colourless. The organic layer was removed, washed with 30 mL H_2O, dried over $MgSO_4$, and filtered. Rotary evaporation of the solvent yielded **36** as a white solid, which was used in the next step without purification. ^{1}H NMR analysis (500 MHz, $CDCl_3$) of the aryl region suggested a mixture of two compounds; major: δ 7.52 (s, 2H), 8.06 (s, 1H); minor: δ 7.63 (s, 2H), 7.94 (s, 1H). In addition there was a pronounced singlet at δ 4.54, which is attributed to the BOH of the desired product.

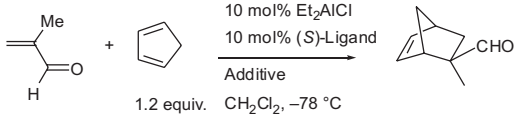
Suzuki coupling of (S)-8 with 36 — Synthesis of (S)-11 (14)



(*S*)-8 **(*S*)-11**

Ethanol, aq Na_2CO_3 (2 mol/L), and benzene were sparged (>10 min) with inert gas (Ar or N_2) prior to use. Optically pure (*S*)-**8** (66 mg, 75.9 µmol, based on MW 872.6, containing two equiv. of EtOAc) was dissolved in a minimum of CH_2Cl_2 in a 25 mL RB flask, the solvent was removed by rotory evaporator, and then the ethyl acetate was removed on high vacuum. To the flask was added $Pd(PPh_3)_4$ (6 mg, 5.2 µmol) and the solids were covered with Ar. Benzene (4 mL) and aq Na_2CO_3 (2 mL 2 mol/L) was added. To the vigorously stirred mixture was added a solution of crude boronic acid **36** (89 mg, ~304 µmol, based on 80% purity) in EtOH (2 mL). The mixture was refluxed for 14 h and then stirred at RT for 11 h. The reaction mixture was partitioned between 50 mL ether and 25 mL brine containing a pipette tip of HCl. The organic layer was dried over $MgSO_4$, filtered, and adsorbed onto a small amount of SiO_2. Purification by chromatography on silica gel (hexane–EtOAc, 9:1) afforded 70.0 mg of (*S*)-**11** as a clear, colourless solid film (100% yield). $[\alpha]_D$ 565° (*c* 1.0, THF). R_f = 0.42 (hexane–EtOAc, 9:1). Chiral HPLC retention time: 5.7 min. IR (neat film, NaCl, cm^{-1}): 3486 (m, sharp), 2962 (s, sharp), 2863 (w), 1594 (m, sharp). ^{1}H NMR (500 MHz, $CDCl_3$) δ: 1.35 (s, 36H), 6.55 (s, 2H), 6.69 (d, 4H, *J* = 7.2 Hz), 6.94 (t, 4H, *J* = 7. 5 Hz), 7.04 (t, 2H, *J* = 6.6 Hz), 7.37 (s, 2H), 7.56 (s, 4 H), 7.43 (s, 2H), 7.64 (d, 2H, *J* = 8.7 Hz), 7.81 (d, 2H, *J* = 8.8 Hz), 7.85 (d, 2H, *J* = 7.7 Hz), 7.96 (d, 2H, *J* = 8.1 Hz), 9.95 (s, 2H). ^{13}C NMR (75 MHz, $CDCl_3$) δ: 31.6, 115.8, 118.4, 121.4, 122.3, 123.4, 126.2, 126.9, 127.6, 127.7, 128.8, 128.9, 129.1, 130.6, 131.8, 135.6, 139.8, 141.2, 141.3, 141.8, 151.2, 153.7 (2 C not located). EI-MS *m/z* (%): 916 [M^+ + 1] (30), 915 [M^+] (42), 710 (69), 709 (87), 576 (63), 575 (82), 574 (86), 481 (26), 259 (50), 183 (33), 57 (100).

Diels–Alder reaction of methacrolein and cyclopentadiene



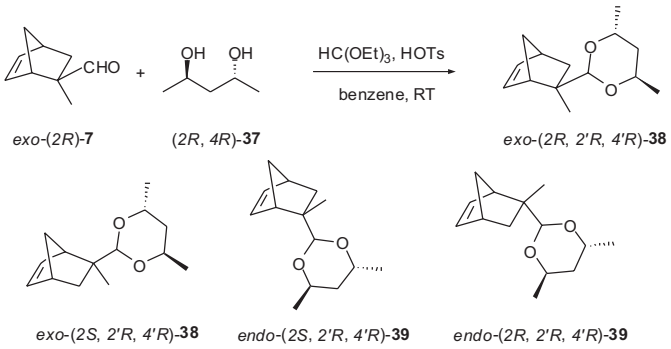
5 **6** **(*2R*)-7**

A sample of the desired ligand (45–75 mg) was added to a 5 mL RB flask containing a stirbar and the flask was flushed with Argon. Methylene chloride (1 to 2 mL) was added by syringe followed by 1 equiv. Et_2AlCl (1 mol/L solution in hexane), which turned the solution a deep blood-red color. After stirring at RT for 0.5 h the flask was cooled to –78 °C. Methacrolein (10 equiv. relative to ligand) was then added by syringe. After stirring at –78 °C for 0.5–0.75 h, 12–14 equiv. of cyclopentadiene was added. If an additive was used, it was added 15 min before the cyclopentadiene was added. After 0.5 h at –78 °C, the reaction was quenched by the addition of 1 mL brine. The mixture was then partitioned between 20 mL CH_2Cl_2 and 10 mL H_2O and stirred vigorously. The organic layer was dried over $MgSO_4$, filtered, and then taken to near dryness on the rotory evaporator. The yield of the exo product **7** was determined on this concd CH_2Cl_2 solution by ^{1}H NMR using the ligand as an internal standard. The product was separated from the ligand by bulb-to-bulb distillation under high vacuum into a –78 °C trap prior to the measurement of the exo–endo ratio and the ee%, which were each determined by one of the two methods indicated below. Catalyst formation for ligands **10** and **11** were much slower as indicated by ^{1}H NMR. For these ligands, catalyst formation required heating at 55 °C for 24 h. ^{1}H NMR for *exo*–**7** (500 MHz, $CDCl_3$) δ: 0.76 (d 1H, *J* = 11.9 Hz), 1.00 (s, 3H), 1.38 (s, 2H), 2.23 (dd, 1H, J = 11.9, 3.5 Hz), 2.80 (s, 1H), 2.87 (s, 1H), 6.06 (dd, 1H, J = 5.2, 2.9 Hz), 6.25 (dd, 1H, J = 5.1 Hz, 2.9 Hz), 9.62 (s, 1H).

© 2006 NRC Canada

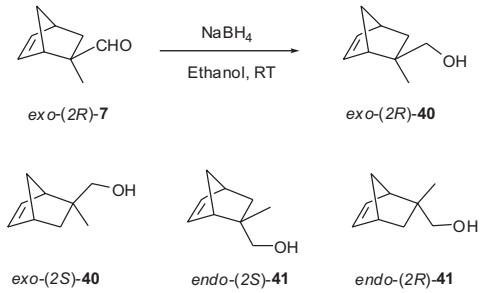
This data matches that previously reported for this compound (19).

Analysis of exo-adduct 7 by conversion to chiral acetals



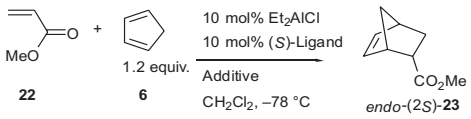
This method was originally developed by Yamamoto (20). A pipette tip of product **7** (~20 mg) was mixed with 25–30 mg (2*R*,4*R*)-(–)-pentanediol, 40 mL triethyl orthoformate, a small crystal of $TsOH{\cdot}H_2O$, and 1 to 2 mL benzene and stirred overnight. The de% of the exo product (and hence ee% of the exo product) and the exo–endo ratio were determined by GC on an Alltech Econocap capillary column (cat. #19646, ser. # 2475–9): 0.32 mm i.d., 0.25 mm film thickness, and 30 m in length. Column temperature was 50 °C for 2 min and then ramped up at 4 °C per min. Under these conditions, the following retention times were observed: (*2R*,*2′R*,*4′R*)-**38** (23.15 min); (*2S*,*2′R*,*4′R*)-**38** (23.25 min), **39** (21.98 and 22.93 min, not assigned). It was previously established that (*S*)-VAPOL is selective for (*2R*,*2′R*,*4′R*)-**38** (4*a*). Spectral data for (*2R*,*2′R*,*4′R*)-**38**: IR (neat, cm^{-1}): 3139 (w), 3059 (m), 2979 (s), 2932 (s), 2878 (s), 2700 (w), 1572 (w), 1451 (s), 1398 (m), 1376 (s), 1333 (s), 1289 (m), 1241 (s), 1181 (m), 1158 (s), 1135 (s), 1093 (m), 1081 (m), 1007 (s), 972 (m), 906 (m), 839 (m), 721 (s). ^{1}HNMR ($CDCl_3$) δ: 0.76 (d, 1H, *J* = 12.0 Hz), 0.86 (s, 3H), 1.19 (d, 3H, *J* = 6.2 Hz), 1.29–1.31 (m, 2H), 1.34 (d, 3H, *J* = 7.1 Hz), 1.60 (d, 1H, *J* = 8.4 Hz), 1.74–1.82 (m, 2H), 2.66 (s, 1H), 3.90–3.94 (m, 1H), 4.27–4.66 (m, 1H), 4.66 (s, 1H), 6.01–6.11 (m, 2H). ^{13}C NMR (CDC_3) δ: 17.25, 18.77, 21.96, 36.87, 37.10, 43.07, 45.45, 47.15, 48.06, 67.68, 67.74, 99.48, 135.54, 137.15. MS *m*/*z* (%): 222 [M^+] (4), 157 (22), 115 (78), 69 (100). HRMS *m*/*z*: calcd. for $C_{14}H_{22}O_2$: 222.1620; found: 222.1662. Anal. calcd. for $C_{14}H_{22}O_2$: C 75.63, H 9.97; found: C 75.88, H 10.26. Spectral data for (*2S*,*2′R*,*4′R*)-**38** (prepared from (*R*)-VAPOL): ^{1}H NMR ($CDCl_3$) δ: 0.74 (dd, 1H, *J* = 2.7, 12.0 Hz), 0.86 (s, 3H), 1.20 (d, 3H, *J* = 6.2 Hz), 1.28–1.33 (m, 2H), 1.36 (d, 3H, *J* = 7.0 Hz), 1.58–1.85 (m, 3H), 2.75 (bs, 2H), 3.89–3.96 (m, 1H), 4.30–4.35 (m, 1H), 4.70 (s, 1H). ^{13}C NMR ($CDCl_3$) δ: 17.26, 18.57, 21.93, 36.83, 37.35, 43.25, 45.48, 47.41, 47.94, 67.43, 67.98, 99.43, 135.74, 137.10. IR (neat, cm^{-1}): 3060 (w), 2972 (s), 2941 (s), 2877 (m), 1449 (m), 1398 (w), 1375 (m), 1333 (m), 1288 (w), 1241 (w), 1217 (w), 1158 (s), 1135 (s), 1102 (w), 1081 (w), 1059 (s), 1024 (m), 1003 (s), 982 (w), 722 (s). MS *m*/*z* (%): 222 [M^+] (18), 157 (70), 115 (100), 69 (13). HRMS calcd. for $C_{14}H_{22}O_2$ *m*/*z*: 222.1620; found: 222.1617. Anal calcd. for $C_{14}H_{22}O_2$: C 75.63, H 9.97; found: C 75.85, H 10.12.

Analysis of exo-adduct 7 by reduction to alcohol 40



The aldehyde **7** (71.7 mg) distilled from the reaction described above was dissolved in 1.2 mL of ethanol and treated with $NaBH_4$ (24 mg). After 1 h the reaction was quenched by the slow addition of water. The reaction mixture was partitioned between 10 mL of H_2O and 10 mL of ethanol. The aqueous phase was extracted with ether (2 × 5 mL) and the combined organic layer was washed with 15 mL of brine and dried over $MgSO_4$. Removal of solvent left 77 mg of crude product, which was purified by chromatography on silica gel with a 5:1 mixture of hexanes – ethyl acetate to give 61 mg of **40** as a white solid. The de% of the exo product (and hence ee% of the exo product) and the exo–endo ratio were determined by GC on an Astec B-MB capillary column (Beta-cyclodextrin Dimethyl, *t*-Butyl, ser. # 9606–29) of 0.25 mm i.d. and 30 m in length. Column temperature was isothermal at 140 °C. Under these conditions, the following retention times were observed: (*2R*)-**40** (6.12 min); (*2S*)-**40** (6.01 min); **41** (5.67 and 5.41 min, not assigned).

Diels–Alder reaction of methacrolein and cyclopentadiene



A sample of the desired ligand (45 mg) was added to a 5 mL RB flask containing a stir bar and the flask was then flushed with argon. Methylene chloride (1 to 2 mL) was added by syringe followed by 1 equiv. Et_2AlCl (1 mol/L solution in hexane), which turned the solution a deep blood-red color. After stirring at RT for 0.5 h, the flask was cooled to –78 °C. Methyl acrylate (10 equiv. relative to ligand) was then added by syringe. After stirring 0.5–0.75 h at –78 °C, 12–14 equiv. of cyclopentadiene was added. If an addtive was used it was added 15 min before methyl acrylate. After 24 h at –78 °C the reaction was quenched by the addition of 1 mL brine. The mixture was then partitioned between 20 mL of CH_2Cl_2 and 10 mL of H_2O and stirred vigorously. The organic layer was dried over $MgSO_4$, filtered, and then taken to near dryness on a rotatory evaporator. The yield of *endo*-**23** was determined on this concentrated CH_2Cl_2 solution by ^{1}H NMR using the ligand as an internal standard. The product was separated from the ligand by bulb-to-bulb distillation under high vacuum into a –78 °C trap prior to the measurement of the exo–endo ratio and the ee%, which were

© 2006 NRC Canada

both determined by the method indicated below. Catalyst formation for ligands **10** and **11** were much slower as indicated by ^{1}H NMR. For these ligands, catalyst formation required heating at 55 °C for 24. Spectral data for *endo*-**23**: ^{1}H NMR (500 MHz, $CDCl_3$) δ: 1.28 (d, 1H), 1.40–1.45 (m, 2H), 1.88–1.96 (m, 1H), 2.92–2.99 (m, 2H), 3.21 (s, 1H), 3.63 (s, 3H), 5.94 (dd, 1H, J = 5.6, 2.8 Hz), 6.20 (dd, 1H, J = 5.6, 3.0 Hz).

Analysis of endo-adduct 23 by GC



endo-(2*S*)-**23** *endo*-(2*R*)-**23** *exo*-(2*R*)-**42** *exo*-(2*S*)-**42**

The methyl ester **23** distilled from the reaction described above was directly assayed for endo–exo selectivity and for enantioselectivity by chiral GC on a J & W Cyclodex-B capillary column (part #1122532, ser. #5094942) of 0.25 mm i.d., 0.25 mm film thickness, and 30 m in length, and with column temperature 90 °C (isothermal). The oven was baked at 200 °C a few minutes before each run, which improved GC peak resolution. Under these conditions, the following retention times were observed: (*2S*)-**23** (16.43 min), (*2R*)-**23** (15.90 min), **42** (12.79 and 12.98 min, not assigned). It was previously shown that (*S*)-VAPOL gives selectively the *endo*-(*2S*) isomer of **23** (4).

Acknowledgment

This work was supported by National Insitute of Health (NIH) Grant GM 63019.

References

1. J.M. Brunel. Chem. Rev. **105**, 857 (2005)
2. (*a*) L. Pu. Chem. Rev. **98**, 2405 (1998); (*b*) P. Kocovsky, S. Vyskocil, and M. Smrcina. Chem. Rev. **103**, 3213 (2003); (*c*) Y. Chen, S. Yekta, and A.K. Yudin. Chem. Rev. **103**, 3155 (2003).
3. J. Bao, W.D. Wulff, J.D. Dominy, M.J. Fumo, E.B. Grant, A.C. Rob, M.C. Whitcomb, S. Yeung, R.L. Ostrander, and A. Rheingold. J. Am. Chem. Soc. **118**, 3392 (1996).
4. (*a*) J. Bao, W.D. Wulff, and A.L. Rheingold. J. Am. Chem. Soc. **115**, 3814 (1993); (*b*) J. Bao and W.D. Wulff. Tetrahedron Lett. **36**, 3321 (1995); (*c*) D.P. Heller, D.R. Goldberg, and W.D. Wulff. J. Am. Chem. Soc. **119**, 10551 (1997).
5. (*a*) J.C. Antilla and W.D. Wulff. J. Am. Chem. Soc. **121**, 5099 (1999); (*b*) J. Antilla and W.D. Wulff. Angew. Chem. Int. Ed. **39**, 4518 (2000); (*c*) C. Loncaric and W.D. Wulff. Org. Lett. **3**, 3675 (2001); (*d*) A.P. Patwardhan, V.R. Pulgam, Y. Zhang, and W.D. Wulff. Angew. Chem. Int. Ed. **44**, 6169 (2005).
6. S. Xue, S. Yu, Y.-H. Deng, and W.D Wulff. Angew. Chem. Int. Ed. **40**, 2271 (2001).
7. C. Bolm, J. Frison, Y. Zhang, and W.D. Wulff. Synlett, 1619 (2004).
8. G.B. Rowland, H. Zhang, E.B. Rowland, S. Chennamadhavuni, Y. Wang, and J.C. Antilla. J. Am. Chem. Soc. **127**, 15696 (2005).
9. E. Napolitano, R. Fiaschi, and E. Mastrorilli. Synthesis, 122 (1986).
10. W.D. Wulff, B.M. Bax, T.A. Brandvold, K.S. Chan, A.M. Gilbert, R.P. Hsung, J. Mitchell, and J. Clardy. Organometallics, **13**, 102 (1994).
11. M. Smrcina, M. Lorenc, V. Hanus, P. Sedmera, and P. Kocovsky. J. Org. Chem. **57**, 1917 (1992).
12. Y. Zhang, S.-M. Yeung, H. Wu, D.P. Heller, C. Wu, and W.D. Wulff. Org. Lett. **5**, 1813 (2003).
13. M. Kumada, K. Tamao, and K. Sumitani. Org. Syn. Coll. Vol. VI. 409 (1988).
14. N. Miyaura, T. Yanagi, and A. Suzuki. Synth. Commun. **11**, 513 (1981).
15. For recent examples and reviews, see: (*a*) A.M. Costa, C. Garcia, P.J. Carroll, and P.J. Walsh. Tetrahedron, **61**, 6442 (2005); (*b*) B.M. Trost, A. Fettes, and B.T. Shireman. J. Am. Chem. Soc. **126**, 2660 (2004); (*c*) M.H. Todd. Chem. Soc. Rev. **31**, 211 (2002).
16. M.S. Newman and S. Seshadri. J. Org. Chem. **27**, 76 (1962).
17. W. Brackman and P.J. Smit. Recl. Trav. Chim. Pays–Bas, **85**, 857 (1966).
18. W.J. Thompson and J. Gaudino. Org. Chem. **49**, 5237 (1984).
19. J.M. Mellor and C.F. Webb. J. Chem. Soc. Perkin Trans. 2, 17 (1974).
20. F. Furuta, S. Shimizu, Y. Miwa, and H. Yamamoto. J. Org. Chem. **54**, 1483 (1989).

© 2006 NRC Canada

BIOGRAPHY / BIOGRAPHIE

Born in Vienna, Alfred Bader fled to England at the age of fourteen, ten months before the outbreak of World War II. Although a Jewish refugee from the Nazis, he was interned in 1940 along with other 'enemy aliens', and sent to a Canadian prisoner of war camp.

Today, Dr. Bader is one of the most respected men in his field. In this heartwarming book, he tell the fascinating story of how he made good in the land of opportunity, the United States.

It was a case of hard study and hard work. Obtaining release in 1941, he was accepted at Queen's University in Kingston, Ontario, where he studied engineering chemistry. There followed a fellowship in organic chemistry at Harvard. He worked in Milwaukee as a research chemist for the Pittsburgh Plate Glass Company and in 1951 co-founded Aldrich, which today, as Sigma-Aldrich, is the world's largest supplier of research chemicals.

He spent forty years building Aldrich's distinctive reputation and the extraordinary story of how he was eventually thrown off the board of Sigma-Aldrich will be of key interest to people in the chemical industry worldwide, as well as to students of business.

After leaving Sigma-Aldrich, he continued a fruitful career as an art collector and dealer, and he has some very pertinent and amusing things to say about his experiences in the art world.

Alfred Bader and his family have earned a reputation as generous benefactors, notably in the fields of chemistry, education, and Jewish interests. Dr. Bader's personal philanthropy has been particularly directed towards helping students of chemistry and art history. He recently gave £6,000,000 to Queen's University to purchase and renovate Herstmonceux Castle in Sussex (the home of the old Royal Greenwich Observatory) – one more 'thank you' to the Canadian institution that had enabled him to take the first step on the road to success, so entertainly described in this book.

(Alfred Bader, Adventures of a Chemist Collector. Weidenfeld & Nicolson, London, 1995)

Né à Vienne, Alfred Bader s'enfuit en Angleterre à l'âge de 14 ans, dix mois avant qu'éclate la Seconde Guerre mondiale. Réfugié juif des nazis, il est quand même interné en 1940 avec d'autres « ressortissants de pays ennemis » et déporté au Canada dans un camp de prisonniers de guerre.

Aujourd'hui, Bader figure parmi les plus respectés de son domaine. Dans ce récit attachant et émouvant, il retrace les événements qui lui ont permis de faire sa marque dans un pays d'avenir, les États-Unis.

C'est l'histoire d'un solide engagement envers les études et de persévérance. Libéré en 1941, il étudie le génie chimique à l'Université Queen's. Il fait un stage postdoctoral en chimie organique à Harvard. Il travaille à Milwaukee à titre de chimiste de recherche pour la *Pittsburgh Plate Glass Company*. En 1951, il cofonde l'*Aldrich Chemical Company*, aujourd'hui la *Sigma-Aldrich Corporation*, le plus important fournisseur de substances chimiques employées dans la recherche du monde entier.

Malgré le fait qu'il consacre quarante ans de sa vie à cultiver la réputation d'excellence d'Aldrich, il se fait exclure du conseil de Sigma-Aldrich, une histoire qui est sfre d'intéresser tous les intervenants de l'industrie, sans compter les étudiants en administration.

Il quitte donc Sigma-Aldrich pour poursuivre une carrière fructueuse en tant que collectionneur et marchand d'Éuvres d'art. Il a d'ailleurs des anecdotes fort amusantes et très pertinentes à raconter à propos de ses expériences dans l'univers des arts.

La très grande réputation de bienfaisance et de bonté d'Alfred Bader et de sa famille, notamment au profit de la chimie, de la pédagogie et de la culture juive, n'est plus à démontrer. Parmi les plus importants bénéficiaires de leur générosité figurent les étudiants en chimie et en histoire de l'art. Un autre grand bénéficiaire de la philanthropie des Bader est l'Université Queen's, qui s'est vu remettre la somme de 6 000 000 £ pour acquérir et rénover le château Herstmonceux, B Sussex (le site de l'Observatoire royal de Greenwich) – une autre façon de « remercier » l'établissement canadien qui lui a permis de faire un premier pas vers la réussite, tel que décrit de manière si divertissante dans cet ouvrage.

(Alfred Bader, Adventures of a Chemist Collector. Weidenfeld & Nicolson, Londres, 1995)

© 2006 NRC Canada

Unwrapped

for Alfred Bader and a city

by Roald Hoffmann

I didn't expect
to receive it
watching "The Third

Man," to hear it
in Anna's schmal-
tzy lines, in her

black and white walk
down the allée. No,
it would have made

more sense for it
to surface in
the angle of cut

of the vines still
strapped to wires.
Or at night. But

if one is in-
clined to sadness,
it plain takes over --

like an arch, all
of-a-sudden
perceived as off-

center, like the
leaping buck in
my lights. Until...

you realize you
have been granted
a gift, the salty,

loosening gift
of the road in
to the father -

no chance, then,
to mourn; the
time rending

gift, Vienna, her;
The gift I wish
would pass from me.

Can. J. Chem. Downloaded from www.nrcresearchpress.com by Renmin University of China on 09/13/12
For personal use only.

© 2006 NRC Canada

TRIBUTE / HOMMAGE

It is a great privilege and honour for us to write the dedication for this Special Issue honouring Alfred Bader. Alfred Bader, a true visionary, has had a profound effect on the way chemists do research. But Alfred Bader's influence is much broader than chemistry as he is an entrepreneur, businessman, art collector, Rembrandt expert, and philanthropist.

Throughout his childhood and teenage years Alfred faced great adversity. He was born in Vienna in 1924 and two weeks after his birth, his father died. In November 1938 following the anti-Jewish demonstrations on Kristallnacht, Alfred's mother sent him to the U.K. He lived in Sussex and entered Brighton Technical College in 1939. In May 1940, the British government, given the escalating conflict with Germany, arrested German and Austrian males including Alfred and put them in internment camps. The Canadian government agreed to accept custody of some of the interned individuals comprising prisoners of war and strongly anti-Nazi refugees as well as German civilians. Alfred Bader was one of those interned in Canada and was sent to a fortress on an island on the Richelieu River near Lake Champlain. While there, he and some others were determined to continue their education and Alfred passed both the Junior and Senior Matriculation exams before being released in 1941. Bader applied to several universities and was accepted by Queen's University in Kingston. Alfred enjoyed his studies at Queen's and to earn money to continue university and go on dates, he worked at Murphy Paint Company in Montreal on the formulation of enamels and lacquers. There, he also learned to appreciate industry and entrepreneurship.

Bader recognized the need for a research chemicals business while he was a graduate student at Harvard working with Louis Fieser, a leading organic chemist. At that time nearly all chemicals came from Eastman Kodak, which had a product list of 4000 chemicals. Although others tried to discourage him, Alfred persevered and together with a friend, Milwaukee attorney Jack Eisendrath, incorporated Aldrich Chemical Company on August 17, 1951, each putting up $250. The first home of Aldrich was a garage they rented for $25 per month. They were two part-time employees, their catalogue was a mimeographed sheet with one offering, and sales in the first year was $1705.

The company moved to 1000 square feet of rented space where Bader single handedly carried out all the syntheses. In 1955 Aldrich expanded into medicinal chemistry, which gave Alfred tremendous satisfaction. Alfred's hard work and determination paid off and by 1958 they had a staff of 12 and purchased a three-story building. What was so impressive was the commitment by Alfred to deliver chemicals in a highly efficient manner. It was clear by then that Bader's vision and integrity coupled with his determination and dedication would lead to a highly successful career.

The company continued to grow at a tremendous rate and by 1962 had sales of one million dollars, up from $5,400 a decade earlier. In 1990, Aldrich merged with Sigma to become Sigma-Aldrich, the 80th largest corporation in the US, employing over 4,000 people with subsidiaries in many European countries, Israel, and Japan. After serving as Chair of the Board from 1980 to 1991 he "officially retired" but became chairman emeritus.

One of Bader's key recommendations to those building a business is "listen carefully to your customers". This personal approach was the cornerstone of Alfred's success. The trademark Aldrich advertisement had a picture of Alfred with the heading "Please Bother Us". He and his wife Isabel travelled tirelessly to laboratories throughout North America and around the world where he listened attentively to problems chemists were having with syntheses and offering advice and proposing solutions. Bader comments in his book *Adventures of a Chemist Collector* "Although all of our visits to universities begin in the hope of getting to know our customers and perhaps finding exciting new compounds, they often become pure personal pleasure for Isabel and me". My (Anne's) first encounter with Alfred Bader was in 1966, discussing with him over breakfast in the Windsor Hotel in Montreal, the possibility of making a diazo compound in larger quantities than the few mg I had amassed after a lengthy process. The research went in another direction and Aldrich did not make the compound but I will never forget my first meeting with Alfred and Howard's and my good fortune in getting to know Alfred and Isabel in the years following.

Bader's vision and accomplishments go far beyond chemistry and the chemicals business. Bader calls himself an "inveterate collector" beginning with stamps at 8, drawings at 10, and paintings at 20. When Alfred was a child in Vienna his mother's apartment was filled with paintings, 19th and 20th century Viennese works. He knew he did not like these but became very interested in painting. Bader has been buying selling, trading, and giving away paintings for many years. When Aldrich was on a firm footing and he could give a little more time to what he calls an enjoyable pastime, he established Alfred Bader Fine Arts and since 1992 has devoted more and more of his time to it. Although he now trades in very expensive art including works by Rembrandt and Rubens, he always considered it much more fun to pay a few thousand dollars for a work that might prove great and valuable after cleaning. He loves discoveries not only of material value but also of great beauty. Bader has shared his love of paintings with others. On his visits to universities and at every Aldrich exhibit booth, he distributed prints of some of the paintings in his vast collection. Chemists will remember the Alchemist well and each year a painting appeared on the cover of the Aldrich catalog. He thus served a very important role in art appreciation for the chemical community

In addition to Bader's impact on chemistry and his contributions to art collecting, art history, and art conservation, his generosity of spirit will leave a lasting impact. He gives back to the discipline of chemistry, to Queen's University that accepted him when other universities did not, and to other institutions and foundations. It started with small no strings attached grants to chemists in need of funding around the world. Many of these have become internationally recognized scientists. He has established prizes, scholarships, and awards for students in Canada, the United States, Britain, and the Czech Republic recalling the benefit such awards provided him when he was a student. He established the Alfred Bader Award in Organic Chemistry for the American Chemical Society (now known as the Aldrich award) and the Canadian Society for Chemistry and the Royal Society of Chemistry in the UK. More recently he endowed the ACS Alfred Bader Award in Bioinorganic or Bioorganic Chemistry and supported the ACS Project Seed to enable undergraduate chemistry students to experience laboratory work.

© 2006 NRC Canada

Bader's donations to Queen's have included: Chairs in Organic Chemistry and Art History, outstanding paintings from his collection for the Agnes Etherington Art Centre, and seed money for a new museum. Bader Lane at Queen's connects the Chemistry Building with the Agnes Etherington Art Centre. Perhaps the most unusual gift to Queen's has been Herstmonceux Castle, a moated castle in Sussex England parts of which date from the 15th century. In addition, Bader has supported many Jewish educational projects and set up charitable foundations in Milwaukee.

Alfred Bader has been recognized for his work by a number of Honorary Doctorates from different universities including Simon Fraser University and the University of Ottawa, an honorary Fellowship in the Royal Society of Chemistry, and the ACS Charles Lathrop Parsons Award, given in recognition of outstanding public service by a member of the ACS. He is also a Honorary Fellow of the Chemical Institute of Canada.

Another facet of Alfred, and Isabel, is their remarkably intense romantic relationship. Several years ago, a new book was published by Isabel entitled "A Canadian in Love". It contains some beautifully composed letters by Isabel to Alfred and at the end of the book, a letter from Alfred to Isabel dated April 18, 1975. One paragraph in the letter states:

"You had not written to me from September 11, 1950 until August 11, 1951, your last letter to me for 24 years. I have read that letter so often that I know it by heart and it has torn me apart these many years. What power you have over me! Your last words to me were "God bless you, Alf" and of course you meant this with all your heart. And God has indeed blessed me by giving me you as a beacon in my life. Whatever important I have done, I have thought of you, and done the right thing. As David said-"Whither shall I go from your spirit, or whither shall I flee from your presence? If I ascend into heaven, you are there, and if I make my bed in hell, behold, you are there". All of us have part of God in us, and the great goodness in you is so plain to me".

Following his retirement from Aldrich, Alfred was able to devote nearly all his time and energy to his activities as an art collector, lecturer, and philanthropist. Alfred says that getting to know people involved in art has enriched his life. Those of us who have been fortunate to know Alfred have had our lives enriched by him.

Anne Alper
Howard Alper

© 2006 NRC Canada

TRIBUTE / HOMMAGE

Nous sommes extrêmement privilégiés et honorés de rédiger la dédicace du présent numéro spécial de la Revue, qui rend hommage à Alfred Bader. Véritable visionnaire, Alfred Bader a certes profondément transformé la façon dont les chimistes réalisent aujourd'hui leurs recherches, mais son influence s'étend beaucoup plus loin puisqu'il est aussi un entrepreneur, un homme d'affaires, un collectionneur d'œuvres d'art, un spécialiste de Rembrandt et un philanthrope.

L'enfance et l'adolescence d'Alfred ont été marquées par l'adversité. Alfred est né à Vienne, en 1924; deux semaines après sa naissance, son père est décédé. En novembre 1938, dans le sillage de la campagne antisémite « Nuit de Cristal », la mère d'Alfred a envoyé son fils au Royaume-Uni. Là-bas, il a vécu au Sussex et est entré au Brighton Technical College en 1939. En mai 1940, aux prises avec un conflit grandissant avec l'Allemagne, le gouvernement britannique a fait arrêter tous les hommes allemands et autrichiens, y compris Alfred, et les a fait placer dans des camps d'internement. Le gouvernement du Canada a accepté de prendre à sa charge quelques-uns de ces détenus, principalement des prisonniers de guerre, des réfugiés antinazis et des civils allemands : c'est ainsi qu'Alfred Bader a été envoyé au Canada, plus précisément dans une forteresse sur une île de la rivière Richelieu, près du lac Champlain. Malgré cet internement, Alfred et quelques autres détenus étaient déterminés à poursuivre leurs études et Alfred est arrivé à obtenir son immatriculation junior et son immatriculation senior avant sa libération, en 1941. Alfred a frappé à la porte de plusieurs universités avant d'être accepté à l'Université Queen's, à Kingston, où il a vécu des jours heureux. Pour financer la poursuite de ses études et ses rendez-vous galants, il a travaillé pour la Murphy Paint Company, à Montréal, où il planchait sur la formulation de peintures-émail et de peintures-laque. C'est auprès de cette société qu'il a nourri un intérêt pour l'industrie et l'entrepreneuriat.

Tandis qu'il était étudiant de troisième cycle à l'Université Harvard, sous la direction de Louis Fieser, chimiste organicien réputé, Alfred a pris conscience de la nécessité de fonder une entreprise de production de produits chimiques spécialisée en recherche. À l'époque, presque tous les produits chimiques provenaient de la société Eastman Kodak, dont le catalogue recensait quelque 4 000 substances. Bien que plusieurs de ses pairs aient tenté de l'en dissuader, Alfred a constitué l'Aldrich Chemical Company le 17 août 1951, avec son ami Jack Eisendrath, un avocat du Milwaukee, chacun ayant investi 250 $ dans le projet. À ses débuts, Aldrich occupait un garage loué à 25 $ par mois; la société comptait deux employés à temps partiel et son catalogue se bornait à une page polycopiée. Ses ventes se sont chiffrées à 1 705 $ la première année.

La société a subséquemment déménagé dans des locaux loués de 1 000 pieds carrés, où Alfred réalisait à lui seul toutes les synthèses. En 1955, Aldrich a étendu ses activités aux produits chimiques médicinaux, ce qui a particulièrement ravi Alfred. L'ardeur et la détermination d'Alfred ont porté fruit et, en 1958, sa société, qui employait 12 personnes, s'est enfin installée dans son propre édifice de trois étages. Une qualité particulièrement admirable chez Alfred était son engagement à fournir des produits chimiques dans la plus grande efficacité. On voyait déjà dans son acuité et son intégrité, conjuguées à sa détermination et à son dévouement, les signes annonciateurs d'une carrière remarquable.

La société a poursuivi son ascension et, en 1962, ses ventes ont atteint le million de dollars, bien loin des 5 400 $ de dix ans auparavant. En 1990, Aldrich a fusionné avec Sigma et est devenue Sigma-Aldrich, la 80e plus importante société américaine, forte de 4 000 effectifs et de filiales dans de nombreux pays d'Europe, en Israël et au Japon. Après avoir occupé la présidence du conseil d'administration de la société de 1980 à 1991, Alfred a « officiellement pris sa retraite », mais est toutefois demeuré président émérite.

Un des principaux conseils qu'Alfred se plaisait à donner aux nouveaux entrepreneurs était le suivant : « Écoutez attentivement vos clients. » Cette attitude était la clé de voûte de son succès. D'ailleurs, toute la publicité d'Aldrich arborait une photo d'Alfred au-dessus de laquelle figurait la phrase « Prière de déranger ». Lui et sa conjointe, Isabel, voyageaient sans relâche d'un laboratoire à l'autre, en Amérique du Nord et partout dans le monde, et Alfred écoutait attentivement les difficultés qu'éprouvaient les chimistes en matière de synthèse, puis leur livrait des conseils ou leur proposait des solutions. Dans son autobiographie *Adventures of a Chemist Collector*, il déclarait : « Bien que toutes nos visites dans les universités soient mues par le désir de mieux connaître nos clients et, peut-être, de découvrir de nouveaux composés prometteurs, elles aboutissent souvent à une délicieuse expérience personnelle pour Isabel et pour moi. » Mon premier contact avec Alfred Bader [c'est Anne qui parle] remonte à 1966, à l'hôtel Windsor de Montréal. À l'occasion d'un petit déjeuner, je m'entretenais avec lui de la possibilité d'accroître ma production actuelle d'un composé diazoïque – à peine quelques milligrammes à la suite d'un long procédé. Les recherches ont pris un autre cours et Aldrich n'est jamais revenu sur la question, mais je n'oublierai jamais notre première rencontre avec Alfred, à Howard et à moi, et la chance qui m'a été donnée de côtoyer ultérieurement Alfred et Isabel au cours des années qui ont suivi.

Le talent et les réalisations d'Alfred vont bien au-delà de la chimie et du commerce des produits chimiques. Alfred se dit un « collectionneur invétéré » : son parcours a commencé avec les timbres, à l'âge de 8 ans, puis s'est poursuivi avec les étampes, à l'âge de 10 ans, et enfin avec les tableaux, à l'âge de 20 ans. Lorsqu'Alfred était enfant, à Vienne, l'appartement de sa mère regorgeait de tableaux, principalement d'œuvres viennoises des XIXe et XXe siècles. Bien que ces écoles ne l'aient pas particulièrement séduit, la peinture a fait vibrer une corde sensible chez lui. Alfred fait le commerce et le don de tableaux depuis nombre d'années. Une fois qu'Aldrich eut été bien établie et qu'il eut davantage de temps à consacrer à ce qu'il estime être un joli passe-temps, Alfred a fondé Alfred Bader Fine Arts et, depuis 1992, il s'emploie de plus en plus à cette activité. Bien qu'il gravite dans les hautes sphères du commerce des œuvres d'art, notamment celui des tableaux de grands maîtres, tels que Rembrandt et Rubens, Alfred tire énormément de plaisir à ne payer que quelques milliers de dollars pour une œuvre d'art qui, au prix de quelques efforts de restauration, est appelée à devenir un objet de grande valeur. C'est non seulement le caractère monnayable des œuvres d'art qui l'anime, mais aussi leur caractère esthétique. Alfred n'hésite jamais à partager son amour de la peinture. Lors de ses visites dans les universités et à tous les

© 2006 NRC Canada

kiosques aménagés par Aldrich, il distribuait des représentations de tableaux tirés de sa vaste collection. Les chimistes ne sauront oublier l'*Alchimiste* et, chaque année, un tableau faisait la page couverture du catalogue d'Aldrich. Alfred a de ce fait beaucoup contribué à l'« éducation artistique » de la collectivité de la chimie.

En plus de ses contributions à la chimie, à la collection et la conservation d'œuvres d'art et à l'enrichissement de l'histoire de l'art, Alfred a fait preuve d'une vaste générosité qui laissera une empreinte indélébile. En effet, il est prodigue avec les membres de la collectivité de la chimie, avec l'Université Queen's, qui lui a ouvert ses portes alors que les autres universités l'avaient repoussé, ainsi qu'avec d'autres institutions et fondations. Tout a commencé par de petites subventions sans condition destinées aux chimistes du monde entier en manque de financement; plusieurs de ces chimistes sont devenus des scientifiques réputés à l'échelle internationale. Alfred a impulsé la création de primes, de bourses et de prix pour les étudiants du Canada, des États-Unis, de la Grande-Bretagne et de la République tchèque, étant reconnaissant de l'aide que de tels appuis financiers lui avaient procurée quand il était lui-même étudiant. Il est le père du prix de chimie organique Alfred Bader de la American Chemical Society (aussi connu sous le nom « Prix Aldrich ») de même que d'autres prix éponymes de la Société canadienne de chimie et de la Royal Society of Chemistry du Royaume-Uni. Plus récemment, il a fondé le prix de chimie bio-inorganique et bio-organique Alfred Bader de l'ACS et financé la fondation de démarrage de l'ACS, qui permet aux étudiants de chimie de premier cycle de se familiariser avec le travail de laboratoire.

Alfred a fait de nombreux dons à l'Université Queen's, dont une chaire en chimie organique, une chaire en histoire de l'art, de superbes tableaux de sa collection privée destinés à l'Agnes Etherington Art Centre et du financement de lancement d'un nouveau musée. (Au fait, la voie Bader, sur le campus de l'Université Queen's, relie la faculté de chimie et l'Agnes Etherington Art Centre). Le don le plus original fait par Alfred à l'Université Queen's est sans contredit le château de Herstmonceux, dans le comté de Sussex, en Angleterre, dont certaines sections datent du XVe siècle. Par ailleurs, Alfred a appuyé plusieurs projets éducatifs pour la communauté juive et a mis sur pied des organisations caritatives à Milwaukee.

Les contributions d'Alfred Bader ont été soulignées par des doctorats honorifiques de plusieurs universités, y compris l'Université Simon Fraser et l'Université d'Ottawa; par un honorariat de la Royal Society of Chemistry de même que par le prix Charles Lathrop Parsons de l'ACS, soulignant l'indéfectible engagement d'un membre de l'ACS au bien public. Alfred est également membre honoraire de l'Institut de chimie du Canada.

Un autre admirable trait d'Alfred et de sa conjointe est leur profonde tendresse l'un pour l'autre. Il y a quelques années, Isabel a publié l'ouvrage, *A Canadian in Love*, dans lequel elle citait de magnifiques lettres qu'elle avait adressées à Alfred. On y retrouvait aussi, en toute fin, une lettre qu'Alfred lui avait écrite le 18 avril 1975. Nous nous permettons d'en traduire un paragraphe :

« Tu ne m'as pas écrit du 11 septembre 1950 au 11 août 1951, ta dernière lettre depuis 24 ans. J'ai tant lu et relu ce mot que je le connais par cœur et cela me bouleverse depuis tout ce temps. Quelle emprise tu as sur moi! Les derniers mots que tu m'as adressés étaient "Que Dieu te bénisse, Alf". Cette imploration, je le savais, venait du creux de ton âme. Et Dieu m'a certes béni en faisant de toi la lumière de ma vie. Tous mes accomplissements, je les sais justes, car continuellement inspirés de toi. Comme l'a dit David "Où irais-je loin de ton esprit; et où fuirais-je loin de ta face? Si je monte aux cieux, tu y es; si je me couche au séjour des morts, t'y voilà." Dieu est présent en chacun de nous et, chez toi, Sa Bonté m'apparaît flagrante. »

Après avoir tiré sa révérence à Aldrich, Alfred a pu consacrer presque tout son temps et son énergie à la collection d'œuvres d'art, à la présentation de conférences et à des activités philanthropiques. Il estime que le fait d'avoir forgé des rapports avec la communauté des arts a enrichi sa vie. Ceux d'entre nous qui ont eu la chance de forger des rapports avec Alfred peuvent aussi affirmer que leur vie en a été enrichie.

Anne Alper
Howard Alper

© 2006 NRC Canada

AWARD LECTURE / CONFÉRENCE D'HONNEUR

Montreal Medal Award Lecture — Coordination chemistry of molecular bowls: Ligands and their complexes derived from resorcinarenes[1]

Richard J. Puddephatt

Abstract: A review is given of the design, synthesis, structures, and properties of octadentate or tetradentate ligands and their coordination compounds, based on the bowl-like resorcinarene skeleton.

Key words: resorcinarene, coordination, phosphine, thiophosphinate, polymer.

Résumé : On présente une revue du développement, de la synthèse, des structures et des propriétés de ligands octadentates ou tétradentates et de leurs composés de coordination apparentés au squelette de résorcinarène qui a la forme d'un bol.

Mots clés : résorcinarène, coordination, phosphine, thiophosphinate, polymère.

[Traduit par la Rédaction]

Introduction

Calixarenes and resorcinarenes (Chart 1) are bowl-shaped molecules that have a rich host–guest chemistry. Consequently, they have potential uses in sensors, catalysts, and in selective separation or extraction processes (1). Chart 1 shows the molecules in flat projection (above) and in the cone conformation (below).

For many potential applications of the molecular bowls, it is advantageous to decorate the lower or upper rim with extra functional groups. If these functional groups can bind metals, an extensive coordination chemistry can be developed (2, 3). The parent calixarenes (Chart 1) can bind metal ions through the oxygen atoms or through the arene groups, but a much greater variety of donor groups can be added by derivatization. Some examples of metal complexes with ligands derived from calixarenes are shown in Chart 2 (4). Chart 2 shows a silver(I) ion bound directly to atoms of the calixarene skeleton and linear gold(I) or square planar platinum(II) centres bound to appended diphenylphosphinite or alkynyl donor groups (4).

The chemistry of complexes derived from calixarenes is extensive and has been well reviewed (1–4). The coordination chemistry of ligands, and their metal complexes, derived from resorcinarenes is developing rapidly and will be the subject of this review. Because this is primarily a review of work carried out in the author's research group, the important contributions to this area of research from other groups cannot be described adequately. However, some recent references are cited for the interested reader (1, 5–13).

Received 2 September 2006. Accepted 27 September 2006. Published on the NRC Research Press Web site at http://canjchem.nrc.ca on 23 November 2006.

R.J. Puddephatt. Department of Chemistry, University of Western Ontario, London, ON N6A 5B7, Canada, (e-mail: pudd@uwo.ca).

[1]This article is an expanded form of a section of the Montreal Medal award lecture, given in Halifax, Nova Scotia, in May 2006.

Resorcinarene ligands with eight donor groups

The hydroxyl groups of a resorcinarene **1** (Scheme 1, R = CH_2CH_2Ph) can be converted to phosphorus-donor diphenylphosphinite groups by the reaction with diphenylchlorophosphine and a base. Ligands of type **2** can be regarded as octopus-like, with the resorcinarene skeleton as the body and the diphenylphosphinite groups as the arms. Ligand **2** phosphorus-donors can then bind eight gold(I) centers in **3** or, by acting as a tetra(bidentate) ligand, it can bind four platinum(II) centres in complex **4** (Scheme 1) (14). Comparing Scheme 1 with Charts 1 and 2, it is clear that calixarenes and resorcinarenes are naturally functionalized at the lower and upper rims of the bowl, respectively. The octa(diphenylphosphinito) ligands are sterically congested, and thus, no host–guest chemistry has been established (14).

Similarly, the resorcinarene **1** can be converted to the octapropargyl derivative **5** (Scheme 2). Ligand **5** provides a route to the octopus-like organometallic derivatives. Thus, the alkyne units can be deprotonated and act as σ-alkynyl ligands in forming the octagold(I) derivative **6** (Scheme 2). Alternatively, the alkynes can act as π-donor ligands in reactions with dicobalt octacarbonyl to give the derivative **7**, which contains sixteen cobalt atoms (15).

Complex **7** is the most highly metallated resorcinarene complex known, and its sterically congested structure is shown in Fig. 1. The complex adopts a boat conformation of

 doi:10.1139/V06-155 © 2006 NRC Canada

Chart 1.

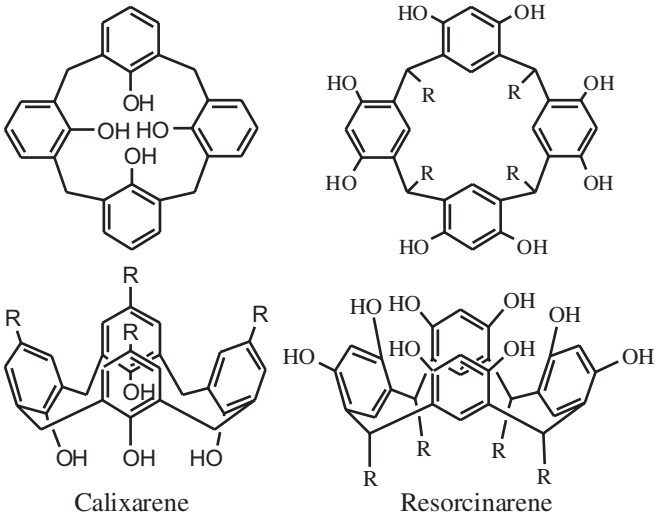
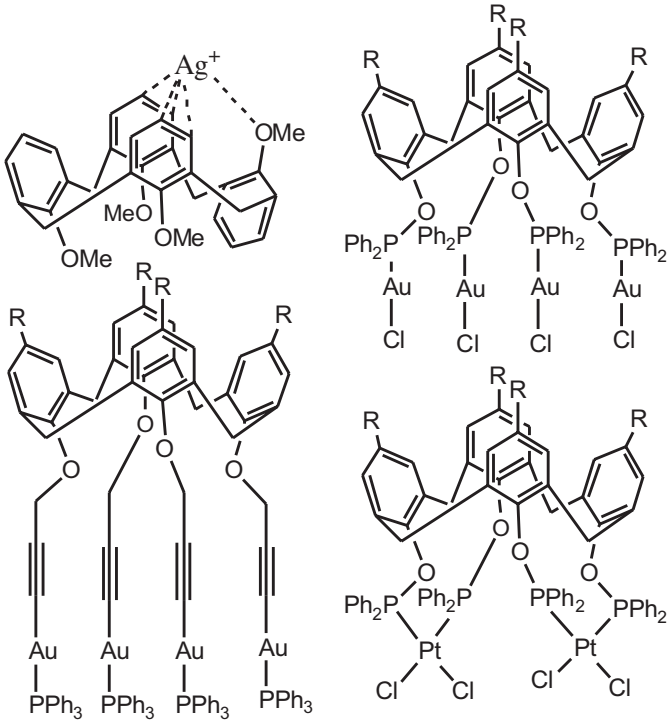


Chart 2.

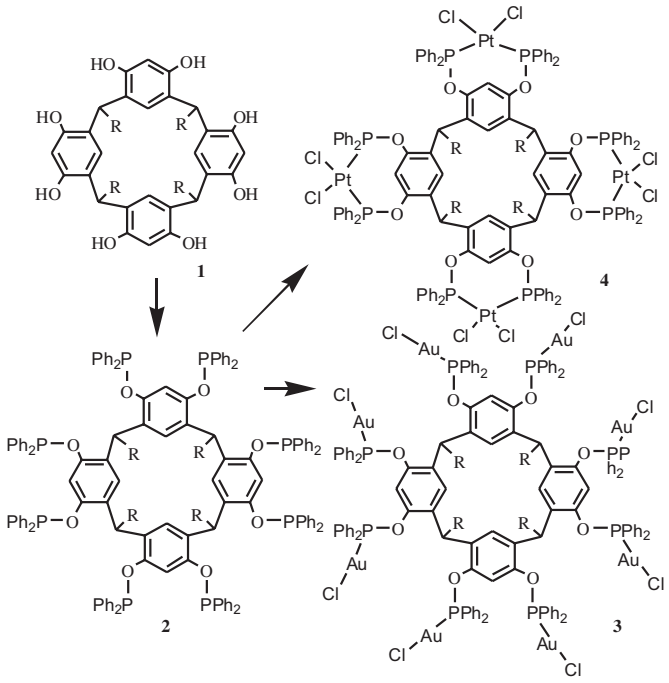


the resorcinarene core in which two opposite aryl rings are flattened to reduce the steric congestion around the upper rim of the original bowl. There is an activation energy in dichloromethane solution of 51 kJ mol^{-1} for the interconversion of the flattened and upright arene rings of complex **7**, as determined by variable temperature NMR of the fluxional complex (15).

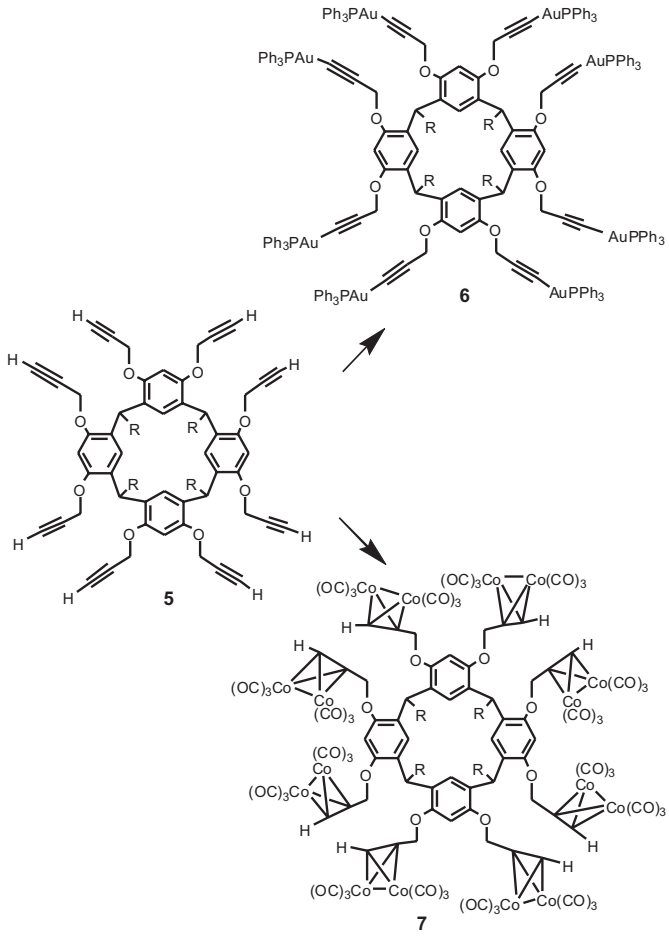
Resorcinarene ligands with four phenylphosphonite groups

The reaction of resorcinarene **1** with phenyldichlorophosphine gave the tetrakis(phenylphosphonite) ligand **8** (Scheme 3) (14, 16). The scheme shows the ligand both in flat projection (left) and in the cone conformation

Scheme 1.

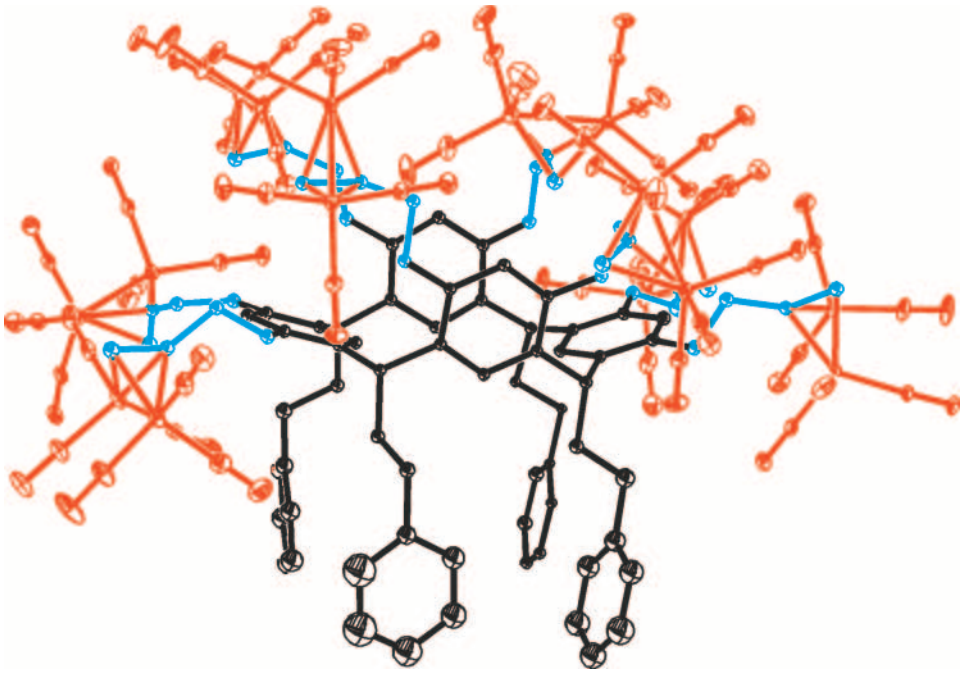


Scheme 2.

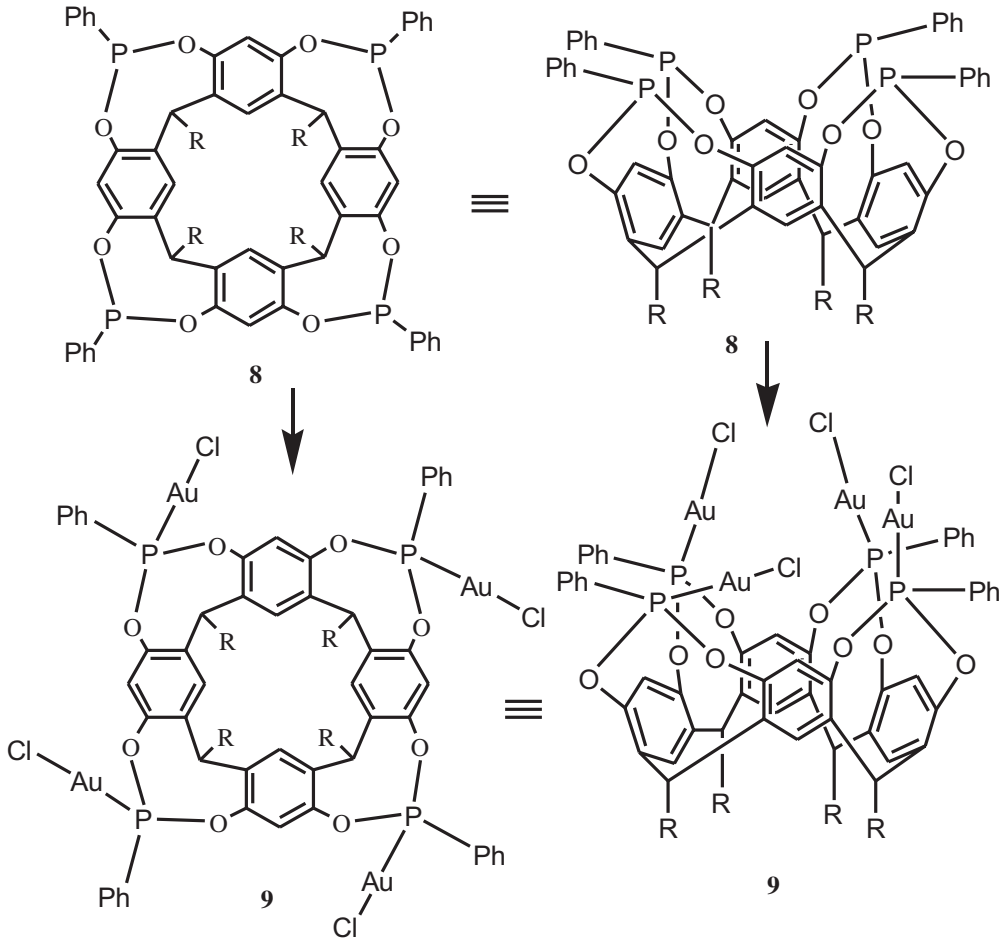


© 2006 NRC Canada

Fig. 1. Structure of the 16-cobalt complex **7**. The propargyloxy groups are shown in blue and the $Co_2(CO)_6$ groups are in red.

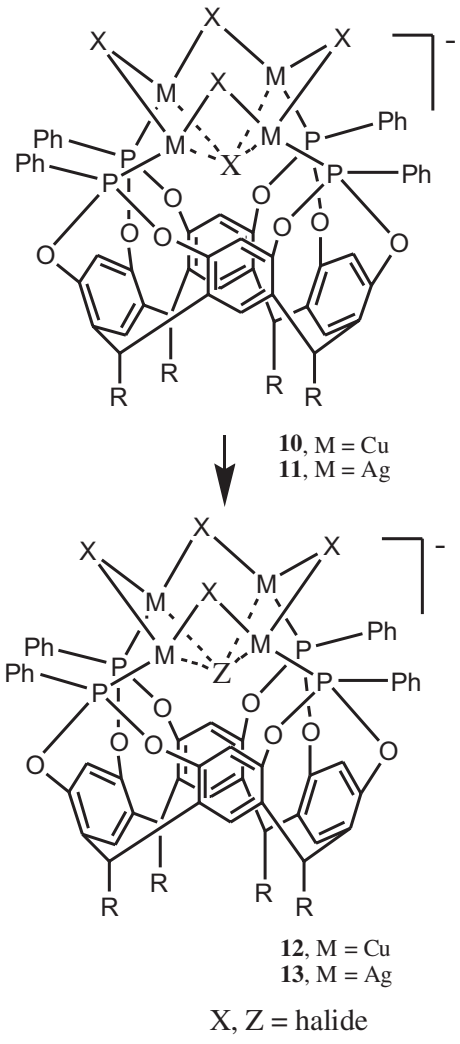


Scheme 3.



© 2006 NRC Canada

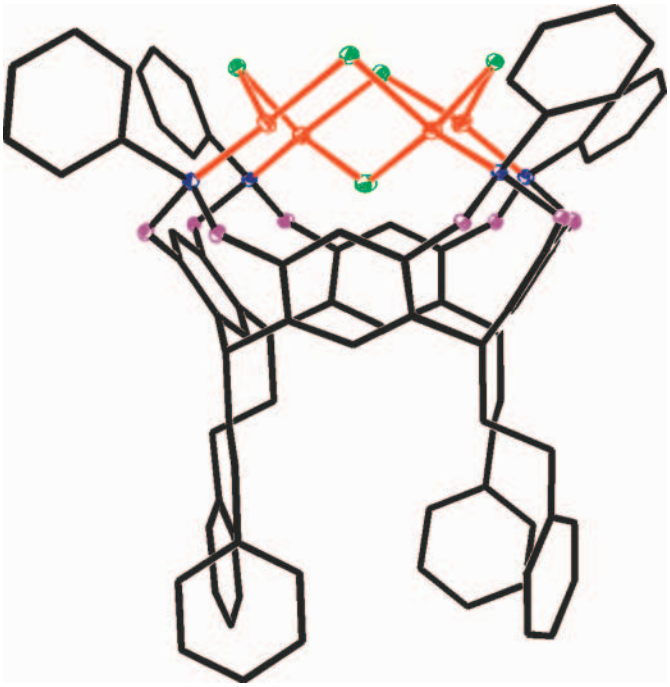
Scheme 4.



(right), which is imposed by the bridging phosphorus atoms. In addition, the ligand **8** adopts a conformation with all phenyl groups directed outwards and all lone pairs on phosphorus directed inwards. When ligand **8** reacts with [AuCl(SMe_2)], the tetragold(I) complex **9** is formed in which three of the AuCl units are directed upwards, extending the depth of the bowl, while the fourth AuCl unit is directed towards the centre of the bowl, occupying the cavity (14, 16). This fourth AuCl unit seems able to move out of the cavity to allow guest molecules, such as primary amines, to enter (14).

The reaction of the tetraphosphonite ligand **8** with precursors to copper(I) or silver(I) halides gave the unusual anionic complexes **10** or **11** (Scheme 4, X = Cl, Br, or I). These complexes contain an $M_4(\mu\text{-}X)_4$ crown unit (M = Cu or Ag) with a more weakly bound halide ion in the centre of the resorcinarene bowl. When X = Cl and M = Cu, the "guest" halide is too small to bind effectively to all copper atoms and tends to bind to two or three copper(I) centres while moving easily among them all. A view of one such complex, in which the guest chloride binds to two copper(I) centres, is shown in Fig. 2. Larger halide ions can bind more strongly in the guest position and can be substituted selectively to

Fig. 2. The structure of one form of complex **10** [M = Cu (red), X = Cl (green)] with the guest chloride weakly bound to two copper(I) centers.



form complexes **12** or **13** (e.g., X = Cl, Z = I) (17, 18). The guest halide could be removed by the reaction of complex **10** with silver(I) ions (18).

Complex **11** (M = Ag, X = Cl) reacts with *t*-BuI or *i*-PrI by overall halide exchange to give *t*-BuCl or *i*-PrCl and complex **13** (Scheme 4, M = Ag, X = Cl, Z = I), and the corresponding reaction with (*S*)-(+)-2-iodooctane occurred with an overall retention of the stereochemistry at the asymmetric carbon centre. It is suggested that a silver(I) centre of complex **11** abstracts the iodide from the alkyl iodide while a chloride ligand is donated to the forming alkyl cation (18).

The anionic complexes **10** and **11** can act as cation receptors by binding primarily through the bridging chloride ligands. Structures of a complex of **10** with cesium(I) ions and of a complex of **11** with mercury(II) ions are shown in Figs. 3 and 4, respectively (19). Overall, these compounds can be considered to form by the inclusion of two units of CsCl or one unit of $HgCl_2$ with the neutral complex [**8**{$M_4(\mu\text{-}Cl)_4$}], with the chloride inside the bowl and the metal ion outside.

Resorcinarene ligands with four diphenylphosphinite groups

It is possible to esterify the hydroxyl groups of opposite arene rings of the resorcinarene **1** and then to introduce diphenylphosphinite groups to the remaining arene rings (as shown in Scheme 5). This reaction sequence gives the tetraphosphinite derivatives **14a**–**14e** (Scheme 5), which, like the tetraphosphonite ligand **8**, have four phosphorus donor groups but are more flexible (20).

Ligands **14** adopt the boat conformation and tend to exist in the conformation with the arene groups having the

© 2006 NRC Canada

Fig. 3. Binding of Cs^+ ions (blue) to the resorcinarene complex **10** [M = Cu (red), X = Cl (green)]. Phenyl groups (Ph) and phenethyl groups (R) are omitted for clarity. Two Cs^+ ions bridge between two anionic units of **10**.

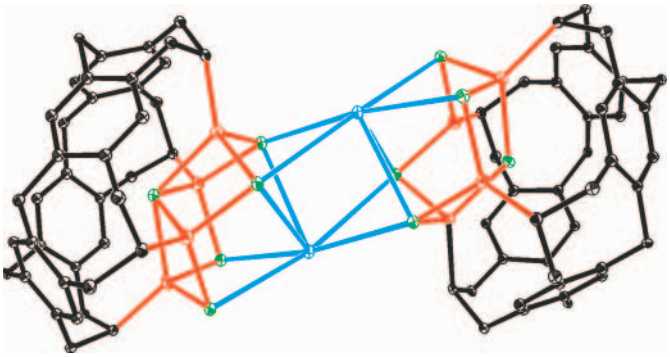
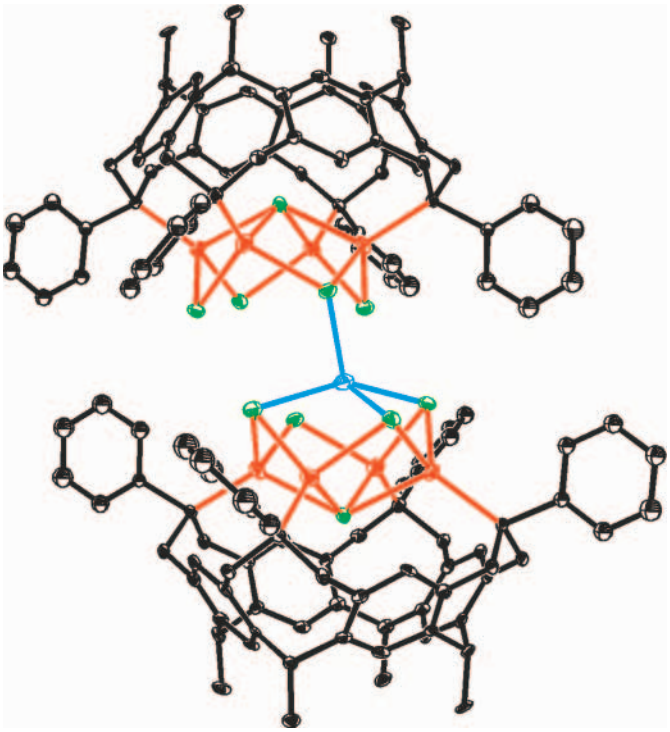
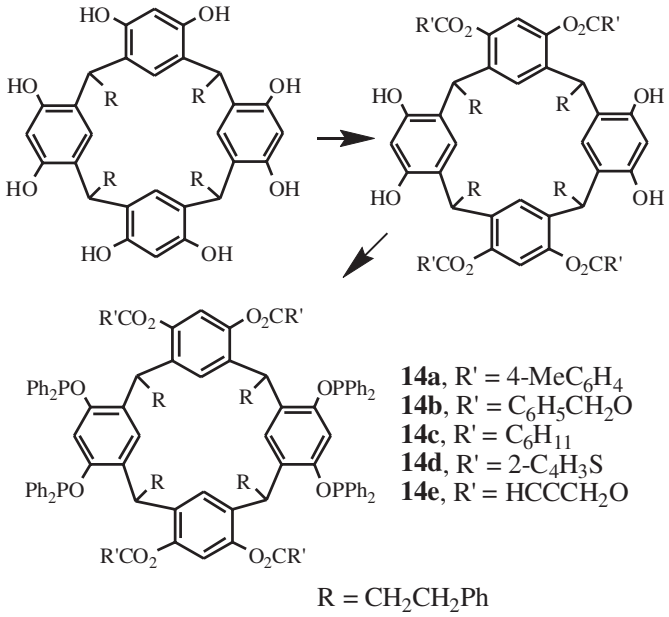


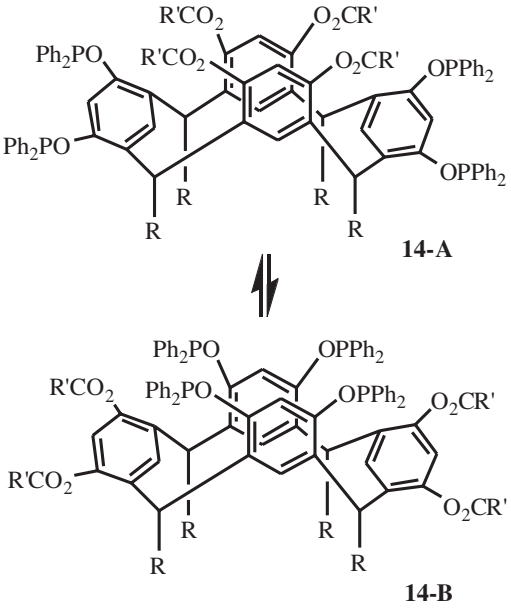
Fig. 4. Binding of Hg^{2+} (blue) between two units of the anionic complex **11** [M = Ag (red), X = Cl (green)].



Scheme 5.



Scheme 6.



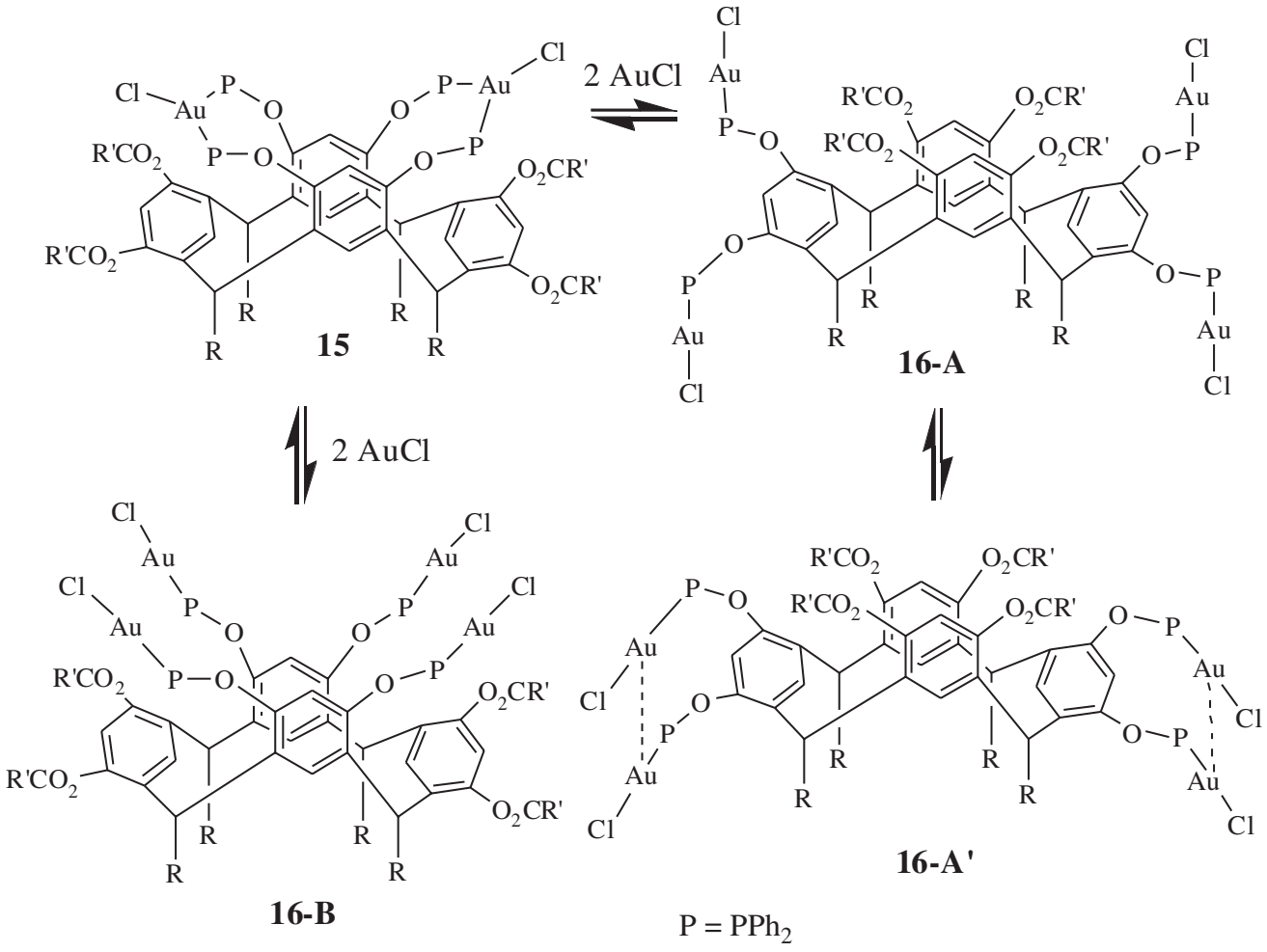
diphenylphosphinite groups in the flattened position (Scheme 6, conformation **14-A**) (20). However, the conformation **14-B**, with diphenylphosphinite groups on the upright arene rings, is easily accessible, and complexes can be formed with the ligands in either conformation.

Ligand **14** can bind to two AuCl units to give complex **15** or to four AuCl units to give complex **15** (Scheme 7) (21). In complex **15**, the ligand must adopt conformation **B** so that the gold atoms can bind between phosphorus donors from opposite arene rings, but complex **16** is flexible and can exist either in conformation **A** or **B** (Scheme 7) depending on the nature of the groups R′ (Scheme 7). Rotation about the P–O bonds is also possible and can lead to different orientations of the P–Au–Cl units (as illustrated for **16-A** and **16-A′** in Scheme 7). The presence of aurophilic bonding may influence the nature of the preferred conformer **16-A** versus **16-A′** both in the solid state and in solution (21).

The tetraphosphinite ligand **14** reacts with copper(I) or silver(I) halides to give the crown cluster complexes **17** (M = Cu or Ag, X = Cl, Br, or I), as shown in Scheme 8 (22). These crown cluster compounds are related to the tetraphosphonite deivatives **10** and **11**, but they contain one extra copper(I) or silver(I) ion bound to chloride ligands in the $M_4(\mu\text{-}Cl)_4$ crown ; thus, the complexes **17** are neutral. The reaction of **17b** (M = Ag, X = Cl) with triflic acid led to loss of silver(I) and chloride ions to give the corresponding disilver complex **18b**. Both complexes **17** and **18** have the arene groups with diphenylphosphinite substituents in the

© 2006 NRC Canada

Scheme 7.



upright position so that the cluster or dimer can be accommodated between opposite arene groups (Scheme 8).

When ligand **14** reacts with silver trifluoroacetate or silver triflate, the primary products are the tetrasilver(I) derivatives **19** shown in Chart 3 and Scheme 9, in which the arene groups with the diphenylphosphinite groups are in the flattened position (23, 24). However, with smaller amounts of silver(I) salts, the disilver(I) complexes **20** or the monosilver complexes **21** may be formed. The conversion of **19** to **20** or **21** requires rearrangement of the resorcinarene boat conformation so that the arene groups with the diphenylphosphinite groups are in the upright position.

Complexes **19** can undergo association in the solid state through intermolecular Ag···O(trifluoroacetate) bridging to give the first supramolecular polymers incorporating resorcinarene units (Fig. 5) or they can undergo partial hydrolysis followed by supramolecular association to give capsule complexes formed by tail-to-tail dimerization of resorcinarene units (23, 24).

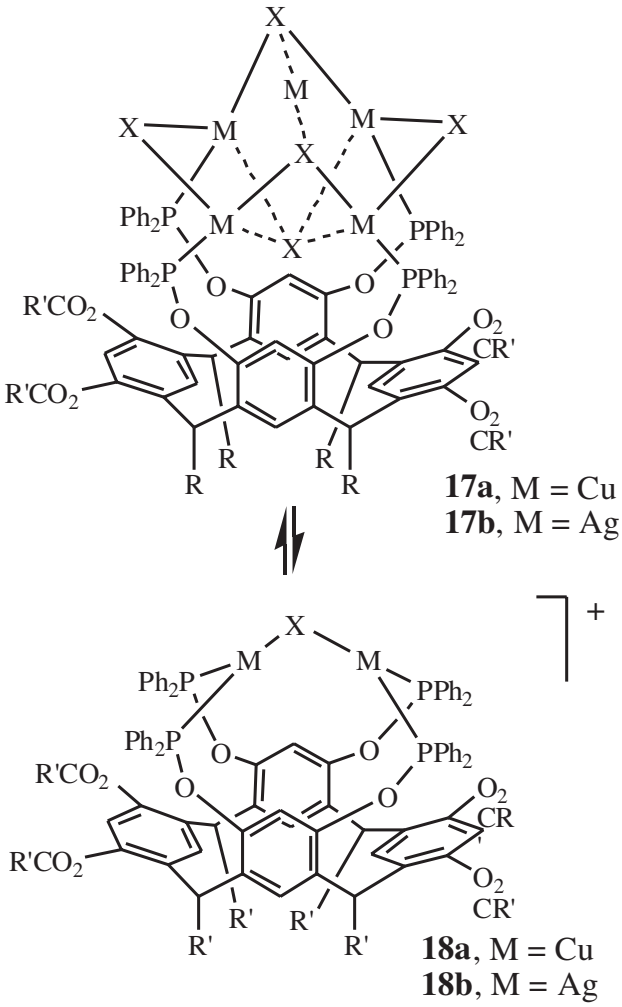
An interesting property of complexes **17** and **18** (Scheme 8) is that they can bind mercury(II) halides in subtle ways. An example, in which an I–Hg^+ unit is substituted for Ag^+ in **17b** (M = Ag, X = I) to give complex **22**, is shown in Scheme 10. The atoms involved in the substitution step are shown in bold in Scheme 10 (25).

Another example, in which three copper(I) iodide units are displaced for each HgI_2 unit added, is shown in Scheme 11 (25). The complex **23** can be formed by the coordination of a $[Hg_2I_6]^{2-}$ ion between two units of complex **18** (Scheme 8, M = Cu, X = I).

The two phosphorus donors on a given arene group of the ligand **14** do not chelate to a single metal ion acceptor in any known complex because the bite distance is too great. However, they are well suited to bind to two metal centres connected by a bridging ligand. These complexes usually form with the arene groups bearing the diphenylphosphinite donors in the flattened position. The tetrasilver(I) complexes **19** (Scheme 9) are examples of this type of complex, and two further examples are shown in Chart 4 (26, 27). The metal centres can have tetrahedral stereochemistry, as in the tetramercury(II) complexes **24** (X = Cl, Br, or I), or square planar stereochemistry, as in the tetrarhodium(I) complex **25**. In solution, complexes **24** exist as a mixture of two conformers, one of which has the arene groups bearing the diphenylphosphinite groups in the upright position. The stereochemistry of the dimercury(II) and dirhodium(I) units in complexes **24** and **25**, with the *syn* arrangement of the phosphorus donors, is very unusual and is imposed by the geometry of the ligand **14** (26, 27).

© 2006 NRC Canada

Scheme 8.



Scheme 9.

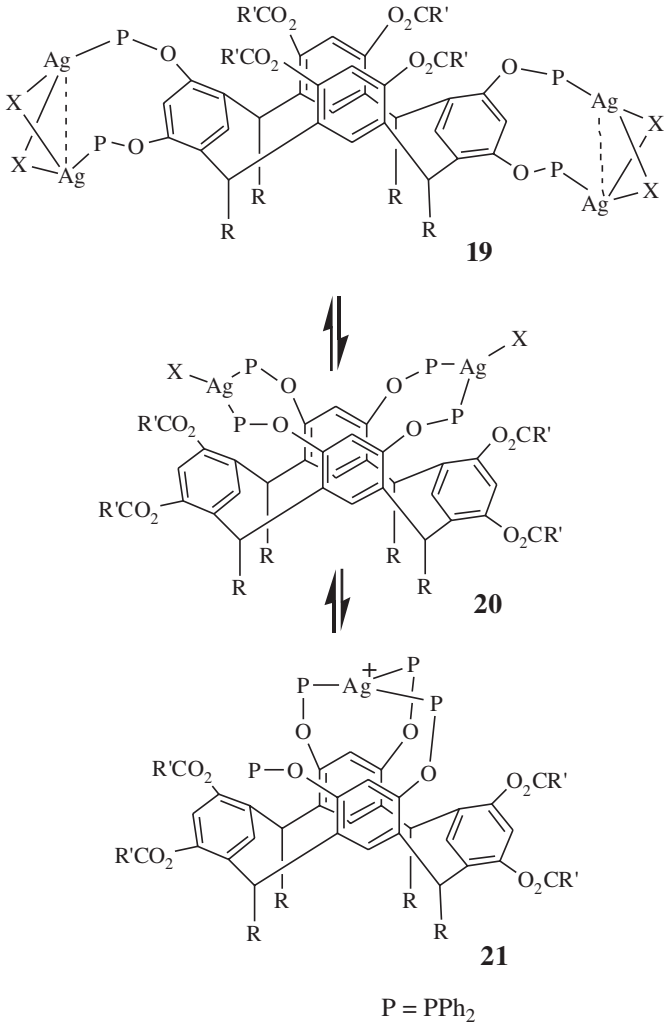
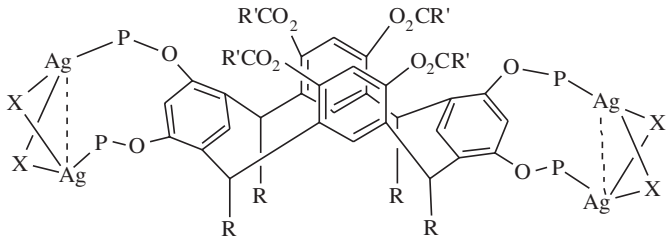


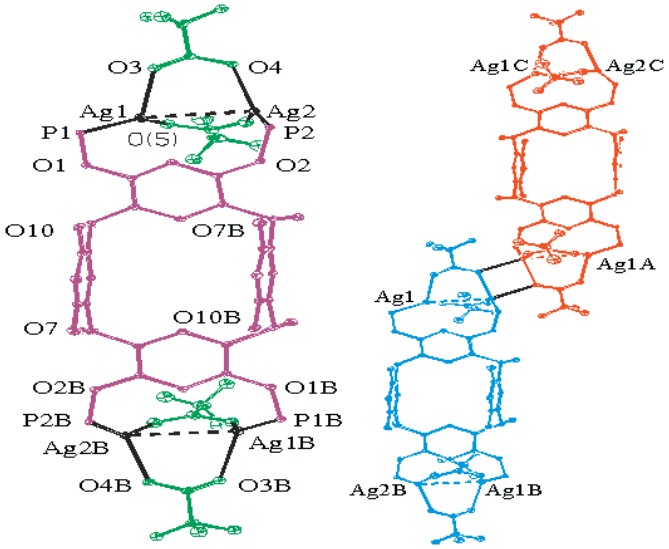
Chart 3.



Resorcinarene ligands with four thiophosphinate groups

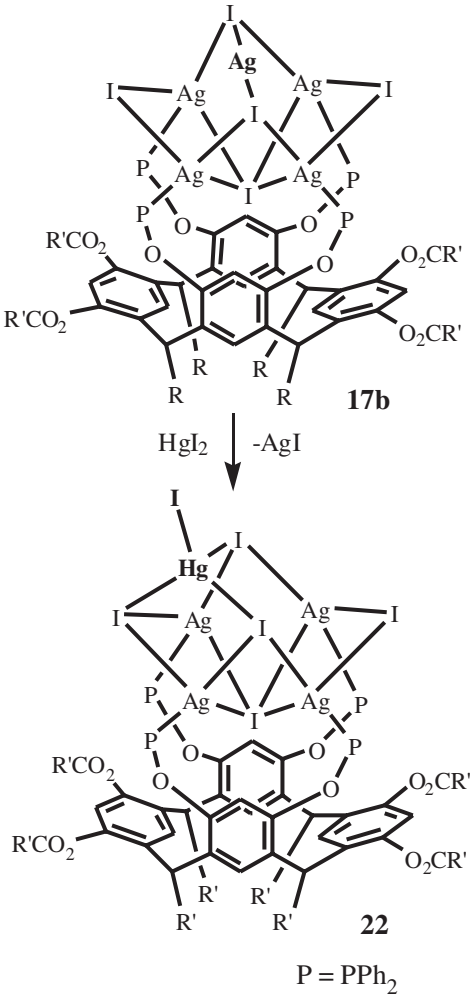
Ligands **14** react with sulfur to give the corresponding tetrakis(thiophosphonite) ligands **26** (Chart 5) (28). These ligands react with silver(I) or gold(I) compounds to give the corresponding cationic complexes **27** or **28** (Chart 5), provided that the anions present are weakly coordinating. In these complexes **27** and **28**, the arene groups bearing the thiophosphinate groups are in the flattened position of the resorcinarene boat, and the two thiophosphinate donors on a

Fig. 5. The silver trifluoroacetate complex **19** (left) and its supramolecular association through intermolecular Ag···O-bonding to give a side-by-side polymer. The phenyl (Ph) and phenethyl groups (R) have been omitted for clarity.

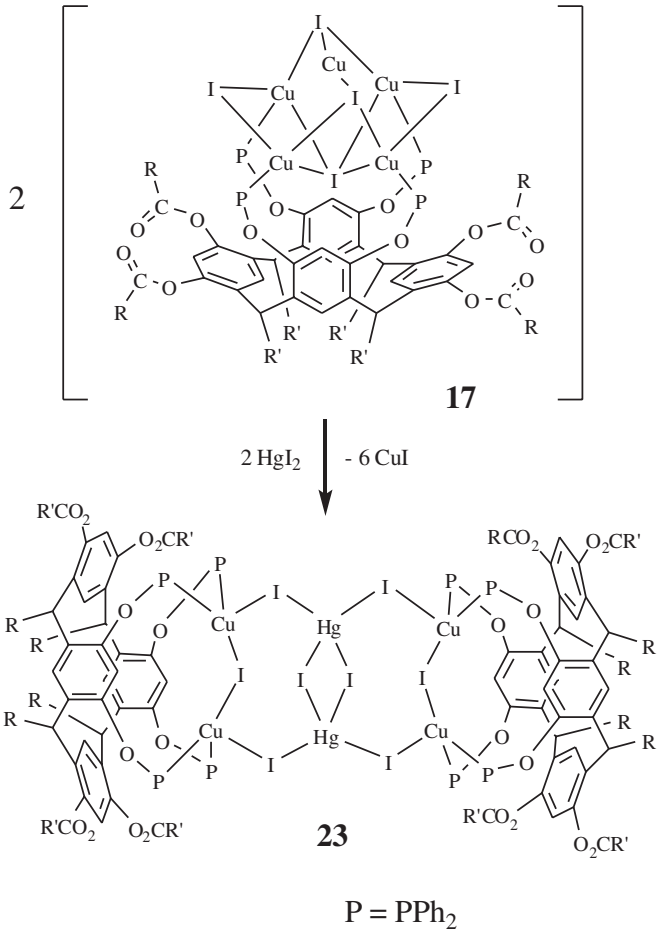


© 2006 NRC Canada

Scheme 10.



Scheme 11.



given arene group chelate to the metal atom to give a 10-membered ring. This behaviour is different from that of the precursor ligand **14**, which cannot form such chelate complexes.

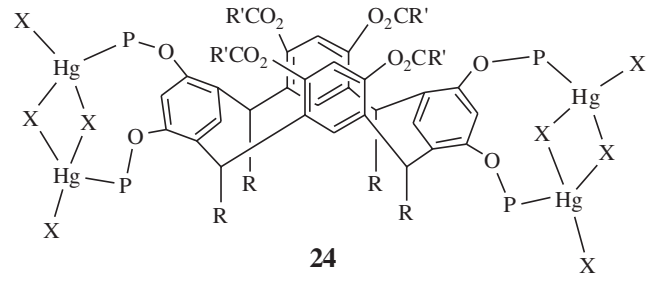
In cases when the anion is more strongly coordinating, there can be an equilibrium between the chelate and monodentate ligation by **26**. Thus, with gold(I) chloride there is a complex equilibrium in solution and crystallization gives a 1:1 mixture of complexes **28** and **29** (Chart 5). In the solid state, these complexes associate through aurophilic bonding to give a supramolecular polymer shown in Fig. 6 (28).

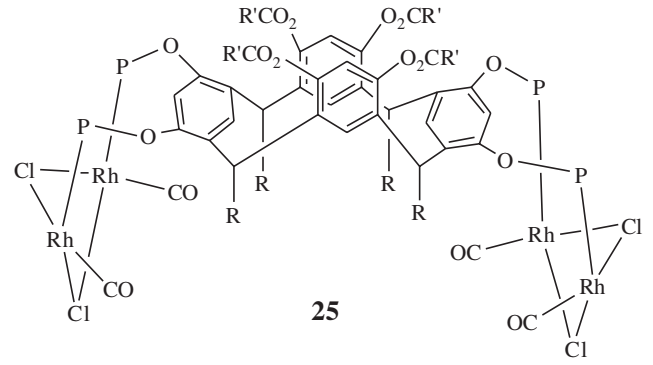
The tetrakis(thiophosphonate) ligand **26** reacts with palladium(II) chloride to give complex **30** (Chart 6). In this complex a $Pd_2Cl_2(\mu\text{-}Cl)_2$ unit is bound to a thiophosphonate donor from two opposite arene groups, which are in the upright position. There are two free thiophosphonate groups. The structure is rigid in solution, and there is no easy exchange between the free and coordinated thiophosphonate groups (28).

Summary

The resorcinarene skeleton has been shown to be an excellent platform for developing new and unusual coordination chemistry of both main group and transition elements. It is

Chart 4.





© 2006 NRC Canada

Fig. 6. The supramolecular polymer formed by Au–Au bonding between units of complexes **28** and **29**. Some substituents on phosphorus atoms and resorcinarene groups are omitted for clarity.

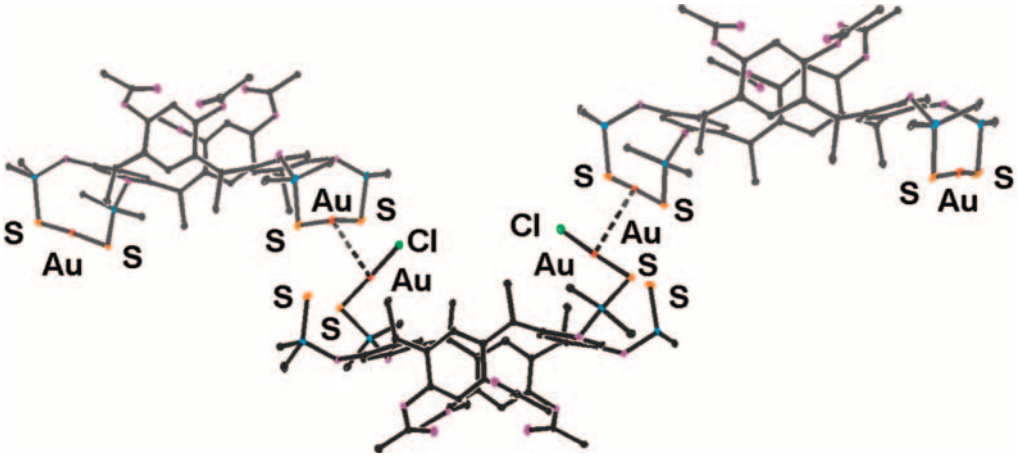
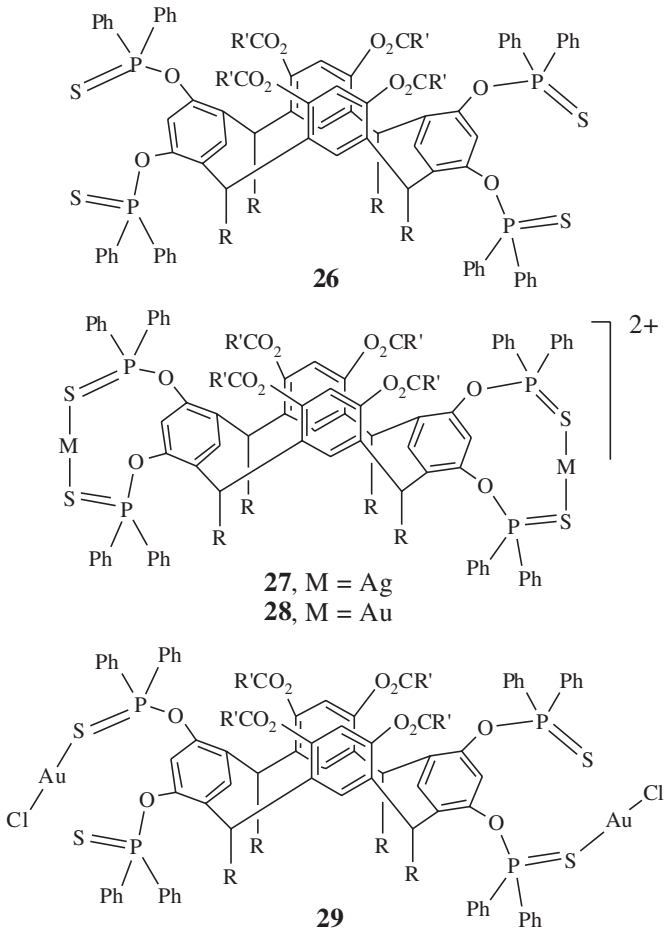
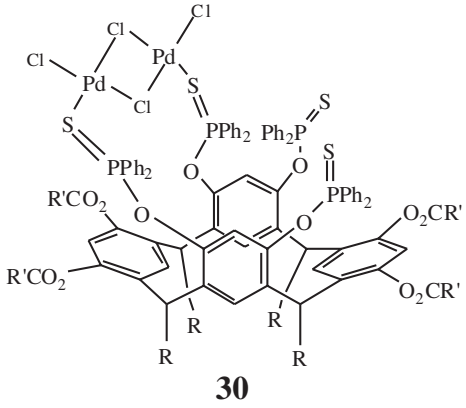


Chart 5.



easy to introduce eight donor groups at the upper rim of the resorcinarene bowl and to coordinate eight, or even 16, metal atoms to these donors. The complexes with eight or more metal atoms are sterically congested, and a more versatile chemistry is found for ligands with four donor groups incorporated. Metal cluster complexes that can act as unusual hosts for anion or salt inclusion have been discovered. Moreover, the unusual bite distances between the donor atoms in the tetradentate ligands leads to very unusual coordination geometries in many of the complexes formed. Clearly, there is a considerable scope for further exploitation of ligands derived from resorcinarenes.

Chart 6.



Acknowledgments

RJP thanks the Natural Sciences and Engineering Research Council of Canada (NSERC) for financial support and the Government of Canada for a Canada Research Chair. Particular thanks are due to the excellent students whose names are given in the references. In particular, Jon Rourke began the work, and Wei Xu and Dana Eisler carried it forward, while J.J. Vittal, Ljubica Manojlovic-Muir, and Ken Muir solved challenging X-ray structures.

References

1. (*a*) C.D. Gutsche. Calixarenes revisited. Monographs in supramolecular chemistry. Royal Society of Chemistry, Cambridge, UK. 1998; (*b*) D.J. Cram and J.M. Cram. Container. Molecules and their guests. Royal Society of Chemistry, Cambridge, UK. 1994
2. (*a*) C. Wieser, C.B. Dieleman, and D. Matt. Coord. Chem. Rev. **165**, 93 (1997); (*b*) C. Jeunesse, D. Armspach, and D. Matt. Chem. Commun. 5603 (2005).

© 2006 NRC Canada

3. P.D. Harvey. Coord. Chem. Rev. **233–234**, 289 (2002).
4. (*a*) W. Xu, R.J. Puddephatt, Lj. Manojlovic-Muir, K.W. Muir, and C.S. Frampton. J. Inclusion Phenom. 19, 277 (1994); (*b*) W. Xu, R.J. Puddephatt, K.W. Muir, and A.A. Torabi. Organometallics, **13**, 3054 (1994); (*c*) W. Xu, J.J. Vittal, and R.J. Puddephatt. Can. J. Chem. **74**, 766 (1996).
5. E.E. Nifantyev, V.I. Maslennikova, and R.V. Merkulov. Acc. Chem. Res. **38**, 108 (2005).
6. (*a*) Q.-F. Zhang, R.D. Adams, and D. Fenske. J. Mol. Struct. **741**, 129 (2005); (*b*) A. Vollbrecht, I. Neda, H. Thonnessen, P.G. Jones, R.K. Harris, L.A. Crowe, and R. Schmutzler. Chem. Ber. **130**, 1715 (1997); (*c*) I. Neda, T. Kaukorat, and R. Schmutzler. Main Group Chem. News, **6**, 4 (1998).
7. (*a*) S.E. Matthews and P.D. Beer. Supramol. Chem. **17**, 411 (2005). (*b*) O.D. Fox, M.G.B. Drew, E.J.S. Wilkinson, and P.D. Beer. Chem. Commun. 391 (2000).
8. (*a*) B. Bibal, J.P. Declercq, J.P. Dutasta, B. Tinant, and A.G.L. Valade. Tetrahedron, **59**, 5849 (2003); (*b*) B. Bibal, B. Tinant, J.P. Declercq, and J.P. Dutasta. Chem. Commun. 432 (2002).
9. A.F.D. de Namor, J.K. Chaaban, O.E. Piro, and E.E. Castellano. J. Phys. Chem. B, **110**, 2442 (2006).
10. (*a*) J.S. Gardner, Q.P. Peterson, J.O. Walker, B.D. Jensen, B. Adhikary, R.G. Harrison, and J.D. Lamb. J. Membr. Sci. **277**, 165 (2006); (*b*) R.G. Harrison, J.L. Burrows, and L.D. Hansen. Chem.—Eur. J. **11**, 5881 (2005).
11. A.R. Mustafina, V.V. Skripacheva, A.T. Gubaidullin, S.K. Latipov, A.V. Toropchina, V.V. Yanilkin, S.E. Solovieva, I.S. Antipin, and A.I. Konovalov. Inorg. Chem. **44**, 4017 (2005).
12. A.L. Maksimov, D.A. Sakharov, T.Y. Filippova, A.Y. Zhuchkova, and E.A. Karakhanov. Ind. Eng. Chem. Res. **44**, 8644 (2005).
13. G. Arnott and R. Hunter. Tetrahedron, **62**, 992 (2006).
14. W. Xu, J.P. Rourke, J.J. Vittal, and R.J. Puddephatt. Inorg. Chem. **34**, 323 (1995).
15. D.J. Eisler, W. Hong, M.C. Jennings, and R.J. Puddephatt. Organometallics, **21**, 3955 (2002).
16. W. Xu, J.P. Rourke, J.J. Vittal, and R.J. Puddephatt. Chem. Commun. 145 (1993).
17. W. Xu, J.J. Vittal, and R.J. Puddephatt. J. Am. Chem. Soc. **115**, 6456 (1993).
18. W. Xu, J.J. Vittal, and R.J. Puddephatt. J. Am. Chem. Soc. **117**, 8362 (1995).
19. W. Xu, J.J. Vittal, and R.J. Puddephatt. Inorg. Chem. **36**, 86 (1997).
20. D.J. Eisler and R.J. Puddephatt. Can. J. Chem. **82**, 185 (2004).
21. D.J. Eisler and R.J. Puddephatt. Inorg. Chem. **42**, 6352 (2003).
22. D.J. Eisler, C.W. Kirby, and R.J. Puddephatt. Inorg. Chem. **42**, 7626 (2003).
23. D.J. Eisler and R.J. Puddephatt. Cryst. Growth Des. **5**, 57 (2005).
24. D.J. Eisler and R.J. Puddephatt. Inorg. Chem. **44**, 4666 (2005).
25. D.J. Eisler and R.J. Puddephatt. Inorg. Chem. **42**, 8192 (2003).
26. D.J. Eisler and R.J. Puddephatt. Dalton Trans. 3567 (2003).
27. D.J. Eisler and R.J. Puddephatt. Can. J. Chem. **82**, 1423 (2004).
28. D.J. Eisler and R.J. Puddephatt. Inorg. Chem. **45**, 7295 (2006).

© 2006 NRC Canada

Synthesis of β-hydroxy dithiocarbamate derivatives via regioselective addition of dithiocarbamate anion to epoxide in water

Azim Ziyaei-Halimjani and Mohammad R. Saidi

Abstract: The reactions of different dithiocarbamate anions with epoxides were investigated in water. With this method, β-hydroxy dithiocarbamate derivatives were synthesized in high yields. The reaction was also carried out in DMF in the presence of lithium perchlorate with a simple work-up procedure, and the results are compared.

Key words: hydroxy dithiocarbamate, dithiocarbamate anion, epoxide, water.

Résumé : On a étudié les réactions de divers anions dithiocarbamates avec des époxydes dans l'eau. De cette façon, on a réalisé la synthèse de dérivés β-hydroxydithiocarbamates avec des rendements élevés. La réaction a aussi été effectuée dans le DMF, en présence de perchlorate de lithium, en utilisant un traitement conclusif simple et on compare les résultats.

Mots clés : hydroxydithiocarbamate, anion dithiocarbamate, époxyde, eau.

[Traduit par la Rédaction]

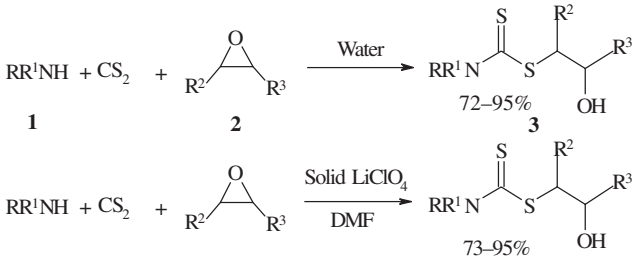
Introduction

Dithiocarbonyl-containing compounds such as xanthates and dithiocarbamate have been successful in their role as important synthesis precursors (1, 2), protecting groups (3*a*), and chain transfer agents (3*b*), and are of considerable biological and medical interest (4, 5). Also, the superconductivity of different transition metal complexes of dithiocarbamates makes these compounds more interesting (6–9). The reported procedure for the preparation of these compounds employs harsh reaction conditions, such as the use of a strong base, high temperature, and long reaction times (10, 11). Different modifications have been reported, such as using thiophosgene (12), chlorothioformate, and isothiocyanates, which are costly and toxic (13). The preparation of dithiocarbamate derivatives from the reaction of an amine, inexpensive and readily available CS_2, and a nucleophile acceptor were also investigated using a strong base as an activator (14–18). They were also prepared by the reaction of an amine, CS_2, and alkyl halides (19), and by the addition of amines and carbon disulfide to α,β-unsaturated compounds (20).

Results and discussion

As a result of environmental consideration in recent years, water has become an attractive solvent in the preparation of organic compounds (21). We recently reported a one-pot procedure for the Michael addition of the dithiocarbamate anion to α,β-unsaturated olefins mediated by solid lithium perchlorate (22). As part of our research in organic synthesis in water and under solvent-free conditions (23), we report the ring-opening of epoxides with a variety of dithiocarbamate anions in water at room temperature. To the best of our knowledge, there are no reports for the addition of dithiocarbamate to epoxides for the preparation of β-hydroxy dithiocarbamate derivatives. The reactions were carried out at room temperature without adding any other solvent or catalyst. By mixing amine **1** and CS_2 in water, then adding epoxide **2** into the reaction mixture, the β-hydroxy dithiocarbamates **3** derivatives are formed in high yields. All epoxides showed very high regioselectivity with the exception of styrene oxide. The procedure for these reactions is very simple, and the products were extracted from the aqueous solution after the completion of the reaction (Scheme 1). To show the generality and scope of this new protocol, structurally diverse amines were treated with various epoxides, and the results are shown in Table 1. The role of water as a reaction medium is still unclear. Hydrophobic and hydrogen bonding interactions and polarity are probably the main factors that influence the reactivity and selectivity of the process.

Scheme 1.



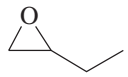
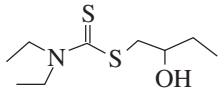
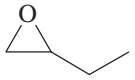
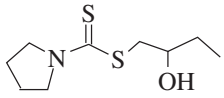
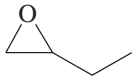
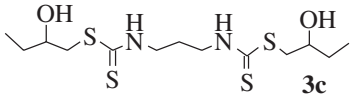
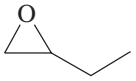
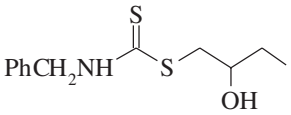
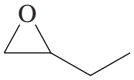
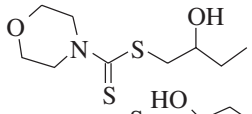
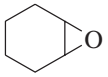
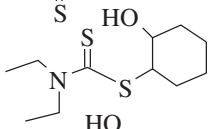
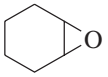
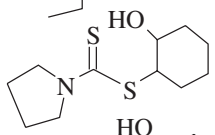
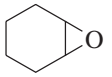
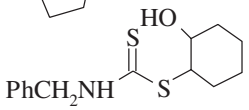
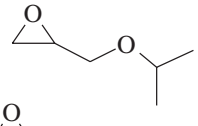
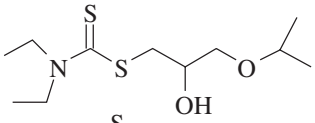
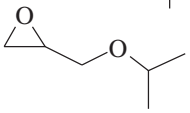
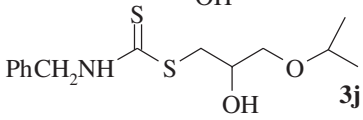
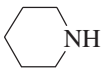
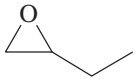
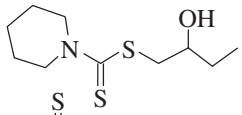
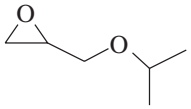
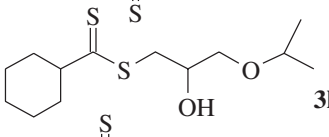
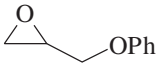
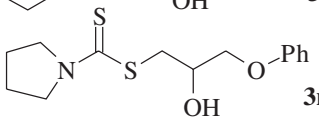
Received 19 April 2006. Accepted 6 September 2006. Published on the NRC Research Press Web site at http://canjchem.nrc.ca on 3 November 2006.

A. Ziyaei-Halimjani and M.R. Saidi.[1] Department of Chemistry, Sharif University of Technology, P.O. Box 11365-9516 Tehran, Iran.

[1]Corresponding author (e-mail: saidi@sharif.edu).

 doi:10.1139/V06-150 © 2006 NRC Canada

Table 1. Addition of dithiocarbamates to epoxides in water and DMF.

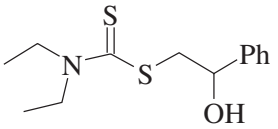
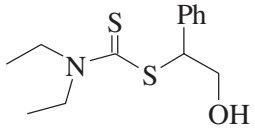
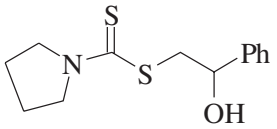
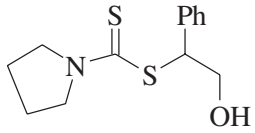
Entry	Amine	Epoxide	Product		Yield[a] in water (DMF) %
1				**3a**	93(89)
2				**3b**	85(95)
3				**3c**	(91)88
4				**3d**	95(93)
5				**3e**	93(90)
6				**3f**	(73)
7				**3g**	89(81)
8				**3h**	(75)
9				**3i**	95(95)
10				**3j**	90(90)
11				**3k**	76
12				**3l**	80
13				**3m**	72

Note: The molar ratio of the amine:CS_2:epoxide is 6:16:8.
[a]Isolated yield.

For comparison, the same reactions were also carried out in an organic solvent. After testing different organic solvents, we found that the best was *N,N*-dimethylformamide (DMF). The preparation of β-hydroxy dithiocarbamates **3** in DMF was accelerated by the presence of anhydrous lithium perchlorate at room temperature, with good to excellent yields in a short reaction time. Without adding lithium perchlorate, the reaction time is much longer. Under these mild conditions, both in water and DMF, the reactions are regioselective, except for styrene oxide. Also, we did not observe any direct addition of amine to epoxide in water or in DMF.

© 2006 NRC Canada

Table 2. Addition of dithiocarbamates to styrene oxide in water and DMF.

Amine	Product	Yield[a] in water (DMF) %
NH	 **4a** 70(12)[b]  **4b** 30(88)[b]	90(81)
NH	 **5a** 78(14)[b]  **5b** 22(86)[b]	85(85)

[a]Isolated yield.
[b]The % of regioisomers in water and (DMF).

Table 1 shows that primary and secondary amines can react with carbon disulfide and different epoxides in water and DMF to give the corresponding β-hydroxy dithioarbamate derivatives. All reactions with aliphatic epoxides are regioselective, and NMR (^{1}H & ^{13}C) spectra of the crude products showed only one regioisomer. The reactions in water were done in one-pot and completed overnight, while the one-pot reaction in DMF and in the presence of anhydrous lithium perchlorate was completed within 1.5 h. In general, the isolated yields are higher in water.

As shown in Table 2, the addition of dithiocarbamate to styrene oxide was not regioselective. In general, the reaction in DMF gave a more S_N2 type reaction (attack of the anion on the β-position of the styrene oxide), while the reaction in water gave a more S_N1 type reaction compared with DMF (attack on the α-position of the styrene oxide). The addition of dithiocarbamate (Table 2, entry 3) with two equivalents of an epoxide gave the corresponding bis(dithiocarbamate) in an excellent yield.

In conclusion, we have shown the first clean, mild, efficient, and neutral method for the preparation of β-hydroxy dithiocarbamate derivatives in water without using any catalyst or in DMF in the presence of solid lithium perchlorate as a catalyst. The procedures for these reactions are very simple, with good to excellent yields, and the work-up system is very easy. Therefore, they can serve as a new method for the preparation of substituted dithiocarbamates and bis(dithiocarbamates).

Experimental

A typical procedure for the synthsis of β-hydroxy dithiocarbamate in water

To a mixture of pyrrolidine (0.43 g, 6 mmol, 0.5 mL) and water (20 mL) in a 50 mL round bottom flask, CS_2 (1 mL, 16 mmol) was added dropwise over 2 min at room temperature, and the mixture was stirred for 20 min. Then, 1,2-epoxybutane (0.58 g, 8 mmol) was added, and the mixture was stirred vigorously at room temperature overnight (18 h). After completion of the reaction, the mixture was extracted with ethyl acetate (2 × 20 mL). The combined organic layers were washed with water (2 × 20 mL), dried over $MgSO_4$, and concentrated under reduced pressure. The resulting residue was purified by flash column chromatography (light petroleum – ethyl acetate, 9:1) if needed. The products were pure in most cases and did not need any further purification.

General procedure for the synthsis of β-hydroxy dithiocarbamate in DMF in the presence of $LiClO_4$

To a solution of an amine (3 mmol), anhydrous lithium perchlorate (0.4 g, 4 mmol), and anhydrous DMF (8 mL), carbon disulfide (0.36 ml, 0.46 g, 6 mmol) was added slowly at room temperature. The mixture was stirred for 30 min, and then an epoxide (4 mmol) was added. The reaction mixture was stirred for about 1.5 h at room temperature, and the reaction was monitored by TLC. After completion of the reaction, the solution was poured into water, and the organic materials were extracted with ethyl acetate (3 × 10 mL). The combined organic layers were washed with water (2 × 20 mL) and dried over Na_2SO_4. The solvent was removed using a rotary evaporator. Flash chromatography of the residue using silica gel (light petroleum – ethyl acetate, 9:1) afforded the pure product.

Spectroscopic data for dithiocarbamate derivatives

Compound 3a

IR (cm^{-1}): 3400 (OH), 1210 (C=S). ^{1}H NMR (500 MHz, $CDCl_3$ + CCl_4) δ: 0.86 (t, J = 7.4 Hz, 3H), 1.21 (s, 6H), 1.50 (m, 2H), 3.05 (br, 1H), 3.20 (dd, J = 7.4 and 6.5 Hz, 1H), 3.47 (dd, J = 10.5 and 3.6 Hz, 1H), 3.66 (m, 3H), 3.90 (br, 2H). ^{13}C NMR (125 MHz, $CDCl_3$ + CCl_4) δ: 10.3, 11.9, 12.9, 29.8, 43.7, 47.2, 50.1, 72.5, 196.2. Anal. calcd. for $C_9H_{19}NOS_2$: C 48.87, H 8.60, N 6.34; found: C 48.78, H 8.42, N 6.43.

Compound 3b

IR (cm^{-1}): 3500 (OH), 1225 (C=S). ^{1}H NMR (500 MHz, $CDCl_3$) δ: 0.82 (t, J = 7.4 Hz, 3H), 1.42 (m, 2H), 1.84 (t, J = 6.8 Hz, 2H), 1.94 (t, J = 6.8 Hz, 2H), 3.15 (br, 1H), 3.27 (dd, J = 7.4 and 6.7 Hz, 1H), 3.47–3.73 (m, 4H), 3.76 (br, 2H). ^{13}C NMR (125 MHz, $CDCl_3$) δ: 10.3, 24.7, 25.4, 29.7,

© 2006 NRC Canada

43.0, 51.2, 55.7, 72.4, 193.8. Anal. calcd. for $C_9H_{17}NOS_2$: C 49.32, H 7.76, N 6.39; found: C 49.15, H 7.71, N 6.17.

Compound 3c

IR (cm^{-1}): 3250–3450 (NH and OH), 1215 (C=S). ^1H NMR (500 MHz, $CDCl_3$) δ: 0.99 (br s, 6H), 1.57 (m, 4H), 2.03 (br s, 2H), 3.19 (br, 2H), 3.35 (br, 2H), 3.7–4.1 (br, 6H), 8.6 and 9.22 (br, 2H). ^{13}C NMR (125 MHz, $CDCl_3$) δ: 10.3, 27.7, 29.6, 42.0, 44.3, 72.9, 198.2.

Compound 3d

IR (cm^{-1}): 3300–3500 (NH and OH), 1225 (C=S). ^1H NMR (500 MHz, $CDCl_3$ + CCl_4) δ: 0.92 (t, *J* = 7.4 Hz, 3H), 1.47 (m, 2H), 2.7 (br, 1H), 3.09 (dd, *J* = 7.5 and 6.8 Hz, 1H), 3.42 (dd, *J* = 13.2 and 3 Hz, 1H), 3.63 (m, 1H), 4.54 and 4.78 (br, 2H), 7.21–7.28 (m, 5H), 7.94 (br, 1H). ^{13}C NMR (125 MHz, $CDCl_3$ + CCl_4) δ: 10.3, 29.8, 42.3, 51.6, 73.2, 128.1, 128.6, 129.1, 136.7, 196.2. Anal. calcd. for $C_{12}H_{17}NOS_2$: C 56.43, H 6.66, N 5.49; found: C 56.51, H 6.68, N 5.19.

Compound 3e

IR (cm^{-1}): 3450 (OH), 1215 (C=S). ^1H NMR (500 MHz, $CDCl_3$ + CCl_4) δ: 1.01 (t, *J* = 7.4 Hz, 3H), 1.56 (m, 2H), 2.7 (br, 1H), 3.34 (dd, *J* = 7.6 and 6.4 Hz, 1H), 3.62–3.76 (m, 6H), 4.10 (br, 4H). ^{13}C NMR (125 MHz, $CDCl_3$ + CCl_4) δ: 10.3, 29.9, 43.7, 50.9, 51.7, 66.5, 72.9, 198.1. Anal. calcd. for $C_9H_{17}NO_2S_2$: C 45.96, H 7.23, N 5.96; found: C 45.66, H 7.10, N 5.56.

Compound 3f

IR (cm^{-1}): 3500 (OH), 1230 (C=S). ^1H NMR (500 MHz, $CDCl_3$) δ: 1.31–1.39 (br, 6H), 1.46–1.54 (m, 4H), 1.80 (m, 2H), 2.21 (m, 2H), 3.15 (m, 1H), 3.81 (m, 1H), 4.05 (br, 2H), 4.45 (br, 2H).

Compound 3g

IR (cm^{-1}): 3500 (OH), 1230 (C=S). ^1H NMR (500 MHz, $CDCl_3$ + CCl_4) δ: 1.28–1.46 (m, 4H), 1.71 (m, 2H), 1.95–2.05 (m, 4H), 2.10 (m, 2H), 3.4 (br, 1H), 3.5 (m, 1H), 3.65 (br, 2H), 3.98 (br, 2H), 4.04 (m, 1H). ^{13}C NMR (125 MHz, $CDCl_3$ + CCl_4) δ: 24.5, 26.4, 32.2, 36.0, 36.6, 51.2, 55.3, 56.4, 74.7, 193.3. Anal. calcd. for $C_{11}H_{19}NOS_2$: C 53.87, H 7.75, N 5.71; found: C 54.13, H 7.82, N 5.53.

Compound 3h

IR (cm^{-1}): 3250–3500 (NH and OH), 1220 (C=S). ^1H NMR (500 MHz, $CDCl_3$) δ: 1.29–1.48 (m, 4H), 1.78 (m, 2H), 2.13 (m, 2H), 3.50 (m, 1H), 3.71 (m, 1H), 4.82–4.94 (m, 2H), 7.30–7.41 (m, 5H), 8.07 (br, 1H).

Compound 3i

IR (cm^{-1}): 3500 (OH), 1230 (C=S). ^1H NMR (500 MHz, $CDCl_3$ + CCl_4) δ: 0.96–1.12 (br, 12H), 3.20–3.43 (br, 6H), 3.61 (br, 2H), 3.82 (br, 3H). ^{13}C NMR (125 MHz, $CDCl_3$ + CCl_4) δ: 11.9, 12.6, 22.4, 40.4, 47.06, 49.8, 70.0, 71.2, 72.3, 195.6. Anal. calcd. for $C_{11}H_{23}NO_2S_2$: C 49.78, H 8.67, N 5.28; found: C 49.72, H 8.67, N 4.74.

Compound 3j

IR (cm^{-1}): 3350–3500 (NH and OH), 1225 (C=S). ^1H NMR (500 MHz, $CDCl_3$ + CCl_4) δ: 1.15 (d, *J* = 5.9 Hz, 6H), 3.20 (dd, *J* = 7.6 and 6.7 Hz, 1H), 3.3–3.55 (br, 5H), 3.95 (br, CHOH, 1H), 4.30 and 4.80 (br, 2H), 7.27 (m, 5H), 8.20 and 8.50 (br, 1H). ^{13}C NMR (125 MHz, $CDCl_3$ + CCl_4) δ: 22.1, 39.1, 51.4, 70.5, 70.9, 72.5, 127.2, 128.2, 129.8, 136.8, 197.9. Anal. calcd. for $C_{14}H_{21}NO_2S_2$: C 56.16, H 7.02, N 4.67; found: C 55.78, H 7.26, N 4.08.

Compound 3k

IR (cm^{-1}): 3500(OH) and 1240(C=S). ^1H NMR (500 MHz, $CDCl_3$ + CCl_4) δ: 0.86 (t, *J* = 7.3 Hz, 3H), 1.44–1.56 (br, 6H), 3.20 (dd, *J* = 7.5 and 6.3 Hz, 1H), 3.41 (m, 2H), 3.61 (m, 1H), 3.82 (br, 2H), 4.12 (br, 2H). ^{13}C NMR (125 MHz, $CDCl_3$ + CCl_4) δ: 10.3, 20.9, 26.13, 29.4, 45.0, 51.5, 55.4, 72.2, 196.1. Anal. calcd. for $C_{10}H_{19}NOS_2$: C 51.50, H 8.15, N 6.01; found: C 51.77, H 8.15, N 6.03.

Compound 3l

IR (cm^{-1}): 3450 (OH) and 1210 (C=S). ^1H NMR (500 MHz, $CDCl_3$ + CCl_4) δ: 1.09 (d, *J* = 5.9 Hz, 6H), 1.62 (br, 6H), 3.13 (br, 1H), 3.30 (m, 2H), 3.44 (dd, *J* = 7.4 and 4.2 Hz, 1H), 3.54 (m, 2H), 3.90 (br, 3H), 4.20 (br, 2H). ^{13}C NMR (125 MHz, $CDCl_3$ + CCl_4) δ: 22.5, 24.7, 25.8, 26.4, 40.4, 51.6, 53.5, 70.2, 71.2, 72.4, 196.1. Anal. calcd. for $C_{12}H_{23}NO_2S_2$: C 51.95, H 8.30, N 5.05; found: C 51.49, H 8.11, N 4.93.

Compound 3m

IR (cm^{-1}): 3500 (OH) and 1230 (C=S). ^1H NMR (500 MHz, $CDCl_3$ + CCl_4) δ: 1.94–2.07 (m, 4H), 3.5–3.8 (br, 5H), 3.90 (t, *J* = 6.6 Hz, 2H), 4.05 (t, *J* = 6.6 Hz, 2H), 4.26 (m, 1H), 6.92 (m, 3H), 7.25 (m, 2H). ^{13}C NMR (125 MHz, $CDCl_3$ + CCl_4) δ: 24.7, 26.5, 39.7, 51.1, 55.7, 70.0, 70.9, 115.0, 121.3, 129.0, 158.9, 193.2. Anal. calcd. for $C_{14}H_{19}NO_2S_2$: C 56.56, H 6.40, N 4.71; found: C 56.56, H 6.35, N 4.81.

Compound 4a

IR (cm^{-1}): 3500 (OH), 1210 (C=S). ^1H NMR (500 MHz, $CDCl_3$ + CCl_4) δ: 1.14–1.29 (br, 6H), 3.06 (br, 1H), 3.48 (dd, *J* = 8.6 and 5.6 Hz, 1H), 3.79 (dd, *J* = 11.3 and 3.1 Hz, 1H), 4.06 (br, 2H), 5.30 (t, *J* = 6.6 Hz, 1H), 7.25–7.4 (m, 5H). ^{13}C NMR (125 MHz, $CDCl_3$ + CCl_4) δ: 12.1, 13.1, 45.8, 47.3, 50.1, 73.2, 127.2, 128.5, 129.0, 138.7, 194.6. Anal. calcd. for $C_{13}H_{19}NOS_2$: C 57.96, H 7.06, N 5.2; found: C 58.28, H 6.99, N 4.89.

Compound 4b

IR (cm^{-1}): 3500 (OH), 1215 (C=S). ^1H NMR (500 MHz, $CDCl_3$ + CCl_4) δ: 1.14–1.29 (br, 6H), 3.06 (br, 1H), 3.73 (d, *J* = 7.7 Hz, 2H), 3.97 (br, 4H), 4.96 (br, 1H), 7.25–7.42 (m, 5H). ^{13}C NMR (125 MHz, $CDCl_3$ + CCl_4) δ: 12.1, 13.1, 51.5, 52.7, 57.8, 66.1, 125.9, 128.1, 128.8, 143.8, 196.0. Anal. calcd. for $C_{13}H_{19}NOS_2$: C 57.96, H 7.06, N 5.2; found: C 58.28, H 6.99, N 4.89.

Compound 5a

IR (cm^{-1}): 3400 (OH), 1220 (C=S). ^1H NMR (500 MHz, CDCl3) δ: 1.80–1.95 (br, 4H), 3.40 (dd, *J* = 9.0 and 5.0 Hz, 1H), 3.6 (br, 1H), 3.8 (br, 2H), 4.0 (br, 2H), 5.41 (t, *J* = 6.4 Hz, 1H), 7.2–7.4 (m, 5H). ^{13}C NMR (125 MHz, $CDCl_3$ + CCl_4) δ: 24.6, 26.5, 45.3, 51.1, 55.5, 73.2, 125.9, 127.2,

© 2006 NRC Canada

128.7, 138.8, 191.7. Anal. calcd. for $C_{13}H_{17}NOS_2$: C 58.40, H 6.36, N 5.24; found: C 58.51, H 6.19, N 4.84.

Compound 5b

IR (cm^{-1}): 3500 (OH), 1230 (C=S). ^{1}H NMR (500 MHz, $CDCl_3$ + CCl_4) δ: 1.8–1.95 (br, 4H), 3.5 (d, J = 5.7 Hz, 2H), 3.8 (br, 2H), 4.0 (br, 2H), 4.90 (br, 1H), 7.2–7.4 (m, 5H). ^{13}C NMR (125 MHz, $CDCl_3$ + CCl_4) δ: 24.7, 26.5, 51.1, 55.6, 57.1, 66.0, 126.3, 128.0, 129.1, 143.2, 193.0. Anal. calcd. for $C_{13}H_{17}NOS_2$: C 58.40, H 6.36, N 5.24; found: C 58.51, H 6.19, N 4.84.

Acknowledgments

We are grateful to the Research Council of Sharif University of Technology for financial support. We also thank Volkswagen-Stiftung, Federal Republic of Germany, for financial support towards the purchase of chemicals. We are also grateful to the staff of the Giessen University for the CHN analysis.

References

1. A.D. Dunn and W.D. Rudorf. Carbon disulfide in organic chemistry. Ellis Harwood, Chichester, UK. 1989. pp. 226–67.
2. C.H. Depuy and R.W. King. Chem. Rev. **60**, 431 (1960).
3. (*a*) T.W. Greene and P.G.M. Wuts. Protective groups in organic synthesis. 3rd ed. Wiley-Interscience, New York. 1999. pp. 484–86; (*b*) R.T.A. Mayadunne, E. Rizzardo, J. Chiefari, and Y.K. Chong. Macromalecules, **32**, 6977 (1999).
4. B.H. Alexander, S.I. Gertler, T.A. Oda, R.T. Brown, R.W. Ihndris, and M. Beroza. J. Org. Chem. **25**, 626 (1960).
5. G.D. Thorn and R.A. Ludwing. The Dithiocarbamates and related compounds. Elsevier, Amsterdam. 1962.
6. J.L. Serrano, L. Garcia, J. Perez, E. Perez, G. Sanchez, J. Garcia, G. Lopez, G. Garcia, and E. Molins. Inorg. Chim. Acta, **355**, 33 (2003).
7. A. Ariafard, M.M. Amini, R. Fazaeli, and H.R. Aghabozorg. J. Mol. Struct. **636**, 49 (2003).
8. B.W. Wenclawiak, S. Uttich, H. Deiseroth, and D. Schmitz. Inorg. Chim. Acta, **348**, 1, (2003).
9. K.-H. Yih, G.-H. Lee, S.-L. Huang, and Y. Wang. J. Organomet. Chem. **665**, 114 (2003).
10. A.W. M. Lee, W.H. Chan, H.C. Wang, and M.S. Wang. Synth. Commun. **19**, 547 (1989).
11. I. Degani and R. Fochi. Synthesis, 365 (1978).
12. T.R. Burke, Jr., B.S. Bajwa, A.E. Jacobson, K.C. Rice, R.A. Streaty, and W.A. Klee. J. Med. Chem. **27**, 1570 (1984).
13. W. Walter and K.D. Bode. Angew. Chem., Int. Ed. Engl. **6**, 281 (1967).
14. (*a*) E. Lieber and R. Orlowski. J. Org. Chem. **22**, 88 (1957); (*b*) C.M. Buess. J. Am. Chem. Soc. **77**, 6613 (1955).
15. (*a*) D.L. Fox, J.T. Ruxer, J.M. Oliver, K.L. Alford, and R.N. Salvatore. Tetrahedron Lett. **45**, 401 (2004); (*b*) R.N. Salvatore, J.A. Ledger, and K.W. Jung. Tetrahedron Lett. **42**, 6023 (2001).
16. R.N. Salvatore, S. Sahab, and K.W. Jung. Tetrahedron Lett. **42**, 2055 (2001).
17. R.N. Salvatore, S.I. Shin, A.S. Nagle, and K.W. Jung. J. Org. Chem. **66**, 1035 (2001).
18. W. McGhee, D. Riley, K. Christ, Y. Pan, and B. Parnas. J. Org. Chem. **60**, 2820 (1995).
19. (*a*) B. Guo, Z. Ge, T. Cheng, and R Li. Synth. Commun. **31**, 3021 (2001); (*b*) R.-T. Li, M.-S. Cai. Synth. Commun. **29**, 65 (1999); (*c*) Z. Ge, R. Li, and T. Cheng. Synth. Commun. **29**, 3191 (1999).
20. N. Azizi, F. Aryanasab, L. Torkiyan, A. Ziyaei, and M.R. Saidi. J. Org. Chem. **71**, 3634 (2006).
21. (*a*) P.A. Grieco (Editor). Organic synthesis in water. Blackie Academic and Professional, London. 1998; (*b*) C.J. Li and T.H. Chang. *In* Organic reactions in aqueous media. Wiley, New York. 1997; (*c*) S. Narayan, J. Muldoon, M.G. Finn, V.V. Fokin, H.C. Kolb, and K. B. Sharpless. Angew. Chem., Int. Ed. Engl. **44**, 3275 (2005).
22. A. Ziyaei-Halimjani, and M.R. Saidi. Journal of Sulfur Chemistry, **26**, 149 (2005).
23. (*a*) N. Azizi and M.R. Saidi. Org. Lett. **7**, 3649 (2005); (*b*) A. Ziyaei-Halimjani, N. Azizi, and M.R. Saidi. J. Mol. Catalysis A, **238**, 138 (2005); (*c*) A. Ziyaei-Halimjani, N. Azizi, and M.R. Saidi. J. Sci. I. R. Iran, **16**, 37 (2005); (*d*) F. Rajabi and M.R. Saidi. Synth. Commun. **35**, 483 (2005); (*e*) N. Azizi and M.R. Saidi. Can. J. Chem. **83**, 505 (2005); (*f*) F. Rajabi and M.R. Saidi. Synth. Commun. **34**, 4179 (2004). (*g*) N. Azizi and M.R. Saidi. Synth. Commun. **34**, 1207 (2004); (*h*) N. Azizi and M.R. Saidi. Organometallics, **23**, 1457 (2004); (*i*) N. Azizi and M.R. Saidi. Tetrahedron, **60**, 383 (2004); (*j*) N. Azizi, F. Rajabi, and M.R. Saidi. Tetrahedron Lett. **45**, 9233 (2004); (*k*) N. Azizi and M.R. Saidi. Eur. J. Org. Chem. 4630 (2003). (*l*) N. Azizi and M.R. Saidi. J. Organomet. Chem. **688**, 283 (2003).

© 2006 NRC Canada

Reactivity of mesoporous palladium yttria-stablilized zirconia for solution phase reactions

Carl Poulin, Matthew A. Brown, Yamile A. Wasslen, Catherine M. Grgicak, Keith Fagnou, and Javier B. Giorgi

Abstract: A reduced mesoporous 5% Pd-YSZ precatalyst was observed to be very active for the Heck reaction providing up to 770,000 TON. Three-phase tests have experimentally confirmed that a leached homogeneous species is responsible for the activity. Residual Pd concentration in solution is minimal (<0.10 ppm) and therefore this material has potential applications because it can be easily removed by filtration. This paper describes the synthesis, structural characterization, and catalytic activity of the mesoporous Pd-YSZ material. The material was prepared using an amphiphillic surfactant templating method resulting in a homogeneous dispersion of Pd in an ordered mesoporous structure. Material properties were fully characterized using X-ray diffraction, surface area analysis, and electron microscopy.

Key words: mesoporous catalysts, palladium, yttria-stabilized zirconia, Heck reaction, Pd-YSZ.

Résumé : On a observé qu'un précatalyseur 5% Pd-YSZ mésoporeux réduit est très actif pour la réaction de Heck qui peuvent fournir jusqu'à 770,000 TON. Des essais en trois phases ont permis de confirmer expérimentalement qu'une espèce homogène lessivée est responsable pour cette activité. La concentration résiduelle de palladiium dans la solution est minimale (<0,10 ppm); ce matériau a donc des applications potentielles compte tenu du fait qu'il peut être récupéré par filtration. Dans ce travail, on décrit la synthèse, la caractérisation de la structure et l'activité catalytique du matériel mésoporeux Pd-YSZ. Ce produit a été préparé en faisant appel à la méthode de matrice à agent de surface amphiphile qui fournit une dispersion homogène du palladium dans une structure mésoporeuse ordonnée. Les propriétés du matériau ont été complètement caractérisées à l'aide de la diffraction des rayons X, l'analyse de la superficie de la surface et la microscopie électronique.

Mots clés : catalyseurs mésoporeux, palladium, yttrium stabilisé par du zirconium, réaction de Heck, Pd-YSZ.

[Traduit par la Rédaction]

Introduction

Palladium-catalyzed transformations have become widespread in the construction of new carbon–carbon and carbon–heteroatom bonds (1–5). Recent advances in the development of new homogeneous palladium catalysts have enabled these transformations to be carried out even with very deactivated substrates such as aryl chlorides under mild conditions (6). In the context of product purity, however, the use of homogeneous catalysts has detractions including the fact that the palladium must be removed from the organic product at the end of the reaction (7, 8). This can sometimes be very challenging and costly. With this challenge in mind, chemists have been studying the use of heterogeneous palladium catalyst systems as viable alternatives to the more intensely studied homogeneous catalysts (9). In recent years, a variety of heterogeneous supports have appeared including carbon, silicates, zeolites, and block copolymers (10–16). Alternatively, homogeneous catalysts have been "heterogenized" via immobilization of active homogeneous catalysts on various solid supports (17–26). With all of these heterogeneous catalysts, however, there is debate with respect to the true nature of the active catalyst (27). Some catalysts do appear to function as true heterogeneous catalysts (28, 29), while others have been shown to be catalyst reservoirs (precatalysts) from which an active catalyst leaches into solution (28, 30–38). Analysis of these reactions is further complicated by a third option in which a release and capture mechanism involving catalyst leaching and subsequent readsorption onto the matrix support occurs upon reaction completion. Since the question of catalyst form is of paramount importance, more studies are warranted in this area, particularly when new catalysts and (or) supports are being designed and studied. Simple coupling reactions such as Heck or Suzuki can be used as the standard to test catalyst performance of heterogeneous catalysts.

In the design of heterogeneous catalysts, maximization of the active surface area is the key to performance together with the nature of the catalytic species. Metal catalysts such as palladium have been shown to be in their most active state when speciated as nanoparticles (39). In this state, a maximum of palladium sites are exposed while the catalytic properties are controlled by the electronic structure of the

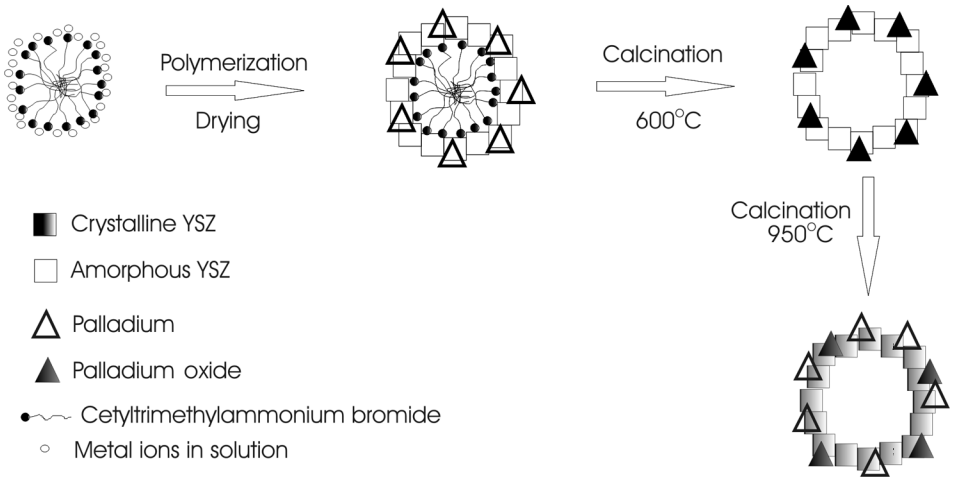
Received 15 July 2006. Accepted 9 September 2006. Published on the NRC Research Press Web site at http://canjchem.nrc.ca on 8 November 2006.

C. Poulin, M.A. Brown, Y.A. Wasslen, C.M. Grgicak, K. Fagnou, J.B. Giorgi.[1] Center for Catalysis Research and Innovation, Department of Chemistry, University of Ottawa, 10 Marie Curie, Ottawa, ON K1N 6N5, Canada.

[1]Corresponding author (e-mail: jgiorgi@uottawa.ca).

 doi:10.1139/V06-154 © 2006 NRC Canada

Fig. 1. Mechanism of formation of mesoporous Pd-YSZ.



nanoparticle and influenced by its support. The optimization of the active surface area was revolutionized with the discovery of mesoporous structures, which provide a maximum total surface area with channels of the appropriate size for reactant transport (40–42). Examples of the improved performance of mesoporous silica-based catalysts date back to their petrochemical origins (43) and enhanced properties continue to surface, as recently demonstrated for ethane hydrogenolysis and ethylene hydrogenation (44), hydrogenation of phenyl acetylene (45), and anti-stokes luminescence of encapsulated dyes (46). A particularly appropriate example has recently used mercaptopropyl modified silica to anchor Pd atoms to the SBA-15 zeolitic framework (16). The modified zeolite is an excellent Pd scavenger and has been used successfully as a Pd catalyst for low-turnover high-yield coupling reactions with minimal Pd leaching.

A considerable effort has been made over the past 15 years to obtain mesoporous metal oxide materials that possess enhanced properties in catalysis, charge transport, and host–guest affinities. Since the family of silicate mesoporous molecular sieves was first synthesized (40–42), efforts have been made toward the synthesis of mesoporous transition metal oxide materials (47–50) and, in particular, mesoporous yttria and zirconia materials have been recently developed (51–53). The general synthetic methodology to prepare mesoporous oxides uses an amphiphillic surfactant as a template. In solution, the surfactant agglomerates into micelles and the inorganic oxide framework grows around it. Upon removal of the organic species, a mesoporous framework remains. In many cases, the mesoporous framework is impregnated with the metal catalyst, however we used this methodology to create not only the support framework but also the homogeneous distribution of the nanoparticle-catalyst within the framework. Coproduction of the catalyst with the support produces a homogeneous distribution of the metal and is particularly suitable for high metal loadings where metallic connectivity and (or) conductivity is desired. For low metal loadings, coproduction ensures a homogeneous distribution of the catalyst in the porous framework. The obstacle of relatively low solubility of the metal precursors can be overcome by the synthesis of yttrium and zirconium glycolates as precursors for the preparation of yttria-stabilized zirconia (YSZ) with mesoporous structure (54–56).

In this paper, we report the synthesis and characterization of a versatile palladium catalyst supported on a mesoporous yttria-stabilized zirconia (YSZ) framework. These materials, which are characterized by a high surface area, have the potential to be used in a liquid–solid regime for the catalysis of organic reactions (57, 58), which has been validated by demonstrating high turn-over numbers in the Heck reaction. Catalyst structure along with reaction kinetics and mechanisms are discussed.

Experimental

Pd-YSZ preparation

The general synthesis involves the formation of yttrium and zirconium glycolates separately by reaction of $ZrCl_4$/$(OEt)_3$ with ethylene glycol. The solutions are combined and a Pd^{+2} source is added in appropriate proportion according to the desired loading. Cetyltrimethylammonium bromide (CTAB) is added as a template to form the mesoporous structure. The solution is allowed to age and finally the resulting precipitate is filtered, washed, and dried. This "as-synthesized" (dried) material consists of the micellar CTAB array around which the Pd-YSZ matrix has been formed. Upon calcination, the organic component is eliminated giving rise to the porous structure (Fig. 1).

Details of the procedure are as follows. Zirconium ethoxide (5.0 g, Strem Chemicals Inc., 99.9+%) and 2.4 equiv. of NaOH (1.8 g) were added to a flask containing excess ethylene glycol (51 mL, spectroscopic grade, Sigma-Aldrich Chemical Ltd.). The resulting mixture was then refluxed at 180 °C under flowing nitrogen for 24 h. Excess ethylene glycol was distilled off leaving a thick yellowish gel (zirconium glycolate). Separately, yttrium glycolate was prepared by adding yttrium acetate tetrahydrate (1.2 g, Alfa Aesar, 99.9%) to ethylene glycol (31 mL) and stirring. The zirconium and yttrium glycolates were then mixed in a dropwise fashion while the zirconium glycolate was still hot (~50 °C). The resulting solution was added to a polypropylene bottle containing a Pd^{+2} source ($Pd(NO_3)_2$, Sigma-Aldrich Chemical Ltd., 99.999%, 2.0 mL solution 10 wt% in

© 2006 NRC Canada

10 wt% nitric acid), cetyltrimethylammonium bromide (CTAB, Sigma-Aldrich Chemical Ltd., 4.1 g), NaOH (1.7 g), and water (120 mL). The mixtures were stirred at RT for 25 min and then put into an oven for 5 days at 80 °C. The solid products obtained were collected by vacuum filtration and washed two times with water to remove residual chlorine and CTAB. Samples were then dried at 120 °C for 6 h and denoted as-synthesized. This procedure produces a Pd loading of 5%; for different loading the Pd concentration is simply adjusted.

Calcination to 600 °C or 950 °C was performed in air for 2 h to ensure the crystallization of the YSZ. The calcination procedure also produces PdO. When reduced Pd is required, reduction was performed at 500 °C under H_2 flow for 2 h for samples previously calcined to 600 °C, and at 800 °C under N_2 flow for 2 h for samples previously calcined to 950 °C. A reduced material containing 5 mol% Pd and calcined to 950 °C prior to reduction shall be denoted as 5%Pd-YSZ950 and one precalcined to 600 °C as 5%Pd-YSZ600.

Pd-YSZ characterization

Powder composition and crystallite sizes were determined by X-ray diffraction (XRD) (Phillips PW1830) using Cu K_α radiation with a wavelength of 1.54 Å. Crystalline phases were assigned using the Powder Diffraction File database (ICCD, 2001). The crystallite size analysis of each phase was performed using the Williamson–Hall methodology, which takes into account crystallite strain (59). Vibrational characterization of the powders prior to calcination was determined using Attenuated Total Reflection Fourier transform IR spectroscopy (ATR-FTIR) (Bruker Equinox 55). The BET surface area of the calcined powders were determined after reduction in flowing H_2 (5% in N_2) at 500 °C for 2 h, using a Quantachrome Autosorb 1-C instrument. A BJH analysis provides pore size information and the average pore size was calculated using the Kelvin equation.

General procedure for the Heck reaction of butylacrylate with iodobenzene

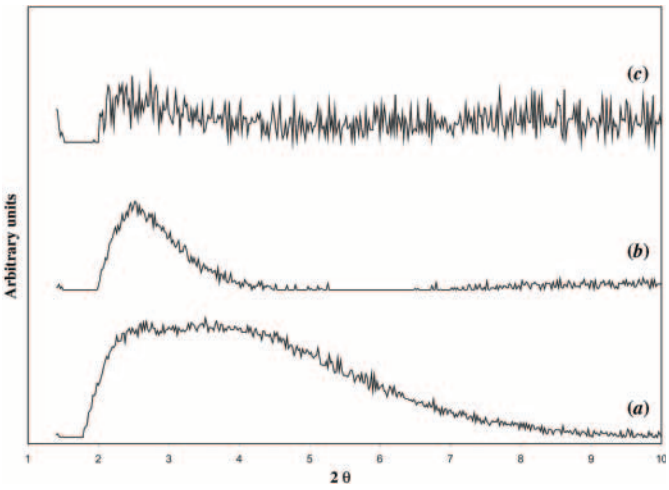
To a round-bottomed flask fitted with a reflux condenser was added iodobenzene (4.0 mmol, 0.45 mL), butylacrylate (4.8 mmol, 0.69 mL), *N,N*-diisopropylethylamine (DIPEA) (8 mmol, 1.4 mL), and *N,N*-dimethylformamide (DMF) (1.4 mL). To this solution was added the precatalyst 5% Pd-YSZ (0.004 mmol, 9.7 mg). The reaction was then heated to 140 °C. Reaction progress was monitored by GC-MS analysis of the crude reaction mixture against a decane internal standard. For all reactions, the mol ratio iodobenzene–butylacrylate–DIPEA was kept at 1:1.2:2.

Triple phase test

Preparation of resin

To a mixture of Wang resin (0.3 equiv.) and iodobenzene (1 equiv.) in DMF (0.1 mol/L) was added dicyclohexylcarbodiimide (1 equiv.) and a few grains of 4-dimethylaminopyridine as catalyst. The reaction mixture was heated at 60 °C for 4 days. The solution was filtered and washed twice with each of the following solvents: water, methanol, dichloromethane (DCM), and diethyl ether.

Fig. 2. Small angle XRD pattern of 20%Pd-YSZ for (*a*) as-synthesized, (*b*) calcined to 600 °C, and (*c*) calcined to 950 °C.



Capping of the unreacted hydroxyls on the resin

To a suspension of the resin (1 equiv.) in dichloromethane (0.1 mol/L) was added acetic anhydride (5 equiv.) and pyridine (5 equiv.). The reaction was stirred for 24 h at RT. The reaction mixture was filtered and washed twice with each of the following solvents: water, methanol, DCM, and ether to afford the acetate protected resin.

Reaction and cleavage of compound from the resin

To a mixture of acetate protected resin (1 equiv.) was added butyl acrylate (3 equiv.), DIPEA (3 equiv.), Pd-YSZ (0.05 equiv.) in DMF (0.16 mol/L). The reaction mixture was heated at 130 °C for 3 h. The resin (1 equiv.) was filtered and washed thoroughly before being stirred in a 1:1 mixture of trifluoroacetic acid and dichloromethane (0.5 mol/L) for 2 h. The resulting mixture was filtered and washed twice with each of the following solvents: methanol, DCM, and ether. The filtrate was put under reduced pressure at 70 °C to remove the volatiles as well as the trifluoroacetic acid. This afforded compound **5** (eq. [1]).

Thiol scavenger test

To a suspension of thiol resin (0.5 equiv.) was added iodobenzene (1 equiv.), butyl acrylate (1.2 equiv.), DIPEA (2 equiv.), and Pd-YSZ (0.01 equiv.) in DMF (2.7 mol/L). The reaction mixture was heated to 130 °C and monitored by GC. After prolonged reaction time, no greater than 2% conversion was detected.

Results and discussion

Pd-YSZ material properties

The as-synthesized material containing the residual hydrocarbon micelles possesses long-range order with d-spacing of 40 Å, as seen by the low-angle peak in the XRD pattern (Fig. 2). Upon calcination in air to 600 °C, the hydrocarbon is eliminated leaving a porous mesostructure with d-spacing of 41 Å. The low-angle peak is decreased in intensity, consistent with a partial disruption of the long-range order. The observed change in d-spacing is consistent with a thickening of the pore walls as the crystals of YSZ become larger (56).

© 2006 NRC Canada

Finally, upon calcination to 950 °C the material is described as having lost its long-range order.

The shape of the low-angle peak for the as-synthesized material is observed as very broad and asymmetrical. Such a shape has been observed by Ozin and coworkers (54–56) in similar materials and discussed in terms of a poor long-range order of the mesoporous structure. An alternative explanation is the superposition of two peaks for different orientations of the long-range order structure (53). Kim et al. (53) assigned their peak at $2\theta \approx 3.9°$ to the (110) reflection of a hexagonal arrangement of meso-zirconyl chloride. In this case, the metastable structure present when the surfactant is still in the pores is disturbed when the organic component is removed, leaving a single peak in the XRD pattern of the calcined samples.

The mesoporous structure of the material calcined to 600 °C is also reflected by the intermediate surface area, typically in the range of 150 $m^2\ g^{-1}$, and a slightly asymmetric pore size distribution that peaks at 19 Å in diameter with an average pore size diameter of 26 Å, as calculated by the Kelvin equation. This value is smaller than those obtained for perfectly structured mesoporous materials such as zeolites, but it is an order of magnitude larger than most commercial YSZ catalyst powders (Maketech Materials 70% NiO/8YSZ, 9.8 $m^2\ g^{-1}$ and 34% NiO/8YSZ, 6.63 $m^2\ g^{-1}$). The surface area decreases to ~10 $m^2\ g^{-1}$ upon calcination to 950 °C indicating the predominant collapse of the porous structure.

Removal of the pore-forming molecule CTAB from the material is achieved during the calcination process and is complete by 600 °C. This is illustrated in Fig. 3, which shows ATR-FTIR spectra of a sample as-synthesized and after calcination. The two peaks present at 2850 and 2916 cm^{-1} in the as-synthesized sample are characteristic of the C–H stretching modes in the CTAB long chain. These peaks are removed upon calcination. The regions around 1500 and 3400 cm^{-1} are characteristic of water and can be seen to decrease substantially upon calcination. Peaks at ~1000 cm^{-1} are associated with yttrium and (or) zirconium species, but their identification is difficult due to the large broadening (60).

It is interesting to note that the CTAB species are not removed at a single temperature and in fact they appear to be partially decomposed and trapped within the porous structure. Thermogravimetric analysis in helium shows weight loss at several distinct temperatures (Fig. 4). Correlation of the weight loss with mass analysis shows that in the temperature range below 60 °C, water is the main component desorbed. The hydrocarbon moieties represented by the ethyl group (*m*/*e* = 29) are desorbed in the subsequent two peaks at 280 and 440 °C. Trapping and decomposition of the CTAB is suggested by the simultaneous observation of zirconium (*m*/*e* = 91) and the tertiary amine group (*m*/*e* = 57), which come out from the matrix at 440 °C. These observations have direct implications on the stability of the mesoporous structure. The binding and (or) trapping of CTAB to the YSZ network is sufficiently strong that the removal of the surfactant disrupts the pores. A more inert surfactant may improve the thermal stability of the YSZ porous structure.

Palladium and YSZ crystallites are present in the material as individual phases as seen from their characteristic powder diffraction pattern. The large width of their peaks suggests extremely small crystallite sizes, particularly for YSZ. Increasing the calcination temperature results in an increase in size of the YSZ crystallites, as observed by a decrease in peak widths in the XRD patterns (Fig. 5).

During the calcination process, the crystallites of palladium originally present (Fig. 5) also increase in size. However, as the temperature rises Pd is oxidized to PdO. At a temperature of 840 °C, PdO is reduced to Pd once again. The reduction of PdO to Pd can be readily observed in the TGA experiment performed in air as a sharp decrease in mass (Fig. 6). It is interesting to note that the reoxidation of Pd to PdO during cooling occurs more gradually around 650 °C, a hysteresis of 190 °C. The observed temperature of PdO reduction in air is high for zirconia-based catalysts, but it is consistent with literature (61–63) for other Pd-oxide catalysts. The ratio of oxidized vs. metallic palladium observed in the XRD (at RT, after calcination to 950 °C, Fig. 5) depends on the sample cooling rate in air. Calcination to

Fig. 3. ATR-FTIR of 20%Pd-YSZ for (*a*) as-synthesized and (*b*) calcined to 600 °C. The CTAB spectrum is shown for comparison.

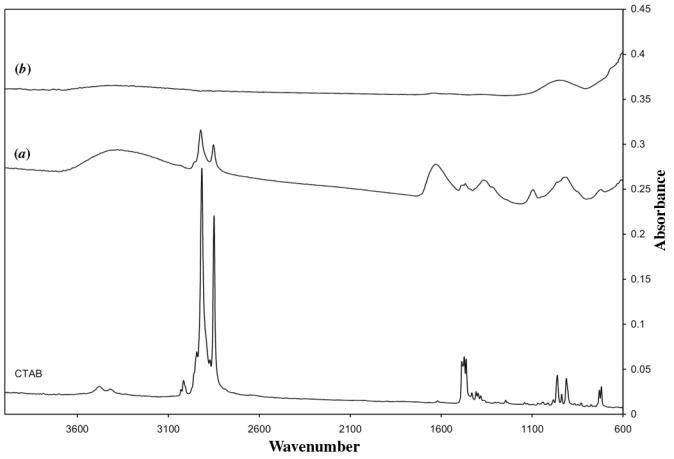
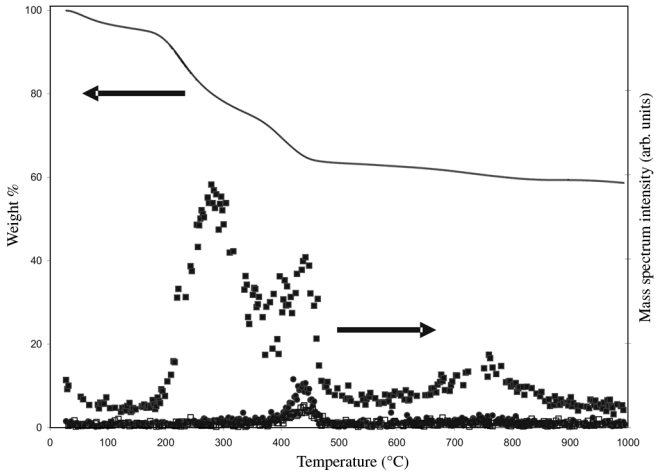


Fig. 4. Thermogravimetric analysis of 20%Pd-YSZ in Helium. The evolution of *m*/*e* = 29 (■), *m*/*e* = 57 (●), and *m*/*e* = 91 (□) as a function of temperature are also shown.



© 2006 NRC Canada

Fig. 5. XRD pattern of 20%Pd-YSZ for (*a*) as-synthesized, (*b*) calcined to 600 °C, and (*c*) calcined to 950 °C, with Pd (▲), PdO (■), YSZ (●) peaks.

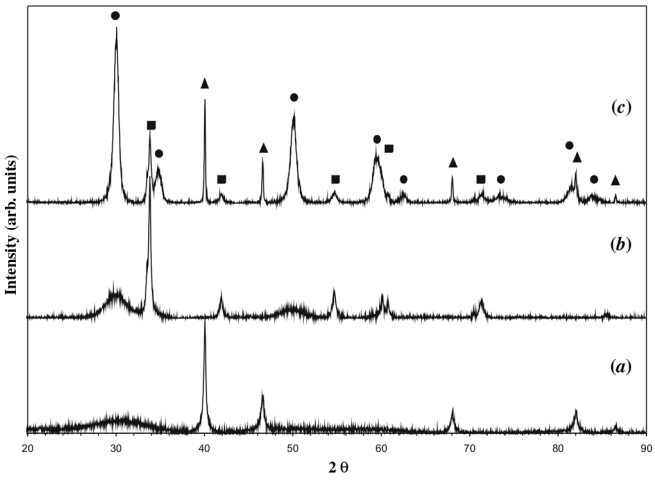


Fig. 6. Thermogravimetric analysis of 20%Pd-YSZ in air. Heating and cooling traces are shown. PdO→Pd (■) upon heating, T = 860 °C, Pd→PdO upon cooling (▲), T = 680 °C.

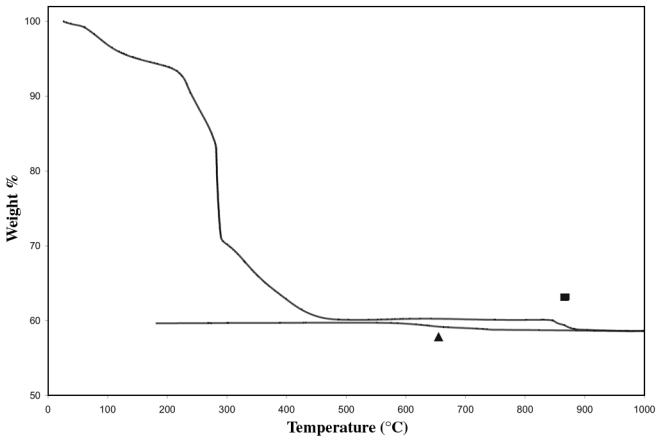


Table 1. Crystallite sizes for selected materials.

Sample composition	Conditions	Pd crystallites (nm±esd)[a]	PdO crystallites (nm±esd)[a]	YSZ crystallites (nm±esd)[a]
5% Pd-YSZ	Calc. 600 °C	Not present	9.3±2.7	5.0±0.5
	Calc. 950 °C	29.8±9.4[b]	21.6±1.4[b]	14.1±0.2
20% Pd-YSZ	As-synthesized	41.8±6.9	Not present	Amorphous
	Calc. 600 °C	Not present	39.6±6.5	4.2±0.1[b,c]
	Calc. 950 °C	133±32	14.8±1.1	21.8±1.1
50% Pd-YSZ	As-synthesized	34.8±4.0	Not present	Amorphous
	Calc. 600 °C	Not present	19.9±2.9	4.7±0.1[b,c]
	Calc. 950 °C	90±16	22.3±2.0	21.1±1.2

Note: Crystallite sizes were measured by XRD using the Williamson–Hall analysis. Multiple peak analysis consisted of, 4 peaks for Pd, 6 peaks for YSZ, and 4 peaks for PdO.

[a]Estimated standard deviation is based on the peak fitting/refinement routine (JADE diffraction analysis).

[b]Single peak analysis (111) performed by Scherrer method.

[c]Only a few broad peaks are available for analysis. YSZ is mostly amorphous in these samples.

600 °C in air produces only the PdO phase. To obtain metallic Pd exclusively, the samples can be calcined and cooled in an inert atmosphere.

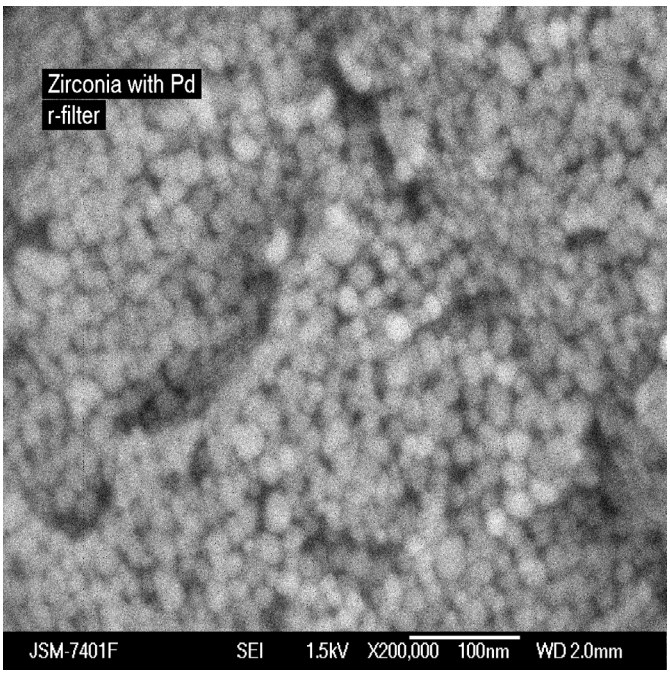
Palladium sintering effects in heterogeneous catalysis are a general concern for temperature treatments above 800 °C because coarsening leads to a decrease in catalytic activity (61–63). In these mesoporous Pd-YSZ materials, palladium crystallites remain constant in size up to ~800 °C during the oxidation and subsequent reduction process. Calcination to higher temperatures does increase the Pd crystallite size, but only to a limited extent (Table 1). The ultimate average crystallite size upon calcination depends on the palladium content with a maximum coarsening of three-fold observed for 20% Pd loading. The observed increase in crystallite size compares very well to increases of over 10-fold for Pd-Al_2O_3 (64, 65) and nanoengineered 3%Pd-YSZ (66) catalysts at similar temperatures. For all samples, the YSZ average crystallite size after calcination to 950 °C is around 20 nm, regardless of Pd loading. The relatively stable mesostructure of the YSZ, which partially survives the calcination process, seems to be responsible for the low degree of sintering of palladium. Figure 7 shows an SEM image of 5%Pd-YSZ950R (reduced palladium) where the homogeneous nature and the small particle size of the material can be assessed.

Application to the Heck Reaction

A 5 mol% material with the highest possible surface area was chosen for catalytic experiments. The mesoporous 5 mol% Pd-YSZ framework possesses long-range order with a d-spacing of 40 Å (by XRD). Crystallites sizes of 10 nm and 5 nm for Pd and YSZ respectively were measured for samples calcined to 600 °C. This highly reactive 5%Pd-YSZ600R has a total surface area of 150 m^2/g with an average pore size diameter of 26 Å. For comparison, a 5% Pd loading material calcinated to 950 °C in the reduced form was chosen (5%Pd-YSZ950R). Higher temperatures during the material preparation process disrupt the long-range order of the mesoporous structure and lead to the overall reduction of surface area to 10 m^2/g. However, up to 1000 °C the increase in the crystallite size of the two components is relatively small, ~2×. Generally, catalytic materials with smaller total surface areas are not expected to perform as well under reaction conditions. However, for selected reactions the

© 2006 NRC Canada

Fig. 7. Scanning electron micrograph of 5%Pd-YSZ950. Image is taken with an r-filter for improved contrast. High palladium concentration areas appear brighter, although Pd is homogeneously distributed in this sample as confirmed by energy dispersion measurements.



high-temperature treatment may be preferred because it adds mechanical, chemical, and thermal stability to the catalysts, which have a direct impact on the reusability of the catalysts.

Preliminary work showed that both of these precatalysts were active for the Heck reaction, even prior to the reduction step. The subsequent sections compare the performance of these two precatalysts and provide a discussion of their effectiveness and the reaction mechanism involved for a standard Heck coupling reaction.

Reaction optimization

With an active catalyst in hand, the reaction conditions were optimized with respect to solvent, base, temperature, and concentration. In early screens, dimethylformamide (DMF) emerged as the optimal solvent. A base scan also revealed that the best outcomes were achieved with organic bases such as diisopropylethylamine (DIPEA). Inorganic bases such as potassium bicarbonate lead to lower turn-over numbers (TONs) and slower reaction. All subsequent optimization studies were performed in DMF with DIPEA as base.

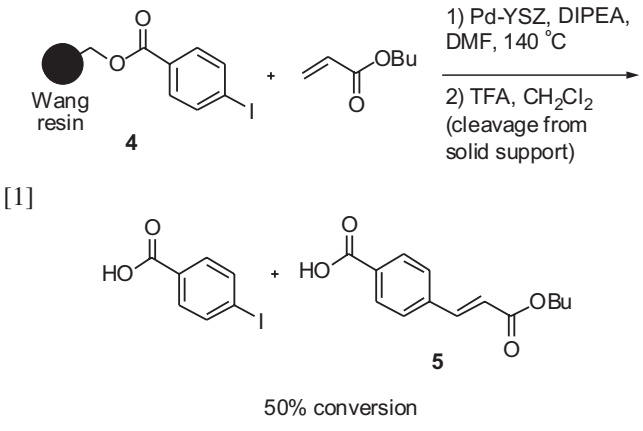
Initial optimization reactions were performed with 5%Pd-YSZ950R (reduced Pd). From three experiments performed at 120, 130, and 140 °C, it was determined that faster reactions and improved TONs were achieved at 140 °C. For example, after 60 min of reaction time less than 10% conversion was observed at 120 °C compared with 47% and 65% conversion at 130 and 140 °C, respectively (Table 2, entries 1–3).

These reactions are very sensitive to concentration as illustrated in Table 2, entries 4–7. Four different iodobenzene concentrations were assayed (0.2, 0.5, 1.0, and 1.2 mol/L) and each of the reactions was analyzed after 30 min. At these intervals, neither reaction at 0.2 and 0.5 mol/L showed any conversion to product. On the other hand, reactions performed at 1.0 and 1.2 mol/L had progressed to 35% and 75% conversion after 30 min, respectively, showing that a faster initial reaction occurs at elevated concentration. It is interesting to note that in Table 2, entries 4–7, the substrate to catalyst ratio (S/C) is kept constant and therefore the effect of concentration is different from the homeopathic effect described by de Vries (27) where a large S/C ratio prevents Pd nucleation and subsequent deactivation of the catalytic species.

A comparison of the two precatalysts 5%Pd-YSZ950R and 5%Pd-YSZ600R was carried out. From these experiments (Table 2, entries 8–11), the 5%Pd-YSZ600R emerges as a superior catalyst as evidenced by the percentage conversion at 30 min (Table 2, entry 10 vs. 8) and 60 min (Table 2, entry 11 vs. 9). With these conditions in hand, reactions were performed to determine the maximal TON that could be achieved with this new catalyst. We were delighted to see that under optimal conditions, up to 770,000 TON could be achieved after approximately 7 days (Table 2, entry 12).

Elucidation of the active species

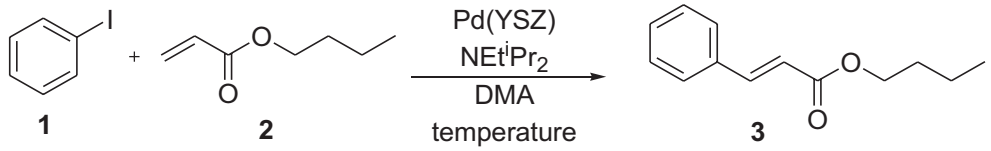
With an active catalyst in hand, we were interested in determining unequivocally if this was a heterogeneous catalyst or if palladium was leaching off of the support to produce an active homogeneous species. Two different approaches were taken to answer this question based on the three-phase test concept (67–70). In the first case, the aryl halide was anchored to a Wang resin (71). If the true catalyst in these processes was purely heterogeneous then interaction between the supported substrate and the matrix bound catalyst should not be possible, thus preventing reaction. In contrast, if palladium leaching occurs and if this soluble palladium species is catalytically active, then Heck reaction at the solid-supported **4** should be observed. When supported **4** was reacted under standard conditions followed by separation of the solid phase, washing of the Wang resin, and cleavage of the substrate–product mixture from the solid support via treatment with trifluoroacetic acid in dichloromethane (72, 73), approximately 50% conversion to **5** was observed (eq. [1]). This lends strong support to the notion that a homogeneous active catalyst is generated under the reaction conditions via leaching from the YSZ support.



[1]

© 2006 NRC Canada

Table 2. Heck reaction optimization.



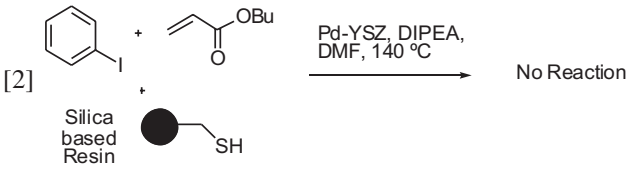
Entry	Catalyst	Substrate–Catalyst Ratio	Temp (°C)	Conc. [B][a]	Reaction Time (min)	% Conc.[b]
1	A	100	140	0.2	60	65
2	A	100	130	0.2	60	47
3	A	100	120	0.2	60	9
4	A	1 000	140	0.2	30	0
5	A	1 000	140	0.5	30	0
6	A	1 000	140	1.0	30	35
7	A	1 000	140	1.2	30	75
8	A	1 000	130	0.5	30	13
9	A	1 000	130	0.5	60	49
10	B	1 000	130	0.5	30	41
11	B	1 000	130	0.5	60	61
12	B	1 000 000	140	1.0	7 days	77

Note: Catalyst A: 5%Pd-YSZ950R and B: 5%Pd-YSZ600R. Conditions: Iodobenzene, butylacrylate, *N,N*-diisopropylethylamine (DIPEA), and *N,N*-dimethylformamide (DMF) added to a round-bottomed flask followed by the addition of the catalyst and heating to the indicated temperature.

[a]Concentration of iodobenzene.

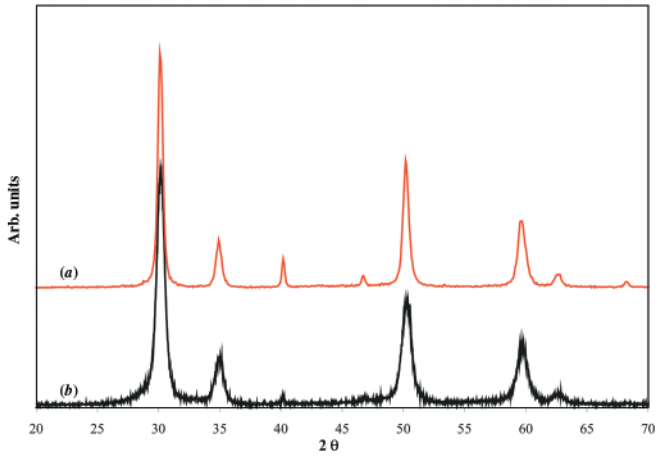
[b]Determined by GC-MS analysis of the crude reaction mixture against a decane internal standard.

To determine if an active heterogeneous catalyst species was also contributing to the direct arylation reaction, another three-phase test was conducted. In this experiment **1** was reacted under standard conditions in the presence of a silica supported thiol-based scavenger resin. Since thiols are known to have a very high affinity for palladium, the presence of this heterogeneous metal scavenger should sequester the homogeneous catalyst as it is produced. On the other hand, a heterogeneous palladium species that is catalytically active should not be poisoned by the presence of the heterogeneous metal scavenger. After 16 h, less than 5% of the desired product had been formed while an identical reaction run in parallel without the scavenger resin reached 100% conversion (eq. [2]). This indicates that the heterogeneous palladium is not catalytically active on the timescale examined and that the observed reactivity arises from the in situ generation of a homogeneous catalyst.



Having shown that the mechanism of reaction is homogeneous, we investigated how much Pd is lost during the process. As it was not possible to identify Pd in solution, we determined the amount of palladium before and after reaction to obtain an upper limit to the amount of palladium remaining in solution after reaction. Figure 8 shows the XRD pattern of catalysts 5%Pd-YSZ950R before and after undergoing a reaction. XRD was chosen to search for PdO, which could have been formed during reaction, but was not observed. Although XRD is not a traditional quantitative technique, we can clearly see that the ratio of Pd to YSZ has

Fig. 8. Powder XRD pattern of 5%Pd-YSZ950. Diffractograms have been normalized to the peak at 2θ = 30° (the most intense YSZ peak) for (*a*) before undergoing reaction and (*b*) after undergoing reaction.



decreased substantially. Since YSZ is not affected by the reaction, it can be considered as an internal standard for the XRD measurement allowing us to use the intensity ratio of the variable (Pd) to the standard (YSZ) for quantization purposes. A quantitative value can be obtained by measuring the intensity ratio of the most intense peaks for Pd and YSZ (at 40 and 30 °, respectively) and comparing this to a calibration curve obtained for variable amounts of Pd in YSZ. The technique cannot measure atomic Pd in the sample, but after a sintering treatment to allow palladium aggregation, no change was observed. If we consider that all the Pd not present in crystalline form in our sample has remained in solution, we obtain an upper limit to the amount of Pd leached. Estimating that about 80% of the Pd was lost during reac-

© 2006 NRC Canada

tion, this would correspond to ~0.10 ppm of Pd in the final solution (e.g., Table 2, entry 12). This value is consistent with best effort for Pd on activated carbon (0.05 ppm) (74) and only slightly worse than the mercaptopropyl-modified silica (0.003 ppm), which is a Pd scavenger (16).

Structure–reactivity analysis

The activity of different precatalysts can be analyzed in terms of total number of turn-overs and how fast that TON can be achieved, namely kinetics. In fact, the optimization of reaction parameters will be most sensitive to the kinetics of reaction. For these reasons, we chose the lower surface area catalyst, which we expected would be slower, to optimize the other reaction parameters. Table 2 (entries 1–9) shows a subset of the reaction optimization data for the Heck reaction using 5%Pd-YSZ950R.

Our previous work demonstrated that if reactions were allowed sufficient time (24 h), the conversion for 100:1 (substrate–catalyst) reactions was >95% for a wide range of conditions. Therefore, the difference in reactivity for the two catalysts was assessed by comparison of the percentage conversion vs. time for different catalysts and conditions. For example, entries 8–11 in Table 2 for a substrate–catalyst ratio of 1000:1 show that after 0.5 h of reaction 5%Pd-YSZ600R has a TON 3× higher than 5%Pd-YSZ950R. This result is consistent with the heterogeneous catalysis literature since more active catalyst is usually exposed in higher surface area materials. In this case, because of the homogeneous nature of the reaction mechanism the higher surface area and smaller Pd particle size of 5%Pd-YSZ600R facilitate the extraction of Pd to solution, thereby making the reaction faster.

However, the support seems to be playing a more important role than simply controlling the surface area of available palladium. It is interesting to note that the activity of the catalyst is also reflected in the total number of turn-overs. 5%Pd-YSZ600R attains 770,000 turn-overs after 7 days, approximately twice as much as 5%Pd-YSZ950R. This effect may be accounted for by the mesoporous structure of 5%Pd-YSZ600R, which may be preventing the active homogeneous Pd species from diffusing into the bulk of the solution (encapsulation) where it can be easily de-activated (27).

Despite the homogeneous nature of the catalysts due to leaching of Pd into solution, 5%Pd-YSZ600R compares well with other heterogeneous precatalysts discussed in the literature. While TONs for homogeneously catalyzed Heck reactions have been documented in excess of 8.0×10^6 (75), TONs with heterogenous precatalysts are typically much lower. In rare cases, TONs in slight excess of 10^6 have been obtained demonstrating that the Pd-YSZ catalyst examined in these studies compares favourably with other catalyst systems. The highest value we have found in the literature is slightly higher (TON 1,150,000 (29, 76)) for a complex polymer-based ligand-coordinated palladium catalyst. In contrast, palladium supported on activated carbon, with similar cost per gram of catalyst as our precatalyst, has been shown to achieve TONs of 36,000 (74, 77).

Conclusions

Pd-YSZ has been prepared using an amphiphillic surfactant templating method resulting in a homogeneous dispersion of Pd on an ordered mesoporous structure. The Pd particle size and composition properties are easily controllable. The material is resistant to high temperatures, although some coarsening is observed and the long-range order is maintained only up to intermediate temperatures.

Reduced Pd-YSZ showed high activity for the Heck reaction. Up to 770,000 TON were achieved with a 5% Pd-loaded catalyst having a surface area of 150 m^2/g. This result compares favourably with other heterogeneous precatalysts in this reaction. Three-phase tests were conducted to ascertain the nature of the active catalyst species. These tests revealed that a homogeneous catalyst is leaching from the solid support and that the palladium that remains on the matrix is not responsible for the observed reactivity. Despite the homogeneous nature of the active species, the heterogeneous precatalyst remains interesting because it can be easily filtered out leaving behind only residual amounts of Pd (<0.10 ppm).

Acknowledgments

The authors thankfully acknowledge funding from the Natural Sciences and Engineering Research Council of Canada (NSERC) and the contribution of the Center for Catalysis Research and Innovation at the University of Ottawa.

References

1. J. Tsuji. Palladium reagents and catalysts: innovations in organic synthesis. John Wiley & Sons, New York, 1995.
2. G. Poli, G. Giambastiani, and A. Heumann. Tetrahedron, **56**, 5959 (2000).
3. J. Tsuji. Transistion metal reagents and catalysts: innovations in organic synthesis. John Wiley & Sons, New York, 2000.
4. F. Diederich and P.J. Stang. Metal catalyzed cross-coupling reactions. Wiley-VCH, New York, 1998.
5. E.-I. Negishi and A. De Meijere. Handbook of organopalladium chemistry for organic synthesis. Wiley-VCH, New York, 2002.
6. A.F. Littke and G.C. Fu. Angew. Chem. Int. Ed. **41**, 4176 (2002).
7. C.E. Garrett and K. Prasad. Adv. Synth. Catal. **346**, 889 (2004).
8. K. Konigsberger, G.-P. Chen, R.R. Wu, M.J. Girgis, K. Prasad, O. Repic, and T.J. Blacklock. Org. Process Res. Dev. **7**, 733 (2003).
9. M.L. Toebes, J.A. van Dillen, and K.P. de Jong. J. Mol. Catal. A: Chem. **173**, 75 (2001).
10. H.-U. Blaser, A. Indolese, A. Schnyder, H. Steiner, and M. Studer. J. Mol. Catal. A: Chem. **173**, 3 (2001).
11. A.L. Dantas Ramos, P. da Silva Alves, D.A.G. Aranda, and M. Schmal. Appl. Catal. A: Gen. **277**, 71 (2004).
12. C.P. Mehnert and J.Y. Ying. Chem. Commun. (Cambridge), 2215 (1997).
13. C.P. Mehnert, D.W. Weaver, and J.Y. Ying. J. Am. Chem. Soc. **120**, 12289 (1998).
14. M.K. Richmond, S.L. Scott, and H. Alper. J. Am. Chem. Soc. **123**, 10521 (2005).
15. K. Okumura, K. Nota, K. Yoshida, and M. Niwa. J. Catal. **231**, 245 (2005).
16. C.M. Crudden, M. Sateesh, and R. Lewis. J. Am. Chem. Soc. **127**, 10045 (2005).
17. N.E. Leadbeater and M. Marco. Chem. Rev. **102**, 3217 (2002).

© 2006 NRC Canada

18. C.A. McNamara, M.J. Dixon, and M. Bradley. Chem. Rev. **102**, 3275 (2002).
19. B. Cetinkaya, N. Gurbuz, T. Seckin, and I. Ozdemir. J. Mol. Catal. A: Chem. **184**, 31 (2002).
20. S.C. Schurer, S. Gessler, N. Buschmann, and S. Blechert. Angew. Chem. Int. Ed. **39**, 3898 (2000).
21. J. Schwarz, V.P.W. Bohm, M.G. Gardiner, M. Grosche, W.A. Herrmann, W. Hieringer, and G. Raudaschl-Sieber. Chem. Eur. J. **6**, 1773 (2000).
22. M. Mayr, M.R. Buchmeiser, and K. Wurst. Adv. Synth. Catal. **344**, 712 (2002).
23. W.A. Herrmann, C. Brossmer, K. Oefele, C.-P. Reisinger, T. Priermerier, M. Beller, and H. Fischer. Angew. Chem. Int. Ed. Engl. **34**, 1844 (1995).
24. M. Beller, H. Fischer, W.A. Herrmann, K. Oefele, and C. Brossmer. Angew. Chem. Int. Ed. Engl. **34**, 1848 (1995).
25. C. Baleizao, A. Corma, H. Garcia, and A. Leyva. Chem. Commun. (Cambridge), 606 (2003).
26. C. Baleizao, A. Corma, H. Garcia, and A. Leyva. J. Org. Chem. **69**, 439 (2004).
27. J. de Vries. J. Chem. Soc. Dalton Trans. 421 (2006).
28. B.M. Choudary, S. Madhi, N. Chowdari, M.L. Kantam, and B. Sreedhar. J. Am. Chem. Soc. **124**, 14127 (2002).
29. Y.M.A. Yamada, K. Takeda, H. Takahashi, and S. Ikegami. Tetrahedron, **60**, 4097 (2004).
30. A. Cwik, Z. Hell, and F. Figueras. Adv. Synth. Catal. **348**, 523 (2006).
31. A. Corma, D. Das, H. Garcia, and A. Leyva. J. Catal. **229**, 322 (2005).
32. C. Rocaboy and J.A. Gladysz. Org. Lett. **4**, 1993 (2002).
33. D.E. Bergbreiter, P.L. Osburn, and J.D. Frels. Adv. Synth. Catal. **347**, 172 (2005).
34. K. Yu, W. Sommer, M. Weck, and C.W. Jones. Adv. Synth. Catal. **347**, 161 (2005).
35. C.C. Cassol, A.P. Umpierre, G. Machado, S.I. Wolke, and J. Dupont. J. Am. Chem. Soc. **127**, 3298 (2005).
36. M. Nowotny, U. Hanefeld, H. van Koningsveld, and T. Maschmeyer. Chem. Commun. (Cambridge), 1877 (2000).
37. R.B. Bedford, C.S.J. Cazin, M.B. Hursthouse, M.E. Light, K.J. Pike, and S. Wimperis. J. Organomet. Chem. **633**, 173 (2001).
38. Y. Ji, S. Jain, and R.J. Davis. J. Phys. Chem. B, **109**, 17232 (2005).
39. M. Che and C.O. Bennett. Adv. Catal. **36**, 55 (1989).
40. J.S. Beck, J.C. Vartuli, W.J. Roth, M.E. Leonowicz, C.T. Kresge, K.D. Schmitt, C.T.-W. Chu, D.H. Olson, E.W. Sheppard, S.B. McCullen, J.B. Higgins, and J.L. Schlenker. J. Am. Chem. Soc. **114**, 10834 (1992).
41. J.S. Beck, J.C. Vartuli, G.J. Kennedy, C.T. Kresge, W.J. Roth, and S.E. Schramm. Chem. Mater. **6**, 1816 (1994).
42. C.T. Kresge, M.E. Leonowitcz, W.J. Roth, J.C. Vartuli, and J.S. Beck. Nature (London), **359**, 710 (1992).
43. B.P. Pelrine, K.D. Schmitt, and J.C. Vartuli. Mobil Oil Corp., USA. US 5105051 A 19920414. 1992. p. 17.
44. R.M. Rioux, G. Song, J.D. Hoefelmeyer, P. Yang, and G.A. Somorjai. J. Phys. Chem. B, **109**, 2193 (2005).
45. N. Marin-Astorga, G. Pecchi, T.J. Pinnavaia, G. Alvez-Manoli, and P. Reyes. J. Mol. Catal. A: Chem. **247**, 145 (2006).
46. M.H. Bartl, B.J. Scott, G. Wirnsberger, A. Popitsch, and G.D. Stucky. Chem. Phys. Chem. **4**, 392 (2003).
47. D.M. Antonelli and J.Y. Ying. Chem. Mater. **8**, 874 (1996).
48. D. Grosso, G.J.d.A.A. Soler Illia, E.L. Crepaldi, B. Charleux, and C. Sanchez. Adv. Func. Mater. **13**, 37 (2003).
49. B. Lee, D. Lu, J.N. Kondo, and K. Domen. J. Am. Chem. Soc. **124**, 11256 (2002).
50. P. Yang, D. Zhao, D.I. Margolese, B.F. Chmelka, and G.D. Stucky. Chem. Mater. **11**, 2813 (1999).
51. M. Yada, H. Kitamura, M. Machida, and T. Kijima. Inorg. Chem. **37**, 6470 (1998).
52. M.S. Wong and J.Y. Ying. Chem. Mater. **10**, 2067 (1998).
53. A. Kim, P. Bruinsma, Y. Chen, L.-Q. Wang, and J. Liu. Chem. Comm. (Cambridge), 161 (1997).
54. M. Mamak, N. Coombs, and G. Ozin. Adv. Mater. **12**, 198 (2000).
55. M. Mamak, N. Coombs, and G. Ozin. J. AM. Chem. Soc., **122**, 8932 (2000).
56. M. Mamak, N. Coombs, and G.A. Ozin. Chem. Mater. **13**, 3564 (2001).
57. V. Calo, A. Nacci, A. Monopoli, A. Detomaso, and P. Iliade. Organometallics, **22**, 4193 (2003).
58. T.H. Galow, U. Drechsler, J.A. Hanson, and V.M. Rotello. Chem. Commun. (Cambridge), 1076 (2002).
59. G. Williamson and W. Hall. Acta Metall. **1**, 22 (1953).
60. C.M. Grgicak, R.G. Green, W.-F. Du, and J.B. Giorgi. J. Am. Ceram. Soc. **88**, 3081 (2005).
61. R.J. Farrauto, J.K. Lampert, M.C. Hobson, and E.M. Waterman. Appl. Catal. B, **6**, 263 (1995).
62. K.-I. Fujimoto, F.H. Ribeiro, M. Avalos-Borja, and E. Iglesia. J. Catal. **179**, 431 (1998).
63. R.J. Farrauto, M.C. Hobson, T. Kennelly, and E.M. Waterman. Appl. Catal. A, **81**, 227 (1992).
64. M. Lyubovsky and L. Pfefferle. Catal. Today, **47**, 29 (1999).
65. O. Leonte, M. Birjega, D. Macovei, P. Pausescu, N. Popescu-Pogrion, and M. Georgescu. **28**, 347 (1986).
66. O. Vasylkiv, Y. Sakka, Y. Maeda, and V.V. Skorokhod. J. Eur. Ceram. Soc. **24**, 469 (2004).
67. I.W. Davies, L. Matty, D.L. Hughes, and P.J. Reider. J. Am. Chem. Soc. **123**, 10139 (2001).
68. J. Rebek and F. Gavina. J. Am. Chem. Soc. **96**, 7112 (1974).
69. J. Rebek, D. Brown, and S. Zimmerman. J. Am. Chem. Soc. **97**, 454 (1975).
70. J.J. Rebek. Tetrahedron, **35**, 723 (1979).
71. A. Bianco, J. Furrer, D. Limal, G. Guichard, K. Elbayed, J. Raya, M. Piotto, and J.-P. Briand. J. Comb. Chem. **2**, 681 (2000).
72. Y. Wang and S.R. Wilson. Tetrahedron Lett. **38**, 4021 (1997).
73. A.S. Kiselyov and R.W. Armstrong. Tetrahedron Lett. **38**, 6163 (1997).
74. R.G. Heindenreich, J.G. E. Krauter, J. Pietsch, and K. Kohler. J. Mol. Catal. A: Chem. **182–183**, 499 (2002).
75. F. Miyazaki, K. Yamaguchi, and M. Shibasaki. Tetrahedron Lett. **40**, 7379 (1999).
76. Y.M.A. Yamada, K. Takeda, H. Takahashi, and S. Ikegami. Tetrahedron Lett. **44**, 2379 (2003).
77. R.G. Heindenreich, K. Kohler, J.G.E. Krauter, and J. Pietsch. Synlett, **7**, 1118 (2002).

© 2006 NRC Canada

A highly efficient carbon–sulfur bond formation reaction via microwave-assisted nucleophilic substitution of thiols to polychloroalkanes without a transition-metal catalyst

Yi-Ju Cao, Yuan-Yuan Lai, Hong Cao, Xiao-Ning Xing, Xiang Wang, and Wen-Jing Xiao

Abstract: An efficient carbon–sulfur bond formation reaction has been developed under microwave irradiation. This reaction affords a novel and rapid synthesis of thioacetals and sulfides under mild conditions. This method is particularly noteworthy given its experimental simplicity and high generality, and no transition-metal catalysts were needed under our conditions.

Key words: microwave, sulfide, thiol, nucleophilic substitution.

Résumé : Faisant appel à des irradiations microondes, on a mis au point une méthode efficace pour la formation de liaisons carbone–soufre. Cette réaction fournit une nouvelle méthode rapide de synthèse de thioacétals et de sulfures dans des conditions douces. La méthode est particulièrement remarquable en raison de sa simplicité, de son caractère général et du fait que, dans nos conditions, aucun catalyseur métallique n'est nécessaire.

Mots clés : microonde, sulfure, thiol, substitution nucléophile.

[Traduit par la Rédaction]

Introduction

The formation of a C–S bond is an important organic reaction (1). For example, the formation of thioacetals provides an excellent method to protect the carbonyl group (2) and can serve to generate umpoled carbonyls (3). Furthermore, some 1,3-dithiolane compounds exhibit remarkable biological activities, which include anticonvulsant (4), radioprotective (5), hepatoprotective (6), anti-tumor (7), and anti-HIV activities (8). In addition, sulfides and their derivatives are also biologically active compounds (9), as well as attractive building blocks in the synthesis of sulfur-containing functional monomers (10). Consequently, numerous synthetic methods for dithioacetals and sulfides have been developed. Representative examples for the preparation of thioacetals include the condensation of a carbonyl compound with thiols in the presence of various Lewis acid catalysts (2, 11) and the reaction of thiols with diiodomethane, dibromomethane, or dichloromethane under strongly basic conditions (12). Sulfide formation is generally carried out by the condensation of activated alkyl halides with alkali metal thiolates (13) or by the reduction of sulfones or sulfoxides using strong reducing agents such as DIBAL–H or $LiAlH_4$ (14). However, many of these clasical methods are limited by their moderate yields, harsh reaction conditions, and tedious work up. Thus, methods for the introduction of a carbon–sulfur bond with the use of transition metal catalysts have been recently developed (15, 16). Among them, the most promising and straightforward methods for the preparation of dithioacetals and sulfides are Tanaka's rhodium-catalyzed reaction of polychloroalkanes with thiols (15*a*) and Ogawa's palladium-catalyzed hydrothiolation of alkynes with thiols (15*h*). Although these methods successfully yield versatile dithioacetals or sulfides, they require a long reaction time, use of expensive catalysts, and vigorous conditions. In particular, the use of transition metals leads to the generation of waste and has a number of hazards associated with it (17). Accordingly, the development of more efficient methods is still in demand.

In the past few years, the utilization of microwave irradiation in organic synthesis has become increasingly popular within the pharmaceutical and academic arenas (18). By taking advantage of this efficient source of energy, compound libraries and optimization can be assembled in a fraction of the time required by classical thermal methods (19). Microwave-assisted protocols have been widely applied to the formation of a variety of carbon–heteroatom and carbon–carbon bonds (20). To the best of our knowledge, the direct metal-free substitution of thiols to polychloroalkanes using

Received 14 June 2006. Accepted 12 September 2006. Published on the NRC Research Press Web site at http://canjchem.nrc.ca on 15 November 2006.

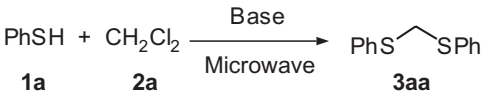
Y.-J. Cao, Y.-Y. Lai, H. Cao, X.-N. Xing, X. Wang,[1] and W.-J. Xiao.[2] Key Laboratory of Pesticide & Chemical Biology, Ministry of Education, College of Chemistry, Central China Normal University, 152 Luoyu Road, Wuhan, Hubei 430079, People's Republic of China.

[1]Current address: Department of Chemistry, Kaili College, 22 Wenhua North Road, Kaili, Guizhou 556000, People's Republic of China.

[2]Corresponding author (e-mail: wxiao@mail.ccnu.edu.cn).

 doi:10.1139/V06-151 © 2006 NRC Canada

Table 1. Optimization of the reaction conditions.



Entry	Base (equiv.)[a]	Temp. (°C)	Yield (%)[b]
1	K_2CO_3 (1.0)	150	75
2	Cs_2CO_3 (1.0)	150	87
3	DMAP[c] (1.0)	150	72
4	DBU[d] (1.0)	150	89
5	Et_3N (1.0)	150	66
6	DBU (2.0)	150	95
7	DBU (3.0)	150	94
8	DBU (4.0)	150	95
9	DBU (2.0)	60	27
10	DBU (2.0)	90	77
11	DBU (2.0)	120	86

Note: All reactions were conducted using thiophenol **1a** (0.5 mmol) and CH_2Cl_2 (2 mL) in the presence of a base at a certain temperature under microwave irradiation for 20 min.

[a]Based on thiophenol.

[b]Isolated yields based on thiophenol.

[c]4-Methyl aminopyridine.

[d]1,8-Diazabicyclo[5,4,0]undec-7-ene.

high-speed microwave techniques has not been described. Herein, we would like to report our preliminary investigation on the microwave-assisted C–S bond formation reactions, which constitute one of the most efficient and rapid syntheses of dithioacetals and sulfides. Compared with Tanaka's procedure (15*a*), the superiorities of our method include (1) a shorter reaction time and higher yields, (2) a broader substrate scope, and (3) the exclusion of transition-metal catalysts.

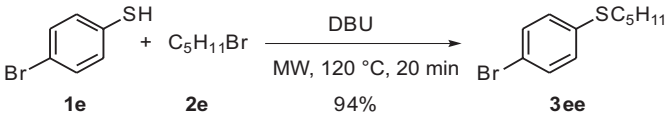
Results and discussion

As a starting point for the development of our microwave-mediated methodology, we chose to study the reaction of thiophenol with dichloromethane for the optimization of reaction conditions, and the results are summarized in Table 1. It was found that the reaction was significantly influenced by the base employed and the temperature (Table 1, entries 1–5 and 9–11). Although both inorganic and organic bases could be used in the reaction, DBU and Cs_2CO_3 are obviously much better than others (Table 1, entries 1–5). Increasing the loading of DBU from 1.0 to 2.0 equiv., based on thiophenol, could dramatically improve the reaction yield (Table 1, entries 4 and 6); however, further increasing the loading of DBU to 4.0 equiv. did not affect the reaction (Table 1, entries 6–8). The reaction temperature is another critical factor for the successful formation of dithioacetals, with the best result being attained at 150 °C (Table 1, entry 6). Decreasing the temperature from this value has been shown to be detrimental to the reaction (Table 1, entries 9–11).

Encouraged by the previous results, we further examined the microwave-assisted reactions of various thiols with polychloroalkanes. From the results shown in Table 2, it can be concluded that both aliphatic and aromatic thiols with an electron-donating or electron-withdrawing group readily undergo this transformation to afford the corresponding dithioacetals or sulfides in good to excellent yiels (Table 2, entries 1–6, 12, and 13). 1,2-Ethanedithiol can also be employed successfully in the reaction (Table 2, entries 7 and 14). In addition to dichloromethane, chloroform, 1,1-dichloropropane, and 1,2-dichloroethane are effective for this microwave-assisted, direct C–S bond formation reaction (Table 2, entries 8–14). 1,3-Dithiolane and 1,4-dithiane can be easily prepared in good isolated yields by the reaction of 1,2-ethanedithiol with dichloromethane and 1,2-dichloroethane, respectively (Table 2, entries 7 and 14).

Next, we investigated the microwave-assisted reaction of *p*-bromothiophenol with pentyl bromide. As expected, the reaction also gave excellent yields and short reaction time in the presence of DBU under microwave irradiation (eq. [1]).

[1]



Conclusions

In conclusion, we established a rapid and efficient method for the synthesis of dithioacetals and sulfides by the direct substitution reaction of thiols with polychloroalkanes without any transition-metal catalyst under microwave irradiation. Particularly, the methodology presented here is attractive because of its shorter reaction time, higher yields, broader substrates scope, and the experimental simplicity. Furthermore, the reaction was developed to meet the increasing demand for green chemistry and environment-friendly chemical processes.

Experimental section

General methods

Unless otherwise noted, materials were purchased from commercial suppliers and used without further purification. Solvents and liquid organic bases were freshly distilled according to the known procedures (21). Column chromatography was performed using 200–300 mesh silica gel. ^{1}H NMR spectra were recorded on Varian Mercury 400 (400 MHz) spectrometers. Chemical shifts are reported in ppm from TMS with the solvent resonance as the internal standard ($CDCl_3$, δ 7.24). Data are reported as follows: chemical

© 2006 NRC Canada

Table 2. Microwave-assisted reactions of thiols with polychloroalkanes.

Entry	Thiol	Polychloro-alkane	Product		Yield (%)[a]
1	PhSH **1a**	CH_2Cl_2 **2a**	PhS, PhS	**3aa**	95
2	*p*-Me-C_6H_4SH **1b**	CH_2Cl_2 **2a**	*p*-Me-C_6H_4S, *p*-Me-C_6H_4S	**3ba**	94
3	*p*-MeO-C_6H_4SH **1c**	CH_2Cl_2 **2a**	*p*-MeO-C_6H_4S, *p*-MeO-C_6H_4S	**3ca**	95
4	*p*-Cl-C_6H_4SH **1d**	CH_2Cl_2 **2a**	*p*-Cl-C_6H_4S, *p*-Cl-C_6H_4S	**3da**	90
5	*p*-Br-C_6H_4SH **1e**	CH_2Cl_2 **2a**	*p*-Br-C_6H_4S, *p*-Br-C_6H_4S	**3ea**	93
6[b]	*n*-C_8H_7SH **1f**	CH_2Cl_2 **2a**	*n*-C_8H_{17}S, *n*-C_8H_{17}S	**3fa**	86
7	HS, SH **1g**	CH_2Cl_2 **2a**	S, S	**3ga**	72
8	PhSH **1a**	Cl, Cl **2b**	SPh, SPh	**3ab**	79
9	PhSH **1a**	Cl, Cl **2c**	Cl, SPh	**3ac**	89
10[b]	PhSH **1a**	Cl, Cl **2c**	PhS, SPh	**3ac'**	91
11	PhSH **1a**	$CHCl_3$ **2d**	PhS, SPh, SPh	**3ad**	72
12	*p*-Br-C_6H_4SH **1e**	Cl, Cl **2b**	SC_6H_4-Br-*p*, SC_6H_4-Br-*p*	**3eb**	95
13	*p*-Br-C_6H_4SH **1e**	Cl, Cl **2c**	Cl, SC_6H_4-Br-*p*	**3ec**	92
14	HS, SH **1g**	Cl, Cl **2c**	S, S	**3gc**	81

Note: For the detailed experimental procedure, see supporting information.[3]
[a]Isolated yields based on thiols.
[b]THF as the solvent.

shift, multiplicity (s = singlet, d = doublet, t = triplet, q = quartet, br = broad, and m = multiplet), coupling constants (Hz). ^{13}C NMR spectra were recorded on Varian Mercury 400 (100 MHz) with complete proton decoupling spectrophotometers ($CDCl_3$: 77.7). Elemental analysis was performed on a Vario EL III instrument. All experiments were performed in a SmithSynthesizer producing controlled irradiation at 2450 MHz with a power of 0–300 W.

[3] Supplementary data for this article are available on the journal Web site (http://canjcehm.nrc.ca) or may be purchased from the Depository of Unpublished Data, Document Delivery, CISTI, National Research Council Canada, Ottawa, ON K1A 0S2, Canada. DUD 5095. For more information on obtaining material, refer to http://cisti-icist.nrc-cnrc.gc.ca/irm/unpub_e.shtml.

© 2006 NRC Canada

Typical procedure for the microwave-assisted reaction of thiol with polychloroalkane

A 5.0 mL process vial was charged with polychloroalkane (2 mL), thiol (0.5 mmol), and DBU (1.0 mmol). The vial was then capped with a Teflon septum and irradiated with microwave to 150 °C for 20 min. After cooling, the reaction mixture was poured into water and extracted with dichloromethane (3 × 5 mL). The combined organic phase was dried over $MgSO_4$ and then filtered. The solvent was evaporated, and the residue was purified by flash chromatography to give the desired dithioacetals or sulfides in good to excellent yields (72%–95%).

Di(phenylthio)methane (3aa) (22)

White solid; mp 30–34 °C; yield 95%. ^{1}H NMR (400 MHz, $CDCl_3$) δ: 7.43–7.27 (m, 10H), 4.34 (s, 2H). ^{13}C NMR (100 MHz, $CDCl_3$) δ: 135.1, 130.8, 129.1, 127.2, 40.5.

Di(p-tolylthio)methane (3ba) (23)

White solid; mp 40–42 °C; yield 94%. ^{1}H NMR (400 MHz, $CDCl_3$) δ: 7.34–7.32 (d, J = 6.4 Hz, 4H), 7.13–7.11 (d, J = 6.8 Hz, 4H), 4.26 (s, 2H) 2.33 (s, 6H). ^{13}C NMR (100 MHz, $CDCl_3$) δ: 137.4, 131.5, 131.3, 129.7, 41.9, 21.1.

Di(4-methoxyphenylthio)methane (3ca)

White solid; mp 66–67 °C; yield 95%. ^{1}H NMR (400 MHz, $CDCl_3$) δ: 7.40 (dd, J = 2.4, 6.4 Hz, 4H), 6.85 (d, J = 9.2 Hz, 4H), 4.15 (s, 2H), 3.81 (s, 6H). ^{13}C NMR (100 MHz, $CDCl_3$) δ: 159.6, 134.4, 125.2, 114.6, 55.3, 44.5. Anal. calcd. for $C_{15}H_{16}O_2S_2$: C 61.61, H 5.52; found: C 61.69, H 5.48.

Di(4-chlorophenylthio)methane (3da) (23)

White solid; mp 42–43 °C; yield 90%. ^{1}H NMR (400 MHz, $CDCl_3$) δ: 7.33 (d, J = 6.8 Hz, 4H), 7.12 (d, J = 6.8 Hz, 4H), 4.26 (s, 2H). ^{13}C NMR (100 MHz, $CDCl_3$) δ: 133.6, 133.0, 132.4, 129.1, 41.2.

Di(4-bromophenylthio)methane (3ea)

White solid; mp 70.5–72.0 °C; yield 93%. ^{1}H NMR (400 MHz, $CDCl_3$) δ: 7.3 (d, J = 8.4 Hz, 4H), 7.26 (d, J = 8.4 Hz, 4H), 4.28 (s, 2H). ^{13}C NMR (100 MHz, $CDCl_3$) δ: 133.6, 132.5, 132.1, 121.5, 40.8. Anal. calcd. for $C_{13}H_{10}Br_2S_2$: C 40.02, H 2.58; found: C 40.21, H 2.61.

Di(octylthio)methane (3fa) (15a)

Colorless oil; yield 86%. ^{1}H NMR (400 MHz, $CDCl_3$) δ: 3.64 (t, J = 1.2 Hz, 2H), 2.62 (t, J = 6.8 Hz, 4H), 1.55–1.60 (m, 4H), 1.27–1.38 (m, 20H), 0.88 (t, J = 7.2 Hz, 6H). ^{13}C NMR (100 MHz, $CDCl_3$) δ: 35.4, 31.8, 30.8, 29.2, 29.2, 28.9, 22.6, 14.0.

1,3-Dithiolane (3ga) (24)

Colorless oil; yield 72%. ^{1}H NMR (400 MHz, $CDCl_3$) δ: 3.86 (d, J = 0.4 Hz, 2H), 3.16 (d, J = 0.8Hz, 4H). ^{13}C NMR (100 MHz, $CDCl_3$) δ: 8.0, 34.3.

1,1-Di(phenylthio)propane (3ab)

Pale yellow oil; yield 79%. ^{1}H NMR (400 MHz, $CDCl_3$) δ: 7.47–7.24 (m, 10H), 4.35 (t, J = 6.4 Hz, 1H), 1.88 (m, 2H), 1.13 (t, J = 7.2 Hz, 3H). ^{13}C NMR (100 MHz, $CDCl_3$) δ: 134.5, 132.8, 128.7, 59.9, 28.8, 11.5. Anal. calcd. for $C_{15}H_{16}S_2$: C 69.18, H 6.19; found: C 69.04, H 6.32.

1-Chloro-2-phenylthioethane (3ac) (25)

Colorless oil; yield 89%. ^{1}H NMR (400 MHz, $CDCl_3$) δ: 7.40–7.24 (m, 5H), 3.61 (t, J = 4.2 Hz, 2H), 3.21 (t, J = 4.2 Hz, 2H). ^{13}C NMR (100 MHz, $CDCl_3$) δ: 134.3, 130.5, 129.3, 127.1, 42.1, 35.9.

1,2-Di(phenylthio)ethane (3ac′) (26)

White solid; mp 92–93 °C; yield 91%. ^{1}H NMR (400 MHz, $CDCl_3$) δ: 7.32–7.21 (m, 10H), 3.08 (d, J = 2.4 Hz, 4H). ^{13}C NMR (100 MHz, $CDCl_3$) δ: 135.0, 130.0, 129.0, 126.5, 33.4.

Tris(phenylthio)methane (3ad)

Pale yellow oil; yield 72%. ^{1}H NMR (400 MHz, $CDCl_3$) δ: 7.49–7.30(m, 15H), 5.41 (s, 1H). ^{13}C NMR (100 MHz, $CDCl_3$) δ: 134.1, 133.1, 129.1, 128.5, 64.9. Anal. calcd. for $C_{19}H_{16}S_3$: C 67.02, H 4.74; found: C 67.30, H 4.86.

1,1-Di(4-bromophenylthio)propane (3eb)

Colorless oil; yield 95%. ^{1}H NMR (400 MHz, $CDCl_3$) δ: 7.43–7.28(m, 8H), 4.28 (t, J = 6.6 Hz, 1H), 1.84 (m, 2H), 1.12 (t, J = 7.4 Hz, 3H). ^{13}C NMR (100 MHz, $CDCl_3$) δ: 137.4, 133.1, 132.0, 122.1, 60.3, 28.8, 11.8. Anal. calcd. for $C_{15}H_{14}Br_2S_2$: C 43.08, H 3.37; found: C 43.29, H 3.30.

1-Chloro-2-(4-bromophenylthio)ethane (3ec)

White solid; mp 134–136 °C; yield 92%. ^{1}HNMR (400 MHz, $CDCl_3$) δ: 7.45–7.23 (m, 4H), 3.60 (m, 2H), 3.20 (m, 2H). ^{13}C NMR (100 MHz, $CDCl_3$) δ: 133.5, 132.3, 132.0, 121.1, 42.1, 36.2. Anal. calcd. for C_8H_8BrClS: C 38.19, H 3.21; found: C 38.07, H 3.33.

1,4-Dithiane (3gc) (27)

White solid; yield 81%. ^{1}H NMR (400 MHz, $CDCl_3$) δ: 2.90 (s, 8H). ^{13}C NMR (100 MHz, $CDCl_3$) δ: 29.1

4-Bromophenylthiopentane (3ee)

Colorless oil; yield 94%. ^{1}H NMR (400 MHz, $CDCl_3$) δ: 7.40–7.16 (m, 4H), 2.89 (t, J = 7.4 Hz, 2H), 1.67–1.25 (m, 6H), 0.91 (t, J = 5.4 Hz, 3H). ^{13}C NMR (100 MHz, $CDCl_3$) δ: 136.3, 131.8, 130.3, 119.3, 33.6, 30.9, 28.7, 22.2, 13.9. Anal. calcd. for $C_{11}H_{15}BrS$: C 50.97, H 5.83; found: C 51.04, H 5.77.

Acknowledgment

We are grateful to the National Key Project for Basic Research of China (2004CCA00100), the Natural Science Foundation of China (20472021 and 20672040), the Hubei Province Science Fund for Distinguished Young Scholar (2004ABB011), and Central China Normal University for the financial support of this research.

References

1. (*a*) R.J. Gremlyn. An introduction to organosulfur chemistry. Wiley, New York. 1996; (*b*) A. Thuillier and P. Metzner. Sulfur reagents in organic synthesis. Academic Press, New York. 1994; (*c*) T.-Y. Luh and C.-F. Lee. Eur. J. Org. Chem. 3875 (2005).

© 2006 NRC Canada

2. T.W. Green and P.G.M. Wuts. Protective groups in organic synthesis. 3rd ed. John Wiley and Sons, New York. 1999.
3. P. Caubere and P. Coutrot. *In* Comprehensive organic synthesis. *Edited by* B.M. Trost and I. Fleming. Pergamon Press, Oxford. 1991. p. 835.
4. (*a*) M. Taroua, C. Ribuot, M.H. Pera, G. Taillandier, M. Fatome, J.D. Laval, P. Demenge, and G. Leclerc. Eur. J. Med. Chem. **31**, 589 (1996); (*b*) S. Pandey, S.N. Suryawanshi, S. Gupta, and V.M.L. Srivastava. Eur. J. Med. Chem. **40**, 751 (2005).
5. M. Taroua, M.H. Pera, G. Taillandier, M. Fatome, J.D. Laval, and G. Leclerc. Eur. J. Med. Chem. **29**, 621 (1994).
6. V.J. Ram, N. Haque, S.K. Singh, M. Nath, A. Shoeb, S.C. Tripathi, and G.K. Patnaik. Bioorg. Med. Chem. Lett. **4**, 1453 (1994).
7. T. Ashizawa, K. Kawashima, Y. Kanda, K. Gomi, M. Okabe, K. Ueda, and T. Tamaoki. Anti-Cancer Drugs, **10**, 829 (1999).
8. N. Nguyen-Ba, W.L. Brown, L. Chan, N. Lee, L. Brasili, D. Lafleur, and B. Zacharie. Chem. Commun. 1245 (1999).
9. (*a*) K.C. Nicolaou, G. Skokotas, P. Maligres, G. Zuccarello, E.J. Schweiger, K. Toshima, and S. Wendeborn. Angew. Chem., Int. Ed. Engl. **28**, 1272 (1989); (*b*) K.C. Nicolaou and W.-M. Dai. Angew. Chem., Int. Ed. Engl. **30**, 1387 (1991).
10. (*a*) R. Prabharasuth and D.L. Van Vranken. J. Org. Chem. **66**, 5256 (2001); (*b*) T.M. Mitzel, C. Palomo, and K. Jendza. J. Org. Chem. **67**, 136 (2002); (*c*) Y. Sawada and A. Oku. J. Org. Chem. **69**, 2899 (2004); (*d*) D.-W. Dong, Y.-O. Yang, H.-F. Yu, Q. Liu, J. Liu, M. Wang, and J. Zhu. J. Org. Chem. **70**, 4535 (2005).
11. For recent examples, see: (*a*) R.C. Besra, S. Rudrawar, and A.K. Chakraborti. Tetrahedron Lett. **46**, 6213 (2005); (*b*) S.K. De. Synthesis, **17**, 2837 (2004).
12. (*a*) N. Ona, H. Miyake, T. Saito, and A. Kaji. Synthesis, **11**, 952 (1980); (*b*) E. Weissflog. Phosphorus Sulfur **12**, 89 (1981) ; (*c*) B. Bertaina, E. Rouvier, J. Fayn, and A. Cambon. J. Fluorine Chem. **66**, 287 (1994); (*d*) H.J.M. Dou, M. Ludwikow, P. Hassanaly, J. Kister, and J. Metzger. J. Heterocycl. Chem. **17**, 393 (1980); (*e*) J.H. Zaidi, F. Naeem, K.M. Khan, R. Iqbal, and Z. Ullah. Synth. Commun. 2641 (2004).
13. (*a*) A.W. Herriott. Synth. Commun. 447 (1975); (*b*) J.S. Bradshaw, J.A. South, and R.H. Hales. J. Org. Chem. **37**, 2381 (1972); (*c*) Y. Guindon, R. Frenette, R. Fortin, and J. Rokach. J. Org. Chem. **48**, 1357 (1983).
14. (*a*) J. Lindley. Tetrahedron, **40**, 1433 (1984); (*b*) A. Van Bierbeek and M. Gingras. Tetrahedron Lett. **39**, 6283 (1998).
15. For representative reports, see: (*a*) K. Tanaka and K. Ajiki. Org. Lett. **7**, 1537 (2005); (*b*) F. Gendre, M. Yang, and P. Diaz. Org. Lett. **7**, 2719 (2005); (*c*) W.-J. Xiao and H. Alper. J. Org. Chem. **70**, 1802 (2005); (*d*) T. Kondo, A. Baba, Y. Nishi, and T. Mitsudo. Tetrahedron Lett. **45**, 1469 (2004); (*e*) M. Arisawa and M. Yamaguchi. J. Am. Chem. Soc. **125**, 6624 (2003); (*f*) T. Kondo, Y. Kanda, A. Baba, K. Fukuda, A. Nakamura, K. Wada, Y. Morisaki, and T. Mitsudo, J. Am. Chem. Soc. **124**, 12960 (2002); (*g*) W.-J. Xiao and H. Alper, J. Org. Chem. **66**, 6229 (2001); (*h*) A. Ogawa, T. Ikeda, K. Kimura, and T. Hirao. J. Am. Chem. Soc. **121**, 5108 (1999); (*i*) W.-J. Xiao and H. Alper. J. Org. Chem. **62**, 3422 (1997).
16. For recent reviews, see: (*a*) A. Ogawa. *In* Main group metals in organic synthesis. *Edited by* H. Yamamoto and K. Oshima. Wiley-VCH, Weinheim. 2004. p. 813; (*b*) A. Ogawa. *In* Handbook of organopalladium chemistry for organic synthesis. *Edited by* E. Negishi. Wiley-Interscience, New York. 2002. Chapter VII.6.; (*c*) B.E. Ali and H. Alper. *In* Handbook of organopalladium chemistry for organic synthesis. *Edited by* E. Negishi. Wiley-Interscience, New York. 2002. Chapter VI.2.1.1.2.; (*d*) H. Kuniyasu and H. Kurosawa. Chem. Eur. J. **8**, 2660 (2002).
17. N.E. Leadbeater and M. Marco. Angew. Chem., Int. Ed. **42**, 1407 (2003).
18. G. Majetich and K. Wheless. *In* Microwave-enhanced chemistry: Fundamentals, sample preparation, and applications. *Edited by* H.M. Kingston and S.J. Haswell. American Chemical Society, Washington, DC. 1997.
19. (*a*) B.L. Hayes. Microwave synthesis: Chemistry at the speed of light. CEM Publishing, Matthews, NC. 2002. (*b*) H. Cao and W.-J. Xiao. Can. J. Chem. **83**, 826 (2005); (*c*) Q. Yang, X.-Y. Li, H. Wu, and W.-J. Xiao. Tetrahedron Lett. **47**, 3893 (2006).
20. M. Larhed, C. Moberg, and A. Hallberg. Acc. Chem. Res. **35**, 717 (2002).
21. W.L.F. Armarego and D.D. Perrin. Purifications of laboratory chemicals. Butterworth-Heinemann, Oxford, UK. 1997.
22. K. Kobayashi, M. Kawakita, K. Yokota, T. Mannami, K. Yamamoto, O. Morikawa, and H. Konishi. Bull. Chem. Soc. Jpn. **68**, 1401 (1995).
23. N. Ono, H. Miyake, T. Saito, and A. Kaji. Synth. Commun. 952 (1980).
24. J. Klaveness, F. Rise, and K. Undheim. Acta Chem. Scand. **40**, 398 (1986).
25. L. De Luca, G. Giacomelli, and A. Porcheddu. Org. Lett. **4**, 553 (2002).
26. T. Kondo, S.-Y. Uenoyama, K.-L. Fujita, and T.-A. Mitsudo. J. Am. Chem. Soc. **121**, 482 (1999).
27. E. Haslam. Tetrahedron, **36**, 2409 (1980).

© 2006 NRC Canada

Interaction of dimethyltin(IV)dichloride with 5′-AMP and 5′-GMP

Farrokh Gharib, Elnaz Farzad, and Mostafa Mohammadpour Amini

Abstract: The formation constants of the species formed in the systems H^+ + dimethyltin(IV) + 5′-AMP and 5′-GMP, H^+ + 5′-AMP, and H^+ + 5′-GMP have been determined in aqueous solution in the pH range of 1.5–9 at constant temperature (25 °C) and constant ionic strength (0.1 mol dm^{-3}, $NaClO_4$) using spectrophotometric and potentiometric techniques. ^1H and ^{31}P NMR investigations in aqueous solution confirmed the species formation and led us to propose their structures. The precipitated complexes of AMP and GMP by $Me_2Sn(IV)^{2+}$ at low pH values were characterized by elemental analysis and FTIR spectroscopy, which ruled out purine moiety (N-1 and N-7) coordination and a bidentated coordination of the phosphate group is concluded in both cases.

Key words: dimethyltin(IV)dichloride, guanosine 5′-monophosphate, adenosine 5′-monophosphate, stability and protonation constants.

Résumé : Faisant appel à des techniques spectrophotométriques et potentiométriques et opérant en solution aqueuse, à des pH allant de 1,5 à 9, à température (25 °C) et une force ionique constante (0,1 mol dm^{-3} $NaClO_4$), on a déterminé les constantes de formation des espèces qui se forment dans les systèmes H^+ + diméthyléthain(IV) + 5′-AMP (ou + 5′-GMP) et H^+ + 5′-AMP et H^+ + 5′-GMP. Des études par RMN du ^1H et du ^{31}P en solutions aqueuses ont confirmé la formation de ces espèces et permis de proposer leurs structures. Les complexes qui précipitent par réaction du AMP ou du GMP avec du $Me_2Sn(IV)^{2+}$, à des pH faibles, ont été caractérisés par analyse élémentaire et par des méthodes de spectroscopie IR à transformée de Fourier, ce qui a permis d'éliminer la possibilité de coordination dans les positions N-1 et N-7 de la purine et de conclure que dans les deux cas il y a coordination bidentate du groupe phosphate.

Mots clés : dichlorure de diméthylétain(IV), 5′-monophosphate de guanosine, 5′-monophosphate d'adénosine, constante de protonation, constante de stabilité.

[Traduit par la Rédaction]

Introduction

Many organometallic compounds exhibit antitumour activity against several human cancer cells in vitro (1). The mechanism of the antitumour activity of cisplatin, which has already been used clinically in cancer chromotherapy, is believed to be due mainly to the formation of an internal crosslink with DNA involving the N-7 sites of two guanine residues (2). To find a metal-based anticancer drug with higher activity and lower toxicity, many organometallic compounds have been synthesized and tested (1, 3). Organotin(IV) complexes have been shown to have high antitumour activity in vitro in a wide variety of human tumors (4–5), but the antitumour action of the complexes of these types is not well understood. The activity of these compounds led to the hypothesis that these drugs hydrolyze easily in aqueous media and transport the active part (R_2Sn) inside the cells where it possibly reacts with DNA (6). To obtain more information on the molecular basis of the anticancer activity of organotin(IV) compounds, a number of studies have been performed on their interactions with some amino acids, dipeptides, and nucleotides (7–17). Several investigations of the last group indicated that purine moiety is not involved in the coordination, confirming that the interactions are limited to the phosphate site of the ligand. On the other hand, some authors have suggested that the N-1 or N-7 atoms of the base interact with $(CH_3)_2Sn(IV)^{2+}$. Recently, Surdy et al. (18) performed pH-metric titration and Mössbauer studies of dimethyltin(IV) with two classes of amino acids and dipeptides, having either only nitrogen or nitrogen and oxygen donor atoms. According to their results, for the two imidazol-containing N-donor ligands that do not contain carboxylate groups (histamine and glycyl-histamine), no evidence of complex formation was observed with dimethyltin(IV) cation. However, for the ligands containing carboxylate and nitrogen donor groups, complexation occurred and several species were detected. Interactions between mononucleotides and some dialkyltin(IV) derivatives were also investigated (16). In the solid complexes formed in the physiological pH range, dissociation of the N-donor ligands and nucleotide coordination through only the phosphate group were observed (19). Investigation of the solid complexes of adenosine and related ligands formed by $Bu_2Sn(IV)$ proved the coordination through the sugar moiety and phosphate group of the ligands, but the base moiety did not participate in complex formation (17).

Received 24 April 2006. Accepted 24 September 2006. Published on the NRC Research Press Web site at http://canjchem.nrc.ca on 16 November 2006.

F. Gharib,[1] E. Farzad, and M.M. Amini. Chemistry Department, Shahid Beheshti University, Tehran, Evin, Iran.

[1]Corresponding author (e-mail: f-gharib@cc.sbu.ac.ir).

 doi:10.1139/V06-152 © 2006 NRC Canada

Since water is a crucial part of the cellular organization of all animals, we decided to study dimethyltin(IV) ions with adenosine 5′-monophosphate (AMP) and guanosine 5′-monophosphate (GMP) in aqueous solution. Since the organotin cations are strong Lewis acids, it follows that the hydrolytic equilibria should be examined in the presence of noncomplexing anions prior to the study of the interactions of organotin cations with the ligands.

Accepting the hypothesis that R_2Sn^{2+} is the usual active species for antitumour action of organotins (20), a good antitumour agent should be easily dissociable following administration to animals. This requires weak bonds between tin and the donor atom of the coordinated ligands, which are readily hydrolysable. If the compound is hydrolytically unstable the R_2Sn moiety will be released too quickly, but if it is too stable it may be released too slowly and consequently lower activity will be observed. Therefore, there is a relationship between the stability of the organotin compounds and their antitumour activity.

The present work is concerned with the equilibrium of complex formation between $Me_2Sn(IV)^{2+}$ with AMP and GMP in a wide pH range. The formation of three complex species is proposed, of which two were isolated in solid states and characterized using FTIR spectroscopy. To verify the different donor groups in the complexes, ^{1}H NMR and ^{31}P NMR spectroscopy was used in D_2O–H_2O solutions.

Experimental

Chemicals

Dimethyltin(IV)dichloride, sodium salts of adenosine, and guanosine 5′-monophosphate were obtained from Merck and Fluka, respectively, as reagent grade materials and were used without further purification. Sodium perchlorate was obtained from Merck and was dried under vacuum at RT for at least 48 h before use. NaOH solution was prepared from a titrisol solution (Merck) and its concentration was determined by several titrations with standard HCl solution. Perchloric acid (Merck) was used as supplied. The aqueous stock solutions of the ligands were freshly prepared daily and their concentrations were determined each time by titration with NaOH solution. All dilute solutions were prepared from double-distilled water with conductance equal to 1.3 ± 0.1 μS.

Measurements

All measurements were carried out at 25 °C. The ionic strength was maintained at 0.1 mol dm^{-3} with sodium perchlorate. An Eyela pH meter, PHM 2000, was used for pH measurements. The hydrogen ion concentration was measured with an Ingold UO 3234 glass electrode and an Ingold UO 3236 calomel electrode. The pH meter was calibrated for the relevant H^+ concentration with a solution perchloric acid (0.01 mol dm^{-3}) containing sodium perchlorate (0.09 mol dm^{-3}, for adjusting the ionic strength to 0.1 mol dm^{-3}). For this standard solution, we set $-\log[H^+] = 2.00$ (21). Junction potential corrections calculated from eq. [1]

$$[1] \qquad -\log[H^+]_{real} = -\log[H^+]_{measured} + a + b[H^+]_{measured}$$

where a and b were determined by measuring the hydrogen ion concentration for two different solutions of $HClO_4$ with sufficient $NaClO_4$ to adjust the ionic media.

Procedure

Fifty cm^3 of an acidic solution of dimethyltin(IV)dichloride (2.0×10^{-3} mol dm^{-3}) was titrated with an alkali solution (0.1 mol dm^{-3}, NaOH) of the ligands ($1.91–1.97 \times 10^{-3}$ mol dm^{-3} of GMP and $1.78 –1.87 \times 10^{-3}$ mol dm^{-3} of AMP), both of the same ionic strength. The absorbance and $-\log[H^+]$ were measured after the addition of a few drops of titrant and this procedure was extended up to the required $-\log[H^+]$. To exclude carbon dioxide from the system, a steam of purified nitrogen was passed through a sodium chloride solution and then bubbled slowly through the reaction solution. In all cases, the procedure was repeated at least three times and the resulting average values and corresponding deviations from the average are shown in the text and tables.

Spectroscopy measurements

Spectrophotometric measurements were performed on a UV–vis Shimadzu 2100 spectrophotometer using a Pentium 4 computer and thermostated matched 10 mm quartz cells. The measurement cell was of flow type. A Masterflex pump allowed circulation of the solution under study from the potentiometric cell to the spectrophotometric cell so the absorbance and $-\log[H^+]$ of the solution could be measured simultaneously.

^{1}H NMR spectra of the ligand and the complexes were recorded on a Bruker DRX-300 MHz spectrometer in H_2O–D_2O (1:1 by volume) using TMS as an external reference. ^{31}P NMR spectra were recorded on the same spectrometer in H_2O–D_2O (1:9 by volume) operating at RT. The chemical shifts are given relative to phosphoric acid. The solutions were prepared by mixing $Me_2Sn(IV)$ with Na_2(5′-GMP or AMP) in H_2O–D_2O solution to give a 1:1 mole ratio. The concentration of the NMR samples was 1 mmol/L in both ^{1}H and ^{31}P NMR.

Other methods

FTIR spectra were obtained on a Bruker Bomem 100 spectrometer in the range 4000–500 cm^{-1} using KBr pellets. Samples for microanalysis were dried in vacuum to constant mass. Elemental analysis (C, H, N) was performed with a Fison Instruments CHNSO-1108 elemental analyzer.

The stepwise acidity constants of AMP^{-2} and GMP^{-2}

The results obtained using potentiometric pH titrations for the various acidity constants of the proton donors of the ligands, eqs. [2–5], are listed in Table 1 together with some previously reported values. The nucleosides 5′-monophosphate shown in Scheme 1 may bind with two protons at the phosphate group and one at the purine moiety. It was proposed (22) that $H_3(AMP)^+$ and $H_3(GMP)^+$ release their first proton from $-P(O)(OH)_2$, the second one from H^+(N-1) in the case of AMP and H^+(N-7) from GMP, and the third one again from the phosphate group. A fourth proton is released from H^+(N-1) in GMP in the alkaline pH range and from the ribose group in AMP (pH > 13). The fourth deprotonation of AMP was not considered further in this work. The given

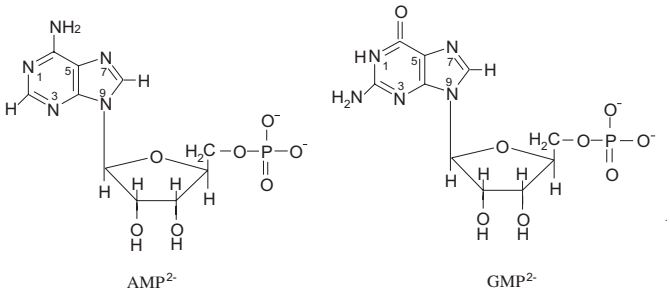
© 2006 NRC Canada

Table 1. Protonation constants of different species of GMP and AMP considered in this work.

Species	log $K^{H}_{H3(NMP)}$	log $K^{H}_{H2(NMP)}$	log $K^{H}_{H(NMP)}$	log $K^{H}_{(NMP)}$	Reference
GMP	—	2.48±0.05	6.28±0.08	9.60±0.09	This work
AMP	—	3.94±0.04	6.31±0.06	—	This work
GMP	0.3	2.48	6.25	9.49	22
AMP	0.4	3.84	6.21	—	22
AMP	—	3.98	6.38	—	23

Note: Measurements made by potentiometric pH titrations in aqueous solution at 25 °C and ionic strength 0.1 mol dm^{-3} ($NaClO_4$).

Scheme 1. Structures of adenosine 5′-monophosphate (AMP) and guanosine 5′-monophosphate (GMP).



acidity constants agree well, as far as available, with those reported in recent compilations (22–23).

[2*a*] $H_3(NMP)^+ \leftrightarrows H_2(NMP) + H^+$

[2*b*] $K^{H}_{H3(NMP)} = [H_2(NMP)][H^+] / [H_3(NMP)^+]$

[3*a*] $H_2(NMP) \leftrightarrows H(NMP)^- + H^+$

[3*b*] $K^{H}_{H2(NMP)} = [H(NMP)^-][H^+] / [H_2(NMP)]$

[4*a*] $H(NMP)^- \leftrightarrows (NMP)^{-2} + H^+$

[4*b*] $K^{H}_{H(NMP)} = [(NMP)^{-2}][H^+] / [H(NMP)^-]$

[5*a*] $(NMP)^{-2} \leftrightarrows (NMP\text{-}H)^{-3} + H^+$

[5*b*] $K^{H}_{(NMP)} = [(NMP\text{-}H)^{-3}][H^+] / [(NMP)^{-2}]$

The release of the first proton from $H_3(NMP)^+$ occurs at very low pH. A comparison of the protonation constants listed in Table 1 and those reported by ^1H NMR shift experiments (24) shows that the second proton in H_2(AMP) and H_2(GMP) are released mainly from H^+(N-1) and H^+(N-7), respectively, and the next from the phosphate group; these assignments agree with previous conclusions (25).

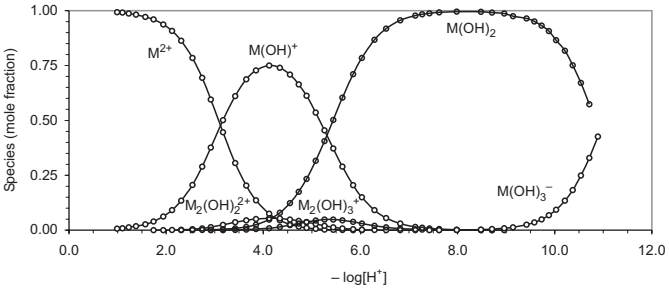
Hydrolysis of dimethyltin(IV)dichloride

The hydrolysis of $Me_2Sn(IV)^{+2}$ has been investigated in different media by several authors (26–27). We performed earlier spectrophotometric titrations to obtain these data in various ionic strengths (0.1–1.0 mol dm^{-3}) in $NaClO_4$ and NaCl media (28). The species mole fractions of the observed hydrolyzed species of $Me_2Sn(IV)^{2+}$ in different pH and constant ionic strength (0.1 mol dm^{-3} sodium perchlorate) are shown in Fig. 1. Hydrolysis reactions are (where $M^{2+} = Me_2Sn^{2+}$),

$$M^{2+} + OH^- \Phi M(OH)^+$$

$$M^{2+} + 2OH^- \Phi M(OH)_2$$

Fig. 1. Distribution mole fraction of hydrolytic species of $Me_2Sn(IV)^{2+}$ vs. hydrogen ion concentration at 25 °C and ionic strength 0.1 mol dm^{-3} ($NaClO_4$) ($[Me_2Sn(IV)^{2+}] = 4 \times 10^{-3}$ mol dm^{-3}).



$$M^{2+} + 3OH^- \Phi M(OH)_3^-$$

$$2M^{2+} + 2OH^- \Phi M_2(OH)_2^{2+}$$

$$2M^{2+} + 3OH^- \Phi M_2(OH)_3^+$$

The hydrolysis constants of the hydrolyzed species are determined as before (28) and are listed in Table 2. The detected species and their formation constants are in good agreement with those reported earlier and show the strong tendency of dimethyltin(IV) to hydrolysis in aqueous solution to form various hydrolyzed species (26–28).

Complexation of AMP and GMP by dimethyltin(IV)

One of the main obstacles in studying metal ion systems with nucleotide derivatives in solution is the known self-association of AMP and GMP (29). This means that low concentrations of the ligands must be employed in the experiments, a condition usually fulfilled with UV spectroscopic studies. In similar studies, Sigel and coworkers (22, 30) have demonstrated that in 5 mmol/L and 1 mmol/L solutions, about 95% and 97% of the total GMP or AMP exists in the monomeric form, respectively. With the indicated problems in mind we decided to study the complexes of AMP and GMP with dimethyltin(IV) in aqueous solution by evaluating precise stability data from spectrophotometric titrations.

The complex $M_xH_yL_z^{(2x+y-nz)}$ that formed is characterized by its stoichiometry (x:y:z), where M and L represent the metal ion and AMP or GMP, respectively. To determine the stability constant of the complexation, eq. [6] is defined by β_{xyz} where

[6] $xM^{2+} + yH^+ + zL^{n-} \leftrightarrows M_xH_yL_z^{(2x+y-nz)}$

[7] $\beta_{xyz} = [M_xH_yL_z^{(2x+y-nz)}] / ([M^{2+}]^x[H^+]^y[L^{n-}]^z)$

© 2006 NRC Canada

Table 2. Average values of hydrolysis constants β_{pq} for $Me_2Sn(IV)^{2+}$ species.

$-\log \beta_{11}$	$-\log \beta_{12}$	$-\log \beta_{13}$	$-\log \beta_{22}$	$-\log \beta_{23}$	Reference
3.12±0.03	8.43±0.04	19.45±0.09	4.86±0.05	9.74±0.08	This work
3.25	8.54	—	5.05	9.81	26
3.12	8.45	19.48	5.2	9.7	27

Note: Measurements of β_{pq} made in aqueous solution at 25 °C and ionic strength 0.1 mol dm^{-3} ($NaClO_4$), where p and q represent $Me_2Sn(IV)$ and hydroxyl ions, respectively. Some literature values are also listed.

The method of determining the stability constant is based on the relation A = f(pH) (21, 31). The absorbance A and $-\log[H^+]$ were measured for a solution containing dimethyltin(IV) and AMP or GMP. Treatments of the spectrophotometric data (each 5 nm) obtained during the titrations, as a function of the H^+ concentration, were analysed by computer program (32). The program calculates the stability constants for different stoichiometry models. The degree of refinement guides the user to a choice between the models.

Considering the protonation constants of the ligands, the predominant species for complexation is H_2L in acidic pH. In this case, the spectrophotometric titration data were analyzed by using the absorbance of AMP or GMP in the presence of dimethyltin(IV) at wavelengths in the UV range that are given by,

$$[8] \quad A = \varepsilon_M[(CH_3)_2Sn(IV)^{2+}] + \Sigma\varepsilon_C[\text{complex}]$$

where ε_M and ε_C are the molar absorbance coefficients of the metal ion and each complex, respectively. For the mass balance

$$[9] \quad [(CH_3)_2Sn(IV)^{2+}] = C_M - \Sigma[\text{complex}]$$

$$[10] \quad [H_2L] = C_L - \Sigma[\text{complex}]$$

where C_M and C_L are the total concentrations of the metal ion and each ligand, respectively. Substituting eqs. [7], [9], and [10] into eq. [8] gives the final equation for fitting. Using a suitable computer program (31) we fitted the data to the final equation to estimate the formation constant of eq. [6]. We used the Gauss–Newton nonlinear least-squares method in the computer program to refine the absorbance by minimizing the error squares sum from eq. [11],

$$[11] \quad U = \Sigma(a_i - b_i)^2 \qquad (i = 1, 2, 3, \ldots)$$

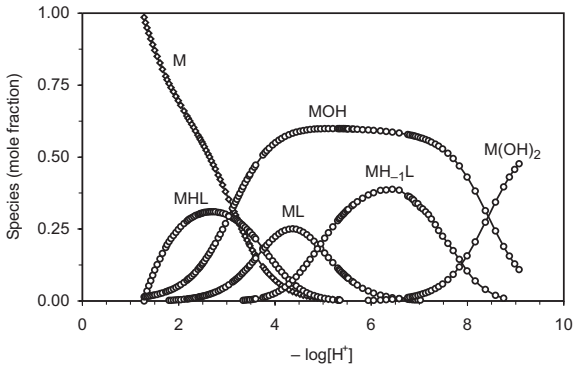
Here, a_i is an experimental absorbance and b_i is a calculated one. The computer program used two different kinds of fit, (*a*) graphical and (*b*) numerical. The final selection of the species was based on both graphical and numerical methods and on various statistical criteria, i.e., sums of squared residuals and differences of C_M(exp) and C_L(exp) values from calculated ones.

Different models, including ML, MHL, $MH_{-1}L$, and several polynuclear and protonated species were tested by the program. As expected, polynuclear complexes were systematically rejected by the computer program, as were MH_2L_2, MHL_2, and ML_2 (the charges were omitted for simplicity). A value for the MH_3L species (in both cases of GMP and AMP) was also calculated by the program, but the species was not considered further because the estimated error in its formation constant was unacceptable and its inclusion does not improve the goodness of the fit. The chosen models, formed by MHL, ML, and $MH_{-1}L$ for AMP and GMP, besides the hydrolysis products of $Me_2Sn(IV)^{2+}$, resulted in satisfactory numerical and graphical fits. The calculated average values of the stability constants for various wavelengths are listed in Table 3.

Table 3. Average values of the stability constants for the systems $Me_2Sn(IV)^{2+}$ + AMP and GMP at 25 °C and ionic strength 0.1 mol dm^{-3} ($NaClO_4$).

Species	$\log \beta_{111}$	$\log \beta_{101}$	$\log \beta_{1-11}$
AMP	5.69±0.11	2.56±0.01	8.47±0.05
GMP	5.59±0.09	4.19±0.04	7.75±0.06

Fig. 2. Species distribution diagram of the $Me_2Sn(IV)$-AMP system ($[Me_2Sn(IV)] = 2 \times 10^{-3}$ mol dm^{-3} and [AMP] = 1.87×10^{-3} mol dm^{-3}) at 280 nm, 25 °C and 0.1 mol dm^{-3} $NaClO_4$.



During the spectrophotometric titration of AMP and GMP by dimethyltin(IV), no precipitation was observed (under the conditions of the UV–vis measurements). The species distribution curves depicted in Figs. 2 and 3 reveal similar behaviour for the two ligands towards $(CH_3)_2Sn(IV)^{2+}$ and demonstrate that complexes with a 1:1 ligand to metal ion ratio were formed. There was no evidence of the presence of polynuclear species in solution.

Figures 4 and 5 exhibit the ^1H NMR spectra of methyl signals at different pH values. As can be seen, the $^2J(Sn\text{-}^1H)$ values increase with increasing pH in NMR titration, which indicate that a complex species besides $(CH_3)_2Sn(IV)$ exists in solution. This species is most probably MH_2L, which forms on the monodentate coordination of the ligands through their phosphate groups. At such a low pH value (<1), it was very difficult to fit the species matrix and determine the stability constant of this species. However, at higher pH (pH ≅ 1.5–4.5 for AMP and 1.5–3 for GMP) the MHL species is formed from MH_2L on deprotonation of H^+(N-1) and H^+(N-7) on the purine bases of AMP and GMP, respectively (MH_2L Φ MHL + H^+). The species formed at different pH values were found to be in different protonation

© 2006 NRC Canada

Fig. 3. Species distribution diagram of the $Me_2Sn(IV)$-GMP system ([$Me_2Sn(IV)$] = 2 × 10^{-3} mol dm^{-3} and [GMP] = 1.97 × 10^{-3} mol dm^{-3}) at 295 nm, 25 °C and 0.1 mol dm^{-3} $NaClO_4$.

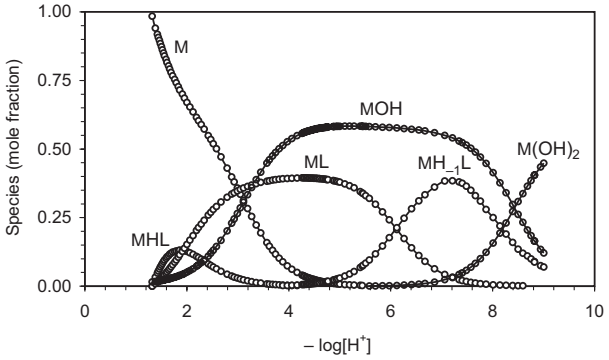
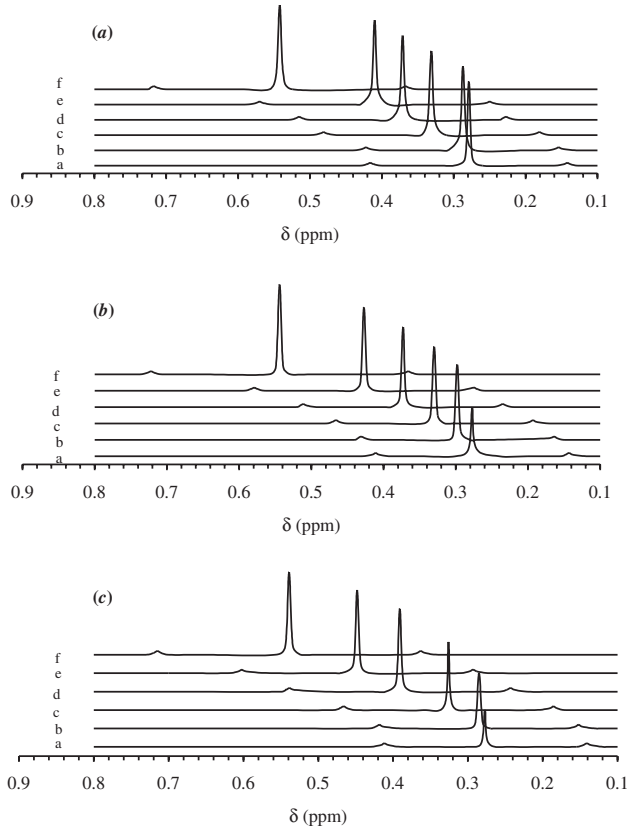
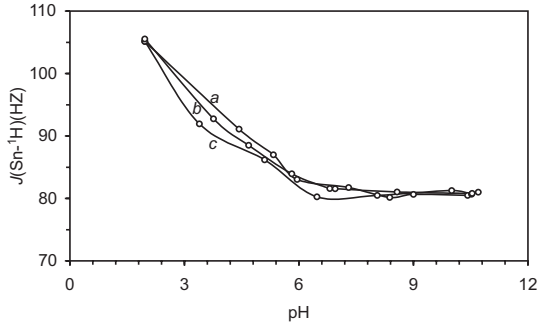


Fig. 4. ^1H NMR spectra as a function of pH in the Me proton range for (*A*) $Me_2Sn(IV)$ alone, (*B*) the 1:1 $Me_2Sn(IV)$-AMP system, and (*C*) the 1:1 $Me_2Sn(IV)$-GMP system. In (*a*) curves a–f represent pH 10.01, 8.05, 6.47, 5.1, 3.39, and 1.96, respectively; in (*b*) curves a–f represent pH 9.01, 8.38, 7.3, 5.95, 4.43, and 1.96, respectively; in (*c*) curves a–f represent pH 8.57, 6.95, 5.81, 4.68, 3.76, and 1.97, respectively.



states. In the acidic and neutral pH range, two deprotonation processes take place for both systems (pH ≅ 2.5–6 and 4–8 for AMP; pH ≅ 2–7 and 4.5–9 for GMP, respectively) resulting in formation of the ML and $MH_{-1}L$ species, MHL Φ ML + H^+, and ML Φ $MH_{-1}L$ + H^+. The first reaction is due to the deprotonation of the second OH of the phosphate group and the second reaction is attributed to the deprotonation of a coordinated H_2O molecule, resulting in the formation of a

Fig. 5. Measured coupling constants, $^2J(Sn\text{-}^1H)$, of Me protons as a function of pH in solutions of (*a*) 1:1 $Me_2Sn(IV)$-AMP system, (*b*) 1:1 $Me_2Sn(IV)$-GMP system, and (*c*) $Me_2Sn(IV)$ alone.



mixed hydroxo complex (Figs. 2 and 3). Evaluation of the titration curves shows that only the hydrolyzed species, $M(OH)_2$, is present at higher pH (pH ≅ 8–9).

Lockhart and Manders studied the correlation of $^2J(Sn\text{-}^1H)$ and the Me–Sn–Me angle in 25 methyltin(IV) compounds (33). They proposed an empirical quadratic expression in terms of $^2J(Sn\text{-}^1H)$ to determine the C–Sn–C angle. It was found that these values provide useful information on the C–Sn–C bond angle of the compounds in a sample and indirectly on the possible coordination numbers and geometry around the Sn atom.

Two-bond coupling, $^2J(Sn\text{-}^1H)$, of the $Me_2Sn(IV)^{2+}$ alone and its complexes with AMP and GMP were determined via the ^1H NMR spectra at different pH. It can be seen (Fig. 4) that the signals of the methyl protons in $Me_2Sn(IV)^{2+}$ are sharp for both systems and have the same chemical shift as in the solution of $Me_2Sn(IV)^{2+}$ alone. The ^1H NMR titration vs. pH of 1:1 mixtures of $Me_2Sn(IV)^{2+}$ and GMP or AMP, on the other hand, do not show any shift of the adjacent to N-1 and N-7 protons of the ligands in the pH range 1.5–9, thus excluding Sn(IV) interaction with the nitrogen of the purine ring. In similar studies, the same results were observed by Yang et al. (34) and Jankovics et al. (19) in ^1H NMR and ^{119}Sn Mössbauer spectra for the systems $Et_2Sn(IV)^{2+}$ + 5′-GMP, 5′-IMP, and $Me_2Sn(IV)^{2+}$+ R5P, GIP, G6P, respectively. At higher pH the $^2J(Sn\text{-}^1H)$ values of $Me_2Sn(IV)^{2+}$ are somewhat smaller than complex systems (Fig. 5), possibly because of a slight distortion of C–Sn–C angle by the coordinated ligand (33). Using the quadratic equation of Lockhart and Manders (33), the average C–Sn–C bond angle at low pH (<2) and higher pH values (>6) for the two species calculated from the coupling constant are 175 and 135 °, respectively. On this basis, $Me_2Sn(IV)^{2+}$ and their complexes with AMP and GMP are proposed to have an octahedral structure at low pH and a distorted trigonal bipyramidal structure at higher pH, as shown in Scheme 2.

Figures 6 and 7 present the ^{31}P NMR chemical shifts (δ) of the $Me_2Sn(IV)^{2+}$ and the complexes with AMP and GMP in 1:1 stoichiometries in aqueous solution as a function of pH. For the free ligand the chemical shifts of P slightly increase with increasing pH up to two and this can be attributed to the deprotonation of P-OH and delocalization of negative charge over the P moiety. Interestingly, a further increase of pH to four has no effect on chemical shifts. However, pH values higher than five facilitate further deprotonation and the delocalization of remaining P-OH and

© 2006 NRC Canada

Table 4. IR absorption bands of the free ligands and the complexes in KBr (cm^{-1}).

Assignment	GMP	GMP + $Me_2Sn(IV)$	AMP	AMP + $Me_2Sn(IV)$
ν (OH), ν (NH_2)	3356, s, b	3353, s, b	3335, s, b	3336, s, b
ν (CH)	2945, m	2940, m	2942, m, b	2940, w, b
ν (C=O)	1677, s	1680, s		
δ (NH_2)			1641, s	1648, s
Bands of the purine skeleton	1530, m	1531, m	1609, m	1609, m
	1500, m	1498, m	1578, m	1577, m
			1481, m	1481, m
ν (*P* = O)	1204, w	1230, w	1250, m	1242, w
ν_{as} (PO_3)	1084, s	1104, s	1070, s	1095, s
ν_{sym} (PO_3)	979, s	999, s	978, s	995, m

Note: s = strong, m = medium, w = weak, b = broad.

Fig. 6. The ^{31}P chemical shifts vs. pH of (*a*) GMP and (*b*) the mixtures with $Me_2Sn(IV)$.

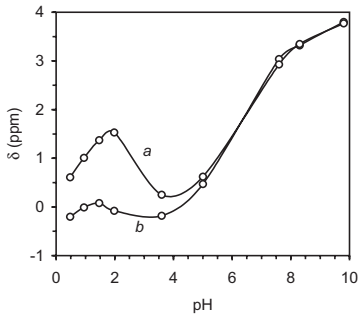
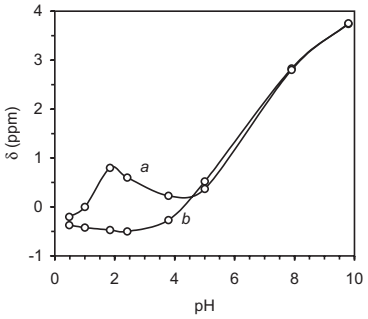


Fig. 7. The ^{31}P chemical shifts vs. pH of (*a*) AMP and (*b*) the mixtures with $Me_2Sn(IV)$.

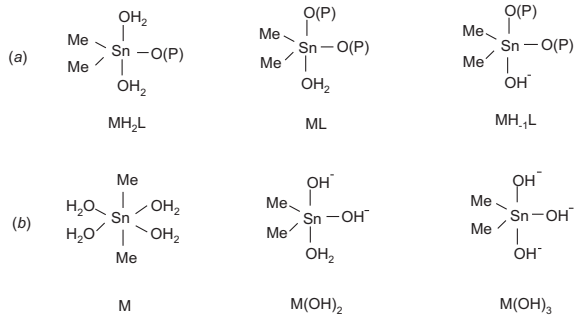


consequently large down field shifts accrue. It is seen that the presence of $Me_2Sn(IV)^{2+}$ causes an upfield shift in ^{31}P NMR signals of AMP and GMP to a maximum of about 1.5–2 ppm at pH ~2 for both systems, indicating a Sn(IV) interaction with the pyrophosphate groups. At about pH 3, precipitation starts at higher concentrations. In aqueous solution, it has been suggested that $Me_2Sn(IV)^{2+}$ reacts with phosphate ions to form solid complexes (11, 34). At pH > 6.5, the ^{31}P NMR chemical shift of the free ligands and their mixtures with $Me_2Sn(IV)^{2+}$ present no significant difference and this leads to the conclusion that no tin–phosphate interaction is taking place.

Characterization of the $Me_2Sn(IV)^{2+}$-AMP and GMP precipitates

When the concentration of the ligands is higher than 0.005 mol dm^{-3}, a white precipitate is formed in the pH range 3–5 during the titration of both GMP and AMP by dimethyltin(IV). The hydrolysis products of dimethyltin(IV) are soluble at this concentration and there was no precipitation during the titration of the ligands alone. So, we concluded that the solid products were attributed to the formation of MHL and ML species. The precipitates were collected by filtration, dried at RT by vacuum, and characterized by means of FTIR. The metal to ligand ratio in $Me_2Sn(IV)^{2+}$-AMP and -GMP were determined by elemental analysis (found C 27.03, H 4.02, N 13.06 and C 26.24, H 3.92, N 12.75 for AMP and GMP, respectively, that were calculated for Me_2Sn-AMP,$2H_2O$ [$C_{12}H_{22}N_5O_9PSn$] C 27.18, H 4.15, N 13.22 and Me_2Sn-GMP,$2H_2O$ [$C_{12}H_{22}N_5O_{10}PSn$] C 26.39, H 4.03, N 12.83). These results indicate the formation of complexes with 1:1 metal to ligand ratio. The characteristic IR bands of GMP, AMP, dimethyltin(IV)-GMP, and dimethyltin(IV)-AMP are listed in Table 4.

Scheme 2. Proposed structure of (*a*) the complexes and (*b*) the hydrolyzed species of dimethyltin(IV).



The intensive and broad band in the region 3500–2600 cm^{-1} due to ν(OH) and ν(NH_2) stretching vibrations of the sugar OH groups and the purine moiety is observed in the spectra of the ligands and the precipitates (19). The intensity of the band is lower in the spectra of the complexes, but their shapes are identical. From this, coordination of the ligands through their sugar moiety can be excluded (19). The skeleton vibrations of the purine rings of the nucleotides in the region 1609–1481 cm^{-1} do not shift in the complexes, indicating the nonexistence of any metal ion with the ring nitrogen atoms interactions (34). On the other hand, considerable changes were observed in phosphate stretching in the range 1200–970 cm^{-1} of the free ligands and the complexes. This can be explained by the binding of tin to the oxygen of the phosphate.

© 2006 NRC Canada

The arrangement mentioned above confirms that the phosphate group in both cases coordinate to dimethyltin(IV) and the ring nitrogen atoms do not participate in the coordination. These findings are in agreement with earlier results for similar systems (6, 9, 17, 34).

Acknowledgements

Financial support by the Research Council of Shahid Beheshti University is gratefully acknowledged.

References

1. B.K. Keppler. Metal complexes in cancer chemotherapy. VCH, Weinheim, Germany. 1993.
2. S.E. Sharman and S.J. Lippard. Chem. Rev. **87**, 1153 (1987).
3. M. Bloemink and J. Reedijik. Metal ions in biology. Marcel Dekker, New York. 1996.
4. M. Gielen, M. Biesemans, and R. Willem. Appl. Organomet. Chem. **19**, 440 (2005).
5. M. Gielen. Appl. Organomet. Chem. **16**, 481 (2002).
6. A.J. Crowe. Drugs Future, **12**, 255 (1987).
7. M.J. Hynes and M. O'Dowd. J. Chem. Soc. Dalton Trans. 563 (1987).
8. G. Arena, R. Cali, A. Contino, N. Loretta, S. Musumeci, and R. Purello. J. Chem. Soc. Dalton Trans. 2039 (1992).
9. A. Jancso, L. Nagy, E. Moldrheim, and E. Sletten. J. Chem. Soc. Dalton Trans.1587 (1999).
10. L. Ghys, M. Biesemans, M. Gielen, A. Garoufis, N. Hadjiliadis, R. Willem, and J.C. Martins. Eur. J. Inorg. Chem. 513 (2000).
11. R. Barbieri, A. Silvestri, and V. Piro. J. Chem. Soc. Dalton Trans. 3605 (1990).
12. R. Barbieri and A. Silvestri. J. Inorg. Biochem. **41**, 31 (1991).
13. V. Piro, F. Di Simone, G. Madonia, A. Silvestri, A.M. Giuliani, G. Ruisi, and R. Barbieri. Appl. Organomet. Chem. **6**, 537 (1992).
14. R. Barbieri, A. Silvestri, A.M. Giuliani, V. Piro, F. Di Simone, and G. Madonia. J. Chem. Soc. Dalton Trans. 585 (1992).
15. R. Barbieri, G. Alonzo, and R.H. Herber. J. Chem. Soc. Dalton Trans. 789 (1987).
16. C. Pettinari, F. Marchetti, and Q. Li. Main Group Met. Chem. **24**, 53 (2001).
17. K. Gajda-Schrantz, L. Nagy, E. Kuzmann, A.A. Christy, H. Barat-Jankovics, E. Sletten, and A. Vertes. J. Radioanal. Nucl. Chem. **247**, 79 (2001).
18. P. Surdy, P. Rubini, N. Buzas, B. Henry, L. Pellerito, and T. Gajda. Inorg. Chem. **38**, 346 (1999).
19. H. Jankovics, L. Nagy, N. Buzas, L. Pellerito, and R. Barbieri. J. Inorg. Biochem. **92**, 55 (2002).
20. J.M. Tsangaris and D.R. Williams. Appl. Organomet. Chem. **6**, 3 (1992).
21. P. Lagrange, K. Schneider, K. Zare, and J. Lagrange. Polyhedron, **13**, 861 (1994).
22. H. Sigel, S.S. Massoud, and N.A. Corfu. J. Am. Chem. Soc. **116**, 2958 (1994).
23. M.M. Taqui Khan and E. Martel. J. Am. Chem. Soc. **67**, 1083 (1963).
24. N.A. Corfu and H. Sigel. Eur. J. Biochem. **199**, 659 (1991).
25. H. Sigel. Chem. Soc. Rev. **22**, 255 (1993).
26. R.S. Tobias and C.E. Friedline. Inorg. Chem. **4**, 215 (1965).
27. C. De Stefano, C. Foti, A. Gianguzza, M. Martino, L. Pellerito, and S. Sammartano. J. Chem. Eng. Data, **41**, 511 (1996).
28. F. Gharib, M.M. Amini, and A. Haghgou. Main Group Met. Chem. **26**, 381 (2003).
29. F. Gharib, T. Kheradmand, and P. Amani. Anal. Sci. **21**, 945 (2005).
30. H. Sigel, S.S. Massoud, and R. Tribolet. J. Am. Chem. Soc. **110**, 6857 (1988).
31. F. Gharib. J. Chem. Eng. Data, **50**, 196 (2005).
32. D.C. Harris. J. Chem. Educ. **75**, 119 (1998).
33. T.P. Lockhart and W. Mandars. Inorg. Chem. **25**, 892 (1986).
34. Z. Yang, T. Bakas, A. Sanchez-Diaz, C. Charalampopoulos, J. Tsangaris, and N. Hadjiliadis. J. Inorg. Biochem. **72**, 133 (1998).

© 2006 NRC Canada

Efficient Ru^{III}-catalyzed condensation of indoles and aldehydes or ketones

Khalil Tabatabaeian, Manouchehr Mamaghani, Nosratollah Mahmoodi, and Alireza Khorshidi

Abstract: Synthesis of bis(indolyl)methanes through condensation of indoles and various aldehydes or ketones, using Ru^{III} as catalyst, is reported. It was found that the catalytic system involving Ru^{III} affords the products smoothly under very mild conditions in good to high yields.

Key words: aldehydes, ketones, bis(indolyl)methanes, indoles, ruthenium.

Résumé : Utilisant du Ru(III) comme catalyseur, on a réalisé la synthèse de bis(indolyl)méthanes par le biais de la condensation d'indoles et de divers aldéhydes ou cétones. On a trouvé que le système catalytique impliquant du Ru(III) permet d'obtenir facilement les produits dans des conditions douces et avec des rendements allant de bon à élevés.

Mots clés : aldéhydes, cétones, bis(indolyl)méthanes, indoles, ruthénium.

[Traduit par la Rédaction]

Introduction

Transition metal-catalyzed C–H bond activation has received considerable attention in synthetic organic chemistry since the cleavage of an unreactive C–H bond and subsequent addition of the C–H unit into unsaturated substrates could lead to the formation of a new C–C bond (1). The formation of a C–C bond is one of the most fundamental projects in organic chemistry. Much effort has naturally been devoted to developing more convenient and efficient strategies for the formation of C–C bonds. During the last two decades, many successful applications of catalytic C–H bond activation directed toward the construction of C–C bonds have been reported in synthetic communities (2).

The development of new efficient synthetic methods leading to indole derivatives continues to receive much attention in organic synthesis because of their biological activities (3). Various indole derivatives occur in many pharmacologically and biologically active compounds (4). Among of them, bis(indolyl)methanes possess a wide range of biological activity and their synthesis has received a considerable amount of interest (5, 6). Generally, bis(indolyl)methanes are prepared by the condensation of indoles with various aldehydes or ketones in the presence of either protic (7) or Lewis acids (8–10). On the other hand, Ru^{III} salts are well-known to catalyze many organic transformations, including aldol and Michael reactions (11), oxidation reactions of alkanes (12), oxidative cyanation of amines (13), and many others (14). We found that Ruthenium (III) chloride hydrate is a very effective catalyst for the double addition of indoles to aldehydes or ketones, yielding bis(indolyl) derivatives in high yields. The ruthenium catalyst was used in low concentrations (as low as 1.2 mol%) and a relatively easy work-up affords catalytic formation of a carbon–carbon bond under mild reaction conditions. To the best of our knowledge, this is the first report on the use of Ru^{III} salts as catalyst for the condensation of indoles with various aldehydes or ketones.

Received 12 July 2006. Accepted 2 October 2006. Published on the NRC Research Press Web site at http://canjchem.nrc.ca on 17 November 2006.

K. Tabatabaeian,[1] M. Mamaghani, N. Mahmoodi, and A. Khorshidi. Department of Chemistry, Faculty of Sciences, The University of Guilan, P. O. Box 41335–1914, Iran.

[1]Corresponding author (email: Taba@guilan.ac.ir).

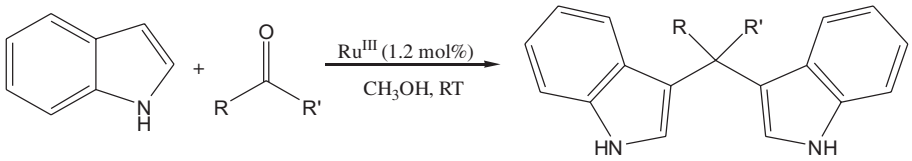
Results and discussion

Typical results of the ruthenium-catalyzed condensation of indoles and aldehydes or ketones are shown in Tables 1 and 2 and they indicate the scope of the reaction. Treatment of benzaldehyde (1.2 mmol) with indole (2 mmol) in the presence of $RuCl_3 \cdot nH_2O$ catalyst (1.2 mol%) in methanol (2 mL) at RT for 27 min gave the corresponding 3,3′-bis(indolyl)phenylmethane in 92% yield (product 1a). No attempts were made to characterize byproducts since they are formed in trace amounts (using GLC analysis). The reaction can be used for substituted aromatic aldehydes with either electron-donating or electron-withdrawing groups (Table 1, entries b–e). Furthermore, the reaction of indole with aliphatic aldehydes furnished high yields of the corresponding product class (Table 1, entries f and g).

Encouraged by these results, we studied the condensation reaction between indole and some ketones. The method is highly chemoselective, as ketones do not participate in the reaction in ambient conditions. This selectivity might be useful in the reaction of multifunctional carbonyl compounds with indole since they have both aldehyde and ketone functionalities. However, the method is still effective enough to afford the condensation products of indole and ketones through reflux of the reaction mixture (Table 1, entries h–l) in good yields.

 doi:10.1139/V06-159 © 2006 NRC Canada

Table 1. Ru^{III}-catalyzed condensation of indole and aldehydes or ketones.



Entry	R	R′	Product	Time (min)	Yield (%)[a]
a	C_6H_5	H	**1a**	27	92[c]
b	4-pr^i-C_6H_4	H	**1b**	25	93
c	4-OHC_6H_4	H	**1c**	30	82[d]
d	2-ClC_6H_4	H	**1d**	30	88[c]
e	3-$NO_2C_6H_4$	H	**1e**	30	85[e]
f	CH_3	H	**1f**	30	73
g	$CH_3(CH_2)_3$	H	**1g**	30	87
h	C_6H_5	CH_3	**1h**	180[b]	68[d]
i	4-$CH_3OC_6H_4$	CH_3	**1i**	60[b]	72
j	3,4-$(CH_3O)_2C_6H_3$	CH_3	**1j**	120[b]	77
k	4-$NO_2C_6H_4$	CH_3	**1k**	120[b]	73
l	C_6H_5	C_6H_5	**1l**	180[b]	51

Note: All products were characterized by ^1H NMR, ^{13}C NMR, and IR data.
[a]Isolated yields.
[b]Reflux.
[cde]Identified by comparison with authentic samples (15, 16, 8).

With regard to the indole moiety, the present protocol is noteworthy because substituted indoles underwent smooth reactions with aromatic aldehydes giving excellent yields of products (Table 2). For example, treatment of 1-, 2-, and 5-substituted indoles with various aromatic aldehydes gave corresponding products **2a**–**2f**, most of them insoluble in the reaction media (solvent methanol) and this makes the work-up even easier (see Experimental section). Also, the reaction times for 1- and 2-substituted indoles are much less than those of unsubstituted substrates.

The reaction of indole and benzaldehyde was taken as a representative example and the progress of the reaction was monitored by GLC technique. To examine the influence of the catalyst concentration, we also carried out the reaction of benzaldehyde and indole in different catalyst concentrations. Due to the decomposition of the products under chromatographic conditions, decrease in the corresponding aldehyde peak areas was selected as a measure of reaction coordinate. Also, the peak of methanol was used as internal standard. The results are summarized in Table 3.

These results reveal that the Ru^{III} system is at least four times more effective than the previously reported catalytic system using Fe^{III} in ionic liquids (15) in terms of utilized catalyst concentration (1.2% vs. 5%). Also, the catalytic activity is nearly ten times greater in terms of reaction time (3 min vs. 30 min in ~5 mol% of catalyst).

Conclusion

In brief, we have developed a convenient method for the synthesis of bis(indolyl)methanes using the condensation reaction of indoles and aldehydes or ketones in the presence of $RuCl_3 \cdot nH_2O$ as efficient catalyst. With regard to the previous works, the present protocol has several advantages. As the reaction solvent, methanol has lower toxicity in contrast to CH_3CN (8–10). In the reaction of substituted indoles with aromatic aldehydes, the products are mainly insoluble in methanol, therefore simple filtration of the reaction mixture and rinsing with methanol provides completely pure products. The unique feature of the reaction is selectivity between ketones and aldehydes at ambient temperature while the other methods catalyze the reaction of both aldehydes and ketones at room temperature (8–10) or only catalyze the reaction of aldehydes (15). Further manipulation of this reaction is underway.

Experimental

General

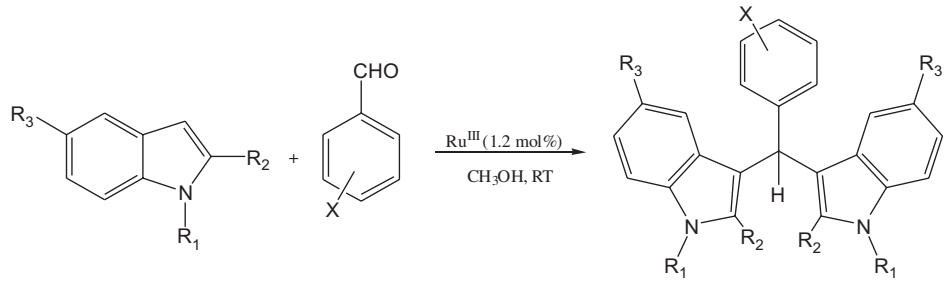
IR spectra were recorded on a Shimadzu FTIR-8400S spectrometer. ^1H NMR spectra were obtained on a Bruker DRX-500 Avance and ^{13}C NMR spectra were obtained on a Bruker DRX-125 Avance. Chemical shifts of ^1H and ^{13}C NMR spectra were expressed in parts per million downfield from tetramethylsilane. Analytical GLC evaluations of product mixtures were carried out on a Varian CP-3800 chromatograph (using a split/splitless injector, CP Sil 8CB column, FID assembly). Melting points were measured on a BÜCHI Melting Point B-540 and are uncorrected. Elemental analyses were made with a Carlo-Erba EA1110 CNNO-S analyzer and agreed with the calculated values.

Materials

HPLC grade methanol was used as solvent and all other materials were purchased from Merck and used without further purification.

© 2006 NRC Canada

Table 2. Ru^{III}-catalyzed condensation of substituted indoles and aldehydes.



Entry	R_1	R_2	R_3	X	Product	Time (min)	Yield (%)[a]
a	CH_3	H	H	H	**2a**	5	98
b	CH_3	H	H	4-pr^i-C_6H_4	**2b**	3	98
c	CH_3	H	H	3-(CH_3O)-4-$(HO)C_6H_3$	**2c**	10	95
d	H	CH_3	H	H	**2d**	3	98[b]
e	H	CH_3	H	4-pr^i-C_6H_4	**2e**	10	96
f	H	H	Br	H	**2f**	30	75

Note: All products were characterized by ^1H NMR, ^{13}C NMR, and IR data.
[a]Isolated yields.
[b]Identified by comparison with authentic samples (17).

Table 3. $RuCl_3 \cdot nH_2O$-catalyzed condensation of benzaldehyde and indole in different catalyst concentrations.

Entry	Reaction time (min)	Aldehyde consumption (%)	Catalyst concentration (mol% Ru/aldehyde)
1	27	98	1.2
2	3	91.6	1.9
3	15	97.8	1.9
4	27	97.8	1.9
5	3	96.7	3.8
6	15	97.2	3.8
7	27	97.6	3.8
8	3	98	5.6
9	15	98.3	5.6
10	27	98.3	5.6

Ruthenium-catalyzed condensation of benzaldehyde and indole

A 20 mL flask equipped with a magnetic stirring bar was charged with methanol (2 mL), benzaldehyde (127.4 mg, 1.2 mmol), and indole (234.4 mg, 2 mmol). $RuCl_3 \cdot nH_2O$ (3 mg, 0.014 mmol) was added into the flask and the reaction mixture was stirred at RT. After 0.5 h, the reaction mixture was purified by preparative TLC (petroleum ether – ethyl acetate, 10:4) providing a pure product (296 mg, 92%). The same procedure was also used for the other products listed in Tables 1 and 2. In the case of entries a–e in Table 2, simple filtration of the reaction mixture and treatment with methanol provided pure products.

3,3-Bis(indolyl)-4-isopropylphenylmethane (1b)

Solid, mp 153 to 154 °C. IR (KBr, cm^{-1}) υ: 422, 468, 497, 586, 599, 744, 752, 792, 1010, 1089, 1215, 1338, 1417, 1456, 1510, 2867, 2962, 3051, 3421 (NH). ^1H NMR (500 MHz, $CDCl_3$, 25 °C, ppm) δ: 1.29 (d, 6H, J = 7.00 Hz, $(CH_3)_2CH$), 2.93 (sept, J = 7.00 Hz, -$CH(CH_3)_2$), 5.91 (s, 1H, Ar-CH), 6.7 (s, 2H), 7.06 (t, J = 7.5 Hz, 2H), 7.18 (d, J = 8.00 Hz, 2H), 7.21 (t, J = 7.5 Hz, 2H), 7.3 (d, J = 7.3 Hz, 2H), 7.39 (d, J = 8.00 Hz, 2H), 7.46 (d, J = 7.9 Hz, 2H), 7.91 (br, s, 2H, NH). ^{13}C NMR (125 MHz, $CDCl_3$, 25 °C, ppm) δ: 24.51, 34.11, 40.2, 111.46, 119.6, 120.42, 120.44, 122.3, 124.0, 126.66, 127.6, 128.98, 137.12, 141.7, 146.92. Anal. calcd. for $C_{26}H_{24}N_2$: C 85.68, H 6.64, N 7.69; found: C 85.74, H 6.67, N 7.65.

3,3′-Bis(indolyl)methylmethane (1f)

Solid, mp 157–159 °C. IR (KBr, cm^{-1}) υ: 424, 499, 578, 740, 756, 815, 1018, 1097, 1220, 1334, 1421, 1456, 2837, 2925, 2956, 3417 (NH). ^1H NMR (500 MHz, $CDCl_3$, 25 °C, ppm) δ: 1.87 (d, J = 7.06 Hz, 3H), 4.74 (q, J = 6.96 Hz, 1H), 6.96 (d, J= 2.06 Hz, 2H), 7.10 (t, J = 7.53 Hz, 2H), 7.23 (t, J = 7.30 Hz, 2H), 7.39 (d, J = 8.15 Hz, 2H), 7.64 (d, J = 7.92 Hz, 2H), 7.89 (br, s, 2H, NH). ^{13}C NMR (125 MHz, $CDCl_3$, 25 °C, ppm) δ: 22.17, 28.62, 111.50, 119.46, 120.18, 121.64, 122.13, 122.22, 127.36, 137.09. Anal. calcd. for $C_{18}H_{16}N_2$: C 83.04, H 6.19, N 10.76; found: C 83.11, H 6.24, N 10.78.

3,3′-Bis(indolyl)butylmethane (1g)

Viscous liquid. IR (KBr, cm^{-1}) υ: 424, 487, 582, 740, 800, 929, 1010, 1093, 1218, 1244, 1336, 1417, 1456, 2856, 2927, 2954, 3055, 3415 (NH). ^1H NMR (500 MHz, $CDCl_3$, 25 °C, ppm) δ: 0.97 (t, J = 6.95 Hz, 3H), 1.44–1.49 (m, 4H), 2.27–2.33 (m, 2H), 4.55 (t, J = 7.40 Hz, 1H), 6.98 (d, J = 2.08 Hz, 2H), 7.14 (t, J = 7.43 Hz, 2H), 7.24 (t, J = 7.35 Hz, 2H), 7.36 (d, J = 8.12 Hz, 2H), 7.70 (d, J = 7.90 Hz, 2H), 7.84 (br, s, 2H, NH). ^{13}C NMR (125 MHz, $CDCl_3$, 25 °C, ppm) δ: 14.64, 23.33, 31.03, 34.42, 36.09, 111.59, 119.44, 120.14, 120.97, 121.93, 122.16, 127.63, 137.02. Anal. calcd. for $C_{21}H_{22}N_2$: C 83.40, H 7.33, N 9.26; found: C 83.43, H 7.36, N 9.25.

© 2006 NRC Canada

3,3′-Bis(indolyl)methyl-4-methoxyphenylmethane (1i)

Solid, mp 225–227 °C. IR (KBr, cm^{-1}) υ: 428, 457, 588, 613, 742, 783, 823, 844, 1004, 1026, 1080, 1097, 1178, 1244, 1290, 1336, 1369, 1411, 1456, 1508, 1604, 2831, 2935, 2977, 3058, 3413 (NH). ^{1}H NMR (500 MHz, $(CD_3)_2SO$, 25 °C, ppm) δ: 2.05 (s, 3H), 3.52 (s, 3H), 6.42 (d, *J* = 2.35 Hz, 2H), 6.50 (d, *J* = 8.76 Hz, 2H), 6.58 (t, *J* = 7.82 Hz, 2H), 6.80 (t, *J* = 7.75 Hz, 2H), 7.00 (d, *J* = 8.00 Hz, 2H), 7.05 (d, *J* = 8.76 Hz, 2H), 7.10 (d, *J* = 8.12 Hz, 2H), 9.58 (br, s, 2H, NH). ^{13}C NMR (125 MHz, $(CD_3)_2SO$, 25 °C, ppm) δ: 29.30, 43.19, 55.32, 111.67, 113.05, 118.36, 120.96, 121.94, 123.89, 124.22, 126.64, 129.28, 137.60, 140.97, 157.52. Anal. calcd. for $C_{25}H_{22}N_2O$: C 81.94, H 6.05, N 7.64; found: C 81.87, H 6.11, N 7.66.

3,3′-Bis(indolyl)methyl-3,4-dimethoxyphenylmethane (1j)

Solid, mp 218–220 °C. IR (KBr, cm^{-1}) υ: 424, 478, 547, 580, 605, 655, 738, 746, 763, 783, 817, 873, 1004, 1022, 1095, 1110, 1139, 1228, 1245, 1253, 1334, 1409, 1444, 1460, 1506, 1593, 2839, 2933, 2960, 3355, 3413. ^{1}H NMR (500 MHz, $(CD_3)_2SO$, 25 °C, ppm) δ: 1.75 (s, 3H), 3.09 (s, 3H), 3.29 (s, 3H), 6.17 (d, *J* = 2.40 Hz, 2H), 6.22 (d, *J* = 8.48 Hz, 1H), 6.27 (t, *J* = 7.5 Hz, 2H), 6.35 (dd, *J* = 8.50 Hz, *J* = 2.11 Hz, 1H), 6.44–6.50 (m, 3H), 6.69 (d, *J* = 8.03 Hz, 2H), 6.81 (d, *J* = 8.11 Hz, 2H), 9.78 (br, s, 2H, NH). ^{13}C NMR (125 MHz, $(CD_3)_2SO$, 25 °C, ppm) δ: 29.22, 43.19, 55.69, 55.72, 110.51, 111.52, 112.39, 118.02, 120.32, 120.63, 121.57, 123.55, 123.59, 126.37, 137.35, 141.36, 146.72, 147.83. Anal. calcd. for $C_{26}H_{24}N_2O_2$: C 78.76, H 6.10, N 7.07; found: C 78.81, H 6.11, N 7.10.

3,3′-Bis(indolyl)methyl-4-nitrophenylmethane (1k)

Solid, mp 250 to 251 °C. IR (KBr, cm^{-1}) υ: 422, 457, 551, 582, 636, 700, 744, 770, 808, 862, 1008, 1107, 1245, 1338, 1409, 1458, 1504, 1591, 2923, 2981, 3045, 3409 (NH). ^{1}H NMR (500 MHz, $(CD_3)_2SO$, 25 °C, ppm) δ: 2.04 (s, 3H), 6.42 (d, *J* = 2.42 Hz, 2H), 6.54 (t, *J* = 7.60 Hz, 2H), 6.76 (t, *J* = 7.60 Hz, 2H), 6.87 (d, *J* = 8.07 Hz, 2H), 7.07 (d, *J* = 8.17 Hz, 2H), 7.28 (d, *J* = 8.94 Hz, 2H), 7.75 (d, *J* = 8.87 Hz, 2H), 9.98 (br, s, 2H, NH). ^{13}C NMR (125 MHz, $(CD_3)_2SO$, 25 °C, ppm) δ: 29.16, 44.25, 111.91, 118.64, 121.22, 121.37, 122.24, 123.02, 124.01, 126.16, 129.32, 137.59, 145.99, 156.70. Anal. calcd. for $C_{24}H_{19}N_3O_2$: C 75.57, H 5.02, N 11.02; found: C 75.52, H 5.05, N 11.06.

3,3′-Bis(indolyl)diphenylmethane (1l)

Solid. IR (KBr, cm^{-1}) υ: 426, 487, 580, 607, 624, 702, 742, 815, 1012, 1033, 1101, 1242, 1336, 1373, 1413, 1456, 1485, 1606, 1720, 2850, 2920, 3053, 3407 (NH). ^{1}H NMR (500 MHz, $CDCl_3$, 25 °C, ppm) δ: 6.80–6.85 (m, 4H), 6.87 (d, *J* = 2.47 Hz, 2H), 7.10–7.15 (m, 3H), 7.20–7.27 (m, 5H), 7.34–7.37 (m, 6H), 7.95 (br, s, 2H, NH). ^{13}C NMR (125 MHz, $CDCl_3$, 25 °C, ppm) δ: 54.65, 111.61, 112.30, 119.48, 120.05, 121.96, 122.96, 126.39, 127.89, 128.16, 130.56, 137.26, 146.39. Anal. calcd. for $C_{29}H_{22}N_2$: C 87.41, H 5.56, N 7.03; found: C 87.44, H 5.60, N 6.99.

3,3′-Bis(1-methyl-indolyl)phenylmethane (2a)

Solid, mp 199–201 °C. IR (KBr, cm^{-1}) υ: 428, 518, 572, 702, 742, 769, 800, 1010, 1118, 1130, 1150, 1199, 1224, 1238, 1328, 1369, 1425, 1475, 2933, 3020, 3053. ^{1}H NMR (500 MHz, $CDCl_3$, 25 °C, ppm) δ: 3.73 (s, 6H), 5.95 (s, 1H), 6.59 (s, 2H), 7.06 (t, *J* = 7.72 Hz, 2H), 7.21–7.28 (m, 3H), 7.31–7.37 (m, 4H), 7.41 (d, *J* = 5.32 Hz, 2H), 7.44 (d, *J* = 7.90 Hz, 2H). ^{13}C NMR (125 MHz, $CDCl_3$, 25 °C, ppm) δ: 33.11, 40.52, 109.48, 118.70, 119.07, 120.48, 121.85, 126.45, 127.90, 128.63, 128.70, 129.13, 137.85, 144.89. Anal. calcd. for $C_{25}H_{22}N_2$: C 85.68, H 6.33, N 7.99; found: C 85.69, H 6.33, N 8.01.

3,3′-Bis(1-methyl-indolyl)-4-isopropylphenylmethane (2b)

Solid, mp 147–149 °C. IR (KBr, cm^{-1}) υ: 426, 567, 595, 676, 738, 767, 804, 860, 1010, 1105, 1153, 1222, 1261, 1326, 1369, 1421, 1465, 1510, 1548, 1612, 2871, 2925, 2958, 3049. ^{1}H NMR (500 MHz, $CDCl_3$, 25 °C, ppm) δ: 1.30 (d, *J* = 6.90 Hz, 6H), 2.95 (sep, *J* = 6.90 Hz, 1H), 3.74 (s, 6H), 5.92 (s, 1H), 6.62 (s, 2H), 7.06 (t, *J* = 7.20 Hz, 2H), 7.18 (d, *J* = 7.90 Hz, 2H), 7.26 (t, *J* = 8.00 Hz, 2H), 7.31–7.35 (m, 4H), 7.46 (d, *J* = 7.90 Hz, 2H). ^{13}C NMR (125 MHz, $CDCl_3$, 25 °C, ppm) δ: 24.50, 33.11, 34.09, 40.09, 109.45, 118.97, 118.99, 120.54, 121.78, 126.63, 127.97, 128.61, 128.90, 137.84, 142.12, 146.76. Anal. calcd. for $C_{28}H_{28}N_2$: C 85.67, H 7.19, N 7.14; found: C 85.70, H 7.20, N 7.15.

3,3′-Bis(1-methyl-indolyl)-3-methoxy-4-hydroxyphenylmethane (2c)

Solid, mp 147–149 °C. IR (KBr, cm^{-1}) υ: 426, 505, 690, 738, 779, 804, 869, 1010, 1026, 1116, 1199, 1220, 1251, 1267, 1326, 1369, 1427, 1508, 1612, 2935, 3490. ^{1}H NMR (500 MHz, $CDCl_3$, 25 °C, ppm) δ: 3.74 (s, 6H), 3.84 (s, 3H), 5.56 (s, 1H), 5.88 (s, 1H), 6.59 (s, 2H), 6.86 (d, *J* = 8.14 Hz, 1H), 6.89 (d, *J* = 8.14 Hz, 1H), 6.96 (s, 1H), 7.07 (t, *J* = 7.35 Hz, 2H), 7.27 (t, *J* = 7.21 Hz, 2H), 7.36 (d, *J* = 8.12 Hz, 2H), 7.46 (d, *J* = 7.85 Hz, 2H). ^{13}C NMR (125 MHz, $CDCl_3$, 25 °C, ppm) δ: 33.13, 40.22, 56.35, 109.50, 111.86, 114.41, 118.94, 119.05, 120.51, 121.68, 121.84, 127.88, 128.68, 136.99, 137.85, 144.20, 146.75. Anal. calcd. for $C_{26}H_{24}N_2O_2$: C 78.76, H 6.10, N 7.07; found: C 78.81, H 6.15, N 7.10.

3,3′-Bis(2-methyl-indolyl)-4-isopropylphenylmethane (2e)

Solid, mp 224–226 °C. IR (KBr, cm^{-1}) υ: 451, 493, 582, 599, 740, 784, 833, 1016, 1220, 1244, 1299, 1342, 1423, 1458, 1510, 2920, 2956, 3049, 3396 (NH), 3438. ^{1}H NMR (500 MHz, $(CD_3)_2SO$, 25 °C, ppm) δ: 0.94 (d, *J* = 6.90 Hz, 6H), 1.78 (s, 6H), 2.59 (sep, *J* = 6.90 Hz, 1H), 5.63 (s, 1H), 6.44 (t, *J* = 8.04 Hz, 2H), 6.62–6.65 (m, 4H), 6.77 (d, *J* = 8.12 Hz, 2H), 6.86 (d, *J* = 8.04 Hz, 2H), 6.93 (d, *J* = 8.05 Hz, 2H), 9.50 (br, s, 2H, NH). ^{13}C NMR (125 MHz, $(CD_3)_2SO$, 25 °C, ppm) δ: 12.51, 24.36, 33.72, 38.93, 110.44, 113.13, 118.36, 119.16, 119.96, 126.04, 128.99, 129.03, 132.41, 135.49, 141.68, 146.35. Anal. calcd. for $C_{28}H_{28}N_2$: C 85.67, H 7.19, N 7.14; found: C 85.69, H 7.17, N 7.14.

3,3′-Bis(5-bromo-indolyl)phenylmethane (2f)

Solid, mp 246–248 °C. IR (KBr, cm^{-1}) υ: 420, 487, 584, 609, 659, 703, 732, 750, 771, 800, 858, 871, 881, 979, 1099, 1217, 1334, 1417, 1442, 1460, 1560, 1596, 3417 (NH). ^{1}H NMR (500 MHz, $(CD_3)_2SO$, 25 °C, ppm) δ: 5.14 (s, 1H), 6.11 (d, *J* = 1.94 Hz, 2H), 6.52 (dd, *J* = 8.57, *J* = 10.73 Hz, 2H), 6.59 (t, *J* = 7.00 Hz, 1H), 6.65–6.71 (m, 6H), 6.75 (d, *J* = 1.40 Hz, 2H), 10.13 (br, s, 2H, NH). ^{13}C NMR

© 2006 NRC Canada

(125 MHz, $(CD_3)_2SO$, 25 °C, ppm) δ: 39.75, 111.35, 113.31, 117.72, 121.43, 123.68, 125.33, 126.19, 128.22, 128.39, 128.47, 135.56, 143.94. Anal. calcd. for $C_{23}H_{16}Br_2N_2$: C 57.53, H 3.36, N 5.83; found: C 57.46, H 3.31, N 5.85.

Acknowledgement

The authors are grateful to the Research Council of Guilan University for the partial support of this study.

References

1. C. Jia, T. Kitamura, and Y. Fujiwara. Acc. Chem. Res. **34**, 633 (2001).
2. V. Ritleng, C. Sirlin, and M. Pfeffer. Chem. Rev. **102**, 1731 (2002).
3. C. Aubry, A. Patel, S. Mahale, B. Chaudhuri, J.-D. Marechal, M.J. Sutcliffe, and P.R. Jenkins. Tetrahedron Lett. **46**, 1423 (2005).
4. H.-C. Zhang, H. Ye, A.F. Moretto, K.K. Brumfield, and B.E. Maryanoff. Org. Lett. **2**, 89 (2000).
5. T.R. Garbe, M. Kobayashi, N. Shimizu, N. Takesue, M. Ozawa, and H. Yukawa. J. Nat. Prod. **63**, 596 (2000).
6. J.K. Porter, C.W. Bacon, J.D. Robins, D.S. Himmelsbach, and H.C. Higman. J. Agric. Food Chem. **25**, 88 (1977).
7. M. Roomi and S. MacDonald. Can. J. Chem. **48**, 139 (1970).
8. R. Nagarajan and P.T. Perumal. Tetrahedron, **58,** 1229 (2002).
9. J.S. Yadav, B.V. Subba Reddy, C.V.S.R. Murthy, G.M. Kumar, and C. Madan. Synthesis, **5**, 783 (2001).
10. B.P. Bandgar and K.A. Shaikh. Tetrahedron Lett. **44**, 1959 (2003).
11. S.-I. Murahashi, T. Naota, H. Taki, M. Mizuno, H. Takaya, S. Komiya, Y. Mizuho, N. Oyasato, M. Harioka, M. Hirano, and A. Fukuoka. J. Am. Chem. Soc. **117**, 12436 (1995).
12. N. Komiya, S. Noji, and S.-I. Murahashi. Chem. Commun. (Cambridge), 65 (2001).
13. S.-I. Murahashi, N. Komiya, H. Terai, and T. Nakae. J. Am. Chem. Soc. **125**, 15312 (2003).
14. S.-I. Murahashi. Ruthenium in organic synthesis. Wiley-VCH, New York. 2004.
15. S.-J. Ji, M.-F. Zhou, D.-G. Gu, Z.-Q. Jiang, and T.-P. Loh. Eur. J. Org. Chem. **7**, 1584 (2004).
16. B.P. Bandgar, S.V. Bettigeri, and N.S. Joshi. Monatsh. Chem. **135**, 1265 (2004).
17. A.V. Reddy, K. Ravinder, V.L.N. Reddy, T.V. Goud, V. Ravikanth, and Y. Venkateswarlu. Synth. Commun. **33**, 3687 (2003).

© 2006 NRC Canada

Phenolic compounds from *Mammea siamensis* seeds

Surat Laphookhieo, Wisanu Maneerat, and Rattana Kiattansakul

Abstract: The investigation of dichloromethane and acetone extracts of the seeds of *Mammea siamensis* led to the isolation of a novel phenolic compound, siamensone A (**1**), together with three known compounds, suragin B (**2**), mammea E/BB (**3**), and δ-tocotrienol (**4**). The structures of the isolates were characterized by spectroscopic methods, and all compounds were reported for the first time as metabolites of *M. siamensis*.

Key words: Mammea siamensis, siamensone, coumarins.

Résumé : Une étude des produits d'extraction des graines de *Mammea siamensis* par le dichlorométhane et l'acétone a permis d'isoler un nouveau produit phénolique, la siamensone A (**1**), aux côtés de trois composés déjà connus, la suragine B (**2**), la mammea E/BB (**3**) et le δ-tocotriénol (**4**). Les structures des composés isolés ont été déterminées par des méthodes spectroscopiques et tous les composés ont été caractérisés pour la première fois comme métabolites de *M. siamensis*.

Mots clés : Mammea siamensis, siamensone, coumarines.

[Traduit par la Rédaction]

Introduction

Mammea belongs to the family of Guttiferae, typically found in several southeast asian countries. Two species are found in Thailand, *M. siamensis* (syn. *Ochrocarpus siamensis*) and *M. harmandii* (1). The flowers of *M. siamensis* have been used as a heart tonic in local medicine. A number of secondary metabolites have been isolated from both species (2–8). Our previous phytochemical studies of Thai medicinal plants led to the isolation and identification of xanthones (9), triterpenoids (10–12), cardenolide glycosides (13), and diterpenes (14). As a continuation of our studies on Thai medicinal plants, we now report the isolation of a novel chromone, siamensone A (**1**) and three other known compounds (**2**–**4**) from the seeds of *M. siamensis*. In addition, the ^{13}C NMR spectral data of **2** and **3** is also reported for the first time.

Results and discussion

The dichloromethane and acetones extracts of the seeds of *M. siamensis* were subjected to column chromatography to give a new compound (**1**) together with three other known compounds (**2**–**4**) shown in Chart 1. Their structures were elucidated using 1D and 2D NMR spectroscopic data and compared with those reported in the literature.

Siamensone A (**1**), yellowish solid, is a 6,8-dihydroxy-2-*sec*-butyl-4*H*-chromen-4-one. Its molecular formula of $C_{13}H_{14}O_4$ with a molecular ion $[M]^+$ at *m/z* 234.0877 (calc. $C_{13}H_{14}O_4$ *m/z* 234.0892) was established by HR-EIMS analysis. This compound exhibited UV absorption maxima at 225, 248, 300, and 337 nm, suggesting the presence of conjugation in the molecule. The IR spectrum showed absorption bands of OH stretching at 3399 cm^{-1} and C=O stretching at 1714 cm^{-1}. The ^{13}C NMR spectrum also showed the resonance of a carbonyl carbon at δ: 182.7 (C-4). The ^{1}H NMR spectrum (Table 1) displayed the characteristic signals of *meta*-coupled aromatic protons at δ: 6.32 (d, *J* = 2.1 Hz, H-5) and 6.24 (d, *J* = 2.1 Hz, H-7) and a singlet signal of an olefinic proton at δ: 6.00 (*s*, H-3). With combination of the COSY spectrum, a *sec*-butyl moiety was evident from ^{1}H NMR signals at δ: 2.58 (sextet, *J* = 6.9 Hz, H-1′), 1.70–1.80 (m, H-2′a), 1.55–1.65 (m, H-2′b), 1.27 (d, *J* = 6.9 Hz, Me-4′), and 0.93 (t, *J* = 7.5 Hz, Me-3′). The *sec*-butyl moiety was located at C-2 position based on Heteronuclear Multiple Bond Correlations (HMBC) (Table 1). The singlet methine proton signal at δ: 6.00 (H-3) correlated to C-1′ (40.4), and a sextet methine proton at δ: 2.58 (H-1′) correlated to C-2 (174.2) and C-3 (106.7). The other HMBC correlations were summarized in Table 1. Therefore, compound **1** was deduced to be siamensone A.

The remaining compounds were characterized as suragin B (**2**) (15, 16), mammea E/BB (**3**) (16), and δ-tocotrienol (**4**) (17) by the analysis of 1D and 2D NMR data and by comparison with their reported physical and spectroscopic data. In addition, the complete assignments of ^{13}C NMR of

Received 30 July 2006. Accepted 6 October 2006. Published on the NRC Research Press Web site at http://canjchem.nrc.ca on 16 November 2006.

S. Laphookhieo[1] and W. Maneerat. School of Science, Mae Fah Luang University, Tasud, Muang, Chiang Rai 57100, Thailand.
R. Kiattansakul. Faculty of Arts and Sciences, Prince of Songkla University, Muang, Suratthani 84100, Thailand.

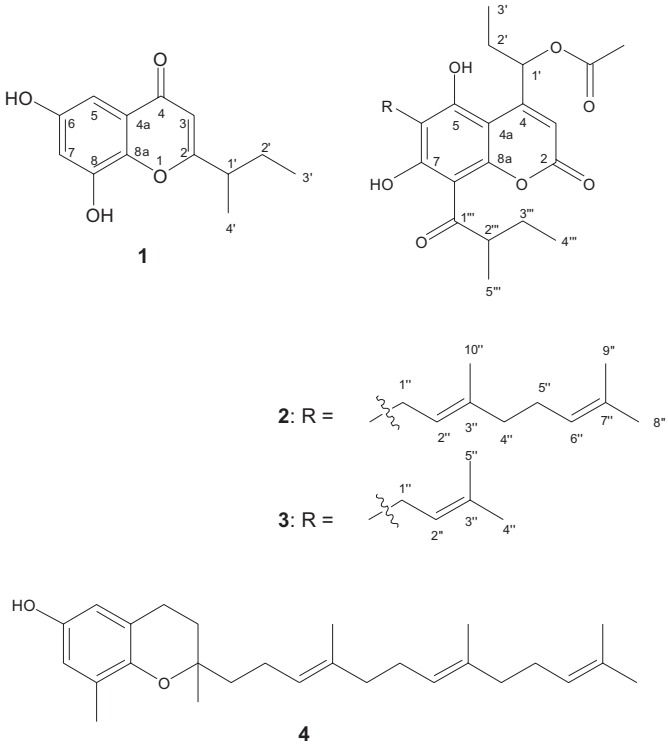
[1]Corresponding author (e-mail: surat@mfu.ac.th or laphookhieo@yahoo.com).

 doi:10.1139/V06-157 © 2006 NRC Canada

Table 1. ^{1}H (300 MHz), ^{13}C NMR (75 MHz), COSY, and HMBC spectral data of siamensone A (**1**) in $CDCl_3$.

C/H	δ_C	δ_H (J in Hz)	^{1}H–^{1}H COSY	HMBC Correlations $^{1}H \rightarrow ^{13}C$
2	174.2			
3	106.7	6.00 (s)		C-2, C-4, C-4a, C-1′
4	182.7			
4a	105.0			
5	94.2	6.32 (d, J = 2.1)	H-7	C-4, C-4a, C-6, C-7, C-8a
6	163.2			
7	99.0	6.24 (d, J = 2.1)	H-5	C-5, C-6, C-8, C-8a
8	161.8			
8a	158.3			
1′	40.4	2.58 (sextet, J = 6.9)	H-2′, H-4′	C-2, C-3, C-2′, C-3′, C-4′
2′	27.5	1.70–1.80 (m)	H-1′, H-3′	C-2, C-1′, C-3′, C-4′
		1.55–1.65 (m)		
3′	11.5	0.93 (t, J = 7.5)	H-2′	C-1′, C-2′
4′	17.7	1.27 (d, J = 6.9)	H-1′	C-1′, C-2′

Chart 1.



suragin B (**2**) and mammea E/BB (**3**) are also reported here for the first time (Table 2).

Experimental section

General experimental procedures

Melting points were determined using a Fisher–Johns melting point apparatus. The optical rotation $[\alpha]_D$ values were determined with a JASCO P-1020 polarimeter. UV spectra were measured with a UV-160A spectrophotometers (Shimadzu, Kyoto, Japan). The IR spectra were measured with a PerkinElmer FTS FTIR spectrophotometer. The ^{1}H and ^{13}C NMR spectra were recorded using 400 and/or 300 MHz Bruker FTNMR Ultra Shield spectrometers. Chemical shifts were recorded in ppm (δ) in $CDCl_3$ with tetramethylsilane (TMS) as an internal reference. The EIMS was obtained from a MAT 95 XL mass spectrometer. Quick column chromatography (QCC) (18, 19) and column chromatography (CC) were carried out on silica gel 60 H (Merck, Rahway, NJ; 5–40 μm) and silica gel 100 (Merck, Rahway, NJ; 63–200 μm), respectively. Precoated plates of silica gel 60 F_{254} were used for analytical purposes.

Plant material

The seeds of *M. siamensis* were collected from Mae Fah Luang University, Tasud, Muang, Chiang Rai province, northern part of Thailand in August 2005. Plant identification was made by Professor Puangpen Sirirugsa, Department of Biology, Faculty of Science, Prince of Songkla University, and the voucher specimen (No. SC09) was deposited at Prince of Songkla University Herbarium.

Extraction and isolation

The seeds (224.5 g) of *M. siamensis* were extracted with dichloromethane and acetone, respectively, at room temperature (each for 5 days) and evaporated under reduced pressure to provide dichloromethane extract (44.4 g) and acetone extract (30.5 g). The dichloromethane extract (44.4 g) was chromatographed by QCC (column size: 12 × 16 cm) and eluted with EtOAc–hexane mixtures to give seven fractions (F1–F7). Fraction F4 (3.35 g) was separated by CC with EtOAc–hexane (3:17) followed by RP-18 preparative TLC with MeOH–H_2O (4:1) to afford five subfractions (F4a–F4e). Subfraction F4d (1.02 g) was purified by RP-18 CC with MeOH–H_2O (4:1) followed by CC with EtOAc–hexane (1:3) to afford compound **1** (12.7 mg).

The acetone extract (30.5 g) was chromatographed by QCC (column size: 12 × 16 cm) and eluted with hexane–acetone (5:1) to give seventeen fractions (F1–F17), of which fractions F8–F10 (1.5 g) gave compound **2**. Fraction F2 (4 g) was subjected to repeated QCC with hexane–acetone mixtures (95% hexane–acetone to 100% acetone) to afford compound **2** (104 mg) and 5 subfractions (F2-1–F2-5). A portion (450 mg) of subfraction F2-2 (1.05 g) was subjected to repeated CC with 10% EtOAc–hexane to afford fourteen subfractions (F2-2A–F2-2N). Compound **4** (7.7 mg) was ob-

© 2006 NRC Canada

Table 2. ^{1}H (400 MHz) and ^{13}C NMR (100 MHz) spectral data of **2** and **3** in $CDCl_3$.

	2		**3**	
C/H	δ_C	δ_H (J in Hz)	δ_C	δ_H (J in Hz)
2	159.3		159.7	
3	106.3	6.28 (s)	106.3	6.28 (s)
4	157.2	—	155.7	—
4a	100.3	—	100.3	—
5	158.2	—	158.3	—
6	110.2	—	110.1	—
7	165.5	—	165.9	—
8	104.6	—	104.3	—
8a	156.0	—	156.5	—
1′	73.7	6.49 (dd, J = 2.1, 8.0)	73.7	6.50 (dd, J = 2.7, 8.1)
2′	27.1	1.88–1.98 (m)	27.1	1.89–2.01 (m)
3′	10.1	1.00 (t, J = 7.2)	10.1	1.01 (t, J = 7.5)
1″	21.0	3.48 (dd, J = 4.4, 16.5)	21.6	3.49 (dd, J = 7.6, 16.6)
		3.52 (dd, J = 4.4, 16.5)		3.55 (dd, J = 6.4, 16.6)
2″	123.2	5.24 (t, J = 7.1)	119.1	5.25 (t, J = 7.0)
3″	142.4	—	138.9	—
4″	40.4	2.08–2.18 (m)	18.0	1.81 (s)
5″	26.3	2.08–2.18 (m)	25.9	1.87 (s)
6″	119.7	5.04–5.11 (m)		—
7″	132.2	—		—
8″	18.8	1.67 (s)		—
9″	25.5	1.59 (s)		—
10″	16.4	1.87 (s)		—
1‴	210.7	—	210.7	—
2‴	46.5	3.91 (sextet, J = 7.0)	47.0	3.80 (sextet, J = 6.6)
3‴	28.7	1.42–1.50 (m)	28.7	1.40–1.46 (m)
		1.81–1.87 (m)		1.83–1.88 (m)
4‴	11.7	0.98 (t, J = 7.4)	11.7	0.98 (t, J = 7.5)
5‴	16.6	1.24 (d, J = 7.0)	16.6	1.26 (d, J = 6.6)
CH_3CO	21.0	2.19 (s)	21.0	2.19 (s)
CH_3CO	170.3	—	170.5	—
5–OH		7.21 (s)		7.18 (s)
7–OH		14.64 (s)		14.64 (s)

tained from subfraction F2-2G by repeated CC with 90% hexane–acetone. Repeated CC of subfraction F2-4 with 10% EtOAc–hexane gave compound **3** (11.0 mg).

Siamensone A (6,8-dihydroxy-2-*sec*-butyl-4*H*-chromen-4-one)

Yellowish solid; mp 177–178 °C. $[\alpha]^{27}_D$ –25.0° (*c* 1.35, MeOH). UV (MeOH) λ_{max} (log ε): 225 (4.14), 248 (3.92), 300 (3.42), 337 (3.41). IR (neat): 3399, 1714, 1609. ^{1}H and ^{13}C NMR: see Table 1. EIMS *m*/*z* (%): 234 ([M^+], 90), 233 (100), 177 (19), 176 (23). HR-EIMS *m*/*z*: [M^+] calcd. for $C_{13}H_{14}O_4$, 234.0892; found, 234.0877.

Acknowledgments

The authors are grateful to Mae Fah Luang University for partial financial support.

References

1. T. Smitinand. Thai Plant Names. Prachachon Publisher, Bangkok. 2001. p. 343.
2. C. Thebtaranonth, S. Imraporn, and N. Padungkul. Phytochemistry, **20**, 2305 (1981).
3. O. Poobrasert, H.L. Constant, C.W.W. Beecher, N.R. Farnsworth, A.D. Kinghorn, J.M. Pezzuto, G.A. Cordell, T. Santisuk, and V. Reutrakul. Phytochemistry, **47**, 1661 (1998).
4. W. Kaweetripob, C. Mahidol, H. Prawat, and S. Ruchirawat. Pharm. Biol. **38**, 55 (2000).
5. V. Prachyawarakorn, C. Mahidol, and S. Ruchirawat. Pharm. Biol. **38**, 58 (2000).
6. C. Mahidol, W. Kaweetripob, H. Prawat, and S. Ruchirawat. J. Nat. Prod. **65**, 757 (2002).
7. V. Reutrakul, P. Leewanich, P. Tuchinda, M. Pohmakotr, T. Jaipetch, S. Sophasan, and T. Santisuk. Planta Med. **69**, 1048 (2003).
8. V. Prachyawarakorn, C. Mahidol, and S. Ruchirawat. Phytochemistry, **67**, 924 (2006).
9. S. Laphookhieo, J.K. Syers, R. Kiattansakul, and K. Chantrapromma. Chem. Pharm. Bull. **54**, 745 (2006).
10. S. Laphookhieo, C. Karalai, and C. Ponglimanont. Chem. Pharm. Bull. **52**, 883 (2004).
11. S. Laphookhieo, C. Karalai, C. Ponglimanont, and K. Chantrapromma. J. Nat. Prod. **67**, 886 (2004).
12. C. Karalai and S. Laphookhieo. Aust. J. Chem. **58**, 556 (2005).

© 2006 NRC Canada

13. S. Laphookhieo, S. Cheenpracha, C. Karalai, S. Chantrapromma, C. Ponglimanont, Y. Rat-a-pa, and K. Chantrapromma. Phytochemistry, **65**, 507 (2004).
14. S. Cheenpracha, C. Karalai, C. Ponglimanont, K. Chantrapromma, and S. Laphookhieo, Helv. Chim. Acta, **89**, 1062 (2006).
15. B.S. Joshi, V.N. Kamat, T.R. Govindachari, and A.K. Ganguly. Tetrahedron, **25**, 1453 (1969).
16. L. Combie, R.C.F. Jones, and C.J. Palmer. J. Chem. Soc., Perkin Trans. 1, 345 (1987).
17. S.H. Goh, N.F. Hew, A.S.H. Ong, Y.M. Choo, and S. Brumby. J. Am. Oil Chem. Soc. **67**, 250 (1990).
18. J.C. Coll, G.B. Hawes, N. Liyanage, W. Oberhänsli, and R. J. Wells. Aust. J. Chem. **30**, 1305 (1977).
19. J.C. Coll and B.F. Bowden. J. Nat. Prod. **49**, 934 (1986).

© 2006 NRC Canada

Medium effects on the α-effect in DMSO–H_2O mixtures — Comparative studies of *p*-nitrophenyl benzoate and acetate — Dissection of ground-state and transition-state effects

Ik-Hwan Um, Young-Hee Shin, Jeong-Yoon Han, and Erwin Buncel

Abstract: In a study of the origin of the α-effect and its dependence on the nature of the reaction medium as well as structural effects, we report herein a kinetic study of the reactions of *p*-nitrophenyl benzoate (PNPB) with butan-2,3-dione monoximate (Ox^-, α-nucleophile) and *p*-chlorophenoxide (*p*-$ClPhO^-$, the reference nucleophile) in dimethyl sulfoxide (DMSO)–H_2O mixtures of varying compositions at 25.0 ± 0.1 °C. The second-order rate constants (k_N) decrease modestly on addition of DMSO to the medium up to 10 mol% DMSO but increase significantly beyond that point for both nucleophiles. Ox^- is more reactive than *p*-$ClPhO^-$ in all solvent mixtures studied (i.e., the α-effect). The α-effect increases as the DMSO content in the medium increases up to 40 mol% DMSO and then decreases beyond that point resulting in a bell-shaped α-effect profile. The bell-shaped α-effect profile obtained for the current reaction is similar to that found previously for the corresponding reaction of *p*-nitrophenyl acetate (PNPA), differing notably however, in the magnitude of the α-effect beyond 40 mol% DMSO. The PNPB/*p*-$ClPhO^-$ reaction gains greater rate enhancement than the PNPA/*p*-$ClPhO^-$ reaction in the DMSO-rich region, resulting in the smaller α-effect for PNPB beyond 40 mol% DMSO. It is proposed that the observed modulation of the α-effect by the solvent medium is explicable as a ground-state effect in the H_2O-rich region and a transition-state effect in the DMSO-rich region.

Key words: medium effect, the α-effect, ground state, transition state, solvation, desolvation.

Résumé : Dans le cadre d'une étude sur l'origine de l'effet α et de sa dépendance sur la nature du milieu réactionnel ainsi que des effets structuraux, on a réalisé une étude cinétique des réactions du benzoate de *p*-nitrophényle (BPNP) avec le monoximate de la butane-2,3-dione (Ox^-, α-nucléophile) et le *p*-chlorophénolate (*p*-$ClPhO^-$, le nucléophile de référence), dans des mélanges de diméthylsulfoxyde (DMSO)–eau (H_2O) de compositions variables, à 25,0 ± 0,1 °C. Jusqu'à une concentration de 10 mole %, les constantes de vitesse du deuxième ordre (k_N) diminuent légèrement par addition de DMSO; au-delà de ce point, elles augmentent toutefois d'une façon significative pour les deux nucléophiles. Le nucléophile Ox^- est plus réactif que le *p*-$ClPhO^-$ dans tous les mélanges de solvant étudiés, c'est-à-dire qu'il présente l'effet α. Jusqu'à une concentration de 40 mole % de DMSO, l'effet α augmente avec une augmentation de la concentration de DMSO; au-delà de ce point, il diminue ce qui conduit à un profil d'effet α qui est en forme de cloche. Le profil d'effet α en forme de cloche qui est obtenu pour cette réaction est semblable à celui qui a été observé antérieurement pour la réaction correspondante de l'acétate de *p*-nitrophényle (APNP); il diffère toutefois dans l'amplitude de l'effet α au-delà de la concentration de 40 mole % en DMSO. Dans la région riche en DMSO comportant plus de 40 mole % de DMSO, la réaction du BPNP–*p*-$ClPhO^-$ conduit à une augmentation beaucoup plus grande de la vitesse que celle observée pour la réaction du APNP–*p*-$ClPhO^-$. On propose donc que la modulation observée de l'effet α par la nature du solvant (figure 2) peut être expliquée par un effet de l'état fondamental dans la région riche en eau et un effet de l'état de transition dans la région riche en DMSO.

Mots clés : effet de solvant, effet α, état fondamental, état de transition, solvatation, désolvatation.

[Traduit par la Rédaction]

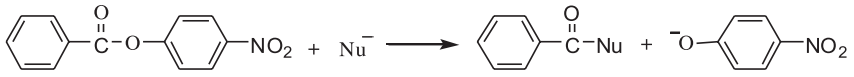
Received 14 August 2006. Accepted 10 October 2006. Published on the NRC Research Press Web site at http://canjchem.nrc.ca on 16 November 2006.

I.-H. Um,[1] Y.-H. Shin, and J.-Y. Han. Division of Nano Sciences and Department of Chemistry, Ewha Womans University, Seoul 120–750, Korea.
E. Buncel.[2] Department of Chemistry, Queen's University, Kingston, ON K7L 3N6, Canada and Division of Nano Sciences and Department of Chemistry, Ewha Womans University, Seoul 120–750, Korea.

[1]Corresponding author (e-mail: ihum@ewha.ac.kr).
[2]Corresponding author (e-mail: buncele@queensu.ca)

 doi:10.1139/V06-156 © 2006 NRC Canada

Scheme 1.



Nu^- : Ox^- and *p*-$ClPhO^-$
Solvent : 0, 10, 20, 30, 40, 50, 60, 70, 80, 90 mol% DMSO in H_2O

Introduction

Nucleophiles possessing one or more nonbonding electron pairs at the position α to the nucleophilic center exhibit enhanced reactivity compared with reference nucleophiles of similar basicity (the α-effect) (1). Various proposals have been advanced to account for the α-effect phenomenon, including destabilization of the ground state (GS) through electronic repulsion between nonbonding electron pairs, stabilization of product (thermodynamic α-effect), stabilization of the transition state (TS), a TS having aromatic or radicaloid character, as well as a solvent medium effect (1–11). However, up to this time there is no general agreement as to which factor(s) are predominant as the origin(s) of this phenomenon. Our studies have been largely directed toward elucidating the role of the solvent medium (7–10).

In the best known protic polar solvent, water, anionic nucleophiles are expected to be highly solvated through H-bonding (12, 13). Transfer to an aprotic polar solvent such as DMSO should result in loss of H-bonding, however, ion–dipole and polarizability interactions could become dominant (12, 13). The generally observed increased nucleophilic reactivity of small (hard) anions in DMSO with respect to water was first highlighted in studies by Parker (13). However, this effect may operate differentially when comparing two nucleophiles, as must be the case when considering the α-effect. Differential solvation could be exhibited in imbalanced transition states as well as in differences in ground state solvation and desolvation (14). To probe such differential effects, we have combined kinetic and thermodynamic studies for α-effect systems as a function of incremental modulation of the solvent medium from pure water to DMSO (7, 9).

The definition of the α-effect adopted recently is a positive deviation exhibited by an α-nucleophile from a Brønsted-type nucleophilicity plot (1*a*, 1*b*). According to this definition, the reference nucleophile is one which possesses the same basicity as the α-nucleophile but does not deviate from the Brønsted-type plot.

Some years ago, we performed nucleophilic substitution reactions of *p*-nitrophenyl acetate (PNPA) with butan-2,3-dione monoximate (Ox^-, α-nucleophile) and *p*-chlorophenoxide (*p*-$ClPhO^-$, the reference nucleophile) in dimethyl sulfoxide (DMSO)–H_2O mixtures at 25.0 ± 0.1 °C (7*a*). The pK_a of the conjugate acids of the two nucleophiles has been reported to vary in a parallel manner in the DMSO–H_2O mixtures studied. Unexpectedly, we found that the α-effect increases as the DMSO content in the medium increases up to ca. 50 mol% DMSO and then decreases on further addition of DMSO, resulting in a bell-shaped α-effect profile (7*a*). Such a bell-shaped α-effect profile cannot be accounted for in terms of basicity changes with solvent variation and was also found for the corresponding reactions of substrates with different electrophilic centers (i.e., *p*-nitrophenyl diphenylphosphinate and benzenesulfonate) and with different leaving groups (i.e., substituted phenyl acetates) (7*c*–7*e*).

However, a contrasting result was reported by Moss et al. (11) for the reactions of PNPA with *o*-iodosylbenzoate as the α-effect nucleophile and *p*-$ClPhO^-$ as reference nucleophile, i.e., the α-effect decreased steadily as the mol% DMSO was increased. Since the basicity of *o*-iodosylbenzoate was not determined in the DMSO–H_2O mixtures, one cannot exclude the possibility that the decreasing α-effect trend could be due to variation in pK_a for the conjugate acid of *o*-iodosylbenzoate with mol% DMSO. In fact, we have recently shown that variation of the basicity of the α-nucleophile is an important factor in determining the magnitude of the α-effect in the reactions of PNPA with Ox^- and *p*-$ClPhO^-$ in MeCN–H_2O mixtures (8). While the α-effect increases continuously as the mol% MeCN in the medium increases, Ox^- becomes more basic than *p*-$ClPhO^-$ with increasing mol% MeCN in the medium. Accordingly, the increasing basicity difference between Ox^- and *p*-$ClPhO^-$ was held responsible for the increasing α-effect in MeCN–H_2O mixtures (8).

There has been an upsurgence of interest in recent years in studies of solvent effects on reaction kinetics, equilibria, and chemistry more generally (12). For example, renewed interest has been engendered by studies into environmentally benign or "green" solvents including ionic solvents and supercritical water (15). Any practical use of such new media will require an in-depth examination of the physical organic chemistry of these systems. DMSO has emerged as the prototypical aprotic solvent of choice for a wide range of reactions (12, 13). One may cite a few landmark studies: those of Cram in the area of stereocontrol in isotopic H exchange and carbanion chemistry more generally (16), Cox and Stewart on the H_- basicity scale (17), and Parker (13) on nucleophilic reactivity, as well as the extensive investigations of Bordwell (18) into acidities in DMSO. Studies of mixed solvent systems have yielded a wealth of information on structure–reactivity relationships (19). In this context, we have focused on DMSO–H_2O mixed media and more recently on MeCN–H_2O media (7–9).

As mentioned above, one key difference between H_2O and DMSO is the enhanced polarizability of the latter solvent, which may be expected to extend to DMSO-rich media as well. To test the significance of this factor we have extended our study to *p*-nitrophenyl benzoate (PNPB) as the substrate. Here, a change of a methyl in PNPA for a phenyl group in PNPB provides a test compound that should exhibit greater polarizability interactions with the DMSO solvent component. The reaction studied is that of PNPB with Ox^- and *p*-$ClPhO^-$ anions (Scheme 1) as part of the α-effect phenomenon, as modulated by systematic change of mol% DMSO in DMSO–H_2O mixtures.

© 2006 NRC Canada

Table 1. Summary of second-order rate constants for reactions of PNPB with Ox^- and *p*-$ClPhO^-$ in various DMSO–H_2O mixtures at 25.0 ± 0.1 °C.

DMSO (mol%)	pK_a (OxH)	k_{Ox-} ($(mol/L)^{-1}s^{-1}$)	pK_a (*p*-ClPhOH)	$k_{p\text{-}ClPhO-}$ ($(mol/L)^{-1}s^{-1}$)	α-effect $k_{Ox-}/k_{p\text{-}ClPhO-}$
0	9.44	22.5	9.38	0.255	88
10	10.04	20	9.94	0.144	139
20	10.68	34.2	10.58	0.185	185
30	11.33	75.7	11.21	0.347	218
40	12.06	186	11.93	0.814	229
50	12.86	455	12.73	2.21	206
60	13.69	1070	13.54	5.73	187
70	14.51	2360	14.34	15.5	152
80	15.32	5360	15.14	44.8	120
90	16.14	11700	15.95	162	72

Note: The pK_a data were taken from ref. 7*b*.

Results

The kinetic study was performed spectrophotometrically under pseudo-first-order conditions with the nucleophile in excess. All the reactions in this study obeyed pseudo-first-order kinetics and pseudo-first-order rate constants (k_{obsd}) were obtained from plots of ln (A_∞–A_t) vs. *t*, which were linear over 90% of the total reaction. Second-order rate constants (k_{Nu}) were determined from the slopes of the linear plots of k_{obsd} vs. the nucleophile concentration. These plots had only small intercept values, indicating that the contribution of hydroxide and (or) water to k_{obsd} is negligible (see Supplementary data for detailed kinetic data).[3] It is estimated from replicate runs that the uncertainty in the rate constants is less than ±3%. The k_{Nu} values determined are summarized in Table 1 for the reactions of PNPB with Ox^- and *p*-$ClPhO^-$ in DMSO–H_2O mixtures of varying compositions.

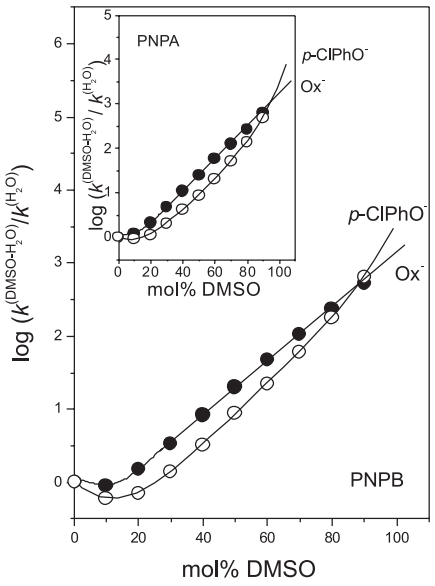
Discussion

Effect of medium on reactivity

The rate data presented in Table 1 and exhibited in Fig. 1 show a nonuniform behaviour as the DMSO content of the medium is varied. Now, it is well-known that the properties of DMSO–H_2O mixtures exhibit anomalous behavior up to 33 mol% DMSO (7, 12, 20). This has been interpreted as resulting from rigidification of water–water H bonding induced by the addition of DMSO or the strong tendency of DMSO to form complexes with two water molecules (7, 12, 20). In the present system we have observed that the reactivity of *p*-$ClPhO^-$ and Ox^- decreases modestly in the low DMSO region (<20 mol% DMSO) but increases significantly in the high DMSO region. This initial decline in reactivity is more significant for *p*-$ClPhO^-$ than for Ox^-.

Focusing on the high DMSO region, it is generally accepted that GS destabilization of anionic nucleophiles is responsible for the rate enhancement in this region relative to pure water (12, 13). Loss of H bonding in going to DMSO-rich media will effectively destabilize the anionic nucleophile (see Introduction). This desolvation of the anion enhances reactivity. For *p*-$ClPhO^-$ and Ox^-, in fact, we have recently found through calorimetric measurements that these anions become desolvated to the extent of 10.2 and 13.2 kcal/mol (1 cal = 4.184 J), respectively, as the medium is changed from pure water to 90 mol% DMSO (7*b*).

Fig. 1. Logarithmic plots of relative rate constants, $\log k^{(DMSO-H_2O)}/k^{(H_2O)}$, vs. mol% DMSO for reactions of PNPB (and PNPA in inset) with Ox^- (●) and *p*-$ClPhO^-$ (○) at 25.0 ± 0.1 °C. The data for reactions of PNPA were taken from ref. 7*a*.

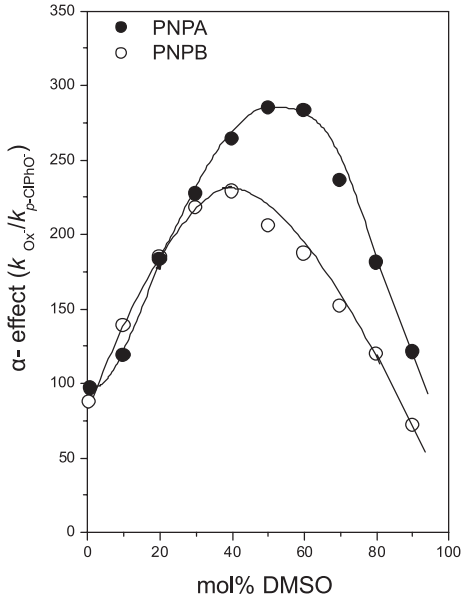


The effect of medium change on reactivity can be expressed as the ratio of the second-order rate constant in DMSO–H_2O mixtures over the corresponding rate constant in pure H_2O, i.e., $k^{(DMSO-H_2O)}/k^{(H_2O)}$. As shown in Fig. 1, this rate constant ratio decreases as the medium changes from H_2O to 10 mol% DMSO with both Ox^- and *p*-$ClPhO^-$. Beyond 10 mol% DMSO the relative rate for Ox^- increases linearly as the mol% DMSO increases, while *p*-$ClPhO^-$ exhibits slightly upward curvature resulting in a crossover.

[3] Supplementary data for this article are available on the journal Web site (http://canjchem.nrc.ca) or may be purchased from the Depository of Unpublished Data, Document Delivery, CISTI, National Research Council Canada, Ottawa, ON K1A 0R6, Canada. DUD 5097. For more information on obtaining material refer to http://cisti-icist.nrc-cnrc.gc.ca/irm/unpub_e.shtml.

© 2006 NRC Canada

Fig. 2. Plots of the α-effect ($k_{Ox^-}/k_{p\text{-}ClPhO^-}$) vs. mol% DMSO for reactions of PNPA with Ox^- and *p*-$ClPhO^-$ (●) and PNPB with Ox^- and *p*-$ClPhO^-$ (○) at 25.0 ± 0.1 °C. The data for reactions of PNPA were taken from ref. 7*a*.



Recalling that our calorimetric study has shown that Ox^- is more destabilized than *p*-$ClPhO^-$ throughout the range of DMSO–H_2O mixtures studied, we conclude that destabilization of the anionic nucleophile GS cannot be solely responsible for the rate enhancement in the high DMSO region.

The bell-shaped α-effect

As shown in Table 1, Ox^- exhibits much larger k_N values than *p*-$ClPhO^-$ for the reaction of PNPB in all the medium compositions investigated (i.e., the α-effect). Interestingly, as illustrated in Fig. 2 up to 40 mol% DMSO the magnitude of the α-effect ($k_{Ox^-}/k_{p\text{-}ClPhO^-}$) increases as the DMSO content in the medium increases. Beyond that point there is a decrease in the α-effect, resulting in a bell-shaped α-effect profile. The bell-shaped α-effect profile found for PNPB is similar to that found previously for the comparable reactions of PNPA, differing notably however in the magnitude of the α-effect beyond 40 mol% DMSO; the PNPB system exhibits a much smaller α-effect than the PNPA system in this DMSO-rich region.

The origin of the bell-shaped α-effect

A further striking aspect of the α-effect plots in Fig. 2 is that up to 30 mol% DMSO the plots for PNPB and PNPA are virtually superimposable but diverge thereafter; the PNPB curve reaches a maximum at 40 mol% DMSO while the maximum for PNPA is found at 50 mol% DMSO. Also the α-effect maximum occurs at 230 for PNPB and at 285 for PNPA. While the advent of the maximum in the bell-shaped α-effect profile at a lower DMSO content with PNPB, relative to PNPA, is concordant with the higher polarizability associated with the change from Me to Ph, the different response of the two systems to medium change beyond 40 mol% DMSO bears further analysis.

Dissection of medium effect into GS and TS contributions

Studies of the relationship between the magnitude of the α-effect, Brønsted basicity, and medium effects have revealed a remarkable behaviour of oximate reactivity that is, however, still not fully understood (2, 21). Terrier et al. (2*a*) studied the reaction of PNPA with a series of pyridinium carbaldoximates in H_2O and found that the Brønsted-type plot is linear for reactions of low basic oximates ($pK_a < \sim 8$), but levels off for more basic oximates ($pK_a \geq 8$). In a study of reactions of PNPB with a series of acetophenone oximates in 20 and 90 mol% DMSO, we observed that in 20 mol% DMSO the Hammett plot is linear with $\rho = +0.20$, but in 90 mol% DMSO $\rho = -0.15$ (21). The positive ρ value obtained for the reactions in 20 mol% DMSO is striking since it corresponds to a decrease in reactivity of the oximate with a stronger base strengthening substituent. A similar result has recently been found by Terrier and coworkers (2*b*) for reactions of bis(*p*-nitrophenyl)phenylphosphonate with a series of oximates in H_2O. The Brønsted-type plot exhibited a negative β_{nuc} value in the region of $pK_a > \sim 9$, indicating that more basic oximates become less reactive.

We have recently reported (7*b*) from a calorimetric study that both Ox^- and *p*-$ClPhO^-$ become desolvated on addition of DMSO to water and the former experiences higher desolvation than the latter. The difference in desolvation energy between Ox^- and *p*-$ClPhO^-$ ($\Delta\Delta H_{sol}$) became large as the DMSO content in the medium increased up to 40 mol% DMSO and then remained nearly constant beyond that point. Thus, $\Delta\Delta H_{sol}$ increased from 0 to 0.6, 1.8, and 3.2 kcal/mol as the medium changes from pure water to 10, 20, and 40 mol% DMSO, in turn, but remained nearly constant on further addition of DMSO (7*b*). The increasing trend in $\Delta\Delta H_{sol}$ up to 40 mol% DMSO was found to parallel the increasing α-effect trend observed over that medium range, indicating that the difference in GS desolvation between Ox^- and *p*-$ClPhO^-$ may be responsible for the increasing α-effect trend for the reactions of PNPA in this solvent region. However, since $\Delta\Delta H_{sol}$ remains constant beyond 40 mol% DMSO the GS effect cannot account for the decreasing α-effect trend in that medium range.

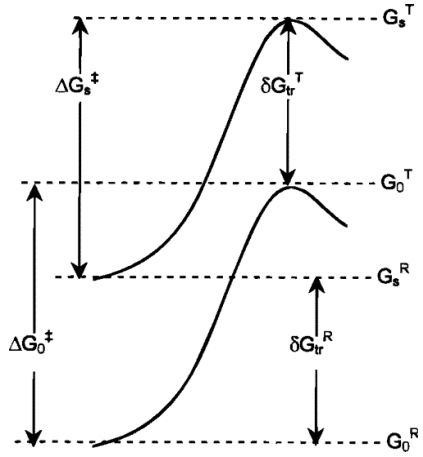
Previously, we introduced a methodology for the dissection of medium effects into GS and TS contributions (see also refs. 12, 13, 22, 23). Figure 3 shows a qualitative two-dimensional energy profile for a reaction carried out in two different media, H_2O and a DMSO–H_2O mixture. δG_{tr}^{T} can be evaluated from the measurable transfer free energies of reactants (δG_{tr}^{R}) and the kinetic activation parameters ($\delta G_{tr}^{\ddagger}$) as given by eq. [1].

$$[1] \qquad \delta\Delta G_{tr}^{\ddagger} = \delta G_{tr}^{T} - \delta G_{tr}^{R}$$

This methodology can be applied to enthalpy and entropy parameters as well. This allows the dissection of the effect of medium on the α-effect into GS and TS effects through the combination of the calorimetrically measured enthalpies of solution (ΔH_{sol}) and the kinetically determined activation parameters. For the reaction of PNPA with Ox^- and *p*-$ClPhO^-$, we have found that in the DMSO-rich region the TS becomes more stabilized for *p*-$ClPhO^-$ than for Ox^- resulting in a smaller α-effect (7*b*). Accordingly, differential solvation of the two TSs was proposed to be responsible for the de-

© 2006 NRC Canada

Fig. 3. Illustration of the relationship between the transfer free energies of reactants (δG_{tr}^{R}) and the transition state (δG_{tr}^{T}) and the free energies of activation for a reaction occurring in the two-solvent systems.



creasing α-effect trend for the reactions of PNPA beyond the break point of 40–50 mol% DMSO (7*b*). For the current PNPB system, one can also conclude that the origin of the increasing and decreasing α-effect trend found with medium change can be attributed to the same factors as for the PNPA system, i.e., dominant GS effect in the H_2O-rich region and TS effect in the DMSO-rich region, which demonstrates the generality of this methodology.

The effect of medium change on reactivity can be illustrated in a different way via Fig. 4, showing a plot of the logarithmic relative rate constants for the reactions of PNPA and PNPB with Ox^- and *p*-$ClPhO^-$ vs. the transfer enthalpies from H_2O to DMSO–H_2O mixtures ($\Delta\Delta H_{tr}$) for the two nucleophiles (Table 2). $\Delta\Delta H_{tr}$ represents the extent of GS desolvation for Ox^- and *p*-$ClPhO^-$ ions as the medium changes from H_2O to DMSO–H_2O mixtures (7*b*). Accordingly, if the GS effect were solely responsible for the relative rate constants one should have observed a linear correlation between $\Delta\Delta H_{tr}$ and $\log k^{(DMSO-H_2O)}/k^{(H_2O)}$. Contrariwise, Fig. 4 exhibits nonlinear correlations, i.e., the increase in the relative rate constant is small on changing $\Delta\Delta H_{tr}$ from 0 to 8 kcal/mol for *p*-$ClPhO^-$ and from 0 to 11 kcal/mol for Ox^-. However, for *p*-$ClPhO^-$ the relative rate constant increases significantly as $\Delta\Delta H_{tr}$ changes from 8 to 10 kcal/mol while for Ox^- the change is from 11 to 13 kcal/mol. These results further emphasize that the GS effect is not solely responsible for the medium effect on reactivity but that a TS effect also contributes to the rate enhancement in the DMSO-rich region.

Notably in Fig. 4, the curved lines for the reactions of PNPA and PNPB with *p*-$ClPhO^-$ cross over those for the corresponding reactions for Ox^- at $\Delta\Delta H_{tr}$ = 6–7 kcal/mol. The points for the reactions of *p*-$ClPhO^-$ lie below those for the reactions with Ox^- up to $\Delta\Delta H_{tr}$ = ~6 kcal/mol but exceed them beyond that point. Such a crossover indicates that in the DMSO-rich region the reactions with *p*-$ClPhO^-$ attain almost the same rate enhancements as those with Ox^- but with smaller $\Delta\Delta H_{tr}$ values.

Interestingly, further scrutiny of Fig. 4 reveals that the points for the reactions of PNPA with Ox^- fall above

Fig. 4. Plots of $\log k^{(DMSO-H2O)}/k^{(H2O)}$ vs. transfer enthalpies ($\Delta\Delta H_{tr}$) for reactions of PNPA (○) and PNPB (●) with Ox^- and *p*-$ClPhO^-$ at 25.0 ± 0.1 °C. The data for reaction of PNPA were taken from ref. 7*b*.

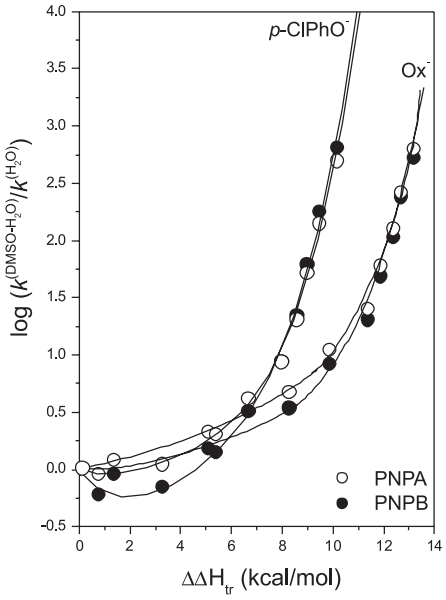


Table 2. Transfer enthalpies ($\Delta\Delta H_{tr}$, kcal/mol) from 0 to 90 mol% DMSO for single ions of *p*-$ClPhO^-$ and Ox^- at 25.0 °C.

	$\Delta\Delta H_{tr}$ (kcal/mol)	
DMSO (mol%)	*p*-$ClPhO^-$	Ox^-
0	0	0
10	0.8	1.4
20	3.3	5.1
30	5.4	8.3
40	6.7	9.9
50	8.0	11.4
60	8.6	11.9
70	9.0	12.4
80	9.5	12.7
90	10.2	13.2

Note: Data were taken from ref. 7*b*.

those for the reactions of PNPB with Ox^- throughout the whole $\Delta\Delta H_{tr}$ range. However, a contrasting result is shown for the reactions with *p*-$ClPhO^-$, i.e., the points for the reactions of PNPA lie above those for the reactions of PNPB up to $\Delta\Delta H_{tr}$ = ~7 kcal/mol, but are situated below beyond that point. This result indicates that the reactions of PNPB with *p*-$ClPhO^-$ gain greater rate enhancement than the corresponding reactions of PNPA with the same $\Delta\Delta H_{tr}$ value in the DMSO-rich medium. The contrasting α-effect behaviour for the PNPB and PNPA systems, as exhibited in Fig. 2 for the DMSO-rich region, is therefore accounted for.

Conclusions

Through the combination of kinetic data with calorimetrically determined GS solvation of Ox^- and *p*-$ClPhO^-$, which allowed dissection of the medium effect on TS and GS con-

© 2006 NRC Canada

tributions, the present study leads to the following conclusions. (*i*) The bell-shaped α-effect profile obtained for the reaction of PNPB with Ox^- and *p*-$ClPhO^-$ is similar to that previously found for the corresponding reaction with PNPA, differing notably however, in the magnitude of the α-effect beyond 40 mol% DMSO; the PNPB system exhibits a much smaller α-effect than the PNPA system in this DMSO-rich region. (*ii*) The dominant GS effect in the H_2O-rich region and TS effect in the DMSO-rich region are proposed to be responsible for the origin of the increasing and decreasing α-effect trends, respectively. (*iii*) The effect of medium change on reactivity is more significant for the reaction with *p*-$ClPhO^-$ than for that with Ox^- in DMSO-rich region. (*iv*) The reaction of PNPB with *p*-$ClPhO^-$ gains greater rate enhancements than the corresponding reaction of PNPA in DMSO-rich region, which is responsible for the smaller α-effect found for the reaction of PNPB beyond 40 mol% DMSO. (*v*) Concordant with the increased polarizability effected on going from PNPA to PNPB with the change Me → Ph, is the advent of the maximum in the bell-shaped α-effect profile (Fig. 2) at a lower DMSO content with PNPB than with PNPA (40 vs. 50 mol% DMSO) and similarly the smaller magnitude of the α-effect (230 vs. 285).

Experimental section

Materials

PNPB was readily prepared from the reaction of benzoyl chloride with *p*-nitrophenol in the presence of triethyl amine in anhydrous ether. Butan-2,3-dione monoxime and phenols used are of the highest quality available and were recrystallized before use. DMSO was refluxed over calcium hydride, distilled, collecting the fraction of bp 64–66 °C (6–7 mm Hg, 1 mm Hg = 133.322 4 Pa) and stored under nitrogen. Doubly glass distilled water was further boiled and cooled under nitrogen just before use.

Kinetics

Kinetic studies were performed with a UV–vis spectrophotometer for slow reactions ($t_{1/2} \geq 10$ s) and a stopped-flow spectrophotometer for fast reactions ($t_{1/2} < 10$ s) with a constant temperature circulating bath at 25.0 ± 0.1 °C. Typically, the reaction was initiated by adding 5 μL of ca. 0.02 mol/L of substrate solution in MeCN by 10 μL gastight syringe to a 10 mm quartz UV cell containing 2.50 mL of the thermostated reaction mixture made up of reaction medium and an aliquot of the nucleophile stock solution. The nucleophile stock solution of ca. 0.2 mol/L was prepared by dissolving 2 equiv. of oxime (or phenol) and 1 equiv. of standardized NaOH solution to make a self buffered solution. Generally, the nucleophile concentration was varied over the range, $1–100 \times 10^{-3}$ mol/L, while the substrate concentration was 4×10^{-5} mol/L. All the solutions were transferred by gastight syringes under nitrogen. The reactions were followed by monitoring the appearance of *p*-nitrophenoxide ions at 410 nm.

Product analysis

p-Nitrophenoxide ion was liberated quantitatively and identified as one of the reaction products in the reactions of PNPB by comparison of the UV–vis spectra after completion of the reactions with those of the authentic samples under the same reaction conditions.

Acknowledgement

The authors are grateful for the financial support from Korea Science and Engineering Foundation (KOSEF-F01–2005–000–10033–0) and Natural Sciences and Engineering Research Council of Canada (NSERC) (EB). Y.H. Kim is also grateful for the BK 21 Fellowship.

References

1. For reviews see: (*a*) E. Buncel and I.H. Um. Tetrahedron, **60**, 7801 (2004); (*b*) E. Buncel and S. Hoz. Isr. J. Chem. **26**, 313 (1985); (*c*) A.P. Grekov and V.Y. Veselov. Usp. Khim. **47**, 1200 (1978); (*d*) N.J. Fina and J.O. Edwards. Int. J. Chem. Kinet. **5**, 1 (1973).
2. (*a*) F. Terrier, E. Le Guevel, A.P. Chatrouse, G. Moutiers, and E. Buncel. Chem. Commun. (Cambridge), 600 (2003); (*b*) E. Buncel, C. Cannes, A.P. Chatrousse, and F. Terrier. J. Am. Chem. Soc. **124**, 8766 (2002); (*c*) A.P. Moutiers, E. Le Guevel, L. Villien, and F. Terrier. J. Chem. Soc. Perkin Trans. 2, 7 (1997); (*d*) F. Terrier, G. Moutiers, L. Xiao, E. Le Guvel, and F. Guir. J. Org. Chem. **60**, 1748 (1995); (*e*) F. Terrier, P. McCormack, E. Kizilian, J.C. Halle, P. Demerseman, F. Guir, and C. Lion. J. Chem. Soc. Perkin Trans. 2, 153 (1991); (*f*) G. Moutiers, E. Le Guevel, C. Cannes, F. Terrier, and E. Buncel. Eur. J. Org. Chem. **17**, 3279 (2001).
3. (*a*) C.F. Bernasconi and C. Murray. J. Am. Chem. Soc. **108**, 5251 (1986); (*b*) C.F. Bernasconi and A. Leyes. J. Am. Chem. Soc. **117**, 1703 (1995); (*c*) C.F. Bernasconi and M. Stronach. J. Org. Chem. **56**, 1993 (1991); (*d*) D. Herschlag and W. P. Jencks. J. Am. Chem. Soc. **112**, 1951 (1990); (*e*) D.J. Palling and W.P. Jencks. J. Am. Chem. Soc. **106**, 4869 (1984); (*f*) H.J. Dixon, and T.C. Bruice. J. Am. Chem. Soc. **94**, 2052 (1972); (*g*) H.J. Dixon and T.C. Bruice. J. Am. Chem. Soc. **93**, 6592 (1971).
4. (*a*) K.R. Fountain. J. Phys. Org. Chem. **18**, 481 (2005); (*b*) K.R. Fountain, C.J. Felkerson, J.D. Driskell, and B.D. Lamp. J. Org. Chem. **68**, 1810 (2003); (*c*) K.R. Fountain, D.B. Tad-y, T.W. Paul, and M.V. Golynskiy. J. Org. Chem. **64**, 6547 (1999); (*d*) K.R. Fountain, and K.D. Patel. J. Org. Chem. **62**, 4795 (1997).
5. (*a*) Y. Ren and H. Yamataka. Org. Lett. **8**, 119 (2006); (*b*) J.D. Evanseck, J.F. Blake, and W.L. Jorgensen. J. Am. Chem. Soc. **109**, 2349 (1987); (*c*) S. Hoz and E. Buncel. Tetrahedron Lett. **25**, 3411 (1984); (*d*) E. Buncel and S. Hoz. Tetrahedron Lett. **24**, 4777 (1983); (*e*) S. Hoz. J. Org. Chem. **47**, 3545 (1982).
6. (*a*) C.H. DePuy, E.W. Della, J. Filley, J.J. Grabowski, and V.M. Bierbaum. J. Am. Chem. Soc. **105**, 2481 (1983); (*b*) S. Wolfe, D.J. Mitchell, and H.B. Schlegel. J. Am. Chem. Soc. **103**, 7694 (1981).
7. (*a*) E. Buncel and I.H. Um. J. Chem. Soc. Chem. Commun. 595 (1986); (*b*) I.H. Um and E. Buncel. J. Org. Chem. **65**, 577 (2000); (*c*) R.M. Tarkka and E. Buncel. J. Am. Chem. Soc. **117**, 1503 (1995); (*d*) I.H. Um, J.Y. Hong, and E. Buncel. Chem. Commun. (Cambridge), 27 (2001); (*e*) I.H. Um, S.J. Hwang, and E. Buncel. J. Org. Chem. **71**, 915 (2006).
8. (*a*) I.H. Um, Y.M. Park, and E. Buncel. Chem. Commun. (Cambridge), 1917 (2000); (*b*) I.H. Um, E.J. Lee, and E. Buncel. J. Org. Chem. **66**, 4859 (2001).
9. I.H. Um and E. Buncel. J. Am. Chem. Soc. **123**, 11111 (2001).

© 2006 NRC Canada

10. (*a*) I.H. Um, J.S. Lee, and S.M. Yuk. J. Org. Chem. **63**, 9152 (1998); (*b*) I.H. Um, H.W. Lee, J.S. Lee, H.J. Moon, and D.S. Kwon. J. Org. Chem. **62**, 5939 (1997).
11. R.A. Moss, S. Swarup, and S. Ganguli. J. Chem. Soc. Chem. Commun. 860 (1987).
12. (*a*) E. Buncel, R. Stairs, and H. Wilson. The role of the solvent in chemical reactions. Oxford University Press, Oxford, UK. 2003. (*b*) E. Buncel and H. Wilson. Adv. Phys. Org. Chem. **14**, 133 (1977); (*c*) E. Buncel and H. Wilson. Acc. Chem. Res. **12**, 42 (1979).
13. A.J. Parker. Chem. Rev. **69**, 1 (1969).
14. C.F. Bernasconi. Adv. Phys. Org. Chem. **27**, 119 (1992).
15. (*a*) R.D. Rogers and K.R. Seddon. Ionic liquid IIIA: fundamentals, progress, challenges, and opportunities — Properties and structure. Adv. Chem. Ser. 901, American Chemical Society, Washington D.C. 2005; (*b*) R.D. Rogers and K.R. Seddon. Ionic liquid *IIIB*: fundamentals, progress, challenges, and opportunities-transformations and processes. Adv. Chem. Ser. 902, American Chemical Society, Washington D.C. 2005
16. (*a*) D.J. Cram. Pure Appl. Chem. **7**, 155 (1963); (*b*) E. Buncel and J.M. Dust. Carbanion chemistry. Structures and mechanisms. Oxford University Press-ACS, Oxford and Washington D.C. 2003.
17. R.A. Cox and R. Stewart. J. Am. Chem. Soc. **98**, 488 (1976).
18. F.G. Bordwell. Acc. Chem. Res. **21**, 456 (1988).
19. (*a*) E. Grunwald and S. Winstein. J. Am. Chem. Soc. **70**, 846 (1948); (*b*) T.W. Bentley and P.v.R. Schleyer. Adv. Phys. Org. Chem. **14**, 1 (1977).
20. (*a*) D.E. Bowen, M.A. Priesand, and M.P. Eastman. J. Phys. Chem. **78**, 2611 (1974); (*b*) E.A. Symons. Can. J. Chem. **24**, 3940 (1971), and refs. therein.
21. I.H. Um, S.J. Oh, and D.S. Kwon. Tetrahedron Lett. **36**, 6903 (1995).
22. P. Harberfied, J. Friedman, and M.F. Pinkston. J. Am. Chem. Soc. **94**, 71 (1972).
23. C.D. Ritchie. *In* Solute-solvent interactions. *Edited by* J.F. Coetzee and C.D. Ritchie. Marcel Dekker, New York. 1969.

© 2006 NRC Canada

Morphology of surfactant–polymer complexes on mica substrate visualized by atomic force microscopy

Feng Zhao, Yukou Du, Jingkun Xu, and Shufeng Liu

Abstract: The morphology of surfactant–polymer complexes formed in two dimensions has been studied. We found that the morphology of hexadecyltrimethylammonium bromide – modified partially hydrated polyacrylamide (CTAB–MHPAM) complexes transferred to mica from the interface between air and MHPAM aqueous solution shows pearl necklace structures, and it is orientationally aligned. On the addition of salt, this structure is altered to the dendritic fractal structure with a smaller fractal dimension about 1.1 ± 0.01. These structures have potential applications in the fabrication of materials in the nanoscale. The mechanism of the formation of different patterns has been discussed.

Key words: morphology, Surfactant–polymer complexes, Dendritic fractal structure.

Résumé : On a étudié la morphologie des complexes agent de surface–polymère qui se forment en deux dimensions. On a trouvé que la morphologie des complexes du bromure de hexadécyltriméthylammonium – polyacrylamide hydraté partiellement modifié (CTAB–MHPAM) transférés à du mica à partir d'une interface entre de l'air et une solution aqueuse de MHPAM présente des structures en forme de collier de perle et qu'ils ont une orientation alignée. Par addition de sel, cette structure est modifiée en structure fractale dendritique avec une dimension fractale plus petite d'environ 1,1 ± 0,01. Ces structures offrent des possibilités d'application dans la fabrication de matériaux à l'échelle nano. On discute du mécanisme de formation des différents patrons.

Mots clés : morphologie, complexes agent de surface–polymère, structure fractale dendritique.

[Traduit par la Rédaction]

Introduction

Modification of interfaces is important in a broad range of applications in biotechnology and materials science (1–4). To establish a relationship between the applications and the properties of the surfaces, it is necessary to have additional information about their structures and morphologies. Significant efforts have been made to understand these features (5–9). However, the studies have predominately focused on the relatively simple or ordered structures at interfaces, and little is known about the highly disordered and complicated structures (fractal structures), at least on some length scales. The analysis of these structures is usually a difficult task owing to the complexity of the system. However, such fractal patterns play an important role in many physical processes (10). Campion et al. (11) reported a large enhancement of Raman scattering from the metallic fractal clusters. Safonov et al. (12) reported the formation of silver nanoparticle fractal aggregates with highly localized, laser-excited optical modes. Recently, Kimberly et al. (13) described the synthesis of branching fractal "nanotree". The process involves the self-assembled growth of nanoparticles via the vapor–liquid–solid growth mode followed by the sequential seeding of branching structures. More recently, Lauhon et al. (14) reported a new route to generate the fractal nanowire structure based on the vapor-phase deposition and a self-assembly of a catalyst on the surface of a growing nanowire.

Recently, some fractal patterns are reported at air–liquid and solid–liquid interfaces (15–20). Fractals are often statistically self-similar and defined by an average cluster size and a fractal dimension (21–23). Fractal dimension is a measure of the surface and structural irregularities of a given solid. The value of this dimension can vary from two to three. The lower limiting value of two corresponds to a perfectly regular smooth surface, whereas the upper limiting value of three relates to the maximum allowed complexity of the surface (24). The diffusion limited cluster aggregation (DLCA) model (25) and reaction limited cluster aggregation (RLCA) model (26) are widely used to characterize such irregular patterns at the interface. The corresponding fractal dimensions are 1.45 and 1.55 in two dimension (d = 2). In this study, we report the dendritic fractal pattern of CTAB–MHPAM complex films transferred to mica surface from the interface between the air and aqueous MHPAM solution. Without adding salt to subphase, the pearl necklace structure

Received 28 May 2006. Accepted 17 September 2006. Published on the NRC Research Press Web site at http://canjchem.nrc.ca on 18 November 2006.

F. Zhao,[1] J. Xu, and S. Liu. Jiangxi Key Laboratory of Organic Chemistry, Jiangxi Science and Technology Normal University, Nanchang 330013, People's Republic of China. **Y. Du.** Department of Chemistry and Chemical Engineering, Suzhou University, Su Zhou 215006, People's Republic of China.

[1]Corresponding author (e-mail: zhf19752003@yahoo.com.cn).

 doi:10.1139/V06-153 © 2006 NRC Canada

Fig 1. Structure of MHPAM.

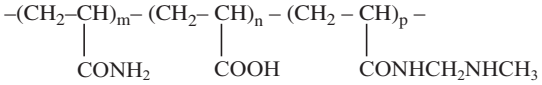
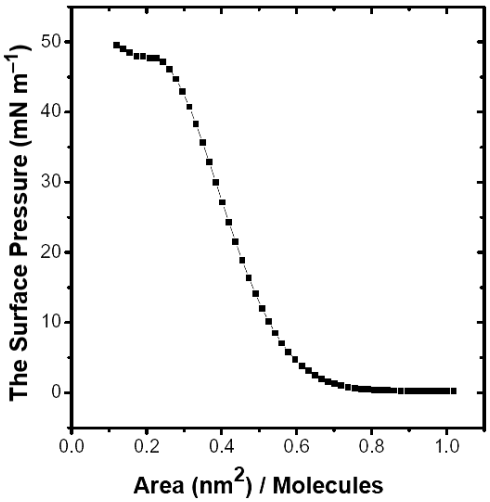


Fig 2. Isotherm of surface pressure versus mean molecular area.



on mica surface was observed. On the addition of salt, a well-defined dendritic fractal structure was formed with a small fractal dimension (D = 1.1 ± 0.02).

Experimental section

Materials

Hexadecyltrimethylammonium bromide (CTAB) was of analytical reagent grade (Beijing Xi Zhong Chemical Factory, Beijing, China) and was purified by extraction with diethylether followed by recrystallization from anhydrous ethanol. After recrystallization, there was no minimum in the plot of surface tension vs concentration.

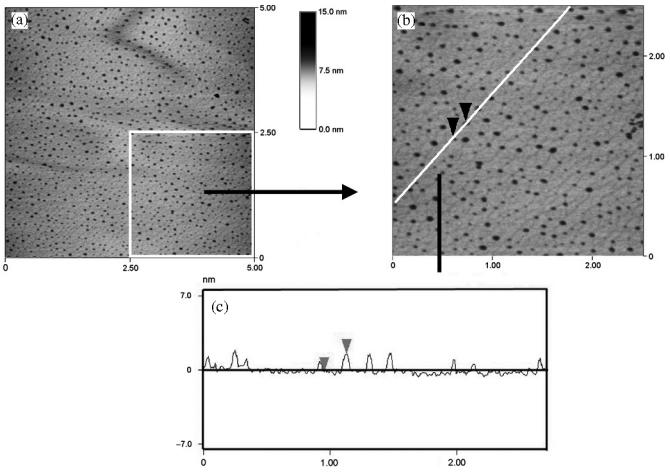
Modified partially hydrated polyacrylamide (MHPAM) with a weight average molecular weigh of 0.8×10^7g mol^{-1} was obtained from Beijing Hengju Chemical Agent Co. Ltd. (Beijing, China) and used without further purification. The values of the repeated units (m, n, p) are about 109825, 15294, and 7018. The structure of MHPAM is shown in Fig. 1.

Preparation of CTAB–MHPAM complexes

The surface pressure (π) – surface area (A) isotherm of a spread film was obtained using an LB trough (length 700 mm ± width 40 mm, FACE HBM, Japan) equipped with a Wilhelmy plate for monitoring the surface pressure. The entire film balance is placed in a container to avoid contamination and air flows. The accuracy of the surface pressure measurements is ±0.1 mN/m. Before each experiment, the trough was thoroughly cleaned with acetone and dichloromethane. The surface area was compressed by moving a Teflon barrier at the speed of 20–25 cm^2/min.

Owing to the good solubility in water, either CTAB or MHPAM molecules cannot form a stable monolayer at the air–water interface. However, the strong electrostatic interactions between the negatively charged COO$^-$ groups along

Fig. 3. (a) AFM image of CTAB–MHPAM complexes on mica surfaces transferred from the interface between the air and MHPAM aqueous solution. (b) Enlarged and contrast-enhanced AFM image from (a). (c) Cross-section indicated by arrows on image (b). (Note: to observe the structures more clearly, the above images were treated with nvert function in Adobe Photoshop 6.0; therefore, the brighter regions in AFM images are bare mica substrate, and the darker regions are the complex films, which is different from the conventional AFM images. AFM images in Fig. 6 are also similar).



MHPAM chains and CTA$^+$ headgroups make CTAB–MHPAM complexes form stable film at the air–water interface. The CTAB–MHPAM complex films were prepared as following.

CTAB was dissolved in chloroform to make a 1.0 mmol/L solution and then spread on the subphase MHPAM aqueous solution interface (c = 0.01 mg/mL). Five minutes was allowed for solvent evaporation before compression was started. The π–A isotherm is shown in Fig. 2, which implied co-adsorption of MHPAM and CTAB molecules at the air–water interface and the formation of a stable CTAB–polymer complex films. Then, the CTAB–MHPAM complex films were compressed to the surface pressure of 12 mNm^{-1}. The freshly cleaved mica slide was brought down horizontally by hand to touch the monolayer and lifted carefully after a contact time of a few seconds. This is the so-called "horizontal lifting method (HLM)" described in detail elsewhere (27). Finally, the mica slide was dried in air and imaged with AFM.

Atomic force microscopy (AFM)

CTAB–MHPAM complex films on mica surfaces were characterized using a Digital Instrument Nanoscope IIIa multimode system (Santa Barbara, CA) with the tapping mode. AFM cantilevers were conductive silicon cantilevers with a typical resonance frequency of 300 kHz, spring constant of 35 N m^{-1}. The AFM image is shown in the height mode after flattening.

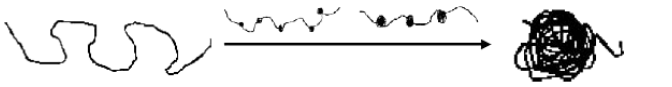
Results and discussion

Morphology of CTAB–MHPAM complex films on mica surfaces

Figure 3 shows AFM images morphology of CTAB–MHPAM complex films transferred to mica surfaces from

© 2006 NRC Canada

Fig 4. A representative schematic drawing of the conformational transition of a polymer.



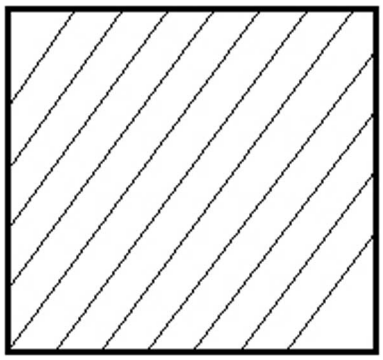
a: The high charge density *b: The low charge density*

the interface between air and MHPAM aqueous solution. Figs. 3*a* and 3*b* clearly confirm the existence of pearl necklace structures. We believe the pearl necklace structure morphology results from the compromise between short-range attraction and long-range repulsion (28) along the polymer chains. The coil-to-globule conformational transition of the polymer chains has been predicted by Dobrynin–Rubinstein–Obukhov (DRO) theory (29). In the process of transition, a sequence of intermediate configurations, which consist of chains bearing individual smaller sub-globules along the chains, similar to a pearl necklace, may be formed (28). In the past, direct visualization of the pearl necklace structure of the polymer chains has been lacking; a few papers (28, 30–31) recently reported direct experimental evidences of such structure. Particularly, Kirwan et al. (30) depicted the coil-to-globule conformational transition of single poly(vinylamine) molecules through a sequence of pearl necklace structures on mica surface. In our experiments, the formation of pearl necklace structures is similar to what they observed. However, it should be noted that the pearl necklace structures visualized by Kirwan et al. formed through single polymer molecule chains,whereas the structures reported here resulted from many polymer molecule chains through the mutual entanglement.

The negatively charged COO^- groups, along each MHPAM long chain complex with CTA^+ ions, and the long-range Coulombic repulsion forces decrease owing to the effect of neutralization of charged groups, analogous to the decrease of the polyelectrolyte density, which results in the collapse of the MHPAM chains. However, the positively charged $CH_2N^+H_2CH_3$ groups (pK_a = 9.1–10.2, in our experiments, pH = 6.18) attached to the MHPAM chains will hinder the collapse of MHPAM, thus the long coil MHPAM chains may form a necklace with compact globules joined by narrow strings (29) because of the equilibrium interaction between short-range attraction and long-range repulsion along the chains. A representative schematic of conformational transition of a polymer is shown in Fig. 4.

In addition, it should be emphasized that one can observe the orientational adsorption of the pearl necklace structure to mica. The phenomenon obtained in the present investigation is related to the combination of the properties of mica surfaces and adsorption behavior of polymer. Mica is a layered aluminosilicate mineral. Each layer is strongly negatively charged due to isomorphism substitution where some silicon atoms are replaced by aluminum. These charges are compensated for by monovalent ions, mostly potassium (32, 33). Mica has crystalline substrate features (Fig. 5). The adsorption behavior of polymer to surface is a two-step process: an initial adsorption in terms of the diffusion-limited adsorption and the slow reorganization of the adsorbed chains to minimize the surface free energy (34). In the case of adsorption of CTAB–MHPAM complexes to mica surfaces, the aggregation of CTAB–MHPAM complex chains with the positively charged $CH_2N^+H_2CH_3$ groups was mainly along the mica crystal axes, and the thermal fluctuations of the complex chains on mica surface eventually resulted in the morphology of orientational adsorption on mica substrate.

Fig 5. A schematic representation of the mica surface crystal axes.



Effect of salt on the morphology of CTAB–MHPAM complex films

Figure 6 shows morphological changes of CTAB–MHPAM on mica at various subphase NaCl concentrations. Here, we show that the addition of salt causes a sequential conformational transition from the pearl necklace structure to the dendritic structure.

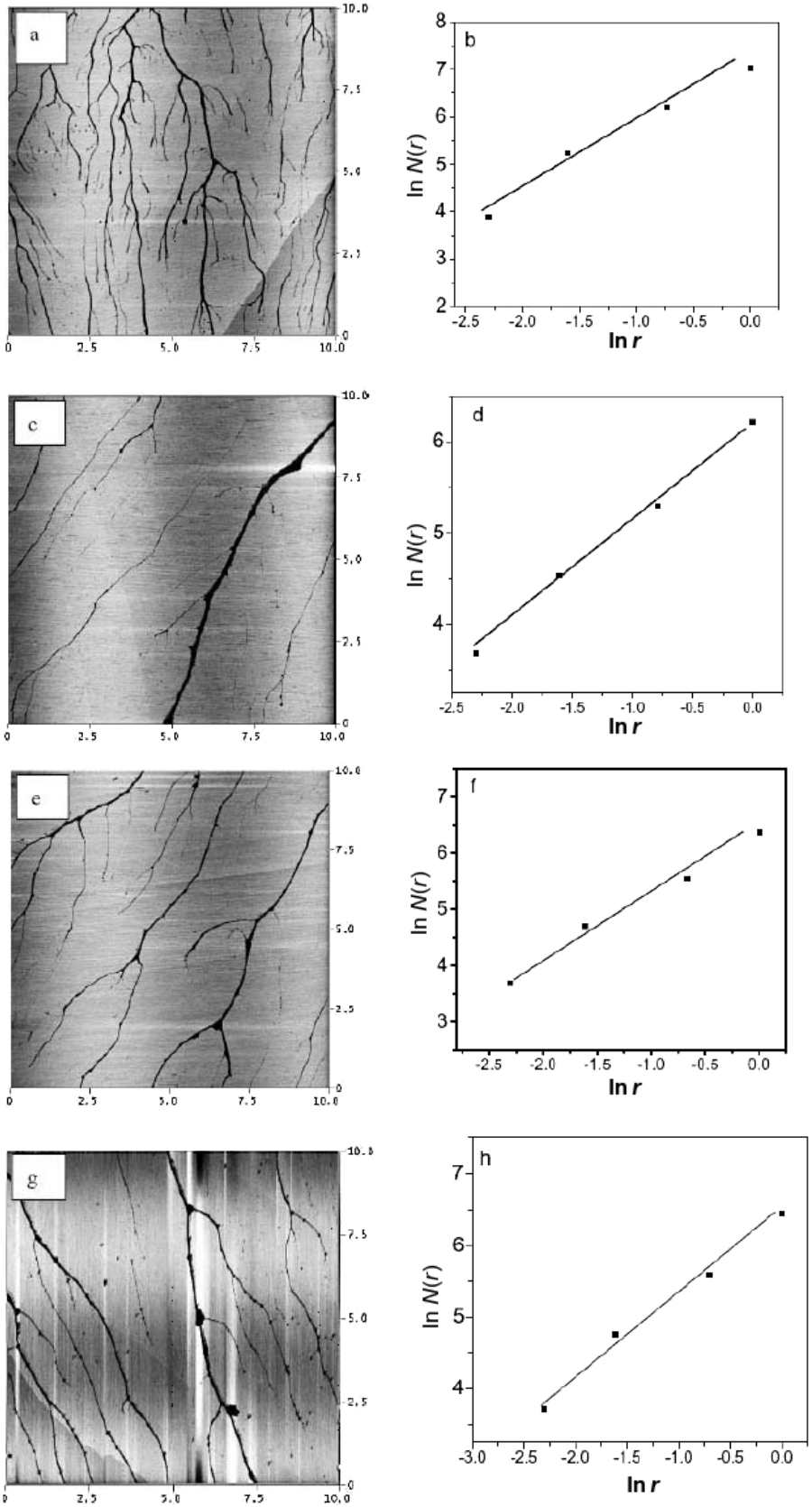
The structures in our systems are quite similar to fractal patterns observed in other systems, particularly the metal dendrites grown by electrodeposition (9, 20), two-dimension crystallites grown on a rough surface (35), and dendritic crystal grown (36). As a result, we performed the fractal dimension analysis for the images of Fig. 6 by the box-counting method (21–23), which quantifies the total number of occupied boxes ($N_{(r)}$) (squares containing any portion of the image) at varying box sizes *r*. The logarithm of the number of occupied boxes is plotted against the log of the box sizes. The absolute value of the slope of the resulting line is the fractal dimension *D*, as shown in detail by the early literature (37), and the corresponding results are shown in Figs. 6*b*, 6*d*, 6*f*, and 6*h*.

With the increase of salt concentration, the fractal dimensions of the dendritic structure decrease continuously. It clearly shows that at salt concentration ~0.73 mmol/L, a stable fractal structure is formed, and its fractal dimension is 1.1 ± 0.02 (Fig. 7). In two-dimensional systems, fractal dimensions ranging from 1.2 to 1.74 have been obtained under different experimental conditions (19, 38–39). However, the smaller fractal dimension (D = 1.1 ± 0.02) was obtained in our experiments. The well-refined dendritic fractal structure on mica substrate holds great promise for potential fundamental and technological applications. The fractal dimension *D* of 1.41–1.09 is reasonable compared with the diffusion-limited cluster aggregation (DLCA) (D = 1.45), indicating that the self-complexation and adsorption on mica surfaces seems to be a DLCA process, but the interactions between the adsorbed molecules and mica surfaces also played an important role in the morphology formation.

The driving force for the occurrence of dendritic patterns on mica may be the interaction between the background (mica surface) and the aggregated particles (CTAB–MHPAM complexes) (40, 41). When NaCl is added to the subphase

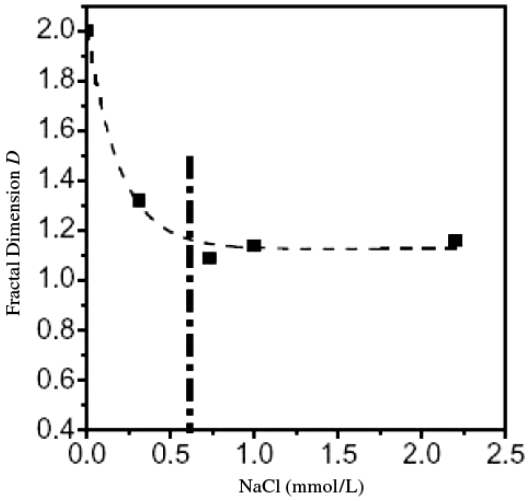
© 2006 NRC Canada

Fig 6. AFM images of CTAB–MHPAM complexes on mica surfaces at various NaCl concentrations (a: 0.31 mmol/L, c: 0.73 mmol/L, e: 1.0 mmol/L, g: 2.2 mmol/L, z scale = 10 nm) and fractal dimension analysis of dendritic structure by using the box counting method (b, d, f, h).



© 2006 NRC Canada

Fig 7. A plot of fractal dimension versus NaCl concentration.



MHPAM aqueous solution, it screens the electrostatic repulsion barrier between the CTAB–MHPAM complex chains and enhances the aggregation of CTAB–MHPAM complex chains. On the other hand, they cannot grow strictly along the mica crystal axes owing to uncertain conditions, such as liquid convection, and defects of mica crystal axes. Consequently, the aggregation patterns were not very regular orientational lattice-like structures. Similar mechanism had been proposed earlier in several papers to describe the adsorption of other surfactants (33, 42).

Moreover, such fractal dendritic patterns could have potential applications as self-assembly templates for the formation of fractal metallic nanoparticles because the functional group, CH_2NHCH_3, has a high affinity for metal nanoparticles (43). Therefore, it is reasonable to expect that dendritic metallic nanoparticle aggregations can be achieved by applying this pattern as a template.

Conclusions

We demonstrated the morphological formation of surfactant–polymer complexes on mica substrates by AFM. At the air–MHPAM aqueous solution interface, CTAB–MHPAM complexes, adsorbed to mica surfaces, appear as a pearl necklace structure with orientational lattice-like array. On the addition of salt, a well-defined dendritic fractal structure eventually formed with a smaller fractal dimension. Such fractal structures enable the complexes to have potential applications as self-assembly templates for the formation of fractal nanoparticles.

References

1. C. Ionescu-Zanetti, R. Khurana, J.R. Gillespie, J.S Petrick, L.C. Trabachino, L.J Minert, S.A Carter, and A.L Fink. PNAS, **96**, 13175 (1999).
2. J. Kumaki, Y. Nishikawa, and T. Hashimoto. J Am Chem Soc. **118**, 3321 (1996).
3. V. Percec, C.H. Ahn, G. Ungar, D.J.P. Yeardley, M. Moller, and S.S Sheiko. Nature (London), **391**, 161 (1998).
4. J. Kumaki and T. Hashimoto. J. Am. Chem. Soc. **125**, 4907 (2003).
5. I.I. Potemkin, E.Y. Kramarenko, A.R. Khokhlov, R.G. Winkler, P. Reineker, P. Eibeck, J.P. Spatz, and M. Moller. Langmuir, **15**, 7290 (1999).
6. J.P. Spatz, S. Sheiko, and M. Moller. Macromolecules, **29**, 3220 (2003).
7. G.B. Webber, E.J. Wanless, S.P. Armes, F.L. Baines, S. Biggs. Langmuir, **17**, 5551 (2001).
8. A. Kiriy, G. Gorodyska, S. Minko, M. Stamm, and C. Tsitsilianis. Macromolecules, **36**, 8704 (2003).
9. R.M. Brady and R.C. Ball. Fractal growth of copper electrodeposits. Nature (London), **309**, 225 (1984).
10. D.P. Tsai, J. Kovacs, Z.H. Wang, M. Moskovits, V.M. Shalaev, J.S. Suh, and R. Botet. Phys. Rev. Lett. **72**, 4149 (1994).
11. A. Campion and P. Kambhampati. Chem. Soc. Rev. **27**, 241 (1998).
12. V.P. Safonov, V.M. Shalaev, V.A. Markel, Y.E. Danilova, N.N. Lepeshkin, W. Kim, S.G. Rautian, and R.L. Armstrong. Phys. Rev. Lett. **80**, 1102 (1998).
13. K.A. Dick, K. Deppert, M.W. Larsson, T. Martensson, W. Seifert, L.R. Wallenberg, and L. Samuelson. Nature Material, **3**, 380 (2004).
14. S.J. May, J.G. Zheng, B.W. Wessels, and L.J. Lauhon. Adv Mater. **17**, 598 (2005).
15. Y.D. Jin and S.J. Dong. Angew. Chem., Int. Ed Engl. **41**, 1040 (2002).
16. I. Lee, J.S. Ahn, T.R. Hendricks, M.F. Rubner, and P.T. Hammond. Langmuir, **20**, 2478 (2004).
17. N. Koneripalli1, F.S. Bates, and G.H. Fredrickson. Phys. Rev. Lett. **81**, 1861 (1998).
18. S.H. Lee, H. Kang, J. Cho, Y.S. Kim, and K. Char. Macromolecules, **34**, 8405 (2001).
19. S. Wang and H. Xin. J. Phys. Chem. B, **104**, 5681 (2000).
20. M. Matsushita, M. Sano, Y. Hayakawa, H. Honjo, and Y. Sawada. Phys. Rev Lett. **53**, 286 (1984).
21. B.B. Mandelbrot. The fractal geometry of nature. Freeman, San Franciso, CA. 1982.
22. T. Vicsek. Fractal growth phenomena. World Scientific, Teaneek, NJ. 1989.
23. H. Takayasu. Fractal in the physical science. Manchester University Press, New York. 1990.
24. A. Gil, G.Y. Cherkashinin, and S.A.J. Korili. J. Chem. Eng. Data, **49**, 639 (2004).
25. T.A. Witten and L.M. Sander. Phys Rev Lett. **47**, 1400 (1983).
26. P. Meakin. Phys. Rev. Lett. **51**, 1119 (1985).
27. P. Liljeroth, D. Vanmaekelbergh, V. Ruiz, K. Kontturi, H. Jiang, E. Kauppinen, and B.M. Quinn. J. Am. Chem. Soc. **126**, 7126 (2004).
28. S. Minko, A. Kiriy, G. Gorodyska, and M. Stamm. J. Am. Chem. Soc. **124**, 3218 (2002).
29. A.V. Dobrynin, M. Rubinstein, and S.P. Obukhov. Macromolecules, **29**, 2974 (1996).
30. L.J. Kirwan, G. Papastavrou, and M. Borkovec. Nano. Lett. **4**, 149 (2004).
31. Y. Roiter and S. Minko. J. Am. Chem. Soc. **127**, 15688 (2004).
32. A. Dedinaite, P.M Claesson, and M. Bergstrom. Langmuir, **16**, 5257 (2000).
33. W.A. Ducker and E.J. Wanless. Langmuir, **15**, 160 (1999).
34. A. Kiriy, G. Gorodyska, S. Minko, W. Jaeger, P. Stepanek, and M. Stamm. J. Am. Chem. Soc. **124**, 13454 (2002).
35. E. Ben-Jacob, G. Deutscher, P. Garik, N.D. Goldenfeld, and Y. Lareah. Phys. Rev. Lett. **57**, 1903 (1986).

© 2006 NRC Canada

36. J.F. Spengler and W.T. Coakley. Langmuir, **19**, 3635 (2003).
37. V.A. Kimler, M. Tracy-bee, C. Ollie, R.M. Langer, J.M. Montante, C.C. Marks, D.C. Freeman, R.A. Hough, and J. Taylor. Pigment Cell Res. **17**, 165 (2004).
38. A.T. Skjeltorp. Phys. Rev. Lett. **58**, 1444 (1987).
39. A.J. Hurd and D.W. Schaefer. Phys. Rev. Lett. **54**, 1043 (1985).
40. H. Brune, C. Romainczyk, H. Roer, and K. Kern. Nature (London), **369**, 469 (1994).
41. H. Honjo, and S. Ohat. Phys. Rev A, **36**, 4555 (1987).
42. R.E. Lamont and W.A. Ducker. J. Am. Chem. Soc. **120**, 7602 (1998).
43. M. Noh, J. Thiel, and D.C. Johnson. Adv. Mater. **8**, 596 (1998).

© 2006 NRC Canada

Ytterbium perfluorooctanesulfonate catalyzed synthesis of acylals from aldehydes and acetic anhydride in a fluorous biphasic system

Wen-Bin Yi, Ya-Qing Yin, and Chun Cai

Abstract: Ytterbium perfluorooctanesulfonate [$Yb(OPf)_3$] catalyses the highly efficient synthesis of acylals from aldehydes and acetic anhydride in a fluorous biphase system (FBS) composed of toluene and perfluorodecalin. The fluorous phase containing the fluorous catalyst is easily separated and can be reused several times without significant loss of catalytic activity.

Key words: acylals, ytterbium perfluorooctanesulfonate, fluorous biphasic catalysis.

Résumé : Le perfluorooctanesulfonate d'ytterbium [$Yb(OPf)_3$] catalyse d'une façon très efficace la synthèse d'acylals à partir d'aldéhydes et d'anhydride acétique dans un système fluoré biphasique (SFB) formé de toluène et de perfluorodécaline. La phase fluorée qui contient le catalyseur fluoré se sépare facilement et elle peut être réutilisée plusieurs fois sans perte significative de son activité catalytique.

Mots clés : acylals, perfluorooctanesulfonate d'ytterbium, catalyseur fluoré biphasique.

[Traduit par la Rédaction]

Introduction

Recently, transition metal-catalyzed reactions in a fluorous biphasic system (FBS) have become among the most important methods for facile catalyst separation from the reaction mixture and recycling of the catalyst (1–3). In this catalytic system, the metal catalyst coordinated by perfluoroalkylated ligands can dissolve into the fluorous phase containing the product after the reaction (1). Furthermore, FBS has the advantage of possible use for water-sensitive reactions unlike aqueous biphase systems (4, 5). In our continued interest in the utility of lanthanide perfluorooctanesulfonates-catalyzed reactions in fluorous media (6–8), we report herein our newest results on a successful approach to FBS, i.e., perfluorodecalin–toluene system for the synthesis of 1,1-diacetates (acylals), efficient protecting groups for aldehydes (9) catalyzed by a ytterbium perfluorooctanesulfonate [$Yb(OPf)_3$] complex.

Rare earth (III) perfluorooctanesulfonates ($RE(OPf)_3$, RE = Sc,Y, La, Lu), a novel series of Lewis acids, have been of special interest because of their characteristic features such as low hygroscopicity, ease of handling, robustness for recycling, and high solubility in fluorous solvent (10–12). A catalytic amount of $RE(OPf)_3$ successfully promotes several synthetically useful reactions such as Friedel–Crafts acylation (13) and alkylation (6), aldol condensation (8), nitration (14), Mannich reaction (15), and Diels–Alder reactions (10). The catalyst immobilized in the fluorous phase was recovered by simple phase separation and reused directly for the next reaction without a significant loss of catalytic activity.

The acylals were prepared from aldehydes and acetic anhydride employing fluorous phase technology. The reaction of benzaldehyde with acetic anhydride in a FBS was examined with various Lewis acid catalysts (Scheme 1) and the results are summarized in Table 1. We found that the $Yb(OPf)_3$ and $Sc(OPf)_3$ complexes had similar activity for the reaction with a quantitive conversion to acylal product in the presence of 0.3 mol% catalyst at 80 °C over 2 h, while other lanthanide perflates such as $Eu(OPf)_3$, $Tm(OPf)_3$, or $La(OPf)_3$, yielded desired product in 62%, 51%, or 39%, respectively. This could be ascribed to the higher Lewis acidity of $Yb(OPf)_3$ and $Sc(OPf)_3$ relative to other lanthanide perflates (10). Heptadecafluorooctanesulfonic acid ($C_8F_{17}SO_3H$, PfOH) can itself promote the reaction, but it was found to be less effective than $RE(OPf)_3$. When the reaction was finished, the reaction mixture was cooled to RT. The fluorous phase with $RE(OPf)_3$ catalysts can separate from the organic layer and return to the bottom layer. In addition, based on ^{19}F NMR, UV–vis, and GC-MS data, no loss of catalyst or fluorous solvent to the organic phase was detected and no organic compounds were found in the fluorous phase. There were no significant differences between the UV–vis spectra of the initial and recovered fluorous phases, which may indicate that the fluorous lanthanide catalyst is recovered unaltered after the reaction process has taken place. $RE(OPf)_3$ was completely (>99%) recovered, as determined by atomic emission spectrometry (ICP) and was then reused (Table 1, entries 3 and 4). The separated fluorous phase could be re-

Received 3 September 2006. Accepted 16 October 2006. Published on the NRC Research Press Web site at http://canjchem.nrc.ca on 23 November 2006.

W.-B. Yi, Y.-Q. Yin, and C. Cai.[1] Chemical Engineering College, Nanjing University of Science & Technology, Nanjing 210094, China.

[1]Corresponding author (e-mail address: c.cai@mail.njust.edu.cn).

 © 2006 NRC Canada

Scheme 1. $Yb(OPf)_3$-catalysed synthesis of acylals in FBS.

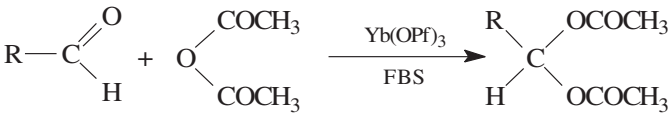


Table 1. Reaction of benzaldehyde with acetic anhydride in FBS.

Entry	Catalyst	Yield (%)[a]
1	$Sc(OPf)_3$	99
2	$Eu(OPf)_3$	62
3	$Tm(OPf)_3$[b]	51, 50, 51, 52, 50
4	$Yb(OPf)_3$[b]	99, 99, 98, 96, 97
5	$La(OPf)_3$	39
6	PfOH	27

[a]Isolated yield.
[b]The fluorous phase was run for five consecutive cycles.

used for the next reaction without any specific treatment and the recycling work-up procedure was accomplished by simple phase separation. For example, in the $Yb(OPf)_3$-catalyzed reaction of aldehydes and acetic anhydride, the yields from the first run to the fifth run were 99%, 99%, 98%, 96%, and 97%, respectively.

We decided to use the relatively cheap and similarly active catalyst $Yb(OPf)_3$ for the synthesis of other acylals (Scheme 1). The results are summarized in Table 2. All isolated pure products gave satisfactory spectral analysis for ^1H NMR, IR, and MS. The aromatic aldehydes, cinnamaldehyde and 1-naphthylaldehyde that have an electron-withdrawing group, are worth mentioning as they almost gave quantitative yields in the presence of 0.3 mol% catalyst, which is less than those of the reported methods (21–27). The nature of the substituents on the aromatic ring seems to have no effect on the reaction system. It is worth noting that hydroxyl groups in 2-hydroxy- and 4-hydroxybenzaldehyde were also acetylised to afford the corresponding triacetates under these conditions. Notably, in the cases of 4-hydroxy- and 4-(dimethylamino)-benzaldehyde, only 41% of 4-hydroxy-benzaldehyde was converted to acylals, while 4-(dimethylamino)-benzaldehyde failed to give the expected acylals even though the reaction mixtures were stirred for 24 h. Such reactions may have suffered from the tautomerization that occurred in the catalysis of $Yb(OPf)_3$, which decreased the reactivity of the aldehyde groups (17). However, such tautomerization does not happen in 2-hydroxy-benzaldehyde because the intramolecular hydrogen bond between hydroxyl and aldehyde groups prevents the formation of a quinoid structure (20). The reaction of heterocyclic aldehydes such as furyl aldehyde also gave quantitive conversion to products. Greater reaction times were required for aliphatic aldehydes than aromatic aldehydes to obtain excellent yields, while ketones such as butanone, acetophenone, and benzophenone were practically unchanged in the reaction (Scheme 2). Therefore, the present procedure is a selective preparation of acylals of aldehydes in the presence of ketones.

It was reported that the mechanism of the title reaction could involve either intermolecular or intramolecular transfer of the second acetate group after initial attack by acetic anhydride (Scheme 3) (19). To test this aspect of the conversion in an FBS, we prepared acetic propionic anhydride for the geminal acylation reaction (Scheme 4). Analysis of the products by GC-MS showed a nearly 1:1:2 ratio of geminal diacetate, geminal dipropionate, and mixed acetate–propionate, respectively. This result supports the intermolecular pathway of Scheme 3.

In summary, the efficiency of $Yb(OPf)_3$ as a Lewis acid catalyst in FBS as an ecofriendly reaction system was demonstrated for the conversion of aldehydes into geminal diacetates. The versatility of this reaction system benefits greatly from both the efficient Lewis acidity of $Yb(OPf)_3$ and the unique solution properties of FBS. We believe that the following properties endow the catalytic approach with great potential for synthetic applications: (*i*) the amount of catalyst used is minute, (*ii*) the catalyst, which is completely immobilized in the fluorous phase, can be recovered and reused, and (*iii*) fluorous biphasic catalytic technique allows high yields and purities of the resultant 1,1-diacetates and indeed they can be used directly, without purification, for many reactions.

Experimental section

Melting points were obtained with a Shimadzu DSC-50 thermal analyzer. IR spectra were recorded on a Bomem MB154S IR analyzer. UV–vis spectra were obtained with a UV-1601 apparatus. ^1H NMR and ^{19}F NMR spectra were recorded with Bruker Advance RX300. Mass spectra were recorded on a Saturn 2000GC-MS instrument. Inductively coupled plasma (ICP) spectra were measured on an Ultima2C apparatus. Elemental analyses were performed on a Yanagimoto MT3CHN recorder. The perfluorodecalin (octadecafluorodecahydronaphthalene) and rare earth (III) salts were purchased from Sigma-Aldrich Co. Heptadecafluorooctanesulfonic acid was commercially obtained from ARCOS Co. Commercially available reagents were used without further purification.

Typical procedure for the preparation of rare earth (III) perfluorooctanesulfonates

$RE(OPf)_3$ compounds were prepared according to literature methods (6). In method A, a mixture of a solution of heptadecafluorooctanesulfonic acid (PfOH, 0.77 g, 1.5 mmol) in water (5 mL) and a solution of $YbCl_3{\cdot}6H_2O$ (0.2 g, 0.5 mmol) in water (0.8 mL) was stirred at RT for 18 h. In method B, a mixture of a solution of PfOH (0.77 g, 1.5 mmol) in water (5 mL) and of Yb_2O_3 (0.12 g, 0.25 mmol) powder was stirred at boiling for 3 h.

In both methods, the resulting gelatinlike solid was collected, washed, and dried at 150 °C in vacuum to give a white solid that shrinks at around 380–450 °C. IR (KBr, cm^{-1}) υ: 1237 (CF_3), 1152 (CF_2), 1081 (SO_2), 1059 (SO_2), 747 (S-O), 652 (C-S). ICP (%) calcd. for $C_{24}O_9F_{51}S_3Yb{\cdot}H_2O$: Yb

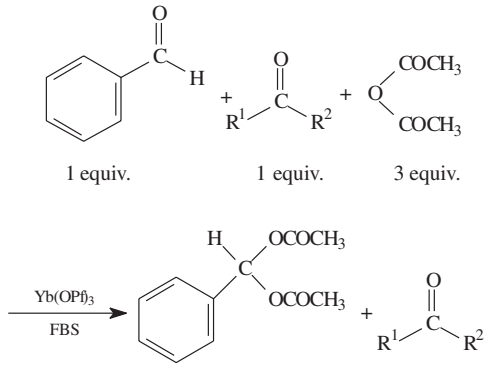
© 2006 NRC Canada

Table 2. $Yb(OPf)_3$-catalyzed synthesis of acylals in FBS.

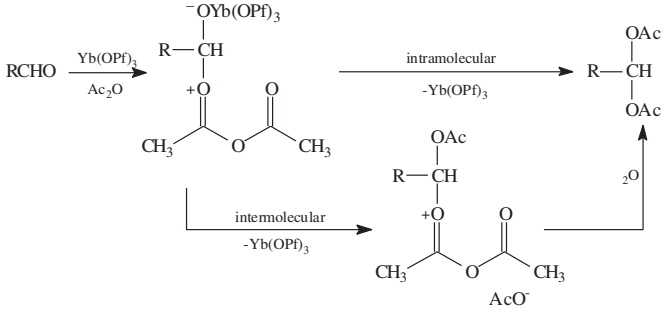
Entry	R^1	Time (h)	Yield (%)[a]	Mp or bp (XXX mmHg)[b] (°C)
1	4-ClPh	2	98	81~82 [Lit. value (16) 80~81]
2	3-ClPh	2	97	65~66 [Lit. value (17) 65~66]
3	2-ClPh	2	97	55~56 [Lit. value (18) 56~57]
4	4-NO_2Ph	2	99	126~127 [Lit. value (17) 125~126]
5	3-NO_2Ph	2	99	64~66 [Lit. value (17) 65~66]
6	2-NO_2Ph	2	98	90~91 [Lit. value (17) 91~9]
7	4-MePh	3	92	76~78 [Lit. value (19) 78~80]
8	4-MeOPh	4	90	64~65 [Lit. value (20) 64~65]
9	4-HOPh	12	41[c]	88~90 [Lit. value (20) 89~90]
10	2-HOPh	4	91[c]	103~104 [Lit. value (20) 104~105]
11	4-$(Me)_2$NPh	24	—	—
12	Cinnamyl	2	99	84~85 [Lit. value (17) 83~84]
13	1-Naphthyl	2	97	105~106 [Lit. value (18) 105~106]
14	Furyl	3	98	52~53 [Lit. value (17) 50~51]
15	C_2H_5	8	60	116~118 (8.0) [Lit. value (19) 115~118 (8.0)]
16	n-C_5H_{11}	8	61	129~130 (2.1) [Lit. value (19) 128~129 (2.0)]
17	$PhCH_2CH_2$	12	64	186~190 (0.7) [Lit. value (19) 185~190 (0.7)]

Note: All reactions were carried out at 80 °C in the presence of 0.3 mol% catalyst.
[a]Isolated yields.
[b]1 mmHg = 133. 322 4 Pa.
[c]5 equiv. of acetic anhydride was used.

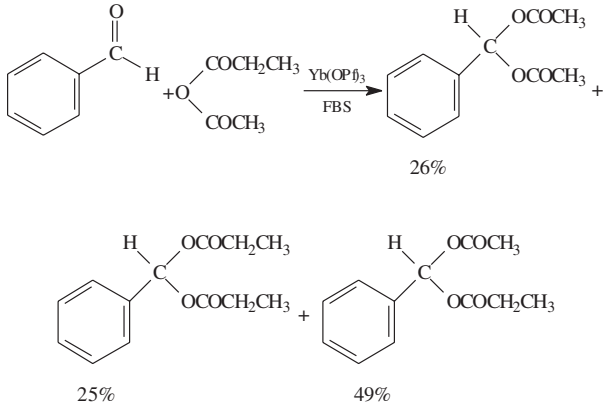
Scheme 2. Selective preparation of acylals of aldehydes in the presence of ketones.



Scheme 3. The possible mechanism of the conversion of aldehydes into acylals.



Scheme 4. Reaction of benzaldehyde with acetic propionic anhydride.



10.24; found: Yb 9.99. Anal. calcd. for $C_{24}O_9F_{51}S_3Yb{\cdot}H_2O$: C 17.21, H 0.10; found: C 17.03, H 0.18.

Typical procedure for synthesis of acylals in FBS

The aldehyde (10 mmol) or ketone (10 mmol) was slowly added into a mixture of $Yb(OPf)_3$ (50 mg, 0.03 mmol), toluene (2 mL), and perfluorodecalin ($C_{10}F_{18}$, cis and trans mixture, 2 mL) containing acetic anhydride (20 mmol). The mixture was stirred at 80 °C for the time indicated in Table 2. The fluorous layer on the bottom was then separated for the next reaction. The reaction mixture (organic phase) was washed subsequently with brine (10 mL), 5% $NaHCO_3$ solution (10 mL), and water (2 × 10 mL), and dried over $MgSO_4$. The solvent was removed under reduced pressure and the residue was purified by a silica gel column chroma-

© 2006 NRC Canada

tography or by recrystallization from cyclohexane solution to give the acylals.

The acylals of the following selected aldehydes show the IR, ^{1}H NMR, and MS (EI) spectra as given below.

2-Hydroxybenzaldehyde

See Table 2, entry 10. IR ($CHCl_3$, cm^{-1}) υ: 2960, 1740. ^{1}H NMR (500 MHz, TMS, $CDCl_3$) δ: 2.09 (s, 6H), 2.33 (s, 3H), 7.06–7.69 (m, 4H), 7.91 (s, 1H). MS (EI) *m*/*z*: 224 (M^+).

Cinnamaldehyde

See Table 2, entry 12. IR ($CHCl_3$, cm^{-1}) υ: 1755, 1660. ^{1}H NMR (500 MHz, TMS, $CDCl_3$) δ: 2.12 (s, 6H), 5.92 (dd, J = 16.7 Hz, 1H), 6.87 (d, J = 16 Hz, 1H), 7.1–7.6 (m, 6H). MS (EI) *m*/*z*: 234 (M^+).

1-Nathphylaldehyde

See Table 2, entry 13. IR ($CHCl_3$, cm^{-1}) υ: 1760. ^{1}H NMR (500 MHz, TMS, $CDCl_3$) δ: 2.13 (s, 6H), 7.45–7.59 (m, 3H), 7.70 (d, J = 6.9 Hz, 1H), 7.89–7.92 (m, 2H), 8.24–8.27 (m, 2H). MS (EI) *m*/*z*: 258 (M^+).

Hexanal

See Table 2, entry 16. IR ($CHCl_3$, cm^{-1}) υ: 2950, 2860, 1750. ^{1}H NMR (500 MHz, TMS, $CDCl_3$) δ: 2.13 (s, 6H), 7.45–7.59 (m, 3H), 7.70 (d, J = 6.9 Hz, 1H), 7.89–7.92 (m, 2H), 8.24–8.27 (m, 2H). MS (EI) *m*/*z*: 202 (M^+)

Acknowledgements

We thank the National Defense Committee of Science and Technology (40406020103) for financial support. We also thank the Zhen-Ya Rare Earth Co. Ltd. for providing several kinds of rare earth oxides.

References

1. T.H. Horváth and J. Rabai. Science (Washington, D.C.), 266, 72 (1994).
2. J.A. Gladysz, D.P. Curran, and I.T. Horváth (*Editors*). Handbook of fluorous chemistry, Wiley-VCH, Weinheim, Germany. 2004.
3. K. Mikami (*Editor*). Green reaction media in organic synthesis. Blackwell, Oxford. 2005.
4. B. Cornils and W.A. Herrmann. Aqueous-phase organometallic catalysis. Wiley-VCH, New York. 1998. p. 208.
5. B.E. Hanson. Coord. Chem. Rev. **185–186**, 795 (1999).
6. W.B. Yi and C. Cai. J. Fluorine Chem. **126**, 831 (2005).
7. W.B. Yi and C. Cai. J. Fluorine Chem. **126**, 1191 (2005).
8. W.B. Yi and C. Cai. J. Fluorine Chem. **126**, 1553 (2005).
9. T.W. Greene and P.G.M. Wats. Protective groups in organic synthesis. 3rd ed. Vol. 4. Wiley, New York. 1999.
10. T. Hananmoto, Y. Sugimoto, Z.J. Yong and J. Inanaga. Bull. Chem. Soc. Jpn. **70**, 1421 (1997).
11. K. Mikami, Y. Mikami, H. Matsuzawa, Y. Matsumoto, J. Nishikido, F. Yamamoto, and H. Nakajima. Tetrahedron, **58**, 4015 (2002).
12. K. Mikami, Y. Mikami, Y. Matsumoto, J. Nishikido, F. Yamamoto, and H. Nakajima. Tetrahedron Lett. **42**, 289 (2001).
13. M. Shi and S.C. Cui. J. Fluorine Chem. **116**, 143 (2002).
14. M. Shi and S.C. Cui. Chem. Commun. (Cambridge), **994** (2002).
15. M. Shi, S.C. Cui, and Y.H. Liu. Tetrahedron, **61**, 4965 (2005).
16. J.K. Michie and J.A. Miller. Synthesis, **824** (1981).
17. T.S. Jin, G.L. Feng, M.N. Yang, and T.S. Li. Synth. Commun. **34**, 1645 (2004).
18. F. Freeman and E.M. Karchefski. J. Chem. Eng. Data, **22**, 355 (1977).
19. S.K. Kanwarpal, S.B. Balkrishna, R.P. Deshpande, S.N. Rajadhyaksha, and W.P. Harold. J. Org. Chem. **48**, 1765 (1983).
20. T.S. Li, Z.H. Zhang, and Y.J. Gao. Synth. Commun. **28**, 4665 (1998).
21. Y.Q. Li. Chin. Chem. Lett. **12**, 565 (2001).
22. J.S. Yadav, B.V.S. Reddy, and C. Srinivas. Synth. Commun. **32**, 1175 (2002).
23. B.C. Nanu, J. Dutta, and A. Das. Chem. Lett. **32**, 366 (2003).
24. H. Firouzabadi, N. Iranpoor, F. Nowrouzi, and K. Amani. Tetrahedron Lett. **44**, 3951 (2003).
25. K.L. Chandra, P. Saravanan, and V.K. Singh. Synlett, 359 (2004).
26. A.K. Chakraborti, R. Thilagavathi, and R. Kumar. Synthesis, 831 (2004).
27. M. Salavati-Niasari and S. Hydarzadeh. J. Mol. Catal. A: Chem. **237**, 254 (2005).

© 2006 NRC Canada

Expanding the scope of the Newman–Kwart rearrangement — A computational assessment

Heiko Jacobsen and James P. Donahue

Abstract: The Newman–Kwart rearrangement (NKR) has been studied for a variety of thioncarbamates using density functional (B3LYP) and ab initio (MP2) methodologies. The results confirm and support the generally accepted mechanism that the NKR proceeds through a four-membered cyclic transition state. The presence of a π system connected via an oxygen linkage to a thiocarbonyl functionality is identified as a crucial structural element for the NKR. The calculations further suggest that the NKR might also be feasible for thioncarbamates derived from π system containing groups other than phenols such as ethenol, ethenediol, and butadienol. The NKR is compared with the Schönberg rearrangements of thioncarbonates.

Key words: density functional calculations, localized orbital locator, oxygen–sulfur transposition, thiols.

Résumé : Faisant appel à des méthodologies ab initio (MP2) et de densité fonctionnelle (B3LYP), on a étudié le réarrangement de Newman–Kwart (RNK) d'une variété de thioncarbamates. Les résultats confirment et sont en accord avec le mécanisme généralement accepté selon lequel le RNK se produit par le biais d'un état de transition impliquant un cycle à quatre chaînons. On a identifié que la présence d'un système π lié à une fonctionnalité thiocarbonyle par le biais d'une liaison oxygène est un élément crucial au RNK. Les calculs suggèrent de plus que le RNK pourrait aussi être possible avec des thioncarbamates dérivés de groupes contenant des systèmes π autres que les phénols, tels l'éthénol, l'éthènediol ou le butènediol. On a comparé le RNK aux réarrangements de Schönberg des thioncarbonates.

Mots clés : calculs de densité fonctionnelle, locateur d'orbitale localisée, transposition oxygène–soufre, thiols.

[Traduit par la Rédaction]

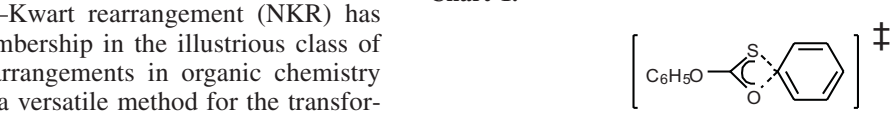
Introduction

By now, the Newman–Kwart rearrangement (NKR) has firmly established its membership in the illustrious class of the most well-known rearrangements in organic chemistry (1). The NKR represents a versatile method for the transformation of phenols to the corresponding thiophenols as outlined in Scheme 1.

Phenols **1** are first converted to thioncarbamates **2**. These compounds, when heated, rearrange to the corresponding thiolcarbamates **3**, which then can be easily changed into the desired thiophenols **4**. The key step in NKR is the O→S transposition, which relates this reaction to the Schönberg rearrangement (2) of diaryl thioncarbonates to diaryl thiolcarbonates. Tarbell and coworkers (3) have studied the Schönberg rearrangement in detail, addressing the scope as well as the kinetics (4) of this transformation. He proposed (3) that this first order reaction involves a four-membered cyclic transition state (Chart 1).

When talking about the Schönberg rearrangement, a caveat is in order. This rearrangement should not be mistaken for the Schönberg reaction (5, 6), i.e., the reaction of diarylthioketones with diazomethane at room temperature (7).

Chart 1.



Kwart and Evans (8) have expanded the Schönberg rearrangement and studied the vapour phase rearrangement not only of thioncarbonates but also of thioncarbamates. Newman and Karnes (9) have then established a synthetic protocol for the conversion of phenols to thiophenols via dialkylthioncarbamates, which has evolved into a standard procedure in organic chemistry. The NKR has not only found wide applications in synthetic protocols such as the syntheses of benzothiophenes (10), azulenethiols (11), isoflavons (12), and biaryl dithiols (13), to list but a few representative examples, but has also emerged as key procedure in the field of supramolecular chemistry (14–17). Partly because of its importance in medicinal chemistry, the NKR remains a central focus of ongoing research activities (18–20). Very recently, Moseley and et al. (21) have re-evaluated the NKR employing microwave technology. Microwave heating

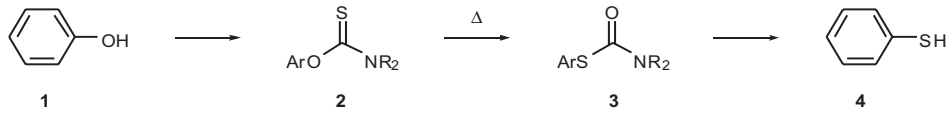
Received 12 July 2006. Accepted 5 October 2006. Published on the NRC Research Press Web site at http://.nrc.ca on 23 November 2006.

H. Jacobsen.[1,2] KemKom, Libellenweg 2, 25197 Leck, Nordfriesland, Germany.
J.P. Donahue. Department of Chemistry, Tulane University, 6400 Freret St., New Orleans, LA 70118.

[1]Corresponding author (e-mail: jacobsen@kemkom.com).
[2]Present address: Department of Chemistry, Tulane University, 6400 Freret St., New Orleans, LA 70118.

 doi:10.1139/V06-161 © 2006 NRC Canada

Scheme 1.



has proven to be ideal for investigating this high temperature rearrangement and has facilitated the confirmation of many aspects of this valuable reaction.

The NKR is well established for phenols and substituent influences on the kinetics of the reaction have been studied in detail (22–24). Electron-withdrawing groups are known to aid the rearrangement, either by reducing the reaction time or lowering the required temperature. Thus far however, no reports are to be found in the literature as to whether this methodology might be employed for other alcohols as well.

Inspired by the broad potential of the Newman–Kwart rearrangement, we have undertaken a computational study to explore whether and how the scope of the NKR might be expanded. The goals of the present study are twofold. Firstly, we seek to identify structural elements that are essential requirements for the NKR. The computational investigation therefore centers on the mechanism of the O→S transposition step. Secondly, we want to develop an electronic picture of the NKR that provides a deeper understanding of this important reaction. Not only shall we follow the traditional molecular orbital approach to chemical bonding, but we will employ arguments based on the charge density distribution ρ of a molecular system (25). In this context, the newly proposed localized orbital locator LOL (26, 27) will be of special importance in our analysis. We will briefly outline our computational approach before discussing our results in detail.

Computational methodology

Pratt and coworkers (28) have recently proposed a strategy for evaluating barrier heights for gas-phase reactions. Based on an extensive study of representative lithium enolate reactions, they found that transition-state geometry optimization with B3LYP followed by single-point MP2 calculations generally provided acceptable results in comparison with higher level ab initio methods. In this study, we adopt the approach as advocated by Pratt and coworkers. Geometries for reactants, products, and transition states have been optimized in density functional calculations employing the hybrid functional B3LYP. Final energies were determined in Møller–Plesset MP2 single-point calculations.

Regarding the choice of basis set, Truhlar and coworkers (29) have found that the addition of diffuse functions is of importance when calculating reaction energies and reaction barrier heights with density functional theory. It was shown that diffuse basis functions are vital to describe the relative energies between reactants, products, and transition states in isogyric reactions. Therefore, we employed a 6–31+G** basis for all calculations presented in the present work.

Enthalpies H at zero K were obtained as the sum of total electronic energies E_{elec} and zero-point vibrational energies ZPVE. Rate constants k were calculated according to transition-state theory, $k = (k_B \cdot T/h) \times \exp(-\Delta G^{\ddagger}/R \cdot T)$ (30). For calculations at the MP2–B3LYP level of theory, corrections for ZPVE, for H, and for entropy S were calculated from B3LYP frequencies.

The results presented in this work were obtained using the Gaussian03 program system, revision C.02 (31). B3LYP density functional calculations are based on Becke's three parameter hybrid functional (32) together with the correlation functional of Lee et al. (33). Local minima on potential energy surfaces were characterized by real frequencies only, while transition states were characterized by one imaginary frequency corresponding to a molecular displacement along the reaction coordinate.

Topological analyses of molecular electron densities have been carried out with a modified version of the program MORPHY (34). Bond orders have been evaluated using the program FUZZY (35).

Results and discussion[3]

We have studied the O→S transposition step of the NKR for nine representative molecules, **2a**–**2i** (Chart 2). The set of molecules includes phenols, substituted phenols, ethenylic alcohols, alkyl alcohols, as well as thioncarbonates. The molecules were chosen to identify the structural elements required for the NKR and to make a comparison with experimental results to judge the quality of the calculations.

Energetics of NKR

Representative geometries along the reaction coordinate of the O→S transposition of **2a** are depicted in Fig. 1. Of special interest is the geometry of the cyclic transition state and we will return to this aspect at a later point in our discussion.

Reaction enthalpies ΔH_{NKR} for the transformation **2**→**3** are reported in Table 1 and we will base our discussion on the values obtained from MP2–B3LYP calculations. The NKR is calculated to be exothermic with ΔH_{NKR} values ranging from –51 to –76 kJ/mol. The formation of the C=O double bond provides the thermodynamic driving force for this reaction. The enthalpy of activation $\Delta H^{\ddagger}_{NKR}$ for the prototypical substrate **2a** amounts to 151 kJ/mol. Introducing electron-withdrawing substituents like a nitro group into the aromatic ring, compound **2b**, substantially lowers the activation enthalpy by 14 kJ/mol. When the aromatic ring is replaced by a C=C double bond as in **2c**, the activation energy increases by 8 kJ/mol. Expanding the conjugated π system by adding another double bond, as is the case for compound

[3] Supplementary data for this article are available on the journal Web site (http://canjchem.nrc.ca) or may be purchased from the Depository of Unpublished Data, Document Delivery, CISTI, National Research Council Canada, Ottawa, ON K1A 0R6, Canada. DUD 5105. For more information on obtaining material refer to http://cisti-icist.nrc-cnrc.gc.ca/irm/unpub_e.shtml.

© 2006 NRC Canada

Chart 2.

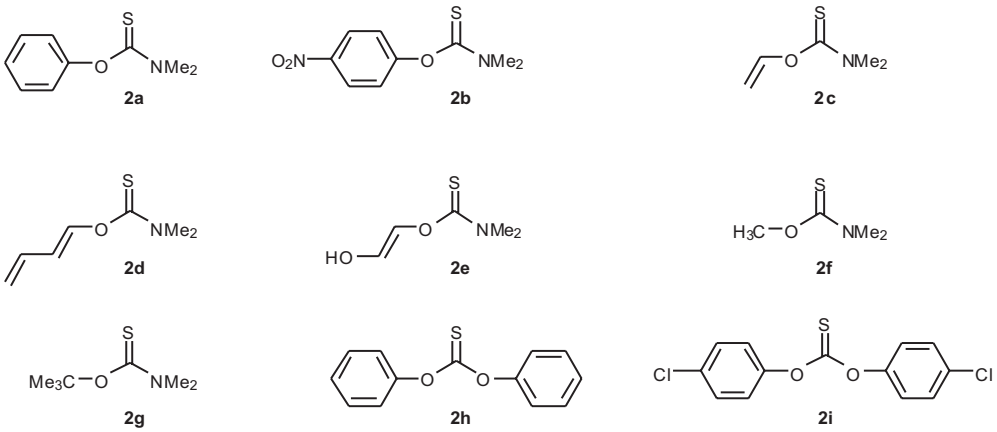
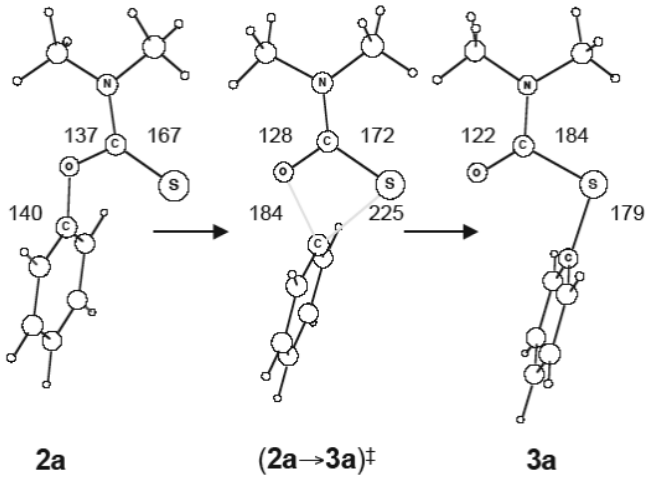


Table 1. Reaction enthalpies ΔH_{NKR} and enthalpies of activation $\Delta H^{\ddagger}_{NKR}$ (in kJ/mol) for the **2**→**3** transformation step in the NKR, obtained from density functional B3LYP and Møller–Plesset MP2 calculations.

	B3LYP–B3LYP		MP2–B3LYP	
	ΔH_{NKR} (**2**→**3**)	$\Delta H^{\ddagger}_{NKR}$ (**2**→**3**)	ΔH_{NKR} (**2**→**3**)	$\Delta H^{\ddagger}_{NKR}$ (**2**→**3**)
a	–46	156	–56	151
b	–45	136	–55	137
c	–46	160	–52	159
d	–49	159	–57	151
e	–59	175	–70	175
f	–57	190	–60	225
g	–45	158	–51	218
h	–66	168	–74	167
i	–68	170	–76	167

Fig. 1. Optimized geometries of reactant, transition state, and product for the NKR **2a**→**3a**. Selected bond distances are given in pm.



2d, is equivalent to adding an electron-withdrawing substitutent to the C=C double bond. As expected, $\Delta H^{\ddagger}_{NKR}$ decreases by 8 kJ/mol when going from **2c** to **2d**. The activation energy for compound **2d** is comparable to that of the aromatic system **2a**. Adding electron-donating substituents to the conjugated π system now has the opposite effect. Introducing a hydroxyl group to the C=C double bond in **2c** furnishes compound **2e**. This substitution causes an increase in $\Delta H^{\ddagger}_{NKR}$ by 16 kJ/mol.

The presence of a π system connected via an oxygen linkage to a thiocarbonyl functionality appears to be a crucial structural element for the Newman–Kwart rearrangement. When the aryl or ethenyl group is replaced by an alkyl group like methyl or *tert*-butyl as in **2f** and **2g**, the activation enthalpy $\Delta H^{\ddagger}_{NKR}$ increases substantially and takes on values of 225 and 218 kJ/mol, respectively.

The activation enthalpies for thioncarbonates **2h** and **2i** are higher than those for aryl or ethenyl thioncarbamates. The presence of a nitrogen atom couples the π system of adjacent the O- and S-atoms more effectively, and thus facilitates the thiocarbonyl to carbonyl transformation.

The results of B3LYP and MP2–B3LYP calculations are in qualitative agreement and also in good quantitative agreement. An exception is the activation enthalpy $\Delta H^{\ddagger}_{NKR}$ for the alkyl compounds **2f** and **2g**. The density functional approach appears to underestimate the activation barriers by 35–60 kJ/mol.

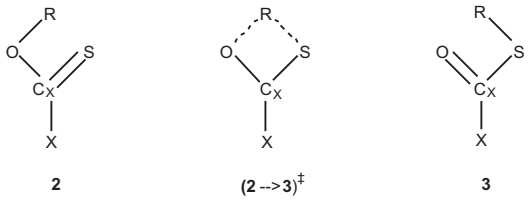
The **2a**→**3a** rearrangement has also been computationally investigated by Woodward and coworkers (36). The authors employed 6–31G* basis sets and report activation energies E_a of 162 and 160 kJ/mol obtained from B3LYP–MP2 calculations, respectively. These results are in good agreement with values of the present study.

© 2006 NRC Canada

Table 2. Selected bond distances (in pm) of reactants **2**, transition states $(\mathbf{2}\rightarrow\mathbf{3})^{\ddagger}$, and products **3** for the **2**→**3** transformation step in the NKR.

	2			$(\mathbf{2}\rightarrow\mathbf{3})^{\ddagger}$				**3**		
	O–R	O–C_X	S=C_X	O···R	O–C_X	S–C_X	S···R	O=C_X	S–C_X	S–R
a	140	137	167	184	128	172	225	122	184	179
b	139	138	167	176	129	172	215	122	185	179
c	138	137	167	182	129	172	222	122	184	177
d	138	137	167	179	129	172	218	122	184	176
e	139	136	167	183	129	172	224	122	184	177
f	144	135	168	208	127	173	258	122	182	182
g	148	135	168	246	126	175	301	123	182	188
h	140	134	164	187	126	171	231	120	180	179
i	140	135	164	186	126	170	229	120	180	179

Chart 3.



Next, we turn to the geometries of reactants **2**, products **3**, and transition states $(\mathbf{2}\rightarrow\mathbf{3})^{\ddagger}$ (Chart 3). Here, X represents a dimethyl amide (**a**–**g**) or phenoxy (**h**, **i**) functionality.

Selected bond distances are compiled in Table 2. All transition state structures display O–C_X distances between 126 and 129 pm, and have S–C_X separations between 170 and 175 pm. These bond distances reflect the change of bond character; a C–O single bond is converted into a C=O double bond whereas a C=S double bond transforms into a C–S single bond. The O–C_X and S–C_X distances formally indicate bonds of order 1.5 and characterize the transition state as a resonance structure. The distances O···R and S···R are indicative of a concerted process of bond cleavage and bond formation. Comparing related aryl and ethenyl thioncarbamates, it appears that transition states with lower activation barriers have shorter O···C and S···C distances.

Alkyl compounds **2f** and **2g** undergo the O→S transpositions via transition states with extremely long O–C and S–C separations. The processes of bond cleavage and bond formation do not proceed in a synchronous fashion but constitute a sequential reaction. Since the process of bond cleavage is not supported by additional bond forming interaction, the transition states for compounds **2f** and **2g** are at high energies.

To assess the feasibility of a Newman–Kwart rearrangement for the compounds investigated in this work, we have calculated rate constants k for **2**→**3** transformations at various temperatures. The synthetic protocol developed by Newman and Karnes (9) prescribes temperatures in the range of 170–270 °C, a temperature range that we have adopted in our calculations as well. The values for k at different temperatures are collected in Table 3.

For the nitro compound **2b**, Newman and Karnes (9) report a reaction temperature of 180 °C. From inspection of the data presented in Table 3, we estimate that the rate constant k should have a value of 1.0×10^{-5} s^{-1} or greater for a Newman–Kwart rearrangement to be of synthetic value. The data in Table 3 suggest that thioncarbamates **2c**, **2d**, **2e** derived from ethenol, butadienol, and ethenediol should undergo O→S transpositions at temperatures above 250, 175, and 275 °C, respectively. The data further suggest that alkyl compounds such as **2f** and **2g** cannot be subjected to the NKR.

Although the activation enthalpies for compounds **2h** and **2i** are almost identical, entropic contributions cause slight differences in reaction rates. The chloro compound **2i** displays somewhat smaller k values compared with the unsubstituted compound **2h**. Powers and Tarbell (4) have investigated the gas-phase kinetics of the rearrangement of bis-(4-chlorophenyl)thioncarbonate **2i**. They report values for the rate constant k of 6.2×10^{-5} s^{-1} and 2.08×10^{-4} s^{-1} at 251.4 and 269.3 °C, respectively. The results of our calculations are in good agreement with the experimental data.

Solution kinetics of the NKR have also been investigated. Relles and Pizzolato (22) measured rate constants k (in s^{-1}) for the rearrangement **2a**→**3a** in diphenyl ether solutions (0.3 mol/L) of $8.0 \pm 0.25 \times 10^{-5}$ and $5.70 \pm 0.20 \times 10^{-4}$ at temperatures of 232.3 and 258.2 °C, respectively. For the same reaction in diphenyl ether, Miyazaki and coworkers (24) report a k value of 5.92×10^{-6} at a temperature of 200.5 ± 0.1 °C.

Arrhenius plots of $\ln k$ vs. $1/T$ for measured and calculated rate constants are depicted in Fig. 2. Inspection of Fig. 2 suggests that the main difference between gas-phase and solution kinetics is caused by different pre-exponential factors, which in turn are related to the entropy of activation $\Delta S^{\ddagger}_{NKR}$. An enhanced entropic barrier causes the NKR to proceed somewhat slower in solution than in the gas phase.

Electronic structure of NKR transition states

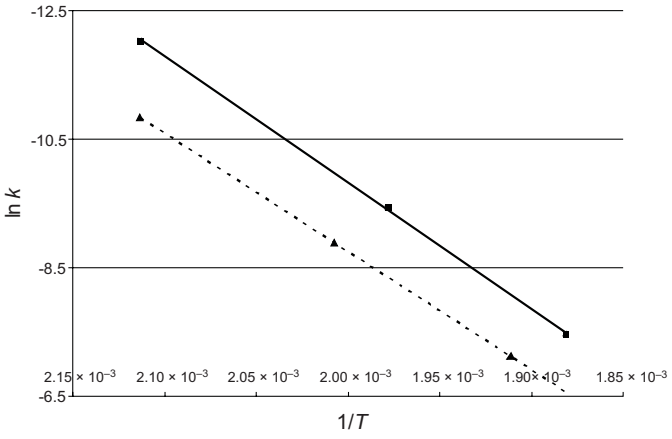
The nature of the chemical bond constitutes one of the central subjects of chemistry and provides valuable insight and information not only for a chemical molecule but also for the cause of chemical reactions. Since the early days of quantum chemistry this problem has been tackled mainly on the grounds of orbital models, which have evolved into a standard tool in chemistry. We therefore begin with an analysis of the electronic structure of NKR transition states in terms of their relevant frontier orbitals. We will restrict our analysis to compounds **2a**, the prototypical Newman–Kwart reagent, **2c**, in which the migrating phenol group has been

© 2006 NRC Canada

Table 3. Calculated rate constants k (in s^{-1}) for the Newman–Kwart rearrangement at selected temperatures (in °C).

T	**2a→3a**	**2b→3b**	**2c→3c**	**2d→3d**	**2e→3e**	**2f→3f**	**2g→3g**	**2h→3h**	**2i→3i**
175	2.22×10^{-6}	8.99×10^{-6}	1.16×10^{-8}	4.01×10^{-6}	3.64×10^{-9}	3.94×10^{-14}	6.51×10^{-13}	1.13×10^{-7}	6.51×10^{-8}
200	1.95×10^{-5}	6.45×10^{-5}	1.26×10^{-7}	3.56×10^{-5}	4.46×10^{-8}	1.01×10^{-12}	1.52×10^{-11}	1.26×10^{-6}	7.30×10^{-7}
225	1.38×10^{-4}	3.80×10^{-4}	1.08×10^{-6}	2.54×10^{-4}	4.25×10^{-7}	1.86×10^{-11}	2.60×10^{-10}	1.11×10^{-5}	6.43×10^{-6}
250	8.11×10^{-4}	1.89×10^{-3}	7.58×10^{-6}	1.51×10^{-3}	3.28×10^{-6}	2.62×10^{-10}	3.38×10^{-9}	7.93×10^{-5}	4.60×10^{-5}
275	4.07×10^{-3}	8.16×10^{-3}	4.45×10^{-5}	7.60×10^{-3}	2.10×10^{-5}	2.90×10^{-9}	3.49×10^{-8}	4.75×10^{-4}	2.76×10^{-4}

Fig. 2. Arrhenius plots $\ln k$ vs. $1/T$ (in K^{-1}) of rate constants from experiment (solid line, ■) and computation (broken line, ▲).



replaced by ethenyl, and **2f**, having a methyl group. A frontier Kohn–Sham (KS) orbital diagram for the corresponding transition states is displayed in Fig. 3.

The lowest unoccupied and the highest occupied orbitals kso1 and kso2 are similar for the three transition states (**2a→3a**)‡, (**2c→3c**)‡, and (**2f→3f**)‡. For kso1, lone-pair p orbitals at oxygen and sulfur interact in antibonding fashion with a p orbital of the migrating group, which is oriented towards the two chalcogen atoms. For kso2, we again see major contributions for chalcogen lone-pair p orbitals; in cases where the migrating ligand binds to the chalcogen atom through an sp_2-carbon atom that contributes to an extended π system, the chalcogen lone-pair orbitals undergo antibonding interaction with the migrating group. This then is the reason that the highest occupied molecular orbitals for the transition states (**2a→3a**)‡ and (**2c→3c**)‡ are higher in energy than for (**2f→3f**)‡. Of special interest is orbital kso3, which contains significant bonding interaction of sulfur lone-pair orbitals with p_π orbitals of the migrating group. For the transition state (**2f→3f**)‡, a kso3-type orbital surface at 0.075 au is not to be found among the frontier orbitals. Instead, we see bonding contributions between a p orbital at oxygen and an sp_3-type orbital of the migrating group, orbital kso4. Similar orbitals are present for (**2a→3a**)‡ and (**2c→3c**)‡. This orbital analysis is in accord with our previous observation that the presence of a π system connected via an oxygen linkage to a thiocarbonyl functionality appears to be a crucial structural element for the NKR.

The conclusions emerging from our orbital analysis are not new. Miyazaki and coworkers (24) already pointed out that a four-membered cyclic transition state is formed by nucleophilic attack of lone-pair electrons of the thiocarbonyl sulfur atom on the migrating ring. However, the question arises as to how well these simple molecular orbital arguments correlate with the nature of the chemical bonds of the transition states in question. Do we indeed have a four-membered cyclic transition state and if so, is this transition state topology also present in systems that have migrating groups without π systems at the chalcogen-bonded atom?

Orbitals are not unique and it is desirable to have orbital-independent descriptions of chemical bonding. One such picture is supplied by the electronic charge density ρ(r) of a chemical system. Bader (25) has revolutionized the field of interpretation of ρ(r) in terms of physical and chemical principles and his theory of "atoms in molecules" (AIM) not only allows for a description of the topology of a chemical system but also for an assessment of the quality of chemical bonds. In a topological analysis of the electronic charge density ρ(r), gradient paths of the gradient vector field ∇ρ(r), which originate at a bond critical point and terminate at the nuclei, might be used to define a chemical bond and to establish a molecular graph (37). Such graphs in the O–C_X–S plane of transition states (**2a→3a**)‡, (**2c→3c**)‡, and (**2f→3f**)‡ are displayed in Fig. 4. We reiterate the fact that the chemical bonds, which define the molecular graph, are derived from the electron density of the calculated molecules and are not based on structural criteria of optimized molecular geometries. The AIM approach provides a clear and unambiguous definition of a chemical bond and is applicable whenever the electron density ρ(r) is known, be it from theory or experiment.

From Fig. 4, it is evident that the three representative transition states all possess a four-membered cyclic ring, which includes the two chalcogen atoms as well as the migrating functional group R. Even for the transition state (**2f→3f**)‡, with long R–O and R–S separations of 208 and 238 pm, we find bond paths connecting the migrating R group with both O and S atoms. The presence of a four-membered ring system is further corroborated by the occurrence of a ring critical point.

When assessing the quality of a chemical bond, Bader advocates the use of the topology of the Laplacian of the electron density $\nabla^2\rho$. The function L, which is the negative of the Laplacian, can be used to map out regions where electronic charge is locally concentrated, $L > 0$, or depleted, $L < 0$ (38). This analysis leads naturally to the identification of covalent bonds and electron lone pairs. Becke and Edgecombe (39) have introduced a different approach to the identification of localized electronic groups in atomic and molecular systems. This function is based on the kinetic energy density τ and is commonly known as electron localization function ELF. Very recently, Schmider and Becke (26) have formulated a localized orbital locator LOL (26,27). LOL is similar in definition and structure to the electron localization function

© 2006 NRC Canada

Fig. 3. KS frontier orbital diagram for transition states (**2a→3a**)‡ (left), (**2c→3c**)‡ (middle), and (**2f→3f**)‡ (right). For orbital energy levels represented by solid lines, a corresponding orbital surface plot at 0.075 au is shown. The occupation of the highest occupied orbitals is designated by a double arrow. The molecular orientation is that of Chart 3.

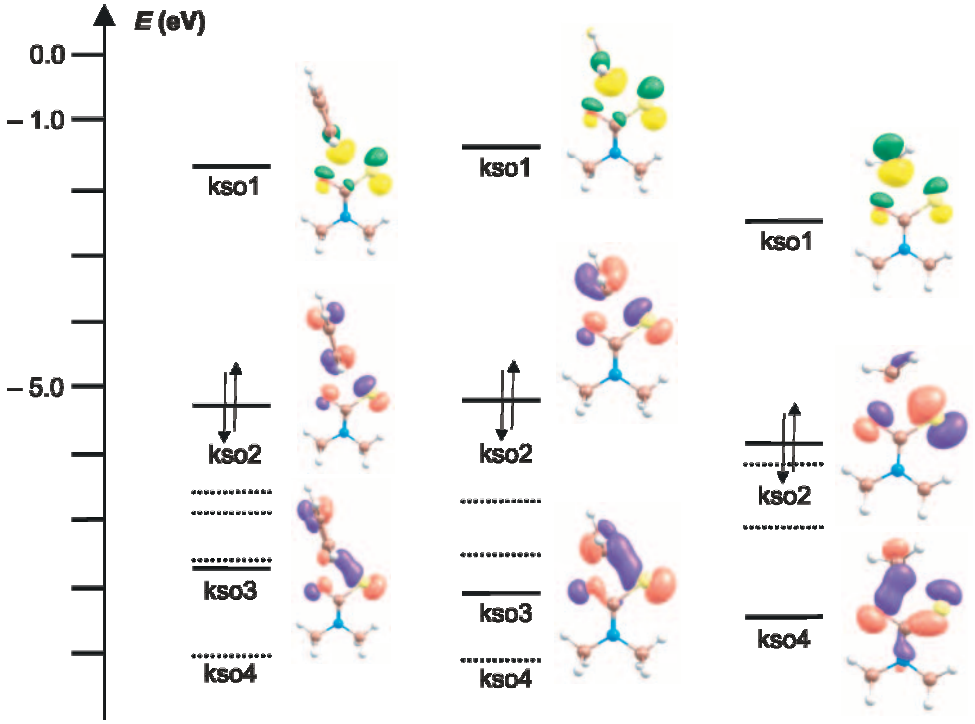
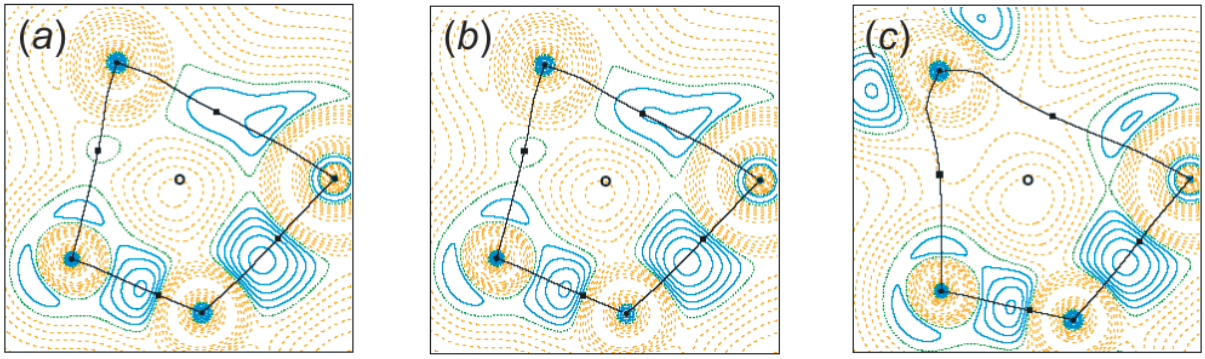


Fig. 4. Molecular graphs and LOL contour maps in the O–CX–-S plane for *a*) (**2a→3a**)‡, *b*) (**2c→3c**)‡, and *c*) (**2f→3f**)‡. Also shown are bond critical points (■) and ring critical points (○). The molecular orientation is that of Chart 3. ν contours are equally spaced by 0.05 units. Contours with ν = 1/2 are plotted as dotted lines (green), with ν > 1/2 as solid lines (blue), and with ν < 1/2 as dashed lines (yellow).



ELF, but is a simpler function and generates simplified pictures that are easier to interpret.

The localized orbital locator ν is a measure of the relative value of the local kinetic energy τ in a mapping onto the finite range [0,1]. A value of $\nu = 1/2$ indicates that the kinetic energy content of the corresponding region is what would be expected from a spin-neutral electron gas of that density and values of ν > 1/2 indicate regions where electrons are localized. Such regions do not only occur in bonds but also at places in the molecule that are usually associated with lone pairs. Only covalent bonds show up as a closed region of large ν values between the bound atoms. Closed-shell interactions do not show that feature.

LOL contour plots are also shown in Fig. 4. For the transition states (**2a→3a**)‡ and (**2c→3c**)‡, we find a region of significant electron localization along the S–R bonds and only marginal electron localization along the O–R bonds. For the transition state (**2f→3f**)‡, on the other hand, no regions of electron localization are to be found along S–R or O–R bonds. This picture supports our previous notion of the course of the NKR. For systems that have migrating groups without π systems at the chalcogen-bonded atom, the steps of O–R bond cleavage and S–R bond formation occur in a sequential matter; in the transition states, the bonds between chalcogen atoms and the migrating group are essentially broken. On the other hand, for systems that have migrating groups with π systems at the chalcogen-bonded atom, the steps of O–R bond cleavage and S–R bond formation occur

© 2006 NRC Canada

Table 4. FBO values of selected atoms of reactants **2**, transition states $(\mathbf{2}\rightarrow\mathbf{3})^{\ddagger}$, and products **3**.

	2				$(\mathbf{2}\rightarrow\mathbf{3})^{\ddagger}$				**3**			
	O–R	O–C_X	S=C_X	S/R	O⋯R	O–C_X	S–C_X	S⋯R	O/R	O=C_X	S–C_X	S–R
a	1.20	1.32	1.65	0.10	0.61	1.64	1.36	0.66	0.05	2.04	1.10	1.16
b	1.27	1.29	1.65	0.10	0.68	1.60	1.35	0.74	0.05	2.04	1.09	1.18
c	1.27	1.32	1.64	0.10	0.65	1.65	1.37	0.72	0.04	2.03	1.11	1.24
d	1.28	1.32	1.64	0.10	0.68	1.63	1.36	0.76	0.04	2.03	1.11	1.25
e	1.25	1.34	1.64	0.11	0.65	1.65	1.36	0.72	0.06	2.04	1.10	1.24
f	1.19	1.39	1.63	0.12	0.47	1.73	1.39	0.57	0.06	2.02	1.15	1.20
g	1.06	1.40	1.60	0.04	0.21	1.81	1.37	0.30	0.02	2.01	1.04	1.15
h	1.19	1.38	1.73	0.20	0.58	1.74	1.42	0.62	0.04	2.13	1.17	1.16
i	1.20	1.38	1.75	0.09	0.59	1.73	1.42	0.63	0.04	2.13	1.17	1.15

Note: The molecular orientation is that of Chart 3.

in a concerted manner, which then leads to a decrease in activation energy.

We recall that the LOL maps out the covalent character of a chemical bond. However, there exist other bonding interactions such as electrostatic attraction. Molecular properties then are often analyzed in terms of charge or electron distribution and in the context of density functional theory one might say that the charge distribution determines all molecular properties (30). The most popular indicators of electron distribution in a molecule are electron population and bond order. Various definitions for bond orders have been suggested and are used in bonding analysis, all of which have their particular advantages and drawbacks. Recently, Mayer and Salvador (40) have proposed bond order indices in terms of fuzzy atoms. The fuzzy bond order (FBO) scheme is based on divisions of the three-dimensional physical space into atomic regions in which the regions assigned to the individual atoms have no sharp boundaries but exhibit a continuous transition from one to another. In a comparative study, Solà and coworkers (41) have analyzed the behaviour of various bond order schemes. They found that, especially for polar bonds, the bond orders obtained with the FBO approach are in good agreement with the formally predicted bond orders. We thus decided to evaluate bond orders using the fuzzy atom approach and the results of an FBO analysis are collected in Table 4. The bond orders presented here are derived from B3LYP calculations.

When we compare the transition state bond orders of molecules with (**2a**, **2b**, **2c**, **2d**, **2e**) and without (**2f**, **2g**) supporting π systems, we see that the latter group shows lower O⋯R and higher O–C_X bond orders. It appears that for the latter group the transition state represents a structure in which the O–R bond cleavage has proceeded to a more complete degree. At the same time, we see that molecules without supporting π system have smaller values for the S⋯R bond order. This observation is in agreement with our conclusions obtained from the LOL analysis: In the absence of a supporting π system, the processes of bond formation and bond cleavage occur in a sequential fashion.

Comparing thioncarbamates and thioncarbonates, we find for the latter somewhat larger FBO values for the O–C_X and S=C_X bonds. Making the simplified assumption that a larger FBO value corresponds to a larger bond strength, the introduction of a carbamate group then reduces the O–C_X and S=C_X bonds. Since these bonds need to be fully or partially broken during the course of the NKR, it follows that introduction of a carbamate group lowers the activation barrier for the NKR.

Conclusion

Our computational studies confirm and support the mechanism of the NKR that was developed in the early kinetic investigations, i.e., the NKR proceeds through a four-membered cyclic transition state. The presence of a π system connected via an oxygen linkage to a thiocarbonyl functionality is identified as crucial structural element for the NKR. This allows the processes of bond cleavage and bond formation to proceed in a synchronous fashion, which in turn lowers the activation energy associated with this reaction. Our calculations further suggest that the NKR might also be feasible for thioncarbamates derived from π system-containing groups other than phenols, such as ethenol, ethenediol, and butadienol. Experimental work is currently under way in our laboratories addressing the question whether the NKR can indeed be expanded according to the predictions that emerged from the present computational assessment.

Acknowledgments

KemKom thanks Professor L. Cavallo for providing access to the MoLNaC Computing Facilities at Dipartimento di Chimica, Università di Salerno.

References

1. S. Moulay. Chem. Educ. Res. Pract. **3**, 33 (2002).
2. A. Schönberg and L. Vargha. Ber. Dtsch. Chem. Ges. **63**, 178 (1930).
3. H.R. Al-Kazimi, D.S. Tarbell, and D. Plant. J. Am. Chem. Soc. **77**, 2479 (1955).
4. D.H. Powers and D.S. Tarbell. J. Am. Chem. Soc. **78**, 70 (1956).
5. A. Schönberg and L. Vargha. Liebigs Ann. Chem. **483**, 176 (1930).
6. A. Schönberg and L. Vargha. Ber. Dtsch. Chem. Ges. **64**, 1390 (1931).
7. R. Huisgen, I. Kalvinsch, X.Y. Li, and G. Mloston. Eur. J. Org. Chem. 1685 (2000).

© 2006 NRC Canada

8. H. Kwart and R. Evans. J. Org. Chem. **31**, 410 (1966.)
9. M.S. Newman and H.A. Karnes. J. Org. Chem. **31**, 3980 (1966).
10. C.K. Lau, P.C. Bélanger, C. Dufresne, and J. Scheigetz. J. Org. Chem. **52**, 1670 (1987).
11. T. Asao, S. Ito, and N. Morita. Tetrahedron Lett. **30**, 6345–6348 (1989).
12. A. Levai and O. Sebock. Synth. Commun. **22**, 1735 (1992).
13. S. Cossu, O. DeLucchi, D. Fabbri, G. Valle, G.F. Painter, and R.A. J. Smith. Tetrahedron, **53**, 6073 (1997).
14. D.J. Cram, R.C. Helgeson, K.Koga, E.P. Kyba, K. Madan, L.R. Sousa, M.G. Siegel, P. Moreau, G.W. Gokel, J.M. Timko, and G.D.Y. Sogah. J. Org. Chem. **43**, 2758 (1978).
15. Y. Ting, W. Verboom, L.C. Groenen, J.-D. van Loon, and D.N. Reinhoudt. J. Chem. Soc. Chem. Commun. 1432 (1990).
16. P. Rao, M.W. Hosseini, A. De Cian, and J. Fischer. Chem. Commun. (Cambridge), 2169 (1999).
17. V.V. Kane, A. Gerdes, W.Grahn, L. Ernst, I. Dix, P.G. Jones, and H. Hopf. Tetrahedron Lett. **42**, 373 (2001)
18. B.M. Davis and M.M. Joullie. Compounds for the treatment of Alzheimer's disease. U.S. Patent 6-569-848. 27 May 2003.
19. F.E. Boyer, Jr., J.M. Domagala, E.L. Ellsworth, C.A. Gajda, S.E. Hagen, M.J. Lovdahl, E.A. Lunney, L.J. Markoski, J.V.N.V. Prasad, and B.D. Tait. HIV protease inhibitors. U.S. Patent 6-852-711. 8 Feb 2005.
20. B.J. Auerbach, L.D. Bratton, G.F. Filzen, A.G. Geyer, B.K. Trivedi, and P.C. Unangst. Compounds that modulate PPAR activity and methods for their preparation. U.S. Patent 6-875-780. 5 April 2005.
21. J.D. Moseley, R.F. Sankey, O.N. Tang, and J.P. Gilday. Tetrahedron, **62**, 4685 (2006).
22. H.M. Relles and G. Pizzolato. J. Org. Chem. **33**, 2249 (1968).
23. K.Miyazaki. Tetrahedron Lett. **23**, 2793 (1968).
24. A. Kaji, Y. Araki, and K. Miyazaki. Bull. Chem. Soc. Jpn. **44**, 1393 (1971).
25. R.W.F. Bader. Atoms in molecules. A quantum theory. Clarendon Press, Oxford, UK. 1990.
26. H.L. Schmider and A.D. Becke. THEOCHEM. **527**, 51 (2000)
27. H.L. Schmider and A.D. Becke. J. Chem. Phys. **116**, 3184 (2002).
28. L.M. Pratt, N. Văn Nguỹên, and B. Ramachandran. J. Org. Chem. **70**, 4279 (2005).
29. B.J. Lynch, Y. Zhao, and D.G. Truhlar. J. Phys. Chem. A, **107**, 1384 (2003).
30. C.J. Cramer. Essentials of computational chemistry. John Wiley and Sons, New York, NY. 2002.
31. M.J. Frisch, G.W. Trucks, H.B. Schlegel, G.E. Scuseria, M.A. Robb, J.R. Cheeseman, J.A. Montgomery, Jr., T. Vreven, K.N. Kudin, J.C. Burant, J.M. Millam, S.S. Iyengar, J. Tomasi, V. Barone, B. Mennucci, M. Cossi, G. Scalmani, N. Rega, G.A. Petersson, H. Nakatsuji, M. Hada, M. Ehara, K. Toyota, R. Fukuda, J. Hasegawa, M. Ishida, T. Nakajima, Y. Honda, O. Kitao, H. Nakai, M. Klene, X. Li, J.E. Knox, H.P. Hratchian, J.B. Cross, V. Bakken, C. Adamo, J. Jaramillo, R. Gomperts, R.E. Stratmann, O. Yazyev, A.J. Austin, R. Cammi, C. Pomelli, J.W. Ochterski, P.Y. Ayala, K. Morokuma, G.A. Voth, P. Salvador, J.J. Dannenberg, V.G. Zakrzewski, S. Dapprich, A.D. Daniels, M.C. Strain, O. Farkas, D.K. Malick, A.D. Rabuck, K. Raghavachari, J.B. Foresman, J.V. Ortiz, Q. Cui, A.G. Baboul, S. Clifford, J. Cioslowski, B.B. Stefanov, G. Liu, A. Liashenko, P. Piskorz, I. Komaromi, R.L. Martin, D.J. Fox, T. Keith, M.A. Al-Laham, C.Y. Peng, A. Nanayakkara, M. Challacombe, P.M.W. Gill, B. Johnson, W. Chen, M.W. Wong, C. Gonzalez, and J.A. Pople. Gaussian 03 [computer program]. Rev. C.02. Gaussian Inc., Wallingford, CT. 2004.
32. A.D. Becke. J. Chem. Phys. **98**, 5648 (1993).
33. C. Lee, W. Yang, and R.G. Parr. Phys. Rev. B, **37**, 785 (1988).
34. P.L.A. Popelier. Comput. Phys. Commun. **93**, 212 (1996).
35. I. Mayer and P. Salvador. FUZZY [computer program]. Version 1.0. Girona. 2003.
36. V. Albrow, K. Biswas, A. Crane, N. Chaplin, T. Easun, S. Gladiali, B. Lygo, and S. Woodward. Tetrahedron: Asymmetry, **14**, 2813 (2003).
37. R.F.W. Bader. J. Phys. Chem. A, **102**, 7314 (1998).
38. R.J. Gillespie and P.L.A. Popelier. Chemical bonding and molecular geometry. Oxford University Press, Oxford, UK. 2001.
39. A.D. Becke and K.E. Edgecombe. J. Chem. Phys. **92**, 5397 (1990).
40. I. Mayer and P. Salvador. Chem. Phys. Lett. **383**, 368 (2004).
41. E. Matito, J. Poater, M. Solà, M. Duran, and P. Salvador. J. Phys. Chem. A, **109**, 9904 (2005).

© 2006 NRC Canada

Metal(II) Schiff base complexes as catalysts for the high-regioselective conversion of epoxides to β-hydroxy nitriles in glycol solvents

Hossein Naeimi and Mohsen Moradian

Abstract: A facile preparation of 3-hydroxy propanenitrile derivatives is described involving ring opening of epoxides with potassium cyanide in glycol solvents in the presence of Schiff base complexes as catalysts. This method occurs under neutral and mild conditions with high yields and high regioselectivity. Thus, several β-Hydroxy nitriles, useful intermediates toward biologically-active molecules, are easily obtained at room temperature.

Key words: β-hydroxy nitrile, Schiff base, epoxide, glycol, catalyst.

Résumé : On décrit une préparation facile de dérivés du 3-hydroxypropanenitrile qui implique l'ouverture d'époxydes à l'aide de cyanure de potassium dans des solvants à base de glycol, en présence de complexes de bases de Schiff comme catalyseurs. Cette méthode implique des conditions neutres et douces et conduit à des rendements et une régiosélectivité élevés. Opérant à température ambiante, on an a ainsi préparé plusieurs β-hydroxynitriles utiles comme intermédiaires dans la synthèse de molécules biologiquement actives.

Mots clés : β-hydroxynitrile, base de Schiff, époxyde, glycol, catalyseur.

[Traduit par la Rédaction]

Introduction

β-hydroxy nitriles are important reagents as well as technical products in organic chemistry. They have been extensively investigated and employed for the preparation of intermediates of many naturally occurring bioactive compounds (1–4).

β-Hydroxy nitriles can be prepared by the reaction of epoxides with the toxic volatile HCN (5), NaCN (6, 7), KCN (8), LiCN (9), cyanide exchange resin (10*b*), and TBAF–TMSCN in CH_3CN (11–13). The reaction of epoxides with NaCN, KCN, or HCN usually requires extended times (6, 7*b*, 7*c*, 8*c*), protic solvents (5–7, 8*a*, 8*b*), or additives (7*a*, 8*c*), e.g., Zr-catalyzed one-pot synthesis of β-cyanohydrins from olefins via epoxidation of the olefins and nucleophilic ring opening of the epoxides (10*a*). Some of these reactions afford mixtures of regioisomers (8*c*, 10*b*, 11) or stereoisomers (5). By using trimethylsilylcyanide (TMSCN) in the preparation of β-hydroxy nitriles, the iso-nitrile has been formed (12, 13*d*) as the main product.

In the literature, ring opening of epoxides with cyanide ion as a nucleophile has been carried out by employing nonvolatile alkali cyanides in the presence of perchlorate salts (14) or $Yb(CN)_3$ (12, 14). Some methods employ acetone cyanohydrin in the presence of various bases (15) or lanthanide alkoxides (16), alkyl aluminum cyanides (17), and $Ce(OTf)_4$ (18). In most methods referred to in the literature, the reaction conditions are usually severe; some reagents are commercially unavailable and have to be prepared from alkali cyanides. In addition, the use of alkyl aluminum cyanides presents difficulty in large scale reactions.

To overcome these limitations, we developed a new approach of oxirane ring opening with potassium cyanide in glycol solvents using Schiff base complexes as catalysts at room temperature to afford β-hydroxy nitriles.

Received 6 September 2006. Accepted 2 October 2006. Published on the NRC Research Press Web site at http://canjchem.nrc.ca on 29 November 2006.

H. Naeimi[1] and M. Moradian. Chemistry Department, Faculty of Sciences, Kashan University, Kashan 87317, Islamic Republic of Iran.
[1]Corresponding author (e-mail: naeimi@kashanu.ac.ir).

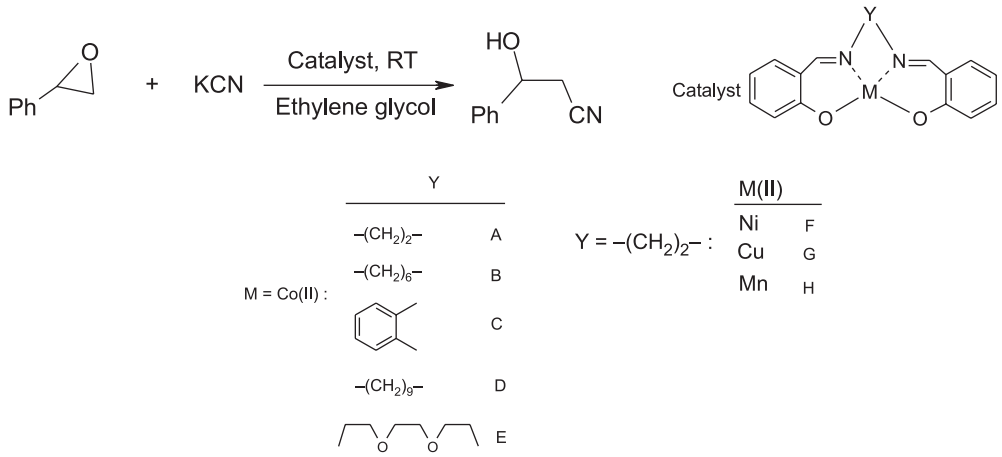
Results and discussion

Metal(II)-salen complexes are promising catalysts for various reactions. These complexes have shown wide applicability and are now used as catalysts for a variety of enantioselective reactions, such as oxidation (19), aziridination (20), cyclopropanation (21), the Diels–Alder reaction (22), and the conversion of 1,2-epoxyethanes to 2-haloethanols with molecular halogen (23).

In this study, the reaction of styrene oxide with potassium cyanide in the presence of some Schiff base complexes of metal(II) was carried out. The preparation and characterization of these complexes were according to the procedure reported in the literature (23–25). On this basis, the syntheses of these metal complexes were essentially the same and involved heating and stirring of stoichiometric amounts of the appropriate tetradentate ligand and metal acetate in a suitable solvent, such as methanol, ethanol, or water–methanol mixtures. The desired complexes crystallized upon cooling and were recrystallized from chloroform. The complexes are easy to prepare and cheap. All of the used metal chelates in this study are insoluble in water but soluble in most organic

 doi:10.1139/V06-158 © 2006 NRC Canada

Scheme 1.



solvents. They are stable in water, even at high pH and temperature.

The IR spectrum of the Schiff base exhibits a band at 1625 cm^{-1} assigned to υ(C=N) of azomethine (26). This band shifts to a lower wavenumber by about 10–15 cm^{-1} on the chelation of the ligand with a metal ion. In the ^1H NMR spectra of the Schiff bases (26), the broad signals around 12.5–13.1 ppm are assigned to the protons of the hydroxyl groups in the free ligands. Protons of CH=N have the same chemical shifts (8.5–8.9 ppm). The signal around 6.0–6.65 ppm is assigned to the protons of the NCHN, and signals around 6.6–7.90 ppm are assigned to the protons of aromatic rings (CH=CH). In the ^1H NMR spectra of the Schiff base complexes, all of these signals exhibit a 0.6 ppm shift to a lower field and the broad signal around 12.5–13.1 ppm disappeared. In the IR spectrum, the appearance of two or three bands in the low frequency region (between 420 and 540 cm^{-1}) indicates the coordination of phenolic oxygen in addition to azomethine nitrogen (24).

To examine the effects of the ligands on the catalyst, a variety of ligands were employed in the reaction (Scheme 1).

After a solution of styrene oxide and a catalyst (molar ratio is 10:1) in ethylene glycol was stirred at room temperature, 1.2 mol of potassium cyanide was added to the flask. In this reaction, 3-hydroxy-3-phenyl propanenitrile was obtained as a product and its yield was determined by GC and TLC analysis. The results of the reactions of styrene oxide with potassium cyanide in the presence of the previously mentioned catalysts are given in Table 1.

As shown in Table 1, in these reactions, β-hydroxy nitriles were prepared as products in good to excellent yields with high regioselectivity. In each case, cleavage of the epoxide ring occurs. After completion of the reaction, by addition of water and work-up with CH_2Cl_2, propanenitriles are obtained.

In comparison, the cleavage behaviour of styrene oxide with potassium cyanide in the absence of the catalyst is given in Table 1 (entry 9). This reaction in ethylene glycol in the absence of the catalyst has afforded the product with very low yield and low regioselectivity even with an extended reaction time to overnight. As seen in Table 1, the yields of the reactions with this new method are quite fair, and the reaction time is short. It is of great importance that the reaction is largely affected by the various ligands of the complexes. The complex catalysts **A** and **B** are the most effective ones in these reactions (Table 1, entries 1 and 2), while the complex catalysts **C**, **D**, and **E** have shown lower catalytic performance. This can be related to the low ability of their ligands to coordinate the metal(II) ions.

Table 1. The reaction of styrene oxide with KCN in the presence of various complex catalysts in ethylene glycol.

Entry	Catalyst	Time (h)	Yield (%)[a]
1	A	2.4	98[b]
2	B	2.6	95
3	C	3.0	90
4	D	3.2	88
5	E	3.2	85
6	F	3.8	68
7	G	4.3	63
8	H	4.5	55
9	–	Overnight	20

Note: The reactions were carried out at room temperature.
[a]GC yield based on epoxide.
[b]The only formed *trans*-isomer.

Because H_2-salen is the most effective ligand for the reaction, we studied the catalytic effect of the first-row transition metal(II) with the ligand of *N*,*N*′-ethylenedisalicylideneamine (H_2-salen) on the formation of 3-hydroxy-3-phenyl propanenitrile (Table 1, entries 1, 6, 7, and 8). On the other hand, because the first-row transition metal(II) complexes of simple Schiff base are known to be sparingly soluble in common organic solvents, the different of the used complexes may be attributed to their own solubility or their adducts with epoxide in the reaction solution.

From the previous studies, the Co(II)-salen **A** was the best catalyst used in this reaction (see Table 1). To study the solvent effect on the reaction, nucleophilic cleavage of styrene oxide with potassium cyanide by catalyst **A** has been carried out in various glycol solvents. The results shown in Table 2 indicated that ethylene glycol is the most convenient solvent in this reaction. It was found that these reactions appeared to be largely dependent on the nature of the solvent.

The results of the reactions of some representative

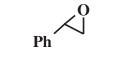
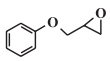
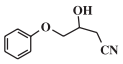
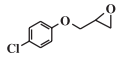
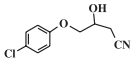
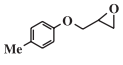
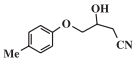
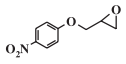
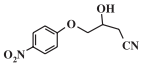
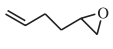
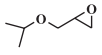
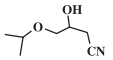
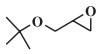
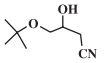
© 2006 NRC Canada

Table 2. Ring cleavage of styrene oxide by KCN in the presence of 0.1 mol of catalyst **A** in various solvents at room temperature.

Entry	Solvent	Time (h)	Yield (%)[a]
1	Ethylene glycol	2.4	98
2	Glycerol anhydrous	2.5	90
3	Triethylene glycol anhydrous	3	75
4	Triethylene glycol dimethyl ether	4	75
5	Tetraethylene glycol	4	65

[a]GC yields.

Table 3. Reaction of various epoxides with cyanide in the presence of 0.1 mol of catalyst **A** in ethylene glycol at room temperature.

Entry	Substrate	Product	Time (h)	Yield (%)[a]
1			2.4	92
2			2.7	90
3			2.8	93
4			2.6	88
5			3.0	93
6			2.2	84
7			2.2	83
8			2.3	80
9			2.5	85
10			2.2	82

[a]Isolated yields based on epoxide.

epoxides in the presence of complex **A** as the catalyst are summarized in Table 3. In these reactions, the optimum amount of the catalyst used for all of the epoxides was 0.1 mol for 1 mol of epoxide. As can be seen, at the same amount of the catalyst, the ring opening of various epoxides have been carried out with 80%–93% yields, and the reaction time was 2.2–3.0 h.

As shown in Table 3 (entry 6, in which only the trans isomer is obtained), the reactions are completely anti-stereoselective. As for the regioselectivity, an attack of the nucleophile preferentially occurs at the less-substituted oxirane carbon. An anti-Markovnikov type regioselectivity is generally observed in these reactions. In many cases, this type of regioselectivity appears to be the opposite of that observed in ring opening of the same epoxides with aqueous hydrogen cyanide under classic acidic conditions. The previously mentioned regiochemical mode can be viewed as occurring via a nucleophilic attack by a cyanide ion on the less sterically hindered oxirane carbon. This mechanism closely resembles the S_N2 model for aliphatic nucleophilic displacement.

The structure of β-hydroxy nitrile products has been assigned by spectroscopic data. In the IR spectra, the C–N stretching vibrations of the nitrile groups appear in the region between 2250 and 2274 cm^{-1}. The hydroxyl group O–H bond stretching frequency is found in the region between 3400 and 3477 cm^{-1} as a strong broad band. The C–H stretching vibrations of the alkyl groups appear in the region between 2877 and 2960 cm^{-1}. In the ^1H NMR spectra, OH protons have chemical shifts between 4.20–4.55 ppm as a singlet broad peak. The signals around 6.5–8.4 ppm are assigned to the protons of CH=CH of the aromatic rings.

Conclusion

This new method for the preparation of β-hydroxy nitriles have some advantages, such as high regioselectivity, high yields, short reaction times relative to other procedures, and work-up simplicity. The nucleophilic attack by the cyanide ion on the epoxides occurs at the primary carbon atom. Thus, we have not so far detected secondary cyano derivatives.

Experimental section

Column chromatography was carried out using 100–200 mesh silica gel (Acme India Ltd., Maharashtra, India). TLC analyses were performed on Merck 60 PF254 silica gel plates. Melting points were determined in open capillaries using an Electrothermal Mk3 apparatus. IR spectra were recorded using a PerkinElmer FT-IR 550 spectrometer and values are reported as υ in cm^{-1}. ^1H and ^{13}C NMR spectra were recorded on a Bruker DRX-400 spectrometer for samples as indicated with tetramethylsilane as internal reference. Mass spectra were recorded on a Finnigan MAT 44S with an ionization voltage of 70 eV. The elemental analyses (CHN) were obtained from a Carlo ERBA Model EA 1108 analyzer carried out on PerkinElmer 240c analyzer.

General procedure for the cleavage of epoxide into β-hydroxy nitriles

To a solution of epoxide (20 mmol) in ethylene glycol (30 mL), KCN (22 mmol) was added and the mixture was stirred for 5 min at room temperature. Then, catalyst **A** (as the modified catalyst) (2.0 mmol) was added, and stirring was continued to completion of the reaction as indicated by TLC. Then, 100 mL water and 20 mL CH_2Cl_2 were added to the reaction mixture while stirring. After being stable, the organic phase was collected and concentrated to dry under reduced pressure. The product was washed with brine and dried over anhyd Na_2SO_4. Evaporation and purification by column chromatography employing EtOAc–hexane (3:7) as the eluent afforded the pure β-hydroxy nitriles.

3-Hydroxy-3-phenylpropanenitrile

Yield: 92%; liquid. IR (Neat, cm^{-1}): 3445, 3062, 3034, 2899, 2255, 1604, 1495, 1456, 1412, 1329, 1204, 1081, 1059, 1028, 940, 867, 757. ^1H NMR (400 MHz, $CDCl_3$) δ: 2.67–2.84 (2H, m), 4.25 (1H, t, J = 5.98 Hz), 4.35 (1H,

© 2006 NRC Canada

br s), 7.35 (5H, m). ^{13}C NMR (100.6 MHz, $CDCl_3$) δ: 22.8, 69.8, 117.4, 125.5, 128.7, 128.8, 141.1. MS (70 eV): 147 (M^+), 121, 107, 105, 91, 79, 77. Anal. calcd.for C_9H_9NO: C 73.45, H 6.16, N 9.52; found: C 73.17, H 6.13, N 9.24.

3-Hydroxy-4-phenoxybutanenitrile

Yield: 90%; mp 58–61 °C. IR (Neat, cm^{-1}): 3437, 3066, 2930, 2256, 1228, 1047. ^{1}H NMR (400 MHz, $CDCl_3$) δ: 2.60–2.84 (2H, m), 3.96–4.12 (2H, m), 4.20 (1H, m), 4.35 (1H, br s), 6.77–7.00 (3H, m), 7.14–7.29 (2H, m). ^{13}C NMR (100.6 MHz, $CDCl_3$) δ: 21.7, 62.5, 69.1, 113.1, 117.1, 126.6, 130.3, 155.8. MS (70 eV): 177, 119, 107, 94, 77.

3-Hydroxy-4-(4-chlorophenoxy)butanenitrile

Yield: 93%; mp 65–68 °C. IR (KBr, cm^{-1}): 3438, 3098, 2879, 2255, 1242, 1092, 1043. ^{1}H NMR (400 MHz, $CDCl_3$) δ: 2.55–2.67 (2H, m), 3.86–4.07 (2H, m), 4.37 (1H, m), 4.39 (1H, br s), 6.84 (2H, m), 7.24 (2H, m). ^{13}C NMR (100.6 MHz, $CDCl_3$) δ: 20.6, 64.1, 68.9, 114.4, 115.3, 124.6, 127.3, 154.9. MS (70 eV): 211, 141, 128, 94.

3-Hydroxy-4-(4-methylphenoxy)butanenitrile

Yield: 88%; mp 54–58 °C. IR (Neat, cm^{-1}): 3477, 3028, 2931, 2254, 1193, 1044. ^{1}H NMR (400 MHz, $CDCl_3$) δ: 2.22 (3H, s), 2.69–2.88 (2H, m), 3.68–3.81 (2H, m), 4.42 (1H, m), 4.54 (1H, br s), 6.73–6.94 (2H, m), 7.06–7.19 (2H, m). ^{13}C NMR (100.6 MHz, $CDCl_3$) δ: 20.6, 21.3, 67.1, 73.9, 124.6, 116.1, 128.6, 129.1,158.0. MS (70 eV): 191, 139, 108, 91, 77.

3-Hydroxy-4-(4-nitrophenoxy)butanenitrile

Yield: 93%; mp 71–74 °C. IR (KBr, cm^{-1}): 3401, 3023, 2938, 2274, 1240, 1102, 1052. ^{1}H NMR (400 MHz, $CDCl_3$) δ: 2.43–2.58 (2H, m), 3.78–3.89 (2H, m), 4.30 (1H, m), 4.62 (1H, br s), 7.24 (2H, m), 8.08 (2H, m). ^{13}C NMR (100.6 MHz, $CDCl_3$) δ: 21.0, 22.5, 68.1, 74.2, 117.7, 125.3, 132.6, 139.1, 155.0. Anal. calcd. for $C_{10}H_{10}N_2O_4$: C 54.06, H 4.54, N 12.61; found: C 54.02, H 4.49, N 12.49.

2-Hydroxy-1-cyclohexanecarbonitrile

Yield: 84%; liquid. IR (KBr, cm^{-1}): 3425, 2960, 2885, 2254, 1189, 1082, 1038, 948, 870, 790. ^{1}H NMR (400 MHz, $CDCl_3$) δ: 1.2–1.4 (3H, m), 1.7–1.9 (3H, m), 2.15 (1H, m), 2.3 (1H, m), 2.4 (1H, s), 2.5 (1H, m), 3.6–3.8 (1H, m). ^{13}C NMR (100.6 MHz, $CDCl_3$) δ: 20.6, 23.3, 24.1, 26.9, 33.4, 60.3, 118.6. Anal. calcd. for $C_7H_{11}NO$: C 67.17, H 8.86, N 11.19; found: C 67.05, H 8.81, N 10.94.

3-Hydroxy-6-heptenenitrile

Yield: 83%; liquid. IR (KBr, cm^{-1}): 3401, 3023, 2938, 2274, 1240, 1102, 1052. ^{1}H NMR (400 MHz, $CDCl_3$) δ: 2.14 (2H, m), 2.41 (2H, m), 2.67–2.85 (2H, m), 3.91 (1H, m), 4.21 (1H, br), 4.87 (1H, dd, J_1 = 9.6 Hz, J_2 = 2.1 Hz), 4.94 (1H, dd, J_1 = 16.3 Hz, J_2 = 2.1 Hz), 5.69 (1H, m). ^{13}C NMR (100.6 MHz, $CDCl_3$) δ: 28.3, 30.4, 36.3, 66.16, 114.3, 119.8, 137.0. Anal. calcd. for $C_7H_{11}NO$: C 67.17, H 8.86, N 11.19; found: C 67.15, H 8.70, N 11.02.

3-Hydroxy-4-isopropoxybutanenitrile

Yield: 80%; liquid. IR (KBr, cm^{-1}): 3445, 2924, 2899, 2253, 1602, 1495, 1412, 1329, 1028, 868. ^{1}H NMR (400 MHz, $CDCl_3$) δ: 1.21 (6H, d, J = 6.1 Hz), 2.64–2.75 (2H, m), 3.24 (2H, m), 3.6 (1H, m), 3.7 (1H, m), 3.98 (1H, br). ^{13}C NMR (100.6 MHz, $CDCl_3$) δ: 21.9, 22.7, 65.3, 70.6, 72.1, 117.8. Anal. calcd. for $C_7H_{13}NO_2$: C 58.72, H 9.15, N 9.78; found: C 58.62, H 9.08, N 9.57.

4-(Tert-butoxy)-3-hydroxybutanenitrile

Yield: 85% ; liquid. IR (KBr, cm^{-1}): 3432, 2933, 2894, 2258, 1594, 1483, 1440, 1354, 1031, 890. ^{1}H NMR (400 MHz, $CDCl_3$) δ: 1.14 (9H, s), 2.36–2.48 (2H, m), 3.14 (2H, m), 3.88 (1H, m), 4.14 (1H, br). ^{13}C NMR (100.6 MHz, $CDCl_3$) δ: 22.1, 27.4, 66.5, 68.5, 73.2, 117.8. Anal. calcd. for $C_8H_{15}NO_2$: C 61.12, H 9.62, N 8.91; found: C 62.01, H 9.55, N 8.78.

3-Hydroxybutanenitrile

Yield: 82%; liquid. IR (KBr, cm^{-1}): 3419, 2916, 2887, 2251, 1519, 1474, 1365, 1033, 890, 745. ^{1}H NMR (400 MHz, $CDCl_3$) δ: 1.74 (3H, d, J = 5.3 Hz), 2.34–2.47 (2H, m), 4.07 (1H, m), 4.25 (1H, br). ^{13}C NMR (100.6 MHz, $CDCl_3$) δ: 21.6, 25.3, 63.7, 119.0.

Acknowledgement

We gratefully acknowledge the support for this work by the Kashan University Research Council.

References

1. G. Dittus. *In* Methoden der organishen chemie (Huben–Weyl). *Edited by* E. Mulle. Thieme Verlag, Stuttgart. 1965. p. 451.
2. D.C. Ha and D.J. Hart. Tetrahedron Lett. **28**, 4489 (1987).
3. (*a*) W. Seidel and D. Seebach. Tetrahedron Lett. **23**, 159 (1982); (*b*) A.I. Meyers and R.A. Amos. J. Am. Chem. Soc. **102**, 870 (1980).
4. A. Kramer and H. Pfander. Helv. Chim. Acta, **65**, 293 (1982).
5. (*a*) F. Fülöp, I. Huber, G. Bernáth, H. Hönig, and P. Seufer-Wasserthal. Synthesis, 43 (1991), and refs. cited therein; (*b*) J.G. Smith. Synthesis, 629 (1984); (*c*) W. Nagata, M. Yoshioka, and T. Okumura. J. Chem. Soc. **17**, 2365 (1970).
6. A. Kamal, G.B. Ramesh Khanna, and R. Ramu. Tetrahedron Asymmetry, **13**, 2039 (2002).
7. (*a*) N. Iranpoor, H. Firouzabadi, and M. Shekarize. Org. Biomol. Chem. **1**, 724 (2003); (*b*) A. Kamal and G.B. Ramesh Khanna. Tetrahedron Asymmetry, **12**, 405 (2001); (*c*) O. Pàmies, J.-E. Bäckvall. Adv. Synth. Catal. **343**, 726 (2001).
8. For examples, see: (*a*) J. Jin and S.M. Weinreb. J. Am. Chem. Soc. **119**, 2050 (1997); (*b*) T. Itoh, K. Mitsukura, W. Kanphai, Y. Takagi, H. Kihara, and H. Tsukube. J. Org. Chem. **62**, 9165 (1997); (*c*) M. Chini, P. Crotti, L. Favero, and F. Macchia. Tetrahedron Lett. **32**, 4775 (1991).
9. (*a*) J.A. Ciaccio, C. Stanescu, and J. Bontemps. Tetrahedron Lett. **33**, 1431 (1992); (*b*) J.A. Ciaccio, M. Smrtka, and W. Maio. *In* Proceedings of the 226th ACS National Meeting, New York. American Chemical Society, Washington D.C. 2003. ORGN–123.
10. (*a*) S. Yamasaki, M. Kanai, and M. Shibasaki. J. Am. Chem. Soc. **123**, 1256 (2001); (*b*) B. Tamami, N. Iranpoor, and R. Rezaei. Synth. Commun. **33**, 3153 (2003).
11. H. Konno, E. Toshiro, and N. Hinoda. Synthesis, 2161 (2003).
12. S. Matsubara, H. Onishi, and K. Utimoto. Tetrahedron Lett. **31**, 6209 (1990).
13. (*a*) M.B. Sassaman, G.K.S. Prakash, and G.A. Olah. J. Org. Chem. **55**, 2016 (1990); (*b*) A.E. Vougioukas and H.B. Kagan.

© 2006 NRC Canada

Tetrahedron Lett. **28**, 5513 (1987); (*c*) M. Hayashi, M. Tamura, and N. Oguni. Synlett, 663 (1992); (*d*) K. Imi, N. Yanagihara, and K. Utimoto. J. Org. Chem. **52**, 1013 (1987); (*e*) K. Sugita, A. Ohta, M. Onaka, and Y. Izumi. Chem. Lett. **3**, 481 (1990).
14. M. Chini, P. Crotti, L. Favero, and F. Macchia. Tetrahedron Lett. **32**, 4775 (1991).
15. A. Tsuruoka, S. Negi, M. Yanagisawa, K. Nara, T. Naito, and N. Minami. Synth. Commun. **27**, 3547 (1997).
16. H. Ohno, A. Mori, and S. Inoue. Chem. Lett. 975 (1993).
17. (*a*) W. Nagata, M. Yoshioka, and T. Okumura. Tetrahedron Lett. 847 (1966); (*b*) J.C. Mullis and W.P. Weber. J. Org. Chem. **47**, 2873 (1982).
18. N. Iranpoor and M. Shekarriz. Synth. Commun. **29**, 2249 (1999).
19. (*a*) T. Katsuki. J. Mol. Catal. A, **113**, 87 (1996); (*b*) E.N. Jacobsen. *In* Catalytic asymmetric synthesis. *Edited by* I. Ojima. VCH Publishers Inc., New York. 1993. pp. 159–202.
20. (*a*) T. Katsuki, K. Noda, N. Hosoya, and R. Irie. Synlett, 469 (1993); (*b*) T. Katsuki and H. Nishikori. Tetrahedron Lett. **37**, 9245 (1996); (*c*) T. Katsuki, K. Hori, H. Sugihara, and N. Ito. Tetrahedron Lett. **40**, 5207 (1999).
21. (*a*) T. Katsuki and T. Fukuda. Synlett, 825 (1995); (*b*) T. Katsuki and T. Fukuda. Tetrahedron, **53**, 7201 (1997); (*c*) T. Katsuki, T. Uchida, and B. Saha. Synlett, 114 (2001).
22. T. Katsuki and Y. Yamashita. Synlett, 829 (1995); (*b*) E.N. Jacobsen, J. Branalt, and S.E. Schaus. J. Org. Chem. **63**, 403 (1998).
23. H. Sharghi and H. Naeimi. Bull. Chem. Soc. Jpn. **72**, 1525 (1999).
24. (*a*) R.H. Holm, G.W. Everett, and A. Chakravorty, Jr. Prog. Inorg. Chem. **7**, 83 (1966); (*b*) B. Mahapatra and D. Panda. Transition Metal. Chem. (London), **9**, 280 (1984).
25. H. Naeimi. Ph.D. thesis, Shiraz University, Shiraz, Iran. 1997.
26. H. Sharghi and H. Naeimi Khaledi. Iran. J. Chem. Chem. Eng. **18**, 72 (1999).

© 2006 NRC Canada

Principal component analysis of solvent effects on equilibria and kinetics — A hemisphere model

Robert A. Stairs and Erwin Buncel

Abstract: Principal Component Analysis (PCA) was applied to 17 selected properties relating to the properties of solvents and their effect on solute spectra and equilibria and rates of reactions in solution. The analysis showed affinities and contrasts among the parameters. Using the first three principal components (PC's) as unit vectors in the Cartesian directions, the properties were represented as vectors in this space with their directions being represented as points on the unit hemisphere; their magnitudes are lost in the process of correlation. Properties that fell into recognizable groups included the following: (*i*) those purporting to measure acidity (**A**) (α, AN, SA, and A_j), closely associated with E_T^N, *Z*, *S*, and $A(^{14}N)$, which are usually considered to be measures of polarity; (*ii*) properties supposed to measure basicity (**B**) (β, SB, and DN); (*iii*) polarity group (**P**), including pure (di-)polarity properties ($\beta_\mu^{1/2}$ and Q_v) and those measuring some combinations of polarity and polarizability (π*, π^*_{azo}, SPP, and $-\chi_R$). The space spanned by the three PCs of the properties provided a frame in which solvent effects on equilibria and on rates of reactions could be represented. Eight equilibria, represented by $\log_{10}(K)$ measured in different solvents, and 10 reaction rates, similarly represented by $\log_{10}(k)$, were correlated with the three PCs of the solvent properties. This enabled plotting of their directions in the hemisphere to show which groups of properties were most strongly correlated with the rate of each reaction. A separate plot showed the magnitudes and sense of the effects. These finding are considered in the light of the mechanisms proposed for the reactions.

Key words: Chemometrics, Principal Component Analysis, solvent effects on equilibria and rates.

Résumé : On a appliqué l'analyse du composant principal à dix-sept propriétés choisies apparentées aux propriétés de solvants et leurs effets sur les spectres ainsi que les équilibres et vitesses de réaction de solutés en solution afin de mettre en évidence les affinités et les contrastes entre les paramètres. Utilisant les trois premiers composants principaux (CP) comme vecteurs unitaires dans les directions cartésiennes, on a représenté les propriétés sous la forme de vecteurs dans cet espace dans lequel leurs directions sont représentées sous la forme de points sur l'hémisphère unitaire; leurs amplitudes sont toutefois perdues dans le processus de corrélation. Les propriétés qui peuvent être regroupées dans groupes reconnaissables sont les suivantes: (*i*) celles qui se rapportent à une mesure de l'acidité (**A**) (α, AN, SA et A_j) avec E_T^N, *Z*, *S* et $A(^{14}N)$, qui sont généralement considérées comme une mesure de la polarité; (*ii*) les propriétés qui sont sensées mesurer la basicité (**B**) (β, SB et DN); (*iii*) le groupe de polarité (**P**), y compris les propriétés de (di-)polarité pure ($\beta_\mu^{1/2}$ et Q_v) et celles qui mesurent des combinaisons de polarité et de polarisabilité (π*, π^*_{azo}, SPP et $-\chi_R$). L'espace couvert par les trois composants principaux des propriétés fournit un cadre dans lequel on peut représenter les effets de solvant sur les équilibres et les vitesses de réaction. On a pu établir une corrélation entre les trois composants principaux des propriétés de solvant et huit équilibres, représentés par $\log_{10}(K)$ mesurés dans différents solvants, et dix vitesses de réaction, représentées principalement par $\log_{10}(k)$. Ceci a permis de tracer leurs directions dans l'hémisphère et de montrer quelle est la nature des groupes de propriétés qui sont les plus reliés aux vitesses de chacune des réactions. Une courbe différente montre l'amplitude et le sens de ces effets. On discute de ces résultats à la lumière des mécanismes proposés pour les réactions.

Mots clés : chimiométrie, analyse du composant principal, effets de solvant sur les équilibres et les vitesses de réaction.

[Traduit par la Rédaction]

Introduction

Buncel et al. (1) described an application of Principal Component Analysis (PCA) to a selected group of properties that have been used to correlate the effects of solvents on spectra and on equilibria and rates of reactions in solution. This paper reports an extension of that study with a modified graphical method of representing the results. The result will first be applied to the consideration of solvent effects on equilibrium constants of a set of reactions, and second, to

Received 13 June 2006. Accepted 21 September 2006. Published on the NRC Research Press Web site at http://canjchem.nrc.ca on 1 December 2006.

R.A. Stairs.[1] Department of Chemistry, Trent University, Peterborough, ON K9J 7B8, Canada.
E. Buncel. Department of Chemistry, Queen's University, Kingston, ON K7L 3N6, Canada.

[1]Corresponding author (e-mail: rstairs@trentu.ca).

 doi:10.1139/V06-160 © 2006 NRC Canada

Table 1. Summary of the procedure to prepare a hemisphere plot of the solvent property data.

Step	Do	Keep (file name)
1	Enter raw data (file or keyboard): m properties, n solvents	File of raw data n x m: **X** (f$.dat) (f$ is forename for particular data set.)
2	Correlate pairwise	Matrix of correlation coefficients m x m (Stored as lower triangular): **R** (f$.cor)
3	Find eigenfunctions and eigenvalues of correlation matrix	Eigenvalues: λ_i (i = 1, 2, …, n) (f$.lam), First three eigenfunctions: **Q** : m x 3 (f$.q)
4	Prepare table of reduced data (zero mean and unit norm)	File of reduced data: **Y** : n x m (f$.red)
5	Calculate the first three principal components (PCs): **QY** = **Z**. If the data contain gaps, they may not be mutually orthogonal; orthogonalize. Create augmented data matrix adding the three **z** column vectors before the **y** vectors	Augmented data: [**Z**|**Y**]: n x (3 + m) (f$.aug)
6	Correlate again to obtain correlation coefficients between the **y** vectors and the three **z** vectors	Correlation coefficients $r_{j,k}$ (j = 1, 2, …, m; k = 1, 2, 3)
7	Interpret the coefficients $r_{j,k}$ as direction cosines to $\mathbf{z}_1$('N'), $\mathbf{z}_2$('G') and $\mathbf{z}_3$('E') (on the equator at long. 0 and 90° E); calculate latitude and longitude of each **y**, and uncertainties	Lats., Longs., and uncertainties (m x 3) for export for plotting (f$.lat)

Table 2. Analysis of reaction rate data for the hemisphere display.

Step	Do	Keep
1	Enter (from file or keyboard) data on m' reaction equilibrium or rate constants in the same set of solvents as were used for the solvent properties	File of reaction rates (speeds) in solvents. **S**: (n x m')
2	Create table n x (3 + m') of the previous three **z** vectors and the m' **s** vectors	File of **z**'s and rates (n x (3 + m'))
3	Correlate and interpret $r_{j,k}$ as direction cosines	
4	Calculate lats., longs., and uncertainties	Table of lats., longs., and uncertainties for export to plotting program
5	Prepare file of vectors parallel to reaction vectors; calculate magnitudes of solvent effects	

solvent effects on the rate constants of a separate set of reactions.

The properties that are most susceptible to this treatment are those that are considered in the method of *Linear Free Energy Relationship* (LFER) (2, 3), i.e., quantities that have the dimension of energy, or that are proportional to energies, such as changes in spectral frequencies or in the logarithms of rate or equilibrium constants. Some other properties are often included, such as functions of dipole moment or relative permittivity as polarity measures or functions of refractive index as a measure of polarizability.

The list of values of a physical property x_i for a set of n substances can be treated as a vector in n-dimensional space, i.e., we may write $(x_1, x_2, \ldots, x_n) = \mathbf{X}$. Given a data set containing values of m properties of the n substances, the actual number of really distinct properties may be less than m. Among the many parameters that have been introduced over the years to attempt to relate reaction rates in solvents to solvent properties, there is a great deal of redundancy or overlap. Buncel et al. (*loc. cit*. p. 135) list 10 that purport to measure acidity without being nearly exhaustive.

The PCA statistical procedure (4, 5) is a way of finding a minimal set of vectors, *principal components*, that are linear combinations of the original properties such that the first contains the largest portion of the variance of all the data, the second, orthogonal to the first, contains the next largest portion, and so on. If all the various kinds of measurements actually measure only, say, three really distinct properties, only the first three vectors will be important. Part of the remainder of the variance of the data will represent error, though some contribution from properties of less significance will necessarily be lost.

Methodology

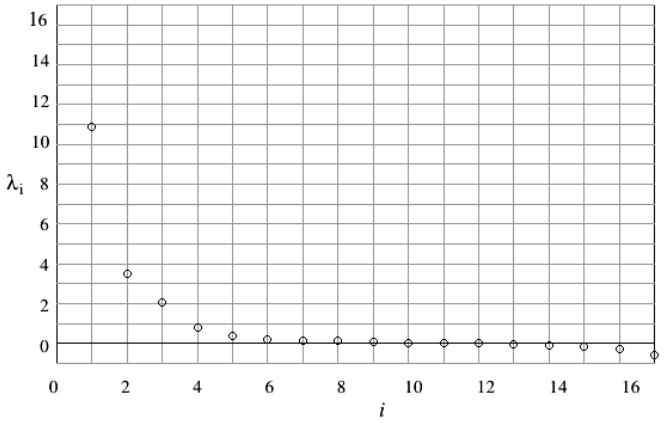
The method employed in this study is summarized in Tables 1 and 2. It begins with pairwise correlation of all the m properties, generating the $m \times m$ correlation matrix **R**, which contains the correlation coefficients $r_{j,k}$, defined by eq. [1]. Here, all the summations are over the $n_{j,k}$ substances for which both properties are known. It is symmetric, and all the diagonal elements $r_{j,j}$ are unity.

$$[1] \qquad r_{j,k} = \frac{n_{j,k}\sum_i x_{i,j}x_{i,k} - \sum_i x_{i,j}\sum_i x_{i,k}}{\left[\left(n_{j,k}\sum_i x_{i,j}^2 - \left(\sum_i x_{i,j}\right)^2\right)\left(n_{j,k}\sum_i x_{i,k}^2 - \left(\sum_i x_{i,k}\right)^2\right)\right]^{1/2}}$$

The matrix **R** has m eigenvalues λ_j and m eigenvectors $\mathbf{V}_j$, which satisfy eq. [2].

© 2006 NRC Canada

Fig. 1. The scree plot (so called from a fancied resemblance to the pile of debris fallen from a cliff face), the eigenvalues λ_i of the correlation matrix in descending order.



[2] $$\mathbf{R}\mathbf{V}_j = \lambda_j \mathbf{V}_j$$

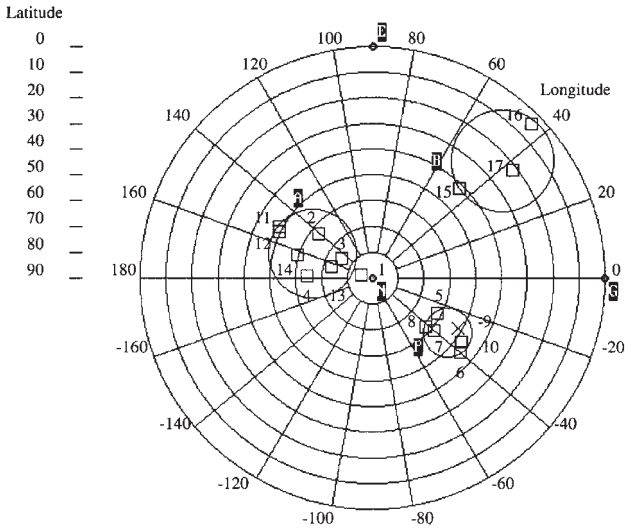
The m constants λ_j are solutions of the secular equation [3], where **I** is the identity matrix, and are the only values of the constant that permit solutions of eq. [2] to find the eigenvectors $\mathbf{V}_j$.

[3] $$|\mathbf{R} - \lambda \mathbf{I}| = 0$$

Each eigenvector is then used as a set of weighting factors to generate a new variable, a linear combination of the original properties, from the original data set. If the eigenvalues are listed in decreasing order, the first few, with their associated eigenvectors, are all that we need to consider. The magnitude of an eigenvalue shows the portion of the variance of the data that the corresponding new parameter contains. Any eigenvalue whose magnitude is less than unity, i.e., that represents less than one whole "property", is usually considered negligible. Some of the remaining variance is normally experimental error. If the data are complete, in the sense of having no gaps, the eigenvalues will be all positive. Missing data create a problem in that some eigenvalues may be negative. As long as the negative eigenvalues are small in magnitude, this does not do great harm to the analysis; however, it does represent increased error.

Using the eigenvectors corresponding to the largest eigenvalues as weighting functions, we create the first, second, and so forth, PC's as vectors in the n-dimensional space that are linear combinations of the m normalized vectors representing the original properties. If only two eigenvalues are larger than unity, one may expect to be able to represent the properties as vectors in two dimensions. In what follows, it will be seen that we were faced with three eigenvalues larger than unity. A suitable projection may represent an aspect of a three-dimensional figure in two dimensions. Here, we shall use the fact that the variance magnitudes of the different properties have been discarded in the normalization process. In fact, the magnitudes are lost in the correlation process. We set up a coordinate system using the first three PC's, as unit vectors in the *z, x*, and *y* directions, to be the *base vectors*. In geographical terms, we place the first at the North Pole (labelled N in Fig. 2), the second on the equator on the Greenwich meridian (G), and the third on the equator at 90° East longitude (E).[2]

Fig. 2. The 17 properties in the hemispheric projection: *(a)* acid–polar: 1. E_T^N, 2. *Z*, 3. *S*, 4. $A(^{14}N)$; (*b*) dipolar: 5. Q_v, 6. $\beta_\mu^{1/2}$; (*c*) polar–polarizable: 7. π*, 8. π^*_{azo}, 9. χ_R (–ve), 10. SPP; (*d*) acid (HBD): 11. α, 12. SA, 13. A_j, 14. AN; (*e*) base (HBA): 15. β, 16. DN, 17. SB.



The angle α between two vectors $\mathbf{X}_j$ and $\mathbf{X}_k$ is defined by eq. [4]:

[4] $$\cos a = \frac{\mathbf{X}_j \cdot \mathbf{X}_k}{|\mathbf{X}_j||\mathbf{X}_k|}$$

From eq. [1], if both $x_{i,j}$ and $x_{i,k}$ are normalized as above, the norms $|\mathbf{X}_j| = \Sigma x_{i,j}^2$ and $|\mathbf{X}_k| = \Sigma x_{i,k}^2$ are each equal to 1, the sums $\Sigma x_{i,j}$ and $\Sigma x_{i,k}$ are zero, and $\cos \alpha = r_{j,k}$. This means that if the vector representing each property is placed in the coordinate system, its termination will lie on the unit sphere, and the three correlation coefficients with the base vectors will be the direction cosines that define its position. If there is no error, the sum of the squares of the three direction cosines is equal to unity (6). The departure of this sum from unity (eq. [5]) may be taken as a rough indication of uncertainty.

[5] $$s_j \approx \sqrt{\left|1 - \sum_{i=1}^{3} r_i^2\right|}$$

Solvent property parameters

There are many parameters in the literature that relate to solvent properties that are relevant to this work. They include solvatochromic parameters (based on the change in frequency of spectral features), parameters based on changes in equilibrium or rate constants, direct measures of physical properties such as dielectric constant, or parameters derived therefrom. We selected a miscellaneous set, chiefly because

[2] A.A. Milne. Winnie-the-Pooh. Dutton, New York. 1926. p. 133. "There's a South Pole", said Christopher Robin, "and I expect there's an East Pole and a West Pole, though people don't like talking about them."

© 2006 NRC Canada

Table 3. Set of 10 nonspecific solvent property parameters.

Entry	Property		Basis	Reference
1	E_T^N	Polarity	Charge-transfer (CT) absorption frequency of a dye	(7)
2	Z	Polarity	CT frequency of a pyridinium iodide	(8)
3	S	Polarity	composite	(9)
4	$A(^{14}N)$	Polarity	ESR hyperfine splitting	(10)
5	Q_v	Polarity	$(\varepsilon_r - 1)/(\varepsilon_r + 2) - (n^2 - 1)/(n^2 + 2)$	(11)
6	$\beta_\mu^{1/2}$	Dipolarity	$\mu/v^{1/2}$	(12) (Square root of the parameter)
7	π^*	Polarity–polarizability	$\pi\rightarrow\pi^*$ transitions in seven nitroaromatics	(13)
8	π^*_{azo}	Polarity	$n\rightarrow\pi^*$ and $\pi\rightarrow\pi^*$ transitions in six azo-merocyanine dyes	(14)
9	χ_R	Polarity	$\pi\rightarrow\pi^*$ transition in a merocyanine dye	(15)
10	SPP	Polarity	Differential UV–vis shift between 2-(dimethylamino)- and 2-fluoro-7-nitrofluorene	(16)

Table 4. Acidity (11–14) and basicity (15–17) parameters.

Entry	Property		Basis	Reference
11	α	H-bonding donor strength	Enhanced solvatochromism in HBD solvents of Reichardt's dye 30 relative to 4-nitroanisole	(17)
12	SA	Solvent acidity	Comparison of solvatochromism of an unhindered with a sterically hindered stilbazolium betaine dye	(16)
13	A_j	Acity: anion-solvating tendency	Bilinear correlation (with B_j) of many effects.	(18)
14	AN	Electron pair acceptor number (Lewis acidity)	^{31}P NMR shifts in triethylphosphane oxide	(19)
15	β	HBA strength	Enhanced solvatochromism in HBA solvents of 4-nitroaniline relative to *N,N*-diethyl-4-nitroaniline	(17)
16	DN	Donor number (Lewis basicity)	$-\Delta H$ of adduct formation with SbF_5 in dilute solution in 1,2-dichloroethane	(19)
17	SB	Solvent basicity	Solvatochromism of 5-nitroindoline with *N*-methyl-5-nitroindoline	(16)

they were known for a reasonably large number of solvents, to minimize the number of gaps in data. They are listed in Tables 3 and 4. Similarly, a set of solvents (listed in Table 6) was chosen for which most of the chosen properties had been reported, with the additional criterion that at least some of the equilibria and rates of reactions to be discussed later had been measured in them.

When this set of parameters for the chosen 20 solvents was subjected to PCA, the scree plot (Fig. 1) showed that three components have eigenvalues greater than unity, i.e., there are three distinct properties embodied in the 20 parameters. The first is dominant, representing 64% of the total variance of the data. The next two represent 21% and 12%, respectively, leaving 3% of the variance that we neglect in using only the first three. Some of this is error, but some is undoubtedly lost information. The last few eigenvalues are negative, as expected with a data set containing gaps, but none is large. The plotting errors have not been shown in Fig. 2, the representation of the 17 parameters on the hemisphere as the resulting picture would have been too confusing. Estimates of error are listed in Table 5, with the mean latitudes and longitudes.

The properties fall for the most part into three recognizable groups, which we have labelled **A** for acid, **B** for basic, and **P** for polarity. Polarity measures based on physical

Table 5. The properties on the hemisphere.

Entry	Symbol	Mean Latitude	Mean Longitude	Uncertainty[a]
1	E_T^N	85.3	165.9	1.1
2	Z	62.7	141.1	10.4
3	S	75.5	148.1	1.5
4	$A(^{14}N)$	64.3	177.7	0.9
5	Q_v	61.4	–28.6	8.6
6	$\beta_\mu^{1/2}$	45.1	–40.2	
7	π^*	58.8	–40.6	11.2
8	π^*_{azo}	62.1	–42.4	1.4
9	χ_R	51.3	–30.2	10.5
10	SPP	47.5	–35.6	1.8
11	α	48.4	151.6	1.7
12	SA	49.4	153.6	19.5
13	A_j	73.2	164.8	2.0
14	AN	59.2	162.63	4.2
15	β	41.8	45.6	3.1
16	DN	4.2	44.1	20.4
17	SB	21.2	37.6	9.2

[a]Expressed in degrees on a great circle.

© 2006 NRC Canada

Table 6. Equilibria: $\log_{10}(K)$ of eight reactions in different solvents.

		PCs			Reactions							
Entry	Solvents	$z_{i,1}$	$z_{i,2}$	$z_{i,3}$	*A*	*B*	*C*	*D*	*E*	*F*	*G*	*H*
1	Cyclohexane	–0.336	–0.307	0.135	0.22				–0.09			
2	tetrachloromethane	–0.303	–0.198	0.075	–0.54				–0.05	–0.23		
3	Toluene	–0.214	–0.150	0.036	–0.41	–1.12						
4	Benzene	–0.263	–0.084	–0.003	–0.58	–0.91	0.10	–4.39	0.14	0.07		
5	Diethyl ether	–0.227	0.094	0.311	–0.40	0.51						
6	1,4-dioxane	–0.204	0.008	0.165	–0.89	0.45						
7	Chlorobenzene	–0.123	0.005	–0.146								
8	Chloroform	–0.075	–0.053	–0.177	–1.06	–1.28	0.58	–4.01	0.09	0.55		
9	Dichloromethane	–0.058	0.040	–0.205	–1.06				0.19			
10	Nitrobenzene	0.038	0.084	–0.476								
11	Acetone	–0.044	0.242	–0.017	–0.89	0.63	–0.37	–2.87	0.41	0.14	5.89	
12	*N,N*-Dimethylformamide	0.044	0.445	0.169		1.93			0.58		4.19	–12.4
13	Dimethyl sulfoxide	0.141	0.546	0.145	–1.28	1.97			0.72	0.55	3.35	
14	Acetonitrile	0.034	0.131	–0.181	–1.30	0.36			0.50	0.35	5.52	–13.0
15	Nitromethane	0.048	–0.031	–0.521								
16	Acetic acid	0.225	–0.321	0.273			0.91					
17	Ethanol	0.234	0.030	0.246	–0.87	2.23	–0.35	–2.07				–8.0
18	Methanol	0.312	–0.068	0.187	–1.16	2.17	–0.18			0.55	6.00	
19	Formamide	0.255	–0.047	0.042					0.75			–6.0
20	Water	0.516	–0.366	–0.060	–1.16	1.28					1.98	–4.3

properties (Q_v on dielectric constant, $\beta_\mu^{1/2}$ on dipole moment, and molecular volume) and those based on solvatochromism (π^*, π^*_{azo}, SPP, and so forth) with a different set of solvents and properties (1) were found to form distinct sets, but here they were indistinguishable. Interestingly, Reichardt's E_T^N and Kosower's *Z*, which are usually considered to measure polarity, fell close to the **A** region rather than the **P** region. The theoretical study by Matyushov et al. (20) showed that while π^* contains positive contributions from both dipolarity and polarizability, E_T^N is negatively correlated with polarizability, so it is not surprising that they fall into different groups.

The equilibria

The eight equilibria were discussed by Reichardt (21) (Chapter 4). The processes comprise keto–enol equilibria (*A* and *B*), azo–hydrazone (*C*), spiropyran–merocyanine (*D*), rotational *gauche–cis* (*E*) and valence (*F*) isomerism, host–guest complexation (*G*), and electron-transfer equilibrium (radical disproportionation) (*H*). The original reports for the equilibria and also for the rate processes, discussed later, are supplemented and updated by various cognate references that were provided to facilitate further studies in this area. The equilibria were chosen because their equilibrium constants had been measured in at least four of the solvents listed, and they covered a range of different reaction types. A 20 × 11 table (Table 6) was created, having the first three PC's from the analysis of the 17 solvent properties for columns 1, 2, and 3, and for the remaining columns, the common logarithms of the equilibrium constants were listed. The 20 rows correspond to the 20 solvents. There were many more gaps than data, which was regrettable, as too few data points make the correlation less meaningful (22); two points only lead inevitably to a correlation coefficient $r = \pm 1$ exactly. The correlation coefficients $r_{i,j}$ (i = 1, 2, 3; j = 1, 2, …, 8) between the three PC's and the each of the rates (logarithmic) were treated as before as direction cosines, i.e., as cosines of the angular distances between a particular vector and the vectors in each of the three Cartesian axial directions. One may imagine drawing arcs with these distances, two at a time, with great-circle radii on the spherical surface, and finding three estimates of the position of the vector by their intersections. The best estimate of position lies at the centroid of the resulting triangle (the navigator's "cocked hat"). If any two of these cosines squared sum to more than unity, the angles sum to less than 90°, and the arcs fail to intersect. It was decided, to ensure finding at least approximate positions for the eight points, to divide each triplet of correlation coefficients by the quantity $\sqrt{\sum_i r_{i,j}^2}$. This ensures that all three arcs intersect in a common point. Some of the points so determined are subject to large errors, but all meaning is not lost. Figure 3 shows the positions of the eight reactions, *A–H*, in the frame defined by the 17 solvent properties, in hemispheric projection.

As previously noted, the magnitudes of the effects are lost in the correlation process (Table 7). A unit vector in the same direction as the vector representing a given reaction may be constructed as a linear combination of the three base vectors, weighted by the three correlation coefficients, as in eq. [6].

$$[6] \qquad \mathbf{Z}_j = \sum \mathbf{X}_i \, r_{i,j} \qquad (i = 1, 2, 3)$$

i.e., $\mathbf{Z}_j$ is a unit vector parallel to the vector representing the *j*'th reaction. The slope of the least-squares line representing the plot of the *j*'th reaction (as logarithms of equilibrium or rate constants) vs. the elements of the "parallel" vector was taken as a measure of the sensitivity of the reaction to solvent change. Figure 4 summarises the magnitudes and the senses of the effects on the equilibria, and Fig. 5 shows the individual plots. The effects of solvent change on reactions *B, D*, and especially *H* are strongly positive while on *E* it

© 2006 NRC Canada

Table 7. Equilibria: Locations on the hemisphere and magnitude of effect.

Reaction	Latitude	Longitude	Error (°)	Magnitude	Error	n^b
A^a	52.7	–20.9	9.1	–1.57	0.78	14
B	44.6	65.7	8.1	5.62	1.41	12
C^a	3.7	4	15.0	–2.58	1.57	6
D	43.8	52.5	35.3	4.25	0.56	4
E	50.1	13.3	22.2	0.99	0.38	10
F^a	36.8	–36.8	58.5	–1.08	0.31	4
G^a	71.9	–178.1	26.8	–2.73	4.87	6
H	47.3	175.4	29.0	10.68	4.38	5

[a]These points are plotted as antipodes, i.e., for the reverse reaction.
[b]Number of points correlated.

Fig. 3. The 8 equilibria, *A–H,* in hemispheric projection. Reactions *B* and *D* fall close to region **B**; *H* and the negative of *G* are in region **A**; the negatives of *F* and *A* are near the polar region, **P**. *E* and the negative of *C* lie between the basic **B** and the polar regions, *C* being almost orthogonal to the **A** region.

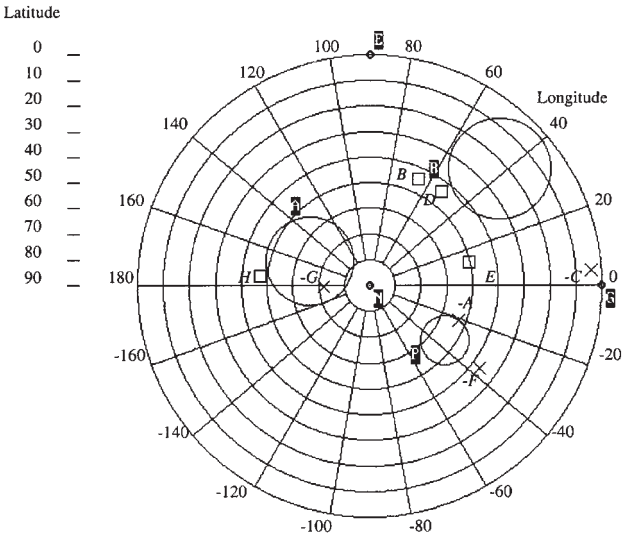


Fig. 4. Magnitude of equilibrium solvent effects: slope of $\log(K_j)$ vs. z_{ij}, the appropriate parallel vector elements, multiplied by the sign of the correlation with the first PC. Error bars are at one standard deviation of slope.

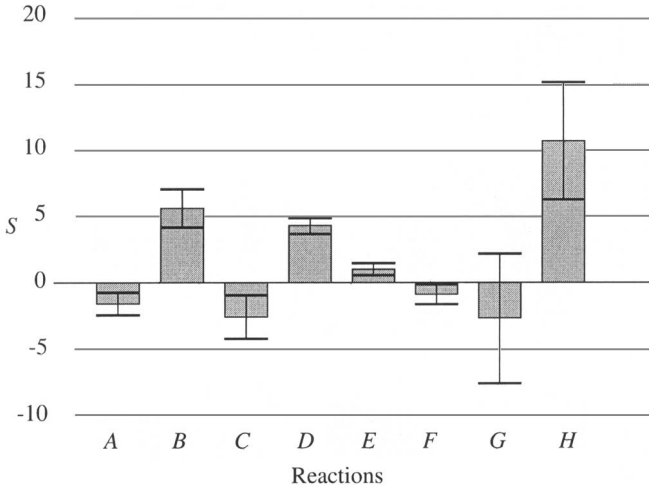
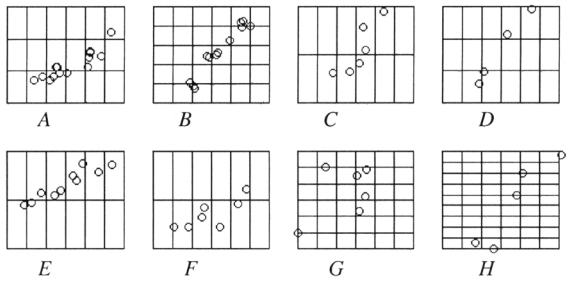
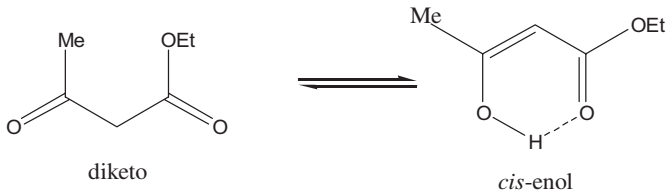


Fig. 5. Logarithms of equilibrium constants vs. the appropriate "parallel" vector components. All the horizontal scales run from –0.6 to 0.6; the vertical scales vary, the grid lines being at one-unit intervals.



Scheme 1.



was weakly positive but probably real. Reactions *A* and *C* show a reverse effect. The apparently negative effect on *G* is subject to a very large uncertainty. When these values are considered together with the locations of the reactions on the hemisphere, shown in Fig. 3, it becomes possible to discuss the implications. We consider each reaction in turn (Numbers in square brackets [xxx] refer to the page xxx in Reichard) (21).

A. Keto–enol equilibrium of ethyl acetoacetate [107] (23)

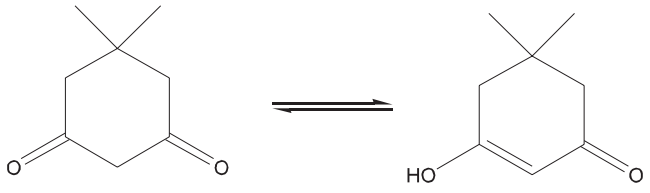
K_T = [*cis*-enol]/[diketo]. Increasing polarity of the solvent favours the diketo form (Scheme 1), though not strongly. The overall dipole moment of the diketo form may not be large, but isolated carbonyl groups can act as separate dipoles. The polarity of the *cis*-enol form is reduced by intramolecular H-bond formation.

B. Keto–enol equilibrium of 5,5-dimethylcyclohexane-1,3-dione [107] (23)

K_T'' = [*trans*-enol]/[diketo]. In contrast with *A*, the cyclic enol cannot form an intramolecular H-bond (Scheme 2), so the hydroxyl group is free to interact with basic (H-bond ac-

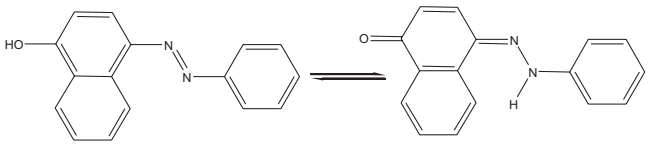
© 2006 NRC Canada

Scheme 2.

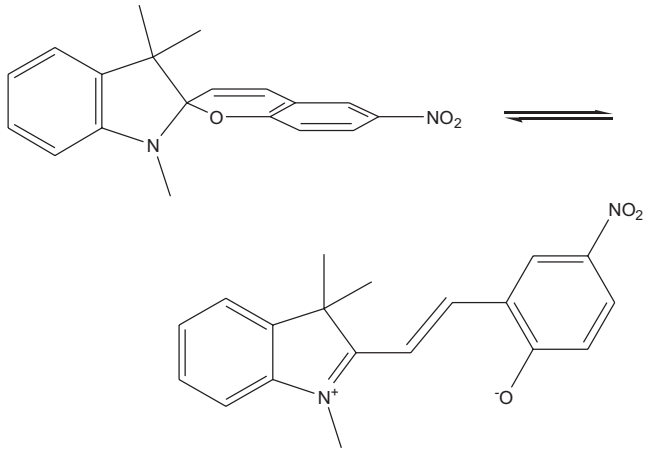


diketo *trans*-enol

Scheme 3.



Scheme 4.



ceptor, HBA) solvents, as shown by the strong positive effect, in the **B** region of the hemisphere.

C. Azo–hydrazone tautomerism [117] (24)

This point is plotted in Fig. 3 as its "antipodes", i.e., inversely. There appears to be a slight positive effect of acidity and negative effects of polarity and basicity. While the hydrazone form may have a larger net dipole moment, the acidic OH group on the azo form carries a local dipole moment (Scheme 3), so that the combined effects of solvent polarity and basicity work to reverse the reaction.

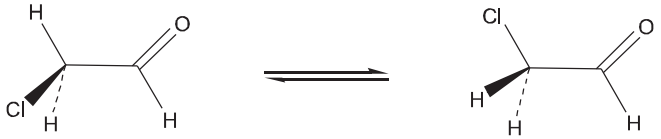
D. Neutral–zwitterion. [124] (25)

A fairly strong positive effect, favouring the zwitterionic form, as expected. The location of the point on the hemisphere in the **B** region suggests that solvation of the charge-localized positive nitrogen site by basic solvents is more important than solvation of the charge-delocalized negative oxygen by acid solvents (Scheme 4). The uncertainty of position (~35°) is large, but the polar region is 60° away.

E. Gauche–cis rotational equilibrium of chloroacetaldehyde. [126–127] (26)

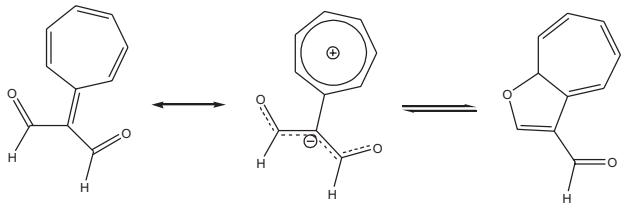
The more polar *cis* rotamer is favoured by solvent polarity as expected (Scheme 5), and it is also unexpectedly favoured

Scheme 5.

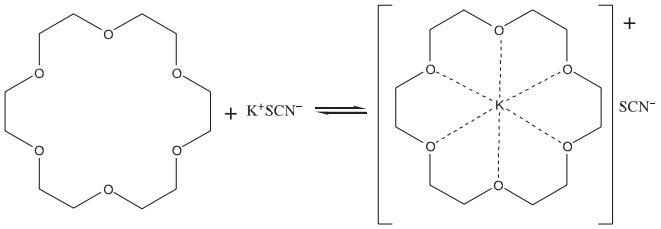


gauche *cis*

Scheme 6.



Scheme 7.



by solvent basicity. Apparently the aldehyde is more acidic in the *cis* form.

F. Valence isomerism equilibrium between 8,8-diformylheptafulvene and 8aH-cyclohepta[b]furan-3-carbaldehyde [136] (27)

Though the uncertainty of position is large, the antipodal position close to the **P** region clearly shows that the former more polar substance is favoured (Scheme 6). The effect is not large but real (see Fig. 4).

G. Host–guest complexation of K^+ (present as thiocyanate) by a crown ether [140] (28)

The antipodal point falls in the **A** region, though with a large uncertainty (27°). If the effect is real, it would be attributable to the coordination of K^+ by EPD (basic) solvents (Scheme 7). The uncertainty of magnitude is so large that the reality of the effect becomes doubtful. K^+ is a weak, hard acid; this analysis did not consider hardness or softness of solvents, and there are perhaps other relevant properties of the solvents in the 3% of the variance previously noted as unaccounted for.

H. Disproportion of 1-ethyl-4-(methoxycarbonyl)pyridinyl radical to form an ion pair [137] (29)

The equilibrium constant is written as K = [ion pair]/[radical] (28), which does not fit the form of the equilibrium reaction: $2R^{\cdot} = (pair)$. Nevertheless, the position of the point in the **A** region (recalling that this region encompasses both the acid parameters and the polar $E_T^{\tilde{N}}$ family) and the strength of the effect show that the ion pair is clearly favoured by increasing solvent polarity reinforced by solvent acidity, owing in part to the basic N in the pyridinyl anion (Scheme 8).

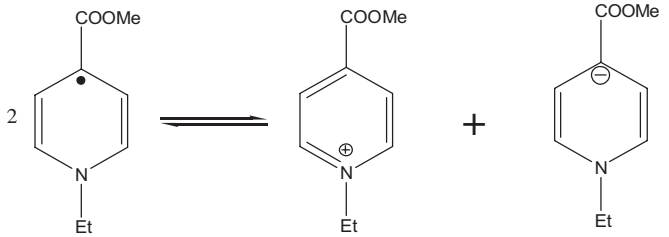
© 2006 NRC Canada

Table 8. Rate constants (in some cases relative) as common logarithms for 10 reacting ions in the same set of solvents.

	Reaction									
Solvents (as in Table 6)	*a*[a]	*b*	*c*[a]	*d*[a]	*e*[a]	*f*[a]	*g*	*h*	*i*[a]	*j*[a]
1	0.00						0.00	2.52[c]		1.81[d]
2				–0.75	0.00					
3										
4	0.30					1.60		2.08	0.54	
5						0.00				1.49
6						0.40		1.86		
7	0.70			1.16[b]			1.11		0.70	
8					2.78	2.09				
9				2.40		1.76				
10					3.45				1.04	
11	1.11	4.9	2.04	2.87			1.63			0.92
12	1.46	4.5	0.85							
13	1.70	3.9	0.60	4.62[b]						
14		3.9	2.71	5.44			2.21	1.40		
15		3.5	3.68						0.82	
16				4.28[b]	3.14					
17				4.68				1.04		0.32
18		0.00		5.77[b]						0.00
19		0.8								
20										

[a]These constants are relative. The standard solvent has log k = 0.00.
[b]Adjusted values: see text.
[c]Solvent was methylcyclohexane.
[d]Solvent was *n*-pentane.

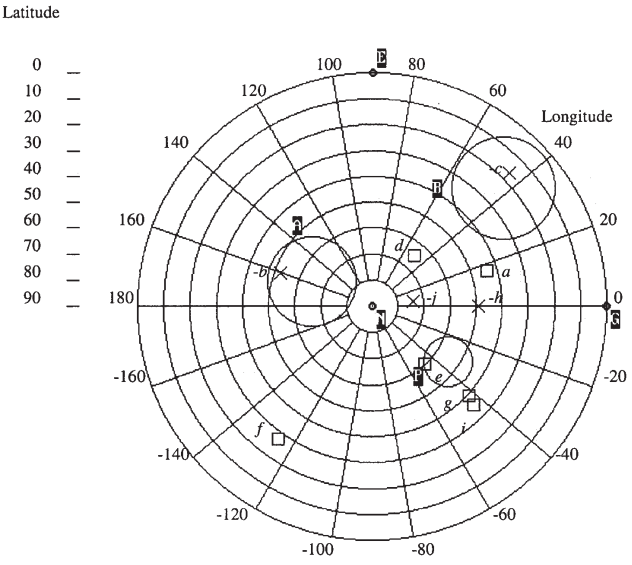
Scheme 8.



The reaction rates

In an exactly analogous fashion, we have placed 10 rate processes on the hemisphere defined by the 17 solvent properties. Again, they were chosen somewhat randomly from those discussed by Reichardt (21) (Chapter 5), and the choice was subject to each having been studied in at least four of the solvents in the set of 20, and illustrating a variety of types. These include nucleophilic aromatic substitution S_NAr (*a, b*), electrophilic aromatic substitution S_EAr (*c*), electrophilic aliphatic substitution S_E2 (*d*), electrophilic addition to alkene (*e*), epoxidation of alkene (*f*), alkene cycloaddition (*g*), sulfoxide racemization (*h*), Diels–Alder cycloaddition (*i*), and azoalkane thermolysis (*j*). The reactions and their measured rate constants (in most cases relative to the rate constants in a standard solvent) as common logarithms are listed in Table 8. The ratio of gaps to data is still large, though slightly better than the corresponding ratio for the equilibria. Figure 6 shows their positions on the hemisphere. Again, we did not attempt to show the error circles, the radii of which are listed in Table 9. Figure 7 shows the magnitudes and senses of the effects, and Fig. 8 shows the individual plots. The reactions are labelled with lowercase letters, conforming to the use of lower case for the symbol *k* for rate constants.

Fig. 6. The 10 rates in hemispheric projection. The clear cases: reactions *e, g,* and (slightly) *i* are accelerated by solvent polarity; *c* is retarded by basicity and *b* by acidity. Reactions *a* and *h* are affected by both polarity and basicity, *a* being accelerated and *h* retarded. Reactions *d* and the negative of *j* fall into the space between the three distinguishable regions, so *d* appears to be accelerated by acidity, basicity, and polarity, though the uncertainty of the slope is very large, while *j* is retarded. Reaction *f* lies 130° away from region **B**, meaning that it is retarded by basicity; it is also somewhat accelerated by acidity–polarity.



© 2006 NRC Canada

Table 9. Rates of reactions: positions, magnitudes.

Reaction	Latitude	Longitude	Error (°)	Magnitude	Error	n^b
a	43.8	16.8	48.2	1.84	0.18	6
b[a]	52.2	160.3	19.3	–8.88	1.43	7
c[a]	16.5	44.2	49.5	–3.64	0.29	5
d	64.9	50.1	0.3	8.06	4.64	9[c]
e	60.0	–47.8	1.1	6.05	2.36	4
f	27.4	–125.4	34.1	4.14	1.15	5
g	39.3	–42.3	66.4	3.13	0.75	4
h[a]	49.0	0.2	29.8	–2.16	0.24	5
i	35.5	–43.8	60.9	0.77	0.31	4
j[a]	74.2	6.4	3.3	–2.59	0.43	5

[a]These points are plotted as antipodes, i.e., representing retardation.
[b]Number of points correlated.
[c]Some of these points were adjusted, see text.

Fig. 7. Magnitude and sense of solvent effects on rates. Slope of the plot of log (*k*) vs. elements of the parallel vector, multiplied by the sign of the correlation with the first PC. Errors bars at one standard deviation of slope.

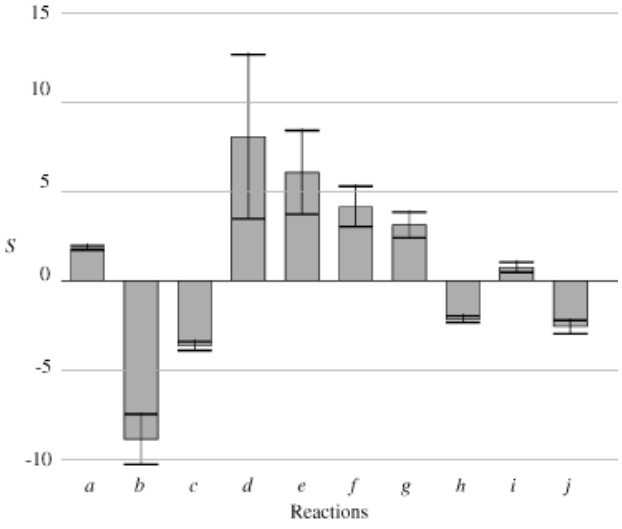
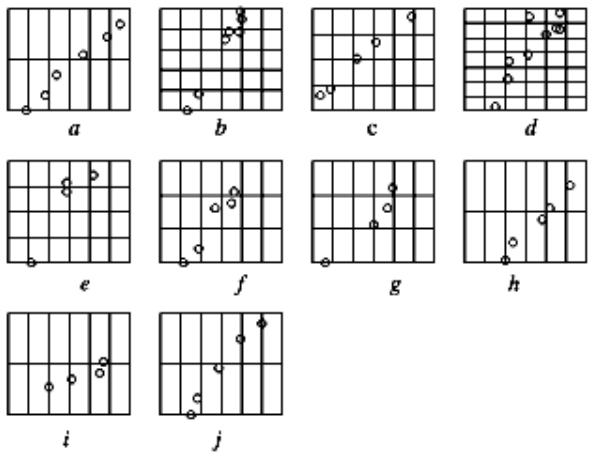
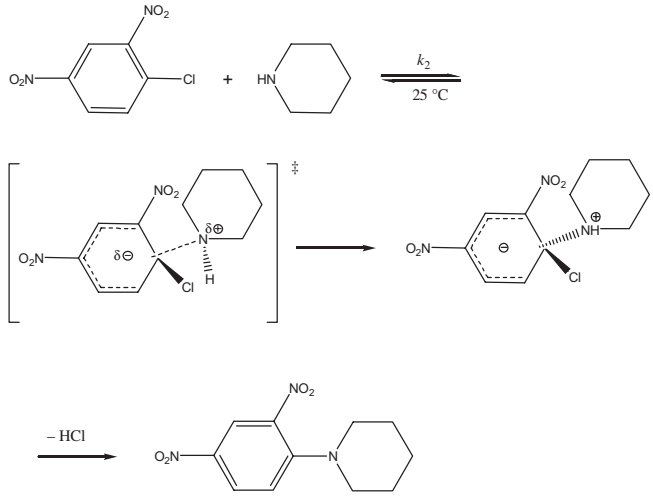


Fig. 8. Kinetic solvent effects: log (*k*) for the 10 reaction rates vs. elements of the appropriate **Z** vectors. Scales are as in



Scheme 9.



a. S_NAr reaction of 1-chloro-2,4-dinitrobenzene with piperidine [174] (30)

Falling between the **B** and **P** regions with a large uncertainty of the position (48°), this reaction appears to be accelerated by both polarity and basicity. If there is an effect of acidity, it appears small (though the list of solvents used does not include notably acidic ones). The mechanism described (*loc. cit.*) shows a polar transition state agreeing with the effect of polarity (Scheme 9). The influence of solvent basicity is invoked only for the second step.

b. S_NAr reaction of 4-fluoro-1-nitrobenzene with azide ion [249] (31)

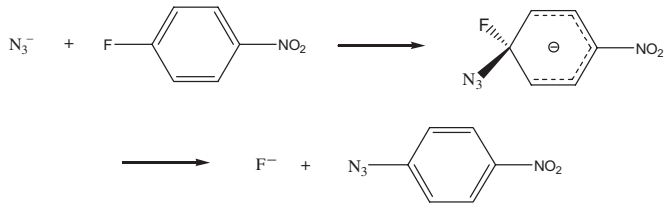
Very strongly retarded by acidity. HN_3 is a weak acid (p*K* in water at 25° is 4.74), so interaction of azide with solvent (HBD) acidity is to be expected (Scheme 10).

c. S_EAr azo coupling of 4-nitrobenzenediazonium tetrafluoroborate with N,N-dimethylaniline [174] (32)

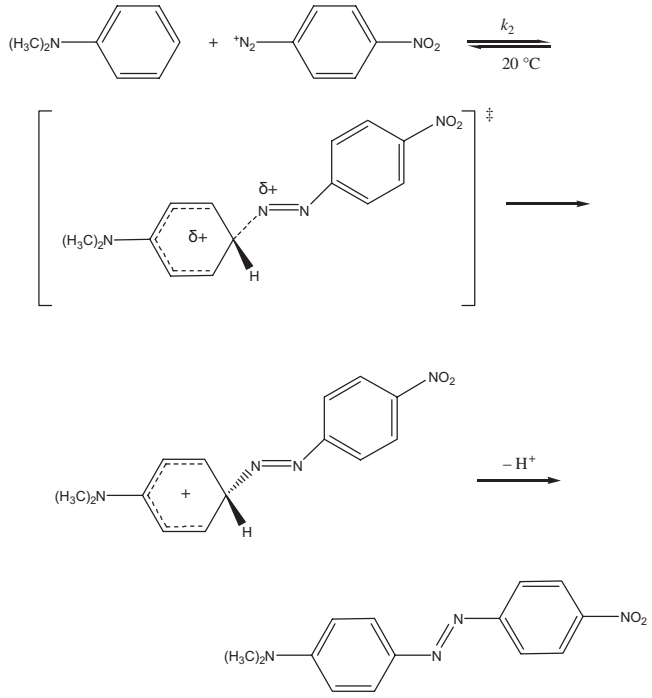
Moderate retardation; the negative point falls in the **B** region with large uncertainty (50°) suggesting coordination of the positive diazonium group by basic solvents. One would have expected a retardation also by polarity, owing to charge dispersal in the transition state (Scheme 11).

© 2006 NRC Canada

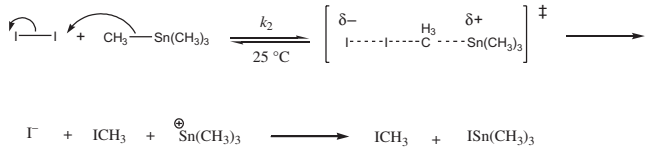
Scheme 10.



Scheme 11.



Scheme 12.



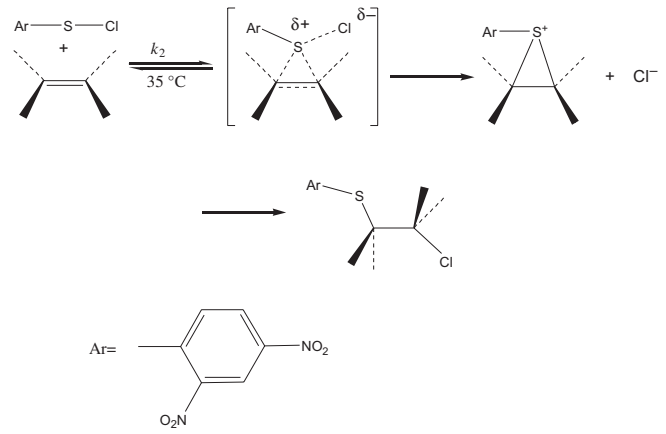
d. S_E2 cleavage of tetramethyltin by iodine [175] (33)

Large but rather uncertain positive effect between **A** and **B** with small position uncertainty. A push–pull effect of acidity on $I^{\delta-}$ and basicity on $Sn^{\delta+}$ is suggested (Scheme 12). To extend the range of solvents, we included the point for tetrachloromethane at 50 °C and four points from Gielen (33*a*) at 20 °C adjusting each to the temperature of Fukuzumi and Kochi's work (33*b*) at 25 °C by using the rule-of-thumb assumption that rates double for each 10 °C rise in temperature. This rough procedure reduced the uncertainty of the slope by half compared with using only the five points at 25 °C.

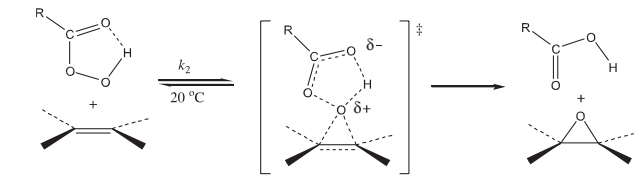
e. Addition of chloro-2,4-dinitrophenylsulfane to cyclohexene [177] (34)

Precisely located in **P** region with fairly large acceleration. The reactants are relatively non-polar, but there is a considerable charge separation in the transition state (Scheme 13).

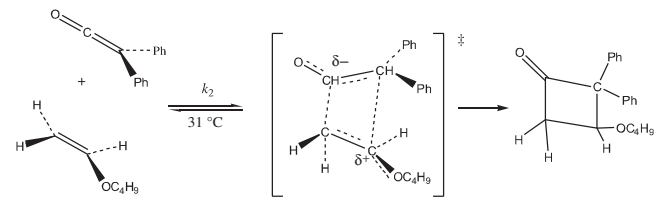
Scheme 13.



Scheme 14.



Scheme 15.



f. Epoxidation of cyclohexene with peroxybenzoic acid [177] (35)

Fairly large acceleration. The position is away from the **B** region but closer to the **A** and **P** regions. Thus, it shows that acidity and polarity have positive effects (the postulated transition state is more polar than the reactants), but basicity (HBA) has a retarding effect owing to interaction with the peroxyacid (Scheme 14).

g. Cycloaddition of diphenylketene to n-butyl vinyl ether [181] (36)

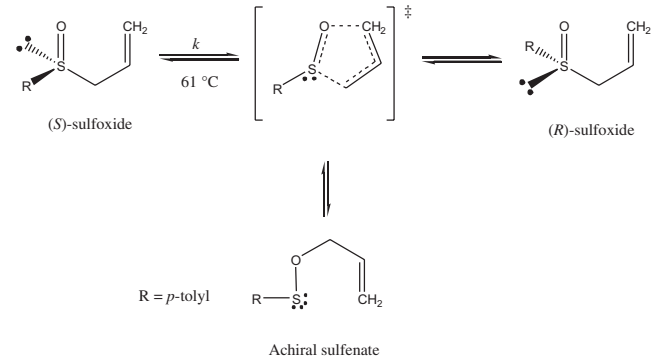
Moderately large acceleration with the point falling on the edge of the **P** region. Although the uncertainty of magnitude is not large, the position uncertainty is very large (66°). The mechanism described shows a substantial charge separation in the transition state (Scheme 15).

h. Thermal racemization of p-tolyl allyl sulfoxide [184] (37)

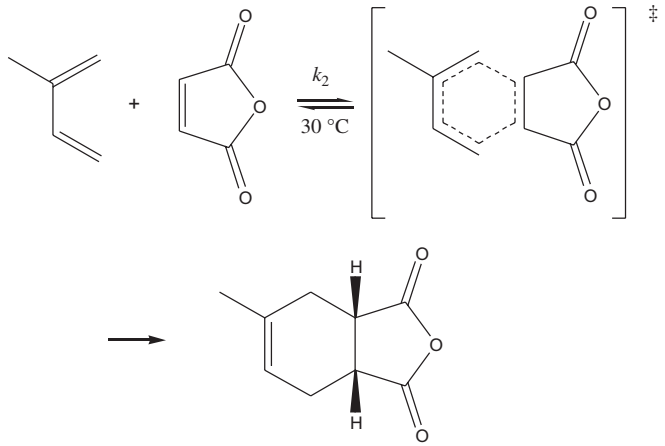
Moderate retardation with the point falling on the basic side of the polar (**P**) region. The sulfoxide is rather polar, and the proposed intermediate is much less so (Scheme 16). Thus, a decrease of polarity in the transition state is reason-

© 2006 NRC Canada

Scheme 16.



Scheme 17.



able. The position uncertainty is enough (30°) to cast doubt on the effect of basicity, but it may be real.

i. Diels–Alder cycloaddition of isoprene and maleic anhydride [188] (38)

A slight, but probably real acceleration by polarity, though the position is very uncertain (60°). Polarizability, which is given scant consideration in this work, may be a factor (Scheme 17).

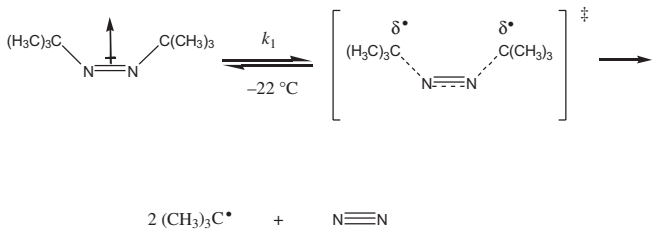
j. Thermolysis of cis-2,2′-dimethyl-2,2′-azopropane [203] (39)

Moderate retardation with the point falling between the polar, acid, and basic regions. The positive end of the dipole in the starting molecule is accessible to polar solvent molecules in spite of the bulky *t*-butyl groups (Scheme 18), so an effect of solvent polarity is to be expected. Why the point lies towards the acid region is less understandable.

Conclusions

With respect to both equilibria and rate processes, this analysis has largely borne out the conclusions of the authors of the various studies as to the nature and magnitude of solvent effects on the reactions and the probable reasons for them. In some cases, the positions of the points on the hemisphere plot have raised interesting questions. For instance, among the equilibria, the importance of solvent basicity might have gone unnoticed with reactions *C, D*, and *E* but

Scheme 18.



especially with reaction *B*. Among the rates, the importance of solvent basicity emerged with reactions *a* and *b*. In reaction *c*, the possibility of push–pull action by base at one end and acid at the other end of the activated complex was raised. In the case of reaction *b*, the puzzling location of the point, remote from any of the recognised areas, was seen to be due to influences from all three factors, acceleration by acidity, polarity, and retardation by basicity. In short, subtleties that might otherwise have been missed have emerged in several cases at least as possibilities to be further examined.

We suggest that in examining a new reaction, it would be worthwhile to measure its rate or equilibrium in an assortment of solvents of different characters, and to use a suitable set of properties of those same solvents to create the frame in which the reaction is then placed. The nature and strength of the solvent effects on the reaction should immediately emerge pointing the way to further study.

Acknowledgements

This work was supported in part by an institutional grant to Trent University (RAS) and a Discovery Grant (EB) from the Natural Sciences and Engineering Research Council of Canada. The authors wish to thank Ms. Jan Myland and Ms. Jessica Butler for computer assistance, Professors Andrew Vreugdenhil, Errol Lewars, and Raymond March for help and suggestions, and Professor Dr. Christian Reichardt for discussion and insightful comments.

References

1. E. Buncel, R. Stairs, and H. Wilson. The role of the solvent in chemical reactions. Oxford University Press, Oxford, UK. 2003.
2. N.B. Chapman and J. Shorter (*Editors*). Advances in linear free energy relationships: correlation analysis in chemistry – recent advances. Plenum, London. 1972.
3. L.P. Hammett. Physical organic chemistry, 2nd ed. McGraw–Hill, New York. 1970.
4. B. Eliasson, D. Johnels, U. Edlund, and M. Sjöström. Acta Chem. Scand. B, **36**,155 (1982).
5. D.E. Johnson. Applied multivariate methods for data analysis. Brooks/Cole, Pacific Grove, California. 1988.
6. H.S.M. Coxeter. Introduction to geometry. Wiley, New York and London. 1961, p. 128, eq. [8.84].
7. K. Dimroth and C Reichardt. Justus Liebigs Ann. Chem. **727**, 93 (1969).
8. E.M. Kosower. J. Am. Chem. Soc. **80**, 3253 (1958).
9. S. Brownstein. Can. J. Chem. **38**, 1590 (1960).
10. B.R. Knauer and J.J. Napier. J. Am. Chem. Soc. **98**, 4395 (1974).

© 2006 NRC Canada

11. I.A. Koppel and V.A. Pal'm. *In* Advances in linear free energy relationships. *Edited by* N.B. Chapman and J. Shorter. Plenum, New York and London. 1972. pp. 203ff.
12. M. Dutkiewicz. J. Chem. Soc., Faraday Trans. 2237 (1990).
13. M.J. Kamlet, J.-L. M. Abboud, and R.W. Taft. J. Am. Chem. Soc. **99**, 6027 (1977).
14. E. Buncel and S. Rajagopal. J. Org. Chem. **54**, 798 (1989).
15. L.G.S. Brooker, A.C. Craig, D.W. Heseltine, P.W. Jenkins, and L.L. Lincoln. J. Am. Chem. Soc. **87**, 2443 (1965).
16. J. Catalán. *In* Handbook of solvents. *Edited by* G. Wypych. Chem. Tec., Toronto, and William Andrew Publishing, New York. 2001. pp. 583ff.
17. M.J. Kamlet and R.W. Taft. J. Am. Chem. Soc. **98**, 377; 2886 (1976).
18. C.G. Swain, M.S. Swain, A.L. Powell, and S. Alunni. J. Am. Chem. Soc. **105**, 502 (1983).
19. (*a*) U. Mayer, V. Gutmann, and W. Gerger. Monatsh. Chem. **106**, 1235 (1975); **(*b*)** U. Mayer, V. Gutmann, and W. Gerger. Monatsh. Chem. **108**, 489 (1977).
20. D.V. Matyushov, R. Schmidt, and B.M. Ladanyi. J. Phys. Chem. **101**, 1035 (1997).
21. C. Reichardt. Solvents and solvent effects in organic chemistry. 3rd ed. Wiley–VCH, Weinheim, Germany. 2003.
22. F.J. Gravetter and L.-A. Forzano. Research methods for the behavioural sciences. 2nd ed. Thomson Nelson, New York. 2005. p. 477.
23. (*a*) S.G. Mills and P. Beak. J. Org. Chem. **50**, 1216 (1985); (*b*) Z. Rapopport (*Editor*). The chemistry of enols: the chemistry of functional groups. Wiley–Interscience, New York; (*c*) M.J. Pellerite and J.L. Brauman. *In* Comprehensive carbanion chemistry, Part A. *Edited by* E. Buncel and T. Durst. Elsevier, Amsterdam. 1988.
24. (*a*) S. Kishimoto, S. Kitahara, O. Manabe, and H. Hiyama. J. Org. Chem., **43**, 3882 (1978); (*b*) K.-S. Cheon, P.M. Kazmaier, S.-R. Keum, K.-T. Park, and E. Buncel. Can. J. Chem. **82**, 551 (2004).
25. (*a*) J.B. Flannery. J. Am. Chem. Soc. **90**, 5660 (1969); kinetic aspects of this reaction were studied by: (*b*) J.T.C. Wojtic, A.Wasey, P.M. Kazmaier, S. Hoz, and E. Buncel. J. Phys. Chem. **104**, 9046 (2000); and by: (*c*) S. Swansburg, E. Buncel, and R.P. Lemieux. J. Am. Chem. Soc. **122**, 6594 (2000).
26. (*a*) G.J. Karabatsos and D.J. Fenoglio. J. Am. Chem. Soc. **91**, 1124 (1969); (*b*) E.L. Eliel, S.H. Wilen, and L.N. Mander. Stereochemistry of organic compounds. Wiley–Interscience, New York. 1944; (*c*) R.J. Abraham and E. Breitschneider. *In* Internal rotation in molecules. *Edited by* W.J. Orville-Thomas. Wiley–Interscience, New York. 1947. pp. 481ff.
27. (*a*) C. Reichardt, K.-W. Yun, W. Massa, R.E. Schmidt, O. Exner, and E.-U. Würthwein. Justus Liebigs Ann. Chem. **1985**, (1997); (*b*) N.E. Takenada, R. Hamlin, and D.M. Lemal. J. Am. Chem Soc. **112**, 6715 (1990).
28. (*a*) V.P. Solov'ev, N.N. Strakhova, O.A. Raevsky, V. Rüdiger, and H.-J. Schneider. J. Org. Chem. **61**, 5221 (1996); (*b*) F. Vögtle. Supramolecular chemistry, Wiley, Chichester. 1993; (*c*) J.-M. Lehn. Supramolecular chemistry: concepts and perspectives. VCH, Weinheim, Germany. 1995.
29. (*a*) M. Mohammed, R. Iqbal, A.Y. Khan, M. Bhatti, K. Zahir, and R. Jahan. J. Phys. Chem. **85**, 2816 (1981); (*b*) R.A. Ransdell and C.C. Wamser. J. Phys. Chem. **96**, 10572 (1992); (*c*) E. Kiepek, Y. Zhou, S. Hoz, E. Rozental, P.M. Kazmaier, and E. Buncel. Can J. Chem. **83**, 1448 (2005).
30. (*a*) F. Terrier. Nucleophilic aromatic displacement. VCH, Weinheim and New York. 1991; (*b*) E. Buncel, J.M. Durst, and F. Terrier. Chem. Rev. **95**, 2261 (1995).
31. R. Alexander, E.C.F. Ko, A.J. Parker, and T.J. Broxton. J. Am. Chem. Soc. **90**, 5049 (1968).
32. (*a*) L. Bagal, S.A. Skvortsov, and A.V. El'tov. J. Org. Chem. USSR, **14**, 328 (1978); (*b*) I. Szele and H. Zollinger. Top. Curr. Chem. **112**,1 (1983).
33. (*a*) M. Gielen. Acc. Chem. Res. **6**, 198 (1973); (*b*) S. Fukuzumi and J.K. Kochi. J. Phys. Chem. **84**, 2254 (1980).
34. (*a*) G.A. Jones, C.J.M. Stirling, and N.G. Bromby. J. Chem. Soc.; Perkin Trans. 2, 385 (1983); (*b*) D.S. Campbell and D.R. Hogg. J. Chem. Soc. B, **1967**, 889; (*c*) M.-F. Ruasse. Adv. Phys. Org. Chem. **28**, 207 (1993); (*d*) G. Modena, F. Rivetti, and U. Tonnelato. J. Org. Chem. **43**, 1521 (1978).
35. (*a*) R. Renolen and J. Ugelstad. J. Chim. Phys. Phys.-Chim. Biol. **57**, 634 (1960); (*b*) R.S. Brown. Acc. Chem. Res. **30**, 131 (1977).
36. (*a*) R. Huisgen, L.A. Feiler, and P. Otto. Tetrahedron Lett. 4485 (1968); (*b*) G. Swieton, J.v. Jouanne, H. Kelm, and R. Huisgen. J. Chem. Soc., Perkin Trans. 2, 37 (1983).
37. P. Bickart, F.W. Carson, J. Jacobus, E.G. Miller, and K. Mislow. J. Am. Chem. Soc. **90**, 4869 (1968).
38. (*a*) M.J.S. Dewar and R.S. Pyron. J. Am. Chem. Soc. **92**, 3098 (1970); (*b*) P.S. Engel. Chem. Rev. **80**, 99 (1980).
39. A. Schulz and C. Rüchardt. Tetrahedron Lett. 3883 (1976).

© 2006 NRC Canada

Absolute configuration assignments by experimental and theoretical approaches of *ent*-labdane- and *cis-ent*-clerodane-type diterpenes isolated from *Croton glabellus*[1]

Abraham García, Teresa Ramírez-Apan, J. Antonio Cogordan, and Guillermo Delgado

Abstract: The bioassay-guided fractionation of the moderately cytotoxic extract from *Croton glabellus* resulted in the isolation of bioactive compounds, which were characterized as austroinulin (2), 6-*O*-acetylaustroinulin (**3**), the acetonide artifact of **2** (**4**), and 3-*O*-methylkaempferol (**9**). In addition, a new natural *cis-ent*-clerodane lactone diterpene named marrubiagenin (**1**), *trans*-dehydrocrotonin (**6**), the epimeric mixture of cajucarinolide (**7/8**), and 5,7,3′,4′-tetrahydroxy-3-methoxyflavonoid (**10**) were also characterized and identified as nonbioactive compounds. The structures of all compounds were determined by analyses of their physical and spectroscopic data and by comparison with those reported in the literature. The absolute configuration assignment of **3** was carried out by means of the modified Mosher method and by the experimental and theoretical circular dichroism method establishing that **3** belongs to the *ent*-labdane diterpene series. Furthermore, the absolute configuration of **1** was established by analysis of its chiroptical properties concluding that **1** belongs to the *cis-ent*-clerodane diterpene series.

Key words: Croton glabellus, *ent*-labdane-type diterpenes, *cis-ent*-clerodane-type diterpenes, circular dichroism, TD-DFT.

Résumé : Un fractionnement orienté par des bioessais du mélange modérément cytotoxique extrait de *Croton glabellus* a permis d'isoler et de caractériser des composants bioactifs, dont l'austroinuline (**2**), la 6-*O*-acétylautroinuline (**3**), l'acétonide **4**, un artefact du composé **2** et le 3-*O*-méthylkaempférol (**9**). On a aussi isolé et caractérisé des composés qui ne sont pas bioréactifs, dont une nouvelle lactone diterpénique naturelle de la famille du *cis-ent*-clérodane dénommée marrubiagénine (**1**) ainsi que des produits déjà connus, dont la *trans*-déshydrocrotonine (**6**), un mélange d'épimères du cajucarinolide (**7/8**) et le 5,7,3′,4′-tétrahydroxy-3-méthoxyflavonoide (**10**). Les structures de tous les composés ont été déterminées sur la base d'analyses de données spectroscopiques et physiques et par comparaison avec les données rapportées dans la littérature. L'attribution de la configuration absolue du composé **3** a été faite sur la base de la méthode de Mosher modifiée et par la méthode de dichroïsme circulaire théorique et expérimentale et elle a permis d'établir qu'il appartient à la série diterpénique du *ent*-labdane. De plus, en se basant sur ses propriétés chiroptiques, on a établi que la configuration absolue du composé **1** le situe dans la série diterpénique *cis-ent*-clérodane.

Mots clés : Croton glabellus, diterpène de type *ent*-labdane, diterpènes de type *cis-ent*-clérodane, dichroïsme circulaire, TD-DFT.

[Traduit par la Rédaction]

Introduction

Croton glabellus (Euphorbiaceae) is a plant widely distributed from Mexico to South America whose infusions of leaves and bark are mainly used against cancer and wound infections (1). Previous reports on the chemical constituents of *Croton* species have illustrated the predominance of *cis*- and *trans*-clerodane-type diterpenes (2–4) and some labdane-type diterpenes (5) that are principally confined to the chemistry of *Stevia* (Compositae) (6–9). It has also been reported that some clerodane-type diterpenes possess cytotoxic properties (10).

In the search of new bioactive constituents from the family Euphorbiaceae (11), the CH_2Cl_2–MeOH extract obtained from the leaves of *C. glabellus* was studied because of its moderate cytotoxic properties exhibited against five human tumor cell lines. Chemical investigations of the organic extract led to the purification and characterization of a new natural *cis*-clerodane lactone diterpene (**1**), three *ent*-labdane-type diterpenes (**2**–**4**) (7, 8), three clerodane-type diterpenes (**6**–**8**) (2–4), two 3-*O*-methylflavonoids (**9**, **10**) (12, 13), together with β-sitosterol, β-sitosteryl β-*D*-

Received 6 July 2006. Accepted 3 October 2006. Published on the NRC Research Press Web site at http://canjchem.nrc.ca on 1 December 2006.

A. García, T. Ramírez-Apan, J.A. Cogordan, and G. Delgado.[2] Instituto de Química, Universidad Nacional Autónoma de México. Ciudad Universitaria, Circuito Exterior, Coyoacán 04510. México, D.F.

[1]Taken in part from the PhD thesis of AG.

[2]Corresponding author: (e-mail: delgado@servidor.unam.mx).

 doi:10.1139/V06-164 © 2006 NRC Canada

Table 1. Cytotoxic activities of compounds **2**–**4**, **9**, and the synthetic derivatives **2a** and **2b**.

Compound	U251	PC3	K562	HCT15	MCF7
2	34.2±7.06	Nd	18.30±1.80	33.94±8.92	Nd
2a	Nd	32.13±1.76	31.34±3.25	Nd	Nd
2b	Nd	60.77±5.46	29.82±1.24	44.12±5.10	46.82±6.02
3	Nd	Nd	19.83±0.56	31.93±7.30	Nd
4	Nd	27.93±2.14	37.56±10.5	Nd	32.95±5.48
9	18.32±6.07	Nd	16.64±4.20	20.69±1.23	Nd
Adriamycin	0.32±0.02	0.19±0.01	0.28±0.01	0.23±0.02	0.14±0.01

Note: IC_{50} values are given in μmol/L with ± standard error. Adriamycin was used as the positive control. Nd = Not determined.

glucopyranoside, and sucrose. Compounds **2**–**4** and **9** exhibited moderate cytotoxic properties, with **9** being the most active.

This paper reports the stereostructural determination of **1**, **3**, and **7/8** and the absolute configuration assignments of **1** and **3** by circular dichroism (CD), the application of the exciton chirality method for **3** (14), and the diene helicity rule (quadrant diene rule) for a derivative of **1** (15). The relative configuration of **3** was corroborated by an X-ray analysis and its absolute configuration was established by the application of the empirically modified Mosher method (16) and confirmed by the theoretical simulation of the electronic circular dichroism (ECD) spectrum of its derivative **2b**, using the time dependent density functional theory (TD-DFT) approach. Additionally, the cytotoxic activity of the isolated compounds is reported.

Results and discussion

The bioassay-guided fractionation of the moderately cytotoxic extract from the leaves of *C. glabellus*, using the K562 (leukemia, IC_{50} = 17.79 ± 2.97 μg/mL) and HCT15 (colon cancer, IC_{50} = 31.93 ± 7.3 μg/mL) tumor cell lines as the pilot cells, led to the isolation and characterization of austroinulin (**2**) (8), 6-*O*-acetylaustroinulin (**3**) (7), an acetonide artifact (**4**, formed during the isolation process by reaction of the diol and acetone), and 3-*O*-methylkaempferol (**9**) (12) as the bioactive constituents (Table 1). After the isolation and purification process, a new natural *cis-ent*-clerodane-type diterpene (**1,** previously characterized as the aglycone of marrubiaside), *trans*-dehydrocrotonin (**6**) (2, 3), the epimeric mixture of cajucarinolide (**7/8**) (4), 5,7,3′,4′-tetrahydroxy-3-methoxyflavonoid (**10**) (13), β-sitosterol, β-sitosteryl β-*D*-glucopyranoside, and sucrose were also isolated and characterized. The structures of all compounds were established by means of a careful revision of their physical and spectroscopic properties and by comparison with those reported in literature for related metabolites.

Compound **1** was isolated as optically pure colourless needles ($[\alpha]_D^{25}$ +54.4) and presented the molecular formula $C_{20}H_{28}O_4$, which was established by HRMS–FAB (*m/z*: 333.2076 $[M + H]^+$) and confirmed by 20 carbon signals observed in the ^{13}C NMR spectrum. The IR spectrum exhibited absorption bands for carboxylic acid (HO, 3500–2636 and 1779 cm^{-1}; C=O, 1679 cm^{-1}) and lactone ring functionalities (C=O, 1746 cm^{-1}). The ^1H NMR spectrum (Table 2) showed two vinylic proton signals at δ: 6.82 (t, *J* = 4.0 Hz, H-3) and δ: 5.86 (quint, *J* = 1.5 Hz, H-14), which were positioned β and α to carbonyl groups, respectively; also, a singlet was observed at δ: 4.76 (2H, d, *J* = 2.0 Hz, H-16) that was attributed to two chemically equivalent oxymethylene protons. In addition, the ^1H NMR spectrum exhibited three simple signals at δ: 1.25 (3H, s, H_3-19), 0.83 (3H, s, H_3-20), and 0.78 (3H, d, *J* = 6.5 Hz, H_3-17), which correspond to three methyls. The *cis*-clerodane skeleton of **1** was confirmed by analyses of its HSQC and HMBC spectra, whereas its *cis*-decalin fusion was established by an analysis of the NOESY spectrum, which showed relevant NOE interactions between H-10β (δ: 1.40) and H_3-19 (δ: 1.25). Thus, the OR, MS, IR, and NMR data observed for **1** were quite identical to those reported for the *cis*-clerodane-type diterpenes named marrubiagenin (17, 18) and amphiacric acid (19).

Marrubiagenin was reported at first by Tschesche and Plenio (17) as the acid hydrolysis derivative from the

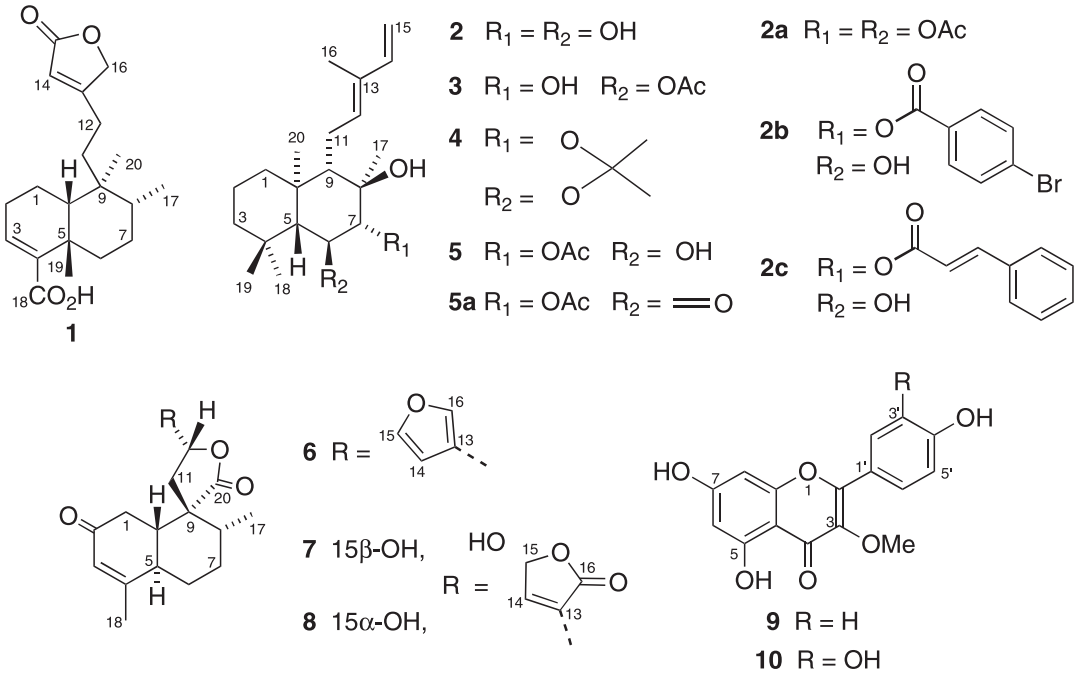
Table 2. ^1H (500 MHz) and ^{13}C (125 MHz) NMR data for marrubiagenin (**1**).

Position	^1H	^{13}C
1β	2.06 m	17.0
1α	1.79 br dd (15.5, 9.0)	
2α	2.46 ddd (13.0, 9.0, 4.0)	24.3
2β	2.27 m	
3	6.82 t (4.0)	142.1
4		137.3
5		36.3
6β	2.75 ddd (17.0, 11.5, 3.5)	36.7
6α	1.11 ddd (16.5, 13.5, 3.0)	
7α	1.18 dddd (16.0, 14.0, 14.0, 2.0)	28.5
7β	1.32 m	
8β	1.47 m	37.9
9		40.3
10β	1.40 dd (6.5, 1.0)	45.5
11a	1.73 dd (10.5, 7.0)	35.2
11b	1.55 dd (10.5, 7.0)	
12 (2H)	2.27 m	22.2
13		170.9
14	5.86 quint (1.5)	115.1
15		174.0
16 (2H)	4.76 d (2.0)	73.1
17	0.78 d (6.5)	15.9
18		171.7
19	1.25 s	33.4
20	0.83 s	17.9

Note: Spectra were recorded in $CDCl_3$. δ values are given in ppm and *J* values are in Hz.

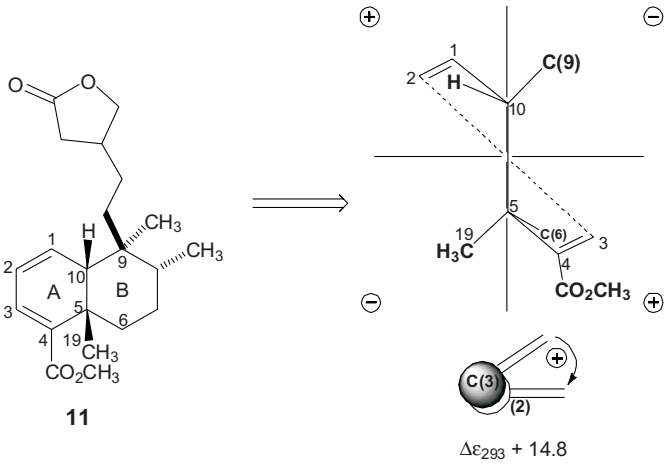
© 2006 NRC Canada

Fig. 1. Natural products (**2**, **3**, **6–10**) isolated from *C. glabellus*, derivatives **2a–2c** and **4**, and compounds **5** and **5a** taken from ref. 8.



diterpene glucoside marrubiaside isolated from *Leonurus marrubiastrum* and then presumably by Tonn and coworkers (18) as a constituent of *Baccaris sagittalis*. However, the configuration of the substance from *Baccharis* was not determined. Amphiacric acid ($[\alpha]_D^{25}$ – 60.5°) (19) and the substance from *Baccharis* ($[\alpha]_D^{25}$ –58°) (18) exhibited negative optical rotation values, which are opposite to that found for **1** ($[\alpha]_D^{25}$ +54.4°) in this study. The enantiomeric relative configurations reported for amphiacric acid and the substance from *Baccharis* are not consistent with their negative values of optical rotation; therefore, they should be referred to as the same compound. Although the optical rotation for marrubiagenin was not reported by Tschesche and Plenio (17), we compared the observed molar ellipticity (included in the paper) with that found for **1** (this study) and that reported for amphiacric acid (19). Compound **1** ($[\theta]_{242}$ +18 886) and marrubiagenin ($[\theta]_{243}$ +21 054) (17) exhibited first positive Cotton effects in their circular dichroism (CD) spectra, whereas amphiacric acid ($[\theta]_{235}$ –14 900) (19) showed a first negative Cotton effect. These differences confirmed that they are enantiomers. The *cis*-β-decalin fusion of marrubiagenin was established by the analysis of the CD data for its diene derivative **11** and we took those data into account to establish the absolute configurations of **1** and to define the corresponding configuration for amphiacric acid.[3] Diene derivative **11** showed a positive Cotton effect at 293 (Δε +14.8, reported in ref. 17), which can be attributed to the $\pi \rightarrow \pi^*$ electric transition band of the conjugated diene chromophore. Applying the diene helicity rule (15), it can be deduced that the diene derivative **11** contributes to the positive Cotton effect and has the absolute configuration depicted for **1** in Fig. 1. Neither the conformational change of ring B (chair to boat) nor the presence of the alkyl lactone

Fig. 2. Model deduced by application of the diene helicity rule and quadrant diene rule for derivative **11** (Δε value was taken from ref. 17).



fragment bonded to C-9 contribute to the CD properties of **1**, **11**, and several synthetic derivatives from marrubiasid (17); therefore, they do not interfere with the application of the diene helicity rule. Furthermore, the application of the quadrant diene rule (Fig. 2) determines that the allylic hydrogen at C-10 and the helicity of the diene system constitute the main positive contributions to the first Cotton effect. Therefore, it can be established that **1** (this study) and marrubiagenin have the same absolute configuration (5*S*,10*R*), whereas the corresponding configuration for amphiacric acid and the substance from *Baccharis* should be referred as 5*R*,10*S* (see the configuration depicted for

[3] Derivative **11** was obtained by chemical derivatization from the natural product named marrubiasid (17). CD data were taken from the same reference and were analyzed here to establish the absolute configuration of **1**.

© 2006 NRC Canada

amphiacric acid in ref. 19). Therefore, marrubiagenin (**1**) represents a new natural product assigned to the *cis-ent*-clerodane diterpene series (*cis*-β).

Compound **3** showed a positive optical rotation sign ($[\alpha]_D^{25}$ +34.2) and presented the molecular formula $C_{22}H_{36}O_4$, which was deduced from the HRMS–FAB (364 [M^+] (1%); *m/z*: 347.2589, [$M - H_2O + H]^+$) and the ^{13}C NMR and DEPT spectra. All the spectrometric, spectroscopic, and optical data observed for **3** were quite identical to those reported for 6-*O*-acetylaustroinulin whose absolute configuration remains ambiguous (7, 8), notwithstanding that some attempts have been directed towards this challenge. In 1987, Bohlmann and coworkers (8) assigned the absolute configuration of 7-*O*-acetylaustroinulin (**5**), an isomer of **3**, by the CD method and application of the octant rule for its oxidized derivative **5a** (20, 21), which exhibited a negative Cotton effect in the CD spectrum ($\Delta\varepsilon_{295}$ –1.5). The authors concluded that the Cotton effect was principally due to the methyl group at position C-4 and that **5a** belongs to the *ent*-labdane diterpene series; however, they did not analyze the dominant (negative or positive) contribution due to the free rotating conjugated diene fragment at position C-9. Bohlmann's conclusion was contradicted by Ishibashi and coworkers (22) who proposed that **2** belongs to the normal labdane diterpene series according to the results obtained by the application of the modified Mosher method. To clarify these inconsistencies, we attempted three approaches towards the assignment of the absolute configuration of the structural analogue **3** based on the application of the modified Mosher method for its hydrolyzed derivative **2**, followed by the analysis of the experimental CD method for its esterified derivative **2b**, and finally by the theoretical simulation of the ECD spectrum for **2b**.

First, a conformational study of **3** and its structural analogues **2**, **2a**–**2c**, and **4** led to the analysis of CD data for **5a** and allowed us to confirm the previous configurational assignment by Bohlmann and coworkers (8). For this purpose, the solid-state conformation of **3** obtained by an X-ray analysis of a single crystal (Table 3)[4] was compared with its preferred conformation in solution by a NOESY spectrum analysis. Relevant NOE interactions between H-14 and H_2-11, between H-11_a and H_3-20, between H-11_b and H_3-17, and between H-12, H_3-16, and H-9 established that the conformation of **3**, in solution and at room temperature (Fig. 3), is the same as that found in the solid state (Fig. 4, X-ray analysis not previously reported). Analyses of NOESY spectra of compounds **2**–**4** and the synthetic derivatives **2a**–**2c** indicated that the orientation of the planar *trans*-conjugated-diene unit does not change because of the presence or absence of functional groups at C-6 or C-7, which allowed us to establish the same main conformation for all compounds. In this context, the major part of the molecular volume (the diene fragment, the acetoxy group, and part of the decalin skeleton) of the minimum energy structure of **5a** (Fig. 5), which was generated using the MMX force field as implemented in the PCMODEL program (23), is located in negative octants. According to the absolute configuration of **5**, depicted in Fig. 1, a negative Cotton effect is predicted for the $n \rightarrow \pi^*$ ketone transition in the CD curve, which can be corroborated by the sign of the reported molar ellipticity $[\theta]_{295}$ –4 900 (8). This CD analysis supports the proposed absolute configuration for **5** (8) and suggests that **2** and **3**, which were reported as constituents of the same source as that of **5** (8), have the same absolute configuration. To ascertain the latter and to determine whether or not the conclusion of Ishibashi and coworkers (22) should be considered, **3** was subjected to alkaline hydrolysis to give **2**, which was then reacted in situ with the *R*-(+)- and *S*-(–)-α-methoxy-α-trifluoromethylphenylacetyl chloride to obtain its corresponding diastereoisomers according to the modified Mosher method (**2d** and **2e**, Fig. 6) (16). Chemical derivatization of **3**, to furnish **2b** and **2c**, revealed the preferred esterification of the secondary hydroxyl at position

Table 3. X-ray crystallographic information for 6-*O*-acetylaustroinulin (**3**).

Compound	**3**
Empirical formula	$C_{22}H_{36}O_4$
Formula mass	364.51
Colour, shape	Colourless, prism
Crystal dimension (mm^3)	0.488 × 0.144 × 0.114
Crystal system	Orthorhombic
Space group	$P\ 2_12_12_1$
Z	4
a (Å)	6.0067(4)
b (Å)	18.178(1)
c (Å)	19.173(1)
α (°)	90
β (°)	90
γ (°)	90
Collection ranges	$-7 \le h \le 7$, $-23 \le k \le 23$, $-24 \le l \le 24$
Temperature (K)	294(2)
Volume ($Å^3$)	2093.5(2)
$D_{calcd.}$ ($Mg\ m^{-3}$)	1.156
Radiation	Mo Kα (λ= 0.710 73 Å)
Absorption coefficient (μ) (mm^{-1})	0.077
F(000)	800
θ Range for data collection (°)	2.12–27.50
Observed reflections.	21 049
Independent reflections	4806 [R_{int} = 0.0766]
Data/restraints/parameters	4806/0/247
Goodness-of-fit on F^2	1
Final *R* indices [$I > 2\sigma(I)$]	*R*1 = 0.0603, *wR*2 = 0.0644
R indices (all data)	*R*1 = 0.1188, *wR*2 = 0.0733
Largest diff. peak and hole (e $Å^3$)	0.137 and –0.168

[4] Supplementary data for this article are available on the journal Web site (http://canjchem.nrc.ca) or may be purchased from the Depository of Unpublished Data, Document Delivery, CISTI, National Research Council Canada, Ottawa, ON K1A 0R6, Canada. DUD 5107. For more information on obtaining material refer to http://cisti-icist.nrc-cnrc.gc.ca/irm/unpub_e.shtml. CCDC 603409 contains the crystallographic data for this manuscript. These data can be obtained, free of charge, via http://www.ccdc.cam.ac.uk/conts/retrieving.html (Or from the Cambridge Crystallographic Data Centre, 12 Union Road, Cambridge CB2 1EZ, UK; fax +44 1223 336033; or deposit@ccdc.cam.ac.uk).

© 2006 NRC Canada

Fig. 3. Key NOESY interactions of **3**.

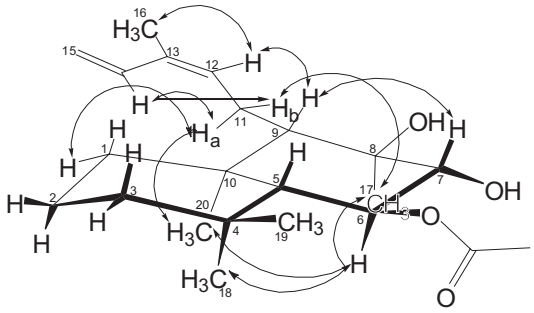
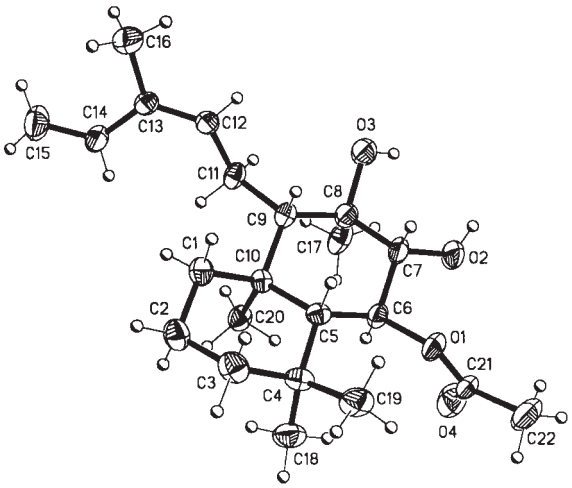


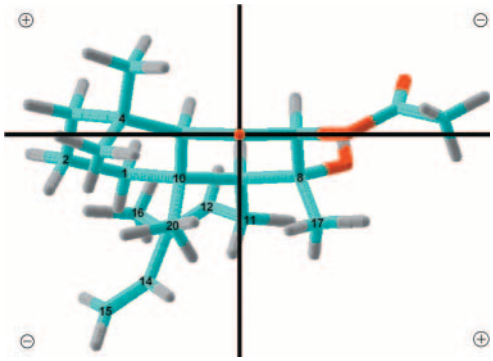
Fig. 4. ORTEP view of the X-ray diffraction structure of **3**.



C-7 and the same happened with the formation of Mosher esters. The difference between the chemical shifts of selected hydrogens of the *S*-MTPA (**2d**) and the *R*-MTPA (**2e**) established the 7*R* absolute configuration for **3** (Fig. 6). This result indicates that **3** belongs to the *ent*-labdane diterpene series, as initially proposed by Bohlmann and coworkers (8) and it does not agree with the absolute configuration of **2** proposed by Ishibashi and coworkers (22).

To support our conclusion, **3** was hydrolyzed and esterified to obtain the 7-*p*-bromobenzoylated derivative **2b**, which was then subjected to several unsuccessful crystallization processes where the crystals formed were not suitable for an X-ray diffraction analysis. Nevertheless, considering the *trans*-conjugated-diene and the benzoate chromophores in **2b** and according to the exciton chirality method applied for a diene-benzoate system (14), it was decided to analyze **2b** by the CD method. The CD spectrum of **2b** showed a first positive Cotton effect at 247 nm and a second negative Cotton effect at 231 nm, which were attributed to the $\pi \rightarrow \pi^*$ intramolecular charge transfer bands of the *p*-bromobenzoate and the planar *trans*-conjugated-diene chromophores. According to the exciton chirality method, the CD spectrum of **2b** showed the characteristic exciton-split CD curves due to the interactions between both chromophores (Fig. 7). The exciton splitting was corroborated by an analysis of the CD data of derivative **2c**, which exhibited bisignated CD curves with similar intensities

Fig. 5. Application of the octant rule for the minimum energy structure (PCMODEL) of **5a**.



($[\theta]_{276}$ +6737 and $[\theta]_{266}$ +6961, $[\theta]_{237}$ −15667) (Fig. 7). The positive chirality between the electric transition moments of the benzoate and the *trans*-conjugated-diene chromophores in derivatives **2b** and **2c** allowed us to assign the absolute configuration of **3** as shown in Fig. 1. Thus, it was possible to reinforce that **3** belongs to the *ent*-labdane-type diterpene as was deduced in this work by the application of the modified Mosher method.

The absolute configuration, deduced from experimental CD data, was confirmed by means of the calculated ECD spectrum of the derivative **2b** (24). Following the computational details (described in the experimental section), rotatory strengths were calculated for the velocity and length formalisms. The velocity and length rotatory strengths exhibited similar values. Thus, the computed velocity data were used to reproduce the experimental ECD spectrum. Calculated excitation energies showed a bathochromic shift of ca. 0.4 eV relative to transitions in the experimental CD of **2b**, whereas the intensities of the two Cotton effects are in agreement with the experimental ones (Fig. 8). Our computed ECD spectrum of **2b**, illustrated in Fig. 8, exhibited the characteristic exciton-split CD curves due to the electric dipole – electric dipole interaction of the *p*-bromobenzoate and the *trans*-conjugated-diene chromophores. This exciton splitting can be attributed to the $\pi \rightarrow \pi^*$ transitions of the interacting electric transition moments of the benzoate-diene chromophores of **2b**. The first positive Cotton effect at ca. 274 nm and the second negative Cotton effect at ca. 256 nm from the theoretically computed ECD spectrum of **2b** are in agreement with the experimental CD curves (Fig. 8).

After the isolation and purification process of natural compounds, a white amorphous solid was isolated and characterized by detailed NMR analyses as the acetonide artifact (**4**, formed during the isolation process since acetone was used as a component of the eluting system for chromatographies; see the Experimental section).

Compounds **7** and **8** were isolated as a beige amorphous solid (238–240 °C), which was composed of an epimeric mixture of cajucarinolide as can be deduced from the duplicated pattern of signals in the ^{1}H and ^{13}C NMR spectra (Fig. 9) and their comparison with those reported for cajucarinolide (4). One set of these NMR data was quite identical to those reported for the clerodane-type diterpene named cajucarinolide (4); however, an additional hemiacetal

© 2006 NRC Canada

Fig. 6. Application of the modified Mosher method to determine the absolute configuration at C-7 of **3**. $\Delta\delta$ ($\delta_S - \delta_R$) values are given in ppm.

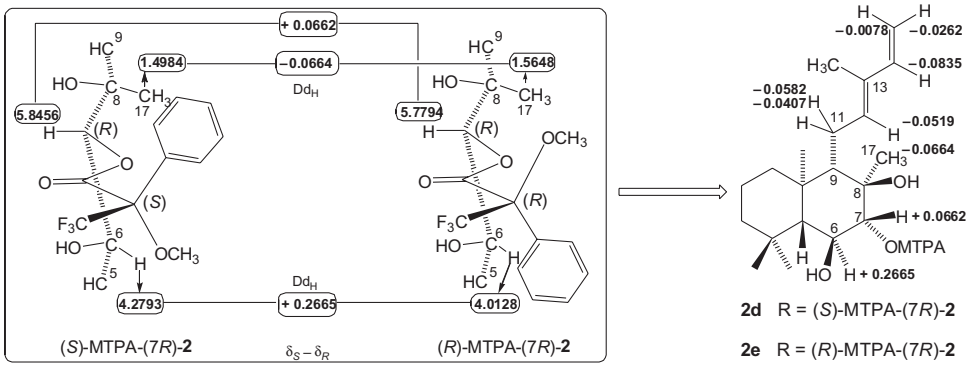


Fig. 7. CD spectra of synthetic derivatives **2b** (red line in the Web version; line *a* in the print version) and **2c** (blue line in the Web version; line *b* in the print version).

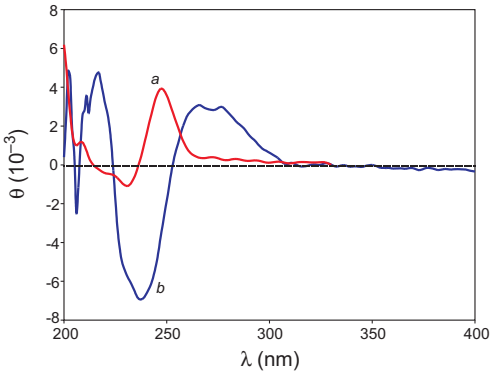
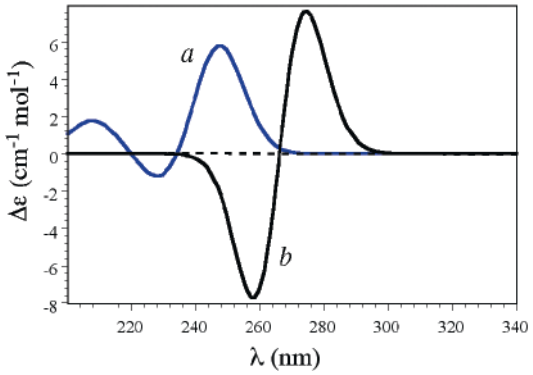


Fig. 8. Comparison between the experimental (blue line in the Web version; line *a* in the print version) and the theoretical CD spectrum (black line in the Web version; line *b* in the print version) of **2b**.

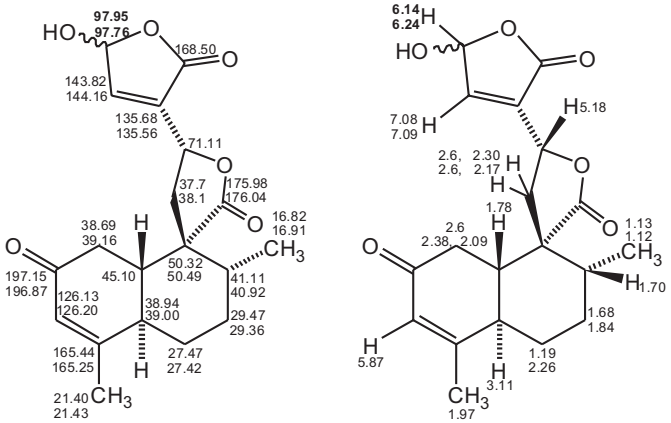


group (δ: 6.14, H-15 and δ: 97.76, C-15) suggested the presence of its epimer at C-15. This functional group allowed us to establish that the second set of proton signals corresponds to the epimer of cajucarinolide and not to the presence of its isomer named isocajucarinolide (4), which was reported to have a vinylic proton positioned α to carbonyl group at δ: 6.12 (H-14) and an hemiacetal proton at δ: 6.19 (H-16) [data taken from ref. 4]. This vinylic proton (H-14, δ: 6.12) was not observed for the mixture **7/8**; instead, two vinylic protons β to carbonyl group (δ: 7.09 and 7.08) and two hemiacetal protons (δ: 6.24 and 6.14) were found. These spectroscopic data support the epimeric mixture at C-15 of cajucarinolide (**7/8**), which could not be separated because of the minute amounts of substance available.

Conclusions

The bioassay-guided fractionation of the moderately cytotoxic extract from the aerial parts of *C. glabellus* led us to the isolation of the bioactive constituents **2**–**4** and **9**, which exhibited moderate cytotoxicities against the U251, K562, and HCT15 cell lines (Table 1). The leukemia cell line (K562) was the most sensitive to the tested compounds, with **9** being more potent than the *ent*-labdane-type diterpenes. It is interesting to mention that clerodane-type diterpenes (**1**, **6**–**8**) did not show remarkable cytotoxic activities (these compounds were tested at 50 µmol/L and exhibited ca. 20% tumor cell growth inhibition and no further

Fig. 9. ^{13}C and ^{1}H NMR chemical shifts for the epimeric mixture at C-15 of **7/8**.



experiments were carried out), contrary to those exhibited for the *ent*-labdane series (**2**–**4**). In addition, it can be noted that the functional group variation at C-6 or C-7 in the *ent*-labdane-type diterpenes did not modify their cytotoxic properties noticeably.

Additionally, the applicability of the circular dichroism method and its rules in the determination of the absolute configurations of chiral molecules was extended here for the

© 2006 NRC Canada

analysis of **1** and **3** by the diene helicity rule (quadrant diene rule) and the exciton chirality method, respectively. Furthermore, the theoretical ECD simulation of **2b** by TD-DFT/B3LYP/H–W showed that the two Cotton effects between 230 and 280 nm are due to the dipole–dipole coupling of the *p*-bromobenzoate and the *trans*-conjugated-diene chromophores, which is in agreement with the experimental spectrum in that region. The experimental and theoretical ECD results support the *ent*-labdane classification of **3**, which was also determined by the modified Mosher method. These conclusions do not agree with previous assignments (22), which should be re-examined.

Experimental

General experimental procedures

Uncorrected melting points were determined on a Fisher-Johns apparatus. Optical rotations were measured on a PerkinElmer 341 polarimeter. IR spectra were recorded on a Nicolet Magna FT-IR 750 spectrometer. UV spectra were performed on a Shimadzu-UV160 spectrophotometer. Circular dichroism spectra were recorded on a Jasco-J720 spectropolarimeter. ^{1}H and ^{13}C NMR spectra were recorded on a Varian Unity Plus 500 spectrometer (at 500 and 125 MHz) and on a Bruker Avance 300 spectrometer (at 300 and 75 MHz). EI and HR–FAB mass spectra were measured on Jeol JMS-AX505HA and JMX-SX102A mass spectrometers, respectively. Column chromatography (CC) was performed using silica gel 60 (70–230 mesh). Thin layer chromatography (TLC) and preparative TLC (PTLC) were performed using the silica gel 60 F_{254} (Merck) plates.

Plant material

C. glabellus was collected in Los Tuxtlas, Veracruz, México, on April 2003 and authenticated by M. Sc. Verónica Juárez Jaimes (Instituto de Biología, UNAM). A voucher specimen was deposited in the National Herbarium, UNAM, with the register number MEXU-1104456.

Extraction and separation

The leaves (5.5 kg) of *C. glabellus* were dried at RT and extracted with a mixture of CH_2Cl_2–MeOH (1:1) for 48 h, three times. The crude extract was evaluated against five human tumor cell lines showing major bioactivity against K562 and HCT15 cells (IC_{50} = 17.79 ± 2.97 and IC_{50} = 31.93 ± 7.3, respectively). Then, the crude extract (270 g) was dissolved in a mixture of CH_2Cl_2–MeOH (1:1), adsorbed in silica gel 60, and subjected to CC (silica gel 60, hexane, hexane–AcOEt, AcOEt–MeOH, and MeOH). Seventeen main fractions (A–Q) were obtained according to their similarity pattern in TLC. Fractions E–L showed 90%–100% tumor cell growth inhibition; thus, these fractions were processed until the isolation and purification of the bioactive constituents. β-sitosterol (32.9 mg) (CC, Hex–AcOEt 9:1) was obtained from D. Forty-five milligrams of **3** (CC, Hex–AcOEt 7:3) and 32 mg of **6** (PTLC, Hex–AcOEt 75:25) were isolated from E. Nine hundred fifty-two milligrams of **3** (CC, Hex–AcOEt 7:3) were obtained from F. Sixteen milligrams of **2** (CC, Hex–Acetone 3:2 and PTLC, Hex–Acetone 3:2), 4.11 g of **3** (CC, Hex–AcOEt 7:3), 28 mg of **4** (CC, Hex–Acetone 3:2), 3.6 mg of **1** (CC, Hex–Acetone 4:1), and 23 mg of **9** (CC, Hex–Acetone 7:3) were isolated from G. Thirty-five milligrams of **2** (CC, Hex–Acetone 3:2), 436 mg of **3**, 5.3 mg of the epimeric mixture of **7/8** (CC, Hex–Acetone 3:2), and 38 mg of **9** (CC, Hex–Acetone 3:2) were isolated from H and I. Five milligrams of **10** (CC, Hex–AcOEt 1:1) and 57 mg of **2** were obtained from J. β-sitosteryl (1.45 g) β-*D*-glucopyranoside (CC, AcOEt) was isolated from K and L. Four hundred milligrams of sucrose (CC, AcOEt–MeOH 3:2) was obtained from fraction O.

Marrubiagenin (1)

Colourless needles; mp 174 to 175 °C. $[\alpha]_D^{25}$ +54.4° (*c* 0.18, $CHCl_3$). UV–vis (MeOH, *c* 3 × 10^{-5} mol/L) nm (log ε): 225 (3.68); (lit. value (19) (log ε): (MeOH) 208 (4.30)), (lit. value (17) (log ε): (CH_3CN) 209 (4.30)). CD (MeOH, *c* 3 × 10^{-5} mol/L): $[\theta]_{210}$ –13 240, $[\theta]_{216}$ –9 946, $[\theta]_{242}$ +18 886; (lit. value (19) (MeOH, *c* 3 × 10^{-5} mol/L) $[\theta]_{205}$ +5 300, $[\theta]_{215}$ 0, $[\theta]_{235}$ –14 900); (lit. value (17) (MeOH) Δε: 243 (+6.38) = $[\theta]_{243}$ +21 054, 215 (–2.16) = $[\theta]_{215}$ –7 128). IR ($CHCl_3$, cm^{-1}) ν_{max}: 3500–2636, 1779 (CO-OH), 1746 (C=O lactone ring), 1679 (C=O α,β-unsaturated acid), 1635 (C=C), 1267, 1173 (C-O). ^{1}H NMR ($CDCl_3$, 500 MHz) and ^{13}C NMR ($CDCl_3$, 125 MHz) see Table 2. EIMS 332 (7, $[M^+]$), 333 (2, $[M + H]^+$), 314 (67, $[M - H_2O]^+$), 299 (100, $[M - CH_3 - H_2O]^+$), 271 (15), 203 (31), 125 (22), 111 (19, $[C_6H_7O_2]^+$), 98 (16, $[C_5H_6O_2]^+$), 91 (19), 69 (24), 57 (23), 55 (23), 41 (17), 28 (14). HRMS–FAB *m/z* calcd. for $C_{20}H_{29}O_4$: 333.2066 $[M + H]^+$; found: 333.2076.

Austroinulin (2)

White powder; mp 76–78 °C. $[\alpha]_D^{25}$ +24.77° (*c* 0.44, MeOH). EIMS, IR, ^{1}H and ^{13}C NMR data were identical to those reported (8).

6-*O*-Acetylaustroinulin (3)

Colourless crystals; mp 162–165 °C. $[\alpha]_D^{25}$ +34.2° (*c* 1.0, $CHCl_3$). IR ($CHCl_3$, cm^{-1}) ν_{max}: 3581 (OH), 2932, 2875, 1726 (C=O), 1253 (C-O), 1641, 975 y 909 (C=C). ^{1}H NMR ($CDCl_3$, 500 MHz) δ: 6.87 (ddd, *J* = 17.1, 10.8, 0.9 Hz, H-14), 5.44 (t, *J* = 7.2 Hz, H-12), 5.19 (d, *J* = 17.4 Hz, H-15), 5.12 (dd, *J* = 11.4, 9.9 Hz, H-6α), 5.10 (dd, *J* = 11.4, 2.1 Hz, H-15), 3.46 (d, *J* = 10.2 Hz, H-7β), 2.48 (ddd, *J* = 15.9, 4.5, 1.2 Hz, H-11a), 2.25 (dt, *J* = 16.2, 6.0 Hz, H-11b), 2.12 (s, H_3C-Ac), 1.79 (d, *J* = 1.2 Hz, H3–16), 1.61 (dtd, *J* = 13.0, 5.0, 1.5 Hz, H-1a), 1.56 (ddt, *J* = 13.5, 13.0, 4.0 Hz, H-2a), 1.41 (dt, *J* = 14.5, 5.0 Hz, H-2b), 1.40 (d, *J* = 11.0 Hz, H-5β), 1.39 (t, *J* = 5.5 Hz, H-9β), 1.34 (dtd, *J* = 13.5, 5.0, 1.5 Hz, H-3a), 1.23 (s, H-17); 1.22 (m, H-3b), 1.01 (s, H-18), 0.96 (s, H-20), 0.95–0.97 (m, H-1b), 0.87 (s, H-19). ^{13}C NMR ($CDCl_3$, 75 MHz) δ: 171.8 (C=O), 133.6 (C-12), 133.2 (C-14), 131.0 (C-13), 113.8 (C-15), 83.7 (C-7), 76.9 (C-8), 73.2 (C-6), 59.2 (C-9), 56.5 (C-5), 43.4 (C-3), 39.8 (C-1), 39.4 (C-10), 36.0 (C-18), 33.3 (C-4), 22.8 (C-11), 22.2 (C-19), 21.8 (CH_3-CO_2), 19.9 (C-16), 19.5 (C-17), 18.0 (C-2), 16.8 (C-20). EIMS *m/z*: 364 (not observed), 346 (10, $[M - H_2O]^+$), 286 (65, 346 – $C_2H_4O_2$), 205 (95), 137 (67), 81 (93), 43 (100), 18 (10). MS–FAB *m/z*: 364 (1, $[M^+]$), 347 (17, $[M - H_2O]^+$), 287 (55, 347 – $C_2H_4O_2$), 205 (25), 81 (100), 69 (38), 43 (35), 29 (7). HRMS–FAB *m/z* calcd. for $C_{22}H_{34}O_3$: 347.2586 $[M - H_2O + H]^+$; found: 347.2589.

© 2006 NRC Canada

6,7-Diacetylaustroinulin (2a)

Compound **2** (5 mg) was esterified with acetic anhydride and pyridine to afford 4 mg of **2a**. The same procedure was applied to **3** (62.5 mg). ^{1}H NMR ($CDCl_3$, 300 MHz) δ: 6.85 (ddd, *J* = 17.2, 10.8, 0.8 Hz, H-14), 5.43 (t, *J* = 7.4 Hz, H-12), 5.29 (dd, *J* = 10.0, 9.8 Hz, H-6α), 5.19 (d, *J* = 16.8 Hz, H-15), 5.10 (dd, *J* = 10.8, 1.5 Hz, H-15), 4.90 (d, *J* = 10.0 Hz, H-7β), 2.45 (m, H-11a), 2.24 (m, H-11b), 2.06 (s, H_3C(2′)-Ac), 2.01 (s, H_3C(2″)-Ac), 1.78 (d, *J* = 1.2 Hz, H-16), 1.70–1.18 (m, H-1a, H-2a, H2b, H-9, H-5, H-3a, H-3b), 1.22 (s, H-17), 0.97 (s, H-18), 0.95 (s, H-20), 0.95–0.97 (m, H-1b), 0.88 (s, H-19).

7-*p*-Bromobenzoylaustroinulin (2b)

Compound **3** (60 mg) was hydrolyzed with KOH–MeOH (10%) to obtain **2** (36 mg). Then **2** was reacted with *p*-bromobenzoyl chloride in anhydrous pyridine to obtain derivative **2b** (29 mg). UV–vis (*c* 1.98 × 10^{-5} mol/L, EtOH) (log ε): 204 (4.48), 215 (4.17), 241 (4.62). CD (*c* 1.98 × 10^{-5} mol/L, EtOH): $[\theta]_{247}$ +9962, $[\theta]_{231}$ –2760, $[\theta]_{208}$ +2987. ^{1}H NMR ($CDCl_3$, 300 MHz) δ: 7.94 (2H, d, *J* = 9.0 Hz, AA′MM′), 7.58 (2H, d, *J* = 8.7 Hz, AA′MM′), 6.86 (ddd, *J* = 17.4, 10.8, 0.9 Hz, H-14), 5.45 (t, *J* = 7.8 Hz, H-12), 5.20 (d, *J* = 17.1 Hz, H-15_{trans}), 5.10 (dt, *J* = 10.8, 1.8 Hz, H-15_{cis}), 5.02 (d, *J* = 9.9 Hz, H-7β), 3.89 (dd, *J* = 11.2, 9.8 Hz, H-6α), 2.50 (dt, *J* = 15.6, 5.1 Hz, H-11a), 2.23 (dt, *J* = 16.2, 6.0 Hz, H-11b), 1.78 (d, *J* = 1.2 Hz, H_3-16), 1.32 (s, H_3-17), 1.27 (d, *J* = 11.1 Hz, H-5), 1.17 (s, H_3-18), 1.01 (s, H_3-20), 0.96 (s, H_3-19). MS–FAB *m/z*: 504 (2, $[M^+]$), 505 (3), 507 (2), 487 (7, 505 – H_2O), 489 (3, 507 – H_2O), 183 (100, $[C_7H_4OBr]^+$), 185 (97, $[C_7H_4OBr]^+$), 81 (67, $[C_6H_9]^+$).

7-(*E*)-Cinnamoylaustroinulin (2c)

Compound **3** (40 mg) was subjected to alkaline hydrolysis to obtain **2** (31 mg), which was further reacted with (*E*)-cinnamoyl chloride in anhydrous pyridine to give **2c** (23 mg). UV–vis (*c* 4.42 × 10^{-5} mol/L, MeOH) (log ε): 238 (4.34), 277 (4.37). CD (*c* 4.42 × 10^{-5} mol/L, MeOH): $[\theta]_{276}$ +6 737, $[\theta]_{266}$ +6 961, $[\theta]_{237}$ –15 667, $[\theta]_{217}$ –10 710. ^{1}H NMR ($CDCl_3$, 300 MHz) δ: 7.74 (d, *J* = 15.9 Hz, AB), 7.53 (m, 2H), 7.39 (m, 2H), 6.87 (ddd, *J* = 17.1, 10.5, 0.6 Hz, H-14), 6.52 (d, *J* = 16.2 Hz, AB), 5.46 (t, *J* = 7.5 Hz, H-12), 5.19 (dd, *J* = 17.1, 0.6 Hz, H-15_{trans}), 5.10 (dt, *J* = 10.8, 1.5 Hz, H-15_{cis}), 4.90 (d, *J* = 9.9 Hz, H-7β), 3.85 (dd, *J* = 11.1, 9.9 Hz, H-6α), 2.50 (dt, *J* = 15.9, 6.0 Hz, H-11a), 2.23 (dt, *J* = 16.2, 5.7 Hz, H-11b), 1.78 (d, *J* = 1.5 Hz, H_3-16), 1.27 (s, H_3-17), 1.17 (s, H_3-18), 1.02 (s, H_3-19), 0.96 (s, H_3-20).

Preparation of the (*S*)-MTPA and (*R*)-MTPA ester derivatives (2d and 2e) of 3

Compound **3** (35 mg) was hydrolyzed with KOH–MeOH (10%) to afford **2** (16 mg). Then, 2.0 mg of **2** were reacted in situ (into a NMR tube) with 6 μL of the (*R*)-(–)-α-methoxy-α-(trifluoromethyl)phenylacetyl chloride in 0.5 mL of anhydrous pyridine-d_5 (16). The NMR tube was shaken carefully to mix the sample and the reaction was monitored every 2 h by ^{1}H NMR until the (*S*)-MTPA ester derivative (**2d**) of **2** was formed. ^{1}H NMR (pyridine-d_5, 300 MHz) δ: 7.1784 (ddd, *J* = 17.11, 10.83 Hz, H-14), 5.7429 (t, *J* = 7.6 Hz, H-12), 5.8456 (d, *J* = 9.9 Hz, H-7β), 5.2474 (dd, *J* = 17.13 Hz, H-15 *trans*), 5.1285 (dt, *J* = 10.86 Hz, H-15 *cis*), 4.2793 (dd, *J* = 11.0, 10.83 Hz, H-6α), 2.8732 (m, H.11a), 2.3764 (m, H-11b). The procedure described for **2d** was applied to afford the (*R*)-MTPA ester derivative (**2e**) of **2** from the reaction mixture of (*S*)-(+)-α-methoxy-α-(trifluoromethyl)phenylacetyl chloride (6 μL), anhydrous pyridine-d_5 (0.5 mL), and **2** (2.0 mg). ^{1}H NMR (pyridine-d_5, 300 MHz) δ: 7.2619 (ddd, *J* = 17.31, 10.77, 0.78 Hz, H-14), 5.7948 (t, *J* = 7.64 Hz, H-12), 5.7794 (d, *J* = 9.24 Hz, H-7β), 5.2552 (dd, *J* = 17.46, 2.37 Hz, H-15 *trans*), 5.1547 (dt, *J* = 10.89, 1.59 Hz, H-15 *cis*), 4.0128 (dd, *J* = 10.0, 8.97 Hz, H-6a), 2.9314 (m, H.11a), 2.4171 (m, H-11b).

6,7-Isopropylidendioxy-austroinulin (4)

White powder; mp 106–108 °C. $[\alpha]_D^{25}$ +40° (*c* 0.075, MeOH). IR ($CHCl_3$, cm^{-1}) ν_{max}: 3460 (OH), 2985, 2921, 2874, 1370; 1230 (C-O), 1642, 1091, 896 (C=C). ^{1}H NMR (CD_3COCD_3, 500 MHz) δ: 6.95 (ddd, *J* = 17.5, 11.0, 1.0 Hz, H-14), 5.48 (t, *J* = 7.0 Hz, H-12), 5.13 (dd, *J* = 17.0, 1.0 Hz, H-15), 5.03 (dt, *J* = 10.8, 1.5 Hz, H-15), 3.61 (dd, *J* = 11.0, 9.0 Hz, H-6α), 3.49 (OH), 3.42 (d, *J* = 9.5 Hz, H-7β), 2.50 (m, H-11a), 2.27 (m, H-11b), 1.74 (d, *J* = 0.5 Hz, H-16), 1.64–1.58 (2H, m, H-1a, H-2a), 1.42–1.34 (3H, m, H-2b, H-9β, H-3a), 1.35 (d, *J* = 0.5 Hz, H_3-2′), 1.33 (d, *J* = 0.5 Hz, H_3-3′), 1.26 (d, *J* = 11.5 Hz, H-5β), 1.16 (m, H-3b), 1.18 (s, H-17), 1.04 (s, H-18), 0.97 (s, H-20), 0.96 (s, H-19), 0.93 (d, H-1b). ^{13}C NMR (CD_3COCD_3, 125 MHz) δ: 135.7 (C-12), 135.0 (C-14), 130.5 (C-13), 113.5 (C-15), 108.9 (C-1′), 90.8 (C-7), 76.6 (C-6), 75.0 (C-8), 61.5 (C-9), 56.7 (C-5), 42.7 (C-3), 41.5 (C-10), 40.8 (C-1), 35.3 (C-18), 34.1 (C-4), 27.6 (C-3′), 27.1 (C-2′), 23.0 (C-11), 22.5 (C-19), 20.0 (C-16), 19.0 (C-2), 18.6 (C17), 17.0 (C-20). EIMS *m/z*: 362 (1, $[M^+]$), 361 (1, $[M - H]^+$), 344 (10, $[M - H_2O]^+$), 286 (10), 195 (65), 137 (50), 81 (82), 43 (100), 41 (42), 18 (12). HRMS–FAB *m/z* calcd. for $C_{23}H_{39}O_3$: 363.2899 $[M + H]^+$; found: 363.2889.

***trans*-Dehydrocrotonin (6)**

White solid; mp 135 °C (137 to 138 °C). $[\alpha]_D^{25}$ +13° (*c* 0.075, $CHCl_3$). EIMS, IR, ^{1}H and ^{13}C NMR data were identical to those reported (2, 3).

Epimeric mixture of cajucarinolide (7, 8)

Beige powder; mp 238–240 °C. UV–vis (*c* 2.02 × 10^{-5} mol/L, MeOH) (log ε): 205 (4.15), 235 (4.60). CD (*c* 2.02 × 10^{-5} mol/L, MeOH): $[\theta]_{324}$ –8 399, $[\theta]_{271}$ +2 506, $[\theta]_{243}$ –41 300, $[\theta]_{222}$ +56 754. IR ($CHCl_3$, cm^{-1}) ν_{max}: 3273 (OH), 2962, 2859, 1753 (C=O γ-lactone ring), 1661 (C=O α,β-unsaturated), 1213, 1107 (C-O), 1620 (C=C), 755. ^{1}H NMR ($CDCl_3$–DMSO-*d*6 3:1, 300 MHz) δ: 7.08 (2H, t, *J* = 1.2 Hz, H-14′, H-14), 6.24 (t, *J* = 1.2 Hz, H-15′), 6.14 (dd, *J* = 1.2, 1.8 Hz, H-15), 5.87 (2H, s, H-3′, H-3), 5.19 (2H, m, H-12′, H-12), 3.09 (2H, s, H-5′, H-5), 2.60 (m, H-11a), 2.58 (m, H-1a), 2.51 (m, H-11a′), 2.34 (2H, m, H_2-1′), 2.29 (m, H-11b′), 2.23 (2H, m, H-6a′, H-6a), 2.16 (m, H-11b), 2.12 (m, H-1b), 1.97 (6H, d, *J* = 1.0 Hz, H_3-18′, H_3-18), 1.82 (2H, m, H-7a′, H-7a), 1.77 (2H, m, H-10′, H10), 1.70 (2H, m, H-8′, H-8), 1.68 (2H, m, H-7b′, H-7b), 1.19 (2H, td, *J* = 12.6, 3.3 Hz, H-6b′, H6b), 1.13 (3H, d, *J* = 6.6 Hz, H_3-17), 1.12 (3H, d, *J* = 6.6 Hz, H_3-17′). ^{13}C NMR ($CDCl_3$–DMSO-*d*6 3:1, 75 MHz) δ: 197.5 (C-2′), 197.3

© 2006 NRC Canada

(C-2), 176.5 (C-20′), 176.4 (C-20), 168.5 (C-16′, C-16), 165.9 (C-4′), 165.6 (C-4), 144.7 (C-16′), 144.2 (C-14), 136.2 (C-13′), 136.0 (C-13), 126.6 (C-3′), 126.5 (C-3), 98.4 (C-15′), 98.2 (C-15), 71.5 (C-12′, C-12), 50.9 (C-9′), 50.7 (C-9), 45.5 (C-10′, C-10), 41.5 (C-8′), 41.3 (C-8), 39.6 (C-1′), 39.4 (C-5′, C-5), 39.1 (C-1), 38.6 (C-11′), 38.2 (C-11), 29.9 (C-7′), 29.8 (C-7), 27.9 (C-6′), 27.9 (C-6), 21.8 (C-18′, C-18), 17.3 (C-17′), 17.2 (C-17). MS–FAB: 693 (4, $[2(M) + H]^+$), 347 (82, $[M + H]^+$), 259 (51), 243 (100), 154 (80), 136 (68), 91 (32), 77 (30), 55 (25), 43 (18), 41 (21).

3-*O*-Methylkaempferol (9)

Yellow powder; mp 268–270 °C. MS–FAB, IR, ^{1}H and ^{13}C NMR data were identical to those reported (12).

5,7,3′,4′-Tetrahydroxy-3-methoxyflavonoid (10)

White powder; mp 254–256 °C (252–255 °C). EIMS, IR, ^{1}H and ^{13}C NMR data were identical to those published (13).

Computational details

First, a minimum energy structure of **2b** was obtained using the PCMODEL program. Then, geometry optimization was carried out by means of density functional theory employing the hybrid functional B3LYP. To reduce the computational effort for all our quantum mechanical calculations, we employed the Hay and Wadt (H–W) effective core potentials (ECP) together with their associated double-ζ basis sets (25). The optimized geometry was used to carry out theoretical ECD calculations within the time-dependent DFT formalism.[5] Our TD-DFT computations were calculated for singlet states and solved for 10 states. We only considered the spectrum in the [200, 300] nm interval. Rotatory strengths were calculated in the velocity and length formalisms. All these quantum mechanical computations were carried out with the suite of programs in Gaussian 03 (26). The ECD spectrum was simulated by overlapping Gaussian functions for each transition according to (see ref. 24),

$$\Delta\varepsilon(E) = \left(\frac{1}{2.297^{-39}}\right)\left(\frac{1}{\sqrt{2\pi\sigma}}\right) \times \sum_a (\Delta E_{0a})(R_{0a}) \exp\left[-\left(\frac{(E - \Delta E_{0a})}{2\sigma}\right)^2\right]$$

where σ is the width of the band at 1/*e* height and ΔE_{0a} and R_{0a} are the excitations energies and rotatory strengths for transitions 0 to a, respectively. A σ value of 0.2 eV was used.

Cytotoxicity assay

Colon (HCT-15), breast (MCF-7), leukemia (K-562 CML), central nervous system (U-251 Glia), and prostate (PC-3) human tumor cell lines were supplied by National Cancer Institute (NCI), USA. The cytotoxicity of the tumors cells with the test compounds was determined using the protein-binding dye sulforhodamine B (SRB) in microculture assay to measure cell growth (27). The cell lines were cultured in RPMI-1640 (Sigma Chemical Co. Ltd., St. Louis, Missouri), supplemented with 10% fetal bovine serum, 2 μM L-glutamine, 100 IU/mL penicillin G, 100 μg/mL streptomycin sulfate, and 0.25 μg/mL amphotericin B (Gibco). They were maintained at 37 °C in a 5% CO_2 atmosphere with 95% humidity. For the assay, 5×10^4 cell/mL (K562, MCF-7), 7.5×10^4 cell/well (U251, PC-3), 10×10^4 cell/well (HCT-15), and 100 μL/well of these cell suspensions were seeded in 96-well microtiter plates and incubated to allow the cell attachment. After 24 h, 100 μL of each test compound and positive substance were added to each well. After additional 48 h, adherent cell cultures were fixed in situ by adding 50 μL of cold 50% (*wt*/*vol*) trichloroacetic acid (TCA) and incubated for 60 min at 4 °C. The supernatant was discarded and the plates were washed three times with water and air-dried. Cultures fixed with TCA were stained for 30 min with 100 μL of 0.4% SRB solution. Protein-bound dye was extracted with 10 μmol/L unbuffered tris base and the optical densities were read on an Ultra Microplate Reader (Elx 808, BIO-TEK Instruments, Inc.) with a test wavelength of 515 nm. Results were expressed as inhibitory concentration 50 (IC_{50}) values and they were calculated according to the protocol of Monks (27), where a dose-response curve was plotted for each compound and the concentration giving 50% inhibition (IC_{50}) was estimated from linear regression equations. The IC_{50} values (mean ± standard error) for **2**–**4**, the synthetic derivatives **2a** and **2b**, and **9** are shown in Table 1.

Acknowledgments

AG acknowledges Consejo Nacional de Ciencia y Tecnología (CONACYT) and Universidad Nacional Autónoma de México (UNAM) for the PhD scholarships. The authors thank Héctor Ríos, Nieves Zavala, Rubén A. Toscano, Luis Velasco, and Eréndira García for their technical assistance.

References

1. A. Arqueta-Villamar, L.M. Cano-Asseleih, and M.E. Rodarte. Atlas de las Plantas de la Medicina Tradicional Mexicana. Tomo I. Instituto Nacional Indigenista. México, D.F. 1994, p. 348.
2. H. Itokawa, Y. Ichihara, H. Kojima, K. Watanabe, and K. Takeya. Phytochemistry, **28**, 1667 (1989).
3. I. Kubo, Y. Asaka, and K. Shibata. Phytochemistry, **30**, 2545 (1991).
4. Y. Ichihara, K. Takeya, Y. Hitotsuyanagi, H. Morita, S. Okuyama, M. Suganuma, H. Fujiki, M. Motidome, and H. Itokawa. Planta Med. **58**, 549 (1992).
5. B.T. Ngadjui, B.M. Abegaz, F. Keumedijo, G.N. Folefoc, and G.W.F. Kapche. Phytochemistry, **60**, 345 (2000).
6. A. Ortega, R. Martínez, and L.C. García. Rev. Latinoam. Quím. **11**, 45 (1980).
7. M. Scholichin, K. Yamasaki, R. Miyaka, S. Yahara, and O. Tanaka. Phytochemistry, **19**, 326 (1980).

[5] Cartesian coordinates of the fully optimized geometry of **2b** at the DFT/B3LYP/H–W level of theory are available as Supplementary material.

© 2006 NRC Canada

8. C. Zdero, F. Bohlmann, and G. Schmeda-Hirschmann. Phytochemistry, **26**, 463 (1987).
9. M. Darise, H. Kohda, K. Mizutani, R. Kasai, and O. Tanaka. Agric. Biol. Chem. **47**, 133 (1983).
10. B. Rodríguez, M.C. De la Torre, M. Bruno, F. Piozzi, G. Savona, M.S.J. Simmonds, W.M. Blaney, and A. Perales. Phytochemistry, **33**, 309 (1993).
11. A. García and G. Delgado. Helv. Chim. Acta, **89**, 16 (2006).
12. Y. Wang, M. Hamburger, J. Gucho, and K. Hosttetmann. Phytochemistry, **28**, 2323 (1989).
13. A. Grouiller and H. Pacheco. Bull. Soc. Chim. Fr. **6**, 1938 (1967).
14. (*a*) N. Berova, K. Nakanishi, and R.W. Woody. *In* Circular dichroism — principles and applications. *Edited by* N. Berova, K. Nakanishi, and R.W. Woody. Wiley-VCH, New York. 2000. pp. 361–398; (*b*) M.A. Adams, K. Nakanishi, W.C. Still, E.V. Arnold, J. Clardy, and C.J. Persoons. J. Am. Chem. Soc. **101**, 2495 (1979); (*c*) N. Harada, S. Lai-Chen, and K. Nakanishi. J. Am. Chem. Soc. **97**, 5345 (1975).
15. R.M. Moriarty, H.E. Paaren, U. Weiss, and W.B. Whalley. J. Am. Chem. Soc. **101**, 6804 (1979).
16. I. Ohtani, T. Kusumi, Y. Kashman, and H. Kakisawa. J. Am. Chem. Soc. **113**, 4092 (1991).
17. R. Tschesche and H.U. Plenio. Chem. Ber. **106**, 2929 (1973).
18. D.A. Cifuente, E.J. Borkowski, M.E. Sosa, J.C. Gianello, O.S. Giordano, and C.E. Tonn. Phytochemistry, **61**, 899 (2002).
19. F.M. Harraz, M.J. Pcolinski, and R.W. Doskotch. J. Nat. Prod. **59**, 5 (1996).
20. D.N. Kirk and W.J. Klyne. J. Chem. Soc. Perkin Trans. 1, 1076 (1974).
21. D.A. Lightner and J.E. Gurst. *In* Organic conformational analysis and stereochemistry from circular dichroism spectroscopy. Wiley-VCH, New York. 2000. pp. 63–94.
22. T. Ohtsuki, T. Koyano, T. Kowithayakorn, N. Yamaguchi, and M. Ishibashi. Planta Med. **70**, 1170 (2004).
23. U. Burkert and N.L. Allinger. Molecular mechanics. ACS Monograph 177. American Chemical Society, Washington, DC. 1982.
24. C. Diedrich and S. Grimme. J. Phys. Chem. A, **107**, 2524 (2003).
25. (*a*) J. Hay and W.R. Wadt. J. Chem. Phys. **82**, 270 (1985); (*b*) J. Hay and W.R. Wadt. J. Chem. Phys. **82**, 284 (1985).
26. M.J. Frisch, G.W. Trucks, H.B. Schlegel, G.E. Scuseria, M.A. Robb, J.R. Cheeseman, J.A. Montgomery, T. Vreven, K.N. Kudin, J.C. Burant, J.M. Millam, S.S. Lyengar, J. Tomasi, V. Barone, B. Mennucci, M. Cossi, G. Scalmani, N. Rega, G. A. Petersson, H. Nakatsuji, M. Hada, M. Ehara, K. Toyota, R. Fukuda, J. Hasegawa, M. Ishida, T. Nakajima, Y. Honda, O. Kitao, H. Nakai, M. Klene, X. Li, J.E. Knox, H.P. Hratchian, J.B. Cross, C. Adamo, J. Jaramillo, R. Gomperts, R.E. Stratmann, O. Yazyev, R.E. Stratmann, A.J. Austin, R. Cammi, C. Pomelli, J. Ochterski, P.Y. Ayala, K. Morokuma, G.A. Voht, P. Salvador, J.J. Dannenberg, V.G. Zakrzewski, S. Dapprich, A.D. Daniels, M.C. Strain, O. Farkas, D.K. Malick, A.D. Rabuck, K. Raghavachari, K. Raghavachari, J.B. Foresman, J.V. Ortiz, Q. Cui, A.G. Baboul, S. Clifford, J. Cioslowski, B.B. Stefanov, G. Liu, A. Liashenko, P. Piskorz, I. Komaromi, R.L. Martin, D.J. Fox, T. Keith, M.A. Al-Laham, C.Y. Peng, A. Nanayakkara, M. Challacombe, P.M.W. Gill, B.G. Johnson, W. Chen, M.W. Wong, C. Gonzalez, and J.A. Pople. Gaussian 03 [computer program]. Revision B. 05. Gaussian, Inc., Pittsburgh, Penn. 2003.
27. A. Monks, D. Scudiero, P. Skehan, R. Shoemaker, K. Paull, D. Vistica, C. Hose, J. Langley, P. Cronise, A. Vaigro-Wolff, M. Gray-Goodrich, H. Campbell, J. Mayo, and M. Boyd. J. Natl. Cancer Inst. **83**, 757 (1991).

© 2006 NRC Canada

The absolute configuration of a nitroxide spin labeled derivative of podophyllotoxin determined by the crystal structure

Baohan Zhou, Guodong Yin, Xianggao Meng, Yitao Li, and Anxin Wu

Abstract: The crystal structure of the nitroxide spin labeled derivative of podophyllotoxin was first reported. X-ray analysis demonstrated that four contiguous chiral centers in the molecule, C1, C2, C3, and C4, adopt *cis*- (1:2), *trans*- (2:3), and *cis*- (3:4) arrangement.

Key words: crystal structure, synthesis, nitroxyl radical, podophyllotoxin.

Résumé : On a déterminé pour la première fois la structure cristalline d'un dérivé de la podophyllotoxine portant un groupe nitroxyde comme marqueur de spin. Les analyses par diffraction des rayons X ont permis de démontrer que quatre centres chiraux contigus de la molécule, C1, C2, C3 et C4, adoptent des arrangements *cis*- (1,2), *trans*- (2,3) et *cis*- (3,4).

Mots clés : structure cristalline, synthèse, radical nitroxyle, podophyllotoxine.

[Traduit par la Rédaction]

Introduction

Podophyllotoxin (**1**) and its many related derivatives are well known to possess pronounced antitumor and antiviral properties. However, the clinical application of podophyllotoxin and its analogues in the treatment of cancer has been limited by severe toxic side effects during the administration of the drugs (1–4). It was previously found that the introduction of a stable nitroxyl radical into the molecule of podophyllotoxin could result in novel compounds that have significant antitumor activity with marked decrease in toxicity compared with podophyllotoxin itself (5–7). Though the structure of spin-labeled podophyllotoxin derivatives can be indirectly characterized by mp, ESR, IR, MS, and HR-MS spectral analyses, its elaborate structure can't be confirmed by ^{1}H NMR because of its paramagnetic properties. Moreover, there are four contiguous chiral centers in the molecule, and its absolute configuration was not determined until now. In this paper, we synthesized one nitroxide spin labeled derivative of podophyllotoxin (**3**), first reported the crystal structure, and confirmed its absolute configuration.

Experimental section

4-[4″-(2″,2″,6″,6″-tetramethyl-1″-piperidinyloxy)amino]-4′-demethylepipodophyllotoxin (**3**) was prepared as shown in Scheme 1 (8). Podophyllotoxin (**1**), commercial agent (J & K Chemical Ltd., Shanghai, China), was used as a starting material.

The demethylation and bromination of **1** gave 4-bromo-4′-demethyl-epipodophyllotoxin (**2**). 33 g of **1** was suspended in 300 mL of 1,2-dichloroethane and 30 mL of ether and cooled to 0 °C. A current of dry hydrobromide was passed in until an increased mass of 82.5 g was obtained. After standing at 0–2 °C for 20 h, the solvent was removed under vacuum. The residue was recrystallized from acetone to give 12 g of **2**: 36% yield; mp 180–190 °C (dec.). A solution of **2** (2.77 g, 6 mmol) and 2,2,6,6-tetramethyl-1-piperidinyloxy-4-amine (2.57 g, 15 mmol) in 35 mL of dry THF and 2 drops of dry pyridine was refluxed under N_2 for 4 h. After filtering off the insoluble solids and removing the solvent under reduced pressure, the crude product was chromatographed twice through silica gel using CH_2Cl_2–acetone–Et_2NH (40:1:1, *v*/*v*) as an eluent to obtain 1.07 g (32% yield). Crystallization from acetone–hexane afforded the spin-labeled derivative of podophyllotoxin (**3**): red solid; mp 218–220 °C. UV (methanol) λ_{max} (nm): 283, 242, 220. IR (cm^{-1}): 3338 υ(NH), 1757 υ(C=O), 1609 υ(C=C), 1516 υ(C=C), 1479 $\delta_S(CH_3)$. ESR: 3 Lines, A_n = 16.2 G, ΔH_o = 2.66 G, g_o = 2.0061. MS–FAB *m*/*z* (%): 554 (13), 553 (16), 537 (7), 383 (100). Anal. calcd. (%): C 65.08, H 6.74, N 5.06; found: C 65.36, H 6.505, N 4.035.

A red crystal of the synthesized compound **3** was mounted on a glass fiber in a random orientation at 292(2) K. The determination of the unit cell and the data collection were performed with Mo Kα radiation (λ = 0.71073 Å) on a Bruker SMART APEX-CCD diffactometer with a ψ-ω scan mode. The structure was solved by direct methods with SHELXS-97 program and expanded by Fourier technique. The non-hydrogen atoms were refined anisotropically, and the hydrogen atoms were determined by theoretical calculations.

Received 28 February 2006. Accepted 18 September 2006. Published on the NRC Research Press Web site at http://canjchem.nrc.ca on 1 December 2006.

B. Zhou, G. Yin, X. Meng, Y. Li, and A. Wu.[1] Key Laboratory of Pesticide and Chemical Biology, Ministry of Education, College of Chemistry, Central China Normal University, Wuhan 430079, People's Republic of China.

[1]Corresponding author (e-mail: chwuax@mail.ccnu.edu.cn).

 doi:10.1139/V06-167 © 2006 NRC Canada

Scheme 1.

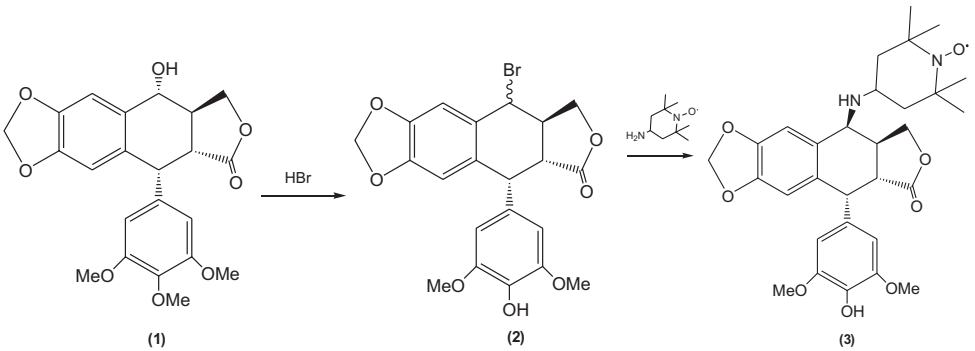


Table 1. Crystal data and structure refinement for **3**.

Empirical formula	$C_{30}H_{37}N_2O_8$
Formula weight	553.62
Temperature	292(2) K
Wavelength (Å)	0.71073
Crystal system	Orthorhombic
Space group	$P2_12_12_1$
a (Å)	8.1082(6)
b (Å)	19.3396(13)
c (Å)	42.130(3)
$\alpha = \beta = \gamma$	90°
Volume (Å^3)	6606.4(8)
Z	4
D_{calcd} (mg/m^3)	1.222
Absorption coefficient (μ) (mm^{-1})	0.087
F(000)	2576
Crystal size (mm^3)	0.30 × 0.20 × 0.20
θ range for data collection (°)	2.16–25.00
Limiting indices	$-9 \le h \le 9$, $-19 \le k \le 23$, $-50 \le l \le 48$
Reflections collected	33402
Independent reflections	6467 (R_{int} = 0.0851)
Refinement method	Full-matrix least-squares on F^2
Data/restraints/parameters	6467/0/853
Goodness-of-fit on F^2	1.023
Final R indices ($I > 2\sigma(I)$)	R_1 = 0.0614, wR_2 = 0.1453
R indices (all data)	R_1 = 0.1039, wR_2 = 0.1692
Extinction coefficient	0.0002(4)
Largest diff. Peak and hole (e Å^{-3})	0.189 and –0.188

Crystal data and structure refinement for compound **3** are listed in Table 1. The selected bond lengths and bond angles are given in Table 2 and 3, respectively. The other tables of CIF have been deposited as supplementary material.[2]

Results and discussion

Figure 1 shows the molecular structure of compound **3**, and the atomic numbering of the same compound is shown in Fig. 2.

Because the tumor-damaging potency of podophyllotoxin and related compounds is closely associated with their stereochemistry (9, 10), the determination of their absolute configuration might shed further light on the mechanism of their action, a question of importance in the search for effective chemotherapeutic agents. Synthetic organic chemists have been attracted to the stereochemical challenge represented by the four contiguous chiral centers of podophyllotoxin, the rigid *trans*-lactone, and the axially locked 1-aryl substituent. The early syntheses (11–14) generated

[2] Supplementary data for this article are available on the journal Web site or may be purchased from the Depository of Unpublished Data, Document Delivery, CISTI, National Research Council Canada, Ottawa, ON K1A 0S2, Canada. DUD 5111. For more information on obtaining material, refer to http://cisti-icist.nrc-cnrc.gc.ca/irm/unpub_e.shtml. CCDC 298236 contains the crystallographic data for this manuscript. These data can be obtained, free of charge, via ww.ccdc.cam.ac.uk/conts/retrieving.html (or from the Cambridge Crystallographic Data Centre, 12 Union Road, Cambridge CB2 1EZ, UK; fax +44 1223 336033; or deposit@ccdc.cam.ac.uk).

© 2006 NRC Canada

Table 2. Selected Bond lengths (Å).

Bond	Distance
C1—N1	1.472(6)
C1—C9	1.525(7)
C1—C2	1.541(7)
C2—C3	1.513(7)
C2—C12	1.522(7)
C3—C13	1.497(8)
C3—C4	1.524(7)
C4—C10	1.516(8)
C4—C1′	1.523(6)
C5—C6	1.349(9)
C5—C10	1.406(7)
C6—O2	1.388(7)
C7—C8	1.359(8)
C7—O1	1.374(7)
C8—C9	1.424(8)
C9—C10	1.398(7)
C11—O1	1.409(11)
C11—O2	1.434(11)
C12—O3	1.444(8)
C13—O4	1.205(7)
C13—O3	1.362(8)
C6—C7	1.381(9)

Table 3. Selected bond angles (°).

Angle	(°)
N1–C1–C9	110.1(4)
N1–C1–C2	110.6(4)
C9–C1–C2	107.8(4)
C3–C2–C12	101.2(4)
C3–C2–C1	108.6(4)
C12–C2–C1	119.7(4)
C13–C3–C2	103.6(4)
C13–C3–C4	120.0(5)
C2–C3–C4	113.3(4)
C10–C4–C1′	113.2(4)
C10–C4–C3	108.2(4)
C1′–C4–C3	114.0(4)

much new and interesting chemistry but led to the inactive *cis*-lactone.

X-ray analysis demonstrated that four contiguous chiral centers in the molecule, C1, C2, C3, and C4, adopt *cis*-(1:2), *trans*- (2:3), and *cis*- (3:4) arrangement (Fig. 1). The angles of C3–C2–C12, C3–C2–C1, and C13–C3–C2 are 101.2(4)°,108.6(4)°, and 103.6(4)°, respectively, which are less than the normal 109.5° angle. The angles of C12–C2–C1, C13–C3–C4, and C2–C3–C4 are 119.7(4)°, 120.0(5)°, and 113.3(4)°, respectively, which are much larger than the normal 109.5° angle. These results show that C2 and C3 are distorted atoms. Perhaps because the *trans*-lactone is a rigid ring and can not rotate freely. The six-membered ring containing N–O radical adopts a chair conformation, and the bond length of N—O is 1.270(5) Å, which is in the normal range of nitroxyl radicals (1.25–1.31 Å) (15, 16).

Fig. 1. Molecular structure of compound **3**.

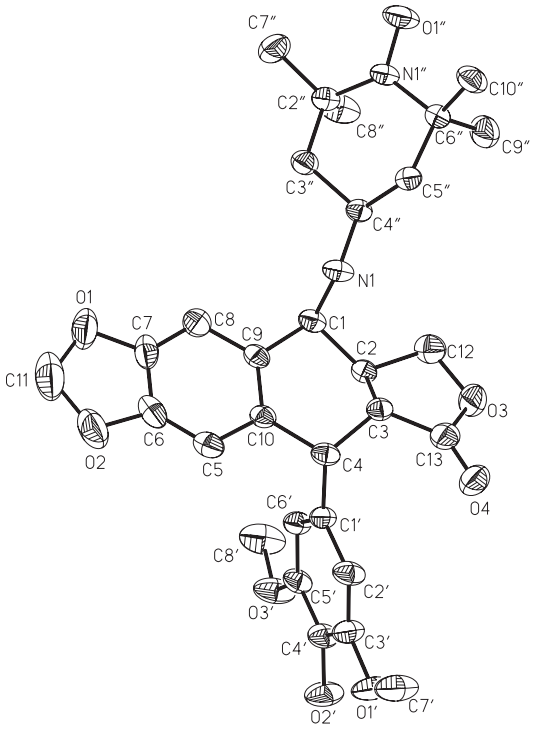
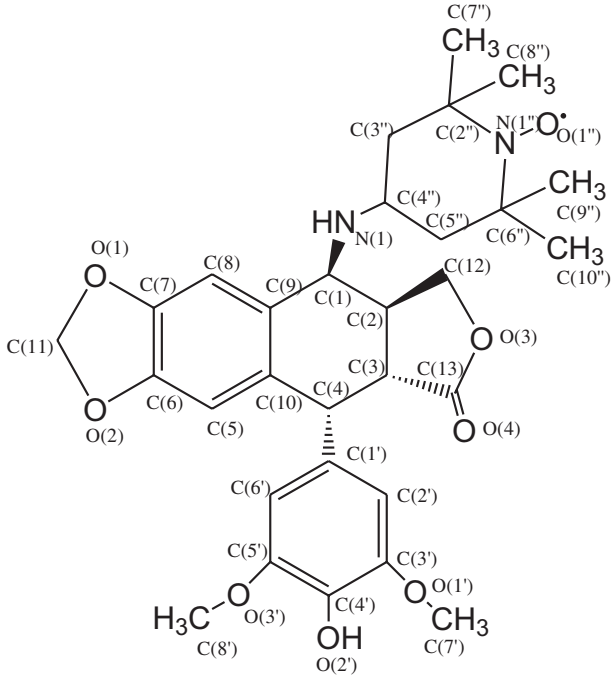


Fig. 2. Atomic numbering of compound **3**.



Acknowledgement

The Project was sponsored by the Scientific Research Foundation for the Returned Overseas Chinese Scholars, State Education Ministry (No. [2005] 383).

© 2006 NRC Canada

References

1. Y. Damayanthi and J.W. Lown. Curr. Med. Chem. **5,** 205 (1998).
2. C. Keller-Juslen, M. Kuhn, A. Von Wartburg, and H. Stahelin. J. Med. Chem. **14**, 936 (1971).
3. S.G. Weiss, M. Tin-Wa, R.E. Perdue, Jr. and N.R. Farnsworth. J. Pharm. Sci. **64**, 95 (1975).
4. Z.Q. Xia, M.A. Costa, J. Proctor, L.B. Davin, and N.G. Lewis. Phytochemistry, **55**, 537 (2000).
5. J.Z. Wang, X. Tian, H. Tsumura, K. Shimura, and H. Ito. Anti-Cancer Drug Des. **8**, 193 (1993).
6. X. Tian, F.M. Zhang, and W.G. Li. Life Sci. **70**, 2433 (2002).
7. X. Tian, Y.G. Wang, M.G. Yang, and Y.Z. Chen. Life Sci. **60**, 511 (1997).
8. Y.Z. Chen, Y.G. Wang, J.X. Li, X. Tian, Z.P. Jia, and P.Y. Zhang. Life Sci. **45**, 2569 (1989).
9. A.W. Schrecker and J.L. Hartwell. J. Org. Chem. **21**, 381 (1956).
10. J.L. Hartwell, A.W. Schrecker, and J. Leiter. Proc. Am. Assoc. Cancer Research, **1**, 19 (1954).
11. S.P. Forsey, D. Rajapaksa, N.J. Taylor, and R. Rodrigo. J. Org. Chem. **54**, 4280 (1989).
12. A.S. Kende, L.S. Liebeskind, J.E. Mills, P.S. Rutledge, and D.P. Curran. J. Am. Chem. Soc. **99**, 7802 (1977).
13. A.S. Kende, M.L. King, and D.P. Curran. J. Org. Chem. **46**, 2826 (1981).
14. W.S. Murphy and S.J. Wattanasin. J. Chem. Soc., Perkin Trans. 1, 271 (1982).
15. O.P. Anderson and T.C. Kuecher. Inorg.Chem. **19**, 1417 (1980).
16. C. Benelli, D. Gatteschi, C. Zanchini, R.J. Doedens, M.H. Dickman, and L.C. Porter. Inorg. Chem. **25**, 3453 (1986).

© 2006 NRC Canada

The energetics of the $X_2 + X^- \rightarrow X_3^-$ equilibrium (X = Cl, Br, I) in aqueous and nonaqueous solution

Evan Crawford, J. Scott McIndoe, and (the late) Dennis G. Tuck

Abstract: The magnitude of the stability constants (*K*) for the formation of X_3^- from X^- and X_2 (X = Cl, Br, I) in aqueous and nonaqueous solution depends strongly on both X and solvent. Thermodynamic arguments establish that for aqueous solutions this is not the result of differing bond strengths in the X_3^- anion but rather depends on the solvation energies of the relevant anions and halogens. The experimental results for *K* in different organic solvents can also be rationalized in terms which emphasise solvation effects. Electrospray ionization mass spectrometry (ESI-MS) has been used to qualitatively probe relative bond strengths in the absence of solvent.

Key words: trihalides, stability constants, solvation, electrospray ionization, mass spectrometry.

Résumé : En solutions aqueuses ou non aqueuses, l'amplitude des constants de stabilité (*K*) pour la formation de X_3^- à partir de X^- et X_2 (X = Cl, Br, I) dépend fortement de la nature de X ainsi que de celle du solvant. Des arguments thermodynamiques permettent d'établir que, dans les cas de solutions aqueuses, cette situation ne résulte pas de différences dans les forces de liaison dans l'anion X_3^-, mais plutôt des énergies de solvatation des anions et des halogènes appropriés. Les résultats expérimentaux pour les valeurs de *K* dans divers solvants organiques peuvent aussi être rationalisés en fonction d'effets qui mettent l'accent sur la solvatation. On a utilisé la spectrométrie de masse avec ionisation par électronébulisation pour évaluer qualitativement les forces relatives des liaisons en absence de solvant.

Mots clés : trihalogénures, constantes de stabilité, solvatation, ionisation par électronébulisation, spectrométrie de masse.

[Traduit par la Rédaction]

Introduction

Many polyhalide anions have been characterized in recent years and the X_3^- ions (X = Cl, Br, I) have been the focus of special interest. Over the last 100 years, many different techniques have been used in attempts to establish reliable values for the equilibrium constant for the formation of these ions in aqueous and nonaqueous solutions. The related X_2Y^- anions (X ≠ Y = Cl, Br, I, SCN) are also known and their dissociative and redistribution equilibria in solution have been investigated (1).

One feature which has aroused interest is that in aqueous solution the equilibrium constants for

[1] $$X_2 + X^- \rightleftharpoons X_3^-$$

[2] $$K_3 = \frac{[X_3^-]}{[X_2][X^-]}$$

are in the order I > Br > Cl, which has prompted speculation about the bonding in the X_3^- anions. A second point is that in nonaqueous solvents this order is reversed and the numerical values are all higher by several orders of magnitude. A recent paper by Landrum et al. (2) has shown that there is, in fact, little difference between the bonding energies in the three trihalide ions (X = Cl, Br, I) and these results form the basis of a satisfactory analysis of those factors that do affect the value of K_3 in different solvents.

The present paper addresses the energetics of the $X_2 + X^- \rightarrow X_3^-$ equilibrium in three related ways. In the first place, we show that the value reported by Landrum et al. (2) for the binding energy of I_3^- is compatible with related experimental values; secondly, we compare this and other calculated binding energies for X_3^- and X_2Y^- anions (X ≠ Y = Cl, Br, I) with mass spectrometric determinations of the decomposition potential; and finally, the effect of solvent on the stability constants of the X_3^- anions is discussed in terms of the relevant solvation parameters.

Received 1 August 2006. Accepted 24 October 2006. Published on the NRC Research Press Web site at http://canjchem.nrc.ca on 7 December 2006.

E. Crawford and J.S. McIndoe.[1] Department of Chemistry, University of Victoria, Victoria, BC V8W 3V6, Canada.
D.G. Tuck.[2] Department of Chemistry, University of Cambridge, Lensfield Road, Cambridge CB2 1EW, UK.

[1]Corresponding author (e-mail: mcindoe@uvic.ca).
[2]Sadly, Dennis Tuck died on June 5, 2003. His permanent address was: Department of Chemistry and Biochemistry, University of Windsor, Windsor, ON N9B 3P4, Canada.

The bonding energy of $I_3^-{}_{(g)}$

The bonding in the X_3^- anions has been the subject of a number of theoretical treatments prompted by the fact that X^-, X_2, and X_3^- are all closed shell species. Landrum et al. (2) have reviewed previous attempts at estimating the bonding energy for

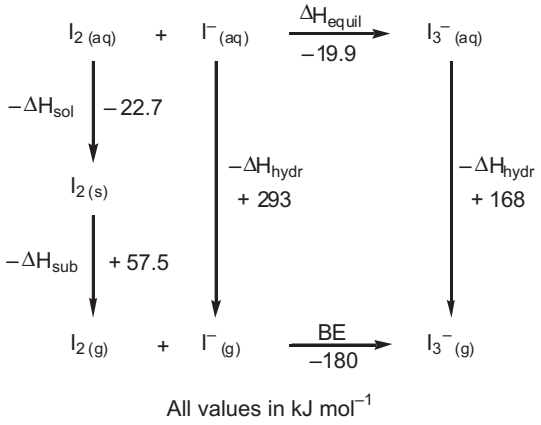
[3] $$X_2 + X^- \longrightarrow X_3^-$$

 doi:10.1139/V06-165 © 2006 NRC Canada

Table 1. Thermodynamic parameters in the $X_2 + X^- \rightarrow X_3^-$ cycle (in kJ mol^{-1}) (Scheme 1).

	Cl	Br	I	Reference
$\Delta EB(X_3^-{}_{(g)})$	–164	–166	–180	2, and text
$\Delta H_f^\circ(X_{2(g)})$	0	29.6	57.5	1b, 1c
$\Delta H_{soln}(X_{2(g)})$	23.3	2.6	22.7	1b, 1c
$\Delta H_{hydr}(X^-_{(g)})$	–368	–335	–293	7
ΔH°_{equil}	~8	–12.8	–19.9	4, 9, 10
$\Delta H_{hydr}(X_3^-{}_{(g)})$	–225	–210	–168	7, 16, and text
$\Delta H[X_{2(s)} \rightarrow X_2(aq)]$	23.3	32.2	80.2	—
$\Delta H_{hydr}(X^-) - \Delta H_{hydr}(X_3^-)$	–143	–125	–125	—

Scheme 1.



for which a range of values have been proposed. Their calculations give –164, –166, and –157 kJ mol^{-1} for Cl_3^-, Br_3^-, and I_3^-, respectively, and this small range of values immediately emphasizes that factors other than bond energy must affect the value of K_3. The authors comment on the lack of experimental data against which these numbers can be tested. Fortunately, it is possible to obtain a value for the iodine system from published information and this provides a starting point for the present discussion. The appropriate thermodynamic cycle is shown in Scheme 1.

The thermodynamic parameters for the formation of I_3^- in aqueous solution (eq. [1], X = I) have been studied by several authors using a variety of experimental techniques, and the results have been reviewed by Ramette and Sandford (3) who recommend the spectrophotometric results of Daniele (4), namely K_3 = 723 at 25 °C, ΔH° = –19.9 kJ mol^{-1}, ΔG° = –16.3 kJ mol^{-1}, ΔS° = –12.0 J K^{-1} mol^{-1}. These values are used in Scheme 1 and later. The enthalpy of solution of I_2 in water reported by Ramette and Sandford is ΔH° = +22.7 kJ mol^{-1} for

$$[4] \qquad I_{2(s)} \rightleftharpoons I_{2(aq)}$$

with ΔG° = +16.4 kJ mol^{-1}. Earlier studies by Davies and Gwynne (5) gave ΔH° = +25.7 kJ mol^{-1}; the lower value is used in Scheme 1. The standard enthalpy of formation of $I_{2(g)}$ (i.e., ΔH_{sub}) is +57.5 kJ mol^{-1}. The thermodynamics of the hydration of ions has been reviewed by Marcus (6); the work of Halliwell and Nyburg (7) gives values for the halide ions and for I_3^- (ΔH_{hydr} (I^-) = –293 ± 4 kJ mol^{-1}, ΔH_{hydr} (I_3^-) = –168 ± 20 kJ mol^{-1}).

The resultant value for the dissociation energy of I_3^- is 180 kJ mol^{-1}, ca. 8% higher than the 157 kJ mol^{-1} calculated by Landrum et al. (2). The largest experimental uncertainties are in the enthalpies of hydration; any errors related to the fact that these necessarily depend on ΔH°_{hydr} of the proton fortunately cancel in the summation around the cycle. The largest uncertainty in the calculation of the bond energy relates to the size of the basis set and to possible relativistic effects.[3] In general, the agreement between the two approaches seems satisfactory.

Equilibrium constants in aqueous solution

As noted earlier, there is a wide range of values for K_3 in contrast to the calculated bond energies. For X = I, the value quoted (4) earlier is K_3 = 723. For X = Br, Dubois and Garnier (8) found K_3 = 16.3 at 25 °C, in good agreement with an earlier result (1*a*), which gave ΔH = –12.8 kJ mol^{-1}. The corresponding values (9) for X = Cl are K_3 = 0.191 ± 0.016 and ΔH = –8 kJ mol^{-1}, again in keeping with earlier investigation (1*a*, 10) of this experimentally difficult system.

To identify the reasons for the differences in K_3, it is necessary to use the hydration enthalpies of Cl^- and Br^- and the enthalpies of solutions of $Cl_{2(g)}$ and $Br_{2(g)}$, which are available from the sources used for iodine. The corresponding terms for Cl_3^- and Br_3^- are not available and so must be estimated, which can be done by using a cycle analogous to that in Scheme 1, but now relying upon the calculations of Landrum et al. (2) for the Cl_3^- and Br_3^- dissociation energies. The relevant numerical values are shown in Table 1 and the appropriate summation leads to ΔH_{hydr} ($Cl_3^-{}_{(g)}$) = –219 kJ mol^{-1} and $\Delta H_{hydr}(Br_3^-{}_{(g)})$ = –214 kJ mol^{-1}. The size dependence of the resultant ΔH_{hydr} for X_3^- is shown in Fig. 1, using the calculated X–X distances as a measure of ionic size; the analogous values for X^- are plotted against r(X^-) for comparison.

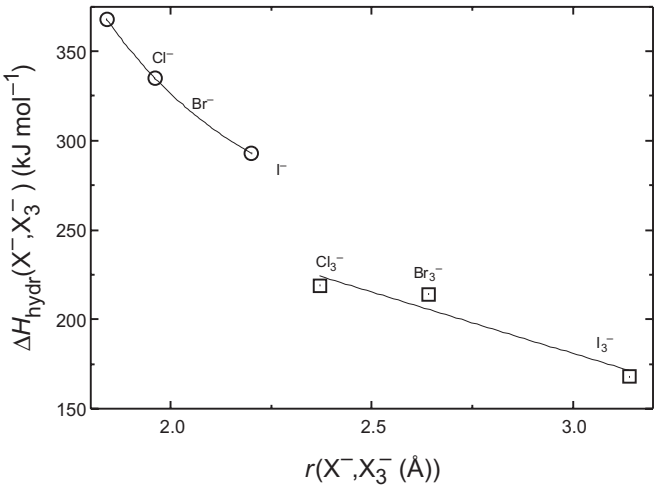
The value for $\Delta H_{hydr}(Cl_3^-)$ appears to be lower than one would predict from Fig. 1 and this may well be related to the large uncertainty in ΔH_{equil} for the formation of $Cl_3^-{}_{(aq)}$. In what follows, we assume the values of the enthalpy of hydration to be –168, –210, and –225 kJ mol^{-1} for I_3^-, Br_3^-, and Cl_3^-, respectively, derived from Fig. 1.

Table 1 makes it immediately obvious that the $X_3^-{}_{(g)}$ bonding energies are not the dominant terms determining the

[3] Private communications from Prof. Hoffmann and Dr. Goldberg.

© 2006 NRC Canada

Fig. 1. Size dependence of ΔH_{hydr} for X^- (circles) and X_3^- (squares) anions (X = Cl, Br, I).



value of $\Delta H°_{equil}$ for eq.[1]. The derived parameters given in the last two lines of this Table show that while the differences between the enthalpy of hydration of $X^-_{(g)}$ and $X_3^-{}_{(g)}$ are similar, there is a much larger variation in the enthalpy of solution of the elements from their standard states. In sum, the important enthalpy terms relate to the solution and hydration of the various solute species and do not reflect differences in the bond energy of the X_3^- anions.

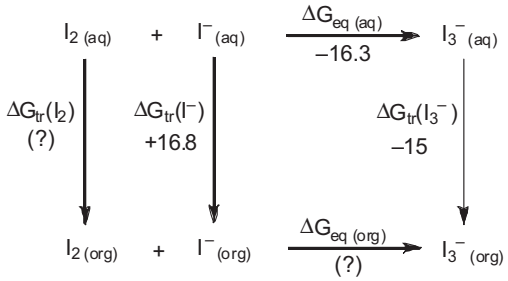
This last conclusion is relevant to the purported estimate of the stability of X_3^- based on the thermal stabilities of crystalline $M^+X_3^-$ salts (ref. 1*a*, p. 241). These results are better understood as a reflection of the different lattice energies of the salts in question and must depend only slightly on the bond energy of X_3^-. Equally, they can have little to do with the symmetry of the cation involved (ref. 1*b*) other than to the extent that this affects the lattice energy.

Comparison of aqueous and nonaqueous solutions

As noted earlier, K_3 is substantially larger for all three trihalide anions in nonaqueous solutions, and in the order Cl > Br > I. It is immediately obvious from the previous discussion that neither of these conclusions can be the result of bond energy factors and therefore it is incumbent to examine the solvation energies involved. As in the aqueous solution case, the I_3^- equilibrium is the only case for which adequate data are available and these are free energy rather than enthalpy values. A comparison of aqueous and nonaqueous systems can be made through the cycle shown in Scheme 2.

Where the numerical values refer to acetonitrile, Nelson and Iwamoto (11) have measured K_3 for Cl, Br, and I^- in this and other polar solvents and we use their value of log K_3 = 6.6 for the formation of I_3^-. The free energy of transfer of I^- from H_2O to CH_3CN is given as +16.8 kJ mol^{-1} by Marcus (6) and the corresponding ΔG_{tr} for I_3^- is –15 kJ mol^{-1}. There appears to be no direct measurement of $\Delta G_{tr}(I_2)$ from aqueous solution to acetonitrile, but Hildebrand et al. (12) have published an extensive set of values for the solubility of I_2 in organic solvents and their data show that iodine is more soluble in polar organic solvents than in water by a factor of

Scheme 2.



ca. 10^3. The value of ΔG_{tr} calculated from the result for ethanol at 25 °C is –18.6 kJ mol^{-1} and in the absence of other information this value is used for acetonitrile in the first iteration. The equilibrium constant for K_3 for I_3^- in aqueous solution is 723, with $\Delta G°$ = –16.3 kJ mol^{-1} (see earlier), so that Scheme 2 gives $\Delta G°$ for eq. [1] in acetonitrile as –29.5 kJ mol^{-1} and log $K_3(CH_3CN)$ = 5.2. As noted above, the reported experimental value is log K_3 = 6.6 and the agreement seems reasonable given the uncertainty in ΔG_{tr}. Nelson and Iwamoto do not give values for their equilibrium constants, so that the reality of the difference cannot be explored.

The agreement justifies an extension of the argument to seek an explanation of the order of K_3 in organic solvents. Ideally, a series of cycles analogous to Scheme 2 for each solvent and each halogen would lead to a detailed understanding of the factors involved, but unfortunately the numerical data required for this approach are not available; in particular, there is an absence of results for the solution properties of X_3^-. It is however possible to go some way in comparing the equilibrium constants for the three different trihalides, in acetonitrile in the first place, with the corresponding aqueous systems by using Scheme 2. The appropriate numerical data are in Table 2, in which the final column is the sum

[5*a*] $\Delta G°(CH_3CN) - \Delta G°(H_2O) + \Delta G_{tr}(X^-)$

which from Scheme 2 obviously equates to

[5*b*] $\Delta G_{tr}(X_3^-) - \Delta G_{tr}(X_2)$

The value of K_3 taken for the iodine system is that reported by Nelson and Iwamoto (log K= 6.6) and not that calculated in the paragraph above.

The values for bromine and iodine in the final column of Table 2 are quite close and as noted earlier any conclusions about the value for chlorine are conditioned by the experimental uncertainties. Beyond that, an inspection of the parameters in this table suggests that the single most significant factor predicting the order Cl > Br > I for K in acetonitrile and the change from the reverse order in water is the free energy of transfer of X^- from aqueous to nonaqueous solution.

To further examine this conclusion and its possible application to other solvents (e.g., S), we make the assumption that the term in eq. [5*b*], which equates to the last column of Table 2, is effectively constant within experimental error and lies in the range 0 ± 15 kJ mol^{-1}, corresponding to ±2.6 in

© 2006 NRC Canada

Table 2. Thermodynamic parameters (in kJ mol^{-1}) for $X_2 + X^- \rightarrow X_3^-$ in water and in acetonitrile.

X	K_{aq}[a]	$\Delta G°(H_2O)$ (A)	log $K(CH_3CN)$[b]	$\Delta G°(CH_3CN)$ (B)	$\Delta G_{tr}(X^-)$[c] (C)	(B)+(C)–(A)
Cl	0.19	4.1	10	–57	42.1	–19
Br	16.3	–6.9	7	–40	31.3	–1.8
I	721	–16.3	6.6	–38	16.8	–4.8

[a]See text.
[b]Ref. 13.
[c]$H_2O \rightarrow CH_3CN$; ref. 6.

the accumulated errors for log $K(H_2O)$ and log $K(S)$. Experimental values have been reported for K_3 for each trihalide in the solvents acetonitrile, nitromethane, and acetone, and Marcus has published ΔG values for the transfer of X^- from aqueous to nonaqueous solution for these and other solvents. Equation [5] can be rewritten as

$$[6] \quad \Delta G°(H_2O) - \Delta G°(S) = -\Delta G_{tr}(X) - [\Delta G_{tr}(X_2) - \Delta G_{tr}(X_3)]$$

and following the assumption above that the term in square brackets is effectively constant within the uncertainties of the data, we have

$$[7] \quad RT \log [K_3(S) / K_3(H_2O)] = -\Delta G_{tr}(X^-) - \text{constant}$$

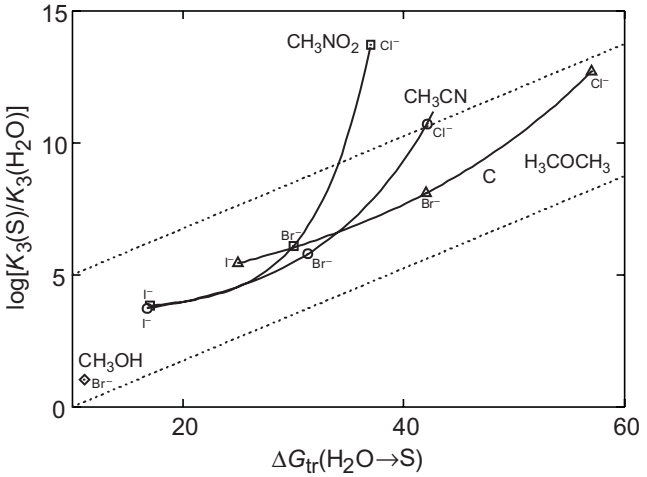
Figure 2 shows a plot of log $[K_3(S) / K_3(H_2O)]$ against $\Delta G_{tr}(X^-)$ for acetonitrile, nitromethane, and acetone, using the data in Table 2, and in refs. 6 and 11.

With one exception, the points fall within a band (indicated with dotted lines on Fig. 2) with a slope of 2.303*RT* on log $[K_3(S) / K_3(H_2O)]$. The exception is for Cl^-–CH_3NO_2 and the value for Cl^-–CH_3CN is barely within the upper limit. Given the experimental problems in measuring K_3 for the Cl_3^- system in aqueous solution and apparently in organic solvents (9), it is not surprising that this is where the largest deviations are found. In spite of the considerable assumptions made in deriving eq. [8], it is reasonable to conclude that the main factor predicting the value of K_3 in organic solvents relates to the free energy of transfer of X^- from H_2O to the solvent in question. In essence, since the X^- anions are much less strongly solvated in organic solvents than in water, equilibrium (3) is driven to the right relative to the situation in aqueous solution. This conclusion is in keeping with that reached earlier that solvation forces are more important than bond energies in both aqueous and nonaqueous systems.

The Br_3^- system in aqueous methanol

Two papers by Dubois and coworkers (8, 14) report results for the Br_2–Br^-–Br_3^- system in water, methanol, and aqueous methanol over the whole range of compositions. The ratio $K_3(MeOH)$–$K_3(H_2O)$ is 176:16.3; ΔG_{tr} for Br^- from H_2O to MeOH is +11.1 kJ mol^{-1}, leading to the point shown in Fig. 2. Dubois and Garnier (8) show that the change in log K_3 with H_2O–CH_3OH mole ratio is a linear function of the reciprocal of the dielectric constant of the solvent mixture. Any comparison of this conclusion with the arguments used in deriving Fig. 2 is negated by the absence of the necessary data (e.g., ΔH_{sol} of Br_2 in H_2O–MeOH mixtures). It is clear, however, that within the limits of the argument the change in K_3 with solvent composition is explicable in terms of the changing free energy of solvation of the Br^- ion, even in a system involving a highly polar nonaqueous solvent.

Fig. 2. Log $(K_3(S) / K_3(H_2O))$ as a function of ΔG_{tr} $(H_2O \rightarrow S)$ for X^- ions (X = Cl, Br, I). The dotted lines have slope = 2.303RT.



Mass spectrometry

We were interested in the speciation of Br_3^- in methanol. One useful technique for the analysis of charged species in polar solvents is electrospray ionization mass spectrometry (ESI-MS) (15). This technique is most prominent in the study of biomolecules (16) but has also become widely used in the analysis of a huge range of inorganic compounds (17). The power of the technique is probably best demonstrated in the analysis of complex mixtures, because the extensive fragmentation common to other mass spectrometric ionization methods is essentially absent from ESI mass spectra. A result of this is that each signal in the spectrum is due to a different parent ion corresponding to a unique solution species. We have already demonstrated the utility of the technique with respect to solutions of polyhalides (1*d*).

Examination of the negative-ion ESI mass spectrum of Br_3^- in methanol revealed rather complicated solution speciation (Fig. 3). While Br_3^- can be observed in the spectrum, it makes up only a small percentage of the total ion current. Close inspection of the isotope patterns revealed a complex series of polybrominated ions. These could not be assigned to simple combinations of Br, solvent, and counterion and so other possibilities were considered. The key to this puzzle was an ion at 517 m/*z* that had the exact

© 2006 NRC Canada

Table 3. Results of MS–MS decomposition studies of X_3^- and X_2Y^- species.

Anion	*m/z*	Product ion(s)	Neutral fragment	E_{COM} (eV) 50% decomposition	E_{COM} (eV) 50% appearance	Bonding *E* [a] (kJ mol^{-1})
Br_2I^-	254.7	Br^-	BrI	1.7	1.4	
I_3^-	380.7	I^-	I_2	1.5	1	157
Cl_2I^-	196.8	Cl^-	ClI	1.4	1	
Br_2Cl^-	192.6	Br^-	BrCl	1.4	0.7	
ClI_2^-	289.8	I^-	ClI	1.2	0.8	155, 119
Br_3^-	236.5	Br^-	Br_2	1.2	0.9	166
BrI_2^-	332.7	I^- (58%)	IBr (58%)	1.1	1.4	153, 141
		Br^- (42%)	I_2 (42%)		1.1	
$BrCl_2^-$	148.9	Cl^-	BrCl	1	0.6	
$[Br_2(SCN)]^-$	217.8	SCN^- (30%)	Br_2 (30%)	0.8	0.4	
		Br^- (70%)	BrSCN (70%)		0.6	
$[I_2(SCN)]^-$	311.8	SCN^- (98%)	I_2 (98%)	0.6	0.4	
		I^- (2%)	ISCN (2%)		3.0	
$[I(SCN)_2]^-$	242.8	SCN^-	ISCN	0.5	0.3	

[a]Values from ref. 2.

Fig. 3. Negative-ion ESI-MS of $[NBu_4][Br_3]$ in methanol. The inset shows the calculated (grey bars) and experimental isotope pattern of $[AuBr_4]^-$.

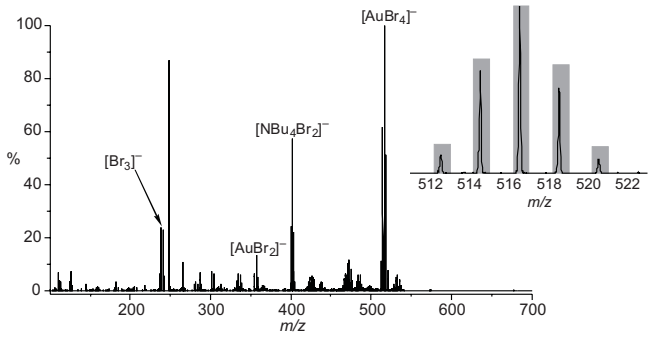
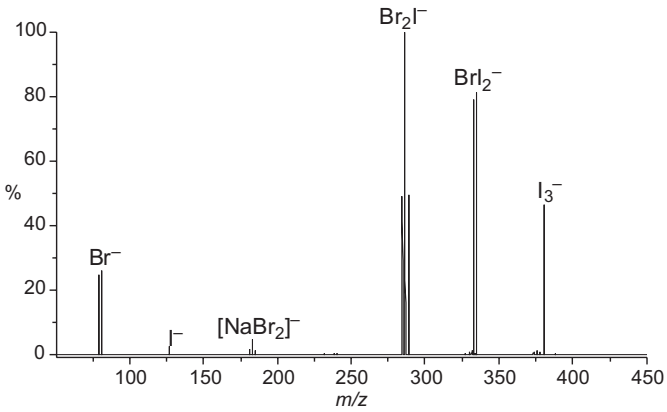


Fig. 4. Negative-ion ESI-MS of NaBr + I_2 in acetonitrile.



isotope pattern for Br_4, with all other contributors being monoisotopic (see inset pattern in Fig. 3). A single isotope with the correct mass is ^{197}Au and the pattern matches perfectly for $[AuBr_4]^-$. Chemically, this is perfectly reasonable as this complex is quite stable (18), but where did it come from? The answer provided itself when the mass spectrometer stopped functioning and after dismantling the source we found that the stainless steel capillary from which the spray emerges had been completely corroded. $[AuBr_4]^-$ is present in an appreciable quantity; its abundance in the spectrum is surprising and suggests that corrosion elsewhere in the source is an issue because it is unlikely the stainless steel capillary contains sufficient gold to provide the strength of signal observed (the brass components of the ion block assembly are a likely source of the gold; some parts may also be gold-plated, though this information is proprietary). Br_3^- in methanol is clearly too reactive to be studied routinely using ESI-MS and viable conclusions cannot be drawn using this method of analysis.

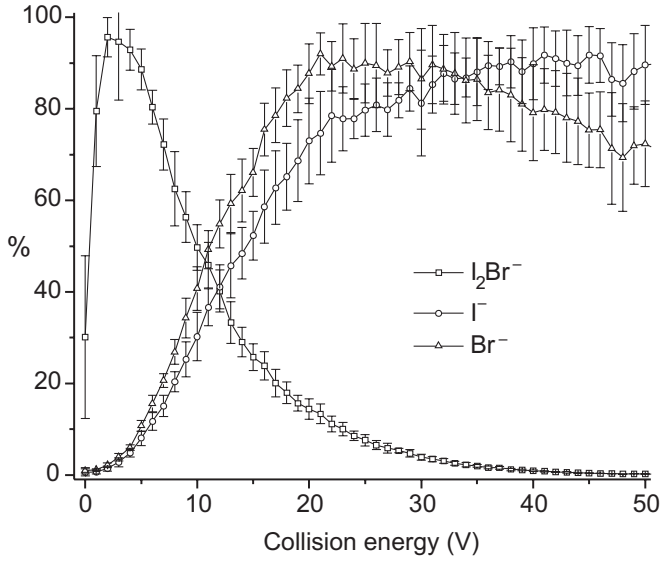
However, we found ESI-MS of acetonitrile solutions of X_3^- (X = I, Br, Cl, and the pseudohalide SCN) to provide entirely explicable spectra (Fig. 4), with no sign of any species attributable to corrosion of parts of the source. Prominent peaks in the negative-ion mode include X^-, X_3^-, and $[CX_2]^-$ (C = cation) (Fig. 4). The thiocyanates were investigated, but spectra were dominated by $X_2(SCN)^-$ ions and an $X(SCN)_2^-$ ion was detected only in the case of X = I.

All X_3^- species undergo collision-induced dissociation (CID) in the argon-filled collision cell of the mass spectrometer to form X_2 (neutral, so not observed) and X^- in a simple MS–MS experiment. As collision energies may be smoothly varied, this process offers qualitative insight into the relative bonding energy by assessing the voltage required to fragment X_3^-. Table 3 summarizes the results obtained from these experiments. Figure 5 illustrates the type of raw data obtained for each of the species using I_2Br^- as the example (only I_2Br^-, $I_2(SCN)^-$, and $Br_2(SCN)^-$ generated both possible X^- ions upon CID; the remainder exclusively formed the ions listed in Table 3).

Essentially, X_3^- was selected using the first mass analyser (MS1) of a hybrid quadrupole time-of-flight (Q-TOF) mass spectrometer. The ion was fragmented in the collision cell using a collision voltage that increased by an increment of

© 2006 NRC Canada

Fig. 5. Breakdown graph of I_2Br^- showing traces for the disappearance of $I_2Br^-$and the appearance of I^- and Br^-. The error bars represent the variability between five independent experiments. The collision energy, E_{LAB} is the value of the offset voltage for the central hexapole.



1 V for each spectrum that was recorded, in exactly the same way as in energy-dependent ESI mass spectra (EDESI-MS) (19). However, the simplicity of the spectra are such that breakdown graphs (20) convey the same information in a readily comprehensible fashion. Half of the maximum intensity of the X_3^- ion was used as a convenient point to assess the relative energy required to break apart the X_2 and X^- fragments (Table 3, 50% decomposition). Half of the maximum intensity of the X^- ion was also recorded (Table 3, 50% appearance; also see Fig. 6). The energies are recorded as centre-of-mass, where $E_{COM} = E_{LAB}(m / (m + M))$, where E_{LAB} is the value of the offset voltage for the central hexapole (the collision energy), m is the mass of the stationary Ar atom, and M is the mass of the precursor ion.

Figure 7 shows a spectrum obtained by summing all spectra used in the collection of the breakdown graphs depicted in Fig. 5 (note that all ions appear monoisotopic because of the fact that the lowest mass isotopomer of X_3^- was selected for fragmentation in all cases). Note that trace amounts of $I_2^{\bullet-}$ and $IBr^{\bullet-}$ are also present; these imply loss of $Br^{\bullet}$ and $I^{\bullet}$, respectively. The radical decomposition channel was always a minor one.

There is sufficient error in the values obtained for appearance and decomposition voltages (ca. ±0.3 V) that in-depth analysis of the values obtained is not prudent; the experiments we describe are very much qualitative. However, two useful general conclusions can be drawn. First, all mixed species X_2Y^- tended to lose XY as the primary neutral fragment, generating X^-. Three examples also lost X_2, namely $I_2(SCN)^-$, $Br_2(SCN)^-$, and BrI_2^-, but in all of these cases this decomposition pathway was in competition with XY loss. On purely statistical grounds, one would expect that X_2Y^- species should produce XY as the neutral fragment twice as often as X_2; the selectivity for the mixed fragment suggests that the XY bond is marginally stronger than the X_2 bond

Fig. 6. Breakdown plots of the appearance of I^- from I_3^-, BrI_2^-, ClI_2^-, and $I_2(SCN)^-$. $E_{COM} = E_{LAB}(m / (m + M))$, where E_{LAB} is the value of the offset voltage for the central hexapole, m is the mass of the stationary Ar atom, and M is the mass of the precursor ion. Dotted lines indicate the 50% appearance potential for each trace. Note that for BrI_2^- and $I_2(SCN)^-$, Br^- and SCN^- were being concurrently generated.

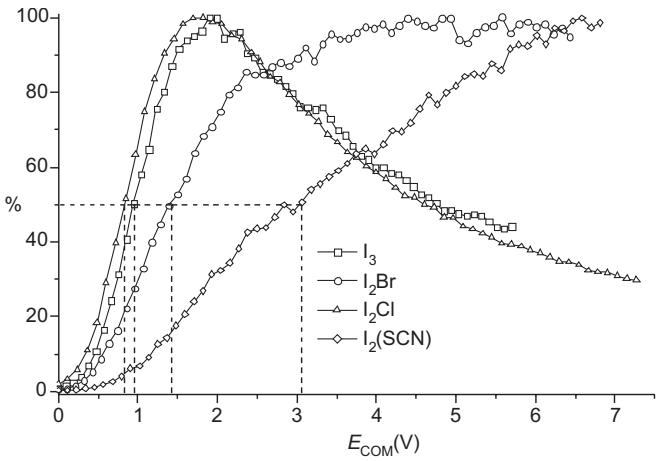
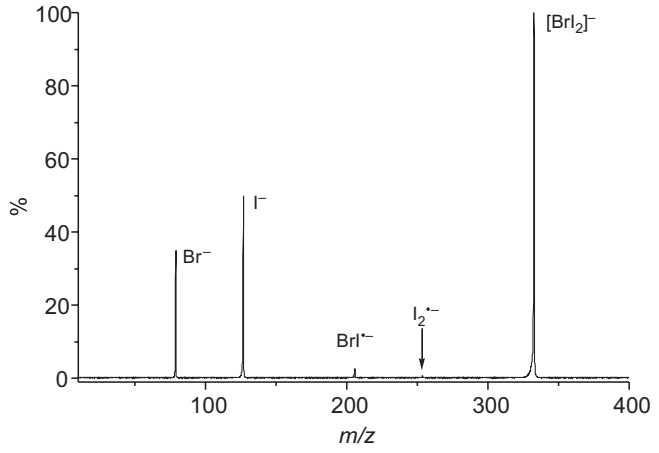


Fig. 7. ESI-MS–MS of BrI_2^- summed over collision voltages of 0–50 V.



(though in the case of BrI_2^-, I-Br, and I-I it must be of comparable strength). Second, the thiocyanate-containing species $I_2(SCN)^-$, $Br_2(SCN)^-$, and $(SCN)_2I^-$ clearly have the lowest bonding energies, being the easiest to decompose. Both $I_2(SCN)^-$ and $Br_2(SCN)^-$ produced both possible decomposition products (SCN^- and the appropriate halide ion), though in the case of $I_2(SCN)^-$, I^- was a very minor product and the spectrum was dominated by the appearance of SCN^-. The remaining species have values that are not dramatically different to one another and accurate quantitative assessments of the bond energies are required, e.g., by guided ion beam tandem mass spectrometry (21), before any firm conclusions can be drawn about the exact ordering of bond strengths.

General conclusion

The variation of K_3 in the Cl, Br, I triad is not a function

© 2006 NRC Canada

of any wide variation in the X_3^- bonding energy, but rather reflects the solvation energies of the solutes in question. Within the limits of the available thermodynamic information, it is possible to rationalize the range of equilibrium constants and the effect of changes of solvent on these constants. ESI-MS–MS studies confirm that bond strengths do not vary wildly between different species and also suggest that for mixed X_2Y^- trihalides the XY bond is marginally stronger than the X_2 bond. Mixed halogen–thiocyanate species exhibit the weakest bonding.

Experimental

Electrospray ionization mass spectra were collected using a Waters Micromass Q-Tof micro with Z-Spray source with the following settings: the nebuliser tip was set at 2900 V and 100 °C and nitrogen was used as the bath gas; samples were introduced directly to the source at 5 μL min^{-1} as acetonitrile solutions via a syringe pump; data collection was carried out in continuum mode. For the breakdown graphs, the cone voltage was set at 15 V and MS1 was set at the appropriate *m*/*z* value for the species of interest. The collision voltage was initially set at 0 V and spectra collected at every 1 V increment until MS2 showed no change in the daughter ion spectrum (typically ~ 60 V). The collision gas was argon at a pressure of 10^{-4} mbar (1 bar = 100 kPa).

All chemicals were purchased from Sigma-Aldrich (99% purity or better) and used as received. Solutions of the trihalides were typically prepared by adding the appropriate potassium or sodium (pseudo)halide salt to an acetonitrile solution of I_2 or Br_2. To get spectra of $[Cl_2Br]^-$ and $[Br_2Cl]^-$, equimolar amounts of Br_2 and $[Et_4N]Cl{\cdot}H_2O$ were heated to complete liquification. The cooled solid was then dissolved in acetonitrile. The spectrum of $[Br_2(SCN)]^-$ was collected by mixing an acetonitrile solution of Br_2 with 0.2 mL of a saturated acetonitrile solution of KSCN. Solution concentrations of each species were of the order of ca. 0.1 mg mL^{-1}.

Acknowledgements

This work was carried out with the help of financial support to DGT from the Royal Society of Chemistry (Journals Travel Grant). JSM gratefully acknowledges the support of Natural Sciences and Engineering Research Council of Canada (NSERC), Canada Foundation for Innovation (CFI), and British Columbia Knowledge Development Fund (BCKDF). The University of Victoria is thanked for a summer undergraduate research award to EC. We also thank the referees for their extremely helpful comments and suggestions.

References

1. (*a*) A.I. Popov. *In* Halogen chemistry. Vol. 1. *Edited by* V. Gutmann. Academic Press, New York, 1967. p. 225; (*b*) A.J. Downs and C.J. Adams. *In* Comprehensive inorganic chemistry. Vol. II. *Edited by* G. Wilkinson. Pergamon Press, Oxford, UK, 1976 ; (*c*) N.N. Greenwood and A. Earnshaw. Chemistry of the elements. 2nd ed. Butterworth, Oxford. 1997. p. 800; (*d*) J.S. McIndoe and D.G. Tuck. J. Chem. Soc. Dalton Trans. 244 (2003).
2. G.A. Landrum, N. Goldberg, and R. Hoffmann. J. Chem. Soc. Dalton Trans. 3605 (1997).
3. R.W. Ramette and R.W. Sandford. J. Am. Chem. Soc. **87**, 5001 (1965).
4. G. Daniele. Gazz. Chim. Ital. **90**, 1068 (1960).
5. M. Davies and E. Gwynne. J. Am. Chem. Soc. **74**, 2748 (1952).
6. Y. Marcus. Ionic solvation. Wiley-Interscience, New York. 1985. p. 107.
7. D.F. Halliwell and S.C. Nyburg. Trans. Faraday Soc. **59**, 1126 (1963).
8. J.E. Dubois and F. Garnier. Bull. Soc. Chim. Fr. 1715 (1965).
9. G. Zimmerman and F.C. Strong. J. Am. Chem. Soc. **79**, 2063 (1957).
10. M.S. Sherrill and E.F. Izard. J. Am. Chem. Soc. **53**, 1667 (1931).
11. I.V. Nelson and R.I. Iwamoto. J. Electroanal. Chem. **7**, 218 (1964).
12. J.H. Hildebrand, H.A. Benesi, and L.M. Mower. J. Am. Chem. Soc. **72**, 1017 (1950).
13. A.G. Sharpe. Halogen chemistry. Vol. 1. *Edited by* V. Gutmann. Academic Press, New York. 1967. p. 11.
14. J.E. Dubois and H. Herzog. Bull. Soc. Chim. Fr. 57 (1963).
15. J.B. Fenn, M. Mann, C.K. Meng, S.F. Wong, and C.M. Whitehouse. Mass Spectrom. Rev. **9**, 37 (1990).
16. R.B. Cole (*Editor*). Electrospray ionization mass spectrometry: Fundamentals, instrumentation and applications. John Wiley & Sons, New York. 1997.
17. (*a*) W. Henderson and J.S. McIndoe. Mass spectrometry of inorganic and organometallic compounds: Tools, techniques and tips. John Wiley & Sons, Chichester, NY. 2005; (*b*) W. Henderson, L.J. McCaffery, and B.K. Nicholson. Polyhedron, **17**, 4291 (1998); (*c*) R. Colton, A. D'Agostino, and J.C. Traeger. Mass Spectrom. Rev. **14**, 79 (1995); (*d*) J.C. Traeger. Int. J. Mass Spectrom. **200**, 387 (2000).
18. N.N. Greenwood and A. Earnshaw. Advanced inorganic chemistry. 5th ed. Wiley-Interscience, New York. 1988. p. 951.
19. (*a*) P.J. Dyson, B.F.G. Johnson, J.S. McIndoe, and P.R.R. Langridge-Smith. Rapid Commun. Mass Spectrom. **14**, 311 (2000); (*b*) P.J. Dyson, A.K. Hearley, B.F.G. Johnson, J.S. McIndoe, P.R.R. Langridge-Smith, and C. Whyte. Rapid Commun. Mass Spectrom. **15**, 895 (2001); (*c*) C.P.G. Butcher, P.J. Dyson, B.F.G. Johnson, P.R.R. Langridge-Smith, J.S. McIndoe, and C. Whyte. Rapid Commun. Mass Spectrom. **16**, 1595 (2002); (*d*) S.L.G. Husheer, O. Forest, M. Henderson, and J.S. McIndoe. Rapid Commun. Mass Spectrom. **19**, 1352 (2005).
20. (*a*) A.G. Harrison. Rapid Commun. Mass Spectrom. **13**, 1663 (1999); (*b*) N.N. Dookeran, T. Yalcin, and A.G. Harrison. J. Mass Spectrom. **31**, 500 (1996); (*c*) W. Weinmann, M. Stoertzel, S. Vogt, M. Svoboda, and A. Schreiber. J. Mass Spectrom. **36**, 1013 (2001); (*d*) M. Begala, G. Delogu, E. Maccioni, G. Podda, G. Tocco, E. Quezada, E. Uriarte, M.A. Fedrigo, D. Favretto, and P. Traldi. Rapid Commun. Mass Spectrom. **15**, 1000 (2001).
21. P.B. Armentrout. J. Am. Soc. Mass Spectrom. **13**, 419 (2002).

© 2006 NRC Canada

Carbonate radical anion — Thermochemistry[1]

D.A. Armstrong, W.L. Waltz, and A. Rauk

Abstract: High level ab initio calculations along with isodesmic reactions have been used to derive a set of self-consistent free energies of formation for carbonate and nitrate species in the gas phase and in aqueous solution. The results show that $HCO_3^{\cdot}$ is a strong acid, $pK_a = -4.1$, and that $E°(CO_3^{\cdot-}/CO_3^{2})$ = 1.23 ± 0.15 V.

Key words: carbonate radical anion, theoretical, thermochemistry, acidity, reduction potentials.

Résumé : On a utilizé des calculs théoriques *ab initio* de haut niveau associés à des réactions isodesmiques pour déduire un ensemble d'énergies libres autocohérentes pour les espèces carbonate et nitrate en phase gazeuse et en solution aqueuse. Les résultats montrent que le $HCO_3^{\cdot}$ est un acide fort, $pK_a = -4,1$, et que la valeur de $E°(CO_3^{\cdot-}/CO^{2-})$ = 1,23 ± 0,15 V.

Mots clés : anion radical carbonate, théorique, thermochimie, acidité, potentiels de réduction.

[Traduit par la Rédaction]

Introduction

The production of carbonate radicals by the reaction of $^{\cdot}OH$ with bicarbonate or carbonate ions in aqueous solution has been known for many years and rate constants for its reactions with many inorganic and organic species have been reported (1, 2). During the last decade it has also been shown that carbonate radicals are produced in living cells, where they can cause damage to important constituents, including DNA (3, 4). There is, therefore, a need to understand the structure of the radical and the thermodynamic properties that control its rate of formation and reactivity. Shkrob (5) has recently reviewed earlier work on the structure of $CO_3^{\cdot-}$. He also performed CIS-B3LYP/6-311+G(d) calculations and showed that the experimentally observed optical, Raman, and magnetic properties of carbonate radical in aqueous solution can be accounted for by a trigonally distorted C_{2v} $CO_3^{\cdot-}$ structure, a consequence of a complex with a single water molecule. In terms of the thermochemistry, several experimental studies[3] reported evidence for pK_a in the range of 8–10. This was attributed to the presence of $HCO_3^{\cdot}$ at lower values of pH and its ionization in reaction [1].

[1] $$HCO_3^{\cdot} = H^+ + CO_3^{\cdot-}$$

However, that evidence is not supported by the early ESR work (6) or the recent Raman spectroscopic (7) and optical pulse radiolysis studies (8). These imply that $HCO_3^{\cdot}$ is strongly acidic with pK_a probably below 0.0. Redox equilibrium experiments carried out with $Br_2^{\cdot-}$ and $(SCN)_2^{\cdot-}$ at values of pH above 10 demonstrate that $E°(CO_3^{\cdot-}/CO_3^{2-})$ is 1.58 ± 0.03 V vs. the standard hydrogen electrode (9, 10).[4] In short, at the present time there is considerable information available on the carbonate radical anion with direct spectroscopic observations pointing to $CO_3^{\cdot-}$ as the only significant species in the pH region 0–14. However, while H abstraction appears to be one of the most important reactions of $CO_3^{\cdot-}$ (3, 4), there appears to be no data on the bond dissociation enthalpy (BDE) of HCO_3^-, the parameter that controls the barrier to H-atom abstraction reactions.

The purpose of this study was to use ab initio methods to examine the thermochemical properties of $HCO_3^{\cdot}$ and $CO_3^{\cdot-}$ species in some detail. These include the BDE of HCO_3^- and $\Delta G_{(acid;g)}$ of $HCO_3^{\cdot}$, the free energy of reaction [1] in the gaseous phase. Using corrections to calculated free energies of solution based on the structurally similar nitrate species HNO_3, NO_3^-, and $NO_3^{\cdot}$, values of $\Delta_f G_{(aq)}°$ for $HCO_3^{\cdot}$ and $CO_3^{\cdot-}$ were also derived. These are clearly free of any of the "medium effects" that have created problems in the interpretation of some of the experimental data. The calculated values are found to be in excellent accord with the experimental $E°(CO_3^{\cdot-}/CO_3^{2-})$ cited above. Also, the results indicate unequivocally that the pK_a for $HCO_3^{\cdot}$ is negative.

Computational details

The ab initio calculations were performed with the Gaussian 98 and Gaussian 03 molecular orbital packages

Received 5 September 2006. Accepted 16 October 2006. Published on the NRC Research Press Web site at http://canjchem.nrc.ca on 7 December 2006.

D.A. Armstrong and A. Rauk.[2] Department of Chemistry, University of Saskatchewan, Saskatoon, SK S7N 5C9, Canada.
W.L. Waltz. Department of Chemistry, University of Calgary, Calgary, AB T2N 1N4, Canada.

[1]This article is dedicated to the memory of the late David A. Armstrong (1930–2006)
[2]Corresponding author (e-mail: rauk@ucalgary.ca).
[3]See refs. 1, 2, and 6–8 for citations of those studies.
[4]This is the average of the two sets of results. Note that some data in ref. 10 are at pH 8.5. They are consistent with those at higher pH, again suggesting the absence of pK_a in this region.

 doi:10.1139/V06-168 © 2006 NRC Canada

(11–13). Geometry optimizations and vibrational frequency calculations were carried out at the B3LYP-LB level, where LB denotes the large basis set, 6-311+G(3df,2p). Zero-point energies (ZPEs) were scaled with the factor 0.9806 (14). Values of $H° - H_0°$ and entropies were evaluated by standard methods of statistical thermodynamics based on the rigid rotor harmonic oscillator model (15, 16). The electronic energies used to obtain heats of formation were calculated by application of the CBS-RAD procedure (17) to the B3LYP-LB structures. CBS-RAD is a high-level theoretical procedure for obtaining thermochemical values for radicals to experimental accuracy. The CBS-RAD–B3LYP combination employed here has been found to yield good reaction enthalpies and barriers for the addition of C-centred radicals to alkenes (18) and to the β-scission reactions of alkoxy radicals (19). Gaseous phase free energies of formation were obtained from the entropies and heats of formation (16). Free energies of solvation were calculated with the integral equation following a polarizable continuum model procedure implemented as SCRF = IEFPCM in Gaussian 03 (20, 21). The cavity was defined from the united atom Hartree–Fock (UAHF) radii, scaled according to program defaults. The free energy of solvation evaluated in this manner is further subject to correction by reference to experimental values on related systems as described below.

UV–vis spectroscopic properties were calculated by time-dependent density functional theory (22) using the B3LYP Hamiltonian and the LB basis in the polarizable continuum medium implemented as SCRF = CPCM in Gaussian 98 and 03 (23), with the molecular cavity defined by the 0.001 electrons/bohr^3 (1 bohr = 0.529×10^{-10} m) isodensity surface (24).

Results

Structure and IR–Raman spectra of $CO_3^{\cdot-}$

The ground electronic state of $CO_3^{\cdot-}$ is $^1A_1'$, with D_{3h} symmetry and r_{CO} = 1.270 Å. At the B3LYP-LB level of theory, the predicted vibrational modes are (cm^{-1}): E′ 374.6 (O–C–O bend); A_2'' 837.0 (out-of-plane bend); A_1' 1097.4 (sym str); E′ 1278.7 (asym str). At the same level of theory, the presence of a single water molecule coordinated by a single H bond to one of the O atoms reduces the symmetry approximately to C_{2v} (actually C_s), with the unique O–C–O angle contracted to 114.2°. The predicted vibrational modes are (cm^{-1}): 367.2, 506.1 (O–C–O bend); 828.1 (out-of-plane bend); 1097.8 (sym C–O str); 1184.1, 1453.7 (asym C–O str). Thus, in the H-bonded complex, the O–C–O in-plane bends and asymmetric C–O stretches are strongly split, while the out-of-plane umbrella motion and the symmetric C–O stretching motions are hardly perturbed. Given the breadth of the bands in the experimental Raman spectrum, the calculated frequencies agree well with those observed (cm^{-1}): 485, 701, 1063, 1166, 1372, and 1426 (7). The three C–O stretching modes all have high Raman intensities, in units of Å^4 AMU^{-1} (depolarization ratios), 64.4(0.57), 137.7(0.87), and 426.7(0.78), respectively. Thus, the calculations of the IR–Raman spectrum of the single-water complex support the suggestion that the structure of the carbonate radical anion is distorted toward C_{2v} by interaction with water (7).

UV–vis spectra of $CO_3^{\cdot-}$

The electronic spectrum of D_{3h} $CO_3^{\cdot-}$ predicted at the TD-B3LYP-LB level in an aqueous environment shows the following bands (nm, oscillator strength): E″ 828.6, 0.0000; E′ 608.2, 0.0606; A_1'' 205.7, 0.0000. In the lower C_s symmetry environment of the H_2O–$CO_3^{\cdot-}$ complex, one finds in the same spectral range (nm, oscillator strength): A″ 942.5, 0.0000; A″ 699.6, 0.0000; A′ 596.0, 0.0236; A′ 569.3, 0.0403; A″ 360.2, 0.0000; A′ 231.6, 0.0177; A″ 203.62, 0.0000. Thus, the degeneracy of the E″ state is strongly split by the explicit solvation but the transitions, though formally allowed, do not gain any intensity. Both components of the E′ state are blue-shifted but also not much affected in intensity. The calculated absorption spectrum of either the D_{3h} or the C_{2v} form of $CO_3^{\cdot-}$ agrees well with the experimental observation of a broad absorbance at 600 nm (25).

Gas phase heats and free energies of formation

Values of the electronic energies (EEs), zero-point energy levels (ZPEs), thermal corrections ($H° - H_0°$), entropies ($S°$), and $\Delta_f H°$ values derived from the CBS-RAD level EEs are given in Table 1 for $HCO_3^{\cdot}$, $CO_3^{\cdot-}$, and several other species of relevance to this study. The column under the heading $\Delta_f H°$ (Rec.) contains values of $\Delta_f H°$ from the literature for HNO_3, NO_3^-, the formyloxyl radical (HC(O)O$^{\cdot}$), bicarbonate (HCO_3^-), and the recommended values derived here for $HCO_3^{\cdot}$ and $CO_3^{\cdot-}$. It can be seen that the CBS-RAD energies lead to $\Delta_f H°$ being underestimated by 3–8 kJ mol^{-1} for HNO_3 and NO_3^-, but overestimated by 8 kJ mol^{-1} for HCO_3^-. A correction for $HCO_3^{\cdot}$ and $CO_3^{\cdot-}$ is obviously desired but the direction is uncertain. Assuming that the error for $HCO_3^{\cdot}$ is similar to that for $HCO_2^{\cdot}$, 11.6 kJ mol^{-1}, one derives $\Delta_f H°$ of $HCO_3^{\cdot}$ = –365.7 kJ mol^{-1}. Alternatively one can use the isodesmic reaction

[2] $$HCO_3^{\cdot} + CH_4 = HCO_2^{\cdot} + CH_3OH$$

for which $\Delta\Delta H°$ (CBS-RAD) (= $\Delta_f H°(HCO_2^{\cdot}) + \Delta_f H°(CH_3OH) - \Delta_f H°(CH_4) - \Delta_f H°(HCO_3^{\cdot})$ is 110.7 kJ mol^{-1}. Combining this with the values of $\Delta_f H°$ (Rec.) for CH_4, $HCO_2^{\cdot}$, and CH_3OH leads to $\Delta_f H°$ of $HCO_3^{\cdot}$ = –364.1 kJ mol^{-1}, which differs from the CBS-RAD value by 13.2 kJ mol^{-1}. We chose to take the mean of these two corrections, 12.4 kJ mol^{-1}, giving the recommended value of $\Delta_f H°$ ($\Delta_f H°$ (Rec.)) of $HCO_3^{\cdot}$ = –364.9 kJ mol^{-1} in Table 1. One may note here that $\Delta_f H°$ (Rec.) of $HCO_2^{\cdot}$ = –127.0 kJ mol^{-1} reported in our previous study (26) is bracketed by –129.7 ± 12.6 from photoelectron spectroscopy (27) and –126.4 ± 1.7 from a computational coupled cluster study (28).

Proceeding in the same manner, the error for $CO_3^{\cdot-}$ should be similar to that for NO_3^- (8.3 kJ mol^{-1}) and the isoelectronic $NO_3^{\cdot}$ (6.2 kJ mol^{-1}) (29). Use of the isodesmic reaction,

[3] $$HCO_3^{\cdot-} + NO_3^{\cdot} = CO_3^{\cdot-} + HNO_3$$

leads to –3.2 kJ mol^{-1}. The correction is again taken as the mean (3.8 kJ mol^{-1}), giving $\Delta_f H°$ (Rec.) of $CO_3^{\cdot-}$ = –564.8 kJ mol^{-1}. $\Delta_f H°$ (Rec.) of NO_3^- in Table 1 is supported by a calculation from $\Delta_f H^0$ (Rec.) of HNO_3 and the proton affinity (30), as well as from the energy of formation of

© 2006 NRC Canada

Table 1. Values of electronic energies (EE in Hartrees), ZPEs, and $H° - H_0°$ (in kJ mol^{-1}), and S° (in J mol^{-1} K^{-1}) for carbonate radical and related species.

Species	EE[a]	ZPE	$H° - H_0°$	$S°$	$\Delta_f H°$ (Calc.)	$\Delta_f H°$ (Rec.)[b]
HCO_3^-	–264.159 33	68.5	11.8	266.4	–736.3	–743.9
HNO_3	–280.576 02	69.4	11.7	265.9	–138.1	–135.0
$HCO_2^{\cdot}$	–188.851 80	41.8	10.8	244.7	–138.6	–127.0
$HCO_3^{\cdot}$	–264.022 56	66.4	12.0	273.0	–377.3	–364.9[c]
NO_3^-	–280.062 41	36.5	10.8	245.7	–315.3	–307.0
$NO_3^{\cdot}$	–279.917 68	27.8	13.0	245.7	67.5	73.7[d]
$CO_3^{\cdot -}$	–263.514 91	31.4	12.0	257.8	–568.6	–564.8[c]
CH_3OH	–115.538 07	135.1	11.3	239.7	–201.8	–201.0
CH_4	–40.409 51	117.0	10.0	186.0	–73.8	–74.6
H_2	–1.165 7	26.6	8.68	130.3	—	0.0
H^+	0.0	0.0	6.20	108.8	—	1530.0

Note: $H° - H_0°$ and S° $\Delta_f G°$ at 298 K and 1 atm (1 atm = 101.326 kPa).

[a]CBS-RAD EEs (include ZPEs).
[b]From ref. 7, unless stated otherwise, and are consistent with values in ref. 10 to within ≤0.5 kJ mol^{-1}.
[c]This study; see text.
[d]Ref. 29.

Table 2. Recommended values of $\Delta_f H_{(g)}°$, $\Delta_f G_{(g)}°$, and $\Delta_f G_{(aq)}°$ (in kJ mol^{-1}) and values of $\Delta G_{(soln)}°$ for carbonate radicals and related species at 1 mol/L conc. and 298 K.

				$\Delta G_{(soln)}°$	
Species	$\Delta_f H_{(g)}°$ (Rec.)[a]	$\Delta_f G_{(aq)}°$	$\Delta G_{(soln)}°$	Rec.	IEFPCM
HCO_3^-	–743.9	–703.0	–586.8[b]	–304.7	–333.6
$HCO_3^{\cdot}$	–364.9	–346.8	–389.1	–42.3	–32.7
$CO_3^{\cdot -}$	–564.8	–557.7	–409.2	–269.4	276.8
HNO_3	–135.0	–66.7	–100.9[b]	4.2	–24.6
NO_3^-	–307.0	–252.1	–108.74[b]	–274.5	–281.4
CO_3^{2-}	—	—	–527.81[b]	—	—
CO_2	–393.5[b]	–386.5[b]	–386.0[b]	0.5	—
H^+	1530.0[c]	1524.9[c]	0.0	–1107.0[d]	—

[a]From Table 1 unless stated otherwise.
[b]Experimental data from ref. 32.
[c]From ref. 37 with $\Delta_f G_{(g)}°$ corrected for 1 mol/L conc.
[d]Ref. 35.

$NO_3^{\cdot}$ from NO_2 + O ($^3P_2$) (29) and the EA of $NO_3^{\cdot}$ (3.937 eV) (31). The uncertainties in the calculated $\Delta_f H°$ (Rec.) values are taken to be ±5 kJ mol^{-1}.

Bond dissociation enthalpies (BDE)

From the $\Delta_f H^0$ (Rec.) values in Table 1 and using $\Delta_f H°(H^{\cdot})$ = 218.0 kJ mol^{-1}, one finds that BDE(OH) of HCO_3^-, namely $\Delta H_{(rxn)}$ for

[4] $$HCO_3^- = CO_3^{\cdot -} + H^{\cdot}$$

is 397 kJ mol^{-1} (387 kJ mol^{-1} by direct calculation from the CBS-RAD values). This is 30 kJ mol^{-1} lower than BDE(OH) of HNO_3 (426 kJ mol^{-1}) and 83 kJ mol^{-1} lower than BDE(OH) of HCO_2H (470 kJ mol^{-1}). Thus, the formation of $CO_3^{\cdot -}$ as a result of H atom abstraction from bicarbonate anion by hydroxyl radical is exothermic by 100 kJ mol^{-1}.

Aqueous phase free energies of formation

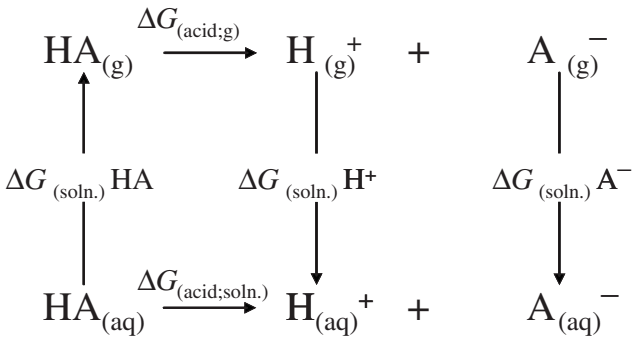
Table 2 summarizes the values of $\Delta_f G_{(g)}$ obtained from the $\Delta_f H°$ (Rec.) in Table 1 and lists $\Delta_f G_{(aq)}°$, and the free energies of solution, $\Delta G_{(soln)}$. The values of $\Delta_f G_{(aq)}°$ for the $HCO_3^{\cdot}$ and $CO_3^{\cdot -}$ radicals were obtained from the gas phase results and the IEFPCM free energies of solution by using corrections derived from the structurally similar HNO_3 and NO_3^- species. The data for other species except HNO_3 are from standard tables (32). $\Delta_f G_{(aq)}°$ for HNO_3 was derived from the value for NO_3^- and pK_a (= –1.37) (33). Comparison with $\Delta_f G_{(g)}{}^0$ of HNO_3 gave a $\Delta G_{(soln)}$ (–34.2 kJ mol^{-1}) 9.6 kJ mol^{-1} more negative than calculated by the polarizable continuum model. Applying the same correction to the IEFPCM result for $HCO_3^{\cdot}$ gave $\Delta G_{(soln)}$ = –42.2 kJ mol^{-1} and hence, from $\Delta_f G_{(g)}°$, $\Delta_f G_{(aq)}°$ = –367.7 kJ mol^{-1}. In a similar vein, $\Delta_f G_{(aq)}°$ for the two anion species NO_3^- and $CO_3^{\cdot -}$ can be derived from their $\Delta_f G_{(aq)}°$ values and the $\Delta G_{(Rxn)}$ for,

[5] $$H^+_{(g)} + A^-_{(g)} = H^+_{(aq)} + A^-_{(aq)}$$

in which A^- is NO_3^- or $CO_3^{\cdot -}$. The result for NO_3^-

© 2006 NRC Canada

Scheme 1.



(–115.6 kJ mol^{-1}) is in error by –6.9 kJ mol^{-1} from the accepted –108.7 in Table 2. Applying this correction to the $CO_3^{\cdot-}$ data leads to $\Delta_f G_{(soln)}$ = –269.4 kJ mol^{-1} and the $\Delta_f G_{(aq)}^\circ$ value in Table 2, –409.4 kJ mol^{-1}. This is 26 kJ mol^{-1} more negative than the estimate based on a review of early data in ref. (34). The $\Delta_f G_{(aq)}^\circ$ value of $HCO_3^\cdot$ in that paper is badly in error because of the erroneous pK_a of 7.6, which was accepted at that time. For $CO_3^{\cdot-}$ and $HCO_3^\cdot$ the uncertainties in the calculated $\Delta G_{(soln)}$ and $\Delta_f G_{(aq)}^\circ$ values are estimated to be ±5 and ±7 kJ mol^{-1}, respectively, the latter being the combination of the uncertainties in $\Delta_f G_{(g)}^\circ$ and $\Delta G_{(soln)}$.

The pK_a of $HCO_3^\cdot$

The pK_a values of the two acid species HNO_3 and $HCO_3^\cdot$ were evaluated using the thermochemical cycle in Scheme 1. IEFPCM free energies of solution were used for the HA and A^- species and –1107 kJ mol^{-1} for H^+ (35). The value of $\Delta G_{(acid;g)}$ for HNO_3 derived directly from our CBS-RAD energies was 3.2 kJ mol^{-1} lower than the experimental value reported in ref. 30 (1330 ± 1 kJ mol^{-1}), which is acceptable for calculations at this level. The value derived from the $\Delta_f H_{(g)}$ (Rec.) data in Table 1 (1339.5 kJ mol^{-1}) was in less good agreement. However, for consistency we used $\Delta G_{(acid;g)}$ from the $\Delta_f H_{(g)}$ (Rec.) values for all species. For HNO_3, the resulting $\Delta G_{(acid;aq)}$ (–7.8 kJ mol^{-1}) was in perfect agreement with the pK_a value, –1.37. $\Delta G_{(acid;g)}$ for $HCO_3^\cdot$ was found to be 1306.9 kJ mol^{-1}. Using this result, $\Delta G_{(acid;aq)}$ for $HCO_3^\cdot$ was found to be –27.2 kJ mol^{-1}, which is similar to the –20.1 kJ mol^{-1} difference between the $\Delta_f G_{(aq)}^\circ$ values of $CO_3^{\cdot-}$ and $HCO_3^\cdot$ in Table 2 and clearly more negative than the experimental value of –7.8 kJ mol^{-1} for HNO_3. $HCO_3^\cdot$ is therefore a very strong acid with pK_a = –4.1 ± 1 and $CO_3^{\cdot-}$ will be the only important form of the radical over the pH range 0–14. This conclusion is in agreement with the conclusions in ref. 8.

Reduction potentials

Because of the very low radical pK_a, reactions [6] and [7] are the important redox half reactions. The E° values calculated from the $\Delta_f G_{(aq)}^\circ$ values in Table 2 are given beside the equations below.

[6] $CO_3^{\cdot-}{}_{(aq)} + H^+{}_{(aq)} + e^- = HCO_3^-{}_{(aq)}$; E° = 1.84 ± 0.1 V

[7] $CO_3^{\cdot-}{}_{(aq)} + e^- = CO_3^{2-}{}_{(aq)}$; E° = 1.23 ± 0.1 V

The E° value for reaction [7] is in modest agreement with the experimental value of 1.58 ± 0.03 V noted above from refs. 8 and 9. The experimental data are therefore consistent with the monomeric $CO_3^{\cdot-}$ form of the radical.

Other equilibria

By using the $\Delta_f G_{(aq)}^\circ$ values in Table 2 and further information in refs. 32–34, we may examine other possible reactions involving $CO_3^{\cdot-}$. These include the reactions for formation by $^\cdot OH$ at different pH values and the decomposition to CO_2 and $O^{\cdot-}$. The reactions are listed below with the $\Delta G_{(Rxn.)}^\circ$ values in kJ mol^{-1} beside them.

[8] $^\cdot OH + CO_2 = H^+ + CO_3^{\cdot-}$; $\Delta G_{(Rxn.)}$ = –49

[9] $^\cdot OH + HCO_3^- = H_2O + CO_3^{\cdot-}$; $\Delta G_{(Rxn.)}$ = –85

[10] $^\cdot OH + CO_3^{2-} = OH^- + CO_3^{\cdot-}$; $\Delta G_{(Rxn.)}$ = –220

[11] $O^{\cdot-} + H_2O + CO_3^{2-} = 2OH^- + CO_3^{\cdot-}$; $\Delta G_{(Rxn.)}$ = –53

[12] $CO_3^{\cdot-} = CO_2 + O^{\cdot-}$; $\Delta G_{(Rxn.)}$ = 117

Formation from carbonate (reaction 10) is clearly the most favoured. The electron transfer is fast with $k_{10} = 3.7 \times 10^8$ (mol/L)$^{-1}$ s^{-1} (36). Formation by hydrogen atom transfer from bicarbonate (reaction 9) is also favoured, although is probably much slower than electron transfer. Lastly, the radical is clearly stable to decomposition to $CO_2 + O^{\cdot-}$.

Self-association

Finally, we examine the possibility of dimerization of $CO_3^{\cdot-}$ according to reaction [13],

[13] $2\ CO_3^{\cdot-} = O_2COOCO_2^{2-}$; $\Delta G_{(Rxn.)}$ = –65

In the gaseous phase, the dimeric dianion is a local minimum with C_2 symmetry. Like hydrogen peroxide, the peroxy link is twisted with C–O–O–C dihedral angle = 140°. The dimer is unstable toward dissociation into two carbonate radical anions by 220 kJ mol^{-1} at the CBS-RAD level.[5] In aqueous solution, however, the much greater free energy of solution of the dianion ($\Delta G_{(soln)}$ = –913 kJ mol^{-1}) compared with the two $CO_3^{\cdot-}$ radicals (IEFPCM value, –276.8 kJ mol^{-1} in Table 2) makes the dimer more stable by 65 kJ mol^{-1} at the uncorrected IEFPCM level. This result suggests that if the $CO_3^{\cdot-}$ radical concentration is higher than nanomolar then the major species at equilibrium would be the dimer dianion. Whether equilibrium could be achieved, given the reactivity of $CO_3^{\cdot-}$, is doubtful however. Although we are not able to determine it, we expect that there will be a substantial barrier to dimerization because of the coulombic repulsion and solvent reorganization that must be overcome. Nevertheless, in the absence of substrates, dimerization would provide a route to the decay of the $CO_3^{\cdot-}$ radical in aqueous solution.

Conclusions

The present ab initio calculations along with isodesmic reactions have been used to derive a set of self-consistent free

[5] The CBS-RAD energy of $O_2COOCO_2^{2-}$ is –526.929 454 hartrees (1 hartree = 2625.5 kJ/mol).

© 2006 NRC Canada

energies of formation for carbonate and nitrate species in the gas phase. By using IEFPCM-calculated free energies of solution and making corrections based on the experimental values for the nitrate system, these have been extended to the aqueous phase. The results show that $HCO_3^{\cdot}$ is a strong acid and that $E^{\circ}(CO_3^{\cdot -}/CO_3^{2-}) = 1.23 \pm 0.15$ V. These findings do not support earlier data indicating a pK_a of $HCO_3^{\cdot}$ in the region of 7–10, but are in excellent agreement with the experimental findings in refs. 7 and 8. Attention is currently being directed toward medium effects, which are likely to be the origin of the conflicting results from earlier studies.

Acknowledgement

The financial support of the Natural Sciences and Engineering Research Council of Canada (NSERC), the University of Saskatchewan, and the University of Calgary is gratefully acknowledged. The authors are also indebted to Mr. Patrick Brunelle for assistance with the computer network.

References

1. J.P. Keene, Y. Raef, and A.J. Swallow. *In* Pulse radiolysis. *Edited by* M. Ebert, J.P. Keene, A.J. Swallow, and J.H. Baxendale. Academic Press, New York. 1965. p. 99.
2. (*a*) G.V. Buxton, C.L. Greenstock, W.P. Helman, and A.B. Ross. J. Phys. Chem. Ref. Data, 17, 513 (1988); (*b*) Th. Umschlag and H. Herrmann. Acta Hydroch. Hydrob. **27**, 214–222 (1999).
3. O. Augusto, M.G. Bonini, A.M. Amanso, E. Linares, C.C.X. Santos, and S.L. De Menezes. Free Radical Biol. Med. **32**, 841 (2002).
4. A. Joffe, N.E. Geacintov, and V. Shafirovich. Chem. Res. Toxicol. **16**, 1528 (2003).
5. I.A. Shkrob. J. Phys. Chem. A, **106**, 11871 (2002).
6. O.P. Chawla and R.W. Fessenden. J. Phys. Chem. **79**, 2693 (1975).
7. (*a*) R.H. Bisby, S.A. Johnson, A.W. Parker, and S.M. Tavender. J. Chem. Soc. Faraday Trans. **94**, 2069 (1998); (*b*) S.M. Tavender, S.A. Johnson, D. Balsom, A.W. Parker, and R.H. Bisby. Laser Chem. **19**, 311 (1999).
8. G. Czapski, S.V. Lymar, and H.A. Schwarz. J. Phys. Chem. A, **103**, 3447 (1999).
9. R.E. Huie, C.L. Clifton, and P. Neta. Radiat. Phys. Chem. **38**, 477 (1991).
10. S.V. Lymar, H.A. Schwarz, and G. Czapski. Radiat. Phys. Chem. **59**, 387 (2000).
11. M.J. Frisch, G.W. Trucks, H.B. Schlegel, G.E. Scuseria, M.A. Robb, J.R. Cheeseman, V.G. Zakrzewski, J.A. Montgomery, Jr., R.E. Stratmann, J.C. Burant, S. Dapprich, J.M. Millam, A.D. Daniels, K.N. Kudin, M.C. Strain, O. Farkas, J. Tomasi, V. Barone, M. Cossi, R. Cammi, B. Mennucci, C. Pomelli, C. Adamo, S. Clifford, J. Ochterski, G.A. Petersson, P.Y. Ayala, Q. Cui, K. Morokuma, P. Salvador, J.J. Dannenberg, D.K. Malick, A.D. Rabuck, K. Raghavachari, J.B. Foresman, J. Cioslowski, J.V. Ortiz, A.G. Baboul, B.B. Stefanov, G. Liu, A. Liashenko, P. Piskorz, I. Komaromi, R. Gomperts, R.L. Martin, D.J. Fox, T. Keith, M.A. Al-Laham, C.Y. Peng, A. Nanayakkara, M. Challacombe, P.M.W. Gill, B. Johnson, W. Chen, M.W. Wong, J.L. Andres, C. Gonzalez, M. Head-Gordon, E.S. Replogle, and J.A. Pople. Gaussian 98 [computer program]. Revision A.11. Gaussian, Inc., Pittsburgh, Penn. 2001.
12. L.A. Curtiss, K. Raghavachari, and J.A Pople, J. Chem. Phys. **98**, 1293 (1993).
13. M.J. Frisch, G.W. Trucks, H.B. Schlegel, G.E. Scuseria, M.A. Robb, J.R. Cheeseman, J.A. Montgomery, Jr., T. Vreven, K.N. Kudin, J.C. Burant, J.M. Millam, S.S. Iyengar, J. Tomasi, V. Barone, B. Mennucci, M. Cossi, G. Scalmani, N. Rega, G.A. Petersson, H. Nakatsuji, M. Hada, M. Ehara, K. Toyota, R. Fukuda, J. Hasegawa, M. Ishida, T. Nakajima, Y. Honda, O. Kitao, H. Nakai, M. Klene, X. Li, J.E. Knox, H.P. Hratchian, J.B. Cross, C. Adamo, J. Jaramillo, R. Gomperts, R.E. Stratmann, O. Yazyev, A.J. Austin, R. Cammi, C. Pomelli, J.W. Ochterski, P.Y. Ayala, K. Morokuma, G.A. Voth, P. Salvador, J.J. Dannenberg, V.G. Zakrzewski, S. Dapprich, A.D. Daniels, M.C. Strain, O. Farkas, D.K. Malick, A.D. Rabuck, K. Raghavachari, J.B. Foresman, J.V. Ortiz, Q. Cui, A.G. Baboul, S. Clifford, J. Cioslowski, B.B. Stefanov, G. Liu, A. Liashenko, P. Piskorz, I. Komaromi, R.L. Martin, D.J. Fox, T. Keith, M.A. Al-Laham, C.Y. Peng, A. Nanayakkara, M. Challacombe, P.M.W. Gill, B. Johnson, W. Chen, M.W. Wong, C. Gonzalez, and J.A. Pople. Gaussian 03 [computer program]. Revision C.02. Gaussian, Inc., Wallingford, Conn. 2004.
14. A.P. Scott and L. Radom. J. Phys. Chem. **100**, 16502 (1996).
15. D.A. McQuarrie. Statistical thermodynamics. Harper and Row, New York. 1973.
16. (*a*) J.W. Ochterski. Thermochemistry in Gaussian [online]. Available from http://www.gaussian.com/g_whitepap/thermo.htm. 2000.
17. P.M. Mayer, C.J. Parkinson, D.M. Smith, and L. Radom. J. Chem. Phys. **108**, 604 (1998).
18. (*a*) H. Fischer and L. Radom. Angew. Chem. Int. Ed. **40**, 1340 (2001); (*b*) M.W. Wong and L. Radom. J. Phys. Chem. **99**, 8582 (1995); (*c*) M.W. Wong and L. Radom. J. Phys. Chem. A, **102**, 2237 (1998).
19. A. Rauk, R.J. Boyd, S.L. Boyd, D.J. Henry, and L. Radom. Can. J. Chem. **81**, 1 (2003).
20. (*a*) M.T. Cancès, B. Mennucci, and J. Tomasi. J. Chem. Phys. **107**, 3032 (1997); (*b*) B. Mennucci and J.Tomasi. J. Chem. Phys. **106**, 5151 (1997); (*c*) B. Mennucci, E. Cancès, and J. Tomasi. J. Phys. Chem. B, **101**, 10506 (1997).
21. (*a*) J. Tomasi, B. Mennucci, and E. Cancès. THEOCHEM, **464**, 211 (1999); (*b*) E. Cancès and B. Mennucci. J. Chem. Phys. **114**, 4744 (2001).
22. (*a*) R.E. Stratmann, G.E. Scuseria, and M.J. Frisch. J. Chem. Phys. **109**, 8218 (1998); (*b*) R. Bauernschmitt and R. Ahlrichs. Chem. Phys. Lett. **256**, 454 (1996); (*c*) M.E. Casida, C. Jamorski, K.C. Casida, and D.R. Salahub. J. Chem. Phys. **108**, 4439 (1998).
23. (*a*) V. Barone and M. Cossi. J. Phys. Chem. A, **102**, 1995 (1998); (*b*) M. Cossi, N. Rega, G. Scalmani, and V. Barone. J. Comput. Chem. **24**, 669 (2003).
24. (*a*) B.O. Leung, D.L. Reid, D.A. Armstrong, and A. Rauk. J. Phys. Chem. A, **108**, 2720 (2004); (*b*) C. Zhan, J. Bentley, and D.M. Chipman. J. Chem. Phys. **108**, 177 (1998).
25. S.-N. Chen, V.W. Cope, and M.Z. Hoffman. J. Chem. Phys. **77**, 1111 (1973).
26. D. Yu, A. Rauk, and D.A. Armstrong. J. Chem. Soc. Perkin Trans. 2, 2207 (1994).
27. E.H. Kim, S.E. Bradforth, D.W. Arnold, R.B. Metz, and D.M. Neumark. J. Chem. Phys. **103**, 7801 (1995).
28. D. Feller and D.A. Dixon. J. Phys. Chem. **107**, 1604 (2003).

© 2006 NRC Canada

29. H.F. Davis, B. Kim, H.S. Johnston, and Y.T. Lee. J. Chem. Phys. **97**, 2172 (1993).
30. S.G. Lias, J.E. Bartmess, J.F. Liebman, J.L. Holmes, R.D. Levin, and W.G. Mallard. J. Phys. Chem. Ref. Data. **17**(Suppl. No. 1), 789 (1988).
31. A. Weaver, D.W. Arnold, S.E. Bradforth, and D.M. Neumark. J. Chem. Phys. **94**, 1740 (1991).
32. D.D. Wagman, W.H. Evans, V.B. Parker, R.H. Schumm, I. Halow, S.M. Bailey, K.L. Churney, and R.L. Nuttal. J. Chem. Phys. Ref. Data, **11**(Suppl. No. 2), (1982).
33. (*a*) R.P. Bell. The proton in chemistry. 2nd Ed. Chapman and Hall, London. 1959; (*b*) O. Reddick and D.C. Hood. Discuss. Faraday Soc. **24**, 87 (1957).
34. D.M. Stanbury. Adv. Inorg. Chem. **33**, 69 (1989).
35. M.D. Liptak, K.C. Gross, P.G. Seybold, S. Feldgus, and G.C. Shields. J. Am. Chem. Soc. **124**, 6421 (2002).
36. D. Behar, G. Czapski, and I. Duchovny. J. Phys. Chem. **74**, 2206 (1970).
37. J.E. Bartness. J. Phys. Chem. **98**, 6420 (1994).

© 2006 NRC Canada

Intramolecular amidation — An efficient synthesis of 3-aryl-2-quinolinones

Yinggang Luo, Feiyan Tao, Yan Liu, Bogang Li, and Guolin Zhang

Abstract: To reveal the scope of the syntheses of 3-aryl-2-quinolinones from 2-nitro-α-phenylcinnamic acids, the isomerization of (*E*)-2-amino-α-phenylcinnamic acids was studied. The results showed that (*E*)-2-amino-α-phenylcinnamic acids were isomerized to its (*Z*)-forms under sunlight in organic solvents. The reaction temperature and the functional groups at both phenyl rings have no effect on the isomerization of (*E*)-2-amino-α-phenylcinnamic acids and the following intramolecular spontaneous amidation of (*Z*)-2-amino-α-phenylcinnamic acids. Various 3-aryl-2-quinolinones prepared in high total yields indicated that the syntheses of 3-aryl-2-quinolinones from Perkin condensation products 2-nitro-α-phenylcinnamic acids via reduction, sunlight-induced isomerization of (*E*)-2-amino-α-phenylcinnamic acids, and the following intramolecular amidation is an efficient procedure.

Key words: 3-aryl-2-quinolinones, isomerization, amidation.

Résumé : Afin d'évaluer la portée des synthèses de 3-aryl-2-quinoléinones à partir d'acides 2-nitro–phénylcinnamiques, on a étudié l'isomérisation des acides (*E*)-2-amino-α-phénylcinnamiques. Les résultats montrent que les acides (*E*)-2-amino-α-phénylcinnamiques en solution dans des solvants organiques s'isomérisent en formes (*Z*) sous l'influence de la lumière du jour, que la température de la réaction et les groupes fonctionnels sur l'un ou l'autre des groupes phényles n'ont aucune influence sur l'isomérisation des acides (*E*)-2-amino-α-phénylcinnamiques et sur l'amidation spontanée intramoléculaire des acides (*Z*)-2-amino-α-phénylcinnamiqued. Les synthèses de 3-aryl-2-quinoléinones à partir des acides 2-nitro-α-phénylcinnamiques qui ont été obtenus comme produits de condensation de Perkin, puis soumis à une réduction, une isomérisation induite par la lumière des acides (*E*)-2-amino-α-phénylcinnamiques et une amidation intramoléculaire s'avèrent efficaces.

Mots clés : 3-aryl-2-quinoléinones, isomérisation, amidation.

[Traduit par la Rédaction]

Introduction

3-Aryl-2-quinolinones could inhibit the migration of tumor cells with no cytotoxicity in vitro or in vivo. The combination of 3-aryl-2-quinolinones and doxorubicin (or etoposide), two drugs routinely used in clinic, led to additive in vivo benefits compared with individual administration of the drugs (1). 3-Aryl-2-quinolinones were also efficient tools in the treatment of osteoporosis (2). They were selective non-competitive antagonists of *N*-methyl-D-aspartate receptors and (or) antagonists of 2-amino-3-hydroxy-5-methyl-4-isoxazolepropionic acid receptors (3). They could serve as precursors of a new class for nonpeptide gonadotropin releasing hormone receptor antagonists (4).

Received 30 March 2006. Accepted 20 October 2006. Published on the NRC Research Press Web site at http://canjchem.nrc.ca on 7 December 2006.

Y. Luo, Y. Liu, B. Li, and G. Zhang.[1] Chengdu Institute of Biology, The Chinese Academy of Sciences, Chengdu 610041, People's Republic of China.
F. Tao. Chengdu Institute of Biology, The Chinese Academy of Sciences, Chengdu 610041, People's Republic of China; Graduate School of the Chinese Academy of Sciences, Beijing 10049, People's Republic of China.

[1]Corresponding author (e-mail: zhanggl@cib.ac.cn).

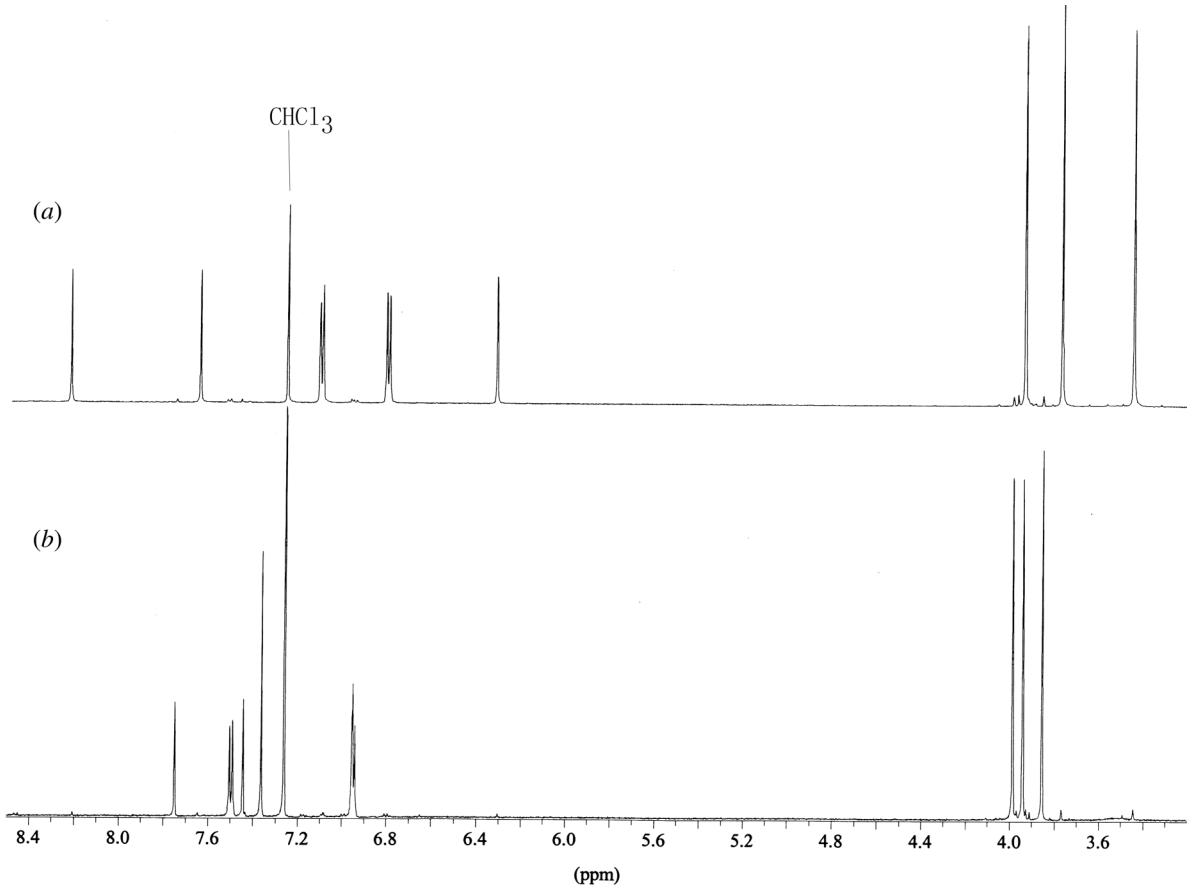
To date, the condensation of anilines with arylmalonate or its analogues (1, 2*a*) and the palladium-catalyzed annulation of *o*-iodoaniline derivatives with aryl substituted terminal alkynes or 2-phenylacrylic acid were introduced into the syntheses of 3-aryl-2-quinolinones (5, 6). The total yields ranged from 9.10 to 40.85% for the former strategy (1, 2) and from 20 to 42% for the latter one (5, 6). Recently, palladium-catalyzed amidation of *o*-carbonyl-substituted aryl halides for quinolinones (7*a*) and a rapid assembly of 4-fluoroquinolinones were reported (7*b*).

3-Aryl-2-quinolinones, a small-amount by-product in Pschorr's phenanthrene synthesis, were obtained from the reduction of (*Z*)-2-nitro-α-phenylcinnamic acids originally formed in Perkin condensation (8). (*E*)-2-Amino-α-phenylcinnamic acids could be converted to 3-aryl-2-quinolinones by treatment with acetic anhydride and concentrated sulfuric acid or zinc chloride (8*a*, 9) or by exposure to ultraviolet (8*a*) or sunlight (10). The methyl esters of (*E*)-2-amino-α-phenylcinnamic acids were converted to 3-aryl-2-quinolinones by heating or by standing at room temperature (10).

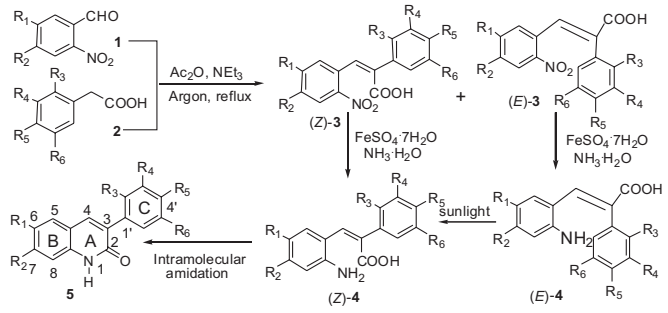
However, the scope of the preparation of 3-aryl-2-quinolinones from 2-amino-α-phenylcinnamic acids including the detailed process of the isomerization of the (*E*)-2-amino-α-phenylcinnamic acids, the effect of the functional groups at aryl moieties on the isomerization, and the following spontaneous intramolecular amidation has not been reported.

 doi:10.1139/V06-163 © 2006 NRC Canada

Fig. 1. ^{1}H NMR spectra of the isomers of compound **3d** in $CDCl_3$: (*a*) (*E*)-**3d**; (*b*) (*Z*)-**3d**.



Scheme 1.



Herein, we report our investigations concerning these problems.

Results and discussion

Perkin condensation of 2-nitro-benzaldehydes (**1**) and phenylacetic acids (**2**) gave a mixture of the (*E*)- and (*Z*)-isomers of 2-nitro-α-phenylcinnamic acids (**3**) (Scheme 1). The ratio of (*E*)- and (*Z*)-isomers could be determined by proton integration in the ^{1}H NMR spectra without separation (8*c*). Taken as an example, Fig. 1 shows the ^{1}H NMR spectra of (*E*)-**3d** and (*Z*)-**3d**, which could be separated by silica gel column chromatography or fractional crystallization.

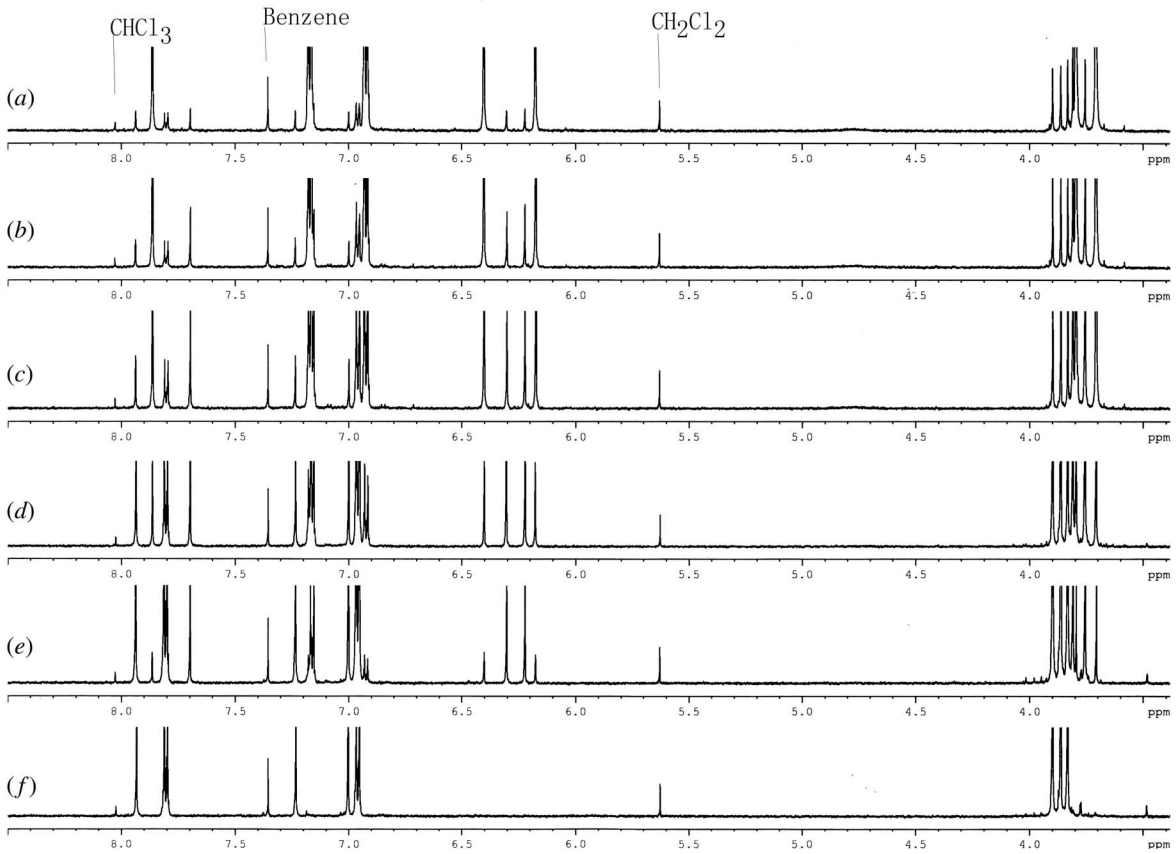
Reduction of the mixture of (*E*)-**3** and (*Z*)-**3** by ferrous sulfate in aq. ammonia led to the formation of (*E*)-**4** and 3-aryl-2-quinolinones (**5**); thus, indicating that (*Z*)-**4** spontaneously cyclized to give the intramolecular amidation products **5**. Roy and Bhaduri (8*c*) suggested that only (*Z*)-**3d** could be converted to 3-aryl-2-quinolinone by reduction. To confirm their conclusion, the (*E*)-**3d** and (*Z*)-**3d** were isolated and characterized on the basis of NMR, IR, UV, and mass spectral data. The stereochemistry of (*E*)-**3d** was confirmed by X-ray crystallographic analysis (Fig. S1, the ORTEP drawing of CCDC 264443, see supplementary data).[2] Reduction of (*Z*)-**3d** by ferrous sulfate in aqueous ammonia with or without exposure to sunlight led to 3-aryl-2-quinolinone (**5d**), whereas the reduction of (*E*)-**3d** under the same conditions afforded only (*E*)-**4d**.

However, 3-aryl-2-quinolinone (**5d**) was obtained when (*E*)-**4d** was dissolved in acetone and was left standing under sunlight at room temperature. Initially, only (*E*)-**4d** was observed in the ^{1}H NMR spectrum, and it was stable without exposure to sunlight. When the acetone solution of (*E*)-**4d**

[2] Supplementary data for this article are available on the journal Web site or may be purchased from the Depository of Unpublished Data, Document Delivery, CISTI, National Research Council Canada, Ottawa, ON K1A 0S2, Canada. DUD 5108. For more information on obtaining material refer to http://cisti-icist.nrc.cnrc.gc.ca/irm/unpub_e.shtml. CCDC 264442 and 264443 contain the crystallographic data for this manuscript. These data can be obtained, free of charge, via ww.ccdc.cam.ac.uk/conts/retrieving.html (or from the Cambridge Crystallographic Data Centre, 12 Union Road, Cambridge CB2 1EZ, UK; fax +44 1223 336033; or deposit@ccdc.cam.ac.uk).

© 2006 NRC Canada

Fig. 2. Conversion of (*E*)-**4d** to **5d** in acetone-d_6 monitored by ^{1}H NMR spectra: (*a*) 10 min, (*b*) 30 min, (*c*) 60 min, (*d*) 90 min, (*e*) 10 h, and (*f*) 16 h.



was left standing under sunlight, the ratio of (*E*)-**4d**, (*Z*)-**4d**, and **5d** changed from 100:0:0 to 0:0:100 in 16 h (Fig. 2), suggesting that the isomerization of (*E*)-**4d** to (*Z*)-**4d** is a sunlight-induced process and the formation of **5d** from (*Z*)-**4d** is an intramolecular spontaneous amidation.

(*E*)-**4d** kept unchanged in H_2O, 5% HCl (aq.), 5% NaOH (aq.), or 25% aq. ammonia under sunlight, indicating that sunlight could not induce the isomerization of (*E*)-**4d** to its (*Z*)-isomer in acidic, basic, or neutral aqueous media. The conversion of (*E*)-**4d** to **5d** in protic and polar aprotic solvents was very easy and fast (10–18 h), but it was difficult in nonpolar aprotic solvents (>48 h).[2]

To investigate the scope of this method, 26 3-aryl-2-quinolinones with electron-withdrawing and electron-donating groups on the rings B and C were synthesized (Scheme 1 and Table 1). The functional groups have no effect on the isomerization of (*E*)-**4** to (*Z*)-**4** or on the subsequent intramolecular amidation of (*Z*)-**4** to 3-aryl-2-quinolinones in view of the total yields of the title compounds (Table 1). The same conversion rate of (*E*)-**4d** to **5d** was observed when the acetone solution of (*E*)-**4d** was exposed to sunlight with stirring under reflux at room temperature or at 0 °C, indicating that the temperature has no effect on this process.

In the case of **3f**–**3h** and **3n**–**3p**, the hydroxyl groups were acetylated during Perkin reaction. The acetyl groups were removed during reduction, which was concluded from their ^{1}H NMR spectral data (Table 1, entries 6–8 and 14–16).

All 3-aryl-2-quinolinones were identified by ^{1}H and ^{13}C NMR, UV, IR, ESIMS, and HR-ESIMS data. The basic skeleton of 3-aryl-2-quinolinone, compound **5i**, was confirmed by X-ray crystallographic analysis (Fig. S2, the ORTEP drawing of CCDC 264442).[2]

In conclusion, it is an efficient procedure to prepare 3-aryl-2-quinolinones from Perkin condensation products (*Z*)- and (*E*)-2-nitro-α-phenylcinnamic acids via reduction, sunlight-induced isomerization of (*E*)-2-amino-α-phenylcinnamic acids to its (*Z*)-forms, and the spontaneous intramolecular amidation of the latter.

Experimental

General

All reagents were commercial and were used without purification. The 2-nitrobenzaldehydes with electron-withdrawing groups such as 4-bromo (11), 5-bromo (12), 5-chloro (12), and 4-acetyl (13) were prepared according to the literature. 2-Benzyloxyphenylacetic acid was prepared according to the reported procedure (14). Acetic anhydride was obtained by fractional distillation. Triethylamine was refluxed for 6 h with the freshly distilled acetic anhydride, then distilled, refluxed with CaH_2, and distilled again. Melting points were recorded on an X-6 apparatus and were uncorrected. IR spectra were recorded on a PerkinElmer Spectrum One spectrometer using KBr discs, and ν_{max} is given in cm^{-1}. UV spectra were recorded in MeOH (1 mg in

© 2006 NRC Canada

Table 1. The prepared 3-aryl-2-quinolinones bearing different functional groups.

Entry	Compound	R1	R2	R3	R4	R5	R6	Yield[a] (%)
1	**5a**	OMe	OMe	H	H	H	H	88.9
2	**5b**	OMe	OMe	OMe	H	H	H	88.4
3	**5c**	OMe	OMe	H	OMe	H	H	86.8
4	**5d**	OMe	OMe	H	H	OMe	H	88.4
5	**5e**	OMe	OMe	H	OMe	H	OMe	88.0
6	**5f**	OMe	OMe	OH	H	H	H	85.9
7	**5g**	OMe	OMe	H	OH	H	H	87.5
8	**5h**	OMe	OMe	H	H	OH	H	89.2
9	**5i**	H	H	H	H	H	H	88.2
10	**5j**	H	H	OMe	H	H	H	85.7
11	**5k**	H	H	H	OMe	H	H	89.6
12	**5l**	H	H	H	H	OMe	H	87.6
13	**5m**	H	H	H	OMe	H	OMe	89.0
14	**5n**	H	H	OH	H	H	H	86.5
15	**5o**	H	H	H	OH	H	H	88.6
16	**5p**	H	H	H	H	OH	H	88.6
17	**5q**	Cl	H	H	H	OMe	H	89.3
18	**5r**	Cl	H	H	Cl	H	H	83.6
19	**5s**	Br	H	H	H	OMe	H	89.4
20	**5t**	H	Br	H	H	OMe	H	88.0
21	**5u**	Br	H	H	Cl	H	H	87.0
22	**5v**	H	CH_3CO	H	H	OMe	H	95.6
23	**5w**	H	CH_3CO	H	H	F	H	82.7
24	**5x**	OMe	OMe	H	Cl	H	H	84.0
25	**5y**	OMe	OMe	H	H	F	H	86.0
26	**5z**	OMe	OMe	OBn	H	H	H	84.7

[a]Isolated total yield starting from compound **1**.

50 mL) on a PerkinElmer Lambda 35 spectrometer. NMR spectra were recorded on a Bruker Avance 600 spectrometer (^{1}H NMR: 600 MHz; ^{13}C NMR: 150 MHz) at room temperature in DMSO-d_6, when not mentioned. The chemical shifts (δ) are reported in ppm relative to tetramethylsilane as an internal standard, and the coupling constants (*J*) are given in Hz. HR-ESIMS spectra were obtained on a Bio TOF IIIQ mass spectrometer. Column chromatography (CC) was performed on self-packed open column with silica gel (200–300 mesh) from Qingdao Ocean Chemical Engineering Company (QOCEC, Qingdao, P.R. China). TLC analyses were carried out on plates precoated with 10–40 μ of silica gel GF_{254} from QOCEC and were visualized under an ultraviolet lamp.

General procedure for preparation of substituted 2-nitro-α-phenylcinnamic acids 3.

Compounds **3** were prepared according to Lebrun et al. (15*a*) with some modifications. A solution of 2-nitrobenzaldehyde (**1**, 0.2 mmol), NEt_3 (0.5 mL), substituted phenylacetic acid (**2**, 0.22 mmol), and Ac_2O (0.5 mL) was refluxed under argon for 30 min (TLC analysis). When the reaction was completed, water (10 mL) was added to the reaction mixture. During the addition, the temperature of the mixture should be maintained at 100–110 °C. Then, the reaction mixture was cooled to room temperature and then to 0 °C. The precipitate from the cold solution was collected by filtration. The mother liquor was partitioned between water and ethyl acetate. The organic layers were combined, washed with brine, dried over anhyd. Na_2SO_4, and concentrated to give a residue. The residue and the precipitate were pure enough for the next step. For compound **3d**, the two isomers can be separated by column chromatography over silica gel and eluted with petroleum ether (bp 60–90 °C) : acetone : acetic acid (5:1:0.025) (the value of $R_{f\text{-}(E)\text{-}\mathbf{3d}}$ > the value of $R_{f\text{-}(Z)\text{-}\mathbf{3d}}$) or by fractional crystallization from ethanol, in which (*E*)-**3d** crystallized from ethanol and (*Z*)-**3d** was left in the mother liquor.

General procedure for preparation of substituted 2-amino-α-phenylcinnamic acids 4

Compounds **4** were prepared according to Bradsher et al. (15*b*) with some modifications. A solution of **3** in 10% aq. ammonia was added dropwise in the course of 3 to 6 min to a solution of 440 mg of $FeSO_4 \cdot 7H_2O$ in 1.3 mL of H_2O and 0.03 mL of 25% aq. ammonia (several drops of *n*-butanol was added to the solution before heating to prevent foaming) under reflux. A total of 0.5 mL of concd. aq. ammonia was added slowly to the mixture within 85 min. When the reaction was completed, the reaction solution was cooled to 40–50 °C and filtered. The dark residue was washed six times with 10% aq. ammonia solution at about 50 °C, then washed 10 times with ethyl acetate. The combined basic solution was acidified carefully with acetic acid to pH = 6.0 and then extracted with ethyl acetate. The combined organic layers were washed with brine, dried over anhyd. Na_2SO_4, and con-

© 2006 NRC Canada

centrated to give a residue. For compound (*E*)-**4d**, the residue was subjected to column chromatography over silica gel and eluted with petroleum ether (bp 60–90 °C) : acetone : acetic acid (2:1:0.025) to give (*E*)-**4d** and **5d**.

General procedure for the preparation of 3-aryl-2-quinolinones 5

The previously obtained residue was dissolved in acetone and was left standing under sunlight at room temperature until (*E*)-**4** was converted to 3-aryl-2-quinolinones (**5**, TLC analysis). Most of the 3-aryl-2-quinolones were crystallized or precipitated from the solution. The mother liquor was subjected to silica gel column chromatography and eluted with petroleum ether (bp 60–90 °C) : acetone (5:2) to give another portion of 3-aryl-2-quinolinones.

*6,7-Dimethoxy-3-(4-methoxyphenyl)-quinolin-2(1*H*)-one (5d)*

White solid (55 mg); mp 259–260 °C (lit. 247–249 °C (16)). UV λ_{max} (log ε): 239 (4.40), 299 (3.88), 360 nm (4.23). IR ν_{max}: 3436, 1650, 1628, 1571, 1509, 1448, 1421, 1395, 1264, 1245, 1212, 1178, 1153, 1037, 1005, 929, 843, 830, 795, 755, 605 cm^{-1}. ^{1}H NMR: δ 11.72 (1H, s, NH), 7.95 (1H, s), 7.72 (2H, d, *J* = 8.8 Hz), 7.25 (1H, s), 6.98 (2H, d, *J* = 8.8 Hz), 6.87 (1H, s), 3.83, 3.80 and 3.79 (each 3H, s, H-6, 7, 4′-O*Me*). ^{13}C NMR: δ 161.4, 159.2, 152.1, 145.4, 136.5, 134.2, 130.1, 129.5, 128.4, 113.8, 113.4, 109.3, 97.7, 56.2, 56.0, 55.6. ESIMS (positive ion mode) *m*/*z*: 312 ([M + H]$^+$, 100). HR-ESIMS (positive ion mode) *m*/*z*: 312.1221 ([M + H]$^+$ calcd. for $C_{18}H_{18}NO_4$, 312.1230; error 3.12 ppm).

*6,7-Dimethoxy-3-(2-hydroxyphenyl)-quinolin-2(1*H*)-one (5f)*

Off-yellow solid (51 mg); mp 204.5–205.5 °C. UV λ_{max} (log ε): 240 (4.51), 298 (3.96), 361 nm (4.42). IR ν_{max}: 3434, 1644, 1625, 1611, 1568, 1516, 1490, 1474, 1443, 1414, 1394, 1352, 1293, 1277, 1252, 1215, 1160, 1039, 1012, 932, 916, 857, 832, 817, 761, 741, 724, 688, 608 cm^{-1}. ^{1}H NMR: δ 12.33 (1H, s, NH), 10.1 (1H, s, OH), 8.10 (1H, s), 7.38 (1H, dd, *J* = 7.6, 1.4 Hz), 7.35 (1H, s), 7.24 (1H, td, *J* = 7.9, 1.4 Hz), 6.97 (1H, s), 6.92 (1H, dd, *J* = 7.3, 1.4 Hz), 6.90 (1H, td, *J* = 7.9, 1.4 Hz), 3.87 and 3.82 (each 3H, s, H-6, 7-O*Me*). ^{13}C NMR: δ 162.6, 156.2, 152.9, 146.1, 140.7, 134.0, 131.3, 129.7, 127.8, 125.1, 120.0, 118.1, 114.0, 109.2, 97.8, 56.3, 56.2. ESIMS (negative ion mode) *m*/*z*: 296 ([M – H]$^-$, 25). HR-ESIMS (positive ion mode) *m*/*z*: 320.0881 ([M + Na]$^+$ calcd. for $C_{17}H_{15}NO_4Na$, 320.0893; error 3.74 ppm).

*3-Phenyl-quinolin-2(1*H*)-one (5i)*

Granule crystals (39 mg); mp 226.2–227 °C (lit. white solid; mp 230–231 °C (5)). UV λ_{max} (log ε): 239 (4.24), 290 (3.97), and 339 nm (3.96). IR ν_{max}: 3436, 1656, 1599, 1567, 1497, 1444, 1429, 1368, 1310, 1227, 1126, 1073, 1029, 985, 946, 909, 880, 788, 752, 730, 698 cm^{-1}. ^{1}H NMR: δ 11.94 (1H, s, NH), 8.09 (1H, s), 7.73 (3H, m), 7.38 (5H, m), 7.19 (1H, br s). ^{13}C NMR: δ 161.5, 138.8, 138.1, 136.7, 132.0, 130.7, 129.1, 128.6, 128.4, 128.3, 122.4, 120.0, 115.1. ESIMS (positive ion mode) *m*/*z*: 222 ([M + H]$^+$, 100). ESIMS (negative ion mode) *m*/*z*: 220 ([M – H]$^-$, 100). HR-ESIMS (positive ion mode) *m*/*z*: 244.0739 ([M + Na]$^+$ calcd. for $C_{15}H_{11}NONa$, 244.0733; error –2.43 ppm).

*3-(2-Hydroxyphenyl)-quinolin-2(1*H*)-one (5n)*

White solid (41 mg); mp 272–274 °C. UV λ_{max} (log ε): 239 (4.34), 269 (3.97), 292 (3.99), 342 nm (4.18). IR ν_{max}: 3436, 1641, 1603, 1573, 1553, 1490, 1476, 1424, 1379, 1292, 1256, 1233, 1196, 1161, 1109, 1048, 995, 952, 943, 927, 911, 847, 807, 750, 718, 676 cm^{-1}. ^{1}H NMR: δ 12.23 (1H, s, NH), 9.73 (1H, s, OH), 8.08 (1H, s), 7.76 (1H, d, *J* = 7.86 Hz), 7.55 (1H, t, *J* = 8.1 Hz), 7.40 (1H, d, *J* = 8.22 Hz), 7.35 (1H, d, *J* = 7.44), 7.25 (1H, t, *J* = 7.32 Hz), 7.24 (1H, t, *J* = 7.74 Hz), 6.91 (1H, d, *J* = 8.1 Hz), 6.88 (1H, t, *J* = 7.32 Hz). ^{13}C NMR: δ 162.5, 155.9, 140.5, 138.4, 131.6, 131.1, 130.8, 129.8, 128.5, 124.5, 122.7, 120.2, 119.6, 117.3, 115.5. ESIMS (positive ion mode) *m*/*z*: 238 ([M + H]$^+$, 100). ESIMS (negative ion mode) *m*/*z*: 236 ([M – H]$^-$, 100). HR-ESIMS (positive ion mode) *m*/*z*: 260.0682 ([M + Na]$^+$ calcd. for $C_{15}H_{11}NO_2Na$, 260.0682; error 0.10 ppm).

*7-Bromo-3-(4-methoxyphenyl)-quinolin-2(1*H*)-one (5t)*

White solid (58 mg); mp 222–225 °C. UV λ_{max} (log ε): 237 (4.38), 299 (3.95), 316 (4.01), 346 nm (4.22). IR ν_{max}: 3436, 2924, 2853, 1657, 1607, 1564, 1512, 1462, 1393, 1255, 1179, 1071, 1033, 988, 945, 826, 617, 555 cm^{-1}. ^{1}H NMR: δ 11.98 (1H, s, NH), 8.07 (1H, s), 7.74 (2H, d, *J* = 8.6 Hz), 7.67 (1H, d, *J* = 8.2 Hz), 7.49 (1H, s), 7.35 (1H, dd, *J* = 8.2, 1.3 Hz), 7.00 (2H, d, *J* = 8.6 Hz), 3.80 (3H, s, H-4′-O*Me*). ^{13}C NMR: δ 161.5, 160.0, 139.5, 136.2, 131.9, 130.4, 128.6, 125.2, 123.2, 119.2, 117.3, 113.9, 55.6. ESIMS (positive ion mode) *m*/*z*: 352 ([M + Na]$^+$, 100). HR-ESIMS (positive ion mode) *m*/*z*: 351.9936 ([M + Na]$^+$calcd. for $C_{16}H_{12}{}^{79}BrNNaO_2$, 351.9944; error 2.17 ppm).

*6-Bromo-3-(3-chlorophenyl)-quinolin-2(1*H*)-one (5u)*

White solid (58 mg); mp 258–261 °C. UV λ_{max} (log ε): 242 (4.65), 291 (4.18), 350 nm (4.10). IR ν_{max}: 3435, 2972, 2924, 1727, 1663, 1567, 1477, 1426, 1282, 1227, 1103, 924, 867, 813, 791, 763, 687, 605, 567, 516, 468 cm^{-1}. ^{1}H NMR: δ 12.20 (1H, s, NH), 8.20 (1H, s), 7.99 (1H, d, *J* = 1.8 Hz), 7.85 (1H, s), 7.71 (1H, d, *J* = 7.0 Hz), 7.68 (1H, dd, *J* = 8.7, 2.0 Hz), 7.46–7.50 (2H, m), 7.29 (1H, d, *J* = 8.7 Hz). ^{13}C NMR: δ 161.0, 138.3, 138.0, 137.7, 133.5, 133.1, 131.4, 130.6, 130.4, 128.9, 128.4, 127.8, 121.6, 117.4, 114.02. HR-ESIMS (positive ion mode) *m*/*z*: 355.9449 ([M + Na]$^+$calcd. for $C_{15}H_9{}^{79}Br{}^{35}ClNNaO$, 355.9448; error –0.32 ppm).

*7-Acetyl-3-(4-methoxyphenyl)-quinolin-2(1*H*)-one (5v)*

Off-yellow solid (56 mg); mp 243–245 °C. UV λ_{max} (log ε): 238 (4.31), 274 (3.83), 339 (4.04), 366 nm (4.11). IR ν_{max}: 3435, 2930, 1689, 1663, 1607, 1564, 1518, 1500, 1396, 1369, 1302, 1251, 1222, 1180, 1112, 1033, 913, 872, 820, 638, 621, 591 cm^{-1}. ^{1}H NMR: δ 12.11 (1H, s, NH), 8.14 (1H, s), 7.88 (1H, s), 7.85 (1H, d, *J* = 7.6 Hz), 7.77 (2H, d, *J* = 8.3 Hz), 7.76 (1H, d, *J* = 7.6 Hz), 7.01 (2H, d, *J* = 7.5 Hz), 3.81 (3H, s, H-4′-O*Me*), 2.62 (3H, s, 7-C*H*$_3$CO–). ^{13}C NMR: δ 198.0, 161.7, 159.9, 138.2, 137.4, 135.9, 133.8, 130.5, 128.7, 128.5, 123.5, 121.8, 114.9, 113.9, 55.7, 27.3. HR-ESIMS (positive ion mode) *m*/*z*: 316.0939 ([M + Na]$^+$calcd. for $C_{18}H_{15}NNaO_3$, 316.0944; error –1.48 ppm).

*7-Acetyl-3-(4-fluorophenyl)-quinolin-2(1*H*)-one (5w)*

White solid (46 mg); mp 293–296 °C. UV λ_{max} (log ε): 238 (4.34), 312 (4.15), 360 nm (4.03). IR ν_{max}: 3435, 2930,

© 2006 NRC Canada

2844, 1664, 1603, 1564, 1501, 1398, 1371, 1301, 1222, 1163, 1114, 877, 826, 806, 635, 593, 549, 522, 468 cm^{-1}. ^1H NMR: δ 12.17 (1H, s, NH), 8.20 (1H, s), 7.88 (1H, s), 7.83–7.86 (3H, m), 7.76 (1H, d, *J* = 8.1 Hz), 7.28 (2H, t, *J* = 8.8 Hz), 2.62 (3H, s, 7-C*H*$_3$CO–). ^{13}C NMR: δ 197.9, 163.4, 161.7, 138.5, 137.8, 137.2, 133.1, 132.6, 131.4, 131.3, 129.0, 123.2, 121.8, 115.4, 115.3, 115.0, 27.4. HR-ESIMS (positive ion mode) *m/z*: 304.0740 ([M + Na]$^+$calcd. for $C_{17}H_{12}FNNaO_2$, 304.0744; error 1.53 ppm).

3-(3-Chlorophenyl)-6,7-dimethoxy-quinolin-2(1H)-one (5x)

White needle crystal (53 mg); mp 247–248 °C. UV λ_{max} (log ε): 238 (4.32), 298 (3.79), 362 nm (4.06). IR ν_{max}: 3436, 2925, 1664, 1630, 1594, 1572, 1508, 1491, 1470, 1421, 1389, 1276, 1263, 1243, 1211, 1158, 1021, 928, 834, 785, 754, 701, 674, 606, 575, 542 cm^{-1}. ^1H NMR: δ 11.87 (1H, s, NH), 8.12 (1H, s), 7.88 (1H, s), 7.72 (1H, d, *J* = 7.6 Hz), 7.45 (1H, t, *J* = 7.6 Hz), 7.40 (1H, d, *J* = 7.6 Hz), 7.28 (1H, s), 6.88 (1H, s), 3.80 and 3.83 (each 3H, s, H-6, 7-O*Me*). ^{13}C NMR: δ 161.0, 152.8, 145.5, 139.2, 138.4, 134.8, 133.0, 130.3, 128.6, 127.6, 127.3, 126.8, 113.2, 109.4, 56.2, 56.1. HR-ESIMS (positive ion mode) *m/z*: 338.0556, ([M + Na]$^+$calcd. for $C_{17}H_{14}{}^{35}ClNNaO_3$, 338.0554 ; error –0.40 ppm).

3-(2-Benzyloxyphenyl)-6,7-Dimethoxy-quinolin-2(1H)-one (5z)

White solid (66 mg); mp 160–162 °C. UV λ_{max} (log ε): 238 (3.83), 291 (3.24), 350 nm (3.56). IR ν_{max}: 3435, 2910, 2826, 1668, 1650, 1576, 1510, 1464, 1448, 1398, 1266, 1245, 1153, 1124, 1043, 1018, 918, 838, 783, 758, 731, 691, 677, 605, 574, 462 cm^{-1}. ^1H NMR ($CDCl_3$): δ 12.12 (1H, s, NH), 7.84 (1H, s), 7.51 (1H, dd, *J* = 7.0, 1.5Hz), 7.33–7.35 (3H, m), 7.19–7.21 (2H, m), 7.16 (1H, m), 7.05–7.07 (2H, m), 6.88 (1H, s), 6.81 (1H, s), 5.12 (2H, s, C*H*$_2$), 3.90 and 3.91 (each 3H, s, H-6, 7-O*Me*). ^{13}C NMR ($CDCl_3$): δ 162.8, 156.6, 152.3, 145.8, 140.0, 137.2, 134.0, 131.5, 129.3, 128.3, 127.5, 127.2, 126.9, 126.3, 120.9, 113.5, 113.2, 107.9, 70.7, 56.2. HR-ESIMS (positive ion mode) *m/z*: 388.1558 ([M + H]$^+$calcd. for $C_{24}H_{22}NO_4$, 388.1543; error –3.79 ppm).

For the physicochemical data of 3-aryl-2-quinolinones (**5a**–**5c**, **5e**, **5g**–**5h**, **5j**–**5m**, **5o**–**5s**, and **5y**), see supplementary data.[2]

Acknowledgement

This work was supported by National Natural Science Foundation of China (20442006).

References

1. B. Joseph, F. Darro, A. Bard, B. Lesur, F. Collignon, C. Decaestecker, A. Frydman, G. Guillaumet, and R. Kiss. J. Med. Chem. **45**, 2543 (2002).
2. (*a*) M. Croisy, C. Huel, and E. Bisagni. Heterocycles, **45**, 683 (1997); (*b*) M.X. Xu, W.H. Duan, and H. Zheng. Acta Pharmacol. Sin. **30**, 792 (1995).
3. (*a*) P.D. Lesson, R. Baker, R.W. Carling, J.J. Kulagowski, I.M. Mawer, M.P. Ridgill, M. Rowley, J.D. Smith, and I. Standsfield. Bioorg. Med. Chem. Lett. **3**, 299 (1993); (*b*) R.W. Carling, P.D. Leeson, K.W. Moore, and M. Rowley. WO 9311115, 1993.
4. (*a*) J.L. Jiang, R.J. DeVita, M.T. Goulet, M.J. Wyvratt, J.L. Lo, N. Ren, J.B. Yudkovitz, J.S. Cui, Y.T. Yang, K. Cheng, and S.P. Rohrer. Bioorg. Med. Chem. Lett. **14**, 1795 (2004); (*b*) R.J. DeVita, T.F. Walsh, J.R. Young, J.L. Jiang, F. Ujjainwalla, R.B. Toupence, M. Parikh, S.X. Huang, J.A. Fair, M.T. Goulet, M.J. Wyvratt, J.L. Lo, N. Ren, J.B. Yudkovitz, Y.T. Yang, K. Cheng, J.S. Cui, G. Mount, S.P. Rohrer, J.M. Schaeffer, L. Rhodes, J.E. Drisko, E. McGowan, D.E. MacIntyre, S. Vincent, J.R. Carlin, J. Cameron, and R.G. Smith. J. Med. Chem. **44**, 917 (2001); (*c*) J.R. Young, S.X. Huang, I. Chen, T.F. Walsh, R.J. DeVita, M.J. Wyvratt, M.T. Goulet, N. Ren, J.L. Lo, Y.T. Yang, J.B. Yudkovitz, K. Cheng, and R.G. Smith. Bioorg. Med. Chem. Lett. **10**, 1723 (2000); (*d*) T.F. Walsh, R.B. Toupence, J.R. Young, S.X. Huang, F. Ujjainwalla, R.J. DeVita, M.T. Goulet, M.J. Wyvratt, M.H. Fisher, J.L. Lo, N. Ren, J.B. Yudkovitz, Y.T. Yang, K. Cheng, and R.G. Smith. Bioorg. Med. Chem. Lett. **10**, 443 (2000); (*e*) R.J. DeVita, M.T. Goulet, M.J. Wyvratt, M.H. Fisher, J.L. Lo, Y.T. Yang, K. Cheng, and R.G. Smith. Bioorg. Med. Chem. Lett. **9**, 2621 (1999); (*f*) R.J. DeVita, D.D. Hollings, M.T. Goulet, M.J. Wyvratt, M.H. Fisher, J.L. Lo, Y.T. Yang, K. Cheng, and R.G. Smith. Bioorg. Med. Chem. Lett. **9**, 2615 (1999).
5. D.V. Kadnikov and R.C. Larock. J. Organomet. Chem. **687**, 425 (2003).
6. M.O. Terpko and R.F. Heck. J. Am. Chem. Soc. **101**, 5281 (1979).
7. (*a*) P.J. Manley and M.T. Bilodeau. Org. Lett. **6**, 2433 (2004); (*b*) A.S. Kiselyov, E.L. Piatnitski, and J. Doody. Org. Lett. **6**, 4061 (2004).
8. (*a*) J.W. Gulland and C.J. Virden. J. Chem. Soc. 1478 (1928); (*b*) G.L. Buchanan, J.W. Cook, and J.D. Loudon. J. Chem. Soc. 325 (1944); (*c*) J. Roy and A.P. Bhaduri. Indian J. Chem. **16B**, 744 (1978).
9. (*a*) D.H. Hey and J.M. Osbond. J. Chem. Soc. 3164 (1949); (*b*) D.H. Hey and J.M. Osbond. J. Chem. Soc. 3172 (1949); (*c*) K. Hino, Y. Nagai, and H. Uno. Chem. Pharm. Bull. **35**, 2819 (1987).
10. (*a*) M. Pailer, A. Schleppnik, and M. Meller. Monatsh. Chem. **96**, 1695 (1965); (*b*) M. Pailer and G. Willvonseder. Monatsh. Chem. **109**, 511 (1978).
11. A.T. Hewson, K. Hughes, S.K. Richardson, D.A. Sharpe and A.H. Wadsworth. J. Chem. Soc., Perkin Trans. 1, **6**, 1565 (1991).
12. (*a*) J.S. Buck and W.S. Ide. Org. Syn. Coll. **2**, 130 (1943); (*b*) E.J. Alford and K. Schofield. J. Chem. Soc. 2102 (1952).
13. (*a*) C.R. Noller and R. Adams. J. Am. Chem. Soc. **46**, 1889 (1924); (*b*) O.L. Brady and J.N.E. Day. J. Chem. Soc., 114 (1934); (*c*) A. Kalir. Org. Syn. Coll. **5**, 825 (1973).
14. D. Rakowitz, A. Gmeiner, N. Schröer, and B. Matuszczak. Eur. J. Pharm. Sci. **27**, 188 (2006).
15. (*a*) S. Lebrun, A. Couture, E. Deniau, and P. Grandclaudon. Tetrahedron, **55**, 2659 (1999); (*b*) C.K. Bradsher and H. Berger. J. Am. Chem. Soc. **80**, 930 (1958).
16. G. Uray, K.S. Niederreiter, F. Belaj, and W.M.F. Fabian. Helv. Chim. Acta, **82**, 1408 (1999).

© 2006 NRC Canada

Scaled quantum mechanical force fields for trifluoromethyl selenium derivatives. I. The CF_3SeCN and CF_3SeCH_3 molecules

L.E. Fernández and E.L. Varetti

Abstract: Force fields and vibrational properties were calculated for the trifluoromethyl selenium derivatives, CF_3SeCN and CF_3SeCH_3, by means of density functional theory (DFT) techniques. The existing experimental data and assignments for these molecules were confirmed by the theoretical results. These data were subsequently used in the definition of scaled quantum mechanical force fields for such chemical species. The obtained force constants are compared with results previously published for similar compounds.

Key words: trifluoromethyl selenium, force constants, structure, DFT calculation.

Résumé : Faisant appel à des techniques de la théorie de la fonctionnelle de densité (« DFT »), on a calculé les champs de force et les propriétés vibrationnelles de dérivés trifluorométhylsélénium, soit le CF_3SeCN et le CF_3SeCH_3. Les données expérimentales et les attributions pour ces composés ont été confirmées par les résultats théoriques. On a subséquemment utilisé ces données dans la définition d'un champ de force normalisé en mécanique quantique pour de telles espèces. On a comparé les constantes de force obtenues avec les résultats publiés antérieurement pour des composés semblables.

Mots clés : trifluorométhylsélénium, constantes de force, calculs selon la théorie de la fonctionnelle de densité.

[Traduit par la Rédaction]

Introduction

A theoretical study of the vibrational properties of the selenium compounds, CF_3SeX (X = H, D, Cl, or Br), was recently performed in our laboratory (1). Similar calculations are now made on other two simple CF_3Se derivatives, i.e., CF_3SeCN and CF_3SeCH_3. These molecules were prepared from $(CF_3Se)_2Hg$ by Dale et al. (2) and by Emeléus and Welchman (3). The molecular parameters for CF_3SeCN were obtained by the electron diffraction method (4), but no structural study is known for the CF_3SeCH_3 molecule. IR and Raman spectra were reported for these two molecules by Marsden (5) and by Clase et al. (6), and normal coordinate analyses were also published (7).

In the present work, quantum chemical calculations were performed on the mentioned molecules to obtain the corresponding force constants, which were scaled to reproduce the experimental frequencies. Such adjustment was made using the formalism of the scaled quantum mechanical (SQM) force field, as defined by Pulay et al. (8).

Received 4 September 2006. Accepted 7 November 2006. Published on the NRC Research Press Web site at http://canjchem.nrc.ca on 13 December 2006.

L.E. Fernández. Instituto de Química y Física, Facultad de Bioquímica, Química y Farmacia, Universidad, Nacional de Tucumán, San Lorenzo 456, 4000 S.M. de Tucumán, República Argentina.
E.L. Varetti.[1,2] Centro de Química Inorgánica (CEQUINOR, CONICET-UNLP), Departamento de Química, Facultad de Ciencias Exactas, Universidad Nacional de La Plata, C. Correo 962, 1900 La Plata, República Argentina.

[1]Member of the Carrera del Investigador Científico, CONICET, República Argentina.
[2]Corresponding author (e-mail: varetti@quimica.unlp.edu.ar).

Calculation procedure

Optimized structures and vibrational wavenumbers for CF_3SeCN and CF_3SeCH_3 were obtained with density functional theory (DFT) methods using the B3LYP functional (9, 10) together with the 6-311G* basis set. This theoretical data facilitated the comparison of the results with those obtained in previous work in which the same combination of functional and basis sets was used. The natural bond orbitals (NBO) formalism (11) was used for the calculation of the atomic charges, which appear in Fig. 1. The calculations were made with the Gaussian 98 set of programs (12).

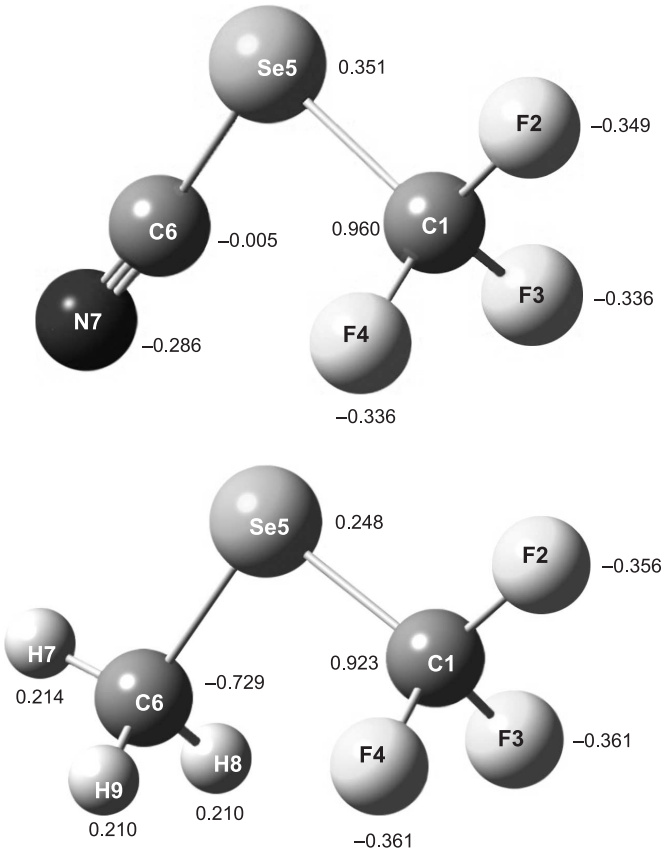
Structural results

The molecular conformations of the two molecules were investigated starting with initial, staggered structures having FCSeC dihedral angles of 180°. The respective CF_3 group was rotated around the Se–C bond from 0° to 60°, in steps of 5°, and the structure was optimized with that dihedral angle frozen. These calculations showed that only a single conformer exists for both compounds, corresponding to the structures of symmetry Cs shown in Fig. 1. The potential energy curve shows maxima for structures in which the trifluoromethyl group is rotated 60° with respect to the most stable conformation.

An additional series of calculations were performed for the CF_3SeCH_3 molecule in which the CF_3 and CH_3 groups

 doi:10.1139/V06-171 © 2006 NRC Canada

Fig. 1. The calculated molecular structure and atomic charges for the molecules CF_3SeCN and CF_3SeCH_3.



were rotated simultaneously in the same or opposite directions in steps of 10°. These calculations confirmed the existence of only one minimum in the potential energy surface.

The most stable conformations predicted for these molecules were fully optimized, and their structures are shown in Fig. 1. As mentioned before, structural geometrical parameters were reported only for CF_3SeCN (4), and these values are shown in Table 1 together with the calculated values. The (mean) calculated and experimental distances and angles do not differ by more than 0.020 Å and 3.4°, respectively. The theoretical tilt angles existing between the C–Se bonds and the ideal symmetry axis of the CX_3 group, with X = F or H, also appear in Table 1; this angle is calculated for the CF_3 groups as $1/3[2\alpha(F3,4–C–Se) – 2\alpha(F2–C–Se)]$ (13). Clearly, CF_3SeCN shows a tilt angle that is considerably larger than those calculated for $SeCF_3$ and $SeCH_3$ in CF_3SeCH_3. This theoretical result could be explained by taking into account the calculated electric charges on the atoms. In fact, the F3, F4, and N7 atoms of CF_3SeCN (Fig. 1) show negative charges of –0.34 (F) and –0.29 (N); whereas, in CF_3SeCH_3 the charges are positive for H8 and H9 (+0.21) and negative for F3 and F4 (–0.36). Therefore, the repulsive forces between the F and N atoms in the former molecule could explain the relatively large tilt angle of the $SeCF_3$ moiety and the predicted value of 176.6° for the Se–C–N angle; whereas, the attractive forces between the mentioned H and F atoms in the latter molecule could be the cause of the notably smaller calculated tilt angles.

Table 1. Optimized geometric parameters for the molecules CF_3SeCN and CF_3SeCH_3 and experimental data for CF_3SeCN.

	CF_3SeCN		CF_3SeCH_3
	Calculated	Experimental (4)	Calculated
Bond lengths (Å)			
C1—F2	1.339	1.332	1.342
C1—F3,4	1.33		1.346
Se—CF_3	2.004	1.984	1.968
Se—CN	1.846	1.854	—
C≡N	1.157	1.152	—
Se—CH_3	—	—	1.971
C6—H7	—	—	1.089
C6—H8,9	—	—	1.087
Bond angles (°)			
F3–C1–F4	108.6	109.4	106.7
F2–C1–F3,4	109.1		108.1
F2–C1–Se5	105.6	109.6	108.7
F3,4–C1–Se5	112.2		112.6
Tilt Se–CF_3	4.37	—	2.62
C–Se–C	95.6	92.2	95.4
Se–C–N	176.6	180.0 (fixed)	—
H8–C6–H9	—	—	111.1
H7–C6–H8,9	—	—	109.8
H7–C6–Se5	—	—	106.1
H8,9–C6–Se5	—	—	110.0
Tilt Se–CH_3	—	—	2.55

Vibrational results

The normal modes of vibration of the CF_3SeCN and CF_3SeCH_3 molecules, with Cs symmetry, are classified as $10A' + 5A''$ and $13A' + 8A''$, respectively.

The atomic displacements calculated for each vibrational mode, represented graphically with the program Moldraw (14), confirmed the assignment of bands proposed by Clase et al. (6) for both molecules. In fact, these authors corrected and completed a previous study made on CF_3SeCN and related molecules by Marsden (5). The experimental wavenumbers for each molecule reported in ref. 6 appear in Tables 2 and 3 together with the corresponding qualitative intensities. In most cases, the observed values agree with the calculated IR and Raman band intensities. That agreement is particularly clear for the bands due to the CF_3 stretching vibrations where the strongly polarized C–F bonds produce very strong IR bands and weak or very weak Raman bands. The agreement between measured and calculated wavenumbers was evaluated by means of the root-mean-square deviation (RMSD), which was equal to 29 cm^{-1} for CF_3SeCN and 55 cm^{-1} for CF_3SeCH_3. After the force field scaling procedure, these values fell to 8 and 7 cm^{-1}, respectively.

Force constants

The force fields in Cartesian coordinates, as generated by the Gaussian programs for the two molecules, were transformed to the set of non-redundant coordinates defined in Tables 4 and 5. Such coordinates consider the local symmetry of the CF_3 and CH_3 groups and follow the proposals of Fogarasi et al. (15). The resulting force constants were sub-

© 2006 NRC Canada

Table 2. Experimental and calculated wavenumbers, IR and Raman intensities and, potential energy distribution (PED) for CF_3SeCN.

Mode	Experimental (6)[a]	Calcd.[b]	Calcd. SQM[c]	IR intensity (km mol^{-1})	Raman intensity (Å^4 (amu)$^{-1}$)	PED (contributions ≥ 10%)	Main coordinate
A′							
ν_1	2178 (s)	2274	2185	2.14	109.75	95 S_1	ν(C≡N)
ν_2	1201 vs. (vvw)	1190	1196	225.92	0.73	101 S_2 + 19 S_5	ν(CF_3) antisymm.
ν_3	1103 vs. (vw)	1079	1090	523.6	5.89	76 S_3 + 49 S_4 + 22 S_8	ν(CF_3) symm.
ν_4	747 vs. (vs)	742	752	32.83	6.79	47 S_4 + 31 S_3 + 14 S_8	δ(CF_3) symm.
ν_5	543 (m)	551	553	1.14	0.77	50 S_5 + 22 S_6	δ(CF_3) antisymm.
ν_6	534 s (m)	534	536	3.08	3.38	72 S_6 + 19 S_5	ν(Se–C(N))
ν_7	390 m (vvw)	402	397	2.46	0.94	37 S_7 + 11 S_5 + 24 S_{10}	δ(SeCN) in plane
ν_8	315 m (vs)	300	316	1.1	6.86	66 S_8 + 11 S4	ν((F_3)C–Se)
ν_9	272 vw (m)	267	267	0.57	3.01	84 S_9 + 23 S_7	ρ(CF_3)
ν_{10}	118 (m)	98	97	3.77	3.29	78 S_{10} + 32 S_7 + 19 S_9	δ(CSeC)
A″							
ν_{11}	1197 vs	1199	1205	270.59	0.61	102 S_{11} + 18 S_{12}	ν(CF_3) antisymm.
ν_{12}	—	529	532	1.44	0.99	77 S_{12}	δ(CF_3) antisymm.
ν_{13}	356 w (vvw)	359	344	1.35	1.88	98 S_{13}	δ(SeCN) out of plane
ν_{14}	282 (vvw)	273	275	0.03	1.16	96 S_{14} + 11 S_{12}	ρ(CF_3)
ν_{15}	—	33	34	1.49	1.24	103 S_{15}	Torsion (CF_3)
RMSD (cm^{-1})	29	8					

[a]Qualitative intensities for IR and Raman (in parentheses) observed bands: w, weak; m, medium; s, strong; v, very.
[b]B3LYP/6-311G* calculations.
[c]From SQM force field.

Table 3. Experimental and calculated wavenumbers, IR and Raman intensities, and potential energy distribution (PED) for CF_3SeCH_3.

Mode	Experimental (6)[a]	Calcd.[b]	Calcd. SQM[c]	IR intensity (km mol^{-1})	Raman intensity (Å^4 (amu)$^{-1}$)	PED (contributions ≥ 10%)	Main coordinate
A′							
ν_1	3035 w (w)	3161	3039	3.38	56.62	100 S_1	ν(CH_3) antisymm.
ν_2	2955 s (s)	3069	2950	13.33	113.22	100 S_2	ν(CH_3) symm.
ν_3	1438 s	1497	1440	12.32	7.81	96 S_3	δ(CH_3) antisymm.
ν_4	1288 vs	1337	1284	11.39	0.36	105 S_4	δ(CH_3) symm.
ν_5	1157 vs	1161	1167	241.27	0.8	96 S_5 + 18 S_{10}	ν(CF_3) antisymm.
ν_6	1117 vs (vw)	1097	1106	438.34	1.28	70 S_6 + 49 S_8 + 24 S_{11}	ν(CF_3) symm.
ν_7	916	939	903	17.36	3.76	88 S_7	ρ(CH_3)
ν_8	740 vs (s)	735	742	15.64	4.29	42 S_8 + 35 S_6 + 12 S_{11}	δ(CF_3) symm.
ν_9	597	577	599	0.68	20.64	107 S_9	ν(Se–CH_3)
ν_{10}	533 w (vw)	538	541	0.29	1.22	73 S_{10}	δ(CF_3) antisymm.
ν_{11}	339 s (ms)	331	338	2.15	4.12	53 S_{11} + 13 S_8 + 11 S_{12}	ν(Se–CF_3)
ν_{12}	302 m (m)	295	298	0.6	3.41	61 S_{12} + 18 S_{11} + 11 S_{10}	ρ(CF_3)
ν_{13}	148 (m)	156	150	1.82	1.28	95 S_{13} + 33 S_{12}	δ(CSeC)
A″							
ν_{14}	3036 w (w)	3172	3050	3.38	56.62	100 S_{14}	ν(CH_3) antisymm.
ν_{15}	1431 s (vw)	1484	1427	6.31	10.49	95 S_{15}	δ(CH_3) antisymm.
ν_{16}	1141 vs	1133	1140	263.8	0.7	100 S_{16} + 19 S_{18}	ν(CF_3) antisymm.
ν_{17}	911	934	897	4.63	3.43	95 S_{17}	ρ(CH_3)
ν_{18}	536	526	529	0.55	0.95	73 S_{18}	δ(CF_3) antisymm.
ν_9	289 (w)	283	285	0	1.19	94 S_{19} + 13 S_{18}	ρ(CF_3)
ν_{20}	—	129	129	0.04	0.03	108 S_{20}	Torsion (CH_3)
ν_{21}	—	51	49	0.87	1.17	106 S_{21}	Torsion (CF_3)
RMSD (cm^{-1})	55	7					

[a]Qualitative intensities for IR and Raman (in parentheses) observed bands: w, weak; m, medium; s, strong; v, very.
[b]B3LYP/6-311G* calculations.
[c]From SQM force field.

© 2006 NRC Canada

Table 4. Natural internal (local symmetry) coordinates for CF_3SeCN.

Definition (according to Fig. 1)	Description[a]
A′	
S_1 = d(6–7)	ν(C≡N)
S_2 = 2r(1–2) – r(1–3) – r(1–4)	ν(CF_3) antisymm.
S_3 = r(1–2) + r(1–3) + r(1–4)	ν(CF_3) symm.
S_4 = α(2–1–3) + α(2–1–4) + α(3–1–4) – β(2–1–5) – β(3–1–5) – β(4–1–5)	δ(CF_3) symm.
S_5 = 2α(3–1–4) – α(2–1–3) – α(2–1–4)	δ(CF_3) antisymm.
S_6 = l(5–6)	ν(Se–CN)
S_7 = δ(5–6–7)	δ(SeCN) in plane
S_8 = t(1–5)	ν(Se–CF_3)
S_9 = 2β(2–1–5) – β(3–1–5) – β(4–1–5)	ρ(CF_3)
S_{10} = γ(1–5–6)	δ(CSeC)
A″	
S_{11} = r(1–3) – r(1–4)	ν(CF_3) antisymm.
S_{12} = α(2–1–3) – α(2–1–4)	δ(CF_3) antisymm.
S_{13} = δ(5–6–7)	δ(SeCN) out of plane
S_{14} = β(3–1–5) – β(4–1–5)	ρ(CF_3)
S_{15} = Στ[F*i*–C1–Se5–C6)]	Torsion (CF_3)

[a] ν, stretching; δ, deformation; ρ, rocking.

Table 5. Natural internal (local symmetry) coordinates for CF_3SeCH_3.

Definition (according to Fig. 1)	Description[a]
A′	
S_1 = 2d(7–6) – d(8–6) – d(9–6)	ν(CH_3) antisymm.
S_2 = d(7–6) + d(8–6) + d(9–6)	ν(CH_3) symm.
S_3 = 2ψ(8–6–9) – ψ(8–6–7) – ψ(9–6–7)	δ(CH_3) antisymm.
S_4 = ψ(7–6–9) + ψ(7–6–8) + ψ(8–6–9) – φ(7–6–5) – φ(8–6–5) – φ(9–6–5)	δ(CH_3) symm.
S_5 = 2r(1–2) – r(1–3) – r(1–4)	ν(CF_3) antisymm.
S_6 = r(1–2) + r(1–3) + r(1–4)	ν(CF_3) symm.
S_7 = 2φ(7–6–5) – φ(8–6–5) – φ(9–6–5)	ρ(CH_3)
S_8 = α(2–1–3) + α(4–1–2) + α(4–1–3) – β(2–1–5) – β(3–1–5) – β(4–1–5)	δ(CF_3) symm.
S_9 = l(6–5)	ν(Se–CH_3)
S_{10} = 2α(3–1–4) – α(3–1–2) – α(4–1–2)	δ(CF_3) antisymm.
S_{11} = t(1–5)	ν(Se–CF_3)
S_{12} = 2β(2–1–5) – β(3–1–5) – β(4–1–5)	ρ(CF_3)
S_{13} = δ(1–5–6)	δ(CSeC)
A″	
S_{14} = d(8–6) – d(9–6)	ν(CH_3) antisymm.
S_{15} = ψ(8–6–7) – ψ(9–6–7)	δ(CH_3) antisymm.
S_{16} = r(1–3) – r(1–4)	ν(CF_3) antisymm.
S_{17} = φ(8–6–5) – φ(9–6–5)	ρ(CH_3)
S_{18} = α(3–1–2) – α(4–1–2)	δ(CF_3) antisymm.
S_{19} = β(3–1–5) – β(4–1–5)	ρ(CF_3)
S_{20} = Στ[H*i*–C6–Se5–C1)]	Torsion (CH_3)
S_{21} = Στ[F*i*–C1–Se5–C6)]	Torsion (CF_3)

[a] ν, stretching; δ, deformation; ρ, rocking.

sequently scaled according to the scheme of Pulay et al. (8), in which the main force constants are multiplied by scale factors (e.g., f_i and f_j), and the corresponding interaction constants are multiplied by $(f_i \times f_j)^{1/2}$, adjusting the scale factors to reproduce the experimental wavenumbers as accurately as possible.

The final scaling factors corresponding to each force constant for the two studied species appear in Table 6. Obviously, most of these factors are greater than one. This is the case when heavy atoms (after the second row of the Periodic Table) appear in the molecule. This fact has been reported for many molecules containing non-metallic heavy atoms

© 2006 NRC Canada

Table 6. Final scaling factors for the force field of the molecules CF_3SeCN and CF_3SeCH_3.

Coordinates[a]	CF_3SeCN	CF_3SeCH_3
$\nu(CF_3)$, $\delta(CF_3)$, $\rho(CF_3)$, Torsion (CF_3)	1.011	1.013
ν(Se–CN)	1.011	—
ν(Se–CH_3)	—	1.075
ν(Se–CF_3)	1.155	1.075
$\nu(CH_3)$, $\delta(CH_3)$, $\rho(CH_3)$	—	0.924
δ(CSeC)	1.011	0.924
ν(C≡N), δ(SeCN)	0.919	—
Torsion (CH_3)	—	1.013

[a] ν, stretching; δ, deformation; ρ, rocking.

Table 7. Symmetry force constants for the molecule CF_3SeCN.

Force constant[a]	This work	Reference (7)
F1,1	17.321	16.982
F2,2	5.348	5.259
F3,3	7.833	7.461
F4,4	1.639	1.733
F5,5	1.518	1.584
F6,6	3.526	3.452
F7,7	0.24	0.332
F8,8	2.583	2.482
F9,9	0.884	0.83
F10,10	0.973	0.828
F11,11	5.416	5.259
F12,12	1.454	1.584
F13,13	0.311	0.332
F14,14	0.85	0.83
F15,15	0.012	—
F3,8	0.675	0.393
F4,8	–0.437	–0.434
F5,6	–0.016	0.061
F3,4	0.64	0.65
F2,5	–0.63	–0.5
F1,7	0.021	–0.5
F2,9	0.547	0.5
F1,11	0	0.5

[a] Units are mdyn $Å^{-1}$ (1 dyn = 10 μN) for stretchings and stretch–stretch interactions, mdyn Å for bend and bend–bend interactions, and mdyn for strech–bend interactions.

Table 8. Symmetry force constants for the molecule CF_3SeCH_3.

Force constant[a]	This work	Reference (7)
F1,1	4.96	4.9
F2,2	5.057	4.834
F3,3	0.519	0.514
F4,4	0.527	0.588
F5,5	5.103	4.83
F6,6	7.471	7.461
F7,7	0.546	0.58
F8,8	1.633	1.792
F9,9	2.746	2.642
F10,10	1.574	1.549
F11,11	2.742	2.714
F12,12	0.9	0.93
F13,13	0.916	0.663
F14,14	4.976	4.9
F15,15	0.507	0.514
F6,11	0.628	0.221
F8,11	–0.405	–0.566
F6,8	0.655	0.65
F5,10	–0.645	–0.5
F2,1	–0.014	–0.5
F5,12	0.514	0.5
F2,4	0.13	0.5
F9,4	–0.35	–0.261
F1,3	–0.135	–0.041
F16,15	–0.011	–0.041
F16,16	4.898	4.83
F17,17	0.545	0.58
F18,18	1.502	1.549
F19,19	0.905	0.93
F20,20	0.011	—
F21,21	0.017	—

[a] Units are mdyn $Å^{-1}$ (1 dyn = 10 μN) for stretchings and stretch–stretch interactions, mdyn Å for bend and bend–bend interactions, and mdyn for strech–bend interactions.

(16) as well as for several CF_3SO_2X molecules (17). To prove that the scaling factors are transferable between related molecules, a subsequent calculation was performed using the mean factors for common coordinates previously obtained for the CF_3SeX series (1) and adjusting only the factors that affect the non-common coordinates. In that calculation, the final RMSD values did not differ by more than 1 cm^{-1} from those obtained with the scaling factors of Table 6.

The main force constants in symmetry coordinates as well as some interaction constants for the studied molecules are reproduced in Tables 7 and 8 together with the corresponding values calculated by Wahi et al. (7). Clearly, no large differences appear between both sets of main force constants, based in the same vibrational band assignments. However, there are significant disagreements between the sets of interaction constants, probably because most of these values were fixed in the traditional procedure of refinement performed by these authors. On the other hand, the theoretical approach used in the present work produces a complete force constants matrix. The SQM matrices are available as supplementary data.[3] The SQM force fields were used to calculate the potential energy distributions (PED) that appear in Tables 2 and 3. The PED show that some coordinates are strongly mixed in both molecules, as is the case with S_3 ($\nu(CF_3)$ symm.), S_4 ($\delta(CF_3)$ symm.), and S_8 (ν(C–Se)) for CF_3SeCN and the corresponding S_6, S_8, and S_{11} coordinates for CF_3SeCH_3, which appear to be contributing in different proportions to the modes ν_3 and ν_4 for the first

[3] Supplementary data for this article are available on the journal Web site or may be purchased from the Depository of Unpublished Data, Document Delivery, CISTI, National Research Council Canada, Ottawa, ON K1A 0S2, Canada. DUD 5112. For more information on obtaining material, refer to http://cisti-icist.nrc-cnrc.gc.ca/irm/unpub_e.shtml.

© 2006 NRC Canada

Table 9. Internal force constants for CF_3SeCN, CF_3SeCH_3, and the related molecules CF_3SeX.

	This work		Reference (1)			
Force constant[a]	CF_3SeCN	CF_3SeCH_3	CF_3SeH	CF_3SeD	CF_3SeCl	CF_3SeBr
Bond stretchings						
f (C–F) [b]	6.167	5.841	5.928	6.004	6.033	5.976
f (Se–CF_3)	2.583	2.742	2.8	2.84	2.529	2.69
f (Se–CN)	3.526	—				
f (C≡N)	17.321	—				
f (Se–CH_3)	—	2.746				
f (C–H)[b]	—	4.996				
f (C–F/C–F)[b]	0.802	0.789	0.826	0.844	0.824	0.818
f (C–F/Se–CF_3)	0.39	0.362	0.387	0.392	0.364	0.372
f (C–H/CH)[b]	—	0.032				
f (Se–CN/CN)	0.199	—				
Deformations						
f (F–C–F)[b]	1.269	1.304	1.305	1.291	1.295	1.252
f (F–C–Se)[b]	0.854	0.874	0.931	0.936	0.845	0.868
f (C–Se–C)	0.973	0.916				
f (Se–C≡N)	0.24	—				
f (H–C–H)[b]	—	0.431				
f (H–C–Se)[b]	—	0.452				

[a]Units are mdyn $Å^{-1}$ (1 dyn = 10 μN) for stretchings and stretch–stretch interactions and mdyn Å rad^{-2} (1 dyn = 10 μN) (1 rad = 10 mGy) for angular deformations.
[b]Mean values.

molecule and ν_6 and ν_8 for the latter. A similar observation was made for the CF_3SeX molecules (1).

The internal force constants calculated from the corresponding SQM force fields for these molecules are shown in Table 9. As expected, these force constants are close to the values previously obtained for other selenium derivates using the same calculation procedure (1).

Acknowledgements

Research grants from the following institutions in R. Argentina are gratefully acknowledged: CONICET (Consejo Nacional de Investigaciones Científicas y Técnicas), ANPCYT (Agencia Nacional de Promoción Científica y Tecnológica, BID 1728/OC-AR, PICT 11127), UNLP (Universidad Nacional de La Plata), and CIUNT (Consejo de Investigaciones de la Universidad Nacional de Tucumán). We thank Dr. G. Arteca, Laurentian University, Canada, for providing access to some published articles.

References

1. L.E. Fernández and E.L. Varetti. J. Mol. Struct.: THEOCHEM, **761**, 217 (2006).
2. J.W. Dale, H.J. Emeléus, and R.N. Haszeldine. J. Chem. Soc. 2939 (1958).
3. H J. Emeléus and N. Welchman. J. Chem. Soc. 1268 (1963).
4. C.J. Marsden and G.M. Sheldrick. J. Mol. Struct. **10**, 413 (1971).
5. C.J. Marsden. J. Fluorine Chem. **5**, 401 (1975).
6. H.J. Clase, P.K. Wahi, and D.R.L. Bomford. Can. J. Spectrosc. **22**, 92 (1977).
7. P.K. Wahi and N.D. Patel. Can. J. Spectrosc. **22**, 88 (1977).
8. P. Pulay, G. Fogarasi, G. Pongor, J.E. Boggs, and A.Vargha. J. Am. Chem. Soc. **105**, 7037 (1983).
9. A.D. Becke. J. Chem. Phys. **98**, 5648 (1993).
10. C. Lee, W. Yang, and R.G. Parr. Phys. Rev. B, **37**, 785 (1988).
11. A.E. Reed, L.A. Curtiss, and F. Weinhold. Chem. Rev. **88**, 899 (1988).
12. M.J. Frisch, G.W. Trucks, H.B. Schlegel, G.E. Scuseria, M.A. Robb, J.R. Cheeseman, V.G. Zakrzewski, J.A. Montgomery, Jr., R.E. Stratmann, J.C. Burant, S. Dapprich, J.M. Millam, A.D. Daniels, K.N. Kudin, M.C. Strain, O. Farkas, J.Tomasi, V. Barone, M. Cossi, R. Cammi, B. Mennucci, C. Pomelli, C. Adamo, S. Clifford, J. Ochterski, G.A. Petersson, P.Y. Ayala, Q. Cui, K. Morokuma, D.K. Malick, A.D. Rabuck, K. Raghavachari, J.B. Foresman, J. Cioslowski, J.V. Ortiz, A.G. Baboul, B.B. Stefanov, G. Liu, A. Liashenko, P. Piskorz, I. Komaromi, R. Gomperts, R.L. Martin, D.J. Fox, T. Keith, M.A. Al-Laham, C.Y. Peng, A. Nanayakkara, C. Gonzalez, M. Challacombe, P.M.W. Gill, B. Johnson, W. Chen, M.W. Wong, J.L. Andres, C. Gonzalez, Head-M. Gordon, E.S. Replogle, and J.A. Pople. GAUSSIAN 98 [computer program]. Revision a.7. Gaussian, Inc., Pittsburgh, PA. 1998.
13. J.S. Francisco. Spectrochim. Acta, **40**A, 923 (1984).
14. P. Ugliengo, D. Viterbo, and G. Chiari. Z. Kristallogr. **207**, 9 (1993).
15. G. Fogarasi, X. Zhou, P.W. Taylor, and P. Pulay. J. Am. Chem. Soc. **114**, 8191 (1992).
16. F. Kalincsák and G. Pongor. Spectrochim. Acta, **58**A, 999 (2002).
17. L.E. Fernández, A. Ben Altabef, and E.L. Varetti. J. Mol. Struct. **612**, 1 (2002).

© 2006 NRC Canada

Regioselective synthesis of biologically interesting pentacyclic polyheterocycles by sequential thio-Claisen and $AlCl_3$ catalyzed oxy-Claisen rearrangement of 4-(4′-aryloxybut-2′-ynylthio)-1-phenyl-1,8-naphthyridin-2(1*H*)-one

K.C. Majumdar and R. Islam

Abstract: A number of 4-aryloxymethyl-6-phenyl-2*H*-thiopyrano[3,2-*c*][1,8]naphthyridin-5(6*H*)-ones were regioselectively synthesized in 82%–95% yields by the thermal Claisen rearrangement of 4-(4′-aryloxybut-2′-ynylthio)-1-phenyl-[1,8]naphthyridin-2(1*H*)-ones. These products were then subjected to a second Claisen rearrangement in the presence of a Lewis acid catalyst, anhyd. $AlCl_3$, to give hitherto unreported pentacyclic heterocycles in 75%–90% yields. The same final products were also obtained in low yield upon refluxing 4-aryloxymethyl-6-phenyl-2*H*-thiopyrano-[3,2-*c*][1,8]naphthyridin-5(6*H*)-ones in *N,N*-diethyl aniline for 12–14 h. This method was found to be more effective than thermal Claisen rearrangement.

Key words: [3,3] sigmatropic rearrangement, regioselective synthesis, phase transfer catalysis, sequential Claisen rearrangement, Lewis acid catalyzed Claisen rearrangement, single crystal X-ray.

Résumé : On a réalisé des synthèses régiosélectives de 4-aryloxyméthyl-6-phényl-2*H*-thiopyrano[3,2-*c*][1,8]naphtyridin-5(6*H*)-ones, avec des rendements allant de 82 % à 95 %, en soumettant des 4-(4'-aryloxybut-2'-ynylthio)-1-phényl[1,8]naphtyridin-2(1*H*)-ones à un réarrangement de Claisen thermique. Ces produits ont ensuite été soumis à un deuxième réarrangement de Claisen, en présence d'un acide de Lewis comme catalyseur, le trichlorure d'aluminium, pour conduire à la formation d'hétérocycles pentacycliques non rapportés jusqu'à maintenant, avec des rendements allant de 75 % à 90 %. On a aussi obtenu ces produits avec de faibles rendements en portant les 4-aryloxyméthyl-6-phényl-2*H*-thiopyrano[3,2-*c*][1,8]naphtyridin-5(6*H*)-ones au reflux dans la *N,N*-diéthylaniline pendant 12 à 14 h. On a trouvé que cette méthode est plus efficace que le réarrangement thermique de Claisen.

Mots clés : réarrangement sigmatropique [3,3], synthèse régiosélective, catalyse par transfert de phase, réarrangements de Claisen séquentiels, réarrangement de Claisen catalysé par un acide de Lewis, diffraction des rayons X par un cristal unique.

[Traduit par la Rédaction]

Introduction

1,8-Naphthyridinones and their derivatives have attracted considerable attention primarily because the 1,8-naphthyridine skeleton is present in many compounds that have been isolated from natural substances and exhibited various medicinal and biological activities (1, 2). 4-Hydroxy-1-phenyl-1,8-naphthyridin-2(1*H*)-one and its derivatives have been used as inhibitors of sulfidopeptide leukotrienes, the major component of SRS-A release (3). 2-Oxo-1,8-naphthyridin-3-carboxylic acid derivatives possess potent gastric antisecretary properties and anti-inflammatory activities (4–6). A series of novel imidazo[4,5-*c*][1,8]naphthyridin-4(5*H*)-ones exhibited potent bronchodilator activity (7). The attractive bioactivities of these 1,8-naphthyidinones, such as the cytoprotective, anti-inflammatory, and antiallergic activity of some 2,3-fused and 3,4-fused furo- and pyrano-tricyclic compounds, justify the great interest in the naphthyridinone moiety as a target in organic synthesis. It is well-documented that the Claisen rearrangement (8) is an excellent method for carbon–carbon bond formation and has been successfully employed for the synthesis of a number of potentially bioactive thieno[3,2-*d*]pyrimidinone and dihydrothieno[3,2-*d*]pyrimidinone derivatives (9). We have previously reported the sequential [3,3] sigmatropic rearrangement of suitably substituted but-2-ynes to give interesting results, e.g., easy access to [6,6] and [6,5] fused polyhetrocycles (10). In view of the medicinal importance of 1,8-

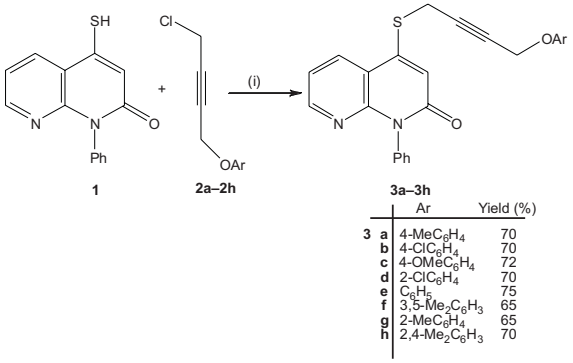
Received 16 October 2006. Accepted 23 October 2006. Published on the NRC Research Press Web site at http://canjchem.nrc.ca on 19 December 2006.

K.C. Majumdar[1] and R. Islam. Department of Chemistry, University of Kalyani, Kalyani 741235, W.B. India.

[1]Corresponding author (e-mail: kcm_ku@yahoo.co.in).

 doi:10.1139/V06-174 © 2006 NRC Canada

Scheme 1. Reagent and conditions: (*i*) BTEAC, $CHCl_3$, 1% aq. NaOH, 8–10 h, stirring, RT.



		Ar	Yield (%)
3	a	4-MeC_6H_4	70
	b	4-ClC_6H_4	70
	c	4-$OMeC_6H_4$	72
	d	2-ClC_6H_4	70
	e	C_6H_5	75
	f	3,5-$Me_2C_6H_3$	65
	g	2-MeC_6H_4	65
	h	2,4-$Me_2C_6H_3$	70

naphthyridine and its derivatives, we became interested in synthesizing a number of polyheterocycles derived from 4-hydroxy-1-phenyl-1,8-naphthyridin-2(1*H*)-one. Here, we report our focused attention on the synthesis of furothiopyrano heterocyclic ring-fused 1,8-napthyridin-2(1*H*)-one by the application of thio-Claisen and oxy-Claisen rearrangement.

Results and discussion

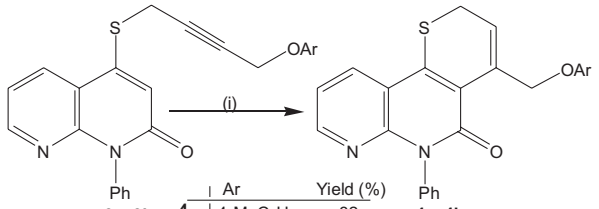
The starting materials, 4-(4′-aryloxybut-2′-ynylthio)-1-phenyl-[1,8]naphthyridin-2(1*H*)-ones (**3a**–**3h**) were synthesized by phase transfer catalyzed alkylation (11) of 4-mercapto-1-phenyl-1,8-naphthyridin-2(1*H*)-one (**3**) with 1-aryloxy-4-chlorobut-2-ynes (**2a**–**2h**) in 65%–75% yield. 4-Mercapto-1-phenyl-1,8-naphthyridin-2(1*H*)-one (**1**) was prepared according to published procedure (12) (Scheme 1).

The substrates **3a**–**3h** contain the propynylthio-1,8-naphthyridinone moiety as well as the aryl prop-2-ynyl ether moiety, which suggests two different possible [3,3] sigmatropic rearrangements. The aliphatic Claisen rearrangement has the lower activation energy since the aromatic counterpart has to disturb its aromatic sextet in the transition state. Substrate **3a** was heated in chlorobenzene (132 °C) and the reaction was monitored by TLC until complete conversion. Complete conversion was achieved in 4 h giving a white solid in 95% yield. The product **4a** was characterized from elemental analysis and spectroscopic data as 4-(4′-methylphenoxymethyl)-6-phenyl-2*H*-thiopyrano[3,2-*c*][1,8]naphthyridin-5(6*H*)-one. Its ^{1}H NMR spectrum (600 MHz) showed two two-proton doublets at δ: 3.43 (J = 5.4 Hz, -SCH_2), 5.17 (J = 1.2 Hz, -OCH_2) respectively, one proton triple triplet (tt) at δ: 6.28–6.31 (J = 1.8 Hz, 6 Hz, =CH), and a multiplet for twelve aromatic protons at δ: 6.83–8.43. Substrates **3b**–**3h** under similar treatment afforded compounds **4b**–**4h** in 82%–90% yield (Scheme 2).

The formation of products **4a**–**4h** from the substrates **3a**–**3h** is easily rationalized by the initial [3,3] sigmatropic rearrangement of the sulfides **3a**–**3h** to give **5.** This was followed by enolization to **6** and subsequent [1,5] hydrogen shift and electrocyclic ring closure (ECR) to give products **4a**–**4h** (Scheme 3).

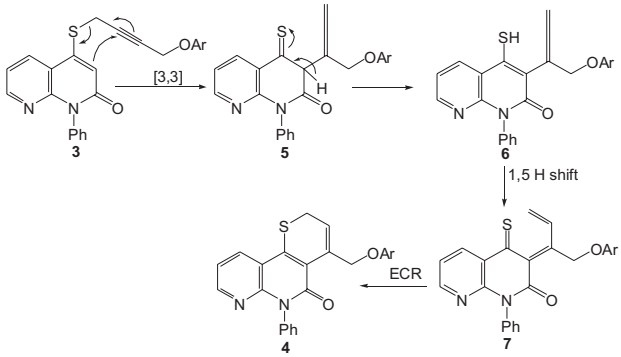
Compounds **4a**–**4h** contain allyl aryl ether moieties favourable for a further [3,3] sigmatropic rearrangement. Compounds **4a**, **4d**, and **4f** were refluxed in *N*,*N*-diethyl aniline to perform Claisen rearrangement of allyl aryl ether to

Scheme 2. Reagent and conditions: (*i*) Chlorobenzene, reflux, 4–6 h.

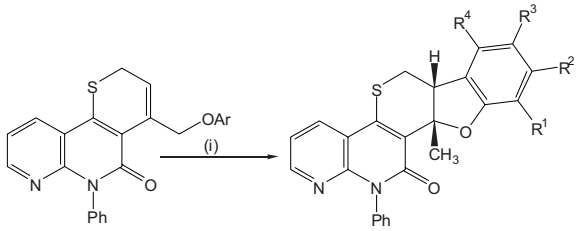


		Ar	Yield (%)
4	a	4-MeC_6H_4	82
	b	4-ClC_6H_4	82
	c	4-$OMeC_6H_4$	90
	d	2-ClC_6H_4	95
	e	C_6H_5	85
	f	3,5-$Me_2C_6H_3$	85
	g	2-MeC_6H_4	90
	h	2,4-$Me_2C_6H_3$	85

Scheme 3.



Scheme 4. Reagent and conditions: (*i*) *N*,*N*-Diethyl aniline, reflux, 12–14 h.



		R^1	R^2	R^3	R^4	Yield (%)
8	a	H	H	CH_3	H	30
	d	Cl	H	H	H	25
	f	H	CH_3	H	CH_3	28

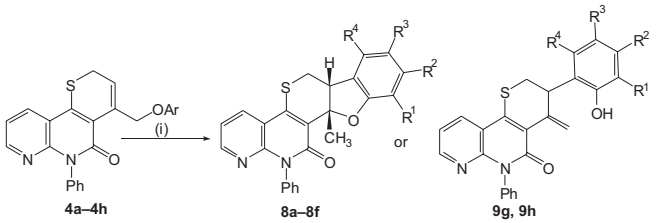
afford the cyclized products in 25% to 30% yields. The products were characterized as **8a**, **8d**, and **8f** from their elemental analyses and spectroscopic data (Scheme 4).

The thermal rearrangement required very high temperature and afforded products in poor yield because of decomposition, so we attempted Lewis acid catalyzed Claisen rearrangement. Among different catalysts reported in literature (13), $AlCl_3$ and its derivatives are known to be efficient for Claisen rearrangement.

Substrate **4a**, upon treatment with anhyd. $AlCl_3$ in dry dichloromethane at RT for 1 h, afforded the cyclized product **8a** in 90% yield. Compound **8a** was characterized from elemental analysis and spectroscopic data. The ^{1}H NMR (500 MHz) spectrum showed δ_H: 1.86 (s, 3H, CH_3 of ring junction), 2.31 (s, 3H, $ArCH_3$), 2.84–2.89 (t, 1H, J =

© 2006 NRC Canada

Scheme 5. Reagent and conditions: (*i*) $AlCl_3$ (1 equiv.), Dry CH_2Cl_2, stirring, 2 h, RT.



		R^1	R^2	R^3	R^4	Yield(%)
8	a	H	H	CH_3	H	90
	b	H	H	Cl	H	88
	c	H	H	OCH_3	H	80
	d	Cl	H	H	H	85
	e	H	H	H	H	85
	f	H	CH_3	H	CH_3	90

		R^1	R^2	R^3	R^4	Yield(%)
9	g	CH_3	H	H	H	87
	h	CH_3	H	CH_3	H	75

Scheme 6.

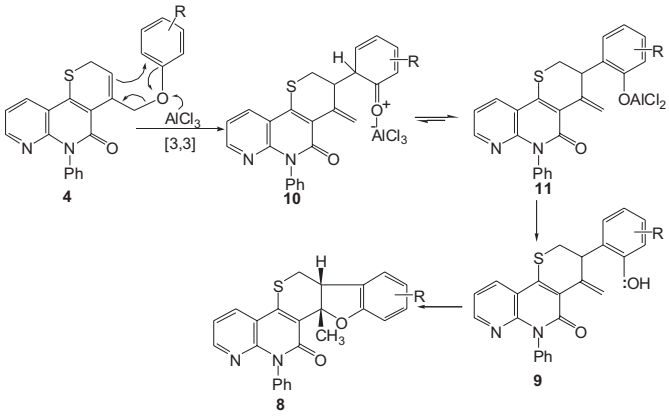
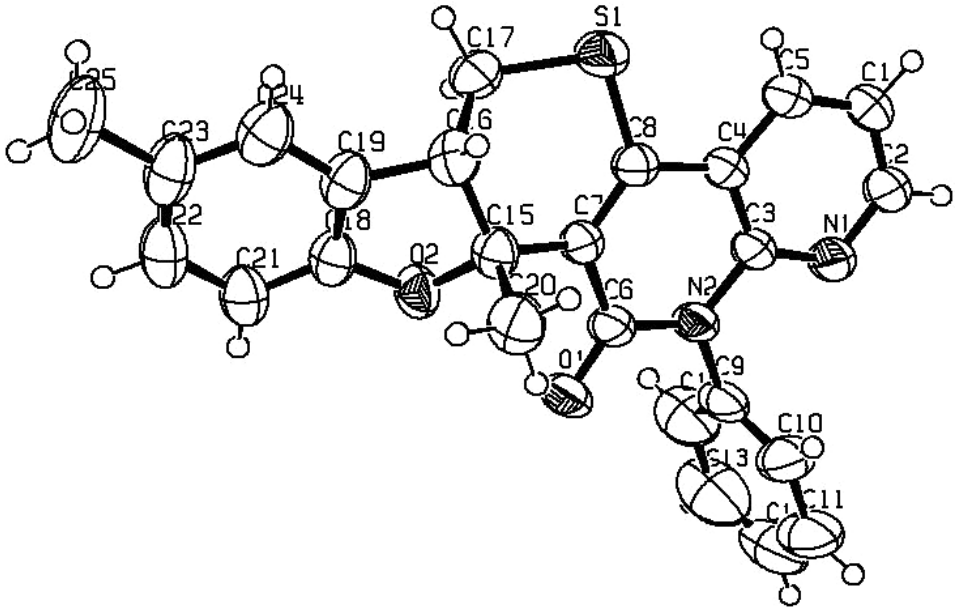


Fig. 1. Single crystal X-ray structure of compound **8a**.



12.3 Hz, SC**H**$_2$), 3.11–3.15 (dd, 1H, *J* = 3.7 Hz, 13.2 Hz, SCH_2), 3.46–3.49 (dd, 1H, *J* = 3.7 Hz, 11.2 Hz, ring juncture H), 6.84–6.85 (d, 1H, *J* = 8.1 Hz, ArH), 6.97–6.99 (d, 1H, *J* = 7.9 Hz, ArH), 7.09 (s, 1H, ArH), 7.14–7.16 (dd, 1H, *J* = 4.6 Hz, 7.8 Hz, ArH), 7.29–7.30 (d, 2H, *J* = 7.5 Hz, ArH), 7.44–7.47 (t, 1H, *J* = 7.4 Hz, ArH), 7.53–7.55 (m, 2H, ArH), 8.26–8.27 (d, 1H, *J* = 7 Hz, ArH), 8.43–8.44 (d, 1H, *J* = 3.3 Hz, ArH). Compounds **4b**–**4h** were also similarly treated to give products **8a**–**8f**, **9g**, and **9h** in 75%–90% yields (Scheme 5). The products were characterized from their elemental analyses and spectroscopic data.

We also examined whether the charge accelerated [3,3] sigmatropic rearrangement is applicable to the sulfides **3a**–**3f**. The substrates **3a**–**3f**, when treated with anhyd. $AlCl_3$ in dichloromethane at RT, showed a tendency to decompose and no traceable product was obtained, although they are quite stable in dichloromethane at RT.

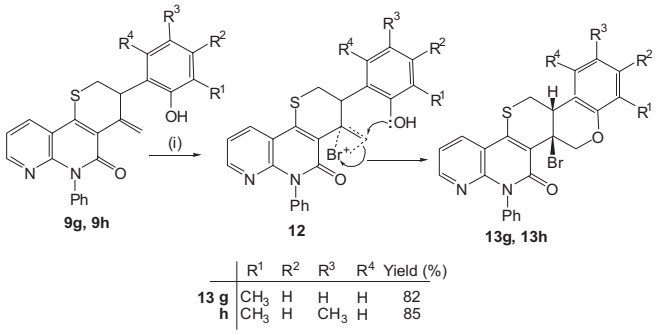
The formation of products **8a**–**8f**, **9g,** and **9h** from **4a**–**4h** is shown in Scheme 6. The isolation of the intermediate **9g** and **9h** indicates that the formation of both the thermal and catalytic rearrangement may follow the [3,3] sigmatropic rearrangement pathway. The use of a Lewis acid catalyst avoids the problem of high temperature that led to decomposition. The formation of products **8** from **4** can be rationalized by a series of steps involving an initial charge accelerated [3,3] sigmatropic rearrangement to give **10,** an ether–oxygen–$AlCl_3$ complex that may pass through a charge-delocalized transition state followed by rapid tautomerization to intermediate **11**, and proton exchange to give the intermediate **9**, which on *5-exo*-cyclization gives the products **8**, analogous to the product usually obtained in the thermal rearrangement (Scheme 6). The single crystal X-ray analysis of **8a** showed the cis stereochemistry at the ring juncture (Fig. 1).

The compounds **9g** and **9h**, upon treatment with pyridine hydrotribromide in chloroform, afforded compounds **13g** and **13h**. The formation of products **13g** and **13h** is thought to occur through the intermediate bromonium ion followed by a "6-endo" attack of the phenolic OH on the bromonium ion **12** (Scheme 7) (10*b*).

In summary, it has been possible to successfully perform the sequential Claisen rearrangement of 4-(4′-aryloxybut-2′-

© 2006 NRC Canada

Scheme 7. Reagent and conditions: (*i*) $PyHBr_3$, $CHCl_3$, 1 h, RT.



	R^1	R^2	R^3	R^4	Yield (%)
13 g	CH_3	H	H	H	82
h	CH_3	H	CH_3	H	85

ynylthio)-1-phenyl-1,8-naphthyridin-2(1*H*)-ones. The method is facile, operationally simple, and allows rapid access to two complex biologically significant heterocyclic systems.

Experimental[2]

Melting points were determined in an open capillary and are uncorrected. IR spectra were recorded on a PerkinElmer L 120–000A spectrometer (ν_{max} in cm^{-1}) on KBr disks. UV absorption spectra were recorded in EtOH on a Shimadzu UV-2401PC spectrophotometer (λ_{max} in nm). ^1H NMR (300 MHz, 400 MHz, 500 MHz, 600 MHz) and ^{13}C NMR (75.5 MHz, 125.7 MHz) spectra were recorded on a Bruker DPX-300, Varian-400 FT-NMR, Bruker DPX-500, and Varian-600 MHz spectrometers in $CDCl_3$ (chemical shifts in δ) with TMS as internal standard. Elemental analyses and mass spectra were recorded on a Leco 932 CHNS analyzer and on a JEOL JMS-600 instrument, respectively. ^1H NMR and ^{13}C NMR spectra were recorded at the Indian Institute of Chemical Biology, Kolkata, and Bose Institute, Kolkata. Silica gel [60–120 mesh, Spectrochem, India] was used for chromatographic separation. Silica gel G [E-Merck, India] was used for TLC. Petroleum ether refers to the fraction boiling between 60–80 °C.

The 1-aryloxy-4-chlorobut-2-ynes (**2a**–**2f**) were prepared according to published procedures (14–16).

Single crystal X-ray study was performed on a Bruker APEX CCD diffractometer equipped with an Oxford Instruments low-temperature attachment. Data were collected using monochromated Mo Kα radiation (λ_a = 0.710 69 Å). The frames were integrated in the Bruker SAINT Software package and the data were corrected for absorption using the SADABS program. The structure was solved and refined with the SHELX suite of programs. ORTEP-III was used to produce the diagram. Pertinent crystallographic data for compound **8a** is summarized in Table 1.

Table 1. Crystallographic data for compound **8a**.

Compound	**8a**
Empirical formula	$C_{25}H_{20}N_2O_2S$
Formula weight	412.5
Crystal system	Monoclinic
Space group	$P2_1/c$
a (Å)	8.4181(2)
b (Å)	20.3559 (6)
c (Å)	14.1321 (4)
α (°)	90
β (°)	95.269 (2)
γ (°)	90
V ($Å^3$)	2411.42 (11)
Z	5
ρ_{calcd} (g cm^{-3})	1.424
μ (mm^{-1})	0.194
F(000)	1085
Reflections collected	20 896
Reflections independent	5886
Goodness-of-fit	1.257
Final *R* indices [$I > 2\sigma(I)$][a]	*R*1 = 0.0950, *wR*2 = 0.3021

General procedure for the preparation of 4-(4′-aryloxy-2′-but-ynylthio)-1-phenyl-1,8-naphthyridin-2 (1*H*)-one (3a–3f)

To a mixture of 4-mercapto-1-phenyl-1,8-naphthyridin-2(1*H*)-one **1** (0.50 g, 2 mmol) and 1-aryloxy-4-chloro-2-butyne **2a**–**2f** (2.4 mmol) was added a solution of benzyl triethyl ammonium chloride (BTEAC) in 1% aq. NaOH (50 mL) and the mixture was stirred at RT for 8–10 h. The reaction mixture was then diluted with water (100 mL) and the organic layer was extracted with chloroform (3 × 25 mL). The organic layer was repeatedly washed with saturated brine and dried (Na_2SO_4). The solvent was removed and the viscous mass was chromatographed over silica gel using petroleum ether – ethyl acetate (3:1) as eluant to afford the products **3a**–**3f.**

Compounds **3d**–**3h** have already been reported (12).

Compound 3a

Yield 70%; solid; mp 112–114 °C. UV–vis (EtOH) λ_{max} (nm): 205, 222, 309, 327. IR (KBr, cm^{-1}) ν_{max}: 2918, 1655, 1578, 1509, 1436. ^1H NMR (600 MHz, $CDCl_3$) δ_H: 2.26 (s, 3H, CH_3), 3.86–3.87 (t, 2H, *J* = 1.8 Hz, SCH_2), 4.68–4.69 (t, 2H, *J* = 1.8 Hz, OCH_2), 6.73 (s, 1H, =CH), 6.83–6.85 (m, 2H, ArH), 7.06–7.07 (d, 1H, *J* = 8.4 Hz, ArH), 7.14–7.17 (dd, 1H, *J* = 4.2 Hz, 7.8 Hz, ArH), 7.26–7.28 (m, 3H, ArH), 7.48–7.51 (t, 1H, *J* = 7.8 Hz, ArH), 7.56–7.59 (t, 2H, *J* = 7.8 Hz, ArH), 8.11–8.12 (dd, 1H, *J* = 1.8 Hz, 7.8 Hz, ArH), 8.45–8.46 (dd, 1H, *J* = 1.8 Hz, 4.2 Hz, ArH). MS *m*/*z*: 412 (M^+). Anal. calcd. for $C_{25}H_{20}N_2O_2S$: C 72.81, H 4.85, N 6.79; found: C 73.04, H 4.60, N 6.96.

Compound 3b

Yield 70%; solid; mp 148–150 °C. UV–vis (EtOH) λ_{max} (nm): 200, 223, 327. IR (KBr, cm^{-1}) ν_{max}: 2921, 1662, 1578, 1488, 1435. ^1H NMR (300 MHz, $CDCl_3$) δ_H: 3.86 (t, 2H, *J* = 1.8 Hz, SCH_2), 4.69 (t, 2H, *J* = 1.8 Hz, OCH_2), 6.72 (s, 1H, =CH), 6.86–6.89 (m, 2H, ArH), 7.14–7.29 (m, 5H, ArH),

[2] Supplementary data for this article are available on the journal Web site (http://canjchem.nrc.ca) or may be purchased from the Depository of Unpublished Data, Document Delivery, CISTI, National Research Council Canada, Ottawa, ON K1A 0R6, Canada. DUD 5113. For more information on obtaining material refer to http://cisti-icist.nrc-cnrc.gc.ca/irm/unpub_e.shtml. CCDC 627102 contains the crystallographic data for this manuscript. These data can be obtained, free of charge, via http://www.ccdc.cam.ac.uk/conts/retrieving.html (Or from the Cambridge Crystallographic Data Centre, 12 Union Road, Cambridge CB2 1EZ, UK; fax +44 1223 336033; or deposit@ccdc.cam.ac.uk).

© 2006 NRC Canada

7.47–7.60 (m, 3H, ArH), 8.09–8.12 (dd, 1H, *J* = 1.5 Hz, 7.8 Hz, ArH), 8.45–8.47 (dd, 1H, *J* = 1.6 Hz, 4.6 Hz, ArH). MS *m/z*: 432, 434 (M^+). Anal. calcd. for $C_{24}H_{17}N_2O_2SCl$: C 66.58, H 3.93, N 6.47; found: C 66.78, H 3.75, N 6.23.

Compound 3c

Yield 72%; solid; mp 155–157 °C. UV–vis (EtOH) λ_{max} (nm): 222, 298, 327. IR (KBr, cm^{-1}) ν_{max}: 2962, 1647, 1582, 1512, 1432. ^1H NMR (400 MHz, $CDCl_3$) δ_H: 3.72 (s, 3H, OCH_3), 3.86 (t, 2H, *J* = 2 Hz, SCH_2), 4.66 (t, 2H, *J* = 2 Hz, OCH_2), 6.72 (s, 1H, =CH), 6.79–6.81 (d, 2H, *J* = 8.8 Hz, ArH), 6.88–6.90 (d, 1H, *J* = 8.8 Hz, ArH), 7.14–7.17 (dd, 1H, *J* = 4.4 Hz, 8.4 Hz, ArH), 7.25–7.28 (m, 3H, ArH), 7.47–7.51 (t, 1H, *J* = 7.6 Hz, ArH), 7.55–7.59 (t, 2H, *J* = 7.6 Hz, ArH), 8.10–8.12 (d, 1H, *J* = 8.4 Hz, ArH), 8.45–8.46 (d, 1H, *J* = 3.6 Hz, ArH). MS *m/z*: 428 (M^+). Anal. calcd. for $C_{25}H_{20}N_2O_3S$: C 70.09, H 4.67, N 6.54; found: C 70.32, H 4.88, N 6.36.

General procedure for the preparation of compounds 4a–4h

Compounds **3a**–**3h** (1 mmol) were refluxed in chlorobenzene (5 mL) for 4–6 h. The reaction was monitored by TLC. The chlorobenzene was removed at reduced pressure and the residual mass was chromatographed over silica gel. Elution of the column with petroleum ether removed residual chlorobenzene and the rearranged products **4a**–**4h** were obtained by eluting the column with petroleum ether – ethyl acetate (4:1).

Compound 4a

Yield 82%; solid; mp 175–177 °C. UV–vis (EtOH) λ_{max} (nm): 204, 225, 343. IR (KBr, cm^{-1}) ν_{max}: 2925, 1646, 1629, 1582, 1509, 1443. ^1H NMR (600 MHz, $CDCl_3$) δ_H: 2.26 (s, 3H, CH_3), 3.43–3.44 (d, 2H, *J* = 5.4 Hz, SCH_2), 5.17 (d, 2H, *J* = 1.2 Hz, OCH_2), 6.28–6.31 (tt, 1H, *J* = 1.8 Hz, 6 Hz, =CH), 6.83–6.85 (m, 2H, ArH), 7.02–7.04 (d, 1H, *J* = 8.4 Hz, ArH), 7.17–7.20 (dd, 1H, *J* = 4.8 Hz, 7.8 Hz, ArH), 7.26–7.28 (m, 3H, ArH), 7.48–7.50 (tt, 1H, *J* = 1.2 Hz, 4.8 Hz, ArH), 7.56–7.58 (m, 2H, ArH), 8.30–8.31 (dd, 1H, *J* = 1.8 Hz, 7.8 Hz, ArH), 8.42–8.43 (dd, 1H, *J* = 1.8 Hz, 4.8 Hz, ArH). ^{13}C NMR (125.7 MHz, $CDCl_3$) δ_c: 20.87, 24.95, 69.02, 115.34, 115.44, 117.54, 118.61, 125.54, 128.97, 129.29, 129.95, 130.19, 130.31, 134.16, 136.95, 137.51, 146.18, 149.36, 150.69, 156.90, 160.45. MS *m/z*: 412 (M^+). Anal. calcd. for $C_{25}H_{20}N_2O_2S$: C 72.81, H 4.85, N 6.79; found: C 73.07, H 5.02, N 6.58.

Compound 4b

Yield 82%; solid; mp 204–206 °C. UV–vis (EtOH) λ_{max} (nm): 205, 226, 342. IR (KBr, cm^{-1}) ν_{max}: 2961, 2921, 1646, 1576, 1491, 1443. ^1H NMR (500 MHz, $CDCl_3$) δ_H: 3.43 (d, 2H, *J* = 6 Hz, SCH_2), 5.17 (s, 2H, OCH_2), 6.25–6.27 (t, 1H, *J* = 6 Hz, =CH), 6.85–6.87 (d, 2H, *J* = 8.8 Hz, ArH), 7.17–7.20 (m, 3H, ArH), 7.24–7.25 (m, 2H, ArH), 7.47–7.50 (t, 1H, *J* = 7.4 Hz, ArH), 7.55–7.58 (t, 2H, *J* = 7.4 Hz, ArH), 8.30–8.31 (dd, 1H, *J* = 1.3 Hz, 7.9 Hz, ArH), 8.43–8.44 (dd, 1H, *J* = 1.3 Hz, 4.5 Hz, ArH). MS *m/z*: 432, 434 (M^+). Anal. calcd. for $C_{24}H_{17}N_2O_2SCl$: C 66.58, H 3.93, N 6.47; found: C 66.35, H 4.12, N 6.64.

Compound 4c

Yield 90%; solid; mp 180–182 °C. UV–vis (EtOH) λ_{max} (nm): 204, 226, 344. IR (KBr, cm^{-1}) ν_{max}: 2928, 1645, 1578, 1508, 1442. ^1H NMR (400 MHz, $CDCl_3$) δ_H: 3.43 (d, 2H, *J* = 6 Hz, SCH_2), 3.73 (s, 3H, OCH_3), 5.14 (d, 2H, *J* = 2 Hz, OCH_2), 6.28–6.31 (t, 1H, *J* = 6 Hz, =CH), 6.76–6.79 (dd, 2H, *J* = 2.4 Hz, 6.8 Hz, ArH), 6.86–6.88 (dd, 2H, *J* = 2.4 Hz, 6.8 Hz, ArH), 7.17–7.20 (dd, 1H, *J* = 4.4 Hz, 7.6 Hz, ArH), 7.25–7.27 (m, 2H, ArH), 7.46–7.50 (t, 1H, *J* = 8 Hz, ArH), 7.55–7.58 (t, 2H, *J* = 8 Hz, ArH), 8.29–8.31 (dd, 1H, *J* = 1.6 Hz, 7.6 Hz, ArH), 8.42–8.43 (dd, 1H, *J* = 1.6 Hz, 4.4 Hz, ArH). MS *m/z*: 428 (M^+). Anal. calcd. for $C_{25}H_{20}N_2O_3S$: C 70.09, H 4.67, N 6.54; found: C 69.91, H 4.91, N 6.76.

Compound 4d

Yield 95%; solid; mp 212–214 °C. UV–vis (EtOH) λ_{max} (nm): 204, 223, 343. IR (KBr, cm^{-1}) ν_{max}: 2924, 1651, 1579, 1485, 1444. ^1H NMR (600 MHz, $CDCl_3$) δ_H: 3.46 (d, 2H, *J* = 6 Hz, SCH_2), 5.26 (d, 2H, *J* = 1.8 Hz, OCH_2), 6.43–6.45 (tt, 1H, *J* = 1.8 Hz, 6 Hz, =CH), 6.84–6.87 (dt, 1H, *J* = 1.2 Hz, 7.8 Hz, ArH), 6.98–6.99 (dd, 1H, *J* = 1.2 Hz, 8.4 Hz, ArH), 7.13–7.16 (dt, 1H, *J* = 1.8 Hz, 8.4 Hz, ArH), 7.18–7.20 (dd, 1H, *J* = 4.2 Hz, 7.8 Hz, ArH), 7.28–7.29 (m, 2H, ArH), 7.33–7.34 (dd, 1H, *J* = 1.2 Hz, 7.8 Hz, ArH), 7.48–7.50 (t, 1H, *J* = 7.8 Hz, ArH), 7.56–7.59 (m, 2H, ArH), 8.31–8.32 (dd, 1H, *J* = 1.8 Hz, 7.8 Hz, ArH), 8.43–8.44 (dd, 1H, *J* = 1.8 Hz, 4.8 Hz, ArH). MS *m/z*: 432, 434 (M^+). Anal. calcd. for $C_{24}H_{17}N_2O_2SCl$: C 66.58, H 3.93, N 6.47; found: C 66.80, H 3.68, N 6.26.

Compound 4e

Yield 85%; solid; mp 186–188 °C. UV–vis (EtOH) λ_{max} (nm): 206, 222, 337. IR (KBr, cm^{-1}) ν_{max}: 2921, 1655, 1574, 1443. ^1H NMR (400 MHz, $CDCl_3$) δ_H: 3.43 (d, 2H, *J* = 6 Hz, SCH_2), 5.19 (s, 2H, OCH_2), 6.28–6.31 (t, 1H, *J* = 6 Hz, =CH), 6.91–6.94 (m, 3H, ArH), 7.17–7.27 (m, 5H, ArH), 7.46–7.50 (t, 1H, *J* = 8 Hz, ArH), 7.54–7.58 (t, 2H, *J* = 8 Hz, ArH), 8.29–8.31 (dd, 1H, *J* = 1.6 Hz, 8 Hz, ArH), 8.42–8.43 (dd, 1H, *J* = 1.6 Hz, 4.4 Hz, ArH). MS *m/z*: 398 (M^+). Anal. calcd. for $C_{24}H_{18}N_2O_2S$: C 72.36, H 4.52, N 7.03; found: C 72.57, H 4.35, N 7.22.

Compound 4f

Yield 85%; solid; mp 165–167 °C. UV–vis (EtOH) λ_{max} (nm): 206, 224, 341. IR (KBr, cm^{-1}) ν_{max}: 2913, 1663, 1583, 1448. ^1H NMR (600 MHz, $CDCl_3$) δ_H: 2.25 (s, 6H, CH_3), 3.44–3.45 (d, 2H, *J* = 6 Hz, SCH_2), 5.15 (d, 2H, *J* = 2 Hz, OCH_2), 6.31–6.33 (t, 1H, *J* = 6 Hz, =CH), 6.57 (s, 1H, ArH), 6.58 (s, 1H, ArH), 7.18–7.20 (dd, 1H, *J* = 4.8 Hz, 7.8 Hz, ArH), 7.27–7.28 (m, 3H, ArH), 7.48–7.50 (t, 1H, *J* = 7.2 Hz, ArH), 7.56–7.59 (t, 2H, *J* = 7.8 Hz, ArH), 8.30–8.31 (dd, 1H, *J* = 1.2 Hz, 7.8 Hz, ArH), 8.42–8.43 (dd, 1H, *J* = 1.2 Hz, 4.8 Hz, ArH). MS *m/z*: 426 (M^+). Anal. calcd. for $C_{26}H_{22}N_2O_2S$: C 73.23, H 5.16, N 6.57; found: C 73.04, H 5.39, N 6.78.

Compound 4g

Yield 90%; solid; mp 195–197 °C. UV–vis (EtOH) λ_{max} (nm): 204, 223, 339. IR (KBr, cm^{-1}) ν_{max}: 2924, 1653, 1575, 1492, 1443. ^1H NMR (600 MHz, $CDCl_3$) δ_H: 2.26 (s, 3H,

© 2006 NRC Canada

CH_3), 3.45–3.46 (d, 2H, J = 6 Hz, SCH_2), 5.20 (d, 2H, J = 1.2 Hz, OCH_2), 6.34–6.36 (tt, 1H, J = 1.8 Hz, 6 Hz, =CH), 6.81–6.87 (m, 1H, ArH), 7.07–7.12 (m, 2H, ArH), 7.18–7.20 (dd, 1H, J = 4.8 Hz, 7.8 Hz, ArH), 7.26–7.28 (m, 3H, ArH), 7.48–7.51 (m, 1H, ArH), 7.56–7.59 (m, 2H, ArH), 8.31–8.32 (dd, 1H, J = 1.8 Hz, 7.8 Hz, ArH), 8.43–8.44 (dd, 1H, J = 1.8 Hz, 4.8 Hz, ArH). MS m/z: 412 (M^+). Anal. calcd. for $C_{25}H_{20}N_2O_2S$: C 72.81, H 4.85, N 6.79; found: C 72.55, H 5.02, N 7.02.

Compound 4h

Yield 85%; solid; mp 178–180 °C. UV–vis (EtOH) λ_{max} (nm): 200, 226, 341. IR (KBr, cm^{-1}) ν_{max}: 2918, 1651, 1579, 1503, 1444. ^1H NMR (300 MHz, $CDCl_3$) δ_H = 2.22 (s, 3H, CH_3), 2.26 (s, 3H, CH_3), 3.43 (d, 2H, J = 6 Hz, SCH_2), 5.16 (s, 2H, OCH_2), 6.32–6.36 (t, 1H, J = 6 Hz, =CH), 6.74–6.93 (m, 3H, ArH), 7.16–7.28 (m, 3H, ArH), 7.47–7.60 (m, 3H, ArH), 8.30–8.32 (d, 1H, J = 7.8 Hz, ArH), 8.42–8.44 (dd, 1H, J = 1.2 Hz, 4.4 Hz, ArH). MS m/z: 426 (M^+). Anal. calcd. for $C_{26}H_{22}N_2O_2S$: C 73.23, H 5.16, N 6.57; found: C 73.49, H 5.40, N 6.38.

General procedure for the preparation of 8a–8f, 9g, and 9h

Compound **4a**–**4f** (0.5 mmol) was dissolved in dry dichloromethane (10 mL) and anhyd. $AlCl_3$ (0.06 g, 0.5 mmol) was added. The reaction mixture was stirred at RT for 0.5–2.0 h. Crushed ice was added to the reaction mixture and was extracted with dichloromethane. The combined extracts were washed with water (20 mL), brine (20 mL), and dried (Na_2SO_4). The solvent was removed and the residual viscous mass was chromatographed over silica gel using petroleum ether – ethyl acetate (3:1) as eluant to afford the products **8a**–**8f**, **9g**, and **9h**.

Compound 8a

Yield 90%; solid; mp 150–152 °C. UV–vis (EtOH) λ_{max} (nm): 206, 224, 296, 320, 332. IR (KBr, cm^{-1}) ν_{max}: 2924, 1655, 1583, 1488, 1441. ^1H NMR (500 MHz, $CDCl_3$) δ_H: 1.86 (s, 3H, CH_3 of ring junction), 2.31 (s, 3H, $ArCH_3$), 2.84–2.89 (t, 1H, J = 12.3 Hz, SCH_2), 3.11–3.15 (dd, 1H, J = 3.7 Hz, 13.2 Hz, SCH_2), 3.46–3.49 (dd, 1H, J = 3.7 Hz, 11.2 Hz, ring juncture H), 6.84–6.85 (d, 1H, J = 8.1 Hz, ArH), 6.97–6.99 (d, 1H, J = 7.9 Hz, ArH), 7.09 (s, 1H, ArH), 7.14–7.16 (dd, 1H, J = 4.6 Hz, 7.8 Hz, ArH), 7.29–7.30 (d, 2H, J = 7.5 Hz, ArH), 7.44–7.47 (t, 1H, J = 7.4 Hz, ArH), 7.53–7.55 (m, 2H, ArH), 8.26–8.27 (d, 1H, J = 7 Hz, ArH), 8.43–8.44 (d, 1H, J = 3.3 Hz, ArH). ^{13}C NMR (125.7 MHz, $CDCl_3$) δ_c: 21.26, 24.75, 29.28, 52.04, 86.05, 111.26, 114.83, 118.30, 125.10, 127.08, 128.68, 128.81, 129.68, 129.71, 130.14, 130.38, 134.30, 137.53, 145.85, 149.45, 151.03, 155.71, 160.56. MS m/z: 412 (M^+). Anal. calcd. for $C_{25}H_{20}N_2O_2S$: C 72.81, H 4.85, N 6.79; found: C 72.58, H 4.64, N 6.98.

Compound 8b

Yield 88%; solid; mp 260–262 °C. UV–vis (EtOH) λ_{max} (nm): 205, 224, 301, 321, 332. IR (KBr, cm^{-1}) ν_{max}: 2921, 1652, 1583, 1470, 1442. ^1H NMR (500 MHz, $CDCl_3$) δ_H: 1.88 (s, 3H, CH_3 of ring junction), 2.85–2.90 (t, 1H, J = 12.2 Hz, SCH_2), 3.12–3.15 (dd, 1H, J = 2.6 Hz, 13 Hz, SCH_2), 3.52–3.54 (d, 1H, J = 8.5 Hz, ring juncture H), 6.87–6.88 (d, 1H, J = 8.3 Hz, ArH), 7.13–7.17 (m, 2H, ArH), 7.25–7.30 (m, 3H, ArH), 7.41–7.55 (m, 3H, ArH), 8.25–8.27 (d, 1H, J = 7.4 Hz, ArH), 8.45–8.46 (m, 1H, ArH). ^{13}C NMR (125.7 MHz, $CDCl_3$) δ_c: 24.75, 29.03, 51.92, 86.99, 112.72, 114.70, 118.39, 124.77, 125.71, 126.55, 128.63, 128.74, 129.49, 129.69, 130.62, 134.30, 137.42, 145.97, 149.45, 151.22, 156.58, 160.44. MS m/z: 432, 434 (M^+). Anal. calcd. for $C_{24}H_{17}N_2O_2SCl$: C 66.58, H 3.93, N 6.47; found: C 66.84, H 4.14, N 6.69.

Compound 8c

Yield 80%; solid; mp 226–228 °C. UV–vis (EtOH) λ_{max} (nm): 204, 224, 333. IR (KBr, cm^{-1}) ν_{max}: 2938, 1650, 1582, 1484, 1441. ^1H NMR (500 MHz, $CDCl_3$) δ_H: 1.87 (s, 3H, CH_3 of ring junction), 2.86–2.91 (dd, 1H, J = 11.5 Hz, 13 Hz, SCH_2), 3.13–3.16 (dd, 1H, J = 3.8 Hz, 13 Hz, SCH_2), 3.48–3.51 (dd, 1H, J = 3.8 Hz, 11.3 Hz, ring juncture H), 3.78 (s, 3H, OCH_3), 6.71–6.71 (dd, 1H, J = 2.5 Hz, 8.7 Hz, ArH), 6.86–6.92 (m, 2H, ArH), 7.14–7.16 (dd, 1H, J = 4.6 Hz, 7.9 Hz, ArH), 7.29–7.30 (d, 2H, J = 7.4 Hz, ArH), 7.44–7.47 (t, 1H, J = 7.4 Hz, ArH), 7.50–7.60 (m, 2H, ArH), 8.25–8.27 (dd, 1H, J = 1.4 Hz, 7.9 Hz, ArH), 8.43–8.44 (dd, 1H, J = 1.4 Hz, 4.5 Hz, ArH). ^{13}C NMR (125.7 MHz, $CDCl_3$) δ_c: 24.72, 29.12, 52.35, 56.45, 86.18, 111.08, 111.69, 114.35, 118.30, 126.94, 127.05, 128.68, 129.67, 129.74, 134.27, 137.51, 145.76, 149.45, 151.04, 151.91, 154.65, 160.53. MS m/z: 428 (M^+). Anal. calcd. for $C_{25}H_{20}N_2O_3S$: C 70.09, H 4.67, N 6.54; found: C 69.85, H 4.48, N 6.72.

Compound 8d

Yield 85%; solid; mp 162–164 °C. UV–vis (EtOH) λ_{max} (nm): 206, 224, 290, 321, 332. IR (KBr, cm^{-1}) ν_{max}: 2926, 1655, 1584, 1444. ^1H NMR (600 MHz, $CDCl_3$) δ_H: 1.92 (s, 3H, CH_3 of ring junction), 2.90–2.94 (dd, 1H, J = 11.4 Hz, 13.2 Hz, SCH_2), 3.13–3.16 (dd, 1H, J = 3.6 Hz, 13.2 Hz, SCH_2), 3.58–3.61 (dd, 1H, J = 3.6 Hz, 11.4 Hz, ring juncture H), 6.84–6.86 (t, 1H, J = 7.8 Hz, ArH), 7.13–7.16 (dd, 1H, J = 4.8 Hz, 7.8 Hz, ArH), 7.17–7.19 (m, 2H, ArH), 7.29–7.30 (d, 2H, J = 6.6 Hz, ArH), 7.45–7.48 (t, 1H, J = 8.4 Hz, ArH), 7.55–7.57 (t, 2H, J = 8.4 Hz, ArH), 8.24–8.25 (dd, 1H, J = 1.8 Hz, 7.8 Hz, ArH), 8.43–8.44 (dd, 1H, J = 1.8 Hz, 4.8 Hz, ArH). MS m/z: 432, 434 (M^+). Anal. calcd. for $C_{24}H_{17}N_2O_2SCl$: C 66.58, H 3.93, N 6.47; found: C 66.32, H 4.15, N 6.66.

Compound 8e

Yield 85%; solid; mp 214–216 °C. UV–vis (EtOH) λ_{max} (nm): 203, 224, 287, 332. IR (KBr, cm^{-1}) ν_{max}: 2919, 1644, 1583, 1461, 1443. ^1H NMR (500 MHz, $CDCl_3$) δ_H: 1.88 (s, 3H, CH_3 of ring junction), 2.85–2.89 (t, 1H, J = 12.3 Hz, SCH_2), 3.13–3.16 (d, 1H, J = 10.5 Hz, SCH_2), 3.52 (d, 1H, J = 8.8 Hz, ring juncture H), 6.90–6.97 (m, 2H, ArH), 7.15–7.20 (m, 2H, ArH), 7.25–7.30 (m, 3H, ArH), 7.46–7.55 (m, 3H, ArH), 8.26–8.27 (d, 1H, J = 7.5 Hz, ArH), 8.44 (d, 1H, J = 2.1 Hz, ArH). MS m/z: 398 (M^+). Anal. calcd. for $C_{24}H_{18}N_2O_2S$: C 72.36, H 4.52, N 7.03; found: C 72.54, H 4.77, N 6.81.

Compound 8f

Yield 90%; solid; mp 284–286 °C. UV–vis (EtOH) λ_{max}

© 2006 NRC Canada

(nm): 207, 224, 288, 320, 332. IR (KBr, cm^{-1}) ν_{max}: 2925, 1655, 1584, 1441. ^1H NMR (500 MHz, $CDCl_3$) δ_H: 1.79 (s, 3H, CH_3 of ring junction), 2.26 (s, 3H, $ArCH_3$), 2.36 (s, 3H, $ArCH_3$), 2.68–2.74 (t, 1H, J = 12.6 Hz, SCH_2), 3.07–3.11 (dd, 1H, J = 3.8 Hz, 13.1 Hz, SCH_2), 3.39–3.43 (dd, 1H, J = 3.8 Hz, 12.4 Hz, ring juncture H), 6.55 (s, 1H, ArH), 6.62 (s, 1H, ArH), 7.15–7.17 (dd, 1H, J = 4.6 Hz, 7.9 Hz, ArH), 7.30–7.31 (d, 2H, J = 7.4 Hz, ArH), 7.45–7.48 (t, 1H, J = 7.4 Hz, ArH), 7.53–7.57 (t, 2H, J = 7.8 Hz, ArH), 8.28–8.30 (dd, 1H, J = 1.6 Hz, 7.9 Hz, ArH), 8.44–8.45 (dd, 1H, J = 1.6 Hz, 4.6 Hz, ArH). MS m/z: 426 (M^+). Anal. calcd. for $C_{26}H_{22}N_2O_2S$: C 73.23, H 5.16, N 6.57; found: C 73.47, H 4.97, N 6.35.

Compound 9g

Yield 87%; solid; mp 128–130 °C. UV–vis (EtOH) λ_{max} (nm): 205, 224, 337. IR (KBr, cm^{-1}) ν_{max}: 3475, 2921, 1638, 1579, 1444, 1281. ^1H NMR:(300 MHz, $CDCl_3$) δ_H: 2.27 (s, 3H, $ArCH_3$), 3.39–3.44 (dd, 1H, J = 3.3 Hz, 12.2 Hz, SCH_2), 3.66–3.73 (dd, 1H, J = 8.4 Hz, 12.3 Hz, SCH_2), 4.33–4.36 (dd, 1H, J = 3.1 Hz, 5 Hz, ring juncture H), 5.02 (s, 1H, OH), 5.41 (s, 1H, $=CH_2$), 6.70 (s, 1H, $=CH_2$), 6.79–6.84 (t, 1H, J = 7.3 Hz, ArH), 6.95–7.15 (m, 3H, ArH), 7.26–7.31 (m, 2H, ArH), 7.48–7.60 (m, 3H, ArH), 8.21–8.24 (d, 1H, J = 8.1 Hz, ArH), 8.42–8.43 (d, 1H, J = 3.2 Hz, ArH). MS m/z: 412 (M^+). Anal. calcd. for $C_{25}H_{20}N_2O_2S$: C 72.81, H 4.85, N 6.79; found: C 72.99, H 5.10, N 6.55.

Compound 9h

Yield 75%; solid; mp 230–232 °C. UV–vis (EtOH) λ_{max} (nm): 205, 224, 337, 344. IR (KBr, cm^{-1}) ν_{max}: 3475, 2921, 1640, 1579, 1444, 1281. ^1H NMR (300 MHz, $CDCl_3$) δ_H: 2.11 (s, 3H, $ArCH_3$), 2.22 (s, 3H, $ArCH_3$), 3.35–3.59 (d, 1H, J = 11 Hz, -SCH_2) 3.65–3.72 (t, 1H, J = 9.8 Hz, SCH_2), 4.28–4.30 (d, 1H, J = 6.5 Hz, ring juncture H) 4.84 (s, 1H, OH), 5.37 (s, 1H, $=CH_2$), 6.65 (s, 1H, $=CH_2$), 6.77 (s, 1H, ArH), 6.88 (s, 1H, ArH), 7.13–7.15 (m, 1H, ArH), 7.26–7.30 (m, 2H, ArH), 7.48–7.58 (m, 3H, ArH), 8.22–8.24 (d, 1H, J = 7.9 Hz, ArH), 8.43–8.44 (d, 1H, J = 3.1 Hz, ArH). MS m/z: 426 (M^+). Anal. calcd. for $C_{26}H_{22}N_2O_2S$: C 73.23, H 5.16, N 6.57; found: C 73.09, H 5.33, N 6.71.

General procedure for the preparation of compounds 8a, 8d, and 8f

A mixture of compounds **4a**, **4d**, and **4f** (1 mmol) in *N,N*-diethylaniline (5 mL) was refluxed for 12–14 h. The reaction mixture was cooled, poured into ice-cold 6 (N) HCl (30 mL), and extracted with $CHCl_3$ (3 × 20 mL). The $CHCl_3$ layer was washed with water and dried over Na_2SO_4. Removal of $CHCl_3$ gave a viscous liquid, which was chromatographed over silica gel. Elution of the column with petroleum ether – ethyl acetate (4:1) furnished products **10a**, **10d**, and **4f**.

General procedure for the cyclization of the compounds 9g and 9h

The brominating agent, solid pyridine hydrobromide perbromide (0.16 g, 0.5 mmol), was added to a chloroform solution (20 mL) of the compounds **9g** and **9h** (0.5 mmol). The reaction mixture was then stirred for 1 h on a magnetic stirrer at 0–5 °C. After the completion of the reaction (monitored by TLC), the mixture was washed with 5% aq. $NaHCO_3$ (3 × 25 mL) and water (3 × 25 mL), and dried (Na_2SO_4). The residual mass after removal of the solvent was subjected to column chromatography over silica gel using petroleum ether – ethyl acetate (6:1) as eluant to give cyclized products **13g** and **13h**.

Compound 13g

Yield 82%; solid; mp 146–148 °C. UV–vis (EtOH) λ_{max} (nm): 207, 224, 286, 323, 334. IR (KBr, cm^{-1}) ν_{max}: 2923, 1651, 1584, 1443. ^1H NMR (300 MHz, $CDCl_3$) δ_H: 2.22 (s, 3H, $ArCH_3$), 2.82 (t, 1H, J = 12.6 Hz, SCH_2), 3.18–3.23 (dd, 1H, J = 4 Hz, 13 Hz, SCH_2), 3.54–3.57 (d, 1H, J = 9.5 Hz, OCH_2), 3.97–4.02 (dd, 1H, J = 4 Hz, 13 Hz, ring juncture H), 4.89–4.92 (d, 1H, J = 9.5 Hz, OCH_2), 6.58–6.90 (t, 1H, J = 7.3 Hz, ArH), 7.01–7.04 (d, 1H, J = 7.3 Hz, ArH), 7.14–7.33 (m, 4H, ArH), 7.49–7.61 (m, 3H, ArH), 8.30–8.33 (d, 1H, J = 8.1 Hz, ArH), 8.46–8.47 (d, 1H, J = 2.8 Hz, ArH). MS m/z: 490, 492 (M^+). Anal. calcd. for $C_{25}H_{19}N_2O_2SBr$: C 61.09, H 3.86, N 5.70; found: C 61.27, H 4.07, N 5.86.

Compound 13h

Yield 85%; solid; mp 140–142 °C. UV–vis (EtOH) λ_{max} (nm): 207, 224, 294, 334. IR (KBr, cm^{-1}) ν_{max}: 2924, 1655, 1584, 1443. ^1H NMR (500 MHz, $CDCl_3$) δ_H: 2.18 (s, 3H, $ArCH_3$), 2.29 (s, 3H, $ArCH_3$), 2.83–2.88 (dd, 1H, J = 12.4 Hz, 13 Hz, SCH_2), 3.17–3.20 (dd, 1H, J = 4.2 Hz, 13.2 Hz, SCH_2), 3.54–3.56 (d, 1H, J = 9.6 Hz, OCH_2), 3.93–3.96 (dd, 1H, J = 4.2 Hz, 12.2 Hz, ring juncture H), 4.89–4.91 (d, 1H, J = 9.6 Hz, OCH_2), 6.84 (s, 1H, ArH), 6.95 (s, 1H, ArH), 7.16–7.18 (dd, 1H, J = 4.6 Hz, 8 Hz, ArH), 7.28–7.32 (m, 2H, ArH), 7.46–7.50 (m, 1H, ArH), 7.56–7.59 (t, 2H, J = 7.8 Hz, ArH), 8.30–8.32 (dd, 1H, J = 1.6 Hz, 7.9 Hz, ArH), 8.45–8.47 (dd, 1H, J = 1.6 Hz, 4.6 Hz, ArH). MS m/z: 504, 506 (M^+). Anal. calcd. for $C_{26}H_{21}N_2O_2SBr$: C 61.78, H 4.15, N 5.54; found: C 61.57, H 4.38, N 5.36.

Acknowledgements

We thank the Council of Scientific and Industrial Research (CSIR, New Delhi) for financial assistance. RI is thankful to CSIR (New Delhi) for a Junior Research Fellowship. We are grateful to Professor A.T. Khan of the Indian Institute of Technology, Guwahati, for the X-ray crystallographic analysis of compound **8a**. We also thank the Department of Science and Technology (DST, New Delhi) for providing a UV–vis spectrophotometer and an FT-IR spectrometer under the Fund for Improvement of S&T Infrastructure in Universities and Higher Educational Institutions (DST-FIST) programme.

References

1. V.P. Litvinov, S.V. Roman, and V.D. Dyachenko. Russ. Chem. Rev. 69, 201 (2000).
2. V.P. Litvinov. Russ. Chem. Rev. **73**, 637 (2004).
3. M.H. Sherlock, J.J. Kaminski, W.C. Tom, J.F. Lee, S.C. Wong, W. Kreutner, R.W. Bryant, A.T. McPhail. J. Med. Chem. **31**, 2108 (1988).
4. A.A. Santilli, A.C. Scotese, R.F. Bauer, and S.C. Bell. J. Med. Chem. **30**, 2270 (1987).
5. K. Chen, S.C. Kuo, M.C. Hsieh, A. Merger, C.M. Lin, E. Hamel, and K.H. Lee. J. Med. Chem. **40**, 3049 (1997).

© 2006 NRC Canada

6. T. Kuroda, F. Suzuki, T. Tamure, K. Ohmori, and H. Hosoe. J. Med. Chem. **35**, 1130 (1992).
7. F. Suzuki, T. Kuroda, T. Kawakita, H. Manabe, S. Kitamura, K. Ohmori, M. Ichimura, H. Kase, and S. Ichikawa. J. Med. Chem. **35**, 4866 (1992).
8. For a recent review, see: Ana M. Martin Castro. Chem. Rev. **104**, 2939 (2004).
9. (*a*) C. Mohan, P. Singh, and M.P. Mahajan. Tetrahedron, **61**, 10774 (2005); (*b*) C. Mohan, V. Kumar, and M.P. Mahajan. Tetrahedron Lett. **45**, 6075 (2004).
10. (*a*) K.C. Majumdar and U. Das. J. Org. Chem. **63**, 9997 (1998); (*b*) K.C. Majumdar, U.K. Kundu, and S.K. Ghosh. Org. Lett. **4**, 2629 (2002); (*c*) K.C. Majumdar, U.K. Kundu, and S.K. Ghosh. J. Chem. Soc. Perkin Trans 1, 2139 (2002); (*d*) K.C. Majumdar and S.K. Ghosh. Tetrahedron Lett. **43**, 2115 (2003); (*e*) K.C. Majumdar, M. Ghosh, M. Jana, and D. Saha. Tetrahedron Lett. **43**, 2111 (2002); (*f*) K.C. Majumdar, A. Bandopadhyay, and A. Biswas. Tetrahedron, **59**, 5289 (2003).
11. (*a*) C.M. Starks and C. Liotta. Phase transfer catalysis. Academic Press, New York. 1978; (*b*) E.V. Dehmlow and S.S. Dehmlow. Phase transfer catalysis. 3rd ed. VCH, New York. 1993.
12. K.C. Majumdar and R. Islam. Heteroat. Chem. 2006 (In Press).
13. (*a*) P.R. Lutz. Chem. Rev. **84**, 205 (1984); (*b*) D.K. Bates and M.W. Janes. J. Org. Chem. **43**, 3856 (1978); (*c*) J. Borgulya, R. Madeja, P. Fahrni, H.J. Hansen, H. Schmid, and R. Barner. Helv. Chim. Acta, 56 (1973); (*c*) K.C. Majumdar and S. Alam. J. Chem. Res. 281 (2006); (*d*) K.C. Majumdar and S.K. Chattopadhyay. Can. J. Chem. **84**, 469 (2006).
14. K.C. Majumdar and B.S. Thyagarajan. Int. J. Sulfur Chem. Part A, **2**, 67 (1972).
15. K.C. Majumdar and B.S. Thyagarajan. Int. J. Sulfur Chem. Part A, **2**, 93 (1972).
16. J.B. Hillard, K.V. Reddy, K.C. Majumdar, and B.S. Thyagarajan. J. Heterocycl. Chem. **11**, 369 (1974).

© 2006 NRC Canada

Electrocatalytic hydrogenation of catechol on Rh–Al_2O_3 in different media — pH-Dependent reduction mechanism for intermediate formation

Anne Brisach-Wittmeyer, Nicolas-Alexandre Bouchard, Raymond Breault, and Hugues Ménard

Abstract: The electrocatalytic hydrogenation of catechol was carried out in aqueous media in different pH ranges with Rh–Al_2O_3 powder catalyst. The reactions were conducted in an H-cell used as a dynamic cell, with a reticulated vitreous carbon electrode in contact with the catalyst powder as the working electrode. It was shown that the final product is 1,2-cyclohexanediol (cis and trans isomers) and that several intermediates are detected depending on the pH of the solution. Different media, from pH 5 to 13, were studied. One of the intermediates is 1,2-cyclohexanedione, detected at all pH values. The other is 2-hydroxycyclohexan-1-one, only observed at pH ≤ 7. To determine the mechanism of the reactions involved, the electrocatalytic hydrogenation of these intermediates to form the final 1,2-cyclohexanediol product was also conducted, and their UV spectroscopy and cyclic voltammetry data recorded. The influence of the nature of the solution was screened by measuring the Henry constant of each molecule.

Key words: electrocatalytic hydrogenation of catechol, pH-dependent reduction mechanism, UV–vis spectroscopy, cyclic voltammetry, Henry constants.

Résumé : L'hydrogénation électrocatalytique du catéchol a été menée en milieu aqueux à différents pH sur des poudres de Rh–Al_2O_3 comme catalyseur. Les réactions ont été réalisées dans une cellule en H utilisée en mode dynamique avec des électrodes de carbone vitreux réticulé en contact avec le catalyseur comme électrodes de travail. Il a été montré que le produit final est le 1,2-cyclohexanediol (isomers cis et trans) et que plusieurs intermédiaires sont détectés dépendamment du pH de la solution. Divers milieux de pH 5 à 13 ont été étudiés. Un des intermédiaires est la 1,2-cyclohexanedione, formée quel que soit le pH. L'autre est la 2-hydroxycyclohexan-1-one, uniquement observée à pH ≤ 7. Afin de déterminer le mécanisme des réactions impliquées, l'hydrogénation électrocatalytique de ces intermédiaires en 1,2-cyclohexanediol a été réalisée ainsi que la spectroscopie UV-visible et la voltampérométrie cyclique. L'influence de la nature du milieu a été évaluée en mesurant les constantes de Henry pour chacune de ces molécules.

Mots clés : hydrogénation électrocatalytique du catéchol, mécanisme de réduction dépendant du pH, spectroscopie UV–vis, voltampérométrie cyclique, constantes de Henry.

Introduction

Catechol is known to inhibit gibbsite precipitation (1–4). The scope of this work was to investigate the use of electrocatalytic hydrogenation (ECH) (Fig. 1, I) to transform catechol into an inactive molecule by hydrogenation of its aromatic ring. Since gibbsite crystal growth occurs in alkaline media in the Bayer process, the hydrogenation of catechol at high pH was of particular interest.

Received 20 August 2006. Accepted 2 November 2006. Published on the NRC Research Press Web site at http://canjchem.nrc.ca on 6 January 2007.

A. Brisach-Wittmeyer, N.-A. Bouchard, and H. Ménard.[1] Laboratoire de Science des Matériaux d'Électrodes, Université de Sherbrooke, Sherbrooke, QC J1K 2R1, Canada.
R. Breault. Alcan International Limited, Arvida Research and Development Centre, Jonquière, QC G7S 4K8, Canada.

[1]Corresponding author (e-mail: Hugues.Menard@USherbrooke.ca).

Several papers have been devoted to the electrocatalytic hydrogenation of phenol (5–12). It was shown that the addition of six electrons per molecule leads to cyclohexanol via cyclohexanone as intermediate product. It was also shown that catechol, a benzyl group bearing two adjacent hydroxyl groups, can be reduced to 1,2-cyclohexanediol (Fig.1, IV) in H_3BO_3 on Rh–Al_2O_3 (13). Similar electrochemical techniques to the one used for ECH of phenol (14) and catechol (13) were used here with various catalysts. The highest efficiency was observed with 5% Rh–Al_2O_3 as the catalyst, and all the results presented here were obtained using this catalyst.

In sodium hydroxide (1 mol/L), good conversion rates from catechol to 1,2-cyclohexanediol by total reduction with six electrons were obtained in this work, and the formation of the 1,2-cyclohexanedione (Fig. 1, II) intermediate was detected. However, the final molecule presented two forms, cis and trans (Fig. 1, IVa and IVb). This suggested that the catechol hydrogenation occurred via more than one intermediate. To study its mechanism, the ECH of catechol was investigated at different pH values to try to detect intermedi-

 doi:10.1139/V06-169 © 2006 NRC Canada

Fig. 1. Proposed ECH mechanism for the reduction of catechol into 1,2-cyclohexanediol depending on the pH of the media.

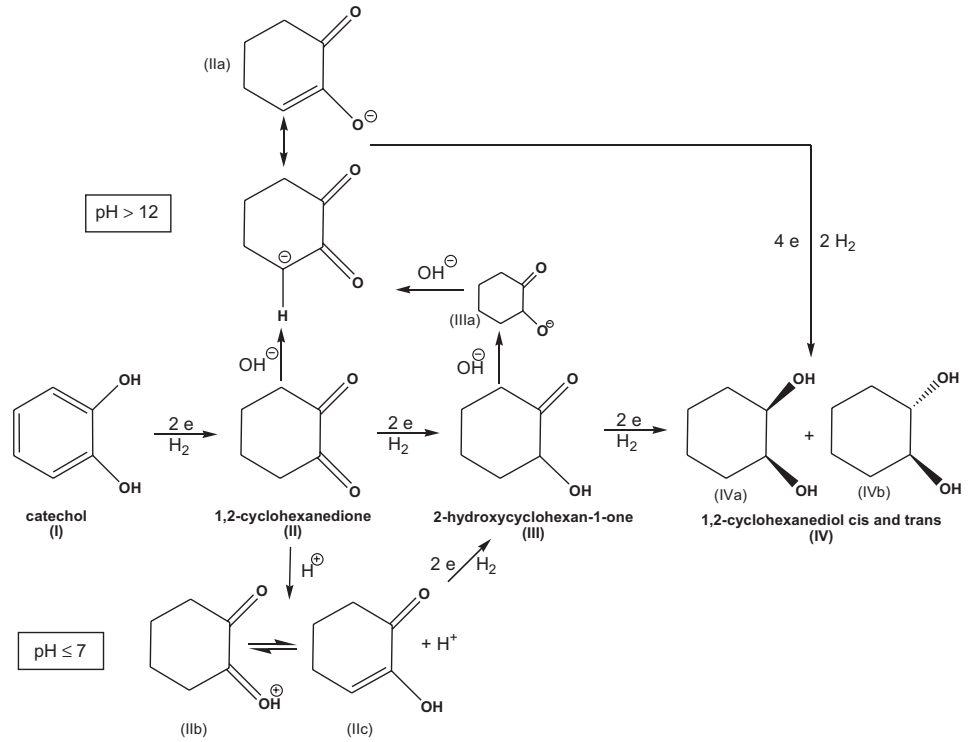
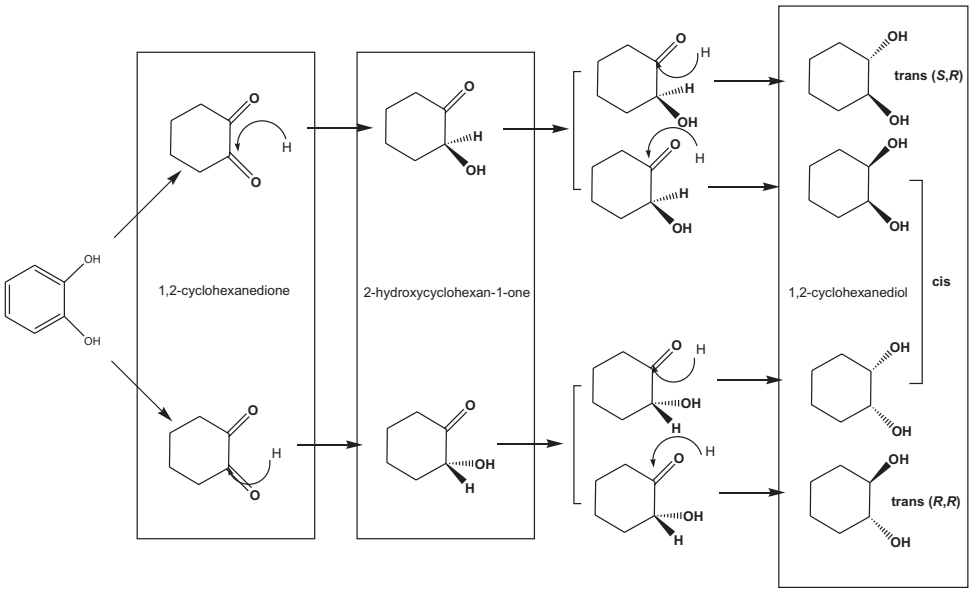


Fig. 2. Possible pathway for the formation of the different isomers of 1,2-cyclohexanediol. For clarity, only the protons involved in the formation of the isomers are indicated.



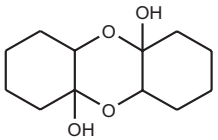
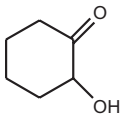
ates as performed in earlier work on molecules such as 2-methyl-1-hydroxybenzene (15). The influence of solution pH on the reactivity appears to be of great importance (16) and was also investigated. Three pH zones were investigated: pH 13 with NaOH (1 mol/L), pH 7 with phosphate buffer (0.5 mol/L), and pH 5 with acetate buffer (0.5 mol/L).

An additional intermediate was observed in media with pH ≤ 7 and was identified as 2-hydroxycyclohexan-1-one (Fig. 1, III). Its presence explains the formation of cis-trans, (*S*-*R*), and (*R*-*R*) isomers of 1,2-cyclohexanediol (17) as depicted in Fig. 2. To determine the role of reaction kinetics in the different media, the direct ECH of 1,2-cyclohexanone and 2-hydroxycyclohexan-1-one into 1,2-cyclohexanediol was also studied.

The stability of these intermediates was examined using UV absorption spectra (18, 19) and voltammetric data (18, 20–22) in the different media. To understand the influence of the solution medium on reactivity, a newly improved method developed by our group (23, 24) was used to determine the adsorption strength by evaluating Henry constants.

© 2006 NRC Canada

Table 1. Characterization of 2-hydrocyclohexan 1-one (monomer and dimer) by IR spectroscopy.

		Wave number (cm^{-1})	
Phase	Product	Commercial	Formed
Solid		OH stretch: 3376, 3335; C–H stretch: 2927, 2857; CH_2 deformation: 1454; C–O–C stretch: 1258, 1221; C–OH stretch: 1093; C–C stretch: 942.	OH stretch: 3600, 3000; C–H stretch: 2933, 2873; CH_2 deformation: 1454; C–OH stretch: 1117; C–C stretch: 956.
Liquid (in 0.001 mol/L)		OH stretch: 3400; C–H stretch: 2844; C=O stretch: 1701; C–OH stretch: 1097; C–C stretch: 810.	OH and C–H stretch: unreadable; C=O stretch: 1662; C–OH stretch: 1260; C–C stretch: 805.

Experimental

Electrolysis

The electrolysis was carried out in a two-compartment glass H-cell having a Nafion-117 membrane (Dupont de Nemours) as the separator. The cathodic compartment was filled with 28 mL of NaOH (1 mol/L), phosphate buffer (0.5 mol/L of KH_2PO_4 and 10 mol/L of NaOH) or acetate buffer (0.5 mol/L of CH_3COOH and 10 mol/L of NaOH). Catalyst powder (5% Rh–Al_2O_3, 200 mg) was added to the catholyte. The solution was stirred to force the catalyst to pass through the RVC electrode. A N_2 flow was maintained over the solution. The anodic compartment was filled with the corresponding electrolyte; the counter electrode was a platinum grid. The working electrode was conditioned before starting the ECH process by polarization with 50 C. The chemisorbed hydrogen radicals formed during this time are immediately usable by unsaturated molecules, so some efficiencies may depend on the ECH mechanism and on the quantity of hydrogen available. After polarization, 2 mL of catechol (0.15 mol/L), 1,2-cyclohexanedione (0.15 mol/L) or 2-hydroxycyclohexan-1-one (0.05 mol/L) solution in water was added to the catholyte, giving a total volume of 30 mL. The electrocatalytic hydrogenation was performed under galvanostatic control (i = 10 or 5 mA) using an EG&G Princeton Avanced Research power supply model 273. The commercial 5% Rh–Al_2O_3 powder was purchased from Alfa Aesar and used as received.

During the ECH reaction, aliquots of 200 μL were withdrawn from the catholyte, acidified to pH 5 with HCl (2 mol/L) and filtered with Millipore filters (0.45 μm). The solution analyses were performed on an HPLC Agilent 1100 series liquid chromatograph equipped with a model G1362 refractive index detector.

UV spectroscopy and cyclic voltammetry

UV–vis spectra were recorded on an Agilent 845x UV spectrophotometer. Voltammetric measurements were performed under a nitrogen atmosphere at RT in a three-electrode cell connected to a potentio–galvanostat (EG&G Princeton Avanced Research model 273). Data were quantified on a personal computer using Echem software, version 4.23 (eDAQ Inc., Colorado Springs, Colorado). The working electrode was a hanging mercury drop, the auxiliary electrode was a platinum grid, and the reference electrode was a saturated calomel electrode (SCE).

Quantification

The 1,2-cyclohexanediol cis and trans isomers were quantified by HPLC analysis and compared with available commercial molecules. With this technique, it was not possible to distinguish the (*S*-*R*) and (*R*-*R*) stereoisomers. All other molecules involved in the ECH process (catechol, 1,2-cyclohexanedione, and 2-hydroxycyclohexan-1-one) were analysed by comparison with commercially available molecules.

Henry's Law constants (k_H)

The chromatographic parameters were obtained using an Agilent 1100 series HPLC equipped with a diode array detector (G1315B). The dead volume τ_0 was determined by injecting 5 μL of deuterium oxide (D_2O). The mobile phases were 0.01 mol/L NaOH, 0.05 mol/L phosphate buffer or 0.05 mol/L acetate buffer, filtered through 0.45 μm Milipore filters. The flow rate was 1.00 mL/min. The columns (15 cm) were filled with the sieved Al_2O_3, whose average particle size was between 25 and 35 μm. The parameters used to determine the dynamic adsorption isotherms were collected from the HPLC elution chromatograph and the Henry constants were calculated from the well-known equation, $Q_e = k_H C_e$, according to previous works (23, 24).

Characterization

The isolated 2-hydroxycyclohexan-1-one intermediate was characterized by comparison with the commercially obtained dimer using IR spectroscopy (Bomen MB 104 spectrometer in HATR mode) and Mass Spectroscopy (electrospray MS Agilent G1946A). Solid IR spectrospcopy (Table 1) showed that 2-hydroxycyclohexan-1-one is dimeric in its solid state, proved by the absence of a C=O stretch (25). Liquid-phase IR spectra under the ECH conditions with NaOH in solution showed that the 2-hydroxycyclohexan-1-one dimer reforms to the monomer under these conditions. The MS experiments confirmed these assumptions. Previous synthesis work showed that the 2-hydroxycyclohexan-1-one monomer is liquid at RT whereas the dimer is solid (26–28), and that the monomer easily dimerizes at RT (29).

Results

Preliminary remarks

As demonstrated by the reaction mechanism shown in Fig. 1, 6 F (faraday where 1 F = 96 495.7 C) are necessary to totally hydrogenate one mole of catechol. In the same

© 2006 NRC Canada

way, it takes 4 F to transform one mole of 1,2-cyclohexanedione into one mole of 1,2-cyclohexanediol and 2 F for the conversion of one mole of 2-hydroxycyclohexan-1-one. Under the conditions used in the present study, it was calculated that it takes 174 C (Coulombs) for the total conversion of 3.00×10^{-4} mol of catechol, 116 C for 3.00×10^{-4} mol of 1,2-cyclohexanedione, and 19 C for 1.00×10^{-4} mol of (i.e., 58 C for 3.00×10^{-4} mol) 2-hydroxycyclohexan-1-one. The relative efficiencies of the ECH processes in the different media were evaluated by comparing the residual concentration of the starting material at the designated value of the current.

In addition, since the charge used is a function of time ($Q_{(C)} = i_{(A)} \times t_{(s)}$) and the applied current is a constant, the slopes of the curves ($\chi = f(Q)$) have been used to indicate the reaction rate in the ECH processes.

ECH of catechol at pH 13

The electrochemical hydrogenation of catechol in an alkaline medium was conducted in NaOH (1 mol/L). The initial and final pH values were 13. After 6 F (Fig. 3*a*), 68% of the catechol was reduced. The intermediate product is 1,2-cyclohexanedione. The low quantity detected indicates that it is a transient species, and that it is not necessary to transform all the catechol into 1,2-cyclohexanedione to form the final product.

ECH of catechol at pH 7

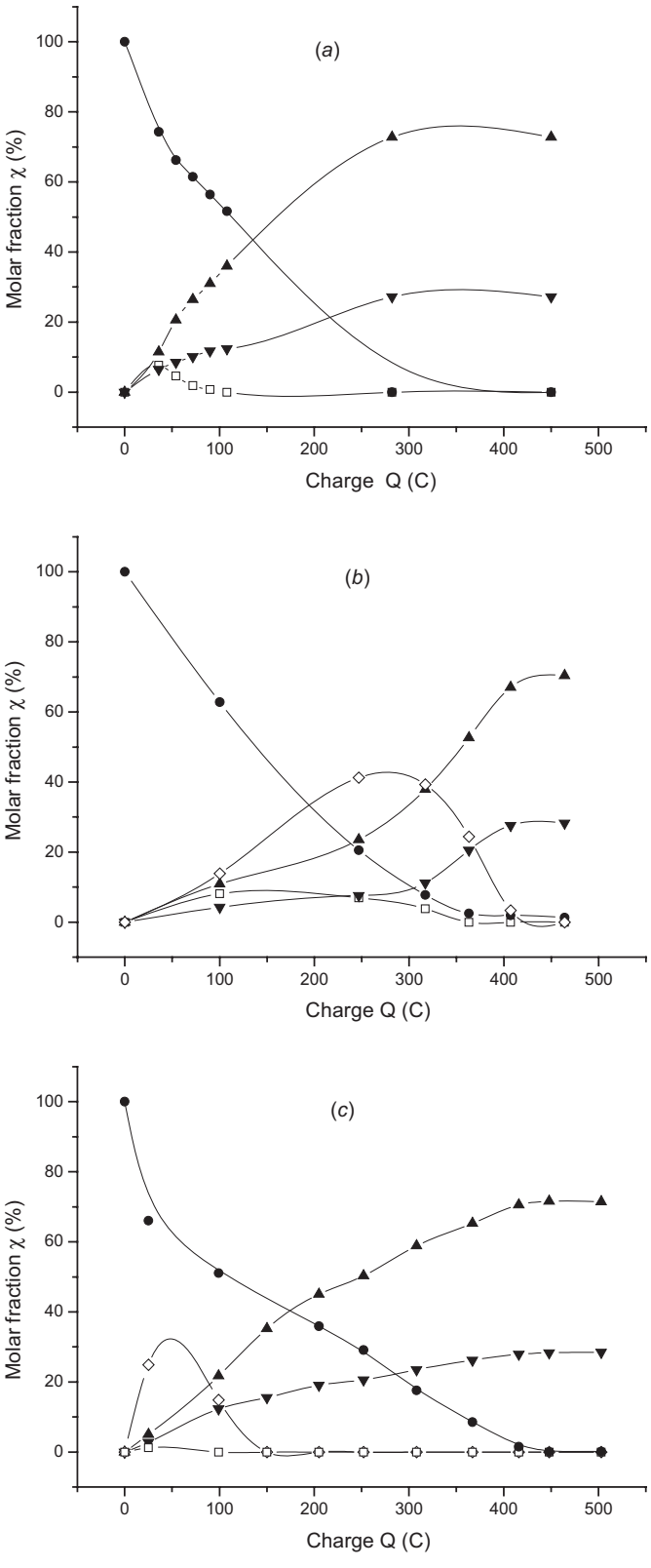
The electrochemical hydrogenation of catechol was conducted in phosphate buffer (0.5 mol/L) with the initial and final pH being 7. After 6 F were passed (Fig. 3*b*), 62% of the catechol was completely reduced. The intermediate products were 1,2-cyclohexanedione and 2-hydroxycyclohexan-1-one. Both molecules seemed to form together. That is, 2-hydroxycyclohexan-1-one forms immediately after 1,2-cyclohexanedione is produced without any separation of the two steps. The low quantities detected for 1,2-cyclohexanedione indicate that this product is a transient species with a very short lifetime. The formation and disappearance of 2-hydroxycyclohexan-1-one could clearly be detected, allowing preparation and characterization of this molecule. It was not necessary to transform all the catechol into 1,2-cyclohexanedione and 2-hydroxycyclohexan-1-one to form the final 1,2-cyclohexanediol product.

ECH of catechol at pH 5

The electrochemical hydrogenation of catechol was conducted in acetate buffer (0.5 mol/L); the initial and final pH values were 5. After a charge of 174 C was passed (Fig. 3*c*), 60% of the catechol had completely disappeared. The intermediate products were 1,2-cyclohexanedione (a trace detected) and 2-hydroxycyclohexan-1-one, as observed at pH 7. The low quantities of 1,2-cyclohexanedione detected indicate that this product is a transient species in this medium with a very short lifetime compared with that of 2-hydroxycyclohexan-1-one. In this case, 2-hydroxycyclohexan-1-one is rapidly formed and also very rapidly transformed into 1,2-cyclohexanediol. It can be assumed that 1,2-cyclohexanedione is also quickly converted to 2-hydroxycyclohexan-1-one.

The next main question was to determine if 1,2-cyclohexanedione effectively transforms into 2-hydroxycyclohexan-1-

Fig. 3. ECH of catechol (0.01 mol/L) in (*a*) NaOH (1 mol/L), (*b*) phosphate buffer (0.5 mol/L, pH 7), (*c*) acetate buffer (0.5 mol/L, pH 5). Working electrode: RVC 80 PPI packed with 5% $Rh–Al_2O_3$, polarized at 10 mA for 50 C; auxiliary electrode: Pt grid; i = 10 mA. Catechol (–●–); 1,2-cyclohexanedione (–□–); 2-hydroxycyclohexan-1-one (–◇–); *trans*-1,2-cyclohexanediol (–▼–); *cis*-1,2-cyclohexanediol (–▲–).



© 2006 NRC Canada

one in alkaline medium, as suggested by the formation of different isomers of 1,2-cyclohexanediol. It was also of interest to discover the role of formation kinetics for the different products in the global mechanism. The reactivity of 1,2-cyclohexanedione and 2-hydroxycyclohexan-1-one in the different media was therefore examined.

ECH of 1,2-cyclohexanedione and 2-hydroxycyclohexanone at pH 13

1,2-cyclohexanedione transforms into 2-hydroxycyclohexan-1-one and afterwards into *cis*- and *trans*-1,2-cyclohexanediol in NaOH (Fig. 4, I*a*). These reactions are very fast. It is obvious that all the 1,2-cyclohexanedione must be transformed into 2-hydroxycyclohexan-1-one to allow the formation of 1,2-cyclohexanediol, but this step takes place in a very short time (38 C). The reaction needs less than 2 F; this can be explained by the presence of reactive H adsorbed on the catalyst during the cathodic polarization of 50 C performed before electrolysis. In addition, 58% of 2-hydroxycyclohexan-1-one was consumed after 58 C (Fig. 4, I*a*).

ECH of 1,2-cyclohexanedione and 2-hydroxycyclohexanone at pH 7

At pH 7, 2-hydroxycyclohexan-1-one is also formed very rapidly, and 1,2-cyclohexanediol appears in solution when all 1,2-cyclohexanedione is consumed (Fig. 4, I*b*). Moreover, the reaction is very efficient, with 98% of the 1,2-cyclohexanedione transformed after 4 F. But in this case the transformation of 2-hydroxycyclohexan-1-one into 1,2-cyclohexanediol is much slower than in the other media (Fig. 4, II*a* compared with II*b* and II*c*). The direct transformation from 2-hydroxycyclohexan-1-one into 1,2-cyclohexanediol correlates with results observed for the direct reduction of 1,2-cyclohexanedione (Fig. 4, I*b* and II*b*), and its reduction when formed from catechol (Fig. 3*b*). That is, the reaction is very slow.

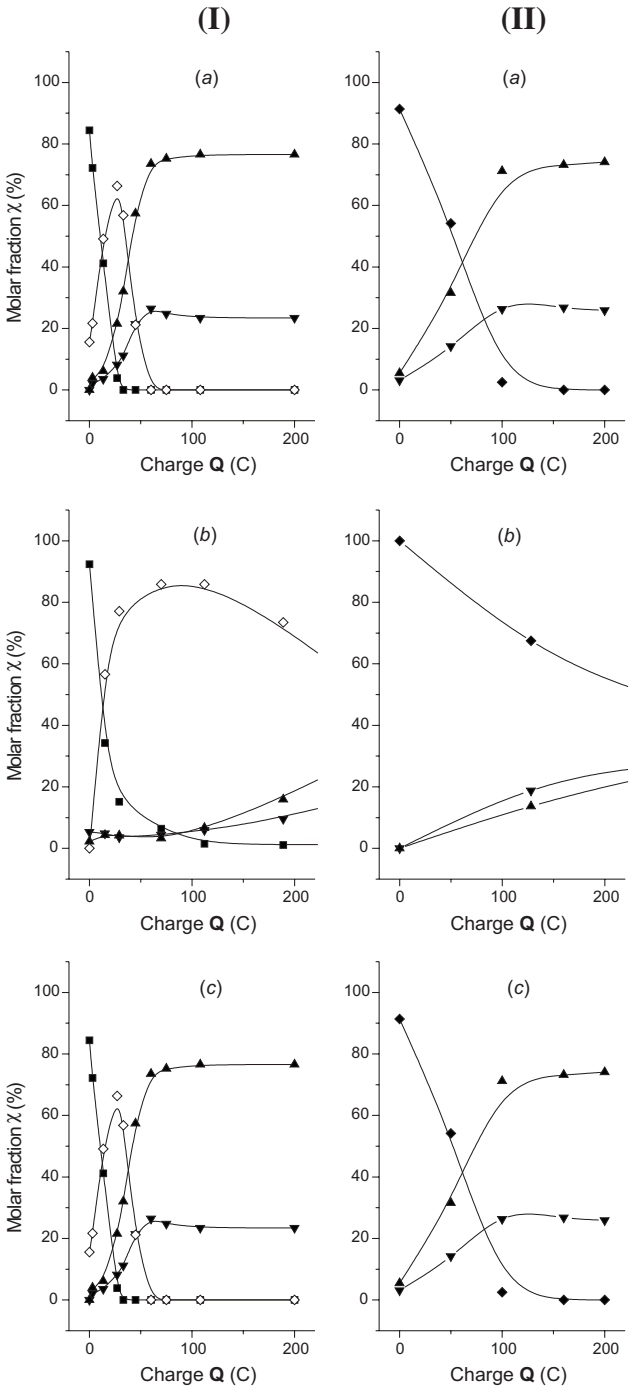
ECH of 1,2-cyclohexanedione and 2-hydroxycyclohexanone at pH 5

At pH 5, 2-hydroxycyclohexan-1-one is, once again, formed very rapidly from 1,2-cyclohexanedione, and 1,2-cyclohexanediol appears in solution when all 1,2-cyclohexanedione is consumed (Fig. 4, I*c*). The process is again very efficient with 99% of 1,2-cyclohexanedione consumed after 4 F. 2-Hydroxycyclohexan-1-one is also very rapidly hydrogenated into 1,2-cyclohexanediol in this process (Fig. 4, II*c*). Its direct transformation into 1,2-cyclohexanediol is the fastest among the experiments done on this molecule in the different media (Fig. 4, II*c* compared with II*b* and II*c*). It is particularly interesting to note that the reaction is much more efficient in an acetate than a phosphate buffer, considering that the pH conditions are comparable taking into account the pK_a of catechol (pK_{a1} = 9.45) (30).

UV spectroscopy

The UV spectra of 1,2-cyclohexanedione and 2-hydroxycyclohexan-1-one in the three media showed typical behaviour. In sodium hydroxide, both 1,2-cyclohexanedione and 2-hydroxycyclohexan-1-one present a band at 300 nm (Fig. 5) that corresponds to carbanion-enolate (Fig. 1, IIa) (18). In phosphate and acetate buffers, i.e., at pH ≤ 7, 1,2-cyclohexanedione exibits a band near 260 nm corresponding to its protonated form (Fig. 1, IIb) in equilibrium with the

Fig. 4. ECH of (I) 1,2-cyclohexanedione (0.01 mol/L) and (II) 2-hydrocyclohexan-1-one (0.0013 mol/L) in (*a*) NaOH (1 mol/L), (*b*) phosphate buffer (0.5 mol/L), (*c*) acetate buffer (0.5 mol/L). Working electrode: RVC 80 PPI packed with 5% Rh–Al_2O_3, polarized at 5 mA for 50 C; auxiliary electrode: Pt grid; i = 5 mA. 1,2-Cyclohexanedione (–■–); 2-hydroxycyclohexan-1-one (I) (–◇–) or 2-hydroxycyclohexan-1-one (II) (–◆–); *trans*-1,2-cyclohexanediol (–▼–); *cis*-1,2-cyclohexanediol (–▲–).



© 2006 NRC Canada

Table 2. Henry constants of catechol, 1,2-cyclohexanedione, 2-hydrocyclohexan-1-one and 1,2-cyclohexanediol in NaOH (0.01 mol/L), phosphate buffer (0.05 mol/L), and acetate buffer (0.05 mol/L).

	NaOH (±0.01)	Phosphate buffer (±0.01)	Acetate buffer (±0.01)
Catechol	0.12	0.12	7.14
1,2-Cyclohexanedione	0	0.01	0.40
2-Hydroxycyclohexan-1-one	0	0	0.40
1,2-Cyclohexanediol	—	—	0.07

Note: All values in (L g^{-1}). The Henry constants for 1,2-cyclohexanediol in sodium hydroxide and phosphate buffer could not be determined because of the detection limit of the RID detector used.

Fig. 5. UV spectra of 1,2-cyclohexanedione and 2-hydroxycyclohexan-1-one respectively in, NaOH, pH 13 (—) and (—); phosphate buffer, pH 7 (——) and (——); acetate buffer, pH 5 (–···) and (–···).

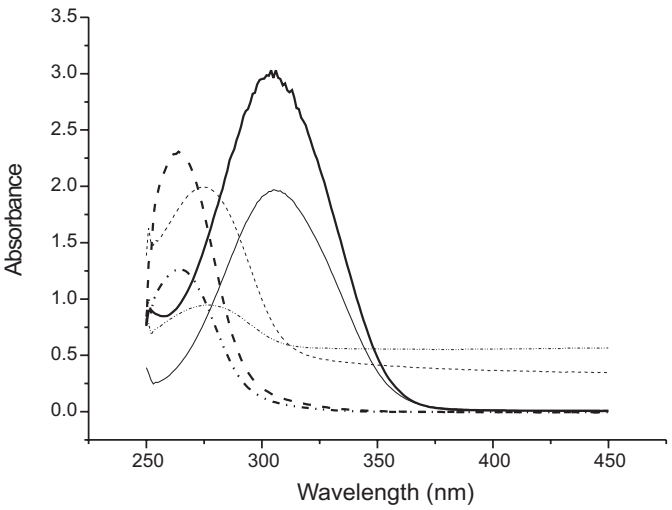
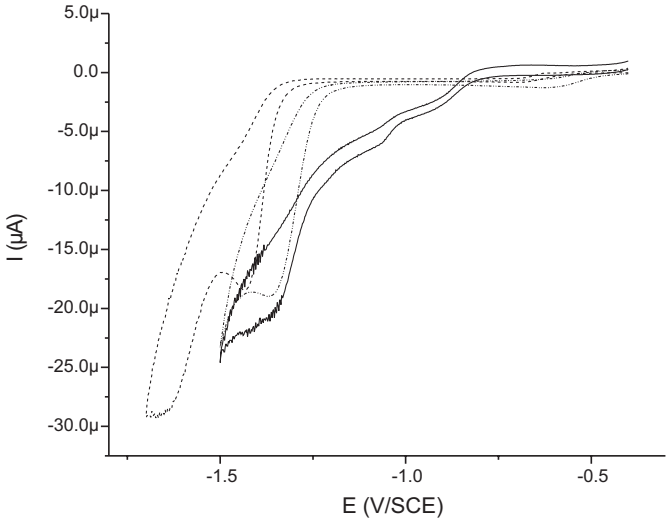


Fig. 6. Voltammetric curves of 1,2-cyclohexanedione in NaOH, pH 13 (—), phosphate buffer, pH 7 (——), and acetate buffer, pH 5 (–···). Working electrode : Hg; auxiliary electrode: Pt grid; reference electrode: Ag–AgCl. Scan rate: 100 mV s^{-1}.



enol form (Fig. 1, IIc) in solution (18). 2-Hydroxycyclohexan-1-one shows a band near 270 nm. The difference of 10 nm between the enol forms of 1,2-cyclohexanedione (Fig. 1, IIc) and 2-hydroxycyclohexan-1-one (Fig. 1, III) could be explained by the slight difference in their structure (Fig. 1).

Cyclic voltammetry

Because of the low solubility of 2-hydroxycyclohexan-1-one in the solutions (in particular in acidic media), it was not feasible to record results for this product. However, the cyclic voltammetry curves of 1,2-cyclohexanedione recorded in the different media fit well with those reported in the literature (Fig. 6) (18). In sodium hydroxide solutions, three reduction waves were observed at –0.81, –1.05, and –1.25 V/SCE. The first and second waves correspond to electron transfers onto 1,2-cyclohexanedione, whereas the third is a reduction process occurring onto the enol form (Fig. 1, IIc). In the phosphate buffer, two reduction waves were observed at –1.39 and –1.59 V/SCE, corresponding to electron transfers onto the protonated form (Fig. 1, IIb) and the enol form (Fig. 1, IIc) in solution equilibrium. In the acetate buffer, only one wave was observed at –1.30 V/SCE, as expected for the reduction of the protonated form (Fig. 1, IIb). All the reported electron transfers were irreversible.

Henry constants

The influence of the bulk chemical nature on the adsorption of the intermediates onto the catalyst surface was investigated by measuring the Henry constants (Table 2). These values, given in L g^{-1}, reflect adsorption of the target molecule on a given support for a given eluent.

It was observed that catechol is most highly adsorbed, whatever the solvent, whereas 1,2-cyclohexanediol is the least adsorbed among the products (Table 2). The adsorption propensity of 1,2-cyclohexanedione and 2-hydroxycyclohexan-1-one follows the order, acetate buffer > phosphate buffer > sodium hydroxide. The medium having the highest adsorption (acetate buffer) also shows the fastest reduction of 2-hydroxycyclohexan-1-one into 1,2-cyclohexanediol (Fig. 4, II*c*).

Discussion

It was clearly shown that the final product of the total ECH of catechol consists of two forms of 1,2-cyclohexanediol: the cis and the trans isomers. This result

© 2006 NRC Canada

indicates that the catechol is transformed into 1,2-cyclohexanedione and then is hydrogenated into 2-hydroxycyclohexan-1-one. 2-Hydroxycyclohexan-1-one gives the cis and trans isomers, regardless of the medium (Fig. 2). On the contrary, when varying the medium, changes in the transformation rate of 2-hydroxycyclohexan-1-one were observed. In sodium hydroxide, only 1,2-cyclohexanedione was detected, whereas in media with pH ≤ 7, 2-hydroxycyclohexan-1-one was detected, although 1,2-cyclohexanedione was poorly observed because of its rapid hydrogenation. These differences are explained by the pH variations. Indeed, the pK_a of 1,2-cyclohexanedione is equal to 9.7 (22), so in NaOH (1 mol/L, pH 13) the carbanion-enolate (Fig. 1, IIa) is easily formed from 1,2-cyclohexanedione and from 2-hydroxycyclohexan-1-one. However, when the ECH is conducted at pH ≤ 7, the enol (Fig. 1, IIc), with pK_a equal to 10.3 (22), is rapidly formed. Subsequently, it easily transforms into 2-hydroxycyclohexan-1-one (31), which remains the most stable molecule in solution in these pH ranges (Fig. 1). These results are supported by the UV spectroscopic data (Fig. 5), which show the highest stability for carbanion-enolate (Fig. 1, IIa) at pH 13. At pH ≤ 7, the coexistence of two species (with enol (Fig. 1, IIc) clearly identified) was observed.

The cyclic voltammetry data for 1,2-cyclohexanedione (Fig. 6) are consistent with the UV results (Fig. 5) for pH ≤ 7, as they show in these media that the reducible species are the protonated and enol intermediates (Fig. 1, IIb and IIc). It is also clear that at pH 5, the most stable species in solution is the enol form (Fig. 1, IIc). In sodium hydroxide solutions, both the neutral (Fig. 1, II) and the anionic form (Fig. 1, IIa) can be reduced. All these observations fit well with the ECH results.

The kinetics of the first step in the electrohydrogenation of catechol indicate that the process is pH-independent, as its efficiency is similar in all the media. In all cases, 35% of catechol remains in solution above 200 C. Then, the reduction mechanism kinetics are governed by the formation of the intermediates. At pH 13, the first hydrogenation step of catechol is as fast as the conversion of the intermediate 1,2-cyclohexanedione (or its stable form IIa in Fig. 1), and this intermediate is consumed as soon as it is produced to form 1,2-cyclohexanediol directly. At pH ≤ 7, the transformation of catechol into the enol form (Fig. 1, IIc), then into 2-hydroxycyclohexan-1-one seems to be faster than that of 2-hydroxycyclohexan-1-one into 1,2-cyclohexanediol, because a large quantity of this intermediate can be detected. This difference in kinetics can also be explained by the pH of the solution. Indeed, at pH ≤ 7, the most stable form of 1,2-cyclohexanedione is the enol form (Fig. 1, IIc) (or the protonated form IIb), which can react very fast to give 2-hydroxycyclohexan-1-one (31).

However, great variations are observed in the kinetics of intermediate formation between phosphate and acetate buffers. These are explained by the difference in adsorption in these media. Comparing the Henry constants (Table 2), it is remarkable that the intermediates 1,2-cyclohexanedione and 2-hydroxycyclohexan-1-one are more highly adsorbed on alumina covered by acetate than by phosphate. Their hydrogenation is also favoured in the acetate media (Fig. 4). This effect has been pointed out and further explained in recent papers (32, 33).

Conclusions

The work presented in this paper clearly shows that catechol can be hydrogenated by an electrochemical process into 1,2-cyclohexanediol, particularly at high pH values. The pH of the electrolyte plays an important role in the ECH process. It has been demonstrated that the rate of the primary conversion of catechol into 1,2-cyclohexanedione is independent of the pH of the media, although pK_{a1} of the catechol is reached in the basic medium. However, the pH of the medium plays a key role in the conversion mechanism of the identified intermediates 1,2-cyclohexanedione and 2-hydroxycyclohexan-1-one. In some cases (phosphate and acetate buffers, pH ≤ 7), it was even possible to isolate one of the intermediates (2-hydroxycyclohexan-1-one). Its formation explains the cis–trans and the (*S*-*R*) and (*R*-*R*) forms of the final product 1,2-cyclohexanediol. UV spectroscopy and cyclic voltammetry enable the determination of which species coexist in the different media. It has also been demonstrated that adsorption of the different molecules on the catalyst support depends on the nature of the bulk solution. Hydrogenation of the intermediates is fastest in acetate buffer coinciding with the medium where they adsorb most.

Acknowledgements

This work was financially supported by Alcan International Limited, the Natural and Engineering Research Council of Canada (NSERC), and the Lavoisier program (French Ministry of Foreign Affairs). The authors thank M. Lyndon Armstrong from Alcan International Limited for its collaboration and Mr. Alain Desponts from Université de Sherbrooke for the IR spectroscopy experiments.

References

1. L. Armstrong. Proceedings of the International Alumina Quality Workshop, Hunter Valley, Australia. 17–21 October 1993. 283 (1993).
2. L. Armstrong, J. Hunter, K. McCormick, and H. Warren. Light Met. 37 (1996).
3. F. Picard, D. Audet, H. Boily, and J. Larocque. Proceedings of the 6th International Alumina Quality Workshop, Brisbane, Australia. 8–13 September 2002. 46 (2002).
4. N.A. Bouchard, A. Brisach-Wittmeyer, R. Breault, and H. Ménard. J. Appl. Electrochem. In press.
5. L.L. Miller and L. Christensen. J. Org. Chem. 43, 2059 (1978).
6. K. Sasaki, A. Kunai, J. Harada, and S. Nakabori. Electrochim. Acta, **28**, 671 (1983).
7. K. Amouzegar and O. Savadogo. Electrochim. Acta, **39**, 557 (1994).
8. K. Amouzegar and O. Savadogo. J. Appl. Electrochem. **27**, 539 (1997).
9. K. Amouzegar and O. Savadogo. Electrochim. Acta, **43**, 503 (1998).
10. H. Ilikti, N. Rekik, and M. Thomalla. J. Appl. Electrochem. **32**, 603 (2002).
11. F. Laplante, L. Brossard, and H. Ménard. Can. J. Chem. **81**, 258 (2003).
12. A. Chagnes, F. Laplante, F. Kerdouss, P. Proulx, and H. Ménard. Can. J. Chem. **82**, 641 (2004).
13. H. Ménard, P. Dabo, A. Cyr, L. Brossard, and J. Lessard. Can. Patent CA 2273688, 4 June 1999.

© 2006 NRC Canada

14. F. Laplante, L. Brossard, and H. Ménard. Can. J. Chem. **81**, 258 (2003).
15. L.L. Miller and L. Christensen. J. Org. Chem. **43**, 2059 (1978).
16. M.A. Casadei and P. Proulx. Electrochim. Acta, **33**, 117 (1988).
17. P. Boutoute, G. Mousset, and H. Veschambre. New J. Chem. **22**, 247 (1998).
18. J.P. Segretario, N. Sleszynski, and P. Zuman. J. Electroanal. Chem. **214**, 259 (1986).
19. H.S. French and M.E.T. Holden. J. Am. Chem. Soc. **67**, 1239 (2006).
20. M.A. Zon and J.M.R. Mellado. J. Electroanal. Chem. **338**, 229 (1992).
21. M.R. Montoya, M.A. Zon, and J.M.R. Mellado. J. Electroanal. Chem. **353**, 217 (1993).
22. M.R. Montoya and J.M.R. Mellado. J. Electroanal. Chem. **371**, 215 (1994).
23. F. Laplante, N.A. Bouchard, P. Dubé, H. Ménard, and L. Brossard. Can. J. Chem. **81**, 1039 (2003).
24. N.A. Bouchard, R. Breault, F. Picard, Y. Chouinard, and H. Ménard. Light Met. 197 (2005).
25. M. Schulz, R. Kluge, L. Sivilai, and B. Kamm. Tetrahedron, **46**, 2371 (1990).
26. P.D. Bartlett and R.H. Rosenwald. J. Am. Chem. Soc. **56**, 1990 (1934).
27. P.D. Bartlett and G.F. Woods. J. Am. Chem. Soc. **62**, 2933 (1940).
28. P. Boutoute, G. Mousset, and H. Veschambre. New J. Chem. **22**, 247 (1998).
29. T. Maki, K. Fukae, H. Harasawa, T. Ohishi, Y. Matsumura, and O. Onomura. Tetrahedron Lett. **39**, 651 (1998).
30. X. Ma, X. Zhang, J. Tan, W. Chen, and C. Wang. Acta Pharmacol. Sin. **25**, 950 (2004).
31. P. Dabo, B. Mahdavi, H. Menard, and J. Lessard. Electrochim. Acta, **42**, 1457 (1997).
32. M.C. Cirtiu, N.A. Bouchard, H.O. Hassani, P. Rowntree, and H. Ménard. Langmuir, **22**, 6414 (2006).
33. M.C. Cirtiu, A. Brisach-Wittmeyer, and H. Ménard. Catal. Commun. **8**, 751 (2001).

© 2006 NRC Canada

Dynamic NMR spectroscopy of 2,2′-dimethyl-1-picrylhydrazine in various solvents

K.C. Brown, M. El-Bermani, Y. Upadrashta, and J.A. Weil

Abstract: We have studied the ^{1}H NMR spectra of 2,2′-dimethyl-1-(2,4,6-trinitrophenyl)hydrazine at 300 and 500 MHz in seven liquid solvents, with a view to learning details of the internal conformational changes taking place as a function of temperature and of the solvent. These molecules in liquid solution occur as interconverting enantiomorphic pairs (atropisomers). Advanced techniques for obtaining the correct activation energies and pseudo-thermodynamic parameters have been utilized, and these parameters are listed and discussed. Our results point to a transformation between the pair of atropisomers that is not quite as complicated as one might have encountered in that the solvent does not affect $\Delta G^{\ddagger}$ in any major fashion. Molecular orbital calculations clarified some of the chemical shifts observed for both ^{1}H and ^{13}C. One goal of this study was to enable a detailed comparison with similar results available for 2,2′-diphenyl-1-(2,4,6-trinitrophenyl)hydrazine.

Key words: dynamic NMR, dimethylpicrylhydrazine, hindered rotation, atropisomers, activation parameters.

Résumé : A fin de préciser les détails des changements conformationnels qui se produisent en fonction de la température et du solvant, on a étudié les spectres de résonance magnétique nucléaire du proton de la 2,2′-diméthyl-1-(2,4,6-trinitrophényl)hydrazine à 300 et 500 MHz, dans sept solvants liquides. En solution dans des liquides, ces molécules existent sous la forme de paires énantiomorphes (atropisomères) qui s'interconvertissent. On a utilisé des techniques avancées afin d'obtenir les énergies correctes d'activation et les paramètres pseudo-thermodynamiques qu'on rapporte et qu'on discute. Les résultats obtenus tendent à montrer qu'il se produit une transformation entre la paire d'atropisomères qui n'est pas tout à fait aussi compliquée que celle attendue; en effet, le solvant n'affecte pas le $\Delta G^{\ddagger}$ d'une façon importante. Des calculs d'orbitales moléculaires ont permis de clarifier quelques-uns des déplacements chimiques observés, tant pour le ^{1}H que pour le ^{13}C. Un des buts de ce travail était d'établir une comparaison détaillée avec des résultats semblables disponibles pour la 2,2′-diphényl-1-(2,4,6-trinitrophényl)hydrazine.

Mots clés : RMN dynamique, diméthylpicrylhydrazine, rotation empêchée, atropisomères, paramètres d'activation.

[Traduit par la Rédaction]

Introduction

The dynamic internal motions of organic amines have been a source of interest leading to numerous NMR spectroscopic studies since the beginnings of that research field in the 1950s. For instance, see the recent review by Bain (1). In particular, various substituted diacyl and diaryl-2,4,6-trinitrophenyl (picryl) hydrazines have yielded detailed information derived from thermal NMR studies (2–8). With these molecules, the NMR spectra of the protons 3 and 5 in the picryl ring have been used as fine probes for the internal conformational changes, in various solvents (4). Similar work has also been published utilizing the ^{13}C NMR spectra of the picryl carbon nuclei (6).

The molecule of interest in the present work, 2,2′-dimethyl-1-picrylhydrazine, is denoted as DMPH-H herein. The notation emphasizes the importance of the hydrazinic proton. This hydrazine was chosen in part to investigate the effect of size and internal steric interaction reduction in going from 2,2′-diphenyl (DPPH-H) to 2,2′-dimethyl hydrazines on the internal conformation rates and barrier energies. Figure 1 depicts the molecular structures of one of the pair of atropisomers of DMPH-H, as obtained from our recent X-ray diffraction studies (9).

The unique property of the molecule of prime interest herein is that the two nitro groups located at ring positions 2 and 6 have different orientations, one out-of-plane (phenyl) and the other (close to being) in-plane because of the H-bonding between hydrazinic nitrogen atom N1 and an oxygen ion on either nearby nitro group. The two non-superimposable enantiomers (atropisomers), which interchange dynamically and can be labeled with (*R*) and (*S*) chirality at N1, have equal energies. The planes of the two nitro groups are far from being orthogonal.

The stability of each DMPH-H molecule towards transforming to its conformer is of course the result of several

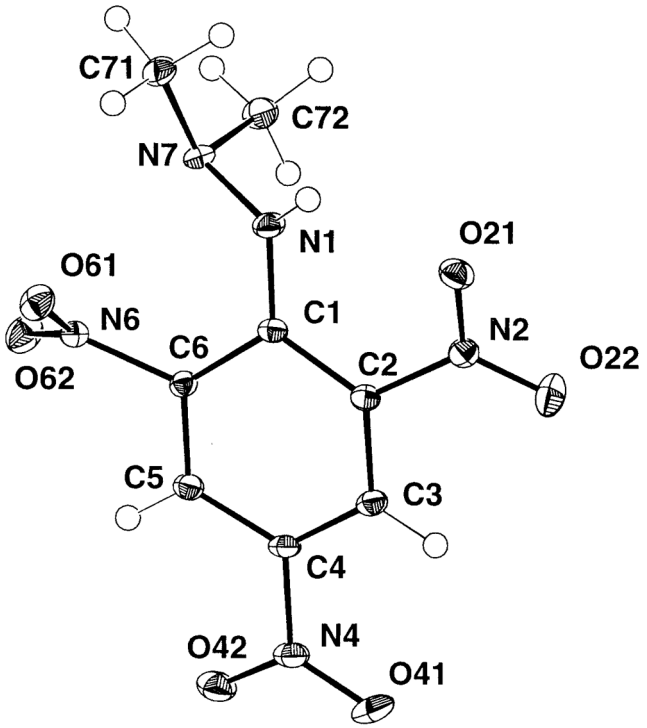
Received 08 June 2006. Accepted 26 October 2006. Published on the NRC Research Press Web site at http://canjchem.nrc.ca on 5 January 2007.

K.C. Brown, M. El-Bermani, Y. Upadrashta, and J.A. Weil.[1] Department of Chemistry, 110 Science Place, University of Saskatchewan, Saskatoon, SK S7N 5C9, Canada.

[1]Corresponding author (e-mail: john.weil@usask.ca).

 doi:10.1139/V06-172 © 2006 NRC Canada

Fig. 1. A stereoscopic view of the molecular structure of one of the atropisomers of DMPH-H (configuration (*R*) at N1), as obtained from X-ray diffraction data taken at 123(2) K.



factors. We believe that the presence of the hydrogen-bond between the N1 proton and an oxygen anion from the adjacent nitro group (on C2 or C6) is vital. Another important factor is the partial double-bond nature of the C1–N1 bond. This can be estimated qualitatively from the known C–N bond lengths via the empirical relation:

$$\mathrm{DB} = 100\ (D_s - D_x)/(D_s - D_d),$$

where D_s is a typical single-bond length (0.147 nm), D_d is a typical double-bond length estimated to be 0.127 nm, and D_x is the observed value of 0.134 nm (9). This yields DB ≈ 60%. The corresponding value of DB for DPPH-H is just slightly smaller, as D_x is 0.135 nm in that case (10).

More correctly, there are various possible isomers with asymmetric centres at the picryl hydrazinic nitrogen, local mirror-plane symmetry at the dimethyl nitrogen, and two situations for the out-of-plane nitro groups. Thus, 2^c isomers would exist, where c is the number of asymmetric centres in the molecule. Note that when transforming from (*R*) to (*S*) configuration at the hydrazinic nitrogen N1, other important atropisomer characteristics (the HN–O bond direction and nitro group planes) also switch.

Mathematical model of the dynamic lineshape

Previously, we have been quite successful in modeling the NMR absorption lineshapes over the whole range of temperatures in which the conformation effect displays itself, beginning from a low-temperature limit showing a sharp-lined AB quartet to a high-temperature limit of a single narrow peak (2, 4, 5, 11, 8, 12). All five limiting lines are Lorentzian in shape. The mathematical expression, $V_\tau(\nu)$, for the lineshape is a function of the mean first-order rate constant k_T, which equals the inverse of the mean lifetime τ_T, both varying with temperature. The relation, derived from density-matrix considerations (2, 13) is

$$[1] \qquad V_\tau = C\left(\frac{r_+ b_+ - s a_+}{a_+^{\,2} + b_+^{\,2}} + \frac{r_- b_- - s a_-}{a_-^{\,2} + b_-^{\,2}}\right)$$

$$[1a] \qquad a_\pm = 4\pi^2\,(\nu_o - \nu \pm J/2)^2 - (\tau^{-1} + \tau_2^{-1})^2 - \pi^2(\nu_A - \nu_B)^2 - \pi^2 J^2 + \tau^{-2}$$

$$[1b] \qquad b_\pm = 4\pi(\nu_o - \nu \pm J/2)\,(\tau^{-1} + \tau_2^{-1}) \mp 2\pi J\tau^{-1}$$

$$[1c] \qquad r_\pm = 2\pi(\nu_o - \nu \pm J)$$

$$[1d] \qquad s = 2\tau^{-1} + \tau_2^{-1}$$

Thus, the parameters required include: ν_o, τ_2, and coupling constant J. Note that the chemical shift difference $\nu_A - \nu_B$ between peaks A (picryl proton 3) and B (picryl proton 5) is proportional to the frequency ν_o of the excitation magnetic field. For the circumstances holding herein, the value of J (taken in frequency units, hertz) is small compared with $\nu_A - \nu_B$, and it affects V_τ less and less as τ (as well as T) increases. Parameter τ_2 is taken to be the inverse of πw, where w (alias $w_{1/2}$ and w_T) is the total width (in hertz) at half-height of the individual line for the limit $\tau \to \infty$, as well as of the single line occurring at $\tau = 0$. The question arises: Should the parameters $\nu_A - \nu_B$, τ_2, and J be taken as a function of temperature in fitting the spectral data to find the kinetic parameter $\tau = k^{-1}$? Unfortunately, a common assumption in the literature has been to take all three to be independent of T. We have investigated this point (see later) and found it to be important. We shall emphasize this functionality by writing the parameters as $\nu_A - \nu_B \equiv \delta_T$, and w_T. We assume that these do not depend on the mean lifetime τ of the molecular configuration.

The τ_T values obtained by lineshape fitting are used to attain tables of τ_T vs. T for each solvent. From these data, Arrhenius-type plots were constructed, from which (slope and intercept) the relevant pseudo-thermodynamic parameters $\Delta H^\ddagger$, $\Delta S^\ddagger$, and $\Delta G^\ddagger$ were estimated via equations given in ref. 5. Similarly, Eyring-type plots were made and used.

It is informative to define the coalescence of the line set to be the particular τ and also the particular T yielding the point at which the central minimum in function V_τ becomes a maximum. Note that this point depends on ν_o, so the choice of ν_o affects the feasibility of any given study (via the melting and boiling points of the solvent used) and also affects the potential accuracy of the dynamic analysis. The mean lifetime at coalescence has been shown to obey the relation

$$[2] \qquad \tau_{coa} = 4\tau_2\,[(1 + 8\sigma^2)^{1/2} - 1]^{-1}$$

where auxiliary parameter $\sigma \equiv \pi\tau_2\,\delta = \delta/w$ is dimensionless (8).

It has also been of some interest to enquire whether the area under the total absorption lineshape indeed is independent of τ_T. The actual experimental area is proportional to the concentration of molecules in the solution studied. As shown explicitly in ref. 8, contour integration of the normalized lineshape function, eq. [1] with $C = 1$, demonstrates that the area is indeed constant, independent of all the parameters,

© 2006 NRC Canada

with the value unity. Thus, the lineshapes at different temperatures can be directly compared (see later).

Experimental

The DMPH-H was prepared as described in ref. 9. Among the solvents used for the NMR studies were tetrachloromethane (carbon tetrachloride), trichloromethane-d_1 (chloroform-d_1), dichloromethane-d_2 (methylenechloride-d_2), toluene-d_8, ethanenitrile-d_3 (acetonitrile-d_1), 2-propanone-d_6 (acetone-d_6), and tetrahydrofuran-d_8 as well as *N*,*N*-dimethylformamide-d_7. These were used partly to reach down to ~200 K and also because they differ appreciably in H-bonding capability. Tetramethylsilane (TMS) was used as a line-position standard.

The ^{1}H NMR experiments were carried out on a Bruker AMX-300 spectrometer operating at 300.13 MHz and a Bruker Avance DRX System (located at the Saskatchewan Structural Sciences Centre on the University of Saskatchewan campus) working at 500.13 MHz. Some ^{13}C NMR experiments were also performed using the Avance machine. Our ^{1}H spin-lattice relaxation time (τ_1) measurements were carried out with the usual inversion-recovery pulse scheme (14), for DMPH-H at selected temperatures and in two solvents.

A computer program incorporating the above theoretical results (see eq. [1]) and others has been written by us and is called DYNAMAP. This program, written in the Maple V (Release 5) language, simulates the magnetic resonance spectra arising from a two-spin system (denoted by AB in NMR language). The program is equally applicable to frequency-swept and magnetic-field-swept spectra. DYNAMAP is available upon request, from us. The spectral scanning variable is the ordinary frequency ν, rather than the angular frequency $2\pi\nu$ that is sometimes used. A well-known computer program that can accomplish spectral simulation of the Master equation is available, and it is called DNMR (Windows version: WinDNMR) (5, 15). The results from DYNAMAP are consistent with it.

Much of the matching of the experimental and simulated spectra was done visually, using a Porta-Trace Model 1012–1 light-box (Gagne Inc., Johnson City, NY, USA) to superimpose and best-fit the pairs of spectra. This turned out to be sufficiently accurate and the most convenient method.

Fittings of the chemical-shift, linewidth, and rate-constant thermal data were accomplished by using the commercial scientific graphing program OriginLab, Version 7.5 (16) (see Figs. 2*a,* 3–5). This yields some indication of the data quality, for instance, χ (goodness of fit) and R (multiple correlation coefficient).

Some modest modeling calculations applying molecular orbital techniques, using Hartree–Fock bases performing geometry optimizations at the 6-311G* level, were carried out with the commercial program Spartan′04, Quantum Mechanics Module, Release 123 (17).

The various statistical curve fittings and error analyses performed were done in accordance with the treatise by Bevington (18), which also defines the symbols used.

NMR parameters

Of course, the computed line positions depend on the level of sophistication of the theory programmed. We found that the program Spartan yielded mediocre chemical-shift data when we utilized inadequate basis sets. A case in point is restricted Hartree–Fock calculations using basis 3-21G* (single-point) on a trial basis and following with 6-311G* (geometry-optimized) predictions. The latter yielded results far closer to our observed ^{1}H NMR data and thus proved to be quite informative, as discussed later in this paper. No J splittings were included.

Methyl protons

The six lines occurred within the chemical-shift range 2.2–2.9 ppm, relative to 0 for TMS. One methyl proton was predicted to be sufficiently close to an oxygen (see Fig. 1) so as to be shifted away from the other methyls and from TMS. Because we observed a single methyl peak, we concluded that in reality both methyl groups are rotating sufficiently to yield only a single line, even at our lower temperatures, experimentally at 2.10 ppm in acetonitrile-d_3 and 2.19 in chloroform-d_1. The average predicted by Spartan was 2.37 ppm.

Hydrazinic proton

The predicted location for the single peak was 7.23 ppm, while our data yielded 9.0 ppm for both of the previously mentioned solvents. Thus, less shielding should have been predicted by the theory.

Picryl protons

The chemical shift difference for the two picryl protons (labeled 3 and 5 in Fig. 1) was predicted to be 10.265 – 9.278 = 0.987 ppm, with an average center at 9.7725 ppm. Experimental work gave differences and centers at 0.66 and 8.90 ppm, respectively, for acetonitrile and 0.75 and 8.85 ppm for chloroform. The agreement is sufficiently good that the identification of proton 3 (peak A) as being adjacent to (between) two nitro groups "in-plane" with the picryl ring and proton 5 (peak B) as being adjacent to the one out-of-plane nitro group is meaningful (see Fig. 1). This identification was previously suggested by us (4). We note then that the existence of the chemical-shift difference is very successfully predicted by molecular orbital (MO) theory.

Turning now to the ^{13}C NMR spectra calculated via Spartan, we find that a pleasing consistency with experiment values is also attained. The shifts, relative to TMS, are found to be at δ 157.35, 129.39, 141.46, 131.96, 142.46, and 140.00 ppm, and they can be attributed to the ring carbons C (i = 1, …, 6; see Fig. 1). Two methyl peaks are predicted to occur at 42.87 and 41.62 ppm. These data are to be compared with the measured values.

We plan for further results, including energetics and molecular geometric configurations, obtained from Spartan and other programs to appear in a future publication, incorporating results both for several relevant hydrazines and their corresponding hydrazyl free radicals.

From the experimental picryl ^{1}H NMR spectra taken at temperatures sufficiently low that intramolecular motions are too slow to manifest themselves, one can arrive at the picryl chemical shifts δ 3–5 ppm, proton coupling constants J 3–5 Hz, and individual linewidths (full widths at half-height) w, using standard techniques, including lineshape fitting of the AB quartet. Such shift data are to be found in Table 1 of ref. 7

© 2006 NRC Canada

for the various solvents at one temperature (300 K).[2] Careful investigation has disclosed that δ 3–5 ppm and w depend quite appreciably on sample temperature and on the solvent, as discussed later.

Long-range coupling between the N–H and one picryl proton

The presence of a very small long-range (five-bond) coupling between the N–H and one (peak B) of the picryl protons is discernible (4) in some solvents (e.g., acetone) at low temperatures, but that did not appear to interfere with our dynamic measurements.

Measurements of τ_1

The inversion-recovery results show that the τ_1 values at lower temperatures (~240 K) are appreciably longer for the picryl protons than for the methyl protons of DMPH-H. We assume that this is explainable via the considerable rotational motion of the methyls even at the lowest temperatures used.

We discerned no dramatic shortening of the τ_1 times away from their typical (order of magnitude is 1–10 s) values for the picryl protons as the temperature was raised towards and through the coalescence region.

^{13}C NMR results

At a sufficiently low temperature (216 K) and in $CDCl_3$, DMPH-H molecules show six sharp picryl carbon peaks that can be attributed to C1–C6 at 141.90, 139.42, 127.02, 134.82, 126.20, and 131.62 ppm, respectively, as well as a single CH_3 peak at 48.05 ppm from TMS. At a higher T (320 K), C1 occurs at 141.42 ppm, C2 and C6 are broadened out of sight, C3 and C5 merge to give a sharp peak at 125.73 ppm, C4 at 135.84 ppm, and CH_3 at 48.68 ppm. These data are consistent with those reported for the analogous molecule diphenylpicrylhydrazine (DPPH-H) (19). At an intermediate temperature (e.g., 296 K), one finds C2 and C6 as a broad line at ~132 ppm and C3 and C5 as a broad doublet (close to coalescing) centered at 125.64 ppm. Modeling the latter lineshape using the previously mentioned formalism yields results consistent with the kinetic data derived from the ^{1}H measurements.

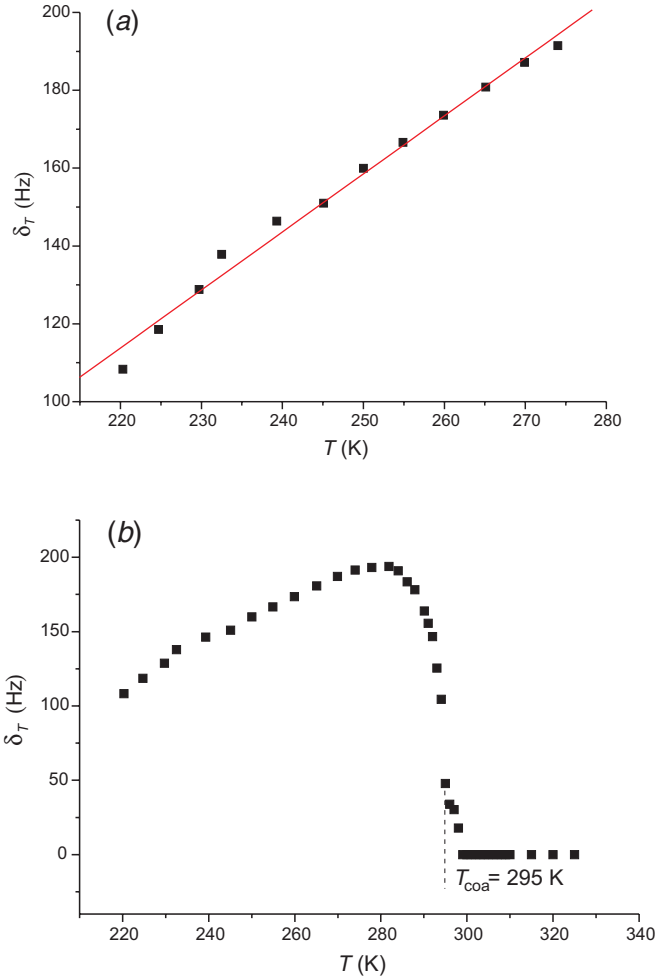
Thermal properties of the parameters

As previously discussed, parameters $\nu_A - \nu_B = \delta_T$ and $w_T = (\pi\ \tau_{2T})^{-1}$ depend on the temperature. The possible dependence of J on T is of no appreciable import for our work and will not be considered herein. We note recent papers (11, 12), other than the present one, which report tackling evaluation of such thermal effects in DNMR.

The picryl chemical-shift difference

We have prepared for the demands of the present work by studying the ^{1}H chemical shift difference δ_T, already discussed in a previous publication (7), as a function of solvent, using temperature ranges well below T_{coa}. We found a substantial dependence on temperature, which allowed extrapolation into the dynamic region for use in accurately evaluating the kinetic parameters obtained by fitting (e.g., see Fig. 2*b*, which shows the course of the AB splitting collapse with increasing temperature, and Fig. 2*a*, which shows only the portion of these data kept for shift extrapolation). Furthermore, the dependence of δ_T was found to correlate well with the Kamlet–Taft solvolytic parameter β, which measures the proton-acceptor basicity of the solvent. The slopes are positive for some solvents and negative for others (see ref. 7, Table 1). Thus, the shift parameter δ_T is markedly affected by the hydrogen-bonding capabilities of the solvent molecules.

Fig. 2. Temperature-dependent nominal chemical-shift difference between picryl proton lines A and B. The NMR spectra were measured at 500.13 MHz for DMPH-H in 2-propanone-d_6. (*a*) No. of data points shown is 12 (T range is limited to 220–280 K). (*b*) No. of data points is 42. Linear regression parameters: slope = 1.49 ± 0.05 Hz/K, intercept $\delta_{T=0}$ = –214 ± 13 Hz, SD = ±3.1 Hz, r = 0.9940.



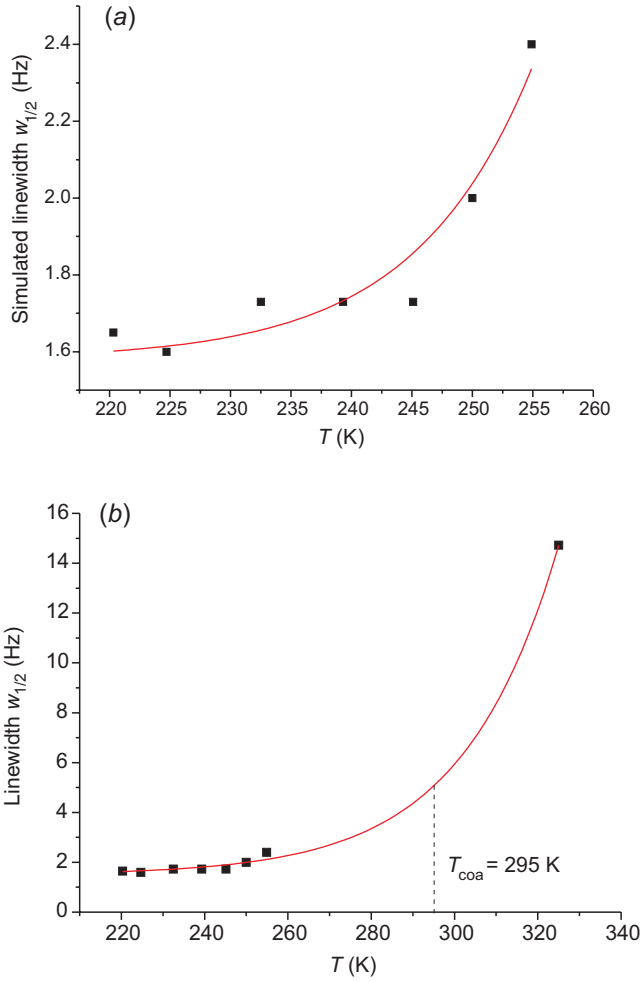
The inherent picryl-peak linewidths

The thermal variation of w_T has been estimated by lineshape fitting (using the program DYNAMAP) at a limited set of lowest liquid-phase temperatures (see Figs. 3*a* and 3*b*) as well as by measuring the linewidths (the full

[2] Note the difference in definition for the shift-difference symbol δ.

© 2006 NRC Canada

Fig. 3. Temperature-dependent linewidth curves $w_{1/2}$ (Hz). The NMR spectra were measured at 500.13 MHz for DMPH-H in 2-propanone-d_6. The curve fitting is to a first-degree exponential growth equation $w = w_e + w_f \exp(T/T_e)$. (*a*) No. of data points is 7, $w_e = 1.580 \pm 0.081$ Hz, $w_f = (3.320 \pm 31.29)10^{-12}$ Hz, $T_e = 9.75 \pm 3.50$ K, $\chi^2 = 0.0074$, $R^2 = 0.9370$. (*b*) High-T limit value included. No. of data points is 8, $w_e = 1.49 \pm 0.17$ Hz, $w_f = (9.14 \pm 16.8)10^{-6}$ Hz, $T_e = 22.9 \pm 3.0$ K, $\chi^2 = 0.0240$, $R^2 = 0.9992$.

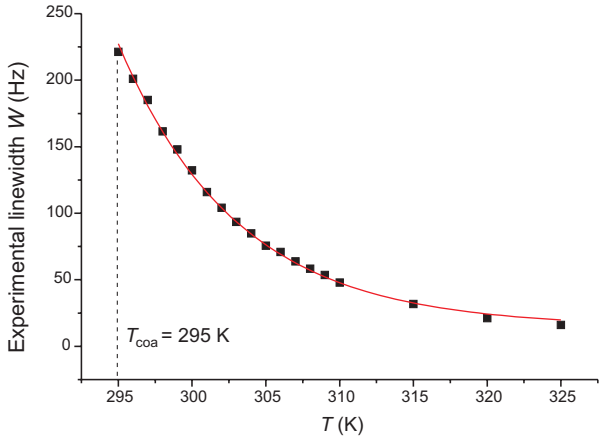


widths $W_T = \Delta\nu_{1/2}$ at half-height of the coalesced line) as a function of T to obtain the limiting high-T value W_∞ of widths W_T. As the mean lifetime τ moves towards zero, the limit W_∞ turns out to be just the (fixed) input parameter w.

In fact, the actual thermal data for W can be nicely represented by a descending exponential function, as shown in Fig. 4. One can derive an analytic functional expression obtained from eq. [1] for $W = \Delta\nu_{1/2}$ (see ref. 8 and eq. [4]).

The values of w_T actually used for the dynamic analysis were taken from a non-linear plot connecting the low-T values of w_T and limiting high-T value W_∞. Typically, w_T increased by a factor of ~5 with increasing temperature in the ranges of interest.

Fig. 4. Experimental temperature-dependent linewidth W (Hz). The NMR spectra were measured at 500.13 MHz for DMPH-H in 2-propanone-d_6. The curve fitting is to a first-degree exponential decay equation $W = W_\infty + W_F \exp(-T/T_E)$. No. of data points is 19. Parameters: $W_\infty = 14.72 \pm 2.19$ Hz, $W_F = (1.61 \pm 1.67)10^{18}$ Hz, $T_E = 8.07 \pm 0.23$ K, $\chi^2 = 7.2682$, $R^2 = 0.9983$.



Some typical values of widths w, W, and W_∞ are to be found in Tables 1 and 2 for the various solvents employed. Figures 3–4 give visual indications.

Sensitivity considerations

All the points given in Tables 3*a*–3*b* have been given equal weighting factors in arriving at the slopes and intercepts of the Arrhenius (Fig. 5) and Eyring plots. This is routine in the literature, using the equation

$$[3] \qquad \ln(k_T) = \ln(k_\infty) - \Delta E/(RT)$$

where the first-order rate constant is $k_T = 1/\tau_T$, and ΔE is the molar activation energy.

However, it is true that the sensitivity of the points to the value of τ_T derived at each temperature varies greatly, with maximum sensitivity in the region where line coalescence occurs. We have herein attempted to take this consideration into account to discover how important this might be.[3] Ideally, one would wish to utilize expressions for the first derivatives $dV_\tau/d\tau$ at each temperature for this purpose.

In Arrhenius and Eyring fittings, it is tempting to try to obtain useful weighting factors given by a normalized Gaussian distribution function

$$[4] \qquad \Sigma \equiv \exp\{-[(T^{-1} - T_{coa}^{-1})/T_o^{-1}]^2\}$$

centered at the coalescence temperature (see the discussion and Fig. 2 in ref. 8). However, the choice of the appropriate drop-off factor T_o is not obvious.

[3] Perhaps another tractable way to accomplish this is to computer-generate lineshapes using a set of appropriate input parameters, and do so at a convenient set of values of $k_T = 1/\tau_T$ chosen over the fitting range. Then, at each k_T value, increment and also decrement by some suitably small value δ_k, and find the difference in fit by subtracting the lineshape at k from that at $\pm\delta_k$. Such curve needs to be integrated somehow (remove negative contributions by shifting and taking the magnitude, …) to produce a number. Average these two numbers to yield a non-negative number Δ. This is a measure of the sensitivity but needs to be normalized by dividing it by the largest $= \Delta_{max}$ of the set to yield the desired sensitivity factors $\Sigma \equiv \Delta/\Delta_{max}$.

© 2006 NRC Canada

Table 1. Picryl ^{1}H NMR linewidths (measured at 500.13 MHz) for DMPH-H in various liquid solvents.

Solvent	mp [a] (K)	bp [a] (K)	Kamlet–Taft parameter β	Temperature [b] (K)	Linewidth [b] w (Hz)	Temperature [c] (K)	Linewidth [c] W (Hz)	Number of data points [d] (n_W) for $T \geq T_{coa}$	Limiting linewidth W_∞ [e] (Hz)
Tetrachloromethane	250	349	~0	256	3.65	314	59.6	6	61±14
Trichloromethane-d_1	209	335	~0	235	1.85	320	85.4	5	54±42
Dichloromethane-d_2	178	313	~0	220	2.20	___ [f]	___ [f]	___ [f]	___ [f]
Toluene-d_8	178	384	0.11	200	2.55	360	11.4	6	10.5±0.2
Ethanenitrile-d_3	231	352	0.31	240	1.51	320	38.0	7	27±7
2-Propanone-d_6	179	328	0.48	220	1.63	325	16.1	19	15±2
2-Propanone-d_6 [g]	179	328	0.48	230	2.03	325	9.6	5	6.7±0.9
Tetrahydrofuran-d_8	168	337	0.55	220	1.88	302	68.5	6	66±15
N,*N*-Dimethyl-formamide-d_7	213	425	0.69	230	2.52	340	7.89	12	6.1±0.6

[a]For the deuterated solvents when applicable.
[b]Lowest experimental temperature.
[c]Highest experimental temperature.
[d]n_W is the number of data points in the W vs. T plot.
[e]From exponential fitting of high-T data.
[f]Incomplete data since T_{coa} occurs above this solvent's boiling point for 500 MHz ^{1}H NMR.
[g]These spectra have been measured at 300.13 MHz.

We have constructed and tried out an intuitively derived and thus empirical relation

$$[5] \qquad T_o^{-1} = \left\{3n/[10(\ln(2))^{1/2}(n-1)]\right\}(T_1^{-1} - T_n^{-1}),$$

where $2([\ln(2)]^{1/2}T_o^{-1}$ is the full width at half height of the Gaussian (eq. [4]), and n is the total number of points used, e.g., in the Arrhenius plot of $\ln(k_T)$ vs. T^{-1} (Fig. 5). The Eyring plot of $\ln(k_T/T)$ vs. T^{-1} looks much the same as Fig. 5. Quantities T_1 and T_n are the temperatures of the first and last points used ($T_1 < T_n$).

Arrhenius and Eyring activation energies, and pseudo-thermodynamic parameters

The rate constants fitted (20) to the quite general semi-empirical relation

$$[6a] \qquad k_T \approx k_b\, h^{-1}T^\alpha \exp[-\Delta G^\ddagger(RT)^{-1}]$$

$$[6b] \qquad \approx k_b\, h^{-1}T^\alpha \exp(\Delta S^\ddagger R^{-1}) \exp[(-\Delta H^\ddagger (RT)^{-1}]$$

where k_b and h are the Boltzmann and Planck constants, and α is a small ($\alpha < 3$) non-negative number. In the simplified version termed the Arrhenius model,

$$[6c] \qquad k_T = k_\infty \exp[-\Delta E (RT)^{-1}]$$

where α is taken to be unity, and $\Delta E = \Delta H^\ddagger - RT$ (see ref. 5).

It is evident from Table 3*a* that the activation energy ΔE_{Ar} depends on the Kamlet–Taft β parameter, i.e., it is quite appreciably affected by hydrogen-bonding between the DMPH-H molecules and the solvent molecules. Similarly, the energy quantities $\Delta H^\ddagger$ and $T\Delta S^\ddagger$ depend on β in a linear fashion, as may be seen in Fig. 6 and Table 3*a*. These energies can be derived from our data by standard techniques (5).

We have, for good measure, also carried out analysis of some of our data using Eyring plots, $\ln(k_T/T)$ vs. $1/T$, as was done, for instance, by Olsen et al. (11). As seen from Tables 2 and 3, all the resulting activation energies ΔE_{Ey} (Table 3*b*) turn out to be approximately identical to their Arrhenius equivalents with much the same dependence on β. The Gibbs free activation energies $\Delta G_{Ey}^\ddagger$ too are very close to the $\Delta G_{Ar}^\ddagger$ values and independent of β.

Enthalpy–entropy cancellation

Previously, we have already observed that the Gibbs isothermal energy change

$$[7] \qquad \Delta G^\ddagger = \Delta H^\ddagger - T\Delta S^\ddagger$$

for the kinetic process is the most reliable among these three pseudo-thermodynamic quantities (5, 11, 13). Furthermore, it is close to constant for the picrylhydrazines so far investigated in various solvents. On the other hand, the enthalpy change $\Delta H^\ddagger$ and the entropy change $\Delta S^\ddagger$ vary appreciably with β (see Fig. 6) but in the same fashion. Thus, our systems appear to display cancellations of some of the active internal and environmental parameters, and thus, the errors in these, i.e., $\Delta H^\ddagger$ and $T\Delta S^\ddagger$ seem to be proportional to these parameters with virtually identical coefficients. Such "isokinetic" effects are well-known and have been previously detailed in the literature (21–23).

© 2006 NRC Canada

Table 2. NMR spectral properties at line coalescence (measured at 500.13 MHz) for DMPH-H picryl peaks (^{1}H) in various solvents.

Solvent	T_{coa}[b] (K)	δ (s^{-1}) at $T = T_{coa}$	w (s^{-1}) at $T = T_{coa}$	W (s^{-1}) at $T = T_{coa}$	$\tau_2 \times 10^3$ (s) at $T = T_{coa}$	$\tau_{coa} \times 10^3$ (s) Experimental[b]	$\tau_{coa} \times 10^3$ (s) Theoretical[c]
Tetrachloromethane	300	374	35.3	260	9.02	0.8	1.2
Trichloromethane-d_1	308	374	29.2	314	10.9	1.0	1.2
Toluene-d_8	296	343	7.7	281	41	1.0	1.3
Ethanenitrile-d_3	302	262	11.8	231	27.0	1.5	1.0
2-Propanone-d_6	295	226	5.1	221	63	2.1	2.0
2-Propanone-d_6[a]	290	132	5.4	101	59	2.8	3.4
Tetrahydrofuran-d_8	292	205	30.1	182	10.6	1.9	2.2
N,*N*-Dimethylformamide-d_7	292	113	3.05	89	104	3.2	4.0

Note: Here, δ and w at T_{coa} were obtained by extrapolating the measured thermal data.
[a]These spectra have been measured at 300.13 MHz.
[b]Judged visually, see text.
[c]See eq. [2].

Table 3*a*. Kamlet–Taft parameter β, coalescence temperature T_{coa}, coalescence mean lifetime τ_{coa}, number n of data points used for the Arrhenius plot, rate constant k_T calculated for T_o = 298.15 K, natural logarithm of the frequency factor k_∞, Arrhenius-type activation energy ΔE_{Ar}, enthalpy difference $\Delta H_{Ar}^{\ddagger}$ of activation, entropy difference $\Delta S_{Ar}^{\ddagger}$ of activation, and Gibbs free-energy difference $\Delta G_{Ar}^{\ddagger}$ of activation for DMPH-H in various solvents.

Solvent	β	T_{coa} (K)	$\tau_{coa} \times 10^3$ (s)	n	k_T (s^{-1})	$\ln(k_\infty)$ (k_∞ in s^{-1})	ΔE_{Ar}[a] (kJ mol^{-1})	$\Delta H_{Ar}^{\ddagger}$[a] (kJ mol^{-1})	$\Delta S_{Ar}^{\ddagger}$[a] (J K^{-1} mol^{-1})	$\Delta G_{Ar}^{\ddagger}$[a] (kJ mol^{-1})
Tetrachloromethane	~0	300	0.84	13	811.8±0.1	41.0±0.7	85.0±1.7	82.6±1.7	87.7±5.6	56.4 ±3.4
Trichloromethane-d_1	~0	308	0.992	11	308.98 ±0.02	39.8±0.5	84.5±1.2	82.0±1.2	77.8±3.8	58.8 ±2.3
Toluene-d_8	0.11	296	1.045	9	1081.9±0.3	36.7±0.4	73.6±1.0	71.1±1.0	51.6±3.5	55.7 ±2.00
Ethanenitrile-d_3	0.31	302	1.52	23	467.2±0.1	38.9±0.4	81.1±1.0	78.7±1.0	70.0±3.5	57.8 ±2.0
2-Propanone-d_6	0.48	295	2.06	32	739.9±0.4	37.2±0.3	75.9±0.8	73.4±0.8	56.3±2.7	56.6 ±1.6
2-Propanone-d_6[b]	0.48	290	2.80	7	724.2±0.3	35.3±1.2	71.1±0.7	68.6±0.7	39.9±9.6	56.7 ±3.6
Tetrahydrofuran-d_8	0.55	292	1.876	19	922.2±0.4	36.2±0.3	72.9±0.7	70.4±0.7	48.1±2.3	56.1 ±1.4
N,*N*-Dimethylformamide-d_7	0.69	292	3.24	24	577.0±0.5	33.3±0.4	66.8±0.9	64.3±0.9	23.6±3.2	57.3±1.9

Note: The pseudo-thermodynamic parameters were obtained using the relation set out in ref. 5. The ^{1}H NMR measurements were taken at 500.13 MHz. The data in columns 8 and 9 are related via $\Delta H_{Ar}^{\ddagger} = \Delta E_{Ar} - RT_o$.
[a]No sensitivity correction included.
[b]These measurements were taken at 300.13 MHz.

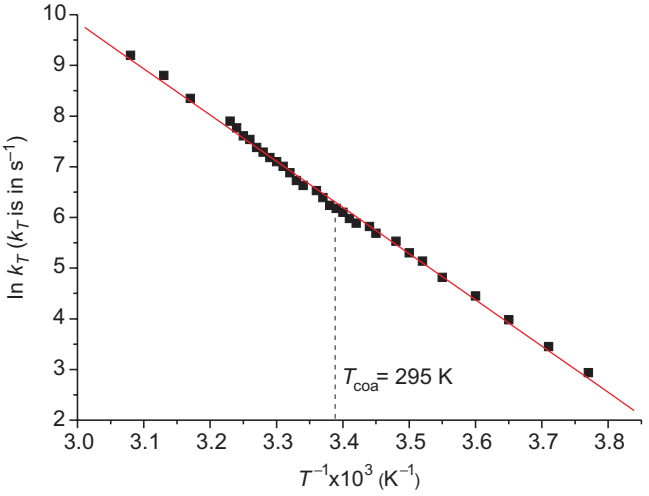
Table 3*b*. Number (n) of data points used for the Eyring plot, rate constant k_T calculated for T_o = 298.15 K, natural logarithm of the limiting frequency factor k_∞, Eyring-type activation energy ΔE_{Ey}, enthalpy difference $\Delta H_{Ey}^{\ddagger}$ of activation, entropy difference $\Delta S_{Ey}^{\ddagger}$ of activation, and Gibbs free-energy difference $\Delta G_{Ey}^{\ddagger}$ of activation for DMPH-H in various solvents.

Solvent	n	k_T/T_o (s^{-1} K^{-1})	$\ln(k_\infty/T_o)$ (k_∞/T_o in s^{-1} K^{-1})	ΔE_{Ey}[a] (kJ mol^{-1})	$\Delta H_{Ey}^{\ddagger}$[a] (kJ mol^{-1})	$\Delta S_{Ey}^{\ddagger}$[a] (J K^{-1} mol^{-1})	$\Delta G_{Ey}^{\ddagger}$[a] (kJ mol^{-1})
Tetrachloromethane	13	2.7±1.6	34.4±0.7	85.2±1.9	82.7±1.9	88.1 ±5.7	56.4 ±3.6
Trichloromethane-d_1	11	1.05±0.5	33.1±0.5	84.5±1.4	82.0±1.4	77.9 ±3.7	58.8 ±2.5
Toluene-d_8	9	3.7±1.6	30.0±0.5	73.6±1.4	71.1±1.4	51.8 ±3.8	55.7 ±2.5
Ethanenitrile-d_3	23	1.5±0.5	32.2±0.4	81.3±1.3	78.8±1.3	70.3 ±3.5	57.8 ±1.9
2-Propanone-d_6	32	2.6±0.7	30.55±0.3	75.9±1.1	73.4±1.1	56.5 ±2.7	56.6 ±1.5
2-Propanone-d_6[b]	7	2.5±2.4	28.6±1.1	71.1±2.8	68.6±2.8	40.2 ±9.5	56.6 ±5.6
Tetrahydrofuran-d_8	19	3.1±0.8	29.6±0.3	73.1±1.1	70.6±1.1	48.8 ±2.2	56.1 ±1.8
N,*N*-Dimethylformamide-d_7	24	1.9±0.7	26.6±0.4	66.9±0.9	64.4±0.9	24.0 ±3.2	57.2 ±1.9

Note: The pseudo-thermodynamic parameters were obtained using the relation set out in ref. 5. The ^{1}H NMR measurements were taken at 500.13 MHz. The data in columns 5 and 6 are related via $\Delta H_{Ey}^{\ddagger} = \Delta E_{Ey} - RT_o$.
[a]No sensitivity correction included.
[b]These measurements were taken at 300.13 MHz.

© 2006 NRC Canada

Fig. 5. Arrhenius plot of $\ln(k_T)$ against T^{-1} (K^{-1}). The NMR spectra were measured at 500.13 MHz for DMPH-H in 2-propanone-d_6. No. of data points is 32. Parameters: slope m = –9.13 ± 0.10 K, intercept b = 37.23 ± 0.32, SD = ±0.09, r = –0.9983. The analogous Eyring plot (not shown) of $\ln(k_T/T)$) against T^{-1} has linear-fitting parameters: slope $-\Delta E_{Ar}/R$ = –9.41 ± 0.10 K, intercept $\ln(k_\infty)$ = 36.96 ± 0.34, SD = ±0.09, r = –0.9983.



In summary, because of the cancellation of terms as described above, the Gibbs free energy does not vary appreciably with the hydrogen-bonding capabilities of the solvents used, as is evident in Fig. 7 and Tables 3*a* and 3*b*.

Discussion

The data-fitting performed to obtain the thermal dependence of the parameters (chemical shift difference δ and linewidth w) seem adequate for our purposes. However, we note that some of the resulting parameters are not all that well characterized (see the captions for Figs. 2 and 3).

We wished to compare the values of ΔE_{Ar} and the other pseudo-thermodynamic energies for the two cases of fittings of the lineshapes done: (*i*) keeping the values of δ and w fixed at their low-T values, as compared with (*ii*) using δ and w values evaluated at each temperature. We used the data taken for DMPH-H in acetone-d_6 (32 points) for this purpose and obtained the Arrhenius results set out in Table 3*a*. A substantial increase (3.4%) in the activation energy was obtained. Thus, our efforts to use thermally varying input parameters appear worthwhile, yielding more accurate ΔE_{Ar} values (Table 3*a*).

Using the weighting factors derived as previously discussed (see eqs. [4] and [5]), we also did linear fittings (OriginLab) incorporating these. For the acetone-d_6 data cited above, we found ΔE_{Ar} = 76.58 kJ mol^{-1}, with the use of T_o = 386.7 K, as compared with 75.91 kJ mol^{-1} unweighted. This constitutes a 0.9% increase. With the DMF-d_7 data, a 4.4 % increase was obtained. The complete set of results is available in Table 4.

We note a couple of aspects of the data recorded in Table 4: (*i*) the values of ΔE_{Ar} are increased appreciably by applying the weighting-factor scheme, as is $\Delta H^{\ddagger}$ (of course) and $T\Delta S_{Ar}{}^{\ddagger}$, by equal amounts, and (*ii*) thus, $\Delta G_{Ar}{}^{\ddagger}$ is not affected by weighting the Arrhenius points (cancellation effect). However, it is lowered by ~1.5 kJ mol^{-1} (2.8%, acetone data) when the temperature dependence of δ and w are not neglected.

Fig. 6. Plot of the Arrhenius molar enthalpy change $\Delta H^{\ddagger}$ and the entropy parameter $T\Delta S^{\ddagger}$ against the Kamlet–Taft parameters β of the solvents at standard temperature T_o = 298.15 K. Numbering of the data points is according to the solvent order in Tables 2 and 3.

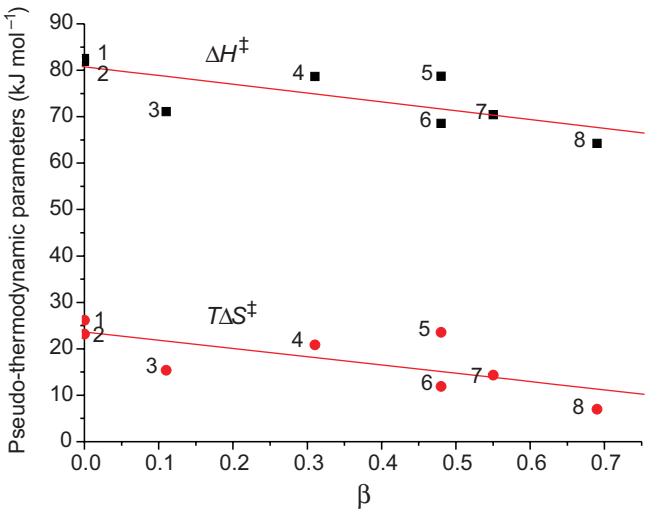
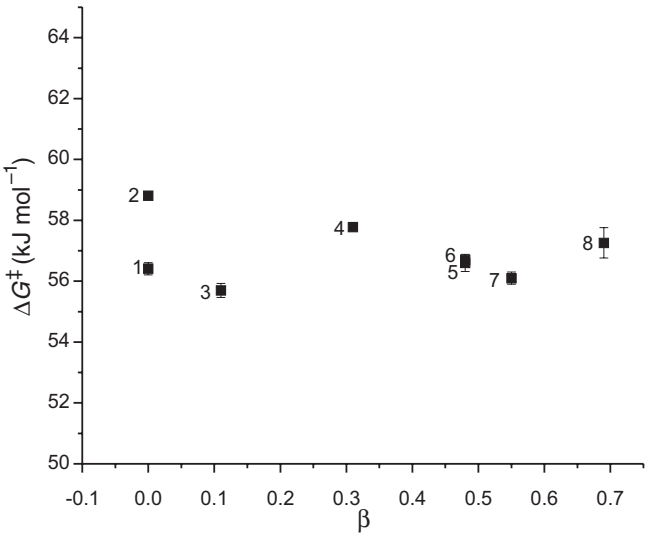


Fig. 7. Plot of the Arrhenius molar Gibbs free energy change $\Delta G^{\ddagger}$ against the Kamlet–Taft parameters β of the solvents at standard temperature T_o = 298.15 K. Numbering of the data points is according to the solvent order in Tables 2 and 3.



The choice of ν_o optimal for dynamic studies is sometimes affected by the physical properties of the solvent to be studied. Thus, CCl_2D_2 boils at such a relatively low temperature that T_{coa} at 500 MHz is above T_{boil} (see Table 4). Hence, increasing the chemical-shift difference δ by going to a higher ν_o is not always beneficial.

Judging from the single example we have, ^{1}H NMR spectra of DMPH-H in acetone-d_6 taken at 300 and 500 MHz, the energies $\Delta H^{\ddagger}$ and $T\Delta S^{\ddagger}$ may contain frequency-

© 2006 NRC Canada

Table 4. Effect of thermal fitting of parameters and of applying the data weighting scheme on the Arrhenius-type molar activation energies for DMPH-H in two solvents at standard temperature T_o = 298.15 K.

δ and w vary with T [a]	Weighted points [a]	ΔE_{Ar}	$\Delta H_{Ar}^{\ddagger}$	$T_o \Delta S_{Ar}^{\ddagger}$	$\Delta G_{Ar}^{\ddagger}$
2-Propanone-d_6					
+	–	75.9±0.8	73.4±0.8	16.8±0.8	56.6±1.6
–	–	73.4±1.0	70.9±1.0	12.7±0.4	58.2±1.6
+	+	74.3±4.2	71.8±4.2	15.2±0.4	56.7±8.6
–	+	71.5±5.0	69.0±5.0	10.5±4.7	58.5±9.7
***N*,*N*-Dimethylformamide-d_7**					
+	–	66.8±0.9	64.3±0.9	7.0±1.0	57.3±1.9
+	+	65.3±6.4	62.8±6.4	5.4±0.3	57.2±6.7

Note: The ^{1}H NMR spectra were measured at 500.13 MHz.

[a]In this table, + and – denote: Yes (effect included) and No (effect not included), respectively.

dependent contributions that cancel (see Tables 3*a* and 3*b*). This point should perhaps be investigated further.

Among the solvents used, one (DMF) itself undergoes conformerization between two atropisomers, as is discernible via ^{1}H NMR (13). It would be amusing to know whether the solvent molecules surrounding any given solute molecule transfer configurations in concert with the transformation of the latter.

Comparisons of DPPH-H and DMPH-H

Comparison with the hydrazine DPPH-H (4) shows clearly that $\Delta G_{Ar}^{\ddagger}$ does depend on the Kamlet–Taft β, whereas this is not the case with DMPH-H. Thus, the latter appears to be less effectively hydrogen-bonded to solvents. For the three solvents (CCl_4, CH_3CN, and CH_3COCH_3) measured for both solutes, $\Delta G_{Ar}^{\ddagger}$ is 9 kJ mol^{-1} lower in case of CCl_4 but 6–7 kJ mol^{-1} greater for the other two (CH_3-containing) solvents.

DMPH-H has been reported to be quite inert and not to yield the corresponding (unknown) hydrazyl free radical, DMPH$^{\bullet}$ on providing strong oxidation conditions (24). This is in contradistinction to the well-known result of easily oxidizing 2,2′-diphenyl-1-picrylhydrazine DPPH-H to yield the ubiquitous stable free radical DPPH$^{\bullet}$. Thus, the presence of the aromatic groups and the resulting electron delocalization appears to be essential for stability of the hydrazyl species. We can now confirm the previously mentioned situation and plan to do further work in this area.

One simple way to understand this result qualitatively is to consider the unpaired electron to be confined in a "box". The smaller the box, the higher the energy.

Summary

In this work, we have taken into account, as best as we could, the thermal behavior of the parameters entering into the analysis throughout the dynamic region. Thus, we have used different values of δ_T and W_T at each temperature at which lineshape simulation using eq. [1] was carried out. This approach should become universal in the area of dynamic NMR measurements. Similarly, giving weighting factors to the various points utilized for an Arrhenius plot seems to be uncommon. We can summarize by stating that both the two improvements cited appear to be of modest import, amounting to 1–5 kJ mol^{-1} in the activation-energy parameters.

Acknowledgments

We thank the University of Saskatchewan, including the Saskatchewan Structural Sciences Centre, for the use of its facilities, and we are grateful to Professor J.W. Quail for his assistance in producing Fig. 1. We also wish to thank D.F. Howarth and R.J. Clark for their help with parts of this project. We acknowledge partial support from the Natural Sciences and Engineering Research Council (NSERC) of Canada.

References

1. A.D. Bain. Prog. Nucl. Magn. Reson. Spectrosc. **43**, 63 (2003).
2. J. Heidberg, J.A. Weil, G.A. Janusonis, and J.K. Anderson. J. Chem. Phys. **41**, 1033 (1964).
3. J.A. Weil, A. Blum, A.H. Heiss, and J.K. Kinnaird. J. Chem. Phys. **46**, 3132 (1967). Note: p. 3139 (col. 1, par. 1), change C–CN_3 to C–CH_3; p. 3143 (col. 2, par. below figs.), change H6 to H4 in 2,6-dinitroanilines.
4. R.L. Tyson and J.A. Weil. J. Phys. Chem. **94**, 3951 (1990). Note: p. 3957, col. 1 in Table IX, acetonitrile-d_6 should read acetonitrile-d_3; col. 6 header in the same table "$\Delta H^{\ddagger}$" should read "$\Delta G^{\ddagger}$".
5. K.C. Brown, R.L. Tyson, and J.A. Weil. J. Chem. Educ. **75**, 1632 (1998).
6. K.C. Brown, B.R. Nelson, J.W. Quail, B.E. Robertson, J.A. Weil, and Z. Zimpel. Can. J. Chem. **77**, 1295 (1999).
7. K.C. Brown, M. El-Bermani, and J.A. Weil. Can. J. Chem. **82**, 1707 (2004).
8. J.A. Weil, Y. Upadrashta, and T.G. Steele. Appl. Magn. Reson. **29**, 531 (2005).
9. J.W. Quail, J.A. Weil, and M.P. Singh. Acta Crystallogr. C, **56**, 235 (2000). Note: On p. 236, "achiral" should read "chiral".
10. H. Wang, R.J. Barton, B.E. Robertson, and J.A. Weil. J. Inclusion Phenom. Mol. Recognit. Chem. **10**, 203 (1991).
11. R.A. Olsen, L. Liu, N. Ghaden, A. Johns, M. E. Hatcher, and L.J. Mueller. J. Am. Chem. Soc. **125**, 10125 (2003).

© 2006 NRC Canada

12. G.M. Leskowitz, N. Ghaderi, R.A. Olsen, K. Pederson, M.E. Hatcher, and L.J. Mueller. J. Phys. Chem. A, **109**, 1152 (2005).
13. J. Sandström. Dynamic NMR spectroscopy. Academic Press, London, UK. 1982.
14. J.K.M. Sanders and B.K. Hunter. Modern NMR spectroscopy. 2nd ed. Oxford University Press, Oxford, UK. 1993.
15. JCE Software. WinDNMR 3D. Version 2 [computer program]. 1995.
16. Redacom AG. OriginLab. Version 7.5 [computer program]. Nidau, Switzerland. 2004.
17. Wavefunction, Inc. Spartan′04. Release 123 [computer program]. Irvine, CA, USA. 2004.
18. P.R. Bevington. Data reduction and error analysis for the physical sciences. McGraw-Hill, New York, NY, USA. 1969.
19. P.F. Currie, J.W. Quail, A.C.M. Rusk, and J.A. Weil. Can. J. Chem. **61**, 1760 (1983).
20. G.W. Castellan. Physical chemistry. 2nd ed. Addison-Wesley, Reading, MA, USA. 1971.
21. M.V. Rekharsky and Y. Inoue. Chem. Rev. **98**, 1875 (1998).
22. M.S. Searle, M.S. Westwell, and D.H. Williams. J. Chem. Soc., Perkin Trans. 2, 141 (1995).
23. J.E. Leffler. J. Org. Chem. **20**, 1202 (1955).
24. R.H. Poirier and F. Benington. J. Org. Chem. **19**, 1157 (1964).

© 2006 NRC Canada

Effect of *N*-cetyl-*N*,*N*,*N*-trimethylammonium bromide and orthophenylenediamine on the corrosion inhibition of carbon steel in 1 mol/L HCl

B. Ramesh Babu, A.K. Parande, and P.L. Ramasamy

Abstract: Inhibition studies of *N*-cetyl-*N*,*N*,*N*-trimethylammonium bromide (CTAB) and orthophenylenediamine (OPD) have shown that they were effective inhibitors of corrosion of carbon steel in HCl. The inhibitive behaviour of OPD with CTAB on the corrosion of carbon steel in 1 mol/L HCl was studied by gravimetric weight loss, potentiodynamic polarization, and electrochemical impedance measurements. Inhibition efficiency (IE) was found to increase with the increase in concentration of CTAB and it was also found that CTAB was effective only when used above a concentration of 100 mmol/L. Furthermore, the addition of 20 mmol/L of OPD to CTAB slightly increased the IE. The adsorption of these compounds on carbon steel in 1 mol/L HCl obeyed Langmuir's adsorption isotherm. These inhibitors reduced the permeation current. The IE was observed as high for 200 mmol/L of CTAB with 20 mmol/L of OPD in all the techniques studied. Scanning electron microscopy clearly showed that the inhibition was due to a polymolecular film formed by the physical adsorption of the inhibitor on the metal surface.

Key words: carbon steel, corrosion, inhibitors, impedance, potentiodynamic polarization.

Résumé : Des études d'inhibition ont permis de montrer que le bromure de *N*-cétyl-*N*,*N*,*N*-triméthylammonium (BCTA) et de l'orthophénylènediamine (OPD) sont des inhibiteurs efficaces de corrosion de l'acier au carbone dans l'acide chlorhydrique. On a étudié le comportement inhibiteur de l'OPD en présence de BCTA sur l'inhibition de la corrosion de l'acier au carbone dans de l'acide chlorhydrique 1 mol/L à l'aide de mesures gravimétrique, galvanostatique et d'impédance. On a trouvé que l'efficacité de l'inhibition (EI) augmente avec une augmentation de la concentration du BCTA et on a aussi observé que le BCTA n'est efficace que lorsque sa concentration est supérieure à 100 mmol/L. De plus, l'addition de 20 mmol/L d'OPD au BCTA augmente aussi l'efficacité de l'inhibition. L'adsorption de ces composés sur de l'acier au carbone dans de l'acide chlorhydrique 1 mol/L obéit à une isotherme d'adsorption de Langmuir. Ces inhibiteurs réduisent le courant de perméation. Dans toutes les techniques étudiées, on a observé une efficacité d'inhibition jusqu'à des valeurs de 200 mmol/L de BCTA avec 20 mmol/L d'OPD. La microscopie électronique à balayage a montré clairement que l'inhibition est due à un film polymoléculaire qui se forme par une adsorption physique de l'inhibiteur sur la surface métallique.

Mots clés : acier au carbone, corrosion, inhibiteurs, impédance, galvanostatique, polarisation.

Introduction

Corrosion of steel in acidic solutions has practical importance (1–7). For example, corrosion is of significant concern in the acid pickling of iron and steel, chemical cleaning of scale in metallurgy and other industries, and in oil recovery and other petrochemical processes. One of the most important means of corrosion protection is the use of organic inhibitors (8–15). Surfactants are used as corrosion inhibitors. These surfactants can be used either alone or in mixtures with other compounds. *N*-Cetyl-*N*,*N*,*N*-trimethylammonium bromide (CTAB), a cationic surfactant, has been used in controlling the corrosion of carbon steel in an aqueous solution containing chlorine ions (16). Orthophenylenediamine (OPD), a nonionic surfactant, has been used as inhibitor for the corrosion of carbon steel in HCl (17). Several studies of surfactant mixtures focused on synergism in both micelle and monolayer formation at the air–water interface (18, 19). Surfactants have been used as corrosion inhibitors either alone (20) or in combination with other compounds to improve their performance as inhibitors (21, 22). CTAB is a cationic surfactant, whereas OPD is a nonionic surfactant. The aim of the present investigation was to study the combined effect of cationic (CTAB) and nonionic (OPD) surfactants on the corrosion inhibition of carbon steel in 1 mol/L HCl. The present work was carried out to investigate the following: (*i*) the inhibition effect of CTAB alone in the corrosion of carbon steel in 1 mol/L HCl and (*ii*) the combined

Received 23 December 2005. Accepted 19 October 2006. Published on the NRC Research Press Web site at http://canjchem.nrc.ca on 5 January 2007.

B.R. Babu,[1] A.K. Parande, and P.L. Ramasamy. Central Electrochemical Research Institute, Karaikudi 630 006, India.

[1]Corresponding author (e-mail: akbabu_2001@yahoo.com).

 doi:10.1139/V06-175 © 2006 NRC Canada

inhibition effect of OPD with CTAB in the corrosion of carbon steel in 1 mol/L HCl. The results are reported and discussed.

Experimental

Materials used

Carbon steel specimens

The chemical composition (wt%) of the carbon steel used in these tests was C 0.07%, P 0.08%, Mn 0.034%, S 0.04%, with the remainder being iron. Test specimens of size 5 cm × 3 cm × 0.2 cm were used for gravimetric studies. The specimens, embedded in epoxy resins with an exposed area of 1 cm^2 were used for potentiodynamic and impedance measurements. The specimens were polished with different grades of emery paper and degreased with trichloroethylene before use.

Reagents

AR chemicals of HCl, orthophynylenediamine, and *N*-cetyl-*N*,*N*,*N*-trimethyl ammonium bromide were used for this study. Table 1 shows the structures of CTAB and OPD.

Techniques adopted

Gravimetric test

The weighed specimens were exposed in 150 mL of 1 mol/L HCl containing different concentrations of inhibitor for a period of 3 days. After 3 days of exposure, the specimens were removed, washed, dried, and weighed. The experiments were conducted at 30 ± 1 °C using a temperature control bath (Siskin Juloba, India). The inhibition efficiency (IE) was calculated using the formula,

$$[1] \qquad IE = 100\ [1 - W_2 / W_1]\%$$

where W_1 = the initial weight of the specimen and W_2 = final weight of the specimen.

Potentiodynamic polarization

A three-electrode cell assembly, consisting of a carbon steel electrode with an exposed area of 1 cm^2 as working electrode, a saturated calomel electrode as reference electrode, and a platinum foil as counter electrode, was used for potentiodynamic polarization studies. The scan range was –650 to –400 mV; the scan rate was 1 mV sec^{-1} and an Electrochemical Analyzer (IM6) was used to generate the scans. From the polarization curves, b_a, b_c, E_{corr}, and I_{corr} values were calculated for carbon steel in uninhibited and inhibited hydrochloric acid. The corrosion IE was calculated using the equation,

$$[2] \qquad IE = 100\ [1 - I_{corr(W)} / I_{corr(WO)}]\%$$

where $I_{corr\ (W)}$ = corrosion current in the presence of inhibitor and $I_{corr\ (WO)}$ = corrosion current without inhibitor.

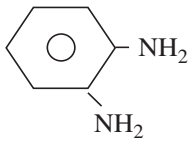
Electrochemical impedance spectroscopy

Electrochemical impedance spectroscopy (EIS) measurements were carried out using the three-electrode cell assembly, as mentioned in polarization studies, after 15 min of immersion. Experiments were carried out using Solartron SI 1287 in the frequency range of 60 KHz to 10 MHz. The applied sinusoidal wave voltage was 5 mV. Nyquist plots were drawn from these results. From the plots, values of polarization resistance, R_p, were calculated. After substituting R_p values in the Stern–Geary equation, the corrosion rate was calculated using,

$$[3] \qquad I_{corr} = \frac{b_a b_c}{2.303\,(b_a + b_c)} \left(1/R_p \right)$$

The IE was calculated using the value of I_{corr} for various systems studied.

Table 1. Structures of CTAB and OPD.

Compound	Structure
N-Cetyl-*N*,*N*,*N*-trimethyl ammonium bromide	$CH_3(CH_2)_{15}N^+ (CH_3)_3\ Br$
Orthophenylenediamine (OPD)	

Hydrogen permeation studies

The hydrogen permeation studies were carried out using a Devanathan and Stachurski two-compartment cell as described elsewhere (23). Permeation current was obtained for a concentration of 1 mol/L HCl, 1 mol/L HCl with 200 mmol/L CTAB, and 200 mmol/L CTAB and 20 mmol/L OPD in 1 mol/L HCl.

Scanning electron microscopy

Micrographs were made of carbon steel specimens using an Hitachi Model-S-3000 H. Carbon steel specimens of size 1 cm^2 were dipped in 1 mol/L HCl with and without inhibitors for surface analysis.

Results and discussion

Mechanism of corrosion inhibition

It has been hypothesized that the mechanism of iron dissolution occurs in two consecutive steps and involves the participation of a species $(FeOH)_{ads}$ as shown here,

$$[4] \qquad Fe + H_2O \leftrightarrow (FeOH)_{ads} + H^+ + e$$

$$[5] \qquad Fe(OH)_{ads} \xrightarrow{rds} (FeOH)^+ + e$$

where rds refers to rate determining step, and

$$[6] \qquad (FeOH)^+ + H^+ \rightarrow Fe^{2+} + H_2O$$

The dissolution of iron in HCl solution has been studied extensively. One of the mechanisms of breakdown of passivity involves the diffusion of Cl^- through the protective oxide layer. The reaction sequence is supposed to involve the following steps,

$$[7] \qquad Fe + Cl^- + H_2O \leftrightarrow (FeClOH)^-_{ads} + H^+ + e^-$$

$$[8] \qquad (FeClOH)^-_{ads} \xrightarrow{rds} FeClOH + e$$

$$[9] \qquad FeClOH + H^+ \leftrightarrow Fe^{2+} + Cl^- + H_2O$$

© 2006 NRC Canada

where $(FeClOH)^{-}_{ads}$ was treated as per Langmuir's isotherm.

It is well-known that the passive film consists of hydrated iron oxides, $Fe_2O_3 \cdot H_2O$. When the aggressive Cl^- anion attacks the passive film, the Cl^- ions tend to diffuse towards the metal (they meet with bound water molecules, which are the cementing elements of the passive layer) and form chloride-containing iron complexes, which in turn increase the dissolution rate. It has also been confirmed that the presence of chlorides accelerates the formation of corrosion products because of the corresponding cyclic processes of rusting.

In the case of chlorides, the process (Fig. 1) takes place in three phases, reactions [10–12], with the net formation of ferric hydroxide iron with water and oxygen in the presence of acid.

[10] $FeCl_3 + 3H_2O \rightarrow Fe(OH)_3 + 3HCl$

[11] $Fe + 2HCl \rightarrow FeCl_2 + H_2$

[12] $FeCl_2 + HCl + \frac{1}{4}O_2 \rightarrow FeCl_3 + \frac{1}{2}H_2O$

The circle of ongoing corrosion is closed, as the ferric chloride consumed in reaction [10] reappears in reaction [12]. The net reaction, which is the sum of reactions [10–12] is

[13] $Fe + 2.5H_2O + 0.25O_2 \rightarrow Fe(OH)_3 + H_2$

Inhibition efficiency by gravimetric method

The IE calculated for 50, 100, 150, 200, and 250 mmol/L concentrations of CTAB alone in 1 mol/L HCl and the addition of 20 mmol/L OPD with different concentrations of CTAB were reported in Table 2. From the table, it is seen that the IE increases from 50 to 200 mmol/L of CTAB alone and similarly from 50 to 200 mmol/L of CTAB with 20 mmol/L of OPD. The optimum concentration of CTAB and OPD was found to be 200 mmol/L. A further increase in inhibitor does not show any increase in the IE, and there is a decrease in IE at 250 mmol/L of CTAB both alone and with OPD.

Inhibition efficiency by potentiodynamic polarization

Figures 2 and 3 show the polarization curves for carbon steel in 1 mol/L HCl with and without inhibitors. The corrosion parameters such as b_a, b_c, E_{corr}, I_{corr}, and IE collected for 1 mol/L HCl containing different concentrations of CTAB with and without OPD were reported in Table 3. The addition of CTAB and OPD influence the b_c values with less potential difference. Similarly, the E_{corr} values are found to be little changed when compared with blank. This indicates that the studied compounds are of mixed type of inhibitor. From the table it was found that as the concentration of the inhibitor increased from 50 to 200 mmol/L, the IE increased markedly compared with using CTAB alone. The addition of OPD in different concentrations of CTAB increased IE, but no further improvement was found with the addition of OPD to 250 mmol/L CTAB.

Because CTAB has a long chain molecule, the surface coverage area, θ, also leads to an increase in IE when used alone. Hence, it is a good inhibitor. The addition of OPD increases the IE to a lesser extent. The availability of an electron in the benzene ring in OPD and a nitrogen atom plays a vital role in the adsorption of the inhibitor to the steel surface. The nitrogen atoms present in OPD enhance its efficiency. The combination of both has a synergistic effect.

The value of the anodic Tafel slope was reduced from 130 mV dec^{-1} to 110 mV dec^{-1}. The value of the cathodic Tafel slope was between 70 mV dec^{-1} and 60 mV dec^{-1}. These data show that the inhibitors, CTAB and OPD, inhibit the corrosion of carbon steel acting as mixed inhibitors.

Fig. 1. Reaction of chloride with iron.

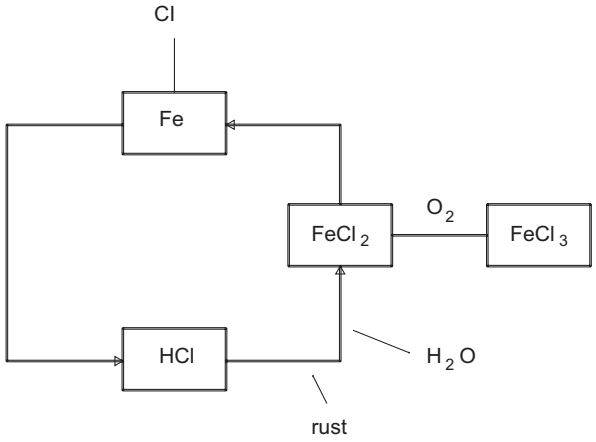


Table 2. Inhibition efficiencies (IE) of CTAB and OPD for the corrosion of carbon steel in 1 mol/L HCl as determined by the gravimetric method.

Inhibitor	CTAB concn. (mmol/L)	IE (%)
CTAB	50	60.4
	100	67.2
	150	78.6
	200	89.2
	250	85.6
CTAB and 20 mmol/L OPD	50	64.3
	100	72.5
	150	81.9
	200	92.3
	250	91.4

Electrochemical impedance spectroscopy (EIS) studies

AC impedance technique has been widely used as a tool in the investigation of the protective properties of organic inhibitors for metals. The technique is based on the measurement of the impedance of the double layer at the metal–solution interface. The charge transfer resistance, R_t, and the double layer capacitance, C_{dl}, are calculated by determining the equivalent electrical circuit of the metal–solution interface. In general for a corrosion system, the equivalent circuit diagram is as given in Fig. 4. C_{dl} is the double layer capacitance, R_t the charge transfer resistance, and R_s is the solution resistance.

The impedance of the circuit given in Fig. 4 can be calculated using,

[14] $$Z = R_s + \frac{R_t}{1 + j\omega C_{dl} R_t}$$

© 2006 NRC Canada

Table 3. Potentiodynamic polarization parameters for carbon steel in 1 mol/L HCl in the presence of inhibitors.

Inhibitor	CTAB Conc. (mmol/L)	E_{corr} (mV)	I_{corr} (mA cm^{-2})	b_a (mV dec^{-1})	b_c (mV dec^{-1})	IE (%)
Blank	—	–520	3.2	130	70	—
CTAB	50	–518	1.04	118	60	67.5
	100	–516	0.99	110	64	69.0
	150	–512	0.75	120	66	76.5
	200	–506	0.68	126	68	78.7
	250	–510	0.73	121	66	77.1
CTAB and 20mmol/L OPD	50	–516	0.89	120	64	72.1
	100	–512	0.67	118	66	79.0
	150	–504	0.54	126	67	83.1
	200	–498	0.48	128	72	85.0
	250	–500	0.52	124	66	83.7

Fig. 2. Polarization curves for carbon steel in blank and in different concentrations of CTAB. (*a*) Blank, (*b*) 50 mmol/L, (*c*) 100 mmol/L, (*d*) 150 mmol/L, (*e*) 200 mmol/L, and (*f*) 250 mmol/L C.

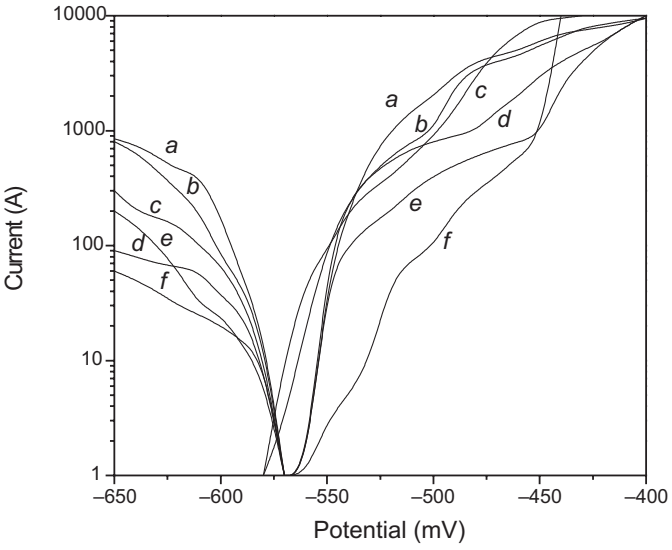
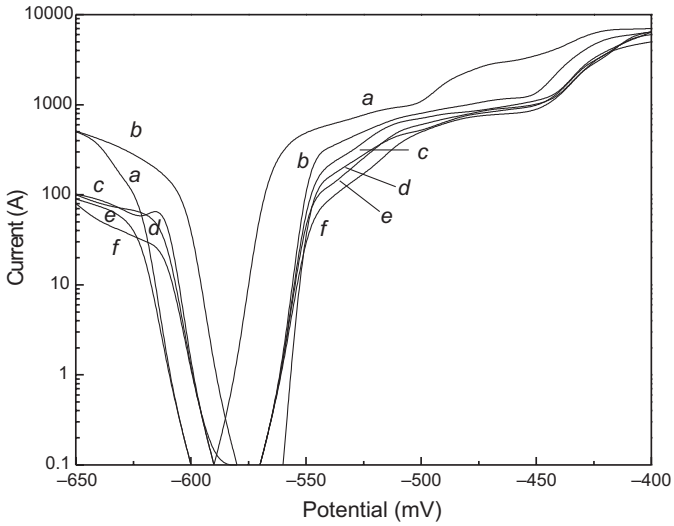


Fig. 3. Polarization curves for carbon steel in blank and in different concentrations of CTAB with OPD. (*a*) Blank, (*b*) 50 mmol/L CTAB and 20 mmol/L OPD, (*c*) 100 mmol/L CTAB and 20 mmol/L OPD, (*d*) 150 mmol/L CTAB and 20 mmol/L OPD, (*e*) 200 mmol/L CTAB and 20 mmol/L OPD, and (*f*) 250 mmol/L CTAB and 20 mmol/L OPD.



$$[15] \quad Z = R_s + \frac{R_t}{1+\omega^2 C_{dl}^2 R_t^2} - \frac{j\omega C_{dl} R_t^2}{1+\omega^2 C_{dl}^2 R_t^2}$$

where R_s is the solution resistance, R_t the charge transfer resistance, j is the imaginary unit ($\sqrt{-1}$), ω is the angular frequency ($\omega = 2\pi f$), and C_{dl} is the double layer capacitance. Equation [15] can be expressed as

$$[16] \quad Z = Z' - jZ''$$

where

$$[17] \quad Z = Z' - jZ''$$

$$[18] \quad Z' = R_s + \frac{R_t}{1+\omega^2 C_{dl}^2 R_t^2}$$

Eliminating ω between eqs. [17] and [18] gives the following equation for a semicircle,

$$[19] \quad \left[Z' - \left(\frac{R_s + R_t}{2}\right)\right]^2 + (Z'')^2 = \left(\frac{R_t}{2}\right)^2$$

According to eq. [19], the experimental data should give a Nyquist plot in the shape of a semicircle. In a real corrosion system, semicircular Nyquist plots can be obtained only with a few metals, and most of the experimental plots deviate from a semicircle.

The value of R_t will be determined from the following equation,

$$[20] \quad I_{corr} = \frac{b_a b_c}{2.3(b_a + b_c)} \frac{1}{R_t}$$

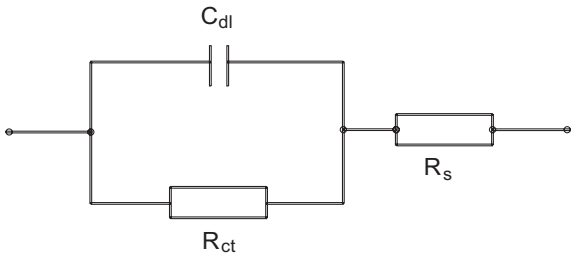
The values of C_{dl} and R_p derived from Nyquist plots, which have been shown in Fig. 5 for CTAB with and without OPD systems, were reported in Table 4.

© 2006 NRC Canada

Table 4. Impedance parameters for the corrosion of carbon steel in 1 mol/L HCl in the presence of inhibitors.

Inhibitor	CTAB Conc. (mmol/L)	R_P (Ω cm^2)	C_{dl} (μF cm^{-2})	I_{corr} (mA cm^{-2})
Blank	—	4.3	318	4.59
CTAB	50	13.7	154	1.34
	100	15.2	146	1.2
	150	17.8	133	1.08
	200	19.7	117	0.87
	250	20.1	114	0.89
CTAB and 20mmol/L OPD	50	14.2	144	1.28
	100	15.8	131	1.16
	150	18.5	125	1.04
	200	22.1	110	0.78
	250	21.8	113	0.84

Fig. 4. Equivalent circuit diagram for the corrosion system.



The C_{dl} value decreased with the addition of CTAB and it was further reduced by the addition of OPD. The data show that the greater the adsorption of inhibitor, the smaller C_{dl} values that were obtained. C_{dl} indirectly measures the water uptake by the passive film. From the data, 200 mmol/L of CTAB with 20 mmol/L of OPD showed the smallest values of C_{dl} when compared with other concentrations studied. This was explained by the presence of the cations present in the surfactant, which have better adsorption properties than a neutral surfactant.

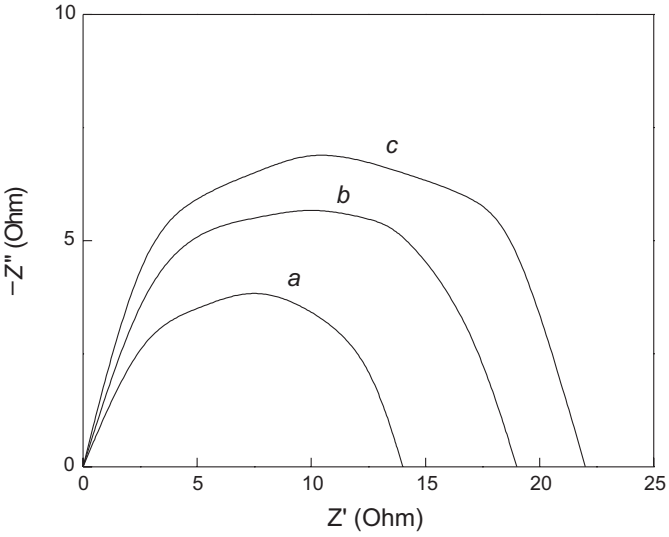
The R_p value for blank was reported as 4.3 Ω cm^2. The addition of CTAB increased the R_p values by 4–5 times in different concentrations. Furthermore, the addition of 20 mmol/L of OPD with different concentrations of CTAB increased the R_p values from 14.2 to 22.1 Ω cm^2. This data showed that the greater the surface coverage of the adsorbed inhibitor, the greater R_p values that were obtained.

The I_{corr} value measured for blank was 4.59 mA cm^{-2}. The I_{corr} values were decreased drastically from 1.34 to 0.87 mA cm^{-2} for different concentrations of CTAB alone. The addition of OPD in CTAB decreased the I_{corr} values further. From the Table 4, the C_{dl} value for the blank was reported as 318 μF cm^{-2}.

Adsorption isotherm

The interaction between the inhibitors and the steel surface can be described by the adsorption isotherm. During corrosion inhibition of metals, the nature of the inhibitor on the corroding surface has been deduced in terms of the adsorption characteristics of the inhibitor. The adsorption of organic inhibitors at an electrolyte–electrode interface may take place through displacement of adsorbed water molecules. The steel electrode is corroding uniformly and the corrosion rate in the absence of inhibitors is representative of the total number of corroding sites. Therefore, the corrosion rate in the presence of inhibitors may be assumed to represent the number of potentially corroding sites that remain after blockage because of inhibitor adsorption.

Fig. 5. Typical Nyquist plots for carbon steel in blank, CTAB, and OPD. (*a*) Blank, (*b*) 150 mmol/L CTAB, and (*c*) 150 mmol/L CTAB and 20 mmol/L OPD.

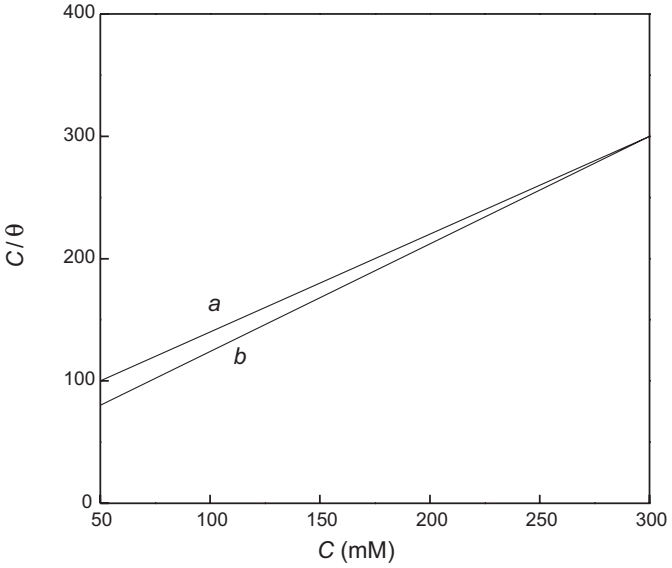


The surface coverage suggests that a chemical bond is formed between the metal atoms and the inhibitor molecules. The surface coverage is the function of the electronic density of the functional atom of the organic inhibitor; the molecules may be adsorbed on the metal–solution interface by the formation of either electrostatic or covalent bonds between the adsorbates and the metal surface atoms. Surface coverage data (θ) was used in determining inhibitor adsorption characteristics, which resulted in fitting the data to different isotherm type models, including Frumkin, Temkin, and Langmuir.

The simplest adsorption isotherm, the Langmuir isotherm, is based on the assumption that all adsorption sites are equivalent and that particle binding occurs independently from nearby sites, whether occupied or not. The degree of

© 2006 NRC Canada

Fig. 6. Langmuir's adsorption isotherm for carbon steel in HCl with inhibitors, (*a*) CTAB alone and (*b*) CTAB with 20 mmol/L OPD.



surface coverage (θ) for different concentrations of the inhibitor in 1 mol/L HCl has been evaluated from weight loss measurements. The plot of C/θ against C yields a straight line (Fig. 6), clearly suggesting that the inhibitors obey Langmuir's adsorption isotherm.

Hydrogen permeation studies

Plots of hydrogen permeation current vs. time for carbon steel in 1 mol/L HCl in the presence and absence of inhibitors are shown in Fig. 7.

In acid solutions, hydrogen permeation through metals takes place in the following manner,

[21] $M + H_3O^+ + e^- \rightarrow H_2O + MH_{ads}$ (discharge step)

where M is the cathode metal surface, followed either by

[22] $MH_{ads} + MH_{ads} \rightarrow 2M + H_2 \uparrow$

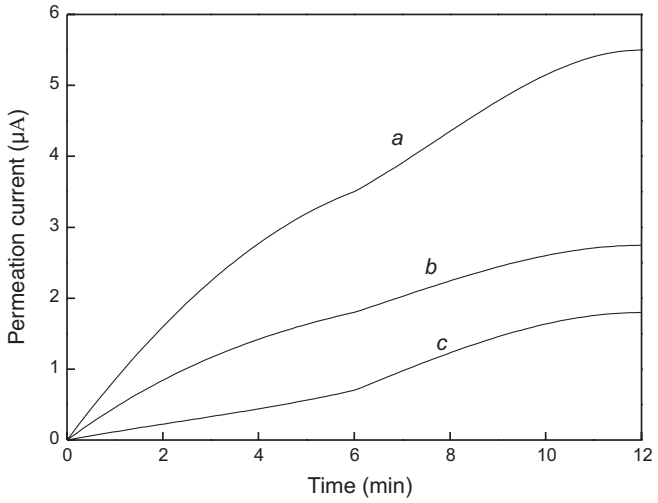
or electrochemical desorption by

[23] $MH_{ads} + H_3O^+ + e^- \rightarrow M + H_2O + H_2 \uparrow$

When the metal is immersed in acidic solutions, hydrogen gas is liberated on the steel surface. Some of the atomic hydrogen liberated during the process permeates through the metal (while the remainder is evolved as a fraction of the diffused hydrogen atoms – gas) and becomes occluded in the metal crystal lattice defects. The fraction of the diffused hydrogen atoms – gas that enters the metal produces some detrimental effects on the mechanical properties of steel, such as a decrease in ductility and loss of mechanical strength, leading to hydrogen embrittlement. Thus, the selection and design of inhibitors should take into account these detrimental effects. Inhibitors should either prevent hydrogen adsorption or favour H–H recombination.

The hydrogen permeation was controlled by the diffusion of hydrogen through the metal and the adsorption of the organic compound on the surface of the metal. The attainment

Fig. 7. Plots of hydrogen permeation current against time for carbon steel in HCl with CTAB and OPD inhibitors. (*a*) 1 mol/L HCl, (*b*) 1 mol/L HCl with 200 mmol/L CTAB, and (*c*) 1 mol/L HCl with 200 mmol/L CTAB and 20 mmol/L OPD.



of steady-state hydrogen permeation current density indicated a stable hydrogen surface coverage on the cathodic side of the membrane and saturation of the hydrogen traps present in the metal and a stable hydrogen concentration within the metal. The organic compounds were investigated for their ability to inhibit the rate at which hydrogen permeates through carbon steel in 1 mol/L HCl.

The transient curve shown in Fig. 7 for hydrogen permeation was controlled by the diffusion of hydrogen through the metal and the adsorption of the organic compound on the surface of the metal. The addition of CTAB alone reduces the permeation current compared with the blank. A further slight reduction in the permeation current was achieved by the addition of 20 mmol/L OPD with CTAB. This corresponds to higher IE values of the inhibitors and lesser permeation of hydrogen through the metal. It is expected that a system that induces maximum cathodic polarization will show lesser permeation current. Hence, CTAB with OPD exhibited a reduced permeation current.

The organic compounds possess high IE and, in addition, they reduce hydrogen permeation through the metal. This is to be expected since hydrogen arises from a corrosion reaction and any inhibition of this will necessarily lead to reduced hydrogen production and, therefore, reduced hydrogen uptake by the metal.

Scanning electron microscopy

Micrographs were made of carbon steel specimens in 1 mol/L HCl in the presence and absence of inhibitors and are shown in Figs. 8 and 9. The morphology of the specimen surface shows a characteristic corrosion pitting of mild steel in hydrochloric acid. These areas are highly oxidized. It was found that an uncovered surface of mild steel in acid corroded severely. Deep pits were observed throughout the specimen surface, which was immersed in HCl only, as clearly shown in Figs. 8*a*–8*c*. There was less pit formation in Fig. 9, which was made with CTAB alone in HCl. The addition of CTAB and OPD in HCl controlled the formation of

© 2006 NRC Canada

Fig. 8. SEM photographs for carbon steel dipped in 1 mol/L HCl.

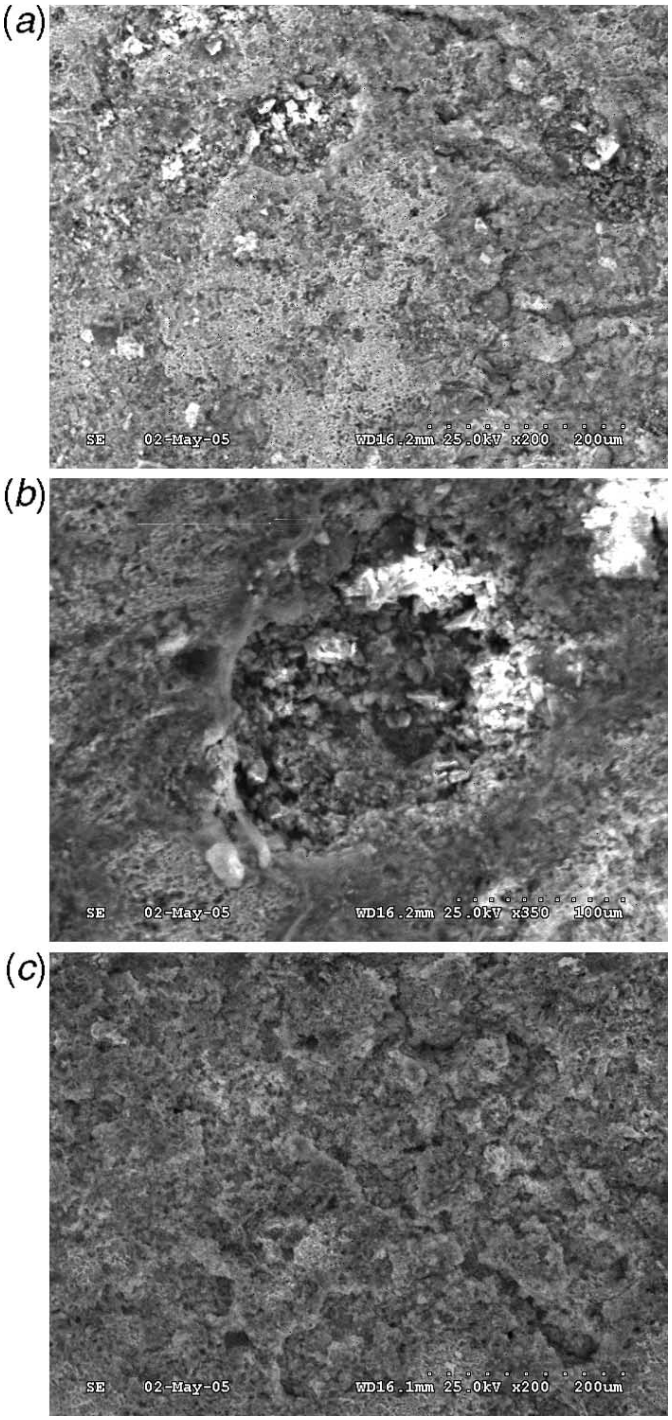
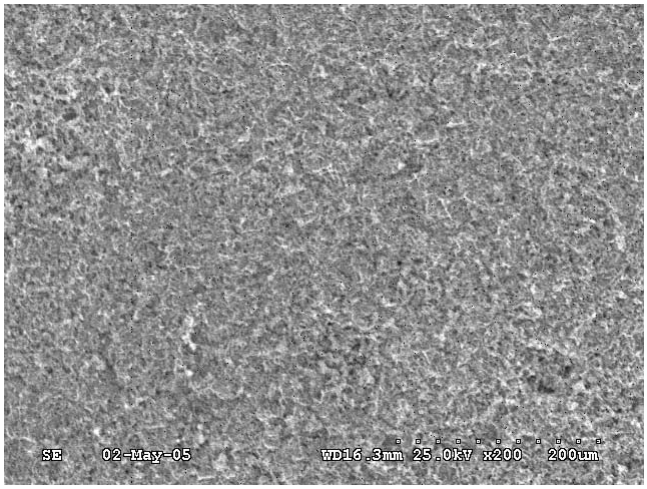


Fig. 9. SEM photograph for carbon steel dipped in 1 mol/L HCl with 200 mmol/L CTAB.



Fig. 10. SEM photograph for carbon steel dipped in 1 mol/L HCl with 200 mmol/L CTAB and 20 mmol/L OPD.



pits and protected the carbon steel from corrosion as shown in Fig. 10. These figures clearly show that the corrosion was less pronounced in the presence of inhibitors.

The increase in IE in all the techniques can be explained in the following way. Inhibition of corrosion can be attributed to the strong adsorption of the compound on the metal surface by the electron transfer from the organic molecule to the metal surface to form a coordinate type of link. This process is facilitated by the presence of low-energy vacant electron orbitals present in iron, as observed in the metals of the transition group.

As far as the inhibition process is concerned, it is generally assumed that the adsorption of the inhibitors at the metal solution interface is the first step in the action mechanism of inhibitors in aggressive acid media. Inhibition of corrosion of mild steel in HCl solution by the inhibitors can be explained on the basis of adsorption. Four types of adsorption may take place involving organic molecules at the metal solution interface: (*i*) electrostatic attraction between charged molecules and the charged metal, (*ii*) interaction of unshared electron pairs in the molecule with the metal, (*iii*) interaction of π electrons with the metal, and (*iv*) a combination of the above. It is apparent that the adsorption of these organic inhibitors on the metal surface could occur directly on the basis of donor acceptor interaction. Moreover, the presence of inhibitors in the organic structures makes the

© 2006 NRC Canada

formation of dπ–dπ bond which enhances the adsorption of the compounds on the metal surface. These compounds inhibit the corrosion by controlling both the anodic and cathodic reactions. In an acidic solution, these compounds can exist as protonated species. These protonated species may adsorb on the cathodic sites of the mild steel surface and decrease the evolution of hydrogen. The adsorption of these compounds on anodic sites may decrease anodic dissolution of mild steel.

The formation of positively charged species in an acidic medium also facilitates the adsorption of the compound on the metal surface through electrostatic interactions between the organic molecule and the metal surface. Adsorbed molecules of the organic compound decrease the anodic and cathode reaction sites, resulting in a decrease in the active surface area, an increase in polarization resistance R_p, and a decrease in the rate of diffusion of ions to or from the metal surface. In addition, the organic compound may react with adsorbed corrosion intermediates of the steel forming products that passivate the steel surface. This indicates an increase in the energy barrier for proton discharge, leading to less gas evolution.

The mechanism of inhibition in CTAB may be attributed to the the micelles that are formed at these concentrations of CTAB, a cationic surfactant. Above a certain concentration range, these surfactant molecules aggregate in aqueous solution to form particles of colloidal dimensions called micelles. At concentrations of less than 100 mmol/L, CTAB does not effectively inhibit corrosion. However, it shows excellent corrosion inhibition properties at concentrations greater than 100 ppm. This is due to the fact that the micelle concentration takes place over a narrow range of surfactant concentration, the critical micelle concentration, and is accompanied by distinct changes in various physical properties such as surface tension, light scattering, electrical conductivity, solubility capacity, viscosity, and osmotic pressure for a wide variety of solutes. Below and up to the critical micelle concentration, the monomeric surfactant acts as a strong electrolyte, fully dissociated and aggregated. Aggregation begins at the critical concentration, at first with the formation of relatively small micelles that grow rapidly over a very limited concentration range to a size, which for a given surfactant remains approximately constant with further increase in surfactant concentration. Micelles are pictured as liquidlike, spherical in shape, their interior approximating that of liquid hydrocarbons but with hydrophilic end chains constrained to micelle surface. Above the critical micelle concentration, increases in the surfactant concentration lead to an increase in the number of micelles with little, if any, increase in the number of monomer surfactants (23).

With the hydrocarbon chains forming the inner hydrophilic core of the spherical micelles, the polar head groups of ionic micelles align together in a compact manner at the micelle surface. The ionic head groups of the surfactants and a portion of the counter ions form a compact "Stern" layer at the micelle surface at which about 60%–75% of the micelle charge is believed to be neutralized. The remaining ions form a diffuse Guoy–Chapman layer (24).

The addition of OPD in CTAB increases the IE in all the tests and this is due to adsorption of amines through electrostatic interaction between the positively charged amine and the negatively charged metal surface. In addition, in the case of aromatic amines the π electron interaction between the aromatic molecules and the positively charged metals may also play a role.

The concentration of inhibitor has a very great influence on the corrosion of carbon steel. This may be due to the formation of Fe^{2+} and Fe^{3+} complex species with ions like OH^- and Cl^-. For example, Fe^{2+} and Fe^{3+} ions formed from the metal dissolution should be able to form a corrosion product but the film of inhibitor on the surface prevents them. At low concentrations of these additives, the Fe^{2+} and Fe^{3+} ions resulting from metal dissolution should have formed an insoluble protective film of the type $Fe(OH)_3 – FeCl_3$ on the steel surface, but this is converted to a soluble one only at higher currents and temperatures.

The strong influence of the H^+ ion in this medium also helps in the oxidation of Fe^{++}. On the other hand, the solubility of a protective $Fe(OH)_3 – FeCl_3$ film is able to incorporate the inhibitor molecules to form a protective stable film. This incorporation of inhibitor molecules in the protective layer stabilizes the protective layer on the steel surface and decreases the corrosion rate.

Conclusions

The following conclusions can be made: (*i*) the IE calculated by gravimetric and potentiodynamic methods revealed that the combined inhibition effect of OPD and CTAB is better than the CTAB alone; (*ii*) potentiodynamic polarization data showed that the values of E_{corr} decreased using CTAB alone and decreased further with the addition of OPD; (*iii*) CTAB and OPD influence the b_c values but not specific changes in b_a values, showing that inhibitors are of mixed type; (*iv*) the R_p values obtained from EIS studies showed that the addition of OPD in CTAB increases R_p values; (*v*) the adsorption isotherm data showed that inhibitors obey Langmuir's adsorption isotherm; (*vi*) the IE was observed as high for 200 mmol/L of CTAB with 20 mmol/L of OPD in all the techniques studied; and (*vii*) micrographs clearly indicate that these inhibitors control the corrosion of carbon steel in 1 mol/L HCl.

Acknowledgement

The authors thank the Director of the Central Electrochemical Research Institute, Karaikudi 630 006, India for his kind help in carrying out this work.

References

1. A. Chetouani, A. Aouniti, B. Hammouti, N. Benchat, T. Benhadda, and S. Kertit. Corros. Sci. 45, 1675 (2003).
2. K. Tebbji, H. Oudda, B. Hammouti, M. Benkaddour, M. El Kodadi, F. Malek, and A. Ramdani. Appl. Surf. Sci. **241**, 326 (2005).
3. A. Dafali, B. Hammouti, R. Touzani, S. Kertit, A. Ramdani, and K. El Kacemi. Anti-Corros. Methods Mater. **49**, 96 (2002).
4. A. El-Ouafi, B. Hammouti, H. Oudda, S. Kertit, R. Touzani, and A. Ramdani. Anti-Corros. Methods Mater. **49**, 199 (2002).
5. K. Tebbji, H. Oudda, B. Hammouti, M. Benkaddour, M. El Kodadi, and A. Ramdani. Colloids Surf. A, **259**, 157 (2005).

© 2006 NRC Canada

6. M. Elayyachy, M. El Kodadi, B. Hammouti, A. Ramdani, and A. El Idrissi. Pigm. Resin Technol. **33**, 375 (2004).
7. A. Popova, E. Sokolova, S. Raicheva, and M. Chritov. Corros. Sci. **45**, 33 (2003).
8. H.-L. Wang, R.-B. Liu, and J. Xin. Corros. Sci. **46**, 10, 2455 (2004).
9. S. Bilgiç. Mater. Chem. Phys. **76**, 52 (2002).
10. Sk.A. Ali, M.T. Saeed, and S.U. Rahman. Corros. Sci. **45**, 253 (2003).
11. J. Cruz, R. Martínez, J. Genesca, and E. García-Ochoa. J. Electroanal. Chem. **566**, 111 (2004).
12. C.K. Emregül and O. Atakol. Mater. Chem. Phys. **83**, 373 (2004).
13. S.S. Abd El Rehim, H.H. Hassan, and M.A. Amin. Mater. Chem. Phys. **78**, 337 (2003).
14. B. El Medí, B. Mernari, M. Trainsnel, F. Bentiss, and M. Lagrenée. Chem. Phys. **77**, 489 (2003).
15. M. El Azhar, M. Traisnel, B. Mernari, L. Gengembre, F. Bentiss, and M. Lagrenée. Appl. Surf. Sci. **185**, 197 (2002).
16. P. Morales-Gil, G. Negrón-Silva, M. Romero-Romo, C. Ángel-Chávez, and M. Polomar-Pardavé. Electrochim. Acta, **49**, 4733 (2004).
17. P. Manjula, S. Manonmani, P. Jayaram, and S. Rajendran. Anti-Corros. Methods Mater. **48**, 319 (2001).
18. B. Ramesh Babu and R. Holze. Br. Corros. J. **35**, 204 (2000).
19. M.E. Haque, A.R. Das, and S.P. Moulik. J. Phys. Chem. **99**, 14032 (1995).
20. P.K. Jana and S.P. Moulik. J. Phys. Chem. **95**, 9525 (1991).
21. A.A. Abdel Fattah, K.M. Atia, F.S. Ahmed, and M.I. Roushdy. Corr. Prev. Control, **33**, 67 (1986).
22. F.B. Growcock and W.W. Frenier. J. Electrochem. Soc. **135**, 817 (1988).
23. K.N. Srinivasan, M. Selvam, and S. Venkatakrishna Iyer. J. Appl. Electrochem, **23**, 358 (1993).
24. F.B. Growcock, V.P. Lopp, and R.J. Josinski. J. Electrochem. Soc. **135**, 823 (1988).

© 2006 NRC Canada

Synthesis and coordination chemistry of the diamido-arsine ligand [NAsN] (NAsN = $PhAs(CH_2SiMe_2NPh)_2$))

Christopher D. Carmichael, Michael P. Shaver, and Michael D. Fryzuk

Abstract: The preparation and characterization of the diamido-arsine ligand $[NAsN]Li_2(THF)$ (**1**) (where NAsN = $PhAs(CH_2SiMe_2NPh)_2$), the protonated ligand precursor $[NAsN]H_2$ (**2**), and its coordination chemistry with tantalum is presented. The complex $[NAsN]TaMe_3$ (**3**) can be synthesized from **1** and $TaMe_3Cl_2$. Hydrogenation of **3** did not produce the desired tetrahydride $([NAsN]Ta)_2(\mu\text{-}H)_4$, instead, activation of Ta–N bonds in the complex produced a modest yield of the free ligand **2**. In an attempt to understand the unusual reactivity of **3**, a density functional theory investigation of the model complexes 'NAsN'$Li_2(OMe_2)_2$ (**4**) and 'NAsN'$TaMe_3$ (**5**) (where 'NAsN' = $MeAs(CH_2SiH_2NMe)_2$) and their phosphine analogs 'NPN'$Li_2(OMe_2)$ (**7**), 'NPN'$TaMe_3$ (**8**), and a related niobium complex 'NPN'$NbMe_3$ (**10**) (where 'NPN' = $MeP(CH_2SiH_2NMe)_2$) was undertaken. The difference between the chemistry supported by the As and P ligands originates from the poor binding of As to Ta in these systems and is likely due to a mismatch of the soft As donor and the hard Ta(V) metal centre.

Key words: arsine ligand, tridentate, tantalum, hydrogenation, DFT calculations.

Résumé : On a décrit la synthèse et la caractérisation du coordinat diamido-arsine $[NAsN]Li_2(THF)$ (**1**) [dans lequel NAsN= $PhAs(CH_2SiMe_2NPh)_2$], de son précurseur protoné $[NAsN]H_2$ (**2**) et sa chimie de coordination avec le tantale. On a synthétisé les complexes $[NAsN]TaMe_3$ (**3**) par réaction du composé **1** avec le $TaMe_3Cl_2$. L'hydrogénation du composé **3** ne conduit pas à la formation de l'hydrure recherché de formule $([NAsN]Ta)_2(\mu\text{-}H)_4$; on observe plutôt une activation des liaisons Ta–N dans le complexe qui conduit à la formation du coordinat libre (**2**) avec un faible rendement. Dans le but d'essayer de comprendre la réactivité inhabituelle du composé **3**, on a entrepris une étude basée sur la théorie de la fonctionnelle de la densité des complexes modèles 'NAsN'$Li_2(OMe_2)_2$ (**4**) et 'NAsN'$TaMe_3$ (**5**) [dans lesquels 'NAsN' = $MeAs(CH_2SiH_2NMe)_2$], des phosphines analogues 'NPN'$Li_2(OMe_2)_2$ (**7**) et 'NPN'$TaMe_3$ (**8**) et d'un complexe du niobium apparenté 'NPN'$NbMe_3$ (**10**) dans lesquels 'NPN' = $MeP(CH_2SiH_2NMe)_2$. La différence entre la chimie supportée par les coordinats de As ou de P tire son origine de la faible liaison du As au Ta dans ces systèmes qui est probablement causée par mauvaise adaptation du donneur doux As et du centre métallique dur du Ta(V).

Mots-clés : coordinat arsine, tridentate, tantale, hydrogénation, calculs sur la base de la théorie de la fonctionnelle de la densité.

[Traduit par la Rédaction]

Introduction

Our interest in small molecule activation has centered around the design, synthesis, and coordination chemistry of a variety of mixed donor ancillary ligands in an attempt to generate reactive metal complexes (1–3). One of the key design criteria has been to utilize multidentate ligand sets that can support changes in oxidation state of the central metal. For this reason, we have concentrated on combinations of hard and soft donors, in particular, amido- and phosphine-based systems as shown in Chart 1 (4, 5).

Recently, we have disclosed the use of the [NPN] system shown (Chart 1) (where NPN = $PhP(CH_2SiMe_2NPh)_2$) as an ancillary ligand for the activation and functionalization of molecular nitrogen by early transition metals (6). In particular, the side-on end-on bound dinitrogen complex $([NPN]Ta)_2(\mu\text{-}H)_2(\mu\text{-}\eta^1\text{:}\eta^2\text{-}N_2)$ and its reactivity with boranes, alanes, and silanes has been extensively studied (7–9). Reactivity patterns in the [NPN] system can be altered by changing the substituents at both nitrogen and phosphorus (10, 11). Presumably, a change in the neutral donor atom in the ligand from phosphorus to arsenic should also affect reactivity patterns of the resultant complexes. Previously, we have reported profound changes in reductive stability of the $[As_2N_2]$ analogue (12) of the macrocyclic $[P_2N_2]$ system shown in Chart 1.

In comparison with phosphines, arsines are known to be modest σ donors and π acceptors (13). From an NMR spectroscopic point of view ^{75}As (I = 3/2), unlike ^{31}P, is not a

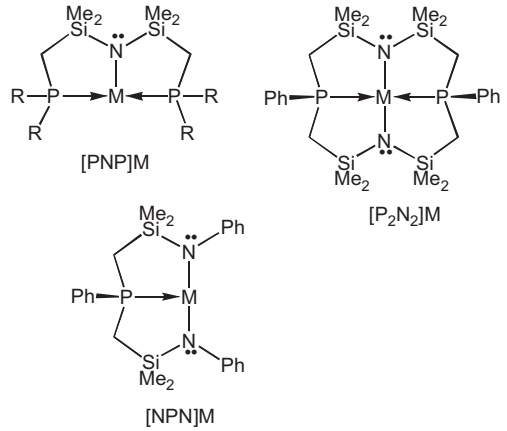
Received 25 September 2006. Accepted 7 November 2006. Published on the NRC Research Press Web site at http://canjchem.nrc.ca on 6 January 2007.

C.D. Carmichael, M.P. Shaver, and M.D. Fryzuk.[1] Department of Chemistry, The University of British Columbia, 2036 Main Mall, Vancouver, BC V6T 1Z1, Canada.

[1]Corresponding author (e-mail: fryzuk@chem.ubc.ca).

 doi:10.1139/V06-173 © 2006 NRC Canada

Chart 1. Related amido-phosphine ligand systems with different ratios of phosphine to amido donors.



useful nucleus because of its quadrupolar nature (14). Although the majority of arsine coordination chemistry has been limited to the late transition metals by the modest electron-donating and -accepting properties of arsenic, there are examples of both monodentate and bidentate arsine ligands bound to early transition metals (15, 16), and in particular there are a few reports of arsine–tantalum complexes (17–19).

In this paper, the successful synthesis of a diamido-arsine ligand, [NAsN] (where NAsN = $PhAs(CH_2SiMe_2NPh)_2$), its coordination chemistry to Ta(V) to generate $[NAsN]TaMe_3$, and attempts to hydrogenate this trimethyl complex are reported. We also include the results of a density functional theory (DFT) investigation of the model complexes '$NAsN'Li_2(OMe_2)_2$ and '$NAsN'TaMe_3$ (where 'NAsN' = $MeAs(CH_2SiH_2NMe)_2$). The results are compared with the analogous series of model complexes using the 'NPN' ligand, '$NPN'Li_2(OMe)$ (**6**), '$NPN'TaMe_3$ (**7**), and the related niobium complex '$NPN'NbMe_3$ (**8**) (where 'NPN' = $MeP(CH_2SiH_2NMe)_2$).

Results and discussion

Synthesis

The synthesis of $[NAsN]Li_2(THF)_2$ (**1**) is shown in eq. [1] and is analogous to that described for $[NPN]Li_2(THF)_2$. Thus, the addition of 4 equiv. of BuLi to a mixture of 2 equiv. of $PhNHSiMe_2CH_2Cl$ and 1 equiv. of $PhAsH_2$ in diethyl ether leads to the formation of the dilithiated diamidophosphine as a diethyl ether adduct. Addition of 4 equiv. of THF to a hexanes slurry of the first species and subsequent precipitation affords the bis THF adduct **1** in 78% yield.

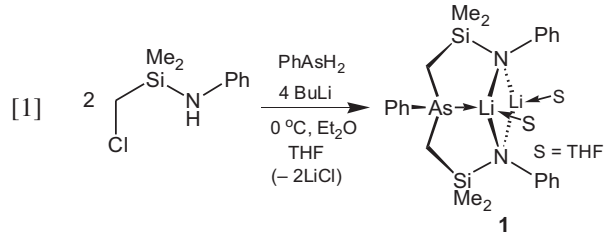


Fig. 1. Molecular structure (ORTEP) of $[NAsN]Li_2(THF)_2$ (**1**). Ellipsoids are drawn at 50% probability.

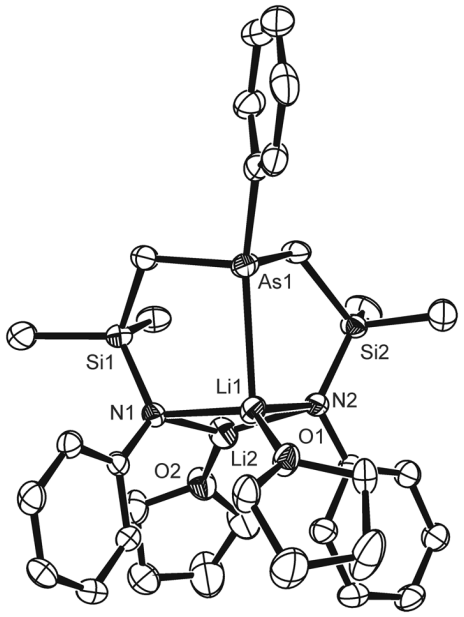


Table 1. Selected bond distances and angles for $[NAsN]Li_2(THF)_2$ (**1**).

Bond distances (Å)	
N(1)—Li(1)	2.089(9)
N(2)—Li(1)	2.045(9)
N(1)—Li(2)	1.984(9)
N(2)—Li(2)	2.020(9)
As(1)—Li(1)	2.686(8)
O(1)—Li(1)	1.872(8)
O(2)—Li(2)	1.880(9)
Bond angles (°)	
As(1)–Li(1)–N(1)	92.5(3)
As(1)–Li(1)–N(2)	95.0(3)
O(1)–Li(1)–N(1)	128.4(4)
O(1)–Li(1)–N(2)	120.3(4)
O(2)–Li(2)–N(2)	131.1(5)
Li(1)–N(1)–Li(2)	75.2(3)
Li(1)–N(2)–Li(2)	75.5(4)

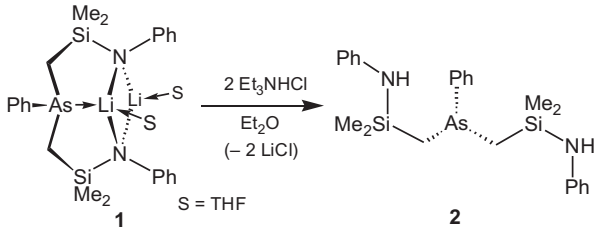
X-ray quality crystals of **1** were grown from a saturated THF solution at –40 °C. X-ray diffraction studies determined the crystal to be a two-component twin; the two orientations of the lattice are related by a rotation of 7.77° normal to 0.03, –1.00, and –1.39. The solid-state molecular structure of **1** is presented in Fig. 1, and selected bond distances and angles are given in Table 1. The structure contains a Li_2N_2 core, like the similar $[NPN]Li_2(THF)_2$ (20) and macrocyclic $[E_2N_2]Li_2$(1,4-dioxane) (E = P, As) complexes (12, 21), and the bond distances and angles of the core agree well with these complexes. The Li(1)–As(1) bond distance of 2.686(6) Å agrees well with the macrocyclic $[As_2N_2]Li_2$(1,4-dioxane) (12) and other similar molecules (22–24).

The ambient temperature ^1H NMR spectrum of **1** displays resonances due to two types of silyl methyl protons, and the

© 2006 NRC Canada

CH_2 ring proton signals appear as a pair of AB doublets, as expected from the solid-state structure. However, the $^7Li\{^1H\}$ spectrum is comprised of a narrow singlet indicating there is only a single lithium environment in solution, whereas two distinct lithium environments would be expected on the basis of the X-ray structure. Substituted variations of the $[NPN]Li_2$ system with only one coordinated solvent donor also show only a single environment in the $^7Li\{^1H\}$ NMR spectrum (10, 11); a fluxional process that exchanges the lithium environments through migration of the phosphine and donor solvent from one lithium to another has been postulated to explain this behaviour (11). Complex **1** is the first observation of a $^7Li\{^1H\}$ singlet in the $[NEN]Li_2$ (E = P, As) ligand family with two coordinated solvent molecules. It is possible that a fluxional process involving arsenic migration can exchange the lithium environments, however, variable temperature ^1H NMR experiments performed on **1** (290–190 K) did not show decoalescence of any resonances. Another possibility for the observed singlet is that arsenic may not be coordinated to either of the lithium ions in solution.

The synthesis of the protonated ligand precursor $[NAsN]H_2$ (**2**) is outlined in eq. [2]. Reaction of **1** with 2 equiv. of NEt_3HCl affords **2** in 96% yield as a colourless oil. Allowing the oil to stand for several weeks produced X-ray quality crystals of **2**.

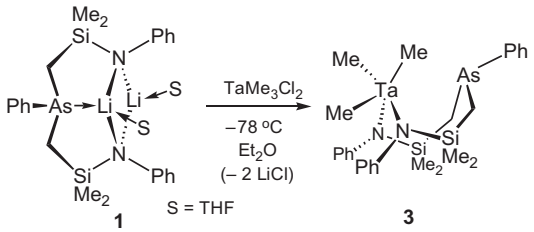
[2] 

Selected bond distances and angles are collected in Table 2. The asymmetric unit contains two independent molecules, one of which is shown in Fig. 2. The hydrogen atoms bound to N(1) and N(2) were located within the diffraction pattern and refined isotropically. Delocalization of the nitrogen lone pair into the aromatic ring is evidenced by the planarity around the nitrogen atoms ($\Sigma(°)$ 360°). This is also reflected in the short C–N bonds (1.412(4) and 1.401(4) Å) (25–27), compared with nonconjugated examples (28, 29) and indicates partial double bond character. The acute angles about the central arsenic atom have also been observed in solid-state structures of other arsine molecules (30–32). In solution, the silylamine arms are equivalent, and the compound assumes C_s symmetry with the silylmethyl proton resonances appearing as two singlets in the ^1H NMR spectrum, the signals due to methylene protons as a pair of AB doublets, and the NH resonances as a broad singlet.

The synthesis of $[NAsN]TaMe_3$ (**3**) is outlined in eq. [3]. Reaction of dilithio **1** with $TaMe_3Cl_2$ affords **3** as a pale yellow solid in 63% yield after washing with minimal pentane. The product is quite soluble in pentane, and the necessity of removing soluble coloured by-products contributes to the modest yield. Solutions of **3** are photochemically and thermally sensitive, and appropriate precautions must be taken during the reaction; however, the isolated and dried solid

Table 2. Selected bond distances and angles for $[NAsN]H_2$ (**2**).

Bond distances (Å)	
N(1)—Si(1)	1.747(3)
N(1)—C(13)	1.412(4)
As(1)—C(1)	1.997(3)
As(1)—C(7)	1.972(3)
Si(2)—N(2)	1.741(3)
N(2)—C(19)	1.401(4)
As(1)—C(2)	1.990(3)
Bond angles (°)	
C(1)–As(1)–C(2)	99.87(13)
C(1)–As(1)–C(7)	98.08(13)
C(2)–As(1)–C(7)	99.97(12)
Si(1)–N(1)–C(13)	133.7(3)
Si(2)–N(2)–C(19)	133.7(2)

[3] 

can be stored for extended periods of time in the dark at –40 °C.

Crystals of **3** suitable for X-ray diffraction experiments were grown by slow evaporation of a concentrated benzene solution. The solid-state molecular structure of **3** is presented in Fig. 3, and selected bond distances and angles are detailed in Table 3. The most striking feature of the structure is that arsenic is not coordinated to tantalum (Ta···As = 4.55 Å), which makes the tantalum five-coordinate. The geometry about the tantalum center is a distorted square pyramid with N(1) in the apical position, and the methyl groups are all cis disposed. There is a distinct lack of symmetry in the molecule; this can be observed in the phenyl amido groups and the phenyl group bound to arsenic. Comparing the bonding to the structurally characterized $[NPN]TaMe_3$ complex (20), the Ta–N and Ta–C bonds are slightly shorter on average, perhaps because of the five-coordinate nature of **3**. The Ta–N distances are, however, not significantly different from other [NPN]Ta complexes (33–35), and both Ta–N and Ta–C match those of similar complexes in the literature (36–41). Very few coordination complexes containing tantalum arsenic interactions have been characterized in the solid state. There are two examples using the diars ligand (o-$C_6H_4(AsMe_2)_2$) (17, 42) and three examples of tantalum arsenic clusters (19, 43). The absence of nonchelating examples suggests that interactions between arsenic and tantalum are weak and a stabilizing force is necessary for coordination. The fact that arsenic does not coordinate in **3**, despite the chelating nature of the ligand, confirms the poor coordinating ability of arsenic donors to high oxidation state metal centres such as Ta(V).

NMR data provide some insight into the structure of **3** in solution. The ambient temperature ^1H NMR spectrum of **3**

© 2006 NRC Canada

Fig. 2. Molecular structure (ORTEP) of $[NAsN]H_2$ (**2**). Ellipsoids are drawn at 50% probability.

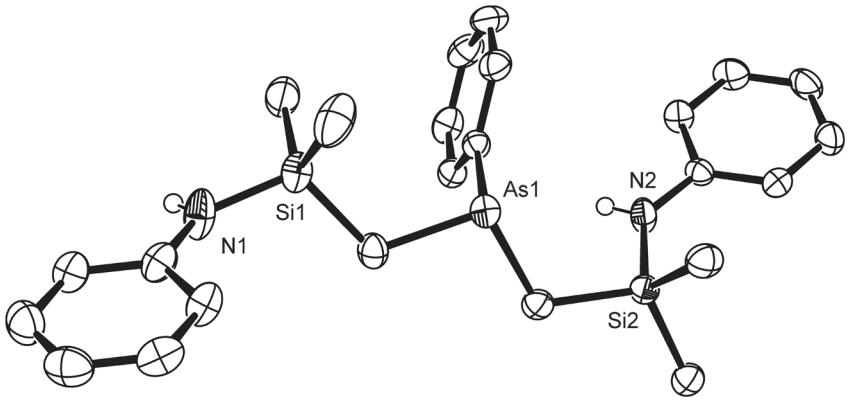


Fig. 3. Molecular structure (ORTEP) of $[NAsN]TaMe_3$ (**3**). Ellipsoids are drawn at 50% probability.

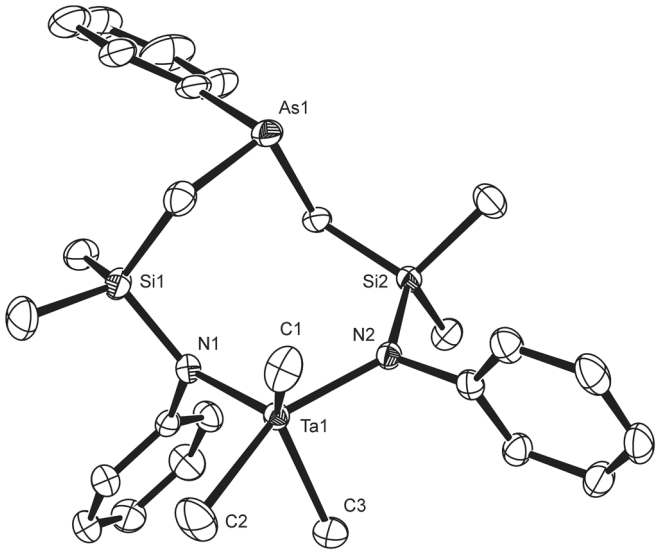


Table 3. Selected bond distances and angles for $[NAsN]TaMe_3$ (**3**).

Bond distances (Å)	
Ta(1)—C(1)	2.189(2)
Ta(1)—C(2)	2.223(2)
Ta(1)—C(3)	2.176(2)
Ta(1)—N(1)	1.948(2)
Ta(1)—N(2)	2.014(2)
Ta(1)···As(1)	4.550(2)
Bond angles (°)	
C(1)–Ta(1)–C(2)	77.53(11)
C(1)–Ta(1)–C(3)	126.43(10)
C(2)–Ta(1)–C(3)	78.71(11)
N(1)–Ta(1)–C(1)	117.20(8)
N(1)–Ta(1)–C(2)	98.83(9)
N(2)–Ta(1)–C(1)	87.39(8)
N(2)–Ta(1)–C(2)	149.72(8)
N(2)–Ta(1)–C(3)	89.88(8)
N(1)–Ta(1)–C(3)	113.44(9)
N(1)–Ta(1)–N(2)	111.44(7)

shows only two silyl methyl resonances, and the methylene resonances appear as a pair of AB doublets, consistent with a C_s symmetry. A single resonance is observed for the three tantalum-bound methyl groups, indicating that a fluxional process must be exchanging the methyl groups in solution. If the complex is five-coordinate in solution and approximates the distorted square pyramid of the solid-state structure, the Ta-methyl groups can be made equivalent through a standard Berry pseudo rotation.

Variable temperature ^{1}H NMR experiments performed in d_8-toluene show that, at 195 K, two resonances are observed for the tantalum-bound methyl groups at δ 1.36 and 1.03, in a 2:1 ratio. A similar 2:1 ratio of methyl resonances has been observed at low temperature in the octahedral complex $[NPN]TaMe_3$, but at significantly different shifts of δ 0.40 and –0.05 (20). This was attributed to cis and trans conformation of the methyls in relation to the phosphine donor. The difference in the shift of the methyl resonances is as pronounced in the RT spectra, where $[NPN]TaMe_3$ has a doublet at δ 0.55 because of phosphorus coupling, and the resonance in **3** is a singlet at δ 1.09. The low temperature ^{1}H spectrum of $[NPN]TaMe_3$ also shows hindered rotation of the amido phenyl groups; however, **3** shows no evidence of this, even at 185 K. There are significant differences in the chemical shifts of the methylene resonances of these two complexes, with $[NPN]TaMe_3$ displaying two multiplets at δ 1.23 and 1.18 and **3** having AB doublets at δ 1.82 and 1.25. The spectral differences suggest that **3** may be five-coordinate in solution; lowering the temperature slows the Berry pseudo rotation and results in the two Ta-methyl signals. However, a six-coordinate structure where the low temperature methyl signals are due to cis and trans conformations relative to the arsine donor cannot be definitively ruled out.

Reaction of **3** with donating solvents such as THF, pyridine, and PMe_3 does not produce solvent adduct complexes, which would be expected if **3** were five-coordinate in solution. This is not conclusive, however, because it is possible that the phenylarsine unit, while not coordinated to the tantalum center can still effectively block access to the open coordination site for a potential ligand.

Hydrogenation of **3** performed under one or four atmospheres (1 atm = 101.325 kPa) of hydrogen in the absence of light does not produce the dinuclear tetrahydride analog of $([NPN]Ta)_2(\mu\text{-}H)_4$, namely $([NAsN]Ta)_2(\mu\text{-}H)_4$. When a diethyl ether solution of **3** is exposed to H_2 (4 atm), a subtle

© 2006 NRC Canada

colour change from pale yellow to pale tan is observed over 24 h, and a colourless solid is deposited on the sides of the flask. In contrast, hydrogenation of [NPN]$TaMe_3$ results in a deep purple-red solution and formation of the dinuclear tetrahydride (20). Evaporation of the solvent from the reaction of **3** with H_2 leaves an oily brown residue, and examination of the soluble material by ^{1}H NMR indicates that a single material displaying two resonances in the silylmethyl region, a pair of doublets in the methylene region, and a broad resonance at δ 3.1 is the major product. The spectrum closely matches that of the protonated ligand precursor [NAsN]H_2 (**2**). No resonances attributable to tantalum hydrides are observed, nor are resonances due to the starting material **3**. ^{1}H NMR spectra obtained in the presence of an internal standard (ferrocene) indicates a 33% yield of **2**.

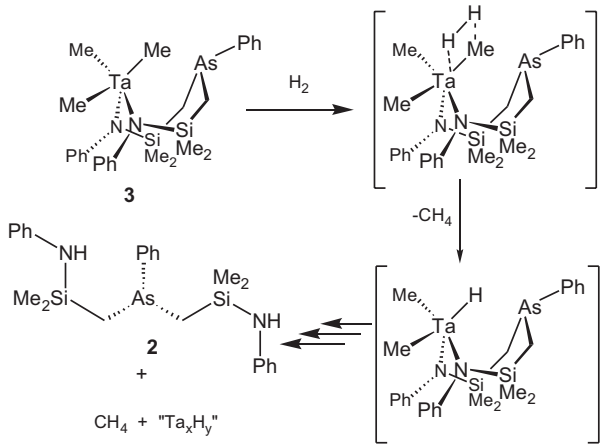
Reaction of **3** with 4 atm of deuterium (D_2) produces the same colour change and precipitate; however, a ^{1}H NMR spectrum of the soluble material indicates the broad N–H resonance is present, although with significantly smaller integration relative to the methylene and silylmethyl resonances. Integration of the spectrum against an internal standard shows a 32% yield of deuterated **2** (D_2-**2**). The trace amount of **2** is due to thermal decomposition of **3**. A solution of **3** in benzene or THF produces approximately 1% of **2** by integration over the course of 24 h at RT. Although the reaction of **3** with adventitious water cannot be completely ruled out, the degree of deuteration suggests the product is formed by reaction of **3** with H_2–D_2 exclusively.

Hydrogenations performed under lower pressure (1 atm) of hydrogen primarily produce unidentified products from which small amounts of **2** (<5%) can be identified, while deuterations produce similar small amounts of D_2-**2** and a trace of **2** from thermal decomposition of **3**. Following the reaction by ^{1}H NMR spectroscopy does not show any intermediates; the formation of **2** is complete in the first 24–48 h of the reaction, and no resonances attributable to tantalum hydrides are observed. Further reaction time leads to decomposition of the remaining **3**. It is not known why the reaction stops producing **2**, as dissolved hydrogen remains visible in ^{1}H NMR spectrum.

Elemental analyses of the isolated materials, while not reproducible from reaction to reaction, are consistently low in carbon and hydrogen relative to the trimethyl complex **3**, suggesting possible loss of methane. Methane gas can be detected in the headspace of four atmosphere hydrogenations by GC-MS; however, it could not be quantified because of limitations in the four-atmosphere apparatus. Methane was not detected in the one-atmosphere experiments, presumably because not enough methane is produced in such small-scale reactions to permit detection.

Monitoring the hydrogenation reaction of **3** by ^{1}H NMR spectroscopy does not reveal any hydride containing intermediates. However, the detection of methane suggests that the hydrogenation of **3** begins with a σ-bond metathesis of Ta–C bonds producing methane and a tantalum hydride, as shown in Scheme 1. This type of mechanism follows directly from that postulated previously for the hydrogenation of [NPN]$TaMe_3$; however, in that case, further hydrogenation results in the evolution of two additional equivalents of methane and the eventual formation of the dinuclear tetrahydride ([NPN]Ta)$_2$(μ-H)$_4$. The hydrogenation of **3** follows a different reaction pathway leading to the free ligand **2**. It is possible that the amide could be removed from the metal center by reductive N–H formation followed by tantalum amine dissociation affording a Ta(III) dihydride species containing a dangling amine. However, the absence of intense colours in this reaction, typical of low valent tantalum complexes, suggests that any Ta(III) is present only as a transient species. It seems more probable that the mechanism parallels that of [NPN]$TaMe_3$ with further metathesis of tantalum methyl bonds to produce a transient trihydride. At this point, it is possible that a partially open coordination site permits coordination of an additional equivalent of H_2 followed by hydrogenation of the Ta–N bonds. This is supported by the H_2 pressure dependence of the reaction, which suggests that it may be necessary to force the H_2 into the tantalum coordination sphere, perhaps by fully displacing the arsenic donor. However, this steric argument is not supported by previous work with the macrocyclic [P_2N_2] ligand, which has shown that a sterically congested seven-coordinate alkyl complex, [P_2N_2]$TaMe_3$, can be cleanly hydrogenated to yield the dinuclear tetrahydride ([P_2N_2]Ta)$_2$(μ-H)$_4$ (44). Another possibility is the direct hydrogenation of Ta–N bonds in preference to the Ta–C bonds. The fact that Ta–N bonds are significantly stronger than Ta–C bonds suggests that this would not be the preferred reaction (45–48).

Scheme 1.



Previous work in the Fryzuk group performed using ruthenium has shown that the Ru–N bond can activate H_2 to generate Ru-H and N-H moieties (49), including a system supported by the [NPN] ligand (50). The hydrogenation of metal-amide bonds has also been implicated in the regeneration of the active catalytic species for the hydrogenation of ketones and imines via the metal-ligand bifunctional mechanism (51–53). However, this chemistry is virtually unknown for the early transition metals. There are examples of imide hydrogenation in substituted cyclopentadienyl titanium systems (54, 55) and a molybdenum system that formally adds molecular hydrogen across the Si–N bond of a diamido ligand via transfer of H from a coordinated dihydrogen complex (56).

DFT calculations

The observation that the simple substitution of arsenic for phosphorus in the ancillary ligand leads to such a profound difference in the hydrogenation reactivity between

© 2006 NRC Canada

[NAsN]$TaMe_3$, **3**, and [NPN]$TaMe_3$ was unexpected. In an attempt to probe this chemistry further, density functional theory (DFT) calculations were performed on model complexes of **1**, **3**, and their phosphine analogs along with the niobium complex [NPN]$NbMe_3$.

The literature contains many examples of theoretical investigations conducted on transition metal complexes, including reactivity studies (57). Comparative studies have been performed on the activation of methane C–H bonds via oxidative addition and σ-bond metathesis in platinum and rhodium systems (58, 59). Generally, σ-bond metathesis reactions have been studied for high oxidation state early transition metals and lanthanides because oxidative addition is not possible. Investigations conducted on the reaction of Cp_2LnH complexes with H–H (60) and Si–H bonds (61) have shown the reactions proceed via σ-bond metathesis. Similarly, DFT studies on zirconium systems have suggested that a variety of bond activation processes progress through the same mechanism (62–64).

Geometry optimizations and DFT calculations were performed with the Gaussian 98 software package (65) using the B3LYP hybrid functional (66) and the LANL2DZ basis set (67, 68). While care must be taken with DFT calculations of systems with phosphines to incorporate the role of d-type functions in correlated wave functions to account for extra polarization (69), the effect of phosphorus atom d-type functions on the calculated M–P bond distances in diamidodiphosphine systems was studied systematically and found to have a negligible influence (70, 71). For the arsenic systems, the LANL2DZ basis set was augmented with diffusion and polarization functions (denoted LANL2DZdp) (72) to better account for the filled 3d-orbitals of arsenic. Recent results using these additional functions have illustrated their utility in modeling arsenic ligands bound to main group elements (73). Rather than use the [NPN] or [NAsN] framework, a simplified version of the ligand, 'NEN' (where 'NEN' = $MeE(CH_2SiH_2NMe)_2$ and E = P, As), was utilized to reduce calculation complexity. This simplified ligand uses methyl groups on amide and neutral donors and a secondary silane backbone instead of a bis(methylsilyl) backbone.

The model complex 'NAsN'$Li_2(OMe_2)_2$ (**4**) is depicted in Fig. 4 with selected optimized bond distances; 'NPN'$Li_2(OMe_2)$ (**5**) is depicted in Fig. 5 along with bond data. The bond distances and angles of **4** compare well to the solid-state structure for **1**, while those of **5** compare well with [NPN]$Li_2(THF)_2$ (20) and the variant ^{CyMes}[NPN]Li_2(THF) (11) with a cyclohexyl phosphine and the bulky mesityl amide. The N_2Li_2 cores are more square in the model complexes, with distances up to 0.1 Å longer and angles closer to 90°; they differ only slightly despite the fact that the [NPN] derivative has two donor solvent molecules and the model complex only has one. This suggests that the presence or absence of the second solvent molecule does not greatly influence the structure of the ligand. Comparing E–Li distances finds that both are longer in the model complexes with the P–Li distance of **7** marginally longer and the As–Li distance of **4** approximately 0.4 Å longer than in **1**. The longer Li–As distance in the model complex could be due to limitations in the DFT method for modeling the bonding of a soft ligand like arsenic with a hard metal such as lithium. Alternatively, the longer distance in the model complex could be due to the removal of the silylmethyls in the 'NAsN' ligand. It is possible that the silylmethyl groups of **1** could force the arsenic closer to the lithium ion by tightening the angle between the methylene and amide attached to silicon.

Fig. 4. Calculated geometry for 'NAsN'$Li_2(OMe_2)_2$ (**4**) with selected optimized bond distances (Å). Values in brackets are experimental values for **1**.

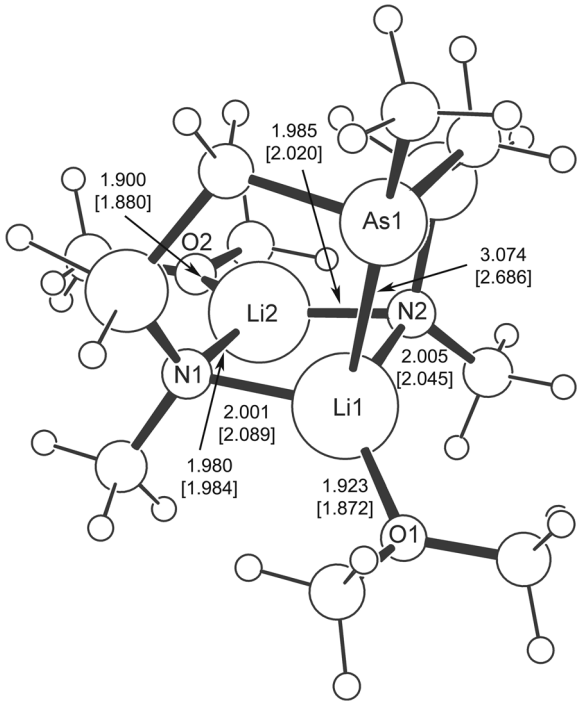
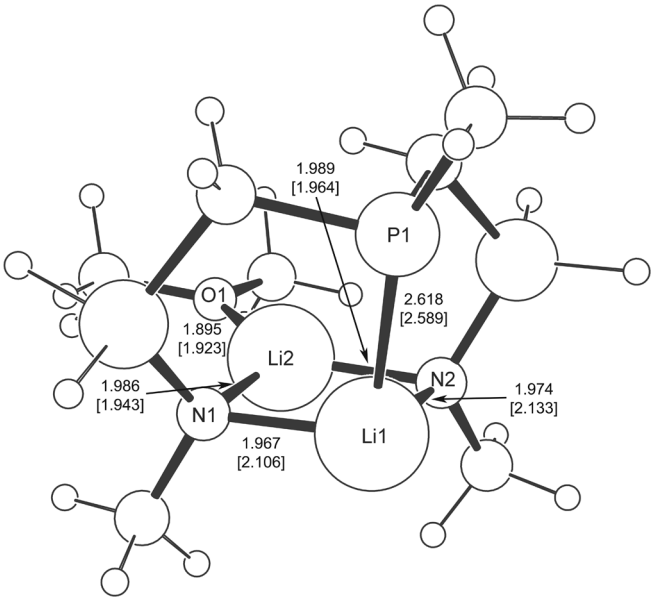


Fig. 5. Calculated geometry for 'NPN'Li_2(OMe) (**5**) with selected optimized bond distances (Å). Values in brackets are experimental values for ^{CyMes}[NPN]Li_2(THF) (11) .



The calculated geometry for the model complex 'NAsN'$TaMe_3$ (**6**) is depicted in Fig. 6 along with selected optimized bond distances; the phosphine analogue 'NPN'$TaMe_3$ (**7**) is similarly depicted in Fig. 7. The Ta–N

© 2006 NRC Canada

Fig. 6. Calculated geometry for 'NAsN'TaMe$_3$ (**6**) with selected optimized bond distances (Å). Values in brackets are experimental values for **3**.

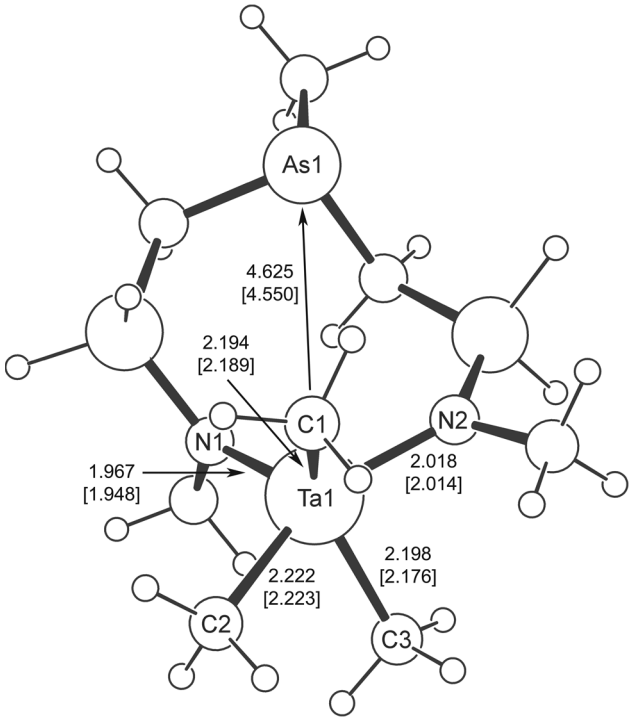
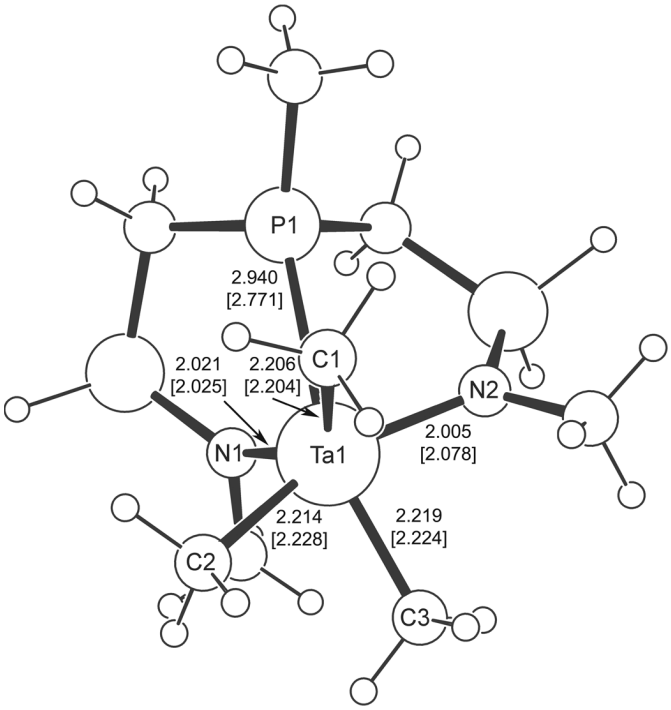
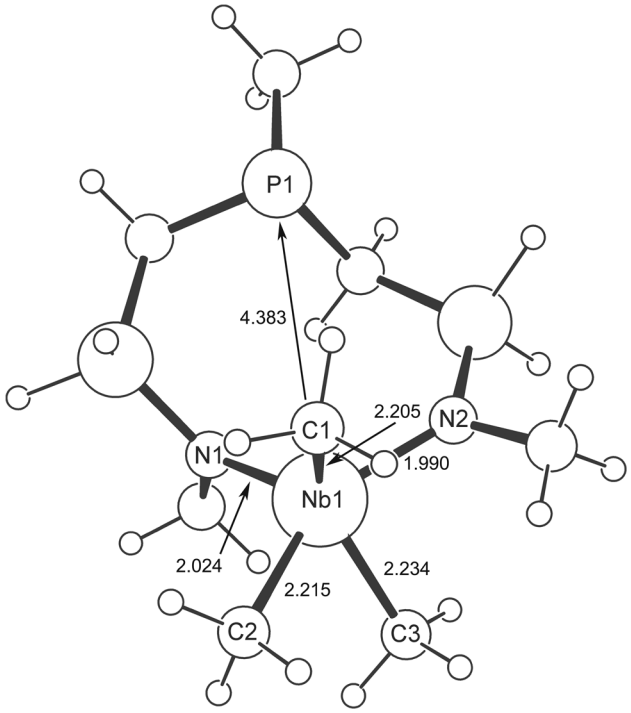


Fig. 7. Calculated geometry for 'NPN'TaMe$_3$ (**7**) with selected optimized bond distances (Å). Values in brackets are experimental values for [NPN]TaMe$_3$.



and Ta–C bond distances and angles of model complex **6** compare very well with **3**; the Ta(1)–As(1) distance is 0.07 Å longer in the model complex. This reinforces the five-coordinate nature of **3** and indicates that the lack of interaction between tantalum and arsenic is not a solid-state phenomenon. The bond distances and angles of the model complex **7** also compare well with the solid-state structure of [NPN]TaMe$_3$ (20) with the Ta–P length of the model complex slightly elongated from the solid-state structure. Comparing bond angles of the ligands surrounding tantalum for **6** and **7** reveals great similarity. This is surprising given the difference in coordination number and suggests that even in the ^{R}[NPN]TaMe$_3$ complexes, the interaction between the tantalum and phosphorus is weak and the interaction has little influence on the geometry of the other ligands about the metal center. The favorable comparison of model complex distances and angles to solid-state structures for the tantalum trimethyl complexes indicates that the level of calculation employed can adequately model the interaction of phosphorus and, more importantly, arsenic with tantalum.

Fig. 8. Calculated geometry for 'NPN'NbMe$_3$ (**10**) with selected optimized bond distances (Å).



Ligand dissociation is not restricted to the [NAsN] tantalum trimethyl complex. Hydrogenation of niobium trimethyl complexes supported by different versions of the [NPN] ligand failed to produce the corresponding dinuclear tetrahydride complex of niobium, ([NPN]Nb)$_2$(μ-H)$_4$ (11). This was initially attributed to the thermal instability of the niobium trimethyl species. However, a DFT calculation on a model complex as part of this work shows that other factors may be involved. The model complex 'NPN'NbMe$_3$ (**8**) is depicted in Fig. 8 along with selected optimized bond distances. The Nb–N and Nb–C bond distances compare well with the 'NPN'TaMe$_3$ and 'NAsN'TaMe$_3$ model complexes, other ^{R}[NPN]Nb complexes (10), and to the literature (74–77). The Nb–P distance clearly indicates that there is no interaction between the niobium and phosphorus.

While not definitive, there is a correlation between the reactivity of the three trimethyl complexes and their structures determined by DFT optimization. In the case of

© 2006 NRC Canada

[NPN]$TaMe_3$, the reaction with H_2 produces the dinuclear tetrahydride species ([NPN]Ta)$_2$(μ-H)$_4$, for which the model complex 'NPN'$TaMe_3$ shows phosphine ligand binding. In the arsine analog [NAsN]$TaMe_3$ and the niobium congener [NPN]$NbMe_3$ the analgous reaction with H_2 does not generate hydride species, and free ligand is observed. For both of these latter examples, DFT analysis shows that the neutral donor does not coordinate to the metal. Such coordinative unsaturation may facilitate side reactions that exclude formation of the anticipated dinuclear hydride species.

Conclusions

In this report, the synthesis of a mixed donor diamidoarsine ligand [NAsN] and our attempts to utilize this ligand in dinitrogen coordination are described. The lithium complex [NAsN]$Li_2(THF)_2$ (**1**) is a useful reagent for the generation of the tantalum trimethyl [NAsN]$TaMe_3$ (**3**). The solid-state structure of **3** shows that the arsine donor does not interact with the Ta(V) center. Unfortunately, solution NMR spectroscopy does not provide definitive evidence to support the solid-state structure. However, DFT studies on simplified models of the dilithio precursor 'NAsN'$Li_2(THF)_2$ and 'NAsN'$TaMe_3$ show good correlations with the solid-state structures. Hydrogenation of **3** performed under four atmospheres of hydrogen did not produce the anticipated dinuclear tetrahydride ([NAsN]Ta)$_2$(μ-H)$_4$; instead, a modest yield of the protonated ligand precursor [NAsN]H_2 (**2**) was obtained. The observation of methane in the reaction mixture suggests that the reaction may proceed through the anticipated σ-bond metathesis mechanism but was perhaps followed by hydrogenation of the tantalum amide bonds leading to the release of the ligand from the metal center as **2**.

Density functional theory calculations carried out on the trimethyl model complex **5** reveal a five-coordinate complex similar to the solid-state structure. Since the arsenic donor does not bind to the tantalum(V) centre, it is proposed that this is the reason that hydride formation does not occur. The fact that the DFT calculations reproduce the same structure observed in the solid-state was incentive to examine the trimethylniobium(V) complex that incorporates the NPN ligand system; this complex also does not undergo hydrogenation, and this is correlated to the fact that the phosphine donor is not bound to the metal. Although these are only two examples, they exemplify the possibility that σ-bond metathesis processes of group 5 alkyl complexes depend on the ancillary ligand set present.

Experimental

General procedures

All manipulations were performed under an atmosphere of dry oxygen-free dinitrogen or argon by means of standard Schlenk or glovebox techniques (Vacuum Atmospheres HE-553–2 glovebox equipped with a MO-40–2H purification system and a –40 °C freezer) unless specified. Anhydrous hexanes and toluene were purchased from Sigma-Aldrich, sparged with dinitrogen, and further dried by passage through a tower of silica followed by passage through a tower of Ridox (or Q-5) catalyst prior to use (78). Anhydrous pentane, benzene, tetrahydrofuran, and diethyl ether were purchased from Sigma-Aldrich, sparged with dinitrogen, and passed through an Innovative Technologies SPS Pure-Solv 400-4 apparatus. All organic solvents were tested with the addition of sodium benzophenone ketyl prior to use to ensure absence of oxygen and water. Alternatively, anhydrous diethyl ether was stored over sieves and distilled from sodium benzophenone ketyl under argon. Tetrahydrofuran was refluxed over CaH_2 prior to distillation from sodium benzophenone ketyl under argon, and pentane was stored over sieves and distilled from sodium benzophenone ketyl solubilized by tetraglyme under dry dinitrogen prior to storage over a potassium mirror. Nitrogen gas was dried and deoxygenated by passage through a column containing activated molecular sieves and MnO.

Deuterated benzene was dried by refluxing with molten sodium–potassium alloy in a sealed vessel under partial pressure, then trap-to-trap distilled, and freeze-pump-thaw-degassed three times. Deuterated tetrahydrofuran and toluene were dried by refluxing with molten potassium metal or sodium–potassium alloy in a sealed vessel under vacuum, then trap-to-trap distilled, and freeze-pump-thaw-degassed three times. ^1H, $^{13}C\{^1H\}$, and $^7Li\{^1H\}$ NMR spectra were recorded on either a Bruker AMX-500 instrument operating at 500.13 MHz for ^1H spectra, a Bruker AVA-400 instrument operating at 400.13 MHz for ^1H spectra, or a Bruker AVA-300 instrument operating at 300.13 MHz for ^1H spectra. ^1H NMR spectra were referenced to residual protons in deuterated solvent as follows: C_6D_5H (δ 7.15), C_4D_7HO (δ 3.58), and C_7D_7H (δ 2.09) with respect to tetramethylsilane at δ 0.0. $^{13}C\{^1H\}$ NMR spectra were referenced to $^{13}CC_5D_6$ (δ 128.4). $^7Li\{^1H\}$ NMR spectra were referenced to external LiCl (0.3 mol/L solution in MeOH at δ 0.0). Elemental analyses were performed by Mr. M. Lakha, and mass spectrometry by Mr. M. Lapawa, all at The University of British Columbia, Department of Chemistry.

Materials

The compounds $PhAsH_2$ (12), $PhNHSiMe_2CH_2Cl$ (33), and $TaMe_3Cl_2$ (79) were prepared according to literature procedures. Et_3NHCl was prepared by the reaction of triethylamine and aqueous hydrochloric acid and recrystallized from ethanol. Solutions of BuLi (1.6 mol/L) in hexanes were purchased from Acros Chemicals (Geel, Belgium) and used as received. High purity hydrogen gas was purchased from PRAXAIR (Danbury, Conn.) and used as received. Deuterium gas was purchased from Cambridge Isotopes (Andover, Mass.) and used as received. All other reagents were obtained from a commercial source and purified by appropriate methods (80).

Synthesis of [NAsN]$Li_2(THF)_2$ (1)

To a solution of $PhAsH_2$ (2.0 g, 13.0 mmol) and $PhNHSiMe_2CH_2Cl$ (5.2 g, 26.0 mmol) in Et_2O (100 mL) at 0 °C was added a 1.6 mol/L solution of BuLi in hexanes (32.5 mL, 52.0 mmol) dropwise. The solution was warmed to ambient temperature, stirred for 2 h, and then evaporated to dryness. The residue was extracted into toluene (50 mL), the solution filtered through Celite, and the toluene removed. The colourless residue was slurried in hexanes (20 mL), THF was added (3.7 g, 52 mmol), and the solution cooled to

© 2006 NRC Canada

–40 °C. The resultant colourless crystals were collected, rinsed with a small amount of hexanes, and dried under vacuum. Yield 6.50 g (78%). ^{1}H NMR (400 MHz, C_6D_6, 25 °C) δ: 7.71 (d, $^3J_{HH}$ = 7.1 Hz, 2H, *o*-AsPh), 7.23 (m, 6H, *m*-AsPh and *m*-NPh), 7.15 (t, $^3J_{HH}$ = 7.3 Hz, 1H, *p*-AsPh), 6.86 (d, $^3J_{HH}$ = 7.9 Hz, 4H, *o*-NPh), 6.74 (t, $^3J_{HH}$ = 7.2 Hz, 2H, *p*-NPh), 3.35 (m, 8H, THF-OCH_2CH$_2$), 1.27 (AB d, $^2J_{HH}$ = 13.7 Hz, 2H, CH_2), 1.20, AB d, $^2J_{HH}$ = 13.7 Hz, 2H, CH_2), 1.11 (s, 8H, THF-OCH$_2$CH_2), 0.49 (s, 6H, SiCH_3), 0.42 (s, 6H, SiCH_3). ^{1}H NMR (500 MHz, d_8-THF), 25 °C) δ: 7.59 (d, $^3J_{HH}$ = 7.3 Hz, 2H, *o*-AsPh), 7.29 (t, $^3J_{HH}$ = 7.3 Hz, 2H, *m*-AsPh), 7.23 (t, $^3J_{HH}$ = 7.3 Hz, 1H, *p*-AsPh), 6.85 (t, $^3J_{HH}$ = 7.8 Hz, 4H, *m*-NPh), 6.53 (d, $^3J_{HH}$ = 7.7 Hz, 4H, *o*-NPh), 6.33 (t, $^3J_{HH}$ = 7.7 Hz, 2H, *p*-NPh), 3.62 (m, 8H, THF-OCH_2CH$_2$), 1.77 (m, 8H, THF-OCH$_2$CH_2), 1.15 (AB d, $^2J_{HH}$ = 13.7 Hz, 2H, SiCH_2As), 1.07 (AB d, $^2J_{HH}$ = 13.7 Hz, 2H SiCH_2As), 0.15 (s, 6H, SiCH_3), 0.13 (s, 6H, SiCH_3). ^{7}Li{^{1}H} NMR (155.5 MHz, C_6D_6, 25 °C) δ: –1.47 (s). MS (EI) *m*/*z*: 492 (20) [M – (THF)$_2$]$^+$; 387 (45) [M – NPh(THF)$_2$]$^+$. Anal. calcd. for $C_{32}H_{47}AsN_2O_2Si_2Li_2$: C 60.36, H 7.44, N 4.40; found: C, 60.00, H 7.46, N 4.73.

Synthesis of [NAsN]H$_2$ (2)

To a mixture of **1** (1.0 g, 1.5 mmol) and Et$_3$NHCl (0.43 g, 3.11 mmol) was added Et$_2$O (50 mL). The solution was stirred for 12 h and then evaporated to dryness. The residue was extracted into toluene (25 mL), the resulting solution was filtered through Celite, and the solvent removed under vacuum to yield a colourless oil that solidified upon extended standing, producing X-ray quality crystals of **2**. Yield 0.69 g (96%). ^{1}H NMR (400 MHz, C_4D_8O, 25 °C) δ: 7.61 (m, 2H, *o*-AsPh), 7.28 (m, 3H, *m*/*p*-AsPh), 6.98 (m, 4H, *m*-NPh), 6.54 (m, 6H, *o*/*p*-NPh), 4.22 (br s, 2H, N*H*), 1.24 (AB d, $^2J_{HH}$ = 13.6 Hz, 2H, SiCH_2As), 1.17 (AB d, $^2J_{HH}$ = 13.6 Hz, 2H, SiCH_2As), 0.17 (s, 6H, SiCH_3), 0.07 (s, 6H, SiCH_3). ^{1}H NMR (300 MHz, C_6D_6, 25 °C) δ: 7.57 (m, 2H, AsPh *o*-*H*), 7.19 (m, 7H, AsPh *m*/*p*-*H* and NPh *m*-*H*), 6.82 (m, 2H, NPh *p*-*H*), 6.58 (m, 4H, NPh *o*-*H*), 3.09 (br s, 2H, N*H*), 1.13 (AB d, $^2J_{HH}$ = 13.6 Hz, 2H, SiCH_2As), 1.02 (AB d, $^2J_{HH}$ = 13.6 Hz, 2H, SiCH_2As), 0.23 (s, 6H, SiCH_3), 0.18 (s, 6H, SiCH_3). MS (EI) *m*/*z*: 387 (55) [M – NHPh]$^+$. Anal. calcd. for $C_{24}H_{33}AsN_2Si_2$: C 59.98, H 6.92, N 5.83; found: C 60.14, H 7.15, N 6.06.

Synthesis of [NAsN]TaMe$_3$ (3)

A solution of TaMe$_3$Cl$_2$ (0.47 g, 1.57 mmol) in Et$_2$O (10 mL) was added dropwise to a stirred solution of **1** (1.00 g, 1.57 mmol) in Et$_2$O (25 mL) at –78 °C in the dark. The solution was stirred for 20 min at –78 °C, warmed to –20 °C, and then evaporated to dryness. The residue was extracted into toluene (15 mL), the resulting solution was filtered through Celite, and the solvent removed under vacuum. The resulting solid was washed with a minimal amount of cold pentane and further dried to give **3** as a pale yellow solid that was stored in the dark at –40 °C. Yield 0.69 g (63%). Crystals of **3** suitable for X-ray diffraction experiments were grown by slow evaporation of a concentrated benzene solution. ^{1}H NMR (300 MHz, C_6D_6, 25 °C) δ: 7.62 (d, $^3J_{HH}$ = 6.8 Hz, 2H, *o*-AsPh), 7.21 (m, 11H, *m*/*p*-AsPh and *o*/*m*-NPh), 7.03 (t, $^3J_{HH}$ = 6.8 Hz, 2H, *p*-NPh), 1.82 (AB d, $^2J_{HH}$ = 14.1 Hz, 2H, SiCH_2As), 1.25 (AB d, $^2J_{HH}$ = 14.1 Hz, 2H, SiCH_2As), 1.24 (s, 9H, TaCH_3), 0.37 (s, 6H, ring SiCH_3), 0.02 (s, 6H, ring SiCH_3). ^{1}H NMR (500 MHz, C_4D_8O, 25 °C) δ: 7.63 (d, $^3J_{HH}$ = 7.0 Hz, 2H, *o*-AsPh), 7.33 (m, 2H, *m*-AsPh), 7.28 (m, 5H, *p*-AsPh and *m*-NPh), 7.16 (m, 2H, *p*-NPh), 7.07 (d, $^3J_{HH}$ = 7.3 Hz, 4H, *o*-NPh), 1.87 (AB d, $^2J_{HH}$ = 14.2 Hz, 2H, SiCH_2As), 1.40 (AB d, $^2J_{HH}$ = 14.2 Hz, 2H, SiCH_2As), 0.69 (s, 9H, TaCH_3), 0.27 (s, 6H, ring SiCH_3), –0.02 (s, 6H, ring SiCH_3). ^{13}C{^{1}H} NMR (75.4 MHz, C_6D_6, 25 °C) δ: 144.8 (s, NPh *i*-*C*), 141.4 (s, AsPh *i*-*C*), 132.1 (s, AsPh *o*-*C*), 129.9 (s, AsPh *p*-*C*), 129.5 (s, NPh *p*-*C*), 129.2 (s, AsPh *m*-*C*), 128.6 (s, NPh *m*-*C*), 126.1 (s, NPh o-C), 63.6 (s, Ta*C*H$_3$), 13.2 (s, Si*C*H$_2$As), 2.1 (s, Si*C*H$_3$), 1.5 (s, Si*C*H$_3$). MS (EI) *m*/*z*: 689 (100) [M – Me]$^+$, 673 (92) [M – HMe$_2$]$^+$. Anal. calcd. for $C_{27}H_{40}AsN_2Si_2Ta$: C 46.02, H 5.72, N 3.98; found: C 46.22, H 5.62, N 4.29.

Hydrogenation of [NAsN]TaMe$_3$

Hydrogen gas was admitted to a Kontes valve equipped thick-walled bomb fully immersed in liquid nitrogen containing a freeze-pump-thaw degassed solution of **3** (35 mg, 0.050 mmol) in diethyl ether (10 mL). The bomb was sealed and allowed to warm to RT. The solution was stirred for 48 h during which a colour change from pale yellow to pale tan was noted and a colourless precipitate was deposited on the side of the flask. Removal of the solvent under vacuum gave an oily brown residue. ^{1}H NMR (300 MHz, C_6D_6, 25 °C) showed resonances attributable to **2** in 33% yield relative to an internal standard (ferrocene). Elemental analysis of the isolated material returned data indicating the solids were depleted in carbon and hydrogen relative to **3**; a representative analysis found: C 43.33, H 5.20, N 4.32. Deuteration experiments were conducted using the same procedure.

Calculations

Calculations were performed using the Gaussian 98 suite of programs on either a dual 450MHz Pentium II workstation using G98 Rev. A.9 (65) or a dual 1.0 GHz Pentium III workstation using G98 Rev. A.11.4 (81). Calculations were performed using the B3LYP functional (66). The basis functions and effective core potentials were those of the LANL2DZ basis set (67), augmented with polarization functions (p,d) developed for arsenic (72). No geometric constraints were set in the optimization of the complexes. Geometric illustrations were created using ORTEP-III for Windows (82). Orbital depictions were created using the Molden program (83). The Supplementary data for this article contains further details on the calculations including pictures of orbitals, calculated bond distances, and archival output summaries.[2]

[2] Supplementary data for this article are available on the Web site or may be purchased from the Depository of Unpublished Data, Document Delivery, CISTI, National Research Council of Canada, Ottawa, ON K1A 0S2, CANADA. DUD 5114. For more information on obtaining material refer to http://cisti-icist.nrc-cnrc.gc.ca/irm/unpub_e.shtml. Crystallographic data for this manuscript are contained in CCDC 621660, 621661, and 621662. These data can obtained, free of charge, via www.ccdc.cam.ac.uk/conts.retrieving.html (or from the Cambridge Crystallographic Data Centre, 12 Union Road, Cambridge CB2 1EZ, UK; fax +44 1223 336033; or deposit@ccdc.cam.ac.uk.

© 2006 NRC Canada

Table 4. Crystallographic and structure refinement data for $[NAsN]Li_2(THF)_2$ (**1**), $[NAsN]H_2$ (**2**), and $[NAsN]TaMe_3$ (**3**).

Compound	$[NAsN]Li_2(THF)_2$, (**1**)	$[NAsN]H_2$, (**2**)	$[NAsN]TaMe_3$, (**3**)
Formula	$C_{32}H_{47}AsLi_2N_2O_2Si_2$	$C_{24}H_{33}AsN_2Si_2$	$C_{27}H_{40}AsN_2Si_2Ta$
Fw	636.70	480.62	704.66
CCDC Number	621660	621661	621662
Colour, habit	Colourless, irregular	Colourless, platelet	Colourless, irregular
Crystal size (mm)	0.20 × 0.15 × 0.05	0.25 × 0.20 × 0.05	0.5 × 0.4 × 0.3
Crystal system	Triclinic	Triclinic	Monoclinic
Space group	*P*-1 (No. 2)	*P*-1 (No. 2)	$P2_1/a$ (No. 14)
a (Å)	10.005(2)	9.8456(3)	16.9447(3)
b (Å)	12.103(3)	11.751 0(3)	9.972 40(10)
c (Å)	15.287(3)	23.8216(5)	17.9460(3)
α (°)	83.135(14)	95.2940(10)	90
β (°)	74.071(12)	96.130 0(10)	104.029 0(10)
γ (°)	73.759(14)	109.8230(10)	90
V (Å^3)	1708.9(7)	2553.48(11)	2942.05(8)
Z	2	4	4
T (°C)	–100±1	–100±1	–100±1
ρ_{calc} (g/cm^3)	1.237	1.250	1.591
F(000)	672	1008	1400
μ (Mo Kα) (mm^{-1})	1.094	1.437	4.951
Transmission factors	0.8372–1.0000	0.7706–1.0000	0.3767–1.0000
$2\theta_{max}$ (°)	55.74	49.94	55.74
Total reflections	9 247	53 634	41 381
Unique reflections	5564	8829	7033
R_{merge}	0.0774	0.0514	0.0293
Reflections with $I \geq 2\sigma(I)$	3618	6818	6155
No. of variables	374	547	305
R (F^2, all data)	0.0970	0.0569	0.0225
R_w (F^2, all data)	0.1165	0.0933	0.0393
R (*F*, $I > 2\sigma(I)$)	0.0524	0.0374	0.0168
R_w (*F*, $I > 2\sigma(I)$)	0.1042	0.0857	0.0355
Gof	0.949	1.017	1.078

Crystallography

In all cases, suitable crystals were selected and mounted on a glass fibre using Paratone-N oil or an acceptable substitute and freezing to –100 °C. Data collection for **1** was made on a Rigaku ADSC CCD area detector with graphite monochromated Mo Kα radiation. Data for **2** and **3** were collected on a Bruker X8 area detector with monochromated Mo Kα radiation. Crystallographic data[2] appear in Table 4. Data for **1** was determined to be a two-component twin (components related by a rotation of 7.77° normal to 0.03, –1.00, and –1.39) using the Twinsolve module of the CrystalClear software package, version 1.3.6 SP0 (84), and corrected for Lorentz and polarization effects and absorption. Data for **2** and **3** was processed and integrated using the Bruker SAINT software package (85) and corrected for absorption effects using the multiscan technique (SADABS) (86). Neutral atom scattering factors for all non-hydrogen atoms were taken from Cromer and Waber (87). Anomalous dispersion effects were included in F_{calc} (88); the values for $\Delta f''$ and $\Delta f'''$ were those of Creagh and McAuley (89). The values for the mass attenuation coefficients are those of Creagh and Hubbell (90).

All structures were solved by direct methods using the program SIR97 (91). All non-hydrogen atoms were refined anisotropically by least-squares procedures on F^2 using SHELXL-97 (92). Hydrogen atoms were included but not refined; their positional parameters were calculated with fixed C–H bond distances of 0.99 Å for sp^2 C, 0.98 Å for sp^3 C, and 0.95 Å for aromatic sp C, with U_{iso} set to 1.2 times the U_{eq} of the attached sp or sp^2 C and 1.5 times the U_{eq} values of the attached sp^3 C atom. Methyl hydrogen torsion angles were determined by electron density. Structure solution and refinements were conducted using the WinGX software package, version 1.64.05 (93). Structure illustrations were created using ORTEP-III for Windows (82).

Acknowledgement

Dr. B.O. Patrick is gratefully thanked for crystallography assistance. We thank the Natural Sciences and Engineering Research Council (NSERC) of Canada for generous financial support.

References

1. D.M.A. Minaham, W.E. Hill, and C.A. McAuliffe. Coord. Chem. Rev. **55**, 31 (1984).

© 2006 NRC Canada

2. H. Butenschon. Chem. Rev. **100**, 1527 (2000).
3. A.L. Gavrilova and B. Bosnich. Chem Rev. **104**, 349 (2004).
4. M.D. Fryzuk. Can. J. Chem. **70**, 2839 (1992).
5. M.D. Fryzuk. Chem. Rec. **3**, 2 (2003).
6. M.D. Fryzuk, P. Yu, and B.O. Patrick. Can. J. Chem. **79**, 1194 (2001).
7. B.A. MacKay, S.A. Johnson, B.O. Patrick, and M.D. Fryzuk. Can. J. Chem. **83**, 315 (2005).
8. B.A. MacKay, R.F. Munha, and M.D. Fryzuk. J. Am. Chem. Soc. **128**, 9472 (2006).
9. B.A. MacKay, B.O. Patrick, and M.D. Fryzuk. Organometallics, **24**, 3836 (2005).
10. M.D. Fryzuk, M.P. Shaver, and B.O. Patrick. Inorg. Chim. Acta, **350**, 293 (2003).
11. M.P. Shaver, R.K. Thomson, B.O. Patrick, and M.D. Fryzuk. Can. J. Chem. **81**, 1431 (2003).
12. C.D. Carmichael and M.D. Fryzuk. J. Chem. Soc. Dalton Trans. 452 (2005).
13. N.N. Greenwood and A. Earnshaw. Chemistry of the elements. 2nd ed. Butterworth-Hienemann, Oxford. 1997.
14. R.K. Harris. *In* NMR and the periodic table. *Edited by* R.K. Harris and B.E. Mann. Academic Press, London. 1978. pp. 379–382.
15. R. Hart, W. Levason, B. Patel, and G. Reid. Eur. J. Inorg. Chem. 2927 (2001).
16. W. Levason, M.L. Matthews, B. Patel, G. Reid, and M. Webster. J. Chem. Soc. Dalton Trans. 3305 (2004).
17. J.C. Dewan, D.L. Kepert, C.L. Raston, and A.H. White. J. Chem. Soc. Dalton Trans. 2031 (1975).
18. R.R. Schrock, L.J. Guggenberger, and A.D. English. J. Am. Chem. Soc. **98**, 903 (1976).
19. K. Mast, J. Meiers, O.J. Scherer, and G. Wolmershauser. Z. Anorg. Allg. Chem. **625**, 70 (1999).
20. M.D. Fryzuk, S.A. Johnson, B.O. Patrick, A. Albinati, S.A. Mason, and T.F. Koetzle. J. Am. Chem. Soc. **123**, 3960 (2001).
21. M.D. Fryzuk, J.B. Love, and S.J. Rettig. Organometallics, **17**, 846 (1998).
22. A. Bashall, A.D. Bond, A.D. Hopkins, S.J. Kidd, M. McPartlin, A. Steiner, R. Wolf, A.D. Woods, and D.S. Wright. J. Chem. Soc. Dalton Trans. 343 (2002).
23. M. Driess, U. Hoffmanns, S. Martin, K. Merz, and H. Pritzkow. Angew. Chem. Int. Ed. **38**, 2733 (1999).
24. A. Bashall, F. Garcia, A.A. Hopkins, J.A. Wood, M. McPartlin, A.D. Woods, and D. S. Wright. J. Chem. Soc. Dalton Trans. 1143 (2003).
25. M. Weidenbruch, S. Olthoff, W. Saak, and H. Marsmann. Eur. J. Inorg. Chem. 1755 (1998).
26. G.B. Deacon, C.M. Forsyth, and N.M. Scott. J. Chem. Soc. Dalton Trans. 2494 (2001).
27. R. Murugavel, N. Palanisami, and R.J. Butcher. J. Organomet. Chem. **675**, 65 (2003).
28. B. Eichhorn and H. Noth. Z. Naturforsch. B Chem. Sci. **55**, 352 (2000).
29. M. Westerhausen, T. Bollwein, K. Karaghhiosoff, S. Schneiderbauer, M. Vogt, and H. Noth. Organometallics, **21**, 906 (2002).
30. R.G. Cunninghame, L.R. Hanton, S.D. Jensen, B.H. Robinson, and J. Simpson. Organometallics, **6**, 1470 (1987).
31. S. Kamepalli, C.J. Carmalt, R.D. Culp, C.H. Cowley, R.A. Jones, and N.C. Norman. Inorg. Chem. **35**, 6179 (1996).
32. B. Carlson, G.D. Phelan, W. Kaminsky, L. Dalton, X. Jiang, S. Liu, and A.K.-Y. Jen. J. Am. Chem. Soc. **124**, 14162 (2002).
33. M.D. Fryzuk, S.A. Johnson, and S.J. Rettig. J. Am. Chem. Soc. **120**, 11024 (1998).
34. M.D. Fryzuk, B.A. MacKay, S.A. Johnson, and B.O. Patrick. Angew. Chem. Int. Ed. **41**, 3709 (2002).
35. M.D. Fryzuk, B.A. MacKay, and B.O. Patrick. J. Am. Chem. Soc. **125**, 3234 (2003).
36. S.M. Pugh, A.J. Blake, L.H. Gade, and P. Mountford. Inorg. Chem. **40**, 3992 (2001).
37. J.P. Araujo, D.K. Wicht, P.J. Bonitatebus., Jr., and R.R. Schrock. Organometallics, **20**, 5682 (2001).
38. J.A.R. Schmidt, S.A. Chmura, and J. Arnold. Organometallics, **20**, 1062 (2001).
39. M.D. Fryzuk, S.A. Johnson, and S.J. Rettig. Organometallics, **18**, 4059 (1999).
40. R.R. Schrock, J. Lee, L.-C. Liang, and W.M. Davis. Inorg. Chim. Acta, **270**, 353 (1998).
41. K.S. Cook, W. Piers, S.J. Rettig, and R. McDonald. Organometallics, **19**, 2243 (2000).
42. M.G.B. Drew, A.P. Wolters, and J.D. Wilkins. Acta Crystallogr. Sect. B: Struct. Crystallogr. Cryst. Chem. **31**, 324 (1975).
43. K. Mast, O.J. Scherer, and G. Wolmershauser. Z. Anorg. Allg. Chem. **625**, 1475 (1999).
44. M.D. Fryzuk, S.A. Johnson, and S.J. Rettig. Organometallics, **19**, 3931 (2000).
45. F.A. Adedeji, K.J. Cavell, S. Cavell, J.A. Connor, G. Pilcher, H.A. Skinner, and M. Zafarani-Moattar. J. Chem. Soc. Faraday Trans. 603 (1979).
46. L. Luo, L. Li, and T.J. Marks. J. Am. Chem. Soc. **119**, 8574 (1997).
47. J.A. Kerr. *In* CRC handbook of chemistry and physics. Vol. 84. *Edited by* D.R. Lide. CRC Press, Boca Raton, Fla. 2003.
48. E. Durgun, S.D.S. Ciraci, and O. Gulersen. J. Phys. Chem. B, **108**, 575 (2004).
49. M.D. Fryzuk, C.D. Montgomery, and S.J. Rettig. Organometallics, **10**, 467 (1991).
50. M.D. Fryzuk, M.J. Petrella, R.C. Coffin, and B.O. Patrick. C.R. Acad. Sci. Ser. IIc: Chim. **5**, 451 (2002).
51. M. Yamakawa, H. Ito, and R. Noyori. J. Am. Chem. Soc. **122**, 1466 (2000).
52. R. Noyori, M. Yamakawa, and S. Hashiguchi. J. Org. Chem. **66**, 7931 (2001).
53. K. Abdur-Rashid, M. Faatz, A.J. Lough, and R.H. Morris. J. Am. Chem. Soc. **123**, 7473 (2001).
54. J.L. Polse, R.A. Andersen, and R.G. Bergman. J. Am. Chem. Soc. **120**, 13405 (1998).
55. T.E. Hanna, I. Keresztes, E. Lobkovsky, W.H. Bernskoetter, and P.J. Chirik. Organometallics, **23**, 3448 (2004).
56. T.M. Cameron, C.G. Ortiz, I. Ghiviriga, K.A. Abboud, and J.M. Boncella. J. Am. Chem. Soc. **124**, 922 (2002).
57. S. Niu and M.B. Hall. Chem. Rev. **100**, 353 (2000).
58. T.M. Gilbert, I. Hristov, and T. Ziegler. Organometallics, **20**, 1183 (2001).
59. I.H. Hristov and T. Ziegler. Organometallics, **22**, 3513 (2003).
60. L. Maron and O. Eisenstein. J. Am. Chem. Soc. **123**, 1036 (2001).
61. L. Perrin, L. Maron, and O. Eisenstein. Inorg. Chem. **41**, 4355 (2002).
62. I. Hyla-Kryspin and R. Gleiter. J. Mol. Catal. A: Chem. **160**, 115 (2000).
63. L.A. Watson, D.V. Yandulov, and K.G. Caulton. J. Am. Chem. Soc. **123**, 603 (2001).
64. S. Sakaki, T. Takayama, M. Sumimoto, and M. Sugimoto. J. Am. Chem. Soc. **126**, 3332 (2004).
65. M.J. Frisch, G.W. Trucks, H.B. Schlegel, G.E. Scuseria, M.A. Robb, J.R. Cheeseman, V.G. Zakarzewski, J.A. Montgomery,

© 2006 NRC Canada

R.E. Stratmann, J.C. Burant, S. Dapprich, J.M. Millam, A.D. Daniels, K.N. Kudin, M.C. Strain, O. Farkas, J. Tomasi, V.A. Petersson, P.Y. Ayala, Q. Cui, K. Morokuma, D.K. Malick, A.D. Rabuck, K. Raghavachari, J.B. Foresman, J. Cioslowski, J.V. Ortiz, B.B. Stefanov, G. Lui, A. Liashenko, P. Piskorz, I. Komaromi, R. Gomperts, R.L. Martin, D.J. Fox, T. Kieth, M.A. Al-Laham, C.Y. Peng, A. Nanajakkara, C. Gonzalez, M. Challacombe, P.M.W. Gill, B.G. Johnson, W. Chen, M.W. Wong, J.L. Andres, M. Head-Gordon, E.S. Repogle, and J.A. Pople. Gaussian 98. Rev A.9 [computer program]. Gaussian Inc., Pittsburg, Pa. 1998.

66. A.D. Becke. J. Chem. Phys. **98**, 5648 (1993).
67. P.J. Hay and W.R. Wadt. J. Chem. Phys. **82**, 270 (1985).
68. F.A. Cotton and X. Feng. J. Am. Chem. Soc. **119**, 7514 (1997).
69. E. Magnusson. J. Am. Chem. Soc. **115**, 1051 (1993).
70. H. Basch, D.G. Musaev, and K. Morokuma. J. Am. Chem. Soc. **121**, 5754 (1999).
71. H. Basch, D.G. Musaev, K. Morokuma, M.D. Fryzuk, J.B. Love, W.W. Seidel, A. Albinati, T.F. Koetzle, W.T. Klooster, S.A. Mason, and J. Eckert. J. Am. Chem. Soc. **121**, 523 (1999).
72. C.E. Check, T.O. Faust, J.M. Bailey, B.J. Wright, T.M. Gilbert, and L.S. Sunderlin. J. Phys. Chem. A, **105**, 8111 (2001).
73. M.F. Mahon, N.L. Moldovan, K.C. Molloy, A. Muresan, I. Silaghi-Dumitrescu, and L. Silaghi-Dumitrescu. J. Chem. Soc. Dalton Trans. 4017 (2004).
74. S.M. Pugh, D.J.M. Trosch, M.E.G. Skinner, L.H. Gade, and P. Mountford. Organometallics, **20**, 3531 (2001).
75. M.D. Fryzuk, C.M. Kozak, and B.O. Patrick. Inorg. Chim. Acta, **345**, 53 (2003).
76. S. Kleinhenz, V. Pfennig, and K. Seppelt. Chem. Eur. J. **4**, 1687 (1998).
77. M.J. Humphries, M.L.H. Green, R.E. Douthwaite, and J.H. Rees. J. Chem. Soc. Dalton Trans. 4555 (2000).
78. A.B. Pangborn, M.A. Giardello, R.H. Grubbs, R.K. Rosen, and F.J. Timmers. Organometallics, **15**, 1518 (1996).
79. R.R. Schrock and P.R. Sharp. J. Am. Chem. Soc. **100**, 2389 (1978).
80. D.D. Perrin and W.L.F. Amarego. Purification of laboratory chemicals. 3rd ed. Butterworth-Heinemann, Oxford. 1994.
81. M.J. Frisch, G.W. Trucks, H.B. Schlegel, G.E. Scuseria, M.A. Robb, J.R. Cheeseman, J.A. Zakrzewski, J.A. Montgomery, R.E. Stratmann, J.C. Burant, S. Dapprich, J.M. Millam, A.D. Daniels, K.N. Kudin, M.C. Strain, O. Farkas, J. Tomasi, V. Barone, M. Cossi, R. Cammi, B. Mennucci, C. Pomelli, C. Adamo, S. Clifford, J. Ochterski, G.A. Petersson, P.Y. Ayala, Q. Cui, K. Morokuma, P. Salvador, J.J. Dannenberg, D.K. Malick, A.D. Rabuck, K. Raghavachari, J.B. Foresman, J. Cioslowski, J.V. Ortiz, A.G. Baboul, B.B. Stefanov, G. Liu, A. Liashenko, P. Piskorz, I. Komaromi, R. Gomperts, R.L. Martin, D.J. Fox, T. Kieth, M.A. Al-Laham, C.Y. Peng, A. Nanayakkara, M. Challacombe, P.M.W. Gill, B. Johnson, W. Chen, M.W. Won, J.L. Andres, C. Gonzalez, M. Head-Gordon, E.S. Repogle, and J.A. Pople. Gaussian 98. Rev. A.11.4 [computer program]. Gaussian Inc., Pittsburg, Pa. 2001.
82. L.J. Farrugia. J. Appl. Crystallogr. **30**, 565 (1997).
83. G. Schaftenaar. CAOS/CAMM center. Molden [computer program]. University of Nijmegen, The Netherlands. 1991.
84. CrystalClear [computer program]. Rigaku Corporation, The Woodlands, Tex. 2002–2004.
85. SAINT. Version 7.03A [computer program]. Bruker Analytical X-ray Systems Inc., Madison, Wis. 1997–2003.
86. G.M. Sheldrick. SADABS. Version 2.05 [computer program]. Bruker Analytical X-ray Systems Inc., Madison, Wis. 2003.
87. D.T. Cromer and J.T. Waber. International tables for X-ray crystallography. Vol. IV. Kynoch Press, Birmingham, UK. 1974.
88. J.A. Ibers and W.C. Hamilton. Acta Crystallogr. **17**, 781 (1964).
89. D.C. Creagh and W.J. McAuley. *In* International tables for crystallography. Vol. C. *Edited by* A.J.C Wilson. Kluwer Academic Publishers, Boston, Mass. 1992. pp. 219–222.
90. D.C. Creagh and J.H. Hubbell. *In* International tables for crystallography. Vol. C. *Edited by* A.J.C. Wilson. Kluwer Academic Publishers, Boston, Mass. 1992. pp. 200–206.
91. A. Altomare, M.C. Burla, G. Cammali, M. Cascarano, C. Giacovazzo, A. Guagliardi, A.G.G. Moliterni, G. Polidori, and A. Spagna. J. Appl. Crystallogr. **32**, 115 (1999).
92. G.M. Sheldrick. SHELXL-97 [computer program]. University of Gottingen, Gottingen, Germany. 1998.
93. L.J. Farrugia. J. Appl. Crystallogr. **32**, 837 (1999).

© 2006 NRC Canada

Reactions of α-isobutyl-α-(methylthio)methylene Meldrum's acid with primary amines in aqueous DMSO

Supriya Biswas, Mahammad Ali, Zvi Rappoport, and Hatim Salim

Abstract: The aminolysis of α-isobutyl-α-(methylthio)methylene Meldrum's acid **7** with primary amines, namely, *n*-butylamine, glycinamide, and methoxyethylamine in DMSO–H_2O (50:50, *v/v*) at 20 °C is overall second-order but first-order in both **7** and amines. The reaction with aminoacetonitrile (AA) is overall third-order, first-order in substrate, and second-order in amine at low amine concentration, while at high amine concentration and high pH the dependence on amine is first-order. A general three-step mechanism has been proposed for all these reactions. For the former group of amines, the first step is a rate-limiting attack of the amine to form the tetrahedral intermediate ($\mathbf{T_A^{\pm}}$), followed by a fast acid–base equilibrium and a fast RNH_3^+- or H_2O-assisted leaving group expulsion. For AA, general base catalysis was confirmed from the dependence of k_A on $[AA]_f$ and on $[OH^-]$. For all four amines, a good Brønsted plot of log k_1 vs. pK_a^{AH} in DMSO–H_2O (50:50, *v/v*) with $\beta_{nuc} = 0.34 \pm 0.02$ was observed. These observations are consistent with the suggested mechanism.

Key words: nucleophilic vinylic substitution reactions, primary amines, α-isobutyl-α-(methylthio)methylene Meldrum's acid, three-step mechanism.

Résumé : L'aminolyse du dérivé α-isobutyl-α-(méthylthio)méthylène de l'acide de Meldrum (**7**) avec des amines primaires telles la butylamine, le glycinamide et la méthoxyéthylamine, dans des solutions contenant 50% de DMSO et 50% d'eau, à 20 °C, est une réaction globalement du deuxième ordre, du premier ordre en composés **7** et du premier ordre en amines. À faible concentration d'amine, la réaction avec l'aminoacétonitrile (AA) est globalement du troisième ordre, soit du premier ordre en substrat et du deuxième ordre en amine; à des concentrations plus élevées d'amine et à des pH plus élevés, la dépendance sur l'amine est toutefois du premier ordre. D'une façon générale, on suggère que la réaction se produit par un mécanisme en trois étapes. Pour le premier groupe d'amines, la première étape est une attaque cinétiquement limitante de l'amine qui conduit à la formation de l'intermédiaire tétraédrique ($\mathbf{T_A^{\pm}}$) et qui est suivie par un équilibre acide-base rapide et une expulsion rapide du groupe partant assistée par RNH_3^+ ou H_2O. Dans le cas de l'aminoacétonitrile, on a confirmé l'existence d'une catalyse basique générale à partir de la dépendance de k_A sur les $[AA]_f$ et $[OH^-]$. Pour les quatre amines, dans des solutions contenant 50% de DMSO et 50% d'eau, on a observé une bonne corrélation de Brønsted entre log k_1 et pK_a^{AH} avec $\beta_{nuc} = 0{,}34 \pm 0{,}02$. Ces résultats sont en accord avec le mécanisme suggéré.

Mots clés : réactions de substitution vinylique nucléophile, amines primaires, dérivé α-isobutyl-α-(méthylthio)méthylène de l'acide de Meldrum, mécanisme en trois étapes.

[Traduit par la Rédaction]

Introduction

The mechanism of the addition–elimination variant of nucleophilic vinylic substitution (S_NV) reactions of electrophilic alkenes (**1**), where X and Y are the activating substituents (1), with anionic nucleophiles (Nu^-) may occur either in a single-step (concerted type) process via a transition state (**2**) or in a two-step process via an intermediate (**3**, $\mathbf{T_{Nu}^-}$), which expels the leaving group (LG^-) to form the product **4** (Scheme 1). Whereas the concerted route is relatively rare (1*h*), reactions with most anionic nucleophiles proceed by a two-step mechanism (1).

The reactions with amine nucleophiles go through a two-step route with the involvement of acid–base equilibrium as an additional step, as depicted in Scheme 2 (2).

In the reactions of **6-SMe-Z** (Chart 1) with a series of secondary amines (2), it was shown that general-acid-catalyzed MeS^- departure (k_3^{AH}, $k_3^{H_2O}$) from $\mathbf{T_A^-}$ is rate-limiting for piperidine, while with piperazine, 1-(2-hydroxyethyl-piperazine), and morpholine deprotonation of $\mathbf{T_A^{\pm}}$ to $\mathbf{T_A^-}$ is

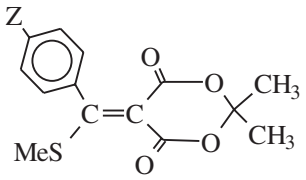
Received 29 June 2006. Accepted 10 October 2006. Published on the NRC Research Press Web site at http://canjchem.nrc.ca on 6 January 2007.

S. Biswas and M. Ali.[1] Department of Chemistry, Jadavpur University, Kolkata 700 032, India.
Z. Rappoport and H. Salim. Department of Organic Chemistry, the Hebrew University of Jerusalem, Jerusalem 91904, Israel.

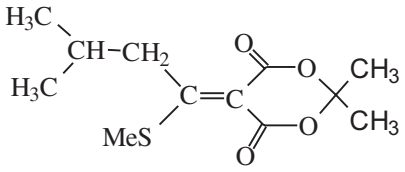
[1]Corresponding author (e-mail: mali@chemistry.jdvu.ac.in).

 doi:10.1139/V06-166 © 2006 NRC Canada

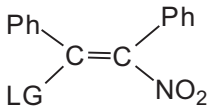
Chart 1.



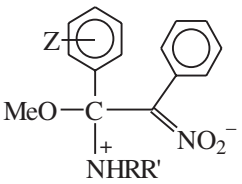
6-SMe-Z



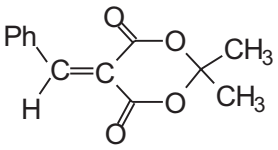
7



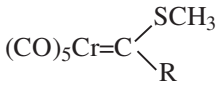
9-OMe (LG = MeO)
9-SMe (LG = SMe)



10

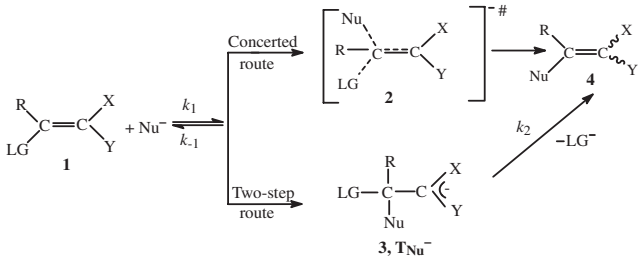


11-H

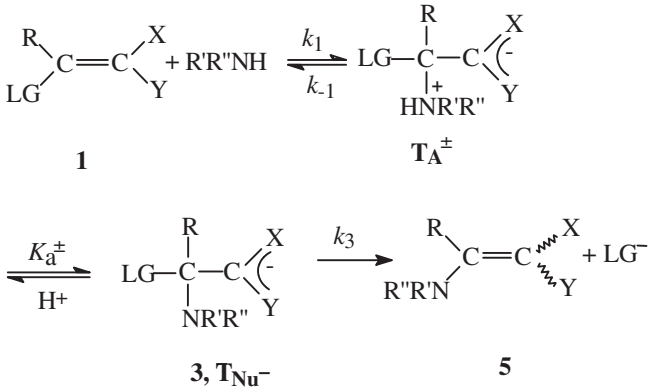


12 for **R** = **Me**
13 for **R** = **Ph**

Scheme 1.



Scheme 2.



rate-limiting. This conclusion is based on the k_3^{OH}/k_3^{A} ratios of 18:36, indicating the independence of k_1 values on the amine pK_a^{AH} for the former, while for the latter, the ratio was 179, higher than the observed limit of 5:25 (2, 3) manifesting the dependence of k_3^{OH}/k_3^{A} ratio on pK_a^{AH} of the amines.

In the present paper, we examine how the change from a substituted phenyl group in **6-SMe-Z** (**Z** = **H**) to the isobutyl group in **7** (see Chart 1) affects the rate-limiting step(s) and how the overall reactivity changes in the reactions with a series of primary amines.

Results and discussion

General features

All reactions were conducted in DMSO–H_2O (50:50, *v*/*v*) at 20 °C, at an ionic strength of 0.5 mol dm^{-3} maintained with KCl. Pseudo-first-order conditions were applied throughout, with the substrate being the minor component. Rates were measured for the reactions of **7** with *n*-butylamine, glycinamide, methoxyethylamine, and aminoacetonitrile. The representative Fig. 1 shows time-resolved spectra of the reaction with aminoacetonitrile. The presence of an isosbestic point indicates a clean reaction. As observed in the literature, the formation of amine-substituted product **8** produces a blue shift in the UV–vis spectrum (2), and the spectrum of the reaction mixture at infinite time is identical with that of the synthetically prepared **8**. This was further supported by ^{1}H NMR and HR-MS studies.

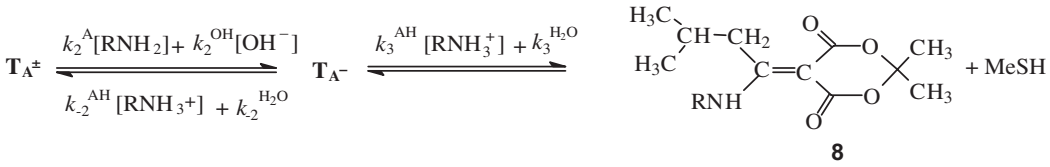
Based on the observations from the reaction of aliphatic primary (4) and alicyclic secondary amines with **6-SMe-Z** (2), we adopt Scheme 3 for the reactions of primary aliphatic amines (RNH_2) with **7**.

As the intermediate does not accumulate to a detectable level, a steady-state approximation to $\mathbf{T_A}^{\pm}$ leads us to derive an expression for the second-order rate constant, k_A, as given by eq. [1].

$$[1] \qquad k_A = \frac{k_1\left(\frac{k_3^{A}}{k_{-1}}[RNH_2] + \frac{k_3^{OH}}{k_{-1}}[OH^-]\right)}{1 + \left(\frac{k_3^{A}}{k_{-1}}[RNH_2] + \frac{k_3^{OH}}{k_{-1}}[OH^-]\right)}$$

The rate constants corresponding to the conversion of $\mathbf{T_A}^{\pm}$ via $\mathbf{T_A}^{-}$ and then to product **8** are shown in eq. [2].

© 2006 NRC Canada

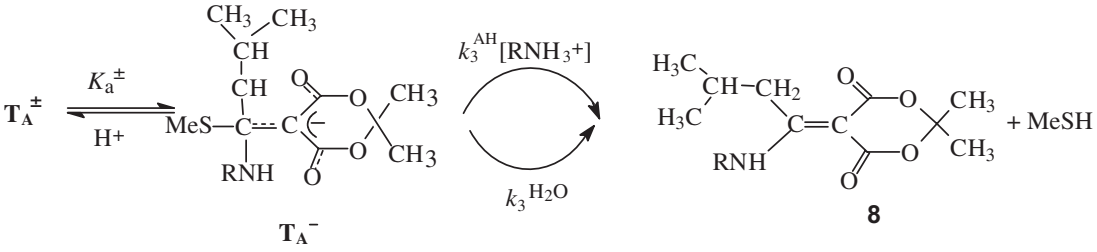
[2] 

Three cases may arise:

(*i*) When the acid-catalyzed conversion of $\mathbf{T_A^-}$ to $\mathbf{T_A^{\pm}}$ is much faster than its reversal, eq. [3] applies.

[3] $$k_{-2}^{AH}[RNH_3^+] + k_{-2}^{H_2O} \gg k_2^{A}[RNH_2] + k_2^{OH}[OH^-]$$

The interconversion of $\mathbf{T_A^-}$ and $\mathbf{T_A^{\pm}}$ can be treated as a rapid pre-equilibrium followed by a rate-limiting MeS^- departure (eq. [4]) and eqs. [5] and [6] hold, where K_a^{AH} is the acidity constant and K_w is the ionic product of the solvent (pK_w = 15.89 in DMSO–H_2O (50:50, *v*/*v*) at 20 °C, μ = 0.50 mol dm^{-3} KCl) (5).

[4] 

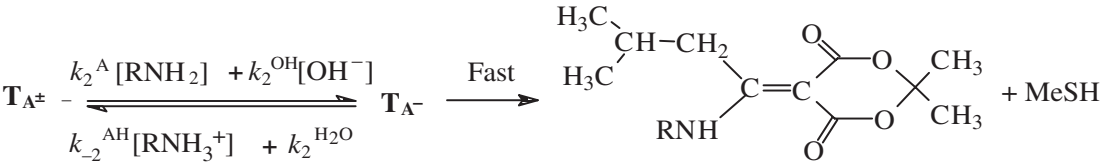
[5] $$k_3^{A} = k_3^{AH}K_a^{\pm}/k_a^{AH}$$

[6] $$k_3^{OH} = k_3^{H_2O}K_a^{\pm}/K_w$$

(*ii*) When the inequality in eq. [7] holds, $\mathbf{T_A^{\pm}}$ deprotonation is the rate-limiting step for the conversion

[7] $$k_{-2}^{AH}[RNH_3^+] + k_{-2}^{H_2O} \ll k_3^{AH}[RNH_3^+] + k_3^{H_2O}$$

of $\mathbf{T_A^{\pm}}$ to **8**, and eq. [8] and relationships [9] and [10] then hold.

[8] 

[9] $$k_3^{A} = k_2^{A}$$

[10] $$k_3^{OH} = k_2^{OH}$$

(*iii*) The nucleophilic attack becomes the rate-limiting step either via a concerted route or through the formation of $\mathbf{T_A^{\pm}}$ (Scheme 2) with subsequent faster steps. For reactions with amines, it is generally accepted that the nucleophilic vinylic substitution (S_NV) occurs through the formation of $\mathbf{T_A^{\pm}}$ (2, 6–7), and eqs. [11] and [12] hold (at high pH, this condition is easily met).

[11] $$\left(\frac{k_3^{A}}{k_{-1}}[RNH_2] + \frac{k_3^{OH}}{k_{-1}}[OH^-]\right) \gg 1$$

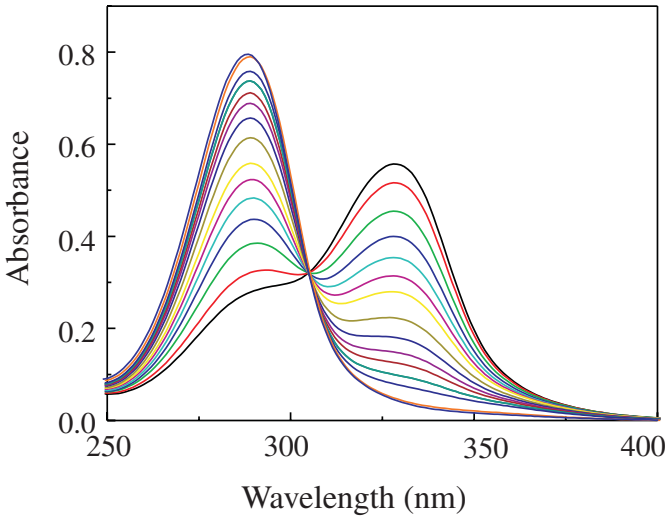
[12] $$k_A = k_1$$

Reactions of *n*-$BuNH_2$, $MeOCH_2CH_2NH_2$, and $NH_2COCH_2NH_2$

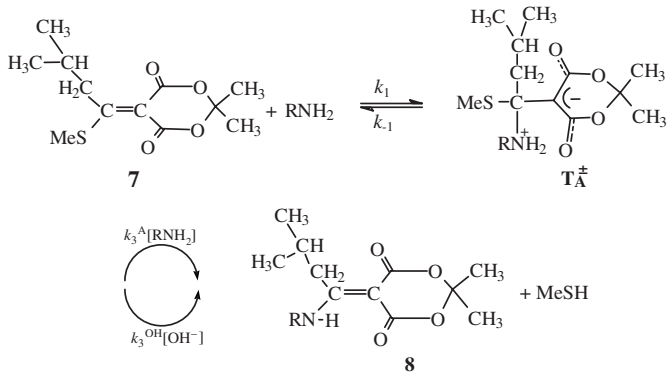
For the reactions of these three primary amines, a strict second-order kinetics (eq. [12] with $k_A = k_1$) was observed under all conditions. All the plots of k_{obs} vs. $[RNH_2]_f$ at pH ~ pK_a of the amines, where $[RNH_2]$:$[RNH_3^+]$ is 1:1, are linear with negligible or no intercept on the rate axis (Fig. 2). A contribution from H_2O or OH^--catalyzed hydrolysis ($k_1^{H_2O}$, k_1^{OH}) of **7** was excluded by the small values of the independently determined k_1^{OH} = 3.27 ± 0.01 dm^3 $mol^{-1}s^{-1}$ and $k_1^{H_2O}$ = (5.52 ± 0.03) × 10^{-6} dm^3 $mol^{-1}s^{-1}$.

© 2006 NRC Canada

Fig. 1. Time resolved spectra generated from a kinetic trace for the reaction between **7** and H_2NCH_2CN in DMSO–H_2O (50:50, *v*/*v*) with $[H_2NCH_2CN]$ = 0.02 mol dm^{-3} at pH 5.30 and 20 °C.



Scheme 3.



[13] $k_{obs} = k_A[RNH_2]$

Consequently, experimental eq. [13] fits the previously mentioned situation (*iii*), and k_A can be identified as k_1 according to eq. [12].

In few cases, reactions were carried out at pH where $[RNH_2]$:$[RNH_3^+]$ ~ 9:1, and no significant changes were observed in slope (k_A) values. Consequently, k_A is pH-independent, showing no general base catalysis.

Reaction with H_2NCH_2CN

The kinetics were performed under pseudo-first-order conditions with **7** as the minor component. A plot of the observed pseudo-first-order rate constants, k_{obs}, vs. $[H_2NCH_2CN]_f$ showed upward curvatures with an increasing slope (Fig. 3), while a plot of k_A ($k_A = k_{obs}/[H_2NCH_2CN]_f$) showed an initial rapid increase in k_A with the increase in [amine] followed by leveling off at higher amine concentration (Fig. 4), which is reminiscent of the reactions of **6-SMe-Z** with secondary amines (2). To check for a general base catalysis in this reaction, a variation of $[NMM]_f$ (NMM is *N*-methylmorpholine) in the range of 0.0005–0.10 mol dm^{-3} at pH 7.40 with $[H_2NCH_2CN]_f$ = 0.002 mol dm^{-3} and pH variation in the range of 6.70–8.45 at constant $[NMM]_f$ = 0.002 mol dm^{-3} and $[H_2NCH_2CN]_f$ = 0.002 mol dm^{-3} were carried out. The k_A value remained almost independent of $[NMM]_f$ with a value 2.26 ± 0.04 dm^3 mol^{-1} s^{-1}, while it increased with $[OH^-]$ at the low $[OH^-]$ region and became independent at high $[OH^-]$ (Fig. 5). This behaviour seems to be a special case of Scheme 2, where only OH^- catalysis but not amine catalysis occurs, particularly at high pH. This can be understood if eqs. [14] and [15] hold throughout the whole concentration ranges used, and if simultaneously the ratio ($k_3^{H_2O}K_a^{\pm}/k_{-1}K_w$) $[OH^-]$ changes from <1 to >1 as $[OH^-]$ is increased and eq. [3] changes to eq. [16].

[14] $$\frac{k_3^{AH}K_a^{\pm}}{k_{-1}k_a^{AH}}[RNH_2] << 2$$

Fig. 2. Plot of k_{obs} vs. $[RNH_2]_f$ for the reaction of **7** with primary amines in DMSO–H_2O (50:50, *v*/*v*) at 20 °C.

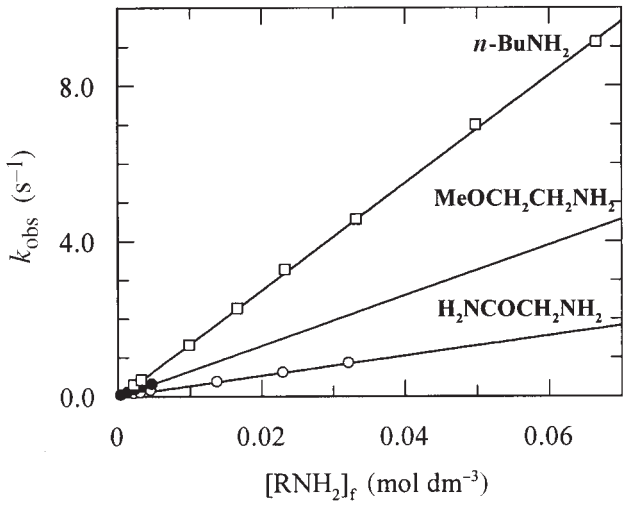
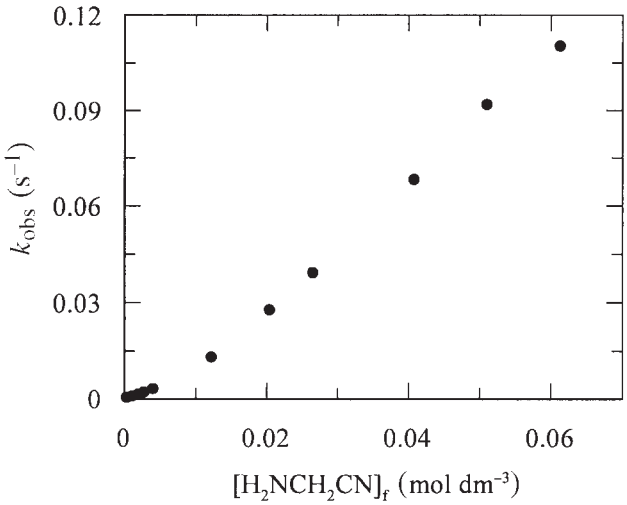


Fig. 3. Plot of k_{obs} vs. $[H_2NCH_2CN]_f$ for the reaction of **7** with aminoacetonitrile in DMSO–H_2O (50:50, *v*/*v*) at 20 °C.



© 2006 NRC Canada

Table 1. Comparison of rate constants for the nucleophilic attack on **6-SMe-H** and **7** by nucleophiles in DMSO–H_2O (50:50, *v*/*v*) at 20 °C.

Amine or other nucleophile	pK_a^{AH}	k_1 (**7**) ($dm^3\ mol^{-1}\ s^{-1}$)	k_1 (**6-SMe-H**) ($dm^3\ mol^{-1}\ s^{-1}$)	k_1(**7**)/k_1 (**6-SMe-H**)
n-Butylamine	10.61	138.4	5.36	25.8
Methoxyethylamine	9.63	65.0	2.63	24.7
Glycinamide	8.28	26.1	1.30	22.9
Aminoacetonitrile	5.39	2.38	0.12	20.3
OH^-	17.30	3.27	0.63	5.2
H_2O	17.33	5.52×10^{-6}	2.80×10^{-6}	2.0

Fig. 4. Plot of k_A vs. $[aminoacetonitrile]_f$ for the reaction of **7** with aminoacetonitrile in DMSO–H_2O (50:50, *v*/*v*) at 20 °C.

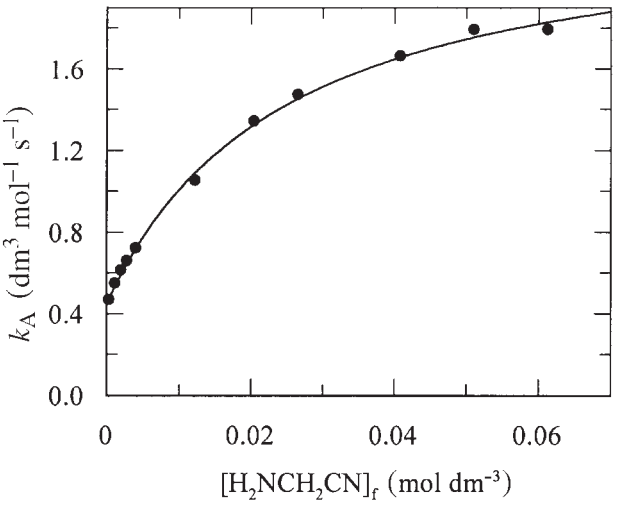
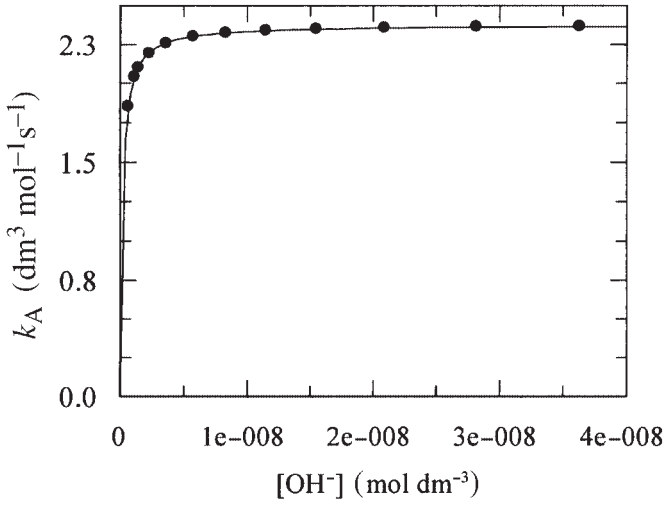


Fig. 5. Plot of k_{obs} vs. $[OH^-]$ for the reaction of **7** with aminoacetonitrile with $[H_2NCH_2CN]_f$ = 0.002 mol dm^{-3} in DMSO–H_2O (50:50, *v*/*v*) at 20 °C.



$$[15]\quad \frac{k_3^{AH}K_a^{\pm}}{k_{-1}k_a^{AH}}[RNH_2] << \frac{k_3^{H_2O}K_a^{\pm}}{k_{-1}K_w}[OH^-]$$

$$[16]\quad k_A = \frac{k_1\left(\frac{k_3^{H_2O}K_a^{\pm}}{k_{-1}K_w}[OH^-]\right)}{1+\left(\frac{k_3^{H_2O}K_a^{\pm}}{k_{-1}K_w}[OH^-]\right)}$$

A non-linear least-squares fit of the data to eq. [3] for $[H_2NCH_2CN]_f$ gives k_1 = 2.37 ± 0.07 $dm^3\ mol^{-1}\ s^{-1}$ and k_3^A/k_{-1} = 50.8 ± 5.15 s^{-1}. Similar treatment for the change in $[OH^-]$ (eq. [16]) yields k_1 = 2.48 ± 0.05 $dm^3\ mol^{-1}\ s^{-1}$ and k_3^{OH}/k_{-1}= 8.13 ± 0.78 × 10^8 s^{-1} (Table 1). The k_1 value obtained from the variation of $[H_2NCH_2CN]_f$ at constant pH is almost the same as that obtained from the variation of $[OH^-]$ at constant $[NMM]_f$ and $[H_2NCH_2CN]_f$, thus confirming the proposed mechanism.

The rate-limiting step

The catalysis by both OH^- and H_2NCH_2CN demonstrates a general base catalysis, which is most likely accounted by Scheme 2. The lack of NMM catalysis may be attributed to its bulkiness, which precludes its closer approach to $\mathbf{T_A^{\pm}}$ in the transition state. Either the conversion of $\mathbf{T_A^{\pm}}$ to $\mathbf{T_A^-}$ or LG departure from $\mathbf{T_A^-}$ is rate-limiting. The very high k_3^{OH}/k_3^A ratio (3.28×10^8) implies a rapid acid–base equilibrium between $\mathbf{T_A^{\pm}}$ and $\mathbf{T_A^-}$ followed by a rate-limiting, general-acid-catalyzed LG departure (2). Similar observations were encountered in the aminolysis of the electrophilic β-methoxy-α-nitrostilbene (**9-OMe**) (see Chart 1) where the deprotonation of the corresponding zwitterionic intermediate (**10**) is fast, and methoxide ion departure is rate determining (7).

Based on the reaction in eq. [8], the reaction of OH^- is expected to be a diffusion-controlled proton transfer with a k_2^{OH} value around 10^{10} $dm^3\ mol^{-1}\ s^{-1}$ (8); hence, k_2^{OH} should be independent of the amine basicity. k_2^A is also expected to be essentially independent of the amine basicity irrespective of whether the reaction is diffusion-controlled ($K_a^{AH} >> K_a^{\pm}$) or diffusion-separation-controlled ($K_a^{BH} < K_a^{\pm}$) (9). In the latter case, k_2^A is independent of the amine basicity because the pK_a *difference* ($K_a^{\pm} - K_a^{AH}$) should be constant. Furthermore, if $K_a^{AH} < K_a^{\pm}$ of $\mathbf{T_A^{\pm}}$, the proton transfer from $\mathbf{T_A^{\pm}}$ to RNH_2 will be thermodynamically favorable and close to diffusion controlled limit. Hence, k_3^{OH}/k_3^A ratios should be independent of the amine basicity and have values of 5–25 (3). Because this contrasts our experimental observation, we ascribe the very high k_3^{OH}/k_3^A value for the H_2NCH_2CN reac-

© 2006 NRC Canada

tion to a rate-limiting leaving group departure rather than to a rate-limiting proton transfer from $\mathbf{T_A^{\pm}}$.

The nucleophilic attack step (k_1)

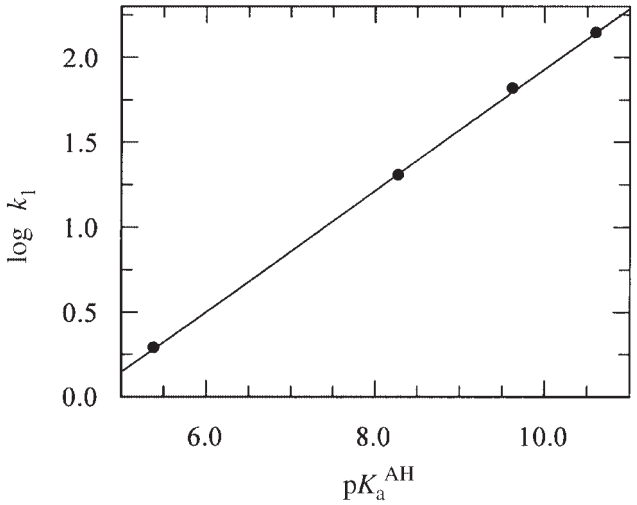
The good linearity of a Brønsted plot of $\log(k_1)$ vs. pK_a^{AH} ($\beta_{nuc} = 0.34 \pm 0.004$) for the reaction of **7** with the four primary amines is shown in Fig. 6. The corresponding β_{nuc} for k_1 values for the reaction of secondary amines with **6-SMe-H** is 0.41. It was found that the k_1 values for the reactions with secondary amines are smaller than those for the primary amines of comparable basicity. For example, for the **11-H**–HEPA (HEPA is *N*-(2-hydroxyethyl)piperazine) reaction ($pK_a^{AH} = 9.51$), k_1 is 1.06 ± 0.34 dm^3 mol^{-1} s^{-1}, while for **11-H**–$MeOCH_2CH_2NH_2$ reaction ($pK_a^{AH} = 9.63$), k_1 is 2.63 ± 0.05 dm^3 mol^{-1} s^{-1}. These results reflect a strong steric effect that reduces the reactivity of the bulkier secondary amines. When steric effects are absent, secondary amines generally react faster than primary amines of comparable basicity (9, 10).

The substitution reactions of **7** are 20–26 times faster than the **6-SMe-H**–RNH_2 reactions. Hence, the formation of $\mathbf{T_A^{\pm}}$ with RNH_2 is thermodynamically more favorable for **7** than for **6-SMe-H**. However, based on both inductive and steric effects a reverse trend is expected. We ascribe this discrepancy to an additional effect, i.e., π-donation by the phenyl group (Ph), which may reduce the reactivity of **6-SMe-H** (11). A similar reactivity trend, which was observed for the reactions of H_2NCH_2CN and morpholine with the Fischer carbene complexes **12** and **13** (see Chart 1) was attributed to a different π-donation effect of the Ph group which lowers the reactivity of **13** over **12** (12–15).

The higher β_{nuc} value for **6-SMe-H**–RR′NH (0.41 ± 0.01) compared with that for the **6-SMe-H**–RNH_2 reactions (0.32 ± 0.01) (4) implies that at the transition state, C–N bond formation is more advanced with the secondary amines. Similarly, the β_{nuc} value for the **7**–RNH_2 reaction (0.34 ± 0.02) is almost the same as that for **6-SMe-H**–RNH_2 reaction and manifests the fact that the bond formations in the transition states progress equally in both reactions.

In the reaction of **14-H** with piperidine or morpholine (16) (eq. [17]), $\beta_{nuc}(k_1) = 0.14$, suggesting that the C–N bond is less advanced than in the reaction of **11-H** and **7** with both primary and secondary amines. This is again consistent with the Hammond–Leffler (17, 18) principle, because **14-H** (19) and **15-H** (16) are much more reactive, e.g., k_1 for the **14-H**-morpholine reaction (3.19×10^5 dm^3 mol^{-1} s^{-1}) is much higher than k_1 for the addition of morpholine to **11-H** (0.49 dm^3 mol^{-1} s^{-1}), and K_1 for the same reaction is also higher for **15-H** (7.76×10^4 dm^3 mol^{-1}) than for **11-H**, which is ~1.9×10^{-8} dm^3 mol^{-1}. The inverse correlation between β_{nuc} and the reactivity of electrophilic olefins (PhCH=CXY) appears to be quite general and has been observed before (20).

Fig. 6. Brønsted Plot for the reaction of **7** with primary amines.



Conclusions

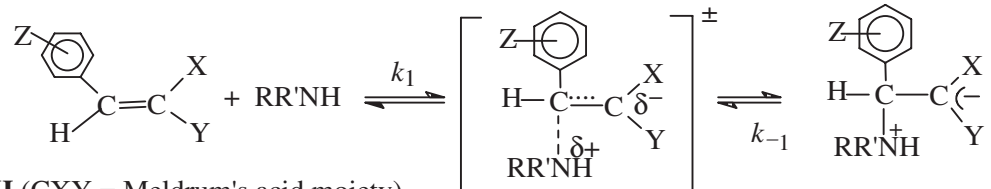
(1) In the reactions of **7** with the more basic amines, namely, $H_2NCH_2CONH_2$, $MeOCH_2CH_2NH_2$, and *n*-$BuNH_2$, no base catalysis is observed; thus, implying a rate-limiting k_1 step because of the strong electronic push from the nitrogen lone pair in the product leading to the stabilization of the transition state resulting from the developing product resonance. For the less basic amine, H_2NCH_2CN, general base catalysis is observed as the electronic push is not so prominent here.

(2) The k_1 values for **6-SMe-H**–RNH_2 reactions are lower than those for the **7**–RNH_2 reactions, suggesting that a strong π-donation by the phenyl group reduces the reactivity of **6-SMe-H**.

Experimental section

Compound **7** was synthesized by following the literature method (20). DMSO was refluxed over CaH_2 and distilled under vacuum. Reagent grade amines were purchased from Aldrich chemicals (USA). The solid amines were recrystallized from a water–ethanol solution, and the liquids were distilled over CaH_2 before use.

[17]



14-H (CXY = Meldrum's acid moiety)

15-H (CXY = $CHNO_2$)

© 2006 NRC Canada

Synthesis of α-isobutyl-α-(*n*-butylamino)methylene Meldrum's acid (6)

Compound **7** was prepared analogous to the procedure reported for the synthesis of 2,2-dimethyl-5-[piperidino(*p*-methoxyphenyl)methylene-1,3-dioxane-4,6-dione (21). $CaCl_2$-protected MeCN solution (15 mL) containing 1 mmol of each of **7** and *n*-butylamine was stirred for 48 h at room temperature. The solvent was evaporated, and the remaining solid was recrystallized from EtOH to give α-isobutyl-α-(*n*-butylamino)methylene Meldrum's acid in 35% yield. ^{1}H NMR (300 MHz, $CDCl_3$, ppm) δ: 1.00 (2Me of *i*-Bu), 1.02 (Me), 1.24 (CH_2), 1.41 (CH_2), 1.67 (2Me of Meldrum's acid moiety), 2.04 (CH_2 of *i*-Bu), 2.58 (NH), 2.68 (CH of *i*-Bu), 3.45 (CH_2 α- to NH). ES-MS *m*/*z*: 284 (MH^+), 241 ($MH^+ - CMe_2$), 226($MH^+ - OCMe_2$), 197 ($MH^+ - HCMe_2$–$CH_3(CH_2)_2$), 171 (MH^+ – *i*-BuN–CMe_2), 114 (M – MA–CH_2–CH_2, MA is Meldrum's acid moiety).

Kinetics and pH measurements

Details of the kinetic and pH measurements are reported elsewhere (2, 4). Most reactions were followed by monitoring the disappearance of the substrates around 330 nm using a Hewlett-Packard 8453 Agilent UV–vis spectrophotometer. The pH in DMSO–H_2O (50:50, *v*/*v*) at an ionic strength of 0.50 mol dm^{-3} KCl at 20 °C was determined by a digital pH-meter (Systronics–335, India) equipped with a glass electrode and a reference electrode calibrated with standard aq. buffers in DMSO–H_2O (50:50, *v*/*v*) before use. Stock solutions of the substrates were prepared in anhyd. acetonitrile. The pseudo-first-order rate constants (k_{obs}, s^{-1}) were obtained by fitting the kinetic traces with a suitable computer-fit program and the results were within an error limit of ±5%.

Acknowledgment

This work was supported by grants SR/S1/IC-19/2002 from the Department of Science and Technology (DST), New Delhi and F.12–22/2003(SR) from University Grant Commission (UGC), New Delhi.

References

1. For reviews, see: (*a*) Z. Rappoport. Adv. Phys. Org. Chem. **7**, 1 (1969); (*b*) G. Modena. Acc. Chem. Res. **4**, 73 (1971); (*c*) S.I. Miller. Tetrahedron, **33**, 1211 (1977); (*d*) Z. Rappoport. Acc. Chem. Res. **14**, 7 (1981); (*e*) Z. Rappoport. Recl. Trav. Chim. Pays–Bas, **104**, 3092 (1985); (*f*) B. A. Shainyan. Usp. Khim. **55**, 942 (1986); (*g*) Z. Rappoport. Acc. Chem. Res. **25**, 474 (1992); (*h*) T. Okuyama and G. Lodder. Adv. Phys. Org. Chem. **37**, 1 (2002).
2. C.F. Bernasconi, M. Ali, K. Nguyen, V. Ruddat, and Z. Rappoport. J. Org. Chem. **69**, 9248 (2004).
3. (*a*) C.F. Bernasconi and M.W. Stronach. J. Org. Chem. **56**, 1993 (1991); (*b*) C.F. Bernasconi and M.W. Stronach. J. Am. Chem. Soc. **113**, 2222 (1991).
4. M. Ali, S. Biswas, Z. Rappoport, and C.F. Bernasconi. J. Phys. Org. Chem. In press.
5. J.-C. Hallé, R. Gaboriaud, and R. Schaal. Bull. Soc. Chim. Fr. 2047 (1970).
6. C.F. Bernasconi, A.E. Leyes, Z. Rappoport, and I. Eventova. J. Am. Chem. Soc. **115**, 7513 (1993); (*b*) C.F. Bernasconi, A.E. Leyes, I. Eventova, and Z. Rappoport. J. Am. Chem. Soc. **117**, 1703 (1995).
7. C.F. Bernasconi, J. Fassberg, R.B. Killion, Jr. and Z. Rappoport. J. Org. Chem. **55**, 4569 (1990).
8. M. Eigen. Angew. Chem., Int. Ed. Engl. **3**, 1 (1964).
9. W.P. Jencks. Catalysis in chemistry and enzymology. McGraw-Hill, New York. 1969. p. 95.
10. C.F. Bernasconi, C.J. Murray, J.P. Fox, and D.J. Carre. J. Am. Chem. Soc. **105**, 4349 (1983).
11. C.F. Bernasconi, S.D. Brown, M. Ali, Z. Rappoport, H. Yamataka, and H. Salim. J. Org. Chem. **71**, 4795 (2006).
12. C.F. Bernasconi and S. Bhattacharya. Organometallics, **22**, 426 (2003).
13. M. Ali. New J. Chem. **28**, 412 (2004).
14. M. Ali and D. Maiti. J. Organeomet. Chem. **689**, 3520 (2004).
15. M. Ali, S. Gangopadhyay, and M. Mizanuddin. J. Organomet. Chem. **690**, 4878 (2005).
16. C.F. Bernasconi and M. Panda. J. Org. Chem. **52**, 3042 (1987).
17. G.S. Hammond. J. Am. Chem. Soc. **77**, 334 (1955).
18. J.E. Leffler and E. Grunwald. Rates and equilibria of organic reactions. Wiley, New York. 1963. p. 156.
19. C.F. Bernasconi, R.F. Renfrow, and P.R. Tia. J. Am. Chem. Soc. **108**, 454 (1986).
20. C.F. Bernasconi. Tetrahedron, **45**, 4017 (1989).
21. M. Beit-Yannai and Z. Rappoport. J. Chem. Soc., Perkin Trans. 2. 1534 (2001).

© 2006 NRC Canada

Chlorine atom initiated reactions of selected tropospheric halocarbons — Kinetic and product studies

Anisha Garib, Qadir K. Timerghazin, and Parisa A. Ariya

Abstract: Halogens are suggested as important atmospheric oxidants in the marine boundary layer. The room-temperature kinetics of the chlorine-initiated reactions of three biogenic brominated hydrocarbons and four anthropogenic chlorinated ethenes was investigated by gas chromatography with flame ionization detection (GC–FID) at a pressure of 1 atm (1 atm = 101.325 kPa) in air, using the relative rate technique. The rate constants ($\times 10^{13}$ cm^3 molecule^{-1} s^{-1}) for CH_2Br_2, $CHBr_2Cl$, and $CHBr_3$ reactions at 298 ± 2 K were found to be 4.25 ± 0.65, 2.03 ± 0.31, and 2.81 ± 0.41, respectively, using methane as a reference compound. Room temperature rate constants ($\pm 10^{11}$ cm^3 molecule^{-1} s^{-1}) obtained for 1,1-dichloroethene, *cis*-dichloroethene, *trans*-dichloroethene, and trichloroethene using ethene as a reference are 13.4 ± 3.3, 9.1 ± 2.3, 7.4 ± 1.8, and 7.7 ± 1.9, respectively. The rate constants of chlorine-atom reactions with various hydrocarbons obtained in this work and taken from literature were correlated with corresponding rate constants of the OH radical available in the literature. The temperature dependences for the reactions of chlorine atoms with chlorinated ethenes were studied within the 298–358 K range. The corresponding Arrhenius expressions for the rate constants are (cm^3 molecule^{-1} s^{-1}): ln k = (–25.26 ± 0.17) – (758 ± 55)/T for 1,1-dichloroethene, ln k = (–25.79 ± 0.10) – (799 ± 34)/T for *cis*-dichloroethene, ln k = (–26.74 ± 0.09) – (1018 ± 28)/T for *trans*-dichloroethene, and ln k = (–26.10 ± 0.26) – (846 ± 83)/T for trichloroethene. In addition, product studies for the chlorine-initiated gas phase oxidation reactions of $CHBr_3$ and $CHBr_2Cl$ were performed using gas chromatography with mass spectrometric detection (GC–MS). The only identified product for the reaction of $CHBr_3$ with Cl reaction was $COBr_2$, while for the $CHBr_2Cl$ + Cl reaction, COBrCl and $COCl_2$ were observed, indicating the possibility of halogen atom release. The atmospheric implications of the results obtained are discussed.

Key words: tropospheric reactions, kinetics, chlorine atoms, chlorinated hydrocarbons, brominated hydrocarbons.

Résumé : Il a été suggéré que les halogènes sont des oxydants atmosphériques importants dans les interfaces marines. Faisant appel à la chromatographie en phase gazeuse avec détection à ionisation de flamme (CG–DIF), à une pression de une atmosphère dans l'air et utilisant la technique de la vitesse relative, on a étudié la cinétique, à la température ambiante, de réactions initiées par le chlore de trois hydrocarbures bromés biogéniques et de quatre éthènes chlorés anthropogéniques. Utilisant le méthane comme composé de référence, on a établi que les constantes de vitesse ($\times 10^{13}$ cm^3 molécule^{-1} s^{-1}), à 298 ± 2 K, pour les réactions du CH_2Br_2, du $CHBr_2Cl$ et du $CHBr_3$ sont respectivement de 4,25 ± 0,65, 2,03 ± 0,31 et 2,81 ± 0,41. Utilisant l'éthène comme produit de référence, les constantes de vitesse à la température ambiante ($\times 10^{11}$ cm^3 molécule^{-1} s^{-1}) pour les réactions du 1,1-dichloroéthène, du *cis*-1,2-dichloroéthène, du *trans*-1,2-dichloroéthène et du trichloroéthène sont respectivement de 13,4 ± 3,3, 9,1 ± 2,3, 7,4 ± 1,8 et 7,7 ± 1,9. On a établi une corrélation entre les constantes de vitesses des réactions des atomes de chlore avec les divers composés étudiés dans ce travail ou tirées des travaux publiés dans la littérature et les constantes de vitesse correspondantes des réactions du radical HO tirées de la littérature. Opérant entre 298 et 358 K, on a étudié les relations entre les constantes des vitesses de réactions des atomes de chlore avec les divers dérivés halogénés. Les expressions d'Arrhenius correspondantes pour les constantes de vitesses sont (cm^3 molécule^{-1} s^{-1}): ln k = (–25,26 ± 0,17) – (758 ± 55)/T pour le 1,1-dichloroéthène, ln k = (–25,79 ± 0,10) – (799 ± 34)/T pour le *cis*-1,2-dichloroéthène, ln k = (–26,74 ± 0,09) – (1018 ± 28)/T pour le *trans*-1,2-dichloroéthène et ln k = (–26,10 ± 0,26) – (846 ± 83)/T pour le trichloroéthène. De plus, faisant appel à la chromatographie en phase gazeuse avec détection par spectrométrie de masse (CG–SM), on a réalisé une étude des produits obtenus lors des en réactions en phase gazeuse initiées par le chlore du $CHBr_3$ et du $CHBr_2Cl$. Le seul produit identifié pour la réaction de $CHBr_3$ avec le chlore est le $COBr_2$ alors que pour

Received 14 August 2006. Accepted 24 October 2006. Published on the NRC Research Press Web site at http://canjchem.nrc.ca on 10 January 2007.

A. Garib and P.A. Ariya.[1] Departments of Chemistry and Atmospheric and Oceanic Sciences, McGill University, 801 Sherbrooke St. W., Montréal, QC H3A 2K6, Canada.
Q.K. Timerghazin. Departments of Chemistry and Atmospheric and Oceanic Sciences, McGill University, 801 Sherbrooke St. W., Montréal, QC H3A 2K6, Canada; Centre for Research in Molecular Modeling and Department of Chemistry and Biochemistry, Concordia University, 7141 Sherbrooke St. W., Montréal, QC H4B 1R6, Canada.

[1]Corresponding author (e-mail: parisa.ariya@mcgill.ca).

 doi:10.1139/V06-170 © 2006 NRC Canada

la réaction du chlore avec le $CHBr_2Cl$, on a observé la formation de COBrCl et de $COCl_2$, ce qui indique la possibilité d'émission d'un atome d'halogène. On discute des implications atmosphériques de ces résultats.

Mots clés : réactions troposphériques, cinétiques, atomes de chlore, hydrocarbures halogénés, hydrocarbures bromés.

[Traduit par la Rédaction]

Introduction

Analysis of ozone-depletion events (1) along with concomitant decreases of the C_2–C_6 hydrocarbon concentrations observed in the Arctic marine boundary layer (MBL) during polar sunrise studies provided convincing evidence of the involvement of chlorine chemistry in these processes (2, 3). The abundance of active chlorine in the marine troposphere and its important role as an atmospheric oxidant has been intensively studied during the last decade (4–6). The OH radical is considered to be a major oxidant and a natural "cleanser" of the troposphere during daytime (6). Its concentration in the MBL is estimated to be approximately 100 times higher than that of active chlorine (7). However, the concentration of Cl atoms may significantly increase during sunrise (8), and for most of the non-methane hydrocarbons (NMHCs) the reaction rates of oxidation by chlorine atoms are about two orders of magnitude larger than the corresponding reactions with OH radicals. Hence, even if [Cl] is lower than [OH], the role of Cl atoms as oxidants for hydrocarbons might still be significant (4).

The mechanism of active chlorine release in the troposphere is still a matter of debate; several proposed mechanisms suggest that heterogeneous reactions are responsible for the formation of Cl atoms. These include reactions of sea-salt aerosols with NO_x species (4), sulfur-containing compounds (9), or the release of halogens through the cycles involving halide ions (10). Various forms of chlorine-containing compounds, such as HOCl, BrCl, and Cl_2, have been repeatedly observed in the atmosphere (11–13). Whereas the concentration of chlorine atoms in the troposphere was estimated to be 10^4–10^5 atoms cm^{-3} during the day in the MBL (14), the molecular chlorine concentration is suggested to be as high as 150 parts per trillion (ppt) (13). Impey et al. (11) reported measurements of photolyzable chlorine of 100 ppt in the boundary layer at Alert (82.5°N, 62.3°W) using a photo-halogen detector (PHD) during the Polar Sunrise Experiment. Thus, photolysis of molecular chlorine or BrCl by sunlight at the Arctic dawn is also believed to form Cl atoms (15).

There is a great variety of biogenic and anthropogenic hydrocarbons emitted into the troposphere, including a large number of chlorinated and brominated species. Whereas the latter compounds are mostly of anthropogenic source, most of the brominated hydrocarbons are of biogenic origin. Trichloroethene, one of the most abundant chlorinated ethenes (emission rate of 197×10^9 g $year^{-1}$) (16), is used industrially as a degreasing, dry-cleaning agent, and solvent (17). It is also emitted by fossil fuel production and combustion. Dichloroethenes, on the other hand, are used in the manufacturing of various plastics (18). The major biogenic bromine-containing species is bromoform ($CHBr_3$) (19) with a concentration in the troposphere within 10–20 ppt (19, 20). Other important brominated hydrocarbons include dibromomethane (CH_2Br_2) and chlorodibromomethane ($CHBr_2Cl$). These compounds are mainly emitted by marine organisms such as algae and phytoplankton (16). According to a recent estimate, marine algae are responsible for up to 70% of global bromoform production (19).

Although a number of experimental and theoretical papers on the chlorine atom initiated oxidation of halocarbons (e.g., see refs. 21–24) have been published, there is still a lack of information on the kinetics of these reactions, especially at the conditions relevant for tropospheric chemistry. The goal of the current work is to provide a self-consistent set of kinetic data for chlorine-initiated reactions of seven halocarbons at an atmospheric pressure of ~760 torr (1 torr = 133.3224 Pa) and over a temperature range of 298–358 K. Product studies of chlorine-initiated reactions of selected brominated hydrocarbons were performed to assess the possibility of regeneration of the halogen atoms as well as their importance in the chemistry of the troposphere.

Experimental

Kinetic studies

Rate constants were determined using the relative rate technique, in which rate constants of two reactions are measured simultaneously and one of the reaction rate constants (a reference) is known.

[1] Cl + reactant → product

$$\frac{-\mathrm{d[reactant]}}{\mathrm{d}t} = k[\mathrm{Cl}][\mathrm{reactant}]$$

[2] Cl + reference → product

$$\frac{-\mathrm{d[reference]}}{\mathrm{d}t} = k_{\mathrm{ref}}[\mathrm{Cl}][\mathrm{reference}]$$

Provided that the reference and the reactant are lost solely by reactions [1] and [2], and there are no significant secondary reactions leading to the reformation of reference and reactant, the following equation applies

$$[3] \qquad \ln\left(\frac{[\mathrm{reactant}]_{t_1}}{[\mathrm{reactant}]_{t_2}}\right) = \frac{k}{k_{\mathrm{ref}}} \ln\left(\frac{[\mathrm{reference}]_{t_1}}{[\mathrm{reference}]_{t_2}}\right)$$

where t_1 and t_2 refer to initial and final concentrations, respectively. Hence, a plot of $\ln([\mathrm{reactant}]_{t_1}/[\mathrm{reactant}]_{t_2})$ against $\ln([\mathrm{reference}]_{t_1}/[\mathrm{reference}]_{t_2})$ is expected to yield a straight line with slope k/k_{ref} and zero intercept. Since k_{ref} is known, the rate constant k for the molecule or atom of interest can be calculated.

All reactants were injected using Hamilton microsyringes into an evacuated (~10^{-3} torr) 3 L double-walled Pyrex glass flask. To avoid undesired side-reactions at the surfaces of the

© 2006 NRC Canada

reaction vessel, the inner walls were deactivated by dimethyldichlorosilane (DMDCS) (25, 26). DMDCS was deposited on the flask walls via a toluene solution, and the toluene was removed by drying and subsequent pumping. The flask was then filled to 760 torr with Ultra Pure air as a diluent. The concentrations of organic reactants ranged from 50 to 150 ppm (where 1 ppm = 2.46×10^{13} molecules cm^{-3}), while that of molecular chlorine was approximately twice as much. Also, 200–500 ppm benzene was added to all reaction flasks to act both as an OH scavenger ($k_{OH} = 1.3 \times 10^{-12}$ cm^3 $molecule^{-1}$ s^{-1}) (27) and an internal reference. Under our experimental conditions, no significant change in the benzene signal was observed throughout the course of the experiments. The reaction mixtures were mixed in the dark using a magnetic stirring bar until all hydrocarbon concentrations were stable.

The reactants were monitored using a gas chromatograph equipped with a flame ionization detector (GC–FID), model HP 6890 equipped with a 5% phenyl-methyl siloxane DB1 capillary column (30 m × 25 mm × 25 μm). Irradiations of reaction mixtures ranging from a few minutes to 30 min were performed in a 0.75 m^3 photolytic box equipped with nine UV tubes (GE Black Light, model F20T12-BL) positioned vertically on the sides of the box. Molecular chlorine was photolyzed to yield two chlorine atoms

$$[4] \qquad Cl_2 + h\nu\ (300 \le \lambda \le 400\ nm) \rightarrow 2\ Cl$$

Immediately following the irradiation, 100 μL of the gas mixture was introduced into the injection port of the GC–FID. For the reactions of the brominated hydrocarbons, the chosen reference molecule was methane, and in the case of chlorinated ethenes, ethene was used as a reference molecule. The reaction flask was thermostated (±1 K) by means of a water circulator (Neslab RTE 111). Identical conditions were maintained for temperature-dependence studies carried out within 298–358 K. Reported experimental uncertainties include a calculated uncertainty of ±2σ. We evaluated an accumulative error of about 12%, which includes uncertainties associated with kinetic plots (~5%–10%), as well as concentration measurements (<5%), and instrument and human errors (~10%).

Product studies

The gas-phase products of the chlorine-initiated reactions of CH_2Br_2, $CHBr_2Cl$, and $CHBr_3$ were investigated using a gas chromatograph with a mass selective detector (GC–MSD, model HP 6890/5973) equipped with a cross-linked 5% phenyl-methyl siloxane HP-5MS (30 m × 0.25 mm × 1.00 μm) capillary column. The experimental setup was identical to the procedure described in the *Kinetic studies* section. Each Cl reaction system was treated separately. Typical concentrations of reactants were 50–200 ppm, while $[Cl_2] \approx 2 \times$ [reactant]. All GC–MS runs were performed in SCAN mode.

Materials

Unless otherwise indicated, all reactants were used as received. Benzene (99.9+%), bromoform (99+%), molecular chlorine (99.5+%), chlorodibromomethane (98%), *cis*-1,2-dichloroethene (97%), dibromomethane (99.6%), 1,1-dichloroethene (99%), ethene gas (99+%), methane gas (99+%), *trans*-1,2-dichloroethene (98%), and trichloroethene (98%) were supplied by Sigma-Aldrich (Oakville, Canada). Ultra Pure air (containing <1 ppm hydrocarbons) was obtained from Matheson Tri-Gas (Newark, USA). Carrier gases for GC (hydrogen, helium, and air) were also supplied by Matheson Tri-Gas. Dimethyldichlorosilane (5% DMDCS in toluene) was obtained from Supelco (Oakville, Ontario, Canada).

Fig. 1. Relative rate plots for the brominated hydrocarbons and the reference compound (methane) at 298 ± 2 K.

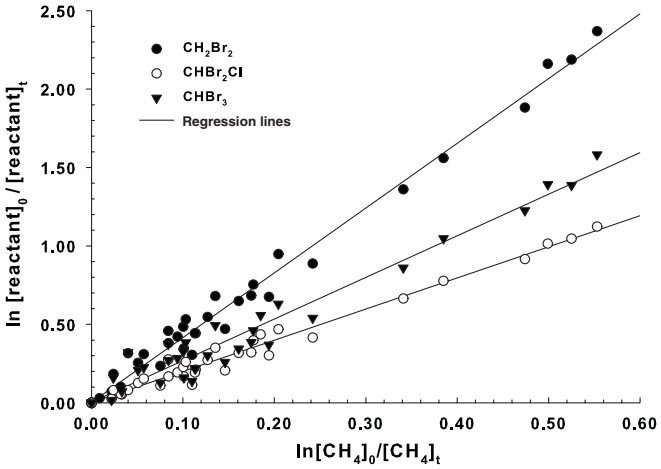
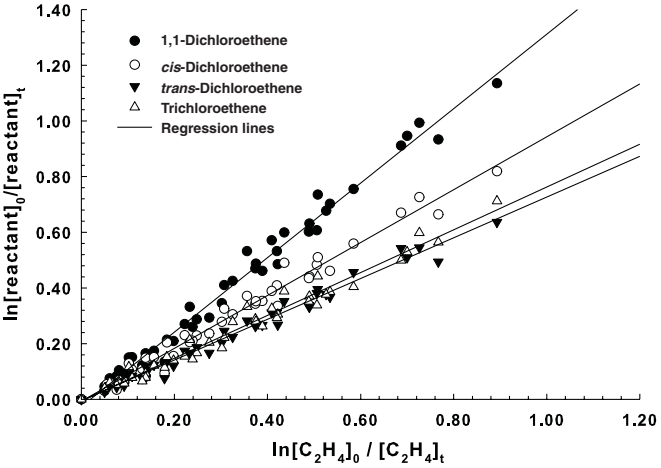


Fig. 2. Relative rate plots for the chlorinated ethenes and the reference compound (ethene) at 298 ± 2 K.



Results and discussion

Reaction rate constants

Prior to starting the kinetic studies, we carried out a series of experiments to verify that "dark" reactions are not significant; no such reactions were observed within experimental uncertainties. Also, aging the gas samples after irradiation for up to 1 h showed that no observable reformation of reactants occurred. To evaluate possible surface catalysis reactions, selected experiments were carried out in 2 to 5 L flasks. However, no change outside experimental errors was

© 2006 NRC Canada

Table 1. Room-temperature rate constants for the reactions of brominated hydrocarbons with chlorine atoms.

Compound	k/k_{ref}	k ($\times 10^{13}$ cm^3 molecule^{-1} s^{-1})	Technique	Ref.
CH_2Br_2	4.25±0.50[a]	4.25±0.65		This work
		4.2±0.6		Recommended value (29)
		5.30±1.6	Competitive photochlorination	(32)
		4.10±0.18	UV resonance fluorescence	(30)
		4.3±0.3	FTIR[b]	(31)
		4.20±0.21[c]	VLPR[d]	(23)
$CHBr_2Cl$	2.03±0.14	2.03±0.31		This work
		2.2±0.6		(34)
$CHBr_3$	2.81±0.20	2.81±0.41		This work
		2.8±1.5		Recommended value (29)
		2.7±0.2	FTIR	(33)
		3.04±0.24[c]	VLPR	(23)

[a]Accumulated uncertainties. Rate constants were obtained using methane as the reference compound.
[b]Fourier transform infrared spectroscopy.
[c]Rate constant measured at 303 K.
[d]Very low pressure reactor.

observed. Each kinetic experiment was repeated several times at different reactant concentrations. Conversions of reactants ranged from 30% to 50%. Kinetic plots in Figs. 1 and 2 show the combined results from several experiments. The good linearity of the plots ($r^2 \geq 0.98$) confirms that secondary reactions are negligible. The rate constants for chlorine atom initiated reactions of chlorinated ethenes were measured within the 298–358 K temperature range and at an approximate pressure of 760 torr. The kinetic experiment at each temperature was repeated at least twice. The experimental rate constant ratios have been put on an absolute basis using respective reference rate constants.

Reactions of brominated methanes

For the reactions of bromomethanes, the generally accepted value for the room-temperature rate constant of the reference Cl + CH_4 reaction ($k_{methane}$ = (1.0 ± 0.2) × 10^{-13} in cm^3 molecule^{-1} s^{-1}) was used (28, 29). The room-temperature rate constants for the reactions of bromomethanes are presented in Table 1. The kinetics of the reaction of CH_2Br_2 with chlorine atoms at room temperature is relatively well studied (Table 1), and its rate constant obtained in this work agrees well with the previously published values (23, 29–32), within the uncertainty limits. For the reaction of bromoform, our value is also in agreement with the rate constants from the literature (23, 29, 33). The only value available in the literature for the Cl + $CHBr_2Cl$ reaction rate constant, measured by Bilde et al. (34), is in good agreement with the value reported in the present work.

Reactions of chlorinated ethenes

For the reactions of chlorinated ethenes, the Arrhenius expression for the reference C_2H_4 + Cl reaction rate constant from our previous work (26) (k_{ethene} = (0.39 ± 0.22) × 10^{-11} exp[(966 ± 180)/T] (cm^3 molecule^{-1} s^{-1})) has been used. It should be noted that this Arrhenius expression was obtained at very similar conditions to those used in this work, with both air and N_2 as diluent gases (no considerable differences were found for the rate constants measured in air and N_2) (26). For the room-temperature measurements, the rate constant of k_{ethene} = (10.0 ± 4.0) × 10^{-11} cm^3 molecule^{-1} s^{-1}, calculated from this expression, was used for consistency; it agrees well with the recommended value of k_{ethene} = (10.6 ± 0.3) × 10^{-11} (28, 35).

The relative rate constants (k/k_{ethene}), obtained at room temperature in this work (Table 2), are in good agreement (within the accumulated error bars) with the data reported by Atkinson and Aschmann (21), who also employed the relative rate technique with ethene as a reference compound; the slight disagreements in the absolute values are mainly due to the different reference rate constants used (21). The only case where our rate constant does not agree with the value found by Atkinson and Aschmann (21) is for the *trans*-dichloroethene: the value measured in this work appears to be lower than the literature value. For the trichloroethene reaction, the rate constant measured in the present work is also consistent with the results of Catoire et al. (24).

Chlorinated alkenes are highly reactive toward chlorine atoms: the rate constants of the chlorine-initiated reactions of chlorinated ethenes are greater than those of brominated hydrocarbons by about two orders of magnitude. Radical reactions with unsaturated hydrocarbons proceed via the addition of a radical (Cl in our case) to the double bond forming a carbon-centered radical. This chlorinated alkyl radical formed in the addition reaction rapidly reacts with molecular oxygen to form a peroxy radical, and subsequent reactions lead to the formation of oxygenated chlorine-containing products (6). It should be stressed, however, that the reactions involving unsaturated hydrocarbons are pressure dependent (25, 36, 37); therefore, our results are valid at or near atmospheric pressure.

The temperature dependence studies (Table 2) show that the reactions of chlorinated ethenes have small negative activation energies from approximately –1.5 to –2.0 kcal mol^{-1} (i.e., E_A/R from appoximately –750 to –1000 K^{-1}, Table 3, Fig. 3). Similar small activation energies were observed previously for chlorine-atom reactions with other alkenes, such as ethene (–1.9 kcal mol^{-1}), propene (–1.7 kcal mol^{-1}),

© 2006 NRC Canada

Table 2. Rate constants for the reactions of chloroethenes with chlorine atoms.

Compound	T (K)	k/k_{ref}	k ($\times 10^{13}$ cm^3 molecule^{-1} s^{-1})	Technique	Ref.
1,1-Dichloroethene	273	1.34±0.14	13.4±3.3	GC–FID	This work
	273	1.32±0.01	14.00±0.20	GC–FID	(21)
	318	1.46±0.12	11.9±2.5	GC–FID	This work
	328	1.47±0.09	10.9±2.1	GC–FID	This work
	338	1.49±0.14	10.1±3.4	GC–FID	This work
	348	1.49±0.13	9.3±3.3	GC–FID	This work
***cis*-Dichloroethene**	273	0.91±0.13	9.1±2.3	GC–FID	This work
	273	0.910±0.009	9.65±0.10	GC–FID	(21)
	318	0.97±0.08	7.9±1.9	GC–FID	This work
	328	0.97±0.11	7.2±2.2	GC–FID	This work
	338	0.99±0.10	6.7±2.4	GC–FID	This work
	348	0.99±0.14	6.2±3.2	GC–FID	This work
***trans*-Dichloroethene**	273	0.74±0.11	7.4±1.8	GC–FID	This work
	273	0.904±0.016	9.58±0.18	GC–FID	(21)
	318	0.74±0.10	6.0±1.6	GC–FID	This work
	328	0.74±0.06	5.5±1.4	GC–FID	This work
	338	0.74±0.12	5.0±1.9	GC–FID	This work
	348	0.72±0.11	4.5±1.7	GC–FID	This work
Trichloroethene	273	0.77±0.09	7.7±1.9	GC–FID	This work
	273	0.76±0.01	8.08±0.10	GC–FID	(21)
	273	1.27±0.04	7.20±0.80	FTIR[a]	(24)
	318	0.82±0.12	6.7±2.6	GC–FID	This work
	328	0.85±0.08	6.3±1.9	GC–FID	This work
	338	0.83±0.10	5.6±2.3	GC–FID	This work
	348	0.82±0.07	5.1±1.6	GC–FID	This work

Note: Accumulated uncertainties. Rate constants were obtained using ethene as the reference compound, unless specified otherwise.
[a]Rate constant obtained using ethane as the reference molecule (k_{ethane} = 5.7 × 10^{-11} cm^3 molecule^{-1} s^{-1}, ref. 52).

Table 3. Pre-exponential factors and activation energies for the reactions of chlorine atoms with chloroethenes.

Compound	A ($\times 10^{11}$ cm^3 molecule^{-1} s^{-1})	$E_A R^{-1}$ (K)	T range (K)	Ref.
1,1-Dichloroethene	1.07±0.20	–758±55	298–348	This work
***cis*-Dichloroethene**	0.63±0.07	–799±34	298–348	This work
	9.2±0.3[a,b]	–430±80[a,b]	308–386	(39)
***trans*-Dichloroethene**	0.24±0.05	–1018±28	298–348	This work
	3.1±0.1[a,b]	–680±100[a,b]	308–386	(39)
Trichloroethene	0.46±0.13	–846±83	298–348	This work
	1.1±0.7[b,c]	–1050±350[b,c]	313–406	(40)

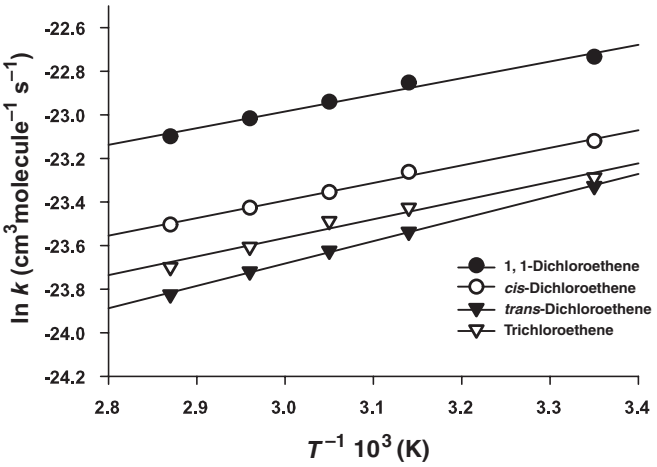
[a]Estimation from three-point temperature dependence.
[b]The values presented are recalculated using the relative rate data from refs. 51 and 52, and the IUPAC recommended (28) (1.4 × 10^{-10} cm^3 molecule^{-1} s^{-1}, T = 200–700 K) value for the reference Cl + C_3H_8 reaction rate.
[c]Estimation from the four-point temperature dependence.

1-butene (–2.0 kcal mol^{-1}), 1-pentene (–1.5 kcal mol^{-1}) (26), and cyclic diene γ-terpenine (–4.2 kcal mol^{-1}) (38). Temperature-dependence studies of the rate constants for chlorine-atom reactions with *cis*-dichloroethene, *trans*-dichloroethene, and trichloroethene were reported in early works by Knox and co-workers (39, 40). The Arrhenius parameters estimated from three- (*cis*-dichloroethene, *trans*-dichloroethene) and four-point (trichloroethene) temperature dependencies taken from refs. 39 and 40 are given in Table 3. It should be noted that the absolute rate constants were recalculated from the relative rate data by Knox and co-workers using a revised rate constant for the reference reaction C_3H_8 + Cl (1.4 × 10^{-10} cm^3 molecule^{-1} s^{-1}, T = 200–700 K) (29). As in the present work, the results of these early studies show negative activation energies for the reaction of chlorine atoms with chlorinated ethenes; however, the absolute values of the activation parameters are significantly different from our results.

As was shown in the case of OH radical addition to unsaturated compounds, the negative activation energies can be explained by reversible formation of a pre-reactive complex

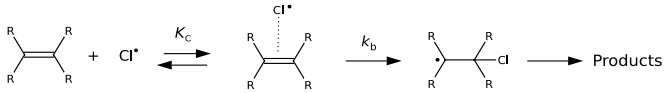
© 2006 NRC Canada

Fig. 3. Arrhenius plots for the reactions of chlorinated ethenes with Cl atoms (298–358 K).



(41). Indeed, the existence of a π-complex formed by the chlorine atom with a C=C double bond has been predicted by quantum-chemical calculations (42). If the reaction mechanism involves the formation of a pre-reactive π-complex at the first step

[5]



then the net rate of the reaction, ν_{net}, is given by

[6] $$\nu_{net} = k_b K_C[\text{alkene}][\text{Cl}] = k_{eff}[\text{alkene}][\text{Cl}]$$

where K_C is the equilibrium constant of the π-complex formation, k_b is the rate constant of the formation of the chlorinated alkyl radical from the pre-reactive complex, and k_{eff} is the effective rate constant. Thus, the dependence of the effective rate constant on the temperature can be expressed as follows (38);

[7] $$k_{eff} = k_b K_C = A\ \exp(-E_A/RT)\ \exp(-\Delta G_C/RT)$$

where ΔG_C is free energy change of the formation of π-complex from the reagents and E_A is the activation energy for the transformation of the π-complex into the chlorinated alkyl radical. Therefore,

[8] $$k_{eff} = A\ \exp(-E_A/RT - \Delta H_C/RT + \Delta S_C/R)$$

where ΔS_C and ΔH_C refer to the entropy and enthalpy change of the formation of the π-complex, respectively. The effective rate constant and activation energy can be described as

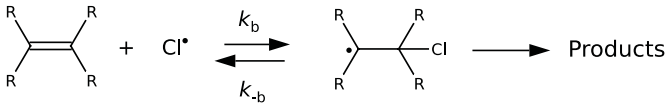
[9] $$k_{eff} = A\ \exp[-(E_A + \Delta H_C)/RT + \Delta S_C/R] = A'\ \exp(-E_{eff}/RT)$$

[10] $$E_{eff} = E_A + \Delta H_C$$

[11] $$A' = A\ \exp(\Delta S_C/R)$$

Consequently, depending on the magnitudes of E_A and ΔH_C values, the effective activation energy (E_{eff}) can become negative (eq. [10]). Braña et al. (42) estimated the binding energy of the chlorine–ethene π-complex from quantum-chemical calculations to be in the range of 3 to 7 kcal mol^{-1}, which makes a negative temperature dependence of the effective rate constant possible, if the activation energy of the π-complex transformation into carbon-centered radical is sufficiently low. Unfortunately, no reliable theoretical data on this reaction are available at the moment because the correct treatment of this transformation requires high-level, multi-reference calculations (43).

[12]



Alternatively, the reversible formation of an unstable radical adduct can account for the negative activation energies in a similar way as the formation of a pre-reactive complex because the enthalpy of formation of a chloroalkyl radical adduct from the reaction of a chlorine atom with an alkene is relatively small (15–20 kcal mol^{-1}) (38).

However, this is less likely because of the high reactivity of chloroalkyl radicals, which would be readily scavenged in reactions with O_2 and (or) other molecules.

Correlation between the reaction rate constants of Cl and OH radicals

We attempted to correlate available experimental rate constants, k_{Cl} (obtained in this work and taken from the literature), for the reactions of chlorine atoms with various hydrocarbons (halogenated or not) with the corresponding rate constants for the OH radical, k_{OH}, (Table 4 and Fig. 4). For the two sets of compounds, saturated and unsaturated, we obtained fairly good correlations: the r^2 values are 0.90 and 0.96, respectively. Obviously, these two sets of rate constants give different correlations because of the different reaction mechanisms: the hydrogen-atom abstraction mechanism for saturated hydrocarbons and the addition to the double bond for unsaturated hydrocarbons (44). Linearity of correlation plots suggests that the reaction mechanism does not change within each series and that the mechanisms of the Cl and OH reactions are similar. It should be mentioned that Bierbach et al. (45) reported very similar correlations among the rate constants for bromine atom reactions and the corresponding reactions of OH, NO_3, and oxygen atoms.

Product studies of chlorine-initiated oxidation of brominated hydrocarbons

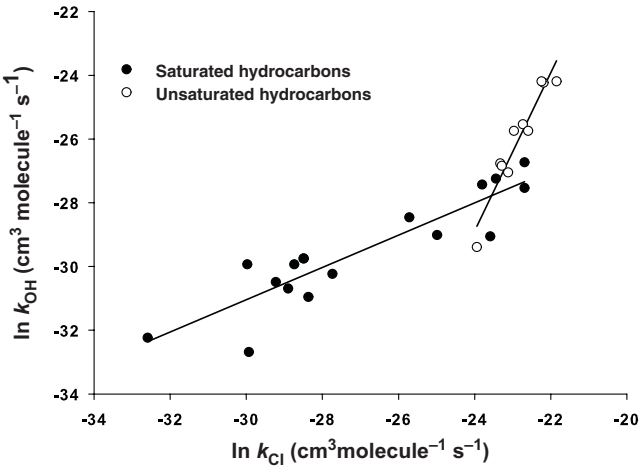
For the reaction of chlorine atoms with $CHBr_3$ (Scheme 1), the only product observed is carbonyl dibromide ($COBr_2$) (Fig. 5). A plausible mechanism involves the initial abstraction of the hydrogen atom from bromoform to yield a brominated alkyl radical (CBr_3). Calculations by McGivern et al. (46) have shown that the reaction of the CBr_3 radical with molecular oxygen to form a peroxy radical (CBr_3O_2) is exoergic (–16.7 kcal mol^{-1}), and its barrier is very small. The initial Br atom abstraction by a chlorine atom from $CHBr_3$ is unlikely because this process is quite endothermic (17 to 18 kcal mol^{-1}) (34). Eventual re-

© 2006 NRC Canada

Table 4. Hydrocarbon rate constants included in the correlation plot.

Compound	k_{Cl} (cm^3 $molecule^{-1}$ s^{-1})	Ref.	k_{OH} (cm^3 $molecule^{-1}$ s^{-1})	Ref.
CH_4	1.0×10^{-13}	(28)	6.4×10^{-15}	(28)
C_2H_6	5.7×10^{-11}	(29)	2.4×10^{-13}	(29)
C_3H_8	1.4×10^{-10}	(29)	1.1×10^{-12}	(29)
$CHBr_3$	2.81×10^{-13}	This work	4.68×10^{-14}	(51)
CH_2Br_2	4.25×10^{-13}	This work	1.20×10^{-13}	(31)
$CHBr_2Cl$	2.03×10^{-13}	This work	5.75×10^{-14}	(51)
CH_3Cl	4.78×10^{-13}	(53)	3.6×10^{-14}	(29)
CH_2Cl_2	3.3×10^{-13}	(29)	1.0×10^{-13}	(29)
$CHCl_3$	9.6×10^{-14}	(29)	1.0×10^{-13}	(29)
CH_2BrCl	4.20×10^{-13}	(48)	1.20×10^{-13}	(34)
CH_3I	9.00×10^{-13}	(54)	7.43×10^{-14}	(49)
1-C_3H_7I	6.60×10^{-11}	(55)	1.47×10^{-12}	(55)
2-C_3H_7I	4.60×10^{-11}	(55)	1.22×10^{-12}	(55)
C_2H_5Cl	6.79×10^{-12}	(56)	4.37×10^{-13}	(51)
CH_3CCl_3	7.0×10^{-15}	(29)	1.0×10^{-14}	(29)
C_2H_5Br	1.41×10^{-11}	(57)	2.51×10^{-13}	(49)
C_4H_9Br	1.40×10^{-10}	(57)	2.45×10^{-12}	(57)
C_2H_4	10.6×10^{-11}	(28)	6.59×10^{-12}	(58)
1,1-$C_2H_2Cl_2$	13.4×10^{-11}	This work	8.12×10^{-12}	(59)
cis-$C_2H_2Cl_2$	9.1×10^{-11}	This work	1.79×10^{-12}	(59)
trans-$C_2H_2Cl_2$	7.4×10^{-11}	This work	2.37×10^{-12}	(59)
C_2HCl_3	7.7×10^{-11}	This work	2.20×10^{-12}	(49)
C_2H_3Cl	1.54×10^{-10}	(60)	6.60×10^{-12}	(61)
C_2Cl_4	4.00×10^{-11}	(62)	1.72×10^{-13}	(49)
C_3H_6	2.31×10^{-10}	(36)	2.99×10^{-11}	(63)
1-C_4H_8	2.19×10^{-10}	(64)	3.12×10^{-11}	(65)
1-C_5H_{10}	3.25×10^{-10}	(66)	3.12×10^{-11}	(65)

Fig. 4. Correlation plots between room temperature rate constants for the reactions of Cl and OH radicals with saturated and unsaturated hydrocarbons.



action of two brominated peroxy radicals yields a brominated alkoxy radical (CBr_3O), which later decomposes into a carbonyl dibromide molecule and a bromine atom. Therefore, our results suggest that the reaction of a chlorine atom with a $CHBr_3$ molecule in atmosphere may lead to the formation of a bromine atom.

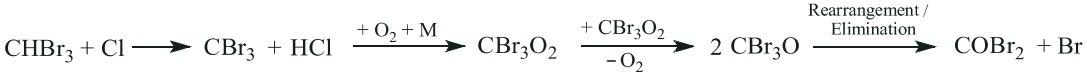
In previous studies of the reaction of a chlorine atom with $CHBr_3$ using FTIR spectroscopy by Kamboures et al. (33) and Weller et al. (47), the formation of $COBr_2$ was also confirmed. In the study performed by Kambanis et al. (23) using a quadrupole mass spectrometer, the experiments were done in a very low pressure reactor in the absence of molecular oxygen; therefore, no $COBr_2$ was observed. However, quantitative production of HCl was reported in this case, which supports the hydrogen-abstraction mechanism as the first step of the reaction.

Our GC–MS study of the chlorine-atom initiated reaction of $CHBr_2Cl$ in the air shows the formation of two products: carbonyl bromochloride (COBrCl), as the main product, and phosgene ($COCl_2$) in small amounts (Fig. 6). The first step of the reaction can involve either hydrogen- or bromine-atom abstraction, with subsequent reaction of the haloalkyl radicals with O_2 and recombination of peroxy radicals, leading to the CBr_2ClO or CHBrClO alkoxy-radicals, respectively (Scheme 2).

Further elimination of a bromine atom from the CBr_2ClO radical leads to the formation of CBrClO, which is the main product observed in this work. The reasons for the formation of small amounts of phosgene ($COCl_2$) detected in our experiments are not clear at the moment. It is possible that side reactions of the radicals formed during the reaction with some impurities in the starting compounds, which are unde-

© 2006 NRC Canada

Scheme 1.



Scheme 2.

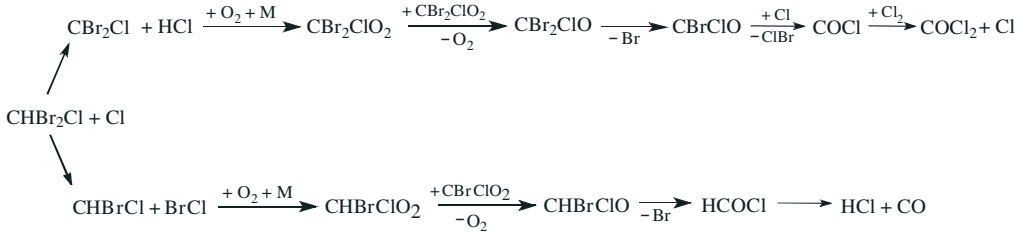


Fig. 5. Chromatogram of the products for the $CHBr_3$ + Cl reaction, and mass spectrum of the product ($COBr_2$).

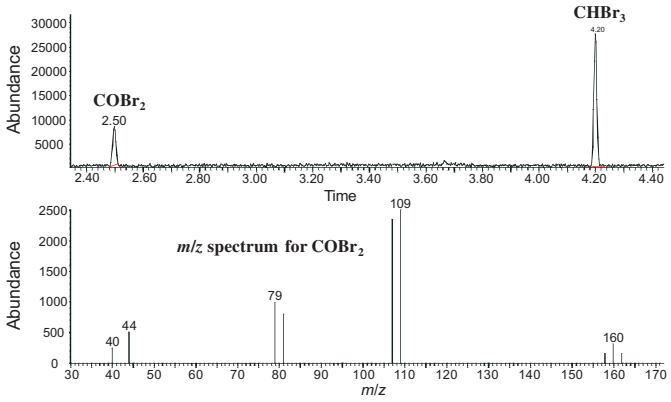
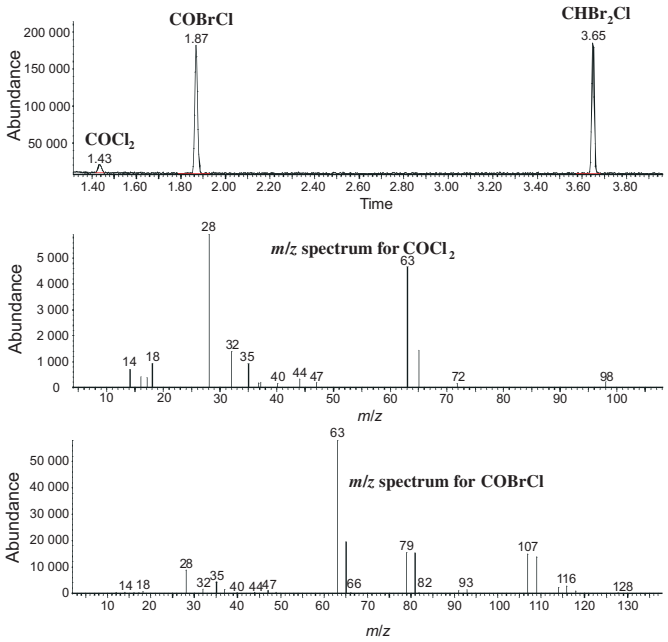


Fig. 6. Chromatogram and mass spectra of the products for the $CHBr_2Cl$ + Cl reaction.



tectable with the GC–MS setup used in this study, are responsible for the $COCl_2$ formation. We also can not exclude side reactions of the radicals between each other.

It should be noted that in the FTIR study by Bilde et al. (34), carbonyl bromochloride was the only product observed for the $CHBr_2Cl$ + Cl reaction. Also, the absence of HCOCl among the products led Bilde et al. (34) to conclude that the bromine-atom abstraction mechanism is not operational because it is has been shown that the CHBrClO alkoxy radical decomposes quickly and quantitatively to HCOCl (48). However, under the experimental conditions used in both studies, HCOCl would probably not be observed because of its thermal instability toward the decomposition into CO and HCl. Therefore, we cannot completely rule out the bromine-atom abstraction route, although it does not seem to play an important role in the reaction, at least at atmospheric conditions.

We also attempted gas-phase product studies for the CH_2Br_2 + Cl reaction, but no visible product peaks were detected even for high (~80%) conversions of CH_2Br_2. This can be explained by the formation of HCOBr as the main product of the reaction, as observed in ref. 31, which also reports that HCOBr easily undergoes thermal decomposition to give CO and HBr, which are not detectable at our experimental conditions. Therefore, the lack of observable products in our work indirectly supports the formation of HCOBr.

Table 5. Tropospheric lifetimes of studied halocarbons.

Compound	τ_{Cl}	τ_{OH}
CH_2Br_2	7–70 years	0.7–7 years
$CHBr_2Cl$	14–140 years	0.3–3 years
1,1-Dichloroethene	1–14 days	7–75 days
cis-Dichloroethene	6–65 days	10–100 days
trans-Dichloroethene	5–50 days	14–140 days
Trichloroethene	5–55 days	13–130 days

Atmospheric implications

Tropospheric lifetimes of the halogenated hydrocarbons with respect to removal by chlorine atoms can be estimated from the reaction rate constants measured in our study and the chlorine-atom concentration (2) of 10^3–10^4 atoms cm^{-3}. Table 5 shows calculated lifetimes for the hydrocarbons studied in this work in the reactions with Cl and OH (assuming OH concentration (31, 49–51) of 10^5–10^6 radical cm^{-3}). Reaction with OH radicals seems to be the major sink for

© 2006 NRC Canada

the brominated hydrocarbons. In the case of chlorinated ethenes, the chlorine-initiated reactions become as important as the OH-initiated reactions. In the MBL, chlorine atoms can indeed act as a potentially important tropospheric oxidant, which also can lead to release and (or) regeneration of halogen atoms.

Concluding remarks

Rate constants of the chlorine-initiated reactions of several saturated and unsaturated halogenated hydrocarbons were measured within the 298–358 K temperature range. Generally, our kinetic results are in agreement with literature values. The reactions of chlorinated ethenes appear to proceed by chlorine-atom addition to the double bond via the formation of a pre-reactive complex, which leads to negative activation energies for the overall process. The product studies are in agreement with the hydrogen-atom abstraction as the first step of the reactions of the brominated hydrocarbons with chlorine atoms and suggest regeneration of halogen atoms, confirming that these reactions may be important in regulating the tropospheric ozone budget. Chlorine-initiated reactions of the halocarbons studied may only become important sinks in the MBL depending on the relative concentrations of Cl with respect to OH.

Acknowledgements

We sincerely thank the following agencies for financial support: Natural Sciences and Engineering Research Council of Canada (NSERC), Fond pour la Formation des Chercheurs et l'Aide à la Recherche (FCAR), Surface Ocean Lower Atmosphere Study (SOLAS-Canada), Canadian Foundation for Innovation (CFI), Environment Canada and Centre for Climate, and Global Change Research (C^2GCR) of McGill University. We would like to thank anonymous reviewers for helpful comments.

References

1. L.A. Barrie, J.W. Bottenheim, R.C. Schnell, P.J. Crutzen, and R.A. Rasmussen. Nature (London), **334**, 138 (1988); J.W. Bottenheim, L.A. Barrie, E. Atlas, L.E. Heidt, H. Niki, R.A. Rasmussen, and P.B. Shepson. J. Geophys. Res. D, Atmos. **95**, 18555 (1990).
2. B.T. Jobson, H. Niki, Y. Yokouchi, J. Bottenheim, F. Hopper, and R. Leaitch. J. Geophys. Res. D, Atmos. **99**, 23 (1994).
3. P.A. Ariya, B.T. Jobson, R. Sander, H. Niki, G.W. Harris, J.F. Hopper, and K.G. Anlauf. J. Geophys. Res. D, Atmos. **103**, 13169 (1998); P.A. Ariya, H. Niki, G.W. Harris, K.G. Anlauf, and D.E.J. Worthy. Atmos. Environ. **33**, 931 (1999); B. Ramacher, J. Rudolph, and R. Koppmann. J. Geophys. Res. D, Atmos. **104**, 3633 (1999).
4. D.O. De Haan, T. Brauers, K. Oum, J. Stutz, T. Nordmeyer, and B.J. Finlayson-Pitts. Int. Rev. Phys. Chem. **18**, 343 (1999).
5. T.E. Graedel and W.C. Keene. Global Biogeochem. Cycles, **9**, 47 (1995); W.C. Keene, A.A.P. Pszenny, D.J. Jacob, R.A. Duce, J.N. Galloway, J.J. Schultz-Tokos, H. Sievering, and J.F. Boatman. Global Biogeochem. Cycles, **4**, 407 (1990); C.A. Taatjes. Int. Rev. Phys. Chem. **18**, 419 (1999); K.L. Foster, R.A. Plastridge, J.W. Bottenheim, P.B. Shepson, B.J. Finlayson-Pitts, and C.W. Spicer. Science (Washington, D.C.), **291**, 471 (2001).
6. B.J. Finlayson-Pitts and J.N. Pitts. Chemistry of the upper and lower atmosphere: Theory, experiments, and applications. John Wiley and Sons. 1999.
7. H.B. Singh and J.F. Kasting. J. Atmos. Chem. **7**, 261 (1988).
8. W.C. Keene. Environ. Toxicol. Chem. (Dordrecht, Netherlands), **1**, 363 (1995).
9. M. Mozurkewich. J. Geophys. Res. D, Atmos. **100**, 14 (1995).
10. R. Vogt, P.J. Crutzen, and R. Sander. Nature (London), **383**, 327 (1996).
11. G.A. Impey, P.B. Shepson, D.R. Hastie, L.A. Barrie, and K.G. Anlauf. J. Geophys. Res. D, Atmos. **102**, 16005 (1997).
12. G.A. Impey, C.M. Mihele, K.G. Anlauf, L.A. Barrie, D.R. Hastie, and P.B. Shepson. J. Atmos. Chem. **34**, 21 (1999).
13. C.W. Spicer, E.G. Chapman, B.J. Finlayson-Pitts, R.A. Plastridge, J.M. Hubbe, J.D. Fast, and C.M. Berkowitz. Nature (London), **394**, 353 (1998).
14. A.A.P. Pszenny, W.C. Keene, D.J. Jacob, S. Fan, J.R. Maben, M.P. Zetwo, M. Springer-Young, and J.N. Galloway. Geophys. Res. Lett. **20**, 699 (1993).
15. B.J. Finlayson-Pitts, C.J. Keoshian, B. Buehler, and A.A. Ezell. Int. J. Chem. Kinet. **31**, 491 (1999).
16. B. Quack and E. Suess. J. Geophys. Res. D, Atmos. **104**, 1663 (1999).
17. P. Warneck. Chemistry of the natural atmosphere. International geophysics series. Vol. 41. Academic Press, New York. 1988.
18. C.E. Canosa-Mas, T.J. Dillon, H. Sidebottom, K.C. Thompson, and R.P. Wayne. Phys. Chem. Chem. Phys. **3**, 542 (2001).
19. L.J. Carpenter and P.S. Liss. J. Geophys. Res. D, Atmos. **105**, 20539 (2000).
20. T. Class and K. Ballschmiter. J. Atmos. Chem. **6**, 35 (1988); L.J. Carpenter, W.T. Sturges, S.A. Penkett, P.S. Liss, B. Alicke, K. Hebestreit, and U. Platt. J. Geophys. Res. D, Atmos. **104**, 1679 (1999).
21. R. Atkinson and S.M. Aschmann. Int. J. Chem. Kinet. **19**, 1097 (1987).
22. J.M. Nicovich, S. Wang, M.L. McKee, and P.H. Wine. J. Phys. Chem. **100**, 680 (1996).
23. K.G. Kambanis, Y.G. Lazarou, and P. Papagiannakopoulos. J. Phys. Chem. A, **101**, 8496 (1997).
24. V. Catoire, P.A. Ariya, H. Niki, and G.W. Harris. Int. J. Chem. Kinet. **29**, 695 (1997).
25. J.S. Pilgrim, A. McIlroy, and C.A. Taatjes. J. Phys. Chem. A, **101**, 1873 (1997).
26. S. Coquet and P.A. Ariya. Int. J. Chem. Kinet. **32**, 478 (2000).
27. O. Sokolov, M.D. Hurley, T.J. Wallington, E.W. Kaiser, J. Platz, O.J. Nielsen, F. Berho, M.-T. Rayez, and R. Lesclaux. J. Phys. Chem. A, **102**, 10671 (1998).
28. R. Atkinson, D.L. Baulch, R.A. Cox, J.N. Crowley, R.F. Hampson, Jr., J.A. Kerr, M.J. Rossi, and J. Troe. IUPAC Subcommittee on Gas Kinetic Data Evaluation for Atmospheric Chemistry [online]. Centre for Atmospheric Science, Cambridge Univeristy, UK. Available from http://www.iupac-kinetic.ch.cam.ac.uk. 2003.
29. S.P. Sander, R.R. Friedl, D.M. Golden, D.M. Kurylo, R.E. Huie, V.L. Orkin, G.K. Moortgat, A.R. Ravishankara, C.E. Kolb, M.J. Molina, and B. Finlayson-Pitts. Chemical kinetics and photochemical data for use in stratospheric modeling, evaluation number 14. JPL Publication 02–25, Jet Propulsion Laboratory, California Institute of Technology, Pasadena, Calif. 2003.
30. T. Gierczak, L. Goldfarb, D. Sueper, and A.R. Ravishankara. Int. J. Chem. Kinet. **26**, 719 (1994).

© 2006 NRC Canada

31. J.J. Orlando, G.S. Tyndall, T.J. Wallington, and M. Dill. Int. J. Chem. Kinet. **28**, 433 (1996).
32. E. Tschuikow-Roux, F. Faraji, S. Paddison, J. Niedzielski, and K. Miyokawa. J. Phys. Chem. **92**, 1488 (1988).
33. M.A. Kamboures, J.C. Hansen, and J.S. Francisco. Chem. Phys. Lett. **353**, 335 (2002).
34. M. Bilde, T.J. Wallington, C. Ferronato, J.J. Orlando, G.S. Tyndall, E. Estupinan, and S. Haberkorn. J. Phys. Chem. A, **102**, 1976 (1998).
35. R. Atkinson and S.M. Aschmann. Int. J. Chem. Kinet. **17**, 33 (1985).
36. J. Stutz, M.J. Ezell, and B.J. Finlayson-Pitts. J. Phys. Chem. A, **101**, 9187 (1997).
37. O. Sokolov, M.D. Hurley, T.J. Wallington, E.W. Kaiser, J. Platz, O.J. Nielsen, F. Berho, M.T. Rayez, and R. Lesclaux. J. Phys. Chem. A, **102**, 10671 (1998); E.W. Kaiser and T.J. Wallington. J. Phys. Chem. **100**, 4111 (1996).
38. Q.K. Timerghazin and P.A. Ariya. Phys. Chem. Chem. Phys. **3**, 3981 (2001).
39. J.H. Knox and J. Riddick. Trans. Faraday Soc. **62**, 1190 (1965).
40. J.H. Knox and K.C. Waugh. Trans. Faraday Soc. **65**, 1585 (1969).
41. D.L. Singleton and R.J. Cvetanovic. J. Am. Chem. Soc. **98**, 6812 (1976); M. Mozurkewich and S.W. Benson. J. Phys. Chem. **88**, 6429 (1984); J.R. Alvarez-Idaboy, N. Mora-Diez, and A. Vivier-Bunge. J. Am. Chem. Soc. **122**, 3715 (2000).
42. P. Braña, B. Menendez, T. Fernandez, and J.A. Sordo. J. Phys. Chem. A, **104**, 10842 (2000).
43. B. Engels, S.D. Peyerimihoff, and P.S. Skell. J. Phys. Chem. **94**, 1267 (1990).
44. R.W.S. Aird, C.E. Canosa-Mas, D.J. Cook, G. Marston, P.S. Monks, R.P. Wayne, and E. Ljungstroem. J. Chem. Soc. Faraday Trans. **88**, 1093 (1992).
45. A. Bierbach, I. Barnes, and K.H. Becker. Int. J. Chem. Kinet. **28**, 565 (1996).
46. W.S. McGivern, J.S. Francisco, and S.W. North. J. Phys. Chem. A, **106**, 6395 (2002).
47. R. Weller, H. Lorenzen-Schmidt, and O. Schrems. Ber. Bunsen-Ges. **96**, 409 (1992).
48. M. Bilde, J. Sehested, O.J. Nielsen, and T.J. Wallington. J. Phys. Chem. A, **101**, 5477 (1997).
49. W.B. DeMore, S.P. Sander, D.M. Golden, R.F. Hampson, M.J. Kurylo, C.J. Howard, A.R. Ravishankara, C.E. Kolb, and M.J. Molina. Chemical kinetics and photochemical data for use in stratospheric modeling, Evaluation Number 12. JPL Publ. 97-4, Jet Propulsion Laboratory, Pasadena, Calif. 1997.
50. R. Atkinson. J. Phys. Chem. Ref. Data, **26**, 215 (1997).
51. C. Chiorboli, R. Piazza, M.L. Tosato, and V. Carassiti. Coord. Chem. Rev. **125**, 241 (1993).
52. P.A. Hooshiyar and H. Niki. Int. J. Chem. Kinet. **27**, 1197 (1995).
53. T.J. Wallington, J.M. Andino, J.C. Ball, and S.M. Japar. J. Atmos. Chem. **10**, 301 (1990).
54. M. Bilde and T.J. Wallington. J. Phys. Chem. A, **102**, 1550 (1998).
55. E.S.N. Cotter, N.J. Booth, C.E. Canosa-Mas, D.J. Gray, D.E. Shallcross, and R.P. Wayne. Phys. Chem. Chem. Phys. **3**, 402 (2001).
56. E.W. Kaiser, L. Rimai, E. Schwab, and E.C. Lim. J. Phys. Chem. **96**, 303 (1992).
57. T. Donaghy, I. Shanahan, M. Hande, and S. Fitzpatrick. Int. J. Chem. Kinet. **25**, 273 (1993).
58. W. Kloepffer, R. Frank, E.G. Kohl, and F. Haag. Chem. Ztg. **110**, 57 (1986).
59. E.C. Tuazon, R. Atkinson, S.M. Aschmann, M.A. Goodman, and A.M. Winer. Int. J. Chem. Kinet. **20**, 241 (1988).
60. R.S. Iyer and F.S. Rowland. J. Phys. Chem. **89**, 3730 (1985).
61. R.A. Perry, R. Atkinson, and J.N. Pitts, Jr. J. Chem. Phys. **67**, 458 (1977).
62. L.P. Thuener, I. Barnes, K.H. Becker, T.J. Wallington, L.K. Christensen, J.J. Orlando, and B. Ramacher. J. Phys. Chem. A, **103**, 8657 (1999).
63. R. Zellner and K. Lorenz. J. Phys. Chem. **88**, 984 (1984).
64. J. Stutz, M.J. Ezell, A.A. Ezell, and B.J. Finlayson-Pitts. J. Phys. Chem. A, **102**, 8510 (1998).
65. R. Atkinson and S.M. Aschmann. Int. J. Chem. Kinet. **16**, 1175 (1984).
66. T.J. Wallington, L.M. Skewes, and W.O. Siegl. J. Phys. Chem. **93**, 3649 (1989).

© 2006 NRC Canada

COMMUNICATION / COMMUNICATION

Diastereoselective addition of chlorotitanium enolates of *N*-acyl thiazolidinethione to activated imines — A novel synthesis of β-lactams[1]

Marike Herold-Dublin and Dennis C. Liotta

Abstract: We report a novel methodology for preparing enantiomerically pure β-lactams, starting from nitriles in diastereomeric ratios up to 10:1. The power of the methodology was demonstrated by the efficient synthesis of the cholesterol absorption inhibitor **SCH 48462**.

Key words: β-lactam, *N*-metalloaldimine, titanium Lewis acids, cholesterol absorption inhibitor.

Résumé : Nous rapportons une nouvelle méthode de préparation des β-lactames énantiomériquement pures à partir de nitriles avec des rapports diastereomériques allant jusqu'à 10 : 1. L'efficacité de la méthode a été démontrée par la synthèse de l'inhibiteur d'absorption du cholestérol **SCH 48462**.

Mots clés : β-lactame, *N*-metalloaldimine, acides de Lewis à base de titane, inhibiteur d'absorption du cholestérol.

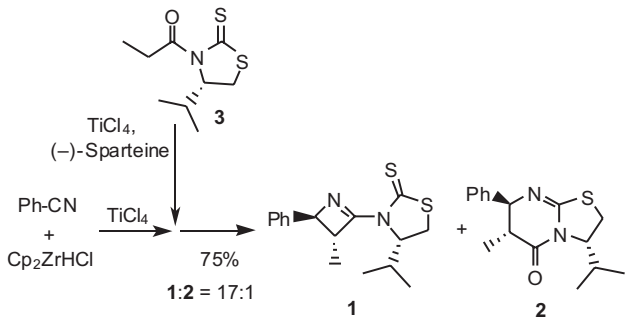
[Traduit par la Rédaction]

Introduction

The biological importance of β-lactams has been clearly demonstrated over the last five decades, particularly regarding the central role they play as antibiotics (1). The search continues for new β-lactams that exhibit a broader spectrum of antibacterial activity and a better resistance profile. Furthermore, the relevance of β-lactams in many important non-antibiotic uses, such as cholesterol absorption inhibitors (2) or a variety of enzyme inhibitors (3–6), continues to expand at a surprising rate.

Recently, our research group reported a diastereoselective, one-pot procedure for preparing novel azetine derivatives (**1**) from readily accessible nitriles (Scheme 1) (7). The diastereoselective additions of chlorotitanium enolates of *N*-propionyl-thiazolidine-2-thione (**3**) to various metalloaldimines, derived from the hydrometallation of the corresponding nitriles, resulted in the preferred formation of azetine **1** over tetrahydropyrimidinone derivatives (**2**) for both enolizable and non-enolizable substrates. Here, we describe an efficient, diastereoselective one-pot procedure for preparing β-lactams starting from nitriles.

Scheme 1. Diastereoselective synthesis of azetine derivatives, starting from nitriles.



Results and discussion

In the synthesis of azetine derivative **1**, a β-lactam side-product could be detected in a low percent. The formation of a β-lactam can mechanistically be explained as follows (Scheme 2).

Received 8 December 2005. Accepted 6 October 2006. Published on the NRC Research Press Web site at http://canjchem.nrc.ca on 5 January 2007.

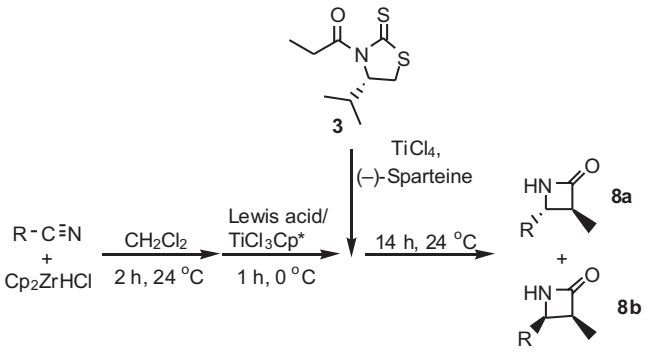
M. Herold-Dublin, D.C. Liotta.[2] Department of Chemistry, Emory University, 1521 Dickey Drive, Atlanta, GA 30322, USA.

[1]This article is part of a Special Issue dedicated to Dr. Alfred Bader.

[2]Corresponding author (e-mail: dliotta@emory.edu).

 doi:10.1139/V06-179 © 2006 NRC Canada

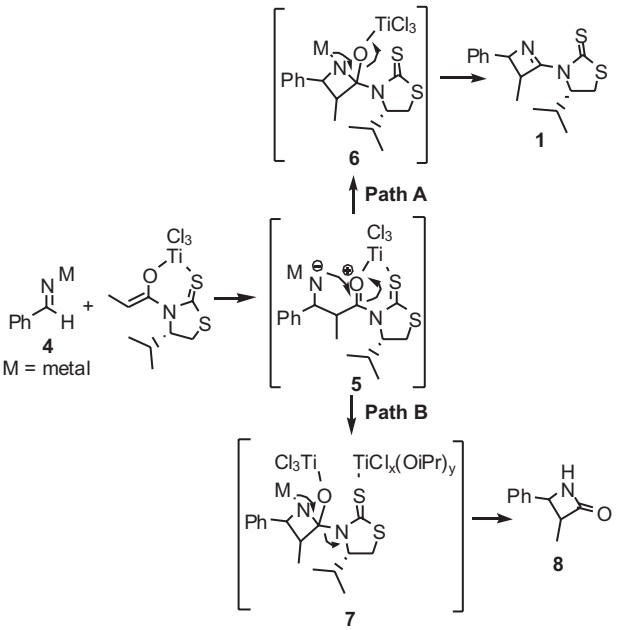
Table 1. Formation of β-lactam in the presence of titanium Lewis acids.



Entry	Nitrile (R)	Lewis acid	Yield (%)[a]	*anti:syn* Ratio[b]
1	Ph	$TiCl_3(OiPr)$	70	4:1
2	Ph	$TiCl_2(OiPr)_2$	89	2:1
3	Ph	$TiCl(OiPr)_3$	80	1:2
4	Ph	$TiCl_3Cp^*$	<50[b]	7:1
5	Ph	$TiCl_3Cp^*/TiCl_3(OiPr)$	81	7:1
6	*p*-MeO–Ph	$TiCl_3Cp^*/TiCl_2(OiPr)_2$	76	7:1
7	*p*-Me–Ph	$TiCl_3Cp^*/TiCl_2(OiPr)_2$	70	6:1
8	*p*-CF_3–Ph	$TiCl_3Cp^*/TiCl_2(OiPr)_2$	74	1:3
9	2-Thienyl	$TiCl_3Cp^*/TiCl_3(OiPr)$	65	8:1

[a]Isolated material after silica gel chromatography.
[b]Determined by ^{1}H NMR analysis of the crude reaction mixture; ~5% error of the stated values.

Scheme 2. Proposed mechanism for the formation of lactam **8** and azetine **1**.



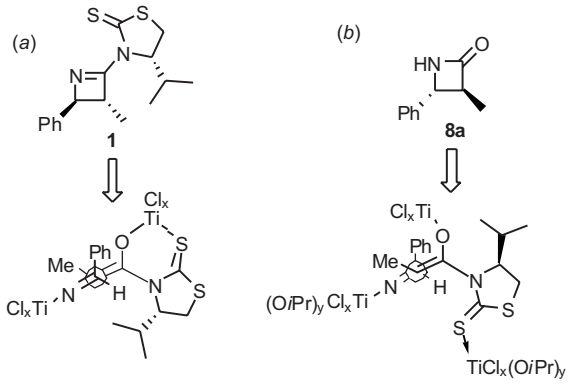
The nitrile is converted in situ to the *N*-metalloaldimine species (**4**), thereby activating it for attack by the titanium enolate. After the C–C bond formation, the resulting zwitterion (**5**) undergoes ring closure by nitrogen attack at the carbonyl group (8).[3] When the oxygen in intermediate (**6**) coordinates with a second titanium Lewis acid, it becomes the preferred leaving group, leading to the formation of the azetine **1** (path A). Alternatively, Lewis acid coordination with the chiral auxiliary converts it to a reasonable leaving group, resulting in the production of the β-lactam (**8**) (path B). In principle, redirecting the reaction to favor the lactam over the azetine could be achieved by employing a Lewis acid that is more thiaphilic than oxaphilic (i.e., one that would preferably coordinate to the thiocarbonyl group of the chiral auxiliary). In this way, the thiazolidine-2-thione could be activated as a leaving group, thereby leading to lactam formation.

In our initial investigation, we chose the thiaphilic Lewis acid, titanium trichloroisopropoxide, and were gratified to find that a mixture of *syn* and *anti* β-lactams was formed in a 70% yield (Table 1, entry 1). Each of these isomers was produced in an enantiomerically pure form as confirmed by chiral HPLC studies. The absolute stereochemistry of the β-lactams was elucidated using X-ray crystallography. The yields (but not the diastereomeric ratios) could be improved by increasing the isopropoxide content of the Lewis acid (Table 1, entries 2 and 3). To increase the diastereoselectivity of the lactam formation, a screening of other titanium Lewis acids was conducted. Although the use of pentamethylcyclopentadienyl titanium trichloride increased the ratio of the lactam diastereoselectivity (Table 1, entry 4),

[3]Consistent with literature results from both Crimmins laboratory (see ref. 8) and our own, we have never observed any stereoinduction resulting from the use of sparteine in titanium addition reactions. We use it primarily because we obtain better chemical yields relative to other tertiaty amines, e.g. triethylamine and Huenig's base.

© 2006 NRC Canada

Scheme 3. Proposed transition-states for the formation of (*a*) azetine and (*b*) lactam.

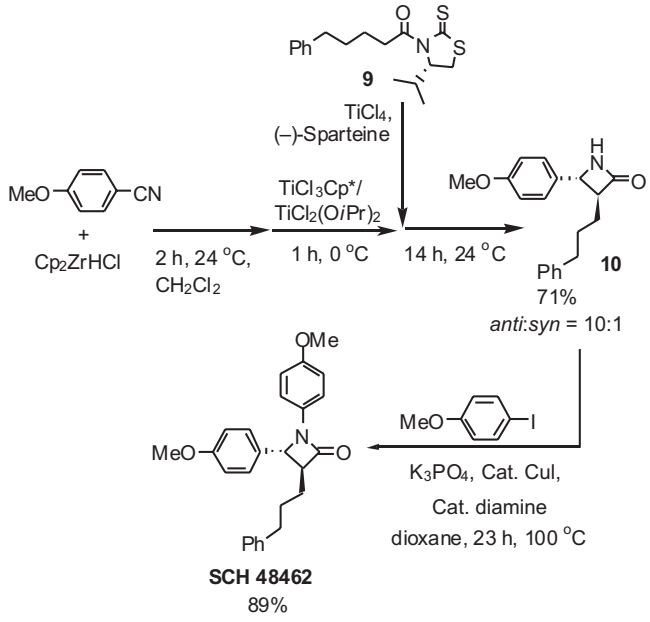


dihydropyrimidinone **2** was also produced in significant quantities (**8**:**2** ratio was 2:1). Because we observed high lactam yields and only traces of dihydropyrimidinone (Table 1, entries 1–3), we speculated that the 6-membered ring formation might be suppressed by adding titanium trichlorodiisopropoxide to the reaction mixture. Indeed, a combination of the Lewis acids, pentamethylcyclopentadienyl titanium trichloride and titanium trichloride isopropoxide, resulted in an efficient formation of the mixture of lactams in a good diastereomeric ratio with nearly complete suppression of dihydropyrimidinone (Table 1, entry 5). The process works well with other non-enolizable nitriles (Table 1, entries 6–9) but resulted in poor yields (0–20%) when attempted with several enolizable nitriles. The diastereoselectivity is highly dependent on the electronic properties of the nitriles, favoring *syn*-lactam fromation for nitriles with electron withdrawing substituents (Table 1, entry 8).

Interestingly, the absolute stereochemistries observed in the formation of *anti*-azetine derivatives are opposite to those observed in the *anti*-lactams (Scheme 3). To explain the difference in the stereochemical outcome, we propose the competing transition-states shown in Scheme 3 as our models. In the azetine formation, we postulate an open transition-state that minimizes dipole interactions (9) between the (*Z*)-titanium enolate (10–12) and the titanium imine.[4] As a consequence, the thiazolidinethione blocks the *re* side of the enolate, and the imine must approach from the *si* side. Diastereomeric transition-states presumably create larger dipole and steric interactions. In case of the lactam formation; however, the coordination of an additional thiaphilic Lewis acid to the thiocarbonyl group of the chiral auxiliary eliminates chelation, thereby allowing it to rotate 180° to minimize dipole effects of the thiocarbonyl group and the carbonyl group of the enolate. As a consequence, the thiazolidinethione blocks the *si* side of the enolate and the imine has to attack from the *re* side. The *syn*-lactam is presumably formed by attack on the other face of the imine.

To probe the scope of this newly developed methodology, we applied it to the synthesis of the cholesterol absorption inhibitor **SCH 48462** (Scheme 4) (2, 13–15). Using the combination of titanium dichlorodiisopropoxide and pentamethyl cyclopentadienyl titanium trichloride, the reaction proceeded in 71% yield and gave improved diastereoselectivity (an *anti* to *syn* ratio of 10:1). In the second step of the synthesis, the β-lactam **10** was readily *N*-arylated (89% yield) by using copper catalysis as described by Klapars et al. (16) (63% overall yield for the two-pot process).

Scheme 4. Synthesis of the cholesterol inhibitor **SCH 48462**.



Conclusions

In summary, we have developed a novel methodology for the preparation of enantiomerically pure β-lactams, starting from nitriles in diastereomeric ratios up to 10:1. The power of the methodology was demonstrated by the efficient synthesis of the cholesterol absorption inhibitor **SCH 48462**.

Experimental section

General procedure for β-lactam formation

The nitrile (1.72 mmol) and Cp_2ZrHCl (445.00 mg, 1.72 mmol) were dissolved in dry dichloromethane (2 mL) in a 50-mL flask and stirred for 2 h under argon at room temperature. The respective titanium Lewis acid (3.45 mmol) was added, and the reaction mixture was stirred for 1 h at 0 °C. During this time, titanium enolate of compound **3** or **9** was generated by dissolving **3** or **9** (1.15 mmol) in dry dichloromethane (5 mL) at 0 °C under argon, then dropwise addition of titanium tetrachloride (0.13 mL, 1.15 mmol), stirring for 5 min, and the addition of (–)-sparteine (0.66 mL, 2.87 mmol). The brown solution was stirred 40 min at 0 °C and then added to the first reaction mixture via a cannula. The reaction mixture was stirred for 14 h at room temperature. It was then quenched with 20 mL saturated aq. ammonium chloride solution with continuous stirring, and dichloromethane (30 mL) and distilled water

[4] We considered and rejected Zimmerman–Traxler-like transition-states primarily because the absolute stereochemistries of the newly formed stereogenic centers would have been derived from an unfavorable *trans* diaxial substituent pattern.

© 2006 NRC Canada

(30 mL) were added. The organic phase was separated, and the aq. phase extracted with dichloromethane (2 × 30 mL). The combined organic phases were washed with saturated aq. sodium bicarbonate solution, then with brine, dried with anhyd. magnesium sulfate, and finally concentrated under vacuum. The product mixture was purified by silica gel flash chromatography (EtOAc:hexanes was 1:10 – 1:3).

For spectroscopic and physical data of **8a**, **8b**, **9**, **10**, and **SCH 48462**, refer to the supplementary data.[5]

Acknowledgments

We would like to thank Dr. Kenneth Hardcastle (Department of Chemistry, Emory University) for obtaining the X-ray structures.

References

1. G. Burton, N.F. Osborne, M.J. Pearson, and R. Southgate. *In* Burger's medicinal chemistry and drug discovery. Vol. 4. *Edited by* M.E. Wolff. Wiley & Sons, New York. 1995. p. 277.
2. D.A. Burnett. Curr. Med. Chem. **11**, 1873 (2004).
3. R.M. Adlington, J.E. Baldwin, B.N. Chen, S.L. Cooper, W. McCoul, G.J. Pritchard, T.J. Howe, G.W. Becker, R.B. Hermann, A.M. McNulty, and B.L. Neubauer. Bioorg. Med. Chem. Lett. **7**, 1689 (1997).
4. W.T. Han, A.K. Trehan, J.J.K. Wright, M.E. Federici, S.M. Seiler, and N.A. Meanwell. Bioorg. Med. Chem. **3**, 1123 (1995).
5. A.D. Borthwick, G. Weingarten, T.M. Haley, M. Tomaszewski, W. Wang, Z. Hu, J. Bedard, H. Jin, L. Yuen, and T.S. Mansour. Bioorg. Med. Chem. Lett. **8**, 365 (1998).
6. W.W. Ogilvie, C. Yoakim, F. Do, B. Hache, L. Lagace, J. Naud, J.A. O'Meara, and R. Deziel. Bioorg. Med. Chem. **7**, 1521 (1999).
7. N.B. Ambhaikar, M. Herold, and D.C. Liotta. Heterocycles, **62**, 217 (2004).
8. (*a*) M.T. Crimmins and K. Chaudhary. Org. Lett. **2**, 775 (2000); (*b*) M.T. Crimmins, B.W. King, E.A. Tabet, and K. Chaudhary. J. Org. Chem. **66**, 894 (2001); (*c*) M.T. Crimmins, B.W. King, and E.A. Tabet. J. Am. Chem. Soc. **119**, 7883 (1997).)
9. H. Danda, M.M. Hansen, and C.H. Heathcock. J. Org. Chem. **55**, 173 (1990).
10. D.A. Evans, J. Bartroli, and T.L. Shih. J. Am. Chem. Soc. **103**, 2127 (1981).
11. D.A. Evans, F. Urpi, T.C. Somers, J.S. Clark, and M.T. Bilodeau. J. Am. Chem. Soc. **112**, 8215 (1990).
12. W.A. Kleschick, C.T. Buse, and C.H. Heathcock. J. Am. Chem. Soc. **99**, 247 (1977).
13. D.A. Burnett. Tetrahedron Lett. **35**, 7339 (1994).
14. D.A. Burnett, M.A. Caplen, H.R. Davis, R.E. Burrier, and J.W. Clader. J. Med. Chem. **37**, 1733 (1994).
15. J.W. Clader, D.A. Burnett, M.A. Caplen, M.S. Domalski, S. Dugar, W. Vaccaro, R.R. Sher, M.E. Browne, H.R. Zhao, R.E. Burrier, B. Salisbury, and H.R. Davis. J. Med. Chem. **39**, 3684 (1996).
16. A. Klapars, X.H. Huang, and S.L. Buchwald. J. Am. Chem. Soc. **124**, 7421 (2002).

[5] Supplementary data for this article are available on the journal Web site or may be purchased from the Depository of Unpublished Data, Document Delivery, CISTI, National Research Council Canada, Ottawa, ON K1A 0S2, Canada. DUD 5116. For more information on obtaining material, refer to http://cisti-icist.nrc-cnrc.gc.ca/irm/unpub_e.shtml. CCDC 628790 and 628791 contain the crystallographic data for this manuscript. These data can be obtained, free of charge, via http://www.ccdc.cam.ac.uk/conts/retrieving.html (or from the Cambridge Crystallographic Data Centre, 12 Union Road, Cambridge CB2 1EZ, UK; fax +44 1223 336033; or deposit@ccdc.cam.ac.uk).

© 2006 NRC Canada